Canadian Journal of Chemistry

Published by
THE NATIONAL RESEARCH COUNCIL OF CANADA

Volume 55 Number 1 January 1, 1977

Journal canadien de chimie

Publié par
LE CONSEIL NATIONAL DE RECHERCHES DU CANADA

Volume 55 numéro 1 janvier 1, 1977

Crystal and molecular structure of difluoroboron *N*-methylacethydroxamate (2,2-difluoro-4,5-dimethyl-1,3-dioxa-4-azonia-2-boranatacyclopent-4-ene)

STEVEN J. RETTIG AND JAMES TROTTER

Department of Chemistry, University of British Columbia, 2075 Wesbrook Place, Vancouver, B.C., Canada V6T 1W5

AND

W. KLIEGEL AND D. NANNINGA

Institut für Pharmazeutische Chemie der Technischen Universität, 33 Braunschweig, Bundesrepublik Deutschland

Received July 9, 1976

STEVEN J. RETTIG, JAMES TROTTER, W. KLIEGEL, and D. NANNINGA. Can. J. Chem. **55**, 1 (1977).

Crystals of difluoroboron *N*-methylacethydroxamate are monoclinic, $a = 5.097(1)$, $b = 10.653(2)$, $c = 11.520(2)$ Å, $\beta = 103.57(2)°$, $Z = 4$, space group $P2_1/c$. The structure was solved by direct methods and was refined by full-matrix least squares procedures to a final R of 0.056 and R_w of 0.077 for 988 reflections with $I \geq 3\sigma(I)$. The structure features a planar five-membered BO_2CN ring. Bond lengths (corrected for libration) are: B—F, 1.374(3) and 1.381(3), O—B, 1.496(3) and 1.497(3), O—N, 1.349(2), O—C, 1.346(2), C—N, 1.298(3) and 1.458(3), and C—C, 1.468(3) Å.

STEVEN J. RETTIG, JAMES TROTTER, W. KLIEGEL et D. NANNINGA. Can. J. Chem. **55**, 1 (1977).

Les cristaux du *N*-méthylacethydroxamate de difluorobore sont monocliniques, $a = 5.097(1)$, $b = 10.653(2)$, $c = 11.520(2)$ Å, $\beta = 103.57(2)°$, $Z = 4$, groupe d'espace $P2_1/c$. On a résolu la structure par des méthodes directes et on l'a affinée par la méthode des moindres carrés (matrice complète) jusqu'à une valeur de R de 0.056 et de R_w de 0.077 pour 988 réflexions avec $I \geq 3\sigma(I)$. La structure comprends un plan cycle BO_2CN à cinq membres. Les longueurs de liasons (corrigées pour la libration) sont: B—F, 1.374(3) et 1.381(3), O—B, 1.496(3) et 1.497(3), O—N, 1.349(2), O—C, 1.346(2), C—N, 1.298(3) et 1.458(3), and C—C, 1.468(3) Å.

Introduction

The formulae **1***a–c*, describing the different tautomeric and mesomeric forms of an isolated molecule of hydroxamic acid with intramolecular chelate type hydrogen bonding, have been discussed for hydroxamic acid and its anions (1–10), and may be summarized in **1***d*, which features chelation of the proton by a bidentate zwitterionic ligand. Replacement of the proton by a metal cation should allow fixation of this structure which is otherwise difficult to establish due to the formation of both inter- and intramolecular hydrogen bonds (4).

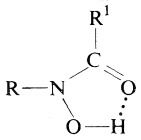

1*a*

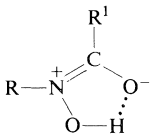

1*b*

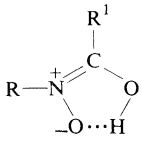

1*c*

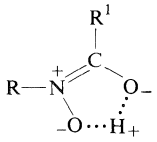

1*d*

Metal hydroxamates are well known (11–15), but structural formulations are (as with hydroxamic acid or hydroxamate anions) still subject to some controversy (6, 15). Spectroscopic data do not provide sufficient information for a definitive formulation. Evidence for at least partial C—N double bond and C—O single bond character is mainly given by X-ray crystallographic studies of organotin (16–18), iron (19), and zinc (20) complexes of hydroxamic acids and a nickel thiohydroxamate (15, 21). Chelated protons are also easily displaced by "pseudo-metal" cations (22) X_2B^+ which are well established (23–27) as remarkable acceptors in the formation of chelate complexes. The bidentate dianionic ligand in **1***d* should be well suited for the synthesis of boron chelates and in fact hydroxamic acids and their *N*-substituted derivatives readily form X_2B-chelates **2** (8, 9, 26, 28–31).[1] The uv spectrum of the anion **3** suggests the presence of C=N double bonding (8, 9) whereas for a cyclic thiohydroxamate the thione form, analogous to **2***a*, is favored but not unambiguously proven (30).

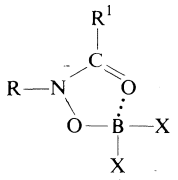

2*a*

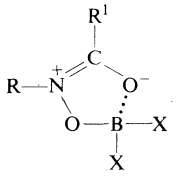

2*b*

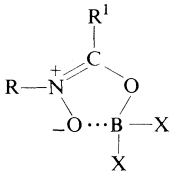

2*c*

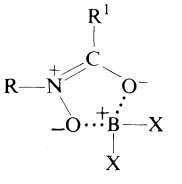

2*d*

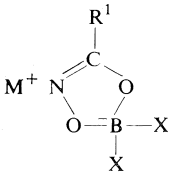

3

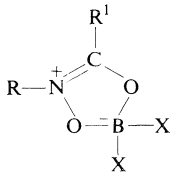

4*a*

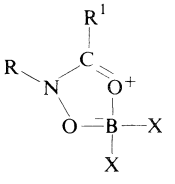

4*b*

[1]W. Kliegel and D. Nanninga, unpublished results.

With the assumption that a betainic structure **4***a* represents the best formal description of the chelates **2***a–d*, the study of complexes of *N*-substituted[2] hydroxamic acids with electron-accepting boron compounds seemed very useful. One of the simplest molecules of this type is the *N*-methylacethydroxamate of the extremely electron-deficient difluoroborenium ion (**2** or **4**, R = R′ = Me, X = F). The ir spectrum of *N*-methylacethydroxamic acid (**1**, R = R′ = Me) (32) displays an absorption around 1625 cm^{-1} which can be assigned to C=O of the hydroxamic or to C=N of the hydroximic form (33). In the difluoroboron chelate **2** or **4***a* this band is shifted to a higher frequency (about 1675 cm^{-1}) into the region of $C{=}N^+$ vibrations of iminium salts, which is a general effect (34) associated with quaternization of a C=N group. The iminium structure **2***b–d* or **4***a* is also supported by the ^{1}H-nmr spectrum, which shows a low field shift of the *N*-methyl protons at δ = 3.70 ppm which can be compared with the values for *N*-methyl protons in nitrones **6** (R = Me) of 3.70 ppm. (δ (ppm) for *N*-methyl protons in *N*-methyl-C-...-nitrones: (*a*) -*tert*-butyl-, 3.65;[3] (*b*) -phenyl-, 3.86 (35); (*c*) -phenyl-, 3.83; -*p*-tolyl-, 3.80; -methyl-C-phenyl-, 3.65; -methyl-C-*p*-tolyl-, 3.65 (36).)

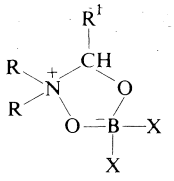

5

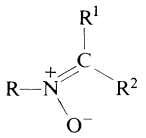

6

Formally **4***a* can be derived by the elimination of R—H from the boron-nitrogen betaine **5** (26, 37), the structure of which has been confirmed by X-ray analysis of the diphenylboron derivative (38). Structure **5** may also be regarded as a formal reduction derivative of **4***a*. Definitive information on the boron-nitrogen betaine character of **4***a* could be expected from an analysis of bond distances. To this end an X-ray crystallographic analysis of difluoroboron *N*-methylacethydroxamate has been undertaken.

[2]In *N*-unsubstituted hydroxamates (R = H) the position of the proton within the complex is unclear (21).

[3]W. Kliegel, unpublished results.

Experimental

2,2-Difluoro-4,5-dimethyl-1,3-dioxa-4-azonia-2-boranata-cyclopent-4-ene

Boron trifluoride – diethyl ether complex (1.42 g, 10 mmol) was added to a solution of 0.45 g (5 mmol) of *N*-methylacethydroxamic acid (39) in 20 ml of anhydrous diethyl ether. A white solid, which had precipitated during 30 min of refluxing, was filtered off after the solution had been allowed to stand at room temperature for 10 h. After recrystallization from ethyl acetate/diethyl ether or chloroform/ethyl acetate 0.53 g (77%) of colourless crystalline material, mp 91 °C, was obtained. *Anal.* calcd. for $C_3H_6BF_2NO_2$: C 26.32, H 4.42, B 7.90, N 10.23; found: C 26.31, H 4.25, B 7.53, N 10.26; ir (1/300 KBr) 1675 cm^{-1} (C=N); ^{1}H-nmr (60 MHz, $CDCl_3$/TMS) δ (ppm) 2.53 (s, 3, C—CH_3), 3.70 (s, 3, N—CH_3).

X-Ray Crystallographic Analysis

Crystals suitable for X-ray analysis were obtained by recrystallization from chloroform/ethyl acetate. The crystal chosen for study was mounted with a^* parallel to the goniostat axis and had dimensions of *ca.* 0.4 × 0.2 × 0.3 mm. Unit-cell and space group data were obtained from film and diffractometer measurements. The unit-cell parameters were refined by a least-squares treatment of $\sin^2\theta$ values for 18 reflections measured on a diffractometer with Cu K_α radiation. Crystal data are:

$C_3H_6BF_2NO_2$ f.w. = 136.9

Monoclinic, $a = 5.097(1)$, $b = 10.653(2)$, $c = 11.520(2)$ Å, $\beta = 103.57(2)°$, $V = 608.0(2)$ Å^3, $Z = 4$, $\rho_c = 1.4954(5)$ g cm^{-3}, $F(000) = 280$ (22 °C, Cu K_α, $\lambda = 1.54178$ Å, $\mu = 14.1$ cm^{-1}). Absent reflections: $0k0$, $k \neq 2n$, and $h0l$, $l \neq 2n$ define uniquely the space group $P2_1/c$ (C_{2h}^5, No. 14).

Intensities were measured on a Datex-automated General Electric XRD 6 diffractometer, with a scintillation counter, Cu K_α (nickel filter and pulse height analyser), and a θ–2θ scan at 4° min^{-1} over a range of (1.80 + 0.86 tan θ) degrees in 2θ, with 10 s background counts being measured at each end of the scan. Data were measured to 2θ = 146° (minimum interplanar spacing 0.81 Å). The intensity of the check reflection, measured every 50 reflections throughout the data collection, remained constant to with ±4%. Lorentz and polarization corrections and check reflection scaling were applied, and the structure amplitudes were derived. No absorption correction was made in view of the low value of μ. Of the 1223 independent reflections measured, 230 had intensities less than $3\sigma(I)$ above background where $\sigma^2(I) = S + B + (0.06S)^2$ with S = scan count and B = time averaged background count. These reflections were given zero weight in the refinement but were included in the structure factor calculations.

The structure was solved by direct methods. Eight sets of signs for 168 reflections with $|E| \geq 1.50$ were determined by a computer program which uses Sayre relationships in an iterative procedure (40). One set of signs was outstanding in that it converged in six cycles to a set having the highest consistency index, 0.72, with 84 positive and 84 negative signs. The positions of the nine nonhydrogen atoms were easily located among the 13 highest peaks on an *E*-map calculated from this set of signs.

Two cycles of isotropic followed by two cycles of anisotropic full-matrix least-squares refinement of the nonhydrogen atoms gave $R = 0.085$. An electron density difference map calculated at this point gave the coordinates of the six hydrogen atoms which were included in all subsequent cycles of refinement with isotropic thermal parameters. The entire structure was refined for six cycles giving a final R of 0.056 and R_w of 0.077 for 978 reflections with $I \geq 3\sigma(I)$ (15 reflections which had $|F_o| - |F_c| > 3\sigma(F)$ were removed from the data set in the final stages of refinement).

The least-squares refinement was based on the minimization of $\Sigma w[|F_o| - |F_c/(1 + gI)|]^2$ where g is the extinction parameter and I the uncorrected intensity. The final value of g was 4.1×10^{-8}. The scattering factors of ref. 41 were used for the nonhydrogen atoms and those of ref. 42 for the hydrogen atoms. Anomalous scattering factors from ref. 43 were used for the nonhydrogen atoms. The anisotropic thermal parameters employed in the refinement are U_{ij} in the expression:

$$f = f^o \exp[-2\pi^2(U_{11}h^2a^{*2} + U_{22}k^2b^{*2} + U_{33}l^2c^{*2} + 2U_{12}hka^*b^* + 2U_{13}hla^*c^* + 2U_{23}klb^*c^*)]$$

where f^o is the tabulated scattering factor and f is that corrected for thermal motion. The weighting scheme: $w = 1/\sigma^2(F)$ where $\sigma^2(F)$ is derived from the previously defined $\sigma^2(I)$ gave uniform average values of $w(|F_o| - |F_c|)^2$ over ranges of $|F_o|$ and was employed in the final stages of refinement.

Near the end of the refinement it became apparent that there may be some ambiguity in the identification of the ring carbon and nitrogen atoms. A parallel refinement with C(1) and N interchanged was carried out. The ratios of the final R and R_w values (for all 993 observed planes) are 1.068 and 1.038 respectively. Hamilton's test (44) indicates that this ratio is significant at a confidence level of >99.5%, indicating correct assignment of C(1) and N and also that these atoms are most likely not disordered. The behavior of the thermal parameters of C(1) and N upon interchange of scattering factors further supports this conclusion. The mean values of U_{ii} (from the parallel refinements mentioned above) for C(1) and N as shown in Fig. 1 are 5.22 and 5.87 Å^2 and when interchanged are 4.75 and 6.56 Å^2 respectively. On the final cycle of refinement the mean parameter shift was 0.05σ and no parameter shift was greater than 0.26σ. The mean error in an observation of unit weight was 1.913. The final positional and thermal parameters appear in Tables 1 and 2 respectively. Measured and calculated structure factors have been placed in the Depository of Unpublished Data.[4]

The ellipsoids of thermal motion for the nonhydrogen atoms are shown in Fig. 1. The thermal motion has been analysed in terms of the rigid-body modes of translation (**T**), libration (**L**), and screw (**S**) motion (45) using the computer program MGTLS. The rms standard error in the temperature factors σU_{ij} (derived from the least-squares analysis) is 0.0011 Å^2. The rms ΔU_{ij} value for the entire molecule treated as a rigid-body is 0.0034 Å^2. This

[4]The structure factor table is available, at a nominal charge, from the Depository of Unpublished Data, CISTI, National Research Council of Canada, Ottawa, Canada K1A 0S2.

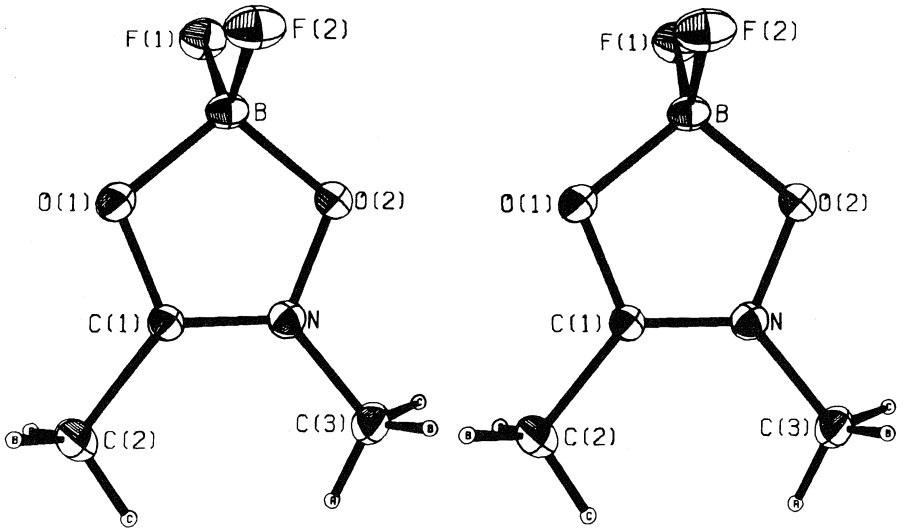

FIG. 1. A stereo view of the difluoroboron *N*-methylacethydroxamate molecule. 50% ellipsoids are shown for the nonhydrogen atoms. Hydrogen atoms have been assigned artificially small temperature factors for clarity.

TABLE 1. Final positional parameters (fractional × 10^4, H × 10^3) with estimated standard deviations in parentheses

Atom	*x*	*y*	*z*
F(1)	7884(3)	1697(2)	3069(1)
F(2)	4611(3)	459(1)	3388(2)
O(1)	4472(3)	2613(2)	3849(1)
O(2)	3467(3)	1980(1)	1882(1)
N	2056(4)	2997(2)	2056(1)
C(1)	2608(4)	3341(2)	3151(2)
C(2)	1410(7)	4346(3)	3718(3)
C(3)	129(6)	3521(3)	1043(3)
B	5199(5)	1636(2)	3063(2)
H(2*a*)	269(14)	497(5)	390(5)
H(2*b*)	97(9)	402(4)	443(4)
H(2*c*)	−1(10)	471(4)	312(4)
H(3*a*)	−64(7)	426(4)	119(3)
H(3*b*)	−87(7)	302(3)	79(3)
H(3*c*)	74(9)	359(4)	32(4)

value indicates some independent motion of the atoms but the derived rigid-body parameters are otherwise physically reasonable.

The appropriate bond distances have been corrected for libration (46, 47), using shape parameters q^2 of 0.08 for all atoms involved. The bond distances not involving hydrogen atoms were also corrected for independent motion based on the ΔU_{ij} (48, 49). Corrected bond lengths appear in Table 3 along with the uncorrected values.

Results and Discussion

Figure 1 shows a general view of the difluoroboron *N*-methylacethydroxamate molecule with the crystallographic numbering scheme and Fig. 2 shows the packing arrangement viewed down *a**. Bond angles are listed in Table 4 and deviations of atoms from the least-squares mean plane defined by the five-membered BO_2CN ring are given in Table 5. The corrected bond distances will be employed throughout the discussion.

The crystal structure (Fig. 2) consists of discrete molecules of difluoroboron *N*-methylacethydroxamate. The shortest nonbonded intermolecular distance not involving hydrogen (F(1)...C(1) $(1 + x, y, z) = 2.961(2)$ Å) corresponds to a normal van der Waals contact. In view of recent comments on the importance of weak hydrogen bonds (50), the geometry of three such C—H...F interactions appears in Table 6. These weak intermolecular C—H...F interactions may be responsible for a close intramolecular contact between H(2*c*) and H(3*a*) (2.22(6) Å), both of which interact with the same fluorine atom (see Table 6).

The five-membered BO_2CN ring is essentially, but not rigorously ($\chi^2 = 10.7$), planar with all five ring atoms lying within ±0.004 Å of the mean plane (see Table 5). The substituent atoms C(2) and C(3) are both significantly displaced from the mean plane of the BO_2CN ring, by −0.082(4) and −0.028(3) Å respectively.

In contrast to the organotin (16–18) and iron (19) hydroxamates in which the metal–oxygen bond from C—O is significantly longer than that from N—O, the O—B bonds in difluoroboron *N*-methylacethydroxamate, 1.496(3) and 1.497(3)

TABLE 2. Final thermal parameters and their estimated standard deviations

(*a*) Anisotropic thermal parameters ($U_{ij} \times 10^3$ Å^2)

Atom	U_{11}	U_{22}	U_{33}	U_{12}	U_{13}	U_{23}
F(1)	51(1)	98(1)	110(1)	2(1)	24(1)	2(1)
F(2)	81(1)	69(1)	130(1)	5(1)	24(1)	28(1)
O(1)	71(1)	83(1)	55(1)	18(1)	9(1)	5(1)
O(2)	69(1)	66(1)	64(1)	9(1)	14(1)	−6(1)
N	58(1)	56(1)	60(1)	0(1)	13(1)	2(1)
C(1)	51(1)	53(1)	53(1)	1(1)	14(1)	−1(1)
C(2)	95(2)	74(2)	77(2)	20(1)	25(1)	−9(1)
C(3)	81(2)	72(2)	67(1)	5(1)	−2(1)	3(1)
B	48(1)	63(1)	75(1)	4(1)	16(1)	5(1)

(*b*) Isotropic thermal parameters ($U \times 100$)

Atom	U (Å^2)	Atom	U (Å^2)
H(2*a*)	15(2)	H(3*a*)	9(1)
H(2*b*)	13(1)	H(3*b*)	8(1)
H(2*c*)	12(1)	H(3*c*)	12(1)

TABLE 3. Bond lengths (Å) with estimated standard deviations in parentheses

(*a*) Nonhydrogen atoms

	Distance			Distance	
Bond	Uncorr.	Corr.	Bond	Uncorr.	Corr.
F(1)—B	1.369(3)	1.381	O(1)—C(1)	1.338(2)	1.346
F(2)—B	1.362(3)	1.374	C(1)—N	1.280(2)	1.298
O(1)—B	1.482(3)	1.496	C(3)—N	1.450(3)	1.458
O(2)—B	1.484(3)	1.497	C(1)—C(2)	1.460(3)	1.468
O(2)—N	1.342(2)	1.349			

(*b*) Bonds involving hydrogen atoms

Bond	Distance	Bond	Distance
C(2)—H(2*a*)	0.92(6)	C(3)—H(3*a*)	0.92(4)
C(2)—H(2*b*)	0.97(5)	C(3)—H(3*b*)	0.75(3)
C(2)—H(2*c*)	0.96(5)	C(3)—H(3*c*)	0.96(4)

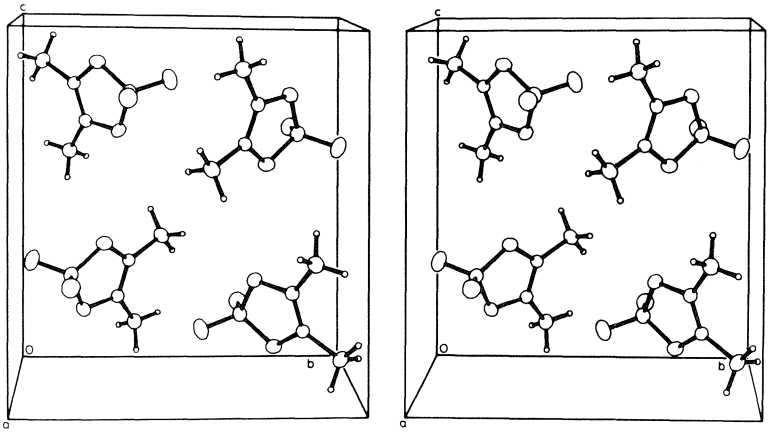

FIG. 2. The crystal structure viewed down a^*.

TABLE 4. Bond angles (deg) with estimated standard deviations in parentheses

(*a*) Nonhydrogen atoms

Bonds	Angle (deg)	Bonds	Angle (deg)
C(1)—O(1)—B	106.5(2)	N —C(1)—C(2)	129.2(2)
N —O(2)—B	106.6(2)	F(1)—B —F(2)	109.0(2)
O(2)—N —C(1)	112.2(2)	F(1)—B —O(1)	110.9(2)
O(2)—N —C(3)	118.4(2)	F(1)—B —O(2)	111.9(2)
C(1)—N —C(3)	129.4(2)	F(2)—B —O(1)	112.1(2)
O(1)—C(1)—N	112.8(2)	F(2)—B —O(2)	110.9(2)
O(1)—C(1)—C(2)	118.0(2)	O(1)—B —O(2)	101.9(2)

(*b*) Angles involving hydrogen atoms

Bonds	Angle (deg)	Bonds	Angle (deg)
C(1) —C(2)—H(2*a*)	106(4)	N —C(3)—H(3*a*)	115(2)
C(1) —C(2)—H(2*b*)	109(3)	N —C(3)—H(3*b*)	108(2)
C(1) —C(2)—H(2*c*)	108(3)	N —C(3)—H(3*c*)	116(3)
H(2*a*)—C(2)—H(2*b*)	111(4)	H(3*a*)—C(3)—H(3*b*)	114(4)
H(2*a*)—C(2)—H(2*c*)	104(4)	H(3*a*)—C(3)—H(3*c*)	110(4)
H(2*b*)—C(2)—H(2*c*)	118(4)	H(3*b*)—C(3)—H(3*c*)	93(4)

TABLE 5. Weighted least-squares plane in the form $lX + mY + nZ = p$ where x, y, z are orthogonal Å coordinates with respect to a, b, and c^*

Ring atoms	BO_2CN
χ^2	10.7
Equation	$0.7876X + 0.5914Y - 0.1731Z = 1.8742$
Deviation (Å) of atoms from plane	
O(1)	0.002(2)
O(2)	−0.001(2)
N	0.003(2)
C(1)	−0.004(2)
B	−0.002(3)
C(2)	−0.082(4)
C(3)	−0.028(3)
F(1)	1.111(2)
F(2)	−1.111(2)

Å, are essentially equal in length. The O—B distances are somewhat longer than those of 1.485(3) and 1.490(3) Å in the related molecule (benzoylacetonato)difluoroboron (51), the difference possibly being due to σ-hybridization effects arising from angular constraints at boron imposed by the different chelate ring sizes (5- *vs.* 6-membered rings). The O—B—O angle in the present structure is 101.9(2)° *vs.* 111.4° in (benzoylacetonato)difluoroboron. The B—F bond lengths (Table 3) do not differ significantly from one another and their mean value of 1.378 Å compares well with the unique distance of 1.376(2) Å in (benzoylacetonato)difluoroboron (51).

The C—N and N—O bonds are shorter and the C—O bond longer than those in all other hydroxamate chelates cited (15–20) as well as in acethydroxamic acid hemihydrate (52). The C—N and N—O distances of 1.298(3) and 1.349(2) Å are similar to corresponding bond lengths of 1.29–1.30 and 1.33–1.37 Å in the *cis*- and *trans*-nickel(II) thiohydroxamate complexes (21). The C—N distance is shorter than that in pyridine-*N*-oxide (53) (1.34 Å) and about the same as that in the dimethylformamide complex $SbCl_5.HCON(CH_3)_2$ (54) (1.29(1) Å), in which at least partial C=N double bond character is assumed. The N—O distance of 1.349(2) Å compares well with the N—O distance of 1.35(2) Å in pyridine-*N*-oxide (53). The C—O distance of 1.346(2) Å is comparable to phenolic C—O distances. The C(1)—C(2) bond length of 1.468(3) Å is shorter than the value of 1.51 Å expected for a $C(sp^2)$—$C(sp^3)$ single bond. Other bond distances in the molecule are as expected.

In view of the equivalence of the two O—B bond distances and their covalent character as deduced from the bond lengths, the overall structure of difluoroboron *N*-methylacethydroxamate appears to be best described by the resonance forms **4***a* and **4***b*. The C—N and C—O bond lengths indicate bond orders of approximately 1.75 and 1.25 respectively, thus the overall structure may be thought of as a 3:1 hybrid of **4***a* and **4***b*, *i.e.* the B–N betainic form **4***a* is the most important contributor to the structure.

TABLE 6. C—H...F interactions*

D—H...A	H...A (Å)	D...A (Å)	∠DHA (deg)	∠XAH (deg)
C(3)—H(3*c*)...F(1)[1]	2.67(4)	3.355(3)	128(3)	108(1)
C(3)—H(3*a*)...F(2)[2]	2.53(4)	3.358(4)	150(3)	138.8(8)
C(2)—H(2*c*)...F(2)[2]	2.69(5)	3.636(4)	169(3)	108.1(9)

*Superscripts refer to atoms at positions: [1] $x-1, 1/2-y, z-1/2$; [2] $-x, 1/2+y, 1/2-z$. The H...F...H angle at F(2) is 50(1)°.

Acknowledgements

We thank the National Research Council of Canada for financial support and the University of British Columbia Computing Centre for assistance.

1. D. MONNIER and C. JEGGE. Helv. Chim. Acta, **40**, 513 (1957).
2. R. T. COUTTS. Can. J. Pharm. Sci. **2**, 1, 27 (1967).
3. Y. K. AGRAWAL and S. G. TANDON. J. Ind. Chem. Soc. **49**, 911 (1972).
4. H. G. AURICH and J. TROSKEN. Chem. Ber. **106**, 3483 (1973).
5. L. BAUER and O. EXNER. Angew. Chem. Int. Ed. Engl. **13**, 376 (1974).
6. O. EXNER. Dan. Tidsskr. Farm. **42**, 145 (1968).
7. G. M. STEINBERG and R. SWIDLER. J. Org. Chem. **30**, 2362 (1965).
8. J. HASE, K. KOBASHI, and K. KUKAMI. Chem. Pharm. Bull. **15**, 534 (1967).
9. K. KOBASHI, N. TERASHIMA, and J. HASE. Chem. Pharm. Bull. **21**, 2303 (1973).
10. N. P. BUU-HOI, G. LAMBELIN, and C. GILLET. Res. Progr. Org. Biol. Med. Chem. **2**, 1 (1973).
11. H. L. YALE. Chem. Rev. **33**, 209 (1943).
12. F. MATHIS. Bull. Soc. Chim. Fr. Doc. 9 (1953).
13. F. UMLAND. Theorie und Praktische Anwendung von Komplexbildern. Akademische Verlagsgesellschaft, Frankfurt. 1971.
14. A. K. MAJUMDAR. *N*-Benzoylphenylhydroxylamine and its analogues. Pergamon Press, Oxford. 1972.
15. S. MIZUKAMI and K. NAGATA. Coord. Chem. Rev. **3**, 267 (1968).
16. T. J. KING and P. G. HARRISON. J. Chem. Soc. Chem. Commun. 815 (1972).
17. P. G. HARRISON and T. J. KING. J. Chem. Soc. Dalton Trans. 2298 (1974).
18. P. G. HARRISON, T. J. KING, and J. A. RICHARDS. J. Chem. Soc. Dalton Trans. 826 (1975).
19. A. ZALKIN, J. D. FORRESTER, and D. H. TEMPLETON. J. Am. Chem. Soc. **88**, 1810 (1966).
20. S. GOTTLICHER and P. OCHSENREITER. Chem. Ber. **107**, 391 (1974).
21. T. SATO, K. NAGATA, Y. TSUKUDA, M. SHIRO, and M. KOYAMA. J. Chem. Soc. B, 989 (1968); 125 (1969).
22. L. H. TOPORCER, R. E. DESSY, and S. I. E. GREEN. Inorg. Chem. **4**, 1649 (1965).
23. E. HOHAUS and F. UMLAND. Chem. Ber. **102**, 4025 (1969).
24. I. BALLY and A. T. BALABAN. Stud. Cerc. Chim. **17**, 431 (1969).
25. A. T. BALABAN. CNRS, Colloq. Int. **191**, 233 (1970).
26. W. KLIEGEL. Organomet. Chem. Rev. Sect. A, **8**, 153 (1972).
27. O. P. SHITOV, S. L. IOFFE, V. A. TARTAKOVSKIJ, and S. S. NOVIKOV. Russ. Chem. Rev. **39**, 905 (1970).
28. A. L. GREEN. J. Chem. Soc. 2566 (1956).
29. F. UMLAND and C. SCHLEYERBACH. Angew. Chem. **77**, 426 (1965).
30. E. HOHAUS and F. UMLAND. Naturwiss. **56**, 636 (1969).
31. F. UMLAND, E. HOHAUS, and K. BRODTE. Chem. Ber. **106**, 2427 (1973).
32. H. ULRICH and A. A. R. SAYIGH. J. Chem. Soc. 1098 (1963).
33. P. A. S. SMITH. The chemistry of open-chain nitrogen compounds. Vol. 2. Benjamin, New York. 1966. p. 68.
34. C. SANDORFY. *In* The chemistry of the carbon–nitrogen double bond. *Edited by* S. Patai. Interscience Publ., London. 1970. p. 37.
35. K. KOYANO and H. SUZUKI. Tetrahedron Lett. 1859 (1968).
36. R. W. KLUIBER and W. DEW. HORROCKS. Inorg. Chim. Acta, **4**, 183 (1970).
37. W. KLIEGEL. Z. Chem. **9**, 112 (1969).
38. S. J. RETTIG, J. TROTTER, and W. KLIEGEL. Can. J. Chem. **52**, 2531 (1974).
39. O. EXNER. Collect. Czech. Chem. Commun. **16**, 266 (1951).
40. R. E. LONG. Ph. D. Thesis, University of California at Los Angeles, Los Angeles, California. 1965.
41. D. T. CROMER and J. B. MANN. Acta Crystallogr. Sect. A, **24**, 321 (1968).
42. R. F. STEWART, E. R. DAVIDSON, and W. T. SIMPSON. J. Chem. Phys. **42**, 3175 (1965).
43. D. T. CROMER and D. LIBERMAN. J. Chem. Phys. **53**, 1891 (1970).
44. W. C. HAMILTON. Acta Crystallogr. **18**, 502 (1965).
45. V. SCHOMAKER and K. N. TRUEBLOOD. Acta Crystallogr. Sect. B, **24**, 63 (1968).
46. D. W. J. CRUICKSHANK. Acta Crystallogr. **14**, 896 (1961).
47. D. W. J. CRUICKSHANK. Acta Crystallogr. **9**, 747 (1956); **9**, 754 (1956).
48. W. R. BUSING and H. A. LEVY. Acta Crystallogr. **17**, 142 (1964).
49. C. K. JOHNSON. *In* Crystallographic computing. *Edited by* F. Ahmed. Munksgaard, Copenhagen. 1970. pp. 207–226.
50. I. D. BROWN. Canadian Crystallography Conference, Hamilton, Ontario, May 1976; I. D. BROWN and R. D. SHANNON. Acta Crystallogr. Sect. A, **29**, 266 (1973).
51. A. W. HANSON and E. W. MACAULAY. Acta Crystallogr. Sect. B, **28**, 1961 (1972).
52. B. H. BRACHER and R. W. H. SMALL. Acta Crystallogr. Sect. B, **26**, 1705 (1970).
53. D. ULKU, B. P. HUDDLE, and J. C. MORROW. Acta Crystallogr. Sect. B, **27**, 432 (1971).
54. L. BRUN and C.-I. BRANDEN. Acta Crystallogr. **20**, 749 (1966).

Structure of the type XXVII *Streptococcus pneumoniae* (pneumococcal) capsular polysaccharide[1]

LARRY G. BENNETT[2] AND CLAUDE T. BISHOP

Division of Biological Sciences, National Research Council of Canada, Ottawa, Ont., Canada K1A 0R6

Received July 26, 1976

LARRY G. BENNETT and CLAUDE T. BISHOP. Can. J. Chem. **55**, 8 (1977).

The type XXVII *Streptococcus pneumoniae* (pneumococcus) capsular polysaccharide contains equimolar amounts of D-glucose, D-galactose, L-rhamnose, 2-amino-2-deoxy-D-glucose, acetyl, pyruvic acid, phosphate, and choline. Structural investigations involving methylation studies and characterization of oligosaccharides obtained by three different degradations indicate the structure of the complete repeating unit to be

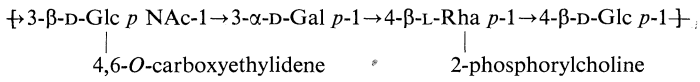

LARRY G. BENNETT et CLAUDE T. BISHOP. Can. J. Chem. **55**, 8 (1977).

Le polysaccharide capsulaire du *Streptococcus pneumoniae* (pneumococcus) de type XXVII contient des quantités équimolaires de D-glucose, de D-galactose, de L-rhamnose, d'amino-2 déoxy-2 D-glucose, d'acétyle, d'acide pyruvique, de phosphate et de choline. Des études structurales impliquant des méthylations et la caractérisation d'oligosaccharides obtenus par trois dégradations différentes indiquent que la structure de l'unité complète de base pourrait être

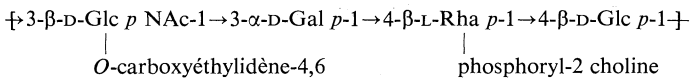

[Traduit par le journal]

Introduction

The type specific capsular polysaccharide of type XXVII *Streptococcus pneumoniae* (pneumococcus) has been reported to contain glucose, galactose, rhamnose, and glucosamine (1) as well as 7.02% acetyl, 3.12% phosphorus (2), and 8.7% pyruvic acid (3). However, the relative amounts, sequence, and linkages of the monosaccharides and the locations of the other substituents are unknown. A number of cross-reactions of anti-XXVII serum have been recorded (4–7) but the only structural bases that could be deduced from these was the common presence of pyruvic acid in the type XXVII polysaccharide and in the cross-reacting polysaccharides. The present paper reports the results of a structural study of the type XXVII polysaccharide as part of a continuing program on structure–specificity relations in polysaccharide antigens of bacteria.

Results and Discussion

The type XXVII polysaccharide was from the collection of pneumococcal polysaccharides prepared by Brown (2). Table 1 gives the results of analysis of this product; the constituents, reported as percent of hydrolysed material, accounted for 91.7% of the polysaccharide on an anhydrous basis.

Elemental analysis of the type XXVII polysaccharide showed twice as much nitrogen as could be accounted for by the glucosamine content (N, calculated from glucosamine, 1.33%; found, 2.7%). The absence of amino acids in hydrolysates precluded protein or peptides as the source of this extra nitrogen, but the initial clue as to its identity was found in the ^{13}C nmr spectrum of the polysaccharide. An outstanding feature of this spectrum (Fig. 1) was the high intensity resonance at 55.1 ppm. The observation that this signal was three times the intensity of the signals from three equivalent methyl-carbons at 18.1, 23.4, and 25.6 ppm (for assignments see below), suggested a structure with

[1]Issued as NRCC No. 15527.

[2]NRCC Research Associate 1975–1977.

TABLE 1. Composition of type XXVII pneumococcal polysaccharide. Elemental analysis: C 37.7, H 6.0, N 2.7, P 2.9; ash 9.9 (%)

Constituents	%	Molar ratio
Acetyl	5.0	1.16
Choline	13.1	1.08
Phosphate	8.9	0.94
Pyruvate	9.0	1.02
Glucose	18.1	1.00
Galactose	16.5	0.92
Rhamnose	17.4	1.06
Glucosamine	17.0	0.95

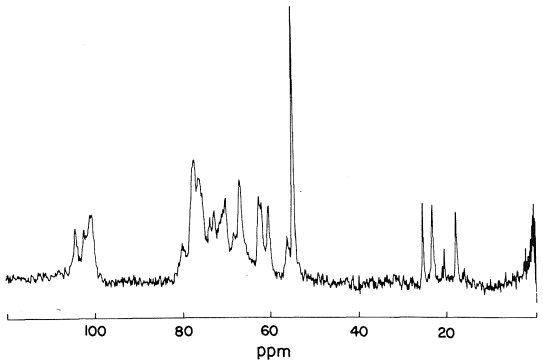

FIG. 1. ^{13}C nmr spectrum of pneumococcal type XXVII polysaccharide.

three carbons of identical electronic environment. Choline is such a compound, and its ^{13}C nmr spectrum exhibits a triplet at 55.0, 55.2, and 55.4 ppm attributed to the trimethylammonium carbons. Thus, the resonance at 55.1 ppm in the spectrum of the type XXVII polysaccharide was assigned tentatively to the trimethylammonium carbons of choline. Confirmation of the presence of choline in acid hydrolysates of the polysaccharide was obtained on thin-layer chromatograms (8) by Dragendorff's reagent (9) and by quantitative analysis (10) that showed a choline content of 13.1%.

The identification of choline, not previously reported as a constituent of the type XXVII polysaccharide, was cause for concern that the preparation was contaminated by C-substance that is known to contain choline (11–13): however, ribitol, *N*-acetyl-D-galactosamine, and *N*-acetyldiaminotrideoxyhexose, the other major components of C-substance (12, 14, 15) were not present. Furthermore, the amount of choline (13.1%) and its stoichiometric relation with the other components (Table 1) indicated that it could not have arisen from a minor contaminant. Finally, the type XXVII polysaccharide gave a single precipitin band on immunodiffusion against homologous antiserum (Fig. 2) and showed a cross-reaction with myeloma proteins specific for phosphorylcholine (16); the resulting spur formation where the precipitin bands merge (Fig. 2*A*) indicated partial identity of reaction (complete cross-over of the bands would have indicated non-identity). Thus, the myeloma proteins and *some* of the homologous antibody proteins had reacted with a common determinant in the polysaccharide. Confirmation that this determinant was phosphorylcholine was given by the ability of that compound to dissolve the precipitin bands formed with the myeloma protein (Fig. 2*B*).

Evidence that the choline was bound to the type XXVII polysaccharide through a phosphodiester linkage was provided by inhibition studies of the homologous precipitin reaction. Table 2 shows the results of inhibition by phosphorylcholine and choline in homologous precipitations of type XXVII and type VIII. While both phosphorylcholine and choline were good inhibitors of the type XXVII system, it was clear from the inhibition at the two lowest concentrations that phosphorylcholine was the better inhibitor. The lack of inhibition in the type VIII homologous precipitation showed that the results for type XXVII were indeed specific and were not caused by non-specific, ionic dissociation of the precipitated complex.

The ^{13}C nmr spectrum (Fig. 1) provided other information in addition to the detection of choline: the methyl carbon region between 15

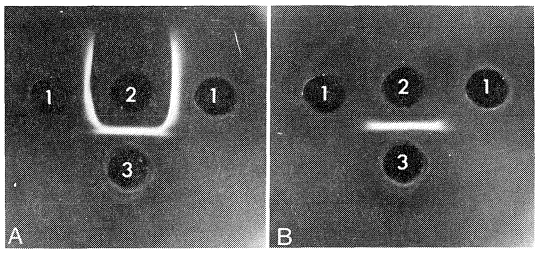

FIG. 2. Immunodiffusion of pneumococcal type XXVII polysaccharide against homologous antiserum and myeloma proteins specific for phosphorylcholine. (*A*) Wells: *1* – myeloma proteins, *2* – type XXVII polysaccharide, *3* – anti-type XXVII serum. (*B*) Same as *A*, 3 h after flooding with phosphorylcholine solution (5 mg/ml).

TABLE 2. Inhibition of type XXVII and of type VIII homologous precipitations by phosphorylcholine and by choline

Inhibitor (μmol)	% Inhibition	
	Type XXVII	Type VIII
Phosphorylcholine		
0.1	9.1	+0.8
0.5	16.3	−3.0
2.0	20.2	+0.8
5.0	22.3	+2.6
20.0	23.9	0.0
Choline		
0.1	3.2	+1.3
0.5	9.3	+1.3
2.0	14.3	−1.3
5.0	21.0	−0.8
20.0	20.7	−2.9

and 30 ppm showed four distinct resonant frequencies. These were assigned to rhamnose *C*-methyl at 18.1 ppm (17), to *N*-acetyl methyl at 23.4 ppm (18), and to pyruvic acid *C*-methyl at 25.6 ppm, the last being made by comparison with the ^{13}C nmr spectrum of methyl 4,6-*O*-carboxyethylidene-α-D-galactopyranoside (19) that showed a *C*-methyl resonance at 26.4 ppm. The equivalent intensities of these three signals and the triple-strength intensity of the choline methyl carbon peak showed that rhamnose, *N*-acetyl glucosamine, pyruvic acid, and choline were present in equimolar amounts in the polysaccharide. The smaller signal at 20.8 ppm in the ^{13}C nmr spectrum might be attributed to the methyl carbons of *O*-acetyl groups (20); however, neither the structural nor serological significance of *O*-acetyl groups was assessed because of the relatively small amount and the uncertainty in detecting their serological role in the presence of the major determinants, pyruvate and phosphorylcholine.

Methylation studies provided information about some of the linkages in the polysaccharide. Complete methylation was difficult to achieve, probably because of the pyruvate and phosphorylcholine substituents. However, three major components were detected by gas–liquid chromatography of the partially methylated alditol acetates. The three derivatives, identified by gas chromatography – mass spectrometry (21), were 1,3,5-tri-*O*-acetyl-2,4,6-tri-*O*-methyl galactitol, 1,4,5-tri-*O*-acetyl-2,3,6-tri-*O*-methyl glucitol, and 1,2,4,5-tetra-*O*-acetyl-3-*O*-methyl rhamnitol in a ratio of 1:1:0.6. Two smaller components were identified as 1,4,5-tri-*O*-acetyl-2,3-di-*O*-methyl rhamnitol and 1,3,4,5-tetra-*O*-acetyl-2-*O*-methyl rhamnitol. The sum of all rhamnitol derivatives was equal to an equimolar ratio with respect to the galactitol and glucitol derivatives. These results indicated that glucose and galactose were present as 1→4 and 1→3 linked units, respectively. The presence of 3-*O*-methyl rhamnitol as a major component indicated that rhamnose was disubstituted at C-2 and C-4, and was either a branch point or the site of a non-sugar substituent. As no products representing a non-reducing terminal unit were detected, it was concluded that the polysaccharide was not branched. Reported difficulty in methylation of phosphorylated sugars, and problems of phosphate migration during methylation (22), provide a probable interpretation of the rhamnose derivatives that were found. Thus, the 3-*O*-methyl rhamnitol and the smaller quantities of the 2,3-di-*O*-methyl and 2-*O*-methyl derivatives could have arisen from a 1→4 linked rhamnose residue that bore a phosphorylcholine group at C-2. Dephosphorylation would account for the 2,3-di-*O*-methyl and a 2→3 phosphate migration would yield the 2-*O*-methyl rhamnitol. Each of these reactions would be expected to occur to some extent under the strongly basic conditions of methylation. This interpretation was supported by oxidation of the dephosphorylated polysaccharide by periodate as described below.

The conditions under which the three non-sugar substituents, pyruvic acid, choline, and phosphate, could be removed from the polysaccharide provided information about their modes of linkage. Hydrolysis by acid (0.01 *N* hydrochloric at 100 °C) released pyruvic acid but choline and phosphate were stable. Gel chromatography showed that depyruvylation caused some degradation by hydrolysis of either glycosidic bonds or phosphodiester linkages between sugar units. Incubation of the depyruvylated product with alkaline phosphatase did not release phosphate, thus eliminating the latter alternative. Alkaline hydrolysis (0.01 *N* sodium hydroxide at 100 °C) released choline, but pyruvate and phosphate were stable. This lability of choline and stability of phosphate has been observed with phosphorylcholine groups in C-substance (12).

Dephosphorylation of the native type XXVII polysaccharide by 48% hydrofluoric acid at

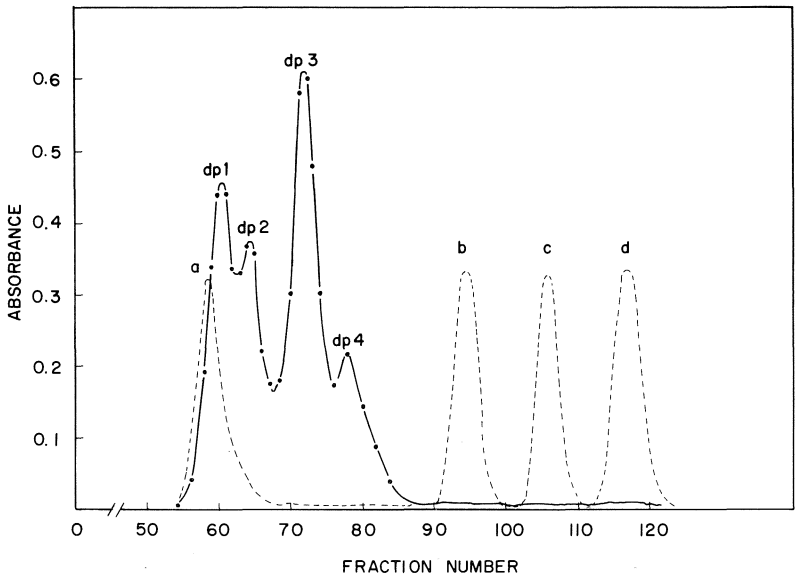

FIG. 3. Bio-Gel P-2 chromatography of dephosphorylated pneumococcal type XXVII oligosaccharides (●—●, phenol-sulfuric assay) and standards [---, (*a*) blue dextran, (*b*) 3-*O*-(2-acetamido-2-deoxy-β-D-glucopyranosyl)-L-rhamnose, (*c*) 2-acetamido-2-deoxy-D-glucose, (*d*) D-galactose].

4 °C (23) yielded a mixture of oligosaccharides that was resolved by gel filtration in Bio-Gel P-2 (Fig. 3). The major component (dp 3) was a tetrasaccharide that contained equimolar proportions of glucosamine, galactose, glucose, rhamnose, and pyruvate but no choline or phosphate. Oxidation of this by periodate, followed by reduction and hydrolysis, yielded glucosamine, galactose, pyruvic acid, glycerol, and 4-deoxyerythritol. The last was identified by gas chromatography – mass spectrometry of its triacetate as compared with a standard obtained from 4-*O*-β-D-glucopyranosyl-L-rhamnose (24) by the same sequence of reactions. The 4-deoxyerythritol could have arisen only from a 4-*O*-substituted rhamnose residue in the dephosphorylated tetrasaccharide and the point of linkage in the linear polymer was thereby established. Furthermore, as the rhamnose in the polysaccharide was not susceptible to periodate before dephosphorylation and yielded mainly 3-*O*-methyl rhamnose on methylation, the phosphorylcholine was located at the C-2 hydroxyl of this sugar. Oxidation of the dephosphorylated tetrasaccharide by periodate also contributed information about the sequence of sugars. The glycerol in the hydrolysate after reduction must have come from glucose, the only sugar other than rhamnose to be oxidized. The glucose must therefore have been the nonreducing terminal unit in the oligosaccharide; a 1→6 linked glucose residue that would also have given rise to glycerol was ruled out because the results of methylation showed that glucose was 4-*O*-linked in the repeating unit. Similarly, galactose was 3-*O*-substituted in the repeating unit (methylation results) and could not represent the reducing end of the tetrasaccharide because it would then have been susceptible to oxidation by periodate. Degradation of the native polysaccharide described below gave a glucosaminylgalactose disaccharide that located the amino sugar as being attached glycosidically (1→3) to galactose. The tetrasaccharide sequence was therefore glucosyl-glucosaminyl-galactosyl-rhamnose.

The evidence so far showed that in the repeating unit glucose and galactose were glycosidically monosubstituted, and rhamnose was substituted by a glycosidic bond at the 4-*O*-position and by phosphorylcholine at the 2-*O*-position. Thus glucosamine was the only residue that could bear the pyruvate substituent. As the pyruvate was stable in alkali it must have been present as a ketal bridging the 3,4, 3,6, or 4,6 hydroxyls with the latter most likely for steric reasons. The presence of pyruvate and glycosidic attachment of the adjacent sugar residue to the

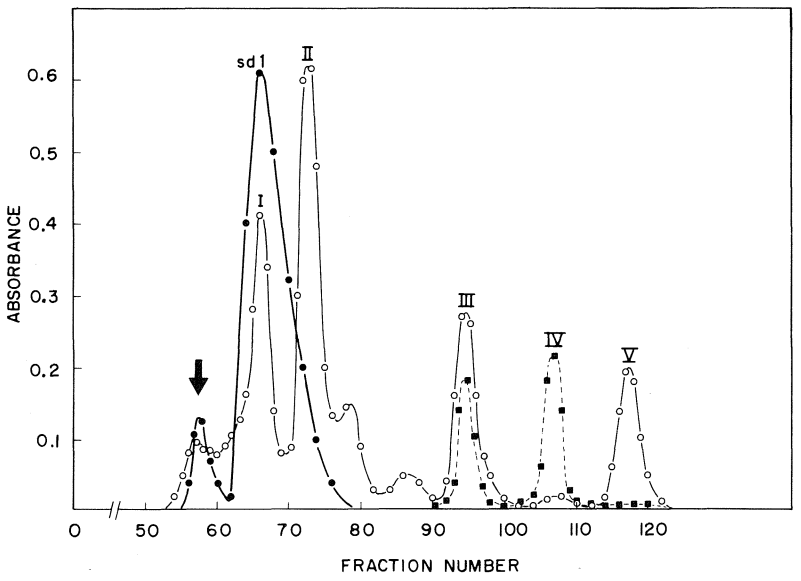

FIG. 4. Bio-Gel P-2 chromatography of hydrolysates (*a*) and (*b*) of periodate oxidized, reduced, pneumococcal type XXVII polysaccharide. Hydrolysate (*a*) ●—●; hydrolysate (*b*) ○—○ (phenol–sulfuric) and ■---■ (amino sugar). The arrow indicates the void volume.

remaining hydroxyl would mean that glucosamine was fully substituted in the native polysaccharide. In support of this, it was noted that no methyl ethers of glucosamine were identified in the methylation analysis.

Confirmation of the foregoing deduction was obtained by the following degradations. The native polysaccharide, when oxidized by periodate, consumed 1 mol of oxidant per 4 mol of monosaccharide. Analysis of the products after reduction and hydrolysis showed that all the glucose had been oxidized and had given rise to erythritol; a direct confirmation of the methylation study showing that glucose was monosubstituted glycosidically at the 4-*O*-position. Periodate oxidation of the 85% depyruvylated polysaccharide (0.01 *N* hydrochloric acid, 60 min, 100 °C) gave the same results as the native polysaccharide. Thus, depyruvylation did not expose a glycol group and the possibility that pyruvate was linked in glucosamine as a 3,4-ketal was ruled out.

The periodate-oxidized, reduced, native polysaccharide was subjected to mild hydrolysis (25) under two sets of conditions: (*a*) 1 *N* hydrochloric acid at 23 °C for 24 h, (*b*) 0.1 *N* hydrochloric acid at 100 °C for 1 h. The products of these partial hydrolyses were separated by elution from Bio-Gel P-2 (Fig. 4). Hydrolysis (*a*) gave a single oligosaccharide (peak sd 1, Fig. 4) in about 90% yield. This product contained equimolar amounts of glucosamine, galactose, rhamnose, erythritol, phosphate, choline, and pyruvate. It was therefore an erythritol glycoside of a trisaccharide that represented the intact repeating unit of the polysaccharide with erythritol in the position of the oxidized glucose residue. Further periodate oxidation, reduction, and hydrolysis of this non-reducing erythritol glycoside resulted in the loss of erythritol with the concomitant appearance of glycerol. However, when the compound was depyruvylated (0.01 *N* hydrochloric acid at 100 °C for 1 h) and then exposed to periodate, erythritol disappeared as before but there was also loss of glucosamine that corresponded quantitatively with the amount of depyruvylation. Because depyruvylation of the native polysaccharide did not expose glucosamine to periodate as it did in the erythritol glycoside, it was concluded that glucosamine formed the other non-reducing terminal unit in the latter. Thus, the oxidation of glucosamine in the depyruvylated erythritol glycoside must have occurred at adjacent hydroxyl groups, one of which was exposed by the hydrolysis of the oxidized polysaccharide, the other by the subsequent depyruvylation. The most likely interpretation was that glucosamine was 3-*O*-linked

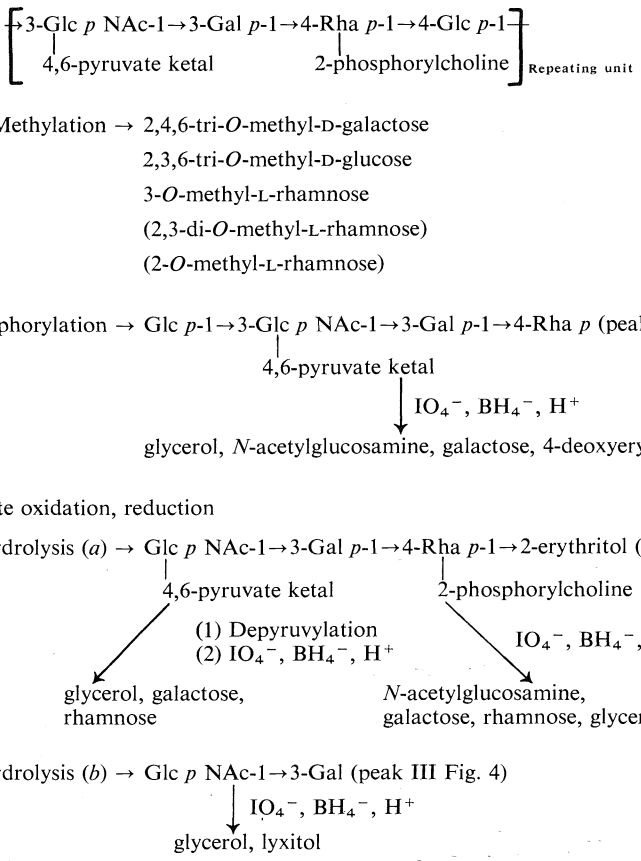

FIG. 5. Structural analysis of pneumococcal type XXVII polysaccharide.

in the polysaccharide and carried a 4,6-pyruvate ketal. The alternative of a 4-*O*-linked glucosamine with a 3,6-pyruvate ketal was considered unlikely on steric grounds, nor have 3,6-pyruvate ketals been found in polysaccharides.

Hydrolysis (*b*) of the oxidized, reduced polysaccharide gave a mixture that was resolved into five components (peaks I–V, Fig. 4). Peaks IV and V contained *N*-acetylglucosamine and galactose respectively. Peak III was a disaccharide composed of *N*-acetylglucosamine and galactose. Borohydride reduction converted the galactose moiety to galactitol showing that the compound was a glucosaminyl-galactose. Periodate oxidation, reduction, and hydrolysis yielded glycerol and lyxitol. Clearly, the glycerol came from the non-reducing terminal *N*-acetylglucosamine and the lyxitol must have arisen from oxidation (at the C_1—C_2 glycol) of a 3-*O*-linked galactopyranose residue. The characterization of this disaccharide, together with the identification of the reducing and non-reducing terminal residues in the tetrasaccharide from dephosphorylation as rhamnose and glucose respectively, unequivocally established the sequence in the repeating unit. The results of this structural analysis are summarized in Fig. 5.

The relative susceptibilities of the sugars in the polysaccharide to oxidation by chromium trioxide were investigated to permit assignment of anomeric configurations to the glycosidic bonds (26–28). It was necessary to depyruvylate and dephosphorylate the polysaccharide so that a sufficient number of acetyl groups could be introduced for extractability into chloroform after the oxidation. Even though this caused some depolymerization, enough glycosidic bonds were left intact to permit a clear interpretation of the results. Thus, glucosamine, glucose, and rhamnose were oxidized and their glycosidic linkages were therefore in the β-configuration. The galactose was not oxidized so its glycosidic linkage was α.

The enantiomorphic forms of glucose and

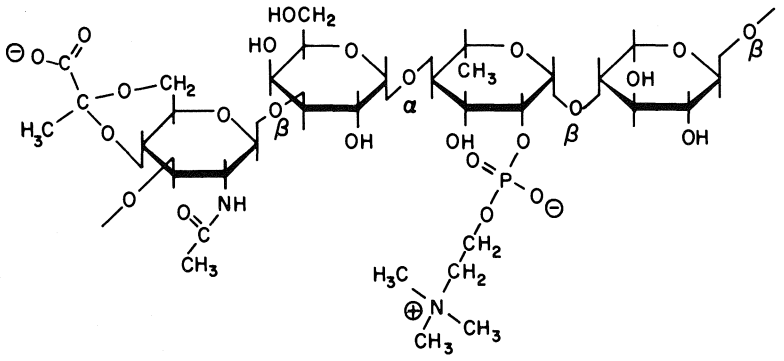

FIG. 6. The repeating unit of pneumococcal type XXVII capsular polysaccharide. The configuration at the asymmetric carbon of the pyruvate ketal has not yet been determined.

galactose were established as D by the susceptibility of these two sugars to enzymic oxidation by their specific oxidases. If it is assumed that the glucosamine is also D, a reasonable assumption because the L-form has not been found in nature, then the enantiomorphic form of rhamnose may be deduced from the specific rotation of the polysaccharide ($[\alpha]_D$ +53.2°) (2). This rotation may be regarded as the sum of rotations of the four constituent sugars in the anomeric configuration given above. For the corresponding methyl glycosides these are: β-D-glucopyranoside −34.2°, α-D-galactopyranoside +179.3°, β-D-glucosamine −44°, and β-L-rhamnopyranoside +95.4° for a total contribution of (196.5°)/4 = +49.1°. The corresponding calculated rotation using the value for β-D-rhamnopyranoside is +5.7°. It was therefore concluded that rhamnose was present as the L-enantiomer and the full structure of the repeating unit is shown in Fig. 6.

Experimental

Biological Materials

The pneumococcal type XXVII capsular polysaccharide and type specific anti-XXVII and anti-VIII horse sera were generously provided by Dr. Kenneth Amiraian, New York State Department of Health, Albany, New York. Mouse serum from BALB/c mice bearing plasmacytoma MOPC603, as the source of myeloma proteins specific for phosphorylcholine, was a gift from Dr. N. M. Young of these laboratories.

^{13}C Nuclear Magnetic Resonance

The spectrum of the type XXVII polysaccharide (100 mg in 1.0 ml D_2O) was measured in a 12 mm tube at 30 °C on a Varian XL-100 spectrometer at 25.16 MHz. Spectra were obtained using a pulsed Fourier transform mode with complete proton decoupling. Chemical shifts are reported as parts per million downfield relative to an external tetramethylsilane standard. The ^2H resonance of the D_2O provided the field frequency lock. Spectra of phosphorylcholine and of methyl 4,6-*O*-carboxyethylidene-α-D-galactopyranoside (19) in D_2O were determined in 10 mm tubes on a Varian CFT-20 spectrometer.

Immunodiffusion

Double diffusion studies (29) were done at 4 °C in plastic petri plates (1.5 × 5 cm) containing 1% agarose in 0.8% sodium chloride solution. The precipitin bands (Fig. 2) were allowed to form during 4 days. The plate was then flooded with 5 ml of aqueous phosphorylcholine (5 mg/ml). Disappearance of the precipitin bands specific for phosphorylcholine determinants was complete in 3 h (Fig. 2*B*).

Quantitative Precipitins

The relative amounts of antigen and antiserum used for inhibition studies were those at maximum precipitation. The system used was 0.5 *M* sodium bicarbonate, p*H* 7.5 (100 µl), undiluted antiserum (100 µl), antigen (25 µg in 100 µl water), and varying amounts of inhibitor in water (200 µl). Mixtures were incubated at 4 °C for 5 days after which the precipitates were washed twice with 0.1 *M* sodium bicarbonate, p*H* 7.5 (1.0 ml), and dissolved in 0.1 *N* sodium hydroxide for estimation of protein (30).

Other Analytical Methods

For analysis of neutral sugars the polysaccharide was hydrolysed by *N* hydrochloric acid at 100 °C for 10 h. The hydrolysate was neutralized (Dowex 1-X8, HCO_3^- form) and concentrated by evaporation under diminished pressure at 40 °C. Sugars were separated by thin-layer chromatography on silica gel 60 in ethyl acetate:isopropanol:acetic acid:water, 3:5:1:1, and analysed by a micromodification (31) of the phenol – sulfuric acid method (32) with the minor but significant change that the silica gel was simply pelletized by centrifugation before absorbances were measured.

Alditols from studies on periodate oxidation and their methyl ethers from methylations were analysed by gas–liquid chromatography with a Hewlett-Packard Model 402 gas chromatograph. The glass U-tube columns (150 × 0.3 cm) were packed with 3% ECNSS-M on 80–100 mesh Gas-Chrom Q (33) which was also used in a Finnigan Model 9500 gas chromatograph-3100D mass spectrometer when that system was used to identify products (21).

TABLE 3. Characterization of partially methylated alditols

Alditol	T_R*	*m/e*	Molar ratio
1,4,5-Tri-*O*-acetyl-2,3-di-*O*-methyl rhamnitol	1.00	117, 203	0.2
1,3,4,5-Tetra-*O*-acetyl-2-*O*-methyl rhamnitol	1.54	117	0.2
1,2,4,5-Tetra-*O*-acetyl-3-*O*-methyl rhamnitol	1.88	189, 203	0.6
1,3,5-Tri-*O*-acetyl-2,4,6-tri-*O*-methyl galactitol	2.26	45, 117, 161, 233	1.0
1,4,5-Tri-*O*-acetyl-2,3,6-tri-*O*-methyl glucitol	2.53	45, 117, 233	1.0

*Retention times relative to that of 1,5-di-*O*-acetyl-2,3,4,6-tetra-*O*-methyl glucitol.

Analyses for amino sugars and amino acids were done on an automatic amino acid analyzer following hydrolysis by 3 *N* hydrochloric acid at 100 °C for 10 h. Phosphate (34), pyruvic acid (35), and choline (10) were assayed by published procedures. Acetyl was determined as acetic acid by gas chromatography on Chromosorb 102 with propionic acid as an internal standard.

Methylation

Because of its limited solubility in dimethyl sulfoxide the type XXVII polysaccharide (5 mg) was acetylated prior to methylation. The acetylation and methylations by the Hakomori (36) and Purdie and Irvine (37) methods were as described by Choi and Meyer (38). Two methylations by the Hakomori procedure gave incomplete methylation as shown by hydroxyl absorption in the infrared and by a multiplicity of components after hydrolysis. The partially methylated polysaccharide was therefore remethylated with methyl iodide:methanol (1:1) and silver oxide (37). The product, recovered by extraction with chloroform and methanol, was dissolved in 80% aqueous methanol and deionized (mixed resin column: Rexyn 101 (H^+) and Dowex 1 (OH^-)). Infrared spectroscopy showed only minor hydroxyl absorption, and three major components were present after hydrolysis. The methylated polysaccharide was hydrolysed, first in 2.5% methanolic hydrogen chloride at 100 °C for 20 h, then in 2 *N* hydrochloric acid at 100 °C for 6 h. The hydrolysis products were reduced ($NaBH_4$), acetylated, and analysed by gas chromatography – mass spectrometry (21). The characterization of the partially methylated alditols is detailed in Table 3.

Hydrolysis of Substituent Groups

(i) Acid Hydrolysis

The type XXVII polysaccharide (8 mg) was dissolved in 0.01 *N* hydrochloric acid (8.0 ml) and the solution was heated at 100 °C. At intervals the solution was cooled and aliquots (100 and 400 µl) were removed, the former for analysis of free pyruvic acid (35). The other aliquot was neutralized (4 µl of *N* sodium hydroxide) and incubated 5 days with alkaline phosphatase (100 µl, 0.1% solution in 0.5 *M* Tris, p*H* 10.3), after which 200 µl was assayed for free choline (10) and 300 µl was assayed for free phosphate (34).

(ii) Alkaline Hydrolysis

The same quantities and conditions used for acid hydrolysis were employed for hydrolysis of the polysaccharide in 0.01 *N* sodium hydroxide. Release of pyruvic acid, choline, and phosphate were monitored as described above.

(iii) Dephosphorylation

A solution of the polysaccharide (10 mg) in 48% hydrofluoric acid kept at 4 °C for 3 days was neutralized with sodium carbonate and insoluble sodium fluoride was removed by centrifugation. The supernatant was deionized (mixed resin, Rexyn 101 (H^+) and Dowex 1-X8 (OH^-)) and freeze dried. The product recovered (8 mg) was free of both phosphate and choline.

Periodate Oxidation

Periodate oxidations, borohydride reductions, and hydrolysis of the products were done by standard procedures (25). In brief, oxidations were done with 0.01 *M* sodium metaperiodate in the dark at room temperature for 50 h; consumption of oxidant was monitored spectrophotometrically (39). Oxidized products were reduced with sodium borohydride and hydrolysed with *N* hydrochloric acid at 100 °C for 10 h. Components in these hydrolysates were analysed by thin-layer chromatography and by gas–liquid chromatography after further reduction and acetylation to alditol acetates. Glucosamine was determined colorimetrically (40). Results are given in the preceding section.

Isolation of Oligosaccharides

(i) From Dephosphorylation

Dephosphorylated oligosaccharides (8 mg) were eluted from Bio-Gel P-2 (minus 400 mesh, 120 × 1.2 cm) with 0.1 *M* pyridine acetate buffer, p*H* 6.0. Fractions (0.85 ml) were monitored by the phenol – sulfuric acid method (32) and the elution pattern is shown in Fig. 3. Fractions containing only peak dp 3 were combined and freeze dried to yield a product shown to be a tetrasaccharide as described above.

(ii) From Periodate Oxidation

Portions (10 mg) of periodate-oxidized, borohydride-reduced, polysaccharide were hydrolysed (*a*) by *N* hydrochloric acid (5 ml) at room temperature for 24 h, (*b*) by 0.1 *N* hydrochloric acid (5 ml) at 100 °C for 1 h, neutralized (0.5 *N* sodium hydroxide), and fractionated on Bio-Gel P-2 as described above. Fractions were monitored for neutral sugars as in (*i*) and for amino sugars by a modified Elson–Morgan assay (40). The elution patterns are shown in Fig. 4. Hydrolysis (*a*) gave only one component (sd 1) apart from a small peak at the void volume. Analysis and further degradation studies as described above and summarized in Fig. 5 showed this to be an erythritol glycoside of a trisaccharide. Hydrolysis (*b*) gave 5 components on elution from Bio-Gel P-2 (peaks I–V, Fig. 4). Peaks IV and V were identified by chromatography as *N*-acetylglucosamine and galactose, respectively. Peak III, as described above, was shown to be the disaccharide, Glc *p* NAc 1→3 Gal. Peaks I and II from this elution were not examined further.

Chromium Trioxide Oxidations

The polysaccharide (5.5 mg) was depyruvylated and dephosphorylated as described above. The deionized product (3 mg) was reduced ($NaBH_4$), acetylated, and divided into three equal portions for oxidations of 0, 1, and 2 h as described by Laine and Renkonen (28). After hydrolysis the glucosamine contents were determined colorimetrically (40); neutral sugars were analysed directly by thin-layer chromatography and as alditol acetates by gas–liquid chromatography with addition of inositol as internal quantitative standard. The results showed a 75% loss of glucosamine and the almost total loss of glucose and rhamnose in the 2 h oxidations; galactose was not affected.

Enzymic Oxidations

An hydrolysate of the polysaccharide was incubated separately with D-glucose oxidase and D-galactose oxidase (Glucostat and Galactostat reagents, Worthington). Thin-layer chromatography failed to show glucose and galactose.

Acknowledgements

The authors gratefully acknowledge the generosity of Dr. Kenneth Amiraian, New York State Department of Health, Albany, N.Y., for donations of polysaccharide and antisera. The mouse myeloma antiserum specific for phosphorylcholine was provided by Dr. N. M. Young of these laboratories. The methyl 4,6-*O*-carboxyethylidene-α-D-galactopyranoside was a gift from Dr. P. A. J. Gorin, National Research Council of Canada, Prairie Regional Laboratory, Saskatoon, and Dr. I. C. P. Smith of these laboratories determined the ^{13}C nmr spectrum. Finally, we are grateful for the skilled technical assistance of Mr. F. P. Cooper with methylations and gas chromatography – mass spectrometry and Mr. H. Seguin with microanalysis.

1. Z. A. SHABAROVA, J. G. BUCHANAN, and J. BADDILEY. Biochim. Biophys. Acta, **57**, 146 (1962).
2. R. BROWN. J. Immunol. **37**, 445 (1939).
3. W. F. DUDMAN and M. HEIDELBERGER. Science, **164**, 954 (1969).
4. M. HEIDELBERGER, W. F. DUDMAN, and W. NIMMICH. J. Immunol. **104**, 1321 (1970).
5. M. HEIDELBERGER and W. NIMMICH. J. Immunol. **109**, 1337 (1972).
6. M. HEIDELBERGER. *In* Research in immunochemistry and immunobiology. Vol. 3. *Edited by* J. B. G. KWAPINSKI. University Park Press, Baltimore. 1973.
7. M. HEIDELBERGER and W. NIMMICH. Immunochemistry, **13**, 67 (1976).
8. J.-V. HÖLTJE and A. TOMASZ. J. Biol. Chem. **250**, 6072 (1975).
9. M. KATES. *In* Laboratory techniques in biochemistry and molecular biology. Vol. 3. *Edited by* T. S. Work and E. Work. American Elsevier Publishing Co., Inc., New York. 1972.
10. M. HAYASHI, T. UNEMOTO, and K. MIYAKI. Chem. Pharm. Bull. **10**, 533 (1962).
11. A. TOMASZ. Science, **157**, 694 (1967).
12. D. E. BRUNDISH and J. BADDILEY. Biochem. J. **110**, 573 (1968).
13. J. L. MOSSER and A. TOMASZ. J. Biol. Chem. **245**, 287 (1970).
14. T.-Y. LIU and E. C. GOTSCHLICH. J. Biol. Chem. **238**, 1928 (1963).
15. E. C. GOTSCHLICH and T.-Y. LIU. J. Biol. Chem. **242**, 463 (1967).
16. M. A. LEON and N. M. YOUNG. Biochemistry, **10**, 1424 (1971).
17. J. B. STOTHERS. *In* Organic chemistry: a series of monographs. Vol. 24. *Edited by* E. T. Blomquist and H. Wasserman. Academic Press, New York. 1972.
18. D. R. BUNDLE, H. J. JENNINGS, and I. C. P. SMITH. Can. J. Chem. **51**, 3812 (1973).
19. P. A. J. GORIN and T. ISHIKAWA. Can. J. Chem. **45**, 521 (1967).
20. A. K. BHATTACHARJEE, H. J. JENNINGS, C. P. KENNY, A. MARTIN, and I. C. P. SMITH. J. Biol. Chem. **250**, 1926 (1975).
21. H. BJÖRNDAL, C. G. HELLERQVIST, B. LINDBERG, and S. SVENSSON. Angew. Chem. Intl. Ed. Engl. **9**, 610 (1970).
22. D. M. BROWN, D. I. MAGRATH, and A. R. TODD. J. Chem. Soc. 1442 (1954).
23. P. PREHM, S. STIRM, B. JANN, and K. JANN. Eur. J. Biochem. **56**, 41 (1975).
24. R. R. KING and C. T. BISHOP. Can. J. Chem. **52**, 3913 (1974).
25. I. J. GOLDSTEIN, G. W. HAY, B. A. LEWIS, and F. SMITH. Methods Carbohydr. Chem. **5**, 361 (1965).
26. S. J. ANGYAL and K. JONES. Aust. J. Chem. **23**, 1209 (1970).
27. J. HOFFMAN, B. LINDBERG, and S. SVENSSON. Acta Chem. Scand. **26**, 661 (1972).
28. R. A. LAINE and O. RENKONEN. J. Lipid Res. **16**, 102 (1975).
29. O. OUCHTERLONY. Acta Pathol. Microbiol. Scand. **25**, 186 (1948).
30. O. H. LOWRY, N. J. ROSEBROUGH, A. L. FARR, and R. J. RANDALL. J. Biol. Chem. **193**, 265 (1951).
31. G. W. HAY, B. A. LEWIS, and F. SMITH. J. Chromatog. **11**, 479 (1963).
32. M. DUBOIS, K. A. GILLES, J. K. HAMILTON, P. A. REBERS, and F. SMITH. Anal. Chem. **28**, 350 (1956).
33. J. S. SAWARDEKER, J. H. SLONEKER, and A. JEANES. Anal. Chem. **37**, 1602 (1965).
34. P. S. CHEN, T. Y. TORIBARA, and H. WARNER. Anal. Chem. **28**, 1756 (1956).
35. J. H. SLONEKER and D. G. ORENTAS. Nature, **194**, 478 (1962).
36. S. HAKOMORI. J. Biochem. (Tokyo), **55**, 205 (1964).
37. T. PURDIE and J. C. IRVINE. J. Chem. Soc. **83**, 1021 (1903).
38. H. U. CHOI and K. MEYER. Carbohydr. Res. **40**, 77 (1975).
39. G. O. ASPINALL and R. J. FERRIER. Chem. Ind. 1216 (1957).
40. R. GATT and E. R. BERMAN. Anal. Biochem. **15**, 167 (1965).

Molecular inclusions in the paraffin layers of the nickel cyanide *n*-alkylamine systems

Y. MATHEY, R. SETTON, AND C. MAZIERES

Laboratoire de Physicochimie Minérale, Université de Paris Sud, 91405 Orsay, France

Received May 10, 1976

Y. MATHEY, R. SETTON, and C. MAZIERES. Can. J. Chem. **55**, 17 (1977).

The layered $Ni(C_nH_{2n+1}NH_2)_2Ni(CN)_4$ acts as a host structure for amines, yielding $Ni(C_nH_{2n+1}NH_2)_2Ni(CN)_4,xC_nH_{2n+1}NH_2$ (with $0 \leq x \leq 0.4$ and $12 \leq n \leq 16$) which are easily prepared by various procedures including solid–solid reaction. The guest can be removed and re-included; it can be replaced by aromatics. Phase transitions of the clathrate (with amines as guest) occur in the range 55–85 °C, obviously related to the transitions previously observed in the parent compound $Ni(C_nH_{2n+1}NH_2)_2Ni(CN)_4$.

Y. MATHEY, R. SETTON et C. MAZIERES. Can. J. Chem. **55**, 17 (1977).

La préparation et les caractéristiques de composés d'inclusion $Ni(C_nH_{2n+1}NH_2)_2Ni(CN)_4$, $xC_nH_{2n+1}NH_2$ avec $0 \leq x \leq 0.4$ et $12 \leq n \leq 16$ sont décrites. Les molécules d'amines incluses dans les couches paraffiniques du système peuvent être déplacées puis réinsérées. L'inclusion d'aromatiques, dans le même système, a été réalisée. L'existence de deux transitions pour le clathrate d'amines dans l'intervalle 55–85 °C est interprétée en relation avec le comportement de la structure d'accueil $Ni(C_nH_{2n+1}NH_2)_2Ni(CN)_4$.

The method of preparation which was given (1) after the original description by Weiss (2) of the nickel cyanide *n*-alkylamine compounds always leads to products for which the $RNH_2/Ni(CN)_2$ ratio (with $R = C_nH_{2n+1}$) can vary between 1 (parent compound) and about 1.20. A moderate heating (2 h at 100 °C, for instance) yields the parent compound $Ni(C_nH_{2n+1}NH_2)_2Ni(CN)_4$ which has already been described (1–3).

The ease of formation of the Ni cyanide *n*-alkylamines compounds will first be demonstrated; then, using *n*-dodecylamine as an example, it will be shown that the excess of amine molecules is not held by superficial adsorption but rather as the guest in a true layered inclusion compound conveniently described as $Ni(C_nH_{2n+1}NH_2)_2Ni(CN)_4,xC_nH_{2n+1}NH_2$)with $0 \leq x \leq 0.4$. The process of inclusion is progressive and reversible but a point exists beyond which the polymeric cyanide host structure breaks down. Furthermore, the same type of compound can exist with aromatic hydrocarbons as the included species.

Experimental

Preparation

The compounds $Ni(C_nH_{2n+1}NH_2)_2Ni(CN)_4,xC_nH_{2n+1}NH_2$ (which will hereafter be noted $NiNiC_n,xC_n$) have been prepared with normal alkylamines with $n = 12$ to 16.

In the case of *n*-dodecylamine (given as an example), one of the following three preparations can be used; all of them leading to a light violet product. (*A*) 'Quasi-anhydrous' nickel cyanide was prepared by dehydrating the hydrated cyanide at 160 °C; 0.5 mol of the yellow powder thus obtained was suspended in dry hexane and refluxed for 2 h with 0.65 mol of $n\text{-}C_{12}H_{25}NH_2$. The solid was then filtered, washed with hexane and dried.[1] (*B*) Freshly prepared hydrated cyanide $Ni(H_2O)_2Ni(CN)_4 \cdot yH_2O$ (0.5 mol) (4) was added to 65 ml of a 10 *M* solution of *n*-dodecylamine in hexane and the mixture refluxed, filtered, washed, and dried as above. (*C*) A mixture of 0.65 mol of solid $C_{12}H_{25}NH_2$ and 0.5 mol of quasi-anhydrous nickel cyanide was gently heated until it suddenly changes from yellow to light violet indicating coordination of the amine on the available Ni sites.

Analysis

Nickel was estimated by EDTA complexometry (5). Thermogravimetric analysis (TGA) gave the total amine content and hence *x*. These results were in good agreement with those calculated from elementary analysis using the hypothesis of one Ni to each two CN groups (Table 1).

Note

The maximum value of *x* found was 0.4; this value did not seem to depend on the mode of preparation. However, the use of excess quantities of amine led to much larger values of *x* (up to $x = 4$) but X-ray diffraction and infrared absorption showed that the compounds thus obtained were no longer of the $NiNiC_n,xC_n$ type here described.

[1]This method of preparation is analogous to that given by Walker and Hawthorne (1) in which the excess amine is removed by heating to yield the stoichiometric parent compound $NiNiC_n$ in its form I (3).

TABLE 1. Elementary analysis results

	Ni		C		N		H	
x*	Calcd.	Found	Calcd.	Found	Calcd.	Found	Calcd.	Found
0	19.8	19.8	56.8	56.1	14.2	13.7	9.2	9.2
0.15	18.9	18.8	57.7	57.3	13.9	13.8	9.4	9.4
0.35	17.9	17.4	58.9	58.7	13.5	13.3	9.7	9.7

*Content included dodecylamine.

Physical Properties

X-Ray diffraction patterns were obtained by reflexion, on a diffractometer ($\lambda K_{\alpha 1}Cu$); ir spectra were obtained on Nujol mulls or KBr pellets; thermal analyses were obtained in air on samples ranging from 10–15 mg (TGA) to a few micrograms (DTA).

Results

Whatever the value of x (between 0 and 0.4) or n (between 12 and 16) the compounds are light violet powders. A part of the X-ray diffraction pattern of the $NiNiC_{12}$, $\sim 0.4C_{12}$ compound is compared to the diffractogram given by form I of the parent $NiNiC_{12}$ compound in Fig. 1. Thermal treatment of the compounds singles out

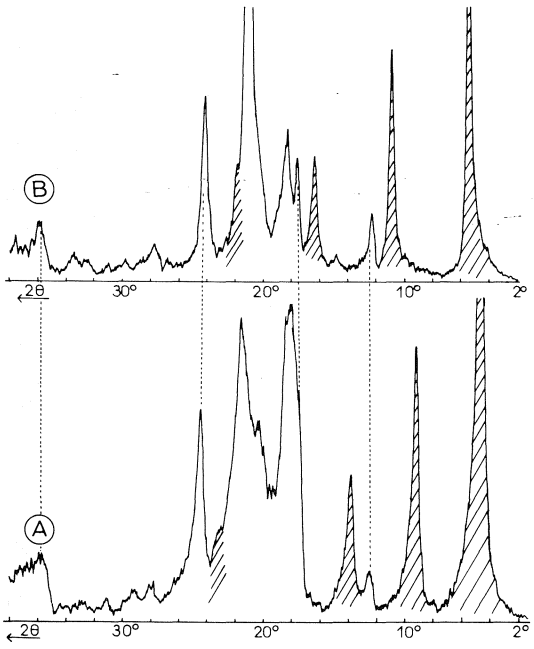

FIG. 1. X-Ray diffractogram ($\lambda K_{\alpha 1}Cu$) of (*A*) $NiNiC_n$, xC_n inclusion compound, for $n = 12$ and $x \approx 0.4$; (*B*) $NiNiC_{12}$, the parent compound (form I). The shading refers to the first category of lines (see text) In *A*, the 4th harmonic (around 19°) is occulted by other reflections. The lines of the second category are shown linked in the two diagrams.

TABLE 2. Maximum values (in Å) observed for the largest interplane distance in $NiNiC_n,xC_n$ with $12 \leq n \leq 16$ and $x \approx 0.4$

	d (Å)	
n	$NiNiC_n$	$NiNiC_n,xC_n$
12	16.2	19.3
13	17.1	20.5
14	18.0	21.2
15	18.9	22.3
16	19.7	23.2

three categories of lines: (*i*) The first line (smallest value of the diffraction angle) and its harmonics, with intensities strongly enhanced by preferential orientation of the powder on the holder. The corresponding value of the interlayer spacing is slightly dependent on the value of x and differs with n. It is always greater than that of the corresponding parent compound but tends discontinously to this latter value during the heat treatment (Table 2); an incomplete heat treatment leads to two phases. (*ii*) A few lines whose positions do not depend on n and which are not much affected by the heat treatments. They correspond to distances very close to those characteristic of the polymeric nickel cyanide plane already met in $NiNiC_n$. (*iii*) Some strong lines which are not linked with the value of n and are considerably modified by the heat treatment.

The ir spectra obtained on as-prepared and heat-treated compounds are quite similar but, in the latter case, the spectrum is less complex, particularly in the extension vibrations ν(C—C) and ν(C—N) of the $C_nH_{2n+1}NH_2$ chain and ν(N—H) of the NH_2 group; also the very intense ν(C≡N) vibration splits (2162 and 2156 cm^{-1}).

The different methods of physical analysis show that below 85 °C, modifications occur without any loss of mass; above this threshold, loss of mass occurs leading to $NiNiC_n$ (I) with $x = 0$. Depending on the previous thermal his-

tory, three types of thermograms can thus be distinguished:

Heating to 75 °C (maximum)

The DTA curve of Fig. 2*A* shows a first endotherm starting at 55 °C and another rather weaker one at about 65 °C. The reverse signals can be observed on cooling and the cycle is reproducible any number of times. There is no loss of mass from the sample; X-ray diffraction pattern and ir spectra of the sample at room temperature show no variations.

Heating to 85 °C

At room temperature no loss of mass or any modification of the ir spectrum are observed after a first heating to 85 °C, but the X-ray diffraction pattern is permanently modified with the largest value of *d*, the interplanar distance, changing from 19.30 to 19.05 Å. Similarly, the DTA curve shows a significant reduction of the first endotherm (Fig. 2*A'*). Identical thermograms are obtained during further heating cycles limited to a maximum temperature of 85 °C.

Heating to Beyond 85 °C

This entails decomposition and leads to $NiNiC_{12}$ (I) whose characteristics have already been described (3) (Fig. 2*B*). It is important to note that the removal of the excess amine is still, in a way, reversible since *x* can be increased again through the action of a solution of $n\text{-}C_{12}H_{25}NH_2$ in hexane. The products thus obtained, corresponding to the formula $NiNiC_{12}$, $x'C_{12}$, are analogous to those obtained by procedures *A*, *B*, or *C*, with the value of x' independent of the previous value of *x*. Also in this case, there exists a limiting value of x' beyond which profound modifications of the system occur. Thus, the products obtained from $NiNiC_{12}$ and a quantity of amine equivalent to $x' = 4$ correspond to the expected formula but their characteristics are quite different from those described above. X-Ray diffraction yields a value of 24.9 Å and the ir spectrum shows two peaks for $\nu(C{\equiv}N)$ at 2152 and 2123 cm^{-1}, both intense, two for $\nu_{as}(N{-}H)$ at 3334 and 3316 cm^{-1} and two for $\nu_s(N{-}H)$ at 3270 and 3254. The product is identical to that described in the Note in Experimental section.

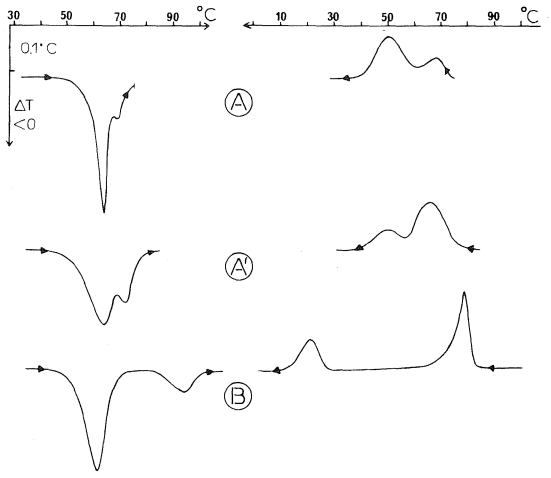

FIG. 2. Differential thermal analysis. (*A*) Of $NiNiC_n$, xC_n with $x \approx 0.4$. First heating and cooling cycle. if $t < 75$ °C, this cycle is reproducible. (*A'*) After a first heating to 85 °C, this cycle is reproducible if $t_{max} \leq 85$ °C. (*B*) After a first heating to 100 °C (2 h). The thermogram is that of the parent compound.

Discussion

The analogy between the X-ray diffraction pattern and the ir spectra of $NiNiC_n$ and $NiNiC_n,xC_n$ (particularly with regard to the structure in the Ni planes) as well as the analogy of the DTA curves suggests that the excess amine of $NiNiC_n,xC_n$ (with $0 \leq x \leq 0.4$) leaves most of the crystalline lamellar structure of the parent compound unchanged. Apparently, the excess molecules are trapped between the layers, and this both modifies the interlayer spacing and increases the complexity of organization of the paraffinic system. Since the coordinated and non-coordinated alkyl chains are identical and must probably both be in their fully extended *trans* conformation, the axes of the mean repulsion cylinder are likely to be parallel so as to obtain closest packing in the interlayer spacing. Furthermore, since the increase in the interlamellar distances with *n* (when $x \approx 0.4$) is slightly greater than that observed for the parent compound (Table 2), the angle between the chains and the cyanide planes must have been slightly increased. The problem of the structural relationship between the various parts of the lattice has not, however, yet been solved owing to the lack of single-crystal data (3).

The thermal evolution of $NiNiC_{12},xC_{12}$ can be interpreted as follows: at about 75 °C the system of planes and chains settles irreversibly with d_{max} changing from 19.30 to 19.05 Å. When this more compact $NiNiC_{12},xC_{12}$ is heated once again from room temperature, a first transition occurs at about 55 °C, strikingly similar to the I → II transition of the parent compound (3).

The second transition, starting at about 65 °C, could be homologous to the II → III transition which, in $NiNiC_{12}$, occurs at 85 °C. The decrease in the transition temperature could be the result of an increase in freedom of the terminal CH_3 groups.

The $NiNiC_n,xC_n$ system therefore shows the following properties: reproducibility of the spectral and structural properties, possibility of obtaining x values between ~ 0.4 and 0, decomposition leading to the parent compound $NiNiC_n$, possibility of regeneration. These features are characteristic of an inclusion compound in which the parent lattice plays the role of a host structure. For $n = 12$, the maximum value of x seems to be about 0.4; beyond this value, the Ni—CN bonds in the polymeric cyanide phase break down, as shown by the profound modifications of the ir spectra in which two intense ν(C—N) bands appear separated by 30 cm^{-1}. In other words, an excess of amine seems to lead to $[Ni(RNH_2)_x]^{2+}[Ni(CN)_4]^{2-}$ but the structural relationship between the square planar anions and the bulky cations has not yet been ascertained.

A similarity can be drawn between the host structure and that of the Hofmann clathrate (6) $Ni(NH_3)_2Ni(CN)_4,2C_6H_6$. This has led us to attempt the inclusion of aromatics: (*1*) With benzene, for $n \leq 12$ one can obtain $NiNiC_n$, xC_6H_6 but the stability of this compound is low even at room temperature. In fact benzene seems to diffuse into and out of the $NiNiC_n$ structure. Naphthalene and anthracene can be included, their diffusion out being slow enough to permit observation of their inclusion. (*2*) If one tries to regenerate $NiNiC_{12},x'C_{12}$ by reacting $NiNiC_{12}$ with $C_{12}H_{25}NH_2$ dissolved in benzene (instead of hexane), the inclusion of the amine doesn't occur. The extreme ease with which benzene apparently diffuses into the structure probably prevents the bulkier amine molecules from penetrating between the layers. (*3*) The stability of the aromatic inclusion compounds can be markedly improved by adjusting the size of host site to that of the included molecule, thus, anthracene can be better included in $NiNiC_8$ than in $NiNiC_{12}$. The differences in the uv spectrum of the aromatic molecules brought about by inclusion suggest that the distribution and orientation in the aliphatic chains could be studied along the lines of the numerous results (7) obtained following the work of Shpolskii (8) in this field.

1. G. F. WALKER and D. G. HAWTHORNE. Trans. Faraday Soc. **63**, 166 (1967).
2. A. WEISS. Chem. Ber. **91**, 487 (1958).
3. Y. MATHEY and C. MAZIERES. J. Phys. Lett. **36**, L-243 (1975).
4. Y. MATHEY and C. MAZIERES. Can. J. Chem. **52**, 3637 (1974).
5. G. SCHWARZENBACH. Complexometric titrations. Interscience Publ., New York. 1960.
6. J. H. RAYNER and H. M. POWELL. J. Chem. Soc. 319 (1952).
7. M. LAMOTTE and J. J. JOUSSOT-DUBIEN. J. Chem. Phys. **61**, 1893 (1974).
8. E. V. SHPOLSKII. Sov. Phys. Usp. **5**, 522 (1962).

1,2,3,4,7,8,9,10-Octahydrodicyclohepta[*de*,*ij*]naphthalene and 2,7-dimethylpyrene: a short novel synthesis

DAVID E. LAYCOCK,[1] ROSEMARY J. WAIN,[2] AND ROBERT H. WIGHTMAN[3]

Department of Chemistry, Carleton University, Ottawa, Ont., Canada K1S 5B6

Received July 12, 1976

DAVID E. LAYCOCK, ROSEMARY J. WAIN, and ROBERT H. WIGHTMAN. Can. J. Chem. **55**, 21 (1977).

The preparation of two tetracyclic benzenoid hydrocarbons is described using a four step synthesis involving 'aromatization' of a Diels–Alder dianhydride adduct.

DAVID E. LAYCOCK, ROSEMARY J. WAIN et ROBERT H. WIGHTMAN. Can. J. Chem. **55**, 21 (1977).

On décrit la préparation de deux hydrocarbures benzénoïdes tétracycliques qui se font par l'intermédiaire d'une synthèse en quatre étapes impliquant 'l'aromatisation' d'un adduit dianhydride de Diels–Alder.

[Traduit par le journal]

Introduction

Bis-annelation of the naphthalene nucleus via the peri positions has led to some interesting tetracyclic polyunsaturated hydrocarbons including acepleiadylene **1** (1), pyracylene **2** (2) and pyrene **3** (3). These compounds have received much chemical (1, 4) and theoretical (5–7) attention to ascertain their degree of 'aromatic' character. The next higher homologue 'dipleiadiene' **4** has not yet been synthesized (for synthesis of a similar system, see ref. 8) although it has received considerable theoretical attention (9, 10). One approach to **4** would seem to be via its octahydro derivative **8** and this manuscript describes a short synthetic route for this compound as well as an interesting rearrangement by-product, 2,7-dimethylpyrene **9**.

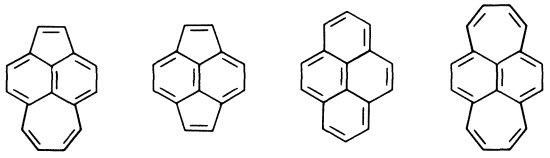

1 **2** **3** **4**

Fischer *et al.* have reported the only synthesis of **8** in a lengthy sequence starting with benzosuberone and involving ten steps with a 7% overall yield (11). Our synthesis outlined in Scheme 1 can provide the compound quickly in four steps from cycloheptanone despite one very low yield step. Interestingly, the sequence also provides a source of 2,7-dimethylpyrene **9** for which there is only one reported synthesis with an acceptable yield (12).

Results and Discussion

1,2,3,4,7,8,9,10-Octahydrodicyclohepta[de,ij]-naphthalene

The synthesis of **8** was based on the observation that mono Diels–Alder adducts of maleic anhydride and bicyclic dienes could be converted directly to benzenoid hydrocarbons in yields of 60–70% by heating with phosphorus pentoxide (13). This procedure has been used previously by us to synthesize a series of bis *meta*-annelated benzenoid hydrocarbons (14).

A substantial improvement over reported yields (~50%) of 1-chlorocycloheptene **5** (15) from cycloheptanone was achieved by modifications in the work-up (see Experimental). The product should be used immediately after distillation but can be stored under nitrogen atmosphere in the cold (0 °C) and dark. Conversion to the diene **6** was accomplished with potassium *tert*-butoxide in tetrahydrofuran at 70 °C as reported by Bottini *et al.* (16). The method is a distinct improvement over the original procedure of Ball and Landor (15) both in yields and experimental ease. We have found that cmr provided an easy and direct verification of the absence of double bond isomers noted by previous workers

[1]Taken in part from the thesis presented by D.E.L. in partial fulfillment of the requirements of the M.Sc. degree at Carleton University, Ottawa, Canada, May 1976.

[2]Taken in part from the thesis presented by R.J.W. in partial fulfillment of the requirements of the M.Phil. (external) degree for the University of London, U.K., April 1972.

[3]Author to whom correspondence should be addressed.

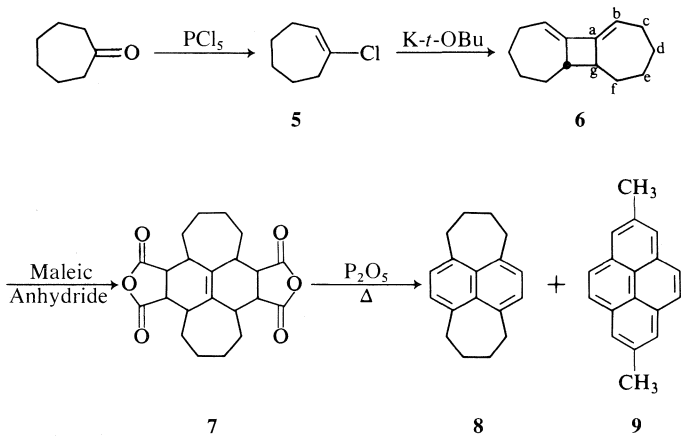

SCHEME 1

(15, 16). The presence of only seven lines in the spectrum must indicate the required (symmetrical) product. The *anti* configuration for **6** indicated on the formula is based on assignments from chemical degradations of **6** (17), a Woodward–Hoffman conrotatory [2 + 2] dimerization of the cycloallene proposed as the intermediate between compounds such as **5** and **6** (16, 18), and possible pmr evidence (19). It should be possible to confirm this stereochemical assignment by cmr if the other isomer of **6** could be obtained (20).

The dianhydride **7** was obtained as described by Ball and Landor (15) although we were never able to achieve the yields nor, consistently, the sharp melting points reported by the earlier workers. This may be due to mixtures of conformational/configurational isomers such as have been reported for similar products (21). Nonetheless the reaction product when foamed and dried gave spectral data (ir, nmr, ms) consistent with the proposed structure and gave products identical to the crystalline material when subjected to the final reaction conditions. Upon heating the dianhydride **7** with phosphorus pentoxide at 360 °C an orange hydrocarbon-soluble solid was obtained in 13% yield which was disappointingly low when compared to our previous experiences (14). Gas–liquid chromatographic analysis of this product indicated two major components which were easily separated and purified by column chromatography on alumina to yield **8** with petroleum ether elution and **9** from the benzene fraction.

Various attempts were made to improve the yield of the Diels–Alder/aromatization sequence. Cycloadditions with the diene **6** were investigated using ethylene, acrylic acid, dimethylacetylene dicarboxylate, and tetracyanoethylene (22) as dienophiles with no useful derivatives obtained. Attempted conversion of the dianhydride to hydrocarbon products using bis triphenylphosphine nickel dicarbonyl (23), Pd/C at 350 °C (14), or lead tetraacetate with dimethyl sulfoxide in pyridine (24) were also unsuccessful.

2,7-Dimethylpyrene

At first glance the formation of **9** bears some similarity to reported pyrolytic (500 °C) rearrangement of benzcycloheptadiene to methylnaphthalene (25). However, treatment of **8** at 360 °C or with phosphorus pentoxide at 360 °C returned essentially quantitative amounts of starting material with no evidence for **9**. Perhaps this result offers some clue to the mechanism of the 'oxidative decarboxylation' reaction with phosphorus pentoxide.

Experimental

General Details

All reactions were carried out under nitrogen. Melting points were obtained on a Fisher-Johns melting point apparatus. Refractive indices were taken on an Officine Galileo Di Milano (Jo. 50532) refractometer. Analytical glc data were obtained on a Hewlett Packard F&M 402 instrument using ¼ in. × 6 ft columns packed with 5% SE54 on Chromosorb W, an oven temperature of 225 °C, and flow rate of nitrogen at 70 ml/min. Infrared spectra were recorded on a Perkin-Elmer 237B spectrophotometer. Ultraviolet spectra were obtained in 95% EtOH on a Perkin-Elmer Coleman-124 spectrophotometer. ^{13}C nmr data were obtained on a Varian XL-100 (100 MHz) instrument and proton nmr spectra were recorded on a Varian T-60 (60 MHz) instrument; all values are recorded in ppm (δ) with reference to TMS. All nmr were taken in $CDCl_3$ with 1% TMS. Low resolution mass spectra were carried out at Trent University in Peterborough.

1-Chlorocycloheptene (5) (15)

Cycloheptanone (225 g, 1.8 mol) was added dropwise to phosphorus pentachloride (454 g, 2.2 mol) over 3 h at 0 °C. The reaction mixture was then poured on ice (1000 g) and after 1 h extracted with methylene chloride (3 × 200 ml); the combined organic layers were washed with water (2 × 200 ml), dried over anhydrous sodium sulfate, filtered, and evaporated *in vacuo*. Distillation of the resulting oil yielded 1-chlorocycloheptene, 196 g (79%) as a clear colourless oil; bp 54–59 °C/14 torr, η_D^{20} 1.4840 (lit. (26) bp 75 °C/26 torr, η_D^{21} 1.4844); nmr 5.95 (1H, t, olefinic C*H*), 2.5 (2H, m, CH_2 α to CCl), 2.1 (2H, m, allylic CH_2), 1.6 (6H, m, other CH_2).

Tricyclic Diene (6) (16)

Freshly distilled 1-chlorocycloheptene (**5**) (196 g, 1.5 mol) was added dropwise over 1 h to a stirred dispersion of potassium *tert*-butoxide (370 g, 3.3 mol) in 1 litre dry THF at 66–70 °C. After 2 h at this temperature the mixture was poured into 1 litre of water and extracted with ether (3 × 200 ml); the combined ether extracts were washed with water (1 × 200 ml), dried, filtered, and evaporated to give a reddish oil. Upon distillation the diene **6** was obtained, as a clear colourless oil, 67 g (49%), bp 150–162 °C/14 torr (lit. (15, 16) 142 °C/14 torr, 123–137 °C/4 torr); η_D^{20} 1.5408; nmr 5.8 (2H, m, olefinic C*H*), 2.6–0.9 (18H, m, other *H*); ir 1660 cm^{-1} (C=C); uv λ_{max} (ε) 260 (17 500), sh 270, sh 254 nm; ^{13}Cmr (±0.2 ppm), 145.8 (C_a), 118.2 (C_b), 48.7 (C_g), 33.4 (C_e), 30.9 (C_c), 29.7 (C_f or C_d), 28.9 (C_d or C_f).

Dianhydride 7 (15)

Freshly distilled diene **6** (29.0 g, 0.154 mol) and maleic anhydride (58 g, 0.465 mol) were refluxed in dry benzene (200 ml) for 8 h. Removal of benzene *in vacuo* followed by trituration with ether furnished a residual yellow oil which, after repeated evaporations with acetone, yielded yellow foam, 16.5 g (28%). A small portion could be crystallized in benzene – petroleum ether (60–100 °C) as needles mp 263–267 °C, softening at 230 °C (lit. (15) 267 °C); ir 1760, 1850 cm^{-1} (anhydride); ms *m/e* 384 (M^+); nmr 3.3 (4H, m, C*H* α to C=O), 2.9–2.4 (4H, m, allylic C*H*), 2.3–1.2 (16H, m, other *H*).

Substituted Naphthalene (8) and 2,7-Dimethylpyrene (9)

Dry powdered dianhydride **7** (15 g, 0.039 mol) was mixed thoroughly with phosphorus pentoxide (15.0 g, 0.15 mol) and placed in a long Pyrex tube with a Hickman still attached. The apparatus was then placed vertically in a furnace at 360 °C for 15 min. Orange crystals were recovered from the still and chromatographed on an alumina column. Elution with petroleum ether gave clear colourless needles, recrystallized from hexane to yield **8**, 0.5 g (6%): mp 143 °C (lit (11) 143 °C); glc 6.5 min; nmr 7.0 (4H, s, aromatic *H*), 3.15 (8H, m benzylic CH_2), 2.0 (8H, m, other CH_2).

Subsequent elution with benzene furnished, after recrystallization from hexane, 2,7-dimethylpyrene **9**, 0.3 g (4%), as clear colourless crystals: mp 233 °C (lit. 12, 27) 234 °C, 238 °C); glc 8.75 min; nmr 7.95 (8H, s, ring *H*'s), 2.75 (6H, s, CH_3's); ms *m/e* 230 °C (M^+); uv λ_{max} (ε) 247 (20 000), 267 (5900), 277 (9500), sh 237 nm.

Acknowledgments

We acknowledge with thanks the National Research Council of Canada which provided the operating grants to finance much of this work and Dr. G. W. Buchanan of Carleton University for his assistance in obtaining and interpreting the cmr spectra.

1. V. Boekelheide and G. K. Vick. J. Am. Chem. Soc. **78**, 653 (1956).
2. B. M. Trost and G. M. Bright. J. Am. Chem. Soc. **89**, 4244 (1967).
3. E. Clar. Ber. **69**, 1671 (1936).
4. B. M. Trost, C. M. Bright, C. Frihart, and D. Bertelli. J. Am. Chem. Soc. **93**, 737 (1971).
5. B. Pullman, A. Pullman, G. Bertier, and J. Pontis. J. Chim. Phys. **20**, 49 (1952); Chem. Abstr. **46**, 6486b (1952).
6. R. Zahradnik and J. Michl. Coll. Czech. Chem. Commun. **30**, 3550 (1965).
7. G. Binsch and E. Heilbronner. Tetrahedron, **24**, 1215 (1968).
8. V. Boekelheide and R. H. Mitchell. Chem. Commun. 1557 (1970).
9. R. Zahradnik, J. Michl, and J. Pancier. Tetrahedron, **22**, 1355 (1966).
10. C. A. Coulson and R. B. Mallion. J. Am. Chem. Soc. **98**, 592 (1976).
11. A. Fischer, D. P. A. Leonard, and D. A. K. Happer. Can. J. Chem. **48**, 1446 (1970).
12. R. H. Mitchell and R. J. Carruthers. Can. J. Chem. **52**, 3054 (1974).
13. V. R. Skvarchenko, R. Ya. Levina, and O. Yu. Okhlobystin. Doklady Akad. Nauk S.S.S.R. **99**, 789 (1954); Chem. Abstr. **49**, 5414e (1955).
14. R. H. Wightman, R. J. Wain, and D. H. Lake. Can. J. Chem. **49**, 1360 (1971).
15. W. J. Ball and S. R. Landor. J. Chem. Soc. 2298 (1962).
16. A. T. Bottini, K. A. Frost II, B. R. Anderson, and V. Dev. Tetrahedron, **29**, 1975 (1973).
17. R. Criegee and H. J. Reinhardt. Chem. Ber. **101**, 102 (1968).
18. K. G. Untch and D. J. Martin. J. Am. Chem. Soc. **87**, 4501 (1965).
19. W. R. Moore and W. R. Moser. J. Am. Chem. Soc. **92**, 5469 (1970).
20. W. R. Moore, L. N. Bell, and G. P. Daumit. J. Org. Chem. **36**, 1694 (1971).
21. H. Christol and M. Levy. Bull. Soc. Chim. Fr., 3046 (1964).
22. G. Wittig and J. Meske-Schuller. Ann. Chem. **711**, 76 (1968).
23. B. M. Trost and F. Chen. Tetrahedron Lett. 2603 (1971).
24. N. B. Chapman, S. Sotheeswaran, and K. J. Toyne. J. Chem. Soc. Chem. Commun. 214 (1965).
25. M. Pomerantz and A. S. Ross. J. Am. Chem. Soc. **97**, 5850 (1975).
26. E. A. Braude, W. F. Forbes, and E. A. Evans. J. Chem. Soc. 2202 (1953).
27. M. Orchin, L. Reggel, and R. A. Friedel. J. Am. Chem. Soc. **74**, 1094 (1952).

Gas phase ion equilibria studies of the proton in hydrogen sulfide and hydrogen sulfide – water mixtures. Stabilities of the hydrogen bonded complexes: $H^+(H_2S)_x(H_2O)_y$

KENZO HIRAOKA AND PAUL KEBARLE

Chemistry Department, University of Alberta, Edmonton, Alta., Canada T6G 2E1

Received July 6, 1976

KENZO HIRAOKA and PAUL KEBARLE. Can. J. Chem. **55**, 24 (1977).

The temperature dependence of the equilibria $(n,n+1)$ $H^+(H_2S)_n + H_2S \rightleftharpoons H^+(H_2S)_{n+1}$ was measured for $n = 1$ to 5 in a pulsed electron beam mass spectrometer with a high pressure ion source. The $\Delta H_{n+1,n}$ values obtained were (2,1) 15.4, (3,2) 9.1, (4,3) 8.4, (5,4) 6.7 kcal/mol. Possible structures of the clustered ions are proposed.

Addition of water vapor leads to mixed cluster ions such as $H^+(H_2S)_x(H_2O)_y$, with $x + y$ from 1 to 6, observed as the ion source temperature was decreased to -100 °C. The temperature dependence of the equilibria for the exchange reactions $H^+(H_2S)(H_2O) + H_2O \rightleftharpoons H^+(H_2O)_2 + H_2S$, $H^+(H_2S)(H_2O)_2 + H_2O \rightleftharpoons H^+(H_2O)_3 + H_2S$, and the association reaction $H^+(H_2S)(H_2O) + H_2S \rightleftharpoons H^+(H_2S)_2(H_2O)$ were also measured. For all ions measured, the hydration process is energetically more favorable than the solvation by H_2S.

KENZO HIRAKOA et PAUL KEBARLE. Can. J. Chem. **55**, 24 (1977).

La relation qui existe entre la température et l'équlibre $(n,n+1)$ $H^+(H_2S)_n + H^+(H_2S)_{n+1}$ a été mesurée pour $n = 1$ jusqu'à 5 dans un spectromètre de masse avec un faisceau d'électrons pulsés et une source ionique à haute pression. Les valeurs de $\Delta H_{n+1,n}$ obtenues sont (2,1) 15.4, (3,2) 9.1, (4,3) 8.4, (5,4) 6.7 kcal/mol. On propose des structures possibles pour les ions agglomérés.

L'addition de vapeur d'eau conduit à des ions mixtes sous forme d'agglomérats tels que $H^+(H_2S)_x(H_2O)_y$ où $x + y$ varie de 1 à 6; on peut observer ces ions lorsque la température de la source ionique est abaissée jusqu'à -100 °C. Les relations entre la température et l'équilibre pour les réactions d'échange $H^+(H_2S)(H_2O) + H_2O \rightleftharpoons H^+(H_2O)_2 + H_2S$, $H^+(H_2S)(H_2O)_2$ $H_2O \rightleftharpoons H^+(H_2O)_3 + H_2S$ et pour la réaction d'association $H^+(H_2S)(H_2O) + H_2S \rightleftharpoons H^+(H_2S)_2(H_2O)$ ont aussi été mesurées. Pour tous les ions mesurés, le processus d'hydratation est plus favorisé, au point de vue énergétique, que la réaction de solvatation par H_2S.

[Traduit par le journal]

Introduction

Several years ago, a study of the gas phase equilibria of the proton in water, methanol, dimethyl ether (1) and mixtures thereof (2) was made in this laboratory. This study provided thermochemical information giving special insights in the solvation processes and suggested possible structures of the hydrogen bonded clusters.

The present work deals with hydrogen sulfide and mixtures of hydrogen sulfide and water. A number of spectroscopic studies of hydrogen bonding to the sulfur atom in solution have been reported (3). However, few thermochemical data were obtained by this method. Lowder *et al.* (4) estimated the energy of hydrogen bonding in $H_2S....HSH$ in the gas phase from quantitative infrared intensity measurements as 1.7 ± 0.3 kcal/mol. This can be compared with the energy of hydrogen bonding of water $H_2O...OH_2$ which is ~ 5 kcal/mol (5). Apart from a qualitative study of Hopkins and Bone (6), no quantitative information on the hydrogen bonding in ionic species like $(H_2S...H...SH_2)^+$ etc. has been published. In order to investigate the intrinsic hydrogen bonding ability of hydrogen sulfide, we studied the equilibrium reaction of the proton in hydrogen sulfide and mixtures of hydrogen sulfide and water in methane carrier gas.

Experimental

The high pressure ion source mass spectrometer with which the measurements were done was described earlier (7). Only a brief account of the procedures followed will be given here.

The 2000 V ionizing electron beam (10^{-8} Å) was pulsed 'on' for 10–100 μs and 'off' for 2–4 ms. The ions escaping from the field free ion source into an evacuated region were magnetically mass analyzed and collected in a multichannel analyzer as a function of their arrival time after the electron pulse.

The $H^+(H_2S)_n + H_2S \rightleftharpoons H^+(H_2S)_{n+1}$ measurements were done with CH_4 gas at a pressure of 4 torr containing known small amounts of H_2S (50 to 600 mtorr). The CH_4 gas (Linde UHP) was further purified by passing it through a Dry Ice – acetone-cooled trap containing molecular sieve 5 Å. Downstream of this trap, H_2S (Matheson C.P. Grade) was added to the CH_4 stream through a calibrated capillary. The mixed gas was passed in slow flow through the thermostated ion source.

For the measurements of equilibria of the mixed cluster ions of H_2S and H_2O, only a very small amount of H_2O (< 1 mtorr) needed to be introduced since more than a few mtorr of water easily converted all mixed cluster ions to fully hydrated ions. This made it difficult to determine the water pressure directly. We had to determine the water pressure by measuring the equilibrium ion intensities of $H^+(H_2O)_n$ and $H^+(H_2O)_{n+1}$ and using the expression:

$$p = \frac{I_{n+1}}{I_n} \times \frac{1}{K_{n,n+1}}$$

The equilibrium constants $K_{n+1,n}$ were obtained in this laboratory before (7, 8). The water concentration resulting from this procedure is accurate to only some 20–50%. This introduces a similar error in the equilibrium constants for the exchange reactions $H^+SW + W \rightleftharpoons H^+W_2 + S$ and $H^+SW_2 + W \rightleftharpoons H^+W_3 + S$ (where S stands for H_2S and W for H_2O).

The cluster ions H^+S_n and H^+W_n, and mixed cluster ions $H^+S_xW_y$ were the major ions observed in the mixed H_2S, water experiment with some minor ions such as CHS^+, CH_3S^+, $CH_3SH_2^+$, $C_2H_5SH_2^+$, $C_3H_5SH_2^+$, and $C_3H_7SH_2^+$. The total of the minor ions was less than 1% of the total ions. The minor ions might be produced from the impurities, possibly mercaptans present in the hydrogen sulfide gas, by reaction of the primary ions of methane with hydrogen sulfide. No investigation was made of the mechanism by which these ions were formed.

Results and Discussion

The experimentally obtained van't Hoff plots for the reactions $(n,n+1)$ $H^+(H_2S)_n + H_2S = H^+(H_2S)_{n+1}$ are shown in Fig. 1 together with the corresponding results for water which are given for comparison.

An examination of the dependence of the equilibrium constants on the H_2S pressure was made at all the temperatures shown in the van't Hoff plots. One example of these determinations is given in Fig. 2 for the reaction (1,2).

(1,2) $\quad H^+(H_2S) + H_2S \rightleftharpoons H^+(H_2S)_2$

The results show that the equilibrium constants are independent of H_2S pressure in the experimentally covered pressure range, where the pressure changes by a factor of five to six.

The van't Hoff plots for the exchange reactions $H^+SW + W \rightleftharpoons H^+W_2 + S$ and $H^+SW_2 + W \rightleftharpoons H^+W_3 + S$, and the addition reaction

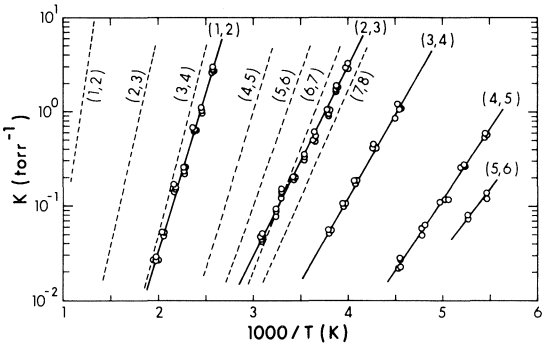

FIG. 1. van't Hoff plots for the reactions $H^+(H_2S)_n + H_2S \rightleftharpoons H^+(H_2S)_{n+1}$ $(n,n+1)$. (---) plots for the reaction $H^+(H_2O) + H_2O = H^+(H_2O)_{n+1}$, refs. 7 and 8.

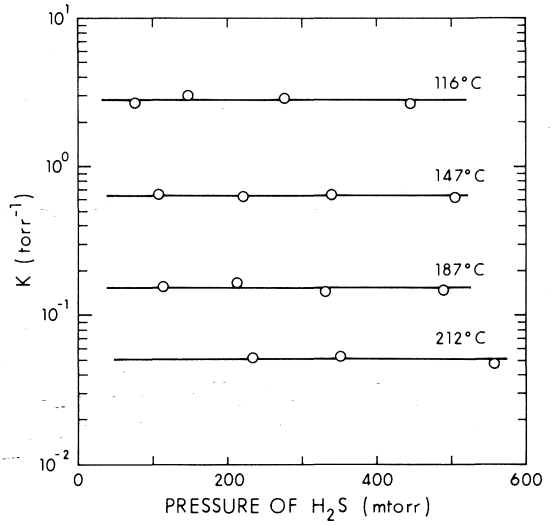

FIG. 2. Pressure dependence of the equilibrium constant $K_{1,2}$ for the reaction $H^+(H_2S) + H_2S \rightleftharpoons H^+(H_2S)_2$.

$H^+SW + S \rightleftharpoons H^+S_2W$ are shown in Fig. 3. The corresponding ΔH^0, ΔG^0, and ΔS^0 values are summarized in Fig. 4 and Table 1. Included are results obtained earlier for pure protonated water (7, 8). Some of the values shown in Fig. 4 are marked by an asterisk. Such values were obtained not by direct measurement of the equilibrium but by the application of thermodynamic cycles. This was done for cases where the direct measurement of the equilibrium was difficult.

The van't Hoff plots for pure hydrogen sulfide were shown in Fig. 1. The vertical distance between two adjacent van't Hoff lines taken at some $(1/T)$ is proportional to the free energy difference. Big gaps between two van't Hoff lines

TABLE 1. Thermochemical data from protonated clusters in equilibria; hydrogen sulfide, hydrogen sulfide – water mixture[a]

Reaction	$-\Delta H^0$	$-\Delta G^0$	$-\Delta S^0$
	(1) Addition Reaction		
$H^+S + S \rightleftharpoons H^+S_2$	15.4±0.5	8.1±0.4	24.4±1.5
$H^+S_2 + S \rightleftharpoons H^+S_3$	9.1±0.5	2.8±0.1	20.9±2.1
$H^+S_3 + S \rightleftharpoons H^+S_4$	8.4±0.5	1.0±0.2	24.5±1.8
$H^+S_4 + S \rightleftharpoons H^+S_5$	6.7±0.3	−0.7±0.2	24.7±1.4
$H^+S_5 + S \rightleftharpoons H^+S_6$[b]	~6.1[b]	~−1.1[b]	(24)
$H^+SW + S \rightleftharpoons H^+S_2W$	13.3±0.4	6.8±0.2	21.7±1.3
	(2) Exchange Reaction		
$H^+SW + W \rightleftharpoons H^+W_2 + S$	6.7±1	7.1±0.5	−1.2±2
$H^+SW_2 + W \rightleftharpoons H^+W_3 + S$	5.9±1	6.3±0.6	−1.3±2

[a]All values are in kcal/mol, ΔG^0 values for 300 K, ΔS^0 in eu, standard state 1 atm. Only data from directly measured equilibria are shown. Data for related reactions can be obtained from thermodynamic cycles as shown in Fig. 4. S and W are hydrogen sulfide and water.
[b]The values ΔH^0 and ΔG^0 are estimated by assuming $-\Delta S^0 = 24$ eu and ΔG measured at a different temperature.

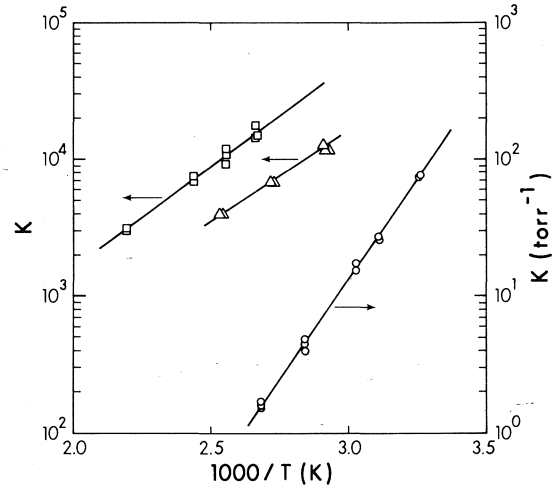

FIG. 3. van't Hoff plots for hydrogen sulfide (S) and water (W): Exchange reactions: $H^+SW + W \rightleftharpoons H^+W_2 + S$ (□) and $H^+SW_2 + W \rightleftharpoons H^+W_3 + S$ (△). Association reaction $H^+SW + S \rightleftharpoons H^+S_2W$ (○).

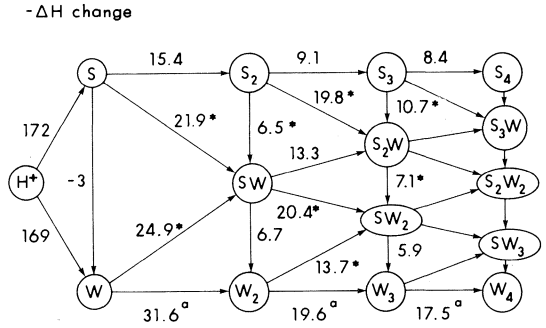

FIG. 4. Enthalpy changes for addition and exchange reactions of protonated clusters containing hydrogen sulfide (S) and water (W). The value corresponds to $-\Delta H$ (kcal/mol). The proton is omitted from the clusters. Values with an asterisk were obtained indirectly from cycles involving directly measured values. The pure water values taken from refs. 7 and 8 are indicated with the superscript [a].

thus indicate a big drop of stability towards dissociation of one molecule. Easily noticed in Fig. 1 is a big gap between (1,2) and (2,3). This is followed by a smaller gap between (2,3) and (3,4) and a big gap again between (3,4) and (4,5).

A similar pattern can be observed in Fig. 5 which shows the measured enthalpy changes for the $(n,n+1)$ reactions in function of n. A decrease of $\Delta H_{n+1,n}$ with n is observed as is generally the case for ion clusters. The results of Fig. 5 show that the decrease is not regular. The fall off between the first three interactions $\Delta H_{2,1}$, $\Delta H_{3,2}$ and $\Delta H_{4,3}$ is rather smooth, then an appreciable decrease occurs between $\Delta H_{4,3}$ and $\Delta H_{5,4}$ followed by an only small decrease to $\Delta H_{6,5}$. This means that the first incoming molecule reacts most strongly, relatively strong interactions occur also for the second and third molecule, while the next two molecules, *i.e.* fourth and fifth, experience weaker interactions. This pattern of interactions is qualitatively very similar to the changes observed earlier for the proton hydrates $H^+(H_2O)_n$, except that the binding energies for the H_2S clusters are very much lower. For the proton hydrates the stability decrease between $H_3O^+(H_2O)_3$ and $H_3O^+(H_2O)_4$ was very much less pronounced than the stability decrease observed between $H_3S^+(H_2S)_3$ and $H_3S^+(H_2S)_4$ observed in the present results. In the earlier studies (1, 2, 7, 8), it was concluded that the Eigen

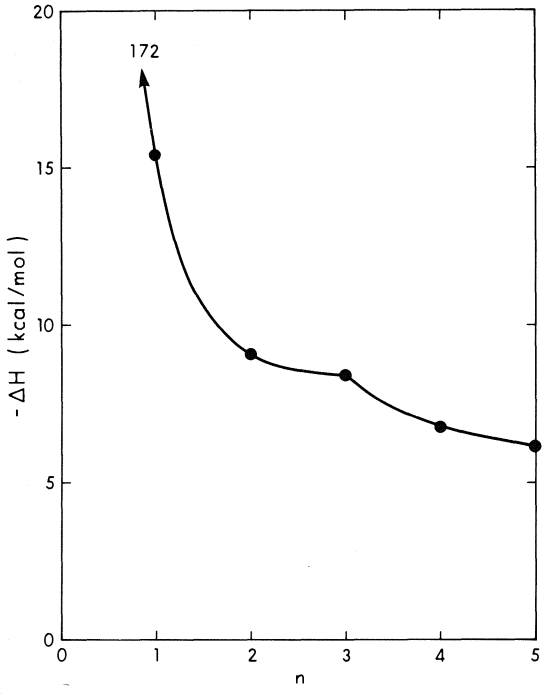

FIG. 5. Plot of experimental $-\Delta H_{n,n+1}$ *vs.* n for the reactions $H^+(H_2S)_n + H_2S \rightleftharpoons H^+(H_2S)_{n+1}$. The number 172 is the proton affinity of hydrogen sulfide obtained in this laboratory (14).

structure (9) $H_3O^+(H_2O)_3$ does not have a really special prominence. It is therefore interesting to compare the water and hydrogen sulfide systems and also examine why the Eigen-type structure should show relatively greater stability in the H_2S system. (The Eigen type structure, H_3S^+-$(H_2S)_3$ is shown in Fig. 6.)

Yamabe *et al.* (10) have examined the electronic structure of H_3S^+ by *ab initio* MO calculations (STO 3G). Their results predict that H_3S^+ has C_{3v} structure with an HSH angle of 94°. The calculated net positive charges on H and S are 0.150 and 0.550 respectively. Comparable calculations for H_3O^+ by Almlöf and Wahlgren (11) predict an HOH angle of 117° and net positive charges on H and O of 0.328 and 0.015 respectively. Thus nearly all the positive charge in H_3O^+ is on the hydrogens. The near planarity of this molecule may be considered to be a consequence of the H^+ repulsions. H_3S^+ is quite different with much more charge on the sulfur atom, consequent smaller hydrogen repulsions and pyramidal structure. The above differences may be considered to largely reflect the higher electronegativity of the oxygen atom. The dipole

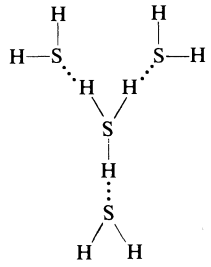

FIG. 6. Structure of cluster $H_3S^+(H_2S)_3$.

moments of H_2S and H_2O are 1.1 and 1.8 D respectively. Considering the much smaller partial positive charges on the H atoms in H_3S^+, the smaller permanent dipole of H_2S and the greater bulkiness of the S atom one has no trouble understanding that the $H^+(H_2S)_n$ clusters are held much more weakly than the corresponding water clusters. The shorter bonds in the water clusters lead to a fairly efficient positive charge transfer from the 'inner' hydrogen atoms of the H_3O to the outer hydrogen atoms in the water molecules of the Eigen structure. This charge dispersal, which is characteristic of 'strong hydrogen bonds', is achieved by a small amount of electron transfer from the outer molecules to the H_3O and by a considerable internal polarization of the outer water molecules. For this reason bonding of the $H_3O(H_2O)_3^+$ to an additional water molecule *i.e.* $-\Delta H_{4,5}^0$ and $-\Delta G_{4,5}^0$ is not weakened appreciably. In the $H_3S(H_2S)_3^+$ system positive charge transfer to the periphery should be much smaller because of the weaker hydrogen bonding, *i.e.* longer bonds with attendant big decrease in electron transfer and polarization. In addition to this comes the smaller permanent dipole of H_2S. Therefore the large drop off at the (4,5) stage is expected. Other solvents with weak bonding abilities have been also observed to show distinct drop off the enthalpy and free energy change after completion of the first shell. For example recent measurements of the solvation of the proton by hydrogen (12) and methane (13) gas showed breaks after the completion of the first 'shell' that were even more distinct than that observed for the hydrogen sulfide system.

Figure 4 shows the enthalpy changes for addition and exchange reactions of protonated clusters containing hydrogen sulfide and water. The proton affinity of hydrogen sulfide is 3 kcal/mol higher than that of water (14). Since the chemical bonding ability of sulfur is much lower,

the slightly better accommodation of the proton by H_2S should be mostly due to the higher polarizability of the H_2S. This slight edge of H_2S is lost when the interactions occur at larger distances and for reasons outlined above the interactions with water when more than one molecule is present are more favorable. Thus we see from Fig. 4 that the addition of one H_2S molecule to H_3S^+ brings only 15.4 kcal/mol exothermicity while the addition of a water molecule ($S \rightarrow SW$) brings a whole 21.9 kcal/mol. The exchange reaction $H^+S_2 + W \rightleftharpoons HSW^+ + S$ is exothermic by $\sim$6.5 kcal while the further exchange $HSW^+ + W \rightleftharpoons HW_2{}^+$ releases an additional $\sim$6.7 kcal/mol. These and the other data in Fig. 4 graphically show how H_2S rapidly becomes a less desired species as the clusters grow. Thus the very weak bonding of H_2S in an acidic aqueous solution is foreshadowed by these results.

It is interesting to compare the present pair for $H^+(H_2O)_n$ and $H^+(H_2S)_n$ with the $H^+(NH_3)_n$ and $H^+(PH_3)_n$ systems for which results were obtained earlier (15, 16). The bonding in the phosphine system was found (16) to be much weaker than that in the ammonia system. This is a result that could have been expected for reasons very similar to those pointed out in the present work for the water and hydrogen sulfide systems. A further analogy could have been expected, namely that the relative drop off in stability between inner- and outer-shell should have been more pronounced for the phosphine system. This, however, was not observed (16). While there is a significant drop off in stability between $NH_4{}^+(NH_3)_4$ and $NH_4{}^+(NH_3)_5$ the change for the corresponding phosphine species seems to be small and continuous (16). The reasons for this result are not very clear.

1. E. P. GRIMSRUD and P. KEBARLE. J. Am. Chem. Soc. **95**, 7939 (1973).
2. K. HIRAOKA, E. P. GRIMSRUD, and P. KEBARLE. J. Am. Chem. Soc. **96**, 3359 (1974).
3. M. P. MERTES. Mechanism of reactions of sulfur compounds. Vol. 2. Intrascience Research Foundation, Santa Monica, Calif. 1968. p. 27.
4. J. E. LOWDER, L. A. KENNEDY, K. G. P. SULZMANN, and S. S. PENNER. J. Quant. Spectrosc. Radiat. Transfer, **10**, 17 (1970).
5. J. S. ROWLINSON. Trans. Faraday Soc. **47**, 120 (1951); J. D. LAMBERT. Discuss. Faraday Soc. **15**, 226 (1953).
6. J. M. HOPKINS and L. I. BONE. J. Chem. Phys. **58**, 1473 (1973).
7. A. J. CUNNINGHAM, J. D. PAYZANT, and P. KEBARLE. J. Am. Chem. Soc. **94**, 7627 (1972).
8. P. KEBARLE, S. K. SEARLES, A. ZOLLA, J. SCARBOROUGH, and M. ARSHADI. J. Am. Chem. Soc. **89**, 6393 (1967).
9. E. WICKE, M. EIGEN, and T. L. ACKERMANN. Z. Phys. Chem. Frankfurt am Main, **1**, 340 (1954).
10. T. YAMABE, TO AOYAGI, S. NAGATA, H. SAKAI, and K. FUKUI. Chem. Phys. Lett. **28**, 182 (1974).
11. J. ALMLÖF and V. WAHLGREN. Theoret. Chim. Acta, **28**, 161 (1973).
12. K. HIRAOKA and P. KEBARLE. J. Chem. Phys. **62**, 2267 (1975).
13. K. HIRAOKA and P. KEBARLE. J. Am. Chem. Soc. **97**, 4179 (1975).
14. R. YAMDAGNI and P. KEBARLE. J. Am. Chem. Soc. **98**, 1320 (1976).
15. S. K. SEARLES and P. KEBARLE. J. Phys. Chem. **72**, 742 (1968).
16. J. W. LONG and J. L. FRANKLIN. J. Am. Chem. Soc. **96**, 2320 (1974).

Photoisomerization of 1-triphenylmethylcyclopentadiene. Di-π-methane rearrangement to 5,6,6-triphenylbicyclo[3.1.0]hex-2-ene

STEFAN WEIGL AND JOHN WARKENTIN

Department of Chemistry, McMaster University, Hamilton, Ont., Canada L8S 4M1

Received August 4, 1976

STEFAN WEIGL and JOHN WARKENTIN. Can. J. Chem. **55**, 29 (1977).

Triphenylmethylcyclopentadiene exists as a mixture of isomers, the minor and major components of which are shown to be 1-triphenylmethylcyclopentadiene (**1**) and 2-triphenylmethylcyclopentadiene (**2**), respectively.

Direct irradiation of a mixture of **1** and **2** led to formation of 5,6,6,-triphenylbicyclo[3.1.0]hex-2-ene (**3**) via rearrangement of **1**. Acetophenone-sensitized irradiation of the same mixture gave **3** as well as a two component mixture of photodimers of **1** and/or **2**. Results are interpreted in terms of the di-π-methane rearrangement mechanism.

STEFAN WEIGL et JOHN WARKENTIN. Can. J. Chem. **55**, 29 (1977).

Le triphénylméthylcyclopentadiène existe sous forme de mélange d'isomères; les composants mineurs et majeurs sont respectivement le triphénylméthyl-1 cyclopentadiène (**1**) et le triphénylméthyl-2 cyclopentadiène (**2**).

L'irradiation directe d'un mélange de **1** et de **2** conduit à la formation de triphényl-5,6,6 bicyclo[3.1.0] hexène-2 (**3**), par l'intermédiaire d'un réarrangement de **1**. Une irradiation sensibilisée par l'acétophénone du même mélange conduit à **3** ainsi qu'à un mélange à deux composants des photodimères de **1** et/ou **2**. On interprète les résultats en terme d'un mécanisme de réarrangement di-π-méthane.

[Traduit par le journal]

Introduction

There are many potential photoreactions of the triphenylmethylcyclopentadiene system. First, monosubstituted cyclopentadienes are interconverted by thermal [1,5]-sigmatropic hydrogen migration and are obtained as mixtures of isomers (1–6), any one or all of which could be photolabile. Second, all three possible isomers have the endocyclic di-π-methane system of cyclopentadiene itself but, in the cases of 1- and 2-triphenylmethylcyclopentadienes, **1** and **2**, respectively, there is an additional di-π-methane system consisting of a double bond of the diene moiety and a phenyl group. Potential photoproducts, therefore, include four triphenylmethylbicyclo[2.1.0]pent-2-enes from the known electrocyclic reaction of the diene singlet (6, 7), eq. 1, two bicyclo[3.1.0]hex-2-enes from di-π-methane rearrangement[1] with phenyl migration, eqs. 2 and 3, and a bicyclo[2.1.1]hex-2-ene from

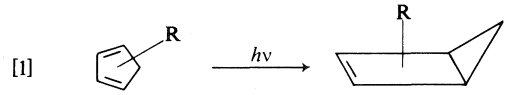

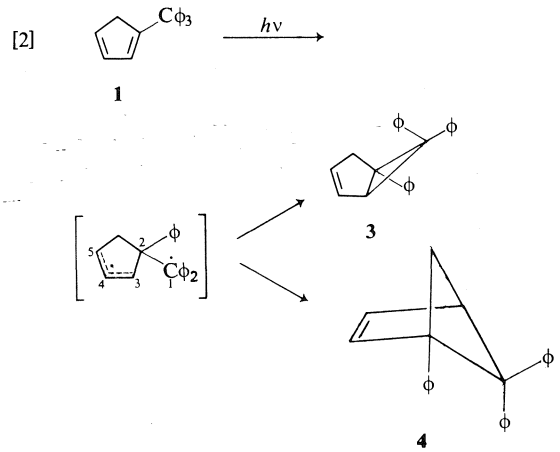

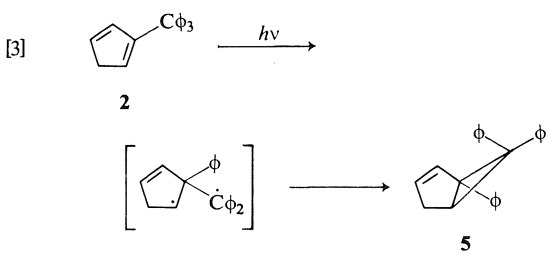

a variant (unprecedented) of that rearrangement, eq. 2. Finally, some of the potential photopathways might require either the singlet or the triplet excited state of the precursor.

[1]Photochemical rearrangement of systems having a single sp^3-hybridized carbon flanked by two π-systems (*e.g.* vinyl and phenyl) has been named *di-π-methane rearrangement* by Zimmerman and co-workers, who first recognized its generality (8).

In this paper we report the identities of the isomers present in triphenylmethylcyclopentadiene and the structure and origin of the photorearrangement product.

Methods, Results, and Discussion

Isomers of Triphenylmethylcyclopentadiene

Riemschneider and Nehrin (9), as well as Werner *et al.* (10) had established that **1** and **2** are the major isomers in triphenylmethylcyclopentadiene mixtures and the equilibrium ratio had been established at 3.8:1 (10). However, neither group was able to establish whether **1** or **2** is the predominant isomer. We speculated that the large trityl group might slow Diels–Alder reaction of **1** more than that of **2**. That postulate turned out to be correct, for treatment of the mixture of **1** and **2** with tetracyanoethylene (**6**) led to rapid consumption of the major isomer only, with formation of 5,5,6,6-tetracyano-2-triphenylmethylbicyclo[2.2.1]hept-2-ene (**7**). Long reaction times led to total conversion of dienes to **7**, presumably by prior rearrangement of **1** to **2**, followed by reaction with **6**. Thus, the major component in the mixture of **1** and **2** is isomer **2**. Methylcyclopentadiene also contains more 2- than 1-isomer at equilibrium but the ratio is only 1.20:1 (2, 4). Since this ratio is opposite in sense to that expected from a hyperconjugative effect of the methyl group (4), and since the effect of replacing the methyl group with the larger triphenylmethyl group is to increase the fraction of 2-substituted diene in the equilibrium mixture, we suggest that the reason for the predominance of 2-alkyl cyclopentadienes over the 1-isomers has to do with greater steric hindrance in the latter.

The pmr spectrum of the cyclopentadiene portion of **2** was assigned with the aid of decoupling and the data are gathered in Table 1.

TABLE 1. Nuclear magnetic resonance spectra of **1** and **2**

Nucleus	Chemical shift (δ)[a] **1**	**2**	J(Hz)[b]
H_1	—	6.08	$J_{1,3} = 1.40$
H_2	6.05–6.40[c]	—	$J_{1,4} = 2.05$
H_3	6.05–6.40[c]	6.20	
H_4	6.05–6.40[c]	6.33	$J_{3,4} = 5.29$
H_5	2.89	3.03	$J_{1,5} = 1.83$[d], $J_{4,5} = 1.85$[d]
C_1	154.2[e]	130.1[e]	$J_{3,5} = 0.92$[d]
C_2	128.3[e]	152.4[e]	
C_3	132.7[e]	136.9[e]	
C_4	131.3[e]	131.9[e]	
C_5	44.5[e]	40.6[e]	
C_6	62.2[e]	60.9[e]	

[a] ^{1}H spectra: 100 MHz, $CDCl_3$, TMS. ^{13}C spectra: 90 MHz, $CDCl_3$, TMS.
[b] Determined by decoupling, except where otherwise indicated.
[c] Not resolved from other signals in the vinyl region.
[d] Estimated by computer simulation of the vinylic signals.
[e] Assignments based on relative intensities and the known isomer ratio (**2**:**1** = 4.5), as well as by analogy, using methylcyclopentadiene spectra as models (11).

Identity of Photoproduct ***3***

The structure of the photorearrangement product followed from molecular weight and composition data (see Experimental) and from its spectra. A cyclopropane ring was inferred from ir bands at 3.25 and 9.80 μm (12). The uv spectrum (cyclohexane, max 275 (350); plateaus 267 (850), 260 (1205) and 227 nm (ε 20 153)) is similar to that of 6,6-diphenylbicyclo[3.1.0]hex-2-ene (13) (uv, cyclohexane, max 276 (700); plateaus 268 (1145), 260 (1560), and 227 nm (ε 12 800)) and indicated that the cyclopropane ring bears two or more phenyl substituents. Particularly useful in the structure elucidation were the ^{1}H and ^{13}C nmr spectra (Table 2). Off-resonance decoupling of the ^{13}C spectrum showed that the four high-field signals must be attributed to two quaternary, one tertiary, and one secondary carbon. Decoupling of the ^{1}H spectrum showed that the methine proton resonating at 3.21 δ is coupled weakly (1.5 Hz) to the methylene protons. That feature rules out the isomeric 1,6,6-triphenylbicyclo[3.1.0]hex-2-ene (**5**), in which the methine and methylene protons would be vicinally coupled. Model bicyclo[3.1.0]hex-2-enes show approximately 7 Hz coupling to one of the methylene protons and 0–2 Hz coupling to the other (14, 15). In the case of accidental magnetic equivalence of the methylene protons, one would expect the vicinal coupling constant to the cyclopropyl proton to be of 3–4 Hz magnitude. Clearly, the observed spectrum is not compatible with structure **5** but does fit **3**.

Bicyclo[2.1.1]hexene system **4** can be ruled out, not only on the basis of the ir and uv data cited above but also on the basis of the ^{1}H spectrum, in which one would expect to see strongly differentiated methylene protons.

Photochemistry

Direct irradiation of a solution of **1** and **2** in benzene (see Experimental) yielded **3** cleanly, with 45% conversion. Chromatographic separation of unreacted starting material revealed that the latter was depleted in isomer **1** (**2**:**1** $\geqslant$ 10).

TABLE 2. Nuclear magnetic resonance spectra of **3**

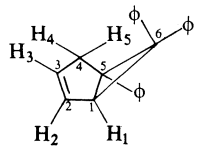

Nucleus	Chemical shift (δ)[a]	*J*(Hz)
H_1	3.21 q[b]	$J_{1,2} = 2.0, J_{1,3} \simeq 0.0$
H_2	5.91 m	$J_{1,4} = J_{1,5} = 1.5$
H_3	5.19 m	$J_{2,3} = 5.5, J_{2,4} = J_{2,5} = 2.0$
H_4, H_5	2.83 q[b]	$J_{3,4} = J_{3,5} = 2.0$
ArH	6.75–7.30 m	
C_1	40.54 d[c,d]	
C_4	42.06 t[c]	
C_5	44.31 s[c]	
C_6	48.18 s[c]	

[a]^{1}H spectra: 100 MHz, CCl_4, TMS. ^{13}C spectra: 90 MHz, $CDCl_3$, TMS.
[b]Pseudo quartet.
[c]Off-resonance decoupled.
[d]C_2 and C_3 signals mixed in with aromatics.

Control experiments showed that **1** and **2** elute together from the column that was employed and that the chromatographic process itself did not alter the ratio (**2**:**1** ≃ 4.5) in an unirradiated sample. The simplest explanation for the change in isomer ratio as a result of irradiation is that **1** is more reactive than **2** in the di-π-methane rearrangement. The fact that only one product (**3**) was detectable suggests that **2** does not undergo any photorearrangement on direct irradiation, with the possible exception of [1,3]-sigmatropic shifts which would interconvert it with **1**.

Formation of **3** can be interpreted in terms of the di-π-methane rearrangement (8, 16). The process is most easily visualized in terms of diradical intermediates [1] although such pictures do not necessarily represent actual minima on the potential energy surface but are more likely points on the energy surface of a concerted process (8, 16, 17). The fact that **4** is not obtained is understandable because the 1,5-overlap required to reach it is expected to be poor, relative to 1,3-overlap required in the transition state leading to **3** (eq. 2, arbitrary numbering in bracketed structure). A diradical representation is also useful for rationalizing the inefficient di-π-methane rearrangement of **2**, for which an unconjugated, as opposed to an allylic, radical site develops along the reaction coordinate [2].

Acetophenone sensitized reaction of **1** and **2** led to **3** and two other major products. Although the latter were not separated from each other, analyses and osmometric molecular weight determination of the mixture indicated that they are dimers of **1** and/or **2**. A melting point determination on a microscope-equipped hot stage showed two crystalline solids melting at 199 and 234 °C, respectively.

Sensitized photodimerization of cyclopentadiene to form both the *exo* and *endo* (4 + 2) cycloadducts as well as a (2 + 2) cycloadduct has been reported (18) and sensitized addition of cyclopentadiene to alkenes, such as *cis*- and *trans*-but-2-ene is also well known (19). Formation of dimers from use of a triplet sensitizer in the present case was therefore expected and the interesting results are, first, that only two of the many possible dimers can be detected and, second, that **3** is formed. The former result can be attributed to the large steric requirements of the trityl groups which would make for exceedingly crowded transition states for some potential cycloadditions. The latter result implies that both the singlet and the triplet excited states of **1** undergo the di-π-methane rearrangement. Sensitized reaction must involve the triplet, for the sensitizer absorbs nearly all of the light and the products include dimers typical of triplet diene reactions. Unsensitized rearrangement could also involve the triplet as the rearranging species but, if that were the case, dimers should be formed in that reaction also. We conclude that the singlet of **1** undergoes rearrangement more rapidly than intersystem crossing, that the triplet of **1** undergoes the same rearrangement in competition with intermolecular cycloadditions, and that neither excited state of **2** rearranges. Presumably, the triplet of **2** also adds to **1** and/or **2**.

Generalizations concerning structure–multiplicity relationships for the di-π-methane rearrangement have been proposed by Zimmerman and co-workers (8, 17). They proposed that an unconstrained system (*e.g.* one having at least one of the π-moieties capable of causing geometric change via rotation) is capable of fast deactivation of its triplet excited state. That deactivation stops (or slows) rearrangement and such a system therefore rearranges from the singlet state only. A constrained di-π-methane, being unable to deactivate as rapidly after intersystem crossing, does rearrange from the triplet state. It may or may not rearrange to the same product from the singlet state, depending on what other singlet reactions are possible.

At least one example has been reported of a

system which undergoes di-π-methane rearrangement from both the singlet and the triplet manifolds (20). Compound **1** appears to be another system which behaves in that way.

We do not have an explanation for the apparent failure of **1** and/or **2** to form bicyclo[2.1.0] hex-2-enes [1] in the direct irradiation. For the case of **1**, the alternative di-π-methane reaction may simply be faster but that rationale is an unlikely one for the case of **2**, which does not undergo di-π-methane rearrangement. One possibility is that some or all of the substituted bicyclo[2.1.0]hex-2-enes [1] are simply too labile, thermally, to accumulate to detectable concentration levels.

Experimental

Triphenylmethylcyclopentadienes (1 and 2)

Treatment of cyclopentadienyl magnesium bromide, prepared from cyclopentadiene (10.0 g, 0.15 mol) and a slight excess of ethylmagnesium bromide, with triphenylchloromethane (26.0 g, 0.095 mol) as described in the literature (3) afforded a mixture of **1** and **2** (11.5 g, 40%), mp 197–199 °C after crystallization of the crude product from benzene. The pmr spectrum consisted of signals at δ 2.89 (m), 3.03 (m), 6.08 (m), 6.10–6.39 (m), and 7.15 (s). Integration of the signals at 2.89 and 3.03 δ, attributable to **1** and **2**, respectively, gave the ratio **2**:**1** = 4.5.

Reaction with Tetracyanoethylene (6)

A mixture of **1** and **2** (**2**:**1** ≃ 4.5) (0.500 g, 1.62 mmol) in dry benzene (8 ml) was added during 10 min to a stirring solution of **6** (0.209 g, 1.63 mmol) in dry benzene (7 ml), at 20 °C. After a further 20 min an aliquot was removed and the solvent was evaporated from it at reduced pressure. The pmr spectrum ($CDCl_3$) had, in addition to the signals listed below for **7**, a signal at 2.89 δ but none at 3.03 δ. An aliquot taken after 4 days did not absorb at 2.89 δ. Evaporation of the solvent from the main reaction mixture at that time afforded a residue which was recrystallized from benzene – petroleum ether to yield 0.576 g (82%) of **7** as colorless crystals: mp, decomposition at 206 °C; pmr ($CDCl_3$, δ) 2.38 (AB quartet, 2H, J_{AB} = 11.4 Hz, additional fine coupling, H_7), 3.95 (m, 1H, H_4), 4.44 (m, 1H, H_1), 6.13 (m, 1H, H_3), 7.05–7.40 (m, 15H); ^{13}C nmr ($CDCl_3$, δ, off resonance decoupled) 58.78 (d, C_1), 55.88 (d, C_4), 46.85 (s, C_5 or C_6), 47.98 (s, C_6 or C_5), 48.89 (t, C_7), 109.82, 111.47, 112.06, and 112.22 (s, CN), 63.39 (s, ϕ_3C). *Anal.* calcd. for $C_{30}H_{20}N_4$: C 82.54, H 4.62, N 12.84; found: C 82.23, H 4.85, N 12.99.

Direct Irradiation of 1 and 2

A Hanovia type L 450 W lamp was used in a water-cooled, quartz immersion apparatus fitted with magnetic stirrer and argon purging tubes. In a typical experiment, the mixture of **1** and **2** (2.05 g, 6.7 mmol) in 400 ml of cyclohexane (spectroquality, Matheson, Coleman and Bell) was irradiated for 12 h. The solvent was distilled off at reduced pressure and the orange residue was chromatographed on silica gel (Woelm, activity grade 1, 2.2 × 33 cm column) using CCl_4 as eluant. Product **3**, still contaminated with a trace of starting material, was further purified by preparative thin layer chromatography (silica gel, 50:50 hexane–cyclohexane). Crystallization from benzene gave **3** as colorless prisms: mp 108–109 °C; molecular ion (*m/e*) 308; ir (CCl_4 and CS_2) 3.27, 3.30, 13.21, 13.61, 13.87, 14.34, and 14.53 (strong), 3.24, 3.44, 6.28, 6.74, 9.38 and 9.80 (medium), 3.53, 7.04, 7.30, 7.48, 7.58, 7.67, 7.87, 8.62, 8.78, 9.94, 10.72, 10.87, 10.99, 11.11, 12.69, and 12.85 μm (weak). *Anal.* calcd. for $C_{24}H_{20}$: C 93.46, H 6.54, found: C 93.18, H 6.50. The nmr spectra of **3** are in Table 2.

Sensitized Irradiation of 1 and 2

The apparatus was the same as that described above except for a Pyrex sleeve around the lamp. A solution of **1** and **2** (10.0 g, 29.2 mmol) and freshly-distilled acetophenone (5.03 g, 41.8 mmol) in 500 ml of benzene was irradiated for 12 h. Vacuum distillation of the solvent and tlc of the residue showed four components, two of which were acetophenone and starting material (**1** and **2**). Column chromatography on neutral Alumina (80–200 mesh, Brockman, activity grade 1, 4.0 × 63 cm column) with hexane–cyclohexane (50:50) separated **1** and **2** (together) from the other components. A second component was eluted with 10% benzene – 90% hexane, and was followed by a fraction containing a third component contaminated with the second. That fraction was rechromatographed on a 2.2 × 55 cm column to yield pure third component.

Recrystallization of the second component from benzene gave colorless prisms of **3**, mp 108–109 °C, spectra as described above. Recrystallization of the third component from benzene gave granular crystals: mp 199–234 °C; mw (osmometric) 616, mw (ms) 616 (parent ion). Examination of the crystals with a microscope (Kofler hot stage) revealed two distinct types with sharp melting points of 199 and 234 °C.

Acknowledgments

The authors are grateful to Mr. Brian Sayer for the nmr spectra and to the National Research Council of Canada for financial support.

1. K. Alder and H. Holzrichter. Ann. **524**, 145 (1936).
2. V. A. Moronov, E. V. Sobolev, and A. N. Elizarova. Tetrahedron, **19**, 1939 (1963).
3. R. Riemschneider, A. Reisch, and H. Hovak. Monatsh. **91**, 805 (1960).
4. S. Mclean and P. Haynes. Tetrahedron Lett. 2385 (1964); Tetrahedron, **21**, 2329 (1965).
5. S. Mclean, C. J. Webster, and R. J. D. Rutherford. Can. J. Chem. **47**, 1555 (1969).
6. S. Mclean and D. M. Findlay. Can. J. Chem. **48**, 3107 (1970).
7. J. I. Brauman, L. E. Ellis, and E. E. van Tamelen. J. Am. Chem. Soc. **88**, 846 (1966).
8. H. E. Zimmerman and P. S. Mariano. J. Am. Chem. Soc. **91**, 1718 (1969) and references cited therein.

9. R. RIEMSCHNEIDER and R. NEHRIN. Monatsh. **91**, 824 (1960).
10. H. WERNER, G. MATTMANN, A. SALZER, and T. WINKLER. J. Organomet. Chem. **25**, 461 (1970).
11. Y. K. GRISHIN, N. M. SERGEYER, and Y. A. USTYNYUK. Org. Magn. Reson. **4**, 377 (1972).
12. J. M. DERFER, E. E. PICKETT, and C. E. BOORD. J. Am. Chem. Soc. **71**, 2484 (1949).
13. H. E. ZIMMERMAN, D. S. CRUMRINE, D. DÖPP, and P. S. HUYFFER. J. Am. Chem. Soc. **91**, 434 (1969).
14. M. P. SCHNEIDER and R. J. CRAWFORD. Can. J. Chem. **48**, 628 (1970).
15. J. MEINWALD and P. H. MAZZOCHI. J. Am. Chem. Soc. **89**, 1755 (1967).
16. H. E. ZIMMERMAN and G. E. SAMUELSON. J. Am. Chem. Soc. **91**, 5307 (1969).
17. H. E. ZIMMERMAN and A. C. PRATT. J. Am. Chem. Soc. **92**, 6267 (1970).
18. N. J. TURRO and G. S. HAMMOND. J. Am. Chem. Soc. **84**, 2841 (1962).
19. B. D. KRAMER and P. D. BARTLETT. J. Am. Chem. Soc. **94**, 3934 (1972) and references cited therein.
20. R. C. HAHN and L. J. ROTHMAN. J. Am. Chem. Soc. **91**, 2409 (1969).

La formation de biphénylènes par pyrolyse de mélanges de précurseurs de benzynes

ANDRÉ MARTINEAU ET DON C. DEJONGH[1]

Département de chimie, Université de Montréal, C.P. 6210, Succ. A, Montréal (Qué.), Canada H3C 3V1

Reçu le 25 mai 1976

ANDRÉ MARTINEAU et DON C. DEJONGH. Can. J. Chem. **55**, 34 (1977).

Nous décrivons une nouvelle méthode d'obtention des biphénylènes substitués sur un cycle. La pyrolyse en phase gazeuse de mélanges de précurseurs de benzynes appropriés est utilisée pour ces synthèses. La rencontre de deux benzynes provenant de sources différentes conduit à la formation des dits biphénylènes. Les divers composés sont sublimés dans un courant d'azote, puis entraînés dans une colonne de quartz non garnie, chauffée extérieurement par un four.

La pyrolyse simultanée de la ninhydrine et de l'anhydride tétrachlorophtalique (rapport molaire 2:1), à 800 °C, donne le tétrachloro-1,2,3,4 biphénylène avec un rendement de 31%. La pyrolyse du mélange anhydride phtalique – anhydride méthyl-4 phtalique, à 850 °C, conduit à la formation du méthyl-2 biphénylène (rapport molaire 9:1) (16%).

ANDRÉ MARTINEAU and DON C. DEJONGH. Can. J. Chem. **55**, 34 (1977).

A new method of forming biphenylenes substituted on one ring is described using gas-phase pyrolysis of mixtures of precursors of appropriate benzynes. The reaction of two benzynes coming from two different sources leads to the formation of the biphenylenes. The mixture of compounds is sublimed into a current of nitrogen and led into an unpacked quartz column heated externally by a furnace.

The simultaneous pyrolysis of ninhydrin and tetrachlorophthalic anhydride (molar ratio, 2:1) at 800 °C gives 1,2,3,4-tetrachlorobiphenylene in a 31% yield. The pyrolysis of a mixture of phthalic anhydride and 4-methylphthalic anhydride at 850 °C leads to the formation of 2-methylbiphenylene (molar ratio, 9:1) (16%).

Introduction

Plusieurs méthodes d'obtention des biphénylènes sont connues dans la littérature; trois d'entre elles sont retenues pour l'intérêt qu'elles ont suscité chez plusieurs chercheurs. La première méthode fut proposée par Lothrop. Il obtint le biphénylène (**1**) par distillation du diiodo-2,2′ biphényle sur de l'oxyde cuivreux (1). Par la suite, certains biphénylènes substitués ont été obtenus par cette méthode (2–7).

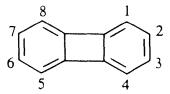

1

La deuxième méthode concerne la substitution électrophile sur le biphénylène. Un grand nombre de biphénylènes nouveaux ont pu être obtenus de cette façon (3, 8–10). Il faut cependant noter que les règles de substitutions ne permettent que la synthèse de certains biphénylènes.

Vers 1965, certains chercheurs ont commencé à préparer le benzyne dans la phase gazeuse par pyrolyse à haute température de produits simples. Brown et Solly ont fait la pyrolyse en phase gazeuse de l'indanetrione (**2**) dans une colonne de quartz garnie d'hélices de Pyrex (11, 12). À 600 °C sous une pression de 0.2 torr, ils ont obtenu le biphénylène avec un rendement de 40%; le biphényle, le naphtalène, le fluorène, le phénanthrène, l'anthracène et le triphénylène furent aussi présents. La même pyrolyse à 500 °C a conduit à la formation du biphénylène (17%), de la benzocyclobutènedione (**3**) (11%) et de la fluorènone (**4**) (1.2%) [1].

[1] 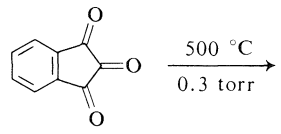

2

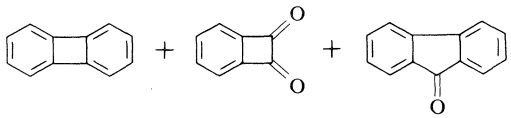

1 (17%) **3** (11%) **4** (1.2%)

[1]A qui toute demande d'information devra être adressée.

D'autre part, Cava *et al.* ont entrepris la pyrolyse des anhydrides phtalique (**5**), tétrachlorophtalique (**6**) et tétrabromophtalique (13). Les pyrolyses furent faites dans un courant d'azote, les anhydrides étant entraînés sur un fil de Nichrome chauffé à 800 °C. Pour la pyrolyse de l'anhydride phtalique (**5**), un rendement de biphénylène situé entre 10 et 15%, basé sur l'anhydride non récupéré (33% récupéré), fut obtenu. La pyrolyse de l'anhydride tétrachlorophtalique (**6**) dans les mêmes conditions a conduit à la formation de l'hexachlorobenzène (**7**) (34%) et de l'octachlorobiphénylène (**8**) (30%), éq. 2. Enfin, la pyrolyse de l'anhydride tétrabromophtalique n'a conduit qu'à la formation de l'hexabromobenzène (20%).

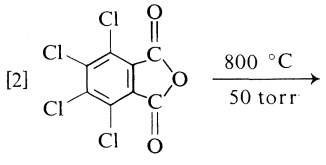

6

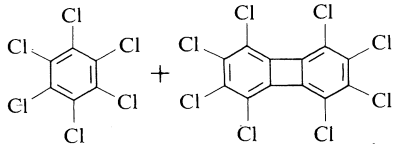

7 (34%) **8** (30%)

Brown et coll. ont aussi fait la pyrolyse de l'anhydride phtalique (14, 15). Leur pyrolyse a été faite dans une colonne non garnie, à 760 °C, sous une pression de 0.3 torr, et a conduit à la formation du biphénylène (9%), du triphénylène (1.5%) et de petites quantités de naphtalène, de biphényle et de fluorène; 71% du produit de départ a été récupéré. A 830 °C, dans les mêmes conditions, le rendement de biphénylène monte à 17% et les produits mineurs sont presque absents.

La pyrolyse de certains anhydrides phtaliques substitués a été faite et les biphénylènes correspondants ont été obtenus (15). Ainsi furent obtenus le dichloro-2,6 (15%), le tétrachloro-2,3,6,7 (6.5%), le tétrachloro-1,4,5,8 (4%), l'octachloro (**8**) (26%) et le tétraméthyl-2,3,6,7 (3%) biphénylène. D'autre part, parmi les composés polycarbonylés, la pyrolyse de l'anhydride *o*-sulfobenzoïque (15) a été faite. A 730 °C, dans une colonne garnie de tubes de quartz, le biphénylène a été obtenu; un rendement de 5.5% a été calculé.

On trouve dans la littérature d'autres préparations de biphénylènes par pyrolyse de composés précurseurs de benzyne ou du diradical-2,2′ biphényle (16–21). Par exemple, la pyrolyse du dioxyde-1,1 de méthyl-5 benzothiadiazole (**9**) conduit à la formation des diméthyl-2,6 (**10**) et diméthyl-2,7 (**11**) biphénylènes (17), [3]. Aussi, Adger *et al.* ont fait la pyrolyse de benzotriazines-1,2,3 (21). Ils pensaient obtenir les benzazètes correspondants, mais ont obtenu le biphénylène.

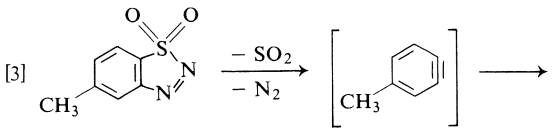

9

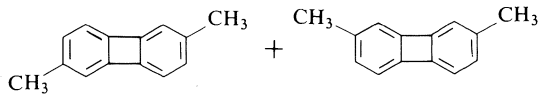

10 **11**

Fields et Meyerson ont fait la pyrolyse de plusieurs anhydrides aromatiques et hétérocycliques, dans le benzène et la pyridine (22). La formation de produits formés par réaction des benzynes avec le solvant a été constatée.

Parmi les différentes méthodes énumérées jusqu'ici impliquant la pyrolyse en phase gazeuse, on remarque que toutes impliquent la décomposition d'un seul composé à la fois. Ceci a pour effet de conduire à la formation du biphénylène, quand le produit de départ n'est pas substitué, et, dans le cas contraire, à la formation de biphénylènes substitués symétriquement sur les deux cycles.

Partant de ce que l'obtention des différents biphénylènes se fait par un intermédiaire benzyne, nous nous sommes proposés d'obtenir certains biphénylènes substitués sur un cycle par pyrolyse de mélange de diverses sources de benzyne et de benzynes substitués.

Partie théorique

Notre démarche nous a d'abord conduit à examiner deux sources de benzyne: les pyrolyses de l'anhydride phtalique (**5**) et de la ninhydrine (**12**) ont été faites à différentes températures avec notre appareillage. Nous avons ensuite entrepris la pyrolyse de deux anhydrides phtaliques substitués; dans un premier cas, les halogènes sont utilisés comme substituants et, dans l'autre, un groupement aliphatique. Ainsi, les pyrolyses des

anhydrides tétrachlorophtalique (**6**) et méthyl-4 phtalique (**13**) ont été faites pour examiner leur comportement individuel avec la chaleur. En dernier lieu, la pyrolyse d'un mélange composé de ninhydrine et d'anhydride tétrachlorophtalique a été entreprise d'une part et, d'autre part, la pyrolyse du mélange anhydride phtalique – anhydride méthyl-4 phtalique. La pyrolyse se produit dans un courant d'azote; les produits sont condensés dans une série de trappes refroidies et, par la suite, sont analysés dans la plupart des cas par cpg.

Sources de benzyne

Nous avons décidé de réexaminer le comportement de l'anhydride phtalique (**5**) avec la chaleur dans les conditions dictées par notre appareillage. La pyrolyse du composé **5** a été faite à différentes températures. Les produits obtenus à 825 °C sont des traces de naphtalène et de fluorène, le biphénylène (5%) et de l'anhydride phtalique récupéré. Ceci représente le meilleur rendement de **1** que nous ayions obtenu à partir de **5** seul. Donc nos résultats montrent des rendements de biphénylène assez faibles. L'augmentation de la température de pyrolyse fait se consommer plus de produit de départ, sans pour autant augmenter de façon appréciable les rendements de **1**. D'autre part, les rendements de **1** sont plus petits que ceux obtenus (15%) par Cava *et al.* à 800 °C avec le fil de Nichrome (13).

Comme deuxième source de benzyne, nous avons examiné la pyrolyse de la ninhydrine (**12**). On trouve dans la littérature la pyrolyse du composé **12** sous sa forme déshydratée (indanetrione-1,2,3 (**2**)), (11, 12). Nous avons tout de même pyrolysé le composé **12**, en supposant que la déshydratation se ferait "in situ" et que l'eau ainsi formée ne gênerait pas la formation du biphénylène.

A 700 °C, le composé **1** uniquement est obtenu (40%), tandis qu'à 800 °C, c'est encore le seul produit obtenu mais son rendement diminue (32%). Lorsque la pyrolyse est faite à 600 °C, deux produits sont présents: le composé **1** avec un rendement de 19%, inférieur à ce qu'il est à 700 °C, et la benzocyclobutènedione (**3**) (39%). Dans chacun des cas, aucun produit de départ n'est récupéré. Ceci est en accord avec les résultats obtenus par Brown et Solly (11, 12).

Sur la base de ces résultats, il ressort que la ninhydrine (**12**) est un meilleur précurseur de benzyne que l'anhydride phtalique (**5**) dans le cas de notre appareillage. De plus, la pyrolyse du composé **12** se fait à des températures plus basses et avec une efficacité plus grande, si l'on tient compte du produit de départ récupéré. Etant donné ces résultats, le plus grand intervalle de température dans lequel le composé **12** se pyrolyse peut être une variable importante dans la pyrolyse de mélanges.

Pyrolyse des anhydrides substitués

La pyrolyse de l'anhydride tétrachlorophtalique (**6**) est déjà connue dans la littérature (13, 15). Dans un premier cas, un fil de Nichrome chauffé à 800 °C est utilisé (13). Les produits obtenus sont l'hexachlorobenzène (**7**) et l'octachlorobiphénylène (**8**) avec des rendements respectifs de 34% et 30%. Dans un autre cas, la pyrolyse a été faite à 700 °C avec une colonne de quartz garnie (15). Les mêmes produits sont obtenus; des rendements respectifs de 31% et 26% ont été calculés pour les composés **7** et **8**. Avant de faire la pyrolyse de mélange impliquant la ninhydrine et l'anhydride tétrachlorophtalique, nous avons voulu refaire la pyrolyse du composé **6** pour vérifier si les mêmes produits sont obtenus dans les conditions dictées par notre appareillage.

La pyrolyse du composé **6** a été faite à 800 °C. Les produits obtenus les plus importants sont l'hexachlorobenzène (**7**, 44%) et l'octachlorobiphénylène (**8**, 32%). Les produits mineurs sont le pentachlorobenzène (3%) et le décachlorobiphényle (3%).

Un deuxième anhydride substitué a été examiné; le choix de l'anhydride méthyl-4 phtalique (**13**) a été fait. Nous voulions voir si la différence des substituants pouvait faire varier les conditions d'obtention des biphénylènes substitués sur un cycle. La démarche entreprise pour l'anhydride tétrachlorophtalique a été utilisée à nouveau. Une pyrolyse du composé **13** seul a été faite pour voir si le biphénylène correspondant était obtenu. Le choix de la température a été fait par analogie avec les résultats obtenus pour les pyrolyses des composés **5** et **6**.

Ainsi, la pyrolyse de l'anhydride **13** a été faite à 825 °C. A cette température, une grande partie du produit de départ est récupérée. Le diméthylbiphénylène a, d'autre part, été obtenu. La pyrolyse du dioxyde-1,1 de méthyl-5 benzothiadiazole (**9**) passe par le même intermédiaire, méthyl-4 benzyne, que dans notre cas et conduit à la formation des composés **10** et **11** (17). Sur

cette base, nous supposons que ces deux isomères sont aussi présents dans nos produits de pyrolyse. De plus, le diméthylfluorène a été obtenu. Sur la même base que précédemment, nous présumons que trois isomères sont présents. Aucune détermination des quantités de produits n'a été faite, puisque le but de cette pyrolyse était de voir si le biphénylène attendu était formé. Cependant, on remarque en plus d'une grande récupération du produit de départ qu'on obtient d'après le chromatogramme, une quantité relativement grande de diméthylbiphénylène. Les quantités relatives de diméthylfluorène sont plus petites.

Compte tenu que les biphénylènes désirés ont été formés, nous avons été encouragés à faire les pyrolyses de mélanges. Les températures utilisées, 800 °C pour le composé **6** et 825 °C pour l'anhydride **13**, serviront de base pour les pyrolyses de mélanges.

Pyrolyse des mélanges

Notre première préoccupation dans la pyrolyse des mélanges est de trouver les conditions de température maximales pour l'obtention des biphénylènes substitués sur un cycle. Concernant la synthèse du tétrachloro-1,2,3,4 biphénylène (**14**), nous nous sommes basés sur les résultats obtenus pour les pyrolyses des composés seuls. Les rendements élevés du biphénylène dans la pyrolyse de la ninhydrine à 700 et 800 °C, et l'absence de l'anhydride tétrachlorophtalique récupéré dans la pyrolyse de ce dernier à 800 °C, nous ont conduits à faire la pyrolyse du mélange de ces composés à 800 °C. Des pyrolyses qualitatives ont cependant été faites pour s'assurer de la validité de notre choix. Des quantités relatives maximums du composé **14** sont obtenues pour des températures de pyrolyse de 750 et 800 °C. On note cependant à 750 °C la présence de l'anhydride tétrachlorophtalique dans les produits de pyrolyse; à 800 °C, aucune quantité de composé **6** n'est récupérée. La pyrolyse quantitative du mélange des composés **6** et **12** a donc été faite à 800 °C (voir tableau 1).

Une investigation sur le rendement du composé **14** en fonction des proportions relatives de chacun des composés de départ a été faite. Des mélanges de composés **6** et **12** ont été pyrolysés à 800 °C avec des rapports molaires respectifs de 1:2, de 1:3 et de 1:9; les résultats sont résumés dans le tableau 1. Parmi les produits obtenus, les plus importants sont le biphénylène (**1**) et le tétrachloro-1,2,3,4 biphénylène (**14**). Les produits mineurs sont le tétrachloro-1,2,3,4 naphtalène (**15**), l'octachlorobiphénylène (**8**) et le décachlorobiphényle. Ces produits sont en accord avec les résultats attendus (schéma 1).

Uniquement les rendements des produits **1** et **14** ont été calculés. Bien qu'aucune détermination précise de la quantité de tétrachloro-1,2,3,4 naphtalène (**15**) n'ait été faite, elle est apparue environ six fois plus petite que la quantité de produit **14**, indépendamment du rapport des composants du mélange.

On note que le rendement de biphénylène augmente avec la quantité de ninhydrine initialement pesée. D'autre part, on constate que le rendement de tétrachloro-1,2,3,4 biphénylène (**14**) ne varie pas avec le pourcentage de ninhydrine employée.

On note dans la pyrolyse d'un même mélange, un certain écart dans la reproductibilité des résultats. Nous sommes portés à croire que le facteur responsable de ces différences est la sublimation individuelle des composés formant le mélange. La synthèse du tétrachloro-1,2,3,4 biphénylène implique la rencontre de benzynes provenant de sources différentes et une variation dans la sublimation aura un effet sur les rendements des produits obtenus. Cet effet est dû à ce que les composés formant le mélange ne se subliment pas à la même température.

Quand nous avons entrepris la pyrolyse d'un mélange conduisant à la formation du méthyl-2 biphénylène (**16**), nous nous sommes d'abord intéressés à la température à laquelle il faudrait pyrolyser ce mélange. La ninhydrine (**12**) s'étant avérée une meilleure source de benzyne que l'anhydride phtalique dans nos pyrolyses préliminaires, nous avions pensé l'utiliser à nouveau dans la pyrolyse impliquant l'anhydride méthyl-4 phtalique (**13**). Le choix de la température pour la pyrolyse du mélange ninhydrine – anhydride méthyl-4 phtalique a été fait sur la base des résultats obtenus pour les pyrolyses des composés seuls. La présence satisfaisante des diméthylbiphénylènes dans les produits de la pyrolyse du composé **13** à 825 °C et le rendement important de biphénylène (32%) dans la pyrolyse du composé **12** à 800 °C nous ont conduits à pyrolyser le mélange de ces deux composés à 825 °C.

En se basant sur les résultats obtenus dans la section précédente, la quantité de ninhydrine employée dans une première pyrolyse a été mise

TABLEAU 1. Pyrolyses du mélange ninhydrine (**12**) – anhydride tétrachlorophtalique (**6**)*

6 (mg)	**12** (mg)	Rapport molaire	Rendement de **1** (%)	Rendement de **14** (%)
288.3	360.7	1:2	20	20
284.4	356.2	1:2	17 } 21 ± 4	38 } 31 ± 9
286.0	355.7	1:2	25	34
284.1	533.9	1:3	26	24
284.1	533.5	1:3	39 } 37 ± 10	37 } 29 ± 7
284.2	534.1	1:3	46	27
143.4	802.1	1:9	47	31
142.4	800.7	1:9	63 } 60 ± 12	38 } 33 ± 5
142.4	800.7	1:9	71	29

*Les pyrolyses ont été faites à 800 °C, sous une pression de 0.2 torr avec un débit d'azote de 90 ml/min.

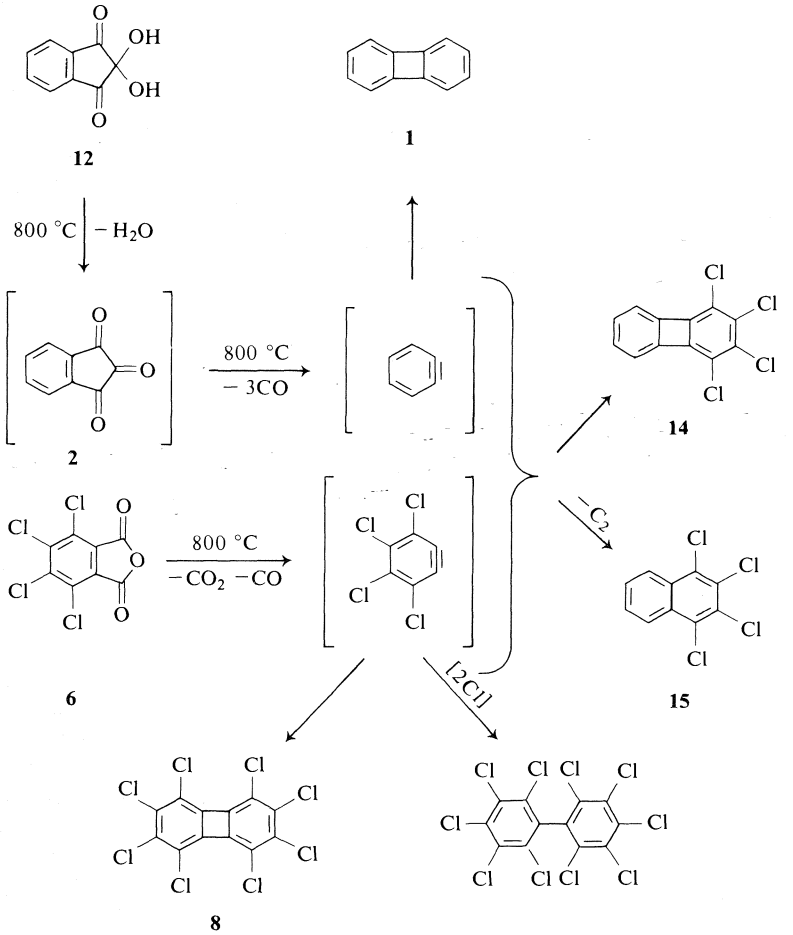

SCHÉMA 1

au double de celle de l'anhydride. L'analyse des produits de pyrolyse a montré la présence d'une faible quantité de méthyl-2 biphénylène. Aucune étude quantitative n'a été faite dans ce cas. Nous avions noté, au cours de la pyrolyse, que l'anhydride **13** se sublimait en premier et que le composé **12** (après déshydratation "in situ") se sublimait beaucoup plus tard. Cette observation expliquait en quelque sorte pourquoi si peu de méthyl-2 biphénylène avait été formé.

TABLEAU 2. Pyrolyse du mélange anhydride phtalique (**5**) – anhydride méthyl-4 phtalique (**13**)*

			Récupéré (%)		Rendements (%)		
5 (mg)	**13** (mg)	Rapport molaire	**5**	**13**	**1**†	**16**‡§	**10** + **11**‡
665.7	243.5	3:1	15	2	15	11	10
677.9	247.7	3:1	35	6	17	9	21
999.8	123.8	9:1	8	Trace	32	16	7
1002.6	123.6	9:1	14	Trace	15	16	10

*Ces pyrolyses ont été faites à 850 °C sous une pression de 0.2 torr avec un débit d'azote de 90 ml/min.
†Ces rendements sont basés sur les quantités d'anhydride phtalique non récupérées.
‡Ces rendements sont basés sur les quantités d'anhydride méthyl-4 phtalique non récupérées.
§Les temps de rétention du fluorène, formé dans les pyrolyses conduisant au benzyne (11, 12, 15) et de **16** se recouvrent sur plusieurs colonnes.

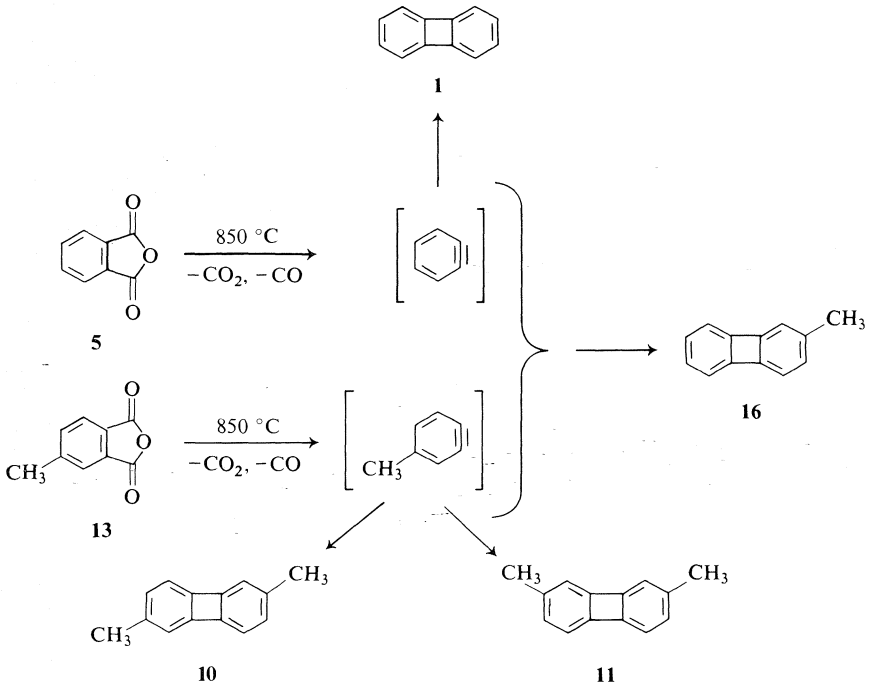

SCHÉMA 2

Les contraintes de la sublimation des produits de départ nous ont conduits à remplacer la ninhydrine dans le mélange par l'anhydride phtalique. De nouvelles conditions de température ont dû être choisies. Les grandes quantités de produit de départ récupéré dans les pyrolyses séparées des anhydrides **5** et **13** à 800 et 825 °C nous ont amenés à penser que la pyrolyse devrait se faire à une température supérieure; une température de 850 °C a été choisie. On avait constaté, dans la pyrolyse du composé **5** à 850 °C, que le rendement de biphénylène était le même que celui obtenu à 825 °C; de plus, la quantité d'anhydride récupéré avait grandement diminué en passant d'une température à l'autre.

La pyrolyse du mélange anhydride phtalique – anhydride méthyl-4 phtalique a été faite à 850 °C et les deux anhydrides ont été pesés pour qu'un rapport molaire de ceux-ci soit de 3:1 respectivement; les résultats sont résumés dans le tableau 2. Les produits obtenus sont le biphénylène (**1**), le méthyl-2 biphénylène (**16**) et un mélange de diméthyl-2,6 (**10**) et diméthyl-2,7 (**11**) biphénylènes. Certaines quantités des deux produits de départ ont été récupérées. Les produits sont en accord avec les résultats attendus (schéma 2).

Dans cette dernière pyrolyse la quantité de diméthylbiphénylène est relativement grande par rapport à celle du méthyl-2 biphénylène. C'est pourquoi nous avons fait une pyrolyse où les

deux composants du mélange sont présents dans un rapport molaire de 9:1. Les mêmes produits sont obtenus mais avec des rendements différents; les résultats sont résumés dans le tableau 2.

Conclusions

La synthèse des biphénylènes substitués sur un cycle implique la rencontre de benzynes provenant de sources différentes. Partant de ce fait, il est important que les deux produits de départ entrent dans la zone de pyrolyse en même temps, comme mis en évidence avec la pyrolyse du mélange impliquant l'anhydride méthyl-4 phtalique. Quand la ninhydrine est employée pour l'obtention du méthyl-2 biphénylène, le trop grand écart dans les températures de sublimation des deux produits fait que ceux-ci entrent successivement dans la zone de pyrolyse. De ce fait, la différence des températures de sublimation des produits formant le mélange est plus importante que le rendement des produits attendus dans les pyrolyses individuelles.

D'autre part, on a pu remarquer avec les résultats obtenus pour les pyrolyses de chaque mélange que dans le premier cas, le rendement du biphénylène substitué sur un cycle ne dépend pas du rapport molaire des deux composants du mélange et que dans l'autre cas, ce rendement varie avec le rapport molaire des deux anhydrides de départ. Nous pensons que le facteur important est l'efficacité de la source de benzyne à se fragmenter dans la zone de pyrolyse. En effet, dans le cas où la ninhydrine est employée, la fragmentation efficace de cette dernière fait que la concentration de benzyne présent dans la zone de pyrolyse est grande même si peu de ninhydrine est employé. Dans le cas où l'anhydride phtalique est utilisé, il faut une quantité plus grande de ce dernier pour que la même quantité de benzyne obtenue avec une quantité moindre de ninhydrine soit présente dans la zone de pyrolyse.

Somme toute, la méthode que nous avons décrite comporte des avantages et des désavantages. Les principaux avantages de notre méthode sont qu'elle utilise comme source de benzynes des produits commerciaux facilement accessibles et que la synthèse des biphénylènes substitués sur un cycle se fait en une étape. Pour ces raisons, si l'on considère en plus les rendements, notre méthode est plus avantageuse que celle proposée par Lothrop (1, 2). Un des principaux désavantages de la méthode est qu'il nous est impossible d'utiliser des anhydrides phtaliques dont le substituant se décompose pendant la pyrolyse; ainsi les anhydrides portant un groupement nitro ne pourront être utilisés.

Les contraintes de notre montage font que seulement 1 à 2 g de mélange peuvent être pyrolysés à la fois. Ainsi l'obtention d'une grande quantité de produit nécessite plusieurs pyrolyses. Pourtant, nous n'avons pas essayé de construire un appareillage à plus grande échelle.

En conclusion, ce travail a permis d'obtenir des biphénylènes substitués sur un cycle et a permis d'ouvrir la voie pour de nouvelles synthèses de biphénylènes.

Partie expérimentale

Les spectres de masse ont été pris à basse résolution sur un appareil Hitachi modèle RMU-6D vendu par la compagnie Perkin-Elmer et/ou un appareil de la compagnie Associated Electrical Industries (A.E.I.) modèle MS-902.

Les points de fusion ont été mesurés à l'aide d'un appareil Buchi et/ou Mel-Temp; les valeurs rapportées ne sont pas corrigées.

Les spectres de résonance magnétique nucléaire du proton ont été pris sur un spectromètre Brucker de 90 MHz, modèle WH-90 fonctionnant par transformée de Fourier.

Les spectres ultraviolets ont été enregistrés sur un appareil Cary, modèle 14 et/ou 17.

Les analyses par chromatographie en phase gazeuse (cpg) ont été faites par un appareil de la compagnie Hewlett-Packard modèle 5750. Cet appareil contient deux colonnes et est muni d'un système de programmation de température. Dans la plupart de nos analyses, une colonne de cuivre mesurant 9 pieds de longueur par 0.25 po de diamètre est utilisée. Le garnissage de la colonne consiste en du SE-54, 10%, sur Chromosorb W. Une programmation de 6 °C/min de 90 à 270 °C est utilisée. Dans certains cas, une colonne mesurant 6 pieds de longueur, contenant du SE-30, 10%, sur Chromosorb W a été nécessaire. La programmation employée est la même que précédemment.

Produits

L'anhydride phtalique provient de la compagnie Matheson, Coleman et Bell. Avant son utilisation, il a été purifié par cristallisation dans un mélange benzène–éthanol. La ninhydrine a été achetée de la compagnie Pierce Chemical; les anhydrides tétrachlorophtalique et méthyl-4 phtalique proviennent de la compagnie Eastman Kodak; après vérification de leur pureté, ils ont été utilisés comme tels.

Montage et procédure

Le montage pour la pyrolyse et la procédure ont déjà été décrits précédemment (23). Le produit ou le mélange de produits est d'abord sublimé dans un courant d'azote, puis entraîné sous forme vapeur dans une colonne de quartz de ~60 cm, dont la zone chauffée par un four extérieur mesure 30 cm. La vitesse d'entrée du produit dans la zone chauffée est réglée par un débitmètre. Un vide de l'ordre de 0.1 torr est maintenu. Les produits

formés sont condensés dans une série de trappes. La colonne et les trappes sont par la suite lavées. La solution provenant du lavage est concentrée, placée dans un ballon jaugé de 25 ml et le volume total est amené jusqu'à la ligne de jauge. Les produits obtenus sont dans la plupart des cas séparés par cpg. Leurs rendements sont déterminés en comparant les surfaces sous la courbe du chromatogramme des produits de pyrolyse avec les surfaces des pics de composés standards de concentrations connues.

Sources de benzynes

Dans les pyrolyses de l'anhydride **5** et de la ninhydrine, le chloroforme et l'acétone ont été utilisés pour le lavage des trappes. Les analyses de la solution de chaque pyrolyse ont été faites par cpg en utilisant une colonne de SE-54, 10% sur Chromosorb W mesurant 9 pieds. Une programmation de 6 °C/min à partir de 90 jusqu'à 270 °C a été utilisée.

Dans la pyrolyse de l'anhydride phtalique, le chromatogramme montre la présence de trois produits dont deux d'entre eux sont l'anhydride phtalique et le naphtalène; ils ont été identifiés par leur spectre de masse (24, 25) et par leur temps de rétention qui sont identiques à ceux d'échantillons commerciaux.

Le troisième produit, un solide jaune, a été identifié comme étant le biphénylène. Le spectre de masse obtenu donne la fragmentation suivante: *m/e* (%) 153(13.7), 152(100), 151(15.1), 150(11.7), 126(6.4), 76(14.9), 75(5.7), 74(4.8), 63(9.4) (litt. (26) *m/e* (%) 153(14.0), 152(100.0), 151(18.0), 150(10.0), 126(7.1), 76(9.1), 75(4.9), 74(4.5), 63(6.0)). Un spectre ultraviolet qualitatif a été enregistré et les absorptions suivantes ont été obtenues: λ_{max} (MeOH) nm 239, 247, 327, 330, 339, 348 et 358 (litt. (3) (EtOH) 239, 248, 326, 330, 339, 343, 348, et 358). Une trace de fluorène a aussi été détectée.

Dans la pyrolyse de la ninhydrine à 700 et 800 °C, uniquement le biphénylène a été obtenu; il a été identifié par ses spectres de masse et ultraviolet. A 600 °C, en plus du biphénylène, est présente la benzocyclobutènedione. Le spectre de masse de ce dernier donne les pics suivants: *m/e* (%) 133(1.6), 132(16.3), 105(8.0), 104(78.3), 78(5.4), 77(12.4), 76(100.0), 75(10.1), 74(16.3), 73(7.7), 50(45.7). Le spectre ultraviolet qualitatif du même composé donne les absorptions suivantes: λ_{max} (MeOH) 224, 247, 284, 291, 299 (litt. (12) 225, 286, 292, 301; litt. (27) 220, 286, 292, 301).

Pyrolyse des anhydrides substitués

Pyrolyse de l'anhydride tétrachlorophtalique

Dans la pyrolyse de l'anhydride tétrachlorophtalique, le benzène et l'acétone ont été utilisés comme solvants pour le lavage des trappes. L'analyse de la solution de pyrolyse par cpg a été faite sur une colonne de SE-54, 10%, sur Chromosorb W mesurant 9 pieds, dans les mêmes conditions de programmation que précédemment.

Le chromatogramme obtenu montre la présence de deux produits dont l'hexachlorobenzène; pf 227 °C (litt. (28) pf 230 °C). Le spectre de masse d'un échantillon de ce composé a été enregistré à 70 eV; il est comparable à celui trouvé dans la littérature (29). Une série de pics dont les valeurs de *m/e* sont situées entre 282 et 292 correspond à l'ion moléculaire et ses pics isotopiques. Le calcul des intensités relatives des pics isotopiques de l'ion moléculaire montre que le composé possède 6 atomes de chlore (30). Le même calcul fait pour les ions fragments indique la perte respective de 1, 2 et 3 atomes de chlore.

Le second produit est le pentachlorobenzène; pf 85 °C (litt. (31) pf 86 °C). Le spectre de masse de ce composé, un solide de couleur blanche a été pris à 70 eV. Une série de pics dont les valeurs sont situées entre 248 et 256 correspond à l'ion moléculaire et ses pics isotopiques. Le calcul des intensités relatives des pics isotopiques de l'ion moléculaire montre que le composé possède 5 atomes de chlore (30). Les autres séries de pics correspondent à la perte respective de 1, 2, 3 et 4 atomes de chlore.

La prise de spectres de masse du mélange de pyrolyse, en fonction de la température, nous a permis de détecter la présence de l'octachlorobiphénylène et du décachlorobiphényle.

Par la suite, nous avons fait la sublimation du mélange des produits de pyrolyse. Après avoir chauffé le mélange à 90 °C sous la pression atmosphérique, une première fraction contenant l'hexachlorobenzène et le pentachlorobenzène a été recueuillie. Le poids de cette fraction a été déterminé et les quantités respectives de chacun des composés ont été trouvées par calcul du rapport des surfaces sous la courbe du chromatogramme. Le résidu a été par la suite sublimé à 120 °C sous une pression de 0.6 torr; une deuxième fraction contenant l'octachlorobiphénylène et le décachlorobiphényle a été recueuillie.

Le spectre de masse de la deuxième fraction à 70 eV montre la présence d'une série de pics entre *m/e* 424 et 434 ainsi qu'entre *m/e* 494 et 506. L'intensité relative des deux massifs varie avec le temps indiquant la présence de deux produits. Le spectre ultraviolet de cette fraction donne les absorptions suivantes: λ_{max} (dioxanne) nm 224, 243, 265, 278, 288, 302, 324, 333, 350, 370, 392, 425, 450. Le spectre ultraviolet de l'octachlorobiphénylène est donné dans la littérature (13): λ_{max} (dioxanne) 225, 243, 268, 279, 290, 354, 375, 393, 428, 452. De même le spectre ultraviolet du décachlorobiphényle est connu (32): λ_{max} (isooctane) nm 280, 292, 301.

Les quantités relatives de l'octachlorobiphénylène et du décachlorobiphényle ont été calculées par spectrométrie de masse à 11 eV. La méthode consiste à enregistrer des spectres de masse du mélange à 11 eV à partir du moment de son introduction dans l'appareil jusqu'à disparition presque complète des pics de chaque composé; l'étape suivante consiste à faire un graphique donnant l'intensité des ions en fonction du temps et ceci pour chaque produit. Etant donné que le nombre d'atomes de chlore dans chaque molécule est différent, nous avons additionné les intensités de tous les pics formant chaque massif pour fin de comparaison. Le rapport des quantités respectives est de 9:1 pour l'octachlorobiphénylène et le décachlorobiphényle respectivement.

Pyrolyse de l'anhydride méthyl-4 phtalique

La pyrolyse de l'anhydride méthyl-4 phtalique a été faite à 825 °C, avec un débit d'azote de 90 ml par min, sous une pression de 0.3 torr. Le benzène et l'acétone ont été utilisés comme solvants pour le lavage des trappes. Les analyses de cpg ont été faites en utilisant une colonne de SE-54, 10% sur Chromosorb W; les conditions de programmation sont les mêmes que précédemment.

Le chromatogramme montre la présence de trois produits. Le premier composé est l'anhydride méthyl-4 phtalique; son pf est de 88 °C (litt. (33) pf 88.5–89 °C). Le spectre de masse de ce composé pris à 20 eV montre trois pics; *m/e* (%) 162(23.3), 118(100), 90(27.8). Le spectre de masse pris à 70 eV donne la fragmentation suivante:

m/e (%) 163(1.8), 162(16.1), 119(8.8), 118(100.0), 91(5.6), 90(67.1), 89(48.4), 88(0.6), 87(1.1), 86(1.6), 85(1.2), 77(0.6), 76(0.2), 75(1.2), 74(2.4), 73(0.5), 64(6.3), 63(22.1), 62(9.6), 61(2.9), 51(4.2), 50(7.9).

Le deuxième produit est le diméthylbiphénylène. Un spectre de masse de ce produit a été enregistré à 70 eV: *m/e* (%) 181(14.3), 180(100.0), 179(30.0), 178(24.4), 177(7.0), 176(8.7), 166(11.1), 165(58.5), 164(4.2), 163(6.6), 162(6.3), 90(18.8), 89(27.2), 88(9.8), 87(5.6), 86(3.5), 64(3.9), 63(15.7), 62(5.9). Le spectre de rmn montre un singulet à δ 2.15 ppm (6H) et un singulet élargi à δ 6.50 (6H). Le spectre de rmn du diméthyl-2,7 est connu dans la littérature (34); les protons des groupes méthyle apparaissent à δ 2.12 ppm, tandis que les protons aromatiques apparaissent à δ 6.50 ppm. Nous croyons que les deux isomères sont présents et que la grande symétrie de ceux-ci ne nous permet pas de les différencier dans le mélange par la spectroscopie de rmn.

Le troisième composé a été identifié comme étant le diméthylfluorène par son spectre de masse et par analogie avec les pyrolyses de composés similaires trouvées dans la littérature (11, 12, 15) (trois isomères sont attendus). Le spectre de masse de ce composé a été enregistré à 70 eV: *m/e* (%) 195(17.3), 194(100.0), 193(15.0), 192(5.3), 191(7.5), 190(3.0), 189(9.0), 180(23.3), 179(95.5), 178(35.3), 177(7.5), 176(8.3), 166(3.8), 165(12.8), 164(3.0), 163(3.8), 162(3.0).

Pyrolyse des mélanges:

Pyrolyse du mélange ninhydrine – anhydride tétrachlorophtalique

Dans la pyrolyse des mélanges ninhydrine – anhydride tétrachlorophtalique, le benzène et l'acétone ont été utilisés comme solvants pour le lavage des trappes. Les analyses par chromatographie en phase gazeuse ont été faites en utilisant une colonne de SE-54, 10% sur Chromosorb W mesurant 9 pieds de longueur.

Des pyrolyses qualitatives de mélanges ont été faites à différentes températures selon la procédure décrite plus haut. L'analyse des chromatogrammes obtenus pour chaque pyrolyse par comparaison des surfaces sous la courbe montre que la température de choix est 800 °C.

Dans les pyrolyses quantitatives, le chromatogramme obtenu par injection d'une quantité de chaque solution montre la présence de trois produits; leur temps de rétention respectif est de 18.7, 28.7 et 32.4 min. Le second composé est présent en faible quantité; donc, après identification des trois composés uniquement les rendements des deux autres produits ont été déterminés (voir tableau 1).

Le premier composé a été identifié comme étant le biphénylène par ses spectres de masse et ultraviolet. Le second composé, un solide blanc, a été identifié comme étant le tétrachloro-1,2,3,4 naphtalène. Le point de fusion d'un échantillon collectionné du chromatographe en phase gazeuse est voisin de celui trouvé dans la littérature: 196 °C (litt. (35) pf 200–201 °C); le spectre de masse de ce composé montre une série de pics entre *m/e* 264 et 270 qui correspond à l'ion moléculaire et ses pics isotopiques. Trois autres séries de pics sont obtenus par perte successive de 1, 2 et 3 atomes de chlore. Enfin, il y a deux séries de pics débutant à *m/e* 132 et 97 correspondant à $(M)^{++}$ et $(M - Cl_2)^{++}$.

Le troisième composé est le tétrachloro-1,2,3,4 biphénylène; pf 175 °C (litt. (36) pf 176 °C). Son spectre de masse a été enregistré à 70 eV. Une série de pics entre *m/e* 288 et 294 correspond à l'ion moléculaire et ses pics isotopiques. Un calcul de l'intensité relative de cette série de pics montre que le composé contient quatre atomes de chlore: trouvé, *m/e* (%) 288(80.0), 290(100.0), 292(47.0), 294(10.3), calculé (30), *m/e* (%), 288(77.16), 290(100.0), 292(48.60), 294(10.50). Le reste du spectre a la même allure que celui du tétrachloro-1,2,3,4 naphtalène; les trois séries de pics suivant l'ion moléculaire correspondent respectivement à $(M - Cl)^+$, $(M - 2Cl)^+$ et $(M - 3Cl)^+$. Les deux dernières séries correspondent à $(M)^{++}$ et $(M - 2Cl)^{++}$. Un spectre ultraviolet qualitatif du même composé a été enregistré: λ_{max} (MeOH) nm 256 ép., 263, 335, 352 ép, 355, 371, (litt. (36) λ_{max} (EtOH) nm 258 ép., 265, 339, 353 ép, 357, 375).

Pyrolyse du mélange anhydride phtalique – anhydride méthyl-4 phtalique

Au départ, des pyrolyses qualitatives de mélange impliquant la ninhydrine et l'anhydride méthyl-4 phtalique ont été faites. Après avoir remarqué la formation d'une faible quantité de méthyl-2 biphénylène, nous avons abandonné la pyrolyse de ce mélange. Aucune étude quantitative n'a été faite dans ce cas. Par la suite, nous avons remplacé la ninhydrine par l'anhydride phtalique.

Dans la pyrolyse du mélange anhydride phtalique – anhydride méthyl-4 phtalique, le benzène et l'acétone ont été utilisés comme solvants pour le lavage des trappes. L'analyse des produits de pyrolyse a été faite par chromatographie en phase gazeuse, utilisant une colonne de 6 pieds contenant du SE-30, 10% sur Chromosorb W. La programmation de température est la même qu'utilisée précédemment. Les rendements des produits sont donnés dans le tableau 2.

Le chromatogramme montre la présence de cinq produits dont les temps de rétention respectifs sont de 14.8, 17.8, 18.4, 20.8 et 23.0 min. Les deux premiers ont été identifiés comme étant les deux anhydrides de départ (le premier étant l'anhydride phtalique). Les spectres de masse et les temps de rétention mesurés correspondent à ceux d'échantillons commerciaux. Le troisième produit est le biphénylène; il a été identifié par ses spectres de masse et ultraviolet. Le cinquième produit est le diméthylbiphénylène; il a été identifié par ses spectres de masse et de rmn. Comme dans la pyrolyse de l'anhydride méthyl-4 phtalique, nous supposons que deux isomères sont présents.

Le dernier produit est le méthyl-2 biphénylène (**16**): spectre de masse (70 eV), ion moléculaire, *m/e* (%) 166(100.0). Un spectre rmn a été enregistré dans le $CDCl_3$: **16**, δ 2.15 (s, 3H), 6.5–7.0 ppm (m, 7H). Il y a un recouvrement des pics du composé **16** et du fluorène, trouvé également en petite quantité dans notre pyrolyse de l'anhydride phtalique (**5**) ainsi que dans d'autres pyrolyses de **2** (11, 12) et de **5** (15). Il est possible de distinguer ces deux produits dans un mélange des deux par moyen du spectre rmn: le fluorène, δ 3.76 (s, 2H) et 7.2–7.7 ppm (m, 8H). Le spectre uv de **16** formé dans cette pyrolyse s'accorde bien avec celui de la littérature (8): λ_{max} (EtOH) nm 242, 250, 298, 343, 361.

1. W. C. Lothrop. J. Am. Chem. Soc. **63**, 1187 (1941).
2. W. C. Lothrop. J. Am. Chem. Soc. **64**, 1698 (1942).
3. W. Baker, M. P. V. Boardland et J. F. W. McOmie. J. Chem. Soc. 1476 (1954).
4. W. Baker, J. W. Barton et J. F. W. McOmie. J. Chem. Soc. 2658 (1958).

5. W. BAKER, J. W. BARTON, J. F. W. MCOMIE, R. J. PENNECK et M. L. WATTS. J. Chem. Soc. 3986 (1961).
6. J. M. BLATCHY, J. F. W. MCOMIE et M. L. WATTS. J. Chem. Soc. 5085 (1962).
7. W. BAKER, N. J. MCLEAN et J. F. W. MCOMIE. J. Chem. Soc. 922 (1963).
8. W. BAKER, J. W. BARTON et J. F. W. MCOMIE. J. Chem. Soc. 2666 (1958).
9. W. BAKER, J. F. W. MCOMIE, D. R. PRESTON et V. ROGERS. J. Chem. Soc. 414 (1960).
10. J. M. BLATCHY, J. F. W. MCOMIE et S. D. THATTE. J. Chem. Soc. 5090 (1962).
11. R. F. C. BROWN et R. K. SOLLY. Chem. Ind. (London), 1462 (1965).
12. R. F. C. BROWN et R. K. SOLLY. Aust. J. Chem. **19**, 1045 (1966).
13. M. P. CAVA, M. J. MITCHELL, D. C. DEJONGH et R. Y. VANFOSSEN. Tetrahedron Lett. 2947 (1966).
14. R. F. C. BROWN, D. V. GARDNER, J. F. W. MCOMIE et R. K. SOLLY. Chem. Commun. 407 (1966).
15. R. F. C. BROWN, D. V. GARDNER, J. F. W. MCOMIE et R. K. SOLLY. Aust. J. Chem. **20**, 139 (1966).
16. E. K. FIELDS et S. MEYERSON. Tetrahedron Lett. 719 (1971).
17. G. V. NUNEZ. Bol. Soc. Quim. Peru, **31**, 6 (1965).
18. P. DE CHAMPLAIN et P. DE MAYO. Can. J. Chem. **50**, 270 (1972).
19. J. A. H. MCBRIDE. Chem. Commun. 1219 (1972).
20. M. P. DAVID et J. F. W. MCOMIE. Tetrahedron Lett. 1361 (1973).
21. B. M. ADGER, M. KEATING et C. W. REES. J. Chem. Soc. Perkin Trans. I, 41 (1975).
22. E. K. FIELDS et S. MEYERSON. Chem. Commun. 474 (1965); J. Org. Chem. **31**, 3307 (1966).
23. (*a*) D. C. DEJONGH et M. L. THOMSON. J. Org. Chem. **38**, 1356 (1973). (*b*) D. C. DEJONGH, D. C. K. LIN et M. L. THOMSON. Advances in mass spectrometry. Vol. 6. *Edité par* A. R. West. Applied Science Publishers, Barking, England. 1974. Chapt. 12.
24. F. W. MCLAFFERTY et R. S. GOHLKE. Anal. Chem. **31**, 2076 (1959).
25. F. L. MOHLER, V. H. DIBELER, L. WILLIAMSON et H. DEAN. J. Res. Natl. Bur. Stand. **48**, 188 (1952).
26. J. H. D. ELAND et C. J. DANBY. J. Chem. Soc. 5935 (1965).
27. M. P. CAVA, D. R. NAPIER et R. J. POHL. J. Am. Chem. Soc. **85**, 2076 (1963).
28. R. C. WEAST (*éditeur*). Handbook of chemistry and physics. 52è éd. Chemical Rubber Co. 1971. p. C-159.
29. O. HUTZINGER, W. D. JAMIESON et S. SAFE. J. Assoc. Off. Anal. Chem. **54**, 178 (1971).
30. R. BINKS, J. S. LITTLER et R. L. CLEAVER. Tables for use in high resolution mass spectrometry. Heyden-Sadtler. 1970. p. 122–124.
31. R. C. WEAST (*éditeur*). Handbook of chemistry and physics. 52è éd. Chemical Rubber Co. 1971. p. C-164.
32. M. BALLISTER. J. PALLARI et J. RIERA. J. Quant. Spectrosc. Radiat. Transfer, **4**, 819 (1964).
33. W. N. PRICHARD. J. Am. Chem. Soc. **78**, 6137 (1956).
34. P. R. CONSTANTINE, G. E. HALL, C. R. HARRISON, J. F. W. MCOMIE et R. J. G. SEARLE. J. Chem. Soc. C. 1767 (1966).
35. J. W. WILT et E. VASILIAUSKAS. J. Org. Chem. **35**, 2410 (1970).
36. A. J. BOULTON et J. F. W. MCOMIE. J. Chem. Soc. 2549 (1965).

Conformational analysis of substituted 1,2-oxathiane 2-oxides by ^{13}C and ^{1}H nuclear magnetic resonance spectroscopy

G. W. BUCHANAN

Department of Chemistry, Carleton University, Ottawa, Ont., Canada K1S 5B6

AND

N. K. SHARMA, F. DE REINACH-HIRTZBACH, AND T. DURST

Department of Chemistry, University of Ottawa, Ottawa, Ont., Canada K1N 6N5

Received March 26, 1976

G. W. BUCHANAN, N. K. SHARMA, F. DE REINACH-HIRTZBACH, and T. DURST. Can. J. Chem. **55**, 44 (1977).

^{1}H and ^{13}C nmr results for 1,2-oxathiane 2-oxide and eight derivatives are reported. It is concluded that these molecules have a high preference for chair forms with axial S=O groups, even when a sterically bulky group such as phenyl is substituted in a *syn*-axial orientation to the exocyclic oxygen.

G. W. BUCHANAN, N. K. SHARMA, F. DE REINACH-HIRTZBACH et T. DURST. Can. J. Chem. **55**, 44 (1977).

On rapporte des données de rmn ^{1}H et ^{13}C pour l'oxyde-2 d'oxathianne-1,2 et pour huit de ses dérivés. On en conclut que ces molécules ont une grande préférence pour des formes chaises avec des groupes S=O axiaux même lorsqu'un groupe stériquement encombrant tel que le phényle est substitué dans une orientation *syn*-axiale par rapport à l'oxygène exocyclique.
[Traduit par le journal]

Introduction

In recent years there has been considerable interest in the stereochemistry of 6-membered organic heterocycles containing the S=O function. For thiane oxide it has been established (1) that the preferred conformation is a chair in which there is a slight preponderance (0.2 kcal/mol) of the form in which the S=O is axial.

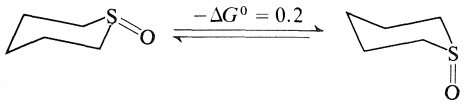

When heteroatoms with lone pairs of electrons are introduced into the ring, adjacent to the S=O group, the equilibria become more biased toward the axial S=O forms. In the case of trimethylene sulfite, this preference has been estimated to be *ca.* 2.1 kcal/mol (2), although no direct measure of $-\Delta G^0$ for the parent compound has been possible since its ^{1}H nmr spectrum is temperature independent from -150 to $+150\,^{\circ}C$.

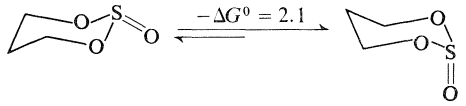

On the basis of dipole moments (2), ^{1}H nmr (3) and ^{13}C nmr (4), substitution of potentially axial CH_3 groups at both C-4 and C-6 of the sulfites is deemed to alter the ring conformation such that non-chair forms, or chairs with equatorial S=O functions, can contribute.

Compounds intermediate between the thiane oxides and the trimethylene sulfites, namely the 1,2-oxathiane 2-oxides (sultines) have, by contrast, received rather little attention. To date, the only report has been that of Harpp and Gleason (5) who found that the ^{1}H spectrum of 1,2-oxathiane 2-oxide is temperature independent from -90 to $+150\,^{\circ}C$. They concluded that the molecule adopts a chair conformation with a considerable preference for the form having an axial S=O moiety (*ca.* 2 kcal/mol).

For all these systems the ^{1}H nmr spectra are difficult to analyze completely, and thus the structural information available is somewhat limited. Recently it has been demonstrated that ^{13}C nmr offers an attractive alternative for the study of sulfur heterocycles (4, 6–8) since the spectra are first order and the chemical shift differences are an order of magnitude greater than those in the ^{1}H spectra. We now report the

TABLE 1. ^{1}H spectral data of 1,2-oxathiane 2-oxides*

Compound	Area of adsorption (assignment)
1,2-Oxathiane 2-oxide (**1**)	1.5–2.2 (4e, 5a, 5e); 2.2–3.0 (3a, 3e, 4a); 3.6–3.8 (6e); 4.3–4.7 (6a)
3-Methyl-1,2-oxathiane 2-oxide (**2**)	1.08 (CH_3); 1.4–2.2 (4e, 5a, 5e); 2.2–3.0 (3a, 4a); 3.3–3.8 (6e); 4.0–4.6 (6a)
4-Methyl-1,2-oxathiane 2-oxide (**3**)	1.0 (CH_3); 1.3–1.9 (5a, 5e); 2.3–2.8 (3a, 3e, 4a); 3.75–4.0 (6e); 4.4–4.7 (6a)
5-Methyl-1,2-oxathiane 2-oxide (**4**)	0.87 (CH_3); 1.6–2.4 (4e, 5a); 2.6–3.0 (3a, 3e, 4a); 3.6–3.8 (6e); 4.0–4.5 (6a)
6-Methyl-1,2-oxathiane 2-oxide (**5**)	1.22 (CH_3); 1.45–2.0 (4e, 5a, 5e); 2.3–2.8 (3a, 3e, 4a); 4.5–4.9 (6a)
6-Phenyl-1,2-oxathiane 2-oxide (**6**)	1.2–2.2 (4e, 5a, 5e); 2.5–2.9 (3a, 3e, 4a); 5.37 (6a); 7.3 (phenyl)
6,6-Dimethyl-1,2-oxathiane 2-oxide (**7**)	1.25 (CH_3-equatorial); 1.57 (CH_3-axial); 1.6–1.9 (4e, 5a, 5e); 2.3–2.8 (3a, 3e, 4a)
cis-6-Methyl-6-phenyl-1,2-oxathiane 2-oxide (**8**)	1.90 (CH_3); ~2.25 (4e, 5a, 5e); ~2.75 (3a, 3e, 4a); 7.2 (5H)
trans-6-Methyl-6-phenyl-1,2-oxathiane 2-oxide (**9**)	1.58 (CH_3); 1.7–3.2 (all other ring H); 7.1–7.5 (5H)

*0.05–0.10 *M* solutions in $CDCl_3$.

results of an examination of 1,2-oxathiane 2-oxide and eight derivatives, using ^{1}H and ^{13}C nmr, which permits some detailed conformational conclusions.

Results and Discussion

(a) ^{1}H Spectra

Table 1 contains a summary of the ^{1}H data for the nine compounds examined. A discussion of part of the 100 MHz ^{1}H spectrum of **1** has been published (5). The axial C-6 proton is the

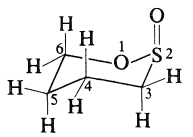

1

most deshielded (δ = 4.42) due to the well known (9–13) *syn*-axial deshielding effect of the sulfinyl oxygen. This proton exhibits an 11.5 Hz vicinal coupling with the *trans*-diaxial H on C-5, indicative of a chair-type geometry. The C-4 axial hydrogen is also deshielded relative to its equatorial counterpart for the same reason as the axial C-6 hydrogen, and to a similar extent. The close spatial relationship between the S=O group and the C-4 and C-6 axial hydrogens was verified by the observation that these hydrogens underwent the largest downfield shift, *ca.* 8 ppm, upon addition of approximately 0.5 equiv. of $Eu(FOD)_3$.

The chemical shift differences referred to above were observed for all the monosubstituted 1,2-oxathiane 2-oxides which we have thus far been able to isolate. On the basis of these observations and the ^{13}C spectra discussed below, the preferred conformations of these compounds (**2**–**6**) are chair forms having the substituent in an equatorial and the S=O in the axial position.

The proton spectrum of 6,6-dimethyl-1,2-oxathiane 2-oxide (7) showed two methyl signals at 1.25 and 1.57 ppm, assigned to the equatorial and axial methyl groups respectively. The chemical shift difference between the CH_3 groups of **6** (0.32 ppm) is somewhat smaller than for the CH_3 groups of the corresponding sulfite **10** (3), but considerably larger than that in the sulfite **11** which has an equatorial S=O bond (3). On this basis, **7** is suggested to have a conformation similar to that of **10**. The methyl proton assignments in **7** were confirmed by $Eu(FOD)_3$ studies which showed downfield shifts of *ca.* 3.0 and 1.5 ppm for the δ = 1.57 and the δ = 1.25 resonances respectively upon addition of 0.3

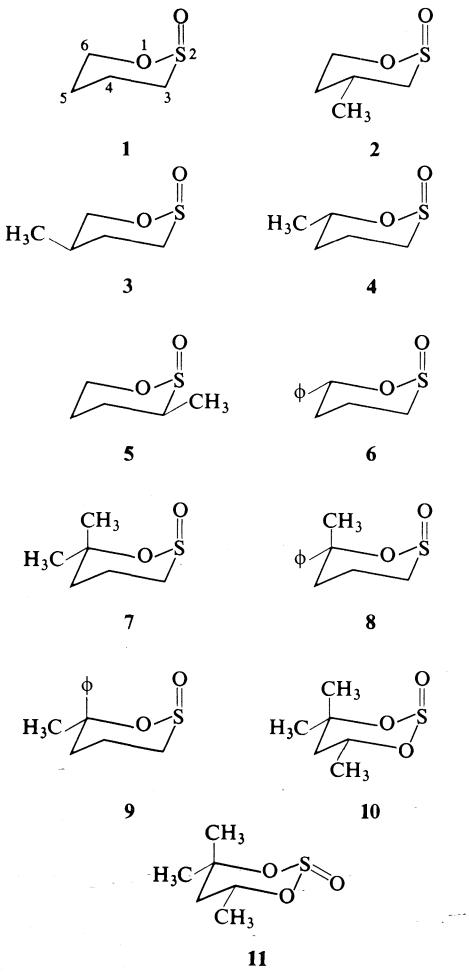

FIG. 1. Structures and numbering scheme for compounds discussed in the text.

equiv. of the shift reagent, indicating that the $\delta = 1.57$ resonance arises from the axial methyl.

Examination of the data for the 6-methyl-6-phenyl isomers **8** and **9** suggests that **8** exists mainly in the chair form having both the S=O and the CH_3 axial. For **9**, the CH_3 group is shielded by 0.32 ppm relative to **8**, resulting from the removal of the deshielding *syn*-axial S=O --- CH_3 interaction present in **8**. Interestingly in **8** the phenyl protons appear as a singlet at

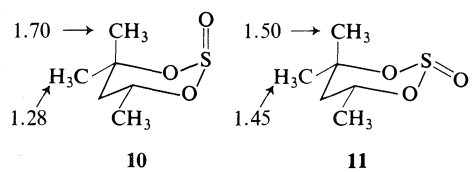

$\delta = 7.2$ whereas in **9** a multiplet in the range 7.1–7.5 ppm is found. In 2-phenyl-1,3-dithiane which contains an axial phenyl group (14) resolved *ortho* aromatic protons are also observed. Further evidence for the existence of **9** in a chair with axial S=O is obtained from the effect of addition of *ca.* 0.3 equiv. of $Eu(FOD)_3$. The protons most affected (downfield shift of *ca.* 4 ppm) are those in the *ortho* aromatic position. The axial proton (H_3) was next most affected (downfield shift of *ca.* 3 ppm) as expected on the basis of its *syn*-axial relation to the S=O, assuming the exocyclic oxygen to be the site of complexation (3). Furthermore, the lanthanide

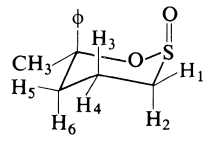

shifted spectrum of **9** permitted measurement of several of the coupling constants. In addition to large geminal couplings (13.0 and 14.5 Hz for J_{12} and J_{56} respectively), J_{23} and J_{36} are 11.0 Hz which typify axial–axial couplings in chair forms and are similar to values found in related molecules such as sulfites (3). Smaller couplings (3.0–6.5 Hz) are noted for interactions involving equatorial protons as expected on the basis of dihedral angle considerations. Of course it can be argued that the shift reagent perturbs the geometry of the substrate and renders conformational conclusions somewhat tenuous. Nevertheless, it seems clear that the lanthanide complexed system **9** exists in a chair with axial S=O and we thus can suggest that the geometry of the free substrate is similar.

(b) ^{13}C Spectra

^{13}C chemical shifts for compounds **1**–**9** are presented in Table 2. Assignments have been made using results for model compounds (4, 7), well-established trends of alkyl substitution (15), selective ^1H decoupling, and single frequency off resonance (SFORD) decoupling experiments.

For **1** it is interesting to compare the ring carbon shifts with those for trimethylene sulfite **12** and the two chair forms of thiane oxide **13** and **14**. Not surprisingly (15, 16), the C-5 shift of **1** is near that of C-5 of **12** and C-4 of **13** and **14**. Also, C-6 of **1** resonates at a similar position

TABLE 2. ^{13}C chemical shifts of 1,2-oxathiane-2-oxides (δ_c from TMS ± 0.1)*

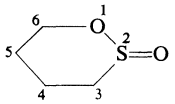

Compound	Substituent	Position C-3	C-4	C-5	C-6	CH_3	C-quat.	C-*o*	C-*m*	C-*p*
1	—	49.5	13.6	24.5	58.5					
2	4-CH_3	56.4	20.1	33.1	59.1	21.9				
3	5-CH_3	50.0	17.6	29.8	63.7	21.8				
4	6-CH_3	48.7	14.3	32.0	65.2	21.5				
5	3-CH_3	53.4	20.8	24.9	58.6	15.1				
6	6-ϕ	48.8	14.8	31.9	69.9		139.9	126.5	128.6	128.6
7	6,6-diCH_3	49.6	11.4	36.0	81.3	31.8(*c*)† 28.4(*t*)†				
8	6-CH_3(*c*)† 6-ϕ(*t*)†	49.9	12.3	35.1	83.5	30.5	146.2	124.1	128.4	127.3
9	6-CH_3(*t*)† 6-ϕ(*c*)†	50.8	12.8	33.7	82.5	32.8	145.1	124.9	128.0	127.2

*0.05–0.10 *M* solutions in $CDCl_3$.
†(*c*) and (*t*) denote *cis* and *trans* relative to the S=O bond.

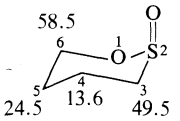

1

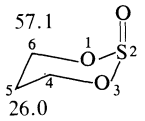

12

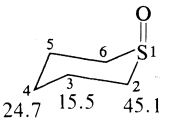

13

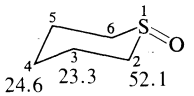

14

to C-4,6 of **12** (4). Notably C-4 of **1** is highly shielded (δ = 13.6) which reflects its *gauche*-γ relationship to the exocyclic oxygen atom (4). An equatorial S=O bond as in **14** is manifested by the absence of the upfield γ shift and the effect is pronounced (7–9 ppm) for both sulfites and sulfoxides (4, 7). Thus the ^{13}C data for **1** are supportive of a chair conformation with an axial S=O function.

For the mono-CH_3 derivatives **2**, **3**, and **4**, several pieces of evidence favor the concept of chair forms with equatorial CH_3 groups and axial S=O bonds. Initially, the alkyl substituent effects on the ring carbon shifts are similar to those in the related sulfites (4) where the corresponding chair forms are likely. For example in **4**, the introduction of the CH_3 at C-6 deshields C-6 by +6.7 ppm (α effect), C-5 by +7.5 ppm (β effect), and C-4 by +0.7 ppm (*trans*-γ effect) relative to **1**.

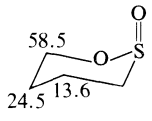

1

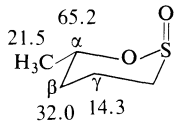

4

Comparing the corresponding sulfites **12** and **15**, the results are +7.0, +7.3, and +0.3 ppm for the α, β, and *trans*-γ effects respectively.

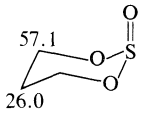

12

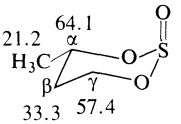

15

Small deshielding γ-effects for **2** (+0.6 ppm) and **3** (+0.5 ppm) relative to **1** again reflect the introduction of equatorial CH_3's into the ring. If the CH_3 groups were axial, pronounced shielding effects (4–6 ppm) would be expected at the γ-carbons (17, 18).

Finally, the close correspondance in the CH_3 shifts for **2**, **3**, and **4** with **15** and other sulfites (4) with equatorial methyl groups support this argument.

Results for the 3-CH_3 derivative **5** also indicate a chair geometry with axial S=O and equatorial CH_3. Compared to **2**, **3**, and **4**, the CH_3 group is shielded by *ca.* 6 ppm, due to its *gauche*-γ

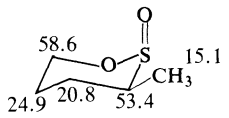

5

relationship to the exocyclic oxygens. Also the small deshielding *trans*-γ effect at C-5 (+0.4 ppm) relative to **1** is consistent with the *trans*-γ shifts noted in **2**, **3**, and **4**.

Comparison of the ring carbon shieldings for the 6-phenyl compound **6** with the 6-CH_3 system **4** reveals a marked similarity at the C-3, 4, and 5 positions. Thus for **6** a chair form with an equatorial phenyl group is dominant. The deshielding effect at C-6 (+4.7 ppm) relative to **4** is a consequence of the two β carbons of the aromatic ring.

Compound **7** exhibits a *gauche*-γ upfield shift of 2.2 ppm at C-4 relative to **1** which is indicative of a substantial contribution from a pure axial CH_3 at C-6. It is interesting to compare the C-6 shift and the gem-CH_3 shifts of **7** with a related sulfite **10** which is mainly a chair form with an axial S=O bond (4). Clearly there is marked

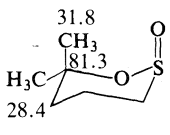

7

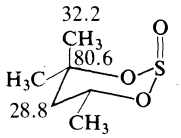

10

similarity in the data suggesting like geometries for **7** and **10**. The deshielding of the axial CH_3's in these compounds compared to their equatorial counterparts may be attributed to a 'δ' interaction with the axial S=O function (4, 19) or to the anisotropic property of the S=O moiety (20).

With the exception of C-6, the ring carbon chemical shifts for **8** are within 1 ppm of those for **7** which can be taken to indicate similar ring conformations. The deshielding at C-6 of **8** relative to **7** is no doubt a consequence of the β deshielding influence of the *ortho*-aromatic carbons. By contrast the CH_3 of **8** is shielded by 1.3 ppm relative to the axial CH_3 of **7**. This is presumably a manifestation of the minor γ interactions of the CH_3 with the *ortho*-aromatic carbons.

Compound **9**, if it were in a chair form with an axial S=O would have the structure **9***a*. An alternate possibility is that ring reversal might occur to render **9***b*. If this were the case, the

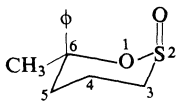

9*a*

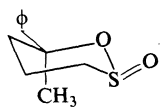

9*b*

C-4 resonance of **9** should be deshielded by 7–9 ppm compared to **8**, using the previous results for trimethylene sulfites (4) and thiane oxides (7) as analogies since there is a marked influence of S=O stereochemistry on γ-carbon shieldings. This large deshielding is not found and accordingly **9***b* seems unlikely.

Examination of the shift data for **8** and **9** in Table 2 reveals a marked similarity in the shieldings and accordingly similar chair conformations of these molecules can be suggested. If **9** were to adopt a twist shape then all the ^{13}C shifts would be expected to go upfield (21) and such a trend is not observed.

The only somewhat puzzling feature of the spectrum of **9** is the 2.3 ppm deshielding of the methyl resonance relative to **8**. We can offer no clear rationale for this finding other than to note that the CH_3 is *trans*-coplanar to a γ sulfur atom. Recently (22) deshielding *trans*-γ shifts have been reported for CH_3's *trans* and γ to oxygen atoms, when both the CH_3 and the O are bonded to quaternary sites.

In conclusion, it is clear that ^1H and ^{13}C nmr are useful complementary tools for the study of 1,2-oxathiane 2-oxide stereochemistry. Our results indicate a pronounced tendency for these molecules to adopt chair forms with axial S=O functions.

Experimental

Spectra

The ^{13}C chemical shifts were obtained using a Varian XL-100-12 nmr spectrometer in the Fourier transform mode via previously described procedures (23). Over the concentration range employed (0.05–0.10 *M* solutions) the ^{13}C shifts vary less than ±0.1 ppm. ^1H spectra were obtained on a Varian T-60 spectrometer using TMS as an internal reference for the $CDCl_3$ solutions. The $Eu(FOD)_3$ experiments on **9** were carried out using a Varian HA-100 nmr spectrometer and CD_2Cl_2 as solvent.

Materials

Preparation and purification of these sultines has been described previously (24).

1. J. B. Lambert and R. G. Keske. J. Org. Chem. **31**, 3429 (1966).
2. G. Wood, J. M. McIntosh, and M. H. Miskow. Can. J. Chem. **49**, 1202 (1971).
3. G. Wood, G. W. Buchanan, and M. H. Miskow. Can. J. Chem. **50**, 521 (1972).

4. G. W. BUCHANAN, J. B. STOTHERS, and G. WOOD. Can. J. Chem. **51**, 3746 (1973); **53**, 2359 (1975).
5. D. N. HARPP and J. G. GLEASON. J. Org. Chem. **36**, 1314 (1971).
6. W. A. SZAREK, D. M. VYAS, A. M. SEPULCHRE, S. D. GERO, and G. LUKACS. Can. J. Chem. **52**, 2041 (1974).
7. G. W. BUCHANAN and T. DURST. Tetrahedron Lett. 1683 (1975).
8. D. M. FRIEZE and S. A. EVANS. J. Org. Chem. **40**, 2690 (1975).
9. J. G. TILLETTE. Q. Rep. Sulfur Chem. **2**, 227 (1967).
10. C. R. JOHNSON and W. O. SIGEL. J. Am. Chem. Soc. **91**, 2796 (1969).
11. E. T. STROM, B. S. SNOWDEN, and P. A. TOLDEN. Chem. Commun. 50 (1969).
12. C. R. JOHNSON. Tetrahedron Lett. 1879 (1969).
13. A. B. FOSTER, J. M. DUXBURY, T. D. INCH, and J. M. WEBBER. Chem. Commun. 881 (1967).
14. A. KALFF and E. HAVINGA. Rec. Trav. Chim. **85**, 467 (1966).
15. J. B. STOTHERS. Carbon-13 NMR spectroscopy. Academic Press, New York, N.Y. 1972.
16. G. C. LEVY and G. L. NELSON. Carbon-13 nuclear magnetic resonance for organic chemists. Wiley-Interscience, New York, N.Y. 1972.
17. F. A. L. ANET, C. H. BRADLEY, and G. W. BUCHANAN. J. Am. Chem. Soc. **93**, 258 (1971).
18. D. K. DALLING and D. M. GRANT. J. Am. Chem. Soc. **89**, 6612 (1967).
19. S. H. GROVER, J. P. GUTHRIE, J. B. STOTHERS, and C. T. TAN. J. Magn. Reson. **10**, 227 (1973).
20. R. D. G. COOPER, P. V. DEMARCO, J. C. CHENG, and N. D. JONES. J. Am. Chem. Soc. **91**, 1408 (1969).
21. G. M. KELLIE and F. G. RIDDELL. J. Chem. Soc. Perkin Trans. II, 2384 (1972).
22. W. A. AYER, L. M. BROWNE, S. FUNG, and J. B. STOTHERS. Can. J. Chem. **54**, 3272 (1976).
23. G. W. BUCHANAN, C. REYES-ZAMORA, and D. E. CLARKE. Can. J. Chem. **52**, 3895 (1974).
24. N. K. SHARMA, F. DE REINACH-HIRTZBACH, and T. DURST. Can. J. Chem. **54**, 3012 (1976).

Nuclear magnetic resonance studies. XXX.[1] Hydrogen–deuterium exchange in bicyclo[3.2.1] and -[2.2.2]octenes through allylic and vinylic anions

A. K. CHENG AND J. B. STOTHERS

Department of Chemistry, University of Western Ontario, London, Ont., Canada N6A 5B7

Received July 26, 1976

A. K. CHENG and J. B. STOTHERS. Can. J. Chem. **55**, 50 (1977).

Bicyclo[3.2.1]oct-2-ene undergoes hydrogen–deuterium exchange through allyl and vinyl carbanionic intermediates under strongly basic conditions, *tert*-BuO^-/*tert*-BuOD at 185 °C. Only allylic exchange had been observed in previous studies with *tert*-BuO^-/DMSO. Since the 2-*tert*-butoxybicyclo[3.2.1]octanes are stable under these conditions an addition–elimination sequence cannot account for exchange at C-3. The relative rates of exchange at C-2, -3, and -4, and the stereoselectivity at the allylic site were determined by ^2H nmr. For comparison, the rate of olefinic exchange in bicyclo[2.2.2]octene was also measured.

A. K. CHENG et J. B. STOTHERS. Can. J. Chem. **55**, 50 (1977).

Dans des conditions basiques fortes impliquant le *tert*-BuO^-/*tert*-BuOD à 185 °C, le bicyclo-[3.2.1]octène-2 subit des échanges hydrogène–deutérium par l'intermédiaire de carbanions allyliques et vinyliques. On avait observé uniquement des échanges allyliques dans des études antérieures avec le *tert*-BuO^-/DMSO. Puisque les *tert*-butoxy-2 bicyclo[3.2.1]octanes sont stables dans ces conditions, on ne peut pas faire appel à une séquence d'addition–élimination pour expliquer l'échange en position C-3. On a déterminé, par rmn du ^2H, les vitesses relatives d'échanges en positions C-2, C-3 et C-4 et la stéréosélectivité au site allylique. Pour fins de comparaison, on a aussi déterminé la vitesse de l'échange des protons oléfiniques du bicyclo-[2.2.2]octène.

[Traduit par le journal]

In earlier work on the behavior of bicyclic ketones in a strongly basic medium, *tert*-butoxide/*tert*-butyl alcohol at 185 °C, we had found that the α,α-dimethyl derivatives of bicyclo-[2.2.2]octenone, bicyclo[3.2.1]oct-2-en-6-one and its Δ^3 isomer undergo hydrogen–deuterium exchange at both olefinic carbons (1). Since these ketones are interconvertible through the common β-enolate **1**, exchange at one of the olefinic centres is readily explicable in terms of the allylic nature of this intermediate. Exchange at the second olefinic carbon, however, requires a different mechanism, perhaps by direct exchange through a vinyl carbanion with a possible activating effect arising from the neighboring carbonyl group. To shed further light on the nature of these processes we have examined the reactivity of bicyclo[3.2.1]oct-2-ene (**2**) and bicyclo-[2.2.2]octene (**3**) under the same conditions to compare their behavior with that of the ketones. The [3.2.1] olefin has been studied previously (2) as a model system for assessing long range π participation in the anion formed from bicyclo-[3.2.1]octadiene. The monoene, with *tert*-butoxide/dimethyl sulfoxide as the base, was found to exhibit only allylic exchange. A comparison of the behavior of this olefin in these two media has proved interesting and we wish to present our results in this paper. Through the use of ^2H nmr spectra, the relative rates of exchange and the stereoselectivity at the allylic methylene site were readily measured in a straightforward fashion.

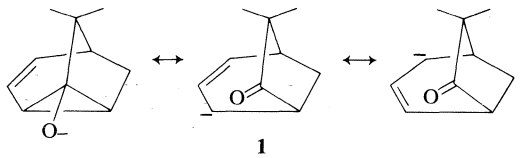

1

Experimental

Materials

With one exception, the compounds employed in this study have been described in the literature and samples were synthesized having essentially the same physical constants. Bicyclo[3.2.1]oct-2-ene (**2**) was obtained from 3-chlorobicyclo[3.2.1]oct-2-ene by Birch reduction (3). This chloroolefin had been prepared by reaction of bicycloheptene with dichlorocarbene followed by reduction with lithium aluminum hydride (4). Epoxidation of **2** with *m*-chloroperbenzoic acid in methylene chloride at room temperature (5) afforded *exo*-2,3-epoxy-**2** (6) in more than 80% yield. Bicyclo[2.2.2]octene (**3**) was pre-

[1]For part XXIX, see ref. 17 and for part XXVIII see ref. 18.

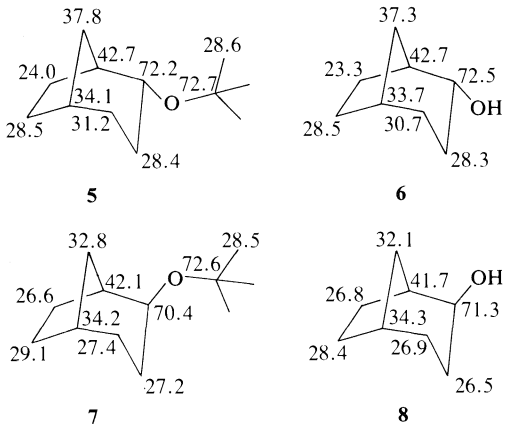

pared by Wolff–Kishner reduction of the corresponding enone which was available from earlier studies (7).

2-tert-Butoxybicyclo[3.2.1]octanes

To a solution of 1 g of *endo*-tricyclo[3.2.1.$0^{2,4}$]oct-6-ene (**4**) (8), in 15 ml of dry *tert*-butyl alcohol was added *p*-toluenesulfonic acid (80 mg) and the temperature raised to 60 °C. After stirring for 4 days, the reaction mixture was cooled and poured into water. Our synthesis was adapted from that reported for methanol addition (9). The product, isolated by pentane extraction, was analyzed by gc on a 15% DEGS column at 90 °C and found to contain three major components in a ratio of 6:2:2, constituting >95% of the total. Hydrogenation of the product in ether at 45 psi over PtO_2 afforded a 2:1 mixture of two compounds, separable by preparative gc on a 15% Carbowax 20M column. The proton spectra of each contained a sharp singlet at 1.15 ppm (9H, $(CH_3)_3C$) and a broad multiplet near 3.4 ppm (1H, $-CH(OR)-$) with no absorption at lower field. The ^{13}C spectrum of the minor product in $CDCl_3$ contained 10 signals which were assigned to the individual carbons in *endo*-2-*tert*-butoxybicyclo[3.2.1]octane as shown in **5** by comparison with the results for **6**, measured in $CDCl_3$ (10); the latter are in reasonable agreement with those recently reported (11) for an unspecified solvent. The ^{13}C spectrum of the major product **7** similarly accorded well with that for *exo*-bicyclo[3.2.1]octan-2-ol (**8**) (10, 11).

Precise mass measurements for the two products gave the following results: *Mol. wt.* calcd. for $C_{12}H_{22}O$: 182.1669; found for **5** (*m/e*): 182.1670; found for **7** (*m/e*): 182.1662.

Spectra

Proton spectra of each of the compounds included in this study were obtained to confirm their identity and purity. These spectra were recorded with a Varian HA-100 spectrometer which was also used for the spin decoupling experiments. ^2H and ^{13}C spectra were obtained with a Varian XL-100-15 system operating in the Fourier transform mode at 15.4 and 25.2 MHz, respectively. The determination and integration of the ^2H spectra have been described previously (12); the precision of the computer-fitted integration data is judged to be 1%. Total deuterium content for each sample was measured with a Varian M-66 instrument; a MAT 311A was used for the precise mass measurements of ethers **5** and **7**.

Exchange Experiments

The general procedure followed was essentially as described previously (12). Typically, the olefin (ether) was added to the base, prepared by dissolving potassium metal in *tert*-butyl alcohol-*O-d*, (99% deuterated and <0.005 *M* in water) to give a solution with a molar ratio of substrate: base:alcohol of 1:4:40, 1.2 *M* in *tert*-BuO^-. Aliquots were placed in glass tubes under nitrogen which were sealed after degassing. After heating at 185 ± 3 °C for various times, the tubes were opened and the products recovered by pentane extraction. Preparative gc was used to isolate samples for analysis.

Results

Following the method used for our examination of the bicyclic ketones (1), samples of **2** dissolved in *tert*-butoxide/*tert*-butyl alcohol-*O-d* were heated in sealed tubes for varying periods of time at 185 °C. After recovery of the olefin, the deuterium content of each sample was determined by mass spectrometry. The results are collected in Table 1, from which it is apparent that up to four deuterium atoms were incorporated. The ^2H spectrum of each sample clearly showed that four sites are involved in the exchange processes and the relative ^2H content at each site was measured by integration using the curve fitting technique described previously (12). These data are included in Table 1. The assignments for the individual signals were made from proton spectra of the olefin and the corresponding epoxide.

The ^2H spectra of the samples of **2**-d_x contained two signals at higher field, 0.53 ppm apart, the allylic methylene deuterons, and two at 3.52 and 4.06 ppm from the highest field signal, the olefinic nuclei. In the proton spectrum of **2**, the lowest field absorption (δ 5.79) was essentially a 'triplet' with spacings of ~8 Hz, and each component broadened by long range coupling. The more shielded of the olefinic patterns at δ 5.26 was essentially a doublet ($J \sim 8$ Hz) of multiplets. Thus, H-2 is the less shielded. To identify the *exo*- and *endo*-4-protons, the ^1H spectrum of the *exo*-epoxide of **2** was examined with varying amounts of the shift reagent, $Eu(fod)_3$, added. As the shift reagent concentration increased, absorption patterns attributable to six nonequivalent protons were shifted sufficiently to permit assignment through spin-decoupling experiments. With 0.74 equiv. of $Eu(fod)_3$, the epoxy protons exhibited the largest shifts to δ 17.15 and 16.89 and the other patterns were: a doublet, $J \sim 11$ Hz, at δ 12.22, a doublet of doublets, $J \sim 4.5$ and 16 Hz, at δ 9.48, an

TABLE 1. Deuterium incorporation in **2** at 185 °C

Time (h)	^{2}H content by mass spectrometry* 1D	2D	3D	4D	Total atoms ^{2}H	^{2}H assay by ^{2}H nmr† C-2	C-3	C-4 *exo*	C-4 *endo*
4	0.012				0.012	0.001	0.001	0.006	0.004
8	0.034				0.034	0.004	0.004	0.017	0.009
12	0.058	0.005			0.068	0.008	0.008	0.037	0.016
30	0.165	0.018			0.201	0.026	0.024	0.104	0.047
98	0.339	0.056	0.007		0.473	0.073	0.061	0.231	0.109
210	0.456	0.217	0.048		1.036	0.218	0.144	0.428	0.247
220	0.452	0.230	0.051	0.004	1.082	0.226	0.156	0.431	0.270
390	0.413	0.304	0.094	0.013	1.354	0.317	0.209	0.478	0.351

*Atoms ^{2}H ±0.001.
†See Experimental.

ill-defined quartet, δ 8.99, and a doublet of multiplets at δ 6.14 having the large J of 16 Hz. Spin-decoupling showed that the 16 Hz coupling was common to the δ 6.14 and 9.48 patterns, thereby identifying the 4-protons, since a geminal coupling of ~16 Hz and substantial shifts in the presence of Eu(fod)$_3$ were expected for these nuclei. The absorption giving the larger relative shift must arise from the *exo*-proton. Irradiation of the lowest field signal changed the quartet at δ 8.99 into a triplet, showing it to arise from H-1. The remaining doublet, δ 12.22, was assigned to the *syn*-8-proton, whose geminal coupling of 11 Hz agreed well with several model systems, and was shown to be coupled to a proton near 5.3 ppm. With this information, a sample of **2**-d_x from the 200 h base treatment was converted to the *exo*-epoxide and its ^{2}H spectrum recorded. The relative intensities of the four signals showed that the shielding order is the same as in the olefin. With Eu(fod)$_3$, the more intense of the two methylene signals exhibited the larger shift showing that *exo*-deuteration at C-4 is preferred. Thus the assignments of the four signals in the ^{2}H spectra of the olefins were completed.

From the deuterium incorporation results (Table 1) for the runs up to 220 h, first-order rate constants for exchange at the four sites were estimated to be: C-2, 3.3×10^{-7}; C-3, 2.1×10^{-7}; *exo*-C-4, 7.2×10^{-7} and *endo*-C-4, 3.9×10^{-7} s^{-1}.

Since exchange at the olefinic sites could occur through an addition–elimination sequence, the stability of the *tert*-butoxy ethers potentially involved in this process was of interest. A sample of *exo*-2-*tert*-butoxybicyclo[3.2.1]octane (**7**) was treated for 221 h under the same conditions employed for the olefin exchange studies. A gas chromatogram of the product was identical to that of the starting material indicating the presence of a single component having a retention time different from that of bicyclo[3.2.1]octene, and the proton spectrum showed no change from that of the starting material. Similarly, a 72:28 mixture of the *exo*- and *endo*-2-*tert*-butoxybicyclo[3.2.1]octanes was unchanged after treatment for 221 h. Thus the observed exchange at C-3 cannot involve addition–elimination.

In the manner described for **2**, samples of bicyclo[2.2.2]octene (**3**) were subjected to the exchange conditions for various times. The deuterium contents of the **3**-d_x samples thus obtained were measured by mass spectrometry and these data are given in Table 2. No species containing three deuterium atoms were observed and examination of the ^{2}H spectrum of **3**-d_x from the longest reaction time showed only olefinic absorption. From the mass spectrometric data a first-order rate constant for deuterium incorporation at C-2 (or C-3) can be estimated as 5.6×10^{-7} s^{-1}.

TABLE 2. Deuterium incorporation in **3** at 185 °C

Time	^{2}H content by mass spectrometry* 0D	1D	2D	Total atoms ^{2}H
5	0.960	0.040		0.040
37	0.724	0.250	0.026	0.303
124	0.605	0.340	0.054	0.449
210	0.323	0.493	0.184	0.861
393	0.190	0.486	0.324	1.133

*Atoms ^{2}H ±0.001.

Discussion

The striking feature of the present results for the [3.2.1] olefin **2** compared to the earlier data (2) is the finding of exchange at C-3 at a rate nearly comparable to that exhibited for the process proceeding through an allylic carbanion. In the earlier study, with *tert*-butoxide – dimethyl sulfoxide as the base–solvent system, only allylic exchange was observed. A crude comparison of the total exchange rates in the two systems may be made from first-order plots of the disappearance of nondeuterated material *vs.* time which gives $k_1 = 2 \times 10^{-7}$ s^{-1} in *tert*-BuO$^-$/DMSO at 60 °C and $k_1 = 1.7 \times 10^{-6}$ s^{-1} in *tert*-BuO$^-$/*tert*-BuOD at 185 °C. Although the temperature difference is 125 °C, the overall rates differ by less than an order of magnitude. As noted above, the observed rate of deuterium incorporation at C-3 (2×10^{-7} s^{-1}) is approximately 50% of that observed for the *endo*-allylic site (3.9×10^{-7} s^{-1}). Unfortunately the ratio of *exo*:*endo* incorporation for **2** in *tert*-BuO$^-$/DMSO was not determined. In fact, the mass spectrometric results reported (2) indicate no species with more than two deuterium atoms. This indicates that the *exo*:*endo* ratio of protonation of the allylic anion is much higher than that found in *tert*-BuO$^-$/*tert*-BuOD, assuming that *exo*-protonation (deuteration) of the anion is the preferred process as seems usual in these systems. It may be noted that pronounced differences in *exo*/*endo* protonation upon quenching the corresponding dienyl anion with ROH and with DMSO have been reported (13).

This contrast in behavior of **2** in the two base–solvent systems could be the result of a number of factors. Perhaps the simplest explanation would be an addition–elimination process in *tert*-BuO$^-$/*tert*-BuOD which would be much less likely in *tert*-BuO$^-$/DMSO. However, the stability of **5** and **7** under the reaction conditions preclude this notion. Another possibility could be a marked difference in the intramolecularity of the exchange processes in the two media since it has been shown that the extent of intramolecularity (internal return) in *tert*-BuO$^-$/*tert*-BuOD at 200 °C can be much less than that found for similar substrates in *tert*-BuO$^-$/DMSO (14). Unfortunately, this suggestion cannot be tested experimentally for **2** but it seems unlikely that this can be the sole factor responsible for the lack of observable exchange at C-3. This would require a major difference in the extent of intramolecularity for the two (or more) exchange processes in *tert*-BuO$^-$/DMSO, *e.g.* allylic and vinylic exchange. The higher temperature may be responsible for the C-3 exchange observed in *tert*-BuO$^-$/*tert*-BuOD. If C-3 exchange is 10 times slower than allylic exchange in DMSO compared with a difference of 2–3 in *tert*-BuOD, one can estimate that an activation enthalpy difference ($\Delta\Delta H^{\neq}$) of 3–4 kcal/mol for the allylic and vinylic exchange processes could render C-3 exchange unobservable at the lower temperature for the reaction times chosen, all other factors being equal. However, other factors may not be equal since the stabilities of the localized and delocalized carbanions may differ in the two solvents. The change from a nonpolar protic to a polar aprotic solvent tends to diminish the stability of a localized carbanion, to judge from pK_a values (15) and this feature may preclude C-3 exchange in DMSO.

It is interesting that exchange at the olefinic carbons in bicyclo[2.2.2]octene (**3**) is *ca.* 3 times faster than that at C-3 in **2**. Presumably there is greater *s* character in the C—H bond in **3** than in **2** which would render the olefinic hydrogens in **3** more acidic. It may be noted that the rate of olefinic exchange in 3,3-dimethylbicyclo[2.2.2]-oct-5-en-2-one is much faster than that for **3**, by a factor of ~100 at C-5 and even more at C-6 at 185 °C. In fact, measurements at lower temperatures will be required to obtain these rate constants for the ketone. Clearly, the polarity of the carbonyl group markedly accelerates olefinic exchange. We have presented ^{13}C data which indicates an appreciable polarization of the double bond by the carbonyl group in the ketone (16).

While the ^{2}H assays for the individual sites of exchange in **2** (Table 1) permit one to estimate rate constants for the appearance of deuterium at these sites, it would be useful to check their relative magnitudes and to determine the rate constant for direct exchange at C-2. The observed deuterium incorporation at C-2 can arise through a combination of allylic and vinylic exchange. The available pathways for allylic exchange can be set out as in Scheme 1 in terms of the rate constants for *exo*- and *endo*-proton abstraction, k_{-X} and k_{-N}, respectively, and the ratio, *R*, of *exo*:*endo* protonation (deuteration). In this scheme, the following abbreviations are used: $k_- = (k_{-X} + k_{-N})$; $k_X = 1/(1 + 1/R)$; $k_N = 1/(1 + R)$ and the primed *k*'s include a factor

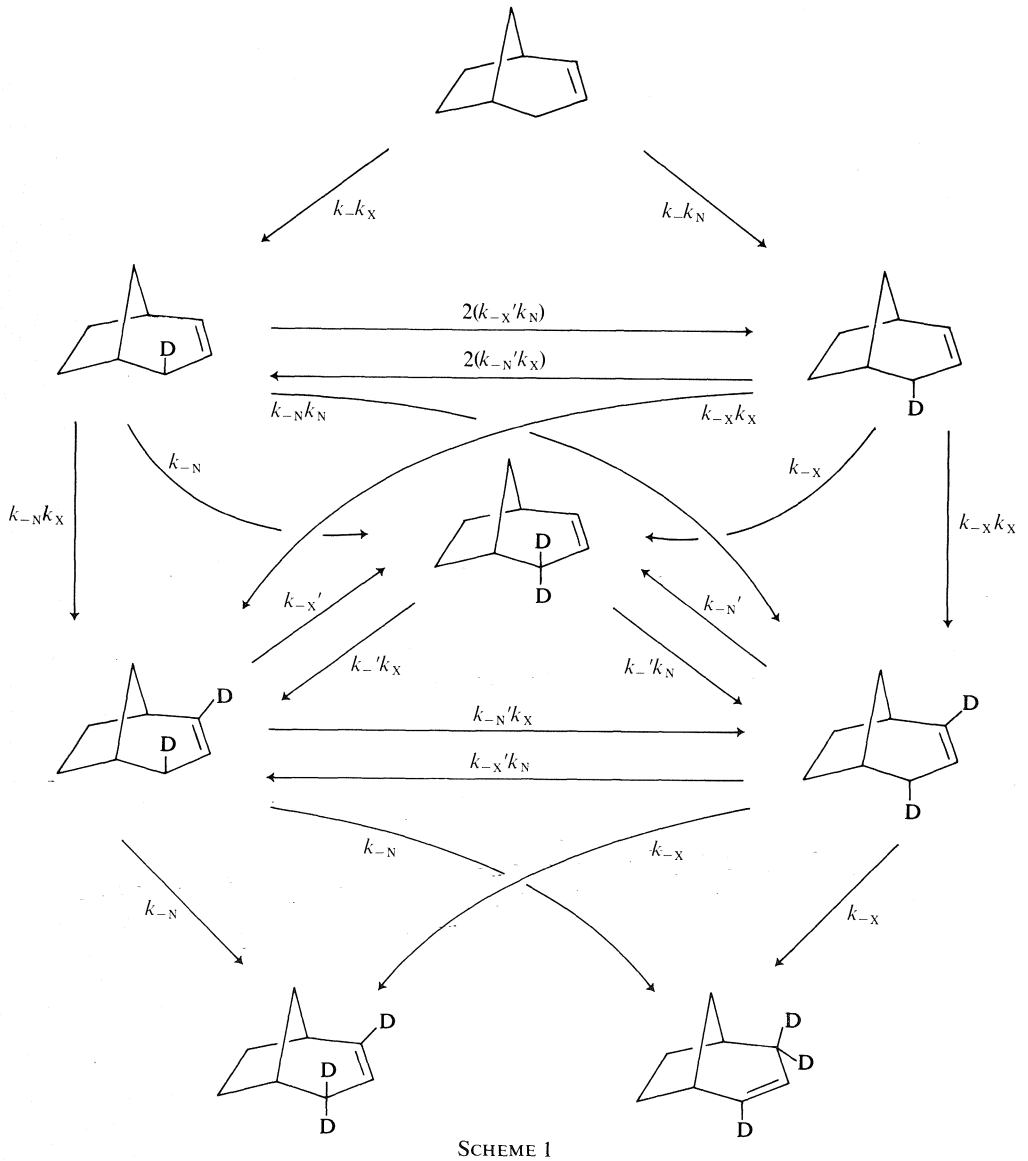

SCHEME 1

k_D/k_H for a primary kinetic isotope effect on the abstraction process. To reduce the complexity of the Scheme, only one enantiomer for A, B, C, D, and E are shown but the rate expressions include the contributions of A′, B′, C′, D′, and E′. These rate equations were numerically integrated using the MIMIC simulation language of the CDC computer and data for ^2H incorporation at C-4 were generated. A good fit with the experimental values was obtained with rate constants of 8.3×10^{-7} s^{-1} and 3.6×10^{-7} s^{-1} for *exo*- and *endo*-proton abstraction, respectively, and a ratio of 2.3 for the *exo*:*endo* deuteration (k_X/k_N). The calculated ^2H content at C-2 was lower than that observed, as expected, since direct vinyl exchange also leads to ^2H incorporation, as observed for C-3. Expansion of the MIMIC analysis to include vinyl exchange at C-2 gave a rate constant of 1.6×10^{-7} s^{-1} which compares favorably with the value of 2.1×10^{-7} s^{-1}, noted earlier for C-3 exchange, indicating no striking reactivity difference between the two olefinic sites.

Acknowledgements

We are grateful to the National Research

Council of Canada for financial support, to Ms. Marlene Brown for technical assistance, and to Prof. D. H. Hunter for helpful discussions.

1. D. M. HUDYMA, J. B. STOTHERS, and C. T. TAN. Org. Magn. Reson. **6**, 614 (1974).
2. J. M. BROWN and J. L. OCCOLOWITZ. Chem. Commun. 376 (1965); J. Chem. Soc. (B), 411 (1968).
3. M. C. HOFF, K. N. GREENLEE, and C. E. BOORD. J. Am. Chem. Soc. **73**, 3329 (1951).
4. C. W. JEFFORD, J. GUNSHER, and D. T. HILL. Org. Synth. **51**, 60 (1971).
5. N. N. SCHWARTZ and J. H. BLUMBERG. J. Org. Chem. **29**, 1976 (1964).
6. R. R. SAUERS, H. M. HOW, and H. FEILICH. Tetrahedron, **21**, 983 (1965).
7. K. R. STEPHENS, J. B. STOTHERS, and C. T. TAN. *In* Mass spectrometry and NMR spectroscopy in pesticide chemistry. *Edited by* R. Haque and F. J. Biros. Plenum Press, New York. 1973.
8. G. L. CLOSS and K. D. KRANTZ. J. Org. Chem. **31**, 638 (1966).
9. M. A. BATTISTE, J. M. COXON, and R. EDELMAN. Abstracts of the 164th National Meeting of the American Chemical Society, New York, N.Y. 1972. ORGN. 133.
10. C. T. TAN. Ph.D. thesis, University of Western Ontario, London, Ont. 1976.
11. E. LIPPMAA, T. PEHK, N. A. BELIKOVA, A. A. BOBYLEVA, A. N. KALINICHENKO, M. D. ORDUBADI, and A. F. PLATÉ. Org. Magn. Reson. **8**, 74 (1976).
12. A. L. JOHNSON, J. B. STOTHERS, and C. T. TAN. Can. J. Chem. **53**, 212 (1975).
13. J. M. BROWN and E. N. CAIN. J. Am. Chem. Soc. **92**, 3821 (1970).
14. D. H. HUNTER. *In* Isotopes in organic chemistry. Vol. 1. *Edited by* E. Buncel and C. C. Lee. Elsevier, Amsterdam. 1975. p. 142 ff.
15. J. F. COETZEE and C. D. RITCHIE. Solute–solvent interactions. M. Dekker, New York, N.Y. 1969.
16. J. B. STOTHERS, J. R. SWENSON, and C. T. TAN. Can. J. Chem. **53**, 581 (1975).
17. M. B. RAMPERSAD and J. B. STOTHERS. J. Chem. Soc. Chem. Commun. 709 (1976).
18. A. L. JOHNSON, N. O. PETERSEN, M. B. RAMPERSAD, and J. B. STOTHERS. Can. J. Chem. **52**, 4143 (1974).

The thermal and photochemical rearrangement of 1,2(4*H*)-diazepine derivatives[1,2]

DAVID JOHN HARRIS,[3] M. T. THOMAS, AND VICTOR SNIECKUS[4]

Guelph–Waterloo Center for Graduate Work in Chemistry, Department of Chemistry, University of Waterloo, Waterloo, Ont., Canada N2L 3G1

AND

NOGA FRIEDMAN, KJELD SCHAUMBURG, KENNETH B. TOMER, AND OLE BUCHARDT[4]

Chemical Laboratory II, University of Copenhagen, The H.C.Ørsted Institute, Universitetsparken 5, DK-2100 Copenhagen Ø, Denmark

Received July 29, 1976

DAVID JOHN HARRIS, M. T. THOMAS, VICTOR SNIECKUS, NOGA FRIEDMAN, KJELD SCHAUMBURG, KENNETH B. TOMER, and OLE BUCHARDT. Can. J. Chem. **55**, 56 (1977).

Thermolysis of 3,5,7-triphenyl-1,2(4*H*)-diazepine (**1**) gives, besides the known 2,4,6-triphenylpyridine (**2**), 3,5,6-triphenyl-1,2(4*H*)-diazepine (**3**) and 3,5,6-triphenyl-1,2(1*H*)-diazepine (**4**) whose structures are deduced on the basis of spectroscopic and chemical evidence. Neat thermolysis of **1** and the related 5-(*p*-methoxyphenyl)-3,7-diphenyl-1,2(4*H*)-diazepine (**24***a*) and 5-(*p*-chlorophenyl)-3,7-diphenyl-1,2(4*H*)-diazepine (**24***c*) gives only the corresponding pyridine derivatives **2**, **26***a*, and **26***c* in low yields. Photolysis of **1** in ethanol affords the somewhat unstable 3,5,7-triphenyl-1,2-diazabicyclo[3.2.0]hepta-2,6-diene (**21**) which upon thermolysis undergoes cycloreversion to **1** and upon hydrolysis provides 3,5-diphenylpyrazole (**23**) and acetophenone. In contrast, photolysis of **1** as well as of **24***a* and **24***c* in acetone results in the formation of the pyridine (**26***a*, **26***c*) and pyrazole (**25***a*, **25***c*) derivatives respectively in low yields. Irradiation of 5-(*p*-dimethylaminophenyl)-3,7-diphenyl-1,2(4*H*)-diazepine (**24***d*) under these conditions gives the photo-oxygenation product **24***e*. The observed thermolysis and photolysis results of **1** are compared and contrasted with those reported for the closely related 4,4-dimethyl-3,7-diphenyl-1,2(4*H*)-diazepine (**16**).

DAVID JOHN HARRIS, M. T. THOMAS, VICTOR SNIECKUS, NOGA FRIEDMAN, KJELD SCHAUMBURG, KENNETH B. TOMER et OLE BUCHARDT. Can. J. Chem. **55**, 56 (1977).

La thermolyse de la triphényl-3,5,7 (4*H*)-diazépine-1,2 (**1**) conduit, en plus de la triphényl-2,4,6 pyridine (**2**) qui est connue, à la triphényl-3,5,6 (4*H*)-diazépine-1,2 (**3**) et à la triphényl-3,5,6 (1*H*)-diazépine-1,2 (**4**) pour lesquelles on a déduit les structures en se basant sur des données spectroscopiques et chimiques. Les thermolyses en phase liquid de **1** et de la *p*-méthoxyphényl-5 diphényl-3,7 (4*H*)-diazépine-1,2 (**24***a*) et de la *p*-chlorophényl-5 diphényl-3,7 (4*H*)-diazépine-1,2 (**24***c*) qui lui sont reliées conduisent uniquement aux dérivés pyridiniques correspondants **2**, **26***a* et **26***c*, avec de faibles rendements. La photolyse de **1** dans l'éthanol conduit au triphényl-3,5,7 diaza-1,2 bicyclo[3.2.0]heptadiène-2,6 (**21**) qui est assez instable et qui par thermolyse subit une cycloréversion pour conduire à **1** et qui par hydrolyse fournit le diphényl-3,5 pyrazole (**23**) et l'acétophénone. Par opposition, les photolyses de **1** ainsi que de **24***a* et de **24***c* dans l'acétone conduisent respectivement à la formation de pyridines (**26***a* et **26***c*) et de dérivés pyrazoles (**25***a* et **25***c*), avec de faibles rendements. L'irradiation de la *p*-diméthylaminophényl-5 diphényl-3,7 (4*H*)-diazépine-1,2 (**24***d*) dans de telles conditions conduit à un produit de photo-oxygénation **24***e*. On compare les résultats observés pour la thermolyse et la photolyse **1** avec ceux rapportés pour la diméthyl-4,4 diphényl-3,7 (4*H*)-diazépine-1,2 (**16**) qui a une structure très analogue; on note qu'ils sont en opposition.

[Traduit par le journal]

The ready accessibility of 1,2(4*H*)-diazepines (**1**) from the reaction of hydrazine with pyrylium (2) and thiapyrylium (3) salts invited the investigation of their thermal and photochemical behaviour as part of our continuing interest in the chemistry of seven-membered heterocyclic systems (1, 4). Studies concerning the photochemistry of acyclic azines (5), pyrazoles (6), and pyrazolines (7) and, in particular, other simple and condensed diazepines (8) and the thermolysis of acyclic azines (9) and diazepines (10, 11) have been recently reported.

[1]This work was initiated independently in both laboratories. Decision for a cooperative project was reached in order to avoid duplication of results.

[2]Part IV in the series "The chemistry of seven-membered heterocyclic systems"; for previous paper, see ref. 1.

[3]National Research Council of Canada Postgraduate Scholar, 1973–1976.

[4]Authors to whom correspondence may be addressed.

Thermolysis

The thermolysis of 3,5,7-triphenyl-1,2,(4*H*)-diazepine (**1**) in refluxing bromobenzene followed by preparative layer chromatography yielded 2,4,6-triphenylpyridine (**2**) (2.5%) and two new isomeric 1,2-diazepines which are assigned structures **3** (14%) and **4** (19%) respectively on the basis of the following evidence (Scheme 1).

The ir, uv, and the mass spectral fragmentation pattern of **3** are very similar to those of **1** (2). Comparison of the nmr spectra of **1** and **3** clearly shows that in both compounds a methylene group is present with a large chemical shift difference between the two geminal protons. In **1**, δ 4.16 and 2.41 (2, 12); in **3**, δ 4.63 and 2.0. For both methylene groups, $J_{gem} = 11 \pm 1$ Hz. Furthermore, both compounds behave similarly under temperature variation: for **1**, $\Delta G^{\ddagger}$(343 K) = 17.6 kcal/mol, $T_c = 366$ K; for **3**, the exchange-broadened doublets observed at 305 K become sharp doublets at 273 K and a value of $T_c = 370$ K may be estimated. Reference to the recently determined X-ray crystal structure of the diazepinium picrate **5** (13) is useful in the analysis of the large chemical shift difference between the C_4-geminal protons in **1** and therefore in **3**.[5] The 1,2(4*H*)-diazepine conformation is such (*cf.* **5**) that H_B is close to and almost coplanar with the C_3 and C_5 phenyl groups whereas H_A is not. A rough estimate of the ring current effect based on the model of Haigh and Mallion (16) predicts a difference in shielding

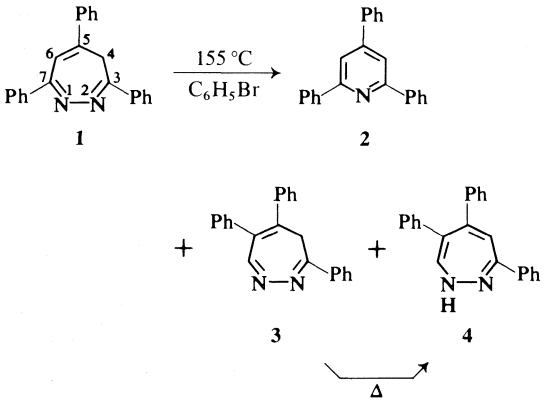

SCHEME 1

[5]There are valid arguments that (*a*) the conformation of the protonated form **5** and **1** are similar (14) and (*b*) the conformation of a (4*H*)-diazepine in the solid state and in solution should be comparable (13, 15).

$\delta_B - \delta_A \approx 2$ ppm which is in qualitative agreement with the observed values (*vide supra*). A further consequence of the conformational representation **5** is the expected larger coupling between H_6 and H_B than between H_6 and H_A due to the coplanarity of the atoms H_6–C_6–C_5–C_4–H_B. In agreement with this expectation, we have found previously (2, 12) that the low-field methylene proton (H_B) in **1** exhibits $J = 2.4$ Hz while the high-field methylene proton (H_A) shows $J = 1.6$ Hz.

The above analysis leads to the deduction that the thermolysis product must exhibit a structure which embodies a methylene group flanked by two phenyl-bearing sp^2-carbons within a 1,2(4*H*)-diazepine framework. This rules out a number of mechanistically reasonable structures (see below) and leaves for examination the two possible formulations, **3** and **6**. Structure **6** would be expected to show long range coupling between the C_5-methylene and H_7 similar to the ABX coupling pattern observed for compound **1** (δ (H_6) 6.45) (2, 12). Since no such absorption and pattern was observed, structure **6** is eliminated[6] and therefore the 3,5,6-triphenyl-1,2(4*H*)-diazepine structure **3** is assigned to the thermolysis product. The spectrum of **3** recorded after addition of Eu(DPM)$_3$ shift reagent showed a sharp singlet at δ 7.56. This downfield shift, independent of other signals, is assigned to the C_7-proton and is undoubtedly due to coordination of europium at N_1 by analogy with rhodium coordination of **1** (19).[7]

The ir spectrum of the other new thermolysis product (**4**) shows the presence of NH (ν_{max} 3425 cm^{-1}) and the mass spectrum exhibits the base

[6]It may be expected that **6** should exist predominantly in its corresponding valence isomer form **i** on the basis of several independent studies on such diazanorcaradienes (11*a*, 17). Structure **i** and, incidentally, **ii** and **12** (Scheme 2), the potential valence isomers of **3** and **1** respectively are eliminated since they should all show typically high field absorption due to the cyclopropane protons (δ < 2, J_{gem} = 3–6 Hz) (18).

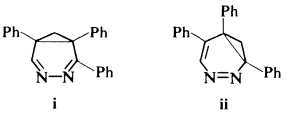

[7]The methylene signal of **3** was also influenced by the addition of Eu(DPM)$_3$: H_A was shifted strongly downfield while H_B was almost unaffected which is again reasonable if binding of the shift reagent at N_1 is assumed (*cf.* **5**). A similar effect on the methylene protons of **1** was observed.

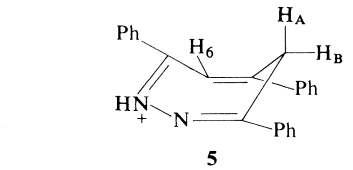

5

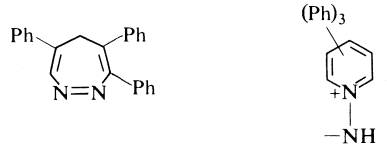

6 7

peak at m/e 321 ($M^+ - 1$). The nmr spectrum portrays, besides absorption for the aromatic protons at δ 7.9–6.85 (m, 16H), a doublet at δ 6.72 (J = 3 Hz) and a broad singlet at δ 8.9. A D_2O exchange experiment collapsed the signal at δ 6.75 into a sharp singlet and removed the broad NH signal at δ 8.9. This observation rules out a 1-iminopyridinium ylide type structure (**7**)[8] and directs consideration of a 1,2(1*H*)-diazepine formulation possessing a hydrogen at C_7. In 3,4,5-triphenyl-1,2(1*H*)-diazepine (**8**), $J_{6,7}$ substantially larger than 3 Hz would be expected. In 4,5,6-triphenyl-1,2(1*H*)-diazepine (**9**), NH-prototropy should make H_3 and H_7 equivalent with an identical chemical shift and coupling constant to NH.[9] The observed spectrum rules out both of these possibilities. There remain structures **4** and **10**, R = H for consideration. In previous work, we have observed that, in general, 3,5,7-triphenyl-1,2(1*H*)-diazepines (*e.g.* **10**, R = Me, CO_2Et, COMe) show $J_{4,6}$ = 1.5–2.0 Hz (3, 4). Since the D_2O exchange experiment resulted in the observation of a sharp singlet for C_7—H with a line width of less than 0.8 Hz, **10**, R = H is eliminated and structure **4** is assigned to this thermolysis product. That the C_4—H signal in **4** falls under the envelope of the phenyl absorption is also reasonable on the basis of our previous observations (3, 4).

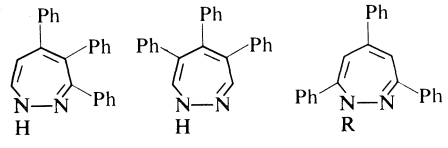

8 9 10

[8]In addition, ylide **7** would not be expected to be stable in refluxing bromobenzene (14, 20).

[9]We have observed this phenomenon recently in the irontricarbonyl complex of the parent 1,2(1*H*)-diazepine (21).

The interrelationship of **3** and **4** was established by thermolysis of **3** which gave **4** as the exclusive product. It was also shown that **4** was stable under these conditions and that refluxing **1** for an extended period of time led to increased amounts of **4** at the expense of **3**. The conversion of **3** into **4** provides supportive chemical evidence and may be viewed as a thermally allowed [1,5]-sigmatropic shift (see Scheme 2). Interconversion of other structures which have been discussed, *e.g.* **6** → **4**, could only proceed by a more complicated series of rearrangements.

Neat thermolysis (220 °C) was also performed on **1** to give 2,4,6-triphenylpyridine (**2**) as the only isolable product. Furthermore, these conditions were applied to 5-(*p*-methoxyphenyl)- and 5-(*p*-chlorophenyl)-3,7-diphenyl-1,2(4*H*)-diazepines, **24***a* and **24***c* respectively and led to the formation of the corresponding pyridine derivatives, **26***a* and **26***c* in low yields (see Experimental).

The mechanism for the formation of products from the thermolysis of **1** is given in Scheme 2. The formation of 2,4,6-triphenylpyridine (**2**) may be viewed as proceeding by a [1,5]-sigmatropic hydrogen shift to the 1,2(1*H*)-diazepine **10**, R = H followed by valence isomerization to **11** and loss of the elements of (NH). [1,5]-Sigmatropic shifts have been observed in a related 1,2-diazepine (15) and are more widely documented in azepines derivatives (22). Valence isomerization of **10**, R = H into **11** and thence rearrangement to **2** (possibly via the intermediate *N*-iminopyridinium ylide, *cf.* **7**) is expected to be facile on the basis of previous thermolysis results of 1-substituted 1,2(1*H*)-diazepines (**10**, R = Me, etc.) (11*b*, 14). The 5,6-dihydro derivative of **1** also yields the pyridine **2** presumably by an oxidative process (10). The formation of **3** and **4** may be described by the sequence of valence isomerizations and [1,5]-sigmatropic shifts (intermediates **12**–**14**) shown in Scheme 2 although a radical mechanism is not excluded.

Contrasting significantly with our results are those reported by Zimmerman and Eberbach on the thermolysis of the closely related dimethyl-1,2(4*H*)-diazepine **16** which gave diazanorcaradiene (**17**) and pyridazine (**18**) products (Scheme 3) (11*a*). Clearly, an identical valence isomerization step, **16** → **19** and **1** → **12** may be invoked to rationalize the thermolysis results of **1** and **16** respectively. However, whereas **19** then

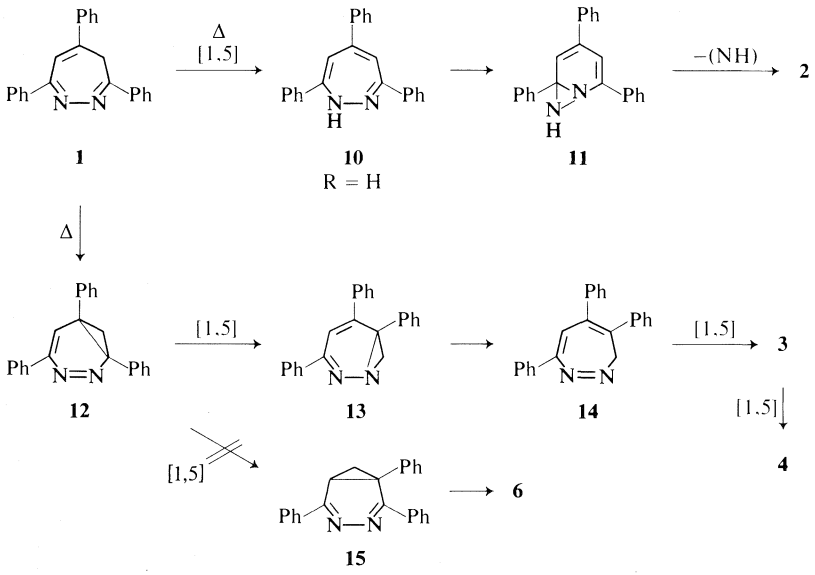

SCHEME 2

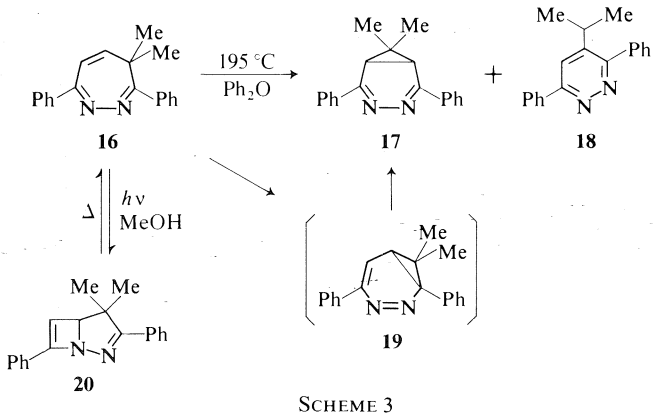

SCHEME 3

may directly proceed to **17** by a C-to-C [1,5]-sigmatropic shift ('walk' rearrangement (11*a*)), intermediate **12** avoids the analogous pathway to **15** in favor of a C-to-N [1,5]-sigmatropic shift to **13** which then continues via **14** to product. In both cases, **1** and **16**, no evidence is available to distinguish between a concerted or non-concerted process. If a concerted process is operative, their different behavior may be a consequence of perturbation on the MO correlation diagrams and thus on the energy requirements caused by the absence of symmetry (N-atoms) and presence or lack of electronic effects (C_5-phenyl in **12**) (23). If a non-concerted process applies, there may be expected to be little difference in stability of the two hypothetical dipolar or diradical species from **12** en route to **13** or **15**. On the other hand, there should be a distinct preference in **19** for C—C cleavage of the cyclopropane ring at the more highly substituted and congested side, a rationalization which is consistent with the observed formation of **17**.[10] It may also be noted that the C–C [1,5]-sigmatropic shift, **19** → **17** is favored over the alternate C–N shift for steric reasons.

Photolysis

When 3,5,7-triphenyl-1,2(4*H*)-diazepine (**1**) was irradiated in ethanol with a Pyrex-filtered immersion lamp, a single, somewhat unstable

[10]Compound **18** probably arises from **17** (11*a*).

product was isolated to which the 3,5,7-triphenyl-1,2-diazabicyclo[3.2.0]hepta-2,6-diene structure **21** is assigned on the basis of the following evidence (Scheme 4). Its 60 MHz nmr spectrum consists of a multiplet at δ 7.1–7.8 due to the aromatic protons, a singlet at δ 6.4 assigned to the vinyl hydrogen, and an AB quartet at δ 3.8 and 3.2 (J = 17.5 Hz) attributed to the C_4 methylene protons. Since no allylic coupling between the vinyl proton signal and the methylene absorption was evident (confirmed by 100 MHz nmr), the structural possibility resulting from the alternate photochemical electrocyclic closure of **1** is eliminated.

Chemical confirmation of structure **21** was obtained as follows. Upon reflux in toluene solution, the photoisomer underwent partial thermal reversion to a 2:1 mixture of **1**:**21**. Such cycloreversions have been observed in the analogous case **20** → **16** (Scheme 3) (11*a*) and other closely related systems (8*a*). In further support of structure, brief treatment of **21** with ethanolic hydrochloric acid gave acetophenone and 3,5-diphenylpyrazole (**23**). This reaction most likely occurs through the intermediacy of 5-phenacyl-3,5-diphenyl-2-pyrazoline (**22**), which has been shown to undergo fragmentation to the same two products upon acid treatment (24).

Irradiation of the readily available (2) compounds **24***a* and **24***b* under conditions similar to those employed for **1** gave crude material whose nmr spectra exhibited peaks consistent with diazabicyclo[3.2.0]heptadiene structures analogous to **21** (see Experimental). However, attempted purification of these products resulted in mixtures of at least eight components (tlc analysis) which were not characterized. Finally, photolysis of **24***c* yielded a complex reaction mixture containing no detectable bicyclic isomer (nmr analysis).

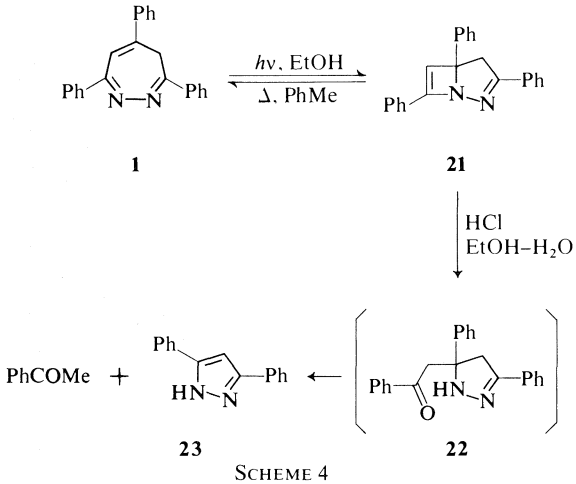

SCHEME 4

When the parent diazepine (**1**) was irradiated (253.7 nm) in acetone solution, the same pyrazole derivative (**23**) as well as 2,4,6-triphenylpyridine (**2**) were isolated in low yields. Under these conditions, but longer irradiation times, the 5-*p*-methoxyphenyl- and 5-*p*-chlorophenyl-1,2-(4*H*)-diazepines, **24***a* and **24***c* afforded the corresponding pyrazole (**25***a* and **25***c*) and pyridine (**26***a* and **26***c*) derivatives respectively.[11] In neither case was there observed a significant build up of the respective diazabicyclo[3.2.0]-heptadiene derivatives. The pyrazoles **25** and pyridines **26** are known compounds and were fully characterized by comparison with authentic samples synthesized independently (see Experimental). Since it is known that *N*-substituted pyrazoles undergo photochemical rearrangement (6), the stability of the NH-pyrazole **23** to our irradiation conditions was tested. It was shown that **23** is stable to prolonged irradiation in acetone solution.

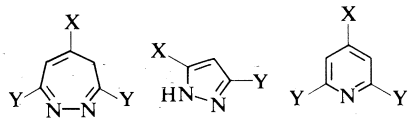

24 **25** **26**

a, X = *p*-$MeOC_6H_4$, Y = Ph
b, X = *p*-$MeOC_6H_4$, Y = *p*-MeC_6H_4
c, X = *p*-ClC_6H_4, Y = Ph
d, X = *p*-$Me_2NC_6H_4$, Y = Ph
e, X = *p*-Me(CHO)NC_6H_4, Y = Ph

Photolysis of **24***d* in acetone did not produce rearranged products but resulted instead in photo-oxidation to give the *N*-formyl derivative **24***e*. Structure **24***e* was assigned on the basis of spectral evidence. Its ir spectrum exhibits amide

[11] An additional minor product from the photolysis of **24***a* could not be obtained in pure form (contaminated with **26***a* even after several preparative tlc separations) but it was definitely shown *not* to be the pyridazine **iii** by independent synthesis (25). Compound **iii** could arise by a valence isomerization analogous to **1** → **12** followed by [CH_2] loss.

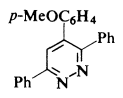

iii

carbonyl absorption at 1675 cm^{-1} and its mass spectrum shows the correct molecular ion at *m/e* 379. In comparison with the starting material (**24***d*), the nmr spectrum of **24***e* shows the loss of one N-Me group and the appearance of a singlet at δ 8.70 readily assigned to a formyl proton. Whereas compound **24***d* shows two-proton absorption at δ 6.80 due to the *ortho* hydrogens of the *p*-dimethylaminophenyl group, in **24***e* this multiplet is shifted under the aromatic proton envelope (δ 8.10–7.10) as expected on the basis of the deshielding influence of the N—CHO function.

The photochemical formation of the diazabicyclo[3.2.0]heptadiene **21** (Scheme 4) may be expected to occur by an allowed 4π electrocyclization and has direct parallel, in contrast to the thermolysis results (*vide supra*), with the photolysis of **16** to give **20** (Scheme 3) (11*a*). These reactions represent additions to an expanding list of cases which involve electrocyclization of azabutadiene units within diverse molecular frameworks (8*a*).[12]

The results obtained by irradiation in acetone may be mechanistically interpreted by reference to the reaction of **1** to produce 3,5-diphenylpyrazole (**23**) and 2,4,6-triphenylpyridine (**2**). The formation of compound **23** may be explained by postulating the intermediacy of **21** (Scheme 4) which undergoes loss of phenyl acetylene to form product. Precedence for such fragmentation is available (11*b*). The pyridine derivative **2** may arise by a photosensitized [1,3]-sigmatropic hydrogen shift to form the 1,2(1*H*)-diazepine **10**, R = H which suffers thermal ring contraction and [NH] loss in a manner similar to that already postulated (Scheme 2). Finally, the transformation **24***d* → **24***e* may be interpreted as an acetone photosensitized oxygenation, a reaction which has been widely documented for tertiary amines in the recent literature (27).

Experimental

General Methods

Melting points were measured on a Mel-Temp apparatus or a Reichert mp Microscope and are uncorrected. Microanalyses were performed by the microanalysis department at the University of Copenhagen. Infrared spectra were determined with Beckman IR-10 and Perkin-Elmer 337 spectrophotometers. Ultraviolet spectra were obtained on a Perkin-Elmer 137 spectrophotometer. Routine nmr spectra were recorded on a Varian T-60 spectrometer with Me_4Si as internal standard. For comparison and interpretation purposes, the nmr spectra of **1–4** were obtained in frequency sweep mode at 32 °C on the Varian HA-100 spectrometer equipped with a Spectra 100 system. Integration was performed on averaged spectra. Samples were prepared in C_6D_5Br (25 mg/400 μl). For shift reagent experiments, **3** was dissolved in $CDCl_3$–CCl_4 (1:4), $Eu(DPM)_3$ was added, and the solution was subjected to filtration. The filtrate was subsequently diluted with additional solvent while the dependence of the signals was followed. Starting concentrations: [**3**] = 0.135 *M*; $[Eu(DPM)_3] = 9.0 \times 10^{-2}$ *M*. Variable temperature spectra of **3** were determined on the Varian A-60A spectrometer using $CDCl_3$ for $T = -40$ to $+50$ °C and C_6D_5Br for the $T = +30$ to $+125$ °C temperature ranges. Mass spectra were recorded on an AEI MS902 spectrometer.

Irradiations were carried out as follows:

Method A: A solution of the sample was placed in a water-cooled (25–35 °C) Pyrex container and photolysis was performed using a Hanovia Q-700 medium pressure mercury arc as internal light source.

Method B: Irradiations were carried out in quartz or Vycor vessels placed centrally in a Rayonet Photochemical Reactor equipped with RUL-2537 Å lamps and cooled internally (15–20 °C) by a cold-finger condenser.

All solvents were dried and distilled before use. Thin layer chromatography was carried out with Merck silica gel GF 254 and column chromatography was effected with Merck silica gel (0.05–0.2 mm). Preparative tlc was performed with Merck PF 254-336 silica gel using 20 × 100 cm plates coated with a 1.5–2.0 mm layer of adsorbent. Fractions were scraped from the plates and isolated by extraction with $CHCl_3$ in a Soxhlet apparatus.

Thermolysis of 3,5,7-Triphenyl-1,2(4H)-diazepine (1) in Bromobenzene

A solution of **1** (2, 3) (1.0 g) in bromobenzene (30 ml) was refluxed under a nitrogen atmosphere for 9 days. The solvent was removed under reduced pressure and the residue was subjected to preparative tlc using ethyl acetate – benzene (5:95) as eluent. Two successive elutions gave the following fractions:

(*a*) Starting material (**1**): 550 mg (55%).

(*b*) *2,4,6-Triphenylpyridine (2)*: 25 mg (2.5%) identified by comparison with an authentic sample (28).

(*c*) *3,5,6-Triphenyl-1,2(4H)-diazepine (3)*: 136 mg (14%); mp 163–164 °C (EtOH); ir ν_{max} (KBr) 1593, 1270, 1200, 925 cm^{-1}; uv λ_{max} (EtOH) 274 (ε 29 400), 312 (sh, 12 200), 360 (6 900) nm; nmr ($CDCl_3$) δ 8.13 (m, 2H), 7.82 (m, 2H) and 7.08–7.53 (m, 12H) aromatic H, 4.63 (br d, 1H, C_4-H_A), 2.0 (br d, 1H, C_4–H_B); mass spectrum *m/e* 322 (M^+). *Anal.* calcd. for $C_{23}H_{18}N_2$: C 85.68, H 5.63, N 8.69; found: C 85.50, H 5.69, N 8.55.

(*d*) *3,5,6-Triphenyl-1,2(1H)-diazepine (4)*: 190 mg (19%), mp 209–210 °C (EtOH–H_2O); ν_{max} (KBr) 3425, 1600, 1495, 1460, 900 cm^{-1}; uv λ_{max} (EtOH) 244 (ε 27 200) 285 (19 000) nm; nmr (C_6D_5Br) δ 6.72 (d, 1H, J = 3 Hz, H_7), 6.9–7.45 and 7.8–8.0 (m, 15H, aromatic H), 8.9 (br s, 1H, exchangeable with D_2O, NH); mass spectrum *m/e* 322 (M^+), 321 (100%). *Anal.* calcd. for $C_{23}H_{18}N_2$: C 85.68, H 5.63, N 8.69; found: C 85.11, H 5.76, N 8.40.

When a solution of **1** (1.9 g) in bromobenzene (30 ml)

[12]The mechanistic details of 1-azabutadiene → azetine electrocyclization are under study by CNDO calculations by Prof. J. P. Snyder, University of Copenhagen (personal communication, May, 1974; see also ref. 26).

was refluxed under nitrogen for 36 days and the crude reaction mixture was processed and separated by preparative tlc as described above, there was obtained compound **4** (250 mg, 25%) as the major product in addition to minor amounts (< 5% each) of starting material and compound **3**.

*Thermolysis of 3,5,6-Triphenyl-1,2(4H)-diazepine (**3**) in Bromobenzene*

Compound **3** (25 mg) in bromobenzene (2 ml) was refluxed under a nitrogen atmosphere for 4 days. Thin layer chromatography (ethyl acetate – benzene, 5:95) showed the complete disappearance of starting material and the formation of *3,5,6-triphenyl-1,2(1H)-diazepine* (**4**) as the only product.

*Thermolysis of 3,5,6-Triphenyl-1,2(1H)-diazepine (**4**) in Bromobenzene*

Compound **4** (25 mg) in bromobenzene (2 ml) was refluxed under nitrogen for 4 days after which time starting material was completely recovered.

*Neat Thermolysis of 1,2(4H)-diazepines **1**, **24b**, and **24c***
*3,5,7-Triphenyl-1,2(4H)-diazepine (**1**)*

Compound **1** (246 mg) was pyrolyzed in a sealed evacuated tube at 220 °C (Wood's metal bath) for 1.5 h. The resulting dark brown oil was subjected to column chromatography (CH_2Cl_2 eluent to give 19 mg (8%) of *2,4,6-triphenylpyridine* (**2**) and 82 mg of recovered **1**. The pyridine **2** was identified by mp and mixture mp comparison with an authentic sample (28).

Pyrolysis of **1** at 220 °C for 4 h (complete disappearance of starting material by tlc) resulted in the formation of 25% of **2**. Numerous minor products evidenced by tlc were in insufficient quantities for isolation.

*5-(p-Methoxyphenyl)-3,7-diphenyl-1,2(4H)-diazepine (**24a**)*

Compound **24***a* (2) (240 mg) was pyrolyzed under the first set of conditions described for **1** above to give 23 mg (10%) of 4-(*p*-methoxyphenyl)-2,6-diphenylpyridine (**26***a*), identified by mp and mixture mp comparison with an authentic sample (29) prepared by a literature method (28), and 85 mg of recovered **1**.

*5-(p-Chlorophenyl)-3,7-diphenyl-1,2(4H)-diazepine (**24c**)*

Pyrolysis of compound **24***c* (2, 3) (240 mg) as described for **1** above (1.5 h) gave 19 mg (10%) of 4-(*p*-chlorophenyl)-2,6-diphenylpyridine (**26***c*) and 83 mg of recovered **1**. Compound **26***c* was identified by mp and mixture mp comparison with an authentic sample (30) synthesized by a literature procedure (28).

*Photolysis of 3,5,7-Triphenyl-1,2(4H)-diazepine (**1**) in Ethanol*

A solution of **1** (300 mg) in ethanol (250 ml) was irradiated for 4 h according to *Method A* outlined in General Methods. The photolysate was carefully taken to dryness *in vacuo* at room temperature and the residue was recrystallized from benzene – petroleum ether (60–90 °C) to give 200 mg (67%) of *3,5,7-triphenyl-1,2-diazabicyclo[3.2.0]hepta-2,6-diene* (**21**), mp 161–163 °C; uv λ_{max} (EtOH) 254 (ε 25 700) nm; nmr ($CDCl_3$) δ 7.1–7.8 (m, 15H, aromatic H), 6.4 (s, 1H, C_6-H), 3.8 (d, 1H, J = 17.5 Hz) and 3.2 (d, 1H, J = 17.5 Hz), CH_2; mass spectrum *m/e* 322 (M^+). *Anal.* calcd. for $C_{23}H_{18}N_2$: C 85.68, H 5.63, N 8.69; found: C 84.36, H 5.73, N 8.34.

Reproducibility of the above experimental conditions was found to be somewhat problematic. On several occasions, attempts to isolate **21** by evaporation of solvent *in vacuo* resulted in complex mixtures of products which no longer contained **21** (nmr evidence) even though tlc of the photolysate showed that it was the major constituent. See also photolysis of **24***a* and **24***b* below.

*Photolysis of 5-(p-Methoxyphenyl)-3,7-diphenyl-1,2(4H)-diazepine (**24a**) in Ethanol*

A solution of **24***a* (200 mg) in ethanol (250 ml) was irradiated according to *Method A* until no more starting material was present (tlc). Evaporation to dryness under reduced pressure gave material whose nmr spectrum ($CDCl_3$) is consistent with *5-(p-methoxyphenyl)-3,7-diphenyl-1,2-diazabicyclo[3.2.0]hepta-2,6-diene*: δ 6.75–7.8 (m, 14H, aromatic H), 6.35 (s, 1H, C_6-H), 3.68 (d, 1H, J = 17.5 Hz) and 3.15 (d, 1H, J = 17.5 Hz), CH_2, 3.65 (s, 3H, OCH_3). Attempted recrystallization from benzene – petroleum ether (60–90 °C) resulted in extensive decomposition (tlc analysis).

*Photolysis of 5-(p-Methoxyphenyl-3,7-di-(p-methylphenyl)-1,2(4H)-diazepine (**24b**) in Ethanol*

Irradiation of **24***b* (2) and work-up was carried out as described for compound **24***a* to give crude material whose nmr spectrum ($CDCl_3$) was consistent with *5-(p-methoxyphenyl)-3,7-di-(p-methylphenyl)-1,2-diazabicyclo[3.2.0]hepta-2,6-diene*: δ 6.7–7.7 (m, 12H, aromatic H), 6.3 (s, 1H, C_6—H), 3.73 (d, 1H, J = 17.5 Hz) and 3.2 (d, 1H, J = 17.5 Hz), CH_2, 3.65 (s, 3H, OCH_3), 2.3 (s, 6H $2 \times CH_3$). Attempted recrystallization from ether – petroleum ether resulted in decomposition to at least eight new products (tlc analysis).

*Thermolysis of Compound **21***

A solution of **21** (30 mg) in toluene (5 ml) was refluxed for 24 h and then evaporated to dryness *in vacuo*. Nuclear magnetic resonance examination of the crude material showed the presence of compounds **21** and **1** in a ratio of 1:2.

*Hydrolysis of Compound **21***

A solution of **21** (50 mg) in ethanol (50 ml) containing concentrated hydrochloric acid (1 ml) was refluxed for 3 h. The solvent was removed under reduced pressure and the resulting residue was treated, in part, with 2,4-dinitrophenylhydrazine solution to give *acetophenone 2,4-dinitrophenylhydrazone*, mp 148 °C, shown to be identical by mp, mixture mp, and ir spectral comparison with an authentic sample. The remaining portion of the residue was recrystallized from ether to give *3,5-diphenylpyrazole* (**23**), identified by nmr and mass spectral and tlc comparison with an authentic sample (31).

*Photolysis of Compounds **1**, **24a**, **24c**, and **24d** in Acetone*
*3,5,7-Triphenyl-1,2(4H)-diazepine (**1**)*

A solution of **1** (200 mg) in anhydrous degassed acetone (200 ml) was irradiated in a quartz tube under nitrogen for 19 h according to *Method B* (General Methods). The solvent was removed *in vacuo* and the resulting oil was subjected to column chromatography to give in order of elution (eluent): 16 mg (8.5%) of *2,4,6-triphenylpyridine* (2) (methylene chloride), 72 mg (36%) of **1** (methylene chloride – ether, 9:1), and 24 mg (20%) of *3,5-diphenylpyrazole* (**23**) (ether).

Compound **1** was found to be stable under the following photochemical conditions (Rayonet apparatus): methylene chloride, 350 nm, 16 h; acetonitrile, 253.7 nm, 12 h; benzene, 253.7 nm, benzophenone sensitization, 24 h.

*Photochemical Stability of 3,5-Diphenylpyrazole (**23**)*

Irradiation of **23** (100 mg) in dry acetone (70 ml) for 24 h under nitrogen using *Method B* resulted in high yield recovery of starting material.

*5-(p-Methoxyphenyl)-3,7-diphenyl-1,2(4H)-diazepine (**24a**)*

Irradiation (Vycor) of **24***a* (1.0 g) for 286 h in anhydrous acetone (500 ml) according to *Method B* gave, after chromatography (benzene eluent), 31 mg (13%) of *4-(p-methoxyphenyl)-2,6-diphenylpyridine* (**26***b*), 10 mg (1%) of *5-(p-methoxyphenyl)-3-phenylpyrazole* (**25***b*), and 500 mg (50%) of starting material. Compound **26***b* was characterized as indicated above while **25***b* was identified by comparison (mp and mixture mp) with an authentic sample prepared by a known method (31).

*5-(p-Chlorophenyl)-3,7-diphenyl-1,2(4H)-diazepine (**24c**)*

A solution of compound **24***c* (1.0 g) was irradiated (*Method B*, Vycor) in anhydrous acetone (500 ml) for 262 h and processed as described for **24***a* above to give 31 mg (12%) of *4-p-chlorophenyl-2,6-diphenylpyridine* (**26***c*) and 10 mg (1%) of *5-(p-chlorophenyl)-3-phenylpyrazole* (**25***c*) in addition to 400 mg of recovered starting material (**24***c*). The pyridine (**26***c*) (30) and pyrazole (**25***c*) (32) derivatives were characterized by mp and mixture mp comparison with authentic samples synthesized independently by the methods of Dimroth and Wolf (28) and Widman (32) respectively.

*5-(p-Dimethylaminophenyl)-3,7-diphenyl-1,2(4H)-diazepine (**24d**)*

A solution of **24***d* (3) (500 mg) in anhydrous acetone (600 ml) was irradiated (*Method B*, quartz) for 24 h. Chromatography gave the following fractions in order of elution (eluent): 127 mg (25%) of starting material (ether – methylene chloride, 5:95), 43 mg (9%) of compound **24***e* (ether – methylene chloride, 10:90). Recrystallization from ethanol gave pure **24***e*, mp 190–191 °C; ir ν_{max} (CH_2Cl_2) 1675 cm^{-1}; nmr ($CDCl_3$) δ 8.70 (s, 1H, CHO), 8.10–7.10 (m, 14H, aromatic H), 6.75 (br s, 1H, C_6-H), 4.45 (br d, 1H, J = 12 Hz, C_4-H_A), 3.40 (s, 3H, CH_3), 2.70 (br d, 1H, J = 12 Hz, C_4-H_B); mass spectrum *m/e* 379 (M^+). *Anal.* calcd. for $C_{25}H_{21}N_3O$: C 79.13, H 5.58, N 11.07; found: C 78.66, H 5.28, N 10.74.

Acknowledgments

This work was supported by 'Statens naturvidenskabelige Forskningsrad,' Denmark (to O.B.) and by the National Research Council of Canada (to V.S.). We also thank Bristol Laboratories, Syracuse for continued support. V.S. is indebted to the H.C. Ørsted Foundation for a Fellowship at the University of Copenhagen (1973) which made part of this work possible. The assistance of C. Bender and M. Kaufman (Chem. 13 News Award holders, University of Waterloo) in the preparation of starting materials is gratefully acknowledged.

1. C. L. Pedersen and O. Buchardt. Acta Chem. Scand. **27**, 271 (1973).
2. O. Buchardt, C. L. Pedersen, U. Svanholm, A. M. Duffield, and A. T. Balaban. Acta Chem. Scand. **23**, 3125 (1969).
3. D. J. Harris, G.Y.-P. Kan, V. Snieckus, and E. Klingsberg. Can. J. Chem. **52**, 2798 (1974).
4. D. J. Harris, G.Y.-P. Kan, V. Snieckus, and O. Buchardt. Synthesis, 603 (1975) and references cited therein.
5. J. Gorse III and R. W. Binkley. J. Org. Chem. **37**, 575 (1972) and references cited therein.
6. A. Lablanche-Combier and M. A. Remy. Bull. Soc. Chim. Fr. 679 (1971).
7. L. Schrader. Chem. Ber. **104**, 941 (1971); H. J. Rosenkranz and H. Schmid. Helv. Chim. Acta, **51**, 1628 (1968).
8. (*a*) V. Snieckus and D. J. Harris. *In* Photochemistry of heterocyclic compounds. *Edited by* O. Buchardt. Wiley, New York. 1976. p. 288; (*b*) J. P. Luttringer, N. Perol, and J. Streith. Tetrahedron, **31**, 2435 (1975); (*c*) J. Kurita and T. Tsuchiya. J. Chem. Soc. Chem. Commun. 936 (1974); (*d*) A. A. Reid, H. R. Sood, and J. T. Sharp. J. Chem. Soc. Perkin Trans. I, 362 (1976).
9. W. T. Flowers, D. R. Taylor, A. E. Tipping, and C. N. Wright. J. Chem. Soc. C, 1986 (1971).
10. G. Hasenheuttl, C. Opalka, and J. G. Krause. Chem. Ind. London, 1356 (1971).
11. (*a*) H. E. Zimmerman and W. Eberbach. J. Am. Chem. Soc. **95**, 3970 (1973); (*b*) G. Kan, M. T. Thomas, and V. Snieckus. Chem. Commun. 1022 (1971); (*c*) J. Streith and J.-M. Cassal. Bull. Soc. Chim. Fr. 2175 (1969); J. N. Done, J. H. Knox, R. McEwen, and J. T. Sharp. J. Chem. Soc. Chem. Commun. 532 (1974).
12. U. Svanholm. Acta Chem. Scand. **25**, 640 (1971).
13. R. Gerdil. Helv. Chim. Acta, **55**, 2159 (1972).
14. D. J. Harris, M. T. Thomas, V. Snieckus, and E. Klingsberg. Can. J. Chem. **52**, 2805 (1974).
15. J. N. Brown, R. L. Towns, and L. M. Trefonas. J. Am. Chem. Soc. **92**, 7436 (1970).
16. C. W. Haigh and R. B. Mallion. Org. Magn. Reson., **4**, 203 (1972).
17. G. Maier. Valenzisomerisieurungen. Verlag Chemie, Weinheim. 1972. p. 208.
18. G. Maier. Chem. Ber. **98**, 2438 (1965); **98**, 2446 (1965).
19. D. P. Madden, A. J. Carty, and T. Birchall. Inorg. Chem. **11**, 1453 (1972).
20. V. Snieckus and G. Kan. Chem. Commun. 172 (1970).
21. A. J. Carty, C. R. Jablonski, and V. Snieckus. Inorg. Chem. **15**, 601 (1976); A. J. Carty, R. F. Hobson, H. A. Patel, and V. Snieckus. J. Am. Chem. Soc. **95**, 6835 (1973).
22. A. Padwa, J. Smolanoff, and A. Tremper. J. Org. Chem. **41**, 543 (1976); A. Hassner and D. J. Anderson. J. Org. Chem. **39**, 3070 (1974) and references cited therein.
23. R. B. Woodward and R. Hoffmann. The conserva-

tion of orbital symmetry. Academic Press. New York. 1970. pp. 32, 37.
24. A. T. BALABAN. Tetrahedron, **24**, 5059 (1968).
25. D. J. HARRIS. Ph.D. Thesis, University of Waterloo, Waterloo, Ontario. 1976.
26. B. SCHILLING and J. P. SNYDER. J. Am. Chem. Soc. **97**, 4422 (1975).
27. F. KHUONG-HUU, D. HERLEM, and Y. HUBERT-BRIERRE. Tetrahedron Lett. 359 (1975); I. SAITO, S. ABE, Y. TAKAHASHI, and T. MATSUURA. Tetrahedron Lett. 4001 (1974); G. H. PARSONS, JR. and S. G. COHEN. J. Am. Chem. Soc. **96**, 2948 (1974); K. GOLLNICK and J. H. E. LINDNER. Tetrahedron Lett. 1903 (1973).
28. K. DIMROTH and K. H. WOLF. *In* Newer methods of preparative organic chemistry. Vol. III. *Edited by* W. Foerst. Academic Press, Inc. New York. 1964. p. 413.
29. M. WEISS. J. Am. Chem. Soc. **74**, 200 (1952).
30. R. L. FRANK and R. P. SEVEN. J. Am. Chem. Soc. **71**, 2629 (1949).
31. C. F. BEAM, R. S. FOOTE, and C. R. HAUSER. J. Chem. Soc. C, 1658 (1971).
32. O. WIDMAN. Chem. Ber. **49**, 477 (1916).

A three-coordinate complex of mercury: crystal structure of bis(iodo-*N*,*N*-diethyldithiocarbamatomercury(II))

CHUNG CHIEH

Guelph–Waterloo Centre for Graduate Work in Chemistry, University of Waterloo, Waterloo, Ont., Canada N2L 3G1

Received July 9, 1976

CHUNG CHIEH. Can. J. Chem. **55**, 65 (1977).

Reaction of mercuric iodide with *N*,*N*,*N*′,*N*′-tetraethylthiuramdisulfide (TETD), $Et_2N-\overset{\overset{S}{\|}}{C}-S-S-\overset{\overset{S}{\|}}{C}-NEt_2$, gave bis(iodo-*N*,*N*-diethyldithiocarbamatomercury(II)) and diiodo-*N*,*N*,*N*′,*N*′-tetraethylthiuramdisulfidemercury(II). The crystal of the former was monoclinic with $a = 7.645(3)$, $b = 7.787(4)$, $c = 18.005(7)$ Å and $\beta = 102.08(4)°$. The space group was $P2_1/c$, with two dimeric molecules per unit cell. Diffractometer measured intensities of 1727 observed reflections were used to determine the structure; the final *R* factor being 0.059. The mercuric ion was three-coordinated with two Hg—S distances of 2.422(4) and 2.644(4) Å and one Hg—I distance of 2.641(1) Å. The dimer had a centre of symmetry and formed an eight-membered ring.

CHUNG CHIEH. Can. J. Chem. **55**, 65 (1977).

La réaction de l'iodure mercurique avec le disulfure de *N*,*N*,*N*′,*N*′-tétraéthylthiourame (TETD) $Et_2N-\overset{\overset{S}{\|}}{C}-S-S-\overset{\overset{S}{\|}}{C}-NEt_2$, conduit aux bis(iodo *N*,*N*-diéthyldithiocarbamatomercure(II)), $Et_2-N-C-S-S-C-N-Et_2$, et au diiodo *N*,*N*,*N*′,*N*′-tétraéthylthiouramdisulfure de mercure(II). Les cristaux de premier sont monocliniques avec $a = 7.645(3)$, $b = 7.787(4)$, $c = 18.005(7)$ Å et $\beta = 102.08(4)°$. Le groupe d'espace est $P2_1/c$ et comporte deux molécules dimères par maille. On a utilisé les intensités mesurées à l'aide d'un diffractomètre pour 1727 réflexions observées pour déterminer la structure; le facteur final *R* est de 0.059. L'ion mercurique est tricoordonnée avec deux distances Hg—S de 2.422(4) et 2.644(4) Å et une distance Hg—I de 2.641(1) Å. Le dimère a un centre de symétrie et forme un cycle à huit chaînons.

[Traduit par le journal]

Introduction

Disulfuram has been used for the treatment of chronic alcoholism at a dose of 0.5 g per day. The chemical abstract name for the compound is tetraethylthioperoxydicarbonic diamide; however, it is better known as tetraethylthiuram disulfide (TETD),

$$Et_2NCS-SCNEt_2 \quad (1).$$

There has been a considerable interest in the interaction of heavy metal ions with biologically active compounds (2, 3). The interactions of TETD with mercurials are being studied. Reaction of TETD with methylmercury chloride gave bis(*N*,*N*-diethyldithiocarbamato)mercury-(II), $(Et_2NCS_2)_2Hg$, and methyl *N*,*N*-diethyldithiocarbamatomercury(II), $(Et_2NCS_2)HgMe$. The former was also obtained as a product in the reaction of TETD with mercuric chloride in chloroform–ethanol (1:1 by volume) mixed solution. Both α- and β-forms of $(Et_2NCS_2)_2Hg$ were obtained and X-ray diffraction data confirmed that they had the structures as reported by Iwasaki (4). The structure of Et_2NCS_2HgMe had been reported (5). The reactions of TETD with mercuric bromide and mercuric iodide also gave two kinds of products in each case. Compounds of HgX_2.TETD were obtained for X = Br and I. Their gross structures were obtained by X-ray diffraction methods. Further refinements are now being carried out. The existence of compounds of this type was claimed through nmr studies (6). Another compound obtained in the reaction of TETD with HgI_2 had cell constants similar to those of $(Et_2NCS_2)HgMe$ (5) and it was originally thought that they not only had similar formula but also similar structure, with CH_3 and I playing the same role. However the Raman spectrum of them, Fig. 1 and Fig. 5 of ref. 5, were quite different and the structure determination was carried out. It revealed that the compound had the empirical formula (Et_2NCS_2)-

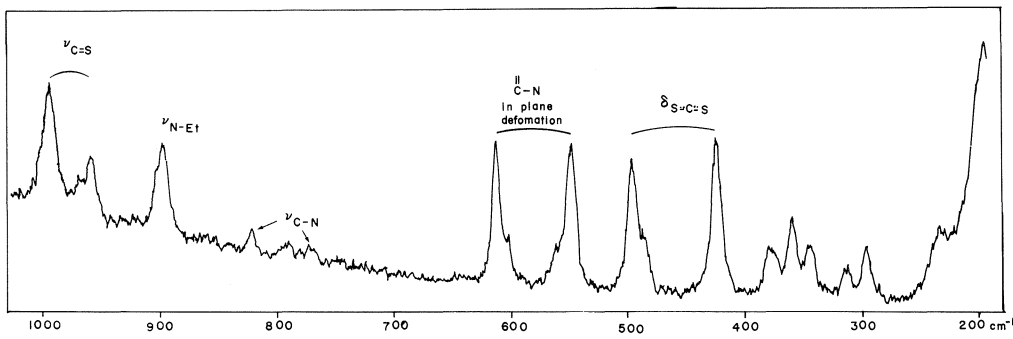

FIG. 1. Raman spectrum of bis(iodo-*N*,*N*-diethyldithiocarbamatomercury(II)) and partial assignments.

HgI which is similar to $(Et_2NCS_2)HgMe$; however, the two structures were different.

Experimental

The room temperature stable red form of mercuric iodide was purchased from Fisher Scientific Co., and tetraethylthiuram disulfide from Sigma Chemical Company, St. Louis, Missouri. The solvents used were standard reagent grade chemicals. Raman spectra of solids were obtained by Dr. S. Y. Tang on a Jarrel-Ash 25-100 spectrometer with argon ion laser excitation.

Several methods of preparation had been tried. For $((Et_2NCS_2)HgI)_2$, the following method was found to be the best. To 20 ml ethanolic solution of 0.235 g HgI_2, 20 ml chloroform solution of 0.154 g TETD were added. There was a small amount of small deep yellow square plates formed when the solutions were mixed. These small plates were identified as HgI_2.TETD as mentioned in the Introduction. The mixture was covered and left at room temperature for 3 days. Then, it was placed in a cool room (0 °C) and partly covered only to allow slow evaporation. After a week, the solution was reduced to about 0.5 ml. Yellow hexagonal prismatic crystals were obtained after filtration. A few square plate-like crystals were visible even to the naked eye. Due to the presence of a mixture, elemental analysis was not performed.

Crystals grown from the reactions described above were subjected to X-ray diffraction studies. Cell constants and space group were determined from photographic measurements; however, the former were refined by least-squares methods based on the 2θ values of 30 reflections measured on a G.E. XRD-6 diffractometer.

Crystal Data

$C_5H_{10}HgINS_2$ fw = 475.7

Monoclinic, $a = 7.645(3)$, $b = 7.787(4)$, $c = 18.005(7)$ Å, $\beta = 102.08(4)°$, $V = 1048.1$ Å^3, $\rho_0 = 3.00(1)$, $Z = 4$, $\rho_c = 3.014$, μ(Mo-K$_\alpha$) = 182.9 cm^{-1}; mp = 136 °C, space group $P2_1/c$.

Crystallographic Measurement

The crystal used for intensity measurement was a hexagonal prism with cross sections and length of 0.10 and 0.12 mm respectively. It was mounted with a^* along the φ axis of the goniostat. Intensities of 3052 independent reflections with $2\theta < 60°$ (Zr-filtered Mo-K$_\alpha$ radiation) were measured using θ–2θ scan method at room temperature (25 ± 3°). The scan speed was 2°/min and the 2θ range was $\pm(0.9 + 0.41 \tan\theta)$. Stationary background counts of 10 s each were taken at the limits of scan. Four standard reflections (104, 040, 202, 011) which had values evenly spread around the φ-circle were measured after each 100 reflections. The intensities of these reflections showed a fluctuation of ±2% during data collection. Of the reflections collected, 1727 had net intensities greater than $2\sigma_{(I)}$ were considered as observed. Majority of the unobserved reflections had 2θ greater than 45°. No absorption correction was made; however, the crystal used was uniform in dimension μR(Mo-K$_\alpha$) = 1.10, and the intensity of reflection 200, which had $\chi = 90°$, showed very little variation when φ was varied. Lorentz and polarization corrections were applied and only the observed reflections were used in the structure analyses.

Solution and Refinement

The structure was solved by the heavy-atom method and refined by full-matrix least-squares. The solution was straightforward and the refinement was smooth. The atomic scattering curves were taken from ref. 7 with dispersion corrections made for Hg and I atoms. The function minimized was $\Sigma w(|F_o| - |F_c|)^2$ where $w = (60 - |F_o| + 0.005F^2)^{-1/2}$ in the final stage of refinement. This weighting scheme gave lighter weight for both strong and weak reflections than the medium intense reflections; the variation of $\Sigma w\Delta F^2/n$ *vs.* ranges of F_o was small. An extinction coefficient of Zachariasen type was included in the 92-variable refinements. In the last cycle of refinement, the shifts of parameters were less than a quarter of their standard deviations. The difference Fourier showed some ripples around the mercury atom but was otherwise featureless. The final R $(= \Sigma(|F_o| - |F_c|)/\Sigma F_o)$ and weighted R_w $(= (\Sigma w(|F_o| - |F_c|)^2/\Sigma wF_o^2)^{1/2}$ were 0.059 and 0.051 respectively. The atomic coordinates and temperature factors are listed in Table 1.[1]

Results and Discussion

The crystal consists of dimeric molecules as shown in Fig. 2. The dimer has a centre of inversion which coincides with the centre of

[1]Photocopies of the table of structure factors may be obtained at a nominal charge, upon request, from the Depository of Unpublished Data, CISTI, National Research Council of Canada, Ottawa, Canada K1A 0S2.

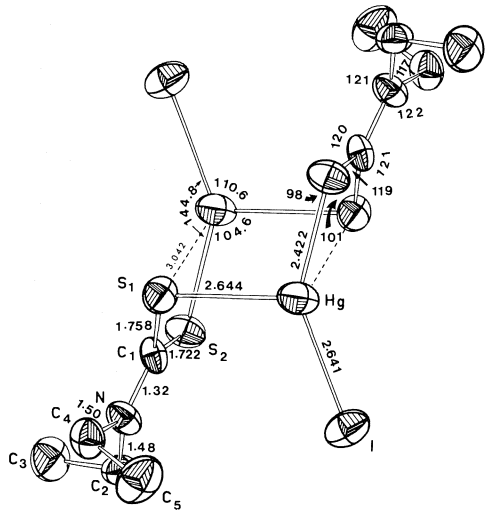

FIG. 2. Molecular structure with atomic labels and important bond distances and angles. The esd's are: σ_{Hg-I}, 0.001; σ_{Hg-S}, 0.004; σ_{C-S}, 0.015; and $\sigma_{C-C \text{ or } C-N}$, 0.02 Å. For the angles, the esd depends mainly on the centre atom: σ_{Hg}, ~0.1, σ_S, ~0.5 and $\sigma_{C \text{ or } N}$, ~0.7°.

symmetry of the space group $P2_1/c$; therefore, atoms of only half of the diagram are labelled. The important bond lengths and angles are also given separately in the two halves of the dimer. Around the mercuric ion, three bond lengths are noted: one Hg—I, 2.641(1), and two Hg—S distances of 2.644(4) and 2.422(4) Å. However, there is an additional short Hg...S contact of 3.042(4) Å. The mercury atom is coplanar with the three coordinated atoms, plane *5* of Table 2. It is interesting to compare with the coordination of Hg in diiodo-*N*,*N*,*N'*,*N'*-tetramethylthiuram-disulfidemercury(II), $HgI_2(S_2CNMe_2)_2$, in which there are two almost equal Hg—I distances of 2.661(2) and 2.654(2) Å. However, the two Hg—S distances of 2.651(7) and 2.882(7) Å are significantly different (8). The mercury atom is 0.305 ± 1 Å out of the plane containing the two iodine and the short-distant sulfur atoms.

Grdenic (9) derived the following mercury radii: van der Waals radius, 1.50; ionic radius, 1.04; digonal covalent radius, 1.30; and tetrahedral covalent radius, 1.48 Å. No three coordinated covalent radius was available, probably due to the fact that three coordinated mercury is not common; however the anions HgX_3^- (X = Cl, Br, and I) have a coordination number of 3 for mercury atom and the anion is planar (9). In particular, for HgI_3^- the three Hg—I distances are 2.71, 2.71, and 2.65 Å (average 2.69 Å)

TABLE 1. Final parameters (esd's) × 10^5 for Hg, I, and S, but × 10^4 for N and C, $\pm|x,y,z;x,\frac{1}{2}-y,\frac{1}{2}+z|$
T.F. = exp $\{-2\pi^2(a^{*2}h^2U_{11}+\ldots+2a^*b^*hkU_{12}+\ldots+)\times 10^{-4}\}$

Atom	x	y	z	U_{11}	U_{22}	U_{33}	U_{12}	U_{13}	U_{23}
Hg	27640(1)	52015(1)	51898(04)	465(3)	468(4)	674(5)	−87(3)	157(2)	−123(3)
I	10603(2)	24906(2)	55635(07)	516(6)	561(7)	689(7)	−28(5)	99(5)	191(6)
S_1	34805(5)	47995(5)	38258(22)	567(22)	374(19)	489(21)	65(17)	209(18)	−3(18)
S_2	60779(5)	19773(5)	44072(25)	465(21)	372(20)	595(24)	31(16)	22(19)	−64(18)
C_1	4062(17)	2613(18)	3854(07)	379(68)	360(71)	263(66)	114(57)	68(53)	−53(59)
N	2998(15)	1467(16)	3443(07)	374(67)	499(77)	446(74)	−18(56)	49(56)	−84(59)
C_2	3466(20)	−0387(19)	3476(09)	519(85)	328(73)	586(96)	−62(66)	211(73)	−56(69)
C_3	4529(26)	−0805(24)	2864(11)	557(90)	539(98)	723(99)	111(92)	339(96)	−73(71)
C_4	1343(19)	1975(23)	2880(09)	391(60)	672(99)	425(89)	41(76)	21(70)	−6(70)
C_5	−0314(22)	1887(31)	3253(12)	416(87)	1080(105)	891(99)	−22(99)	136(91)	234(98)

TABLE 2. (*a*) Least-squares planes for the molecule in the form $lX+mY+nZ=p$ where X, Y, Z, are coordinates in Å referred to orthogonal axes a, b, and c^*

Plane	Part of molecule	l	m	n	p	Displacement (Å) Maximum	Other atoms
1	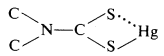	0.6258	0.1112	0.7720	3.9	0.11,Hg	1.4,C_3;−1.3,C_5
2	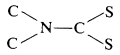	−0.6536	−0.1345	0.7448	3.7	0.07,C_4	−0.3,Hg
3		−0.6243	−0.1442	0.7677	3.9	0.01,C_1	−0.2,Hg
4		−0.6869	−0.1131	0.7179	3.5	0.03,N	−0.4,Hg
5		0.8086	−0.4137	0.4183	2.3	0.01,Hg	−0.005,S,I

(*b*) Interplanar angles

Planes	Angle (deg)
2,3	2.3
2,4	2.7
2,5	99.3
3,4	4.9

and the three I—Hg—I angles are 123.3, 123.6, and 112.8° (10). Taking the single-bond covalent radius for I as 1.33 Å (11), the trigonal radius for mercury is then 1.36 Å. By taking into account the influence of the electronegativity difference (12) (Schomaker–Stevenson coefficient = 0.03), the mean value for trigonal radius is then 1.38 Å. The single-bond covalent radius for sulfur is 1.04 Å (11). The sum of trigonal mercury radius and single-bond sulfur covalent radius is 2.42 Å which agrees very well with the shortest Hg—S distance, 2.422 Å, found for the title compound. The lengthening of the other Hg—S distance, 2.644 Å, may be due to the fact that S_1 is in close contact with another mercury atom. The Hg—I distance of 2.641(1) Å is slightly shorter than those found for HgI_3^- ion. The three bonds are not evenly spread in space around the mercury atom with angles of 144.8°, 110.6°, and 104.6°, of which the sum is 360°. From the above discussion, it can be concluded that the mercury atom is three-coordinated. The additional short Hg...S contact, 3.042 Å, is less than the sum of van der Waals radii for Hg and S, 3.35 Å, but this type of interaction is not uncommon in crystal structures (9, 13). It is true that in coordination compounds, the mercury atom is either linearly two- or tetrahedrally four-coordinated (14). This tendency still remains in the present compound as the angle between the shortest Hg—S and Hg—I bonds is 144.8°, much greater than 120°. Perhaps intramolecular forces prevent Hg...S_1 contact to be closer than 3.04 Å.

The part of 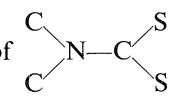 in the ligand, diethyldithiocarbamate, is usually found to be planar (4). The equations for mean planes of various parts of the molecule are listed in Table 2. The unlabelled mercury atom is almost coplanar with labelled dithiocarbamate, excluding

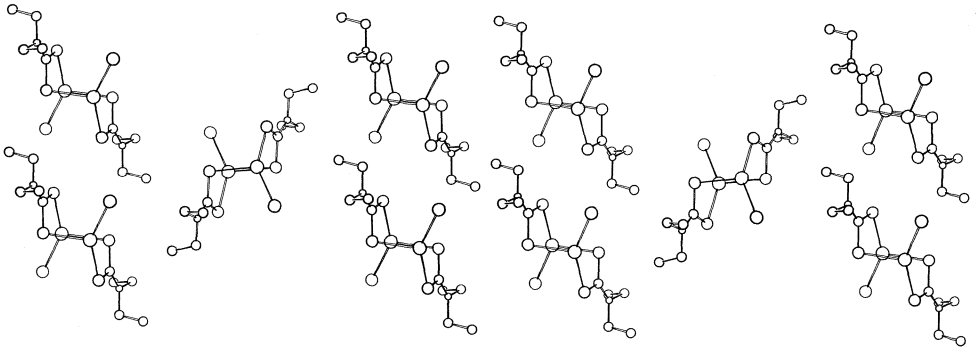

FIG. 3. Stereoscopic view of the molecular packing in bis(iodo-*N*,*N*-diethyldithiocarbamatomercury-(II)). Atoms are represented by the size of the ring in descending order of Hg > I > S > C > N. The direction of viewing is from *a* axis.

the terminal CH_3 groups. When Hg^{2+} is included in the mean plane calculation, the maximum displacement from the plane is only 0.11 Å. When Hg^{2+} is excluded from the least-squares plane calculation, the deviation becomes −0.3 Å. The planarity of 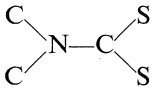 and the short N—C distance of 1.32(2) Å suggest that partial double bond character exists between N and C_1.

Absorption bands in the range from 560 to 608 cm^{-1} were assigned to C—N in plane deformation in ref. 15 for similar compounds; the band at 615 cm^{-1}, Fig. 1, was assigned accordingly. The band caused by $\nu_{(C-N)}$, usually found for other compounds, is very weak. Assignments for bands in the region between 200 and 400 cm^{-1} are very difficult. Coleman, Koenig, and Shelton gave all kinds of composite contributions for bands in this region for tetramethylthiuram disulfide (15). Meić studied the vibrational spectra of CH_3HgI and CD_3HgI as well as other halo-complexes and assigned a band at 173 cm^{-1} for $\nu_{(Hg-I)}$ (16). Two very strong Raman bands at 173 and 139 cm^{-1} were observed for $((Et_2NCS_2)HgI)_2$. The one at 139 cm^{-1} was 30 times as strong as the strongest band of Fig. 1, and ten times stronger than the band at 173 cm^{-1}. It was anticipated that the stretching mode of Hg—I be a strong band in Raman and a shift in frequency was also expected due to a change from two- to three-coordinated mercury; therefore, the band at 139 cm^{-1} could be assigned to $\nu_{(Hg-I)}$.

A packing diagram is shown in Fig. 3. The viewing direction is from the *a*-axis. All intermolecular distances are van der Waals type. The mercuric ion has no further close contact other than the one indicated in Fig. 2. The next closest intermolecular distance between mercury and iodine atoms is 3.5 Å. The dimers interlock into one another and this may be responsible for the hardness of the crystals.

Acknowledgement

This work is supported by the National Research Council of Canada.

1. N. G. NASH and R. D. DALEY. Analytical profiles of drug substances. Vol. 4. *Edited by* K. Florey. Academic Press, New York. 1975. pp. 169–191.
2. P. L. J. HUBERT and A. L. BEAUCHAMP. Inorg. Chem. **15**, 322 (1976).
3. D. R. WILLIAMS. Inorg. Chim. Acta Rev. **6**, 123 (1972).
4. H. IWASAKI. Acta Crystallogr. B**29**, 2115 (1973).
5. C. CHIEH and L. P. C. LEUNG. Can. J. Chem. **54**, 3077 (1976).
6. H. C. BRINKOFF, A. M. GROTENS, and J. J. STEGGERDA. Recl. Trav. Chim. Pays-Bas, **89**, 11 (1970).
7. International Tables for X-ray Crystallography, Vol. III. Kynoch Press, Birmingham. 1962. p. 201.
8. P. T. BEURSKENS, J. A. CRAS, J. H. NOORDIK, and A. M. SPRUIJT. J. Cryst. Mol. Struct. **1**, 93 (1971).
9. D. GRDENIC. Q. Rev. **19**, 303 (1965).
10. R. H. FENN, J. W. H. OLDHAM, and D. C. PHILLIPS. Nature, **198**, 381 (1963).
11. F. A. COTTON and G. WILKINSON. Advanced inorganic chemistry. 3rd ed. John Wiley and Sons, Inc. 1972.
12. L. PAULING. The nature of the chemical bond. 3rd ed. Cornell University Press, Ithaca. 1960.
13. Y. S. WONG. Ph.D. Thesis, University of Waterloo. Waterloo. Ont. 1975.
14. A. F. WELLS. Structural inorganic chemistry. 4th ed. Claredon Press, Oxford. 1975.
15. M. M. COLEMAN, J. L. KOENIG, and J. K. SHELTON. J. Polym. Sci. Polym. Phys. Ed. **12(5)**, 1001 (1974).
16. Z. MEIĆ. J. Mol. Struct. **23**, 131 (1974).

Synthesis and electron spin resonance studies of a Co(II) complex with a tetradentate macrocyclic Schiff base ligand

AMIKAM REUVENI, VINCENZO MALATESTA,[1] AND BRUCE R. MCGARVEY

Department of Chemistry, University of Windsor, Windsor, Ont., Canada N9B 3P4

Received June 4, 1976

AMIKAM REUVENI, VINCENZO MALATESTA, and BRUCE R. MCGARVEY. Can. J. Chem. **55**, 70 (1977).

The synthesis, physical properties, and electron spin resonance of frozen solutions of $CoTAAB(NO_3)_2$ (TAAB = tetrabenzo[*b,f,j,n*] [1,5,9,13]tetraazacyclohexadecine) are reported. The spin Hamiltonian parameters were elucidated by simulation of spectra assuming axial g and ^{59}Co hyperfine tensors and including nuclear quadrupole and Zeeman contributions. Electron spin resonance spectra in solvents such as methanol, acetone, and dimethylformamide are typical for a low spin complex ($S = 1/2$) and are nearly identical with $|A_{\parallel}| \gg |A_{\perp}|$ and $g_{\perp} \gg g_{\parallel}$. In pyridine and quinoline a complex with a molar ratio solvent/ligand of 1:1 is formed with the solvent which gives $|A_{\parallel}| \approx |A_{\perp}|$ and $g_{\perp}$ much closer to $g_{\parallel}$. In strong Lewis bases, such as piperidine, a 2:1 complex is formed and no esr signal is found. Evidence is presented to show that these 2:1 complexes with strong Lewis bases are $S = 1/2$ complexes with a low lying $S = 3/2$ state that is partially populated at room temperatures. This behaviour is accounted for in terms of a theory derived for a $^2A_1$ ground state with a low lying quartet state which could become the ground state in strong basic solvents.

AMIKAM REUVENI, VINCENZO MALATESTA et BRUCE R. MCGARVEY. Can. J. Chem. **55**, 70 (1977).

On rapporte la synthèse, les propriétés physiques et les résonances paramagnétiques électroniques de solutions surgelées de $CoTAAB(NO_3)_2$ (TAAB = tétrabenzo[*b,f,j,n*] [1,5,9,13]-tétraazacyclohexadécine). On a élucidé les paramètres du hamiltonien de spin par simulation de spectres en faisant l'hypothèse que g est axial, en utilisant des tenseurs hyperfins pour ^{59}Co, et en incluant des contributions nucléaires quadrupolaires et de Zeeman. Les spectres de résonance paramagnétique électronique dans des solvants tels que le méthanol, l'acétone et la diméthylformamide sont typiques pour un complexe de spin bas ($S = 1/2$); ils sont pratiquement identiques et $|A_{\parallel}| \gg |A_{\perp}|$ et $g_{\perp} \gg g_{\parallel}$. Dans la pyridine et la quinoléine il y a formation d'un complexe avec un rapport molaire solvant-ligand de 1:1 qui donne $|A_{\parallel}| \approx |A_{\perp}|$ et $g_{\perp}$ beaucoup plus proche de $g_{\parallel}$. Dans des bases de Lewis fortes, telles que la pipéridine, il y a formation d'un complexe 2:1 et on ne trouve aucun signal rpe. On présente des données pour montrer que ces complexes 2:1 avec des bases de Lewis fortes sont des complexes $S = 1/2$ avec un état $S = 3/2$ peu élevé et qu'un peuplement partiel à température de la pièce. On tient compte de ce comportement en termes d'une théorie dérivée d'un état fondamental $^2A_1$ avec un état quadruplet peu élevé qui peut devenir l'état fondamental dans les solvants basiques forts.

[Traduit par le journal]

Introduction

Planar low spin Co(II) complexes of the types CoN_4, CoN_2O_2, and CoS_4 have been the subject of many esr studies. The theory for the spin Hamiltonian parameters for these d^7 complexes was the subject of a recent study (1) which showed that contributions of low-lying quartet states to the magnetic parameters could be significant for some systems. Most of the esr studies on frozen solutions (see references in ref. 1) have involved low symmetry complexes and have proven of little value since the three principal g and A values could not be assigned unambiguously to the molecular axes. A few single crystal studies have appeared (2–7). Most of these complexes can bond to Lewis bases to form five- and six-coordinated species. Several of the five-coordinated complexes have demonstrated the ability to bond reversibly to molecular oxygen.

Transition metal complexes of the tridentate, tribenzo[*b,f,j*][1,5,9]triazacycloduodecine, abbreviated TRI, **1**, and tetradentate, tetrabenzo-[*b,f,j,n*][1,5,9,12]tetraazacyclohexadecine, abbreviated TAAB, **2**, have been made (8–11) by the condensation of *o*-aminobenzaldehyde in the presence of different metal ions.

[1]Present address: Department of Chemistry, University of Guelph, Guelph, Ontario.

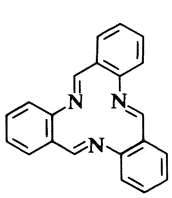

1

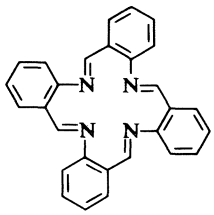

2

We report here the synthesis of Co(II)TAAB-$(NO_3)_2 \cdot H_2O$, its isolation for the first time, and an esr study of the Co(II)TAAB^{2+} complex in frozen solutions of various solvents and Lewis bases. The TAAB ligand is similar to the porphyrin and phthalocyanine ligands in that it is a planar, conjugated tetradentate ligand with a fourfold symmetry axis. It differs from the porphyrin, phthalocyanine, and most planar tetradentate ligands studied in that it is neutral in charge. We therefore will expect to find the complex with the fifth and sixth coordination sites occupied by either a polar solvent molecule or the anions required for charge balance.

Experimental

Synthesis of Co(II)TAAB$(NO_3)_2 \cdot H_2O$

The synthesis follows that used by Melson and Busch (8) except that care is taken to keep oxygen out by degassing all solvents and carrying out all steps under prepurified N_2. A solution of 2.9 g (0.024 mol) of *o*-aminobenzaldehyde (freshly prepared by the method of Smith and Opie (12)) in 40 ml of ethanol was heated and stirred. While the *o*-aminobenzaldehyde solution was under reflux, a solution of 1.75 g of $Co(NO_3)_2 \cdot 6H_2O$ in 30 ml of absolute ethanol was added. The color of the solution changed from pale yellow to reddish brown and within 15–20 min it turned green and a precipitate began forming. After refluxing for 5 h the solution was cooled and filtered. The dark green solid was washed with chilled ethanol and ether. The green solid was recrystallized from acetonitrile to give dark green crystals which analyzed as CoTAAB$(NO_3)_2 \cdot H_2O$. Calculated for $C_{28}H_{20}N_6O_6$-$Co \cdot H_2O$: C 54.82, H 3.61, N 13.70, Co 9.61. Found: C 54.30, H 3.29, N 13.63, Co 9.63.

Physical Measurements

Electron spin resonance spectra were taken with a Varian E-12 spectrometer. All spectra were taken at X-band at liquid nitrogen temperatures using a finger-Dewar. Infrared absorption spectra were obtained using a Beckman IR-12 spectrophotometer. Electron Ionization mass spectra were obtained at various temperatures up to 270 °C using a Varian-MAT CH5 spectrometer. Magnetic susceptibilities of methanol and piperidine solutions were measured using the nmr shift technique (13). Magnetic susceptibilities of powder (in air) were measured by Professor A. B. P. Lever of York University using the Faraday method at temperatures from 82 K to room temperature. Nuclear magnetic resonance spectra were taken using a JEOL C68JEL Spectrometer. Chemical analysis was done by Galbraith Laboratories Inc., Knoxville, Tenn.

Results

Properties of CoTAAB$(NO_3)_2$

CoTAAB$(NO_3)_2$ is soluble in water. Addition of concentrated solutions of $HClO_4$ or HBr to the water solution produced green precipitates which are presumed to be the corresponding perchlorate and bromide salts. When O_2 was bubbled through an HBr solution of the bromide a red–brown solid resulted whose ir was identical to that of [CoTAABBr_2]Br reported by Cummings and Busch (11). The synthesis of Co-TAABBr_2 directly from $CoBr_2$ was attempted yielding a green precipitate whose esr in acetone was identical to the bromide produced from the nitrate and which oxidized to [CoTAABBr_2]Br, but a suitable recrystallization solvent was not found so no analysis was attempted.

In the reaction between $Co(NO_3)_2$ or $CoBr_2$ with *o*-aminobenzaldehyde considerable amounts of cobalt remain in the ethanol solution. Evaporation of this green filtrate under vacuum yields a light green solid. Examination of this solid by tlc reveals it to be a mixture. Frozen solution esr spectra of acetone solutions give only the signal found for CoTAAB$(NO_3)_2$. Magnetic susceptibility measurements reveal a much larger susceptibility than that found for CoTAAB$(NO_3)_2$ suggesting the presence of a high spin complex. Finally acetone and ethanol solutions of this solid turn brown within minutes after exposure to air while similar solutions of CoTAAB$(NO_3)_2$ oxidize much more slowly. Cummings and Busch (11) have shown that under similar preparative conditions, but in the presence of oxidizing agents, a mixture of Co(TRI)$_2X_3$ and Co-TAABX_3 is produced. We presume, therefore, that a main constituent of the ethanol solution after reflux is a Co(TRI)$_2^{2+}$ compound since this complex is octahedrally coordinated and would be expected to be high spin. This would account for the high susceptibility and our failure to detect any other esr signals at liquid nitrogen temperatures.

The ir spectrum of CoTAAB$(NO_3)_2$ is similar to that reported by Cummings and Busch (11) for [CoTAAB$(NO_3)_2$]NO_3 except only three bands attributable to NO_3^- are found at 1365, 1310, and 1031 cm^{-1}. The first two are obviously asymmetric stretches and the 1031 cm^{-1} is the

symmetric stretch. Since these frequencies are those normally found in ionic nitrates we can conclude that neither nitrate ion is really coordinated to the cobaltous ion. Electron ionization mass spectra, between 100 and 270 °C, of $CoTAAB(NO_3)_2$ did not give the m/e peak at 412 attributed by Cummings and Busch (11) to $(TAAB)^+$.

The magnetic susceptibilities at 298 K of methanol and piperidine solutions were found from nmr measurement of these solutions in a concentric double tube with TMS in the annulus (13). (Calibration was made with acetone, methanol, and carbon tetrachloride, respectively, in the inner tube.) The susceptibility of the methanol solution was found to be 1.67 ± 0.05 B.M., a value very close to that expected for an $S = 1/2$ state (1.73 B.M.). The piperidine solution gave a susceptibility of 2.25 ± 0.05 B.M., indicating a presence of an $S > 1/2$ state.

The magnetic susceptibility of powdered $CoTAAB(NO_3)_2$ has been measured between 82 and 298 K and is given in Table 1. Ligand and anion corrections were calculated from Pascal's constants (14). The effective magnetic moment increases with temperature to a value at room temperature considerably larger than that expected for an $S = 1/2$ system with the g values found for the complex from the esr studies. Attempts to fit the data to a simple model assuming a ground state doublet and an excited quartet state were made, but no satisfactory fit of all the data could be made. It seems reasonable, however, that the only way to account for these results is to assume some population at room temperature of excited states with a spin higher than 1/2. The same may be said for the piperidine solution of the complex.

TABLE 1. Magnetic susceptibilities of $CoTAAB(NO_3)_2$ powder at various temperatures

T (K)	μ_{eff} (B.M.)	χ_M (cgs × 10^6)
82.2	2.28	7880
87.3	2.30	7550
105.3	2.32	6370
121.8	2.32	5520
138.7	2.33	4900
156.3	2.37	4490
173.4	2.38	4080
191.4	2.40	3760
209.4	2.41	3470
227.5	2.46	3310
245.5	2.46	3070
263.2	2.50	2950
298.2	2.65	2950

Electron Spin Resonance

The esr results were fitted to the spin Hamiltonian

$$[1]\quad \mathcal{H} = \beta[g_{\parallel}H_zS_z + g_{\perp}(H_xS_x + H_yS_y)] + A_{\parallel}S_zI_z + A_{\perp}(S_xI_x + S_yI_y) + Q'[I_z^2 - \tfrac{1}{3}I(I+1)] - g_N\beta_N\mathbf{H}\cdot\mathbf{I}$$

where symbols have their usual meaning. The esr studies were all done in frozen solutions involving $CoTAAB(NO_3)_2$ in most cases (esr of the powdered compound gave a very broad line). Spectra of the perchlorate and bromide salts in acetone and methanol were identical to the nitrate. The solvents used for making the frozen solutions could be divided into three groups according to the spin Hamiltonian parameters observed: (*i*) Solutions in methanol, acetone, and dimethylformamide which gave $|A_{\parallel}| \gg |A_{\perp}|$, and $g_{\perp} \gg g_{\parallel}$. (*ii*) Solutions in pyridine and quinoline which gave $|A_{\parallel}| \approx |A_{\perp}|$, $g_{\perp}$ much closer to $g_{\parallel}$ than in (*i*). (*iii*) Solutions in piperidine, aliphatic amines, pyrrolidine, and morpholine which gave no esr spectrum at all.

The magnetic parameters were obtained by comparing the experimental spectra with simulated spectra obtained from a computer program which numerically integrates over expressions for the resonance fields predicted by the spin Hamiltonian given in eq. 1, solved to second order. Forbidden transitions ($\Delta m_I = \pm 1, \pm 2$) were included with the allowed transitions

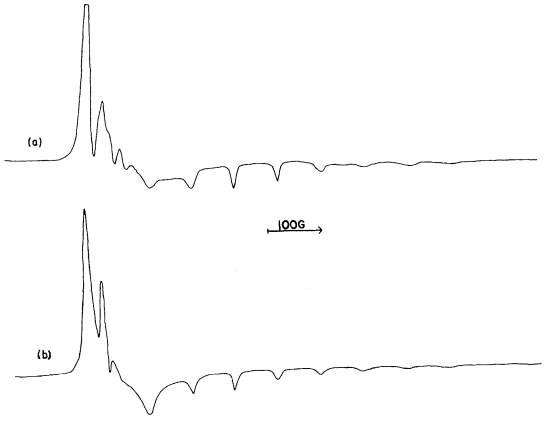

FIG. 1. (*a*) Electron spin resonance spectrum of a frozen solution of $CoTAAB(NO_3)_2$ in dimethylformamide. (*b*) Simulated spectrum of the dimethylformamide solution.

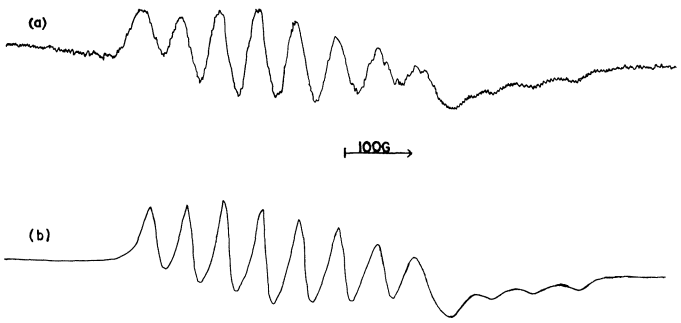

FIG. 2. (*a*) Electron spin resonance spectrum of a frozen solution of $CoTAAB(NO_3)_2$ in pyridine. (*b*) Simulated spectrum of the pyridine solution.

($\Delta m_I = 0$) (15) in the calculation. A Lorentzian line shape was assumed and it was found necessary to assume a different line width for each hyperfine line to get good agreement between calculated and experimental spectra. Our program for frozen solution spectra appears to be different from most reported programs in that it calculates the derivative directly rather than numerically differentiating an absorption curve.

Figure 1(*a*) shows a spectrum of a frozen solution of $CoTAAB(NO_3)_2$ in DMF. The lower trace (*b*) is the simulated spectrum. Figure 2 shows, similarly, a spectrum of a frozen solution of the complex in pyridine. The magnetic parameters for different frozen solutions are given in Table 2.

Addition of pyridine stepwise to a solution of $CoTAAB(NO_3)_2$ in acetone gives a complete conversion to the pyridine-type spectrum at a molar ratio of 1:1, indicating that the spectrum observed in pyridine is of a complex formed by addition of one pyridine molecule to $CoTAAB^{2+}$. A similar experiment using piperidine gives complete disappearance of the acetone esr spectrum at a molar ratio of 2:1, indicating the formation of a complex having two molecules of piperidine. Addition of acetone to the residue obtained after evaporation of a piperidine solution of $CoTAAB(NO_3)_2$ restores the acetone esr signal. This indicates that the reaction between piperidine and the complex is reversible in nature and that the disappearance of the esr spectrum in piperidine is not due to some irreversible process such as oxidation which converts Co(II) to diamagnetic Co(III). The nmr spectrum of $CoTAAB(NO_3)_2$ in piperidine shows an upfield shift of all piperidine lines relative to the neat solvent with the NH line shifted most. The lines are also slightly broadened. Further shifts and broadening occur in mixed piperidine–CD_3COCD_3 solvents. These nmr shifts indicate that the piperidine complex is paramagnetic with a much shorter spin relaxation time than the $S = 1/2$ complex in pyridine or acetone. The only reasonable explanation for the lack of an esr spectrum and the nmr shifts is to postulate either an $S = 3/2$ ground state for the piperidine complex or a low lying $S = 3/2$ state that is close enough in energy to produce a very short electronic T_1 making esr detection at liquid N_2 temperatures impossible. The latter explanation is favored by the nmr susceptibility measurements.

TABLE 2. Spin Hamiltonian parameters for $CoTAAB(NO_3)_2$ in frozen solutions[a]

Solvent	$g_\parallel$	$g_\perp$	$A_\parallel$[b]	$A_\perp$[b]
Acetone	2.0259	2.2762	75.3	12.9
Methanol	2.0275	2.2720	75.3	12.3
Dimethyl formamide	2.0244	2.2772	75.8	12.1
Pyridine	2.0562	2.1949	59.4	58.3
Quinoline	2.0547	2.1968	60.5	59.4

[a] Q' was found to be $-0.00015\ cm^{-1}$.
[b] Values in $10^{-4}\ cm^{-1}$.

Discussion

The spin Hamiltonian parameters fit the theoretical equations for an $^2A_1$ ground-state, where in the case of axial symmetry we have, by perturbation methods (1), for an electron in a d_z^2 orbital:

$$[2] \quad g_\parallel = g_e + 2c_3^2 - 3c_1^2$$

$$[3] \quad g_\perp = g_e + \tfrac{2}{3}c_3^2 - 6c_1^2 + 6c_1$$

TABLE 3. Computed parameters for $CoTAAB(NO_3)_2$ using perturbation and exact equations

	Perturbation calculation				Exact calculation				
Solvent	c_1	c_3	P^a	K^a	c_1	c_3	P^a	K^a	K(ave)^b
Methanol	0.045	0.125	206.0	−32.5	0.047	0.118	235.5	−19.6	−24.3
Pyridine	0.030	0.168	228.7	−51.3	0.033	0.109	227.9	−40.7	−47.5

[a]In 10^{-4} cm^{-1}.
[b]See ref. 1, p. 2509.

$$[4] \quad A_{\parallel} = K + P\left\{\frac{4}{7} - \frac{4}{7}c_3 - \frac{6}{7}c_1 + \frac{2}{63}{c_3}^2 + \frac{15}{7}{c_1}^2\right\}$$

$$[5] \quad A_{\perp} = K + P\left\{-\frac{2}{7} + \frac{45}{7}c_1 + \frac{2}{7}c_3 + \frac{4}{21}{c_3}^2 - \frac{57}{14}{c_1}^2\right\}$$

$$[6] \quad \begin{cases} c_1 = \xi/\Delta(^2B_1) \\ c_3 = \xi/\Delta(^4B_1) \end{cases}$$

$$[7] \quad P = g_e g_N \beta_e \beta_N \langle r^{-3} \rangle$$

K is the Fermi contact interaction, ξ is the spin–orbit interaction constant for one d electron. $\Delta(^2B_1)$ is the energy difference between the $^2B_1$ state and the ground state and $\Delta(^4B_1)$ is defined likewise. These equations can serve to obtain c_1 and c_3 from the g-values and P and K from $A_{\parallel}$ and $A_{\perp}$. In this case we can also solve exactly for the magnetic parameters. The results of these exact calculations are given in eqs. 48–56 of ref. 1. Table 3 gives values for methanol and pyridine frozen solutions obtained by using both methods of calculation.

Table 1 of ref. 1 contains a large number of results of such calculations for axial complexes of Co(II) with porphyrins and phthalocyanines, our values are within the range of values given there. It was found (1) that in the range $c_1 < 0.05$ it was necessary to take $A_{\parallel} > 0$ and $A_{\perp} < 0$ in order to obtain P in the expected range, this choice of signs was also used here.

The $CoTAAB(NO_3)_2$ forms three types of complexes with the solvents investigated here. In acetone, methanol, and dimethylformamide the ground state is a doublet. In piperidine, where two solvent molecules are attached to the planar $CoTAAB^{2+}$, there is obviously a low-lying $S = 3/2$ state, which is partially populated. It is close enough in energy to the ground state to result in an electronic T_1 too short to allow observation of esr spectra even at 77 K. The magnetic susceptibility measured in the solution and the paramagnetic shifts observed in the nmr spectrum of the complex are strong indications that there is indeed a paramagnetic species here which is not a pure $S = 1/2$ state. The magnetic susceptibility of the powdered complex is about the same as that measured in the piperidine solution, suggesting an arrangement in the solid where molecules are stacked such that the fifth and sixth coordination sites are occupied by nitrogen atoms from adjacent molecules. That the species in piperidine is indeed a reversibly formed complex and not a product of some irreversible chemical change is manifested by retrieving the acetone-complex on redissolving in acetone the residue left after evaporating the piperidine from its solution. The pyridine-complex, which is formed with one solvent molecule is apparently an intermediate case between the acetone-type complex and the piperidine-type one. The low-lying quartet state is closer to the $S = 1/2$ ground state than in the acetone complex but still farther than in the piperidine case so that esr spectra (with different magnetic parameters) could be observed.

Acknowledgement

This work was supported by a grant from the National Research Council of Canada.

1. B. R. McGARVEY. Can. J. Chem. **53**, 2498 (1975).
2. V. MALATESTA and B. R. McGARVEY. Can. J. Chem. **53**, 3791 (1975).
3. O. VON ZELEWSKY and H. FIERZ. Helv. Chim. Acta, **56**, 977 (1973).
4. V. P. CHACKO and P. T. MANOHARAN. J. Magn. Reson. **16**, 75 (1974).
5. A. H. MAKI, N. EDELSTEIN, A. DAVIDSON, and R. H. HOLM. J. Am. Chem. Soc. **86**, 4580 (1964).

6. A. K. GREGSON, R. L. MARTIN, and S. MITRA. Chem. Phys. Lett. **5**, 310 (1970).
7. F. CARIATI, F. MORAZZONI, C. BUSETTO, G. DEL PIERO, and A. ZAZZETTA. Private communication.
8. G. A. MELSON and D. H. BUSCH. Proc. Chem. Soc., London, 223 (1963); J. Am. Chem. Soc. **86**, 4830 (1964); **86**, 4834 (1964); **87**, 1706 (1965).
9. L. T. TAYLOR, S. C. VERGEZ, and D. H. BUSCH. J. Am. Chem. Soc. **88**, 3170 (1966).
10. L. T. TAYLOR and D. H. BUSCH. J. Am. Chem. Soc. **89**, 5372 (1967).
11. S. C. CUMMINGS and D. H. BUSCH. J. Am. Chem. Soc. **92**, 1924 (1970); Inorg. Chem. **10**, 1220 (1971).
12. D. E. SMITH and J. W. OPIE. Org. Synth. Coll. Vol. **111**, 56 (1955).
13. N. C. LI, L. JOHNSON, and J. SHOOLERY. J. Phys. Chem. **65**, 1902 (1961).
14. B. N. FIGGIS and J. LEWIS. Modern coordination chemistry. Interscience, New York. 1960. p. 403.
15. L. D. ROLLMAN and S. I. CHEN. Electron spin resonance of metal complexes. *Edited by* Teh Fu Yen. Plenum Press, New York. 1969. pp. 175–200.

Excess volumes of an alcohol + methylethylketone

KALLURU S. REDDY AND PULIGUNDLA R. NAIDU
Sri Venkateswara University Chemical Laboratory, Tirupati 517502, India

Received August 11, 1976

KALLURU S. REDDY and PULIGUNDLA R. NAIDU. Can. J. Chem. **55**, 76 (1977).

Excess volume data for mixtures of 1-propanol, 1-butanol, 1-pentanol, and 1-hexanol with methylethylketone were determined at 303.15 and 313.15 K. These volumes are negative with 1-propanol and increasingly positive with the higher homologs, suggesting that the structure-making effect of the ketone outweighs the structure-breaking effect in the first mixture of the series while the structure-breaking effect dominates in the other three mixtures. Further, the temperature coefficient of V^E was found to be positive in all four mixtures.

KALLURU S. REDDY et PULIGUNDLA R. NAIDU. Can. J. Chem. **55**, 76 (1977).

On a déterminé, à 303.15 et à 313.15 K, les données concernant les volumes d'excès pour des mélanges de propanol-1, de butanol-1, de pentanol-1 et d'hexanol-1 avec la butanone-2. Ces volumes qui sont négatifs avec le propanol-1 augmentent d'une façon algébrique lorsque l'on passe aux homologues supérieurs; ces résultats suggèrent que l'effet de formation de structure de la cétone contrebalance l'effet de brisure de structure dans le premier mélange de la série alors que l'effet de brisure de structure domine dans les trois autres mélanges. De plus on a trouvé que le coefficient de température de V^E est positif dans les quatre mélanges.

[Traduit par le journal]

Introduction

These measurements were made as part of a study of excess volumes of alcohol solutions containing a ketone as a common component (1). The systems studied include: 1-propanol, 1-butanol, 1-pentanol, and 1-hexanol with methylethylketone. An attempt has been made to interpret the results on the basis of structure-breaking and structure-making effects of the common solvent, methylethylketone.

Experimental

The dilatometer used for measuring excess volumes was similar to that described by Rao and Naidu (2). The mixing cell contained two bulbs of two different capacities and were connected through a U-tube having mercury to separate the two components. One end of the bulb was fitted with a capillary (1 mm id) and the other end of the second bulb was fixed with ground glass stopper. The V^E values were accurate to ± 0.003 cm^3 mol^{-1}.

The alcohols were purified by the method described by Rao and Naidu (2). Methylethylketone was dried over potassium carbonate for 3 days, then boiled for 2 h and distilled (3). The purity of methylethylketone was checked by comparing the values of density ρ with that reported in the literature $\rho^{303.15} = 0.79443$ g cm^{-3} (lit. (4) 0.79452 g cm^{-3}).

Results

Excess volume data[1] determined at 303.15 and 313.15 K are presented in Figs. 1 to 4. These results may be expressed by an emperical equation of the form

$$[1] \quad \frac{V^E}{X_A X_B}\ \text{cm}^3\ \text{mol}^{-1} = a_0 + a_1(X_A - X_B) + a_2(X_A - X_B)^2$$

The values of a_0, a_1, and a_2 obtained by method of least-squares are given in Table 1 along with the standard deviation $\sigma(V^E)$.

Discussion

The values of V^E are negative for the mixture 1-propanol and methylethylketone at 303.15 and 313.15 K. The negative values for V^E suggest

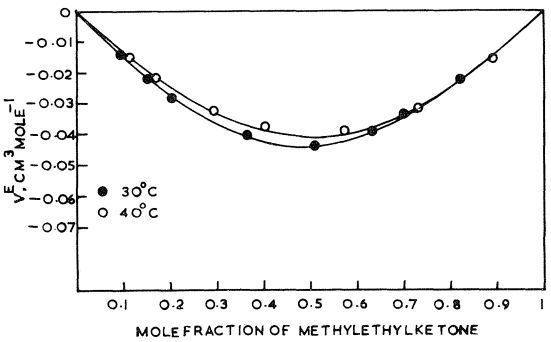

FIG. 1. Plot of V^E as a function of composition for methylethylketone and 1-propanol system.

[1]Complete set of actual experimental data is available upon request, at a nominal charge, from the Depository of Unpublished Data, CISTI, National Research Council of Canada, Ottawa, Canada K1A 0S2.

TABLE 1. Standard deviation $\sigma(V^E)$ and values of the constants in eq. 1

System	Temperature (K)	a_0	a_1	a_2	$\sigma(V^E)$ ($cm^3\ mol^{-1}$)
Methylethylketone + 1-propanol	303.15	−0.1709	0.0122	0.0118	0.001
Methylethylketone + 1-butanol	303.15	0.0598	0.0283	0.0156	0.002
Methylethylketone + 1-pentanol	303.15	0.1615	0.0662	−0.0960	0.004
Methylethylketone + 1-hexanol	303.15	0.3133	0.0051	0.1721	0.002
Methylethylketone + 1-propanol	313.15	−0.1897	0.0030	0.0614	0.006
Methylethylketone + 1-butanol	313.15	0.1218	0.0157	−0.0206	0.002
Methylethylketone + 1-pentanol	313.15	0.2170	0.0132	0.0802	0.005
Methylethylketone + 1-hexanol	313.15	0.3073	−0.0683	−0.0031	0.006

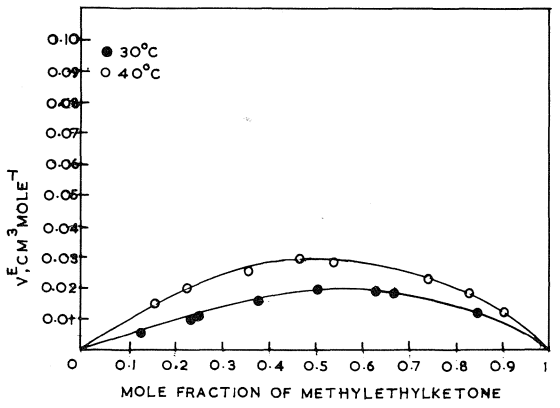

FIG. 2. Plot of V^E as a function of composition for methylethylketone and 1-butanol system.

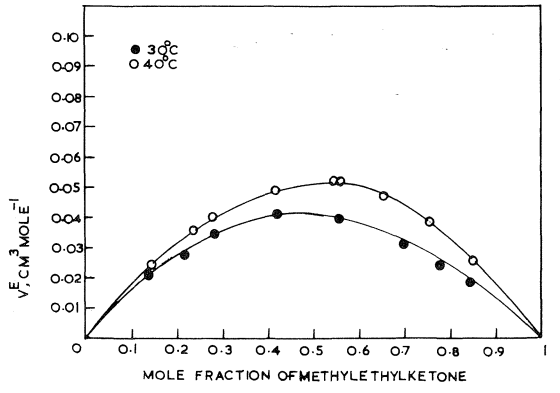

FIG. 3. Plot of V^E as a function of composition for methylethylketone and 1-pentanol system.

that the structure-making effect, hydrogen bond formation between the components, outweighs the structure-breaking effect. V^E is positive for the mixtures of 1-butanol, 1-pentanol, and 1-hexanol with methylethylketone at 303.15 and

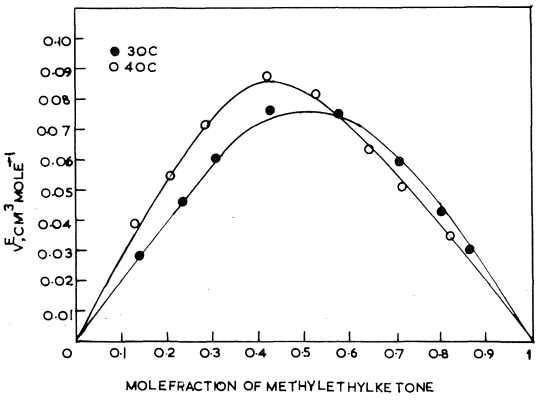

FIG. 4. Plot of V^E as a function of composition for methylethylketone and 1-hexanol system.

313.15 K. In these systems the structure-breaking effect is dominant over structure-making effect.

The algebraic values of V^E of the four systems fall in the order:

1-propanol < 1-butanol < 1-pentanol < 1-hexanol

This order is similar to that observed in the earlier work (1). This shows that the individual alcohol behaves in the same way towards the two ketones.

Finally, a comparison between V^E values determined at 303.15 and 313.15 K shows that V^E becomes more positive with increase in temperature in the four mixtures.

1. K. S. REDDY, M. V. P. RAO, and P. R. NAIDU. Can. J. Chem. **54**, 2676 (1976)
2. M. V. P. RAO and P. R. NAIDU. Can. J. Chem. **52**, 788 (1974).
3. P. R. NAIDU. Aust. J. Chem. **23**, 967 (1970).
4. J. TIMMERMANS. Physico-chemical constants of pure organic compounds. Elsevier Publishing Co., Amsterdam. 1950.

Pulsed nuclear magnetic resonance study of deuteron lineshapes in clathrate hydrates[1]

JOHN A. RIPMEESTER

Division of Chemistry, National Research Council of Canada, Ottawa, Ont., Canada K1A 0R9

Received June 28, 1976

JOHN A. RIPMEESTER. Can. J. Chem. **55**, 78 (1977).

D nmr lineshape information was obtained from the echo response following a pair of phase shifted pulses using a method first proposed by Clark. In this manner the D quadrupole coupling constant and asymmetry parameter for D_2O in *p*-dioxane·$17D_2O$ were found to be 217 kHz and 0.10 at 63 K. The D nmr lineshape for ethylene oxide-d_4·$7H_2O$ shows that at 17 K the guest molecules are held rigidly in their cages. At higher temperatures the doublet lineshape collapses to a broad structureless line characteristic of molecules for which the reorientational modes vary from cage to cage.

JOHN A. RIPMEESTER. Can. J. Chem. **55**, 78 (1977).

On a obtenu de l'information sur les formes des lignes de D rmn à partir de la réponse écho qui peut être dérivée en une paire de pulsations déplacées en phase et utilisant une méthode qui avait été développée originalement par Clark. On a trouvé, de cette manière, que la constante de couplage quadrupolaire D et que le paramètre d'asymétrie du D_2O dans le complexe *p*-dioxanne·$17D_2O$ sont de 217 kHz et de 0.10 à 63 K. La forme des lignes D rmn de l'oxyde d'éthylène d_4·$7H_2O$ montre qu'à 17 K, les molécules hôtes sont tenues rigidement dans leurs cages. A des températures plus élevées la forme des lignes du doublet disparait et devient une ligne large sans structure, caractéristique de molécules pour lesquelles des modes de réorientation varient d'une cage à l'autre

[Traduit par le journal]

Introduction

In the study of clathrate hydrates, selective deuteration of either guest or host molecules has been used extensively to separate the respective contributions to the ^1H nmr spectrum (1). Relatively little use has been made of D nmr lineshape information, presumably because of experimental difficulties in recording the weak, very broad D nmr spectral lines.

In this publication it is shown that a method first suggested by Clark (2), in which the resonance line is swept while the free induction decay (FID) is integrated, can also be applied to very wide D nmr powder spectra. For such lines, which can be ~300 kHz wide, the FID decays in a time of the same order as the instrument recovery time, and the lineshape can be obtained by integrating the echo response of the spin system to a pair of phase shifted pulses as the magnetic field is swept.

In the following sections the principle of the method is described, some experimental details are given, and results of the technique as applied to two clathrate hydrate systems are discussed.

[1]NRCC No. 15567. Presented at the 58th Annual Meeting of the Chemical Institute of Canada, Toronto, Ontario, 1975.

Theory

The quadrupolar Hamiltonian in a coordinate frame rotating at the Larmor frequency ω can be written as (4)

$$[1] \qquad \mathcal{H} = \Delta\omega\hbar\boldsymbol{I}_z + a\hbar\boldsymbol{I}_z^2$$

where $\Delta\omega = \omega_0 - \omega$ and

$$a\hbar = \frac{3eQV_{zz}}{4I(2I-1)}$$

where Q is the nuclear quadrupole moment and V_{zz} is the electric field gradient in the direction of the external magnetic field. The response of the spin system to rf pulses can be obtained from (3)

$$[2] \qquad S(t) = \mathrm{Tr}\,[\rho(t)\boldsymbol{I}_+]$$

where $\rho(t)$ is the density matrix in the rotating frame and $\boldsymbol{I}_+ = \boldsymbol{I}_x + i\boldsymbol{I}_y$. The equilibrium density matrix in the high temperature, high field approximation is proportional to I_z, and becomes I_y after rotation by a sufficiently intense 90° pulse about the rotating frame x axis. After a second pulse of length $t = \theta/\gamma H_1$, where H_1 is the rf field strength, and shifted in phase with respect to the first by an angle ϕ at time τ, the spin system response can be found from

[3] $$S(t) = \mathrm{Tr}\{\exp[(-i/\hbar)\mathscr{H}(t-\tau)]\boldsymbol{R} \times \exp[(-i/\hbar)\mathscr{H}\tau]\boldsymbol{\rho}(0)\exp[(i/\hbar)\mathscr{H}\tau]\boldsymbol{R}^{-1} \times \exp[(i/\hbar)\mathscr{H}(t-\tau)]\boldsymbol{I}_+\}$$

with

$$\boldsymbol{R} = \exp(i\phi\boldsymbol{I}_z)\exp(-i\theta\boldsymbol{I}_y)\exp(-i\phi\boldsymbol{I}_z)$$

For $I = 1$, this expression can be evaluated to give

[4] $$S(t) = e^{-i2\phi}\cos\{\Delta\omega(t-2\tau)\}\{F(t) \times \cos\theta(1-\cos\theta) - \sin^2\theta F(t-2\tau)\} + \cos\Delta\omega t\{\cos\theta(1+\cos\theta)F(t) + \sin^2\theta F(t-2\tau)\}$$

Equation 4 is similar to the expression found by Metzger and Gaines (4) for the two pulse response of two half integral spins tightly coupled by the nuclear dipolar interaction. Here $F(t)$ is the Fourier transform of the lineshape function

[5] $$F(t) = \int_{-\infty}^{\infty} f(\Delta\omega)\cos\Delta\omega t\, d\Delta\omega$$

$F(t-2\tau)$, the echo response, consists of two FID's back to back centred at $t = 2\tau$ if relaxation effects are neglected. If both ϕ and θ for the second pulse are 90°

[6] $$S(t) = F(t-2\tau)\{\cos\Delta\omega(t-2\tau) + \cos\Delta\omega t\}$$

If the spin echo signal is then integrated using the boxcar integrator, the boxcar response will be

[7] $$V(\Delta\omega) = K\int_{t'}^{t''} F(t-2\tau) \times \{\cos\Delta\omega(t-2\tau) + \cos\Delta\omega t\}\, dt$$

Here K is a constant to take into account the gain of the integrator. If the entire spin echo is integrated, the limits of integration t' and t'' can be expanded to $-\infty$ and $+\infty$, respectively. On expanding expression 7 one gets

[8] $$V(\Delta\omega) = K(1+\cos 2\Delta\omega\tau) \times \int_{-\infty}^{\infty} F(t-2\tau)\cos\Delta\omega t\, dt$$

It can be seen that the boxcar response is proportional to the absorption line intensity at $\Delta\omega$. The entire absorption line shape can therefore be obtained by plotting $V(\Delta\omega)$ as $\Delta\omega$ is swept through resonance. According to eqs. 6 and 8 both the spin echo amplitude and the boxcar response are modulated. Often, by judicious choice of the pulse spacing τ, the modulating $\cos 2\Delta\omega\tau$ term can be made to vary with $\Delta\omega$ much more rapidly than the spin echo fine structure information, and the modulated absorption line shape envelope can still provide lineshape information.

Time averaging can be used to good advantage to remove the modulation. Instead of averaging successive scans, the usual time averaging technique, the resonance line is scanned only once and m successive boxcar output signals are added.

At constant sweep rate, the signal is sampled at constant intervals of $\Delta\omega$, say $\Delta'\omega$. The averaged signal will then be

[9] $$V(m\Delta'\omega) = K\sum_{n=1}^{m}(1+\cos 2n\Delta'\omega\tau) \times \int_{-\infty}^{\infty} F(t-2\tau)\cos 2n\Delta'\omega\tau\, dt$$

If m and τ are adjusted so that $2m\Delta\omega\tau = \pi$ the $\cos 2\Delta\omega\tau$ modulation will be averaged out. Naturally the signal response will be averaged over the interval $m\Delta'\omega$.

Experimental Methods

Pulsed D nmr measurements were performed at 9.2 MHz using a Bruker SXP spectrometer. D quadrupole echoes were generated using $90°_{x}$–τ–$90°_{90°}$ pulse sequences. The H_1 field amplitude was about 60 G, and the FID could be observed after a recovery time of 20–25 μs measured from the center of the rf pulse. The quadrupole echoes centred at a time $t = 2\tau$ were integrated using a Bruker B-KR Z15 pulse gated (boxcar) integrator. Time averaging was effected using a Digital Equipment Corporation PDP 8-L computer.

The experimental conditions used to obtain each spectrum can be summarized by specifying τ, the pulse spacing, $\Delta t = t'' - t'$, the integrator gate width, T_c, the integrator time constant, m (eq. 9), the number of successive integrator responses added, N_t, the total number of points taken to define the spectrum and t, the total time taken to accumulate each spectrum. In addition, each spectrum could be subjected to one or more cycles of digital smoothing.

The clathrate hydrate samples were the same as used in other studies (5, 6).

Results and Discussion

p-Dioxane forms a clathrate hydrate in which the *p*-dioxane guest molecules occupy the large structure II cages (5). The water molecules making up the clathrate cages form a fully hydrogen bonded network, with each water molecule bonded to four others (7).

The right portion of Fig. 1*a* shows half of the

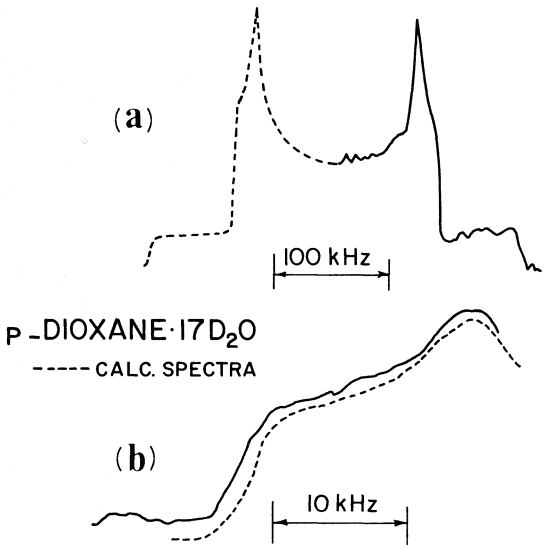

FIG. 1. Experimental and calculated D nmr lineshapes for *p*-dioxane·17D_2O (see text).

D nmr spectrum for *p*-dioxane·17D_2O recorded at 63 K. The total time taken to obtain the spectrum was 30 min, with the other experimental parameters as follows: $N_t = 225$, $\tau = 220$ μs, $\Delta t = 300$ μs, $T_c = 1$ ms, $m = 8$. The spectrum is a typical spin 1 powder doublet with fine structure in the vicinity of the singularity due to a non-zero asymmetry parameter (8). This fine structure is illustrated in Fig. 1*b* where the spectral region near the singularity was recorded on an expanded scale. The recording time was 20 min, with $N_t = 100$, $m = 12$, and the remaining parameters the same as for Fig. 1*a*.

The dashed portions of Fig. 1 (*a*) and (*b*) were calculated (8) using a quadrupole coupling constant of 217 kHz and an asymmetry parameter of 0.10. Internuclear dipolar broadening was accounted for by folding the powder pattern with a Gaussian function using a broadening parameter of 1.6 kHz. As structure II clathrate hydrates have three inequivalent sites for the O atoms of the water molecules (7), the parameters characterizing the *p*-dioxane·17D_2O spectrum must be average values. Not surprisingly, the D nmr parameters for the deuteriohydrate are nearly the same as those obtained for D_2O ice I_h (9); for OD bonds parallel to the *c* direction the quadrupole coupling constant and asymmetry parameter were 213.3 kHz and 0.100, and for the non-*c* bonds the values were 216.4 kHz and 0.100 (the last value assumed).

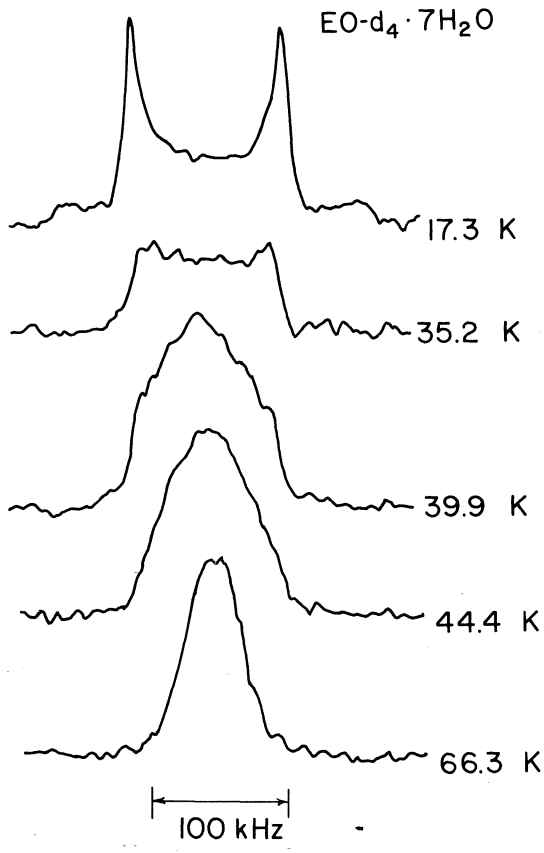

FIG. 2. D nmr lineshapes obtained for ethylene oxide-d_4·7H_2O at various temperatures.

Figure 2 shows a number of D spectra obtained for ethylene oxide-d_4·7H_2O, a structure I clathrate hydrate (10). From the exact composition of the hydrate, EO·6.89H_2O (11), about 90% of the EO molecules are in the large structure I cage, the remainder in the smaller cage (12).

The 17.3 K spectrum is again a typical powder doublet from which a quadrupole coupling constant of 163 kHz for the deuterons in EO-d_4 can be derived. The total accumulation time for this spectrum was 50 min with the other experimental parameters $N_t = 200$, $\tau = 220$ μs, $\Delta t = 300$ μs, $T_c = 1$ ms, $m = 30$. The other spectra were obtained under identical conditions but in a much shorter time, 10 min. The doublet structure can be seen to collapse with rise of temperature from 17.3 to 40 K, the spectrum at the highest temperature being a broad featureless line. This disappearance of fine structure corresponds to the onset of slow guest molecule reorientations which were also observed in this

temperature range by dielectric and CW ^{1}H nmr methods (13). The width and shape of the D nmr line at 66.3 K indicate that the EO molecules reorient about axes which vary from cage to cage, and that, in general, the motions are not random.

The lineshapes presented here illustrate the relative ease with which D nmr spectra may be recorded using a pulsed nmr spectrometer, even for very wide powder spectra. It should be possible to obtain good results with this technique provided that T_2 is constant for all components of the spectrum so that the degree of refocusing is the same for all the spins.

1. S. K. GARG and D. W. DAVIDSON. Physics and chemistry of ice. *Edited by* E. Whalley, S. J. Jones, and L. W. Gold. Royal Soc. Canada, Ottawa. 1973. p. 56.
2. W. G. CLARK. Rev. Sci. Instrum. **35**, 316 (1964).
3. I. SOLOMON. Phys. Rev. **110**, 61 (1958).
4. D. S. METZGER and J. R. GAINES. Phys. Rev. **147**, 644 (1966).
5. S. R. GOUGH, J. A. RIPMEESTER, and D. W. DAVIDSON. Can. J. Chem. **53**, 2215 (1975).
6. J. A. RIPMEESTER. Can. J. Chem. **54**, 3677 (1976).
7. T. C. W. MAK and R. K. MCMULLAN. J. Chem. Phys. **42**, 2732 (1965).
8. R. G. BARNES and J. W. BLOOM. J. Chem. Phys. **57**, 3082 (1972).
9. P. WALDSTEIN, S. W. RABIDEAU, and J. A. JACKSON. J. Chem. Phys. **41**, 3407 (1964).
10. M. VON STACKELBERG and B. MEUTHEN. Z. Elektrochem. **62**, 130 (1958).
11. D. N. GLEW and N. S. RATH. J. Chem. Phys. **44**, 1710 (1966).
12. R. K. MCMULLAN and G. A. JEFFREY. J. Chem. Phys. **42**, 2725 (1965).
13. S. K. GARG, B. MORRIS, and D. W. DAVIDSON. J. Chem. Soc. Faraday Trans. II, **68**, 481 (1972).

Reactions of dicarbonyl compounds with β-ketoglutaric acid: synthesis of 4-hydroxy-3,4-diphenylcyclopent-2-enone-2-carboxylic acid

JAMES OEHLDRICH AND JAMES M. COOK

Department of Chemistry, University of Wisconsin–Milwaukee, Milwaukee, WI, U.S.A. 53201

Received August 3, 1976

JAMES OEHLDRICH and JAMES M. COOK. Can. J. Chem. **55**, 82 (1977).

Reaction of β-ketoglutaric acid with benzil in ethanolic KOH furnished the 1:1 adduct **7**. Hydrolysis and partial decarboxylation gave the monoacid **8**, the structure of which was erroneously reported to be **5** in the earlier literature.

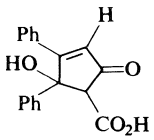

5

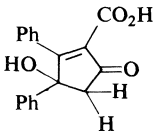

8

JAMES OEHLDRICH et JAMES M. COOK. Can. J. Chem. **55**, 82 (1977).

La réaction de l'acide β-cétoglutarique avec le benzile en présence de KOH en milieu éthanolique conduit à l'adduit 1:1, **7**. L'hydrolyse et la décarboxylation partielle conduisent au monoacide **8**; il avait été rapporté par erreur dans une référence antérieure que cet acide avait la structure **5**.

[Traduit par le journal]

In 1968 Weiss and Edwards (1) reported that reaction of aliphatic or alicyclic 1,2-dicarbonyl compounds with dimethyl β-ketoglutarate provided 1:2 adducts of the type represented by tetramethyl bicyclo[3.3.0]octane-3,7-dione-2,4,-6,8-tetracarboxylate **1**. We have investigated the analogous reaction of dimethyl-β-ketoglutarate with aromatic α-diketones. This procedure yielded 1:1 adducts (2–4) of type **2** instead of compounds having the 1:2 stoichiometry observed in aliphatic or alicyclic cases (1, 2). This reaction of aromatic α-diketones has been extended to phenanthrenequinone which also gave adducts of 1:1 stoichiometry (5).

In the course of this work we have had occasion to reexamine the reaction of benzil **3** with β-ketoglutaric acid **4**, which was first carried out by Japp and Lander (6). These authors reported that this condensation furnished a 1:1 adduct, which was formulated as **5** because of its conversion to the monoketone **6** by treatment with hydroiodic acid. The monoketone **6** had been prepared by another route (7).

In our laboratory, benzil **3** was stirred with β-ketoglutaric acid **4** in alcoholic potassium hydroxide under the conditions reported by Japp and Lander (6). Upon acidification of the potassium salt isolated from this reaction, followed by treatment with ethanol to remove excess benzil, a new compound (mp 248–250 °C) was obtained which appeared to be the diacid **7** ($C_{19}H_{14}O_6$). Esterification of this substance with methanolic

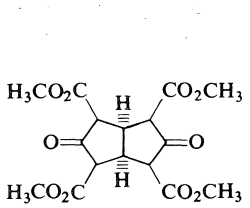

1

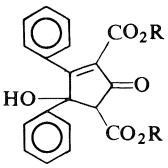

2, R = CH_3
7, R = H

hydrogen chloride furnished dimethyl-4-hydroxy-3,4-diphenylcyclopent-2-enone-2,5-dicarboxylate **2**, identical in all respects with an authentic sample prepared by the procedure outlined in refs. 2, 3, and 4.

Decarboxylation of the diacid **7** in hot glacial acetic acid provided the monoacid **8** (mp 167–168 °C); the structure of which was incorrectly reported to be **5** by Japp and Lander (6). The nmr spectrum of this acid did not contain a signal in the vinyl region; this observation suggested structure **8** for this compound. This was confirmed by the appearance of two overlapping singlets (representing two protons) at δ 2.99 and 3.01 in the spectrum, which are clearly due to the

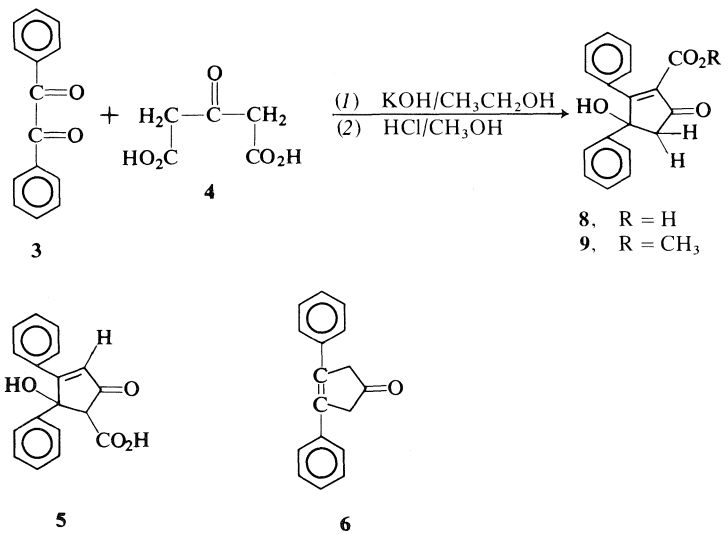

3 4 8, R = H 9, R = CH_3 5 6

SCHEME 1

methylene protons of the monoacid **8**. This signal for α-methylene protons is not possible for the structure **5** reported in 1897 by Japp. The electron impact mass spectra of the diacid **7** and the monoacid **8** are very similar, a fact which indicates that thermal decarboxylation of **7** to **8** occurs readily, as would be anticipated. Esterification of the monoacid in methanolic hydrogen chloride gave the ester **9** (142–144 °C) in 92% yield. The nmr spectrum of this ester also contained a signal for the α-methylene protons (δ 2.97). We would therefore like to propose structure **8** for the monoacid instead of structure **5** reported earlier (6) for this compound.

β-Keto acids are quite difficult to isolate in good yield; however, presumably the strain which occurs when **7** is decarboxylated through the high energy cyclopentadiene intermediate precludes facile decarboxylation and allows isolation of this diacid.

Experimental

Microanalyses were performed (UWM) on an F & M Scientific Corporation Carbon, Hydrogen, Nitrogen Analyzer model 185. Melting points were taken on a Thomas Hoover apparatus and are uncorrected. Nuclear magnetic resonance spectra were recorded on Varian T-60 and HA-100 spectrometers. Infrared spectra were taken on a Beckman Acculab-1 instrument; ultraviolet spectra were recorded on a Cary 17 spectrophotometer and mass spectra were taken on a Finnigan 1015 or AEI MS902 instrument.

Analytical tlc plates used were E. Merck-Brinkmann uv active silica gel on plastic. The spray reagent was composed of 2,4-dinitrophenylhydrazine, ethanol, and sulfuric acid. The citrate–phosphate buffer (p*H* 6.8) was prepared by dissolving $Na_2HPO_4 \cdot 7H_2O$ (11.67 g) and citric acid (3.68 g) in water (900.00 ml).

4-Hydroxy-3,4-diphenylcyclopent-2-enone-2,5-dicarboxylic Acid, 7

Benzil (11.5 g, 0.05 mol) and 3-ketoglutaric acid (7.5 g, 0.05 mol) were dissolved in a small amount of warm ethanol. A prefiltered solution of potassium hydroxide (8.5 g, 0.15 mol), water (10 ml), and ethanol (50 ml) was added. The mixture was stirred for 1 h after which time a white solid precipitated. The precipitate was filtered and washed with a small amount of ethanol; the crystals were then dissolved in the smallest amount of water possible and the resulting solution was acidified to p*H* 1 with 6 *M* H_2SO_4. White crystals (11.5 g, 68%) formed and were filtered from the solution, washed with water, and dried *in vacuo*: mp 248–250 °C with decomposition; ir (KBr) 3300 (br OH), 1727 (C=O), and 1673 cm^{-1} (enol form of β-keto acid); nmr (DMSO-d_6) δ 2.74 (1H, s), 7.60 (10H, m); mass spectrum *m/e* 294(25), 277(19), 276(87), 250(20), 234(54), 232(28), 220(20), 208(20), 206(21), 205(33), 203(29), 202(25), 191(22), 278(33), 249(20), 131(21), 129(39), 106(43), 105(100), 103(25), 102(46), 101(25), 91(54), 89(21), 78(41), 77(100), 76(31). (Molecular ion not observed, $M^+ - CO_2$ was found.) *Anal.* calcd. for $C_{19}H_{14}O_6 \cdot 3H_2O$: C 58.16, H 5.14; found: C 58.38, H 5.03.

Dimethyl 4-Hydroxy-3,4-diphenylcyclopent-2-enone-2,5-dicarboxylate, 2

The diacid **7** (0.5 g, 1.48 mmol) was dissolved in methanolic hydrogen chloride (20 ml). This solution was stirred for 24 h and the solvent was then evaporated under reduced pressure. The crystals (0.51 g, 94%) were recrystallized from benzene: mp 138–140 °C, ir (KBr) 3480 (OH) and 1745 cm^{-1} (ester C=O), M^+ at *m/e* 366; nmr identical with that reported by White (4*b*). *Anal.* calcd. for $C_{21}H_{18}O_6$: C 68.85, H 4.95; found: C 69.00, H 5.06.

*4-Hydroxy-3,4-diphenylcyclopent-2-enone-2-carboxylic Acid, **8***

The diacid **7** (0.50 g, 1.48 mmol) was dissolved in hot glacial acetic acid and diluted with enough hot water to cause the solution to become turbid. This mixture was allowed to cool to room temperature and crystallize. The crystals (0.31 g, 71%) were recrystallized from benzene; mp 167–168 °C, ir (KBr) 3400 (OH), 1685 (acid C=O), and 1675 cm^{-1} (enol form of β-keto acid), nmr (acetone-d_6) δ 2.99, 3.01 (2H, overlapping signal, methylene protons) 5.78 (1H, s, OH, D_2O exchangeable), 7.25 (10H, m, aryl protons); mass spectrum *m/e* 294(36), 277(25), 276(97), 234(63), 232(27), 206(29), 205(37), 203(27), 202(21), 191(21), 178(30), 129(38), 105(100), 103(30), 91(44), 78(40), 77(96), 76(21). *Anal.* calcd. for $C_{18}H_{14}O_4$: C 73.46, H 4.79; found: C 73.17, H 4.56.

*Methyl 4-Hydroxy-3,4-diphenylcyclopent-2-enone-2-carboxylate, **9***

The monoacid **8** (0.25 g, 0.85 mmol) was placed in methanolic hydrogen chloride (10 ml) and stirred for 24 h. The solvent was then evaporated under reduced pressure. The crystals (0.24 g, 92%) were recrystallized from methanol: mp 142–144 °C, ir ($CHCl_3$) 3600 (OH) and 1735 cm^{-1} (ester C=O); nmr ($CDCl_3$) δ 2.97 (2H, s, methylene protons), 3.66 (3H, s, OCH_3), 3.85 (1H, s, OH, D_2O exchangeable), 7.20 (10H, m, aryl protons). *Anal.* calcd. for $C_{19}H_{16}O_4$: C 74.01, H 5.23; found: C 73.92, H 4.98.

1. U. Weiss and J. M. Edwards. Tetrahedron Lett. 4885 (1968).
2. D. Yang and J. M. Cook. J. Org. Chem. **41**, 1903 (1976).
3. R. C. Cookson, J. B. Henstock, J. Hudec, and B. R. D. Whitear. J. Chem. Soc. (C), 1986 (1967).
4. (*a*) B. Eistert and A. J. Tommen. Chem. Ber. **104**, 3048 (1971); (*b*) D. M. White. J. Org. Chem. **39**, 1951 (1974).
5. D. Yang, J. Oehldrich, and J. M. Cook. Presented at the 10th Middle Atlantic Regional Meeting of the American Chemical Society, Philadelphia, PA, 1976, Abstract K-41.
6. F. R. Japp and G. D. Lander. J. Chem. Soc. **71**, 139 (1897).
7. F. R. Japp and G. D. Lander. Proc. Chem. Soc. 109 (1896).

The reaction of diphenylethylenes with boron trifluoride and water[1]

STANLEY BYWATER AND DENIS J. WORSFOLD

Chemistry Division, National Research Council of Canada, Ottawa, Canada K1A 0R9

Received July 9, 1976

STANLEY BYWATER and DENIS J. WORSFOLD. Can. J. Chem. **55**, 85 (1977).

The concentrations have been measured of carbenium ions formed when diphenylethylene and diphenylpropene react with boron trifluoride and water in methylene chloride solution. With both these olefins it appeared necessary that two boron trifluoride molecules should be present for every water molecule to form the carbenium ion. Also the ionic species formed showed a very high degree of ionic dissociation. Diphenylethylene rapidly formed the cyclized dimer, and as a side reaction formed some triphenylmethylcarbenium ions. The diphenylpropene gave a diphenylcarbenium ion that appeared stable, but the accompanying anion was thought to be unstable and rearranged to a more stable form which disrupted the dependences on the concentrations of original reactants.

STANLEY BYWATER et DENIS J. WORSFOLD. Can. J. Chem. **55**, 85 (1977).

On a mesuré les concentrations d'ions carbénium qui sont formés lorsque le diphényléthylène et le diphénylpropène réagissent avec le trifluorure de bore et l'eau en solution dans le chlorure de méthylène. Avec ces deux oléfines, il semble nécessaire que deux molécules de trifluorure de bore soient présentes pour chaque molécule d'eau si l'on veut former un ion carbénium. De plus les espèces ioniques formées présentent un très haut degré de dissociation ionique. Le diphényléthylène forme rapidement un dimère cyclique et une réaction secondaire forme aussi des ions triphénylméthylcarbénium. Le diphénylpropène conduit à l'ion diphénylcarbénium qui semble stable mais il nous est apparu que l'anion qui l'accompagne est instable et qu'il se réarrange pour donner une forme plus stable; ce réarrangement brise la dépendance sur les concentrations des réactifs originaux.

[Traduit par le journal]

1,1-Diphenylethylene (DPE) has been used by several authors in model systems of cationic polymerization. Its basic reactions in these systems parallel those found with other monomers, but with the simplifying factor that only a reversible dimerization occurs. Evans *et al.* (1–3) studied principally the kinetics of these systems in benzene, whereas Sigwalt and co-workers (4, 5) took advantage of the relatively high concentrations of the diphenylcarbenium ion formed in methylene chloride solution to make a spectroscopic study of the active centres. The uv spectra obtained at low temperatures were complex, and three forms of active centre were suggested.

An attempt has been made here to use this system to describe the behaviour of boron trifluoride and water as a catalyst–cocatalyst system in the initiation reaction of cationic polymerizations of olefins by spectroscopic measurements of the carbenium ion concentration. Because of the activity of this catalyst, however, the subsequent cyclization reaction found for this monomer complicates the system. Some work has also been done using 1,1-diphenylpropene (DPP) for which the reaction goes no further than the initiation reaction, subsequent dimerization or cyclization is negligible.

[1]NRCC No. 15585.

Experimental

All reactions were done in all-glass appartus, with break seals separating reactants, and glass covered breakers. The reaction vessel contained 1 cm quartz uv cells with removable 9 mm quartz blocks to convert them at will to 1 mm cells. All manipulations were made under a vacuum of 10^{-3} P. The monomers were treated with butyl lithium. The solvent was methylene chloride, dried over calcium hydride after treatment with sulphuric acid and fractional distillation.

No attempt was made to have rigorously dry systems as water was added to most reactions. The residual water in the DPE systems was estimated to be less than 10^{-4} *M* as judged from spectra observed in systems where no water was added and the intercept on the abscissa of Fig. 3. Then solid DPP was more difficult to dry, and the residual water level appeared somewhat higher.

All reactions were carried out at 20 °C, unless otherwise stated. Concentrations of ions in methylene chloride solution were determined from the optical spectra at λ_{max} = 436 nm for DPE and 438 nm for DPP, using extinction coefficients of 35 000 as determined from H_2SO_4 solutions. Values of extinction coefficients between 35 000 and 39 000 are reported in the literature for

DPE. The absorption of DPP dissolved in H_2SO_4 was very similar to that of DPE in the same solvent having maxima at 319 and 434 nm attributable to the diphenylethylcarbenium ion. The maxima were displaced slightly in methylene chloride under our reaction conditions.

Results and Discussion

When DPE is added to a solution of BF_3 in methylene chloride in the presence of small amounts of water at 20 °C, the characteristic uv spectrum of the diphenylcarbenium ion is observed, although the shorter wavelength band is obscured by excess DPE. If lower temperatures are used, however, the spectrum is complicated by auxilliary peaks which were attributed by Sigwalt and co-workers (5) to complexes between DPE and the ions. To avoid this complication measurements were confined to 20 °C.

At 20 °C, however, due to the great reactivity of this Friedel–Crafts catalyst the presence of the final product of the reaction, the cyclic dimer (3-methyl-1,1,3-triphenylindane), leads to the formation of some triphenylcarbenium ions. This reaction has been noted previously with perchloric acid catalysis (6). Hence, very soon after the start of the reaction, the uv spectrum of the diphenylcarbenium ion is replaced slowly by that of the triphenylcarbenium ion. It is, however, possible by measuring a series of spectra to extrapolate back to zero time to get the initial diphenylcarbenium ion spectrum (Fig. 1). In Fig. 2 is plotted the disappearance of the monomer in a typical experiment, measured by vpc, together with the concentrations of the diphenyl- and triphenylcarbenium ions. The sole product found was the cyclic dimer, identified by vpc and tlc by comparison with an authentic sample. The product which produced the spectrum characteristic of triarylcarbenium ions could not be isolated or identified because of its very low concentration.

Difficulty was found in establishing proper equilibrium between BF_3 in the vapour phase and that in solution in the 1 mm optical cell, particularly as the initial stages of the reaction were important. This led to undesirable irreproducibility of the results. From the optical density at zero time it was possible to calculate the concentration of carbenium ions as a function of concentration of BF_3, H_2O, and DPE. At a fixed concentration of the BF_3 and DPE, the concentration of the carbenium ion was found to increase as the water concentration was increased to a maximum near a 2:1 ratio of BF_3–H_2O and

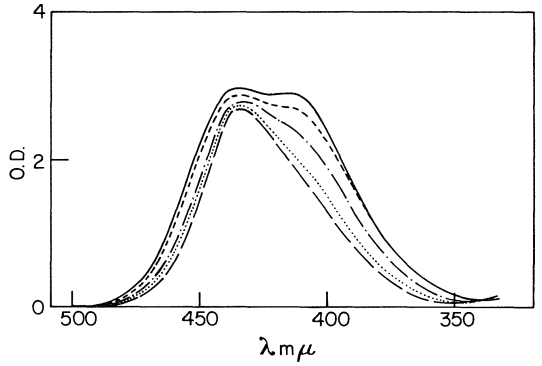

FIG. 1. Spectra of reaction mixture at times, from bottom to top, 1.5, 6, 20, 60 and 105 min from start of reaction. Reaction conditions $[BF_3]_0 = 2.56 \times 10^{-3}$ *M*, $[H_2O]_0 = 4.42 \times 10^{-4}$ *M*, $[DPE]_0 = 2.84 \times 10^{-2}$ *M*, 20 °C, methylene chloride solution.

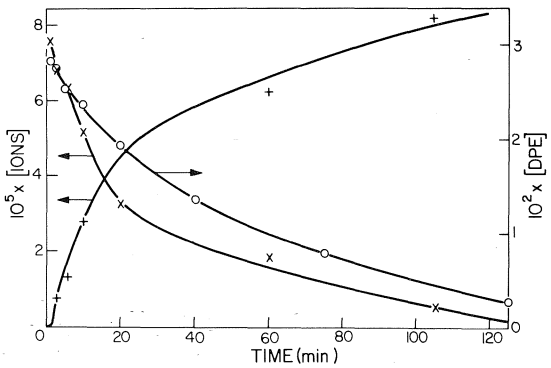

FIG. 2. Changes of concentration with time of DPE (○), diphenylcarbenium ion (×) and, triphenylcarbenium ion (+). Reaction conditions as in Fig. 1.

then to decrease (Fig. 3). If the BF_3 concentration was varied, a non-linear relationship was found as in Fig. 4 with very low ion concentrations formed when the BF_3 concentration was less than that of the water. The dependence on the DPE concentration was quite small under the conditions chosen, a forty-fold increase in $[DPE]_0$ caused only a four-fold increase in carbenium ion concentration.

At 20 °C the concentration of carbenium ions was small compared with the water concentration if the BF_3 was in excess. Initiation of the reaction at −30 °C led to much higher carbenium ion concentrations but the spectrum at this temperature showed the extra absorption band at 520 nm described by Sigwalt and co-workers (4). On cooling of these solutions to −70 °C, the total absorption increased, corresponding to a carbenium ion concentration approaching that

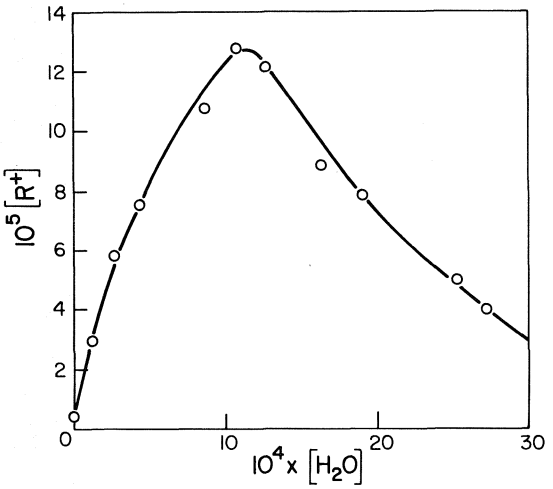

FIG. 3. Initial concentrations of diphenylcarbenium ions formed in reaction of DPE with BF_3 at varying added H_2O concentrations. $[DPE]_0 = 2.84 \times 10^{-2}$ *M*, $[BF_3]_0 = 2.56 \times 10^{-3}$ *M*, 20 °C.

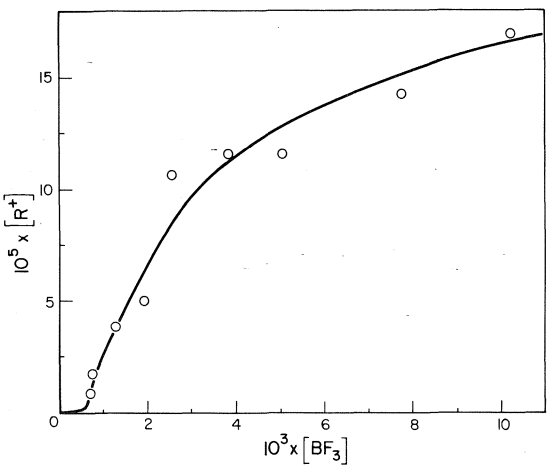

FIG. 4. Initial concentrations of diphenylcarbenium ions formed in reaction of DPE with H_2O and varying BF_3 concentrations. $[DPE]_0 = 2.84 \times 10^{-2}$ *M*, $[H_2O]_0 = 8.3 \times 10^{-4}$ *M*, 20 °C.

of the added water. Subsequent warming of the solutions to 0 °C and then to 20 °C caused a reduction in ion concentration; disappearance of the 520 nm band and finally spectral evolution of the type shown in Fig. 1. Despite the complications at low and high temperatures, the large differences in absorption at different temperatures suggest a temperature dependent equilibrium between BF_3, H_2O, DPE, and carbenium ions. At 20 °C carbenium ion formation was unfavoured, and the concentration of ions was in the range 10^{-5}–10^{-4} *M*. If the dissociation constant of the carbenium salt was similar to that of triphenylcarbenium salts in solvents with dielectric constant comparable to that of methylene chloride, *i.e.*, in the region $K_D = 2 \times 10^{-4}$ *M* (7), a concentration of salt of 5×10^{-5} *M* would be 80% dissociated into free ions.

Boron trifluoride as a catalyst has been studied extensively by Eastham and co-workers (8–10). In the system BF_3/H_2O, it was shown that the presence of both $BF_3 \cdot H_2O$ and excess BF_3 was necessary for catalytic activity to be evident. If it is assumed that the catalytic activity is reflected be the concentration of carbenium ions, the dependence of the carbenium ion concentration on H_2O and BF_3 shown in this study is in agreement with that found by Eastham. Negligible concentrations of carbenium ions would be expected until appreciable amounts of free BF_3 are present in solution. This condition requires $[BF_3]_0 \geqslant [H_2O]_0$ where the subscript zero refers to *added* concentrations. In this range the concentration of $BF_3 \cdot 2H_2O$ can be neglected with respect to the concentrations of BF_3 and $BF_3 \cdot H_2O$ according to the measurements of Clayton and Eastham (9).

The overall equation describing this scheme is

$$BF_3 \cdot H_2O + BF_3 + M \overset{K}{\rightleftharpoons} R^+ + A^-$$

where M = DPE, R^+ = the carbenium ion, and A^- the corresponding anion. Because of the high degree of ionic dissociation and the comparatively small concentration of carbenium ion, the carbenium ion concentration would be *approximately* governed by the equation

$$[R^+]^2 = aK\,[H_2O]_0([BF_3]_0 - [H_2O]_0)[M]_0$$

when $[BF_3]_0 \gg [H_2O]_0$, *a* is the fraction of the total free BF_3 that is in solution and in equilibrium with that in the vapour phase. The above equation predicts a maximum concentration of carbenium ions will occur when $[BF_3]_0 = 2[H_2O]_0$. It will become increasingly inaccurate as $[H_2O]_0$ approaches $[BF_3]_0$ due to the neglect of the presence of $BF_3 \cdot 2H_2O$. Overestimation of the carbenium ion concentration will result when $[H_2O]_0$ is greater than about 75% of $[BF_3]_0$ (9).

The dependence of $[R^+]$ on [M] should be a simple half power. The dependence found was lower than this which raises the possibility of preliminary complexing between DPE and BF_3 or $BF_3 \cdot H_2O$. Total complexing would give zero

order in [M] under the present conditions where DPE is in large excess. This is not the case and so an equilibrium would have to exist. Complexes between other Friedel–Crafts reagents and aromatic hydrocarbons have been demonstrated, also between BF_3 and olefins at low temperatures (11, 12).

Neglecting this deviation, the term aK has been calculated from the data obtained and was found to be a constant with a fairly large random error, $aK = 0.245 \pm 0.087$. The value of a is not known but from results of Clayton and Eastham (9) must be about 0.3 for the reaction vessels used.

A similar study was made using DPP as the monomer at 20 °C. It is reasonable to assume that the extra species formed with DPE leading to new spectral bands are associated with the presence in this system of the dimer cation. A monomer which would only form monomer cations might therefore show simpler behaviour. No dimerization could, in fact, be detected with DPP by tlc, and glc indicated less than 1% in 24 h. Only the main absorption band at 438 nm corresponding to the diphenylethylcarbenium ion was observed. Several days elapsed before noticeable changes in peak shape became apparent. It was also found that on lowering the temperature of the reaction mixture, although there was a great increase in optical density, the shape of the absorption band remained unchanged. Conversely, on re-warming the solution, the absorption decreased markedly. No longer wavelength band appeared at low temperatures as it did with DPE.

The concentration of ions formed was considerably lower with DPP than with DPE. In contrast with the DPE system, a 1 cm cell could be used to measure the absorption, and a cell was constructed incorporating a stirrer that circulated the solvent through the cell to improve the equilibrium between the liquid and vapour phases. Several additions of BF_3 were made to each reaction mixture of given water concentration.

It was found, as with DPE, that when the concentration of BF_3 was less than that of the water, little or no carbenium ion was formed. When a small excess of BF_3 was added, the absorption appeared instantly, but would then decrease with a half life time of about 10 min. The final value was the measured value. On adding more BF_3 a point would come when there was no decrease with time, and the absorption remained constant for this BF_3 concentration. The reaction mixture also became a little cloudy, particularly on standing, although it would tend to clear at higher $BF_3 : H_2O$ ratios.

The equilibrium carbenium ion concentration was measured as a function of the concentration of reactants. Although the results were in some ways similar to those found for DPE, there were some marked differences. Once again, for a fixed $[BF_3]_0$, $[R^+]$ went through a maximum with increasing water concentration (Fig. 5), but except at low $[BF_3]_0$, this maximum did not correspond to $[BF_3]_0 = 2[H_2O]_0$. The dependence on $[DPP]_0$ was far closer to a half power than for DPE. In addition it was not found possible to fit the results to the equation which was satisfactory for the DPE results. There were gross systematic variations in the constants aK found. Empirically a better constant was found by substituting the term $([BF_3]_0 - [H_2O])$ in the equation for $[R^+]$ by $([BF_3]_0 - 2[H_2O]_0)$. It should be noted that with DPE the diphenylmethylcarbenium ion concentrations had to be found by extrapolation to zero time. On the other hand, in the DPP experiments it was possible to allow sufficient time for steady values to be obtained. This could be taken to imply that in the DPP experiments the system was closer to

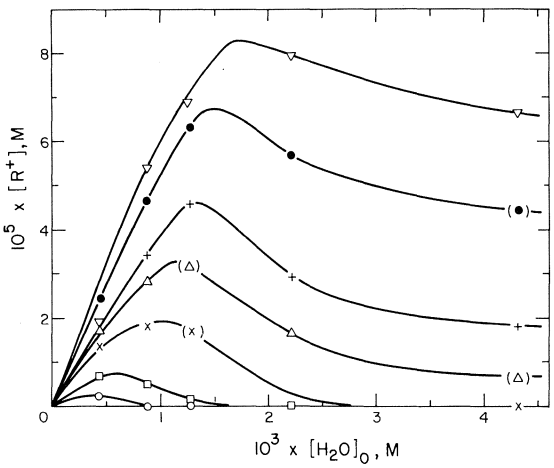

FIG. 5. Steady state concentrations of diphenylcarbenium ions formed in the reaction of DPP with BF_3 at varying added H_2O concentrations. $[DPP]_0 = 2.8 \times 10^{-2}$ *M*, $[BF_3]_0$ = ○, 0.639; □, 1.28; ×, 2.56; △, 3.83; +, 5 11; ●, 7.67; ▽, 10.22×10^{-3} *M*. Points in parentheses interpolated.

true equilibrium. Alternatively the DPP experiments could be affected by reactions described later associated with the cloudiness developed in the systems.

Confirmation of the high degree of dissociation into free ions was sought by conductance measurements. A reaction vessel incorporating both a conductivity cell and an optical cell was used, and incremental additions of BF_3 were made to vary the carbenium ion concentration. The ion concentration was in the range 10^{-5} to 10^{-4} *M*. Difficulty was again experienced maintaining an equilibrium between the vapour and solution in such a complex apparatus. The degree of ionic dissociation over this range was over 0.9, assuming $\Lambda_0 = 89$ ohm^{-1} cm^2 by extrapolation to infinite dilution, and a very approximate K_D of 4×10^{-4} *M* was found. This is in the range found for triphenylcarbenium salts, but in such a complex system it is uncertain whether such a calculation is legitimate.

A further test of the high degree of ionic dissociation was made by adding the salt Bu_4NBF_4 to a reaction mixture which normally would be expected to have a concentration of carbenium ions of 1.34×10^{-5} *M*. When the concentration of ammonium salt was 2.1×10^{-3} *M*, the absorption due to the carbenium ion could not be measured, but at a concentration of 2.3×10^{-4} *M* salt, the ion gave a small absorption (*ca.* 8×10^{-7} *M*). This is in agreement with a high degree of ionic dissociation. Although the tetrafluoroborate salt added is not necessarily a true common-ion salt, as it is in such large excess, its presence would cause the effective proton acid to be HBF_4 instead of $BF_3 \cdot H_2O$. Thus on the usual assumption that the free cation and its ion-pair have nearly identical absorptions, addition of a large excess of tetrafluoroborate would cause a drastic reduction in absorption as the total carbenium ion concentration is reduced to the small equilibrium concentration of ion-pairs. Had the carbenium ions been present largely in the form of ion-pairs, only a small reduction in absorption would have been observed as the free carbenium ions were removed from solution.

The differences between the dependences of the carbenium ion concentration on the reactants in the DPE and DPP systems is suggested to be associated with the formation of the cloudiness in the latter system as it came to equilibrium. Typical reactions that occur are described by Eastham and co-workers for the reaction of triphenylcarbinol with BF_3. The triphenylcarbenium ion formed and the BF_3OH^- ion rearranged to fluoroborate ions and H_3BO_3, with the boric acid precipitating (13),

$$3Ph_3COH + 7BF_3 \rightarrow 3Ph_3CB_2F_7 + B(OH)_3$$

The anions expected to be formed initially in solution in the DPP system resemble closely those in the triphenylcarbinol case, and the reaction might follow the same course. This is in accord with the decline in the carbenium ion absorption found when BF_3 is added initially in excess to the DPP + water solution. The resultant 1,1-diphenylpropylfluoroborate could be expected to have a constant of formation (*K*) from DPP and its acid component different from the original BF_3OH^- compound, and hence give a different carbenium ion concentration.

Attempts to isolate boric acid from the DPP system failed, as the precipitate was not crystalline as was that found with triphenylcarbinol, so it is probable that these secondary reactions are more complex in this case. Nevertheless a similar rearrangement to a fluoroborate ion is probable. At lower temperatures (-30 °C , it is possible to eliminate the initial decline in the carbenium ion concentration, but difficulties caused by heterogeneity still occurred.

It has been suggested here that an equilibrium is established between this Friedel–Crafts reagent, olefins, and the carbenium ion. Because of the high degree of ionic dissociation, the dependence of the carbenium ion concentration appears as a half power of the effective reagents. In studies of kinetics of systems using this type of catalyst–cocatalyst system, such half powers do not appear, and linear dependences are found (8–10). This indicates that equilibrium is not established in these reactions between the ion and the reactant, so that the formation of the ion is the rate determining process.

With DPE, the initial rapid formation of the carbenium ion is studied as it is comparatively shortlived. If however, the ion is longlived as is the ion formed by DPP, secondary reactions of the counter ion take place in this catalyst system and complicate the dependences on the reactants.

1. A. G. Evans, N. Jones, and H. J. Thomas. J. Chem. Soc. 1824 (1955).
2. A. G. Evans and J. Lewis. J. Chem. Soc. 2975 (1957).

3. A. G. EVANS and E. D. OWENS. J. Chem. Soc. 4123 (1959).
4. G. SAUVET, J. P. VAIRON, and P. SIGWALT. Bull. Soc. Chim. 4031 (1970).
5. G. SAUVET, J. P. VAIRON, and P. SIGWALT. J. Polym. Sci. Symposium, **52**, 173 (1975).
6. S. BYWATER, A. F. JOHNSON, and D. J. WORSFOLD. Can. J. Chem. **42**, 1255 (1964).
7. P. M. BOWYER, A. LEDWITH, and D. C. SHERRINGTON. J. Chem. Soc. B, 1511 (1971).
8. A. M. EASTHAM. J. Am. Chem. Soc. **78**, 6040 (1956).
9. J. M. CLAYTON and A. M. EASTHAM. J. Am. Chem. Soc. **79**, 5368 (1957).
10. T. SZELL and A. M. EASTHAM. J. Chem. Soc. B, 30 (1966).
11. T. B. BOGOMOLOVA, A. R. GANTMAKHER, and YE. B. LYUDVIG. Vysokomol. Soed. A**14**, 2210 (1972).
12. L. ELÉGANT, J. CASSAN, and M. AZZARO. Bull. Soc. Chim. Fr. 2675 (1968).
13. P. J. BURCHILL, S. BROWNSTEIN, and A. M. EASTHAM. Can. J. Chem. **45**, 17 (1967).

Chalkogenides of the transition elements. XI. Mössbauer ^{57}Fe spectrum of the spinel $Co_{2.94}Fe_{0.06}S_4$ between 10 K and room temperature[1]

F. W. D. WOODHAMS

Department of Natural Philosophy, University of Aberdeen, Aberdeen, Scotland AB9 2UE

AND

OSVALD KNOP

Department of Chemistry, Dalhousie University, Halifax, N.S., Canada B3H 4J3

Received April 13, 1976

F. W. D. WOODHAMS and OSVALD KNOP. Can. J. Chem. **55**, 91 (1977).

Mössbauer spectra of ^{57}Fe probe atoms in the spinel $Co_{2.94}Fe_{0.06}S_4$ indicate the existence of a magnetic transition at $T_{tr} \approx 95$ K in the parent phase Co_3S_4. The spectrum observed below T_{tr} consists of a six-line magnetic spectrum and a two-line quadrupole spectrum. Above T_{tr} the six-line spectrum collapses to a single line superposed on the two-line quadrupole spectrum. Consideration of the Mössbauer parameters and of the area ratio of the component spectra suggests that the atomic occupancy of the spinel lattice is $[Co_{0.968}Fe_{0.032}][Co_{0.986}Fe_{0.014}]_2S_4$, the Fe atoms having preference for the tetrahedrally coordinated cation sites.

F. W. D. WOODHAMS et OSVALD KNOP. Can. J. Chem. **55**, 91 (1977).

Les spectres Mössbauer du ^{57}Fe dans la spinelle $Co_{2.94}Fe_{0.06}S_4$ témoignent de l'existence d'une transition magnétique à $T_{tr} \approx 95$ K dans la phase mère Co_3S_4. Au-dessous de T_{tr} on observe un spectre magnétique à six composantes superposé à un doublet quadrupolaire, tandis qu'au-dessus de T_{tr} les six composantes du spectre magnétique fusionnent, ce qui produit une bande unique superposée au spectre quadrupolaire. Les valeurs des paramètres Mössbauer et le rapport de l'aire du spectre magnétique à celle du spectre quadrupolaire suggèrent une répartition des atomes du Co et du Fe sur le réseau spinelle suivant $[Co_{0.968}Fe_{0.032}][Co_{0.986}Fe_{0.014}]_2S_4$, les atomes Fe préférant des sites à coordinence tétraèdrique.

Only a very limited amount of work has been done to determine the nature of the spin states of the Co atoms at the A and B sites in the spinel Co_3S_4. Heidelberg *et al.* (2) stated the magnetic susceptibility (in 10^{-6} emu/g) of the sulfide to be 3.4 and independent of temperature between 300 and 800 K,[2] while Lotgering (footnote 1 of ref. 4) found a small temperature dependence: 3.1 (700 K), 3.6 (295 K), 4.6 (77 K), and 6.9 (20 K). It is not clear whether this represents spontaneous magnetic behaviour from ions with a small spin, or Pauli-paramagnetic behaviour (*cf.* Co_9S_8 and pentlandite, ref. 1). There was no evidence in the susceptibility data (*cf.* also ref. 5) to indicate the onset of magnetic order. Bouchard *et al.* (6) measured the resistivity of Co_3S_4 between -180 and $+150$ °C and found that the resistivity increased with temperature; the room-temperature value was small, 3×10^{-4} ohm cm. From this they concluded that Co_3S_4 is metallic. The existence of metallic conduction is not inconsistent with spontaneous magnetic behaviour. Goodenough (7) has shown that if the strength of the interaction between neighbouring atoms, as measured by the parameter b, is such that $b_c < b < b_m$, then both spontaneous magnetism and metallic conduction are observed (*cf.* the pyrite CoS_2, ref. 8). Goodenough himself concluded from the magnetic and electrical properties that Co_3S_4 was a Pauli paramagnet but that the small temperature dependence of χ indicated a narrow conduction band and thus $b \approx b_m$, *i.e.* close to the border between metallic with a localized spin and metallic with no localized spin. Locher (4) has suggested that the Co atoms at the A sites might be present as Co^{1+} ($3d^8$), which would be qualitatively consistent with the observed low χ values. His suggestion is based on a comparison of the nmr spectra of ^{59}Co in the metallic spinel $CuCo_2S_4$ and in Co_3S_4. It was estimated that $2.5 \pm 1.5\%$ of the Co atoms in $CuCo_2S_4$ were in the A sites; these and the Co(A) atoms in Co_3S_4 showed a zero quadrupole interaction, while the splitting at 77 K at Co(B) was closely similar in both sulfides. In Co_3S_4 the

[1]For Part X, see ref. 1.

[2]Serres (3) reported 1.27×10^{-6} emu/g for natural linnéite between 19 and 115 °C.

change in the splitting from 295 to 77 K was small compared with $CuCo_2S_4$.

Replacing some of the Co in Co_3S_4 by ^{57}Fe offers the possibility of utilizing this nuclide as a Mössbauer probe to investigate the behaviour of the Fe atoms in the host structure and, indirectly, the magnetic properties of the Co_3S_4 matrix. In this paper we describe the results of such Mössbauer experiments with $Co_{2.94}Fe_{0.06}S_4$, *i.e.* at 2% replacement of Co by Fe.

Experimental

A sample of $Co_{2.94}{}^{57}Fe_{0.06}S_4$ was prepared by direct synthesis from high-purity elements in an evacuated, sealed silica-glass tube. The ^{57}Fe content of the iron powder was about 92%; the powder was freshly reduced with H_2 before use. On completion of reaction the sulfide was kept at 500 °C for 24 h. The cooled mass was then reground under acetone, resealed, and annealed at 600 °C/6 days → 550 °C/2 days → 400 °C/1 day followed by cooling with the furnace. A sample of Co_3S_4 was prepared for comparison (600 °C/24 h; reground, 600 °C/4 days → 550 °C/2 days → 400 °C/1 day → room temperature). Overexposed X-ray powder photographs contained only lines of the spinel phase. The patterns were identical with those reported in ref. 9.

Mössbauer spectra of the Fe-containing sample at temperatures between 10 K and ambient were obtained with a conventional constant-acceleration transducer system coupled to a 400-channel multichannel analyzer, operated in its multiscaler mode. The source used was ^{57}Co in Pd and had an initial strength of 25 mCi. Calibration of the spectrometer was carried out using an enriched ^{57}Fe foil and the calibration data given by Stevens and Preston (10). The low-temperature spectra were obtained with the source and absorber mounted in a vertical configuration in a commercial liquid-helium cryostat (Oxford Instrument Company Ltd.). This cryostat maintained the source temperature at that of the main refrigerant (He or N_2) but allowed the absorber temperature to be maintained at any temperature between that of the main refrigerant and ambient. The absorber temperature was measured with a AuFe/chromel thermocouple and the desired temperature was maintained with a proportional temperature controller coupled to a small heating coil mounted close to the absorber. The temperature stability was better than ± 0.5 K throughout the period required to obtain a spectrum.

All chemical shifts quoted in this paper are relative to metallic iron at room temperature.

Results and Discussion

A representative selection of the Mössbauer ^{57}Fe spectra is shown in Figs. 1 to 3. Below 80 K the spectra consisted of two components: a six-line magnetic spectrum (6LMS) and superposed on this a two-line quadrupole spectrum (2LQS) typical of Fe atoms not ordered magnetically, in sites of symmetry lower than cubic. The presence of a 6LMS at only 2% replacement of the Co by Fe is an immediate indication that the structure of the sulfide is magnetically ordered and that the Co atoms participate in the ordering. Thus Co_3S_4 must fall within Goodenough's region $b_c < b < b_m$.

As the temperature of the sample was increased from 10 K the splitting of the 6LMS decreased, until at 93 K the six lines overlapped to such an extent that only a broad envelope was observed. Above 97 K the 6LMS collapsed to a single line superposed on the 2LQS, the net result being that only a broad, non-Lorentzian-shaped resonance line appeared. This would fix the magnetic transition temperature T_{tr} at about 95 K. Thus in demonstrating the existence of magnetic ordering and in yielding an estimate of T_{tr} the ^{57}Fe probe provides information concerning the behaviour of *cobalt* atoms in Co_3S_4.

Spectra below T_{tr} were fitted by least-squares to a model comprising a 6LMS and a 2LQS. As lines 3 and 4 of the 6LMS were not well resolved from the 2LQS, constraints had to be applied to obtain a sensible fit: the areas of the six lines were constrained in the ratio 3:2:1:1:2:3, the ratio appropriate for an unmagnetized absorber, the widths of the pairs of lines 1–6, 2–5, and 3–4 were constrained to be equal, and the relative positions of lines 3 and 4 were fixed with respect to lines 1 and 6 using the known ratio of the magnetic moments of the excited and ground states. No constraints were applied to the two lines of the 2LQS. This model will be referred to as model *a*.

The Mössbauer parameters obtained from these computer fits are given in Table 1. The parameter ε of the 6LMS is the difference in the splitting between lines 1–2 and 5–6. The fits of model *a* to the 10, 60, and 70 K spectra (Fig. 1) are acceptable except in the region of the resonance positions of the 2LQS lines. Moreover, there is a very noticeable difference in the widths and the intensities of the two component lines of the 2LQS, a feature to which we shall return below.

We assign the two spectra on the assumption that they arise from ^{57}Fe atoms substituting for Co atoms in the A and B sites of the spinel structure. However, the assignment is not straightforward, as it cannot be made directly from the area ratio R of the two spectra, $R =$ (area of 6LMS)/(area of 2LQS). The value of R at 10, 60, and 70 K is about 1.2, whereas a value of 2 would be expected if the 6LMS originated

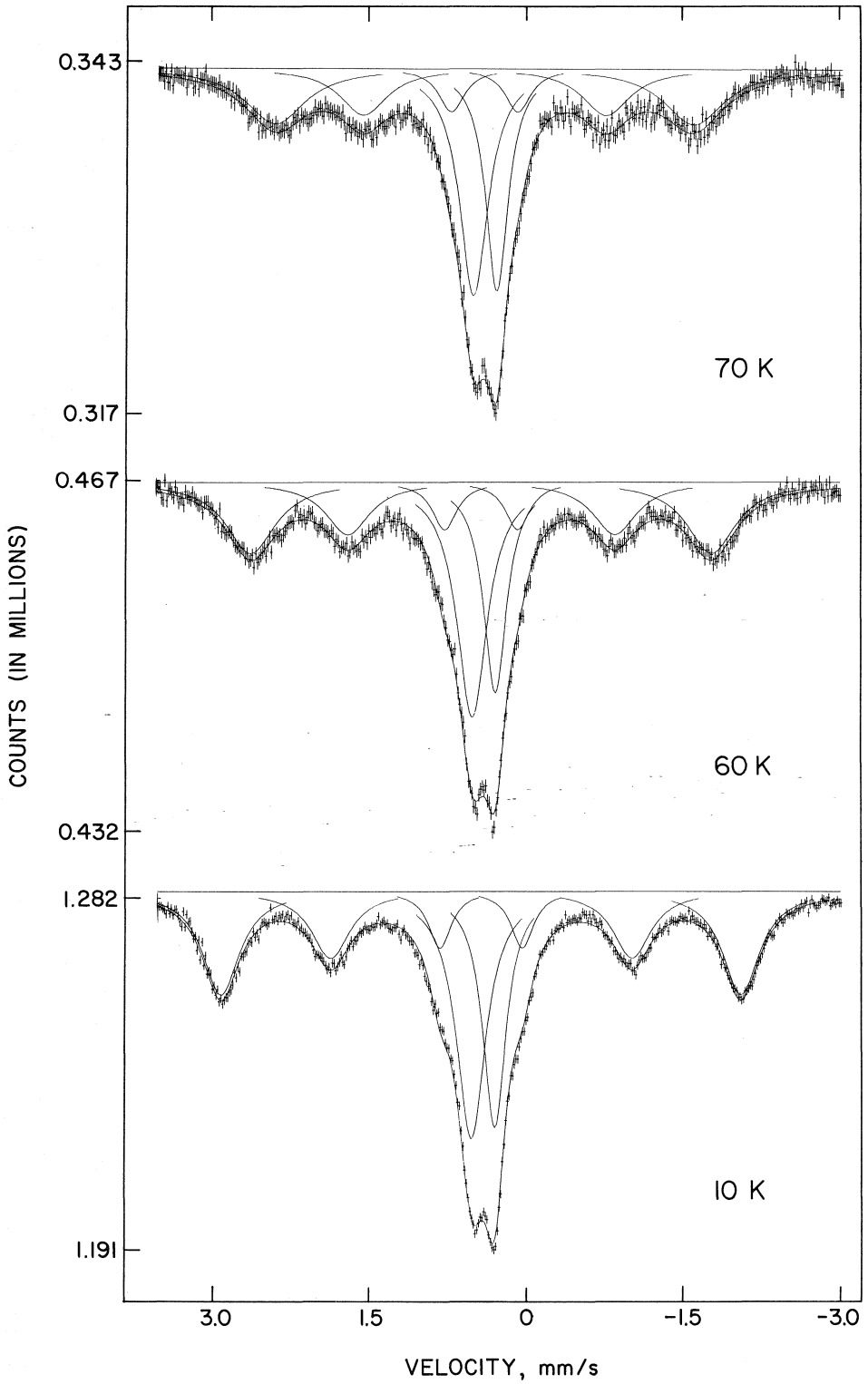

FIG. 1. Mössbauer ^{57}Fe spectra of $Co_{2.94}{}^{57}Fe_{0.06}S_4$ at 10, 60 and 70 K fitted to model *a* (see text).

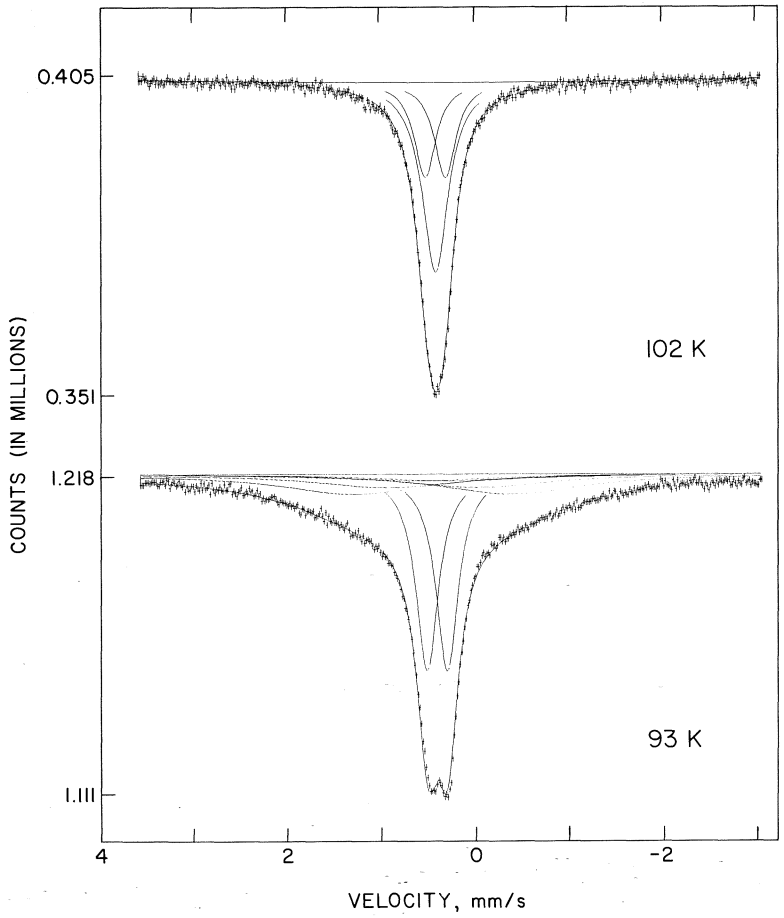

FIG. 2. Mössbauer ^{57}Fe spectra of $Co_{2.94}{}^{57}Fe_{0.06}S_4$ below (93 K) and above (102 K) the magnetic transition temperature $T_{tr} \approx 95$ K, fitted to model *b*.

from Fe(B), and 0.5 if from Fe(A), assuming the Fe atoms to be distributed at random over the A and B sites. The observed ratio is too small to be considered as a 2:1 ratio reduced by differences in the recoil-free fractions of the ^{57}Fe atoms at the two sites, or by vacancies at the A sites. It must then be due to a marked preference of Fe atoms for one type of site. Assignment of the two spectra has therefore been made from a consideration of the quadrupole splittings and the important observation that there is no, or at least only a very small, hyperfine magnetic field at one of the sites.

The fact that $\varepsilon = 0$, within experimental error, indicates that there is either no electric field gradient (EFG) at the Fe atom that gives rise to the 6LMS, or if there is, then the angle between the hyperfine magnetic field and the principal axis of the EFG is close to arc cos $(1/\sqrt{3})$. The 2LQS has an essentially temperature-independent quadrupole splitting of about 0.22 mm/s.

The symmetry at the A site is $\bar{4}3m$–T_d, so that no EFG is expected except for a contribution from disordered local environments of an Fe(A) due to other probe atoms (see below). The symmetry at a B site is $\bar{3}m$–D_{3d}, so that here an EFG is expected giving a non-zero quadrupole splitting; indeed, a non-zero nmr quadrupole interaction has been previously reported (4) at Co(B) in pure Co_3S_4 at 295 and 77 K. On this basis we assign the 6LMS observed below T_{tr} as arising from Fe atoms in the tetrahedrally coordinated A sites, and the 2LQS from Fe atoms in the trigonally distorted octahedral B

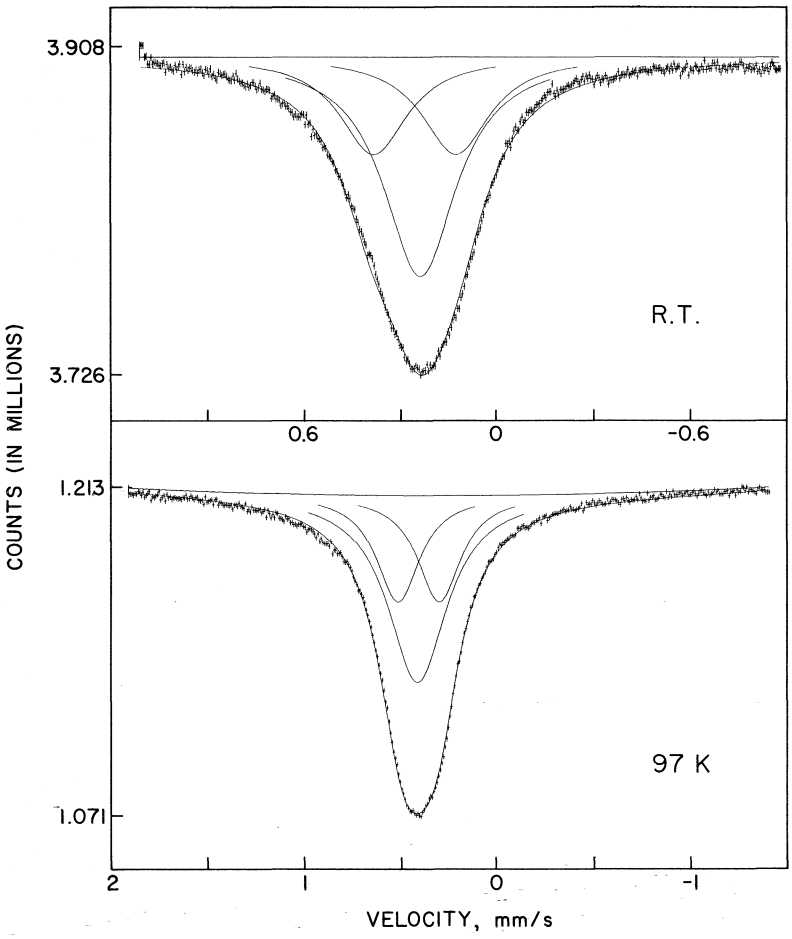

FIG. 3. Mössbauer ^{57}Fe spectra of $Co_{2.94}{}^{57}Fe_{0.06}S_4$ at 97 K and room temperature using a narrow velocity sweep. The spectra are fitted to model *b* with additional constraints (see text and Table 1). Note the different velocity scales.

sites. The site occupancy should thus be formulated as $[Co_{0.968}Fe_{0.032}][Co_{0.986}Fe_{0.014}]_2S_4$, the probe atoms preferring the A sites.[3]

An unusual feature is the closeness of the chemical shifts at Fe(A) and Fe(B) at all temperatures (Table 1). These shifts are, however, close to the measured chemical shifts in other sulfides containing Fe in tetrahedral sites (*cf.* Fig. 4 of ref. 11). The similarity of the room-temperature shifts at Fe(A) in $Co_{2.94}Fe_{0.06}S_4$ and in Fe_3S_4, 0.26(2) mm/s (12), is paralleled by the similarity of the shortest M(A)—S distances in these two spinels, 2.18(5) and 2.15(2) Å, respectively (13).

The magnitude of the hyperfine magnetic field *B* at Fe(A), extrapolated to 0 K, is about 16 T and thus much smaller than that observed in other Fe sulfides. For example, the field at both Fe(A) and Fe(B) in Fe_3S_4 is 31 T (12), while in troilite, FeS, it is 31 T at room temperature (14) and in orthorhombic cubanite, $CuFe_2S_3$, it is about 33 T (15, 16); in chalcopyrite, $CuFeS_2$, the value is about 37 T at 77 K (15). Since the similarity of δ[Fe(A)] in $Co_{2.94}Fe_{0.06}S_4$ and Fe_3S_4 would lead us to expect that covalency effects might be comparable in the two sulfides, the smallness of *B* in $Co_{2.94}Fe_{0.06}S_4$ might be

[3]A similar preference of Fe for tetrahedrally coordinated sites is observed in natural (untreated) pentlandite, $(Fe, Ni)_{9\pm\delta}S_8$ (11).

TABLE 1. Mössbauer parameters (mm/s) of ^{57}Fe in $Co_{2.94}Fe_{0.06}S_4$[a]

T (K)	δ	Δ or ε	B (T)[b]	Γ_1	Γ_2	Γ_3	R
			Two-line quadrupole spectrum (2LQS)				
10	0.412(3)[c]	0.223(6)		0.268(6)	0.341(7)		1.21(4)
60	0.395(4)[c]	0.220(8)		0.265(9)	0.350(9)		1.17(5)
70	0.400(5)[c]	0.220(10)		0.258(9)	0.331(10)		1.18(5)
93	0.407(1)[d]	0.213(2)		0.286(4)			1.29(7)
97	0.402(1)[e]	[0.213]		0.272(3)			[1.2]
102	0.405(2)[e]	[0.213]		0.276(5)			[1.2]
r.t.[g]	0.251(2)[e]	[0.213]					[1.2]
	0.248(3)[f]	0.254(6)		0.255(5)			[1.2]
			Six-line magnetic-field spectrum (6LMS)				
10	0.428(3)[c]	0.011(11)	15.41(2)	0.434(9)	0.446(10)	0.263(9)	
60	0 420(5)[c]	0.001(14)	13.65(4)	0.574(16)	0.518(16)	0.286(14)	
70	0.410(8)[c]	0.015(19)	12.39(5)	0.703(22)	0.558(20)	0.300(17)	
93	0.467(10)[d]	—	5.20(28)		1.84(12)		
97	0.408(1)[e]	—	—		0.371(3)		
102	0.407(1)[e]	—	—		0.333(3)		
r.t.	0.226(1)[e]	—	—		0.319(3)		
	0.231(1)[f]	—	—		0.272(5)		

[a]The chemical shifts are relative to metallic Fe at room temperature. The errors quoted are the computer-generated single standard deviations. Δ refers to 2LQS, ε refers to 6LMS (see text). R is the ratio of the area under the 6LMS (or the collapsed 6LMS) to the area under the 2LQS.
[b]Hyperfine magnetic field at Fe(A).
[c]Model *a* (see text).
[d]Model *b* (see text).
[e]R and Δ constrained to the values in brackets.
[f]The constraint on Δ relaxed.
[g]r.t. = room temperature.

taken as evidence that the moment localized at the A site is much less than it is in Fe_3S_4. This would be consistent with the metallic nature of Co_3S_4, the small dependence of its χ on temperature, and with $b \approx b_m$.

The appearance of the 2LQS below T_{tr} shows that the Fe atoms that give rise to this spectrum do not participate in the magnetic order. This is entirely consistent with the proposed assignment that the 2LQS arises from Fe(B) atoms, if they have a low-spin $S = 0$ t_{2g}^6 configuration. The chemical shift of the 2LQS at room temperature, 0.250(5) mm/s, is reasonably close to that of the pyrite FeS_2, 0.305(3) mm/s (17), which is known to contain Fe atoms with an $S = 0$ configuration in an octahedral coordination of sulfur atoms. The shift is smaller than that observed at Fe(B) in Fe_3S_4, 0.55(2) mm/s (12). This is not surprising, as the configuration of Fe(B) in Fe_3S_4 has been suggested by Spender *et al.* (18) to be intermediate between high-spin ferric and high-spin ferrous; the low-spin d^6 Fe(B) configuration in $Co_{2.94}Fe_{0.06}S_4$ is more highly covalent than Fe in the high-spin states and yields a correspondingly smaller δ. Support for this is found in the observed Fe(B)—S distances. In Fe_3S_4, the shortest Fe(B)—S distance, 2.46(1) Å, is noticeably larger than the comparable Co(B)—S distance in Co_3S_4, 2.27(3) Å (*cf.* ref. 13), and the Fe—S distance in pyrite, 2.26 Å. The quadrupole splitting, ~0.22 mm/s at room temperature, is smaller than that of cubic FeS_2, 0.613(4) mm/s, (17), so that any lattice and molecular-orbital contributions are less than in pyrite.

The 2LQS below T_{tr} is similar in appearance to the ^{57}Fe spectrum of the pyrite $Co_{0.98}Fe_{0.02}S_2$ at 91 K that we have previously analyzed in detail (8). That spectrum was shown to be due to a supertransferred hyperfine magnetic field of about 0.6 to 0.7 T at the Fe sites in addition to the quadrupole interaction. The fact that a similar spectrum is observed at Fe(B) in $Co_{2.94}Fe_{0.06}S_4$ is not particularly surprising.

In the 93 K spectrum, which was the highest-temperature magnetic spectrum still showing a resolved quadrupole spectrum (Fig. 2), the hyperfine magnetic field at Fe(A) has decreased to such an extent that only a broad envelope of the collapsed 6LMS is seen. To obtain a sensible fit to this spectrum additional constraints were necessary. The widths of all six lines of the 6LMS were now constrained to be equal and the relative line

positions to be consistent with those of a pure magnetic interaction; the two lines of the 2LQS were constrained to have equal areas and widths. As Fig. 2 shows, this model, model *b*, gave a satisfactory fit. The ratio R again turned out to be close to the value of 1.2 observed in the well-resolved low-temperature spectra.

Above T_{tr} the area ratio R and Δ had to be constrained to values extracted from the low-temperature spectra; the two lines of the quadrupole doublet were constrained to have equal line widths and areas (Table 1). In the room-temperature spectrum the velocity sweep was small and it was possible to obtain a reasonable fit without constraining Δ. This resulted in a somewhat higher Δ value.

Some comment is justified concerning the absence of any measurable quadrupole splitting in the 6LMS and the appreciable, and unequal, line widths of the 6LMS components, which show an increase with increasing temperature as the hyperfine magnetic field at Fe(A) decreases. This line-width behaviour is an indication that either there are a number of hyperfine magnetic fields or there is a hyperfine-field distribution, leading to a number of closely overlapping six-line spectra. Examination of the Co_3S_4 structure shows that a Co(A) atom is surrounded by four Co(A) atoms at 4.07 Å, at the corners of a regular tetrahedron, and by twelve Co(B) atoms at 3.90 Å, at the corners of a regular truncated tetrahedron. The frequency of 4Co(A) + 12Co(B) environments of the Fe(A) atoms in $Co_{2.94}Fe_{0.06}S_4$, assuming an Fe(A):Fe(B) ratio of 1.2 but a random distribution over the A and B sites, will be 0.742, *i.e.* 74.2% of the Fe(A) atoms will have only Co atoms as their nearest metal-atom neighbours out to a distance of 6 Å. A 10% fraction of the Fe(A) atoms will have 1Fe(A) + 3Co(A) + 12Co(B) as their nearest metal-atom neighbours, and 12.4% will have 4Co(A) + 1Fe(B) + 11Co(B). As the magnetic moments of the Fe(A), Co(A), and Co(B) atoms will almost certainly be different, and non-zero,[4] these three environments of Fe(A) atoms will be expected to give three different hyperfine magnetic fields at Fe(A). If more distant metal-atom neighbours are included a *distribution* of magnetic fields at Fe(A) will result.

The second and third of the Fe(A) environments just enumerated are non-cubic if the charges on the Fe and Co atoms are different, and will give rise to an EFG at Fe(A). However, the resulting quadrupole splitting is difficult to estimate from a point-charge lattice sum because of the uncertainty in assigning effective charges to the metal atoms and in the absence of an estimate of the shortest Fe—Fe distances. Moreover, the principal axis of the Fe(A)—$Co(A)_3$-$Fe(A)_1$ tetrahedron is the threefold axis passing through the two Fe atoms. If the hyperfine magnetic field is parallel to a crystallographic axis (*i.e.* to an edge of the unit cell or to a $\bar{4}$ axis), the angle of the field with the threefold axis of the tetrahedron, and thus with the principal axis of the EFG, is arc cos $(1/\sqrt{3})$. Then if the effective charges on the Fe(A) and Co(A) atoms were similar, the q_{latt} contribution from any such tetrahedron to Δ would be close to zero. The EFG in the Fe(A)—$Co(B)_{11}Fe(B)_1$ truncated tetrahedron does not have axial symmetry; the Fe(A)—Fe(B) vector is 29.5° off the nearest threefold axis. The q_{latt} contribution to Δ from this environment is not likely to be large. These considerations explain why Δ is not resolved in the 6LMS and why it is almost certainly 'swamped' by the range of hyperfine magnetic fields expected at Fe(A). Further evidence for this conclusion is available from the spectra obtained above T_{tr}: the single line arising from Fe(A) atoms is not noticeably broadened.

It is interesting to note that the recently reported (19) room-temperature spectrum of the paramagnetic phase of the spinel $Fe_{1.06}Cr_{1.94}S_4$ consisted of a singlet and a quadrupole doublet having the same δ and an area ratio of 70:30. The appearance of the doublet was explained by formulating the site occupancy as $[Fe^{2+}_{0.94}Fe^{3+}_{0.06}][Fe^{2+}_{0.03}Cr^{3+}_{0.97}]_2S_4$, in which case the Fe^{2+}(A) atoms would occur in the structure either surrounded by $12Cr^{3+}$ or by $11Cr^{3+}$ + $1Fe^{2+}$ nearest-neighbour B atoms, in an abundance ratio of 69:26. The observed Δ produced at an Fe^{2+}(A) atom by the $11Cr^{3+}$ + $1Fe^{2+}$ environment was 0.73 mm/s. Since the authors considered a distribution $[Fe^{2+}][Fe^{3+}_{0.03}Cr^{3+}_{0.97}]_2S_4$ unlikely on the grounds that the M(B) atoms would have equal charge and practically equal ionic radii and hence would not produce an EFG at Fe(A), the spectrum was taken as experimental evidence of a preference of the Fe^{2+} ions for B sites in sulfospinels.

[4]The magnetic moment of Fe(B) is zero, see above.

Our results support this conclusion to the extent that the Fe(B) atoms in $Co_{2.94}Fe_{0.06}S_4$ have a t_{2g}^6 configuration, $S = 0$; the effective ionic radii for 6-coordination of Fe^{2+}_{LS} and Co^{3+}_{HS} are closely similar (20).

Acknowledgments

We wish to thank Dr. C.-H. Huang for the preparation of the two samples and to the National Research Council of Canada for a grant in aid of research to one of us (O.K.).

1. O. KNOP, C.-H. HUANG, K. I. G. REID, J. S. CARLOW, and F. W. D. WOODHAMS. J. Solid State Chem. **16**, 97 (1976).
2. R. F. HEIDELBERG, A. H. LUXEM, S. TALHOUK, and J. J. BANEWICZ. Inorg. Chem. **5**, 194 (1966).
3. A. SERRES. J. Phys. Radium, **14**, 689 (1953).
4. P. R. LOCHER. Z. Angew. Phys. **24**, 277 (1968).
5. F. K. LOTGERING. Philips Res. Repts. **11**, 337 (1956).
6. R. J. BOUCHARD, P. A. RUSSO, and A. WOLD. Inorg. Chem. **4**, 685 (1965).
7. J. B. GOODENOUGH. Solid State Commun. **5**, 577 (1967).
8. F. W. D. WOODHAMS, P. S. WHITE, and O. KNOP. J. Solid State Chem. **5**, 334 (1972).
9. O. KNOP, K. I. G. REID, SUTARNO, and Y. NAKAGAWA. Can. J. Chem. **46**, 3463 (1968).
10. J. G. STEVENS and R. S. PRESTON. Mössbauer Effect Data Index for 1970. *Edited by* J. G. Stevens and V. E. Stevens. IFI/Plenum, New York. 1972. Appendix G.
11. O. KNOP, C.-H. HUANG, and F. W. D. WOODHAMS. Am. Mineral. **55**, 1115 (1970).
12. J. M. D. COEY, M. R. SPENDER, and A. H. MORRISH. Solid State Commun. **8**, 1605 (1970).
13. C.-H. HUANG and O. KNOP. Can. J. Chem. **49**, 598 (1971).
14. N. N. GREENWOOD and T. C. GIBB. Mössbauer spectroscopy. Chapman and Hall, London. 1971.
15. N. N. GREENWOOD and H. J. WHITFIELD. J. Chem. Soc. A, 1697 (1968).
16. E. F. MAKAROV, A. S. MARFUNIN, A. E. MKRTCHYAN, V. A. POVITSKII, and R. A. STUKAN. Fiz. Tverd. Tela, **10**, 913 (1968); Sov. Phys. – Solid State, **10**, 717 (1968).
17. P. S. WHITE. Ph.D. thesis. Dalhousie University, Halifax, Nova Scotia. 1972.
18. M. R. SPENDER, J. M. D. COEY, and A. H. MORRISH. Can. J. Phys. **50**, 2313 (1972).
19. F. K. LOTGERING, A. M. VAN DIEPEN, and J. F. OLIJHOEK. Solid State Commun. **17**, 1149 (1975).
20. R. D. SHANNON. Acta Cryst. A**32**, 751 (1976).

Transition state enthalpies of transfer in aqueous dimethyl sulfoxide solutions. The hydroxide catalyzed ionization of chloroform[1]

JOHN R. JONES
Chemistry Department, University of Surrey, Guildford, England GU2 5XH
AND
RICHARD FUCHS
Department of Chemistry, University of Houston, Houston, Texas 77004

Received June 28, 1976

JOHN R. JONES and RICHARD FUCHS. Can. J. Chem. **55**, 99 (1977).

The accelerating effect of added dimethyl sulfoxide on the rate of hydroxide-catalyzed ionization of chloroform in water has been examined in terms of the solvation of reactants and transition state. Enthalpies of solution of chloroform in water, DMSO, and mixtures of the two have been measured. From these, together with enthalpies of activation for the detritiation of chloroform, and enthalpies of transfer of hydroxide ion from water to aqueous DMSO mixtures, transition state enthalpies of transfer have been calculated. The reaction is accelerated by small concentrations of DMSO because of increased transition state solvation, but by large DMSO concentrations due to reduced solvation of hydroxide ion. Transition state solvation is unlike that of the reactants, but resembles that expected for CCl_3^- ion.

JOHN R. JONES et RICHARD FUCHS. Can. J. Chem. **55**, 99 (1977).

L'addition de diméthylsulfoxyde dans l'eau augmente la vitesse d'ionisation, catalysée par les ions hydroxyles, du chloroforme; on a étudié cet effet d'accélération en termes de solvatation des réactifs et d'état de transition. On a aussi mesuré les enthalpies de solution du chloroforme dans l'eau, dans le DMSO et dans des mélanges des deux. A partir de ces données et à l'aide des enthalpies d'activation pour la détritiation du chloroforme et des enthalpies de transfert de l'ion hydroxyle de l'eau vers des mélanges aqueux de DMSO, on a calculé les enthalpies de l'état de transition du transfert. La réaction est accélérée par des faibles concentrations de DMSO parce qu'il y a augmentation dans la solvatation de l'état de transition; toutefois dans le cas de concentrations élevées de DMSO, l'accélération est due à une solvatation réduite de l'ion hydroxyle. La solvatation de l'état de transition ne ressemble pas à celle des réactifs mais ressemble plutôt à celle attendue pour l'ion CCl_3^-.

[Traduit par le journal]

Dimethyl sulfoxide – water mixtures containing a fixed concentration of hydroxide ions (usually 0.010 *M*) are finding increasing use in physical organic chemistry (1). Many reactions are greatly accelerated in such media (2) which have also been used to study the acidities of weak acids (3) and kinetic hydrogen isotope effects (4).

In analyzing the effects of changing the composition of the reaction medium on reaction rates it is necessary to be able to assess the importance of solvent – solute interactions. This can best be done by taking a reaction of well defined mechanism and varying the nature of the substrate. Unfortunately, in many kinds of chemical reactions there are severe limitations on the choice of substrate. This restriction probably applies less to the ionization of carbon acids than most other types of reaction and we have recently shown (5) how a carbonyl-activated carbon acid (D-α-methyl-α-phenylacetophenone) responds to changes in medium composition. Such an analysis requires enthalpies of activation in a series of dimethyl sulfoxide – water mixtures, and corresponding heats of solution for the substrate. The present paper is concerned with a different type of carbon acid (chloroform) for which data of the first kind are available (6). We have consequently measured heats of solution for chloroform in water, dimethyl sulfoxide, and mixtures of the two, as well as for deuteriated chloroform in a particular medium as it is implicit in the analysis of the data that the heats of solution are not subjected to isotope effects.

The hydroxide-catalysed rate of detritiation of chloroform in water has a value of 0.165 l mol^{-1} s^{-1}, somewhat higher than that observed

[1]Work at the University of Houston was supported by the Robert A. Welch Foundation Grant E-136.

for acetone (0.0024) (7) and acetophenone (0.0054) (8). This suggests a pK_a *ca.* 20, and on this basis the rate acceleration upon addition of dimethyl sulfoxide should, if expressed in terms of a log $k - H_-$ relationship (9), result in a slope of 0.4–0.45. The much higher value near unity (6) is unlike that of other carbon acids, and probably occurs because the process of ionization of chloroform is accompanied by little charge delocalization and solvent reorganization.

Experimental

Materials

Reagent grade dimethyl sulfoxide was purified by a previously reported procedure (10). Mixtures with deionized water were prepared by weight. Reagent grade chloroform (stabilized with 0.75% ethanol) was stored over 4A molecular sieves to remove water and ethanol. The dried chloroform was examined by gas chromatography (DC-710 on Chromosorb W). No remaining ethanol was found under conditions which will detect less than 0.1%. Deuteriated chloroform was commercially available and of 99.8% isotopic purity.

Calorimetry

The procedure employed was the same as that outlined previously (11). The accuracy of the ΔH_s measurements is ± 0.10 kcal mol^{-1} in water and the most highly aqueous solvent mixtures and ± 0.05 kcal mol^{-1} in the other solvents. The values of ΔH_s reported are averages of 3–6 determinations in the concentration range of 3–10 $\times$ 10^{-3} *M*. No effect of concentration on ΔH_s was observed.

Results and Discussion

The measured enthalpies of solution (ΔH_s) in water, dimethyl sulfoxide, and mixtures of the two solvents are listed in Table 1. These slowly increase until a maximum is reached at mole fraction DMSO of 0.17. The value of ΔH_s for deuteriated chloroform in a medium of mole fraction DMSO equal to 0.13 is, within experimental error, equal to that obtained for chloroform itself. It is reasonable to assume that the identity of values is carried over to the other solvent mixtures and to tritiated chloroform.

TABLE 1. Enthalpies of solution of chloroform in DMSO–water mixtures

χ_{DMSO}[a]	ΔH_s[b]	χ_{DMSO}[a]	ΔH_s[b]
0.000	1.08	0.171	1.98
0.027	1.12	0.203	1.86
0.059	1.36	0.236	1.75
0.090	1.59	0.330	1.19
0.130	1.81 (1.83)[c]	1.000	−2.04

[a]Mole fraction DMSO.
[b]In kcal mol^{-1}.
[c]Value for $CDCl_3$.

Single ion enthalpies of transfer (from water to DMSO–water mixtures) for hydroxide ion can be calculated using the extrathermodynamic assumption $\Delta H_{tr}(Ph_4P^+) = \Delta H_{tr}(Ph_4B^-)$ (11, 12). The absolute values of ΔH_{tr} for anions are dependent on the accuracy of the assumption, but the relative values of $\Delta H_{tr}(OH^-)$ and ΔH_{tr}^{ts} are independent of the assumption (12). The enthalpy of transfer of chloroform is obtained from the enthalpies of solution: $\Delta H_{tr} = \Delta H_s(S) - \Delta H_s(H_2O)$. The sum of the two enthalpies of transfer ($\sum\Delta H_{tr}$(reactants)) together with changes in the measured enthalpies of activation (6) ($\Delta H_{tr}^{\neq} = \Delta H^{\neq}(S) - \Delta H^{\neq}(H_2O)$) can be used to derive the transition state enthalpy of transfer for the ionization of chloroform $\Delta H_{tr}^{ts} = \sum\Delta H_{tr}$(reactants) + $\Delta H_{tr}^{\neq}$. The results (Table 2) indicate that in the more aqueous solvent mixtures (up to DMSO mole fraction 0.13) the enthalpies of transfer for chloroform and hydroxide ion are small, with both species being slightly better solvated than in water. Further increase in the concentration of dimethyl sulfoxide however brings about a considerable change, the hydroxide ion becoming increasingly desolvated and chloroform solvation remaining approximately constant. In other words the initial rate acceleration is brought about by increasing transition state solvation but subsequent rate increases arise mainly from hydroxide ion desolvation.

Although the results are not directly comparable with those for the ionization of D-α-methyl-α-phenylacetophenone (5) (where because of solubility difficulties mixtures of higher mole fraction dimethyl sulfoxide had to be used) it appears that the loss of transition state solvation with increasing DMSO concentration is smaller in chloroform ionization. Recent findings (13) on hydroxide-catalysed isotopic exchange of molecular deuterium indicate that the loss of transition state solvation with increasing [DMSO] approaches that of hydroxide ion. The dependence of enthalpies of transfer of the transition state on structure is to be expected, as has been well established for stable ions. In the ionization of chloroform the available evidence (5, 14) suggests that the transition state is very product-like ($\bar{C}Cl_3 \ldots \overset{+}{H}\bar{O}H$). It is interesting therefore that ΔH_{tr}^{ts} resembles ΔH_{tr} for the iodide ion (11) (Table 2) with the difference that at mole fractions dimethyl sulfoxide in excess of 0.13 the transition state values become less exothermic.

TABLE 2. Enthalpies of transfer[a] of reactants and transition state in the ionization of chloroform

χ_{DMSO}[b]	$\Delta H^{\neq}$[c]	$\Delta H_{tr}^{\neq}$	ΔH_{tr} (OH^-)[d]	$\Sigma\Delta H_{tr}$ (reactants)	ΔH_{tr}^{ts}	ΔH_{tr} (I^-)[e]
0.000	23.2	0.0	0.0	0.0	0.0	0.0
0.027	22.5	−0.7	−0.2	−0.2	−0.9	−0.6
0.059	21.6	−1.6	−0.6	−0.3	−1.9	−1.3
0.090	21.1	−2.1	−0.8	−0.3	−2.4	−1.7
0.130	20.2	−3.0	0.0	0.7	−2.3	−2.0
0.171	19.0	−4.2	2.2	3.1	−1.1	−1.8
0.203	18.0	−5.2	4.0	4.8	−0.4	−1.5
0.236	16.5	−6.7	5.4	6.1	−0.6	−1.3

[a]From water to indicated solvent, kcal mol^{-1}.
[b]Mole fraction DMSO.
[c]Reference 6.
[d]Reference 12.
[e]Reference 11.

This suggests that the transition state is a 'harder' anion than iodide, *i.e.* is less polarizable, with more localized charge and probably better solvated by water than dimethyl sulfoxide. This would be expected for a species resembling CCl_3^-.

The above analysis is based entirely on considerations of enthalpy changes. This would seem to be a good approximation as the results of Margolin and Long (14) show that the enthalpy of activation for the detritiation of chloroform decreases by 3 kcal mol^{-1} in going from water to a medium of mole fraction dimethyl sulfoxide 0.13 with but a small (3.4 eu) decrease in the entropy of activation. However, for media of still higher dimethyl sulfoxide content $\Delta S^{\neq}$ rapidly decreases. Consequently our interpretation of the results in these solutions is less firmly based.

1. E. BUNCEL and H. WILSON. Adv. Phys. Org. Chem. In press.
2. J. R. JONES. Progr. Phys. Org. Chem. **9**, 241 (1972).
3. D. DOLMAN and R. STEWART. Can. J. Chem. **45**, 911 (1967); D. W. EARLS, J. R. JONES, T. G. RUMNEY, and A. F. COCKERILL. J. Chem. Soc. Perkin II, 1806 (1974).
4. R. P. BELL and B. G. COX. J. Chem. Soc. (B), 176 (1970); D. W. EARLS, J. R. JONES, and T. G. RUMNEY. J. Chem. Soc. Faraday I, 925 (1972).
5. D. K. JAISWAL, J. R. JONES, and R. FUCHS. J. Chem. Soc. Perkin II, 103 (1976).
6. Z. MARGOLIN and F. A. LONG. J. Am. Chem. Soc. **95**, 2757 (1973).
7. J. R. JONES. Trans. Faraday Soc. **61**, 95 (1965).
8. J. R. JONES, R. E. MARKS, and S. C. SUBBA RAO. Trans. Faraday Soc. **63**, 111 (1967).
9. D. W. EARLS, J. R. JONES, T. G. RUMNEY, and A. F. COCKERILL. J. Chem. Soc. Perkin II, 1806 (1974).
10. R. FUCHS, J. L. BEAR, and R. F. RODEWALD. J. Am. Chem. Soc. **91**, 5797 (1969).
11. R. FUCHS and C. P. HAGAN. J. Phys. Chem. **77**, 1797 (1973).
12. R. FUCHS, C. P. HAGAN, and R. F. RODEWALD. J. Phys. Chem. **78**, 1509 (1974).
13. E. BUNCEL and E. A. SYMONS. J. Am. Chem. Soc. **97**, 656 (1976).
14. Z. MARGOLIN and F. A. LONG. J. Am. Chem. Soc. **94**, 5108 (1972).

Kinetic studies of Dakin oxidation of *o*- and *p*-hydroxyacetophenones[1]

M. B. HOCKING AND J. H. ONG

Department of Chemistry, University of Victoria, Victoria, B.C., Canada V8W 2Y2

Received May 20, 1976

M. B. HOCKING and J. H. ONG. Can. J. Chem. **55**, 102 (1977).

Rates of oxidation of aqueous *o*-, and *p*-hydroxyacetophenone with alkaline hydrogen peroxide to yield catechol and hydroquinone, respectively, have been followed spectrophotometrically. Both ketones showed smooth pseudo first-order behaviour, the *ortho* isomer yielding rate constants in the range 2.6 to 6.6 × 10^{-2} min^{-1} at 0 °C, and the *para* isomer of 0.73 to 7.10 × 10^{-2} min^{-1} at 35 °C for the concentrations of hydrogen peroxide and base used. The order in hydrogen peroxide was, unexpectedly, found to be 1.4. A simple test established that this fractional order was probably not the result of hydrogen peroxide involvement in simultaneous first- and second-order processes of differing rates. Other plausible pathways to explain this are proposed.

M. B. HOCKING et J. H. ONG. Can. J. Chem. **55**, 102 (1977).

L'oxydation, par le peroxyde d'hydrogène en solution alcaline aqueuse, de l'*ortho* et de la *para*-hydroxyacétophénone conduit au catéchol et à l'hydroquinone; on a déterminé les vitesses de ces réactions d'une façon spectrophotométrique. Les deux cétones présentent un comportement régulier du pseudo premier ordre, pour les concentrations de peroxyde d'hydrogène et de base utilisées, les constantes de vitesse de l'isomère *ortho* sont de l'ordre de 2.6 à 6.6 × 10^{-2} min^{-1} à 0 °C alors que celles de l'isomère *para* devient de 0.73 à 7.10 × 10^{-2} min^{-1} à 35 °C. On a trouvé d'une façon inattendue que l'ordre en peroxyde d'hydrogène est de 1.4. Un test simple a établi que cet ordre fractionnel n'est probablement pas dû à l'implication du peroxyde d'hydrogène dans des processus simultanés du premier et du second ordre de vitesse différentes. On propose d'autres chemins plausibles pour expliquer ces résultats.

[Traduit par le journal]

Introduction

Dakin oxidation (1) as a means to obtain a predictable variety of hydroxylated aromatic nuclei (**2**) from appropriate *ortho*- or *para*-hydroxylated aldehydes or ketones (**1**) has been known for many years (1) but no experimentally well-supported mechanism has yet been presented. The reaction path which is generally accepted (2, 3) as a plausible description of the process is given in Scheme 1. The ionic basis is founded on the resemblance of this reaction to the Baeyer–Villiger oxidation of bis-aromatic ketones **5** with peracids (4), which is experimentally well documented by evidence which includes isolated intermediates and rearrangement products.

These general conclusions may be made from the extensive mechanistic experiments concerning the Baeyer–Villiger reaction. The migratory aptitude is greatest for groups R or R′ best able to

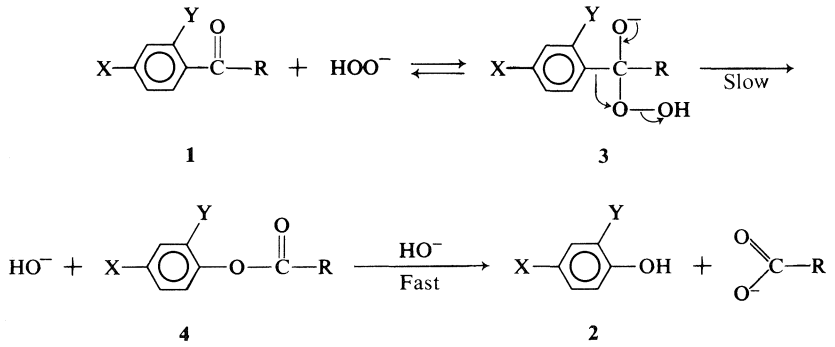

SCHEME 1

[1]Presented at the First Chemical Congress of the North American Continent, Mexico City, Nov. 30, 1975.

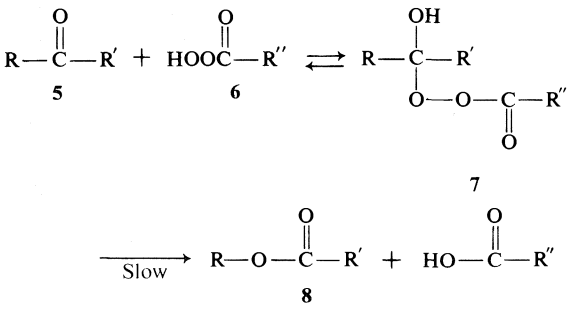

stabilize a positive charge (5–8), although vinyl (4, pp. 117 and 18; 9) and cyclopropyl (10) groups have been shown to migrate in preference to methyl. Migration proceeds with retention of configuration (11–13). ^{18}O labelling of the carbonyl carbon in the substrate **5** gives ^{18}O in the carbonyl of the ester **8** (14, 15). A migration cage **9** has been proposed for the group R (16), with a highly negative $\Delta S^{\ddagger}$ of -30 to -45 eu (5, 17–19), and it is accepted that no free (electron deficient) oxygen species or carbonium ion is

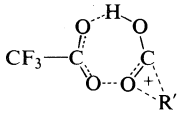

formed during the rearrangement process (16, 20). The collapse of **8** to products is acid-catalyzed and is the rate-determining step of the process (6).

That the initial step of Dakin oxidation is via nucleophilic attack of the ketone carbonyl by hydroperoxide anion is plausible and well accepted (2, 3, 21). The alkaline solution present has led to the adoption of hydroxyl ion as the leaving group coincident to migration. In contrast, the acidic solutions of Baeyer–Villiger oxidations involve departure of a carboxylate anion, which being a delocalized, 'softer' anion than hydroxide is much more acceptable as a leaving group than the highly localized hydroxyl ion, and specifically in this type of reaction (21, p. 120; 22, 23).

From a stereochemical point of view, as from leaving group considerations, there are contrasting aspects to the two processes. A hydroxyphenonium ion is the intermediate or transition state required by the currently held Dakin mechanism, which dictates phenolate migration with inversion of configuration. Unfortunately configurational changes cannot be observed with Dakin reaction substrates, but with the Baeyer–Villiger reaction where configurational changes are observable retention has been demonstrated, probably via a closely associated three-center transition state (24).

While a very strong electron-donating substituent such as OH (or $-O^-$) is required on the aromatic nucleus for Dakin oxidation to occur at all (25, 26), Baeyer–Villiger reactions have been shown to proceed with migration of acyl aromatic groups (24, pp. 242 and 243; 27).

With all these contrasting features, it is evident that the mechanism for the Dakin reaction cannot simply be adopted from an analogy with the Baeyer–Villiger oxidation, but to have any real hope of understanding must be experimentally examined using the conditions required for the Dakin reaction itself.

Experimental

Melting points were determined at calibration immersions using thermometers calibrated against National Bureau of Standards thermometers. Melting points and boiling points are not corrected. Ultraviolet spectra were obtained on a Cary Model 17 spectrophotometer at room temperature and nmr spectra on a Perkin-Elmer R12A spectrometer at 37 °C. p*H* measurements were taken using a Fisher Accumet Model 310 p*H* meter calibrated at measuring temperature in p*H* 11.10 buffer using a high p*H* electrode (type H5586-1, Canlab).

Materials

Commercial *p*-hydroxyacetophenone was purified by recrystallization from water followed by sublimation at 160 °C/0.5 torr, white crystals mp 109–110 °C (lit. (28) mp 109–110 °C). The cut of redistilled *o*-hydroxyacetophenone used boiled at 120–122 °C/15 torr (lit. (29) bp 106–107 °C/17 torr) and was a pale yellow oil which gave only one peak on glc 25% SE 30 on Chromosorb G, AW-DMCS, column temperature 115 °C. All inorganic salts, ethylenediamine tetraacetic acid (EDTA), and hydrogen peroxide used were reagent grade materials. The strength of the initial batch of 30% hydrogen peroxide was accurately determined by titration (30) to be 9.62 *M*, about 1% above labelled, and the strength was periodically checked both during use and on changing to a new lot number. Hydrogen peroxide was briefly sparged with nitrogen before use. Quadruply distilled water, the second stage from alkaline $KMnO_4$ in Pyrex and the third and fourth stages from quartz ware (conductance 0.8×10^{-6} S), purged with nitrogen (to avoid radical interference from dissolved oxygen) was employed in the kinetic runs.

Hydroquinone monoacetate was prepared by acetylation of hydroquinone with acetic anhydride in aqueous sodium carbonate at 0 °C according to the method of Olcott and incorporating the improvements of Bunton and Hellyer (31). When the reaction was complete, diester was filtered off and the filtrate was extracted with ether. The ether extracts were dried (Na_2SO_4) and the ether evaporated. The residual solid obtained gave a low

yield of monoester on trituration with 60–90 °C petroleum ether (PE). Recrystallization several times from 60–90 °C PE yielded colourless plates mp 57–59 °C (lit. (31) mp 62–63 °C); 60 MHz nmr (37 °C, CCl_4, internal TMS) δ 2.21 (s, 3H), 7.60 (d, 4H), 5.75 (br s, 1 H), *m/e* 152 (m^+) was observed.

Competitive Oxidation/Hydrolyses

The oxidation of *p*-hydroxyacetophenone (136 mg; 1 mmol) in 2.6 ml of 0.375 *M* sodium hydroxide in water, with 214 mg of 30% hydrogen peroxide at 37 °C was followed by the loss of the ketone methyl and the appearance of acetate ion methyl in repetitive nmr spectra. No other methyl was observed.

p-Hydroxyacetophenone (136 mg) was then oxidized competitively while hydroquinone monoacetate (152 mg; 1 mmol) was hydrolyzed in 5.2 ml of 0.375 *M* sodium hydroxide in water with the addition of 214 mg of 30% hydrogen peroxide. By nmr, the relative changes in peak height *vs.* time, which had previously been checked by integration and found to be a reliable measure of concentration at the scanning rates used, were recorded (Table 1).

Alternate Oxidizing Agents

tert-Butylhydroperoxide reacted only very slowly with *p*-hydroxyacetophenone in dilute aqueous sodium hydroxide or sodium hydroxide – sodium acetate at room temperature so that proton nmr examination at intervals during 2 days showed only *tert*-butylhydroperoxide methyl and acetyl methyl protons, with only a trace of *tert*-butanol and acetate ion. Heating the same initial compositions 3 days at 85 °C still gave only a small acetate ion peak, even though small amounts of acetone (32) and *tert*-butanol were produced.

Hydrogen disulfide (33) could not be induced to react with *p*-hydroxyacetophenone in 0.2 *M* Na_3PO_4 in water at room temperature or on heating at 60 °C for 5 h, when monitored in the same way as the *tert*-butylhydroperoxide experiments.

Kinetic Preliminaries

Buffer selection was guided by the 11.65 pK_a of hydrogen peroxide at 25 °C (34) together with the requirement of a high hydroperoxide anion concentration. Solutions of 2.5 g of sodium and potassium carbonates or phosphates in 50 ml of water gave p*H* readings at 20 °C of 11.8 and 12.6 for the change in anion, and each dropped 0.05, 0.04, 0.04, and 0.03 p*H* units for each 10 ml addition of water. Addition of hydrogen peroxide to these solutions showed noticeable spontaneous peroxide decomposition, probably from traces of iron or manganese in the buffer salts. This could not be cured by use of the highest purity reagents available, by adsorptive pretreatment of the solutions with MgO, or by solution passage through 'Chelex 100' chelating resin[2] (35), and could only be reduced somewhat by the addition of small amounts of the standard peroxide stabilizers Na_2SnO_3, $Na_4P_2O_7$, or 8-hydroxyquinoline. It could, however, be prevented for a period of 2 h or more by the addition of 20–30 mg of EDTA.

Using proton nmr to follow directly ketone loss during the reaction failed because the initial concentrations required for analysis were sufficiently high that the temperature could not be held constant. Gravimetric determinations by either bromination or lead salt formation were insufficiently reproducible and were tedious. Gas–liquid chromatographic determination of ketone directly from the aqueous reaction solutions using a flame ionization detector gave problems with time measurement and was less accurate than uv. Ultraviolet determination of the ketone directly from the aqueous kinetic solutions was not possible because of interference by broad buffer absorption, but three extractions with chloroform of acidified blank samples saturated with NaCl gave quantitative recovery of ketone for absorbance measurement without interference.

TABLE 1. Relative aqueous oxidation/hydrolysis rates of *p*-hydroxyacetophenone and hydroquinone monoacetate by proton nmr

	Methyl proton peak heights (mm)*		
Time (min)	Ketone (δ 2.95 ppm)	Ester (δ 2.68 ppm)	Acetate ion (δ 2.32 ppm)
0	45	45	0
1	10	21	59
2	8	22	60
6	5	22	63
20	6	23	61
1000	5	13	72

*Normalized to constant total methyl integral. Shifts reported from external neat TMS.

Kinetic Runs

For a typical run a solution of 1–3 × 10^{-4} mol of the hydroxyacetophenone, 2.5 g of Na_2CO_3 or $Na_3PO_4 \cdot 12H_2O$, and ~10^{-5} mol EDTA in 40 ml H_2O in an alkaline hydrogen peroxide pretreated (30) new polyethylene flask, was equilibrated in a thermostatted water bath. To this was added 10 ml of previously thermally-equilibrated 30% hydrogen peroxide, usually corresponding to more than 100× excess. To follow the progress of the reaction, 5 ml aliquots of the reaction solution were transferred to 25 ml glass vials and were then rapidly chilled in a dry ice – acetone bath and acidified to p*H* 1 with HCl or $HClO_4$ (*p*- and *o*-ketone respectively), which effectively stopped the reaction. In this way, duplicate experimental samples extracted and analyzed immediately or after up to 2 h refrigerated storage gave agreement of ketone concentrations within 1.0%.

Quenching by sparging with SO_2 or addition of sodium sulfite was found to be too slow acting and produced significant heat. It was also a procedure which did not allow monitoring of peroxide disappearance.

For runs with *p*-hydroxyacetophenone, the chloroform extracts of the chilled acidified and salted aliquots were scanned in the region of 268 nm (λ_{max} for the ketone) to follow the loss in optical density and to determine the rate of ketone loss (*e.g.* Table 2). Product hydroquinone was further oxidized under the reaction conditions used, and did not interfere spectrophotometrically. Duplicate samples from a single run were reproducible in ketone concentrations to within 0.5%, and pseudo first-order rate constants of whole kinetic runs were reproducible to better than 1% (Table 1).

For runs with *o*-hydroxyacetophenone, aliquots satu-

[2]Purchased from Bio-Rad Laboratories (Canada) Ltd., Mississauga, Ontario.

TABLE 2. Absorbance readings for oxidation of 21 mg *p*-hydroxyacetophenone with buffered* 1.35 *M* hydrogen peroxide at 35 °C (run 5, Table 3)

Time elapsed (min)	Absorbance $CHCl_3$ extracts
0	0.5765
5	0.4710
10	0.3900
15	0.3113
20	0.2506
25	0.2000
30	0.1570
35	0.1276
40	0.10325

*Na_2CO_3 (2.500 g) in total solution volume of 50 ml, p*H* before H_2O_2 addition = 11.8.

rated with NaCl generated a yellow colour which, it was suspected, might interfere with the ketone analysis; therefore, the chilled aliquots were simply extracted with chloroform to recover unreacted ketone and the loss of optical density of the peak at 253 nm was followed. Blank tests with known amounts of ketone established that the extraction procedure was quantitative and reproducible without salting. Catechol, the oxidation product was relatively stable under the extraction conditions at 0 °C and was seen in the $CHCl_3$ phase by a peak at λ_{max} 277.5 nm and a shoulder at 282.5 nm. Its presence did not interfere with the ketone determination. In this way duplicate sample runs gave pseudo first-order rate constants reproducible to better than 4% for $1\frac{1}{2}$ half-lives, and better than 6% for whole kinetic runs.

Hydrogen peroxide concentration and p*H* were monitored during the course of several of the kinetic runs and neither changed significantly. For hydrogen peroxide typical results, when oxidizing *p*-hydroxyacetophenone (41.3 mg) titres of 10 ml of 30% H_2O_2 (reaction concentration, 1.92 *M*) in 0.13 *M* Na_3PO_4 (40 ml) KI/thiosulfate (0.0994 *M*) with aliquots taken initially and after 15, 75, and 135 min, were 9.92; 10.10, 9.98 (duplicate); 9.96; and 9.69, 9.92 ml (duplicate), respectively. While nitrogen purging of the water used and brief nitrogen sparging of the hydrogen peroxide eliminated any significant interference of oxygen-induced radical formation in the initial rates, in prolonged runs a rate enhancement occurred when spontaneous peroxide decomposition was observed.

Results and Discussion

Kinetic study of any system comprising substituted phenols and hydrogen peroxide has to contend with the formation of phenoxy radicals and secondary products, either of which may interfere. This may be minimized, allowing useful kinetic interpretation if the reaction being studied is fast and only the 'initial rate' data are considered. Experiments aimed at reducing this type of interference here by use of the alternative oxidizing agents *tert*-butylhydroperoxide and hydrogen disulfide only succeeded in generating small amounts of *tert*-butanol and acetone (a rearrangement product (32)) from the former and no reaction with the latter.

With the proper choice of buffer, absolute and relative concentrations, and temperature oxidation of *p*-hydroxyacetophenone with alkaline hydrogen peroxide was kinetically well-behaved yielding smooth concentration *vs.* time curves. From these, an initial rate test using the general expression $dx/dt = k[\text{ketone}]^n$ gave 0.971 for the order of the reaction, *n* (first 10 min). Runs 1 and 2 (Table 3) followed through $2\frac{1}{2}$ half-lives gave pseudo first-order rate constants of 7.10×10^{-2} min^{-1} and 7.14×10^{-2} min^{-1}, agreement to within 0.6% and also, from the different initial ketone concentration, confirmation of first-order behaviour with respect to ketone. Even to $4\frac{1}{2}$–5 half-lives, the rate constants for the same runs showed less than 7% deviation from each other, kinetically very predictable behaviour (Fig. 1), but the first-order plots became slightly concave-down curves.

A decrease in the initial peroxide concentration in order to determine the effect on rate accentuated the concavity observed in the later stages of runs 1 and 2 (see Table 3, runs 4 and 5).

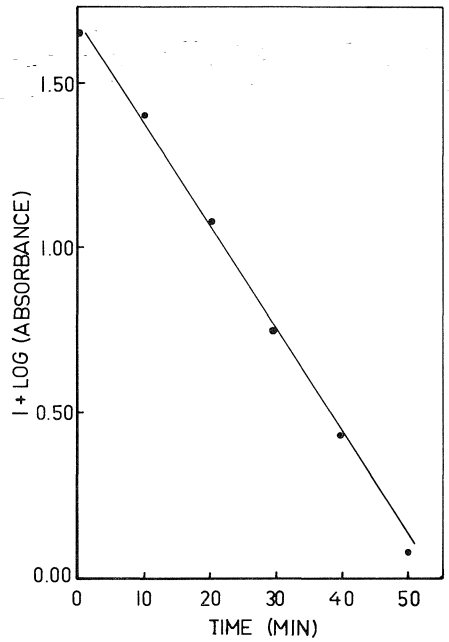

FIG. 1. Loss of *p*-hydroxyacetophenone with time, when oxidized with hydrogen peroxide in the presence of Na_2CO_3, $LiNO_3$, and EDTA at 35 °C (run 2, Table 3).

TABLE 3. Pseudo first-order rate constants for the oxidation of *p*-hydroxyacetophenone* at 35 °C

Run No.	$[H_2O_2]$ (M)†	[*p*-Ketone] ($M \times 10^3$)	Reaction time (min)	No. of half-lives for calc. k	k ($min^{-1} \times 10^2$)	$t_{1/2}$ (min)
1‡	1.923	2.938	30	2.5	7.10	9.76
1‡	1.923	2.938	50	>5	7.37	9.40
2‡	1.923	7.344	25	2.5	7.14	9.70
2‡	1.923	7.344	40	4.5	7.84	8.80
3	1.923	3.966	25	2.5	6.55	10.58
3	1.923	3.966	40	4	6.94	9.98
4	0.962	3.085	40§	1.5	2.62	26.4
5	1.346	3.085	40	>2.5	4.35	15.9
5	1.346	3.085	35	>2	4.40	15.7
6	0.385	2.023	60	0.67	0.73	94.6

*Oxidized in 0.4630 M Na_2CO_3 (2.50 g Na_2CO_3 in 40+ ml of water, plus reagents tabulated, giving in all cases a total solution volume of 50 ml). pH before H_2O_2 addition = 11.8.
†Solutions with 1.923 and 0.962 M H_2O_2 present gave pH readings of 9.9 and 10.5 respectively.
‡$LiNO_3$ (250 mg, 0.0725 M) was also present in these runs as part of salt effect study.
§Reaction followed for 70 min but curvature was evident in kinetic plots at times greater than shown (see Experimental and Discussion).

While the rate of initial ketone loss with time was slower for smaller (~41:1 $[H_2O_2]$:[*p*-ketone]) excesses of hydrogen peroxide present, this initial rate was found to increase as the run progressed, possibly an indication of kinetic influence by the products of the reaction. The more than 100 molar excess of hydrogen peroxide normally used was probably instrumental in oxidizing the initial product (hydroquinone) before it could exert kinetic influence in most runs.

The much more significant result emerging when the hydrogen peroxide concentration was varied was that the pseudo first-order rate constant obeyed the relation $k_{obs} = k[H_2O_2]^{1.4}$ (Fig. 2), where $k = 2.82 \times 10^{-3}$ min^{-1} $mol^{-1.4}$. Thus, the Dakin oxidation is clearly not first-order in hydrogen peroxide. The mechanism currently accepted requires at least some modification to yield an acceptable pathway consistent with this.

If the Dakin reaction is assumed to proceed via a purely ionic route, Scheme 2 is one way in which the observed order in hydrogen peroxide may be rationalized. Hydroperoxide anion attack on the carbonyl carbon of **10** is straightforward (20, p. 218; 36), and the process of peroxy anion displacement by **11** has been invoked for *p*-cyanobenzoic acid hydrolysis in the presence of hydrogen peroxide, with the comment it is expected that this type of process "... will increase in importance... at higher pH values". (37). Hydrotrioxide intermediates like **12** have also been observed, for example benzaldehyde hydrotrioxide has been shown to have a half-life

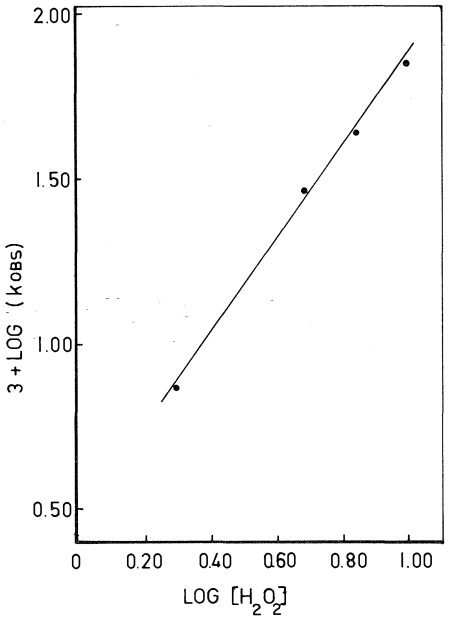

FIG. 2. Order in hydrogen peroxide from Dakin oxidation of *p*-hydroxyacetophenone at 35 °C.

of 400 s at 12 °C (38). For more than a first-order dependence on hydrogen peroxide, hydrotrioxide decomposition must be the slow step of the sequence.

Theoretical considerations too support the proposed pathway. A readily polarizable hydroperoxide anion (39) presents a more energetically favourable leaving group (38) to the hydrotrioxide intermediate **12**, than hydroxide

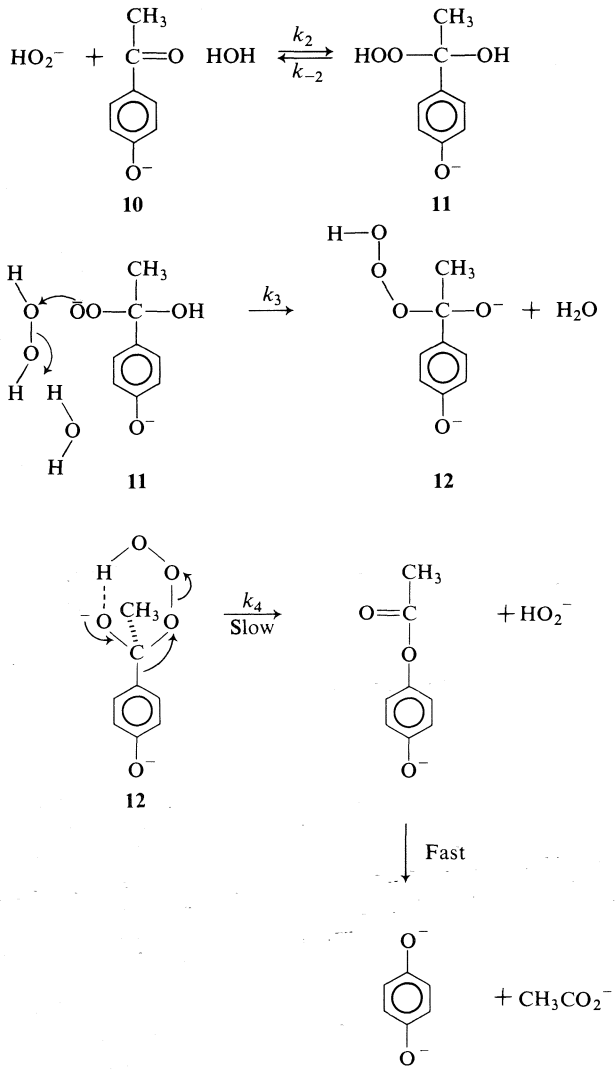

SCHEME 2. Proposed pathway to incorporate $[H_2O_2]$[1,4] in Dakin oxidation kinetics

$$H_2O_2 + B \underset{k_{-1}}{\overset{k_1}{\rightleftharpoons}} HO_2^- + HB$$

ion does to the alternative intermediate **3**. Also, the much less stable hydrotrioxide intermediate **12** favours significant progression of hydroperoxide anion departure prior to phenyl migration, facilitating the slow step of the reaction.

Even though mildly alkaline competitive oxidation/hydrolyses could be readily followed (Table 1), final step ester hydrolysis under the kinetic reaction conditions was found to be extremely fast. At 35 °C, by nmr, using 0.1 to 0.5 *M* buffer concentrations, the ester was completely hydrolyzed before it could be placed in the spectrometer. The possibility of mechanistic ester intermediacy in the Dakin reaction, therefore, could not be ruled out.

From the slow step of the sequence

$$\text{Rate} = k_4\,[\mathbf{12}]$$

and invoking a series of pre-equilibria between starting ketone and **12**, this becomes

$$\text{Rate} = \frac{k_4 k_3 k_2 k_1}{k_{-3} k_{-2} k_{-1}} [H_2O_2]^2[\mathbf{10}]\frac{[B]}{[BH]}$$

TABLE 4. Effect of temperature on the rates of oxidation of *p*-hydroxyacetophenone*

[*p*-Hydroxyacetophenone] ($M \times 10^3$)	Temperature (°C)	Reaction time (min)	k (min^{-1})
3.966	40	20	0.017
3.231	35	45	0.012
4.99	25	50	0.0046

*Runs in 50 ml total solution volume, 1.923 M in H_2O_2 (10 ml; 30%) and 0.1316 M in Na_3PO_4. pH was 12.6 prior to H_2O_2 addition, and 10.1 subsequently. Calculated values from data: E_{act} = 65.7 kJ/mol (15.7 kcal/mol); $\Delta S^{\ddagger}$ = −16.3 eu.

TABLE 5. Observed rates of oxidation of *o*-hydroxyacetophenone with hydrogen peroxide in water at 0 °C

Run No.*	[H_2O_2] (M)	[*o*-Ketone] ($M \times 10^3$)	Reaction time (min)	k ($min^{-1} \times 10^2$)	$t_{1/2}$ (min)
1†	1.923	7.344	20	6.6	10.5
2	0.962	5.875	35	5.1	13.0
3‡	0.481	11.75	15	2.6	26.0
p-Ketone	1.923			0.037§	

*Each run in 50 ml total solution volume, buffered by 0.1316 M Na_3PO_4. pH = 12.6 before H_2O_2 addition.
†10 ml 30% H_2O_2 present, pH = 10.1.
‡5 ml 30% H_2O_2 present, pH = 10.7.
§Value calculated for this temperature from the three values experimentally determined at higher temperatures.

This simplifies to

$$\text{Rate} = k'[H_2O_2]^2[\mathbf{10}]\frac{[B]}{[BH]}$$

where

$$k' = \frac{k_4k_3k_2k_1}{k_{-3}k_{-2}k_{-1}}$$

For a constant [B]/[BH],

$$\text{Rate} = k''[H_2O_2]^2\,[\mathbf{10}],$$

where $k'' = k'[B]/[BH]$. With a large excess of hydrogen peroxide

$$\text{Rate} = k_{obs}\,[\mathbf{10}]$$

where $k_{obs} = k''[H_2O_2]^2$ and is the pseudo first-order rate constant with respect to ketone experimentally observed.

The possibility that the fractional order in hydrogen peroxide might be the consequence of competing reactions involving terms first-order and second-order in hydrogen peroxide was examined by letting $k_{obs} = k_x[H_2O_2] + k_y[H_2O_2]^2$. Rearranging, this gives

$$\frac{k_{obs}}{[H_2O_2]} = k_x + k_y[H_2O_2]$$

Plotting the data on coordinates [H_2O_2] *vs.* $k_{obs}/[H_2O_2]$ gave a scatter diagram, suggesting that this was not the explanation for the observed fractional order in hydrogen peroxide. Kinetic information from the *p*-ketone was insufficient to permit further speculation on the reason for this fractional order.

The enthalpy of activation for the oxidation of *p*-hydroxyacetophenone calculated from observed rates at 40, 35, and 25 °C (Table 4), was 65.7 kJ/mol (15.7 kcal/mol) and the entropy change, −16.3 eu. While these values are not readily interpreted mechanistically (22, p. 121; 40) they fall between the values for nucleophilic displacement of iodide from methyl iodide, $\Delta S^{\ddagger} = -10$ eu, and the more crowded neopentyl iodide, $\Delta S^{\ddagger} = -20$ eu (41).

o-Hydroxyacetophenone was found to oxidize about 180 times faster than the *p*-isomer (Table 5), which required decreasing the reaction temperature to 0 °C to allow the same kinetic methods to be used. Similarly faster *ortho* than *para* ketone oxidation has been observed for chloramine oxidation of hydroxyacetophenones (42), and for the Baeyer–Villiger oxidation of nitroacetophenones (24).

For a large excess of hydrogen peroxide, good pseudo first-order plots were obtained for the rate of disappearance of *o*-hydroxyacetophenone up to 2–3 half-lives. However, decreasing the

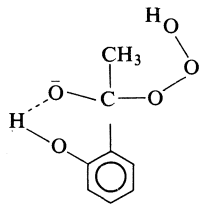

13

initial hydrogen peroxide concentration gave a more significant deviation from first-order linearity than seen for the *p*-ketone. Since catechol is not nearly as readily oxidized as hydroquinone under these conditions,[3] and since it has been found to be catalytically active for oxidations with hydrogen peroxide (43), it is possible that catechol or its oxidation products were responsible for the more significant kinetic interference found with the *o*-ketone.

o-Hydroxyacetophenone is more susceptible to hydroperoxide anion attack than *para* because of intramolecular hydrogen bonding. For the phenyl migration step, the phenonium ion requires the phenyl group to be perpendicular to the bond between the migration origin and the migration terminus (44) requiring rupture of the hydrogen bond in **13**, and consequent loss of stabilization energy of the order of 5 kcal (45) in the process. Thus, if phenyl migration was the rate determining step, the *ortho* isomer would be expected to react more slowly than the *para*.

Because *o*-hydroxyacetophenone was found to react faster than the *para* isomer possibly a variant of Scheme 2 operates to account for this, or other alternatives may be operating for both ketones. A spirocyclic epoxide intermediate (46) (Scheme 3) or a resonance-stabilized phenolate radical intermediate (Scheme 4), such as has been invoked by Kratzl for air oxidation of phenols in the presence of amine–copper complexes (47), are other less likely possibilities under consideration. Further synthetic and electron spin resonance experiments are underway to attempt to identify and isolate if possible, key intermediates in this system to better establish the pathway involved.

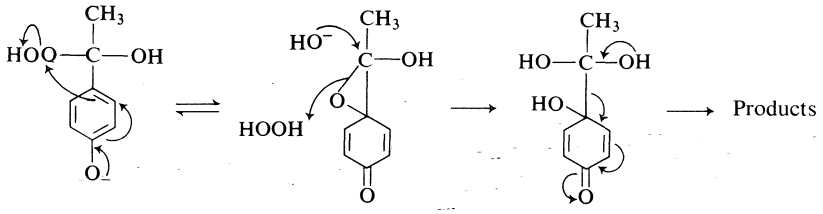

SCHEME 3. Proposed involvement of a spirocyclic epoxide intermediate in Dakin oxidation.

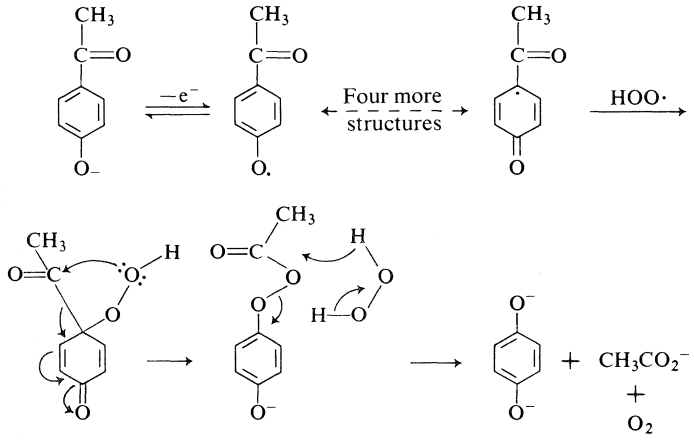

SCHEME 4. Suggested involvement of a phenolate radical intermediate in Dakin oxidation.

[3]M. B. Hocking, unpublished results.

Acknowledgements

The authors are grateful to the National Research Council of Canada and the University of Victoria for financial support of this work.

1. H. D. DAKIN. Am. Chem. J. **42**, 477 (1909).
2. C. A. BUNTON. *In* Peroxide reaction mechanisms. *Edited by* J. O. Edwards. Interscience Publishers, New York. 1962. p. 14.
3. J. B. LEE and B. C. UFF. Q. Rev. (London), **21**, 429 (1967).
4. H. O. HOUSE. Modern synthetic reactions. W. A. Benjamin, Inc., New York. 1965. p. 123.
5. S. L. FRIESS and A. H. SOLOWAY. J. Am. Chem. Soc. **73**, 3968 (1951).
6. M. F. HAWTHORNE, W. D. EMMONS, and K. S. MCCALLUM. J. Am. Chem. Soc. **80**, 6393 (1958).
7. S. L. FRIESS and N. FARNHAM. J. Am. Chem. Soc. **72**, 5518 (1950).
8. W. VON E. DOERING and L. SPEERS. J. Am. Chem. Soc. **72**, 5515 (1950).
9. H. M. WALTON. J. Org. Chem. **22**, 1161 (1957).
10. W. D. EMMONS and G. B. LUCAS. J. Am. Chem. Soc. **77**, 2287 (1955).
11. K. MISLOW and J. BRENNER. J. Am. Chem. Soc. **75**, 2318 (1953).
12. R. B. TURNER. J. Am. Chem. Soc. **72**, 878 (1950).
13. T. F. GALLAGHER and T. H. KRITCHEVSKY. J. Am. Chem. Soc. **72**, 882 (1950).
14. W. VON E. DOERING and E. DORFMAN. J. Am. Chem. Soc. **75**, 5595 (1953).
15. C. A. BUNTON, T. A. LEWIS, and D. R. LLEWELLYN. J. Chem. Soc. 1226 (1956).
16. YA. K. SYRKIN and I. I. MOISEEV. Usp. Khim. 425 (1960); Russ. Chem. Rev. **27**, 193 (1960).
17. S. L. FRIESS and R. PINSON, JR. J. Am. Chem. Soc. **74**, 1302 (1952).
18. S. L. FRIESS and P. E. FRANKENBURG. J. Am. Chem. Soc. **74**, 2679 (1952).
19. J. C. WRIGHT, A. FRY. At the South West Regional Meeting, Am. Chem. Soc. 1967, reported in Chem. Eng. News, **46**, 28 (1968).
20. R. CURCI and J. O. EDWARDS. *In* Organic peroxides. Vol. 1. *Edited by* D. Swern. Wiley–Interscience, Toronto. 1970. p. 242.
21. R. STEWART. Oxidation mechanisms, applications to organic chemistry. W. A. Benjamin Inc., New York. 1964. p. 31.
22. K. M. IBNE-RASA and J. O. EDWARDS. J. Am. Chem. Soc. **84**, 763 (1962).
23. S. N. LEWIS. *In* Oxidation, techniques and applications in organic synthesis. *Edited by* R. L. Augustine. Marcel Dekker, New York. 1969. p. 237.
24. E. E. SMISSMAN, J. P. LI, and Z. H. ISRAILI. J. Org. Chem. **33**, 4231 (1968).
25. J. PLIML. Chemie (Prague), **10**, 647 (1958).
26. M. HUDLICKY. Chem. Listy, **46**, 567 (1952). Chem. Abstr. **46**, 11104d (1952).
27. L. J. CHIN. Selection of oxidants in synthesis, oxidation at the carbon atom. Marcel Dekker, New York. 1971. p. 119.
28. R. C. WEAST (*editor*). Handbook of Chemistry and Physics. 51st ed. The Chemical Rubber Publishing Co., Cleveland. 1970. p. C-94.
29. K. VON AUWERS. Justus Liebigs Ann. Chem. **408**, 245 (1915).
30. M. B. HOCKING. Can. J. Chem. **51**, 2384 (1973).
31. H. S. OLCOTT. J. Am. Chem. Soc. **59**, 392 (1937); C. A. BUNTON and J. HELLYER. J. Am. Chem. Soc. **89**, 6252 (1967).
32. M. S. KHARASCH, A. FONO, and W. NUDENBERG. J. Org. Chem. **15**, 763 (1950).
33. E. MULLER and J. B. HYNE. Can. J. Chem. **46**, 2341 (1968); T. WIEWIOROWSKI. Endeavour, **29**, 9 (1970).
34. W. C. SCHUMB, C. N. SATTERFIELD, and R. L. WENTWORTH. Hydrogen peroxide. Reinhold Publishing Corp., New York. 1955. p. 393.
35. G. SHMUCKLER. Talanta, **12**, 281 (1965).
36. J. O. EDWARDS. *In* Peroxide reaction mechanisms. *Edited by* J. O. Edwards. Interscience Publishers, New York. 1962. p. 14.
37. J. E. MCISAAC, JR., R. E. BALL, and E. J. BEHRMAN. J. Org. Chem. **36**, 3048 (1971).
38. F. E. STARY, D. E. EMGE, and R. W. MURRAY. J. Am. Chem. Soc. **96**, 5671 (1974).
39. R. CURCI and J. O. EDWARDS. *In* Peroxide reaction mechanisms. *Edited by* J. O. Edwards. Interscience Publishers, New York. 1962. pp. 248, 249.
40. W. F. SLIWINSKI, T. M. SU, and P. v. R. SCHLEYER. J. Am. Chem. Soc. **94**, 133 (1972).
41. J. A. HIRSCH. Concepts in theoretical organic chemistry. Allyn and Bacon, Inc., Boston. 1974. p. 124.
42. R. A. CROCHET, F. R. SULLIVAN, and P. KOVACIC. J. Org. Chem. **39**, 3094 (1974).
43. G. A. HAMILTON, J. W. HANIFIN, JR., and J. P. FRIEDMAN. J. Am. Chem. Soc. **88**, 5629 (1966).
44. C. D. GUTSCHE and D. J. PASTO. Fundamentals of organic chemistry. Prentice-Hall, Inc., Englewood Cliffs. 1975. p. 1045.
45. E. S. GOULD. Mechanism and structure in organic chemistry. Henry Holt and Co., New York. 1959. p. 575.
46. M. S. NEWMAN. Acc. Chem. Res. **7**, 85 (1974).
47. K. KRATZL, W. SCHÄFER, P. CLAUS, J. GRATZL, and P. SCHILLING. Monatsh. Chem. A, **98**, 891 (1967).

X-Ray structure of tris(acetonitrile)tricarbonylrhenium(I) tetrafluoroborate

LILLIAN Y. Y. CHAN, E. E. ISAACS, AND W. A. G. GRAHAM
Department of Chemistry, University of Alberta, Edmonton, Alta., Canada T6G 2E1

Received July 21, 1976

LILLIAN Y. Y. CHAN, E. E. ISAACS, and W. A. G. GRAHAM. Can. J. Chem. **55**, 111 (1977).

Reaction of $[n\text{-}Bu_4N]_2[Re_4(CO)_{16}]$ with $AgBF_4$ in acetonitrile affords the compound $[(CH_3CN)_3Re(CO)_3][BF_4]$. The latter crystallizes in monoclinic space group $P2_1/c$ with unit cell dimensions $a = 11.021(5)$ Å, $b = 11.136(5)$ Å, $c = 12.980(6)$ Å, $\beta = 96.906(25)°$, and four molecules per unit cell. Data were collected by counter methods and the structure was refined using least-squares procedures to give $R = 0.041$. The rhenium cation is approximately octahedrally coordinated by six facially arranged ligands. The mean rhenium–nitrogen distance is 2.13 Å, and the mean rhenium–nitrogen–carbon angle in the coordinated acetonitrile is 174.7°.

LILLIAN Y. Y. CHAN, E. E. ISAACS et W. A. G. GRAHAM. Can. J. Chem. **55**, 111 (1977).

La réaction de $[n\text{-}Bu_4N]_2[Re(CO)_{16}]$ avec $AgBF_4$ dans l'acétonitrile conduit à un composé $[(CH_3CN)_3Re(CO)_3][BF_4]$. Ce dernier cristallise sous forme monoclinique avec un groupe d'espace $P2_1/c$ avec des dimensions de maille $a = 11.021(5)$ Å, $b = 11.136(5)$ Å, $c = 12.980(6)$ Å, $\beta = 96.906(25)°$ et il y a quatre molécules par maille. On a récolté les données par la méthode des compteurs et la structure a été affinée par la méthode des moindres carrés jusqu'à une valeur de $R = 0.041$. Le cation rhénium est coordonné approximativement d'une façon octaédrique par six ligands arrangés d'une façon faciale. La distance moyenne rhénium/azote est de 2.13 Å et l'angle moyen rhénium–azote–carbone dans l'acétonitrile coordonné est de 174.7°.

(Traduit par le journal]

Introduction

A number of polynuclear rhenium carbonyl anions are known through the work of Kaesz and co-workers (1–3). The electrochemistry of these species has been little investigated and it seemed to us that the oxidation of the tetranuclear anion $[Re_4(CO)_{16}]^{2-}$ (1) might lead to the formation, via rhenium–rhenium bond formation, of new neutral polynuclear carbonyls of rhenium. However, this expectation was not fulfilled under the conditions of our experiments. Using silver tetrafluoroborate in acetonitrile, the product was $[(CH_3CN)_3Re(CO)_3][BF_4]$. We describe here this unexpected reaction, and, more importantly, the crystal structure of the product.

Experimental

Preparation of $[(CH_3CN)_3Re(CO)_3][BF_4]$

To 10 ml of an acetonitrile solution of $[n\text{-}Bu_4N]_2[Re_4(CO)_{16}]$ (1) (0.25 g, 0.15 mmol), $AgBF_4$ (0.8 g, 5.1 mmol) was added and the mixture stirred for 24 h. The initial red color was lost as the solution became colorless with the deposition of Ag metal. The solution was filtered through Celite and the solvent removed *in vacuo*. The brown residue was washed with several portions of water and then dried by pumping overnight. Two recrystallizations from dichloromethane–heptane afforded 0.2 g (58% yield) of product. *Anal.* calcd. for $C_9H_9N_3O_3ReBF_4$: C 22.50, H 1.89, N 8.75; found: C 22.56, H 2.14, N 8.49; mp 171–173 °C.

The conductivity measurement performed on a 3.5×10^{-3} *M* nitromethane solution gave a value of 104.5 ohm^{-1} cm^2 mol^{-1}.

The crystals for the X-ray determination were obtained by slow recrystallization from acetone–ethanol.

Crystal Structure

Preliminary X-ray studies of single crystals of the compound with Weissenberg and precession photographs showed the systematic absences *h0l*, $l = 2n + 1$, and *0k0*, $k = 2n + 1$, which indicate the monoclinic space group $P2_1/c$. A single crystal was ground to a sphere (diameter 0.155 mm) for diffractometer use. The lattice parameters and their estimated standard deviations were obtained at 22 °C as $a = 11.021(5)$ Å, $b = 11.136(5)$ Å, $c = 12.980(6)$ Å, and $\beta = 96.906(25)°$, by a least-squares refinement using 2θ values for 12 high-angle reflections that had been accurately centered on a Picker automatic FACS 1 diffractometer (Mo $K_{\alpha 1}$ radiation, $\lambda = 0.70926$ Å). The observed density by flotation is 2.03 g cm^{-3}, in good agreement with that calculated, 2.02 g cm^{-3}, for four molecules per unit cell.

Intensity data were collected using graphite monochromated Mo K_α radiation ($\mu = 82.20$ cm^{-1}) and the θ–2θ scan method (2° base width, 2° min^{-1} scan rate, 20 s background counts at each scan limit). The intensity data were reduced using the procedure of Doedens and Ibers (4) with a *p* factor of 0.03. The independent Re atom was recovered from a Patterson map and a difference Fourier map based on the Re atom position revealed all of the remaining non-hydrogen atoms. Following several cycles

TABLE 1

(*a*) Atomic parameters for $[(CH_3CN)_3Re(CO)_3][BF_4]$

Atom	*x*	*y*	*z*	*B* (Å²)
Re	0.05599(7)	0.24302(10)	−0.14183(7)	[a]
C6	−0.062(2)	0.178(2)	−0.242(2)	5.3(5)
O6	−0.134(2)	0.136(2)	−0.307(2)	[a]
C4	−0.049(2)	0.380(2)	−0.131(2)	5.7(5)
O4	−0.106(2)	0.463(2)	−0.125(2)	[a]
C5	−0.026(2)	0.170(2)	−0.036(2)	4.7(5)
O5	−0.073(2)	0.124(2)	0.029(2)	[a]
N1	0.178(2)	0.095(2)	−0.149(2)	4.2(4)
C1	0.249(2)	0.017(2)	−0.148(2)	3.9(4)
M1	0.331(2)	−0.086(2)	−0.148(2)	5.3(5)
N3	0.197(2)	0.318(2)	−0.035(2)	5.1(4)
C3	0.277(2)	0.359(2)	0.016(2)	5.3(5)
M3	0.375(3)	0.415(3)	0.079(2)	7.8(7)
N2	0.160(2)	0.325(2)	−0.251(2)	4.5(4)
C2	0.224(2)	0.371(2)	−0.301(2)	4.4(5)
M2	0.311(3)	0.440(2)	−0.359(2)	6.3(6)
B	0.537(3)	0.242(5)	−0.127(2)	6.2(6)
F1	0.652(2)	0.245(3)	−0.108(2)	[a]
F2	0.489(3)	0.174(2)	−0.056(2)	[a]
F3	0.476(2)	0.343(2)	−0.147(2)	[a]
F4	0.515(2)	0.173(3)	−0.206(2)	[a]

[a]Anisotropic thermal parameters were used.

(*b*) Anisotropic temperature factors (× 10^5) for $[(CH_3CN)_3Re(CO)_3][BF_4]$

Atom	β_{11}	β_{22}	β_{33}	β_{12}	β_{23}	β_{13}
Re	863(8)	741(8)	806(7)	40(17)	261(5)	60(16)
F1	1197(150)	2570(243)	3784(280)	−301(301)	7(166)	1470(312)
F2	3588(331)	2687(286)	1755(182)	−14(249)	753(222)	1196(210)
F3	1615(213)	1200(176)	3209(288)	264(153)	628(220)	382(212)
F4	5905(682)	3085(343)	2218(271)	−787(378)	−113(341)	−1277(249)
O6	1667(226)	1215(177)	1530(173)	172(168)	−244(166)	−266(152)
O4	1541(195)	1245(188)	1656(178)	666(168)	455(152)	101(147)
O5	1670(217)	1969(232)	1316(164)	131(183)	896(158)	516(163)

of full-matrix least-squares refinement using isotropic thermal parameters, anisotropic thermal parameters were allowed for rhenium, oxygen, and fluorine (as indicated from a difference map) whereupon the *R* value dropped to 4.8%. Examination of the structure factors at this stage showed extinction effects, and a secondary extinction parameter was introduced in the refinement. Finally, refinement converged at $R_1 = 4.1\%$ and $R_2 = 3.9\%$. A final electron density difference map showed no peaks or troughs exceeding ± 0.6 electrons $Å^{-3}$.[1]

The scattering factors used were taken from Cromer and co-worker (5) with anomalous dispersion included for the rhenium atom. Table 1 lists atomic positions and thermal parameters, and Table 2 the interatomic distances and angles. A drawing of the $[(CH_3CN)_3Re(CO)_3][BF_4]$ structure is shown in Fig. 1, with a packing diagram in Fig. 2.

[1]Photocopies of the table of structure factors may be obtained at a nominal charge, upon request, from the Depository of Unpublished Data, CISTI, National Research Council of Canada, Ottawa, Canada K1A 0S2.

Results and Discussion

The reaction of $[n\text{-}Bu_4N]_2[Re_4(CO)_{16}]$ with $AgBF_4$ in acetonitrile solution resulted in the formation of the title compound, a process which can be represented by the following equation:

$$[n\text{-}Bu_4N]_2[Re_4(CO)_{16}] + 6AgBF_4 + 12CH_3CN \rightarrow 4[(CH_3CN)_3Re(CO)_3][BF_4] + 6Ag + 4CO + 2n\text{-}Bu_4NBF_4$$

The infrared spectrum in dichloromethane shows two strong carbonyl stretching bands at 2052 and 1951 cm^{-1}, the latter of greater half width. These are clearly the A_1 and E modes expected for the facial (C_{3v}) isomer. In addition, the solid state infrared spectrum (KBr disc) showed weak bands at 2315 and 2290 cm^{-1} due to the coordinated acetonitrile ligands.

TABLE 2

(*a*) Interatomic distances for $[(CH_3CN)_3Re(CO)_3][BF_4]$

Bond	Distance (Å)	Bond	Distance (Å)
Re—N1	2.134(16)	C1—M1	1.462(25)
Re—N2	2.133(16)	C2—M2	1.505(27)
Re—N3	2.125(18)	C3—M3	1.425(29)
Re—C4	1.931(24)	C4—O4	1.129(23)
Re—C5	1.916(23)	C5—O5	1.157(22)
Re—C6	1.867(23)	C6—O6	1.183(23)
N1—C1	1.167(20)	B—F1	1.268(27)
N2—C2	1.132(21)	B—F2	1.354(34)
N3—C3	1.133(23)	B—F3	1.318(41)
		B—F4	1.281(34)

(*b*) Bond angles for $[(CH_3CN)_3Re(CO)_3][BF_4]$

Bonds	Angle (deg)	Bonds	Angle (deg)
Re—N1—C1	176.2(1.5)	N2—Re—C5	175.4(0.8)
Re—N2—C2	173.4(1.6)	N2—Re—C6	95.2(0.8)
Re—N3—C3	174.5(1.8)	N3—C3—M3	178.1(2.4)
Re—C4—O4	177.5(2.0)	N3—Re—C4	92.2(0.8)
Re—C5—O5	177.8(1.9)	N3—Re—C5	93.8(0.7)
Re—C6—O6	178.1(2.0)	N3—Re—C6	176.9(0.8)
N1—C1—M1	176.5(1.9)	C4—Re—C5	86.8(0.9)
N1—Re—N2	84.8(0.6)	C4—Re—C6	89.0(0.9)
N1—Re—N3	85.0(0.6)	C5—Re—C6	89.1(0.9)
N1—Re—C4	177.2(0.8)	F1—B —F2	110.1(2.8)
N1—Re—C5	93.4(0.7)	F1—B —F3	112.2(2.3)
N1—Re—C6	93.7(0.8)	F1—B —F4	105.2(3.1)
N2—C2—M2	174.8(2.2)	F2—B —F3	119.4(3.8)
N2—Re—N3	81.9(0.6)	F2—B —F4	99.0(3.3)
N2—Re—C4	94.8(0.8)	F3—B —F4	108.7(2.7)

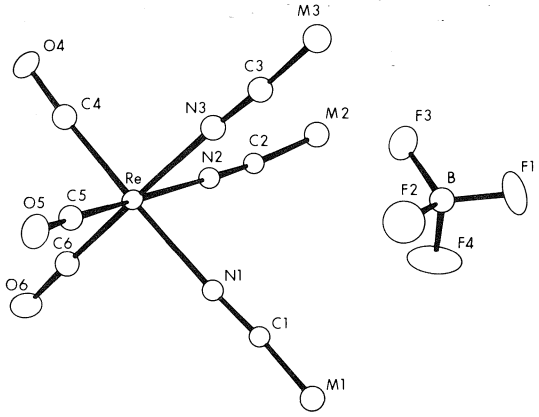

FIG. 1. The structure of $[(CH_3CN)_3Re(CO)_3][BF_4]$. Methyl groups are represented by M.

The preparation of the hexafluorophosphate salt of $[(CH_3CN)_3Re(CO)_3]^+$ has been reported by Reimann and Singleton (6) who obtained it in almost quantitative yield by reaction of $Re(CO)_5Br$ with $AgPF_6$ in acetonitrile. Their method would be preferred for synthesis of salts of this cation in terms of the ease of availability of starting materials.

The structure consists of discrete cations and anions with no unusual non-bonded contacts. It is interesting to note the ligands about the rhenium atom together with the BF_4^- group are so arranged that there is an approximate three-fold axis passing through the two moieties. The bond angles at rhenium deviate slightly from octahedral, averaging 88.3° for OC—Re—CO and 83.9° for CH_3CN—Re—$NCCH_3$.

The average N—C—CH_3 angle is 174.7°, and the average N—CCH_3 and NC—CH_3 distances of 1.14 and 1.46 Å, respectively, are essentially the same as those in the free ligand (7). The average Re—N bond length in $[(CH_3CN)_3Re(CO)_3]^+$ is 2.13 Å. Using a value of 1.52 Å as the covalent radius of Re(I), a figure derived from the reported Re(I)—Cl distance of 2.51 Å (8), the predicted Re(I)—N distance is 2.22 Å; this might be considered reasonable agreement, if

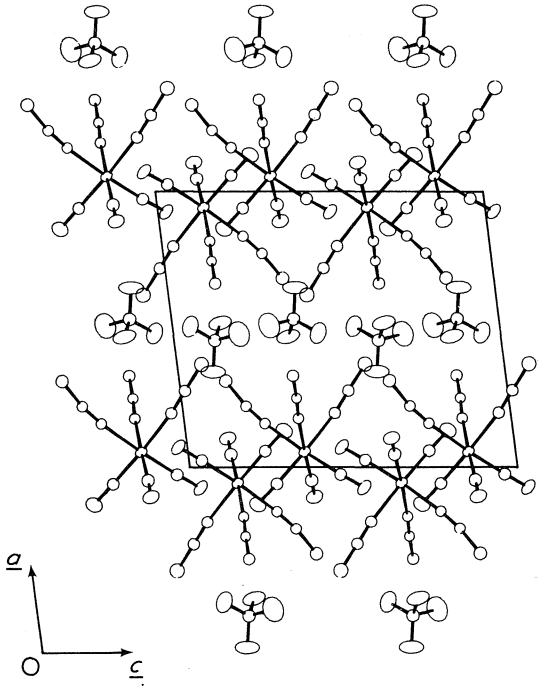

FIG. 2. Packing diagram and unit cell for $[(CH_3CN)_3Re(CO)_3][BF_4]$, shown in projection along the *b* axis.

allowance is made for uncertainties in the choice of appropriate covalent radii for both N and Re(I) in the circumstances. In acetonitrile complexes of copper(II), the Cu(II)—N bond length is 1.96–1.97 Å (9); if an adjustment is made for the larger size of Re(I) (1.52 Å *vs.* 1.28 Å) (10), one estimates Re(I)—N as 2.22 Å. This may indicate a stronger ligand–metal interaction in the $[(CH_3CN)_3Re(CO)_3]^+$ cation than in the Cu(II) complexes. It is of interest that the Re(V)—N distance in $[ReBr_4—O(CH_3CN)]^-$ was 2.31 Å (10), which was taken to indicate a very weak interaction between rhenium and the acetonitrile ligand relative to the same Cu(II) complexes.

The average Re—CO distance of 1.91 Å is comparable to other reported terminal Re—CO values, *e.g.*, 1.95 Å in $Ph_2SiH_2Re_2(CO)_8$ (11), 1.91 Å in $[Re_4(CO)_{16}]^{2-}$ (1), and 1.85 Å in $(\eta\text{-}C_5H_5)_2Re_2(CO)_5$ (12).

Acknowledgements

We thank the National Research Council of Canada for financial support, for a postgraduate scholarship to E.E.I., and a Postdoctoral Fellowship to L.Y.Y.C.

1. R. BAU, B. FONTAL, H. D. KAESZ, and M. R. CHURCHILL. J. Am. Chem. Soc. **89**, 6374 (1967).
2. M. R. CHURCHILL, P. H. BIRD, H. D. KAESZ, R. BAU, and B. FONTAL. J. Am. Chem. Soc. **90**, 7135 (1968).
3. H. D. KAESZ, B. FONTAL, R. BAU, S. W. KIRTLEY, and M. R. CHURCHILL. J. Am. Chem. Soc. **91**, 1021 (1969).
4. R. J. DOEDENS and J. A. IBERS. Inorg. Chem. **6**, 204 (1967).
5. D. T. CROMER and J. B. MANN. Acta Crystallogr. **A24**, 321 (1968); D. T. CROMER. Acta Crystallogr. **18**, 17 (1965).
6. R. H. REIMANN and E. SINGLETON. J. Organomet. Chem. **59**, C24 (1973).
7. M. D. DANFORD and R. L. LIVINGSTON. J. Am. Chem. Soc. **77**, 2944 (1955).
8. M. C. FREDETTE and C. J. L. LOCK. Can. J. Chem. **51**, 1116 (1973).
9. R. D. WILLETT and R. E. RUNDLE. J. Chem. Phys. **40**, 838 (1964).
10. F. A. COTTON and S. J. LIPPARD. Inorg. Chem. **5**, 416 (1966).
11. J. K. HOYANO, M. ELDER, and W. A. G. GRAHAM. J. Am. Chem. Soc. **91**, 4568 (1969); M. ELDER. Inorg. Chem. **9**, 762 (1970).
12. A. S. FOUST, J. K. HOYANO, and W. A. G. GRAHAM. J. Organomet. Chem. **32**, C65 (1971).

Orbital ground state, crystal field splittings, and magnetic hyperfine interactions in iron(II) fluorosulphate

JOHN R. SAMS, ROBERT C. THOMPSON, AND TSANG BIK TSIN

Department of Chemistry, University of British Columbia, Vancouver, B.C., Canada V6T 1W5

Received July 5, 1976

JOHN R. SAMS, ROBERT C. THOMPSON, and TSANG BIK TSIN. Can. J. Chem. **55**, 115 (1977).

Magnetic susceptibilities between 80 and 300 K and ^{57}Fe Mössbauer parameters between 4.2 and 295 K are reported for $Fe(SO_3F)_2$. These data have been analysed via a crystal field model including spin–orbit and spin–spin coupling. The compound is trigonally distorted by an elongation along the [111] axis of the FeO_6 octahedron, and the ground state is the orbital doublet $[(\sqrt{2/3}|x^2 - y^2\rangle - \sqrt{1/3}|xz\rangle),(\sqrt{2/3}|xy\rangle + \sqrt{1/3}|yz\rangle)]$. The quadrupole coupling constant e^2qQ is positive, and no rhombic distortion could be detected. The electronic spectrum shows a splitting of the ^5E_g excited level, presumably by a dynamic Jahn–Teller effect, and $10Dq \simeq 8000\ cm^{-1}$. Attempts to fit a low-temperature magnetic perturbation Mössbauer spectrum using a pseudo-spin Hamiltonian were only partially successful, but suggest that the **g** tensor is highly anisotropic with $g_{\parallel} \gg g_{\perp}$, and that the internal hyperfine field is small. Spin relaxation in $Fe(SO_3F)_2$ is fast at all temperatures down to 4.2 K and in applied magnetic fields of up to 5.0 *T*.

JOHN R. SAMS, ROBERT C. THOMPSON et TSANG BIK TSIN. Can. J. Chem. **55**, 115 (1977).

On rapporte les susceptibilités magnétiques, entre 80 et 300 K, et les paramètres de Mössbauer du ^{57}Fe, entre 4.2 et 295 K, dans $Fe(SO_3F)_2$. On a analysé ces données par l'intermédiaire d'un modèle de champ de cristal impliquant des couplages spin–orbite et spin–spin. Le composé est déformé d'une façon trigonale par une élongation le long de l'axe [111] de l'octaèdre FeO_6 et l'état fondamental est l'orbitale sous forme de doublet $[(\sqrt{2/3}|x^2 - y^2\rangle - \sqrt{1/3}|xz\rangle),(\sqrt{2/3}|xy\rangle + \sqrt{1/3}|yz\rangle)]$. La constante de couplage quadrupolaire e^2qQ est positive et on n'a pas pu détecter aucune distorsion rhombique. Le spectre électronique montre une coupure de l'état excité ^5E_g qui est probablement dû à un effet Jahn–Teller dynamique et $10Dq \simeq 8000\ cm^{-1}$. Les essais pour ajuster une perturbation magnétique à basse température du spectre de Mössbauer en faisant appel à un hamiltonien pseudo-spin n'ont connu que des succès partiels; ils suggèrent toutefois que le tenseur **g** est hautement anisotropique avec $g_{\parallel} \gg g_{\perp}$ et que le champ hyperfin interne est petit. La relaxation de spin du $Fe(SO_3F)_2$ est rapide à toutes les températures jusqu'à 4.2 K et dans des champs magnétiques appliqués jusqu'à 5.0 *T*.

[Traduit par le journal]

Introduction

In a recent study (1, 2) of some octahedrally coordinated high-spin iron(II) complexes, $Fe(pyO)_6(ClO_4)_2$ (pyO = C_5H_5NO) was found to have an unusual orbital ground state. The $Fe(pyO)_6^{2+}$ cation is distorted by a trigonal elongation along the [111] direction of the octahedron, and the ground state is the $[(\sqrt{2/3}|x^2 - y^2\rangle - \sqrt{1/3}|xz\rangle),(\sqrt{2/3}|xy\rangle + \sqrt{1/3}|yz\rangle)]$ orbital doublet. A detailed fit of the temperature dependence of the Mössbauer quadrupole splitting in terms of a crystal field model which included spin–orbit and spin–spin coupling, showed that the axial crystal field splitting $3Ds$ was 455 cm^{-1} (2), with the ground doublet separated by 110 cm^{-1} from the next lowest lying spin–orbit-split state.

One of the most interesting features of this complex is that it is the only known example of an octahedral paramagnetic iron(II) derivative in which the spin–lattice relaxation rate at low temperatures is slow compared to the nuclear Larmor precession frequency. Thus, at temperatures below 30 K the two lines of the Mössbauer spectrum broaden asymmetrically, signaling the onset of paramagnetic hyperfine splitting (1, 2). Mössbauer measurements at 4.2 K in applied magnetic fields ranging from 1 to 50 kG have unequivocally confirmed the existence of slow spin relaxation in the complex (3). These measurements also established that any Jahn–Teller-induced rhombic splitting of the ground doublet must be less than 15 cm^{-1}.

For purposes of comparison we were interested in studying another trigonally distorted octahedral iron(II) complex. In particular, we wished to know if the existence of a ground doublet well isolated from all higher lying states is generally to be expected for a trigonally elongated complex, and if this could be in-

fluencing the spin relaxation rate. The ir spectrum of $Fe(SO_3F)_2$ (4) shows clearly that the anion maintains C_{3v} symmetry even though the ν_2 band is shifted upwards by 147 cm^{-1} compared to its position in $CsSO_3F$ (5), indicating significant cation–anion interaction. This means that the metal–anion coordination must involve terdentate fluorosulphate groups with all three oxygen atoms coordinated in an equivalent manner. Thus the structure of $Fe(SO_3F)_2$ is presumably of the terdentate bridging type proposed for $Co(SO_3F)_2$ (6), and should involve a trigonal distortion of the Fe—O_6 octahedron. $Fe(SO_3F)_2$ therefore seemed an attractive compound to investigate, and this paper reports detailed measurements of its susceptibility and Mössbauer spectra over wide ranges of temperature.

Experimental

Iron(II) fluorosulphate was prepared as described previously (4), and its identity and purity were confirmed by chemical analysis and ir spectroscopy. Electronic spectra over the range 5–33 kK were obtained on samples mulled in Nujol and hexachlorobutadiene, using a Cary model 14 spectrophotometer. Magnetic susceptibility and ^{57}Fe Mössbauer spectra were measured as fully described elsewhere (2). The Doppler velocity scale was calibrated with a metallic iron foil absorber, and isomer shifts are quoted relative to the centroid of the iron foil spectrum.

TABLE 1. Effective magnetic moments of $Fe(SO_3F)_2$

T (K)	μ_{eff} (BM)	T (K)	μ_{eff} (BM)
300	5.53	175	5.54
276	5.54	150	5.52
251	5.55	127	5.51
226	5.55	103	5.51
201	5.56	79	5.43

TABLE 2. ^{57}Fe Mössbauer parameters for $Fe(SO_3F)_2$*

T† (K)	δ‡ (mm s^{-1})	ΔE_Q (mm s^{-1})	Γ_1 (mm s^{-1})	Γ_2 (mm s^{-1})
293	1.37	1.28	0.30	0.28
250	1.40	1.40	0.33	0.32
220	1.42	1.48	0.32	0.34
180	1.44	1.54	0.34	0.34
160	1.46	1.60	0.32	0.32
130	1.48	1.67	0.33	0.34
115	1.49	1.71	0.35	0.34
100	1.49	1.73	0.35	0.34
85	1.50	1.77	0.33	0.32
84	1.49	1.77	0.32	0.34
60	1.50	1.84	0.32	0.31
30	1.50	1.92	0.34	0.33
7.7	1.50	1.94	0.35	0.35
4.2	1.50	1.92	0.31	0.32

*Estimated precision of the parameters is ± 0.01 mm s^{-1}.
†Measured with a Pt resistance thermometer for $T \geq 30$ K, and a Ge thermometer for $T < 30$ K.
‡Relative to the centroid of a metallic iron foil spectrum.

Results

Magnetic moments of $Fe(SO_3F)_2$ between 78 and 300 K and Mössbauer parameters between 4.2 and 295 K are given in Tables 1 and 2, respectively. The μ_{eff} values are in the range expected for a high-spin iron(II) complex. It will be noted that the values increase initially with decreasing temperature, pass through a maximum and then decline at low temperature. Similar behaviour was found for $Fe(pyO)_6(ClO_4)_2$, whereas for two similar solvates having tetragonal distortions and orbital singlet ground states, μ_{eff} decreased monotonically with decreasing temperature (2).

The electronic spectrum of $Fe(SO_3F)_2$ consists of a broad band, similar in appearance to that observed for $FeSiF_6.6H_2O$ (7), with a principal absorption at 8800 cm^{-1} and a broad shoulder at approximately 7100 cm^{-1}.

The Mössbauer isomer shift δ is very high, the usual range for octahedral $S = 2$ iron(II) complexes at *ca.* 80 K being 1.1–1.3 mm s^{-1}. The only other high-spin iron(II) compounds which show comparable shifts are the fluorides FeF_2 (8), $CsFeF_3$ (9), and Rb_2FeF_4 (10). As a general rule, high isomer shifts are associated with high ionicity. Using either the Walker–Wertheim–Jaccarino (11) model, or its modified form given by Danon (12), the derived electron configuration for the Fe^{2+} ion in $Fe(SO_3F)_2$ is $3d^{6.00}$ $4s^{0.00}$. The temperature dependence of δ presumably arises from a second-order Doppler shift, and is not chemically significant.

The quadrupole splitting $|\Delta E_Q|$ of $Fe(SO_3F)_2$ is much smaller than that of FeF_2 (8) where the ground state is essentially an orbital singlet (13), but somewhat larger than those of the other anhydrous iron(II) dihalides, all of which are trigonally distorted with doublet ground states (14–17). $|\Delta E_Q|$ for $Fe(SO_3F)_2$ also shows a strong temperature dependence, a point we shall return to below.

The Mössbauer spectrum of the compound remained a sharp symmetric doublet down to 4.2 K, and there was no indication of either

magnetic ordering or of the asymmetric line broadening found for $Fe(pyO)_6(ClO_4)_2$. Thus it is clear that in the absence of an applied magnetic field the electronic spin relaxation in $Fe(SO_3F)_2$ is fast compared to the nuclear precession frequency, so that the internal field sensed by the nucleus is zero.

Discussion

As suggested above, the fact of C_{3v} symmetry for the SO_3F^- ion in $Fe(SO_3F)_2$ strongly suggests an Fe—O_6 octahedron which is either undistorted or distorted along the threefold (C_3) axis, since a tetragonal distortion along the C_4 axis of the octahedron would be expected to result in a lowering of the anion symmetry to C_s. Of course the ir data cannot differentiate between D_{3h} and O_h symmetries for the cation because the anion symmetry would be identical in either case. The Mössbauer data are definitive on this point, however, since a pure $^5T_{2g}$ state cannot show a quadrupole splitting. Thus the cation must have symmetry lower than O_h.

In view of the small $|\Delta E_Q|$ values observed, it might be thought that the crystal field distortion may be too small to be sensed by ir spectroscopy, and that the ir data do not in fact rule out a tetragonal distortion. Indeed, it is sometimes assumed (18) that a small $|\Delta E_Q|$ necessarily implies a small distortion for octahedral Fe^{2+} ions. This view completely ignores the fact that an orbital doublet ground state will produce a quadrupole splitting roughly half that produced by a singlet ground state, and that no matter how large the distortion $|\Delta E_Q|$ will never be much greater than 2 mm s^{-1} for a doublet state. This is an important point. For an octahedral high-spin iron(II) complex a quadrupole splitting substantially larger than 2 mm s^{-1} is conclusive proof of an orbital singlet ground state. On the other hand, if the quadrupole splitting is less than *ca.* 2 mm s^{-1} two possibilities exist: either the orbital ground state is a singlet and the crystal field splitting is very small, or the ground state is a doublet. Only by detailed analysis of the temperature dependence of ΔE_Q over a wide range of T can these cases be distinguished, as we now describe.

Orbital Ground State

For simplicity we consider only those iron 3*d* orbitals transforming as t_{2g}, and ignore the higher lying e_g orbitals. In the presence of an axial crystal field the threefold degeneracy of the t_{2g} subset is partially lifted to produce a singlet and a doublet, separated by $3Ds$. The nature of these orbital states depends upon the symmetry of the axial field (*i.e.*, the choice of quantization axis). For a tetragonal distortion the singlet is $|xy\rangle$ and the doublet ($|xz\rangle$, $|yz\rangle$). However, if the distortion is along the trigonal axis the singlet is $|z^2\rangle$ and the doublet $[(\sqrt{2/3}|x^2 - y^2\rangle - \sqrt{1/3}|xz\rangle),(\sqrt{2/3}|xy\rangle + \sqrt{1/3}|yz\rangle)]$. In both cases the singlet lies lower if the distortion corresponds to a compression along the quantization axis, and higher for an elongation along this axis. If there is a rhombic field as well, the doublet will be split by $12Dr$. Each of these orbital states also has a fivefold spin degeneracy which will be split by the spin–orbit coupling.

If we assume there is no rhombic distortion, and we shall see that this is a good approximation for $Fe(SO_3F)_2$, then there are four possible orbital ground states. A knowledge of the sign of the quadrupole coupling constant e^2qQ will eliminate two of these possibilities, since for the $|z^2\rangle$ and ($|xz\rangle$,$|yz\rangle$) states e^2qQ will be negative, whereas it is positive for the other two states.

A Mössbauer spectrum of $Fe(SO_3F)_2$ recorded at 195.3 $\pm$ 0.1 K in the presence of a longitudinal applied magnetic field of 5.0 T revealed that e^2qQ was positive, and the asymmetry parameter η of the electric field gradient (EFG) tensor was nearly or exactly zero. (As discussed elsewhere (1, 2), this measurement was made at elevated temperature to avoid any possible ambiguity which might arise from induced magnetization in the specimen due to spin polarization by the applied field.) The fact that $\eta \simeq 0$ is consistent with the absence of a significantly large rhombic distortion, whilst $e^2qQ > 0$ limits the possible ground states to $[(\sqrt{2/3}|x^2 - y^2\rangle - \sqrt{1/3}|xz\rangle), (\sqrt{2/3}|xy\rangle + \sqrt{1/3}|yz\rangle)]$ or $|xy\rangle$.

Both the ir data and the fact that ΔE_Q does not exceed 2.0 mm s^{-1} favour the former ground state. However, in order to establish this unequivocally, we have attempted to fit the temperature dependence of ΔE_Q, using the crystal field model described below, for both these ground states. With $|xy\rangle$ taken to be the ground state we were not able to obtain a satisfactory representation of the observed ΔE_Q *vs.* T behaviour, for any reasonable choice of parameter values. With the doublet ground state on the other hand, a very satisfactory fit of the data was achieved (*vide infra*), which thus establishes that

the orbital ground state is in fact the $[(\sqrt{2/3}|x^2 - y^2\rangle - \sqrt{1/3}|xz\rangle),(\sqrt{2/3}|xy\rangle + \sqrt{1/3}|yz\rangle)]$ doublet. Thus, the Fe—O_6 octahedron in $Fe(SO_3F)_2$ is distorted by a trigonal elongation along the [111] axis, and the point-group symmetry of the iron environment is effectively D_{3h}.

Crystal Field Parameters

The value of $10Dq$ for $Fe(SO_3F)_2$ should be obtainable from its electronic spectrum. For a regular octahedral complex the spectrum should consist of a single absorption, at an energy $10Dq$, arising from the $^5T_{2g} \rightarrow {}^5E_g$ transition. The structure observed here (principal band at 8800 cm^{-1} and shoulder at 7100 cm^{-1}) suggests a splitting of the excited level by some 1700 cm^{-1}. As discussed above the distortion of this complex from regular O_h symmetry is trigonal in nature, and since such a distortion cannot lift the degeneracy of the ^5E_g level, this cannot be the cause of the band splitting.

A similar situation exists for $FeSiF_6.6H_2O$ which contains trigonally distorted $[Fe(H_2O)_6]^{2+}$ octahedra. The spectrum of this compound consists of a principal band at 10 300 cm^{-1} with a shoulder at 8700 cm^{-1}, and the band splitting in this case has been attributed to the removal of the excited state degeneracy by a dynamic Jahn–Teller effect (7). If one assumes that the band splitting in $Fe(SO_3F)_2$ is also due to this effect, the value of $10Dq$ for the complex must be about 8000 cm^{-1} (approximate centre of the absorption band). This value is not unreasonable when compared with previously measured $10Dq$ values of 7650 cm^{-1} for $Co(SO_3F)_2$ (6) and 7340 cm^{-1} for $Ni(SO_3F)_2$ (19).

The effects of the noncubic part of the crystal field together with spin–orbit and spin–spin splitting can be treated via the Hamiltonian

$$[1] \quad \mathcal{H} = Ds(\hat{L}_z^2 - 2) + Dr(\hat{L}_+^2 + \hat{L}_-^2) - \lambda[\hat{L}_z\hat{S}_z + \tfrac{1}{2}(\hat{L}_+\hat{S}_- + \hat{L}_-\hat{S}_+)] - D\sigma(\hat{S}_z^2 - 2)$$

where the $\hat{L}_i$ and $\hat{S}_i$ are orbital and spin angular momentum shift operators, respectively, Ds and Dr the axial and rhombic field splitting parameters, and λ and $D\sigma$ the spin–orbit and spin–spin coupling constants. The cubic field term has been omitted from [1] because in our calculations we ignore the e_g orbitals, and $\mathcal{H}$ operates only on a basis set of 15 t_{2g} wave functions. We have shown elsewhere (2) that this appears to be a valid truncation if $10Dq \gtrsim 9000$ cm^{-1}. Although we estimate $10Dq$ for $Fe(SO_3F)_2$ to be only ~ 8000 cm^{-1}, this approximation is retained here. (The reason for doing this is simply that it allows one to truncate the 25×25 matrices which one would otherwise need to diagonalize to 15×15 matrices, thereby reducing the computation time by a factor of nearly three.) The basis sets used were

$$\sqrt{1/2}(|2,2\rangle - |2,-2\rangle)|M_s\rangle$$
$$\sqrt{1/2}(|2,1\rangle \pm |2,-1\rangle)|M_s\rangle$$

for tetragonal symmetry, and

$$|2,0\rangle|M_s\rangle$$
$$(\sqrt{2/3}|2,\pm 2\rangle \mp \sqrt{1/3}|2,\mp 1\rangle)|M_s\rangle$$

for trigonal symmetry, where we have used the notation $|L,M_L\rangle|M_s\rangle$, M_L being the z component of the total orbital angular momentum L, and $M_s = 0, \pm 1, \pm 2$ the z component of spin angular momentum.

For particular choices of Ds/λ, Dr/λ, and $D\sigma/\lambda$ the 15×15 matrix was diagonalized to obtain the eigenvalues ε_i/λ and corresponding eigenvectors $|i\rangle$. These quantities were then used to calculate quadrupole splittings and magnetic moments as described in detail previously (2). The only change from our earlier procedure is that the numerical factor appearing in eq. 8 of ref. 2 has been altered from 4.1 to 4.5, as suggested recently by König *et al.* (20).

In fitting the Mössbauer data, since the EFG at Fe has effectively axial symmetry ($\eta \simeq 0$), we have set $Dr = 0$. The remaining parameter values were refined by least-squares techniques. As mentioned above, we were unable to obtain a satisfactory fit using an orbital singlet ground state. The main difficulty here was that in order to fit the approximate magnitude of ΔE_Q one must use quite small values of Ds, and this in turn leads to a much more pronounced temperature dependence than that observed experimentally. No reasonable choices of λ and $D\sigma$ could rectify this problem. For the doublet ground state, the Mössbauer quadrupole splittings are adequately fitted by the crystal field model using the following parameter values: $Ds = 96$ cm^{-1}, $\lambda = -90$ cm^{-1}, and $D\sigma = 22$ cm^{-1}. In treating the magnetic moment data we employed these same values of Ds, λ, and $D\sigma$, and fitted the μ_{eff} *vs.* T curve merely by adjusting the orbital reduction factor κ. The value of κ so found was 0.95. Figure 1 compares the experi-

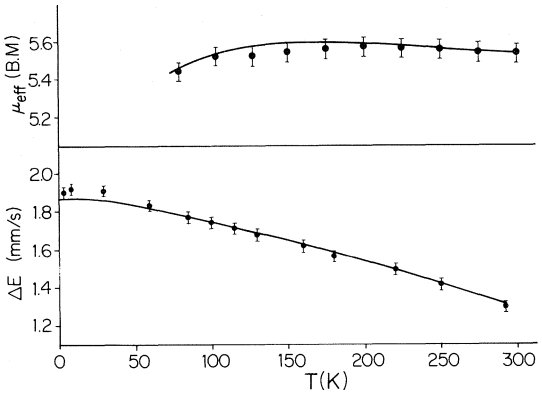

FIG. 1. Comparison of observed and calculated effective magnetic moments (upper) and quadrupole splittings (lower) as functions of temperature for $Fe(SO_3F)_2$. The parameters used to compute the theoretical curves are given in the text.

mental ΔE_Q and μ_{eff} data with theoretical curves computed from these parameter values.

The *Ds* value found for $Fe(SO_3F)_2$ is somewhat larger than those reported for $FeCl_2$ (48 cm^{-1}), $FeBr_2$ (58 cm^{-1}), and FeI_2 (61 cm^{-1}) (15, 17), all of which have orbital doublet ground states. The larger distortion here is perhaps not surprising in view of the polyatomic nature of the anion. Inclusion of the spin–spin coupling term, $D\sigma(\hat{S}_z^2 - 2)$, is necessary to account for the behaviour of ΔE_Q at temperatures below *ca.* 80 K. If this term is omitted from the Hamiltonian [1] the theoretical ΔE_Q values decrease rather than increase as the temperature is lowered from 80 to 4.2 K. The magnitude of $D\sigma$ for $Fe(SO_3F)_2$ is very similar to those obtained for other high-spin Fe^{2+} complexes (2).

The λ and κ values found here are slightly lower than one might expect. In view of the very high isomer shift of $Fe(SO_3F)_2$ which suggests high ionicity, values of these parameters closer to the free-ion values ($\lambda_0 = -103\ cm^{-1}$, $\kappa_0 = 1.00$) would appear more reasonable. We suspect the low values we obtain may be more artificial than real, and perhaps result from our neglect of the iron e_g orbitals in the crystal field model used. This omission appears to have no significant effect on the results for tetragonally distorted complexes (2), presumably because under D_{4h} symmetry E_g goes over into $A_{1g} + B_{1g}$ and there is no mixing with the ground term. However, the E_g term remains degenerate under D_{3h} (trigonal distortion) and there is now a symmetry-allowed mixing with the E_g component of T_{2g}. Clearly any effect on κ and λ is not very large, and we feel that more elaborate calculations employing a full basis set of 25 spin–orbit wavefunctions are hardly justified.

Spin Relaxation and Magnetic Hyperfine Interaction

As noticed above, electronic spin relaxation in $Fe(SO_3F)_2$ at 4.2 K in zero magnetic field is fast relative to the nuclear precession frequency, so that the Mössbauer spectrum remains a symmetric doublet under these conditions.

The *d* orbital energy level diagram for the compound, obtained from the eigenvalues calculated in the crystal field treatment above, is shown in Fig. 2. This diagram is similar in appearance to that of $Fe(pyO)_6(ClO_4)_2$ (3), for which spin–lattice relaxation is slow. In particular, the ground spin–orbit-split doublet in $Fe(SO_3F)_2$ lies 96 cm^{-1} below the next lowest lying state, compared to 110 cm^{-1} in $Fe(pyO)_6(ClO_4)_2$. In both cases the ground state is effectively isolated at 4.2 K ($kT \simeq 2.9\ cm^{-1}$) and there will be no mixing with higher levels. We have shown (3) that a ground state of this type

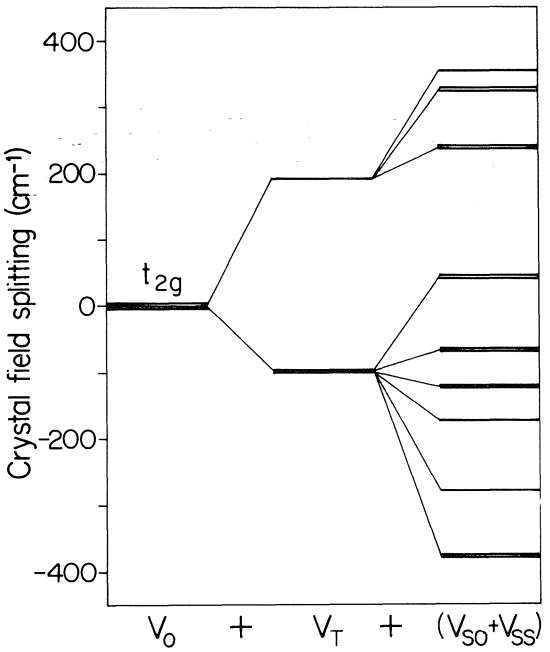

FIG. 2. Energy level diagram for the t_{2g} subset of ferrous 3*d* orbitals in $Fe(SO_3F)_2$, obtained by fitting the temperature dependence of the quadrupole splitting via the crystal field model described in the text. The effects of the trigonal distortion (V_T), spin–orbit coupling (V_{so}), and spin–spin coupling (V_{ss}) are shown.

can be accurately treated as a Kramer's doublet, and that the magnetic properties of such a state in the presence of an applied field $\boldsymbol{H}$ can be described in terms of a pseudo-spin ($S = \frac{1}{2}$) Hamiltonian,

$$[2] \quad \mathscr{H} = \beta \boldsymbol{H} \,.\, \mathsf{g} \,.\, \boldsymbol{S} + \boldsymbol{I} \,.\, \mathsf{A} \,.\, \boldsymbol{S} - g_n \beta_n \boldsymbol{I} \,.\, \boldsymbol{H} + \mathscr{H}_Q$$

where β and β_n are the Bohr and nuclear magnetons, respectively, g_n the nuclear g-factor and $\mathscr{H}_Q$ the nuclear quadrupole coupling Hamiltonian. The first three terms in [2] describe respectively the electronic Zeeman interaction, the magnetic hyperfine interaction between the nuclear spin $\boldsymbol{I}$ and electron spin $\boldsymbol{S}$, and the direct nuclear Zeeman interaction with the external field. Thus, in principle, Mössbauer measurements on such a system at 4.2 K in large applied fields enable one to deduce the components of both the g and A tensors and the magnitude of the internal hyperfine field.

The spectrum shown in Fig. 3 was obtained at 4.2 K with an applied longitudinal magnetic field of 5.0 T, and is unusual from several points of view. Rather than a well-resolved hyperfine pattern of six or more lines, one sees only two comparatively featureless absorption envelopes. These envelopes have very different intensities, and their small widths suggest that the internal magnetic field along the trigonal axis is quite small.

Because of these unusual features we have made a great effort to fit the spectrum using the Hamiltonian of [2]. From our previous experience with $Fe(pyO)_6(ClO_4)_2$ (3) and the predictions of Griffith (21), we expected a highly anisotropic g tensor with $g_\parallel \gg g_\perp \simeq 0$. Therefore most of the theoretical spectra calculated employed one of the following sets of g values: $g_\perp = 0$, $g_\parallel = 9$; $g_\perp = 0.5$, $g_\parallel = 9$; $g_\perp = 0.8$, $g_\parallel = 9$; $g_\perp = 1$, $g_\parallel = 9$; and $g_\perp = 2$, $g_\parallel = 8$. However, several other seemingly less realistic sets of values were also tried, including $g_\perp = g_\parallel = 2$ and sets with $g_\perp > g_\parallel$. For a given combination of g values the A tensor components $A_\perp$ and $A_\parallel$ were systematically varied, and spectra were calculated in both slow and fast relaxation limits (3) in attempting to simulate the observed spectrum. Altogether, more than 300 spectra were generated, but in no case were we able to obtain a really satisfactory fit. One of the main difficulties was in trying to reproduce the relative intensities of the two absorption envelopes.

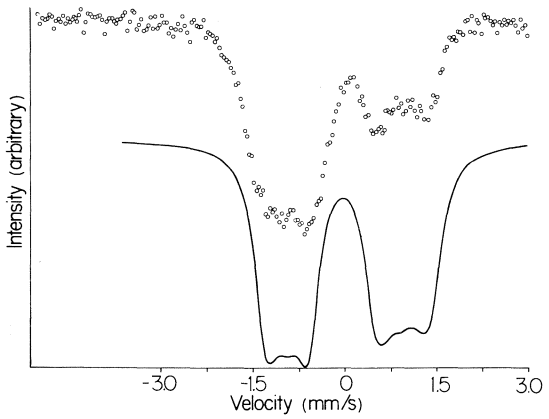

FIG. 3. ^{57}Fe Mössbauer spectrum of $Fe(SO_3F)_2$ at 4.2 K in a longitudinal applied magnetic field of 5.0 T. The solid line is a theoretical spectrum computed from the $S = 1/2$ pseudo-spin Hamiltonian, using parameter values given in the text and a fast relaxation limit. The velocity scale is relative to the centroid of the zero-field spectrum

The solid line shown in Fig. 3 represents our most successful attempt at simulating the widths and shapes of the two envelopes, but the intensities are clearly wrong. This spectrum, computed in the fast relaxation limit, employs the parameters: $g_\perp = 1$, $g_\parallel = 9$, $A_\perp = +1.50$ mm s^{-1}, $A_\parallel = +0.78$ mm s^{-1}, and ΔE_Q and Γ values obtained from the zero-field spectrum. Although these parameter values should not be taken too seriously in view of the inadequacies of the fit, certain rather firm conclusions did emerge during the course of our calculations. Firstly, it appears necessary to use a very anisotropic g tensor with $g_\parallel \gg g_\perp$ as expected (3, 21). Spectra computed with isotropic g values or with $g_\perp > g_\parallel$ were far less successful. Secondly, the easy axis of magnetisation is parallel to the z axis of the EFG, and the hyperfine field along this axis is apparently small ($\gtrsim 6T$) and positive. Thirdly, in almost all cases spectra computed in the slow relaxation limit showed substantially more fine structure than did the fast relaxation spectra, and in order to duplicate the rather featureless character of the measured spectrum it seems necessary to use the fast relaxation limit. Thus, at 4.2 K spin relaxation in $Fe(SO_3F)_2$ remains fast even in the presence of a large applied field.

The rather marked difference between theoretical and experimental intensity ratios of the two absorption envelopes remains a mystery, and we are not able to offer a satisfactory explanation at this time. The zero-field spectra rule

out the possibility of an anisotropy of the recoilless fraction, and this would not be expected to be important in a highly ionic compound at 4.2 K in any case. Preferential orientation of the crystallites also seems highly improbable. Spectra at 4.2 K in zero applied field were recorded for three different samples of $Fe(SO_3F)_2$, and in each instance the intensities and areas of the two lines were identical within experimental error.

Conclusions

The present study has shown that $Fe(SO_3F)_2$ is distorted by an elongation along the C_3 axis of the Fe—O_6 octahedron, with a trigonal field splitting $3Ds$ of about 290 cm^{-1}. The $10Dq$ value is about 8000 cm^{-1}, and there appears to be substantial Jahn–Teller splitting of the ^5E_g level. The quadrupole coupling constant is positive and the electric field gradient has effectively axial symmetry, consistent with a nearly degenerate $[(\sqrt{2/3}|x^2 - y^2\rangle - \sqrt{1/3}|xz\rangle),(\sqrt{2/3}|xy\rangle + \sqrt{1/3}|yz\rangle)]$ orbital doublet ground state. The trigonal axis of the crystalline field, the z axis of the EFG and the easy axis of magnetisation are colinear, and the hyperfine field along this axis is apparently small. Spin relaxation in the complex is fast relative to the ^{57}Fe nuclear precession frequency at all temperatures down to 4.2 K and in applied magnetic fields of up to 5.0 T.

Acknowledgements

Financial support from the National Research Council of Canada is gratefully acknowledged. We thank Mrs. A. Sallos and Ms. B. Krizan for technical assistance, and T.B.T. thanks NRCC for the award of a postdoctoral fellowship.

1. J. R. Sams and T. B. Tsin. J. Chem. Phys. **62**, 734 (1975).
2. J. R. Sams and T. B. Tsin. Inorg. Chem. **14**, 1573 (1975).
3. J. R. Sams and T. B. Tsin. Chem. Phys. In press.
4. C. S. Alleyne, K. O'Sullivan Mailer, and R. C. Thompson. Can. J. Chem. **52**, 336 (1974).
5. A. Ruoff, J. B. Milne, G. Kaufmann, and M. Leroy. Z. Anorg. Allg. Chem. **372**, 119 (1970).
6. J. M. Taylor and R. C. Thompson. Can. J. Chem. **49**, 511 (1971).
7. F. A. Cotton and M. D. Meyers. J. Am. Chem. Soc. **82**, 5023 (1960).
8. G. K. Wertheim and D. N. E. Buchanan. Phys. Rev. **161**, 478 (1967).
9. M. Eibschutz, L. Holmes, H. J. Guggenheim, and H. J. Levinstein. J. Appl. Phys. **40**, 1312 (1969).
10. G. K. Wertheim, H. J. Guggenheim, H. J. Levinstein, D. N. E. Buchanan, and R. C. Sherwood. Phys. Rev. **173**, 614 (1968).
11. L. R. Walker, G. K. Wertheim, and V. Jaccarino. Phys. Rev. Lett. **6**, 98 (1961).
12. J. Danon. *In* Applications of the Mössbauer effect in chemistry and solid state physics. Int. Atomic Energy Agency, Vienna. 1966. p. 89.
13. R. Ingalls. Phys. Rev. **133**, A787 (1964).
14. K. Ono, A. Ito, and T. Fujita. J. Phys. Soc. Jpn. **19**, 2119 (1964).
15. E. Pfletschinger. Z. Phys. **209**, 119 (1968).
16. D. J. Simkin. Phys. Rev. **177**, 1008 (1969).
17. T. Fujita, A. Ito, and K. Ono. J. Phys. Soc. Jpn. **21**, 1734 (1966).
18. J. Reedijk and A. M. van der Kraan. Rec. Trav. Chim. Pays Bas, **88**, 828 (1969).
19. D. A. Edwards, M. J. Stiff, and A. A. Woolf. Inorg. Nucl. Chem. Lett. **3**, 427 (1967).
20. E. König, G. Ritter, and H. S. Goodwin. Chem. Phys. **5**, 211 (1974).
21. J. S. Griffith. The theory of transition metal ions. Cambridge University Press, Cambridge. 1964. pp. 355–360.

Electrophilic additions of iodonium nitrate to unsaturated substrates

J. WILLIAM LOWN AND ALUMMOOTTIL V. JOSHUA[1]

Department of Chemistry, University of Alberta, Edmonton, Alta., Canada T6G 2G2

Received June 14, 1976

J. WILLIAM LOWN and ALUMMOOTTIL V. JOSHUA. Can. J. Chem. **55**, 122 (1977).

Iodonium nitrate (generated by reaction of iodine chloride with silver nitrate in chloroform–pyridine) reacts with a variety of unsaturated substrates to form the following: 1,4-conjugate addition products of the type alkenyl pyridinium nitrates; alkyliodopyridinium nitrates; products of aromatic iodination of both phenols and anilines; substituted benzodihydrofurans; tetrahydrofurans and tetrahydropyrans; polycyclic bridged ethers; lactones; thiazolines.

J. WILLIAM LOWN et ALUMMOOTTIL V. JOSHUA. Can. J. Chem. **55**, 122 (1977).

Le nitrate d'iodonium (formé par réaction du chlorure d'iode avec le nitrate d'argent dans le chloroforme et la pyridine) réagit avec un grand nombre de substrats non-saturés pour former ceux qui suivent: des produits d'addition conjugué-1,4 du type nitrate d'alkényl pyridinium; des nitrates d'alkyliodopyridinium; des produits d'iodation aromatique des phénoles et d'anilines; des benzodihydrofurannes substitués; des tétrahydrofurannes et des tétrahydropyrannes; des éthers polycycliques pontés; des lactones; des thiazolines.

[Traduit par le journal]

In previous publications we reported on the chemical versatility of the addition reactions of the pseudo halogen iodonium nitrate (1–3). For example, iodonium nitrate (generated by reaction of iodine chloride with silver nitrate in chloroform–pyridine solution) readily undergoes addition to alkenes to form (*i*) iodoalkyl nitrates, (*ii*) iodoalkylpyridinium nitrates, or (*iii*) alkenylpyridinium iodides (1, 3). With olefinic alcohols, iodonium nitrate affords (*iv*) hydroxyiodoalkyl nitrates, (*v*) hydroxyiodoalkylpyridinium nitrates, or (*vi*) three, four, and five membered cyclic ethers depending on the substrate and the reaction conditions (2). It was established that these electrophilic additions proceed via a discrete pyridine complex $(I{\cdot}2Py)^+NO_3^-$ (in which the iodine is bonded to the nitrogens of the pyridine rings), *trans*-stereospecifically and often regiospecifically (1).

In a continuation of our investigations we report several further examples of the synthetic utility of this reagent.

Reactions with Conjugated Systems

2,3-Dimethyl-1,3-butadiene reacts with iodonium nitrate to afford the 1,2-addition product *N*-[3-(4-iodo-2,3-dimethyl)but-1-enyl]pyridinium nitrate **1** in 60% yield and compound **2**, the product of 1,4-conjugate addition, in 5.5% yield. The sole formation of the pyridinium salt is consistent with the observation that this is the major type of product obtained when a stabilized (*e.g.* allylic) cation intermediate is involved (1). The nmr spectrum of **1** was consistent with a 1,2-addition since it showed the terminal vinylic protons. Product **2** is envisaged as arising from 1,4-addition followed by displacement of the allylic iodine by pyridine. Alkenyl pyridinium salts of the general type represented by **1** and **2** were found to possess significant oral antidiabetic properties which will be reported elsewhere.

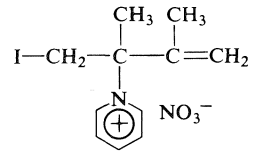

1

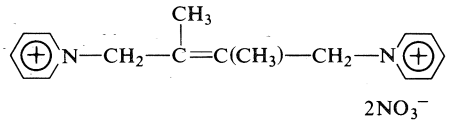

2

Iodonium nitrate is generally unreactive towards α,β-unsaturated ketones and esters unless activated by electron-releasing substituents. Thus chalcone is recovered unchanged on treatment with iodonium nitrate. In contrast, *p*-methoxychalcone **3** did react to afford the iodopyridinium nitrate **4** as the sole product in 91% yield.

[1]NRCC scholarship holder 1974–1975.

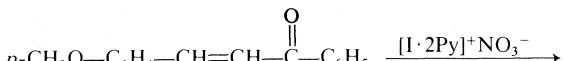

3

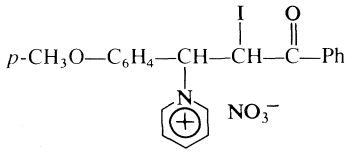

4

Reactions with Phenols and Anilines

Reaction of 2-allylphenol **5** with 1 mol equiv. of iodonium nitrate did not give the expected double bond addition product, but instead gave the aromatic iodination products **6**, **7**, and **8** together with the corresponding amount of pyridinium nitrate. With 2 equiv. of iodonium nitrate the diiodinated product **8** was obtained in 74.5% yield.

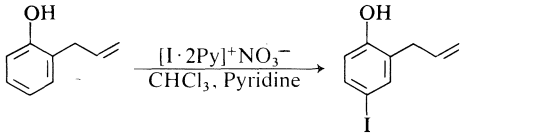

5 6

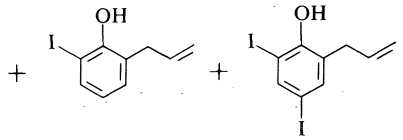

7 8

In the reaction between allylphenols and iodonium nitrate no addition to the double bond takes place until all the available positions *ortho* and *para* to the hydroxy group are substituted with iodine; subsequently addition occurs readily. Thus 2-allylphenol on reaction with 3 equiv. of INO_3 in chloroform–pyridine gave **9** in 13% yield and a substituted benzo[*b*]furan **10**. The regiochemistry of **9** is evident from the nmr

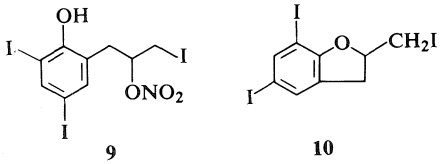

9 10

spectrum which showed characteristic absorptions for the $—CH_2I$ and $—CHONO_2$ groups at δ_{TMS} 3.33 and 5–5.5 respectively. The same type of products, **11** and **12**, were isolated from the addition of iodonium nitrate to 2-allyl-6-methylphenol in almost the same ratio (15% and 33.5% respectively).

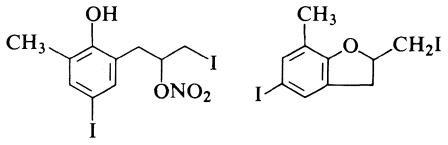

11 12

Phenol reacted with 3 mol equiv. of INO_3 to give 2,4,6-triiodophenol **13** in 94% yield. Similarly, *para*-cresol afforded a 90% yield of 2,6-diiodo-4-methylphenol **14** with 2 equiv. of INO_3.

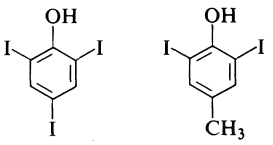

13 14

Aromatic primary amines react with INO_3 to give the corresponding iodinated products in low yield. This reaction is accompanied by tar formation probably due to oxidation of the amino group. It was also observed that a maximum of two iodine atoms can be introduced. Thus aniline with 3 equiv. of INO_3 gave 2,4-diiodoaniline **15** in 46% yield and *para*-toluidine

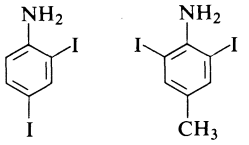

15 16

gave the corresponding diiodo compound **16** in 23% yield. Reactions of secondary and tertiary aromatic amines with INO_3 are cleaner and the iodinated products are obtained in good to excellent yields. For example, *N*-methylaniline with an excess of INO_3 gave a 78% yield of 2,4-diiodo-*N*-methylaniline **17**. In the case of *N*,*N*-dimethylaniline the reaction was regiospecific in that only the *para* iodinated product **18** was formed in 94.5% yield.

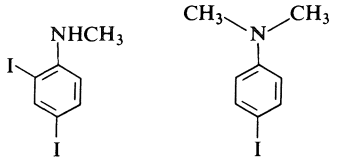

17 18

Only two of the three available *ortho* and *para* positions in aromatic 1°- and 2°-amines can be substituted with INO_3 in contrast to phenol. This may be due to the deactivation of the ring as a result of the introduction of the two iodine atoms. Steric factors may also play a role (*cf.* aniline and *N,N*-dimethylaniline).

This convenient method compares favorably with alternative methods of aromatic iodination. For example, iodine will only react with aromatic amines because the iodide precipitates as a salt; otherwise an oxidizing agent must be added to oxidize the iodide ion to iodine (4–6). Iodine chloride has also been used and tends to be a better iodinating agent (4). Recently another route to aromatic iodination has been developed using thallium trifluoroacetate and potassium iodide but tends to be more specialized in its applications (7).

Additions to Olefinic Alcohols

The behavior of neighbouring groups in electrophilic addition (4) of pseudo-halogens is often unpredictable. For example, whereas participation and subsequent migration of phenyl group have been observed in the addition of bromine (9), iodine chloride, iodine isocyanate, iodine azide (10), and bromine azide (11) to triphenylpropene, no participation by hydroxy group occurs in the addition of iodine isocyanate to 1,1-dimethylallyl alcohol (10, 11). Therefore we examined the reaction of iodonium nitrate with unsaturated substrates bearing potential neighbouring groups.

Reaction of 1-allylcyclohexanol with INO_3 in chloroform–pyridine gave a normal addition product **19**. The Markovnikov nature of the

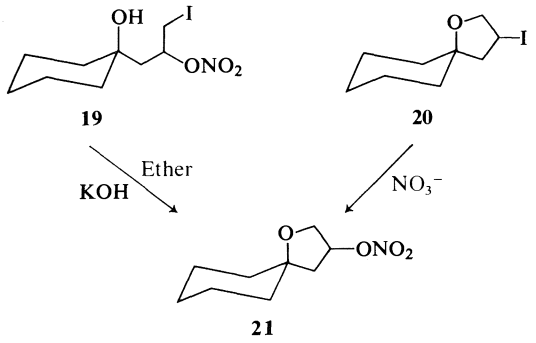

19 **20** **21**

addition was evident from the nmr spectrum which showed absorptions at δ 3.4 (d) and 5.23 (quintet) characteristic of $—CH_2I$ and $—CHONO_2$ (3). In addition to compound **19**, a spiro ether was isolated in 10% yield which proved to be **21** and not the expected product **20**. This was confirmed by the base-catalyzed cyclization of **19** to the spiro ether **21** which was characterized by its nmr and ir spectra and elemental analysis. The formation of spiro ether **21** in the addition of INO_3 to 1-allylcyclohexanol is explicable on the basis of the scheme outlined for the reaction of INO_3 with hex-5-en-3-ol (2).

Olefinic compounds which can give rise to five- or six-membered cyclic structures by neighbouring group participation in the addition of electrophilic reagents are generally expected to follow this path in preference to other reaction pathways as exemplified by the formation of five-membered cyclic ethers (12, 13) and lactones (14) in the electrophilic addition of iodine to pent-4-en-1-ol and 4-pentenoic acid respectively. Addition of INO_3 in chloroform–pyridine to pent-4-en-1-ol gave as the major product 2-iodomethyltetrahydrofuran **22** in 60% yield. In addition a small amount (6%) of isomeric hydroxyiodoalkyl nitrates **23** and **24** was produced in a ratio of approximately 9:1 as determined by comparing the intensities of $CHONO_2$

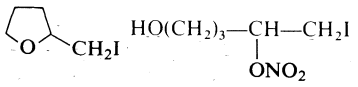

22 **23**

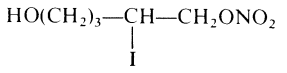

24

and $—CH_2ONO_2$ absorptions in the nmr spectrum. The ir spectrum showed intense hydroxy and nitrate absorptions. The structure of **22** was evident from the nmr and ir spectra. The ir spectrum showed no hydroxyl absorption. The cyclic ether and the iodonitrate esters were readily separable by chromatography on Florisil.

As the distance between the olefinic centre and the neighbouring hydroxy group increases, the propensity for participation decreases, as evi-

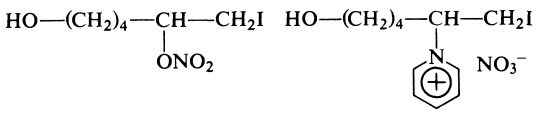

25 **26**

denced by the addition of INO_3 to hex-5-en-1-ol. The major products isolated were the hydroxy-iodoalkyl nitrate **25** and the pyridinium salt **26** formed in 21% and 39% yields respectively corresponding to regiospecific Markovnikov addition.

The cyclic ether 2-iodomethyl tetrahydropyran **27** was also formed in 17% yield. The behavior of pent-4-en-1-ol and hex-5-en-1-ol towards INO_3 is consistent with their behaviour towards bromine and iodine in that their propensity for

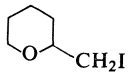

27

participation by a neighbouring hydroxyl group decreases if the resulting cyclic structure is six-membered rather than five-membered (13).

Reactions with Bicyclic Olefinic Alcohols

The behavior of bicyclic olefinic alcohols towards INO_3 was examined. It was anticipated that in such rigid ring systems ring closure by the neighbouring hydroxy group would be preferred to other modes of reaction namely addition and/or rearrangement, provided the participating group has the correct stereochemistry and the resulting ring system is stable. The three isomeric 5-norbornene-2,3-dimethanols namely, *endo-cis*-5-norbornene-2,3-dimethanol, *exo-cis*-5-norbornene-2,3-dimethanol, and *trans*-5-norbornene-2,3-dimethanol were synthesized according to literature procedures (15, 16). Reaction of *endo-cis*-5-norbornene-2,3-dimethanol with iodonium nitrate in chloroform–pyridine gave a cyclized product **28***A* in 74% yield and a

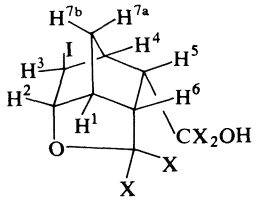

28
A X = H
B X = D

stoichiometric amount of pyridinium nitrate. Similarly addition of INO_3 to the deuterated analog (>95% deuterium) gave the corresponding cyclic ether **28***B*. Structural assignments for **28***A* and **28***B* are based on nmr and ir spectra and elemental analysis. Assignments of the various absorptions in the nmr spectra were made by comparison with other models (17–21) and extensive decoupling.

Reaction of iodonium nitrate with *trans*-5-norbornene-2,3-dimethanol in chloroform–pyridine gave the cyclized product **29** in 86% yield together with a corresponding amount of pyridinium nitrate. Compound **29** contained only one hydroxyl group as shown by the formation of a mono *para*-nitrobenzoyl derivative **30** in 70% yield, which was characterized by its nmr and ir spectra and elemental analysis.

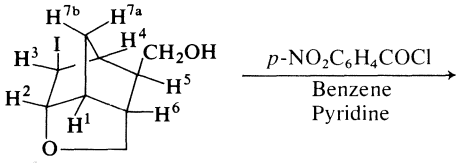

29

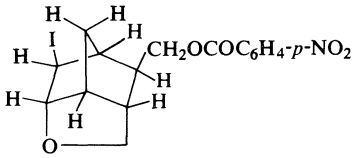

30

Reaction of *exo-cis*-5-norbornen-2,3-dimethanol with INO_3 gave a mixture of products from which the major product **31** was isolated in 40%

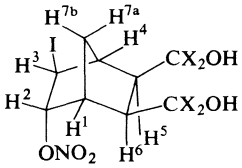

31
A X = H
B X = D

yield by chromatography on Florisil. The ir spectrum showed intense absorption at 1630 cm^{-1} indicating the presence of a ONO_2 group. The assignments of the various absorptions in the nmr spectrum were made by extensive decoupling and by comparison of the spectrum with that of **31***B* prepared from the deuterium analog. Thus the nmr spectrum of **31***B* showed δ 5.5 (q, 1H, H^2, $J_{2,3}$ = 2.8 Hz; $J_{1,2}$ = 2 Hz); 3.82 (t, 1H, H^3, $J_{2,3} = J_{3,7a}$ = 2.8 Hz). The methylene signal of the hydroxylmethyl groups in **31***A* appeared as a multiplet at δ 3.3–4.

Anti-7-norbornenol (19), on reaction with INO_3 in chloroform–pyridine gave **32** as the sole product indicating a preference for addition. Compound **32** was characterized as its *para*-nitrobenzoyl derivative **33**. *syn*-7-Norbornenol

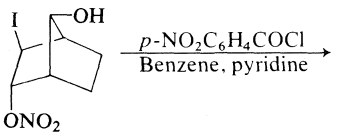

32

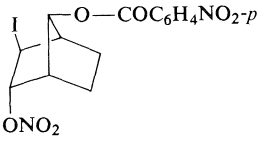

33

(24) reacted more slowly than **32** with INO_3 to give a mixture of several products as shown by the nmr spectrum of the crude reaction products, which could not be separated and characterized.

Like the hydroxyl group, the carboxyl group can also participate in INO_3 additions if such participation can lead to five- or six-membered ring structures (14, 25). An example is provided by the addition of INO_3 to 4-pentenoic acid which gave the iodolactone **34** together with a stoichiometric amount of pyridinium nitrate. Compound **34** has also been obtained in the addition of iodine and iodine cyanide to 4-pentenoic acid.

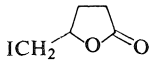

34

An example of participation by a neighbouring sulfur is provided in the addition of INO_3 to the allylthiourea **35** which gave a cyclized product assigned the thiazoline structure **36**. The more

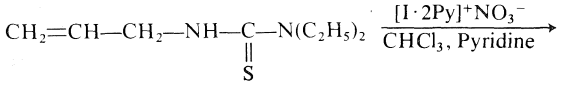

35

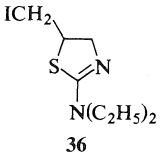

36

quantitative aspects of these reactions of iodonium nitrate are discussed in the following paper (31).

Experimental

Melting points were determined on a Fisher-Johns apparatus and are uncorrected. The ir spectra were recorded on a Perkin-Elmer model 421 spectrophotometer, and only the principal, sharply defined peaks are reported. The ^1H nmr spectra were recorded on Varian A-60 and A-100 analytical spectrometers. The spectra were measured on approximately 10–15% (w/v) solutions in appropriate deuterated solvents with tetramethylsilane as standard. Line positions are reported in ppm from the reference. Noise decoupled ^{13}C nmr spectra were obtained at 25.15 MHz in 12 mm spinning tubes on a Varian HA-100-15 instrument. Mass spectra were determined on an Associated Electrical Industries MS-9 double focussing high resolution mass spectrometer. The ionization energy, in general, was 70 eV. Peak measurements were made by comparison with perfluorotributylamine at a resolving power of 15000. Kieselgel DF-5 (Camag, Switzerland) and Eastman Kodak precoated sheets were used for thin layer chromatography.

The gc analyses were performed with an Aerograph model A-700 gas chromatograph. The lc analyses were made with a Waters Associates model ALC-100 liquid chromatograph. Microanalyses were carried out by Mrs. D. Mahlow of this department.

General Procedure for the Reaction of Iodonium Nitrate with Unsaturated Substrates

Silver nitrate, 6.8 g (0.04 mol) was dissolved in a mixture of 50 ml of anhydrous chloroform and 15 ml of anhydrous pyridine. Iodine monochloride, 6.5 g (0.4 mol) in 20 ml of dry chloroform, was added dropwise to the stirred solution. The silver chloride produced was collected and washed with a mixture of 10 ml of chloroform and 10 ml of pyridine. A 0.04 mol quantity of the unsaturated substance was added all at once to the yellow filtrate. The mixture was stirred at room temperature for 3 h, then poured into an excess of ether and chilled. The resulting precipitate was collected and the filtrate concentrated *in vacuo*. The oil obtained was taken up in 50 ml of ether and washed with 50 ml of 5% cold hydrochloric acid to remove pyridine and then with 25 ml of cold water to remove any remaining pyridinium salt. If the ether solution was colored with iodine, it was washed with 20 ml of 5% sodium thiosulfate solution and then with 20 ml of water. The ether layer was dried ($MgSO_4$) and evaporated *in vacuo*. Further purification of the iodonitrate ester so obtained was effected by distillation under reduced pressure.

The ether insoluble residue, after washing several times with ether, was extracted with a 50:50 mixture of ethanol–isopropanol and filtered. Ether was added to the filtrate dropwise until the solution turned cloudy. The solution contained in a small beaker was placed in a larger beaker containing a little ether; the large beaker was covered with plastic film and kept in the refrigerator overnight. The resulting precipitate was collected and washed with ether containing a little ethanol and then with ether to

afford the iodopyridinium nitrate. In a few instances, when the iodopyridinium salt was difficult to purify and very dark in color (contamination with iodine and tarry materials), the purification was carried out by chromatography on silica gel, eluting with $CHCl_3$, 5% CH_3OH in $CHCl_3$ (v/v), 10% CH_3OH in $CHCl_3$ (v/v), and 30% CH_3OH in $CHCl_3$ (v/v), the iodopyridinium salt being collected with the last mixture of solvents.

Reaction of Iodonium Nitrate with 2,3-Dimethyl-1,3-butadiene in Chloroform–Pyridine

To a solution of iodonium nitrate (0.04 mol) in 60 ml of chloroform and 25 ml of pyridine was added 3.28 g (0.04 mol) of 2,3-dimethyl-1,3-butadiene all at once. The mixture was stirred at room temperature for 3 h, then poured into an excess of ether and chilled. The resulting precipitate was collected. Evaporation of the filtrate *in vacuo* did not give any identifiable material.

The ether insoluble residue after washing several times with ether was extracted with ethanol at room temperature and filtered. Ether was added dropwise to the filtrate till it turned cloudy. Crystallization by the method discussed before gave 8.4 g (60%) of *N-[3-(4-iodo-2,3-dimethyl)-butenyl]pyridinium nitrate* **1**; mp 106–108 °C. *Anal.* calcd. for $C_{11}H_{15}N_2O_3I$: C 37.73, H 4.32, N 8.00; found: C 37.70, H 4.03, N 7.91. The nmr spectrum δ_{TMS} ($(CD_3)_2SO$) 1.67 (s, 3H, CH_3—C=C), 2.03 (s, 3H, CH_3—C(—)=N$^+$(=)—), 4.3 (s, 2H, —CH_2I), 5.28 (s, 1H, one olefinic hydrogen), 5.41 (m, 1H, other olefinic hydrogen), 8.2–9.3 (m, 5H, pyridine hydrogens).

The ethanol insoluble residue was extracted with hot methanol and filtered. Addition of ether and filtration gave 0.8 g (5.5%) of *N,N'-[1,4-(2,3-dimethylbut-2-enyl)]dipyridinium dinitrate* **2** mp 261–263 °C (dec.). *Anal.* calcd. for $C_{16}H_{20}N_4O_6$: C 52.97, H 5.49, N 15.38; found: C 52.43, H 5.51, N 15.33. The nmr spectrum δ_{TMS} ($(CD_3)_2SO$) 1.82 (s, 6H, 2—CH_3), 5.4 (s, 4H, —CH_2—N$^+$(=)—), 7.9–8.8 (m, 10H, Py).

Reaction with p-Methoxychalcone

A similar reaction between iodonium nitrate (0.40 mol) and *p*-methoxychalcone (0.04 mol) in chloroform–pyridine afforded *N-[1-(2-iodo-2-benzoyl-1-para-methoxyphenyl-ethyl)]pyridinium nitrate* **4** mp 178–179 °C (dec.) in 91% yield. *Anal.* calcd. for $C_{21}H_{19}N_2O_6I$: C 49.79, H 3.75, N 5.53; found: C 49.73, H 3.72, N 5.57.

General Procedure for the Reaction of Iodonium Nitrate with Phenols and Anilines.

The procedure was similar to that described above. Addition of the reaction mixture to an excess of ether resulted in the precipitation of an equivalent amount of pyridinium nitrate which was collected. The filtrate was concentrated *in vacuo* and the residual oil taken up in ether. The ether extract was washed with water, sodium thiosulfate solution, and then with water. Evaporation *in vacuo* after drying ($MgSO_4$) gave the iodinated compound. Purification was effected either by crystallization from a suitable solvent or chromatography on Florisil. Addition to 2-allylphenol gave 4,6-diiodo-2-allylphenol **8** in 74.5% yield. *Mol. Wt.* calcd. for $C_6H_8OI_2$: 385.8664; found (ms): 385.8688. Infrared ν_{max} ($CHCl_3$) 3845 (OH), 1633 (C=C) cm^{-1}; nmr δ_{TMS} ($CDCl_3$) 7.8 (d, 1H, H^3, $J_{3,5}$ = 2 Hz), 7.4 (d, 1H, H^5, $J_{5,3}$ = 2 Hz), 5.5–6.3 (m, 1H, C*H*=CH_2), 5.4 (s, 1H, —OH), 4.8–5.3 (m, 2H, =CH_2), 3.4 (d, 2H, —CH_2—).

Similarly phenol gave 2,4,6-triiodophenol (26) **13** in 94% yield; 4-methylphenol gave 2,6-diiodo-4-methylphenol **14** (27) in 90% yield, aniline gave 2,4-diiodoaniline **15** (28) in 46% yield, 4-methylaniline gave 2,4-diiodo-*N*-methylaniline **16** (29) in 23% yield, and *N,N*-dimethylaniline gave 4-iodo-*N,N*-dimethylaniline **18** (30) in 95% yield. *N*-methylaniline afforded 2,4-diiodo-*N*-methylaniline **17** in 78% yield. *Mol. Wt.* calcd. for $C_7H_7NI_2$: 358.8660; found (ms): 358.8662. Infrared ν_{max} ($CHCl_3$) 3405 (NH) cm^{-1}; nmr δ_{TMS} ($CDCl_3$) 7.85 (d, 1H, H^3, $J_{3,5}$ = 2 Hz), 7.4 (q, 1H, H^5, $J_{5,3}$ = 2 Hz, $J_{5,6}$ = 8.5 Hz), 6.27 (d, 1H, H^6, $J_{5,6}$ = 8.5 Hz), 6.2 (brs, 1H, —NH—), 2.83 (s, 3H, CH_3).

General Procedure for the Reaction of Iodonium Nitrate with Unsaturated Alcohols

The procedure in chloroform–pyridine was similar to that discussed before. When the reactions were carried out in chloroform–*sym*-collidine the following procedure was adopted. The reaction mixture was added to sufficient ether to precipitate the collidinium salt. The precipitate was collected and the ethereal layer was washed several times successively with (*a*) cold hydrochloric acid (5%) saturated with sodium chloride, (*b*) saturated aqueous sodium chloride, (*c*) sodium bicarbonate (5%) saturated with sodium chloride until neutral, and finally (*d*) saturated sodium chloride solution containing sodium thiosulfate. The ether layer was dried ($MgSO_4$) and concentrated *in vacuo*. The residual oil was distilled under reduced pressure. The iodopyridinium salts were purified by the crystallization procedure described before.

Hex-1-en-3-ol with INO_3 gave an isomeric mixture of 3-hydroxy-1-iodohex-2-yl nitrate and 3-hydroxy-2-iodohex-1-yl nitrate bp 90 °C/0.1 torr in a yield of 34%. *Anal.* calcd. for $C_6H_{12}NO_4I$: C 24.95, H 4.2, N 4.85; found: C 24.95, H 4.2, N 4.85. This product was formed together with a 16% yield of the corresponding iodopyridinium salt.

1-Allylcyclohexanol similarly gave 4-hydroxy-4,4-pentamethylene-1-iodobut-2-yl nitrate **19** in 55% yield. *Mol. Wt.* calcd. for $C_9H_{16}NO_3I$: 329.0124; found (ms): 329.0113. This product was formed together with a 15% yield of the corresponding iodopyridinium salt and 10% of the spiro ether **21**.

2-Allylphenol with INO_3 gave 3-(2-hydroxy-3,5-diiodo)phenol-1-iodoprop-2-yl nitrate **9** in 13% yield. *Mol. Wt.* calcd. for $C_9H_8NO_4I_3$: 574.7587; found (ms): 574.7598. The nmr δ_{TMS} ($CDCl_3$) 5.0–5.5 (2H, m, —$CHONO_2$), 3.33 (2H, m, —CH_2I), 3.1 (m, 2H, —CH_2—), 7.45, 7.9 (2d, 2H, aromatic protons, J = 2 Hz). In addition was formed 2-iodomethyl-5,7-diiodobenzo-[*b*]2,3-dihydrofuran **10** in 33% yield. *Mol. Wt.* calcd. for $C_9H_7OI_3$: 511.7631; found (ms): 511.7631. The nmr δ_{TMS} ($CDCl_3$) 3.1–3.5 (4H, m, —CH_2I), 4.9 (m, 1H, —CH—O), 7.4, 7.75 (2d, 2H, aromatic protons, J = 1 Hz).

Similarly 2-allyl-6-methylphenol gave 3-(2-hydroxy-5-

iodo-3-methyl)phenyl-1-iodoprop-2-yl nitrate **11** in 15% yield. *Mol. Wt.* calcd. for $C_{10}H_{11}NO_4I_2$: 462.8778; found (ms): 462.8773. The nmr δ_{TMS} ($CDCl_3$) 5.2 (1H, quint, J = 6 Hz, —$CHONO_2$), 3.33 (2H, m, —CH_2I), 2.2 (s, 3H, CH_3), 3.1 (m, 2H, CH_2), 7.4 (s, 2H, aromatic hydrogens). In addition was formed 2-iodomethyl-5-iodo-6-methylbenzo[*b*]2,3-dihydrofuran **12** in 33.5% yield. *Mol. Wt.* calcd. for $C_{10}H_{10}OI_2$: 399.8822; found (ms): 399.8828. The nmr δ_{TMS} ($CDCl_3$) 3.33 (2H, m, —CH_2I), 3.04 (m, 2H, —CH_2—), 7.3 (s, 2H, aromatic protons), 4.8 (m, 1H, —CH—O), 2.14 (s, 3H, —CH_3).

Base-catalyzed Cyclization of 1-Iodo-4-hydroxy-4,4-pentamethylenebut-2-yl Nitrate

To a stirred solution of 7.1 g (0.0215 mol) of 1-iodo-4-hydroxy-4,4-pentamethylenebut-2-yl nitrate **19** in 50 ml of ether was added 2.25 g (0.04 mol) of powdered potassium hydroxide. The mixture was stirred at room temperature overnight and then filtered. The ether solution was washed with 25 ml portions of water twice and dried ($MgSO_4$). Removal of the ether *in vacuo* gave 3.8 g (88%) of *5,5-pentamethylenetetrahydrofuran-3-yl nitrate* **21**, which was purified by distillation under reduced pressure; bp 66–67 °C/0.07 torr. *Anal.* calcd. for $C_9H_{15}NO_4$: (mol. wt. 201.1001) C 53.72, H 7.46, N 6.97; found: (M, ms, 201.0995) C 53.97, H 7.43, N 6.82. The nmr spectrum δ_{TMS} ($CDCl_3$) 1.57 (br s, 10H, cyclohexane ring hydrogens), 1.9–2.15 (m, 2H, —CH_2—), 4.7 (m, 2H, —CH_2—O), 5.5 (m, 1H, —CH—ONO_2). The ir spectrum ν_{max} (liquid film), 1630, 1275 cm^{-1} (—ONO_2).

Addition of Iodonium Nitrate to Pent-4-en-1-ol in Chloroform–Pyridine

To a solution of iodonium nitrate (0.02 mol) in 30 ml of chloroform and 12.5 ml of pyridine was added 1.55 g (0.018 mol) of pent-4-en-1-ol; the mixture was stirred at room temperature for 3 h and then poured into an excess of ether and chilled. The precipitated pyridinium nitrate was collected and the filtrate concentrated *in vacuo*. The residual oil was taken up in ether and washed successively with 40 ml of cold 5% hydrochloric acid, 25 ml of water, 25 ml of 5% sodium thiosulfate solution, and finally with 25 ml of water. The ether layer was dried ($MgSO_4$) and concentrated *in vacuo*. The residual oil was chromatographed on 75 g of Florisil and eluted with petroleum ether – chloroform (9:1) and then with chloroform–methanol (9:1). Evaporation of the first fraction gave 2.29 g (60%) of *2-iodomethyltetrahydrofuran* **22**. The nmr spectrum δ_{TMS} ($CDCl_3$) 3.25 (d, 2H, —CH_2—I, J = 6 Hz), 1.5–2.3 (m, 4H, 2 —CH_2—), 3.6–4.1 (m, 3H, —CH—O, —CH_2—O).

Evaporation of the second fraction gave a mixture of *5-hydroxy-1-iodopent-2-yl nitrate* **23** and *5-hydroxy-2-iodopent-1-yl nitrate* **24**, 0.3 g (6%).

Addition of Iodonium Nitrate to Hex-5-en-1-ol in Chloroform–Pyridine

The reaction was carried out by the general procedure described before. The oil obtained on evaporation of the dried ($MgSO_4$) ether solution was chromatographed on Florisil and eluted with petroleum ether – chloroform (1:1) and then with chloroform–methanol (9:1). Evaporation of the first fraction gave 0.7 g (17%) of *2-iodomethyltetrahydropyran* **27**. The nmr spectrum δ_{TMS} ($CDCl_3$) 3.23 (s, 2H, —CH_2—I), 0.8–2.5 (m, 6H, 3 —CH_2—), 3.1–3.7 (m, 2H, —CH_2—O), 3.9–4.25 (m, 1H, —CH—O).

Evaporation of the second fraction gave 1.115 g (21%) of *6-hydroxy-1-iodohexyl nitrate* **25**.

The ether insoluble residue was extracted with ethanol and a small amount of ether added. The precipitated pyridinium nitrate was collected and more ether added to the filtrate. The resulting oil was separated by decantation and the excess solvents removed *in vacuo* to afford 2.6 g (39%) of *N-[2-(6-hydroxyl-1-iodohexyl)]pyridinium nitrate* **26** as an oil.

Addition of Iodonium Nitrate to endo-cis-5-Norbornene-2,3-dimethanol in Chloroform–Pyridine

Reaction of iodonium nitrate (0.03 mol) in 40 ml of chloroform and 20 ml of pyridine with 4.16 g (0.027 mol) of *endo-cis*-5-norbornene-2,3-dimethanol (15, 16) at room temperature for 2½ h and work-up by the usual procedure gave the cyclic ether **28***A*. Yield 5.58 g (74%). Purification was effected by recrystallization from ether–hexane; mp 54.5–55.5 °C. *Anal.* calcd. for $C_9H_{13}O_2I$: (mol. wt. 279.9961) C 38.56, H 4.64; found: (279.9971, ms) C 37.87, H 4.68. The nmr spectrum δ_{TMS} ($CDCl_3$) see text. The ir spectrum ν_{max} ($CHCl_3$) 3620, 3450 cm^{-1} (—OH). Similarly reaction of *endo-cis*-5-norbornene-2,3-dimethanol-d_4 with iodonium nitrate gave **28***B* (70%).

Addition of Iodonium Nitrate to trans-5-Norbornene-2,3-dimethanol in Chloroform–Pyridine

Reaction of iodonium nitrate (0.02 mol) in 30 ml of chloroform and 15 ml of pyridine with 2.772 g (0.018 mol) of *trans*-5-norbornene-2,3-dimethanol (15, 16) at room temperature for 3 h and work-up by the usual procedure gave 4.315 g (86%) of the cyclic ether **29**. The nmr spectrum δ_{TMS} ($CDCl_3$) 1.5–2.7 (m, 6H, H^1, H^6, H^5, H^4, H^7, H^{7a}), 3.65 (d, 1H, CH—I, $J_{3,7a}$ = 2.3 Hz), 4.73 (d, 1H, CH—O, $J_{1,2}$ = 5 Hz). The ir spectrum ν_{max} (liquid film) 3400 cm^{-1} (—OH).

para-Nitrobenzoylation of Cyclic Ether 29

To a solution of 0.650 g (2.32 mmol) of **29** and 0.237 g (3 mmol) of pyridine in 25 ml of anhydrous benzene was added a solution of 0.431 g (2.32 mmol) of *para*-nitrobenzoyl chloride in 10 ml of anhydrous benzene dropwise and the mixture stirred at room temperature overnight. The precipitated pyridinium chloride was collected and the filtrate washed with 20 ml of 5% sodium bicarbonate solution and then with 20 ml of water. Removal of the solvent *in vacuo* after drying ($MgSO_4$) gave an oil which was crystallized from benzene–hexane to afford 0.7 g (70%) of the *para*-nitrobenzoyl derivative **30**; mp 105–105.5 °C. *Anal.* calcd. for $C_6H_{16}NO_5I$: C 44.75, H 3.73, N 3.26; found: C 45.13, H 3.74, N 3.29. The nmr spectrum δ_{TMS} ($CDCl_3$) 1.7–2.85 (m, 6H, H^1, H^6, H^5, H^4, H^7, H^{7a}), 3.7 (d, 1H, CH—I, J = 2 Hz), 3.8 (d, 2H, —CH_2—O, J = 2 Hz), 4.33 (d, 2H, —CH_2—O—C(=O)—, J = 8 Hz), 4.8 (d, 1H, CH—O, J = 4.5 Hz), 8.35 (m, 4H, aromatic hydrogens). The ir spectrum ν_{max} ($CHCl_3$) 1735 cm^{-1} (C=O), 1530 cm^{-1} (—NO_2).

Addition of Iodonium Nitrate to exo-cis-5-Norbornene-2,3-dimethanol in Chloroform–Pyridine

The reaction was carried out as before with iodonium

nitrate (0.02 mol) in chloroform–pyridine and the olefinic alcohol, 2.772 g (0.018 mol). The oil obtained after evaporation of the dried ($MgSO_4$) solution was chromatographed on Florisil and eluted with chloroform, chloroform–methanol (19:1), and chloroform–methanol (9:1). Evaporation of the last fraction gave 2.45 g (40%) of the adduct, **31***A*, which was recrystallized from chloroform–hexane; mp 86–88 °C. *Anal.* calcd. for $C_9H_{14}NO_5$: C 31.5, H 4.08, N 4.08; found: C 31.38, H 3.99, N 3.75. The nmr spectrum δ_{TMS} ($CDCl_3$) 1.5–2.6 (m, 6H, H^1, H^6, H^5, H^4, H^{7a}, H^{7b}), 6.2 (s, 2H, 2 —OH), 3.3–4.0 (m, 5H, 2 $—CH_2—O$, —CH—I), 5.5 (m, 1H, *CH*—ONO_2). The ir spectrum ν_{max} ($CHCl_3$) 3600, 3430 cm^{-1} (—OH), 1637 (O—NO_2).

Similarly reaction of 1.386 g (9 mmol) of *exo-cis*-5-norbornene-2,3-dimethanol-d_4 with iodonium nitrate (0.01 mol) in chloroform–pyridine and work-up by the method described above gave 1.13 g (36%) of the adduct **31***B*. The nmr spectrum δ_{TMS} ($CDCl_3$) 1.5–2.6 (m, 6H, H^1, H^6, H^5, H^4, H^{7a}, H^{7b}), 3.82 (t, 1H, —CH—I), 5.5 (m, 1H, —CH—ONO_2).

Addition of Iodonium Nitrate to anti-7-Norbornenol in Chloroform–Pyridine

The reaction was carried out according to the general procedure. Thus reaction of iodonium nitrate (0.01 mol) and 0.99 g (0.9 mmol) of *anti*-7-norbornenol (23) gave 2 g (74.3%) of *anti*-7-hydroxy-*exo*-3-iodo-*endo*-norborn-2-yl nitrate **32**. The nmr spectrum δ_{TMS} ($CDCl_3$) 1.2–2.5 (m, 4H, $—CH_2—$), 2.2 (s, 1H, —OH), 2.6 (m, 2H, H^1, H^4), 3.6 (d, 1H, —CH—I, J = 3 Hz), 4.8 (m, 1H, —C*H*—OH), 5.6 (m, 1H, —CH—ONO_2). The ir spectrum ν_{max} ($CHCl_3$) 3600 cm^{-1} (—OH), 1637, 1275 cm^{-1} (—ONO_2).

*para-Nitrobenzoylation of Adduct **32***

The reaction was carried out as described before. Thus from 1 g (3.344 mmol) of adduct **32** and 0.625 g (3.344 mmol) of *para*-nitrobenzoyl chloride was formed 0.77 g (51.4%) of *anti-7-para-nitrobenzoyloxy-exo-3-iodo-endo-norborn-2-yl nitrate*, **33**; mp 119, 120 °C (benzene–hexane). *Anal.* calcd. for $C_4H_{13}N_2O_7$: C 37.5, H 2.9, N 6.25; found: C 38.06, H 2.94, N 5.88. The nmr spectrum δ_{TMS} ($CDCl_3$) 1.45–2.25 (m, 4H, 2 $—CH_2—$), 2.9 (m, 2H, H^1, H^4), 3.75 (d, 1H, —CH—I, J = 3 Hz), 5.6 (m, 2H, *CH*—ONO_2, —*CH*—O—C(=O)—). The ir spectrum ν_{max} ($CHCl_3$) 1733 cm^{-1} (>C=O), 1645 cm^{-1} (ONO_2), 1525 (—NO_2).

Addition of Iodonium Nitrate to 4-Pentenoic Acid in Chloroform–Pyridine

The addition was carried out as described before. Thus reaction of iodonium nitrate (0.04 mol) in 60 ml of chloroform and 25 ml of pyridine with 3.6 g (0.036 mol) of 4-pentenoic acid and work-up by the usual procedure gave 4.9 g (60%) of 5-iodomethylbutyrolactone, **34**. Purification was effected by chromatography on Florisil and elution with chloroform. *Anal.* calcd. for $C_5H_7O_2I$: (mol. wt. 225.9491) C 26.56, H 3.10, I 56.2; found: (225.9486, ms) C 27.01, H 3.18, I 58.28. The nmr spectrum δ_{TMS} ($CDCl_3$) 1.7–2.8 (m, 4H, 2 $—CH_2—$), 3.4 (t, 2H, $—CH_2I$, J = 4 Hz, 6.5 Hz), 4.6 (m, 1H, —CH—O). The ir spectrum ν_{max} (liquid film) 1775 cm^{-1} (>C=O).

Addition of Iodonium Nitrate to 3-Allyl-1,1-diethyl-2-thiourea in Chloroform–Pyridine

To a stirred solution of iodonium nitrate (0.02 mol) in 40 ml of chloroform and 15 ml of pyridine was added 3.49 g (0.02 mol) of 3-allyl-1,1-diethyl-2-thiourea all at once. An exothermic reaction took place and the color changed to dark brown. The mixture was stirred at room temperature for 3 h, then poured into an excess of ether and chilled. The resulting residue was collected, washed several times with ether, extracted with cold methanol, filtered, and reprecipitated with ether. The residue was chromatographed on 100 g of silica gel and eluted with benzene–methanol (85:15). Evaporation of the eluate gave an oily residue (3.3 g) which solidified slowly on standing to give *2-diethylamino-5-iodomethyl-2-thiazoline*, **36**. *Mol. Wt.* calcd. for $C_8H_{15}N_2SI$: 298.0001; found (ms): 298.0003. The nmr spectrum δ_{TMS} $(CD_3)_2SO$ 1.03 (t, 6H, 2 $CH_3—CH_2—$, J = 6.5 Hz), 3.3–4.6 (m, 9H, $—CH_2—$, CH_2I, 2 $—N—CH_2—$, —CH—). The ir spectrum ν_{max} ($CHCl_3$) 1597–1625 (—C=N—).

Acknowledgments

This research was supported by the National Research Council of Canada and the Chemistry Department of the University of Alberta.

1. J. W. Lown and A. V. Joshua. J. Chem. Soc. Perkin Trans. 1, 2680 (1973).
2. U. E. Diner, M. Worsley, and J. W. Lown. J. Chem. Soc. (C), 3131 (1971).
3. U. E. Diner and J. W. Lown. Can. J. Chem. **49**, 403 (1971).
4. J. March. Advanced organic chemistry, reactions, mechanisms and structure. McGraw-Hill, New York. 1968. p. 405.
5. E. Grovenstein and N. S. Aprahamian. J. Am. Chem. Soc. **84**, 212 (1962).
6. L. Schutte and E. Havinga. Tetrahedron, **26**, 2297 (1970).
7. E. C. Taylor, F. Kienzle, R. L. Robey, and A. McKillop. J. Am. Chem. Soc. **92**, 2175 (1970).
8. B. Capon. Q. Rev. **18**, 45 (1964).
9. R. O. C. Norman and C. B. Thomas. J. Chem. Soc. (B), 598 (1967).
10. A. Hassner and J. S. Teeter. J. Org. Chem. **35**, 3397 (1970).
11. A. Hassner and J. S. Teeter. J. Org. Chem. **36**, 2176 (1971).
12. D. L. H. Williams. Tetrahedron Lett. 2001 (1967).
13. D. L. H. Williams, E. Bienvenue-Goetz, and J. E. Dubois. J. Chem. Soc. (B), 517 (1969).
14. E. E. van Tamelyn and M. Shamma. J. Am. Chem. Soc. **76**, 2315 (1954).
15. H. N. Miller and K. W. Greenlee. J. Org. Chem. **26**, 3734 (1961).
16. D. Craig. J. Am. Chem. Soc. **73**, 4889 (1951).
17. A. Factor and T. G. Traylor. J. Org. Chem. **33**, 2607 (1968).

18. F. A. L. ANET. Can. J. Chem. **39**, 789 (1961).
19. P. LASZLO and P. R. SCHLEYER. J. Am. Chem. Soc. **85**, 2709 (1963).
20. P. LASZLO and P. R. SCHLEYER. J. Am. Chem. Soc. **86**, 1171 (1964).
21. P. M. SUBRAMANIAN, M. E. EMERSON, and N. A. LEBEL. J. Org. Chem. **30**, 2624 (1965).
22. J. MEINWALD, Y. C. MEINWALD, and T. N. BAKER. J. Am. Chem. Soc. **86**, 4074 (1964).
23. P. R. STORY. J. Org. Chem. **26**, 287 (1961).
24. W. C. BAIRD. J. Org. Chem. **31**, 2411 (1966).
25. R. T. ARNOLD and K. L. LINDSAY. J. Am. Chem. Soc. **75**, 1048 (1954).
26. J. E. MARSH. J. Chem. Soc. 3164 (1927).
27. R. L. DATTA and N. PROSAD. J. Am. Chem. Soc. **39**, 443 (1917).
28. E. ELBS and H. VOLK. J. Prakt. Chem. **99**, 270 (1919).
29. H. L. WHEELER and L. M. LIDDLE. Am. Chem. J. **42**, 449 (1909).
30. F. AITKEN and T. H. READE. J. Chem. Soc. 1896 (1926).
31. J. W. LOWN and A. V. JOSHUA. Can. J. Chem. This issue.

Kinetics and energetics of the addition of iodonium nitrate to unsaturated systems

J. William Lown and Alummoottil V. Joshua[1]

Department of Chemistry, University of Alberta, Edmonton, Alta., Canada T6G 2G2

Received June 17, 1976

J. William Lown and Alummoottil V. Joshua. Can. J. Chem. **55**, 131 (1977).

The stereochemistry of the products of addition of iodonium nitrate to a series of cycloalk-2-en-1-ols indicates that the intermediate iodonium ion is formed *cis* to the neighbouring hydroxyl in the case of five-, six-, and seven-membered cyclic alkenols and *trans* to the hydroxyl in the case of cycloct-2-en-1-ol. The rates and Arrhenius parameters for the second-order additions of iodonium nitrate to these and other unsaturated substrates have been determined. An α-hydroxy group enhances the rate of addition over the corresponding alkene when the iodonium ion is formed *cis* to the hydroxyl and has the opposite effect when it is formed *trans* to the hydroxyl. This evidence for neighbouring hydroxyl group participation in additions of iodonium nitrate is in contrast to the known chemistry of iodine isocyanate and iodine azide. The effects of structural changes of the substrate on the kinetic and energetic parameters in iodonium nitrate additions are discussed and compared with those of other pseudo-halogens.

J. William Lown et Alummoottil V. Joshua. Can. J. Chem. **55**, 131 (1977).

La stéréochimie des produits d'addition du nitrate d'iodonium à une série de cycloalcène-2 ols-1 indique que l'ion iodonium intermédiaire est formé en position *cis* par rapport au groupement hydroxyle voisin dans le cas des alkanols cycliques à cinq, six et sept chaînons et *trans* par rapport au groupe hydroxyle dans le cas du cyclooctène-2 ol-1. On a déterminé les vitesses et les paramètres d'Arrhénius pour les additions du second ordre du nitrate d'iodonium à ces substrats insaturés et à d'autres substrats. Un groupe hydroxyle en α augmente la vitesse d'addition par rapport à l'alcène correspondant lorsque l'ion idononium se forme *cis* par rapport à l'hydroxyle et présente l'effet opposé quand il est formé *trans* par rapport à l'hydroxyle. Ces indications concernant la participation du groupe hydroxyle voisin à l'addition du nitrate d'iodonium est en opposition avec la chimie connue de l'isocyanate d'iode et de l'azoture d'iode. On discute des effets produits par des changements structuraux dans le substrat sur les paramètres cinétiques et énergétiques des additions de nitrate d'iodonium et on les compare avec ceux d'autres pseudo-halogènes.

[Traduit par le journal]

Introduction

In previous papers we have explored the chemical behavior of iodonium nitrate, particularly in electrophilic additions to a wide range of unsaturated substrates (1–4). Iodonium nitrate (generated by the reaction of iodine chloride with silver nitrate in chloroform–pyridine) like

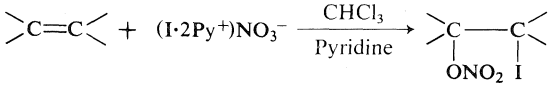

other pseudohalogens has all the characteristics of an electrophilic reagent which is consistent with the qualitative observation that electron-donating groups facilitate the reaction while electron-withdrawing groups considerably retard or even arrest it (1, 2).

But iodonium nitrate differs from the other pseudohalogens in that in this reagent the iodine is complexed to two pyridine groups through nitrogen (1, 2). The effect of this complexation may alter its relative electrophilicity compared to other iodine containing pseudohalogens such as iodine isocyanate, iodine chloride, and iodine azide depending on the electronic and steric environments in the olefinic substrate. It was also observed that iodonium nitrate in both chloroform–pyridine and chloroform–*sym*-collidine added to suitable olefinic substrates gives cyclized and/or addition products depending upon the structure of the substrate (2, 3). These results were in contrast to the known chemistry of iodine isocyanate (5) and iodine azide (6). Also, addition of INO_3 to cyclohex-2-en-1-ol gives products derived from intermediate iodonium ions which are formed *cis* to the hydroxyl group, signifying some compensating interaction

[1]NRCC scholarship holder 1974–1975.

between the iodine and hydroxyl group (3) (see below).

Therefore we undertook a kinetic study of the addition of iodonium nitrate to olefins of varying nucleophilic character to allow comparison with other pseudo-halogens and with a view to obtaining thermodynamic evidence for neighboring group participation and for the stereodirectional character of these electrophilic additions.

Results and Discussion

Stereochemical Directing Influence of Neighboring Hydroxyl Groups in the Addition of Pseudohalogens to Cycloalk-2-en-1-ols.

Addition of iodonium nitrate to cyclohex-2-en-1-ol in chloroform–pyridine gave an iodonitrate ester **1** in 36% yield and the iodopyridinium nitrate **2** in 29% yield. Examination of the appropriate coupling constants in the nmr spectrum of **1** showed it to be 3-hydroxy-2-iodocyclohexyl nitrate with the stereochemistry shown in which the hydroxy group is axial. Assuming both the iodonitrate ester and the iodopyridinium salt are formed from the same intermediate iodonium ion, structure **2** is proposed for the salt. Parallel reaction of iodonium

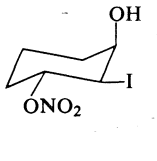

1

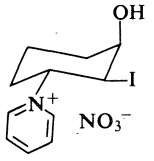

2

nitrate in chloroform–*sym*-collidine with cyclohex-2-en-1-ol gave **1** in 55% yield (3).

The stereochemistry of the two possible products favors an intermediate of type **3** and proves that the iodonium ion is formed *cis* to the hydroxyl group. This is in agreement with the observed stereochemistry of epoxidation of cyclohex-2-en-1-ols in which the oxirane ring is formed *cis* to the hydroxy group (7, 8). Apparently the epoxidation reagent becomes associated in some way with the hydroxy group in the molecule prior to attacking the double bond and is therefore constrained to approach the latter from the side of the ring which bears the hydroxy group.

The above result prompted us to investigate the stereochemical directing influence of hydroxy groups in the addition of other pseudohalogens to cyclohex-2-en-1-ol and also in the addition

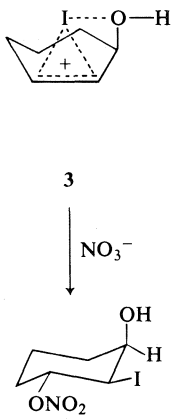

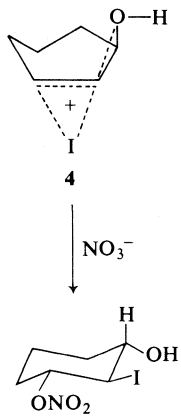

of iodonium nitrate to cycloalk-2-en-1-ols of various ring sizes.

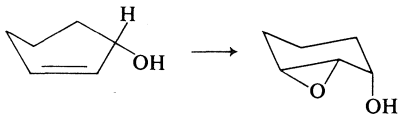

Reaction of iodine azide with cyclohex-2-en-1-ol produced an unstable adduct in 86% yield. The ir spectrum of the adduct showed strong absorption at 2100 cm^{-1} indicating the presence of an azide group in the molecule. The nmr spectrum showed the following significant absorptions: δ_{TMS} ($CDCl_3$) 4.3 (q, 1H, —CH—I, J = 8.5 Hz and 2.5 Hz), 3.7–4.15 (m, 2H, —C*H*—OH and —CH—N_3). On the basis of the nmr spectrum structure **5** is assigned to the

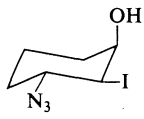

5

adduct, which is derived from an intermediate iodonium ion formed *cis* to the hydroxy group.

Addition of iodine monochloride to cyclohex-2-en-1-ol gave a product in about 90% yield, but no stereochemical information could be gathered from the nmr spectrum.

Cyclohept-2-en-1-ol (9) with iodonium nitrate produced four products. The two iodonitrate esters were formed in a combined yield of 59% and in a ratio of approximately 80:20 (obtained by comparing the nmr intensity of —CH—I of the major product with the total intensity of —CH—ONO_2 at δ_{TMS} ($CDCl_3$) 5.2–5.6). The major product is assigned structure **6** in which the iodine is *cis* to the hydroxyl group, and the

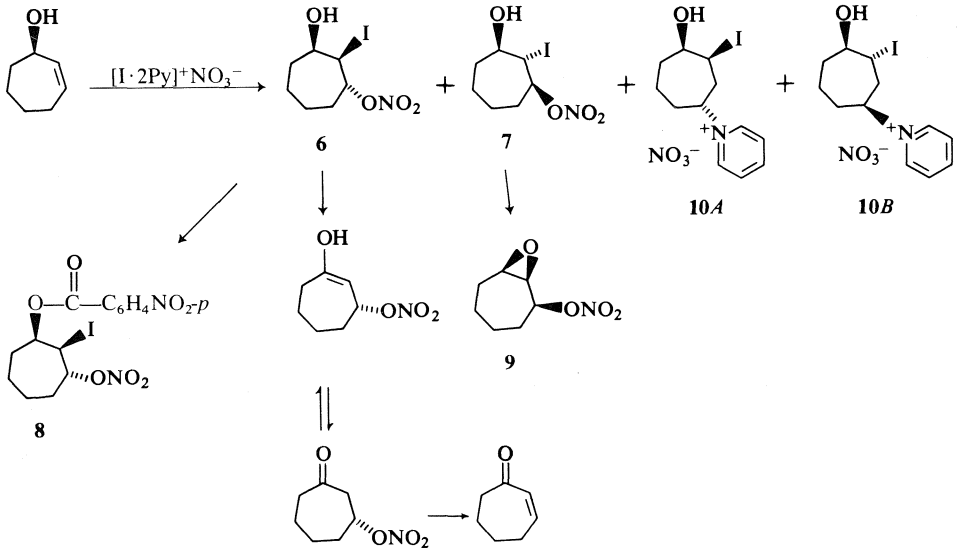

SCHEME 1

minor product as **7**. The major product had the —CH—I absorption in the nmr spectrum at δ_{TMS} ($CDCl_3$) 4.57 (q), with coupling constants of 2.25 Hz and 6.75 Hz. The nmr spectrum of the cycloheptene – iodonium nitrate adduct showed absorptions at δ_{TMS} ($CDCl_3$) 4.33 (sextet, 1H, —CH—I, $J_{a,a}$ = 7 Hz, $J_{a,e}$ = 5 Hz), and 5.36 (sextet, 1H, —CH—ONO_2, $J_{a,a}$ = 7 Hz, $J_{a,e}$ = 3.5 Hz). This indicates that in **6** the hydroxy group is pseudo-axial and iodine and nitrate groups equatorial. Esterification of the hydroxyl group with *para*-nitrobenzoyl chloride in the presence of pyridine allowed separation of the major product as a crystalline derivative **8** which had in the nmr spectrum absorptions at δ_{TMS} ($CDCl_3$) 4.77 (q, 1H, CH—I, J = 2.5 Hz and 6.5 Hz), 4.96 (m, 1H, —CH—O), and 5.5 (m, 1H, —CH—ONO_2). Treatment of the mixture of iodonitrate esters with potassium hydroxide in ether produced cycloheptenone as the major product by elimination of both hydrogen iodide and nitric acid from **6** and another compound which is assigned the epoxy nitrate structure **9** derived from **7** by base-catalyzed cyclization. The transformations are illustrated in Scheme 1.

The iodopyridinium nitrate salts **10***A* and **10***B* were formed in 27% and 8% yields respectively. They were easily separated by fractional crystallization from ethanol.

Reaction of iodonium nitrate with cyclooct-2-en-1-ol in chloroform–pyridine gave an iodonitrate ester in 60% yield. No iodopyridinium nitrate was isolated in this case. The reaction was considerably slower and traces of cyclooctenol could be detected in the reaction mixture even after 24 h.

The assignment of structure **11** to the iodonitrate ester is based on a comparison of the coupling constants in the nmr spectrum of **11** with those in the spectrum of the cyclooctene – iodonium nitrate adduct. Thus the nmr spectrum of **11** showed absorptions at δ_{TMS} ($CDCl_3$) 4.43 (t, 1H, —CHI, J = 9 Hz), and 5.3 (sextet, 1H, —CH—ONO_2, J = 9 Hz and 4.5 Hz). The corresponding coupling constant $J_{CHI-CH-ONO_2}$ in the spectrum of 2-iodocyclooctyl nitrate was 10 Hz. A coupling constant of 9 Hz indicates a *trans* configuration of iodine and hydroxyl groups.

Treatment of adduct **11** with potassium hydroxide in ether gave a cyclized product assigned as the epoxy nitrate **12** on the basis of nmr and ir spectra and mass spectral fragmentation pattern.

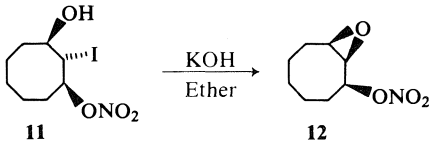

11 **12**

Cyclopent-2-en-1-ol (17) with iodonium nitrate in chloroform–pyridine produced an iodonitrate ester **13** in 52% yield and the corresponding iodopyridinium nitrate **14** in 22% yield. No stereochemical information could be gathered from the nmr spectra of the products and comparison with that of the cyclopentene – iodonium nitrate adducts. Treatment of the iodonitrate ester with base did not produce any cyclized product. This may indicate that the iodonium ion is formed *cis* to the hydroxy group.

The second-order rate constants and thermodynamic factors for the addition of iodonium nitrate to a range of selected unsaturated substrates were determined by estimation of unreacted iodonium nitrate with thiosulfate at

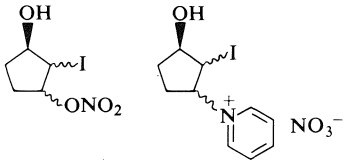

13 **14**

appropriate intervals. The kinetic data support an addition of iodonium ion *cis* to the hydroxyl group in the case of cyclopent-2-en-1-ol (see below).

In electrophilic epoxidation reactions cyclohept-2-en-1-ol gave a mixture of *cis* and *trans*-3-hydroxycycloheptene oxides in a ratio of 2:1 (9, 10). On the other hand, cyclooct-2-en-1-ol (18) gave the *trans* isomer stereospecifically (11). No information is available on the stereochemistry of epoxidation cyclopent-2-en-1-ol.

A comparison of the relative yields of iodonitrate esters and iodopyridinium salts for olefinic alcohols and alkenes of comparable structure (3) reveals that in general introduction of the hydroxy function results in a marked increase in the proportion of the iodopyridinium salt relative to that of the iodonitrate. This suggests that the hydroxy function contributes to the increased stabilization of the intermediate iodonium ion rather than to its inductive destabilization. This finding is born out by the kinetic results.

Figure 1 represents a typical standard and weighted least-squares plot for the determination of second-order rate constants for the addition of iodonium nitrate to various substrates.

The second-order rate constants at 0 °C for

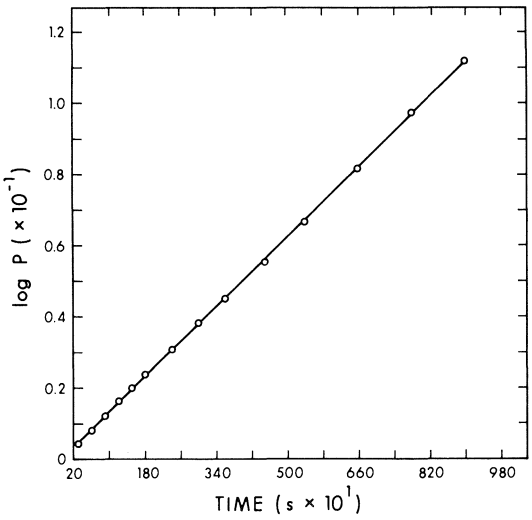

FIG. 1. Plot of log P against time (s) for the addition of iodonium nitrate to cyclooct-2-en-1-ol at 37 °C in 70% chloroform and 30% pyridine.

the reaction of iodonium nitrate with some cyclic olefins and the corresponding olefinic alcohols (hydroxy group in the α-carbon atom) along with their concentrations are given in Table 1. For the monocyclic olefins the order of increasing rate of reaction is cyclooctene < cycloheptene < cyclohexene < cyclopentene. Norbornadiene is approximately 2.5 times as

TABLE 1. Second-order rate constants, k (l mol^{-1} s^{-1}), for the addition of iodonium nitrate at 0 °C in 70% chloroform and 30% pyridine

Substrate	k
Cyclopentene	$7.96 \pm 0.06 \times 10^{-3}$
Cyclopent-2-en-1-ol	$1.12 \pm 0.01 \times 10^{-2}$
Cyclohexene	$7.08 \pm 0.12 \times 10^{-3}$
Cyclohex-2-en-1-ol	$1.17 \pm 0.01 \times 10^{-2}$
Cycloheptene	$4.24 \pm 0.04 \times 10^{-3}$
Cyclohept-2-en-1-ol	$9.50 \pm 0.27 \times 10^{-3}$
Cyclooctene	3.36×10^{-4}*
Cyclooct-2-en-1-ol	2.21×10^{-5}*
Norbornylene	$3.24 \pm 0.06 \times 10^{-3}$
Norbornadiene	$8.14 \pm 0.07 \times 10^{-3}$
Hex-1-ene	$3.09 \pm 0.03 \times 10^{-3}$
Allyl alcohol	$9.04 \pm 0.17 \times 10^{-3}$
But-3-en-1-ol	$7.44 \pm 0.06 \times 10^{-3}$
Pent-4-en-1-ol	$3.98 \pm 0.02 \times 10^{-3}$
Hex-5-en-1-ol	$2.83 \pm 0.03 \times 10^{-3}$
Z-Hex-3-en-1-ol	$4.18 \pm 0.05 \times 10^{-2}$
Hex-1-en-3-ol	$7.71 \pm 0.14 \times 10^{-3}$
3-Methylbut-3-en-1-ol	$3.95 \pm 0.10 \times 10^{-2}$
3,3-Dimethylbut-1-ene	$1.12 \pm 0.03 \times 10^{-3}$

*Obtained by extrapolation to 0 °C.

reactive as norbornylene towards iodonium nitrate.

The effect of an α-hydroxy group in the monocyclic olefin systems on the rate of reaction is also evident. In the five-, six-, and seven-membered cyclic systems, where the iodonium ion is formed *cis* to the hydroxyl group, the alcohols are more reactive than the corresponding olefins, whereas with the eight-membered case where the iodonium ion is formed *trans* to the hydroxyl the reverse situation obtains. Since the only product of reaction of cyclooct-2-en-1-ol with iodonium nitrate corresponds to addition of the iodonium ion *trans* to the hydroxyl group, the rate ratio between cyclooctene and cyclooct-2-en-1-ol = 15.5 provides an estimate of the combined statistical, steric hindrance, and inductive withdrawal effects of the α-hydroxyl in the absence of neighboring group rate enhancement. By contrast cyclohex-2-en-1-ol is some 15.5 × 1.5 ≈ 23 times as reactive as cyclohexene and cyclopent-2-en-1-ol is some 15.5 × 1.4 ≈ 22 times as reactive as cyclopentene. Both cases indicate rate enhancement due to the neighboring hydroxyl group. Cyclohept-2-en-1-ol represents an intermediate situation leading to addition both *cis* and *trans* to the hydroxyl group with the former favored by at least a factor of 4.

The order of decreasing reactivity for the linear unsubstituted olefinic alcohols is allyl alcohol > but-3-en-1-ol > pent-4-en-1-ol > hex-5-en-1-ol. The rate constant for hex-5-en-1-ol is comparable with that for hex-1-ene indicating that the hydroxy group does not have any profound influence on the reaction rate when it is far removed from the reaction centre. The rate constants for the other three olefinic alcohols show that the stabilization of the intermediate iodonium ion by the hydroxy group is a maximum when it is α to the olefinic center and that the effect decreases as the distance between the hydroxy group and the olefinic center increases, whereas for bromination in methanol, water, acetic acid, and trifluoroacetic acid and for iodination in water the reverse has been observed (12, 13). The drastically reduced extent of hydroxy participation for bromination in trifluoroacetic acid solvent has been attributed to hydrogen bonding between the solvent and the hydroxy substituent which reduces its nucleophilicity and hence its effectiveness as a neighboring group (12). The results for addition of

TABLE 2. Rate coefficients for the addition of halogens and iodonium nitrate to olefinic alcohols, k (l mol^{-1} min^{-1})

Olefin	Bromination			Iodination			
	CH_3OH	H_2O (0.02 M NaBr)	CH_3COOH (0.2 M NaBr)	CF_3COOH (0.1 M NaBr)	H_2O (0.0167 M KI)	Iodonium nitrate (addition at 0 °C)
CH_2=CH—CH_2—OH	284 ± 4	1.35 × 10^7	251	3480	0.011 ± 0.0005	0.542 ± 0.010
CH_2=CH—$(CH_2)_2$—OH	525 ± 4	6.9 ± 0.2 × 10^7	594	17 000	0.023 ± 0.001	0.446 ± 0.003
CH_2=CH—$(CH_2)_3$—OH	2630 ± 50	31 ± 1.4 × 10^7	4020	38 900	2.2 ± 0.1	0.239 ± 0.001
CH_2=CH—$(CH_2)_4$—OH	1730 ± 30	37 ± 1.5 × 10^7	1595	51 500	0.38 ± 0.02	0.170 ± 0.002
CH_2=CH—$(CH_2)_4$—H	2090	—	1730	101 000	—	0.185 ± 0.002

TABLE 3. Activation parameters for the addition of iodonium nitrate in 70% chloroform and 30% pyridine

Substrate	E_a (kcal mol^{-1})	$\Delta S^{\neq}$ (eu)	$\Delta H^{\neq}$ (kcal mol^{-1})
Cyclohexene	16.89±0.6	−9.554±0.566	16.13±0.61
Cyclohex-2-en-1-ol	15.92±1.39	−8.486±1.075	16.19±1.3
Cycloheptene	15.20±0.42	−16.01 ±1.033	14.56±0.54
Cyclohept-2-en-1-ol	17.93±0.16	−3.877±0.047	17.40±0.14
Cyclooctene	17.52±0.89	−12.45 ±1.045	16.87±0.89
Cyclooct-2-en-1-ol	21.36±0.9	−3.685±0.25	20.82±0.89
Allyl Alcohol	15.31±0.7	−13.34 ±1.03	14.78±0.7
But-3-en-1-ol	15.60±0.49	−13.15 ±0.71	15.07±0.49
Pent-4-en-1-ol	17.14±0.38	−8.48 ±0.30	16.61±0.36

bromine, iodine, and iodonium nitrate are summarized in Table 2.

For the determination of activation parameters, both log k and log k/T were plotted against $1/T$. This gave good Arrhenius-type plots. A representative example of a standard and weighted least-squares plot is given in Fig. 2. The E_a values (see Table 3) are larger than those for the addition of iodine in hexane to cyclohexene (5.3 kcal mol^{-1}) and for the addition of iodine monobromide to cyclohexene in carbon tetrachloride (8.2 kcal mol^{-1}) (16). On the other hand $\Delta S^{\neq}$ values are comparatively lower for the addition of iodonium nitrate than for the addition of sulfenyl chloride (14) or bromine (15). This may indicate that in this bimolecular reaction, there is no large increase in polarity in the transition state compared to the reactants. This is not unexpected since the reacting pseudohalogen itself is considerably polarized as $[I{\cdot}2Py]^+NO_3^-$.

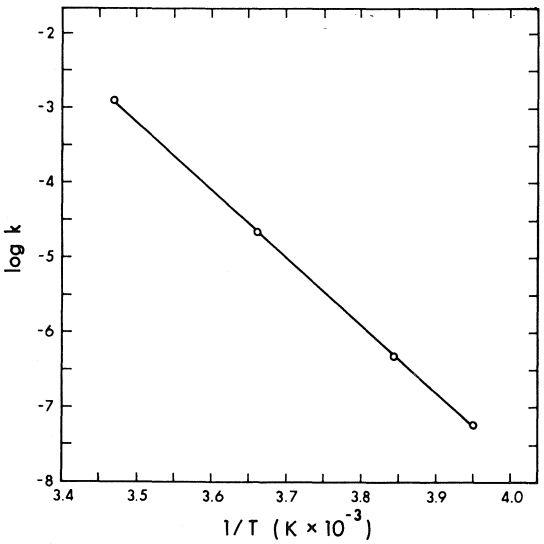

FIG. 2. Plot of log k against $1/T$ for the addition of iodonium nitrate to cyclohept-2-en-1-ol in 70% chloroform and 30% pyridine.

For the linear olefinic alcohols the E_a and $\Delta H^{\neq}$ values increase steadily from allyl alcohol to pent-4-en-1-ol whereas the $\Delta S^{\neq}$ values show a tendency to become less negative. This may suggest that the transition state for allyl alcohol is more favored both by energetics and entropically than those for its higher homologues. This signifies considerable stabilization of the intermediate iodonium ion by the neighbouring hydroxy group. This enhanced stabilization afforded the iodonium ion by the hydroxy group can be envisaged in a number of ways; participation to carbon **15**, participation to iodine **16**, or participation to the slightly positively charged pyridine nitrogen which may be still attached to the iodine in the transition state **17**. Since no

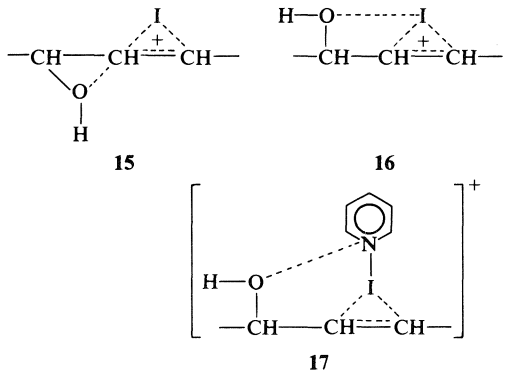

such interaction to carbon or halogen has been observed in the iodination and bromination of allyl alcohol (13), the participation may be to the nitrogen as in **17**.

It was also observed that pent-4-en-1-ol with

iodonium nitrate gives a substantial amount of cyclized product. Hex-5-en-1-ol behaved similarly, although to a lesser extent. This result signifies considerable participation to the carbon by the hydroxy group in the transition state. Thus it is reasonable to assume that in allyl alcohol and but-3-en-1-ol, the hydroxy group stabilizes the iodonium ion by participation to nitrogen, whereas in pent-4-en-1-ol and hex-4-

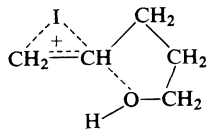

18

en-1-ol, the stabilization is by participation to carbon. In the latter two compounds participation to nitrogen will be unfavorable entropically.

Experimental

Melting points were determined on a Fisher-Johns apparatus and are uncorrected. The ir spectra were recorded on a Perkin-Elmer model 421 spectrophotometer, and only the principal, sharply defined peaks are reported. The nmr spectra were recorded on Varian A-60 and A-100 analytical spectrometers. The spectra were measured on approximately 10–15% (w/v) solutions in appropriate deuterated solvents with tetramethylsilane as standard. Line positions are reported in ppm from the reference. Mass spectra were determined on an Associated Electrical Industries MS-9 double focussing high resolution mass spectrometer. The ionization energy, in general, was 70 eV. Peak measurements were made by comparison with perfluorotributylamine at a resolving power of 15 000. Kieselgel DF-5 (Camag, Switzerland) and Eastman Kodak precoated sheets were used for thin layer chromatography.

The gc analyses were performed with an Aerograph model A-700 gas chromatograph. The lc analyses were made with a Waters Associates model ALC-100 liquid chromatograph. Microanalyses were carried out by Mrs. D. Mahlow of this department.

Materials

Chloroform and pyridine were freshly distilled. All olefinic substrates were fractionally distilled before use and purities were determined by gas chromatography on a Varian Autoprep instrument. The iodonium nitrate–pyridine complex required for kinetic studies was prepared as follows. A solution of iodonium nitrate in chloroform–pyridine was prepared in the usual way. The solution was poured into an excess of anhydrous ether with stirring. The precipitated solid was collected and washed several times with ether. The product was recrystallized several times from anhydrous acetonitrile or acetonitrile–ether. It was not possible to remove all silver salts from the complex because of their solubility in acetonitrile. An approximate purity of 95% was achieved by this method.

The presence of silver salts was shown not to interfere with the reaction by studying kinetics with samples of complex containing different amounts of silver salts.

General Procedure for the Reaction of Iodonium Nitrate with Unsaturated Substrates

The procedure in chloroform–pyridine was similar to that discussed before (1). When the reactions were carried out in chloroform–*sym*-collidine the following procedure was adopted. The reaction mixture was added to sufficient ether to precipitate the collidinium salt. The precipitate was collected and the ethereal layer was washed several times successively with (*a*) cold hydrochloric acid (5%) saturated with sodium chloride, (*b*) saturated aqueous sodium chloride, (*c*) sodium bicarbonate (5%) saturated with sodium chloride until neutral, and finally (*d*) saturated sodium chloride solution containing sodium thiosulfate. The ether layer was dried ($MgSO_4$) and concentrated *in vacuo*. The residual oil was distilled under reduced pressure. The iodopyridinium salts were purified by the crystallization procedure described before (4).

Allyl alcohol gave an isomeric mixture of (*a*) 3-hydroxy-1-iodo-2-propyl nitrate and (*b*) 3-hydroxy-2-iodo-1-propyl nitrate in 30% yield, bp 78 °C/0.15 torr. *Anal.* calcd. for $C_3H_4NO_4I$: N 5.8; found: N 5.7. The nmr (*a*) 5.15 (0.8H, m, $—CHONO_2$), 3.42 (1.6H, d, J = 6 Hz, $—CH_2I$), 3.3 (s, 1H, OH); (*b*) 4.35 (0.2H, m, —CHI), 4.83(0.4H, t, J = 6Hz, 7 Hz, $—CH_2ONO_2$), 3.95 (m, 2H, CH_2OH). In addition were formed the corresponding pyridinium nitrates in 23% yield, mp 48–52 °C. *Anal.* calcd. for $C_8H_{11}N_2O_4I$: C 29.45, H 3.4, N 8.6; found: C 30.2, H 3.18, N 8.8. The nmr (*a*) 4.1 (1.5H, d, J = 5 Hz, $—CH_2I$), 3.85 (m, 2H, CH_2OH), 5.83 (s, 1H, OH); (*b*) 4.5–5.41 (m, pyr).

1,1-Dimethylallyl alcohol gave 3-hydroxy-2-iodo-3-methyl-1-butyl nitrate in 20% yield, bp 70 °C/0.15 torr. *Anal.* calcd. for $C_5H_{10}NO_4I$: C 21.8, H 3.65, N 5.00; found: C 22.1, H 3.7, N 4.55. 2,3-Epoxy-1-iodo-3-methylbutane was also produced, bp 52 °C/6 torr in 5% yield. *Anal.* calcd. for C_5H_9OI: C 28.3, H 4.3; found: C 28.5, H 4.2. The corresponding pyridinium salt was also formed in 40% yield.

Hex-1-en-3-ol gave an isomeric mixture of (*a*) 3-hydroxy-1-iodo-2-hexyl nitrate and (*b*) 3-hydroxy-2-iodo-1-hexyl nitrate in 34% yield, bp 90° C/0.1 torr. *Anal.* calcd. for $C_6H_{12}NO_4I$: C 24.95, H 4.2, N 4.85; found: C 24.95, H 4.2, N 4.7. The nmr (*a*) 4.95 (0.5H, m, $CHONO_2$), 3.47 (1H, d, J = 6 Hz, $—CH_2I$), 0.97 (m, 3H, CH_3), 1.5 (m, 4H, $2—CH_2$); (*b*) 4.4 (0.5H, m, CHI), 4.87 (1H, d, J = 7.5 Hz), 2.43 (s, 1H, OH), 3.0, 3.9 (m, 1H, C*H*OH). In addition was formed the corresponding pyridinium salt *N*-[1-(3-hydroxy-2-iodohexyl)]pyridinium nitrate in 16% yield, mp 80–85 °C. *Anal.* calcd. for $C_{11}H_{17}N_2O_4I$: C 35.9, H 4.65, N 7.61; found: C 36.15, H 4.7, N 7.2. Also formed was the corresponding 3-iodo-2-propyloxetan, bp 72 °C/2 torr in 11% yield (in the reaction in *sym*-collidine). *Anal.* calcd. for $C_6H_{11}OI$: C 31.9, H 2.9; found: C 31.75, H 4.75.

Hex-5-en-3-ol gave an isomeric mixture of 3-hydroxy-1-iodo-2-hexyl nitrate and 3-hydroxy-2-iodo-1-hexyl nitrate in 10% yield, bp 65 °C/0.1 torr. *Anal.* calcd. for $C_6H_{12}NO_4I$: N 4.85; found: N 5.0. In addition was found *N*-[3-(5-ethyltetrahydrofurfuranyl)]pyridinium nitrate in 20% yield, bp 60 °C/1 torr. *Anal.* calcd. for $C_6H_{11}NO_4$: N 8.7; found: N 8.1.

2-Cyclohexenol gave 3-hydroxy-2-iodo-cyclohexyl ni-

trate, bp 90 °C/0.05 torr in 36% yield. *Anal.* calcd. for $C_6H_{10}NO_4I$: C 25.1, H 3.5, N 4.9; found: C 25.3, H 3.4, N 4.2. The nmr 4.48 (1H, q, $J_{1,2} = 8.5$ Hz, $J_{2,3} = 2.5$ Hz, CHI), 5.4 (1H, m, —$CHONO_2$), 1.78 (m, 4H, $2CH_2$), 2.3 (m, 3H, —CH_2, OH), 3.8 (m, 1H, —*CH*OH). The pyridinium salt, *N*-[1-(3-hydroxy-2-iodocyclohexyl)]pyridinium nitrate, mp 166–168 °C, was found in 29% yield. *Anal.* calcd. for $C_{11}H_{15}N_2O_4I$: C 36.1, H 4.1, N 7.65; found: C 36.1, H 4.8, N 8.0.

2-Cyclopentenol gave 3-hydroxy-2-iodocyclopentyl nitrate, mp 46–47 °C in 52% yield. *Anal.* calcd. for $C_5H_8NO_4I$: C 21.98, H 2.93, N 5.13; found: C 21.97, H 2.98, N 5.04. The nmr 4.33 (1H, t, $J = 4.5$ Hz, —CHI), 5.6 (1H, m, —CH—ONO_2), 1.7–2.8 (m, 5H, 2—CH_2, OH), 3.83 (s, 1H, C*H*OH, $J = 5$ Hz). *N*-[1-(3-Hydroxy-2-iodocyclopentyl)]pyridinium nitrate, mp 137–139 °C was formed in 22% yield. *Anal.* calcd. for $C_{10}H_{13}N_2O_4I$: C 34.1, H 3.69, N 7.96; found: C 34.14, H 3.68, N 7.91.

2-Cycloheptenol gave 3-hydroxy-2-iodocycloheptyl nitrate in 59% yield. *Mol. Wt.* calcd. for $C_7H_{12}NO_4I$: 300.9811; found (ms): 300.9811. The nmr 4.57 (1H, q, $J = 2.25$ Hz, 6.75 Hz, CHI), 5.5 (1H, m, $CHONO_2$), 1.5–2.5 (m, 9H, $4CH_2$, OH), 3.76 (m, 1H, CHO). *N*-[1-(3-Hydroxy-2-iodocycloheptyl)]pyridinium nitrate, mp 148 °C, was formed in 59% yield. *Anal.* calcd. for $C_{12}H_{17}N_2O_4I$: C 37.9, H 4.47, N 7.37; found: C 37.92, H 4.89, N 7.22.

1-Hexene gave 1-iodo-2-hexyl nitrate, bp 80 °C/0.5 torr, in 41% yield. *Anal.* calcd. for $C_6H_{12}NO_3I$: C 26.39, H 4.42, N 5.12; found: C 26.35, H 4.79, N 4.73. The nmr 4.9 (1H, m, $CHONO_2$), 3.35 (2H, d, $J = 5.5$ Hz, CH_2I), 1.3 (m, 9H, $3CH_2$—CH_3). *N*-[2-(1-Iodohexyl)]pyridinium nitrate was formed in 42% yield as an oil.

3,3-Dimethyl-1-butene gave 2-iodo-3,3-dimethyl-1-butyl nitrate, bp 55 °C/0.2 torr, in 26% yield. *Anal.* calcd. for $C_6H_{12}NO_3I$: C 26.39, H 4.42, N 5.12; found: C 26.37, H 4.80, N 4.70. The nmr 4.17 (1H, m, CHI), 4.8 (2H, m, CH_2ONO_2) 1.15 (s, 9H, —$C(CH_3)_3$). *N*-[1-(2-Iodo-3,3-dimethylbutyl)]pyridinium nitrate, mp 133 °C, was formed in 49% yield. *Anal.* calcd. for $C_{11}H_{17}N_2O_3I$: C 35.90, H 4.65, N 7.50; found: C 36.10, H 4.70, N 4.60.

3,4-Dimethyl-1-hexene gave an isomeric mixture of 1-iodo-3,4-dimethyl-2-hexyl nitrate and 2-iodo-3,4-dimethyl-1-hexyl nitrate bp 93–97 °C/0.5 torr, in 75% yield. *Anal.* calcd. for $C_8H_{16}NO_3I$: C 31.90, H 5.35, N 4.65; found: C 32.30, H 5.60, N 4.67. The nmr 4.8 (1H, m, CHI), 5.0 (2H, m, $CHONO_2$), 3.4 (1.4H, m, CH_2I), 4.4 (0.6H, m, CH_2ONO_2), 0.8–2 (m, 13H, 2—CH—, —CH_2—, $3CH_3$).

Cyclopentene gave 2-iodocyclopentyl nitrate, bp 40 °C/0.5 torr, in 54% yield. *Anal.* calcd. for $C_5H_8NO_3I$: C 23.35, H 3.11, N 5.45; found: C 23.48, H 3.19, N 5.42. The nmr 4.2 (1H, m, —CHI), 5.4 (1H, m, —$CHONO_2$), 2.0 (m, 6H, $3CH_2$—). *N*-(2-Iodocyclopentyl)pyridinium nitrate was also formed as an oil in 9% yield. *Anal.* calcd. for $C_{10}H_{13}N_2O_3I$: C 35.73, H 3.89, N 8.33; found: C 34.13, H 3.96, N 8.94.

Cyclohexene formed 2-iodocyclohexyl nitrate, bp 113 °C/1.3 torr, in 60% yield. *Anal.* calcd. for $C_6H_{10}NO_3I$: C 26.58, H 3.72, N 5.16; found: C 26.84, H 3.87, N 4.98. The nmr 4.17 (1H, m, —CH—I), 5.15 (1H, m, —CH—ONO_2), 1.7 (m, 8H, 4—CH_2—). *N*-(2-Iodocyclohexyl)-pyridinium nitrate, bp 145–150 °C, was formed in 40% yield. *Anal.* calcd. for $C_{11}H_{15}N_2O_3I$: C 37.73, H 4.32, N 8.00; found: C 37.77, H 4.80, N 7.97.

Cycloheptene gave 2-iodocycloheptyl nitrate, bp 113 °C/1.3 torr, in 60% yield. *Anal.* calcd. for $C_7H_{12}NO_3I$: C 29.50, H 4.21, N 4.91; found: C 29.93, H 4.52, N 4.84. The nmr 4.33 (1H, m, —CHI), 5.36 (1H, m, —$CHONO_2$), 1.5–2.4 (m, 10H, 5—CH_2). *N*-(2-Iodocycloheptyl)pyridinium nitrate, bp 140–142 °C, was also formed in 40% yield. *Anal.* calcd. for $C_{12}H_{17}N_2O_3I$: C 39.60, H 4.67; found: C 39.82, H 4.87.

Cyclooctene similarly gave 2-iodocyclooctyl nitrate, bp 97 °C/0.02 torr, in 79% yield. *Anal.* calcd. for $C_8H_{14}NO_3I$: C 33.62, H 4.90, N 4.90; found: C 32.71, H 5.08, N 4.37. The nmr 4.3 (1H, m, —CHI), 5.4 (1H, m, —$CHONO_2$), 1.1–2.3 (m, 12H, $6CH_2$—). *N*-(2-Iodocyclooctyl)pyridinium nitrate, bp 152–153 °C, was formed in 5.5% yield. *Anal.* calcd. for $C_{13}H_{19}N_2O_3I$: C 41.27, H 4.03, N 7.41; found: C 41.36, H 4.99, N 7.36.

Norbornene gave 2-iodonorborn-3-yl nitrate, bp 83 °C/0.3 torr, in 60% yield. *Anal.* calcd. for $C_7H_{10}NO_3I$: C 29.70, H 3.56, N 4.95; found: C 30.55, H 3.50, N 4.33. The nmr 3.75 (1H, m, —CH—I), 5.5 (1H, m, —$CHONO_2$), 1.3–2.8 (m, 8H, 2—CH—, 3—CH_2—). Nortricyclanyl iodide was also produced in 40% yield, bp 40 °C/0.15 torr. Molecular ion 220.

Norbornadiene gave tricyclo[2.2.1.$0^{2,6}$]-5-iodohept-3-yl nitrate, bp 75 °C/0.08 torr, in 64% yield. *Anal.* calcd. for $C_7H_8NO_3I$: C 29.92, H 2.87, N 4.93; found: C 30.05, H 3.18, N 5.05. The nmr 4.25 (1H, m, —CHI), 5.03 (1H, m, —$CHONO_2$), 1.75, 2.5 (m, 6H, 4—CH—, —CH_2).

1,5-Hexadiene gave 6-iodohex-1-en-5-yl nitrate, bp 62 °C/0.35 torr, in 85% yield. *Anal.* calcd. C 26.59; H 3.72, N 5.16; found: C 26.51, H 3.34, N 4.89. The nmr 4.9 (1H, m, —$CHONO_2$), 3.35 (2H, d, $J = 5.5$ Hz, —CHI), 2.0 (m, 4H, $2CH_2$), 5.5, 5.6 (m, 3H, —CH=CH_2).

Treatment of Cyclohept-2-en-1-ol Iodonium Nitrate Adducts with Potassium Hydroxide in Ether

A solution of 2.5 g (8.3 mmol) of the adducts in 50 ml of ether was stirred with 0.6 g of powdered potassium hydroxide for 3 h. Work-up according to the procedure described before gave 1 g of cyclohept-2-en-1-one and a small amount of 2,3-epoxycyclohept-1-yl nitrate **9**. Separation was achieved by chromatography on Florisil and elution with benzene–hexane (50:50). Evaporation of the first fraction gave the epoxy nitrate. The nmr spectrum δ_{TMS} ($CDCl_3$) 0.8–2.5 (m, 8H, 4—CH_2—), 3.2 (m, 2H, 2—CH—O), 5.25 (m, 1H, —CH—ONO_2). The ir spectrum ν_{max} ($CHCl_3$) 1630 cm^{-1}, 1270 cm^{-1} (ONO_2), 1310, 960 cm^{-1} 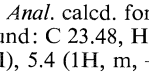 .

Evaporation of the second fraction gave cyclohept-2-en-1-one, which was identical with an authentic sample.

para-Nitrobenzoylation of 3-Hydroxy-3-iodocycloheptyl Nitrate

To a solution of 2 g (6.63 mmol) of adducts **6** and **7** and 0.79 g (0.01 mol) of pyridine in 30 ml of anhydrous benzene was added a solution of 1.245 g (0.00663 mol) of *para*-nitrobenzoyl chloride in 10 ml of benzene dropwise and the mixture stirred for 3 h. Work-up by the usual procedure gave an oil which was crystallized from benzene–hexane to afford 1.5 g (50%) of *3-para-nitrobenzoyloxy-2-iodocycloheptyl nitrate*, **8** mp 103–104 °C. *Anal.* calcd. for $C_{14}H_{15}N_2O_7I$: C 37.34, H 3.33, N 6.22; found: C 37.4, H 3.41, N 6.25. The nmr spectrum δ_{TMS} ($CDCl_3$) 1.7–2.5 (m, 8H, 4—CH_2—), 4.77 (q, 1H,

—CH—I, J = 2.5 Hz), 4.96 (m, 1H, —CH—O), 5.5 (m, 1H, —CH—ONO_2), 8.27 (m, 4H, aromatic hydrogens). The ir spectrum ν_{max} ($CHCl_3$) 1730 cm^{-1} (>C=O), 1640 (—ONO_2), 1530 (—NO_2).

Treatment of 3-Hydroxy-2-iodocyclooctyl Nitrate with Potassium Hydroxide in Ether

To a solution of 2 g (6.35 mmol) of 3-hydroxy-2-iodocyclooctyl nitrate in 50 ml of ether was added 0.56 g (0.01 mol) of powdered potassium hydroxide. The mixture was stirred at room temperature for 3 h. Work-up by the usual procedure gave 1 g (84%) of 2,3-epoxycyclooctyl nitrate, **12**. Purification was achieved by chromatography on Florisil and elution with benzene–hexane (50:50). The nmr spectrum δ_{TMS} ($CDCl_3$) 1.1–2.4 (m, 10H, 5—CH_2—), 2.88 (q, 1H, H^3), 3.08 (t, 1H, H^2, J = 4 Hz), 5.63 (sextet 1H, —CH—ONO_2, J = 5 Hz, 3.33 Hz). The ir spectrum ν_{max} ($CHCl_3$) 1640 cm^{-1} (ONO_2), 1280 cm^{-1}. (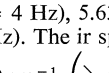). The mass spectrum, *m/e* 141 ($M - NO_2$), 125 ($M - ONO_2$).

Addition of Iodine Azide to Cyclohex-2-en-1-ol

This reaction was carried out by the procedure of Hassner and Teeter (19). Thus the reaction of 3.92 g (0.04 mol) of cyclohex-2-en-1-ol with iodine azide generated from 5.2 g (0.08 mol) of sodium azide and 9.8 g (0.06 mol) of iodine monochloride in 70 ml of anhydrous acetonitrile at 0 °C for 24 h and work-up by the usual procedure gave 9.2 g (86%) of 3-hydroxy-2-iodo-1-azidocyclohexane, **5**, as a dark brown oil. The nmr spectrum δ_{TMS} ($CDCl_3$) 1–2.5 (m, 6H, 3—CH_2—), 2.85 (s, 1H, —OH), 3.9 (m, 2H, —C*H*—OH, —CH—N_3), 4.3 (q, 1H, —CH—I, $J_{1,2}$ = 9.5 Hz, $J_{2,3}$ = 2.5 Hz). The ir spectrum ν_{max} (liquid film) 3425 cm^{-1} (—OH), 2100 cm^{-1} (—N_3).

Addition of Iodine Monochloride to Cyclohex-2-en-1-ol

To a stirred solution of 8.1 g (0.05 mol) of iodine monochloride in 60 ml of anhydrous acetonitrile at 0 °C was added a solution of 3.92 g (0.04 mol) of cyclohex-2-en-1-ol in 10 ml of anhydrous acetonitrile and the mixture stirred at 0–5 °C for 24 h. The solution was added to 50 ml of saturated sodium bisulfite solution and the mixture extracted with 50 ml of ether. Removal of the solvent *in vacuo* after drying ($MgSO_4$) gave 9.4 g (90%) of the adduct as a dark brown oil. The nmr spectrum δ_{TMS} ($CDCl_3$) 1.2–2.6 (m, 7H, 3—CH_2—, —OH), 3.2–3.8 (m, 3H, —CH—I, —CH—Cl, —C*H*—OH). The ir spectrum ν_{max} (liquid film) 3420 cm^{-1} (—OH).

Estimation of Iodonium Nitrate

Iodonium nitrate can be estimated quantitatively with thiosulfate. The reaction may be formulated as:

$$2Na_2S_2O_3 + INO_3 \rightarrow NaI + NaNO_3 + Na_2S_4O_6$$

The method is as follows:

A known volume of iodonium nitrate solution in chloroform–pyridine (70:30) is thoroughly shaken with an excess of a known volume of standard sodium thiosulfate solution. The completion of the reaction between sodium thiosulfate and iodonium nitrate is indicated by the change in color of the iodonium nitrate solution from light yellow to colorless (*ca.* 15–20 s). The excess of sodium thiosulfate is then determined by titration with standard iodine solution using starch as the indicator. The titre values were quite reproducible within experimental limits. The end point is indicated by the first appearance of the blue color. It was found that the color faded gradually.

In some additions, where cyclization (*e.g.* pent-4-en-1-ol, hex-5-en-1-ol) or rearrangement (*e.g.* norbornylene) occurs, pyridinium nitrate (Py·HNO_3) is an additional product in the reaction. It was found that the titre values were unchanged in the presence of added pyridinium nitrate.

Stoichiometry of the Reaction

The stoichiometry of the addition reactions was shown to be 1:1 by allowing a known excess of iodonium nitrate in chloroform–pyridine to react with a known amount of *e.g.* cyclohexene to completion and then determining the excess of iodonium nitrate by the method described above.

Kinetic Measurements

All kinetic studies were done in chloroform–pyridine (70:30 v/v) at temperatures between −20.5 to 45 °C. Chloroform and pyridine were freshly distilled. The progress of the reaction was followed by the rate of disappearance of iodonium nitrate. An accurately weighed amount of olefin was made up to 50 ml with chloroform–pyridine (70:30) at the temperature at which kinetic measurements were made. The olefin solution and the iodonium nitrate solution (50 ml) were equilibrated at the desired temperature. The two solutions were mixed thoroughly. Portions (5 ml) of the reaction mixture were withdrawn at intervals and the unreacted iodonium nitrate was estimated by the method described before. Whenever possible the kinetics were followed up to 80–85% of the reaction except at very low temperatures where they were followed up to 50–60%.

In all the kinetic runs a slight excess (10–25%) of iodonium nitrate was used. The initial concentration of iodonium nitrate was determined by titrating 5 ml of the stock solution. This was checked by titrating a sample after completion of the reaction. Good agreement was observed within experimental error.

A typical kinetic run may be represented as follows:

Time (min)	I_2* (ml)	Time (min)	I_2* (ml)
5	1.3	50	11.9
10	2.85	60	13.6
20	5.45	80	16.4
30	7.8	100	18.8
40	9.9	120	20.7

*I_2 ≡ excess thiosulfate.

Determination of Rate Constants

The second-order rate constants for the addition of iodonium nitrate to various olefinic substrates were determined by plotting log P against time: $P = (c_b^0 \times c_a)/(c_a^0 \times c_b)$, where c_a^0 = initial concentration of iodonium nitrate, c_b^0 = initial concentration of unsaturated substrate, c_a and c_b are concentrations of iodonium nitrate and olefin respectively at any given time.

Good second-order plots (straight lines) were obtained up to about 80–85% of the reaction: k = Slope $(2.303/c_a^0 - c_b^0)$.

Acknowledgments

This research was supported by the National Research Council of Canada and the Chemistry Department of the University of Alberta.

1. J. W. Lown and A. V. Joshua. Can. J. Chem. This issue.
2. J. W. Lown and A. V. Joshua. J. Chem. Soc. Perkin Trans. 1, 2680 (1973).
3. U. E. Diner, M. Worsley, and J. W. Lown. J. Chem. Soc. (C), 3131 (1971).
4. U. E. Diner and J. W. Lown. Can. J. Chem. **49**, 403 (1971).
5. A. Hassner, R. P. Hoblitt, C. Heathcock, J. E. Kropp, and M. Lorber. J. Am. Chem. Soc. **92**, 1326 (1970).
6. A. Hassner, R. G. Isbister, and A. Friederang. Tetrahedron Lett. 2939 (1969).
7. H. B. Henbest and R. A. L. Wilson. J. Chem. Soc. 1958 (1957).
8. H. B. Henbest. Proc. Chem. Soc. 159 (1963).
9. A. C. Cope, T. A. Liss, and G. W. Wood. J. Am. Chem. Soc. **79**, 6287 (1957).
10. A. C. Cope, J. K. Heeren, and V. Seeman. J. Org. Chem. **28**, 516 (1963).
11. A. C. Cope, A. H. Keough, P. E. Peterson, H. E. Simmons, and G. W. Wood. J. Am. Chem. Soc. **79**, 3900 (1957).
12. S. R. Hooley and D. L. H. Williams. J. Chem. Soc. Perkin Trans. II, 503 (1975).
13. D. L. H. Williams, E. Bienvenue-Goetz, and J. E. Dubois. J. Chem. Soc. (B), 517 (1969).
14. W. L. Orr and N. Kharasch. J. Am. Chem. Soc. **78**, 1201 (1956).
15. K. Yates and W. V. Wright. Can. J. Chem. **45**, 167 (1967).
16. G. B. Sergeev and T'Ung-Ha Ch'Eng. Vestn. Mosk. Yu. Khim. **24**, 62 (1969); Chem. Abstr. **70**, 105634h (1969).
17. K. Alder and F. H. Flock. Chem. Ber. **89**, 1732 (1956).
18. A. C. Cope, M. R. Kinter, and R. T. Keller. J. Am. Chem. Soc. **76**, 2757 (1954).
19. A. Hassner and J. S. Teeter. J. Org. Chem. **35**, 3397 (1970).

Hydroxyl proton resonances of methyl 4,6-*O*-benzylidene-α- and β-D-glucopyranosides and their derivatives in dimethyl sulfoxide solution[1]

YÔTARO KONDO AND KEISUKE KITAMURA[2]

Department of Agricultural Biochemistry, Tottori University, Tottori 680, Japan

Received June 7, 1976

YÔTARO KONDO and KEISUKE KITAMURA. Can. J. Chem. **55**, 141 (1977).

Proton magnetic resonance spectra of methyl 4,6-*O*-benzylidene-α- and β-D-glucopyranosides (**1** and **10**) and their mono-substituted derivatives are determined in dimethyl sulfoxide solution. Assignments of the hydroxyl group resonances of **1** and **10** are confirmed by means of INDOR techniques. It is shown that the position of the hydroxyl substituent of the mono-substituted derivatives of **1** and **10** can be determined by using the coupling constants $J_{H-C-O-H}$. It is proposed that the vicinal diols of **1** and **10** give 1:1 associations with dimethyl sulfoxide molecules, and the C—H and O—H bonds at position 2 of the mono-substituted derivatives of **1** are approximately *anti*.

YÔTARO KONDO et KEISUKE KITAMURA. Can. J. Chem. **55**, 141 (1977).

On a déterminé les spectres rmp, dans des solutions de diméthylsulfoxyde, des *O*-benzylidène-4,6-α- et β-D-glucopyrannosides de méthyle (**1** et **10**) et de leurs dérivés monosubstitués. L'attribution des résonances des groupes hydroxyles de **1** et de **10** a pu être confirmée en faisant appel à des techniques INDOR. On montre que la position d'un substituant hydroxyle des dérivés monosubstitués de **1** et de **10** peut être déterminée en faisant appel aux constantes de couplage $J_{H-C-O-H}$. On croit que les diols vicinaux de **1** et de **10** donnent des associations 1:1 avec les molécules de diméthylsulfoxyde et que les liaisons C—H et O—H en position 2 des dérivés mono-substitués de **1** sont approximativement *anti*.

[Traduit par le journal]

It is well known that the pmr spectra of alcohols (1, 2) and carbohydrates (3–9) in dimethyl sulfoxide (DMSO) solution display well resolved signals of the hydroxyl groups and that the derived coupling constants $J_{H-C-O-H}$ provide valuable information on configuration and conformation of these compounds (2–9).

This communication describes assignments of the vicinal diols in the pmr spectra of methyl 4,6-*O*-benzylidene-α- and β-D-glucopyranosides in dimethyl sulfoxide solution and characterization of 'isolated' hydroxyl groups of their mono-substituted derivatives.

The pmr spectrum of methyl 4,6-*O*-benzylidene-α-D-glucopyranoside (**1**) in DMSO-d_6, together with the INDOR spectra, are shown in Fig. 1. The signals of the hydroxyl groups appeared at τ 4.85 and 5.04 as doublets (J = 4.5 and 6.5 Hz, respectively) which disappeared on addition of D_2O. The signal of H-1 occurred at τ 5.37 as a doublet ($J_{1,2}$ = 3.8 Hz). The signals of the hydroxyl groups at C-2 and C-3 were assigned by using INDOR (internuclear double resonance) techniques (10–13).

Six different INDOR spectra are shown in Fig. 1. Monitoring the frequency of line 1 and varying the INDOR frequency gave rise to three pairs of 'negative–positive' peaks (spectrum 1), whereas that of line 2 gave rise to three pairs of 'positive–negative' peaks (spectrum 2) in the same region of τ 6.20–6.60. Monitoring lines 3 and 4 (spectra 3 and 4) resulted in responses in the same region of τ 6.50–6.80. When the H-1 peaks (lines 5 and 6) were monitored, perturbation patterns similar to the INDOR spectra 3 and 4 were observed at frequencies corresponding to the H-2 proton. These indicate that peaks 3, 4, 5, and 6 come from the H-2 resonance. Accordingly, the doublet at higher field (τ 5.04) was assigned to the 2-OH resonance and another doublet at lower field (τ 4.85) to the 3-OH.

The pmr and INDOR spectra of methyl 4,6,-*O*-benzylidene-β-D-glucopyranoside (**10**) in DMSO-d_6 are shown in Fig. 2. The signals of two hydroxyl groups occurred as overlapped pair doublets at τ 4.67 (J = 5.0 Hz) and 4.70 (J = 3.5 Hz). The signal of H-1 appeared at τ 5.75 as a doublet ($J_{1,2}$ = 7.8 Hz). Assignment of the

[1]Presented at the Annual Meeting of the Agricultural Chemical Society of Japan, July, 1975.

[2]Kyoto College of Pharmacy, Kyoto 607, Japan.

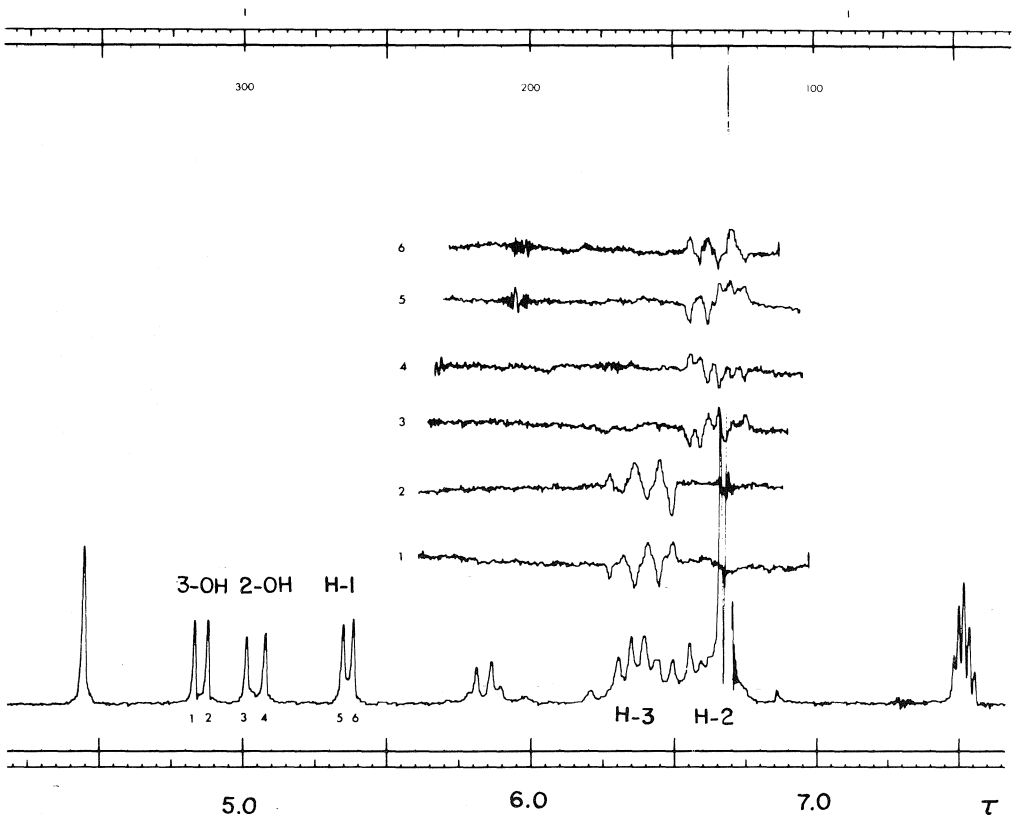

FIG. 1. Proton magnetic resonance and INDOR spectra of methyl 4,6-*O*-benzylidene-α-D-glucopyranoside (**1**) in DMSO-d_6.

hydroxyl groups at C-2 and C-3 was facilitated by combined use of INDOR and double-resonance techniques.

When lines 1 and 2 were monitored, perturbations were observed (spectra 1 and 2) at the same frequencies as when lines 4 and 5 were monitored (spectra 4 and 5). It follows that the doublet at lower field (τ 4.67) was due to the 2-OH resonance and hence, by inference, that the doublet to higher field (τ 4.70) must be due to the 3-OH. The perturbations observed in Fig. 2, obtained by monitoring transition 3 must, then, arise from the H-3 resonance. These assignments were confirmed by double-resonance experiments (Fig. 2). On irradiation of the H-2 resonance at the region 7, the 2-OH doublet at lower field collapsed to a singlet, whereas irradiation of H-3 at the region 6 changes the 3-OH doublet at higher field to a sharp singlet. The 2-OH signal in compound **1** appeared at higher field as compared with that in compound **10**. This large up-field shift (0.37 ppm) may be caused by the shielding of the axial methoxyl group in compound **1**, indicating the axial methoxyl group has a strong influence on the neighboring hydroxyl group rather than the equatorial methoxyl group.

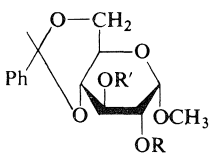

1 R = R′ = H
2 R = Ac, R′ = H
3 R = CH_3, R′ = H
4 R = Ts, R′ = H
5 R = Ben, R′ = H
6 R = H, R′ = Ac
7 R = H, R′ = CH_3
8 R = H, R′ = Ts
9 R = H, R′ = Ben

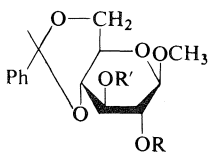

10 R = R′ = H
11 R = Ac, R′ = H
12 R = CH_3, R′ = H
13 R = Ts, R′ = H
14 R = Ben, R′ = H
15 R = H, R′ = Ac
16 R = H, R′ = CH_3
17 R = H, R′ = Ts
18 R = H, R′ = Ben

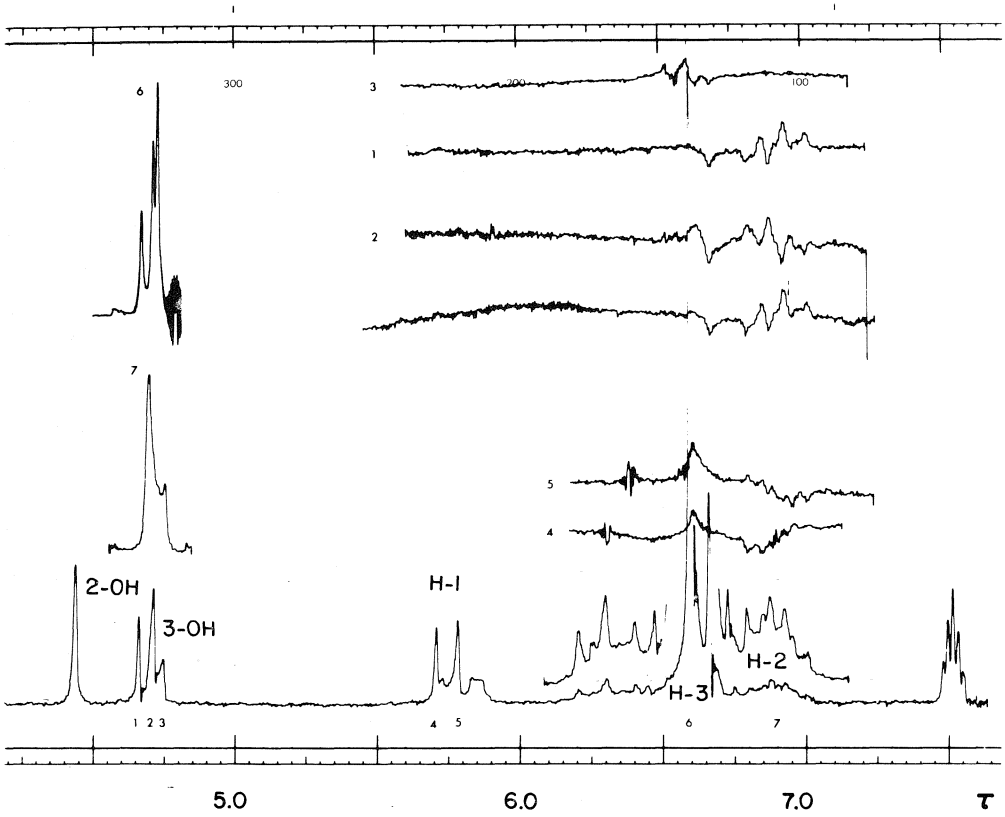

FIG. 2. Proton magnetic resonance and INDOR spectra of methyl 4,6-*O*-benzylidene-β-D-glucopyranoside (**10**) in DMSO-d_6.

It is noteworthy that H–O–C–H(2) couplings are larger than H–O–C–H(3) in vicinal diols of both anomers **1** and **10**. Provided that a similar correlation holds for 'isolated' hydroxyl groups of mono-substituted derivatives of compounds **1** and **10**, this relationship may be useful for determination of the position of the substituents in compounds **1** and **10**. To confirm this, we selected mono-substituted (acetyl, benzoyl, methyl, and benzyl) derivatives of compounds **1** and **10**. The coupling constants $J_{H-C-O-H}$ for these compounds are presented in Tables 1 and 2. For mono-substituted derivatives (**2–9**) with α-D-configuration, the coupling constants of positions 2 and 3 were found to be 7.0–8.0 and 5.0–5.3 Hz, respectively, while compounds **11–18** with β-D-configuration showed coupling constants of 5.5–6.0 and 4.5–5.2 Hz for the 2- and 3-OH signals, respectively. This shows that in these mono-substituted derivatives, the coupling constants at position 2 of the α- and β-D-anomers are larger than those at position 3, in agreement with the results obtained with the original diols **1** and **10**. Consequently, it is possible to predict directly the location of the substituents in a series of mono-substituted derivatives of **1** and **10** from the coupling constants of 'isolated' hydroxyl groups.

TABLE 1. Proton magnetic resonance parameters for mono-substituted derivatives of methyl 4,6-*O*-benzylidene-α-D-glucopyranoside (**1**) in DMSO-d_6

	Coupling constants (Hz)	
Compound	$J_{H,OH}$	$J_{1,2}$
2	5.0	3.5
3	5.0	3.5
4	5.3	3.5
5	5.0	3.7
6	7.0	3.5
7	7.0	3.5
8	8.0	3.7
9	7.0	3.0

TABLE 2. Proton magnetic resonance parameters for mono-substituted derivatives of methyl 4,6-*O*-benzylidene-β-D-glucopyranoside (**10**) in DMSO-d_6

Compound	Coupling constants (Hz)	
	$J_{H,OH}$	$J_{1,2}$
11	4.8	7.5
12	4.5	8.0
13	5.0	7.8
14	5.2	7.6
15	5.5	7.7
16	5.5	*
17	6.0	7.6
18	5.5	8.0

*Unresolved.

It is interesting to note that H–O–C–H(2) couplings in the α-D-anomers **6–9** (7.0–8.0 Hz) are especially large. This indicates that the C—H and O—H bonds are approximately an *anti*-conformation, because it is well known that Karplus type of relation for H–C–C–H system is also applicable for H–O–C–H system and the coupling constants are larger for *anti*-conformers than *gauche* (9, 14).

Casu *et al.* (5) postulated 1:1 and 2:1 complex models (Fig. 3 *a* and *b*, respectively) for the complex formation of DMSO molecules with a vicinal diol. Inspection of molecular models of the association of compounds **1** and **10** with DMSO offers an explanation for their observed difference in the coupling constants. In a 2:1 association, the DMSO molecule that is sufficiently far from the glucosidic methoxyl moiety in **1** and **10**, has little influence on the geometry of the seven-membered ring, so that a significant change of the coupling constants of hydroxyl groups would not be expected to be caused by the configurational change at C-1. However, a considerable difference in coupling constants at position 2 and 3 was observed for the α- and β-D-anomers **1** and **10**. This observation may be explained by the steric hindrance of the glucosidic methoxyl group in a 1:1 association to the neighboring DMSO molecule at C-2. This effect is expected to be especially significant in the α-D-anomer with the axial methoxyl group. Accordingly, 1:1 associations of DMSO molecules with vicinal diols of methyl 4,6-*O*-benzylidene-α- and β-D-glucopyranosides are responsible for the difference in the coupling constants.

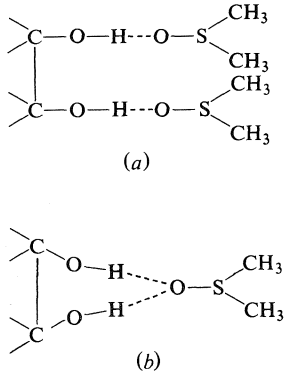

FIG. 3. Association of a vicinal diol with DMSO molecules.

Experimental

Proton magnetic resonance spectra were measured on a Hitachi–Perkin-Elmer 90 MHz spectrometer with tetramethylsilane as an internal reference. The solutions used contained 30 mg of compound in 0.4 ml DMSO-d_6. Chemical shifts were measured at the 800 Hz sweep-width and coupling constants obtained directly from the spectra recorded at the 400 Hz or 200 Hz sweep-widths. INDOR spectra were measured on a Varian HA-100D spectrometer which was modified as reported by van Deursen (13), *i.e.*, an additional oscillator was used for irradiation.

The sugar derivatives used were prepared by the literature procedures (15).

1. O. L. CHAPMAN and R. W. KING. J. Am. Chem. Soc. **86**, 1256 (1964).
2. J. J. UEBEL and H. W. GOODWIN. J. Org. Chem. **31**, 2040 (1966).
3. B. CASU, M. REGGIANI, G. G. GALLO, and A. VIGEVANI. Tetrahedron Lett. 2839 (1964).
4. B. CASU, M. REGGIANI, G. G. GALLO, and A. VIGEVANI. Tetrahedron Lett. 2253 (1965).
5. B. CASU, M. REGGIANI, G. G. GALLO, and A. VIGEVANI. Tetrahedron, **22**, 3061 (1966).
6. A. S. PERLIN. Can. J. Chem. **44**, 539 (1966).
7. J. C. JOCHIMS, G. TAIGEL, A. SEELIGER, P. LUTZ, and H. E. DRIESEN. Tetrahedron Lett. 4363 (1967).
8. G. KOTOWYCZ and R. U. LEMIEUX. Chem. Rev. **73**, 669 (1973).
9. V. S. R. RAO. J. Indian Inst. Sci. **55**, 253 (1973).
10. R. BURTON, L. D. HALL, and P. R. STEINER. Can. J. Chem. **48**, 2679 (1970).
11. B. COXON. Carbohydr. Res. **18**, 427 (1971).
12. V. J. KOWALEWSKI. Progress in nuclear magnetic resonance spectroscopy. Vol. 5. *Edited by* J. W. Emsley, J. Feeney, and L. H. Sutcliffe. Pergamon Press, New York. 1966. p. 1.
13. F. W. VAN DEURSEN. Org. Magn. Reson. **3**, 221 (1971).
14. R. R. FRASER, M. KAUFMAN, P. MORAND, and G. GOVIL. Can. J. Chem. **47**, 403 (1969).
15. Y. KONDO. Agr. Biol. Chem. **39**, 1879 (1975).

Aliphatic diazo compounds. X. The reaction of α-diazoacetophenone with methanolic sodium methoxide[1]

PETER YATES AND R. J. MAYFIELD

Lash Miller Chemical Laboratories, Department of Chemistry, University of Toronto, Toronto, Ont., Canada M5S 1A1

Received June 8, 1976

PETER YATES and R. J. MAYFIELD. Can. J. Chem. **55**, 145 (1977).

The reaction of α-diazoacetophenone (**1**) with methanolic sodium methoxide in dilute solution gives 3-benzoyl-5-hydroxy-4-phenylpyrazole (**4**), 3-benzoyl-4-hydroxy-5-phenylpyrazole (**5**), 3-benzoyl-5-methoxy-4-phenylpyrazole (**9**), 3-benzoyl-4-phenylpyrazole (**6**), 5-benzoyltetrazole (**7**), 3,6-dibenzoyldihydro-*s*-tetrazine (**10**), *cis*- and *trans*-β-benzoyl-α-phenylacrylic acid, acetophenone, methyl benzoate, and benzoic acid. The pyrazoles **4**, **5**, and **9** are considered to arise via reaction of **1** to give α-methoxyacetophenone followed by further reaction of the anion of the latter with **1**. Evidence in accord with this view was obtained by a study of the products formed when **1** was treated with methanolic sodium methoxide in the presence of 2-methoxy-4′-methylacetophenone. Acetophenone is considered to arise by reduction of **1** via phenylglyoxal 2-monohydrazone (**37**); condensation of **1** with the enolate ion derived from acetophenone then can give the pyrazole **6**, while condensation of **1** with **37** could give the tetrazole **7**.

PETER YATES et R. J. MAYFIELD. Can. J. Chem. **55**, 145 (1977).

La réaction de l'α-diazoacétophénone (**1**) avec une solution diluée de méthylate de sodium dans le méthanol conduit au benzoyl-3 hydroxy-5 phényl-4 pyrazole (**4**) au benzoyl-3 hydroxy-4 phényl-5 pyrazole (**5**), au benzoyl-3 méthoxy-5 phényl-4 pyrazole (**9**), au benzoyl-3 phényl-4 pyrazole (**6**), au benzoyl-5 tétrazole (**7**), au dibenzoyl-3,6 dihydro *s*-tétrazine (**10**), aux acides β-benzoyl α-phénylacrylique *cis* et *trans*, à l'acétophénone, au benzoate de méthyle et à l'acide benzoïque. On considère que les pyrazoles **4**, **5** et **9** proviennent d'une réaction de **1** conduisant à l'α-méthoxyacétophénone dont l'anion réagirait par la suite avec **1**. On a obtenu des données en accord avec ces vues par une étude des produits formés lorsque l'on traite **1** avec une solution méthanolique de méthylate de sodium en présence de méthoxy-2 méthyl-4′ acétophénone. On considère que l'acétophénone provient d'une réduction de **1** par l'intermédiaire de la monohydrazone du phénylglyoxal-2 (**37**); la condensation de **1** avec l'ion énolate dérivé de l'acétophénone conduit alors au pyrazole **6** alors que la condensation de **1** avec **37** donne le tétrazole **7**.

[Traduit par le journal]

Treatment of a 0.1 *M* solution of α-diazoacetophenone (**1**) with 0.15 *M* potassium *tert*-butoxide in *tert*-butyl alcohol has been shown to give 5-benzoyl-2-phenacyltetrazole (**2**), a dimer of **1**, in good yield (1). The only other products formed are 2-phenacyltetrazole (**3**) and benzoic acid, which are considered to arise by cleavage of **2**.

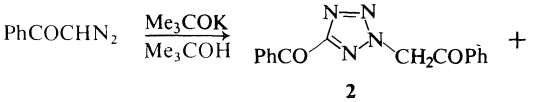

2

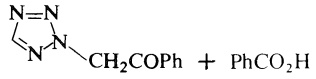

3

In contrast, treatment of a 5 *M* solution of **1** in methanol with 7 *M* methanolic sodium methoxide has been found to give an exceedingly complex product mixture that includes the pyrazoles **4**–**6**, the tetrazole **7**, and the N_5 compound **8***a* or **8***b*, together with methyl benzoate and benzoic acid (2) (Table 1).

We now report on an investigation of the reaction of **1** and sodium methoxide in dilute solution that has shed further light on the reactions of α-diazo ketones with bases.[2]

Products and their Identification

The products obtained were compounds **4**–**7**, methyl benzoate and benzoic acid, and five

[1]For paper IX, see ref. 1.

[2]A preliminary study of the reaction of **1** with methanolic sodium methoxide of intermediate concentration has been carried out previously (3).

TABLE 1. Products from reaction of α-diazoacetophenone (**1**) with methanolic sodium methoxide

Product	Yield(%) Dilute[a]	Concentrated[b]
4	11	3
5	6	4
6	—[c]	1
7	4	10
8*a*(*b*)	—	5
9	4	—
10	1[d]	—
11	6	—
12	—[c]	—
$PhCO_2CH_3$	1	—[e]
$PhCO_2H$	3	—[e]
$PhCOCH_3$	7	—

[a]See Experimental section for reaction conditions.
[b]Reference 2.
[c]Trace.
[d]Isolated in run during which reaction mixture became neutral.
[e]Detected, but not isolated.

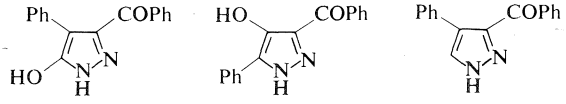

4 **5** **6**

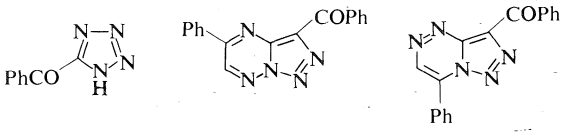

7 ***8a*** ***8b***

compounds not previously detected from the reaction in concentrated solution (Table 1). Although acetophenone was not isolated from the reaction in concentrated solution, it has been isolated from the reaction mixture obtained on treatment of **1** with aqueous sodium hydroxide (3).

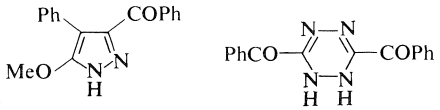

9 **10**

11 **12**

The pyrazole **9** was identified by comparison with an authentic sample obtained, together with the dimethylation products **13** and **14**, by methylation of the sodium salt of **4** with methyl iodide in dimethyl sulfoxide. In order to determine whether the product mixtures from the reaction of **1** with sodium methoxide also contained **15**, the methyl ether of **5**, this was prepared by methylation of **5** with diazomethane. The pmr spectra of the neutral fractions from the reaction of **1** with sodium methoxide failed to show the presence of **15**.

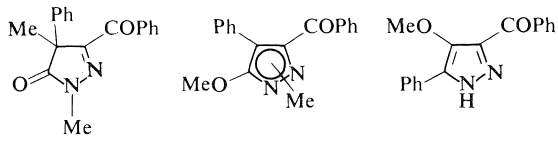

13 **14** **15**

The dihydrotetrazine **10**[3] has previously been obtained from **1** by treatment with potassium hydroxide in dimethyl sulfoxide (4). It was obtained in the present work in one run only, when a reaction of **1** was carried out with very dilute methanolic sodium methoxide and the reaction mixture became neutral during the course of the reaction, suggesting that it is a product of the reaction of **1** with methanolic sodium methoxide but is not normally observed because of its own base sensitivity (*vide infra*).

The lactol **11** of *cis*-β-benzoyl-α-phenylacrylic acid was identified by comparison with an authentic sample (5). The corresponding *trans* acid, **12**, was isolated as its methyl ester which was also identified by comparison with an authentic sample (5).

Formation of Pyrazoles

Pyrazoles are known to be formed on treatment of α-diazo carbonyl compounds with

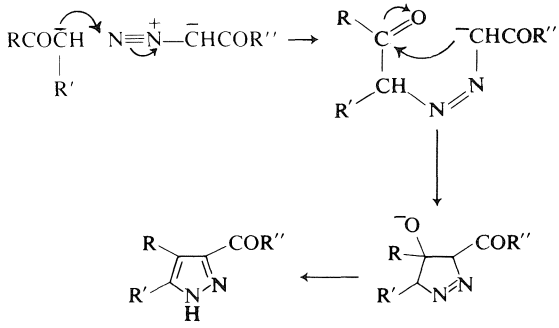

SCHEME I

[3]This is either the 1,2- or 1,4-dihydro compound (4).

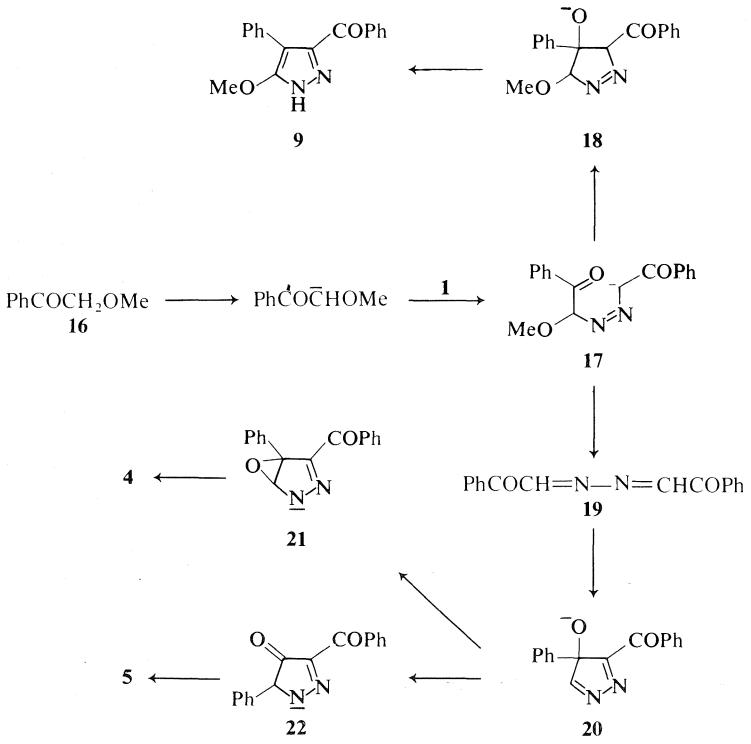

SCHEME 2

enolate ions, a reaction that can readily be interpreted as involving initial terminal addition (3) of the enolate ion to the α-diazo carbonyl compound, followed by aldol condensation and dehydration (*cf.* ref. 6) (Scheme 1).

The occurrence of acetophenone in the reaction mixture from **1** and methanolic sodium methoxide clearly suggests that the pyrazole **6** arises by the condensation of **1** with acetophenone as in Scheme 1, as has previously been suggested for the reaction in aqueous base (3).

The other pyrazoles formed, *i.e.*, **4**, **5**, and **9**, are all in a higher oxidation state than **6**, and their formation via Scheme 1 from **1** and an enolate ion in a higher oxidation state than that of acetophenone seems likely. In the case of the methoxypyrazole **9**,[4] the route in Scheme 1 could involve the condensation of **1** with the enolate ion of α-methoxyacetophenone (**16**)[5] to give **17**, and the conversion of this to **9** via **18** (Scheme 2). When **16** was added to the initial solution of **1** and methanolic sodium methoxide, the yield of **9** was considerably increased. Furthermore, there was an increase in the yields of the two hydroxypyrazoles **4** and **5**.[6] Thus the intermediacy of α-methoxyacetophenone is implicated in the formation of all three of the pyrazoles, **4**, **5**, and **9**. To account for this we propose that **17** is converted to the azine **19**, which undergoes base-catalyzed cyclization to **20**, which gives **4** and **5**, via **21** and **22**, respectively (Scheme 2).

These pathways together with the pathway via **18** to **9** account for the circumstance that, while both the 5-hydroxypyrazole **4** and the corresponding 5-methoxypyrazole **9** are formed, the 4-hydroxypyrazole **5** is not accompanied by the corresponding 4-methoxypyrazole, **15**.[7] Scheme 2 also accounts for the following observations made when 2-methoxy-4′-methyl-

[4]The observation that a 5-methoxypyrazole of type **9** is formed in the reaction of an α-diazo ketone with methanolic sodium methoxide was first made by Dr. A. L. Crowther in the case of α-diazopinacolone (P. Yates, A. L. Crowther, and P. A. Gilbert, unpublished results).

[5]The origin of α-methoxyacetophenone is discussed subsequently.

[6]We thank Dr. R. G. F. Giles for the original observation of this effect.

[7]The possibility that **9** and **15** were both formed but that **15** preferentially underwent further reaction was excluded by the observation that both **9** and **15** are stable under the reaction conditions.

acetophenone (**23**) was added to the initial solution of **1** and methanolic sodium methoxide. From the weak acid fraction was obtained a crystalline mixture of the hydroxypyrazoles **24** and **25**. The pmr spectrum of the mixture showed two overlapping singlets at δ 2.35 and 2.39 (11:9). Baeyer–Villiger oxidation of the mixture followed by hydrolysis gave a 1:1 mixture of the carboxylic acids **26** and **27**, together with a mixture of phenol and *p*-cresol (1:1). From the acid fraction of the original reaction mixture was obtained a mixture of the two hydroxypyrazoles **28** and **29**. The pmr spectrum of the

p-$CH_3C_6H_4COCH_2OMe$

23

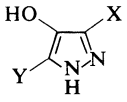

24 X = PhCO, Y = *p*-MeC_6H_4
25 X = *p*-MeC_6H_4CO, Y = Ph
26 X = CO_2H, Y = *p*-MeC_6H_4
27 X = CO_2H, Y = Ph

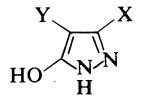

28 X = PhCO, Y = *p*-MeC_6H_4
29 X = *p*-MeC_6H_4CO, Y = Ph
30 X = CO_2H, Y = *p*-MeC_6H_4
31 X = CO_2H, Y = Ph

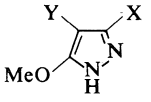

32 X = PhCO, Y = *p*-MeC_6H_4
33 X = *p*-MeC_6H_4CO, Y = Ph

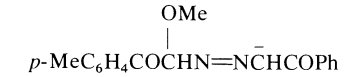

34

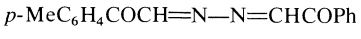

35

mixture showed two overlapping singlets at δ 2.23 and 2.30 (11:4). Baeyer–Villiger oxidation of the mixture followed by hydrolysis gave a mixture of carboxylic acids considered to be **30** and **31**, together with a mixture of phenol and *p*-cresol (2:1). From the neutral fraction of the original reaction mixture was obtained a single 5-methoxypyrazole, **32**; the presence of the isomeric 5-methoxypyrazole, **33**, could not be detected. The assignment of structure **32** to the methoxypyrazole is based on comparison of its pmr spectrum with the spectra of **9** and **15** and of the mixture of **32** and **33** obtained by methylation of the 11:4 mixture of hydroxypyrazoles **28** and **29** (see Table 2). These results are readily accommodated in terms of Scheme 2. Thus, the terminal adduct **34** formed from **1** and the anion of **23** can give the single 5-methoxypyrazole **32** and the azine **35**, which can give **24**, **25**, **28**, and **29** via two analogues of **20**.

Formation of N_4 Compounds and Other Products

5-Benzoyltetrazole (**7**) was isolated from the product mixtures formed on treatment of **1** with both concentrated and dilute methanolic sodium methoxide. Its structural relationship to 2-phenacyl-5-benzoyltetrazole (**2**) the major product from the reaction of **1** with potassium *tert*-butoxide in *tert*-butyl alcohol suggested that it might arise via cleavage of **2**. However, treatment of **2** with methanolic sodium methoxide led not to **7** but to 5-benzoyl-2-methyltetrazole (**36**). This is in interesting contrast to its reaction with potassium *tert*-butoxide and *tert*-butyl alcohol which gives 2-phenacyltetrazole (**3**) (1). Presumably cleavage to give **36** is inhibited in this case by enolate anion formation at the methylene group.

With the exclusion of **2** as the source of **7** in methanolic sodium methoxide, we propose that the formation of **7** involves base-catalyzed reaction of **1** with phenylglyoxal 2-monohydrazone (**37**), itself formed by reduction of **1** by methanolic sodium methoxide; the resulting intermediate, **38**, could then form **7** by cyclization to **39** followed by elimination of acetophenone (Scheme 3). The latter could also arise via Wolff–Kishner reduction of **37**. In these terms the formation of **7** requires that the base also be a reducing agent.

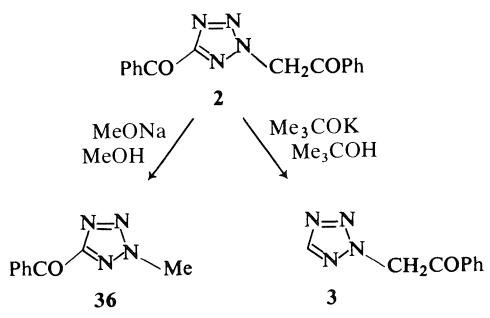

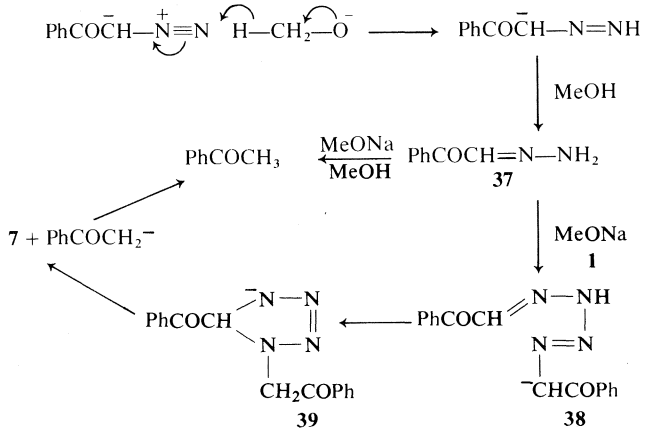

SCHEME 3

TABLE 2. Proton magnetic resonance spectra of methoxypyrazoles

Compound[a]	δ
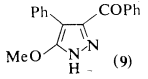 (9)	4.03 (s, 3H) 7.1–7.4 (m, 8H) 7.67 (d of d, 2H)[b]
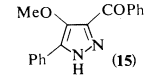 (15)	3.60 (s, 3H) 7.3–7.5 (m, 6H) 7.8–8.1 (m, 4H)
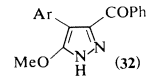 (32)	2.25 (s, 3H) 4.04 (s, 3H) 6.8–7.4 (m, 7H) 7.67 (d of d, 2H)[b]
32 + 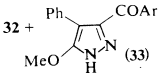 (33) (11:4)	2.25, 2.28 (two s (11:4), 3H) 4.03 (s, 3H) 6.9–7.7 (m, 9H)

[a]Ar = *p*-$CH_3C_6H_4$.
[b]First order approximation: J = 7.5 and 2 Hz.

The other type of N_4 product, **10**, has not been observed previously in the reaction of **1** with methanolic sodium methoxide; as mentioned above, this might be due to the fact that it usually reacts further under the basic reaction conditions. In order to investigate this possibility the reaction of **10** with dilute methanolic sodium methoxide was investigated. All of the products isolated were also obtained from the reaction of **1** with dilute methanolic sodium methoxide. However, the relative product yields suggest strongly that **10** is not a major intermediate in the reaction of **1** with sodium methoxide, nor a major source of compounds other than methyl benzoate in that reaction. This follows from the very much greater yield of methyl benzoate in the case of the reaction of **10** with sodium methoxide.

The cleavage product, methyl benzoate, could also arise by attack of methoxide ion on either **1** itself or on **40**, its adduct with methanol (*i.e.*, a protonation product of the terminal adduct **41**) (3). The formation of benzoic acid is attributable to hydrolysis of methyl benzoate by hydroxide ion produced from water formed, for example, in the formation of the pyrazoles **6** and **9**. The putative intermediate, α-methoxyacetophenone (**16**), could also arise from **41**; protonation of this on carbon would give **42**, which could give **16** either directly by loss of nitrogen or by a displacement reaction with methoxide ion. The adduct **42** could serve as a further source of methyl benzoate.

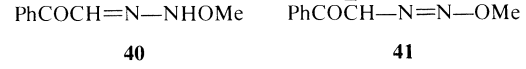

40 **41**

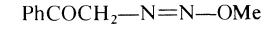

42

It is recognized that the mechanistic proposals made here are speculative; however, the multiplicity of the reactions involved makes it difficult to delineate definitively the origin of all the products, particularly since these may often arise by more than one pathway.[8]

[8]A discussion of some additional mechanistic proposals and ancillary experimental results are available, at a nominal charge, from the Depository of Unpublished Data, CISTI, National Research Council of Canada, Ottawa, Canada K1A 0S2.

Experimental

Solutions in organic solvents were dried over anhydrous magnesium sulfate. Chromatographic columns were packed in petroleum ether (bp 60–70 °C); the mixture to be separated was pre-absorbed on the column material and the resulting powder was placed as a thin band on top of the column. Melting points are uncorrected. Infrared spectra were recorded with chloroform as solvent, unless otherwise specified; pmr spectra were recorded with deuterochloroform as solvent. Known compounds were identified by mp and mixture mp determinations, and by spectroscopic and vpc comparison with authentic samples.

*Reaction of α-Diazoacetophenone (**1**) with Methanolic Sodium Methoxide*

(*i*) A solution of **1** (1.32 g, 9.0 mmol) in anhydrous methanolic sodium methoxide (0.4 *M*, 450 ml), was boiled under reflux for 5.5 h. The resulting mixture was separated into acid (soluble in aqueous 5% $NaHCO_3$), weak acid (soluble in aqueous 3% KOH), and neutral fractions. The *acid fraction* (0.40 g) was triturated with petroleum ether – ether (1:1) and the resulting pale yellow precipitate was filtered to give **4** (0.12 g, 11%), mp 246–248 °C. The filtrate was stripped of solvent and treated with an ethereal solution of diazomethane. Evaporation of solvent left a pale yellow oil whose pmr spectrum showed methyl benzoate (δ 3.90 (s)) to be the major component, accompanied by smaller amounts of the two *N*-methyl derivatives of 5-benzoyltetrazole (**7**) (δ 4.28 (s) and 4.40 (s)). In another run the residue obtained on removal of the solvent was examined by vpc (10 ft, 10% SE 30), and ir and pmr spectroscopy, which showed the presence of benzoic acid and **7**. The *weak acid fraction* (0.26 g) was treated with warm benzene to yield a pale brown precipitate of **5** (0.065 g, 6%), mp 206–208 °C. The *neutral fraction* (0.48 g) was chromatographed on alumina. Elution with ether – petroleum ether (4–10% v:v) gave a mixture of acetophenone (0.070 g, 7%) and methyl benzoate (0.010 g, 1%) as determined by vpc (SE 30). Unchanged α-diazoacetophenone (0.090 g) was eluted subsequently. Elution with ether – petroleum ether (10–25% v:v) afforded small amounts of unidentified products. Elution with methanol–ether (2% v:v) yielded 3-benzoyl-5-methoxy-4-phenylpyrazole (**9**) (0.050 g, 4%) as a yellow glass, which on crystallization from ether – petroleum ether gave yellow prisms, mp 143–144 °C.

(*ii*) A solution of **1** (1.00 g, 6.8 mmol) in anhydrous methanolic sodium methoxide (0.01 *M*, 17.5 ml) was boiled under reflux. An aliquot (2 ml), taken after a reaction time of 6.25 h, deposited on cooling in dry ice – methanol red-brown needles of **10** (0.005 g), mp 182–183 °C (lit. (4) mp 182–183 °C). After this reaction time the mixture was found to have p*H ca.* 6.5. A further amount of methanolic sodium methoxide was added to bring the concentration to 0.025 *M*. The mixture was boiled for a further 47 h, and then cooled (dry ice – ethanol). A further quantity of **10** (0.004 g), mp 179–181 °C, was deposited. The reaction mixture was separated into acid, weak acid, and neutral fractions; these were shown to contain **4**, benzoic acid, **7**, and α-diazoacetophenone.

(*iii*) To a boiling solution of methanolic sodium methoxide (0.4 *M*, 100 ml) was added dropwise over a 7 h period, a solution of **1** (2.92 g, 0.020 mol) in anhydrous methanol (100 ml). Heating was continued at 45–50 °C for a further 22 h. The *acid fraction* (0.90 g) was triturated with ether – petroleum ether (1:1) to give **4** (0.30 g, 11%), mp 246–248 °C. The filtrate was stripped of solvent, and the residue was chromatographed on silica gel. The first fraction was eluted with ether – petroleum ether (13–25% v:v) and afforded benzoic acid (0.07 g, 3%), mp 121–122 °C. Elution with ether – petroleum ether (25–35% v:v) yielded a pale yellow oil (0.28 g) that was a mixture. 5-Benzoyltetrazole (**7**) (0.075 g, 4%) was isolated by a combination of fractional crystallization and precipitation as its silver salt from a hot aqueous solution of the oil. On cooling the aqueous solution a cream solid precipitated, which on crystallization from benzene–cyclohexane gave the lactol form of *cis*-β-benzoyl-α-phenylacrylic acid (**11**) (0.15 g, 6%) as colorless plates, mp 122–123 °C (lit. (5) mp 123–124 °C). Methylation of **11** with an ethereal solution of diazomethane gave methyl *cis*-β-benzoyl-α-phenylacrylate as a viscous oil. The *weak acid* (0.60 g) and the *neutral fractions* (1.09 g) were shown to contain **5**, **7**, acetophenone, methyl benzoate, and unchanged α-diazoacetophenone as in (*i*).

(*iv*) A solution of α-diazoacetophenone (2.92 g) in anhydrous methanolic sodium methoxide (0.4 *M*, 200 ml) was boiled under reflux for 23.5 h. The *acid fraction* (0.48 g) was triturated with warm ether – petroleum ether (1:1), to give **4** (0.18 g, 7%), mp 245–247 °C. The filtrate was stripped of solvent, and the residue was treated with ethereal diazomethane. Removal of the ether left a viscous yellow oil, which was chromatographed on silica gel. The first fractions eluted with ether – petroleum ether (5% v:v) gave methyl benzoate. Elution with ether – petroleum ether (20% v:v) yielded the methyl ester of *trans*-β-benzoyl-α-phenylacrylic acid (**12**) (0.01 g) as a viscous oil that partially crystallized. Elution with ether – petroleum ether (25–30% v:v) gave the methyl ester of *cis*-β-benzoyl-α-phenylacrylic acid (**11**) (0.13 g) as a viscous pale yellow oil. The final fractions were eluted with ether – petroleum ether (30–35% v:v) to give 5-benzoyl-1-methyltetrazole (0.09 g) as a colorless oil that slowly crystallized. The *weak acid* (0.68 g) and *neutral fractions* (0.71 g) contained the same products as the corresponding fractions in *iii*. In another run with 0.2 *M* methanolic sodium methoxide and 0.2 *M* α-diazoacetophenone, 3-benzoyl-4-phenylpyrazole (**6**), mp 197–198 °C, was isolated from the neutral fraction.

*3-Benzoyl-5-methoxy-4-phenylpyrazole (**9**)*

To a stirred solution of the sodium salt of **4** (0.38 g) in dimethyl sulfoxide (5 ml) was added dropwise a solution of methyl iodide (0.30 g) in ether (5 ml). After addition was complete, stirring was continued for 0.5 h, the mixture was poured into water, and then extracted with ether. The ethereal extract was washed with aqueous 5% KOH and water, and dried. Evaporation of the ether left a viscous oil (0.24 g), which was chromatographed on alumina. Elution with ether – petroleum ether (10–15% v:v) afforded **13** as a pale yellow viscous oil (0.10 g); λ_{max} (CCl_4) 6.05, 7.60, 7.82, 9.40, 10.68, 10.86 μm; δ 3.87 (s, 3H), 4.00 (s, 3H), 7.0–7.4 (m, 8H), 7.73 (d of d, 2H). Elution with ether – petroleum ether (40–50% v:v) gave **14** as cream crystals (0.04 g); λ_{max} (CCl_4) 5.76, 6.05, 8.10, 9.85, 10.82, 11.10 μm; δ 1.95 (s, 3H), 3.52 (s, 3H), 7.25–7.6 (m, 8H), 8.13 (d of d, 2H). Elution with ether gave **9**

(0.05 g, 24%) which, after recrystallization from ether – petroleum ether, was obtained as pale yellow prisms, mp 145–146 °C; λ_{max} 3.00, 3.05–3.25, 6.09, 7.05, 7.70, 9.32, 9.75, 10.96 μm; δ 4.03 (s, 3H), 7.1–7.4 (m, 8H), 7.67 (d of d, 2H). *Anal.* calcd. for $C_{17}H_{14}N_2O_2$: C 73.36, H 5.07, N 10.07; found: C 73.19, H 5.15, N 9.97.

*3-Benzoyl-4-methoxy-5-phenylpyrazole (**15**)*

A solution of **5** (0.50 g, 1.9 mmol) in anhydrous ether was treated with an ethereal solution of diazomethane (10 ml, 2.56 mmol). The resulting mixture was stirred at 5–10 °C for 6 h and then allowed to stand at room temperature for a further 18 h. The reaction mixture was extracted with aqueous 3% KOH and the ethereal layer was separated and dried. Evaporation of the ether left a viscous colorless oil which was chromatographed on alumina. Elution with ether – petroleum ether gave small quantities of several unidentified compounds. Elution with methanol–ether (2% v:v) gave an oil that slowly crystallized. Recrystallization from benzene–cyclohexane afforded **15** (0.22 g, 42%) as colorless needles, mp 143–144.5 °C; λ_{max} 3.00, 3.15–3.40, 6.08, 7.28, 9.90, 11.00 μm; δ 3.60 (s, 3H), 7.3–7.5 (m, 6H), 7.8–8.1 (m, 4H). *Anal.* calcd. for $C_{17}H_{14}N_2O_2$: C 73.36, H 5.07, N 10.07; found: C 73.52, H 5.04, N 9.84.

Reaction of α-Diazoacetophenone with α-Methoxyacetophenone and Methanolic Sodium Methoxide

To a stirred solution of sodium methoxide in anhydrous methanol (5.5 *M*, 6.5 ml) was added dropwise a solution of α-diazoacetophenone (4.90 g, 0.034 mol) and α-methoxyacetophenone (4.70 g, 0.031 mol) in anhydrous methanol (5.5 ml). The mixture was kept at 0 °C during the addition and allowed to stand at room temperature for 1 h after completion of the addition. The *acid fraction* was treated with a little warm ether to give a precipitate of **4** (0.63 g, 7%)[9], mp 248–250 °C. The filtrate was stripped of solvent to give a pale yellow oil (0.25 g) that slowly crystallized. Its pmr and ir spectra showed that it consisted mainly of benzoic acid and **7**. The *weak acid fraction* was triturated with a small amount of hot benzene to give **5** (0.50 g, 5.5%)[9], mp 206–208 °C. The *neutral fraction* was obtained as a yellow-orange glass (5.7 g) that slowly crystallized on standing at room temperature for several days. Its pmr spectrum exhibited a singlet at δ 3.93 besides aromatic proton signals. It was chromatographed on silica gel. Elution with ether – petroleum ether mixtures (0–35% v:v) afforded some biphenyl (shown to be present as an impurity in the α-methoxyacetophenone used in this experiment), a small amount of methyl benzoate, and small quantities of yellow oils. Elution with ether – petroleum ether (40% v:v) gave **9** (2.20 g, 24%)[9] as a pale yellow glass that slowly crystallized. Recrystallization from ether – petroleum ether yielded pale yellow prisms, mp 145–146 °C.

*2-Methoxy-4′-methylacetophenone (**23**)*

A solution of *p*-tolylmagnesium bromide in anhydrous ether (350 ml) was prepared from magnesium (8.8 g) and *p*-bromotoluene (61.6 g). Methoxyacetonitrile (21.3 g) in anhydrous ether (50 ml) was slowly added to the cooled (ice–salt bath), well stirred Grignard solution and, after completion of the addition, the mixture was allowed to stand at room temperature for 2 h. The complex was decomposed by the addition of water (200 ml), cracked ice, and cold 12 *N* sulfuric acid (100 ml). The solution was extracted with ether, and the extract was dried and stripped of solvent to give a colorless liquid. Distillation gave **23** (32 g, 54%), bp 83–88 °C/0.15 torr (lit. (7) bp 127 °C/3.0 torr); λ_{max} (film) 5.90, 6.24, 8.10, 8.32, 8.85, 12.30 μm; δ 2.37 (s, 3H), 3.35 (s, 3H), 4.45 (s, 2H), 7.18 (d, 2H, J = 8 Hz), 7.80 (d, 2H, J = 8 Hz).

*Reaction of α-Diazoacetophenone with **23** and Methanolic Sodium Methoxide*

α-Diazoacetophenone (4.05 g, 0.028 mol) and **23** (4.50 g, 0.027 mol) in anhydrous methanol (5.5 ml) were added dropwise to a stirred solution of methanolic sodium methoxide (5.5 *M*, 6.5 ml), which was kept at 0 °C. After the addition the mixture was allowed to stand at room temperature for 1 h and then poured into water. The *acid fraction* (0.67 g) was triturated with warm ether – petroleum ether (1:1) to give a yellow solid (0.38 g), mp 195–207 °C, which could not be purified by recrystallization. Its pmr spectrum (DMSO-d_6) exhibited overlapping singlets at δ 2.23 and 2.30 (ratio 11:4) in addition to aromatic proton signals, assigned to 3-benzoyl-5-hydroxy-4-(*p*-tolyl)pyrazole (**28**) and 5-hydroxy-4-phenyl-3-(*p*-toluyl)pyrazole (**29**), respectively. The filtrate was evaporated to dryness and treated with an ethereal solution of diazomethane. The resulting yellow oil was shown to consist mainly of methyl benzoate and methyl *p*-toluate (major product) by pmr spectroscopy and vpc. The *weak acid fraction* (1.16 g) was digested with warm benzene and the resulting solution allowed to stand for several hours to give a yellow-brown solid (0.51 g), mp 191–194 °C. Its pmr spectrum showed overlapping singlets at δ 2.35 and 2.39 (ratio 11:9) in addition to aromatic proton signals, and these were assigned to 3-benzoyl-4-hydroxy-5-(*p*-tolyl)pyrazole (**24**) and 4-hydroxy-5-phenyl-(3-*p*-toluyl)pyrazole (**25**), respectively. The *neutral fraction* (4.92 g) was chromatographed on alumina. Elution with ether – petroleum ether (10% v:v) afforded a mixture of bi-*p*-tolyl and methyl benzoate; the former was present as an impurity in the starting material **23**. Elution with ether – petroleum ether (10–12% v:v) gave unchanged **23** (0.16 g). Elution with ether – petroleum ether (20–25% v:v) gave a yellow oil (1.44 g) that slowly crystallized. Recrystallization from ether–hexane afforded pale yellow prisms of 3-benzoyl-5-methoxy-4-(*p*-tolyl)pyrazole (**32**), mp 126–127 °C; λ_{max} 3.00, 3.20, 6.10, 6.72, 7.75, 9.30, 11.00 μm; δ 2.25 (s, 3H), 4.04 (s, 3H), 6.8–7.4 (m, 7H), 7.67 (d of d, 2H). *Anal.* calcd. for $C_{18}H_{16}N_2O_2$: C 73.95, H 5.52, N 9.58; found: C 74.01, H 5.47, N 9.38.

*Baeyer–Villiger Oxidation of the Mixture of **24** and **25***

To a solution of glacial acetic acid (2.0 ml) and concentrated H_2SO_4 (1.0 ml) was added the mixture of **24** and **25** (0.20 g). The solution was cooled to 0 °C, 40% peracetic acid (0.3 ml) was added, and the mixture was stirred at room temperature for 24 h. It was then poured into excess water to give a fawn solid; λ_{max} (Nujol) 5.85 μm. This was dissolved in aqueous KOH (10 ml) and the solution was boiled under reflux for 2 h. This was acidified and steam distilled. The distillate was acidified and extracted with several portions of ether. The extract was dried and stripped of solvent to give a colorless oil

[9]Calculated on the basis of the conversion of 1 mol of **1** to 1 mol of pyrazole.

(0.03 g) that possessed a distinct phenolic odor. Infrared and nmr spectroscopy and vpc analysis of the oil showed it to be a *ca.* 1:1 mixture of phenol and *p*-cresol. The steam involatile components of the above mixture were isolated by extraction with ether. The ethereal extract was dried and stripped of solvent to give a fawn solid (0.06 g); λ_{max} (Nujol) 3.0–4.8, 5.98, 8.05, 10.30, 12.15 μm; this ir spectrum was identical with that of a 1:1 mixture of 4-hydroxy-5-(*p*-tolyl)pyrazole-3-carboxylic acid (**26**) and 4-hydroxy-5-phenylpyrazole-3-carboxylic acid (**27**).

*4-Hydroxy-5-(p-tolyl)pyrazole-3-carboxylic Acid (**26**)*

To a stirred solution of anhydrous methanolic sodium methoxide (5 *M*, 20 ml) at room temperature was added dropwise a mixture of methyl *p*-tolylacetate (2.20 g, 13.4 mmol) and ethyl diazoacetate (1.60 g, 14.0 mmol). After addition was complete, the mixture was stirred for an additional 1 h. The reaction mixture was diluted with water (5 ml) and boiled under reflux for 2 h. The resulting dark-brown solution was neutralized with dilute HCl, poured into aqueous 5% $NaHCO_3$ (150 ml), and extracted with ether. The aqueous layer was acidified and extracted with several portions of ether. The ethereal extract was dried and stripped of solvent to give an orange-brown gum, which after several washings with boiling cyclohexane solidified to an orange-brown solid (0.95 g), which was chromatographed on silica gel. Elution with ether – petroleum ether (30% v:v) afforded **26** (0.50 g, 17%) as a cream solid, mp 221–222 °C (dec.); λ_{max} (Nujol) 3.04, 3.0–4.8, 6.00, 8.05, 10.30, 12.15 μm. *Anal.* calcd. for $C_{11}H_{10}N_2O_3$: C 60.54, H 4.62, N 12.84; found: C 60.53, H 4.68, N 12.79.

*4-Hydroxy-5-phenylpyrazole-3-carboxylic Acid (**27**)*

Compound **27** was prepared from anhydrous methanolic sodium methoxide (5 *M*, 20 ml), methyl phenylacetate (3.00 g, 20.0 mmol), and ethyl diazoacetate (2.30 g, 20.0 mmol) by the procedure described above for the preparation of **26**. The orange-brown crude solid product (1.50 g) was chromatographed on silica gel; elution with ether – petroleum ether (60–80% v:v) gave **27** (0.53 g, 13%) as a cream solid, mp 212–213 °C (dec.); λ_{max} (Nujol) 3.00, 3.0–4.8, 5.98, 10.30 μm. *Anal.* calcd. for $C_{10}H_8N_2O_3$: C 58.82, H 3.95, N 13.72; found: C 58.96, H 4.13, N 13.60.

*Baeyer–Villiger Oxidation of the Mixture of **28** and **29***

The mixture of **28** and **29** (0.15 g) was oxidized with glacial acetic acid (2 ml), concentrated H_2SO_4 (1 ml), and peracetic acid (0.3 ml) by a procedure similar to that described above. When poured into water, the reaction mixture gave a fawn precipitate, which was dried; λ_{max} (Nujol) 3.08, 3.24 (br), 5.80, 7.94, 8.34 μm. This was subjected to alkaline hydrolysis followed by steam distillation as described above. The steam distillate was acidified and extracted with ether. The ethereal extract was dried and stripped of solvent to give a colorless oil (0.025 g) with a distinct phenolic odor. Infrared and pmr spectroscopy and vpc showed the oil to be a 2:1 mixture of phenol and *p*-cresol. The steam involatile constituents were obtained as a fawn solid (0.055 g); λ_{max} 3–4, 5.90 μm. This is considered to be a mixture of **30** and **31**, but attempts to separate the components were unsuccessful.

*Methylation of the Mixture of **28** and **29***

Sodium methoxide (0.019 g, 0.36 mmol) was added to a solution of the mixture of **28** and **29** (0.10 g, 0.36 mmol) in dimethyl sulfoxide (5 ml). The resulting orange solution was treated dropwise with a solution of methyl iodide (0.051 g, 0.36 mmol) in dimethyl sulfoxide (2 ml). The mixture was stirred at room temperature for 2 h, when the orange color had faded to a pale yellow color. It was poured into aqueous 3% KOH and extracted with ether. The ethereal layer was washed with several portions of water, dried, and stripped of solvent to give a mixture of **32** and **33** as a viscous oil (0.04 g) that slowly crystallized (mp 80–90 °C); δ 2.25 and 2.28 (overlapping s (11:4), 3H), 4.03 (s, 3H), 6.9–7.7 (m, 9H).

*Reaction of **2** with Methanolic Sodium Methoxide*

Compound **2** (0.100 g) was dissolved in anhydrous methanolic sodium methoxide (0.3 *M*, 20 ml), and the solution was boiled under reflux for 3.5 h. The reaction mixture was poured into water, and the aqueous solution was neutralized and extracted with ether. The ethereal extract was dried and stripped of solvent to give a colorless oil (0.084 g); δ 3.90 (s), 4.48 (s) and 6.30 (s) (ratio 7:11:12), 7.5–7.8 (m), 8.00 (d of d) and 8.37 (d of d) (ratio 5:8). The oil was chromatographed on silica gel. Elution with ether – petroleum ether (5% v:v) gave methyl benzoate (0.01 g, 20%). Elution with ether – petroleum ether (40–50% v:v) afforded **36** (0.02 g, 30%) as a colorless oil; after crystallization from ether – petroleum ether this had mp 41–43 °C (lit. (8) mp 45.4–46 °C); λ_{max} 6.00, 6.30, 7.35, 10.90 μm; δ 4.48 (s, 3H), 7.5–7.7 (m, 3H), 8.37 (d of d, 2H). The final fraction from the column was eluted with ether – petroleum ether (50% v:v) and gave unchanged **2** (0.04 g).

Acknowledgments

We thank the National Research Council of Canada for support of this work and Mr. G. J. Köves for technical assistance.

1. P. Yates, R. G. F. Giles, and D. G. Farnum. Can. J. Chem. **47**, 3997 (1969).
2. P. Yates and D. G. Farnum. J. Am. Chem. Soc. **85**, 2967 (1963).
3. P. Yates and B. L. Shapiro. J. Am. Chem. Soc. **81**, 212 (1959).
4. P. Yates, O. Meresz, and H. Morrison. Tetrahedron Lett. 77 (1967); 1575 (1967).
5. C. P. Kohler, W. D. Peterson, and C. L. Bickel. J. Am. Chem. Soc. **56**, 2000 (1934).
6. R. Huisgen. Angew. Chem. **67**, 439 (1955).
7. I. E. El-Kholy, F. K. Rafia, and G. Soliman. J. Chem. Soc. 2588 (1959).
8. O. Gryszkiewicz-Trochimowski. C. R. **246**, 2627 (1958).

Isotope effect studies of the decomposition of 2-propanol on hafnium(IV) oxide

IAN M. HOODLESS

Department of Chemistry, Lakehead University, Thunder Bay, Ont., Canada P7B 5E1

Received July 6, 1976

IAN M. HOODLESS. Can. J. Chem. **55**, 153 (1977).

The catalytic decomposition of 2-propanol on hafnium dioxide has been investigated over the temperature range 355–397 °C by a micropulse reactor technique. The major reaction is one of dehydration to propene but dehydrogenation also occurs to a small extent. Isotope effect measurements with deuterio-2-propanols indicate that the rate-limiting step in dehydration involves cleavage of the β-carbon–hydrogen while in the dehydrogenation reaction it is cleavage of the α-carbon–hydrogen bond.

IAN M. HOODLESS. Can. J. Chem. **55**, 153 (1977).

On a étudié, à des températures allant de 355–397 °C et utilisant une technique de réacteur micropulsé, la décomposition catalytique du propanol-2 sur le dioxyde d'hafnium. La réaction principale conduit au propène par déshydratation; il y a toutefois une petite quantité de déshydrogénation. Des mesures d'effets isotopiques à l'aide de deutériopropanols-2 indiquent que l'étape déterminante dans la déshydratation implique le bris du lien carbone-β hydrogène alors que dans la réaction de déshydrogénation, l'étape déterminante implique le bris du lien carbone-α hydrogène.

[Traduit par le journal]

Introduction

The mechanism of the catalytic decomposition of secondary alcohols on metal oxide surfaces has been the subject of numerous studies. Dehydration and dehydrogenation are the predominant modes of decomposition but there is still some controversy in regard to the identification of the rate-determining step in these reactions. Desorption of one of the products, the ketone in the case of dehydrogenation and water in the case of dehydration, has been proposed by some workers as the rate-controlling stage while others favour the surface reaction of the adsorbed alcohol as rate controlling (1). One method of investigation of the rate-determining stage in a reaction is by kinetic isotope effect measurements; the present paper describes the application of this method to the investigation of 2-propanol decomposition on a HfO_2 catalyst. HfO_2 is an insulator oxide and previous work (2) has indicated that it catalyses both the dehydration and dehydrogenation of 2-propanol.

Experimental

The decomposition of 2-propanol was investigated by a micropulse reactor technique. The reactor was a 10 mm diameter Pyrex-glass tube containing the powdered catalyst mounted on a sintered glass disc sealed across the tube. Pulses of the alcohol (2 μl each) were injected into a preheated helium carrier-gas stream and passed over the catalyst; the reaction products and unreacted alcohol emerging from the reactor were collected in a trap, cooled with liquid nitrogen, before being admitted to a Pye series 104 gas chromatograph. Quantitative analysis for 2-propanol, acetone, and propene was carried out using a 6 ft column of 10% Carbowax 20M on Chromosorb G at 85 °C and a katharometer as detector. A trapping time of 4 min was employed in all the experiments; tests in which the trapping time was increased by a factor of six did not lead to an increased recovery of products or the alcohol. The general procedure was that at a particular reaction temperature the catalyst would be subjected to approximately twenty pulses of the alcohol; typically pulses 1–4 would be 2-propanol, pulses 5–7, a deuterio-alcohol, pulses 8–10, 2-propanol and so on. The time interval between pulses was approximately 15 min. On the basis of the results over the whole temperature range the mean error in the estimation of propene is 10%, while that for acetone is 13%.

Materials

The catalyst samples were HfO_2 (special grade, Alfa Inorganics Incorporated) and had a surface area of approximately 0.4 $m^2\ g^{-1}$, as measured by the BET method using krypton as the adsorbate. Prior to any alcohol pulses the catalysts were conditioned in the reactor by annealing at 500 °C for 4 h in the helium carrier-gas stream. The reactants were Spectranalyzed 2-propanol (Fisher Scientific Company) and the deuterio-alcohols (Merck, Sharp and Dohme); 2-propanol-d_1 ($(CH_3)_2CHOD$) and 2-propanol-d_6 ($(CD_3)_2CHOH$) had a minimum isotopic purity of 99 atom% D while for 2-propanol-2d_1 ($(CH_3)_2CDOH$) it was 98 atom% D.

Results

The decomposition of 2-propanol was investigated over the temperature range 355 to 397 °C. The predominant reaction was dehydration of the alcohol to propene; small amounts of acetone and propane were also formed. In comparative experiments over the same temperature range but in the absence of the catalyst, no decomposition of the alcohol was detected.

The kinetics of the dehydration reaction were briefly examined on four samples of the catalyst and with varying reactant–catalyst contact times. Plots of conversion to propene against reciprocal space velocity obtained by varying the amount of catalyst at a constant flow rate (Fig. 1) or by varying the carrier-gas flow rate (Fig. 2) are shown. The results are consistent with zero-order kinetics, which have frequently been reported (1*c*) for this type of reaction. Furthermore, since the curves pass through the origin, product desorption is unlikely to be the rate-controlling process (3). In independent experiments we have shown that water does inhibit the reaction; injections of 2 μl of water on to the catalyst prior to the alcohol injections reduced the subsequent propene production only with the first alcohol pulse. Apparently the time interval between alcohol injections is sufficient to permit the desorption of water from the catalyst at these reaction temperatures. The limited temperature range investigated does not permit accurate evaluation of the activation energy for the dehydration reaction but the present results yield a value of 32 kcal mol^{-1}. The extent of conversion to acetone is too small to enable identification of the kinetics or the determination of the activation energy for this reaction.

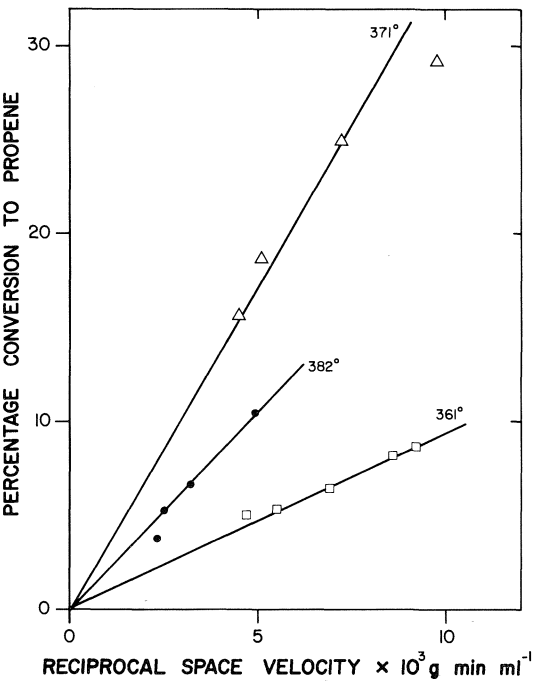

FIG. 2. Dehydration of 2-propanol over HfO_2. Space velocity was varied by flow rate: □, catalyst wt. = 0.42 g; ●, catalyst wt. = 0.166 g; △ (1 μl alcohol injections), catalyst wt. = 0.338 g.

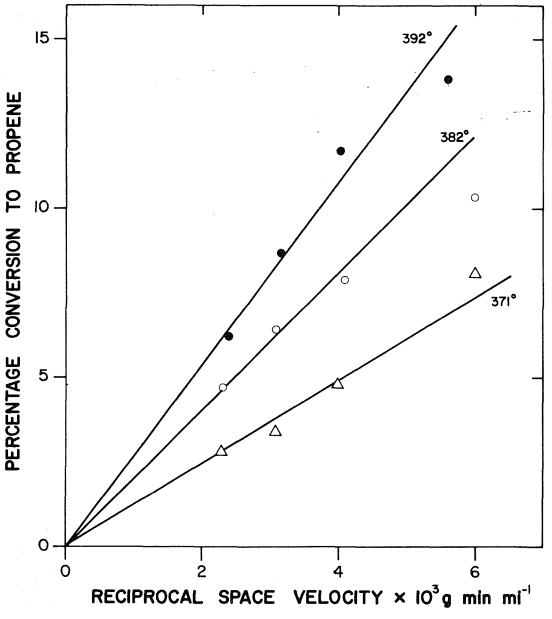

FIG. 1. Dehydration of 2-propanol over HfO_2. Space velocity was varied by catalyst weights (0.166 g, 0.230 g, 0.284 g, and 0.42 g).

Substitution of deuterium for hydrogen leads to significant changes in the degree of conversion of alcohol. Some results for one catalyst sample are given in Table 1 and a more complete set of results for two catalyst samples is shown in Fig. 3 as a plot of the ratio of the fractional conversions of the alcohol and deuterio-alcohols as a function of temperature. With 2-propanol-d_6 the propene yield is reduced while the acetone yield is reduced with 2-propanol-2d_1 as the reactant; the substitution of deuterium in the hydroxyl group does not appear to affect

TABLE 1. Conversion of 2-propanol and deuterated 2-propanols on HfO_2 (weight of catalyst, 0.42 g; 2 μl pulses)

Reactant	Reaction temp. (°C)	Flow rate (ml min^{-1})	Conversion to propene (%)	Conversion to acetone (%)
2-Propanol	361	69.8	5.7	0.7
	371	69.8	8.1	1.0
	382	69.8	10.3	1.3
	387	69.8	12.9	1.6
	392	75.0	13.8	1.6
2-Propanol-d_6	361	69.8	3.8	0.7
	371	69.8	5.1	1.1
	382	69.8	6.7	1.4
	387	69.8	8.9	1.7
	392	75.0	8.7	1.7
2-Propanol-2d_1	361	69.8	4.6	0.3_8
	382	69.8	9.0	0.7_5
	387	69.8	11.3	0.9
	392	75.0	13.5	1.1
2-Propanol-d_1	371	75.0	8.4	1.0

the rate of either the dehydration or the dehydrogenation reactions.

Discussion

The present work has shown that there is a significant kinetic isotope effect in the production of propene when there is deuterium substitution at the β-hydrogens of the alcohol and in the production of acetone when the deuterium substitution is at the α-hydrogen. These observations rule out desorption of acetone in the case of dehydrogenation and desorption of water in the case of dehydration as being the rate-determining steps in the reactions under the present experimental conditions. The magnitude of the isotope effect for the acetone formation compares favourably with some recent studies of the same reaction on a predominantly dehydrogenating catalyst. Nondek and Sedláček (6) have compared the rate constants for the reaction of 2-propanol, 2-propanol-d_1, and 2-propanol-2d_1 on a chromia catalyst. With 2-propanol-2d_1 and a reaction temperature of 350 °C they obtained an isotope effect of 1.94 which compares with a value of 2.1_4 obtained by extrapolation of the present results. As with the present work, substitution of deuterium in the hydroxyl group had no significant influence on the reaction rate. This observation contrasts with that obtained using molten indium as a catalyst for 2-propanol dehydrogenation; at a reaction temperature of 460 °C substitution of deuterium in the hydroxyl group gives rise to a significant isotope effect (7). With a basic oxide transfer of the hydrogen, presumably as a proton, from the hydroxyl group to the catalyst would more easily be achieved and hence the rate-limiting step would be fission of the α-carbon–hydrogen bond.

The isotope effect observed in formation of propene from 2-propanol-d_6 is somewhat unusual in that, over the temperature range under investigation, it appears to be temperature independent; a value of 1.5_2 is obtained for the magnitude of the effect. A simplified model (8) for the calculation of isotope effects gives

$$[1]\quad \frac{k_H}{k_D} = \left(\frac{m_D}{m_H}\right)^{1/2} \frac{h\nu_D}{h\nu_H} \times e^{(h\nu_H - h\nu_D)/2RT} \frac{1 - e^{-h\nu_H/RT}}{1 - e^{-h\nu_D/RT}}$$

where k_H/k_D is the kinetic isotope effect, m_H and m_D are the reduced masses of the normal and deuterated substrates and ν_H and ν_D are the frequencies of the stretching vibrations of the C—H and C—D bonds undergoing reaction. The model assumes that the C—H and C—D bonds in question are completely broken in the activated complex. At moderate temperatures eq. 1 can be approximated to

$$[2]\quad \frac{k_H}{k_D} = e^{(h\nu_H - h\nu_D)/2RT}$$

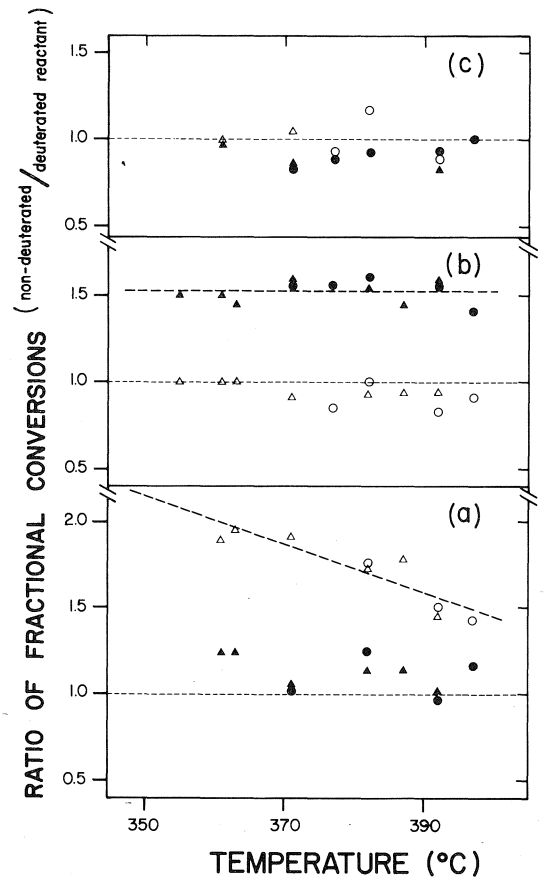

FIG. 3. Isotope effect (fractional conversion of 2-propanol/fractional conversion of deuterated 2-propanol) as a function of temperature for decomposition of 2-propanol; (*a*) 2-propanol-2d_1, (*b*) 2-propanol-d_6, (*c*) 2-propanol-d_1. Shaded symbols are for conversion to propene and open symbols for conversion to acetone; ▲/△, catalyst wt. = 0.42 g: ●/○, catalyst wt. = 0.23 g.

Comparison of the ir spectra of 2-propanol and 2-propanol-d_6 shows that the insertion of deuterium in the methyl group reduces its C—H stretching frequencies by 738 cm^{-1}. Substitution of this value in eq. 2 gives a value of 2.26 for the isotope effect at a reaction temperature of 375 °C and the decrease in the value of k_H/k_D over the interval 350–400 °C is less than 4%. Such a small temperature dependence could be obscured by errors in the experimental determination of the isotope effect. Because of the model employed, the values from eq. 3 correspond to a maximum possible isotope effect and the relatively low value obtained in the present work could indicate incomplete bond fission in the transition state.

The mechanism of the dehydration of alcohols on oxides, particularly alumina, has been extensively investigated and Pines and Manassen (9) have proposed that tertiary alcohols are dehydrated via a carbonium ion mechanism while primary and secondary alcohols are dehydrated via a concerted mechanism. In the latter case a transition state involving two-point attachment of the alcohol to the catalyst surface would be anticipated and the isotope effect would be lower than that predicted by eq. 3. The transition state would involve the weakening of the C_α—O and C_β—H bonds of the alcohol and the rate and extent of this bond loosening is important in identifying the detailed reaction mechanism. If the weakening of the C_α—O and C_β—H bonds proceeds to approximately equal extents in the transition state an E2-like mechanism applies, while a marked weakening of only one of the bonds in the transition state is characteristic of an E1-like mechanism. This aspect of the reaction mechanism has been investigated by Knözinger and co-workers (4, 5, 10) using isotope effect measurements. They conclude that with increasing reaction temperature there is a trend from an E2- to an E1-like mechanism. A similar trend is observed with increasing acidic nature of the catalyst. In one such study the dehydration of 2-propanol, 2-propanol-d_1, and 2-propanol-d_6 was investigated on some oxide catalysts at a reaction temperature of 300 °C (5). Substitution of deuterium in the hydroxyl group led to an increase in the isotope effect from 1.01 to 1.47 for the catalyst sequence Al_2O_3, ZrO_2, TiO_2, SiO_2 while the reverse trend from an isotope effect of 1.44 to 1.04 was observed for deuterium substitution at the β-carbon. Comparison of this study with the present results suggests that the dehydration reaction on HfO_2 occurs by a predominantly E2-type mechanism.

Acknowledgements

The author wishes to thank Mrs. D. Garred for assistance in the experimental work. Support of this work by the National Research Council of Canada is gratefully acknowledged.

1. (*a*) O. V. KRYLOV. Russ. J. Phys. Chem. **39**, 1554 (1965); (*b*) Y. DECHATRE and S. J. TEICHNER. Bull. Soc. Chim. Fr. 2804 (1967); (*c*) H. KNÖZINGER. The chemistry of the hydroxyl group. *Edited by* S. Patai, Interscience Publishers. 1971. Chapt. 12.
2. I. P. KONENKO, A. A. TOLSTOPYATOVA, and A. A. BALANDIN. Izv. Akad. Nauk. SSSR, Ser. Khim. 496 (1967).
3. J. A. S. BETT and W. K. HALL. J. Catal. **10**, 105 (1968).
4. H. KNÖZINGER and A. SCHEGLILA. J. Catal. **17**, 252 (1970).
5. K. KOCHLOEFL and H. KNÖZINGER. Proc. 5th Int. Congr. Catal. Vol. 2. North-Holland Publ. Co., Amsterdam. 1972. p. 1171.
6. L. NONDEK and J. SEDLÁČEK. J. Catal. **40**, 34 (1975).
7. A. MIYAMOTO and Y. OGINO. J. Catal. **37**, 133 (1975).
8. K. B. WIBERG. Chem. Rev. **55**, 713 (1955).
9. H. PINES and J. MANASSEN. Adv. Catal. **16**, 49 (1966).
10. H. KNÖZINGER and A. SCHEGLILA. Z. Phys. Chem. Frankfurt, **63**, 197 (1969).

Heat capacities of weak electrolytes and ion association reactions: method and application to aqueous $MgSO_4$ and HIO_3 at 298 K

EARL M. WOOLLEY[1] AND LOREN G. HEPLER

Department of Chemistry, University of Lethbridge, Lethbridge, Alta., Canada T1K 3M4

Received July 6, 1976

EARL M. WOOLLEY and LOREN G. HEPLER. Can. J. Chem. **55**, 158 (1977).

Analysis of heat capacities for weak electrolytes (or 'almost strong' electrolytes) in terms of the various solute species is shown to require allowance for the thermal effects associated with the shift of the association or dissociation equilibrium when the temperature changes during a calorimetric measurement. This shift of equilibrium state is related to changes in the equilibrium constant and activity coefficient with temperature, as expressed by thermodynamic equations we have derived. These equations have been applied to aqueous $MgSO_4$ and HIO_3 to obtain the contributions of the solute species to the apparent molal heat capacities, which are then analyzed to yield heat capacities of $MgSO_4$ (aq, undiss.) and HIO_3 (aq, undiss.) and ΔC_p^0 values for the association reactions of the ions to form these species.

EARL M. WOOLLEY et LOREN G. HEPLER. Can. J. Chem. **55**, 158 (1977).

L'analyse des capacités calorifiques des électrolytes faibles (ou des électrolytes presque forts) en termes des diverses espèces solutées démontre que l'on doit faire appel à des facteurs thermiques associés avec le déplacement de l'équilibre d'association ou de dissociation quand la température change durant une mesure calorimétrique. Ce déplacement de l'état d'équilibre est relié à des changements, avec la température, de la constante d'équilibre et de coefficient d'activité tel qu'exprimés par les équations thermodynamiques que nous avons dérivés. On a appliqué ces équations au $MgSO_4$ et HIO_3 en solutions aqueuses pour obtenir les contributions des espèces solutées aux capacités calorifiques molales apparentes qui ont ensuite été analysées pour obtenir les capacités calorifiques de $MgSO_4$ (aqueux et non-dissocié) et de HIO_3 (aqueux et non-dissocié) et les valeurs de ΔC_p^0 pour les réactions d'association des ions pour former ces espèces.

[Traduit par le journal]

Introduction

It has been known for a long time that heat capacities are useful or even essential for various important thermodynamic calculations. Also, it has gradually become apparent that theoretical analysis of heat capacities can lead to knowledge of the microscopic properties of various systems. For specific applications of these generalities to solutions, the quantities that are usually desired are the partial molal heat capacities of solute species at infinite dilution. In principle, these desired partial molal heat capacities can be obtained from results of heat capacity measurements on solutions of finite concentration, with results of the measurements expressed as apparent molal heat capacities, which are then extrapolated to infinite dilution.

There are no special problems associated with data treatment for nonelectrolytes or for those electrolytes that are completely dissociated in the usual moderately dilute concentration range of the heat capacity measurements. But there are significant unresolved problems in the treatment of experimental results for weak electrolytes or for 'almost strong' electrolytes that are partly associated in the concentration range of the heat capacity measurements. In this paper we show how to analyze measured heat capacities (expressed as apparent molal heat capacities) to obtain heat capacities of the undissociated species and the sum of the heat capacities of the ions. We illustrate the method by application to heat capacities for aqueous magnesium sulfate and iodic acid at 298 K, followed by brief discussion of other systems.

Method of Data Analysis and Results

We are here concerned with analysis of heat capacities of solutions in which there is an equilibrium between ions and a neutral species as in

[1] $$M^{n+}(aq) + X^{n-}(aq) \rightleftharpoons MX(aq, undiss.)$$

[1]On leave from Department of Chemistry, Brigham Young University, Provo, Utah, U.S.A.

The measured heat capacities are to be analyzed in terms of contributions from the various solute species, partly along the lines previously described by Perron, Desnoyers, and Millero (1). It is also necessary to consider the thermal effects associated with the shift of the equilibrium represented by equation 1 when the temperature increases during a measurement of heat capacity. This shift of equilibrium state is related to the change in the equilibrium constant with temperature and also to the change of activity coefficient with temperature.

Letting $C_p^{\,s}$ and $C_p^{\,w}$ represent the heat capacity of a solution of molality m that contains 1 kg of water and the heat capacity of 1 kg of pure water, respectively, we express the experimental apparent molal heat capacity ϕ_C^{exp} as

$$[2] \qquad \phi_C^{exp} = (C_p^{\,s} - C_p^{\,w})/m$$

The heat capacity of a solution that contains $M^{n+}(aq)$, $X^{n-}(aq)$, and MX(aq, undiss.) in equilibrium with each other can be expressed as

$$[3] \qquad C_p^{\,s} = (dH_{sp}/dT) + (dH_r/dT)$$

in which subscripts sp and r indicate contributions to the total enthalpy from the solute *sp*ecies (and their interactions with solvent and each other) and from the *r*eaction represented by eq. 1. Combination of eqs. 2 and 3 leads to

$$[4] \quad \phi_C^{exp} = [(dH_{sp}/dT) + (dH_r/dT) - C_p^{\,w}]/m$$

We now define the contribution to the apparent molal heat capacity from the solute species as

$$[5] \qquad \phi_C^{sp} = [(dH_{sp}/dT) - C_p^{\,w}]/m$$

and combine with eq. 4 to obtain

$$[6] \qquad \phi_C^{sp} = \phi_C^{exp} - [(dH_r/dT)/m]$$

We shall later express ϕ_C^{sp} as a sum of contributions from the various solute species and thence obtain some desired partial molal heat capacities, but first we evaluate (dH_r/dT) so that we can obtain ϕ_C^{sp} values from the experimental results represented here by ϕ_C^{exp}.

The thermodynamic equilibrium constant for the reaction represented by eq. 1 is

$$[7] \qquad K_f = a_{MX}/a_M a_X$$

in which we have omitted charges on M^{n+} and X^{n-}. This equilibrium constant can also be expressed in terms of the fraction of ions associated, the mean activity coefficient of free ions, and the activity coefficient of undissociated MX (represented by α, $\gamma_\pm^{\,i}$, and γ^u, respectively):

$$[8] \qquad K_f = \alpha\gamma^u/(1 - \alpha)^2 m(\gamma_\pm^{\,i})^2$$

We take the activity coefficient of the neutral MX to be unity and express the activity coefficient of the ions in terms of the stoichiometric (experimental) mean activity coefficient ($\gamma_\pm^{\,st}$) as

$$[9] \qquad \gamma_\pm^{\,i} = \gamma_\pm^{\,st}/(1 - \alpha)$$

to obtain

$$[10] \qquad K_f = \alpha/m(\gamma_\pm^{\,st})^2$$

and thence

$$[11] \qquad \alpha = K_f m(\gamma_\pm^{\,st})^2$$

Differentiation of α with respect to temperature (at constant molality) leads to

$$[12] \quad d\alpha/dT = 2K_f m(\gamma_\pm^{\,st})^2(d \ln \gamma_\pm^{\,st}/dT) + m(\gamma_\pm^{\,st})^2 K_f(d \ln K_f/dT)$$

We now substitute $-\bar{L}_2/2RT^2$ for $d \ln \gamma_\pm^{\,st}/dT$ and $\Delta H_r^{\,0}/RT^2$ for $d \ln K_f/dT$ to obtain

$$[13] \quad d\alpha/dT = K_f m(\gamma_\pm^{\,st})^2(\Delta H_r^{\,0} - \bar{L}_2)/RT^2 = \alpha(\Delta H_r^{\,0} - \bar{L}_2)/RT^2$$

The quantity (dH_r/dT) in eq. 6 can be expressed as

$$[14] \quad dH_r/dT = (dH_r/d\alpha m)(d\alpha m/dT) = m\Delta H_r(d\alpha/dT)$$

in which ΔH_r represents the molar enthalpy of the association reaction. Combination of eqs. 13 and 14 with 6 now leads to

$$[15] \quad \phi_C^{sp} = \phi_C^{exp} - m\Delta H_r K_f(\gamma_\pm^{\,st})^2 \times (\Delta H_r^{\,0} - \bar{L}_2)/RT^2 = \phi_C^{exp} - \alpha\Delta H_r(\Delta H_r^{\,0} - \bar{L}_2)/RT^2$$

Note that ΔH_r represents the enthalpy of the association reaction at the molality of the heat capacity measurement while $\Delta H_r^{\,0}$ represents the standard state (infinite dilution) enthalpy of the same reaction. Our procedure for obtaining ΔH_r values from $\Delta H_r^{\,0}$ and other information is given in Appendix I.

Now that we have eq. 15 to permit evaluation of ϕ_C^{sp} from experimental results expressed as ϕ_C^{exp} at various molalities, we can proceed to relate ϕ_C^{sp} to ϕ_C values for the various solute species as follows.

The contribution of electrically neutral MX (aq, undiss.) to ϕ_C^{sp} is represented by $\phi_{C(MX)}$, an initially unknown quantity that is taken to be independent of concentration. Similarly, the sum of the contributions of $M^{n+}(aq)$ and $X^{n-}(aq)$ to ϕ_C^{sp} is represented by $\phi_{C(M^{n+},X^{n-})}$. It is now possible to express ϕ_C^{sp} in terms of these quantities and α as

$$[16]\quad \phi_C^{sp} = \alpha\phi_{C(MX)} + (1-\alpha)\phi_{C(M^{n+},X^{n-})}$$

Extended Debye–Hückel theory leads to

$$[17]\quad \phi_{C(M^{n+},X^{n-})} = \phi^0_{C(M^{n+},X^{n-})} + A_C[(1-\alpha)m]^{1/2} + B_C(1-\alpha)m$$

in which A_C is known and B_C is an empirical parameter. Substitution of eq. 17 in eq. 16 and rearrangement leads to

$$[18]\quad \left[\frac{\phi_C^{sp} - (1-\alpha)\phi^0_{C(M^{n+},X^{n-})} - (1-\alpha)^{3/2}A_C m^{1/2}}{\alpha}\right] = \phi_{C(MX)} + B_C\left[\frac{(1-\alpha)^2 m}{\alpha}\right]$$

A graph of the term in brackets on the left side of this equation *vs*, the term in brackets on the right side should lead to a straight line. The intercept of this line will give us the desired value of $\phi_{C(MX)}$ while the slope will give the parameter B_C that is of no immediate interest to us.

To make use of eq. 18, we must have a value of $\phi^0_{C(M^{n+},X^{n-})}$. Because we are here concerned with solutes that are incompletely dissociated into $M^{n+}(aq)$ and $X^{n-}(aq)$ in the concentration range of the heat capacity measurements, we cannot obtain the desired $\phi^0_{C(M^{n+},X^{n-})}$ values by straightforward extrapolation of ϕ_C^{exp} (or even ϕ_C^{sp}) to zero concentration. Instead, we make use of heat capacity results for other electrolytes involving M^{n+} and X^{n-} ions whose heat capacities can be extrapolated to zero concentration without troublesome complications due to association or dissociation reactions. We illustrate this procedure as follows for both magnesium sulfate and iodic acid.

Combination of ϕ_C^0 values for aqueous $MgCl_2$ (2), NaCl (2, 3), and Na_2SO_4 (2, 4) and similar combination of ϕ_C^0 values for $MgCl_2$ (2), KCl (2, 3), and K_2SO_4 (2) lead to $\phi^0_{C(Mg^{2+},SO_4^{2-})} = -293$ J K^{-1} mol^{-1}. Similarly, combinations of ϕ_C^0 values for aqueous (HCl (3), KCl (2, 3), KIO_3 (4)) and (HBr (3), KBr (2, 3), KIO_3 (4)) lead to $\phi^0_{C(H^+,IO_3^-)} = -74$ J K^{-1} mol^{-1}.

For further specific application of our data treatment procedure to magnesium sulfate, we use the following auxiliary thermodynamic quantities. Sillén and Martell (5) and Pitzer (6) have reviewed various evaluations of K_f; we select $K_f = 200$. Sillén (5), Larson (7), and Leung and Millero (8) have all reported results of various evaluations of ΔH_r^0; we select $\Delta H_r^0 = 1.2$ kcal mol^{-1} = 5.0 kJ mol^{-1}. Stoichiometric activity coefficients from Pitzer (6) and from Millero and Masterton (9) are in good agreement with each other. Self-consistent heats of dilution and related quantities (ϕ_L^{exp} and $\bar{L}_2$) are from ref. 10 and Harned and Owen (11). We have used results of our measurements (4) of heat capacities (expressed as ϕ_C^{exp}) of aqueous magnesium sulfate.

A graph for magnesium sulfate based on eq. 18 (also using eqs. 15 and I-8) is shown in Fig. 1, from which we obtain $\phi^0_{C(MgSO_4)} = -168$ J K^{-1} mol^{-1} (= −40 cal K^{-1} mol^{-1}). We estimate that the *total* uncertainty in this value is about ±15 J K^{-1} mol^{-1} or ±4 cal K^{-1} mol^{-1}. Combination of this $\phi^0_{C(MgSO_4)}$ for undissociated $MgSO_4$ with $\phi^0_{C(Mg^{2+},SO_4^{2-})} = -293$ J K^{-1} mol^{-1} cited earlier leads to $\Delta C_p^0 = 125$ J K^{-1}

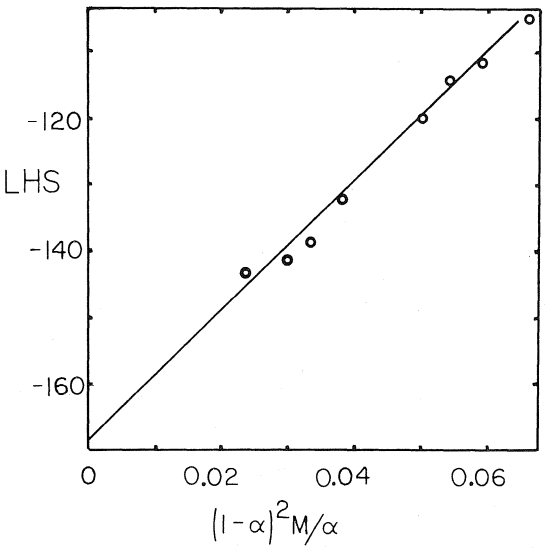

FIG. 1. Plot of the left hand side of eq. 18 for $MgSO_4$, yielding $\phi^0_{C(MgSO_4)} = -168$ J K^{-1} mol^{-1} and $B_C = 930$.

mol^{-1} (= 30 cal K^{-1} mol^{-1}) for the association reaction represented by eq. 1.

Several years ago Helgeson (12) and Marshall (13) carefully analyzed equilibrium results to obtain information about this ΔC_p^0. Helgeson (12) reported ΔC_p^0 = 19 cal K^{-1} mol^{-1} as an average value for a wide temperature range, while Marshall (13) reported ΔC_p^0 = 3 cal K^{-1} mol^{-1} for 25 °C and ΔC_p^0 = 25 cal K^{-1} mol^{-1} as an average value for the temperature range 0–200 °C. Uncertainties in all of these values based on d ln $K/dT = \Delta H^0/RT^2$ and $d\Delta H^0/dT = \Delta C_p^0$ are large.

More recently, Perron *et al.* (1) have reported ΔC_p^0 = 85 J K^{-1} mol^{-1} for the association reaction represented by eq. 1. Because our eq. 15 had not yet been derived, they made no distinction between ϕ_C^{exp} and ϕ_C^{sp}. Furthermore, there appear to be inconsistencies between $\phi^0_{C(Mg^{2+},SO_4^{2-})}$ values used in their eqs. 9–13.

For iodic acid (HIO_3) we use K(ionization) = 0.157 and thence K_f = 1/0.157 = 6.37 from the results of Pethybridge and Prue (14), from whom we also obtain activity coefficients. Further activity coefficients have been based on the work of Goldman, Bates, and Robinson (15). For the enthalpy of ionization we have ΔH^0_{ioniz} = −2.4 kcal mol^{-1} from earlier reviews (16) and therefore use ΔH_r^0 = 2.4 kcal mol (= 10.0 kJ mol^{-1}). Because there are no reliable ϕ_L^{exp} values for aqueous iodic acid known to us, we use eq. I-5 with ϕ_L^i based on the Debye–Hückel theory and the ion size parameter from Pethybridge and Prue (14) to obtain the connection between ΔH_r^0 and ΔH_r values and the $\bar{L}_2$ values needed for application of eq. 15 to ϕ_C^{exp} values (4) to obtain ϕ_C^{sp} values.

A graph for iodic acid based on eq. 18 (also using eq. 15 and I-5) is shown in Fig. 2, from which we obtain $\phi^0_{C(HIO_3)}$ = −40 J K^{-1} mol^{-1} (= −10 cal K^{-1} mol^{-1}). We estimate that the *total* uncertainty in this value is about ±8 J K^{-1} mol^{-1} or ±2 cal K^{-1} mol^{-1}. Combination of this $\phi^0_{C(HIO_3)}$ for undissociated HIO_3 with $\phi^0_{C(H^+,IO_3^-)}$ = −74 J K^{-1} mol^{-1} cited earlier leads to ΔC_p^0 = 34 J K^{-1} mol^{-1} for the association reaction represented by eq. 1 or to ΔC_p^0 = −34 J K^{-1} mol^{-1} (= −8 cal K^{-1} mol^{-1}) for the ionization of HIO_3(aq, undiss.). We know of no results with which to compare this value, but we note that is is of "reasonable" magnitude as compared to "similar" reactions (16).

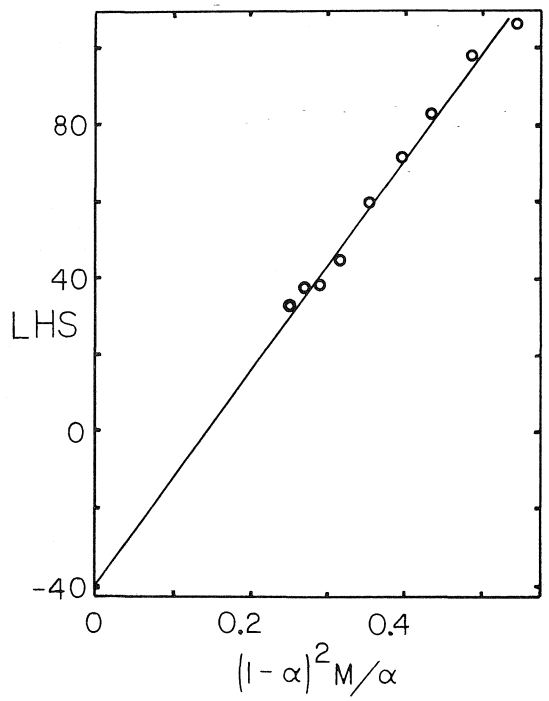

FIG. 2. Plot of the left hand side of eq. 18 for HIO_3, yielding $\phi^0_{C(HIO_3)}$ = −40 J K^{-1} mol^{-1} and B_C = 274.

Discussion

The magnitude of the hitherto unrecognized difference between ϕ_C^{exp} and ϕ_C^{sp} depends on the concentration range of the heat capacity measurements and on the various thermodynamic quantities that appear in eq. 15. For magnesium sulfate and iodic acid solutions treated here, the difference between ϕ_C^{exp} and ϕ_C^{sp} ranges from less than 1 to 22 J K^{-1} mol^{-1}. Thus the distinction between ϕ_C^{exp} and ϕ_C^{sp} should not be ignored for these solutes.

For quite strong electrolytes that are fully dissociated in the practical concentration range of heat capacity measurements there is no need or opportunity for the treatment described here. For much weaker electrolytes, such as acetic acid, there is again no need for the treatment described here. In this case it is possible to obtain ΔC_p^0 for association of H^+ with Ac^- or dissociation of HAc by way of combination of results of heat capacity measurements on solutions of acetic acid, sodium acetate, sodium chloride, and hydrochloric acid. It is only for 'intermediate' electrolytes, such as magnesium sulfate and iodic acid, that a treatment such as the one described here is needed.

It should be noted that eq. 15 cannot be applied to very weak electrolytes for which $\alpha \cong 1$, due to complications associated with eq. 9. Instead, it is proper to consider [1′]

[1′] $\quad HX(aq, undiss.) \rightleftharpoons H^+(aq) + X^-(aq)$

We now define α' as the fraction of HX dissociated. Following the procedure given earlier in this paper, with $\gamma_\pm \cong 1$ (or calculated from the Debye–Hückel theory) and small α', we obtain

$$[15'] \quad \phi_C^{sp} \cong \phi_C^{exp} - [\alpha'(\Delta H^0_{ioniz})^2]/2RT^2$$

in which ΔH^0_{ioniz} represents the standard enthalpy of ionization of HX(aq). The term in brackets is very small so that ϕ_C^{exp} can be attributed to HX(aq, undiss.) in straightforward fashion as stated in the paragraph above.

NOTE ADDED IN PROOF:

In considering the dimensional consistency of eq. 14 (and some other equations) it is necessary to remember that we are concerned with the heat capacity of a solution that contains 1 kg of solvent. We therefore express dH_r/dT in terms of energy K^{-1} (kg solvent)$^{-1}$, which is consistent with expressing $m\Delta H_r(d\alpha/dT)$ in terms of (mol solute) (kg solvent)$^{-1}$ energy (mol solute)$^{-1}$ K^{-1}.

Acknowledgments

We thank the National Research Council of Canada for support of this research and Brigham Young University for sabbatical leave support to E.M.W. We are also grateful to Professors Frank Millero and Jacques Desnoyers for stimulating and useful discussions.

1. G. PERRON, J. E. DESNOYERS, and F. J. MILLERO. Can. J. Chem. **53**, 1134 (1975).
2. J. E. DESNOYERS, C. DE VISSER, G. PERRON, and P. PICKER. J. Solution Chem. In press.
3. P. P. SINGH, E. M. WOOLLEY, K. G. MCCURDY, and L. G. HEPLER. Can. J. Chem. In press.
4. P. P. SINGH, E. M. WOOLLEY, K. G. MCCURDY, and L. G. HEPLER. In preparation.
5. L. G. SILLÉN and A. E. MARTELL. Stability constants of metal–ion complexes. Special Publ. No. 17. The Chemical Society, London. 1964; L. G. SILLÉN and A. E. MARTELL. Stability constants of metal–ion complexes. Supplement No. 1. Special Publ. No. 25. The Chemical Society, London. 1971.
6. K. S. PITZER. J. Chem. Soc. Faraday Trans. II, **68**, 101 (1972).
7. J. W. LARSON. J. Phys. Chem. **74**, 3392 (1970).
8. W. H. LEUNG and F. J. MILLERO. J. Solution Chem. **4**, 145 (1975).
9. F. J. MILLERO and W. L. MASTERTON. J. Phys. Chem. **78**, 1287 (1974).
10. V. B. PARKER, D. D. WAGMAN, and W. H. EVANS. National Bureau of Standards Technical Note 270-6. U.S. Government Printing Office, Washington, D.C. 1971.
11. H. S. HARNED and B. B. OWEN. The physical chemistry of electrolytic solutions. 3rd ed. Reinhold Publ. Corp., New York. 1958.
12. H. C. HELGESON. J. Phys. Chem. **71**, 3121 (1967).
13. W. L. MARSHALL. J. Phys. Chem. **71**, 3584 (1967).
14. A. D. PETHYBRIDGE and J. E. PRUE. Trans. Faraday Soc. **63**, 2019 (1967).
15. S. GOLDMAN, R. G. BATES, and R. A. ROBINSON. J. Solution Chem. **3**, 593 (1974).
16. J. W. LARSON and L. G. HEPLER. *In* Solute–solvent interactions. *Edited by* J. F. Coetzee and C. D. Ritchie, Marcel Dekker, Inc., New York. 1970; D. D. WAGMAN, W. H. EVANS, V. B. PARKER, I. HALOW, S. M. BAILEY, and R. H. SCHUMM. National Bureau of Standards Technical Note 270-3. U.S. Government Printing Office, Washington, D.C. 1968.
17. H. P. HOPKINS, JR., C.-H. WU, and L. G. HEPLER. J. Phys. Chem. **69**, 2244 (1965); H. P. HOPKINS, JR. and C. A. WULFF. J. Phys. Chem. **69**, 6 (1965); **69**, 9 (1965).

Appendix I

We first consider a solution of magnesium sulfate of stoichiometric molality m. The concentrations of Mg^{2+} and SO_4^{2-} ions are both $(1 - \alpha)m$ and the concentration of undissociated $MgSO_4$ is αm. Dilution of the ions in this solution to $m = 0$ is represented by

[I-1] $$Mg^{2+}[(1 - \alpha)m] + SO_4^{2-}[(1 - \alpha)m] \rightleftharpoons Mg^{2+}(m = 0) + SO_4^{2-}(m = 0)$$

The enthalpy change for this dilution is $-\phi_L^i[(1 - \alpha)m]$, where ϕ_L^i is the relative apparent molal enthalpy of the ions at the indicated molality of ions. We also write

[I-2] $$Mg^{2+}(m = 0) + SO_4^{2-}(m = 0) \rightleftharpoons MgSO_4(m = 0) \qquad \Delta H_r^0$$

for the standard state formation of $MgSO_4$(aq, undiss.). Next we have

[I-3] $$MgSO_4(m = 0) \rightleftharpoons MgSO_4(\alpha m)$$

for the change in concentration of undissociated $MgSO_4$ from zero concentration to the concentra-

tion represented by αm. The enthalpy of this process is represented by $\phi_L{}^u$. Combination of the three equations above and the corresponding enthalpies leads to

[I-4] $$Mg^{2+}[(1 - \alpha)m] + SO_4{}^{2-}[(1 - \alpha)m] \rightleftharpoons MgSO_4(\alpha m)$$

and

[I-5] $$\Delta H_r = \Delta H_r{}^0 - \phi_L{}^i[(1 - \alpha)m] + \phi_L{}^u(\alpha m)$$

To eliminate $\phi_L{}^i$ from eq. I-5, we consider three processes similar to those above, but now for an amount of solution of stoichiometric molality m such that the solution contains 1 mol of magnesium sulfate and therefore $(1 - \alpha)$ mol of Mg^{2+}, $(1 - \alpha)$ mol of $SO_4{}^{2-}$, and (αm) mol of undissociated $MgSO_4$. The corresponding enthalpies will be $-(1 - \alpha)\phi_L{}^i[(1 - \alpha)m]$, $\alpha\Delta H_r{}^0$, and $\alpha\phi_L{}^u(\alpha m)$. Combination of equations and enthalpies for these three processes leads to

[I-6] $$(1 - \alpha)Mg^{2+}[(1 - \alpha)m] + (1 - \alpha)SO_4{}^{2-}[(1 - \alpha)m] + \alpha MgSO_4(\alpha m) \rightleftharpoons Mg^{2+}(m = 0) + SO_4{}^{2-}(m = 0)$$

and the corresponding *exp*erimental enthalpy of dilution represented by

[I-7] $$-\phi_L{}^{exp} = -(1 - \alpha)\phi_L{}^i[(1 - \alpha)m] - \alpha\Delta H_r{}^0 - \alpha\phi_L{}^u$$

Finally, we combine eqs. I-5 and I-7 with $\phi_L{}^u = 0$ to obtain

[I-8] $$\Delta H_r = (\Delta H_r{}^0 - \phi_L{}^{exp})/(1 - \alpha)$$

Equation I-7 above is equivalent to equations used by earlier investigators (7, 8, 17) of the thermodynamics of ion pair formation.

Rearrangements involving alkoxycarbonyl group migration between nitrogen and oxygen. III. Reactions of modified isoquinoline Reissert compounds with aldehydes

M. D. ROZWADOWSKA

Institute of Chemistry, Adam Mickiewicz University, Grunwaldzka 6, 60–780 Poznań, Poland

Received June 8, 1976

M. D. ROZWADOWSKA. Can. J. Chem. **55**, 164 (1977).

The condensation reaction of modified Reissert compounds with aldehydes was investigated. In the reaction of the *N*-ethoxycarbonyl Reissert analog **1***b*, ethoxycarbonyl group migration takes place and carbonates of 1-isoquinolylphenylcarbinols (**2***b*, *c*) are formed. No alkoxycarbonyl group migration was observed in the case of the dihydro-Reissert derivative **6**, but the cyclic urethane **7** and the amide **8** were obtained.

M. D. ROZWADOWSKA. Can. J. Chem. **55**, 164 (1977).

On a examiné la réaction de condensation de composés de Reissert modifiés avec des aldéhydes. Dans la réaction de l'analogue *N*-éthoxycarbonylé de Reissert (**1***b*), il y a migration du groupe éthoxycarbonyle et formation de carbonates de l'isoquinolyl-1 phénylcarbinoles (**2***b*, *c*). On n'observe aucune migration du groupe alkoxycarbonyle dans le cas du dérivé dihydro-Reissert **6** mais on obtient l'uréthane cyclique **7** et l'amide **8**.

[Traduit par le journal]

Introduction

Rearrangement reactions involving acyl group migration are well known, and have been the subject of several reviews (1–4). They are common in acylated 1,2-amino alcohols, where an intramolecular mechanism with a 5-membered cyclic intermediate hydroxyoxazolidine is postulated. Significant contributions to the elucidation of the mechanism of this reaction are due mainly to Fodor and co-workers (5, 6) and to Welsh (7).

These migrations are reversible and p*H*-dependent. It has been well established that in acidic conditions N → O migration occurs, whereas in alkaline solutions the opposite O → N takes place. The structure of the products is determined by the direction of ring opening in the intermediate hydroxyoxazolidine. The cleavage of either C—N or C—O bonds furnishes the *O*-acyl or *N*-acyl derivatives, respectively. In acidic media the positive nitrogen attracts the bonding electrons giving rise to an *O*-acyl amine. In alkaline conditions the C—O bond, being more polarized, is broken and an *N*-acyl alcohol is formed. This can be considered as a general rule and is applicable to most of the acylated aliphatic amino alcohols. There are, however, exceptions. For instance, in reaction of Reissert compounds with aldehydes N → O acyl migration takes place in strongly alkaline conditions (8, 9). The aromatization of the system is postulated as the driving force for this transformation.

In connection with our studies of alkoxycarbonyl group migration (10, 11), this reaction was chosen, but modified *N*-ethoxycarbonyl and dihydro-Reissert compounds were used.

Results and Discussion

The name 'isoquinoline Reissert compounds' has been reserved for 1-cyano-2-benzoyl-1,2-dihydroisoquinolines (8, 9). However, some modified Reissert compounds have been prepared. Thus 1,2,3,4-tetrahydro derivatives, called 'dihydro-Reissert compounds' have been described (9, 12–15), and others, having acetyl (9, 16), sulfonyl (17), alkoxycarbonyl (9, 18, 19), carbamoyl (20), and phosphate (21) substituents in the place of benzoyl group are also known.

Reissert compounds are easily converted into their conjugate bases, which are valuable intermediates in organic synthesis (8, 9). In condensation reactions with aldehydes, these compounds (**1***a*) are transformed into secondary alcohols, or their esters, containing a 1-isoquinolyl or 2-quinolyl group bonded to the carbinol carbon atom (Scheme 1, **2**, **3**) (9, 21, 23–26).

In the course of this reaction the acyl group is shifted from nitrogen to oxygen in alkaline solution. However, an example was described by Popp *et al.* (18) in which migration of the alkoxycarbonyl group was not observed in this

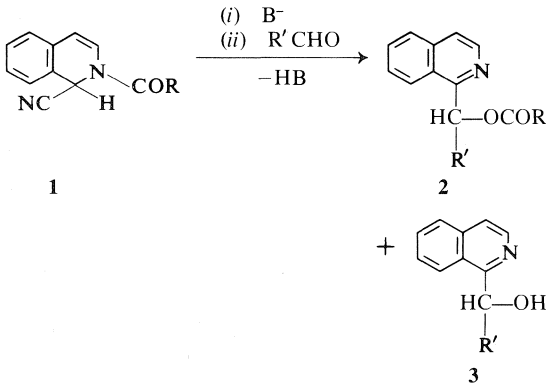

1 2 3

a, $R = C_6H_5$
b, $R = OC_2H_5$, $R' = C_6H_5$
c, $R = OC_2H_5$, $R' = C_6H_3(OCH_2O)$

SCHEME 1

process. This involved the reaction of *N*-alkoxycarbonyl analogs of Reissert compounds with benzaldehyde in which the anions were generated by the action of *n*-butyllithium at −40 °C. As a result the cyclic urethane **4** was formed in moderate yield. This difference can be easily ex-

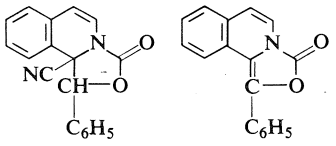

4 **5**

plained, when one considers that the oxyanion *C* (Scheme 2) can alternatively lose alkoxide and give the product **4**. When the reaction was carried out using sodium hydride in *N*,*N*-dimethylformamide, the authors were able to isolate the carbinol **3***b* with 47% yield, although in one case **5** was isolated and easily hydrolized by base to **3***b*.

It was of interest to see whether there is a general tendency for *N*-alkoxycarbonyl Reissert compounds to form a cyclic urethane in reactions with aromatic aldehydes and not the fully aromatic isoquinoline formed by the rearrangement–elimination process. Therefore *N*-ethoxycarbonyl-1,2-dihydroisoquinaldonitrile (**1***b*) was prepared from isoquinoline, potassium cyanide and ethyl chloroformate, and reacted with aromatic aldehydes using two different reaction conditions. Treatment of **1***b* with benzaldehyde in a two-phase catalytic system according to the Makosza method (27) described by Jończyk (22), using triethylbenzylammonium chloride (TEBA) as a phase-transfer agent, resulted, depending on the time of the reaction, in either of the two compounds **2***b* or **3***b*, or both of them. When the reaction time was 30 min the ethyl carbonate of 1-isoquinolylphenylcarbinol (**2***b*) was formed in high yield (96%). After 24 h the hydrolysis product of **2***b*, 1-isoquinolylphenylcarbinol (**3***b*), was isolated in 91% yield. With times varying from 30 min to 24 h mixtures of **2***b* and **3***b* were obtained.

Reaction with piperonal in the place of benzaldehyde gave carbonate **2***c* or carbinol **3***c* depending on the reaction time.

When the reaction of **1***b* and benzaldehyde was carried out with sodium hydride in DMF at −40 °C, carbonate **2***b* was obtained almost quantitatively.

The structure of carbonates **2***b* and **2***c* was established on the bases of elemental analysis, spectral data (ir, nmr, uv, ms), and chemical transformations. All these data are in accordance with structures **2***b*, *c* except for one: compounds **2***b* and **2***c* do not show basic properties in that they are not soluble in aqueous solutions of acids. Table 1 lists the pK_a values (measured in methylcellosolve) of several compounds related to the carbonates. As expected, carbinols **3***b*, *c* exhibit pK_a values (4.1) similar to that of the parent isoquinoline (3.85). The values for carbonates **2***b*, *c* (approximately 2.1) are comparable with that of *N*-ethoxycarbonylquinaldonitrile (**1***b*) (approximately 2.1).

On the other hand, carbonate **2***b* under the action of hydrogen chloride in dry ether forms a crystalline hydrochloride which on dissolution in aqueous solvents is hydrolized to the free base.

Because of the diverse behaviour of these compounds a careful analysis of their spectra seemed to be necessary.

A strong absorption band in the carbonyl frequency region, centered at 1745 cm^{-1}, is pres-

TABLE 1. pK_a values of carbonates **2***b*, *c* and related compounds

Compound	pK_a
Reissert analog **1***b*	~2.1
Carbonate **2***b*	~2.1
Carbonate **2***c*	~2.1
Carbinol **3***b*	~4.1
Carbinol **3***c*	~4.1
Isoquinoline	~3.85

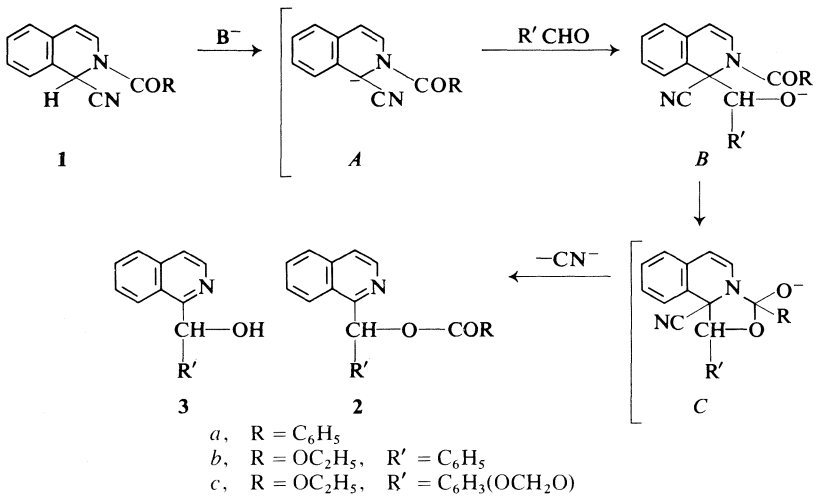

SCHEME 2

ent in the ir spectra of carbonates **2***b*, *c*, which if compared with the spectrum of the starting *N*-ethoxycarbonylisoquinaldonitrile (**1***b*) is shifted 20 cm^{-1} to shorter wavelength. This position corresponds better to the carbonate absorption (1750 cm^{-1}) described in the literature (28) than to a disubstituted urethane (1720 cm^{-1}) (28).

The nmr spectra of 1,2-dihydroisoquinolines exhibit signals characteristic of olefinic protons, giving rise to an AB quartet located in the region between 5.95–6.9 δ with a coupling constant $J = 8$ Hz (15, 29). As is evident from Table 2, the *N*-ethoxycarbonyl Reissert analog **1***b* shows such a quartet centered at 6.0 δ and 6.9 δ, with $J = 8$ Hz. Neither in the spectra of carbonates **2***b*, *c* nor in those of carbinols **3***b*, *c* is an absorption present around 5.95–6.9 δ (except for a sharp singlet near 6 δ, corresponding to two methylenedioxy group protons in **2***c* and **3***c*). On the other hand, the C_3 proton in the spectra of these compounds, as in spectra of other isoquinoline derivatives, appears as a doublet at *ca.* 8.6 δ with $J = 6$ Hz.

Other spectral evidence that suggests a fully aromatic system for carbonates **2***b*, *c* can be seen from their uv spectra which are practically superimposable with those of the corresponding carbinols **3***b*, *c* and isoquinoline, but which differ significantly from that of the starting Reissert compound **4***b* (see Experimental).

In their mass spectra the two carbonates show the common feature of the initial loss of ethoxycarbonyl and carbonate groups (73 and 89 mass units respectively) followed by the substituent attached to the C_1 carbon atom giving rise to the isoquinoline fragment ion (129-1 *m/e*) (30). In the mass spectra of carbinols the molecular ion is also the parent. The second most intense peak is that at 129 mass units, which corresponds to the isoquinoline ion.

Reduction of **2***b* with sodium borohydride yielded carbinol **3***b*, also obtained by alkaline hydrolysis of **2***b*. Reaction of **3***b* with ethyl chloroformate under Gadamer–Knoch conditions yielded **2***b*.

In view of the spectral and experimental results, the structures **2***b*, *c* for the carbonates formed in the reaction of 2-ethoxycarbonylisoquinaldonitrile (**1***b*) with aromatic aldehydes seem to be confirmed.

The mechanism of this reaction is shown in Scheme 2. In the first step the attack of the carbanion *A* on the carbon atom of the aldehyde carbonyl takes place. The resulting oxyanion *B* then undergoes rearrangement (via *C*) with simultaneous release of the cyanide ion, giving the final product **2***a*.

Taking into consideration the observations made on the reaction of *N*-alkoxycarbonyl Reissert analogs with aldehydes, one comes to a conclusion that this reaction may proceed via three different mechanisms, giving rise to three different intermediates (**2**, **4**, **5**) formed on the route from Reissert compound **1** to 1-isoquinolylphenylcarbinol (**3**). These mechanisms probably show the same initial course, involving the formation of oxyanion *C* (see Scheme 2) which can then be transformed to either carbonate **2***b*, *c*

due to alkoxycarbonyl group migration and elimination of the cyanide ion, or to the cyclic urethane **4** or **5** by the loss of alkoxide ion. Formation of **5** requires the additional elimination of a molecule of hydrogen cyanide.

It is evident from the results presented in this paper as well as from those reported by Popp *et al.* (18) that the course of this reaction and thus the structure of the products depend on the experimental conditions. Factors such as type and amount of base used for the generation of the anion, solvent, temperature, and time of reaction seem to have a significant influence on the direction of this process. A more detailed study must, however, be undertaken in order to examine the relation between experimental conditions and the course of this reaction.

The reaction of dihydro isoquinoline Reissert compounds in which formation of their anions is needed, such as alkylation and acylation have been investigated in two cases (14, 15). The behaviour of these compounds in condensation reactions with aldehydes has not been examined.

In connection with our interest of alkoxycarbonyl group migration, 2-ethoxycarbonyl-6,7-methylenedioxy-1,2,3,4-tetrahydroisoquinaldonitrile (**6**) was synthesized and subjected to reaction with benzaldehyde in a two-phase catalytic system with TEBA as catalyst. When acetonitrile was used as solvent two compounds were isolated: the cyclic urethane **7** and dihydroisocarbostiril **8**, while in benzene only **7** was formed.

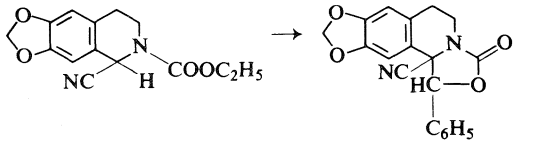

6

7

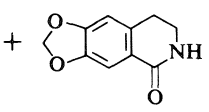

8

In the ir spectra of **7** and **8** strong absorption bands are present in the carbonyl region, centered at 1760 and 1660 cm^{-1} respectively, while in the spectrum of **8** an additional broad band around 3200 cm^{-1} suggests N—H stretching vibrations.

The nmr spectra of **7** and **8** (Table 2) do not exhibit the resonances characteristic of ethoxy group protons, but rather a singlet at 5.36 δ in the

TABLE 2. Nuclear magnetic resonance data of carbonates **2***b*, *c* and related compounds. Chemical shift in ppm (δ) relative to TMS

Compound	OH	O-CH_2-CH_3	O-CH_2-CH_3	*H*-C_α-OR/H	C_1-H	C_3-H	C_4-H	Aromatic	-O-CH_2-O-
Reissert analog **1***b*	—	1.33t *J* = 7 Hz	4.4q *J* = 7 Hz	—	6.4*	6.95d* *J* = 8 Hz	6.0 *J* = 8 Hz	7–7.5	—
Carbonate **2***b*	—	1.23t *J* = 7 Hz	4.2q *J* = 7 Hz	7–8.4†	—	8.7d *J* = 6 Hz	7–8.4†	7–8.4	—
Carbonate **2***c*	—	1.26t *J* = 7 Hz	4.2q *J* = 7 Hz	6.6–8.4†	—	8.6 *J* = 6 Hz	6.6–8.4†	6.6–8.4	5.85
Carbinol **3***b*	~6‡	—	—	6.35	—	8.55 *J* = 6 Hz	7.2–8.2†	7.2–8.2	—
Carbinol **3***c*	~6‡	—	—	6.30	—	8.6 *J* = 6 Hz	6.6–8.2†	6.6–8.2	5.90
Dihydro Reissert analog **6**	—	1.33t *J* = 7 Hz	4.31q *J* = 7 Hz	—	6.0	—	2.6–3.6	6.66; 6.78	6.00
Urethane **7**	—	—	—	5.36	—	—	2.7–4.5	6.66; 6.7; 7.6	6.00
Noroxyhydrastinine	—	—	—	—	—	—	2.75–3.8	6.68; 7.5	6.00

*Broad due to the long-range spin coupling with C_3-H (31).
†Hidden among aromatic protons signals.
‡Disappears after treatment with D_2O.

spectrum of **7** may be attributed to the proton attached to the C_α carbon atom.

Further support for **7** and **8** as correct structures was adduced from their mass spectra. Both compounds show molecular ions and the base peak (200 *m/e*) in the spectrum of **7** is probably derived from the 6,7-methylenedioxy-3,4-dihydroisoquinaldonitrile ion, formed from **7** by the cleavage of bonds between nitrogen and the urethane carbonyl and between the C_1 and C_α carbon atoms.

The molecular ion in the spectrum of **8** is at the same time the base peak. The loss of 29 mass units ($NHCH_2$) provides the fragment *m/e* 162, which in turn appears to lose a molecule of carbon monoxide giving rise to an ion *m/e* 134.

6,7-Methylenedioxy-1-oxo-1,2,3,4-tetrahydroisoquinoline (**8**) is probably formed from **7** via dihydroquinaldonitrile and subsequent displacement of nitrile by hydroxide ion.

Two conclusions may be drawn from the reactions described above. First, no alkoxycarbonyl group migration is observed in the reaction of dihydro-Reissert compounds with aldehydes, even under conditions when this group migrates readily in normal Reissert compounds. Secondly, there seems to be a general tendency of the alkoxycarbonyl group to lose alkoxide ion from the intermediate oxyanion *C* (Scheme 2) and form a stable 5-membered carbamate.

Experimental

Melting points were determined on a Kofler block and are uncorrected. The ir spectra were determined in chloroform solution using 0.1 mm cells and a ~0.2 *M* sample concentration on a Unicam SP 200G spectrophotometer. The uv spectra in 96% ethanol were recorded on a Specord UV–VIS spectrophotometer. The nmr spectra were measured on a Varian Associates A-60 spectrometer with TMS as an internal standard. Sample concentrations were approximately 19% w/v in $CDCl_3$. Chemical shifts are given in δ units. The mass spectra were obtained on a Jeol MS 100-D instrument. Only those signals of use in structure assignment are given in this paper. The pK_a values were measured in methylcellosolve on a Radiometer Titrigraph Module PMA 943. Purity of all compounds prepared was checked by tlc on alumina plates (Woelm, neutral).

2-Ethoxycarbonyl-1,2-dihydroisoquinaldonitrile (1b)

To a vigorously stirred mixture of 0.05 mol of iso quinoline (freshly distilled from zinc dust) and 0.15 mol of potassium cyanide in 60 ml of water was added 0.1 mol of ethyl chloroformate over a period of 1 h with ice cooling. The temperature was allowed to rise to room temperature and stirring was continued overnight. The mixture was then extracted with benzene and the organic layer washed with water, dilute HCl, water, dilute NaOH, and water again, then dried. Evaporation of the solvent left a dark oil (7.8 g) which was passed through silica gel (MN, 100–200 mesh ASTM). Benzene eluted 6.5 g (57%) of a colorless oil, that solidified, mp 82–85 °C. After recrystallization from ether–hexane mp 83–85 °C; uv λ_{max} 285 nm (ε 12 000); ir 1725 (urethane C=O), 1620 cm^{-1} (C=C); nmr 1.33 (t, J = 7 Hz, 3H, -OCH_2 -CH_3), 4.36 (q, J = 7 Hz, 2H, -O-CH_2-CH_3), 6.0 (d, J = 8 Hz, 1H, C_4-H), 6.38 (br s, 1H, C_1-H), 6.95 (d, J = 8 Hz, 1H, C_3-H), 6.75–7.5 δ (m, 4H, aromatic); ms *m/e* 228 (M^+, 32%), 155 ($M - COOC_2H_5$, 16%), 129 ($M - COOC_2H_5 - CN$, 100%). *Anal.* calcd. for $C_{13}H_{12}O_2N_2$ (228): C 68.42, H 5.26, N 12.28; found: C 68.35, H 5.44, N 12.12.

Condensation of the Reissert Analog 1b with Aromatic Aldehydes

(1) In a Two Phase System Using TEBA as Phase-transfer Agent

Compound **1***b* (1.27 g, 5.57 mmol), 3 ml of benzene, 50% NaOH (2.3 ml), TEBA (45 mg), and freshly distilled benzaldehyde (0.69 ml, 7.28 mmol) were stirred at room temperature for 30 min. The mixture was diluted with water and extracted with benzene. The organic layer was washed with dilute HCl, and water, dried, and the solvents evaporated *in vacuo*. Carbonate **2***b* (1.65 g, 96%) was obtained as a colorless oil which crystallized from ethanol: mp 93–94.5 °C; uv λ_{max} 324 (4080), 311 (3440), 286 (4160), 274 (5040), 261 (3760), 255 nm (ε 3000); ir 1745 cm^{-1} (carbonate C=O); nmr 1.23 (t, J = 7 Hz, 3H, -O-CH_2-CH_3), 4.23 (q, J = 7 Hz, 2H, -O-CH_2-CH_3), 7–8.45 (m, 11H, aromatic + C_α-H), 8.7 δ (d, J = 6 Hz, 1H, C_3-H); ms *m/e* 307 (M^+, 29%), 234 ($M - COOC_2H_5$, 61%), 218 ($M - OCOOC_2H_5$, 100%), 128 ($M - C_1$ – substituent, 36%). *Anal.* calcd. for $C_{19}H_{17}O_3N$ (307): C 74.26, H 5.54, N 4.65; found: C 74.20, H 5.55, N 4.39.

Hydrochloride of 2b—HCl gas was bubbled through a solution of carbonate **2***b* in ether for 5 min. A white solid precipitated in quantitative yield that was recrystallized from anhydrous methanol, mp around 100 °C; ir (KBr) 3450 and 1640 (water of crystallization), 3100–2500 ($^+$N—H), 1750 cm^{-1} (carbonate C=O). *Anal.* calcd. for $C_{19}H_{17}O_3N \cdot HCl \cdot H_2O$ (361.5): C 63.07, H 5.53, N 3.87; found: C 63.02, H 5.51, N 3.68.

Treatment of **1***b* (880 mg, 4 mmol) with piperonal (675 mg, 4.5 mmol) with the same reaction conditions afforded 1.24 g of an oil, which after chromatography on alumina (Woelm, neutral, activity grade II°) yielded 440 mg (32%) of carbonate **2***c*, which, crystallized from ether–hexane, mp 98–100 °C; uv λ_{max} 321 (4960), 308 (4640), 285 (8480), 275 (7600), 259 (4320), 252 nm (ε 3840); ir 1745 cm^{-1} (carbonate C=O); nmr 1.26 (t, J = 7 Hz, 3H, -O-CH_2-CH_3), 4.2 (q, J = 7 Hz, 2H, -O-CH_2-CH_3), 5.9 (s, 2H, -O-CH_2-O-), 6.66–8.35 (m, 9H, aromatic + C_α-H), 8.63 δ (d, J = 6 Hz, 1H, C_3-H); ms *m/e* 351 (M^+, 18%), 278 ($M - COOC_2H_5$, 34%), 262 ($M - OCOOC_2H_5$, 100%), 128 ($M - C_1$ – substituent, 21%). *Anal.* calcd. for $C_{20}H_{17}O_5N$ (351): C 68.37, H 4.81, N 3.98; found: C 68.11, H 4.99, N 3.89.

When this reaction was carried out in the same conditions, but over 24 h carbinols **3***b* or **3***a* were obtained in yields of 91 and 48%, respectively.

Carbinol 3b—**3***b* mp 107–109 °C (lit. (26) mp 108.5–109.5 °C); uv λ_{max} 320 (4080), 308 (3280), 282 (4240),

271 (5200), 261 (4800), 254 nm (ε 4000); ir 3500–3150 cm^{-1} (carbinol OH); nmr 6.0 (br, 1H, exchangable with D_2O, OH), 6.35 (s, 1H, C_α-H), 7.2–8.2 (m, 10H, aromatic), 8.55 δ (d, J = 6 Hz, 1H, C_3-H); ms *m/e* 235 (M^+, 100%), 218 (M − OH), 129 (M − C_6H_5CHO).

Carbinol 3c—**3***c* mp 91–93 °C; uv λ_{max} 320 (4640), 307 (4160), 282 (7520), 272 (6720), 259 (6380), 251 nm (ε 3040); ir (KBr) cm^{-1} 3350–3150 (carbinol OH); nmr 6 (br, 1H, exchangable with D_2O, OH), 5.9 (s, 2H, -O-CH_2-O-), 6.30 (s, 1H, C_α-H), 6.6–8.2 (m, 8H, aromatic), 8.6 δ (d, J = 6 Hz, 1H, C_3-H); ms *m/e* 279 (M^+, 100%), 262 (M − OH, 12%), 129 (M − C_1 − substituent, 95%). *Anal.* calcd. for $C_{17}H_{13}O_3N$ (279): C 73.11, H 4.66, N 5.02; found: C 73.05, H 4.70, N 4.91.

(2) In Dimethylformamide with Sodium Hydride

To a solution of **1***b* (456 mg, 2 mmol) and of benzaldehyde (206 mg, 2 mmol) in 6 ml of DMF cooled to −40 °C was added with stirring 96 mg (2 mmol) of 50% sodium hydride in oil dispersion in one portion. This mixture was stirred at −40 to −30 °C for 1 h, and then at room temperature overnight. Ice (12 g) was added and the mixture was extracted with ether. The ethereal solution was washed with water, dilute HCl, and water. Drying and evaporation of the solvent gave a residue (600 mg), which was purified by the filtration through alumina to yield carbonate **2***b* (590 mg, 96%).

Sodium Borohydride Reduction of Carbonate 2b

A methanolic solution of carbonate **2***b* (154 mg, 0.5 mmol) was treated with sodium borohydride (33 mg, 1 mmol) at room temperature with stirring overnight. After the usual work-up was isolated 80 mg (68%) of carbinol **3***b*.

Base-catalyzed Hydrolysis of Carbonate 2b

2*b* (170 mg, 0.55 mmol) was dissolved in acetonitrile (0.5 ml) and 0.8 ml of 50% NaOH was added. The mixture was stirred overnight. Water was added and the mixture extracted with benzene. The combined organic layers were extracted with dilute HCl, the acidic solution neutralized, and extracted with ether. Work-up resulted in 80 mg (61.5%) of pure carbinol **3***b*.

Carbonates **2***b*, *c* are resistant toward acid-catalyzed hydrolysis.

Reaction of Carbinol 3b with Ethyl Chloroformate

Carbinol **3***b* (130 mg, 0.55 mmol) was dissolved in 6.5 ml of ether and three portions of reagent, consisting of 0.5 ml of 50% KOH and 0.15 ml of ethyl chloroformate each, were added to the mixture at 1 h intervals. Stirring was continued for 20 h at ambient temperature. The organic layer was separated, washed with water and dilute HCl, dried, and the solvent evaporated to yield carbonate **2***b* (140 mg, 82%).

2-Ethoxycarbonyl-6,7-methylenedioxy-1,2,3,4-tetrahydroisoquinaldonitrile (6)

To a vigorously stirred mixture of 6,7-methylenedioxy-3,4-dihydroisoquinoline (32) (320 mg, 1.8 mmol) in methylene chloride (2.5 ml) and sodium cyanide (271 mg, 4.5 mmol), in 2.5 ml of water was added gradually ethyl chloroformate (0.68 ml, 3.7 mmol) in 1.25 ml of methylene chloride. Stirring was continued overnight, then the organic layer was separated and washed with water, dilute HCl, water, dilute NaOH, and water. Removal of the solvent yielded a yellow oil (500 mg) which was chromatographed on alumina (Woelm, neutral, activity II°). Benzene eluted 355 mg of a colorless oil, that crystallized from ether–hexane giving 150 mg (30%) of crystals, mp 103–105 °C; ir 1710 cm^{-1} (carbamate C=O); nmr 1.33 (t, J = 7 Hz, 3H, -O-CH_2-CH_3), 4.31 (q, J = 7 Hz, 2H, -O-CH_2-CH_3), 6.0 (s, 3H, C_1-H + -O-CH_2-O-), 6.66–6.78 δ (m, 2H, aromatic); ms *m/e* 274 (M^+, 45%), 274 (M − HCN, 45%), 200 (M − $HCOOC_2H_5$, 68%), 174 (M − HCN − $COOC_2H_2$, 100%). *Anal.* calcd. for $C_{14}H_{14}O_4N$ (274): C 61.31, H 5.10, N 10.21; found: C 61.63, H 5.19, N 10.07.

Reaction of Dihydro-Reissert Analog 6 with Benzaldehyde

Compound **6** (210 mg, 0.76 mmol), 1.5 ml of benzene, 0.3 ml of 50% NaOH, 0.1 ml (1 mmol) of benzaldehyde, and TEBA (8 mg) were stirred at room temperature for 30 min in an argon atmosphere. A little water and ether was added, causing precipitation of a white solid which was filtered off, washed with water and ether, dried, and recrystallized from ethyl acetate. Fine crystals (117 mg) were collected; mp 221–222.5 °C (sealed capillary). The remaining filtrate (water–ether) was separated and the aqueous layer extracted three times with ether. The combined ether extracts were worked-up in the usual manner, giving an additional 100 mg of carbamate **7**. Total yield 217 mg (79%); ir 1760 cm^{-1} (carbamate C=O); nmr 5.36 (s, 1H, C_α-H), 6.0 (s, 2H, -O-CH_2-O-), 6.6, 6.7 (2s, 2H, aromatic), 7.6 δ (s, 5H, aromatic); ms *m/e* 334 (M^+, 24%), 200 (M − CO − PHCHO, 100%). *Anal.* calcd. for $C_{19}H_{14}O_4N_2$ (334): C 68.25, H 4.19, N 8.38; found: C 68.28, H 4.28, N 8.37.

When in the same reaction, acetonitrile was used as solvent, and the products were worked-up by extraction with ether, a mixture of two compounds was obtained. They were separated by column chromatography on alumina (Woelm, neutral, activity II°). Benzene eluted 120 mg of urethane **7**, while ether eluted compound **8** (110 mg, overall yield 73%).

Compound **8** after crystallization from ethyl acetate showed mp 185.5–186.5 °C (lit. (33) mp 185–186 °C); ir 3200–2900 (br, N—H), 1660 cm^{-1} (amide C=O); nmr 6.0 (s, 2H, -O-CH_2-O-), 6.68, 7.5 δ (2s, 2H, aromatic); ms, *m/e* 191 (M^+, 100%), 162 (M − CHNH, 89%), 134 (M − CHNH − CO, 78%). *Anal.* calcd. for $C_{10}H_9O_3N$ (191): C 62.82, H 4.71, N 7.32; found: C 62.63, H 4.73, N 7.30.

Acknowledgment

The author wishes to thank Dr. J. W. Apsimon for correcting the English of this manuscript.

1. L. V. Pavlova and F. J. Rachinskij. Usp. Khim. **37**, 1369 (1968).
2. R. M. Acheson. Acc. Chem. Res. **4**, 177 (1971).
3. Y. Akabori. Kagaku No Ryoiki, **19**, 270 (1965); Chem. Abstr. **63**, 16631 (1965).
4. P. de Mayo. Molecular rearrangements. Interscience, N.Y. 1963, 1964. pp. 763, 937, 992, 995, 1121.
5. K. Koczka and G. Fodor. Acta Chim. Acad. Sci. Hung. **13**, 83 (1957).
6. G. Fodor and J. Kiss. J. Am. Chem. Soc. **72**, 3495 (1950).
7. L. H. Welsh. J. Am. Chem. Soc. **71**, 3500 (1949).

8. W. E. McEwen and R. L. Cobb. Chem. Rev. **55**, 511 (1955).
9. F. D. Popp. Adv. Heterocycl. Chem. **9**, 1 (1968).
10. M. D. Rozwadowska. Bull. Acad. Pol. Sci. Ser. Sci. Chim. **24**, 101 (1976).
11. M. D. Rozwadowska. Bull. Acad. Pol. Sci. Ser. Sci. Chim. **24**, 685 (1976).
12. J. W. Elliott and J. O. Leflore. J. Org. Chem. **28**, 3181 (1963).
13. H. W. Gibson and F. D. Popp. J. Chem. Soc. C, 1860 (1966).
14. M. Shamma and C. D. Jones. J. Org. Chem. **35**, 3119 (1970).
15. H. Böhme and P.-K. Stöcker. Chem. Ber. **105**, 1578 (1972).
16. H. Böhme and R. Schweitzer. Arch. Pharmaz. **303**, 225 (1970).
17. J. M. Wefer, A. Catala, and F. D. Popp. J. Org. Chem. **30**, 3075 (1965).
18. F. D. Popp, L. E. Katz, C. W. Klinowski, and J. M. Wefer. J. Org. Chem. **33**, 4447 (1968).
19. R. Hull. J. Chem. Soc. 1777 (1968).
20. F. D. Popp, J. M. Wefer, and A. Catala. J. Heterocycl. Chem. **2**, 317 (1965).
21. D. M. Spatz and F. D. Popp. J. Heterocycl. Chem. **5**, 497 (1968).
22. A. Jończyk. Bull. Acad. Pol. Sci. Ser. Sci. Chim. **22**, 849 (1974).
23. F. E. Granchelli and J. L. Neumeyer. Tetrahedron, 3701 (1974).
24. R. Picirilli and F. D. Popp. Can. J. Chem. **47**, 3261 (1969).
25. S. M. Kupchan, A. J. Liepa, V. Kameswaran, and K. Sempuku. J. Am. Chem. Soc. **95**, 2995 (1973).
26. L. R. Walters, N. T. Iyer, and W. E. McEwen. J. Am. Chem. Soc. 1177 (1958).
27. M. Mąkosza. Tetrahedron Lett. 677 (1969).
28. K. Nakanishi. Infrared absorption spectroscopy. Holden-Day Inc., San Francisco. 1964.
29. R. Bramley and M. D. Johnson. J. Chem. Soc. 1372 (1965).
30. F. D. Popp, K. T. Potts, and R. Armbruster. Org. Mass Spectrom. **3**, 1075 (1970); Chem. Abstr. **73**, 92633s (1970).
31. S. R. Chhabra, I. R. Kershaw, and C. Uff. Tetrahedron Lett. 3199 (1967).
32. E. Späth and N. Polgar. Monatsh. Chem. **51**, 190 (1929).
33. F. L. Pyman. J. Chem. Soc. **99**, 1690 (1911).

Gas phase competitive anionic cleavage of esters[1]

M. COMISAROW

Department of Chemistry, University of British Columbia, Vancouver, B.C., Canada V6T 1W5

Received August 30, 1976

M. COMISAROW. Can. J. Chem. **55**, 171 (1977).

The gas phase reaction of deuteriomethoxide with methyl benzoate and with methyl trifluoroacetate yields the corresponding carboxylate anions and not protiomethoxide ion. These results are opposite to what would be expected based upon the known reactions in solution of anions with esters. The reasons for the different behavior between the gas phase and the solution phase are discussed.

M. COMISAROW. Can. J. Chem. **55**, 171 (1971).

La réaction en phase gazeuse du deutérométhylate avec le benzoate de méthyle et le trifluoroacétate de méthyle conduit aux anions carboxylates correspondants et non pas à l'ion protiométhylate. Ces résultats sont en opposition avec ceux que l'on pourrait attendre en se basant sur les réactions connues en solution des anions avec les esters. On discute des raisons pour le comportement différent entre la phase gazeuse et la phase en solution.

[Traduit par le journal]

It is well known that the base catalyzed hydrolysis of carboxylic acid esters usually proceeds via the acyl cleavage $B_{AC}2$ mechanism; the alkyl cleavage $B_{AL}2$ mechanism only occurring in special cases (1). The same mechanistic preference holds for base catalyzed alcoholysis (1). For instance, the reaction of methoxide in methanol with methyl benzoate at 100 °C yields exchanged methyl benzoate 430 000 times faster than it yields dimethyl ether (1). This communication reports an investigation using ion cyclotron resonance techniques (2) of the gas phase reaction of methoxide ion with some carboxylic acid methyl esters[2] and shows that in the *gas phase*, the reaction products are strikingly different from those observed *in solution*.

When deuteriomethoxide ion **1**, formed by dissociative electron capture by deuteriomethyl nitrite (4), is reacted in the gas phase with methyltrifluoroacetate **2**, trifluoroacetate ion **3**, is the only product of the reaction as shown by pressure dependence studies and double resonance experiments.[3,4]

$$[1]^{5}\quad \underset{\substack{\mathbf{1}\\ m=34}}{CD_3O^-} + \underset{\mathbf{2}}{CF_3COCH_3} \xrightarrow{k_{carboxylate}} \underset{\substack{\mathbf{3}\\ m=113}}{CF_3CO^-} + CD_3OCH_3$$

Similarly, methyl benzoate **4**, reacts with deuteriomethoxide ion to yield only benzoate anion **5**.

[1]Reported at 57th Canadian Chemical Conference, Regina, Saskatchewan, June 3–5, 1974.

[2]The reaction of alkoxide ions with formate esters yields clustered alkoxide ions (3).

[3]The reactions were carried out on a home-built 'drift cell' ICR spectrometer of conventional design. A dynamic pressure balance was maintained in the cell by bleeding in the reagents via separate inlet systems while pumping on the vacuum system with an ion pump. Double irradiation in the source region of the drift cell was used for double resonance experiments. The techniques used are well described in ref. 2.

[4]Typical pressures of the reagents were CD_3ONO, 10^{-6} torr; ester, 10^{-6} to 5×10^{-5} torr.

[5]All ion structures and the structures of the neutral products are presumed.

$$[2]^5\quad \underset{\underset{m=34}{\mathbf{1}}}{CD_3O^-} + \underset{\mathbf{4}}{C_6H_5\overset{\overset{O}{\|}}{C}OCH_3} \xrightarrow{k_{carboxylate}} \underset{\mathbf{5}\ m=121}{C_6H_5\overset{\overset{O}{\|}}{C}O^-} + CD_3OCH_3$$

Under the experimental conditions,[4] no protiomethoxide ion, **6**, was observable with either the trifluoroacetate or benzoate systems and from the estimated maximum possible yield of protiomethoxide, the rate of the alkoxide-forming reaction 3 may be estimated to be *at least* thirty times *slower* than the corresponding carboxylate-forming reaction 1 or 2.

$$[3]^5\quad \underset{\underset{m=34}{\mathbf{1}}}{R\overset{\overset{O}{\|}}{C}OCH_3} + {}^-OCD_3 \xrightarrow{k_{alkoxide}} \underset{\mathbf{6}\ m=31}{R\overset{\overset{O}{\|}}{C}OCD_3} + {}^-OCH_3$$

$$R = CF_3, C_6H_5$$

The enthalpy change, ΔH_1, for reaction 1 can be determined from the thermodynamic cycle

$$\begin{array}{ccc} CF_3\overset{\overset{O}{\|}}{C}OCH_3 + {}^-OCD_3 & \xrightarrow{\Delta H_1} & CF_3\overset{\overset{O}{\|}}{C}O^- + CH_3OCD_3 \\ \downarrow \Delta H_a & & \uparrow \Delta H_c \\ CF_3\overset{\overset{O}{\|}}{C}O\cdot + \cdot CH_3 + {}^-OCD_3 & \xrightarrow{\Delta H_b} & CF_3\overset{\overset{O}{\|}}{C}O^- + \cdot CH_3 + \cdot OCD_3 \end{array}$$

where ΔH_a is the methyl–oxygen bond strength in methyltrifluoroacetate **2**, ΔH_c is minus the methyl–oxygen bond strength in dimethyl ether, and ΔH_b is the difference in electron affinities between methoxide radical and trifluoroacetate radical;

$$\Delta H_b = EA(CH_3O\cdot) - EA(CF_3COO\cdot)$$

Assuming[6]

$$\Delta H_a = -\Delta H_c$$

yields

$$\Delta H_1 = \Delta H_b$$

Therefore

$$\begin{aligned}\Delta H_1 &= EA(CH_3O\cdot) - EA(CF_3COO\cdot)\\ &= 32.5 \text{ (ref. 5)} - 103.4 \text{ (ref. 6)}\\ &= -70.9 \text{ kcal}\end{aligned}$$

Reaction 2 may similarly be estimated[7] to be exothermic by 53.8 kcal. Neglecting the secondary isotope effect, reaction 3 is, of course, thermoneutral.

The present results do not provide any direct evidence regarding the details of the molecular rearrangements which convert the reactants into products in the *gas phase* reactions 1 and 2. One possible mechanism, however, is that the deuteriomethoxide ion attacks the ester at the carbonyl carbon to form the tetrahedral intermediate, **7**, which then decomposes to products.

$$R-\underset{\underset{OCD_3}{|}}{\overset{\overset{O^-}{|}}{C}}-O-CH_3 \rightarrow RCOO^- + CD_3OCH_3$$

7

The formation of a tetrahedral intermediate has been suggested as the first step in the gas phase reactions of hydroxide ion and fluoride ion with formate esters (9). Another possible mechanism for the gas phase reactions 1 and 2 is S_N2 displacement upon the methyl group in the ester via the complex, **8** (9).

$$R-\overset{\overset{O}{\|}}{C}O^{\delta-}\cdots CH_3\cdots {}^{\delta-}OCD_3$$

8

The striking feature of the above results is the preference for carboxylate formation in the gas phase. In the case of methyl benzoate, the ratio $k_{carboxylate}/k_{alkoxide}$ is seven orders of magnitude

[6]This approximation could be in error by several kilocalories without changing any of the conclusions of this paper.

[7]Yamdagni and Kebarle (7) quote the difference between the O—H bond energy in benzoic acid and the electron affinity of benzoate radical as 23.7 kcal. Assuming that the O—H bond strength in benzoic acid is 110 kcal (8), estimation of the electron affinity of the benzoate radical would be 86.3 kcal.

greater in the gas phase than in methanol solution. Since the gas phase reaction yields the most exothermic products, the presence of the protic methanol solvent must be responsible for the observation of the formation of the thermoneutral products when the reaction of methoxide with methyl esters is carried out in solution. The change in product ratio when methanol solvent is 'added' to the gas phase systems can be explained by postulating a preferential stabilization by the protic methanol solvent of the transition state for the alkoxide-forming reaction, relative to the transition state for the carboxylate-forming reaction. Since *in solution* the alkoxide-forming reaction proceeds via the tetrahedral intermediate, **7**, in which negative charge is localized on one atom whereas carboxylate is formed via the transition state, **8**, in which the negative charge is spread out over three atoms, this preferential stabilization by the protic solvent is not surprising. Analogous considerations should apply to other (anion) – (acid derivative) reactions, and may explain why in solution the rate of the addition–elimination reaction is faster than many S_N2 reactions (10).

Acknowledgement

This research was supported by the National Research Council of Canada.

1. J. KOSKIKALLIO. *In* The chemistry of carboxylic acids and esters. *Edited by* S. Patai. Interscience Publishers. New York. 1969. Chapt. 3 and references therein.
2. J. L. BEAUCHAMP. Ann. Rev. Phys. Chem. **22**, 527 (1971).
3. L. K. BLAIR, P. C. ISOLANI, and J. M. RIVEROS. J. Am. Chem. Soc. **95**, 1057 (1973).
4. K. JAGER and A. HENGLEIN. Z. Naturforsch. A, **22**, 700 (1967).
5. D. K. BOHME, E. LEE-RUFF, and L. B. YOUNG. J. Am. Chem. Soc. **94**, 5153 (1972).
6. K. HIRAOKA, R. YAMDAGNI, and P. KEBARLE. J. Am. Chem. Soc. **95**, 6833 (1973).
7. R. YAMDAGNI and P. KEBARLE. Can. J. Chem. **52**, 861 (1974).
8. V. I. VEDENEYEV *et al.* Bond energies, ionization potentials, and electron affinities. E. Arnold Publishers Ltd., London, 1966.
9. J. F. G. FAIGLE, P. C. ISOLANI, and J. M. RIVEROS. J. Am. Chem. Soc. **98**, 2049 (1976).
10. J. HINE. Physical organic chemistry. McGraw-Hill, New York. 1962. p. 276.

On the mechanisms of acid-catalyzed enolization and hydrogen isotope exchange of cyclic ketones

NICK HENRY WERSTIUK AND SUJIT BANERJEE

Department of Chemistry, McMaster University, Hamilton, Ont., Canada L8S 4M1

Received May 3, 1976

NICK HENRY WERSTIUK and SUJIT BANERJEE. Can. J. Chem. **55**, 173 (1977).

The acid-catalyzed hydrogen isotope exchange of norcamphor **1** in DOAc–DCl–D_2O is shown to follow the general theory (4) for exchange of a diastereotopic proton pair α to a carbonyl group. That is, the less reactive proton undergoes exchange via two channels. Through an analysis of a combination of the rate data for acid-catalyzed bromination and the pK_{BH+} values for a series of cyclic and bicyclic ketones, we establish that the reactivity order in the former is controlled by ketone basicity and not, as has been suggested previously, by angle strain developed in a very enol-like transition state.

NICK HENRY WERSTIUK et SUJIT BANERJEE. Can. J. Chem. **55**, 173 (1977).

Dans le cas du norcamphre **1**, on démontre que l'échange isotopique de l'hydrogène, catalysé par les acides dans le DOAc–DCl–D_2O, suit la théorie générale (4) de l'échange d'une paire de protons diastéréotopes en α d'un groupement carbonyle. Ceci implique que le proton moins réactif subit un échange par deux voies. Faisant appel à une analyse d'une combinaison des données concernant les vitesses pour la bromation catalysée par les acides et les valeurs de pK_{BH+} d'une série de cétone cyclique et bicyclique, on établit que l'ordre de réactivité dans le premier cas est contrôlé par la basicité de la cétone et non pas, comme il avait été suggéré antérieurement, par la tension d'angle développée dans un état de transition ressemblant beaucoup à un énol.

[Traduit par le journal]

greater in the gas phase than in methanol solution. Since the gas phase reaction yields the most exothermic products, the presence of the protic methanol solvent must be responsible for the observation of the formation of the thermoneutral products when the reaction of methoxide with methyl esters is carried out in solution. The change in product ratio when methanol solvent is 'added' to the gas phase systems can be explained by postulating a preferential stabilization by the protic methanol solvent of the transition state for the alkoxide-forming reaction, relative to the transition state for the carboxylate-forming reaction. Since *in solution* the alkoxide-forming reaction proceeds via the tetrahedral intermediate, **7**, in which negative charge is localized on one atom whereas carboxylate is formed via the transition state, **8**, in which the negative charge is spread out over three atoms, this preferential stabilization by the protic solvent is not surprising. Analogous considerations should apply to other (anion) – (acid derivative) reactions, and may explain why in solution the rate of the addition–elimination reaction is faster than many S_N2 reactions (10).

Acknowledgement

This research was supported by the National Research Council of Canada.

1. J. KOSKIKALLIO. *In* The chemistry of carboxylic acids and esters. *Edited by* S. Patai. Interscience Publishers. New York. 1969. Chapt. 3 and references therein.
2. J. L. BEAUCHAMP. Ann. Rev. Phys. Chem. **22**, 527 (1971).
3. L. K. BLAIR, P. C. ISOLANI, and J. M. RIVEROS. J. Am. Chem. Soc. **95**, 1057 (1973).
4. K. JAGER and A. HENGLEIN. Z. Naturforsch. A, **22**, 700 (1967).
5. D. K. BOHME, E. LEE-RUFF, and L. B. YOUNG. J. Am. Chem. Soc. **94**, 5153 (1972).
6. K. HIRAOKA, R. YAMDAGNI, and P. KEBARLE. J. Am. Chem. Soc. **95**, 6833 (1973).
7. R. YAMDAGNI and P. KEBARLE. Can. J. Chem. **52**, 861 (1974).
8. V. I. VEDENEYEV *et al.* Bond energies, ionization potentials, and electron affinities. E. Arnold Publishers Ltd., London, 1966.
9. J. F. G. FAIGLE, P. C. ISOLANI, and J. M. RIVEROS. J. Am. Chem. Soc. **98**, 2049 (1976).
10. J. HINE. Physical organic chemistry. McGraw-Hill, New York. 1962. p. 276.

On the mechanisms of acid-catalyzed enolization and hydrogen isotope exchange of cyclic ketones

NICK HENRY WERSTIUK AND SUJIT BANERJEE

Department of Chemistry, McMaster University, Hamilton, Ont., Canada L8S 4M1

Received May 3, 1976

NICK HENRY WERSTIUK and SUJIT BANERJEE. Can. J. Chem. **55**, 173 (1977).

The acid-catalyzed hydrogen isotope exchange of norcamphor **1** in DOAc–DCl–D_2O is shown to follow the general theory (4) for exchange of a diastereotopic proton pair α to a carbonyl group. That is, the less reactive proton undergoes exchange via two channels. Through an analysis of a combination of the rate data for acid-catalyzed bromination and the pK_{BH+} values for a series of cyclic and bicyclic ketones, we establish that the reactivity order in the former is controlled by ketone basicity and not, as has been suggested previously, by angle strain developed in a very enol-like transition state.

NICK HENRY WERSTIUK et SUJIT BANERJEE. Can. J. Chem. **55**, 173 (1977).

Dans le cas du norcamphre **1**, on démontre que l'échange isotopique de l'hydrogène, catalysé par les acides dans le DOAc–DCl–D_2O, suit la théorie générale (4) de l'échange d'une paire de protons diastéréotopes en α d'un groupement carbonyle. Ceci implique que le proton moins réactif subit un échange par deux voies. Faisant appel à une analyse d'une combinaison des données concernant les vitesses pour la bromation catalysée par les acides et les valeurs de pK_{BH+} d'une série de cétone cyclique et bicyclique, on établit que l'ordre de réactivité dans le premier cas est contrôlé par la basicité de la cétone et non pas, comme il avait été suggéré antérieurement, par la tension d'angle développée dans un état de transition ressemblant beaucoup à un énol.

[Traduit par le journal]

The generally accepted mechanism for acid-catalyzed enolization (exchange) of ketones, as described in Scheme 1 involves a rapid equilibrium protonation of the ketone B, and proton transfer from the conjugate acid BD^+ to produce enol E (1).

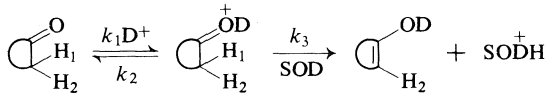

B BD^+ E

SCHEME 1

Up to the present, a diastereotopic proton pair H_1 (fast) and H_2 (slow) would have been expected to exchange by separate one-channel processes. Also, the implication in the literature is that the development of double bond character is advanced in acid-catalyzed enolization and it is greater than that developed in the base-catalyzed process (2, 3). Thus, it has been suggested (3) that bond-angle strain developed in a very enol-like transition state in the former, controls the order of reactivity[1] in a series of cyclic ketones.

As a continuation of our study on the enolization of bicyclic ketones (4, 5) we now establish that (*a*) acid-catalyzed hydrogen isotope exchange of a diastereotopic proton pair follows the general mechanism proposed previously (4), and (*b*) the range of reactivity in acid-catalyzed enolization of cyclic and bicyclic ketones primarily results from a variation of pK_{BH^+} with ketone structure.

That acid-catalyzed exchange in norcamphor **1** is describable by the theory documented for base-catalyzed exchange (4) is established by the data in Table 1. That the less reactive proton exchanges via two channels is determined by the fact that $(k_{exo}/k_{endo})^{D\rightarrow H} = 29$ (entries 5 and 6). The intrinsic selectivity factor s is obtained from either the H → D ($i = 5.4$, $s = 191$) or D → H ($i = 5.4$, $s = 186$) exchange data.[2]

[1]The range of reactivity for acid-catalyzed enolization in the series of cyclobutanone, cyclopentanone, cyclohexanone, and cycloheptanone (1:150:743:101) (3) is much greater than that for base-catalyzed enolization (15:9.9:1.0:1.7) (6).

[2]Theory (4) predicts that $(k_{exo}/k_{endo})^{H\rightarrow D} = si/(i+1)$, and $(k_{exo}/k_{endo})^{D\rightarrow H} = s/(i+1)$, where s = intrinsic selectivity, $i = i_{exo} \simeq i_{endo}$, $k_{H\rightarrow D}(endo)/k_{D\rightarrow H}(endo) = i_{solv}$ (solvent isotope effect) and $k_{H\rightarrow D}(exo)/k_{D\rightarrow H}(exo) = i_{exo} \times i_{solv}$. From entries 3 and 6, $i_{solv} \simeq 1.99$, and from entries 2 and 5, $i_{exo} \times i_{solv} = 10.65$. Therefore the K.I.E. $i = 5.4$ at 100 °C.

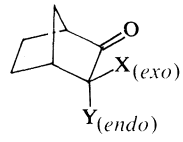

1*a* X = Y = H
b X = D, Y = H
c X = Y = D
d X = H, Y = D

To establish whether acid-catalyzed enolization (exchange) is sensitive to torsional or bond-angle strain effects in the transition state, we utilized data that were available in the literature (Table 2). Bank and co-workers (8) have shown that the rates of base-catalyzed isomerization (*tert*-BuO^-, DMSO) of the exocyclic olefins correlate with torsional strain energy differences between transition state and ground state. Furthermore, they have established that angle strain factors are of major importance in endocyclic olefin isomerization. Schriesheim and co-workers (6, 7) have shown that the rates of base-catalyzed bromination of the corresponding ketones correlate with the rates of isomerization of the corresponding exocyclic olefins, thereby establishing that torsional strain effects are important in determining the reactivity order in base-catalyzed enolization.

We have utilized Bank's isomerization data to estimate the importance of torsional and bond-angle strain effects on the rates of acid-catalyzed enolization. Thus a plot of $\log k^{acid}_{bromination}$ (Table 2) *vs.* $\log^{exo\rightarrow endo}_{isomerization}$ (8)[3] reveals no obvious

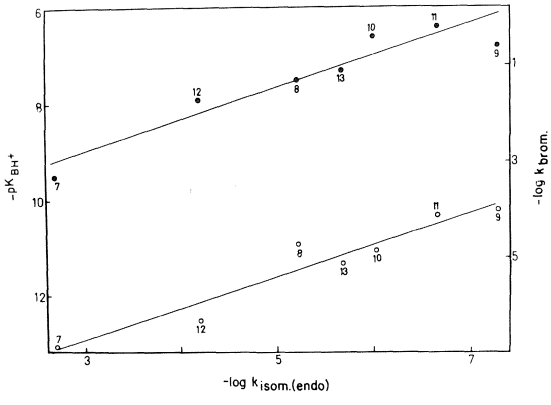

FIG. 1. Correlation of $\log k^{acid}_{bromination}$ (○) and pK_{BH^+} (●) with $\log k^{exo\rightarrow endo}_{isomerization}$. Numbers refer to entries in Table 2.

[3]The available *exo* → *endo* isomerization rate data (8) are not included in Table 2.

TABLE 1. Rate constants for acid-catalyzed exchange

Entry	Substrate	Temperature (°C)	Medium[a,b]	$k \times 10^5$ (s^{-1})	Site	$\frac{k_{exo}}{k_{endo}}$
1	**1***a*	75.0	A	44.8[c]	*exo*	
2	**1***a*	100.0	A	386.0[c,e]	*exo*	156
3	**1***b*	100.0	A	2.47[d]	*endo*	
4	**1***c*	75.0	B	4.20[d]	*exo*	
5	**1***c*	100.0	B	36.2[d]	*exo*	29
6	**1***d*	100.0	B	1.24[d]	*endo*	

[a]A: 90% DOAc – 10% 2.08 *N* DCl–D_2O.
[b]B: 90% HOAc – 10% 2.00 *N* HCl–H_2O.
[c]Single determination.
[d]Mean of two determinations.
[e]Obtained from *exo* rate at 75 °C.

TABLE 2. Data for the base-catalyzed isomerization of *endo* olefins and the acid-catalyzed bromination of ketones

Entry	Substrates (olefins or ketones)	$\log k^{endo \rightarrow exo}_{isomerization}$[a]	$\log k^{acid}_{bromination}$[b]	pK_{BH^+}[c]	$\log k_3 - H_x$
7		−2.701	−6.884	−9.5	2.6
8		−5.205	−4.707	−7.5	2.8
9		−7.284	−3.985	−6.8	2.8
10		−6.018	−4.877	−6.6	1.7
11		−6.662	−4.104	−6.2	2.1
12		−4.193	−6.333[d]	−7.9[f]	1.6
13	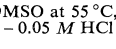	−5.680	−5.129[e]	−7.3[f]	2.2

[a]In KO-*t*-Bu–DMSO at 55 °C, on per H basis (6).
[b]In 90% HOAc – 0.05 *M* HCl at 29.9 °C, on per H basis (3).
[c]See ref. 9.
[d]This work in 90% HOAc – 10% 2.00 *N* HCl at 40.0 °C. Rates converted to conditions in footnote *b* by comparison with cyclohexanone.
[e]This work in 90% DOAc – 10% 2.08 *N* DCl at 40.0 °C. Rates corrected for solvent isotope effect (based on norcamphor) and converted to the conditions in footnote *b*, by comparison with cyclohexanone.
[f]Estimated from a plot of pK_{BH^+} *vs.* $\nu_{C=O}$ (9).

correlation (correlation coefficient 0.46)[4], whereas a linear relationship (correlation coefficient 0.96) exists between $\log k^{acid}_{bromination}$ and $\log k^{exo \rightarrow endo}_{isomerization}$ (Fig. 1). Consequently, the reactivity of the ketones in the present series is controlled by bond-angle strain effects rather than by torsional strain factors.

For the process

$$B \underset{}{\overset{H^+}{\rightleftharpoons}} BH^+ \overset{k_3}{\longrightarrow} E$$

where B, BH^+, and E represent ketone, protonated ketone, and enol, respectively, and where protonation of the substrate follows the acidity function H_x,[5]

$$\log k_{obs} = \log k_3 + pK_{BH^+} - H_x$$

Since ketone pK_{BH^+} values are available (9), and the value for H_x is constant, the data (Table 2) establish that the deprotonation rate constant k_3 changes only minimally (a factor of 10). Consequently, we establish that ketone basicity, controlled by bond-angle strain effects as illus-

[4]To minimize the length of the text, the plot of $\log k^{acid}_{bromination}$ *vs.* $\log k^{exo \rightarrow endo}_{isomerization}$ is not included.

[5]Since the acidity function for protonation of these ketones has not been defined, we use H_x only in an illustrative sense.

trated in Fig. 1 by the plot of pK_{BH^+} *vs.* log $k^{endo \rightarrow exo}_{isomerization}$, determines the reactivity of the ketones towards acid-catalyzed enolization. Thus, it is clear that a deprotonation transition state in which unsaturation is highly developed *is not required* to account for the order of reactivity in cyclic ketones.

Acknowledgment

Financial support of the National Research Council of Canada is acknowledged.

1. G. E. LIENHARD and T. C. WANG. J. Am. Chem. Soc. **91**, 1146 (1969) and references therein.
2. W. D. EMMONS and M. F. HAWTHORNE. J. Am. Chem. Soc. **78**, 5593 (1956).
3. H. SHECHTER, M. J. COLLINS, R. DESSY, Y. OKUZUMI, and A. CHEN. J. Am. Chem. Soc. **84**, 2905 (1962).
4. S. BANERJEE and N. H. WERSTIUK. Can. J. Chem. **53**, 1099 (1975).
5. N. H. WERSTIUK and R. TAILLEFER. Can. J. Chem. **48**, 3966 (1970).
6. A. SCHRIESHEIM, R. J. MULLER, and C. A. ROWE, JR. J. Am. Chem. Soc. **84**, 3164 (1962).
7. A. SCHRIESHEIM, C. A. ROWE, JR., and L. A. NASLUND. J. Am. Chem. Soc. **85**, 2111 (1963).
8. S. BANK, C. A. ROWE, JR., A. SCHRIESHEIM, and L. A. NASLUND. J. Am. Chem. Soc. **89**, 6897 (1967).
9. H. J. CAMPBELL and J. T. EDWARD. Can. J. Chem. **38**, 2109 (1960).

Canadian Journal of Chemistry

Published by
THE NATIONAL RESEARCH COUNCIL OF CANADA

Journal canadien de chimie

Publié par
LE CONSEIL NATIONAL DE RECHERCHES DU CANADA

Volume 55 Number 2 January 15, 1977

Volume 55 numéro 2 15 janvier 1977

Chemistry of metal hydrides. Part XIX. Stereochemical changes at platinum during the insertion of acetylenes with platinum(II) hydrides

H. C. CLARK,[1] P. L. FIESS, AND C. S. WONG[1]

Department of Chemistry, University of Western Ontario, London, Ont., Canada N6A 3K7

Received July 21, 1976

H. C. CLARK, P. L. FIESS, and C. S. WONG. Can. J. Chem. **55**, 177 (1977).

The reactions of *trans*-$[PtH(PEt_3)_2(acetone)]^+$ and *trans*-$[PtH(PEt_3)_2(CO)]^+$ with a variety of acetylenes are described. The geometries of the products with respect to the platinum centre and to the stereochemistry of the alkenyl group have been determined on the basis of their ^1H nmr parameters. For reactions with the cation containing acetone, and particularly from a variable temperature ^1H nmr study of its reaction with 2-butyne in the presence of water, the insertion pathway is shown to be entirely analogous to that for olefin insertion, involving an initial displacement of the *trans* ligand by acetylene, isomerization to a *cis*-like intermediate, migratory insertion rearrangement, and re-combination with an appropriate ligand to give either *cis* or *trans* platinum products. The insertion pathway with the carbonyl cation is dependent on the nature of the acetylene; for non-activated or weakly activated acetylenes insertion occurs via five-coordinate intermediates, but with strongly activated acetylenes, the same mechanism as with the acetone cation appears to occur, involving reversible loss of carbon monoxide.

H. C. CLARK, P. L. FIESS et C. S. WONG. Can. J. Chem. **55**, 177 (1977).

On décrit les réactions de $[PtH(PEt_3)_2(acétone)]^+$ *trans* et $[PtH(PEt_3)_2(CO)]^+$ *trans* avec divers acétylènes. On a déterminé, en se basant sur les paramètres de leurs spectres rmn du proton, les géométries des produits par rapport au platine et la stéréochimie des groupes alkényles. Pour les réactions avec le cation contenant l'acétone et particulièrement à partir d'une étude, par rmn du proton à température variable, de sa réaction avec le butyne-2 en présence d'eau on démontre que le chemin de l'insertion est complètement analogue à celui de l'insertion de l'oléfine et qu'il implique un déplacement initial du ligand *trans* par l'acétylène, une isomérisation impliquant un intermédiaire "*cis*", un réarrangement d'insertion migratoire et une recombinaison avec un ligand approprié pour donner des produits de platine soit *cis* soit *trans*. Le chemin d'insertion avec le cation carbonylé dépend de la nature de l'acétylène; pour des acétylènes non-activés ou faiblement activés, l'insertion se produit par des intermédiaires penta-coordonnés mais pour les acétylènes qui sont fortement activés, il semble que le mécanisme soit le même que celui du cation contenant l'acétone et qu'il implique une perte réversible du monoxyde de carbone.

[Traduit par le journal]

Introduction

There have been numerous reports in the literature of reactions involving the insertion of acetylenes in transition metal – hydrogen bonds (see, for example, ref. 1). While stable alkenyl products have been characterized, few investigations of the mechanism of such processes appear to have been conducted. This contrasts with the comparable insertions of olefins into metal–hydrogen bonds, which are of considerable importance in relation to the metal-catalyzed isomerizations and hydrogenations of olefins, and which have been extensively studied in recent years.

For Pt(II) hydrides, it has been demonstrated

[1]Present address: Department of Chemistry, University of Guelph, Guelph, Ont. Canada N1G 2W1.

that insertions proceed via a common mechanism in which the determining factor is the relative ease of displacement of the ligand *trans* to the hydridic hydrogen (2). Thus, for $-SnCl_3$ as a *trans* ligand which is not readily displaced, insertion proceeds via a five-coordinate intermediate (3). With —Cl, $-NO_3$, or acetone as readily displaceable *trans* ligands, such five-coordinate species occur only as transition states and insertion proceeds (4) by initial displacement of the *trans* ligand, isomerization of the resulting *trans* olefinic complex to its *cis* isomer, migratory rearrangement to the alkyl (or alkenyl) product, and finally recombination with a suitable ligand to give either the *cis* or *trans* product. Hence the nature of the *trans* ligand, in determining the relative stabilities of four- and five-coordinate species, controls the mechanistic pathway for insertion. Kinetic data (3, 4), the isolations (5, 6) of stable *trans*-hydrido(olefin)platinum(II) species, and the observation that, depending on the reaction conditions, both *cis* and *trans* platinum isomers of the alkenyl product may be obtained (7) with the formation of this *cis* isomer being kinetically controlled, all provide strong support for this general mechanism.

Most of the previous work described above relates to olefin insertions. Although qualitative studies have been conducted leading to the characterization of the alkenyl products formed by insertion with some acetylenes (3, 7), intermediates such as *trans*-hydrido(acetylene)platinum(II) species have not been identified. On the other hand, both cationic (8) and neutral (9) methylplatinum(II) acetylene complexes have been isolated as stable complexes, suggesting that comparable hydrido analogues should perhaps have a reasonable stability. Also, the presently available data do not indicate whether acetylenes, compared with olefins, have a greater or lesser preference for a five-coordinate versus a four-coordinate pathway for insertion. Again, the use of unsymmetrically substituted acetylenes, $R_1C{\equiv}CR_2$, in reactions with Pt(II) hydrides may provide much more detailed information about the actual migratory insertion step than is accessible from studies of olefin insertions.

Further data are therefore presented here concerning acetylene insertions in the Pt—H bond, particularly in terms of the stereochemical changes which occur at the platinum centre during the insertion process. In the following paper, the nature of the actual migratory insertion step is considered.

Experimental

Reactions were carried out in 50 ml round-bottomed flasks under standard conditions. Where gaseous acetylenes were used, standard vacuum techniques were employed to transfer slightly greater than equimolar amounts into the reaction mixture.

Infrared spectra were recorded using Nujol mulls between NaCl optics on a Perkin-Elmer 621 spectrometer. ^1H and ^{19}F nmr spectra were recorded on Varian T-60 and HA-100 spectrometers, with chemical shifts being reported relative to TMS and $CFCl_3$ (Freon 11) respectively. Melting points were recorded on a Thomas Hoover instrument. Microanalyses were carried out by Chemalytics Inc., Tempe, Arizona, and Midwest Microlab Ltd., Indianapolis, Indiana.

trans-Chlorohydridobis(triethylphosphine)platinum(II) was prepared using the procedure of Parshall (10), and *trans*-$PtH(CO)(PEt_3)_2^+PF_6^-$ following the method of Church and Mays (11).

Reactions with trans-$PtH(PEt_3)_2(acetone)^+PF_6^-$

Since common procedures were employed for numerous reactions, only typical experiments will be described. *trans*-Chlorohydridobis(triethylphosphine)platinum(II) (0.2 mmol) was dissolved in acetone and an acetone solution of silver hexafluorophosphate was added (0.2 mmol). The thick precipitate of silver chloride was removed by centrifugation and the resulting clear solution was diluted to 25 ml with acetone, in a 50 ml round-bottomed flask. The acetylene (0.2 mmol) was added with stirring, this usually being accompanied by a color change. After 5 min, pyridine (0.2 mmol) was added turning the solution to a pale yellow color. The solution was passed through a short florisil column (100–200 mesh) and then evaporated to dryness under vacuum. The resulting solid or oil was taken up in the minimum amount of methanol, and diethyl ether was added dropwise to induce crystallization of the alkenyl product. When gaseous acetylenes were being used, similar procedures were employed except that standard high vacuum techniques were used for transfers of acetylenes.

The products obtained in such reactions, together with characterization data, are described in Table 1.

Reaction of trans-$[PtH(PEt_3)_2(CH_3OH)]^+PF_6^-$ with $CH{\equiv}CCH_2CH_2OH$

A solution of *trans*-$[PtHCl(PEt_3)_2]$ (0.1 g, 0.21 mmol) in methanol (25 ml) was prepared in a 50 ml round-bottomed flask fitted with a magnetic stirring bar. 3-Butyne-1-ol (0.018 ml, 0.21 mmol) was added followed by silver hexafluorophosphate (0.053 g, 0.21 mmol) in methanol (5 ml). The thick white precipitate of silver chloride which formed rapidly was removed by centrifugation to give a clear pale yellow solution. This was through a short florisil column and then evaporated under reduced pressure to *ca.* one-third of its original volume. Diethyl ether (20 ml) was added to ensure crystallization of white crystalline *trans*-$[PtH\{\overline{CH_2CH_2O\ddot{C}CH_2}\}(PEt_3)_2]^+PF_6^-$; yield 92%; mp 128–130 °C. *Anal.* calcd. for $C_{16}H_{37}F_6OP_3Pt$: C 29.67, H 5.72; found: C 29.58, H 5.47.

Reactions of trans-$[PtH(PEt_3)_2(acetone)]^+PF_6^-$ with 2-Butyne over −60 to 32 °C Temperature Range in the Presence of Water

trans-$[PtHCl(PEt_3)_2]$ was dissolved in acetone-d_6 and

TABLE 1. Characterization data for the products* of the reaction *A*

trans-PtH(PEt_3)$_2$(acetone)$^+PF_6^-$ + $R_1C{\equiv}CR_2$ $\xrightarrow{+py}$ Ptpy(PEt_3)$_2$(alkenyl)$^+PF_6^-$

Alkenyl	Configuration at Pt	Yield (%)	Melting point (°C)	Analysis (%) Calculated C	Calculated H	Found C	Found H
$(CH_3OOC)C{=}CH(COOCH_3)$	*cis*	84	207–208	34.59	5.30	34.68	5.09
$C_6H_5C{=}CHC_6H_5$	*trans*	82	174–175	44.61	5.55	44.85	5.44
$CH_3C{=}CHCH_3$	*trans*	73	150–151	35.50	5.96	35.14	5.82
$CH_3C{=}CHCOOCH_3$							
$(CH_3OOC)C{=}CHCH_3$	*trans*	66		35.01	5.61	34.84	5.70
$(CH_3OOC)C{=}CHC_6H_5$	*trans*	67	173–174	39.71	5.43	39.70	5.44
$CH_3C{=}CHC_6H_5$	*trans*	77	90–91	40.41	5.74	39.82	5.57
$C_2H_5C{=}CHC_6H_5$							
$C_6H_5C{=}CHC_2H_5$	*trans*	85		41.22	5.89	40.98	5.72
$C_2H_5C{=}CHC_2H_5$	*trans*	66	119–120	37.40	6.28	37.18	6.14
$CF_3C{=}CHC_6H_5$	*cis* and *trans*						
$C_6H_5C{=}CHCF_3$	*trans*	87		37.78	5.00	37.66	5.10
$CF_3C{=}CHCF_3$	*cis*	61	168–169	30.81	4.43	31.19	4.42
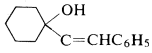	*trans*	67	148–150	43.46	6.12	43.78	5.78
$CF_3C{=}CH_2$	*cis*	31	127–130	32.01	4.97	32.34	5.02
$HC{=}CHC_6H_5$	*trans*	27	178–180	36.47	5.39	36.27	5.23

an equimolar amount of silver hexafluorophosphate in acetone-d_6 was added. The precipitated silver chloride was removed by centrifugation and the remaining clear solution was pipetted into an nmr tube. Sufficient water was added to provide an approximate H_2O:Pt ratio of 0.8:1. The solution was cooled to −60 °C and 2-butyne was added. After the ^1H nmr spectrum had been recorded, the temperature was raised to −30 °C, the spectrum re-run, and the process repeated at −20, −10, 0, and 32 °C.

Reactions with trans-PtH(CO)(PEt_3)$_2^+PF_6^-$

For qualitative observations of the rates of these reactions, 50 mg of the carbonyl salt was dissolved in 0.3 ml $CDCl_3$ in an nmr tube. A measured quantity of acetylene was then introduced (dimethylacetylenedicarboxylate, 15 µl; $CF_3C{\equiv}CC_6H_5$, 20 µl; C_4H_6, 15 µl; $C_6H_5C{\equiv}CC_6H_5$, 20 mg; $CH_3C{\equiv}CCOOCH_3$, 40 µl). The reaction was followed by nmr by monitoring the disappearance of the Pt–H signal and the formation of the product. The reaction time reported was the time after which no Pt—H signal was observed. The possible error in determining the reaction time is the interval of recording (may be as much as 12 h in slower reactions). Authentic samples of the products were prepared in larger quantities as described below.

Reaction with C_4F_6 was carried out in a sealed nmr tube. *trans*-PtH(CO)(PEt_3)$_2PF_6$ (105 mg) was dissolved in 0.3 ml $CDCl_3$. About 100 µl of C_4F_6 was condensed in and the tube sealed. On warming to room temperature, some C_4F_6 remained as a separate layer. The reaction was followed by periodically observing the ^1H nmr spectrum until the Pt—H signal had completely disappeared. Recrystallization of the product from acetone/ether yielded *cis*-Pt(PEt_3)$_2$($CF_3C{=}CHCF_3$)(CO)$^+PF_6^-$ (59%).

For the preparation of large quantities of the alkenyl products, *trans*-PtH(CO)(PEt_3)$_2PF_6$ was allowed to react with the appropriate acetylene in acetone solution for periods of time from 15 h to 2 days (heated to 54 °C when using $CF_3C{\equiv}CC_6H_5$). Solvent was removed under vacuum and the product recrystallized from methanol/ether. Yields with the various acetylenes were as follows: C_4H_6, 73%; $CH_3C{\equiv}CCOOCH_3$, 52%; $C_6H_5C{\equiv}CC_6H_5$, 78%; $CF_3C{\equiv}CC_6H_5$, 78%; $CH_3OOCC{\equiv}CCOOCH_3$, 49%. Characterization data are presented in Table 2.

Results and Discussion

The reactions which have now been investigated fall into two classes, the first of which is concerned with acetylenes interacting with *trans*-[PtH(PEt_3)$_2$(acetone)]$^+PF_6^-$. These reactions were all conducted in acetone, the Pt(II) cation being generated by the treatment of an acetone solution of *trans*-PtHCl(PEt_3)$_2$ with an equimolar amount of silver hexafluorophosphate. After removal of the precipitated silver chloride, treatment with the stoichiometric amount of acetylene (Table 1) gave the alkenyl insertion product according to *A*, reaction generally being complete in a matter of minutes. The products were isolated, following the addition of pyridine,

[*A*] *trans*-[PtH(PEt_3)$_2$(acetone)]$^+PF_6$ + $R_1C{\equiv}CR_2$ $\xrightarrow{py}$ *trans(cis)*- 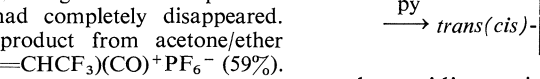

as the pyridine-cation. With only two exceptions

TABLE 2. Characterization data for the products of the reaction *B*
trans-PtH(CO)$(PEt_3)_2^+PF_6$ + $R_1C{\equiv}CR_2$ → *trans*-(*cis*)Pt(CO)$(PEt_3)_2$(alkenyl)$^+PF_6^-$

Alkenyl	Solvent	Reaction time	Mp (°C)	Analysis (%) Calcd. C	Calcd. H	Found C	Found H
$(CH_3)C{=}CH(CH_3)$	$CDCl_3$	< 2 days	(dec. ~140)	30.96	5.66	31.28	5.83
$(C_6H_5)C{=}CH(C_6H_5)$	$CDCl_3$	2 days	132–135	41.38	5.27	41.75	5.45
$(CH_3OOC)C{=}CH(CH_3)$	$CDCl_3$	2½ days	124–127	30.73	5.30	31.13	5.29
$(CF_3)C{=}CH(C_6H_5)$	$CDCl_3$	~2 weeks	87–89	34.07	4.68	34.70	4.94
$(CF_3)C{=}CH(CF_3)$	$CDCl_3$	7 days	118–119	26.61	4.07	27.38	4.23
$(CH_3OOC)C{=}CH(COOCH_3)$	$CDCl_3$	2½ days	119–121	30.53	4.99	30.80	5.08

the yields are high (> 60%) and there is no indication of the formation of secondary products. The alkenyl derivatives are all air-stable, white crystalline materials with melting points in the 100–200 °C range.

The second group reactions is described by reaction *B*

[*B*] *trans*-[PtH(CO)$(PEt_3)_2$]$^+PF_6^-$ + $R_1C{\equiv}CR_2$
→ *trans*(*cis*)-[Pt(CO)(PEt_3)(alkenyl)]$^+PF_6^-$

These were all conducted in $CDCl_3$ as solvent, and of course did not require the addition of a neutral ligand such as pyridine for product isolation. Reactions in general were very slow, requiring periods of days or weeks and yields tended to be lower (49–78%) than for reactions with the acetone cation in [*A*]. The products are again all air-stable, crystalline solids with moderately high melting points.

Stereochemistry of Reaction Products

The nmr spectra of the products provided for the ready determination of the stereochemistry at platinum and also the disposition of substituents about the alkenyl C=C bond. The gross geometry about platinum was determined by examination of the P—CH_2—CH_3 signals (11–13). For a *trans* configuration at platinum, a 1:4:6:4:1 quintet was expected and observed. Coupling from the two methylene protons ($J(CH_2$–$CH_3)$ ~8 Hz) equivalent to virtual coupling (12, 14) from two equivalent phosphorus nuclei (J(P–CH_2–CH_3) ~ 8 Hz) produces an overlapping triplet of triplets forming the observed pattern. For a *cis* configuration a 1:2:2:2:1 quintet might be expected but a 1:3:4:4:3:1 sextet was observed. Coupling from the *cis* phosphorus nucleus is apparently too small to be observed and coupling from the other phosphorus is approximately twice that from the methylene protons (J(P–CH_2–CH_3) ~16 Hz; $J(CH_2$–$CH_3)$ ~8 Hz). The resulting overlap of the expected doublet of triplets should have produced the expected 1:2:2:2:1 quintet, but due to the strong *trans* influence of the pyridine ligand, the methyl resonance of the phosphine *trans* to pyridine is shifted about ~8 Hz producing the observed overlapping doublet of pentets.

These assignments could be confirmed by examination of the magnitude of the phosphorus coupling to the vinylic proton. For the *trans* isomer $^4J(P–H_v)$ ~1.5–4 Hz (15, 16). Where observable, this results in a splitting of the vinylic proton resonance into a triplet from virtual coupling to two equivalent phosphorus nuclei. For the *cis* isomer, coupling from the *cis* phosphorus atom is too small to be resolvable, so that the vinylic proton resonance is split into a doublet from coupling to only the *trans* phosphorus nucleus ($^4J(P–H_v)$ ~10 Hz) (7, 17).

The disposition of platinum and hydrogen in the alkenyl function may be determined from the magnitude of $^3J(Pr–H_v)$, for which it has been shown (7, 17–19) that the order observed is *trans* > *cis* ≫ geminal. However, it has also been found (16) that the value of $^3J(Pt–H_v)$ for a particular vinylic configuration varies considerably according to the *trans*-influence of the ligand *trans* to the vinylic group. Thus, for the complexes reported here (Table 3), when the configuration at platinum was *cis* (*i.e.* phosphines *trans* to the vinylic group), the ranges of values are $^3J(Pt–H_{v(trans)})$, 90–120 Hz; $^3J(Pt–H_{v(cis)})$, 35–60 Hz; $^3J(Pt–H_{v(gem)})$ 10–20 Hz. In those of our complexes with a *trans* configuration at platinum (*i.e.* pyridine *trans* to the vinylic group), the ranges are: $^3J(Pt–H_{v(trans)})$, 120–160 Hz; $^3J(Pt–H_{v(cis)})$, 80–105 Hz; and $^2J(Pt–H_{v(gem)})$, 25–30 Hz.

TABLE 3. ^{1}H nmr parameters for $[Ptpy(PEt_3)_2(R_1C{=}CHR_2)]PF_6$

R_1	R_2	Geometry at Pt	Vinyl proton δ	$^3J(Pt\text{–}H_v)$	$^4J(P\text{–}H_v)$	Other couplings
CH_3	CH_3	*trans*	5.4	64		$^3J(H\text{–}H_v)$ 6.4 Hz $^4J(H\text{–}H_v)$ 1.8 Hz
$COOCH_3$	CH_3	*trans*	5.78	82	3	$^3J(H\text{–}H_v)$ 7 Hz
CH_3	$COOH_3$	*trans*	6.12	84		$^4J(H\text{–}H_v)$ 1 Hz
CH_3	C_6H_5	*trans*	6.59	74		$^4J(H\text{–}H_v)$ 1.4 Hz
$COOCH_3$	C_6H_5	*trans*	6.80	92	3	
C_6H_5	C_2H_5	*trans*	5.63	78	1.5	$^3J(H\text{–}H_v)$ 7 Hz
C_2H_5	C_6H_5	*trans*	6.76	74.5	1.5	$^4J(H\text{–}H_v)$ 1.5 Hz
C_2H_5	C_2H_5	*trans*	4.92	70	1.5	$^3J(H\text{–}H_v)$ 7 Hz $^4J(H\text{–}H_v)$ 1.5 Hz
C_6H_5	CF_3	*trans*	5.92	85	1.5	$^3J(F\text{–}H_v)$ 9.9 Hz
CF_3 CF_3	C_6H_5 C_6H_5	*cis* *trans*	Not observable			
CF_3	CF_3	*cis*	6.44	63	10	$^3J(F\text{–}H_v)$ 9.6 Hz
	C_6H_5	*trans*	6.67	100		
CF_3	H	*cis*	5.74	85	1.5	$^3J(F\text{–}H_v)$ 9.9 Hz
H	C_6H_5	*trans*	6.62	72		
$COOCH_3$	$COOCH_3$	*cis*	5.89	60	10	

Consideration of the data in Table 3 shows that the products of reaction *A*, with few exceptions, had the *trans* configuration at the platinum centre. The only instances where *cis* isomers can be isolated as part or all of the product occurred where R_1 and R_2, and in some cases only R_1, was a strongly electron-withdrawing substituent, either $—COOCH_3$ or CF_3. It has been established (7) by variable temperature studies that *cis* isomers are the kinetically controlled products and the *trans* ones are thermodynamically more stable. This point is further verified by a variable temperature ^{1}H nmr study of the reaction of $PtH(PEt_3)_2(H_2O)^+PF_6^-$ and 2-butyne (see below). The nmr parameters of Table 3 also show that all the products have the *cis* arrangement of platinum and the vinylic hydrogen about the double bond.

For the products of symmetrically substituted acetylenes, the nmr parameters thus readily allow for the complete determination of stereochemistry. For products of other acetylenes, further analysis of their nmr spectra is necessary, although in all cases, the data of Table 3 show Pt and the vinylic proton to have the *cis* arrangement about the alkenyl double bond. Thus the proton nmr spectrum of the reaction product of *trans*-$[PtH(PEt_3)_2(acetone)]^+PF_6^-$ with methyl propiolate showed two vinylic proton resonances H_v(**A**) and H_v(**B**) at δ5.78 and δ6.12 respectively, indicating formation of two isomeric products **A** and **B**. For isomer **A**, a 1:3:3:1 quartet of triplets was observed, the quartet splitting of 7 Hz being consistent with coupling of a vinylic proton to a geminal methyl group. The triplet splitting of 3 Hz was attributable to virtual coupling to two phosphorus nuclei, *trans* to each other and *cis* to the vinylic group. Isomer **A** was thus assigned the vinylic configuration $—[(COOCH_3)C{=}CHCH_3]$. For isomer **B**, the observed 1:3:3:1 quartet arose from coupling (~1 Hz) of the vinylic proton to a *trans* methyl group, and coupling to ^{31}P was not resolved. This isomer was therefore assigned the configuration $[—(CH_3)C{=}CH(COOCH_3)]$. Irradiation experiments at the vinylic proton resonances indicated that the vinylic methyl resonances for **A** and **B** were at δ1.88 and δ1.97 respectively and hence obscured by the phosphine ethyl resonances. The $P—CH_2—CH_3$ resonance exhibited a 1:4:6:4:1 quintet at ~δ1.12 indicative of *trans* configurations of the phosphines in both isomers. Integration of the vinylic hydrogen resonances indicate a 5:1 ratio of **A** to **B**, and this was confirmed by the similar integration ratio found for the $—COOCH_3$ resonances at δ3.74 and δ3.59 respectively. Only for isomer **A** was coupling (4 Hz) observed between ^{195}Pt and $—COOCH_3$ which in this isomer is geminal.

For the reaction product obtained with 1-

phenyl-1-propyne, the vinylic proton resonance appeared as a 1:3:3:1 quartet at δ6.59 with coupling to ^{195}Pt (^3J(Pt–H) = 74 Hz) giving rise to satellites of one quarter total intensity. The quartet splitting of 1.4 Hz is that expected for coupling to a *trans* methyl group and the configuration of the vinylic group was therefore assigned as [$(CH_3)C{=}CHC_6H_5$]. The methyl resonance appeared at δ2.25 as a broad 1:4:1 triplet due to coupling with ^{195}Pt (^3J(Pt–H) = 46 Hz); any splitting due to coupling to the vinylic proton was not well resolved. The phosphine P—CH_2—CH_3 resonance was a 1:4:6:4:1 pentet at δ1.12 indicative of *trans* phosphines.

The spectrum of the product obtained with methylphenylpropiolate shows the resonance for the vinylic proton as a broad triplet at δ6.80, with coupling to ^{195}Pt (^3J(Pt–H) = 92 Hz) giving rise to satellites of one-quarter total intensity. The triplet resonance and the magnitude of the splitting, 3 Hz, indicate a *trans* configuration of the phosphines about the platinum. The —$COOCH_3$ resonance appeared as a 1:4:1 triplet at δ3.74 due to coupling to ^{195}Pt. Such coupling has only been observed for configurations containing the Pt and —$COOCH_3$ attached to the same carbon atom (*e.g.* as described above, such coupling is observed for the configuration **1** but not for **2**

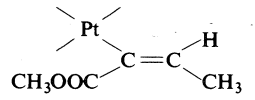

1

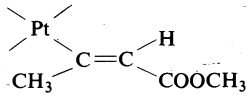

2

The product is therefore tentatively assigned configuration **3**.

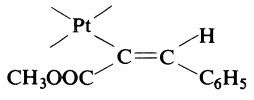

3

The vinylic insertion product of 1-phenyl-1-butyne gave a proton nmr spectrum showing two vinylic proton resonances at δ5.63 and 6.76, indicating the formation of two isomeric products, **A** and **B**, respectively. Satellites of one quarter intensity were observed for each isomer due to coupling to ^{195}Pt. For isomer **A**, the vinylic proton resonance appeared as a triplet of triplets, the larger triplet splitting of 7 Hz being attributable to coupling to a geminal ethyl (*i.e.* methylene) group so that the configuration **4** is assigned.

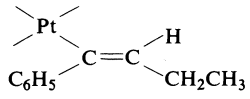

4

The smaller triplet of 1.5 Hz arises from coupling to the two equivalent, mutually *trans* phosphorus nuclei.

For isomer **B**, the vinylic proton resonance appears as a 1:4:6:4:1 pentet. Coupling to the methylene protons of a *trans* ethyl group ~1.5 Hz combined with coupling to the two mutually *trans* phosphines (~1.5 Hz) would lead to a pentet resonance. Isomer **B** is therefore assigned configuration **5**.

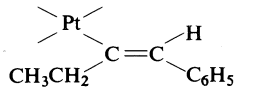

5

Integration of the vinylic resonances gave a ratio of **A**:**B** = 2:3.

The product obtained from 1-phenyl-1-perfluoropropyne showed the presence of three CF_3 resonances in a 1:7:2 ratio at δ − 43.65, −43.95, and − 50.85 respectively in its ^{19}F nmr spectrum, indicating the presence of three isomeric products **A**, **B** and **C**. The **B** resonance at δ − 43.95 was a 1:4:1 triplet of doublets due to coupling to ^{195}Pt = 89 Hz. The chemical shift is that expected for a CF_3 group attached to the α-carbon, the doublet splitting of 9 Hz being due to coupling the phosphine *trans* to the vinylic group. The other phosphine in the *cis* position does not cause observable coupling. Resonance **B** is therefore attributable to *cis*-[Pt{$C(CF_3)$=CHC_6H_5}py$(PEt_3)_2$]$^+PF_6^-$. The **A** resonance at δ − 43.65, a singlet with one quarter intensity satellites (^3J(Pt–H) = 144 Hz), because of its very similar chemical shift, is assigned to the isomer, *trans*-[Pt{$C(CF_3)$=CHC_6H_5}py$(PEt_3)_2$]-PF_6. Vinylic proton resonances for these two isomers were not observed, but presumably were obscured by the broad phenyl resonance at δ7.3, but for **C** a vinylic proton resonance was observed as a quartet of triplets at δ5.92 with satellites of one quarter intensity due to ^{195}Pt coupling. The quartet splitting of 9.9 Hz is consistent with that expected for coupling of the vinylic proton to a geminal CF_3 group, and the further splitting into

triplets would be expected for coupling of the vinylic proton to two *cis* phosphorus nuclei (^4J(P–H) = 1.5 Hz). Product **C** is therefore identified as *trans*-[Pt{C(C_6H_5)=CHCF_3}py-(PEt_3)$_2$]$^+PF_6^-$. The ^{19}F nmr spectrum for this product showed a 1:6:10:7:7:10:6:1 octet at δ − 50.85, this resulting from coupling to ^{195}Pt(^4J(Pt–F) = 7 Hz), to two equivalent P nuclei *cis* to the vinylic group (^5J(P–F) = 3.5 Hz) and to the vinylic proton (^3J(H–F) = 9.9 Hz).

The ^{19}F nmr spectrum of the product obtained with 3,3,3-trifluoropropyne showed the CF_3 resonance as a 1:4:1 triplet of doublets at δ − 52.8. The triplet pattern is due to coupling to ^{195}Pt(^3J(Pt–F) = 69 Hz), the magnitude of which is consistent with other data given above for compounds containing both Pt and CF_3 on the α-carbon. The doublet splitting of 8 Hz is consistent with coupling to one *trans* phosphorus nuclei, thus indicating a mutually *cis* phosphine arrangement. This was confirmed by examination of the ^{1}H nmr spectrum in which the phosphine methyl resonance appeared as a characteristic 1:3:4:4:3:1 sextet at δ1.2. Also in the ^{1}H nmr spectrum, two vinylic proton resonances, H_v(**A**) and H_v(**B**), were observed at δ5.74 and 6.15 with coupling to platinum of 58 Hz and 101 Hz respectively. From the magnitudes of these couplings, assignments could thus be made of H_v(**A**) and H_v(**B**) to protons respectively *cis* and *trans* across the alkenyl bond with respect to platinum, as previously discussed. The H_v(**A**) resonance was a doublet flanked by satellites of one quarter intensity due to coupling to ^{195}Pt. The doublet splitting of 8 Hz arises from coupling to a *trans* phosphine, this again confirming the mutually *cis* arrangement of the two phosphines. As in other comparable cases (21), no coupling of the proton to the *trans* CF_3 group was observable. The H_v(**B**) resonance consisted of a doublet of quartets, flanked by satellites of one quarter intensity due to ^{195}Pt coupling. The quartet splitting of 2 Hz is consistent with coupling of the vinylic proton to a *cis* CF_3 across an alkenyl bond (20). The doublet splitting 16 Hz arises from coupling to the phosphorus *trans* to the alkenyl group.

For the reaction product obtained with phenylacetylene, two vinylic proton resonances, H_v(**A**) and H_v(**B**) in a 1:1 ratio, were observed at δ6.62 and 7.60 respectively. (The product was isolated as the carbonyl cation rather than as the pyridine analog, to avoid overlap of the second vinylic proton resonance with those of pyridine.) The resonance at δ6.62 was a doublet of triplets with satellites of one quarter intensity due to coupling to ^{195}Pt(^3J(Pt–H_v(**A**)) = 60 Hz; 72 Hz with pyridine as *trans* ligand.) The comparable coupling for H_v(**B**) was 17 Hz so that H_v(**A**) and H_v(**B**) were assigned to the *cis* and geminal protons respectively relative to platinum. Moreover the doublet splitting of both H_v(**A**) and H_v(**B**) of 18.5 Hz is fully consistent with coupling between *trans* protons on an alkenyl group. Both H_v(**A**) and H_v(**B**) resonances showed a triplet character due to couplings to two equivalent phosphines *cis* to the alkenyl group. This mutually *trans* geometry of the phosphines is also shown by the phosphine methyl resonance which appeared as the characteristic 1:4:6:4:1 pentet at δ1.12.

For the reaction product with 1-cyclohexanolphenylacetylene the vinylic proton resonance appeared as a broad 1:4:1 triplet at δ6.67 due to coupling with ^{195}Pt(^3J(Pt–H_v) = 100 Hz). The product is assigned the vinylic configuration

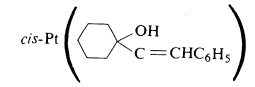

solely on the argument that in related vinylic products containing the =CHC_6H_5 group the vinylic proton resonance shows much the same chemical shift, whereas in cases where the phenyl group is on the α-carbon, this resonance is shifted to much higher field. The phenyl resonance is a broad multiplet centered at δ7.49, and the phosphine methyl resonance as a 1:4:6:4:1 pentet at δ1.01 characteristic of mutually *trans* phosphine ligands.

The reaction with CH≡CCH_2CH_2OH gave a product whose proton spectrum showed a triple hydride resonance at δ − 6.83, flanked by triplet satellites of one quarter intensity due to coupling with ^{195}Pt (^1J(Pt–H) = 616 Hz). The smaller triplet splitting of 18 Hz is indicative of coupling to two equivalent phosphines and this was confirmed by the characteristic 1:4:6:4:1 pentet resonance observed for the phosphine methyl protons at δ1.09. The α-alkoxy protons, —OCH_2R, appeared as a 1:4:1 triplet of triplets at δ5.65 (21) due to coupling to ^{195}Pt (^4J(Pt–H) = 15 Hz). The smaller triplet splitting of 4 Hz is consistent with coupling to the two protons on the β-carbon. The α-carbene protons, —CCH_2R appeared as a 1:4:1 triplet of triplets at δ3.22 due to coupling to ^{195}Pt (^3J(Pt–H) = 14 Hz), and

TABLE 4. Spectroscopic data for $Pt(PEt_3)_2(CO)(alkenyl)^+PF_6^-$

	Infrared			Nuclear magnetic resonance parameters				
				Vinyl			Other	^{19}F
Alkenyl	ν(CO)	ν(C=C)	δ	^3J(Pt–H)	^4J(P–H)	Other	δ	δ (rel. $CFCl_3$)
$CH_3C{=}CHCH_3$	2072	1610	5.38	53	1.6	^3J(H–H) = 5.3	CH_3 1.79 CH_3 1.64	
$(C_6H_5)C{=}CH(C_6H_5)$	2100	1595	6.47	68	N.R.[b]		C_6H_5 7.12	
$(CH_3OOC)C{=}CH(CH_3)$	2095	1600	5.79	69	2.0	^3J(H–H) = 6.9	CH_3OOC 3.64	
$(CF_3)C{=}CH(C_6H_5)$	2113	1592 1570	6.78	73.6	N.R.		C_6H_5 7.26	CF_3 −47.92 ^3J(Pt–F) = 111 J(P–F) N.R.
$(CH_3OOC)C{=}CH(COOCH_3)$	(*trans*)[a] 2116	1591	5.89	74.8	2.1		CH_3OOC 3.77 ^5J(Pt–H) = 2.5 CH_3OOC 3.69	
$(CF_3)C{=}CH(CF_3)$	(*trans*)[c] 2103 2116	1625	6.40	79.5	N.R.	^3J(H–F) = 9.7		CF_3 −50.55 ^3J(Pt–F) = 110 ^5J(F–F) = 12.05 CF_3 −59.33 J(P–F) N.R.
$(CH_3OOC)C{=}CH(COOCH_3)$	(*cis*) 2142	1604	6.21	61.4	8.3 1.0		CH_3OOC 3.75 ^5J(Pt–H) = 1.6 CH_3OOC 3.64	
$(CF_3)C{=}CH(CF_3)$	(*cis*) 2135	1624	6.59	6.5	9.5	J(H–F) = 9.5		CF_3 −53.01 ^3J(Pt–F) = 83, ^4J(P–H) = 6.6 ^5J(F–F) = 12.0 CF_3 −58.79

[a]Geometry about Pt centre.
[b]N.R. = not resolved.
[c]Prepared by reacting CO with *trans*-$Pt(PEt_3)_2(CF_3C{=}CHCF_3)(acetone)^+PF_6^-$.

to the two protons on the adjacent carbon (^3J(H–H) = 1.5 Hz).

The reactions of acetylenes with the platinum(II) carbonyl cation gave products with the *trans*- geometry at platinum with non-activated acetylene or with mildly activated acetylenes, as is shown by the data of Table 4. Reactions with $CH_3C{\equiv}CCH_3$, $C_6H_5C{\equiv}CC_6H_5$, $CH_3C{\equiv}CCOOCH_3$, $CF_3C{\equiv}CC_6H_5$ gave only the *trans* isomers as products, but with more activated acetylenes such as $CH_3OOCC{\equiv}CCOOCH_3$ and $CF_3C{\equiv}CCF_3$, the *cis* isomers are the major products; from relative intensities in their nmr spectra, the relative amounts were, for $CH_3OOCC{\equiv}CCOOCH_3$, 12:1 (*cis*:*trans*) and for $CF_3C{\equiv}CCF_3$, no *trans* isomer was detected. Only for the unsymmetrical acetylenes $CH_3C{\equiv}CCOOCH_3$ and $CF_3C{\equiv}CC_6H_5$ does any question of the geometry of the vinylic group arise, since in all cases the ^3J(Pt–H) and ^4J(P–H) data clearly reveal both the *trans* (or *cis*) geometry at platinum as well as the *cis* arrangement of Pt and H about the C=C bond. For the product with $CF_3C{\equiv}CC_6H_5$, both the chemical shift (Table 4) for the CF_3 group and also the J(Pt–F) value of 111 Hz are indicative of a stereochemistry with CF_3 on the α-carbon. The product with $CH_3OOCC{\equiv}CCH_3$ showed, in its proton spectrum, a coupling of 6.9 Hz between the methyl and vinylic protons consistent with an arrangement containing the methyl group geminal to the vinylic hydrogen.

That the reactions of acetylenes with *trans*-$[PtH(PEt_3)_2(acetone)]^+PF_6^-$ proceed via the same route established previously (4, 6) for olefins is demonstrated by the ^{1}H nmr study of the reaction with 2-butyne in the presence of water. The presence of small amounts of water, which is a better donor than acetone, should allow species such as *trans*-$[PtH(PEt_3)_2(H_2O)]^+$ and its subsequent reaction products to be observed readily. Because of the close proximity of protons in the aquo ligand with the metal centre, they are extremely sensitive to changes in the metal coordination sphere, particularly to the ligand *trans* to the aquo ligand thus providing further information about the stereochemical course of the reaction. At −60 °C, the ^{1}H nmr spectrum (see Fig. 1) of this reaction mixture showed a broad resonance at δ7.10 clearly attributable to coordinated H_2O, in addition to the expected resonances for the phosphine protons, for free water, and for 2-butyne. At high field, in addition to the hydride signal of *trans*-$[PtH(PEt_3)_2(acetone)]^+$ (δ − 24.71, ^1J(PtH) = 1360 Hz, ^2J(PH) = 15 Hz), there was another signal at δ − 24.82 which was assigned to the hydridic hydrogen of *trans*-$[PtH(PEt_3)_2(H_2O)]^+$. At −30 °C, the signal of the coordinated water diminished in intensity, and a new resonance at δ2.21 developed with fine structure due to coupling to ^{195}Pt. This could be assigned to coordinated 2-butyne with ^3J(PtH) = 21 Hz in the species *trans*-$[PtH(PEt_3)_2(C_4H_6)]^+$ (step 1 in Scheme 1). Its hydride signal appears at δ − 12.06 with ^1J(PtH) = 1320 Hz, ^2J(PH) = 13 Hz. At −20 °C, all the resonances associated with *trans*-$[PtH(PEt_3)_2(acetone)]^+$, *trans*-$[PtH(PEt_3)_2(H_2O)]^+$ (δ6.72), and *trans*-$[PtH(PEt_3)_2(C_4H_6)]^+$ (δ2.16) could be observed, as well as new peaks at δ5.50 and δ7.20. The transient existence of the latter two peaks (see below) and the unusual low field of the latter lead us to assign them as the $-C(CH_3){=}CH(CH_3)$ and the coordinated water in *cis*-$[Pt(PEt_3)_2(CH_3C{=}CHCH_3)(H_2O)]^+$ (step 3 in Scheme 1). At 10 °C, isomerization of the *cis* vinyl complex to the *trans* isomer occurred (step 4 in Scheme 1) as is evidenced by the gradual disappearance of the resonance at δ7.20 and the simultaneous appearance of the resonance at δ6.18; the vinyl hydride signal also shifted to slightly higher field to δ5.32. These changes in positions of the resonances are in accordance with the greater *trans*-influence of PEt_3 compared with that of a vinyl group or of water. At 32 °C, the spectrum also showed the presence of *trans*-$[Pt(PEt_3)_2(cis\text{-}C(CH_3){=}CHCH_3)(C_4H_6)]^+$, ($H_v$5.32 with ^3J(PtH) = 90 Hz, and C_4H_6 δ1.91 with J(PtH) masked by the phosphine signals).

This experiment thus provides conclusive evidence for an insertion process (Scheme 1) which is initiated by acetylene displacement of the *trans* ligand, in this case water and acetone. The detection of the existence of the thermodynamically less stable *cis* product, *cis*-$[Pt(PEt_3)_2(cis\text{-}C(CH_3){=}CH(CH_3))(H_2O)]^+$, implies a *trans*-to-*cis* isomerization (step 2, Scheme 1) must have occurred. Interestingly, in this experiment we also observed interaction with a second acetylene unit in the formation of *trans*-$[Pt(PEt_3)_2(cis\text{-}(CH_3){=}CH(CH_3))(C_4H_6)]^+$.

Further evidence for this mechanism comes from the observation that the reaction of the hydrido cation with 3-butyne-1-ol gave the *trans*-hydrido carbene complex, the cyclic carbene resulting from rearrangement of the co-

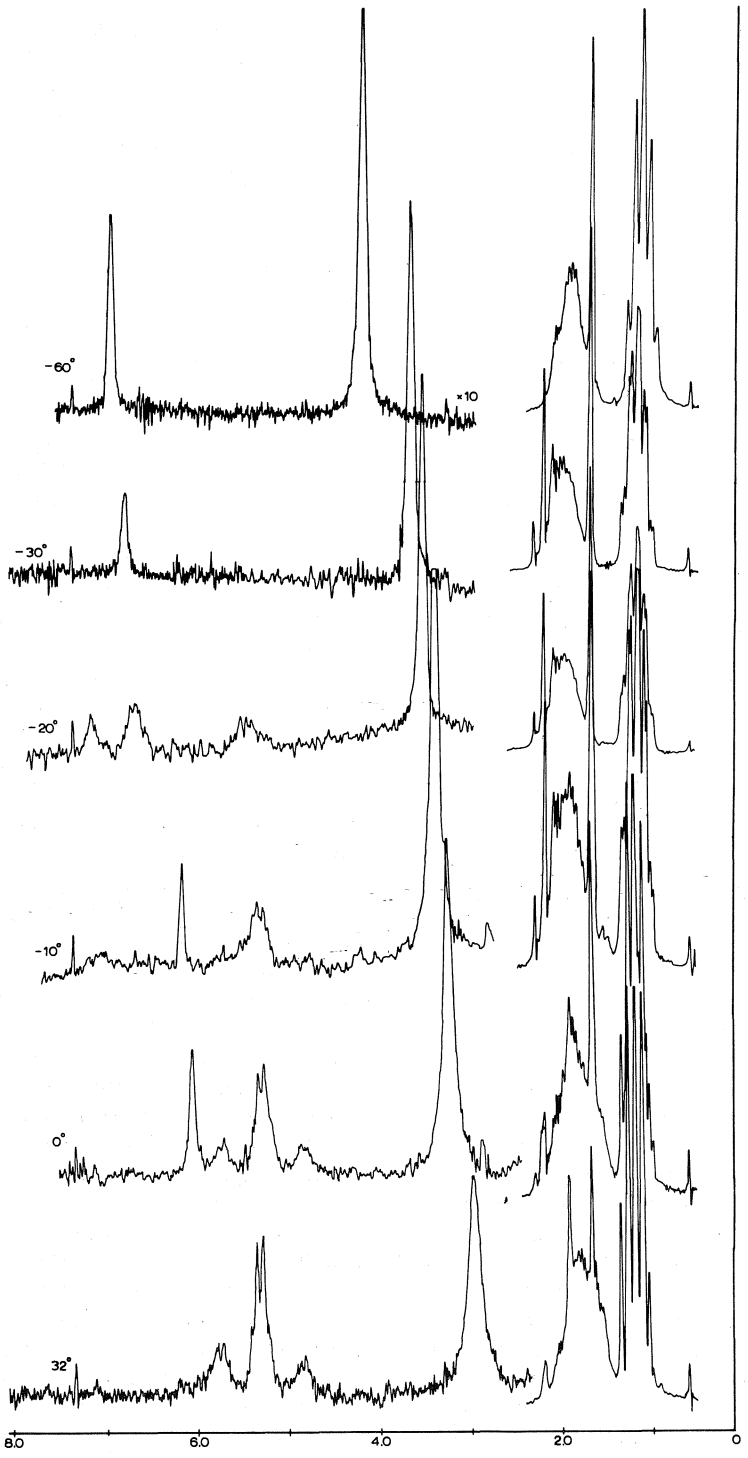

FIG. 1. Variable-temperature ^1H nmr spectrum of a CD_3COCD_3/H_2O solution containing *trans*-$[PtH(PEt_3)_2(acetone)]^+PF_6^-$ and 2-butyne.

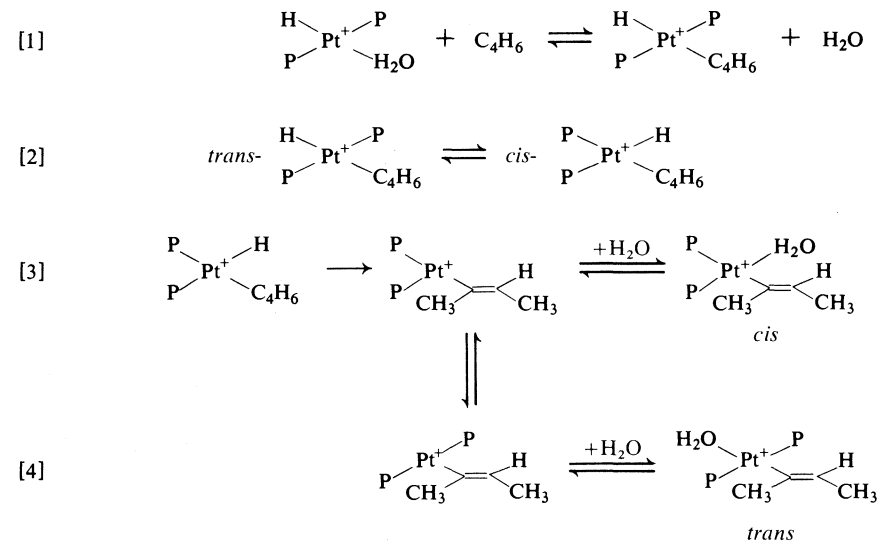

SCHEME 1. Proposed mechanism for the reaction of $PtH(PEt_3)_2(H_2O)^+PF_6^-$ with 2-butyne.

ordinated acetylene. It has previously been found that such carbene formation (for both cyclic and non-cyclic carbenes) occurs via co-ordinated acetylene intermediates for both Pt(II) (22), and rhodium(III) and iridium(III) systems (23).

In contrast, all currently available evidence indicates that the mechanism by which the carbonyl platinum(II) cation undergoes insertion with acetylenes (except for the highly activated perfluorobut-2-yne and dimethylacetylene dicarboxylate) must be described differently. Firstly, reactions with the hydrido(acetone)platinum cation require reaction times in the order of minutes, whereas hydrido(acetone)platinum cations takes days for their completion. Secondly, the reaction products with the hydrido(carbonyl) cation all retain CO as a ligand, and the final stereochemistry at platinum seems to depend on the nature of the acetylene employed. Hence, for reactions of non-activated or only weakly-activated acetylenes with the hydrido(carbonyl) cation where *trans* (at Pt) products are obtained, we conclude that five-coordinate, presumably trigonal bipyramidal intermediates (**6**) are involved,

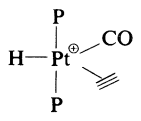

6

With C_4F_6 and dimethylacetylene dicarboxylate, reactions with the hydrido(carbonyl) cation are slower than for the non-activated acetylenes, and *cis*-platinum alkenyl products, rather than *trans*, are formed. We therefore conclude that with these acetylenes, reaction may very well proceed via a four-coordinate cationic mechanism involving the displacement of CO from the coordination sphere by the acetylene. This interpretation is supported by our observation that *trans*-$PtH(PEt_3)_2(acetone)^+PF_6^-$ catalyzes the hydration of dimethylacetylene dicarboxylate in aqueous acetone solution to form dimethyloxosuccinate; *trans*-$PtH(CO)(PEt_3)_2^+PF_6^-$ shows the same catalytic effect when the reaction is carried out in an open atmosphere (under nitrogen purge), but the same compound is catalytically inactive in a closed atmosphere. This indicates that the active catalyst which is generated in an open atmosphere does not contain a CO ligand. We are currently studying further this interesting catalytic hydration reaction.

Again, therefore, as is the case for olefin insertion, the nature of the ligand *trans* to hydride largely determines the mechanistic course of the insertion process. A readily displaced *trans* ligand results in an insertion mechanism which proceeds via a four-coordinate intermediate, while a less readily displaced ligand such as CO requires the involvement of a five-coordinate

intermediate. However, the present results also indicate that the mechanistic pathway is also dependent on the nature of the acetylene. Because of the better coordinating ability of some acetylenes (*e.g.* C_4F_6) compared with olefins, the normally less readily displaced CO ligand may also be displaced in certain cases. Other than this, the behaviour of acetylenes towards insertion into platinum(II) hydrides and presumably other square planar d^8 metal hydrides is essentially the same as that of olefins.

Acknowledgement

The continued financial support of the National Research Council of Canada is gratefully acknowledged.

1. H. C. CLARK and W. S. TSANG. J. Am. Chem. Soc. **89**, 529 (1967).
2. H. C. CLARK, C. R. JABLONSKI, and C. S. WONG. Inorg. Chem. **14**, 1332 (1975).
3. H. C. CLARK, C. R. JABLONSKI, J. HALPERN, A. MANTOVANI, and T. A. WEIL. Inorg. Chem. **13**, 1541 (1974).
4. H. C. CLARK and C. S. WONG. J. Am. Chem. Soc. **96**, 7213 (1974).
5. A. J. DEEMING, B. F. G. JOHNSON, and J. LEWIS. J. Chem. Soc. D, 598 (1970).
6. H. C. CLARK and H. KUROSAWA. Inorg. Chem. **11**, 1275 (1972).
7. H. C. CLARK and C. S. WONG. J. Organomet. Chem. **92**, C31 (1975).
8. M. H. CHISHOLM and H. C. CLARK. Inorg. Chem. **10**, 2557 (1971).
9. H. C. CLARK and R. J. PUDDEPHATT. Inorg. Chem. **10**, 18 (1971).
10. G. W. PARSHALL. Inorg. Synth. **12**, 27 (1970).
11. M. J. CHURCH and M. J. MAYS. J. Chem. Soc. A, 3074 (1968).
12. E. W. RANDALL and D. SHAW. Mol. Phys. **10**, 41 (1965).
13. H. C. CLARK, K. R. DIXON, and W. J. JACOBS. J. Am. Chem. Soc. **90**, 2259 (1968).
14. J. M. JENKINS and B. L. SHAW. J. Chem. Soc. A, 770 (1966).
15. T. G. APPLETON, M. H. CHISHOLM, H. C. CLARK, and K. YASUFUKU. J. Am. Chem. Soc. **96**, 6600 (1974).
16. T. G. APPLETON, M. H. CHISHOLM, H. C. CLARK, and L. E. MANZER. Can. J. Chem. **51**, 2243 (1973).
17. M. A. BENNETT, G. B. ROBERTSON, P. O. WHIMP, and T. YOSHIDA. J. Am. Chem. Soc. **95**, 3028 (1973).
18. B. E. MANN, B. L. SHAW, and N. I. TUCKER. J. Chem. Soc. A, 2667 (1971).
19. B. F. G. JOHNSON, J. LEWIS, J. D. JONES, and K. A. TAYLOR. J. Chem. Soc. Dalton, **34** (1974).
20. T. G. APPLETON, H. C. CLARK, and L. E. MANZER. Coord. Chem. Rev. **10**, 335 (1973).
21. H. C. CLARK and W. S. TSANG. J. Am. Chem. Soc. **89**, 533 (1967).
22. M. H. CHISHOLM and H. C. CLARK. Inorg. Chem. **10**, 1711 (1971).
23. H. C. CLARK and K. J. REIMER. Inorg. Chem. **14**, 2133 (1975).

Chemistry of metal hydrides. Part XX. The nature of the insertion rearrangement of acetylenes with platinum(II) hydrides

T. G. ATTIG,[1] H. C. CLARK,[2] AND C. S. WONG[2]

Department of Chemistry, University of Western Ontario, London, Ont., Canada N6A 3K7

Received July 21, 1976

T. G. ATTIG, H. C. CLARK, and C. S. WONG. Can. J. Chem. **55**, 189 (1977).

The reactions of platinum(II) hydrides, *trans*-$PtHXL_2$, where X = NO_3, Cl or CH_3OH, and L = PEt_3 or tricyclohexylphosphine, with disubstituted acetylenes, $R_1C{\equiv}CR_2$, have been examined under a variety of conditions. From spectroscopic parameters, the gross geometry at platinum as well as the geometry of the resulting alkenyl groups in the products have been determined. The observation that all alkenyl groups have a *cis* geometry is consistent with a migratory insertion step involving a four-centred transition state, in which the disposition of the acetylene relative to the Pt—H bond appears to be dependent on the Pt—H bond polarity. Evidence is presented to demonstrate that this polarity depends on several factors including solvent, and ligands on Pt(II). For L = tricyclohexylphosphine, the occurrence of a side reaction which competes with insertion and which leads to a Pt(0) acetylene complex is also demonstrated, and other interesting reactions are described.

T. G. ATTIG, H. C. CLARK et C. S. WONG. Can. J. Chem. **55**, 189 (1977).

On a étudié, dans diverses conditions, les réactions des hydrures de platine(II), $PtHXL_2$ *trans* (où X = NO_3, Cl ou CH_3OH et L = PEt_3 ou tricyclohexylphosphine) avec les acétylènes disubstitués $R_1C{\equiv}CR_2$. En se basant sur des paramètres spectroscopiques, on a déterminé, pour les produits, la géométrie globale au niveau du platine de même que la géométrie des groupes alkényles résultants. Le fait que tous les groupes alkényles possèdent une géométrie *cis* est en accord avec une étape d'insertion migratoire impliquant un état de transition à quatre centres dans lequel l'orientation de l'acétylène par rapport au lien Pt—H semble dépendre de la polarité du lien Pt—H. On présente des données pour démontrer que cette polarité dépend de plusieurs facteurs incluant le solvant et les ligands attachés au Pt(II). Pour L = tricyclohexylphosphine, l'existence d'une réaction secondaire qui est en compétition avec l'insertion et qui conduit à un complexe Pt(0) acétylène peut aussi être démontrée et on décrit d'autres réactions intéressantes.

[Traduit par le journal]

Introduction

In the preceding and earlier papers (1, 3), the mechanisms of insertion of olefins and acetylenes into the Pt—H bond of platinum(II) hydrides have been discussed with particular reference to the stereochemistry at the platinum centre. Evidence has been presented for a mechanistic pathway which may involve either four- or five-coordinate intermediates, the determining factors being the nature of the ligand *trans* to hydride in the original reactant and the coordinating ability of the organic substrate. This pathway brings the hydridic hydrogen and the coordinated unsaturate into *cis* positions with respect to each other, and it is from this arrangement that the alkyl or alkenyl product is thought to be formed. In the absence of any direct evidence, it has usually been assumed (4) that a simple four-centred transition state is involved. Recent semiempirical SCF-MO calculations (5) appear to be consistent with this, although unfortunately many of the models used for these calculations are inconsistent with recent experimental work (2, 6). The purpose of this paper is to present and discuss evidence concerning the nature of the actual insertion step and of the transition states that may be involved. The reactions of platinum(II) hydrides with disubstituted acetylenes are particularly valuable in this connection, in that their reaction rates can be conveniently followed, and also the nmr parameters of the resulting alkenyl derivatives allow their stereochemistry to be readily determined. It follows that the *cis* or *trans* geometry about the C=C alkenyl bond, and the locations of the acetylenic substituents on the α- and β-carbons of the alkenyl group, as well as the ligand and solvent effects on this stereochemistry, provide considerable information on the nature of the migratory insertion step.

[1]Present address: Department of Chemistry, University of Kentucky, Lexington, Kentucky 40506.

[2]Present address: Department of Chemistry, University of Guelph, Guelph, Ont., Canada N1G 2W1.

TABLE 1. Analytical nmr spectroscopic and other parameters obtained

Reaction	R_1	R_2	Hydride[a]	Solvent[b]	Gross geometry[c]	Yield	M.P. (°C)	Analytical data: Calcd C	Calcd H	Calcd Other	Found C	Found H	Found Other
1	CH_3	C_6H_5	*1*	MeOH MeOD[n]	*trans*	81	103–104	41.30	6.39	2.29(N)	41.70	6.55	2.24(N)
2	CH_3	C_6H_5	*2*	MeOH	*trans*	60	104–105	43.18	6.68	6.08(Cl)	43.55	6.60	6.22(Cl)
3	C_6H_5	CF_3	*1*	MeOH	*trans*	81	140–143	37.96	5.46		38.24	5.73	
4	C_6H_5	CF_3	*2*	MeOH MeOD[x]	*trans*	63	116–118	39.53	5.69		39.67	5.90	
5	C_6H_5	C_6H_5	*2*	MeOH MeOD[n]	*trans*	80	132–133	48.33	6.40		48.71	6.64	
6	CH_3	$COOCH_3$	*1* *3*	MeOH MeOD[x]	*trans* *trans*	71	132–134	34.46	6.29		34.90	6.38	
7	CH_3	$COOCH_3$	*2*	MeOH MeOD[x]	*cis*	71	123–125	36.07	6.54	6.28(Cl)	36.12	6.50	6.19(Cl)
8	CH_3	$COOCH_3$	*1*	C_6H_6	*cis*	Not isolated							
9	CF_3	CF_3	*1* *3*	MeOH MeOD[x]	*cis* *cis*	76	121–123	29.27	4.76		29.56	5.07	
10	CF_3	CF_3	*2* *2*	MeOH MeOD	*cis*	70	132–134	30.50	4.92		30.79	5.06	
11	$COOCH_3$	$COOCH_3$	*1* *3*	MeOH MeOD[x]	*cis* *cis*	48	115–116	33.96	5.86		34.68	6.23	
12	$COOCH_3$	$COOCH_3$	*2*	MeOH MeOD[x]	*cis*	87	136–138	35.43	6.07	5.82(Cl)	35.99	6.08	5.98(Cl)
13	CH_3	CH_3	*3*	MeOD[n]	*trans*	80[d]	111–112	36.82	7.15		37.22	7.49	
14	$COOCH_3$	$COOCH_3$	*4*	CH_2Cl_2	*trans*	80[d]	257–258	53.98	7.87		53.66	8.02	
15	$COOCH_3$	C_6H_5	*4*	CH_2Cl_2	*trans*	76[d]	244–247	56.13[e]	7.70		55.78	7.85	
16	$COOCH_3$ CH_3	CH_3 $COOCH_3$	*4*	CH_2Cl_2	*trans*	75[d]	208–215	55.30	8.26		55.03	8.41	
17	CF_3	CF_3	*4*	CH_2Cl_2	*trans*	56[d]	238–240	50.34	7.08	11.96(F)	50.38	7.22	11.99(F)
18	CF_3	C_6H_5	*4*	CH_2Cl_2	*trans*	64[d]	128–135	56.15	7.54	5.92(F)	56.10	7.77	6.10(F)
19	CH_3	C_6H_5	*4*	CH_2Cl_2	*trans*	77[d]	197–200	58.78[f]	8.46		58.83	8.40	

[a] *1* = *trans*-$PtH(PEt_3)_2NO_3$; *2* = *trans*-$PtH(PEt_3)_2Cl$; *3* = *trans*-$PtH(PEt_3)_2(MeOD)^+PF_6^-$; *4* = *trans*-$PtH(Pcy_3)_2(MeOH)^+PF_6^-$
Vinyl products isolated as the chlorocomplex.
[b] Deuterium exchange reactions: x = exchange, n = no exchange.
[c] Geometry at Pt for insertion product.
[d] As chlorocomplex.
[e] Product analyses as $PtCl(Pcy_3)_2[C(COOCH_3) = CHC_6H_5].0.5CH_2Cl_2$.
[f] Product analyses as $PtCl(Pcy_3)_2[C(CH_3) = CHC_6H_5].CH_3OH$.

Results and Discussion

In addition to the reactions described earlier (1), we have now investigated a substantial number of reactions of disubstituted acetylenes with platinum(II) hydrides. Table 1 gives details of some of the systems examined, the reaction conditions used and the yields and nature of the alkenyl products. The Pt(II) hydrides used contained either triethylphosphine or tricyclohexylphosphine as ligand, the latter introducing additional steric constraints due to its size and also placing greater electron density on Pt because of its higher basicity. Both cationic and neutral hydrides were used, the latter having either NO_3^- or Cl^- as anionic ligand.

As can be seen from Table 1, the yields of the alkenyl products are high, averaging about 70–75% with few exceptions. The reasonable assumption is therefore made that these are generally clean reactions with the alkenyl insertion compounds as the only major products. The rates of these reactions vary substantially. For triethylphosphine cationic hydrides, insertion is often complete in less than 30 min, in contrast to the reactions of neutral chlorides where complete insertion may require 24 h.

the reaction *trans*-$PtHL_2X + R_1C{\equiv}CR_2 \rightarrow PtL_2X$ 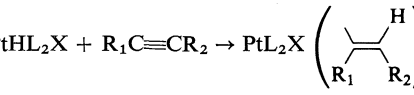

Nuclear magnetic resonance parameters					
	Vinyl				^{19}F
δ	^3J(PH)	^4J(PH)	Other	Other	δ(rel $CFCl_3$)
.64	91.5			CH_3 δ2.22 (^3J(PtH)56.0)	
.75	90.0			CH_3 δ2.27 (^3J(PtH)56.5)	
.85	102.0	1.2	^3J(HF)9.6		−55.50 (^4J(PtF)7.2,^5J(PF)3.6)
.97	98.5	1.2	^3J(HF)3.8		−54.72 (^4J(PtF)7.2,^5J(PF)3.6)
.92	98.2				
.18	88.0		^4J(HH)1.2	$COOCH_3$ δ3.68; CH_3 δ2.63 (^3J(PtH)53.2)	
.22	43.7	10.6	^4J(HH)1.6	$COOCH_3$ δ3.66; CH_3 δ2.70 (^3J(PtH)26.7,^4J(PH)6.7,^4J(HH)1.6)	
.42	38.5	10.0	^4J(HH)1.6	$COOCH_3$ δ3.46; CH_3 δ2.46 (^3J(PtH)27,^4J(PH)6.4)	
.24	56.6	9.5	^3J(HF)9.5		−52.24 (^5J(FF)12.5,^3J(PtF)86.8,^4J(PF)7.6); −59.52 (^4J(PtF)5)
.99	61.8	9.8	^3J(HF)9.8		−51.43 (^5J(FF)12.1,^3J(PtF)91.5,^4J(PF)9.0); −58.66 (^4J(PtF)7,^5J(PF)1.7)
18	55.6	10.0		$COOCH_3$ δ3.82; δ3.70	
07	60.5	10.0		$COOCH_3$ δ3.86; δ3.70	
51[d]	108.5		^3J(HH)6.5 ^4J(HH)1.5	CH_3 δ1.96 (^3J(PtH)54); CH_3 δ1.66	
12	102	1.3		$COOCH_3$ δ3.60; δ3.67 (^5J(PtH)3.0)	
64	107			$COOCH_3$ δ3.53 (^5J(PtH)3.0)	
76	98		^3J(HH)7	$COOCH_3$ δ3.52	
25	83			CH_3 δ2.64 (^3J(PtH)48); $COOCH_3$ δ3.52	
01	101		^3J(HF)10		−49.80 (^3J(PtF)138,^5J(FF)12); −57.75
92	100				−45.85 (^3J(PtF)143.5)
59	88			CH_3 δ2.33 (^3J(PtH)52)	

More electron-withdrawing substituents on the acetylene generally accelerate the insertion process.

The arguments given below depend critically on the determination of the stereochemistry of each reaction product. For these Pt(II) alkenyl derivatives, such stereochemical determination can be achieved unambiguously on the basis of the observed nmr parameters, in terms both of *cis* or *trans* geometry about platinum and of the *cis* or *trans* disposition of Pt and H in the alkenyl group.

Consideration of ^3J(PtH) and ^4J(PH) data distinguishes clearly between the four isomeric possibilities. We have been able to prepare (7) the four possible isomers from the insertion of dimethylacetylene dicarboxylate with Pt(II) hydrides, and the data shown in Table 2, together with previously published values (8–11), allow a ready determination of stereochemistry. Additional information can also be obtained from the relative intensities of the P—CH_2CH_3 quintet signals (8, 12–14) and in favorable cases the couplings of Pt and P with protons on the α-carbon help to confirm stereochemistry. Table 1 contains the nmr data on which the

stereochemical conclusions are based. The question of kinetically or thermodynamically controlled products has been discussed in the preceding paper (1). We further note that although *cis*-to-*trans* isomerization (about the Pt centre) of the complexes in solution can be achieved by heating, no isomerization of the vinylic groups of the complexes shown in Table 2 has been observed even after heating in benzene at 70 °C for 3 days. It is, therefore, concluded that the geometry of the vinylic group is kinetically (rather than thermodynamically) controlled.[3]

In considering the nature of the insertion step, [1], two models may be proposed which rep-

[1] 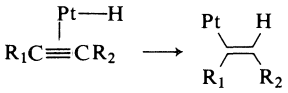

resent the extreme descriptions of the transition state. In the first model, the commonly held assumption is made that the Pt—H bond remains intact while the appropriate geometry of the transition state is attained. This suggests (but does not necessarily require) a four-centred transition state, **1**.

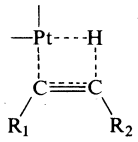

1

In all of the reactions described earlier (1), as well as those given in Table 1, the alkenyl groups have *cis* dispositions. Thus, in Table 1, for *trans* (at Pt) complexes, ^3J(PtH) is in the range 83–108.5 Hz and for *cis* (at Pt) complexes, the corresponding range is 38.6 to 61.8 Hz. These values taken in conjunction with the related ^4J(PH) values, and by comparison with the data of Table 2, confirm the *cis* stereochemistry for the alkenyl group. This is consistent with a four-centred transition state, although not proof of it. It is interesting that a recent theoretical study (5) of the ethylene–

[3]Intramolecular (C=C) isomerizations have been observed for several vinylic Rh(III) complexes (15). But their rearrangements corresponded to a *cis*-to-*trans* isomerization only and required up to 24 h reaction time. This result is, therefore, not in conflict with our conclusion that the *cis* geometry of the vinylic groups in our isolated products are kinetically controlled.

TABLE 2. Coupling constant data for $PtCl(PEt_3)_2(C(COOCH_3)=CH(COOCH_3)$

Isomer	^3J(Pt–H)	^4J(P–H)
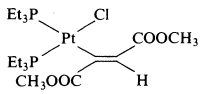	80.5	16.6 1.1
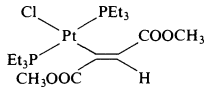	138.0	1.6
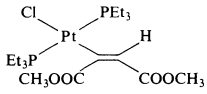	102.2	1.5
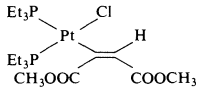	60.5	10.0

platinum hydride insertion, despite weaknesses in the choice of models, also suggests the likelihood of a four-centre transition state.

For a disubstituted acetylene inserting into Pt—H via such a transition complex, the disposition of the acetylenic substituents in the alkenyl product would then depend primarily on the polarity of the Pt—H bond. Since in the majority of products described in Table 1 the more electron-withdrawing acetylenic substituent is placed on the β-carbon, polarization of the transition state may be described by **2**.

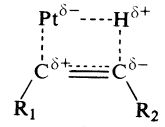

2

However, our data show that there are three circumstances under which the reverse configuration of the alkenyl group with the more electron-withdrawing substituent on the α-carbon may be obtained.

Firstly, this occurs, for example, in the insertion (1) of $CH_3OOCC{\equiv}CCH_3$ or $CF_3C{\equiv}CC_6H_5$ with *trans*-$[PtH(PEt_3)_2(CO)]PF_6$. Since in these reactions CO remains on Pt during the insertion, a five-coordinate intermediate must be involved and in contrast to those cases involving a four-coordinate intermediate these ligands including CO must place much greater electron density into the platinum center.

Secondly, with tricyclohexylphosphine as

ligand, the alkenyl group tends (reactions 15 and 18 of Table 1) to have the stereochemistry with the more electron-withdrawing acetylenic substituent on the α-carbon. Thus from $CH_3C{\equiv}CCOOCH_3$ and *trans*-$[PtH(Pcy_3)_2(MeOH)]PF_6$ in dichloromethane a mixture of the two isomers is obtained, while with $CF_3C{\equiv}CC_6H_5$ the only product has CF_3 on the α-carbon. Since tricyclohexylphosphine is more basic than triethylphosphine (16), it will increase the electron density on platinum as did CO in the previous case. These two effects indicate that with ligands placing increased density on to platinum, a reversal of polarity may occur leading to formation of the other alkenyl isomer.

[2] $Pt^{\delta+}H^{\delta-} + RC{\equiv}CR' \rightarrow$ 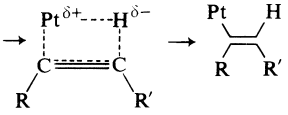 $\rightarrow$

R = $COOCH_3$, or CF_3

The third exceptional circumstance leading to this configuration of the alkenyl group appears to be caused by either an anion or solvent effect. An examination of Table 1 and of previous data (1) shows that for all neutral hydrido-complexes (*i.e.*, X = Cl or NO_3) the resulting alkenyl product always has the more electron-withdrawing acetylenic substituent on the β-carbon. On the other hand, for these neutral complexes the rate of formation of the insertion product does show some solvent dependence; $CH_3C{\equiv}CCOOCH_3$ and *trans*-$[PtHCl(PEt_3)_2]$ react completely within 24 h in methanol, 7 days in $CHCl_3$, but scarcely react at all in acetone, even over a period of 2 weeks. We have no obvious explanation for this unusual effect in acetone.

For cationic hydrido complexes, with methanol or DMSO as solvent, the same geometry of the alkenyl product is obtained as for the neutral complexes, but in acetone or methylene chloride, some of the alkenyl product has the reversed geometry with the more electron-withdrawing substituent on the α-carbon. Obviously, charge separation is less favoured in non-polar solvents, so that the Pt—H bond is less polarized, resulting in less selective insertions. The presence of coordinating anions may also play a role in affecting the polarity of the Pt—H bond, and we tentatively attribute this to an ion-pairing effect, $\overset{\delta-}{Pt}—\overset{\delta+}{H}—Cl^-$.

It is interesting that in protonation studies of $Pt(PPh_3)_2(CH_3C{\equiv}CC_6H_5)$, Shaw and coworkers report (9), without comment, the formation of the two alkenyl derivatives containing $Pt[C(CH_3){=}CHC_6H_5]$ and $Pt[C(C_6H_5){=}CHCH_3]$. From our results as described above, it is clear that by appropriate ligand and solvent changes the polarity of the Pt—H bond can be readily reversed so that the formation of one or other alkenyl isomer can be achieved in a controlled fashion.

The second model for the insertion step involves actual migration of the hydridic hydrogen to the coordinated acetylene. In its extreme form, it could be regarded as a stepwise process involving prior cleavage of the Pt—H bond. Such bond cleavage might be heterolytic or homolytic; the latter possibility will be considered in a later paper.

That facile Pt—H cleavage may occur in the course of such insertion reactions can be demonstrated from reactions 1 and 2 of Table 3. In particular, treatment of *trans*-$[PtH(Pcy_3)_2(MeOH)]PF_6$ with $CF_3C{\equiv}CCF_3$ or $H_3COOCC{\equiv}CCOOCH_3$ was found to be markedly solvent dependent. In dichloromethane the *cis*-alkenyl insertion product is obtained, but in a 1:8 dichloromethane:methanol mixture the platinum(0) acetylene complex, $(Pcy_3)_2Pt(RC{\equiv}CR)$, R = CF_3, or $COOCH_3$, is immediately precipitated. If this precipitate is not removed and more dichloromethane is added to the solvent mixture, the precipitate re-dissolves and the final product is the expected *cis*-alkenyl insertion derivative.

[3] *trans*-$[PtH(Pcy_3)(MeOH)]PF_6 + RC{\equiv}CR \xrightarrow[NaCl]{CH_2Cl_2}$ *trans*- 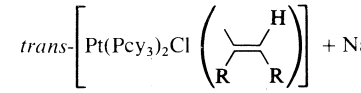 + $NaPF_6$

1:8 CH_2Cl_2:MeOH ↘ ↗ CH_2Cl_2

$Pt(Pcy_3)_2(RC{\equiv}CR) + H^+ + PF_6^-$

TABLE 3. Reactions of *trans*-PtH(CH_3OH)(PCy_3)$_2PF_6$ with $R_1C{\equiv}CR_2$ in methanol

No.	R_1	R_2	Product	Yield (%)	MP (°C)	Analysis Calc. C	Calc. H	Calc. F	Found C	Found H	Found F	Nuclear magnetic resonance parameters ^1H	Nuclear magnetic resonance parameters ^{19}F
1	$COOCH_3$	$COOCH_3$	$Pt(PCy_3)_2[CH_3COOC{\equiv}CCOOCH_3]$	81	212–215	56.17	8.08		56.11	8.33		δ3.77s, $COOCH_3$	
2	CF_3	CF_3	$Pt(PCy_3)_2[CF_3C{\equiv}CCF_3]$	81		52.34	7.25	12.42	53.38	8.10	12.40		δ52.65, CF_3, *J*(Pt–F) 58.8 Hz, *J*(P–F) 9.8 Hz
3	CF_3	C_6H_5	*trans*-$PtH(PCy_3)_2[C(CF_3){=}C(OCH_3)CF_3]$	70	210–211	54.12	7.44	5.46	54.59	7.56	5.32[a]	δ−10.36, Pt—*H*, *J*(Pt–H) 620 Hz, *J*(P–H) 16 Hz, *J*(HF) 3 Hz; δ3.46s, OCH_3	δ46.36, C*F*, *J*(Pt–F) 101.5 Hz, *J*(F–H) 3 Hz
4	CH_3	CH_3	*trans*-$[PtH(CH_3C{\equiv}CCH_3)(PCy_3)_2]PF_6$	92	153–157	50.25	7.70		50.12	7.74		δ−11.53, Pt—*H*, *J*(Pt–H) 1300 Hz, *J*(PH) 14 Hz	
5	$COOCH_3$	C_6H_5	$C_6H_5COCH_2COOCH_3$			67.41	5.66		68.11	6.10		[b]*keto* δ3.97s, CH_3; δ3.72s, $COOCH_3$ *enol* δ12.45s, O*H*; δ5.63s C*H*; δ3.72s, $COOCH_3$	
			Z and E, $C_6H_5C(OCH_3){=}CHCOOCH_3$			68.74	6.30		68.64	6.53		δ5.45s olefinic C*H*; δ3.78s, δ3.68 OCH_3 δ5.18s olefinic C*H*; δ3.73s, δ3.53s OCH_3	

[a]As the CH_2Cl_2 solvate.
[b]79% keto, 21% enol.

Also, although *trans*-$[PtH(Pcy_3)_2(MeOH)]^+$ in methanol-*d* shows no H–D exchange over a 3 h period, when the above reaction with $H_3COOCC{\equiv}CCOOCH_3$ is carried out in a 1:1 mixture of CH_3OD and CH_2Cl_2 (the composition of the solvent mixture chosen so as to prevent actual precipitation of the Pt(0) acetylene complex) the *cis*-alkenyl insertion product has an 85% deuterium incorporation.

An obvious interpretation is that the insertion process occurs by a sequence of steps involving (*a*) reductive elimination of H^+ and formation of the Pt(0) complex, (*b*) rapid H–D exchange between the H^+ and the deuterated methanol solvent, (*c*) protonation of the coordinated acetylene to give the alkenyl 'insertion' product. The insertion 'step' is then the summation of a series of reactions and does not involve a four-centred transition state. It is by no means clear, however, that the conversion of the Pt(0) complex to the *cis*-alkenyl product involves protonation of the coordinated acetylene; it is at least equally probable that protonation involves reformation of the Pt—H bond and that insertion occurs *only* via a four centre transition state to give the *cis*-alkenyl product. This would also imply that in the majority of cases an equilibrium exists between the hydrido(acetylene)platinum(II) cation and the platinum(0) acetylene complex, and that the low solubility of the latter compound favors its precipitation in methanol-rich solvent mixtures.

[4] *trans*-$[PtH(Pcy_3)_2(MeOH)]PF_6$ + $RC{\equiv}CR \rightarrow$ *trans*-$[PtH(Pcy_3)_2(RC{\equiv}CR]PF_6$

[5] $[PtH(Pcy_3)_2(RC{\equiv}CR)]PF_6 \rightleftharpoons Pt(Pcy_3)_2(RC{\equiv}CR) + H^+ + PF_6^-$

[6] $[Pt(CR{=}CHR)(solvent)(Pcy_3)_2]PF_6$

Although the starting compound of equilibrium [5] has the *trans* configuration, this geometry at platinum is not necessarily regenerated in the protonation of the Pt(0) acetylene complex, nor does the product of [6] necessarily have the *trans* geometry.

This is consistent with other results given in Table 1 concerning acetylene insertions conducted in methanol-*d*. While none of these hydridoplatinum(II) species undergo H–D exchange themselves with methanol-*d*, the presence of acetylene does induce such exchange but only in some instances. As Table 1 indicates, for such systems with $CF_3C{\equiv}CC_6H_5$, $CF_3C{\equiv}CCF_3$, $CH_3C{\equiv}CCOOCH_3$, or $CH_3OOCC{\equiv}CCOOCH_3$, H–D exchange was essentially complete (*i.e.*, D incorporation into the alkenyl group better than *ca.* 90%) but for acetylenes such as $CH_3C{\equiv}CC_6H_5$, $C_6H_5C{\equiv}CC_6H_5$, or $CH_3C{\equiv}CCH_3$, no such exchange occurred (*i.e.*, D incorporation into the alkenyl group less than *ca.* 10%). Apparently, the generalization can be made that H–D exchange only occurs in those systems in which the acetylene has electron-withdrawing substituents. This can be explained in terms of the equilibria:

[7] *trans*-$[PtH(PR_3)_2X] + R_1C{\equiv}CR_2 \rightleftharpoons$ *trans*-$[PtH(PR_3)_2(R_1C{\equiv}CR_2)]X \rightleftharpoons Pt(PR_3)_2(R_1C{\equiv}CR_2) + H^+ + X^-$

The presence of acetylenic electron-withdrawing substituents assists in the stabilization of both hydridoacetylenic cations and of Pt(0) acetylene complexes, thus pushing the overall equilibria in the direction most favorable for H–D exchange with the methanol-*d* solvent. For the reactions described above involving tricyclohexylphosphine hydrido cations, not only are the acetylenes strongly electron-withdrawing, but also the low solubilities of the corresponding bis(tricyclohexylphosphine)acetyleneplatinum(0) complexes push the equilibria to the right favoring extensive H–D exchange. With regard to the actual insertion process then, such formation of Pt(0) acetylene complexes appears to represent only a side reaction which is relatively unimportant in terms of the mechanism of formation of alkenyl insertion products.

For the tricyclohexylphosphine complex a number of other interesting reactions were observed. With 2-butyne, in dichloromethane, reaction (see Table 3) with *trans*-$[PtH(Pcy_3)_2(MeOH)]PF_6$ gave the hydrido(acetylene) cation, *trans*-$[PtH(Pcy_3)(CH_3C{\equiv}CCH_3)]^+$. In the preceding paper (1), we reported that with triethylphosphine hydridoplatinum(II) species, the existence of the analogous hydrido(acetylene) cation could only be observed at low temperature. In the present case, presumably the steric bulk of the tricyclohexylphosphine ligands stabilize the hydrido(acetylene) species. Presum-

ably, also, insertion proceeds via the previously described mechanism involving an isomerization to the *cis*-platinum complex and insertion to the alkenyl product. Since platinum(II) species are known (19) with two tricyclohexylphosphine ligands in approximately *cis* positions, the bulk of the phosphine might well slow this *trans–cis* isomerization but not totally prevent it. The formation of a $Pt(Pcy_3)_2$(acetylene) complex and its recombination with H^+ possibly provide a route for the *trans*-to-*cis* isomerization of the $PtH(Pcy_3)_2$(acetylene) complex. If this is the case, then the inability of $CH_3C{\equiv}CCH_3$ to insert is because of its inability to form the Pt(0) acetylene complex. It is interesting also that reactions in methanol-rich solvent mixture of *trans*-$[PtH(Pcy_3)_2(MeOH)]^+$ with $CH_3C{\equiv}CC_6H_5$ and $CH_3C{\equiv}CCH_3$ gave only starting materials. This is consistent with the relatively low donor properties of these acetylenes and their inability to displace methanol from platinum.

In 1:8 dichloromethane methanol mixtures, the reaction of *trans*-$[PtH(Pcy_3)_2(MeOH)]PF_6$ with $C_6H_5C{\equiv}CCOOCH_3$ led to interesting products (Table 3). An approximately 25-fold excess of the latter acetylene was converted at room temperature to a mixture of **E** and **Z** isomers of $C_6H_5(CH_3O)C{=}CHCOOCH_3$, and $C_6H_5COCH_2COOCH_3$. The mode of formation of the latter compound as well as its abundance relative to the other purely organic products have yet to be determined. However, it is clear that the above two olefinic isomers result from the catalyzed addition of methanol and water to the acetylene. The platinum-containing catalyst is recovered as

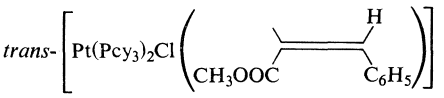

with the final addition of NaCl. This catalyzed conversion of the acetylene therefore appears to be essentially quantitative other than the amount consumed in the Pt(II)-alkenyl formation. At the present stage, the efficiency of the original hydride as catalyst has yet to be determined and indeed the fact that the actual catalyst is the original hydride must be verified. Similar behaviour is observed for reactions with $CH_3C{\equiv}CCOOCH_3$, while using ethanol rather than methanol appears to lead to the ethoxy analogues. Work on these reactions is continuing. In this connection, it is interesting to note the formation of *trans*-$PtH[C(CF_3){=}C(OCH_3)(C_6H_5)(Pcy_3)_2$ from the reaction of the cationic hydride with $CF_3C{\equiv}CC_6H_5$ in methanol. This presumably results from nucleophilic attack on the coordinated acetylene and is comparable to the analogous reactions (18) of cationic methylplatinum(II) species.

Experimental

The general procedures and instrumentation employed in these studies have been described previously (see, for example, refs. 3, 8, and 11). Previously reported methods (17, 19) were used for the preparation of *trans*-$[PtHCl(PEt_3)_2]$ and *trans*-$[PtHCl(Pcy_3)_2]$. The source and method of purification for each acetylene were as follows: $CF_3C{\equiv}CC_6H_5$ was prepared and purified as described (20); $CH_3C{\equiv}CCOOCH_3$ was obtained by the methylation of tetrolic acid (Farchan) with methanol using sulfuric acid as catalyst and was purified by distillation under partial vacuum and characterized by nmr; $CF_3C{\equiv}CCF_3$ (PCR Inc.) was used without further purification; $CH_3C{\equiv}CC_6H_5$ and $CH_3OOCC{\equiv}CCOOCH_3$ (Aldrich) were distilled before using, and $PhC{\equiv}CPh$ was purified by recrystallization from methanol; 2-butyne was kindly provided by Dr. K. Yasufuku.

Preparation of Pt(alkenyl)Cl(PEt$_3$)$_2$ Derivatives

To a solution of 150 mg of *trans*-$PtHCl(PEt_3)_2$ in 1 ml of methanol was added two- to three-fold excess of acetylene. After 24 h, the solution was evaporated to dryness and the residue recrystallized from an appropriate solvent mixture ($CH_3C{\equiv}CC_6H_5$, ether/hexane; $CH_3C{\equiv}CCOOCH_3$, methanol/ether/hexane; $C_6H_5C{\equiv}CC_6H_5$, methanol; $CH_3OOCC{\equiv}CCOOCH_3$, methanol/ether/hexane; $CF_3C{\equiv}CC_6H_5$, methanol/pentane).

Preparation of trans-Pt(CH$_3$C=CHCH$_3$)Cl(PEt$_3$)$_2$

246 mg of *trans*-$PtHCl(PEt_3)_2$ in 9 ml of methanol was treated with 126 mg $AgPF_6$ in 1 ml of methanol. The white precipitate of AgCl was separated by centrifugation. Excess of 2-butyne (70 μl) was then added. After 1 h, the reaction mixture was quenched with an aqueous methanolic solution of NaCl. The solution was evaporated to dryness under vacuum, extracted with ether and passed through a short florisil column. Recrystallization in acetone/H_2O yield *trans*-$Pt(CH_3C{=}CHCH_3)Cl(PEt_3)_2$ as white crystals 220 mg (80%).

Preparation of cis-Pt(CF$_3$C=CHCF$_3$)X(PEt$_3$)$_2$ (X = Cl or NO$_3$)

C_4F_6 was passed into a solution of 150 mg of *trans*-$PtHX(PEt_3)_2$ in methanol for 5 min. Evaporation of the solvent after 3 h (X = Cl; ½ h for X = NO_3) gave white crystals which were recrystallized from methanol/ether/hexane (for X = Cl; CH_2Cl_2/ether for X = NO_3).

Preparation of Pt(alkenyl)NO$_3$(PEt$_3$)$_2$

To a solution of 150 mg of *trans*-$PtH(NO_3)(PEt_3)$ in 1 ml of methanol was added 1 equivalent of acetylene. After ½ h, the solution was evaporated to dryness

under vacuum and chromatographed through a florisil column with benzene. After evaporation to dryness under vacuum, the residue was recrystallized from an appropriate solvent mixture (for $CH_3C{\equiv}CCOOCH_3$, CH_2Cl_2/ether/hexane, for $CH_3OOCC{\equiv}CCOOCH_3$, methanol/ether/hexane; for $CH_3C{\equiv}CC_6H_5$, ether/hexane; for $CF_3C{\equiv}CC_6H_5$, methanol).

Preparation of $PtCl(CR_1{=}CHR_2)(Pcy_3)_2$

To a solution of 250 mg of *trans*-$PtH(Pcy_3)_2(CH_3OH)PF_6$ (prepared from *trans*-$PtHCl(Pcy_3)_2$ as previously described (16)) in 5 ml CH_2Cl_2 was added 1 equivalent of acetylene. After being stirred for 1 h, a methanolic NaCl solution was added and the solvent was removed. The product was extracted with CH_2Cl_2, and precipitated as white crystals upon the addition of hexane or methanol.

Preparation of $PtCl(CF_3C{=}CHCF_3)(Pcy_3)_2$

In a thick-walled nmr tube containing 200 mg of *trans*-$PtH(Pcy_3)_2(CH_3OH)PF_6$ in 0.5 ml CH_2Cl_2, were condensed 2 equivalents of hexafluoro-2-butyne at -196 °C. The tube was sealed and allowed to warm to room temperature and to stand for 12 h. After similar working with methanolic NaCl the white crystals of $PtCl(CF_3C{=}CHCF_3)(Pcy_3)_2$ were obtained upon addition of methanol.

Preparation of $Pt(Pcy_3)_2(CF_3C{\equiv}CCF_3)$

In a thick-walled nmr tube containing 200 mg (0.252 mmol) of *trans*-$PtH(Pcy_3)_2(CH_3OH)PF_6$ in 0.25 ml CH_2Cl_2 and 1 ml CH_3OH was condensed 1.5 equivalents of hexafluoro-2-butyne at -196 °C and the tube sealed. After standing at room temperature for 1 day the tube was opened and the solution concentrated to afford 196 mg (81%) of white crystals of $Pt(Pcy_3)_2(CF_3C{\equiv}CCF_3)$; $\nu(C{\equiv}C)_{Nujol}$ 1727 cm^{-1}.

Preparation of $Pt(Pcy_3)_2(CH_3CO_2C{\equiv}CCO_2CH_3)$

To a solution of 100 mg (0.126 mmol) of *trans*-$PtH(Pcy_3)_2(CH_3OH)PF_6$ in 1 ml CH_2Cl_2 and 10 ml CH_3OH were added 15.5 µl of dimethylacetylenedicarboxylate. After 5 min the product began precipitating from the solution as white crystals. Recrystallization from CH_2Cl_2–hexane afforded 91.7 mg (81%) of $Pt(Pcy_3)_2(CH_3CO_2C{\equiv}CCO_2CH_3)$ $\nu(C{\equiv}C)_{Nujol}$ 1768 cm^{-1}, ν(CO) 1677, 1693 cm^{-1}.

When CH_2Cl_2 is added to the reaction mixture, after precipitation of $Pt(Pcy_3)_2(CH_3CO_2C{\equiv}CCO_2CH_3)$, to redissolve the precipitate and the solution allowed to stir for 2 h, the vinylic product *trans*-$PtCl(C(CO_2CH_3){=}CHCO_2CH_3)(Pcy_3)_2$ is obtained after methanolic NaCl workup.

Preparation of $trans\text{-}PtCl(C(CO_2CH_3){=}CDCO_2CH_3)(Pcy_3)_2$

To a solution of 177 mg *trans*-$PtH(Pcy_3)_2(CH_3OH)PF_6$ in 1 ml CH_2Cl_2 and 2 ml CH_3OD were added 1 equivalent of dimethylacetylenedicarboxylate. After stirring for 1 h the reaction mixture was quenched with methanolic NaCl and worked up as above to afford 151 mg (85%) of *trans*-$PtCl(C(CO_2CH_3){=}CDCO_2CH_3)(Pcy_3)_2$ containing 85% deuterium on the β-carbon at the vinyl group as determined from relative intensities in its ^1H nmr spectrum.

Preparation of $trans\text{-}PtH(C(CF_3){=}C(OCH_3)(C_6H_5))(Pcy_3)_2$

To a solution of 295 mg of *trans*-$PtH(Pcy_3)_2(CH_3OH)PF_6$ in 2 ml CH_2Cl_2 and 6 ml methanol was added 1 equivalent of $CF_3C{\equiv}CC_6H_5$. The solution was allowed to stir for 2 days during which the product slowly precipitated from the solution. The solution was concentrated slightly and the white crystals filtered to afford 329 mg (70%) of *trans*-$PtH(C(CF_3){=}C(OCH_3)(C_6H_5))(Pcy_3)_2{\cdot}CH_2Cl_2$. $\nu(Pt{-}H)_{Nujol}$ 2071 cm^{-1}.

Preparation of $[trans\text{-}PtH(CH_3C{\equiv}CCH_3)(Pcy_3)_2]PF_6$

A suspension of 236 mg of *trans*-$PtH(Pcy_3)_2(CH_3OH)PF_6$ in 5 ml 2-butyne was stirred for 2 days. The white crystals were filtered to afford 223 mg (92%) of *trans*-$PtH(CH_3C{\equiv}CCH_3)(Pcy_3)_2PF_6$. $\nu(PtH)_{Nujol}$ 2206 cm^{-1}.

Reaction of $CH_3CO_2C{\equiv}CC_6H_5$ *with* $trans\text{-}PtH(Pcy_3)_2(CH_3OH)PF_6$ *in* CH_3OH

To a solution of 200 mg of *trans*-$PtH(Pcy_3)_2(CH_3OH)PF_6$ in 1 ml CH_2Cl_2, 10 ml CH_3OH, was added 4 ml of $CH_3CO_2C{\equiv}CC_6H_5$ and the solution was allowed to stir at room temperature for 4 days. The solvent was removed and the organic products were vaccum distilled from the residue at 88 °C to afford a mixture of methyl benzoylacetate and **Z** and **E** methylmethoxycinnamate.

Deuterium Exchange Experiments

trans-$PtH(PEt_3)_2(MeOD)PF_6$ was prepared by the addition of 1 equivalent of $AgPF_6$ to a solution of *trans*-$PtHCl(PEt_3)_2$ in methanol-*d*. After the removal of the AgCl, slight excess of acetylene was introduced. After 1 h the reaction mixture was evaporated to dryness and its nmr spectrum recorded in $CDCl_3$. The absence of an alkenyl proton signal in the product spectrum indicated exchange.

The exchange reactions of the nitrato and chloro complexes were carried out as described above for the preparation of the corresponding vinyl complexes except that methanol-*d* was used instead of methanol. The nmr spectrum was recorded in $CDCl_3$.

Acknowledgement

The financial support of this work by the National Research Council of Canada is gratefully acknowledged.

1. H. C. Clark, P. L. Fiess, and C. S. Wong. Can. J. Chem. This issue.
2. H. C. Clark and C. S. Wong. J. Am. Chem. Soc. **96**, 7213 (1974).
3. H. C. Clark, C. R. Jablonski, and C. S. Wong. Inorg. Chem. **14**, 1322 (1975).
4. M. L. H. Green and D. J. Jones. *In* Advances in inorganic chemistry and radiochemistry. Vol. 7. *Edited by* H. J. Emeleus and A. G. Sharpe. Academic Press, New York. 1965.
5. S. Sakaki, H. Kato, H. Kanai, and K. Tarama. Bull. Chem. Soc. Jpn. **48**, 813 (1975).
6. H. C. Clark, C. R. Jablonski, J. Halpern, A. Mantovani, and T. A. Weil. Inorg. Chem. **13**, 1541 (1974).
7. C. S. Wong. Unpublished results.

8. H. C. CLARK and C. S. WONG. J. Organomet. Chem. **92**, C31 (1975).
9. B. E. MANN, B. L. SHAW, and N. I. TUCKER. J. Chem. Soc. A, 2667 (1971).
10. M. A. BENNETT, G. B. ROBERTSON, P. O. WHIMP, and T. YOSHIDA. J. Am. Chem. Soc. **95**, 3028 (1973).
11. T. G. APPLETON, M. H. CHISHOLM, H. C. CLARK, and L. E. MANZER. Can. J. Chem. **51**, 2243 (1973).
12. E. W. RANDALL and D. SHAW. Mol. Phys. **10**, 41 (1965).
13. M. J. CHURCH and M. J. MAYS. J. Chem. Soc. A, 3074 (1968).
14. H. C. CLARK, K. R. DIXON, and W. J. JACOBS. J. Am. Chem. Soc. **90**, 2259 (1968).
15. D. W. HART and J. SCHWARTZ. J. Organomet. Chem. **87**, C11 (1975).
16. W. A. HENDERSON, JR. and C. A. STREULI. J. Am. Chem. Soc. **82**, 5791 (1960).
17. T. G. ATTIG and H. C. CLARK. Can. J. Chem. **53**, 3466 (1975).
18. M. H. CHISHOLM and H. C. CLARK. Inorg. Chem. **10**, 2557 (1971).
19. J. CHATT and B. L. SHAW. J. Chem. Soc. 5075 (1962).
20. L. M. YAGUPOL'SKII and Y. A. FIALKOV. Zh. Obshche; Khim. **30**, 1291 (1960).

The silver–pyrazole electrode and its application to determine the stability of Cd(II), Zn(II), Ni(II), Co(II) pyrazole complexes

MARIE-JOSÉ BLAIS AND GUY BERTHON[1]

Laboratoire de Thermodynamique Chimique et Electrochimie de l'Université, 40, Avenue du Recteur Pineau, 86022 Poitiers, France

Received July 22, 1976

MARIE-JOSÉ BLAIS and GUY BERTHON. Can. J. Chem. **55**, 199 (1977).

The silver–pyrazole metal-complex electrode was investigated and used to determine free concentrations of pyrazole in the presence of Cd^{2+}, Zn^{2+}, Ni^{2+}, or Co^{2+} ion, under different pyrazole/divalent metal concentration ratios. The stability constants of the complexes formed between these ions and pyrazole were calculated.

MARIE-JOSÉ BLAIS et GUY BERTHON. Can. J. Chem. **55**, 199 (1977).

L'électrode métal-complexe argent–pyrazole a été étudiée et utilisée pour déterminer les concentrations de pyrazole à l'équilibre en présence des ions Cd^{2+}, Zn^{2+}, Ni^{2+}, Co^{2+}, pour différents rapports de concentrations globales ligand/métal divalent. Les constantes de stabilité des complexes formés entre ces ions et le pyrazole ont été calculées.

Introduction

The proton ionisation constant of pyrazole is low (pK_a about 2.5 (1)) and hence its determination in solution is not easy by means of classical acid–base titration.

Indeed, two kinds of difficulties appear in such a case: the first arises from the closeness of the pK_a to the acidic pH limit of the solution, which reduces the possibility of accurate determination of the equivalence volume, even if the Gran procedure is used; the second is occasioned by the poor reproductibility of glass electrode measurements in the very acidic medium obtained at the end of the titration. In partially aqueous or non-aqueous solvents, the problem is still more complicated because of the necessary choice of an appropriate pH scale.

The usefulness of a selective electrode, which could be directly used as an indicator of pyrazole, is therefore evident.

In the present work, such an indicator is the Ag/Ag^+, pyrazole electrode.

First, we calculated the stability constants of the complexes formed between silver ion and pyrazole, which characterize the standard potential of this electrode. Then, we tested the reliance of the method by verifying its accuracy in some determinations of pyrazole in solutions of known titre.

Finally, we determined free concentrations of

[1]To whom correspondence should be addressed.

TABLE 1. Application of the silver–pyrazole electrode to some pyrazole determinations

$E_{[9]}-E_{[10]}$ (mV)	$C_A \times 10^3$ (mol l^{-1})	$C_{A(calc.)} \times 10^3$ (mol l^{-1})	$\Delta C_A/C_A$ (%)
14.30	3.846	3.829	−0.44
21.20	5.660	5.668	+0.14
27.20	7.407	7.369	−0.51
32.75	9.091	9.060	−0.34
37.50	10.714	10.617	−0.90
38.10	10.714	10.822	+1.01
42.05	12.281	12.218	−0.51
42.55	12.281	12.401	+0.98
46.00	13.793	13.705	−0.64
46.40	13.793	13.861	+0.49
49.55	15.254	15.126	−0.84
49.95	15.254	15.292	+0.25
52.90	16.667	16.551	−0.69
53.40	16.667	16.771	+0.62
55.90	18.033	17.897	−0.75
56.30	18.033	18.081	+0.27
58.40	19.355	19.416	+0.31
61.05	20.634	20.583	−0.25
63.65	21.875	21.729	−0.67
63.95	21.875	21.889	+0.06
65.85	23.077	22.912	−0.71
66.25	23.077	23.141	+0.28
67.85	24.242	24.035	−0.85
68.35	24.242	24.327	+0.35
70.30	25.373	25.474	+0.40
70.50	25.373	25.594	+0.87
71.80	26.470	26.377	−0.35
72.10	26.470	26.570	+0.38
73.80	27.536	27.636	+0.36
73.90	27.536	27.682	+0.53
75.55	28.571	28.765	+0.68
75.45	28.571	28.703	+0.46

pyrazole in the presence of Cd^{2+}, Zn^{2+}, Ni^{2+}, or Co^{2+} ion, and computed the stability constants of the complexes formed in these systems.

Theoretical Considerations

Let us consider the electrochemical equilibrium of a metal M with a solution including M^{z+} ions of this metal and a ligand A, which are liable to form complexes between themselves. They define the following electrode

[1] $$M/M^{z+},A$$

which is reversible to the metal ions.

The related potential may be expressed by

[2] $$E = E_M{}^0 + \frac{RT}{zF}\ln [M^{z+}]$$

or writing the free metal ion concentration in terms of

[3] $$E = E_M{}^0 + \frac{RT}{zF}\ln \frac{[M^{z+}]_T}{\sum_0^N \beta_n[A]^n}$$

where $[M^{z+}]_T$, [A], and β_n represent the total metal ion concentration, the free ligand concentration, and the stoichiometric stability constants, respectively.

If $[M^{z+}]_T$ is $\ll [A]_T$ then $[A] \simeq [A]_T$ and eq. 3 may be rearranged to give

[4] $$E = E^1 - \frac{RT}{zF}\ln \sum_0^N \beta_n[A]_T{}^n$$

Thus the electrode may be considered to be reversible to the ligand under consideration and may be used as a ligand indicator electrode.

From a practical point of view, one may consider a concentration cell of the type

[5] $$\underset{1}{M/M^{z+},A}//\underset{2}{M^{z+}/M}$$

the emf of which may be expressed by

[6] $$E_2 - E_1 = \frac{RT}{zF}\ln \frac{[M_2{}^{z+}]}{[M_1{}^{z+}]}$$

$$= \frac{RT}{zF}\ln \frac{[M_2{}^{z+}]\sum_0^N \beta_n[A]_T{}^n}{[M_1{}^{z+}]_T}$$

$$= \frac{RT}{zF}\ln \frac{[M_2{}^{z+}]}{[M_1{}^{z+}]_T} + \frac{RT}{zF}\ln \sum_0^N \beta_n[A]_T{}^n$$

If $[M_2{}^{z+}] = [M_1{}^{z+}]_T$, then

[7] $$E_1 = E_2 - \frac{RT}{zF}\ln \sum_0^N \beta_n[A]_T{}^n$$

From that last equation, it appears (on condition that $[M^{z+}]_T \ll [A]_T$ and the β_n constants are known for a known temperature, solvent and ionic strength) that the electrode

[8] $$M/[M(A)_{\bar{n}}]^{z+},A$$

can be used to determine any concentration of the ligand A, in the range of $[A]_T$ where the complexation of M with A is significant ($\bar{n} > 0$).

The Silver–Pyrazole Electrode

In order to determine the characteristic equilibrium constants of the silver–pyrazole electrode, the following cells were studied

[9] $$\underset{(0.5\,M)}{Ag/Ag^+,KNO_3}//\underset{(sat)}{KNO_3}//\underset{(sat)}{KCl/Hg_2Cl_2}–Hg$$

[10] $$Ag/[Ag(pyrazole)_{\bar{n}}]^+,\underset{(0.5\,M)}{pyrazole,KNO_3}//\underset{(sat)}{KNO_3}//\underset{(sat)}{KCl/Hg_2Cl_2}–Hg$$

The total silver concentration, C_{Ag}, was the same in eqs. 9 and 10, and remained always negligible in regard to that of pyrazole, C_A.

The temperature of the cells was controlled under the limits of 25 ± 0.05 °C.

Potential measurements were made by means of a Beckman Research pH-meter, the precision of which was ±0.05 mV. This apparatus was equipped with a Beckman silver electrode No. 39261 D7 and a Beckman calomel electrode No. 4970.

Determination of the Stability Constants of the Silver–Pyrazole System

A total silver concentration of 10^{-5} *M* was used, whereas the total concentrations of pyrazole varied from 10^{-3} to 3×10^{-2} *M*.

The formation constants obtained by means of the Leden method (8) are

$$\log \beta_1 = 2.110 \pm 0.005$$

$$\log \beta_2 = 4.235 \pm 0.005$$

which may be compared with 2.04 and 4.45 (7), that were determined in water–ethanol 20% solvent, at the ionic strength of 0.1 *M* KNO_3.

Testing of Applicability of the Electrode. Titration of Pyrazole Solutions

Equation 7, which may be rewritten in the form

[11] $$C_A = \frac{-\beta_1 + \sqrt{\beta_1^2 + 4\beta_2\left[\exp\left(\frac{E_{[9]} - E_{[10]}}{RT/F}\right) - 1\right]}}{2\beta_2}$$

and the previously determined values of β_1 and β_2 were used to determine a series of pyrazole concentrations in solutions which contained known concentrations of pyrazole. The comparison of known and calculated values is reported in the Table 1. The accuracy one obtained is generally better than 1%.

Application of Silver–Pyrazole Electrode to Determine Stability Constants of Complexes Formed by Cd(II), Zn(II), Ni(II), Co(II) Ions with Pyrazole

In those cases, we studied cells of the type [9] and

[12] $$Ag/[Ag(pyrazole)_{\bar{n}}]^+,\underset{(0.5\,M)}{pyrazole,M^{2+}},\underset{(sat)}{KNO_3}//\underset{(sat)}{KNO_3}//\underset{(sat)}{KCl/Hg_2Cl_2}–Hg$$

where C_{Ag} was always equal to 10^{-5} *M*.

An equation similar to [11] was used to analyze experimental emf data by calculating the free pyrazole concentrations [A] in the presence of a second metallic ion, and the average coordination number of the complexed metal then calculated from

[13] $$\bar{n}_M = \frac{C_A - [A]}{C_M}$$

These measurements were made for different ratios C_A/C_M in each system under consideration and are given in Fig. 1. Since, according to the results, none of the systems gave rise to polynuclear complexes, the calculation of the related stability constants was made from the pairs of ($\bar{n}$, [A]) values; first, graphically by the Fronaeus method (9) in order to determine the maximum degree of complexation in the investigated range of [A] concentrations (actually, the maximum value of $\bar{n}$ experimentally reached is determined by the appearance of precipitates of the complexes) and secondly, by means of a IRIS 45 CII computer, using a least-squares minimisation program (2).

The results are given in Table 2, where they may be compared to those earlier obtained by other authors from different methods (polarography, p*H*-metry) under several experimental conditions.

The agreement is generally satisfying and thus the accuracy of the constants we have calculated is rather good.

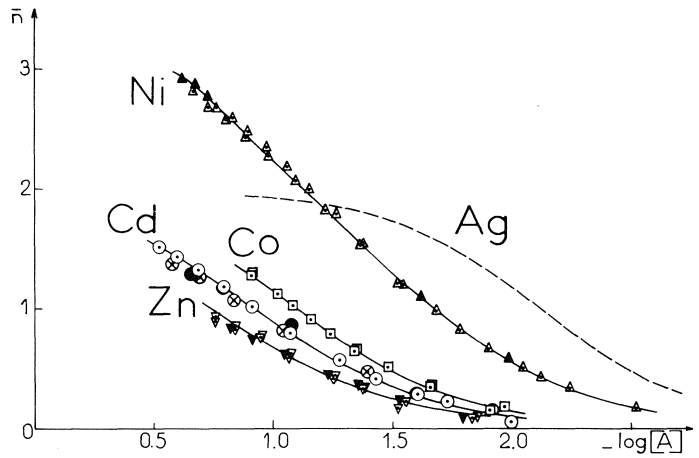

FIG. 1. Formation curves $\bar{n} = f(-\log [A])$ of the systems: Cd(II)–pyrazole ($C_{Cd} = 0.25\ M$ ○, $0.125\ M$ ⊗, $0.05\ M$ ●); Zn(II)–pyrazole ($C_{Zn} = 0.05\ M$ ▽, $0.04\ M$ ▼); Ni(II)–pyrazole ($C_{Ni} = 0.10\ M$ △, $0.05\ M$ ▲); Co(II)–pyrazole ($C_{Co} = 0.05\ M$ □). The averaged curves are drawn from the results of Table 2. The dashed line represents the formation curve of the Ag(I)–pyrazole reference system.

TABLE 2. Stability constants of the complexes formed by some transition metals with pyrazole (temperature 25 °C, solvent water, ionic strength 0.5 M KNO_3)*

M(II)	$\log \beta_1$	$\log \beta_2$	$\log \beta_3$	$\log \beta_4$
Cd(II)	1.11†	1.81†		
	1.02 ± 0.03‡	1.85 ± 0.03‡		
	1.50 (3)	2.18 (3)		
	1.11 (4)	1.60 (4)		
Zn(II)	0.95†	1.53†		
	0.92 ± 0.03‡	1.49 ± 0.05‡		
Ni(II)	1.79†	3.20†	4.11†	4.43†
	1.78 ± 0.01‡	3.25 ± 0.03‡	4.02 ± 0.08‡	4.53 ± 0.09‡
	1.88 (6)	3.28 (6)	4.18 (6)	4.61 (6)
Co(II)	1.23†	2.08†	2.32†	
	1.15 ± 0.03‡	2.20 ± 0.02‡		
	1.50 (5)	1.78 (5)	2.23 (5)	

*Reference numbers in parentheses.
†Fronaeus method.
‡Least-squares.

Conclusion

One can conclude from these results that the silver–pyrazole electrode is a suitable indicator of pyrazole. Practically, it is applicable from a concentration of pyrazole near $5 \times 10^{-3}\ M$ until relatively high values (about $1\ M$), under the experimental conditions defined here (25 °C, $\mu = 0.5\ M$ KNO_3).

1. D. D. PERRIN. Dissociation constants of organic bases in aqueous solutions. Supplement 1972. Butterworths, London. 1972.
2. G. BERTHON and C. LUCA. Chim. Anal. Paris, **52**, 391 (1970).
3. A. C. ANDREWS and J. K. ROMARY. Inorg. Chem. **2**, 1060 (1963).
4. D. R. CROW. J. Polarog. Soc. **11**, 22, 67 (1965).
5. D. R. CROW and J. V. WESTWOOD. J. Inorg. Nucl. Chem. **30**, 179 (1968).
6. T. R. MUSGRAVE and E. R. HUMBURG. J. Inorg. Nucl. Chem. **32**, 2229 (1970).
7. S. N. PODDAR, S. M. BHATTACHARYA and S. ROY CHOWDHURY. Indian J. Chem. **12**, 754 (1974).
8. I. LEDEN. Z. Phys. Chem. **188**A, 160 (1941).
9. S. FRONAEUS. Komplexsystem hos Koppar. Gleerupska Universitets-Bokhandeln, Lund. 1948.

Ozone yields from the Febetron radiolysis of oxygen – rare gas mixtures[1]

A. W. BOYD, O. A. MILLER, AND E. B. SELKIRK

Physical Chemistry Branch, Chalk River Nuclear Laboratories, Atomic Energy of Canada Limited, Chalk River, Ont., Canada K0J 1J0

Received June 25, 1976

A. W. BOYD, O. A. MILLER, and E. B. SELKIRK. Can. J. Chem. **55**, 203 (1977).

Ozone yields have been measured from the Febetron irradiation of mixtures containing 1–50 mol% oxygen and each of the five rare gases. The maximum values of $G(O_3)$ calculated using the energy absorbed only in the rare gas are obtained with the addition of less than 10% oxygen and are for: He, 16; Ne, 14; Ar, 11; Kr, 10; Xe, 12; each with an uncertainty of less than ±10%. On the addition of 0.2 mol% SF_6 these yields are reduced to 6, 5, 1, 2, and 2.5 respectively. These values are compared with those derived from ion and excited state yields and the contributions of subexcitation electrons.

A. W. BOYD, O. A. MILLER et E. B. SELKIRK. Can. J. Chem. **55**, 203 (1977).

On a mesuré les rendements en ozone obtenus par irradiation par le Febetron de mélanges contenant de 1 à 50 mol% d'oxygène et chacun des cinq gaz rares. On obtient les valeurs maximales de $G(O_3)$, calculées en utilisant uniquement l'énergie absorbée dans les gaz rares, lors de l'addition de moins de 10% d'oxygène et ces valeurs maximums sont de 16, He; 14, Ne; 11, Ar; 10, Kr; 12, Xe et dans chaque cas le facteur d'incertitude est moins que ±10%. Lors de l'addition de 0.2 mol% de SF_6, on réduit respectivement ces rendements à des valeurs de 6, 5, 1, 2 et 2.5. On compare ces valeurs avec celles obtenues à partir des rendements pour des états ioniques et excités et les contributions des électrons sous-excités.

[Traduit par le journal]

Introduction

The yields of ions and excited states and their reactions in irradiated rare gases are necessary to predict the radiolytic behaviour of mixtures of the rare gases with other materials. They are also important to the understanding of rare gas lasers. Values for many of these quantities are available: the total ion yields from W values; the ion distribution and energy from mass spectrometry; the reactions of ions and excited states from mass spectrometry, flowing afterglow, and beam techniques. The yields of the excited states are not readily determined experimentally in the pure gases. The present values are either calculated from binary collision theory (1, 2) or from partial excitation cross section measurements (3, 4). The two sets of values are not in agreement.

A possible method of obtaining excited state yields is from the measurement of the ozone yields in rare gas – O_2 mixtures. The yield of ozone in pure O_2 is well established (5) and there is good agreement between this value and the yields and reactions of the ions and excited states in oxygen (6). Combining the measured yields in the mixtures with the data for the pure components could then give values for the rare gas excited state yields.

We have therefore measured the yields of ozone from the irradiation of mixtures of each of the five rare gases with oxygen. We used the short intense pulses available from Febetrons because as we have shown, these result in a suppression of charge transfer to products or impurities (7). Previous measurements of these mixtures have been made using ^{60}Co γ-rays (8) but at the dose rates from these sources there is no contribution of ion neutralization to the ozone yield.

Experimental

The radiation source used is a Febetron 705. The oxygen – rare gas mixtures were contained in a single pass cell 16 cm long and 9 cm diameter with an electron window (0.025 cm thick, 6 cm diameter Al) at right angles to the optical path. The analyzing light was from a 300 W Xe arc and was dispersed by a 3/4 m Spex Czerny-Turner monochromator after passage through the cell. The ozone was measured at 254 nm and an interference filter with a transmission peak at 250 nm was used to eliminate scattered light from the monochromator.

Measurements were made both with and without a 0.005 cm thick 2.5 cm diameter Ta scattering foil placed ~1.5 cm in front of the electron beam window and within

[1]AECL No. 5628.

0.3 cm of the optical cell window. The average dose calculated from the yield of ozone $G(O_3) = 12.8 \pm 0.6$ (5) and its extinction coefficient $\varepsilon_{254nm} = 135\ cm^{-1}$ STP (9) and the observed optical density in pure O_2 was 0.2 Mrad/pulse with the foil and 0.5 Mrad/pulse without it.

Both Matheson UHP and CP grades of oxygen were found to give the same ozone yields. The rare gases were Matheson research purity. Substitution of Matheson purified grade for He and Ar did not change the observed yields. The sulphur hexafluoride was Matheson CP grade.

Results

The yields of ozone as a function of mol% oxygen in each of the five rare gases with and without the addition of 0.2 to 1 mol% SF_6 are shown in Figs. 1 to 3. These yields were determined using pressures of 50 to 220 kPa (375 to 1650 torr) and each one is the average of at least three measurements. They are based on $G(O_3) = 12.8$ in pure O_2 and $G(O_3) = 6.3$ in O_2 with 0.2 to 3 mol% SF_6 (5).

The values given $G(O_3)_{He}$, $G(O_3)_{Ne}$, etc. are the yields of O_3 due to energy absorbed only by the rare gas and were calculated as follows. The optical density (O.D.) of the O_3 observed in the mixture was first corrected by subtracting the O.D. of the O_3 resulting from energy absorbed in the O_2. This was assumed to be the O.D. of ozone obtained in pure O_2 under the same conditions multiplied by the mole fraction of O_2 in the mixture. The yield of ozone from the energy absorbed in the rare gas is then directly proportional to the ratio of the energy absorbed in the rare gas to the energy absorbed in pure O_2 with both gases at the same pressure. It is given by

$$G(O_3)_x = \frac{\text{Net O.D.}}{\text{O.D. pure } O_2} \times \frac{\text{Stopping power } O_2 \times \text{density } O_2}{\text{Stopping power X} \times \text{density X}} \times 12.8$$

The ratios (O_2/X) of stopping powers used are: He, 0.909; Ne, 1.05; Ar, 1.21; Kr, 1.38; Xe, 1.50 (10–12).

There appears to be no significant difference

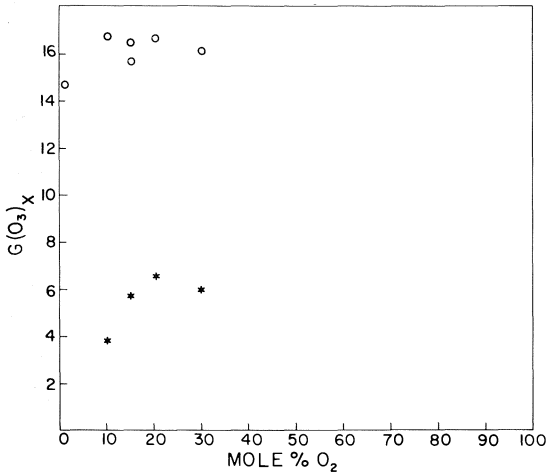

FIG. 1. Ozone yields from the Febetron radiolysis of $He–O_2$ and $He–O_2–SF_6$ mixtures. ○, $G(O_3)_{He}$ (see text) for $He–O_2$ mixtures; ×, $G(O_3)_{He}$ for $He - O_2 - 0.2\%\ SF_6$ mixtures.

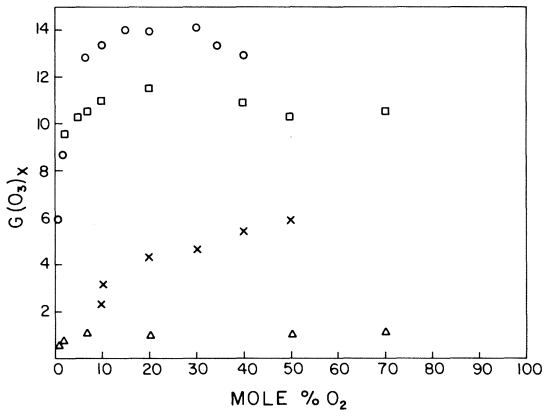

FIG. 2. Ozone yields from the Febetron radiolysis of $Ne–O_2$, $Ne–O_2–SF_6$, $Ar–O_2$, and $Ar–O_2–SF_6$ mixtures. ○, $G(O_3)_{Ne}$ for $Ne–O_2$ mixtures; ×, $G(O_3)_{Ne}$ for $Ne–O_2 - 0.2\%\ SF_6$ mixtures; □, $G(O_3)_{Ar}$ for $Ar–O_2$ mixtures; △, $G(O_3)_{Ar}$ for $Ar - O_2 - 1\%\ SF_6$ mixtures.

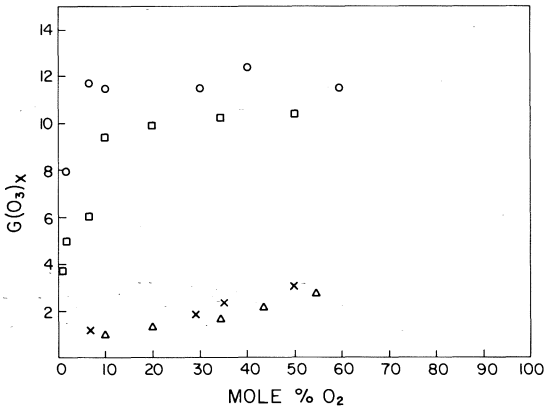

FIG. 3. Ozone yields from the Febetron radiolysis of $Kr–O_2$, $Kr–O_2–SF_6$, $Xe–O_2$, and $Xe–O_2–SF_6$ mixtures. □, $G(O_3)_{Kr}$ for $Kr–O_2$ mixtures; △, $G(O_3)_{Kr}$ for $Kr - O_2 - 1\%\ SF_6$ mixtures; ○, $G(O_3)_{Xe}$ for $Xe–O_2$ mixtures; ×, $G(O_3)_{Xe}$ for $Xe - O_2 - 1\%\ SF_6$ mixtures.

between the yields of the two dose rates of 0.2 and 0.5 Mrad/pulse.

In all the O_2 rare gas mixtures and O_2 with SF_6 the ozone concentration as shown by the oscilloscope traces rose to a maximum value within 1–2 ms and remained constant at this value for several hundred milliseconds. In the rare gas – O_2 – SF_6 mixtures there was a fall-off in the ozone concentration over a period of 300–500 ms. The extent of this fall-off appeared to be greater in Xe and Kr mixtures than in Ar or Ne and was very small in mixtures with He.

Discussion

To provide a basis for the comparison of calculated excited state yields in the rare gases and those derived from the ozone yields, we shall first summarize the primary yields and the mechanism of ozone production in O_2 and list the yields and the reactions in the rare gases.

The following summary of O_2 radiolysis is taken from ref. 6.

The primary processes of ionization and excitation and their yields and energies are:

Processes	G	Threshold energy (eV)
$O_2 \rightsquigarrow O^+ + O + e$	1.22	18.8
$O_2 \rightsquigarrow O_2^+ + e$	2.06	12.08
$O_2 \rightsquigarrow O + O$	2.0	5.2

The ions and atoms thus formed may undergo the following reactions:

[1] $$O^+ + O_2 \rightarrow O_2^+ + O$$
$$k_1 = 2 \times 10^{-11}\ \text{cm}^3\ \text{molecule}^{-1}\ \text{s}^{-1}$$

[2] $$O_2^+ + \text{e(or } O_2^- \text{ or } O_2^-(O_2)_n) \rightarrow O + O$$
$$k_2 \simeq 2 \times 10^{-6}\ \text{cm}^3\ \text{molecule}^{-1}\ \text{s}^{-1}$$

[3] $$O + 2O_2 \rightarrow O_3 + O_2$$
$$k_3 = 3 \times 10^{-34}\ \text{cm}^6\ \text{molecule}^{-2}\ \text{s}^{-1}$$

[4] $$e + SF_6^- \rightarrow SF_6^-$$
$$k_4 = 2.4 \times 10^{-7}\ \text{cm}^3\ \text{molecule}^{-1}\ \text{s}^{-1}$$

[5] $$O_2^+ + SF_6^- \rightarrow \text{Products (no O atoms)}$$
$$k_5 \simeq 2 \times 10^{-6}\ \text{cm}^3\ \text{molecule}^{-1}\ \text{s}^{-1}$$

[6] $$O_2^- + O_3 \rightarrow O_3^- + O_2$$
$$k_6 = 3 \times 10^{-10}\ \text{cm}^3\ \text{molecule}^{-1}\ \text{s}^{-1}$$

[7] $$O_2^+ + O_3^- \rightarrow O_2 + \text{products}$$
$$k_7 \approx 2 \times 10^{-6}\ \text{cm}^3\ \text{molecule}^{-1}\ \text{s}^{-1}$$

With Febetron pulses because of the high ion concentration, reaction 6 cannot compete with reaction 2 so that each neutralization of a positive ion gives two O_3 molecules. However, because of the high value of k_4, only a small amount of SF_6 is needed to capture all the electrons and replace reaction 2 by reaction 5. At low dose rates in pure O_2 reaction 2 is replaced by reaction 6 and this like [5] results in no contribution to the O_3 yield from the neutralization.

The maximum calculated value of the ozone yield from the above processes and reactions is $G(O_3)_{calc} = 2(1.22) + 2(3.28) + 2(2.0) = 13$. This is reduced by $2(3.28 = 6.56$ on the addition of SF_6 or at low dose rates.

The measured and calculated values of ion and excited state yields in the rare gases are listed in Table 1. These can be divided into three categories. The first is the experimental ion pair yields which are well established and known within an uncertainty of less than $\pm 5\%$. The second category is the calculated values for all five gases of G_i and G_{ex} by Sato, Okazaki, and Ohno (2). These were obtained using binary collision theory in which several approximations are made. They provide the only reported results for excited state yields in Ne, Kr, and Xe. The third category comprises the calculations of Alkhazov (3) and Douthat (14) on He and of Eggarter (4) for Ar. For the comparison with our results we will of course use the experimental ion pair yields.

The rate constants for the reactions in the rare gas – O_2 mixtures are given in Table 2. The available rate data indicate that at concentrations of O_2 more than about 5%, all the rare gas ions react with O_2. The rate constants for the reactions to form the dimeric ion *e.g.*, [9], [15] are one to two orders of magnitude less than those for charge transfer to O_2 and neutralization of single rare gas atoms is a much slower process than formation of the dimeric ion. The rate constants listed for excited state reactions also indicate that these react only with O_2 at concentrations of the latter of 10% or more.

He–O_2

The maximum yields of ozone in He–O_2 mixtures calculated from the data in Tables 1 and 2 and the subexcitation electron contribution are compared with our experimental yields in Table 3.

The total energy of subexcitation electrons in He is estimated by Alkhazov (3) to be 15 eV. We have calculated the ionization and excitation of O_2 by these electrons using cross sections com-

TABLE 1. Ion and excited state yields in irradiated rare gases

Process	Threshold energy (eV)	G, yields per 100 eV[f]	
		Experimental	Calculated
$He \rightsquigarrow He^+ + e$	24.58	2.41(W = 41.5 eV) (13)	2.42 (1), 2.27 (3) 2.24 (14)
$He \rightsquigarrow He^*$ T[a]	19.8	—	0.13 (1), 0.2[b] (3)
$He \rightsquigarrow He^*$ S[c]	20.6	—	0.91 (1), 1.44[b] (3)
$Ne \rightsquigarrow Ne^+ + e$	21.56	2.76(W = 3.62 eV) (13)	2.19 (2)
$Ne \rightsquigarrow Ne^*$ T[a]	16.7	—	0.07 (2)
$Ne \rightsquigarrow Ne^*$ S[c]	16.8	—	1.55 (2)
$Ar \rightsquigarrow Ar^+ + e$	15.75	3.82(W = 26.2 eV) (13)	2.81 (2), 3.72 (4)
$Ar \rightsquigarrow Ar^*$ T[a]	11.6	—	0.13 (2)
$Ar \rightsquigarrow Ar^*$ S[c]	11.8	—	1.92 (2)
$Ar \rightsquigarrow Ar^*$ I			0.4[d]
$Ar \rightsquigarrow Ar^*$ II			0.6[e]
$Kr \rightsquigarrow Kr^+ + e$	14.00	4.11(W = 24.3 eV) (13)	3.20 (2)
$Kr \rightsquigarrow Kr^*$ T[a]	9.9		0.23 (2)
$Kr \rightsquigarrow Kr^*$ S[c]	10.6		1.64 (2)
$Xe \rightsquigarrow Xe^+ + e$	12.13	4.56(W = 21.9 eV) (13)	3.45 (2)
$Xe \rightsquigarrow Xe^*$ T[a]	8.3	—	0.39 (2)
$Xe \rightsquigarrow Xe^*$ S[c]	9.6		1.51 (2)

[a]Triplet states.
[b]Normalized to G ion pair = 2.41.
[c]Singlet states.
[d]Calculated for Ar* states with energy < 12 eV from cross section data in ref. 4 and slowing down spectrum in ref. 2.
[e]Calculated for Ar* states with energy > 12 eV from cross section data in ref. 4 and slowing down spectrum in ref. 2.
[f]Reference numbers in parentheses.

TABLE 2. Reactions of rare gas ions and excited states in mixtures with O_2

Reaction	Rate constant (cm^3 molecule^{-1} s^{-1})	Reference
[8] $He^+ + O_2 \rightarrow O^+ + O + He$	1.5×10^{-9}	15, 16
[9] $He^+ + 2He \rightarrow He_2^+ + He$	3×10^{-12}[a]	17
[10] $He_2^+ + e \rightarrow 2He$	$<10^{-8}$	18
[11] $He^* T + O_2 \rightarrow$ Products	2.5×10^{-10}	19
$He^* T + O_2 \rightarrow He + O_2^+$	0.94 ± 6%	20
$He^* T + O_2 \rightarrow He + O^+ + O$	0.06 ± 15%	20
[12] $He^* S + O_2 \rightarrow$ Products	5.6×10^{-10}	19
$He^* S + O_2 \rightarrow He + O_2^+$	0.75 ± 6%	20
$He + O^+ + O$	0.25 ± 10%	20
[13] $Ne^+ + O_2 \rightarrow O^+ + O + Ne$	5.8×10^{-11}	21, 22
[14] $Ne^* T + O_2 \rightarrow O_2^+ + Ne$ 0.997	2.3×10^{-10}	20
$\rightarrow NeO_2^+$ 0.003		
[15] $Ne^* S + O_2 \rightarrow O_2^+ + Ne$		[c]
[16] $Ar^+(^2P_{3\,2}, {}^2P_{1\,2}) + O_2 \rightarrow O_2^+ + Ar$	5.7×10^{-11}	21
[17] $Ar^+(^2P_{3\,2}) + 2Ar \rightarrow Ar_2^+ + Ar$	5.6×10^{-12}[a]	23
[18] $Ar(^3P_2) + O_2 \rightarrow O + O + Ar$[b]	1.8×10^{-10}	24
[19] $Ar^* S + O_2 \rightarrow O_2^+ + Ar$	3.0×10^{-10}	25
$Ar^* S + O_2 \rightarrow O + O + Ar$		[c]
[20] $Ar^* I + O_2 \rightarrow O + O + Ar$		[c]
[21] $Ar^* II + O_2 \rightarrow O_2^+ + Ar$		[c]
[22] $Kr^+(^2P_{3\,2}, {}^2P_{1\,2}) + O_2 + O_2^+ + Kr$	3×10^{-11}	21
[23] $Kr^* S, T + O_2 \rightarrow O + O + Kr$		[c]
[24] $Xe^+(^2P_{3\,2}, {}^2P_{1\,2}) + O_2 \rightarrow O_2^+ + Xe$	1.1×10^{-10}	21
[25] $Xe(^3P_2) + O_2 \rightarrow O + O + Xe$[b]	2.2×10^{-10}	26

[a]Second order rate constant at 100 kPa.
[b]Assumed products.
[c]Assumed reaction.

TABLE 3. Ozone yields in $He–O_2$ mixtures[a]

Ion or excited state	Yield	Reaction[b]	$G(O_3)_{He}$ $He–O_2$	$G(O_3)_{He}$ $H_2–O_2–SF_6$
He^+	2.41	[8]	9.64	4.82
He* T	0.13 (1) 0.20	[11]	0.28 0.42	0.015 0.024
He* S	0.91 (1) 1.44 (3)	[12]	2.28 3.6	0.46 0.72
		Subtotal	12.2 (1) 13.7 (3)	5.3 (1) 5.6 (3)
Subexcitation electrons			2.8	—
		Total	15.0 to 16.5	5.3 to 5.6
Experimental (Fig. 1)			16.2±0.7	6±1

[a]Reference number in parentheses.
[b]Ozone is produced as a result of the reactions listed and two or more of reactions 1 to 5.

piled by Kieffer (27) and the spectrum of the electrons calculated by Douthat (14). Over the energy range from 5 to 20 eV we assumed that the significant loss processes were ionization or dissociative excitation. Ionization was calculated to be less than 5% of neutral dissociation.

The yield of O_3 in the presence of SF_6 is reduced by the suppression of dissociative neutralization of O_2^+ and by inelastic collisions of the subexcitation electrons with the SF_6. There are several large resonances for the dissociative electron attachment to SF_6 in the region below 20 eV (28) and these should largely suppress dissociation of oxygen by these electrons.

The uncertainties in our experimental yields and in the calculated subexcitation electron contribution produce a wide range of excited state yields in He. Assuming the subexcitation contribution to $G(O_3)$ to be 2.8 ± 0.5 then $G(\text{He* T + S}) = 1.5 \pm 0.5$. It should be noted that excited state yields can also be derived from an energy balance. The energy available for excited state formation per 100 eV absorbed in He is $100 - [2.41(41.5) + 15]$. The first term in the brackets is the energy required for ionization, the second is that required for subexcitation electrons. Taking the average energy per excited state as 20 eV the yield is $G(\text{He*}) = 1.3$.

Ne–O_2

The maximum yields of ozone calculated from the data in Tables 1 and 2 and the subexcitation electron contribution for $Ne–O_2$ mixtures are compared with our experimental data in Table 4.

TABLE 4. Ozone yields in $Ne–O_2$ mixtures

Ion or excited state	Yield	Reaction[a]	$G(O_3)_{Ne}$ $Ne–O_2$	$G(O_3)_{Ne}$ $Ne–O_2–SF_6$
Ne^+	2.76	[13]	11.04	5.52
Ne* T	0.07	[14]	0.14	0
Ne* S	1.55	[15]	3.1	0
		Subtotal	14.28	5.52
Subexcitation electrons (See Discussion)			2.5	—
		Total	16.8	5.5
Experimental (Fig. 2)			13.7±0.6	5±1

[a]Ozone is produced as a result of the reaction listed and two or more of reactions 1 to 5.

The total energy of the subexcitation electrons is estimated to be the same as in He (29) but no spectrum for these is available. The value given is calculated assuming a spectrum similar to that for He. The contribution of these electrons to the production of O_2^+ is negligible.

It seems unlikely that the excited state yield in Ne is less than 1 and that the contribution of subexcitation electrons to the O_3 yield is less than 2. Using these minimum values the calculated yield is $G(O_3) = 15$ which is still significantly larger than the experimental value. A possible explanation of the discrepancy is that reaction 13 produces some O_2^+ at higher pressures. The value in Table 2 was measured at a total pressure of less than 0.3 kPa (22). Since the reaction is believed to proceed through the NeO_2^+ ion (30) the ratio of O_2^+ to O^+ could be pressure dependent.

Ar–O_2

The yields of ozone calculated from the data in Tables 1 and 2 and the subexcitation electrons in $Ar–O_2$ mixtures are compared with our experimental yields in Table 5.

The total energy of the subexcitation electrons was taken to be 15 eV and their spectrum was again assumed to have a shape similar to that in He.

The yield of the excited states in Ar below the ionization potential of O_2 from the O_3 yields is taken to be one-half the yield in the presence of SF_6 and is $G(\text{Ar* I}) = 0.5 \pm 0.1$ in good agreement with the yields calculated from the cross sections in ref. 4 and the slowing down spectrum in ref. 2. The calculation of $G(Ar^+)$ using the ionization cross sections of Ar and the slowing down spectrum in ref. 2 gave the same value as that calculated by Eggarter (4).

TABLE 5. Ozone yields in $Ar–O_2$ mixtures

Ion or excited state	Yield	Reaction[a]	$G(O_3)_{Ar}$ $Ar + O_2$	$Ar + O_2 + SF_6$
Ar^+	3.82	[16]	7.64	0
Ar* T	0.13 (2)	[18]	0.26	0.26
Ar* S	1.92 (2)	[19]	3.94	?
Ar* I	0.4[b]	[20]	0.8	0.8
Ar* II	0.6[b]	[21]	1.2	—
		Subtotal	11.84 (2) 9.64 (4)	0.8
Subexcitation electrons (see Discussion)			2	—
		Total	13.8 (2) 11.6 (4)	
Experimental (Fig. 2)			11±0.6	1.0±0.2

[a]Ozone is produced as a result of this reaction and two or more of reactions 1 to 5.
[b]Calculated from both refs. 2 and 4; see Discussion.

TABLE 6. Ozone yields in $Kr–O_2$ mixtures

Ion or excited state	Yield	Reaction[a]	$G(O_3)_{Kr}$ $Kr + O_2$	$Kr + O_2 + SF_6$
Kr^+	4.11	[22]	8.22	0
Kr* S,T	1.87	[23]	3.74	3.74
		Total	11.96	3.74
Experimental (Fig. 3)			10.0±0.5	2.0±0.5

[a]Ozone is produced as a result of this reaction and two or more of reactions 1 to 5.

It can be seen that as with He the subexcitation electron contribution is necessary for good agreement between the calculated and experimental yields. The uncertainty in this contribution and the experimental uncertainty do not allow a precise value of $G(Ar^*\ II)$ to be derived from the measured $G(O_3)$ value.

$Kr–O_2$

The yields of ozone calculated from the data in Tables 1 and 2 for $Kr–O_2$ mixtures are compared with our experimental yields in Table 6. Although there will be some contribution from the subexcitation electrons to the ozone yield it should be smaller than the uncertainties in the calculated excited state yields or the measured ozone yield.

The excited state yields of ref. 2 again appear to be too high. We have assumed that reaction 23 is the sole pathway for the loss of energy of the excited states of Kr but this does not seem unreasonable in view of the rate constants found for reactions 11, 12, 14, 19, and 25. Our results indicate a total yield of $G(Kr^*) = 0.9 \pm 0.25$.

$Xe–O_2$

The yields of ozone calculated from the data in Tables 1 and 2 for $Xe–O_2$ mixtures are compared with our experimental yields in Table 7. The contribution of subexcitation electrons will be less than in $Kr–O_2$ mixtures.

Assuming all the excited states of Xe react as in [25] our results give a value of $G(Xe^*) = 1.3 \pm 0.2$.

Comparison with Reference 8

The yields of O_3 from irradiations of rare gas–oxygen mixtures at low dose rates (8) are compared with our data in Table 8. As we have discussed, the yield from dissociative neutralization is suppressed at these dose rates and they should be comparable to our values for mixtures with SF_6. A further correction needs to be made for the elimination of the contribution of the subexcitation yield by the SF_6. The difference between the values in the first and third columns is probably not much greater than the sum of the experimental uncertainties for Ar, Kr, and Xe. We have no explanation for the much greater differences for He and Ne.

TABLE 7. Ozone yields in $Xe–O_2$ mixtures

Ion or excited state	Yield	Reaction[a]	$G(O_3)_{Xe}$ $Xe + O_2$	$Xe + O_2 + SF_6$
Xe^+	4.56	[24]	9.12	0
Xe* S,T	1.9	[25]	3.8	3.8
		Total	12.92	3.8
Experimental (Fig. 3)			11.7±0.3	2.5±0.5

[a]Ozone is produced as a result of this reaction and two or more of reactions 1 to 5.

TABLE 8. Comparison with low dose rate yields

Rare gas	Low dose rate[a] (8)	$G(O_3)_{Kr}$ Febetron[b]	Corrected Febetron[c]
He	3.4	6	9
Ne	4.4	5	7.5
Ar	2.2	1	3
Kr	3.2	2	2–2.5
Xe	4.6	2.5	2.5–3.0

[a]These values have been corrected as discussed previously (5).
[b]These are for mixtures containing SF_6.
[c]The contributions of subexcitation electrons have been added to the measured Febetron values for mixtures containing SF_6.

Conclusions

The agreement between the experimentally determined yields of ozone in rare gas – O_2 mixtures due to energy absorbed in the rare gas and the values calculated from ion and excited state yields and subexcitation electrons is somewhat different for each rare gas.

In helium the value of the excited state yield is probably close to $G(He^* S + T) = 1.3$ and the agreement between the calculated and experimental ozone yields supports the rather large contribution we calculated due to subexcitation electrons.

In neon the minimum calculated value of $G(O_3)$ assuming four ozones per Ne^+ ion is significantly larger than the experimental value. Resolution of this discrepancy requires measurements of the pressure dependence of the products of the $Ne^+ + O_2$ reaction.

In argon as in helium, the excited state yields appear to be well known. The results support the importance of the contribution of subexcitation electrons to the O_3 yield and the suppression of this contribution by SF_6.

The excited state yields in Kr and Xe derived from our results can be compared only with the calculated values of Sato *et al.* (2). The differences between their values and ours may be due to inefficient energy transfer from the rare gas excited state to O_2 or to the difficulties of accurate yield calculations for these large atoms.

Acknowledgements

We are most grateful to Dr. C. Willis for many helpful discussions on the calculation of subexcitation electron yields. We also thank Drs. M. Bourène and J. LeCalvé for their comments.

1. S. Ohno. Chem. Lett. 817 (1973).
2. S. Sato, K. Okazaki, and S. Ohno. Bull. Chem. Soc. Jpn. **47**, 2174 (1974).
3. G. D. Alkhazov. Sov. Phys. Tech. Phys. **16**, 1995 (1972).
4. E. Eggarter. J. Chem. Phys. **62**, 833 (1975).
5. C. Willis, A. W. Boyd, M. J. Young, and D. A. Armstrong. Can. J. Chem. **48**, 1505 (1970).
6. C. Willis and A. W. Boyd. Int. J. Radiat. Phys. Chem. **8**, 71 (1976).
7. A. W. Boyd, C. Willis, and O. A. Miller. Can. J. Chem. **51**, 1228 (1973).
8. G. R. A. Johnson and J. M. Warman. Discuss. Faraday Soc. **37**, 87 (1964).
9. W. B. DeMore and O. Raper. J. Phys. Chem. **68**, 412 (1964).
10. G. G. Meisels. J. Chem. Phys. **41**, 51 (1964).
11. A. T. Nelms. National Bureau of Standards Circular 577, Washington, D.C. 1956.
12. M. J. Berger and S. M. Seltzer. NASA Report SP-3012. 1964.
13. I. T. Myers. Radiation dosimetry. Vol. 1. Fundamentals. *Edited by* F. H. Attix and W. C. Roesch. Academic Press, New York. 1968. Chapt. 7.
14. D. A. Douthat. Radiat. Res. **61**, 1 (1975).
15. F. C. Fehsenfeld, A. L. Schmeltekopf, P. D. Golden, H. I. Schiff, and E. E. Ferguson. J. Chem. Phys. **44**, 4087 (1966).
16. P. Warneck. J. Chem. Phys. **47**, 4279 (1967).
17. E. C. Beaty and P. L. Patterson. Phys. Rev. A, **137**, 346 (1965).
18. J. N. Bardsley and M. A. Biondi. Adv. At. Mol. Phys. **6**, 1 (1970).
19. W. Lindinger, A. L. Schmeltekopf, and F. C. Fehsenfeld. J. Chem. Phys. **61**, 2890 (1974).
20. J. P. Riola, J. S. Howard, R. D. Rundel, and R. F. Stebbings. J. Phys. B, **7**, 376 (1974).
21. J. B. Laudenslager, W. T. Huntress, and M. T. Bowers. J. Chem. Phys. **61**, 4600 (1974).
22. R. C. Bolden, R. S. Hemsworth, M. J. Shaw, and N. D. Twiddy. J. Phys. B, **3**, 45 (1970).
23. W. F. Liu and D. C. Conway. J. Chem. Phys. **60**, 784 (1974).
24. M. Bourène and J. LeCalvé. J. Chem. Phys. **58**, 1452 (1972).
25. O. J. Dunn and R. A. Young. J. Chem. Phys. **62**, 1996 (1975).
26. J. E. Velazco and D. W. Setser. Chem. Phys. Lett. **25**, 197 (1974).
27. L. J. Kieffer. Report of the Joint Institute for Laboratory Astrophysics, Boulder, Colorado, COM-74-11661. 1973.
28. P. W. Harland and J. C. J. Thynne. J. Phys. Chem. **75**, 3517 (1971).
29. C. E. Klots. Fundamental processes in radiation chemistry. *Edited by* P. Ausloos. Wiley, New York, 1968. p. 1.
30. T. L. Budzynski and T. L. Bailey. Int. J. Mass. Spectrom. Ion Phys. **18**, 317 (1975).

The intra- and intermolecular copper(I) catalyzed couplings of vinyl Grignards. A facile synthesis of pleiadiene and a synthesis of a conjugated 14-membered ring system[1]

REGINALD H. MITCHELL,[2] BHUPENDRA N. GHOSE, AND MARY E. WILLIAMS

Department of Chemistry, University of Victoria, Victoria, B.C., Canada V8W 2Y2

Received July 6, 1976

REGINALD H. MITCHELL, BHUPENDRA N. GHOSE, and MARY E. WILLIAMS. Can. J. Chem. **55**, 210 (1977).

Pleiadiene, **27**, can be efficiently prepared in 45% yield by copper catalyzed intramolecular coupling of the bis-Grignard reagent of 1,8-*trans*-(β-bromovinyl)naphthalene, **5**. Also obtained in 6% yield is the unsaturated 14-membered ring compound **28**. Whereas the bis(β-bromovinyl) compound **5** is readily available from 1,8-divinylnaphthalene, α-bromovinyl compounds are obtained from divinylbenzenes. On coupling the Grignard reagent from 1,4-bis(β-bromovinyl)-benzene, only linear dimeric products were obtained.

REGINALD H. MITCHELL, BHUPENDRA N. GHOSE et MARY E. WILLIAMS. Can. J. Chem. **55**, 210 (1977).

En effectuant un couplage intramoléculaire, catalysé par le cuivre, du réactif de Grignard double obtenu à partir du bis(β-bromovinyl)-1,8-*trans* naphtalène, **5**, on peut préparer d'une façon efficace le pléiadiène **27**, avec un rendement de 45%. On obtient aussi avec un rendement de 6% le composé **28** qui est insaturé et qui possède un cycle à 14 chaînons. Alors que le composé **5** peut etre obtenu facilement à partir du divinyl-1,8 naphtalène, les composés α-bromovinyliques ne peuvent être obtenus qu'à partir du divinylbenzène. Par couplage du réactif de Grignard obtenu à partir du bis(β-bromovinyl)-1,4 benzène, on obtient uniquement des produits dimères linéaires.

[Traduit par le journal]

Introduction

Extensive use (for a review see ref. 1) has been made of the copper induced coupling of acetylenes to diynes using the procedures known as the Glaser (2) and Eglinton (3) couplings. It is, however, only much more recently that the analogous coupling of vinyl compounds has been observed. In 1966 Whitesides *et al.* reported (4) that vinyllithium compounds on treatment with Cu(I) or Ag(I) coupled to give 1,3-dienes. This was extended in 1967 by Kauffman and Sahm (5) to include vinyl Grignard reagents and by Zweifel and Miller (6) in 1970 for vinyl alanes. Moreover, while the oxidative coupling of diacetylenes has been put to good use in the preparation of a whole variety of novel conjugated macrocyclic compounds (1, 7, 8), reports on the similar use of coupling of bis-vinyl derivatives are absent. Indeed there appears to be only one report (9) of a coupling of a bis-vinyl compound and in this the cyclobutane ring in **1** was formed. We decided

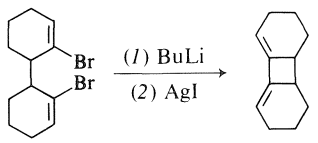

1

that in view of the extensive interest in large conjugated systems (for a review containing many pertinent examples see ref. 10) to investigate the feasibility of coupling vinyl derivatives to obtain such systems.

1,8-Bis(β-bromovinyl)naphthalene, **2**, had attraction as a test for the coupling reaction since the naphthalene nucleus directs the vinyl groups in the same region of space which should facilitate both intra- and intermolecular cyclization at the expense of linear polymer formation. On the other hand, 1,4-bis(β-bromovinyl)benzene, **3**, should be one of the hardest tests to apply since intramolecular cyclization is not

[1]Presented in preliminary form at the 30th Northwest Regional Meeting of the American Chemical Society, University of Hawaii, June 13, 1975.

[2]Author to whom correspondence should be addressed.

probable[3] and intermolecular cyclization is not going to be helped by the severe geometry requirements of the product, the known (12) paracyclophane derivative **4**. This paper reports the results of these tests.

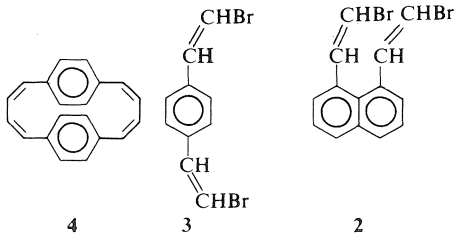

4 3 2

Results and Discussion

I. Synthesis of Bromovinyl Compounds

Mitchell and Sondheimer (7) reported that 1,8-bis(*trans*-β-bromovinyl)naphthalene, **5**, was obtained as a by-product in the dehydrobromination of the tetrabromide **6** to 1,8-diethynylnaphthalene (**7**). We have found that use of potassium *tert*-butoxide in *tert*-butyl alcohol – dioxane for short reaction times yields **5** as the major product, an average yield of 87% from **6** being obtained. The preparation of the precursor for **6**, 1,8-divinylnaphthalene, **8**, was achieved in 98% yield by using the Wittig reaction between the bis-phosphonium salt **9** and formaldehyde with lithium ethoxide as base rather than the much less convenient sodamide – liquid ammonia system previously reported (7). Further, the analogous reactions yielded 1,2-divinylbenzene **10** in 92% yield from **11**, and 1,3-divinylbenzene **12** in 95% yield from **13** using equally simple procedures. These were carried out since we hoped to generate both 1,2- and 1,3-bis(β-bromovinyl)benzene, **14** and **15** respectively from the tetrabromides **16** and **17** to provide further tests for our coupling reaction.

Raphael and co-workers (13) in 1964 reported that the unsymmetric bromide **18** is in fact formed from **16** on treatment with potassium *tert*-butoxide in *tert*-butyl alcohol. Since their aim was the preparation of 1,2-diethynyl benzene, we hoped that by variation of the base we could make the bis(β-bromide) **14** the major product. In fact that was not so. Indeed, the analogous tetrabromide **17** on treatment with a variety of bases gave the bis(α-bromide) **19** as the product.

[3]The smallest *p*-cyclophane derivative yet prepared is [6]paracyclophane (11).

This suggests that the mechanism proposed by Raphael (13) for the dehydrobromination of **16** is not necessary, and a simple steric argument seems more likely. Removal of an α-H (necessary to form the β-bromides **5**, **14**, and **15**) becomes more difficult sterically as we go from the 1,3-benzene **17** to the 1,2-benzene **16** to the 1,8-naphthalene **6** and hence increased formation of β-bromide occurs in this order too. That there can be no doubt of the structures of the bromides **5**, **18**, and **19** follows from their ir and pmr spectra: **5** shows a strong 950 cm^{-1} band in its ir spectrum (*trans* —CH=CH—) and a coupling constant of $J = 14$ Hz for the doublet at τ 3.57 in its pmr spectrum, whereas **19** shows the 892 cm^{-1} band (—CBr=CH_2) and two doublets, $J = 2$ Hz each at τ 3.89 and 4.20. As Raphael (13) has reported, bromide **18** shows both ir bands and both types of doublets.

In order to overcome this problem we decided to investigate alternative routes to the 1,2-, 1,3-, and 1,4-bis(β-bromovinyl)benzenes. With the ready commercial availability of the corresponding benzene dialdehydes we were at first tempted by the Wittig reaction. Use of bromomethyltriphenylphosphonium bromide, however, proved fruitless, despite Kobrich's (14) successful use of this compound. The analogous chloromethyl salt did yield 1,4-bis(β-chlorovinyl)benzene **20** from terephthalaldehyde, albeit in low (20%) yield. However, it turned out that we were unable to convert this compound into its bis-Grignard reagent and hence preferred to seek an alternative source of the bromovinyl compounds. Bachman's (15) method, namely the decarboxylative dehydrobromination of α,β-dibromoacids seemed appropriate, since cinnamic acids can be readily formed from benzaldehydes, especially in light of the more recent paper by Wolinsky and Erickson (16). After following the procedure of Grovenstein and Lee (17) for the preparation of β-bromostyrene from cinnamic acid dibromide we found that we could obtain a better yield more conveniently by adding bromine to an aqueous solution of sodium cinnamate. This procedure also worked, albeit poorly (11% yield), to prepare 1,4-bis(β-bromovinyl)benzene, **21**, from *p*-benzene diacrylic acid, **22**, whereas attempted isolation of the dibromo-acids failed, probably because of low solubility in organic solvents. Use of pyridine or DMF as solvent (16), at least in our hands, did not appear to help. An analogous reaction produced very little of the 1,3-isomer **15**.

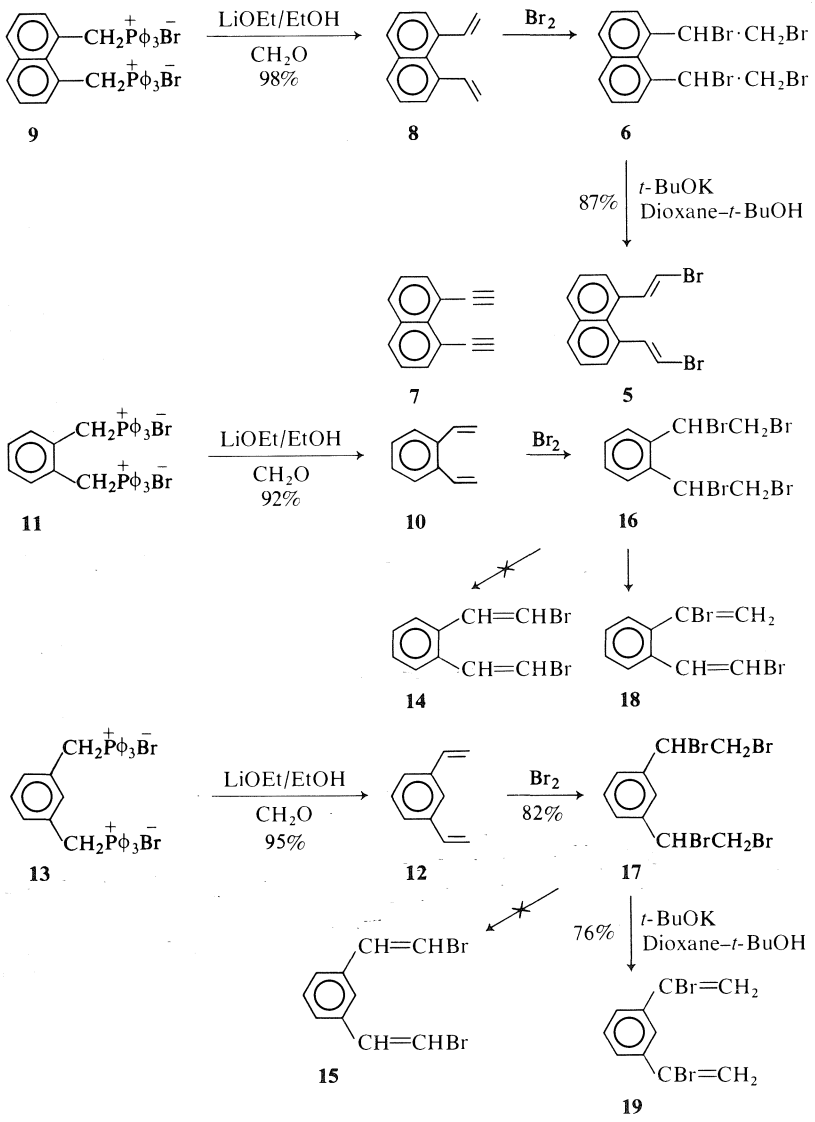

II. Coupling of β-Bromostyrene

Since Yoshino *et al.* (18) have shown that both *cis*- and *trans*-styryl Grignards are formed from either *cis*- or *trans*-β-bromostyrene, **23**, we decided in all couplings to use the mixture of isomers of β-bromovinyl compounds as prepared. Using Kauffman's method (5), namely

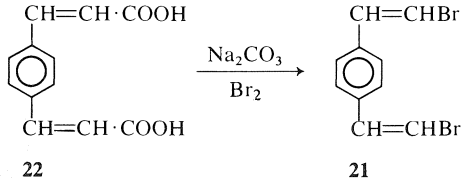

addition of the Grignard reagent to a cold (−50 °C) suspension of CuBr in tetrahydrofuran, and then warming to room temperature, a 65% yield of *trans-trans*-1,4-diphenylbuta-1,3-diene, **24**, could be isolated. Although Seyferth *et al.* (19) describe a method to prepare β-styryllithium in high yield, we found that coupling the resultant product led to both diene **24** and 1,4-diphenylbuta-1,3-diyne, **25**. When lithium/Br exchange was attempted using **23** and *n*-BuLi, diyne **25** was the sole isolated product. Seebach's (20) paper on lithium/Br exchange suggested that acetylene formation could be avoided by use of *tert*-butyllithium; this indeed was the case, how-

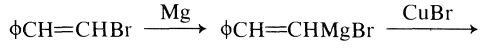

23

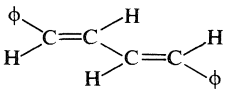

24

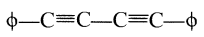

25

ever, the yield of the coupled diene **24**, was only 20%. We concluded therefore that simple coupling of the Grignard reagent was most fruitful.

III. Coupling of 1,8-Bis(β-bromovinyl)naphthalene. Synthesis of Pleiadiene and Cyclic Dimer

It quickly became obvious that ordinary Grignard quality magnesium was not active enough to react with the bis-bromovinylnaphthalene **5**. Since use of *n*- and *tert*-butyllithium and lithium itself failed to generate any vinyllithio-compounds from **5** (rather acetylenes were formed) we decided to activate the magnesium before use. Using the procedure of either Gilman and Kirby (21) (160 °C, I_2) or Rieke and Bales (22) (in which Mg is generated from $MgBr_2$ and K) sufficiently active Mg was formed so that immediate reaction occurred with the bis-bromide **5**. Coupling of bis-Grignard reagent **26** with CuBr and separation of the products by chromatography led to a 39–45% yield of pleiadiene, **27**, about 6% of the cyclic dimer **28**, and 1–2% of linear dimer **29**.

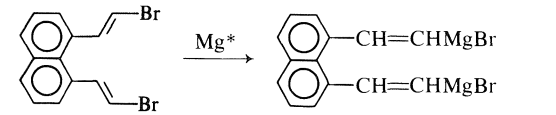

5 26

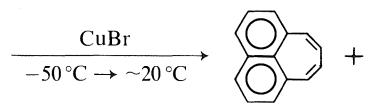

27

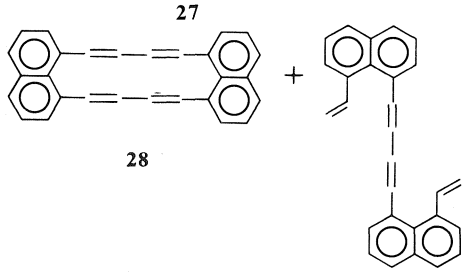

28 29

Pleiadiene (**27**) was readily recognized by its orange-red colour, mp, and pmr spectrum, all identical to that published (23). It has been synthesized by Boekelheide and Vick (24), Meinwald *et al.* (25), Shields *et al.* (23), and most recently by Pagni and co-workers (26) who claim the earlier syntheses to be lengthy and/or low yielding. We believe that the coupling procedure described is at least an equally facile synthesis of this interesting compound. The change of stereochemistry of the carbon–carbon double bonds in the cyclization is consistent with the work of Yoshino (18) noted above.

Structure of the Cyclic Dimer 28

The overall structure of dimer **28** (stereochemistry not indicated) follows from its mass spectrum, in which a clear molecular ion was observed at *m/e* 356. The structure was confirmed by hydrogenation, when one of the products showed uptake of 4 mol of hydrogen to give **30**. There was also obtained a heptacyclic transannular hydrogenation product of possible structure **31**, which showed a molecular ion at *m/e* 360, *i.e.* containing four hydrogen atoms less

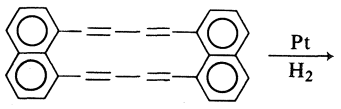

28

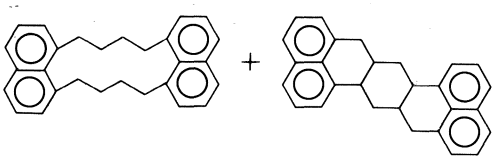

30 31

than **30**. These results are analogous to the case (7) for the hydrogenation of the tetraacetylene **32** in which **30** and a hexacyclic transannular product are formed. In both cases the resultant hydrogenation products are not very stable and

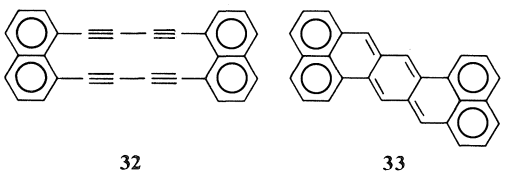

32 33

are rather difficult to characterize; several further conformers of **30** are capable of existence (for an analogous case see ref. 27) as are several isomers of **31**, and hence the pmr spectra of both

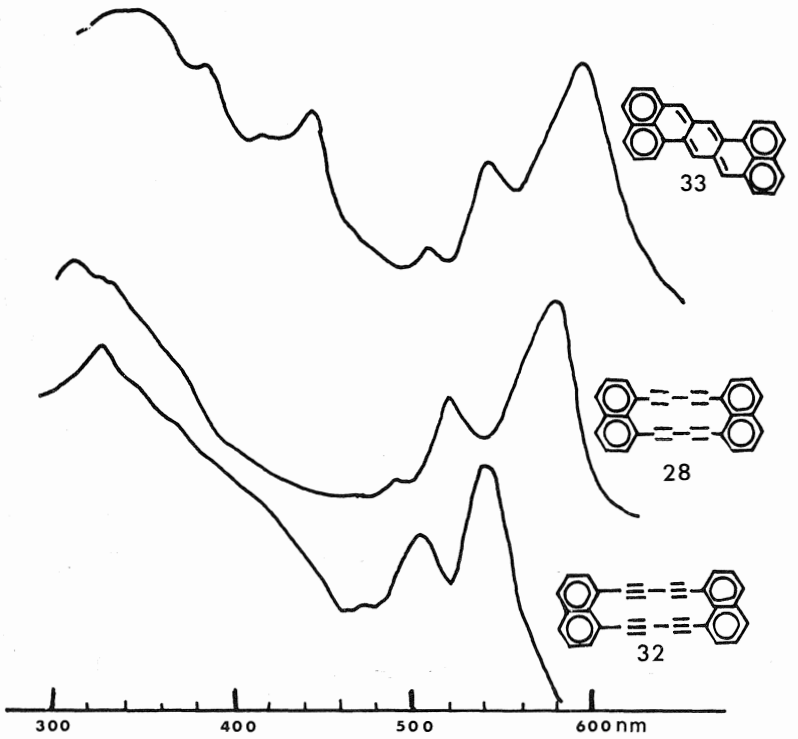

FIG. 1. The uv spectra of **33** (29), **32** (7), and **28**.

are complex. The uv spectra, however, are simple and consistent with the assigned structures and resemble that (7) of 1,8-diethylnaphthalene. The stereochemistry of **28** is more difficult to assign. The ir spectrum has only a very weak band at 970 cm^{-1}, the region associated[4] with *trans* —CH=CH— groups. Since all the protons occur as a broad band in the pmr spectrum (which is not resolved on cooling) coupling constants for the —CH=CH— protons cannot be obtained either. The uv spectra of **28**, the acetylene **32** (7), and heptazethrene, **33**, (29) are, however, all remarkably similar (see Fig. 1), and all three compounds give purple solutions. The acetylene **32** was too unstable to be isolated in the solid state (7), but both **28** and heptazethrene, **33**, form green crystals. Since no ir, mp, or pmr data are reported for **33**, it was at first thought that this was the product from the coupling reaction, especially in light of the report (30) that zethrene itself, **34**, is readily formed from the diene **35**.

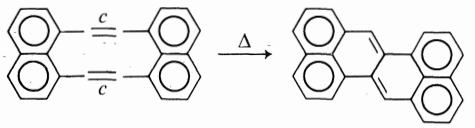

35 **34**

However, the mass spectral evidence and the difference in stability reported for **33** from that found for **28** precludes that. Nevertheless, the similarities between the uv spectra of **28**, **32**, and **33** suggest that they have a very similar π-orbital structure. A *cis-cis*-isomer of **28**, namely **36**,

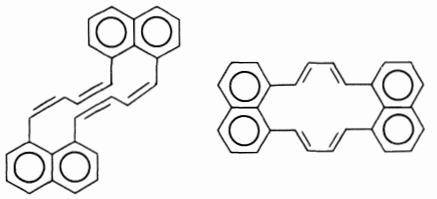

36 **37**

would not be planar or even nearly so, whereas a *trans-trans*-isomer, namely **37** could be, and hence is much more likely to give the observed uv spectrum which indicates that extensive delocali-

[4]By comparison, medium or strong ir bands in the 1000–940 cm^{-1} region are shown for *trans*-stilbene, *trans-trans*-1,4-diphenylbuta-1,3-diene, and many other examples (28).

zation of the π-system occurs. In view of the limited stability of **28**, however, unless other isomers can be synthesized by an alternative route, it is unlikely that the stereochemistry question can be settled quickly.

IV. The Coupling of 1,4-Bis(bromovinyl)benzene

Activated magnesium readily formed the bis-Grignard reagent of **21** and coupling as previously described produced a mixture of yellow compounds from which the linear dimer **38** could be isolated in low (<5%) yield. The structure could be assigned on the basis of the mass

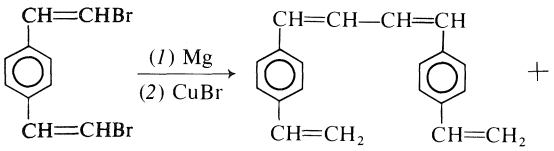

21 **38**

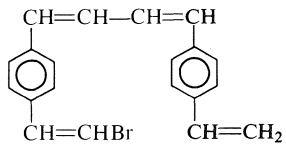

39

spectrum, the molecular ion at *m/e* 258, the pmr spectrum showing the presence of —CH=CH— protons at τ 2.9–4.2 as well as $=CH_2$ at τ 4.3–4.9, and strong ir bands at 1000 and 915 cm^{-1}. It is however, quite likely that more than one isomer is present. Mass spectroscopy also indicated that bromide **39** was formed in the reaction, presumably from the mono-Grignard reagent of **21**. However, we were unable to isolate any compound having the same molecular weight as the known (12) cyclic dimer **4**.

V. Coupling of Alanes

Since acetylenes are readily formed from bromovinyl compounds on treatment with strong base, and because vinylalanes are simple to prepare by addition of R_2AlH to the acetylene, we wondered if coupling the resultant vinylalane would be synthetically more useful than coupling the vinyl Grignard reagent.

Diisobutylaluminium hydride has been reported (31) to add to phenylacetylene in high yield to give diisobutylaluminiumstyryl **40**. When we added **40** to CuBr at −50 °C and then warmed to room temperature, we could only isolate diene **24** in low (6%) yield. This seemed surprising in view of Zweifel's (6) report of good yields from aliphatic-1-alkynes. When we applied

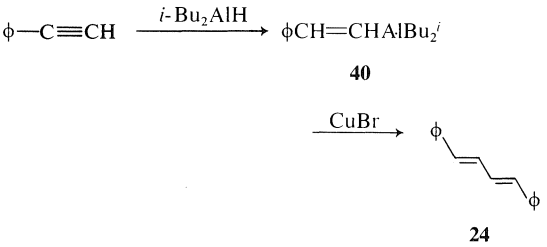

40 **24**

this procedure to 1,8-diethynylnaphthalene, **7**, we obtained a low yield of the previously obtained cyclic dimer **28**, linear dimer **29**, and no detectable pleiadiene, **27**.[5]

For the preparation of the cyclic dimer **28** coupling the alane does not appear to offer an advantage over coupling the Grignard reagent.

Conclusions

We have shown that both an inter- and intramolecular cyclization to yield a fully conjugated diene system are possible by coupling vinyl Grignard reagents with Cu(I), and in so doing have found a useful synthesis of pleiadiene, **27**. If a more general synthesis of β-bromovinyl compounds can be found, it is possible that the reaction can be extended to prepare other interesting examples of macrocyclic conjugated dienes, similar to **28**, of which there are very few reports.

A possible extension of this reaction is by the use of vinyl boranes. It was reported (32) in 1961 that alkyl boranes couple with $AgNO_3$. Despite the fact that Brown *et al.* (33) have reported that phenylacetylene forms a vinylborane with disiamylborane, no reports of the coupling of this compound have appeared. Very recently, however, Yamamoto *et al.* (34) have shown that dialkenyl chloroboranes couple with CH_3Cu to yield 1,3-dienes, at least in the case for those derived from alkyl-1-alkynes. Coupling of boranes derived from aryl-1-alkynes will form part of our next investigation into this area.

Experimental

All melting points were determined on a Kofler hot stage and are uncorrected. The pmr spectra were determined in $CDCl_3$ (unless otherwise stated) on a Perkin-Elmer R12A (60 MHz) or R32 (90 MHz) spectrometer

[5]As pointed out by a referee this is consistent with *cis*-addition of the elements of Al—H to the alkyne.

using tetramethylsilane as internal standard. Mass spectra were determined on a Hitachi–Perkin-Elmer RMU-7 or Finnigan 3300 mass spectrometer at 70 eV. The ir spectra were recorded on a Pye-Unicam SP1000 spectrophotometer and only major bands are reported. The uv spectra were recorded on a Cary 17 spectrophotometer. Microanalyses were performed by this department. All evaporations were carried out under reduced pressure on a rotary evaporator at *ca.* 40 °C. Extracts were dried with anhydrous sodium sulfate.

1,8-Divinylnaphthalene, **8**

A simpler procedure than that previously described (7) by one of us (R.H.M.) is rapid addition of a solution of lithium ethoxide (0.5 mol) in ethanol (150 ml) to a stirred solution of 1,8-bis(triphenylphosphoniomethyl)naphthalene dibromide, **9**, (7), (41.9 g, 50 mmol) and anhydrous formaldehyde (0.5 mol) in absolute ethanol (600 ml) at room temperature under N_2. After 3 h the volume was reduced by evaporation, and H_2O and pentane were added. The organic layer was washed, dried, and filtered through a short column of alumina (to remove any ϕ_3PO). Evaporation of the pentane filtrate yielded 8.12 g (98%) of pure product, identical to previous samples.

1,8-Bis(trans-β-bromovinyl)naphthalene, **5**

By shortening the reaction time of the literature procedure (7) from 24 h to 1 h the yield of the product (obtained by direct recrystallization from hexane) was increased from 28% to 87%.

1,2-Divinylbenzene, **10**

A solution of lithium ethoxide (0.25 mol) in ethanol (125 ml) was added with stirring under N_2 to a solution of *o*-bis(triphenylphosphoniomethyl)benzene dibromide, **11**, (35) (79 g, 0.10 mol) and formaldehyde (0.35 mol) in absolute ethanol (350 ml) at room temperature. After 3 h the volume of solvent was reduced by evaporation and H_2O and pentane were added. The organic extract was washed, dried, and filtered through a short column of alumina to remove any ϕ_3PO. Evaporation of the pentane yielded the product **10**, as a colourless oil, 11.9 g (92%); pmr τ (60 MHz) 2.5–3.3 (6H, m, Ar*H* + ArC*H*=), 4.51 (2H, dd, J = 18 and 2 Hz, *trans* —ArCH=C*H*—) and 4.80 (2H, dd, J = 11 and 2 Hz, *cis* —ArCH=C*H*—).

1,3-Divinylbenzene, **12**

(a) 1,3-Bis(triphenylphosphoniomethyl)benzene Dibromide, **13**

A solution of α,α′-dibromo-*m*-xylene (Aldrich, 66 g, 0.25 mol) and triphenylphosphine (144 g, 0.55 mol) in DMF (400 ml) was heated to 180 °C for 2 h with stirring and then allowed to cool. The product was removed by filtration. Evaporation of the filtrate to 50% (vol.) and addition of benzene precipitated a further quantity of product, 197 g in all (almost quantitative), mp 312–313 °C.

(b) The Wittig Reaction

A solution of lithium ethoxide (0.5 mol) in ethanol (250 ml) was added with stirring under N_2 to a solution of *m*-bis(triphenylphosphoniomethyl)benzene dibromide, **13**, (79 g, 0.10 mol), and formaldehyde (0.56 mol) in absolute ethanol (400 ml) at room temperature. After 2 h the volume of solvent was reduced by evaporation and H_2O and pentane added. The organic layer was washed, dried, and filtered through a short column of silica gel to give, after evaporation of the pentane, the product **12** as a colourless oil, 12.5 g (95%); pmr τ (60 MHz), 2.6–2.9 (4H, m, ArH), 3.39 (2H, dd, J = 11 and 17 Hz, Ar—C*H*=), 4.40 (2H, dd, J = 17 and 1 Hz, *trans* —ArCH=C*H*—) and 4.88 (2H, dd, J = 11 and 1 Hz, *cis* —ArCH=C*H*—).

1,3-Bis(α,β-dibromoethyl)benzene, **17**

Bromine (13 ml, 40 g, 0.25 mol) in CCl_4 (50 ml) was added dropwise to an ice cold solution of *m*-divinylbenzene, **12** (15.6 g, 0.12 mol), in CCl_4 (100 ml). After warming to room temperature the reaction mixture was poured into 10% $NaHSO_3$ solution. The organic layer was washed, dried, and evaporated to yield an oil which, on trituration with pentane at 0 °C, gave white crystals of product, 44.3 g (82%), mp 62–63 °C; pmr τ (60 MHz) 2.63 (4H, s, ArH), 4.90 (2H, dd, J = 10 and 7 Hz, ArC*H*Br—) and 5.8–6.1 (4H, m, —CH_2Br); ms correct M^+ for $C_{10}H_{10}Br_4$.

1,3-Bis(α-bromovinyl)benzene, **19**

A solution of *tert*-BuOK (Aldrich, 5.7 g, 50 mmol) in *tert*-butyl alcohol (75 ml) and dioxane (25 ml) was added over 30 min with stirring to a solution of the tetrabromide **17** (9.0 g, 20 mmol), in dioxane (100 ml) at room temperature. After a further 30 min, H_2O and ether were added. The organic layer was washed, dried, and evaporated and the residual oil was chromatographed on silica gel. Pentane first eluted the product **19** as a colourless oil, 4.4 g (76%); pmr τ (90 MHz) 2.2–2.8 (4H, m, ArH), 3.89 and 4.20 (2H each, d, J = 2 Hz, =CH_2); ir (neat) 1610 and 1478 (—C=C—), 1175 and 892 (—CBr=CH_2) and 800 and 705 cm^{-1} (1,3-benzene); ms correct M^+ for $C_{10}H_8Br_2$. *Anal.* calcd. for $C_{10}H_8Br_2$: C 41.71, H 2.80; found: C 41.73, H 2.77.

1,4-Bis(β-chlorovinyl)benzene, **20**

n-Butyllithium (Alfa, 35 mmol in 18 ml hexane) was injected into a stirred suspension of chloromethyltriphenylphosphonium chloride (Aldrich, 12.11 g, 35 mmol) in dry THF (200 ml) at −60 °C under N_2. After 10 min, terephthaladehyde (Aldrich, 2.35 g, 17.5 mmol) in dry THF (200 ml) was added keeping the temperature below −40 °C. The reaction mixture was then allowed to stir ~12 h without further cooling. After addition of water the aqueous phase was extracted with ether. The extracts were washed, dried, and evaporated. After chromatography of the residual solid on silica gel using pentane as eluant, the product **20** was obtained as a solid mixture of isomers, 1.39 g (20%). Crystallization from $CHCl_3$–hexane gave crystals of a single isomer mp 72–74 °C; pmr τ 2.35 (4H, s, ArH), 3.41 (2H, d, J = 8 Hz, ArC*H*=) and 3.80 (2H, d, J = 8 Hz, =CHCl); ir (KBr) 932 (m) (*trans* —CH=CHCl), 860 (vs), 852 (vs), 825 (vs), 728 (vs), and 670 (s) cm^{-1}; correct M^+ for $C_{10}H_8Cl_2$. *Anal.* calcd. for $C_{10}H_8Cl_2$: C 60.33, H 4.05; found: C 59.98, H 3.83.

The stereochemistry of the double bond is not assigned for this isomer since the ir band at 932 cm^{-1} indicates a *trans* CH=CHCl whereas the coupling constant, J = 8 Hz indicates a *cis* CH=CHCl.

β-Bromostyrene, **23**

This was obtained in 60% yield using the method of Grovenstein and Lee (17) by treating cinnamic acid dibromide with aqueous sodium carbonate or more conveniently by adding bromine (1 mol) dropwise to a hot

(80 °C) solution of sodium cinnamate (1 mol, prepared by dissolving cinnamic acid and sodium carbonate in hot water) with good stirring. After cooling, the reaction was extracted with ether. The extract was washed, dried, and evaporated to yield a pale yellow oil consisting nearly entirely of β-bromostyrene by pmr comparison to an authentic sample (obtained above). Filtration through a short column of silica gel gave pure colourless product in about 85% yield.

1,4-Bis(trans-β-bromovinyl)benzene, ***21***

Bromine (5 ml, 92 mmol) was added dropwise with stirring at room temperature to a solution of *p*-benzene diacrylic acid, **22**, (36) (10.0 g, 46 mmol) and Na_2CO_3 (10 g, 94 mmol) in H_2O (500 ml). Vigorous bubbling ensued as the bromine colour was discharged and an off-white precipitate formed. The total reaction mixture was extracted with ether and the organic layer was washed, dried, and evaporated. Recrystallization of the resulting residue from benzene yielded almost white crystals of product, *ca.* 1.5 g (11% yield), mp 138–140 °C (lit. (37) mp 135 °C); pmr τ (60 MHz) 2.77 (4H, s, ArH), 2.91 (2H, d, J = 14 Hz, Ar*CH*=) and 3.28 (2H, d, J = 14 Hz, =CHBr); ir (KBr) 940 (*trans* —CH=CHBr), 770 and 725 cm^{-1}; ms correct M^+ for $C_{10}H_8Br_2$.

Concentration of the benzene mother liquors and addition of hexane precipitated the addition product of 2 mol of bromine to **21**, the hexabromide

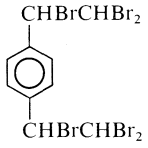

mp 159–162 °C; pmr τ (60 MHz) 2.54 (4H, s, ArH), 4.03 (2H, d, J = 7 Hz, Ar—C*H*Br), and 4.64 (2H, d, J = 7 Hz, —$CHBr_2$); ms, M^+ 608, correct isotope pattern for $C_{10}H_8Br_6$ with subsequent stepwise loss of Br.

The Attempted Preparation of 1,3-Bis(trans-β-bromovinyl)-benzene ***15***

The reaction was carried out exactly as described above for the 1,4-isomer using *m*-benzene diacrylic acid (38). Chromatography of the resulting orange oil on silica gel using pentane as eluant gave a small amount of material which in its pmr spectrum showed peaks at τ (60 MHz) 2.81 (4H, bs, ArH), 2.92 (2H, d, J = 14 Hz, Ar*CH*=) and 3.32 (2H, d, J = 14 Hz, =C*H*Br), consistent with the structure of **15**.

Couplings of β-Bromostyrene, ***23***

(a) With Mg and then CuBr

β-Bromostyrene **23** (2.6 g, 14 mmol) and Mg turnings (0.36 g, 15 mmol) under N_2 in dry THF (50 ml) were heated under reflux for 6 h. The cooled black reaction mixture was then added dropwise over 30 min to a suspension of CuBr (dried over P_2O_5, 2.2 g, 15 mmol) kept at −60 °C under N_2. After the addition the resulting orange solution was allowed to warm to room temperature. It turned brown above −20 °C. After stirring overnight, H_2O and CH_2Cl_2 were added and the organic layer was washed, dried, and evaporated to yield a yellow residue which on crystallization from ethanol yielded *trans-trans*-1,4-diphenylbuta-1,3-diene, **24**, as plates, 1.0 g (65%), mp 152 °C (lit. (39) mp 152–152.5 °C). Identical pmr and ir spectra to those published (Aldrich *IV* 20C and 511E).

(b) With Li and then CuBr

The above reaction was repeated except that the vinyl lithium was prepared in ether at 0 °C under argon. The resulting oil from the coupling reaction contained the diene **24**, the diyne **25**, as well as many other products.

(c) With n-BuLi and then CuBr

A solution of *n*-BuLi (11 mmol in 5 ml hexane) was injected into a solution of β-bromostyrene (2.0 g, 11 mmol) in dry ether (50 ml) at 0 °C under N_2. After stirring for 1 h, this solution was added dropwise to a suspension of CuBr (1.6 g, 11 mmol) in dry ether (50 ml) kept at −60 °C under N_2. After stirring for 1 h the pale yellow solution was allowed to warm to room temperature (it turned brown above −10 °C). After addition of H_2O, the organic layer was washed, dried, and evaporated to yield a brown oil which on chromatography on silica gel using pentane as eluant yielded firstly unchanged bromide, **23** (30%) followed by crystals of 1,4-diphenylbuta-1,3-diyne, **25**, 0.3 g (27%), identical ir spectrum to that published (Aldrich 1257D).

(d) With tert-BuLi and then CuBr

A solution of β-bromostyrene (7.4 g, 40 mmol) in dry THF (50 ml) was added slowly to a solution of *tert*-BuLi (80 mmol) in pentane (100 ml) and dry THF (50 ml) kept at −78 °C. After 1 h, CuBr (5.7 g, 40 mmol) was added and then the reaction mixture was allowed to warm to room temperature. The volume of solvent was reduced and then H_2O and ether were added. The organic layer was washed, dried, and evaporated to yield a pale yellow solid. Recrystallization of this from ethanol yielded colourless plates of 1,4-diphenylbuta-1,3-diene, **24**, 0.82 g (20%) identical to previous samples.

Coupling of 1,8-Bis(β-bromovinyl)naphthalene, ***5***. *Synthesis of Pleiadiene*, ***27***, *and Cyclic Dimer* ***28***

1,2-Dibromoethane (1 ml) was added to a suspension of activated (21) Mg turnings (7.2 g, 30 mmol) in dry THF (100 ml) under N_2 at room temperature. After 15 min a portion of a solution of 1,8-bis(β-bromovinyl)naphthalene, **5**, (7.8 g, 20 mmol) in dry THF (75 ml) was added. The reaction started quickly and an orange colour developed. The remainder of **5** was added slowly and stirring continued for 2 h. The reaction mixture was then cooled to −78 °C and CuBr (7.0 g, 50 mmol) was added. The mixture was allowed to warm slowly to room temperature and was kept overnight. After addition of H_2O and ether the organic layer was washed, dried, and evaporated. The residue was then chromatographed on silica gel. Pentane first eluted a small amount of 1,8-divinylnaphthalene and as a second fraction an orange-red band. After evaporation of solvent and recrystallization from hexane this gave pleiadiene, **27**, 1.4–1.6 g (39–45%) as red crystals mp 91–92 °C (lit. (23) mp 91–92.5 °C) identical pmr spectrum to that published (23); ir (KBr) 3010 (—CH=CH—), 840, 775, 730 cm^{-1}. The third fraction eluted was any unchanged starting bromide **5**. Benzene–pentane (15:85) then eluted the yellow linear dimer **29**, *ca.* 50 mg (1.4%), mp 133 °C (dec.); pmr τ (60 MHz) 2.1–3.4 (18H, m, ArH and —*CH*=) and 4.30, 4.62, and 4.82 (4H, bs (some coupling), $=CH_2$); ir (KBr), 980 (s) (*trans* —CH=CH), 910 (m) ($=CH_2$), and 770 (s) cm^{-1}; ms *m/e*

(relative intensity), M^+ 358(5), 180(50), 179(100), 178(100), 165(100), under CH_4 chemical ionisation: $(MH)^+$ 359(19). The compound decomposes slowly on standing at room temperature.

Eluted next was the cyclic dimer **28**, as green crystals, 224 mg (6.3%) which formed a purple solution. Sometimes further chromatography on silica gel was necessary to purify this compound. Very careful recrystallization from hexane gave 94 mg (2.6%) of green crystals, mp 160–162 °C. On several occasions overheating or use of a different solvent produced dark tars; pmr τ (90 MHz, CD_2Cl_2) 2.1–3.7 (br signal, all protons, not resolved on cooling to −90 °C); ir (KBr) 970 (vw), 832 (m), 773 (s) cm^{-1}; uv (cyclohexane) λ_{max} (log ε_{max}) 578 nm (3.58), 534 (3.24), 497 (2.86), 332 (3.58), 316 (3.63), 305 (3.60), 279 (3.47), and 232 (4.28); (CH_2Cl_2) λ_{max} 582 nm, 536 and 500; (C_6H_5Cl) λ_{max} 592 nm, 545 and 510; ms *m/e* (relative intensity) (source temperature 170 °C) M^+ 356(17), 355(7), 354(10), 353(8), 352(5), 180(27), 179(71), 178(100), 177(20), 176(20), and 165(67), under $(CH_3)_3CH$ chemical ionization $(M + 1)^+$ 357(14). *Anal.* calcd. for $C_{28}H_{20}$: C 94.34, H 5.66; found: C 94.42, H 5.60. The compound can be stored unchanged at −20 °C. Eluted next, very close to the cyclic dimer, was a second green compound of unknown structure, ~20 mg, dec. *ca.* 250 °C, which gave a green solution having λ_{max} (cyclohexane) 592, 546, 506 nm. No molecular ions could be seen in the mass spectrum. The pmr and ir spectra were essentially the same as for **28**.

These results were not changed significantly by preparing the active magnesium from $MgBr_2$ and K (22).

Hydrogenation of the Cyclic Dimer 28

The cyclic dimer **28** (80 mg) and PtO_2 (30 mg) were stirred under an H_2 atmosphere in ethyl acetate (50 ml) for 30 min–2 h. Removal of catalyst and then solvent gave an oil which was chromatographed on silica gel, using pentane–benzene (5:1) as eluant. Eluted first was the product **30** as a yellow oil (~8 mg) which darkened on removal of solvent; pmr τ (60 MHz), 2.3–3.3 (12H, m, ArH); 6.6–7.2 (8H, m, ArCH_2—) and 7.6–8.4 (8H, m, —CH_2—); uv (Et_2O) λ_{max} (relative absorbance) 340 nm (0.07), 324 sh (0.24), 302 sh (0.92), 293 (1.00) and 279 sh (0.79); ms *m/e* (relative intensity) M^+ 364(100), 362(50), 360(47), with a very large number of much stronger cleavage peaks. This was immediately followed by a transannular product, *e.g.* **31**, ~5 mg as an oil; pmr τ 2.2–3.6 (12H, m, ArH) and 4.2–8.9 (12H, m, —CH, —CH_2); uv (ether) λ_{max} (relative absorbance) 300 nm (0.95), 293 (1.00), 280 sh (0.79) with a tail to 450 nm; ms *m/e* (relative intensity), M^+ 360(100), 358(22), 181(41), 180(46), and 179(71).

Coupling of 1,4-Bis(β-bromovinyl)benzene, 21

A few drops of 1,2-dibromoethane were added to a stirred suspension of activated (21) Mg (2.0 g, 8.3 mmol) in dry THF (50 ml) under N_2 at room temperature to which approximately one quarter of the dibromide **21** (1.30 g, 4.5 mmol) had been added. After 15 min stirring the colour of the reaction became yellowish and the remainder of the dibromide was added in dry THF (20 ml). After stirring overnight the yellow reaction mixture was added dropwise to a stirred suspension of CuBr (1.5 g, 10 mmol) in dry THF (100 ml) kept at −50 °C under N_2. The mixture was then allowed to warm slowly to room temperature. After 5 h, H_2O and ether were added, and the organic layer was washed, dried, and evaporated. The resulting bright orange solid (470 mg) was chromatographed on silica gel.

Pentane eluted first any unused starting bromide **21**, followed by the yellow linear dimer **38**, as a yellow solid from hexane, dec. with softening 140 °C; pmr τ (60 MHz) 2.5–2.9 (m, ArH), 2.9–4.2 (m, —CH=) and 4.3–4.9 (m, $=CH_2$); ir (KBr) 1000 and 915 ($=CH_2$), 868 and 822 cm^{-1}; ms *m/e* (relative intensity) M^+ 258(100) and 128(52). Later fractions contained the bromide **39** as indicated by its mass spectrum, molecular ions at *m/e* 338, 336. None of the known (12) cyclic dimer **4** could be detected.

Couplings of Alanes

(a) Derived from Phenylacetylene

i-Bu_2AlH (30 mmol) in hexane was added dropwise over 15 min to a solution of phenylacetylene (3 g, 29 mmol) in dry hexane (20 ml) under N_2. The mixture was then heated to 50 °C for 4 h when it became orange. After cooling, it was added dropwise with stirring to a suspension of CuBr (4.6 g, 32 mmol) in THF (50 ml) under N_2 kept at −50 °C. After 30 min the mixture was allowed to warm to room temperature. H_2O and ether were then added and the organic layer was washed, dried, and evaporated. The resulting solid was chromatographed on silica gel using pentane as eluant to yield the previously obtained diene **24**, 180 mg (6%).

(b) Derived from 1,8-Diethynylnaphthalene, 7

i-Bu_2AlH (50 mmol in hexane) was added to a solution of 1,8-diethynylnaphthalene, **7**, (7) (3.56 g, 20 mmol) in hexane (100 ml) at 0 °C under N_2. On warming to 50 °C the solution turned through yellow and red to brown. After 2 h the solution was cooled to −78 °C, and dry THF (50 ml) added followed by CuBr (7.2 g, 50 mmol). The reaction mixture was allowed to warm to room temperature and then H_2O and ether were added. The organic layer was washed, dried, and evaporated and the residue chromatographed on silica gel to give small amounts of the previously obtained linear **29** and cyclic dimers **28**, but no pleiadiene, **27**.

Acknowledgments

We thank the Research Corporation for a Cottrell Research Grant to initiate this investigation and the National Research Council of Canada and the University of Victoria for their further support.

1. G. Eglinton and W. McCrae. Adv. Org. Chem. Methods and Results, **4**, 225 (1963).
2. C. Glaser. Chem. Ber. **2**, 422 (1869).
3. G. Eglinton and A. R. Galbraith. J. Chem. Soc. 889 (1959).
4. G. M. Whitesides and C. P. Casey. J. Am. Chem. Soc. **88**, 4541 (1966); G. M. Whitesides, C. P. Casey, and J. K. Krieger. J. Am. Chem. Soc. **93**, 1379 (1971).
5. T. Kauffman and W. Sahm. Angew. Chem. Int. Ed. Engl. **6**, 85 (1967).
6. G. Zweifel and R. L. Miller. J. Am. Chem. Soc. **92**, 6678 (1970).

7. R. H. MITCHELL and F. SONDHEIMER. Tetrahedron, **24**, 1397 (1968).
8. G. EGLINTON, R. A. RAPHAEL, O. M. BEHR, and A. R. GALBRAITH. J. Chem. Soc. 3614 (1960); W. OKAMURA and F. SONDHEIMER. J. Am. Chem. Soc. **89**, 5991 (1967).
9. W. R. MOORE, L. N. BELL, and G. P. DAUMIT. J. Org. Chem. **36**, 1694 (1967).
10. K. P. C. VOLLHARDT. Synthesis, 765 (1975).
11. V. V. KANE, A. D. WOLF, and M. JONES, JR. J. Am. Chem. Soc. **96**, 2643 (1974).
12. D. J. CRAM and K. C. DEWHIRST. J. Am. Chem. Soc. **81**, 5963 (1959).
13. O. M. BEHR, G. EGLINTON, I. A. LARDY, and R. A. RAPHAEL. J. Chem. Soc. 1151 (1964).
14. G. KOBRICH. Angew Chem. **74**, 33 (1962).
15. G. B. BACHMAN. J. Am. Chem. Soc. **55**, 4279 (1933); J. K. FARRELL and G. B. BACHMAN. J. Am. Chem. Soc. **57**, 1281 (1935).
16. J. WOLINSKY and K. L. ERICKSON. J. Org. Chem. **30**, 2208 (1965).
17. E. GROVENSTEIN, JR. and D. E. LEE. J. Am. Chem. Soc. **53**, 2639 (1953).
18. T. YOSHINO, Y. MANABE, and Y. KIKUCHI. J. Am. Chem. Soc. **86**, 4670 (1964).
19. D. SEYFERTH, L. G. VAUGHAN, and R. SUZUKI. J. Organomet. Chem. **1**, 437 (1964).
20. D. SEEBACH and H. NEUMANN. Chem. Ber. **107**, 847 (1974).
21. H. GILMAN and R. H. KIRBY. Recl. Trav. Chim. **54**, 577 (1935); Chem. Abstr. 3774 (1935).
22. R. D. RIEKE and S. E. BALES. J. Am. Chem. Soc. **96**, 1775 (1974).
23. J. E. SHIELDS, D. GAVRILOVIC, J. KOPECKÝ, W. HARTMANN, and H. G. HEINE. J. Org. Chem. **39**, 515 (1974).
24. V. BOEKELHEIDE and G. K. VICK. J. Am. Chem. Soc. **78**, 653 (1956).
25. J. MEINWALD, G. E. SAMUELSON, and M. IKEDA. J. Am. Chem. Soc. **92**, 7604 (1970).
26. C. R. WATSON, JR., R. M. PAGNI, J. R. DODD, and J. E. BLOOR. J. Am. Chem. Soc. **98**, 2551 (1976).
27. G. WITTIG, G. KOENIG, and K. CLAUSS. Ann. **593**, 127 (1953).
28. K. LUNDE and L. ZECHMEISTER. Acta Chem. Scand. **8**, 1421 (1954).
29. E. CLAR and I. A. MACPHERSON. Tetrahedron, **18**, 1411 (1962).
30. R. H. MITCHELL and F. SONDHEIMER. J. Am. Chem. Soc. **90**, 528 (1968).
31. G. WILKE and H. MÜLLER. Ann. **629**, 222 (1960).
32. H. C. BROWN and C. H. SNYDER. J. Am. Chem. Soc. **83**, 1002 (1961).
33. H. C. BROWN, D. H. BOWMAN, S. MISUMI, and M. K. UNNI. J. Am. Chem. Soc. **89**, 4531 (1967).
34. Y. YAMAMOTO, H. YATAGAI, and I. MORITANI. J. Am. Chem. Soc. **97**, 5606 (1975).
35. C. E. GRIFFEN, K. R. MARTIN, and B. E. DOUGLAS. J. Org. Chem. **27**, 1627 (1931).
36. P. RUGGLI and W. THEILHEIMER. Helv. Chim. Acta, **24**, 899 (1941).
37. F. EPHRAIM. Chem. Ber. **34**, 2779 (1901).
38. W. REID and F. J. KÖNIGSTEIN. Chem. Ber. **92**, 2532 (1959).
39. E. R. BLOUT and V. W. EAGER. J. Am. Chem. Soc. **67**, 1315 (1945).

Structure and stability of vitamin E – lecithin and phytanic acid – lecithin bilayers studied by ^{13}C and ^{31}P nuclear magnetic resonance[1]

ROBERT J. CUSHLEY AND BRUCE J. FORREST

Department of Chemistry, Simon Fraser University, Burnaby, B.C., Canada V5A 1S6

Received July 21, 1976

ROBERT J. CUSHLEY and BRUCE J. FORREST. Can. J. Chem. **55**, 220 (1977).

^{13}C spin–lattice relaxation studies on lecithin bilayers indicate a marked destabilization of the bilayer structure by incorporated vitamin E (*d,l*-α-tocopherol) and phytanic acid, phytanic acid causing the greatest perturbation.

Kinetic analysis of paramagnetic praseodymium infusion into the lecithin vesicles containing various phytyl compounds has been performed using ^{31}P nmr. Relative rates of Pr^{3+} leakage through the mixed lecithin – phytyl compound bilayer compared with pure lecithin (relative rate = 1.00) were: phytol = 7.8, vitamin E = 47.7, and phytanic acid = 2897.

ROBERT J. CUSHLEY et BRUCE J. FORREST. Can. J. Chem. **55**, 220 (1977).

Des études de relaxation spin–réseau du ^{13}C sur des couches doubles de lécithine indiquent qu'il se produit une déstabilisation importante de la structure de la couche double lors de l'incorporation de vitamine E (*d,l*-α-tocophérol) et d'acide phytanique; l'acide phytanique cause la plus grande perturbation.

Utilisant la rmn du ^{31}P, on a effectué des analyses cinétiques de l'infusion de praséodyme paramagnétique dans des ampoules de lécithine contenant divers composés phytylés. Les vitesses relatives de perte de Pr^{3+} à travers une couche double mixte de lécithine – composé phytylé, par rapport à la lécithine pure (vitesse relative = 1.00), sont: phytol = 7.8, vitamine E = 47.7 et acide phytanique = 2897.

[Traduit par le journal]

Introduction

As part of our continuing study on the effects of branched chain compounds on the structure and stability of model membrane systems, we wish to report the effects of the incorporation of vitamin E (*d,l*-α-tocopherol) and phytanic acid into a model membrane. Previously, we had studied the effects of the intercalation of the related isoprenoid, phytol, 3,7,11,15-tetramethylhexadec-*trans*-2-en-1-ol (1). We found that, at 52 °C, the fluidity of the lecithin bilayer, as shown by ^{13}C T_1 relaxation times, increased greatly due to added phytol and the effect was lessened as the temperature was lowered and the gel–liquid crystalline transition temperature, T_m, was approached. Since any change in the packing of the lipid molecules may greatly alter the properties of the bilayer (2), the perturbation was interpreted in terms of the difficulty in accommodating the phytyl compound in an ordered bilayer structure.

In the present study the isoprenyl compounds phytanic acid and vitamin E have been incorporated into hen egg lecithin bilayers. Despite the obvious physiological importance of these two

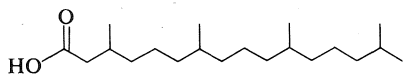

Phytanic acid
3,7,11,15-Tetramethylhexadecanoic acid

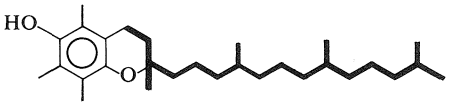

α-Tocopherol
D-2,5,7,8-Tetramethyl-2-(4,8,12-trimethyltridecyl)-6-chromanol

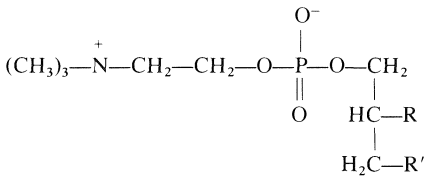

Egg lecithin
R = Oleic (18:1) or linoleic acid (18:2)
R′ = Palmitic (16:0) or stearic acid (18:0)
Dipalmitoyl lecithin: R = R′ = palmitic acid

[1]Presented at the 59th Canadian Chemical Conference of the Chemical Institute of Canada, London, Ontario, June 6–10, 1976.

phytyl compounds, very little is known of their effects at a molecular level. This is in direct contrast to the wealth of information concerning the interactions of cholesterol with membrane systems. To this end, we report herein the effects of incorporated vitamin E and phytanic acid on membrane structure and fluidity evidenced by ^{13}C nmr relaxation studies.

In addition, we have discovered a large permeability increase in the model membrane by means of lanthanide induced shifts (LIS) of the ^{31}P nmr signals which shows a strong correlation with the effects demonstrated by ^{13}C.

Experimental

Lecithin was extracted from fresh egg yolks by the method of Singleton *et al.* (3). Thin layer chromatographic analysis showed a single spot when developed with $CHCl_3$:MeOH:H_2O (65:25:4) and heated. Compounds were obtained from the following sources: *d,l*-α-tocopherol (vitamin E), Sigma Chemical Co.; phytanic acid (99.7%), Analabs; phytol, Aldrich Chemical Co.; praseodymium nitrate (99.9%), Alpha Inorganics.

Lecithin dispersions (10% w/v) were prepared by shaking the dry lipid with D_2O, in the case of the ^{13}C spectra, and with 0.05 *M* Tris buffer, p*H* 7.22 which was 0.05 *M* in KCl in the case of ^{31}P spectra. The dispersions were then sonicated under nitrogen on a Biosonik III probe-type sonicator until translucence (~10 min) while being cooled by a stream of cold water flowing through a jacket surrounding the sample. The vesicle preparations were then centrifuged and passed through a 0.22 μ Millipore filter to remove titanium fragments and to remove large liposomes. The resultant vesicle preparation was subsequently transferred under nitrogen to a 12 mm nmr tube and the nmr spectra were taken immediately.

Mixed vesicle preparations (3:1 mole ratio lecithin:phytyl compound) were prepared in a similar manner by first co-dissolving both components in chloroform followed by exhaustive pumping to obtain the dry mixture. Attempts to incorporate either vitamin E or phytanic acid into the bilayers at higher molar ratios were unsuccessful.

All ^{13}C spectra were determined at 25.2 MHz on a Varian XL-100-15 nmr spectrometer fitted with a TT 100 FT attachment using an internal ^{2}H field-frequency lock, and an 8K dataset, with external TMS as a reference. The sample temperature was kept constant at 11 ± 1 °C. Under these conditions, the vesicles remained stable throughout the course of the experiment. Due to the length of the T_1's to be measured, and in order to circumvent the required waiting period of five times T_1 between pulse sequences, the ^{13}C spin–lattice relaxation times were measured by the homospoil sequence of McDonald and Leigh (4). T_1's for several carbon atoms which were indicated to be < 200 ms were checked by the inversion-recovery method of Vold *et al.* (5) and were found to be in agreement with the homospoil determinations to within experimental error. The percentage error for each measurement is included in Table 1 and averages ±6%; occasionally duplicate runs showed variance in the two runs up to 10%. Thus, our confidence limit is set at ±10%. Therefore, if the variance exceeded the percentage error, the variance is reported in Table 1.

^{31}P spectra were determined at 33 °C using a Varian XL-100-15 spectrometer operating at 40.5 MHz fitted with a TT 100 FT attachment, using an external ^{19}F field-frequency lock and external H_3PO_4 (85%) as a reference. Unless otherwise indicated, running conditions were: data set = 2K zero-filled to 4K; digitizing rate = 2 kHz; pulse width = 10 μs; pulse delay = 0.5 s. Initial spectra were taken and a 150 μl portion of 0.1 *M* $Pr(NO_3)_3 \cdot 5H_2O$ in the aforementioned buffer solution was then added and subsequent spectra taken. Using 3 ml of vesicle solution gave a Pr^{3+} concentration of 0.005 *M*.

Results and Discussion

The ^{13}C spin–lattice relaxation times for egg lecithin, lecithin with 25 mol% incorporated vitamin E, and lecithin with 25 mol% incorporated phytanic acid are shown in Table 1. Assignments are taken from those made previously (1). At the concentrations used, resonances of the phytyl additives were not of sufficient intensity to allow an accurate determination of their relaxation times. An examination of the lecithin T_1's readily reveals a large increase in the fluidity of the lipid bilayer upon addition of the phytyl compounds.

Increases are observed in the relaxation times for each carbon along the lecithin hydrocarbon chain. For example, the T_1 of the main methylene envelope carbons increases from 0.30 to 0.55 s upon vitamin E incorporation, and to 0.81 s upon intercalation of phytanic acid, while the antepenultimate carbon experiences increases from 0.30 to 0.55 s and to 0.90 s for the lecithin – vitamin E, and lecithin – phytanic acid mixed bilayers, respectively. In like fashion, increases are also detected for the penultimate carbon from 0.66 to 0.80 and 1.75 s, and for the terminal carbon from 2.05 to 2.76 and to 2.98 s.

It has recently been pointed out by Seelig and Seelig (6) and Stockton *et al.* (7) that interpretation of ^{13}C T_1's is hampered by the fact that the order parameter, S_{mol}, and τ_c, the rate for segmental motion about individual C—C bonds, cannot be separated in the dipolar correlation time, τ, calculated from T_1 for purely dipolar relaxation

$$\tau = r^6/N\gamma_C{}^2\gamma_H{}^2\,\hbar^2 T_1$$

That is, the relaxation rate is determined by the anisotropy of motion as well as the rate of motion. Nevertheless, the concept of increased motional freedom due to separation of phos-

TABLE 1. ^{13}C relaxation times[a] for lecithin and lecithin – phytyl compound bilayers[c]

Carbon	T_1(s) at 11 °C		
	Lecithin	Lecithin + 25 mol% vitamin E	Lecithin + 25 mol% phytanic acid
$-CH_3$	2.05 ± 0.12	2.76 ± 0.17	2.98 ± 0.25
$-CH_2-CH_3$	0.66 ± 0.04	0.80 ± 0.05	1.75 ± 0.08
$-CH_2-CH_2-CH_3$	0.30 ± 0.02	0.55 ± 0.03	0.90 ± 0.05
$(CH_2)_n$	0.30 ± 0.02	0.45 ± 0.03	0.81 ± 0.05
$-CH_2-C(=O)-C(=O)$	0.12[b] ± 0.01	0.13[b] ± 0.01	0.35 ± 0.02
	1.62 ± 0.12	2.31 ± 0.14	2.01 ± 0.23
$-CH_2-CH=CH-$	0.24 ± 0.02	0.47 ± 0.03	0.58 ± 0.05
$-CH=CH-CH_2-CH=CH-$	0.25 ± 0.02	0.60 ± 0.04	1.06 ± 0.06
$-CH=CH-CH_2-CH_2-$	0.33 ± 0.02	0.53 ± 0.04	0.74 ± 0.04
$-CH=CH-CH_2-CH=CH-$	0.58 ± 0.05	0.71 ± 0.04	1.10 ± 0.07
$-N(CH_3)_3$	0.24 ± 0.03	0.41 ± 0.02	0.39 ± 0.02
$-N-CH_2-$	0.13[b] ± 0.01	0.27 ± 0.02	0.24 ± 0.02
$-P-O-CH_2-$	0.12[b] ± 0.01	0.21 ± 0.01	0.14[b] ± 0.01

[a]Measured by homospoil method.
[b]Measured by inversion-recovery method.
[c]4000 transients; pulse width = 23 μs (90° pulse).

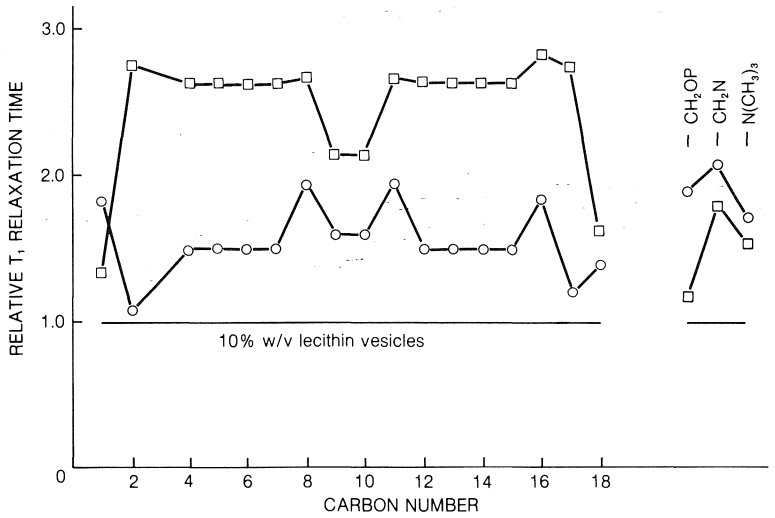

FIG. 1. Plot of the relative ^{13}C T_1 relaxation times for individual fatty acid carbons of lecithin and mixed lecithin – phytyl compounds in sonicated D_2O dispersions: □ 0.33 mol phytanic acid added; ○ 0.33 mol vitamin E added. The ^{13}C T_1 values for 10% w/v lecithin, column 2, Table 1 have been given the relative value of 1.00.

pholipid molecules in the bilayer will result in larger values for ^{13}C T_1's whether due to increased disorder ($< S_{mol}$), *i.e.*, greater excursions of the C—H dipole from the normal to the chain long axis, or increased rate of segmental motion, or both.

The amount of increase in relaxation time is more clearly evinced in Fig. 1. Figure 1 plots the observed ^{13}C T_1 values of lecithin with the incorporation of vitamin E and phytanic acid relative to the T_1 values obtained for egg lecithin alone (relative T_1 value = 1.00). As can be seen from the figure, large increases in T_1 for the hydrocarbon chain carbons of the order of 50–

100% are found for the incorporation of vitamin E and of the order of 150–200% for the incorporation of phytanic acid, even at 11 °C which is close to the transition temperature, $T_m = -5$–0 °C, for egg lecithin. Such increases in T_1, we believe, are a result of increased mobility along the entire acyl chain due to the necessary deviation from normal lipid packing. The deviations are caused by the difficulty in accommodating the highly branched compounds in an ordered bilayer arrangement.

London attractive forces between identical nonpolar molecules leads to an interaction potential of

$$U = -\frac{A\alpha^2}{r^6}$$

where A is a constant, α is the molecular polarizability, and r is the separation of the molecules. Since there is a highly distance dependent nature of the London forces between the hydrocarbon chains of a lecithin bilayer, the incorporation of phytol, α-tocopherol, or phytanic acid results in a large decrease in the interaction of adjacent lipid molecules for even a small expansion of the bilayer.

For the lecithin hydrophilic headgroup the order of T_1 increase is reversed; that is, vitamin E incorporation gives rise to greater increases in T_1 than determined for phytanic acid. The effect is particularly noticeable for the carbon atom adjacent to the choline phosphate moiety. The ^{13}C relaxation time for the choline CH_2—O—P is increased by only 17% by the incorporation of phytanic acid, while the T_1 value for CH_2—O—P is increased by 75% in the presence of vitamin E. The behavior of the headgroup carbons is explained by considering the depth each phytyl compound sits below the membrane surface.

We have previously provided firm evidence that phytol interjects further into the polar region of the lecithin bilayer than does, for instance, cholesterol (1). A linear electric field effect of the polar head groups of the lecithin bilayer was found for the unsaturated C2,C3 bond of intercalated phytol. An electric field calculation based on the surface dipole moment placed the midpoint of the C2,C3 double bond approximately 4.7 Å below the surface and the phytol hydroxyl close enough to hydrogen bond to the phosphate of the lecithin headgroup.

Since the ^{13}C relaxation time for the choline CH_2—O—P does not greatly increase upon incorporation of phytanic acid, in contrast to the effect of α-tocopherol, it is probable that the acid moiety is engaged in hydrogen bonding with the lecithin phosphate. Such an interaction would tend to anchor the carbon atoms of the lipid headgroup and decrease their motional freedom. A similar effect has been noted for the choline CH_2—O—P in mixed phytol–lecithin bilayers (1). Note that the effect is lessened as the trimethylammonium carbons are approached.

In direct contrast to the effect of vitamin E and phytanic acid, the intercalation of cholesterol does not cause any appreciable change in ^{13}C T_1 relaxation times of egg lecithin (8). Also, our own results indicate little effect upon ^{13}C T_1's due to the incorporation of up to 25 mol% of an unbranched C_{16} fatty acid, palmitic acid.

Monolayers of phytol, α-tocopherol, and phytanic acid occupy molecular areas of 55, 60, and 61 Å^2 per molecule at 0.5 dyn/cm, respectively (9). The disruptive effect of the branched phytyl chains of these molecules is understandable when a comparison of the aforementioned molecular areas is made with unbranched stearic acid which occupies 24 Å^2 per molecule (9). Cholesterol is known to form stable monolayers with molecular areas of approximately 40 Å^2 at a surface pressure of 0.5 dyn/cm.

Phytanic acid is expected to cause the greatest expansion of the bilayer not only because of steric factors, but also because the carboxyl moiety extends furthest into the hydrophilic region. In other words, the penetration into the plane of the lecithin headgroup further electrostatically interferes with the normal ionic interaction between the negative phosphate of one lecithin molecule for the now necessarily more distant trimethylammonium group of adjacent lipid molecules.

Although α-tocopherol has nearly the same area requirements as phytanic acid, it is not expected to penetrate as far into the hydrophilic region. With a single hydroxyl function on the bulky hydrophobic chromanol ring system vitamin E is expected to lie lower in the bilayer than phytanic acid or phytol and may parallel that occupied by incorporated cholesterol (10, 11). These authors have shown that the cholesterol hydroxyl is found at the position of the ester carbonyl. We calculate this to be some 7.5 ± 2 Å below the polar surface based on the X-ray data of Hitchcock *et al.* (12). The phytol

TABLE 2. Leak rates for lecithin and mixed lecithin vesicles determined by ^{31}P nuclear magnetic resonance

	^{31}P chemical shift[a] in absence of Pr^{3+} (ppm upfield from 85% H_3PO_4)	Decrease in 'inside' ^{31}P signal intensity upon Pr^{3+} addition (% total/min)	Relative rate	Half-life (day)
Lecithin	0.87	5.35×10^{-3}	1.00	6.5
Lecithin + phytol (25 mol%)	0.85	4.17×10^{-2}	7.79	0.83
Lecithin + vitamin E (25 mol%)	0.79	2.55×10^{-1}	47.66	0.14
Lecithin + phytanic acid (25 mol%)	0.91	15.50	2897	2.2×10^{-3}

[a]800 transients; pulse width = 10 μs (56° flip angle).

hydroxyl, on the other hand, resides some 0–2 Å from the surface based on the field effect measurements. The much larger steric effect of tocopherol *vs.* cholesterol, *vide supra*, would cause a disruptive expansion of the bilayer. Situated lower in the bilayer, vitamin E would not then be expected to interact with or anchor the lecithin headgroup. The large increase of 75, 108, and 71% for the relaxation times of the choline CH_2OP, $\overset{+}{N}CH_2$, and $\overset{+}{N}(CH_3)_3$ carbons, respectively, upon vitamin E incorporation, compared with increases of 17, 85, and 63% for the same three carbons when phytanic acid is added, is simply the consequence of decreased ionic interaction of adjacent lipid molecules due to the sterically induced increased separation with concomitantly decreased H-bonding of the vitamin E hydroxyl to phosphate.

Phytol, in spite of its relatively high position in the bilayer, is not expected to cause as large an electrostatic perturbation in the plane of the lipid headgroups as phytanic acid. In addition, the phytol monolayer area requirement of 55 $Å^2$ is not as large as that for phytanic acid or vitamin E. In summary, the foregoing provides a rationale that the destabilizing effect of the intercalation of isoprenoid compounds into phospholipid bilayer membranes increases in the order phytanic acid > α-tocopherol > phytol.

^{31}P *Nuclear Magnetic Resonance Results*

The permeability of lecithin vesicles can be correlated directly with the membrane fluidity as expressed by ^{13}C T_1 relaxation times. We have studied the effect of the incorporation of phytyl compounds on the permeability of lecithin vesicles using a lanthanide induced shift (LIS) ^{31}P nmr technique.

A number of recent studies have shown LIS of ^{1}H and ^{31}P nmr signals of phospholipid vesicles due to added lanthanide (13–16). The addition of Pr^{3+} results in a downfield shift for the outside phosphorus nuclei.

We have utilized the rate of disappearance of the 'inside' ^{31}P resonance signal to study the permeability changes in model membrane systems. Upon addition of the Pr^{3+} to preformed vesicles, the ^{31}P resonance of the nuclei on the outside of the bilayer is broadened slightly and shifted downfield (LIS) by approximately 8 ppm, while the 'inside' phosphorus resonance is shifted upfield very slightly (17) but remains sharp.

The rate of infusion of praseodymium across the bilayer is proportional to the rate of disappearance of the high field ^{31}P nmr signal. Plots of the disappearance of 'inside' ^{31}P resonance signal as paramagnetic Pr^{3+} crosses the bilayer *vs.* time are shown in Fig. 2.

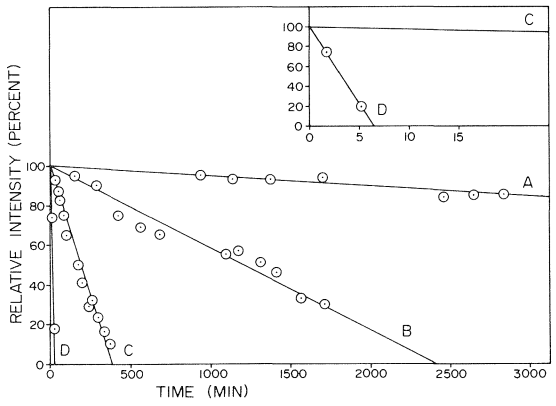

FIG. 2. Percent total of inside phosphorus nmr signal relative to its initial value *vs.* time for (*A*) egg lecithin alone + 0.005 *M* Pr^{3+}, (*B*) egg lecithin with 25 mol% incorporated phytol + 0.005 *M* Pr^{3+}, (*C*) egg lecithin with 25 mol% incorporated vitamin E + 0.005 *M* Pr^{3+}, (*D*) egg lecithin with 25 mol% incorporated phytanic acid + 0.005 *M* Pr^{3+}. Because of the extreme slope with phytanic acid, lines (*C*) and (*D*) are reproduced in the insert using an expanded time scale.

The kinetic data from Fig. 2 are quantified in Table 2 for egg lecithin alone, lecithin with incorporated phytol, lecithin with incorporated α-tocopherol (vitamin E), and lecithin with incorporated phytanic acid. The incorporation of 25 mol% phytol increases the vesicle leak rate by approximately 8 times, 25 mol% vitamin E by approximately 48 times, and 25 mol% phytanic acid by nearly 2900 times over the leak rate obtained with pure egg lecithin vesicles.

The half-life of the 'inside' resonance was calculated from the observed rates and is shown in Table 2, column 5. The addition of 25 mol% phytanic acid to the system is seen to decrease the half-life of the peak unaffected by paramagnetic Pr^{3+} from 6.5 days to about 3 min. Lesser, but significant, effects are seen with the incorporation of phytol and vitamin E which have half-lives of approximately 20 and 3 h, respectively. When 25 mol% palmitic acid was added, no change in the lecithin leak rate was detected.

Because of the potential physiological significance of the above results, a much lower amount of vitamin E (3 mol%) was incorporated. The permeability results still showed an increase of 300%.

In spite of the large increase in permeability, even in the presence of phytanic acid, the vesicles did not rupture. After the complete disappearance of the upfield 'inside' resonance due to Pr^{3+} entering the vesicles, sufficient EDTA was added to complex with all of the Pr^{3+} on the outside of the membrane resulting in reappearance of two ^{31}P resonances. In this case, the upfield peak was due to the 'outside' phosphorus nuclei of intact vesicles since Pr^{3+} inside the vesicles cannot form an EDTA complex.

The ^{31}P results parallel the ^{13}C T_1 relaxation studies on bilayers containing intercalated phytol (1) and ^{13}C studies of bilayers with incorporated vitamin E and phytanic acid reported here. The ^{13}C relaxation studies have shown an increase in the fluidity of the lipid bilayer caused by the intercalation of the branched chain compounds. The increased permeability to ions shown by ^{31}P nmr spectroscopy exactly parallels the order found for mobility increase *viz.* phytanic acid > vitamin E > phytol > lecithin alone.

Conclusion

On a molecular level, incorporation of vitamin E or phytanic acid disrupts the packing of the hydrocarbon region of phospholipid bilayers. In addition, penetration of the carboxyl function of phytanic acid into the plane of the lecithin headgroups causes a further disruption of the electrostatic attraction between adjacent lipid molecules. As we have demonstrated by ^{13}C spin–lattice relaxation measurements, large changes in the 'fluidity' of bilayer membranes can be caused by the incorporation of phytyl compounds.

In addition, the effect of intercalated vitamin E, phytol, and phytanic acid are shown to *increase* the permeability of phosphatidylcholine bilayers to Pr^{3+} by up to 2900 times. The incorporation of cholesterol is known to *decrease* the permeability of phospholipid bilayers to Na^+, K^+, Cl^-, and glucose (18) as well as showing increased order (7).

Several studies (19–22) have indicated that there exists a correlation between membrane 'fluidity' and the regulation of membrane bound co-operative enzymes. While it is possible that a definite level of membrane 'fluidity' is necessary for regulation, it is also probable that too great an increase in the 'fluidity' of biological membranes may lead to a loss of cell function and a failure of compartmentalization.

Thus, Lucy and Dingle (23) observed *in vitro* that the rapid hemolysis by added retinol of rabbit erythrocytes is inhibited by low concentrations of α-tocopherol, as well as other branched chain compounds such as 6-*O*-acetyl-α-tocopherol, squalene, ubiquinone-30, vitamin K_1, and phytol, while *N*,*N'*-diphenyl-*p*-phenylenediamine and hydroquinone were completely without effect. However, in higher concentrations, extensive hemolysis was produced by vitamin E and phytol themselves. This activity was deemed not to be caused by the redox system of α-tocopherol, but rather that it was a function of the isoprenoid side chain (23).

Furthermore, the accumulation of branched chain compounds has been associated with a number of disorders. Patients afflicted with Refsum's disease cannot α-oxidize and decarboxylate phytanic or similar branched chain fatty acids. The resultant buildup of these branched chain compounds in the nervous tissue has been linked with the observed degeneration which often leads to the complete disintegration of the myelin sheaths (24).

It is clear that the incorporation of phytyl compounds has a marked destabilizing effect on

phospholipid bilayers as shown by increased freedom of fatty acid chains, said effect also increasing abruptly their permeability.

Acknowledgement

Financial support of this work by the National Research Council of Canada is gratefully acknowledged.

1. R. J. CUSHLEY and B. J. FORREST. Can. J. Chem. **54**, 2059 (1976).
2. L. L. M. VAN DEENEN. *In* The molecular basis of membrane function. *Edited by* D. C. Tosteson. Prentice Hall, Englewood Cliffs, N.J. 1969. p. 47.
3. W. S. SINGLETON, M. S. GRAY, M. L. BROWN, and J. L. WHITE. J. Am. Oil Chem. Soc. **42**, 53 (1965).
4. G. G. MCDONALD and J. S. LEIGH, JR. J. Magn. Reson. **9**, 358 (1973).
5. R. L. VOLD, J. S. WAUGH, M. P. KLEIN, and D. E. PHELPS. J. Chem. Phys. **48**, 3381 (1968).
6. A. SEELIG and J. SEELIG. Biochemistry, **13**, 4839 (1974).
7. G. W. STOCKTON, C. F. POLNASZEK, A. P. TULLOCH, F. HASAN, and I. C. P. SMITH. Biochemistry, **15**, 954 (1976).
8. P. E. GODICI and F. R. LANDSBERGER. Biochemistry, **14**, 3927 (1975).
9. G. L. GAINES, JR. *In* Insoluble monolayers at liquid–gas interfaces. Interscience Monographs on Physical Chemistry. Vol. 1. *Edited by* I. Prigogine. Interscience, New York, N.Y. 1966. pp. 220–255.
10. N. P. FRANKS. J. Mol. Biol. **100**, 345 (1976).
11. D. L. WORCESTER and N. P. FRANKS. J. Mol. Biol. **100**, 359 (1976).
12. P. B. HITCHCOCK, R. MASON, K. M. THOMAS, and G. G. SHIPLEY. Proc. Natl. Acad. Sci. U.S.A., **71**, 3036 (1974).
13. V. F. BYSTROV, N. I. DUBROVINA, L. I. BARSUKOV, and L. D. BERGELSON. Chem. Phys. Lipids, **6**, 343 (1971).
14. R. J. KOSTELNIK and S. M. CASTELLANO. J. Magn. Reson. **7**, 219 (1972).
15. V. F. BYSTROV, YU. YE. SHAPIRO, A. V. VIKTOROV, L. I. BARSUKOV, and L. D. BERGELSON. FEBS Lett. **25**, 337 (1972).
16. L. I. BARSUKOV, A. M. PARFEN'EVA, A. V. VICTOROV, YU. YE. SHAPIRO, V. F. BYSTROV, and L. D. BERGELSON. Biofizika, **19**, 456 (1974).
17. Y. K. LEVINE, A. G. LEE, N. J. M. BIRDSALL, J. C. METCALFE, and J. D. ROBINSON. Biochim. Biophys. Acta, **291**, 592 (1973).
18. D. PAPAHADJOPOULOS, S. NIR, and S. OHKI. Biochim. Biophys. Acta, **266**, 561 (1972).
19. B. BLOJ, R. D. MORERO, R. N. FARIAS, and R. E. TRUCCO. Biochim. Biophys. Acta, **311**, 67 (1973).
20. B. BLOJ, R. D. MORERO, and R. N. FARIAS. FEBS Lett. **38**, 101 (1973).
21. F. SIÑERIZ, B. BLOJ, R. N. FARIAS, and R. E. TRUCCO. J. Bacteriol. **115**, 723 (1973).
22. R. N. FARIAS, B. BLOJ, R. D. MORERO, F. SIÑERIZ, and R. E. TRUCCO. Biochim. Biophys. Acta, **415**, 231 (1975).
23. J. A. LUCY and J. T. DINGLE. Nature, **204**, 156 (1964).
24. M. C. MACBRINN, and J. S. O'BRIEN. J. Lipid Res. **9**, 552 (1968).

Nuclear magnetic resonance spectra of *o*-hydroxythiobenzamides: the intramolecular OH· · ·S hydrogen bond as a conformational probe[1,2]

ADRIAN O. FULEA[3] AND PETER J. KRUEGER

Department of Chemistry, University of Calgary, Calgary, Alta., Canada T2N 1N4

Received September 15, 1975[4]

ADRIAN O. FULEA and PETER J. KRUEGER. Can. J. Chem. **55**, 227 (1977).

The OH and NCH_2 proton signals of 1-(2′-hydroxythiobenzoyl)-2-methylpiperidine (**2**) are resolved into separate peaks assigned to four conformers (*EA*, *EB*, *ZA*, and *ZB*) in 220 MHz nmr spectra at −50 °C. All have a strong intramolecular OH· · ·S hydrogen bond. The *ZB* and *EB* conformers have the lowest and highest ground state energies, respectively. Exchanges between *A* and *B* conformers have a higher energy barrier than exchanges between *Z* and *E* isomers, but by +40 °C all four conformers interchange rapidly. The nature of all possible interchange processes is considered and a potential energy surface with respect to rotation about the Ph—C(S) and C—N bonds is presented. For the 4-methyl analogue of **2** low temperature nmr spectra exhibit two sharp OH signals arising from *A* and *B* conformers. For 2,6-dimethyl-4-(2′-hydroxythiobenzoyl)morpholine the *A*/*B* OH doublet of the *cis* dimethyl isomer can be distinguished from that of the *trans* isomer. Thus it is demonstrated that the intramolecularly hydrogen bonded OH proton is a good spectroscopic conformational probe. Nuclear magnetic resonance, ir, and uv data all indicate that in the 2,6-dimethylpiperidine analogue of **2** the CNC and Ph—C(S)N planes are perpendicular due to steric interference. Coplanarity of the phenyl ring with the thioamide group is attributed to a very strong intramolecular OH· · ·S hydrogen bond, in equilibrium with a proton transferred O· · ·H—S form in solution. This structure resembles the transition state for rotation in the most readily achieved exchange between conformers of **2**.

ADRIAN O. FULEA et PETER J. KRUEGER. Can. J. Chem. **55**, 227 (1977).

On a déterminé le spectre rmn à 220 MHz et à −50 °C de (l'hydroxy-2′ thiobenzoyl)-1 méthyl-2 pipéridine (**2**); on a pu en résoudre les signaux dus aux protons OH et NCH_2 en pics distincts attribués aux quatre conformères (*EA*, *EB*, *ZA* et *ZB*). Tous ces conformères présentent un pont hydrogène intramoléculaire OH· · ·S qui est très fort. Les conformères *ZB* et *EB* ont respectivement les énergies des états fondamentaux qui sont les plus basses et les plus élevées. Les échanges entre les conformères *A* et *B* ont une barrière d'énergie plus élevée que les échanges entre les isomères *Z* et *E*; toutefois à +40 °C les quatre conformères s'échangent rapidement. On considère la nature de tous les processus possibles pour ces échanges et on propose une surface d'énergie potentielle par rapport à la rotation autour des liens Ph—C(S) et C—N. Pour l'analogue de **2** méthylé en position 4, les spectres rmn à basse température montrent deux signaux OH intenses dérivant des conformères *A* et *B*. Dans le cas de la diméthyl-2,6 (hydroxy-2′ thiobenzoyl)-4 morpholine, on peut distinguer le doublet *A*/*B* du OH de l'isomère diméthyl-*cis* de celui de l'isomère *trans*. Ainsi on a pu démontrer que le proton OH lié par un pont hydrogène intramoléculaire est une bonne sonde spectroscopique conformationnelle. Des données de rmn, ir, et d'uv indiquent toutes que dans la diméthyl-2,6 pipéridine analogue de **2**, les plans CNC et Ph—C(S)N sont perpendiculaires l'un à l'autre dus à des interférences stériques. On attribue la coplanarité du cycle phényle avec le groupe thioamide à un lien hydrogène OH· · ·S intramoléculaire qui est très fort et qui est en équilibre, en solution, avec une forme H—S· · ·O dans laquelle le proton a été transféré. Cette structure ressemble à l'état de transition de rotation dans l'échange qui peut s'effectuer le plus facilement entre les deux conformères de **2**.

[Traduit par le journal]

Introduction

In previous papers (1, 2) we have shown that 1-(2′-hydroxythiobenzoyl)piperidine and 4-(2′-hydroxythiobenzoyl)morpholine exist in two conformers (*A* and *B*) which arise because of different steric interactions between the 6′ aromatic proton and either one or both of the hetero-ring NCH_2 protons *trans* to the thiocarbonyl group. These conformers interchange rapidly on the nmr scale by ring inversion, and

[1]From the Ph.D. thesis of A. O. Fulea.

[2]Presented in part at the 12th European Congress on Molecular Spectroscopy, Strasbourg, France, June 1–5, 1975.

[3]Isaac Walton Killam scholar; on leave of absence from the University of Bucharest.

[4]Revision received April 2, 1976.

also by rotation around the C—N and Ph—C(S) bonds. The last two processes are slow at low temperatures.

Since these conformers play an important role in the elucidation of the origin of the magnetic non-equivalence of the NCH_2 protons in benzamides and thiobenzamides (3), we have now investigated *N*-(*o*-hydroxythiobenzoyl)piperidines and -morpholines in which the hetero ring is biased by one or more methyl groups, freezing the hetero-ring inversion over the temperature range investigated (+40 to −50 °C) and thus providing an opportunity to see both conformers separately in their nmr spectra.

Spectroscopic data on the compounds **1–6** are presented and discussed in this paper.

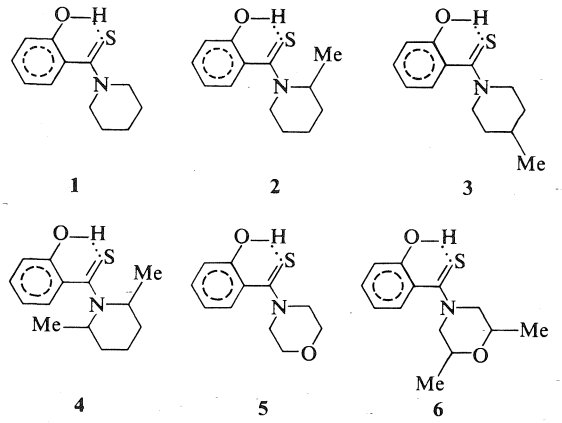

Compounds **1** and **5** are reference compounds for the study of the effect of methyl substitution on conformational dynamics. All of these compounds are characterized by a very strong intramolecular OH···S hydrogen bond. Furthermore, steric hindrance forces the aromatic ring out of planarity with the thioamide group.[5] The details of this have been investigated with a model which is in good agreement with experimental data.

Experimental

Compounds

Samples **1** and **5** were those used in previous investigations; **2**, **3**, **4**, and **6** are new compounds which were prepared by the Willgerodt–Kindler reaction (6) from *o*-hydroxybenzaldehyde, sulfur, and the appropriate methylated piperidine or morpholine, using pyridine as a solvent. A 3 h reflux period gave crystalline material with the characteristics described in Table 1. The 2,6-dimethylmorpholine used as starting material for the synthesis of **6** was a 60/30 = *cis*(ee)/*trans*(ae) mixture, from nmr. Microanalyses were carried out by Chemalytics, Inc., Tempe, Arizona, U.S.A.

Spectra

The 220 MHz ^1H nmr spectra were obtained at the Canadian 220 MHz NMR Centre, Sheridan Park, Ontario, under the direction of Dr. A. E. Grey. The 100 MHz spectra were obtained with a Varian HA-100 spectrometer, with the assistance of Mr. Lawrence Wong. Temperature calibrations for the latter were checked with methanol. An internal TMS reference was used in all cases.

Infrared spectra in solution, using matched 2 or 10 cm cells, were obtained with a Perkin-Elmer Model 621 spectrophotometer, and uv spectra with a Beckman Acta V spectrophotometer by Mrs. Marelle Bertram.

Calculations

Dreiding model dimensions and geometries are used throughout the discussion in this paper, with full recognition of their inherent limitations, particularly with respect to multiple angle deformations that may occur in sterically crowded molecules to relieve strain. The thioamide N atom was considered to be planar, and oriented for maximum π-electron overlap with the C=S group. The following thioamide group bond lengths were used:

$$(Ph)C—C(S) = 1.48 \text{ Å}$$
$$C=S = 1.68 \text{ Å}$$
$$C—N = 1.40 \text{ Å}$$

All non-bonded distances were calculated with the computer programme CART (7). While some distortion of the piperidine ring in compounds of this type has been established (1), it cannot be put on a quantitative basis at present, and this treatment does not take such dis-

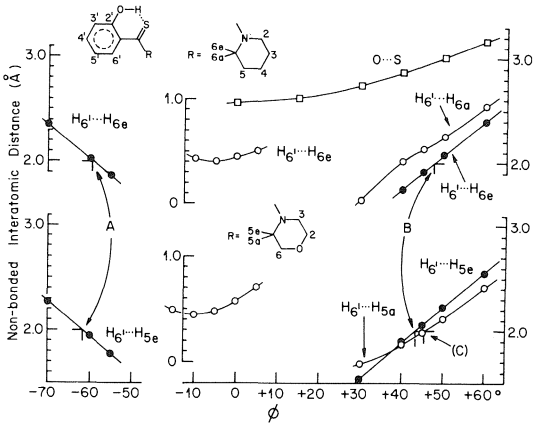

FIG. 1. Selected non-bonded H···H and O···S distances in the *A* and *B* conformers of *N*-(*o*-hydroxythiobenzoyl)morpholines and -piperidines, calculated from Dreiding model geometry, as a function of the phenyl ring rotational angle ϕ. For further details see text.

[5]The phenyl ring twist angle in benzamides and thiobenzamides has been discussed recently (4), and near planarity of the N atom in amides is well established (5).

TABLE 1. Some properties of thiobenzamides synthesized

Compound	Reaction temperature (°C)	Yield (%)	Recrystallization solvent	mp (°C)	Colour
2	90	70	EtOH (aq.)	132–134	White
3[a]	70	49	EtOH (aq.)	136–138	White
4	70	24	Benzene	132–133	Red
6[b]	80	80	Benzene	105–108	Pale green

[a] *Anal.* calcd. for **3**: C 66.34, H 7.28, N 5.95, S 13.62; found: C 66.59, H 7.23, N 5.98, S 14.83.
[b] *Anal.* calcd. for **6**: C 62.12, H 6.82, N 5.57, S 12.76; found: C 61.88, H 6.63, N 5.56, S 12.87.

tortion into consideration. *Greater planarity of the aromatic ring and the thioamide plane probably exists in these molecules than is deduced from the constrained models employed, but this does not alter the essential features of any conclusions, which are based on spectral observations.*

Results and Discussion

Geometry of Model Conformers

The $H_{6'}\cdots H_{6e}$ and corresponding $H_{6'}\cdots H_{5e}$ distances in **1** and **5** are shown in Fig. 1 as a function of the phenyl ring rotational angle (ϕ) out of the thioamide plane.[6] It would fall to less than 0.5 Å when $\phi = 0°$; comparison of this distance with twice the van der Waals radius of hydrogen (2.0 Å)[7] indicates that the phenyl ring must be rotated out of the thioamide plane.

In *ortho*-substituted *N*-thiobenzoylmorpholines and -piperidines with unsubstituted hetero rings we have previously found two conformers (*A* and *B*) arising out of hetero-ring inversion and its relation to the $H_{6'}\cdots H_{5e}$ steric interaction ($H_{6'}\cdots H_{6e}$ in piperidines), which requires extensive rotation of the phenyl ring out of the thioamide plane (1, 2). The ground state energies for *A* and *B* were found to differ by only 0.2 kcal/mol or less. Calculations based on Dreiding model geometries and assuming 'contact' of the $H_{6'}\cdots H_{5e}$ atoms in *N*-thiobenzoylmorpholines ($H_{6'}\cdots H_{6e}$ atoms in *N*-thiobenzoylpiperidines) at a distance of 2.0 Å[8] leads to twist angles ϕ_A and ϕ_B for the two conformers as listed in Table 2, along with other calculated geometric parameters. These are applicable to all the compounds under discussion, regardless of aromatic or hetero-ring substitution.

The data in Table 2 show, first of all, that substitution of a morpholine ring for piperidine introduces significant conformational changes. Secondly, the structural features calculated on the supposition that the phenyl ring will attempt to be as planar as possible with the thioamide group, being hindered only by the steric interference of an *ortho*-aromatic proton with one (or both) *anti* NCH_2 proton of the hetero ring, are very reasonable. Thus the first H···H 'contact' (d = 2.00 Å) when rotating the phenyl ring from $\phi = 90°$ toward planarity in compounds of the type **1** occurs when $\phi_A = 59.5°$ (in conformer *A*) and $\phi_B = 47.5°$ (in conformer *B*). In both cases the aromatic *o*-proton ($H_{6'}$) first touches the H_{6e} atom. In compounds of the type **5** (morpholine ring) $\phi_A = 61.5°$ and $\phi_B = 43.5°$, corresponding to 'contact' with H_{5e}, although it must be noted in the last case (see Fig. 1) that $H_{6'}\cdots H_{5a}$ 'contact' actually occurs *first* as ϕ decreases, leading to the definition of conformer *C* (as in Table 2) with $\phi_C = 45.5°$.[9] Since librations about the C—N bond would allow $H_{6'}$ to slip past H_{5a}, given the angle of approach, conformer *C* is not expected to play a role except perhaps at very low temperatures when librational amplitudes are reduced.

[6] The numbering system is summarized in Fig. 1.

[7] While the Pauling van der Waals radius of hydrogen is 1.2 Å, it has more recently been concluded that 1.0 Å is a more appropriate value (8). The hydrogen disks in Dreiding models therefore have 1.0 Å radii. Non-bonded atomic radii cannot be defined precisely in any event, and are frequently anisometric (9), so that contact distances depend on the angle between the bonds to the approaching atoms. For aromatic protons the consistent van der Waals radius appears to be 1.0 Å (9), and even closer H···H contacts have been reported in bicyclo[3.3.1]nonane (1.7 Å) (10) and in 1,8-bisdehydro[14]annulene (1.85 Å) (11). Large atoms in particular can lead to 'soft' contacts.

[8] This is the low value end of the 'contact range' recommended by Scheraga (12) for use in 'hard sphere potential' calculations of protein conformations.

[9] Previously estimated values of ϕ_A, ϕ_B and other structural parameters were based on direct measurements on Dreiding models; the values given in this paper supercede the earlier values.

TABLE 2. Geometric parameters calculated for conformers of *N*-(*o*-hydroxythiobenzoyl)piperidines and -morpholines[a]

Conformers		Hetero ring	
View along C=S bond[b]	View along (Ph)C—C(S) bond[c,d]	Piperidine (X = CH_2)	Morpholine (X = O)
(A) 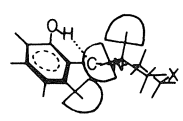	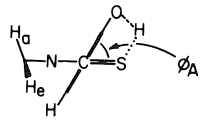	$\phi_A = 59.5°$ $d_{H...H_e} = 2.0$ Å $d_{H...H_a} > 2.0$ Å $d_{O...S} = 3.16$ Å $\Delta d = 0.09$ Å[e]	61.5° 2.0 Å >2.0 Å 3.18 Å 0.07 Å[e]
		0.18 Å decrease	0.26 Å decrease
(B) 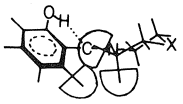	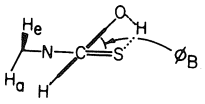	$\phi_B = 47.5°$ $d_{H...H_e} = 2.0$ Å $d_{H...H_a} = 2.0$ Å $d_{O...S} = 2.98$ Å $\Delta d = 0.27$ Å[e]	43.5° 2.0 Å 2.0 Å 2.92 Å 0.33 Å[e]
		$\phi_A - \phi_B = 12°$ $(\cos^2 \phi_B/\cos^2 \phi_A) = 1.8$	18° 2.3
(C) 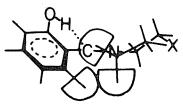	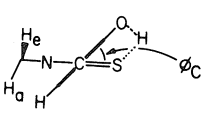	Not applicable	$\phi_C = 45.5°$ $d_{H...H_e} > 2.0$ Å $d_{H...H_a} = 2.0$ Å $d_{O...S} = 2.94$ Å $\Delta d = 0.31$ Å $(\cos^2 \phi_C/\cos^2 \phi_A) = 2.2$

[a]Using Dreiding model geometry, with a planar hetero-ring N atom. While these data are calculated for the *N*-(*o*-hydroxythiobenzoyl) compounds, the ϕ values determined by non-bonded H · · · H contact are also deemed applicable to all other *N*-thiobenzoylpiperidines and -morpholines.

[b]Hydrogen bond to thiocarbonyl S atom which is located directly behind thioamide C atom.

[c]H is the aromatic *o*-proton, H_a and H_e are the *anti* NCH_2 protons of the hetero ring, and ϕ is the dihedral angle between the phenyl ring and thioamide planes.

[d]When $\phi = 55.0°$ a torsion angle of 22.3° is required about the C—O bond for the COH···S atoms to lie in a plane. This corresponds to an ∠ OH···S of 145.8°.

[e]Sum of van der Waals radii of O and S atoms, minus calculated $d_{O...S}$.

Table 2 and Fig. 1 also show that O· · ·S distances are estimated to be 3.16 and 2.98 Å for conformers *A* and *B*, respectively, in the piperidine ring compounds, and 3.18 and 2.92 Å, respectively, in the morpholine ring compounds. These values are 0.07–0.33 Å shorter than the sum of the respective van der Waals radii ($r_O + r_S = 1.40 + 1.85 = 3.25$ Å), and such shortening on strong hydrogen bond formation is well known. Thus, O· · ·O and F· · ·F shortening of 0.25 Å has been documented for intermolecular OH· · ·O and FH· · ·F hydrogen bonds (13). For **1** and **5** in very dilute CCl_4 solution we have observed only minute traces of a 'free' fundamental OH stretching vibration in the infrared spectrum, but very intense and broad intramolecularly OH· · ·S bonded OH peaks displaced by 341 and 350 cm^{-1}, respectively. These attest to very strong hydrogen bonds, the hydroxyl proton being pushed into the S atom electron density as the aromatic ring attempts to achieve the maximum permissible co-planarity with the thioamide group. It is known that the effective radius of a hydrogen atom in a hydrogen bond is negligible (14). In 2-methylmercaptophenol the intramolecular O· · ·S distance is identical with that which we estimate for conformer *B* in the case of a morpholine ring, but the OH frequency shift due to intramolecular OH· · ·S hydrogen bonding is only 149 cm^{-1} (14*b*). From the data in Table 2 it is also expected that the acidity of OH_B will exceed that of OH_A, and the basicity of S_B will exceed that of S_A, for a given compound, due to the dependence of the conjugation on ϕ.

Hamilton and Ibers (15) consider that a good operational criterion for the existence of a hydrogen bond is H· · ·X shortening. Assuming a normal ∠COH and a normal OH bond distance, our model calculations show that the H· · ·S distance in the compounds under consideration falls from 2.23 Å at $\phi = 55°$ to 1.70 Å at $\phi = 0°$ (phenyl ring/thioamide group coplanar). Relative to the sum of the van der Waals radii ($r_H + r_S = 1.0 + 1.85 = 2.85$ Å), this corresponds to 'shrinkage' of 0.5–1.12 Å, which is in line with those of 0.9 and 1.4 Å noted for intermolecular OH· · ·O and OH· · ·F

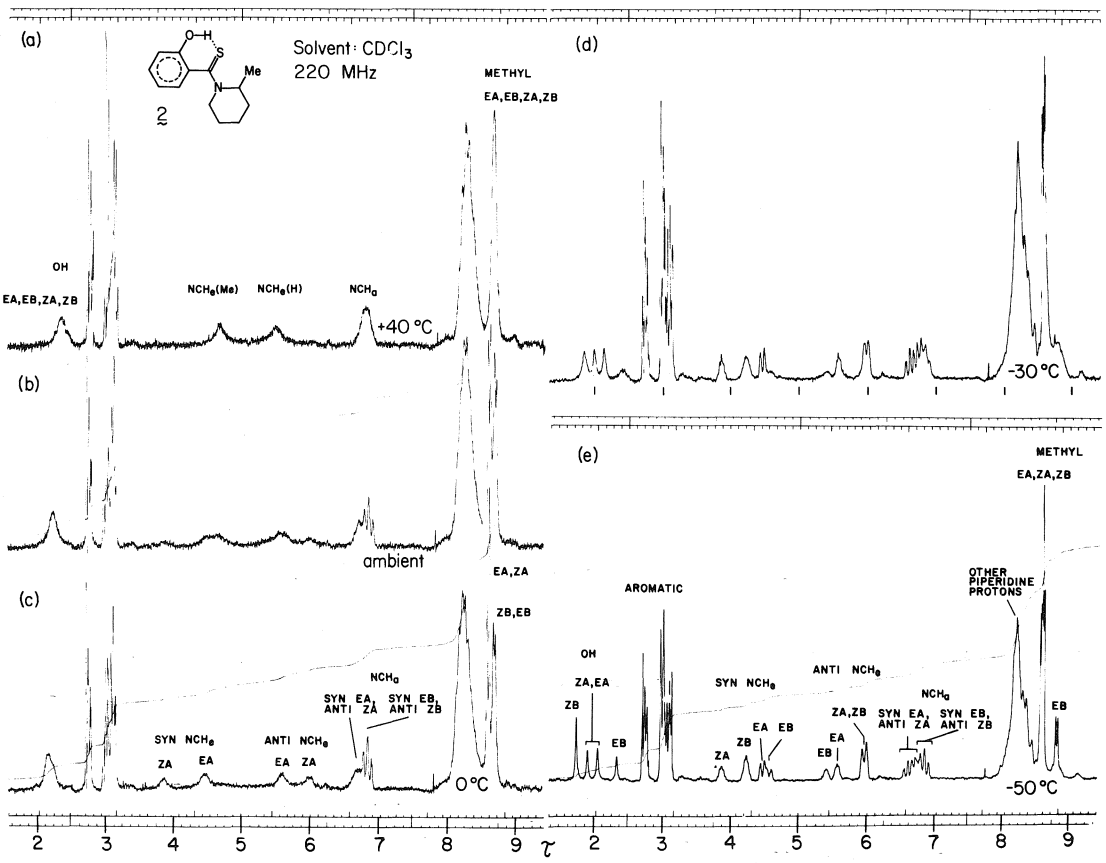

FIG. 2. 220 MHz ^1H nmr spectra of **2**.

hydrogen bonds, respectively (15). Unfortunately crystallographic data for compounds involving OH···S hydrogen bonds is quite meagre (16).

No reference is made to the $H_6\cdots H_{6a}$ and $H_6\cdots H_{5a}$ distances in Fig. 1 since they always exceed 2.0 Å when some other contact set in. As far as the *syn* NCH_2 protons are concerned, the following distances apply in our model: $S\cdots H_{2a} = 3.65$ Å, $S\cdots H_{2e} = 2.39$ Å (in piperidines); $S\cdots H_{3a} = 3.50$ Å, $S\cdots H_{3e} = 2.49$ Å (in morpholines). Distances below 2.85 Å are considered to correspond to 'soft' contacts here.

Conformers of 1-(2'-Hydroxythiobenzoyl)-2-methylpiperidine (2)

The 220 MHz nmr spectra of **2** in $CDCl_3$ at selected temperatures between +40 and −50 °C are given in Fig. 2, and expansions at two low temperatures in the most relevant regions in Fig. 3. Proton signal assignments are indicated in these figures. The most striking characteristic is the progressive resolution of the spectrum into distinctly separate OH and *syn* and *anti* NCH_2 (and NCHR) proton signals characterizing the *A* and *B* conformers of both the *Z* ('zusammen')[10] and *E* ('entgegen')[10] isomers as the temperature is lowered. These four conformers[11] are illustrated in Fig. 4 together with all possible interchange paths, the energy barriers being correlated with the schematic potential energy surface proposed in Fig. 5 to explain the experimental data.

Figure 4 classifies the interchange paths into

[10] *Z* and *E* have the methyl and thiocarbonyl groups on the same and opposite sides of the CN bond, respectively.

[11] Because the *Z* and *E* forms are not physically separable, reference will be made only to the *EA*, *EB*, *ZA*, and *ZB* forms as 'conformers'. These conformers can be interchanged by rotation around the formal single bonds C(S)—Ph and C—N. Each of these conformers has an enantiomer, but that is irrelevant for this study. Their existence might be demonstrated in a chiral solvent.

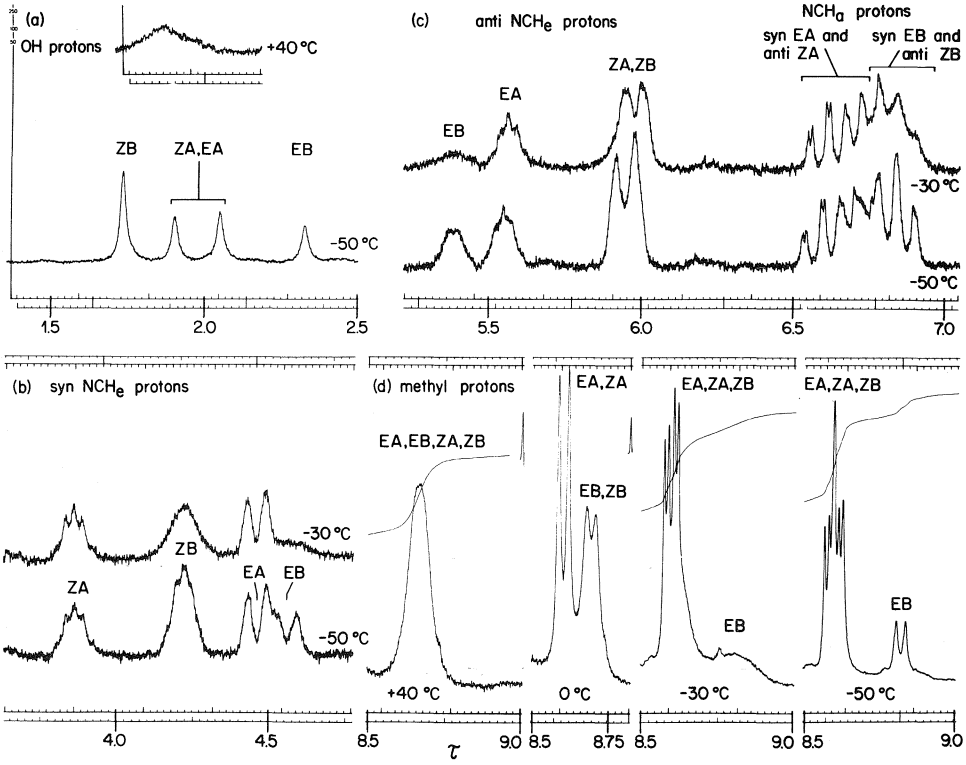

FIG. 3. Expanded scale 220 MHz ^{1}H nmr spectra of **2**: (*a*) OH protons, (*b*) *syn* NCH_e protons, (*c*) *anti* NCH_e and *syn* and *anti* NCH_a protons, and (*d*) methyl protons.

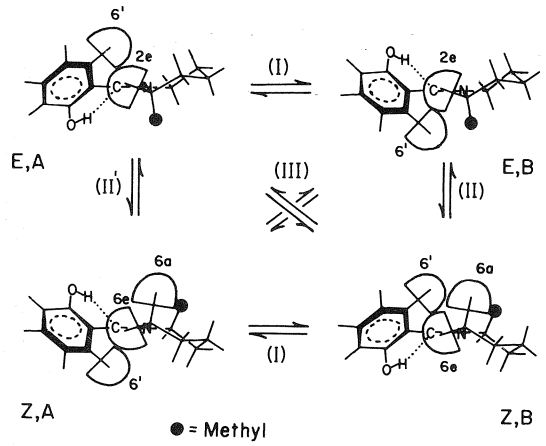

FIG. 4. The four conformers of **2** and their interchange paths, together with the energy barriers for interconversion correlated with the potential energy surface in Fig. 5. The thioamide plane is perpendicular to the paper and the thiocarbonyl S atom is directly behind the thioamide C atom. These sketches are based on photographs of Dreiding models, and selected H disks shown have a radius of 1 Å. For simplicity the methyl group is shown only as a dark circle.

the following processes, based on a comparison of equilibrium geometries for the four conformers calculated on the basis of thioamide group planarity and steric 'contact' between the aromatic *o*-proton and one (or both) *anti* NCH_2 protons of the hetero-ring:

(*I*) (*a*) Rotation about the Ph—C(S) bond ($\Delta\phi = \sim 107°$) and passage of the O atom past the S atom, and $H_{6'}$ past H_{2e} (or past H_{6e}, depending on the isomer involved), or (*b*) rotation about the Ph—C(S) bond in the opposite direction ($\Delta\phi = \sim 253°$) with passage of the O atom past H_{2e} (or H_{6e}), which would be even more difficult than (*a*).

(*II*), (*II'*) Co-operative rotation about the C—N bond ($\Delta\theta = \sim 180°$) and (*a*) about the Ph—C(S) bond ($\Delta\phi = \sim 95° - \sim 119°$) with passage of the O atom past the S atom, or (*b*) about the Ph—C(S) bond in the opposite direction ($\Delta\phi = \sim 241° - \sim 265°$), involving complete breaking of the conjugation of the phenyl ring with the thioamide group. Path (*a*) may be energetically preferable because of

the increased phenyl ring conjugation and the very strong OH· · ·S hydrogen bond stabilizing the planar transition state, as demonstrated later in this paper. This is an example of the 'gear effect' (17).

(*III*) Small angle rotation about the Ph—C(S) bond ($\Delta\phi = \sim 12°$) with maintenance of some conjugation of the phenyl ring with the thioamide group, and $\Delta\phi = \sim 180°$ rotation about the C—N bond.

The angles cited are based on our calculations for **1** and **5** described in the preceding section. Undoubtedly the real angles will be somewhat different, particularly in the case of **2**, but the calculated values are used throughout this discussion for illustrative purposes. Notwithstanding the above classification of pathways, all probably proceed via the energetically favourable 'saddle point' region in Fig. 5, *e.g.* even the $EA \rightleftarrows EB$ conversions which appear to involve no rotation about the C—N bond probably involve an intermediate state where sufficient rotation about this bond has occurred to permit the $H_{6'}$ atom to slip past H_{2e}. Librational motion about the C—N bond may provide the mechanism for this. Cooperative rotation about two bonds in amides has already received some consideration (18).

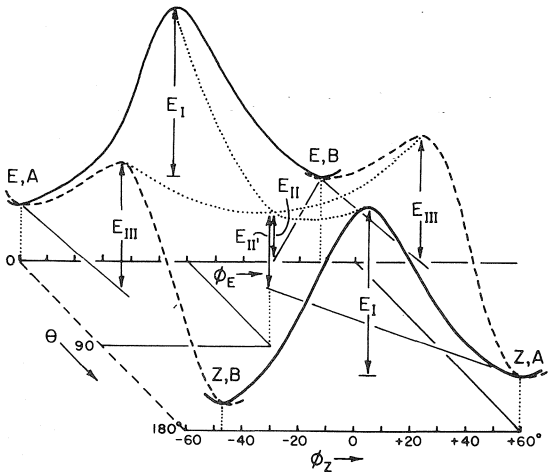

FIG. 5. Potential energy surface proposed for interconversion between all possible pairs of *ZA*, *ZB*, *EA*, and *EB* conformers. The angles θ and φ refer to rotation about C—N and Ph—C(S) bonds, respectively. The θ scale is compressed by a factor 2 relative to the φ scale. Only cuts through the surface are shown for Ph—C(S) rotation interchanging *E* and *Z* isomers, and for C—N rotation relating the $E,A \rightleftarrows Z,B$ and $E,B \rightleftarrows Z,A$ conformers. Tie lines (dotted lines) from the maxima in these cuts are joined to indicate the 'saddle point'.

The assignment of OH and CH proton peaks follows from their relative intensities at −50 °C, the manner in which they coalesce as the temperature is raised, and an assessment of steric plus other factors. The NCH_a signals account for half as many protons as the NCH_e signals; thus the methyl group is axial (19). The *syn* NCH_e proton signal is known to be downfield relative to the *anti* NCH_e signal (19). Further, the $NCH_e(H)$ proton signals are doublets due to coupling with the geminal axial protons, while the $NCH_e(CH_3)$ signals are multiplets due to coupling with the methyl protons. Molecular models show that conformer *EB* is the most sterically hindered conformer in the ground state, and hence its peak should have the lowest intensity. Thus all the *EB* signals can be assigned readily as indicated in the spectrum at −50 °C in Figs. 2*e* and 3. The methyl group signal for this conformer also appears well separated from that of the other three conformers.

The *syn* NCH_e proton doublet of conformer *EA* can be identified next, slightly downfield from the corresponding doublet in *EB*. At −30 °C the *EB* signals begin to broaden, together with the peaks for another conformer, whereas the peaks for the remaining two conformers (one of which is *EA*) are still sharp. Since the chemical shift difference between the *syn* NCH_e protons of *EA* and *EB* is the smallest of all the possible shift differences that can be formed for the four conformers, it follows that the process which interchanges $EB \rightleftarrows EA$ is *not* the one which begins to appear as rapid on the nmr scale at −30 °C (process *I*). Process *II* interchanging $EB \rightleftarrows ZB$ is envisaged as having a lower barrier than process *III* interchanging $EB \rightleftarrows ZA$ for reasons already mentioned, and this is proven later in this paper from the nmr spectra of **6**, where $A \rightleftarrows B$ interchange can be ruled out and coalescence similar to that observed for **2** must be due to $B \rightleftarrows B'$ interchange (where B' is the mirror image of *B*). The interchange $EB \rightleftarrows ZB$ thus remains as the one which first becomes rapid at −30 °C as the temperature is raised.

Taking the selective broadening at −30 °C into account, the OH and *syn* and *anti* NCH_e proton signals of the *ZB* conformer can be

assigned. This OH peak is the strongest of the four OH signals at −50 °C and has the largest chemical shift from TMS. The two central OH peaks of almost equal intensity are thus due to the *EA* and *ZA* conformers, but no specific assignment can be made. In order of increasing chemical shift at −50 °C, the OH protons therefore have the following chemical shifts from TMS (and relative intensities): *EB* = 1688 Hz (1.0); *EA*/*ZA* = 1749 Hz (1.7) and 1781 Hz (1.4); *ZB* = 1818 Hz (2.7). This means that the *EB* conformer is 0.43 kcal/mol less stable than the *ZB* conformer and the *EA*/*ZA* conformers are 0.20/0.28 kcal/mol less stable than *ZB*.

The remaining *syn* NCH_e multiplet (with the largest chemical shift in this group) must arise from *ZA*. The *anti* NCH_e multiplet that remains unidentified belongs to *EA*, and intensity considerations dictate that the *anti* NCH_e proton chemical shifts of the *ZB* and *ZA* conformers (doublet) must be identical. At −30 °C broadening due to the *ZB* contribution to this signal is already evident.

The axial proton signals are more overlapped. However, the broadening at −30 °C permits the identification of the *syn* and *anti* NCH_a proton signals of *EB* and *ZB*. The remaining NCH_2 peaks are assigned to a superposition of the *syn* and *anti* NCH_a signals of *EA* and *ZA*; these broaden at 0 °C and this shows that $\Delta E_{II'} > \Delta E_{II}$.

The commencement of selective broadening around −30 °C as the temperature is raised proves the following:

(*1*) The process *EB* ⇄ *ZB* is becoming rapid, and intermolecular hydrogen exchange processes are ruled out, as in this case all four OH signals should start to coalesce at the same temperature.

(*2*) Because

$$(\tau_{OH}^{EB} - \tau_{OH}^{ZB}) \gg |\tau_{OH}^{ZA} - \tau_{OH}^{EA}|$$

and yet the *EB* and *ZB* conformers interchange at a lower temperature, it follows that $\Delta E_{II'} > \Delta E_{II}$.

(*3*) The exchange *ZB* ⇄ *EB* takes place at a lower temperature than the exchange *EB* ⇄ *EA* in spite of the fact that for the NCH_e protons

$$(\tau_{anti}^{ZB} - \tau_{syn}^{EB}) \gg (\tau_{syn}^{EB} - \tau_{syn}^{EA})$$

which implies that the energy barrier for the latter exchange (ΔE_I) exceeds that for the former (ΔE_{II}).

The relative barrier heights $\Delta E_I > \Delta E_{III} > \Delta E_{II'} > \Delta E_{II}$ are therefore indicated, with the thermodynamic stability of isomers/conformers increasing in the order *E*,*B* < *E*,*A* ≈ *Z*,*A* < *Z*,*B*. These features are incorporated into Fig. 5. While the barriers for *ZA* ⇄ *ZB* and *EA* ⇄ *EB* exchange may be slightly different, they are both referred to here as ΔE_I; similarly those for *EB* ⇄ *ZA* and *EA* ⇄ *ZB* exchange are both labelled ΔE_{III}.

By 0 °C the OH peaks for all four conformers have already coalesced (Fig. 2*c*) and the NCH_e proton signals for the *EB* and *ZB* conformers have broadened to the extent that they are lost in the background. Broad signals are observed for the *syn* and *anti* NCH_e protons of the *EA* and *ZA* conformers, as well as a broad superimposed *syn* and *anti* NCH_a signal for these conformers. On the other hand, the *syn* and *anti* NCH_a signal of *EB* and *ZB* is *sharp* at τ = 6.85 ppm, as are the methyl doublets due to the conformer pairs *ZB*/*EB* and *EA*/*ZA*. These sharp features persist at 20 °C indicating that even at that temperature neither of the barriers ΔE_{III} or ΔE_I have yet been exceeded.

By 40 °C the signals for the OH, NCH_e(H), NCH_e(Me), NCH_a(H) and methyl protons are averaged to one signal each, respectively, for all four conformers (Fig. 2*a*). This means that at least one or both of the energy barriers ΔE_{III} and ΔE_I are now being exceeded by rapid exchange on the nmr scale, bearing in mind that co-operative θ,φ motion may mean that the full barrier heights ΔE_I and ΔE_{III} need never be attained (Fig. 5). Coalescence at 40 °C implies a barrier height of ~17 kcal/mol between *A* and *B* conformers of **2**.

Figure 6*a* shows the OH proton signals for **2** at 100 MHz over a temperature range. At low temperatures the four separate signals are still seen, corresponding to the number of conformers, proving that even at this lower field strength the OH group is a good spectroscopic probe in these compounds.

Conformers of 1-(2′-Hydroxythiobenzoyl)-4-methylpiperidine (3)

For **3** only two OH peaks are observed at 100 MHz at low temperatures, (Fig. 6*b*) in agreement with the expected number of conformers. The

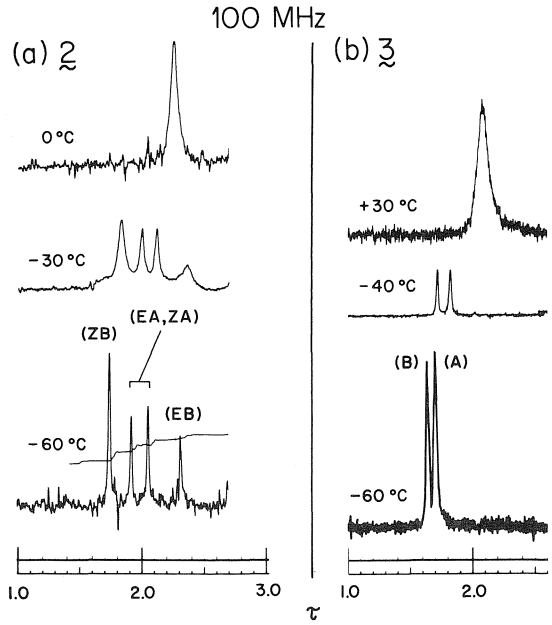

FIG. 6. 100 MHz ^{1}H nmr spectra of (*a*) **2** and (*b*) **3** in $CDCl_3$.

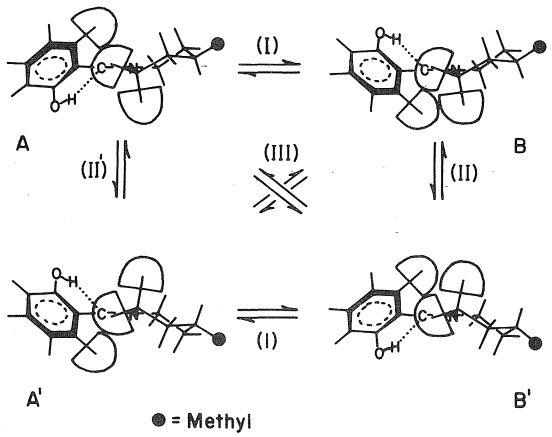

FIG. 7. The *A* and *B* conformers of **3** and their enantiomers *A'* and *B'*, respectively, together with all possible interconversion paths. For further details see caption to Fig. 4 and text.

complete conformational scheme for **3** is presented in Fig. 7. Here processes *II* and *II'* lead to the enantiomers *B'* and *A'* of the conformers *B* and *A*, respectively, and thus only two spectroscopically distinguishable forms of this molecule are expected in non-chiral solvents. The potential energy surface for conformational interconversion in **3** would resemble that presented in Fig. 5 except that it would have a vertical two-fold symmetry axis through the saddle point. At 100 MHz the OH signal splitting is the only evidence for the existence of two conformers of **3**, the hetero-ring protons giving only one signal for both *A* and *B* conformers.

Isomers of 2,6-Dimethyl-4-(2'-hydroxythiobenzoyl)morpholine (6)

The sensitivity of the OH proton to the *A* and *B*, and the *Z* and *E* conformers of **2** having been demonstrated, it was of interest to investigate the existence of *A* and *B* conformers in the *cis* and *trans* dimethyl compound **6**. The 220 MHz spectra of **6** at ambient temperature in $CDCl_3$ and CS_2 solution are shown in Fig. 8*d* and *e*, respectively. In $CDCl_3$ solutions the *syn* NCH_e and the *syn* and *anti* NCH_a proton signals differ in shape and in chemical shift for the *A* and *B* conformers, and the *syn* and *anti* methyl group protons are also distinguishable. From this $A \rightleftarrows B$ (process *I*) and $A' \rightleftarrows B$ (process *III*) exchanges can be ruled out, and $B \rightleftarrows B'$ and/or $A \rightleftarrows A'$ (processes *II* and *II'*) identified as being responsible for the broadening. The great similarity between the *syn* and *anti* NCH_a proton signal patterns for **6** and **2** at 20 °C suggests an identical process in the latter, and this has already been used in the assignment of its nmr signals. At the same temperature in CS_2 solution the *syn* NCH_e proton signals of **6** have merged, but the *syn* and *anti* NCH_a proton signals are still different in *A* and *B*.

From the spectrum of **6** in $CDCl_3$ at 20 °C a lower limit of $\Delta E > 17$ kcal/mol can be predicted for the barrier between *A* and *B* conformers, given that they still give separate *syn* and *anti* NCH_a peaks at this temperature. This barrier is probably $\Delta E_{III'}$ or related to it but lowered by passage through the saddle region in Fig. 5. In a compound like 2,6-dimethyl-4-(4'-nitrothiobenzoyl)morpholine an even higher barrier is expected because of increased 'stiffness' to rotation due to the higher C—N bond order.

The breadth, multiplicity, and temperature dependence of the OH peaks in **6** (Fig. 8*c*) are contrasted with the corresponding signals in **1** and **5**, which are shown on the same scale in Fig. 8*a* and *b*, respectively. Both **1** and **5** exhibit

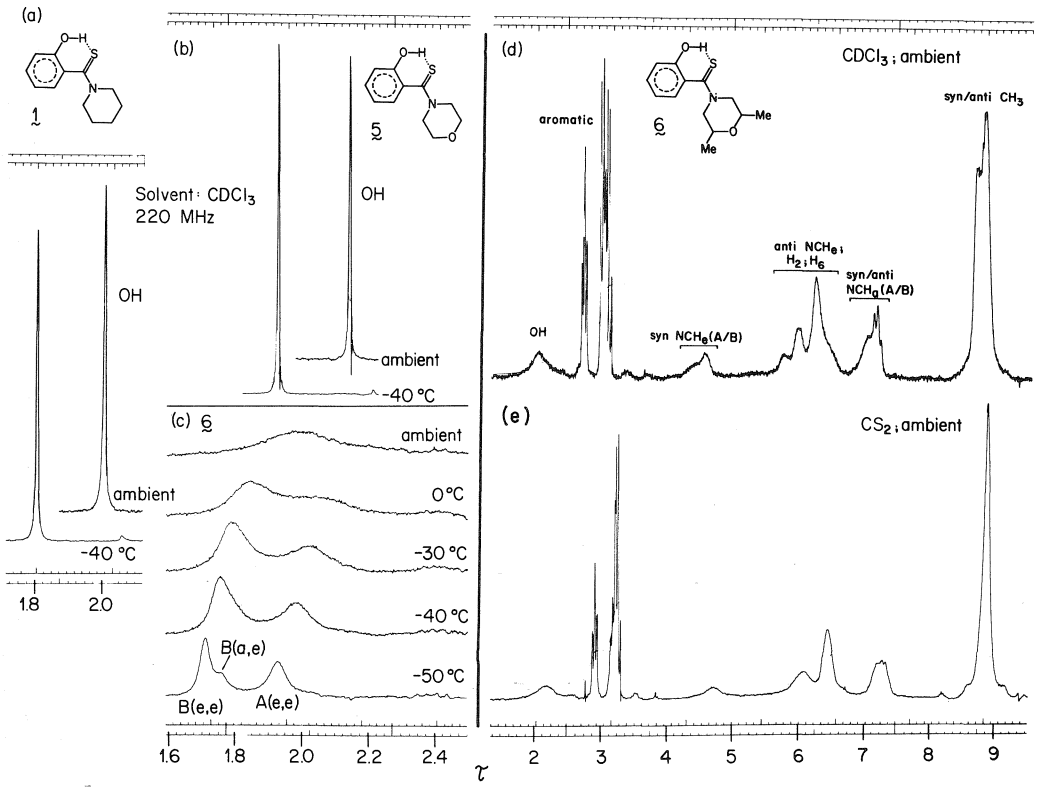

FIG. 8. 220 MHz ^{1}H nmr OH proton signals in (*a*) **1**, (*b*) **5**, and (*c*) **6**; (*d*) (*e*) nmr spectra of **6**.

only a single very sharp OH peak down to −40 °C. The chemical shifts $\tau_{OH}{}^{A}$ and $\tau_{OH}{}^{B}$ should each be approximately the same (if not identical) in **1** and **3**, and in **5** and **6**, as all the factors which can influence this chemical shift in a given conformer remain constant. Thus the shift differences $\tau_{OH}{}^{A} - \tau_{OH}{}^{B}$ should also be the same in **1** and **2**, and in **5** and **6**, respectively. The appearance of only a single peak in **1** and **5** implies that the interchange $A \rightleftarrows B$ by hetero-ring inversion is rapid on the nmr scale, over the temperature range investigated. For **2**, **3**, and **6** this process is frozen on the nmr scale by the biased hetero ring (or a rapidly equilibrating mixture of a major conformer like *A* and a minor conformer of type *B* with an axial methyl group exists).

The 220 MHz OH proton signals of **6** in $CDCl_3$ solution as a function of decreasing temperature are shown in Fig. 8*c*. By −50 °C three peaks are observed. The dominant peaks at 1777 and 1824 Hz from TMS are assigned to the *A* and *B* conformers of **6** with ee methyl groups, while the secondary peak at 1813 Hz arises from the *B* conformer of **6** with ea methyl groups. The latter reflect an ee/ae mixture in the 2,6-dimethylmorpholine used in the synthesis of **6** (see Experimental). The $\tau_{OH}{}^{ae}$ and $\tau_{OH}{}^{ee}$ signals of the *A* conformer may well overlap in Fig. 8*c*.

A smaller proportion of the ae isomer is also seen in the 300 MHz methyl proton signals of 2,6-dimethyl-4-(3′-nitrothiobenzoyl)morpholine (**7**) and (**6**) shown in Fig. 9*a* and *b*, respectively, together with assignments. The a methyl group in **7** now shows up as separate *syn* and *anti* doublets. In **6** the *o*-OH substituent introduces greater rigidity into the molecule and accentuates the difference between the *A* and *B* conformers. Thus at −11 °C the a methyl signals are now split. At −33 °C these signals have collapsed into single lines, but the *syn* e CH_3 signal shows splitting corresponding to the different chemical shifts of *A* and *B* conformers. The *anti* e CH_3 signals are clearly different for the *A* and *B* conformers at both of these temperatures.

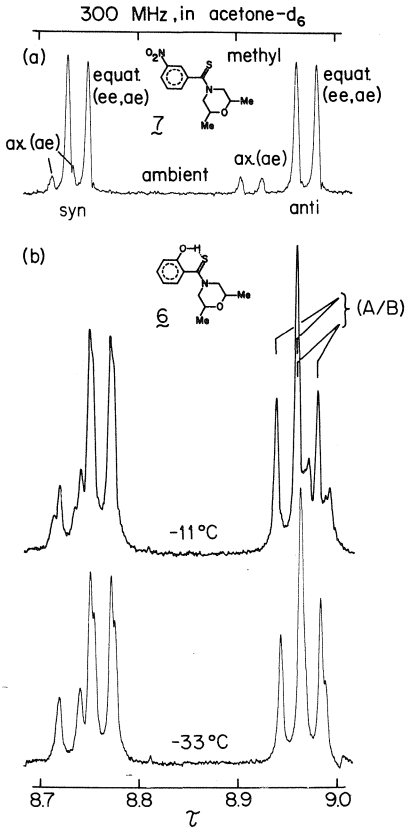

FIG. 9. 300 MHz ^{1}H nmr spectra of (*a*) **7** and (*b*) **6** in the methyl proton region.

1-(2′-Hydroxythiobenzoyl)-2,6-dimethylpiperidine (4): Phenolthione (C—O—H···S=C) and Enethiol-quinonemethide (C=O···H—S—C=C)

2,6-Dimethyl substitution of **1** produces **4**, which is radically different in structure from **2**. In the 220 MHz nmr spectrum of **4** (Fig. 10) both the chemical shift and the signal pattern of the NCH protons show that they are axial, and therefore both methyl groups must be equatorial. At all temperatures investigated the NCH_a protons have the same signal; also the two e CH_3 groups have the same signal. Molecular models indicate that the steric interactions cannot be accommodated in a structure like that of **2** (where the single methyl group is axial in all the conformers) and all spectral data are consistent with **4***a* (Scheme 1) in which the CNC plane is perpendicular to the Ph—C(S)—N plane. This would break the conjugation of the C—N bond and increase the Ph—C=S conjugation, with its planarity being favoured by a very strong intramolecular OH···S hydrogen bond. While another conformer can be envisaged by 180° rotation about the C—N bond, this involves steric H_6···Me interactions leading to an unpopulated high energy form. Rotation about the C—N bond to interchange these conformers is also bound to have a very high energy barrier because of the severe steric interactions in the planar transition state. We believe **4** to be the first amide in which N lone pair electrons are not conjugated with the C=X π-electrons because of mutual orthogonality in the molecular structure. Its ground state structure is a model for the transition state of process *II* in **2**, and the existence of **4** as a stable compound lends strong support to the hypothesis that this type of stabilized transition state is the most important in the low temperature interconversion of $Z \rightleftarrows E$ conformers in **2**.

All the compounds dealt with in this paper are white in colour, except **6** which is pale green, and **4** which is red. That provides further evidence of radically different electronic structure in the last one. Furthermore, in **4** the aromatic proton $H_{6'}$ is very much deshielded relative to the equivalent protons in all other *o*-OH thiobenzamides studied, such a low-field position being quite normal for a δ proton in a quinonemethide.

The OH signal of **4** is very broad in $CDCl_3$, conditions under which **1** and **5** give very sharp bands, and this is indicative of an exchange process. The infrared spectra of **4** in very dilute CCl_4 solution ($c < 10^{-3}$ *M*) provide further evidence as to its structure (Fig. 11). Compound **2** exhibits a very weak 'free' OH peak at 3613 cm^{-1} and an intense broad intramolecularly OH···S bonded band with a maximum ~3270 cm^{-1}, and all other *o*-hydroxythiobenzoylpiperidines and -morpholines are similar. Compound **4** has a trace of 'free' OH at 3616 cm^{-1}, with $\nu_{OH...S} < 3000\ cm^{-1}$ and overlapped by CH stretching bands, *and an intramolecularly hydrogen bonded SH···O band at 2250 cm^{-1}*. No absorption occurs in this region for any other related *o*-hydroxythiobenzamides, and 'free' SH groups normally absorb *weakly* in the range 2550–2600 cm^{-1}. We attribute all of these features to the equilibrium in Scheme 1.

The lack of double bond character in the C—N bond favours **4***b* and **4***d*, and the hydrogen

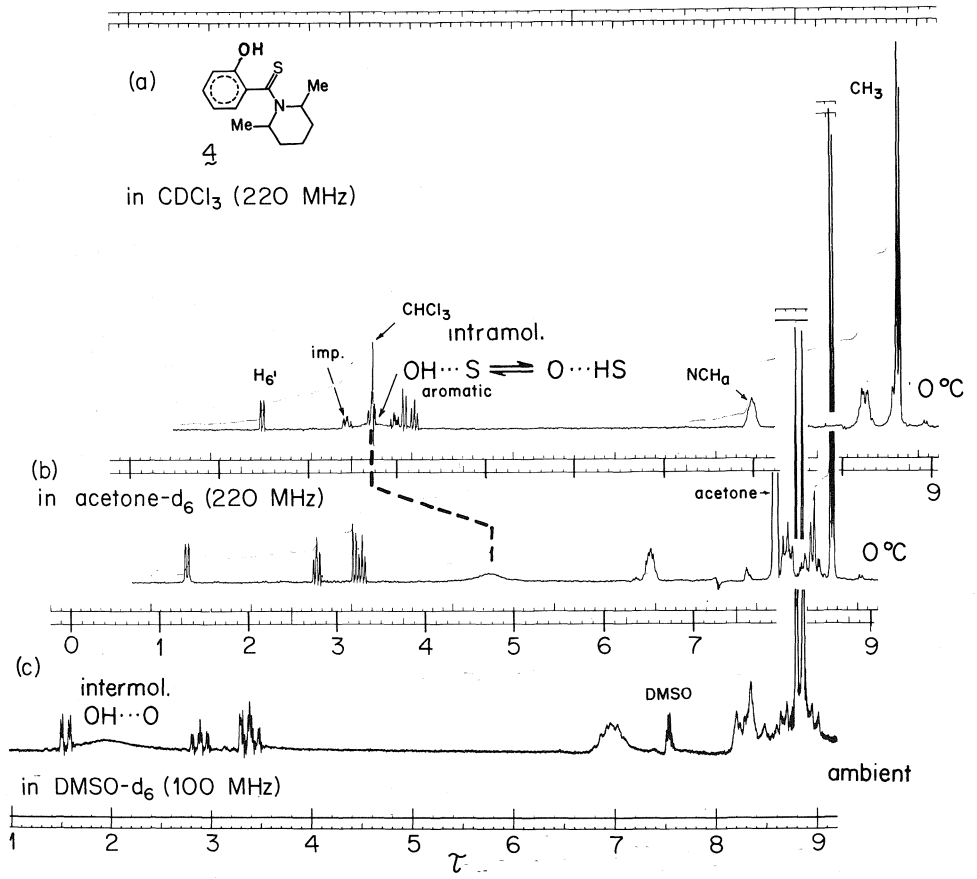

FIG. 10. ^1H nmr spectra of **4**.

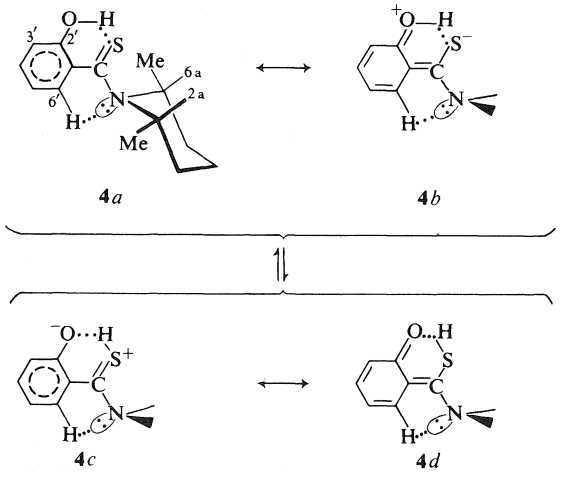

SCHEME 1

bonded proton moves in an unsymmetrical double minimum potential. The planarity of the 2′-hydroxythiobenzoyl moiety in the absence of steric interactions between $H_{6'}$ and H_{2e} lends strong support to the concept that non-planarity of the phenyl ring with the thioamide group which is normally found in *N*-thiobenzoyl-piperidines and -morpholines arises because of $H_{6'}\cdots H_{2e}$ interaction. Trace amounts of 'free' OH probably arise from rotation about the C—O bond, as opposed to rotation about the Ph—C(S) bond.

The intramolecular OH···S hydrogen bond in **4** has all the characteristics of a very strong hydrogen bond corresponding to a short O···S distance, not only in CCl_4 solution (Fig. 11) but also in KBr pellets (Fig. 12). Here the infrared spectra exhibit broad bands at 2750,

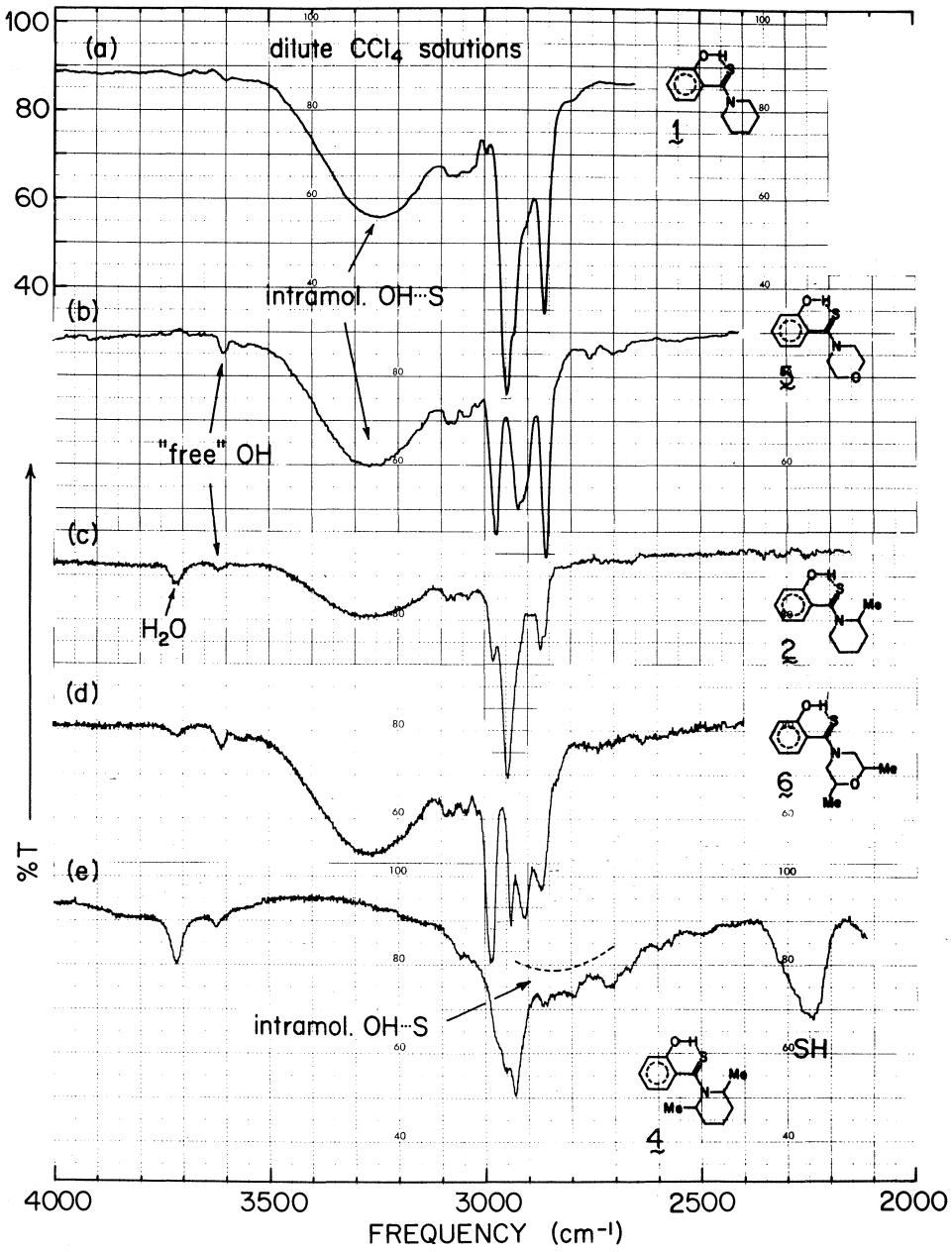

FIG. 11. Infrared spectra of *N*-(*o*-hydroxythiobenzoyl)morpholines and -piperidines in very dilute ($c < 0.003\ M$) CCl_4 solution.

2150, 1400 (?), and 970 cm^{-1}, similar to the "A", "B", "C", and "D" bands observed in strongly intermolecularly hydrogen bonded systems (20). These do not appear in the infrared spectra of KBr pellets of other *o*-hydroxythiobenzoylmorpholines (Fig. 12). Furthermore, the "A" and "B" bands have fine structure similar to that reported by Bellamy and Rogash (21) for strong hydrogen bonds in tautomeric 2-thiopyridone and 2-pyridone dimers. They interpreted the fine structure tentatively in terms of Fermi resonance of the ν_{XH} fundamental

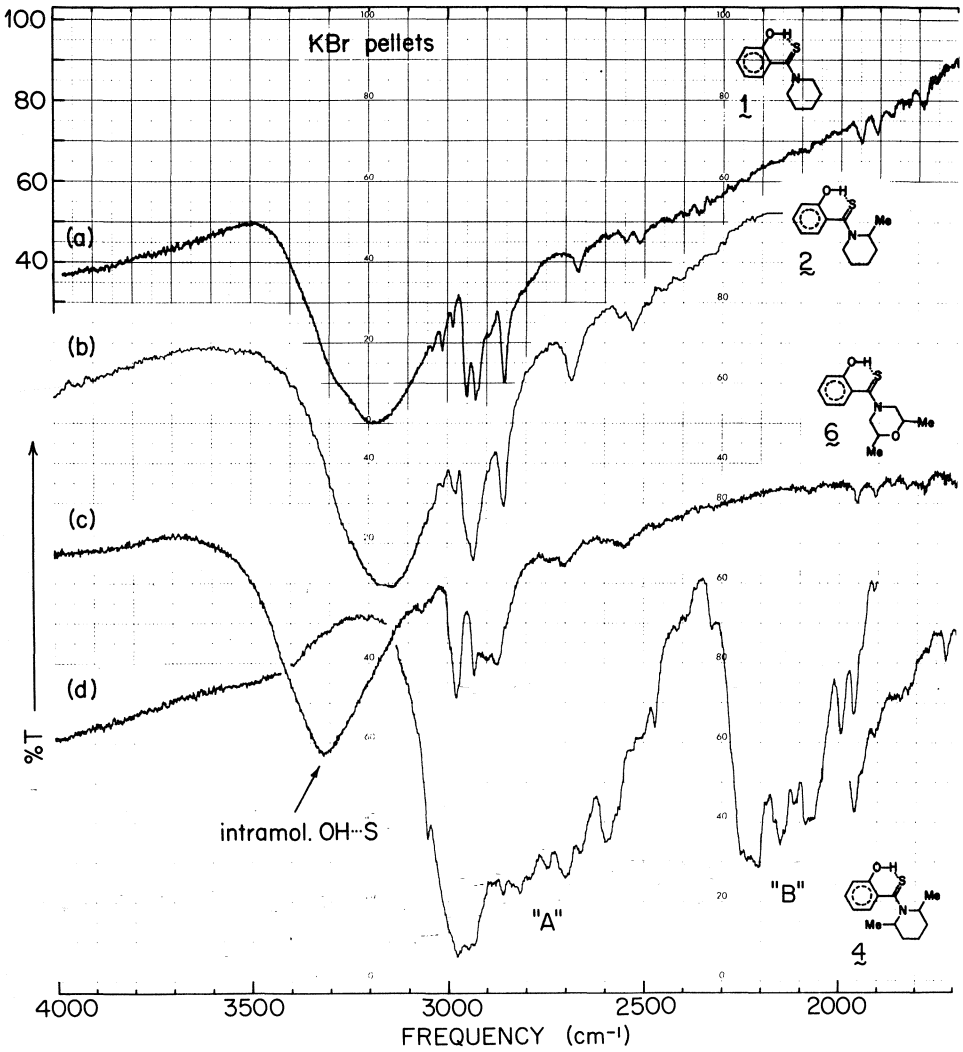

FIG. 12. Infrared spectra of *N*-(*o*-hydroxythiobenzoyl)morpholines and -piperidines in KBr pellets.

vibration with overtones and combinations of lower frequency fundamentals.

The uv spectrum of **4** is significantly different from that of **2**. The following absorption bands are observed in methanol (λ, nm; followed by ε, 1×10^4 l mol^{-1} cm^{-1}): **2**, 281 (1.3), 240 (0.71), 211 (1.7); **4**, 364 (0.80), 293 (0.72), 235 (0.76), 219 (1.4). Most normal *N*-thiobenzoylpiperidines exhibit a very weak $n \rightarrow \pi^*$ band near 350 nm, but it is too weak in **2** to be observed. The large ε value of the 364 nm band in **4** shows that it is due to a $\pi \rightarrow \pi^*$ and not an $n \rightarrow \pi^*$ transition, and its long wavelength (low energy) confirms the high degree of conjugation of the aromatic ring with the thiocarbonyl group, which are coplanar in **4**, but not in **2**.

The broad OH signals in the nmr spectra of **4** in $CDCl_3$ and acetone-d_6 (Fig. 10*a* and *b*; $\tau_{OH/SH}$ ~2.7 and ~4.8 ppm, respectively) reflect the intramolecular $OH\cdots S \rightleftarrows O\cdots HS$ proton transfer equilibrium, which is displaced more to the right in the latter solvent because of its higher dielectric constant.[12] The τ_{OH} signal at ~1.9 ppm in DMSO-d_6 solution (Fig. 10*c*) probably indicates that the intramolecular

[12]In aromatic thiols in $CDCl_3$ solution, τ_{SH} is around 6.5–6.7 ppm, dropping to 5.27 ppm in $O{=}C(SH)CH_3$ (22).

hydrogen bond has ruptured and has been replaced by a very strong intermolecular OH· · ·O bond to the solvent. In both acetone-d_6 and DMSO-d_6 the OH signal moves downfield with decreasing temperature, and the OH integral indicates the equivalent of more than one proton, which may indicate the involvement of traces of water in the hydrogen bonding equilibria.

Conclusions

(*1*) The proton in an intramolecular OH· · ·S hydrogen bond is shown to be a very sensitive conformational probe. To our knowledge this is the first observation of distinctly separate nmr OH signals arising from the *same* OH· · ·S bond, as modulated by different rotational isomeric and conformational geometries.

(*2*) The existence of *A* and *B* conformers in *o*-hydroxythiobenzoylpiperidines and -morpholines is well documented, and the geometrical parameters of these conformers are estimated from a model which is in good agreement with the experimental data.

(*3*) The structural characteristics of a thiobenzamide with no conjugation between the N lone pair electrons and the thiocarbonyl π-electrons is described for the first time, and it is shown to have an intramolecularly hydrogen bonded proton in an unsymmetrical double minimum potential.

(*4*) The complex and still poorly understood infrared "A", "B", "C", and "D" band systems which are well known for very strong intermolecular hydrogen bonds are also shown to arise from an intramolecular hydrogen bond in **4**.

(*5*) This investigation supports the hypothesis of Muller and Reiter (23) that the temperature dependence of the chemical shift of a hydrogen bonded proton can largely be explained by a change in the relative population of vibrational levels of the ν_σ (here $\nu_{O\ldots S}$) stretching mode (13*b*). This vibration lies around 100–200 cm^{-1} in the far infrared (24), and several excited states are expected to be appreciably populated even at low temperatures. The OH proton of **3** yields separate sharp signals for *A* and *B* conformers, respectively at −40 and −60 °C (Fig. 6) and no 'free' OH exists, since that would lead to a different chemical shift from that of OH_A· · ·S and OH_B· · ·S. Furthermore rapid exchange between hydrogen bonded and 'free' OH protons would collapse the hydrogen bonded peaks, which is not the case. The temperature dependence of the OH chemical shift for both conformers between −40 and −60 °C can be accounted for only by decreasing OH· · ·S distance (decreasing excitation of ν_σ) as the temperature decreases, and not by a shift in the hydrogen bonding equilibrium as previously considered (25).

Acknowledgement

The financial assistance of the National Research Council of Canada is gratefully acknowledged.

1. P. J. KRUEGER, A. O. FULEA, C. FULEA, and F. CORNEA. Spectrosc. Lett. **8**, 141 (1975).
2. P. J. KRUEGER and A. O. FULEA. Tetrahedron, **31**, 1813 (1975).
3. A. O. FULEA and P. J. KRUEGER. Tetrahedron Lett. 3135 (1975).
4. G. A. BARAMKI, G. DERDALL, and J. T. EDWARD. Can. J. Spectrosc. **18**, 160 (1973).
5. K. C. RAMEY, D. J. LOUICK, P. W. WHITEHURST, W. B. WISE, R. MUKHERJEE, J. F. ROSEN, and R. M. MORIARTY. Org. Magn. Reson. **3**, 767 (1971), and references cited therein.
6. W. WALTER and J. VOSS. *In* The chemistry of amides. *Edited by* J. Zabicky. Interscience, London. 1970. pp. 426–429, and references cited therein.
7. R. L. HILDERBRANDT. J. Chem. Phys. **51**, 1654 (1969).
8. W. C. HAMILTON, M. FREY, L. GOLIC, P. G. JÖNSSON, T. K. KOETZLE, A. KVICK, M. LEHMAN, and J. J. VERBIST. Abstr. 163rd Am. Chem. Soc. National Meeting, Boston, Mass., April 1972. Paper 065.
9. A. BONDI. J. Phys. Chem. **68**, 441 (1964).
10. G. EGLINTON, J. MARTIN, and W. PARKER. J. Chem. Soc. 1243 (1965).
11. N. A. BAILEY and R. MASON. Proc. R. Soc. Ser. A, **29**, 94 (1966).
12. H. A. SCHERAGA. *In* Advances in physical organic chemistry. Vol. 6. *Edited by* V. Gold. Academic Press, London. 1968. p. 124.
13. G. C. PIMENTEL and A. L. MCCLELLAN. The hydrogen bond. W. H. Freeman, San Francisco. 1960. (*a*) pp. 285–293; (*b*) p. 68.
14. (*a*) S. N. VINOGRADOV and R. H. LINNELL. Hydrogen bonding. Van Nostrand Reinhold, New York. 1971. pp. 176–178; (*b*) L. J. BELLAMY and R. J. PACE. Spectrochim. Acta, Part A, **25**, 319 (1969).
15. W. C. HAMILTON and J. A. IBERS. Hydrogen bonding in solids. W. A. Benjamin, New York. 1968. p. 16.
16. R. SRINIVASAN and K. K. CHACO. *In* Conformation of biopolymers. Vol. 2. *Edited by* G. N. RAMACHANDRAN. Academic Press, New York. 1967. p. 607.
17. C. ROUSSEL, M. CHANON, and J. METZGER. Tetrahedron Lett. 1861 (1971).
18. R. LOZAC'H, L. LEGRAND, and J. SANDSTRÖM. Org. Magn. Reson. **7**, 54 (1975).
19. W. WALTER, E. SCHAUMANN, and H. PAULSEN. Justus Liebigs Ann. Chem. **727**, 61 (1969).

20. J. BELLAMY. Advances in infrared group frequencies. Methuen and Co., London. 1968. pp. 277–280; D. HADZI. Pure Appl. Chem. **11**, 435 (1965); D. HADZI and N. KOLILAROV. J. Chem. Soc. (A), 439 (1966); M. F. CLAYTON and N. SHEPPARD. Chem. Commun. 1431 (1969).
21. L. J. BELLAMY and P. E. ROGASCH. Proc. R. Soc. Part A, **257**, 98 (1960).
22. H. A. SZYMANSKI and R. E. YELLIN. N.m.r. band handbook. Plenum Publishing Co., New York. 1968. p. 398.
23. N. MULLER and R. C. REITER. J. Chem. Phys. **42**, 3265 (1965).
24. K. D. MÖLLER and W. G. ROTHSCHILD. Far-infrared spectroscopy. Wiley–Interscience, New York. 1971. pp. 200–201.
25. U. LIDDEL and N. F. RAMSAY. J. Chem. Phys. **19**, 1608 (1951).

The reaction of certain α-diazocarbonyl compounds with thiophosgene and ethyl chlorodithioformate[1]

PATRICIA DEMAREE, MARIE-CARMEN DORIA, AND JOSEPH M. MUCHOWSKI[2]

Research Laboratories, Syntex, S.A., Apartado Postal 10-820, Mexico 10, D.F.

Received July 27, 1976

PATRICIA DEMAREE, MARIE-CARMEN DORIA, and JOSEPH M. MUCHOWSKI. Can. J. Chem. **55**, 243 (1977).

The reaction of thiophosgene with α-diazocarbonyl compounds produced mixtures of 1,2,3- and 1,3,4-thiadiazoles, in which the latter predominated, irrespective of whether the bis(α-diazoacyl)mercury derivatives or the free diazo compounds were used. In contrast, ethyl chlorodithioformate gave exclusively 1,3,4-thiadiazoles with α-diazocarbonyl compounds in the presence of triethylamine and only 1,2,3-thiadiazoles when the bis(α-diazoacyl)mercury derivatives were used.

PATRICIA DEMAREE, MARIE-CARMEN DORIA et JOSEPH M. MUCHOWSKI. Can. J. Chem. **55**, 243 (1977).

La réaction de thiophosgène avec les composés α-diazocarbonyles conduit à des mélanges de thiadiazoles-1,2,3 et 1,3,4; que l'on utilise des dérivés mercuriques du bis(α-diazoacyl) ou les composés diazos libres le dernier prédomine. Par opposition, le chlorodithioformate d'éthyle conduit uniquement à des thiadiazoles-1,3,4 par réaction avec les composés α-diazocarbonyles en présence de triéthylamine et uniquement à des thiadiazoles-1,2,3 lorsque l'on utilise des dérivés bis(α-diazoacyl) mercure.

[Traduit par le journal]

The reaction of diazoalkanes with thiocarbonyl compounds has been extensively studied (1–5), and diverse products, the nature of which depends on the structure of both reactants, are formed. For example, it has long been known (6, 7) that 1,3,4-thiadiazoles are produced from thiocarboxylic acid chlorides and diazoacetic esters or diazomethane. In addition, Ried and Beck (8) assigned the 1,2,3-structure to the thiadiazoles derived from thiophosgene and diazoketones, but it is now recognized (9) that the reported compounds were, in fact, members of the 1,3,4-series. Nevertheless, 1,2,3-thiadiazoles can arise from certain thioacyl halides, since it has recently been reported (2) that a mixture of 5-ethylthio-1,2,3-thiadiazole and 2-ethylthio-1,3,4-thiadiazole was obtained from ethyl chlorodithioformate and diazomethane. Both of the above types of thiadiazoles were required in connection with other studies and therefore the reaction of thiophosgene and ethyl chlorodithioformate with several diazoacetophenones and ethyl diazoacetate was examined under a variety of conditions.

When diazoacetophenone **1***a* (2 mol) was

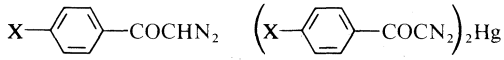

1

a X = H
b X = Cl
c X = CH_3

2

a X = H
b X = Cl

reacted with thiophosgene (1 mol), a complex mixture, from which no pure chlorobenzoylthiadiazole **3***a* or **4***a* could be isolated, was obtained. The presence therein of at least one chlorothiadiazole was established, however, by the isolation of an ethylthiobenzoylthiadiazole, in 10% yield, after treatment of the mixture with ethanolic sodium ethyl mercaptide. The same compound was formed in considerably better yield (25%, see Table 1) from ethyl chlorodithioformate and bis(α-diazophenacyl)mercury **2***a*.

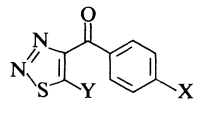

3

a X = H, Y = Cl
b X = Y = Cl
c X = CH_3, Y = Cl
d X = H, Y = SC_2H_5
e X = Cl, Y = SC_2H_5
f X = Cl, Y = NHC_6H_5

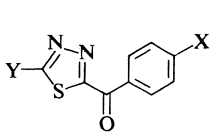

4

a X = H, Y = Cl
b X = Y = Cl
c X = CH_3, Y = Cl
d X = H, Y = SC_2H_5
e X = Cl, Y = SC_2H_5
f X = Cl, Y = NHC_6H_5

[1]Contribution No. 471 from the Syntex Institute of Organic Chemistry.

[2]Author to whom enquiries should be addressed.

TABLE 1. Synthesis of thiadiazoles from thioacyl chlorides and diazo compounds

Diazo compound (No.)		Acylation system	Thiadiazoles (%)[a] 1,2,3- (No.)	1,3,4- (No.)
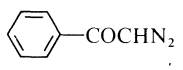	(1*a*)	$CSCl_2$	8 (3*d*)	?[b]
		$ClCS_2C_2H_5/(C_2H_5)_3N$	—	38 (4*d*)
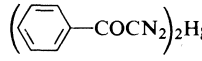	(2*a*)	$ClCS_2C_2H_5$	26 (3*d*)	—
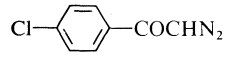	(1*b*)	$CSCl_2$	13 (3*b*)	47 (4*b*)[c]
		$CSCl_2/(C_2H_5)_3N$	4 (3*b*)	25 (4*b*)
		$ClCS_2C_2H_5/(C_2H_5)_3N$	—	36 (4*e*)
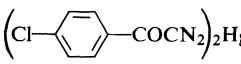	(2*b*)	$CSCl_2$	5 (3*b*)	20 (4*b*)[d]
		$ClCS_2C_2H_5$	25 (3*e*)	—
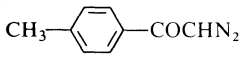	(1*c*)	$CSCl_2$	4 (3*c*)	52 (4*c*)[e]
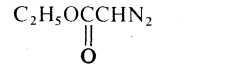		$CSCl_2$	23 (6*a*)	44 (7*a*)
		$CSCl_2/(C_2H_5)_3N$	7 (6*a*)	15 (7*a*)
		$CSCl_2$	20 (6*a*)	40 (7*a*)
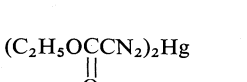	(7)	$ClCS_2C_2H_5$	37 (6*c*)	—
CH_2N_2		$ClCS_2C_2H_5$	19	41[f]

[a]Refers to the percent of product(s) isolated.
[b]See text and footnote 4.
[c]The ratio (3*b*):(4*b*) was 2:3 in the crude product as measured by nmr.
[d]The ratio (3*b*):(4*b*) was 1:6 in the crude product.
[e]The ratio (3*c*):(4*c*) was 1:6 in the crude product.
[f]Data taken from ref. 3. See text for structures of these thiadiazoles. Nuclear magnetic resonance analysis of the crude product indicated a 1:2.3 ratio of the 1,2,3- to the 1,3,4-isomers which was unchanged in the presence of triethylamine.

That this substance was 4-benzoyl-5-ethylthio-1,2,3-thiadiazole **3***d* was strongly supported by the characteristic (10, 11) mass spectrum[3] and conclusively established in the following manner. Sodium borohydride reduction of **3***d* gave an alcohol **5** which was different from that (**6***b*) synthesized by the aerial oxidation (12) of the anion derived from 1-ethylthio-5-benzyl-1,3,4-thiadiazole **6***a*. 2-Ethylthio-5-benzoyl-1,3,4-thiadiazole **4***d*, the ketone isomeric with **3***d*, could be prepared from diazoacetophenone and ethyl chlorodithioformate in the presence of triethylamine, and reduction of this compound with sodium borohydride produced the alcohol **6***b*.

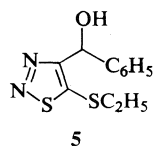

5

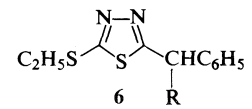

6

a R = H
b R = OH

The reaction of 4-chlorodiazoacetophenone **1***b* and thiophosgene, with or without added triethylamine, gave a mixture of products in which

[3]It has been reported (10, 11) that the loss of N_2 from the molecular ion is characteristic of 1,2,3-thiadiazoles. Both **3***d* and **4***d* showed a peak due to the loss of 28 mass units from this ion and, therefore, it was not possible to distinguish between the two compounds on this basis in the absence of exact mass measurements. An examination of the other fragments of these spectra did, however, make a facile identification of **3***d* possible, because the mass spectrum of this compound showed two sequential losses of 28 mass units ($M^+ - N_2 - C_2H_4$ or $M^+ - C_2H_4 - N_2$). This fragmentation pattern was found in all of the ethylthio-1,2,3-thiadiazoles reported in this paper (see Experimental section). Furthermore, those 1,2,3-thiadiazoles which did not contain the ethylthio moiety did show the expected relatively intense $M^+ - 28$ peaks. The corresponding 1,3,4-thiadiazoles showed either a very weak $M^+ - 28$ absorption or this peak was absent entirely. For those cases where it was considered unsafe to rely on the intensity of the $M^+ - 28$ peak, the 1,3,4-thiadiazoles all lost a ring fragment (NCX) which identified the system without doubt (*e.g.* $M^+ - N{\equiv}C{-}Cl$ for **4***b* or $M^+ - N{\equiv}C{-}SC_2H_5$ for **4***e*).

both the 1,2,3- and the 1,3,4-thiadiazoles **3***b* and **4***b* were present. The structures of these compounds were proved by conversion into the known anilinothiadiazoles **3***f* (9) and **4***f* (13), respectively. Although the isolated yields of **3***b* and **4***b* varied considerably (see Table 1), for a given experiment the ratio in the crude product was nearly constant, as measured by nmr spectroscopy, and was invariant throughout the course of a reaction. For example, the ratio of **3***b*:**4***b* was about 2:3 for the reaction of thiophosgene with 4-chlorodiazoacetophenone, whereas it was 1:6 when the mercuric salt was used.

4-Methyldiazoacetophenone **1***c* and thiophosgene also furnished a mixture of the 1,2,3- and the 1,3,4-thiadiazoles, but the proportion of the 1,3,4-isomer was substantially greater (**3***c*:**4***c* = 1:6) than observed for 4-chlorodiazoacetophenone under the same conditions. In view of the fact that 1,3,4- as well as 1,2,3-thiadiazoles were formed from both of the *para*-substituted diazoacetophenones and thiophosgene, it is highly probable that the 1,3,4-thiadiazole **4***a* was also produced in the corresponding reaction with diazoacetophenone. This substance, without doubt, was selectively deacylated (9) to lower molecular weight compounds under the strongly basic conditions of the thiolate ion displacement reaction.[4]

The formation of 1,2,3-thiadiazoles from thiophosgene and diazoacetophenones, or salts thereof, under all the conditions examined in this study contrasts with the failure of Bacchetti *et al.* (9) to detect these substances.

A study of the reaction of thiophosgene with ethyl diazoacetate and the corresponding mercuric salt **7** showed that a 1:2 mixture of the 1,2,3- and the 1,3,4-thiadiazoles **8***a* and **9***a* was formed in every case. Ethyl-5-chloro-1,2,3-thiadiazole-4-carboxylate **8***a* was a known compound and the physical properties thereof corresponded to those reported (14) for it. The structure of this substance was confirmed by conversion into a mixture of the chloroamide **10** and the amino ester **8***b* with alcoholic ammonia. Ethyl-5-amino-1,2,3-thiadiazole-4-carboxylate **8***b* synthesized in this way was identical to the known compound prepared by the method of Goerdeler and Gnad (14). The identity of the

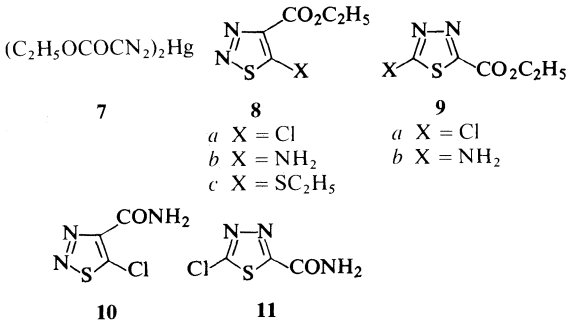

7 **8** **9**

a X = Cl
b X = NH_2
c X = SC_2H_5

a X = Cl
b X = NH_2

10 **11**

1,3,4-thiadiazole **9***a* was established as follows. The ester **9***a* was transformed exclusively into 2-chloro-1,3,4-thiadiazole-5-carboxamide **11** upon reaction with ethanolic ammonia. This substance was also prepared by the aminolysis of crude ethyl-2-chloro-1,3,4-thiadiazole-5-carboxylate **9***a* obtained by a Sandmeyer reaction on the known (15) amine **9***b*.

The data in Table 1 show that under all the conditions examined, α-diazocarbonyl compounds react with thiophosgene to give a mixture of 1,2,3- and 1,3,4-thiadiazoles with the latter predominating. The formation of these products can be interpreted in terms of the two possible modes (3) of dipolar cycloaddition of the diazo compound to the thiocarbonyl group of thiophosgene with subsequent loss of hydrogen chloride [1]. Alternatively, the thiadiazoles could stem from acylation of the dipolar system on carbon or nitrogen followed by either proton loss and cyclization, or cyclization and then proton loss [2]. It was considered that if acylation of the diazo compounds by the thioacyl halides played a significant role in the formation of the thiadiazoles, then utilization of an α-metalated diazo compound[5] might direct the acylation entirely to carbon. The exclusive formation of the 1,2,3-thiadiazoles **3***d*, **3***e*, and **8***c* from ethyl chlorodithioformate and the bis(α-diazoacyl)mercury compounds **2***a*, **2***b*, and **7** respectively, was consistent with this expectation. In contrast, the bis(α-diazoacyl)mercury reagents and thiophosgene gave mixtures in which the 1,3,4-thiadiazole always predominated, and for which the thiadiazole ratio was not greatly different from that observed for the free diazo compound. Indeed, the reaction of thiophosgene with ethyl diazoacetate or the corresponding mercury derivative, repeatedly gave mixtures of

[4]The reaction of **4***b* with ethanolic sodium ethyl mercaptide did not result in the formation of even traces of the ethylthio compound **4***e* (as shown by tlc), presumably for the same reason.

[5]Ethyl lithiodiazoacetate is acylated on carbon with benzoyl chloride (16). The acylation of bis(α-diazoacyl)-mercury compounds has not previously been reported.

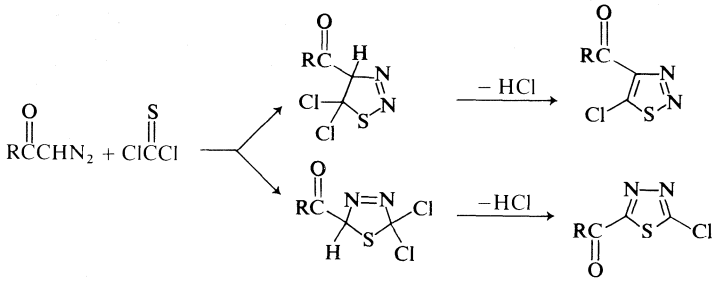

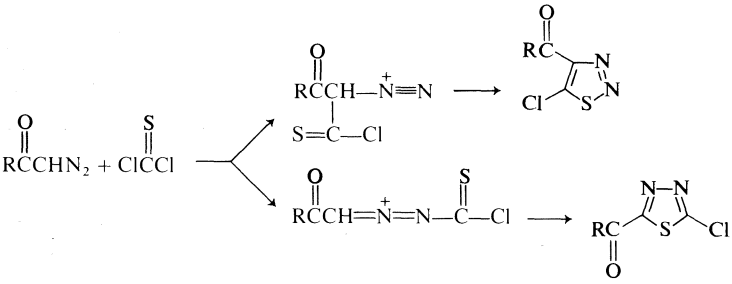

8*a* and **9***a* which were identical in composition and yield.

It is also of considerable interest that, in the presence of an equivalent of triethylamine, the α-diazoketones **1***a* and **1***b* and ethyl chlorodithioformate produced only the 1,3,4-thiadiazoles **4***d* and **4***e*. This result apparently is restricted to the less reactive α-diazocarbonyl compounds since the reaction of diazomethane with this dithioacid chloride gave a 1:2.3 mixture of 5-ethylthio-1,2,3-thiadiazole and 2-ethylthio-1,3,4-thiadiazole in the presence or absence of triethylamine.

Finally, it is noteworthy that compositionally similar mixtures of the 1,2,3- and 1,3,4-thiadiazoles were obtained when thiophosgene was the acylating agent irrespective of whether triethylamine was present or absent.

The results described herein have several consequences of synthetic importance, and some of these will be described in due course.

Experimental

The melting points were determined in a Mel-Temp apparatus and are not corrected. The infrared spectra were measured with a Perkin-Elmer model 237 grating infrared spectrophotometer. The ultraviolet spectra were recorded with a Perkin-Elmer model 402 ultraviolet visible spectrophotometer. The nmr spectra were obtained with a Varian T-60 spectrometer. The chemical shifts are expressed as ppm (δ) from internal tetramethylsilane. The mass spectra were measured with an Atlas CH-4 spectrometer.

4-Benzoyl-5-ethylthio-1,2,3-thiadiazole 3d

(*A*) *Reaction of Ethanethiol with the Crude Reaction Product of Diazoacetophenone and Thiophosgene*

The reaction was carried out in the manner described by Ried and Beck (8) except that a 2:1 molar ratio of diazoacetophenone to thiophosgene was used. The crude product was used directly in the next step.

The crude material from above (1.213 g), dissolved in absolute alcohol (15 ml) was added dropwise to a stirred solution of ethanethiol (0.4 ml, 0.33 g, 5.33 mmol) in absolute alcohol containing sodium ethoxide (prepared from sodium metal (0.125 g, 5.43 mmol)). After 24 h at room temperature, the solvent was removed *in vacuo* and the residue was dissolved in chloroform. The chloroform solution was washed with water, dried over sodium sulfate and evaporated *in vacuo*. The residue was purified by tlc on silica gel using benzene as the developing solvent. The product with R_f 0.55 was taken and after crystallization from alcohol a solid (0.053 g, 8%), mp 93–95 °C, was obtained. After recrystallization from methanol it had mp 97–98 °C; uv (CH_3OH) 250 (12 300), 322 nm (13 500); ir ($CHCl_3$) 1639 cm^{-1}; nmr ($CDCl_3$) 1.52 (t, 3H, J = 7.4 Hz), 3.12 (q, 2H, J = 7.4 Hz), 7.64 (m, 3H), 8.39 (m, 2H); ms (relative intensity) 250(5), 222(2), 194(19), 105(100), 77(50). *Anal.* calcd. for $C_{11}H_{10}N_2OS_2$: C 52.80, H 4.03, N 11.20; found: C 52.86, H 4.10, N 11.37.

(*B*) *From Bis(α-diazophenacyl)mercury 2a and Ethyl Chlorodithioformate*

A suspension of bis(α-diazophenacyl)mercury (17) (0.980 g, 2 mmol) in dry acetonitrile (30 ml) containing ethyl chlorodithioformate (0.4 ml, 0.56 g, 4 mmol) was stirred at room temperature, with protection from light, for 60 h. The mixture was filtered, the filtrate was evaporated *in vacuo*, and the residue was purified by tlc on silica gel (benzene). The product (0.264 g, 26%) was crystallized from methanol to give a solid mp 95–96 °C, identical to the compound prepared via method *A*.

Phenyl(5-ethylthio-1,2,3-thiadiazol-4-yl)carbinol **5**

Sodium borohydride (0.250 g, 6.6 mmol) was added to a stirred solution of 4-benzoyl-5-ethylthio-1,2,3-thiadiazole (1.00 g, 4.0 mmol) in ethanol (50 ml). After 2 h at room temperature the solvent was removed *in vacuo* and water was added to the residue. The mixture was extracted with ethyl acetate and the extract was dried over sodium sulfate and evaporated *in vacuo*. The oily residue (0.867 g, 86%) crystallized spontaneously and after crystallization from aqueous methanol it had mp 63–65 °C; uv (CH_3OH) 307 nm (5250); ir ($CHCl_3$) 3585, 3410 cm^{-1}; nmr ($CDCl_3$) 1.50 (t, 3H, J = 7.4 Hz), 2.57 (s, 1H, W_H = 9 Hz, exchanged with D_2O), 6.15 (s, 1H), 7.28 (m, 5H); ms (relative intensity) 252(1), 224(3), 196(10), 163(46), 162(43), 134(22), 118(66), 107(88), 79(100), 77(74). *Anal.* calcd. for $C_{11}H_{12}N_2OS_2$: C 52.38, H 4.80, N 11.11; found: C 52.26, H 4.87, N 11.25.

2-Ethylthio-5-benzoyl-1,3,4-thiadiazole **4***d*

A mixture of diazoacetophenone (1.46 g, 10 mmol), ethyl chlorodithioformate (1.2 ml, 1.69 g, 12.0 mmol), and triethylamine (1.4 ml, 1.01 g, 10 mmol) in dry acetonitrile (30 ml), was stirred at room temperature for 24 h, at the end of which time additional ethyl chlorodithioformate (0.5 ml) and triethylamine (0.5 ml) were added. After a further 24 h the solvent was removed *in vacuo*, the residue was taken up in ethyl acetate, and this solution was washed with water and dried. Evaporation of the solvent *in vacuo* gave a red oil which was chromatographed on silica gel (300 g). A small amount of the starting material and other nonpolar materials were removed with hexane–dichloromethane (90:10). A nonaromatic product (1.14 g) of intermediate polarity (shown to be triethyldithiocarbamate by direct comparison with an authentic specimen) was eluted with hexane–dichloromethane (75:25) and the required thiadiazole (0.94 g, 38%) was removed from the column with dichloromethane. After evaporative distillation at 114 °C/0.005 torr and crystallization from hexane the product had mp 35–37 °C; uv (CH_3OH) 270 (8320), 326 nm (12 600); ir ($CHCl_3$) 1655 cm^{-1}; nmr ($CDCl_3$) 1.52 (t, 3H, J = 7.3 Hz), 3.42 (q, 2H, J = 7.3 Hz), 7.50 (m, 3H), 8.44 (m, 2H); ms (relative intensity) 250(42), 222(17), 163(6), 136(21), 105(100), 77(50). *Anal.* calcd. for $C_{11}H_{10}N_2OS_2$: C 52.80, H 4.03, N 11.20; found: C 52.73, H 3.95, N 11.23.

Phenyl-(5-ethylthio-1,3,4-thiadiazol-2-yl)carbinol **6***b*

(A) By the Sodium Borohydride Reduction of 2-Ethylthio-5-benzoyl-1,3,4-thiadiazole **4***d*

This reduction was effected in the same manner as described above for compound **3***d*, except that the reaction time was 20 h. The product (80% yield) had mp 67–68 °C after crystallization from benzene–hexane; uv (CH_3OH) 273 nm (6920); ir ($CHCl_3$) 3590, 3300 cm^{-1}; nmr ($CDCl_3$) 1.57 (t, 3H, J = 7.5 Hz), 3.22 (q, 2H, J = 7.5 Hz), 3.67 (s, 1H, exchanged with D_2O), 6.08 (s, 1H), 7.34 (m, 5H); ms (relative intensity) 252(100), 224(36), 219(17), 165(3), 138(24), 107(49), 79(51), 77(51). *Anal.* calcd. for $C_{11}H_{12}N_2OS_2$: C 52.38, H 4.80, N 11.11; found: C 52.37, H 4.90, N 11.12.

(B) By the Oxidation of 2-Ethylthio-5-benzyl-1,3,4-thiadiazole **6***a*

The ethylthio compound **6***a* was prepared from 5-benzyl-1,3,4-thiadiazole-2-thione (18) as follows. A solution of 85% potassium hydroxide (1.1 g, 16.7 mmol) in alcohol (10 ml) was added to the thione (3.4 g, 16.3 mmol) in alcohol (100 ml) containing ethyl iodide (3 ml). The solution was stirred at room temperature for 24 h, the solvent was removed *in vacuo*, and ethyl acetate was added to the residue. The resultant was washed with water, dried, and the solvent was removed *in vacuo*. Evaporative distillation of the residue at 110 °C/0.01 torr gave the product (3.1 g, 80%); uv (CH_3OH) 271 nm (7940); nmr ($CDCl_3$) 1.58 (t, 3H, J = 7.2 Hz), 3.25 (q, 2H, J = 7.2 Hz), 4.32 (s, 2H), 7.24 (s, 5H); ms (relative intensity) 236(50), 221(7), 208(23), 204(18), 149(50), 135(18), 122(12), 116(11), 91(100). *Anal.* calcd. for $C_{11}H_{12}N_2S_2$: C 55.93, H 5.12, N 11.86; found: C 55.69, H 5.16, N 12.06.

To a solution of lithium diisopropylamide (prepared from diisopropylamine (1.7 ml, 1.2 g, 12 mmol) and *n*-butyllithium in hexane (7.5 ml of a 1.6 *M* solution)) in anhydrous tetrahydrofuran (50 ml), maintained in a nitrogen atmosphere at 0 °C, was added a solution of **6***a* (1.9 g, 8.05 mmol) in dry tetrahydrofuran (10 ml). The solution became red in color and after 1 h at 0 °C, oxygen was bubbled through the solution for 20 h at room temperature. The solution was poured into water, and the resultant was extracted with ethyl acetate. The extract was washed with water, dried, and evaporated *in vacuo*. Thin-layer chromatography on silica gel (dichloromethane – ethyl acetate, 9:1) showed the presence of four products as well as starting material. The most polar material (R_f = 0.52), which was the desired product, was obtained pure (0.35 g, 17%) by preparative tlc using the above solvent system. After crystallization from benzene, it had mp 66–67 °C, undepressed on admixture with the compound prepared as described in *A*.

4-(4-Chlorobenzoyl)-5-chloro-1,2,3-thiadiazole **3***b and 2-Chloro-5-(4-chlorobenzoyl)-1,3,4-thiadiazole* **4***b*

(A) From 4-Chlorodiazoacetophenone and Thiophosgene

A solution of 4-chlorodiazoacetophenone (4.16 g, 23.1 mmol) in anhydrous benzene (30 ml) containing thiophosgene (0.88 ml, 1.32 g, 11.5 mmol) was stirred at room temperature, with protection from light, for 20 h. The solvent was removed *in vacuo*, toluene was added to the residue, and the resultant was once more evaporated *in vacuo*. This process was repeated once again with toluene and once with methanol at which point the residue partially crystallized. Hexane and a little methanol were added and the crystalline 1,3,4-thiadiazole **4***b* (0.93 g) was removed by filtration. The solvent was removed *in vacuo*, hexane was added to the residue, and the mixture was scratched until crystallization had occurred. The insoluble material (4-chlorophenacyl chloride and other more polar substances) was removed by filtration and the filtrate was evaporated *in vacuo*. The residue was chromatographed on silica gel using hexane as the eluant. In this way, an additional quantity (0.28 g) of the 1,3,4-thiadiazole and a mixture of both thiadiazoles, contaminated with the phenacyl chloride (1.41 g), was obtained. Hexane and a little methanol were added to the mixture and more of the phenacyl chloride was removed by filtration. Evaporation of the filtrate gave an oil which was separated by tlc on silica gel (hexane – ethyl acetate, 95:5, two developments). In this way there was obtained a further quantity (0.19 g) of the less polar 1,3,4-thiadiazole as well as the more polar 1,2,3-thiadiazole **3***b*

(0.40 g, 13%). The combined yield of the 1,3,4-isomer was 47%. After crystallization from methanol it had mp 106–107 °C (lit. (10, 11) mp 114 °C); uv (CH_3OH) 286 nm (13 500); ir ($CHCl_3$) 1668, 1588 cm^{-1}; nmr ($CDCl_3$) 7.47 (d, 2H, J = 8.4 Hz), 8.44 (d, 2H, J = 8.4 Hz); ms (relative intensity) 260(10), 258(14), 232(2), 230(3), 199(19), 197(38), 172(27), 170(75), 141(33), 139(100), 113(22), 111(71), 75(47).

After crystallization from methanol, the 1,2,3-thiadiazole had mp 88–89 °C; uv (CH_3OH) 214 (15 850), 273 nm (13 200); ir ($CHCl_3$) 1670, 1590 cm^{-1}; nmr ($CDCl_3$) 7.48 (d, 2H, J = 8.6 Hz), 8.11 (d, 2H, J = 8.6 Hz); ms (relative intensity) 260(1), 258(3), 232(11), 230(15), 224(3), 222(2), 141(33), 139(100), 113(15), 111(46), 75(28). *Anal.* calcd. for $C_9H_4Cl_2N_2OS$: C 41.68, H 1.55, N 10.86; found: C 41.88, H 1.75, N 10.62.

(B) From 4-Chlorodiazoacetophenone and Thiophosgene in the Presence of Triethylamine

A solution of the diazoketone (0.45 g, 2.5 mmol) in dry benzene (50 ml) containing thiophosgene (0.19 ml, 2.5 mmol) and triethylamine (0.34 ml, 2.5 mmol) was left at room temperature for 24 h. The solvent was removed *in vacuo*, ethyl acetate was added to the residue, and the solution was washed with water, dried, and evaporated *in vacuo*. The residue was separated by tlc on silica gel (hexane – ethyl acetate, 95:5) to give the 1,3,4-thiadiazole (0.17 g, 25%) and the 1,2,3-thiadiazole (0.027 g, 4%).

(C) From Bis(4-chloro-α-diazophenacyl)mercury 2b[6] *and Thiophosgene*

Thiophosgene (2.3 ml, 30 mmol) was added to a suspension of the diazo mercury reagent (8.4 g, 29.5 mmol) in dry acetonitrile (200 ml) and the mixture was stirred at room temperature, with protection from light, for 48 h. The solvent was evaporated *in vacuo*, chloroform was added to the residue, and the mixture was filtered. The filtrate was evaporated *in vacuo* and the residue was separated by column chromatography on silica gel using hexane – ethyl acetate (98:2) as the eluant. The 1,3,4-thiadiazole (1.55 g, 20%) was eluted first, followed immediately by the 1,2,3-thiadiazole (0.39 g, 5%).

4-(4-Chlorobenzoyl)-5-ethylthio-1,2,3-thiadiazole 3e

The diazo mercury compound **2b** (0.33 g, 6 mmol) was suspended in anhydrous acetonitrile (50 ml) which contained ethyl chlorodithioformate (0.28 ml) and the mixture was stirred at room temperature, with protection from light, for 24 h. After the usual work-up and purification by tlc on silica gel (hexane – ethyl acetate, 95:5), there was obtained the 1,2,3-thiadiazole (0.087 g, 25%), which had mp 110–112 °C after crystallization from methanol; uv (CH_3OH) 270 (12 500), 324 nm (14 100); ir ($CHCl_3$) 1642, 1595 cm^{-1}; nmr ($CDCl_3$) 1.50 (t, 3H, J = 7.2 Hz), 3.25 (q, 2H, J = 7.2 Hz), 7.40 (d, 2H, J = 8.6 Hz), 8.28 (d, 2H, J = 8.6 Hz); ms (relative intensity) 286(0.5), 284(1), 258(0.5), 256(1), 230(5), 228(20), 141(34), 139(100), 113(16), 111(36), 75(17). *Anal.* calcd. for $C_{11}H_9ClN_2OS_2$: C 46.38, H 3.15, N 9.72; found: C 46.17, H 3.06, N 9.74.

2-Ethylthio-5-(4-chlorobenzoyl)-1,3,4-thiadiazole 4e

This compound was prepared from 4-chlorodiazoacetophenone and ethyl chlorodithioformate, in acetonitrile solution containing triethylamine, in the manner described for the synthesis of **4d**, except that the reaction time was 48 h. After the usual work-up, tlc (hexane – ethyl acetate, 95:5) did not show the presence of the 1,2,3-isomer **3e** (which had R_f 0.41) in the product mixture. The 1,3,4-isomer (R_f = 0.50) was purified by preparative tlc using the above solvent system. There was thus obtained, a solid (1.03 g, 36%) which, after crystallization from methanol, had mp 106–107 °C; uv (CH_3OH) 285 (19 300), 333 nm (13 800); ir ($CHCl_3$) 1643, 1580, 1510 cm^{-1}; nmr ($CDCl_3$) 1.51 (t, 3H, J = 7.4 Hz), 3.42 (q, 2H, J = 7.4 Hz), 7.39 (d, 2H, J = 8.6 Hz), 8.40 (d, 2H, J = 8.6 Hz); ms (relative intensity) 286(31), 284(66), 258(12), 256(28), 197(3), 172(7), 170(19), 141(35), 139 (100), 113(17), 111(37), 75(21). *Anal.* calcd. for $C_{11}H_9ClN_2OS_2$: C 46.38, H 3.15, N 9.72; found: C 46.19, H 3.16, N 9.78.

4-(4-Chlorobenzoyl)-5-anilino-1,2,3-thiadiazole 3f

This compound was prepared from **3b** (1 equiv.) and aniline (3 equiv.) in hot methanol according to the method described by Bacchetti *et al.* (9) for the isomeric 1,3,4-compound. The product **3f** obtained in 77% yield had mp 174 °C (lit. (13) mp 179 °C), undepressed on admixture with an authentic specimen prepared from phenylisothiocyanate and 4-chlorodiazoacetophenone.[4]

2-Anilino-5-(4-chlorobenzoyl)-1,3,4-thiadiazole 4f

This compound was prepared from **4b** and aniline as described by Bacchetti *et al.* (9). It had mp 278 °C (lit. (9) mp 278 °C).

4-(4-Methylphenyl)-5-chloro-1,2,3-thiadiazole 3c and 2-Chloro-5-(4-methylphenyl)-1,3,4-thiadiazole 4c

The diazoketone **1c** (1.60 g, 10 mmol) and thiophosgene (0.58 g, 5 mmol) in benzene (30 ml) was left at room temperature for 20 h. The reaction was worked-up in the manner described by Ried and Beck (8) and after crystallization of the crude product from methanol, the 1,3,4-thiadiazole **4c** (0.45 g), mp 93–94 °C (lit. (8) mp 97 °C) was obtained; uv (CH_3OH) 292 nm (12 300); ir ($CHCl_3$) 1653, 1608, 1571 cm^{-1}; nmr ($CDCl_3$) 2.43 (s, 3H), 7.25 (d, 2H, J = 8.3 Hz), 8.32 (d, 2H, J = 8.3 Hz); ms (relative intensity) 240(10), 238(25), 224(4), 210(6), 177(37), 150(82), 119(100), 91(87), 65(46). The mother liquors from the above crystallization were evaporated *in vacuo* and the residue was separated by tlc on silica gel (hexane – ethyl acetate, 96:4). There was obtained a further quantity (0.17 g, total yield 0.62 g or 52% yield) of the 1,3,4-thiadiazole, as well as 4-chlorophenacyl chloride (0.46 g) and a 1:1 mixture (0.24 g) of 4-chlorophenacyl chloride and the 1,2,3-thiadiazole **3c**. This mixture was separated by tlc on silica gel (hexane–acetone, 97:3) to give the 1,2,3-thiadiazole **3c** (0.088 g, *ca.* 90% pure) which, after crystallization from petroleum ether (bp 70–90 °C), had mp 56–58 °C; uv (CH_3OH) 214 (13 500), 273.5 nm (14 800); ir ($CHCl_3$) 1669, 1610 cm^{-1}; nmr ($CDCl_3$) 2.43 (s, 3H), 7.18 (d, 2H, J = 8.2 Hz), 7.88 (d, 2H, J = 8.2 Hz); ms (relative intensity) 240(1), 238(2), 212(6), 210(15), 119(100), 91(58), 65(27). *Anal.* calcd. for $C_{10}H_7ClN_2OS$: C 50.30, H 2.96, N 11.74; found: C 50.47, H 3.01, N 12.16.

Ethyl-5-chloro-1,2,3-thiadiazole-4-carboxylate 8a and Ethyl-2-chloro-1,3,4-thiadiazole-5-carboxylate 9a

(A) From Ethyl Diazoacetate and Thiophosgene

To a stirred solution of ethyl diazoacetate (18.5 ml,

[6]Prepared according to ref. 17 and used without purification.

19.9 g, 175 mmol) in acetonitrile (100 ml) at 0 °C was added thiophosgene (6.7 ml, 87.5 mmol). The reaction was then stirred at room temperature for 20 h and the solvent was removed *in vacuo*. The residue was separated by column chromatography on silica gel (500 g) using hexane – ethyl acetate (96:4) as the eluting solvent. The 1,2,3-thiadiazole **8***a* (3.33 g) was eluted first, then a mixture (2.21 g) of both thiadiazoles followed, and the 1,3,4-thiadiazole **8***a* (5.71 g) was eluted last. The above mixture was separated by tlc on silica gel (hexane – ethyl acetate, 95:5) and in this way additional amounts of the 1,2,3-thiadiazole (0.59 g; total yield 3.92 g or 23%) and the 1,3,4-thiadiazole (1.59 g; total yield 7.31 g or 44%) were obtained.

Ethyl-5-chloro-1,2,3-thiadiazole was further purified by evaporative distillation at 70 °C/0.05 torr. The oil solidified (mp 25 °C; lit. (14) mp 25 °C) on standing; uv (CH_3OH) 225 (5270), 257 nm (3630); ir ($CHCl_3$) 1735 cm^{-1}; ms (relative intensity) 194(1), 192(1), 166(7), 164(18), 149(9), 147(24), 136(6), 121(7), 119(18), 108(28), 105(22), 100(34), 92(100), 84(47). *Anal.* calcd. for $C_5H_5ClN_2O_2S$: C 31.17, H 2.61, N 14.54; found: C 30.91, H 2.65, N 14.86.

Evaporative distillation of ethyl-2-chloro-1,3,4-thiadiazole-5-carboxylate at 110 °C/0.02 torr gave an oil which solidified (mp 29 °C) on standing; uv (CH_3OH) 245 nm (6920); ir 1760, 1730 cm^{-1}; ms (relative intensity) 194(2), 192(5), 165(10), 150(24), 149(26), 148(65), 147(54), 122(39), 121(24), 120(100), 119(22), 93(17), 79(39), 59(82). *Anal.* calcd. for $C_5H_5ClN_2O_2S$: C 31.17, H 2.61, N 14.54; found: C 31.09, H 2.71, N 14.53.

(B) From Ethyl Diazoacetate and the Mercury Derivative **7** *of Ethyl Diazoacetate (19)*

To a suspension of the mercury derivative (3.49 g, 8.2 mmol) in dry acetonitrile (100 ml) was added thiophosgene (1.26 ml, 16.4 mmol) in a dropwise manner. The mixture was stirred at room temperature, with protection from light, for 3 h and the solvent was evaporated *in vacuo*. Chloroform was added to the residue, the mixture was filtered, the filtrate was evaporated *in vacuo*, and the residue was separated by tlc on silica gel (hexane – ethyl acetate, 95:5). Evaporative distillation of the 1,3,4-thiadiazole fraction at 110 °C/0.02 torr gave a liquid (1.26 g, 40%) which solidified mp 29 °C. Evaporative distillation of the 1,2,3-thiadiazole fraction at 70 °C/0.05 torr gave an oil (0.63 g, 20%) which crystallized (mp 25 °C) on standing.

(C) From Ethyl Diazoacetate and Thiophosgene in the Presence of Triethylamine

Thiophosgene (0.77 ml, 10 mmol) was added at 0 °C to a solution of ethyl diazoacetate (1.07 ml, 10 mmol) in acetonitrile (50 ml) containing triethylamine (1.4 ml, 10 mmol). The solution was stirred at room temperature for 22 h, the solvent was removed *in vacuo*, chloroform was added to the residue, and the mixture was filtered. Evaporation of the filtrate *in vacuo* gave a residue which was separated by column chromatography on silica gel in the manner described above. After distillation there was obtained the 1,2,3-thiadiazole (0.13 g, 7%) and the 1,3,4-thiadiazole (0.29 g, 15%).

Ethyl-5-ethylthio-1,2,3-thiadiazole-4-carboxylate **8***c*

(A) From the Mercury Derivative of Ethyl Diazoacetate and Ethyl Chlorodithioformate

Ethyl chlorodithioformate (0.46 ml, 4 mmol) was added to a stirred suspension of the mercury derivative (0.85 g, 2 mmol) in dry acetonitrile (50 ml). The mixture was stirred at room temperature, with protection from light, for 60 h and then the mixture was worked-up in the usual way. The product was purified by tlc on silica gel (hexane – ethyl acetate, 95:5). A solid (0.32 g, 37%) was obtained, which, after crystallization from hexane, had mp 52 °C; uv (CH_3OH) 233 (6310), 300 nm (9550); ir ($CHCl_3$) 1710 cm^{-1}; ms (relative intensity) 218(49), 190(22), 162(14), 144(10), 131(16), 118(66), 103(65), 90(100), 89(93), 73(51). *Anal.* calcd. for $C_7H_{10}N_2O_2S_2$: C 38.53, H 4.65, N 12.84; found: C 38.63, H 4.59, N 12.88.

(B) From Ethyl-5-chloro-1,2,3-thiadiazole-4-carboxylate and Ethanethiol

Ethyl mercaptan (0.22 ml, 3 mmol) was added to a solution of sodium ethoxide (from 0.072 g (3 mmol) of sodium hydride) in absolute ethanol (15 ml). The chlorothiadiazole (0.19 g, 1 mmol) was then added and after 10 min the solvent was removed *in vacuo*. Water was added to the residue and the product was extracted into chloroform. The extract was dried and evaporated *in vacuo* to give a solid (0.18 g, 81%) mp 51 °C, undepressed on admixture with a specimen prepared according to method *A*.

Ethyl-5-amino-1,2,3-thiadiazole-4-carboxylate **8***b and 5-Chloro-1,2,3,-thiadiazole-4-carboxamide* **10**

Ethyl-5-chloro-1,2,3-thiadiazole-4-carboxylate (0.19 g, 1 mmol) was dissolved in a solution of alcoholic ammonia (30 ml, 4.6 *N*) and left at room temperature for 8 h. The solvent was removed *in vacuo* and the residue was separated by tlc on silica gel (dichloromethane – ethyl acetate, 19:1) to give the amino ester **8***b* (0.020 mg, 11.5%) which after crystallization from benzene–hexane had mp 121 °C, (lit. (14) mp 126 °C) undepressed on admixture with an authentic specimen prepared according to Goerdeler and Gnad (14).

The major product (0.097 g, 60%) from this reaction was the carboxamide **10**. After crystallization from benzene it had mp 127–129 °C; uv (CH_3OH) 230 (6310), 242 nm (7240); ir (KBr) 3400, 3305, 1695, 1615 cm^{-1}; ms (relative intensity) 166(0.5), 165(0.3), 164(1), 163(1), 162(0.5), 137(12), 135(33), 109(19), 107(53), 94(36), 92(96), 57(57), 44(100). *Anal.* calcd. for $C_3H_2ClN_3O_2S$: C 22.04, H 1.23, N 25.69; found: C 22.11, H 1.19, N 25.85.

2-Chloro-1,3,4-thiadiazole-5-carboxamide **11**

(A) From Ethyl-2-chloro-1,3,4-thiadiazole-5-carboxylate **9***a and Ammonia*

The ester **8***a* (0.19 g, 1 mmol) was dissolved in an ethanolic ammonia solution (25 ml, 2.06 *N*) and left at room temperature for 16 h. The solvent was removed *in vacuo*, hexane was added to the residue, and a solid (0.16 g, 93%) which had mp 170–171 °C after crystallization from benzene, was obtained; uv (CH_3OH) 222 (5880), 259 nm (3240); ir (KBr) 3400, 3300, 3210, 1675 cm^{-1}; ms (relative intensity) 165(15), 163(40), 122(37), 120(100), 93(22), 79(17), 59(60), 44(97). *Anal.* calcd. for $C_3H_2ClN_3OS$: C 22.04, H 1.23, N 25.69; found: C 22.28, H 1.26, N 25.79.

(B) From the Chloro Compound **9***a obtained from Ethyl-2-amino-1,3,4-thiadiazole-5-carboxylate* **9***b (15)*

Concentrated sulfuric acid (2.02 ml, 6 mmol) was cooled to 0 °C in a nitrogen atmosphere and sodium nitrite (0.35 g, 5.1 mmol) was added portionwise. The reaction was left to react at room temperature and then

it was heated to 75 °C for 30 min. The resultant was cooled to 0 °C, the amine **9***b* (0.80 g, 4.6 mmol), suspended in acetic acid (5 ml), was added (reaction temperature < 5 °C), and after 10 min water (5 ml) was added below 5 °C. A solution of cupric chloride (0.83 g, 6.2 mmol) in water (5 ml) mixed with dichloromethane (5 ml) was then added at 0 °C. After 15 min the organic phase was separated and combined with a dichloromethane extract of the aqueous phase. The organic solution was washed with water, dried, and evaporated. The oil which remained was chromatographed on a column of silica gel (50 g). The column was first eluted with hexane – ethyl acetate (96:4) and then the ratio was changed to 92:8. The chloro compound **9***a* (0.20 g, 22%) had an ir spectrum identical to the material described above. It was converted into the carboxamide **11** in the manner described above. The material obtained in this way was identical to that obtained in the manner described previously.

1. B. EISTERT, M. REGITZ, G. HECK, and H. SCHWALL. Houben-Weyl X/4. 780 (1968).
2. S. HOLM and A. SENNING. Tetrahedron Lett. 2389 (1973).
3. J. M. BEINER, D. LECADET, D. PAQUER, A. THUILLIER, and J. VIALLE. Bull. Soc. Chim. Fr. 1979 (1973).
4. J. M. BEINER, D. LECADET, D. PAQUER, and A. THUILLIER. Bull. Soc. Chim. Fr. 1983 (1973).
5. R. MAYER and H. KRÖBER. Z. Chem. **11**, 426 (1973).
6. H. STAUDINGER and J. SIEGWART. Helv. Chim. Acta, **3**, 840 (1920).
7. T. BACCHETTI and A. ALEMAGNA. Rend. Ist. Lomb. Sci. Lett. Cl. Sci. Mat. Nat. **91**, 617 (1957).
8. W. RIED and B. M. BECK. Ann. Chem. **673**, 124 (1964).
9. T. BACCHETTI, A. ALEMAGNA, and B. DANIELI. Tetrahedron Lett. 3569 (1964); Ann Chim. (Rome), **55**, 615 (1965).
10. B. J. MILLARD and D. L. PAIN. J. Chem. Soc. C, 2042 (1970).
11. K. P. ZELLER, H. MEIER, and E. MÜLLER. Tetrahedron, **28**, 1353 (1972).
12. G. W. MOERSCH and M. L. ZWIESLER. Synthesis, 647 (1971).
13. W. RIED and B. M. BECK. Ann. Chem. **673**, 128 (1964).
14. J. GOERDELER and G. GNAD. Chem. Ber. **99**, 1618 (1966).
15. G. WERBER and F. MAGGIO. Ann. Chim. (Rome), **49**, 2124 (1959).
16. U. SCHÖLLKOPF and H. FRASNELLI. Angew. Chem. Int. Ed. Engl. **9**, 301 (1970).
17. P. YATES and F. X. GARNEAU. Tetrahedron Lett. 71 (1967); P. YATES, F. GARNEAU, and J. P. LOKENSGARD. Tetrahedron, **31**, 1979 (1975).
18. M. M. KOCHBAR, M. SALAHI-ASBAHI, and B. B. WILLIAMS. J. Pharm. Sci. **62**, 335 (1973).
19. E. BUCHNER. Ber. Dtsch. Chem. Ges. **28**, 215 (1895).

1,4-Cycloheptadienes: preparation and comparison of their proton magnetic resonance spectra with those of the corresponding cycloheptatrienes

IVAN PIKULIK AND RONALD F. CHILDS[1]

Department of Chemistry, McMaster University, Hamilton, Ont., Canada L8S 4M1

Received June 7, 1976

IVAN PIKULIK and RONALD F. CHILDS. Can. J. Chem. **55**, 251 (1977).

A general route to 3-substituted cyclohepta-1,4-dienes is described in this paper. 7-Substituted cycloheptatrienes were used as starting materials and these were reacted with 4-phenyl-1,2,4-triazoline-3,5-dione to give 4 + 2 cycloaddition products of the norcaradiene form of the cycloheptatrienes. Catalytic reduction of these adducts gave 9-substituted 4-phenyl-2,4,6-triazatetracyclo[5.3.2.$0^{2,6}$.$0^{8,10}$]dodeca-3,5-diones in good yield. Basic hydrolysis of the heterocyclic ring of these products followed by Cu^{2+} oxidation of the resulting hydrazo compounds gave the copper complexes of substituted 6,7-diazatricyclo[3.2.2.$0^{2,4}$]non-6-enes. The azo compounds, formed on decomplexation of the copper complexes, readily lost nitrogen to give 3-substituted cyclohepta-1,4-dienes. Care had to be taken during these last steps as the cycloheptadienes with carboxylate substituents very readily isomerized to the conjugated isomers. The pmr spectra of the cyclohepta-1,4-dienes and related cycloheptatrienes are compared and discussed in terms of the presence of an induced diamagnetic ring current in the latter systems.

IVAN PIKULIK et RONALD F. CHILDS. Can. J. Chem. **55**, 251 (1977).

On décrit une méthode générale de préparer des cycloheptadiènes-1,4 substitués en position 3. On a utilisé les cycloheptatriènes substitués en position 7 comme produits de départ; par réaction avec la phényl-4 triazoline-1,2,4 dione-3,5 ils donnent les produits de cycloaddition 4 + 2 correspondant à la forme norcaradiène des cycloheptatriènes. La réduction catalytique de ces adduits conduit avec des bons rendements aux phényl-4 triaza-2,4,6-tétracyclo[5.3.2.$0^{2,6}$.$0^{8,10}$]-dodécadiones-3,5 substitués en position 9. L'hydrolyse basique de l'hétérocycle de ces composés, suivie par une oxydation par le Cu^{2+} des composés hydrazo qui en découlent, conduit aux complexes du cuivre des diaza-6,7 tricyclo[3.2.2.$0^{2,4}$]nonènes-6 substitués. Les composés azo, formés par décomplexation des complexes de cuivre, perdent facilement de l'azote pour conduire aux cycloheptadiènes-1,4 substitués en position 3. On a pris beaucoup de soins au cours de ces dernières étapes car les cycloheptadiènes substitués par un groupement carboxylique s'isomérisent très facilement pour donner les isomères conjugués. On discute des spectres rmp des cycloheptadiènes-1,4 et des cycloheptatriènes qui leur ressemblent en terme de la présence d'un courant de cycle diamagnétique induit dans ces derniers systèmes.

[Traduit par le journal]

In the course of our studies of some 7-cycloheptatrienyl- and 7-norcaradienyl methyl zwitterions, it became necessary to determine the composition of some rapidly equilibrating mixtures of these tautomers (1). Such a measurement can be readily made by nmr spectroscopy, provided that the chemical shifts of appropriate nuclei in each individual tautomer are either known or can be reliably estimated. To this end it seemed that zwitterions formed from suitably substituted 1,4-cycloheptadienes would serve as good models for the cycloheptatriene form of these valence tautomeric mixtures. However, only a limited number of cyclohepta-1,4-dienes have been prepared (2) and as compounds with a carbonyl containing substituent at C_3 have not been reported, it was necessary to devise a synthesis of these materials. We describe here a general route to compounds of this type and discuss some of the fundamental differences in the pmr spectra of the 1,4-cycloheptadienes and cycloheptatrienes.

Results and Discussion

Synthesis of Cyclohepta-1,4-dienes

The cycloheptadienyl anion, **1**, has been reported to react with CO_2 to give a mixture of cyclohepta-1,3- and 1,4-diene and a carboxylic acid, tentatively identified as **2** (2). As the protonation of **1** is known to give cyclohepta-1,4-diene as one of the major products (3), this carbonation reaction was reexamined.

The acidic fraction resulting from the reaction of **1** with CO_2 was esterified by treatment with

[1]Author to whom correspondence should be addressed.

diazomethane and the crude product examined by pmr spectroscopy. One major component was present and this was shown to be **3***a* by comparison of its spectroscopic properties with those previously reported (4). This product was thermally unstable and on heating or attempted vpc purification, **3***a* was partially converted to a further ester which was tentatively identified as **4**. The spectroscopic properties of this ester are fully in accord with the assigned structure, however, the pmr spectrum differs somewhat from that previously reported for **4** (5). A comparable mixture of esters was obtained after esterification of the products obtained on the reduction of cycloheptatriene-7-carboxylic acid with lithium and liquid NH_3 (2, 5). No compound with a pmr spectrum consistent with **5***a* could be detected in either of these reactions.

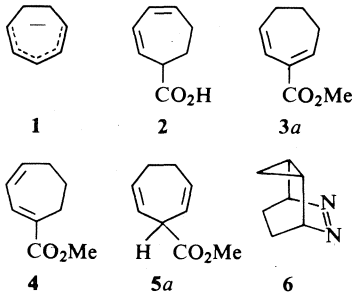

1 **2** **3***a* **4** **5***a* **6**

In view of the complexity of these reactions, a milder, more specific route to compounds such as **5***a* was sought. The azo compound **6** has been reported to decompose at 25 °C to give 1,4-cycloheptadiene and N_2 (6). Although the ease of this N_2 elimination has been shown to be very dependent on the relative configurations of the cyclopropyl ring and azo function (7), substituents on the methylene carbon of the cyclopropyl should not greatly affect this elimination reaction.

The cycloaddition of 4-phenyl-1,2,4-triazoline-3,5-dione to **7***a*, *b*, and *c* proceeded in high yield to give **8***a*, *b*, or *c*, respectively. The spectroscopic properties of these adducts were fully consistent with their assigned structures. The catalytic hydrogenation of the double bond of **8** was readily accomplished using a Pd catalyst. The *anti* relationship of the cyclopropyl ring and the nitrogen bridge of both **8** and **9** was indicated by the considerable downfield shift observed for the resonance of the cyclopropyl proton geminal to the substituent R in the pmr spectra of compounds **9** as compared to those of **8**. In **8** this proton is held in the shielding zone of the carbon–carbon double bond, an effect which is removed on saturation of the double bond (8*a*). Virtually no difference in the resonance positions of the cyclopropyl bridgehead hydrogens was detected in the pmr spectra of **8** and **9**.

It is interesting that no adducts could be detected which were formed from addition of the triazolinedione to the cycloheptatriene forms of **7**. In contrast, when diethyl diazodicarboxylate was reacted with **7***a*, both **13** and **14** were formed.[2] The ratio of **13** to **14** produced was found to be dependent on the temperature at which the cycloaddition was carried out. At +50 °C the ratio of **13** to **14** was 1.7:1 whereas at −5 °C this ratio was 5.7:1. In contrast to these results, no norcaradiene adducts were reported to be formed when cycloheptatriene itself was reacted with diethyl diazodicarboxylate (9). Thus the type of cycloaddition a cycloheptatriene undergoes appears not only to be a function of the dienophile but also the nature of any C_7 substituents on the cycloheptatriene ring.

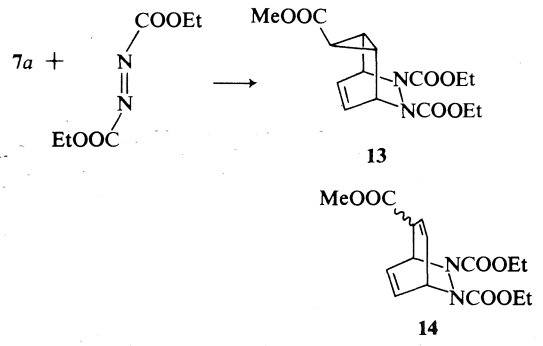

Further structural modification of the cyclopropyl substituent of **9** was possible. For example, reaction of **9***c* with aqueous acid gave **9***e*, obviating the need to prepare **7***e*, a somewhat refractory material (10). Alternatively, treatment of **9***a* with methyllithium gave **9***d* in good yield.

The hydrolysis of **9** to give **10** was straightforward. In the case of **9***a* and *b*, concomitant hydrolysis of the ester also occurred to give **10***f*. The hydrazo compounds **10** were not isolated but were oxidized with cupric chloride to the corresponding azo compounds which subse-

[2]The pmr spectrum of **14** exhibited a temperature dependence arising from inversion of the ester groups about the nitrogen atoms.

TABLE 1. Proton chemical shifts of cyclohepta-1,4-dienes

Compound	Chemical shift*						
	C_1,C_5,H	C_2,C_4,H	C_3H	C_6,C_7,H	CH_3	OH	Other
5*a*	5.79m	5.79m	4.20m	2.25m	3.68s		
5*g*	5.78m	5.78m	4.16m	2.24m		11.2s	
5*c*	5.36	5.80	3.39m	2.15m	3.25s		4.17d
5*d*	5.66	5.66	3.15m	2.21m	1.18s	1.54s	

*In ppm from TMS, $CDCl_3$ as solvent. s, singlet; d, doublet, m, multiplet.

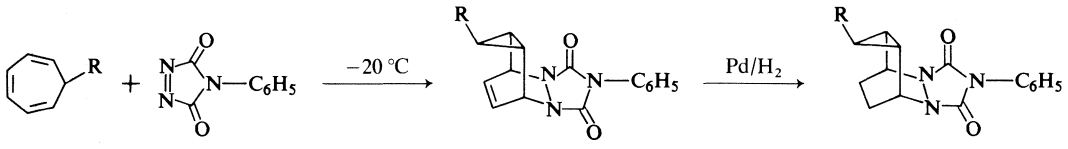

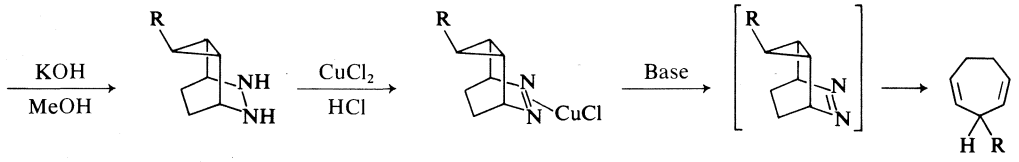

a, R = COOMe
b, R = COOEt
c, R = $CH(OMe)_2$
d, R = $C(Me)_2OH$
e, R = CHO
f, R = COO^-
g, R = COOH

quently formed copper complexes.[3] These complexes were stable and served as storable precursors to the dienes **5**.

The azo compounds **12** which were liberated on treatment of **11** with base, readily lost N_2 when warmed to 35 °C to give **5**. In order to prevent further isomerization of the dienes **5**, it was necessary to use limited quantities of a weak base to break up the copper complexes. The facile loss of N_2 from these azo compounds is in accord with the findings of Allred and Hinshaw (6*a*).

The structures of the 1,4-cycloheptadienes **5** were established from their spectroscopic properties (Table 1) and in the case of **5***c* and **5***d* by their elemental analyses. Compounds **5***a*, *f*, and *g* were unstable and isomerized to their respective conjugated isomers **3***a*, *f*, and *g*. The half-life for rearrangement of **5***a* to **3***a* at room temperature was about 12 h and this isomerization was much more rapid in the presence of base. The ease of isomerization of **5***a* makes it clear why compounds such as **5***a* or **5***g* were never detected as products of the carbonation of **1**. Dienes **5***c* and *d* were found to be relatively stable and could be heated to +60 °C without any detectable rearrangement.

It was not possible to prepare the aldehyde **5***e*. The only product that could be isolated either on the decomposition of **12***e* or the hydrolysis of the acetal **5***c*, was the conjugated aldehyde **3***e*. The structure of **3***e* was established on the basis of a comparison of its spectroscopic properties with those given before for **3***a*.

3

a, R = $COOCH_3$
e, R = CHO
f, R = COO^-
g, R = COOH

15

a, R = $COOCH_3$
c, R = $CH(OMe)_2$
d, R = $C(Me)_2OH$
g, R = COOH
h, R = H

This route to substituted 1,4-cycloheptadienes should be capable of extension to include a wide range of substituents particularly as a large variety of 7-substituted cycloheptatrienes are

[3]It was not possible to prepare **11***c* by this route as hydrolysis of the acetal function occurred. Instead **10***c* was allowed to undergo aerial oxidation to give **12** directly and thence **5***c*.

TABLE 2. Comparison of the proton chemical shifts of 3-substituted cyclohepta-1,4-dienes and 7-substituted cycloheptatrienes

Substituent	Chemical shift*		
	Cycloheptadiene C_3H	Cycloheptatriene C_7H	Δδ†
H	2.80	2.20‡	0.6
COOMe	4.23	2.48§	1.75
COOH	4.16	2.48‖	1.68
$CH(OMe)_2$	3.39	1.95	1.44
$C(Me)_2OH$	3.15	1.85	1.30

*In ppm from TMS.
†δ cycloheptadiene C_3H − δ cycloheptatriene C_7H.
‡Room temperature spectrum, chemical shift given is the average of the two methylene proton resonances (13, 14).
§Reference 1.
‖Reference 33.

available (11). Overall, the yields are high and the route provides a viable entry to this type of molecule.

Comparison of the Proton Magnetic Resonance Spectra of 1,4-Cycloheptadienes and Cycloheptatrienes

As was stated earlier, our principal interest in these 1,4-cycloheptadienes was as model compounds for the corresponding 7-substituted cycloheptatrienes. As can be seen from the data in Table 2, the chemical shifts of the corresponding methine hydrogens of these two systems are by no means comparable. The resonances of the C_7 proton of the cycloheptatrienes all occur considerably further upfield than the corresponding C_3 proton resonances of the cycloheptadienes, the difference ranging from 0.6 ppm for the unsubstituted systems, to 1.75 ppm for the compounds with an ester substituent. The question arises as to what is the origin of this large difference in chemical shift and why does the absolute magnitude of this difference seem to depend on the nature of the substituent.

A consideration of the chemical shifts of these methine hydrogens shows that the 'normal' value is that found for the cycloheptadienes. Using the empirical relationship of Schoolery (12, 8*b*), the chemical shift of a proton attached to a tertiary carbon substituted with two vinyl groups and an ester function is expected to be about δ 4.4. This compares very favourably with the value δ 4.23 found for **5***a* and it would seem that it is the chemical shifts of the cycloheptatrienes which are anomalous.

It is known that the cycloheptatriene ring is not flat but exists in a boat conformation (13–15) with a substituent on C_7 preferentially adopting the pseudo-equatorial position (14, 16). As such it could be argued that the high field position of the C_7 proton resonance is caused by the magnetic anisotropy of the C_3,C_4 double bond. However, the long range shielding effect of a double bond may be estimated using the results of calculations by Tillieu (17) or Pople (18) and in either case the resulting shielding on an axial C_7 proton was found to be less than 0.2 ppm.

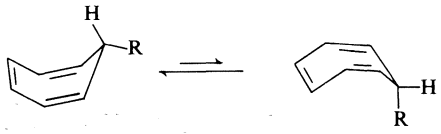

The possibility that the chemical shifts of these cycloheptatrienes are being influenced by the presence in each case of appreciable amounts of their norcaradiene valence tautomers can be discounted. Only in the case of **15***g* has the norcaradiene valence tautomer been directly observed to be in equilibrium with the cycloheptatriene form and even then less than 3% of the norcaradiene form was detected (19). One explanation for the anomalously high-field resonance positions of the C_7 hydrogens of these cycloheptatrienes is that cycloheptatriene ring can support an induced diamagnetic ring current when in a magnetic field.

The question of the aromaticity of cycloheptatriene has been under discussion ever since Doering *et al.* suggested that it could best be regarded as 'pseudo-aromatic' (20). In terms of more modern developments in the understanding of cyclic delocalization, cycloheptatriene is potentially a homoaromatic molecule and could be regarded as homobenzene (21). Homoaromaticity is a well defined and accepted phenomenon

with charged systems, both cationic and anionic, however, its importance in neutral molecules is by no means clearly defined (22).

Evidence for the importance of cyclic delocalization in cycloheptatriene has been claimed on the basis of its spectroscopic properties (23), its resonance energy of 7 kcal/mol (24), its diamagnetic susceptibility exaltation (25), the effect of it as a solvent on the chemical shifts of a solute molecule (26), and work with bridged bicyclic systems (27). However, despite this, there still seems to be a reluctance to accept cycloheptatriene as a bonafide homoaromatic species (28).

The high field chemical shifts of the C_7 protons of these cycloheptatrienes are completely in accord with cycloheptatriene sustaining an induced diamagnetic ring current when in a magnetic field. The presence of such a ring current would result in a shielding of the pseudo-axial and deshielding of the pseudo-equatorial C_7 hydrogens. Although these effects are in opposite directions, they will not be of the same magnitude and will depend very much upon the precise geometry of the molecule in question. Indeed,the low temperature pmr spectrum of cycloheptatriene, where the rate of interconversion of the two boat conformations is slow, exhibits two signals for the C_7 hydrogens, one at δ 1.43, attributed to the pseudo-axial hydrogen and another at δ 2.88 corresponding to the pseudo-equatorial proton (14). It is interesting that the equatorial hydrogen resonates at almost the same place as the corresponding C_3 hydrogens of cyclohepta-1,4-diene (29), suggesting that this hydrogen of cycloheptatriene is located in a nodal region of the magnetic field resulting from the induced ring current.

A substituent on C_7 of a cycloheptatriene preferentially adopts the pseudo-equatorial position. The remaining C_7 methine hydrogen is then largely in the pseudo-axial position and would be expected to be shifted upfield by almost the same amount as is observed for the axial hydrogen of cycloheptatriene itself. As can be seen from Table 2, this is true for **15***a* and **15***g*, however, the differences observed for **15***c* and **15***d* are somewhat smaller than might be expected. This could be the result of several factors, including for example a change in the degree of delocalization of the cycloheptatrienes as a function of the substituent, a change in the conformation of the ring (30), or a change in the axial/equatorial preference of the C_7 substituent.

In conclusion it would seem that the chemical shifts of the C_7 resonances of cycloheptatrienes can be most reasonably explained on the basis of a diamagnetic ring current being induced in these molecules and further more direct evidence for this is presented in the following paper (31). If the presence of such a ring current is a criterion of aromaticity (32), then on this basis these cycloheptatrienes must be regarded as homoaromatic molecules.

Experimental

Proton magnetic resonance spectra were recorded on a Varian HA-100 spectrometer and are referred to internal tetramethylsilane. A Hewlett-Packard 201C audiogenerator was employed for the double irradiation experiments. Infrared spectra were recorded on a Perkin-Elmer 521 spectrometer. Vapour phase chromatography was carried out on a Varian Aerograph A90-P3 instrument using column A (10 ft × ¼ in. column packed with 15% Carbowax on Chromosorb W) or column B (10 ft × ¼ in. column packed with 15% SE-30 on Chromosorb W). Melting points were obtained with a Thomas Hoover capillary melting point apparatus and are uncorrected. Elemental analyses were performed by Galbraith Laboratories in Knoxville, Tennessee.

Reaction of the Cycloheptadienyl Anion with Carbon Dioxide

Cycloheptatriene (10 g, 0.1 mol) was dissolved in liquid ammonia (150 ml) and lithium (1.4 g, 0.20 mol) was added in small pieces to the vigorously stirred solution. The reaction mixture was stirred for 2 h at −40 °C and then poured onto a large excess of crushed dry ice. The dry ice was allowed to evaporate and the volatile portion of the residue removed *in vacuo* at room temperature. This distillate (3.8 g) was separated by vpc (column B, 50 °C) into two fractions which were shown to be the 1,3- and 1,4-cycloheptadiene (in a ratio of 1:3.7) by comparison of their pmr spectra with those of the authentic materials (29). The involatile residue was dissolved in water (20 ml), acidified with HCl, and extracted with ether (3 × 10 ml). The combined ether extracts were washed with water (3 × 10 ml), dried over $MgSO_4$, and treated with diazomethane. The ether was removed and the residual product distilled under reduced pressure to give 2.7 g of an oil. This oil was separated by preparative vpc (column A, 160 °C) into seven fractions. The last two fractions, each 35% of the total, were further purified by vpc to give **3***a*, pmr (CCl_4) δ 1.97 (m, 2, H-6), 2.23 (m, 4, H-5,7), 3.70 (s, 3, OCH_3), 5.86 (m, 1, H-4), 6.39 (d, 1, H-3), 7.04 (t, 1, H-1); uv $\lambda_{max}(CH_3OH)$ 270 nm, ε 2880; ms *m/e* (M^+) calcd. for $C_9H_{12}O_2$: 152.0837; found: 152.0833; and **4**, pmr δ 1.97 (m, 2, H-6), 2.55 (m, 4, H-5,7), 3.70 (s, 3, OCH_3), 5.98 (m, 2, H-3,4), 6.93 (d, 1, H-2), uv $\lambda_{max}(CH_3OH)$ 278 nm; ε 8700. On heating **3***a* at 130 °C for 5 h an equilibrium was set up between **3***a* and **4** with a ratio of 7:3.

9-Methoxycarbonyl-4-phenyl-2,4,6-triazatetracyclo-[5.3.2.0^{2,6}.0^{8,10}]dodec-11-en-3,5-dione ***8a***

A mixture of 4-phenyl-1,2,4-triazoline-3,5-dione (4.25 g, 24.7 mmol) and **7***a* (4.0 g, 24.4 mmol) in CH_2Cl_2 (120 ml)

was cooled in a dry ice – acetone bath at −60 °C. A solution of lead tetraacetate (14.5 g, 33.7 mmol) in methylene chloride (120 ml) was added at once to the rapidly stirred solution. The temperature of the mixture was allowed to rise to +20 °C and the stirring continued for an additional 4 h. The solvent was removed *in vacuo* and the residue was washed with 0.1 *N* HNO_3 (100 ml), 0.1 *N* NaOH (100 ml), and water (100 ml). The remaining brown material was dissolved in boiling methanol (400 ml), treated with charcoal, and the volume was reduced to 300 ml. On cooling this solution to room temperature 6.07 g of **8***a* crystallized and was filtered out. An additional 0.7 g of material was obtained as a second crop, bringing the total yield of **8***a* to 82%. The product was recrystallized from methanol to give pure **8***a*, mp 187 °C; pmr ($CDCl_3$) δ 1.41 (t, 1, J = 3.0 Hz, H-9), 2.19 (m, 2, H-8,10), 3.67 (s, 3, OMe), 5.23 (m, 2, bridgehead protons), 6.15 (t, 2, J = 3.7 Hz, olefinic protons), 7.40 (s, 5, Ph); ir (KBr) 1770, 1730, 1417, 1323, 1240 cm^{-1}. *Anal.* calcd. for $C_{17}H_{15}N_3O_4$: C 62.77, H 4.62; found: C 62.76, H 4.72.

9-Ethoxycarbonyl-4-phenyl-2,4,6-triazatetracyclo-[5.3.2.0^{2,6}.0^{8,10}]dodec-11-en-3,5-dione **8***b*

7-Ethoxycarbonylcycloheptatriene was used as the starting material and the procedure used was the same as that described for the preparation of **8***a*. Yield 73%; mp 172.5 °C; pmr ($CDCl_3$) δ 1.26 (t, 3, Me), 1.45 (t, 1, H-9), 2.23 (d of d's, 2, H-8,10), 4.14 (q, 2, CH_2), 5.25 (m, 2, bridgehead H's), 6.18 (t, 2, olefinic H's), 7.42 (s, 5, Ph); ir (KBr) 1770, 1719, 1500, 1415, 1241 cm^{-1}. *Anal.* calcd. for $C_{18}H_{17}N_3O_4$: C 63.71, H 5.05; found: C 63.81, H 5.13.

9-Dimethoxymethyl-4-phenyl-2,4,6-triazatetracyclo-[5.3.2.0^{2,6}.0^{8,10}]dodec-11-en-3,5-dione **8***c*

The compound **8***c* was prepared from dimethoxymethylcycloheptatriene using the same procedure as that described above for the preparation of **8***a*. Yield 73%; mp 158 °C; pmr ($CDCl_3$) δ 0.97 (d of t's, 1, H-9), 1.76 (m, 2, H-8,10), 3.33 (s, 6, OMe), 4.26 (d, 1, C-9 substituent), 5.22 (m, 2, H-1,7), 6.17 (t, 2, olefinic protons), 7.42 (s, 5, Ph); ir (KBr) 1773, 1755, 1605, 1500, 1398 cm^{-1}. *Anal.* calcd. for $C_{18}H_{19}N_3O_4$: C 63.33, H 5.63; found: C 63.12, H 5.70.

9-Methoxycarbonyl-4-phenyl-2,4,6-triazatetracyclo-[5.3.2.0^{2,6}.0^{8,10}]dodeca-3,5-dione **9***a*

The olefin **8***a* (3 g) was partially dissolved in dioxane (100 ml) and a 5% palladium-on-carbon catalyst (185 mg) added. The mixture was vigorously stirred under H_2 (1 atm) at room temperature, and 1 equiv. of H_2 was absorbed in 10 min (all the solid material dissolved during this reaction). The catalyst was removed by filtration and the solvent removed *in vacuo*. The residue was recrystallized from MeOH to give **9***a* (2.6 g); mp 156 °C; pmr ($CDCl_3$) δ 1.55–2.22 (m, 7, cyclopropyl and methylene protons), 3.66 (s, 3, OMe), 4.7 (br s, 2, bridgehead protons), 7.47 (m, 5, Ph); ir (KBr) 1775, 1720, 1500, 1440, 1410, 1250 cm^{-1}. *Anal.* calcd. for $C_{17}H_{17}N_3O_4$: C 62.38, H 5.23; found: C 62.53, H 5.26.

9-Ethoxycarbonyl-4-phenyl-2,4,6-triazatetracyclo-[5.3.2.0^{2,6}.0^{8,10}]dodeca-3,5-dione **9***b*

Starting with **8***b* the procedure used was the same as that described above for the preparation of **9***a*. Yield 95%; mp 156 °C; pmr ($CDCl_3$) δ 1.27 (t, 3, Me), 1.60–2.20 (m, 7, H-8–12), 4.15 (q, 2, CH_2), 4.73 (br s, 2, bridgehead H's), 7.32–7.62 (m, 5, Ph); ir (KBr) 1770, 1720, 1502, 1409, 1320, 1255 cm^{-1}. *Anal.* calcd. for $C_{18}H_{19}N_3O_4$: C 63.34, H 5.61; found: C 63.23, H 5.52.

9-Dimethoxymethyl-4-phenyl-2,4,5-triazatetracyclo-[5.3.2.0^{2,6}.0^{8,10}]dodeca-3,5-dione **9***c*

Olefin **8***c* was reduced in a directly comparable manner to that described above for reduction of **8***a*, to give 100% yield of **9***c*; mp 121 °C; pmr ($CDCl_3$) δ 1.41 (t, 1, H-9), 1.60–2.20 (m, 6, H-8,10,11,12), 3.34 (s, 6, OMe), 4.22 (br s, 2, bridgehead H's), 7.3–7.7 (m, 5, Ph); ir (KBr) 1750, 1696, 1500, 1430, 1410 cm^{-1}. *Anal.* calcd. for $C_{18}H_{21}N_3O_4$: C 62.93, H 6.18; found: C 62.85, H 6.18.

The Copper Complex of 6,7-Diazatricyclo[3.2.2.0^{2,4}]-nonane-3-carboxylic Acid **11***g*

A solution of **9***a* (2.85 g, 8.81 mmol) in methanol (15 ml) containing KOH (3 g, 65 mmol) was refluxed for 24 h in a nitrogen atmosphere. The reaction mixture was cooled and dissolved in water (500 ml). The solution was titrated with 10% HCl to p*H* 4 and $CuCl_2$ (3 g, 22.3 mmol) was dissolved in the mixture. After 30 min the green solution started turning red and during the following 15 h crystals of **11***g* accumulated on the bottom of the vessel. The complex was filtered off and thoroughly washed with acetone and ether to give **11***g*; yield 1.5 g (64%); mp 147 °C (dec.); ir (KBr) 1697,1470, 1340, 1280 cm^{-1}.

Cyclohepta-1,4-diene-3-carboxylic Acid **5***g and its Rearrangement to* **3***g*

The copper complex **11***g* (0.9 g, 3.22 mmol) was mixed with water (20 ml) containing K_2CO_3 (0.089 g, 6.44 mmol). The red solid immediately turned brown and a slow development of gas was observed. After 1 h of stirring, the precipitate was filtered off and the filtrate was heated to 35 °C until the production of nitrogen was complete (12 h). The solution was cooled to 2 °C, acidified with HCl to p*H* 3, extracted with ether (3 × 15 ml), and the ether extract dried with $MgSO_4$. The solvent was removed *in vacuo* to give **5***g* as a colorless oil; pmr Table 1; ir (film) 3500–2500, 1715, 1421, 1289 cm^{-1}.

Pure **5***g* was heated for 1 h at 45 °C to give **3***g* as a yellow oil; pmr ($CDCl_3$) δ 1.85 (m, 2, H-6), 2.38 (m, 4, H-5,7), 5.91 (d of t, 1, H-4), 6.35 (d of d, 1, H-3), 7.26 (t, 1, H-1), 11.2 (s, 1, OH). On irradiation of the resonance at δ 2.38 the signal at δ 7.26 collapsed to a singlet, that at δ 5.91 to a doublet, and the absorption at δ 1.85 collapsed to a broad singlet: $J_{1,7}$ = 5.3 Hz; $J_{3,4}$ = 11.5 Hz; $J_{4,5}$ = 4.5 Hz; $J_{3,5}$ = 1.0 Hz.

3-Methoxycarbonylcyclohepta-1,4-diene **5***a and its Rearrangement to* **3***a*

The ether solution of **5***g* obtained as above, was treated with a slight excess of diazomethane. The solvent was removed *in vacuo* and the residue distilled to give **5***a* (55%); bp 30 °C/0.1 torr; pmr Table 1; ir (film) 1725, 1465, 1415, and 1295 cm^{-1}.

Kept at room temperature **5***a* rearranged to give **3***a*, which exhibited an identical pmr spectrum to that quoted above.

3-Dimethoxymethylcyclohepta-1,4-diene **5***c*

A solution of acetal **9***c* (2.0 g, 5.8 mmol) in methanol (15 ml) containing KOH (1.5 g, 27 mmol) was refluxed under N_2 for 48 h. Degassed water (30 ml) was added and the mixture extracted with methylene chloride (3 × 15 ml). The combined extract was dried with $MgSO_4$ and the

solvent was removed *in vacuo*, to give an oil, pmr ($CDCl_3$) δ 1.05–2.02 (m, 7), 3.35 (s, 6), 4.20 (m, 4), 3.55 (s, 2), 6.9 (m, 5). This product was dissolved in CH_2Cl_2 and the solution was exposed to air for 8 h. Development of gas was observed during this time. The solvent was removed *in vacuo*, and the mixture of **5***c* and aniline so obtained was separated on a short column of basic alumina eluting with ether. Yield of **5***c* 0.47 g (48%); pmr (Table 1). *Anal.* calcd. for $C_{10}H_{16}O_2$: C 72.26, H 9.70; found: C 71.97, H 9.77.

4-Phenyl-2,4,6-triazatetracyclo[5.3.2.0^{2,6}.0^{8,10}]dodeca-3,5-dione-9-carbaldehyde, **9***e*

Acetal **9***c* (0.8 g) was dissolved in acetone (30 ml), aqueous 37% HCl (0.5 ml) was added, and the solution was kept for 30 min at room temperature. At the end of this time $NaHCO_3$ (0.5 g) was slowly added and the solvent was removed *in vacuo*. The white residue was triturated with methanol, the inorganic salt removed by filtration, and the solvent evaporated *in vacuo* to yield crude **9***e* (0.65 g, 95%). Three recrystallizations from CCl_4–acetone mixtures gave pure **9***e*; mp 204 °C; pmr ($CDCl_3$) δ 1.50–2.30 (m, 7, H-8–12), 4.72 (br s, 2, H-1,7), 7.28–7.62 (m, 5, Ph), 9.72 (d, 1, H-8); ir (KBr) 1770, 1710, 1600, 1500, 1411, 1259 cm^{-1}. *Anal.* calcd. for $C_{16}H_{15}N_3O_3$: C 64.63, H 5.08; found: C 64.60, H 5.00.

Attempted Preparation of 3-Formylcyclohepta-1,4-diene

(*a*) The aldehyde **9***e* was hydrolyzed and treated with $CuCl_2$ as described above for the preparation of **11***g*, to give a copper complex, mp 120–122 °C (dec.); ir (KBr) 1695, 1619, 1401 cm^{-1}. This complex (0.2 g) was stirred with 5% K_2CO_3 solution (10 ml) at 4 °C for 3 h. The organic material was extracted into CH_2Cl_2, (3 × 5 ml), the combined extracts dried over $MgSO_4$, and then heated at 35 °C for 5 h. The solvent was removed *in vacuo* to yield 2-formylcyclohepta-1,3-diene **3***e*, pmr ($CDCl_3$) δ 1.65–2.20 (m, 2, H-6), 2.20–2.90 (m, 4, H-5,7), 6.05–6.60 (m, 2, H-3,4), 6.78 (t, 1, H-1), 9.37 (s, 1, —CHO).

(*b*) Reaction of the acetal **9***c*, using the same procedure as outlined for **9***e*, gave **3***e*, with the same pmr spectrum to that described above. Acetal **5***c* (20 mg) was dissolved in ether (4 ml) containing 3 drops of 37% HCl and stirred at −5 °C for 30 min. The ether solution was washed with 5% aqueous $NaHCO_3$ and water, dried over $MgSO_4$, and the solvent removed *in vacuo* (all operations were carried out at 0 °C). The pmr spectrum of the product was identical to that described above for **3***e*.

9-(2-Hydroxy-2-propyl)-4-phenyl-2,4,6-triazatetracyclo-[5.3.2.0^{2,6}.0^{8,10}]dodeca-3,5-dione, **9***d*

Methyllithium (4 ml, 1.3 *N* in hexane) was added to a vigorously stirred solution of **9***b* (1.4 g, 4.10 mmol) in dry 1,4-dioxane (100 ml). After 15 min, water (15 ml) was added and the volume of the solution was reduced to 30 ml *in vacuo*. Additional water (20 ml) was added and the mixture neutralized with 10% HCl and extracted with CH_2Cl_2 (3 × 20 ml). The organic layer was dried over $MgSO_4$ and reduced to 10 ml. Addition of CCl_4 (10 ml) caused precipitation of 0.2 g of white product. This material was recrystallized from CH_2Cl_2/CCl_4 mixtures to yield **9***d*, mp 147 °C; pmr ($CDCl_3$) δ 1.24 (s, 6, CH_3), 1.46–2.06 (m, 8), 4.66 (br s, 2, H-1,5), 7.30–7.62 (m, 5, ArH); ir (KBr) 3450, 1745, 1700, 1497, 1408, 1278, 1255 cm^{-1}. *Anal.* calcd. for $C_{18}H_{21}N_3O_3$: C 66.04, H 6.47; found: C 66.30, H 6.52.

3-(2-Hydroxy-2-propyl)-1,4-cycloheptadiene **5***d*

9*d* was hydrolyzed and treated with $CuCl_2$ in the same manner to that outlined above for **9***a* to give a copper complex, mp 107–110 °C. This complex was reacted with aqueous K_2CO_3 as described above for **11***g* to give, eventually, an oil which was purified by chromatography on alumina, eluting with ether. The final fraction was distilled (60 °C/0.5 torr) to yield **5***d* (30%); pmr Table 1; ir (film) 3400, 1170, 1450, 1370 cm^{-1}. *Anal.* calcd. for $C_{10}H_{16}O$: C 78.90, H 10.59; found: C 78.70, H 10.71.

1. I. PIKULIK and R. F. CHILDS. Can. J. Chem. **53**, 1818 (1975).
2. A. P. TER BORG and A. F. BICKEL. Recl. Trav. Chim. Pays-Bas, **80**, 1229 (1961).
3. R. B. BATES, W. H. DEINES, D. A. MCCOMBS, and D. E. POTTER. J. Am. Chem. Soc. **91**, 4608 (1969).
4. L. A. PAQUETTE and G. ZON. J. Am. Chem. Soc. **96**, 224 (1974).
5. K. HAFNER and W. RELLENSMAN. Angew. Chem. **72**, 918 (1960).
6. (*a*) E. L. ALLRED and J. C. HINSHAW. J. Chem. Soc. Chem. Commun. 1021 (1969); (*b*) M. MARTIN and W. R. ROTH. Chem. Ber. **102**, 811 (1969).
7. E. L. ALLRED and K. J. VOORHEES. J. Am. Chem. Soc. **95**, 620 (1973); L. A. PAQUETTE and M. J. EPSTEIN. J. Am. Chem. Soc. **95**, 6717 (1973).
8. L. M. JACKMAN and S. STERNHELL. *In* Applications of nuclear magnetic resonance spectroscopy in organic chemistry. Pergamon, Oxford. 1969. (*a*) p. 83; (*b*) p. 182.
9. J. M. CINNAMON and K. WEISS. J. Org. Chem. **26**, 2644 (1961).
10. R. GRIGG, R. HAYES, and A. SWEENEY. J. Chem. Soc. Chem. Commun. 1248 (1971).
11. K. M. HARMON. *In* Carbonium ions. Vol. 4. *Edited* by G. A. Olah and P. von R. Schleyer. Wiley Interscience, N.Y. 1973. p. 157.
12. J. N. SCHOOLERY. Technical Information Bulletin. Varian Associates, Palo Alto, U.S.A. 1959.
13. F. A. L. ANET. J. Am. Chem. Soc. **86**, 458 (1964).
14. F. R. JENSEN and L. A. SMITH. J. Am. Chem. Soc. **86**, 956 (1964).
15. W. TOCHTERMANN. Fortschr. Chem. Forsch. **15**, 378 (1970).
16. H. GÜNTHER, M. GÖRLITZ, and H.-H. HINRICHS. Tetrahedron, **24**, 5665 (1968); H. KESSLER and E. MÜLLER. Z. Naturforsch. Teil B, **22**, 283 (1967); W. E. HEYD and C. A. CUPAS. J. Am. Chem. Soc. **93**, 6086 (1971).
17. J. TILLIEU. Ann. Phys. **2**, 471 (1957); **2**, 631 (1957).
18. J. A. POPLE. J. Chem. Phys. **37**, 60 (1962).
19. R. WEHNER and H. GÜNTHER. J. Am. Chem. Soc. **97**, 923 (1975).
20. W. v. E. DOERING, G. LABER, R. VONDERWAHL, N. F. CHAMBERLAIN, and R. B. WILLIAMS. J. Am. Chem. Soc. **78**, 5448 (1956).
21. S. WINSTEIN. Q. Rev. Chem. Soc. **23**, 141 (1969).
22. M. J. GOLDSTEIN and R. HOFFMANN. J. Am. Chem. Soc. **93**, 6193 (1971).
23. R. E. DAVIS and A. TULINSKY. Tetrahedron Lett. 839 (1962); M. TRAETTEBERG. J. Am. Chem. Soc. **86**, 4265 (1964).
24. R. B. TURNER, W. R. MEADOR, W. v. E. DOERING, L. H. KNOX, J. R. MAYER, and D. W. WILEY. J. Am.

Chem. Soc. **79**, 4127 (1957); J. B. CONN, G. B. KISTIAKOWSKY, and E. A. SMITH. J. Am. Chem. Soc. **61**, 1868 (1939).
25. H. J. DAUBEN, JR., J. D. WILSON, and J. L. LAITY. J. Am. Chem. Soc. **91**, 1991 (1969); and *In* Nonbenzenoid aromatics. Vol. 11. *Edited by* J. P. Snyder. Academic Press, N.Y. 1971. p. 167.
26. F. A. L. ANET and G. E. SCHENCK. J. Am. Chem. Soc. **93**, 556 (1971).
27. E. VOGEL. Proc. XXIIIrd. Int. Cong. Pure. Appl. Chem. **1**, 275 (1971); L. A. PAQUETTE, H. C. BERK, and S. V. LEY. J. Org. Chem. **40**, 902 (1975).
28. K. CONROW. J. Am. Chem. Soc. **83**, 2958 (1961); E. VOGEL, U. H. BRINKER, K. NACHTKAMP, J. WASSEN, and K. MÜLLEN. Angew. Chem. Int. Ed. Engl. **12**, 758 (1973).
29. W. V. E. DOERING and W. R. ROTH. Tetrahedron, **19**, 715 (1963).
30. H. GÜNTHER, M. GÖRLITZ, and H. MEISENHEIMER. Org. Magn. Reson. **6**, 388 (1974).
31. R. F. CHILDS and I. PIKULIK. Can. J. Chem. This issue.
32. P. J. GARRETT. *In* Aromaticity. McGraw Hill, Maidenhead, Berkshire, England. 1971. p. 176.
33. K. TAKAHASHI, H. YAMAMOTO, and T. NOZOE. Bull. Soc. Chem. Jpn. **43**, 200 (1970).

Diamagnetic susceptibilities and susceptibility exaltations of some 7-substituted cycloheptatrienes

RONALD F. CHILDS AND IVAN PIKULIK

Department of Chemistry, McMaster University, Hamilton, Ont., Canada L8S 4M1

Received June 7, 1976

RONALD F. CHILDS and IVAN PIKULIK. Can. J. Chem. **55**, 259 (1977).

The diamagnetic susceptibilities of several 7-substituted cycloheptatrienes have been measured and used in conjunction with estimated values of their susceptibilities (Haberditzl increment system) to obtain the susceptibility exaltations of these compounds. These exaltations were found to be very large and to vary as a function of the size of the C_7 substituent. There was no apparent correlation of the exaltation of a compound with the electronic properties of its substituent. The effect of a substituent on the susceptibility exaltation is interpreted in terms of conformational changes in the seven-membered ring. The magnitude of the susceptibility exaltations of these cycloheptatrienes, for example 7-*tert*-butylcycloheptatriene ($\Lambda = 14.8$), in comparison to that of benzene ($\Lambda = 13.7$) would suggest that the presence of an induced diamagnetic ring current is not a good criterion of its aromaticity.

RONALD F. CHILDS et IVAN PIKULIK. Can. J. Chem. **55**, 259 (1977).

On a mesuré les susceptibilités diamagnétiques de plusieurs cycloheptatriènes substitués en position 7 et on a utilisé ces données, de concert avec les valeurs estimées pour leurs susceptibilités (système additif de Haberditzl), afin d'obtenir les augmentations de susceptibilités de ces composés. On a trouvé que ces exaltations sont très grandes et qu'elles varient en fonction de la grosseur du substituant en position C_7. Il n'y a apparamment aucune corrélation entre l'exaltation d'un composé et les propriétés électroniques de son substituant. On peut interprété l'effet d'un substituant sur l'exaltation de la susceptibilité en termes de changements conformationnels dans le cycle à sept membres. L'amplitude des exaltations des susceptibilités de ces cycloheptatriènes, par exemple pour la *tert*-butyl-7 cycloheptatriènes ($\Lambda = 14.8$) par opposition à celle du benzène ($\Lambda = 13.7$), pourrait suggérer que la présence d'un courant de cycle diamagnétique induit n'est pas un bon critère pour déterminer son aromaticité.

[Traduit par le journal]

The position of the equilibrium between cycloheptatriene and norcaradiene can be changed by the judicious introduction of substituents (1). Particularly dramatic shifts in the equilibrium position have been observed with substitution at C_7, the methylene carbon of these systems (2).

Several explanations have been advanced to account for the effect of a C_7-substituent on the position of this and other closely related equilibria, most of which tend to focus attention on the norcaradiene part of the system (3–6). At this present time the most widely accepted view seems to be that put forward by Hoffmann (4) and Günther (5) which considers the interaction of the molecular orbitals of a C_7 substituent with those of the cyclopropyl function of a norcaradiene. However, the problem is by no means fully resolved. For example, the recent report of Mukai and co-workers (6) on some 7,7-disubstituted systems or the earlier results of Hall and Roberts (7) do not seem to fit in with these proposals.

In the preceeding paper we showed that the large differences in the proton chemical shifts of some 7-substituted cycloheptatrienes and their corresponding cyclohepta-1,4-dienes were consistent with a diamagnetic ring current being induced in the cycloheptatrienes (8). The size of this effect seemed to be dependent on the nature of the substituent, possibly implying that the magnitude of the induced ring current was also determined by substitution at C_7. If this is indeed the case, then it is apparent that the properties of a cycloheptatriene are substituent dependent and this could conceivably have considerable bearing on the cycloheptatriene–norcaradiene equilibrium.

It is difficult on the basis of chemical shift arguments to establish the presence of a diamagnetic ring current in a molecule, particularly as the whole question of the origin of the typically low-field resonances of aromatic protons has been called into question (9). To circumvent this problem we have determined the magnetic susceptibilities and susceptibility exaltations of

TABLE 1. Diamagnetic susceptibilities of cycloheptatrienes and related compounds[a]

Compounds	κ (-10^{-6})	ρ (g/cm^3)	χ $(-10^{-6}$ cm^3/g)	χ_M $(-10^{-6}$ cm^3/mol)	χ_M' $(-10^{-6}$ cm^3/mol)
Cycloheptatriene	0.572[b]	0.8743	0.654	60.3	51.7
Cycloheptatriene				59.8[d]	
7-Methoxycarbonylcycloheptatriene	0.606[c]	1.0419	0.581	87.3	77.8
7-Methylcycloheptatriene	0.597[b]	0.8432	0.708	75.2	63.9
7-Methoxycycloheptatriene	0.592[b]	0.9131	0.648	79.2	71.3[e]
7-Cyanocycloheptatriene	0.628[b]	1.0026	0.626	73.4	61.5
7-Dimethoxymethylcycloheptatriene	0.640[c]	0.9958	0.643	106.8	95.3
7-*tert*-Butylcycloheptatriene	0.654[c]	0.8484	0.771	114.3	99.5
2-Methoxycarbonyl-1,3-cycloheptadiene	0.628[b]	1.0731	0.585	89.0	87.5

[a]All measurements at 36 °C.
[b]Toluene standard.
[c]Acetonitrile standard.
[d]Value reported by Dauben *et al.* (10).
[e]χ_M' calculated assuming a C_2*—C_3 (O) bond increment = 4.6.

a series of 7-substituted cycloheptatrienes and have found the magnitude of the exaltations to be very strongly dependent on the substituent used. The susceptibilities of a limited number of cycloheptatrienes have been reported previously by Dauben *et al.* (10–12), however, unlike the results reported here, no large dependence of the exaltation on substitution was found by these workers.

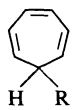

1 R = H
2 R = OCH_3
3 R = CH_3
4 R = $COOCH_3$
5 R = CN
6 R = $CH(OCH_3)_2$
7 R = $C(CH_3)_3$

8

Results and Discussion

Measurement of Magnetic Susceptibility

The diamagnetic susceptibilities of some substituted cycloheptatrienes were measured using the method described by Douglas and Fratiello (13) and more recently utilized by Dauben *et al.* (10). A special nmr tube consisting of two concentric cylinders was used in conjunction with a high resolution nmr spectrometer. All measurements were carried out at a probe temperature of 36 °C, using toluene or nitromethane as the reference material and calibrating the system with a set of pure liquids of known volume magnetic susceptibilities. The cycloheptatrienes used in this study, compounds **1**–**7**, were chosen such that a variety of different types of substituents were present. In each case it is known that the corresponding norcaradiene valence tautomer is not present to any significant extent. The volume magnetic susceptibilities, κ, of cycloheptatrienes **1**–**7** and cycloheptadiene **8** are given in Table 1.

The densities of the various compounds were determined at 36 °C using a calibrated pycnometer. These were used in conjunction with the values of κ to obtain the magnetic susceptibilities per gram, χ ($\chi = \kappa/\rho$), and molar susceptibilities χ_M ($\chi_M = \chi M$; where M = mw).

The reliability of this method of obtaining χ_M was checked by repeating the measurement of the susceptibility and density of cycloheptatriene. As can be seen from the first two entries in Table 1, the value of χ_M obtained in this work differs from that reported by Wilson (10) by only 0.5×10^{-6} cm^3/g, which is within the error limits of this type of experiment (12). Similar cross checks with other compounds of known molar susceptibility proved to be equally as good.

Estimation of Magnetic Susceptibility

In order to determine whether the susceptibility of a compound includes a contribution from an induced diamagnetic ring current, it is necessary to estimate the expected susceptibility, χ_M', in the absence of any ring current. There are several methods available for the calculation of χ_M', the virtues and failures of which have been discussed extensively by Laity (12). The incremental system of Haberditzl (14) which has been shown to give fairly good results for a large number of hydrocarbons, ethers, and alcohols, was used in this work. The estimation of χ_M' for esters is somewhat less reliable,

TABLE 2. Measured and calculated susceptibilities of various nitriles[a]

Compound	χ_M[b]	Calculated susceptibility in absence of C≡N increment[c]	C≡N increment
Acetonitrile	28.0	17.9	10.1
Propionitrile	38.5	29.3	9.2
Butyronitrile	49.4	40.6	8.8
Benzonitrile	65.2	56.6	8.6
Toluonitrile	76.4	68.2	7.7
Phenylacetonitrile	76.9	67.1	9.8

[a]In units of -10^{-6} cm³/mol.
[b]Values taken from data given in ref. 15.
[c]Calculated using Haberditzl increment system (14).

TABLE 3. Diamagnetic susceptibility exaltations and uv spectra of some cycloheptatrienes and related compounds

Compound	Λ (-10^{-6} cm³/mol)	λ_{max} (nm)
Cycloheptatriene	8.5	261[b]
7-Methoxycycloheptatriene	7.9	—
7-Methylcycloheptatriene	11.3	257[c]
7-Methoxycarbonylcycloheptatriene	9.5	(258)[d]
7-Cyanocycloheptatriene	11.8	255[e]
7-Dimethoxymethylcycloheptatriene	11.5	258.5[f]
7-*tert*-Butylcycloheptatriene	14.8	255[g]
1,6-Dimethylcycloheptatriene	8.3[a]	
3,7,7-Trimethylcycloheptatriene	7.1[a]	
2-Methoxycarbonylcyclohepta-1,3-diene	1.5	
Cyclohepta-1,4-diene	1.1[a]	
Cyclohepta-1,3-diene	0.3[a]	
Benzene	13.7[a]	

[a]Value of reported by Dauben *et al.* (11).
[b]Reference 37.
[c]Reference 38.
[d]W. von E. Doering (34).
[e]Value reported for carboxylic acid by Dewar *et al.* (39).
[f]A. C. Cope (35).
[g]W. E. Heyd (33).

however the close agreement of χ_M' with the measured susceptibility χ_M of the cycloheptadiene ester **8** (Table 1), a molecule which cannot sustain an induced ring current, indicates that the Haberditzl system is not grossly in error with molecules of this type.

Some difficulty was encountered in the calculation of χ_M' for **5** as an increment for the C≡N bond has not been reported for the Haberditzl system. Using the known diamagnetic susceptibilities of several nitriles (15) it was possible to estimate a value for the C≡N bond increment by taking the average difference between the measured values of χ_M and the sum of all the other increments involved in these nitriles (Table 2). A value of -8.9×10^{-6} was used as the C≡N bond increment. With the limited number of model compounds used this value is tentative and no great significance should be attached to the absolute magnitude of the difference between χ_M and $\chi_{M'}$ for **5**.

The difference between the observed and calculated susceptibilities is defined as the susceptibility exaltation Λ ($\chi_M - \chi_{M'} = \Lambda$) (16, 11) and values of this parameter are listed in Table 3. This table also includes the susceptibility exaltations of some cycloheptatriene and dienes previously reported by Dauben *et al.* (11).

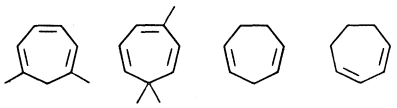

9 **10** **11** **12**

Discussion of Susceptibility Exaltations

It is quite apparent on examination of the

data presented in Table 3 that all the cycloheptatrienes are diatropic, all exhibiting a substantial diamagnetic susceptibility exaltation (17, 18*a*).[1] These exaltations range from a low of 7.1 for the trimethyl compound **10** to a high of 14.8 for the *tert*-butylcycloheptatriene **7**.[2] The sort of discrepancies normally encountered between χ_M and χ_M' for atropic molecules are indicated by the exaltations of the various cycloheptadienes **8**, **11**, and **12** and as can be seen, these are very much smaller than those encountered for the cycloheptatrienes.

A second and most interesting feature of the exaltations of these cycloheptatrienes is that the magnitude of the exaltation is a function of the substituent on the ring. This is particularly noticeable with the change of substituents on C_7. Thus while **9**, with two methyl groups on C_1 and C_6, has almost the same susceptibility exaltation as cycloheptatriene itself, the 7-*tert*-butyl compound **7** has an exaltation which is close to 75% larger than that of **1**. This marked dependence of the exaltation of a cycloheptatriene on the C_7 substituent is different from the very small substituent effects usually encountered with diatropic molecules. For example, the susceptibility exaltation of benzene is not influenced to any significant degree by substitution (12). Clearly some change must be occurring with these cycloheptatrienes as the substituent on C_7 is varied.

Apart from the 7-cyano compound **5** for which there is some uncertainty in χ_M', there would appear to be a correlation between the steric size of a C_7 substituent and the susceptibility exaltations of these mono-substituted cycloheptatrienes. Based on the steric parameters deduced from cyclohexane equilibria, the substituent would be expected to increase in size in the order OMe < COOMe < CH_3 < $CH(OCH_3)_2$ < *tert*-Bu (20) and this is the exact order of increase of the exaltations of the similarly substituted cycloheptatrienes. There does not seem to be any correlation of the susceptibility exaltations with any electronic properties of the substituents. It is interesting that the introduction of a second substituent on C_7, *e.g.* **10** with two C_7 methyl groups, lowers the susceptibility exaltation back to a value slightly less than that of the unsubstituted system **1**.

These changes in the susceptibility exaltation of these cycloheptatrienes could result from conformational changes in the seven-membered ring. The seven-membered ring of cycloheptatriene is non planar and exists as a rapidly equilibrating mixture of two equivalent boat conformations (21). When a substituent is introduced onto the C_7 carbon of a cycloheptatriene, the two boat forms, while still rapidly equilibrating, are no longer of equal energy. The favoured conformation is the one in which the substituent is in the pseudo-equatorial position and this becomes increasingly the preferred conformation as the steric size of the substituent is increased (22).

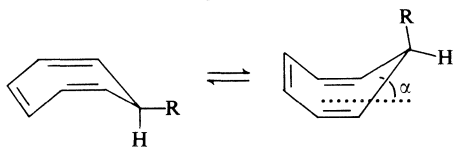

Not only are the two conformations of a C_7 substituted cycloheptatriene no longer of equal energy but it has been suggested that the shape of the boat in each conformation is different (22). Thus with a pseudo-axial substituent, the boat tends to be somewhat flatter and the structural angle α reduced, while with an equatorial substituent the angle α tends to be greater than that found for cycloheptatriene itself. As the larger substituents enhance the population of the conformation in which the group is in the equatorial position, on average the angle α would be expected to increase as the substituent size is increased. One effect of an increase in the angle α is that the lobes of the *p* orbitals on C_1 and C_6 are tipped closer together, Fig. 1, and the possibility of cyclic delocalization enhanced. The magnitude of the magnetic susceptibility exaltations of these 7-substituted cycloheptatrienes parallel these conformational changes.

If such a change in the cyclic delocalization of the π-electrons of a cycloheptatriene is occurring as a function of C_7 substitution, then

[1]The term diatropic was originally defined in terms of the observed deshielding or shielding of the resonances of the peripheral protons in the pmr spectrum of a molecule sustaining an induced diamagnetic ring current (17, 18*a*). Rather than coin a new term, the definition has been extended here to include all molecules which exhibit an induced diamagnetic ring current, irrespective of how this ring current is measured. An alternative term which has been suggested is strobilic (19), however, this does not seem to have been generally accepted.

[2]For simplicity the units of the molar diamagnetic susceptibilities are omitted in the text of this paper. Throughout the units are $-\chi_M \times 10^{-6}$ cm^3 mol^{-1}.

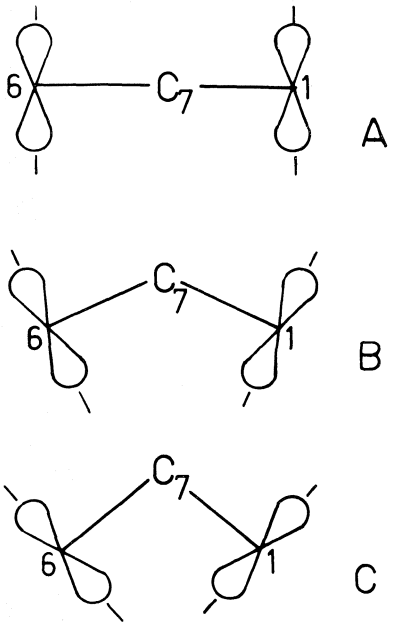

FIG. 1. Schematic representation of changes in the relative alignment of C_1 and C_6 of a cycloheptatriene as the structural angle α is changed; *A*, $\alpha = 0°$; *B*, $\alpha = 30°$; *C*, $\alpha = 55°$.

it should also be reflected in other electronic properties of these molecules. As can be seen from the data in Table 3, the position of the uv absorption maxima of these substituted cycloheptatrienes is increasingly blue shifted as the C_7 group becomes larger. These shifts in λ_{max} are not large but they are in the direction expected if cyclic delocalization were to become more important (23).

The susceptibility exaltation of 7-cyanocycloheptatriene, **5**, is higher and its uv absorption maximum more blue shifted than would be expected simply on the basis of the steric size of the nitrile group. It is interesting, however, that the cyano group of **5** also shows a larger preference for the pseudo-equatorial position than would have been anticipated on just steric grounds (24).

The conformation of the seven-membered ring of a cycloheptatriene with two C_7 substituents would appear to remain much the same as that of the unsubstituted system (25). As can be seen from the results in Table 3 the susceptibility exaltations of **10** and **1** are very similar.

It is instructive to compare the magnitudes of the exaltations of these cycloheptatrienes with their pmr spectra. In the previous paper it was shown that the C_7 proton resonances of 7-substituted cycloheptatrienes occurred substantially further upfield than the comparable resonances of similarly substituted cyclohepta-1,4-dienes (8). The difference in the chemical shifts of these two systems was seemingly inversely related to the size of the substituents, decreasing as the steric bulk of the substituent was increased. This is the exact reverse of the changes that have been found in the susceptibility exaltations of the systems that have been described in this paper. This points out how tenuous are any arguments based on chemical shifts for the presence of an induced ring current in a molecule.

Diatropic or Aromatic?

The question of whether cycloheptatrienes and related molecules are homoaromatic is a long standing, unresolved problem (10, 26–28). Part of this problem is tied up with the confusion which surrounds the term aromatic (29), the difficulty in the quantification of this much cherished term, and the question of the relationship of induced ring currents and pmr spectra (19).

If an aromatic molecule is defined as being "a diatropic molecule in which all the ring atoms are involved in a single conjugated system" (18*b*) and this definition extended to include homoaromaticity by the inclusion of diatropic homo-conjugated systems, then the cycloheptatrienes examined in this work must be considered to be homoaromatic. Indeed, a comparison of the susceptibility exaltations of benzene, 13.7, and the tropylium cation, 17, *vs.* 7-*tert*-butylcycloheptatriene, 14.8, and the homotropylium cation, 21, (11) would suggest that there is as much right to call this substituted cycloheptatriene a homobenzene as there is for the $C_8H_9^+$ cation to be called the homotropylium cation.[3]

This type of quantitative comparison of susceptibility exaltations must, however, be treated with a great deal of caution. Thus benzene, the archetype of all aromatic molecules, with a large resonance energy and showing no

[3]Susceptibility exaltations are related to the area of the ring system involved. In these comparisons, the change in area on going from benzene to cycloheptatriene is very comparable to that involved in going from the tropylium to homotropylium cation.

bond length alternation, would seem to be in an entirely different league to cycloheptatriene. The resonance energy of cycloheptatriene has been reported to be only 7 kcal/mol (27), which is not much greater than that expected for a regular conjugated triene. On the basis of equilibration studies Conrow (28) has suggested that the 1,6-overlap in cycloheptatriene only stabilizes the molecule by some 1–2 kcal/mol relative to systems bearing an exocyclic methylene group in which cyclic delocalization is not possible. Moreover, the several structural studies reported on cycloheptatriene and its derivatives (25) show that the C—C bonds of the seven-membered ring show the alternation in length expected of a linearly conjugated system.

Resonance energy has been advocated and used as a criterion of aromaticity (30). However, with these cycloheptatrienes there does not seem to be any correlation between the magnitude of their resonance energies and diamagnetic ring currents (31). This leads us to question whether the ability of a molecule to support an induced diamagnetic ring current is a useful, or even valid criterion of aromaticity. It would rather seem better, albeit somewhat less glamorous, if molecules exhibiting a diamagnetic ring current irrespective of how this is measured or detected, be termed diatropic.

Experimental

The cycloheptatrienes used in this study were prepared by standard procedures and their purity checked by pmr prior to use. Cycloheptatriene, commercial sample purified by preparative glpc (10 ft × ¼ in. column with 15% Carbowax on Chromosorb W); 7-methoxy and 7-methylcycloheptatrienes were prepared by the procedure of Dauben (32), 7-*tert*-butylcycloheptatriene by the procedure of Heyd (33); 7-cyano-cycloheptatriene by the addition of tropylium tetrafluoroborate to aqueous potassium cyanide according to the procedure of Dauben;[4] and 7-dimethoxymethylcycloheptatriene by the method reported by Cope (35).

Density Determinations

The densities of the cycloheptatrienes were determined at 36 °C using a Lipkin bicapillary pycnometer (0.25 ml, Ace Glass Company) which was calibrated with distilled water.

Diamagnetic Susceptibility Measurements

Volume diamagnetic susceptibilities were determined using the method of Douglass and Fratiello (13). A cell consisting of precision bore, thin wall, concentric, flat bottom tubes was used (Wilmad Glass Company). The reference material, toluene or nitromethane, was placed in the outer tube and the sample in the inner, central tube. With the sample not being spun, the pmr spectrum of each signal of the reference is distorted into a saddle shape; the separation of the two peaks being proportional to the susceptibility of the sample. A Varian HA100 spectrometer operated in the no-lock mode was used for these measurements. Since it was not possible to completely eliminate any drift of the magnetic field under these conditions, the error caused by the drift was reduced by scanning the signal 12 to 18 times alternately on the forward and backward directions and the average separation calculated. It was necessary to tune the spectrometer to a very high degree of field homogeneity.

The sample cell and spectrometer were calibrated with a series of compounds of known susceptibility. The compounds used for this calibration were: CH_2I_2, $CHBr_3$, CH_2Cl_2, H_2O, $C_6H_5CH_3$, CH_3CN, CH_3CH_2OH, and CH_3NO_2, all of which were purified by standard procedures (36) and distilled through a 20 in. glass column filled with glass helices under He. To check that no change in conditions occurred during the measurement of the susceptibilities of the samples, several standard samples were re-run at the end of the measurements. A plot of the separation of the methyl peak of the references (nitromethane and toluene) against the susceptibilities of the standards gave straight lines within each case a correlation coefficient of at least 0.999 and a standard deviation in κ of less than 0.004.

[4]H. J. Dauben, personal communication to S. Winstein; *cf.* ref. 34.

Acknowledgments

We thank the National Research Council of Canada and the Research Corporation (Frederick Gardener Cottrell Grant) for financial support.

1. G. Maier. Angew. Chem. Int. Ed. Engl. **6**, 402 (1967); D. Wendisch. *In* Methoden der Organischen Chemie (Hauben-Weyl). Vol. IV/3. *Edited by* E. Müller. Georg. Thieme Verlag, Stuttgart. 1971. p. 531.
2. E. Ciganek. J. Am. Chem. Soc. **93**, 2207 (1971); H. J. Reich, E. Ciganek, and J. D. Roberts. J. Am. Chem. Soc. **92**, 5166 (1970); W. Betz and J. Daub. Chem. Ber. **107**, 2095 (1974); I. Pikulik and R. F. Childs. Can. J. Chem. **53**, 1818 (1975).
3. E. Ciganek. J. Am. Chem. Soc. **89**, 1454 (1967); R. Huisgen, G. Boche, A. Dahmen, and W. Hechte. Tetrahedron Lett. 5215 (1968); F. G. Klärner. Tetrahedron Lett. 19 (1974).
4. R. Hoffmann. Tetrahedron Lett. 2907 (1970).
5. H. Günther. Tetrahedron Lett. 5173 (1970).
6. H. Tsuruta, S. Mori, and T. Mukai. Chem. Lett. 1127 (1974).
7. G. E. Hall and J. D. Roberts. J. Am. Chem. Soc. **93**, 2203 (1971).
8. I. Pikulik and R. F. Childs. Can. J. Chem. This issue.
9. M. Barfield, D. M. Grant, and D. Ikenberry. J. Am. Chem. Soc. **97**, 6956 (1975) and cited references.
10. H. J. Dauben, Jr., J. D. Wilson, and J. L. Laity. J. Am. Chem. Soc. **90**, 811 (1968); **91**, 1991 (1969).
11. H. J. Dauben, Jr., J. D. Wilson, and J. L. Laity. *In* Non-benzenoid aromatics. Vol. 2. *Edited by* J. P. Snyder. Academic Press, N.Y. 1971. p. 167.

12. J. L, LAITY, Ph.D. Thesis, University of Washington. 1968.
13. D. C. DOUGLASS and A. FRATIELLO. J. Chem. Phys. **39**, 3161 (1963); J. R. ZIMMERMAN and M. R. FOSTER. J. Phys. Chem. **61**, 282 (1957).
14. W. HABERDITZL. *In* Magnetochemie. Akademie-Verlag, Berlin. 1968. p. 115.
15. G. SAURET and R. LALANDE. C. R. **236**, 2066 (1953); C. M. FRENCH. Trans. Faraday Soc. **50**, 1320 (1954); G. W. SMITH. *In* A compilation of diamagnetic susceptibilities. General Motors Corporation Research Report, GMR-317. General Motors Corporation, Detroit, Michigan. 1960.
16. A. PACAULT. Ann. Chem. (Paris), **1**, 567 (1946), Rev. Sci. **86**, 38 (1948); A. PACAULT, J. HOARAU, and A. MARCHAND. Adv. Chem. Phys. **3**, 171 (1961).
17. F. SONDHEIMER. Acc. Chem. Res. **5**, 81 (1972).
18. P. J. GARRETT. *In* Aromaticity. McGraw Hill, Maidenhead, England. 1971. (*a*) p. 177; (*b*) p. 178.
19. J. LABARRE. *In* Aromaticity, pseudo-aromaticity, and anti-aromaticity. *Edited by* E. D. Bergmann and B. Pullman. Israel Academy of Sciences and Humanities, Jerusalem. 1971. p. 55.
20. J. A. HIRSH. *In* Topics in stereochemistry. Vol. 1. *Edited by* N. L. Alinger and E. L. Eliel. Interscience, New York. 1967. p. 199.
21. F. A. L. ANET. J. Am. Chem. Soc. **86**, 458 (1964); F. R. JENSEN and L. A. SMITH. J. Am. Chem. Soc. **86**, 956 (1964).
22. H. GÜNTHER, M. GÖRLITZ, and H. H. HINRICHS. Tetrahedron, **24**, 5665 (1968); H. GÜNTHER, M. GÖRLITZ, and H. MEISENHEIMER. Org. Magn. Reson. **6**, 388 (1974).
23. S. WINSTEIN, C. G. KREITER, and J. I. BRAUMAN. J. Am. Chem. Soc. **88**, 2047 (1966).
24. C. H. BUSHWELLER, M. SHARPE, and S. J. WEININGER. Tetrahedron Lett. 453 (1970).
25. R. E. DAVIS and A. TULINSKY. Tetrahedron Lett. 839 (1962); S. S. BUTCHER. J. Chem. Phys. **42**, 1833 (1965); N. L. ALLINGER and J. T. SPRAGUE. J. Am. Chem. Soc. **95**, 3893 (1973).
26. W. v. E. DOERING, G. LABER, R. VONDERWAHL, N. F. CHAMBERLAIN, and R. B. WILLIAMS. J. Am. Chem. Soc. **78**, 5448 (1956); F. A. L. ANET and G. E. SCHENCK. J. Am. Chem. Soc. **93**, 556 (1971); E. VOGEL, U. H. BRINKER, K. NACHTKAMP, J. WASSEN, and K. MÜLLEN. Angew. Chem. Int. Ed. Engl. **12**, 758 (1973); M. J. GOLDSTEIN and R. HOFFMANN. J. Am. Chem. Soc. **93**, 6193 (1971).
27. R. B. TURNER, W. R. MEADOR, W. v. E. DOERING, L. H. KNOX, J. R. MAYER, and D. W. WILEY. J. Am. Chem. Soc. **79**, 4127 (1957); J. B. CONN, G. B. KISTIAKOWSKY, and E. A. SMITH. J. Am. Chem. Soc. **61**, 1868 (1939).
28. K. CONROW. J. Am. Chem. Soc. **83**, 2958 (1961).
29. D. LLOYD and D. R. MARSHALL. Angew. Chem. Int. Ed. Engl. **11**, 404 (1972); E. D. BERGMANN and J. AGRANAT. *In* Aromaticity, pseudo-aromaticity, and anti-aromaticity. *Edited by* E. D. Bergmann and B. Pullman. Israel Academy of Sciences and Humanities, Jerusalem. 1971. p. 9.
30. M. J. S. DEWAR. Chem. Soc. Spec. Publ. No. 21, 207 (1967).
31. S. W. STALEY and W. G. KINGSLEY. J. Am. Chem. Soc. **95**, 5804 (1973).
32. A. G. HARRISON, L. R. HONNEN, H. J. DAUBEN, and F. P. LOSSING. J. Am. Chem. Soc. **82**, 5593 (1960).
33. W. E. HEYD. Ph.D. Thesis, Case Western Reserve University. 1972.
34. W. v. E. DOERING and L. H. KNOX. J. Am. Chem. Soc. **79**, 352 (1957).
35. A. C. COPE, N. A. NELSON, and D. S. SMITH. J. Am. Chem. Soc. **76**, 1100 (1954).
36. A. WEISSBURGER, E. S. PROSHAUER, J. A. RIDDICK, and E. A. TOPPS, JR. *In* Techniques of organic chemistry. Vol. 7A. Interscience, New York. 1955. pp. 297–459.
37. K. WEISS and M. LALANDE. J. Am. Chem. Soc. **82**, 3117 (1960).
38. K. CONROW, M. E. H. HOWDEN, and D. DAVIS. J. Am. Chem. Soc. **85**, 1929 (1963).
39. M. J. S. DEWAR, C. R. GANELLIN, and R. PETTIT. J. Chem. Soc. 55 (1958).

Milieux hyperbasiques: préparation de carbanions en α d'amides *N,N*-disubstitués. Synthèse de β- et γ-hydroxyamides et de γ-butyrolactones

PIERRE HULLOT, THÉRÈSE CUVIGNY, MARC LARCHEVÊQUE ET HENRI NORMANT

Laboratoire de Synthèse Organique – Laboratoire associé au C.N.R.S. n° 239, Université Pierre et Marie Curie, tour 44–45, 4, place Jussieu – 75230 Paris Cédex 05

Reçu le 6 juillet 1976

PIERRE HULLOT, THÉRÈSE CUVIGNY, MARC LARCHEVÊQUE et HENRI NORMANT. Can. J. Chem. **55**, 266 (1977).

Les carbanions en α d'amides *N,N*-disubstitués sont obtenus avec d'excellents rendements par action des "dialkylamidures activés" en solution dans le HMPT. Ils réagissent avec les aldéhydes et cétones pour conduire à des β-hydroxyamides; avec les époxydes on atteint les γ-hydroxyamides cyclisés in situ en γ-butyrolactones.

PIERRE HULLOT, THÉRÈSE CUVIGNY, MARC LARCHEVÊQUE, and HENRI NORMANT. Can. J. Chem. **55**, 266 (1977).

The α anions of *N,N*-disubstituted carboxamides can be conveniently prepared by treatment with "activated" lithium dialkylamides in HMPT. They react with aldehydes and ketones and lead to β-hydroxyamides; furthermore the ring opening of epoxides affords γ-hydroxyamides which may be cyclized *in situ* to γ-butyrolactones.

Nous avons envisagé dans un précédent mémoire la métallation en α des amides *N,N*-disubstitués à l'aide de bases très puissantes: les dialkylamidures de lithium "activés" préparés in situ par simple agitation du métal dans une solution benzène–amine–HMPT. Nous avons vu que les carbanions, aisément formés à basse température, pouvaient être alkylés dans d'excellentes conditions grâce à la présence du HMPT (1).

D'autre part, nous avons récemment montré que l'autoxydation de ces anions par un courant d'air menait aux α hydroxyamides avec des rendements très satisfaisants (2).

Nous aborderons maintenant la condensation de ces anions avec des dérivés carbonylés et des époxydes divers en vue d'obtenir des β- et γ-hydroxyamides.

I. Synthèse de β-hydroxyamides N,N-disubstitués (3)

Des β-hydroxyamides *N,N*-disubstitués ont déjà été obtenus par diverses méthodes. La condensation des amides avec les cétones aromatiques en présence de potasse donne des résultats satisfaisants (4) mais le procédé ne s'applique pas aux cétones énolisables. Les *N,N*-diméthyl acétamide et propionamide ont été métallés en α à l'aide du dérivé lithié du *s*-trithiane, cependant la réaction ultérieure avec des carbonylés énolisables ne se fait qu'avec des rendements médiocres (5).

L'emploi des amidures de lithium "usuels" (butyllithium + diisopropylamine) a permis la métallation de lactames dont le dérivé lithié ainsi formé a été condensé avec la benzophénone et la cyclohexanone (6) ou encore la méthylvinyl cétone (7) et a fourni les β-hydroxylactames correspondants. Cependant, nous n'avons pas relevé d'étude générale concernant la préparation de β-hydroxyamides *N,N*-disubstitués.

Nous avons réalisé la métallation des amides *N,N*-disubstitués selon le mode opératoire déjà décrit (1). Le carbanion se forme aisément sous l'action des amidures "activés" que l'amide soit linéaire, ramifié ou cyclique. Le dérivé carbonylé est introduit à basse température (−40 à −60 °C), le milieu, initialement violet foncé, se décolore vers la fin de l'addition [1].

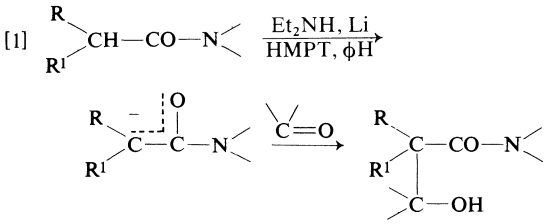

Le tableau 1 résume quelques essais effectués avec les aldéhydes. Les rendements sont satisfaisants, quel que soit l'encombrement de l'amide.

Le *N*-méthyl *N*-phényl butyramide fournit l'hydroxyamide attendu (essai 6). Nous n'obser-

TABLEAU 1. Hydroxyalkylation de R R^1 $\bar{C}$—$CON(Me)_2$ par les aldéhydes

Essai	R	R^1	Aldéhyde	β-Hydroxyamide	Rdt (%)[a]
1	H	H	$CH_3CH{=}CHCHO$	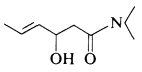	69
2	H	H	PhCHO	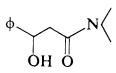	68
3	H	C_2H_5	$(HCHO)_n$[b]	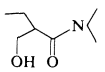	91
4	H	C_2H_5	CH_3CHO	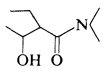	76
5	H	C_2H_5	PhCH=CH—CHO	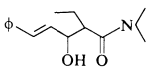	77
6[c]	H	C_2H_5	$(HCHO)_n$[b]	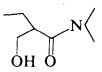	69
7	CH_3	CH_3	C_3H_7CHO	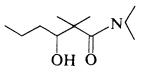	68

[a]En produits distillés.
[b]Polyoxyméthylène non dépolymérisé.
[c]Amide *N*-méthyl *N*-phényl.

vons pas de migration N → C du groupe phényle au cours de la métallation. Par contre, une telle migration est observée quand cet amide est traité par le dérivé lithié du *s*-trithiane (5). Le polyoxyméthylène non dépolymérisé est introduit à +20 °C dans la solution d'amide métallé et fournit ainsi des β-hydroxyamides à fonction alcool primaire avec d'excellents rendements (essais 3 et 6).

Le tableau 2 concerne les cétones. Dans les mêmes conditions que les aldéhydes elles se condensent bien dès −60 °C. Une cétone aussi énolisable que la cyclohexanone conduit au β-hydroxyamide attendu avec un très bon rendement (essai 8, 86%). La différence de comportement de cette cétone avec le dérivé lithié du *N*,*N*-diméthyl acétamide selon le procédé de métallation est frappante: le rendement tombe à 4% si l'on emploie le dérivé lithié du *s*-trithiane (5).

Malgré divers essais dans différentes conditions, nous n'avons pas réussi à condenser le dérivé lithié du *N*,*N*-diméthyl isobutyramide avec la benzophénone (essai 13). Nous pensons que l'encombrement de l'amide est responsable de cet échec (différence avec les essais 9, 10 et 11).

II. Synthèse de γ-hydroxyamides N,N-disubstitués: accès aux γ-butyrolactones

La condensation des époxydes sur les divers amides lithiés formés à l'aide des amidures activés constitue une préparation directe de γ-hydroxyamides *N*,*N*-disubstitués. Ces composés sont des précurseurs immédiats de γ-butyrolactones variées. De telles butyrolactones présentant en γ un ou deux groupes alkyle sont transformées par l'acide polyphosphorique en oxo-3 cyclopentènes dont on connaît l'importance dans la synthèse des prostaglandines (8). Quelques γ-hydroxyamides ont été également obtenus par action d'époxydes sur les *N*,*N*-diméthyl acétamide et propionamide préalablement métallés soit à l'aide des amidures usuels (9) soit avec l'amidure de sodium dans l'ammoniac liquide (10). Ces γ-hydroxyamides ont ensuite été cyclisés à l'aide d'une résine acide à reflux d'acétone (11) ou à reflux d'éthylène glycol en présence de bases fortes (9).

TABLEAU 2. Hydroxyalkylation de $RR^1\bar{C}CON(Me)_2$ par les cétones

Essai	R	R^1	Cétone	β-Hydroxyamide	Rdt (%)[a]
8	H	H		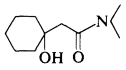	86
9	H	H	Ph_2CO	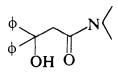	93
10[b]	H	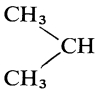	Ph_2CO	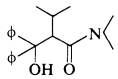	86
11	CH_3	CH_3	CH_3COCH_3	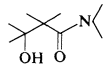	61
12	CH_3	CH_3	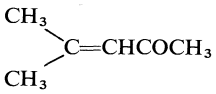	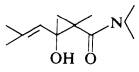	39
13	CH_3	CH_3	Ph_2CO		0
14			Ph_2CO	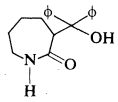	92

[a]En produits distillés.
[b]Amide *N,N*-diéthyl.

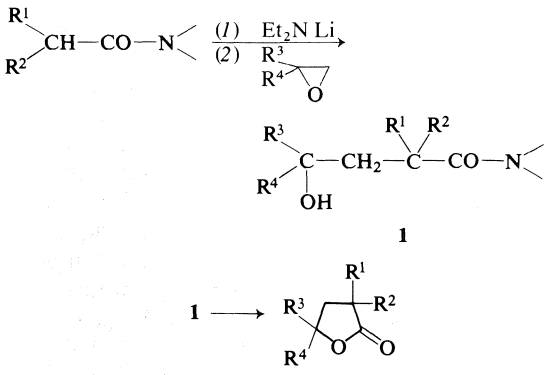

Au cours de cette étude, nous avons utilisé une grande variété d'époxydes: oxydes d'éthylène, de propylène, de butylène, d'isobutylène, de styrène et de cyclohexène et nous les avons opposés aux dérivés lithiés d'amides linéaires: *N,N*-diméthyl acétamide et propionamide, d'amides ramifiés: *N,N*-diméthyl isobutyramide et isovaléramide ou encore cycliques: *N*-méthyl pyrrolidone.

La réaction a lieu dans des conditions douces, l'introduction de l'époxyde est effectuée entre −30 et +15 °C puis retour à température ambiante. Les produits isolés diffèrent selon l'hydrolyse, neutre ou acide.

(A) Hydrolyse neutre

Les résultats obtenus après hydrolyse neutre du mélange réactionnel sont consignés dans le tableau 3. On constate que les rendements en produits obtenus (*a* + *b*) sont généralement satisfaisants et ne sont pas affectés par l'encombrement de l'époxyde ou de l'amide mais, quelles que soient les conditions mises en œuvre, nous n'avons pu isoler les hydroxyamides purs. Ils sont toujours accompagnés d'une quantité plus ou moins importante de lactone.

Remarques—Quelques essais effectués avec les

TABLEAU 3. Hydroxyalkylation de $R^1R^2\bar{C}$—$CON(Me)_2$ et de la *N*-methylpyrrolidone par les époxydes

Essai	R^1	R^2	Epoxyde	Hydroxyamide et lactone A	Hydroxyamide et lactone B	Rdt (%)[a] A	Rdt (%)[a] B
15	H	H		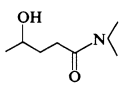		72	22
16	H	H		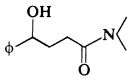		33	33
17	H	H		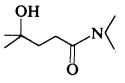		51 27	5 5[b]
18	H	CH_3		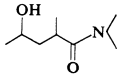		62 30	5 5[b]
19	H	CH_3	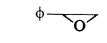	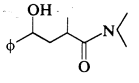		32	49
20	H	CH_3		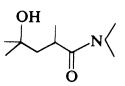		36	3[b]
21	H	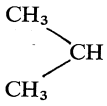		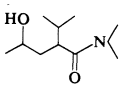		52	5
22	CH_3	CH_3		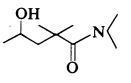		18	38[b]
23	CH_3	CH_3		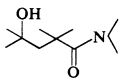		20	40
24						59	
25					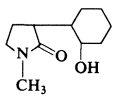	46 54[b]	

[a]En produits distillés.
[b]Métallation par l'amidure usuel (Et_2NH + BuLi).

TABLEAU 4. Préparation de γ-butyrolactones

Essai	R^1	R^2	Epoxyde	Lactone	Rdt (%)[a]
26	H	H			65
27	H	CH_3			56
28	CH_3	CH_3			85
29	CH_3	CH_3			80
30	Hydroxyamide 15				80–90
31	Hydroxyamide 16				80–90
32	Hydroxyamide 17				80–90
33	Hydroxyamide 19				80–90
34	Hydroxyamide 21				80–90
35	Hydroxyamide 23				80–90

[a]En produits distillés.

amidures "usuels" (Et_2NH + BuLi) ont conduit également à des mélanges (essais 17, 18, 19, 22). L'oxyde de styrène susceptible de réagir avec les anions en α et β a donné lieu à une attaque régio-sélective en β (contrôle rmn, essais 16 et 19).

(B) Hydrolyse acide

Les résultats sont résumés dans le tableau 4. On hydrolyse à 0 °C par HCl 4 *N* le mélange réactionnel et agite 24 h à température ambiante. On isole alors les lactones pures avec de bons rendements (essais 26, 27, 28 et 29). Les mélanges

γ-hydroxyamide + lactone isolés précédemment après hydrolyse neutre, conduisent, en milieu acide, aux lactones pures avec des rendements presque quantitatifs (essais 30 à 35).

Nous avons ainsi mis au point en une seule étape une préparation simple et directe de γ-butyrolactones variées à partir des amides *N,N*-disubstitués linéaires ou ramifiés et d'époxydes divers.

Partie expérimentale

La structure des divers hydroxyamides et lactones a été confirmée par ir et rmn. Les spectres infrarouges ont été effectués sur un spectrophotomètre Perkin-Elmer 457 sous forme de film pour les liquides ou dans le Nujol pour les cristaux. Les spectres rmn ont été enregistrés sur un appareil Perkin-Elmer R 12 à 60 MHz, en utilisant le CCl_4–TMS comme solvant.

La pureté des produits a été contrôlée par chromatographie en phase gazeuse (colonnes SE 30 de 3 m et UCON bas de 3 m) et les produits analysés ont donné des résultats satisfaisants à ±0.25%).

Préparation du diéthylamidure de lithium activé

Dans un tétracol de 250 ml on introduit sous argon 10 ml de HMPT, 10 ml de benzène et 4 g (0.055 mol) de diéthylamine. On ajoute alors 0.055 at-g de lithium martelé, le milieu devient rapidement rouge foncé; la température est maintenue à 20 °C à l'aide d'un bain d'eau. Le lithium disparaît en 2–3 h.

β-*Hydroxyamides*

Métallation et hydroxyalkylation du N,N-diméthylacétamide

Le diéthylamidure de lithium dilué de 10 ml d'éther ou de THF pour éviter la prise en masse est refroidi à −60 °C. On introduit 0.055 mol d'amide dilué d'un égal volume d'éther ou de THF. Le milieu devient rapidement violet, on laisse revenir la température à −50 °C pendant 30 min. Le composé carbonylé (0.055 mol) dilué dans 80 ml de THF est introduit à −60 °C. On observe une décoloration rapide de la solution qui devient jaune. On laisse revenir à température ambiante toute la nuit et hydrolyse. Après extraction à l'éther, la couche organique est séchée sur sulfate de magnésium, on chasse sous vide les solvants, puis on distille sous pression réduite le résidu.

Métallation et hydroxyalkylation des amides linéaires, ramifiés ou cycliques

On opère comme précédemment en introduisant l'amide à −20 °C puis la température est ramenée progressivement à +15 °C pendant 1½ h. On introduit alors le dérivé antagoniste. Les températures d'addition et la durée de la réaction seront données pour chaque cas.

Purification

La distillation ne permet pas toujours de séparer le HMPT de l'hydroxyamide. La chromatographie sur colonne d'alumine fournit un produit pur. L'élution se fait à l'aide de solutions hexane–éther (20:80 puis 50:50) et pour finir à l'éther pur. Le HMPT reste fixé sur la colonne.

Les amides de départ ont été obtenus par action du chlorure d'acide sur la diméthylamine, la diéthylamine ou la *N*-méthylaniline anhydres. Le *N*-triméthylsilyl caprolactame a été préparé par action de l'hydrure de sodium en milieu THF sur le caprolactame, suivie d'une alkylation par le triméthylchlorosilane.

Nous remercions vivement la Société Bayer Chemie qui nous a aimablement fourni les oxydes de butylène et d'isobutylène.

Tableau 1

Essai 1—p éb 90 °C/0.01 torr; ir (cm^{-1}) 3350 (OH), 1625 (—CON<); rmn δ 5.53 (2H, m, —C*H*=C*H*—), 4.60 (1H, s, OH), 4.26 (1H, m, —CH—OH), 2.80 (6H, d, NMe_2), 1.52 (3H, d, CH_3). *Anal.* calc. pour $C_8H_{15}NO_2$: C 61.1, H 9.6, N 8.9; trouvé: C 61.2, H 9.5, N 9.0.

Essai 2—p éb 120–130 °C/0.01 torr (litt. (5) 145–147 °C/0.15 torr); ir (cm^{-1}) 3370 (OH), 1620 (—CON<), 3030, 1600, 750, 700 (C_6H_5); rmn δ 7.22 (5H, m, C_6H_5), 5.09 (1H, s, O*H*), 4.96 (1H, t, C*H*—OH), 2.70 (6H, s, NMe_2), 2.43 (2H, d, CH_2). *Anal.* calc. pour $C_{11}H_{15}NO_2$: C 68.4, H 7.8, N 7.3; trouvé: C 68.6, H 7.9, N 7.4.

Essai 3—Le polyoxyméthylène non dépolymérisé est introduit à +20 °C on hydrolyse après 45 min; p éb 130–140 °C/17 torr; ir (cm^{-1}) 3380 (OH), 1620 (—CON<); rmn δ 3.5 (2H, m, C*H*$_2$OH), 3.00 (6H, d, NMe_2), 2.45 (1H, m, CH), 1.45 (2H, m, CH_2), 0.85 (3H, t, CH_3).

Essai 4—L'aldéhyde fraîchement dépolymérisé, distillé, est introduit à −40 °C, on hydrolyse après 1½ h à −20 °C; p éb 80 °C/0.01 torr; ir (cm^{-1}) 3365 (OH), 1625 (—CON<); rmn δ 4.6 (1H, m, C*H*—OH), 3.65 (1H, m, OH), 3.00 (6H, d, NMe_2), 0.9 (8H, m, CH_3 et CH_2).

Essai 5—L'aldéhyde est introduit à −60 °C, l'hydrolyse est effectuée à −45 °C après 2 h; p éb 125 °C/0.01 torr; ir (cm^{-1}) 3390 (OH), 1620 (—CON<); rmn δ 7.2 (5H, m, C_6H_5), 6.8 à 5.85 (2H, m, —CH=CH—), 4.6 (1H, s, OH), 4.29 (1H, m, C*H*—OH), 2.92 (6H, d, NMe_2), 1.65 (2H, m, CH_2), 0.82 (3H, t, CH_3).

Essai 6—L'essai est mené comme en 3; p éb 120–130 °C/0.01 torr; ir (cm^{-1}) 3400 (OH), 1630 (—CON<), 1600, 745, 700 (C_6H_5); rmn δ 7.3 (5H, s, C_6H_5), 4.00 (1H, s, O*H*), 3.57 (2H, m, C*H*$_2$OH), 3.23 (3H, s, NCH_3), 2.54 (1H, m, CH), 1.4 (2H, m, CH_2), 0.74 (3H, t, CH_3).

Essai 7—L'aldéhyde est introduit à −65 °C, on ramène ensuite à température ambiante et hydrolyse après 12 h; p éb 90 °C/0.01 torr; ir (cm^{-1}) 3400 (OH) 1625 (—CON<); rmn δ 4.3 à 4.6 (2H, m, C*H*—O*H*), 3 (6H, s, NMe_2), 1.18 (6H, s, Me_2), 1.2 (13H, m, CH_3 et CH_2).

Tableau 2

Essai 8—La cyclohexanone est introduite à −60 °C, on ramène à +20 °C et hydrolyse après 16 h d'agitation; p éb 103 °C/0.01 torr; ir (cm^{-1}) (Nujol) 3250 (OH), 1615

(—CON<); rmn δ 4.86 (1H, s, OH), 2.95 (6H, d, NMe_2), 2.32 (2H, s, CH_2CO—), 1.46 (10H, m, CH_2). *Anal.* calc. pour $C_{10}H_{19}NO_2$: C 64.8, H 10.3, N 7.5; trouvé: C 64.8, H 9.9, N 7.4.

Essai 9—On opère comme lors de l'essai 8; cristaux blancs, pf 104–105 °C (litt. (5) 103.6–104.1 °C) (éther de pétrole); ir (cm^{-1}) (Nujol) 3250 (OH), 3030, 1600, 1480, 730 (C_6H_5), 1615 (—CON<); rmn δ 7.32 (10H, m, C_6H_5), 3.16 (2H, s, CH_2), 2.85 (6H, d, NMe_2).

Essai 10—On opère comme pour l'essai 8; cristaux blancs, pf 130 °C (éther de pétrole); ir (cm^{-1}) (Nujol) 3250 (OH), 3025, 1570, 1485, 695 (C_6H_5), 1580 (—CON<); rmn δ 7.8 à 6.75 (10H, m, C_6H_5), 1.25 à 0.4 (12H, m, CH_3).

Essai 11—On introduit la cétone à −50 °C, ramène à +20 °C, agite 10 h et hydrolyse; p éb 75–83 °C/0.1 torr; ir (cm^{-1}) 3380 (OH), 1625 (—CON<); rmn δ 3.02 (6H, s, NMe_2), 1.26 (6H, s, Me_2COH), 1.12 (6H, s, Me_2).

Essai 12—La cétone fraîchement distillée est introduite à −60 °C, on hydrolyse à −50 °C au bout d'une heure; p éb 90 °C/0.01 torr, polymères en fin de distillation; ir (cm^{-1}) 3350 (OH), 1600 (—CON< et C=C); rmn δ 5.15 (1H, m, C=CH), 3 (6H, s, NMe_2), 1.85 et 1.65 (6H, d, Me_2C=C), 1.25 (9H, m, CH_3).

Essai 13—La cétone est introduite à −50 °C, on ramène à +20 °C, agite 16 h et hydrolyse. Le résultat est négatif. D'autres essais en faisant varier les températures d'addition et les temps de réaction ont également échoué.

Essai 14—On introduit la cétone à −40 °C, revient à +10 °C, agite 12 h et hydrolyse; cristaux blancs pf 260 °C (éther de pétrole); ir (cm^{-1}) (Nujol) 3310 (OH), 3025, 1595, 1475, 750, 695 (C_6H_5), 1635 (—CON<); rmn (DMSO-d_6) δ 8 à 7.2 (10H, m, C_6H_5), 6.44 (1H, m, NH). *Anal.* calc. pour $C_{19}H_{21}NO_2$: C 77.3, H 7.1, N 4.7; trouvé: C 77.0, H 7.3, N 5.0.

γ-Hydroxyamides

Condensation des époxydes sur le N,N-diméthylacétamide lithié

A l'époxyde à −30 °C (0.055 mol dans 80 ml de THF) on ajoute, goutte à goutte, le carbanion (0.050 mol refroidi à −50 °C). La solution jaune-orange revient à température ambiante en 1½ h et on agite toute la nuit, après hydrolyse on traite comme décrit précédemment.

Amides linéaires, ramifiés ou cycliques

L'amide lithié (0.050 mol à +15 °C) est introduit sur l'époxyde (0.055 mol dans 80 ml de THF) à −30 °C. Dans le cas de l'oxyde de cyclohexène, l'amide lithié est introduit à température ambiante.

Préparation de l'amidure usuel

Une solution de butyllithium dans l'éther (0.055 mol) est ajoutée goutte à goutte à −10 °C à une solution de diéthylamine (0.060 mol dans 30 ml de THF). On revient à température ambiante en 30 min.

Tableau 3

Essais 15 à 23—Les pourcentages respectifs de lactones et d'hydroxyamides ont été déterminés par rmn.

Essai 24—p éb 110–125 °C/0.1 torr; ir (cm^{-1}) 3380 (OH), 1670 (CO—N); rmn δ 3.85 (1H, m, C*H*—OH), 3.6 à 3.2 (2H, m, CH_2N), 2.8 (3H, s, NCH_3), 1.10 (3H, d, CH_3).

Essai 25—p éb 110–140 °C/0.01 torr; ir (cm^{-1}) 3400 (OH), 1670 (—CON—CH_3); rmn δ 4.4 (1H, m, OH), 2.80 (N—CH_3); *Anal.* calc. pour $C_8H_{15}NO_2$: C 61.1, H 9.6, N 8.9; trouvé: C 61.0, H 9.5, N 8.8.

Tableau 4

Nous avons transformé les γ-hydroxyamides en γ-butyrolactones par simple agitation, avec l'acide chlorhydrique 4 *N* pendant 24 h. Nous avons opéré soit directement sur le mélange réactionnel (essais 26 à 29), soit sur le mélange hydroxyamide–lactone déjà distillé (essais 30 à 35).

Essai 26—p éb 115–125 °C/23 torr; ir 1770 cm^{-1}; rmn δ 4.43 (1H, q, CHO), 2.6 à 1.4 (6H, m, CH_2), 0.98 (3H, t, CH_3). *Anal.* calc. pour $C_6H_{10}O_2$: C 63.2, H 8.8; trouvé: C 63.0, H. 8.7.

Essai 27—pf 49 °C (éther de pétrole); rmn δ 2.6 à 1.55 (3H, m, CH, CH_2), 1.4 (6H, d, Me_2), 1.22 (3H, d, CH_3). *Anal.* calc. pour $C_7H_{12}O_2$: C 65.7, H 9.5; trouvé: C 65.8, H 9.5.

Essai 28—p éb 93–105 °C/18 torr (litt. (12) p éb 195.5–197.5 °C; ir 1775 cm^{-1}; rmn δ 4.22 (2H, t, CH_2O), 2.10 (2H, t, CH_2), 1.20 (6H, s, CH_3).

Essai 29—pf 51 °C (litt. (13) 49–51 °C) (éther de pétrole); ir 1775 cm^{-1}; rmn δ 4.8 à 4.27 (1H, m, CH), 2.9 à 2.55 (2H, m, CH_2), 1.44 à 1.34 (3H, d, CH_3), 1.23 (6H, s, CH_3).

Essai 30—p éb 98 °C/21 torr; ir 1763 cm^{-1}. Les spectres ir et rmn sont comparables à ceux d'un échantillon authentique de γ-valérolactone.

Essai 31—p éb 90 °C/0.05 torr; ir 1775 cm^{-1}; rmn δ 7.4 (5H, s, C_6H_5), 5.35 (1H, t, CH—O), 2.75 à 2.10 (4H, m, CH_2).

Essai 32—p éb 80 °C/5 torr; ir 1770 cm^{-1}; rmn δ 2.3 à 1.8 (4H, m, CH_2), 1.4 (6H, s, CH_3).

Essai 33—p éb 125 °C/1.3 torr; ir 1770 cm^{-1}; rmn δ 7.23 (5H, s, C_6H_5), 5.65 à 5.1 (1H, m, CH—O), 3 à 2.10 (3H, m, CH et CH_2), 1.24 et 1.13 (3H, d, CH_3).

Essai 34—p éb 65 °C/0.1 torr; ir 1770 cm^{-1}; rmn δ 4.9 à 4.28 (1H, m, CHO), 1.44 à 1.3 (3H, 2d, CH_3), 1.14 à 0.85 (6H, 2d, $(CH_3)_2C$).

Essai 35—pf 41 °C (litt. (14) 37 °C) (éther de pétrole); ir 1770 cm^{-1}; rmn δ 2.05 (2H, s, CH_2), 1.44 (6H, s, $(CH_3)_2C$—O), 1.27 (6H, s, $(CH_3)_2C$).

1. P. Hullot, Th. Cuvigny, M. Larchevêque et H. Normant. Can. J. Chem. **54**, 1098 (1976).
2. Th. Cuvigny, P. Hullot, M. Larchevêque et H. Normant. C.R. Acad. Sci. Paris C, **281**, 251 (1975).
3. Th. Cuvigny, P. Hullot, M. Larcheveque et H. Normant. C.R. Acad. Sci. Paris C, **279**, 569 (1974).
4. W. Chodkiewicz, P. Cadiot et A. Willemart. Bull. Soc. Chim. Fr. 1586 (1958).

5. D. N. CROUSE et D. SEEBACH. Chem. Ber. **101**, 3113 (1968).
6. T. DURST, R. VAN DEN ELZEN et R. LEGAULT. Can. J. Chem. **52**, 3206 (1974).
7. B. M. TROST et R. A. KUNZ. J. Org. Chem. **39**, 2475 (1974).
8. T. L. HO. Synth. Commun. **4**, 265 (1974).
9. P. L. CREGER. J. Org. Chem. **37**, 1907 (1972).
10. W. SUCROW, M. SLOPIANKA et D. WINKLER. Chem. Ber. **105**, 1621 (1972).
11. W. SUCROW et U. KLEIN. Chem. Ber. **108**, 48 (1975); **108**, 3518 (1975).
12. B. E. HUDSON et C. R. HAUSER. J. Am. Chem. Soc. **63**, 3156 (1941).
13. D. HOCH et P. KARRER. Helv. Chim. Acta, **37**, 397 (1954).
14. D. CURRELL, C. A. GROB et S. W. TAM. Helv. Chim. Acta, **50**, 349 (1967).

An attempted synthesis of an oxacepham derivative using isonitriles as β-lactam forming agents. On the stability of dihydrooxazines and the inadequacy of ammonia as the fourth component in the Ugi reaction

G. JUST, B. Y. CHUNG, AND K. GRÖZINGER

Department of Chemistry, McGill University, Montreal, Que., Canada H3C 3G1

Received June 8, 1976

G. JUST, B. Y. CHUNG, and K. GRÖZINGER. Can. J. Chem. **55**, 274 (1977).

An attempted synthesis of an oxacepham derivative, using isonitriles as β-lactam forming agents, is described. The reasons for the failure of this approach are discussed.

G. JUST, B. Y. CHUNG et K. GRÖZINGER. Can. J. Chem. **55**, 274 (1977).

On décrit un essai de synthèse d'un dérivé oxacéphame où on utilise des isonitriles comme agents formateurs de β-lactames. On décrit les raisons pour l'échec de cette approche.

[Traduit par le journal]

In 1962, Ugi and Wischöffer reported (1) the synthesis of a penam derivative **3** using the reaction of thiazoline **1** with an isonitrile.

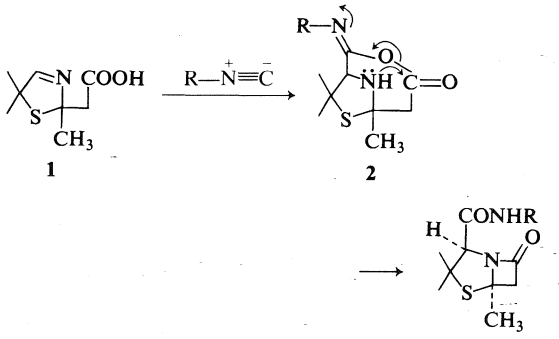

SCHEME 1

This approach to penicillins was not used any further (see, however ref. 2) because of the wrong stereochemistry of the carboxamide group introduced in **3**. We decided to use an analogous procedure to prepare oxacephams **5** and **6** (X = O) in which the stereochemical problem is resolved by the eventual introduction of a double bond.

The main features of the proposed procedure are outlined in Scheme 2.

From previous experience (3, 4) we knew that the hydrolysis of a methyl ester in **4***a* (R = CH_3) was difficult, leading to the decomposition of the ring system. It was therefore obvious that the ring system of type **4** (R = H) could only be built if R were a group removable by non-hydrolytic methods.

We focused our attention on the synthesis of **4** where R = *p*-methoxybenzyl, benzyl, and trichloroethyl, and where -N- was benzamido or phthaloyl. The latter amine-blocking group was chosen because of the crystallinity of many phthalimide containing compounds, and because benzamide esters gave azlactones with considerable ease under relatively mild conditions.

p-Methoxybenzyl 2-benzamido-3-hydroxy acrylate **9** was prepared by condensation of 4-hydroxymethylene-2-phenyl-5-oxazolone **7** (5) with *p*-methoxybenzyl alcohol, and converted to its sodium salt **9***a* with sodium ethoxide in ethanol.

Condensation of the thiazolidine mesylate **10** (6) with the sodium salt **9***a* in 2-butanone at 80 °C gave a 95% yield of the thiazolidine ester **11**. Hydrolysis of the aldehyde protecting group was carried out using mercuric chloride in aqueous tetrahydrofuran. Treatment of the

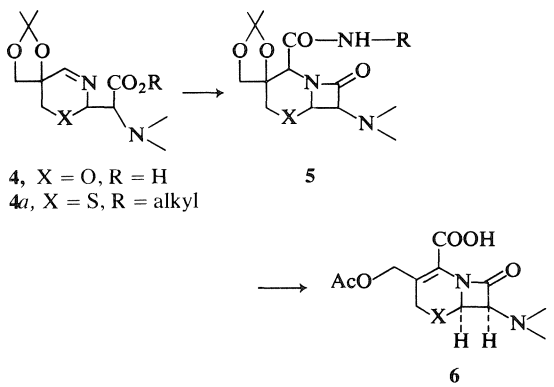

4, X = O, R = H
4*a*, X = S, R = alkyl

5

6

SCHEME 2

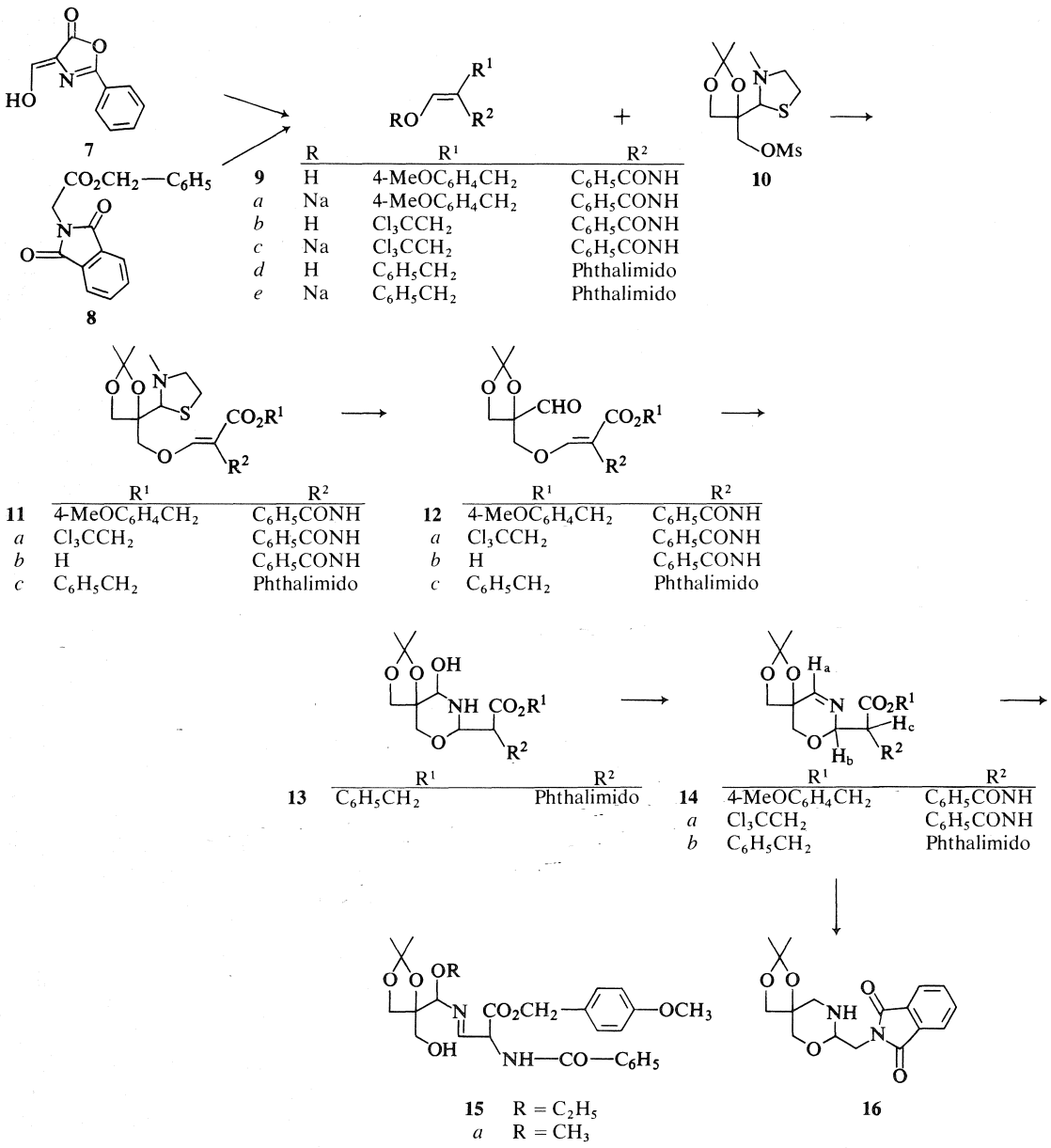

	R	R^1	R^2
9	H	$4\text{-MeOC}_6\text{H}_4\text{CH}_2$	C_6H_5CONH
a	Na	$4\text{-MeOC}_6\text{H}_4\text{CH}_2$	C_6H_5CONH
b	H	Cl_3CCH_2	C_6H_5CONH
c	Na	Cl_3CCH_2	C_6H_5CONH
d	H	$C_6H_5CH_2$	Phthalimido
e	Na	$C_6H_5CH_2$	Phthalimido

	R^1	R^2
11	$4\text{-MeOC}_6\text{H}_4\text{CH}_2$	C_6H_5CONH
a	Cl_3CCH_2	C_6H_5CONH
b	H	C_6H_5CONH
c	$C_6H_5CH_2$	Phthalimido

	R^1	R^2
12	$4\text{-MeOC}_6\text{H}_4\text{CH}_2$	C_6H_5CONH
a	Cl_3CCH_2	C_6H_5CONH
b	H	C_6H_5CONH
c	$C_6H_5CH_2$	Phthalimido

	R^1	R^2
13	$C_6H_5CH_2$	Phthalimido

	R^1	R^2
14	$4\text{-MeOC}_6\text{H}_4\text{CH}_2$	C_6H_5CONH
a	Cl_3CCH_2	C_6H_5CONH
b	$C_6H_5CH_2$	Phthalimido

15 R = C_2H_5
a R = CH_3

SCHEME 3

aldehyde ester **12** with ammonia in tetrahydrofuran gave imine ester **14**, which was purified by column chromatography using ether as eluent. The imine ester **14**, mp 114–117 °C, was eluted first followed by a second fraction, which was identified as the reaction product **15** of ethanol with the imine ester **14**. The pmr spectrum of **15** showed a triplet at δ 1.20 ppm coupled with a methylene group at δ 3.32 ppm (J = 7 Hz), indicating the presence of an ethyl group. An exchangeable triplet at 2.80 ppm, coupled with a methylene group at δ 3.67 ppm (J = 6 Hz) confirmed the presence of a hydroxymethylene group. Furthermore, there were 11 protons downfield, with one representing a CH=N group. The rest of the spectrum was similar to that of the required product, the imine ester **14**. The mass spectrum of **15** showed the

molecular ion peak at *m/e* 514. The base peak at *m/e* 499 represented the loss of a methyl group.

The origin of the ethanol was traced back to the solvent which was used for chromatography. That in fact the imine is very reactive toward alcohol was demonstrated by reacting **14** with 1 equiv. of methanol in tetrahydrofuran; an almost quantitative yield of **15***a* was isolated. The above results excluded all alcohols for the hydrogenolysis of the imine ester **14** and also demonstrated the sensitivity of this compound. Furthermore, stability tests on **14** in solvents such as dioxane, ethyl acetate, and chloroform indicated that the imine ester was not stable long enough to permit hydrogenolysis of the ester group.

In a parallel series, we prepared the analogous compound **14***b*. Phthaloylglycine benzyl ester **8** was formylated with benzyl formate and sodium benzyloxide in refluxing toluene to benzyl 2-phthalimido-3-hydroxy acrylate **9***d* (7) and its sodium salt **9***e* was prepared by treatment of **9***d* with sodium ethoxide. Condensation of the thiazolidine mesylate **10** with **9***e* gave **11***c* in 89% yield. Hydrolysis of the thiazolidine group and treatment of the resulting aldehyde **12***c* with ammonia in ether gave crystalline carbinolamine **13**, mp 108–110 °C, in 40% yield. Proton magnetic resonance studies in DMSO-d_6 of the carbinolamine **13** showed that immediately after dissolving and deuterium exchange, *CH*—OD absorbed at δ 4.28 ppm and ND—*CH*—O showed as a doublet at δ 5.43 ppm. After 20 h, the *CH*=N absorption appeared at δ 7.72 ppm, and H_b resonated downfield at δ 5.68 ppm as a double doublet, coupled with H_c ($J_{b,c}$ = 3 Hz), indicating that elimination of water took place to form the imine **14***b*. Mild hydrogenolysis of **14***b* with palladium on charcoal at atmospheric pressure in ethyl acetate at 20 °C gave the decarboxylated product **16**, mp 151–153 °C, in 50% yield.

The pmr spectrum was consistent with the proposed structure **16**. The two protons, H_a and H_c, which had appeared at δ 7.72 and 4.97 ppm respectively in the imine ester **14***b*, disappeared. Eight protons appeared as multiplets at δ 2.98–4.05 ppm and one exchangeable proton at 1.90 ppm. Also, a double doublet at δ 4.35 ppm was assigned to the N—*CH*—O proton.

The mass spectrum of the product showed a molecular ion ($M^+ + 1 = 333$) and a base peak at *m/e* 317, indicating cleavage of the methyl group of the acetonide, which is an important fragmentation process.

It is known that β-imino acids of type **14** are easily decarboxylated, and there is some experimental evidence (1; 5, p. 759) that similar imine acids lost carbon dioxide even on standing at room temperature. We concluded, on the basis of the spectral data of **16**, that the hydrogenolysis produced the desired imine acid, but that the C=N bond was reduced equally rapidly. Further studies using different catalysts gave essentially the same results, and it was not possible to hydrogenolyze the benzyl esters without reducing the C=N bond. Since we were unable to hydrogenolyze the imine esters **14** or **14***b* to the imine acid **4**, we turned to the use of the 2,2,2-trichloroethyl ester as the acid protecting group.

Treatment of 4-hydroxymethylene-5-oxazolone **7** (5) with 2,2,2-trichloroethanol gave **9***b*, mp 87–88 °C. The sodium salt **9***c* was prepared by treatment of **9***b* with sodium ethoxide in ethanol. Condensation of the thiazolidine mesylate **10** with the sodium salt of the benzamide acrylate **9***c* gave **11***a*, mp 126–128 °C, in 68% yield. Treatment of the thiazolidine ester **11***a* with zinc dust in 90% aqueous acetic acid afforded the thiazolidine acid **11***b*, mp 159–160 °C, in 53% yield. The aldehyde protecting group was removed by treatment of **11***b* with mercuric chloride in aqueous tetrahydrofuran, yielding **12***b* in 93% yield.

However, the aldehyde acid **12***b*, which was initially soluble in ether, decomposed on standing at room temperature within 30 min, and the resulting product was insoluble in ether. The pmr spectrum immediately after dissolving of the aldehyde acid showed the required protons. However, after some time, a broad pmr spectrum was obtained.

Since the above results showed that the aldehyde acid **12***b* was unstable, we attempted a four component condensation using the aldehyde acid **12***b* *in situ*. It is known (8) that ammonia, primary and secondary amines, as well as hydrazine derivatives can be used as the amine component in the Ugi reaction.

The combination of ammonia or primary amines and aldehydes or ketones reacts with carboxylic acids and isonitriles to form the intermediate α-adducts. These undergo O → N

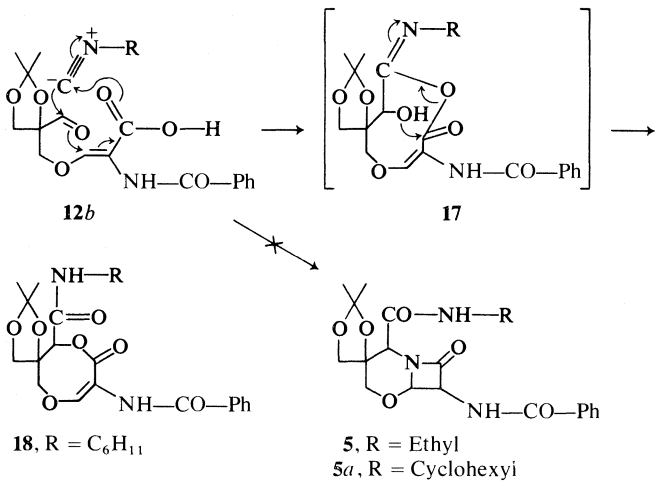

SCHEME 4

acyl transfer by a cyclic mechanism yielding α-acylaminocarbonamides. The formation of the two carbonamide groups in the final product provides the reaction with a strong driving force (see arrows, Scheme 5). In our example, the aldehyde acid **12***b* functions simultaneously as the aldehyde and acid component. Furthermore the reaction with the isonitrile takes place in the aqueous phase (1, 8) and "under dilute conditions", otherwise the formation of resins predominates. Ammonium hydroxide (0.9 equiv.) and cyclohexyl isonitrile (0.9 equiv.) and phosphate buffer (p*H* 6) were added to freshly prepared aldehyde acid **12***b* in petroleum ether. The two-phase system was vigorously stirred for 24 h. After work-up, the mixture was purified by chromatography and the major fraction recrystallized from ether. The product

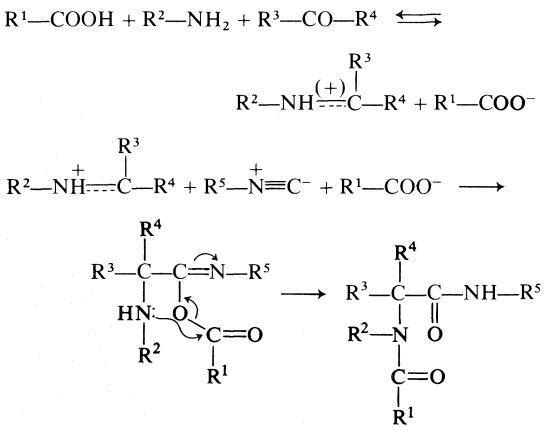

SCHEME 5

showed an absorption at 1730 cm^{-1}, and the mass spectrum showed an ($M^+ + 1$) at *m/e* 458, the cleavage of the methyl group at *m/e* 443, and the loss of acetone at *m/e* 400. The rest of the fragmentation was characteristic for the required product. Although the pmr spectrum was consistent with structure **5** ($C_{24}H_{31}N_3O_6$) microanalysis pointed to $C_{24}H_{30}N_2O_7$, indicating that the isonitrile reacted with the aldehyde in a Passerini-like reaction to give **18**. The ir absorption at 1730 cm^{-1} could now be explained as an α,β-unsaturated lactone and the peak at *m/e* 458 as the molecular ion peak. All other spectral data were consistent with the structure proposed.

Because of the instability of the imine acid **4**, and aldehyde acid **12***b*, we developed a mild method for cleaving the 2,2,2-trichloroethyl esters, involving stirring a tetrahydrofuran solution of the ester with zinc and a 1 *M* phosphate buffer solution for 10 min (9). Using this method the hydrolysis of the 2,2,2-trichloroethyl ester **11***a* could be accomplished smoothly and thiazolidine acid **11***b*, mp 159–160 °C, was obtained within 5 min. It was identical to the acid obtained with zinc – acetic acid.

We then prepared the imine trichloroethyl ester **14***a*. Hydrolysis of the thiazolidine trichloroethyl ester **11***a* with mercuric chloride in aqueous tetrahydrofuran for 5 min gave the aldehyde ester **12***a* in a partially hydrated form. Treatment of **12***a* with ammonia in ether gave the ester **14***a*, mp 157–159 °C, in 66% yield.

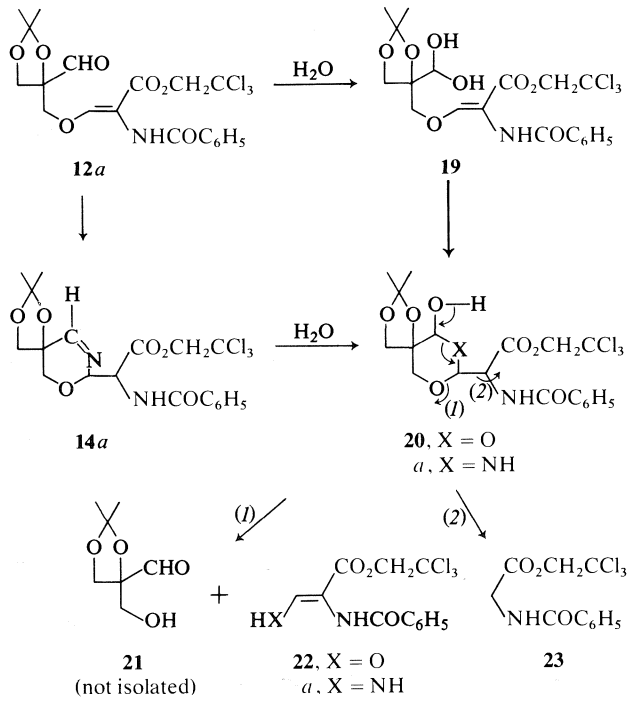

SCHEME 6

Thin layer chromatography of the mother liquors of crystallization indicated the presence of two by-products. These were separated by column chromatography and identified as the acrylate ester **22** and hippuric acid 2,2,2-trichloroethyl ester **23**. Their formation was explained in the following manner: the hydrated aldehyde **19** reacted via the dioxane **20** to give the two products as outlined in Scheme 6.

Since the imine acid **4** was expected to undergo decarboxylation readily, the hydrolysis step and the Ugi reaction were superimposed, without isolation of the intermediate **4**.

We used cyclohexylisonitrile and phosphate buffer solutions at p*H* 4.5, 6.0, or ammonium acetate at p*H* 7.0, which removed the 2,2,2-trichloroethyl ester group in all models studied (9) and subjected the reaction product to the action of isonitriles. Under these reaction conditions, we found no trace of the oxacephalosporin derivative **5** neither by mass spectroscopy (*m/e* 457), nor by infrared spectroscopy (ν 1750–1780 cm^{-1}).

Similar results were obtained when the hydrolysis of the ester group was carried out in the presence of isonitrile.

The failure of these approaches was attributed to the reactivity of the imine esters **14** with water. Stability tests showed that treatment of the imine ester **14***a* with aqueous tetrahydrofuran, using similar conditions to those which are used for the hydrolysis of the ester and subsequent Ugi reaction, resulted in the formation of 2,2,2-trichloroethyl hippurate and 2-benzamido-3-amino acrylate **22** (the latter identified by nmr only).

We believed a possible reason for the instability of the imine acid could be the presence of the spiro moiety. Consequently, our next approach consisted of the removal of the isopropylidene group by 80% trifluoroacetic acid, followed by acetylation with pyridine and acetic anhydride. A crystalline monoacetate, mp 121–122 °C was obtained.

The pmr of the obtained product was different from the expected one **24***a*. Although the isopropylidene group was no longer present, the spectrum showed only one acetyl group at δ 1.85 ppm. Furthermore, the olefinic proton at δ 7.66 ppm was not present. Two protons, H_a, doublet at δ 5.55 ppm ($J_{a,b}$ = 2.5 Hz) and H_b, dd at δ 5.16 ppm ($J_{a,b}$ = 2.5 Hz and $J_{b,NH}$ = 8 Hz) appeared, indicating that one of the hydroxyl groups reacted with the carbon double

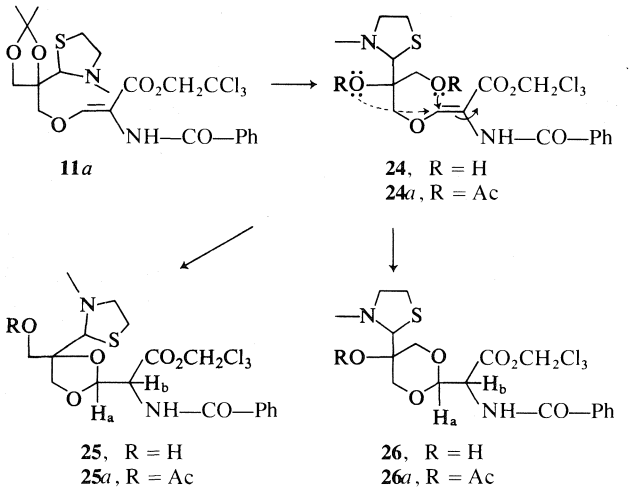

SCHEME 7

bond to form a five- or six-membered ring structure, **25** or **26**. The spectral data did not permit differentiation between these structures. From this result, it is evident that the intermedial diol could have structures **24**, **25**, or **26**.

In summary, the failure of these approaches can be attributed to four factors, all of which became evident as a result of the above studies: (*1*) reaction of the imine esters **14** with water, (*2*) isomerisation of the imine acid **4**, followed by decarboxylation and (*3*) polymerization of the imine acid **4** with isonitrile during the Ugi reaction, (*4*) non-participation of ammonia in the Ugi reaction. Consequently, this scheme had to be abandoned in its present form.

Experimental

Melting points were determined on an Electrothermal block and are corrected.

Mass spectra were obtained on an AEI-MS-902 mass spectrometer at 70 eV using a direct insertion probe. Proton magnetic resonance spectra were recorded on a Varian T-60 spectrometer, using tetramethylsilane as an internal standard. Doublets, triplets, and quartets in the pmr spectral data were recorded as the center of the peaks and multiplets as their range of absorption. Infrared spectra were obtained on a Perkin-Elmer 267B infrared spectrophotometer.

Microanalyses were carried out by Micro-Tech. Laboratories Inc. and C. Daessle, Montreal.

p-Methoxybenzyl 2-Benzamido-3-hydroxy Acrylate ***9***

4-Hydroxymethylene-2-phenyl-5-oxazolone (5) **7** (18.9 g, 0.1 mol) was suspended in benzene (400 ml) and *p*-methoxybenzyl alcohol (15.2 g, 0.11 mol) was added. The mixture was refluxed for 16 h, evaporated, and the residue recrystallized from benzene – petroleum ether. Yield 24.2 g (74%); mp 101–102 °C; pmr ($CDCl_3$): δ 3.82 (s, 3H, OCH_3), 5.20 (s, 2H, O—CH_2), 7.15 (q, 4H, *p*-substituted phenyl), 7.4–8.0 (m, 6H, phenyl, CH=C), 8.50, (s, 1H, NHCO), 12.32 ppm (d, J = 12 Hz, 1H, OH); ir (KBr): 3335 (OH), 1688, 1650, 1600, 1540, 1510, 1388 cm^{-1}; ms (70 eV): *m/e* 327 (M^+), 310 (M^+ − OH). *Anal.* calcd. for $C_{18}H_{17}NO_5$ (327.3): C 66.05, H 5.24, N 4.28; found: C 66.10, H 5.33, N 4.25.

p-Methoxybenzyl 2-Benzamido-3-hydroxy Acrylate Sodium Salt ***9a***

p-Methoxybenzyl 2-benzamido-3-hydroxy acrylate **9** (23 g, 0.07 mol), was suspended in ethanol (200 ml) and an ethanolic solution of sodium ethoxide (1.55 g, 0.075 mol of sodium) was added with vigorous stirring. The suspension dissolved immediately and the sodium salt precipitated. Ethyl ether (200 ml) was added and the white salt collected by filtration, washed with ether, and dried *in vacuo*. Yield 22 g (90%); mp 225–226 °C; ir (KBr): 3400, 3200, 1635, 1600, 1555, 1515, 1485, 1460, 1400, 1358, 1310 cm^{-1}; ms (70 eV): *m/e* 349 (M^+), 300, 243, and 228 ($M^+ - CH_2 - p$-$OMeC_6H_4$). *Anal.* calcd. for $C_{18}H_{16}NO_5Na$ (349.33): C 61.88, H 4.61, N 4.00; found: C 61.46, H 4.54, N 4.11.

p-Methoxybenzyl 2-Benzamido-3-(((2′,2′-dimethyl-4′-(3′′-methylthiazolidine-2′′-yl)-1′,3′-dioxolan 4-yl)-methyl)oxy) Acrylate ***11***

The sodium salt **9a** (22 g, 0.063 mol) was suspended in a solution of the thiazolidine mesylate **10** (12 g, 0.0386 mol) in 2-butanone (300 ml) and the mixture refluxed for 16 h. The salt was filtered off and the filtrate evaporated *in vacuo*. The residue was chromatographed on a silica gel column, eluted with chloroform–methanol (98:2). Evaporation of the solvent gave a colorless oil. Yield 20 g (95%); pmr ($CDCl_3$): δ 1.35, 1.42 (each s, 6H acetonide), 2.28, 2.38 (each s, 3H, N—CH_3), 2.8–3.1 (m, 4H, N—CH_2—CH_2—S), 3.80 (s, 3H, OCH_3), 3.8–4.2 (m, 4H, 2CH_2—O), 4.39, 4.49 (each s, 1H, N—CH—S), 5.18 (2H, CH_2), 7.20 (q, 4H, *p*-methoxyphenyl), 7.29–7.92, ppm (m, 7H, phenyl, NH, C=CH); ir ($CHCl_3$): 3420 (NH), 2980 (CH), 1670 (ester), 1368, 1378 cm^{-1} (*gem*-dimethyl). *Anal.* calcd. for

$C_{28}H_{34}N_2O_7S\cdot\frac{1}{2}H_2O$: C 60.96, H 6.39, N 5.07, S 5.81, found: C 60.59, H 6.14, N 4.95, S 6.05.

p-Methoxybenzyl 2-Benzamido-3-((4′-formyl-2′,2′-dimethyl-1′,3′-dioxolan-4′-yl)methoxy) Acrylate **12**

The thiazolidine ester **11** (20 g, 0.037 mol) was dissolved in acetonitrile (240 ml) and water (60 ml). Mercuric chloride (12 g, 0.0445 mol) was added to this solution. The milky suspension that immediately formed was refluxed for 30 min. The fine precipitate was filtered and the filtrate evaporated. The residue was extracted twice with methylene chloride; the extracts were washed with dilute hydrochloric acid and water and dried. After evaporation of the solvent, the residue was passed through a silica gel column using ether as eluent. Yield 14.6 g (84%), oily residue; pmr ($CDCl_3$): δ 1.38, 1.40 (each s, 6H, acetonide), 3.80 (s, 3H, OCH_3), 3.95–4.30 (m, 2H), 4.10, 4.21 (each s, 2H), 5.15 (s, 2H, CH_2—O), 7.10 (q, 4H, *p*-OCH_3—phenyl), 7.3–7.9 (m, 7H, phenyl, C═CH, NH), 9.70 ppm (s, 1H, CHO); ir ($CHCl_3$): 3410 (NH), 2980 (CH_2), 1700 (ester), 1670 (CO), 1608 (phenyl), 1370 cm^{-1} (*gem*-dimethyl); ms (70 eV): *m/e* 469 (M^+). *Anal.* calcd. for $C_{25}H_{27}NO_8\cdot H_2O$: C 61.59, H 6.00, N 2.87; found: C 60.99, H 5.99, N 2.91.

α-Benzamido-2,2-dimethyl-1,3,7-trioxa-9-azaspiro[4.5]-dec-9-ene-8-acetic Acid p-Methoxybenzyl Ester **14** *and By-product* **15**

The aldehyde ester **12** (14 g, 0.03 mol) was dissolved in dry tetrahydrofuran (75 ml) and 1.1 equiv. of gaseous ammonia in tetrahydrofuran were added. The mixture was kept at room temperature overnight, and then evaporated *in vacuo*. The residue was chromatographed on a silica gel column using ether as eluent.

The first product eluted was crystallized from ether–petroleum ether and its spectral data indicated it to be the required product **14**. Yield 3.0 g (22%); mp 114–117 °C; pmr ($CDCl_3$): δ 1.40 (s, 6H, acetonide), 3.62, 3.75 (each s, 2H, CH_2O), 3.80 (s, 3H, OCH_3), 3.92–4.10 (m, 2H, OCH_2), 5.18 (s, 2H, CH_2—O), 5.3–5.5 (m, 2H), 6.95 (s, 1H, NH), 7.10 (q, 4H, *p*-methoxyphenyl), 7.4–7.9 ppm (m, 6H, phenyl, C═CH); ir (KBr): 3408 (NH), 2983, 2937, 2865 (CH), 1745 (ester), 1659 (amide), 1611 (phenyl), 1578, 1514, 1484, 1379, 1372 cm^{-1}; ms (70 eV) *m/e*: 468 (M^+), 453 ($M^+ - CH_3$), 410 ($M^+ - (CH_3)_2CO$), 347 ($M^+ - CH_2$ – *p*′-methoxyphenyl), 303 ($M^+ - COOCH_2$ – *p*-methoxyphenyl). *Anal.* calcd. for $C_{25}H_{28}N_2O_7\cdot\frac{1}{2}H_2O$: C 62.88, H 6.12, N 5.86; found: C 62.38, H 6.12, N 5.42. The second fraction eluted gave **15** as a colorless oil. Yield 2.3 g (15%); pmr ($CDCl_3$): δ 1.20 (t, J = 7 Hz, 3H, CH_3—CH_2), 1.28 (s, 6H, acetonide), 2.80 (t, J = 6 Hz, 1H, OH), 3.32 (q, J = 7 Hz, 2H, CH_2—CH_3), 3.67 (d, J = 6 Hz, 2H, CH_2—OH), 3.77 (s, 3H, OCH_3), 3.6–3.8 (m, 1H, CH—N═), 4.00 (d, 2H, CH_2O), 4.48 (d, J = 9 Hz, 1H, N—CH—CO), 5.12 (s, 2H, CH_2—phenyl), 6.7–8.0 ppm (m, 11H, phenyl, *p*-methoxyphenyl, NH, N═CH); ir ($CHCl_3$): 3390 (OH), 2970 (CH_2), 1650 (ester, amide) 1370/1380 cm^{-1} (*gem*-dimethyl); uv (EtOH): max 231, 279 nm; ms (70 eV): *m/e* 514 (M^+), 499 ($M^+ - CH_3$), 484 ($M^+ - CH_2$═O), 469 ($M^+ - OEt$), 468 ($M^+ - EtOH$). *Anal.* calcd. for $C_{27}H_{34}N_2O_8$: C 63.02, H 6.66, N 5.44; found: C 62.92, H 6.68, N 5.32.

Treatment of α-Benzamide-2,2-dimethyl-1,3,7-trioxa-9-azaspiro[4.5]dec-9-ene-8-acetic Acid p-Methoxybenzyl Ester with Methanol **15***a*

An excess of methanol (1 ml) was added to a solution of the imine-*p*-methoxybenzyl ester **14** (468 mg, 1 mmol), in 50 ml of tetrahydrofuran. The reaction mixture was stirred at room temperature for 3 h. Evaporation of the solvent and purification by chromatography on silicic acid using ether as eluent gave 422 mg (84%) of **15***a*; pmr ($CDCl_3$): δ 1.37 (s, 6H, acetonide), 2.42 (t, J = 6 Hz, 1H, OH), 3.42 (s, 3H, OCH_3) 3.70 (d, J = 6 Hz, 2H, CH_2O), 3.80 (s, 3H, OCH_3), 3.7–3.9 (m, 1H, C—CHNH), 4.00 (m, 2H, OCH_2), 4.35 (d, 1H, N—CH—NH), 5.14 (s, 2H, CH_2—*p*-methoxy), 6.8–8.0 ppm (m, 11H, phenyl, *p*-methoxyphenyl, NH); ir ($CHCl_3$): 3390 (OH), 2970 (CH_2), 1650 (ester, amide, C═N), 1370, 1380 cm^{-1} (*gem*-dimethyl); uv (EtOH): max 231, 279 nm; ms (70 eV): *m/e* 500 (M^+), 485 ($M^+ - CH_3$), 468 ($M^+ - CH_3OH$). *Anal.* calcd. for $C_{26}H_{32}N_2O_8\cdot\frac{1}{2}H_2O$: C 61.28, H 6.52, N 5.49; found: C 61.50, H 6.44, N 5.52.

Benzyl 2-Phthalimido-3-(((2′,2′-dimethyl-4′-(3′′-methylthiazolidine-2′′-yl)-1′,3′-dioxolan-4′-yl)methyl)oxy) Acrylate **11***c*

The sodium salt **9***e* (13 g, 0.038 mol) was suspended in a solution of the thiazolidine mesylate **10** (7.8 g, 0.025 mol) in 2-butanone (300 ml) and the mixture refluxed for 16 h. The salt was filtered off and the filtrate evaporated *in vacuo*. The residue was chromatographed on a silica gel column using chloroform–methanol (98:2) as eluent. Evaporation of the solvent gave white crystals. Yield 12.0 g (89%); mp 143–145 °C; pmr ($CDCl_3$): δ 1.28, 1.37 (each s, 6H, acetonide), 2.25, 2.35 (each s, 3H, N—CH_3), 2.8–3.12 (m, 4H, N—CH_2—CH_2—S), 3.6–4.37 (m, 5H, two OCH_2 and N—CH—S), 5.1 (s, 2H, CH_2), 7.23 (s, 5H, CH_2—C_6H_5), 7.52–8.0 ppm (m, 5H, phthalimido and C═CH); ir (KBr): 1785/1725 (phthalamido), 1700 (ester), 1658 (C═C), 1465, 1450, 1442, 1380, 1367 cm^{-1}; ms (70 eV): *m/e* 538 (M^+). *Anal.* calcd. for $C_{28}H_{30}N_2O_7S$: C 62.44, H 5.62, N 5.20, S 5.94; found: C 62.59, H 5.51, N 5.40, S 6.02.

Benzyl 2-Phthalimido-3-(((4′-formyl-2′,2′-dimethyl-1′,3′-dioxolan-4′-yl)methyl)oxy) Acrylate **12***c*

The thiazolidine ester **11***c* (8.6 g, 0.016 mol) was dissolved in tetrahydrofuran–water (4:1) (100 ml) and mercuric chloride (1.2 g) was added. The milky suspension that formed immediately was stirred at room temperature for 1 h. The fine suspension was filtered off and the filtrate evaporated. The residue was extracted three times with benzene and the combined extracts were washed with dilute hydrochloric acid and water, and dried over anhydrous sodium sulfate, filtered, and evaporated *in vacuo*. The crude product was passed through a silica gel column using methylene chloride–ether (9:1) as eluent. Evaporation of the solvent gave a white foamy solid. Yield, 6.7 g (90%); pmr ($CDCl_3$): δ 1.38 (s, 6H, acetonide), 3.9–4.0 (m, 2H, OCH_2), 4.20 (m, 2H, OCH_2), 5.10 (s, 2H, CH_2—C_6H_5), 7.34 (s, 5H, phenyl), 7.6–8.1 (m, 5H, phthalimido, C═CH), 9.73 ppm (s, 1H, CHO); ir (KBr): 3480, 3072–2900, 1800/1735 (phthalimido), 1735 (ester), 1720 (aldehyde), 1665 (amide and C═C), 1430, 1395, 1382, 1290, 1100 cm^{-1};

ms (70 eV): *m/e* 465 (M^+). *Anal.* calcd. for $C_{25}H_{23}NO_8$: C 64.51, H 4.98, N 3.01; found: C 64.34, H 5.01, N 3.25.

α-Phthalamido-2,2-dimethyl-10-hydroxy-1,3,7-trioxa-9-azaspiro[4.5]decane-8-acetic Acid Benzyl Ester ***13*** *and Imine* ***14b***

The aldehyde ester **12***c* (6.0 g, 0.013 mol) was dissolved in benzene (50 ml) and refluxed for 30 min using a Dean Stark trap. The solvent was concentrated and the residue dissolved in anhydrous ether (50 ml). Ammonia was passed through the clear solution for 5 min at room temperature. It was then kept overnight. White crystals **13** were collected by filtration. Yield 2.5 g (40%); mp 108–110 °C; pmr (DMSO-d_6): δ 1.34 (s, 6H, acetonide), 3.33–4.00 (m, 5H, two OCH_2, OH), 4.28 (br s, 1H, C*H*—NH), 4.95–5.40 (m, 2H, CH—CH), 5.17 (s, 2H, CH_2—phenyl), 5.95 (d, 1H, J = 4 Hz, NH), 7.28 (s, 5H, phenyl), 7.88 ppm (s, 4H, phthalimido); ir (KBr): 3450, 3330, 3270 (NH, OH), 1780, 1720 (phthalimido), 1740 (ester), 1470, 1450, 1380 cm^{-1}; ms (70 eV): *m/e* 464 ($M^+ - H_2O$), 449 (464 − CH_3), 421 (449 − CO), 406 (421 − CH_3/or 464 $(CH_3)_2CO$). *Anal.* calcd. for $C_{25}H_{26}N_2O_8$ (482.5): C 62.23, H 5.43, N 5.80; found: C 62.44, H 5.45, N 5.81.

The filtrate was chromatographed on a silica gel column using methylene chloride – ether (95:5) as eluent. Evaporation of the major product gave a colorless oil, identified as the imine **14***b*. Yield, 2.0 g (33%); pmr ($CDCl_3$): δ 1.40, (s, 6H, acetonide), 3.4–4.3 (m, 4H, two OCH_2), 4.97 (d, 1H, N—CH—COO), 5.21 (s, 2H, CH_2—phenyl), 5.70 (dd, 1H, N—CH—O), 7.30 (s, 5H, phenyl), 7.6–8.0 ppm (m, 5H, phthalimido and N=CH); ir (KBr): 3500, 2995–2880, 1800, 1730 (phthalimido), 1760 (ester), 1660 (amide and C=N); ms (70 eV): *m/e* 464 (M^+). *Anal.* calcd. for $C_{25}H_{24}N_2O_7$: C 64.65, H 5.21, N 6.03; found: C 64.43, H 5.31, N 6.18.

2,2-Dimethyl-8-phthalimidomethyl-1,3,7-trioxa-9-azaspiro[4.5]decane ***16***

The carbinolamine ester **13** (482 mg, 1 mmol) or **14***b* (464 mg, 1 mmol), was suspended in 25 ml of ethyl acetate and added to 240 mg of palladium on charcoal (10%) in 25 ml of ethyl acetate, previously prehydrogenated with hydrogen. The mixture was hydrogenated at atmospheric pressure, until 24 ml of hydrogen were consumed (6 h). The catalyst was filtered off and the filtrate evaporated to dryness. Addition of ether gave white crystals, recrystallized once from ethyl acetate – ether. Yield 191 mg (50%); mp 151–153 °C; pmr ($CDCl_3$): δ 1.37 (s, 5H, acetonide), 1.90 (br s, 1H, NH), 2.98 (s, 2H, CH_2), 3.45–3.90 (m, 4H, two CH_2), 4.05 (d, 2H, CH_2O), 4.35 (dd, 1H, N—CH—O), 7.6–8.0 ppm (m, 4H, phthalimido); ir (KBr): 3200 (NH), 2980–2860 (CH), 1770, 1705 (phthalimido, amide), 1610 (phenyl), 1460, 1430, 1400 cm^{-1}; ms (70 eV): *m/e* 333 ($M^+ + 1$), 317 ($M^+ - CH_3$). *Anal.* calcd. for $C_{17}H_{20}N_2O_5$: C 61.43, H 6.07, N 8.43; found: C 61.67, H 6.04, N 8.19.

2,2,2-Trichloroethyl 2-Benzamido-3-hydroxy Acrylate ***9b***

4-Hydroxymethylene-2-phenyl-5-oxazolone **7** (5) (69.3 g, 0.365 mol) was suspended in dry benzene (3.5 l) and 2,2,2-trichloroethanol (109 g, 0.73 mol) was added. The suspension was stirred under reflux for 6 h and the clear solution evaporated. The oily residue was triturated with petroleum ether (30–60 °C) and kept overnight in the refrigerator. The red solid was collected by filtration and recrystallized from petroleum ether (60–80 °C). Treatment with charcoal gave pink needles. Yield 95 g, (76.6%); mp 87–88 °C; pmr ($CDCl_3$): δ 4.98 (s, 2H, CH_2—CCl_3), 7.57–8.15 (m, 6H, phenyl and C=CH), 8.6 (br, 1H, NH), 12.7 ppm (br, 1H, OH); ir (KBr): 3380, 1725 (ester), 1665 (amide and C=C), 1615, 1554, 1505, 1463, 1390, 1357, 1325, 1312, 1280, 1268, 1240, 1162, 1115 cm^{-1}. *Anal.* calcd. for $C_{12}H_{10}NO_4Cl_3$: C 42.57, H 2.98, N 4.14, Cl 31.61; found: C 42.83, H 2.74, N 4.27, Cl 31.29.

2,2,2-Trichloroethyl 2-Benzamido-3-hydroxy Acrylate Sodium Salt ***9c***

2,2,2-Trichloroethyl 2-benzamido-3-hydroxy acrylate **9***b* (91 g, 0.27 mol) was added to an ethanolic solution of sodium ethoxide (4.6 g of sodium in 200 ml of ethanol). The mixture was shaken for 10 min and ether (1 litre) added. The precipitated sodium salt was collected by filtration, washed several times with ether, and dried *in vacuo*. Yield 70 g (72%); mp 200–202 °C (dec.); pmr (DMSO-d_6): δ 4.74 (s, 2H, CH_2—CCl_3), 7.3–8.1 (m, 5H, phenyl), 8.42 (s, 1H, NH), 9.12 ppm (s, 1H, C=CH); ir (KBr): 3300 (br, salt), 3070, 2960, 1675, 1640, 1592, 1540, 1500, 1373, 1287, 1160 cm^{-1}. *Anal.* calcd. for $C_{12}H_9NO_4Cl_3Na$: C 39.87, H 2.52, N 3.89, Cl 29.50; found: C 39.90, H 2.63, N 4.13, Cl 29.74.

2,2,2-Trichloroethyl 2-Benzamido-3-(((2′,2′-dimethyl-4′-(3′′-methylthiazolidine-2′′-yl)-1′,3′-dioxolan-4′-yl)-methyl)oxy) Acrylate ***11a***

The sodium salt **9***c* (70 g, 0.195 mol) was suspended in a solution of the thiazolidine mesylate **10** (6) (40 g, 0.130 mol) in dry 2-butanone (1 litre) and the mixture stirred at 80–85 °C (bath temperature) for 12 h. The salt was filtered off and the filtrate evaporated. The red residue was dissolved in ether (50 ml), treated with charcoal, filtered, and evaporated. The yellow oil was further purified by passing through a silica gel column using benzene – ethyl acetate (9:1) as eluent. Evaporation of the solvent gave colorless crystals. On recrystallization from ether, a pure sample was obtained. Yield 48.8 g, (68.5%); mp 126–128 °C; pmr ($CDCl_3$): δ 1.35, 1.46 (each s, 6H, acetonide), 2.37 (s, 3H, N—CH_3), 2.8–3.2 (m, 4H, NCH_2—CH_2—S), 3.93 (q, J = 10 Hz, 2H, OCH_2), 4.24 (s, 2H, OCH_2), 4.46 (s, 1H, NCH—S), 4.84 (s, 2H, CH_2—CCl_3), 7.33–8.0 ppm (m, 7H, phenyl, NH and C=CH); ir (CCl_4): 2990–2800, 1730 (ester), 1698 (amide), 1660 (C=C), 1503, 1480, 1381, 1369, 1210 cm^{-1}; ms (70 eV): *m/e* 554 (M^+). *Anal.* calcd. for $C_{22}H_{27}N_2O_6SCl_3$: C 47.71, H 4.91, N 5.06, S 5.79, Cl 19.20; found: C 47.99, H 5.10, N 5.26, S 5.50, Cl 19.41.

2-Benzamido-3-(((2′,2′-dimethyl-4′-(3′′-methylthiazolidine-2′′-yl)-1′,3′-dioxolan-4′-yl)methyl)oxy) Acrylic Acid ***11b***

Zinc dust (2 g) was added at room temperature to a stirred solution of thiazolidine ester **11***a* (1.0 g, 1.8 mmol) in tetrahydrofuran (10 ml) and a 1*M* potassium dihydro-

gen phosphate solution p*H* 4.2 (2 ml). The acid liberation was followed by tlc (benzene–EtOAc 9:1). After 10 min the mixture was filtered and the tetrahydrofuran was evaporated. The residue was diluted with water (100 ml) and extracted with ether. The organic solution was dried over sodium sulfate, and evaporated *in vacuo* to give 580 mg (74%) of pure thiazolidine acid **11***b*, mp 159–160 °C; pmr ($CDCl_3$): δ 1.40 (s, 6H, acetonide), 2.31, 2.40 (each s, 3H, N—CH_3), 2.90–3.10 (m, 4H, N—CH_2-CH_2—S), 3.65–4.48 (m, 5H, two OCH_2 and N—CH—S), 7.30–7.90 (m, 7H, phenyl, NH and C=CH), 10.23 ppm (s, 1H, COOH); ir (KBr): 3250 (br), 2980, 2940 (CH_2), 1650 (br, amide), 1575, 1510, 1380 cm^{-1}; ms (70 eV): *m/e* 422 (M^+). *Anal.* calcd. for $C_{20}H_{26}N_2O_6S$: C 56.86, H 6.20, N 6.63, S 7.58; found: C 56.75, H 6.42, N 6.45, S 7.79.

2-Benzamido-3-(((4′-formyl-2′,2-dimethyl-1′,3′-dioxolan-4′-yl)methyl)oxy) Acrylic Acid ***12b***

The thiazolidine acid **11***b* (844 mg, 2 mmol), was dissolved in tetrahydrofuran–water (9:1) (10 ml) and mercuric chloride was added. The precipitate that formed immediately was stirred for 30 min. The solid was filtered off and the filtrate was dried over sodium sulfate. Filtration and evaporation of the solvent gave a white solid. Yield 650 mg (93%); mp 55–58 °C (50% hydrated form); pmr ($CDCl_3$): δ 1.43 (s, 6H, acetonide), 3.6–4.2 (m, 4H, two CH_2—O), 5.05 ($\frac{1}{2}$H, 50% hydrated aldehyde), 6.95 (1H, COOH), 7.5–7.9 (m, 7H, phenyl, NH, C=CH), 9.80 ppm ($\frac{1}{2}$H, CH=O); ir ($CHCl_3$): 3410 (OH), 2970, 2870 (CH_2), 1670 (CO), 1600 (phenyl), 1372, 1380 (*gem*-dimethyl); ms (70 eV): 349 (M^+), 334 ($M^+ - CH_3$), 305 ($M^+ - CO_2$), 290 (305 − CH_3), 273 ($M^+ - C_6H_6$), 244 ($M^+ - C_6H_5CO$). Microanalysis was not performed because of instability.

2,2-Dimethyl-9-benzamido-1,3,7,11-tetraoxaspiro[4.7]-dodec-8-ene-10-one-12-carboxycyclohexylamide ***18***

The thiazolidine acid **12***b* (698 mg, 2 mmol), was dissolved in tetrahydrofuran–water (9:1) (10 ml) and mercuric chloride was added. The reaction mixture was stirred at room temperature for 30 min. The solid was filtered off and ammonium hydroxide (1.5 mmol) was added. The p*H* was adjusted to 6.5 by adding phosphate buffer (2 ml). Cyclohexyl isonitrile (655 mg, 6 mmol) was added and the two phases mixed with vigorous stirring for 20 h. The reaction mixture was diluted with water (100 ml) and the aqueous phase extracted with ether. The combined ether extracts were dried over anhydrous sodium sulfate and evaporated *in vacuo*. The residue was washed with petroleum ether to remove the unreacted isonitrile. The residue was purified by chromatography on silica gel using chloroform–methanol (9:1) as eluent, to give 316 mg (36%) of white crystals, mp 254–256 °C; pmr (DMSO-d_6): δ 1.32, 1.40 (each s, 6H, acetonide), 1.0–1.9 (br m, 10H, cyclohexane), 3.20 (s, 1H, CH—N), 4.1–4.4 (m, 4H, two CH_2O), 5.00 (s, 1H, CH—O), 7.45–8.00 ppm (m, 8H, phenyl, 2NH, CH=C); ir (KBr): 3330, 2280 (NH), 2925, 2850 (CH_2), 1732 (lactone), 1637 (amide), 1600 (phenyl), 1370, 1380 cm^{-1} (*gem*-dimethyl); ms (70 eV): 458 (M^+), 443 ($M^+ - CH_3$), 400 ($M^+ - (CH_3)_2CO$). 383 ($M^+ - (CH_3)_2C$  , H transfer), 360 ($M^+ - C_6H_6N$). *Anal.* calcd. for $C_{24}H_{30}N_2O_7$: C 62.87, H 6.60, N 6.11; found: C 62.21, H 6.84, N 5.94.

2,2,2-Trichloroethyl 2-Benzamido-3-(((4′-formyl-2′,2′-dimethyl-1′,3′-dioxolan-4′-yl)methyl)oxy) Acrylate ***12a***

Mercuric chloride (9.7 g, 35 mmol), was added to a solution of the thiazolidine ester **11***a* (19.8 g, 35 mmol), in tetrahydrofuran (200 ml) and water (20 ml); the resulting suspension was stirred for 5 min (tlc benzene – ethyl acetate showed absence of thiazolidine ester). The reaction mixture was filtered and the filtrate evaporated. The residue was chromatographed on silicic acid, first eluted with benzene–ether (9:1), to remove all the mercuric salts, then with benzene–ether (1:1). The main fraction containing the aldehyde ester was concentrated to give a yellowish foamy solid. Yield: 13.5 g, (77%); pmr ($CDCl_3$): δ 1.39, 1.45 (6H, each s, acetonide), 4.10, 4.25 (4H, each s, two CH_2O), 4.80 (2H, s, CH_2CCl_3), 7.2–7.9 (m, 7H, phenyl, NH, C=CH), 9.63 ppm (s, 1H, CHO); ir (KBr): 3340 (br, NH, hydrated form), 1730 (ester, aldehyde), 1650 (amide), 1600 (phenyl), 1380, 3170 cm^{-1} (*gem*-dimethyl); ms (70 eV): *m/e* 481 [M^+, (^{37}Cl)], 479 [M^+(^{35}Cl)], 466 (M^+(^{37}Cl) − CH_3], 464 [M^+ (^{35}Cl) − CH_3]. *Anal.* calcd. for $C_{19}H_{20}NO_7Cl_3$: C 47.47, H 4.19, N 2.90, Cl 22.12; found: C 47.20, H 4.26, N 3.15, Cl 21.98.

α-Benzamido-2,2-dimethyl-1,3,7-trioxa-9-azaspiro[4.5]-dec-9-ene-8-acetic Acid 2,2,2-Trichloroethyl Ester ***14a***

A solution of aldehyde ester **12***a* (15.2 g, 33 mmol) in ether (250 ml) was treated at room temperature with anhydrous ammonia for 1 min (p*H* ≈ 8). After standing for 30 min, the ether was evaporated and the residue chromatographed on silicic acid using ether–benzene (1:1) as eluent. The product first eluted was identified as the imine ester **14***a*. Yield 10.0 g, (66.2%); mp 157–159 °C; pmr ($CDCl_3$): δ 1.42 (s, 6H, acetonide), 3.80 (q, 2H, CH_2O), 4.06 (t, 2H, CH_2O), 4.82 (q, 2H, CH_2—CCl_3), 5.43–5.62 (m, 2H, CO—CH—NH, N—CH—O), 6.77 (d, J = 9 Hz, 1H, NH), 7.3–7.9 ppm (m, 6H, phenyl, CH=N); ir (KBr): 3280 (NH), 3060, 2960, 2870 (CH), 1760 (ester), 1650 (amide), 1600 (aromatic C—H), 1378 cm^{-1} (*gem*-dimethyl); ms (70 eV): *m/e* 478 [M^+ (^{35}Cl)], 480 (M^+ (^{37}Cl)], 464, 463 ($M^+ - CH_3$), 422, 420 (M^+ − acetone). *Anal.* calcd. for $C_{19}H_{21}N_2O_6Cl_3$: C 47.57, H 4.41, N 5.84, Cl 22.17; found: C 47.46, H 4.61, N 6.02, Cl 22.24.

2,2,2-Trichloroethyl α-Benzamido-5-acetoxy-5-(3′-methylthiazolidine-2′-yl)-1,3-dioxacyclohex-2-ylacetic Acid ***26a***

Thiazolidine ester **11***a* (2.2 g, 4 mmol) was added at room temperature to a solution of trifluoroacetic acid (8 ml) and water (2 ml) and the mixture subsequently evaporated to dryness. The residue was neutralized with 2 *N* sodium bicarbonate and extracted with chloroform and the extracts dried over sodium sulfate. Solvent removal left an oil which was treated with a mixture of acetic anhydride (5 ml) and pyridine (5 ml) overnight. Purification on a silica gel column, eluting with chloroform–methanol gave 1.3 g, (59%) of a colorless oil. The product was crystallized from ether, mp 117–119 °C; ir (KBr): 3392 (NH), 1770, 1740 (ester), 1655 (amide),

1522 cm^{-1}; pmr ($CDCl_3$): δ 1.85 (s, 3H, OCH_3), 2.40 (s, 3H, NCH_3), 3.00 (s, 4H, N—CH_2—CH_2—S), 4.00 (s, 2H, OCH_2), 4.20 (s, 1H, N—CH—S), 4.27 (s, 2H, CH_2O), 4.80 (d, 2H, CH_2CCl_3), 5.16 (dd, J = 2 Hz, J = 4 Hz, 1H, C—CH—N), 5.54 (d, J = 2 Hz, 1H, O—CH—O), 6.85 (d, J = 8 Hz, 1H, NH), 7.2–7.0 ppm (m, 5H, phenyl); ms (70 eV): *m/e* 556/554 ($^{37}Cl/^{35}Cl$), 541/539 ($M - CH_3$), 497/495 ($M^+ - OCOCH_3$), 407 ($M^+ - OCH_2CCl_3$), 379 ($M^+ - COOCH_2CCl_3$). *Anal.* calcd. for $C_{21}H_{25}Cl_3N_2O_7S$: C 45.37, H 4.53, Cl 19.13, N 5.03; found: C 45.38, H 4.49, Cl 19.32, N 5.01.

1. I. Ugi and E. Wischöffer. Chem. Ber. **95**, 136 (1962).
2. K. Sjoberg. Dissertation. Institute of Technology, Stockholm, Sweden. 1965.
3. P. A. Rossy. Ph.D. Thesis, McGill University, Montreal, Que. 1972.
4. G. D. Rosebery. Ph. D. Thesis, McGill University, Montreal, Que. 1973.
5. H. T. Clarke, J. R. Johnsen, and R. Robinson (*editors*). The chemistry of penicillin. Princeton University Press, Princeton. 1949. p. 803.
6. G. Just, B. Y. Chung, G. Rosebery, and M. Dupré. Can. J. Chem. **54**, 1260 (1976).
7. J. C. Sheehan and D. A. Johnson. J. Am. Chem. Soc. **76**, 158 (1953).
8. I. Ugi, U. Fetzer, U. Eholzer, H. Knupfer, and K. Offermann. *In* Isonitril Synthesen. Neuere Methoden der präparativen Org. Chemie. Bd. IV. Verlag Chemie. 1966. p. 37.
9. G. Just and K. Grözinger. Synthesis, 457 (1976).

An alternative view of unimolecular reaction theory

HUW OWEN PRITCHARD

Centre for Research in Experimental Space Science, York University, Downsview, Ont., Canada M3J 1P3

Received June 7, 1976

HUW OWEN PRITCHARD. Can. J. Chem. **55**, 284 (1977).

A primitive form of unimolecular reaction theory is constructed, based on the master equation. Application of the theory depends upon the way in which eigenvalues of large stochastic matrices behave as certain of the matrix elements are varied. Some of the required eigenvalue properties have been deduced by numerical experiment, and others are available from earlier work on diatomic dissociation reactions. Comparison of the results from this primitive approach with those of existing theories of unimolecular reactions suggests some reinterpretation of parameters used in those theories: most interestingly, the number of effective oscillators occurring in Kassel theory (or its Slater-theory equivalent) appears to be the ratio, at infinite pressure, of the total rate to the rate of the only reaction channel which survives at the low-pressure limit.

HUW OWEN PRITCHARD. Can. J. Chem. **55**, 284 (1977).

On a construit une forme primitive de la théorie des réactions unimoléculaires qui est basée sur l'équation maîtresse. L'application de la théorie dépend de la façon de se comporter des valeurs de eigen de grandes matrices stochastiques lorsque l'on fait varier certains éléments de la matrice. Faisant appel à des expériences numériques, on a déduit quelques unes des propriétés des valeurs de eigen qui sont requises; d'autres sont disponibles à partir de travaux antérieurs sur des réactions de dissociation diatomique. Une comparaison des résultats obtenus grâce à cette approche primitive avec ceux prévus par les théories de réaction unimoléculaire existante suggère que l'on doit faire quelques réinterprétations des paramètres utilisés dans ces théories: la réinterprétation la plus intéressante a trait au nombre d'oscillateurs effectifs se produisant dans la théorie de Kassel (ou le nombre equivalent dans la théorie de Slater) qui semble être le rapport, à pression infinie, de la vitesse totale par rapport à la vitesse du seul chemin réactionnel qui survie à la limite de basse pression.

[Traduit par le journal]

Introduction

The formulation of the rate of a unimolecular reaction using the master equation is relatively commonplace (1–3). However, despite this general acceptance of its validity, the approach has yielded singularly little in the nature of a concrete predictive theory. The basic reason for this is that in the master-equation approach, there is one differential equation for every discrete state of the molecule, and since an interesting molecule from the point of view of unimolecular reaction theory may have many millions of energy levels, one is faced with a two-fold problem, that of finding solutions for enormously large sets of simultaneous differential equations, whose constant coefficients comprise an even larger number of unknown transition rates between the discrete states (4). The usual method of trying to overcome these difficulties is to partition the set of energy levels into blocks whose size is determined by the average amount of internal energy per collision transferred to the heat bath (2); this is really no more than simulating the real process using a model consisting of (at most) a few hundred levels, which is perfectly acceptable provided (4) that the partitioning is not too restrictive. We then encounter the main obstruction to the formulation of a useful theory of unimolecular reactions, since these sets of simultaneous differential equations, although transformed into matrix notation (2, 4), have to be solved numerically. Unfortunately, there appear to be no useful theorems in existence connecting the eigenvalues with the elements of these transition matrices (5, 6), even for the simplest conceivable changes in the elements. Modern developments in linear algebra, stimulated by complementary computational activity, will clearly lead to some new theorems in this area (7, 8), but it has to be remembered here that in our case, we are interested in the behaviour of the eigenvalue of smallest numerical magnitude, which is the rate constant, rather than in the dominant eigenvalue which is generally more amenable to study.

The aim of this investigation, therefore, was to

set out the simplest and most primitive master-equation formulation which exhibits unimolecular reaction characteristics. The behaviour of the eigenvalues was then examined numerically over a wide range of conditions using matrices of the order of about 30; a few calculations were carried out on much larger matrices, of the order of 300, to confirm that some of the properties of interest were not artefacts of the relatively small size of the transition-rate matrix. It is then conjectured that any 'theorems' so deduced will be valid for the almost infinitely large matrices required for a proper description of the unimolecular reaction problem. The supposition that progress can be made in this way is not entirely without foundation. Earlier work on diatomic dissociation reveals two things: first, that the eigenvalue representing the rate of the reaction is very insensitive to the transition probabilities assumed between the internal states of the molecule, even for systems consisting of quite moderately few energy levels (4, 9); and second, that once one considers the molecule to consist of more than 20 levels or so, the rigid one-to-one dependence (9–11) of certain eigenvalues (relating to the internal relaxation) on specific elements of the matrix disappears, and we enter a regime where network or connectivity effects seem to dominate, with the eigenvalues determined co-operatively by contributions from most of the elements of the matrix (9, 12, 13). Clearly, even in the simplest cases, any connection between eigenvalues and the elements in the matrix is extremely complicated (11) and equally clearly, one can hope to elucidate some of the rules without detailed knowledge of individual matrix elements, or transition probabilities.

Examination of Four Primitive Models

We will consider the simplest possible case, that of a molecule A, infinitely diluted in a heat bath of molecules M, decomposing to give products. The energy levels ε_i of the molecule are assumed to be slightly convergent as the energy increases, and the degeneracy g_i of each level is assumed, for the time being, to be unity. We have three choices for the possible description of the reaction process itself. (*a*) To assume a cut-off at some level which is assumed to be an absorbing barrier (1); this is unnecessarily restrictive, and precludes any discussion of the behaviour of states above the critical level, or of phenomena like chemical activation or the decomposition of ions. (*b*) Following Widom (14) we can restrict ourselves to an isomerisation and include all the internal states of the product molecule as well: this gives, in principle, a totally complete and exact description of the process. However, most unimolecular reactions are studied experimentally far away from equilibrium, *e.g.* methyl isocyanide, cyclopropane, and obviously we can (for now) dispense with the luxury of including all the product states, with a consequent reduction in both the size and complexity of the problem; when we need to include any reference to the product molecules, we can simply treat them as structureless entities. (*c*) We can treat the reaction processes as a series of predissociations from certain energetic states of the molecule: if these predissociating levels are embedded in the total manifold of energy levels, then it is clear that the description can encompass, if necessary, such concepts as chemical activation or decomposition to more than one set of products.

It becomes clear that the present treatment has many similarities to those examined by Valence and Schlag (15) and by Tardy and Rabinovitch (16) a decade ago, but whereas they were forced to circumvent the exact solution of the master-equation problem because of computational limitations, we will go directly for the exact solution. The strategy is that we may be able to discover the behaviour of interest for unimolecular reactions using the exact solutions for relatively small matrices and then make a 'mental extrapolation' to those larger matrices of real interest. It should also be noted that there are strong similarities to some aspects of the papers of Buff and Wilson (17) and of Gilbert and Ross (18).

Figure 1*a* depicts the simplest model of this kind which exhibits unimolecular reaction characteristics. In the actual numerical experiments, a series of $N = 30$ internal energy levels was used, spread over an energy range of 100 kcal/mol: they were slightly convergent, with a quadratic dependence on the index i which would cause the levels to converge at 1000 kcal/mol; in a sense then, the latter figure can be regarded as the heat of atomisation of the molecule, but because the temperature is low, we can truncate the series of levels at a much lower energy value than this. There is one predissociating state, with a decay rate constant k_r, arbitrarily assigned as 10^{13} s^{-1}: in this scheme, this is the 20th level, placed at

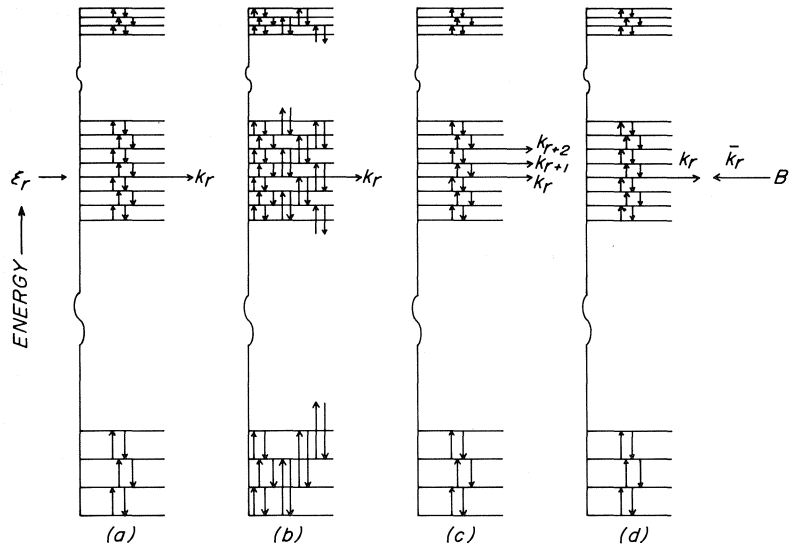

FIG. 1. Schematic representation of four unimolecular reaction models. All models have the same slightly convergent set of energy levels, and the same critical energy ε_r, but with the following variations: (*a*) nearest-neighbour-only transitions, dissipative, one predissociating level (model I); (*b*) one- and two-quantum transitions, dissipative, one predissociating level (model II); (*c*) nearest-neighbour-only transitions, dissipative, two or three predissociating levels (model III); (*d*) nearest-neighbour-only transitions, conservative, one predissociating level giving product molecule B; back-reaction rate constant $\bar{k}_r$ (model IV).

about $\varepsilon = 70$ kcal/mol above the ground state; (note that the subscript r will be reserved for the index i when the state is a predissociating one). Each downward transition was given a transition probability which increased very weakly as the energy gap decreased, and all downward transitions had probabilities of the order of 10^{-3} per collision; upward transition probabilities were generated by detailed balancing from the equilibrium populations $\tilde{n}_i$ for the temperature in question. The temperature T was chosen in the range 500–1000 K to match the practical region in which a reaction with a critical energy of 70 kcal/mol might be studied. The actual numerical details of the model are immaterial, and are only presented for the purposes of clarifying the nature of the model, and as a vehicle for appreciating some of the later discussion; moreover, the philosophy of the experiment is that the model only serves to elucidate some numerical 'theorems', which can then be transferred to more realistic matrices of much larger size.

Most of the numerical experiments were performed upon what may be termed a dissipative model: in these calculations, the product molecules are unspecified and no reverse reaction is included; such dissipative models are models I, II, and III, Figs. 1 *a*, *b*, and *c*. Representing the set of simultaneous differential equations in matrix form, the matrix elements for the dissipative cases are (13)

$$[1] \quad [A]_{ij} \equiv (1 - \delta_{ij})Q_{ji} - \delta_{ij}\left[k_i + \sum_{k=0}^{N-1}(1 - \delta_{ik})Q_{ki}\right]$$

where

$$Q_{ji} = [M]ZP_{ji}$$

$$\tilde{n}_i P_{ji} = \tilde{n}_j P_{ij}$$

and [M] is the concentration of inert molecules, Z is the collision number between M and A, and P_{ji} is the probability per collision of a change in the internal state of A from $i \rightarrow j$. The matrix A_{ij} has N eigenvalues, none of which is zero because the system does not conserve particles: $(N - 1)$ of the eigenvalues represent the internal relaxation times ($\tau_j = -\lambda_j^{-1}$) and the eigenvalue of smallest numerical magnitude λ_N is (minus) the rate constant (k_{uni}) for the loss of particles from the system. Figure 2 shows the behaviour of these N eigenvalues, for fixed P_{ij} and fixed k_r, as a function of the inert gas concentration [M]: such

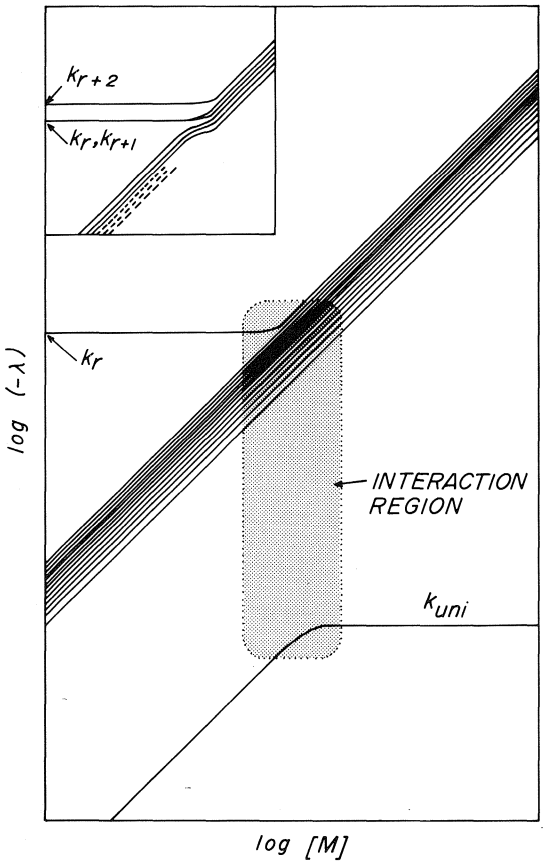

FIG. 2. Schematic representation of the behaviour of the eigenvalues of the reaction-rate matrices as a function of the concentration of M. The inset shows the behaviour of the six eigenvalues of largest numerical magnitude in the interaction region when there are three decay channels, two of them having the same decay constant *i.e.* $k_r = k_{r+1} \neq k_{r+2}$.

behaviour has been shown before for a two-state system (19), and this is the generalisation to an N-state system. The principal features are as follows: There is a bundle of $(N - 2)$ eigenvalues (very closely spaced because all the downward P_{ij} are very similar in numerical magnitude) which appear to be directly proportional to [M]; these are the rates of the internal relaxations of the molecule A in the presence of M. At very low [M], there is an eigenvalue $\lambda_0 = 10^{13}\ s^{-1}$, since this is much faster than any internal process under these conditions; however, as [M] increases and the rates of the internal processes become comparable with $10^{13}\ s^{-1}$, the largest eigenvalue is assimilated into the bundle. In the diagram, the bundle of internal eigenvalues is drawn as though they were all straight lines, but in fact, in the interaction zone (depicted by the shaded area) each member of the bundle exhibits a small displacement such that in the limit of high pressure, λ_j is the continuation of the low-pressure λ_{j-1} (see the inset in Fig. 2 for more details, remembering that the inset actually refers to another calculation of type III); also, for each successive eigenvalue, the centre of the displacement moves slightly to the right as λ decreases in numerical magnitude. Finally, the eigenvalue of smallest numerical magnitude ($\lambda_N = -k_{uni}$) is parallel to the main bundle of internal-relaxation eigenvalues until the interaction region is reached, whence it turns over and becomes independent of [M].

The properties of k_{uni} are as follows:

(a) High pressure

The infinite pressure rate constant is exactly

$$[2] \quad k_{uni,\infty} = \tilde{n}_r k_r; \quad \left(\text{normalisation } \sum_i n_i = 1\right)$$

i.e. the product of the equilibrium population and the predissociation rate constant; this equation also remains true if the state $i = r$ is assigned a degeneracy g_r other than unity.

(b) Low pressure

The identification of the rate constant is not so decisive, and it appears that the low-pressure limiting form is

$$[3] \quad k_{uni,0} \sim 0.26 \tilde{n}_r |\lambda_{N-1}|$$

Obviously, this equation could be written in other suggestive forms, *e.g.* in terms of $\tilde{n}_{r-1}$ which is the state supplying the predissociating one; other possible forms investigated involved the arithmetic or geometric means of the bundle of λ_j, but the relationships here were dependent on the number of levels considered, whereas in the form of [3], it was independent of both the number of levels and the index of the predissociating state, provided $r > \sim 5$, $N > 30$. Equally obviously, the rate of dissipation is simply $n_r k_r$ where n_r is the actual nonequilibrium population of the predissociating state, whence

$$[4] \quad \frac{n_r}{\tilde{n}_r} \sim 0.26 \frac{|\lambda_{N-1}|}{k_r}$$

The coefficient 0.26 is clearly only appropriate for the particular set of energy levels and transition probabilities used in this calculation.

(c) Intermediate pressures

The most interesting property of k_{uni} is that it is exactly a Lindemann fall-off curve: close to a hundred values of k_{uni} as functions of [M] have been obtained during the variety of numerical experiments carried out and in no case, given the high-pressure limit (eq. 2) and the numerical form of the low-pressure limit (eq. 3), did a value of k_{uni} for model I deviate by more than 1 part in 10^6 from Lindemann behaviour, *viz.*

$$k_{uni} = \frac{a[M]}{b + c[M]} \qquad [5]$$

It seems safe to presume therefore that eq. 5 can be regarded as a valid rule for λ_N for *large* matrices of the form [1] with only one dissipative element k_r, given that r is embedded well within the body of the values of the energy-ordering index i; eq. 2 identifies the ratio a/c unambiguously in terms of the properties of the matrix, and eq. 3 gives an approximate form for the ratio $a[M]/b$.

The next interesting question is whether this Lindemann behaviour is specific only to this primitive formulation, or whether it is more general: model I contains two exceedingly restrictive assumptions, that of nearest-neighbour-only transitions, and that of only one allowed predissociating state, and the Lindemann form for λ_N could be confined only to this special case.

The step-ladder or nearest-neighbour approximation (*viz.* $P_{ij} = 0, |i - j| \neq 1$) is a common one in theoretical chemical kinetics, and it is now well established (4, 10) that in diatomic dissociation, the activation flux is essentially step-ladder in form and that the principal result of making the step-ladder approximation is to effect a relatively small decrease in the overall reaction rate. Consequently we will examine this restriction first. This is done using model II, Fig. 1*b*, which includes both one- and two-quantum level transitions: the nearest-neighbour transition probabilities P_{ij} and the predissociating decay rate k_r were kept the same as for model I, and the values of $P_{i-1,i+1}$ were assumed to be quite large, of the order of $0.3P_{i-1,i}$. $P_{i,i+1}$, in order to exaggerate any effect of non-nearest-neighbour transitions. The behaviour of the eigenvalues did not change, of course, from the pattern shown in Fig. 2, except in minor numerical detail. Referring only to λ_N, the high-pressure limiting value remained the same as before *i.e.* eq. 2, as demanded by the physics of the situation, and the low-pressure limiting value was about 1% higher than before, eq. 3; the latter is reasonable since the predissociating level is now fed by two pathways from below, from levels $i = r - 1$ and $i = r - 2$, and the net result is a slightly higher non-equilibrium population n_r. However, in the intermediate-pressure region, the values of $-\lambda_N$ again conformed, to better than 1 part in 10^6, to the Lindemann form, eq. 5. Consequently, we can assume from now on that the step-ladder or nearest-neighbour assumption is only a matter of detail; it will affect the calculated rate somewhat, as it also did in the diatomic dissociation case, but it will not lead to qualitatively invalid results: this of course is a great advantage, because matrix [1] is then only a tridiagonal matrix, and once symmetrised, can be manipulated on a computer with great efficiency. An alternative (but not quite rigorous) rationalisation of this is to say that a full symmetric matrix can always be reduced to tridiagonal form: hence, a nearest-neighbour model, given suitable weighted transition rates, will always mimic the behaviour of the full transition matrix.

A brief digression: it is common in most unimolecular reaction theories to make the assumption, for want of something better, of unit deactivation efficiency, at least for the interesting states. Our model I has deactivation efficiencies which are monotonically increasing as the index i increases, but all of them are close to 10^{-3} per collision in magnitude. The calculation was repeated with all downward transitions $P_{i,i+1}$ having the value of unity, which does no more than shift Fig. 2 to the left by three log units. Alternatively if we make some deactivation probabilities unity, and leave others as 10^{-3}, the thickness of the bundle increases by about three log units, and with it, the width of the (shaded) interaction region. Hence, assumptions about the numerical magnitudes of the transition probabilities themselves also only affect the detail of the calculation, but not the overall picture.

Returning now to the question of more than one decay channel, *i.e.* model III. Calculations were performed using the same standard set of P_{ij}, with k_r having its usual value of 10^{13} s^{-1}, and with various values assigned to $k_{r+1}, k_{r+2}, \ldots$. The pattern of eigenvalue behaviour remains very much as is shown in Fig. 2, except that there is now one eigenvalue, horizontal in the top left-hand portion of the diagram, for each non-zero

value of k_i, and correspondingly one less in the diagonal bundle. At very low pressures, λ_0, λ_1, $\lambda_2, \ldots$ are exactly the values assigned to the k_i in descending order of magnitude. If all the k_i are the same, *e.g.* 10^{13} s^{-1}, then there is a set of degenerate λ_j at this value: this degeneracy begins to split as the interaction region is approached, and each one merges into the corresponding member of the bundle (see inset to Fig. 2). At the high-pressure limit, the obvious result was obtained for the rate constant, *viz.*

$$[6] \qquad -\lambda_N = k_{\text{uni}} = \sum_{i \geqslant r} \tilde{n}_i k_i$$

At the low-pressure limit, a rather startling, but in hindsight very obvious result was obtained, namely that k_{uni} was *exactly* the same as if there was only one decay channel, k_r! The physical explanation is very simple, and in fact is an implicit assumption of earlier master-equation theories (2, 15): level $i = r$ decays to products just as quickly as molecules can be supplied to it from level $i = r - 1$; consequently, in the limit, no molecules can ever find their way into levels $i = r + 1, r + 2, \ldots$, and these decay channels become inoperative at very low pressures.

Moreover, the form of k_{uni} in the intermediate-pressure region can no longer be fitted to the Lindemann form. This is an interesting asymmetry: models I and II have a common high-pressure limit, but different low-pressure limits (arising from additional off-diagonal elements in the matrix); models I and III have a common low-pressure limit, but different high-pressure limits (arising from additional diagonal elements in the matrix); models I and II are Lindemann, model III is not.

Another digression: in order to confirm the interpretation that at the low-pressure limit the steady-state population distribution contains no molecules in states $i > r$, it is necessary to generate the population distribution for a time t in the process for which $|\lambda_j^{-1}| < t < k_{\text{uni}}^{-1}$. This is most easily done using model IV, Fig. 1*d*, which conserves particles. Model IV is identical with model I except for the addition of one more equation representing the concentration of the (unstructured) product molecules B; the equations now conserve particles, and the generation of the population distribution, in principle at least, follows simply in the normal way (20). The equilibrium concentration of B was chosen to be large (as it is in many real isomerisation experiments *e.g.* methyl isocyanide, cyclopropane): this makes $\bar{k}_r$ very small, yielding the result that apart from the introduction of the conservative zero eigenvalue, the remaining N eigenvalues λ_j do not change. It turns out that the calculation of the steady-state population distribution is relatively straightforward in the intermediate pressure range, but is rather ill-conditioned at the pressure extremities, especially at low pressure. At relatively high pressures, where λ_{N-1} is within 0.1% the high-pressure limit, we recover the expected result that all levels below $i = r$ are in thermal equilibrium with each other, all levels above $i = r$ are also in equilibrium with each other, but there is a disparity of the order of 0.1% between the two sets of populations. At relatively low pressures, where $[M]^{-1}\lambda_{N-1}$ is (say) about 1% above the limiting value (it is difficult to get much nearer to the low-pressure limit because of severe cancellation problems) the predicted result is also recovered: levels below $i = r$ are in equilibrium, more or less, with each other, but with the degree of equilibration falling successively as i increases towards r, very much like plots given by Tardy and Rabinovitch some years ago (16); n_r is of course about 1% greater at this pressure than the value given by eq. 4, and all the levels above $i = r$ are very closely in equilibrium with each other, having populations of the order of 0.1% of their normal equilibrium values. Thus, the reason for the common low-pressure limit for models I and III is confirmed.

Now, if the behaviour of k_{uni} for model III does not conform to a Lindemann plot, does it have some other recognisable form? It was found that if two non-zero values of k_i were used *viz.* $k_r = k_{r+1} = 10^{13}$ s^{-1}, the fall-off behaviour of k_{uni} could be represented very well by a Kassel curve. The conformity to a Kassel curve was not exact, but nowhere was the deviation more than 0.1%, and the best value of s for this case was $s = 1.14$, using, of course, the high-pressure Arrhenius parameters appropriate to this model, *i.e.* eq. 6. The most interesting feature of this observation, however, is that at the temperature in question, the rate constant given by eq. 6 was just 1.14 times the value of $k_r\tilde{n}_r$, the single-channel value. Let us therefore introduce the conjecture that

$$[7] \qquad s \cong \sigma = \sum_{i \geqslant r} \tilde{n}_i k_i / \tilde{n}_r k_r \; ?$$

Two model calculations were then constructed

having the value of $\sigma = 2$. This can be done for example by keeping both k_r and k_{r+1} fixed at 10^{13} s^{-1} and increasing the degeneracy g_{r+1} to give the desired result, or by keeping the degeneracy fixed and increasing k_{r+1} correspondingly; either way, the best fit to a Kassel curve was obtained when s was within the range 1.98 to 2.02. The coincidence between s and σ is remarkable and suggestive: however, an attempt to extend eq. 7 to higher values of σ does not lead to a one-to-one correspondence between s and σ; for example, two calculations with $\sigma = 3$ (one with equal contributions to the rate from $i = r$, $r + 1$, and $r + 2$, and the other using only two channels $i = r$ and $r + 1$) both gave good fits to Kassel curves having $s \simeq 2.65$. Considering the density of states in the critical region and the relatively narrow width of the bundle of internal eigenvalues, the calculations for $\sigma = 3$ really are very strained and probably unrealistic, and it would seem therefore not unreasonable at the present juncture to leave conjecture [7] as it stands, to be verified for larger σ at a later stage using much larger matrices.

Relationship to Existing Theories

Rather than compare the present approach specifically and in turn with each of Hinshelwood–Lindemann theory (2), Slater theory (2, 21), and RRK or RRKM theory (2, 3), it seems more economical at this primitive state of development to make associations with the general body of ideas used in these theories, and highlight the shortcomings where they appear. We have constructed an incredibly primitive master-equation formulation of a unimolecular reaction. The fact that this is worth attempting stems from our experience with the master-equation treatment of diatomic dissociation, (*a*) that the step-ladder activation assumption will give results only quantitatively but not qualitatively different from a full network of activation steps, and (*b*) that once the network becomes sufficiently large, the reaction rate is rather insensitive to the internal transition rates. The molecule is represented only as a series of energy levels: they are not subdivided into classes or subgroups which could be regarded as oscillators in the normal sense, and yet fall-off behaviour is found which is often treated using the idea of a number s of coupled oscillators. In a sense, the present model corresponds to complete randomisation of energy and could easily be extended, in principle at least, to accommodate separate interleaving manifolds of energy levels with high transition rates within each manifold and relatively low transition rates between members of different manifolds to examine effects caused by non-randomisation of energy. The concept of oscillators in other theories is associated with both the *shape* of the fall-off curve and the *decline* of the Arrhenius temperature coefficient with pressure; in practice also, there is a correspondence between the complexity of the molecule and the *position* of the fall-off curve on the pressure scale. We have shown that the varying shape of the fall-off curve may have an alternative interpretation: if we use the Kassel s to describe approximately the shape of the fall-off curve, then s appears via the conjecture [7] to be the ratio at infinite pressure of the total rate to the contribution of that particular decay channel which persists at the low-pressure limit.

On the other hand, there is no direct correspondence between the value of σ (or s) and the position of the fall-off. As we showed, the position of the fall-off is adjustable trivially by changing the mean value of the deactivation probabilities in the system. The major determinant of the position of the fall-off curve on the log [M] axis is simply that the top left-hand portion of the interaction region (*cf.* Fig. 2) occurs when

$$[8] \qquad k_r = -\lambda_0' \sim [M]ZP_{ij}(\max)$$

where λ_0' is the eigenvalue of largest numerical magnitude for the unperturbed matrix (*i.e.* all $k_i = 0$), and $P_{ij}(\max)$ is the largest collisional deactivation probability in the system. Thereafter, each successive member of the bundle of eigenvalues exhibits its displacement at a successively higher pressure, and therefore k_{uni} bends over and becomes horizontal at a pressure value higher than that given in [8] by an amount determined in some topological fashion by the *thickness* of the bundle; thus, eq. 8 is the major determinant of the position of the fall-off, with the thickness of the bundle being a secondary factor. Clearly there is some scope for establishing a tenuous connection between σ and the thickness of the bundle of eigenvalues corresponding to the internal processes: this aspect has not been examined in detail, but it seems obvious that the main factor will be the dynamic range of deactivation probabilities for the dominant steps in the network, and this range will probably be greater

for more complex molecules than for simple ones. The necessary relationship which we cannot establish is the one between σ and the k_i required to define the position of the interaction region via eq. 8; this of course is where oscillator-based theories have some strength since, for a fixed deactivation probability, the predicted fall-off pressure decreases with increasing complexity of the molecule.

The present model yields distinctly different Arrhenius temperature coefficients at the high- and low-pressure limits. At the low-pressure limit, when the reaction flux is through only the $i = r$ channel (in the single-step excitation model) or only a few channels just above $i = r$ (in the general multi-step excitation model), the behaviour of the rate constant, to a first approximation, is $\sim \exp(-\varepsilon_r/kT)$. Another factor will be the way in which the depopulation of the predissociating levels and of those below them change with temperature, which will depend to a large extent on the temperature coefficients of the internal relaxation eigenvalues. Making the plausible assumption that any non-equilibrium effects become more severe at higher temperatures, the Arrhenius temperature coefficient would then be just slightly less than ε_r in numerical magnitude (4). At the high-pressure limit, where the rate constant behaves as $\sigma g_r \exp(-\varepsilon_r/kT)$ (from eq. 7), the Arrhenius temperature coefficient will depend on ε_r again, and on the way σ varies with temperature. If σ is small, there will be relatively little scope for deviation from ε_r, if σ is large, there may be considerable scope, so in a sense we recover a relationship between the change in Arrhenius temperature coefficient with pressure and σ (crudely the number of effective oscillators), but not a quantitative one as in other theories. We may distinguish two types of behaviour, one which we may regard as 'normal' and one 'abnormal'. (*a*) If reaction takes place from states immediately above the state $i = r$, and the products $k_i g_i$ for the dominant reactive channels are not very different from the product $k_r g_r$ for the critical level, then the 'activation energy' will be only a little in excess of ε_r, and the frequency factor A_∞ will be of the order $\overline{k_i g_i}$. (*b*) If, because of a peculiar distribution of predissociating rotational states of high J somewhat above the level $i = r$, with $\overline{k_i g_i} \gg k_r g_r$, one can have an Arrhenius temperature coefficient considerably greater than ε_r, and a 'high' frequency factor A_∞. The behaviour of these two cases as the pressure decreases will be different: case (*a*) will exhibit a small decline in 'activation energy' with a relatively constant frequency factor, whereas case (*b*) will exhibit a large decline in 'activation energy' and also a relatively severe change in frequency factor. Obviously σ plays some role in the change in both cases, but not a clearly defined one.

In discussing the results of a similar investigation about 10 years ago, Valance and Schlag (15) concluded that there were three necessary and sufficient conditions for RRK behaviour of the master-equation model: (*i*) the steady-state assumption; (*ii*) the strong-collision assumption; (*iii*) all levels below the critical energy are required to be in equilibrium. We have not established in a detailed sense that the present model gives exactly RRK behaviour, only that it is Kassel-like or Slater-like, but without *any* of these artificial restrictions, which it would seem arise from the partitioning procedure used by Valance and Schlag rather than the physics of the situation: essentially, this partitioning reduced the problem to a two- or three-state problem (admittedly with internal structure within the two or three states concerned) and the risks attendant upon making such drastic assumptions are by now reasonably well recognised (4).

Finally we note that, of course, one of the attractions of the master-equation approach is that it can encompass naturally different efficiencies of colliding molecules in restoring the fallen-off rate, which is not always easy in other approaches. It does not seem entirely unreasonable to envisage at this stage a hybrid theory in which the details of the internal relaxations are treated in the present fashion but the calculation of the lifetimes of the interesting states rests heavily on RRKM-like considerations.

Acknowledgments

I would like to thank the National Research Council of Canada for financial support, and Peggy Hill and Andrew Yau for considerable computational assistance.

1. D. L. BUNKER. Theory of elementary gas reactions. Pergamon Press, London. 1966.
2. P. J. ROBINSON and K. A. HOLBROOK. Unimolecular reactions. Wiley-Interscience, New York. 1972.
3. W. FORST. Theory of unimolecular reactions. Academic Press, New York. 1973.
4. H. O. PRITCHARD. Specialist periodical reports. Reac-

tion kinetics. Vol. 1. The Chemical Society, London. 1975. p. 243.
5. T. MUIR. The theory of determinants in the historical order of development. Vols. 1 to 4. St. Martin's Press, London. 1906, 1911, 1920, and 1923.
6. T. MUIR and W. H. METZLER. A treatise on the theory of determinants. Dover Publications, New York. 1960.
7. H. P. M. v KEMPEN. Linear algebra and its applications. **3**, 263 (1970).
8. R. C. THOMPSON. Linear algebra and its applications. **9**, 243 (1974).
9. D. L. S. MCELWAIN and H. O. PRITCHARD. Thirteenth Symposium (International) on Combustion. The Combustion Institute, Pittsburgh, Pa. 1971. p. 37.
10. D. L. S. MCELWAIN and H. O. PRITCHARD. J. Am. Chem. Soc. **91**, 7693 (1969).
11. R. K. BOYD. Can. J. Chem. **49**, 1401 (1971).
12. D. L. S. MCELWAIN and H. O. PRITCHARD. Can. J. Chem. **49**, 3915 (1971).
13. T. ASHTON, D. L. S. MCELWAIN, and H. O. PRITCHARD. Can. J. Chem. **51**, 237 (1973).
14. B. WIDOM. J. Chem. Phys. **55**, 44 (1971).
15. W. G. VALANCE and E. W. SCHLAG. J. Chem. Phys. **45**, 216 (1966); **45**, 4280 (1966).
16. D. C. TARDY and B. S. RABINOVITCH. J. Chem. Phys. **45**, 3720 (1966).
17. F. P. BUFF and D. J. WILSON. J. Chem. Phys. **32**, 677 (1960).
18. R. G. GILBERT and I. G. ROSS. Aust. J. Chem. **24**, 1541 (1971); J. Chem. Phys. **57**, 2299 (1972).
19. H.-J. BAUER. J. Chem. Phys. **57**, 3130 (1972).
20. H. O. PRITCHARD and N. I. LABIB. Can. J. Chem. **54**, 329 (1976).
21. N. B. SLATER. Theory of unimolecular reactions. Methuen, London. 1959.

The triple helical structure of lentinan, a linear β-(1→3)-D-glucan

TERRY L. BLUHM AND ANATOLE SARKO

Department of Chemistry, State University of New York College of Environmental Science and Forestry, Syracuse, NY 13210

Received June 28, 1976

TERRY L. BLUHM and ANATOLE SARKO. Can. J. Chem. **55**, 293 (1977).

Probable models for the crystalline structure of lentinan, the β-(1→3)-D-glucan of the fungus *Lentinus elodes*, were evaluated by X-ray fiber diffraction and theoretical conformational analysis of single and multiple helices. The X-ray diagram is consistent with a hexagonal unit cell with dimensions $a = b = 15.8$ Å and c (fiber repeat) = 6 Å. Conformational analysis predicts five probable models for this fiber repeat, of which one is a single helix, two are double helices, and two are triple helices. On the basis of packing of these helices into the unit cell and a comparison of their calculated Fourier transforms with the observed X-ray diffraction intensity distribution, all but the two triple helical models are eliminated from consideration. The two triple helices differ only in chirality and both left- and right-handed models are stabilized by interstrand O(2)---O(2) hydrogen bonds, such as are found in the triple helical structure of β-(1→3)-D-xylan. The right-handed triple helix may be the more probable structure of the two, by analogy with the known structure of the β-(1→3)-D-xylan. It is likely that the β-(1→3)-D-glucan of curdlan and those of *Armillaria mellea* and *Lilium longiflorum* also possess the same structure.

TERRY L. BLUHM et ANATOLE SARKO. Can. J. Chem. **55**, 293 (1977).

On a évalué, par diffraction de rayon-X de fibre et par une analyse conformationnelle théorique des hélices simples et multiples, les modèles probables pour la structure cristalline du lentinane, le β-(1→3)-D-glucanne du champignon *Lentinus elodes*. Le diagramme de rayon-X est en accord avec une maille hexagonale ayant des dimensions $a = b = 15.8$ Å et c(répétition de la fibre) = 6 Å. L'analyse conformationnelle prédit cinq modèles probables pour cette répétition de fibre: un correspond à une hélice simple, deux sont des doubles hélices et deux sont des triples hélices. Sur la base de l'entassement de ces hélices dans la maille et par comparaison de la transformation de Fourier calculée avec celle observée pour la distribution des intensités dans la diffraction des rayons-X, on peut éliminer tous les modèles excepté les deux triples hélices. Les deux triples hélices diffèrent uniquement par leur chiralité et les modèles gauches et droits sont aussi stabilisés par des ponts hydrogène O(2)---O(2) entre les chaines comme on en trouve dans la structure triple hélice du β-(1→3)-D-xylane. Il est possible que la triple hélice droite soit la plus probable des deux si l'on se base sur une analogie avec la structure connue du β-(1→3)-D-xylane. Il est probable que le β-(1→3)-D-glucanne du curdlane ainsi que ceux des *Armillaria mellea* et *Lilium longiflorum* possèdent la même structure.

[Traduit par le journal]

Introduction

Although cellulose is the principal structural polysaccharide of the plant world, a number of other β-linked polysaccharides have been found in that capacity. For example, cellulose is replaced by β-(1→4)-mannan in the siphoneous green algae *Codiaceae* (ref. 1, p. 94) and *Dasycladaceae* (2), and by β-(1→3)-xylan in *Caulerpaceae* (3). The β-(1→3)-glucans have similarly been found as the main structural component in baker's yeast, *Saccharomyces cerevisiae* (4), and, along with cellulose, in the pollen tube of *Lilium longiflorum* (5). In the latter, the glucan is fibrillar and crystalline and this is the first known instance of finding this glucan in a structural capacity in higher plants. In addition, β-(1→3)-glucans occur widely in nature as storage polysaccharides, as for example, in brown seaweeds of the species *Laminaria* (6), in unicellular algae such as *Euglena gracilas* (7) and in filamentous green algae such as *Cladophora rupestris* (ref. 1, pp. 196, 197).

Other investigations of the crystalline structure of β-(1→3)-glucans have shown that this polysaccharide can be crystallized in oriented form and that the resulting diffraction diagrams are nearly identical with those obtained from the native crystalline form. For example, Scott and Rees (8) obtained fiber X-ray diffractograms of curdlan, the extra-cellular β-(1→3)-glucan from a mutant of *Alcaligenes faecalis*. Their diffraction data were insufficient for a detailed X-ray analysis of the structure; however, they were able to measure the fiber repeat as between 5.8 and

6.2 Å and the fiber density as 1.43 g/cc. Jelsma and Kreger (9) obtained identical diagrams and fiber repeat data from oriented fungal tissue of *Armillaria mellea* and Herth *et al.* (5) recorded a fiber diagram from the lily pollen tube that appears to be identical with both of the above. Marchessault *et al.* (10) showed that curdlan crystallizes well after annealing and that its diffraction diagrams vary with the degree of hydration of the sample. All diffraction diagrams, however, were similar to those obtained from other β-(1→3)-D-glucans.

On the strength of the similarities between the X-ray diagram of the glucan and that of the β-(1→3)-xylan, the structure of which was shown by Atkins and Parker (11) to be a triple helix, both Jelsma and Kreger (9) as well as Scott and Rees (8) have suggested that the glucan has a similar structure. In fact, Scott and Rees (8) performed a computer modeling analysis using hard-sphere techniques to show that a triple helix for the glucan was possible. In addition, Jelsma and Kreger concluded that a triple helix was in agreement with the observed unit cell (9). Similarly, the triple helix of the β-(1→3)-D-xylan was predicted from conformational calculations by Sathyanarayana and Rao (12).

In this article, we report the results of a conformational analysis of possible single and multiple helices for β-(1→3)-glucan, performed with Lennard–Jones potential energy functions augmented with a term for hydrogen bonds (13). The allowed models were evaluated with the help of X-ray data from a fiber diagram obtained from oriented gels of lentinan, a linear β-(1→3)-glucan isolated from the fungus *Lentinus elodes* (14).

Experimental

Sample

A sample of pure lentinan was obtained from Dr. J. Hamuro of Ajinomoto Co., Inc., Kawasaki, Japan. The polysaccharide was reported to be predominantly linear with some β-(1→6) branching linkages present in the molecule. The average molecular weight was approximately one million. The nmr spectrum of the sample (in DMSO) revealed no inconsistencies with the expected structure and the sample was used without further purification.

X-Ray Diffraction

Fibers of lentinan suitable for X-ray diffraction were prepared by drying of 2% aqueous gels. The material was first dissolved in 1 *N* NaOH overnight at room temperature and subsequently dialyzed 2 days against distilled water. A small amount of the resulting gel was placed between two glass beads held in a fiber stretching clamp, stretched about 50% and left to dry at room temperature. The density of the fibers was measured by flotation in a solution of *p*-xylene/carbon tetrachloride and was 1.547 g/cc (±0.002).

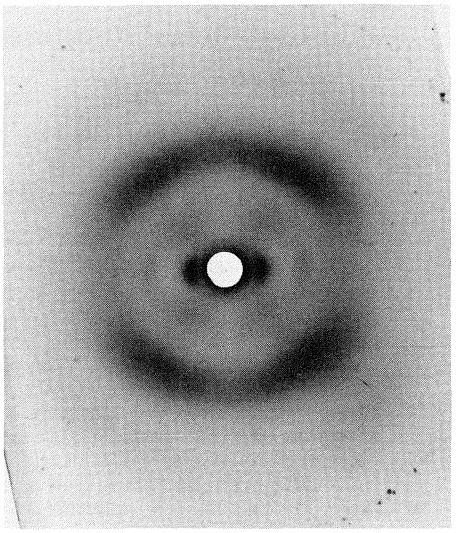

FIG. 1. X-Ray diffractogram of lentinan fiber taken in vacuum. Fiber axis is vertical.

X-Ray diffraction diagrams were obtained in a flat plate camera using CuK_α radiation and at relative humidities ranging from 50% to 100%. A typical fiber diagram of lentinan is shown in Fig. 1.

Conformational Calculations

The conformational analysis was performed for all possible single-strand helices obtainable by rotations of a specified, fixed monomer residue about the bonds linking it to glycosidic oxygens. (The rotational angle about the $C(1)—O_{glyc}$ bond is henceforth referred to as ϕ and the angle about the $C(3)—O_{glyc}$ bond as ψ.) The monomer residue was kept rigid in the *C1* conformation and its atomic coordinates were taken from the average residue of Arnott and Scott (15). The bond angle at the glycosidic oxygen was fixed at 118° and the O(6) hydroxymethyl group was left invariant in the *gg* rotational position.[1] The same conformational analysis was performed for double parallel-stranded, double antiparallel-stranded, and triple parallel-stranded helices in which the strands were translationally in phase, *i.e.* the glycosidic oxygens of each strand were on the same level along the helix axis.

The single-strand helical conformations were created in the usual fashion, by performing ϕ and ψ rotations at 10° intervals in the range −180° to +180° (or at 1° intervals in areas of particular interest). The multi-strand helices were obtained by symmetry operations on the first strand. For example, a double parallel-strand helix with

[1]Refer to ref. 16 for the description of *gt*, *gg*, and *tg* terminology.

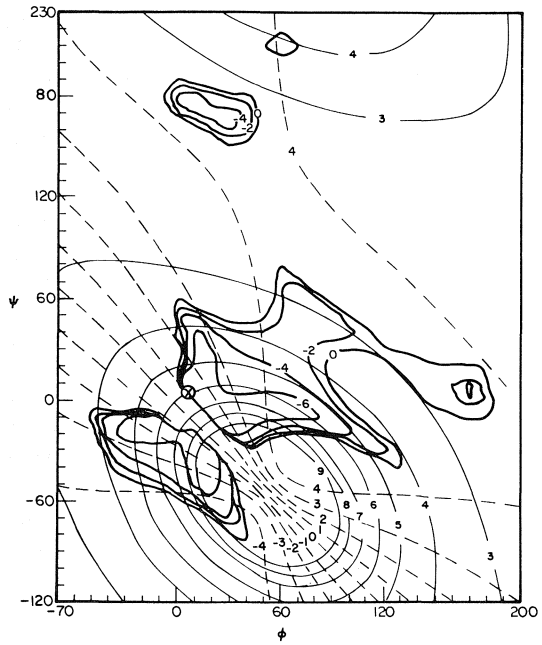

FIG. 2. Conformational energy map for single helical β-(1→3)-D-glucan as a function of rotations about the C(1)—O bond (ϕ) and the C(3′)—O bond (ψ). The (ϕ,ψ) = (0,0) position is with the atom sequence H(1)—C(1)—O—C(3′)—H(3′) in plane and the bonds H(1)—C(1)—O—C(3′) and C(1)—O—C(3′)—H(3′) *cis*. The energy contours are in kcal/mol; the thin solid lines denote constant n; the dashed lines denote constant h (negative h indicates left-handed helices). The conformation denoted by a cross is a minimum energy conformation in agreement with observed X-ray data.

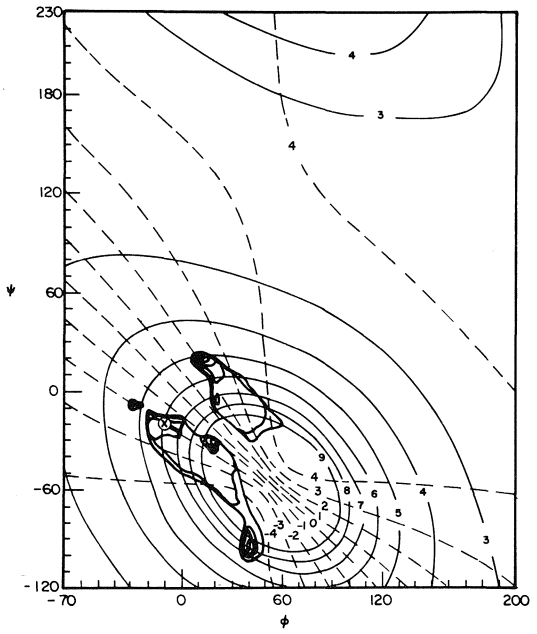

FIG. 3. Conformational energy map for double parallel stranded helical β-(1→3)-D-glucan. (For further explanation see the caption of Fig. 2.)

given ϕ,ψ angles was obtained by first creating the required single strand (by ϕ–ψ rotations), then creating the second strand by imposing a two-fold rotation about the helix axis on the first strand. Similarly, the double antiparallel-strand helix was created by symmetry operations involving two-fold rotation about the helix axis coupled with inversion about an axis at right angles to the helix axis. (The inversion axis was at $z = 0$.) The triple parallel-strand helix was created by a three-fold rotation about the helix axis. All strands of a multiple helix thus possessed the same ϕ,ψ angles.

The probability of the helices was evaluated by calculating their conformational nonbonded energy V_{NB}, using a Lennard–Jones potential energy function augmented with a third term for non-directional hydrogen bonds (13)

$$[1] \quad V_{NB} = \sum_{\substack{i=1 \\ j=1}} A r_{ij}^{-12} + B r_{ij}^{-6} + C r_{ij}^{-3}$$

where the summation is over all pairwise interactions between atoms i and j separated by a distance r_{ij}. In the evaluation of V_{NB} for a given multi-strand helix, the interactions between all atoms of a reference residue and those in the residues in one complete turn of the helix of each strand above and below the reference residue were included in the summation. The conformations with V_{NB} higher than 0 kcal/mol were judged to be improbable. The regions of probable conformations were described as isoenergy contour maps as a function of ϕ and ψ rotations. The resulting maps, with superimposed n (number of residues per turn) and h (axial rise per residue in Å) contours, are shown in Figs. 2–5.

All conformational calculations were done with a CDC 3200 computer.

Results and Discussion

The diffraction diagrams of lentinan showed only poor crystallinity, but they were similar in appearance to the diagrams obtained from native crystalline β-(1→3)-glucans of the pollen tube of *Lilium longiflorum* (5) and the fungus *Armillaria mellea* (9). The patterns were apparently not affected by the relative humidity of the surroundings, as all of them showed two well oriented equatorial reflections at ~14.5 and ~6.7 Å, and a spread of intensity on the first layer line centered at ~4.5 Å. The fiber repeat was ~6 Å. The equatorial reflections and the fiber repeat are in rough agreement with the hexagonal unit cell $a = b = 15.8$ Å and $c = 5.95$ Å proposed for *A. mellea* (9). This unit cell

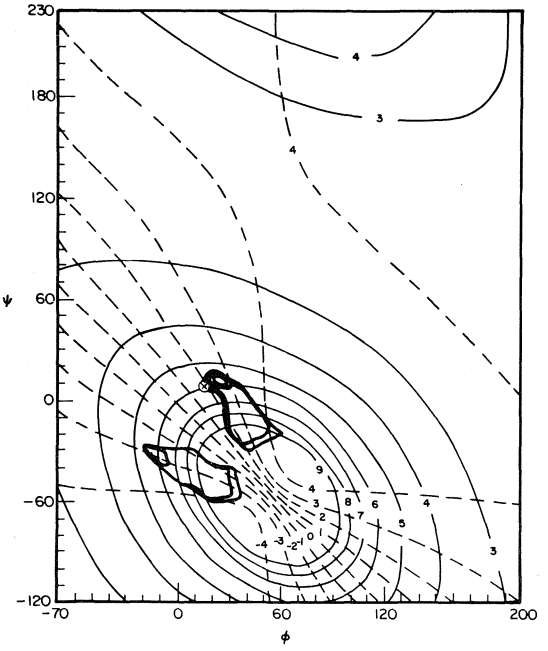

FIG. 4. Conformational energy map for double antiparallel stranded helical β-(1→3)-D-glucan. (For further explanation see the caption of Fig. 2.)

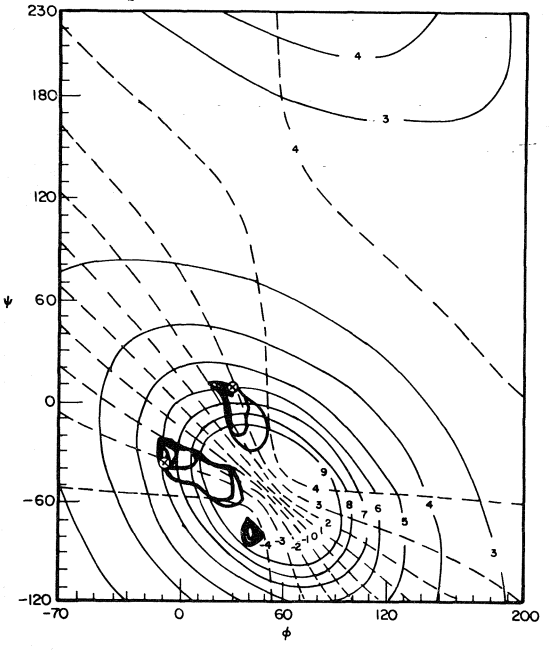

FIG. 5. Conformational energy map for triple all parallel stranded helical β-(1→3)-D-glucan. (For further explanation see the caption of Fig. 2.)

is also in agreement with those obtained on curdlan by Scott and Rees (8) and Marchessault *et al.* (10). It thus appears that regardless of source, all β-(1→3)-glucans that have been studied crystallize in nearly the same hexagonal unit cell. The volume of this cell and the observed density are in agreement with six glucose residues and approximately 12 water molecules per cell. However, as demonstrated by Marchessault *et al.* a lower hydrate can be obtained, with decreased hexagonal unit cell dimensions (10).

As is evident from the conformational energy maps (*cf.* Figs. 2–5), minimum energy conformations that are in agreement with the fiber repeat exist for the single helix as well as all multiple helices. A total of five such conformations were found: one single helix, one parallel-stranded double helix, one antiparallel-stranded double helix, and two triple helices. Their features are shown in Table 1. It must be remembered that the symmetry rules require that for the double parallel helix only layer lines with $l = 2n$ (where n is an integer) be present in the diffraction diagram and, similarly, for the triple helix only layer lines with $l = 3n$. The same is not true for the antiparallel-stranded double helix but the odd-order layer lines are likely to be so weak as to be unobservable. The repeats per turn shown in Table 1 are thus consistent with the observed $c \cong 6$ Å crystal repeat.

The types of hydrogen bonds possible in these conformations have been included in Table 1. The lengths of these bonds do not reflect the most probable values because they result from fixed conformations. When a promising conformation is refined as described below, the hydrogen bond lengths always undergo adjustments toward more reasonable values, provided the structure itself is stereochemically reasonable.

The probability of each of the five helices as a suitable model for the crystal structure of lentinan was tested in two ways: (*1*) by packing analysis, and (*2*) by Fourier transform calculations. In the packing analysis, each model was packed into the unit cell while minimizing the function (17)

$$[2] \quad Y = \sum_{i=1}^{l} \left(\frac{r_i - r_{0i}}{\mathrm{SD}_i^r} \right)^2 + \sum_{i=1}^{m} \left(\frac{\theta_i - \theta_{0i}}{\mathrm{SD}_i^\theta} \right)^2 + \sum_{i=1}^{n} \left(\frac{\phi_i - \phi_{0i}}{\mathrm{SD}_i^\phi} \right)^2 + \frac{1}{W^2} \sum_{\substack{i=1 \\ j=1}}^{N} w_{ij}(d_{ij} - d_{0ij})^2$$

TABLE 1. Helix characteristics of the most probable predicted conformations

Helix type	Handedness	n	h (Å)	Repeat/turn (Å)	ϕ, ψ (deg)	V_{NB} (kcal/mol)	Hydrogen bond type and approximate length (Å)
Single	Right	6	0.98	5.88	6, 5	−8	O(2)---O(2′) intrachain, 2.7
Double parallel	Left	6	2.0	12.0	−11, −20	−14	O(2)---O(2′) intrachain, 3.0
Double antiparallel	Right	6	1.83	10.98	15, 8	−12	O(2)---O(2′) intrachain, 3.1
Triple	Left	6	3.3	19.8	−10, −40	−21	O(2)---O(2) interstrand, 2.5
Triple	Right	6	2.9	17.4	30, 10	−24	O(2)---O(2) interstrand, 2.9

TABLE 2. Packing of the five most probable models

Helix	O(6) rotation	Packing energy (arbitrary units)*		
		Total PE	Interchain	Intrachain
Single	*gg*	15	5	10
Double parallel	*gg*	26	14	12
Double antiparallel	*gg*	62	53	9
Triple (left)	*gt*	15	4	11
Triple (right)	*gt*	15	6	9

*See text.

where r_i are bond lengths, θ_i bond angles, ϕ_i conformation angles and d_{ij} nonbonded distances. The corresponding standard values (r_{0i}, θ_{0i}, ϕ_{0i}) were obtained from known carbohydrate structures (15) and the standard d_{0ij} were previously determined by us from packing of carbohydrate crystal structures (18). In this fashion, both the chain conformation and packing were simultaneously optimized.

The results of this analysis are shown in Table 2. It has been found convenient to compare the packing of different models by comparing values of the last term of eq. 2, which has been termed a 'packing energy', PE. The latter can be subdivided into two parts, one for interchain and the other for intrachain contacts and both are shown in Table 2. The conformational energies described by the first three terms of eq. 2 usually change little and for that reason, are not shown. (Generally, only terms 2, 3, and 4 of eq. 2 were minimized during refinement. Bond lengths were usually left fixed because they varied very little.) It was previously found with other polysaccharides that when PE increases above 20, packing of chains becomes increasingly difficult. With this criterion in mind, it is clear that both the single helix and the two triple helices can pack into the unit cell of lentinan extremely well, but the double helical models are encountering difficulties. When the packing tests were repeated with smaller hexagonal cells, such as the one for the lower hydrate (10), neither the single nor the double helical models could pack, but both triple helices still packed with ease.

As a second test, the Fourier transform of each helix was calculated using the equation:

$$[3] \quad F(R,\psi,Z) = \sum_n \sum_j f_j J_n(2\pi R r_j) \times \exp\{i[n(\psi - \phi_j + \pi/2) - 2\pi Z z_j]\}$$

where $F(R,\psi,Z)$ is the numeric value of the transform at the point in reciprocal space with cylindrical coordinates R,ψ,Z, f_j is the atomic scattering factor and r_j, ϕ_j, z_j are the cylindrical polar coordinates of the jth atom. $J_n(X)$ is the Bessel function of order n and argument X. The transform was calculated for the rotational coordinate ψ ranging from 0° to 60° in 10° increments and for the Z coordinate of all required layer lines. Radial sections of the transforms at ψ identical with best packing position of each model are shown in Fig. 6. The relative magnitudes of the observed intensities are shown for comparison in each transform as vertical lines.

Even a casual comparison of the transforms shows that only the triple helices account in a satisfactory manner for the observed intensities.

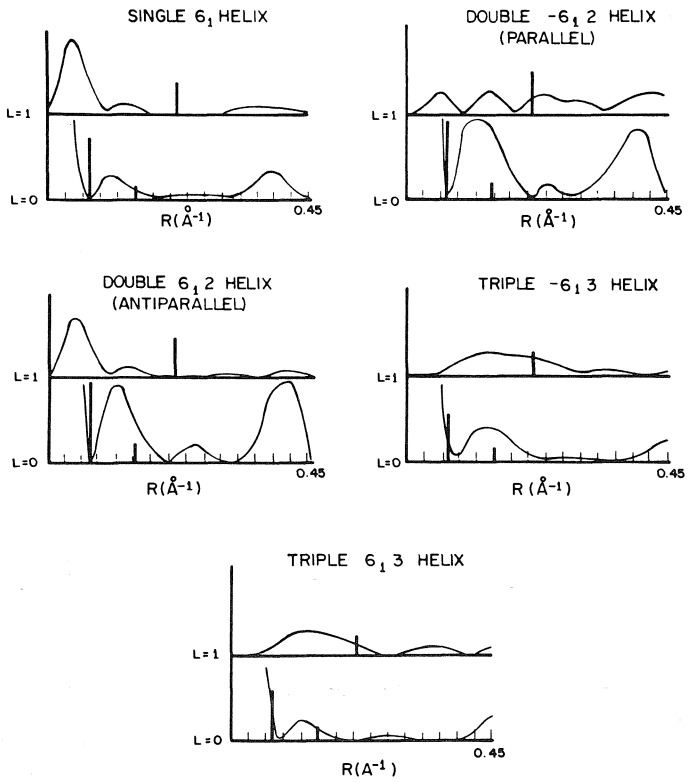

FIG. 6. Predicted intensity distribution on observed layers 0 and 1 for the five probable conformations of β-(1→3)-D-glucan, as calculated from eq. 3. The observed intensities are denoted by vertical lines of approximately correct height as an indication of magnitude.

TABLE 3. Structure amplitudes of equatorial reflections for the triple helical models

Reflection	*F*(calcd) Left-handed helix	*F*(obs)*	*F*(calcd) Right-handed helix
100	69	54	62
110	23	31	38
200	30	37	22

*It was assumed that the reflections (110) and (200) each contributed 50% of the uncorrected intensity occurring at 6.7 Å.

The single helix and the antiparallel double helix can be ruled out immediately because they predict no intensity on the first layer where substantial intensity is present in the X-ray diagram. Likewise, the double parallel helix can be ruled out because the observed high intensity equatorial reflection falls into a trough in the transform. On the other hand, both left- and right-handed triple helices yield transforms that are in good agreement with the observed intensity distribution. This agreement is particularly evident when a comparison is made of calculated and observed structure amplitudes for the equatorial reflections, as shown in Table 3. Furthermore, the triple helix transforms in best agreement with experimental intensity distributions were obtained when the rotational coordinate ψ was nearly identical with the rotational position of the best packing triple helix models. This was true for both left- and right-handed triple helices.

It is thus probable that the crystal structures of β-(1→3)-glucans of lentinan, curdlan, *A. mellea*, and *Lilium longiflorum* are based on a triple helix. The limited X-ray data available from lentinan do not allow determination of the helix chirality, but this should not be a problem with the data available from curdlan (10). In any case, the left- and right-handed triple helices are surprisingly alike, as shown in Fig. 7, both

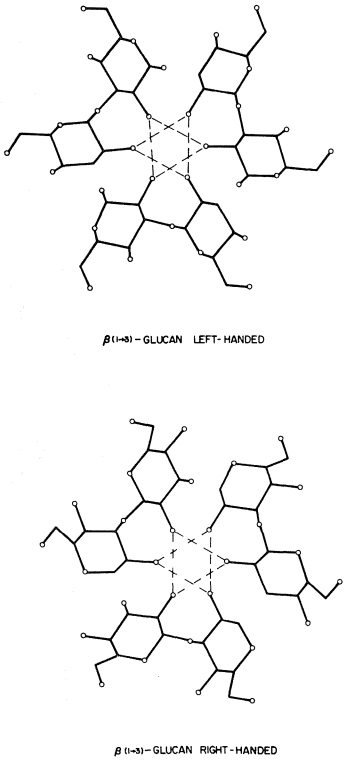

FIG. 7. Projection in the x–y plane of the first two residues of each strand of the left- and right-handed triple helical models.

structures being stabilized by an interstrand O(2)---O(2) hydrogen bond network, as was the case in the structure of β-(1→3)-xylan. Because the latter is right-handed, it is probable that the triple helix of the glucan may also be right-handed.

Acknowledgment

This work has been supported by the National Science Foundation grant No. MPS7501560. We thank Dr. J. Hamuro for the sample of lentinan.

1. E. PERCIVAL and R. H. MCDOWELL. Chemistry and enzymology of marine algal polysaccharides. Academic Press, London. 1967.
2. E. FREI and R. D. PRESTON. Nature, **192**, 939 (1961).
3. I. M. MACHIE and E. PERCIVAL. J. Chem. Soc. 1151 (1959).
4. D. J. MANNERS AND A. J. MASSON. Fed. Bur. Biochem. Soc. Lett. **4(2)**, 122 (1969).
5. W. HERTH, W. W. FRANKE, H. BITTIGER, A. KUPPEL, and G. KEILICH. Cytobiologie, **9**, 344 (1974).
6. G. O. ASPINALL. Polysaccharides, Pergamon Press, Oxford. 1970. pp. 74–80.
7. A. E. CLARKE and B. A. STONE. Biochim. Biophys. Acta, **44**, 161 (1960).
8. W. E. SCOTT and D. A. REES. Private communication; D. A. REES. *In* M.T.P. international review of science: organic chemistry, Series 1. Vol. 7. Carbohydrates. *Edited by* G. O. Aspinall. Butterworths, London. 1973. p. 251.
9. J. JELSMA and D. R. KREGER. Carbohyd. Res. **43**, 200 (1975).
10. R. H. MARCHESSAULT, Y. DESLANDES, K. OGAWA, and P. R. SUNDARARAJAN. Can. J. Chem. This issue.
11. E. D. T. ATKINS and K. D. PARKER. J. Polym. Sci. Part C, **28**, 69 (1969).
12. B. K. SATHYANARAYANA and V. S. R. RAO. Carbohyd. Res. **15**, 137 (1970).
13. J. BLACKWELL, A. SARKO, and R. H. MARCHESSAULT. J. Mol. Biol. **42**, 379 (1969).
14. G. CHIHARA, Y. MAEDA, T. SASAKI, F. FUKUOKA, and G. HAMURO. Nature, **222**, 687 (1969).
15. S. ARNOTT and W. E. SCOTT. J. Chem. Soc., Perkin Trans. II, **2**, 324 (1972).
16. A. SARKO and R. H. MARCHESSAULT. J. Polym. Sci. Part C, **28**, 317 (1969).
17. P. ZUGENMAIER and A. SARKO. Biopolymers. In press.
18. P. ZUGENMAIER and A. SARKO. Acta Crystallogr. **B28**, 3158 (1972).

X-Ray diffraction data for β-(1→3)-D-glucan

R. H. MARCHESSAULT, Y. DESLANDES, K. OGAWA,[1] AND P. R. SUNDARARAJAN[2]

Département de Chimie, Université de Montréal, Montréal, P.Q., Canada H3C 3V1

Received June 28, 1976

R. H. MARCHESSAULT, Y. DESLANDES, K. OGAWA, and P. R. SUNDARARAJAN. Can. J. Chem. **55**, 300 (1977).

The conformation of a bacterial β-(1→3)-D-glucan (curdlan) was studied by X-ray diffraction measurements on fiber diagrams. The glucan fiber, prepared by extruding a dimethyl sulfoxide solution of the glucan into methanol and washing in water (**A**) was of low crystallinity but with a characteristic diffraction and orientation 'as spun'. The same fiber annealed in water, under tension, at 140 °C, in a closed bomb, was of higher crystallinity and occurred as two reversible crystalline polymorphs: one at high relative humidity (**B**) and the other at relative humidities less than 20% (**C**). All three X-ray diagrams displayed the X-shaped patterns characteristic of helical conformations; equatorial diffraction corresponded to hexagonal packing. The fiber axis data for **B** and **C** coupled with a conformational study and density data leads to a proposed three-stranded helical structure with $P6_3$ symmetry.

Curdlan in water forms an irreversible gel when a 2–4% solution is heated above 55 °C. The same gel given the annealing treatment described above undergoes syneresis and the gel properties are lost.

R. H. MARCHESSAULT, Y. DESLANDES, K. OGAWA et P. R. SUNDARARAJAN. Can. J. Chem. **55**, 300 (1977).

La conformation d'un β-(1→3)-D-glucan d'origine bactérienne ("curdlan") a été étudié par diffraction de rayons-X (diagramme à fibre). Les fibres du glucan préparé par extrusion de ce dernier en solution dans le diméthylsulfoxide dans le méthanol et lavés à l'eau (**A**) étaient de faible cristallinité, mais montraient une orientation dès l'extrusion. Les mêmes fibres après avoir été recuites, dans l'eau sous tension, à 140 °C dans une bombe fermée, montraient une haute cristallinité, ainsi que la présence de deux polymorphes cristallins, réversibles: le premier à une humidité relative élevée (**B**) et le second à une humidité relative plus faible que 20% (**C**). Les 3 différents diagrammes montrent un cliché de diffraction caractéristique d'une conformation hélicoidale et correspondent à une maille hexagonale. Les dimensions selon l'axe de la fibre pour **B** et **C**, les valeurs des densités, ainsi qu'une étude conformationnelle nous amènent à proposer une triple-hélice pour la structure du "curdlan", ayant une symétrie $P6_3$.

Le "curdlan" forme dans l'eau un gel irréversible quand une solution de 2–4% est chauffée au dessus de 55 °C. Le même gel exposé au "recuit" décrit précédemment, subit une synérèse et les propriétés du gel sont perdues.

We wish to report X-ray fiber diffraction data which we have obtained from the extracellular bacterial polysaccharide curdlan produced by the Takeda Chemical Co., Osaka, Japan (1). This sample was dissolved in dimethyl sulfoxide (DMSO) and high resolution proton and ^{13}C resonance spectra were recorded and interpreted to show that the polysaccharide was >99% pure β-(1→3)-D-glucan (2). A proof of the chemical homogeneity of this polysaccharide based on chemical methods has also been given (3).

Oriented fibers were prepared by extruding a 10% solution of curdlan in DMSO into methanol at room temperature. The weakly crystalline and oriented fibers were further crystallized by washing in water and annealing in a thermostated, sealed bomb at 143 °C in the presence of H_2O. The fibers which were under a constant load elongated about 70% under these conditions but did not break. The observed X-ray diffraction patterns, after the annealing treatment, were of a quality significantly better than what has been reported so far, both as regards orientation, crystallinity, and number of polymorphs (1, 4, 5).

X-Ray fiber patterns were recorded in a flat film camera at controlled relative humidities (r.h.). Shown in Fig. 1 (and schematically in Fig. 2) are patterns corresponding to: **A**, the extruded fiber washed in water and exposed to X-rays at

[1]On leave from: Radiation Center of Osaka, Prefecture, Sakai, Osaka 593, Japan.

[2]Present address: Xerox of Canada, Mississauga, Ontario, Canada.

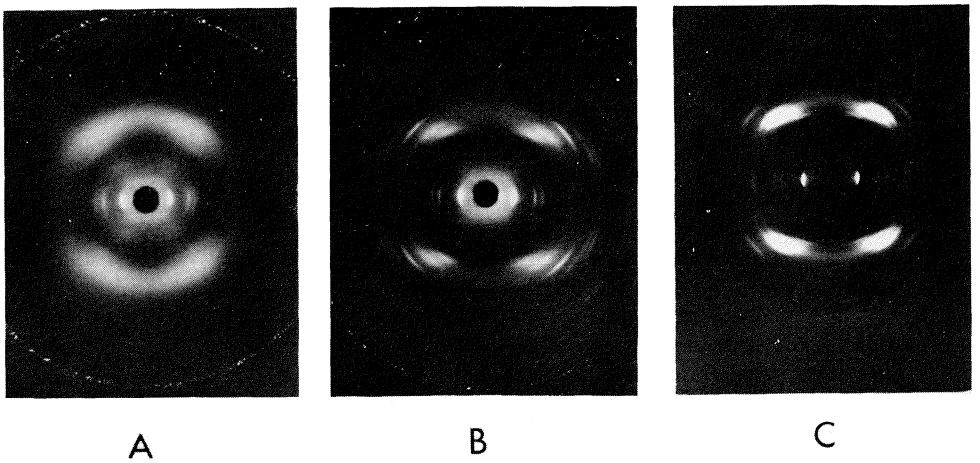

FIG. 1. X-Ray diffraction patterns of oriented curdlan fibers showing the three different polymorphs: **A** as spun, after washing and drying, at 75% r.h.; **B** after annealing in water at 143 °C, at 75% r.h.; **C** same as **B**, at 0% r.h. Data were recorded at same film to sample distance.

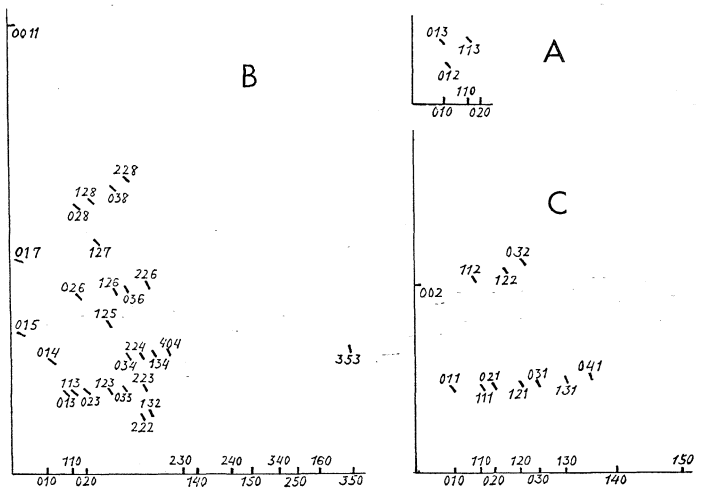

FIG. 2. Indexed schematic display of the X-ray patterns corresponding to those in Fig. 1.

75% r.h., a similar pattern was also observed at 0% r.h.; **B**, the annealed fiber exposed to X-rays at 75% r.h.; **C**, the same fiber as **B** at 0% r.h. It was possible to go reversibly from **B** to **C** simply by adjusting the relative humidity in the camera.

It seemed that 20% r.h. was the changeover point where elements of both patterns **B** and **C** were observed together and there was no obvious evidence of a gradual transition from one phase to the other.

The very extensive change in the patterns on going from **A** to **B** is not unexpected when one considers the annealing treatment. It seems likely that the 'melting' of curdlan crystals in the presence of H_2O occurs somewhere around 140 °C, hence a drastic recrystallization has occurred in going from **A** to **B**.

Although **C** is less rich in diffraction data than **B**, it is a pattern of equal quality as may be judged by the extensive equatorial diffraction and sharpness of the diffraction spots. Since this pattern was recorded at zero r.h., and did not change even after the sample was dried at 60 °C in vacuum, it is believed to be a dehydrated form of **B** which would then correspond to a crystalline hydrate.

TABLE 1. Parameters of curdlan fiber diffraction patterns interpreted as multiple helices

Pattern	Characteristic	Hexagonal base $a = b$ (Å)	Fiber axis c (Å)	Density† (g/cm^3)	Number of glucose units per unit cell	Number of water molecules per unit cell	Number of chains per unit cell
A	Before annealing	17	22	1.45	30	—	4–6
B	Hydrated form* (after annealing)	15.71 ± 0.05	18.82 ± 0.05	1.47	18	36	3
C	Dehydrated* (after annealing)	14.38 ± 0.05	5.79 ± 0.05	1.49	6	0	3

*Lattice parameters were obtained by a least-squares refinement program.
†As measured by flotation in a solution of *p*-xylene and chloroform.

Table 1 gives the unit cell, density, and other data corresponding to the crystal structures of the three samples. The fiber repeat changes drastically from **B** to sample **C**. The latter could correspond to a sixfold helix with a 0.96 Å advance per monomer but both conformational analysis and intensity calculations reject this possibility (4, 6). It is hard to explain the drastic change in the fiber repeat in the transformation **B** $\rightleftharpoons$ **C** unless there is a very close similarity between the helix parameters in the two cases since there is no visible macroscopic rearrangement in the sample. At this point, the data for **C** are best interpreted in terms of three intertwined 6_1 helices with an advance per monomer of 2.89 ± 0.05 Å, *i.e.* a triple helical structure similar to what has been proposed (7) for its crystalline homolog β-(1→3)-D-xylan. This leads to a c value which is 1/3 of the repeat of the individual helices and we propose that this same symmetry, which corresponds to the space group $P6_3$, is present in **C**. Conformational analysis by the virtual bond method (8) for a sixfold helix with a 5.79/2 Å advance per monomer leads to a stereochemically acceptable structure. Fourier transform calculations for triple helices of this kind (4) confirm the above interpretation.

In the case of the hydrated polymorph **B** the $P6_3$ symmetry is lost in the triple strand structure as evidenced by the 18.82 ± 0.05 Å repeat instead of 5.79 ± 0.05 Å repeat. A simple explanation is that addition of water of hydration takes place in a fashion so as to destroy the $P6_3$ symmetry and cause a slight increase in helix pitch which now becomes the fiber repeat. The observed intensification of the apparent 11th order meridional reflection (1.7 ± 0.1 Å) on tilted-fibre photographs characterizes the new molecular periodicity, the significance of which is yet to be established.

The base plane parameters for **B** are similar to those reported by Kreger and Jelsma (5) as well as Bluhm and Sarko (4), while **A** lattice is similar to that reported by Harada (1). The dry form **C** has not been reported to date. The fiber repeat of 18.82 ± 0.05 Å for **B** is reported for the first time thanks to the superior resolution of our patterns.

Evidence so far points to the fact that the β-(1→3)-D-glucan linkage encourages multiple helices (4, 5, 7). In fact at this point we have no definitive interpretation of the helical arrangement in **A** but it would appear that a somewhat irregular and disordered multiple helical structure would be in keeping with the poor quality of the observed data. In view of the importance of gaining a full understanding and definition of the triple helical structure in glucans it would appear that **C** is the pattern whose full interpretation will be most rewarding.

Gelation Phenomenon

Multiple helix interactions have been suggested as a gelling mechanism for polysaccharides (9) and one would expect that the aqueous curdlan system would fall into this category also. Indeed it is reported to form an irreversible gel on heating (1) but the quality of the gel is related to the different types of interactions between chains such as involved in the different crystal structures **A** and **B**. Our original sample is an amorphous, particulate material derived from a spray-drying process. On heating a 2–4% suspension in water, a slight clearing of the suspension occurs at 55 °C then gelation to a resilient gel which resists further change even at the boil. This gel on drying gives an X-ray pattern corresponding to **A** in Fig. 1. When the gel is placed in a sealed bomb with H_2O and heated to 160 °C for 1 h, there is considerable deswelling (syneresis) of the gel and

a pattern corresponding to **B** is obtained. The syneresis can be sufficiently severe to crumple the gel. Finally if the syneresed gel is dried over P_2O_5 it will yield a pattern corresponding to **C**.

Observations in the polarizing microscope show that under 100 °C, the gel was only slightly birefringent and was made of the swollen original particles which filled the container. The cohesion between these particles would seem to be due to a cocrystallization of 'surface solubilized' chains of touching particles. The syneresed gel is highly birefringent and clearly the high temperature has encouraged solution then extensive interaction between the intertwining helices so as to expel the intercrystalline water and form a far less swollen gel. Thus if the degree of crystallinity is too great in multiple stranded structures the 'pseudo-crosslink' effect of the crystallites, which leads to gelation, is lost. In other words, under the right conditions crystallization forces can 'squeeze' the gel dry.

Acknowledgements

We wish to thank the National Research Council of Canada and the Ministère de l'Education du Québec for financial support.

1. T. HARADA, Process Biochem. **9**, 21 (1974).
2. M. VINCENDON. Private communication.
3. I. NAKANISHI, T. KANAMARU, K. KIMURA, A. MATSUKURA, M. ASAI, T. SUZUKI, and S. YAMATODANI. Presented at 278th Meeting of the Kansai Branch of Agr. Chem. Soc. Japan, Osaka, 1972.
4. T. L. BLUHM and A. SARKO. Can. J. Chem. This issue.
5. J. JELSMA and D. R. KREGER. Carbohyd. Res. **43**, 200 (1975).
6. B. K. SATHYANANAYANA and V. S. R. RAO. Biopolymers, **10**, 1605 (1971).
7. E. D. T. ATKINS, K. D. PARKER, and R. D. PRESTON. Proc. Roy. Soc. B, **173**, 209 (1969); E. D. T. ATKINS and K. D. PARKER. J. Polym. Sci. C, **28**, 69 (1969).
8. P. R. SUNDARARAJAN and R. H. MARCHESSAULT. Can. J. Chem. **53**, 3563 (1975).
9. D. A. REES, I. W. STEELE, and F. B. WILLIAMSON. J. Polym. Sci. C**28**, 261 (1969).

The preparation and the crystal and molecular structure of tetradecamethylcycloheptaphosphazene, $(NPMe_2)_7$

KEITH D. GALLICANO, RICHARD T. OAKLEY, NORMAN L. PADDOCK, STEVEN J. RETTIG, AND JAMES TROTTER

Department of Chemistry, University of British Columbia, 2075 Wesbrook Mall, Vancouver, B.C., Canada V6T 1W5

Received July 27, 1976

KEITH D. GALLICANO, RICHARD T. OAKLEY, NORMAN L. PADDOCK, STEVEN J. RETTIG, and JAMES TROTTER. Can. J. Chem. **55**, 304 (1977).

The preparation of tetradecamethylcycloheptaphosphazene, by the methylation of the corresponding fluorophosphazene $(NPF_2)_7$ with methylmagnesium bromide, is reported. Crystals of tetradecamethylcycloheptaphosphazene are monoclinic, $a = 13.160(1)$, $b = 11.685(1)$, $c = 18.576(1)$ Å, $\beta = 108.333(5)°$, $Z = 4$, space group $C2/c$. The structure was solved by direct methods and was refined by full-matrix least squares procedures to a final R of 0.046 and R_w of 0.063 for 2568 reflections with $I \geq 3\sigma(I)$. The molecule has crystallographic C_2 symmetry with mean bond lengths (rms deviations from the mean in parentheses, bonds not involving hydrogen have been corrected for libration) P—N, 1.592(6), P—C, 1.804(11), and C—H, 0.94(7) Å, and mean angles in the 14-membered ring are 132.9° at N and 117.1° at P.

KEITH D. GALLICANO, RICHARD T. OAKLEY, NORMAN L. PADDOCK, STEVEN J. RETTIG et JAMES TROTTER. Can. J. Chem. **55**, 304 (1977).

On rapporte la préparation du tétradécaméthylcycloheptaphosphazène par méthylation du fluorophosphazène correspondant $(NPF_2)_7$ par le bromure de méthylmagnésium. Les cristaux de tétradécaméthylcycloheptaphosphazène sont monocliniques, $a = 13.160(1)$, $b = 11.685(1)$, $c = 18.576(1)$ Å, $\beta = 108.333(5)°$, $Z = 4$, groupe d'espace $C2/c$. On a résolu la structure par les méthodes directes et on l'a affinée par la méthode des moindres carrés (matrice complète) jusqu'à une valeur finale de $R = 0.046$ et $R_w = 0.063$ pour 2568 réflexions avec $I \geq 3\sigma(I)$. La molécule a une symétrie cristallographique C_2 avec des longueurs de liaison moyennes (les déviations rms par rapport à la moyenne sont entre parenthèses et les liens n'impliquant pas d'hydrogène ont été corrigés pour les librations) P—N, 1.592(6), P—C, 1.804(11), et C—H, 0.94(7) Å; les angles moyens dans le cycle à 14 membres sont 132.9° au niveau de l'azote et de 117.1° au niveau du phosphore.

[Traduit par le journal]

Introduction

The methylphosphazenes $(NPMe_2)_{3,4}$ have been known for many years (1), but the preparation of the pentameric compound $(NPMe_2)_5$ has only recently been reported (2). In the present paper the preparation of the heptameric derivative $(NPMe_2)_7$ is described. The method, which employs the action of methylmagnesium bromide on the appropriate fluorophosphazene, is generally applicable to the preparation of methylphosphazenes $(NPMe_2)_n$ of large ring size ($n \geq 6$), and has been used to extend the series of known methylphosphazenes from the trimeric to the decameric derivatives.

Unlike dimethylsiloxanes (3–5), and many phosphazenes of large ring sizes, all the methylphosphazenes $(NPMe_2)_{3-10}$ are crystalline solids at room temperature and, as such, are potentially useful sources of structural information. The molecular structures of $[NP(OMe)_2]_{4,6,8}$ (6–8) and $[NP(NMe_2)_2]_{4,6,8}$ (9–11) all show interesting conformational effects, but their interpretation in terms of nonbonded interactions is complicated by the size and shape of the ligands. In the case of the methylphosphazenes however, the more nearly spherical nature of the methyl ligands and their smaller size greatly reduces the number of nonbonded interactions, and conformational trends are therefore more easily understood. Consequently, the crystal structure determinations of several methylphosphazenes of large ring size are currently being carried out; that of the heptamer $(NPMe_2)_7$ has recently been completed and is reported here.

A comprehensive analysis of the structural data is planned for the series $(NPMe_2)_{3-10}$ upon completion of the structural work.

Experimental

Preparation of $(NPMe_2)_7$

A solution of $(NPF_2)_7$[1] (3.28 g, 5.65 mmol) in 50 ml of diethylether was added, under an atmosphere of nitrogen, to a stirred solution of MeMgBr (from 2.54 g, 104 mmol of magnesium) in 250 ml of ether. No immediate reaction occurred, but, after an induction period of approximately 2 h, precipation of magnesium salts commenced. To ensure the completion of the reaction, the mixture was heated under reflux for a further 48 h. The solvent was then distilled from the reaction vessel, and the reaction mixture dissolved in 200 ml of water. A 1 *M* solution of sodium carbonate (200 ml) was then added to precipitate all the magnesium as its carbonate. The solution was filtered and the solvent evaporated from the filtrate to leave a white solid, which was repeatedly extracted with chloroform. The solvent was distilled from the combined chloroform extracts to leave a white crystalline solid (0.620 g). The original water-insoluble precipitate was recombined with the water-soluble residue and the mixture boiled in 200 ml of ~1 *M* NaOH for 1 h. This mixture was then refiltered, the solvent removed from the filtrate, and the residue extracted with hot chloroform, thereby affording a further 0.523 g of material soluble in chloroform. The two fractions of the product were combined and purified by sublimation *in vacuo* and recrystallization from hexane to give colourless blocks of $(NPMe_2)_7$ (1.14 g, 2.17 mmol, 40% yield); mp 128–130 °C. *Anal.* calcd. for $C_{14}H_{42}N_7P_7$: C 32.01, H 8.06, N 18.66; found: C 31.90, H 7.96, N 18.80.

The methylphosphazenes $(NPMe_2)_n$ (n = 6 and 8–10) have been prepared using a procedure analogous to that just described. The melting points and the ν_{as}(P=N) stretching frequencies of these compounds are given in Table 1.

X-Ray Crystallographic Analysis of $(NPMe_2)_7$

Colourless crystals of $(NPMe_2)_7$ are obtained by recrystallization from hexane. The crystal chosen for study was mounted with (110) perpendicular to the goniostat axis and had dimensions of *ca.* 0.28 × 0.30 × 0.50 mm. Unit-cell and space group data were obtained from film and diffractometer measurements. The unit-cell parameters were refined by a least squares treatment of $\sin^2\theta$ values for 36 reflections measured on a diffractometer with Cu K_α radiation. Crystal data are:
$C_{14}H_{42}N_7P_7$ f.w. = 525.4
Monoclinic, a = 13.160(1), b = 11.685(1), c = 18.576(1) Å, β = 108.333(5)°, V = 2711.6(4) Å^3, Z = 4, ρ_c = 1.2868(2) g cm^{-3}, $F(000)$ = 1120 (22 °C, Cu K_α, λ = 1.54178 Å, μ = 43.1 cm^{-1}). Absent reflections: hkl, $h + k \neq 2n$, $h0l$, $l \neq 2n$, and $0k0$, $k \neq 2n$. Space group $C2/c$ (C_{2h}^6, No. 15) from structure analysis.

[1] $(NPF_2)_{6-10}$ were prepared by fluorination, with KSO_2F, of a mixture of chlorophosphazenes $(NPCl_2)_n$ (n > 5), and separated by vpc (23).

TABLE 1. Melting points and (P=N) stretching frequencies for the methylphosphazenes $(NPMe_2)_n$ (n = 6–10)

n	Melting point* (°C)	ν(P=N)†
6	163–165	1250
7	128–130	1242
8	171–173	1225
9	123–125	1220
10	100–102	1216

*Uncorrected.
†In cm^{-1}, from solutions in carbon tetrachloride.

TABLE 2. Final positional parameters (fractional × 10^4, P × 10^5, H × 10^3) with estimated standard deviations in parentheses

Atom	x	y	z
P(1)	50000	34440(7)	25000
P(2)	37013(5)	49240(5)	12942(3)
P(3)	48941(5)	66985(5)	8315(3)
P(4)	45991(5)	87244(5)	16702(3)
N(1)	4694(2)	4139(2)	1724(1)
N(2)	3919(2)	5834(2)	724(1)
N(3)	5157(2)	7595(2)	1511(1)
N(4)	5000	9197(3)	2500
C(1)	3939(3)	2496(3)	2540(2)
C(2)	3133(3)	5613(3)	1943(2)
C(3)	2636(3)	4042(3)	723(2)
C(4)	6116(2)	5932(3)	946(2)
C(5)	4619(3)	7387(3)	−78(1)
C(6)	4829(3)	9887(3)	1100(2)
C(7)	3169(4)	8591(4)	1351(6)
H(1*a*)	333(3)	301(3)	249(2)
H(1*b*)	417(4)	207(4)	296(3)
H(1*c*)	367(3)	199(4)	212(2)
H(2*a*)	250(2)	609(3)	165(2)
H(2*b*)	367(3)	614(3)	230(2)
H(2*c*)	286(3)	517(3)	215(2)
H(3*a*)	286(3)	359(4)	47(3)
H(3*b*)	243(3)	356(3)	101(2)
H(3*c*)	204(4)	448(4)	41(3)
H(4*a*)	604(3)	543(3)	57(2)
H(4*b*)	666(3)	644(3)	102(2)
H(4*c*)	628(3)	548(3)	140(2)
H(5*a*)	395(3)	778(3)	−17(2)
H(5*b*)	456(4)	683(4)	−47(3)
H(5*c*)	523(3)	794(3)	−4(2)
H(6*a*)	455(4)	1059(4)	118(3)
H(6*b*)	554(4)	995(4)	127(3)
H(6*c*)	459(4)	970(4)	60(3)
H(7*a*)	301(5)	803(5)	177(3)
H(7*b*)	281(4)	931(5)	146(3)
H(7*c*)	324(10)	833(10)	89(7)

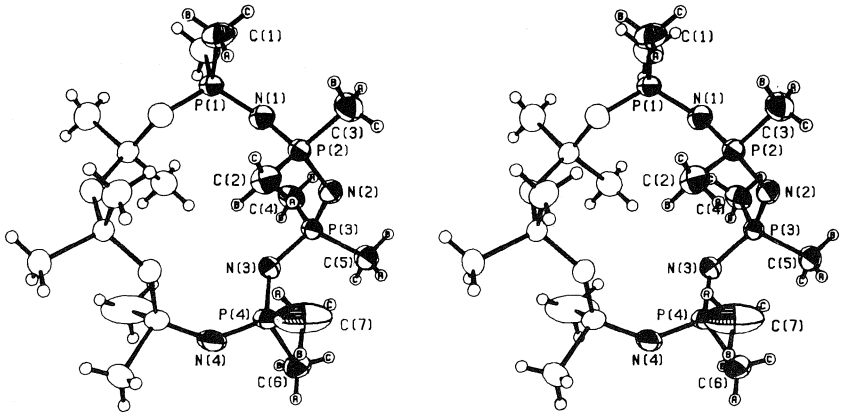

FIG. 1. A stereo view of the tetradecamethylcycloheptaphosphazene molecule; 50% ellipsoids are shown for the nonhydrogen atoms. Hydrogen atoms have been assigned artificially small temperature factors for the sake of clarity.

Intensities were measured on a Datex-automated General Electric XRD 6 diffractometer, with a scintillation counter, Cu K_α (nickel filter and pulse height analyser), and a θ–2θ scan at 4° min^{-1} over a range of (1.80 + 0.86 tan θ) degrees in 2θ, with 10 s background counts being measured at each end of the scan. Data were measured to $2\theta = 160°$ (minimum interplanar spacing 0.78 Å). The intensity of the check reflection, measured every 50 reflections throughout the data collection, decreased slowly to a final value which was 0.97 times the initial value. Lorentz and polarization corrections and check reflection scaling were applied, and the structure amplitudes were derived. An absorption correction was applied by a computer program using a Gaussian integration method (12, 13). Transmission factors ranged from 0.262 to 0.447. Of the 2963 independent reflections measured, 2581 (87%) had intensities greater than $3\sigma(I)$ above background where $\sigma^2(I) = S + B + (0.06S)^2$ with S = scan count and B = time averaged background count. These reflections were used in the solution and refinement of the structure.

The systematic absences allow space groups *Cc* or *C2/c*. The centrosymmetric space group *C2/c* was strongly indicated by the *E*-statistics. The structure was solved by direct methods (14). Fourteen of the 15 nonhydrogen atoms were found among the 20 highest peaks on the *E*-map calculated from the set of signs having the highest consistency index (0.97). Two cycles of isotropic full-matrix least squares refinement of the 14 atoms gave $R = 0.162$. A difference map gave the position of the remaining nonhydrogen atom, C(7). Anisotropic refinement lowered R to 0.066 and a subsequent difference map gave positions for all 21 hydrogen atoms. The entire structure (hydrogen atoms having isotropic thermal parameters) was refined for 8 cycles giving a final R of 0.046 and R_w of 0.063 for 2568 reflections with $I \geq 3\sigma(I)$ (13 reflections which had $|F_o| - |F_c| > 3\sigma(F)$ were removed from the data set in the final stages of refinement).

The least squares refinement was based on the minimization of $\Sigma w[|F_o| - |F_c/(1 + gI)|]^2$ where g is the extinction parameter and I the uncorrected intensity. The final value of g was $1.6(2) \times 10^{-7}$. The scattering factors of ref. 15 were used for the nonhydrogen atoms and those of ref. 16 for the hydrogen atoms. Anomalous scattering factors from ref. 17 were used for the nonhydrogen atoms. The anisotropic thermal parameters employed in the refinement are U_{ij} in the expression:

$$f = f^0 \exp[-2\pi^2(U_{11}h^2a^{*2} + U_{22}k^2b^{*2} + U_{33}l^2c^{*2} + 2U_{12}hka^*b^* + 2U_{13}hla^*c^* + 2U_{23}klb^*c^*)]$$

where f^0 is the tabulated scattering factor and f is that corrected for thermal motion. The weighting scheme: $w = 1/\sigma^2(F)$ where $\sigma^2(F)$ is derived from the previously defined $\sigma^2(I)$ gave uniform average values of $w(|F_o| - |F_c|)^2$ over ranges of $|F_o|$ and was employed in the final stages of refinement.

In the later stages of refinement it became apparent from the large thermal parameters that C(7) and N(4) were most likely disordered. Attempts to refine a split atom disordered model in *C2/c* and an ordered model in *Cc* were unsuccessful. On the final cycle of refinement the mean parameter shift was 0.11σ and the largest shift, 1.0σ, was associated with the x coordinate of H(7*c*). The mean error in an observation of unit weight was 1.625. The final positional and thermal parameters appear in Tables 2 and 3 respectively. Measured and calculated structure factors have been placed in the Depository of Unpublished Data.[2]

The ellipsoids of thermal motion for the nonhydrogen atoms are shown in Fig. 1. The thermal motion has been analysed in terms of the rigid-body modes of translation (**T**), libration (**L**), and screw (**S**) motion (18) using the computer program MGTLS. The rms standard error in the temperature factors σU_{ij} (derived from the least squares analysis) is 0.0017 Å^2. Analysis of all nonhydrogen atoms except C(7) and N(4) with constraints of C_2 symmetry resulted in an rms ΔU_{ij} of 0.0054 Å^2, a

[2]The structure factor table is available, at a nominal charge, from the Depository of Unpublished Data, CISTI, National Research Council of Canada, Ottawa, Canada K1A 0S2.

TABLE 3. Final thermal parameters and their estimated standard deviations

(*a*) Anisotropic thermal parameters ($U_{ij} \times 10^3$, P $\times 10^4$ Å^2)

Atom	U_{11}	U_{22}	U_{33}	U_{12}	U_{13}	U_{23}
P(1)	454(4)	293(4)	427(4)	0	215(3)	0
P(2)	458(3)	351(3)	336(3)	−68(2)	184(2)	−13(2)
P(3)	483(3)	322(3)	299(3)	−39(2)	186(2)	−11(2)
P(4)	627(4)	285(3)	435(3)	−26(2)	301(3)	−12(2)
N(1)	54(1)	42(1)	44(1)	1(1)	25(1)	3(1)
N(2)	53(1)	42(1)	38(1)	−10(1)	17(1)	3(1)
N(3)	54(1)	38(1)	35(1)	4(1)	16(1)	−4(1)
N(4)	230(6)	31(2)	43(2)	0	58(3)	0
C(1)	68(2)	46(1)	71(2)	−12(1)	29(2)	10(1)
C(2)	65(2)	51(1)	53(1)	5(1)	35(1)	4(1)
C(3)	64(2)	58(2)	54(2)	−21(1)	17(1)	−3(1)
C(4)	56(1)	49(1)	55(1)	0(1)	30(1)	−10(1)
C(5)	81(2)	49(1)	36(1)	−14(1)	24(1)	3(1)
C(6)	93(2)	40(1)	48(1)	−1(1)	31(2)	7(1)
C(7)	72(3)	62(2)	240(8)	8(2)	85(4)	2(3)

(*b*) Isotropic thermal parameters ($U \times 10^3$)

Atom	U (Å^2)	Atom	U (Å^2)	Atom	U (Å^2)
H(1*a*)	74(11)	H(3*b*)	74(11)	H(5*c*)	56(8)
H(1*b*)	109(15)	H(3*c*)	101(15)	H(6*a*)	90(14)
H(1*c*)	86(12)	H(4*a*)	80(11)	H(6*b*)	95(15)
H(2*a*)	49(8)	H(4*b*)	68(10)	H(6*c*)	103(14)
H(2*b*)	77(11)	H(4*c*)	60(9)	H(7*a*)	145(21)
H(2*c*)	75(11)	H(5*a*)	54(8)	H(7*b*)	119(17)
H(3*a*)	89(14)	H(5*b*)	99(14)	H(7*c*)	294(58)

TABLE 4. Bond lengths (Å) with estimated standard deviations in parentheses

(*a*) Nonhydrogen atoms

	Distance			Distance	
Bond	Uncorrected	Corrected	Bond	Uncorrected	Corrected
P(1)—N(1)	1.592(2)	1.594	P(1)—C(1)	1.802(3)	1.803
P(2)—N(1)	1.590(2)	1.592	P(2)—C(2)	1.796(3)	1.798
P(2)—N(2)	1.589(2)	1.590	P(2)—C(3)	1.795(3)	1.795
P(3)—N(2)	1.596(2)	1.598	P(3)—C(4)	1.794(3)	1.796
P(3)—N(3)	1.592(2)	1.594	P(3)—C(5)	1.802(3)	1.803
P(4)—N(3)	1.583(2)	1.598	P(4)—C(6)	1.805(3)	1.825
P(4)—N(4)	1.565(1)	1.584	P(4)—C(7)	1.793(5)	1.807

(*b*) Bonds involving hydrogen atoms

Bond	Distance	Bond	Distance
C(1)—H(1*a*)	0.98(4)	C(4)—H(4*c*)	0.96(4)
C(1)—H(1*b*)	0.90(5)	C(5)—H(5*a*)	0.95(3)
C(1)—H(1*c*)	0.96(4)	C(5)—H(5*b*)	0.96(5)
C(2)—H(2*a*)	1.01(3)	C(5)—H(5*c*)	1.02(3)
C(2)—H(2*b*)	1.01(4)	C(6)—H(6*a*)	0.92(5)
C(2)—H(2*c*)	0.80(4)	C(6)—H(6*b*)	0.90(5)
C(3)—H(3*a*)	0.83(5)	C(6)—H(6*c*)	0.90(5)
C(3)—H(3*b*)	0.87(4)	C(7)—H(7*a*)	1.08(6)
C(3)—H(3*c*)	0.96(5)	C(7)—H(7*b*)	1.02(6)
C(4)—H(4*a*)	0.89(4)	C(7)—H(7*c*)	0.94(11)
C(4)—H(4*b*)	0.90(4)		

TABLE 5. Bond angles (deg) with estimated standard deviations in parentheses

(*a*) Nonhydrogen atoms

Bonds	Angle (deg)	Bonds	Angle (deg)
N(1)—P(1)—N(1′)	118.6(2)	N(3)—P(3)—C(4)	105.7(1)
N(1)—P(1)—C(1)	111.9(1)	N(3)—P(3)—C(5)	112.3(1)
N(1)—P(1)—C(1′)	104.8(1)	C(4)—P(3)—C(5)	104.1(2)
C(1)—P(1)—C(1′)	104.1(2)	N(3)—P(4)—N(4)	116.4(1)
N(1)—P(2)—N(2)	115.4(1)	N(3)—P(4)—C(6)	109.5(1)
N(1)—P(2)—C(2)	111.8(1)	N(3)—P(4)—C(7)	111.7(2)
N(1)—P(2)—C(3)	109.4(2)	N(4)—P(4)—C(6)	104.5(2)
N(2)—P(2)—C(2)	110.4(1)	N(4)—P(4)—C(7)	110.6(3)
N(2)—P(2)—C(3)	105.2(1)	C(6)—P(4)—C(7)	103.0(3)
C(2)—P(2)—C(3)	104.0(2)	P(1)—N(1)—P(2)	133.1(1)
N(2)—P(3)—N(3)	118.8(1)	P(2)—N(2)—P(3)	130.3(1)
N(2)—P(3)—C(4)	110.7(1)	P(3)—N(3)—P(4)	134.3(1)
N(2)—P(3)—C(5)	104.4(1)	P(4)—N(4)—P(4′)	135.1(2)

(*b*) Angles involving hydrogen atoms

Bonds	Angle (deg)	Bonds	Angle (deg)
P(1)—C(1)—H(1*a*)	104(2)	H(4*a*)—C(4)—H(4*b*)	116(3)
P(1)—C(1)—H(1*b*)	109(3)	H(4*a*)—C(4)—H(4*c*)	106(3)
P(1)—C(1)—H(1*c*)	116(3)	H(4*b*)—C(4)—H(4*c*)	106(3)
H(1*a*)—C(1)—H(1*b*)	118(4)	P(3)—C(5)—H(5*a*)	106(2)
H(1*a*)—C(1)—H(1*c*)	103(3)	P(3)—C(5)—H(5*b*)	110(3)
H(1*b*)—C(1)—H(1*c*)	108(4)	P(3)—C(5)—H(5*c*)	107(2)
P(2)—C(2)—H(2*a*)	109(2)	H(5*a*)—C(5)—H(5*b*)	110(3)
P(2)—C(2)—H(2*b*)	111(2)	H(5*a*)—C(5)—H(5*c*)	112(3)
P(2)—C(2)—H(2*c*)	113(3)	H(5*b*)—C(5)—H(5*c*)	112(3)
H(2*a*)—C(2)—H(2*b*)	108(3)	P(4)—C(6)—H(6*a*)	115(3)
H(2*a*)—C(2)—H(2*c*)	102(3)	P(4)—C(6)—H(6*b*)	102(3)
H(2*b*)—C(2)—H(2*c*)	114(3)	P(4)—C(6)—H(6*c*)	110(3)
P(2)—C(3)—H(3*a*)	110(3)	H(6*a*)—C(6)—H(6*b*)	107(4)
P(2)—C(3)—H(3*b*)	110(3)	H(6*a*)—C(6)—H(6*c*)	110(4)
P(2)—C(3)—H(3*c*)	113(3)	H(6*b*)—C(6)—H(6*c*)	111(4)
H(3*a*)—C(3)—H(3*b*)	100(4)	P(4)—C(7)—H(7*a*)	104(3)
H(3*a*)—C(3)—H(3*c*)	111(4)	P(4)—C(7)—H(7*b*)	111(3)
H(3*b*)—C(3)—H(3*c*)	111(4)	P(4)—C(7)—H(7*c*)	86(7)
P(3)—C(4)—H(4*a*)	111(3)	H(7*a*)—C(7)—H(7*b*)	99(4)
P(3)—C(4)—H(4*b*)	109(2)	H(7*a*)—C(7)—H(7*c*)	124(8)
P(3)—C(4)—H(4*c*)	109(2)	H(7*b*)—C(7)—H(7*c*)	129(8)

value which indicates some independent motion but the rigid-body parameters resulting from this analysis are otherwise physically reasonable. Analysis of the P(4) tetrahedron without symmetry constraints gave an rms ΔU_{ij} of 0.0019 Å^2 and indicates that N(4) is probably twofold disordered about the C_2 axis as was inferred from the large thermal parameters of N(4) and C(7).

The appropriate bond distances have been corrected for libration (19, 20), using shape parameters q^2 of 0.08 for all atoms involved. Corrected bond lengths appear in Table 4 along with the uncorrected values. Bond angles about P(4) and N(4) in Table 5 are corrected for libration. Corrected angles about other atoms differ by less than 0.5σ from the uncorrected values.

Results and Discussion

Figure 1 shows a view of the molecule with the crystallographic numbering scheme. The unique intraannular torsion angles in the 14-membered ring are listed in Table 6. The mean structural parameters for $(NPMe_2)_7$ are compared with those of the related molecule $(NPMe_2)_4$ (21) in Table 7.

The crystal structure consists of well separated molecules of tetradecamethylcycloheptaphosphazene. The shortest intermolecular nonbonded distance, H(4*c*)···H(7*b*) ($\frac{1}{2} + x$, $y - \frac{1}{2}$, z), 2.41(6) Å, corresponds to a normal van der Waals contact.

Idealized local conformations (22) at each P atom are defined in terms of the intraannular torsion angles about the two P—N bonds. The

TABLE 6. Intra-annular torsion angles (deg), 14-membered ring*

Bond	Value
P(1)—N(1)	−68.7(1)
N(1)—P(2)	156.4(1)
P(2)—N(2)	−46.3(1)
N(2)—P(3)	−57.4(1)
P(3)—N(3)	−72.7(1)
N(3)—P(4)	166.8(1)
P(4)—N(4)	−36.1(1)

*Symmetry related torsion angles have the same signs as those listed above.

TABLE 7. Mean* structural parameters for $(NPMe_2)_n$ ($n = 4$ and 7) (distances in Å and angles in deg)

	Value	
Parameter	$n = 4$	$n = 7$
P—N	1.596(5)	1.592(6)
C—P	1.804(3)	1.804(11)
N—P—N	119.8(2)	117.1(16)
P—N—P	132.0(2)	132.9(20)
C—P—C	104.1(2)	103.9(5)

*Weighted mean values with rms deviations from the mean in parentheses (where appropriate).

ideal *GG* conformation has both torsion angles 60° while the *GT* conformation has one torsion angle of 60° and one of 180°. In $(NPMe_2)_7$ phosphorus atoms P(1) and P(3) have *GG* local conformations and atoms P(2) and P(4) have *GT* local conformations. The adjacent phosphorus atoms, therefore, have alternately *GG* and *GT* local conformations around the 14-membered ring except for the symmetry related pair P(4) and P(4′)[3] which both have *GT* local conformations.

The mean structural parameters for the heptamer are compared with those of the tetramer in Table 7. The mean P—N and P—C bond lengths and the C—P—C and P—N—P angles are nearly the same for all three structures, while the N—P—N angles are seen to decrease with increasing ring size. There are statistically significant variations among the individual values averaged to give the means shown in Table 7 which probably arise from differences between the local conformations of the ring atoms.

[3]Here and elsewhere in this paper primed atoms are related to those in Table 2 by rotation about the twofold axis passing through P(1) and N(4).

Acknowledgements

We thank the National Research Council of Canada for financial support and the University of British Columbia Computing Centre for assistance.

1. H. T. SEARLE. Proc. Chem. Soc. 7 (1959).
2. H. T. SEARLE, J. DYSON, N. L. PADDOCK, and T. N. RANGANANTHAN. J. Chem. Soc. Dalton Trans. 203 (1975).
3. T. ALVIK and J. DALE. Acta Chem. Scand. **25**, 2131 (1971).
4. A. BONDI. Ann. N.Y. Acad. Sci. **53**, 870 (1951).
5. A. BONDI. J. Chem. Phys. **19**, 128 (1951).
6. G. B. ANSELL and G. J. BULLEN. J. Chem. Soc. Chem. Commun. 430 (1966).
7. M. W. DOUGILL and N. L. PADDOCK. J. Chem. Soc. Dalton Trans. 1022 (1974).
8. N. L. PADDOCK, J. TROTTER, and S. H. WHITLOW. J. Chem. Soc. A, 2227 (1968).
9. G. J. BULLEN. J. Chem. Soc. 3193 (1962).
10. A. J. WAGNER and A. VOS. Acta Crystallogr. Sect. B, **24**, 1423 (1968).
11. H. P. CALHOUN, N. L. PADDOCK, and J. TROTTER. J. Chem. Soc. Dalton Trans. 38 (1976).
12. R. E. LONG. Ph. D. Thesis, University of California at Los Angeles, Los Angeles, California. 1965.
13. P. COPPENS, L. LEISEROWITZ, and D. RABINOVITCH. Acta Crystallogr. **18**, 1035 (1965).
14. W. R. BUSING and H. A. LEVY. Acta Crystallogr. **10**, 180 (1957).
15. D. T. CROMER and J. B. MANN. Acta Crystallogr. Sect. A, **24**, 321 (1968).
16. R. F. STEWART, E. R. DAVIDSON, and W. T. SIMPSON. J. Chem. Phys. **42**, 3175 (1965).
17. D. T. CROMER and D. LIBERMAN. J. Chem. Phys. **53**, 1891 (1970).
18. V. SCHOMAKER and K. N. TRUEBLOOD. Acta Crystallogr. Sect. B, **24**, 63 (1968).
19. D. W. J. CRUICKSHANK. Acta Crystallogr. **14**, 896 (1961).
20. D. W. J. CRUICKSHANK. Acta Crystallogr. **9**, 747 (1956); **9**, 754 (1956).
21. M. W. DOUGILL. J. Chem. Soc. 5471 (1961).
22. S. MIZUSHIMA. Structure of molecules and internal rotation. Academic Press, New York. 1954.
23. A. C. CHAPMAN, N. L. PADDOCK, D. H. PAINE, H. T. SEARLE, and D. R. SMITH. J. Chem. Soc. 3608 (1960).

Vibrational analysis and force field for some secondary iodides

G. CROWDER AND ZAHRA NAJAFI
Deparment of Chemistry, West Texas State University, Canyon, Texas 79016
Received August 11, 1976

G. CROWDER and ZAHRA NAJAFI. Can. J. Chem. **55**, 310 (1977).

Normal coordinate calculations were made for 2-iodopropane and the three conformers of 2-iodobutane. A forty-seven parameter modified valence force field was used that fit eighty-four frequencies of those four molecules in the 250–1500 cm^{-1} region with an average error of 4.8 cm^{-1}, or 0.6%. Infrared spectra were obtained for 2-iodopentane and 3-iodopentane, and zero-order normal coordinate calculations were made for three conformers of 2-iodopentane and for five conformers of 3-iodopentane. The S_{HH}, $S_{HH'}$, and S_{CH} conformers of 2-iodopentane are present, along with one or two unidentified ones, and 3-iodopentane exists as a mixture of the S_{HH}, $S_{HH'}$, S_{CH}, and $S_{CH'}$ conformers. The force constants that were determined for the four conformers of 2-iodopropane and 2-iodobutane were transferred to the two secondary iodopentanes with good success. The average difference between observed and calculated wavenumbers for 164 frequencies of seven conformations of these two compounds was 5.8 cm^{-1}.

G. CROWDER et ZAHRA NAJAFI. Can. J. Chem. **55**, 310 (1977).

On a fait des calculs de coordonnées normales pour l'iodo-2 propane et pour les trois conformères de l'iodo-2 butane. On a utilisé un champ de force de valence modifié à 47 paramètres qui permet d'ajuster 84 fréquences de ces quatre molécules dans la région de 250–1500 cm^{-1} avec une erreur moyenne de 4.8 cm^{-1} ou 0.6%. On a déterminé les spectres infrarouges de l'iodo-2 pentane et de l'iodo-3 pentane et on a effectué des calculs de coordonnées normales avec un ordre zéro pour les trois conformères de l'iodo-2 pentane et pour cinq conformères de l'iodo-3 pentane. Les conformères S_{HH}, $S_{HH'}$, et S_{CH} de l'iodo-2 pentane sont présents aux côtés d'une ou deux autres conformations non-identifiées et l'iodo-3 pentane existe sous forme de mélange des conformères S_{HH}, $S_{HH'}$, S_{CH} et $S_{CH'}$. Les constantes de force qui ont pu être déterminées pour les quatre conformères de l'iodo-2 propane et de l'iodo-2 butane ont pu être transferrées aux deux iodopentanes secondaires avec un bon succès. La différence moyenne entre les nombres d'onde observés et calculés pour 164 fréquences de sept conformations de ces deux composés est de 5.8 cm^{-1}.
[Traduit par le journal]

Introduction

Infrared and Raman spectra for 2-iodopropane have been published by Klaboe (1), and he proposed a tentative vibrational assignment in terms of group vibrations. Benedetti and Cecchi (2) made normal coordinate calculations for 2-iodopropane and 2-iodobutane and obtained a force field that fit the frequencies of 2-iodopropane, the S_{HH} conformer of 2-iodobutane, and most of those of the $S_{HH'}$ and S_{CH} conformers of 2-iodobutane, all in the 250–1400 cm^{-1} region, with an average difference between observed and calculated values of 1.1% (fifty-two frequencies).

The calculations for 2-iodopropane and 2-iodobutane have now been repeated for the following reasons: (*1*) Benedetti and Cecchi did not list the calculated results for 2-iodopropane, of which the normal coordinate descriptions of the normal modes are of interest, (*2*) several force constants obtained in the previous work (2) cannot be compared with those of similar compounds, because the C—I stretching force constant was held fixed at the C—Br value that had been obtained for secondary bromides (3), a value obviously too high for the iodides, (*3*) the average error of 1.1% in the previous work seems rather high. A force field that would more accurately reproduce the observed frequencies of these molecular species could be used with more confidence as an aid in making vibrational assignments for other secondary alkyl iodides.

Infrared spectra have been reported for 2-iodopentane and 3-iodopentane only in the region 400–800 cm^{-1} (4). Carbon–iodine stretching bands were assigned to four conformers of 2-iodopentane and five conformers of 3-iodopentane. Gates, Mooney, and Willis (4) assigned the C—I stretch of the S_{CC} conformer of 3-iodopentane to a band at 460 cm^{-1}, contrary to

the normal assignment of the highest-frequency carbon–halogen stretch to a conformer with a carbon *trans* to the halogen.

In an effort to learn more about the conformational behavior of these two compounds, to make vibrational assignments, and to check the transferability of the force constants obtained from 2-iodopropane and 2-iodobutane, infrared spectra have been obtained and zero-order normal coordinate calculations have been made for three conformers of 2-iodopentane and for five conformers of 3-iodopentane.

Experimental

Infrared spectra were obtained with a Beckman IR12 spectrophotometer. The compounds were obtained from Pfaltz & Bauer and were used without further purification.

Normal Coordinate Calculations

Normal coordinate calculations were made with a PDP-10 computer and utilized programs written by Schachtschneider and co-worker (5, 6) for calculation of the **G**-matrix (gmat), solution of the vibrational secular equation (vsec), and for the least-squares refinement of designated force constants to fit the calculated to the observed frequencies (fpert). These references should be consulted for details of the calculations, treatment of the redundancy problem, etc. The molecular parameters used were C—C = 1.54 Å, C—H = 1.09 Å, C—I = 2.135 Å, and all angles were assumed to be tetrahedral.

A forty-seven parameter modified valence force field was used, with initial values being taken from secondary bromides (3), secondary chlorides (7), and primary iodides (8). Calculations were first made for 2-iodopropane, to which thirty-five of the force constants were applicable. Symmetry coordinates were constructed in order to factor the secular equation into two symmetry blocks. The transferred force constant values resulted in an average difference of 14 cm^{-1} between observed and calculated frequencies. Several changes in the force constants were made manually, using the potential energy distributions and **JZ** matrices as guides. Thirteen force constants were then refined by the least-squares program, resulting in an average difference of 1.6 cm^{-1}, or 0.2%, for the twenty frequencies below 1500 cm^{-1}. These force constant values will not be given here, but are available from the author, along with a normal coordinate description of the normal modes obtained with the use of these constants.

The force constants obtained for 2-iodopropane and additional ones transferred from a hydrocarbon force field (9) were used in a zero-order calculation of the frequencies of the S_{HH} conformer of 2-iodobutane. The average difference between calculated and observed wavenumbers was 12.9 cm^{-1}. Several computer runs were then made with the least-squares program adjusting different sets of force constants. In the final run, seventeen constants were refined to fit

TABLE 1. Observed and calculated wavenumbers and approximate normal coordinate descriptions for 2-iodopropane

Wavenumber			Wavenumber		
Obsd.[a]	Calcd.	P.E.D.(%)[b]	Obsd.[a]	Calcd.	P.E.D.(%)[b]
	a'			*a''*	
1468	1462	1(92)	1468	1462	1(91)
1459	1460	1(93)	1459	1459	1(94)
1389	1382	2(102)	1375	1376	2(105)
1210	1206	4(68),8(20)	1325	1327	4(71),9(26)
1153	1144	8(50),9(26),11(11)	1113	1115	9(57),4(16)
1020	1020	8(57),4(33)	937	952	8(75),9(16)
879	877	9(80),8(24)	925	920	8(88),4(13)
499	491	11(62),10(57)	269	272	11(97)
398	397	11(91),8(15)	217	217	13(99)
250	258	10(44),11(41)			
192	192	13(98)			

[a]Observed values from ref. 1.
[b]The coordinate number (see Table 3) is followed by the potential energy in percent. Contributions less than 10% are excluded.

TABLE 2. Observed and calculated wavenumbers and approximate normal coordinate descriptions for 2-iodobutane

Wavenumber			Wavenumber		
Obsd.[a]	Calcd.	P.E.D.(%)[b]	Obsd.[a]	Calcd.	P.E.D.(%)[b]
	S_{HH}			$S_{HH'}$	
1460	1464	1(86)	1460	1463	1(88)
1460	1461	1(91)	1460	1461	1(93)
1453	1460	1(90)	1453	1460	1(92)
1453	1459	1(93)	1453	1459	1(94)
1440	1437	3(73),14(20)	1440	1440	3(72),14(20)
1379	1390	5(35),2(30),4(14)	1379	1379	2(103)
1379	1376	2(73),9(21),5(12)	1354	1351	2(88),9(13)
1354	1347	2(98)	1344	1348	5(67),9(18)
1289	1292	4(45),5(24),6(10)	1311	1324	4(57),9(28)
1270	1258	6(62)	1270	1257	6(66)
1188	1186	4(47),8(23),7(13)	1178	1187	4(46),8(24)
1142	1151	8(37),9(34)	1142	1136	8(29),9(18),4(18)
1101	1093	9(41),8(20)	1118	1111	9(36),4(21),5(15)
1042	1042	4(32),8(22),9(21)	1035	1044	8(45),4(20),9(14)
1021	1021	9(83)	1000	992	8(53),9(27)
993	995	8(63),5(13)	993	980	8(51),9(15),4(15)
947	956	8(71),4(12)	950	949	9(54),8(31)
837	832	9(65),8(41)	816	834	9(73),8(30)
785	787	7(59),8(42)	785	786	7(52),8(40)
487	487	10(45),11(41)	552	567	11(35),12(30),10(16)
447	446	11(33),12(29),10(16)	454	460	11(61),10(38)
336	336	11(79),12(17)	302	300	11(58),10(19),12(13)
265	254	11(48),10(37)	265	265	11(64),10(26)
199[c]	207	13(87)	199[c]	204	13(98)
186[c]	186	11(60),12(22),13(12)	186[c]	179	11(62),12(29)
		S_{CH}			
1460	1463	1(88)	1035	1029	8(40),9(34),4(16)
1460	1460	1(93)	1000[c]	1007	8(48),9(26)
1453	1460	1(92)	976	972	9(45),8(38)
1453	1459	1(93)	950	952	8(60),9(17)
1440	1440	3(72),14(20)	837	839	9(73),8(31)
1379	1380	2(99)	785	774	7(60),8(39)
1354[c]	1364	5(38),9(35),4(22)	579	579	11(43),10(37),8(18)
1344	1346	2(94)	403	389	11(83),7(10)
1311	1311	4(35),5(33),6(16),9(12)		274	12(55),11(30),10(14)
	1240	6(59),4(14),8(12)	265	264	11(65),10(26)
1188	1192	4(64),8(17)	199[c]	212	11(68),10(19)
1142	1139	8(36),9(18),11(12)	199[c]	203	13(97)
1118[c]	1115	9(48),8(17),4(11)			

[a]Observed values from ref. 2.
[b]See footnote *b*, Table 1.
[c]Not used in the refinement procedure.

forty-five frequencies (excluding C—H stretch) of 2-iodopropane and the S_{HH} conformer of 2-iodobutane. The average error was 5.0 cm^{-1}.

The next step was to use the force constant values obtained from 2-iodopropane and S_{HH} 2-iodobutane in a zero-order calculation of the frequencies of the $S_{HH'}$ and S_{CH} conformers of 2-iodobutane. The average error for forty-one frequencies between 200 and 1500 cm^{-1} was 8.1 cm^{-1}. The two calculated C—I stretching frequencies were in error by 35 cm^{-1} each, and exclusion of these two values leaves an average error of 6.7 cm^{-1}.

Finally, force constants were refined in several attempts to simultaneously fit twenty frequencies of 2-iodopropane, twenty-three frequencies of S_{HH} 2-iodobutane, twenty-three frequencies of $S_{HH'}$ 2-iodobutane, and eighteen frequencies of S_{CH} 2-iodobutane. In the final run, nineteen force constants were refined to fit these eighty-four

TABLE 3. Numbering and definitions of symmetry coordinates

Coordinate number	Definition	Coordinate number	Definition
1	Antisymmetric CH_3 bend	8	CH_3 rock
2	Symmetric CH_3 bend	9	C—C stretch
3	CH_2 bend	10	C—I stretch
4	Methine HCC bend	11	CCC, CCI bend (C—C(I)—C)
5	CH_2 wag	12	CCC bend
6	CH_2 twist	13	CH_3 torsion
7	CH_2 rock	14	CH_2 redundancy

frequencies with an average difference between observed and calculated values of 4.8 cm^{-1}, or 0.6%. The observed and calculated wavenumbers are listed in Tables 1 and 2, along with normal coordinate descriptions of the normal modes in terms of the symmetry coordinates whose definitions are given in Table 3. The force constants, their definitions, and their values are listed in Table 4.

Results and Discussion

The normal coordinate descriptions of the normal modes of 2-iodopropane listed in Table 1 support the assignments made by Klaboe (1) except for the two bands observed by him at 250 and 269 cm^{-1}. He assigned these two bands to a'' and a' skeletal bends, respectively, but the reverse assignment was made in the present work, based on the calculations. Both bands are very strong in the Raman spectrum, and Klaboe reported both bands as polarized (1). However, one of these bands must be due to an a'' bend and should be depolarized. Decomposition of the sample may have caused a problem with the polarization data.

It should be noted that calculation of the two methyl torsional frequencies of 2-iodopropane (192 and 217 cm^{-1}) required introduction of F_τ, the interaction constant between the two torsional internal coordinates. The value of F_τ required is approximately 9% of the value of H_τ. Without F_τ, the a' and a'' torsional frequencies were calculated to differ by only 2 cm^{-1}.

There are several differences in the potential energy distributions of the three conformers of 2-iodobutane listed by Benedetti and Cecchi (2) and the distributions listed in Table 2. For example, they found the band to which the transverse CH bend makes its largest contribution to be 1346, 1340, and 1349 cm^{-1}, respectively, in the S_{HH}, $S_{HH'}$, and S_{CH} conformers. The present assignment is 1289, 1311, and 1311 cm^{-1}, in the same order. The calculated values for 2-iodopropane were not given by Benedetti and Cecchi, but with our force field, the two CH bends of 2-iodopropane were calculated at 1202 (a') and 1324 (a'') cm^{-1}, in good agreement with Snyder's (3) values of 1221 and 1322 cm^{-1} for 2-bromopropane.

Another difference between the present work and that of Benedetti and Cecchi that should be pointed out lies in the C—I stretching coordinates. They calculated a larger percentage of C—I stretch to the bands at 487, 454, and 579 cm^{-1} in the three conformers of 2-iodobutane than shown in Table 2. However, this difference was due mainly to their use of a larger value for the C—I stretch force constant (2.312 mdyn/Å) than used in the present work (1.716 mdyn/Å). The effect of using the larger value is to increase the C—I stretching contribution to the higher frequency band and decrease this contribution to the lower-frequency bands to which it contributes. Their value is the C—Br value transferred from a secondary bromides force field, and so cannot give the correct potential energy distributions to the low-frequency bands.

2-Iodopentane

Gates *et al.* (4) show the liquid and solid-state spectra of this compound in the region 400–700 cm^{-1}, and they list the bands observed between 400 and 800 cm^{-1}. They have assigned bands to four separate conformers, namely the S_{HH} (all carbons coplanar), $S_{HH'}$ (fourth carbon oriented on same side of plane as iodine), S_{CH} (fourth carbon *trans* to iodine), and a fourth conformer they call *cis* X—H. We obtained

TABLE 4. Force constants for 2-iodopropane and 2-iodobutane

Force constant	Group	Coordinate(s) involved	Common atom(s)	Value[a]	Standard error
Stretch					
K_r	CH_3	C—H	—	4.699	—
K_d	CH_2	C—H	—	4.554	—
K_ε	CHI	C—H	—	4.588	—
K_R	CH_2—CH_3	C—C	—	4.387	—
$K_R(X)$	C—CHI—C	C—C	—	4.586[b]	—
K_x	CHI	C—I	—	1.716	—
Bend					
H_α	CH_3	H—C—H	—	0.539	—
H_β	CH_2—CH_3	C—C—H	—	0.601[c]	0.007
$H_\beta(X)$	CHI—CH_3	C—C—H	—	0.620[c]	0.004
H_δ	CH_2	H—C—H	—	0.532[c]	0.004
H_γ	C—CH_2—C	C—C—H	—	0.656	—
H_ξ	C—CHI—C	C—C—H	—	0.656	—
H_ε	CHI	I—C—H	—	0.668[c]	0.044
H_ω	C—C—C	C—C—C	—	1.160[c]	0.040
H_Ξ	C—CHI—C	C—C—I	—	0.975[c]	0.053
H_τ	CH_3—CHI	C—C torsion	—	0.0087[b]	—
Stretch–stretch					
F_r	CH_3	CH,CH	C	0.043	—
F_d	CH_2	CH,CH	C	0.006	—
F_R	C—CH_2—C	CC,CC	C	0.064	—
$F_R(X)$	C—CHI—C	CC,CC	C	0.101	—
F_{RX}	C—CHI—C	CC,CI	C	0.121[b]	—
Stretch–bend					
$F_{R\gamma} = F_{R\xi}$	C—CH—C	C—C,CCH	C—C	0.301	—
$F_{R\gamma}' = F_{R\xi}'$	C—CH—C	C—C,CCH	C	0.079	—
$F_{R\omega}$	C—C—C	C—C,CCC	C—C	0.445[c]	0.029
$F_{R\Xi}$	C—C—I	C—C,CCI	C—C	0.265[c]	0.061
$F_{x\varepsilon}$	C—CHI—C	C—I,CCH	C—I	0.226	—
$F_{x\Xi}$	C—C—I	C—I,CCI	C—I	0.278[c]	0.030
$F_{x\omega}$	C—CI—C	C—I,CCC	C	−0.135[c]	0.094
Bend–Bend					
F_β	C—CH_3	CCH,CCH	C—H	0.000	0.002
$F_\beta(X)$	CI—CH_3	CCH,CCH	C—C	−0.014[c]	0.004
F_γ	C—CH_2—C	CCH,CCH	C—C	−0.021	—
$F_\gamma' = F_\xi'$	C—CH—C	CCH,CCH	C—H	0.012	—
$F_{\xi\varepsilon}$	C—CHI—C	CCH,ICH	C—H	0.071[c]	0.019
$F_{\gamma\omega} = F_{\xi\omega}$	C—CH_2—C	CCH,CCC	C—C	−0.031	—
$F_{\omega\Xi}$	C—CHI—C	CCC,CCI	C—C	−0.224[c]	0.076
F_Ξ	C—CHI—C	CCI,CCI	C—I	−0.007[c]	0.048
F_τ	CH_3—CHI—CH_3	CH_3—C,C—CH_3	C	0.0010[b]	—
f_γ^g	—CH—CH—	HCC,CCH *gauche*	C—C	−0.016[c]	0.004 0.004
f_γ^t	—CH—CH—	HCC,CCH *trans*	C—C	0.080	—
f_ω^g	C*—C—C—C^+	C*CC,CCC^+ *gauche*	C—C	0.011	—
f_ω^t	C*—C—C—C^+	C*CC,CCC^+ *trans*	C—C	−0.011	—
$f_{\gamma\omega}^g$	CH—C—C	HCC,CCC *gauche*	C—C	−0.078[c]	0.010
$f_{\gamma\omega}^t$	CH—C—C	HCC,CCC *trans*	C—C	0.049	—
$f_{\gamma\Xi}^g$	CH—C—I	HCC,CCI *gauche*	C—C	−0.037	—

TABLE 4 (*Concluded*)

Force constant	Group	Coordinate(s) involved	Common atom(s)	Value[a]	Standard error
$f_{\gamma\Xi}^{t}$	CH—C—I	HCC,CCI (*trans*)	C—C	0.075[c]	0.048
$f_{\omega\Xi}^{g}$	C—C—C—I	CCC,CCI (*gauche*)	C—C	−0.024	—
$f_{\omega\Xi}^{t}$	C—C—C—I	CCC,CCI (*trans*)	C—C	−0.310[c]	0.069

[a]Stretching constants are in units of mdyn/Å; stretch–bend constants are in units of mdyn/rad; bending constants are in units of mdyn Å/(rad)².
[b]These constants were constrained to the 2-iodopropane value.
[c]These constants were refined.

spectra for this compound and made normal coordinate calculations in order to make vibrational assignments and to check the transferability of the force field determined previously. Calculations were made only for three conformers, namely S_{HH}, $S_{HH'}$, and S_{CH}. The $S_{HH'}$ and S_{CH} conformers are formed from the S_{HH} by rotation about the C_2—C_3 bond. Calculations were not made for the '*cis* X—H' conformer because previous calculations were not made for such a configuration, and interaction force constants were not available.

The observed and calculated wavenumbers are listed in Table 5. There are four observed bands assigned solely to the S_{HH} conformer, and there is little doubt about this form being present. There are five bands assignable to both $S_{HH'}$ and S_{CH} conformers, so one or both of these must also be present. There are two bands assigned solely to the S_{CH} and one solely to $S_{HH'}$, and it seems likely that both of these conformers are present. All other observed bands are due to overlapping bands from more than one conformer.

Gates *et al.* (4) assigned a weak band observed at 559 cm^{-1} to the C—I stretch of the $S_{HH'}$ conformer and the shoulder observed around 480 cm^{-1} to the '*cis* X—H' conformer. The present calculations indicate assignment of the shoulder around 480 cm^{-1} to the S_{HH} conformer, and this assignment seems more logical than the previous assignment. The weak band at 559 cm^{-1} can be explained as a summation band.

Assignment of 71 calculated wavenumbers for all three conformers between 400 and 1500 cm^{-1} to observed bands resulted in an average difference between observed and calculated values of 5.6 cm^{-1}.

There are three bands observed at 768, 795, and 810 cm^{-1} that have not been assigned to the three conformers for which calculations were made. This indicates the presence of one or more additional conformers. Two likely conformers are the ones with the methyl group that is located on the end away from the iodine oriented on either side of the plane of the other four carbons.

3-Iodopentane

Infrared spectra were obtained for this compound in the liquid and solid states, and normal coordinate calculations were made to aid in assigning the observed bands to the different conformers. Calculations were made for the S_{HH}, $S_{HH'}$, S_{CH}, $S_{CH'}$, and S_{CC} conformers.

The liquid-state infrared spectrum in the region 425–700 cm^{-1} is shown by Gates *et al.* (4). The spectrum observed in this region in the present investigation differs in relative intensities for the 461 and 590 cm^{-1} bands, the latter being observed as a shoulder on the 574 cm^{-1} band. Their spectrum shows the 461 cm^{-1} band to be only a little less intense than the one at 485 cm^{-1}, whereas the ratio of the areas of the 485 to 461 cm^{-1} bands in the present work is four to one. The shoulder on the 574 cm^{-1} band is also less intense here than in the spectrum of Gates *et al.*

The solid-state spectrum was obtained for a film which was formed by cooling a liquid film held between salt plates. The sample was solidified several times with no simplification of the spectrum resulting. The solid was annealed with no success in getting it to crystallize. The solid-state spectrum shown by Gates *et al.* also shows their solid to be amorphous.

Gates *et al.* assigned the band they observed

TABLE 5. Observed and calculated wavenumbers for 2-iodopentane

Obsd.	Calcd. S_{HH}	Calcd. $S_{HH'}$	Calcd. S_{CH}
1459	1464	1463	1463
	1461	1461	1461
	1460	1460	1460
	1459	1459	1458
1448	1447	1449	1450
1435	1427	1427	1428
	1413	1402	1401
1380	1379	1379	1379
1339	1346	1347	1346
	1341		
1300		1306	1309
1291	1279	1287	1279
1266	1268	1277	1267
1245	1238	1247	
1219			1230
1183	1178	1182	1178
1138	1139		
1131(sol)		1118	1120
1103			
		1064	1070
1053	1053		
	1050		
1028		1026	1030

Obsd.	Calcd. S_{HH}	Calcd. $S_{HH'}$	Calcd. S_{CH}
1001	1018	1014	1018
980	980	982	983
924	931		
914		911	917
865	876	875	859
840	854	846	847
810			
795			
768			
752	723	722	
743			716
577		581	581
490	489		
ca. 480		484	
423	436		425
417	414		
350		363	372
		276	
	264	263	264
	249		
			227
	155		149
		131	

TABLE 6. Observed and calculated wavenumbers for 3-iodopentane

Obsd. (liquid)	Calcd. S_{HH}	Calcd. $S_{HH'}$	Calcd. S_{CH}	Calcd. $S_{CH'}$
1460	1464	1463	1463	1464
	1462	1462	1462	1462
1455	1460	1460	1460	1461
	1460	1460	1460	1460
1435	1438	1441	1441	1440
	1437	1438	1438	1439
1378	1393	1380	1391	1393
	1377	1375	1376	1376
	1374	1371	1374	
1358	1363			1361
1334		1334	1329	1331
1290			1292	1301
1280	1276			
1265		1266		
	1256			1251
1240		1237		1231
	1224		1225	
1180	1166		1166	
1145		1152		1145
1133	1138	1122		1129
			1118	
	1095	1084	1096	1103
1049	1053			
	1041	1040	1043	1038
		1037		
1028			1032	1029
1022		1014		1015
1015	1011		1010	

Obsd. (liquid)	Calcd. S_{HH}	Calcd. $S_{HH'}$	Calcd. S_{CH}	Calcd. $S_{CH'}$
999				994
979				
915	930		920	
910		899		
905				892
863	863		860	863
838		825		
808	809			
792		797	800	800
768	770	767	761	772
748				
740				
ca. 585				588
572			574	
		546		
				504
482	485			
	474			
457		442	440	
413	401			
358		346	334	
				298
	266		263	269
		215	211	213
		211		
	186		180	181
	182			
		96		

at 461 cm^{-1} to the C—I stretch of the S_{CC} conformer. It seems unlikely from steric considerations that this conformer would be present in an appreciable concentration at room temperature. Moore and Krimm (10) found no evidence for the presence of S_{CC} 3-chloropentane. The band assigned by Gates *et al.* to the C—Cl stretch of the S_{CC} conformer of 3-chloropentane, 534 cm^{-1}, was shown by Moore and Krimm to be due to both $S_{HH'}$ and $S_{CH'}$ conformers. We have found almost the same assignment for 3-iodopentane, except that we have assigned the 461 cm^{-1} band to the $S_{HH'}$ and S_{CH} conformers. The present calculations for the S_{CC} conformer indicate a band at *ca.* 658 cm^{-1}, due to a mixture of C—I stretch, C—C—C bend, and C—C—I bend. There is no observed band in this region of the spectrum.

The observed and calculated wavenumbers for the S_{HH}, $S_{HH'}$, S_{CH}, and $S_{CH'}$ conformers are listed in Table 6. In order to conserve space, the potential energy distributions are not given here, but are available from the author. The transferred force constants resulted in good agreement between observed and calculated wavenumbers, with the average difference being 6.0 cm^{-1} for the 93 values of the four conformers that had observed values assigned to calculated values.

Acknowledgement

The author is grateful to The Robert A. Welch Foundation, Houston, Texas, for financial support of this work.

1. P. KLABOE. Spectrochim. Acta, **26**A, 87 (1970).
2. E. BENEDETTI and P. CECCHI. Spectrochim. Acta, **28**A, 1007 (1972).
3. R. G. SNYDER. J. Mol. Spectrosc. **28**, 273 (1968).
4. P. N. GATES, E. F. MOONEY, and H. A. WILLIS. Spectrochim. Acta, **23**A, 2043 (1967).
5. J. H. SCHACHTSCHNEIDER. Shell Development Co. Tech. Rept., Nos. 231–64 (1964) and 57–65 (1965).
6. J. H. SCHACHTSCHNEIDER and R. G. SNYDER. Spectrochim. Acta, **19**, 117 (1963).
7. C. G. OPASKAR and S. KRIMM. Spectrochim. Acta, **23**A, 2261 (1967).
8. G. A. CROWDER and S. ALI. J. Mol. Struct. **25**, 377 (1975).
9. R. G. SNYDER and J. H. SCHACHTSCHNEIDER. Spectrochim. Acta, **21**, 169 (1965).
10. W. H. MOORE and S. KRIMM. Spectrochim. Acta, **29**A, 2025 (1973).

Photoelectron spectra of substituted oxiranes and thiiranes. Substituent effects on ionization potentials involving σ orbitals

E. J. McAlduff[1] and K. N. Houk[2]

Department of Chemistry, Louisiana State University, Baton Rouge, LA 70803, U.S.A.

Received July 22, 1976

E. J. McAlduff and K. N. Houk. Can. J. Chem. **55**, 318 (1977).

The state assignments corresponding to the second and third ionization potentials of oxirane have been the subject of some uncertainty due to the great sensitivity of Koopmans' theorem predictions to the type of calculation performed for this molecule. In this study, the assignments made by Basch *et al.* for oxirane are confirmed through measurement of the photoelectron spectra of methyl-, 1,1-dimethyl-, 1,2-dimethyl, ethyl-, vinyl-, phenyl-, chloromethyl-, and fluoromethyloxirane. The second and third ionizations of thiirane are confirmed to be of the opposite order from those in oxirane by correlations of these values with those reported here for methyl-, vinyl, and methoxymethylthiirane.

In these compounds, mono-substitution by alkyl groups causes a decrease in ionization potential not obviously related in a simple way to the type of orbital involved. Thus, assignments cannot be made straightforwardly by observing ionization potential changes caused by hyperconjugating or inductive substituents. Alkyl group substitution in both oxirane and thiirane lowers IP's in the same order: $a_2 > b_2 > a_1 > b_1$. The effects of alkyl and heteroalkyl groups on the four lowest IP's of oxirane are linearly related to the electronegativities of the groups, and to the influence of alkyl and heteroalkyl substituents on the π IP of ethylene.

Comparisons of the IP's of ethylheteranes and dimethylheteranes are quite useful in determining the site of localization of orbital density in the various orbitals.

Conjugating substituents, which for symmetry reasons, selectively interact with only a few orbitals make definite assignments possible. Comparisons of experimental ionization potential changes and those predicted by Koopmans' theorem using *ab initio* STO-3G calculations are in good agreement.

E. J. McAlduff et K. N. Houk. Can. J. Chem. **55**, 318 (1977).

Les attributions d'état correspondant aux potentiels d'ionisation second et tierce de l'oxiranne ont fait l'objet de beaucoup d'incertitudes dues à la grande sensibilité des prédictions du théorème de Koopman au type de calcul effectué sur cette molécule. Dans cette étude, les attributions faites par Basch et coll. pour l'oxiranne sont confirmées par des mesures de spectres photoélectroniques du méthyles, du diméthyl-1,1, du diméthyl-1,2, de l'éthyl-, du vinyl-, du phényl-, du chlorométhyl- et du fluorométhyloxiranne. On confirme que les ionisations seconde et tierce du thiirane sont d'un ordre opposé à celles de l'oxiranne par corrélation de ces valeurs avec celles rapportées ici pour le méthyl-, le vinyl et le méthoxyméthylthiirane.

Dans ces composés, la mono-substitution par des groupes alkyles cause une diminution du potentiel d'ionisation qui n'est pas reliée d'une façon apparente ou directe avec le type d'orbitales impliquées. Donc les attributions ne peuvent pas être faites d'une façon directe par les changements des potentiels d'ionisation observés et causés par des substituants qui provoquent de l'hyperconjugaison ou de l'induction. La substitution de groupes alkyles soit dans l'oxiranne ou le thiirane diminue les potentiels d'ionisation dans le même ordre $a_2 > b_2 > a_1 > b_1$. Il y a une relation linéaire entre les effets des groupes alkyles et hétéroalkyles sur les quatre potentiels d'ionisation les plus bas de l'oxiranne et sur les électronégativités des groupes et les influences des substituants alkyles et hétéroalkyles sur les potentiels d'ionisation π de l'éthylène.

Une comparaison des potentiels d'ionisation des éthylhétérannes et diméthylhétérannes est très utile pour déterminer le site de la localisation de la densité orbitale dans les diverses orbitales. Les substituants, provoquant de la conjugaison et qui pour des raisons de symétries interagissent d'une façon sélective avec seulement quelques orbitales, permettent d'obtenir des attributions définitives. Il existe un bon accord entre les changements des potentiels d'ionisation expérimentaux et ceux prédits par le théorème de Koopman utilisant des calculs *ab initio* STO-3G.

[Traduit par le journal]

---

[1]On sabbatical leave from St. Francis Xavier University, Antigonish, Nova Scotia, 1975–1976.

[2]Camille and Henry Dreyfus Teacher–Scholar Grant Recipient 1972–1977; Alfred P. Sloan Foundation Fellow 1975–1977.

Introduction

Photoelectron spectra are often assigned using Koopmans' theorem (1):

$$\mathrm{IP}(i) = -\varepsilon_{\mathrm{SCF}}(i)$$

This useful approximation relates ionization potentials to the negatives of SCF orbital energies. (For discussion of the limitations of Koopmans' theorem, see ref. 2.) Koopmans' theorem ionization potentials differ from experimental vertical ionization potentials by the sum of the amount by which the radical cation is stabilized by reorganization of the MO's upon ejection of one electron and the amount by which the correlation energies of the ground and radical cation states differ. The electron reorganization effect will cause the predicted IP to be too high, while the correlation effect will cause the predicted IP to be too low. Only if the sum of these two effects is a constant, or a linear function of IP, will linear correlations between $-\varepsilon_{\mathrm{SCF}}$ and IP be found.

In spite of this limitation, the assignments of states using Koopmans' theorem are often valid as long as only π states are involved (3). Incorrect assignments may result if π and σ ionizations are similar in energy. In such cases, Koopmans' theorem errors are apparently significantly different for different types of orbitals. An excellent case in point is provided by oxirane, where three different types of *ab initio* SCF calculations give three different orders for the lowest three ionization potentials (4). Our previous work attempted to confirm the order of radical cation states in oxirane by correlations with ionization potentials of dimethyl ether and oxetane. Whereas this procedure proved effective in making assignments for analogous amines and sulfides, it proved less than definitive in the oxygen cases. The study reported here was carried out in order to confirm assignments for oxirane by comparing substituent effects in oxiranes and thiiranes. This goal has been accomplished, and general observations about the effects of substituents on ionization potentials involving σ orbitals and upon the difficulties in applying Koopmans' theorem to systems lacking symmetry were made in the course of this work.

Molecular Orbitals and Radical Cation States of Oxiranes and Thiiranes

The familiar degenerate Walsh orbitals of cyclopropane (of e' symmetry in D_{3h}) give rise to a Jahn–Teller split ionization centered at 10.9 eV in the photoelectron spectrum (5, 6). The degenerate e'' orbitals are combinations of the methylene π_{CH_2} orbitals and give rise to $^2E''$ states centered at 13.2 eV (5). As shown in Fig. 1, the degeneracies of these orbitals (and of the radical ion states arising from them) are removed by inclusion of a heteroatom in the ring as a consequence of the lowered (C_{2v}) symmetry of the resulting molecules. Figure 1 shows the orbital energies calculated for cyclopropane, oxirane, and thiirane by an *ab initio* LCAO-MO-SCF method using the STO-3G basis set (4). The various atomic orbital coefficients are reflected approximately by the shapes and sizes of the lobes drawn in Fig. 1. The experimental vertical ionization potentials are shown in parentheses.

The e'' orbitals of cyclopropane evolve into the b_1 lone pair orbital, and a lower-lying a_2 combination of π_{CH_2} orbitals, while the e' orbitals of cyclopropane evolve into the a_1 and b_2 orbitals of the heterocyclopropanes. The fine-structured ionizations at 10.57 and 9.05 eV in the photoelectron spectra of oxirane (5, 6) and thiirane (6, 7), respectively, represent transitions to the $^2B_1$ radical cation states of these compounds, while the 14.2 and 13.59 eV ionizations arise from transitions to $^2A_2$ states in these molecules (4–7). The assignment of the 11.7 and 13.7 eV ionizations of oxirane and the 11.3 and 11.7 eV ionizations of thiirane are more difficult to make, since various calculations disagree upon the relative energies of the b_2 and a_1 orbitals. Schweig and Thiel have used intensity changes in He(II) spectra to conclude that the order shown in Fig. 1 is, indeed, correct (6).

An assignment of the 11.71 eV transition to the $^2A_1$ state and the 13.7 eV to the $^2B_2$ state of oxirane was made by Basch *et al.* (5) but this order of energy levels has not always been predicted by calculations. Basch *et al.* found that double zeta *ab initio* SCF calculations predicted the b_1 and a_1 orbitals to be accidentally degenerate, with b_2 lower in energy. Direct calculations on the relative energies of the radical cations gave the order $^2B_1 < {}^2A_1 < {}^2B_2 < {}^2A_2$, and this order was also predicted when correlation corrections were taken into account.

Pople and co-workers (8) performed *ab initio* calculation on oxirane using an extended basis set. The orbital energy order $a_1 > b_1 > a_2 > b_2$ was found, in variance with the results of Basch

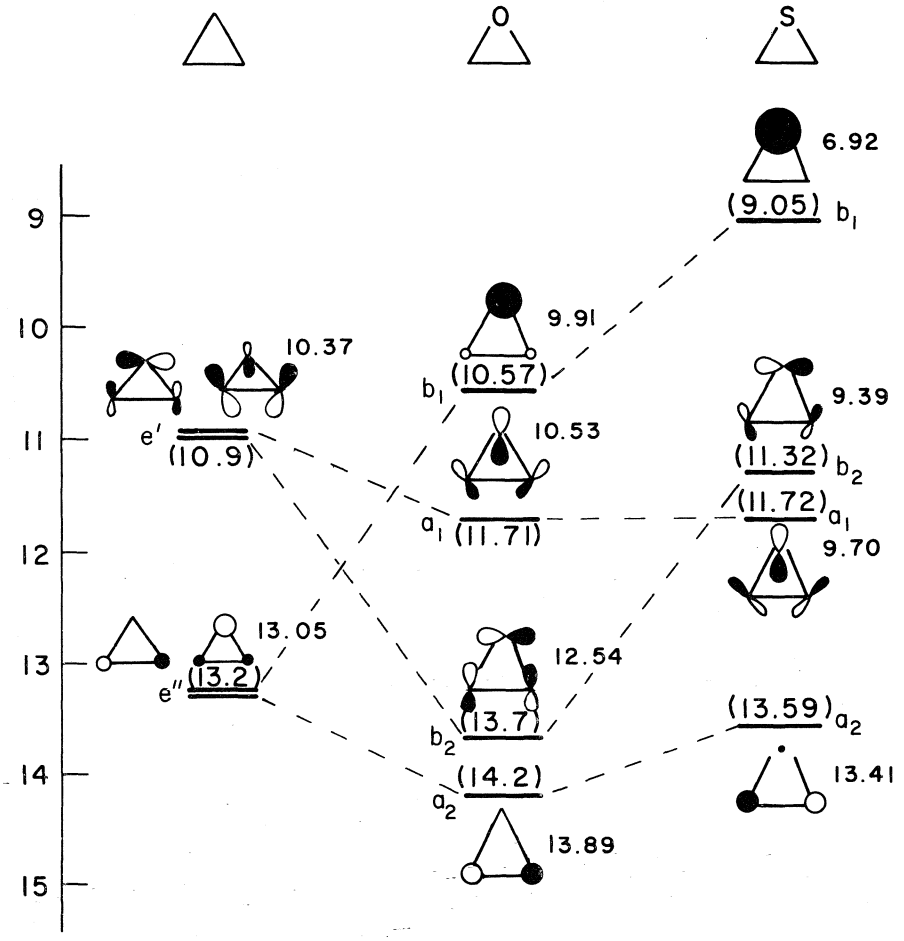

FIG. 1. Molecular orbitals (STO-3G) of cyclopropane, oxirane, and thiirane (negatives of orbital energies are shown next to each orbital, and experimental IP's are given in parentheses).

et al. and with the orbital energies obtained using the STO-3G basis or a minimal Slater basis (4).

For thiirane, less extensive calculations are available, but both semi-empirical (7) and *ab initio* (4) calculations agree on the order $^2B_1 > {}^2B_2 > {}^2A_1 > {}^2A_2$ for the radical cation states. The order of the $^2B_2$ and $^2A_1$ states is curiously different from that in oxirane.

Substitution of heterocyclopropanes with various substituents can clarify these assignments if the substituents cause significant differences in the changes in various ionization potentials. Furthermore, these molecules provide an opportunity to study the effect of substitution on σ orbitals. In particular, most compounds have σ levels that are either at high ionization potential or else lie close together so that their location and assignment proves difficult. However, for oxirane and thiirane the a_1 and b_2 σ levels are resolved from adjacent bands making the study of substituent effects possible.

Results

Alkyl and Halomethyloxiranes

Alkyl groups are generally considered to lower ionization potentials of appended moieties by a combination of inductive and hyperconjugative effects. For π systems, the extent of increase of a given orbital energy (and lowering of the corresponding ionization potential, using Koopmans' theorem) is normally assumed to be proportional

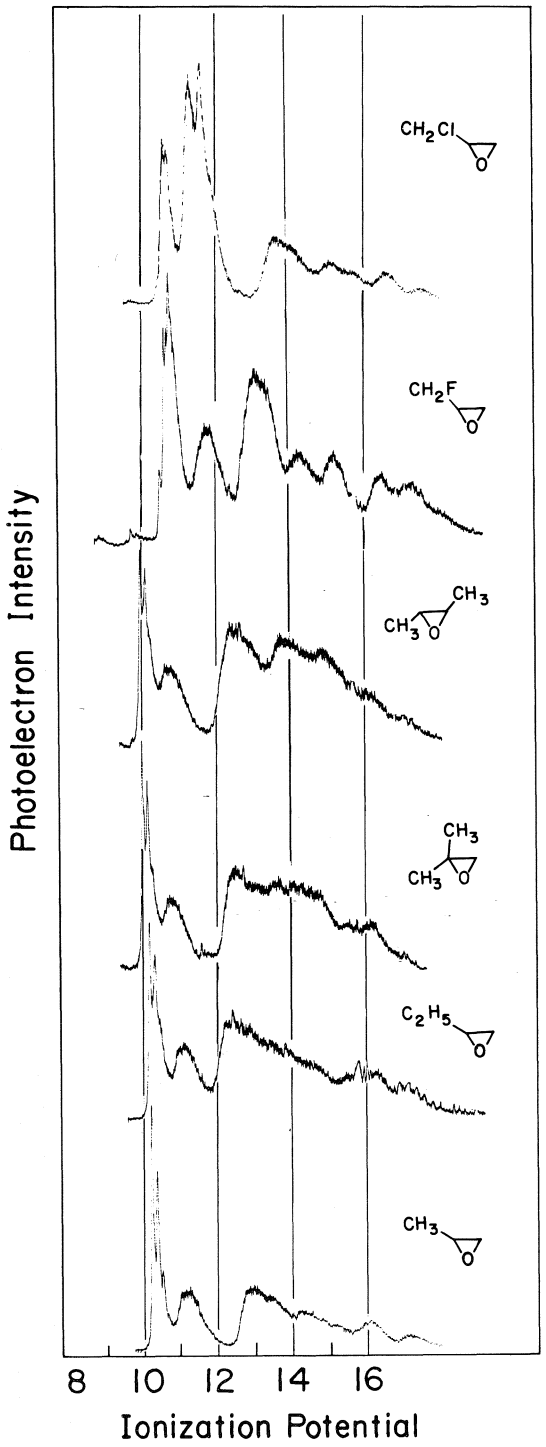

FIG. 2. Photoelectron spectra of alkyl and haloalkyl oxiranes.

to some function of the coefficient in the orbital at the site of substituent attachment (9). However, substitution which destroys the C_{2v} symmetry of the molecule also induces mixing of the formerly orthogonal orbitals, with a resulting further change in orbital energies (9). In the following discussion, we will retain the C_{2v} designations to describe the various orbitals, even though the molecules, and their orbitals, have no symmetry.

The effect of methyl and ethyl substituents on the photoelectron spectra of oxirane can be ascertained by considering the spectra of methyloxirane (propylene oxide) and ethyloxirane (Fig. 2). The assignments given in Fig. 3 are made by assuming that STO-3G and the Basch *et al.* assignment are correct, and that the orders of the first four IP's of oxirane and the two alkyloxiranes are the same. This is supported by calculations discussed below. The first four IP's are lowered by alkyl substitution, but there is no obvious correspondence between the alkyl substituent effect and the shape of the corresponding orbital assuming the shapes in Fig. 1, other than that the b_1 orbital is affected least by alkyl substitution. The ethyl substituent effect is 30% greater than the methyl effect for the first two IP's, and 70% greater on the third and fourth IP's. By comcomparison, the ethyl group lowers the IP of ethylene only 14% more than the methyl group lowers this IP (0.92 *vs.* 0.81 eV) (10).[3]

Methyl substitution cause the b_2 and a_2 ionization potentials to decrease by 0.82 and 0.87 eV, respectively, whereas the b_1 and a_1 are decreased by 0.31 and 0.48 eV. In the case of ethyloxirane the peaks after b_2 are broad and difficult to assign. Assuming that the shoulder on the b_2 peak at 12.7 eV corresponds to ionization from the a_2-like orbital, then ethyl substitution causes a decrease of 1.44 and 1.5 eV in b_2 and a_2 ionization potentials, respectively, whereas the b_1 and a_1 ionization potentials decrease by 0.42 and 0.63 eV, respectively.

Some insight into the mechanism of IP lowering by the substituent may be gained by comparing the first four IP's of oxirane and its alkyl and haloalkyl derivatives.

The photoelectron spectra of the halomethyl-

[3]Ionization potentials reported in ref. 10 are adiabatic; 0.16 eV has been added to all except ethylene to convert them to vertical ionization potentials.

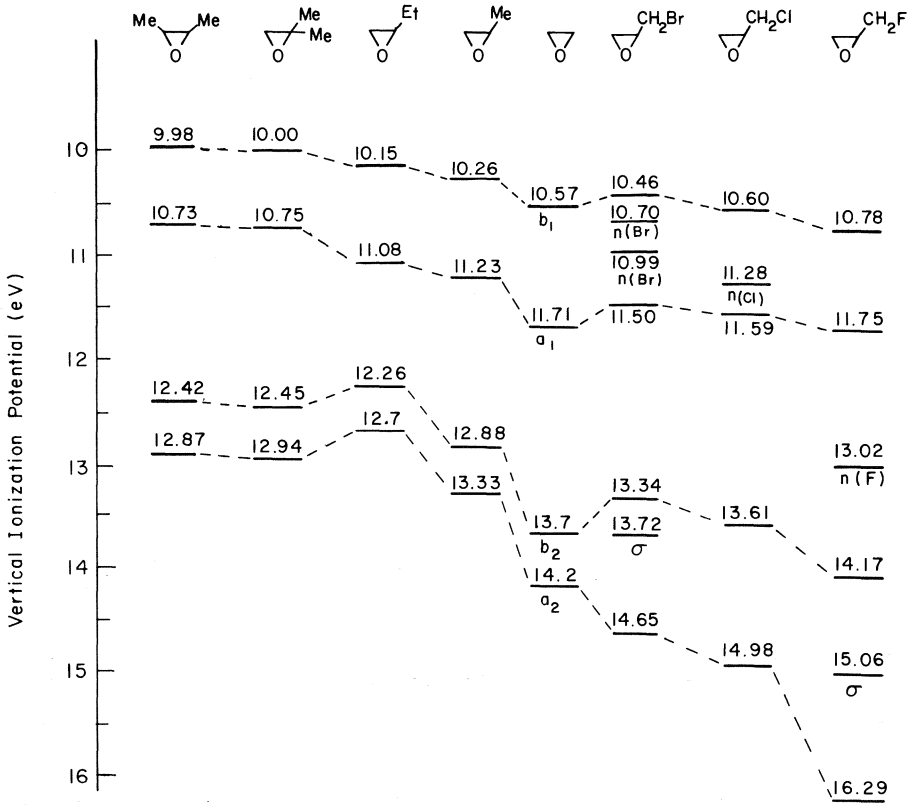

FIG. 3. Correlations between ionization potentials of oxirane and substituted oxiranes.

oxiranes have been reported previously by Baker *et al.* (11). Since these authors did not report the experimental spectra and gave no assignments, we have measured the photoelectron spectra of fluoromethyloxirane and chloromethyloxirane. By comparison of the spectra of halomethyloxiranes with methyloxirane it is possible to assign the first few ionization potentials for fluoromethyloxirane and chloromethyloxirane. We can also assign the bromomethyloxirane spectrum of Baker *et al.* (11). The photoelectron spectra of fluoromethyl- and chloromethyloxirane are shown in Fig. 2 and the correlation diagram with oxirane and methyloxirane in Fig. 3.

Substitution of halogen for hydrogen in methyloxirane stabilizes all levels and increases all ionization potentials. As with alkyl substitution, the third and fourth orbitals, analogous to b_2 and a_2 in oxirane, are lowered to a greater extent than the first two levels which are analogous to b_1 and a_1 in oxirane.

The spectrum of fluoromethyloxirane is in good agreement with that reported by Baker *et al.* (11) except for the peak at 13.17 eV which is found at 13.02 eV in this work. This peak has been assigned to the fluorine lone pair. This is in reasonable agreement with its location in methyl and vinyl fluoride (12). In methyl fluoride, a level due to a methylene-π, fluorine-lone-pair combination orbital occurs as a broad band between 12.5 and 14.5 eV, whereas in vinyl fluoride, the fluorine lone pair is assigned to the band in the region of 13.7 eV.

In fluoromethyloxirane, the band at 14.17 eV is assigned to the level analogous to the b_2 level in oxirane. This represents an increase in IP of 1.29 eV with respect to methyloxirane or 0.56 eV with respect to the same level in chloromethyloxirane.

There is some ambiguity about which of the next two levels at 15.06 and 16.29 eV is to be assigned to the a_2-like orbital. In view of the fact that this orbital has been the one most affected by substitution it has been assigned to the band at

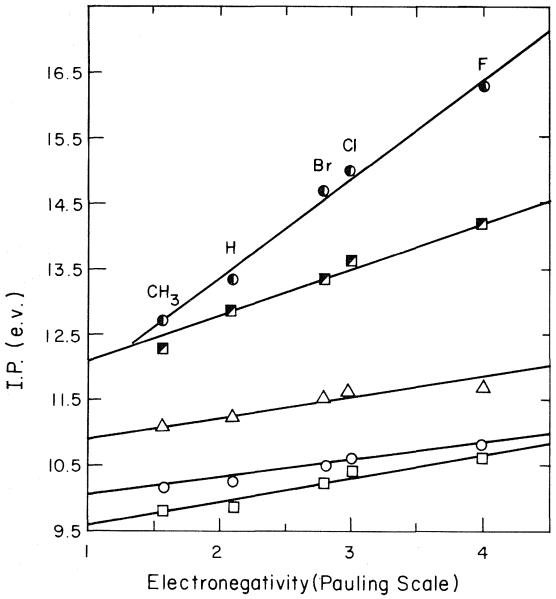

FIG. 4. Plot of IP's of substituted methyl oxiranes and propenes *vs.* substituent electronegativity (Pauling). □, propenes; ○, IP_1; △, IP_2; ◩, IP_3; ◑, IP_4 of methyloxiranes.

16.29 eV. This would represent an increase in ionization potential of 1.31 eV from chloromethyloxirane whereas the alternative assignment would result in an increase of only 0.08 eV.

The spectrum of chloromethyloxirane also agrees well with the peak positions reported by Baker *et al.* (11) except for the band at 13.61 eV which is indicated to be at 13.78 eV by them. The peak at 11.28 eV is assigned to the chlorine lone pair orbital since this peak is absent in the spectrum of fluoromethyloxirane.

The ionization potentials of all four oxirane-like orbitals of the halomethyloxiranes and methyloxirane correlate with electronegativity of the substituent as shown in Fig. 4. The ionization potentials of the π level in propylene and the allyl halides (13) are also plotted as a function of electronegativity for comparison purposes. In order to include the ionization potentials of ethyloxirane in the discussion of $—CH_2X$ substituted oxiranes, an effective electronegativiy of the methyl group is required. This was obtained by assuming that the ionization potential for 1-butene correlates with the plot of propylene and allyl halides *vs.* electronegativity. The π ionization potential of 1-butene (9.79 eV) (10) corresponds to an effective electronegativity of 1.57 for the methyl group. Using this value for the electronegativity of the methyl group, the ionization potentials of ethyloxirane are also included in Fig. 4. It can be seen that the points for ethyloxirane are in reasonable agreement with the lines drawn for the ionization potentials of methyloxirane and the halomethyloxiranes. The value of electronegativity of methyl determined in this way deviates somewhat from literature values (14), which indicate that methyl is nearly the same as, or more electronegative than, nitrogen.

Alternatively, one may think of Fig. 4 as a demonstration of the linear correlation between the first IP of substituted propenes and the first four IP's of the corresponding substituted methyloxiranes.

In Fig. 4, the slopes are 0.27 and 0.28 for the b_1 and a_1-like orbitals and 0.67 and 1.58 for the b_2 and a_2-like orbitals. The slope for the propenes is 0.34, indicating that substituents affect the b_1 and a_1 orbitals of methyloxirane to about the same extent as the π level of propene. The changes in b_2 and a_2 ionization potentials of oxirane brought about by the substituent are considerably larger.

The conclusion drawn from the linear relationship in Fig. 4 is that the combination of inductive and hyperconjugative effects that cause the changes in π ionization potentials from propene to the allyl halides must also be operating in the alkyloxiranes and halomethyloxiranes to produce changes in each of the four oxirane-like orbitals. Further comments are made in the Discussion section.

The STO-3G(15)[4] calculations on oxirane and methyloxirane support the assignments proposed from the experimental data. The calculated (STO-3G) and experiment ionization potentials for oxirane and methyloxirane are listed in Fig. 6. The STO-3G calculations tend to underestimate the ionization potentials with the result that the calculated values are in the range 0.87 to 0.97 of the experimental ones. Despite the disagreement between calculated and experimental values of

[4]The STO-3G calculations were done using the Program Gaussian 70 by Newton *et al.* (15) and R. Ditchfield, Quantum Chemistry Program Exchange, Indiana University, Bloomington, Indiana. The total energies (au) obtained in these calculations are: oxirane, −150.92698; methyloxirane, −189.51265; vinyloxirane, −226.86334; thiirane, −470.27285; methylthiirane, −508.85587; vinylthiirane, −546.20917.

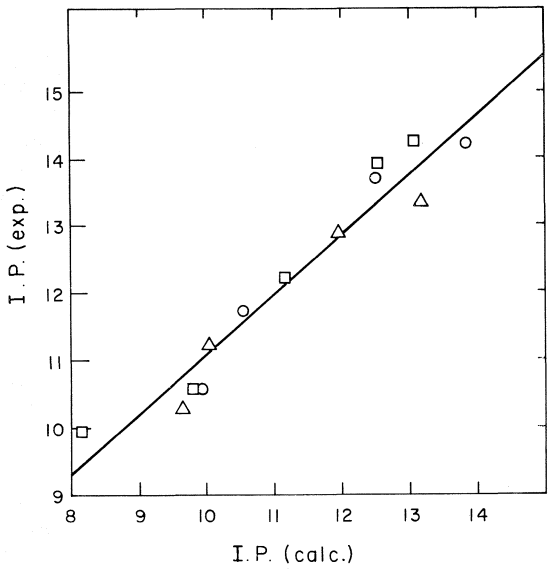

FIG. 5. Correlations between experimental IP's of oxirane, ○; methyloxirane, △; and vinyloxirane, □; and STO-3G orbital energies.

the ionization potentials, a good linear correlation between experimental and calculated ionization potentials is obtained as shown in Fig. 5. This correlation follows the least-squares relationship:

$$\text{IP(exp)} = 0.892\text{IP(calcd)} + 2.15$$

Figure 6 shows the shapes of the first four orbitals of oxirane and methyloxirane and the first five orbitals of vinyloxirane taken from STO-3G calculations. The size of the orbitals of various nuclei is approximately proportional to the square of the coefficient at that nucleus. One can see that the order of energy levels for oxirane agrees with that assigned by Basch *et al.* (5) ($b_1 > a_1 > b_2 > a_2$). From Fig. 6 it is also possible to conclude that even though the C_{2v} symmetry has been lost by addition of the methyl group to oxirane, the order of energy levels remains unchanged; *i.e.* the first one is b_1-like, the second a_1-like, etc.

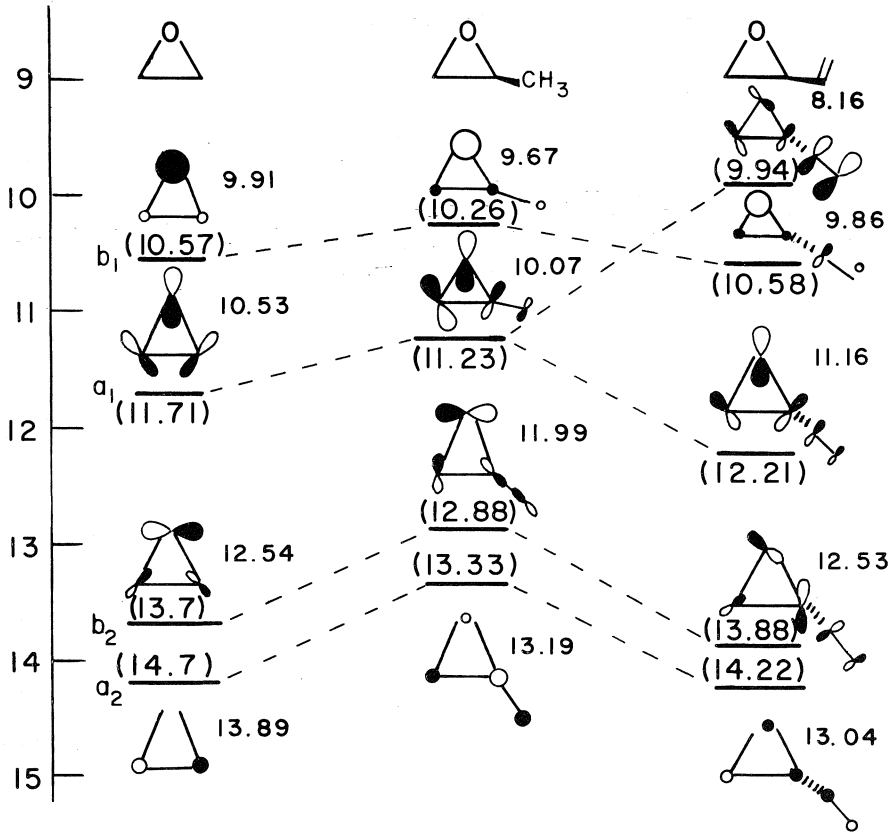

FIG. 6. STO-3G molecular orbitals of oxirane, methyloxirane, and vinyloxirane (negatives of orbital energies are shown next to each orbital, and experimental IP's are given in parentheses).

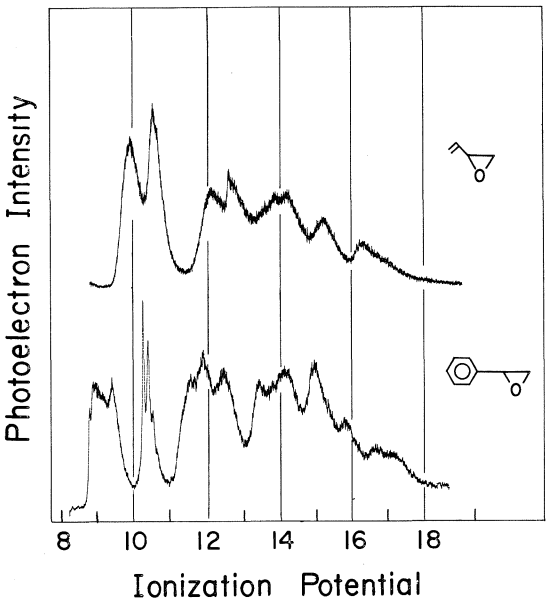

FIG. 7. Photoelectron spectra of vinyloxirane and phenyloxirane.

Disubstituted Oxiranes

The photoelectron spectra of 1,1-dimethyloxirane and *trans*-1,2-dimethyloxirane are shown in Fig. 2. The ionization potentials are correlated with those of oxirane and methyloxirane, and assignments are listed in Fig. 3. From the correlation diagram it can be seen that all four ionization potentials of the disubstituted oxiranes have been decreased relative to methyloxirane. However, the effect of a second methyl substituent on the b_2 and a_2 IP's is less than that of the first methyl. The ionization potentials of 1,1-dimethyloxirane and 1,2-dimethyloxirane are identical within experimental error, and the same order of energy levels is observed for disubstituted oxiranes as was observed for methyloxirane and oxirane (5). The effect of mono-methyl and di-methyl substitution observed here is analogous to that observed in substituted alkenes where the π ionization potential of ethylene decreases 0.62 eV (10) or 0.78 eV (9) upon methylation, but substitution of a second methyl groups has less of an effect. Conversion of propene to 2-methylpropene decreases the IP by 0.50 eV (10) or 0.64 eV (9), and conversion of propene to *trans*-2-butene decreases the IP by 0.62 eV (10) or 0.69 eV (9).

Vinyl and Phenyl Oxiranes

The spectra of these molecules are shown in Fig. 7 and correlations with oxirane and substituent moieties are shown in Fig. 8. Both phenyl and vinyl substituents possess several molecular orbitals whose ionization potentials lie below 15 eV. Vinyloxirane has three ionization potentials virtually unchanged from oxirane. These are located at 10.58 (b_1), 13.88 (b_2), and 14.22 (a_2). Interaction of the ethylenic π orbital at 10.52 eV (12) with a_1 orbitals of oxirane results in two new orbitals, one whose IP is increased by 0.50 eV from that of the a_1 level in oxirane to a value of 12.21 eV. The other ionization in this region corresponds to ionization from the σ levels of the vinyl moiety at 12.71 eV which compares favorably with the corresponding band in ethylene at 12.38 eV (12).

Assignments made in this way correlate exactly with those predicted by the STO-3G calculations (Fig. 6). The only disagreement between the STO-3G calculations and the experimental ionization potentials occurs for the a_2-like orbitals of vinyloxirane where the calculation predicts a decrease in ionization potential of 0.85 eV from oxirane and the observed change is an increase of 0.02 eV. Using the relationship discussed previously between calculated and experimental ionization potentials (IP(exp) = 0.892 IP(calcd) + 2.15) it is possible to predict a value of the a_2-like orbital from the calculated value. A predicted value of 13.78 eV is obtained in this way. From the spectrum of vinyloxirane in Fig. 7, it can be seen that the peak at 13.88 eV is broad and could contain the a_2-like orbital. Thus, there is some uncertainty in the exact position of the a_2-like orbital of vinyloxirane. However, as in the case of oxirane and methyloxirane, the calculations for vinyloxirane support the assignment arrived at from the photoelectron spectra.

In phenyloxirane, the ionization potentials at 10.30, 11.55, 13.42, and 14.08 eV can be assigned to the oxirane moiety. All of these ionization potentials are less than the corresponding ones in oxirane, indicating the superior inductive and/or hyperconjugative donor ability of the phenyl group as compared to the vinyl group. The b_1 and b_2 levels are destabilized by 0.27 and 0.28 eV, respectively, which is somewhat larger than for the a_1 and a_2 whose ionization potentials have decreased by 0.16 and 0.12 eV from those in oxirane.

The first two ionization potentials in phenyloxirane (9.07, 9.47 eV) can be correlated with the

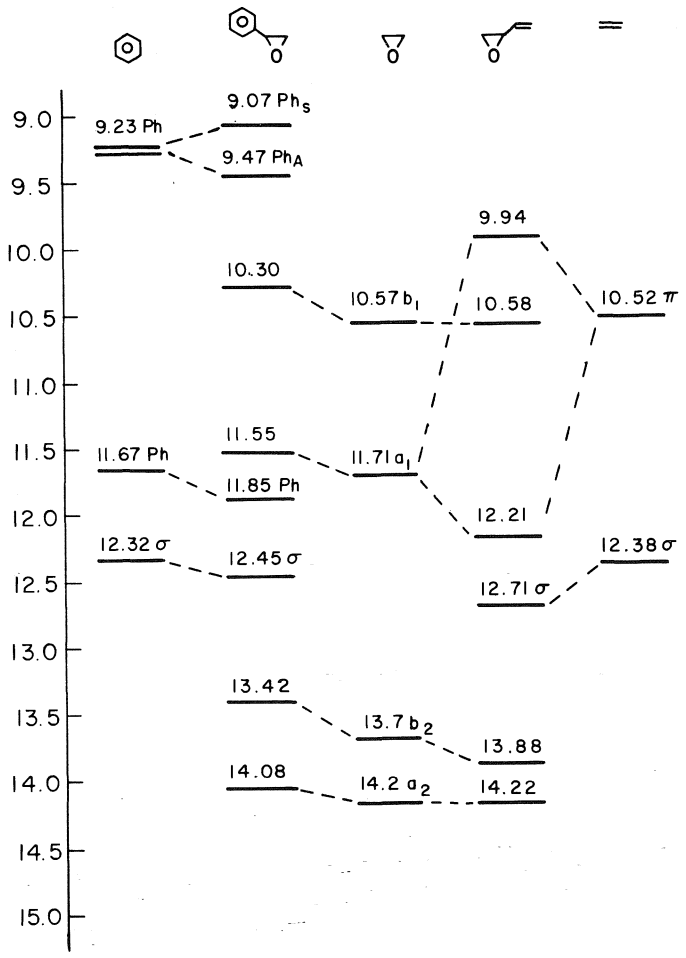

FIG. 8. Correlations between ionization potentials of vinyloxiranes, phenyloxirane, and substituents.

doubly degenerate highest occupied orbitals of benzene at 9.25 eV (12), which split under the influence of a substituent. The symmetric or Ph_S orbital of symmetry b_1 is characterized by being delocalized over the entire phenyl ring and substituent, with the region of highest electron density being at the position of substitution and *para* to it. In phenyloxirane this orbital is that giving rise to the IP at 9.07 eV. The antisymmetric or Ph_A orbital (symmetry a_2) is characterized by a node passing through the position of substitution and *para* to it and high electron density in the *ortho* and *meta* position. The band with IP at 9.47 eV in phenyloxirane is assigned to this orbital.

The ionization potential at 11.85 eV is also due to a phenyl orbital and is analogous to the one at 11.67 eV in benzene. The IP at 12.45 eV in phenyloxirane is assigned to σ ionization and is to be compared to the one at 12.32 eV in benzene (12).

Heilbronner and co-workers (16) have reported the photoelectron spectra of *cis*- and *trans*-diethynyloxirane and *cis*- and *trans*-diethynylthiirane. They assigned the same order to the oxirane and thiirane moiety ionization potentials as reported here. Since the a_1 level of oxirane is of the correct symmetry to interact with the ethynyl groups, the largest changes were observed for this orbital when comparing the photoelectron spectra of oxirane and diethynyloxirane. This is analogous to what has been found here for vinyloxirane.

Thiirane and Alkyl Thiiranes

Two determinations of the photoelectron

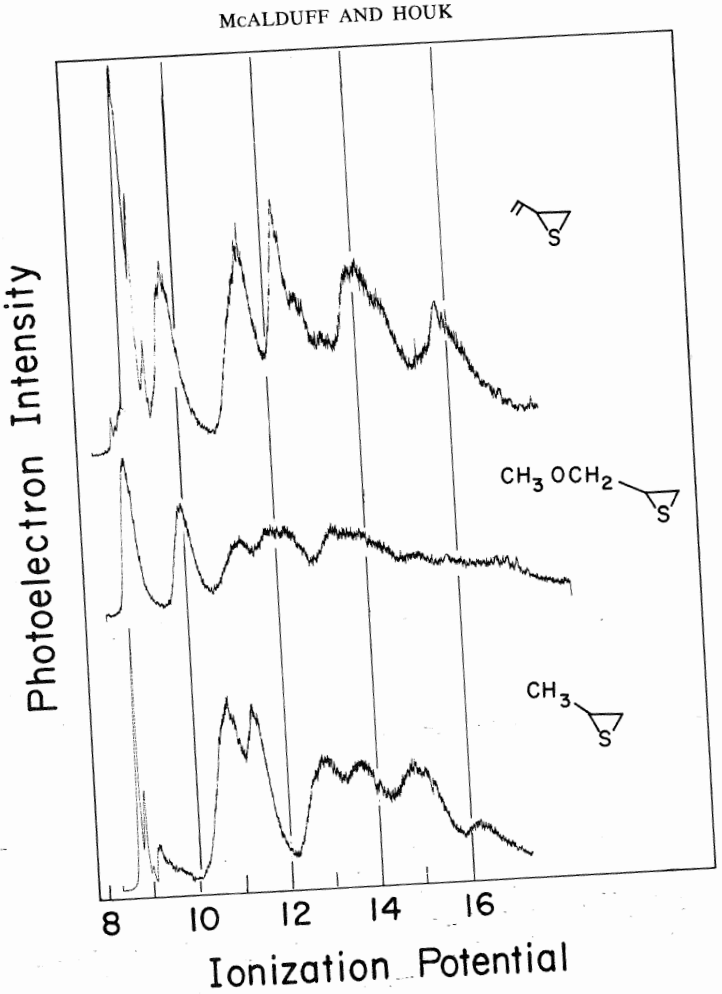

FIG. 9. Photoelectron spectra of thiiranes.

TABLE 1. Effects of methylation on ionization potentials

Parent	Orbital	IP (eV)	IP on methylation (eV)			
			P → Me[a]	Me → Et[b]	Me → 1,1-Me_2[c]	Me → 1,2-Me_2[d]
Ethylene (10)	π	10.52	0.62	0.11	0.50	0.62
Oxirane (5)	b_1	10.57	0.31	0.11	0.26	0.28
	a_1	11.71	0.48	0.15	0.48	0.50
	b_2	13.7	0.82	0.62	0.43	0.46
	a_2	14.2	0.87	0.63	0.39	0.46
Thiirane (7)	b_1	9.05	0.17			
	b_2	11.32	0.56			
	a_1	11.72	0.28			
	a_2	13.59	0.70			

[a]Change in IP upon monomethylation of the parent.
[b]Change in IP upon conversion of a methyl substituent to an ethyl substituent.
[c]Change in IP upon introduction of a second methyl α- to the first.
[d]Change in IP upon introduction of a second methyl β- to the first.

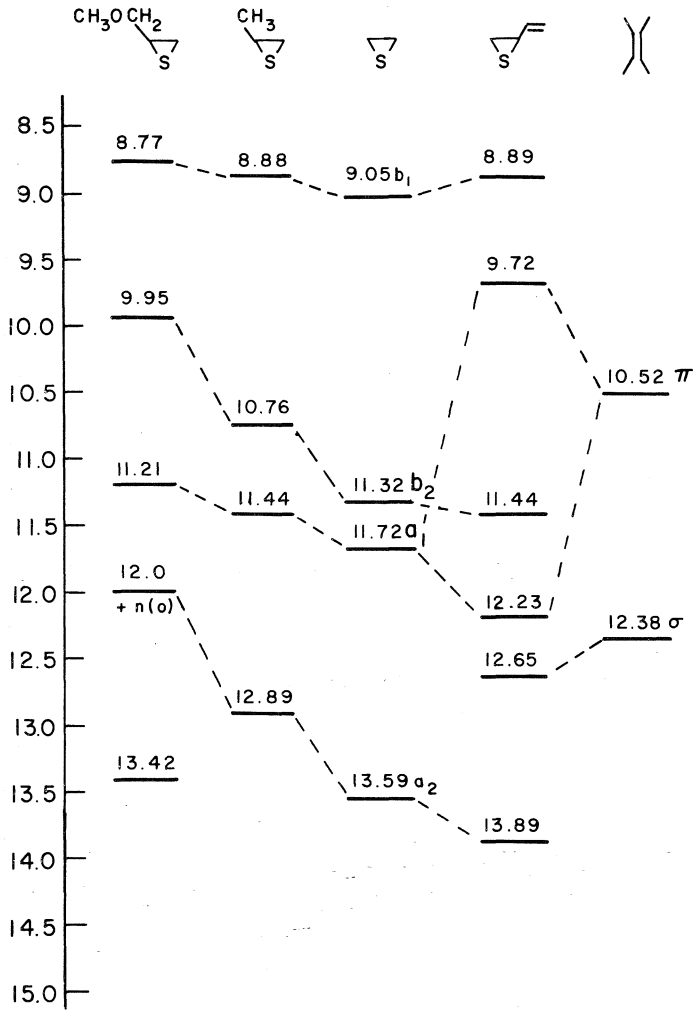

FIG. 10. Correlations between thiirane ionization potentials.

spectra of thiirane have been reported (6, 7). They agree except for the a_1 band which is reported at 11.86 eV by Schweig and Thiel (6) and 11.72 eV by Frost *et al.* (7). We have chosen to compare the latter with our spectra of substituted thiiranes which are shown in Fig. 9. Ionization potentials and assignments are listed in Table 1. Thiirane differs from oxirane in the order of its energy levels. The b_2 level whose ionization potential is 13.7 eV in oxirane has its ionization potential lowered to 11.32 eV in thiirane. This places it at a lower ionization potential than a_1 which is located at 11.72 eV. As with oxirane the first IP at 9.05 eV is associated with the heteroatom lone pair orbital and the fourth ionization potential at 13.59 eV is assigned to an a_2 orbital.

As shown in Fig. 10, methyl substitution on thiirane produces an effect similar to that observed for the alkyl substituted oxiranes, that is, a decrease in all four lowest IP's. The decrease in b_1 and a_1 occurs to a lesser extent than b_2 and a_2 (0.12 and 0.42 eV *vs.* 0.74 and 0.61 eV). As in the oxirane case, the b_2 and a_2 levels undergo greater destabilization upon alkyl substitution.

With methoxymethylthiirane the same phenomena are observed. The ionization potentials at 8.77 and 11.21 eV are analogous to the b_1 and a_1 of thiirane and have decreased less than the ionization potentials at 9.95 and 12.0 eV which

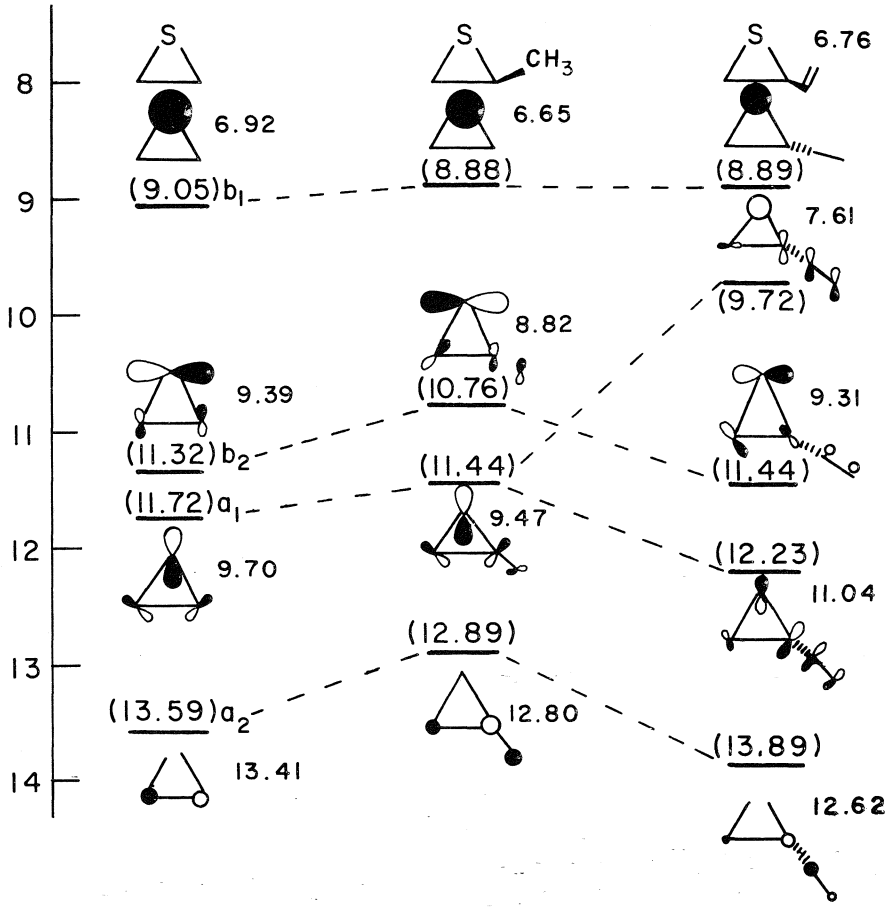

FIG. 11. STO-3G orbitals of thiirane, methylthiirane, and vinylthiirane.

are correlated with the b_2 and a_2 levels of thiirane (Fig. 10). The band at 12.0 eV in methoxymethylthiirane is broad and probably contains two unresolved bands. One of these could correspond to the oxygen lone pair on the methoxy group and the other to the a_2-like orbital.

STO-3G calculations have been performed on thiirane and methylthiirane. Figure 11 represents the shape of the first four orbitals of thiirane and methylthiirane from the STO-3G calculations. The size of the orbital at each nucleus is proportional to the square of the coefficient at that nucleus. As in the case of the oxiranes the calculated order of ionization potentials agrees with the experimental assignments for thiirane (6, 7). The same order is observed both experimentally and in the calculations for methylthiirane as well ($b_1 > b_2 > a_1 > a_2$). Figure 12 shows the correlation between experimental ionization potentials and STO-3G orbital energies for thiirane, methylthiirane, and vinylthiirane. As in the case of the oxiranes, even though the calculated orbital energies do not reproduce the experimental ionization potentials a linear correlation is obtained between them. The following least-squares correlation exists between the calculated and experimental quantities:

$$\text{IP(exp)} = 0.720\text{IP(calcd)} + 4.32$$

Thus, for thiirane and the alkyl-substituted thiiranes there is agreement between the assignments arrived at from the photoelectron spectra and those from the STO-3G calculations.

Vinylthiirane

Vinylthiirane is analogous to vinyloxirane in that the π orbital interacts with the orbital of a_1

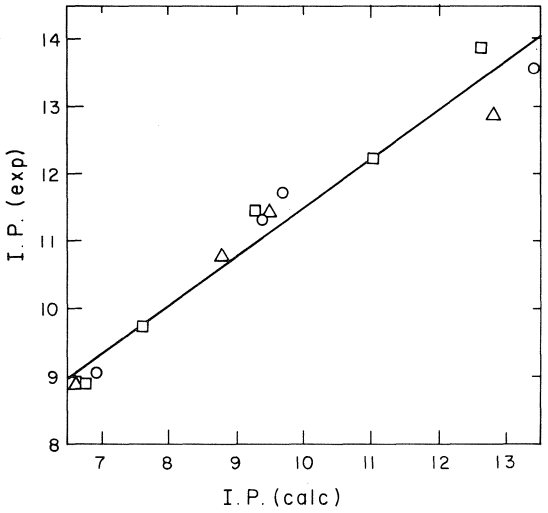

FIG. 12. Correlation between experimental IP's of thiirane, ○; methylthiirane, △; and vinylthiirane, □; and STO-3G orbital energies.

symmetry on the thiirane moiety producing an antibonding and a bonding combination of levels. The antibonding combination which is principally alkene-like is found at 9.72 eV (9.94 eV in vinyloxirane). The bonding combination of the a_1 on thiirane with the vinyl π is found at 12.23 eV which represents an increase of 0.51 eV from the unperturbed a_1 level in thiirane. The other ionization potentials in vinylthiirane are the lone pair on sulfur (b_1-like) at 8.89 eV and the b_2-like ionization potential at 11.44 eV as well as a σ level at 12.65 eV (12.71 eV in vinyloxirane) and the a_2-like level at 13.89 eV. The order $b_2 < a_1$ is obtained in vinylthiirane as it was in thiirane and the alkylthiiranes. As noted previously this is the reverse of the order of these levels in oxirane and the substituted oxiranes.

STO-3G calculations have also been performed on vinylthiirane. The calculated orbital energies are plotted in Fig. 11 and correlated with the experimental ionization potentials in Fig. 12. The shapes of the first five STO-3G orbitals of vinylthiirane are also included in Fig. 11. As can be seen in Fig. 11, the calculated and experimental values agree as to the order of energy levels for vinylthiirane. Thus the first ionization is from the b_1-like level corresponding to the sulfur lone pair and the second is the antibonding combination of the vinyl π and the a_1 orbital of the thiirane moiety. This order is the reverse of that obtained in vinyloxirane.

The third level is the b_2-like and is not changed significantly from thiirane. The fourth level undergoes an increase in ionization potential from thiirane to vinylthiirane and corresponds to the bonding combination of the a_1 and vinyl π orbitals. This increase is predicted in the calculation and realized in the spectrum.

As in the oxirane case, the most serious disagreement between calculated and experimental ionization potentials occurs for the a_2-like level of vinylthiirane where the calculation predicts a 0.79 eV decrease in ionization potential and experimentally an increase of 0.30 eV is observed. Using the least-squares relationship with the STO-3G calculations, the a_2-like ionization potential of vinylthiirane is predicted to occur at 13.41 eV. The band with maximum at 13.89 eV in the photoelectron spectrum of vinylthiirane is a broad one and could possibly result from the overlapping of several bands. Thus the uncertainty in the location of the a_2-like band in vinyloxirane seems to present itself in the case of vinylthiirane as well.

The overall result is that the photoelectron spectra and STO-3G calculation on methylthiirane and vinylthiirane have confirmed the earlier assignment of the order of energy levels in thiirane (6, 7).

Discussion

The first goal of this investigation was to confirm the assignments of IP's of oxirane and thiirane. The spectra of vinyloxirane and vinylthiirane proved to be most useful in this regard. That is, the vinyl moiety leaves three IP's unchanged in both molecules, and has a large influence upon only the second IP of oxirane, and the third of thiirane. These are the IP's which calculations most often assign to ionizations from the a_1 orbitals of the heterocycles. In the parent heterocycles, the a_1 orbitals have identical IP's (11.71 eV in oxirane and 11.72 eV in thiirane) and the densities of these orbitals at carbon are identical in the STO-3G calculations, and provide ideal local symmetry for overlap with a vinyl substituent in a 'bisected' conformation.

In vinyl cyclopropane (17) the first and third IP's at 9.15 and 11.7 eV correspond to the antibonding and bonding interactions of the vinyl π with one of the cyclopropane e' orbitals (b_2 in C_{2v}) centered at 10.9 eV. The other cyclopropane orbital of e' symmetry (a_1 in C_{2v}) is destabilized to

10.65 eV in vinylcyclopropane by the inductive effect of the vinyl substituent. Thus, the influence of the cyclopropyl groups on the vinyl IP (1.37 eV lowering of the vinyl IP; 0.8 eV raising of the cyclopropyl IP) is considerably larger than the effect of thiirane (0.8 eV lowering of vinyl; 0.51 eV raising of the a_1 IP), which, in turn, is larger than the effect of oxirane (0.58 eV lowering of the vinyl IP; 0.50 eV raising of the a_1 IP). These results are comparable quantitative measures of the conjugative power of these three small rings.

The small changes in the remaining three low-energy IP's of oxirane and thiirane upon vinyl substitution indicate that the vinyl moiety exerts a similar inductive effect to that of hydrogen, and that a *C*–vinyl bond hyperconjugates to about the same extent as a C—H bond.

All of the results found in this work are compatible with the assignments made by Basch *et al.* (5) and in our previous work for oxirane (4) ($b_1 > a_1 > b_2 > a_2$), and by all calculations for thiirane ($b_1 > b_2 > a_1 > a_2$) (4).

The influence of alkyl substituents upon the IP's of these molecules is less obviously related to the shapes of the orbitals of the parent molecules. However, the order of decreasing methyl (or other alkyl) influence for oxirane ($a_2(0.9) > b_2(0.8) > a_1(0.5) > b_1(0.3)$) is the same as that for thiirane ($a_2(0.7) > b_2(0.6) > a_1(0.3) > b_1(0.2)$). Furthermore, the effect of the methyl substituent upon the oxirane IP's is 1.3–1.7 times that of the effect on the thiirane IP's. Other alkyl or heteroalkylsubstituents follow the same pattern for oxirane.

The fact that a_2 orbitals are affected most by substitution is reasonable, since this orbital is a symmetry adapted CH bonding orbital in the parent molecules, and becomes largely C—C bonding in the substituted molecules. Thus, the correlation of the a_2 orbital energy with the electronegativities given in Fig. 4 indicates that the largely C—C bonding (but delocalized) orbital has an IP linearly related to the electronegativity of the substituent on this bond.

As indicated by the calculations shown in Figs. 6 and 11, the top three orbitals are polarized, but are less affected by alkyl substitution than is the a_2 orbital. The b_1 (lone pair) orbitals are affected to a very minor extent, but the changes in IP's are reproduced rather well by the calculations. This indicates that a breakdown in Koopmans' theorem (orbital relaxation) cannot

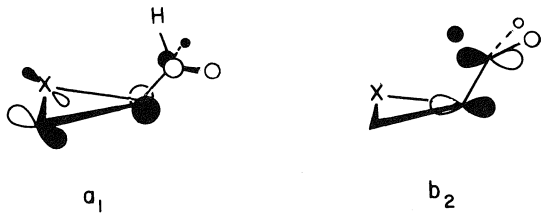

FIG. 13. The a_1 and b_2 orbitals of methyl heteranes, showing the π interaction in the former and $\pi + \sigma$ interactions in the latter.

be the source of the IP change, but instead, the alkyl groups influence the heterocycle lone pair IP's by a combination of a minor increase in hyperconjugative destabilization of the lone pair orbital, and a small inductive effect, reflected in the small increase in charge at the heteroatoms in the calculations on methylheteranes as compared to the parent heteranes: q_O(oxirane) = -0.213; q_O(methyloxirane) = -0.222; q_S(thiirane) = $+0.108$; q_S(methylthiirane) = $+0.078$.

The b_2 orbitals are influenced by alkyl substitution more than the a_1 orbitals in both oxirane and thiirane. This is contrary to the naive expectation that the a_1 should be affected more due to its larger coefficient at carbon (0.25–0.26) than for the b_2 orbital (0.16–0.19). On reflection the experimentally observed trends can be rationalized in the following way: the a_1 orbital can interact only inductively and in a π-hyperconjugative fashion with the alkyl substituent, while the b_2 can interact not only inductively and π-hyperconjugatively, but also in a σ fashion. That is, superimposed on the hyperconjugative interaction between methyl π_{CH_3} orbitals and the heterane b_2 orbitals, there is a change in the b_2 orbital resulting from the substitution of C—C bond for a C—H bond, as shown in Fig. 13.

Finally, we turn to disubstitution on the oxirane ring. Table 1 compares the effects upon IP's arising from monomethylation of ethylene, oxirane and thiirane, as well as upon ethylation, α,α-dimethylation, and *trans*-α,β-dimethylation of ethylene and oxirane. Alkylation of the a_2 and b_2 orbitals of oxirane and thiirane has an effect equal to, or larger than, that upon the π orbital of ethylene. This arises from the fact that substitution causes the a_2 and b_2 orbitals to take on C—C bonding character. This is shown particularly dramatically by the comparison of conversion of methyloxirane to ethyloxirane or either of the dimethyloxiranes. Substitution on the methyl group (Me → Et) causes a much

larger change in b_2 and a_2 IP's than methylation at the ring, compatible with the concept that these orbitals have significant ring-methyl C—C character. By contrast, ring methylation has a much greater influence on the b_1 and a_1 IP's than methylation of the methyl group. The similarity of the ethylene IP changes, and the a_1 changes are quite striking, and fully compatible with the model proposed by Hoffmann *et al.* (18) and Rohmer and Roos (19) in which the a_1 orbital of heteranes is formally constructed by the union of an ethylene π orbital with a vacant a_1 orbital of the heteroatom. The influences of alkyl substituents upon the b_1 IP are smallest, compatible with the weak inductive and hyperconjugative influence discussed earlier. As with the ethylene IP, β-methylation has a larger effect than α-methylation, compatible with the polarization of orbitals away from the site of alkyl substitution.

There is an apparent qualitative agreement between the Hoffmann (18) – Rohmer–Roos (19) model for bonding in oxirane and thiirane and the changes in IP's upon alkyl substitution. These authors described the b_2 orbital of three-membered ring heterocycles as arising from the interaction of a b_2 donor orbital of the heteroatom and the π^* orbital of the ethylene fragment. Because the b_2 orbital of S is higher than that of O, the former should mix in more π^* (carbon) character than the latter. While this shows up in the calculations to a small extent, the IP changes are larger for oxirane than for thiirane, opposite to the expectation based on site of localization of electron density. However, the fact that the b_2 orbital of oxirane is at considerably lower energy than that of thiirane allows great hyperconjugative interaction with the lower lying methyl orbital.

The a_1 orbitals of these molecules formally arise from the union of an a_1 heteroatom acceptor orbital and the π orbital of ethylene. The a_1 acceptor is lower for S than for O, so the thiirane a_1 orbital should have less C—C character than oxirane. This effect is manifested to a small extent in the calculated coefficients, but it is apparent in IP changes upon methylation. The a_1 IP's of oxirane and thiirane are of equal energy, but the change of oxirane a_1 IP upon methylation is 1.7 times that for thiirane.

Experimental

All samples except vinylthiirane were commercially available and were used without further purification. Vinylthiirane was prepared by a standard procedure (20). Photoelectron spectra were recorded on a Perkin-Elmer Ltd., PS-18 Photoelectron Spectrometer using argon and xenon as internal calibrants. Resolution as determined from the argon peak at 15.76 eV was 25–30 meV and the recorded peak positions represent an average of five determinations.

Acknowledgements

Financial support of this research was generously provided by the National Science Foundation and the National Institutes of Health. We are grateful to Andrew Caruso for the preparation of vinylthiirane, and to Ruth W. Gandour for carrying out the STO-3G calculations.

1. T. Koopmans. Physica, **1**, 104 (1934).
2. W. G. Richards. J. Mass. Spectrosc. Ion Phys. **2**, 419 (1969); B. Kellerer, L. S. Cederbaum, and G. Hohlneicher. J. Electron Spectrosc. Relat. Phenom. **3**, 107 (1974).
3. F. Brogli, P. A. Clark, E. Heilbronner, and M. Neuenschwander. Angew. Chem. Int. Ed. Engl. **12**, 422 (1973).
4. P. D. Mollere and K. N. Houk. J. Am. Chem. Soc. In press.
5. H. Basch, M. B. Robin, N. A. Kuebler, C. Baker, and D. W. Turner. J. Chem. Phys. **51**, 52 (1969).
6. A. Schweig and W. Thiel. Chem. Phys. Lett. **21**, 541 (1973).
7. D. C. Frost, T. G. Herring, A. Katrib, and C. A. McDowell. Chem. Phys. Lett. **20**, 401 (1973).
8. W. A. Lathan, L. Radom, P. C. Hariharan, W. J. Hehre, and J. A. Pople. Fortsch.Chem.Forsch. **40**, 1 (1973).
9. M. Beez, G. Bieri, H. Bock, and E. Heilbronner. Helv. Chim. Acta, **56**, 1028 (1973).
10. R. Masclet, D. Grosjean, G. Mouvier, and J. Dubois. J. Electron Spectrosc. **2**, 22 (1973).
11. A. D. Baker, D. Betteridge, N. R. Kemp, and R. E. Kirby. Anal. Chem. **43**, 375 (1971).
12. D. W. Turner, C. Baker, A. D. Baker, and C. R. Brundle. Molecular photoelectron spectroscopy. Wiley-Interscience, New York, N.Y. 1970.
13. G. W. Mines and H. W. Thompson. Spectrochim. Acta, Part A, **29**, 1377 (1973).
14. P. R. Wells. Prog. Phys. Org. Chem. **6**, 111 (1968).
15. M. D. Newton, W. A. Lathan, W. J. Hehre, and J. A. Pople. J. Chem. Phys. **52**, 4064 (1970).
16. F. Brogli, E. Heilbronner, J. Wirz, E. Kloster-Jensen, R. G. Bergman, K. P. C. Vollhardt, and A. J. Ashe, III. Helv. Chim. Acta, **58**, 2620 (1975).
17. P. Brunckmann and M. Klessinger. Chem. Ber. **107**, 1108 (1974).
18. R. Hoffmann, H. Fujimoto, J. R. Swenson, and C.-C. Wan. J. Am. Chem. Soc. **95**, 7644 (1973).
19. M.-M. Rohmer and B. Roos. J. Am. Chem. Soc. **97**, 2025 (1975).
20. F. Lautenschlager and N. V. Schwartz. J. Org. Chem. **34**, 3391 (1969).

Studies of the rhenium–oxygen bond. III. The crystal and molecular structure of 1-oxo-6-ethoxo-2,4-dichloro-3,5-dipyridinerhenium(V)

COLIN JAMES LYNE LOCK[1] AND GRAHAM TURNER

Institute for Materials Research, McMaster University, Hamilton, Ont., Canada L8S 4M1

Received July 16, 1976

COLIN JAMES LYNE LOCK and GRAHAM TURNER. Can. J. Chem. **55**, 333 (1977).

The crystal and molecular structure of the title compound has been examined by single crystal X-ray diffraction. The crystals are monoclinic with $a = 28.045(10)$, $b = 8.766(3)$, $c = 12.376(5)$ Å, $\beta = 91.14(3)°$. The space group is $C2/c$ and there are eight molecules per unit cell. A total of 5053 independent reflections, of which 2860 were observed, were examined on a Syntex $P\bar{1}$ diffractometer. The structure was refined by full matrix least squares to an R_2 value of 0.0449. The ligands form a very rough octahedron around the rhenium atom with Re—Cl(1), 2.441(3); Re—Cl(2), 2.366(3), Re—O(1), 1.684(7); Re—O(2), 1.896(6); Re—N(1), 2.144(7); Re—N(2), 2.132(7) Å. The pyridine rings are a dominant factor in determining the details of the molecular structure.

COLIN JAMES LYNE LOCK et GRAHAM TURNER. Can. J. Chem. **55**, 333 (1977).

On a examiné les structures cristallines et moléculaires du composé mentionné dans le titre par diffraction de rayon-X sur un cristal unique. Les cristaux sont monocliniques avec $a = 28.045(10)$, $b = 8.766(3)$, $c = 12.376(5)$ Å, $\beta = 91.14(3)°$. Le groupe d'espace est $C2/c$ et il y a huit molécules par maille. Utilisant un diffractomètre Syntex $P\bar{1}$, on a examiné un total de 5053 réflexions indépendantes desquelles 2860 ont pu être observées. La structure a été affinée par la méthode des moindres carrés (matrice complète) jusqu'à une valeur de $R_2 = 0.0449$. Les ligands forment approximativement un octaèdre autour de l'atome de rhénium et Re—Cl(1), 2.441(3); Re—Cl(2), 2.366(3), Re—O(1), 1.684(7); Re—O(2), 1.896(6); Re—N(1), 2.144(7); Re—N(2), 2.132(7) Å. Les cycles de pyridine sont un facteur déterminant dans les déterminations des détails de la structure moléculaire.

[Traduit par le journal]

Introduction

The reaction of wet pyridine with oxotrichlorobis(triphenylphosphine)rhenium(V) is postulated to go through the following steps (1).

Chatt and Rowe (2) claimed the structure of **1** was as shown for R = C_6H_5 on the basis that $Z = 4$ for a $C2/c$ monoclinic cell which has an eightfold general position. The molecule thus had a twofold axis of symmetry. There is a possible ambiguity, however, since a simple space group determination will not differentiate $C2/c$ and Cc, with a fourfold general position. There is no indication given by Chatt and Rowe (2) that this ambiguity was resolved by an attempt at crystal structure determination and therefore the structure of **1** must still be considered unknown. We have examined the structure of **5** and shown it is correct (3). More recently we have examined the structure of **3**, and shown that the structure given is incorrect:

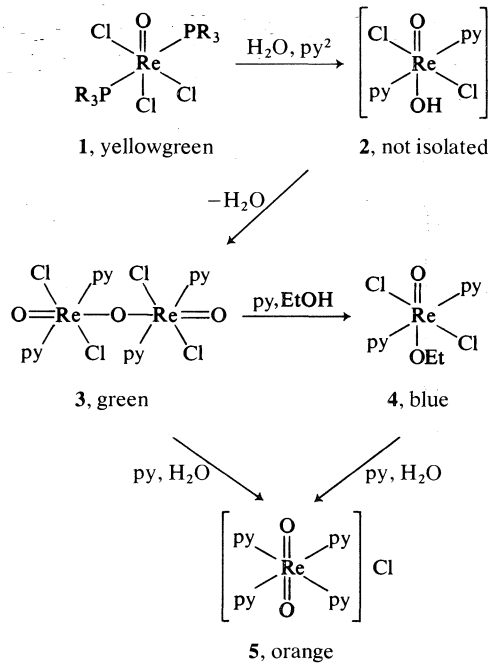

[1]To whom correspondence should be addressed.

[2]py is pyridine, C_5H_5N; Et is the ethyl radical, $C_2H_5\cdot$; en is ethylenediamine, $NH_2\cdot CH_2\cdot CH_2\cdot NH_2$.

the halves of the dimer actually contain *cis* chloro and pyridine groups (4). As a consequence, if the production of **4** is as shown, it seemed possible that the structure postulated was incorrect. We have examined the structure of **4** by single crystal X-ray diffraction and report our results here.

Experiments

Preparation of 1-Oxo-6-ethoxo-2,4-dichloro-3,5-di(pyridine)rhenium(V), $ReCl_2 \cdot O \cdot OC_2H_5(C_5H_5N)_2$

The title compound was prepared by the method of Johnson *et al.* (1). The compound was recrystallized from a 9:1 mixture of 1,1,2,2-tetrachloroethane and absolute ethanol, in a dry atmosphere at 5 °C. The final crystals were blue plates.

Collection of the Diffraction Data

A crystal of the title compound, selected after examination under a polarizing microscope, was mounted with its longest dimension approximately parallel to the goniometer axis. The crystal was bounded by {100}, {010}, and {001}, which were 0.007, 0.018, and 0.022 cm apart, respectively. Precession photographs, using MoKα radiation, of the 0*kl* and *h*0*l* projections showed monoclinic symmetry with C centering. Weissenberg photographs, using CuKα radiation, confirmed the C centering, and revealed an unusually long ***a*** axis. Further precession photographs of 1*kl*, 2*kl*, *h*1*l*, and *h*2*l*, showed the systematic absences, *hkl*, $h + k = 2n + 1$, *h*0*l*, $l = 2n + 1$ ($h = 2n + 1$), and 0*k*0 ($k = 2n + 1$). These absences correspond to the space groups $C2/c$ (#15) or Cc (#9).

The crystal was transferred to a Syntex P$\bar{1}$ diffractometer and unit cell parameters were obtained by least squares refinement of 15 reflections in the range $20° < 2\theta < 30°$. The density of a few single crystals was measured by flotation in a degassed aqueous solution of zinc bromide. Crystal data were:

$C_{12}H_{15}Cl_2N_2O_2Re$ f.w. = 476.2

Monoclinic, $a = 28.045(10)$, $b = 8.766(3)$, $c = 12.376(5)$ Å, $\beta = 91.14(3)°$, $V = 3042(2)$ Å^3, $C2/c(C_{2h}^6$, #15), $\rho_o = 2.10(2)$, $Z = 8$, $\rho_c = 2.08$ (22 °C, $\lambda = 0.70926$ Å), $\mu = 87.98$ cm^{-1}.

Intensities were recorded on the Syntex P$\bar{1}$ diffractometer using graphite monochromatized MoKα radiation for the quadrant defined by *h*, *k*, ±1 up to $2\theta = 55°$. Data were collected using a coupled θ(crystal)–2θ(counter) scan, 1° on either side of the peak. Scan rates were selected by the program supplied with the instrument and varied from 4 to 24°/min. The stability of the system was monitored by measuring a standard reflection, 0,2,2, after every 49 reflections. The counting esd of the standard was 1.3%, and the fluctuation was random (Gaussian). The intensity, *I*, and its esd, σ_I, were calculated as outlined previously (5). A total of 5053 reflections were measured, including 2860 observed, 1567 unobserved, and 626 rejected ($I < \sigma_I$). The intensities were corrected for absorption.[3] After correction for Lorentz and polarization effects, unscaled structure factor amplitudes, *F*, and their standard deviations, σ_F, were calculated as outlined previously (5).

Solution of the Structure

The Patterson map was solved uniquely for one independent rhenium atom at the approximate coordinates $x = 0.11$, $y = 0.25$, $z = 0.02$. This indicated the space group $C2/c$, with an eightfold general position; one cycle of refinement, varying only the scale factor gave $R_1 = 0.30$.[4] A three-dimensional electron density difference map revealed the positions of all the remaining non-hydrogen atoms, except C(2). A further cycle of refinement, using unit weights, followed by a difference map revealed C(2). In further refinement it was necessary to keep the *y* coordinate of the rhenium atom fixed at 0.25. Allowing this parameter to vary by even 0.001 caused the temperature factors of other atoms to blow up or become non-positive definite. This is because in reflections with *k* odd, the rhenium atoms do not contribute to the intensity if *y* is precisely ¼, but this is not so if the rhenium atom moves out of this position. The high scattering power of the rhenium atom tends to swamp other contributions.

In all further refinement the pyridine rings were constrained to the geometry given by Bak *et al.* (6) and refinement was done using the program GROUPLS. In addition, the temperature factors of the rhenium and chlorine atoms were made anisotropic. A weighting scheme of the type $W = [104.4 - 1.016|F_o| + 0.00293|F_o|^2]^{-1}$ was used for further refinement which was stopped at $R_1 = 0.0789$, $R_2 = 0.0453$. At this point a correction was made for secondary extinction by the method of Larsen (7) ($g = 2.93 \times 10^{-8}$), and all reflections, including those previously considered unobserved, were used in further refinement. The weighting scheme was modified to $W = [104.4 - 1.016|F_o| + 0.00293|F_o|^2 + 1390|\sigma/|F_o||^2]^{-1}$ for reasons outlined previously (4). Further refinement was terminated at $R_1 = 0.0713$ and $R_2 = 0.0449$. The maximum shift/error was 0.04 and the average shift/error was 0.007. A final difference map showed no peak higher than 1.02 e/Å^3 at 0.11, 0.20, 0.02 near the rhenium atom and no valley lower than −1.06 e/Å^3 at 0.11, 0.30, 0.02, also near the rhenium atom. The final atom parameters are given in Table 1 and the moduli of F_o and F_c are given in Table 2.[5]

An alternative refinement using anisotropic temperature factors for the oxygen atoms was terminated at

[3]All calculations were carried out on a CDC 6400 computer. The programs DATCO3, ABSORB, DATRDN and ORTEP were taken from the X-RAY 71 package. The full matrix least squares programs, CUDLS and GROUPLS (J. S. Stephens), Fourier program, SYMFOU (J. S. Rutherford), and least squares planes program, PALS (P. G. Ashmore) were written locally.

[4]$R_1 = \dfrac{\sum ||F_o| - |F_c||}{\sum |F_o|}$;

$R_2 = \left[\dfrac{\sum \omega(|F_o| - |F_c|)^2}{\sum \omega F_o^2}\right]^{1/2}$.

[5]Table 2 is available, at a nominal charge, from the Depository of Unpublished Data, CISTI, National Research Council of Canada, Ottawa, Canada, K1A 0S2.

TABLE 1. Atom parameters for $ReOCl_2(OC_2H_5)(C_5H_5N)_2$ ($\times 10^3$)

Atom	x	y	z	U (Å^2)
Re	109.81(1)	250	21.99(3)	*
Cl(1)	158.4(1)	346.8(3)	−124.4(2)	*
Cl(2)	68.2(1)	169.6(4)	176.3(2)	*
O(1)	67.0(3)	208.3(7)	−70.7(5)	43(2)
O(2)	163.1(2)	299.4(7)	111.9(5)	34(1)
C(1)	213.2(6)	310(2)	116(1)	72(4)
C(2)	232(1)	421(1)	187(2)	105(6)
N(1)	139.8(3)	27(1)	2.9(6)	34(2)
C(11)	136.2(4)	−47(1)	−92(1)	40(2)
C(12)	154.7(5)	−193(1)	−109(1)	53(3)
C(13)	178.3(5)	−266(2)	−24(1)	65(3)
C(14)	182.2(5)	−191(2)	75(1)	66(4)
C(15)	162.9(4)	−45(1)	84(1)	48(3)
N(2)	81.8(3)	474(1)	41.6(6)	39(2)
C(21)	84.3(5)	548(1)	136(1)	52(3)
C(22)	65.7(5)	694(1)	153(1)	57(3)
C(23)	43.2(5)	768(2)	66(1)	67(3)
C(24)	40.4(5)	692(1)	−33(1)	55(3)
C(25)	59.9(4)	547(1)	−41(1)	45(3)

Atom	U_{11}	U_{22}	U_{23}	U_{12}	U_{13}	U_{23}
Re	37.1(3)	39.5(2)	29.3(2)	3.7(3)	−3.6(1)	−2.8(2)
Cl(1)	57(2)	53(2)	41(1)	0(1)	11(1)	1(1)
Cl(2)	54(2)	61(2)	37(1)	1(1)	1(1)	7(1)

*Anisotropic temperature factors (Å $\times$ 10^3). Anisotropic temperature factors U_{ij} were obtained from $\beta_{ij} = 2\pi^2 b_i b_j U_{ij}$ where β_{ij}'s appear as a temperature effect through exp $[-(\beta_{11}h^2 + \ldots 2\beta_{12}hk + \ldots)]$ in the structure factor expression and b_j are the reciprocal lattice vectors. Estimated standard deviations are given in parentheses.

$R_1 = 0.0712$ and $R_2 = 0.0448$. This is not significantly better than the above refinement using Hamilton's test (8). A final refinement was tried moving the rhenium atom y parameter to 0.249 or 0.251. In both cases the light atom temperature factors misbehaved, as observed previously. Throughout the refinements the scattering curves used were those from the *International Tables for X-ray Crystallography* (ref. 9, Table 2.2A, p. 72*ff.*) and anomalous dispersion corrections from the same source (ref. 9, Table 2.3.1, pp. 149–150) were applied to the curves for Re and Cl.

Discussion

The molecule is shown in Fig. 1 and selected interatomic distances and angles are given in Table 3. The six bonded ligand atoms form a very rough octahedron about the rhenium atom; that is, although the bond lengths vary markedly, all *cis* angles, except two, are close to 90°. The angles which differ markedly from 90° are O(1)—Re—Cl(2), 97.4(3)° and O(2)—Re—Cl(1), 84.9(3)°. This is apparently caused by non-bonded interactions. The Cl(2)—O(1) distance is normal (13), whereas the other Cl—O distances, particularly Cl(1)—O(1) and Cl(1)—O(2), are more characteristic of systems whereas steric strain is present (10). Re—N(1), 2.144(7), and Re—N(2), 2.132(7), do not differ significantly and the distances agree well with previously determined values (3, 4, 11). Re—Cl(1), 2.441(3) Å, and Re—Cl(2), 2.366(3) Å, do differ significantly, Re—Cl(2) having a distance considered 'normal' by Ibers and co-workers (12). Thus, Re—Cl(1) is long and we shall show below this is caused by steric repulsion. The two Re—O distances differ as would be expected for a structure written formally as

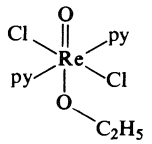

The actual values, however, cast serious doubts on this formulation. Re—O(1), 1.684(7), lies well within the range of distances (1.60(5)–1.73(6) Å) considered to be representative of Re—O triple bonds (13 and references therein),

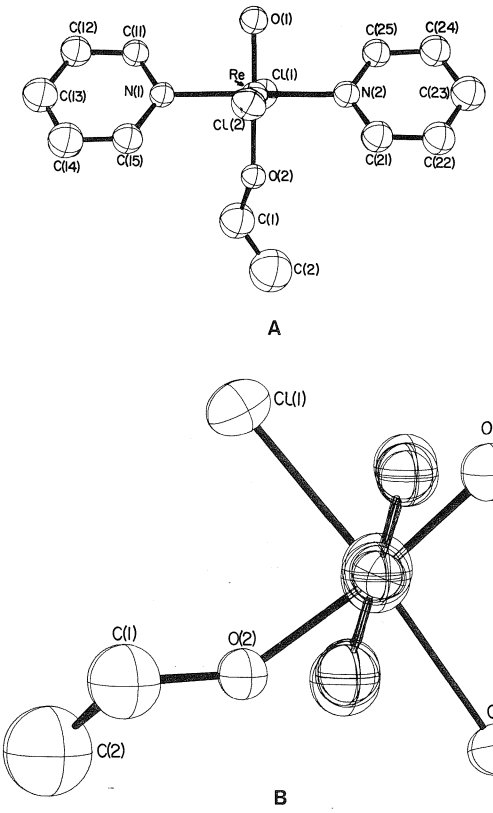

FIG. 1. (*A*) The molecule, $ReOCl(OEt)(C_5H_5N)_2$, oriented such that the plane O(1)N(1)O(2)N(2) lies in the plane of the paper. The numbering of the atoms is as in Table 1. (*B*) The same molecule viewed down the N(1)N(2) vector, and not retouched in the neighbourhood of the pyridine rings, to show the almost complete coplanarity.

and Re—O(2), 1.896(6), is substantially less than 2.04 Å, considered by Cotton and Lippard (14) to be representative of an Re(V)—O single bond. The Re—O(2) distance is closer to the Re—O double bond distance, 1.76–1.78 Å, (3, 15–19) and the Re—O(bridging) distance observed in Re—O—Re systems (19–21) where multiple bonding has been postulated (20). If one uses the above single bond value, the value of 1.765 Å (obtained from accurate redeterminations of the structures of $[ReO_2(en)_2]Cl$ and $[ReO_2(py)_4]Cl{\cdot}2H_2O$, (22)) as the double bond value, and the Pauling bond order – bond length relationship (23), then the Re—O(2) bond has an order of 1.44 and Re—O(1), 2.45. Thus a more realistic picture would be

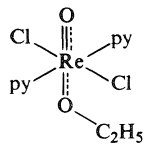

The partial multiple bonding in Re—O(2) is consistent with the very large Re—O(2)—C(1) angle, 144.3(9)°, although this cannot be the only cause since, with an Re—O double bond we would expect Re—O(2)—C(1) to be close to 120°. Again, we shall suggest this is caused by steric repulsion. We note that the Re—O distances observed herein are quite close to those observed by us for the $[ORe(NH_2{\cdot}CH_2{\cdot}CH_2{\cdot}NH_2)_2{\cdot}OH]^{2+}$ ion (11), and thus the multiple bonding postulated here appears to be a general effect for O≡Re—OR systems. This is in complete contrast to the normal behaviour of formally single-bonded groups *trans* to an oxo-ligand in six-coordinate rhenium(V) compounds (13, 14) and is in direct contravention of the model of Porai-Koshits and Shustorovich (24). Normally the *trans* ligands are at distances from the metal even greater than normal metal–ligand single bond distances. We do not consider the effect anomalous; four orbitals are used in bonding along the O—Re—O axis in *trans*-$ReO_2L_4^{n+}$ complexes. In this complex we have gone part way to an O≡Re—X system, but the total bond order still remains close to 4.

The O(2)—C(1) distance (1.41(2) Å) is normal, but the C(1)—C(2) distance (1.40(2) Å) appears to be short (25). We considered the possibility of some inexplicable hydrogen loss to give a vinyl group rather than an ethyl group but proton nmr studies show unambiguously that an ethyl group is present (δ $H(CH_3)$, 1.00; δ $H(CH_2)$, 3.76 ppm downfield relative to TMS, J_{HH} = 7.42 Hz; δ $H(C_5H_5N)$, complex, centered at roughly 7.6 ppm downfield). The shortening of the bond length may be artificial, since both C(1) and C(2), especially C(2), have large temperature factors.

The steric requirements of pyridine, noted previously (3, 4), are again manifest. The pyridine rings are essentially coplanar, as shown in Fig. 1*B*, and are oriented such that the pyridine planes make an angle of 34° with the best plane through O(1)(2)ReN(1)N(2) and 55°

TABLE 3. Selected interatomic distances and angles for $ReOCl_2(OC_2H_5)(C_5H_5N)_2$

Atoms	Distance (Å)	Atoms	Distance (Å)
Re—Cl(1)	2.441(3)	Re—Cl(2)	2.366(3)
Re—O(1)	1.684(7)	Re—O(2)	1.896(6)
Re—N(1)	2.144(7)	Re—N(2)	2.132(7)
O(2)—C(1)	1.41(2)	C(1)—C(2)	1.40(2)
Atoms	**Angle (°)**	**Atoms**	**Angle (°)**
O(1)—Re—N(2)	91.6(3)	O(1)—Re—N(1)	90.2(3)
O(1)—Re—Cl(1)	88.4(2)	O(1)—Re—Cl(2)	97.4(3)
N(2)—Re—Cl(1)	88.7(2)	N(1)—Re—Cl(1)	90.5(2)
N(2)—Re—Cl(2)	89.7(2)	N(1)—Re—Cl(2)	91.1(2)
O(2)—Re—N(1)	88.1(3)	O(2)—Re—N(2)	90.6(3)
O(2)—Re—Cl(1)	84.9(2)	O(2)—Re—Cl(2)	89.4(2)
O(1)—Re—O(2)	173.0(3)	N(1)—Re—N(2)	178.5(3)
Cl(1)—Re—Cl(2)	174.0(1)	Re—O(2)—C(1)	144.3(9)
O(2)—C(1)—C(2)	115(2)	Re—N(1)—C(11)	121(1)
Re—N(1)—C(15)	122(1)	Re—N(2)—C(21)	122(1)
Atoms	**Distance (Å)**	**Atoms**	**Distance (Å)**
	Non-bonded distances		
Cl(1)–O(1)	2.925(8)	Cl(1)–O(2)	2.954(7)
Cl(1)–N(1)	3.263(8)	Cl(1)–N(2)	3.203(9)
Cl(1)–C(1)	3.34(1)	Cl(1)–C(25)	3.45(1)
Cl(2)–O(1)	3.075(7)	Cl(2)–O(2)	3.017(7)
Cl(2)–N(1)	3.222(8)	Cl(1)–N(2)	3.175(9)
Cl(2)–C(15)	3.46(1)	Cl(2)–C(21)	3.39(1)
O(1)–N(1)	2.73(1)	O(1)–N(2)	2.74(1)
O(1)–C(11)	2.98(1)	O(1)–C(25)	3.00(1)
O(2)–N(1)	2.81(1)	O(2)–N(2)	2.87(1)
O(2)–C(15)	3.04(1)	O(2)–C(21)	3.12(1)

with the best plane through N(1)N(2)ReCl(1)-Cl(2). Because of the orientation of the pyridine rings, atom C(1) is constrained, and must lie in the general direction of Cl(1). We noted above the large Re—O(2)—C(1) angle. If this angle was 120°, as would be expected for a double bond – single bond system at an oxygen atom, the C(1)—Cl(1) distance would be 2.65–2.84 Å, depending on the exact features of the model, which is unacceptably short. The Cl(1)—C(1) distance has been increased to a more acceptable 3.34(1) Å, by lengthening the Re—Cl(1) bond, opening up the Re—O(1)—C(1) angle to 144.3(9)° and twisting C(1) out of the Cl(1)-ReO(2) plane. The dihedral angle between the planes ReO(2)C(1) and Cl(1)O(1)ReCl(2)-O(2) is 33°. This final displacement is restricted because C(1) is now only 3.44(1) Å from C(15). The displacement of C(1) out of the Cl(1)Re(2) plane brings one of the hydrogen atoms on C(1) closer to Cl(1) (2.74 Å) than if C(1) had been in the plane (3.09 Å).[6] Presumably a short Cl–H non-bonded distance is preferable to a short Cl–C non-bonded distance.

The packing, shown in Fig. 2, is complex. In the ***a*** direction contact in the plane at $x = \frac{1}{4}$ is primarily between the ethyl groups and pyridine rings on adjacent molecules. In the $x = \frac{1}{2}$ plane, down the $y = \frac{1}{2}$ line contact is between oxygen and chlorine atoms on adjacent molecules. In the same plane and down the $y = 0$ line, however, we have contact between parallel pairs of pyridine rings. A similar contact is observed dominating packing in the ***b*** direction. In the ***c*** direction, contact is between a pyridine ring on one molecule

[6]Calculations are based on an H—C—H angle of 109.8°, a CH distance of 1.000 Å, and C_{2v} symmetry of the bonds about C(1).

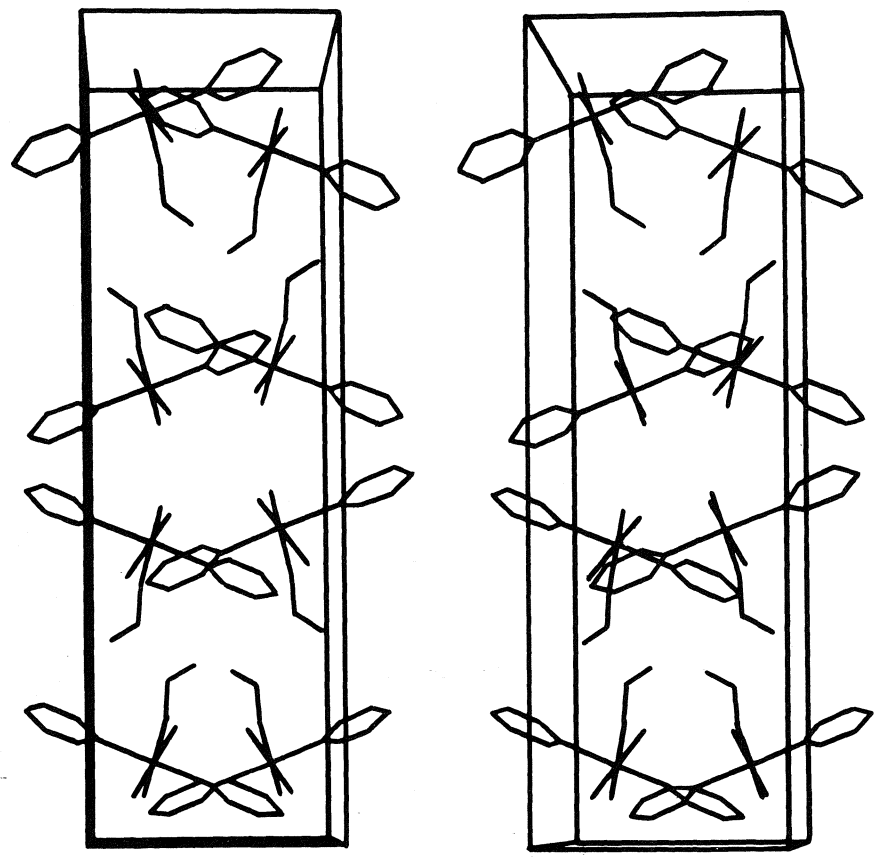

FIG. 2. Stereogram (stereoscopic pair of perspective projections) of $ReOCl_2(OC_2H_5)(C_5H_5N)_2$. The contents of one unit cell are shown. ***a*** and ***b*** are parallel to the side and top of the page respectively and the view is down ***c****.

and chlorine and pyridine groups on another, or a pyridine ring on one molecule and pyridine, chlorine, and ethoxo groups on the other. All contacts mentioned above are equal to or greater than Van der Waals contact distances. There appear to be no features of the packing which would have any dominant effect on the intramolecular structural features.

Finally, we note that the pyridine rings are *trans*, as was correctly postulated by Johnson *et al.* (1). This raises the problem of why the *trans* isomer was obtained from **3**, in which the pyridine rings were arranged *cis*. We have shown that the *cis* arrangement in the dimer is a steric requirement of the structure. It may be that in the monomer species the *trans* arrangement of the pyridine groups is more stable. Octahedral or pseudo-octahedral complexes having two pyridine groups attached to the central metal show both *cis* and *trans* arrangements (26–42). It is notable, however, that *cis* arrangements of the pyridine groups only occur where the remaining coordinated groups are not very large or sterically demanding (26–30). In compounds containing ligands such as halogens the pyridine ligands are *trans* (31–42). It appears therefore, that steric requirements will generally cause pseudo-octahedral complexes which contain two pyridine groups to have a *trans* arrangement of the pydrine groups.

Acknowledgments

We thank the National Research Council of Canada for financial support of this work.

1. N. P. JOHNSON, F. I. M. TAHA, and G. WILKINSON. J. Chem. Soc. 2614 (1964).
2. J. CHATT and G. A. ROWE. J. Chem. Soc. 4019 (1962).

3. C. CALVO, N. KRISHNAMACHARI, and C. J. L. LOCK. J. Cryst. Mol. Struct. **1**, 161 (1971).
4. C. J. L. LOCK and G. TURNER. Can. J. Chem. To be published.
5. R. P. HUGHES, N, KRISHNAMACHARI, C. J. L. LOCK, J. POWELL, and G. TURNER. Inorg. Chem. In press.
6. B. BAK, L. HANEEN-HUGAARD, and J. RASTRUP-ANDERSEN. J. Mol. Spectrosc. **2**, 361 (1958).
7. A. C. LARSEN. Acta Crystallogr. **23**, 664 (1967).
8. W. C. HAMILTON. Acta Crystallogr. **18**, 502 (1965).
9. D. T. CROMER and J. A. WABER. International tables for X-ray crystallography, Vol. IV. *Edited by* J. A. Ibers and W. C. Hamilton. Kynoch Press, Birmingham, 1974.
10. I. D. BROWN, C. J. L. LOCK, and C. WAN. Can. J. Chem. **52**, 1704 (1974).
11. G. BETZNER, I. D. BROWN, C. J. L. LOCK, J. J. PARK, and G. TURNER. To be published.
12. P. W. CORFIELD, R. J. DOEDENS, and J. A. IBERS. Inorg. Chem. **6**, 197 (1967).
13. C. J. L. LOCK and C. WAN. Can. J. Chem. **53**, 1548 (1975).
14. F. A. COTTON and S. J. LIPPARD. Inorg. Chem. **4**, 1621 (1965).
15. T. GLOWIAK, T. LIS, and B. JEZOWSKA-TRZEBIATOWSKA. Bull. Acad. Pol. Sci. Ser. Sci. Chim. **20**, 957 (1972).
16. V. S. SERGIENKO, M. A. PORAI-KOSHITS, and T. S. KHODASHOVA. J. Struct. Chem. **15**, 250 (1974).
17. R. K. MURMANN and E. O. SCHLEMPER. Inorg. Chem. **10**, 2353 (1971).
18. R. H. FENN, A. J. GRAHAM, and N. P. JOHNSON. J. Chem. Soc. A, 2880 (1971).
19. R. SHANDLES, E. O. SCHLEMPER, and R. K. MURMANN. Inorg. Chem. **10**, 2785 (1971).
20. S. R. FLETCHER and A. C. SKAPSKI. J. Chem. Soc. Dalton Trans. 1073 (1972).
21. T. GLOWIAK, T. LIS, and B. JEZOWSKA-TRZEBIATOWSKA. Bull. Acad. Pol. Sci. Ser. Sci. Chim. **20**, 199 (1972).
22. C. J. L. LOCK and G. TURNER. To be published.
23. L. PAULING. The nature of the chemical bond. 3rd ed. Cornell University Press, Ithaca, N.Y. 1960. p. 239.
24. M. A. PORAI-KOSHITS and E. M. SHUSTOROVICH. Acta Crystallogr. Sect. A, **31**, 144 (1975).
25. L. E. SUTTON (*Editor*). Tables of interatomic distances and configurations in molecules and ions supplement 1956–1959. Special Publication No. 18, The Chemical Society, London. 1965.
26. D. L. WEAVER and R. M. TUGGLE. J. Am. Chem. Soc. **91**, 6506 (1969).
27. R. D. GILLARD, M. KEETON, R. MASON, M. F. PILBROW, and D. R. RUSSELL. J. Organometal. Chem. **33**, 247 (1971).
28. J. A. MCGINNETY. J. Organomet. Chem. **59**, 429 (1973).
29. G. INGROSSO, A. IMMIRZI, and L. PORRI. J. Organomet. Chem. **60**, C35 (1973).
30. J. PRADILLA-SORZANO and J. P. FACKLER. Inorg. Chem. **12**, 1174 (1973).
31. J. D. DUNITZ. Acta Crystallogr. **10**, 307 (1957).
32. M. A. PORAI-KOSHITZ and G. N. TISHCENKO. Sov. Phys. Crystallogr. **4**, 2160 (1960).
33. R. C. ELDER. Inorg. Chem. **7**, 1117 (1968); **7**, 2316 (1968).
34. P. PORTA, A. SCAMELLOTTI, and N. VINCIGUERRA. Inorg. Chem. **10**, 541 (1971).
35. C. K. PROUT, M. J. BARROW, and F. J. C. ROSSOTTI. J. Chem. Soc. A, 3326 (1971).
36. A. F. CAMERON, K. P. FORREST, D. W. TAYLOR, and R. H. NUTTALL. J. Chem. Soc. A, 2492 (1972).
37. A. F. CAMERON, D. W. TAYLOR, and R. H. NUTTALL. J. Chem. Soc. Dalton Trans. 422 (1972).
38. M. R. CAIRA, G. V. FAZAKERLEY, P. W. LINDER, and L. R. NASSIMBENI. Acta Crystallogr. Sect. B, **29**, 2898 (1973).
39. P. M. RICHARDS, R. K. QUINN, and B. MOROSIN. J. Chem. Phys. **59**, 4474 (1973).
40. R. J. HOBSON, M. F. C. LADD, and D. C. POVEY. J. Cryst. Mol. Struct. **3**, 337 (1973).
41. P. J. CLARKE and H. J. MILLEDGE. Acta Crystallogr. Sect. B, **31**, 1543 (1975).
42. B. MOROSIN. Acta Crystallogr. Sect. B, **31**, 632 (1975).

Electrical conductivity studies on $Cd_3O_2Cl_2$ and Cd_3OF_4

MAHADEVA NATARAJAN AND ETALO A. SECCO[1]

Chemistry Department, St. Francis Xavier University, Antigonish, N.S., Canada B2G 1C0

Received July 19, 1976

MAHADEVA NATARAJAN and ETALO A. SECCO. Can. J. Chem. **55**, 340 (1977).

Electrical conductivity data on compressed discs of $Cd_3O_2Cl_2$ and Cd_3OF_4 show contrasting electrical behavior. The relative high room temperature conductivity and its quasi-independence of temperature suggest Cd_3OF_4 to be a novel semiconductor compound.

MAHADEVA NATARAJAN et ETALO A. SECCO. Can. J. Chem. **55**, 340 (1977).

Des données de conductivité électrique sur des disques compressés de $Cd_3O_2Cl_2$ et de Cd_3OF_4 montrent des comportements électriques qui sont en opposition. La conductivité relativement élevée à température de la pièce et son indépendance presque totale de la température suggèrent que le Cd_3OF_4 est un nouveau composé semi-conducteur.

[Traduit par le journal]

The cadmium oxyhalides, $Cd_3O_2Cl_2$ and Cd_3OF_4, have been isolated and identified in this laboratory (1, 2). These compounds were expected to possess contrasting electrical conductivity behavior from elementary crystal structure and charge neutrality considerations.

$Cd_3O_2Cl_2$ crystallizes in the monoclinic system (3) in common with $Hg_3O_2Cl_2$ (4) which suggests the structural formula $Cd(OCdCl)_2$. On the other hand, Cd_3OF_4 crystallizes in the cubic system in common with its reactants CdO and CdF_2. With the ionic radii of O^{2-} and F^- given as 1.40 and 1.36 Å, respectively, (5), the oxyfluoride is visualized as a substitution compound with normal F sites in the fluoride lattice replaced by O units. This substitution can be accommodated by singly charged O^- species, F^- vacancies, or Cd^{2+} interstitials.

The inherent defects speculated for oxyfluoride are expected to display characteristic electrical conductivity properties in contrast to the non-defective $Cd_3O_2Cl_2$ and this report includes such a conductivity study.

Experimental

The compounds were prepared according to procedures already described (1, 2) and confirmed by their characteristic DTA and X-ray diffraction patterns. Conductivity measurements were made on compressed polycrystalline discs (13 mm diameter and 2–3 mm thick) held between Pt plates by a spring loaded support (6). Measurements were also made with silver dag painted on the disc contact faces, instead of Pt plates, with no difference in conductivity discernible. The cell was heated at the rate of 20 °C h^{-1} and the temperature was monitored by chromel–alumel thermocouple. The frequency of 1 kHz, unless otherwise specified, employing GR-1608 A Impedance bridge was used in all measurements.

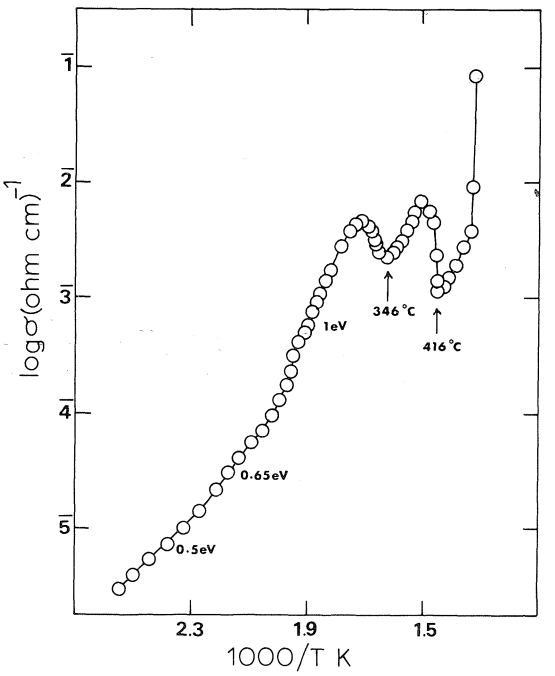

FIG. 1. Logarithm of specific conductivity, σ, *vs.* $10^3/T$ K in vacuum for $Cd_3O_2Cl_2$ preannealed at 220 °C in N_2 for 1 h.

Results and Discussion

The logarithm of conductivity σ *vs.* $1000/T$ K for $Cd_3O_2Cl_2$ is given in Fig. 1. The disc of freshly prepared compound yields $\sigma \approx 10^{-9}$

[1]To whom correspondence should be addressed.

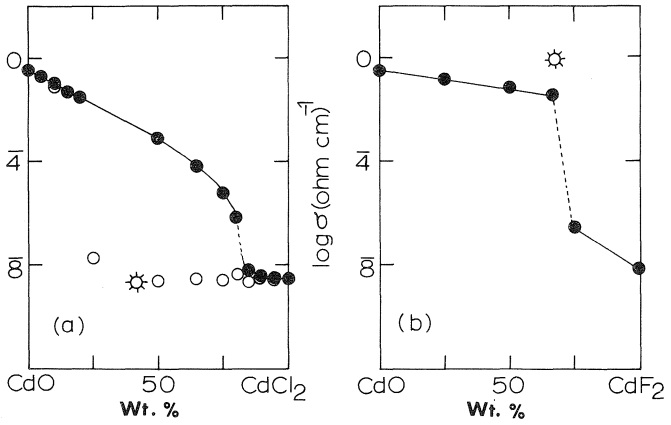

FIG. 2. Logarithm of specific conductivity, σ, *vs.* composition (wt. %) of mixtures, (*a*) $CdO–CdCl_2$, filled circles for unannealed samples, open circles for samples annealed at 500 °C in air for 6 h; (*b*) $CdO–CdF_2$, filled circles for unannealed samples; the spiked circle in each diagram represents the respective compound.

$(ohm\ cm)^{-1}$ at room temperature whereas σ increases to 10^{-6} $(ohm\ cm)^{-1}$ after preannealing at 220 °C for 1 h. The low temperature slope corresponds to an activation energy of 0.5 eV with regional slopes increasing to 0.65 and 1.0 eV at higher temperatures. A pronounced anomaly exists at 346 °C followed by a second effect at 416 °C prior to the sharp rise in conductivity above 460 °C; these latter two effects were observed both in preannealed and unannealed discs. Above 495 °C the compound undergoes trace decomposition with $CdCl_2$ depositing on the cell walls. The characteristic X-ray pattern for $Cd_3O_2Cl_2$ remained unaffected in the temperature region 320–430 °C, thus precluding any phase transition.

Room temperature conductivity measurements were made on $CdO–CdCl_2$ mixtures over the entire composition range; the data are plotted in Fig. 2*a*. The conductivity for annealed and unannealed mixtures remains constant, $\sim 10^{-9}$ $(ohm\ cm)^{-1}$, from $CdCl_2$ to 85% $CdCl_2$. This result supports the earlier suggestion (1) that a solid solution of limited solubility is formed prior to compound formation. The conductivity of the compound (spiked circle) is comparable to $CdCl_2$ and 10^6 lower than the corresponding unannealed composition. Excess CdO in the compound effects a rise in conductivity attaining the unannealed value at ~85% CdO.

Plots of log σ *vs.* $1000/T$ for Cd_3OF_4 under different measurements and preannealed conditions are presented in Fig. 3. Cd_3OF_4 was

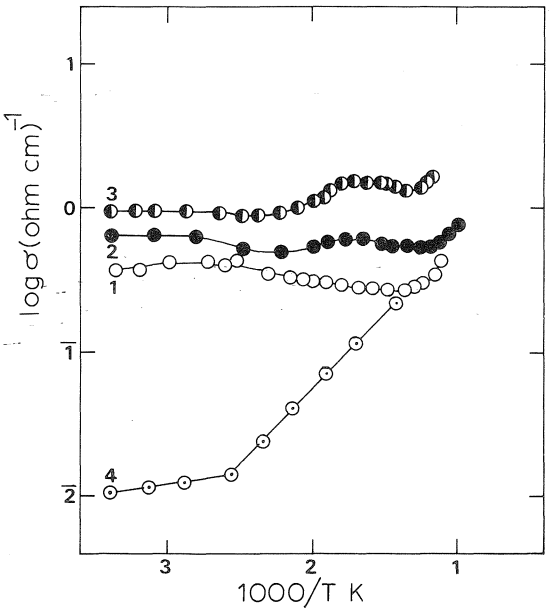

FIG. 3. Logarithm of specific conductivity, σ, *vs.* $10^3/T$ K for Cd_3OF_4 under different conditions of pretreatment and measurement; (*1*) fresh sample in vacuum, (*2*) same sample in N_2 after annealing 1 h at 600 °C, (*3*) same sample in vacuum after annealing in N_2 at 600 °C for ~5 h, (*4*) fused product (prior to compound formation) in N_2.

prepared by prefusing the stoichiometric mixture of CdO and CdF_2 and annealing the fused product at 500 °C for 2 h (2). Curve *1* refers to data obtained in vacuum ($\sim 10^{-4}$ torr) on the freshly prepared compound. Curve *2* represents

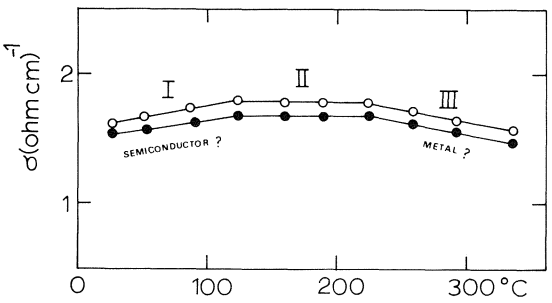

FIG. 4. Specific conductivity, σ, as a function of temperature (°C) at 50 Hz (open circle) and 10 kHz (filled circle).

data obtained in 1 atm N_2 on the same disc from curve *1* after further annealing in N_2 at 600 °C for 1 h and cooled to room temperature. Curve *3* refers to measurements in vacuum on the same disc after prolonged annealing, ~5 h at 600 °C in N_2. The high temperature conductivity is extrapolated to $\sigma_0 \simeq 10 \pm 4$ $(\text{ohm cm})^{-1}$ at $1/T = 0$. The X-ray diffraction pattern of the specimen after curve *3* measurements remained unaltered from its original pattern. Curve *4* represents the conductivity behavior of the fused product, that is, prior to compound formation. The curve shows an initial slope of 0.028 eV with a break at ~100 °C and a second slope of 0.28 eV up to 500 °C. At 500 °C the fused product is completely transformed into the compound.

Figure 2*b* exhibits room temperature conductivities in N_2 for CdO–CdF_2 unannealed mixtures. The conductivity value of Cd_3OF_4, spiked circle, is higher than the CdO value.

Figure 4 shows Cd_3OF_4 conductivity data obtained in vacuum at two frequencies, *viz.* 50 Hz and 10 kHz in the temperature range 25–325 °C. Three σ–*T* regions are identified: region *I*, 25–125 °C, resembles semiconductor behavior; region *II*, 125–225 °C, the conductivity is independent of temperature; and region *III*, 225–325 °C, the gently decreasing conductivity parallels metallic behavior. These data along with curves *1–3* in Fig. 3 suggest a novel semiconductor with an interesting semiconductor–metal transition.

The compound Cd_3OF_4 is visualized as an anion substitution compound incorporating lattice defects. The fused product of 1:2 mole ratio of CdO and CdF_2, however, represents a physical state with a random distribution of defects. At low temperatures, <100 °C, these defects in the fused product behave as so-called shallow impurities where their energies are slightly displaced from the edge of an intrinsic band; similar to shallow donors or acceptors in II–VI compounds (Group III or Group VII substitutional impurities) which exhibit ionization energies of 0.028 eV order of magnitude (7). Above 100 °C the defects become more mobile establishing order in the Cd_3OF_4 lattice with an energy of 0.28 eV. Complete ordering of the lattice is achieved at ~500 °C and the conductivity reaches its maximum value remaining essentially constant on subsequent heat–cool modes, curves *1–3*.

The relatively high room temperature and quasi-constant conductivity presents an interesting case for interpretation. The conductivity behavior of Cd_3OF_4 may be interpreted from the viewpoint of a very heavily doped compound and the discussion implies the presence of electronic defects originating from lattice defects or impurities hitherto unspecified. As the concentration of impurities increases in a semiconductor the quantitative theory of the effect of these impurities on the energy bands becomes a formidable problem. A qualitative appreciation may be had, however, from a simple progression from low to high impurity concentrations. As the impurity concentrations become sufficiently high, appreciable overlap of the wave functions of the carriers at neighboring impurity sites begins to occur, interaction effects give rise to impurity bands in much the same way that the LCAO approach gives energy bands for interacting atoms. We could expect the impurity band to be very wide in Cd_3OF_4 and in fact, overlap the adjacent intrinsic band. When the impurity band overlaps the intrinsic band the impurity activation energy disappears and no freezeout of carriers onto impurity levels at low temperatures should occur; hence, a quasi-independent temperature effect on conductivity.

An alternate mechanism responsible for the unusual conductivity properties of Cd_3OF_4 may reside in the nature of a very fast ionic conductor (8). The three principal features of a fast ionic conductor, *viz.* (*i*) unusually high ionic conductivity value, (*ii*) small temperature dependence of conductivity, and (*iii*) very small value of σ_0, appear consistent with Cd_3OF_4. Assuming the conductivity to be ionic then Cd_3OF_4 exhibits one of the highest values of ionic con-

ductivity $\sigma \approx 1.0$ (ohm cm)$^{-1}$ at 25 °C. With the reasonable assumption of ionic transport, the diffusion coefficient of the mobile species at 25 °C can be estimated as $D \approx 10^{-5}$ cm^2 s^{-1}.

It is hoped that this communication will stimulate further experimental, *e.g.* Hall effect measurements and theoretical studies to elucidate the nature of the electrical species and transport mechanism in Cd_3OF_4.

Acknowledgments

The authors are grateful to the National Research Council of Canada and the University Council for Research for financial support, and to Professor E. M. Clarke, Physics Department, for helpful advice.

1. P. RAMAMURTHY and E. A. SECCO. Can. J. Chem. **47**, 1045 (1969).
2. P. RAMAMURTHY and E. A. SECCO. Can. J. Chem. **48**, 1619 (1970).
3. LEONE WALTER-LEVY and DANIEL GROULT. Bull. Soc. Chim. Fr. 3868 (1970).
4. S. SCAVNICAR. Acta Crystallogr. **8**, 379 (1955).
5. L. PAULING. Nature of chemical bond. 3rd ed. Cornell University Press, Ithaca, New York. 1959. p. 514.
6. MAHADEVA NATARAJAN and ETALO A. SECCO. Can. J. Chem. **52**, 2436 (1974).
7. RICHARD H. BUBE. Electronic properties of crystalline solids. Academic Press, New York. 1974. pp. 322, 344.
8. ROBERT A. HUGGINS. Diffusion in solids. *Edited by* A. S. Nowick and J. J. Burton. Academic Press, New York. 1975. Chapt. 9.

N,N'-Bis(phenylaminomethyl)parabanic acid as a complexing agent. Complexes of some bivalent first row transition metals

ANTONIO COSTANTINO FABRETTI, GIAN CARLO FRANCHINI, CARLO PRETI,[1] AND GIUSEPPE TOSI

Istituto di Chimica Generale ed Inorganica, University of Modena, 41100 Modena, Italy

Received June 24, 1976

ANTONIO COSTANTINO FABRETTI, GIAN CARLO FRANCHINI, CARLO PRETI, and GIUSEPPE TOSI. Can. J. Chem. **55**, 344 (1977).

The preparation of some complexes of *N,N'*-bis(phenylaminomethyl)parabanic acid with halides of cobalt(II), nickel(II), and copper(II) is reported. The complexes of the type MLX_2 seem to have pseudo-tetrahedral and pseudo-octahedral symmetry. The complexes have been studied by means of magnetic susceptibility measurements, infrared and far infrared spectra, electronic and nmr spectra, and conductivity measurements. The ligand behaves as bidentate N-bonded. The various ligand field parameters, *Dq*, *B'*, and β have been evaluated. The *B'* values suggest a strong covalency in the metal–ligand σ bond and *Dq* values show a medium strong ligand field. The presence of metal–nitrogen bonds is suggested. The possible stereochemistries of the complexes are discussed in the light of the experimental results.

ANTONIO COSTANTINO FABRETTI, GIAN CARLO FRANCHINI, CARLO PRETI et GIUSEPPE TOSI. Can. J. Chem. **55**, 344 (1977).

On rapporte la préparation de quelques complexes de l'acide *N,N'*-bis(phénylaminométhyl) parabanique avec les halogénures du cobalt (II), du nickel (II) et du cuivre (II). Il semble que les complexes du type MLX_2 possèdent des symétries pseudo-tétraédriques et pseudo-octaédriques. On a étudié les complexes au moyen de mesures de susceptibilité magnétique, de leurs spectres infrarouges et infrarouges lointains, de leurs spectres électroniques et rmn et de mesures de conductivités. Les ligands se conduisent comme des entités bidentates liées par l'azote. On a évalué les divers paramètres de champ de ligand *Dq*, *B'* et β. Les valeurs de *B'* suggèrent une forte covalence du lien σ métal–ligand et les valeurs de *Dq* montrent un champ de ligand moyennement fort. On peut présumer de la présence de lien métal–azote. A la lumière des résultats expérimentaux, on discute des stéréochimies possibles pour les complexes.

[Traduit par le journal]

N,N'-Bis(phenylaminomethyl)parabanic acid has three carbonyl oxygens, two nitrogen atoms in the ring and two nitrogen atoms exocyclic as potential donors. It is obvious from the structure of the molecule that all the donor atoms cannot coordinate simultaneously to the same metal ion. The complexation may be achieved by coordination with the ligand acting as monodentate or by formation of a chelate structure involving both oxygen and nitrogen atoms. Polymeric structures involving a bridging ligand are also possible, therefore it is of interest to investigate the nature of the complexes formed from this ligand. The parabanic acid, from which this ligand has been obtained, is quite similar to the hydantoin and to the barbituric acid, widely employed as hypnotics and sedatives. We have undertaken a study of the stereochemistries and of the chemical reactivity of the coordination compounds of the derivatives of parabanic acid in order to further our present knowledge in the determination of the relationship existing between chemical structure and biological activity of these drugs. It is well known that the metal complexes of ligands having biological activity are more active than the free ligands (1, 2).

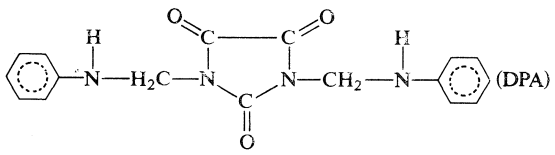

(DPA)

This paper reports the coordinating behaviour of DPA with bivalent cations, Co(II), Ni(II), and Cu(II). The infrared, uv, visible, and nmr spectra, and the magnetic moments of these complexes have been examined. Based on these studies the structures of the complexes have been proposed.

Results and Discussion

According to the method reported in the

[1]To whom correspondence should be addressed.

TABLE 1. Analytical data and other physical properties

Compounds	Colour	Required %			Found %			μ_{eff} (B.M.)	Dec. point (°C)
		C	H	N	C	H	N		
$[Co(DPA)Cl_2]\cdot 2H_2O$	Bright green	41.6	4.1	11.4	41.4	4.0	11.4	4.9	174–176*
$[Co(DPA)Br_2]\cdot 2H_2O$	Green	35.3	3.5	9.7	35.2	3.6	9.5	4.5	191–193*
$[Co(DPA)I_2]\cdot H_2O$	Green	31.2	2.8	8.5	31.3	2.9	8.5	4.6	185–187
$[Ni(DPA)Cl_2]\cdot 2H_2O$	Bright yellow	41.7	4.1	11.4	41.1	4.1	11.5	3.3	127–129
$[Ni(DPA)Br_2]\cdot 2H_2O$	Yellow	35.3	3.5	9.7	35.0	3.3	9.8	3.3	135–137
$[Ni(DPA)I_2]\cdot 4H_2O$	Dark green	28.8	3.4	7.9	29.0	3.1	8.0	3.3	140–142
$[Cu(DPA)Cl_2]\cdot 2H_2O$	Hazel-brown	41.3	4.1	11.3	41.4	3.7	11.7	1.5	110–112*
$[Cu(DPA)Br_2]\cdot H_2O$	Olive green	36.1	3.2	9.9	36.4	3.3	10.4	0.9	105–107*

*Melting point.

TABLE 2. Most important ir bands (cm^{-1})

Compounds	ν(NH)	ν(C=O)	ν(M—X)	ν(M—N)	Other far ir bands
DPA solid	3390vs	1760m,1715vs,1645m	—	—	332s,226ms,184ms
DPA $CHCl_3$ solution	3460ms	1780m,1745vs, —	—	—	—
$[Co(DPA)Cl_2]\cdot 2H_2O$	3360s	1775m,1735vs,1650vs	$324m_t$,$300ms_t$	250m	338m,223m,182m
$[Co(DPA)Br_2]\cdot 2H_2O$	3400s	1780m,1730vs,1655vs	$238m_t$,$216mw_t$	248ms	332m,226ms,184m
$[Co(DPA)I_2]\cdot H_2O$	3400ms	1780m,1735vs,1650vs	$205m_t$	248m	334m,226m,185ms
$[Ni(DPA)Cl_2]\cdot 2H_2O$	3370vs	1770m,1725vs,1650vs	$190ms_b$,$169s_b$	248ms	336ms,228ms,182m
$[Ni(DPA)Br_2]\cdot 2H_2O$	3365vs	1770m,1725vs,1650vs	$158m_b$,$148m_b$	247m	330ms,222ms,186ms
$[Ni(DPA)I_2]\cdot 4H_2O$	3360s	1770m,1722vs,1652vs	$200m_t$,$153vs_t$	244m	328ms,222m,179m
$[Cu(DPA)Cl_2]\cdot 2H_2O$	3385ms	1780m,1725vs,1650m	$300s_b$,$241m_b$	354m	332m,226mw,182ms
$[Cu(DPA)Br_2]\cdot H_2O$	3385ms	1775m,1725vs,1650m	$250m_b$	362ms	334ms,220ms,188m

Experimental section we have obtained complexes of the type $[M(DPA)X_2]$ (M = Co, Ni, X = Cl, Br, I) and $[Cu(DPA)X_2]$ (X = Cl, Br). In Table 1 the coordination compounds obtained are reported together with analytical results, colours, melting points, and magnetic values. The most important ir data are shown in Table 2. The principal features of the visible absorption spectra of this series of complexes are given in Tables 3 and 4. The complexes are microcrystalline, soluble in *N,N'*-dimethylformamide, nitromethane, dimethylsulfoxide. These derivatives are nonelectrolytes, Λ lying in the range 12.7–51.3 ohm^{-1} cm^2 mol^{-1} in nitromethane; the Λ values, even for 1:1 electrolytes, are 75–95 ohm^{-1} cm^2 mol^{-1} in this solvent (3).

It is interesting to point out that all the bands typical of the ligand appear in the ir spectra of the complexes and the ligand can be recovered by chemical decomposition of the compounds.

A formulation of the type $[ML_2][MX_4]$ must be ruled out for these complexes having only one coordinated ligand because these compounds behave as nonelectrolytes and because the typical vibrations for the tetrahalo group $[MX_4]^{2-}$ (X = Cl, Br, I) have not been found in the ir spectra, see below.

Infrared Spectral Studies

The spectra of the ligand in the solid state and in chloroform solution show a difference in the position of the ν(NH) stretching frequency, clearly indicating intermolecular or intramolecular hydrogen bonding between the hydrogen of the NH groups and the oxygen of the keto groups. The ν(NH) in the complexes is shifted towards lower wave numbers by about 80 cm^{-1}. The ν(C=O) vibrational modes are present in the solid state free ligand spectrum as medium bands at 1760 and 1645 cm^{-1}, A_1, while the very strong absorption of the type B_1 is present at 1715 cm^{-1} (4). In the spectrum of the free ligand in chloroform solution only two bands at 1780 and 1745 cm^{-1} are present. On going from the spectra of the free ligand to those of the complexes, these bands are present at the same wave numbers or show very small red shifts. From these facts we can suppose that the coordination centres are the nitrogen atoms of the amino groups of the ligand, but we prefer to use

TABLE 3. Solid state electronic spectra (cm^{-1})

Compounds	Absorption bands
DPA	8115,6895sh,6560,5700,5120
$[Co(DPA)Cl_2]\cdot 2H_2O$	22885,16105sh,15625,14970,8330sh,7510,6725
$[Co(DPA)Br_2]\cdot 2H_2O$	22370,15385,14860,14124,13700,8285,7410,6800,5650
$[Co(DPA)I_2]\cdot H_2O$	22470,16207,15150,14165,13570,12690,8300,7300,6725
$[Ni(DPA)Cl_2]\cdot 2H_2O$	28650,23095,15850,13950,10205,6135,5415
$[Ni(DPA)Br_2]\cdot 2H_2O$	29240,22830,15080,13460,10580,6200,5495
$[Ni(DPA)I_2]\cdot 4H_2O$	17790,11495sh,9390,7500,5390
$[Cu(DPA)Cl_2]\cdot 2H_2O$	23365,16950,13040sh,8300,5980
$[Cu(DPA)Br_2]\cdot H_2O$	23200,16420,13120sh,8250,7120,5870

TABLE 4. Most important visible peaks and crystal field parameters (cm^{-1})

Compounds	ν_3	ν_2	ν_1*	Dq	B'†	β
Cobalt derivatives	$^4A_2(F) \rightarrow {}^4T_1(P)$	$^4A_2(F) \rightarrow {}^4T_1(F)$	$^4A_2(F) \rightarrow {}^4T_2(F)$			
$[Co(DPA)Cl_2]\cdot 2H_2O$	15 565	7 510	3 110	440	658	0.68
$[Co(DPA)Br_2]\cdot 2H_2O$	14 520	7 410	3 040	437	588	0.61
$[Co(DPA)I_2]\cdot H_2O$	14 355	7 300	3 000	430	582	0.60
Nickel derivatives	$^3A_{2g}(F) \rightarrow {}^3T_{1g}(P)$	$^3A_{2g}(F) \rightarrow {}^3T_{1g}(F)$	$^3A_{2g}(F) \rightarrow {}^3T_{2g}(F)$			
$[Ni(DPA)Cl_2]\cdot 2H_2O$	23 095	13 950	5 320	863	744	0.71
$[Ni(DPA)Br_2]\cdot 2H_2O$	22 830	13 460	5 230	823	773	0.74
	$^3T_1(F) \rightarrow {}^3T_1(P)$	$^3T_1(F) \rightarrow {}^3A_2(F)$	$^3T_1(F) \rightarrow {}^3T_2(F)$			
$[Ni(DPA)I_2]\cdot 4H_2O$	17 790	9 390	5 080	508	950	0.91

*Calculated values.
†B is taken to be 967 and 1 041 cm^{-1} for Co^{2+} and Ni^{2+} free ions respectively.

electronic spectra to confirm this hypothesis and to delay the question of the assignment of ν(M—L) until after the discussion of the electronic spectra and nmr measurements.

Medium absorption bands are present in all the complexes in the ranges expected for ν(OH) and δ(HOH), clearly confirming the presence of water of crystallization. We can exclude the presence of coordinated water because from a detailed analysis of the infrared spectra the other vibrational modes such as wagging, twisting, and rocking activated by coordination to the metal have not been found in the expected ranges (5). Furthermore this water is lost near 95–100 °C, while coordinated water is lost near 150–160 °C (5).

As for the metal–halogen stretching modes, Table 2, the bands at 324 and 300 cm^{-1}, 238 and 216 cm^{-1}, and 205 cm^{-1} in the cobalt chloro-, bromo-, and iodo-derivative, respectively, are in accord with the literature data for pseudo-tetrahedral complexes with terminal halides (6–12). In the complexes $[Ni(DPA)Cl_2]$ and $[Ni(DPA)Br_2]$ the values found at 190 and 169 cm^{-1}, and at 158 and 148 cm^{-1} are typical for halide bridged nickel(II) complexes; no bands have been observed for terminal halides. In the iodo-derivative of nickel(II) the vibrational modes at 200 cm^{-1} and 153 cm^{-1} are due to terminal iodide atoms (6, 13–16). In the copper derivatives the bands present at 300 and 242 cm^{-1}, and at 250 cm^{-1} for the chloro- and bromo-derivative respectively are typical for ν(Cu—X) in halide bridged structures. This assignment is supported by the fact that the value of the ratio ν(Cu—Br)/ν(Cu—Cl) equals to 0.83 (6, 17).

We have never observed the wave numbers of the ν(M—X) bands similar to the values reported in the spectra of the halogenometallates of the type $[MX_4]^{2-}$ (M = Co, Ni, Cu; X = Cl, Br, I) (18–22).

These ir results agree very well with the conductivity values.

Electronic Spectral and Magnetic Studies

The spectral data and the values chosen for the energies ν_2 and ν_3 from which the values of

the parameters Dq, B', and β have been derived, are reported in Tables 3 and 4 respectively. With the cobalt halides, complexes of pseudo-tetrahedral geometry are formed, the chloro- and bromo-derivative of nickel have an octahedral polymeric structure while the nickel iodo-complex seems to be tetrahedral. For the copper derivatives, octahedral, polymeric halide-bridged structures seem likely.

The Dq values of the complexes, Table 4, suggest the order Cl > Br > I for the halides in the spectrochemical series and this fact is consistent with the generally accepted sequence. In order to determine the position of the ligand in the spectrochemical series, the Dq values of the complexes were compared with the Dq values of known tetrahedral halide complexes of cobalt(II) and we can suggest the following order for the ligands (7, 15, 16, 23–28):

benzothiazole > benzoxazole-2-thione > 2-methylbenzimidazole > 3-methyl-5-phenylisoxazole > 2-aminobenzimidazole > thiomorpholin-3-thione > thiazolidine-2-thione > 3,5-dimethylisoxazole > DPA > thiazolidine-2-selenone

Table 4 shows that the B' values for the cobalt derivatives are of the order of 60–68% of the free ion value (967 cm^{-1}), which suggests that there is a considerable orbital overlap in the metal–ligand σ bond. The ligands can be placed in the nephelauxetic series in the order:

thiazolidine-2-selenone > thiazolidine-2-thione > thiomorpholin-3-thione > DPA > 2-aminobenzimidazole > 3,5-dimethylisoxazole > benzothiazole > benzoxazole-2-thione > 3-methylbenzimidazole > 3-methyl-5-phenylisoxazole

Our ligand is at the end of the spectrochemica series and almost at the beginning of the nephelauxetic series. This fact can be explained as the former is a measure of the electrical field produced by the ligand while the latter is a measure of the covalency of the metal–ligand bond.

In the cobalt derivatives the bands at 15 565–14 355 cm^{-1} may be assigned as the $^4A_2(F) \rightarrow {}^4T_1(P)$ transition, the second at 7510–7300 cm^{-1} as the $^4A_2(F) \rightarrow {}^4T_1(F)$ transition. These bands passing from the chloro- to the iodo-derivative are shifted towards lower energies. The ν_3 transition is split because of the distorted tetrahedral structure of the complexes; we have calculated the ligand field parameters using only the ν_2 transition and the visually estimated frequency of the centre of gravity of the split bands corresponding to ν_3 using the equations proposed by Underhill and Billing (29). The assignment of ν_1 is made difficult by the presence of vibrational modes in the range where this transition should be expected. The calculated ν_1 wave numbers are reported in Table 4.

From the analysis of the electronic spectra we could determine the mode of bonding of the ligand by comparison of Dq values reported for CoL_4^{2+} and CoX_4^{2-} ions (30, 31). Table 4 shows that Dq values are in good agreement, using the 'law of the average environment', with the literature data for derivatives containing cobalt–nitrogen bonds.

The magnetic susceptibility values, 4.6–4.9 B.M., lie in the range normally accepted for the metal tetrahedrally coordinated in high-spin complexes (32).

The reflectance spectra of $[Ni(DPA)X_2]$ (X = Cl, Br) complexes show two major bands at some 23 000 cm^{-1} and at 13 950–13 460 cm^{-1} and all these are very weak in intensity. This is characteristic of octahedral nickel(II) complexes. These bands may be assigned to the transitions $^3A_{2g}(F) \rightarrow {}^3T_{1g}$ and $^3A_{2g}(F) \rightarrow {}^3T_{1g}(F)$ ν_2. A pseudo-tetrahedral stereochemistry has been assigned to the nickel iodo-derivative on the basis of its electronic spectrum, Table 4 (29). The medium strong band at 9390 cm^{-1} can be attributed to the $^3T_1 \rightarrow {}^3A_2$ transition (ν_2), while the band present at 17 790 cm^{-1} accompanied by a shoulder at 11 495 cm^{-1} may be assigned to the ν_3 transition $^3T_1 \rightarrow {}^3T_1(P)$. The Dq values for these nickel derivatives have been calculated using only ν_2 and ν_3 values, the assignment of ν_1 being very often ambiguous because of the presence of vibrations due to the ligand itself in the region where this band usually lies.

The magnetic moments at room temperature of chloro- and bromo-nickel(II) derivatives lie within the range usually observed for octahedral nickel(II) compounds. The magnetic moment of the iodo-complex is near the lower limit of the range normally accepted for nickel(II) in a pseudo-tetrahedral stereochemistry (32). Comparison of the electronic spectra of our complexes with those of derivatives involving Ni—O bonds and Ni—N bonds confirms that these derivatives are N-bonded as the band energies are at higher values than in O-bonded derivatives (30).

On the basis of the solid state electronic spectra, Table 3, we can assign an octahedral distorted symmetry to the copper(II) derivatives (30); the band at 16 950 and 16 420 cm^{-1}, in the chloro- and bromo-derivative, respectively, accompanied by a shoulder at some 13 000 cm^{-1} and a second band around 23 250 cm^{-1} are in accord with this stereochemistry. The anomalously low effective magnetic moments observed for the copper complexes at room temperature indicate that there is a strong spin–spin interaction between two cupric ions. It is very difficult to decide without complete X-ray analyses whether spin–spin interaction takes place because of σ or δ bond formation or by a superexchange mechanism.

Nuclear Magnetic Resonance Measurements

The ligand has been studied by means of nmr techniques. This spectrum shows a hyperfine structure in hexadeuterodimethylsulfoxide (DMSO-d_6); the chemical shift values of C_6H_5- and CH_2-proton resonances appear in the range 7.09–6.60 ppm and at 4.90 ppm respectively. The NH-proton resonance is at 5.39 ppm.

On going from the spectrum of the free ligand to those of the complexes in freshly-prepared DMSO-d_6 solutions we observe the disappearance of the hyperfine structure of the resonances as a consequence of line broadening because of the presence of a paramagnetic centre. A detailed analysis of the individual bands is, therefore, impossible; it is clear, however, that in all the derivatives studied here the NH-proton resonance is shifted towards lower field of about 2.30 ppm. This chemical shift towards lower fields is ascribed to the electron withdrawing of the metals from the nitrogen atoms and the noticeable deshielding effect supports the hypothesis that the studied complexes are N-bonded.

Conclusions

According to the above reported results, the halogen independent bands in the far ir region in the range 250–244 cm^{-1} for the cobalt(II) and nickel(II) derivatives and at 354 and 362 cm^{-1} for the copper chloro- and bromo-derivative, respectively, can be attributed to the ν(M—N) vibrations, Table 2, according to literature data (15, 19, 33, 34).

The cobalt(II) derivatives contain the metal ion tetrahedrally coordinated in high-spin complexes. The vibrational modes typical of ν(Co—X) for terminal halides only suggest for these complexes either a monomeric structure with DPA acting as a chelating ligand or a dimeric structure involving bridging ligands.

The nickel derivatives show different properties as the size of the halogen increases. The chloro- and bromo-derivatives are bright yellow and yellow, respectively, as opposed to the dark green iodo-derivative, and are less soluble than the iodo-derivative. It is known from literature data that the nickel(II) compounds possess a different stereochemistry on passing from chlorine to iodine; the dark green or dark brown iodo-derivatives have a pseudo-tetrahedral symmetry, whereas the yellow chloro- and bromo-derivatives have a pseudo-octahedral environment with bridging halides. The electronic spectra of our chloro- and bromo-derivatives are typical of the nickel(II) in a pseudo-octahedral symmetry, furthermore in the far ir region only the vibrational modes for ν(Ni—X) for bridging halides are present. It is likely for the nickel to attain a pseudo-octahedral geometry in a polymeric structure involving bridging ligands and bridging halides. Octahedral structures involving bridging ligands and terminal halides having coordinated water must be ruled out because from a detailed analysis of the infrared spectra the water was always uncoordinated lattice water. The iodo-derivative has a pseudo-tetrahedral stereochemistry containing terminal iodine atoms. We can therefore assign to this last complex a tetrahedral dimeric structure involving bridging ligands and terminal halide atoms.

Unfortunately it has not been possible to do vapor phase osmometric molecular weight determinations since the solubility of the complexes is too low for these measurements. Furthermore these experiments require a time longer than that of conductivity and nmr measurements and it is clear that dissociative and solvolytic problems, which could seriously interfere, can not be discounted. Therefore we can propose stereochemistries based upon the reported data only.

Experimental

Preparation of the Ligand

The ligand *N,N'*-bis(phenylaminomethyl)parabanic acid (DPA) was prepared starting with a mixture of 3.50 g (0.0375 mol) of aniline and the same amount of 50% ethanol which was added, drop by drop, to a solution of

2.75 g (0.0158 mol) of *N,N'*-bis(hydroxymethyl)parabanic acid in 75 ml of 50% ethanol, according to the method described by Tanimoto and co-workers (35). The solution turned yellow and a yellow crystalline product separated out. The precipitate was recrystallized from ethanol; mp 72–74 °C, lit. 71–74 °C (35). Anal. calcd. for $C_{17}H_{16}N_4O_3$: C 63.0, H 5.0, N 17.3; found: C 62.6, H 5.0, N 17.2.

Preparation of the Complexes

The complexes were all prepared by reaction of the appropriate metal salt with a small excess of the molten ligand, preliminary studies having shown that in each case only a single product was formed, regardless of the presence of excess ligand. The compounds were purified by means of repeated washing with ethanol. We have obtained complexes only in the metal:ligand ratio reported in Table 1.

Infrared Spectra

The ir spectra have been recorded in the range 4000–100 cm^{-1} with Perkin-Elmer 521 and 225 and Hitachi Perkin-Elmer FIS3 spectrophotometers as KBr discs and Nujol mulls between polyethylene sheets. Atmospheric water was removed from the spectrophotometer housing by flushing dry nitrogen.

Visible and Ultraviolet Spectra

Solid state electronic spectra have been recorded with a Shimadzu MPS-50L spectrophotometer.

Magnetic Susceptibility Measurements

These were carried out by Gouy's method. Molecular susceptibilities were corrected for diamagnetism of the component atoms by use of the Pascal's constants.

Conductivity Measurements

These measurements were carried out with a WTW LBR type conductivity bridge at 25 °C for 10^{-3} *M* solutions in nitromethane.

Nuclear Magnetic Resonance Measurements

The nmr spectra of the ligand and its metal complexes were measured in hexadeuterodimethylsulfoxide (DMSO-d_6) solutions with a Jeol JNM-C 60 HL instrument at 60 MHz; TMS was used as internal standard.

Acknowledgement

Financial support from the Italian National Research Council is gratefully acknowledged.

1. S. Kirschner, Y. K. Wei, D. Francis, and J. G. Bergman. J. Med. Chem. **9**, 369 (1966).
2. A. J. Thomson, R. J. P. Williams, and S. Reslova. Struct. Bonding, Berlin, **11**, 1 (1972).
3. W. J. Geary. Coord. Chem. Rev. **7**, 81 (1971).
4. A. Alemagna and V. Lorenzelli. J. Chim. Phys. **61**, 884 (1964).
5. C. Preti and G. Tosi. Spectrochim. Acta, **31**A, 1139 (1975).
6. W. J. Eilbeck, F. Holmes, C. E. Taylor, and A. E. Underhill. J. Chem. Soc. A, 128 (1968).
7. M. J. M. Campbell, D. W. Card, R. Grzeskowiak, and M. Goldstein. J. Chem. Soc. Dalton, 1687 (1972).
8. J. Reedijk. Rec. Trav. Chim. **90**, 117 (1971).
9. E. J. Duff, M. N. Hughes, and K. J. Rutt. J. Chem. Soc. A, 2354 (1968).
10. E. J. Duff, M. N. Hughes, and K. J. Rutt. J. Chem. Soc. A, 2021 (1969).
11. C. E. Taylor and A. E. Underhill. J. Chem. Soc. A, 368 (1969).
12. W. J. Eilbeck, F. Holmes, C. E. Taylor, and A. E. Underhill. J. Chem. Soc. A, 1189 (1968).
13. C. Postmus, J. R. Ferraro, A. Quattrochi, K. Shobatake, and K. Nakamoto. Inorg. Chem. **8**, 1851 (1969).
14. M. Goldstein and D. W. Unsworth. Spectrochim. Acta, **28**A, 1107 (1972).
15. C. Preti, G. Tosi, D. De Filippo, and G. Verani. Can. J. Chem. **52**, 2021 (1974).
16. C. Preti and G. Tosi. Can. J. Chem. **54**, 85 (1976).
17. M. N. Hughes and K. J. Rutt. Inorg. Chem. **10**, 414 (1971).
18. D. M. Adams. Metal–ligand and related vibrations. E. Arnold, London. 1967.
19. J. R. Ferraro. Low-frequency vibrations of inorganic and coordination compounds. Plenum Press, New York. 1971.
20. K. Nakamoto. Infrared spectra of inorganic and coordination compounds. J. Wiley, New York. 1969.
21. G. E. B. Y. Ahlija and M. Goldstein. Chem. Commun. 359 (1968).
22. R. J. H. Clark and T. M. Dunn. J. Chem. Soc. 1198 (1963).
23. N. N. Y. Chan, M. Goodgame, and M. J. Weeks. J. Chem. Soc. A, 2499 (1968).
24. D. M. L. Goodgame, M. Goodgame, and G. W. Rayner-Canham. Inorg. Chim. Acta, **6**, 245 (1972).
25. M. Massacesi, G. Ponticelli, and C. Preti. J. Inorg. Nucl. Chem. **37**, 1641 (1975).
26. C. Preti and G. Tosi. J. Chem. Soc. Dalton, 685 (1976).
27. D. De Filippo and C. Preti. J. Chem. Soc. A, 1904 (1970).
28. G. Devoto, G. Ponticelli, and C. Preti. J. Inorg. Nucl. Chem. **37**, 1635 (1975).
29. A. E. Underhill and D. E. Billing. Nature, **210**, 834 (1966).
30. A. B. P. Lever. Inorganic electronic spectroscopy. *Edited by* M. F. Lappert. Elsevier, Amsterdam. 1968.
31. B. P. Kennedy and A. B. P. Lever. Can. J. Chem. **50**, 3488 (1972).
32. B. N. Figgis and J. Lewis. Prog. Inorg. Chem. **6**, 37 (1964).
33. I. S. Ahuja. J. Inorg. Nucl. Chem. **29**, 2091 (1967).
34. I. S. Ahuja and P. Rastogi. Inorg. Nucl. Chem. Lett. **5**, 255 (1969).
35. S. Tanimoto, R. Taniyasu, and M. Okano. Bull. Chem. Soc. Jpn. **48**, 357 (1975).

The electronic structures, geometries, and relative energies of some N_2H_2 and $N_2H_2^+$ systems[1]

N. COLIN BAIRD AND DAVID A. WERNETTE[2]

Department of Chemistry, University of Western Ontario, London, Ont., Canada N6A 5B7

Received August 13, 1976

N. COLIN BAIRD and DAVID A. WERNETTE. Can. J. Chem. **55**, 350 (1977).

Ab initio calculations using the 4-31G basis set and extensive configuration interaction are reported for the ^1A_g state of *trans*-diimide (**1**), the $^3A''$ and $^1A_1$ states of 1,1-dihydrodiazine (**2**), and the ground states of the positive ions of these systems and of *cis*-diimide. In all cases the geometries have been optimized. The relative stabilities of these systems are discussed, with particular reference to the heat of formation of *trans*-**1** and to the ionization potentials of **1** and **2**.

N. COLIN BAIRD et DAVID A. WERNETTE. Can. J. Chem. **55**, 350 (1977).

On rapporte des calculs *ab initio* utilisant une base 4-31G et des interactions de configuration étendues pour l'état ^1A_g de la diimide-*trans* (**1**) et les états $^3A''$ et $^1A_1$ de la dihydrodiazine-1,1 (**2**) et pour les états fondamentaux des ions positifs de ces systèmes et de la diimide-*cis*. Dans tous les cas, on a optimisé les géométries. On discute des stabilités relatives de ces systèmes en particulier par rapport à la chaleur de formation de **1**-*trans* et aux potentiels d'ionisation de **1** et de **2**.

[Traduit par le journal]

Introduction

The chemical and physical properties of the dihydrodiazines, N_2H_2, have been the subject of much theoretical interest (1–18), since their size admits to sophisticated *ab initio* treatments whereas experimental results are few and often inconclusive. As a continuation of our own theoretical efforts in this area (10, 11), we wish to report here the results of *ab initio* calculations which include extensive configuration interaction and which were undertaken to determine the structures and relative energies of 1,2-dihydrodiazine ('diimide'), **1**, and its tautomer 1,1-dihydrodiazine ('aminonitrene'), **2**, and the positive ions of these systems.

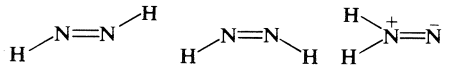

trans-**1** *cis*-**1** **2**

Method of Calculation

The extended 4-31G basis set of Ditchfield, Hehre, and Pople with standard molecular scale factors (19) was employed to expand the molecular orbitals. The single-determinant SCF wavefunctions were constructed using Roothaan's procedures for closed-shell (20) and open-shell (21) systems. To obtain a set of determinants in the configuration interaction (CI) calculations which would provide a reasonably consistent representation for all states and systems considered but which would still be tractable, the following procedure was employed. The set of molecular orbitals (MOs) employed was restricted to the twelve most stable SCF orbitals (*i.e.*, the number of orbitals in a minimal basis set), and the four MOs of lowest energy were kept doubly-occupied.

Determinants corresponding to all configurations (of appropriate spin eigenfunction) which are single or double electron excitations from the other four occupied orbitals of the SCF determinant were included in the CI wavefunction. However, determinants with six unpaired electrons were excluded.

In order to provide as accurate as possible an estimation of the heat of formation of *trans*-diimide, the geometry optimization, and energy calculation for this system and for $N_2 + H_2$ was repeated with only the lowest *two* MOs (essentially 1*s* orbitals on the nitrogens) held doubly-occupied in the CI determinants.

With the methods described above, nitrogen–nitrogen and nitrogen–hydrogen distances, and the bond angles were optimized for the following states:

[1]Research supported by the National Research Council of Canada.

[2]Present address: Department of Chemistry, Ohio State University, Columbus, Ohio 43210.

System	Symmetry assumed	State	Configurations used
N_2H_2 systems			
trans-Diimide ('*trans*-**1**')	C_{2h}	^1A_g	49
1,1-Dihydrodiazine ('triplet nitrene **2**')	C_s	$^3A''$	133
1,1-Dihydrodiazine ('singlet nitrene **2**')	C_{2v}	$^1A_1$	48
$N_2H_2^+$ systems			
trans-Diimide cation	C_{2h}	^2A_g	75
cis-Diimide cation	C_{2v}	$^2B_2$	82
1,1-Dihydrodiazine cation ('nitrene cation **2**$^+$')	C_{2v}	$^2B_2$	75

(Note that 102 configurations resulted when only the lowest two MOs of *trans*-diimide were kept doubly-occupied.)

For all systems, the SCF determinant strongly predominated in the CI wavefunction for the ground state; determinants involving double excitations into the π* orbital were next in importance.

Results and Discussion

The Neutral Molecules

Of particular interest for the neutral species are their geometries, their relative stabilities, their stabilities relative to N_2 and H_2, and the nature of the ground state for the nitrene form.

The optimum geometries calculated in the 4-31G + CI calculations are listed in Table 1. The predicted structure for *trans*-diimide agrees well with the experimental determination (22) with respect to HNN angle (106.5° experimental *vs.* 108° calculated) and nitrogen–hydrogen distance (1.028 Å *vs.* 1.02 Å); however the nitrogen–nitrogen separation of 1.252 Å is overestimated by 0.04 Å and 0.05 Å respectively by the CI calculations with 4 and 2 orbitals always doubly-occupied. A similar overestimation (of 0.027 Å) is obtained for N_2 itself.

The heat of formation ΔH_f of *trans*-diimide is of some interest, since it is a direct measure of the energetic stability of the molecule relative to its decomposition products N_2 and H_2. Table 2 lists all the experimental and theoretical values for ΔH_f (*trans*-**1**) known to the authors. Curiously, the more modern experimental values tend to be considerably lower than the older values, whereas the opposite trend is obtained[3] for the theoretical estimate, the more sophisticated the bases set and use of CI, the higher the calculated energy difference between N_2H_2 and $N_2 + H_2$. (Note that the theoretical results have *not* been corrected for differences in zero-point energies or PV work and thus the experimental and calculated results are not exactly comparable.) Our present value of 66 kcal mol^{-1} is a little larger than those derived from the calculations reported recently by Ahlrichs and Staemmler (1) and which not only included an extensive *sp* basis set and CI but also polarization functions. The best experimental estimate of 36 kcal mol^{-1} indicates that *trans*-diimide is actually 14–30 kcal mol^{-1} more stable than predicted.

The geometries calculated for the singlet and triplet states of the aminonitrene **2** are rather different from each other (see Table 1) but agree quite well with our previous estimates in which a minimal basis set and very little CI were employed. The nitrogen–nitrogen distance of 1.26 Å in the $^1A_1$ state is shorter than that computed for the double bond in diimide itself. In the SCF wavefunction, the population of the p_π orbitals of the nitrene nitrogen totals 0.39e.

Both the rather long nitrogen–nitrogen bond length of 1.39 Å, and the preference for a pyramidal geometry about the amino nitrogen, indicate little stabilization for the three-electron

[3]Plots of ΔH_f against year yield respectable straight lines for both experimental and calculated values. The lines cross in 1973 at a ΔH_f value of 38 kcal mol^{-1}. Curiously this value is identical to that obtained from thermochemical group additivity schemes, see ref. 26 for details.

TABLE 1. Calculated geometries using 4-31G + CI method

System	Geometric parameter	Calculated value for: Neutral molecule	Cation
trans-Diimide (*trans*-**1**)	R_{NN}	1.29 Å (1.30 Å)[a]	1.19 Å
	R_{NH}	1.02 Å	1.02 Å
	∠HNN	108° (108°)[a]	128°
cis-Diimide (cis-**1**)	R_{NN}		1.17 Å
	R_{NH}		1.02 Å
	∠HNN		138°
1,1-Dihydrodiazine (**2**)	R_{NN}	1.26 Å ($^1A_1$) 1.39 Å ($^3A''$)	1.24 Å
	R_{NH}	1.02 Å ($^1A_1$) 1.00 Å ($^3A''$)	1.02 Å
	∠HNN	124° ($^1A_1$) 115° ($^3A''$)	121°
	∠HNH	112° ($^1A_1$) 115° ($^3A''$)	118°
Dinitrogen	R_{NN}	$(1.12_5$ Å)[a]	
Dihydrogen	R_{HH}	0.73_6 Å	

[a]Values in parentheses computed using only two lowest MOs doubly-occupied in all configurations.

TABLE 2. Heats of formation of *trans*-diimide

Method	Reference	ΔH_f (kcal mol^{-1})
Experimental		
Via mass spectrometry	23	55.3
	24	48.7
	25	50.2
Via mass spectrometry on N_2H_2	26	36
Theoretical[a]		
Minimal STO-2G basis, SCF	4	22.3
4-31G basis, SCF level	3	43.4
Extended basis + polarization functions, SCF	2	48.6
Extended basis + polarization functions, SCF	1	71.8[b]
Extended basis + polarization functions + correlation energy estimated	1	49.9[b], 53.6[b]
4-31G basis + extensive CI	This work	66.0

[a]The theoretical values are energy differences, with no corrections for zero-point vibration or PV work effects.
[b]Computed using $D_e(H_2) = 109.5$ kcal mol^{-1}.

π bond in the $^3A''$ state of 1,1-dihydrodiazine. Indeed the unpaired electrons are 90% and 98% localized in the $2p_\pi$ and the $2p_\sigma$ atomic orbitals of the nitrene nitrogen according to the single determinant results.

In Table 3 are listed the energetic separations between the $^3A''$ and $^1A_1$ states of 1,1-dihydrodiazine as calculated by previous workers and by ourselves. All previous work gave the triplet as the more stable state, although the most extensive calculation (that by Ahlrichs and Staemmler (1)) has a T_1–S_0 splitting of only 2.6 kcal mol^{-1}. Our CI results place the singlet *lower* in energy than the triplet, though by only 1.6 kcal mol^{-1}. In our opinion, the closeness in the calculated energies for the singlet and triplet states of the aminonitrene leaves open the question of which is the real ground state; in any event, the lowest excited state should be thermally accessible.

Finally it is worth noting that the CI calculations predict that the neutral *trans*-diimide

TABLE 3. Singlet–triplet energy gap in 1,1-dihydrodiazine

Method of calculation	Reference	Gap[a] (kcal mol^{-1})
STO-3G basis, minimal CI	10	26.3
4-31G unrestricted SCF (using optimum STO-3G geometries)	18	11.7
Extended basis + polarization functions,	1	2.6
4-31G basis, extensive CI	This work	−1.6

[a]A positive gap indicates the triplet is predicted to be more stable than is the singlet state.

molecule is 20.3 kcal mol^{-1} more stable than is the lowest singlet state of 1,1-dihydrodiazine, in fairly good agreement with the 24–26 kcal mol^{-1} values of Ahlrichs and Staemmler (1).

The N_2H_2 Cations

On the basis of qualitative reasoning, one expects the ionization potential for the aminonitrene to be significantly less than for the diimides. In particular, the least tightly-held electron in 1,1-dihydrodiazine occupies a molecular orbital which is almost exclusively $2p$ (nitrene N) in character. (For the triplet state the orbital involved is the $2p_\pi$, whereas for the singlet the electron ionized is one of the in-plane lone pair in $2p_\sigma$.) In contrast, the electron ionized from either isomer of diimide originates from an MO formed by the lone pairs, and to which there is a substantial contribution from the rather stable $2s$ orbitals on the nitrogens.

In agreement with these qualitative arguments, our *ab initio* calculations predict *vertical* ionization potentials for *trans*-diimide and for the singlet state of 1,1-dihydrodiazine to be 9.07 and 7.28 eV respectively. Note that even though Koopman's theorem has not been used, and optimal eigenvectors for the positive ions have been employed, the agreement between the calculated value and the photoelectron spectroscopic value of 10.02 eV for diimide (27) is not very good.

Using restricted open-shell MO theory with CI, the optimum geometries of the cations of both *trans*- and *cis*-diimide, and of the aminonitrene system, were calculated and are listed in Table 1.

The optimum HNN bond angles calculated for the cation of *trans*-diimide is 20° larger than that calculated for the neutral species. A substantial increase in the angles, giving a species closer to the linear geometry, is expected from Walsh's Rules for HAAH systems when a $3a_g$ orbital electron is removed. For the same reason the HNN angles in the *cis*-diimide cation are also large (Table 1). Although the HNN angle calculated for the *trans*-diimide cation agrees well with the 127° value deduced from the photoelectron spectra of diimide, the calculated bond length for the ion is 0.03 Å shorter than is the experimental. In fact the net contraction in the nitrogen–nitrogen separation due to ionization of a strongly-antibonding n_+ electron appears to be exaggerated in the *ab initio* results, the calculated value being 0.10 Å as contrasted with the experimental 0.03 Å.

The structural changes which are calculated to occur upon ionization in the aminonitrene system are much less dramatic than for diimide, since a nonbonding rather than an antibonding electron is removed. The nitrogen–nitrogen bond length decreases slightly (compared to the singlet neutral system) and the HNH angle opens somewhat. In our optimization calculations for H_2NN^+ the ion was assumed to be planar; a few computations with the final NN and NH bond lengths but with a flapped geometry at the amino nitrogen confirmed the assumed preference for a planar structure.

Given that only minor geometry changes occur in the 1,1-dihydrodizaine singlet upon ionization, it is not surprising that the calculated adiabatic ionization potential of 7.23 eV is only 0.05 eV smaller than is the vertical. For *trans*-diimide, the difference between the adiabatic and the vertical is much larger (0.81 eV calculated, 0.43 eV experimental), the former value for *trans*-**1** being 8.26 eV calculated (9.59 eV experimental (27)).

As a consequence of the 23.8 kcal mol^{-1} calculated advantage in adiabatic ionization potential, the 20.3 kcal mol^{-1} advantage held by *trans*-diimide over 1,1-dihydrodiazine in the

neutral molecules is just overcome, and our CI calculations predict the nitrene cation $\mathbf{2}^+$ to be more stable than the *trans*-diimide cation by about 3.5 kcal mol^{-1}. (Given the size of this energy difference, a reversal in stability order in more sophisticated calculations cannot be ruled out, however.) The *trans* isomer of the diimide ion is predicted to be 6.9 kcal mol^{-1} more stable than is the *cis*; this value is close to those obtained in most recent calculations for the energy difference between the *neutral* molecules.

After this work had been completed, Wiberg and co-workers (28) reported the discovery of a second isomer of N_2H_2. From the appearance potentials for N_2H^+, they concluded that the new species is 13 ± 2 kcal mol^{-1} less stable than is *trans*-**1**, a value which is midway between our calculated relative energy (of 20 kcal mol^{-1}) for the aminonitrene isomer **2** and that of 6–9 kcal mol^{-1} usually found (1, 15, 18) for the relative energy of the *cis*-**1** species. While the ionization potential of 9.52 eV found for the new species seems too high to be that for **2** and is close to that expected for *cis*-**1**, the lack of a 380 nm band in the spectrum of the new isomer seems to preclude *cis*-**1** as a candidate. Obviously more experimental and theoretical work is required to characterize the new isomer.

1. R. Ahlrichs and V. Staemmler. Chem. Phys. Lett. **37**, 77 (1976).
2. N. W. Winter and R. M. Pitzer. J. Chem. Phys. **62**, 1269 (1975).
3. L. Radom, W. J. Hehre, and J. A. Pople. J. Am. Chem. Soc. **93**, 289 (1971).
4. L. J. Schaad and H. B. Kinser. J. Phys. Chem. **52**, 1901 (1969).
5. D. W. Genson and R. E. Christoffersen. J. Am. Chem. Soc. **94**, 6904 (1972).
6. R. Ditchfield, J. E. Del Bene, and J. A. Pople. J. Am. Chem. Soc. **94**, 703 (1972).
7. G. Merenyi, G. Wettermark, and B. Ross. Chem. Phys. **1**, 340 (1973).
8. J. M. Lehn and B. Munsch. Theor. Chim. Acta, **12**, 91 (1968).
9. K. Vasudevan, S. D. Peyerimhoff, R. J. Buenker, W. E. Kammer, and H. Hsu. Chem. Phys. **7**, 187 (1975).
10. N. C. Baird and R. F. Barr. Can. J. Chem. **51**, 3303 (1973).
11. N. C. Baird and J. R. Swenson. Can. J. Chem. **51**, 3097 (1973).
12. M. B. Robin, R. R. Hart, and N. A. Kuebler. J. Am. Chem. Soc. **89**, 1564 (1967).
13. D. P. Wong, W. H. Fink, and L. C. Allen. J. Chem. Phys. **52**, 6291 (1970).
14. E. R. Talaty, A. K. Schwartz, and G. Simons. J. Am. Chem. Soc. **97**, 972 (1975).
15. G. Wagniere. Theoret. Chim. Acta, **31**, 269 (1973).
16. J. M. Howell and L. J. Kirschenbaum. J. Am. Chem. Soc. **98**, 877 (1976).
17. L. C. Snyder and H. Basch. Molecular wave functions and properties. Wiley, New York. 1972.
18. W. A. Lathan, L. A. Curtiss, W. J. Hehre. J. B. Lisle, and J. A. Pople. Prog. Phys. Org. Chem. **11**, 175 (1974).
19. R. Ditchfield, W. J. Hehre, and J. A. Pople. J. Chem. Phys. **54**, 724 (1971).
20. C. C. J. Roothaan. Rev. Mod. Phys. **23**, 69 (1951).
21. C. C. J. Roothaan. Rev. Mod. Phys. **32**, 179 (1960).
22. M. Carlotti, J. W. C. Johns, and A. Trombetti. Can. J. Phys. **52**, 340 (1974).
23. P. Smith. J. Chem. Phys. **29**, 683 (1958).
24. S. N. Foner and R. L. Hudson. J. Chem. Phys. **28**, 719 (1958).
25. D. R. Stull (*Editor*). JANAF thermochemical tables. The Dow Chemical Company, Midland, Michigan. 1965.
26. C. Willis, F. P. Lossing, and R. A. Back. Can. J. Chem. **54**, 1 (1976).
27. D. C. Frost, S. T. Lee, C. A. McDowell, and N. P. C. Westwood. J. Chem. Phys. **64**, 4719 (1976).
28. N. Wiberg, G. Fischer, and H. Bachhuber. Angew. Chem. Int. Ed. Engl. **15**, 385 (1976).

Dicyclohexanecarbonylsulphate: a precursor of cyclohexyloxocarbenium ions

E. MONTONERI, L. GIUFFRÉ,[1] M. CASSAGO, E. TEMPESTI, AND M. FORNAROLI

Istituto di Chimica Industriale del Politecnico di Milano, Piazza Leonardo da Vinci 32, 20133 Milano, Italy

Received July 16, 1976

E. MONTONERI, L. GIUFFRÉ, M. CASSAGO, E. TEMPESTI, and M. FORNAROLI. Can. J. Chem. **55**, 355 (1977).

Dicyclohexanecarbonylsulphate (**1**) is the prevailing species in the equimolar solution of cyclohexanecarboxylic anhydride and sulphur trioxide in liquid sulphur dioxide. The ionization of **1** to cyclohexyloxocarbenium ions occurs only in the presence of excess sulphur trioxide. Both **1** and $C_6H_{11}CO^+$ are stable only in solution and at low temperature.

E. MONTONERI, L. GIUFFRÉ, M. CASSAGO, E. TEMPESTI et M. FORNAROLI. Can. J. Chem. **55**, 355 (1977).

Dans une solution équimolaire d'anhydride de l'acide cyclohexanecarboxylique et d'anhydride sulfurique dans l'anhydride sulfureux à l'état liquide, l'espèce principale est le sulfate du dicyclohexanecarbonyl (**1**). L'ionisation de **1** en ion cyclohexyloxocarbénium ne se produit qu'en présence d'un excès d'anhydride sulfurique. Les espèces **1** et $C_6H_{11}CO^+$ ne sont stables qu'en solution et à basse température.

[Traduit par le journal]

Introduction

From the few spectroscopic studies (1–3), which have been made on the interaction of carboxylic anhydrides with strong acids (Lewis and protonic acids), it appears that the employed acid determines the type of carbonyl intermediates formed and their behaviour.

In the presence of metal halides (1, 2), for instance, carboxylic anhydrides form donor–acceptor complexes via the C=O groups mainly (and also via the ethereal oxygen atoms) and no ionization is observed.

Olah *et al.* (3) have shown that, in the presence of HSO_3F—SbF_5, initial protonation of the anhydride is followed, in a large excess of 'magic acid', by ionization to acylium ions.

Other workers (4), however, investigated the behaviour of acetic anhydride toward some typical protonic acids and found that mixed anhydrides form. Of these species only $AcOSO_2CF_3$ was found to ioniz to Ac^+ in the presence of excess CF_3SO_3H. $AcOSO_3H$ (5, 6), however, can ionize as above, if in the presence of excess SO_3.

Although it may be concluded from the above studies that the strength of the excess protonic acid determines the ionization of mixed species, it is not clear if the formation of these last species may take place only after initial protonation of the carboxylic anhydride, and if their ionization may also be obtained in the presence of other aprotic acids.

In relation to these facts, we wish to report the behaviour of cyclohexanecarboxylic anhydride toward sulphur trioxide.

Results and Discussion

Cyclohexanecarboxylic anhydride and sulphur trioxide were mixed over a wide range of $SO_3/(C_6H_{11}CO)_2O$ mole ratios ($0.0 \leq n_S/n_A \leq 5.0$) in liquid SO_2 at -60 °C. The carboxylic anhydride molality always was 2.5. Of the spectroscopic techniques which were tried for studying the system, Raman spectroscopy could not be employed because of the high fluorescence exhibited by the carboxylic anhydride – SO_3 mixtures. Good quality ir and nmr spectra were obtained, however. The spectra recording temperature was -60 °C (ir) and between -78 and -20 °C (nmr). No substantial changes beyond band broadening were observed in the latter spectra on decreasing the temperature within the range reported above.

At ≤ -20 °C the system behaviour was found dependent only on the mole ratio and well consistent with reactions 1 and 2.

$$[1] \qquad (RCO)_2O + SO_3 \rightleftarrows (RCO_2)_2SO_2$$

$$[2] \qquad (RCO_2)_2SO_2 + SO_3 \rightleftarrows 2RCO^+ + S_2O_7^{2-}$$

However, above -20 °C significant changes occurred in the spectra, mainly because of sulphonation of the organic substrate. These

[1]To whom correspondence to be addressed.

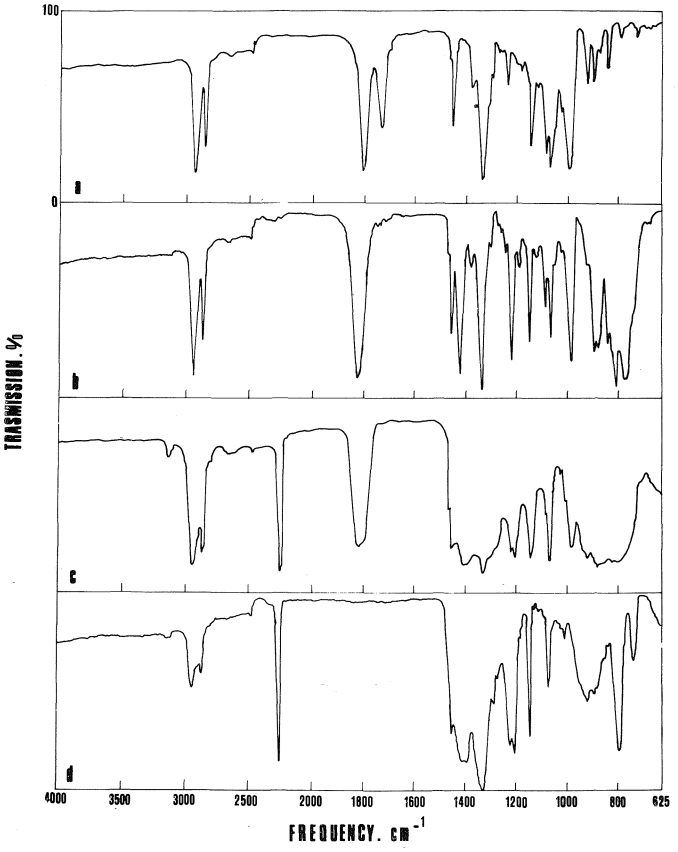

FIG. 1. Infrared spectra of cyclohexanecarboxylic anhydride – sulphur trioxide mixtures in liquid sulphur dioxide at −60 °C and at n_S/n_A = 0.0 (*a*), 1.0 (*b*), 3.0 (*c*), 5.0 (*d*).

changes occurred also if SO_2 was evaporated under vacuum at lower temperature (−50 °C).

Formation and Characterization of Dicyclohexanecarbonylsulphate (1)

The ir spectrum of the cyclohexanecarboxylic anhydride and sulphur trioxide equimolar solution in liquid sulphur dioxide (Fig. 1*b*)

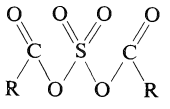

1

exhibits specific new bands compared to those of the carboxylic anhydride (Fig. 1*a*) and of free SO_3 (1390 and 1075 cm^{-1})[2] (*7*) in SO_2. Also in Fig. 1*b* the typical C=O stretching vibration bands of $(C_6H_{11}CO)_2O$ and S=O bands[3] of free SO_3 are absent; this implies that the equimolar addition of SO_3 to $(C_6H_{11}CO)_2O$ is rather quantitative and that at least one new species, which has characteristic absorption frequencies at 1826, 1422, 1220, 895, 882, 808, and 768 cm^{-1}, is prevalently formed.[4]

If this species is assumed to be a donor–acceptor complex, then on the basis of previous work (1, 2), a quite different spectrum from that reported in Fig. 1*b* should be expected. In fact for a donor–acceptor complex such as **2**, for instance, a couple of C=O bands should appear in the region 1700–1500 cm^{-1}. Assuming the ethereal oxygen as the favoured site for SO_3 addition, although not consistent with the reported studies, leads to an alternative structure

[2]The 1075 cm^{-1} band, although forbidden, is also observed by infrared spectroscopy (8).

[3]The 1060–1085 cm^{-1} bands in Fig. 1*b* are most likely due to C—O vibrations, as it is shown later.

[4]The other bands between 995 and 1455 cm^{-1} are common to both $(C_6H_{11}CO)_2O$ and the new species which is formed in the equimolar solution.

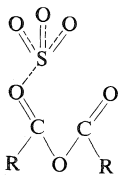

2

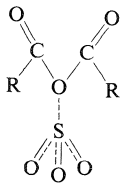

3

such as **3**. This complex may indeed absorb at $>1800\ cm^{-1}$ frequencies but, even in this case, two carbonyl bands should be observed. As to coordinated SO_3, both the S=O bands in each of the exemplified complexes **2** and **3** should fall at frequencies lower than 1390 and $1075\ cm^{-1}$ respectively. An attempt to identify these frequencies in Fig. 1*b* leads to a rather ambiguous interpretation of the spectrum.

Thus compound **1**, dicyclohexanecarbonylsulphate, whose formation may be visualized as in reaction 1, seems more convincing. The new bands, which appear in Fig. 1*b* ($\nu_{C=O}$ 1826; ν_{C-O} 995, 1060–1085; $\nu_{S=O}$ 1422, 1220; ν_{S-O} 895–768 cm^{-1}), have been assumed as the most characteristic ir absorption frequencies of **1**.

The carbonyl groups in the CO—OSO_2—OCO arrangement very likely are not planar, since no coupling of the C=O vibrations is observed (9). The frequency of the resulting single band is higher than the mean absorption frequency of the two C=O bands in pure $(C_6H_{11}CO)_2O$ as expected on the basis of the introduction of the electron-withdrawing SO_3 group in the CO—O—CO bridge (10). Furthermore the $1826\ cm^{-1}$ value is very close to the values reported for other carboxylic–sulphuric mixed anhydrides (4, 11).

Although C—O vibration bands are not generally as diagnostic as C=O bands, some consideration may be allowed in this case. The former bands of cyclohexanecarboxylic anhydride could be tentatively identified in the strong absorption[5] at 995 and 1060–1085 cm^{-1} (Fig. 1*a*). In Fig. 1*b* these bands are still present, but the $995\ cm^{-1}$ band relative to the 1060–1085 cm^{-1} doublet appears more intense than in Fig. 1*a*. This former band is also typical of other cyclic mixed carboxylic–sulphuric species (11*b*) and may be associated with the C—O vibration in the C—O—S bridge. From comparing Fig. 1 *a* and *b* it may therefore be concluded that the C—O bands of both $(C_6H_{11}CO)_2O$ and $(C_6H_{11}CO_2)_2SO_2$ have the same absorption frequencies, although slightly different relative intensities. This conclusion is further substantiated from the discussion of Fig. 1 *c* and *d* below.

The assignment of the 1422 and $1220\ cm^{-1}$ values respectively to the S=O asymmetric and symmetric stretching vibrations of **1** appears justified in view of the linear correlation between these vibration frequencies which has been found valid in a large number of sulphuryl compounds (12). Also the higher mean S=O frequency of **1** ($1321\ cm^{-1}$) compared to dimethylsulphate ($1290\ cm^{-1}$) (13) and dicyclohexylsulphone ($1221\ cm^{-1}$) (14) values reflects well the general dependence of S=O frequencies upon the electronegativity of substituents in $XYSO_2$ compounds (12). The S=O force constant (k = 10.96 dyn/cm), which may be obtained (13) from the 1422 and $1220\ cm^{-1}$ values in Fig. 1*b*, is more consistent with **1** than with **2** and **3**, where SO_3 bonds should lengthen (15) and the obtained k should be <9.50 dyn/cm (16).

Consistent with **1** and with the corresponding frequencies in covalent sulphates, the group

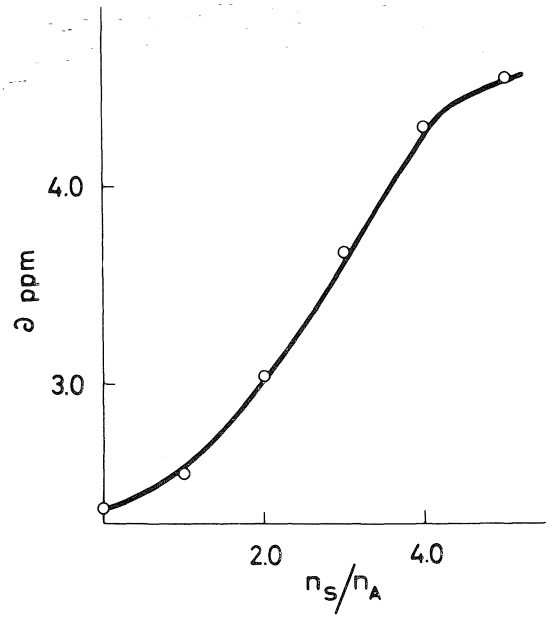

FIG. 2. The α-proton chemical shift (∂) *vs.* n_S/n_A at −20 °C for cyclohexanecarboxylic anhydride – sulphur trioxide mixtures in liquid sulphur dioxide.

[5]A similar spectra feature, although quite less intense, is in fact found for cyclohexanecarboxylic acid, but not for other carbonyl compounds such as cyclohexylamide, cyclohexanone, caprolactam, and dicyclohexylketone.

of bands at 895, 882, 808, and 768 cm^{-1} in Fig. 1*b* is to be clearly related to the S—O stretching vibrations, even considering probable interferences from CH vibrations (10).

In agreement with the infrared data the nmr spectrum of the equimolar solution may well represent that of pure dicyclohexanecarbonylsulphate in liquid SO_2. It was found that the proton chemical shifts in the system are strongly dependent on the mole ratio; in Fig. 2 the α-proton resonance chemical shift is 2.55 ppm (0.18 ppm higher than that of cyclohexanecarboxylic anhydride). The chemical shift is well in the range of values reported for other mixed carboxylic–sulphonic species (17) such as $C_6H_{11}CO_2SO_2X$ (with $X = CH_3$, C_6H_5, $CH_3C_6H_4$, $C_6H_{10}CO_2H$) and almost coincident with the last compound chemical shift (2.52 ppm). Furthermore the 0.18 ppm downfield shift displacement, which is observed in the formation of **1** from $(C_6H_{11}CO)_2O$ as in reaction 1, appears quite consistent with this type of interaction; a downfield chemical shift displacement of the same order of magnitude (0.13 ppm) is in fact reported in the formation of dimethyldisulphate from SO_3 and the corresponding monosulphate (18).

Ionization of Dicyclohexanecarbonylsulphate

The appearance of the known band of the cyclohexyloxocarbenium ion (2260 cm^{-1}) (19) at mole ratios >1.0 (Fig. 1 *c* and *d*) shows that, only in the presence of excess SO_3, **1** ionizes as in reaction 2. At 3.0 mole ratio both **1** and $C_6H_{11}CO^+$ bands are present (Fig. 1*c*), while at 5.0 mole ratio (Fig. 1*d*) only the latter band[6] is observed. This indicates that the ionization of **1** increases on increasing the SO_3 mole ratio and that, at *ca.* 5.0 mole ratio, reaction 2 may be assumed to lie well to the right. In analogy with the ionization of other carboxylic–sulphuric mixed species (6), the 1826 cm^{-1} band broadening which is observed at 3.0 mole ratio seems to imply participation of higher polysulphate mixed species (*e.g.* dicylohexanecarbonyldisulphate) in the formation of cyclohexyloxocarbenium ions. This participation, however, should not be relevant because, if so, a significant frequency shift (*ca.* 20 cm^{-1}) should be observed.

It may also be observed that the bands in the 995–1085 cm^{-1} range, which had been assigned in Fig. 1*a* to the C—O vibrations in the C—O—S bridge of **1**, undergo significant changes as the mole ratio increases above 1.0. These changes are also consistent with the displacement of reaction 2 to the right, which requires breaking of the C—O—S bridge. At 3.0 mole ratio (Fig. 1*c*), in fact, in place of the 1060–1085 cm^{-1} doublet, one band at 1070 cm^{-1} is observed. The intensity of this band is also slightly higher than that of the 995 cm^{-1} band. This may be due to the presence of free SO_3 (8) or to the SO_2 symmetric stretch of the $S_2O_7^{2-}$ ion in reaction 2. At 5.0 mole ratio (in concomitance with the absence of the C=O band of **1**) no absorption at 995 cm^{-1}, but only at 1070 cm^{-1}, is present.[7]

Specifically the other expected (21) absorption bands of $S_2O_7^{2-}$ ($\nu_{S=O\ asym}$ 1230 cm^{-1}; $\nu_{S-O\ asym}$ 795 cm^{-1}; $\nu_{S-O\ sym}$ 738 cm^{-1}) may be recognized in Fig. 1*c* and more evidently in Fig. 1*d*, since there is no interference from the SO frequencies of **1**. These assignments, however, cannot definitely justify the changes observed at >1.0 mole ratios within the regions 1450–1200 and 900–700 cm^{-1}, where the absorption frequencies of free SO_3, $S_3O_{10}^{2-}$, and higher polysulphuric species are also known to occur. Most of these species, as one of the referees pointed out, have rather similar vibrational spectra and further speculation at this point seems unjustified.

In agreement with the above conclusions the interpretation of nmr spectra in the mole ratio range >1.0 may be attempted. There is a strict parallelism between the appearance and intensity increase of the $C_6H_{11}CO^+$ ir band (Fig. 1 *c* and *d*) and the α-proton resonance chemical shift displacement to low fields with increasing SO_3 mole ratio (Fig. 2). The mole ratio dependent chemical shift at $n_S/n_A > 1.0$ is consistent with fast exchange[8] between the species involved in reaction 2. The shape of the curve in Fig. 2 is analogous to that reported

[6]Considering the nonideality of the system, no attempt was made to obtain molar absorptivities.

[7]The weak band at 1005 cm^{-1} may result from a CH vibration of $C_6H_{11}CO^+$; the same band, although more intense, occurs in the spectra of Ac^+ and has been identified as a rocking vibration band (20).

[8]An attempt to freeze out this equilibrium at lower temperatures proved unsuccessful, even at −78 °C. If, in fact, in the mole ratio range $1.0 < n_S/n_A < 5.0$, the exchange rate could have been slowed down sufficiently to observe the α-proton of $C_6H_{11}CO^+$ separately, then the ratio of this band area to the higher field proton bands areas sum should have been < 1/10.

for the formation and ionization of other carboxylic–sulphuric mixed species (5, 6). The slope increase at >1.0 mole ratio is largely accounted for by the formation of the highly deshielded species $C_6H_{11}CO^+$, as in reaction 2. It may also be inferred that this slope increase seems to exclude (as previously observed from ir spectra) a relevant participation of un-ionized organic polysulphuric mixed species in the ionization of **1**. On the basis of the nmr data relative to the formation of dimethylpolysulphate with varying dimethylsulphate/SO_3 mole ratios (18), it may be assumed that the α-proton in a hypothetical species such as dicyclohexanecarbonyldisulphate should not be greatly deshielded (≤ 0.18 ppm) relatively to the α-proton in **1**. Therefore the presence of significant concentrations of this last species should fairly flatten out the plot.

In correspondence with the curve maximum the nmr spectrum is virtually coincident with the spectra of other cyclohexyloxocarbenium salts (*e.g.* $C_6H_{11}CO^+SbF_6^-$) (19) and is a further confirmation that reaction 2 at 5.0 mole ratio lies well to the right.

Experimental

Cyclohexanecarboxylic anhydride (Snia Viscosa) was distilled twice immediately before use. Infrared and nmr spectra were recorded on Perkin-Elmer 157G and Varian NV 14 60 Mz spectrometers respectively. The nmr external reference solution (6% benzene in CS_2) and the sample were placed respectively in 513A-PP outer and sealed 516-1 inner tubes (Wilmad), which were equipped with a Teflon O-ring.

Two sets of runs were made respectively with and without tetramethylsilane (TMS) in the inner tube. TMS was found suitable for internal reference use up to 1.0 $SO_3/(C_6H_{11}CO)_2O$ mole ratio, although two small bands, at 0.47 and 3.28 ppm downfield from TMS, indicated some reaction of the internal standard with SO_3 in the 1.0 mole ratio solution. The TMS band was at 7.87 ppm upfield from the external reference. This value was used to obtain the reported chemical shifts (Fig. 2) from the internal standard even in the remaining mole ratio range, where TMS reacted completely and could not be observed in the spectra. This approximation should however suffice within the limits of our discussion as already evident in a previous work (6).

All other experimental details have been described previously (6).

1. D. Cook. Can. J. Chem. **40**, 445 (1962).
2. P. Hunt and D. P. N. Satchell. J. Chem. Soc. 5437 (1964).
3. G. A. Olah, K. Dunne, and P. Szilagyi. J. Am. Chem. Soc. **94**, 4200 (1972).
4. A. Germain, A. Commeyras, and A. Casadevall. Bull. Soc. Chim. Fr. **7–8**, 2527 (1973).
5. A. Casadevall, A. Commeyras, P. Paillous, and H. Collet. Bull. Soc. Chim. Fr. **2**, 719 (1970).
6. E. Montoneri, M. Fornaroli, L. Giuffré, E. Tempesti, and G. Sioli. J. Chem. Soc. In press.
7. R. J. Gillespie and E. A. Robinson. Can. J. Chem. **39**, 2189 (1961).
8. G. E. Walrafen. J. Chem. Phys. **40**, 2326 (1964).
9. L. J. Bellamy. Advances in ir frequencies. Methuen, London. 1968.
10. R. E. Kagarise. J. Am. Chem. Soc. **77**, 1377 (1955).
11. (*a*) M. H. Karger and Y. Mazur. J. Org. Chem. **36**, 528 (1971); (*b*) R. M. Laird and M. J. Spence. J. Chem. Soc. B, 454 (1971).
12. E. A. Robinson. Can. J. Chem. **39**, 247 (1961).
13. S. Detoni and D. Hadzi. Spectrochim. Acta, **11**, 601 (1957).
14. D. Barnard, J. M. Fabian, and H. P. Koch. J. Chem. Soc. 2442 (1959).
15. R. S. Mulliken. J. Am. Chem. Soc. **74**, 811 (1952).
16. R. J. Gillespie and E. A. Robinson. Can. J. Chem. **41**, 2074 (1963).
17. E. Tempesti, L. Giuffré, G. Sioli, M. Fornaroli, and G. Airoldi. J. Chem. Soc. Perkin Trans. I, 771 (1974).
18. J. R. Van Wazer, D. Grant, and C. H. Dungan. J. Am. Chem. Soc. **87**, 3333 (1965).
19. G. A. Olah and M. B. Comisarow. J. Am. Chem. Soc. **88**, 4442 (1966).
20. P. N. Gates and D. Steele. J. Mol. Structure **1**, 349 (1968).
21. A. Simon and H. Wagner. Z. Anorg. Chem. **311**, 102 (1961).

σ-Aryl complexes of iridium: diphenyliodonium salts as phenylating agents in transition metal chemistry

NICHOLAS FARRELL AND DEREK SUTTON

Department of Chemistry, Simon Fraser University, Burnaby, B.C., Canada V5A 1S6

Received June 10, 1976

NICHOLAS FARRELL and DEREK SUTTON. Can. J. Chem. **55**, 360 (1977).

Diphenyliodonium salts readily react with $[IrX(CO)(PR_3)_2]$ (X = Cl, Br; PR_3 = PPh_3 or $PMePh_2$) to yield iridium(III) σ-phenyl complexes of general composition $[IrXY(C_6H_5)(CO)(PR_3)_2]$ (Y = Cl, BF_4). The possible structures of these compounds, and their occurrence in the decomposition of iridium aryldiazenato complexes, are discussed.

NICHOLAS FARRELL et DEREK SUTTON. Can. J. Chem. **55**, 360 (1977).

Les sels de diphényliodonium réagissent facilement avec $[IrX(CO)(PR_3)_2]$ (X = Cl, Br; PR_3 = PPh_3 ou $PMePh_2$) pour conduire à des complexes σ-phényle d'iridium(III) ayant des compositions générales $[IrXY(C_6H_5)(CO)(PR_3)_2]$ (Y = Cl, BF_4). On discute des structures possibles pour ces composés et de leur présence dans la décomposition des complexes aryldiazénato d'iridium.

[Traduit par le journal]

Introduction

Extrusion of dinitrogen from aryldiazenato (aryldiazo) complexes of transition metals to form σ-aryl derivatives has frequently been reported. Thus, both $[PtCl(N_2C_6H_4p\text{-}F)(PEt_3)_2]$ (1) and $[Pt(N_2C_6H_4p\text{-}$ or $m\text{-}F)(PEt_3)_3]$ (2) have been shown to eliminate dinitrogen and the corresponding aryl complexes have been isolated. Similarly, Robinson and co-workers (3) have cited dinitrogen extrusion as a mode of decomposition for the rhodium(III) species $[RhCl_2(N_2Ar)(PPh_3)_2]$ and in numerous instances aryldiazonium salts have been used by Nesmeyanov's group as precursors for the preparation of metal–aryl complexes (4), two recent examples being the syntheses of $[Fe(\sigma\text{-}C_6H_5)(\eta\text{-}C_5H_5)(CO)_2]$ and $[W(\sigma\text{-}C_6H_5)(\eta\text{-}C_5H_5)(CO)_3]$ (5, 6).

During our investigation of aryldiazenato complexes of iridium(III) (7) several attempts to prepare $[IrCl_2(N_2Ar)(CO)(PPh_3)_2]$ and $[IrCl(N_2Ar)(CO)(PPh_3)_2]BF_4$ (8) gave products with significantly low nitrogen content, which we believed were mixtures of the desired complexes and the σ-aryl analogues resulting from dinitrogen extrusion. In view of this, we considered various ways in which these σ-aryl complexes might be synthesized directly, for comparison.

A literature survey revealed that a few examples of the desired complexes $[IrCl_2(Ar)(CO)(PR_3)_2]$ had been synthesized previously, also by extrusion reactions. Collman and Roper (9) and subsequent investigators (10–12) employed thermal desulfonation of aryl sulfinato complexes to obtain iridium(III) aryl complexes. Deeming and Shaw (13) employed thermal decarbonylation of the related benzoyl complex. We were interested to see whether iridium(III) σ-aryl complexes might be synthesized by direct methods. One possibility is oxidation of an iridium(I) σ-aryl complex. The iridium(I)–aryl complexes $[IrAr(CO)(PPh_3)_2]$ are usually prepared by metathesis of $[IrCl(CO)(PPh_3)_2]$ and the aryl–lithium, silver or Grignard reagent. Thus complexes for Ar = C_6H_5, C_6Cl_5, C_6F_5 have been reported by Rausch and Moser (14), Ar = C_6H_5, C_6Cl_5, C_6F_5, $p\text{-}C_6H_4NMe_2$, *p*-tolyl, and mesityl by Dahlenburg and Nast (15), Ar = C_6F_5 by Bruce and co-workers (16), and Ar = C_6H_5 by Wilkinson and co-workers (17). These complexes are generally much less reactive towards oxidative-addition than the parent Vaska's complex and products from HX and X_2 (X = halogen) addition have been reported for only the perhalophenyl complexes (14, 16).

We considered the possibility of oxidative-addition of phenyl ions to iridium(I) complexes such as $[IrX(CO)(PR_3)_2]$ in preference to attempted oxidation of the above iridium(I)–phenyl complexes. The oxidative-addition of alkyl halides to Vaska's complex and its analogues with $PMePh_2$ and PMe_2Ph is now well documented (18, 19) but aryl halides are much less reactive and no products from simple addition of ArX appear to have been found. However,

TABLE 1. Analytical and spectral data for σ-phenyl complexes of iridium(III)

	Complex	Melting point (°C)	ν(CO) (cm^{-1})	ν(Ir—Cl) (cm^{-1})	Analysis C Found	C Calcd	H Found	H Calcd
1	$[IrCl_2(Ph)(CO)(PPh_3)_2]$	265–270	2055	320, 255	57.8	57.9	4.0	4.0
2	$[IrCl_2(Ph)(CO)(PMePh_2)_2]$	202–205	2057	330, 274, 255	51.2	51.6	4.1	4.1
3	$[IrCl(Ph)(CO)(PPh_3)_2]BF_4 \cdot 0.5C_6H_6$	>250	2044	321, 273, 250	55.9	56.2	3.9	3.9
4	$[IrCl(Ph)(CO)(PMePh_2)_2]BF_4 \cdot 0.5(CH_3)_2CO$	193–197	2048	328, 270, 250	49.6	49.2	3.9	3.9
5	$[IrBr(Ph)(CO)(PPh_3)_2]BF_4$	>250	2047	—	51.9	52.2	3.5	3.6

in view of the widespread use of diphenyliodonium salts as phenylating agents in organic chemistry (20) these appeared to offer considerable potential as phenylating agents for transition metal complexes.

Results and Discussion

The diphenyliodonium salts used were $Ph_2I^+Cl^-$ and $Ph_2I^+BF_4^-$. Both are air-stable white solids, soluble in methanol and reasonably soluble in acetone. Their reactions with $[IrX(CO)(PR_3)_2]$ (X = Cl, Br, PR_3 = PPh_3, $PMePh_2$) proved to be a fast, clean, and convenient route to the required Ir(III)–phenyl complexes. The compounds prepared are listed in Table 1 with spectroscopic and analytical data. All complexes are air-stable, white solids. Those with PPh_3 are only very sparingly soluble in organic solvents, while those with $PMePh_2$ are soluble in chloroform, methanol, and acetone but insoluble in ether and hexane. Compound **2** is also soluble in benzene. The stability contrasts with that of $[Ir(\sigma\text{-}C_6H_5)(CO)(PPh_3)_2]$ which can only be handled in air for short periods (14, 15).

The properties reported here for $[IrCl_2(Ph)(CO)(PPh_3)_2]$ and for $[IrCl_2(Ph)(CO)(PMePh_2)_2]$ may be compared with those reported for the former compound (10) (but synthesised by carbon monoxide displacement of SO_2 from $[IrCl_2(Ph)(SO_2)(PPh_3)_2]$) and the properties of $[IrCl_2(Ph)(CO)(PMe_2Ph)_2]$ synthesised by decarbonylation of the benzoyl complex (13). Kubota and Loeffler (10) assigned structure **B** to $[IrCl_2(Ph)(CO)(PPh_3)_2]$ since only a single ν(Ir—Cl) band was observed, at 319 cm^{-1}, assigned as indicating Cl—Ir—Cl. By contrast $[IrCl_2(Ph)(CO)(PMe_2Ph)_2]$ was assigned structure **A**, since in addition to a band at 315 cm^{-1} (assigned as Cl—Ir—CO) others at 271, 251 cm^{-1} could be assigned as Cl—Ir—Ph. The situation is confused when the compounds $[IrCl_2(C_6F_5)(CO)(PPh_3)_2]$ and $[IrCl_2(C_6F_5)(CO)(PMePh_2)_2]$ are examined. The former has ν(Ir—Cl) at 320 and 290 cm^{-1} and was assigned structure **A**, whilst the latter has only ν(Ir—Cl) at 328 cm^{-1} and was assigned structure **B** (16).

For $[IrCl_2(Ph)(CO)(PPh_3)_2]$ (**1**) we observe ν(Ir—Cl) at 320 cm^{-1} in agreement with Kubota and Loeffler (10), and also a band at 255 cm^{-1}. A value of 320 cm^{-1} is borderline between typical Cl—Ir—Cl and Cl—Ir—CO values (21), but the 255 cm^{-1} band may readily be assigned to Cl—Ir—Ph in view of the *trans*-influencing nature of σ-bonded aryls. Thus we feel our compound to have structure **A**, but cannot neglect the possibility that it is contaminated with isomer **B** (assuming, as is probable, that the phosphines are mutually *trans*). Our value of ν(CO) is some 10 cm^{-1} higher than Kubota and Loeffler's and the band is not symmetric. It is known that the addition of MeX (X = Br, I) to $[IrCl(CO)(PMe_2Ph)_2]$ is solvent dependent and a mixture of isomers is obtained when methanol replaces benzene as solvent (13). The ν(Ir—Cl) values for $[IrCl_2(Ph)(CO)(PMePh_2)_2]$ show a reasonable correspondence with those reported for $[IrCl_2(Ph)(CO)(PMe_2Ph)_2]$ by Deeming and Shaw (13) and we assign our bands as 330 cm^{-1} (Cl—Ir—CO) and 274, 255 cm^{-1} (Cl—Ir—Ph) likewise in favour of structure **A**. Here again, however the high value of the upper band allows its assignment also to Cl—Ir—Cl in structure **B**, and we suspect that both isomers may again indeed be present. The *trans* disposition of the phosphine ligands in **2** is supported by the apparent 1:2:1 triplet ($|^2J_{PH} + {}^4J_{PH}| = 13$ Hz) for the methyl resonance in the ^1H nmr spectrum.

The ir spectra of compounds **3** to **5** exhibit typical broad ν(BF_4) absorptions at *ca.* 1100 cm^{-1}. Compounds **3** and **4** exhibit multiple

ν(Ir—Cl) absorptions in the 250–350 cm^{-1} region (absent in the bromo complex **5**) which are remarkably similar to those of **1** and **2**. This argues against a discrete monomeric pentacoordinate cation being present, and the spectra may be indicative of a chlorine-bridged cation such as structure **C**, not unlike the structure of $[IrCl_2(Me)(CO)_2]_2$ (22). We have not been able to obtain supportive evidence for this structure due to the limited solubility of these tetrafluoroborates and the likelihood of disruption of any halogen bridge bonds in more highly donor solvents

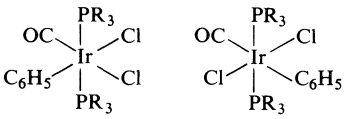

A

B

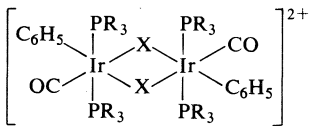

C

The formation of σ-aryl complexes as a source of impurity in the reactions of $[IrCl(CO)(PPh_3)_2]$ with benzenediazonium salts (7) was confirmed by deliberately conducting these reactions under reflux conditions so as to promote dinitrogen extrusion from the initially formed phenyldiazenato complexes. For example, $PhN_2^+BF_4^-$ reacted to give an initial orange solution of the phenyldiazenato complex $\{[IrCl(PhN_2)(CO)(PPh_3)_2]BF_4\}_n$ (7) which gradually lost its colour and precipitated the σ-phenyl complex as a white solid, identified by comparison of its composition, infrared spectrum and melting point with those of **3**.

Experimental

All solvents were dried by usual methods and distilled under nitrogen. The iridium starting materials were prepared by standard literature methods (23, 24). Diphenyliodonium chloride was purchased from Aldrich Chemical Company Inc. and used without further purification. Diphenyliodonium tetrafluoroborate was prepared by metathesis with $AgBF_4$ and recrystallised from methanol–ether. Infrared spectra were recorded on Perkin–Elmer 457 and Beckman IR-12 instruments for samples pressed in KBr discs or as Nujol mulls between polythene windows. Proton nmr spectra were recorded using Varian A60 and HA100 instruments. All τ values are relative to internal TMS. Melting points were recorded on a Fisher-Johns apparatus and are uncorrected. Elemental analyses were carried out by Mr. M. K. Yang of the Simon Fraser University microanalytical laboratory.

Preparation of Iridium(III)–Phenyl Complexes

In a typical synthesis a 10% excess of the salt in methanol was added to a refluxing solution of the iridium(I) complex in benzene under nitrogen. The reaction was considered complete at the disappearance of the yellow colour of $[IrX(CO)(PR_3)_2]$. As expected the more basic diphenylmethylphosphine complexes reacted faster than the triphenylphosphine ones.

Thus, to prepare $[IrCl(Ph)(CO)(PPh_3)_2]BF_4$, a solution of $Ph_2I^+BF_4^-$ (0.06 g) in MeOH (5 ml) was added to a refluxing solution of $[IrCl(CO)(PPh_3)_2]$ (0.1 g) in benzene (10 ml). Reflux was continued for 2.5 h during which time a white solid precipitated from the reaction mixture. The mixture was then evaporated to half-volume, cooled to 8° and the product filtered off, washed with benzene and ether, and dried *in vacuo*. Analytical data are given in Table 1. Complexes **1** and **5** were prepared in a similar manner, in 55–60% yield. Complexes **2** and **4** were precipitated by addition of ether to a cooled solution of the reaction mixture after 1.5 h (by which time only a very pale yellow solution was observed) and then recrystallized from acetone–hexane. ^1H nmr for **2** (τ): 2.25 m 5H (C_6H_5); 2.75 m 20H ($P—C_6H_5$); 7.86 t 6H ($P—CH_3$).

Reaction of [IrCl(CO)(PPh$_3$)$_2$] with Benzenediazonium Tetrafluoroborate

To a refluxing solution of $[IrCl(CO)(PPh_3)_2]$ (0.1 g) in benzene (10 ml) was added $PhN_2^+BF_4^-$ (0.025 g) in acetone (5 ml). Immediately a bright orange solution was obtained which, upon continued reflux, steadily became paler in colour. After 2.5 h the pale yellow solution was evaporated to half-volume and ether added. Upon cooling at 8° a white solid precipitated. This was filtered off and was shown to be $[IrCl(Ph)(CO)(PPh_3)_2]BF_4$ by comparison of mp, ir spectrum, and analysis with that of an authentic sample. Found: C 54.1, H 3.62; calcd. C 54.7, H 3.74.

Acknowledgements

We are grateful to the National Research Council of Canada for support of this work through operating grants and to Johnson Matthey and Co. Ltd. for a generous loan of iridium compounds.

1. G. W. Parshall. J. Am. Chem. Soc. **87**, 2133 (1965).
2. A. W. B. Garner and M. J. Mays. J. Organomet. Chem. **67**, 153 (1974).
3. K. R. Laing, S. D. Robinson, and M. F. Uttley. J. Chem. Soc. Dalton, 2713 (1973).
4. A. N. Nesmeyanov. J. Organomet. Chem. **10**, 1 (1972).
5. A. N. Nesmeyanov, Y. A. Chapovskii, I. V. Polovyanyuk, and L. G. Makarova. J. Organomet. Chem. **7**, 329 (1967).
6. A. N. Nesmeyanov, Y. A. Chapovskii, N. A. Ustynyuk, and L. G. Makarova. Izv. Akad. Nauk. USSR Ser. Khim. 449 (1968).
7. R. E. Cobbledick, F. W. B. Einstein, N. Farrell,

A. B. GILCHRIST, and D. SUTTON. J. Chem. Soc. Dalton. In press.
8. B. L. HAYMORE and J. A. IBERS. J. Am. Chem. Soc. **95**, 3052 (1973).
9. J. P. COLLMAN and W. R. ROPER. J. Am. Chem. Soc. **88**, 180 (1966).
10. M. KUBOTA and B. M. LOEFFLER. Inorg. Chem. **11**, 469 (1972).
11. J. W. KANG and P. M. MAITLIS. J. Organomet. Chem. **26**, 393 (1971).
12. J. BLUM and G. SCHARF. J. Org. Chem. **35**, 1895 (1970).
13. A. J. DEEMING and B. L. SHAW. J. Chem. Soc. A, 1128 (1969).
14. M. D. RAUSCH and G. A. MOSER. Inorg. Chem. **13**, 11 (1974).
15. L. DAHLENBURG and R. NAST. J. Organomet. Chem. **71**, C49 (1974).
16. R. L. BENNETT, M. I. BRUCE, and R. C. F. GARDNER. J. Chem. Soc. Dalton, 2653 (1973).
17. G. YAGUPSKY, C. K. BROWN, and G. WILKINSON. J. Chem. Soc. A, 1392 (1970).
18. J. P. COLLMAN and W. R. ROPER. Adv. Organomet. Chem. **7**, 53 (1968).
19. A. J. DEEMING and B. L. SHAW. J. Chem. Soc. A, 1887 (1968); 2784 (1968).
20. F. M. BERINGER, S. A. GALTON, and S. J. HUANG. J. Am. Chem. Soc. **84**, 2819 (1962).
21. A. R. NORRIS and J. A. VAN KESSELL. Can. J. Chem. **51**, 4145 (1973).
22. N. A. BAILEY, C. J. JONES, and B. L. SHAW. Chem. Commun. 1051 (1967).
23. K. VRIEZE, J. P. COLLMAN, C. T. SEARS, and M. KUBOTA. Inorg. Synth. **11**, 101 (1968).
24. J. P. COLLMAN and J. W. KANG. J. Am. Chem. Soc. **89**, 844 (1967).

The stereochemistry of addition of cyclopropanes to tetrachloro(diethylene)platinum(II)

N. DOMINELLI AND A. C. OEHLSCHLAGER

Department of Chemistry, Simon Fraser University, Burnaby, B.C., Canada V5A 1S6

Received July 2, 1976

N. DOMINELLI and A. C. OEHLSCHLAGER. Can. J. Chem. **55**, 364 (1977).

The synthesis of *trans*-1-*n*-hexyl-*cis*-2,3-dideuterio cyclopropane and *cis*-1-*n*-hexyl-*cis*-2,3-dideuterio cyclopropane are reported. These specifically deuterated cyclopropanes were reacted with tetrachloro(diethylene)diplatinum to yield the product (dichloro(2-*n*-hexylpropane-1,3-diyl)platinum) of addition of Pt^{II} across the cyclopropyl C_2C_3 bond. It was shown by nmr spectroscopic analysis of the deuterated cyclopropanes and the bispyridine derivatives of the adducts that the Pt^{II}–cyclopropane reaction was stereospecific and involved retention of configuration at both reacting carbons. This outcome is interpreted in terms of a concerted cycloaddition mechanism.

N. DOMINELLI et A. C. OEHLSCHLAGER. Can. J. Chem. **55**, 364 (1977).

On rapporte la synthèse du *n*-hexyl-1 *trans* dideutério-2,3 *cis* cyclopropane et du *n*-hexyl-1 *cis* dideutério-2,3 *cis* cyclopropane. On a fait réagir ces molécules de cyclopropanes deutérés d'une façon spécifique avec le tétrachloro(diéthylène)diplatine et l'on obtient le produit (dichloro(*n*-hexyl-2 propanediyl-1,3)platine) provenant de l'addition de Pt^{II} à travers le lien C_2C_3 du cyclopropane. On montre, par des données spectroscopiques rmn des cyclopropanes deutérés et des dérivés bispyridine des adduits, que la réaction du platine avec le cyclopropane est stéréospécifique et implique une rétention de configuration aux niveaux des deux atomes de carbone qui réagissent. On interprète le résultat en terme d'un mécanisme concerté de cycloaddition.

[Traduit par le journal]

Introduction

Many coordinatively unsaturated transition metal complexes with d^7, d^8, or d^{10} electron configurations undergo oxidative addition reactions by insertion of the metal into an X—Y substrate single bond. Owing to the stability of many square planar d^8 complexes of Ir^I, Rh^I, and Pt^{II}, a considerable amount of research has been directed at these complexes (1–4).

The mechanism for oxidative addition reactions is currently under dispute, undoubtedly due to the broad classification of such reactions. Pearson and Muir (5) have proposed a one step concerted mechanism, based on orbital symmetry arguments for the reaction of Ir(CO)-ZL_2 (Z = Cl, I, SCN; L = PPh_3, PPh_2Me) in dichloroethane with CH_3I which explains the occurrence of both *cis* and *trans* addition products.

Evidence for operation of an S_N2 mechanism during oxidative additions of d^8 complexes to alkyl halides has been reported for Rh^I (6), Ir^I (7), and Pd^0 (8, 9) complexes.

Reactions involving insertion of two dimeric d^8 complexes of Rh^I (**1**) and Pt^{II} (**2**) into C—C single bonds have received extensive attention.

A variety of strained hydrocarbons including

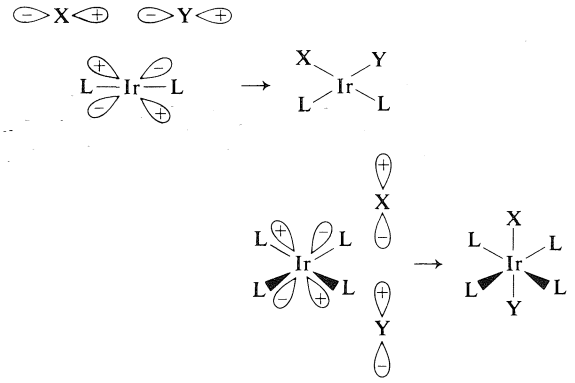

cyclopropanes (10–12), quadracyclane (13), and cubane (14) have been found to react with **1** to

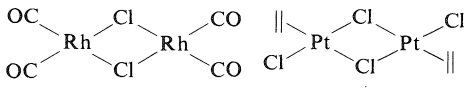

1 **2**

give products in which a rhodium acyl moiety is inserted into a strained C—C bond.

Insertion of the Pt^{II} complex **2** into substituted cyclopropanes has been investigated by several groups (15–23). In this case the reaction led to the formation of polymeric (16) cyclobutyl platinum adducts which reverted to the parent

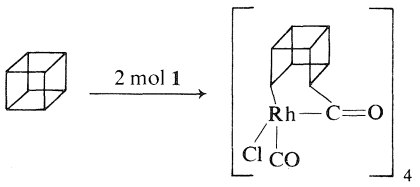

cyclopropanes upon treatment with KCN, triphenylphospine, or carbon monoxide (21–23).

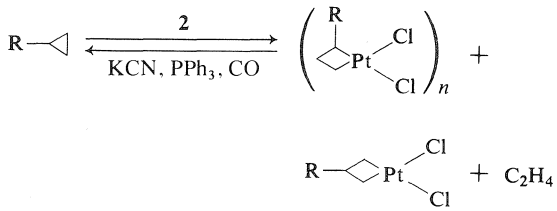

The present investigation was undertaken to determine the stereochemistry of the addition of **2** to the strained C—C bonds of substituted cyclopropanes. Knowledge of the stereochemistry of this addition process is crucial to the understanding of the mechanism of this and related oxidative addition reactions. Our choice of substrates for study was guided by the reports of McQuillin and co-workers (21–23) that **2** reacted with monoalkyl substituted cyclopropanes primarily at the least substituted C—C bond. This observation coupled with their reports (23) of differential shielding of hydrogens *cis* and *trans* to the alkyl substituent both in the parent cyclopropanes and derived metallocyclobutane adducts led us to investigate the reaction of **3** and **4** with **2**.

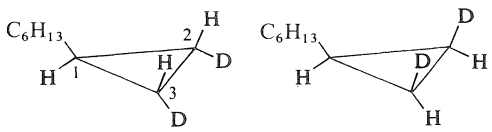

3 **4**

A priori, there are three stereochemical courses which could be observed during addition of Pt^{II} complex, **2**, to the C_2—C_3 bond of a cyclopropane. These are (Fig. 1): (*a*) retention of configuration (R,R) at both carbon centres (C_2 and C_3), (*b*) inversion of configuration (I,I) at both carbon centres (C_2 and C_3), and (*c*) retention of configuration at one carbon centre, and inversion at the other (R,I).

It was anticipated that the distinction between these three possibilities would be evident upon examination of the chemical shifts (23) and vicinal coupling (24, 25) of H_2 and H_3 in **3** and **4** and their Pt^{II} adducts.

Results and Discussion

Our initial efforts were directed at stereospecific syntheses of **3** and **4** and their protio analog *n*-hexylcyclopropane (**5**). Synthesis of **5** was carried out according to the procedure of Simmons and Smith (26). The synthesis of **3** (Fig. 2) proceeded from reaction of a mixture of *cis*- and *trans*-1-chloro-oct-1-enes (27, 28) with dichlorocarbene in the presence of a phase transfer agent (cetyltrimethylammonium bromide (29)). The mixture of hexyltrichlorocyclopropanes thus generated was reduced to the dichloro stage by reaction with tri-*n*-butyltin hydride (30, 31). Deuterium was placed in the molecule stereospecifically *trans* to the hexyl substituent by reduction of the dichlorocyclopropane isomers generated above with sodium in methanol-OD. This reduction is known to yield products in which deuterium is placed in the least hindered position at each chlorine containing carbon (32). In the present case analysis of the hexyldideuteriocyclopropane (**3**) by mass spectroscopy revealed 92% D_2 and 8% D_1. Analysis by nmr revealed the dideuterio species **3** was contaminated with **4** or the isomer in which the deuteriums were *trans* to one another to the extent of 9%. That is, the total contamination due to C_2, C_3 diprotio, and D_2 containing isomers with proton substitution *trans* to the hexyl group was 17% by nmr analysis.

The synthesis of **4** (Fig. 3) proceeded from 1-deuterio-1-chloro-oct-1-ene. This olefin was prepared by reaction of disiamylborane with 1-chlorooct-1-yne (33) followed by hydrolysis of the vinyl borane in acetic acid-OD (34). The deuterated chlorooctene thus produced was reacted with dichlorocarbene as above and the hexyltrichloro cyclopropanes produced were reduced to the dichloro stage by reaction with tri-*n*-butyltin deuteride (30, 31). This sequence placed one deuterium at each of the chlorinated carbons (C_2 and C_3). Reduction of the dichlorodideuterio cyclopropanes with sodium in methanol (32) gave predominantly **4**. Mass spectroscopic analysis revealed that **4** produced by this sequence was 73% D_2 and 27% D_1. Since nuclear magnetic resonance analysis revealed 28% contamination of **4** by isomers containing

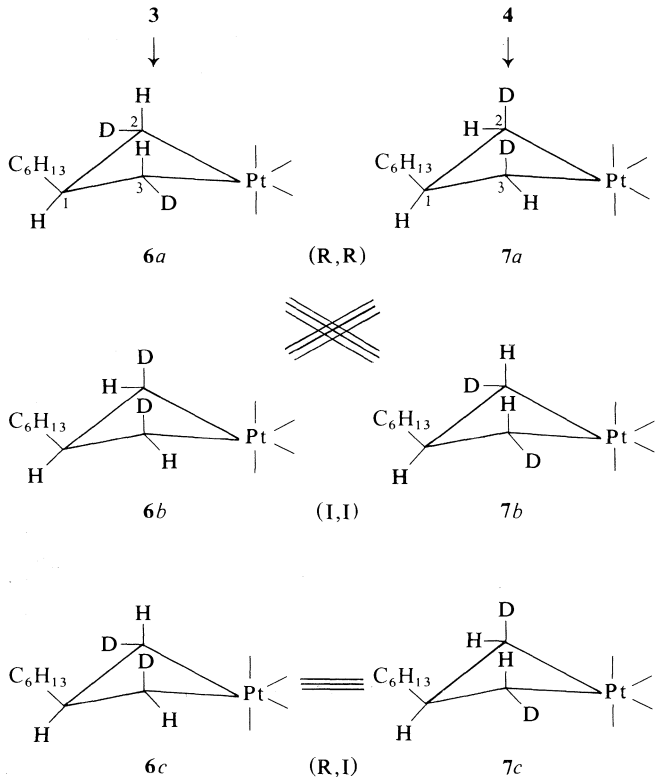

FIG. 1. Possible stereochemical courses of reaction of Pt^{II} complex **2** with deuterated cyclopropanes **3** and **4**.

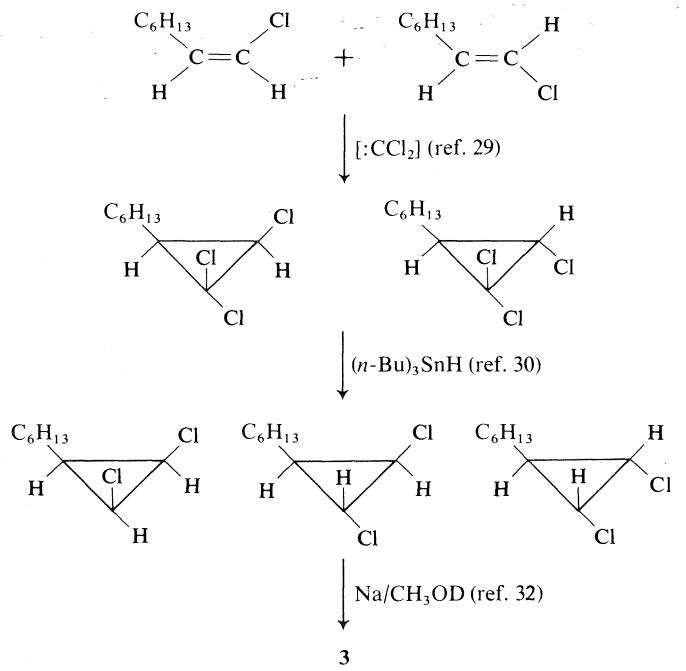

FIG. 2. Synthesis of *trans-n*-hexyl-*cis*-2,3-dideuteriocyclopropane (**3**).

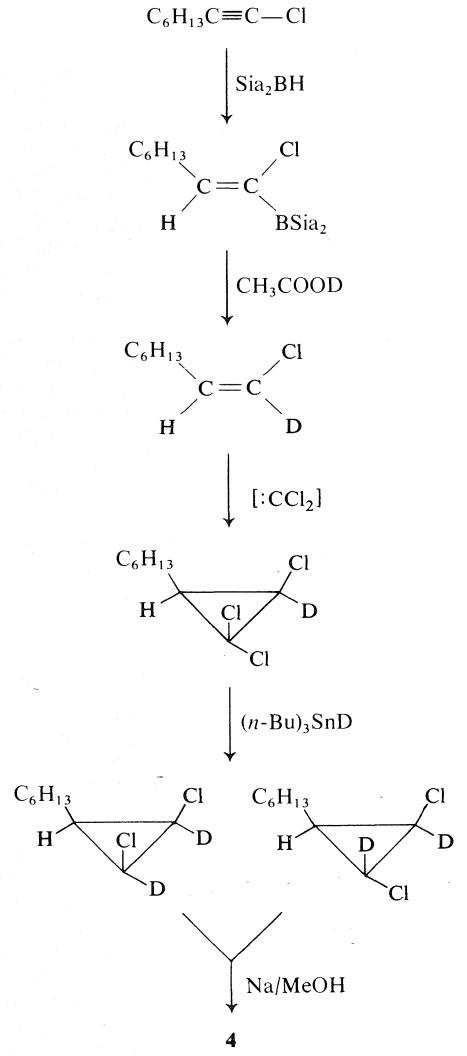

FIG. 3. Synthesis of *cis*-*n*-hexyl-*cis*-2,3-dideuteriocyclopropane **4**.

proton at C_2 and C_3 *cis* to the hexyl group one may deduce that within experimental limits of detection **4** was contaminated only with the monodeuterio species.

Each of **3**, **4**, and **5** were reacted with the Pt^{II} complex, **2**, under the conditions used by Powell and McQuillin (23). The insoluble yellow adducts thus formed were reacted with pyridine to give the corresponding bispyridine adducts (23). These adducts were then analyzed by 220 MHz nmr to determine the stereochemistry of the insertion reaction.

The ^1H nmr spectra of **3**, **4**, and **5** (220 MHz, C_6D_6, internal TMS) revealed the presence of broad multiplets at δ 1.20 assigned to the *n*-hexyl methylene hydrogens, a quartet at δ 1.08 (J = 7 Hz) assigned to the CH_2 group α to the ring, a methyl group appearing as a triplet at δ 0.83 (J = 6.7 Hz), and a one hydrogen multiplet at δ 0.50 attributable to H_1. The ^1H nmr spectrum of **5** revealed the C_2 and C_3 hydrogens *cis* to the hexyl group as a multiplet centered at 0.1 and the hydrogens *trans* to the hexyl group as a multiplet centered at δ 0.27. In the spectrum of **3** the signal due to the *cis*-2,3-hydrogens appears as a doublet ($J_{1,2(3)}$ = 5 Hz) and that due to the *trans*-2,3-hydrogens as a reduced size multiplet (17% of *cis*). The nmr spectrum of **4** revealed the signal of the *cis*-2,3-hydrogens to be 28% that of the *trans*-2,3-hydrogens which gave a doublet signal ($J_{1,2(3)}$ = 8 Hz).

The $PtCl_2(Py)_2$ adducts of **3**–**5** (220 MHz, C_6D_6 external TMS) revealed common ^1H nmr signals due to co-ordinated pyridine (δ 6.5–8.9) and the *n*-hexyl groups (CH_3, δ 0.80; $(CH_2)_4$, δ 1.25; CH_2-ring, δ 1.75). The nmr spectrum of **8**, the adduct of **5**, exhibited a multiplet signal at δ 3.39 assigned to H_1. The ring methylene hydrogen signals appear as quartets at δ 2.95 (*cis*-2,3-H) and δ 3.22 (*trans*-2,3-H) with ^{195}Pt quartet satellites. The couplings of the *cis*-2,3-hydrogens with H_1 was observed to be 9.0 Hz and coupling with ^{195}Pt 86 Hz. Coupling of the *trans*-2,3-hydrogens with H_1 was 7.5 Hz and with ^{195}Pt it was 82 Hz. The above assignments are consistent with the shielding and couplings observed in other three (24) and four (25) membered rings and previously reported for **8** (23).

Examination of the nmr spectrum of the $PtCl_2(Py)_2$ adduct **6** derived from **3** revealed the signals due to the *cis*-2,3-hydrogens as a doublet ($J_{1,2(3)}$ = 9.0 Hz) at δ 2.94 with ^{195}Pt satellites. A signal (δ 3.2) due to *trans*-2,3-hydrogens was unchanged from intensity compared to **3**. This observation unequivocally defines the structure of the adduct of **3** as **6***a*. Similarly the nmr spectrum of the adduct **7** derived from **4** revealed a doublet ($J_{1,2(3)}$ = 7.5 Hz) signal at δ 3.2 with ^{195}Pt satellites due to the *trans*-2,3-hydrogens. Contamination by isomers containing *cis*-2,3-hydrogens was unchanged (28%) from that noted in **4**. These observations define the structure of the adduct of **4** as **7***a*.

Within the limits of detection of our nmr method the addition of Pt^{II} complex **2** adds to cyclopropanes **3** and **4** stereospecifically with retention of configuration at both carbons.

The relatively high degree of stereospecificity noted in the reaction studied coupled with the nonpolar conditions of reaction lead us to the conclusion that the reaction involves a concerted cycloaddition as suggested by Pearson and Muir (5) for oxidative additions of Ir^I to alkyl halides. In the present case the process may be rationalized as involving interaction of the lowest Walsh (35, 36) orbital of the cyclopropane with a vacant orbital on platinum (37). Such a view is consistent with the increase in reactivity of cyclopropanes with **2** upon substitution of the former with electron donating groups (23).

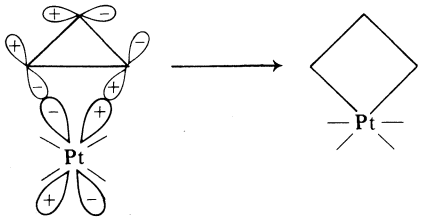

Experimental

Mass spectra were obtained on a Hitachi – Perkin-Elmer RMU-6E double focusing mass spectrometer using an ionization voltage of 80 eV. Nuclear magnetic resonance spectra were obtained on Varian A56/60 and XL100 spectrometers using $CDCl_3$ as solvent and TMS as internal standard (δ 0) unless otherwise stated. Melting point determinations were carried out using a Fisher-Johns melting point apparatus and are uncorrected. Gas–liquid chromatographic analyses were done using a 6 ft × $\frac{1}{8}$ in. stainless steel column packed with 20% SE-30 on Chromosorb G (100/120 mesh) unless otherwise specified.

Synthesis of trans-1-n-Hexyl-cis-2,3-dideuteriocyclopropane, 3

Preparation of cis- and trans-1-Chlorooct-1-ene (28)

A solution of 34.7 g (100 mmol) of (chloromethyl)triphenylphosphonium chloride (27) in 50 ml of dry glyme was prepared and cooled in a dry ice – acetone bath while 60 ml of 2 *M* butyllithium in hexane was added dropwise with stirring over a period of 1 h. The reaction mixture became red and copious quantities of white precipitate formed. While maintaining the reaction mixture at −50 °C, heptanal, (14.9 g, 0.12 *M*), was added. The mixture was allowed to warm to room temperature, then was refluxed for 16 h. The reaction mixture was filtered, the solvent removed *in vacuo*, and the residue distilled under reduced pressure to yield 30–35% of *cis,trans*-1-chlorooct-1-ene: bp 43–67 °C (2.5 mm Hg); glpc analysis showed two major components, nmr (of mixture) δ ($CDCl_3$) 0.9 (3H, t, CH_3, J = 5 Hz), 1.3 (8H, b, $(CH_2)_4$—), 2.1 (2H, m, CH_2—C=C), and 5.9 (2H, m, 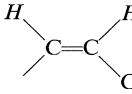); ms (calcd. for $C_8H_{15}Cl$, M^+ 146): 146 (M^+, 18%), 148 (M^+ + 2, 5.7%), M^+/M^+ + 2 = 100/32), 43 (M^+ − $(CH_2)_3CH$=CHCl, 100%).

Preparation of 1,1,2-Trichloro-3-n-hexylcyclopropane (29)

A solution of 1-chlorooct-1-ene (7.5 g) and cetyltrimethylammonium bromide (0.2 g) in 18 g of chloroform was prepared, then heated under an N_2 blanket to 50 °C. A solution of 17 g of NaOH in 17 ml H_2O was added dropwise over a period of 15 min. The reaction progress was monitored by removing samples from the organic layer and analysis by glpc (170 °C). The reaction was allowed to proceed until no further decrease in 1-chlorooct-1-ene was observed after addition of base.

The reaction mixture was diluted with 100 ml H_2O, acidified with 10% H_2SO_4, and extracted with ethyl ether (3 × 100 ml). The solution was dried over anhydrous $MgSO_4$, and solvent removed *in vacuo*, and the residue distilled under reduced pressure to give a 67% yield of 1,1,2-trichloro-3-*n*-hexylcyclopropane; bp 95–96 °C (0.5 mm Hg); nmr δ ($CDCl_3$) 0.9 (3H, t, J = 4.5 Hz, CH_3, 1.5 (11H, b, —(CH_2)—$_n$), 3.1 (0.5H, b, *cis*-), 3.6 (0.5 H, d, J = 8.5 Hz, *trans*-); ms (15 eV, calcd. for $C_9H_{15}Cl_3$, M^+, 228): 193 (M^+ − Cl, 10%), 157 (M^+ − 2Cl, 68%), 122 (100%).

Preparation of 1,2-Dichloro-3-n-hexylcyclopropane

Reduction 1,1,2-trichloro-3-*n*-hexylcyclopropane was accomplished by the use of tri-*n*-butyltin hydride (30, 38) according to the method of Seyferth *et al.* (31). To 1,1,2-trichloro-3-*n*-hexylcyclopropane (4.0 g, 0.02 mol) neat was added tri-*n*-butyltin hydride (5.82 g, 0.02 mol). The reaction was maintained at 115 °C and monitored by glpc (180 °C) by following the disappearance of the starting compound. Gas–liquid phase chromatographic analysis after reaction for 0.5 h revealed the appearance of three new peaks of shorter retention times than the starting trichlorocyclopropane which were attributed to the three possible products of a single reductive process. The reaction was allowed to proceed until the starting material was exhausted (*ca.* 3.5 h). The mixture was distilled at 0.1 mm Hg, collecting fractions of boiling ranges from 65–80 °C. The overall yield of distillate was 80%; nmr δ ($CDCl_3$) 1.0 (3H, t, J = 4.5 Hz, CH_3), 1.4 (11H, broad, d, J = 8 Hz, CH_2) 2.9, 3.2 (2H, m, *cis,trans*,1,2-*H*).

Reduction of 1,2-Dichloro-3-n-hexylcyclopropane to give trans-1-n-Hexyl-cis-2,3-dideuteriocyclopropane

The reaction was carried out according to Willcott and Cargle (32) with minor modification. In a typical reaction, 1,2-dichloro-3-*n*-hexylcyclopropane (2.5 g) in 15 ml of methanol-OD and deuterium oxide (1%) were mixed under nitrogen. Clean pieces (~100 mg each) of sodium were added to the mixture and allowed to react under a positive N_2 atmosphere. The progress of the reaction was followed by glpc (180 °C) and allowed to proceed until the starting material was exhausted or no further consumption of starting material was observed upon further addition of sodium.

The mixture was diluted with water, extracted with hexane, dried over anhydrous $MgSO_4$, and distilled at

atmospheric pressure. Fractions distilling in the range 120–150 °C were collected and pooled giving an overall yield of *trans*-1-*n*-hexyl-*cis*-2,3-dideuteriocyclopropane (**3**) of 30%. Gas–liquid phase chromatographic analysis of the fraction with bp 145–150 °C showed one component with the same retention time as *n*-hexylcyclopropane: ms calcd. for $C_8H_{16}D_2$, M^+, 128; found: M^+, 128; D_0, 0%; D_1, 8%; D_2, 92%.

*Synthesis of cis-1-n-Hexyl-(cis-2,3-dideuteriocyclopropane), **4***

Preparation of cis-1-Chloro-1-deuteriooct-1-ene

The method of preparation of chlorodeuteriooctene was adopted from Brown and Zweifel (34). A solution, under argon, containing sodium borohydride (1.9 g) in 25 ml of dry diglyme and 2-methyl-but-2-ene (9.5 g) was cooled to 0 °C, flushed with argon, and freshly distilled boron trifluoride-etherate (9.2 g) in 10 ml of diglyme was added dropwise while maintaining a temperature below 10 °C. Stirring (0–5 °C) was continued for 2 h. After this time 1-chlorooct-1-yne (33) (7.25 g) was added (at 5–10 °C) and the reaction mixture was stirred for 0.5 h at 0–5 °C, then for 2.5 h at room temperature.

Acetic acid-d_1 (12 ml) was added at 0–5 °C and the reaction mixture stirred for an additional 2.5 h. Dilution with water (150 ml) and extraction with ether yielded an ether extract which was washed with dilute NaOH and subsequently several times with water. Removal of the ether *in vacuo* and distillation of the residue at reduced pressure gave a clear liquid (80%) bp 55–57 °C (8 mm Hg). Gas–liquid phase chromatographic analysis revealed this fraction contained a major component (*ca.* 90%) and a minor amount of starting material; nmr δ ($CDCl_3$) 0.9 (3H, t, J = 4 Hz, $—CH_3$), 1.3 (8H, b, $—CH_2—$), 2.2 (2H, d, J = 7 Hz, $—CH_2—C{=}C_1—$), 5.8 (1H, m, $C_{2\text{-}H}$); ms (calcd. for $C_8H_{14}DCl$, M^+, 147), 147 (M^+, 16%; D_0 21%, D_1 79%, D_2 0%), 43 ($M^+ - (CH_2)_3CH{=}CDCl$), 100%).

Preparation of 1,1,2-Trichloro-2-deuterio-3-n-hexylcyclopropane

A solution containing *cis*-1-chloro-1-deuterio-1-octene (7.5 g) and cetyl trimethylammonium bromide (CTAB) (29), in 20 ml of chloroform was heated to 50–55 °C. A solution of 20 g NaOH in 20 ml of water was added dropwise. The progress of the reaction was monitored by glc (170 °C) and allowed to proceed until no further decrease in concentration of starting material was noted upon further addition of base. The reaction mixture was cooled to room temperature, diluted with water (100 ml), acidified with 10% H_2SO_4, and extracted into ether. Solvent removal and distillation under reduced pressure afforded 1,1,2-trichloro-2-deuterio-3-*n*-hexylcyclopropane as a clear liquid; bp 70–75 °C (0.1 mm Hg). Gas–liquid chromatography at 170 °C showed the product to consist mainly of one component with minor impurities; ms (at 15 eV) (calcd. for $C_9H_{14}DCl_3$, M^+, 229) 194 ($M^+ -$ Cl, 20%), 123 (100%).

Reduction of 1,1,2-Trichloro-2-deuterio-3-n-hexylcyclopropane

The reaction was carried out under nitrogen and using tri-*n*-butyltin deuteride (30, 38). The progress of the reaction was followed by glpc using a 6 ft × $\frac{1}{8}$ in. 5% Carbowax 20M on Chrom G column at 180 °C. Work-up as previously described and distillation gave a main fraction bp 65–80 °C (0.1 mm Hg) consisting of two products (80%) and some unreacted starting material. The distillate was subjected to sodium and alcohol reduction without further purification.

Reduction of 1,2-Dichloro-1,2-dideuterio-3-n-hexylcyclopropane

The crude reduction product (3 g) was added to 25 ml of methanol containing 1% water. While keeping the reaction under N_2, clean pieces of sodium were added to the mixture and allowed to react at room temperature with constant stirring. The progress of the reaction was followed by glpc and terminated when no further reaction of the starting material was observed.

The mixture was diluted with water (100 ml), extracted with ether, the organic layer dried over anhydrous $MgSO_4$ and distilled at atmospheric pressure to give 40% of *cis*-1-*n*-hexyl-*cis*-2,3-dideuteriocyclopropane **4** (95%) pure by glpc; bp 145–150 °C; ms (at 15 eV) (calcd. for $C_9H_{16}D_2$, 128), 128 (M^+; D_0 0%, D_1 27%, D_2 73%).

*Preparation of Tetrachloro(diethylene)diplatinum **2***

The dimeric complex, **2**, was prepared from $K_2(PtCl_4)$ by the method of Chatt and Searle (39). Recrystallization from hot toluene gave a microcrystalline yellow-orange product; mp (darkens) 190 °C, (dec.) 205–210 °C (lit. (39) (dec.) 210 °C); ir ν_{max} (KBr) 1412 (C=C), 1250, 1019, 225, 485, and 335 (PtCl) cm^{-1}.

*Reaction of Complex **2** with Cyclopropanes*

Dichloro(2-n-hexylpropane-1,3-diyl)platinums

In a typical reaction, **2** (200 mg, 0.34 mmol) and an *n*-hexylcyclopropane (**3**, **4**, or **5**) (200 mg, 1.55 mmol) in 5–10 ml of ether was stirred under reflux for 8 h. During the course of the reaction, the orange colored complex, **2**, was replaced by a pale-yellow precipitate. The precipitate was filtered, washed with ether, and dried to give 80–90% yield of a pale-yellow powder; mp 120–125 °C (dec.), (lit. (23) (dec.) 120 °C).

Preparation of trans-Dichlorobispyridine(2-n-hexylpropane-1,3-diyl)platinum

Dichloro(2-*n*-hexylpropane-1,3-diyl)platinums **6**–**8** (100 mg) were individually cooled in an ice–water bath followed by the addition of ice-cold pyridine sufficient for dissolution. The solution was allowed to warm to room temperature then added dropwise and with constant stirring to 100 ml of cold H_2O. The resulting milky suspension was centrifuged, the water decanted, and the yellow precipitate dissolved in $CHCl_3$. Removal of the $CHCl_3$ *in vacuo* gave a pale-yellow solid (70–80%). Recrystallization from benzene – petroleum ether gave a pale-yellow crystalline solid which exhibited one spot on thin layer chromatography (Silcia Gel HF254, $CHCl_3$), mp 124–126 °C (lit. (23) (darkens) 125 °C, (dec.) 220 °C.

Acknowledgements

We wish to thank the National Research Council of Canada for support of this work. Gratitude is also extended to the Canadian 220 MHz Centre, Ontario Research Foundation for nmr spectra.

1. J. A. Osborn, F. H. Jardine, J. F. Young, and G. Wilkinson. J. Chem. Soc. A, 1711 (1966).
2. J. Halpern. Acc. Chem. Res. **7**, 386 (1970).

3. J. P. COLLMAN and W. R. ROPER. Adv. Organomet. Chem. **1**, 53 (1968).
4. A. J. DEEMING. M. T. P. Rev. Inorg. Chem. Ser. I, **9**, 117 (1972).
5. R. G. PEARSON and W. R. MUIR. J. Am. Chem. Soc. **92**, 5519 (1970).
6. J. P. COLLMAN and M. R. MACLAURY. J. Am. Chem. Soc. **96**, 3019 (1974).
7. R. UGO, A. PASINI, A. FUSI, and S. CENINI. J. Am. Chem. Soc. **94**, 7364 (1972).
8. K. S. Y. LAU, R. W. FRIES, and J. K. STILLE. J. Am. Chem. Soc. **96**, 4983 (1974).
9. P. K. WONG, K. S. Y. LAU, and J. K. STILLE. J. Am. Chem. Soc. **96**, 5956 (1974).
10. D. M. ROUNDHILL, D. N. LAWSON, and G. WILKINSON. J. Chem. Soc. A, 845 (1968).
11. K. G. POWELL and F. J. MCQUILLIN. Chem. Commun. 931 (1971).
12. F. J. MCQUILLIN and K. G. POWELL. J. Chem. Soc. Dalton Trans. 2129 (1972).
13. L. CASSAR and J. HALPERN. Chem. Commun. 1082 (1970).
14. L. CASSAR, P. E. EATON, and J. HALPERN. J. Am. Chem. Soc. **92**, 3515 (1970).
15. C. F. H. TIPPER. J. Chem. Soc. 2045 (1955).
16. D. M. ADAMS, J. CHATT, R. G. GUY, and N. SHEPPARD. J. Chem. Soc. 738 (1961).
17. N. BAILEY, R. D. GILLARD, M. KEETON, R. MASON, and D. R. RUSSELL. Chem. Commun. 396 (1966).
18. S. E. BINNS, R. H. CRAIG, R. D. GILLARD, B. T. HEATON, and M. F. PILBROW. J. Chem. Soc. A, 1227 (1969).
19. R. D. GILLARD, M. KEETON, R. MASON, M. F. PILBROW, and D. R. RUSSELL. J. Organomet. Chem. **33**, 247 (1971).
20. P. W. HALL, R. J. PUDDEPHATT, and C. F. H. TIPPER. J. Organomet. Chem. **71**, 145 (1974).
21. W. J. IRWIN and F. J. MCQUILLIN. Tetrahedron Lett. 1937 (1968).
22. K. G. POWELL and F. J. MCQUILLIN. Tetrahedron Lett. 3313 (1971).
23. F. J. MCQUILLIN and K. G. POWELL. J. Chem. Soc. Dalton Trans. 2123 (1972).
24. D. J. PATEL, M. E. HOWDEN, and J. D. ROBERTS. J. Am. Chem. Soc. **85**, 3218 (1963).
25. C. CISTARO, G. FRONZA, R. MANDELLI, S. BRADAMANTE, and G. A. PAGANI. J. Magn. Reson. **15**, 367 (1974).
26. H. E. SIMMONS and R. D. SMITH. J. Am. Chem. Soc. **81**, 4256 (1959).
27. H. HOFFMAN. Angew. Chem. **72**, 77 (1960); G. WITTIG and M. SCHLOSSER. Chem. Ber. **94**, 1373 (1961).
28. D. SEYFERTH, S. O. GRIM, and T. O. READ. J. Am. Chem. Soc. **83**, 1617 (1961).
29. G. L. JOSHE, N. SINGH, and L. M. PANDE. Tetrahedron Lett. 1461 (1972).
30. E. R. BIRNAUM and P. H. JAVORA. J. Organomet. Chem. **9**, 379 (1967).
31. D. SEYFERTH, J. YAMAZAKI, and D. L. ALLESTON. J. Org. Chem. **28**, 703 (1963).
32. H. R. WILLCOTT III and V. A. CARGLE. J. Am. Chem. Soc. **91**, 4310 (1969).
33. H. G. VIEHE. *In* The chemistry of acetylenes. Marcell-Dekker, New York. 1969. p. 673.
34. H. C. BROWN and G. ZWEIFEL. J. Am. Chem. Soc. **83**, 3834 (1961); G. ZWEIFEL, G. M. CLARK, and N. L. POLSTON. J. Am. Chem. Soc. **93**, 3395 (1971).
35. A. D. WALSH. Trans. Faraday Soc. **45**, 179 (1949).
36. R. HOFFMANN. J. Am. Chem. Soc. **90**, 1475 (1967).
37. K. FUKUI. Acc. Chem. Res. **4**, 57 (1971).
38. H. KUIVILA. Synthesis, 499 (1970).
39. J. CHATT and M. L. SEARLE. Inorganic syntheses. Vol. 3. *Edited by* L. F. Andrieth. McGraw-Hill, New York. 1950. p. 210.

The cyclic carbamate unit of maytansine[1]

OLIVER E. EDWARDS AND PAK-TSUN HO

Division of Biological Sciences, National Research Council of Canada, Ottawa, Ont., Canada K1A 0R6

Received September 23, 1976

OLIVER E. EDWARDS and PAK-TSUN HO. Can. J. Chem. **55**, 371 (1977).

An eleven step sequence with control of the relative stereochemistry of four asymmetric centers has converted 3,4-epoxycyclohexene into a highly functionalized model for synthesis of the cyclic carbamate unit of maytansine.

OLIVER E. EDWARDS et PAK-TSUN HO. Can. J. Chem. **55**, 371 (1977).

Une série de onze réactions, impliquant un contrôle de la stéréochimie relative au niveau de quatre centres asymétriques, permet de transformer l'époxy-3,4 cyclohexène en un modèle hautement fonctionnalisé permettant d'effectuer la synthèse de l'unité carbamate cyclique de la maytansine.

[Traduit par le journal]

Maytansine I is an ansa macrolide which has been found to show significant antitumor activity. Following extensive toxicity studies in animals it has recently been found suitable for clinical trials (1). Model studies for the synthesis of the cyclic carbamate unit in maytansine had been reported. However, these approaches provided either no steric control or partial control of the relative stereochemistry (2–5). We now wish to report a relatively efficient new approach to the cyclic carbamate **1** which involved the successful introduction of the required four asymmetric centers with complete stereospecificity.

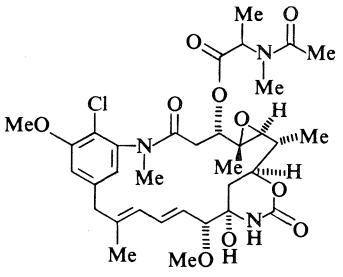

I

The readily available 3,4-epoxycyclohexene was converted to the alcohol **2** by reaction with methyllithium in ether (6).[2] Oxidation of compound **2** by a modified Lemieux periodate–permanganate method (7) followed by heating with acetic acid for 1 h led to the formation of the oily γ-lactone **3** in 71% yield[3]; ν_{max} 1770 (lactone), 1710 cm^{-1} (carboxylic acid); ^1H nmr δ 4.73 (q, 1H, —COOCH—), 1.41 ppm (d, 3H, CH_3CH—). Direct transformation of the carboxylic function of **3** to the corresponding alcohol **4** was accomplished (8) by reaction of **3** with ethyl chloroformate and triethylamine in anhydrous THF at −10 °C followed by reduction of the resulting anhydride with $NaBH_4$ in aqueous THF to yield the hydroxy lactone **4** as

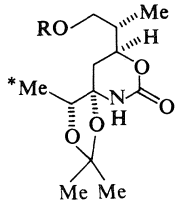

1

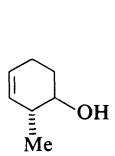

2

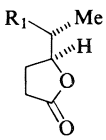

3 R_1 = COOH
4 R_1 = CH_2OH
5 R_1 = CH_2OR

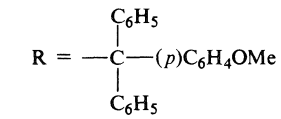

[1]Issued as NRCC No. 15702.

[2]The yield under our conditions (with 2.5 equiv. of methyllithium under argon at −10 °C for 1 h and at room temperature for 2 h, followed by acidic work-up) was improved to 68% after distillation.

[3]Satisfactory physical and spectral data were obtained for all new compounds.

an oil in an isolated yield of 82%. Treatment of compound **4** with *p*-anisyldiphenylmethyl chloride (1.2 equiv.) in anhydrous benzene containing pyridine at room temperature afforded **5** in an almost quantitative yield.

Further elaboration of the lactone **5** was accomplished in the following way. Condensation of acetaldehyde with the lithium enolate from the lactone **5**, generated using lithium diisopropylamide (3 equiv.) in anhydrous tetrahydrofuran under argon at −70 °C, produced a mixture of isomeric alcohols **6** (80% yield). This mixture was dehydrated by conversion to the mesylates followed by elimination using 1,5-diazabicyclo[4.3.0]non-5-ene in anhydrous tetrahydrofuran at 0 °C. The resulting mixture of olefins could easily be separated by chromatography on silica gel to give the α,β-unsaturated lactones **7** and **8** (ratio 4:1) in 86% yield. The desired isomer **7** had ν_{max} 1750 and 1618 cm^{-1} and gave ^1H nmr signals at δ 7.46 (14H, m), 6.79

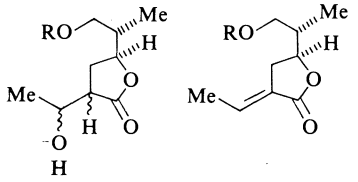

6

7

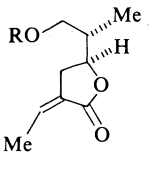

8

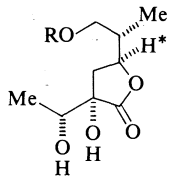

9

(1H, m, C=C*H*CH_3), 4.68 (1H, q, COOC*H*), 3.20 (2H, d, COCH_2), 2.67 (2H, m, C=C—CH_2), 1.87 (3H, br d, C=CHCH_3), and 1.04 (3H, d, CH—CH_3). Its mass spectrum had strong peaks at 442 (M^+), 364, 273, and 169. It had λ_{max} (EtOH) 226 nm (ε 11 600). The minor isomer **8** had ν_{max} 1750 and 1618 cm^{-1}, λ_{max} (EtOH) 228 nm (ε 8000) and gave ^1H nmr signals at δ 7.46 (14H, m), 6.23 (1H, m, C=C*H*CH_3), 4.64 (1H, q, COOC*H*), 3.16 (2H, d, COCH_2), 2.70 (2H, m, C=C—CH_2), 2.17 (3H, br d, C=CHCH_3), 1.03 (3H, d, CHCH_3). Its mass spectrum was essentially identical to that of **7**. The relative stereochemistry of these isomers was clear from the fact that the vinyl hydrogen in **7** and the vinyl methyl in **8** were deshielded by their proximity to the carbonyl oxygen (9).

Since osmium tetroxide is bulky it was anticipated that it would selectively approach the double bond of **7** from the side opposite to the space-filling side chain. This proved to be correct. Osmylation in the presence of pyridine in tetrahydrofuran, followed by reductive work-up using aqueous sodium hydrogen sulfite, converted **7** in 90% yield to a mixture containing 95% of the desired diol **9** accompanied by the isomer **10**.

Compound **9** gave ^1H nmr signals at δ 4.61 (1H, q, COOC*H*), 3.20 (2H, d, COCH_2), 1.20 (3H, d, CHCH_3), and 1.08 (3H, d, CHCH_3) and gave M^+ 476. Isomer **10** gave δ 4.37 (1H, q, COOC*H*), 3.20 (2H, d, COCH_2), 1.32 (3H, d, CHCH_3), and 1.18 (3H, d, CHCH_3) and M^+ 476. The downshield shift of the hydrogen marked by an asterisk in **9** relative to that in **10** is clearly due to its closer proximity to the one hydroxyl group, and hence the relative stereochemistry can be assigned to each.

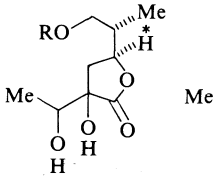

10

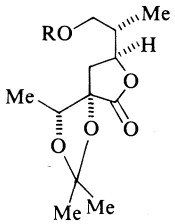

11

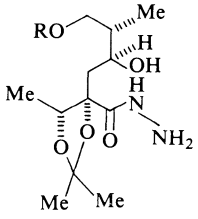

12

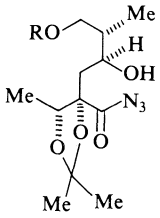

13

The diol **9** was converted into the acetonide **11** by reaction with 2,2-dimethoxypropane catalyzed by *p*-toluenesulfonic acid at room temperature (1 h, 82% yield). Treatment of **11** with excess 100% hydrazine hydrate in absolute ethanol at room temperature for 3 h produced the unstable hydroxy hydrazide **12**. This was immediately treated with a methylene chloride solution of N_2O_4 (4 equiv.) in the presence of a

large excess of sodium acetate.[4] After 5 min at −70 °C the sensitive hydroxy azide **13** was produced. This had ν_{max} 3500, 2140, and 1705 cm^{-1}. Finally, Curtius rearrangement of compound **13** in refluxing xylene gave 75% conversion to the cyclic carbamate **1** with 25% recovery of the lactone **11**. The desired model **1** could be recrystallized from hexane–ether to give a 78% yield (based on unrecovered **11**) with mp 85 °C. It had ν_{max} 3400 and 1710 cm^{-1}, and gave ^1H nmr signals at δ 7.71 (1H, exchanged with D_2O), 4.71 (1H, q, NHCOOC*H*—), 4.01 (1H, q, CH_3CHOC), 3.19 (2H, d, $CHCH_2OC$), 1.48 (3H, s, CH_3C), 1.34 (3H, s, CH_3C), 1.24 (3H, d, CH_3CH—), 1.13 (3H, d, CH_3CH). *Anal.* calcd. for $C_{32}H_{37}O_6N$: C 72.29, H 7.01, N 2.63; found: C 72.25, H 7.19, N 2.56.

It seems probable that the scheme can be modified to place a function on the starred carbon of **1**, thus giving a valuable synthon for construction of maytansine. Further work directed at the synthesis of this interesting molecule is in progress.

[4]Attempts to diazotize **12** either under neutral conditions (pyridine) or by the use of nitrosyl chloride led to quantitative conversion to the lactone **11**. These conditions were successful with a simple model in experiments by Dr. W. Rank, whom we cordially thank.

1. (*a*) S. M. KUPCHAN, Y. KOMODA, W. A. COURT, G. J. THOMAS, R. M. SMITH, A. KARIM, C. J. GILMORE, R. C. HALTIWANGER, and R. F. BRYAN. J. Am. Chem. Soc. **94**, 1354 (1972); (*b*) S. M. KUPCHAN, Y. KOMODA, A. R. BRANFMAN, R. G. DILEY, and V. A. ZIMMERLY. J. Am. Chem. Soc. **96**, 3706 (1974).
2. (*a*) A. I. MEYERS and C. C. SHAW. Tetrahedron Lett. 717 (1974); (*b*) A. I. MEYERS, C. C. SHAW, D. HORNE, L. M. TREFONAS, and R. J. MAJESTE. Tetrahedron Lett. 1745 (1975).
3. E. J. COREY and M. G. BOCK. Tetrahedron Lett. 2643 (1975).
4. W. J. ELLIOTT and J. FRIED. J. Org. Chem. **41**, 2469 (1976).
5. W. A. COURT, O. E. EDWARDS, C. GRIECO, W. RANK, and T. SANO. Can. J. Chem. **53**, 463 (1975).
6. J. STAROSCIK and B. RICKBORN. J. Am. Chem. Soc. **93**, 3046 (1971).
7. C. OVERBERGER and H. KAYE. J. Am. Chem. Soc. **89**, 5640 (1967).
8. K. ISHIZUMI, K. KOGA and S. YAMADA. Chem. Pharm. Bull. Jpn. **16**, 492 (1968).
9. C. PASCUAL, J. MEIER, and W. SIMON. Helv. Chim. Acta, **49**, 164 (1966).

Canadian Journal of Chemistry

Published by
THE NATIONAL RESEARCH COUNCIL OF CANADA

Journal canadien de chimie

Publié par
LE CONSEIL NATIONAL DE RECHERCHES DU CANADA

Volume 55 Number 3 February 1, 1977

Volume 55 numéro 3 1 février 1977

Détermination du mécanisme de dégagement d'hydrogène sur le niobium en milieu alcalin

CHERUBALA P. VIJAYAN ET DOMINIQUE-LOUIS PIRON

Département de Génie Métallurgique, Ecole Polytechnique, Université de Montréal, C.P. 6079, Succursale A, Montréal (Qué.), Canada H3C 3A7

Reçu le 23 août, 1976

CHERUBALA P. VIJAYAN et DOMINIQUE-LOUIS PIRON. Can. J. Chem. **55**, 375 (1977).

Les résultats de ce travail ont permis de déterminer le mécanisme de la réaction de dégagement d'hydrogène sur le niobium immergé dans des solutions alcalines aqueuses à 24 °C. On a mesuré une pente de Tafel de 120 mV/décade (déviation standard de 8 mV/déc.) et un ordre réactionnel de zéro par rapport à la concentration des ions H^+. Ces résultats ont permis d'établir un mécanisme de Heyrovsky. La présence des anions sulfates ou chlorures n'a pas montré d'effets sur les résultats obtenus.

CHERUBALA P. VIJAYAN and DOMINIQUE-LOUIS PIRON. Can. J. Chem. **55**, 375 (1977).

The mechanism of the hydrogen evolution reaction on niobium is evaluated in alkaline media at 24 °C. The reaction order of zero, along with the observed Tafel slopes of 120 mV/decade (standard deviation 8 mV/dec.), indicate the Heyrovsky reaction mechanism to be applicable for the hydrogen evolution reaction. The presence of anions such as sulfate and chloride does not influence the mechanism.

Introduction

L'étude de la cinétique du dégagement d'hydrogène sur le niobium pur (99.85%) en milieu alcalin a été l'objet de la présente investigation. Ce travail constitue donc une étape vers une meilleure compréhension des propriétés électrochimiques de ce métal dont le minerai de pyrochlore est une des richesses du Canada (1).

La résistance à la corrosion du niobium a déjà fait l'objet de certains travaux. Fontana (2) rapporte une vitesse de corrosion de 1.1 mpy à 24 °C dans une solution aqueuse à 5% NaOH.

Tingley et Rogers (3) ont observé dans des solutions d'hydroxyde de sodium à 10% en poids une vitesse de corrosion inférieure à 2 mpy. Dans les limites de leur travail, ces auteurs ont observé que le niobium présente aussi une bonne résistance à la fragilisation. Ce dernier résultat est en contraste avec des observations précédemment rapportées par Taylor (4) dans des solutions de NaOH diluées.

Van Muylder, de Zoubov et Pourbaix (5) ont montré que le niobium est un métal peu noble qui se recouvre d'une couche d'oxyde dans tout le domaine de stabilité de l'eau. Le film ainsi formé peut protéger le niobium en solution aqueuse à n'importe quel p*H*. Il en résulte une résistance à la corrosion qui dépend toutefois de la stabilité et de l'étanchéité de la couche protectrice. Les propriétés électrochimiques sont donc généralement observées sur un revêtement naturel d'oxyde de niobium.

Leavenworth *et al.* (6) considèrent que la corrosion de ce métal en solution d'hydroxyde de sodium se produit par la nucléation et la formation de $Na_8Nb_6O_{19}\cdot 13H_2O$. Leur étude concerne plutôt le comportement anodique.

Le comportement cathodique a été abordé par

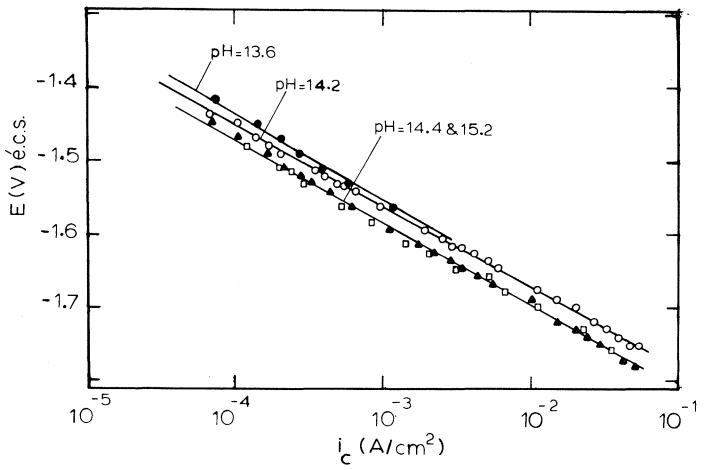

FIG. 1. Polarisation galvanostatique cathodique sur le niobium à 24 °C (bain NaOH).

Piron et Nobe (7) qui ont mesuré une pente de Tafel de 116 mV/décade en solution 1 *N* NaOH à 24 °C, et par Rotinyan et Kozhevnikova (8), qui ont obtenu 120 mV/déc. Lokshtanov et Rotinyan (9) ont obtenu une pente de 135 mV/déc. Piron et Vijayan (10) ont observé une pente de 122 ± 11 mV/déc. L'ordre réactionnel de dégagement d'hydrogène sur le niobium n'a toutefois pas encore été mesuré. Ce résultat a donc été recherché ici afin de pouvoir déterminer le mécanisme de ce procédé d'électrode, en employant la méthode décrite (11) et utilisée par Vetter (12) pour cette même réaction sur d'autres métaux.

Une telle étude est importante pour la compréhension des propriétés électrochimiques du niobium, et en particulier sa résistance à la corrosion. A côté de cet aspect assez fondamental, le présent travail est également un point de départ dans l'évaluation du niobium comme cathode dans de nouveaux électrolyseurs d'eau en relation avec l'économie de l'hydrogène.

Partie expérimentale

Le montage expérimental est analogue à celui décrit précédemment (10). Les solutions sont préparées à partir des produits chimiques NaOH, H_2SO_4, HCl, Na_2SO_4 et NaCl de qualité A.C.S., et de l'eau distillée. Des essais de polarisation galvanostatique sont effectués dans des solutions de p*H* 11.3 à 13.6 contenant des ions SO_4^{2-} ou Cl^-, et dans des solutions 1 *N* à 7 *N* NaOH, p*H* calculé variant entre 13.8 et 15.2, suivant la méthode de Littauer et Tsai (13).

Résultats

Les courbes de polarisation cathodique obtenues à 24 °C en milieu NaOH de normalité variant entre 1 et 7 sont représentées sur la fig. 1. On observe des pentes de Tafel de 114 mV/déc. avec une déviation standard de 9 mV dans un domaine de densité de courant variant entre 10^{-4} et 10^{-2} A/cm^2.

Les résultats de ces mesures montrent un changement non-ordonné par rapport au p*H* dans la position des droites de Tafel. Ceci correspond à une dispersion de 40 mV.

Une pente de Tafel de 120 mV/déc. a aussi été mesurée par Rotinyan et Kozhevnikova (8) dans le même domaine de densité de courant. Toutefois, dans une deuxième série d'essais, Lokshtanov et Rotinyan (9) ont obtenu des pentes de Tafel de 135 mV/déc. en solution 1 *N* NaOH à 20 °C.

Les résultats de polarisations cathodiques du niobium à 24 °C en bain NaOH de p*H* 11.3 à 13.6 contenant des ions sulfates (concentration: 1 équiv./litre) sont représentés sur la fig. 2. La solution de p*H* 13.6 est la solution normale en NaOH à laquelle on a ajouté une concentration normale de Na_2SO_4. La courbe de polarisation cathodique du Nb dans cette solution est identique à la courbe de polarisation du niobium obtenue dans la solution 1 *N* NaOH de la fig. 1 qui ne contient pas de sulfate.

Dans la fig. 2 on observe des pentes de Tafel de 125 mV/déc. avec une déviation standard de 11 mV dans un domaine de densité de courant qui varie entre 10^{-4} et 10^{-2} A/cm^2.

On observe une vibration de la position des droites de Tafel qui change avec le p*H* de

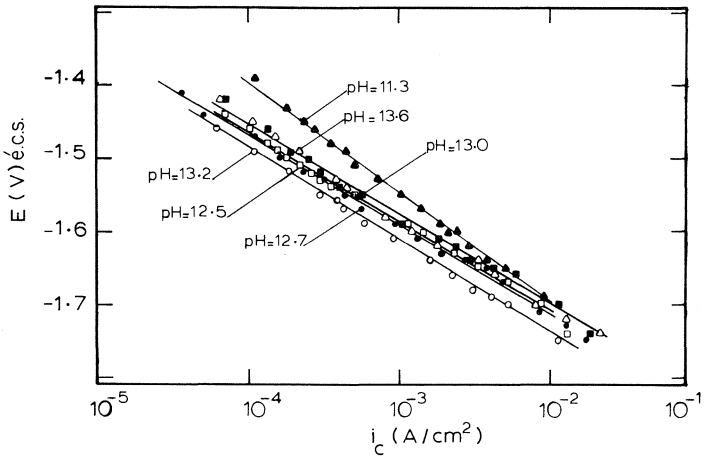

FIG. 2. Polarisation galvanostatique cathodique sur le niobium à 24 °C (bain alcalin contenant des sulfates).

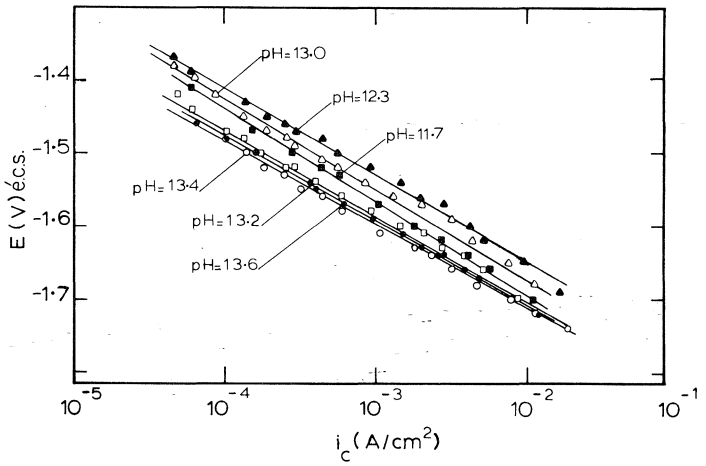

FIG. 3. Polarisation galvanostatique cathodique sur le niobium à 24 °C (bain alcalin contenant des chlorures).

manière désordonnée. Cette dispersion est de 70 mV.

La fig. 3 donne les résultats obtenus à 24 °C lors de la polarisation cathodique en solution de NaOH de p*H* variant entre 11.7 et 13.6 contenant 1 équiv. d'ions chlorures par litre.

Une pente de Tafel de 117 mV/déc., ayant une déviation standard de 6 mV, est observée entre 10^{-4} et 10^{-2} A/cm^2 de densité de courant.

Le changement de la position des pentes de Tafel, désordonnée par rapport au p*H*, se présente encore ici avec une dispersion de 80 mV. Cette dispersion dans la position des droites de Tafel pourrait s'expliquer par une différence de la microrugosité superficielle des électrodes. Ce point de vue semble être renforcé par une dispersion des valeurs de la capacité différentielle. La mesure de ces dernières varie entre 151 et 206 μF/cm^2 pour des électrodes de Nb au repos, après 3 h d'immersion dans une solution normale de NaOH à 25 °C.

L'identité des courbes de polarisation obtenues sur le Nb immergé dans une solution 1 *N* de NaOH ne contenant pas de chlorure (fig. 1) et une solution de même concentration de cette base à laquelle on a ajouté 1 équiv. par litre de NaCl (fig. 3) montre que dans ces conditions l'addition de chlorure n'a pas eu d'effet sur la polarisation.

Les résultats expérimentaux présentés dans les

trois premières figures peuvent être utilisés pour déterminer l'ordre de la réaction de dégagement d'hydrogène. La fig. 4 montre l'ordre réactionnel de zéro par rapport à l'ion H^+ dans un domaine de pH variant entre 11.3 et 15.2. Cette détermination sur le Nb n'ayant pas été publiée précédemment, il convient de la comparer avec les résultats de dégagement d'hydrogène obtenus sur d'autres métaux en milieu alcalin.

Vetter, utilisant les résultats expérimentaux de Lukowzew *et al.* (14) sur le nickel et de Bockris et Watson (15) sur le mercure, a établi également un ordre réactionnel de zéro pour l'ion H^+ dans la réaction de dégagement de l'hydrogène en milieu alcalin.

D'autre part, Bicelli *et al.* (16), travaillant sur le cobalt, ont, eux-aussi, obtenu en milieu alcalin un ordre réactionnel de zéro pour l'ion H^+.

Discussion

Vetter (12) et Bicelli (17) montrent les mécanismes possibles de dégagement d'hydrogène en milieu alcalin. Le mécanisme est en effet en grande partie déterminé par le fait que la fraction θ de la surface couverte par l'hydrogène adsorbé, tend vers zéro, vers l'unité, ou vers des valeurs intermédiaires.

Les résultats obtenus ici (pente de Tafel de 120 mV/déc. et l'ordre réactionnel de zéro) peuvent être expliqués par des mécanismes basés sur des valeurs de θ tendant vers 1 ou zéro, et sur l'hypothèse de Langmuir.

Les calculs de Vijh et Bélanger (18), utilisant la méthode de Stevenson (19) et les résultats d'Ehrlich (20), montrent que l'enthalpie libérée lors de l'adsorption d'hydrogène sur les métaux de transition est très élevée (~80 kcal/mol sur le niobium). Mueller *et al.* (21) aussi arrivent à la même conclusion. Une enthalpie aussi élevée rend l'adsorption de l'hydrogène fort probable sur une fraction importante de la surface du niobium. D'autre part, les résultats expérimentaux de Beeck (22) ont révelé que l'adsorption de l'hydrogène sur les métaux de transition se faisait si facilement qu'elle était instantanée.

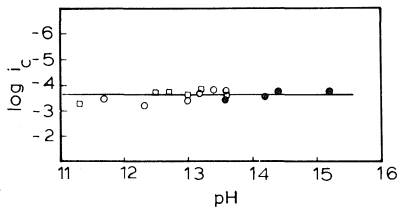

FIG. 4. Ordre réactionnel en milieu alcalin contenant des sulfates □, des chlorures ○, et ni sulfate ni chlorure ●, $E = -1.5$ V (é.c.s.).

La thermodynamique et l'expérience portent donc à penser que des valeurs de θ tendant vers zéro sont fort peu probables ici. De plus, les résultats de la présente investigation ne pouvant s'accorder à des valeurs de θ intermédiaires, il convient donc de conclure à des valeurs de θ tendant vers l'unité. Une conclusion similaire a été utilisée comme point de départ dans le travail de Lokshtanov (9) sur le niobium et aussi par Bicelli *et al.* (16) sur le cobalt.

En considérant les trois mécanismes simples possibles (12), et en les comparant avec les résultats obtenus dans ce travail, il est apparent que le mécanisme de Heyrovsky serait applicable pour le dégagement d'hydrogène sur le niobium.

[1] $$H_2O + e \rightarrow H_{ads} + OH^-$$
(réaction de Volmer, étape rapide)

[2] $$H_{ads} + H_2O + e \rightarrow H_2 + OH^-$$
(réaction de Heyrovsky, étape lente)

Pour ce mécanisme, on écrit la relation suivante, en prenant θ tendant vers l'unité:

$$[3] \quad i_c = -kC_{H_2O} \exp\left(-\frac{(1-\alpha)FE}{RT}\right)$$

où i_c densité de courant cathodique, k une constante, C_{H_2O} concentration de l'eau, α coefficient de transfert, F Faraday, E potentiel de l'électrode, R constante de gaz, T température absolue.

De ceci il résulte que la pente de Tafel est

$$-\frac{2.3RT}{(1-\alpha)F}$$

et l'ordre réactionnel est

$$\left(\frac{\partial \log i_c}{\partial\, pH}\right)_{E,T} = 0$$

On a mesuré une pente moyenne en milieu alcalin de 120 mV/déc. (déviation standard de 8 mV) à 24 ± 1 °C, qui amène une valeur de $\alpha = 0.5$.

Les résultats expérimentaux n'étant pas influencés par la présence d'ions chlorures et sulfates, le mécanisme de dégagement d'hydrogène est, lui-aussi, indépendant de la présence de ces ions.

De plus, il convient de noter que le mécanisme présenté ici permet d'expliquer les résultats expérimentaux sans faire appel à la présence de la

couche d'oxyde superficielle et d'un modèle à doubles barrières plus complexe (23, 24).

Conclusion

En conclusion, la présente étude montre que l'ordre pour la réaction de dégagement d'hydrogène sur le niobium en milieu alcalin est égal à zéro. Le dégagement peut être expliqué par un mécanisme de Heyrovsky. Ce dernier n'est pas influencé par la présence d'ions chlorures et sulfates.

Remerciements

Les auteurs tiennent à remercier la société Noranda pour l'aide financière apportée à ce travail. Ils ont tout particulièrement apprécié les discussions fructueuses qu'ils ont eues avec le Dr. P. Claessens du Centre de Recherche Noranda.

1. Columbium, mineral facts and figures. Bureau of Mines Bulletin 650, U.S. Department of the Interior. 1970.
2. M. G. FONTANA. Ind. Eng. Chem. **44**, 7, 71A (1952).
3. I. I. TINGLEY et R. R. ROGERS. Corrosion, **21**, 132 (1965).
4. D. F. TAYLOR. Ind. Eng. Chem. **42**, 639 (1950).
5. M. POURBAIX. Atlas d'équilibres électrochimiques. Gauthier-Villars & Cie, Paris. 1963. p. 246 ff.
6. H. W. LEAVENWORTH, JR., J. P. CARTER et D. SCHLAIN. Corrosion, **26**, 43 (1970).
7. D. L. PIRON et K. NOBE. Corrosion, **25**, 67 (1969).
8. A. L. ROTINYAN et N. M. KOZHEVNIKOVA. Russ. J. Phys. Chem. **37**, 979 (1963).
9. V. Z. LOKSHTANOV et A. L. ROTINYAN. Elektrokhimiya, **5**, 873 (1969).
10. D. L. PIRON et C. P. VIJAYAN. C.R. Sér. C, **281**, 75 (1975).
11. K. J. VETTER. Z. Phys. Chem. **194**, 284 (1950).
12. K. J. VETTER. Electrochemical kinetics – Theoretical and experimental aspects. Academic Press, New York. 1967. pp. 558, 516 ff.
13. E. L. LITTAUER et K. C. TSAI. J. Electrochem. Soc. **123**, 771 (1976).
14. P. LUKOWZEW, S. LEWINA et A. FRUMKIN. Acta Physicochim. URSS. **11**, 21 (1939).
15. J. O'M. BOCKRIS et R. G. H. WATSON. J. Chim. Phys. **49**, C70 (1952).
16. L. P. BICELLI, C. ROMAGNANI et M. ROSANIA. J. Electroanal. Chem. **63**, 238 (1975).
17. L. P. BICELLI. La chimica e l'industria, **55**, 792 (1973).
18. A. K. VIJH et A. BELANGER. Z. Physik. Chem. Neue Folge, **83**, 173 (1973).
19. D. P. STEVENSON. J. Chem. Phys. **23**, 203 (1955).
20. G. EHRLICH. J. Chem. Phys. **31**, 1111 (1959).
21. W. M. MUELLER, J. P. BLACKLEDGE et G. G. LIBOWITZ (*Editors*). Metal hydrides. Academic Press, New York. 1968. pp. 592 ff.
22. O. BEECK. Advances in catalysis. Vol. II. Academic Press, New York. 1950. pp. 151 ff.
23. N. T. THOMAS. A study of the electrochemical behavior of titanium. Thèse, Université de Californie à Los Angeles. 1970.
24. R. E. MEYER. J. Electrochem. Soc. **107**, 847 (1960).

Trajectory study of dissociation reactions. Br_2 in Ar at 3500 K[1]

D. T. CHANG[2] AND GEORGE BURNS

Lash Miller Chemical Laboratory, University of Toronto, Toronto, Ont., Canada M5S 1A1

Received October 8, 1976

D. T. CHANG and GEORGE BURNS. Can. J. Chem. **55**, 380 (1977).

Dissociation of Br_2 in Ar was studied at 3500 K using classical 3-D trajectory technique, and compared with earlier trajectory calculations. Some of the assumptions used previously were eliminated, while others were studied in some detail. The one-way flux, equilibrium rate coefficient, obtained from over 8400 trajectories, was found to be over an order of magnitude larger than the experimental rate constant. This was taken as an indication that at high temperatures the nonequilibrium effects are important in dissociation reactions. In order to understand these effects better, additional calculations using an improved set of assumptions were performed. The calculated dissociation rate constant for $Br_2 + Ar \rightarrow 2Br + Ar$ reaction, which accounted for nonequilibrium effects, agrees reasonably well with experimental results.

D. T. CHANG et GEORGE BURNS. Can. J. Chem. **55**, 380 (1977).

On a étudié la dissociation de Br_2 dans Ar à 3500 K en faisant appel à la technique classique de trajectoire 3-D et on a comparé ces résultats avec des calculs antérieurs des trajectoires. On a éliminé quelques-unes des hypothèses utilisées auparavant alors que d'autres ont été étudiées en détail. On a trouvé que le flux à sens unique, coefficient de vitesse d'équilibre, obtenu à partir de 8400 trajectoires est au moins dix fois plus grand que la constante de vitesse expérimentale. On en déduit qu'à haute température les effets de non-équilibration sont importants dans les réactions de dissociation. Afin de comprendre mieux ces effets, on a effectué des calculs additionnels en faisant appel à un meilleur ensemble d'hypothèse. Les constantes de vitesse de dissociation, calculées pour la réaction $Br_2 + Ar \rightarrow 2Br + Ar$, qui tiennent compte des effets de non-équilibration sont en bon accord avec les valeurs expérimentales.

[Traduit par le journal]

Dissociation of iodine and bromine molecules was studied earlier (1, 2), using 3-D classical trajectory calculations and Monte Carlo method of sampling. Calculated rate constants agreed reasonably well (1, 2) with experimental data. However, previous calculations incorporated some simplifying assumptions which made results less reliable than they could have been. In the present work, some of these assumptions are removed, and some others studied in greater detail.

The first step in 3-D trajectory computations of dissociation rate is the calculation (1, 2) of k_d^{eq}, the equilibrium one-way flux rate coefficient which is not an observable quantity because it does not include nonequilibrium effects (3). In the past (2), in order to obtain k_d^{eq}, typically several hundred to a few thousand trajectories were run. In the present calculations, it was possible to run 8430 trajectories for the particular case of Br_2 in Ar at 3500 K.

In the earlier studies (1, 2) it was assumed that $\tau(u) = \langle\tau\rangle_i$ for the internal energy range $u_{i-1} < u < u_i$, where $\tau(u)$ is a measure of the vibrational period of the diatomic molecule. Furthermore, earlier (1, 2) it was also assumed that $r = r_{min}(q)$, where r is the initial internuclear separation of the molecule and $r_{min}(q)$ is the position of the minimum of its effective potential at a given value of quadratic angular momentum, q. Both of these assumptions were eliminated in the present work.

In other respects, the present calculations were similar to those performed (2) previously. Specifically, stratified and importance sampling was employed and six energy strata, each one kT wide, around the dissociation limit were used. Within each energy stratum, three annular strata with three different ranges of the impact parameter b ($0 \rightarrow 3$ Å; $3 \rightarrow 5$ Å; $5 \rightarrow 6.5$ Å) were employed. Of the total 8430 trajectories, 279 led to a reaction, and in all but one case, the product was three separated atoms, 2Br + Ar. Only one collision of 8430 led to the formation of BrAr + Br. The most important reaction path involved collisions of Br_2 molecules within

[1]Research sponsored, in part, by the Air Force Office of Scientific Research, Air Force Systems Command, USAF, under grant No. A75-2856. The United States Government is entitled to reproduce and distribute reprints for Government purposes, notwithstanding any copyright notation hereon.

[2]Present address: Singer Stimulation Products, Silver Springs, Maryland 20904.

$\pm 1\,kT$ of the dissociation limit and impact parameters less than 5 Å. The resultant k_d^{eq} was found to be 3.7×10^9 l mol^{-1} s^{-1}, which is larger than 2.3×10^9 l mol^{-1} s^{-1} reported (2) earlier. We attribute this discrepancy predominately to removal of the two assumptions mentioned above and, to some extent, to an improved trajectory size.

Earlier results (1, 2) yield k_r^{eq}, the equilibrium one-way flux recombination rate coefficient obtained from K, the equilibrium constant, via $k_r^{eq} = Kk_d^{eq}$, several times larger than the experimental recombination rate constant, k_r. In addition, k_r^{eq} displays (1, 2) a positive temperature dependence, while a negative temperature dependence of k_r is normally (1, 2) reported. This suggests that both the absolute magnitude and temperature coefficient of k_r is influenced to a significant extent, by the nonequilibrium effects (3). The fact that k_d^{eq}, presently obtained at 3500 K, is also larger than the experimental rate constant (2) also indicates that nonequilibrium effects are important. Presently, no exact method for calculation of nonequilibrium effects in a real system appears to exist. For these reasons further study of nonequilibrium effects for Br_2 + Ar system at 3500 K was undertaken. Again, the purpose of this study was to remove some of the assumptions used (2) and to study other assumptions in some detail.

The nonequilibrium correction factor is related (2) to the observable, steady state dissociation rate constant, k_d, and k_d^{eq} by:

$$f = \frac{k_d}{k_d^{eq}} = \left(\frac{\int_D \phi^{ss}(u)\,du}{\int_D \phi^{eq}(u)\,du}\right)\left(\frac{\langle S^{ss}\rangle}{\langle S^{eq}\rangle}\right)$$

where $\int_D \phi(u)du$ are integrals of the distribution functions in the reactive (dissociative) zone and $\langle S\rangle$ are average cross-sections, at steady state and at equilibrium.

In the present work, the f factors were calculated using the method of successive collisions (3), at first using assumptions employed (2) previously, except that the present calculation did not involve the assumption that $\tau(u) = \langle\tau\rangle_i$ and $r = r_{min}(q)$. For this purpose, an equilibrium ensemble of 800 bromine molecules at 3500 K was generated in the reactive zone, which ranges within $\pm 2kT$ around the dissociative limit and a reflecting barrier (2) at $-3kT$ was assumed. No stratified and importance sampling was attempted, and the whole ensemble was subjected to 31 successive collisions with argon. The average internal energy in the reactive zone reached a reasonably well defined steady state within about 27 collisions, which agrees well with earlier (2) calculations. As previously, fluctuations in $\langle S\rangle$ values, when plotted *vs.* number of collisions, were pronounced, and this alone produced the largest single uncertainty in the f factor. This calculation produced $f = 0.1$ and $k_r = 1.4 \times 10^7$ l^2 mol^{-2} s^{-1} compared to $f = 0.23$ and $k_r = 2.0 \times 10^7$ l^2 mol^{-2} s^{-1}, obtained (2) previously. In view of the uncertainty in $\langle S\rangle_{ss}$, these results are in reasonable agreement.

In order to improve the above calculations of the f factor, we have studied further assumptions previously (2) used. Thus, earlier calculations (2) do not take into account of all collisions which involve unenergized molecules and yield excited molecules in the reactive zone. It merely assumes (2) that the $J_{d\to nd}$ and $J_{nd\to d}$ fluxes, representing de-excitation and excitation of molecules from and into the reactive energy range, are equal. However, one should expect that for Br_2 in Ar at 3500 K, the excitation flux $J_{nd\to d}$ is considerably larger than $J_{d\to nd}$. This assumption may be improved upon by complete elimination of the barrier at $-3kT$. However, such an elimination would make trajectory calculations too expensive and too time consuming. In order to improve calculations, presently another stratum, between $-3kT$ and $-2kT$, is introduced. Although this energy region rarely yields a reactive collision, it contributes significantly to the $J_{nd\to d}$ flux.

It was also realized that upon a sufficient number of collisions, even the *l*owest *e*nergy *s*tratum, $-3kT$ to $-2kT$, (LES) considered, should become depopulated, if it is not allowed to be repopulated from even lower energy strata. In order to deal with this problem in the present work, we assumed that LES remains at equilibrium with all strata which have less energy than $-3kT$. This assumption is arbitrary, but seems reasonable because the LES ($-3kT - 2kT$) stratum is relatively far away from the dissociation limit and is almost in between it and the bottom of the Br_2 potential, where one should expect that molecular distribution functions are well described by the translational temperature of the gas. In order to maintain LES invariant with respect to the number of

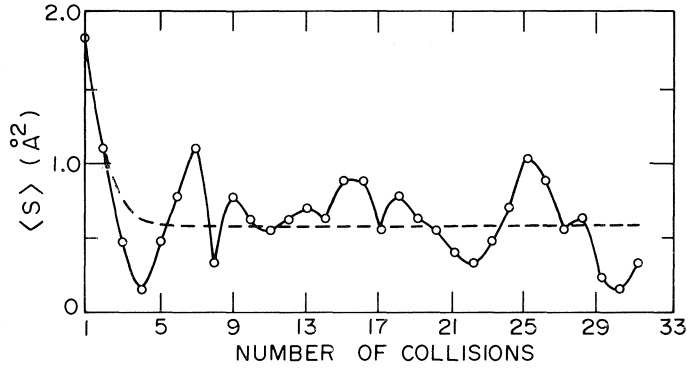

FIG. 1. Reaction cross-section in the dissociative zone ($-3kT$ to $+2kT$) for Br_2 in Ar at 3500 K *vs.* the number of collisions.

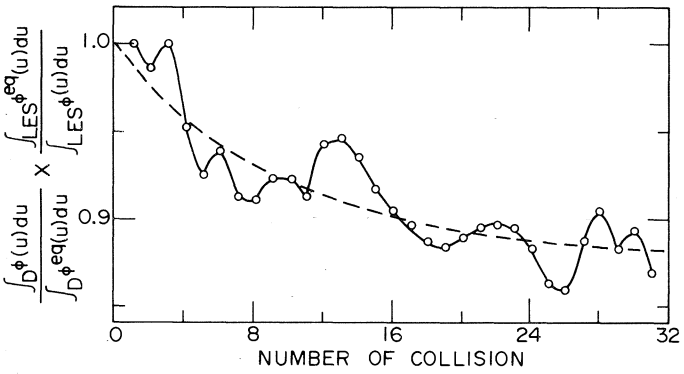

FIG. 2. Corrected normalized distribution function ratio for Br_2 in Ar at 3500 K *vs.* the number of collisions.

collisions, the ratio of the distribution function integrals was multiplied by a correction factor $\int_{LES}\phi^{eq}(u)du/\int_{LES}\phi^{ss}(u)du$, which thus increased the f factor.

In actual calculations, we again generated an equilibrium ensemble of 800 molecules at 3500 K within the dissociative zone, which was now defined by the internal energy of Br_2 from $-3kT$ to $+2kT$. The equilibrium ensemble was then subjected to 31 successive collisions with Ar. The resultant $\langle S\rangle$ and $\{\int_D\phi(u)du/\int_D\phi^{eq}(u)du\}$ $\{\int_{LES}\phi^{eq}(u)du/\int_{LES}\phi(u)du\}$ were plotted *vs.* number of collisions (Figs. 1 and 2). Both curves exhibit appreciable fluctuations, but the $\langle S^{ss}\rangle/\langle S^{eq}\rangle$ ratio, which after 31 collisions is 0.2 ± 0.1, provides the largest uncertainty. The ratios of the integrals of distribution functions (Fig. 2) are of the order of 0.9 at the steady state (30 collisions), and for this reason, fluctuations in Fig. 2 do not affect significantly the calculated values of k_d and k_r. The correction factor $\int_{LES}\phi^{eq}(u)du/\int_{LES}\phi(u)du$ increases the value of the f factor, k_r and k_d by 1.3. The resultant k_r is 3×10^7 l^2 mol^{-2} s^{-1} and is about three times larger than k_r obtained in experiments (2), a fair agreement, considering the precision of the present calculations as well as of the experimental results. Further work on reducing fluctuations in $\langle S\rangle$ is in progress. It should be added that present results do not indicate that the discrepancy between experimental and calculated results is due to nonequilibrium effects only.

Acknowledgements

We would like to acknowledge the support of the Air Force Office of Scientific Research and the National Research Council of Canada.

1. W. H. WONG and GEORGE BURNS. Proc. Roy. Soc. London, Ser. A, **341**, 105 (1974).
2. R. K. BOYD, GEORGE BURNS, D. T. CHANG, R. G. MACDONALD and W. H. WONG. 15th Symposium (International) Combustion, The Combustion Institute, 1975. p. 731.
3. A. GELB, R. KAPRAL, and G. BURNS. J. Chem. Phys. **56**, 4631 (1972).

On the involvement of diazonium ions in the photorearrangement of azoxybenzene[1]

NIGEL J. BUNCE

Guelph–Waterloo Centre for Graduate Work in Chemistry, University of Guelph, Guelph, Ont., Canada N1G 2W1

Received May 10, 1976

NIGEL J. BUNCE. Can. J. Chem. **55**, 383 (1977).

Photolysis of aromatic azoxy compounds in non-basic solvents in the presence of 2-naphthol leads quite generally to azonaphthols in addition to the normal photorearrangement product. Free diazonium ions are implicated as the precursors of the azonaphthols, both the latter and the usual photorearrangement product being derived from the same excited state of the azoxy compound. Variation of the solvent, light intensity, substrate concentration, and percent reaction all cause changes in the product distribution. Such changes can be accommodated by postulating an intermediate which can either afford the normal rearrangement product by loss of a proton to a weak base, or expel a diazonium ion when no base is present.

NIGEL J. BUNCE. Can. J. Chem. **55**, 383 (1977).

La photolyse de composés azoxyaromatiques dans des solvants non-basiques en présence de naphthol-2 conduit généralement à la formation d'azonaphtols aux côtés du produit normal de photoréarrangement. Des ions diazonium libres sont impliqués comme précurseurs des azonaphtols; ces derniers ou de même que les produits habituels de réarrangement se formeraient à partir du même état excité du composé azoxy. Des variations dans le solvant, dans l'intensité de la lumière, dans la concentration du substrat et dans le pourcentage de la réaction causent toujours des changements dans la distribution des produits. On peut accommoder de tels changements en faisant l'hypothèse qu'un intermédiaire peut soit fournir le produit normal par perte d'un proton vers la base faible soit expulsé un ion diazonium quand il n'y a pas de base présente.

[Traduit par le journal]

Apart from *cis–trans* photoisomerization (1), the normal photoreaction of aromatic azoxy compounds is intramolecular rearrangement to an *o*-hydroxyazo compound (2) [1]. 2,2′-Azoxytoluene is known to be unusual in that it gives photo products additional to those predicted by [1] (3), and similar anomalous behaviour has also been observed recently for other *o*-substituted azoxybenzenes (4). The extra products are suppressed when 2,2′-azoxytoluene is photolyzed in the presence of 2-naphthol, and it has been suggested (5) that some intermediate such as **2**, originally proposed by Badger and Buttery (6), has the ability to fragment into a diazonium ion. This may couple with 2-naphthol, giving 1-*o*-tolylazo-2-naphthol **3** as an observed product.

[1] 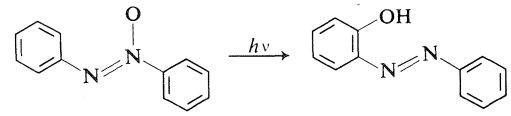

1

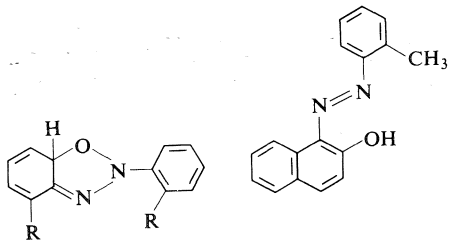

2 **3**

The bulk of the substituent R might be expected to ease the departure of the diazonium ion from **2**. However, in benzene solution, photolysis of even azoxybenzene, which is sterically unencumbered, gave (5) three times as much (60%) of the azonaphthol as of the normal rearrangement product (22%). To the extent that formation of azonaphthol can be considered diagnostic of a diazonium ion precursor, it follows that at least in this solvent, most azoxybenzene molecules photolyze by cleavage to a trappable diazonium ion. Before this assertion can be justified, it must be determined (*i*) whether diazonium ions are *necessarily* the precursors of the azonaphthols and (*ii*) whether both the azonaphthol and the

[1]Presented in part at the 166th National Meeting of the American Chemical Society, Chicago, Illinois, August 1973.

rearrangement product are formed from the same excited state of azoxybenzene. If so, it would be possible that even in the absence of 2-naphthol, the normal product might arise, at least in part, by recombination of a geminate pair of diazonium cation and phenoxide anion.[2] That possibility, that diazonium ions may be intermediates in the azoxybenzene photorearrangement, is the subject of this paper.

Results and Discussion

Although no direct observation of the proposed diazonium ions has been made, it is consistent with their involvement in the photorearrangement that photolysis of *p*-substituted azoxybenzenes in benzene–2-naphthol gave a greater proportion of azonaphthol in the order *p*-Cl < *p*-H < *p*-CH_3, progressively stabilizing the diazonium ion. These results, and comparable ones for *o*-substituents of similar size, are given as product ratios in Table 1. The actual rates of reaction of the different derivatives seem to be subject to a substituent effect, which is currently being investigated.

At this point, it was possible that the naphthol, rather than trapping a free cation, attacks some intermediate such as **2** and abstracts the diazonium moiety with expulsion of the phenol or phenoxide. That this was not the case was shown by varying the concentration of 2-naphthol. The distribution was unchanged over a tenfold range of 2-naphthol concentration; neither was the rate of reaction affected by the naphthol concentration, except when the latter was so high that much of the light was filtered from absorption by azoxybenzene.

Previous sensitization studies of the azoxybenzene photorearrangement have shown that high energy ketone sensitizers retard the photorearrangement (9, 10). In the presence of 2-naphthol, the ratio of photorearrangement product and the azonaphthol was constant with added benzophenone, although their yields drop and photoreduction[3] increases with increasing benzophenone concentration. Potential triplet quenchers such as oxygen and pyrene likewise caused no change in product distribution,[4] so that it was concluded that both products are formed from the same, presumably singlet, excited state. This result meant that 2-naphthol could now be used as a mechanistic probe for the reaction, studying the effects of variation of reaction parameters upon the product distribution, in order to gain information about the intermediate immediately preceding the divergence of the mechanism to the two products.

TABLE 1. Substituent effect upon product ratio in the azoxybenzene photorearrangement[a]

Substituents	Product ratio
4,4′-Cl_2	1.1
None	3.8
4,4′-$(CH_3)_2$	5.3
2,2′-$(CF_3)_2$	0.9
2,2′-$(CH_3)_2$	8.3
2,2′-$(OCH_3)_2$	11.9[b]

[a]In benzene solution; product ratio is azonaphthol:photorearrangement.
[b]Data of ref. 4*b*.

It was suggested above that the size of the group R in intermediate **2** may ease the departure of the diazonium ion. Accordingly, azoxybenzenes substituted in the 2,2′-positions with groups of increasing bulk yield more of the azonaphthol upon photolysis in alcoholic solvents (Table 2). The same kind of steric effect is observed in benzene solution (see first entry to Table 3).

Because the azonaphthol predominates in benzene solution, the rate of azonaphthol formation approximates the overall rate of product formation in this solvent. An experiment was carried out in which azonaphthol production was monitored in the simultaneous photolysis of compounds differing in the bulk of the 2,2′-R_2 groups, and it was found that the quantum efficiencies vary by less than a factor of two, despite the enormous difference in steric hindrance. Thus steric hindrance seems to affect not so much the overall efficiency with which the azoxy compound is transformed to products, as the relative rates of partition of some inter-

[2]Solvent separated diazonium and phenoxide ions are presumably not formed, else *p*-hydroxyazobenzene would be a major product, since azo couplings on phenols invariably involve an available *para* position (7). No more than traces of *p*-hydroxyazobenzene result from photolysis of azoxybenzene (8).

[3]Photoreduction apparently involves not the triplet state of azoxybenzene (*cf.* ref. 9) but rather "chemical sensitization" by benzophenone (10).

[4]High concentrations of piperylene (in benzene) or lithium bromide or 1-bromopropane (in ethanol) cause changes in the product ratio. As shown below, however, the ratio is very sensitive towards solvent changes.

TABLE 2. Effect of *ortho* substitution on the photorearrangement of azoxybenzenes

R	Azonaphthol/hydroxyazo compound: In ethanol	Azonaphthol/hydroxyazo compound: In 2-propanol	Relative rate of azonaphthol formation[a]
H	<0.01	<0.01	1
2,2′-CH_3	0.2	0.7	0.7
2,2′-C_2H_5	0.2	1.1	0.7
2,2′-C_3H_7	1.2	1.4	0.6
2,2′,5,5′-CH_3	1.3	—	0.9

[a]Deviation from run to run was less than 5% over five runs. Solvent was benzene, see text.

mediate between the photorearrangement product and the azonaphthol.

ortho-Substituted azoxybenzenes are known from their electronic spectra (11) to be non-planar in their ground states, and facile deformation about the C—N bonds is compatible with the rather great length of these bonds determined crystallographically (12). Although we have no direct information about the geometry of the excited state, HMO calculations on azoxybenzene do not indicate a large increase in the C—N π-bond orders upon excitation. Thus the excited state is also likely to twist easily, and this is compatible with the aromatic substitution mechanism for photorearrangement (4, 6), in which attack by oxygen on the *ortho* carbon must involve a non-planar transition state such as **4**. This would minimize steric hindrance and explain why bulky substituents have only a small effect on the efficiency of the reaction.

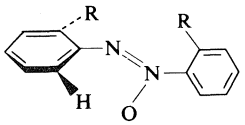

4

This lack of steric interference parallels Tanikaga's (1) observation that 3,3′-disubstituted azoxybenzenes afford equal amounts of both possible photorearrangement products [2], *i.e.*, the 3-substituent offers no hindrance to substitution into the 2-position. Comparable amounts of both products are also obtained in the 3,3′-dimethoxy system (11), and even more strikingly, we now find that even 3,3′-di-*tert*-butylazoxybenzene yields equal amounts of both photorearrangement products.

The effect of solvent upon the product ratio

[2] 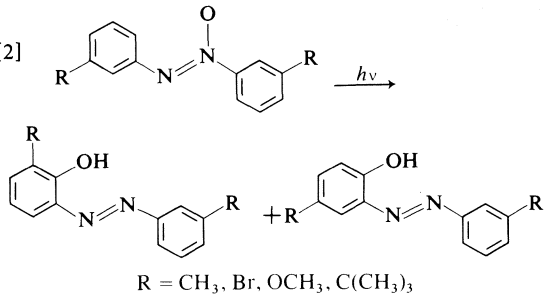

R = CH_3, Br, OCH_3, $C(CH_3)_3$

was now investigated. Since expulsion of the diazonium ion involves separation of charge, it was expected that a higher proportion of diazonium ions, and hence azonaphthol, would be formed in more polar solvents. This was not the case, as Table 3 shows, with the highest proportion of azonaphthol being produced in benzene, while almost none was obtained in ethanol.

Subsequently, it was found that the product spread depends on whether the solvent has basic properties (Table 4). Addition of water to acetonitrile, or of various substances having non-bonded electrons to benzene, results in greatly reduced azonaphthol formation. The conclusion to be drawn is that there is some intermediate that can fulfil a dual role: in the presence of base it is converted to the normal hydroxyazo compound, but when base is absent, a diazonium ion may be expelled, and trapped by 2-naphthol if available. Although there is the possibility that a basic and hence nucleophilic solvent 'Nu' might trap the diazonium ions as ArN=N—Nu and make them unavailable for azonaphthol formation, this seems to be ruled out by the high

TABLE 3. Effect of solvent on the product ratio upon photolysis of azoxybenzene and 2,2′-azoxytoluene with 2-naphthol

Solvent	Product ratios[a]: Azoxybenzene	Product ratios[a]: 2,2′-Azoxytoluene
Benzene	3.9	8.3
Ethyl acetate	0.21	2.6
Dioxane	0.09	—
Diethyl ether	0.07	2.9
Acetone	0.20	—
t-Butyl alcohol	0.007	0.51
2-Propanol	0.005	0.7
Ethanol	0.003	0.18
Methanol	0.003	0.24
Acetonitrile	0.37	—

[a]Product ratio is azonaphthol photorearrangement. All reactions were taken to >40% conversion to minimize the effect of percent conversion on the ratio (see text).

TABLE 4. Effect of adding bases upon the photolysis of azoxybenzene in non-basic solvents

Solvent	Product ratio[a]
Benzene	3.35
Benzene:dioxane 10:1	0.04
Benzene:ethanol 10:1	0.02
Benzene:diethylamine 10:1	0.00
Benzene:pyridine 10:1	0.00
Acetonitrile	0.37
Acetonitrile:water 20:1	0.09
Ethanol	0.18[b]
Ethanol:water 1:1	0.17[b]
Ethanol:0.5 M KOH	0.02[b]

[a]Azonaphthol:photorearrangement.
[b]Substrate was 2,2′-azoxytoluene.

TABLE 5. Acidity data for compounds related to components of azoxybenzene photolysis mixtures

Compound	pK_b
Solvents	
Esters *e.g.* ethyl acetate	20[a]
Nitriles *e.g.* acetonitrile	24[a]
Ketones *e.g.* acetone	21[a]
Alcohols *e.g.* methanol	16[a]
Reaction components	
Azoxybenzene (ground state)	19.2[b]
Azoxybenzene (excited state)	8.7[c]
Phenol	21[a,d]
p-Hydroxyazobenzene	15[e]

[a]Reference 14.
[b]Reference 15.
[c]Reference 16.
[d]Model for 2-naphthol.
[e]Model for *o*-hydroxyazobenzenes and for azonaphthols, ref. 17.

chemical yields of products that can be obtained. Thus photolysis of azoxybenzene in benzene affords **1** and **3** in yields of 22% and 60%; in ethanol, **3** is almost suppressed but the yield of **1** is usually 60–70%.

The complexity of the system increased with the finding that other reaction parameters affect the product distribution. In benzene solution, relatively more photorearrangement occurred as the percent conversion increased, although the rate of reaction declines with conversion due to competing light absorption by the products. This effect, which is most noticeable at small conversions, may be rationalized by noting that the azophenol products which accumulate in the (benzene) solution are the strongest bases present, more so than 2-naphthol (see Table 5). The situation may therefore be similar to that described above under solvent effects. This idea was tested by photolyzing azoxybenzene and 2-naphthol in the presence of *p*-hydroxyazobenzene; increasing the amount of *p*-hydroxy compound decreased the azonaphthol yield.

Especially at low azoxybenzene concentrations, the initial azoxybenzene concentration seems to influence the product spread, with more azonaphthol being formed at low substrate concentrations. Again, this may be an effect of conversion, but it is worth noting that in benzene solutions of azoxybenzene and 2-naphthol, ground state azoxybenzene is the strongest base present (14).

Light intensity was also found to affect the product composition, the amount of azonaphthol being greatest at low light intensities. Although the first excited state of azoxybenzene is a much stronger base than the ground state (17), it is unlikely that it survives long enough in solution to participate in bimolecular acid–base reactions in the absence of molecular association (for which there is no evidence). Likewise, postulation of a biphotonic process leading to photorearrangement but not to azonaphthol seems unlikely in view of the relatively high quantum efficiency of the normal photorearrangement. The effect of light intensity is thus unexplained at present.

These experiments clearly require at least one intermediate to be formed between the disappearance of the excited singlet state of azoxybenzene and the production of the photorearranged isomer. Attempts to trap any intermediates by Diels–Alder reactions have been entirely unsuccessful, neither has it been possible to observe any intermediates by nmr following photolysis at low temperatures. Recently however, it has been disclosed that one, and under some conditions two, intermediates may be observed upon flash photolysis of azoxybenzene (18), though they are as yet unidentified.

Scheme 1 shows a possible pathway for the reaction that is compatible with our observations. Although it is possible that the Badger and Buttery intermediate **2** is the species with the dual reactivity, the intermediate **5** is chosen as that substance on the following grounds. (*i*) The proposed intermediate is the one that would be obtained by electrophilic attack of a diazonium ion at the *ortho* position of the phenol. Azo couplings are known to involve a reversible

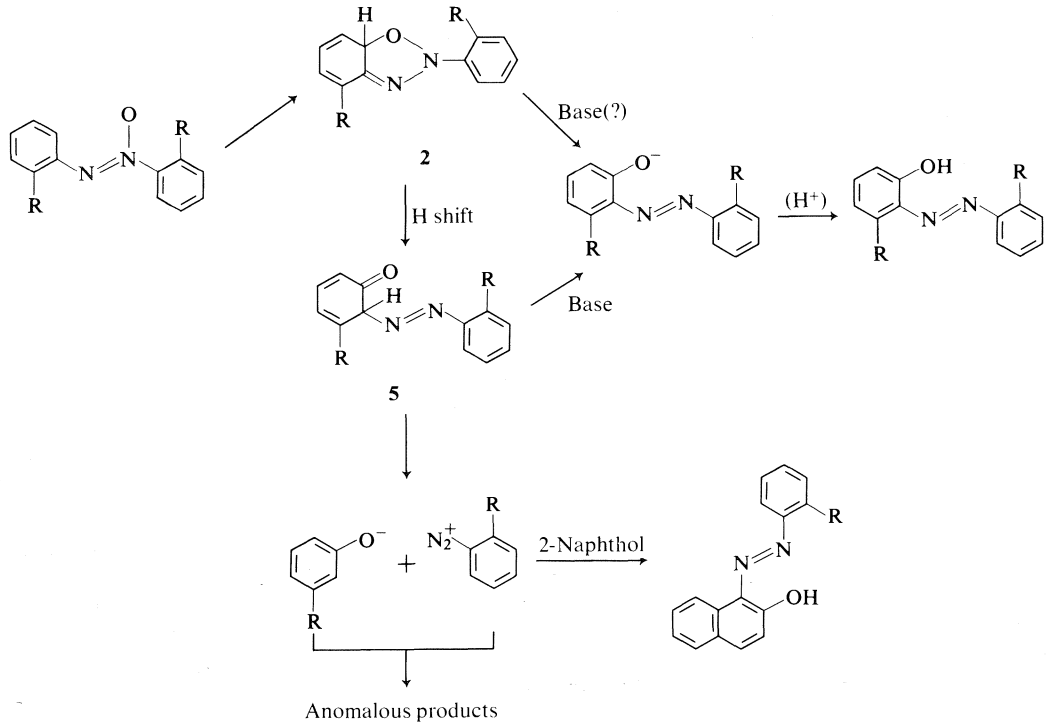

SCHEME 1

addition step (19), the arylazo cation being a relatively good leaving group (20). (*ii*) Considering the resonance structure **6** of intermediate **2**, it might be expected that hydride migration to give **5** would be very facile. It is consistent with

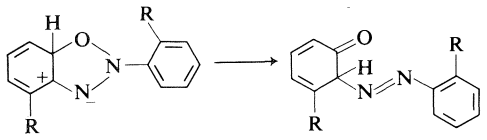

6 **5**

this hypothesis that when 2,2′-azoxytoluene is photolyzed in ethanol-*O*-*d*, the recovered *m*-cresol contains no deuterium, *i.e.*, the hydrogen at C(2) does not come from the solvent. Perhaps related is the observation that 2,2′,4,4′,6,6′-hexamethylazoxybenzene affords no products on photolysis, even those emanating from diazonium ions, although the intermediate corresponding to **2** ought to be able to form, at least in principle, if steric effects are unimportant.

Conclusions

It has been shown that the azonaphthols that had previously been observed upon photolysis of *o*-substituted azoxybenzenes in the presence of 2-naphthol are formed quite generally when aromatic azoxy compounds are illuminated in non-basic solvents, particularly benzene. Free diazonium ions seem to be implicated, and the existence of at least one common intermediate is suggested in that both kinds of product derive from the same excited state of azoxybenzene. The presence in solution of weak bases can provide a self consistent (though probably not a unique) rationalization of the variations in product ratio that result from changes in solvent, substrate concentration, and extent of reaction. (With so many variables to be controlled, it is relatively difficult to obtain reproducible product ratios.) Thus, there exists a central intermediate, possibly **5**, that is capable of losing a proton to a very weak base to afford the *o*-hydroxyazo compound. In the absence of such a base, separation of a diazonium ion occurs and coupling with any available phenol gives the eventual products.

Returning to the original question, of whether diazonium ions are normally intermediates in the azoxybenzene photorearrangement, the answer seems to be no, at least in ethanol, the usual

TABLE 6. Spectral bands used in quantitating reaction components[a]

Compound	λ_{max} (nm)	ε
Azoxybenzene	323	14 500
2,2′-Azoxytoluene	312	11 100
2-Hydroxyazobenzene	325, 375, 410[b]	16 800, 8250, 4500[b]
2-Hydroxy-6,2′-dimethylazobenzene	337	21 000
1-Phenylazo-2-naphthol	475	14 800
1-(*o*-Tolylazo)-2-naphthol	480	18 000
1-(*o*-Ethylphenylazo)-2-naphthol	482	19 600
1-(*o*-Isopropylphenylazo)-2-naphthol	482	19 400
1-(2,5-Dimethylphenylazo)-2-naphthol	482	15 000

[a]In ethanol.
[b]Not a maximum, *cf.* ref. 4.

solvent for the reaction, because ethanol is in this context a relatively strong base. In benzene solution however, diazonium ions are produced; some of these become free and lead by azo couplings to the anomalous products sometimes observed. Thus synthetically, side product formation can be minimized by effecting the photorearrangement in a solvent such as ethanol; in cases where the substrate contains *ortho* substituents, the side products can be suppressed still further by adding a base such as potassium hydroxide to the solvent.

Experimental

Photolytic procedures and methods for the separation and identification of photolysis products have been described in detail previously (4). In this work, photolyses were carried out without deoxygenation and with the light of a Hanovia 450 W medium pressure mercury arc filtered through Pyrex glass, except as noted otherwise. In preparative work, irradiations employed immersion well equipment with capacities of about 325 ml; photolyses on a smaller scale were run in ampoules or test tubes that were illuminated equally where appropriate using a merry-go-round. In either case, product mixtures were resolved by preparative tlc on silica gel (E. Merck #7747); for preparative scale irradiations carried out in the presence of 2-naphthol, the excess 2-naphthol was removed by washing with the stoichiometric amount of ~0.05 *M* aqueous NaOH. This procedure was shown not to affect the azophenols present. After separation, the bands were scraped off and eluted, either into chloroform (Soxhlet extractor) or by packing the sorbent in a short glass column and eluting with methanol, prior to evaporation and purification. In experiments conducted solely to obtain product ratios, the evaporated extracts were dissolved in ethanol, made up volumetrically, and analyzed spectrophotometrically. Absorption bands that were used for this purpose are recorded in Table 6.

Synthesis of Azoxy Compounds

Syntheses of azoxybenzene and 2,2′-azoxytoluene were described previously (4). Several compounds were prepared by reduction of the nitro compound with thallium–ethanol (21). These included 2,2′-diethylazoxybenzene, 2,2′-diisopropylazoxybenzene mp 27–28 °C (lit. (4) oil), 2,2′5,5′-tetramethylazoxybenzene mp 111–112 °C (lit. (22) mp 111 °C), 4,4′-dichloroazoxybenzene mp 155–156 °C (lit. (23) mp 156 °C), 4,4′-dimethylazoxybenzene mp 68.5–70 °C (lit. (24) mp 70 °C), and 3,3′-di-*tert*-butylazoxybenzene mp 49–50 °C, M^+ 310. *Anal.* calcd. for $C_{20}H_{26}N_2O$: C 77.38, H 8.44, N 9.02; found: C 77.65, H 8.47, N 9.17. The *m-tert*-butylnitrobenzene required for the latter preparation was obtained by conventional reactions from acetanilide. A published (24) modification of the Friedel–Crafts reaction gave *p-tert*-butylacetanilide, mp 167–169 °C (lit. (25) mp 169 °C), which was nitrated, deacetylated, diazotized, and deaminated (H_3PO_2).

2,2′-Bistrifluoromethylazoxybenzene was prepared by oxidation of *o*-trifluoromethylaniline with H_2O_2–CH_3CO_2H at room temperature. After purification by column chromatography (alumina) and recrystallization from ethanol, the yield of pale yellow needles, mp 87–88 °C, was 55%. Anal. calcd. for $C_{14}H_8F_6N_2O$: C 50.31, H 2.41; found: C 50.10, H 2.22. M^+ 334.

2,2′,4,4′,6,6′-Hexamethylazoxybenzene was prepared by the general method of Buncel and Cox (11). From oxidation of the azo compound with either H_2O_2–CH_3CO_2H or with *m*-$ClC_6H_4CO_3H$, the compound was obtained as yellow needles from ethanol, mp 89–90.5 °C (lit. (11) mp 63 °C). Elemental analysis and spectroscopic properties (uv, nmr, mass spectrum) agreed with those previously reported. A sample of the material of mp 63 °C was supplied by Dr. E. Buncel, and found to have mixture mp 87–89 °C in several proportions with the present substance. The discrepancy in mp is attributed to a difference in crystal form, the form of mp 63 °C being irregular granules.

1-Arylazo-2-naphthols

Photolysis products were compared with reference materials obtained by coupling the appropriate diazotized aniline with alkaline 2-naphthol. The following unreported reference compounds were prepared.

1-(o-Ethylphenylazo)-2-naphthol, red needles from ethanol, mp 122–123 °C; uv (EtOH) λ_{max} 482 nm (ε 19 600), 420 (11 000), 310 (7200); nmr ($CDCl_3$) δ 1.35 (t, J = 7 Hz, 3H, CH_3), 2.95 (q, J = 7 Hz, CH_2), 6.7–8.7 (m, 10 ArH), 16.5 (s, OH); ms m^+/e 276(M^+, 55%), 262(19), 261(100), 233(10), 143(57), 130(10), 128(10), 120(13), 119(43), 118(13), 115(68), 114(10), 105(20), 103(13). *Anal.* calcd. for $C_{18}H_{16}N_2O$: C 78.24, H 5.84, N 10.14; found: C 78.52, H 5.75, N 9.98.

1-(o-Isopropylphenylazo)-2-naphthol, dark red crystals with green glance from ethanol, mp 133–134 °C; uv (EtOH) λ_{max} 482 nm (ε 19 400), 419 (11 000), 311 (7300); nmr ($CDCl_3$) δ 1.35 (d, J = 6 Hz, 6H, CH_3), 2.50 (septet, J = 6 Hz, CH), 6.7–8.7 (m, 10 ArH), 16.6 (s, OH); ms m^+/e 290(M^+, 16%), 276(36), 158(13), 143(17), 134(12), 133(100), 132(16), 130(15), 118(13), 115(38). *Anal.* calcd. for $C_{19}H_{18}N_2O$: C 78.59, H 6.25, N 9.65; found: C 78.69, H 6.15, N 9.58.

1-(o-Trifluoromethylphenylazo)-2-naphthol, dark red needles from ethanol, mp 157–158 °C, also obtained as bronze platelets, mp 155–156 °C; uv (EtOH) λ_{max} 465 nm (ε 6200), M^+ 316. *Anal.* calcd. for $C_{17}H_{11}F_3N_2O$: C 64.56, H 3.51; found: C 64.12, H 3.42.

Substituted o-Hydroxyazobenzenes

Some of these were available from previous studies (4). All were obtained by photolysis of appropriate azoxy compounds and characterized by nmr (low field OH) and mass spectral fragmentation pattern. The following compounds had not been described previously.

2-Hydroxy-6,2′-diethylazobenzene, red needles from ethanol, mp 62.5–63.5 °C; uv (EtOH) λ_{max} 343 nm (ε 19 000), 240 (7400); ms m^+/e 254(M^+, 60%) 240(20), 239(100), 225(14), 121(71), 120(17), 119(41), 118(15), 106(31), 105(41), 103(36). *Anal.* calcd. for $C_{16}H_{18}N_2O$: C 75.56, H 7.13, N 11.01; found: C 75.32, H 7.13, N 11.04.

2-Hydroxy-2′,3,5′,6-tetramethylazobenzene, red needles from ethanol, mp 148–149 °C; uv (EtOH) 354 nm (ε 19 500); ms m^+/e 254(M^+, 92%), 253(33), 211(16), 149(19), 122(12), 121(100), 120(14), 106(14), 105(86), 103(13). *Anal.* calcd. for $C_{16}H_{18}N_2O$: C 75.56, H 7.13, N 11.01; found: C 75.36, H 7.02, N 11.05. Also obtained from the irradiation of 2,2′,5,5′-tetramethylazoxybenzene was a small yield of 2,2′,5,5′-tetramethylazobenzene, mp 118–119 °C (lit. (26) mp 119 °C), identified by mass spectrometry (M^+ 238) and by comparison with an authentic sample. The authentic sample was obtained by AgO oxidation (27) of 2,5-dimethylaniline; apart from the azocompound (15%) the oxidation also afforded a 5% yield of the previously unreported *1,4,5,8-tetramethylphenazine*, pale yellow needles from ethanol, mp 217–219 °C; uv (EtOH) λ_{max} 363 nm (ε 11 000), 274 (125 000); nmr (C_6D_6) δ 2.35 (s), 6.65 (s), ratio 4:1; ms m^+/e 236(M^+, 100%), 235(26), 221(18), 209(8), 118(M^{++}?, 6). *Anal.* calcd. for $C_{16}H_{16}N_2$: C 81.32, H 6.82, N 11.85; found: C 81.20, H 6.75, N 11.72.

2-Hydroxy-3,3′-di-tert-butylazobenzene and 2-hydroxy-5,3′-di-tert-butylazobenzene: the assignments of these compounds are not certain. More polar isomer: red needles from ethanol, mp 111–113 °C; nmr (CCl_4) δ 1.40, 1.43 (2s, *tert*-butyl), 6.8–8.2 (m, ArH), 12.5 (s, OH); M^+ 310. *Anal.* calcd. for $C_{20}H_{26}N_2O$: C 77.38, H 8.44, N 9.02; found: C 77.24, H 8.63, N 9.13. Less polar isomer: orange crystals from ethanol, mp 91–93 °C; nmr (CCl_4) δ 1.40, 1.42 (2s, *tert*-butyl), 6.8–7.9 (m, ArH), 13.7 (s, OH); M^+ 310. *Anal.* found: C 77.19, H 8.55, N 9.01.

2-Hydroxy-6,2′-bistrifluoromethylazobenzene, orange needles from ethanol, mp 128–130 °C; nmr (CCl_4) δ 7.0–8.1 (m, ArH), 12.6 (s, OH); M^+ 334. *Anal.* calcd. for $C_{14}H_8F_6N_2O$: C 50.31, H 2.41; found: C 50.28, H 2.47. Also obtained in this irradiation was the corresponding azo compound, *2,2′-bistrifluoromethylazobenzene*, mp 126–127 °C, as orange needles from ethanol, M^+ 318. *Anal.* calcd. for $C_{14}H_8F_6N_2$: C 52.84, H 2.53; found: C 53.12, H 2.77.

Electronic Effects on Azonaphthol Formation

The azoxy compound (2 mmol) and 2-naphthol (5 mmol) were irradiated in corked Pyrex test tubes for 28 h in benzene solution (40 ml). The mixtures were worked up by dilute base extraction and preparative tlc to give the results recorded in Table 7.

HMO Calculations on Azoxybenzene

The parameters used were $\alpha_N = \alpha + \beta_0$; $\alpha_{N(O)} = \alpha + 2\beta_0$; $\alpha_O = \alpha + 1.5\beta_0$; $\beta_{C-N} = 0.7\beta_0$; $\beta_{N-N(O)} = \beta_0$; $\beta_{N-O} = 0.8\beta_0$; $\beta_{N(O)-C} = 0.7\beta_0$. π-Bond orders follow, C—N then N(O)—C: ground state, 0.42, 0.31; first n,π* state, 0.38, 0.29; first π,π* state, 0.46, 0.36.

Effect of Varying the 2-Naphthol Concentration

Eight photolysis solutions were prepared by dissolving 2-naphthol (20–208 mg) in 3 ml aliquots of a solution of azoxybenzene (503 mg) in dry benzene (50ml). The solutions were irradiated for 2 h in corked Pyrex ampoules with the 450 W mercury arc, equal illumination being maintained through a merry-go-round which encircled the immersion well. After the usual work-up by preparative tlc, the average ratio of azonaphthol to 2-hydroxyazobenzene was 4.5 ± 0.06. No trend in the ratio was discerned over this concentration range.

Having established the constancy of the product ratio, the rates of reaction were monitored by following the production of the azonaphthol spectrophotometrically. Six aliquots (4 ml) of a solution of azoxybenzene (113 mg) in dry benzene were irradiated in the presence of 2-naphthol (11–158 mg) under similar conditions. After 2 h, the formation of azonaphthol was $3.42 \pm 0.09 \times 10^{-4}$ M. Values lower by more than two standard deviations were obtained when higher concentrations of 2-naphthol were used, probably because of competing light absorption.

Sensitization and Quenching

(i) In the Presence of Benzophenone

In order that light absorption by benzophenone should compete with the azoxy compound, the reactions were carried out in quartz ampoules using the unfiltered light of the 450 W mercury arc. Two millilitre aliquots of a solution of 2,2′-azoxytoluene (301 mg) and 2-naphthol (628 mg) in 25 ml of 2-propanol were irradiated for 1.5 h in sealed degassed quartz ampoules equipped with quartz to Pyrex graded seals. After the usual work-up, the following results were obtained.

	Ph_2CO (mg)			
Products	0	24	51	93
2,2′-Azotoluene	1.15	1.89	2.52	2.94
o-Hydroxyazotoluene	4.49	4.20	3.67	2.89
o-Tolylazonaphthol	7.23	6.38	5.88	4.61

In a similar experiment in which 2 ml aliquots of a solution of azoxybenzene (257 mg) and 2-naphthol (625 mg) dissolved in 25 ml of ethyl acetate were irradiated for 2 h in the presence of benzophenone (0–101 mg), the ratio of azonaphthol to hydroxyazo compound was 0.51 ± 0.04 (six samples).

TABLE 7. Products of irradiation of substituted azoxybenzenes with 2-naphthol

Substituents	Product (mg)			
	Azo compound	*o*-Hydroxyazo compound	Recovered azoxy compound	Azonaphthol
None	—	43[e]	213	169[i]
4,4′-Cl_2	37[c]	39[f]	407	53[j]
4,4′-$(CH_3)_2$	—	8[g]	380	49[k]
2,2′-$(CF_3)_2$[a]	(110)[d]	(206)[d]	250(—)	101(164)[d]
	33			
2,2′-$(CH_3)_2$	—	16[h]	406	140[l]
2,2′-$(OCH_3)_2$[b]	—	10	345	129

[a]Values in parentheses from an irradiation in which 0.70 g of the azoxy compound and 2.0 g 2-naphthol were irradiated in the preparative reactor with 325 ml benzene for 46 h. [b] Experiment described in ref. 4*b*. [c]mp 187–188 °C (lit. 188 °C). Known compounds were further identified by mass spectrometry; unreferenced literature mp's are taken from Beilstein. [d]Compound described in text. [e]mp 79–80 °C (lit. 82 °C). [f]mp 174–176 °C (lit. (1) 176 °C). [g]mp 141–142 °C (lit. 148 °C). [h]mp 95–96 °C (lit. (3) 97 °C). [i]mp 130–131 °C (lit. 133 °C). [j]mp 161–162 °C (lit. 162 °C). [k]mp 132–133 °C (lit. 134 °C). [l]mp 129–130 °C (lit. 131 °C).

(ii) In the Presence of Quenchers

These experiments were done on a similar scale to those above. Some substances which had no effect on the product ratio were oxygen or anthracene (substrate 2,2′-azoxytoluene, solvent 2-propanol, quartz or Pyrex ampoules), *trans*-stilbene (substrate azoxybenzene, ethyl acetate solution), pyrene (substrate azoxybenzene, benzene solution). The relative proportion of azonaphthol was reduced in the presence of 2-methyl-1-butene or piperylene (substrate azoxybenzene, benzene solution), or heavy atom solvents (1-bromopropane or iodoethane in ethylacetate, substrate azoxybenzene; 1-bromopropane in ethanol or 2-propanol, substrate 2,2′-azoxytoluene) but increased when LiBr was added in large quantities (to 3 *M*) to solutions of 2,2′-azoxytoluene and 2-naphthol in ethanol.

Steric Effects

Ratios of *o*-hydroxyazobenzene derivatives to azonaphthols were obtained from experiments in which the azoxy compound (0.01 g/ml) was irradiated preparatively, in the appropriate solvent in the presence of 2-naphthol (0.05 g/ml). The reactions were worked-up by evaporation, extraction of a chloroform solution of the residue with ~0.05 *M* NaOH to remove excess 2-naphthol, and resolution by preparative tlc. Ratios of products are reported in Table 8.

Relative rates of azonaphthol formation were obtained by irradiating benzene solutions (100 ml) of the azoxy compound (0.50 mmol) and 2-naphthol (2.0 g). At 300–320 nm each azoxy compound had an absorbance > 20. Aliquots (3.5 ml) of each of the five solutions were irradiated simultaneously in a Rayonet photochemical reactor equipped with RUL 3000 lamps having maximal output at 300 nm. A 'merry-go-round' apparatus was used to ensure uniform illumination of the samples. Chamber temperature was 40 °C within about 3 min of striking lamps. The illuminated samples were examined by uv in the range 450–550 nm for azonaphthol formation. Table 2 records the average of five such determinations employing different irradiation times.

TABLE 8. Products of irradiation of 2,2′-disubstituted azoxy compounds with 2-naphthol in ethanol[a]

Substituents	Products (mmol)	
	o-Hydroxyazo compound	Azonaphthol
H	0.20	< 0.01
2,2′-$(CH_3)_2$	0.19	0.03
2,2′-$(C_2H_5)_2$	0.17	0.03
2,2′-$(C_3H_7)_2$	0.08	0.10
2,2′5,5′-$(CH_3)_4$	0.07	0.09

[a]The azoxy compound (1 mmol) and 2-naphthol (1.0 g) were irradiated in ethanol (20 ml) for 18 h.

The irradiation of 3,3′-di-*tert*-butylazoxybenzene (0.40 g) was done in ethanol solvent (325 ml) that was 0.25 *M* in KOH. After irradiation for 2 h, the solvent was evaporated and the residue acidified and extracted with chloroform. Preparative tlc yielded the two compounds described above (0.045 g each) and unreacted azoxy compound (0.28 g).

Solvent Effects

The concentrations used were azoxy compound: 10 mg/ml and 2-naphthol: 50 mg/ml. Results of these irradiations are given in Tables 3 and 4.

Variation of Initial Azoxybenzene Concentration

Aliquots (3 ml) of a solution of 2-naphthol (2.5535 g) in benzene (100 ml) were irradiated simultaneously in Pyrex ampoules for 3 h with different quantities of azoxybenzene. The usual work-up procedure afforded the results in Table 9.

Variation in Percent Reaction

In a typical reaction, 2 ml aliquots of a solution of azoxybenzene (253 mg) and 2-naphthol (834 mg) in ethyl acetate (25 ml) were irradiated on a merry-go-round for times varying from 2–100 h. The usual work-up gave the results in Table 10.

TABLE 9. Effect of variation of azoxybenzene concentration

[Azoxybenzene] (mg/ml)	Hydroxyazobenzene (mg)	Azonaphthol (mg)	Ratio
	Run 1		
3	0.49	3.32	5.5
7	0.53	4.15	6.2
12	0.66	4.77	5.8
17	0.71	3.96	4.4
31	1.06	4.35	3.3
49	1.24	5.03	3.2
	Run 2		
5	2.23	12.5	4.5
8	2.64	12.9	3.9
16	6.65	27.3	3.3
21	7.65	34.5	3.6
32	9.08	39.5	3.5
42	9.40	38.1	3.2

TABLE 10. Effect of variation in percent reaction

Irradiation time(h)	Percent reaction	*o*-Hydroxyazobenzene I (mg)	Phenylazonaphthol II (mg)	Ratio II/I
2	5	1.1	0.6	0.42
7	17	3.4	1.3	0.31
21	40	7.7	2.3	0.24
50	52	8.8	2.6	0.23
100	69	11.3	3.2	0.23

TABLE 11. Effect of variation in light intensity

Distance from lamp (in.)	Percent reaction	Hydroxyazo compound I (mg)	Azonaphthol II (mg)	Ratio II/I
1	21	0.60	0.19	0.26
2	20	1.04	0.42	0.33
3	24	1.42	0.77	0.44
4	22	1.15	0.61	0.53

Variation in Light Intensity

The reactant solution contained azoxybenzene (255 mg) and 2-naphthol (626 mg) in 25 ml ethyl acetate. Aliquots (2 ml) were placed in corked Pyrex ampoules which were clamped at a known distance from the lamp and irradiated by trial and error to comparable conversion. Work-up by the usual method gave the results in Table 11.

Effect of Added p-Hydroxyazobenzene

A solution of azoxybenzene (202 mg) and 2-naphthol (486 mg) was prepared with 25 ml benzene. Aliquots of this solution (3 ml) were irradiated with *p*-hydroxyazobenzene for 3 h. The usual analytical procedure gave the results in Table 12.

Attempts to Trap Intermediates

Solutions of azoxybenzene (1 g) in 20 ml of benzene were irradiated in the presence of substances such as maleic anhydride, dimethyl acetylenedicarboxylate, cyclopentadiene, and 1,3-cyclohexadiene. No products additional to those obtained in the absence of these substances were obtained.

Search for Intermediates by Nuclear Magnetic Resonance

This experiment was carried out in the laboratory of Dr. R. F. Childs. Solutions of azoxybenzene in perdeuterated toluene and in perdeuterated acetonitrile were irradiated at −50 °C for periods up to 3 h, then immediately examined by nmr, with the spectrometer probe already cooled to −70 °C. No new resonances were observed.

Irradiation of 2,2′-Azoxytoluene in Ethanol-O-d

Two solutions were prepared, each containing 2,2′-azoxytoluene (0.65 g), 2-naphthol (2.0 g), and ethanol-*O-d* (30 ml). Irradiation in Pyrex test tubes for 46 h gave ~50% conversion of the azoxy compound by tlc. The solvent was evaporated, ethanol (30 ml) added and

TABLE 12. Effect of added *p*-hydroxyazobenzene

p-Hydroxyazobenzene (mg)	Hydroxyazo compound I (mg)	Azonaphthol II (mg)	Ratio II/I
0	0.8	5.0	5.0
27	0.6	1.2	1.6
55	0.6	0.7	1.0
94	0.8	0.6	0.7

evaporated again, and the residue worked up by preparative glc (6 ft × ¼ in., 10% SE30 on Chromosorb W, 60/80, 150 °C). Only the peak corresponding to *m*-cresol was collected. Mass spectral analysis on the ratio of m^+/e 109 to m^+/e 108 gave the following results (average of five determinations): authentic *m*-cresol: 0.130 ± 0.002; reaction product *A*: 0.136 + 0.003; reaction product *B*: 0.132 ± 0.004.

Irradiation of 2,2′,4,4′,6,6′-Hexamethylazoxybenzene

The azoxy compound (5 mg/ml) and 2-naphthol (15 mg/ml) were irradiated together for 16 h. Periodic examination of the progress of the reaction by tlc showed only unchanged reactants and some tarry residue.

Acknowledgements

I wish to thank Mr. Jean-Pierre Schoch for assistance with the preparations of tetramethylazoxybenzene, *m-tert*-butylnitrobenzene and hexamethylazoxybenzene, Dr. E. Buncel for supplying a sample of the latter substance for comparison with our material, and Dr. R. F. Childs in whose laboratory the low temperature photolyses were carried out. I also thank the Ethyl Corporation for donating generous samples of *o*-ethylaniline and *o*-isopropylaniline and the National Research Council of Canada for financial support.

1. R. TANIKAGA. Bull. Chem. Soc. Jpn. **41**, 2151 (1968).
2. G. G. SPENCE, E. C. TAYLOR, and O. BUCHARDT. Chem. Rev. **70**, 231 (1970); E. BUNCEL. *In* Mechanisms of molecular migrations. Vol. I, *Edited by* B. S. Thyagarajan, Interscience. 1969. pp. 104–110.
3. G. E. LEWIS and J. A. REISS. Aust. J. Chem. **19**, 1887 (1966).
4. D. J. W. GOON, N. G. MURRAY, J-P. SCHOCH, and N. J. BUNCE. Can. J. Chem. **51**, 3827 (1973); N. J. BUNCE, D. J. W. GOON, and J-P. SCHOCH. J. Chem. Soc. Perkin Trans. I, 688 (1976).
5. N. J. BUNCE. Bull. Chem. Soc. Jpn. **47**, 725 (1974).
6. G. M. BADGER and R. G. BUTTERY. J. Chem. Soc. 2243 (1954).
7. H. ZOLLINGER. Azo and diazo chemistry. Interscience. 1961. p. 253.
8. M. IWATA and S. EMOTO. Bull. Chem. Soc. Jpn. **43**, 946 (1970).
9. R. TANIKAGA. Bull. Chem. Soc. Jpn. **41**, 1664 (1968).
10. B. M. MONROE and C. C. WAMSER. Mol. Photochem. **2**, 213 (1970).
11. R. A. COX and E. BUNCEL. Can. J. Chem. **51**, 3143 (1973), and references cited therein.
12. W. R. KRIGBAUM, Y. CHATANI, and P. G. BARBER. Acta Crystallogr. Sect. B, **26**, 97 (1970).
13. J. A. BARLTROP and N. J. BUNCE. J. Chem. Soc. (C), 1467 (1968).
14. J. B. HENDRICKSON, D. J. CRAM, and G. S. HAMMOND. Organic chemistry. 3rd ed. McGraw-Hill. 1970. p. 304.
15. E. BUNCEL and B. T. LAWTON. Can. J. Chem. **43**, 862 (1965).
16. H. H. JAFFÉ, D. L. BEVERIDGE, and H. L. JONES. J. Am. Chem. Soc. **86**, 2932 (1964).
17. W. M. J. STRACHAN, A. DOLENKO, and E. BUNCEL. Can. J. Chem. **47**, 3631 (1969).
18. D. GEGIOU-HADJOUDIS and E. HADJOUDIS. Abstracts of the VIII International Conference on Photochemistry, Edmonton, Alta. 1975. Abstract β6.
19. H. ZOLLINGER. Helv. Chim. Acta, **38**, 1597 (1955); **38**, 1617 (1955); R. ERNST, O. A. STAMM, and H. ZOLLINGER. Helv. Chim. Acta, **41**, 2274 (1958); A. GRIMISON and J. H. RIDD. J. Chem. Soc. 3019 (1959).
20. N. J. BUNCE. J. Chem. Soc. Perkin Trans. I, 942 (1974).
21. A. MCKILLOP, R. A. RAPHAEL, and E. C. TAYLOR. J. Org. Chem. **35**, 1670 (1970).
22. E. BAMBERGER. Ber. **33**, 113 (1900).
23. K. HEUMANN. Ber. **5**, 911 (1872).
24. D. LEFORT, C. FOUR, and A. POURCHEZ. Bull. Soc. Chim. Fr. 2378 (1961).
25. G. S. KOLESNIKOV and T. V. SMIRNOVA. Zh. Obshch. Khim. **20**, 1427 (1950); Chem. Abstr. **45**, 2431c (1951).
26. E. NOELTING and T. STRICKER. Ber. **21**, 3138 (1888).
27. B. ORTIZ, P. VILLANUEVA, and F. WALLS. J. Org. Chem. **37**, 2748 (1972).

Electronic excited states of small ring compounds. IV. Bicyclo[2.1.0]pentanes by the photocycloaddition of cyclopropenes to olefins[1]

D. R. ARNOLD AND R. M. MORCHAT

The Photochemistry Unit, Department of Chemistry, University of Western Ontario, London, Ont., Canada N6A 5B7

Received August 10, 1976

D. R. ARNOLD and R. M. MORCHAT. Can. J. Chem. **55**, 393 (1977).

Direct irradiation of the charge-transfer complex between the cyclopropenes 3,3-dimethyl-1,2-diphenylcyclopropene (**3**) and 1,2,3-triphenylcyclopropene (**7**), and the electron deficient olefins dimethyl fumarate (**5**) and maleic anhydride (**11**) resulted in formation of the cycloadducts **6**, **12–15** which are the bicyclo[2.1.0]pentane derivatives. These products were also formed when the reaction was photosensitized by triplet–triplet transfer. The structure of the adducts rests largely upon the interpretation of ^{13}C and ^{1}H nmr spectra. Nuclear Overhauser effect studies were used to assign stereochemistry. The thermal stability of these new bicyclo[2.1.0]-pentane derivatives has been examined, particularly with regard to the ring-flipping process and the rearrangement to the corresponding cyclopentene derivatives.

D. R. ARNOLD et R. M. MORCHAT. Can. J. Chem. **55**, 393 (1977).

L'irradiation directe du complexe de transfert de charge entre les cyclopropènes diméthyl-3,3 diphényl-1,2 cyclopropène (**3**) et triphényl-1,2,3 cyclopropène (**7**), et des oléfines déficientes en électron comme le fumarate de méthyle (**5**) et l'anhydride maléique (**11**) conduit à la formation de cycloadduits **6**, **12–15** qui sont des dérivés bicyclo[2.1.0]pentanes. Ces produits se forment aussi lorsque la réaction est photosensibilisée par le transfert triplet–triplet. La structure des adduits a été déterminée principalement par l'interprétation des spectres rmn du ^{13}C et du ^{1}H. On a utilisé des études d'effet nucléaire Overhauser pour attribuer la stéréochimie. On a examiné la stabilité thermique de ces nouveaux dérivés bicyclo[2.1.0]pentanes particulièrement en ce qui a trait au processus d'inversion de cycle et de réarrangement en dérivés cyclopenténiques correspondants.

[Traduit par le journal]

Introduction

When the vinyl diazo compound **1** was irradiated at long wavelengths ($340 < \lambda < 410$ nm), the cyclopropene **3** formed in nearly quantitative yield, (reaction 1) (1). Less than 1% of the dienes **4***a*, *b* were formed. This reaction is believed to involve the vinylmethylene or vinylcarbene **2** intermediate. In fact, the vinylmethylene (triplet) is produced upon irradiation of **1** at low temperature (4–30 K) and is stable under these conditions (2). On the other hand,

[1] 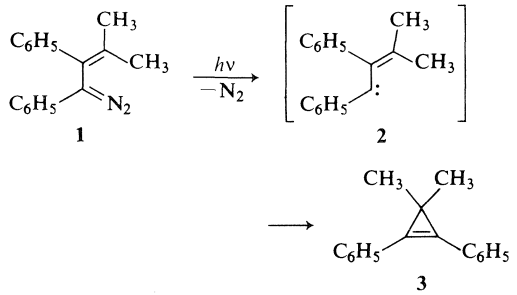

1 **2** **3**

direct irradiation of the cyclopropene **3** produces the dienes **4***a*, *b* in nearly quantitative yield (reaction 2) and with a quantum yield of 0.045 (1). If the same intermediate was involved in reactions 1 and 2, the quantum yield of reaction 2 would require that *at least* 4% of the dienes **4***a*, *b* form during reaction 1.[2] This dichotomy has led us to propose that different pathways are involved in these two reactions.

[2] 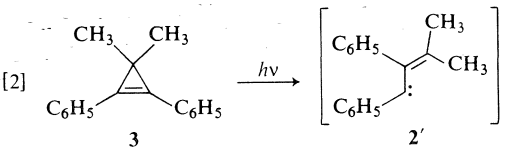

3 **2′**

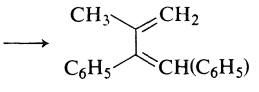

4

(*a*) *cis*

(*b*) *trans*

[1]Contribution No. 159 from the Photochemistry Unit.

[2]That 4% be a lower limit is required since the quantum yield of formation of **2** from **3** may be less than unity.

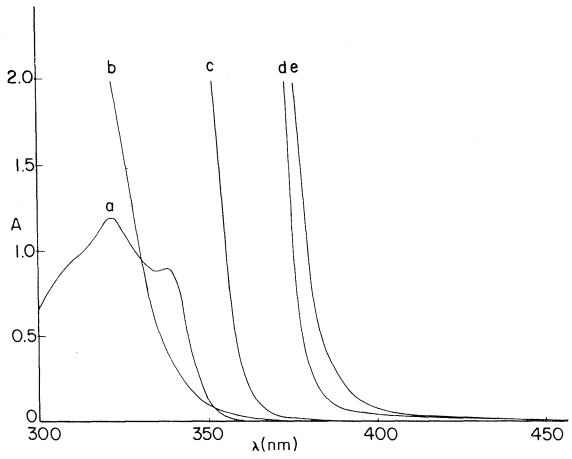

FIG. 1. Absorption curves for (*a*) **3** (2.75×10^{-4} *M*), (*b*) **5** (0.3 *M*), (*c*) filter solution *A* (see Experimental), (*d*) **3** (0.3 *M*), (*e*) **3** (0.3 *M*) and **5** (0.3 *M*). Curves (*a*) 0.1 cm cuvettes, (*b–e*) 1.0 cm cuvettes. Curves *a*, *b*, *d*, and *e* were obtained using benzene solutions.

If two different intermediates are involved during reactions 1 and 2 there are several ways in which they might differ. For example, they might be structural isomers, they might be the singlet (carbene) and triplet (methylene) species, or they might have differing initial energy content. If the difference is due to spin multiplicity, conceivably these species could have different reactivity toward olefins. This criterion has traditionally been applied to distinguish other methylenes and carbenes[3] (3) and in fact there are reported examples of cycloaddition reactions of related vinylmethylenes or vinylcarbenes to olefins (4). We therefore attempted to trap an intermediate by carrying out both reactions 1 and 2 in the presence of dimethyl fumarate **5** (0.3 *M*, the limit of solubility in benzene) which is known to be a good dipolarophile.

In neither case were we able to detect an adduct resulting from trapping an intermediate. Furthermore, the quantum yield for the disappearance of cyclopropene **3** upon irradiation at 340 nm (near the maximum of the absorption of this cyclopropene, Fig. 1) remained 0.04 in the presence of dimethyl fumarate **5** (0.3 *M*).[4] We therefore conclude that if intermediates are involved in reactions 1 or 2, in neither case is the rate of reaction of the intermediate with dimethyl fumarate **5** (0.3 *M*) rapid enough to afford a detectable amount of adduct in competition with the formation of **3** and **4***a*, *b*.

While we were carrying out these experiments with reaction 2, we did, under some conditions, obtain a one-to-one adduct. This adduct has been shown to have the bicyclo[2.1.0]pentane structure **6** (reaction 3). This reaction represents

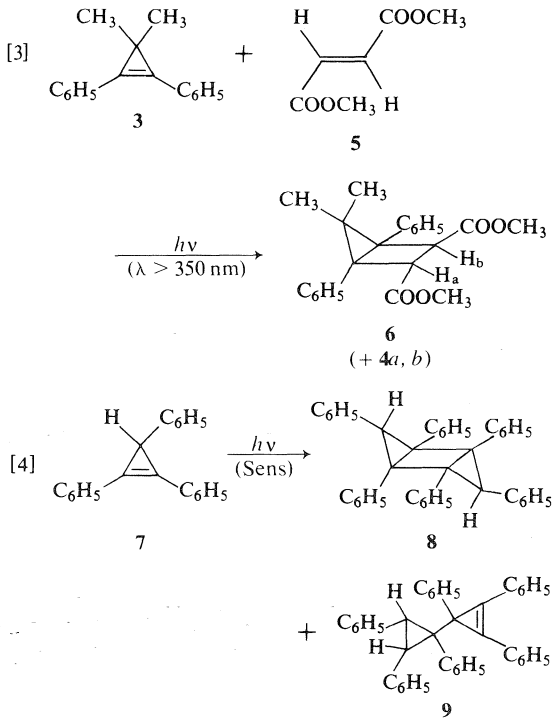

the first example of the photocycloaddition of a cyclopropene to an olefin. Previous work has shown that some cyclopropenes can dimerize to give tricyclo[3.1.0.$0^{2,4}$]hexanes upon irradiation; however, attempts to obtain cross-adducts have hitherto been unsuccessful (5). It has been suggested that the rate of reaction of the excited cyclopropene (triplet) with cyclopropene (ground state) is so rapid that observable cross-adduct formation is precluded (5*a*). The rate constant for the reaction of the triplet state of **7** with **7** (reaction 4) was found to be 1.1×10^8 l mol^{-1} s^{-1} (5*a*). Nevertheless, we have found conditions under which bicyclo-[2.1.0]pentane adducts can be formed from **7** in good yield.

These substituted bicyclo[2.1.0]pentanes are of interest in their own right, particularly with regard to the definition of the factors which

[3]The classic example of the application of this criterion is for the case of methylene *vs.* carbene.

[4]D. R. Arnold and J. A. Pincock, unpublished results.

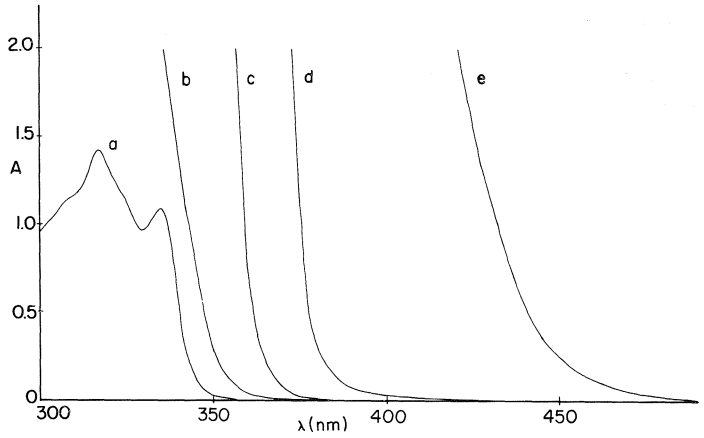

FIG. 2. Absorption curves for (*a*) **3** (3.37×10^{-4} *M*), (*b*) **11** (0.3 *M*), (*c*) filter solution *B* (see Experimental), (*d*) **3** (0.3 *M*), (*e*) **3** (0.3 *M*) and **11** (0.3 *M*). Curves (*a*) 0.1 cm cuvettes, (*b–e*) 1.0 cm cuvettes. Curves *a*, *b*, *d*, and *e* were obtained using benzene solutions.

influence the nature and strength of the central [0] bond in this class of compounds.

We report here: (*1*) the preparation and spectroscopic characterization of the adducts **6**, **12–15**; (*2*) the results of experiments which give an indication of the thermal stability of the central [0] bond in these compounds; and, (*3*) some preliminary results regarding the mechanism of the photocycloaddition reaction. A more thorough study of the scope and mechanism of the photocycloaddition reaction is now in progress and will be described later.

Results

Preparation of Adducts

A benzene solution of 3,3-dimethyl-1,2-diphenylcyclopropene **3** (0.3 *M*) and dimethyl fumarate **5** (0.3 *M*) has absorption at long wavelengths not present in the spectrum of the individual components at this concentration (Fig. 1). We attribute this long wavelength absorption to a charge-transfer complex transition. This solution was irradiated through chemical filter solution *A* which absorbs light of wavelengths shorter than 350 nm, Fig. 1 (reaction 3). The products were the known dienes **4***a*, *b* and the adduct to which we have assigned structure **6**.

When the irradiation was carried out without the filter solution (through Pyrex) so that a wavelength region including the cyclopropene absorption maximum was irradiated, the only products detected were the dienes **4***a*, *b*.

Presumably, if the charge-transfer complex could be irradiated without also exciting the cyclopropene, the ratio of adduct to dienes would increase. Unfortunately, the absorption due to the charge-transfer complex is not sufficiently separated from that of the cyclopropene to allow exclusive excitation at a convenient rate. Using chemical solution filter *B*, with a longer wavelength cut-off (<357 nm, Fig. 2) than that of *A*, some adduct **6** was formed after prolonged (122 h) irradiation; however, the extent of conversion was too small to allow a meaningful ratio of adduct to dienes to be determined. This filter solution was usually used in the sensitizer studies to be discussed below.

There was no evidence for charge-transfer complex formation between the cyclopropene **3** and dimethyl maleate **10**. A benzene solution of **3** (0.3 *M*) and **10** (0.3 *M*) had a long wavelength absorption curve which was superimposable upon that of a benzene solution of **3** (0.3 *M*) alone. When this solution was irradiated (filter *A*), the dienes **4***a*, *b* were the major products. The isomeric adduct(s) with the methyl ester groups *cis* was (were) not detected.

The photocycloaddition reaction can be sensitized by triplet–triplet transfer. For example, a benzene solution of **3** (0.3 *M*), **5** (0.3 *M*), and thioxanthen-9-one (0.01 *M*, $E_T = 65$ kcal mol^{-1} (6)) was irradiated through filter *A*. After 1 h, ^{1}H nmr analysis indicated the reaction was proceeding rapidly with formation of adduct **6** (14%) and *no* dienes (**4***a*, *b*). During this time,

10 (37%) was also formed by sensitized (triplet–triplet) isomerization of **5** (E_T *ca.* 61 kcal mol^{-1} (6)). Further irradiation increased the percentage of **10** to the reported (6) photosensitized stationary state (97% **10**) leaving a small amount of **5**. The photocycloaddition reaction became much less efficient; however, after 45 h all the cyclopropene **3** had been consumed leaving adduct **6** (74%) and dienes **4***a*, *b* (25%). No other adduct was detected.

The photosensitized (triplet–triplet transfer) isomerization of **5** is known to require sensitizers with triplet energy greater than 59 kcal mol^{-1} (6). When benzil (E_T = 54 kcal mol^{-1} (6)) or fluorenone (E_T = 53 kcal mol^{-1} (6)) were used as sensitizers for reaction 3, instead of thioxanthen-9-one, the photocycloaddition (filter *B*) went relatively rapidly (17 h) and completely to adduct **6** (*ca.* 100%) without complications due to sensitized isomerization of **5**.

The long wavelength region in the absorption spectrum of a benzene solution of the cyclopropene **3** (0.3 *M*) and maleic anhydride **11** (0.3 *M*), extends out to 420 nm (Fig. 2) which indicates charge-transfer complex formation occurs. Irradiation (700 h) of this solution through filter solution *A* gives an adduct to which we have assigned structure **12** (80%) along with the dienes **4***a*, *b* (20%) (reaction 5).

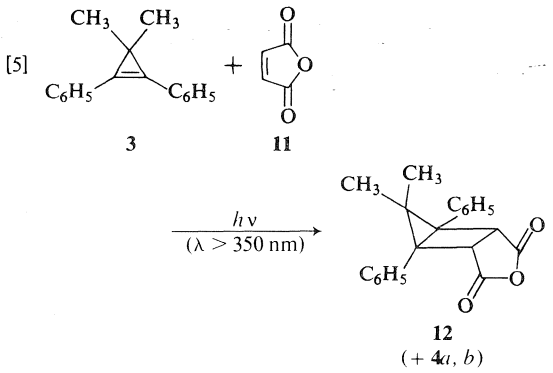

When this irradiation was carried out without the filter (through Pyrex) so that a wavelength region including the cyclopropene absorption maximum was irradiated, the only products detected were the dienes **4***a*, *b*.

The behaviour of cyclopropene **3**, upon both direct and triplet–triplet photosensitized irradiation (in the absence of added olefin), is very different from that of cyclopropene **7**. In contrast to **3**, which gives the dienes **4***a*, *b* upon

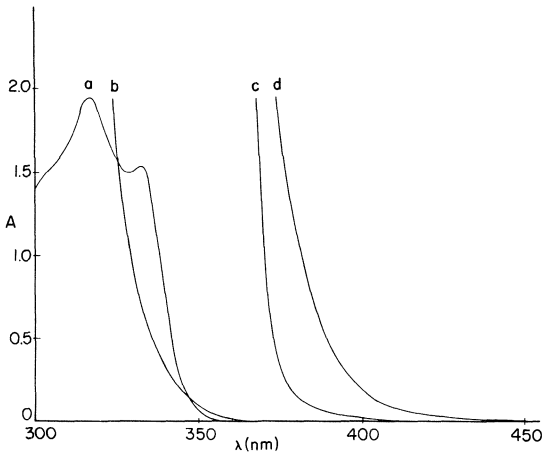

FIG. 3. Absorption curves for (*a*) **7** (6.70×10^{-4} *M*, the absorption maximum (λ = 312 nm) follows Beer's Law over the concentration range 10^{-4}–10^{-7} *M*), (*b*) **5** (0.3 *M*), (*c*) **7** (0.3 *M*), (*d*) **7** (0.3 *M*) and **5** (0.3 *M*). Curves (*a*) 0.1 cm cuvettes, (*b–d*) 1.0 cm cuvettes. The solvent was benzene.

direct irradiation (reaction 2), **7** is known to be stable under these conditions (5*a*). On the other hand, the triplet of **7** gives the dimers **8** and **9** (reaction 4) while no dimers are formed from the triplet of **3**. We therefore turned our attention to the study of the behaviour of **7** upon irradiation, direct and triplet–triplet sensitized, in the presence of **5**, **10**, and **11**.

A benzene solution of the cyclopropene **7** (0.3 *M*) and **5** (0.3 *M*) has long wavelength absorption not present in the spectra of the components (Fig. 3), indicative of charge-transfer complex formation. Irradiation (250 h) of this solution in the long wavelength region, through filter *A*, leads to formation of the one-to-one adduct as the major product (82%) to which we assign structure **13**; small amounts of the dimers **8** (9%) and **9** (9%) are also formed (reaction 6).[5]

These reactions can be sensitized (triplet–triplet transfer) using fluorenone; however, the ratio of adduct **13** to dimer **8** decreases under these conditions. Irradiation of a benzene solution of **7** (0.3 *M*), **5** (0.3 *M*), and fluorenone (0.1 *M*), through filter *B* until 83% of **7** was

[5]We have found that the ratio of the dimers **8**:**9** is not invariant. For example, the ratio of **8**:**9** obtained from reaction 4 depends upon the concentration of **7**; dilute solutions increase this ratio. This leads us to suggest that reaction 4 is more complex than was originally proposed (5*a*).

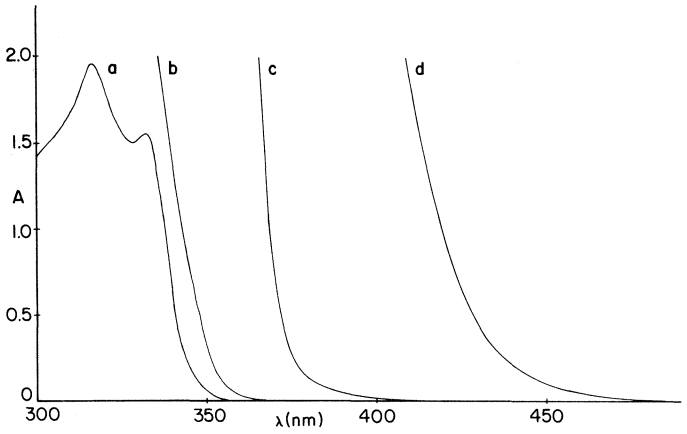

FIG. 4. Absorption curves for (*a*) **7** (6.70×10^{-4} *M*), (*b*) **11** (0.3 *M*), (*c*) **7** (0.3 *M*), (*d*) **7** (0.3 *M*) and **11** (0.3 *M*). Curves (*a*) 0.1 cm cuvettes, (*b–d*) 1.0 cm cuvettes. The solvent was benzene.

[6]

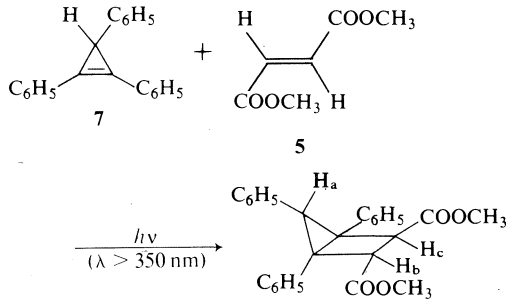

consumed, gave the products **13** (57%), **8** (14%), and **9** (12%). The ratio of **13** to dimer **8** was found to remain essentially constant (**13**/**8** = 3.5 ± 0.5) under sensitized (fluorenone) conditions, when the concentration of equimolar **7** and **5** was varied between 0.3–0.003 *M*.

A benzene solution of **7** (0.3 *M*) and **10** (0.3 *M*) showed only a very small increase in the long wavelength region of the absorption spectrum in comparison to that of the spectra of a benzene solution of **7** (0.3 *M*) alone. When this solution was irradiated (filter *A*) the dimers **8** and **9** were the major products. Some **5** and adduct **13** were also formed; however, no isomeric adduct(s) with the methyl ester groups *cis* was (were) detected.

A benzene solution of **7** (0.3 *M*) and **11** (0.3 *M*) was visibly coloured as a result of the charge-transfer complex absorption. The long wavelength absorption of this solution is shown in Fig. 4. Irradiation (188 h) of this solution through filter *B* gave a good yield (77%) of the adduct to which we have assigned structure **14**, along with some of the dimers, **8** (20%) and **9** (3%) (reaction 7).

This reaction was also sensitized by triplet–triplet transfer when fluorenone was added. The ratio of adduct **14** to dimer **8** again decreased under sensitized irradiation conditions. Irradiation (6 h) of a benzene solution of **7** (0.3 *M*) and **11** (0.3 *M*) and fluorenone (0.1 *M*), through filter *B* until the cyclopropene was consumed gave the following yield of products; **14** (60%), **8** (27%), and **9** (13%).

[7]

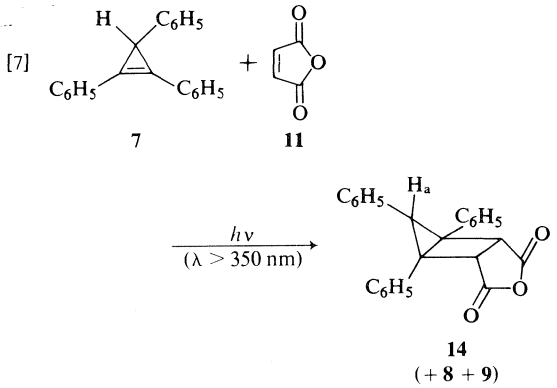

Thermal Stability of the Adducts

The adducts **6** and **12** are surprisingly stable thermally; little or no reaction was observed when solutions (*ortho*-dichlorobenzene) of these adducts were heated for several hours (5–15) at *ca.* 170 °C. In marked contrast, adduct **13** (reaction 6) is quite unstable thermally and rearranges quantitatively, even at room tem-

perature, to an isomer to which we have assigned structure **15**, (reaction 8). The progress of this

[8]

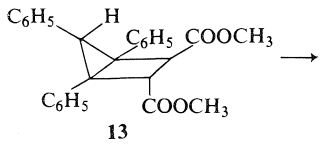

13

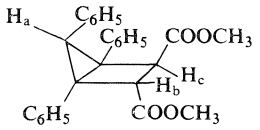

15

reaction was conveniently followed by ^{1}H nmr and the rate of isomerization as a function of temperature was determined. These data are given in Table 1. The kinetic parameters,

TABLE 1. The rate constants for the isomerization **13** to **15** in *ortho*-dichlorobenzene solution, as a function of temperature

T (°C)[a]	10^5k (s^{-1})[b]
71.18	7.53±0.30
72.38	8.19±0.17
77.47	15.22±0.37
81.00	21.57±0.57
84.02	30.45±0.50

[a]Measured with a copper–iron thermocouple (±0.02 °C).
[b]The rate, first order over 2–3 half-lives, was determined from a least-squares plot of at least six concentration measurements. The error limits are the calculated standard deviations.

$E_a = 26.9 \pm 0.6$ kcal mol^{-1} and $\log A = 14.7 \pm 0.4$, were determined from an Arrhenius plot (Fig. 5) of the data in Table 1. Prolonged heating of adduct **15** did cause further reaction ($t_{1/2}$ at 162 °C *ca.* 9 h). The structures of the products (reaction 9) have not been firmly established; however, the ^{1}H nmr, ultraviolet, and mass spectra are consistent with the cyclopentene derivatives **16** and **17**.

Adduct **14** is more thermally stable than **13**. The half-life of **14** at 76 °C is nearly 80 h. The products from **14** have not been fully characterized; however, from the ^{1}H nmr spectrum it is clear that an isomeric bicyclo-[2.1.0]pentane is not among them. We believe the products are isomeric cyclopentene derivatives analogous to **16** and **17** in reaction 9.

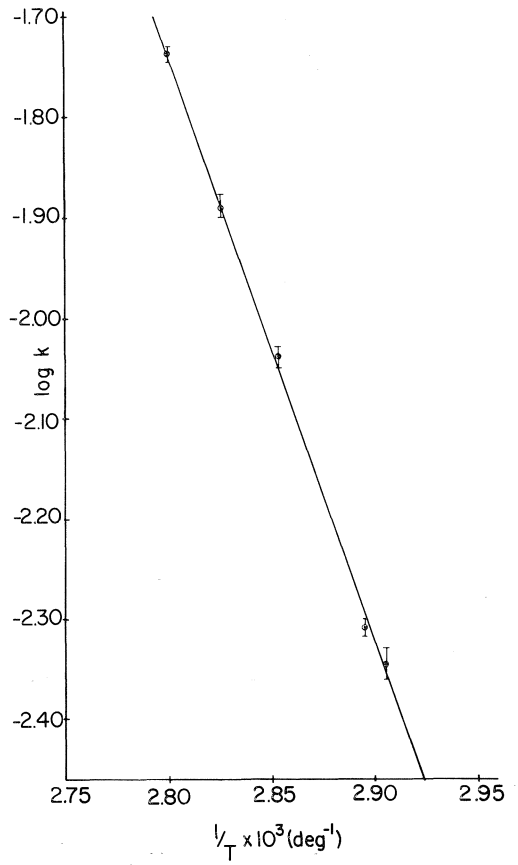

FIG. 5. Arrhenius plot for the isomerization **13** to **15**.

[9]

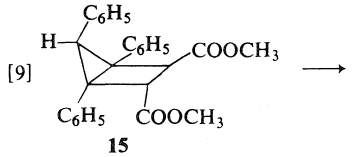

15

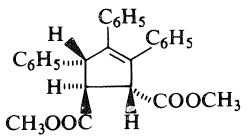

16

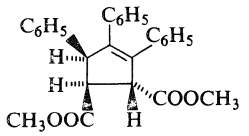

17

Proof of Structure of the Adducts

When adduct **6** was first obtained we initially suspected it to be the substituted cyclopentene derived from the cycloaddition of the vinylcarbene **2** (as a 1,3-dipole) to dimethyl fumarate. The ^{1}H nmr and infrared spectra were superficially in accord with such a structure. This structure was, however, easily ruled out because the ultraviolet spectrum of **6** gave no

indication of extended (*i.e.* styrene like) conjugation. The maximum at 221 nm (ε = 10 100) was typical of the phenyl chromophore. That the adduct was a one-to-one adduct was consistent with the elemental analysis, mass spectrum (*m/e* parent peak), and the molecular weight determined by the isopiestic method.

Convincing evidence for the bicyclo[2.1.0]-pentane structure for **6** came from analysis of the ^{13}C nmr spectrum. The assignments show clearly that only 14 (12 aromatic and 2 carbonyl) carbons are in the region expected for sp^2 hybridized carbon. The remaining nine carbons, (four methyl, three quaternary, and two methine (determined by off-resonance decoupling)) are sp^3 hybridized. The ^1H nmr spectrum is consistent with this assignment. The *trans*-ester stereochemistry is not only required, from the obvious lack of C_s symmetry which would be present in the *cis* isomer, but is consistent with the coupling of protons H_a and H_b (J_{ab} = 4 Hz) expected of the *trans* orientation. Double irradiation technique confirmed coupling between H_a and H_b. The signals due to the ester methyls and the methyls on the methylene bridge were assigned on the basis of chemical shift. The assignment of the *lower* field singlet to the *endo* methyl and the higher field doublet to H_a, also in the *endo*-position, was made by observing an increase in the intensity (18%) of the doublet (3.44 ppm) upon irradiation of the singlet (1.40 ppm). The intensity of the other doublet (4.02 ppm) was not affected by this double irradiation. Furthermore, double irradiation of the high field singlet (0.84 ppm) had no effect on the intensity of either doublet.

The magnitude of the observed increase in signal intensity, (nuclear Overhauser effect, nOe) is similar to that reported for the related structure **18** (7). The *exo* methyl group in **18** also occurs at higher field (0.88 ppm). An

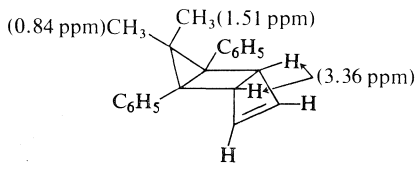

18

nOe experiment revealed a 7% intensity enhancement in the allylic hydrogen absorption (3.36 ppm) upon saturation of the *endo* methyl singlet (1.44 ppm).

The structures of the other adducts were assigned in a similar fashion, and the ^{13}C and ^1H nmr spectral assignments are summarized in the Experimental section.

The stereochemistry of adduct **12** with the anhydride *exo* was established by observing a 8.4% nOe intensity enhancement of the singlet (3.47 ppm) assigned to the two equivalent hydrogens on the ethylene bridge, upon irradiation of the lower field methyl signal (1.50 ppm). No intensity enhancement was observed when the higher field methyl singlet (0.83 ppm) was double irradiated. This requires the anhydride to be in the *exo* position.

The assignment of configuration of adduct **13** having the *exo* phenyl on the methylene bridge was made by observing nOe enhancement (6.5%) of the singlet assigned to hydrogen H_a (3.15 ppm) upon double irradiation of the *higher* field doublet assigned to the *endo* hydrogen H_b (3.49 ppm). Conversely, double irradiation of the doublet (3.49 ppm) led to a 8.5% intensity enhancement of the signal due to H_a. Furthermore, double irradiation of the doublet due to H_c (4.17 ppm) had no effect on the intensity of the signal due to H_a.

The nmr (^{13}C and ^1H) spectra of **15** are similar to those of **13**. The isomeric nature of these compounds was apparent from the mass spectra (70 eV) which appeared to be identical. Isopiestic molecular weight determination confirmed the monomeric structure of **15**. Unlike **13**, however, double irradiation (nOe) of the signal assigned to hydrogen H_a (doublet, J = 0.7 Hz, 3.38 ppm) had no noticeable effect on the intensity of either of the signals assigned to hydrogens H_b (3.56 ppm) or H_c (4.40 ppm). The signal assigned to H_c is a doublet of doublets (J = 4.5 and 0.7 Hz). Double irradiation of this signal causes both the doublet assigned to H_a (J = 0.7 Hz) and the doublet for H_b (J = 4.5 Hz) to collapse to singlets. The configuration of **15** is such that H_a would be expected to be coupled to H_c. From this evidence we conclude that the more stable isomer has the phenyl on the methylene bridge oriented *endo* (**15**). This may be the result of the three phenyls in **13** being in close proximity, the relief of this steric interaction leads to **15** being more stable.

This observation causes us to open to question the structure of the tricyclohexane **8** obtained from reaction 4. The gross structure proposed (5*a*) for this compound is consistent with the

^{13}C nmr spectrum; however, no evidence has been provided which allows assignment of the configuration of the phenyl groups on the methylene bridges. In view of the relative stabilities of **13** and **15**, the phenyl groups on the methylene bridges of **8** may in fact be in the *endo*-position.

The assignment of configuration of adduct **14** having the *exo* phenyl on the methylene bridge and with the anhydride *exo* was established by observing a 11.8% nOe intensity enhancement of the singlet (3.59 ppm) assigned to the two equivalent hydrogens on the ethylene bridge upon irradiation of hydrogen H_a (3.06 ppm); furthermore, double irradiation of the singlet (3.59 ppm) led to a 20% intensity enhancement of the signal due to H_a. No coupling between the hydrogens on the ethylene bridge and H_a was observed; in contrast to **15**, in **14** the configuration is such that H_a would not be expected to be coupled.

Discussion

The long wavelength absorption spectra (Figs. 1–4), give an indication that charge-transfer complex formation occurs between the cyclopropenes **3** and **7** and dimethyl fumarate **5** and maleic anhydride **11**. There is no evidence from the absorption spectrum that a charge-transfer complex forms between **3** and dimethyl maleate **10** and, only a small increase in long wavelength absorption with a mixture of **7** and **10**. These observations are consistent with previous reports that dimethyl maleate is less prone to form charge-transfer complexes with olefins than are either dimethyl fumarate or maleic anhydride (8). The fact that **5** and **11** are reactive in the photocycloaddition reaction, while **10** is not, could be taken as an indication that the excited charge-transfer complex is a necessary intermediate leading to adduct formation. However, several observations negate this conclusion.

The small increase in long wavelength absorption may indicate some charge-transfer complexing occurs between **7** and **10**, yet adduct formation does not occur; however, dimers **8** and **9** are formed. The formation of the dimers **8** and **9**, in this reaction and in reactions 6 and 7, are typical of the triplet of **7** which suggests that irradiation of the charge-transfer complex between **7** and **5**, **10**, and **11** produces the triplet of **7**.

It is known that direct irradiation of **7** does not produce appreciable triplets (5*a*). Obviously, intersystem crossing is not able to compete with other processes which deactivate the excited singlet of **7**. In this connection we have observed intense fluorescence from **3** and **7** in rigid media at low temperature. Furthermore, the cyclopropene ring opening (reaction 2) is a singlet reaction. It may be that carbon–carbon bond breaking (or stretching) is a rapid non-radiative deactivation pathway of the singlet and some thermal activation is required for diene formation. A study of the effect of temperature on the quantum yield of diene formation (reaction 3) might answer this question. In any event, it seems likely that excitation of the charge-transfer complex serves to populate the cyclopropene triplet. There are several examples where irradiation of a charge-transfer complex leads ultimately to the triplet state of one of the components (9). This process has recently been reviewed (9*a*).

The singlet of cyclopropene **3** does not give the adduct with **5** or **11**; in fact, since the quantum yield of the disappearance of **3** upon direct irradiation near the cyclopropene maximum is not affected by **5** (0.3 *M*), the reaction ultimately yielding the dienes **4***a*, *b* is not significantly quenched by this concentration of olefin.

The triplet–triplet transfer sensitization experiments are consistent with adduct formation involving the cyclopropene triplet. The ratio of adduct **13** to dimer **8** does not vary when the concentration of equimolar **7** and **5** changes between 0.3 and 0.003 *M*. If adduct formation involved triplet–triplet transfer excitation of the charge-transfer complex, the amount of adduct formed should have decreased markedly upon dilution. On the other hand, if the cyclopropene triplet were involved the ratio of adduct to dimer should remain constant.

It is significant that the ratio of adduct **13** to dimer **8** is somewhat larger when the charge-transfer complex is excited than when the triplet of the cyclopropene **7** is obtained by triplet–triplet transfer. This observation is consistent with the rate of adduct formation, between the cyclopropene triplet and dimethyl fumarate, being competitive with diffusion, since the cyclopropene triplet formed from the excited charge-transfer complex must initially be next to dimethyl fumarate. Consistent with this view, the reported (5*a*) rate constant of triplet **7** with ground state **7** is close to the

diffusion limit; thus the binding energy between triplet **7** and dimethyl fumarate cannot be significantly larger than the barrier to diffusion.

The observation that dimethyl fumarate **5** leads to the *trans*-adducts **6** and **13** does not require the cycloaddition to be concerted (stereospecific). It may be that the second bond from a diradical intermediate is formed faster than bond rotation which would be required for formation of the *cis*-adducts; or, it may be that the *trans*-isomers are favoured as a result of thermodynamic, not kinetic factors. Knowledge of the extent of concertedness (stereospecificity) of these cycloadditions must await a case where both configurations of olefin undergo reaction.

Dimethyl maleate **10** is known to be less reactive in other cycloaddition reactions than are dimethyl fumarate and maleic anhydride and this can account for the lack of adducts with **10** (10). A qualitative indication of the relative reactivities of dimethyl fumarate **5**, cyclopropene **7**, dimethyl maleate **10**, and maleic anhydride **11** with the triplet of **7**, can be obtained from the observed ratio of adduct to dimer **8** in the triplet–triplet transfer sensitized reactions. These product ratios indicate the relative rate constant of the cycloaddition reaction increases **10** < **7** (6×10^7 l mol^{-1} s^{-1} (*5a*)) < (*ca.* 4 times) **5** < (*ca.* 2 times) **11**. This conclusion, of course, assumes that the rate determining step is not reversible.

The stereochemistry of **13** from reaction 6 and **14** from reaction 7 indicates the photocycloaddition is sensitive to steric factors. The reactants approach minimizing steric hindrance so that the initial product is the less thermodynamically stable isomer.

In the photosensitized dimerization of **7** (reaction 4), two products are formed; the cycloaddition product **8** and the product of a photoene reaction **9** (*5a*).[5] We have not detected the photoene type product incorporating **5** or **11**.

The question regarding the nature and strength of the central bond in substituted bicyclo[2.1.0]-pentane compounds has been of interest for several years (11). We expect that the study of derivatives, readily available by the photocycloaddition reaction reported here, will help answer this question. However, the results of our study of the thermal stability of the adducts **6**, **12**–**15** are not easily explained.

The first reported study of the kinetics of *cis–trans*-isomerization, or ring-flipping process,

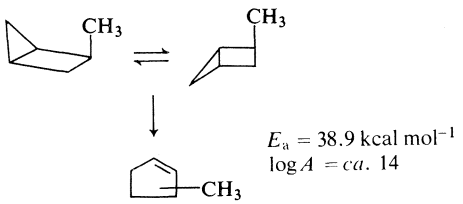

of a bicyclo[2.1.0]pentane was by Chesick who studied the 2-methyl derivative (11*a*). The barrier to isomerization was found to be 38.9 kcal mol^{-1}, significantly greater than the calculated value (19 kcal mol^{-1}) which assumed formation of a strain free cyclic diradical without bonding across the former central bond. The conclusion drawn from this result was that the transition state for the isomerization still maintained considerable strain energy as a result of incomplete rupture of the central bond.

If the radical stabilizing influence of the bridgehead phenyl groups is felt at the transition state for the ring-flipping process, the activation energy should be considerably lower. The thermal stability of the adduct **6** and **13** speak against a large decrease in the strength of the central bond.

The ring-flipping process in the case of **6** is a degenerate process and is therefore amenable to study by variable temperature ^{1}H nmr. Two techniques have been tried: (*1*) the signals due to the methyl groups on the methylene bridge are separated by 34 Hz, rapid exchange would be indicated by line shape analysis; (*2*) double irradiation of either signal would lead to decreased intensity of the other if exchange were occurring at a rate competitive with nuclear spin relaxation (nuclear magnetization transfer (13)). Both of these procedures have been applied in an attempt to detect the ring-flipping process of **6**; in neither case was there any indication of rapid flipping even at 190 °C.[6]

We have used these ^{1}H nmr techniques previously to study the ring-flipping process in the related 2,3-diazabicyclo[2.1.0]pentane system (*e.g.* **19**). We concluded that the diphenyl

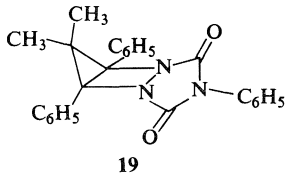

19

[6]The ring-flipping process would have to be very rapid in order to be detected by these techniques (*i.e.* equilibration rate > *ca.* 0.5 s^{-1}).

derivative **19**, analogous to **6**, was isomerizing rapidly even at $-60\,^{\circ}C$ (13). The lack of rapid ring-flipping in the case of **6** now suggests that the urazole moiety plays a major role in decreasing the barrier to the flipping process in **19**.

The isomerization of **13** to **15** (reaction 8) provides the most dramatic indication that the ring-flipping process does occur in these derivatives. The activation energy for this process is 12 kcal mol^{-1} less than that reported for the flipping of 2-methylbicyclo[2.1.0]pentane. Once formed **15** has considerable stability toward further thermal rearrangement (reaction 9). This is consistent with the observation that the isomerization of bicyclo[2.1.0]pentane to cyclopentene has an activation energy 7.7 kcal mol^{-1} greater than the ring-flipping process with the 2-methyl derivative.

Throughout this discussion we have assumed the ring-flipping process involves change of configuration at the central bond; breaking the external cyclopropane bond should also be considered. There are some observations which support isomerization about the central bond. Reaction 9 certainly involves cleavage of the central bond and it seems reasonable to view reaction 8 as involving the same bond.[7] If the external cyclopropane bond were cleaving in reaction 8 there is no apparent reason why adduct **14** would not also rearrange at a low temperature to the *endo*-phenyl isomer analogous to adduct **15**. If, on the other hand, isomerization about the central bond is involved, the rearranged adduct would be less stable as a result of the proximate anhydride function. While adduct **14** is not particularly stable thermally, no isomeric bicyclo[2.1.0]pentane adduct was detected among the products.

Experimental Section

General

The melting points were determined on a Thermolyne hot-stage microscope and were not corrected. The combustion analyses were performed by Chemalytics, Inc., Tempe, Arizona.

Dimethyl fumarate was purchased from Aldrich Chemical Co. and recrystallized once from methanol.

Dimethyl maleate was purified by vapour phase chromatography.

Maleic anhydride was purchased from BDH and purified by recrystallization from chloroform followed by vacuum sublimation.

[7]To our knowledge no cyclobutene or methylene cyclobutane has ever been observed upon thermolysis of any bicyclo[2.1.0]pentane.

1,2,3-Triphenylcyclopropene was prepared from diphenylacetylene in 60–70% yield, via the *syn*-triphenylcyclopropenyl bromide which was reduced with lithium aluminum hydride, by the reported procedure (14).

Preparative thick layer chromatography was carried out on 2 mm layer plates of silica gel GF-254 (E. Merck) and developed with benzene. Bands were detected by viewing under uv light.

Molecular weight determinations by the isopiestic method were performed in benzene solutions using a Mecrolab Model 301A osmometer operating at 37 °C.

Mass spectra were recorded on a Varian M-66 or Mat 311A mass spectrometer and are reported as *m/e* (relative intensity). Unless diagnostically significant only the parent peak and base peak are reported.

The infrared spectra were run in carbon tetrachloride solution using 0.1 cm sodium chloride cells or in KBr disks on either a Beckman IR-5A or 20A spectrometer. The spectra were calibrated using the 1601 cm^{-1} absorption band of polystyrene.

The pmr spectra were determined on dilute solution of deuteriochloroform using tetramethylsilane as an internal reference. The spectra were obtained on a Varian HA-100 spectrometer. The chemical shifts are taken as the center of multiplets and the coupling constants are the result of first-order analysis.

The ultraviolet absorption spectra recorded as absorption against wavelength were run on a Cary 118 spectrometer in methanol using 1.0 cm quartz cuvettes unless otherwise noted.

The ^{13}C spectra were determined on solutions in deuteriochloroform (2–15% w/v) in 5 mm tubes using a Varian XL-100-15 system operating at 25.2 MHz in the Fourier transform mode. With 2000 Hz 'sweep widths' and the available memory core, the peak positions were determined to ± 1 Hz and measured relative to internal tetramethylsilane. Off-resonance decoupling was employed to confirm assignments for methyl, methylene, methine, and quaternary carbons.

Preparative irradiations were performed using a General Electric Co. 1 kW medium pressure mercury vapour arc lamp with a quartz cooling jacket which was immersed in a constant temperature bath maintained at 10 °C. All solutions were placed in Pyrex irradiation tubes, flushed with nitrogen, and sealed with a rubber septum.

Filter Solution A

$BiCl_3$ (200 mg) was dissolved in 10% HCl (150 ml) and this solution was placed in a container such that there was at least 1 cm of filter solution shielding the irradiation vessel. The long wavelength cut-off is shown in Fig. 1. The filter solution was photolabile and was replaced after 24 h irradiation.

Filter Solution B

Same as filter solution A except that a more concentrated solution of $BiCl_3$ was employed (800 mg $BiCl_3$ in 150 ml 10% HCl). The long wavelength cut-off is shown in Fig. 2.

Kinetic Measurements

Isomerizations were carried out in sealed thick-walled nmr tubes. The adduct was dissolved in 0.5 ml *ortho*-dichlorobenzene and placed in the tube which went through two freeze–pump–thaw cycles and was sealed.

The tubes were then placed in an oil-bath maintained

to ±0.02 °C by a Fisher Proportional Controller. The tubes were withdrawn at appropriate intervals and the extent of isomerization determined by analysis of the ^{1}H nmr spectra. At least six values were taken at each temperature. Activation parameters were calculated by standard methods.

Irradiation of 0.3 M 3,3-Dimethyl-1,2-diphenylcyclopropene and 0.3 M Dimethyl Fumarate

A solution containing 1.1 g (4.9 mmol) 3,3-dimethyl-1,2-diphenylcyclopropene and 0.7 g (4.9 mmol) dimethyl fumarate in 17 ml benzene was irradiated through filter solution *A*. Progress of the reaction was monitored by periodic analysis of the ^{1}H nmr spectra. After 355 h irradiation almost all of the cyclopropene had been consumed (>97%) with the subsequent formation of the dienes **4***a*, *b* (11 and 31% respectively) and the photocycloadduct **6** (55%).

Irradiation of 0.3 M 3,3-Dimethyl-1,2-diphenylcyclopropene and 0.3 M Dimethyl Fumarate with 0.1 M Fluorenone Present as Sensitizer

A solution containing 330 mg (1.5 mmol) 3,3-dimethyl-1,2-diphenylcyclopropene, 216 mg (1.5 mmol) dimethyl fumarate, and 90 mg (0.5 mmol) fluorenone in 5 ml benzene was irradiated through filter solution *A*. After 80 h irradiation a ^{1}H nmr spectrum of the reaction mixture revealed that all of the cyclopropene had been consumed. Remaining was the 1:1 adduct **6** (81%) and the dienes **4***a*, *b* (8 and 11% respectively).

By consecutive preparative thick layer chromatographic separations the adduct was isolated pure as a clear viscous liquid, **6**: ir (CCl_4) 2933, 1724, 1595, 1212, 1116, 904, and 698 cm^{-1}; uv λ_{max}(MeOH) 221 nm (ε 10 200); ^{1}H nmr δ_{TMS}($CDCl_3$) 0.84 (s, 3H), 1.40 (s, 3H), 3.38 (s, 3H), 3.44 (d, 1H, J = 4.4 Hz), 3.62 (s, 3H), 4.02 (d, 1H, J = 4.4 Hz), 7.0–7.7 ppm (m, 10H); ^{13}C nmr chemical shifts: bridgehead carbons, 41.6 and 44.7; methine carbons, 45.6 and 46.0; apex carbon, 30.7; *endo* methyl, 16.6; *exo* methyl, 23.1; ester methyls, 51.7 and 51.8; carbonyl carbons, 173.3; aryl carbons attached directly to bicyclopentane nucleus, 135.9 and 137.9; *ortho*, *meta*, and *para* carbons, 124.5–130.8 ppm; ms (70 eV), 364(2, M$^+$), 304(100). *Anal.* calcd. for $C_{23}H_{24}O_4$: C 75.80, H 6.64; found: C 75.99, H 6.68. *Mol. Wt.* calcd. for $C_{23}H_{24}O_4$: 364.42; found (isopiestic): 365.67.

Irradiation of 0.3 M 3,3-Dimethyl-1,2-diphenylcyclopropene and 0.3 M Dimethyl Maleate

A solution containing 410 mg (1.9 mmol) 3,3-dimethyl-1,2-diphenylcyclopropene and 270 mg (1.9 mmol) dimethyl maleate in 6 ml benzene was irradiated through filter solution *A*. Progress of the reaction was monitored by periodic analysis of the ^{1}H nmr spectra. After 285 h irradiation 85% of the cyclopropene had been consumed with the subsequent formation of the dienes **4***a*, *b* (28 and 48% respectively). Also present was the adduct **6** (9%) which comes about from the photocycloaddition of the cyclopropene with dimethyl fumarate (produced via thermal isomerization of dimethyl maleate). No adduct with the esters *cis* was detected.

Irradiation of 0.3 M 3,3-Dimethyl-1,2-diphenylcyclopropene and 0.3 M Dimethyl Fumarate in the Presence of 0.01 M Thioxanthen-9-one as Sensitizer

A solution containing 33 mg (0.15 mmol) 3,3-dimethyl-1,2-diphenylcyclopropene, 22 mg (0.15 mmol) dimethyl fumarate, and 1 mg (0.005 mmol) thioxanthen-9-one in 0.5 ml benzene was irradiated through filter solution *A*. The progress of the reaction was monitored by analysis of the ^{1}H nmr spectra.

Initially the reaction occurred rapidly with formation of adduct **6** (14%) and no dienes **4***a*, *b* being formed, but with 37% of the unconsumed dimethyl fumarate having been isomerized to dimethyl maleate. As the reaction proceeded more dimethyl maleate was formed leaving less dimethyl fumarate available to give the cycloadduct.

After 46 h irradiation all of the cyclopropene had been consumed. Present were the adduct **6** (74%) and the dienes **4***a*, *b* (9 and 17% respectively) with most (>95%) of the unconsumed dimethyl fumarate having been converted to dimethyl maleate.

Irradiation of 0.3 M 3,3-Dimethyl-1,2-diphenylcyclopropene and 0.3 M Dimethyl Fumarate with 0.1 M Benzil as Sensitizer

A solution containing 33 mg (0.15 mmol) 3,3-dimethyl-1,2-diphenylcyclopropene, 21 mg (0.15 mmol) dimethyl fumarate, 10 mg (0.05 mmol) benzil, and 0.5 ml benzene was irradiated through filter solution *B*. After 18 h irradiation a ^{1}H nmr spectrum was taken which indicated that all the cyclopropene had been consumed with *ca.* 100% formation of the 1:1 adduct **6**. There was no appreciable formation of the dienes **4***a*, *b*.

Irradiation of 0.3 M 3,3-Dimethyl-1,2-diphenylcyclopropene and 0.3 M Maleic Anhydride

A solution containing 500 mg (2.3 mmol) 3,3-dimethyl-1,2-diphenylcyclopropene and 220 mg (2.2 mmol) maleic anhydride dissolved in 7.5 ml benzene was irradiated through filter solution *A* for 700 h. After irradiation the solvent was removed on a rotatory evaporator and the reaction mixture analyzed by ^{1}H nmr spectroscopy. The reaction mixture contained some unreacted cyclopropene (5%), the dienes **4***a*, *b* (17%) and the cycloadduct **12** (77%).

The reaction mixture was placed on a column packed with 60–120 mesh silica gel (BDH). Elution with benzene separated the adduct. Recrystallization from $CHCl_3$–hexane afforded pure **12**: mp 182–183 °C; ir (KBr) 2990, 1866, 1790, 1512, 1466, 1257, 1116, 912, 713, and 671 cm^{-1}; uv λ_{max}(MeOH) 220 nm; ^{1}H nmr δ_{TMS}($CDCl_3$) 0.83 (s, 3H), 1.50 (s, 3H), 3.47 (s, 2H), 6.90–7.40 ppm (m, 10H); ^{13}C nmr chemical shifts: bridgehead carbons, 46.2; methine carbons, 47.3; apex carbon, 33.6; *endo* methyl 14.9; *exo* methyl, 22.3; carbonyl carbons, 169.9; aryl carbons attached directly to bicyclohexane nucleus, 133.0; *ortho*, *meta*, and *para* carbons, 127.9–129.8 ppm; ms (70 eV), 318(1, M$^+$), 246(100). *Anal.* calcd. for $C_{21}H_{18}O_3$: C 79.22, H 5.70; found: C 78.90, H 5.73

Direct Irradiation of 0.3 M 3,3-Dimethyl-1,2-diphenylcyclopropene in the Presence of 0.3 M Maleic Anhydride

A solution containing 66 mg (0.3 mmol) 3,3-dimethyl-1,2-diphenylcyclopropene and 30 mg (0.3 mmol) maleic anhydride dissolved in 1 ml chloroform was irradiated for 1 h. Analysis of the ^{1}H nmr spectrum revealed 65% consumption of the cyclopropene and formation of the dienes **4***a*, *b* (23 and 43% respectively) with no formation of a cycloadduct.

Irradiation of 0.3 M 1,2,3-Triphenylcyclopropene with Equimolar and 0.16 M Dimethyl Fumarate in the Presence of 0.1 M Fluorenone as Sensitizer

Two solutions were prepared: (*a*) consisting of 40.1 mg (0.15 mmol) 1,2,3-triphenylcyclopropene, 22.3 mg (0.15 mmol) dimethyl fumarate, 9.9 mg (0.05 mmol) fluorenone in 0.5 ml benzene; and, (*b*) containing 40.7 mg (0.15 mmol) 1,2,3-triphenylcyclopropene, 11.5 mg (0.08 mmol) dimethyl fumarate, 9.9 mg (0.05 mmol) fluorenone in 0.5 ml benzene. Both solutions were irradiated through filter solution *B*. After 1 h irradiation the solvent was removed on a rotatory evaporator and the residues dissolved in $CDCl_3$. The extent of the reaction was determined by analysis of the ^1H nmr spectra.

The spectra revealed that in both solutions *ca.* 73% of the cyclopropene had been consumed. The amount of the adduct **13** decreased from 48% in solution (*a*) to 38% in solution (*b*). There was a corresponding increase in the amount of cyclopropene dimers **8** and **9** from 25% (13% and 12% respectively) in solution (*a*) to 35% (16% and 19% respectively) in solution (*b*).

Concentration Dependence on the Dimerization of 1,2,3-Triphenylcyclopropene in the Presence of Fluorenone as Sensitizer

Three solutions were prepared each containing 40 mg (0.15 mmol) 1,2,3-triphenylcyclopropene and 10 mg (0.05 mmol) fluorenone dissolved in 0.5, 5, and 50 ml benzene. These solutions were irradiated through filter solution *B*. After 5.5 h irradiation all the cyclopropene had been consumed. The solvent was removed on a rotatory evaporator and the residues dissolved in $CDCl_3$. The components of the reaction mixtures were determined by analysis of the ^1H nmr spectra. The concentration of the tricyclohexane dimer **8** increased, in the solutions containing the lower concentrations of cyclopropene, from 65% to 92% to 98% respectively. There was a corresponding decrease in the concentration of the cyclopropylcyclopropene dimer **9** from 35% to 8% to *ca.* 2%.

^{13}C nmr chemical shifts for **8**: bridgehead carbons, 51.5; apex carbons, 48.33; aryl carbons attached directly to tricyclohexane nucleus, 135.2 and 137.2; *ortho*, *meta*, and *para* carbons, 125.7–131.0 ppm.

Concentration Dependence on the Dimerization and Adduct Formation of 1,2,3-Triphenylcyclopropene in the Presence of Dimethyl Fumarate with Fluorenone as Sensitizer

Three solutions were prepared each containing 40 mg (0.15 mmol) 1,2,3-triphenylcyclopropene, 22 mg (0.15 mmol) dimethyl fumarate, and 10 mg (0.05 mmol) fluorenone dissolved in 0.5, 5, and 50 ml benzene. The solutions were irradiated through filter solution *B*. After 5 h the irradiations were stopped, the solvent removed on a rotatory evaporator, and the residues dissolved in $CDCl_3$. The extent of the reaction was determined by analysis of the ^1H nmr spectra.

The spectra revealed that *ca.* 83% of the cyclopropene had been consumed with formation of 57% of the adduct **13** and 26% of the cyclopropene dimers **8** and **9**. The concentration of the tricyclohexane dimer **8** increased in the solutions containing the lower concentration of cyclopropene from 14% to 23% and the concentration of the cyclopropylcyclopropene dimer **9** decreased from 12% to 3%.

Irradiation of 0.3 M 1,2,3-Triphenylcyclopropene and 0.3 M Dimethyl Fumarate

A solution containing 212 mg (0.8 mmol) 1,2,3-triphenylcyclopropene and 130 mg (0.9 mmol) dimethyl fumarate in 3 ml benzene was irradiated through filter solution *A*. Progress of the reaction was monitored by periodic analysis of the ^1H nmr spectrum. After 250 h irradiation all of the cyclopropene had been consumed. Formed were the cycloadduct **13** (82%) and the dimers **8** (9%) and **9** (9%).

By consecutive preparative thick layer chromatographic separations the adduct was isolated pure, **13**: mp 103–104 °C; ir (CCl_4) 3005, 2967, 1728, 1595, 1490, 1431, 1199, 1025, and 690 cm^{-1}; uv λ_{max}(MeOH) 219 nm (ε 21 500); ^1H nmr $\delta_{TMS}(CDCl_3)$ 3.15 (s, 1H), 3.38 (s, 3H), 3.49 (d, 1H, J = 4.2 Hz), 3.68 (s, 3H), 4.17 (d, 1H, J = 4.2 Hz), 6.39–7.43 ppm (m, 15 H); ^{13}C nmr chemical shifts: bridgehead carbons, 43.2 and 44.4; methine carbons, 47.7 and 49.9; apex carbon, 39.9; ester methyls, 51.8 and 51.9; carbonyl carbons, 171.9; aryl carbons attached directly to bicyclopentane nucleus, 136.0, 134.9, and 133.2; *ortho*, *meta*, and *para* carbons, 125.6–131.5 ppm; ms (70 eV), 412(1, M^+), 352(100). *Anal.* calcd. for $C_{27}H_{24}O_4$: C 78.62, H 5.86; found: C 78.55, H 5.55.

Irradiation of 0.3 M 1,2,3-Triphenylcyclopropene and 0.3 M Maleic Anhydride

A solution containing 82 mg (0.3 mmol) 1,2,3-triphenylcyclopropene, 29 mg (0.3 mmol) maleic anhydride in 1 ml benzene was irradiated through filter solution *B*. The solution was irradiated for 188 h, after which analysis of the ^1H nmr spectrum revealed that all the cyclopropene had been consumed with the subsequent formation of the photocycloadduct **14** (77%) and the cyclopropene dimers **8** (20%) and **9** (3%).

The solvent was removed on a rotatory evaporator and the resulting oil dissolved in minimal hot cyclohexane. Cooling of this solution resulted in precipitation of 108 mg slightly yellow crystals. Successive recrystallizations from cyclohexane afforded pure adduct **14**: mp 147–150 °C; ir (CCl_4) 2828, 2717, 1836, 1769, 1504, 1459, 1253, 1118, 1012, 956, and 694 cm^{-1}; uv λ_{max}(MeOH) 218 nm (ε 13 900); ^1H nmr $\delta_{TMS}(CDCl_3)$ 3.06 (s, 1H), 3.59 (s, 2H), 6.34–7.54 ppm (m, 15H); ^{13}C nmr chemical shifts: bridgehead carbons, 46.1; methine carbons, 50.6; apex carbon, 45.0; carbonyl carbons 169.0; aryl carbons attached directly to bicyclopentane nucleus, 134.3 and 132.8; *ortho*, *meta*, and *para* carbons, 124.8–131.1 ppm; ms (70 eV), 366(20, M^+), 294(100).

Exact mass calcd. for $C_{25}H_{18}O_3$: 366.1256; found (ms): 366.1264.

Irradiation of 0.3 M 1,2,3-Triphenylcyclopropene and 0.3 M Maleic Anhydride with 0.1 M Fluorenone Present as Sensitizer

A solution containing 82 mg (0.3 mmol) 1,2,3-triphenylcyclopropene, 30 mg (0.3 mmol) maleic anhydride, 18 mg (0.1 mmol) fluorenone in 1 ml benzene was irradiated through filter solution *B*. The progress of the reaction mixture was followed by analysis of the ^1H nmr spectrum at various time intervals. After 6 h irradiation, ^1H nmr analysis revealed that all of the cyclopropene had been consumed. Products formed were the photocycloadduct **14** (60%) and the two cyclopropene dimers **8** (28%) and **9** (13%).

Thermolysis of ***6***

A solution containing 30 mg (0.08 mmol) **6** dissolved in 0.5 ml *ortho*-dichlorobenzene was placed in a thick-walled nmr tube which was evacuated and sealed. The tube was placed in an oil bath maintained at 170 °C. Periodic checks of the solution by analysis of the ^{1}H nmr spectra revealed that even after 8 h heating no apparent change was observed.

Thermolysis of ***12***

A solution containing 5 mg (0.02 mmol) **12** dissolved in 0.5 ml *ortho*-dichlorobenzene was placed in a thick walled ^{1}H nmr tube which was evacuated and sealed. The nmr tube was placed in an oil bath maintained at 173 °C. Periodic checks of the solution by analysis of the ^{1}H nmr spectra revealed that even after 13 h heating no apparent change was observed.

Isomerization of ***13***

A solution of 31 mg (0.08 *M*) of **13** in 1 ml of *ortho*-dichlorobenzene in a thick walled ^{1}H nmr tube was sealed after three freeze–pump–thaw cycles. The tube was placed in a constant temperature oil bath which was maintained to ±0.02 °C by a Fisher Proportional Temperature Control Unit. The ^{1}H nmr spectra were evaluated periodically. The individual rate constants at each of the five temperatures are listed in Table 1. The rate constants were used in an Arrhenius plot to determine the activation parameters (Fig. 5).

Consecutive preparative thick layer chromatographic separations afforded pure rearranged adduct as a clear viscous oil, **15**: ir (CCl_4) 3040, 2960, 1735, 1600, 1433, 1202, 1006, and 693 cm^{-1}; ^{1}H nmr $\delta_{TMS}(CDCl_3)$ 3.27 (s, 3H), 3.38 (d, 1H, J = 0.7 Hz), 3.45 (s, 3H), 3.56 (d, 1H, J = 4.5 Hz), 4.40 (d of d, 1H, J = 4.5 and 0.7 Hz), 7.26–7.78 ppm (m, 15H); ^{13}C nmr chemical shifts: bridgehead carbons, 41.2; methine carbons, 42.3 and 44.8; apex carbon, 41.9; ester methyls, 51.1 and 51.9; aryl carbons attached directly to bicyclopentane nucleus, 133.6; *ortho*, *meta*, and *para* carbons, 127.4–130.9 ppm; ms (70 eV), 412(1, M$^+$), 352(100). *Anal.* calcd. for $C_{27}H_{24}O_4$: C 78.62, H 5.86; found: C 78.43, H 5.61. *Mol. Wt.* calcd. (isopiestic) of $C_{27}H_{24}O_4$: 412.46; found: 412.80.

Isomerization of ***15***

Heating of the solution used for the isomerization of **13** was continued, at <90 °C, till complete conversion to **15** occurred. This solution was then placed in a constant temperature oil. bath, maintained at 162.2 °C, and the progress of the thermolysis was followed by ^{1}H nmr spectroscopy. The isomerization ($t_{1/2}$ = 8.7 h) resulted in the formation of two products, **16** and **17**, (40 and 60%, respectively). After 69 h heating the tube was opened, the solvent removed on a rotatory evaporator, and the residue chromatographed on preparative tlc silica gel plates. Isolation afforded the two products **16** and **17** pure.

Evidence that these are the 1,2-diphenylcyclopentene isomers was obtained when both products generated a red colour when degassed methylcyclohexane–isopentane (4:1) solutions were irradiated at 5 °C with a 1 kW medium pressure mercury arc lamp, (indicative of dihydrophenanthrene formation).

The physical data are inconclusive in assigning the stereochemistry of the isomers.

Product 1: mp 109–110 °C; ir (CCl_4) 3043, 2945, 1737, 1436, 1204, 1170, 1100, 1033, and 698 cm^{-1}; uv λ_{max}(MeOH) 218 (ε 24 100), 260 (ε 12 900), 324 nm (ε 855); ^{1}H nmr $\delta_{TMS}(CDCl_3)$ 3.26 (s, 3H), 3.46 (s, 3H), 4.14 (d of d, 1H, J = 9.7 and 8.7 Hz), 4.81 (d of d, 1H, J = 9.7 and 0.9 Hz), 4.86 (d of d, 1H, J = 8.7 and 0.9 Hz), 6.94–7.40 ppm (m, 15H), ms (70 eV): 412(7, M$^+$); 352(100). *Exact mass* calcd. for $C_{27}H_{24}O_4$: 412.1674; found (ms): 412.1664.

Product 2: mp 136–137 °C; ir (CCl_4) 2996, 2934, 1726, 1422, 1183, 1158, 1088, 1021, and 687 cm^{-1}; uv λ_{max}(MeOH) 222 (ε 14 600), 251 nm (ε 10 000); ^{1}H nmr $\delta_{TMS}(CDCl_3)$ 3.58 (s, 3H), 3.62 (t, 1H, J = 6.4 Hz), 3.72 (s, 3H), 4.38 (d of d, 1H, J = 6.4 and 1.8 Hz), 4.62 (d of d, 1H, J = 6.4 and 1.8 Hz), 6.89 (m, 5H), 7.26 ppm (m, 10H); ms (70 eV): 412(7, M$^+$), 352(100). *Exact mass* calcd. for $C_{27}H_{24}O_4$: 412.1674; found (ms): 412.1670.

Acknowledgments

This work was supported by a grant from the National Research Council of Canada. We gratefully acknowledge the assistance of H. Schroeder in obtaining the 100 MHz ^{1}H nmr spectra.

1. J. A. Pincock, R. M. Morchat, and D. R. Arnold. J. Am. Chem. Soc. **95**, 7536 (1973).
2. (*a*) G. E. Palmer, J. R. Bolton, and D. R. Arnold. J. Am. Chem. Soc. **96**, 3708 (1974); (*b*) D. R. Arnold, R. W. Humphreys, W. J. Leigh, and G. E. Palmer. J. Am. Chem. Soc. **98**, 6225 (1976).
3. (*a*) H. M. Frey. J. Am. Chem. Soc. **82**, 5947 (1960); (*b*) K. R. Kopecky, G. S. Hammond, and P. A. Leermakers. J. Am. Chem. Soc. **84**, 1015 (1962); (*c*) W. von E. Doering, R. G. Buttery, R. G. Laughlin, and N. Chaudhuri. J. Am. Chem. Soc. **78**, 3224 (1956); (*d*) P. S. Skell and R. C. Woodworth. J. Am. Chem. Soc. **78**, 4496 (1956).
4. (*a*) M. Franck-Newmann and C. Buchecker. Tetrahedron Lett. 2875 (1973); (*b*) M. Franck-Newmann and C. Buchecker. Angew. Chem. **82**, 549 (1970); (*c*) G. L. Closs, L. R. Kaplan, and V. I. Bendall. J. Am. Chem. Soc. **89**, 3376 (1967); (*d*) G. L. Closs and L. R. Kaplan. J. Am. Chem. Soc. **91**, 2168 (1969); (*e*) H. Dürr and W. Schmidt. Justus Liebigs Ann. Chem. **7**, 1140 (1974).
5. (*a*) C. D. DeBoer, D. H. Wadsworth, and W. C. Perkins. J. Am. Chem. Soc. **95**, 861 (1973); (*b*) H. Dürr. Justus Liebigs Ann. Chem. **723**, 102 (1969).
6. G. S. Hammond *et al.* J. Am. Chem. Soc. **86**, 3197 (1964).
7. L. A. Paquette and L. M. Leichter. J. Am. Chem. Soc. **93**, 5128 (1971).
8. A. Cox, P. de Mayo, and R. W. Yip. J. Am. Chem. Soc. **88**, 1043 (1966).
9. (*a*) S. Nagakura *In* Excited states. Vol. 2. *Edited by* E. C. Lim. Academic Press, New York. 1975, p. 321; (*b*) A. Gupta and G. S. Hammond. J. Am. Chem. Soc. **97**, 254 (1975); (*c*) N. Orbach, R. Potashnik, and M. Ottolenghi. J. Phys. Chem. **76**, 1133 (1972).
10. (*a*) R. A. Caldwell. J. Am. Chem. Soc. **95**, 1690 (1973); (*b*) A. Padwa, M. Dharan, J. Smolanoff, and S. I. Wetmore, Jr. J. Am. Chem. Soc. **95**, 1954 (1973); (*c*) R. Huisgen. Angew. Chem. Int. Ed. Engl. **2**, 565 (1963); **2**, 633 (1963).

11. (*a*) J. P. CHESICK. J. Am. Chem. Soc. **84**, 3250 (1962); (*b*) M. J. JORGENSON, T. J. CLARK, and J. CORN. J. Am. Chem. Soc. **90**, 7020 (1968); (*c*) K. MACKENZIE, W. P. LAY, J. R. TELFORD, and D. L. WILLIAMS-SMITH. Chem. Commun. 761 (1969); (*d*) H. KRISTINSSON and G. S. HAMMOND. J. Am. Chem. Soc. **89**, 5970 (1967); (*e*) M. J. JORGENSON and T. J. CLARK. J. Am. Chem. Soc. **90**, 2188 (1968); (*f*) T. H. KINSTLE, R. L. WELCH, and R. W. EXLEY. J. Am. Chem. Soc. **89**, 3660 (1967); (*g*) M. L. HALBERSTADT and J. P. CHESICK. J. Am. Chem. Soc. **84**, 2688 (1962); (*h*) C. STEEL, R. ZAND, P. HURWITZ, and S. G. COHEN. J. Am. Chem. Soc. **86**, 679 (1964); (*i*) J. A. BERSON, W. BAUER, and M. M. CAMPBELL. J. Am. Chem. Soc. **92**, 7515 (1970); (*j*) R. SRINIVASAN. Int. J. Chem. Kinet. **1**, 133 (1969).
12. (*a*) B. M. FUNG. J. Chem. Phys. **49**, 2973 (1968); (*b*) S. FORSÉN and R. A. HOFFMANN. J. Chem. Phys. **40**, 1189 (1964).
13. A. B. EVNIN, D. R. ARNOLD, L. A. KARNISCHKY, and E. STROM. J. Am. Chem. Soc. **92**, 6218 (1970).
14. R. BRESLOW and H. W. CHANG. J. Am. Chem. Soc. **83**, 2367 (1961).

The sulfohaloform reaction. The stepwise conversion of dialkyl sulfides into alkanesulfonyl chlorides

J. STUART GROSSERT AND RICHARD F. LANGLER

Chemistry Department, Dalhousie University, Halifax, N.S., Canada B3H 4J3

Received October 10, 1975[1]

J. STUART GROSSERT and RICHARD F. LANGLER. Can. J. Chem. **55**, 407 (1977).

A thorough examination of the aqueous oxidative chlorination of 1,3,5-trithiane is described. The results are utilized to explore and delineate the scope of a general, stepwise, oxidative cleavage reaction of dialkyl sulfides in which they are successively halogenated and oxidized to α-polychlorosulfoxides; subsequently, these cleave to form sulfinyl chlorides, which hydrolyze and become further oxidized to yield alkanesulfonyl chlorides. The overall stepwise process is named the 'Sulfohaloform reaction' and the structural requirements of the substrates at each step are explored in detail. A practical, general synthesis of sulfonyl chlorides is presented.

J. STUART GROSSERT et RICHARD F. LANGLER. Can. J. Chem. **55**, 407 (1977).

On a examiné la chloruration oxydative du trithiane-1,3,5 effectuée en phase aqueuse. On utilise les résultats obtenus pour explorer et délimiter l'étendue d'une réaction de clivage oxydative générale qui s'opère par étape et au cours de laquelle des sulfures de dialkyles sont successivement halogénés, oxydés en sulfoxyde d'α-polychlorés et par la suite clivés de façon à fournir des chlorures de sulfinyles qui par hydrolyse et oxydation subséquentes peuvent être transformés en chlorures d'alkanesulfonyles. On a appelé ce processus global par étape 'réaction sulfohaloformique' et on a déterminé en détail les conditions de structures du substrat qui sont nécessaires à chaque étape. On présente une synthèse générale et pratique des chlorures de sulfonyle.

[Traduit par le journal]

Introduction

Some time ago, we outlined (1) the preliminary results from a study of the pathway by which 1,3,5-trithiane, **1**, is converted upon treatment with molecular chlorine in aqueous media, into chloromethanesulfonyl chloride, $ClCH_2 \cdot SO_2 \cdot Cl$, **2**. We now wish to report the results in detail.

In 1940, Lee and Dougherty (2) reexamined the chlorination of 1,3,5-trithiane **1** in aqueous medium, which had originally been reported on by Kostsova (3) in 1935. Lee and Dougherty concluded that 1,4-dichloro-2,3-dithiabutane might be an intermediate and showed that no sulfone could be intervening. In a subsequent study, Douglass *et al.* (4) concluded that chloromethanesulfenyl chloride might be a short-lived intermediate.

Results and Discussion

The Aqueous Chlorination of 1,3,5-Trithiane

When we attempted to prepare **2** using the Lee and Dougherty procedure, it became obvious that **2** was grossly contaminated by other products and the mixture could not be separated conveniently. The nature of these other products was revealed by carrying out a partial chlorination of **1**, from which it was ascertained that no **2** had been formed but rather a number of intermediate products as detailed in Table 1. The results suggested the intermediacy of 1,3-dichloro-2-thiapropane, **3**, and this was confirmed by exhaustive chlorination of **3** in aqueous acetic acid from which **2** was isolated in 70% yield. Since Lee and Dougherty had already shown that oxidative chlorination of sulfides into sulfonyl chlorides did not proceed via sulfones, it became apparent that a study of the pathway of this conversion could be fruitful. In particular, the question as to whether C—S bond cleavage and S—Cl bond formation occurred at the sulfenyl or sulfinyl oxidation level was intriguing. Answers to these questions were obtained from a detailed examination of what emerged as a stepwise pathway by which the dichlorosulfide **3** is converted into the sulfonyl chloride **2** upon chlorination in aqueous medium. The study began with chlorination of the dichlorosulfide **3** in glacial acetic acid with varying water–sulfide ratios. This reaction provided the results shown in Scheme 1.

[1]Revision received September 20, 1976.

TABLE 1. Products from partial chlorination of 1,3,5-trithiane (1 mol) in glacial acetic acid containing water (5 mol)

Product*	Yield (g)	Number of moles isolated	Yield (%)
CH_2O	0.52	0.14	14
CO_2	0.57	0.11	11
$ClCH_2OAc$ (41, 42)	2.29	0.18	18
$ClCH_2{\cdot}O{\cdot}CH_2Cl$ (43, 44)	1.49	0.11	22
$ClCH_2{\cdot}S{\cdot}CH_2Cl$ **3** (40)	8.00	0.53	53
$ClCH_2{\cdot}SS{\cdot}CH_2Cl$	†	0.06	6
Unreacted $(CH_2S)_3$ **1**	1.00	0.06	6

*No CCl_4, $CHCl_3$, CH_2Cl_2, HCO_2H, $ClCH_2{\cdot}SO_2{\cdot}Cl$, or $ClCH_2{\cdot}S{\cdot}Cl$ was detected.
†Yield determined on a separate run.

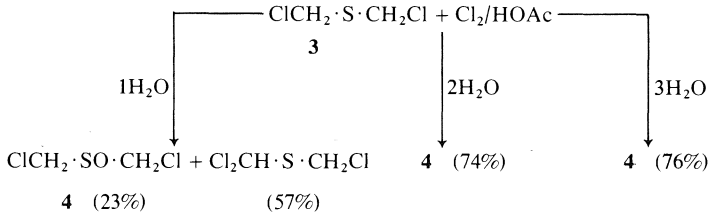

SCHEME 1

These experiments conclusively established 1,3-dichloro-2-thiapropane-2-oxide, **4**, as the next intermediate in the sequence. In a similar manner, chlorination of the dichlorosulfoxide **4** established the intermediacy of 1,1,3-trichloro-2-thiapropane-2-oxide ($Cl_2CH{\cdot}SO{\cdot}CH_2Cl$, **5**) as the subsequent intermediate.

When the trichlorosulfoxide **5** was chlorinated in aqueous acetic acid, only chloromethanesulfonyl chloride, **2**, could be obtained. Although Lee and Dougherty (2) had demonstrated that some sulfones were inert to chlorine–water oxidation, we prepared 1,1,3-trichloro-2-thiapropane-2,2-dioxide and subjected it to chlorination in aqueous acetic acid, from which it was recovered unchanged. Hence it was clear that the intermediate sulfoxide(s) must have reacted with chlorine and cleaved to furnish chloromethanesulfinyl chloride, **6**. Since sulfinyl chlorides are readily hydrolyzed to sulfinic acids (5), it would have been futile to attempt the isolation of **6** from aqueous medium. When the trichlorosulfoxide **5** was chlorinated in dry acetic acid, chloromethanesulfinyl chloride, **6**, could be observed in the nmr of the crude reaction mixture. This was demonstrated by adding authentic **6** to a sample of the crude and following the change in intensity of the chloromethyl signal.

Attempts to isolate the sulfinyl chloride **6** from acetic acid solution were unsuccessful. However, further chlorination led to a good conversion of **6** to the sulfonyl chloride **2** which could be isolated without difficulty.

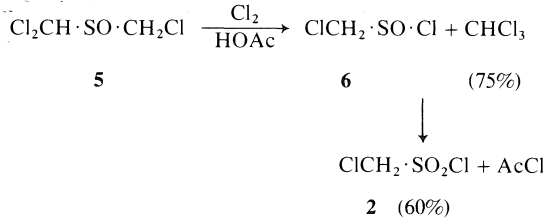

In order to obviate the difficulties experienced in isolating **6** from acetic acid, the trichlorosulfoxide **5** was chlorinated in methylene chloride which permitted the isolation of **6** without complication.

A summary of the pathway for the conversion of 1,3,5-trithiane, **1**, appears in Scheme 2. The grounds for including 1,1,1,3-tetrachloro-2-thiapropane-2-oxide, **7**, in Scheme 2 are presented later.

Mechanisms of Sulfide and Sulfoxide Chlorinations

Mechanisms for the various steps outlined in Scheme 2 are available from previous work. The pathway by which 1,3-dichloro-2-thiapro-

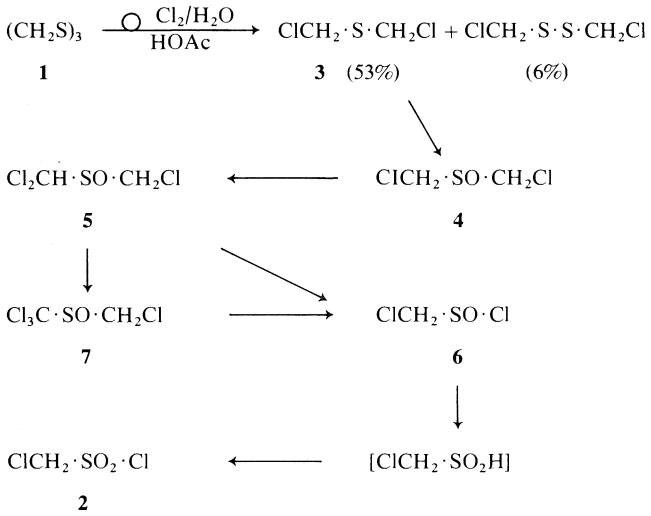

SCHEME 2

pane, **3**, is converted to the corresponding sulfoxide involves chlorosulfonium chloride salt **8** formation prior to nucleophilic attack by water on the sulfur atom of the sulfonium salt. This reaction has ample precedent (6–10). The intermediacy of a species with a sulfur–chlorine bond is supported in a more direct fashion by later work in which chlorination of selected sulfides has been shown to furnish sulfenyl chlorides (11–18).

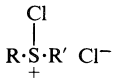

8

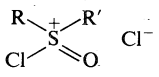

9

The mechanism for the Pummerer rearrangement of chlorosulfonium chlorides has been carefully examined by Wilson *et al.* (13, 14). The mechanism basically involves an E2 type elimination of HCl from the intermediate chlorosulfonium chloride salt with attack by chloride ion on the resultant carbonium-sulfonium ion.

The chlorination of sulfoxides has received a great deal of attention (19–30) since 1968 and this now includes stereochemical studies (24, 27) also. These have led Montanari's group to postulate that the intermediate oxochlorosulfonium chloride **9** undergoes simultaneous proton abstraction and chlorine atom migration to furnish the α-chlorosulfoxide.

Our own observations that α-trichlorosulfoxides, such as **5**, furnish sulfinyl chlorides and chlorocarbons upon chlorination in methylene chloride are the most direct evidence available that the chlorination of sulfoxides proceeds through an intermediate species having a sulfur–chlorine bond.

The Chlorine-induced C—S Cleavage Reaction of α-Polychlorosulfoxides

Although the reactions of sulfides and sulfoxides with chlorine to furnish α-chloro compounds via Pummerer rearrangements and/or to hydrolyze to give sulfoxides or sulfones had been observed previously, the cleavage reaction of the α-polychlorosulfoxide **5** had not been previously reported. We therefore examined it in some detail, by comparison of products formed in three solvents of different polarities.

Chlorination of **5** in methylene chloride furnished chloromethanesulfinyl chloride, **6** (72%), chloroform (53%), and carbon tetrachloride (11%). Direct cleavage of the oxochlorosulfonium chloride salt derived from **5** gives **6** and chloroform. However, the presence of carbon tetrachloride as a product implicated the intermediacy of the tetrachlorosulfoxide **7** (see Scheme 3).[2]

Chlorination of the trichlorosulfoxide **5** in glacial acetic acid furnished chloromethanesulfinyl chloride (isolated as the sulfonyl chloride) and chloroform. No carbon tetrachloride was formed indicating that direct

[2]An alternative formulation in which trichloromethyl carbanion ($:\bar{C}Cl_3$) is displaced by attack of Cl^- at sulfur in **7** is untenable in view of the product distribution when **10** or **11** are chlorinated (*vide infra*).

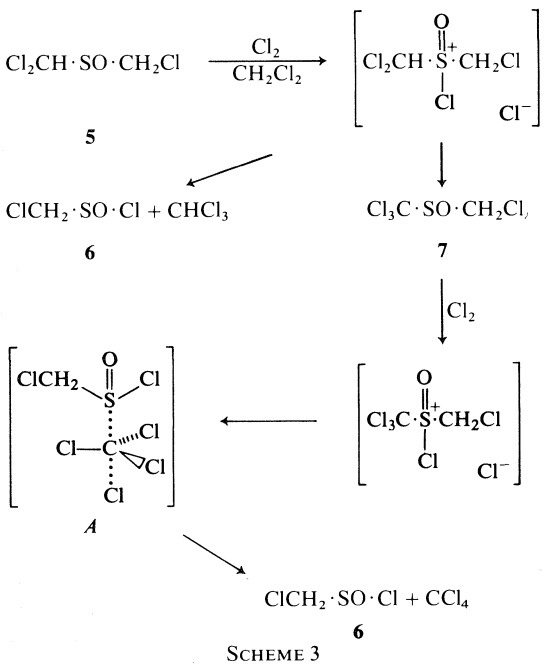

SCHEME 3

cleavage rather than Pummerer-type rearrangement is more favored in acetic acid than in the less polar methylene chloride.

By contrast, the results in [1] showed that chlorination of **5** in water permitted solvolysis to compete with cleavage by chloride ion.

[1] $Cl_2CH\cdot SO\cdot CH_2Cl \xrightarrow[H_2O]{Cl_2}$ (**5**)

$ClCH_2\cdot SO_2Cl + CHCl_3 + CCl_4 + CO_2$

2 (65%) (6%) (10%) (67%)

see footnote 3

The isolation of carbon dioxide indicated that much of the cleavage occurred by nucleophilic attack of water on the most electrophilic carbon atom of the intermediate oxochlorosulfonium chloride salt. The nucleophilic competition observed when the chlorinations were carried out in aqueous media is the basis for treating the cleavage step as an ionic rather than free-radical reaction.

Chlorination of the tetrachlorosulfoxide **7** in water afforded chloromethanesulfonyl chloride **2** (68%), carbon tetrachloride (20%), and carbon dioxide (60%). Simple calculations permit the formulation of a detailed pathway for the chlorination of **5** in water (see Scheme 4).

The reactions which involve sulfinyl chloride intermediates in aqueous medium are assumed to proceed through the sulfinic acids. However, in dry acetic acid, sulfinic acids cannot intervene. Amongst the mechanistic possibilities is the elimination of HCl from the intermediate oxodichlorosulfonium chloride salt **9** to furnish an intermediate analogous to sulfene (31). Should this have been the case, then chlorination of a sulfinyl chloride in acetic acid-d_1 would have furnished monodeuterated sulfonyl chloride. In fact, chlorination of methanesulfinyl chloride in acetic acid-d_1 furnished undeuterated methanesulfonyl chloride, thereby requiring acetolysis of the intermediate oxodichlorosulfonium chloride or, alternatively, the formation of a sulfinate–acetate mixed anhydride before reaction with molecular chlorine.

Hence, the complete pathway for the conversion of 1,3-dichloro-2-thiapropane, **3**, into chloromethanesulfonyl chloride, **2**, has been established and the cleavage step shown to occur on 1,1,3-trichloro-2-thiapropane-2-oxide, **5**. It seemed appropriate at this point to examine the structural requirements of the chlorosulfoxide substrates in general in terms of the cleavage step. It will be shown in the ensuing sections how both α-chlorosulfides and -sulfoxides, or just simply dialkylsulfides, may be subjected to stepwise chlorination, oxidation, and cleavage steps, leading ultimately to sulfonyl chlorides, by a process which we propose is aptly named the 'sulfohaloform reaction'.

Chlorination of Methyl Sulfoxides

In order to complement the work described above on α,α′-polychlorosulfoxides, 1,1-dichloro-2-thiapropane-2-oxide, **10**, was chlorinated in methylene chloride and the results in [2] were obtained.

[2] $Cl_2CH\cdot SO\cdot CH_3 \xrightarrow[CH_2Cl_2]{Cl_2}$ (**10**)

$CH_3\cdot SO\cdot Cl + CCl_4 + CHCl_3$

(76%) (55%) (12%)

Since carbon tetrachloride was formed it is obvious that most of the cleavage reaction was occurring on the more highly chlorinated sulfoxide **11**. Similar results were observed when either **10** or **11** were chlorinated in glacial

[3]Formic acid is readily oxidized to carbon dioxide under the reaction conditions.

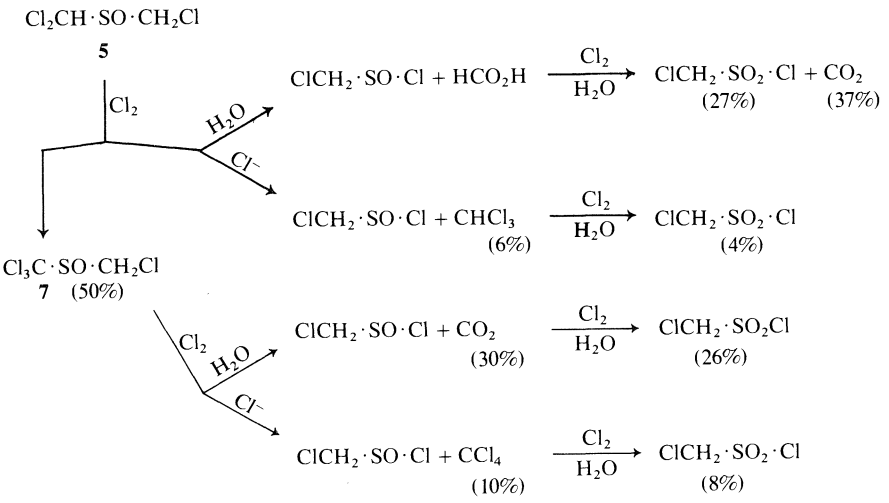

SCHEME 4

acetic acid:

	$CH_3 \cdot SO_2 \cdot Cl$	CCl_4	AcCl
$Cl_2CH \cdot SO \cdot CH_3$ (**10**) Cl_2/HOAc →	75%	76%	67%
$Cl_3C \cdot SO \cdot CH_3$ (**11**) →	86%	70%	70%

Hence, when cleavage occurs via nucleophilic attack by chloride ion, it is necessary for the sulfoxide substrate to have at least three α-chlorine atoms, regardless of the substitution pattern. It is interesting to note that the third chlorine atom is approximately equally effective in promoting smooth chlorinolysis of the sulfoxide (in methylene chloride or acetic acid) either when it is deployed to increase the electrophilicity of the carbon atom undergoing nucleophilic attack (*e.g.* **11**) or when it is located in a position which enhances the electronegativity of the leaving group (*e.g.* **5**).

Chlorination of **10**, **11**, and **7** in water furnished markedly different results, as follows:

Cl_2/H_2O	$CH_3 \cdot SO_2 \cdot Cl$	**2**	CCl_4	CO_2
$Cl_2CH \cdot SO \cdot CH_3$ (**10**) →	70%	40%	22%	68%
$Cl_3C \cdot SO \cdot CH_3$ (**11**) →	50%	24%	20%	56%
$Cl_3C \cdot SO \cdot CH_2Cl$ (**7**) →	0%	68%	20%	60%

The intermediacy of **11** in the chlorination of **10** and of **7** in the chlorination of **11** was established by isolating **11** and **7** from the chlorination. A straightforward analysis permits the formulation of a detailed pathway for the reaction of **10** with chlorine in water (see Scheme 5). It is now evident that, unlike the haloform reaction which requires α-trichloro substrates (ketones) for cleavage to occur in aqueous medium, the sulfohaloform reaction can take place with α-dichloro substrates (sulfoxides) in aqueous medium.

Chlorination of α-Chlorosulfides to Form Sulfonyl Chlorides

Since the isolation of the intermediate sulfoxides in the sulfohaloform reaction was experimentally rather difficult we undertook an examination of the chlorination of α-chlorosulfides in aqueous medium in order to find evidence for the intermediacy of the α-chlorosulfoxides. The chlorination of 1,3-dichloro-2-thiapropane, **3**, in water furnished the corresponding sulfone (4%) and chloromethanesulfonyl chloride **2** (70%).

We have already established that chlorination of **3** proceeds primarily through the corresponding sulfoxide even in dilute aqueous medium. Thus the observation of low yields of the corresponding sulfone in this type of reaction can be taken to implicate the intermediacy of the sulfoxide since the sulfone must, of necessity, have been formed via the sulfoxide. Application of this criterion to 1-chloro-2-thiapropane, **12**, was successful in implicating the intermediacy of the corresponding sulfoxide also, since the sulfone was isolated in 1% yield.

These results along with those from 2-chloro-

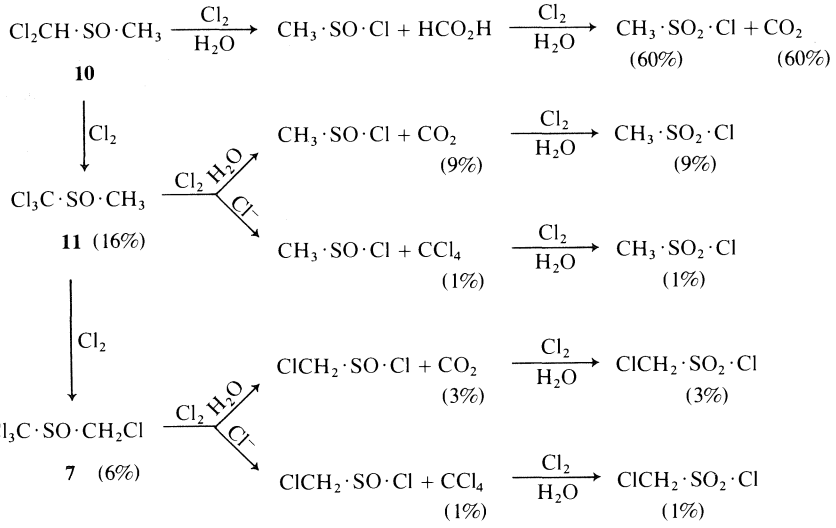

SCHEME 5

3-thiapentane and 4-chloro-5-thianonane are tabulated in Table 2. The process is obviously a potentially useful sulfonyl chloride synthesis.

The overall results from the chlorination of chloromethyl phenyl sulfide in aqueous medium also showed the same behaviour, *i.e.* the formation of chloromethyl phenyl sulfone (2.5%) (along with benzenesulfonyl chloride (68%)) implicated the intermediacy of the chloromethyl sulfoxide. In contrast to the previous cases, the chlorination of chloromethyl phenyl sulfide took a long time to reach completion. Furthermore, analysis of the partially chlorinated reaction mixture indicated that large amounts of trichloromethyl phenyl sulfoxide were present before any significant amount of benzenesulfonyl chloride was formed. This result indicated that the phenyl ring virtually nullifies the electron-withdrawing effect of one chlorine atom. Such an observation can be readily rationalized via resonance forms in which the phenyl ring shares its π electrons with the sulfinyl group of the intermediate oxochlorosulfonium chloride.

TABLE 2. Yields of sulfonyl chlorides prepared by chlorination of α-chlorosulfides in water

Sulfide	Sulfonyl chloride	Yield (%)
$ClCH_2·S·CH_2Cl$	$ClCH_2·SO_2·Cl$	70
$CH_3·S·CH_2Cl$	$CH_3·SO_2·Cl$	75
$Ph·S·CH_2Cl$	$Ph·SO_2·Cl$	67
$CH_3CH_2·S·CHClCH_3$	$CH_3CH_2·SO_2·Cl$	90
n-$C_4H_9·S·CHCl·n·C_3H_7$	n-$C_4H_9·SO_2·Cl$	94

Thus far we had observed that α-polychlorinated sulfoxides could be converted to sulfonyl chlorides without the formation of any sulfones. Chlorination of α-dichloro and simple α-chlorosulfoxides gave rise to minor amounts of sulfones. It appeared, however, that a potential barrier to extending this reaction to unchlorinated sulfides and sulfoxides might be the formation of substantial amounts of unchlorinated sulfones. This problem was solved as follows.

Chlorination of Sulfides to Form Sulfonyl Chlorides

We began this portion of the work by exploring reactions of some conveniently available sulfoxides in order both to maximize sulfone formation and to see if we could find reaction conditions which would suppress it. Such chlorinations of DMSO were illuminating, giving the results in [3] and [4]. Similar results

[3] $CH_3·SO·CH_3 + Cl_2 \xrightarrow{H_2O\text{–}HOAc(1:1)}$

$CH_3·SO_2·Cl + CH_3·SO_2·CH_3 + ClCH_2·SO_2·CH_3$
(48%) (15%) (3%)

[4] $CH_3·SO·CH_3 + Cl_2 \xrightarrow{H_2O}$

$CH_3·SO_2·Cl + CH_3·SO_2·CH_3$
(26%) (70%)

were obtained from the chlorination of di-*n*-propyl sulfoxide in water. Hence, sulfone formation was indeed a major potential complication to the useful formation of sulfonyl chlorides from unchlorinated sulfides and sulfoxides. This was not surprising since the results are consistent with those of Durst and Tin (32) and of Cinquini and co-workers (33), both of whom have observed sulfone formation via nucleophilic attack on oxochlorosulfonium cations.

However, after experimentation, it was found that *chlorination of sulfides in dilute aqueous acetic acid was successful in converting the sulfides into sulfonyl chlorides, in high yield,* without the interference of sulfone formation (see Table 3). By contrast, chlorination of the corresponding sulfoxides under the same conditions furnished significantly larger quantities of sulfones, implying that the reaction pathway from the sulfides does *not* proceed through the corresponding sulfoxides but rather through the corresponding α-chlorosulfides, and hence through the α-chlorosulfoxides, etc.

Since the conditions had been established, which permitted direct chlorination of sulfides to sulfonyl chlorides by controlling the amount of water present in the solvent, one final mechanistic problem remained. In water, the cleavage step is primarily achieved with water functioning as the nucleophile. In dry acetic acid, chloride ion is the exclusive nucleophile. It was not obvious just how competitive chloride ions would be *vis-à-vis* water in dilute aqueous acetic acid, and in order to monitor this, we have chlorinated thiacyclopentane and isolated the ω-chlorinated butanesulfonyl chlorides, as in [5].

The formation of **13** was not unexpected, since chlorination of thiacyclopentane in glacial acetic acid permits its isolation in 28.6% yield as reported by Runge *et al.* (34). Since chloro-

TABLE 3. Yields of sulfonyl chlorides prepared from sulfides and sulfoxides by chlorination in dilute aqueous acetic acid

Sulfides/sulfoxide	Sulfonyl chloride	Yield (%)
$CH_3CH_2{\cdot}S{\cdot}CH_2CH_3$	$CH_3CH_2{\cdot}SO_2{\cdot}Cl$	97
$CH_3(CH_2)_3{\cdot}S{\cdot}(CH_2)_3CH_3$	$CH_3(CH_2)_3{\cdot}SO_2{\cdot}Cl$	86
$PhCH_2{\cdot}S{\cdot}CH_2Ph$	$PhCH_2{\cdot}SO_2{\cdot}Cl$	74
$CH_3(CH_2)_2{\cdot}SO{\cdot}(CH_2)_2CH_3$	$CH_3(CH_2)_2{\cdot}SO_2{\cdot}Cl$	76

[5] 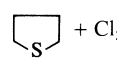 $+ Cl_2 \xrightarrow[HOAc]{H_2O}$

$Cl(CH_2)_4SO_2{\cdot}Cl + Cl_2CH(CH_2)_3{\cdot}SO_2{\cdot}Cl$

13 (8.9%) **14** (4.5%)

sulfonium chloride salts are inert to acetolysis (35), the origin of this monochlorosulfonyl chloride, under either conditions, is undoubtedly through direct chlorinolysis of thiacyclopentane to give 4-chlorobutane sulfenyl chloride. The driving force for this reaction is the release of ring strain and is parallel to the reactions of thiacyclobutane with chlorine in chloroform, or with sulfuryl chloride in pentane (36), which furnish 3-chloropropanesulfenyl chloride. Therefore the formation of **13** is not relevant to a consideration of the normal cleavage step in the sulfohaloform reaction.

However, Runge *et al.* (34) did not report the formation of 4,4-dichlorobutanesulfonyl chloride, **14**, upon chlorinating thiacyclopentane in glacial acetic acid. The sensitivity of α-chloro-chlorosulfonium chloride salts to hydrolysis, implicates the intermediacy of the α-chlorosulfoxide in the formation of **14**. The absence of larger amounts of the ω-dichlorosulfonyl chloride, as well as the failure of any ω-trichlorobutanesulfonyl chloride to form, indicate quite clearly that cleavage by chloride ions in dilute aqueous acetic acid is not an important or competitive process and therefore cleavage by the nucleophilic attack of water remains the major process in the cleavage step in dilute aqueous acetic acid.

The major pathways in the generalized sulfohaloform reaction have therefore been defined, and the overall reaction is outlined in Scheme 6.

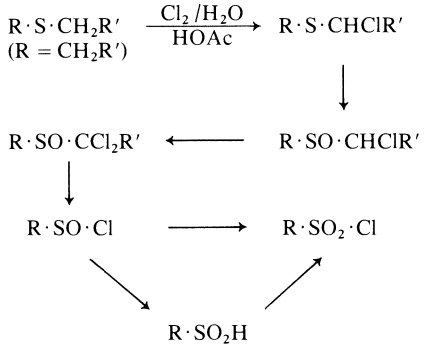

SCHEME 6. The sulfohaloform reaction

Experimental

General

Most experimental details have been described previously (37). Mass spectral samples were directly introduced using an all-glass probe and the spectra run at 70 eV with a source temperature of 150 °C. Elemental analyses were by Dr. F. Pascher (Bonn) or Galbraith Laboratories (Knoxville, Tenn.). Gas–liquid chromatographic analyses were carried out with an N_2 flow rate of 50 ml/min and the column temperature was 40 to 50 °C. Unless otherwise indicated, "washing an organic layer with NaOH" means that a 2.5% w/v solution of NaOH was used to wash the organic layer, usually 100 ml aliquots, until the aqueous layer remained basic. "Standard work-up" of hydrophobic solvents implies that they were dried ($MgSO_4$), filtered, and then rotary evaporated.

Chlorinations

Chlorine flow rates were standardized by the use of a calibrated rotameter. All chlorinations were maintained at 25–30 °C by an ice–water bath. Unless otherwise stated, rates and reaction times are given in the form "232/50". This means a flow rate of 232 ml/min and a reaction time of 50 min. All times are given in minutes.

Yields

It was often necessary to analyze reaction mixtures quantitatively before work-up in order to avoid obtaining yields which reflected losses during work-up. None of the sulfur-containing compounds were detectable on glc. All sulfur compounds were observable in the nmr and integration of the nmr spectrum furnished satisfactory molar ratios. Carbon tetrachloride was detectable on glc and could be interrelated with the sulfur compounds by the addition of methylene chloride which appeared both in the glc trace and the nmr spectrum. The molar ratios, the total sample weight, and the following equation permit the calculation of the weight of each component in any mixture.

$$w_i = x_i a_i T\left(\sum_{c=1}^{n} x_c a_c\right)^{-1}$$

where x_i = mole fraction of 'i'th component, a_i = molecular weight of 'i'th component, w_i = weight (in grams) of the 'i'th component, T = total sample weight (in grams).

CO_2 Determinations

Full details are provided elsewhere (37).

Chlorination of 1,3,5-Trithiane

1,3,5-trithiane (17.11 g) was suspended in glacial acetic acid (38 ml) and distilled water (8 ml) was added. The reaction became non-exothermic by the end of the chlorination (232/40). The reaction mixture was diluted with ice water (25 ml), the organic phase separated, and the aqueous phase set aside.

The organic phase was diluted with $CHCl_3$[4] (150 ml), dried ($MgSO_4$), filtered, and the $CHCl_3$ distilled off.

The residue was fractionated giving the results outlined in Table 4.

[4]An additional run was carried out using ether as the solvent in order to check for the presence of chlorocarbons.

The aqueous phase was diluted to a volume of 150 ml with 95% ethanol, from 100 ml of which authenticated 2,4-dinitrophenylhydrazone of formaldehyde (2.03 g) was isolated (39). The results obtained after isolation and identification of the major products are given in Table 1. Full details of identification methods are provided elsewhere (37).

Preparation of 1,3-Dichloro-2-thiapropane, 3

1,3-Dichloro-2-thiapropane **3** was prepared from 1,3,5-trithiane as described by Truce *et al.* (40). The distilled material from this reaction contains a persistent impurity which showed an ir band at 1523 cm^{-1}. The contaminant was completely removed when the dichlorosulfide was chromatographed on silica gel with CCl_4 using sulfide–silica gel ratios as low as 1:3. In a typical run 1,3,5-trithiane (300 g) furnished crude 1,3-dichloro-2-thiapropane (170 g). After column chromatography and redistillation, high purity dichlorosulfide **3** (121 g, 42.5%) was obtained.

Chlorination of 3 in H_2O/HOAc

1,3-Dichloro-2-thiapropane **3** was dissolved in glacial acetic acid (50 ml) and distilled water added. Following chlorination (232 ml/min), ice water (75 ml) was added and the resultant mixture extracted with $CHCl_3$ (4 × 100 ml). The combined $CHCl_3$ layers were washed first with NaOH then with distilled water. Standard work-up afforded products which were isolated by fractional distillation. 1,3-Dichloro-2-thiapropane-2-oxide, **4**, had mp 36.5–37.5 °C; tlc (37) R_F 0.48 (ether), after recrystallization from CCl_4; ir ($CHCl_3$) 1070 cm^{-1} (ν_{SO}); nmr ($CDCl_3$) δ 4.57 (q, J = 11.0 Hz); ms ions at m/e 146 ($M^{\ddagger}$), 111 and 49. The dichlorosulfoxide **4** was identical with authentic material (45) by nmr, ir, mp, and mixture mp. See Table 5 for details of products obtained.

Chlorination of 1,3-Dichloro-2-thiapropane-2-oxide, 4

1,3-Dichloro-2-thiapropane-2-oxide **4** was chlorinated as described in the previous experiment.

The products were isolated by fractional distillation: 1,1,3-trichloro-2-thiapropane-2-oxide, **5**, had bp 94 °C/0.25 torr; R_F 0.55 on tlc (4:1 $CHCl_3$–ether); ir ($CHCl_3$) 1080 cm^{-1} (ν_{SO}); nmr ($CDCl_3$) δ 4.70 (s, 2H) and 6.60 (s, 1H); ms ions at m/e 180 ($M^{\ddagger}$) 83, 49. Oxidation of **5** (40) furnished material identical to authentic trichlorosulfone by ir, nmr, and bp. Details of the products obtained are found in Table 6.

Preparation of $Cl_2CH{\cdot}S{\cdot}CH_2Cl$

Details are provided elsewhere (37). The product was identical to known material (40).

Preparation of 1,1,3-Trichloro-2-thiapropane-2-oxide, 5

1,1,3-Trichloro-2-thiapropane (24.56 g) was dissolved in glacial acetic acid (100 ml), distilled water (4.4 ml) was added, and the mixture was chlorinated (232/50). The reaction mixture was fractionated, furnishing 1,1,3-trichloro-2-thiapropane-2-oxide (19.6 g, 72.5%).

Chlorination of 5 in H_2O–HOAc

1,1,3-Trichloro-2-thiapropane-2-oxide **5** (16.17 g) was dissolved in glacial acetic acid (50 ml) and distilled water (4.4 ml) was added. Following chlorination (232/39), ice water (75 ml) was added and the organic phase was separated. The aqueous phase was washed with $CHCl_3$ (100 ml) which was combined with the organic phase.

TABLE 4. Fractionation of the products from the chlorination of 1,3,5-trithiane

Fraction	Boiling point (°C/torr)	Components	Weight (g)
1	74–86/760	$CHCl_3$, $ClCH_2OAc$ $ClCH_2{\cdot}O{\cdot}CH_2Cl$*	1.84
2	20–40/25	$ClCH_2OAc$ $ClCH_2{\cdot}O{\cdot}CH_2Cl$	0.71
3	40–68/20	$ClCH_2{\cdot}S{\cdot}CH_2Cl$	5.31
4	70–80/20	$ClCH_2{\cdot}S{\cdot}CH_2Cl$ $ClCH_2{\cdot}S{\cdot}S{\cdot}CH_2Cl$ Unidentified products	3.87
5	Cold trap in vacuum line	$ClCH_2{\cdot}O{\cdot}CH_2Cl$ $ClCH_2OAc$ $ClCH_2{\cdot}S{\cdot}CH_2Cl$	3.23
6	Solid deposited in fractionating column	1,3,5-trithiane	1.0

**CAUTION*: bischloromethyl ether is a potent carcinogen (38).

TABLE 5. Products of the chlorination of **3** in H_2O/HOAc

Weight (g)	Chlorination time (min)	Volume H_2O (ml)	Products	Yield (g)*
15.67	22	2.2	$ClCH_2{\cdot}SO{\cdot}CH_2Cl$ **4**	4.03 (22.7)
			$Cl_2CH{\cdot}S{\cdot}CH_2Cl$	11.29 (56.6)
16.21	20	4.4	$ClCH_2{\cdot}SO{\cdot}CH_2Cl$ **4**	13.47 (74.2)
17.01	30	6.6	$ClCH_2{\cdot}SO{\cdot}CH_2Cl$ **4**	14.52 (76.1)

*Percentage yield in parentheses.

Standard work-up gave a concentrate which was fractionated (glass-bead column, 67 torr), to give chloromethanesulfonyl chloride **2** (8.48 g, 64.0%) and a distillation residue of unreacted **5** (1.80 g, 11.2%).

*Chlorination of **5** in HOAc*

1,1,3-Trichloro-2-thiapropane-2-oxide **5** (15.85 g) was chlorinated (232/30) in glacial acetic acid (50 ml). An nmr spectrum of the reaction mixture showed a molar ratio of 100:73:27, $CHCl_3/ClCH_2{\cdot}SO{\cdot}Cl/ClCH_2{\cdot}SO_2{\cdot}Cl$ respectively. The reaction was chlorinated further with progress being monitored hourly. After 3.5 h the sulfinyl chloride – sulfonyl chloride ratio was 3:7.

Ice water (75 ml) was added to the reaction mixture and the organic phase was removed. The aqueous phase was extracted with ether (100 ml) and the ether layer combined with the organic layer. The combined organic portion was diluted with ether to 200 ml and then divided into equal portions, *A* and *B*.

A. Portion *A* was dried ($MgSO_4$) and concentrated. The bulk of the acetic acid was distilled off at 75 torr. The residue was dissolved in $CHCl_3$ (50 ml) and continuously extracted with water for 1 h. The aqueous phase was discarded and the extraction resumed with fresh water for 1 h. Standard work-up of the $CHCl_3$ gave a residue which was fractionated at reduced pressure to yield chloromethanesulfonyl chloride **2** (3.90 g).

B. Quantitative glc and nmr integration established the yield of $CHCl_3$ to be equal to 75%. The ether solution was extracted with NaOH, washed with distilled water, dried ($MgSO_4$), and fractionated, to furnish pure $CHCl_3$ identical with authentic material by bp, glc, and nmr.

*Chlorination of **5** in CH_2Cl_2*

1,1,3-Trichloro-2-thiapropane-2-oxide **5** (15.34 g) was chlorinated (232/30) in CH_2Cl_2 (50 ml). Methylene chloride (10 ml) was distilled off and the presence of both $CHCl_3$ (53.2%) and CCl_4 (10.7%) was demonstrated (glc). The bulk of the chlorocarbons were distilled off and the residue rectified at reduced pressure affording chloromethanesulfinyl chloride **6** (8.14 g, 71.7%), bp 163.5 °C/760 torr; ir ($CHCl_3$) 1150 cm^{-1} (ν_{SO}); nmr ($CDCl_3$) δ 4.83 (5); ms *m/e* 62, 49. Hydrolysis in distilled water, followed by chlorination in CH_2Cl_2, furnished chloromethanesulfonyl chloride **2** as expected.

*Chlorination of **5** in H_2O*

1,1,3-Trichloro-2-thiapropane-2-oxide **5** (11.32 g) was

TABLE 6. Products of the chlorination of 1,3-dichloro-2-thiapropane-2-oxide, **4**

Weight (g)	Chlorination time (min)	Volume H_2O (ml)	Products	Yield (g)*
16.25	25	2.2	$ClCH_2{\cdot}SO{\cdot}CH_2Cl$ **4**	3.27 (19.8)
			$Cl_2CH{\cdot}SO{\cdot}CH_2Cl$ **5**	10.3 (51.3)
15.40	30	4.4	$Cl_2CH{\cdot}SO{\cdot}CH_2Cl$ **5**	14.20 (74.2)
16.07	30	6.6	$ClCH_2{\cdot}SO{\cdot}CH_2Cl$ **4**	3.25 (20.2)
			$Cl_2CH{\cdot}SO{\cdot}CH_2Cl$ **5**	10.85 (55)

*Percentage yield in parentheses.

chlorinated (232/105) in distilled water (50 ml). The organic phase was pipetted off and dried ($CaCl_2$). Gas–liquid chromatography established the presence of $CHCl_3$ (6.3%) and CCl_4 (10%). The organic phase was distilled at reduced pressure furnishing chloromethanesulfonyl chloride **2** (6.05 g, 64.5%).

In a separate experiment on **5** (1.155 g), the CO_2 was isolated as $BaCO_3$ (0.802 g, 66.6%). Chlorination time was 50 min (116 ml/min).

*Preparation of 1-Chloro-2-thiapropane, **12***

Details of this preparation are given elsewhere (36, 37).

Preparation of $Cl_3C{\cdot}S{\cdot}CH_2Cl$

1-Chloro-2-thiapropane **12** (100 g) was chlorinated (448/330) in CCl_4 (250 ml). The reaction mixture was rectified furnishing 1,1,3-tetrachloro-2-thiapropane (181.9 g, 87.4%); bp 188 °C/760 torr; nmr δ 5.00 (s) ($CDCl_3$).

Preparation of 1,1,1,3-Tetrachloro-2-thiapropane-2-oxide, 7

Distilled water (12 ml) was added to 1,1,1,3-tetrachloro-2-thiapropane (31.19 g) in acetic acid (100 ml). After chlorination (232/50), the reaction mixture was fractionated to give **7** (16.8 g, 50%), bp 78 °C/0.5 torr; R_F 0.65 ($CHCl_3$) which could be crystallized from 95% ethanol at 0 °C but melted upon returning to ambient temperature; ir ($CHCl_3$) 1135 cm^{-1} (ν_{SO}); nmr ($CDCl_3$) δ 4.57 (q, J = 11.0 Hz); ms *m/e* 117, 82, 62, and 49. *Anal.* calcd. for $C_2H_2Cl_4SO$: C 11.13, H 0.93, O 7.41; found: C 11.35, H 0.98, O 7.38. Oxidation of **7** (40) yielded material identical to authentic tetrachlorosulfone by nmr, ir, and mixture mp.

Chlorination of 7 in H_2O

1,1,1,3-Tetrachloro-2-thiapropane-2-oxide **7** (16.56 g) was chlorinated (448/240) in distilled water (50 ml). The organic phase was pipetted off and dried ($CaCl_2$). Gas–liquid chromatography showed that CCl_4 (20%) had been formed. The residue was distilled furnishing chloromethanesulfonyl chloride **2** (7.80 g, 67.5%).

In a separate experiment (Cl_2: 232/50) on **7** (1.030 g) CO_2 was isolated as $BaCO_3$ (0.500 g, 60%).

*Preparation of 1,1-Dichloro-2-thiapropane-2-oxide, **10**[5]*

DMSO (16.21 g) was chlorinated (232/43) in glacial acetic acid (50 ml) and distilled water (6.6 ml). The reaction was repeated on a second portion of DMSO (16.01 g). The combined reaction mixtures were diluted with water (150 ml) and extracted ($CHCl_3$, 6 × 100 ml). The $CHCl_3$ was washed with NaOH then with distilled water (100 ml), dried ($MgSO_4$), and evaporated. The residue was distilled at reduced pressure to yield 1,1-dichloro-2-thiapropane-2-oxide **10**[5] (17.53 g, 28.8%). Recrystallization (CCl_4) of the distilled material afforded pure **10** as bundles of crystals (mp 32–33 °C); R_F 0.49 (ether); ir ($CHCl_3$) 1080 cm^{-1} (ν_{SO}); nmr ($CDCl_3$) δ 3.75 (3H, s) and 6.42 (1H, s); ms *m/e* 146 ($M^{\ddagger}$), 83 and 63. Oxidation of **10** (40) yielded material identical to authentic dichlorosulfone by nmr, ir, and mixture mp.

*Chlorination of **10** in CH_2Cl_2*

1,1-Dichloro-2-thiapropane-2-oxide **10** (16.22 g) was chlorinated (232/25) in CH_2Cl (50 ml). A fraction was distilled at atmospheric pressure (44–75 °C). The residue was rectified at reduced pressure with a −75 °C cold trap in the vacuum line. The fraction from the atmospheric distillation plus the trap material contained $CHCl_3$ (1.5 g, 11.8%) and CCl_4 (8.8 g, 51.8%). The vacuum distillation furnished methanesulfinyl chloride (8.24 g, 76.3%); bp 136.5 °C/760 torr; ir ($CHCl_3$) 1140 cm^{-1} (ν_{SO}); nmr ($CDCl_3$) δ 3.37 (s); ms *m/e* 98 ($M^{\ddagger}$), 82, 63, and 48. Hydrolysis in distilled water, followed by chlorination in CH_2Cl_2 furnished methanesulfonyl chloride.

*Chlorination of **10** in HOAc*

1,1-Dichloro-2-thiapropane-2-oxide **10** (15.81 g) was chlorinated (232/30) in glacial acetic acid (50 ml). Acetyl

[5]*CAUTION:* this sulfoxide ($Cl_2CH{\cdot}SO{\cdot}CH_3$) is very unstable at room temperature and if stored in a tightly stoppered container may generate sufficient gas pressure to explode the container within 4 h. Proper storage for periods of 2 weeks (maximum) requires that the sample be stored in the dark using an explosion-proof container, at or below −32 °C.

chloride was established as being present in a 1:1 ratio with CCl_4 by nmr and glc. The reaction mixture was added to CH_2Cl_2 (100 ml) and ice water (100 ml). The organic phase was separated, dried ($MgSO_4$), filtered, and the CH_2Cl_2 distilled off. A fraction (bp 44–75 °C) was collected at atmospheric pressure and the residue was distilled at 50 torr with a cold trap in the vacuum line. The atmospheric pressure fraction plus the trap material contained CCl_4 (11.10 g, 66.6%). The vacuum distillation afforded methanesulfonyl chloride (9.2 g, 75%).

*Chlorination of **10** in H_2O*

(a) Partial Chlorination

1,1-Dichloro-2-thiapropane-2-oxide **10** (4.30 g) was chlorinated (232/28) in distilled water (25 ml). The reaction mixture was extracted with $CHCl_3$ (100 ml) which was washed with NaOH (50 ml aliquots), then with distilled water (50 ml), followed by a standard work-up. The residue was the trichlorosulfoxide **11** (0.54 g, 10.3%), as established by nmr, ir, and tlc.

(b) Exhaustive Chlorination

1,1-Dichloro-2-thiapropane-2-oxide **10** (16.18 g) was chlorinated (232/85) in distilled water (50 ml). The organic phase was pipetted off and dried over $CaCl_2$. Gas–liquid chromatography established the presence of CCl_4 (2.4%), a sample of which was obtained by distillation at atmospheric pressure and was shown to be identical with authentic material by glc, ms, and bp.

Distillation of the residue at reduced pressure yielded methanesulfonyl chloride (8.84 g, 70.0%).

In a separate experiment on **10**, (1.130 g; Cl_2: 232/50), CO_2 was isolated as $BaCO_3$ (1.067 g, 67.5%).

Preparation of 1,1,1-Trichloro-2-thiapropane

1-Chloro-2-thiapropane (16.01 g) was chlorinated (232/35) in CH_2Cl_2 (50 ml). The reaction mixture was distilled, furnishing 1,1,1-trichloro-2-thiapropane (16.88 g, 61%); bp 148–149 °C; nmr ($CDCl_3$), singlet at δ 2.75.

*Preparation of 1,1,1-Trichloro-2-thiapropane-2-oxide (**11**)*

1,1,1-Trichloro-2-thiapropane (16.36 g) was chlorinated (232/27) in glacial acetic acid (50 ml) and distilled water (6.6 ml). Water (75 ml) was added and the solution was extracted with $CHCl_3$ (4 × 100 ml), which was washed with NaOH, followed by distilled water. After standard work-up, the residue was distilled furnishing **11** (11.00 g, 61.7%) bp 86–88 °C/1.6 torr; crystals (from methanol) had mp 63–65 °C; R_F 0.62 (4:1 chloroform–ether); ir ($CHCl_3$) 1100 cm^{-1} (ν_{SO}); nmr ($CDCl_3$) δ 2.92 (s); ms *m/e* 180 ($M^{\ddagger}$), 117, 82, 63, and 47. *Anal.* calcd. for $C_2H_3Cl_3SO$: C 13.24, H 1.67, O 8.82, S 17.67; found: C 13.26, H 1.56, O 8.74, S 17.27. Oxidation of **11** (40), yielded material identical to authentic trichlorosulfone by nmr, ir, and mixture mp.

*Chlorination of **11** in HOAc*

1,1,1-Trichloro-2-thiapropane-2-oxide **11** (16.83 g) was chlorinated (232/30) in glacial acetic acid (50 ml). Acetyl chloride was established as being present in a 1:1 ratio with CCl_4 by glc on the crude mixture. A small amount of acetyl chloride was distilled off and identified by ir, nmr, and glc. Work-up identical to that described under "Chlorination of **10** in HOAc" afforded CCl_4 (9.95 g, 69.9%) and methanesulfonyl chloride (9.20 g, 86.1%).

*Chlorination of **11** in H_2O*

(a) Partial Chlorination

1,1,1-Trichloro-2-thiapropane-2-oxide **11** (5.01 g) was chlorinated (232/30) in distilled water (25 ml). The organic phase was pipetted off and added to $CHCl_3$ (100 ml), which was washed with NaOH (50 ml aliquots) and then with water. After standard work-up, the residue was a mixture of unreacted **11** (0.75 g) and 1,1,1,3-tetrachloro-2-thiapropane-2-oxide **7** (1.06 g, 18.5%). The sulfoxide mixture was chromatographed on a column of silica gel (180 g). Elution with $CHCl_3$ (1100 ml) furnished **7** and an additional litre of $CHCl_3$ furnished **11**. The tetrachlorosulfoxide **7** was distilled and shown to be identical with authentic material by bp, nmr, ir, and tlc.

(b) Exhaustive Chlorination

1,1,1-Trichloro-2-thiapropane-2-oxide **11** (16.04 g) was chlorinated (448/185) in distilled water (50 ml). The organic phase was pipetted off and dried over $CaCl_2$. Gas–liquid chromatography established that CCl_4 had formed in 20% yield. The aqueous phase was extracted with $CHCl_3$ (2 × 100 ml) which was combined with the original organic phase. Standard work-up gave a residue which was fractionated at reduced pressure to furnish a mixture of methanesulfonyl chloride (5.08 g, 50%) and chloromethanesulfonyl chloride (3.16 g, 23.8%). Further distillation at atmospheric pressure gave four fractions, each of which was still a mixture. Fraction *1* (bp 161–163 °C) contained *ca.* 15% chloromethanesulfonyl chloride and 85% methanesulfonyl chloride.

A portion of fraction *1* (212 mg) was added dropwise to a cooled (5 °C) solution of vanillin (211 mg) in pyridine (0.5 ml). The ice water bath was removed and the solution was stirred at room temperature for 1 h. The reaction mixture was diluted with $CHCl_3$ (50 ml) which was extracted with 2.5% NaOH (50 ml), 2.5% HCl (50 ml), and distilled water (50 ml). Standard work-up gave a pale yellow oil (287 mg) which was dissolved in 95% ethanol (3 ml) and stored in the refrigerator overnight. Colorless crystals were filtered off and dried affording vanillin methanesulfonate (186 mg). After recrystallization, the sulfonate ester was shown to be identical to authentic material by tlc, ir, and mixture mp.

The concentrated mother liquor from the first crystallization was chromatographed on a preparative-layer plate (ether–$CHCl_3$, 1:19). Methanol extraction of the upper band (R_F 0.55, detected by 250 nm uv light) furnished a colorless oil (30.2 mg), which was identical to vanillin chloromethanesulfonate by tlc, nmr, and ir.

In a separate experiment on **11** (1.030 g) carbon dioxide was isolated as $BaCO_3$ (0.928 g, 55.5%). Chlorination time was 45 min.

*Chlorination of **3** in H_2O*

1,3-Dichloro-2-thiapropane **3** (16.41 g) was chlorinated (448/200) in distilled water (50 ml). Ice water (75 ml) was added and the reaction mixture extracted with $CHCl_3$ (2 × 100 ml). The residue from standard work-up of the $CHCl_3$ was distilled at reduced pressure yielding

chloromethanesulfonyl chloride (13.07 g, 70.4%). The distillation residue was covered with sufficient 10% NaOH to establish a pH > 7. The solution was acidified (concentrated HCl) and poured into $CHCl_3$ (200 ml). Standard work-up gave 1,3-dichloro-2,2-dioxide (790 mg, 3.8%); after recrystallization (95% ethanol), this was shown to be identical with authentic dichlorosulfone by nmr, ir, mp, and mixture mp.

Chlorination of ***12*** *in* H_2O

1-Chloro-2-thiapropane **12** (15.76 g) was chlorinated (448/98) in distilled water (50 ml) similarly to the chlorination of **3**. Products were methanesulfonyl chloride (14.10 g, 75.4%) and 1-chloro-2-thiapropane-2,2-dioxide (193 mg, 1.2%). Details are provided elsewhere (37).

Chlorination of $Ph{\cdot}S{\cdot}CH_2Cl$ *in* H_2O

Chloromethyl phenyl sulfide (16.01 g) was chlorinated (448/130) in distilled water (50 ml). By the end of this time all of the organic material had crystallized from solution and all reaction had ceased. The reaction mixture was extracted with $CHCl_3$ (2 × 100 ml), followed by standard work-up. Analytical tlc ($CHCl_3$ eluant) showed a spot at R_F 0.49 (assumed to be $Cl_2CH{\cdot}SO{\cdot}Ph$), a spot at R_F 0.70 (identical to $Cl_3C{\cdot}SO{\cdot}Ph$), and a spot at R_F 0.81 (identical to $Ph{\cdot}SO_2{\cdot}Cl$). The bulk of the material was $Cl_3C{\cdot}SO{\cdot}Ph$ and an ir of the crude showed the expected band at 1100 cm^{-1} (ν_{SO}). The crude product was dissolved in acetic acid – H_2O, 1:1, (50 ml) and chlorination (448/130) was repeated. Repetition of the work-up outlined above furnished crude product which showed about a 1:1 mixture of $Cl_3C{\cdot}SO{\cdot}Ph$ to $Ph{\cdot}SO_2{\cdot}Cl$ on tlc and the complete absence of the product previously observed at R_F 0.49. This new crude product was further chlorinated (448/130) in glacial acetic acid (15 ml) and distilled water (25 ml). The reaction mixture was extracted with $CHCl_3$ (4 × 100 ml) which was dried ($MgSO_4$) and rotary evaporated. Analytical tlc (37) showed the absence of $Cl_3C{\cdot}SO{\cdot}Ph$. The residue was fractionated at reduced pressure providing benzenesulfonyl chloride (12.04 g, 67.3%), identical to authentic material by tlc, nmr, ir, and bp. The distillation residue contained $Ph{\cdot}SO_2{\cdot}CH_2{\cdot}Cl$ (500 mg, 2.5%). Two preparative-layer plates were spotted with residue (100 mg/plate) and eluted with $CHCl_3$. Methanol extraction of the bands at R_F 0.70 furnished chloromethyl phenyl sulfone identical with authentic material by nmr, ir, and tlc.

Preparation of $Ph{\cdot}SO{\cdot}CCl_3$

Trichloromethyl phenyl sulfide (16.20 g) was chlorinated (232/27) in glacial acetic acid (50 ml) and distilled water (6.6 ml). The reaction was rerun on more $Ph{\cdot}SO{\cdot}CCl_3$ (15.96 g). The combined reaction mixtures were diluted with water (100 ml) and extracted with $CHCl_3$ (4 × 100 ml) which was washed with 5% NaOH and then with distilled water. Standard work-up gave a residue which contained unreacted sulfide (10.44 g) and $Ph{\cdot}SO{\cdot}CCl_3$ (20.19 g, 58.9%).

Some crude material (26.33 g) was chromatographed on silica gel (1560 g). Elution with CCl_4 (6 l) furnished trichloromethyl phenyl sulfide (8.86 g). Further elution with diethyl ether (5.2 l) yielded trichloromethyl phenyl sulfoxide (17.35 g). Recrystallization (95% ethanol) to give colorless needles; mp 77–78 °C; R_F 0.61 ($CHCl_3$); ir ($CHCl_3$) 1100 cm^{-1} (ν_{SO}); nmr δ 7.75 (m); ms m/e 242 ($M^{\ddagger}$), 125, 117, 109, 77, and 51. *Anal.* calcd. for $C_7H_5Cl_3OS$: C 34.52, H 2.07, Cl 43.7; found: C 34.79, H 2.28, Cl 42.9. Oxidation of the sulfoxide (40) gave sulfone identical to that obtained by oxidation of the sulfide by tlc, nmr, ir, and mixture mp.

Chlorination of $CH_3CH_2{\cdot}S{\cdot}CHClCH_3$ *in* H_2O

2-Chloro-3-thiapentane (16.77 g) was chlorinated (448/104) in distilled water (50 ml). The reaction mixture was partitioned between ice water (75 ml) and CH_2Cl_2 (10 ml). The aqueous phase was extracted with CH_2Cl_2 (100 ml). Standard work-up of the combined CH_2Cl_2 layers gave a residue which was rectified at reduced pressure giving ethanesulfonyl chloride (15.54 g, 89.6%) bp 90–92 °C/55 torr.

Chlorination of $n\text{-}C_4H_9{\cdot}S{\cdot}CHCl{\cdot}CH_2CH_2CH_3$ *in* H_2O

4-Chloro-5-thianonane (15.95 g) was chlorinated (448/100) in distilled water (50 ml). The reaction mixture was extracted with $CHCl_3$ (2 × 100 ml) which was dried ($MgSO_4$), and evaporated. The residue was fractionated at reduced pressure furnishing 1-butanesulfonyl chloride (13.0 g, 94.3%).

Chlorination of DMSO in 1:1 H_2O–*HOAc*

DMSO (15.91 g) was chlorinated (448/110) in glacial acetic acid (25 ml) and distilled water (25 ml). Products were methanesulfonyl chloride (11.30 g, 48%), dimethyl sulfone (2.78 g, 14.7%), and 1-chloro-2-thiapropane-2,2-dioxide (0.75 g, 2.9%). Details are provided elsewhere (37).

Chlorination of DMSO in H_2O

DMSO (16.11 g) was chlorinated (448/97) in distilled water. Total dimethyl sulfone isolated was 13.64 g (70.3%) and total methanesulfonyl chloride isolated was 6.23 g (26.2%). Details are provided elsewhere (37).

Chlorination of $(n\text{-}C_3H_7)_2SO$ *in* H_2O

Di-*n*-propyl sulfoxide (15.79 g) was chlorinated (448/105) in distilled water (50 ml). Ice water (75 ml) was added and the mixture was extracted with $CHCl_3$ (2 × 100 ml). Standard work-up gave a residue which was fractionated at reduced pressure to yield 1-propanesulfonyl chloride (6.71 g, 39.8%); bp 104–106 °C/65 torr, and di-*n*-propyl sulfone (5.65 g, 31.3%); bp 88 °C/0.1 torr.

Preparation of Sulfonyl Chlorides from the Corresponding Symmetric Sulfide or Sulfoxide

The substrate was dissolved in glacial acetic acid (50 ml) and the appropriate quantity of distilled water was added. Chlorine (448 ml/min) was bubbled through the solution. Chlorination was interrupted as necessary to maintain the reaction at room temperature. Ice water (75 ml) was added to the reaction mixture which was then extracted with $CHCl_3$ (4 × 100 ml). The $CHCl_3$ layers were washed with 2.5% w/v NaOH (3 × 100 ml) and subjected to standard work-up.

Diethyl sulfide (16.01 g, 7.5 ml H_2O_2 108 min chlorination) gave a residue which was fractionated at reduced pressure to yield ethanesulfonyl chloride (22.12 g, 96.6%).

Di-*n*-propyl sulfoxide (16.00 g, 6.6 ml H_2O, 90 min chlorination) gave a residue which was fractionated at reduced pressure to yield di-*n*-propyl sulfone (1.50 g,

8.4%) and 1-propanesulfonyl chloride (12.94 g, 75.6%).

Di-*n*-butyl sulfide (16.00 g, 6.6 ml H_2O, 126 min chlorination) gave a residue which was rectified at reduced pressure to furnish 1-butanesulfonyl chloride (14.74 g, 86.2%).

Dibenzyl sulfide (16.01 g, 6.6 ml H_2O, 75 min chlorination) gave a residue which was crystallized from benzene – low-boiling petroleum ether to yield phenylmethanesulfonyl chloride (8.82 g). The mother liquor furnished another 1.71 g to give a total yield of 73.3%.

Chlorination of Thiacyclopentane in HOAc–H_2O

Thiacyclopentane (15.97 g) was chlorinated (448/106) in glacial acetic acid (50 ml) and distilled water (7.5 ml). Ice water (75 ml) was added and the mixture was extracted with $CHCl_3$ (4 × 100 ml). The $CHCl_3$ was washed with 2.5% w/v NaOH (3 × 100 ml) and distilled water (100 ml), dried ($MgSO_4$), and rotary evaporated. The residue was fractionated at reduced pressure to yield a mixture of sulfonyl chlorides. The mixture contained $Cl(CH_2)_4SO_2Cl$ **13** (3.10 g, 8.9%) and $Cl_2CH(CH_2)_3SO_2Cl$ **14** (1.83 g, 4.5%). A sample (2.01 g) of the distillate was chromatographed on a silica gel column (200 g). Elution with $CHCl_3$ (650 ml) furnished a clean mixture of **13** and **14** (2:1). A second column run on 1.99 g of distillate furnished additional 2:1 mixture. The total chromatographed mixture from chromatography weighed 1.78 g. Strong bands at 1350 and 1162 cm^{-1} were virtually the only bands present in the ir of the 2:1 mixture.

A portion of the chromatographed mixture (1.01 g) was added drop-wise to a cold solution of phenol (419 mg) in pyridine (3 ml) and the reaction mixture was stirred at room temperature for 1 h. Chloroform (100 ml) was added and the solution washed with 2.5% NaOH (50 ml), 2.5% HCl (50 ml), and distilled water (50 ml). The $CHCl_3$ was dried ($MgSO_4$), and rotary evaporated to yield a crude phenate mixture (938 mg), crystallization of which (95% ethanol) afforded three crops. Crops *1* and *2* (150 mg) were mixtures of phenates. Crop *3* (130 mg) was pure $Cl_2CH(CH_2)_3SO_2OPh$. The mother liquor from the third crystallization afforded residual phenate mixture (560 mg).

The mixture (560 mg) was chromatographed on five preparative tlc plates with benzene elution (2×). Each plate had five bands visible under uv light, *i.e.*, R_F 0.97, 0.91, 0.83, 0.77, 0.68.

The band at R_F 0.77 gave $Cl(CH_2)_4SO_2OPh$ (251 mg) as a colorless oil.

The band at R_F 0.83 gave $Cl_2CH(CH_2)_3SO_2OPh$ (138 mg) as fine needles from 95% ethanol, mp 60–61.5 °C; ($CHCl_3$) 1375 and 1140 cm^{-1} (ν_{SO_2}); nmr δ 2.25 (4H, t), 3.34 (2H, t), 5.83 (1H, t), and 7.34 (5H, s); ms *m/e* 125, 94, 65 and 53. *Anal.* calcd. for $C_{10}H_{12}Cl_2O_3S$: C 42.42, H 4.27, Cl 25.04, O 16.95, S 11.32; found: C 42.80, H 3.94, Cl 24.84, O 17.04, S 11.19.

The remaining three bands gave minor quantities and were discarded.

Acknowledgements

We thank Dalhousie University and the National Research Council of Canada for financial support. The award of an NRCC postgraduate fellowship to one of us (R.F.L.) is gratefully acknowledged.

1. J. S. Grossert and R. F. Langler. J. Chem. Soc. Chem. Commun. 49 (1973).
2. S. W. Lee and G. Dougherty. J. Org. Chem. **5**, 81 (1940).
3. A. G. Kostsova. Acta Univ. Voroneg. **8**, 92 (1935); Chem. Abstr. **32**, 6618 (1938).
4. I. B. Douglass, V. G. Simpson, and A. K. Sawyer. J. Org. Chem. **14**, 272 (1949).
5. F. Wudl, D. A. Lightner, and D. J. Cram. J. Am. Chem. Soc. **89**, 4099 (1967).
6. W. E. Lawson and T. P. Dawson. J. Am. Chem. Soc. **49**, 3119 (1927).
7. K. Fries and W. Vogt. Justus Liebigs Ann. Chem. **381**, 337 (1911).
8. T. Zincke and W. Frohneberg. Ber. Dtsch. Chem. Ges. **43**, 837 (1910).
9. T. Zincke and W. Ruppersberg. Ber. Dtsch. Chem. Ges. **48**, 120 (1915).
10. T. Zincke and W. Frohneberg. Ber. Dtsch. Chem. Ges. **42**, 2721 (1909).
11. H. Kwart and L. J. Miller. J. Am. Chem. Soc. **80**, 884 (1958).
12. W. G. Phillips and K. W. Ratts. J. Org. Chem. **36**, 3145 (1971).
13. G. E. Wilson, Jr. and M. G. Huang. J. Org. Chem. **35**, 3002 (1970).
14. G. E. Wilson, Jr. and R. Albert. J. Org. Chem. **38**, 2160 (1973).
15. H. Kwart and R. K. Miller. J. Am. Chem. Soc. **78**, 5008 (1956).
16. H. Kwart and R. W. Body. J. Org. Chem. **30**, 1188 (1965).
17. H. Kwart, R. W. Body, and D. M. Hoffman. Chem. Commun. 765 (1967).
18. H. Kwart and P. S. Strilko. Chem. Commun. 767 (1967).
19. R. N. Loeppky and D. C. K. Chang. Tetrahedron Lett. 5415 (1968).
20. G. Tsuchihashi and S. Iriuchijima. Bull. Chem. Soc. Jpn. **43**, 2271 (1970).
21. M. Cinquini, S. Colonna, and F. Montanari. J. Chem. Soc. D, 607 (1969).
22. S. Iriuchijima and G. Tsuchihashi. Tetrahedron Lett. 5259 (1969).
23. M. Cinquini and S. Colonna. J. Chem. Soc. Perkin Trans. 1, 1883 (1972).
24. M. Cinquini, S. Colonna, R. Fornasier, and F. Montanari. J. Chem. Soc. Perkin Trans. 1, 1886 (1972).
25. M. Cinquini, S. Colonna, and D. Iarossi. Boll. Sci. Fac. Chim. Ind. Bologna, **27**, 197 (1969).
26. M. Cinquini, S. Colonna, and D. Landini. J. Chem. Soc. Perkin Trans. 2, 296 (1972).
27. P. Calzavara, M. Cinquini, S. Colonna, R. Fornasier, and F. Montanari. J. Am. Chem. Soc. **95**, 7431 (1973).
28. J. Klein and H. Stollar. J. Am. Chem. Soc. **95**, 7437 (1973).
29. G. Tsuchihashi and K. Ogura. Bull. Chem. Soc. Jpn. **44**, 1726 (1971).

30. K.-C. TIN and T. DURST. Tetrahedron Lett. 4643 (1970).
31. J. F. KING. Acc. Chem. Res. **8**, 10 (1975), and references therein.
32. T. DURST and K.-C. TIN. Can. J. Chem. **49**, 2374 (1971).
33. R. ANNUNZIATA, M. CINQUINI, and S. COLONNA. J. Chem. Soc. Perkin Trans. 1, 2057 (1972).
34. F. RUNGE, E. PROFFET, and R. DRUZ. J. Prakt. Chem. **2**, 279 (1955).
35. J. S. GROSSERT, W. R. HARDSTAFF, and R. F. LANGLER. J. Chem. Soc. Chem. Commun. 50 (1973).
36. F. G. BORDWELL and B. M. PITT. J. Am. Chem. Soc. **77**, 572 (1955).
37. G. K. CHIP and J. S. GROSSERT. Can. J. Chem. **50**, 1233 (1972); J. S. GROSSERT and R. F. LANGLER. J. Chromatogr. **97**, 83 (1974); R. F. LANGLER. Ph.D. Thesis, Dalhousie University. 1975.
38. Org. React. **19**, 422 (1972).
39. R. L. SHRINER, R. C. FUSON, and D. Y. CURTIN. The systematic identification of organic compounds. 5th ed. Wiley, New York. 1964. p. 126.
40. W. E. TRUCE, G. H. BIRUM, and E. T. MCBEE. J. Am. Chem. Soc. **74**, 3594 (1952).
41. H. E. FRENCH and R. ADAMS. J. Am. Chem. Soc. **43**, 651 (1921).
42. P. M. G. BAVIN. Can. J. Chem. **42**, 704 (1964).
43. F. S. H. HEAD. J. Chem. Soc. 2972 (1963).
44. S. R. BUC. U.S. Patent No. 2704299 (1955); Chem. Abstr. **50**, 1891c (1956).
45. F. G. MANN and W. J. POPE. J. Chem. Soc. Trans. **123**, 1172 (1923).

Intermediate stages of the sulfohaloform reaction. Preparation of α-halosulfoxides and sulfinyl chlorides. Oxygen-transfer reactions

J. STUART GROSSERT, WILLIAM R. HARDSTAFF, AND RICHARD F. LANGLER
Chemistry Department, Dalhousie University, Halifax, N.S., Canada B3H 4J3

Received October 10, 1975[1]

J. STUART GROSSERT, WILLIAM R. HARDSTAFF, and RICHARD F. LANGLER. Can. J. Chem. **55**, 421 (1977).

Details are provided of synthetic routes from dialkyl sulfides to both α-halosulfoxides and sulfinyl chlorides. In the case of the former, oxidation of α-halosulfides to the sulfoxide stage is achieved by chlorine in acetic acid containing controlled amounts of water. Sulfinyl chlorides are prepared by chlorination of α-polyhalosulfoxides in methylene chloride. During investigations into the details of the sulfohaloform reaction, a number of novel redox reactions involving oxygen transfer between sulfur species have been observed and these are presented. They include a reduction of a sulfoxide with thionyl chloride.

J. STUART GROSSERT, WILLIAM R. HARDSTAFF et RICHARD F. LANGLER. Can. J. Chem. **55**, 421 (1977).

On fournit des détails permettant de synthétiser à la fois les α-halosulfoxydes et les chlorures de sulfinyles à partir des sulfures de dialkyles. Dans le premier cas, l'oxydation des sulfures α-halogénés en sulfoxyde est effectuée par du chlore dans de l'acide acétique contenant des quantités contrôlées d'eau. On prépare les chlorures de sulfinyles par chloruration de sulfoxydes α-polyhalogénés dans le chlorure de méthylène. Au cours des études effectuées afin d'élucider les détails de la réaction sulfohaloformique, on a observé un certain nombre de nouvelles réactions d'oxydo réduction impliquant un transfert d'oxygène entre des espèces contenant du soufre; on présente ces nouvelles réactions. Elles comprennent une réduction d'un sulfoxyde par le chlorure de thionyle.

[Traduit par le journal]

Synthesis of α-Polychlorosulfoxides

Sulfoxides are usually synthesized by the controlled oxidation of sulfides (1, 2). Such a reaction always has the potential of giving higher oxidation products, for example, sulfones, and there is ample literature documentation of reactions designed to avoid such complications (2, 3). Initial investigations of the use of halogens in aqueous media to oxidize sulfides demonstrated that molecular bromine afforded much smoother and more readily controlled reactions than did molecular chlorine (ref. 1, p. 216). Since the work of Fries and Vogt in 1911 (4), no further attempts appear to have been made to use chlorine for the oxidation of sulfides to sulfoxides.

The excessive reactivity of chlorine becomes an advantage, however, when the oxidation of heavily chlorinated sulfides is attempted since the

$$R_1R_2R_3C{\cdot}SO{\cdot}CH_2R_4$$

1 $R_1 = Cl; R_2 = R_3 = R_4 = H$

2 $R_1 = R_2 = Cl; R_3 = R_4 = H$

3 $R_1 = R_4 = Cl; R_2 = R_3 = H$

4 $R_1 = R_2 = R_4 = Cl; R_3 = H$

5 $R_1 = R_2 = R_3 = R_4 = Cl$

6 $R_1 = R_2 = R_3 = Cl; R_4 = H$

low nucleophilicity of such sulfides introduces a rate retardation, in comparison to that of unchlorinated sulfides, which makes the reaction easy to control. The complication involved in chlorinating more nucleophilic sulfides and sulfoxides is that the product is often nearly as reactive as the starting material. For example, chlorination of DMSO in aqueous acetic acid, at room temperature, leads to the formation of 1-chloro-2-thiapropane-2-oxide, **1**, which is seriously contaminated with 1,1-dichloro-2-thiapropane-2-oxide, **2**. The desired control for the oxidation of sulfides with chlorine in aqueous media does not obtain until the starting sulfide has at least two α-chlorine atoms. Thus controlled chlorination of 1,3-dichloro-2-thiapropane furnished the corresponding sulfoxide **3** without difficulty (5).

In a typical experiment, the polychlorosulfide

[1]Revision received September 20, 1976.

TABLE 1. Preparation of α-polychlorosulfoxides from α-polychlorosulfides by chlorination (232 ml/min) in glacial HOAc containing 3 equiv. of water

Starting sulfide	Sulfoxide product	Yield (%)	Chlorination time (min)
$ClCH_2{\cdot}S{\cdot}CH_2Cl$	$ClCH_2{\cdot}SO{\cdot}CH_2Cl$ **3**	77	20
$Cl_2CH{\cdot}S{\cdot}CH_2Cl$	$Cl_2CH{\cdot}SO{\cdot}CH_2Cl$ **4**	65	20
$Cl_3C{\cdot}S{\cdot}CH_2Cl$	$Cl_3C{\cdot}SO{\cdot}CH_2Cl$ **5**	50	50
$Cl_3C{\cdot}S{\cdot}CH_3$	$Cl_3C{\cdot}SO{\cdot}CH_3$ **6**	62	27
$Cl_3C{\cdot}S{\cdot}Ph$	$Cl_3C{\cdot}SO{\cdot}Ph$ **7**	63	27

(*ca.* 16 gm) was dissolved in acetic acid (50 ml) and 3 equiv. of water were added. Chlorine was bubbled into the solution and the temperature maintained at 25 to 30 °C. The results obtained on the systems utilized in this study are given in Table 1.

Many reagents available for the conversion of sulfides to sulfoxides give rise to some sulfone as well (2, 6). Although the preparation of α-polychlorosulfoxides utilizing chlorine and aqueous acetic acid is not complicated by sulfone formation, it is normally complicated by sulfonyl chloride formation. However, sulfonyl chloride formation occurs as a minor side reaction and the sulfonyl chloride can be readily removed by washing the sulfoxide with aqueous base. By contrast, sulfones are often difficult to remove from the corresponding sulfoxide, particularly when purification is attempted by recrystallization (6).

A useful modification of this synthetic method involves the conversion of a sulfide to the corresponding α-chlorosulfoxide in one step. Since chlorosulfonium chloride salts are inert to acetolysis (7), the starting sulfide can be chlorinated in glacial acetic acid to furnish the homologous α-chlorosulfide. After the addition of water further chlorination affords the corresponding sulfoxide. In this way, 1,3-dichloro-2-thiapropane has been converted routinely into 1,1,3-trichloro-2-thiapropane-2-oxide, **4**, in 50% yield.

Synthesis of Sulfinyl Chlorides

The development of synthetic methods for the preparation of sulfinyl chlorides has received relatively little attention. Most sulfinyl chlorides have been made by variations of the same reaction developed by Douglass, namely the controlled solvolysis of alkyldichlorosulfonium chloride salts (8, 9). The chief difficulties with this method center around finding a suitable solvent in which to carry out the solvolysis. For example, when acetic acid is employed as the solvent, excess chlorine initiates a slow but smooth transformation of the sulfinyl chloride into the corresponding sulfonyl chloride. However, this problem seems to have been overcome by employing acetic anhydride for the solvent. Using a different synthetic method, some aromatic sulfinyl chlorides have been prepared by reaction between the sulfinic acid and thionyl chloride (10).

Our studies on the cleavage of α-polychlorosulfoxides with chlorine (5) led to the selection of methylene chloride as the solvent in order to prevent solvolysis reactions. The results of the initial examination of this reaction indicated that α-trichlorosulfoxides would undergo facile cleavage when treated with chlorine in methylene chloride, whereas α-dichlorosulfoxides would not undergo cleavage in useful yields.

A summary of the sulfoxide substrates examined is presented in Table 2.

It is noteworthy that the yield of sulfinyl chloride from chlorination of phenyl trichloromethyl sulfoxide was poor and that the compound could not be separated intact from the reaction mixture. This observed poor yield and the long chlorination time are precisely what would have been expected from an alkyl α,α-dichloroalkyl sulfoxide. It appears, therefore, that the phenyl ring acts to suppress the electron-withdrawing effect of approximately one chlorine atom, which may be rationalized by postulating the delocalization in the intermediate oxochlorosulfonium chloride of positive charge on sulfur around the aromatic ring.

In its generalized form, this method of alkanesulfinyl chloride preparation requires that trichloromethyl alkyl sulfoxides be available. Since the chlorination of alkyl methyl sulfides normally

TABLE 2. Preparation of alkanesulfinyl chlorides from α-polychlorosulfoxides by chlorination (232 ml/min) in CH_2Cl_2

Starting sulfoxide	Sulfinyl chloride product	Yield (%)	Chlorination time (min)
$ClCH_2{\cdot}SO{\cdot}CHCl_2$ **4**	$ClCH_2{\cdot}SO{\cdot}Cl$	72	30
$ClCH_2{\cdot}SO{\cdot}CCl_3$ **5**	$ClCH_2{\cdot}SO{\cdot}Cl$	80	50
$CH_3{\cdot}SO{\cdot}CHCl_2$ **2**	$CH_3{\cdot}SO{\cdot}Cl$	76	25
$CH_3{\cdot}SO{\cdot}CCl_3$ **6**	$CH_3{\cdot}SO{\cdot}Cl$	77	25

goes preferentially into the alkyl group (11), it might appear that this method is not generalizable on account of the lack of availability of the intermediate trichloromethyl sulfides. However, this is not so, since both chloromethyl and dichloromethyl alkyl sulfides are available through established methods. Böhme (12, 13) has developed the preparation of chloromethyl alkyl sulfides from alkyl thiols, paraformaldehyde, and HCl. More recently a method for the preparation of dichloromethyl alkyl sulfides from the thiolformates and phosphorus pentachloride has been published by Holsboer and van der Veek (14). These authors have also reported the preparation of a number of trichloromethyl alkyl sulfides from the dichloromethyl alkyl sulfides.

It should be noted that the preferred method for the preparation of methanesulfinyl chloride utilizes 1,1-dichloro-2-thiapropane-2-oxide, **2**, as starting material. Although the chlorination of 1,1,1-trichloro-2-thiapropane-2-oxide, **6**, has been examined and proceeds quite satisfactorily, **6** is considerably less convenient to prepare than is **2**.

Oxygen-transfer Reactions

Most of the reactions which we encountered during our studies on the sulfohaloform reaction (5, 7) involved sulfur behaving as a nucleophile towards electrophilic chlorine. However, we also observed a number of reaction pathways in which sulfoxides acted as nucleophiles at oxygen. This type of reaction by sulfoxides is of course well documented (15, 16), but the reactions described below are novel and warrant a brief discussion.

Although chlorination of 1,3-dichloro-2-thiapropane-2-oxide, **3**, in dilute aqueous acetic acid was a relatively straightforward reaction yielding primarily **4** (5), the use of glacial acetic acid as solvent permitted the observation of a chlorinated sulfoxide behaving as an oxygen nucleophile in a more complex reaction. The products shown in [1] were obtained. The previous report

$$[1]\quad 3 \xrightarrow[HOAc]{Cl_2} 4\ (19\%) + \underset{\mathbf{9}}{ClCH_2{\cdot}SO_2{\cdot}Cl}\ (26\%) + \underset{\mathbf{8}}{Cl_3C{\cdot}S{\cdot}CH_2Cl}\ (26\%) + CHCl_3\ (26\%)$$

(5) established that the chloromethanesulfonyl chloride, **9**, is produced from the corresponding sulfinyl chloride which in turn is produced from the trichlorosulfoxide, **4**. It is also clear that the sulfinyl chloride acquires an oxygen atom from a sulfoxide which is converted to the corresponding α-chlorosulfide. The simplest assumption, since the isolated sulfide is in fact the tetrachlorosulfide **8**, is that oxygen is transferred from the trichlorosulfoxide **4**. Chlorination of the trichlorosulfoxide **4** in glacial HOAc furnishes no tetrachlorosulfide **8** as we have shown previously (5). It therefore follows that the oxygen transfer must have occurred from the dichlorosulfoxide **3**. This reasoning was supported by chlorination of a 1:1 mixture in glacial acetic acid of chloromethanesulfinyl chloride and the dichlorosulfoxide **3** which did indeed furnish the expected mixture of chloromethanesulfonyl chloride **9** and tetrachlorosulfide **8** in a 1:1 ratio. The pathway for the chlorination of the dichlorosulfide **3** in glacial acetic acid is depicted in Scheme 1.

It is interesting to compare the reactions of **3** (*cf.* reaction 1) and **2** (reaction 2) (5) with chlorine in glacial acetic acid. No oxygen-

$$[2]\quad 2 \xrightarrow[HOAc]{Cl_2} CH_3{\cdot}SO_2{\cdot}Cl\ (72\%) + CCl_4\ (72\%) + AcCl\ (72\%)$$

transfer products were observed in [2]. The differences between **2** and **3** may be explained by a number of factors. These include the fact that **2** undergoes rapid further chlorination to the less-nucleophilic trichlorosulfoxide **6** and the fact that in [1], the oxygen transfer arises from the

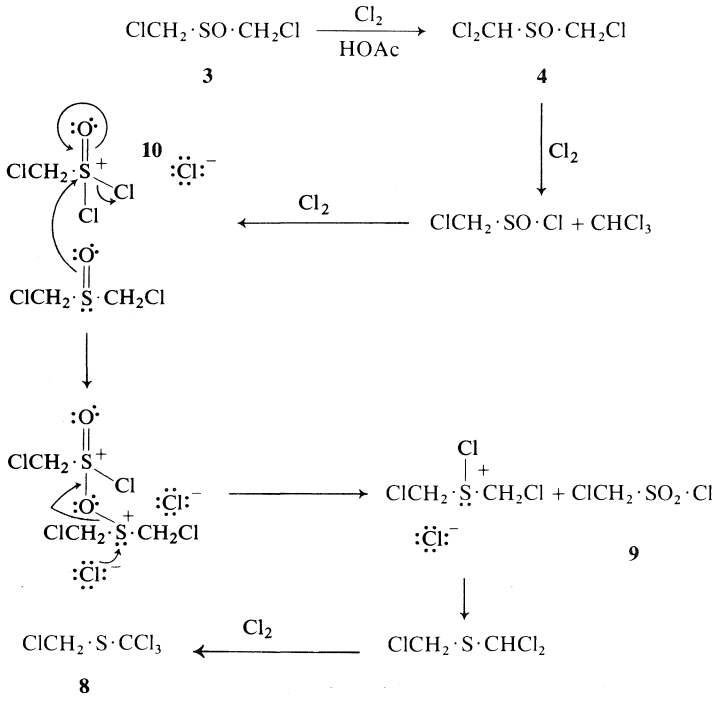

SCHEME 1

more nucleophilic sulfoxide **3** attacking the more electrophilic oxodichlorosulfonium salt **10**. This compares with [2] in which for a comparable process to occur, the predominant sulfoxide would be **6** and the comparable electrophilic species to **10** would be **11** (*cf.* Schemes 1 and 2).

That an oxygen-transfer reaction could occur in the case of dichlorosulfoxide, **2**, was found by a careful examination of its chlorination in methylene chloride solvent. The reaction is depicted in [3].

[3] $2 \xrightarrow[CH_2Cl_2]{Cl_2} CH_3{\cdot}SO{\cdot}Cl\ (75\%) + CH_3{\cdot}SO_2{\cdot}Cl\ (1\%) + \mathbf{8}\ (1\%) + ClCH_2{\cdot}SO{\cdot}Cl\ (3\%)$

The chloromethanesulfinyl chloride must originate from the tetrachlorosulfoxide **5** since methanesulfinyl chloride did not give rise to any chloromethanesulfinyl chloride when chlorinated in methylene chloride. The selective oxidation of methanesulfinyl chloride to the sulfonyl chloride in the presence of chloromethanesulfinyl chloride can be rationalized on the grounds that the concentration of methanesulfinyl chloride is much greater during the reaction and that the methanesulfinyl chloride reacts at a faster rate with

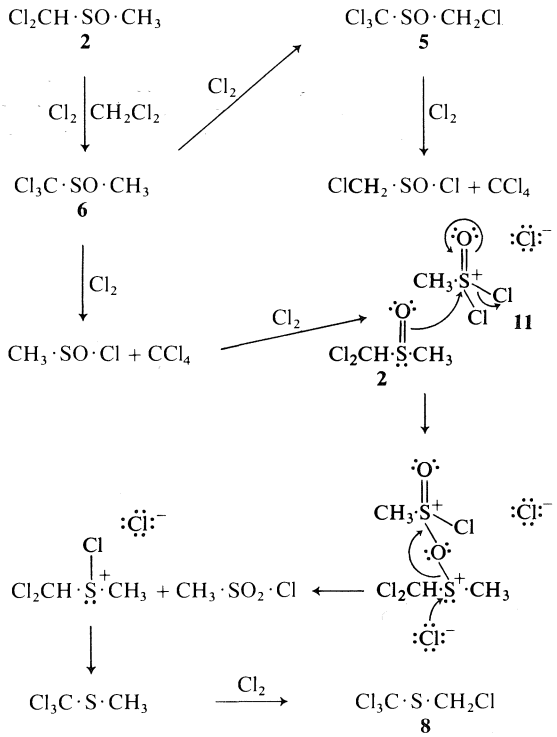

SCHEME 2

chlorine to form the oxodichlorosulfonium chloride salt **11**. A reasonable reaction pathway is outlined in Scheme 2.

It might have been expected that methanesulfinyl chloride would best be prepared by simple chlorination of DMSO, especially in light of the literature report that sulfoxides may be cleanly chlorinated in methylene chloride (17). However, in our hands, DMSO produced a plethora of products with chlorine in either methylene chloride or glacial acetic acid. This is undoubtedly due to oxygen-transfer reactions. We did find that these processes could be suppressed to give a useful reaction by use of a controlled amount of water in the acetic acid (5).

We have also observed a novel oxygen transfer reaction which did not involve molecular chlorine. In 1955, Bordwell and Pitt (18) examined the reaction of sulfoxides with thionyl chloride. Upon subjecting thiacyclopentane-1-oxide to the appropriate conditions, they reported the formation of "a dark colored material with a wide boiling range". A reinvestigation of this reaction furnished the unexpected result that the major isolable product was thiacyclopentane (25% yield). As initially isolated, it was contaminated with a small amount of material that may have been the expected 2-chlorothiacyclopentane (nmr). Redistillation gave thiacyclopentane of satisfactory purity. This apparently unprecedented reduction of a sulfoxide by thionyl chloride (ref. 10, p. 341) can be rationalized as depicted in Scheme 3.

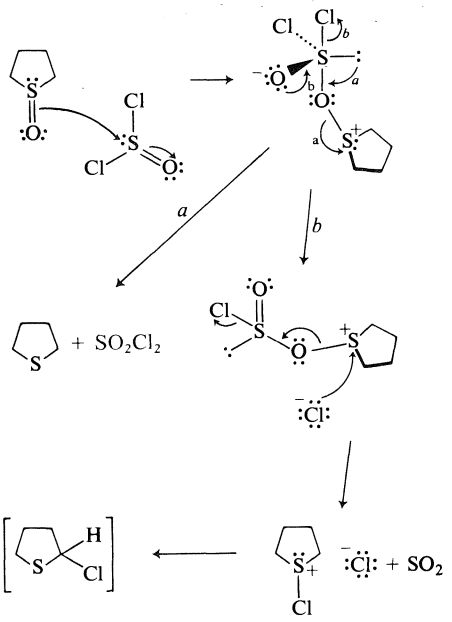

SCHEME 3

Experimental

General

Details have been provided previously (5).

Preparation of $Cl_2CH{\cdot}SO{\cdot}CH_2Cl$, 4

1,3-Dichloro-2-thiapropane (16.00 g) in glacial acetic acid (50 ml) was chlorinated (232 ml/min) for 20 min. Water (6.6 ml) was added and Cl_2 (232 ml/min) was bubbled through the reaction mixture for an additional 35 min. Water (75 ml) was added and the solution was extracted with chloroform (4 × 100 ml). The combined chloroform layers were washed with 2.5% NaOH until the p*H* of the aqueous layer remained basic, and then given a standard work-up. The residue was fractionated at reduced pressure to furnish **4** (11.08 g, 50%).

Chlorination of $Cl_3C{\cdot}SO{\cdot}CH_2Cl$, 5

5 (15.25 g) was dissolved in methylene chloride (50 ml) and chlorine (232 ml/min) was bubbled through the reaction mixture for 50 min. The solvent was distilled off at atmospheric pressure and the residue was rectified at reduced pressure affording chloromethanesulfinyl chloride **9** (7.62 g, 80.3%) bp 94 °C/80 torr.

Chlorination of $Cl_3C{\cdot}SO{\cdot}C_6H_5$, 7

7 (9.64 g) was dissolved in methylene chloride (50 ml) and chlorine (232 ml/min) was bubbled through the reaction mixture for 90 min. The methylene chloride was rotary evaporated to yield an orangish residue (10.02 g). Methanol (50 ml) was added to the residue and the solution stirred at ambient temperature for 60 min. The methanol was rotary evaporated affording a residue containing Ph·SO·OMe (1.90 g, 39%), unreacted $Ph{\cdot}SO{\cdot}CCl_3$ (2.25 g, 23%), as well as at least two other compounds. Some of this residue was chromatographed on two preparative-layer plates (150 mg/plate) which were eluted with carbon tetrachloride. The lowest band (R_F 0.12 detected by uv light) was removed, and chloroform extraction gave a partially crystalline residue (142.7 mg) which was about equal parts $Cl_3C{\cdot}SO{\cdot}Ph$ and Ph·SO·OMe. This residue was rechromatographed (plc, chloroform eluant), the lower band (R_F 0.62) from which furnished methyl benzenesulfinate (66 mg), which was identical with authentic material by tlc, nmr, and ir, and the upper band (R_F 0.83) from which furnished $Ph{\cdot}SO{\cdot}CCl_3$ **7** (67 mg), identical with the starting material by tlc, nmr, and ir.

Chlorination of $ClCH_2{\cdot}SO{\cdot}CH_2Cl$, 3

3 (15.01 g) (5) was dissolved in glacial acetic acid (50 ml) and chlorinated (232 ml/min) for 30 min. The nmr of the crude showed that $Cl_3{\cdot}C{\cdot}S{\cdot}CH_2Cl$ **8** and $ClCH_2{\cdot}SO_2{\cdot}Cl$ **9** were present in a 1:1 ratio. Ice water (75 ml) was added and the solution extracted with chloroform (2 × 100 ml). The chloroform layer was extracted with 2.5% NaOH (100 ml aliquots) until the p*H* of the aqueous layer remained basic. Standard work-up gave a residue which was fractionated at reduced pressure affording $Cl_3C{\cdot}S{\cdot}CH_2Cl$ **8** (5.47 g, 26.4%) and $Cl_2CH{\cdot}SO{\cdot}CH_2Cl$ **4** (3.72 g, 19.6%). Both compounds were identical with authentic samples by nmr, ir, and bp.

The reaction was repeated. After addition of water and chloroform extraction, a portion of the chloroform solution (50 ml) was continuously extracted with water[2] for 24 h. The chloroform was dried ($MgSO_4$), filtered, and concentrated and a portion of the residue (500 mg) was added drop-wise to a chilled solution of vanillin (218 mg) in dry pyridine (1 ml). After the reaction mixture was stirred at ambient temperature for 1 h, work-up in the usual way gave a residue which was chromatographed on five preparative-layer plates using ether–chloroform, 5:95. Extraction of the band visible under uv light furnished vanillin chloromesylate (152 mg) which was identical with authentic material by tlc, ir, and nmr.

Chlorination of $Cl_2CH{\cdot}SO{\cdot}CH_3$, 2

2 (16.81 g) in methylene chloride was chlorinated (232 ml/min) for 25 min. The methylene chloride was distilled off at atmospheric pressure and the residue was fractionated at 34 torr. Methanesulfinyl chloride (bp 52–54 °C/34 torr) was removed and a residue (1.00 g) was obtained. Nuclear magnetic resonance spectra indicated the presence of $Cl_3C{\cdot}S{\cdot}CH_2Cl$ **8** (264 mg, 1.2%), $ClCH_2{\cdot}SO{\cdot}Cl$ (437 mg, 2.9%), $CH_3{\cdot}SO_2{\cdot}Cl$ (163 mg, 1.2%), and $CH_3{\cdot}SO{\cdot}Cl$ (139 mg, 1.2%). The crude residue was treated with vanillin (1.002 g) in pyridine (2.5 ml) as outlined previously, the product of which was evacuated (0.45 torr) and immersed in an oil bath (which had been preheated to 100 °C), for 2 min. Condensation of the distillate in a cold trap (−50 °C) furnished **8** (153 mg) identical to authentic material by nmr, ir, and bp. The residue from the bulb-to-bulb distillation weighed 498 mg. A portion of the residue (200 mg) was chromatographed on two preparative tlc plates (silica gel HF-254) which were developed with 5% ether in chloroform. Vanillin mesylate (32.3 mg, R_F 0.50) was isolated and shown to be identical to authentic material by ir, nmr, and tlc.

The chlorination was rerun and a portion of the distillation residue (250 mg) was chlorinated (232 ml/min) in distilled water (1.7 ml) for 5 min. The reaction mixture was diluted to 10 ml with distilled water and extracted with chloroform (3 × 10 ml). Standard work-up gave a residue which was treated with vanillin (200 mg) in pyridine (1.0 ml) as described previously. Vanillin chloromesylate (48.2 mg, R_F 0.55) was isolated by preparative-layer chromatography, as outlined above and was shown to be identical to authentic material by nmr, ir, and tlc.

Reaction of Thiacyclopentane-1-oxide and $SOCl_2$

Thiacyclopentane-1-oxide (28.85 g) was dissolved in methylene chloride (40 ml) and was added drop-wise over a period of 1¾ h to a gently refluxing solution of thionyl chloride (34.89 g) in methylene chloride (40 ml). Upon completion of the addition the reaction mixture was fractionated and the material (7.32 g) which had bp 90–120 °C was collected. Redistillation furnished clean thiacyclopentane (bp 116–120 °C, 3.65 g) which was identical with authentic material by bp, nmr, and ir.

[2]The water was distilled from 5% NaOH to prevent recycling of the acetic acid.

Acknowledgements

We thank Mr. J. Leahy for technical assistance and the National Research Council of Canada for financial support, as well as for the award of a Postgraduate Fellowship to one of us (R.F.L.).

1. A. Schöberl and A. Wagner. *In* Methoden der organischen Chemie (Houben-Weyl). Vol. 9. *Edited by* E. Müller. G. Thieme. Stuttgart. 1955. p. 211.
2. H. H. Szmant. *In* Organic sulfur compounds. Vol. 1. *Edited by* N. Kharasch. Pergamon. N.Y. 1961. p. 154.
3. G. C. Barrett. *In* Organic compounds of sulphur, selenium, and tellurium. Chem. Soc. Spec. Publ. London. **1**, 71 (1970); **2**, 35 (1973).
4. K. Fries and W. Vogt. Justus Liebig's Ann. Chem. **381**, 337 (1911).
5. J. S. Grossert and R. F. Langler. Can. J. Chem. This issue.
6. F. G. Bordwell and P. J. Bouton. J. Am. Chem. Soc. **79**, 717 (1957).
7. J. S. Grossert, W. R. Hardstaff, and R. F. Langler. J. Chem. Soc. Chem. Commun. 50 (1973).
8. M. L. Kee and I. B. Douglass. Org. Prep. Proc. **2**, 235 (1970).
9. C. G. Venier, H. H. Hsieh, and H. J. Barager III. J. Org. Chem. **38**, 17 (1973).
10. J. S. Pizey. Synthetic reagents. Vol. 1. Ellis Horwood/J. Wiley, Chichester. 1974. p. 336.
11. D. L. Tuleen and T. B. Stephens. J. Org. Chem. **34**, 31 (1969).
12. H. Böhme. Ber. Dtsch. Chem. Ges. **69**, 1610 (1936).
13. H. Böhme, H. Fisher, and R. Frank. Justus Liebig's Ann. Chem. **563**, 54 (1949).
14. D. H. Holsboer and A. P. M. van der Veek. Recl. Trav. Chim. Pays Bas. **91**, 349 (1972).
15. T. Durst. Adv. Org. Chem. **6**, 285 (1969).
16. W. S. MacGregor. Q. Rep. Sulfur Chem. **3**, 149 (1968).
17. K. C. Tin and T. Durst. Tetrahedron Lett. 4643 (1970).
18. F. G. Bordwell and B. P. Pitt. J. Am. Chem. Soc. **77**, 572 (1955).

C-Nucleosides and related compounds. XII. The synthesis of the carbocyclic analogues of D,L-6-azapseudouridine, 2-thio-6-azapseudouridine, and pyrazofurin A. On the cyclization of semicarbazones of α-keto esters

GEORGE JUST AND SUNGGAK KIM[1]

Department of Chemistry, McGill University, Montreal, P.Q., Canada H3C 3G1

Received August 12, 1976

GEORGE JUST and SUNGGAK KIM. Can. J. Chem. **55**, 427 (1977).

The preparation of the title compounds is described. The cyclization of the *syn*- and *anti*-isomers of semicarbazones, thiosemicarbazones, and carbomethoxymethyl hydrazones to azauracils, thioazauracils, and pyrazoles is described. The photochemical isomerization of the hydrazones has been carried out. Whereas both *syn*- and *anti*-isomers of the thiosemicarbazones and carbomethoxymethyl hydrazones cyclize, only the *syn*-isomer of the semicarbazones can be converted to the corresponding azauracil.

GEORGE JUST et SUNGGAK KIM. Can. J. Chem. **55**, 427 (1977).

On décrit la préparation des composés mentionnés dans le titre. On décrit la cyclisation des isomères *syn* et *anti* des semicarbazones, des thiosemicarbazones et des carbométhoxyméthyles hydrazones en azauracils, thioazauracils et pyrazoles. On a effectué les isomérisations photochimiques des hydrazones. Alors que les isomères *syn* ainsi que *anti* des thiosemicarbazones et carbométhoxyméthyles hydrazones peuvent se cycliser, il n'y a que l'isomère *syn* des semicarbazones qui peut être transformé en azauracil correspondant.

[Traduit par le journal]

In the course of the synthesis of the carbocyclic analogue of D,L-pyrazofurin A **17** (1), it was noted that the cyclization of the corresponding hydrazone **10** proceeded in low yield, and that the hydrazone consisted of a mixture of the *syn*- and *anti*-isomers. It occurred to us that perhaps only one isomer underwent cyclization.

The cyclization behaviour of semicarbazones is also a somewhat capricious reaction. It has been reported that semicarbazones of α-keto acids and α-keto esters are cyclized under the influence of aqueous sodium hydroxide directly to the corresponding azauracil in variable yield (2). The reaction is normally carried out at 100 °C. Higher yields are obtained by working at room temperature, but the reaction then often takes several months. The cyclization proceeds best with semicarbazones with a higher alkyl or even better an aryl or aralkyl group in the α-position (3). Furthermore, with the semicarbazones of lower α-keto acids the reaction proceeds with some difficulty or, in case of pyruvic acid, not at all (4).[2]

Bougault observed that the thiosemicarbazone of pyruvic acid underwent a high yield cyclization resulting in the formation of **6**. Replacement of the sulfur atom with an oxygen atom then allowed him to prepare 6-azathymine **4** (5). In contrast with the cyclization of semicarbazones of α-keto acids, the cyclization of thiosemicarbazones proceeds consistently in good yield. The cyclization of the thiosemicarbazones has therefore served as the basis for the synthesis of 6-azauracils.

Since we were interested in the synthesis of 6-azauracils, 4-thio-6-azauracils, and pyrazoles, we decided to investigate the cyclization reactions.

Methyl pyruvate was transformed into its hydrazone **1**, semicarbazone **3**, and thiosemicarbazone **5**. Spectral data indicated them to consist only of one isomer, assigned the *anti* geometry based on data to be discussed later. All cyclization reactions were carried out in a standard manner, involving sodium methoxide in boiling methanol for 2 h, unless specified differently. Thiosemicarbazone **5**-*E* cyclized in 70% yield to thioazauracil **6**, presumably after isomerization to the *syn*-isomer. Pyrazole **2** was obtained in only 30% yield from hydrazone **1**-*E* and the *anti*-semicarbazone **3**-*E* did not react at all.

Irradiation of methanolic solution of the *anti*-

[1]Holder of a McConnell Fellowship, 1974–1976.

[2]Note: Chang (4*c*) prepared **4** from the semicarbazone of pyruvic acid by treatment with sodium ethoxide in ethylene glycol at reflux for 15 h in 51% yield.

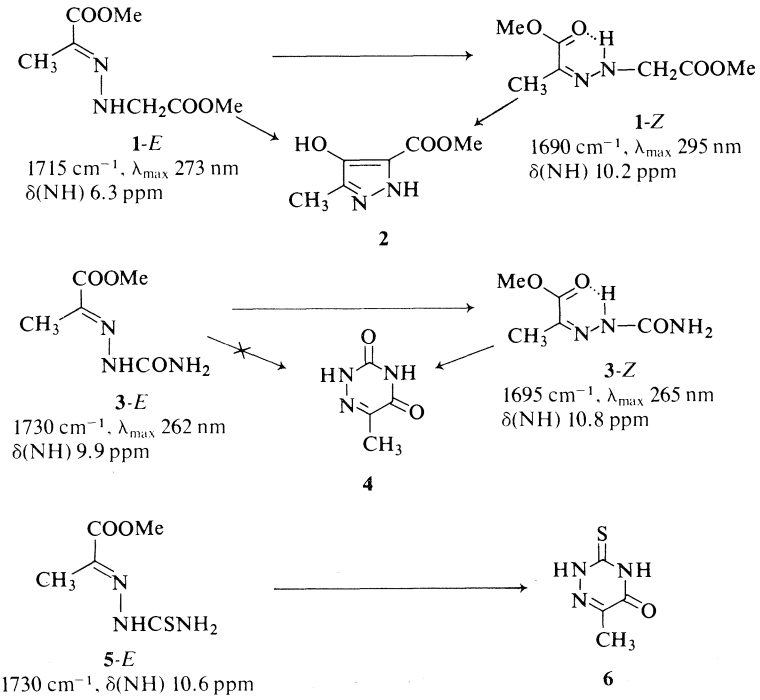

SCHEME 1

semicarbazone **3**-*E*, λ_{max} 262 nm, with 254 nm light for 2 days, shifted the absorption maximum to 265 nm. Purification by tlc gave in 80% yield the crystalline *syn*-isomer **3**-*Z*. Treatment of the *syn*-isomer with sodium methoxide in methanol at room temperature for 30 min gave, after acidification, a crystalline 6-azathymine in 75% yield. During the course of reaction, a precipitate formed. The precipitate turned out to be the sodium salt of **4**. The assignment of the geometry of the semicarbazones is based on the sharply contrasting cyclization behaviour of the two isomers. It is corroborated by the following spectral data. In the *syn*-isomer **3**-*Z*, the NH proton appeared at 10.8 ppm and the carbomethoxy group absorbed at 1695 cm^{-1} due to hydrogen bonding. For the *anti*-isomer, the corresponding bands appeared at 9.9 ppm and 1730 cm^{-1}. It should be noted that the *syn*-isomer absorbed in the ultraviolet at higher wavelength than the *anti*-isomer. Similar spectral data were observed for the hydrazones **1** and **10**, and the semicarbazone **8**. The spectral data are summarized in Scheme 1.

In order to make sure that the poor cyclization yield of hydrazone **1**-*E* was not due to slow conversion of the *anti*-isomer **1**-*E* to the *syn*-isomer **1**-*Z*, a methanolic solution of the *anti*-isomer, λ_{max} 273 nm, was irradiated with 254 nm light for 2 days. Purification by tlc gave the *syn*-isomer in 70% yield as an oil. Treatment of **1**-*Z* with sodium methoxide in methanol gave pyrazole **2** in 35% yield, indicating that *syn–anti* isomerization had occurred during the reaction and that the low yield obtained from the *anti*-isomer was not related to its lack of convertibility to the *syn*-isomer. In the case of the thiosemicarbazones it was obvious that the *anti*-isomer was easily converted to the *syn*-isomer under the reaction conditions, and no further work was done on that system.

These findings were applied to the synthesis of *C*-nucleoside analogues **13**, **14**, and **17**, which fully corroborated the observations made.

The keto ester **7** (1) was converted to its thiosemicarbazone **9**. Spectral data indicated it to consist of the *syn*- and *anti*-isomers in a ratio of approximately 1:1. Treatment of **9** with sodium methoxide in methanol gave **13** in 76% yield. Hydrolysis of protecting groups with 50% aqueous trifluoroacetic acid at room temperature for 30 min gave the crystalline 4-thio-6-azapseudouridine **14** in good yield.

For the preparation of a carbocyclic analogue

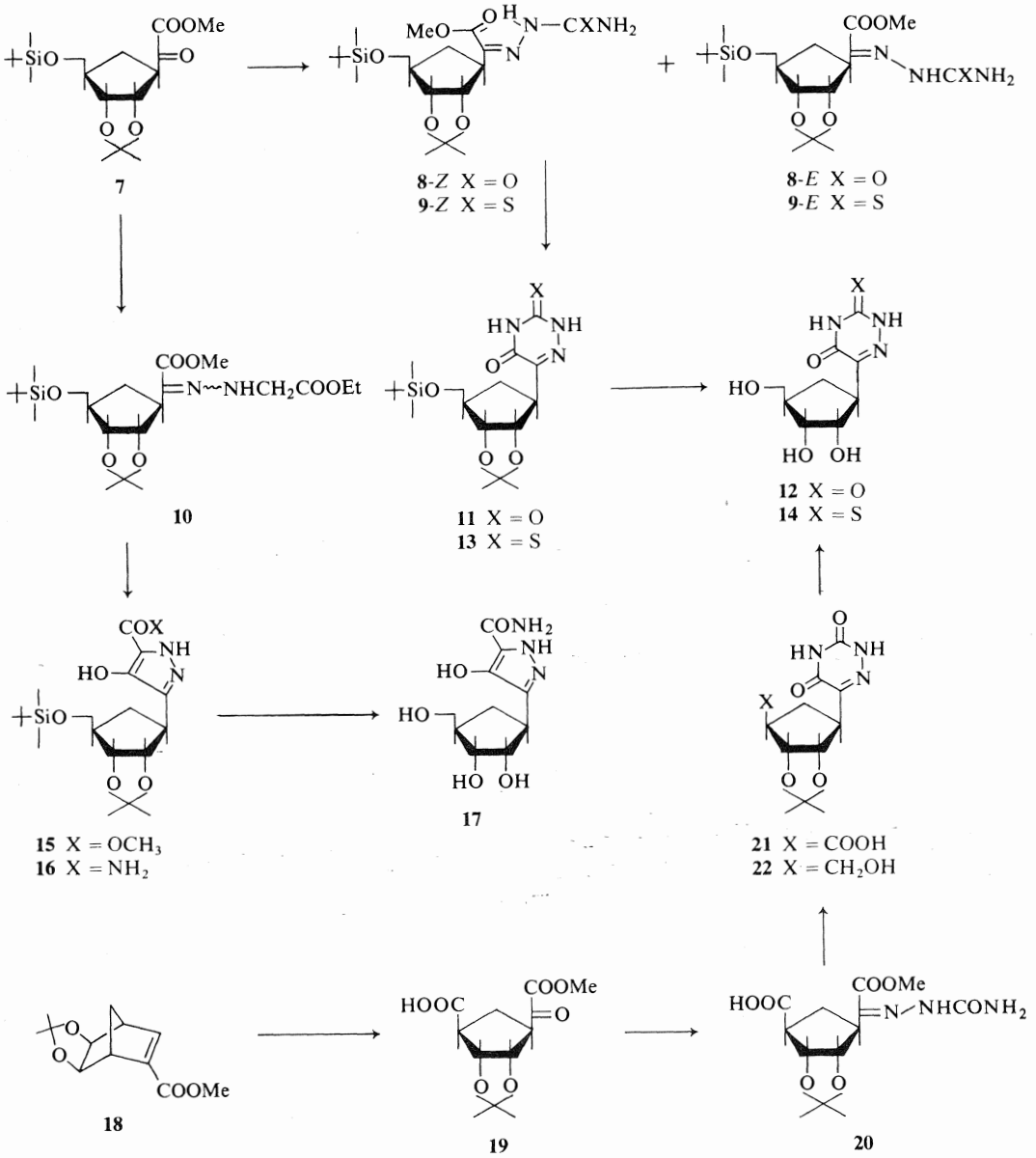

of 6-azapseudouridine, the keto ester **7** was converted to its semicarbazone **8**. Spectral data indicated it to consist of the *syn*- and *anti*-isomers in a ratio of 2:3. Cyclization with sodium methoxide in methanol gave the cyclized product **11** in 30% yield. Pure *anti*-isomer **8**-*E* was recovered in 50% yield. Irradiation of the *anti*-isomer, λ_{max} 263 nm, with 254 nm light for 2 days gave the *syn*-isomer, λ_{max} 272 nm, in quantitative yield. Cyclization of this product resulted in the formation of **11** in 80% yield. Hydrolysis of the protecting groups with 50% aqueous trifluoroacetic acid gave crystalline **12** in 75% yield. The same compound was obtained in the following manner. Olefinic ester **18** (6) was oxidized with potassium permanganate and sodium periodate (7). The resulting keto ester **19** was converted in 78% yield to its crystalline semicarbazone **20**, which consisted of the *syn*-isomer only according to its nmr and uv spectra. It could be cyclized readily using the standard procedure. The resulting cyclized product **21** was

reduced with diborane to give **22**. Treatment of **22** with 90% aqueous trifluoroacetic acid gave **12**, identical in all respects with the product described above.

The carbocyclic analogue of pyrazofurin A was synthesized in the following manner. The keto ester **7** was converted to its hydrazone **10**, which consisted of the *syn*- and *anti*-isomers in a ratio of 6:5, as established by high-pressure liquid chromatography. Cyclization of the mixture gave the crystalline pyrazole **15** in 40% yield. Treatment of **15** with ammonia for 7 days at room temperature gave the amide in 85% yield as a foam. Hydrolysis of the protecting groups gave the crystalline product **17**.

In conclusion, it may be stated that the variability in cyclization behaviours of the semicarbazones of α-keto esters reflects the *syn–anti* isomer ratio of the semicarbazones, which in turn depends to a large extent on the steric bulk of the alkyl or aryl substituent in the keto ester (8). In case of **20**, hydrogen bonding by the carboxyl group of the semicarbazone group seems to stabilize the *syn*-isomer considerably.

Experimental

Melting points were determined on a Gallenkamp block and are uncorrected. Mass spectra were obtained on an AEI-MS-902 mass spectrometer at 70 eV using a direct-insertion probe. Nuclear magnetic resonance spectra were recorded on a Varian Associates T-60 spectrometer. Infrared spectra were obtained on an Unicam SP 1000 and a Perkin–Elmer 257 ir spectrophotometer. Ultraviolet spectra were determined with an Unicam SP 800 spectrophotometer. The photolyses were carried out in Vycor tubes using a Rayonet photochemical reactor equipped with lamps with maximum output at 2537 Å. An Altex Model 300 liquid chromatograph was used for high pressure liquid chromatography. Microanalyses were carried out by Dr. C. Daessle, Montreal and Heterocyclic Chemical Corp., Harrisonville, Mo., U.S.A.

Preparation of Methyl Pyruvate Hydrazone ***1-E***

Methyl pyruvate (1.02 g), methyl hydrazinoacetate hydrochloride (1.68 g, 1.2 equiv.), and sodium acetate (990 mg, 1.2 equiv.) were dissolved in 15 ml of methanol and 5 ml of water. The solution was stirred at room temperature for 6 h. The solution was evaporated under reduced pressure. The residue was taken up in 20 ml of chloroform. The chloroform solution was washed with water, dried over sodium sulfate, and evaporated to dryness *in vacuo*. Yield 1.62 g (86%); mp 70–72 °C; nmr ($CDCl_3$) δ 2.03 (s, 3H, $CH_3C{=}N$), 3.73 (s, 3H, COOMe), 3.80 (s, 3H, COOMe), 4.2 (bs, 2H, $NHCH_2COOMe$), 6.3 (bs, 1H, $NNHCH_2$); ir ($CHCl_3$) 3300 (NH), 1745/1715 (C=O), 1605 cm^{-1} (C=N); uv (MeOH) 273 nm (log ε 4.11).

3(5)-Carbomethoxy-4-hydroxy-5(3)-methylpyrazole ***2***

To a solution of hydrazone **1**-*E* (420 mg) in 5 ml of methanol was added 0.63 *M* sodium methoxide (6.8 ml, 2.5 equiv.). The solution was refluxed for 4 h and evaporated under reduced pressure. The residue was taken up in 10 ml of water, acidified in 0.5 *M* hydrochloric acid and then extracted three times with ethyl acetate. The ethyl acetate solution was dried over sodium sulfate and evaporated to dryness *in vacuo*. The crude product was chromatographed on silica gel plates using chloroform as an eluant (R_f = 0.6). Yield 102 mg (30%); mp 140–142 °C; nmr ($CDCl_3$) δ 2.2 (s, 3H, CH_3), 3.8 (s, 3H, COOMe), 8.4 (b, 2H, NH and OH); ir ($CHCl_3$) 3200–2500, 1720/1690 (C=O), 1640 cm^{-1}; uv λ_{max} 225 (log ε 3.75) and 275 nm (log ε 3.65) in 0.1 *N* HCl; λ_{max} 237 (log ε 3.78) and 317 nm (log ε 3.74) in 0.1 *N* NaOH.

Conversion of the anti-Isomer ***1-E*** *into the syn-Isomer* ***1-Z***

The hydrazone **1**-*E* (320 mg) was dissolved in 20 ml of methanol. The solution was irradiated for 2 days at 254 nm. The solvent was evaporated under reduced pressure and the crude product was chromatographed on silica gel plates using chloroform as an eluant for the separation. The *syn*-isomer was an oil (R_f = 0.7). Yield 225 mg (70%); nmr ($CDCl_3$) δ 2.00 (s, 3H, $CH_3C{=}N$), 3.67 (s, 3H, COOMe), 3.70 (s, 3H, COOMe), 4.13 (d, J = 6 Hz, 2H, $NHCH_2COOMe$), 10.2 (b, 1H, $NNHCH_2$); ir ($CHCl_3$) 330 (NH), 1750/1690 (C=O), 1570 cm^{-1} (C=N); uv (MeOH) 295 nm (log ε 3.97).

Preparation of Pyrazole ***2*** *from the syn-Hydrazone* ***1-Z***

The *syn*-hydrazone **1**-*Z* was treated with sodium methoxide at reflux for 4 h. After usual work-up and separation on silica gel plates, the pyrazole **2** was obtained in 35% yield. Spectral data (nmr, ir, and uv) were identical with those of **2** which was obtained from the *anti*-hydrazone **1**-*E*.

Preparation of the Semicarbazone of Methyl Pyruvate ***3-E***

To a solution of methyl pyruvate (1.02 g) in 20 ml of methanol was slowly added a solution of semicarbazide hydrochloride (1.22 g, 1.1 equiv.) and sodium acetate (900 mg, 1.1 equiv.) in 10 ml of water. The solution was stirred at room temperature for 1 h and the white precipitate was filtered off and washed several times with methanol. Yield 1.40 g (88%); mp 198–200 °C; nmr ($CDCl_3$) δ 2.08 (s, 3H, CH_3—C), 3.77 (s, 3H, COOMe), 6.4 (bs, 2H, $CONH_2$), 9.9 (bs, 1H, NNHCO); ir (KBr) 3540, 3400, 3300–3000, 1730 (COOMe), 1690 ($CONH_2$), 1595 (C=N), 1450 cm^{-1}; uv (MeOH) 262 nm (log ε 4.39).

Conversion of the anti-Semicarbazone ***3-E*** *into the syn-Semicarbazone* ***3-Z***

The *anti*-semicarbazone **3**-*E* (210 mg) was dissolved in 20 ml of methanol. The solution was irradiated at 254 nm for 2 days and separated by chromatography on silica gel plates using ethyl acetate as an eluant (R_f = 0.85). Yield 160 mg (80%); mp 128–130 °C; nmr ($CDCl_3$) δ 2.07 (s, 3H), 3.77 (s, 3H), 6.6 (bs, 2H, $CONH_2$), 10.8 (bs, 1H, NNH); ir (KBr) 3440, 3300, 1695 (C=O), 1600, 1450 cm^{-1}; uv (MeOH) 265 nm (log ε 4.37).

6-Methyl-3,5-dioxo-2,3,4,5-tetrahydro-1,2,4-triazine (6-Azathymine) ***4***

The *syn*-semicarbazone **3**-*Z* (140 mg) was added to 3.0 ml of 0.63 *M* (2.1 equiv.) methanolic sodium meth-

oxide. The solution was stirred at room temperature for 30 min. The formation of a white precipitate was observed after stirring a few minutes. Without filtration of the white precipitate, the reaction mixture was neutralized with Dowex 50W-X8 (H). The resin was filtered and the solvent was evaporated to dryness *in vacuo*. The crude product was crystallized from ethyl ether. Yield 85 mg (75%); mp 209–211 °C (lit. (4*c*) 210–212 °C); nmr (DMSO-d_6, external TMS) δ 2.03 (s, 3H, CH_3), 9.0–11.0 (b, 2H, NHCONH); ir (KBr) 3280, 3200, 1730/1680 (C=O), 1620 (C=N), 1480 cm^{-1}; uv λ_{max} 261 nm (log ε 3.73) in 0.1 *N* HCl; λ_{max} 246 nm (log ε 3.67) in 0.1 *N* NaOH.

Preparation of the Sodium Salt

The *syn*-semicarbazone **3**-*Z* (100 mg) was added to 1.2 ml of 0.6 *M* sodium methoxide (1.2 equiv.). The solution was stirred at room temperature for 10 min and the white precipitate was filtered off and washed with 1 ml of methanol. Drying *in vacuo* gave the sodium salt (45 mg) in 48% yield. Its uv spectrum was identical with that of **4** and the nmr spectrum in D_2O showed a singlet at 2.10 ppm for the methyl group.

Preparation of Thiosemicarbazone **5**-*E of Methyl Pyruvate*

Methyl pyruvate (2.06 g) and thiosemicarbazide (1.83 g, 1 equiv.) were dissolved in 30 ml of 80% aqueous methanol. The solution was stirred at room temperature for 30 min. The precipitate was filtered and washed several times with methanol. Yield 3.50 g (78%); mp 137–138 °C; nmr (DMSO, external TMS) δ 2.0 (s, 3H, CH_3—C), 3.7 (s, 3H, COOMe), 7.6 (bs, 1H), 8.5 (bs, 1H), 10.6 (b, 1H); ir (Nujol) 3540, 3250, 3180, 1730 (C=O), 1640 (C=N) cm^{-1}.

6-Methyl-3-thioxo-5-oxo-2,3,4,5-tetrahydro-1,2,4-triazine ***6***

A solution of the thiosemicarbazone **5**-*E* (285 mg) in 6.6 ml of 0.63 *M* sodium methoxide (2 equiv.) was refluxed for 3 h, cooled, and acidified with concentrated hydrochloric acid. The precipitate was filtered. Yield 155 mg (70%); mp 219–220 °C. (lit. (5*a*) mp 220 °C); uv λ_{max} 272 nm (log ε 4.27) in 0.1 *N* HCl; λ_{max} 265 nm (log ε 4.22) in 0.1 *N* NaOH.

*Methyl-2-(2′α,3′α-dihydroxy-di-O-isopropylidene-4*β*-tert-butyldimethylsiloxymethylcyclopent-1*β*-yl)glyoxylate Semicarbazone* ***8***

The keto ester **7** (290 mg), semicarbazide hydrochloride (135 mg, 1.5 equiv.), and sodium acetate (100 mg, 1.5 equiv.) were dissolved in 10 ml of methanol and 5 ml of water. The solution was stirred at room temperature overnight and then evaporated under reduced pressure to remove most of methanol. The reaction mixture was diluted with 5 ml of water and extracted with methylene chloride. The methylene chloride solution was washed with water, dried over sodium sulfate, and then evaporated to dryness *in vacuo*. Purification on silica gel plates using ethyl acetate as an eluant gave an oily semicarbazone **8** (300 mg) in 90% yield; nmr ($CDCl_3$) δ 0.05 (s, 6H), 0.90 (s, 9H), 1.33 (s, 3H), 1.4–2.5 (m, 6H), 3.0–3.4 (m, 1H), 3.5–3.9 (m, 5H, COOMe, SiO—CH_2), 4.3–4.9 (m, 2H), 6.0 (b, 2H, $CONH_2$), 9.6 (bs, 0.4H, NNHCO), 11.3 (bs, 0.6H, NNHCO); ir ($CHCl_3$) 3540/3430/3400 (NH), 1720 (C=O), 1580 (C=N), 1470, 1395, 1385 cm^{-1}; uv (EtOH) 265 nm (log ε 4.00). *Anal.* calcd. for $C_{19}H_{35}O_6N_3Si$: C 53.15, H 8.16, N 9.79; found: C 52.97, H 8.04, N 9.49.

A mixture of geometrical isomers was separated using high pressure liquid chromatography on a silica gel column using 0.5% methanol in methylene chloride as an eluant at 920 psi. The first fraction, the *syn*-isomer **8**-*Z*: yield 40%; nmr ($CDCl_3$) δ 0.05 (s, 6H), 0.90 (s, 9H), 1.33 (s, 3H), 1.53 (s, 3H), 1.7–2.5 (m, 3H), 3.1–3.5 (m, 1H), 3.67 (bd, J = 4 Hz, SiO—CH_2), 3.86 (s, 3H, COOMe), 4.3–4.8 (m, 2H), 5.8 (b, 2H, $CONH_2$), 11.3 (bs, 1H, NNHCO); ir ($CHCl_3$) 3540/3420/3300 (NH), 1700 (C=O), 1570 (C=N) cm^{-1}; uv (MeOH) 272 nm (log ε 4.01). The second fraction, the *anti*-isomer **8**-*E*: yield 60%; nmr ($CDCl_3$) δ 0.05 (s, 6H), 0.90 (s, 9H), 1.30 (s, 3H), 1.58 (s, 3H), 1.7–2.4 (m, 3H), 3.0–3.4 (m, 1H), 3.73 (bd, J = 4 Hz, 2H), 3.83 (s, 3H, COOMe), 4.3–4.9 (m, 2H), 6.0 (b, 2H, $CONH_2$), 9.6 (bs, NNHCO); ir ($CHCl_3$) 3540/3440/3360 (NH), 1720 (C=O), 1570 cm^{-1}; uv (MeOH) 263 nm (log ε 4.06).

*6-(2′α,3′α-Dihydroxy-di-O-isopropylidene-4′*β*-tert-butyldimethylsiloxymethylcyclopent-1′*β*-yl)-3,5-dioxo-2,3,4,5-tetrahydro-1,2,4-triazine* ***11***

To a solution of a mixture of geometrical isomers of semicarbazone **8** (430 mg) in 10 ml of methanol was added 0.63 *M* sodium methoxide (3.2 ml, 2 equiv.). The solution was refluxed for 2 h and evaporated under reduced pressure. The residue was taken up in 10 ml of water, acidified with 0.5 *M* hydrochloric acid, and immediately extracted three times with ethyl acetate. The ethyl acetate solution was washed with water, dried over sodium sulfate, and evaporated to dryness *in vacuo*. The crude product was separated by chromatography on silica gel plates using ethyl ether and chloroform (5:1) as an eluant. Major product (R_f = 0.5): 215 mg (50%); spectral data (nmr, ir, uv) were identical with those of **8**-*E* which was separated using high pressure liquid chromatography. Minor product **11** (R_f = 0.7): 120 mg (30%); nmr ($CDCl_3$) δ 0.05 (s, 6H), 0.90 (s, 9H), 1.33 (s, 3H), 1.53 (s, 3H), 1.7–2.7 (m, 3H), 3.10–3.85 (m, 3H), 4.2–4.6 (m, 1H), 4.6–5.1 (m, 1H), 10.0–11.0 (b and bs, 2H, NHCONH); ir ($CHCl_3$) 3420, 3380, 3100–3300, 1730/1710 (C=O), 1600 (C=N), 1470, 1460, 1395, 1385 cm^{-1}; uv λ_{max} 265 nm (log ε 3.78) in 0.1 *N* HCl; λ_{max} 255 nm (log ε 3.70) in 0.1 *N* NaOH; ms (150 °C) *m/e* 397 (M^+), 382 ($M^+ - CH_3$), 340 ($M^+ - C(CH_3)_3$), 282 (M^+ – *tert*-butyldimethylsilyl), 140 (B + 28), 139 (B + 27). *Anal.* calcd. for $C_{18}H_{31}O_5N_3Si$: C 54.37, H 7.87, N 10.57; found: C 54.18, H 8.01, N 10.61.

Conversion of **8**-*E into* **8**-*Z*

The *anti*-semicarbazone **8**-*E* (120 mg) was dissolved in 20 ml of methanol. The solution was irradiated at 254 nm for 2 days and evaporated to dryness *in vacuo* to afford the *syn*-semicarbazone **8**-*Z* in essentially quantitative yield. Spectral data (nmr, ir, and uv) were identical with those of **8**-*Z* which was separated using high pressure liquid chromatography.

*Preparation of (***11***) from the syn-Semicarbazone* **8**-*Z*

To a solution of the *syn*-isomer **8**-*Z* (110 mg) obtained from the above reaction in 5 ml of methanol was added 0.8 ml of 0.63 *M* sodium methoxide (2 equiv.). The solution was refluxed for 2 h and evaporated under reduced pressure. The residue was taken up in 10 ml of water.

The resulting solution was acidified with 0.5 *M* hydrochloric acid and extracted three times with ethyl acetate. The ethyl acetate solution was washed with water, dried over sodium sulfate, and evaporated to dryness *in vacuo* to give **11** (81 mg) in 80% yield. Spectral data (nmr, ir, and uv) were identical with those of **11** which obtained from **8**.

6-(2′α,3′α-Dihydroxy-4′β-hydroxymethylcyclopent-1′β-yl)-3,5-dioxo-2,3,4,5-tetrahydro-1,2,4-triazine ***12***

To a solution of **11** (180 mg) in 5 ml of methanol was added 5 ml of 50% aqueous trifluoroacetic acid. The solution was stirred at room temperature for 20 min and evaporated to dryness *in vacuo*. The crude product was crystallized from methanol and ethyl ether. Yield 85 mg (75%); mp 184–186 °C; ir (KBr) 3480/3250/3150 (OH, NH), 1735/1690 (C=O), 1620, 1470 cm^{-1}; uv: λ_{max} 265 nm (log ε 3.80) in 0.1 *N* HCl; λ_{max} 254 nm (log ε 3.74) in 0.1 *N* NaOH; ms (200 °C) *m/e* 244 ($M^+ + 1$), 243 (M^+), 225 ($M^+ - H_2O$), 207 ($M^+ - 2H_2O$), 196, 194, 178, 140 ($B + 28$), 139 ($B + 27$). *Anal.* calcd. for $C_9H_{13}O_5N_3$: C 44.44, H 5.39, N 17.28; found: C 44.38, H 5.19, N 17.02.

Methyl-2-(2α,3α-dihydroxy-di-O-isopropylidene-4β-tert-butyldimethylsiloxymethylcyclopent-1β-yl)glyoxylate Thiosemicarbazone ***9***

To a solution of the keto ester **7** (530 mg) in 20 ml of methanol was added thiosemicarbazide (150 mg, 1.1 equiv.). The reaction mixture was refluxed overnight and evaporated to near dryness under reduced pressure. The residue was taken up in 20 ml of chloroform. The solution was washed with water, dried over sodium sulfate, and evaporated to dryness *in vacuo*. The crude product was purified on silica gel plates using ethyl ether as an eluant. Yield 545 mg (86%); nmr ($CDCl_3$) δ 0.05 (s, 6H), 0.9 (two s, 9H), 1.2–2.8 (m, 10H), 3.4–3.8 (m, 5H), 4.2–4.6 (b, 2H), 4.9–5.1 (b, 1H), 7.0–7.2 (b, 1H), 9.2 (bs, 0.5H), 12.1 (bs, 0.5H); ir ($CHCl_3$) 3540, 3400, 3300, 1730/1710 (C=O), 1580 (C=N), 1480, 1395, 1385 cm^{-1}; uv (MeOH) 273 nm (log ε 3.78) and 315 (log ε 3.68); ms (195 °C) *m/e* 445 (M^+), 430 ($M^+ - CH_3$), 388 ($M^+ - C(CH_3)_3$), 386, 356, 330, 298.

6-(2′α,3′α-Dihydroxy-di-O-isopropylidene-4′β-tert-butyldimethylsiloxycyclopent-1′β-yl)-3-thioxo-5-oxo-2,3,4,5-tetrahydro-1,2,4-triazine ***13***

To a solution of the thiosemicarbazone **9** (200 mg) in 5 ml of methanol was added 0.8 ml of 0.63 *M* sodium methoxide (1.1 equiv.). The solution was refluxed for 3 h and evaporated under reduced pressure. After adding 10 ml of water, the solution was acidified with 0.5 *N* hydrochloric acid and then extracted three times with ethyl acetate. The ethyl acetate solution was dried over sodium sulfate and evaporated to dryness *in vacuo*. Purification of the crude product on silica gel plates using chloroform and ethyl ether (1:2) as an eluant gave the desired product **13** (146 mg) as an oil in 76% yield; nmr ($CDCl_3$) δ 0.05 (s, 6H), 0.93 (s, 9H), 1.43 (s, 3H), 1.67 (s, 3H), 1.8–2.7 (b, 3H), 3.3–3.9 (m, 3H), 4.4–4.7 (m, 1H), 4.9–5.2 (m, 1H), 10.7–12.2 (b, 2H); ir ($CHCl_3$) 3420, 3380, 3200–3300, 1710, 1610, 1530 cm^{-1}; uv λ_{max} 215 (log ε 3.91) and 269 nm (log ε 4.18) in 0.1 *N* HCl; λ_{max} 224 (log ε 4.11), 258 (log ε 4.07) and 310 nm (log ε 3.60) in 0.1 *N* NaOH; ms (185 °C) *m/e* 389 ($M^+ - CH_3$), 356 ($M^+ - C(CH_3)_3$), 298 (M^+-*tert*-butyldimethylsilyl), 280, 206.

6-(2′α,3′α-dihydroxy-4′β-hydroxymethyl-1′β-yl)-3-thioxo-5-oxo-2,3,4,5-tetrahydro-1,2,4-triazine ***14***

To a solution of **13** (110 mg) in 2 ml of tetrahydrofuran was added 5 ml of 50% aqueous trifluoroacetic acid. The solution was stirred at room temperature for 30 min and evaporated to dryness *in vacuo*. The crude product was crystallized from methanol and ethyl ether. Yield 50 mg (72%); mp 163–165 °C; ir (KBr) 3480, 3280, 3100, 1705, 1610, 1560 cm^{-1}; uv λ_{max} 215 (log ε 3.96) and 269 nm (log ε 4.20) in 0.1 *N* HCl; λ_{max} 224 (log ε 4.11), 258 (log ε 4.08), and 310 nm (log ε 3.52) in 0.1 *N* NaOH; ms (190 °C) *m/e* 259 (M^+), 241 ($M^+ - H_2O$), 223 ($M^+ - 2H_2O$), 212, 210, 156 ($B + 28$), 155 ($B + 27$).

Preparation of its Hydrazone ***10*** *from* ***7***

The keto ester **7** (720 mg), ethyl hydrazinoacetate hydrochloride (450 mg, 1.5 equiv.), and sodium acetate (240 mg, 1.5 equiv.) were added in 15 ml of methanol and 5 ml of water. The solution was stirred at room temperature overnight. The solution was evaporated under reduced pressure to remove most of the methanol and 20 ml of chloroform was added to the reaction mixture. The chloroform solution was washed with water, dried over sodium sulfate, and then evaporated to dryness *in vacuo*. The crude product was purified by chromatography on silica gel plates using ethyl ether as an eluant. Yield 850 mg (89%); nmr ($CDCl_3$) δ 0.05 (s, 6H), 0.90 (s, 9H), 1.1–1.7 (m, 9H, O—CH_2CH_3, acetonide), 1.8–2.4 (m, 3H), 3.0–3.3 (m, 1H), 3.5–3.9 (m, 5H, COOMe, SiO—CH_2), 4.0–4.9 (m, 6H), 6.90 (t, $J = 5$ Hz, 0.6H, NH), 10.2 (t, $J = 5$ Hz, 0.4H, NH); ir ($CHCl_3$) 3300 (NH), 1750/1700 (C=O), 1580 (C=N) cm^{-1}; uv (MeOH) 287 nm (log ε 3.93); ms (160 °C) *m/e* 472 (M^+), 457 ($M^+ - CH_3$), 441 ($M^+ - OCH_3$), 415 ($M^+ - C(CH_3)_3$), 357 (M^+ – *tert*-butyldimethylsilyl group) 257, 169. *Anal.* calcd. for $C_{22}H_{40}O_7N_2Si$: C 55.93, H 8.33, N 5.93; found: C 55.98, H 8.68, N 6.06.

A mixture of geometrical isomers (230 mg) was separated using high pressure liquid chromatography on a silica gel column using 0.5% isopropyl alcohol in methylene chloride at 460 psi. The first fraction the *syn*-isomer: yield 120 mg (55%); nmr ($CDCl_3$) δ 0.05 (s, 6H), 0.90 (s, 9H), 1.10–1.53 (m, 9H), 1.67–2.40 (m, 3H), 3.0–3.3 (b, 1H), 3.53 (q, $J = 5$ Hz, SiO—CH_2), 3.77 (s, 3H, COOMe), 4.0–4.7 (m, 6H), 10.2 (t, $J = 5$ Hz, 1H, NH); ir ($CHCl_3$) 3300 (NH), 1750/1700 (C=O), 1560 cm^{-1} (C=N); uv (MeOH) 300 nm (log ε 3.88). The second fraction the *anti*-isomer: yield, 100 mg (45%); nmr ($CDCl_3$) δ 0.05 (s, 6H), 0.90 (s, 9H), 1.1–1.6 (m, 9H), 1.8–2.3 (m, 3H), 2.8–3.1 (b, 1H), 3.4–3.8 (m, 5H, COOMe, SiO—CH_2), 3.9–4.7 (m, 6H), 6.6 (t, $J = 5$ Hz, 1H, NH); ir ($CHCl_3$) 3300 (NH), 1750/1720 (C=O), 1585 cm^{-1} (C=N); uv (MeOH) 275 nm (log ε 3.95).

3(5)-(2′α,3′α-Dihydroxy-O-isopropylidene-4′β-tert-butyldimethylsiloxymethylcyclopent-1′β-yl)-5(3)-carbomethoxy-4-hydroxypyrazole ***15***

To a solution of a mixture of geometrical isomers of hydrazone **10** (340 mg) in 10 ml of methanol was added 0.63 *M* sodium methoxide (3.2 ml, 3 equiv.). The solution was refluxed for 2 h and evaporated under reduced pressure. The residue was taken up in 10 ml of water, acidified

with 0.5 *M* hydrochloric acid, and then immediately extracted three times with ethyl acetate. The ethyl acetate solution was dried over sodium sulfate and evaporated to dryness, followed by chromatography on silica gel plates using ethyl ether – chloroform (5:1) as an eluant (R_f = 0.8). The product was crystallized from petroleum ether (60–80 °C) and ethyl ether. Yield, 120 mg (40%); mp 153–154 °C; nmr ($CDCl_3$) δ 0.05 (s, 6H), 0.90 (s, 9H), 1.30 (s, 3H), 1.47 (s, 3H), 1.9–2.4 (m, 3H), 3.1–3.5 (m, 1H), 3.67 (bd, J = 4 Hz, SiO—CH_2), 3.90 (s, 3H, COOMe), 4.3–4.9 (m, 2H), 8.80–9.25 (b, 2H, NH, OH); ir (KBr) 3420, 1715 (C=O), 1580, 1470 cm^{-1}; ($CHCl_3$) 3440, 1720/1690 (C=O), 1590, 1480 cm^{-1}; uv λ_{max} 230 (log ε 3.62) and 275 nm (log ε 3.50) in 0.1 *N* HCl; λ_{max} 240 (log ε 3.80) and 320 nm (log ε 3.93) in 0.1 *N* NaOH; ms (106 °C), *m/e* 426 (M^+), 411 ($M^+ - CH_3$), 379 ($M^+ - CH_3 - CH_3OH$), 337 ($M^+ - C(CH_3)_3 - CH_3OH$), 311 (M^+-*tert*-butyldimethylsilyl), 279 (M^+ – *tert*-butyldimethylsilyl – CH_3OH), 249, 219, 169 (B + 28), 168 (B + 27). *Anal.* calcd. for $C_{20}H_{24}O_6N_2Si$: C 56.34, H 7.98, N 6.57; found: C 56.59, H 7.69, N 6.71.

3(5)-(2′α,3′α-Dihydroxy-O-isopropylidene-4′β-tert-butyldimethylsiloxymethylcyclopent-1′β-yl)-5(3)-carboxamide-4-hydroxypyrazole ***16***

Pyrazole **15** (340 mg) was dissolved in 20 ml of methanol saturated with ammonia. The flask was well stoppered and allowed to stand for a week. The methanol was evaporated to dryness under reduced pressure and the crude product was chromatographed on silica gel plates using ethyl ether as an eluant to give a foam. Yield 280 mg (85%); nmr ($CDCl_3$) δ 0.05 (s, 6H), 0.90 (s, 9H), 1.35 (s, 3H), 1.58 (s, 3H), 1.8–2.7 (m, 3H), 3.1–3.4 (m, 1H), 3.73 (bs, J = 4 Hz, 2H, SiO—CH_2), 4.4–4.9 (m, 2H), 6.7–7.2 (b, 2H, $CONH_2$), 9.5–10.2 (b, 2H, NH, OH); ir ($CHCl_3$) 3540/3480/3440 (NH, OH), 1680/1630 (C=O), 1590 cm^{-1}; uv λ_{max} 226 (log ε 3.78) and 270 nm (log ε 3.63) in 0.1 *N* HCl; λ_{max} 238 (log ε 3.58) and 312 nm (log ε 3.79) in 0.1 *N* NaOH; ms (180 °C) *m/e* 411 (M^+), 396 ($M^+ - CH_3$), 379 ($M^+ - CH_3 - NH_3$), 354 ($M^+ - C(CH_3)_3$), 337 ($M^+ - C(CH_3)_3 - NH_3$), 296, 279, 153 (B + 27), 137 (B + 27 – NH_3). *Anal.* calcd. for $C_{19}H_{33}O_5N_3Si$: C 55.47, H 8.08, N 10.22; found: C 55.48, H 8.32, N 10.08.

3(5)-2′α,3′α-Dihydroxy-4′β-hydroxymethylcyclopent-1′β-yl)-5(3)-carboxamide-4-hydroxypyrazole ***17***

Amide **16** (440 mg) was dissolved in 5 ml of 50% aqueous trifluoroacetic acid. The solution was stirred at room temperature for 30 min and evaporated to dryness *in vacuo*. The crude product was crystallized from ethyl ether and ethanol. Yield 240 mg (80%); mp 216–218 °C; ir (KBr) 3450/3000–3400 (OH,NH), 1680/1630 (C=O), 1540 cm^{-1}; ms (210 °C) *m/e* 257 (M^+), 240 ($M^+ - NH_3$), 239 ($M^+ - H_2O$), 222 ($M^+ - H_2O - NH_3$), 221 ($M^+ - 2H_2O$), 191, 182, 154 (B + 28), 153 (B + 27), 137 (B + 28 – NH_3), 136 (B + 27 – NH_3); uv λ_{max} = 226 (log ε 3.81) and 270 nm (log ε 3.63) in 0.1 *N* HCl; λ_{max} 235 (log ε 3.71) and 311 nm (log ε 3.93) in 0.1 *N* NaOH. *Anal.* calcd. for $C_{10}H_{15}O_5N_3$: C 46.69, H 5.88, N 16.34; found: C 47.09, H 6.01, N 16.14.

Methyl-2-(2α,3α-dihydroxy-di-O-isopropylidene-4β-carboxycyclopent-1β-yl)glyoxylate ***19***

A mixture of sodium periodate (2.78 g) and potassium permanganate (100 mg) in 30 ml of p*H* 7 phosphate buffer solution and the olefinic ester **18** (670 mg) in 30 ml of acetone was stirred at room temperature for 3 h. The reaction mixture was filtered through Celite and the residue on Celite was washed with chloroform. The filtrate was extracted three times with chloroform. The organic solution was washed with saturated salt solution, dried over sodium sulfate, and evaporated to give the crude keto ester acid (690 mg) as an oil in 85% yield; nmr ($CDCl_3$) δ 1.3 (s, 3H), 1.5 (s, 3H), 2.0–2.6 (m, 2H), 2.8–3.1 (m, 1H), 3.4–3.6 (m, 1H), 3.80 (s, 3H, COOMe), 4.8 (bs, 2H), 9.0 (b, 1H, COOH); ir ($CHCl_3$) 3400–3100, 1740–1710 (C=O), 1395, 1385 cm^{-1}, ms (150 °C) *m/e* 272 (M^+), 257 ($M^+ - CH_3$), 241 ($M^+ - OCH_3$), 213.

Preparation of its Semicarbazone ***20*** *from* ***19***

The keto ester **19** (190 mg), semicarbazide hydrochloride (78 mg), and sodium acetate (58 mg) were dissolved in 10 ml of methanol and 5 ml of water. The solution was stirred at room temperature overnight and then evaporated under reduced pressure to remove most of methanol. The reaction mixture was extracted three times with methylene chloride. The methylene chloride solution was washed with water, dried over sodium sulfate, and then evaporated to dryness to give the semicarbazone (210 mg), which was recrystallized from ethyl ether. Yield 180 mg (78%); mp 141–143 °C; nmr ($CDCl_3$) δ 1.30 (s, 3H), 1.47 (s, 3H), 2.2–2.5 (m, 2H), 2.8–3.0 (m, 1H), 3.2–3.5 (m, 1H), 3.80 (s, 3H, COOMe), 4.67 (m, 1H), 5.10 (m, 1H), 6.0–6.8 (b, 2H, $CONH_2$), 10.2–11.0 (b, 1H), 11.2 (bs, 1H); ir (KBr) 3480, 3250–3400, 2500–2700, 1720 (C=O), 1580 (C=N), 1470, 1390 cm^{-1}; uv (MeOH) 271 nm (log ε 3.92); ms (190 °C) *m/e* 329 (M^+), 314 ($M^+ - CH_3$), 271, 270, 228. *Anal.* calcd. for $C_{13}H_{19}O_7N$: C 47.41, H 5.82, N 12.76; found: C 47.21, H 6.05, N 13.09.

6-(2′α,3′α-Dihydroxy-di-O-isopropylidene-4′β-carboxy-cyclopent-1′β-yl)-3,5-dioxo-2,3,4,5-tetrahydro-1,2,4-triazine ***21***

Semicarbazone **20** (420 mg) was dissolved in 20 ml of methanol containing sodium (100 mg, 3.3 equiv.). The solution was refluxed for 1 h and evaporated under reduced pressure. The residue was taken up in 10 ml of water. The solution was acidified with 0.5 *M* hydrochloric acid and extracted with ethyl acetate. The ethyl acetate solution was dried over sodium sulfate and evaporated to dryness *in vacuo*. The crude product was crystallized from ethyl ether. Yield 300 mg (80%); decomposed above 180 °C; ir (KBr) 3350–3600, 3150–3300, 1700–1740 (C=O), 1620 (C=N), 1390 cm^{-1}; uv λ_{max} 265 nm (log ε 3.62) in 0.1 *N* HCl; λ_{max} 254 nm (log ε 3.60) in 0.1 *N* NaOH; ms (180 °C) *m/e* 297 (M^+), 283 ($M^+ - CH_3$), 239, 222, 210, 140 (B + 28), 139 (B + 27). *Anal.* calcd. for $C_{12}H_{15}O_6N_3$: C 48.48, H 5.09, N 14.14; found: C 48.30, H 5.15, N 14.47.

6-(2′α,3′α-Dihydroxy-di-O-isopropylidene-4′β-hydroxy-methylcyclopent-1′β-yl)-3,5-dioxo-2,3,4,5-tetrahydro-1,2,4-triazine ***22***

To a solution of acid **21** (120 mg) in 5 ml of freshly distilled tetrahydrofuran was added 0.6 ml of 1 *M* diborane (1.5 equiv.) in tetrahydrofuran in an ice bath. The solution was stirred for 2 h in an ice bath under nitrogen atmosphere. A few drops of water were added and the

solvents were evaporated. Boric acid was removed by several coevaporations with methanol under reduced pressure. Purification of the crude product by chromatography on silica gel plates using ethyl acetate as an eluant gave the desired alcohol **22** (95 mg) (which decomposed at above 250 °C) in 83% yield; ir (KBr) 3400–3500/3300 (OH, NH), 1730/1700 (C=O) cm^{-1}; uv λ_{max} 265 nm (log ε 3.70) in 0.1 *N* HCl; λ_{max} 254 nm (log ε 3.57) in 0.1 *N* NaOH; ms (150 °C); *m/e* 268 ($M^+ - CH_3$), 230, 225, 140 ($B + 28$), 139 ($B + 27$). *Anal.* calcd. for $C_{12}H_{17}O_5N_3$: C 50.88, H 6.05, N 14.83; found: C 51.02, H 6.09, N 15.19.

*Preparation of **12** from **22***

Compound **22** (140 mg) was dissolved in 5 ml of 90% aqueous trifluoroacetic acid. The solution was stirred at room temperature for 5 min and evaporated to dryness *in vacuo*. The crude product was crystallized from methanol and ethyl ether to give the crystalline compound **12** (90 mg) in 75% yield. Spectral data (ir and uv) and mp were identical with those of **12**, obtained from **11**.

Acknowledgments

We wish to thank the National Research Council of Canada and the Eli Lilly and Co. for financial support.

1. G. JUST and S. G. KIM. Tetrahedron Lett. 1063 (1976).
2. J. GUT. Advances in heterocyclic chemistry. Vol. I. Academic Press. 1963. pp. 189–251.
3. J. G. ERICKSON, P. F. WILEY, and V. P. WYSTRACK. The chemistry of heterocyclic compounds. Vol. 10. Interscience. 1956. p. 69.
4. (*a*) J. BAILEY. J. Am. Chem. Soc. **28**, 386 (1902); (*b*) J. BOUGAULT. Ann. Chim. **5**, 317 (1916); (*c*) P. K. CHANG. J. Org. Chem. **23**, 1951 (1958).
5. (*a*) J. BOUGAULT and L. DANIEL. C.R. **186**, 1216 (1928); (*b*) J. GUT. Coll. Czech. Chem. Commun. 1588 (1958).
6. G. JUST and G. READER. Tetrahedron Lett. 1521 (1973).
7. R. U. LEMIEUX and E. VON RUDLOFF. Can. J. Chem. **23**, 1701 (1955).
8. G. TRUMMLITZ and J. G. MOFFATT. J. Org. Chem. **38**, 1841 (1973).

Unusual formation of *N*-(1-isoquinolinyl)benzamide from 1-*o*- and 1-*m*-chlorobenzoylisoquinolines

D. Prasad Aysola and Martin S. Gibson

Department of Chemistry, Brock University, St. Catharines, Ont., Canada L2S 3A1

Received July 6, 1976

D. Prasad Aysola and Martin S. Gibson. Can. J. Chem. **55**, 435 (1977).

Syntheses of 1-*o*- and 1-*m*-chlorobenzoylisoquinolines are described, (*a*) from 2-benzoyl-1,2-dihydroisoquinoline-1-carbonitrile and the appropriate chlorobenzaldehyde, and (*b*) from 2-*o*- and 2-*m*-chlorobenzoyl-1,2-dihydroisoquinoline-1-carbonitrile. Treatment of either ketone with potassamide – potassium *tert*-butoxide in ammonia gives *N*-(1-isoquinolinyl)benzamide. The mechanism of this reaction is discussed.

D. Prasad Aysola et Martin S. Gibson. Can. J. Chem. **55**, 435 (1977).

On décrit des synthèses des *o*- et *m*-chlorobenzoyl-1 isoquinoléines à partir: (*a*) du benzoyl-2 dihydro-1,2 isoquinoléine carbonitrile-1 et du chlorobenzaldéhyde approprié et (*b*) des *o*- et *m*-chlorobenzoyl-2 dihydro-1,2 isoquinoléine carbonitriles-1. Le traitement de l'une ou l'autre des deux cétones par de l'amidure ou du *tert*-butylate de potassium dans l'ammoniac conduit au *N*-(isoquinolynyl-1) benzamide. On discute du mécanisme de cette réaction.

[Traduit par le journal]

Bunnett and Hrutfiord have noted that potassamide in ammonia cleaves *o*-chlorobenzophenone to give a mixture of aniline, benzamide, and benzoic acid, but converts *m*-chlorobenzophenone to a mixture of *o*- and *m*-aminobenzophenones (1). Our main interest in these reactions lies in the area of cleavage suppression and heterocyclic synthesis (2), but we have a supplementary interest in problems connected with synthesis of aporphine alkaloids (3), including those of the 7-oxoaporphine sub-group typified by liriodenine (4). To this end we have investigated the behaviour of 1-*o*- and 1-*m*-chlorobenzoylisoquinolines in this type of reaction.

These ketones were prepared from the Reissert compound, 2-benzoyl-1,2-dihydroisoquinoline-1-carbonitrile (5). Treatment with sodium hydride, followed by the appropriate chlorobenzaldehyde, gave the corresponding chlorophenyl-1-isoquinolinylmethyl benzoate. Hydrolysis of the ester to the secondary alcohol, followed by oxidation, gave in each case the desired ketone. We note parenthetically that we have encountered difficulties similar to those reported previously (6) for reactions of the anion of 2-benzoyl-1,2-dihydro-6,7-dimethoxyisoquinoline-1-carbonitrile. However, we find the latter Reissert compound to be stable in refluxing benzene (though not at its melting point) and the earlier reference to its thermal instability would seem to be associated rather with solvolysis in ethanol or ethanolic picric acid.

An alternative synthesis for each of the two ketones was also considered. Reaction of isoquinoline with the corresponding chlorobenzoyl chloride and potassium cyanide in dichloromethane–water (5) gave the corresponding Reissert compound. Treatment of the latter with sodium hydride in dimethylformamide (DMF) (7) gave the desired ketone by expulsion of cyanide ion, but in each case the yield was poor.

A somewhat dirty mixture resulted from reaction of 1-*o*-chlorobenzoylisoquinoline with potassamide – potassium *tert*-butoxide in ammonia, from which a compound, $C_{16}H_{12}N_2O$, was isolated in 17% yield. A similar reaction, conducted in presence of dibenzo-18-crown-6 ether (8), was much cleaner and gave the same product in 77% yield. The same compound was obtained from 1-*m*-chlorobenzoylisoquinoline. This product was isomeric with, but not identical to 1-*o*-aminobenzoylisoquinoline (9) (mixture mp and mass spectrum). The mass spectrum showed peaks at *m/e* 248 (M^+), 171 ($C_9H_7N_2CO$), 143 ($C_9H_7N_2$), 105 (C_6H_5CO), and 77 (C_6H_5). These data suggested that the compound was *N*-(1-isoquinolinyl)benzamide (**1***a*), and identification was subsequently confirmed by direct comparison with an authentic sample (10). Tamura *et al.* (10) have suggested that compound (**1***a*) exists in the enolic form (**1***b*) as the ir spectrum exhibited no CO absorption band in the expected region. We concur in this, noting further that the ir spectrum (KBr) exhibits a broad peak at 2480 cm^{-1}, indicative of a strong O—H· · ·N hydrogen bond (11). The nmr spec-

trum ($CDCl_3$) shows the signal due to the proton involved at unusually high field (δ 15.4 ppm).

We view the formation of **1** in these reactions in terms of a mechanism of the following type (Scheme 1). Amide ion adds reversibly at position 1 in competition with amide ion addition to the carbonyl group. This increases the nucleophilicity of the ring N-atom which bonds to the *ortho*-position of the chlorobenzoyl group; chloride ion is lost by substitution or aryne mechanisms as appropriate. Intramolecular acylation of the angular amino-group (or its conjugate base) is accompanied by regeneration of the isoquinoline system and formation of a carbanion which is protonated to form the phenyl group in the product. Another possibility follows an earlier suggestion (1) that amide ion adds to the carbonyl group and that after deprotonation the amide derived nitrogen then bonds as above to the *ortho*-position of the chlorobenzoyl group. Reformation of the carbonyl group with migration of the 1-isoquinolinyl group to nitrogen and ring cleavage would then produce the same carbanion as that in the above mechanism. This latter mechanism would suggest that benzanilide should be found amongst the products from the reactions of *o*- and *m*-chlorobenzophenones with potassamide, though its presence was not observed (1).

Lastly, we have noted that treatment of either 1-*o*- or 1-*m*-chlorobenzoylisoquinoline with potassium *tert*-butoxide – water in 1,2-dimethoxyethane (12) for 3 h at 20 °C resulted in almost quantitative recovery of the ketone.[1] It seems that neither ketone is very susceptible to cleavage.

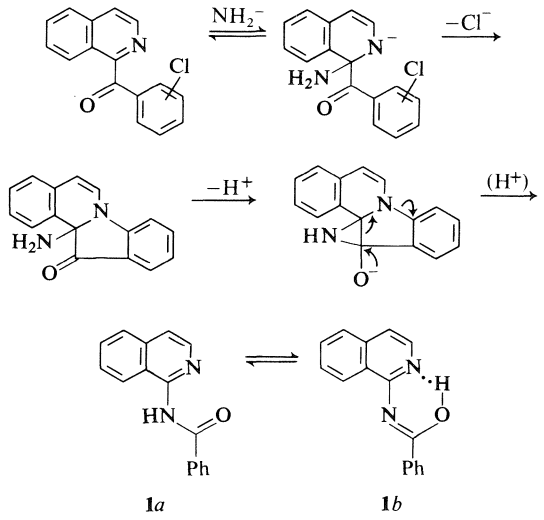

SCHEME 1

Experimental

Mass spectra were determined with an AEI-MS30 double beam mass spectrometer; data are quoted as *m/e* values for the lowest isotopic species. Proton magnetic resonance spectra were recorded on a Bruker WP-60 spectrometer at 60 MHz using tetramethylsilane as internal reference.

Preparation of Reissert Compounds

o-Chlorobenzoyl chloride (14 g, prepared from *o*-chlorobenzoic acid and $SOCl_2$) was added during 1 h under nitrogen to the stirred two-phase system composed of 6,7-dimethoxyisoquinoline (6) (3.5 g) dissolved in CH_2Cl_2 (120 ml) and KCN (12 g) in water (60 ml). More KCN (7 g) in water (30 ml) was added and stirring was continued for 6–8 h. The phases were separated and the aqueous layer was washed with CH_2Cl_2. The CH_2Cl_2 solutions were combined, washed in turn with water, 5% HCl, water, 5% NaOH, and water, dried ($MgSO_4$) and evaporated *in vacuo* to give a brown solid. Crystallization from benzene gave *2-o-chlorobenzoyl-1,2-dihydro-6,7-dimethoxyisoquinoline-1-carbonitrile* as cubes (4.0 g, 61%), mp 174–176 °C; ms *m/e* 354 (M^+, 25%) and 139 (ClC_6H_4CO, 100%). *Anal.* calcd. for $C_{19}H_{15}ClN_2O_3$: C 64.00, H 4.20, N 7.90; found: C 64.09, H 4.21, N 7.76.

Similarly prepared were: 2-benzoyl-1,2-dihydroisoquinoline-1-carbonitrile (65%) (5); 2-*o*-chlorobenzoyl-1,2-dihydroisoquinoline-1-carbonitrile (28%) (13); 2-*m*-chlorobenzoyl-1,2-dihydroisoquinoline-1-carbonitrile (30%) (5); and 2-benzoyl-1,2-dihydro-6,7-dimethoxyisoquinoline-1-carbonitrile (54%) (6).

o-Chlorophenyl-1-isoquinolinylmethyl Benzoate

To a solution of 2-benzoyl-1,2-dihydroisoquinoline-1-carbonitrile (1.3 g) in dry benzene (25 ml) heated under reflux was added 50% sodium hydride dispersion in mineral oil (0.54 g). After 3 min, *o*-chlorobenzaldehyde (0.6 ml) was added. Heating under reflux was continued for 2 h and then the mixture was filtered, washed with water (25 ml), 0.5 *M* HCl (25 ml), and water (25 ml). The benzene solution was dried and evaporated. Trituration of the residue gave *o-chlorophenyl-1-isoquinolinylmethyl benzoate*, which crystallized from ethanol as needles (0.93 g, 50%), mp 104–105 °C; ms *m/e* 373 (M^+, 8%) and 105 (C_6H_5CO, 100%). *Anal.* calcd. for $C_{23}H_{16}ClNO_2$: C 73.90, H 4.28, N 3.75; found: C 73.90, H 4.42, N 3.75.

Similarly prepared was *m-chlorophenyl-1-isoquinolinylmethyl benzoate*, which crystallized from benzene – light petroleum (bp 30–60 °C) as needles (1.27 g, 67%), mp 156–158 °C; ms *m/e* 373 (M^+, 6%) and 105 (C_6H_5CO, 96%). *Anal.* found: C 74.05, H 4.22, N 3.72.

o-Chlorophenyl-1-isoquinolinylmethanol

A solution of *o*-chlorophenyl-1-isoquinolinylmethyl

[1]In a parallel study, Deborah T. Allen has noted that refluxing ethanolic potassium hydroxide slowly reduces 1-benzoylisoquinoline to the corresponding alcohol, with little cleavage; under similar conditions, 2-methyl-1-benzoylisoquinolinium iodide is partially cleaved, the products including 2-methyl-1-isoquinolone and benzoate ion.

benzoate (0.5 g), KOH (3.0 g), ethanol (50 ml), and water (25 ml) was boiled under reflux for 24 h. The mixture was concentrated *in vacuo* and then diluted with water. Extraction with ether gave an oil which solidified on trituration with cold ether. Crystallization from cyclohexane gave *o-chlorophenyl-1-isoquinolinylmethanol* as needles (0.34 g, 95%), mp 115–117 °C; ms *m/e* 269 (M^+, 11%) and 234 ($C_{16}H_{12}NO$, 100%). *Anal.* calcd. for $C_{16}H_{12}ClNO$: C 71.13, H 4.50, N 5.20; found: C 71.20, H 4.44, N 5.27.

m-Chlorophenyl-1-isoquinolinylmethanol was similarly prepared and obtained as an oil (0.3 g, 83%); ms *m/e* 269 (M^+, 31%) and 129 (C_9H_7N, 100%).

1-o-Chlorobenzoylisoquinoline

(a) By Oxidation

A solution of sodium dichromate (0.66 g) in glacial acetic acid (5 ml) was added to *o*-chlorophenyl-1-isoquinolinylmethanol (0.54 g) dissolved in acetic acid (10 ml). The mixture was heated on a steam bath for a few minutes and then diluted with water and basified (NH_4OH). The solid was filtered off and dried. Crystallization from cyclohexane gave *1-o-chlorobenzoylisoquinoline* as needles (0.48 g, 90%), mp 100–103 °C; ms *m/e* 267 (M^+, 4%) and 232 ($C_{16}H_{10}NO$, 100%). *Anal.* calcd. for $C_{16}H_{10}ClNO$: C 72.00, H 3.70, N 5.20; found: C 71.50, H 3.80, N 5.28.

1-m-Chlorobenzoylisoquinoline, similarly prepared, crystallized from cyclohexane as needles (0.48 g, 90%), mp 104–105 °C; ms *m/e* 267 (M^+, 67%) and 266 ($C_{16}H_9ClNO$, 100%). *Anal.* found: C 71.71, H 3.64, N 5.24.

(b) By Rearrangement

Sodium hydride (48 mg, weighed as 50% dispersion in mineral oil and washed free of oil with light petroleum) was suspended in dry DMF (10 ml) and stirred at 18 °C under dry nitrogen. A solution of 2-*o*-chlorobenzoyl-1,2-dihydroisoquinoline-1-carbonitrile (0.97 g) in DMF (15 ml) was added during 10 min and the mixture was then stirred at ambient temperature for 2 h. Ethanol (1 ml) was added and solvents were evaporated *in vacuo* leaving a solid residue. Crystallization from cyclohexane gave 1-*o*-chlorobenzoylisoquinoline (0.1 g, 16%), identical (mp and mixture mp, nmr and mass spectra) with the previous sample.

1-*m*-Chlorobenzoylisoquinoline (52 mg, 13%) was similarly prepared and identified by comparison with the previous sample.

N-(1-Isoquinolinyl)benzamide

(*a*) A solution of 1-*o*-chlorobenzoylisoquinoline (1.0 g) in dry tetrahydrofuran (10 ml) was added dropwise to a stirred solution of potassamide, prepared from potassium (10 g), and potassium *tert*-butoxide (1 g) in redistilled liquid ammonia (150 ml). The resulting brown mixture was stirred for 5 h and then NH_4Cl (28 g) was added in small portions and the ammonia was allowed to evaporate overnight under nitrogen. Water (60 ml) was added and the mixture was extracted with CH_2Cl_2. The extract was washed with water, dried (K_2CO_3), and evaporated. Chromatography on silica gel and elution with benzene–acetone (4:1) gave a buff solid which crystallized from cyclohexane to give colourless crystals of *N*-(1-isoquinolinyl)benzamide (160 mg, 17%), mp 105–106 °C (lit. (10) mp 105.5–106.5 °C). Identity was established by mixture mp, tlc, and spectroscopic correlations with an authentic sample. Spectroscopic data were: ms *m/e* 248 (M^+, 50%), 247(38%), 232(7%), 220(21%), 219(63%), 171(62%), 143(5%), 128(7%), 105(100%), and 77(16%); nmr ($CDCl_3$) δ 15.4 (br s, 1H, exchangeable with D_2O), and 10–8 ppm (10H, aromatic protons). *Anal.* calcd. for $C_{16}H_{12}N_2O$: C 77.45, H 4.69, N 11.43; found: C 77.42, H 4.84, N 11.29.

(*b*) The yield of *N*-(1-isoquinolinyl)benzamide was increased to 77% by increasing the quantity of potassium metal (18 g) and adding dibenzo-18-crown-6 ether (0.1 g) to the reaction mixture.

(*c*) Experiment *a* was repeated, substituting 1-*m*-chlorobenzoylisoquinoline (1.0 g) for the *o*-isomer, to give *N*-(1-isoquinolinyl)benzamide (200 mg, 21%), mp 105–106 °C. Identity was established as in the previous case.

Acknowledgments

We are indebted to Professors Y. Tamura (Osaka University, Japan) and J. L. Neumeyer (Northeastern University, Boston, Mass.) for samples of *N*-(1-isoquinolinyl)benzamide and 1-*o*-nitrobenzoylisoquinoline respectively, I. D. Brindle for helpful discussion, and the National Research Council of Canada for financial support.

1. J. F. BUNNETT and B. F. HRUTFIORD. J. Org. Chem. **27**, 4152 (1962).
2. M. S. GIBSON, S. M. VINES, and J. M. WALTHEW. J. Chem. Soc. Perkin Trans. I, 155 (1975); G. J. CHEN and M. S. GIBSON. J. Chem. Soc. Perkin Trans. I, 1138 (1975).
3. I. AHMAD and M. S. GIBSON. Can. J. Chem. **53**, 3660 (1975).
4. W. I. TAYLOR. Tetrahedron, **14**, 42 (1961); M. SHAMMA. The isoquinoline alkaloids. Academic Press, New York. 1972. Chapt. 13.
5. F. D. POPP and A. SOTO. J. Chem. Soc. 1760 (1963).
6. F. D. POPP and W. E. MCEWEN. J. Am. Chem. Soc. **79**, 3773 (1957).
7. A. H. JACKSON, G. W. STEWART, G. A. CHARNOCK, and J. A. MARTIN. J. Chem. Soc. Perkin Trans. I, 1911 (1974).
8. G. W. GOKEL and H. D. DURST. Synthesis, 168 (1976).
9. F. E. GRANCHELLI and J. L. NEUMEYER. Tetrahedron, **30**, 3701 (1974).
10. Y. TAMURA, S. MATSUGASHITA, H. ISHIBASHI, and M. IKEDA. Tetrahedron, **29**, 2359 (1973).
11. H. H. FREEDMAN. J. Am. Chem. Soc. **83**, 2900 (1961).
12. D. G. DAVIES, M. DERENBERG, and P. HODGE. J. Chem. Soc. C, 455 (1971).
13. H. W. GIBSON. J. Heterocycl. Chem. **7**, 1169 (1970).

Charge distribution in dioxygen complexes of cobalt(III). The crystal structure and absolute configuration of $(+)_{546}$-Δ-*cis*-β-[{2,13-dimethyl-6,9-diphenyl-2,6,9,13-tetraarsatetradecane}(dioxygen)cobalt(III)] perchlorate

DAVID B. CRUMP, ROBERT F. STEPANIAK, AND NICHOLAS C. PAYNE
Department of Chemistry, University of Western Ontario, London, Ont., Canada N6A 5B7

Received May 21, 1976

DAVID B. CRUMP, ROBERT F. STEPANIAK, and NICHOLAS C. PAYNE. Can. J. Chem. **55**, 438 (1977).

The crystal structure and absolute configuration of an optically active dioxygen complex of cobalt(III) have been determined from three dimensional X-ray diffraction data collected by counter techniques. $(+)_{546}$-Δ-*cis*-β-[Co{*R*,*R*-$(CH_3)_2As(CH_2)_3As(C_6H_5)(CH_2)_2As(C_6H_5)(CH_2)_3As(CH_3)_2$}$O_2$]$ClO_4$ crystallizes in the orthorhombic space group $P2_12_12_1$, in a unit cell of dimensions $a = 12.595(7)$, $b = 20.937(10)$, and $c = 11.509(6)$ Å. There are four formula units per cell. The structure was refined on F by full matrix least-squares techniques, and converged with an agreement factor $R = 0.0474$ based on 2988 independent observations collected from two crystals. The absolute configuration of the cation was determined by the Bijvoet absorption edge technique to be Δ. The tetradentate ligand adopts the *cis*-β configuration around the cobalt atom. One six-membered ring has a chair conformation; the other is disordered, and occurs with equal probability in a chair and a distorted boat conformation. The five-membered chelate ring has a *gauche* conformation, of absolute configuration λ. The absolute configurations at the asymmetric arsenic atoms are both *R*. The O—O bond length is 1.424(10) Å. The assignment of formal oxidation states to the cobalt atom and the dioxygen ligand is discussed in light of the molecular geometry and the optical properties of the cation.

DAVID B. CRUMP, ROBERT F. STEPANIAK et NICHOLAS C. PAYNE. Can. J. Chem. **55**, 438 (1977).

On a déterminé la structure cristalline et la configuration absolue d'un complexe dioxygéné optiquement actif du cobalt(III); ces résultats ont été obtenus à partir de données de diffraction de rayon-X en trois dimensions recueillies par la technique des compteurs. Le $(+)_{546}$-Δ-*cis*-β-[Co{*R*,*R*-$(CH_3)_2As(CH_2)_3As(C_6H_5)(CH_2)_2As(C_6H_5)(CH_2)_3As(CH_3)_2$}$O_2$]$ClO_4$ cristallise sous forme orthorhombique avec un groupe d'espace $P2_12_12_1$ et une maille de dimension $a = 12.595(7)$, $b = 20.937(10)$ et $c = 11.509(6)$ Å. Il y a quatre unités de formule par maille. On a affiné la structure sur le fluor par la technique des moindres carrés (matrice complète) jusqu'à un facteur final de $R = 0.0474$ basé sur 2988 observations indépendantes recueillies à partir de deux cristaux. Faisant appel à la technique des absorptions limites de Bijvoet on a établi que la configuration absolue du cation est Δ. Le ligand tétradentate adopte une configuration *cis*-β autour de l'atome de cobalt. Un des cycles à six membres existe sous une conformation chaise; l'autre est désordonné et se produit avec une probabilité égale de conformation chaise et de bateau croisé. Le chélate de cycle à cinq membres a une conformation *gauche* de configuration absolue λ. Les configurations absolues au niveau des atomes d'arsenic asymétriques sont tous les deux *R*. La longueur du lien O—O est de 1.424(10) Å. On discute de l'attribution des états formels d'oxydation au niveau de l'atome de cobalt et du ligand dioxygéné en termes de géométrie moléculaire et de propriétés optiques du cation.

[Traduit par le journal]

Introduction

Dioxygen complexes of group VIII transition metals have been the subject of several recent reviews (1–4). Two different modes of attachment of the O_2 ligand to the metal atom have been demonstrated. Firstly, the diamagnetic 1:1 adducts in which the ligand is 'sideways' bonded with equivalent M—O distances. Secondly, there are complexes with a 'bent' geometry, and two unequal M—O distances. Examples of both geometries have been found for cobalt.

Monomeric complexes evincing the bent geometry are commonly regarded as superoxo compounds of Co(III). Thus, the 1:1 adducts with Co(II) Schiff base complexes have been described as containing the Co(III)—O_2^- group (5–7). The binuclear cobalt amine complexes are considered to be Co(III) complexes of either the superoxide or the peroxide, O_2^{2-}, ligands (8–10). Prior to this study we are aware of only one cobalt complex in which definitive evidence exists for a 'sideways' bonded dioxygen ligand.

Amma and co-workers (11) reported the X-ray structural characterization of the diamagnetic complex $[Co(O_2)\{(C_6H_5)_2PCHCHP(C_6H_5)_2\}_2]$-$BF_4(C_6H_6)_2$. The O_2 ligand is symmetrically bonded, with Co—O bond lengths of 1.871(7) and 1.902(7) Å. The metal coordination geometry was described as either that of a trigonal bipyramid, or a distorted octahedron, with two metal–oxygen bonds. The authors pointed out that conventional coordination numbers and integral oxidation states, *i.e.*, Co(III)—O_2^{2-} or Co(II)—O_2^- represent localised states in a continuum of bonding situations, in a manner analogous to that described for metal–acetylene complexes by Maitlis and co-workers (12), Chatt and Duncanson (13), and Dewar (14).

We present here the first crystal structure analysis of an optically active cobalt dioxygen complex in which the O_2 ligand is 'sideways' bonded to the metal atom. This study was undertaken to determine the geometry of the Co—O_2 bond, and the absolute configuration of the cation. In addition, the results have permitted some conclusions to be drawn as to the charge distribution over the Co—O_2 moiety (15).

Experimental Section

A crystalline sample of $[Co(O_2)(As_4C_{24}H_{38})]ClO_4$ was prepared by Jackson and co-workers (15). The salt forms deep red crystals elongated along [001]. A series of photographs of reciprocal lattice layers $hk(0,1)$, $h(0,1)l$, and $(0,1)kl$, taken with CuKα radiation, indicated the crystals to be orthorhombic, with Laue symmetry *mmm*. There are very few reflections with intensities significantly greater than background for which $\lambda^{-1}\sin\theta$ exceeded 0.40. Systematic absences of h odd, $h00$; k odd, $0k0$; and l odd, $00l$ demonstrated unambiguously the space group to be $P2_12_12_1$ (no. 19, D_2^4) (16). Preliminary cell constants were obtained from the films. The density of the crystals was measured by flotation in a mixture of carbon tetrachloride and ethyl iodide. The values so obtained indicated four formula units per cell. There can be no crystallographic symmetry conditions imposed upon the ions.

The analysis of the structure has taken several years. The collection of intensity data is complicated by the susceptibility of the crystals to X-ray damage. Initially data were collected using Nb filtered Mo radiation, but an examination of the intensities of several standard reflections recorded frequently during the experiment showed a decrease in intensity sometimes approaching 50%, and a deterioration in peak quality as shown by ω-scans (17). These data were sufficient to solve the structure. A second data set was then collected using Cu radiation and a small crystal to minimise absorption effects ($\mu \simeq 100\ cm^{-1}$). Again, radiation damage and the lack of reflections of significant intensity for which $2\theta > 75°$ resulted in unacceptably low precision. Data collected from several other small crystals provided better results, but too few observations to yield acceptable precision. Finally sufficient data were obtained only by using two large crystals, (each approximately 0.4 mm × 0.3 mm × 0.4 mm), which were carefully measured using a filar micrometer eyepiece to facilitate an absorption correction. Crystal data and details of experimental conditions for data collection are summarised in Table 1.

The observations were corrected for background, Lorentz and polarisation effects. A standard deviation σ was assigned to each observation

$$(\sigma(I))^2 = C + \tfrac{1}{4}(t_c/t_b)^2(b_1 + b_2) + (pI)^2$$

where $I = C - \frac{1}{2}(b_1 + b_2)(t_c/t_b)$, C is the total count measured in time t_c, and b_1 and b_2 are background counts, each measured in time t_b. An absorption correction was applied to the data from each crystal.[1] The value of p was chosen to be 0.02.

Structure Solution and Refinement

An initial solution was obtained using 957 observations recorded with MoKα radiation. The Co atom and one As atom were located from a three dimensional Patterson synthesis, and a series of full matrix least-squares refinements and difference Fourier syntheses yielded the positions of the remaining 34 non-hydrogen atoms. When the first set of data collected with Cu radiation became available, the structure was refined with isotropic thermal parameters assigned to the C atoms, and anisotropic parameters to the Co, As, Cl, and O atoms. The phenyl rings were treated as rigid groups. The absolute configuration of the cation was determined to be Δ by the Bijvoet technique (18). Conformational disorder between a chair and a distorted boat was observed in one chelate ring. Refinement converged with 1349 unique observations at $R = 0.067$. The O—O bond length of 1.45 Å had an estimated standard deviation of 0.03 Å, a value considered unacceptably large. The analysis remained at this stage until fresh data were collected using larger crystals.

The final refinement described hereafter was based upon 2654 observations with $F^2 > 0$ collected from crystal 1 within the range $0 < 2\theta \leqslant 90°$, and 1006 observations with $F^2 > 0$ collected from crystal 2 over the range $90 < 2\theta \leqslant 110°$. At greater 2θ values fewer than 1 in 20 observations were significantly different from zero, so no further data were collected. Although the $0kl$ data were collected over the range $0 < 2\theta \leqslant 60°$ for both crystals (60 observations) with a view to scaling the two sets of data, in the final calculations a scale factor was refined for each data set and no other attempt was made to convert the intensities to a common scale.

Refinement was by full matrix least-squares techniques on F, minimizing the function $\Sigma w(|F_o| - |F_c|)^2$, where the weight w is defined as $4F_o^2/\sigma^2(F_o^2)$. The atomic scattering factors for Co, As, Cl, O, and C were taken from Cromer and Waber's tabulation (19); that of H

[1]Computing was carried out on the CDC Cyber 73-14 at the University of Western Ontario. Programs used include local modifications of: orientation matrix and cell refinement, PICK by Ibers; absorption correction, AGNOST, by Cahen and Ibers; Fourier syntheses, FORDAP, by Zalkin; least-squares refinements and structure factor calculations, WOCLS, a version of NUCLS by Ibers; function and error calculations, ORFFE by Busing, Martin, and Levy, and ORTEP, by Johnson.

TABLE 1. Summary of crystal data and experimental conditions for compound $[Co(O_2)\{(CH_3)_2As(CH_2)_3As(C_6H_5)(CH_2)_2As(C_6H_5)(CH_2)_3As(CH_3)_2\}]ClO_4$

Parameter	Value		
	Crystal 1		Crystal 2
Formula weight		816.64	
Formula		$C_{24}H_{38}As_4ClCoO_6$	
Unit cell			
a	12.596(7) Å		12.620(14) Å
b	20.937(10) Å		20.929(19) Å
c	11.509(6) Å		11.508(10) Å
V	3035 Å^3		3040 Å^3
Z		4	
Density			
Observed		1.77(1) g cm^{-3}	
Calculated		1.787 g cm^{-3}	
Space group		$P2_12_12_1$ (D_2^4, orthorhombic)	
Crystal description		Deep red multifaced blocks	
Absorption coefficient		100.05 cm^{-1} (CuKα)	
Crystal faces	{010}, {011}, (1$\bar{1}$0), ($\bar{1}$10), (110), (111), ($\bar{1}\bar{1}$1), (1$\bar{1}$1), ($\bar{1}$1$\bar{1}$)		{010}, {011}, (1$\bar{1}$0), ($\bar{1}$10), ($\bar{1}\bar{1}$0), (1$\bar{1}$1), (1$\bar{1}\bar{1}$), ($\bar{1}\bar{1}$1), (120), (13$\bar{1}$)
Approximate crystal dimensions	0.40 × 0.25 × 0.25 mm		0.35 × 0.20 × 0.20 mm
Crystal volume	0.02701 mm^3		0.01388 mm^3
ω scan, width at half height	0.10°		0.15°
Transmission coefficients	0.063 to 0.199		0.151 to 0.258
Radiation		Cu(λ(Kα_1)1.54056 Å), pre-filtered with 0.018 mm Ni foil	
Temperature		20 °C	
Receiving aperture		5.0 × 5.0 mm, 32 cm from crystal	
Take-off angle		1.5°	
Scan speed		1.0° min^{-1}, 10 s background counts	
Scan range	1.2°		1.5°
2θ limits	$2.5 \leqslant 2\theta \leqslant 90°$		$90° \leqslant 2\theta \leqslant 110°$
Data used in final refinement			
$F_o^2 > 0.0$	2654		1006
p value		0.02	
Final refinement		3660 observations 233 variables	
Error in observation of unit weight		2.44 electrons	
Scale factor	3.072(6)		2.382(15)

from Stewart *et al.* (20). Values of F_c were corrected for the real and imaginary contributions to anomalous dispersion of the Co, As, and Cl atoms. Values of $\Delta f'$ and $\Delta f''$ were taken from Cromer and Liberman (21). The phenyl rings were treated as groups, with D_{6h} symmetry, and a C—C bond length of 1.392 Å (22). Isotropic thermal parameters were assigned to all atoms except the Co, As, Cl, and O atoms. One cycle of least-squares refinement converged at agreement factors

$$R_1 = \frac{\sum (||F_o| - |F_c||)}{\sum |F_o|} = 0.089$$

and

$$R_2 = \left(\frac{\sum w(|F_o| - |F_c|)^2}{\sum wF_o^2}\right)^{1/2} = 0.117$$

An examination of the molecular geometry showed several disturbing features. C(1), C(2), C(3), C(4), and C(5), which comprise one $(CH_3)_2AsCH_2CH_2CH_2$ fragment in the tetradentate ligand, all had abnormally high thermal parameters, and were related by unacceptable bond lengths. The existence of disorder, as observed before, whether static or dynamic, was therefore considered. A difference Fourier synthesis calculated from structure factors computed omitting C(4) showed two peaks so positioned as to indicate a chair/boat conformational disorder. The C atoms bonded to C(4), C(3), and C(5) were then omitted also, and a difference Fourier synthesis computed. Both C(3) and C(5) appeared as single peaks of electron density, though elongated in a direction perpendicular to the plane formed by As(1), As(2), C(3), and C(5). C(4) appeared as two peaks, of electron density 1.81(7) and 1.76(7) e $Å^{-3}$, separated by 1.64 Å. A disorder model was therefore considered in which two chelate rings with ideal boat and chair geometries were superimposed at As(1), As(2), C(3), and C(5). Various attempts were made to refine such disorder models employing rigid group contraints. However a model giving a suitable geometry could be obtained by simply including two atoms of 50% multiplicity for C(4): C(40) and C(41). These atoms were fixed in ideal positions in subsequent refinements, and allotted isotropic thermal parameters. C(3) and C(5) were refined in normal fashion. Two cycles of refinement, with all atoms other than C(40) and C(41) assigned anisotropic thermal parameters, the phenyl C atoms allotted individual isotropic thermal parameters, and using all data with $F^2 > 3\sigma(F^2)$ converged at $R_1 = 0.0654$ and $R_2 = 0.0913$ (2988 observations, 215 variables).

There are 38 H atoms in the cation. A difference Fourier synthesis showed evidence of many of these, though the 12 methyl H atoms were not well resolved. The contributions of the remaining 26 H atoms whose positions could be calculated from the known geometries of the CH_2 and C_6H_5 groups were included in subsequent calculations of F_c. Values of $R_1 = 0.0488$ and $R_2 = 0.0530$ were obtained, a significant improvement.

The absolute configuration of the cation was established by the Bijvoet method. Heretofore, the model chosen was Δ. Accordingly, the enantiomeric model Λ was refined under identical conditions. This model converged at agreement factors $R_1 = 0.0808$ and $R_2 = 0.0941$, confirming that our original choice of the Δ enantiomer was correct at the 0.005 significance level (23). This assignment is confirmed by an examination of Bijvoet pairs of reflections.

In the final model all non-group, non-hydrogen atoms except C(40) and C(41) were assigned anisotropic thermal parameters. Phenyl ring C atoms were given individual isotropic thermal parameters. All data with $F^2 > 0$ were used. H atom positions were calculated prior to the final cycles. Three cycles of least-squares refinement (3660 observations, 233 variables) converged at $R_1 = 0.0557$ and $R_2 = 0.0499$. The error on an observation of unit weight is 2.29 electrons.

A final difference Fourier synthesis on the Δ model contained no peaks greater than 0.77(19) e $Å^{-3}$. This peak, at (−0.12, 0.06, 0.00), was in the neighbourhood of As(4). A comparison of F_o and F_c showed secondary extinction could be neglected. A statistical analysis of the R_2 values of all reflections showed no unusual trends with $|F_o|$, indices, $\lambda^{-1} \sin\theta$ or the χ and ϕ diffractometer setting angles.

The final positional and thermal parameters of the non-group atoms are given in Table 2. The parameters varied for each of the two rigid groups, and the derived positional parameters of the 12 group C atoms are listed in Table 3. Structure amplitudes are tabulated in Table 4, as $10|F_o|$ *vs.* $10|F_c|$ in electrons.[2] Some selected Bijvoet pairs of reflections are given in Table 5, based upon the Δ model, where the difference exceeds 25%. Hydrogen atom parameters are listed in Table 6.[2]

Results and Discussion

The crystal structure is built up from discrete ions, for the closest approaches of anion and cation are 3.32 Å, between O(5) and 2C6, and 3.34 Å, between O(3) and C(8). The shortest non-bonding interaction is 2.4 Å, between O(5) and H2C(6).

The cation is shown in Fig. 1, and some bond distances and bond angles in the inner coordination sphere in Fig. 2. The C atoms are numbered sequentially around the arsine ligand commencing with C(1) and C(2) as the methyl substituents on As(1), and ending with C(11) and C(12) bonded to As(4). A selection of bond distances and bond angles is given in Table 7.

The geometry of the cation may be described either as distorted trigonal bipyramidal, in which case the O_2 ligand is considered to occupy one coordination site, or alternatively, if the ligand occupies two coordination sites, then the geometry is that of a severely distorted octahedron. The angles subtended at the Co atom by the As atoms and the centre of the O_2 moiety (*i.e.* a trigonal bipyramidal geometry) are, in degrees: axial/equatorial, ideal value 90, observed 85.5,

[2]Tables 4 and 6 are available, at a nominal charge, from the Depository of Unpublished Data, CISTI, National Research Council of Canada, Ottawa, Canada K1A 0S2.

TABLE 2. Atom positional and thermal parameters[a]

Atom	x	y	z	U(Å^2) or U_{11}[b]	U_{22}	U_{33}	U_{12}	U_{13}	U_{23}
Co	336.2(13)	498.9(7)	1776.0(12)	619(11)	571(10)	442(8)	2(10)	31(9)	−44(8)
As(1)	−133.1(11)	−570.5(5)	1648.6(10)	1036(11)	596(8)	711(8)	−99(8)	208(9)	−93(7)
As(2)	1257.0(11)	365.6(6)	53.0(9)	766(9)	740(8)	498(6)	−36(9)	116(8)	−99(6)
As(3)	1186.7(11)	1468.3(5)	1893.6(9)	753(9)	638(7)	503(6)	−117(8)	22(8)	−58(6)
As(4)	−1281.7(11)	953.9(6)	1393.4(9)	643(9)	749(8)	661(7)	14(8)	27(8)	80(6)
Cl	307(3)	2962.6(13)	−1742(2)	907(25)	702(17)	615(18)	−52(20)	−7(19)	22(17)
O(1)	229(7)	427(3)	3384(5)	1100(64)	875(50)	523(41)	−61(55)	50(48)	−12(39)
O(2)	1228(8)	211(3)	2961(6)	973(60)	796(52)	786(49)	54(58)	−268(56)	27(39)
O(3)	329(10)	3368(4)	−772(7)	2274(120)	745(54)	776(53)	83(75)	−272(70)	−145(45)
O(4)	193(9)	3331(4)	−2781(6)	1719(93)	900(56)	691(50)	−170(65)	−37(58)	339(41)
O(5)	−543(6)	2516(3)	−1614(7)	867(63)	719(49)	1231(67)	−93(48)	−117(56)	261(52)
O(6)	1274(7)	2605(4)	−1789(7)	740(59)	1496(77)	943(53)	148(68)	69(61)	43(55)
C(1)	−805(12)	−907(6)	3078(10)	1719(156)	941(90)	1053(90)	−27(98)	807(104)	427(77)
C(2)	−1057(14)	−927(6)	446(11)	1557(143)	1167(110)	1250(100)	−430(119)	−436(109)	−532(90)
C(6)	2316(9)	1053(5)	−91(8)	679(81)	869(80)	701(69)	−300(71)	163(69)	−98(67)
C(7)	2506(9)	1387(6)	1028(8)	702(87)	989(92)	587(69)	−310(79)	79(63)	−139(62)
C(8)	514(12)	2180(5)	1148(9)	1167(127)	588(75)	630(70)	−304(85)	80(78)	−66(57)
C(9)	−609(13)	2300(6)	1458(11)	1633(138)	483(72)	829(93)	412(86)	147(96)	66(71)
C(10)	−1353(10)	1833(5)	887(9)	695(83)	797(85)	839(79)	72(79)	−63(76)	147(63)
C(11)	−2287(10)	591(6)	289(11)	945(105)	1347(113)	1105(99)	−29(101)	−492(88)	−159(88)
C(12)	−2137(11)	965(6)	2839(9)	1080(105)	1318(107)	762(80)	347(97)	489(78)	238(75)
C(3)	1113(12)	−1101(5)	1483(10)	1522(133)	587(67)	1240(92)	449(88)	586(112)	218(70)
C(5)	2140(9)	−441(7)	67(10)	814(90)	1661(150)	867(77)	494(107)	158(73)	−149(92)
C(40)	1420	−1020	170	887					
C(41)	2170	−800	1260	887					

[a]All parameters have been multiplied by 10^4. Estimated standard deviations are given in parentheses in this and other tables, and refer to the least significant digits.
[b]$U_{ij} = \beta_{ij}/2\pi^2 a_i^* a_j^*$ (Å^2). The thermal ellipsoid is given by $\exp[-(\beta_{11}h^2 + \beta_{22}k^2 + \beta_{33}l^2 + 2\beta_{12}hk + 2\beta_{13}hl + 2\beta_{23}kl)]$.

TABLE 3

(*a*) Group parameters

	x_g[a]	y_g	z_g	δ	ε	η
Ring(1)	0.0074(4)	0.0440(2)	−0.2529(5)	0.262(5)	−2.924(4)	−1.990(4)
Ring(2)	0.1784(4)	0.2166(2)	0.4390(4)	−1.213(5)	2.740(4)	1.969(4)

(*b*) Derived group atom parameters

Atom	*x*	*y*	*z*	*B*(Å²)	Atom	*x*	*y*	*z*	*B*(Å²)
1C(1)	565(5)[b]	384(3)	−1450(5)	5.0(2)	2C(1)	1561(6)	1841(3)	3364(5)	4.8(2)
1C(2)	562(6)	−131(3)	−2215(7)	6.5(3)	2C(2)	847(5)	1818(3)	4286(7)	6.3(3)
1C(3)	83(6)	−76(3)	−3267(6)	8.1(3)	2C(3)	1070(6)	2143(4)	5312(5)	7.2(3)
1C(4)	−417(6)	496(4)	−3607(5)	7.0(3)	2C(4)	2007(7)	2491(3)	5416(5)	6.0(3)
1C(5)	−414(6)	1012(3)	−2842(7)	7.8(3)	2C(5)	2721(5)	2514(3)	4494(7)	6.9(3)
1C(6)	77(6)	955(3)	−1763(6)	6.1(2)	2C(6)	2498(5)	2189(3)	3467(5)	6.6(3)

[a] x_g, y_g, and z_g are the fractional coordinates of the group origin; δ, ε, and η (radians) are the group orientation angles. See ref. 22.
[b] Derived group atom positional parameters have been multiplied by 10^4.

TABLE 5. Determination of absolute configuration

h	*k*	*l*	$F_c(hkl)$	Observed relationship	$F_c(hk\bar{l})$
1	7	4	13.73	<	25.81
1	7	10	15.47	>	6.67
4	11	1	22.49	>	15.71
4	15	6	11.67	<	17.54
5	2	2	26.19	<	40.21
5	5	2	16.90	>	11.08
5	7	7	17.22	>	7.57
6	3	1	35.99	>	26.77
7	2	8	11.44	<	16.00
8	2	3	8.16	<	16.09

87.4(6), 99.34(8), 90.3, 85.61(7), and 93.36(8); equatorial/equatorial, expected 120, observed 129.0, 121.7, and 109.33(8); axial/axial, expected 180, observed 166.99(9)°. However, if each O atom is considered to occupy one coordination site (an octahedral geometry) the equatorial/equatorial angles, expected 90, are 44.9(3), 99.2(3), 106.6(3), and 109.33(8)°. Of these values, the most unacceptable, 44.9(3)°, arises from the small 'bite' of the dioxygen ligand. Other deviations from idealized values may be attributed to steric strain resulting from the coordination of the tetradentate arsine ligand. A further indication as to the geometry of the coordination sphere may be obtained from several weighted least-squares planes, Table 8. Thus, the atoms in the 'equatorial' plane, Co, As(2), As(4), O(1), and O(2) show deviations from the plane not exceeding 0.040(7) Å (whether it be the equatorial plane of a trigonal bipyramid, or of an octahedron). If an octahedral geometry is assumed,

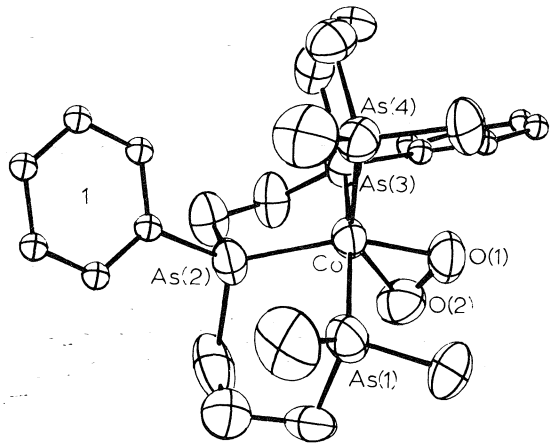

FIG. 1. An overall view of the cation. Atoms are drawn with 50% probability thermal ellipsoids.

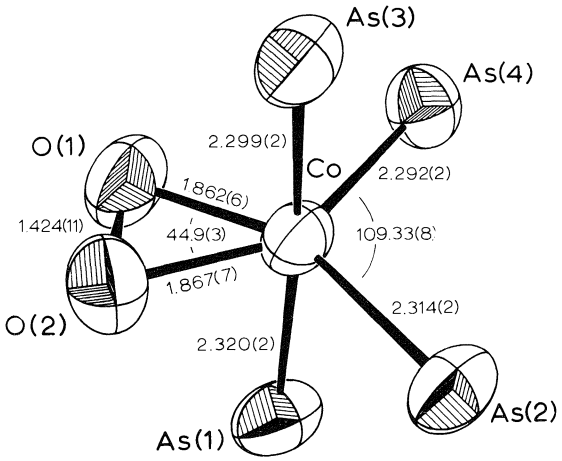

FIG. 2. Inner coordination sphere of the cation.

TABLE 7

(*a*) Selected bond distances (Å)

Bond	Distance	Bond	Distance	Bond	Distance
Co—As(1)	2.320(2)	As(1)—C(1)	1.979(10)	O(1)—O(2)	1.424(10)
Co—As(2)	2.314(2)	As(1)—C(2)	1.956(12)		
Co—As(3)	2.299(2)	As(1)—C(3)	1.932(13)	C(3)—C(40)	1.57
Co—As(4)	2.292(2)	As(2)—C(5)	2.023(14)	C(3)—C(41)	1.50
		As(2)—C(6)	1.970(10)	C(40)—C(5)	1.52
Co—O(1)	1.862(6)	As(2)—1C(1)	1.937(7)	C(41)—C(5)	1.57
Co—O(2)	1.867(7)	As(3)—C(7)	1.944(11)	C(6)—C(7)	1.485(12)
		As(3)—C(8)	1.916(13)	C(8)—C(9)	1.481(16)
Cl—O(3)	1.403(8)	As(3)—2C(1)	1.922(6)	C(9)—C(10)	1.506(17)
Cl—O(4)	1.430(7)	As(4)—C(10)	1.932(11)		
Cl—O(5)	1.429(7)	As(4)—C(11)	1.948(11)		
Cl—O(6)	1.432(8)	As(4)—C(12)	1.982(10)		

(*b*) Selected bond angles (deg)

Bonds	Angle	Bonds	Angle
As(1)—Co—As(2)	87.55(6)	C(7)—As(3)—C(8)	102.5(5)
As(1)—Co—As(3)	166.99(9)	C(7)—As(3)—2C(1)	106.1(4)
As(1)—Co—As(4)	99.34(8)	C(8)—As(3)—2C(1)	100.8(4)
As(2)—Co—As(3)	85.61(7)	Co—As(4)—C(10)	119.7(4)
As(2)—Co—As(4)	109.33(8)	Co—As(4)—C(11)	122.8(4)
As(3)—Co—As(4)	93.36(8)	Co—As(4)—C(12)	109.1(4)
As(1)—Co—O(1)	88.0(2)	C(10)—As(4)—C(11)	98.3(5)
As(1)—Co—O(2)	83.6(2)	C(10)—As(4)—C(12)	102.5(5)
As(2)—Co—O(1)	151.5(3)	C(11)—As(4)—C(12)	101.5(6)
As(2)—Co—O(2)	106.6(3)		
As(3)—Co—O(1)	92.7(2)	As(1)—C(3)—C(40)	103.5
As(3)—Co—O(2)	87.8(2)	As(1)—C(3)—C(41)	119.9
As(4)—Co—O(1)	99.2(3)	C(3)—C(40)—C(5)	108.0
As(4)—Co—O(2)	144.1(3)	C(3)—C(41)—C(5)	109.3
O(1)—Co—O(2)	44.9(3)	As(2)—C(5)—C(40)	109.8
		As(2)—C(5)—C(41)	114.9
Co—As(1)—C(1)	113.5(4)	As(2)—C(6)—C(7)	112.3(7)
Co—As(1)—C(2)	124.4(4)	As(3)—C(7)—C(6)	110.4(8)
Co—As(1)—C(3)	110.7(4)	As(3)—C(8)—C(9)	116.5(8)
C(1)—As(1)—C(2)	101.4(6)	C(8)—C(9)—C(10)	112(1)
C(1)—As(1)—C(3)	103.0(5)	As(4)—C(10)—C(9)	117.3(8)
C(2)—As(1)—C(3)	101.2(6)		
Co—As(2)—C(5)	111.7(3)	O(3)—Cl—O(4)	110.0(5)
Co—As(2)—C(6)	108.9(3)	O(3)—Cl—O(5)	109.2(6)
Co—As(2)—1C(1)	122.5(2)	O(3)—Cl—O(6)	109.2(6)
C(5)—As(2)—C(6)	103.8(5)	O(4)—Cl—O(5)	111.3(6)
C(5)—As(2)—1C(1)	105.7(4)	O(4)—Cl—O(6)	109.6(6)
C(6)—As(2)—1C(1)	102.4(4)	O(5)—Cl—O(6)	107.4(5)
Co—As(3)—C(7)	106.9(3)		
Co—As(3)—C(8)	117.0(4)		
Co—As(3)—2C(1)	121.6(2)		

and the two other planes expected for an octahedron are calculated, then significant deviations of the oxygen atoms result. Overall, the structural data may perhaps be adduced to support the assignment of a trigonal bipyramidal inner coordination sphere.

The arsine ligand adopts the *cis*-β configuration, with a mean Co—As bond length of 2.306(7) Å. The angles subtended at the Co atom by the two six-membered rings are 87.55(6) and 93.36(8)°, both being between axial and equatorial As atoms. The angle subtended by the five-membered ring is 85.61(7)°. The disordered six-membered ring is that which subtends the smaller angle. The disorder model assumed involves the inclusion of two C atoms, C(40) and

TABLE 8. Weighted least-squares planes

	Atom	Deviation (Å)	Atom	Deviation (Å)	Equation
			Co, As(2), As(4), O(1), O(2)		
Plane 1	Co	−0.004(2)	O(2)	0.040(7)	$5.047x + 19.06y + 1.200z - 1.338 = 0$
	As(2)	0.000(1)	O(1)	−0.003(7)	
	As(4)	0.001(1)			
			Co, As(1), As(2), As(3), O(1)		
Plane 2	Co	−0.174(2)	As(1)	0.072(1)	$10.38x - 7.453y + 5.069z - 1.051 = 0$
	As(2)	0.008(1)	O(1)	0.584(8)	
	As(3)	0.047(1)			
			Co, As(1), As(3), As(4), O(2)		
Plane 3	Co	−0.027(1)	As(4)	−0.019(1)	$2.530x - 0.304y - 11.27z + 1.905 = 0$
	As(1)	0.030(1)	O(2)	−1.129(7)	
	As(3)	0.026(1)			

C(41). The four C—C bond lengths involving C(3), C(40), C(41), and C(5) have a mean value of 1.54(1) Å. The mean of the remaining C—C bond lengths is 1.490(8) Å. The average As—C(sp^2) bond length is 1.930(8) and the average As—C(sp^3) bond length is 1.958(10) Å. The five-membered chelate ring adopts the *gauche* conformation of absolute configuration λ (24). The six-membered rings have a chair, and a disordered chair/distorted boat conformation. The absolute configuration at each of the asymmetric As atoms is *R* (25).

The dioxygen ligand is 'π-bonded', with two equivalent Co—O bond lengths of 1.862(6) and 1.867(7), a mean value of 1.865(2) Å. The O—O bond length of 1.424(10) is equivalent to that found by Amma and co-workers (11), 1.420(10) Å, and intermediate between those of 1.28 and 1.49 Å for the superoxide and peroxide ions respectively. The perchlorate ion has the expected tetrahedral structure, with an average Cl—O bond length of 1.424(7) Å, and a mean O—Cl—O angle of 109.5(5)°. The anisotropic thermal parameters of the O atoms are indicative of considerable vibration of the anion, consistent with the absence of any short interionic contacts. However, there was no evidence in the final difference Fourier synthesis of a disordered anion.

It has been noted that conventional coordination numbers and integral oxidation states are inadequate for a discussion of the bonding in these types of compounds (11). We have seen that the inner coordination sphere geometry as deduced from the structural parameters may be viewed either as trigonal bipyramidal, or as

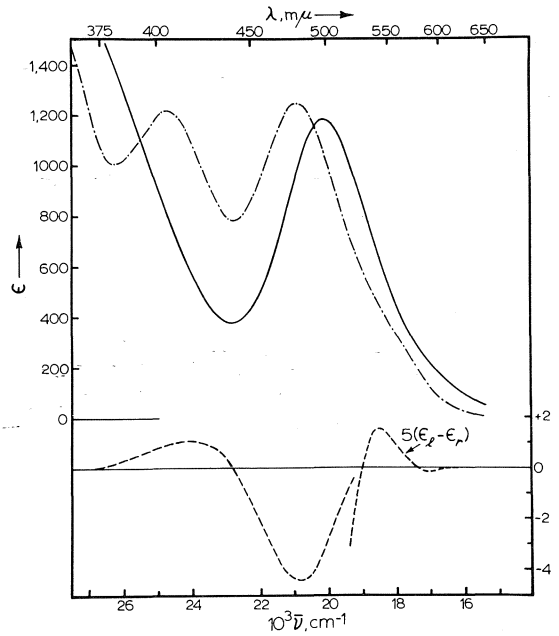

FIG. 3. Optical properties of the cation: —, absorption spectrum of the O_2 complex, in H_2O, 2% v/v CH_3CN. - - -, circular dichroism of the O_2 complex in H_2O, 2% v/v CH_3CN. -·-·-, absorption spectrum of *cis*-$[Co(OH_2)_2(diars)_2](ClO_4)_3$, in 0.5 *M* $HClO_4$.

severely distorted octahedral. However, independent evidence is available for this complex from the optical properties of the cation (15), which are presented in Fig. 3. There is a marked similarity in the electronic spectra between the O_2 complex, and *cis*-$[Co(OH_2)_2(diars)_2](ClO_4)_3$, (diars = *o*-phenylenebis(dimethylarsine)), in which the metal atom is certainly regarded as being in the +3 oxidation state. More convincing, per-

haps, is the circular dichroism spectrum of the O_2 complex, which shows three components under the lower energy band, which may be assigned to the $^1A_{1g} \rightarrow {}^1T_{1g}$ transition of an 'octahedral' Co(III) complex. Therefore the optical properties are best interpreted in light of an octahedral geometry, and a peroxo ligand. A similar formulation has recently been reported by Gray and co-workers (26) for the bis(*cis*-1,2-bis(diphenylphosphine)ethylene)cobalt(III) dioxygen species (11) on the basis of the electronic structure of the complex.

Thus it appears that the charge distribution in this complex is such that, in order for the unipositive cation to contain a Co(III) chromophore, two electrons must have been transferred to the dioxygen ligand. Of the possible bonding schemes, that adopted is closest to the Co(III)—O_2^{2-} description. The chemical and optical properties are characteristic of an octahedral Co(III) chromophore, although the O(1)—Co—O(2) angle of 44.8(3) is far from 90°. The description of the dioxygen ligand as a peroxo species has been further supported by the reaction of resolved *cis*-β-[Co(*R*,*S*-($C_{24}H_{28}As_4$))-$(H_2O)_2]^{3+}$ with hydrogen peroxide in neutral water solution. A dioxygen complex identical with that studied was obtained, with retention of configuration at the Co atom (15).

Acknowledgements

We thank Dr. B. Bosnich and Dr. W. G. Jackson for the crystal sample and the optical spectra, and are grateful to the National Research Council of Canada for financial support of this work.

1. R. G. WILKINS. Adv. Chem. Ser. **100**, 111 (1971).
2. V. J. CHOY and C. J. O'CONNOR. Coord. Chem. Rev. **9**, 145 (1972).
3. J. S. VALENTINE. Chem. Rev. **73**, 235 (1973).
4. L. VASKA. Acc. Chem. Res. **9**, 175 (1976).
5. B. M. HOFFMAN, D. L. DIEMENTE, and F. BASOLO. J. Am. Chem. Soc. **92**, 61 (1970).
6. D. DIEMENTE, B. M. HOFFMAN, and F. BASOLO. Chem. Commun. 467 (1970).
7. G. A. RODLEY and W. T. ROBINSON. Nature (London), **235**, 438 (1972).
8. W. P. SCHAEFER. Inorg. Chem. **7**, 725 (1968).
9. W. P. SCHAEFER and R. E. MARSH. J. Am. Chem. Soc. **88**, 178 (1966).
10. W. P. SCHAEFER and R. E. MARSH. Acta Crystallogr. **21**, 735 (1966).
11. N. W. TERRY III, E. L. AMMA, and L. VASKA. J. Am. Chem. Soc. **94**, 653 (1972).
12. E. O. GREAVES, C. J. L. LOCK, and P. M. MAITLIS. Can. J. Chem. **46**, 3879 (1968).
13. J. CHATT and L. A. DUNCANSON. J. Chem. Soc. 2939 (1953).
14. M. J. S. DEWAR. Bull. Chim. Soc. Fr. **18**, C71 (1951).
15. B. BOSNICH, W. G. JACKSON, S. T. D. LO, and J. W. MCLAREN. Inorg. Chem. **13**, 2605 (1974).
16. International Tables for X-Ray Crystallography. Vol. I. Kynoch Press, Birmingham, England. 1969.
17. T. C. FURNAS. Single crystal orienter instruction manual. General Electric Co., Milwaukee, Wisconsin. 1957.
18. J. M. BIJVOET. Nature (London), **173**, 888 (1954); A. F. PEERDEMAN, A. J. VAN BOMMEL, and J. M. BIJVOET. Proc. K. Ned. Akad. Wet. Ser. B, **54**, 16 (1951); J. TROMMEL and J. M. BIJVOET. Acta Crystallogr. **7**, 703 (1954).
19. D. T. CROMER and J. T. WABER. Acta Crystallogr. **18**, 104 (1965).
20. R. F. STEWART, E. R. DAVIDSON, and W. T. SIMPSON. J. Chem. Phys. **42**, 3175 (1965).
21. D. T. CROMER and D. LIBERMAN. J. Chem. Phys. **53**, 1891 (1970).
22. R. EISENBERG and J. A. IBERS. Inorg. Chem. **4**, 773 (1965).
23. W. C. HAMILTON. Acta Crystallogr. **18**, 17 (1965).
24. IUPAC Information Bulletin No. 33; Inorg. Chem. **9**, 1 (1970).
25. R. S. CAHN, C. K. INGOLD, and V. PRELOG. Angew. Chem. Int. Ed. Engl. **5**, 385 (1966).
26. V. M. MISKOWSKI, J. L. ROBBINS, G. S. HAMMOND, and H. B. GRAY. J. Am. Chem. Soc. **98**, 2477 (1976).

Nuclear magnetic resonance studies. XXXI.[1] Rearrangement and deuterium exchange through β-enolization in bicyclooctanones. An ^2H nuclear magnetic resonance study.

A. K. CHENG, J. B. STOTHERS, AND C. T. TAN[2]

Department of Chemistry, University of Western Ontario, London, Ont., Canada N6A 5B7

Received August 23, 1976

A. K. CHENG, J. B. STOTHERS, and C. T. TAN. Can. J. Chem. **55**, 447 (1977).

The bicyclo[2.2.2]octan-2-one and -[3.2.1]octan-6-one skeletons are interconvertible under strongly basic conditions. Their α,α-dimethyl derivatives in *tert*-BuO^-/*tert*-BuOH at 185 °C undergo very slow interconversion by β-proton abstraction. Using ^2H nmr the stereoselectivity of deuterium incorporation at the β-methylene sites was established. The relative reactivities of β-methyl exchange in the [3.2.1] system were also determined. As models for this process, exchange in the α,α,α′,α′-tetramethyl derivatives of the monocyclic ketones, C_5–C_8, was also studied.

A. K. CHENG, J. B. STOTHERS et C. T. TAN. Can. J. Chem. **55**, 447 (1977).

Dans des conditions fortement basiques, on peut interconvertir les bicyclo[2.2.2]octanone-2 et bicyclo[3.2.1]octanone-6. Leurs dérivés α,α-diméthylés, mis en présence de *tert*-BuO^-/*tert*-BuOH à 185 °C, subissent une interconversion très lente par enlèvement d'un proton en β. Utilisant la rmn du ^2H, on a pu établir la stéréosélectivité de l'incorporation du deutérium au niveau méthylènes β. On a aussi déterminé les réactivités relatives des échanges des méthyles en β dans le système [3.2.1]. Afin d'obtenir des modèles pour ce processus, on a aussi étudié l'échange dans les dérivés α,α,α′,α′-tétraméthylés des cétones monocycliques C_5–C_8.

[Traduit par le journal]

Although it is well-established that enolates can be generated by β-proton abstraction from ketones in strong base, much of the available data has been obtained for systems in which the carbonyl group is in an elaborated norcamphor skeleton (1, 2). Since these β-enolates have synthetic utility (3, 4) it is of interest to define the scope of the process more precisely in terms of the constraints imposed by molecular geometry and to examine the stereochemical features of the process. To this end we have extended our studies to the bicyclooctanone skeleton using the α,α-dimethyl derivatives of bicyclo[2.2.2]octan-2-one (**1**) and bicyclo[3.2.1]octan-6-one (**2**) as substrates. These ketones were chosen since, in principle, these skeletons are interconvertible through a common intermediate, β-enolate **3**, and the methyl substituents preclude possible complications arising through competitive α-enolization. A preliminary report on this system has appeared (4) in which ^{13}C nmr was employed to assay deuterium incorporation from experiments conducted in *tert*-butyl alcohol-*O*-d_1. The several advantages of ^2H nmr as a monitor for hydrogen–deuterium exchange studies (2), however, have led us to a reexamination of this system primarily to obtain information on the stereochemistry of the exchange at the β-methylene sites and more precise data on the stereoselectivity of methyl exchange. As models for comparison of the latter process in a variety of bicyclic systems, we have examined the methyl exchange occurring in the α,α,α′,α′-tetramethyl derivatives of the monocyclic ketones having 5- to 8-membered rings. All of the experiments in this study were conducted under the same strongly basic conditions, *tert*-BuO^-/*tert*-BuOH-(D) at 185 °C, to permit direct comparisons with the results previously reported for a variety of closely related systems.

Experimental

Materials

The preparations of *tert*-butyl alcohol-*O*-d_1, 3,3-dimethylbicyclo[2.2.2]octan-2-one, and 7,7-dimethylbicyclo[3.2.1]octan-6-one have been described (2, 4, 5). The α,α,α′,α′-tetramethyl derivatives of cyclopentanone, cyclohexanone, cycloheptanone, and cyclooctanone were obtained by repeated alkylations with sodium amide and methyl iodide. For the first two ketones, three cycles furnished the tetramethyl derivative as the sole product, each exhibiting the appropriate ^1H, ^{13}C, and infrared spectra and the physical data agreed well with published

[1]For part XXX see ref. 12.

[2]Present address: Department of Pharmacology, University of Toronto, Toronto, Canada.

values (6, 7). After some initial difficulties, our standard methylation procedure was modified slightly to obtain the tetramethyl derivatives of cycloheptanone and cyclooctanone.

To a stirred suspension of 10.5 g (0.269 mol) of freshly powdered sodium amide in 800 ml of anhydrous ether under a nitrogen atmosphere was added, in one portion, a solution of 10 g (0.089 mol) of cycloheptanone in 25 ml of dry ether. The mixture was agitated vigorously for 4 h at room temperature after which 127 g (0.89 mol) of methyl iodide was added slowly. Stirring was continued for another 20 h. Excess sodium amide was hydrolyzed by the addition of water and the product isolated by ether extraction. The ether extracts were washed with water and saturated sodium chloride solution and then dried over anhydrous magnesium sulphate. After removal of the ether by distillation, the residue was recycled through the methylation procedure. A third cycle gave the pure product which was isolated by fractional distillation under reduced pressure.

2,2,7,7-Tetramethylcycloheptanone: ν_{max} ($CDCl_3$) 1695 cm^{-1}; δ_H ($CDCl_3$) 1.16 (s, methyl protons), 1.63 (br s, methylene absorption). *Anal.* calcd. for $C_{11}H_{20}O$: C 78.51, H 11.98; found: C 78.62, H 12.03.

2,2,8,8-Tetramethylcyclooctanone: ν_{max} ($CDCl_3$) 1690 cm^{-1}; δ_H ($CDCl_3$) 1.17 (s, methyl protons), 1.17–1.22 (m, methylene pattern). *Anal.* calcd. for $C_{12}H_{22}O$: C 79.06, H 12.17; found: C 79.08, H 12.28.

Rearrangement and Exchange Experiments

The general procedure has been described (2). To a solution of the base, prepared by dissolving potassium metal in dry *tert*-butyl alcohol under a nitrogen atmosphere, was added the ketone to give a solution containing ketone: *tert*-BuO^- : *tert*-BuOH in a molar ratio of 1:4:40. Aliquots were placed in glass tubes which were sealed after degassing and then heated at 185 ± 3 °C for various periods of time. For the exchange experiments, *tert*-butyl alcohol-*O*-d_1 (99% deuterated and <0.005 *M* in water) was used. After cooling, the tubes were opened and the products were isolated by pentane extraction; the yields for the bicyclic ketones were in the range 70–80%, while the monocyclic ketones were recovered in ~90% yields. Gas chromatography (gc) on a 20% SE-30 column was employed to determine the composition of the total product and preparative gc furnished samples of the major components for nmr and mass spectrometric analysis. Both ^{13}C and ^2H spectra, obtained as previously described (2), were employed to determine the individual sites and extents of deuterium incorporation. The total deuterium content was measured by mass spectrometry. A Varian XL-100-15 system operating in the Fourier transform mode at 25.2 and 15.4 MHz, respectively, was employed for the nmr measurements while a Varian M66 spectrometer furnished the mass spectral data. Shift reagent studies of the proton spectra of the bicyclic ketones, using a Varian HA-100 instrument, were carried out to confirm the assignments in the ^2H spectra.

Results

Analysis of the product obtained upon treatment of **1** under the strongly basic conditions revealed the presence of two ketones, the starting material and **2**, which were readily isolated by preparative gc. The rearrangement of **1** → **2** was found to be very slow, but the equilibrium ratio appears to be approximately 1:4. A large sample of **1** was repeatedly taken through the base treatment a total of nine cycles, each time heated for about 100 h yielding a final mixture containing 60% of **2**. From another series of experiments using various mixtures enriched in **2** it became apparent that the equilibrium concentration of **2** is ~80%. From a series of experiments carried out using *tert*-butyl alcohol-*O*-d_1, samples of **1** and **2** were isolated and their deuterium contents assayed to follow the exchange processes. Initially ^{13}C spectra were employed for these determinations and these results were reported in preliminary form (4). The several advantages of ^2H nmr for this purpose (2), however, led us to reexamine the samples using their ^2H spectra to improve the precision and to determine the stereoselectivity of exchange at the methylene sites. For this purpose, samples of **1**-d_x and **2**-d_x were examined in a solvent mixture of $CHCl_3$/C_6F_6 using $Pr(fod)_3$ as shift reagent to obtain suitable shift dispersion for precise integration. Proton spectra of **1** and **2** were also recorded in the same media to confirm individual assignments.

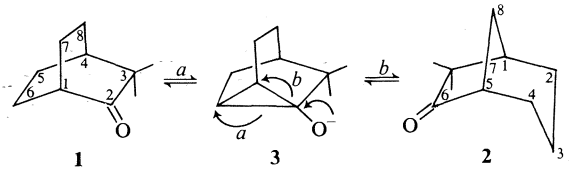

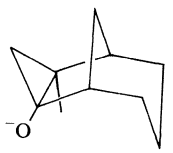

The ^2H spectra of samples of **1**-d_x recovered after treatment with *tert*-BuO^-/*tert*-BuOD consisted of two signals separated by 0.76 ppm with that at higher field presumably arising from the methyl deuterons. Upon addition of $Pr(fod)_3$, these signals moved to higher field with the less shielded absorption splitting into two signals whose separation increased with increasing $Pr(fod)_3$ concentration. Over the range of 0–0.2 equiv. of $Pr(fod)_3$ these signals shifted 0.94, 1.68, and 2.48 ppm with the methyl signal exhibiting the largest change. Proton spectra of **1** were

TABLE 1. Deuterium incorporation in **1** at 185 °C

Time (h)	^{2}H content by mass spectrometry[a]							^{2}H assay by ^{2}H nmr[b]		
	1D	2D	3D	4D	5D	6D	Total Atoms ^{2}H	C-6,7 *exo*	C-6,7 *endo*	CH_3
60	0.412	0.094	0.004				0.61	0.54	0.05	0.03
120	0.486	0.249	0.032				1.08	0.89	0.11	0.07
240	0.212	0.400	0.259	0.090	0.021		2.25	1.56	0.35	0.34
400	0.175	0.320	0.275	0.136	0.044	0.011	2.47	1.32	0.60	0.57

[a]Atoms ^{2}H, ±0.001.
[b]Atoms ^{2}H, ±0.01.

recorded under analogous conditions and it was found that the readily identified methyl singlet exhibited the same change. With increasing [$Pr(fod)_3$], a broad 1-proton singlet showed a larger shift, 3.35 ppm, such that with 0.2 equiv. of $Pr(fod)_3$ it was 0.56 ppm above the methyl signal. Thus it was assigned to the α-bridgehead proton. To unravel the remaining absorptions at lower field, ^{1}H spectra of solutions containing up to 0.8 equiv. of $Pr(fod)_3$ were obtained and the shift dispersion permitted identification of the multiplets. One, an ill-defined 'triplet' with a 32 Hz half-width arising from 2 protons, exhibited the largest shift and its behavior coincided precisely with that of the central signal in the ^{2}H spectra. Because of its sensitivity to $Pr(fod)_3$ it was assigned to the *endo*-6 and -7 nuclei. A second multiplet, integrating for 3 protons with >0.1 equiv. of $Pr(fod)_3$, was discernible and, in the more highly shifted samples, was shown by spin-decoupling to be coupled to the 'triplet'. Since its sensitivity to $Pr(fod)_3$ was different from that of the remaining ^{2}H signal it was tentatively assigned to the 4-, *endo*-5, and -8 protons. The sensitivity of the third ^{2}H absorption, however, was the same as that of the complex multiplet which was least sensitive to added $Pr(fod)_3$ and spin decoupling revealed a strong interaction with the 'triplet' described above. Thus the three ^{2}H signals could be assigned, in order of increased shielding, to the *exo*-6,-7, *endo*-6,-7, and methyl deuterons. In the spectra of the **1**-d_x samples isolated after the longer reaction times, a small signal whose behavior with added $Pr(fod)_3$ paralleled that of the α-bridgehead proton was barely discernible but it could not be reliably integrated. It should be noted that the ^{13}C spectra of these **1**-d_x samples clearly showed that major deuterium incorporation occurred only at C-6, C-7, and the methyl sites; without this information, the foregoing analysis of the ^{2}H spectra would not be unequivocal since the absorption patterns are ill-defined multiplets. Integration by line-shape fitting of the ^{2}H spectra gave the deuterium content at each site and these results are collected in Table 1.

A second series of experiments using **2** as the starting material led to the data collected in Table 2. The individual ^{2}H spectra of these **2**-d_x samples contained four signals whose assignments followed from comparisons of the effect of added $Pr(fod)_3$ on the ^{1}H and ^{2}H spectra. In the absence of $Pr(fod)_3$ the methyl protons are equivalent and the skeletal protons give a complex pattern of essentially three multiplets integrating for 7, 1, and 2 protons in order of decreasing shielding. With addition of the shift reagent, the methyl absorption splits into two singlets and four 1-proton multiplets displaying different sensitivities to [$Pr(fod)_3$] were discernible. A 2-proton multiplet was also clear having the least sensitivity to added reagent. A variety of spin decoupling experiments were carried out to establish the identity of these multiplets and with 0.4–0.7 equiv. of $Pr(fod)_3$ the order of shieldings was found to be: H-5 > *endo*-H-3 ~ *endo*-CH_3 > *endo*-H-4 > *exo*-CH_3 > *syn*-H-8 > *exo*-H-4 ~ *anti*-H-8 > H-1 ~ *endo*-H-2 > *exo*-H-2 ~ *exo*-H-3. The four signals in the ^{2}H spectra could then be assigned to the following sites in order of decreasing shielding: 5 > *endo*-Me > *exo*-Me > *exo*-4. In the initial stages using ^{13}C spectra (4) deuterium incorporation was not detected at the 4-position. Our later refinements of the experimental procedure (2) presumably account for this difference. A spectrum of **2**-d_x isolated after 400 h treatment with *tert*-BuO^-/*tert*-BuOD is shown in Fig. 1. Samples of **2**-d_x formed from **1** after treatment for the

TABLE 2. Deuterium incorporation in **2** at 185 °C

Time (h)	^{2}H content by mass spectrometry[a]								^{2}H assay by ^{2}H nmr[b]				
	1D	2D	3D	4D	5D	6D	7D	Total Atoms ^{2}H	H-3 *exo*	H-4 *exo*	H-5	CH_3 *exo*	CH_3 *endo*
30	0.375	0.411	0.147	0.018	0.002			1.72			0.85	0.87	
60	0.154	0.374	0.338	0.104	0.007	0.004		2.39		0.06	0.76	1.56	0.01_0
120	0.086	0.288	0.388	0.199	0.024	0.007		2.78		0.10	0.73	1.92	0.03_1
240	0.078	0.256	0.379	0.231	0.036	0.009		2.89		0.11	0.65	2.07_5	0.04_6
400	0.085	0.258	0.360	0.217	0.047	0.017	0.005	2.92		0.24	0.58	2.08_4	0.06_5
400[c]	0.057	0.165	0.272	0.266	0.154	0.049	0.008	3.39	0.56	0.69	0.53	1.31	0.32[d]
500[c]	0.043	0.169	0.281	0.277	0.159	0.050	0.008	3.48	0.60	0.68	0.54	1.34	0.32[d]

[a]Atom ^{2}H, ±0.001.
[b]Atom ^{2}H, ±0.02.
[c]Rearrangement product from 3,3-dimethylbicyclo[2.2.2]octan-2-one.
[d]Includes *endo*-^{2}H-3.

longer reaction times were isolated and then ^{2}H spectra recorded; an example is illustrated in Fig. 2. The additional low field signal can be assigned to the *exo*-3 nucleus having been incorporated at the *exo*-6 (7) site in **1** before rearrangement. To optimize the dispersion of the *exo*-3 and -4 signals, as illustrated, the signals for the *endo*-3 and *endo*-methyl sites become essentially equivalent but the relative ^{2}H content at the latter sites is not particularly informative. It can be emphasized, however, that none of the **2**-d_x samples examined contained detectable signals for an *endo*-4 deuterium. If present this signal would have appeared midway between the methyl signals and inspection of the figures reveals no absorption in this region. The results for two samples of **2**-d_x formed from **1** are included in Table 2.

The behavior of four α,α,α′,α′-tetramethyl monocyclic ketones (C_5–C_8) upon treatment with *tert*-BuO^-/*tert*-BuOD at 185 °C was also examined and the ^{2}H assays for these are listed in Table 3. Gas chromatographic analysis of the six-, seven-, and eight-membered ring ketones recovered from the reaction mixtures (~90% yields) revealed the presence of a new peak in the chromatograms of the products from the longer reaction times. In each case, these new component(s) constituted ~1% of the recovered ketone and no attempts were made to isolate these very minor products. Tetramethylcyclopentanone was recovered unchanged with no evidence of rearrangement. The ^{2}H spectra of the recovered tetramethylcyclanones showed that exchange occurred almost entirely at the methyl sites. Only in the cases of the six- and seven-membered rings was there any indication of methylene exchange and this only after >200 h at 185 °C with less than 0.02 atoms ^{2}H incorporation. Although it was not rigorously established, it can be assumed that this very minor process involves the β-methylene sites by analogy with the several results for six- and seven-membered rings incorporated into bicyclic systems (1–4). Since a shift reagent study of the behavior of 2,2,8,8-tetramethylcyclooctanone with added $Pr(fod)_3$ showed that the δ-methylene protons are nearly as sensitive as the methyl protons, indicating their proximity to the carbonyl group, exchange was anticipated to occur at C-5 but even after 375 h at 185 °C no ^{2}H was detected at this site. The presence of a small

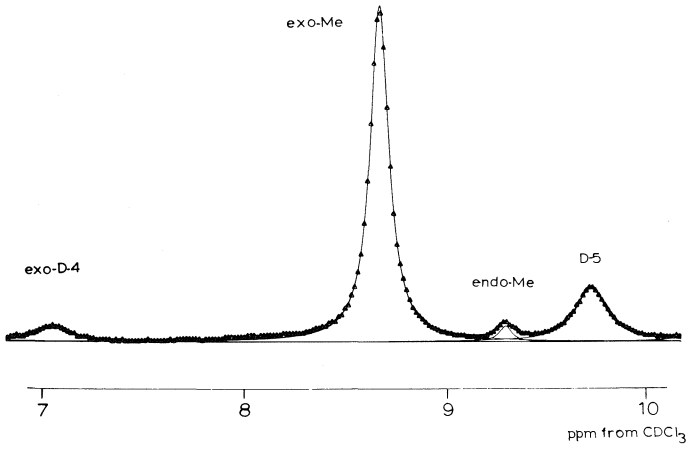

FIG. 1. Observed (△) and computer fitted (full line) ^2H spectra of **2**-d_x isolated after 400 h treatment with *tert*-BuO^-/*tert*-BuOD at 185 °C. The spectrum was obtained in $CHCl_3/C_6F_6$ (4:1) containing 0.3 equiv. of $Pr(fod)_3$.

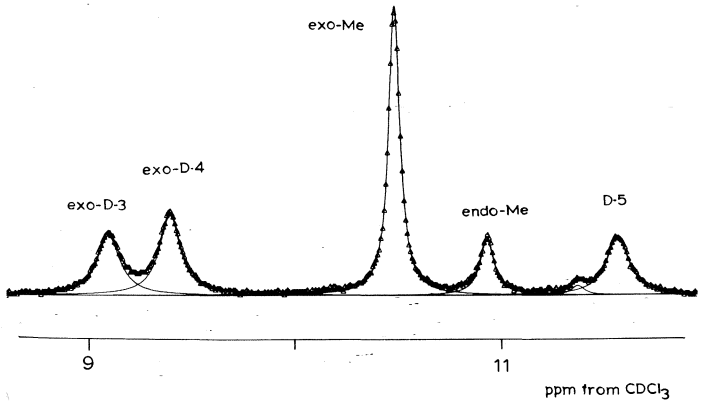

FIG. 2. Observed (△) and computer fitted (full line) ^2H spectra of **2**-d_x obtained after treatment of **1** for 400 h with *tert*-BuO^-/*tert*-BuOD at 185 °C. The spectrum was obtained in $CHCl_3/C_6F_6$ (1:4) containing 0.3 equiv. of $Pr(fod)_3$.

amount (~1%) of a new component could be taken as evidence of very slow isomerization which could conceivably involve a bicyclo[3.3.0]-octan-1-ol intermediate but the second component has not been investigated.

Discussion

From the results for the **1**-d_x samples (Table 1), estimated first-order rate constants for ^2H incorporation are 150×10^{-8}, 17×10^{-8}, and $5 \times 10^{-8}\ s^{-1}$ for the *exo*-6 (7), *endo*-6 (7), and methyl sites, respectively. Clearly *exo*-deuteration is favored over *endo*-deuteration by almost a factor of 10, a somewhat higher degree of stereoselectivity than that found for fenchone (2) but lower than that exhibited by adamantanone (8) both under comparable conditions. It is interesting that the reactivity of bicyclo[2.2.2]-octan-2-one is also intermediate between that of fenchone and adamantanone with the rates of *exo*-deuteration approximately in the order, 700:150:15 and for *endo*-deuteration at the β-methylene site the corresponding order is *ca.* $200:20:1 \times 10^{-8}\ s^{-1}$. Thus, the selectivities for *exo*:*endo* deuteration at this site are approximately 3.5, 7.5, and 15 for fenchone, **1**, and adamantanone, respectively. A similar comparison cannot be made for **2** since we were

TABLE 3. Deuterium in monocyclic ketones 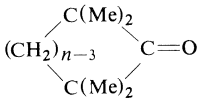 at 185 °C

n	Time (h)	^{2}H content by mass spectrometry[a] 1D	2D	3D	4D	5D	6D	7D	Total atom ^{2}H
5	60	0.392	0.204	0.062	0.013	0.004			1.05
	99[b]	0.345	0.280	0.134	0.042	0.008			1.51
	120	0.251	0.295	0.209	0.102	0.033	0.009		2.10
	120[c]	0.106	0.208	0.251	0.208	0.123	0.061	0.020	3.22
6	60	0.064							0.06
	99[b]	0.161	0.018						0.20
	120	0.290	0.063						0.42
	375[c]	0.363	0.247	0.105	0.028	0.010			1.34
7	99[b]	0.118	0.035						0.19
	399	0.247	0.052	0.011					0.39
	255[c]	0.375	0.207	0.066					0.99
8	99[b]	0.172	0.028						0.23
	375	0.376	0.181	0.066					0.94

[a]Atom ^{2}H, ±0.001.
[b]Using same batch of base, same oven and the same reaction time.
[c]At 215 °C for the first 12 h.

unable to detect measurable amounts of deuterium at the *endo*-C-4 site. The rate constant for *exo*-deuteration, however, is 30×10^{-8} s^{-1} from the data in Table 2, indicating an even greater stereoselectivity for **2** than for the preceding systems. It should be noted that while these crude rate constants may be internally consistent for a given substrate, comparisons from one compound to another are less reliable since competitive experiments were not performed. Such measurements would present major separational difficulties. In any event, the differences seem sufficiently large that the qualitative order of reactivity: fenchone > **1** > **2** > adamantanone is correct and the stereoselectivities for β-methylene exchange in each substrate are certainly reliable. Thus, the most rapidly formed β-enolate exhibits the least selectivity for deuterium capture upon cleavage and in all cases the preferred course is inversion at the β-methylene site, *i.e. exo*-deuteration.

It is apparent from Table 2 that bridgehead exchange at C-5 is the fastest process in **2** in contrast to the almost complete absence of the corresponding process for **1**. This is consistent with earlier observations of bridgehead enolization in [3.2.1] bicyclic systems (9). The barely detectable traces of bridgehead deuterium in samples of **1**-d_x isolated from the longer reaction times presumably arose from small amounts of **2** reformed from **1** in the slow equilibration of the two ketones. The progressively decreasing ^{2}H content at the bridgehead with increasing reaction time (Table 2) reflects the dilution of the deuterium pool by the exchange processes.

The most striking difference between the data for **1** and **2** is the contrast in the relative rates of methyl exchange. In the [3.2.1] system, *exo*-methyl exchange is 100 times faster than *endo*-methyl exchange and the latter is comparable to methyl exchange in the [2.2.2] ketone. For comparison, the *exo*-methyl site in fenchone was also found to be the most reactive but only *ca.* 4 times more rapid than *endo*-methyl exchange. The stereoselectivity of methyl exchange in fenchone and **2**, however, implicates β-enolates such as **4** as intermediates since the inductive effect of the carbonyl group as an activating influence for proton abstraction should be comparable for each methyl site. Formation of **4** could be anticipated to lead to rearrangement of the skeleton to the ring expanded [3.3.1] system but no evidence for this isomerization was obtained. Since cyclopropanols cleave in base to form the product from the more stable carbanion (10), the favored **4** → **2** cleavage is not unexpected. Recently we have observed rearrangement through β-enolates involving methyl sites in acyclic systems which have severely splayed C—C—C bond angles at the carbonyl group (11).

Since it appears that this feature may be the major driving force for cleavage in the less favored direction, it is not surprising that ring expansion does not occur in the bicyclic systems because the skeletal constraints preclude appreciable increases in this bond angle. It is interesting that the rates of methyl exchange in the monocyclic ketones are similar for the six-, seven-, and eight-membered rings and comparable to the values for *endo*-methyl exchange in fenchone and **2**, as well as that for **1** in which the two methyl groups are equivalent, while methyl exchange is significantly faster (*ca.* 10-fold) for tetramethylcyclopentanone. Thus the relative rates for the methyl sites in the systems having five-membered rings are 300, 50, and $20 \times 10^{-8}\ s^{-1}$ for **2**, fenchone, and tetramethylcyclopentanone, respectively, and for the remaining cases the first-order rate constants are in the range $2\text{–}5 \times 10^{-8}\ s^{-1}$. Clearly ring size and stereochemistry govern the reactivity for methyl exchange but it is difficult to be more specific with regard to an interpretation of the observed rates. The 100-fold difference in methyl reactivity for the [3.2.1] system, however, may be useful for tracer studies of selectively deuterated derivatives.

Acknowledgements

We are grateful for the financial assistance provided by the National Research Council of Canada and we wish to acknowledge the technical help of Ms. Lucille Gough, Inára Grikis, and Jane Wheeler. We wish to thank Professors J. P. Guthrie and D. H. Hunter for very valuable discussions.

1. A. NICKON, J. L. LAMBERT, J. E. OLIVER, D. F. COVEY, and J. MORGAN. J. Am. Chem. Soc. **98**, 2593 (1976) and references therein.
2. A. L. JOHNSON, J. B. STOTHERS, and C. T. TAN. Can. J. Chem. **53**, 212 (1975).
3. A. NICKON, H. KWASNIK, T. SWARTZ, R. O. WILLIAMS, and J. B. DIGIORGIO. J. Am. Chem. Soc. **87**, 1615 (1965); R. M. COATES and J. P. CHAN. Chem. Commun. 1481 (1970); A. L. JOHNSON, N. O. PETERSEN, M. B. RAMPERSAD, and J. B. STOTHERS. Can. J. Chem. **52**, 4143 (1974).
4. D. M. HUDYMA, J. B. STOTHERS, and C. T. TAN. Org. Magn. Reson. **6**, 614 (1974).
5. K. R. STEPHENS, J. B. STOTHERS, and C. T. TAN. *In* Mass spectrometry and N.M.R. spectroscopy in pesticide chemistry. *Edited by* R. Haque and J. F. Biros. Plenum Press, New York. 1974. pp. 179–196.
6. L. RAND, W. WAGNER, P. O. WARNER, and L. R. KOVAC. J. Org. Chem. **27**, 1034 (1962).
7. J. A. HENBURROW, A. F. B. CAMERON, J. H. CHAPMAN, R. M. EVANS, B. A. HEMS, A. B. A. JANSEN, and T. WALKER. J. Chem. Soc. 1529 (1968).
8. J. B. STOTHERS and C. T. TAN. J. Chem. Soc. Chem. Commun. 738 (1974).
9. K. W. TURNBULL, S. J. GOULD and D. ARIGONI. Chem. Commun. 597 (1972); D. H. BOWEN and J. MACMILLAN. Tetrahedron Lett. 4111 (1972).
10. C. H. DEPUY. Acc. Chem. Res. **1**, 33 (1968); C. H. DEPUY, F. W. BREITBEIL, and K. R. DEBRUIN. J. Am. Chem. Soc. **88**, 3347 (1966).
11. M. B. RAMPERSAD and J. B. STOTHERS. J. Chem. Soc. Chem. Commun. 709 (1976).
12. A. K. CHENG and J. B. STOTHERS. Can. J. Chem. **55**, 50 (1977).

Décharge triboélectrique dans les alcanes C_1–C_5 à basse pression

JAN A. HERMAN, GILLES MAYRAND ET HADI TARKI
Département de Chimie, Université Laval, Québec (Qué.), Canada G1K 7P4

Reçu le 19 juillet 1976

JAN A. HERMAN, GILLES MAYRAND et HADI TARKI. Can. J. Chem. **55**, 454 (1977).

On a soumis à la décharge triboélectrique les gaz suivants: CH_4, C_2H_6, C_3H_8, n-C_4H_{10}, iso-C_4H_{20} et n-C_5H_{12} et certains produits provenant de leur décomposition ont été mesuré. La proportion des produits insaturés mesurés compte pour environ 75%. Le taux de décomposition augmente avec le nombre d'atomes de carbone du squelette du composé paraffinique. La composition relative des produits provenant de la décomposition du méthane varie en fonction de la pression: la proportion des produits saturés croît avec l'augmentation de la pression. On propose certaines explications du comportement observé des gaz étudiés dans la décharge triboélectrique.

JAN A. HERMAN, GILLES MAYRAND, and HADI TARKI. Can. J. Chem. **55**, 454 (1977).

The following gases were submitted to a triboelectric discharge: CH_4, C_2H_6, C_3H_8, n-C_4H_{10}, iso-C_4H_{10}, and n-C_5H_{12} and their decomposition products were analyzed. The proportion of unsaturated in the products is around 75% of the total. The total yield of decomposition products increases with the number of carbon atoms in the compound submitted to the discharge. The proportion of saturated products formed from methane increases with pressure. Tentative explanations are offered to elucidate the observed behaviour of gases in the tribo-discharges.

Introduction

Selon Harper (1) le nom "triboélectrisation" (anglais: triboelectrification) englobe deux phénomènes distincts de formation d'électricité statique, l'un par séparation de deux phases dissemblables (électrisation de contact), l'autre par frottement de deux matériaux similaires ou non (électrisation par frottement). Dans des nombreux cas, il est difficile de distinguer clairement entre les deux phénomènes; il est alors préférable de parler de triboélectrisation (2). Beaucoup de détails du mécanisme fondamental de triboélectrisation ne sont pas encore élucidés (1, 3), mais le processus lui-même consiste de façon globale en une séparation de charges à l'interface de deux phases suivi d'une recombinaison subséquente des charges pouvant prendre la forme d'une décharge à travers le gaz. Dans le cas particulier du mouvement relatif des surfaces contigues du mercure et du verre la recombinaison est suffisamment énergétique pour produire des états excités jusqu'à 20 eV au-dessus de l'état fondamental des gaz rares, du mercure et aussi de la silice et du bore du verre (4). De la même façon le mouvement du mercure sur le verre recouvert avec des colorants scintillants produit l'émission du spectre caractéristique du colorant et les tensions d'électrisation de contact mesurées dans ces systèmes sont en excès de 20 V, valeur limite de l'électromètre employé dans ces expériences (5). On doit donc s'attendre à des effets chimiques résultant du processus triboélectrique et de telles transformations chimiques ont été récemment décrites (6–8).

Le rôle de certains paramètres (tels la nature des phases misent en contact, le prétraitement des surfaces, la pression, le champ électrique, etc.) a été étudié à plusieures reprises (9, 10), cependant les conséquences chimiques de ces paramètres sont beaucoup moins bien connues. L'étude de Alcock et coll. (8) sur le méthane soumis à la décharge triboélectrique est probablement la plus détaillée à ce sujet. Dans le présent travail nous examinons la décomposition de quelques hydrocarbures gazeux soumis à la décharge triboélectrique. Les gaz utilisés dans ces expériences sont le méthane, l'éthane, le propane, les n- et iso-butanes, le n-pentane. Les expériences sur le méthane sont faite entre 1 et 200 torr de manière à étendre les conclusions de Alcock et coll. (8) à un domaine de pression qui n'a pas été couvert par ces auteurs. La décomposition des autres hydrocarbures dans la décharge triboélectrique est intéressante par comparaison à celle du méthane.

Partie expérimentale

Les cellules de réactions (réacteurs) sont en Pyrex. Elles sont équipées d'un robinet à haut vide en teflon inséré de telle façon sur les réacteurs que le mercure n'entre jamais en contact avec le robinet. Ces réacteurs

de forme cylindrique d'environ 200 cm^3 (diam. int. 5.6 cm) sont soumis à un mouvement de rotation autour de l'axe longitudinale du récipient.

La triboélectrisation est très sensible à la qualité de la surface. Pour cette raison on a adopté une procédure rigoureuse de nettoyage des réacteurs. Ceux-ci sont nettoyés à l'acide sulfurique concentré bouillant, rincés à l'eau distillée et sechés à 450 °C. La cellule propre est ensuite remplie d'une quantité pesée de mercure frais, ou de billes d'acier propres, connectée à une rampe à vide et chauffée à nouveau pour enlever l'humidité et les gaz adsorbés sur le métal. Pendant environ 12 h on pompe sur le réacteur (limite du vide $\sim 10^{-5}$ torr) avant son remplissage par une quantité controllée de gaz.

Les hydrocarbures saturés proviennent de Matheson Co. On les purifie par distillation de piège à piège à -195 °C et par adsorption sur tamis moléculaire à basse température. De façon générale ils ne contiennent que des traces d'autres hydrocarbures. Dans le cas de l'éthane on a pris la précaution supplémentaire de la sécher sur un mirroir de sodium métallique, cependant son comportement dans la décharge triboélectrique n'est guère différent de l'éthane purifié par voie habituelle. Les gaz sont analysés par chromatographie en phase gazeuse. On utilise une colonne de squalane pour analyser les hydrocarbures.

Toutes les expériences sont faites à la température ambiante, soit 23 ± 2 °C.

Résultats

Deux genres de mouvements de réacteurs ont été essayé: (*1*) agitation sur un agitateur de laboratoire, et (*2*) rotation autour de l'axe longitudinal de la cellule de réaction. Des résultats qualitativement similaires ont été obtenus dans les deux cas, mais une comparaison quantitative n'est guère possible. En effet, l'agitation est difficilement reproductible d'une expérience à l'autre malgré les précautions prises dans l'ensemble des manipulations. Il est fréquent de trouver des résultats sur les mêmes réacteurs qui diffèrent de 100%. Cela est dû au moins en partie à la difficulté de positionner les réacteurs de manière rigoureusement reproductible, ce qui entraine des différences dans l'agitation du mercure. L'avantage de l'agitation par rapport à la rotation est une transformation plus grande du gaz soumis à la décharge triboélectrique. Ainsi après quelques heures d'agitation énergique on peut transformer jusqu'à 50% de la quantité initiale du gaz parent, à condition qu'il soit à basse pression.

Par contre, les résultats obtenus par rotation sont reproductibles à 20% près pour une même série d'expériences. L'avantage de cette méthode réside surtout dans la reproductibilité du mouvement du mercure, la connaissance de la vitesse du métal par rapport au verre et celle de la surface totale parcourue au cours de l'expérience. En choisissant une géométrie simple du réacteur on peut mésurer la longueur du contour de l'interface mercure/verre. Chacun de ces paramètres intervient dans le processus triboélectrique, donc influence le taux de décomposition du gaz enfermé dans le réacteur.

(a) Dimensions du réacteur

Le siège de la triboélectrisation est situé à l'endroit de la séparation des phases dissemblables, donc dans le cas présent sur le bord arrière du mercure en mouvement sur la surface isolante. Dans le cas de la rotation d'une cellule, ce contour "actif" de l'interface Hg/verre est facile à déterminer. On s'attend à ce que l'effet chimique soit proportionnel à la longueur de ce contour "actif", et dans le cas de la décomposition du N_2O cela est confirmé (11). D'autre part, pour une longueur constante du contour de l'interface, l'effet chimique est indépendant de la masse du mercure.

(b) Durée de la rotation

Celle-ci est présentée sur la fig. 1 pour l'éthane et le *n*-butane. On a porté sur le graphique le pourcentage de transformation (ordonnées) en fonction du temps de rotation (abcisses) à vitesse constante. Dans le cas du *n*-butane la transformation par unité de temps est plus importante que celle de l'éthane. On voit qu'on s'écarte de la linéarité après environ 3% de transformation du *n*-C_4H_{10}, tandis que dans les mêmes conditions de vitesse le C_2H_6 n'est décomposé que 1.5% après 8 h de rotation. Ces résultats suggèrent que dans les conditions de nos expériences, la linéarité du taux de décomposition des molécules parentes persiste jusqu'à environ 2%. Au-delà de cette limite on doit s'attendre à une diminution de la vitesse de décomposition, due selon toutes vraissemblance, à des dépots polymériques qui modifient les propriétés des surfaces en contact.

(c) Les hydrocarbures paraffiniques C_1 à C_5

La décomposition du CH_4 en fonction de la pression est présentée aux figs. 2 et 3. On constate que la quantité décomposée du méthane à vitesse et à surface parcourue constantes croît avec la pression. Cette constatation est en accord avec les données de Alcock et coll. (8) lesquels ont trouvé une augmentation du taux de conversion jusqu'à 200 torr suivi ensuite d'une brusque chute. La composition relative

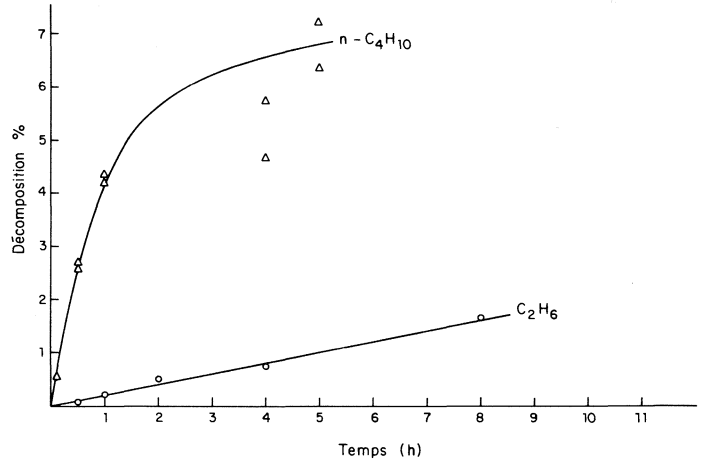

FIG. 1. Décomposition du C_2H_6 et du n-C_4H_{10} en fonction de la durée de rotation. Vitesse: ~21 cm s^{-1}.

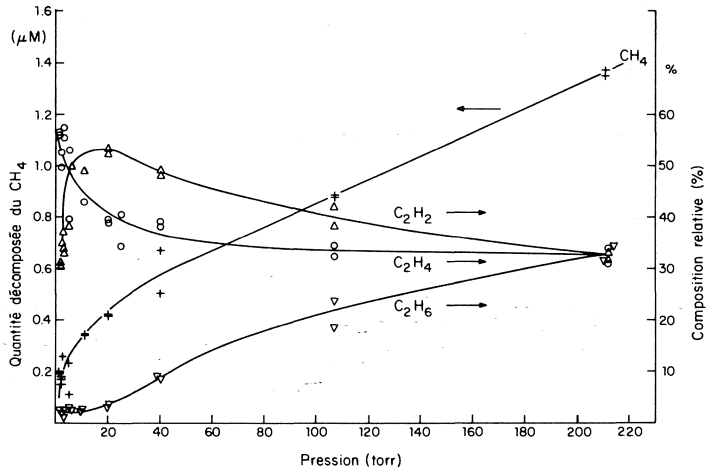

FIG. 2. Quantité (en μM) décomposée du méthane et composition relative des C_2H_2, C_2H_4 et C_2H_6 en fonction de la pression dans une décharge triboélectrique. Vitesse: ~21 cm s^{-1}, durée de rotation: 60 min.

des produits C_2H_2, C_2H_4, C_2H_6 et les C_3 formés dans la décharge triboélectrique change aussi avec la pression. Tandis que les insaturés C_2H_2, C_2H_4, C_3H_6 et C_3H_4 diminuent avec l'augmentation de la pression, les produits saturés: C_2H_6 et C_3H_8 augmentent dans les mêmes conditions.

L'influence du NO sur la décomposition du CH_4 à pression totale 2.6 torr est illustrée à la fig. 4. Des faibles quantités de l'oxyde nitrique baissent de moitié la formation de l'éthane, tandis que l'éthylène montre une faible hausse. L'acétylène diminue très légèrement et de manière progressive. Les résultats relatifs aux C_2H_2 et C_2H_4 sont dans les limites de l'incertitude expérimentale, néamoins la tendance semble réelle dans les deux cas.

La comparaison du comportement chimique dans le processus triboélectrique du CH_4, C_2H_6, C_3H_8, n-C_4H_{10}, iso-C_4H_{10} et n-C_5H_{12} à basse pression (2.5 torr) est présentée dans les tableaux 1 et 2. Dans le tableau 1 sont indiqués les pourcentages absolus et relatifs (entre parenthèses) pour une vitesse de rotation de ~21 cm s^{-1}. Dans l'avant-dernière colonne on trouve le pourcentage globale de transformation. La dernière colonne indique la fraction des produits saturés formés dans la décharge. Dans le tableau

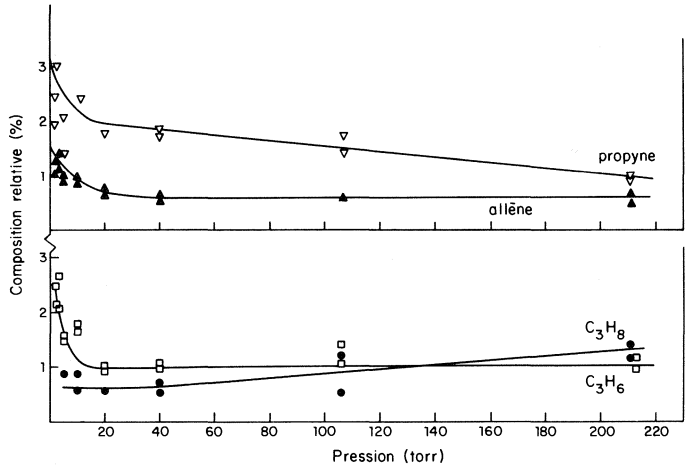

FIG. 3. Variation de la composition relative en fonction de la pression pour les produits mineurs formés dans la décharge triboélectrique dans le méthane. Vitesse: ~21 cm s^{-1}, durée de rotation: 60 min.

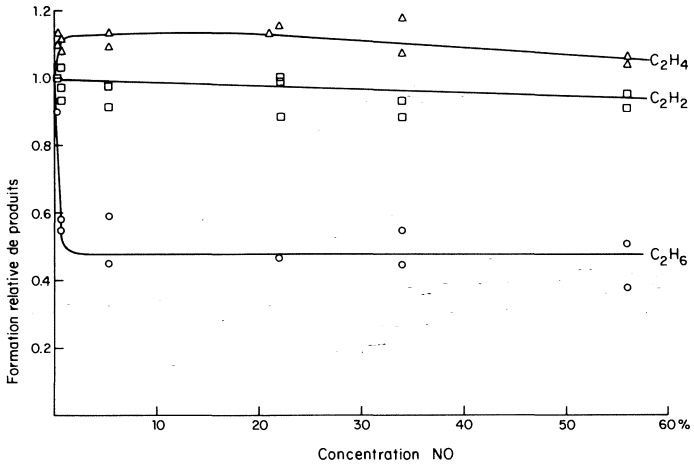

FIG. 4. Formation relative des produits C_2H_2, C_2H_4 et C_2H_6 en fonction de la concentration du NO dans une décharge triboélectrique du méthane. Pression totale: 2.6 torr, vitesse: ~21 cm s^{-1}, durée de rotation: 60 min.

2 sont présentées uniquement les valeurs relatives: (*a*) pour une vitesse de rotation trois fois moindre, soit 6.3 cm s^{-1}, pour les réacteurs Hg/verre, et (*b*) pour les expériences faites dans des réacteurs en verre contenant des billes d'acier. Dans le cas des réacteurs à interface billes d'acier/verre les transformations globales sont environ 30 fois plus faible pour un temps de rotation comparable à celui du tableau 1.

Les données du tableau 1 indiquent que dans la série: méthane–*n*-butane le taux global de transformation (avant-dernière colonne) augmente avec le nombre d'atomes de carbone. Le taux de décomposition du *n*-pentane est plus faible, mais l'analyse n'a pas été faite pour tous les produits en C_5 et supérieurs. La valeur rapportée est donc une valeur par défaut et peu facilement être supérieure à 3%. Dans le cas de l'isobutane, seul alcane ramifié, étudié, celui-ci masque sur le chromatogramme les C_4 insaturés, par conséquent le taux de décomposition de 2.0% n'est qu'un minimum.

Discussion

L'existence de la décharge électrique est prouvée par l'émission des ondes électromagné-

TABLEAU 1. Formation des produits en % à partir des hydrocarbures soumis à la décharge triboélectrique (pression 2.6 torr, durée de rotation: 60 min., vitesse: 20.9 cm s^{-1}, interface Hg/verre)[a]

	Produit																	
	CH_4	C_2H_2	C_2H_4	C_2H_6	C_3H_6	C_3H_8	Propyne	Allène	Cyclo-propane	n-C_4H_{10}	i-C_4H_{10}	i-C_4H_8	1-C_4H_8	2-C_4H_8	Butyne-1-ène-3	C_5 insat.	$-\Delta M^b$ %	% des produits saturés[c]
Méthane	—	0.12	0.11	0.007	0.006	0.008	0.006	0.003	—	—	—	—	—	—	—	—	0.52	7.3
	—	(105)	(100)	(6)	(5)	(7)	(5)	(3)	—	—	—	—	—	—	—	—		
Ethane	0.35	0.44	0.66	—	0.26	0.13	0.034	0.02	0.001	0.013	0.001	—	0.006	0.01	0.004	—	2.0	20
	(53)	(67)	(100)	—	(39)	(20)	(5)	(2)	(0.1)	(2)	(0.2)	—	(1)	(1.4)	(0.6)	—		
Propane	1.21	0.82	1.06	0.30	0.37	—	—	0.03	0.02	0.02	0.03	—	0.03	0.02	0.01	—	2.4	26
	(114)	(78)	(100)	(29)	(35)	—	—	(2)	(2)	(2)	(3)	—	(3)	(1.5)	(1)	—		
n-Butane	1.68	1.47	3.58	0.64	0.60	0.20	0.18	0.09	0.007	—	—	—	0.26	0.06	0.04	—	4.0	22
	(47)	(41)	(100)	(18)	(17)	(6)	(5)	(3)	(0.2)	—	—	—	(7)	(2)	(1)	—		
Isobutane	0.85	0.50	0.80	0.14	0.55	0.23	0.09	0.05	0.002	0.01	—	0.16	—	—	—	—	2.0	23
	(106)	(63)	(100)	(18)	(68)	(29)	(11)	(7)	(012)	(1)	—	(20)	—	—	—	—		
n-Pentane	0.93	0.84	2.08	0.44	0.71	0.27	0.09	0.1	0.005	0.04	—	—	0.14	0.02	0.02	< 0.17[d]	2.6	21
	(45)	(41)	(100)	(21)	(34)	(13)	(5)	(5)	(0.2)	(2)	—	—	(7)	(1)	(1)	< (8)		

[a]Moyenne sur au moins 2 expériences. Entre parenthèses valeurs relatives par rapport à l'éthylène = 100.
[b]Quantité de molécules parents transformées (en %) calculée suivant l'expression: $-\Delta(CH_4) = 2\Sigma C_2 + 3\Sigma C_3$; $-\Delta(C_2H_6) = 0.5C_1 + \Sigma C_2 + 1.5\Sigma C_3 + 2\Sigma C_4$, etc.
[c]Calculé suivant l'expression: (% sat.) = $[2(C_2H_6) + 3(C_3H_8)]100/(-\Delta CH_4)$ pour le méthane, etc.
[d]Analyse partielle des C_5.

TABLEAU 2. Valeurs relatives de formation des produits provenant des hydrocarbures soumis à la décharge triboélectrique (pression 2.6 torr, vitesse pour l'interface Hg/verre: 6.3 cm s^{-1}, vitesse pour l'interface billes d'acier/verre: 19.6 cm s^{-1})

		Produit															
	Interface	CH_4	C_2H_2	C_2H_4	C_2H_6	C_3H_6	C_3H_8	Propyne	Allène	Cyclo-propane	n-C_4H_{10}	i-C_4H_{10}	1-C_4H_8	2-C_4H_8	i-C_4H_8	Butyne-1 3-ène	% des produits saturés[a]
Méthane	Hg/verre	—	64	100	6	3	4	3	2	—	—	—	—	—	—	—	7
Ethane	Hg/verre	47	60	100	—	27	23	5	2	0.3	1	0.3	0.5	0.4	—	0.5	23
Propane	Hg/verre	111	77	100	24	39	—	—	3	1.3	2	2	2	2	—	1	25
n-Butane	Hg/verre	46	45	100	18	17	6	4	3	0.2	—	0.5	7	1.5	—	1	20
Isobutane	Hg/verre	119	76	100	13	64	19	15	8	—	1	—	—	—	22	—	23
Méthane	b.a./verre[b]	—	77	100	—	—	—	—	—	—	—	—	—	—	—	—	—
Propane	b.a./verre	240	13	100	34	60	—	—	—	—	—	—	—	—	—	—	35
n-Butane	b.a./verre	125	1	100	24	84	20	—	—	—	—	—	4	—	—	—	34
Isobutane	b.a./verre	1215	24	100	67	165	1080	—	—	—	—	—	—	—	—	—	86

[a]Calculé suivant la même expression que dans le tableau 1.
[b]b.a. = billes d'acier.

tiques dans la région des MHz accompagnant le mouvement du mercure (ou des billes métalliques) sur le verre. Cette émission d'ondes électromagnétiques est facilement captée par un récepteur radio dans le domaine des ondes courtes. L'effet lumineux qui en principe accompagne le processus triboélectrique est parfois difficilement perceptible, on ne peut donc se fier entièrement à sa présence comme élement caractéristique de ce processus et de plus il ne prouve pas en soit l'existance d'une décharge électrique.

La décharge triboélectrique

En se basant sur la caractéristique des phénomènes triboluminescents accompagnant la rotation d'un système Hg–pyrex Mandeville et coll. concluent qu'on est en présence d'une décharge de Townsend (4). La décharge de Townsend n'a lieu que si la tension de claquage ou de disruption, V_c, est atteinte, et pour une pression donnée elle sera atteinte à une distance critique de séparation métal/verre. Dans un champ uniforme la tension de claquage est donnée par la loi de Paschen: $V_c = f(P \cdot d)$, où P est la pression et d est la distance entre électrodes planes et parallèles. Toujours selon cette loi V_c passe par un minimum et pour la plupart des *n*-paraffines $V_{c,min} \approx 400$ V et correspond à des valeurs $(P \cdot d)$ comprises entre 0.6 et 1 torr · cm (12). La densité moyenne de charges accumulées sur la surface diélectrique par triboélectrisation dans un système métal/verre est de l'ordre de 2 u.e.s./cm^2 (8, 9), ainsi le champ électrique (supposé uniforme) qui en résulte est suffisant pour que V_c soit atteint sur des distances courtes (<1 mm) de séparation des phases en mouvement aux pressions de nos expériences. Pour les champs électriques non-uniformes la tension de claquage passe par un minimum en fonction de la pression, mais sa dépendance par rapport à la distance entre électrodes ne peut être établie, sauf dans le cas des électrodes de symétrie simple. Dans le cas présent le champ électrique est de forme inconnue.

Par ailleurs, Heylen et Lewis ont remarqué qu'une activité considérable en impulsions électriques nettement en dessous du V_c a lieu dans des nombreux hydrocarbures gazeux (12, 13). Cela peut être attribué à ce que le deuxième coefficient de Townsend, α, pour les hydrocarbures est environ 10^5 fois plus faible que pour les gaz atmosphériques (13, 14). Il est difficile à présent de déterminer quel genre de décharge se produit dans le réacteur Hg/verre en rotation, il se peut que les conditions locales favorisent soit l'un soit l'autre mécanisme de décharge et on peut aussi assister à un régime mixte.

La variation du rapport E/P (où E est le champ électrique) détermira l'importance des divers processus primaires de fragmentation des molécules des gaz enfermées dans le réacteur. Or, la complexité physique du système étudié ne permet pas de prédire comment varie le paramètre E/P avec la pression. On peut s'attendre qu'à valeur élevée de E/P (de 200 à 500 V cm^{-1} torr^{-1}) à basse pression (<15 torr) la fragmentation des molécules soit plus prononcée qu'à E/P modéré ($P > 50$ torr). D'autre part, la décharge triboélectrique semble être très localisée. Nous aurons donc une forte densité d'espèces excitées et radicalaires et les réactions qui en suivront favoriseront la recombinaison entre radicaux.

Le méthane

Nos résultats concordent raisonnablement bien avec ceux de Alcock et coll. à 200 torr et 60 min de rotation (8). Dans ces conditions nous trouvons les trois produits principaux: C_2H_2, C_2H_4 et C_2H_6 en proportion 1:1:1 (fig. 2), tandis qu'Alcock donne un rapport 1:1:3. En raison des vitesses de rotation différentes et des difficultés de reproductibilité de ces expériences on doit se contenter d'une telle précision.

La quantité totale du méthane décomposé croit avec la pression au moins jusqu'à 200 torr en raison du nombre croissant de collisions effectives entre électrons accélerés et molécules parentes sur le parcours de la décharge. Simultanément la composition relative des produits formés subit des changements importants comme témoignent les figs. 2 et 3. La présence des spectres des radicaux CH$^\cdot$ (dans l'état $^2\Delta$) et $CH_2^\cdot$ mais l'absence de celui du C_2 (observé dans la décharge à étincelle (15)) dans la décharge triboélectrique du CH_4 est rapporté par Alcock et coll. (8). Ainsi on peut postuler des processus primaires de décomposition suivants:

$$[1] \quad CH_4 + e \rightarrow (CH_4)^* \rightarrow CH^\cdot + H + H_2(2H)$$
$$\rightarrow CH_2^\cdot + H_2(2H)$$
$$\rightarrow CH_3^\cdot + H$$

Les voies subséquentes de réactions de ces intermédiaires dépendent des états d'excitation dans lesquels ils sont formés, états que nous ignorons. De manière générale on peut dire que

les radicaux $CH^{\cdot}$ dans les états $^2\pi$ (16) et $^2\Delta$, ainsi que $^1CH_2$ dans l'état $\tilde{a}_1\,^1A_1$ (17) vont réagir rapidement avec le méthane pour donner des expèces excitées lesquelles peuvent se décomposer ou être stabilisées par collision:

[2] $$CH^{\cdot} + CH_4 \rightarrow (C_2H_5)^* \rightarrow C_2H_4 + H$$
$$\rightarrow C_2H_3^{\cdot} + H_2$$
$$\rightarrow C_2H_2 + H + H_2$$

[3] $$^1CH_2 + CH_4 \rightarrow (C_2H_6)^* \rightarrow 2CH_3^{\cdot}$$
$$\xrightarrow{M} C_2H_6$$

La réactivité avec le méthane du radical $CH^{\cdot}$ dans des états d'excitation supérieurs $\tilde{b}^1B_1$ et $\tilde{c}^1A_1$ (18) n'est pas connue.

La conversion du radical $^1CH_2^{\cdot}$ à l'état triplet $^3B_1$ à la suite de collision avec le méthane (19) et les réactions subséquentes du $^3CH_2^{\cdot}$ avec les radicaux $^3CH_2^{\cdot}$ et $CH_3^{\cdot}$ pour donner de l'acétylène et de l'éthylène (19–21) ne semblent pas être important, même si les constantes de vitesses de ces réactions sont comparables en grandeur à celle de la recombinaison de radicaux méthyl en éthane:

[4] $$CH_3^{\cdot} + CH_3^{\cdot} \rightarrow C_2H_6$$
$$k_4 \approx 4.2 \times 10^{-11}\ \text{cm}^3\ \text{molécule}^{-1}\ \text{s}^{-1}\ (22, 23)$$

Cela est montré par l'effet inhibiteur peu significatif du NO dans la formation du C_2H_2 et du C_2H_4 dans la décharge triboélectrique à basse pression (fig. 4). Ce même capteur de radicaux indique qu'environ 50% de l'éthane est produit à partir d'intermédiaires qui ne sont pas impliqués dans la formation des C_2H_2 et C_2H_4. La même insensibilité à l'action inhibitrice de l'oxygène est rapporté par Alcock et coll. (8). Cela peut être une indication que l'acétylène et l'éthylène sont formés dans les processus [2] et [3] à partir d'intermédiaire peu sensible à l'action de l'oxygène ou de l'oxyde nitrique, confirmant ainsi le mécanisme proposé par Alcock et coll.

En fait il y a une certaine similitude entre les résultats obtenus à 100 torr dans la radiolyse éclair du CH_4 (24) et les résultats présents. Cependant, l'influence du SF_6 est différente dans les deux cas. Des expériences faites en présence du SF_6 (capteur d'électrons thermalisés) n'ont pas indiqué clairement de processus impliquant la neutralisation des charges ou la participation des ions négatifs dans la décharge triboélectrique, mais la présence d'un champ électrique fort peut très bien masquer le cours de ces processus (11).

Le mercure atomique gazeux joue le rôle d'intercepteur de radicaux méthyles

[5] $$Hg + 2CH_2^{\cdot} \rightarrow Hg(CH_3)_2$$

Ce composé identifié par Paoli et Strausz (7) est produit à 10 torr avec un rendement d'environ le double de celui de l'acétylène. C'est donc une espèce (de même que H_2) majeure dans le système.

La variation de la composition relative des hydrocarbures saturés par rapport aux insaturés en fonction de la pression (figs. 2 et 3) peut s'expliquer par l'influence de trois facteurs: (*a*) la diminution du rapport E/P avec l'augmentation de la pression se fera sentir sur le processus [1] en favorisant en proportion croissante les décompositions primaires de moins en moins énergétiques, (*b*) l'accroissement de la pression favorisera les processus de stabilisation par collision, (*c*) la proportion des atomes de mercure gazeux diminuant avec l'augmentation de la pression du CH_4, l'importance de la réaction [5] diminuera en faveur de la recombinaison [4]. L'importance de chacun de ces trois facteurs reste à déterminer, mais *à priori* on peut supposer qu'à basse pression (1–20 torr) le facteur (*b*) aura plus de poids que les deux autres, tandis qu'à pression élevée ce sera le contraire.

L'allure de la formation de l'acétylène qui passe par un maximum à $P \approx 10$ torr (fig. 2) est une indication des dimensions de la trajectoire de la décharge. A basse pression (< 10 torr) le nombre de collision inélastiques menant à des états d'excitation très élevés du CH_4 est faible sur la distance du parcours des électrons entre les deux phases verre–mercure en voie de séparation. Ce nombre de collision très énergétiques entre électrons et molécules parentes augmentera avec la pression, mais simultanément le processus de stabilisation des espèces excitées prend de l'ampleur. Ainsi l'allure de la formation de l'acétylène sera la résultante de ces deux effets opposés.

Les hydrocarbures C_2–C_5

La comparaison des données des tableaux 1 et 2 est intéressante à plusieurs points de vue:

(*a*) le taux absolu de décomposition croissant avec le nombre d'atomes de carbone du composé paraffinique peut être mis en corrélation soit avec le potentiel d'ionisation (25) ou avec le spectre d'excitation électronique du composé (26). L'énergie nécéssaire à ioniser et/ou à exciter étant plus faible à mesure que le nombre de

carbones croît dans le composé permet un accroissement du nombre de collisions effectives entre électrons et molécules parentes sur la distance du parcours des électrons dans la décharge.

(*b*) la fraction des produits saturés gazeux formés dans la tribodécharge à basse pression est d'environ 25% par rapport à celle des produits insaturés. Cependant dans les réacteurs Hg/verre on n'a pas analysé les composés alkylmercuriques, dont la présence a été démontré par De Paoli (7). Par conséquent, la fraction calculée des produits saturés doit être augmentée pour la présence de ces composés. Selon De Paoli pour le propane à $P = 10$ torr, la formation en (RH)Hg(R′H) est à peu de chose près égale à celle du C_2H_2, et en rapportant ce résultat à nos données la fraction de produits saturés devient ~34%. On peut supposer que pour les autres *n*-paraffines (à l'exception du CH_4) le pourcentage de produits saturés gazeux est du même ordre de grandeur. Ce n'est peut être qu'une coincidence, mais pour les systèmes à interface billes d'acier/verre la fraction des produits saturés est d'environ 35%. La diminution des quantités d'acétylène formé dans les réacteurs contenant des billes d'acier est due selon toute vraissemblance à une moindre densité de charges crée au point de contact entre les deux phases solides. La décharge qui en résulte est beaucoup moins énergétique et ne permet pas d'atteindre les niveaux d'excitation élevés des molécules parentes.

(*c*) la production relative de l'acétylène diminue pour le méthane et l'éthane soumis à la tribodécharge à vitesse 3 fois plus lente (tableau 2). Cet effet de vitesse peut s'expliquer en admettant que la densité de charge produite est moindre à faible vitesse de rotation en raison de possibilité accrue de neutralisation de charges par migration de surface. Le rapport E/P serait moindre dans ce cas, et il aura un effet plus marqué pour le hydrocarbures à potentiel d'ionisation plus élevé. On comprendrait ainsi pourquoi le C_3H_8 et les C_4H_{10} ne montrent pas d'effet de vitesse par opposition aux CH_4 et C_2H_6. L'effet de vitesse de rotation fera l'objet d'une étude séparée.

Il serait téméraire de proposer des schémas cinétiques détaillés pour la formation des produits pour chacun des hydrocarbures étudiés. La difficulté réside dans les concentrations élevées d'intermédiaires générés pendant la décomposition induite par une décharge. Les réactions secondaires qui en résulte sont difficile à interpreter. De façon générale, parmi les produits de décomposition d'un système organique soumis à une décharge il y a une importante proportion d'oléfines et d'acétylèniques, proportion qu'on ne retrouve pas pour d'autres modes de déposition d'énergie (27). Dans beaucoup de cas, cet excès de produits insaturés est dû à l'impossibilité de retirer les produits stables de la zone de réaction. Il en est pareillement pour la tribodécharge, surtout pour les réacteurs contenant du mercure. Néamoins, quelques mécanismes réactionnels peuvent être aperçus à travers les données des tableaux 1 et 2. Par exemple, l'élimination des radicaux $CH^{\cdot}$ et $CH_2^{\cdot}$ doit être un important processus primaire pour les paraffines étudiées. L'insertion subséquente de ces intermédiaires dans la molécule parente suivie d'une décomposition conduit au moins en partie aux C_2 insaturés qu'on retrouve régulièrement en quantité abondante parmi les produits. L'élimination d'alcanes à faibles poids moléculaire (CH_4, C_2H_6) à partir de la molécule parente hautement excitée est un autre processus dont on peut soupçonner la présence. Ce processus est observé en photolyse dans l'ultraviolet à vide pour les paraffines C_3–C_6 et il est d'autant plus important que l'énergie des photons incidents est plus élevée (28). Dans le cas de l'isobutane c'est surtout le groupement méthyl qui est impliqué dans ce processus si on en juge d'après la quantité importante du propène formé. En admettant qu'une importante proportion du C_2H_4 provient par élimination directe à partir du *n*-butane et du *n*-pentane, il faut conclure que la rupture de la liaison β(C—C) du squelette carboné serait la plus importante parmi les divers modes de décomposition.

Remarquons que dans la décharge tribo-électrique des C_2–C_5 certains produits mineurs, tels le cyclopropane, le butyne-1-ène-3, sont formés en proportion constante. Les processus qui mènent à leur formation sont probablement les mêmes pour tous les hydrocarbures étudiés et ils impliquent un ou des produits particuliers accumulés dans le système.

Remerciements

Nous remercions le Conseil national de recherches du Canada et le Ministère d'Education du Québec (octroi FCAC) pour l'aide financière qui a permis la poursuite de cette étude.

1. W. R. HARPER. Contact and frictional electrification. Clarendon Press, Oxford. 1967.
2. W. R. HARPER. Phys. Educ. **5**, 87 (1970).
3. L. B. LOEB. Static electrification. Springer-Verlag, Berlin. 1958.
4. G. L. DYBWAD et E. C. MANDEVILLE. Phys. Rev. **161**, 527 (1967).
5. C. P. KESZTHELYI et A. J. BARD. J. Electrochem. Soc. **120**, 1726 (1973).
6. J. H. JOHNSON, R. H. KNIPE et A. S. GORDON. Can. J. Chem. **48**, 3604 (1970).
7. S. DE PAOLI et O. P. STRAUSZ. Can. J. Chem. **48**, 3756 (1970).
8. W. G. ALCOCK, E. J. HAYWARD, B. MILE et B. WARD. Can. J. Chem. **50**, 3813 (1972).
9. J. W. PETERSEN. J. Appl. Phys. **25**, 501 (1954); **25**, 907 (1954).
10. P. E. WAGNER. J. Appl. Phys. **27**, 1301 (1956).
11. J. A. HERMAN. Résultats de ce laboratoire.
12. A. E. D. HEYLEN et T. J. LEWIS. Can. J. Phys. **36**, 721 (1958).
13. A. E. D. HEYLEN et T. J. LEWIS. J. Appl. Phys. **7**, 411 (1956).
14. O. H. LEBLANC et J. C. DEVINS. Nature, **4746**, 219 (1960).
15. L. W. SIECK et R. H. JOHNSEN. J. Phys. Chem. **67**, 2281 (1963).
16. R. GORDEN JR., et P. J. AUSLOOS. J. Chem. Phys. **46**, 4823 (1967).
17. P. J. AUSLOOS, R. GORDEN JR. et S. G. LIAS. J. Chem. Phys. **40**, 1854 (1964).
18. A. R. WECH et D. L. JUDGE. J. Chem. Phys. **57**, 286 (1972).
19. W. BRAUN, A. M. BASS et M. PILLING. J. Chem. Phys. **52**, 5131 (1970).
20. F. S. ROWLAND, P. S. T. LEE, D. C. MONTAGUE et R. L. RUSSEL. Faraday Discuss. **53**, 11 (1972).
21. M. J. PILLING et A. J. ROBERTSON. Chem. Phys. Lett. **33**, 336 (1975).
22. N. BASCO, D. G. L. JAMES et R. D. SUART. Int. J. Chem. Kinet. **2**, 215 (1970).
23. F. K. TRUBY et J. K. RICE. Int. J. Chem. Kinet. **5**, 721 (1973).
24. R. E. REBBERT, S. G. LIAS et P. AUSLOOS. J. Res. Nat. Bur. Stand. A, **77**, 249 (1973).
25. J. L. FRANKLIN et coll. Ionization potentials, appearance potentials and heats of formation of gaseous positive ions. NSRDS-NBS # 26, Washington, D.C. 1969.
26. E. N. LASSETTRE, A. SKEBERLE et A. M. DILLON. J. Chem. Phys. **49**, 2382 (1968).
27. A. KUPPERMAN et M. BURTON. Radiat. Res. **10**, 636 (1959).
28. L. W. SIECK. *Dans* Fundamental processes in radiation chemistry. *Edité par* P. Ausloos, Interscience, New York. 1968.

The effect of reactant purity on the radiolysis of gaseous ethane and propane

JANUSZ GAWŁOWSKI AND JAN NIEDZIELSKI
Laboratory of Radiochemistry and Radiation Chemistry, Warsaw University, Warsaw, Poland
AND
JAN A. HERMAN
Département de Chimie, Université Laval, Québec (Qué), Canada G1K 7P4

Received August 3, 1976

JANUSZ GAWŁOWSKI, JAN NIEDZIELSKI, and JAN A. HERMAN. Can. J. Chem. **55**, 463 (1977).

The yields of products formed in the recombination of free radicals in the radiolysis of gaseous ethane and propane have been determined. The yields of butane from ethane radiolysis, and of 2,3-dimethylbutane from propane radiolysis were found to be much lower than those reported in the literature.

The yields of these products increased markedly in the presence of the traces of water, either desorbed from the walls or introduced with insufficiently dried reagents. The details of experimental procedures warranting the total elimination of water are given.

JANUSZ GAWŁOWSKI, JAN NIEDZIELSKI et JAN A. HERMAN. Can. J. Chem. **55**, 463 (1977).

On a déterminé les rendements des produits formés par recombinaison de radicaux libres dans la radiolyse de l'éthane et du propane gazeux. Les rendements en butane et en 2,3-dimethylbutane dans la radiolyse respectivement de l'éthane et du propane sont beaucoup plus bas que ceux rapportés dans la litterature.

Les rendements de ces produits augmentent substanciellement en présence de trace de vapeur d'eau, soit désorbée des parois, soit introduit avec les réactifs qui non pas étaient suffisamment sechés. On donne les détails expérimentaux, guarantissant une élimination totale de l'eau.

Introduction

Gas-phase radiolysis of saturated hydrocarbons has been studied extensively (1–11). However, there are still many doubts concerning the mechanism of ion neutralization, the effects of scavengers on the yield of products, and so on. This paper presents our preliminary results related to the effects of impurities on the yields of some products, originating from the radiolysis of gaseous ethane and propane.

Experimental

(a) Materials

Phillips research grade ethane and propane were purified from the traces of higher and unsaturated hydrocarbons by passing them through a column filled with activated carbon (ethane at −76 °C, propane at 0 °C), then through a column filled with $Hg(ClO_4)_2$ on firebrick, and finally by the usual freeze–pump–thaw cycles. No impurities could be found in the ethane using gas-chromatography methods, propane contained less than 0.005% ethane (limit of detection $< 10^{-5}$%). Further purification procedures included drying over highly activated molecular sieve 3A, and immediately before use exposure to the action of highly dispersed metallic sodium (12). These drying procedures were not applied in some experiments.

Phillips research grade ethylene and propylene were purified by adsorption in activated carbon, distilled under vacuum, and dried as described above. Triply distilled water was thoroughly degassed by vacuum distillation from the potassium hydroxide solution.

(b) Sample Preparation and Irradiation

Glass ampoules of a volume of about 140 ml, 45 mm in diameter, provided with break-off tips, were used. Ampoules were baked in an oven before pumping, and then evacuated in vacuum. In some experiments the ampoules were heated under vacuum at 350–400 °C.

In a series of separate experiments the ampoules were provided with a small glass tip, into which 2–3 mg of sodium azide were inserted. After prolonged heating of the ampoules under vacuum, sodium azide has been thermally decomposed, and nitrogen formed in such a process has been pumped off. Thus, a sodium mirror has been obtained in the tip, of an area less than 3% of a total area of the ampoule.

Ethane samples were irradiated in a γ-source of the Institute of Radiation Techniques (Lodz) at a dose rate of approx. 0.4 Mrad h^{-1}.

Propane samples were irradiated at the Laval University irradiation facilities, with ^{60}Co rays in AECL Gammacell 220 at a dose rate of about 0.08 Mrad h^{-1}.

(c) Gas-chromatographic Analyses

Propane and butane, originating from the radiolysis of ethane, were analyzed on a 9 m (20% by weight) UCON LB 550X column, operated at room temperature.

Saturated C_5–C_6 hydrocarbons, originating from the radiolysis of propane, were analyzed on a 5 m (20% by weight) isoquinoline column (with 1% DC 550 added), operated at room temperature. An additional short

TABLE 1. The yields of some products from gaseous ethane irradiated at a pressure of 200 torr to a total dose of 0.38 Mrad

	Yield								
					With H_2O		With C_2H_4		With 0.5%
Product	(*i*)*	(*ii*)†	(*iii*)‡	(*iv*)§	0.1%	0.5%	0.1%	0.5%	O_2
C_3H_8	0.67	0.61	0.57	0.60	0.57	0.55	0.60	0.62	0.22
n-C_4H_{10}	1.07	1.12	2.18	2.06	2.35	2.06	1.71	1.81	0.21
$CH_3\cdot$	0.58	0.49	0.40	0.44	0.40	0.37	0.43	0.46	—
$C_2H_5\cdot$	2.50	2.50	4.90	4.61	5.22	4.58	3.82	4.05	—

*Ethane purified by the method described in part (*a*) of the Experimental section.
†Ethane purified as in (*i*) and additionally sodium deposited onto the walls of the small tip attached to the irradiated ampoule.
‡The ampoule not heated in vacuum.
§Ethane purified only by the usual method, without drying over molecular sieves and sodium, the ampoule heated in vacuum.

TABLE 2. The yields of some products from gaseous propane irradiated at a pressure of 400 torr to a total dose of 0.36 Mrad

	Yield (%)					
Initial composition	2,3-Dimethyl butane	2-Methyl pentane	*n*-Hexane	Isopropyl	*n*-Propyl	Comments
C_3H_8*	0.69	0.28	0.043	4.5	0.77	
C_3H_8(Na)†	0.73	0.29	0.037	4.6	0.76	
C_3H_8‡	1.45	0.38	0.03	7.3	0.85	
C_3H_8 + 0.04% H_2O	1.51	0.41	0.028	7.7	0.87	
C_3H_8 + 0.14% C_3H_6	0.74	0.34	0.048	4.7	0.88	
C_3H_8 + 0.2% C_3H_6 + 0.05% H_2O	0.93	0.27	0.027	5.3	0.65	
C_3H_8 + 0.05% H_2O + 1% C_3H_6	0.70	0.26	0.045	4.2	0.66	
C_3H_8§	1.37	0.38	0.08	6.85	0.78	The results of Bone
C_3H_8 + 10^{-2}% C_3H_6§	0.60	0.18	0.04	3.3	0.39	*et al.* obtained at a pressure of 760 torr

*Propane purified by the method described in part (*a*) of the Experimental section.
†Propane purified as in * and additionally sodium deposited onto the walls of the small tip attached to the irradiated ampoule.
‡Propane was not dried over molecular sieves and metallic sodium.
§The results of Bone *et al.* (9) computed using $W_{C_3H_8} = 23.4$ eV.

column filled with $Hg(ClO_4)_2 + HClO_4$ was placed after the isoquinoline column in order to lower the detection limit of analyses, otherwise too high due to the isoquinoline volatility. Further advantage of this column was that it absorbed all olefinic hydrocarbons. Isobutane and butane were resolved in a separate determination using additional 3 m dibutyl phthalate on Chromosorb P, placed after the isoquinoline column. The results for isobutane were not entirely satisfactory owing to a pronounced propane tail.

Results and Discussion

The radiation yields of some products originating from radical processes in ethane and propane are summarized in Tables 1 and 2, and are shown in Fig. 1.

The results of our preliminary experiments were much different than those obtained by many other authors (see Tables 2 and 3). Slight differences in experimental conditions could not explain such big discrepancies as slightly more than half the values for G(*n*-butane) from ethane, and G(2,3-dimethylbutane) from propane radiolysis, compared with the results of earlier investigators. Looking for the impurities which could affect the results we obviously turned our attention to water, known to be extremely difficult to remove from the ampoule walls.

The traces of water were reported to interfere with radiation processes. Hydrogen originating

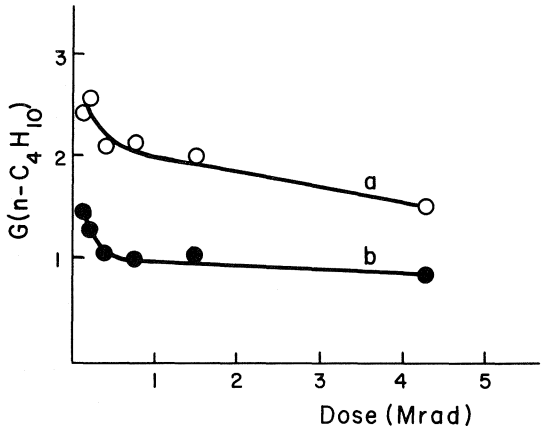

FIG. 1. $G(n\text{-}C_4H_{10})$ as a function of total dose. (*a*) Ampoules not heated in vacuum; (*b*) ampoules heated in vacuum.

from the radiolysis of pure perdeuterated hydrocarbons (propane, cyclohexane, *n*-heptane) contained substantial amounts of HD (7, 10, 13). Ion neutralization on vessel walls, covered with a layer of adsorbed water, as well as reactions of hydrocarbon ions with the traces of desorbed water, followed by neutralization of H_3O^+ ions, were supposed to account for such a surprising result.

In order to check whether these phenomena would occur in our system, we performed four series of experiments: (*1*) ethane and propane purified only using usual method: distillation under vacuum with only middle fraction of the gas retained, thorough degassing, heating of the ampoules in vacuum for many hours before use; (*2*) ethane and propane dried by passing them through a column with molecular sieve 3A at room temperature, and subsequently exposed to the action of metallic sodium deposited onto the walls of a glass bulb; radiolytic vessels were only degassed in a high-vacuum system, no heating of them was applied; (*3*) the ampoules were heated in vacuum, ethane and propane dried as described previously, and the water was purposely introduced into the ampoules; (*4*) all drying procedures previously described were used and additionally a small tip with sodium deposited onto its walls was attached to the ampoules. This should warrant the total elimination of the traces of water present in reactants as well as those desorbed from the walls.

The results of the first two series (*1* and *2*) were much higher than those obtained using highly purified ethane or propane (by the method described in part (*a*) of the Experimental section), and closely resembled those of other authors. Water introduced in series *3* increased the results up to those obtained in series *1* and *2*.

TABLE 3. Ethane radiolysis, the results obtained by different authors

P (torr)	*T* (K)	*G* Propane	*G* Butane	Reference
1100	313	0.75	2.5	6
600	298	0.8	2.5	1
620	298	0.75	2.4	3
200	Room	0.66	1.5	*
200	Room	0.56	2.6	†

*Results of this work (see Fig. 1), extrapolated to zero dose, ampoules heated in vacuum.
†Results of this work (see Fig. 1), extrapolated to zero dose, ampoules not heated in vacuum.

The explanation of these results seems straightforward: the traces of water, either present as impurities or desorbed from the walls, have a pronounced effect on the yields of radiation products. In order to obtain the correct results, meticulous care should be taken when preparing the samples. Our experimental procedures seem to be adequate, since the presence of sodium in series *4* had no effect on the results.

The effect of dose on the yield of *n*-butane from the ampoules heated and unheated under vacuum are shown in Fig. 1. It is interesting to note that the curves are very similar despite the differences in yields in these two experiments.

We have further examined the effects of the presence of unsaturated hydrocarbons. Propylene was found to have no effect on the yield of 2,3-dimethylbutane from the propane radiolysis; this observation is different from that of Bone *et al.* who reported that the presence of propylene reduced the yield of this hydrocarbon to less than one-half. Propylene added to those samples from which the traces of water were not thoroughly removed decreased the yield of 2,3-dimethylbutane. It seems likely that this yield depends on the ratio of water and propylene concentrations.

Ethylene added to irradiated ethane increased the yield of *n*-butane. This result is unexpected and opposed to that described above for the radiolysis of propane. It is also in disagreement with the results of earlier investigations (18) where no influence of ethylene on the yield of *n*-butane could be found. In the presence of water

ethylene had no effect on the yield of *n*-butane within the limit of experimental error.

Unfortunately the explanation of our results is not unambiguous.

(a) Ethane

The main free radicals originating from the irradiated ethane are CH_3 and C_2H_5, the latter one may be formed either in primary processes or in reaction 1 (3, 4)

[1] $$H + C_2H_6 \rightarrow H_2 + C_2H_5$$

Recombination and disproportionation of these radicals leads to a sequence of reactions:

[2] $$CH_3 + CH_3 \rightarrow C_2H_6$$

[3*a*] $$CH_3 + C_2H_5 \rightarrow C_3H_8$$

[3*b*] $$\rightarrow CH_4 + C_2H_4$$

[4*a*] $$C_2H_5 + C_2H_5 \rightarrow n\text{-}C_4H_{10}$$

[4*b*] $$\rightarrow C_2H_6 + C_2H_4$$

On the basis of this mechanism the increase in *n*-butane yield should be ascribed to the increase in the yield of ethyl radicals. The yields of methyl and ethyl radicals were calculated assuming $k_{3b}/k_{3a} = 0.04$ and $k_{4b}/k_{4a} = 0.14$ (14), and taking into account the yields of propane and *n*-butane formed in ionic processes (not scavenged by oxygen), equal to 0.22 and 0.21, respectively (see Table 1). The increase in the yield of ethyl radicals due to the presence of water is equal to 2.1–2.6. Such a marked increment is observed in the presence of the traces of water (either desorbed from the walls or introduced with the ethane insufficiently dried). Thus, water interference must involve a very slow ionic process.

Even though reaction of primary ethane ions $C_2H_6^+$ with water is known to be very fast:

[5] $$C_2H_6^+ + H_2O \rightarrow C_2H_5 + H_3O^+$$

$$k_5 = 1.2 \times 10^{-9} \text{ cc molecule}^{-1} \text{ s}^{-1} \text{ (15)}$$

it cannot compete effectively with condensation reaction 6 under our experimental conditions

[6] $$C_2H_6^+ + C_2H_6 \rightarrow (C_2H_6)_2^+$$

$$k_6 \approx 10^{-10} \text{ cc molecule}^{-1} \text{ s}^{-1} \text{ (16)}$$

Dimeric ion formed in reaction 6 is unreactive towards ethane (16), its structure and heat of formation are unknown, either a chemical bond is formed between the ion and the molecule or the link is due to attractive physical forces. If the latter case is true, the occurrence of reaction 7 may be assumed.

[7] $$(C_2H_6)_2^+ + H_2O \rightarrow C_2H_5 + C_2H_6 + H_3O^+$$

Such reaction may, at least partly, be responsible for the increase in $G_{C_2H_5}$.

Another possible source of ethyl radicals (strictly speaking, of atomic hydrogen, precursor of ethyl radicals in reaction 1) may be neutralization of H_3O^+ ions formed in reaction 7, and in other similar reactions. Reaction of hydrated ions of the type of $C_2H_4(H_2O)_n^+$ may also be involved. Similar mechanism has been advanced by Fujisaki and Gaumann to explain the formation of HD in the radiolysis of gaseous cyclo-C_6D_{12} and *n*-C_7D_{16} (13).

The phenomena described above are far from being well understood. Further studies are needed, especially those concerned with the dependence of G(*n*-butane) on dose, and with the increase in $G_{C_2H_5}$ in the presence of ethylene. The latter result may be tentatively explained by the H atom transfer from $C_2H_6^+$, $(C_2H_6)_2^+$ and other higher order ions. Reaction 8 is exothermic

[8] $$C_2H_6^+ + C_2H_4 \rightarrow C_2H_5^+ + C_2H_5$$

$$\Delta H_8 = -13.3 \text{ kcal mol}^{-1}$$

The enthalpy of analogous reaction involving dimeric $(C_2H_6)_2^+$ ions is unknown.

[9*a*] $$(C_2H_6)_2^+ + C_2H_4 \rightarrow C_2H_5 + C_2H_5^+ + C_2H_6$$

[9*b*] $$\rightarrow C_4H_{11}^+ + C_2H_5$$

Also the assumption that the yield of molecular propane and butane, persisting in the presence of oxygen (and therefore formed in reactions other than [3*a*] and [4*a*]) would be the same in the absence of oxygen is open to serious doubts. Wodetzki *et al.* have reported G(*n*-C_4H_{10}) equal to 0.4 in the presence of NO, but lowered down to 0.1 in the presence of propylene (4).

According to mass-spectrometric evidence ion–molecule reactions in ethane give $C_3H_9^+$ and $C_4H_{11}^+$ ions (16). Oxygenated compounds, formed as a result of radical scavenging by oxygen, may intercept these ions in proton transfer reactions, yielding propane and butane.

(b) Propane

The main free radicals in the radiolysis of gaseous propane are CH_3, C_2H_5, *i*-C_3H_7, and *n*-C_3H_7 (9). The yields of propyl radicals, calculated using the pertinent ratios of k_d/k_r, are in-

cluded in Table 2 (14). The presence of water traces increases the yield of i-C_3H_7 by $\Delta G_{i\text{-}C_3H_7} \approx 2.7$ to 3.1, affecting but slightly the yield of n-propyl radicals.

In this case, the increment in $G_{i\text{-}C_3H_7}$ may also be ascribed to the proton transfer from $(C_3H_8)_2^+$ dimer to the water molecule, ultimately followed by the neutralization of H_3O^+ ions:

[10] $$C_3H_8^+ + C_3H_8 \rightarrow (C_3H_8)_2^+$$

[11] $$(C_3H_8)_2^+ + H_2O \rightarrow i\text{-}C_3H_7 + C_3H_8 + H_3O^+$$

Proton transfer from propane $C_3H_8^+$ ions to the water has been observed in a mass spectrometer

[12] $$C_3H_8^+ + H_2O \rightarrow i\text{-}C_3H_7 + H_3O^+$$

$$k_{12} = 1.4 \times 10^{-9} \text{ cc molecule}^{-1}\text{ s}^{-1} \quad (15)$$

The effect of propylene on the yield of i-C_3H_7 may be explained by the interception of ions by this hydrocarbon, prior to their reaction with water. Higher order unsaturated ions are unlikely to produce atomic hydrogen upon neutralization, according to Bone *et al.* (9). This conclusion is supported by the results of ethylene radiolysis. The yield of atomic hydrogen formed in ethylene radiolysis by the neutralization of ions was assessed as equal to $G_H = 2.9$ (17); in the presence of 1–3% propylene the formation of H atoms by this mechanism was totally suppressed (18). Apparently, higher order ions with inserted propylene molecules do not yield atomic hydrogen upon neutralization, the effect of propylene is exactly similar to that of isobutylene (17).

Conclusions

(*1*) The traces of water, either present as an impurity in insufficiently dried reagents or desorbed from the walls, have a pronounced effect on the yields of some products, originating from the gas-phase radiolysis of ethane and propane.

The yields of products, formed as a result of free radical recombination in pure ethane and propane, are about half as large as those reported hitherto in the literature.

(*2*) Our experimental procedure, including drying of the reactants over molecular sieve, exposing to the action of subtly dispersed sodium, heating of the ampoules in high vacuum, is adequate for removing the traces of water.

1. K. YANG and P. L. GANT. J. Phys. Chem. **65**, 1861 (1961).
2. H. H. CARMICHAEL, R. GORDON JR., and P. AUSLOOS. J. Chem. Phys. **42**, 343 (1965).
3. C. M. WODETZKI, P. A. MCCUSKER, and D. B. PETERSON. J. Phys. Chem. **69**, 1045 (1965).
4. C. M. WODETZKI, P. A. MCCUSKER, and D. B. PETERSON. J. Phys. Chem. **69**, 1056 (1965).
5. N. INOUE, T. UNO, S. SATO, and S. SHIDA. Bull. Chem. Soc. Jpn. **41**, 2005 (1968).
6. P. T. HOLLAND and J. A. STONE. Can. J. Chem. **52**, 221 (1974).
7. J. H. FUTRELL and T. O. TIERNAN. J. Chem. Phys. **37**, 1694 (1962).
8. L. I. BONE, L. W. SIECK, and J. H. FUTRELL. J. Chem. Phys. **44**, 3667 (1966).
9. L. I. BONE, L. W. SIECK, and J. H. FUTRELL. *In* The chemistry of ionization and excitation. *Edited by* G. R. A. Johnson and G. Scholes. Taylor and Francis Ltd., London. 1967. p. 223.
10. N. FUJISAKI, S. SHIDA, and Y. HATANO. J. Chem. Phys. **52**, 556 (1970).
11. G. R. A. JOHNSON and J. M. WARMAN. Trans. Faraday Soc. **61**, 1709 (1965).
12. J. GAWŁOWSKI and J. NIEDZIELSKI. Rocz. Chem. **44**, 685 (1970).
13. N. FUJISAKI and T. GAUMANN. Helv. Chim. Acta, **57**, 2091 (1974).
14. A. F. TROTMAN-DICKENSON and G. S. MILNE. NSROS-NBS 9. U.S. Dept. of Commerce, Wash. D.C. 1967. E. Ratajczak and A. F. Trotman-Dickenson. Supplementary Table 1970. J. A. Kerr and E. Ratajczak. Second Supplement Tables, Univ. of Birmingham. 1972.
15. L. W. SIECK and S. K. SEARLES. J. Phys. Chem. **53**, 2601 (1970).
16. S. L. BENNET, S. G. LIAS, and F. H. FIELD. J. Phys. Chem. **76**, 3919 (1972).
17. J. GAWŁOWSKI and J. NIEDZIELSKI. Int. J. Radiat. Phys. Chem. **5**, 419 (1973).
18. J. GAWŁOWSKI and J. NIEDZIELSKI. Unpublished results.

Nuclear analogs of β-lactam antibiotics. I. Synthesis of *O*-2-isocephams

TERRENCE WILLIAM DOYLE,[1,2] BERNARD BELLEAU, BING-YU LUH, CARRADO F. FERRARI, AND MICHAEL PATRICK CUNNINGHAM[3]

Bristol Laboratories of Canada, 100 Industrial Boulevard, Candiac, Que., Canada J5R 1J1

Received July 8, 1976

TERRENCE WILLIAM DOYLE, BERNARD BELLEAU, BING-YU LUH, CARRADO F. FERRARI, and MICHAEL PATRICK CUNNINGHAM. Can. J. Chem. **55**, 468 (1977).

The preparation by total synthesis of a saturated cephalosporin analog 7-β-phenoxyacetamido-3-ethoxy-*O*-2-isocepham-4-α-carboxylic acid **30**, is described. Compound **30** was prepared via cycloaddition of azidoacetyl chloride to the cinnamylidene Schiff base of ethyl 2-amino-3,3-diethoxypropionate **13***b* to give the *cis*-3-azido-4-styryl β-lactam **15***b*. Ozonolysis of **15***b* followed by sodium borohydride reduction gave the alcohol **18***b*. Boron trifluoride treatment of **18***b* gave ethyl 7-β-azido-3-β-ethoxy-*O*-2-isocephem-4-carboxylate **27**. Reduction of the azido group followed by coupling with phenoxyacetic acid and saponification of the ester gave **30**. The mechanism of the cycloaddition reaction and the stereochemical assignments are also discussed.

TERRENCE WILLIAM DOYLE, BERNARD BELLEAU, BING-YU LUH, CARRADO F. FERRARI et MICHAEL PATRICK CUNNINGHAM. Can. J. Chem. **55**, 468 (1977).

On décrit la préparation, par synthèse totale, d'un analogue d'une céphalosporine saturée soit l'acide β-phénoxyacétamido-7 éthoxy-3 *O*-isocépham-2 α-carboxylique-4 **30**. On a préparé le composé **30** en effectuant une cycloaddition du chlorure d'azidoacétyle sur la base de Schiff dérivée du cinnamaldéhyde et de l'amino-2 diéthoxy-3,3 propionate d'éthyle **13***b* qui conduit à l'azido-3 styryl-4 β-lactame-*cis* **15***b*. L'ozonolyse de **15***b*, suivie par une réduction au borohydrure de sodium, conduit à l'alcool **18***b*. Le traitement de **18***b* par le trifluorure de bore fournit la β-azido-7 β-éthoxy-3 *O*-isocéphème-2 carboxylate-4 d'éthyle **27**. La réduction du groupe azido, suivie par un couplage avec l'acide phénoxyacétique et une saponification de l'ester, conduit à **30**. On discute du mécanisme de la réaction de cycloaddition et des attributions stéréochimiques.

[Traduit par le journal]

Early work on the penicillin and cephalosporin groups of antibiotics (Fig. 1) soon established the following criteria for optimal biological activity (1).

(*1*) The presence of a β-lactam ring fused to a second ring in such a manner as to impart strain to the amide bond of the β-lactam is required. In the penicillins **1** the ring size alone is sufficient to do this. The lack of activity of the Δ^2-cephalosporins **2** relative to the Δ^3-cephalosporins **3** and penicillins leads to the second criterion.

(*2*) In 4–6 fused systems a double bond in conjugation with the β-lactam amide is a requirement either on steric or electronic grounds.

(*3*) An acylated amino function α to the carbonyl of the β-lactam is usually necessary.

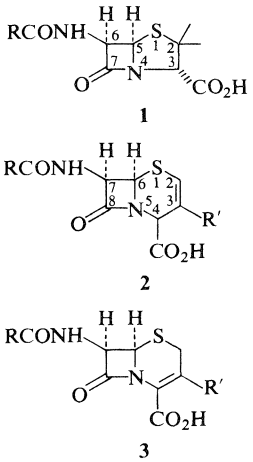

1

2

3

FIGURE 1

(*4*) The protons attached to the bridgehead position and α to the amido side chain must be oriented *cis* to one another.

(*5*) A free carboxylic acid at position 3 in the

[1]Author to whom correspondence concerning this paper may be addressed.

[2]Present address: Bristol Laboratories, P.O. Box 657, Syracuse, New York 13201.

[3]Holder of an NRCC Industrial Postdoctoral Fellowship 1970–1971.

penicillins or position 4 in the cephalosporins seems to be necessary.

At the time we started our research, the role played by the sulfur atom at position 1 in both the penicillins and cephalosporins had not been empirically elucidated. Topp and Christensen (2) have stated, on the basis of molecular orbital calculations of the penicillins and cephalosporins, that it may play a role in transpeptidase enzyme deactivation by controlling the equilibrium conformation which governs binding to the enzyme and in reducing the barrier to reaction with the enzyme.

While a number of nuclear analogs of the penam and cepham systems have been synthesized, the majority of these have involved retention of the sulfur atom at position 1 (for leading references to work carried out prior to 1972 see refs. 1 and 3).[4] Only recently the syntheses of the 1-oxocephalosporin and the desthiacephalosporin systems have been reported (4*i*, *j*) (Fig. 2, **4** and **5**). These compounds exhibited biological activity comparable to that of the natural cephalosporins, thus demonstrating for the first time the non-essential role of the sulfur atom in β-lactam antibiotics (4*i*).

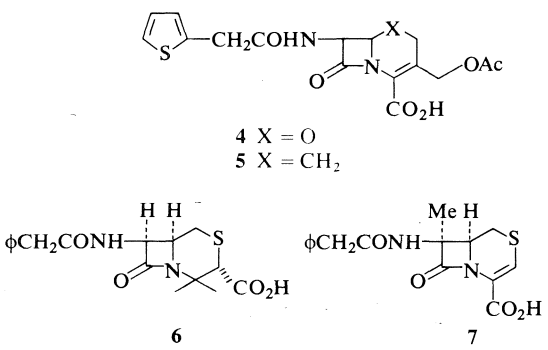

FIGURE 2

Recently, Lowe and co-workers have reported the syntheses of two cephalosporin analogs in which the heteroatom has been transposed from the 1 to the 2 position (4*h*) (Fig. 2, **6** and **7**). The failure of these analogs to exhibit activity is not surprising in view of the fact that they do not fulfill the necessary criteria alluded to earlier. Compound **7** (4*h*) comes closest to doing so but the substitution of the 7α position by a methyl group would be expected to impair the antibacterial activities of the system by analogy with the results in the natural series (5).

For the past several years, we have been engaged with the development of a general synthetic route to nuclear analogs of the cephalosporins of general structure **8** (Fig. 3). In this and the accompanying papers of this series, we would like to report our results in this area.[5]

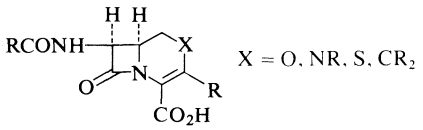

FIGURE 3

A priori one may envisage a number of ways by which the bicyclic systems represented by **8** might be formed (Fig. 4). Formation of the β-lactam amide bond in the latter stages of the synthesis is the classical approach used by Sheehan in his synthesis of penicillin and adapted by Heymes and Dolfini to the synthesis of cephalosporins.[6] Alternatively, the C_6—C_7 bond may be formed onto a preexisting six-membered ring either by ring contraction (4*e*), carbene insertion (4*f*–*h*), or condensation (7) reactions. A third approach is the formation of the C_6—C_7 and C_8—N bonds simultaneously via cycloaddition reactions. This has been used by Bose in his synthesis of epipenicillin, and several nuclear analogs of the penam and cepham systems (3, 4*a*, 4*d*). More recently, Ratcliffe and Christensen have utilized this approach in their total synthesis of cephalothin and cefoxitin (8). A somewhat similar approach has been used by Edwards *et al.* (9) to prepare desacetylcephalothin lactone via

[4]For a list of references to nuclear analogs involving heteroatom substitutions and transpositions which have appeared in the literature recently, see ref. 4.

[5]In order to preserve the numbering system currently in use with the cephalosporins, we propose that the following trivial nomenclature be used for these systems by analogy with that used by Manhas and Bose (3*a*) for **i** and Sheehan and Dadic (6) for **ii**.

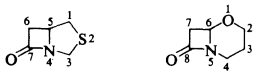

Isopenam **i** *O*-Cepham **ii**

thus:

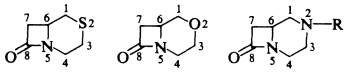

2-Isocepham *O*-2-Isocepham *N*-2-Isocepham

[6]For a review of this work, see K. Heusler in ref. 1.

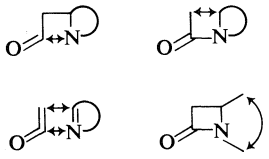

FIGURE 4

furo[3,4-*c*]cephams. The last approach is to build a six-membered ring onto a preformed β-lactam. This approach is perhaps the most versatile with regard to permitting the synthesis of a variety of nuclear types from a common intermediate as has been elegantly demonstrated by Woodward and co-workers in their total synthesis of cephalosporin C and a number of nuclear analogs[6] (10). More recently Kuhlein and Jensen (11) have utilized the approach to prepare a number of analogs of the cephalosporins.

In view of the potential versatility of the approach, the synthesis of a monocyclic β-lactam of general structure **9** became our first target (Fig. 5) wherein R would be either an amino or

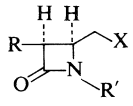

9

FIGURE 5

amido function (or some function readily converted to these) and R′ would either be an easily removed protecting group or would incorporate the requisite functionality for conversion of **9** to **8**.

In principle, the synthesis of structures such as **9** might be approached in a variety of ways.[7] Recently, Hlubucek and Lowe (13) have reported the synthesis of **9** (R = ϕCH_2CONH, R′ = $CH_2\phi$, X = $SCH_2\phi$) as a mixture of *cis* and *trans* isomers. Since we wished to avoid as far as possible the problems associated with *cis–trans* mixtures an approach to compounds such as **9** utilizing the method originally discovered by Staudinger (14) and extended by Bose and co-workers (3, 4*a*, 4*d*, 15) was developed. The addition of ketenes (or substituted acetyl halides in the presence of suitable bases) to Schiff bases yields β-lactams. The stereochemistry of the resultant β-lactams may be controlled by the order of addition of the reagents and by the substitution pattern of both the acid chloride and Schiff base (15*b*, 15*l*). Inasmuch as we wished to avoid working with the highly labile β-substituted acetaldehydes and in view of the possibilities of elimination reactions occurring in competition with cycloaddition we decided to mask the desired substituent at C_4 in the 2-azetidinones as a styryl function.[8] The use of cinnamylidene Schiff bases in the acid chloride – imine formation of β-lactams has been reported only seldom in the literature (14, 16*a*). As early as 1907 Staudinger (14) claimed to have obtained β-lactams from the reactions of dimethyl and diphenyl ketenes with cinnamylidene anil. The work was repeated during the early work on penicillin (16*a*). In contrast to these results Pfleger and Jager (17) have reported that the reaction of phenylketene and ketene with cinnamylidene anil gave dihydropyridones. Similar results with dichloroketene have been reported (18). In a related reaction, Mohan has reported the formation of dihydropyridinone **12***d* from the reaction of an oxazolidinone with this same anil (19) (Fig. 6). While our work was in progress,

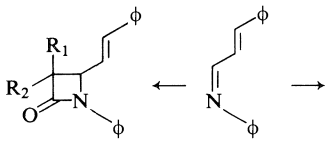

$R_1 = R_2 = Me$
$R_1 = R_2 = \phi$

10

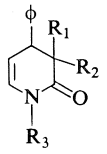

a $R_1 = H$ $R_2 = R_3 = \phi$
b $R_1 = R_2 = H$ $R_3 = \phi$
c $R_1 = R_2 = Cl$ $R_3 = \phi$
d $R_1 = Me$ $R_2 = NHCO\phi$ $R_3 = \phi$

12

FIGURE 6

patents have appeared in which the synthesis of a number of 4-styryl-2-azetidinones via acid chloride – cinnamylidene anil reactions were reported (20).

[7]For a review of methods for the synthesis of β-lactams see refs. 3 and 12.

[8]Bose (4*d*) has observed elimination in the addition of phenoxyacetyl chloride to **iii**.

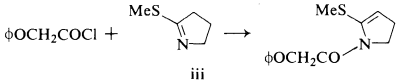

iii

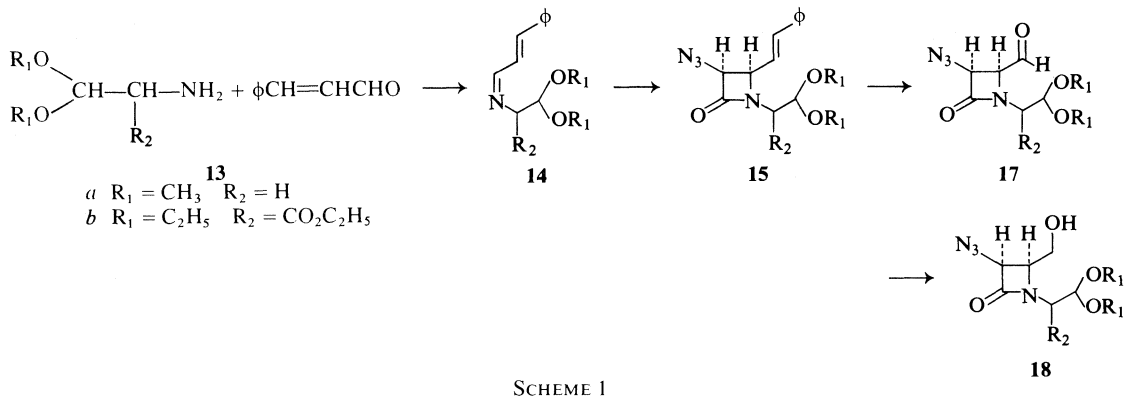

SCHEME 1

Results and Discussion

As a model for future work, the synthesis of **15***a* was studied first (Scheme 1). Treatment of Schiff base **14***a* (derived from cinnamaldehyde and aminoacetaldehyde dimethyl acetal **13***a* in quantitative yield) and an equimolar amount of triethylamine in methylene chloride with an equivalent of azidoacetyl chloride gave *cis*-*N*-(β,β-dimethoxyethyl)-3-azido-4-styryl-2-azetidinone **15***a* in 52.5% yield. That the product was not a dihydropyridone was shown by the β-lactam carbonyl absorption at 1755 cm^{-1} and the nmr spectrum (Table 1). The 5 Hz coupling constant between the C_3—H and the C_4—H was indicative of the *cis* stereochemistry.[9] No trace of the *trans* isomer could be detected by nmr spectroscopy of the crude product. The magnetic non-equivalence of the two protons of the side chain adjacent to the nitrogen and of the two methoxy groups (to a lesser extent) was as expected from the earlier observations of Barrow and Spotswood (21*c*) on *N*-benzyl substituted 2-azetidinones.

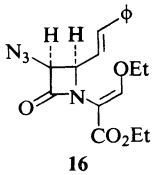

16

Similarly, treatment of Schiff base **14***b* (derived from amine **13***b*[10] and cinnamaldehyde) and triethylamine with azidoacetyl chloride gave *cis*-*N*-(α-carboethoxy-β,β-diethoxyethyl)-3-azido-4-styryl-2-azetidinone **15***b* in high yield. Compound **15***b* was obtained as a mixture (~1:1) of diastereoisomers about the α-carboethoxy function as was indicated by the nmr spectrum of **15***b* (Table 1). Chromatography of the crude product gave a small amount (<5%) of a byproduct **16** which was identified by its nmr and ir spectra and by elemental analysis. Since we envisaged eventually removing the asymmetric center in the side chain of **15***b* no attempt was made to separate the diastereoisomers.

The mechanism of β-lactam formation via the acid chloride – imine route is by no means clear. *A priori*, one may envisage prior formation of an acid chloride – imine complex which undergoes dehydrohalogenation with triethylamine to give β-lactam (Fig. 7). Bose (15*b*, 15*m*) has proposed that with acid chlorides possessing an atom with a free pair of electrons at the α position these atoms are capable of stabilizing transition states such as *B* via the formation of donor–acceptor complexes. Proton abstraction from complex *B* in which the carbon atoms C_3 and C_4 are held in close proximity would lead to β-lactams. This proposal is especially attractive in systems capable of exhibiting extended conjugation such as ours. An examination of Dreiding models indicates that the conformation in which such a donor–acceptor complex would be maximized is as shown in Fig. 8. In such a conformation the C_3—H′ bond axis is aligned with the cationic *p*-orbital at C_4. Removal of C_3—H′ by base with concerted formation of the C_3—C_4 bond would lead to a β-lactam of *cis* stereochemistry. Alternatively, abstraction of C_3—H would give an anion stabilized by the carbonyl. Rotation

[9]The stereochemistry of monocyclic β-lactams may be determined from the coupling constants between C_3—H and C_4—H. *Trans* isomers show *J*'s of approximately 1–2 Hz while the corresponding *cis* isomers have *J* values of approximately 5 Hz (21).

[10]This amine was prepared via a modification of the method reported by Brown in ref. 16*b*.

TABLE 1. Nuclear magnetic resonance spectra of mono cyclic β-lactams[a]

Cmpd.	Aromatic and vinyl protons	C_3-H	C_4-H	OCH_3	$CO_2CH_2CH_3$	CH_2CH_3	Other
15*a*	7.25 (m, 5H, ϕ) 6.64 (d, 1H, ϕ*CH*) J_1=15.5 6.02 (dd, 1H, =C*H*—) J_1=15.5 J_2=8.0	4.75 (d, 1H) J=5.0	4.41 (dd, 1H) J_1=8.0 J_2=5.0	3.30 (s, 3H) 3.26 (s, 3H)	—	—	4.43 (dd, 1H, C*H*(OR)$_2$) J_1=6.0 J_2=4.5 3.53 (dd, 1H)[b] J_1=14.0 J_2=4.5 3.04 (dd, 1H)[b] J_1=14.0 J_2=6.0
15*b*	7.27 (m, 5H, ϕ) 6.62 (d, 1H, ϕCH=)[c] 6.67 (d, 1H, ϕCH=) J=15.0 ~6.20 (m, 1H, =CH—)	5.00 (d)[c] J=5.0 4.85 (d)[c] J=5.0	[d]	—	4.18 (q)[c] 4.06 (q)[c] J=7.0	1.12 (m, 9H)	3.53 (m, 4H, C*H*$_2$CH$_3$)[d]
16	7.56 (m, 5H, ϕ) 7.64 (s, 1H =C*H*OEt) 6.92 (d, 1H, ϕC*H*=) J=16.5 6.38 (ddt, 1H, CH=C*H*—) J_1=16.5 J_2=8.0 J_3=2.75	5.00 (s, 1H) [e]	4.92 (dd, 1H) J=9.0 J=5.0[c]	—	4.32 (q, 2H) 4.27 (q, 2H) J=7.0	1.34 (t, 3H) 1.40 (t, 3H) J=7.0	
18*a*	—	4.69 (d, 1H) J=5.0	[f]	3.40 (s, 6*H*)	—	—	4.47 (t, 1H, C*H*(OR)$_2$) J=5.0 3–3.50 (m, 2H, *CH*$_2$-CH(OR)$_2$)[f]
23*a*		4.24 (d, 1H) J=5.0	[g]	3.43 (s, 6H)	—	—	3.28 (bs, 3H, N*H*$_2$, O*H*) 4.56 (t, 1H, C*H*(OR)$_2$)[g]
23*b*	7.36 (s, 5H) 6.96 (d, 1H, N*H*) J=10	5.49 (dd, 1H) J_1=10.0 J_2=5.0	[h]	3.43 (s, 6H)	—	—	4.53 (t, 1H, CH(OR)$_2$) 3.61 (s, 2H, ϕC*H*$_2$) 3.10 (dd, 1H, J_1=14.5, J_2=4.0)[h,i]
23*c*	6.9–7.6 (m, 5H, ϕ) 8.10 (d, 1H, NH) J=10	5.58 (dd, 1H) J_1=10.0 J_2=5.0	[j]	3.45 (s, 3H) 3.47 (s, 3H)	—	—	4.56 (s, 2H, ϕOC*H*$_2$) 4.58 (t, 1H, C*H*(OR)$_2$) J=4.5 3.20 (dd, 1H)[b] J_1=15.0 J_2=4.0 3.72 (dd, 1H)[b] J_1=15.0 J_2=5.0[j]

TABLE 1 (*Concluded*)

Cmpd.	Aromatic and vinyl protons	C_3-H	C_4-H	OCH_3	$CO_2CH_2CH_3$	CH_2CH_3	Other
25*a*	7.4 (m, 5H, ϕ) 6.74 (d, 1H, ϕC*H*=) *J*=16.0 6.18 (ddt, 1H, =CH—) J_1=16.0 J_2=7.5 J_3=2.0	[k]	[k]	3.32 (s, 3H) 3.36 (s, 3H)	—	—	1.70 (bs, 2H, NH_2) 3.62 (dd, 1H)[b] J_1=14.0 J_2=5.0 3.07 (dd, 1H)[b] J_1=14.0 J_2=6.0[k]
25*b*	7.43 (s, 5H, ϕ) 7.20 (s, 5H, ϕ) 6.70 (d, 1H, ϕC*H*=CH) *J*=16.0 5.98 (dd, 1H, ϕCH=C*H*—) J_1=16.0 J_2=8.0 6.64 (d, 1H, N*H*) *J*=9.0	5.47 (dd, 1H) J_1=9.0 J_2=5.0	4.61 (dd, 1H) J_1=8.0 J_2=5.0	3.38 (s, 3H) 3.42 (s, 3H)	—	—	3.57 (s, 2H, ϕCH_2) 4.58 (dd, 1H, C*H*(OR)$_2$) J_1=6.0 J_2=5.0 3.12 (dd, 1*H*)[b] J_1=14.5 J_2=6.0 3.63 (dd, 1H)[b] J_1=14.5 J_2=5.0
25*c*	7.15 (s, 5H, ϕ) 6.5–7.2 (m, 5H, ϕ) 7.23 (d, 1H, N*H*) *J*=9.0 6.56 (d, 1H, ϕC*H*=CH) *J*=16.0 5.88 (dd, 1H, ϕCH=C*H*) J_1=16.0 J_2=7.5	5.34 (dd, 1H) J_1=9.0 J_2=5.0	—	3.23 (s, 3H) 3.26 (s, 3H)	—	—	4.34 (s, 2H, ϕOCH_2) 4.46 (m, 2H, C*H*(OR)$_2$ and C_4—H) 3.54 (dd, 1H)[b] J_1=14.5 J_2=5.0 3.05 (dd, 1H)[b] J_1=14.5 J_2=6.5
17	9.55 (d)[l] *J*=4.7 9.45 (d)[l] *J*=4.7	4.99(d)[l] 4.95 (d)[l] *J*=6	[m]	—	4.14 (q, 2H) *J*=7	1.18 (m, 9H)	3.59 (m, 4H, O*C*H_2CH$_3$) 4.33 (d) 1H, *J*=4.5, N-C*H*—CO_2Et 4.43 (d, 1H) *J*=4.0, N—C*H*—CO_2Et 4.6–4.9 (m, 2H)[m]
18*b*	—	4.87 (d)[l] 4.81 (d)[l] *J*=4.5	[m]	—	4.15 (q)[l] 4.19(q) *J*=7.0	1.21 (m, 9H)	3.3–4.0 (m, 4H)[m] 4.6–4.8 (m, 2H)[m]

[a]Recorded in $CDCl_3$ at 60 MHz using tetramethylsilane as internal standard unless otherwise noted. The chemical shifts are reported in δ values and *J* values are in Hz. [b]AB quartet for N—CH_2—CH(OMe)$_2$. [c]Two diastereoisomers. [d]A broad multiplet 4.35–4.8 for C_4-H, C*H*(CO_2R)C*H*(OR)$_2$ integrating for 3 protons. [e]Addition of benzene to the sample causes these two overlapping signal sets to resolve into a doublet for C_3-H, *J* = 5.5 Hz and a doublet of doublets for C_4-H, J_1 = 7.0, J_2 = 5.5 Hz. [f]An unresolved multiplet at ~3.80 integrating for 4*H*, assigned to CH_2OH and C_4-*H*. [g]An unresolved multiplet at ~3.80 integrating for 3H, assigned to CH_2OH and C_4-H. The protons N—CH_2—CH(OR)$_2$ appear as an unresolved multiplet at 3–3.6 δ. [h]A broad multiplet centered at 3.85 δ integrating for 5 protons assigned to C_4-H, CH_2—O*H*, and the lower arm of the AB quartet for N—CH_2CH(OR)$_2$. [i]Upfield arm of AB quartet for N—CH_2—CH(OR)$_2$. [j]A broad multiplet centered at ~3.90 δ integrating for 4 protons assigned to C_4-H and CH_2—OH. [k]Complex multiplet from 4.2–4.6 δ integrating for 3 protons assigned to C_3-H, C_4-H, C*H*(OR)$_2$. [l]Two diastereoisomers integrating ~1:1. [m]Assigned to C_4—H and C*H*(OEt)$_2$. [n]Assigned to CH_2—O*H* and N—C*H*(CO_2Et).

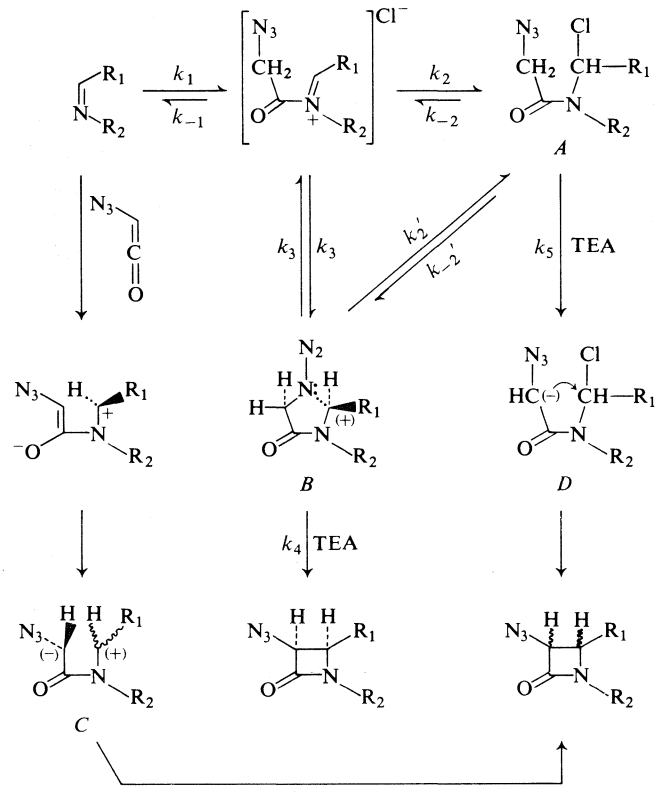

FIGURE 7

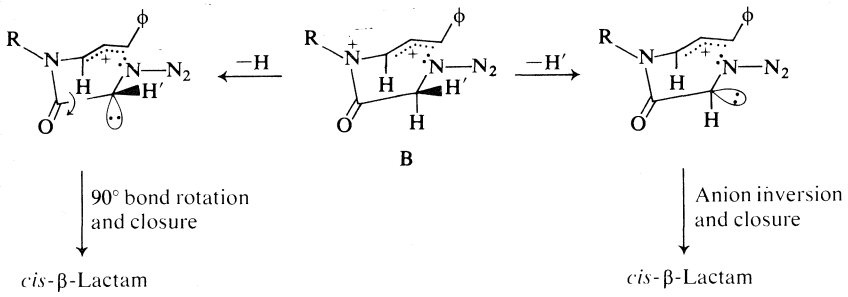

FIGURE 8

through 90° with concomitant C_3—C_4 bond formation would also give a β-lactam of *cis* stereochemistry.

That our β-lactams could arise via ketene addition is unlikely in view of the reports that the additions of aldoketenes generally proceed to give only *trans* adducts (22) with the stereochemistry of the adduct being determined by the energies of the respective transition states leading to intermediates *C*.

That such a degree of selectivity should be exhibited by the presumed azidoketene in the cycloaddition to our cinnamylidene Schiff bases is highly unlikely. Bose has shown (15*m*) that in the addition of acid chlorides to Schiff bases the *trans* stereochemistry generally predominates.

For example, in the addition of azidoacetyl chloride to benzal aniline followed by the addition of triethylamine the *cis–trans* ratio is 1:3 (15*l*). When the order of addition is reversed, the ratio becomes 3:1.[11]

An explanation which accommodates these results would be as follows. When an acid chloride is added to a Schiff base, rapid and reversible formation of an acylimonium ion occurs followed by a slower ($k_1 > k_2$) formation of chloro compound *A*. Where the acid chloride carries a group α to the carbonyl with a pair of free electrons capable of stabilizing the imonium ion one of the conformers of the originally formed acyl imonium ion becomes stabilized as in *B*. The rate with which this occurs would be greater than the formation of *A* depending on the substituents on the acid chloride and on the original Schiff base *e.g.* where R_1 was a simple alkyl function, the rate of formation of *A* would be enhanced whereas when R_1 is aromatic (as in benzalimines) the rate of formation of *A* would be repressed. It has been shown that in the absence of added base (triethylamine) the equilibrium concentrations of the chloride are high. Bose has demonstrated that it is the covalently-bonded form *A* which is produced in the reaction (15*m*). Proton abstraction from *A* would be expected to lead to *D* which would be expected to give both *cis* and *trans* β-lactams (depending on the energies of the transition states leading to the respective isomers) (Fig. 8). If, on the other hand, formation of the initial acylimonium ion were to occur *in the presence of triethylamine* proton abstraction from *B* would lead to exclusively *cis* β-lactam if the assumptions outlined earlier are correct. Where the rate of proton abstraction from *B* and concomitant ring closure to *cis*-β-lactam k_4 is greater than either k_2' or k_2 mixtures of β-lactams in which the *cis* isomer predominates would be obtained. Thus the isomer mixture which is obtained from the acid chloride–imine reaction to form β-lactam is dependant on a number of factors:

(*1*) The equilibrium concentrations of *A* and *B* in the reaction mixture. This would depend upon the degree to which the carbonium ion were to be stabilized by interactions with the lone pair on the amide nitrogen, by the electron pair of the donor atom in *B* and by R_1 itself.

(*2*) The rate with which the equilibrium between *A* and *B* were to be established relative to the rates of proton abstraction from *A* and *B*.

(*3*) The degree to which a conformationally restrained complex *B* could be formed would also affect the stereospecificity of the reaction. One would expect that for disubstituted acid chlorides or for ketoimines that the formation of such a complex would be sterically hindered to some degree. In such cases, the stereochemistry of the adducts might well be governed by steric interactions between the substituents.

In the case of the cinnamylidene Schiff bases the possibility of extended conjugation would tend to stabilize the acylimonium ion *B* thus the high stereospecificity of the reaction.

Ozonolysis of **15***a* in methanol at −78 °C followed by reduction with sodium borohydride gave a mixture of **18***a* and benzyl alcohol. Chromatography of the oil gave pure **18***a* in 77% yield. Treatment of **18***a* with 1 equiv. of boron trifluoride etherate in methylene chloride gave a mixture of the isomeric 3-methoxy-7-azido-*O*-2-isocephams **19** and **20** in 59% yield. On chromatography, there was obtained pure 3-β-methoxy-7-β-azido-*O*-2-isocepham **19** and pure 3-α-methoxy-7-β-azido-*O*-2-isocepham **20** in a ratio of 2:1. The assignment of configuration to each isomer was made on the basis of its nmr spectrum (Table 2). An examination of Dreiding models indicates that the *O*-2-isocepham system may exist in a chair form (C) either of two boat forms (B_1 and B_2) or a twist-boat form (TB) (Fig. 9). The boat forms B_1 and B_2 were eliminated from consideration due to prohibitive steric interactions in each. The chair form C and the twist-boat form were each capable of explaining the pattern of coupling constants observed for **19** and **20** respectively, but led to opposite configurational assignments.

The signals at 2.99 δ and 2.63 δ in compounds **19** and **20** respectively have been assigned to 4-α-protons since we would expect the 4-β-protons to be shifted to lower fields by the β-lactam carbonyls with which they are eclipsed in both conformers. An examination of the

[11]We have observed a similar result in the reaction of azidoacetyl chloride with cinnamylidene anil. Addition of the acid chloride to the Schiff base followed by the addition of triethylamine gave a 29% yield of 1-phenyl-3-azido-4-styryl-2-azetidinone with a *cis–trans* ratio of 3:5. Inverse addition gave an 85% yield of pure *cis* β-lactam (unpublished).

TABLE 2. Nuclear magnetic resonance spectra of *O*-2-isocephams[a]

Cmpd.	Aromatic and vinyl protons	C_7-H	C_3-H	C_4-H	OCH_3	CO_2CH_2—CH_3	CH_3	Other
19	—	4.78 (d, 1H) $J_{76}=5.0$	4.58 (d, 1H) $J_{34\alpha}=3.60$ $J_{34\beta}=0$	2.99 (ddd, 1H)[b] $J_{34\alpha}=3.60$ $J_{4\alpha4\beta}=14.25$ $J_{4\alpha6}=1.5$	3.40 (s, 3H)	—	—	3.5–4.3 (m, 4H)
20	—	4.78 (d, 1H) $J_{76}=4.5$	4.41 (dd, 1H) $J_{34\alpha}=8.0$ $J_{34\beta}=4.0$	2.63 (ddd, 1H)[b] $J_{34\alpha}=8.0$ $J_{4\alpha4\beta}=14.0$ $J_{4\alpha6}=1.5$	3.45 (s, 3H)	—	—	4.15 (m, 2H)[c] 3.80 (m, 2H)[c]
21*a*	—	4.47 (dd, 1H) $J_{67}=4.5$ $J=1.5$	4.71 (d, 1H) $J_{34\alpha}=3.75$	3.08 (ddd, 1H)[b] $J_{34\alpha}=3.75$ $J_{4\alpha4\beta}=14.0$ $J_{4\alpha6}=1.5$	3.47 (s, 3H)	—	—	2.27 (s, 2H, NH_2) 3.6–4.2 (m, 4H)[c]
22*a*	—	4.45 (dd, 1H) $J_{67}=4.5$ $J=1.5$	4.60 (dd, 1H) $J_{34\alpha}=8.0$ $J_{34\beta}=4.75$	2.77 (ddd, 1H)[b] $J_{34\alpha}=8.0$ $J_{4\alpha4\beta}=14.0$ $J_{4\alpha6}=1.5$	3.58 (s, 3H)	—	—	2.18 (s, 2*H*, NH_2) 3.5–4.3 (m, 4H)[c]
21*b*	6.8–7.5 (m, 6H, N*H*, ϕ)	5.11 (m, 1H)[d]	4.58 (m, 1H)[e]	2.95 (ddd, 1H)[b] $J_{34\alpha}=3.0$ $J_{4\alpha4\beta}=14.0$ $J_{4\alpha6}=1.25$	3.30 (s, 3H)	—	—	4.57 (s, 2H, ϕOCH_2) 3.2–3.8 (m, 4H)[c]
22*b*	6.7–7.4 (m, 6*H*, N*H*, ϕ)	5.13 (dd, 1H) $J_1=7.0$ $J_2=4.5$	4.40 (dd, 1H) $J_1=7.5$ $J_2=4.0$	2.70 (ddd, 1H)[b] $J_{34\alpha}=7.5$ $J_{4\alpha4\beta}=13.5$ $J_{4\alpha6}=1.5$	3.40 (s, 3H)	—	—	4.47 (s, 2*H*, ϕOCH_2) 3.4–4.2 (m, 4H)[c]
27	—	4.90 (m, 1H)	5.10 (s, 1H)	4.43 (s, 1H)	—	4.30 (q, 2H) $J=7.0$	1.26 (t, 3H) 1.31 (t, 3H) $J=7.0$	3.4–4.2 (m, 5H)[f]
28	—	4.47 (d, 1H) $J=5.0$	5.08 (s, 1H)	4.42 (s, 1H)	—	4.29 (q, 2H) $J=7.0$	1.26 (t, 3H) 1.31 (t, 3H) $J=7.0$	1.78 (s, 2H, NH_2) 3.6–4.2 (m, 5H)[f]
29	6.9–7.6 (m, 6H, ϕ, N*H*)	5.32 (dd, 1H) $J_1=7.0$ $J_2=5.0$	5.08 (s, 1H)	4.46 (s, 1H)	—	4.30 (q, 2H) $J=7.0$	1.20 (t, 3H) 1.32 (t, 3H) $J=7.0$	4.62 (s, 2*H*, ϕOCH_2) 3.3–4.1 (m, 5H)[f]
30	7.0–7.8 (m, 5H, ϕ) 9.0 (bs, 2H, N*H*) and CO_2H)	5.35 (dd, 1H) $J_1=4.5$ $J_2=6.0$	5.20 (s, 1H)	4.51 (s, 1H)	—	—	1.20 (t, 3H) $J=7.0$	4.67 (s, 2H, ϕOCH_2) 3.3–4.4 (m, 5H)[f]

[a]Recorded in $CDCl_3$ at 60 MHz on a Varian A-60-A spectrometer using tetramethylsilane as internal standard unless otherwise noted. The chemical shifts are in δ (ppm) and *J*'s in Hz. [b]Assigned to C_4-Hα-upfield arm of AB quartet. [c]Assigned to C_6-H, C_1-H_2, and C_4-Hβ. [d]Resolution poor. [e]Obscured by ϕOCH_2 signal. [f]Assigned to C_6-H, C_1-H_2, OCH_2CH_3.

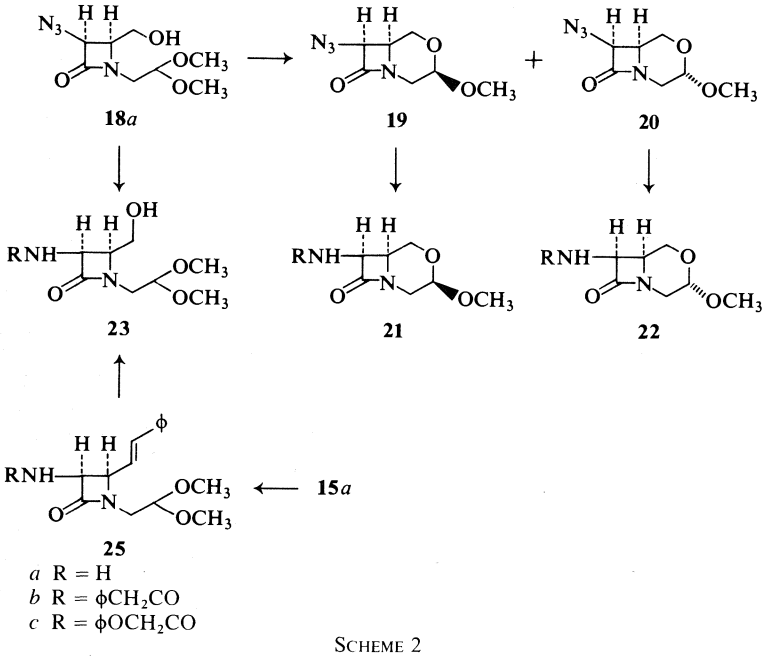

SCHEME 2

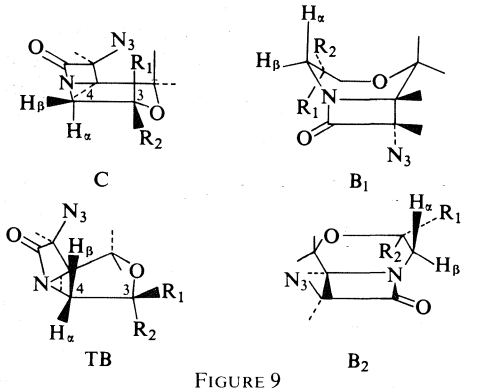

FIGURE 9

splitting patterns in **19** and **20** of the C_3 and $C_4\alpha$ protons indicates that **19** has an axial methoxyl group and **20** an equatorial group. This is further borne out by the relative positions of the C_3 protons in **19** and **20**. The C-3 proton of **20** is at higher field than in **19** which is in accord with the observation that axial protons are usually found at higher fields than equatorial ones in similar systems (23). The preponderance of axial isomer **19** over **20** in this system is in accord with what would be expected on the basis of the anomeric effect (24). To confirm that the isomer ratio produced in the cyclization of **18***a* to **19** and **20** reflects the thermodynamic equilibrium between **19** and **20** each of the isomers was equilibrated in deuteriochloroform with boron trifluoride etherate and the isomer ratios determined by nmr spectroscopy. Treatment of **20** with a catalytic amount of boron trifluoride etherate led to a rapid establishment (~1 h) of an equilibrium between **19** and **20** (66% **19** and 34% **20**). When **19** was treated similarly, the establishment of equilibrium was slower but yielded the same results.

We have assigned the 3-β-methoxy configuration to compound **19** and the 3-α-methoxy configuration to **20**. Although the splitting pattern of **19** could be accommodated by the 3-α-methoxy configuration with twist-boat conformation the observation that the C_4-α proton in **19** appears at lower field than the C_4-α proton in **20** by 20 Hz is better accommodated by the assignment of the 3-β-methoxy configuration in the chair conformation. In the twist-boat conformation, the dihedral angles between the C_4-Hα bond and the C_3-α-methoxy and C_3-β-methoxy C—O bonds are 45° and 75° respectively. In the chair conformation on the other hand the dihedral angle between the 3-β-methoxy C—O bond in **19** and the C_4-Hα bond is 165° and that between the 3-α-methoxy C—O bond in **20** and the C_4-Hα bond is 45°. One would expect that if compounds **19** and **20** were to adopt the twist-boat conformations, the

TABLE 3. $Eu(fod)_3$ shifts $\Delta\delta^{a,b}$

Compound	C_7-H	C_3-Hα	C_3-Hβ	C_4-Hα	β-OCH_3	α-OCH_3
19[c]	6.74 (1.0)	6.50 (0.97)	—	4.75 (0.70)	3.88 (0.58)	—
20[d]	6.23 (1.0)	—	5.20 (0.84)	4.60 (0.74)	—	1.96 (0.32)

[a]Recorded in $CDCl_3$ relative to internal TMS at 60 MHz.
[b]Values extrapolated to 1:1 *M* $Eu(fod)_3$; ratios in parentheses.
[c]Initial concentration 0.001 mol/0.4 ml $CDCl_3$.
[d]Initial concentration 0.00067 mol/0.3 ml $CDCl_3$.

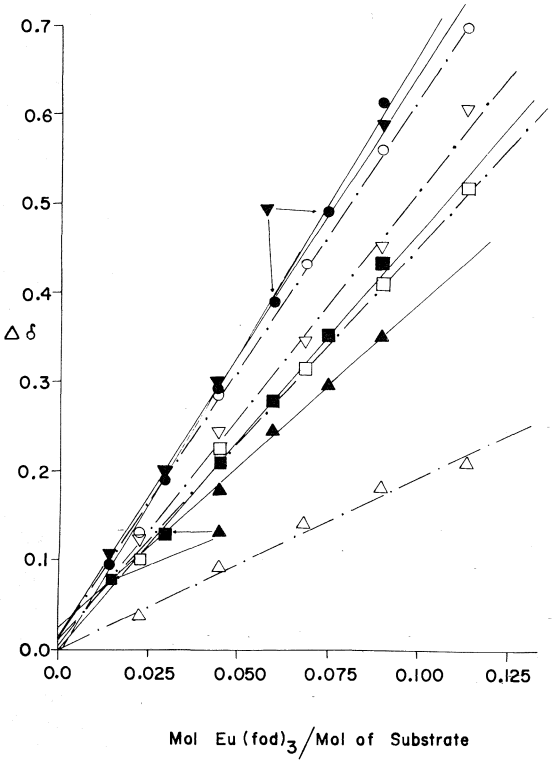

FIG. 10. Shifts in the nmr spectra of **19** and **20** due to the addition of Eu $(fod)_3$: compound **19** —, ● C_7-H, ▼ C_3-Hα, ■ C_4-Hα, ▲ C_3-βOCH_3; compound **20** ----- ○ C_7-H, ▽ C_3-Hβ, □ C_4-Hα, △ C_3-αOCH_3.

difference in chemical shift between the C_4-α protons would be small. On the other hand if **19** and **20** were to adopt the chair conformations, the C_4-α proton would not be expected to be shifted to higher field by the C—O bond whereas it would be expected to do so in **20**.

Incremental addition of $Eu(fod)_3$ caused downfield shifts in the nmr spectra of **19** and **20** (Fig. 10 and Table 3). From the data in Table 3 it is apparent that the primary site of coordination of the $Eu(fod)_3$ is the β-lactam carbonyl since in each isomer C_7-H shows the greatest lanthanide induced shift (LIS) (25*a*).[12] The greater LIS of the 3-β-methoxy in compound **19** over the 3-α-methoxy in compound **20** was as expected. The larger LIS of the 3-α-proton in **19** over the 3-β-proton in **20** may be explained if one assumes that **19** is capable of exhibiting bidentate complexation with the europium.

Reduction of the azido functions of compounds **19** and **20** with triethylamine – hydrogen sulfide[13] in methylene chloride solution gave the amino *O*-2-isocephams **21***a* and **22***a* respectively. These compounds were characterized spectroscopically (ir and nmr) and were coupled with phenoxyacetic acid using *N*-carboethoxy-2-ethoxy-1,2-dihydroquinoline (EEDQ) as the coupling agent (26) to give **21***b* and **22***b* in 77% and 96% yields respectively. The nmr spectra of compounds **21***a*, **21***b*, **22***a*, and **22***b* are recorded in Table 2. Compounds **21***b* and **22***b* exhibited β-lactam carbonyl bands in the ir at 1753 and 1765 cm^{-1} respectively.

Similarly **18***a* was reduced and coupled with phenylacetic acid to yield **23***b* in 38% yield. Compound **23***b* could also be prepared by the reduction of compound **15** followed by coupling of the amine **25***a* with phenylacetic acid to give **25***b* in 34% yield. Ozonolysis of **25***b* in methanol followed by sodium borohydride reduction *in situ* gave **23***b* in 74% yield identical in all respects with the sample prepared from **18***a*. Similarly the coupling of phenoxyacetic acid with **25***a* gave **25***c* in 77.5% yield. Ozonolysis of **25***c* in

[12]The preference for complexation with amides in the presence of acetals has been demonstrated by Wenkert and co-workers (25*b*).

[13]The use of ammonium sulfide in the reduction of azido groups has been demonstrated (9, 27). We have found the hydrogen sulfide – triethylamine procedure to be quite convenient since it permits the operation to be carried out in non-aqueous solution. The yields are generally high, 70–95%, and the method very selective for the azido function. The role of the triethylamine is catalytic although the reaction proceeds faster when at least an equivalent of triethylamine is used.

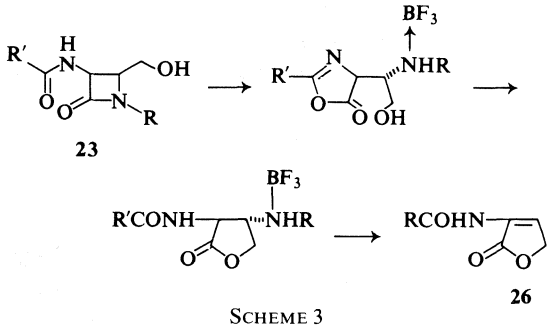

SCHEME 3

methanol followed by sodium borohydride reduction gave **23***c* in 65% yield.

Attempts to cyclize either **23***b* or **23***c* with boron trifluoride etherate led to decomposition and loss of the β-lactam. The decomposition of **23***b* was instantaneous while **23***c* required the addition of slightly greater than 1 equiv. of boron trifluoride etherate. Presumably these compounds undergo a penicilloyl type rearrangement. In the case of **23***c* 1 equiv. of the boron trifluoride is probably bound by the side chain (Scheme 3). In related experiments, low yields of **26** were isolated from the reaction and **26** was identified by spectroscopic methods as part of the product mixtures from the reactions of **23***c* with boron trifluoride etherate.

Treatment of alcohol **18***b* with boron trifluoride etherate gave 3-β-ethoxy-4-α-carboethoxy-7-β-azido-*O*-2-isocepham **27** in 77% yield after chromatography (Scheme 4). While the formation of four configurational isomers of **27** was possible only a single isomer was obtained which has been assigned to the 3-β-ethoxy-4-α-carboethoxy configuration on the basis of its nmr spectrum (Table 2). The axial configuration of the carboethoxy group is not surprising since in the equatorial position a severe interaction with the β-lactam carbonyl would be encountered. In addition in the axial position there is only one *syn–axial* interaction with the C_6 proton. The failure to observe any of the 4-β-carboethoxy isomer may be due to the failure of the side chain on the nitrogen of the β-lactam to adopt a conformation suitable for the cyclization of **18***b* to the 4-β-carboethoxy-3-ethoxy-*O*-2-isocephams due to the carboethoxy–β-lactam carbonyl interaction.

The failure to observe any of the 3-α-ethoxy-4-α-carboethoxy isomer may be due to destabilization of this isomer relative to the 3-β-ethoxy isomer by steric interaction of the ethoxy with the carboethoxy groups in the former case (Fig. 11). Attempts to epimerize **27** to its 4-β-carboethoxy isomer with base failed. Treatment of the anion of **27** with D_2O led to the exchange of the C_4-β proton with no epimerization as determined by nmr spectroscopy.

Reduction of the azido group of **27** with ammonium chloride and zinc in methanol gave 3-β-ethoxy-4-α-carboethoxy-7-β-amino-*O*-2-isocepham **28** in 50% yield. Acylation of the amino function with phenoxyacetic acid and EEDQ proceeded as before to give 7-β-(aminophenoxyacetoyl)-3-β-ethoxy-4-α-carboethoxy-*O*-2-isocepham **29** in 90% yield. Saponification of **29** with dilute alcoholic sodium hydroxide gave 7-β-(aminophenoxyacetoyl)-3-β-ethoxy-*O*-2-isocepham-4-α-carboxylic acid **30** in 55% yield. The ir spectrum of **30** exhibited a β-lactam carbonyl band at 1773 cm^{-1}.

Compound **30** exhibited only weak antibacterial activity which will be discussed in a subsequent publication.

Experimental

The infrared spectra were recorded on a Unicam SP-200G grating, ir spectrometer. The nmr spectra were determined on a Varian A60-A spectrometer using tetramethylsilane as an internal standard. Melting points are uncorrected and were determined on a Gallenkamp melting point apparatus. The analyses were performed by Micro-Tech Laboratories, Skokie, Illinois.

Ethyl α-Amino-β,β-diethoxypropionate ***13b***

To a suspension of 360 g (5 mol) sodium ethoxide in 2800 ml of benzene was added a solution of 393 g (3 mol) ethyl *N*-formylglycinate in 1300 ml of ethyl formate over a period of 2 h at 0–5 °C with vigorous stirring under nitrogen. Stirring was continued for 4 h at 0–5 °C and the suspension was allowed to stand 18 h at 4 °C. The supernatant liquid was carefully decanted from the solid. The residue was taken up in 1.5 l of ethanol and 4.0 l methylene chloride. The solution was cooled to 0–5 °C in an ice bath and a stream of dry hydrogen chloride passed through the solution for 6 h. Cooling was removed after 1 h. Following this, the solution was permitted to stand at ambient temperature (~23 °C) for 18 h then purged of excess hydrogen chloride by passage of a stream of dry nitrogen through the solution. To the solution was added a stream of ammonia until the p*H* of the solution was 9. The suspension was filtered and the filtrate was evaporated at reduced pressure. The oily residue was extracted into petroleum ether (30–60 °C) (6 × 700 ml). The extracts were dried over sodium sulfate and evaporated to give 464 g crude amine which yielded 256 g (42%) of **13***b* on distillation, bp 72–78 °C/0.05 torr (lit. (16*b*) bp 71 °C/1 torr); nmr ($CDCl_3$) δ 4.54 (1H, d, J = 5.0 Hz,, $CH(OR)_2$), 4.16 (2H, q, J = 7.0 Hz, $CO_2CH_2CH_3$)

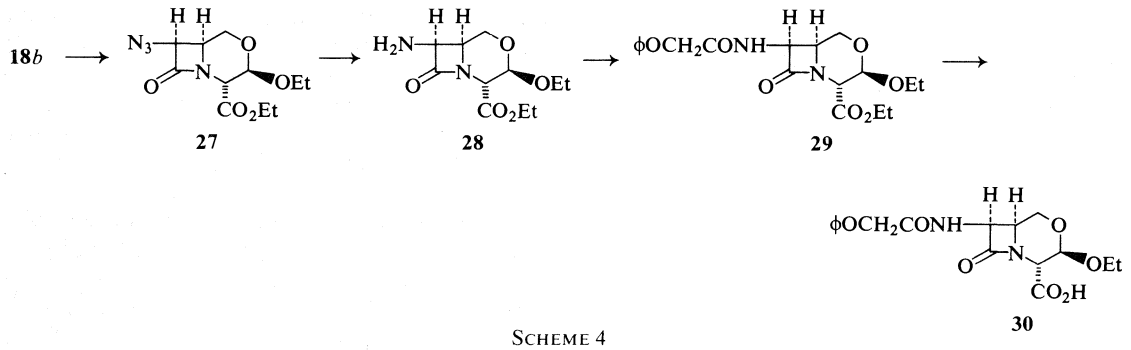

SCHEME 4

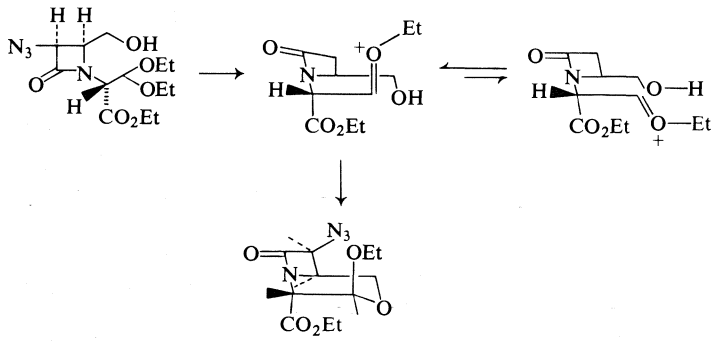

FIGURE 11

3.55 (5H, m, $(OCH_2CH_3)_2$; CH—NH_2), 1.65 (2H, s, NH_2), 1.30 (3H, t, J = 7.0 Hz, $CO_2CH_2CH_3$), 1.19 (6H, t, J = 7.0 Hz, CH_3).

Preparation of Schiff Bases

The Schiff bases **14***a* and **14***b* were prepared via the procedure given for the preparation of **14***a*.

N-Cinnamylidene-β,β-dimethoxy Ethyl Amine ***14a***

To a solution of 13.2 g (0.1 mol) *trans*-cinnamaldehyde in 200 ml dry methylene chloride was added 10.5 g (0.1 mol) aminoacetaldehyde dimethyl acetal. The solution was brought to reflux and the methylene chloride distilled slowly with the constant addition of additional dry methylene chloride so as to maintain the same volume of liquid in the reaction vessel. After the water of reaction ceased to azeotrope (~1 h) the solution was cooled and magnesium sulfate added to complete the reaction. After 1 h, the suspension was filtered and evaporated to yield 21.9 g of **14***a* as a pale yellow oil. The last traces of solvent were removed at low pressure; ir (film) 1640 cm^{-1} (C=N); nmr ($CDCl_3$) δ 8.00 (1H, t, J = 4.0 Hz, CH=N broadened), 7.38 (5H, m, aromatic), 6.94 (2H, d, CH=CH—ϕ), 4.63 (1H, t, J = 5.5 Hz, $CH(OR)_2$), 3.69 (2H, dd, J = 5.5 Hz, J_2 = 1.5 Hz, CH_2—N=), 3.41 (6 H, s, OCH_3).

Ethyl α-Amino-(N-cinnamylidene)-β,β-diethoxy Propionate ***14b***

The Schiff base **14***b* was similarly prepared from 92.5 g (0.46 mol) ethyl α-amino-β,β-diethoxy propionate and 60.8 g (0.46 mol) cinnamaldehyde to give 158 g (quantitative) of **14***b* as a pale yellow oil; ir ($CHCl_3$) 1640 cm^{-1}, 1740 cm^{-1}; nmr ($CDCl_3$) δ 8.08 (1H, dd, J_1 = 3.5 Hz, J_2 = 5.0 Hz, CH=N), 7.35 (5H, m, aromatic), 6.97 (2H, d, J = 5.0 Hz, CH=CH=ϕ), 4.93 (1H, d, J = 7.0 Hz, $CH(OR)_2$), 4.24 (2H, q, J = 7.0 Hz, $CO_2CH_2CH_3$), 3.98 (1H, d, J = 7.0 Hz, CH—N=), 3.62, 3.65 (4H, q, J = 7.0 Hz, OCH_2), 1.20 (9H, m, CH_3).

cis-N-(β,β-Dimethoxyethyl)-3-azido-4-styryl-2-azetidinone ***15a***

A solution of 21.9 g (0.1 mol) Schiff base **14***a* in 500 ml dry methylene chloride was cooled to −10 °C in an ice–methanol bath. To this was added 10.1 g (0.1 mol) triethylamine following which a solution of 12.0 g (0.1 mol) azidoacetylchloride in methylene chloride (100 ml) was added in a dropwise manner over 1 h. After the addition was complete, the solution was stirred an additional 15 min and washed with water (100 ml), 10% hydrochloric acid (100 ml), and brine (100 ml). The organic layer was dried over sodium sulfate, filtered, and evaporated to yield 33.8 g of the crude β-lactam **15***a*. The oil was purified by chromatography over silica gel (10% water w/w) to yield 15.9 g (52.5%) of *cis-N*-(β,β-dimethoxyethyl)-3-azido-4-styryl-2-azetidinone as an oil; ir ($CHCl_3$) 2100 (N_3), 1755 (β-lactam C=O) cm^{-1}. *Anal.* calcd. for $C_{15}H_{18}N_4O_3$: C 59.59, H 6.00, N 18.53; found: C 59.66, H 6.09, N 18.50.

cis-N-(α-Carboethoxy-β,β-diethoxyethyl)-3-azido-4-styryl-2-azetidinone ***15b***

A freshly prepared solution of Schiff base **14***b* (0.46 mol in 1.3 l methylene chloride) was cooled to 0–5 °C with an ice bath. To this 46.1 g (0.46 mol) triethylamine was

added. A solution of 56.0 g (0.46 mol) azidoacetyl chloride in 500 ml methylene chloride was added dropwise over 1 h. The solution was stirred an additional 30 min, washed with water and saturated NaCl solution, and dried over Na_2SO_4. Evaporation of the solution yielded 187.0 g (> 98% crude yield) of compound **15***b* as a reddish oil. Generally this oil was used as such in subsequent reactions. A small sample of the crude product was chromatographed on silica gel (10% water, w/w) using methylene chloride to give pure **15***b* as a mixture of diastereoisomers; ir ($CHCl_3$) 2100 (N_3), 1760 (β-lactam C=O), 1740 (ester C=O) cm^{-1}. *Anal.* calcd. for $C_{20}H_{26}N_4O_5 \cdot \frac{1}{10} CH_2Cl_2$: C 58.50, H 6.35, N 13.64; found: C 58.48, H 6.48, N 13.38.

Further elution of the column with ether gave compound **16**; ir (neat) 2100 (N_3), 1775 (β-lactam C=O), 1720 (ester C=O), 1650 (enol ether >=<) cm^{-1}. *Anal.* calcd. for $C_{18}H_{20}N_4O_4$: C 60.66, H 5.66, N 15.72; found: C 60.78, H 5.73, N 15.91.

cis-N-(β,β-Dimethoxyethyl)-3-azido-4-hydroxymethyl-2-azetidinone ***18a***

A solution of 4.60 g (15.2 mmol) of **15***a* in 200 ml methanol was ozonized at −78 °C (acetone – dry ice bath) until an excess of ozone had been delivered as determined by the development of a faint blue-green color in the solution. The excess ozone was purged by passing a stream of nitrogen through the solution. The solution was allowed to rise to −40 °C at which time was added 500 mg (13 mmol) of sodium borohydride. The temperature of the solution was permitted to rise to 25 °C over 30 min following which 3 ml of 10% hydrochloric acid were added. The solution was evaporated to dryness at reduced pressure and the residue partitioned between brine (100 ml) and a mixture of ether and methylene chloride (5:1) (3 × 100 ml). The combined extracts were dried over magnesium sulfate, filtered, and evaporated at reduced pressure to yield 4.7 g of an oil. The oil was chromatographed on 30 g of silica gel (10% water, w/w) eluted with 15% ether–benzene which was gradually increased to 25% ether–benzene. A total of 2.67 g (76.5%) of pure *cis-N*-(β,β-dimethoxyethyl)-3-azido-4-hydroxymethyl-2-azetidinone **18***a* was collected as an oil; ir ($CHCl_3$) 3450 (OH), 2100 (N_3), 1755 (β-lactam C=O) cm^{-1}. *Anal.* calcd. for $C_8H_{14}N_4O_4$: C 41.74, H 6.13, N 24.34; found: C 41.97, H 6.10, N 24.05.

cis-N-(α-Carboethoxy-β,β-diethoxyethyl)-3-azido-4-hydroxymethyl-2-azetidinone ***18b***

A solution of 43.0 g (0.107 mol) of compound **15***b* in 700 ml of dry methylene chloride was ozonized at −78 °C in an acetone – dry ice bath, until the solution turned bluish-green, at which time the ozone was replaced by a stream of dry nitrogen. When the excess ozone had been purged (as indicated by the disappearance of the blue color) 30 ml of dimethyl sulfide was added. The solution was allowed to come to room temperature (~25 °C) over 1 h. The solution was evaporated to dryness and the residue redissolved in 800 ml CH_2Cl_2. The solution was washed with water and brine and dried over $MgSO_4$. Evaporation of the solution gave an oily residue which was heated *in vacuo* for 18 h at 40–50 °C and 0.1 torr to remove benzaldehyde. This yielded 40.5 g of an oil. The nmr spectrum indicated 76% free aldehyde. The crude aldehyde was used in the next step without further purification.

A solution of 40.3 g of crude aldehyde in 250 ml ethanol – 12.5 ml H_2O was prepared and cooled to 0–5 °C in an ice bath. To this was added 1.56 g (0.041 mol) sodium borohydride and the solution was stirred for 30 min at 0–5 °C. To the solution was added 10% hydrochloric acid to p*H* 4. The reaction mixture was evaporated to dryness at reduced pressure below 35 °C. To the residue was added 200 ml of brine and the solution was extracted with chloroform (3 × 200 ml). The extracts were dried over Na_2SO_4, filtered, and evaporated to yield 37.0 g of crude alcohol. The crude alcohol was filtered through a column of activity III alumina (550 g) using chloroform as an eluent to yield 27.0 g of reasonably pure alcohol (> 90%). The ir and nmr spectra of the oil were compatible with the assigned structure.

The overall yield from compound **15***b* was 67%. A small sample of the alcohol was purified by column chromatography on alumina (activity III); ir ($CHCl_3$) 3300 (OH), 2090 (N_3), 1755 (β-lactam C=O), 1745 (ester C=O) cm^{-1}. *Anal.* calcd. for $C_{13}H_{22}N_4O_6$: C 47.27, H 6.71, N 16.96; found: C 47.26, H 6.85, N 17.15.

α- and β-3-Methoxy-7-β-azido-O-2-isocepham ***20*** *and* ***19***

To a solution of 4.40 g (19.1 mmol) of **18***a* in 40 ml of dry methylene chloride at 25 °C was added a solution of 2.4 ml (19.1 mmol) of boron trifloride etherate in 20 ml methylene chloride over 2 h under an atmosphere of nitrogen. The solution was stirred an additional 30 min then filtered through a pad of activity III alumina. The pad was washed with 300 ml of chloroform–methanol (95:5) and the combined filtrates were evaporated to dryness to yield 4.0 g of an oil. The oil was chromatographed on activity II silica gel (40 g) using benzene–ether (4:1) as eluent. The α-isomer eluted first from the column to give 710 mg of α-3-methoxy-7-β-azido-*O*-2-isocepham **20**. The β-isomer eluted second from the column to yield 1.5 g of an oil which crystallized on standing, mp 73–74 °C. The combined yield was 58.1%; ir of β-isomer ($CHCl_3$) 2100 (N_3), 1772 (β-lactam C=O) cm^{-1}; ir of α-isomer ($CHCl_3$) 2100 (N_3), 1770 (β-lactam C=O) cm^{-1}. *Anal.* calcd. for $C_7H_{10}N_4O_3$: C 42.42, H 5.09, N 28.27; found (for α-isomer): C 42.32, H 5.22, N 28.00; found (for β-isomer): C 42.68, H 5.13, N 28.26.

7-β-(Aminophenoxyacetoyl)-3-α-methoxy-O-2-isocepham ***22b***

To a solution of 400 mg (2 mmol) of **20** in 20 ml methylene chloride at 0 °C was added 0.28 ml triethylamine (2 mmol). A stream of hydrogen sulfide gas was bubbled in for 5 min and the solution allowed to stand for 1 h. Evolution of nitrogen was observed. The solution was evaporated to dryness. An additional 50 ml methylene chloride was added and the solution again evaporated. This procedure was repeated twice more. The resultant yellow oil was taken up in 30 ml methylene chloride and to this was added 310 mg (2 mmol) phenoxyacetic acid followed by 500 mg (2 mmol) EEDQ. The solution was let stand 1 h at room temperature after which it was washed successively with 5% hydrochloric acid (25 ml), water (25 ml), and brine (25 ml). The solution was dried over sodium sulfate, filtered, and evaporated to yield an oil which was purified by chromatography on silica gel (10% water, w/w) (20 g) to yield 587 mg (96%) of 7-β-(aminophenoxyacetoyl)-3-α-methoxy-*O*-2-isocepham **22***b* mp 156–157 °C on elution with benzene–ether (4:1); ir ($CHCl_3$) 3380 (NH), 1765 (β-lactam C=O), 1695

(*CO*NH) cm^{-1}. *Anal.* calcd. for $C_{15}H_{18}N_2O_5$: C 58.82, H 5.92, N 9.15; found: C 58.93, H 6.01, N 9.11.

7-β-(Aminophenoxyacetoyl)-3-β-methoxy-O-2-isocepham ***21b***

From 500 mg (2.5 mmol) of compound **19** was prepared 750 mg of crude **21***b* following the procedure for the preparation of **22***b*. The oil was chromatographed on activity II silica gel (20 g) using benzene–ether (4:1) as the eluting solvent to yield 578 mg (77%) of pure **21***b*, mp 105–106 °C (recrystallized from methanol–ether); ir ($CHCl_3$) 3490 (NH), 1753 (β-lactam C=O), 1680 (*CO*NH) cm^{-1}. *Anal.* calcd. for $C_{15}H_{18}N_2O_5$: C 58.82, H 5.92, N 9.15; found: C 58.80, H 5.91, N 9.08.

cis-N-(β,β-Dimethoxyethyl)-3-amino-4-styryl-2-azetidinone ***25a***

From 2.1 g (6.95 mmol) of **15***a* was prepared 1.34 g (73%) of **25***a* according to the procedure described for **22***b*. The oily amine formed a crystalline oxalate, mp 138–148 °C, recrystallized from methanol–ether; ir (free base) ($CHCl_3$) 3390 (NH_2), 1750 (C=O) cm^{-1}. *Anal.* calcd. for $C_{15}H_{20}N_2O_3 \cdot C_2H_2O_4$: C 55.73, H 6.05, N 7.65; found: C 55.70, H 5.92, N 7.62.

cis-N-(β,β-Dimethoxyethyl)-3-(aminophenylacetoyl)-4-styryl-2-azetidinone ***25b***

From 4.91 g (14.85 mmol) of **15***a* was prepared 4.8 g crude **25***b* according to the method given for the preparation of **22***b*. The oil was purified by column chromatography on silica gel to yield 2.1 g pure **25***b*, mp 121–123 °C (recrystallized from benzene); ir ($CHCl_3$) 3490 (NH), 1755 (C=O), 1680 (NH C=O) cm^{-1}. *Anal.* calcd. for $C_{23}H_{26}N_2O_4$: C 70.03, H 6.64, N 7.10; found: C 70.46, H 6.73, N 7.10.

cis-N-(β,β-Dimethoxyethyl)-3-(aminophenoxyacetoyl)-4-styryl-2-azetidinone ***25c***

To a mixture of 540 mg (1.96 mmol) of amine **25***a* and 304 mg (2.0 mmol) phenoxyacetic acid in 20 ml methylene chloride was added 500 mg (2.02 mmol) EEDQ. The solution was let stand 1.25 h at 25 °C. Upon work-up (see **22***b*) there was obtained 605 mg (77.5%) of pure **25***c* mp 105–106 °C, recrystallized from methylene chloride – ether; ir ($CHCl_3$) 3400 (NH), 1752 (β-lactam C=O), 1690 (amide C=O) cm^{-1}. *Anal.* calcd. for $C_{23}H_{26}N_2O_5$: C 67.30, H 6.38, N 6.83; found: C 67.37, H 6.35, N 6.72.

cis-N-(β,β-Dimethoxyethyl)-3-(aminophenylacetoyl)-4-hydroxymethyl-2-azetidinone ***23b***

From ***18a***

From 2.46 g (10.7 mmol) of **18***a* was prepared 3.5 g of crude **23***b* according to the procedure given for the preparation of **22***b*. The oil was chromatographed on 25 g activity II silica gel using methylene chloride – methanol (19:1) as eluent to yield 1.31 g (38%) pure **23***b*, mp 100–101 °C; ir ($CHCl_3$) 3470 (OH, NH), 1755 (C=O), 1680 (CONH) cm^{-1}. *Anal.* calcd. for $C_{16}H_{22}N_2O_5$: C 59.61, H 6.88, N 8.69; found: C 59.70, H 6.88, N 8.57.

From ***25b***

Into a solution of 394 mg (1 mmol) of **25***b* in 20 ml methanol was passed ozone at −78 °C (acetone – dry ice) until a pale blue color persisted. The excess ozone was purged by passing a stream of dry nitrogen through the solution for 10 min. To the solution was added 38 mg (10 mmol) of sodium borohydride and the solution was let warm to 25 °C over 1 h. On work-up (see **18***a*) there was obtained 250 mg (74%) of **23***b* identical in all respects with that prepared from **18***a*.

cis-N-(β,β-Dimethoxyethyl)-3-(aminophenoxyacetoyl)-4-hydroxymethyl-2-azetidinone ***23c***

The preparation of **23***c* was carried out in a similar manner to the preparation of **23***b* from **25***b*. From 410 mg (1 mmol) of **25***c* there was obtained 220 mg (65%) of **23***c*; mp 120–121.5 °C, recrystallized from ethyl acetate; ir ($CHCl_3$) 3390 (NH), 1760 (β-lactam C=O), 1690 (amide C=O) cm^{-1}. *Anal.* calcd. for $C_{16}H_{22}N_2O_6$: C 56.79, H 6.55, N 8.28; found: C 56.82, H 6.60, N 8.22.

3-β-Ethoxy-4-α-carboethoxy-7-β-azido-O-2-isocepham ***27***

To a solution of 6.20 g (18.8 mmol) of alcohol **18***b* in 100 ml of dry methylene chloride was slowly added a solution of 4.0 g (28.2 mmol, 3.54 ml) boron trifluoride etherate in 20 ml dry methylene chloride over 15 min at 0–5 °C. The cooling bath was removed and stirring was continued for 18 h. The reaction mixture was filtered through a column of activity III alumina (40 g). The column was washed with 300 ml chloroform. The eluted fractions were evaporated to dryness to yield 6.0 g of an oil. The oil was chromatographed on silica gel (10% water, w/w) to yield 4.10 g of **18** as an oil (77%); ir ($CHCl_3$) 2110, 1773, 1746 cm^{-1}. *Anal.* calcd. for $C_{11}H_{16}N_4O_5$: C 46.47, H 5.67, N 19.71; found: C 46.54, H 5.85, N 19.34.

3-β-Ethoxy-4-α-carboethoxy-7-β-amino-O-2-isocepham ***28***

A mixture of 760 mg (2.8 mmol) of compound **27**, 925 mg ammonium chloride (17.1 mmol), and 620 mg (17.1 mmol) zinc powder in 35 ml methanol was stirred at 25 °C for 3 h. The reaction mixture was filtered through Celite and the filtrate evaporated to dryness. The residue was taken up in chloroform and filtered through 30 g of alumina (activity III). Evaporation of the eluent yielded 578 mg of crude amine. The amine was redissolved in 15 ml chloroform and extracted into 10% HCl (2 × 3 ml). The aqueous layer was neutralized with sodium bicarbonate and extracted into chloroform. The extracts were dried over Na_2SO_4, filtered, and evaporated to yield 360 mg (50%) of an oil which crystallized on standing; mp 98.5–99 °C recrystallized from ether; ir ($CHCl_3$) 3420, 1770, 1745 cm^{-1}. *Anal.* calcd. for $C_{11}H_{18}N_2O_5$: C 51.15, H 7.03, N 10.85; found: C 51.16, H 7.01, N 11.03.

7-β-(Aminophenoxyacetoyl)-3-β-ethoxy-4-α-carboethoxy-O-2-isocepham ***29***

A solution of 400 mg (1.55 mmol) of compound **28**, 410 mg (1.64 mmol) EEDQ, and 250 mg (1.69 mmol) phenoxyacetic acid in 20 ml dry methylene chloride was stirred at 25 °C for a period of 1.5 h. The reaction mixture was filtered through a column of alumina (activity III, 8 g) and the eluent evaporated to dryness. The resultant solid was washed with ether and filtered to yield 554 mg (90%), mp 162–164 °C. Recrystallization from chloroform–ether gave analytically pure amide, mp 166.5–167.5 °C; ir ($CHCl_3$) 3550, 1770, 1740 (s), 1692, 1601, 1598 cm^{-1}. *Anal.* calcd. for $C_{19}H_{24}N_2O_7$: C 58.15, H 6.16, N 7.14; found: C 57.93, H 6.23, N 7.34.

7-β-(Aminophenoxyacetoyl)-3-β-ethoxy-O-2-isocepham-4-α-carboxylic Acid ***30***

A solution of 392 mg (1 mmol) compound **29** in 13 ml warm methanol was added to 12 ml, 1% NaOH at 25 °C with stirring over 10 min. After 1 h the methanol was

evaporated and the alkaline solution was extracted with chloroform (2 × 20 ml). The aqueous solution was acidified to p*H* ~4 with 10% HCl and extracted with chloroform (2 × 15 ml). The extracts were washed with water, dried over Na_2SO_4, filtered, and evaporated to give 200 mg (55%) of a white solid. Recrystallization from methanol–ether gave pure acid **30**; mp 150–155 °C; ir ($CHCl_3$) 1775 cm^{-1}. *Anal.* calcd. for $C_{17}H_{20}N_2O_7 \cdot \frac{1}{2}CH_3OH$: C 55.26, H 5.83, N 7.37; found: C 55.08, H 5.53, N 7.48.

Acknowledgements

The financial support of the National Research Council of Canada through its Industrial Research Assistance Program is gratefully acknowledged.

1. E. H. FLYNN (*Editor*). Cephalosporins and penicillins, chemistry and biology. Academic Press, New York and London. 1972.
2. W. C. TOPP and B. G. CHRISTENSEN. J. Med. Chem. **17**, 342 (1974).
3. (*a*) M. S. MANHAS and A. K. BOSE. Synthesis of penicillin, cephalosporin C, and analogs. Marcel Dekker Inc., New York. 1969; (*b*) M. S. MANHAS and A. K. BOSE. Beta-lactams, natural and synthetic. Part 1. Wiley-Interscience, New York, London, Sydney, and Toronto. 1971.
4. (*a*) A. K. BOSE, J. C. KAPUR, J. L. FAHEY, and M. S. MANHAS. J. Org. Chem. **38**, 3437 (1973); (*b*) S. WOLFE, J. B. DUCEP, and G. KANNENGIESSER. Can. J. Chem. **50**, 2902 (1972); (*c*) B. T. GOLDING and D. R. HALL. Chem. Commun. 293 (1973); (*d*) A. K. BOSE and J. L. FAHEY. J. Org. Chem. **39**, 115 (1974); (*e*) G. LOWE and D. D. RIDLEY. Chem. Commun 328 (1973); J. Chem. Soc. Perkin Trans. I, 2024 (1973); (*f*) D. M. BRUNWIN, G. LOWE, and J. PARKER. Chem. Commun. 865 (1971); J. Chem. Soc. C, 3756 (1971); (*g*) G. LOWE and M. V. J. RAMSAY. J. Chem. Soc. Perkin Trans. I, 479 (1973); (*h*) G. LOWE and J. PARKER. Chem. Commun. 577 (1971); D. M. BRUNWIN and G. LOWE. J. Chem. Soc. Perkin Trans. I, 1321 (1973); (*i*) L. D. CAMA and B. G. CHRISTENSEN. J. Am. Chem. Soc. **96**, 7582 (1974); R. N. GUTHIKONDA, L. D. CAMA, and B. G. CHRISTENSEN. J. Am. Chem. Soc. 7584 (1974); (*j*) S. WOLFE, J. B. DUCEP, K. C. TIN, and S. N. LEE. Can. J. Chem. **52**, 3996 (1974).
5. E. H. W. BOHME, H. E. APPLEGATE, B. TOEPLITZ, J. E. DOLFINI, and J. Z. GOUGOUTAS. J. Am. Chem. Soc. **93**, 4324 (1971).
6. J. C. SHEEHAN and M. DADIC. J. Heterocycl. Chem. **5**, 779 (1968).
7. R. HEYMES, G. AMIARD, and G. NOMINE. Bull. Soc. Chim. Fr. 2343 (1973).
8. R. W. RATCLIFFE and B. G. CHRISTENSEN. Tetrahedron Lett. 4645 (1973); 4649 (1973); 4653 (1973).
9. J. A. EDWARDS, A. GUZMAN, R. JOHNSON, P. J. BEEBY, and J. H. FRIED. Tetrahedron Lett. 2031 (1974).
10. R. SCARTAZZINI, H. PETER, H. BICKEL, K. HEUSLER, and R. B. WOODWARD. Helv. Chim. Acta, **55**, 408 (1972); R. SCARTAZZINI and H. BICKEL. Helv. Chim. Acta, **55**, 423 (1972); R. SCARTAZZINI, J. GOSTRELI, H. BICKEL, and R. B. WOODWARD. Helv. Chim. Acta, **55**, 2567 (1972).
11. K. KUHLEIN and H. JENSEN. Ann. Chem. 369 (1974); H. W. SCHNABEL, D. GRIMM, and H. JENSEN. Ann. Chem. 477 (1974).
12. A. K. MUKERJEE and R. C. SRIVASTAVA. Synthesis, 327 (1973).
13. J. R. HLUBUCEK and G. LOWE. J. Chem. Soc. Chem. Commun. 419 (1974).
14. H. STAUDINGER. Ann. Chem. **356**, 51 (1907).
15. (*a*) A. K. BOSE, B. DAYAL, H. P. S. CHAWLA, and M. S. MANHAS. Tetrahedron Lett. 2823 (1972); (*b*) A. K. BOSE, Y. H. CHIANG, and M. S. MANHAS. Tetrahedron Lett. 4091 (1972); (*c*) A. K. BOSE, J. C. KAPUR, S. D. SHARMA, and M. S. MANHAS. Tetrahedron Lett. 2319 (1973); (*d*) A. K. BOSE, H. P. S. CHAWLA, B. DAYAL, and M. S. MANHAS. Tetrahedron Lett. 2506 (1973); (*e*) A. K. BOSE, J. C. KAPUR, B. DAYAL, and M. S. MANHAS. Tetrahedron Lett. 3797 (1973); (*f*) A. K. BOSE, J. C. KAPUR, S. GAMIN, and M. S. MANHAS. Tetrahedron Lett. 1917 (1974); (*g*) A. K. BOSE, S. D. SHARMA, J. C. KAPUR, and M. S. MANHAS. Synthesis, 216 (1973); (*h*) A. K. BOSE, J. L. FAHEY, and M. S. MANHAS. J. Heterocycl. Chem. **10**, 791 (1973); (*i*) A. K. BOSE, M. TSAI, J. C. KAPUR, and M. S. MANHAS. Tetrahedron, **29**, 2355 (1973); (*j*) A. K. BOSE, B. DAYAL, H. P. S. CHAWLA, and M. S. MANHAS. Tetrahedron, **28**, 5977 (1972); (*k*) A. K. BOSE, J. C. KAPUR, B. DAYAL, and M. S. MANHAS. J. Org. Chem. **39**, 312 (1974); (*l*) A. K. BOSE, B. ANJANEYULU, S. K. BHATTACHARYA, and M. S. MANHAS. Tetrahedron, **23**, 4769 (1967); (*m*) A. K. BOSE, G. SPIEGELMAN, and M. S. MANHAS. Tetrahedron Lett. 3167 (1971).
16. H. T. CLARKE. The chemistry of penicillin. Princeton University Press. Princeton, New Jersey. 1949. (*a*) p. 977; (*b*) pp. 473–534.
17. R. PFLEGER and A. JAGER. Chem. Ber. **90**, 2460 (1957).
18. F. DURAN and L. GHOSEZ. Tetrahedron Lett. 245 (1970).
19. S. MOHAN, B. KUMAR, and J. S. SANDHU. Chem. Ind. 671 (1971).
20. R. LATTRELL and G. LOHAUS. Ger. Patent Nos. 2046822 (1970); 2046823 (1970); 2046824 (1970).
21. (*a*) D. A. NELSON. Tetrahedron Lett. 2543 (1970); (*b*) J. DECAZES, J. L. LUCHE, and H. B. KAGAN. Tetrahedron Lett. 3661 (1970); (*c*) K. D. BARROW and T. M. SPOTSWOOD. Tetrahedron Lett. 3325 (1965).
22. (*a*) J. L. LUCHE and H. B. KAGAN. Bull. Soc. Chim. Fr. 2450 (1968); (*b*) J. DECAZES, J. L. LUCHE, and H. B. KAGAN. Tetrahedron Lett. 3666 (1970).
23. E. L. ELIEL and C. A. GIZA. J. Org. Chem. **33**, 3754 (1968) and references therein.
24. E. L. ELIEL, N. L. ALLINGER, S. J. ANGYAL, and G. A. MORRISON. Conformational analysis. Interscience, New York, London, Sydney. 1965.
25. (*a*) R. E. SIEVERS (*Editor*). Nuclear magnetic shift reagents. Academic Press Inc., New York and London. 1973; (*b*) E. WENKERT, D. W. COCHRAN, E. W. HAGAMAN, R. B. LEWIS, and F. M. SCHELL. J. Am. Chem. Soc. **93**, 6271 (1971).
26. B. BELLEAU and G. MALEK. J. Am. Chem. Soc. **90**, 1651 (1968).
27. M. O. FORSTER and H. E. FIERZ. J. Chem. Soc. **93**, 72 (1908); M. O. FORSTER and K. A. N. RAO. J. Chem. Soc. 1943 (1926); K. A. N. RAO and P. R. VENKATARAMAN. J. Indian Chem. Soc. **15**, 194 (1938).

Nuclear analogs of β-lactam antibiotics. II. Synthesis of *O*-2-isocephems[1]

TERRENCE W. DOYLE,[2,3] BERNARD BELLEAU, BING-YU LUH, TERRY THOMAS CONWAY, MARCEL MENARD, JAMES L. DOUGLAS, DANIEL TIM-WU CHU,[4] GARY LIM, LEESON R. MORRIS, PIERRE RIVEST, AND MICHAEL CASEY

Bristol Laboratories of Canada, 100 Industrial Boulevard, Candiac, Que., Canada J5R 1J1

Received July 8, 1976

TERRENCE W. DOYLE, BERNARD BELLEAU, BING-YU LUH, TERRY THOMAS CONWAY, MARCEL MENARD, JAMES L. DOUGLAS, DANIEL TIM-WU CHU, GARY LIM, LEESON R. MORRIS, PIERRE RIVEST, and MICHAEL CASEY. Can. J. Chem. **55**, 484 (1977).

The preparation by total synthesis of a new class of β-lactam antibiotics is reported. Conversion of alcohol **1***b* to its mesylate **9***b* followed by hydrolysis of the acetal to the enol **1***b* and base-catalyzed ring closure gave benzyl 7-β-azido-Δ^3-*O*-2-isocephem-4-carboxylate **8***b*. Similarly prepared were the 3-methyl, 3-benzyl, and 3-phenethyl analogs (**32***b–d*). Reduction of the azides followed by coupling of the resultant amines with phenoxyacetic acid and removal of the benzyl groups by hydrogenolysis gave the acids **35***a–e* which exhibited high antibacterial activity. The structural assignments to the *O*-2-isocephems which were made on the basis of their spectral characteristics (ir, uv, and nmr) are discussed.

TERRENCE W. DOYLE, BERNARD BELLEAU, BING-YU LUH, TERRY THOMAS CONWAY, MARCEL MENARD, JAMES L. DOUGLAS, DANIEL TIM-WU CHU, GARY LIM, LEESON R. MORRIS, PIERRE RIVEST et MICHAEL CASEY. Can. J. Chem. **55**, 484 (1977).

On rapporte la préparation, par synthèse totale, d'une nouvelle classe d'antibiotiques contenant une β-lactame. La conversion de l'alcool **1***b* en mésylate **9***b* suivie par une hydrolyse de l'acétal en énol **1***b* et par la fermeture de cycle catalysée par les bases, conduit à la β-azido-7 Δ^3-*O*-isocéphème-2 carboxylate-4 de benzyle **8***b*. On a préparé par la même procédure les analogues méthyl-3, benzyl-3 et phénéthyl-3 (**32***b–d*). La réduction des azotures, suivie par un couplage des amines qui en résultent avec l'acide phénoxyacétique et l'élimination des groupes benzyles par hydrogénolyse fournit les acides **35***a–e* qui montrent une grande activité antibactérielle. On discute des attributions de structures pour les *O*-isocéphèmes-2 qui ont été faites en se basant sur leurs caractéristiques spectrales (ir, uv et nmr).

[Traduit par le journal]

In the preceding paper the synthesis of **1***a*, its conversion to **2***a*, and the subsequent conversion of **2***a* to **2***e* was described. The low order of antibacterial activity exhibited by **2***e* was as had been anticipated.[5] It remained for us to effect the elimination of a mole of ethanol from **2***e* in order to complete our synthesis of the *O*-2-isocephem nuclear analog of cephalosporin.[6] In this paper we wish to report our efforts in this area and the synthesis of a number of *O*-2-isocephems which exhibit high antibacterial activity.

All efforts to effect direct elimination of ethanol from **2** (Scheme 1) failed as did attempted hydrolysis of **2** to its 3-hydroxy analogs. Treatment of **2***a* with zinc chloride in acetic anhydride gave **3***a* in 85% yield rather than the hoped for 3-acetoxy derivative. This result might have been anticipated from the stereochemistry of **2***a* (Fig. 1). In **2***a* the C_3—O_2 bond and the C_4—H_β bond are *trans* to one another thus facilitating cleavage of the C_3—O_2 bond with formation of the double bond in **3***a* which is formed as a single geometrical isomer. Alternatively, **3***a* could be

[1]For part I of this series see ref. 1.

[2]Author to whom correspondence concerning this paper should be addressed.

[3]Present address: Bristol Laboratories, P.O. Box 657, Syracuse, New York 13201.

[4]NRCC Industrial Postdoctoral Fellow, 1971–1972.

[5]Gutowski *et al.* have reported that compound **i** exhibits low antibacterial activity in comparison with its unsaturated counterpart (2).

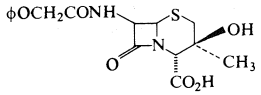

i

[6]See ref. 1 for a review of the literature concerning nuclear analogs of the penicillins and cephalosporins and an explanation of the trivial nomenclature used in this and the accompanying papers.

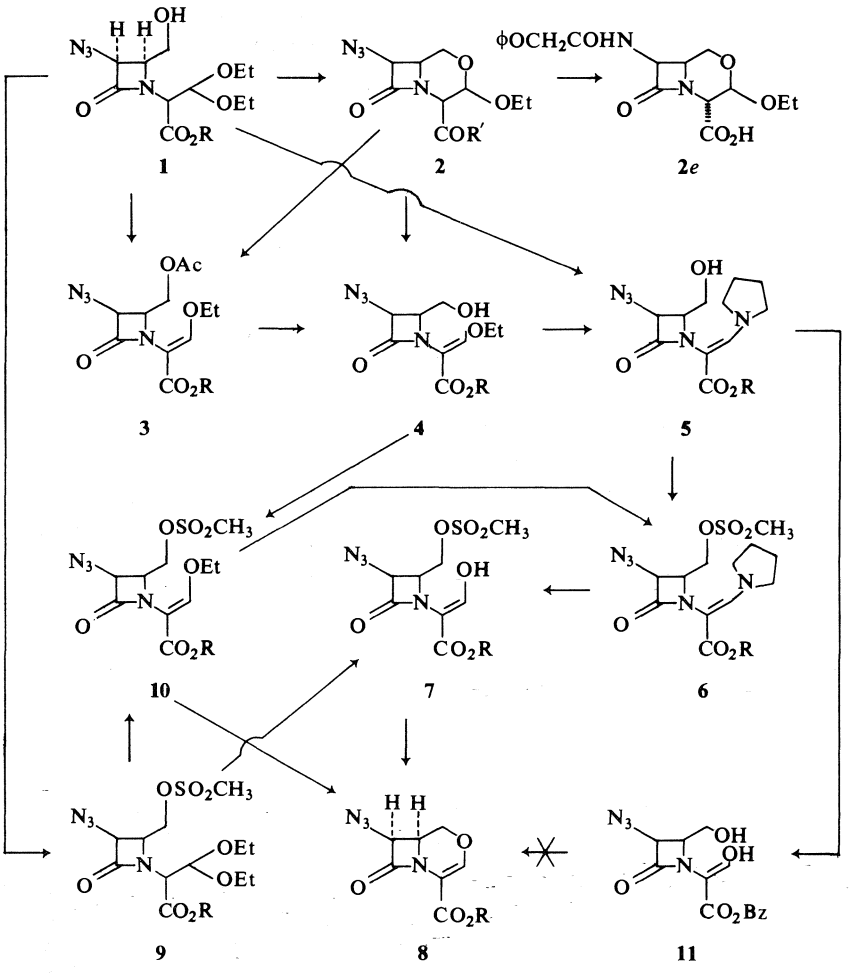

Compounds **1**, **3–10** *a* R = C_2H_5; *b* R = $CH_2\phi$; *c* R = H

Compound **2** *a* R′ = OEt; *b* R′ = OH; *c* R′ = Cl; *d* R′ = $OCH_2\phi$

SCHEME 1

obtained directly from **1***a* in 75% yield. In this case, **3***a* was obtained as a mixture of isomers in which the isomer obtained in major amount (>90%) was identical with that from **2***a*.

Hydrolysis of **3***a* gave **4***a* in 94.5% yield. Compound **4***a* could also be obtained in low yield (26%) by treatment of **2***a* with titanium tetrachloride in methylene chloride.

The nmr and ir spectra (Tables 2 and 4 respectively) of these compounds were in accord with the assigned structures. In the nmr compounds **3***a* and **4***a* showed signals at 7.34 and 7.73 δ respectively for the olefinic proton. In the

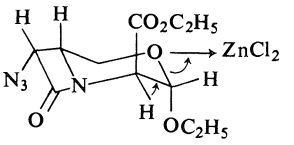

FIGURE 1

ir they exhibited $\diagdown C{=}C \diagup$ stretching frequencies at 1640 and 1645 cm^{-1} for enol ethers in addition to the expected carbonyl bands.

Treatment of compound **4***a* with pyrrolidine – acetic acid in refluxing benzene gave the vin-

ologous urethane **5***a* in 75% yield as a single isomer. The nmr spectrum of **5***a* showed considerable line broadening for all protons with the exception of the signals for the ethyl ester. We attribute this broadening-hindered rotation about the $N\rightarrow C(CO_2R)=CHNC_4H_8$ bond. Compound **5***a* was also prepared directly from **1***a* in 50% yield. Treatment of **5***a* with triethylamine and methane sulfonyl chloride in methylene chloride gave **6***a* in 73.5% yield. Alternatively **6***a* could be prepared by treatment of **4***a* with triethylamine – methane sulfonyl chloride to give **10***a* in 65% yield followed by treatment of **10***a* with pyrrolidine – acetic acid to give **6***a* in 63% yield. Hydrolysis of **6***a* with hydrochloric acid in aqueous acetone gave the enol mesylate **7***a* in 89% yield. The nmr spectrum of **7***a* suggested that it exists as a mixture of geometrical isomers of the enol as well as, to a small extent, the aldehydo form. The enolic hydroxyl appears as a singlet at 12 δ integrating for ~0.85 protons. The signals for the methyl group of the ester appears as a pair of triplets of approximately equal intensities. Compound **7***a* gave a strong ferric chloride test for an enol (deep purple). In the ir spectrum of **7***a* there are bands at 1680 and 1630 cm^{-1} which we assign to the aldehydo and enolic forms respectively.

Treatment of **7***a* with sodium hydride in dimethyl sulfoxide gave ethyl 7-β-azido-Δ^3-*O*-2-isocephem-4-carboxylate **8***a* in 91% yield. Alternatively **7***a* could be converted to **8***a* by refluxing **7***a* with 1 equiv. of triethylamine in chloroform in 47.5% yield. A third route to **8***a* consists of treating **10***a* with aqueous dilute sodium hydroxide in tetrahydrofuran, lyophilizing the resulting solution and taking up the residue in DMSO. The yield of **8***a* from **10***a* by this procedure was 33%. Compound **10***a* was also prepared by mesylation of **1***a* to give **9***a* in 86% yield. Treatment of **9***a* with zinc chloride – acetic anhydride or with triethyloxonium fluoroborate in methylene chloride gave **10***a* in 45% yield. Hydrolysis of the acetal function in **9***a* with trifluoroacetic acid at 50 °C effected the conversion of **9***a* to **7***a* in 58% yield. The overall yield of **8***a* from **1***a* proceeding via the best sequence **1***a* → **9***a* → **7***a* → **8***a* was 45%.

As we required an *O*-2-isocephem carrying an easily deblocked ester function the synthesis of benzyl 7-β-azido-Δ^3-*O*-2-isocephem-4-carboxylate **8***b* was attempted next.

Saponification of **2***a* with dilute sodium hydroxide solution gave **2***b* in 66% yield. The carboxylic acid was converted to its acid chloride **2***c* and subsequently to the benzyl ester **2***d* in 83.5% yield. Treatment of **2***d* with zinc chloride – acetic anhydride gave **3***b* in 94% yield. Alternatively **3***b* could be prepared directly from **1***b* in 41% yield.

The synthesis of **1***b* was accomplished by the following sequences (Scheme 2). Treatment of benzyl nitroacetate (3) **12** with triethylorthoformate in acetic anhydride at 80–90 °C gave a mixture of **13** and **14** in quantitative yield (4). The nmr spectrum of the mixture indicated that the ratio of **13** to **14** was 3:2 and that **13** was present as a mixture of geometric isomers one of which predominates. On distillation, the mixture decomposed extensively and yielded only the starting material **12**. Treatment of the mixture of **13** and **14** with ethanol in the presence of a catalytic amount of sodium ethoxide gave exclusively **14**. The yield of **14** from **12** was quantitative. Reduction of **14** to **15** with aluminum amalgam proceeded in 42.5% yield (not optimized) (5). The ir and nmr spectra of **15** were compatible with the assigned structure.[7] Compound **15** was converted to its cinnamylidene Schiff base **16** in quantitative yield as previously described (1) following which **16** was converted to the β-lactam **17** in 89% yield by treatment with triethylamine–azidoacetylchloride as before (1). The mixture of diastereoisomeric β-lactams could be separated chromatographically, although this was not done generally as the crude product was pure enough for use in the subsequent reactions. The nmr spectra of the isomers of **17** are recorded in Table 2. Compound **17** could also be prepared from the ethyl ester **19** (1). Saponification of **19** with sodium hydroxide gave the corresponding carboxylic acid **20** in 60% yield. Treatment of **20** with triethylamine and benzyl chloroformate gave the mixed anhydride which spontaneously decomposed to the ester **17** in 55% yield. Ozonolysis of **17** at −78 °C gave the aldehyde **18** in 95% yield. The nmr spectrum of crude **18** indicated at least 77% free aldehyde.[8] Reduction of **18** with sodium borohydride in ethanol gave **1***b* in 85% yield.

Hydrolysis of **3***b* gave **4***b* in 87% yield. Com-

[7]In some runs the reduction step stopped at the hydroxylamine stage in which case the hydroxylamine was recycled over fresh aluminum amalgam.

[8]A number of the aldehydes prepared in this manner were found to form hydrates which on reduction gave the desired 4-hydroxymethyl 2-azetidinones.

TABLE 1. Nuclear magnetic resonance spectra of non-β-lactams[a]

Compound	Aromatic and vinyl	$CH_2\phi$	CH_3	O—CH_2—CH_2—O	Other
13	7.33 (s, 5H) 8.27 (s)[c] 7.58 (s)[b]	5.20 (s)	1.24 (t)[b] 1.34 (t)[c]	—	4.20 (q, J=7.0)[b,h] 4.26 (q, J=7.0)[c,h]
14	7.16 (s, 5H)	5.12 (s)	1.06 (t) 1.14 (t) J=7.0	—	3.53 (q, J=7.0)[h] 3.60 (q, J=7.0)[h,d]
15	7.30 (s, 5H)	5.16 (s)	1.15 (t) 1.13 (t) J=7.0	—	1.60 (s, 2H)[e] 4.58 (d, 1H, J=5.0)[f] 3.64 (d, 1H, J=5.0)[g]
16	7.30 (m, 10H) 6.92 (d, 2H)[o] J=4.0	5.16 (s)	1.10 (t) 1.12 (t) J=7.0	—	7.99 (t, 1H, J=4.0)[i] 3.55 (m, 4H)[h] 4.92 (d, 1H, J=7.5)[f] 4.05 (d, 1H, J=7.5)[g]
22*a*	—	—	2.48 (s) 1.39 (t) J=7.0	—	6–8 (bs, 1H)[j] 4.46 (q, 2H, J=7.0)[k]
22*b*	7.50 (s, 5H)	5.43 (s)	2.43 (s)		9.84 (s, 1H)[j]
22*c*	7.26 (s, 5H) 7.16 (s, 5H)	5.25 (s) 4.0 (s)[m]	—		10.14 (s, 1H)[j]
22*d*	7.27 (s, 5H) 7.12 (s, 5H)	5.25 (s)			10.3 (s, 1H)[j] 2.90 (m, 4H)[l]
23*a*	7.43 (s, 5H)	5.37 (s)	1.65 (s)	3.97 (s)	9.12 (s, 1H)[j]
23*b*	7.30 (s, 5H) 7.17 (s, 5H)	5.26 (s) 3.20 (s)[m]	—	3.62 (m)	9.0 (s, 1H)[j]
23*c*	7.28 (m, 5H) 7.12 (s, 5H)	5.25 (s) 2.70 (m)[l]	—	3.87 (s)	2.20 (m, 2H)[l]
24[m]	—	—	2.40 (s) 1.32 (t) J=7.0	—	4.70 (s, 1H)[g] 4.25 (q, 2H, J=7.0)[k]
25*a*	—	—	1.41 (s) 1.31 (t) J=7.0	3.73 (s)	4.07 (s, 1H)[g] 3.26 (s, 2H)[e] 4.30 (q, 2H, J=7.0)[k]
25*b*	7.36 (s, 5H)	5.18 (s)	1.36 (s)	3.91 (s)	3.60 (s, 1H)[g] 1.83 (s, 2H)[e]
25*c*	7.20 (m, 5H) 7.15 (s, 5H)	5.10 (s) 3.99 (s)[m]	—	3.40 (m)	3.58 (s, 1H)[g] 2.38 (s, 2H)[e]
25*d*	7.34 (m, 5H) 7.19 (s, 5H)	5.18 (s) 2.70 (s)[l]	—	3.90 (bs)	3.72 (s, 1H)[g] 1.91 (s, 2H)[e] 2.20 (m, 2H)[l]
26*a*	7.45 (m, 5H) 7.05 (d, 2H)[o] J=4.7	—	1.58 (s) 1.32 (t) J=7.0	4.05 (m, 5H)	4.28 (q, 2H, J=7.0)[k] 8.10 (t, J=4.7)[i]
26*b*	7.30 (10H, s) 6.94 (d, 2H)[o] J=4.0	5.22 (s)	1.53 (s)	3.97 (s)	4.05 (s, 1H)[g] 7.95 (dd, 1H, J=4.0, J=5.0)[i]
26*c*	7.30 (m, 5H) 7.17 (s, 10H) 6.97 (d)[o] J=3.0 6.89 (s, 1H)[o]	5.20 (s) 3.06 (d)[m] J=14.0 3.32 (d)[m] J=14.0	—	3.54 (m)	4.12 (s, 1H)[g] 7.88 (dd, 1H, J_1=5.5, J_2=3.0)[i]
26*d*	7.33 (m, 5H) 7.17 (m, 10H) 7.01 (d, J=3.0) 6.93 (s)[o]	5.21 (s) 2.65 (m, 2H)[l]	—	4.00 (s)	4.17 (s, 1H)[g] 2.40 (m, 2H)[l] 7.95 (dd, J_1=5.5, J_2=3.0)[i]

[a]All spectra were recorded at 60 MHz as $CDCl_3$ solutions using tetramethylsilane as internal reference unless otherwise noted. The chemical shifts are reported in δ units and the coupling constants in Hz. [b]Major isomer. [c]Minor isomer. [d]The proton signals for $CH(OR)_2$ and $CH—NO_2$ are obscured under the $CH(OCH_2—CH_3)$ signals. [e]Assigned to NH_2. [f]Assigned to $CH(OR)_2$. [g]Assigned to $CH—CO_2R$. [h]Assigned to $CH(OCH_2—CH_3)_2$. [i]Assigned to —N=CH—. [j]Assigned to =N—OH. [k]Assigned to $CO_2CH_2—CH_3$. [l]Assigned to $CH_2—CH_2—\phi$. [m]Taken in D_2O. [n]Assigned to $\phi CH_2—C\equiv$. [o]Assigned to $\phi CH=CH$.

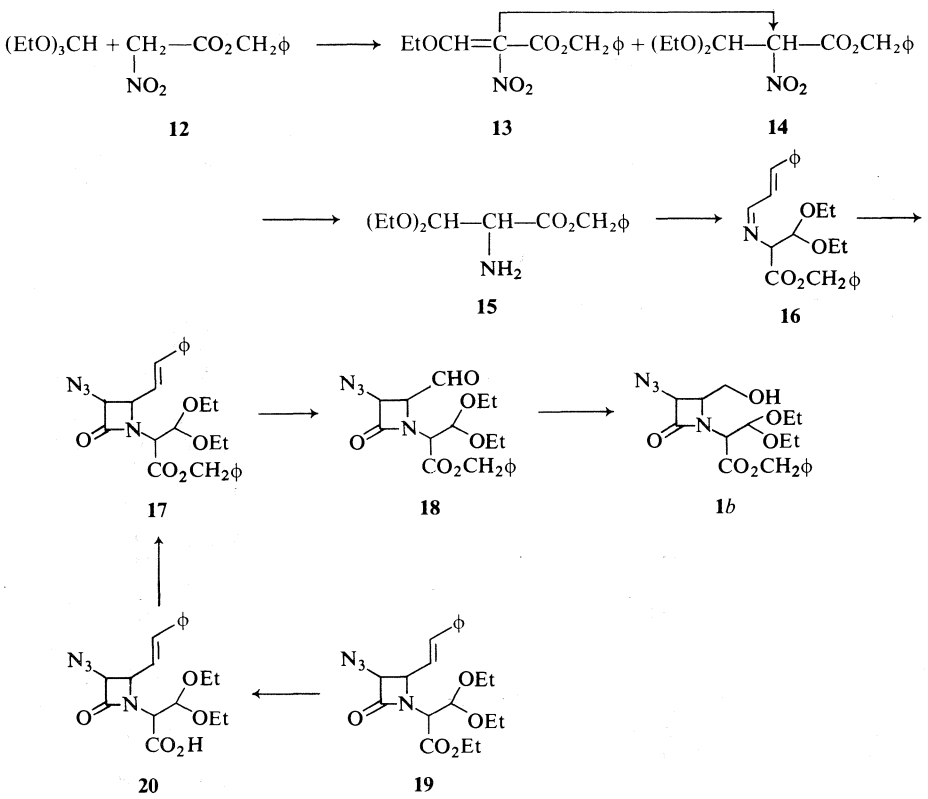

SCHEME 2

pound **4***b* was converted to **5***b* in 71% yield following which it was converted to its mesylate **6***b* in 90% yield. Hydrolysis of **6***b* gave **7***b* (81%) which was converted to **8***b* by treatment with sodium hydride in DMSO in 42% yield. On refluxing **7***b* with 1 equiv. of triethylamine in methylene chloride **8***b* was obtained in 71.5% yield. As in the case of the ethyl ester series compound **4***b* was converted to **10***b* (70%) and thence to **8***b* (40%). The conversion of **1***b* to **9***b* (83.5%) and the hydrolysis of **9***b* to **7***b* (91%) followed by ring closure also gave **8***b* in 54.5% overall yield from **1***b*.

Compound **9***b* could also be obtained from **9***a* via saponification to **9***c* in 55% yield (in addition to **9***c* there was also produced **10***a* in this reaction). Treatment of **9***c* with triethylamine – benzyl chloroformate as before gave **9***b* in 84% yield. Hydrolysis of **5***b* to **11** was carried out in 75% yield. All attempts to prepare **8***b* via the elimination of 1 mol of water from **11** failed.

The structural assignments to **8***a* and **8***b* rest on their mode of synthesis, correct elemental analyses, and their ir, uv, and nmr spectral characteristics. The ir spectra of **8***a* and **8***b* show absorptions at 2110 cm^{-1} for the azide, 1790 cm^{-1} for the β-lactam carbonyl, 1715 cm^{-1} for the α,β-unsaturated ester carbonyl, and an absorption at ~1625 cm^{-1} for the double bond. In the uv spectra of **8***a* and **8***b* there are bands at 268 nm with extinction coefficients of 6800 and 6700 respectively. These values are in accord with those observed in the cephalosporins (6). The pronounced bathochromic shift observed in going from the non-cyclized chromophore in **3**, **4**, and **10** to the chromophores in **8***a* and **8***b* may be explained as being due to participation of the amide lone pair in the chromophore of the latter compounds (the uv spectra are recorded in Table 4). This is further borne out by comparison of the uv spectra of **3**, **4**, and **10** with that of genepin (7) and the simpler dihydropyran system (8) (see Fig. 2) both of which contain the $-O-\overset{R}{C}=\overset{R'}{C}-CO_2CH_2CH_3$ chromophore. The λ_{max} and extinction coefficients for **3**, **4**, and **10** are very similar to those for genepin and the dihydropyran system indicating little contribution of the β-lactam chromophore to the β-alk-

TABLE 2. Nuclear magnetic resonance spectra of monocyclic β-lactams[a]

Compound	Aromatic and olefinic	N_3—CH—	ϕCH_2	CH_3	Other
1*b*[b]	7.27 (s, 5H)	—	5.12 (s)	1.10 (m, 6H)	3.1–4.3 (m, 8H)[c] 4.6–4.7 (m, 2H)[d]
3*a*	7.34 (s, 1H)	4.80 (dd) J_1=3.25 J_2=1.75	—	1.98 (s, 3H)[e] 1.25 (t, 3H)[g] 1.32 (t, 3H)[g] J=7.0	4.30 (m, 3H)[f] 4.11 (q, 2H, J=7.0)[g] 4.09 (q, 2H, J=7.0)[g]
3*b*[h]	7.40 (s, 1H) 7.26 (s, 5H)	4.75 (dd) J_1=3.5 J_2=1.5	5.13 (s)	1.33 (t, 3H)[i] J=7.0 1.95 (s, 3H)[e]	4.25 (m, 3H)[f] 4.10 (q, 2H)[i]
4*a*	7.73 (s, 1H)	4.88 (d) J=5.0	—	1.33 (t, 3H) 1.42 (t, 3H) J=7.0	4.00 (m, 3H)[f] 4.30 (q, 2H)[g] 4.33 (q, 2H)[g]
4*b*	7.45 (s, 1H) 7.28 (s, 5H)	4.66 (d) J=5.0	5.13 (s)	1.31 (t, 3H) J=7.0	4.11 (q, 2H)[i] 4.00 (m, 3H)[f]
5*a*[j]	7.60 (s, 1H)	4.5 (m)[j]	—	1.25 (t, 3H)[k] J=7.0	4.12 (q, 2H)[k] 5.1 (s, O*H*) 3.8 (m, 3H)[f] 3.41 (m, 4H) 1.90 (m, 4H)[l]
5*b*[j]	7.66 (s, 1H) 7.30 (s, 5H)	4.57 (m)[j]	5.13 (s)	—	3.90 (m, 3H)[f] 3.48 (m, 4H) 1.95 (m, 4H)[l]
6*a*[j]	7.51 (s, 1H)	4.83 (dd) J=4.5 J=1.5	—	1.25 (t, 3H) J=7.0 3.00 (s, 3H)[m]	4.40 (m, 3H)[f] 4.10 (q, 2H, J=7.0)[k] 3.42 (m, 4H), 1.90 (m, 4H)[l]
6*b*[j]	7.70 (s, 1H) 7.40 (s, 5H)	4.90 (d) J=5.0	5.17 (s)	3.00 (s, 3H)[m]	4.45 (m, 3H)[f] 3.5 (m, 4H), 1.95 (m, 4H)[l]
7*a*[n]	7.52 (bs, ~1H)	5.01 (d) J=5.0	—	3.04 (s, 3H)[m] 1.30 (t) 1.35 (t) J=7.0	4.18 (q, 2H, J=7.0)[k] 4.5 (m, 3H)[f]
7*b*[n]	7.36 (s, 5H) 7.39 (s, 5H) 7.55 (s, 1H)	4.86 (d, 1H) 4.94 (d, 1H) J=4.5	5.18 (s, 2H) 5.27	2.95 (s, 3H)[m]	4.50 (m, 3H)[f]
9*a*[b]	—	—	—	3.04 (s, 3H)[m] 1.20 (m, 9H)	3.2–3.9 (m, 4H)[o] 4.7–4.9 (m, 2H)[d] 4.16 (q, 2H)[k] 4.2–4.6 (m, 4H)[p]
9*b*[b]	7.38 (s, 5H)	—	5.20 (s)	3.00 (s, 3H)[m] 1.20 (m, 6H)	3.55 (m, 4H)[o] 4.7–4.9 (m, 2H)[d] 4.2–4.6 (m, 4H)[p]
9*c*	—	—	—	3.10 (s, 3H)[m]	3.70 (m, 4H)[o] 5.1–4.9 (m, 2H)[d] 4.2–4.8 (m, 3H)[p] 9.86 (s, 1H, CO_2H)
10*a*	7.46 (s, 1H)	4.95 (dd) J_1=4.0 J_2=1.5	—	3.04 (s, 3H)[m] 1.23 (t, 3H) 1.36 (t, 3H) J=7.0	4.19 (q, 4H, J=7.0)[j] 4.40 (m, 3H)[f]
10*b*	7.68 (s, 1H) 7.51 (s, 5H)	4.94 (dd) J_1=4.2 J_2=1.25	5.25 (s)	2.95 (s, 3H)[m] 1.35 (t, 3H)[i] J=7.0	4.20 (q, 2H, J=7.0)[i] 4.50 (m, 3H)[f]
17[q]	7.28 (s, 5H) 7.25 (m, 5H) 6.60 (d)[u] J=16.0 6.13 (ddt)[v] J_1=16.0 J_2=6.2 J_3=1.5	4.85 (d) J=6.0	5.14 (s, 2H)	1.06 (t, 3H) 1.08 (t, 3H) J=7.0	3.52 (m, 4H)[o] 4.73 (m, 1H)[s] 4.61 (dd, 1H, J_1=8.0, J_2=6.0)[t]

TABLE 2 (*Continued*)

Compound	Aromatic and olefinic	N_3—CH—	ϕCH_2	CH_3	Other
17[r]	7.20 (s, 5H) 7.25 (m, 5H) 6 61 (d)[u] J=16.0 6.17 (ddt)[v] J_1=16.0 J_2=6.2 J_3=1.5	—	5.06 (s, 2H)	1.10 (t, 3H) 1.12 (t, 3H) J=7 0	3.52 (m, 4H)[o] 4.6–4.9 (m, 3H)[w]
18*b*	7.32 (s, 5H) 9.74 (d, J=4.5)[x] 9.63 (d, J=4.5)	4.96 (d, 1H) 4.79 (d, 1H) J=5.5	5.14 (s, 2H) 5.19	0.94 0.97 (t, 6H) 1.14 1.19 J=7.0	3.0–3.9 (m, 5H)[y] 4.78–4.80 (m, 2H)[z] 4.42 (m, 1H)[z]
27*a*[h]	7.38 (m, 5H) 6.77 (d, 1H)[u] J=16.0 6.16 (dd, 1H)[v] J_1=16.0 J_2=8.0	—	—	1.48 (s, 3H) 1.30 (t, 3H)[k] J=7.0	4.23 (q, 2H, J=7.0)[k] 4.27 (s, 1H)[aa] 4.0 (m, 4H)[bb] 4.80 (m, 2H)[cc]
27*b*[h]	7.40 (m, 5H) 6.74 (d, 1H)[u] J=16.0 6.20 (ddd, 1H)[v] J_1=16.0 J_2=8.0 J_3=2.5 7.38 (s, 5H)	—	5.22 (s)	1.48 (s, 3H)	4.35 (s, 1H)[aa] 3.85 (s, 4H)[bb] 4.95 (m, 2H)[cc]
27*e*[h]	7.39 (m, 5H) 6.73 (d, 1H)[u] J=16.0 6.21 (ddd, 1H)[v] J_1=16.0 J_2=8.0 J_3=2.5	—	—	1.47 (s, 3H)	4.36 (s, 1H)[aa] 3.95 (s, 4H)[bb] 4.90 (m, 2H)[cc]
27*d*[b]	7.20 (m, 15H) 6.67 (d, 1H)[u] J=16.0 6.18 (m, 1H)[v]	—	5.20 (2H)	—	3.85 (m, 4H)[bb] 2.10 (m, 2H) 2.68 (m, 2H)[dd] 4.7–5.1 (m, 3H)[cc]
27*c*[b]	7.3 (m, 15H) 6.62 (d, 1H)[u] J=16.0 6.15 (m, 1H)[v]	—	4.98 (s, 2H) 5.13 (s, 2H)	—	4.36 (s), 4.54 (s)[aa] 4.75 (m, 2H)[cc] 2.9–3.9 (m, 6H)[ff]
28*a*[h]	7.35 (s, 5H)	4.95 (d) J=6.0	5.28 (d)[gg] 5.07 (d) J=12.0	1.46 (s, 3H)	3.80 (m, 4H)[bb] 4.73 (s, 1H)[aa] 4.60 (dd, 1H, J_1=6.0, J_2=4.5)[hh] 9.55 (d, 1H)[x]
28*b*[b]	7.16 (s, 5H) 7.28 (s, 5H)	4.84 (d) J=5.5 4.88 (d) J=5.0	5.10 (s) 5.23 (d)[gg] J=9.5 5.01 (d)[gg] J=9.5	—	2.8–3.9 (m, 6H)[ff] 4.42 (dd, J_1=4.0, J_2=5.0)[hh] 4.64 (dd, J_1=4.0, J_2=5.5)[hh] 4.77 (s, 1H)[aa] 9.67 (d, J=4.0) 9.77 (d, J=4.0)[x]
28*c*[b]	7.17 (m, 5H) 7.34 (s, 5H)	4.90 (d) J=4.0 4.89 (d) J=4.0	5.17 (m)	—	3.82 (m, 4H)[bb] 2.64 (m, 2H) 2.0 (m, 2H)[dd] 4.83 (s) 4.87 (s)[aa] 4.3–4.8 (m, 1H)[hh] 9.53 (d, J=3.0) 9.63 (d, J=3.0)[x]

TABLE 2 (*Concluded*)

Compound	Aromatic and olefinic	N_3—CH—	ϕCH_2	CH_3	Other
29*a*[b]	7.32 (s, 5H)	4.66 (d) $J=5.0$ 4.67 (d) $J=5.0$	5.19 (s) 5.35 (d)[gg] $J=12.0$ 5.08 (d)[gg] $J=12.0$	1.35 (s) 1.42 (s)	3.80 (m, 8H)[ii] 4.68 (s)[aa] 4.65 (s)[aa]
29*b*[b]	7.14 (s, 5H) 7.25 (s, 5H)	4.43 (d) $J=5.0$ 4.58 (d) $J=5.0$	2.87 (s) 3.04 (m) 5.08 (m)	—	4.69 (s) 4.72 (s)[aa] 4.0 (m, 3H)[f] 3.35 (m, 4H)[bb]
29*c*[b]	7.17 (m, 5H) 7.33 (s, 5H)	4.89 (d) $J=5.0$ 4.84 (d) $J=5.0$	5.18 (m)	—	4.62 (bs) 4.55 (bs)[aa] 3.84 (m, 5H)[ii] 2.70 (m, 2H) 2.0 (m, 2H)[dd]
30*a*[h]	7.34 (s, 5H)	4.85 (d) $J=5.0$	5.24 (d)[gg] $J=12.0$ 5.04 (d)[gg] $J=12.0$	2.99 (s, 3H)[m] 1.37 (s, 3H)	3.76 (m, 4H)[bb] 4.50 (s, 1H)[aa] 4.3–4.8 (m, 3H)[f]
30*b*[b]	7.15 (s, 5H) 7.26 (s, 5H)	—	5.10 (m) 2.90 (m)	2.91 (s, 3H) 2.94 (s, 3H)	3.50 (m, 4H)[bb] 4.1–4.9 (m, 5H)[jj]
30*c*	7.33 (s, 5H) 7.15 (m, 5H)	—	5.17 (m)	2.92 (s, 3H)	4.2–4.9 (m, 5H)[jj] 3.85 (m, 4H)[bb] 2.67 (m, 2H) 2.0 (m, 2H)[dd]
31*a*	7.30 (s, 5H)	4.84 (d) $J=5.0$	5.24 (s) 5.21 (s)	2.09 (s, 3H) 2.25 (d, $J=3$) 2.92 (s, 3H)[m]	4.25 (m, 3H)[f] 12.0 (s, 1H, enol)
31*b*	7.27 (s, 5H) 7.18 (m, 5H)	4.80 (d) $J=5.0$ 4.65 (d) $J=\sim 5.0$	5.13 (s) 5.24 (s) 3.63 (m)	2.72 (s, 3H)[m] 2.83 (s, 3H)[m]	3.8–4.5 (m, 3H)[f]
31*c*	7.33 (s, 5H) 7.20 (m, 5H)	4.84 (d) $J=5.0$ 4.70 (d) $J=5.0$	5.20 (m)	2.75 (s, 3H)[m] 2.87 (s, 3H)[m]	2.80 (m, 4H)[dd] 3.8–4.6 (m, 3H)[f]

[a]Recorded in $CDCl_3$ at 60 MHz unless otherwise noted. The chemical shifts are recorded in δ units and coupling constants in Hz. [b]A mixture of diastereoisomers. [c]Assigned to $CH(OCH_2—CH_3)_2$, CH_2OH, and the C_4 proton. [d]Assigned to N_3CH and $CH(OR)_2$. [e]Assigned to methyl group of acetate. [f]Assigned to —CH—CH_2—OR. [g]Assigned to $CO_2CH_2—CH_3$ and =CH—O—$CH_2—CH_3$. [h]For single isomer. [i]Assigned to =CH—$OCH_2—CH_3$. [j]Quadrupole broadening of all proton signals was observed. [k]Assigned to $CO_2CH_2—CH_3$. [l]Assigned to pyrrolidine protons. [m]Assigned to mesylate methyl protons. [n]Two geometrical isomers observed in the nmr. [o]Assigned to $CH(OCH_2CH_3)_2$. [p]Assigned to $CH—CO_2R$ and $CH—CH_2—OSO_2CH_3$. [q]Isomer *A*. [r]Isomer *B*. [s]Assigned to $CH(OR)_2$. [t]Assigned to CH—CH=CH—ϕ. [u]Assigned to $\phi CH=CH—$. [v]Assigned to $\phi CH=CH—$. [w]Assigned to CH—CH=$CH\phi$, N_3CH, and $CH(OR)_2$. [x]Assigned to —CHO. [y]Assigned to $CH(OCH_2CH_3)_2$ and $CH—CO_2R$. [z]Assigned to CHCHO and $CH(OR)_2$. [aa]Assigned to $CHCO_2R$. [bb]Assigned to O—$CH_2—CH_2$—O. [cc]Assigned to N_3CH and CH—CH=CH—ϕ. [dd]Assigned to $CH_2CH_2\phi$. [ee]Assigned to N_3CH, CH—C=, and $CH—CO_2R$. [ff]Assigned to O—CH_2CH_2—O and $CH_2\phi$. [gg]Assigned to arms of AB quartet for CH_2—ϕ. [hh]Assigned to CH—CHO. [ii]Assigned to —O—$(CH_2)_2$—O, CH—CH_2—OH. [jj]Assigned to N_3CH, CH—CH_2—OR, $CHCO_2R$.

oxyacrylate chromophore in these systems. In contrast to these observations is the marked bathochromic shift (+23 mm) observed in **8***a* and **8***b* in comparison with **3**, **4**, and **10**.

While the nmr spectra of **8***a* and **8***b* in deuteriochloroform were not first order they provided confirmation of the structures. In **8***a* the C_7—H appears as a doublet J = 5.0 Hz confirming the *cis* stereochemistry of the protons on C_6 and C_7. In **8***b* the C_7—H was partially obscured by the signal of the benzylic protons. The $C_{1\alpha}$ protons in **8***a* and **8***b* appear at 4.63 and 4.58 δ respectively as complex multiplets (six lines). The protons at $C_{1\beta}$ and C_6 appear as sets of overlapping multiplets at ~3.9 and 3.8 δ respectively. In view of the complexity of the nmr spectrum of **8***a* in $CDCl_3$ the spectrum was recorded in $CDCl_3$–C_6D_6 (1:1) at 100 MHz which resulted in aromatic solvent induced shifts (ASIS) and enabled the assignment of each proton in the spectrum as well as an assignment of conformation to **8***a*.[9] The proton signals in the shifted spectrum were assigned on the basis of their coupling constants, spin decoupling experi-

[9]The use of ASIS for the configurational assignments to the isomeric penicillin and cephalosporin sulfoxides has been demonstrated (9).

TABLE 3. Nuclear magnetic resonance spectra of bicyclic β-lactams[a]

Compound	Aromatic	C_7—H	C_3—H	ϕ—CH_2	ϕOCH_2	CH_3	Other
2*b*	—	4.97 (dd) J=4.0 J=1.5	5.21 (s)	—	—	1.30 (t)[c] J=7.0	4.54 (s, 1H, C*H*—CO_2H) 9.70 (s, 1H, CO_2H) 3.4–4.3 (m, 5H)[b]
2*c*	—	4.86 (dd) J=4.0 J=7.0	5.17 (s)	—	—	1.25 (t)[c] J=7.0	4.60 (s, 1H, C*H*COCl) 3.3–4.1 (m, 5H)[b]
2*d*	7.25 (s, 5H)	4.72 (dd) J=4.0 J=1.0	4.99 (s)	5.17 (s)	—	1.23 (t)[c] J=7.0	4.38 (s, 1H, C*H*—CO_2Bz) 3.3–4.1 (m, 5H)[b]
8*a*	—	5.34 (d) J=5.0	7.37 (s)	—	—	1.30 (t) J=7.0	4.29 (q, 2H, OCH_2—CH_3, J=7.0) 4.63 (dt, 1H, J=7.5)[d] 3.94 (m, 1H), 3.82 (m, 1H)[e]
8*b*	7.37 (s, 5H)	5.25 (d) J=5.0	7.37[f]	5.28 (s)	—	—	4.58 (dd, 1H, J_1=9, J_2=3)[d] 3.92 (m, 1H),[e] 3.78 (m, 1H)[e]
32*a*	7.3 (s, 5H)	5.05 (d) J=5.0	—	5.19 (s)	—	2.35 (s)	4.45 (dd, 1H, J_1=9.0, J_2=3.0)[d] 3.25–4.0 (m, 2H)[e]
32*b*	7.21 (m, 5H) 7.10 (s, 5H)	4.95 (d) J=5.0	—	5.18 (s) 4.09 (d)[g] J=14.0 3.75 (d)[g] J=14.0	—	—	4.38 (dd, 1H, J_1=9.0, J_2=3.0)[d] 3.35–3.95 (m, 2H)[e]
32*c*	7.05 (s, 5H) 7.15 (m, 5H)	4.88 (d) J=4.5	—	5.12 (s)	—	—	3.17–3.89 (m, 2H)[e] 4.30 (dd, 1H, J_1=9.5, J_2=3.5)[d] 2.75 (m, 4H, ϕCH_2—CH_2—)
33*a*	—	4.78 (d) J=5.0	7.22 (s)	—	—	1.29 (t) J=7.0	4.57 (dd, 1H, J_1=10, J_2=3.0)[d] 4.22 (q, 2H, OCH_2CH_3, J=7.0) 3.50 (s, 2H, NH_2) 3.65–4.4 (m, 2H)[e]
33*b*	7.40 (m, 5H)	4.83 (d) J=5.0	~7.40	5.30 (s)	—	—	2.45 (s, 2H, NH_2) 4.60 (dd, 1H, J_1=11.0, J_2=3.0)[d] 3.6–4.4 (m, 2H)[e]
33*c*	7.40 (m, 5H)	4.68 (d) J=5.0	—	5.22 (s)	—	2.25 (s)	4.50 (dd, 1H, J_1=7.0, J_2=3.0)[d] 3.5–4.1 (m, 2H)[e] 1.50 (s, 2H, NH_2)
33*e*	7.35 (m, 5H) 7.17 (s, 5H)	4.58 (d) J=5.0	—	5.21 (s)	—	—	1.58 (bs, 2H, NH_2) 2.85 (m, 4H, CH_2CH_2ϕ) 3.3–4.1 (m, 2H)[e] 4.50 (dd, 1H, J=7.0, J=3.0)[d]

TABLE 3 (*Concluded*)

Compound	Aromatic	C_7—H	C_3—H	ϕ—CH_2	ϕOCH_2	CH_3	Other
34*a*	6.7–7.4 (m, 5H)	5.58 (dd) J=7.0 J=4.5	7.23 (s)	—	4.47 (s)	1.28 (t) J=7.0	7.77 (d, 1H, N*H*, J=7.0) 4.23 (q, 2H, OCH_2CH_3, J=7.0) 3.6–4.5 (m, 3H)[d,e]
34*b*	7.39 (s, 5H) 6.8–7.5 (m, 5H)	5.61 (dd) J=7.0 J=4.2	7.32 (s)	5.27 (s)	4.51 (s)	—	7.69 (d, 1H, N*H*, J=7.0) 3.6–4.5 (m, 3H)[d,e]
34*c*	7.30 (s, 5H) 6.7–7.6 (m, 5H)	5.44 (dd) J=6.5 J=4.5	—	5.18 (s)	4.45 (s)	2.25 (s)	3.6–4.3 (m, 3H)[d,e]
34*d*	7.18 (s, 5H) 7.26 (m, 5H) 6.7–7.5 (m, 6H)[h]	5.40 (dd) J=7.0 J=4.0	—	5.23 (s)	4.38 (s)	—	3.6–4.6 (m, 5H)
35*a*	6.7–7.5 (m, 6H)[j]	5.60 (m)	—	—	4.52 (s)	—	7.64 (d, 1H, N*H*, J=~7) 3.7–4.5 (m, 3*H*)[d,e]
35*c*[k]	6.9–7.5 (m, 5H)	5.60 (dd) J=9.0 J=5.0	—	—	4.25 (s)	2.16 (s)	8.85 (d, 1H, N*H*, J=9.0) 3.6–4.25 (m, 3H)[d,e]
35*d*[l]	7.25 (s, 5H) 6.7–7.5 (m, 6H)	5.46 (m)	—	—	4.50 (s)	—	9.0 (1H, CO_2H) 3.6–4.5 (m, 5H)[i]
35*e*	7.28 (s, 5H) 6.8–7.5 (m, 5H)	5.72 (dd) J=9.0 J=5.0	—	—	4.61 (s)	—	8.45 (d, 1H, N*H*, J=9.0) 3.6–4.6 (m, 3H)[d,e] 2.90 (m, 4H, CH_2CH_2ϕ)

[a]Recorded at 60 MHz in $CDCl_3$ with tetramethylsilane as internal reference. The chemical shifts are recorded in δ values and coupling constants in Hz. [b]Assigned to —CO_2-CH_2CH_3, and the protons at C_6 and C_1. [c]Assigned to $CO_2CH_2CH_3$. [d]Assigned to C_1-Hα proton, see text for discussion. [e]Assigned to C_1-Hβ proton and C_6-H, see text for discussion. [f]Obscured by aromatic signal. [g]Arms of AB quartet. [h]CON*H* appears obscured by aromatic resonance. [i]The benzylic protons, the protons at C_1 and the proton at C_6 appear as a complex multiplet. [j]The C_3-proton is obscured by the aromatic signals. [k]Recorded in DMSO-d_6. [l]Recorded in $CDCl_3$, $(CD_3)_2C{=}O$.

TABLE 4. Infrared spectra, uv spectra, and elemental analyses

Compound	Infrared spectrum[a]	Ultraviolet spectrum[b]		Analysis (%)					
				Calculated			Found		
		λ_{max}	ε	C	H	N	C	H	N
1*b*	3460. 2110, 1770, 1745			55.09	6.17	14.28	55.39	6.01	14.43
2*b*	3420, 2120, 1775, 1745			42.19	4.72	21.87	42.18	4.83	22.01
2*c*	2110, 1780, 1750, 1630(w)								
2*d*	2110, 1780, 1755			55.49	5.24	16.18	55.81	5.36	16.40
3*a*	2080, 1775, 1765, 1745, 1710, 1640	245	10730	47.85	5.56	17.17	47.67	5.55	17.23
3*b*	2110, 1780, 1745, 1715, 1645			55.68	5.19	14.43	55.85	5.25	14.16
4*a*	3300, 2080, 1770, 1710, 1645	245	10270	46.48	5.67	19.71	46.23	5.76	19.77
4*b*	3500, 2110, 1770 1710, 1640	245	12200	55.49	5.24	16.18	55.21	5.15	15.96
5*a*	3310, 2120, 1765, 1660, 1620	286	25200	50.48	6.19	22.64	50.64	6.43	22.91
5*b*	3580, 3360, 2110, 1770, 1665, 1620	284	26400	58.21	5.70	18.86	58.23	5.72	19.10
6*a*	2110, 1770, 1685, 1630, 1615	285	29600	43.40	5.46	18.07	43.32	5.39	18.13
6*b*	2120, 1780, 1700, 1640, 1620	282	33000	50.77	5.16	15.58	50.66	5.20	15.65
7*a*	2110, 1775, 1710, 1680, 1630	235	8400	35.92	4.22	16.75	36.05	4.17	16.60
7*b*	2110, 1780, 1710, 1680, 1625	237	9500	43.95	4.30	13.67	43.71	4.24	13.47[c]
8*a*	2110, 1790, 1715, 1625	268	6800	45.38	4.23	23.62	45.13	4.18	23.73
8*b*	2100, 1790, 1715, 1622	268	6700	55.99	4.03	18.66	55.70	4.01	18.72
9*a*	2100, 1780, 1745								
9*b*	2110, 1775, 1745								
10*a*	2100, 1780, 1715, 1645	243	10500	39.77	5.00	15.46	39.72	4.90	15.63
10*b*	2105, 1780, 1715, 1645	244	12300						
11	2120, 1780, 1715, 1630	232	7700	51.38	4.62	17.12	51.16	4.46	17.22[e]
17	2100, 1770, 1745			64.64	6.08	12.06	64.42	6.09	11.96
18	2120, 1780, 1750								
20	2110, 1770, 1730								
22*c*	3550, 3200, 1745, 1695								
22*d*	3550, 3200, 1740, 1715, 1600								
23*b*	3550, 3260, 1740			58.86	5.70	5.28	58.97	5.68	5.12
23*c*	3560, 3240, 1745								
23*d*	3550, 3230, 1740								
25*a*				42.58	7.15	6.21	42.40	7.24	6.37
25*b*				54.26	6.31	4.87	53.96	6.19	4.60
25*c*				62.72	6.08	3.85	62.83	6.14	3.84
27*a*	2100, 1770, 1740[d]			59.06	5.94	14.50	59.08	5.73	14.58
27*b*	2100, 1760, 1735[g]			64.27	5.39	12.49	64.13	5.36	12.48
27*c*	2120, 1770, 1745								
27*d*	2120, 1765, 1745								
27*e*	2108, 1767, 1750[f]			56.98	5.06	15.64	57.06	5.13	15.78

TABLE 4 (*Concluded*)

Compound	Infrared spectrum[a]	Ultraviolet spectrum[b]		Analysis (%)					
				Calculated			Found		
		λ_{max}	ε	C	H	N	C	H	N
28*a*	2120, 1775, 1730, (1740 sh)			54.54	4.84	14.96	54.75	4.87	14.89
28*b*	2110, 1780, 1770, 1745, 1735, 1695								
28*c*	2120, 1780, 1740, 1690								
29*a,c*	3500, 2120, 1765, 1770, 1740								
30*a*	2110, 1775, 1740			47.81	4.88	12.34	47.56	4.93	12.43
32*a*	2110, 1780, 1715, 1610[g]	273	10350	57.62	4.49	17.83	57.31	4.58	17.67
32*b*	2110, 1780, 1715, 1615								
32*c*				65.34	4.98	13.85	65.36	4.96	13.97
33*c*	3400, 1785, 1695, 1670, 1615[g]			62.49	5.59	9.72	62.54	5.51	9.65
34*a*	3410, 1785, 1710, 1695, 1625, 1520	268	11300	58.95	5.24	8.09	58.85	5.25	8.13
34*b*	3410, 3340, 1780, 1710, 1695, 1625, 1525	268	10500	64.70	4.94	6.86	64.62	4.83	6.94
34*c*	3270, 1782, 1710, 1660, 1610, 1530[g]	270, 275	11900, 11600	65.39	5.25	6.63	65.22	5.31	6.86
34*d*	3400, 1780, 1710, 1695, 1615, 1520								
34*e*	3410, 1780, 1710, 1695, 1600, 1520								
35*a*	3420, 3330, 1780, 1695, 1620, 1600, 1530	268	9550	55.06	4.62	8.56	55.19	4.70	9.00
35*b*	1770, 1685, 1630, 1590, 1530[g]	263	6200	49.31	3.82	7.67	49.35	3.94	8.01[e]
35*c*	3340, 1760, 1700, 1655, 1600, 1540[g]	269	10500	57.83	4.85	8.43	57.67	4.97	8.34
		274	9500						
35*d*	3400, 1780, 1695, 1610, 1600, 1520			64.70	4.94	6.86	64.78	4.87	6.80
35*e*	3400, 1778, 1695, 1600, 1520			65.39	5.25	6.63	65.28	5.36	6.56

[a]Recorded as a $CHCl_3$ solution unless otherwise noted. [b]Recorded in ethanol. [c]3/4 hydrate. [d]Liquid film. [e]1/2 hydrate. [f]Single isomer. [g]Nujol mull.

TABLE 5. Nuclear magnetic resonance data and ASIS ($\Delta = \delta(CDCl_3) - \delta(CDCl_3{-}C_6D_6(1:1))$)[a]

Compound	Solvent	H_7	H_6	$H_{1\alpha}$	$H_{1\beta}$	H_3	Other	
8*a*	$CDCl_3$[b]	5.34	3.82	4.63	3.94	7.37	4.29[c]	1.30[d]
	$CDCl_3{-}C_6D_6(1:1)$[b]	4.58[e]	3.08[f]	4.07[g]	3.51[h]	7.17[i]	4.18	1.17
	Δ	+0.76	+0.74	+0.56	+0.43	+0.20	+0.11	+0.13
8*b*	$CDCl_3$[j]	5.25	3.78	4.58	3.92	~7.37	5.28[k]	
	$CDCl_3{-}C_6D_6$[j]	4.45[e]	3.00[f]	3.92[g]	3.37[h]	—	4.96	
	Δ	+0.80	+0.78	+0.66	+0.55	—	+0.32	

[a]Chemical shifts are reported in δ relative to internal TMS. [b]Recorded at 100 MHz. [c]CH_2—CH_3. [d]CH_2—CH_3. [e]Appears as doublet $J = 5.0$ Hz. [f]Appears as doublet of doublets $J_1 = 9.5$, $J_2 = 5.0$, $J_3 = 3.75$ Hz. [g]Appears as doublet of doublets $J_1 = 11.0$, $J_2 = 3.75$ Hz. [h]Appears as doublet of doublets of doublets $J_1 = 11.0$, $J_2 = 9.5$, $J_3 = 0.5$ Hz. [i]Appears as singlet. [j]Recorded at 60 MHz. [k]Assigned to CH_2—φ.

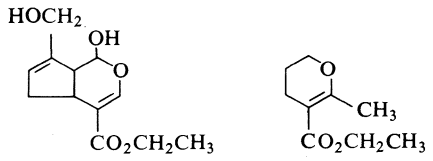

λ = 240
ε = 13 200

λ = 248
ε = 12 500

FIGURE 2

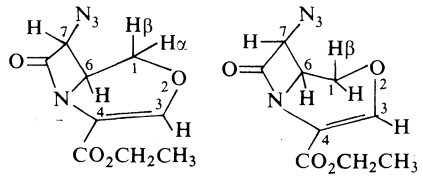

FIGURE 3

ments, and the relative magnitudes of the ASIS (Fig. 3 and Table 5). From the data in Table 3, it is seen that $J_{H6H1\alpha} = 3.75$ Hz and $J_{H6H1\beta} = 9.5$ Hz. Of the two possible conformations for **8** *A* and *B* (Fig. 3) only conformer *A* would be expected to exhibit this splitting pattern for H_6. One would predict for conformer *B* that $J_{6H1\alpha} \simeq 3.20$ Hz and $J_{H6H1\beta} \simeq 0$ Hz.

The assignment of the signals at ~4.6 to $H_{1\alpha}$ and ~3.9 to $H_{1\beta}$ is also in accord with the expectation that the axial proton $H_{1\beta}$ should appear at higher field than the equatorial proton $H_{1\alpha}$. These assignments are also supported by the relative magnitudes of the ASIS for $H_{1\alpha}$ and $H_{1\beta}$. One would expect that complexation of the solute with the C_6D_6 molecules would occur preferentially from the less hindered α face of the molecules and that the ASIS for protons on the α face would be greater than the ASIS for protons on the β-face. Our observations are fully in accord with this prediction, protons H_6 and H_7 show the greatest ASIS. The ASIS for $H_{1\alpha}$ is greater than the ASIS for $H_{1\beta}$ thus adding further evidence for the assignments.

With the experience gained in the synthesis of **8***a* and **8***b* the syntheses of the 3-methyl, 3-benzyl, and 3-phenethyl systems were attempted next.

The syntheses of the starting amines **25***a–d* for these systems were carried out as follows. Oximation of the β-keto esters **21***a–d* (Scheme 3) was achieved using the method of Adkins and Reeve (10) to yield the oximes **22***a–d* in good yields. Reduction of **23***a* with 10% Pd/C in ethanol in the presence of hydrochloric acid gave the amine hydrochloride **24** in 55% yield in accord with the results of Laver *et al.* (11). The amine hydrochloride **24** was readily converted to its ethylene ketal **25***a* in 70% yield. The presence of benzylic ester functions in **22***b–d* precluded the reduction of the oximes via Laver's method. Consequently, compounds **22***b–d* were converted to their ethylene ketals **23***a–c* in 94, 57, and 91% yields respectively. Reduction of **23***a–c* with aluminum amalgam in moist ether (12) gave compounds **25***b–d* in 71, 93, and 68% yields respectively.

Conversion of amines **25***a–d* to their Schiff bases **26***a–d* (Scheme 4) proceeded as before in quantitative yields. Treatment of the Schiff bases **26***a–d* with triethylamine and azidoacetyl chloride as before gave the *cis*-3-azido-4-styryl-*N*-substituted-2-azetidinones **27***a–d* in 98, 94, 100, and 100% crude yields[10] respectively. Saponification of **27***a* with sodium hydroxide in tetrahydrofuran gave the corresponding carboxylic acid **27***e* in 86% yield as a solid. Re-

[10]The crude materials were generally of sufficient purity (as determined by nmr spectroscopy) to be used as such without further purification.

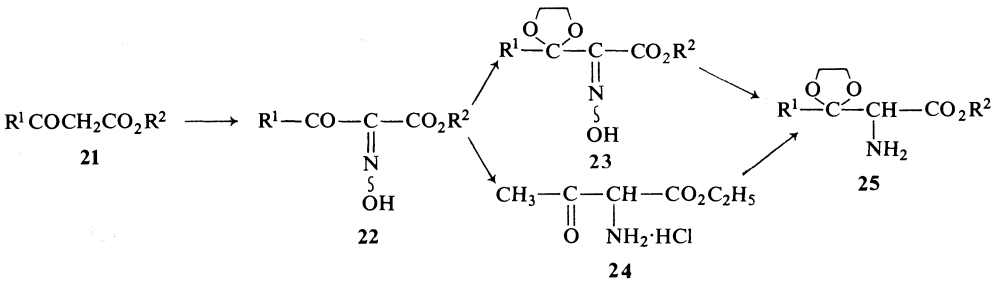

Compounds **21**, **22**, **25**
a $R^1 = Me$ $R^2 = Et$
b $R^1 = Me$ $R^2 = CH_2\phi$
c $R^1 = R^2 = CH_2\phi$
d $R^1 = (CH_2)_2\phi$ $R^2 = CH_2\phi$

Compound **23**
a $R^1 = CH_3$ $R^2 = CH_2\phi$
b $R^1 = CH_2\phi = R^2$
c $R^1 = CH_2CH_2\phi$ $R^2 = CH_2\phi$

SCHEME 3

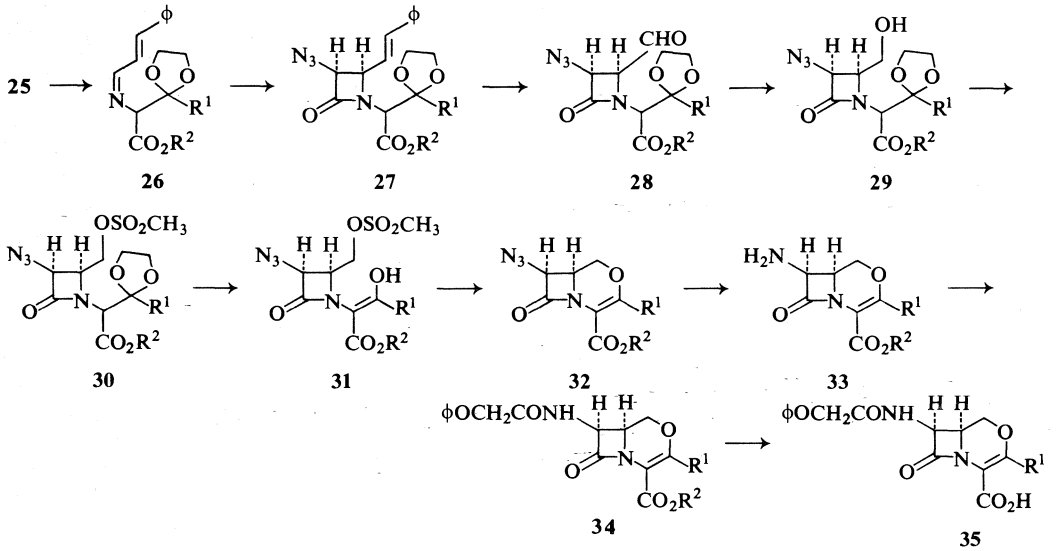

Compounds **33–34**		Compounds **26–27**		Compound **35**	Compounds **28–32**	
R^1	R^2	R^1	R^2		R^1	R^2
a H	C_2H_5	*a* CH_3	CH_2CH_3	*a* $R^1 = H$	*a* CH_3	$CH_2\phi$
b H	$CH_2\phi$	*b* CH_3	$CH_2\phi$	*b* $R^1 = H$	*b* $CH_2\phi$	$CH_2\phi$
c CH_3	$CH_2\phi$	*c* $CH_2\phi$	$CH_2\phi$	*c* $R^1 = CH_3$	*c* $CH_2CH_2\phi$	$CH_2\phi$
d $CH_2\phi$	$CH_2\phi$	*d* $CH_2CH_2\phi$	$CH_2\phi$	*d* $R^1 = CH_2\phi$		
e $(CH_2)_2\phi$	$CH_2\phi$	*e* CH_3	H	*e* $R^1 = CH_2CH_2\phi$		

SCHEME 4

crystallization of **27***e* gave one of the diastereoisomeric acids.[11] Conversion of **27***e* to **27***b* (in 99% yield) was carried out using the triethylamine–benzylchloroformate method used earlier. Ozonolysis of **27***b* (single isomer) in methylene chloride at −78 °C followed by decomposition of the ozonide with dimethyl sulfide gave **28***a* as a crystalline solid in 69% yield. The yield of **28***a* (as a mixture of diastereomers) from **27***b* (isomer mixture) was 71%. Similarly, ozonolysis

[11]Compounds **27***a–d* were produced as mixtures of diastereoisomers epimeric about the carbon directly attached to the nitrogen of the β-lactam and the ester function.

TABLE 6. Biological activities[a]

Compound	*D. pneumoniae*	*S. aureus* Smith	*S. aureus* + 50% serum	*Sal. enteritidis*	*Pr. mirabilis*
2*e*	125	250	> 500	1000	1000
34*a*	> 500	250	> 250	> 500	> 500
35*a*	0.6	0.6	1.0	8	63
35*c*	0.5	0.5	2.0	8	16
35*d*	0.25	0.25	1	32	> 125
35*e*	0.03	0.06	4	8	> 125
36	1	0.5	4	63	125

[a]Expressed as MIC's (μg/ml) and determined by a 2-fold serial dilution assay in Difco nutrient broth by the method of Pursiano *et al.* (20).

of **27***c* and **27***d* gave the aldehydes **28***b* (95% crude yield) and **28***c* (45% purified yield) respectively.

The aldehydes **28***a–c* were reduced to the corresponding alcohols **29***a–c* using sodium borohydride, following which **29***a–c* were converted to their mesylates **30***a–c*. The yields of **30***a–c* from the aldehydes **28***a–c* were 80, 84, and 42% respectively. In the reduction of **28***a* to **29***a* some epimerization of the product was observed in that a mixture of mesylates was obtained epimeric about the ester position in the side chain.

Hydrolysis of **30***a* with 95% trifluoroacetic acid at 25 °C gave the enol **31***a* in greater than 90% yield. Compound **31***a* was converted to benzyl 7-β-azido-3-methyl-Δ^3-*O*-2-isocephem-4-carboxylate **32***a* in 80% yield using triethylamine in refluxing methylene chloride. Similarly, compounds **30***b* and **30***c* were hydrolyzed to the enols **31***b* and **31***c*. In these cases it proved necessary to use higher temperatures (50–55 °C) to effect hydrolysis. The enols were converted to benzyl-7-β-azido-3-benzyl-Δ^3-*O*-2-isocephem-4-carboxylate **32***b* (33%) and benzyl 7-β-azido-3-phenethyl-Δ^3-*O*-2-isocephem-4-carboxylate **32***c* (33%) respectively. The structures of compounds **32***a–c* were confirmed by their elemental analyses, and ir, nmr, and uv spectral characteristics (Tables 3 and 4).

With the appropriately substituted *O*-2-isocephems **8***a–b*, **32***a–c* on hand the conversion of these to their 7-β-(phenoxyacetamido)-Δ^3-*O*-2-isocephem-4-carboxylic acids **35** was examined.

Reduction of **8***a* and **8***b* with hydrogen on 10% Pd/C gave the amines **33***a* and **33***b*. The amines were converted to the amides **34***a* and **34***b* using triethylamine – phenoxyacetyl chloride in 56 and 29% yields respectively. The ir, uv, and nmr spectra of **34***a* and **34***b* confirmed the structural assignments.

Reduction of **32***a* with hydrogen and PtO_2 in ethanol gave **33***c* which was coupled with phenoxyacetic acid using EEDQ (13) to give **34***c* in 65% yield. Compounds **32***b* and **32***c* were reduced to their amines **33***d* and **33***e* using triethylamine – hydrogen sulfide (1) and these were in turn converted to their amides **34***d* and **34***e* using phenoxyacetic acid – EEDQ.

Hydrogenolysis of the benzyl esters **34***b–e* (see Experimental) gave the desired acids **35***a*, **35***c–e* in 70, 84, 20, and 92% yields respectively. Compound **35***a* was also converted to its potassium salt **35***b* in 45% yield (14). The structures of **35***a–e* assigned on the basis of their elemental analyses, ir, uv, and nmr spectral characteristics.

Compounds **35***a*, **35***c*, **35***d*, and **35***e* all exhibited high antibacterial activity. The activities are listed in Table 6 along with those of **2***e*, **34***a*, and the phenoxyacetyl derivative of 7-aminodesacetyl cephalosporanic acid **36** (Fig. 4) for comparison purposes. The activities of these compounds are comparable with or better than those of the comparably substituted natural product (compare **35***c* and **36**).

It should also be noted that **35***a–e* are racemic materials whereas **36** is a single enantiomer. It has been shown (15) that all of the activity in the natural series resides in a single enantiomer, thus the MIC's reported for **35***a–e* are probably too high by a factor of two. A full discussion of structure–activity relationships in this series will be reserved to a later publication.

The obvious modifications of the syntheses reported herein to the syntheses of compounds of general formula **37** have been made and will be reported in subsequent papers of this series (Fig. 5).

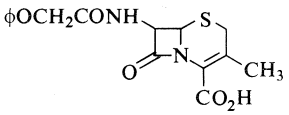

36

FIGURE 4

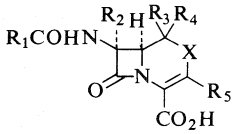

37

FIGURE 5

Experimental

The infrared spectra were recorded on a Unicam SP-200G grating ir spectrophotometer. The uv spectra were recorded on a Unicam SP-800 uv spectrophotometer. The nmr spectra were determined on a Varian A60-A spectrometer using tetramethylsilane as an internal standard. The 100 MHz spectra and spin-decoupling experiments were performed by Dr. Perlin of McGill University whose assistance we gratefully acknowledge. Melting points are uncorrected except where noted and were determined on a Gallenkamp melting point apparatus. The analyses were performed by Micro-Tech Laboratories, Skokie, Illinois.

7-β-Azido-3-β-ethoxy-O-2-isocepham-4-α-carboxylic Acid ***2b***

To a solution of 12.2 g (43 mmol) of compound **2***a* in 180 ml ethanol was added 175 ml 1% sodium hydroxide over a period of 10 min at < 25 °C. The solution was stirred an additional 20 min. The ethanol was evaporated at reduced pressure and the alkaline solution was extracted with ether (2 × 100 ml). The organic layer was discarded and the aqueous solution acidified to p*H* 3–4 with 10% hydrochloric acid. The solution was extracted with chloroform (2 × 100 ml) and the organic layer washed with water (50 ml), brine (50 ml), and dried over $MgSO_4$. Evaporation gave 7.25 g (66%) of acid. Trituration with ether and filtration gave pure acid, mp 114–115 °C.

Benzyl 7-β-Azido-3-β-ethoxy-O-2-isocepham-4-α-carboxylate ***2d***

To a solution of 6.25 g (25.6 mmol) of compound **2***b* in 100 ml of ether was added 5.35 g (25.6 mmol) phosphorous pentachloride. The suspension was refluxed for 15 min after which the clear solution was decanted and evaporated to dryness. The residual oil was taken up in 50 ml benzene and evaporated to dryness at reduced pressure. This procedure was repeated three times to remove phosphorous oxychloride. The residual oil was then pumped in high vacuum (0.05 torr) at 30 °C for 1 h.

The acid chloride was taken up in 20 ml dry methylene chloride and was added to a mixture of 2.7 g (26 mmol) benzyl alcohol and 3.2 g triethylamine in 50 ml dry methylene chloride at 25 °C over a period of 10 min. The solution was stirred for 1 h, washed with water (2 × 20 ml) and brine, and filtered through 20 g of Florisil. The eluent was treated with Norite, dried over $MgSO_4$, filtered, and evaporated to give 7.4 g (83.5%) of crude benzyl ester **2***d*. Trituration with benzene – petroleum ether caused crystallization. The solid was recrystallized from benzene – petroleum ether to yield pure **2***d*, mp 79–79.5 °C.

cis-N-(α-Carboethoxy-β-ethoxyvinyl)-3-azido-4-acetoxymethyl-2-azetidinone ***3a***

From ***1a***

A mixture of 4.8 g (14.5 mmol) compound **1***a*, 2.1 g (15.1 mmol) zinc chloride, and 15 ml acetic anhydride was stirred at 25 °C for 18 h. The solvent was removed at reduced pressure and the residue taken up in $CHCl_3$ (100 ml) – H_2O (20 ml), dried over Na_2SO_4, filtered, and the filtrate passed through 50 g Al_2O_3 (activity III) column. Elution with $CHCl_3$ gave 2.5 g pure acetate. The other fractions were rechromatographed to give an additional 1.1 g (75% total yield).

From ***2a***

Treatment of 1.0 g (3.5 mmol) of **2***a* with 1.1 g zinc chloride in 12 ml of acetic anhydride as above gave **3***a* in 85% yield. The compound was identical in all respects with that obtained from **1***a*.

cis-N-(α-Carbobenzoxy-β-ethoxyvinyl)-3-azido-4-acetoxymethyl-2-azetidinone ***3b***

From ***1b***

A mixture of 3.2 g (8.17 mmol) compound **1***b*, 11 ml acetic anhydride, and 1.12 g (8.2 mmol) zinc chloride was stirred 18 h at 25 °C. The reaction mixture was evaporated at reduced pressure and the residue taken up in 40 ml methylene chloride – 20 ml water. The organic phase was separated, washed with water and brine, dried over $MgSO_4$, filtered, and the filtrate evaporated to yield 3.0 g of an oil. The oil was chromatographed on 50 g silica gel (deactivated, 5% water) by dry column technique using chloroform as an eluent. Evaporation of the eluent gave 1.3 g (41%) of pure **3***b* as an oil.

From ***2d***

Treatment of 104 mg (0.3 mmol) of **2***d* with 82 mg zinc chloride in 3 ml acetic anhydride as in the preparation of **3***a* from **2***a* gave 110 mg pure **3***b* (94%).

cis-N-(α-Carboethoxy-β-ethoxyvinyl)-3-azido-4-hydroxymethyl-2-azetidinone ***4a***

From ***3a***

A solution of 12.18 g (34.8 mmol) of compound **3***a* in 40 ml MeOH and 40 ml 10% HCl was boiled at reflux for 1 h. The methanol was distilled at reduced pressure and the aqueous residue extracted with $CHCl_3$ (3 × 50 ml). The extracts were washed with water and brine, dried over $MgSO_4$, filtered, and the filtrate was evaporated to yield 9.33 g (94.5%) pure alcohol.

From ***2a***

To a solution of 90 mg (0.316 mmol) of **2***a* in 5 ml of methylene chloride was added 3 drops (~ 20 mg) titanium tetrachloride at 25 °C. The solution was let stand for 24 h at 25 °C and filtered through 1.5 g of alumina (activity III). There was obtained 23.7 mg of pure **4***a* (26%) identical in all respects with that obtained from **3***a*.

cis-N-(α-Carbobenzoxy-β-ethoxyvinyl)-3-azido-4-hydroxymethyl-2-azetidinone ***4b***

Hydrolysis of 5.95 g (15.35 mmol) of **3***b* according to the procedure described above for the conversion of **3***a* to **4***a* gave 4.6 g (87%) of **4***b* as an oil.

cis-N-(α-Carboethoxy-β-N-pyrrolidinovinyl)-3-azido-4-hydroxymethyl-2-azetidinone ***5a***

From ***4a***

A solution of 224 mg (0.785 mmol) of **4***a*, 141 mg (2 mmol) pyrrolidine, and 200 mg acetic acid in 15 ml dry benzene was boiled at reflux for 22 h. The solution was washed with 5 ml of saturated sodium bicarbonate solution, washed with water (25 ml), and dried over sodium sulfate. The solution was filtered and evaporated to dryness to give an oil which crystallized on standing. The oil was triturated with ether and filtered to yield 175 mg (72%) pure **5***a*, mp 147–148 °C after recrystallization from benzene.

From ***1a***

Treatment of 2.78 g (8.45 mmol) of **1***a* with 2.5 g pyrrolidine and 2.5 g acetic acid in 50 ml benzene as described above gave 137 g (50%) of pure **5***a* identical in all respects to the sample prepared from **4***a*.

cis-N-(α-Carbobenzoxy-β-N-pyrrolidinovinyl)-3-azido-4-hydroxymethyl-2-azetidinone ***5b***

From ***4b***

In a manner analogous to the preparation of **5***a* from **4***a*, compound **5***b* was prepared from **4***b* in 71% yield; mp 111.5–112.5 °C.

cis-N-(α-Carboethoxy-β-N-pyrrolidinovinyl)-3-azido-4-mesyloxymethyl-2-azetidinone ***6a***

From ***5a***

To a solution of 618 mg (2 mmol) of **5***a* and 404 mg (4 mmol) triethylamine in 15 ml methylene chloride at 0 °C was added 456 mg (4 mmol) methane sulfonyl chloride in 5 ml methylene chloride over 15 min. The solution was allowed to come to 25 °C over 1 h and washed with water (10 ml) and brine (2 × 10 ml). The solution was dried over sodium sulfate and filtered through 4.0 g of alumina (activity III) to give 570 mg of pure **6***a*, mp 138–139 °C.

From ***10a***

Treatment of 181 mg (0.5 mmol) of **10***a* with pyrridineacetic acid according to the procedure given for the preparation of **5***a* gave 125 mg (63%) of **6***a* identical with the sample prepared from **5***a*.

cis-N-(α-Carbobenzoxy-β-N-pyrrolidinovinyl)-3-azido-4-mesyloxymethyl-2-azetidinone ***6b***

A solution of 2.44 g (6.6 mmol) compound **5***b*, 3.9 g (33 mmol) methane sulfonyl chloride, and 3.3 g (33 mmol) triethylamine in 50 ml methylene chloride was stirred at ambient (25 °C) temperature for 74 h. The reaction mixture was washed with water (2 × 10 ml) and brine and dried over Na_2SO_4. The drying agent was filtered and the filtrate evaporated to dryness. The oil was filtered through a silica gel column (deactivated, 15% water) (16 g) with chloroform to give 2.6 g (90%) of crystalline mesylate, mp 116–117 °C.

cis-N-(α-Carboethoxy-β-hydroxyvinyl)-3-azido-4-mesyloxymethyl-2-azetidinone ***7a***

From ***6a***

A solution of 1.27 g (33 mmol) of **6***a* in 20 ml acetone – 5 ml 10% hydrochloric acid was refluxed 20 min and diluted to 100 ml with water. The solution was extracted into methylene chloride (5 × 20 ml). The methylene chloride extracts were extracted with 10% sodium carbonate. The aqueous extracts were acidified with hydrochloric acid and the solution extracted into methylene chloride and dried over sodium sulfate, yielding 0.98 g of pure enol **7***a* as an oil on evaporation (89%).

From ***9a***

A solution of 207 mg (0.51 mmol) of **9***a* in 1 ml of 95% trifluoroacetic acid was warmed to 50 °C for 1 h. The trifluoroacetic acid was removed at reduced pressure and the residue partitioned between methylene chloride – water (50 ml:20 ml). The organic layer was extracted with sodium carbonate as above. Work-up yielded 95 mg (58%) of pure **7***a* identical with that obtained from **6***a*.

cis-N-(α-Carbobenzoxy-β-hydroxyvinyl)-3-azido-4-mesyloxymethyl-2-azetidinone ***7b***

From ***6b***

A solution of 2.28 g (5.26 mmol) compound **6***b* in 25 ml of acetone and 25 ml 10% hydrochloric acid was refluxed 15 min. The acetone was evaporated at reduced pressure and the residue extracted with chloroform (3 × 30 ml). The chloroform layer was washed with water and evaporated to dryness. The residual oil was dissolved in ether (20 ml) and the solution extracted with saturated sodium bicarbonate solution (4 × 8 ml). The bicarbonate was acidified to p*H* 4 with 10% HCl and reextracted with chloroform (3 × 50 ml). The chloroform was washed with water and brine and dried over $MgSO_4$. The drying agent was filtered and the filtrate evaporated to give 1.62 g (81%) of compound **7***b*.

From ***9b***

A solution of 673 mg (1.43 mmol) of **9***b* in 4 ml 95% trifluoroacetic acid was warmed to 50 °C for 25 min. After the work-up (see **9***a* → **7***a*) there was obtained 513 mg (91%) of **7***b* identical with the sample prepared from **6***b*.

Ethyl 7-β-Azido-Δ^3*-O-2-isocephem-4-carboxylate* ***8a***

Method A

To a suspension of 0.0665 g sodium hydride (1.5 mmol) (55% mineral oil dispersion washed three times with petroleum ether) in 2 ml dimethyl sulfoxide (DMSO) was added 500 mg (1.5 mmol) of **7***a* in 4 ml DMSO. The solution was stirred 1 h at 25 °C and then diluted to 30 ml with brine containing 2 ml 10% hydrochloric acid. The aqueous solution was extracted with methylene chloride (5 × 25 ml). The extracts were washed with water (3 × 25 ml) and brine (1 × 25 ml) and dried over sodium sulfate. Evaporation of the extracts gave 327 mg (91.5%) of **8***a*, mp 137–138 °C after recrystallization from benzene.

Method B

A solution of 268 mg (0.8 mmol) of **7***a* and 105 mg triethylamine in 10 ml of chloroform was refluxed for 50 min. The solution was cooled and washed with water,

10% hydrochloric acid, water, and brine. The solution was dried over sodium sulfate, filtered, and evaporated to yield 90 mg (47.5%) of pure **8***a* after crystallization.

From ***10a***

To a solution of 1.83 g (5.00 mmol) of compound **10***a* in 20 ml of tetrahydrofuran was added 20.0 ml of 0.25 *M* sodium hydroxide solution dropwise over 10 min. The resulting solution was concentrated to 20 ml on the rotary evaporator at 30 °C. The concentrate was washed with chloroform (3 × 10 ml). The aqueous layer was evaporated to dryness under high vacuum. The resulting residue was stirred with 7.5 ml of dimethyl sulfoxide for 1 h. Water (30 ml) and saturated sodium chloride (40 ml) followed by a few drops of 10% hydrochloric acid were added to the dimethyl sulfoxide solution. The resulting mixture was extracted with chloroform (3 × 40 ml) and the combined chloroform layers were washed with water and evaporated to give the crude product. Pure compound **8***a* was obtained by recrystallization from benzene–cyclohexane, then chloroform, as colorless crystals, 0.39 g (33% yield).

Benzyl 7-β-Azido-Δ³-O-2-isocephem-4-carboxylate ***8b***

Method A

To a suspension of 198 mg (4.70 mmol) sodium hydride (55% mineral oil dispersion, washed 3× with petroleum ether) in 5 ml dry DMSO was added a solution of 1.62 g (4.27 mmol) compound **7***b* in 5 ml DMSO over 5 min with stirring at 25 °C. After 1 h, the reaction mixture was poured into 50 ml 1% HCl – ice water and was extracted with chloroform (4 × 30 ml). The organic layer was washed with water (3 × 10 ml) and brine and dried over $MgSO_4$. Filtration and evaporation of the filtrate gave 1.2 g of an oil. Trituration with ether caused crystallization; 545 mg (42%) of **8***b*; mp 110 °C.

Method B

A solution of 370 mg (0.935 mmol) of **7***b* and 100 mg triethylamine in 10 ml methylene chloride was refluxed for 4 h. Work-up as in method *B* for **8***a* gave 200 mg (71.5%) of pure **8***b*.

From ***10b***

To a solution of 260 mg (0.64 mmol) of compound in 2.5 ml of tetrahydrofuran was added 2.55 ml of 0.25 *M* sodium hydroxide solution dropwise over 10 min. The solution was concentrated to 2 ml on the rotary evaporator. The concentrate was washed with chloroform (2 × 2 ml), then evaporated to dryness under high vacuum. The residue was stirred with 1 ml of dimethyl sulfoxide for 1 h. Water (1 ml), saturated sodium chloride (1 ml), and one drop of 10% hydrochloric acid were added. The mixture was extracted with chloroform (3 × 2 ml) and the combined chloroform layers were washed with water and evaporated to give crude compound as a yellow solid, 103 mg (54% yield). The nmr spectrum indicated the product to be only 75% pure (*i.e.* a true yield of 40%).

cis-N-(α-Carboethoxy-β,β-diethoxyethyl)-3-azido-4-mesyloxymethyl-2-azetidinone ***9a***

Treatment of 102.0 g (0.308 mol) of **1***a* with 34.3 g (0.34 mol) triethylamine and 39.4 g (0.34 mol) methane sulfonyl chloride according to procedure given for the preparation of **10***a* from **4***a* gave 108.4 g (86%) of **9***a* as an oil.

cis-N-(α-Carbobenzoxy-β,β-diethoxyethyl)-3-azido-4-mesyloxymethyl-2-azetidinone ***9b***

From ***1b***

Treatment of 12.2 g (31.2 mmol) of **1***b* with 3.42 g (34 mmol) triethylamine and 2.90 g (34 mmol) methanesulfonyl chloride as in the above experiment yielded 12.3 g (83.5%) of **9***b* as an oil.

From ***9a***

To a solution of 1.065 g (2.61 mmol) of **9***a* in 25 ml tetrahydrofuran was added 10 ml of 0.25 *N* sodium hydroxide over 5 min. The solution was stirred 30 min at 25 °C following which 3 ml 10% hydrochloric acid was added and the solution diluted to 100 ml with brine. The solution was extracted into ether (4 × 50 ml). The ethereal extracts were extracted with sodium carbonate solution (10%). The ethereal layer was dried over sodium sulfate and evaporated to yield an oil which crystallized on trituration with ether (5 ml). Filtration gave 283 mg (26.6%) pure **10***a*. The alkaline extracts were acidified with 10% hydrochloric acid and extracted into methylene chloride (5 × 20 ml). The extracts were dried over sodium sulfate and evaporated to yield 542 mg (55%) of the desired acid **9***c*. Compound **9***c* was characterized spectroscopically and used without further purification in the next step. The yields of **10***a* from this reaction ranged from10–30% while the yields of **9***c* ranged from 45–70%.

To a solution of 2.64 (7 mmol) of **9***c* and 2.0 g (20 mmol) triethylamine in 30 ml methylene chloride at 0–5 °C was added 2.0 g (11.7 mmol) of benzyl chloroformate. As the solution was stirred gas evolution was observed. After 15 min at 0–5 °C, the solution was refluxed for 30 min. The solution was washed with water (50 ml), 10% hydrochloric acid (10 ml), and brine (50 ml), dried over sodium sulfate, and evaporated to yield 3.07 g of an oil which yielded 2.76 g (84%) of **9***b* on chromatography over silica gel (deactivated with 15% water) using chloroform as eluent.

cis-N-(α-Carboethoxy-β-ethoxyvinyl)-3-azido-4-mesyloxymethyl-2-azetidinone ***10a***

From ***4a***

To a solution of 5.68 g (20 mmol) of **4***a* and 3.0 ml (21 mmol) triethylamine in 50 ml methylene chloride at 0–5 °C was added 2.28 g (20 mmol) methane sulfonyl chloride. The solution was stirred for 30 min at 25 °C after which it was washed with water (2 × 25 ml), 10% hydrochloric acid (2 × 10 ml), and brine (1 × 50 ml), dried over sodium sulfate, and concentrated to give an oil. The oil was triturated with 50 ml ether and the crystalline mesylate isolated by filtration, 4.37 g (60.2%). The mother liquors were chromatographed on a column of 50 g silica gel (deactivated with 15% water). An additional 380 mg (5%) of pure **10***a* was isolated from the latter fractions from ether elution; mp 101–102.5 °C (dec.).

From ***9a***

(A) A mixture of 4.9 g (12 mmol) of compound **9***a*, 10 ml of acetic anhydride, 10 ml of acetic acid, and 1.75 g (13 mmol) of zinc chloride was stirred at 25 °C for 17 h, then evaporated to a tar. A methylene chloride solution of the tar (50 ml) was washed with equal volumes of

water, 5% sodium bicarbonate, and dilute sodium chloride. The methylene chloride solution was filtered through 15 g of alumina (grade III) and evaporated to give an oil. Trituration of the oil with ether gave pure compound **10***a* as a colorless powder, 1.88 g (45% yield).

(B) Treatment of 1.90 g (4.65 mmol) of **9***a* with 2.0 g triethyloxonium fluoroborate in 20 ml methylene chloride for 18 h at 25 °C gave 0.75 g (46.5%) of **10***a*.

*cis-N-(α-Carbobenzoxy-β-ethoxyvinyl)-3-azido-4-mesyloxymethyl-2-azetidinone **10b***

Treatment of 15.2 g (43.8 mmol) of **4***b* with triethylamine and methanesulfonyl chloride as in the procedure for the preparation of **10***a* from **4***a* yielded upon work-up 13.0 g (70.4%) of pure **10***b*, as an oil.

*cis-N-(α-Carbobenzoxy-β-hydroxyvinyl)-3-azido-4-hydroxymethyl-2-azetidinone **11***

A solution of 3.71 g (10 mmol) compound **5***b* in 50 ml of acetone and 25 ml of 10% HCl was boiled at reflux for 30 min. The acetone was removed at reduced pressure and the oily aqueous residue extracted with ether (3 × 35 ml) and methylene chloride (3 × 25 ml). The organic layer was extracted with saturated aqueous $NaHCO_3$ (5 × 20 ml). The aqueous extracts were acidified with 10% HCl and saturated with NaCl. The aqueous layer was extracted thoroughly with ether (3 × 25 ml) then CH_2Cl_2 (3 × 25 ml). The extracts were dried over Na_2SO_4 and concentrated to yield 2.40 g of enol alcohol **11**, 75.5%, as an oil.

*Benzyl α-Amino-β,β-diethoxypropionate **15***

A solution of 62.0 g (0.325 mol) of benzyl nitroacetate **12**, 76.6 g (0.52 mol) triethylorthoformate and 65.0 g (0.64 mol) acetic anhydride was heated to 85–90 °C for 18 h. Following this the excess triethylorthoformate, acetic anhydride, and ethyl acetate were removed by evaporation of the solution at reduced pressure (50 °C/1 torr). There was obtained 85.2 g of an oil the nmr spectrum of which indicated that a mixture of the desired acetal **14** (40%) and the elimination product of **14** (**13**, 60% as *Z* and *E* isomers) had been obtained. To the oil was added 25 ml of ethanol followed by 1.0 g sodium ethoxide. A mildly exothermic reaction ensued. After 15 min the excess ethanol was removed by evaporation at reduced pressure (30 °C/1 torr). There was obtained 95.0 g (100%) of the desired acetal **14** which was used as such in the reduction step.

To 37.5 g aluminum amalgam (19) covered by 450 ml moist ether was added 95.0 g (0.325 mmol) of **14** in 250 ml ether. Initially 50% was added over 10 min. After 10–15 min a violent exothermic reaction ensued which was controlled by ice-bath cooling. When the reaction had subsided the remaining acetal was added over 30 min. After 1 h the reaction had subsided sufficiently that heating became necessary so as to maintain a gentle reflux. The solution was refluxed an additional 2 h then allowed to stand 24 h at 25 °C. The gelatinous aluminum hydroxide was removed by filtration. The filtrate was dried over sodium sulfate and evaporated to give 53.0 g of an oil. The oil was taken up in 1 litre of ether and extracted with 5% hydrochloric acid (5 × 150 ml). The extracts were neutralized with sodium carbonate and the resultant solution extracted with ether. The extracts were dried over sodium sulfate and evaporated to yield 35.0 g (42.5%) of benzyl α-amino-β,β-diethoxypropionate **15**. Compound **15** was characterized by nmr spectroscopy and used as such in the preparation of **17**.

*cis-N-(α-Carbobenzoxy-β,β-diethoxyethyl)-3-azido-4-styryl-2-azetidinone **17***

*From **15***

The cinnamylidene Schiff base **16** of **15** was prepared from 35.0 g (0.13 mol) of **15** and 17.3 g (0.13 mol) cinnamaldehyde by the previously described method (1) in quantitative yield. Treatment of 58.0 g (0.13 mol) of **17** with 13.3 g (0.13 mol) triethylamine followed by 15.7 g (0.13 mol) of azidoacetyl chloride (1) gave 54.14 g (89%) of the desired β-lactam **17** as an oil. A small sample (0.90 g) of the oil was chromatographed on 50 g of silica gel (deactivated with 15% water) using chloroform as eluent. The two isomers of **17** were isolated.

*From **19***

To a solution of 15.5 g (38.6 mmol) of **19** (1) in 300 ml ethanol was added 160 ml of 0.25 *N* sodium hydroxide over 20 min at 25 °C. The solution was stirred an additional 40 min. The solution was acidified to p*H* 3 with 10% hydrochloric acid and extracted into chloroform (3 × 50 ml). The extracts were evaporated to dryness and the resultant oil taken up into 50 ml ether. The ethereal solution was washed once with water and then extracted with saturated sodium bicarbonate (3 × 15 ml). The extracts were made acid with 10% hydrochloric acid and extracted with chloroform. The extracts were dried over sodium sulfate and concentrated to give 8.9 g (60%) of the acid **20**.

Treatment of 8.9 g (23.8 mmol) of **20** with 2.4 g (24 mmol) triethyl amine and 4.6 g (27 mmol) benzylchloroformate according to the procedure given for the conversion of **9***c* to **9***b* gave 6.16 g (55%) of the desired ester **17**.

*cis-N-(α-Carbobenzoxy-β,β-diethoxyethyl)-3-azido-4-hydroxymethyl-2-azetidinone **1b***

A solution of 4.8 g (10.04 mmol) compound **17** in 80 ml dry methylene chloride was prepared and cooled to −78 °C in an acetone – dry ice bath. To this was added ozone until a blue color persisted. The ozone addition was stopped and the excess ozone removed by bubbling dry nitrogen through the solution. To the solution was added 5 ml of dimethyl sulfide and the solution was allowed to come to room temperature over 1 h. The solution was then washed with water (20 ml), saturated $NaHCO_3$ (20 ml), water (10 ml), and brine and dried over $MgSO_4$. The solution was filtered and evaporated to give 5.0 g of an oil. The byproduct benzaldehyde was removed by distillation at 0.05 torr and a bath temperature of ~65 °C. The residual oil 4.0 g (95%) was analyzed by nmr which indicated 77% free aldehyde **18**.

To 3.5 g (9.0 mmol) of compound **18** in 30 ml 95% ethanol at 0–5 °C was added 255 mg (6.0 mmol) of sodium borohydride with stirring. After 30 min at 0–5 °C the solution was stirred an additional 30 min at 25 °C. The solution was acidified to p*H* ≃ 4 with 10% hydrochloric acid and diluted with 40 ml ice water. The aqueous layer was extracted with chloroform (3 × 30 ml). The combined extracts were washed with water (2 × 10 ml) and brine, dried over $MgSO_4$, filtered, and

evaporated to yield 3.4 g crude alcohol **1***b*. The oil was chromatographed on silica gel (5% water) with chloroform to yield 3.0 g pure alcohol **1***b* (85%).

Benzyl γ-Phenylacetoacetate ***21c***

A mixture of 166 g (0.76 mol) of ethyl γ-phenylacetoacetate (16) and 100 g (0.92 mol) benzyl alcohol was heated to 170 °C at atmospheric pressure and the ethanol produced removed by distillation. When the still head temperature began to rise, the pot was cooled and the residue distilled at reduced pressure. Following removal of a forerun (bp 65–80 °C/100 torr) pure **21***c* was obtained 171 g (85%), bp 155–157 °C/0.002 torr.

Benzyl γ-Benzylacetoacetate ***21d***

From 204 g (1.1 mol) phenethyl bromide, 24.30 g (1 mol) magnesium and a trace of iodine in 250 ml of ether was prepared 2-phenylethyl magnesium bromide (17). The pot temperature was maintained at 25–30 °C and 45.2 g (0.40 mol) of ethyl cyanoacetate was added. The solution was stirred 24 h at 20–25 °C following which the excess Grignard reagent was decomposed by addition of saturated ammonium chloride and 10% hydrochloric acid. The phases were separated and the organic phase stirred vigorously with 10% hydrochloric acid for 3 h. The organic phase was washed with brine, dried over sodium sulfate, and concentrated to give 83.5 g of an oil which yielded 12.67 g (21%) of ethyl γ-benzylacetoacetate on distillation, bp 114–122 °C/0.1 torr.

From 12.67 g (50 mmol) of the ethyl ester and 8.1 g (75 mmol) benzyl alcohol was obtained 6.15 g pure **21***d*, bp 160–163 °C/0.1 torr in the same manner as the preparation of **21***c*.

Benzyl Oximinoacetoacetate ***22b***

Treatment of 173 g (0.9 mol) benzylacetoacetate (18) with sodium nitrite – acetic acid according to the method of Adkins and Reeve (10) gave 186.5 g (93.2%) of benzyl oximinoacetoacetate **22***b*; mp 81–82 °C, (lit. (11) mp 79–79.5 °C).

Benzyl γ-Phenyloximinoacetoacetate ***22c***

From 85.5 g (0.32 mol) of benzyl γ-phenylacetoacetate was prepared 92.50 g of oily oxime by the method of Adkins and Reeve (10). Trituration with carbon tetrachloride gave 52.8 g (56%) of pure **22***c*, mp 69–70 °C.

Benzyl γ-Benzyloximinoacetoacetate ***22d***

From 37.0 g (0.13 mmol) of **21***d* was prepared 40.1 g (98%) of **22***d* as a yellow oil by the method of Adkins and Reeve (10). The oil was characterized by its nmr and ir spectra and was used as such in subsequent experiments.

Benzyl Oximinoacetoacetate Ethylene Ketal ***23b***

In a 2 l flask fitted with a Dean Stark water separator and a condenser were placed 186.5 g (0.85 mol) of benzyl oximinoacetoacetate **22***b*, 62 g (1 mol) of ethylene glycol, 800 ml of benzene (reagent grade), and 2 g (10.5 mmol) of *p*-toluenesulfonic acid monohydrate. The reaction mixture was boiled at reflux until 15 ml of water was removed (3 h). The benzene solution was washed once with saturated sodium bicarbonate solution and once with brine. After drying over anhydrous sodium sulfate, the benzene solution was evaporated, leaving 212 g (94%) of benzyl oximinoacetoacetate ethylene ketal **23***b* as a mixture of *syn* and *anti* isomers. Generally, the product was used as such in subsequent reactions but one of the isomers could be crystallized from toluene – petroleum ether (bp 30–60 °C), mp 52 °C.

Benzyl γ-Phenyloximinoacetoacetate Ethylene Ketal ***23c***

From 5.94 g (20 mmol) of **22***c* and 1.36 g (22 mmol) ethylene glycol there was obtained 6.70 g of an oil which crystallized on standing in 20 ml carbon tetrachloride. On filtration 4.0 g (57%) of pure **23***c*, mp 90–92 °C was obtained.

Benzyl γ-Benzyloximinoacetoacetate Ethylene Ketal ***23d***

From 8.48 g (27 mmol) of **22***d* and 1.85 g (30 mmol) of ethylene glycol was obtained 9.40 g crude **23***d* which was used as such in the subsequent reaction.

Ethyl α-Aminoacetoacetate Hydrochloride ***24***

Ethyl α-oximinoacetoacetate **22***a* (10) (80 g; 0.5 mol) was dissolved in a mixture of 200 ml of ethanol and 70 ml of ethanolic HCl (9.28 *N* HCl–EtOH; 1.25 equiv). 10% palladium-on-carbon (8 g) was added carefully and the mixture was hydrogenated in a Parr hydrogenation apparatus starting at 70 psig (11). After absorption of the theoretical amount of hydrogen (1–2 h) the catalyst was filtered off and washed with ethanol. The ethanol was removed *in vacuo* at 40–50 °C leaving a thick red-brown oil. The oil was diluted with 8 volumes of acetone with vigorous stirring. Yellow crystals of the amine hydrochloride **24** separated out on cooling, 49 g (55%), mp 122–123 °C (corr.) (lit. (11) mp 114–116 °C (uncorr.)). This material was used without further purification.

Ethyl α-Aminoacetoacetate Ethylene Ketal ***25a***

To a mixture of 1.75 kg (28.2 mol) of ethylene glycol and 210 g (1.95 mol) *p*-toluenesulfonic acid monohydrate which had been warmed to 90 °C, 460 g (2.54 mol) of amine hydrochloride **24** was added with vigorous mechanical stirring. The mixture was stirred for 40 min at 90 °C, then poured into a mixture of water (2 l), concentrated ammonium hydroxide (650 ml), and ice (1 litre), and extracted four times with 500 ml of methylene chloride. The combined organic extracts were washed with brine, dried (Na_2SO_4), and evaporated to give 491 g of a dark red oil. The oil was diluted to 1.8 l with Et_2O, cooled in an ice bath, and ethanol saturated with hydrogen chloride was added until the p*H* reached 2–3. The resulting solid was filtered off and washed with ether to give 398 g (70%) of a light yellowish solid (70%), mp 153–156 °C (corr.). An analytical sample of **25***a* was recrystallized from 2-propanol–ether to give white crystals, mp 158–160 °C (corr.).

The free base of **25***a* is conveniently prepared from its hydrochloride by neutralization with concentrated ammonium hydroxide and extraction with CH_2Cl_2.

Benzyl α-Aminoacetoacetate Ethylene Ketal ***25b***

Freshly prepared aluminum amalgam (19) (from 27 g of aluminum foil) was covered with 500 ml of diethyl ether. The flask was fitted with a mechanical stirrer, a condenser, and a dropping funnel. A solution of benzyl oximinoacetoacetate ethylene ketal **23***b* (132.5 g; 0.5 mol) in 300 ml of wet diethyl ether was added dropwise at such a rate as to maintain boiling at reflux. After stirring for 4 h, the reaction mixture was filtered through a Buchner funnel. The filtrate was evaporated leaving

110 g of yellowish oil. The oil was dissolved in 800 ml of dry diethyl ether and dry hydrogen chloride gas was bubbled into the solution until no further precipitation occurred. The white precipitate was filtered off and washed once with diethyl ether and then dried *in vacuo*. This provided 108 g of benzyl aminoacetoacetate ethylene ketal hydrochloride, mp 157–158 °C.

To obtain the free base, the hydrochloride salt was suspended in 500 ml of diethyl ether and concentrated ammonium hydroxide was added with shaking until the solid went into solution. The diethyl ether layer was separated and washed twice with brine. After drying over anhydrous sodium sulfate, the solvent was evaporated leaving 90 g (71%) of colorless oil.

Benzyl α-Amino-γ-phenylacetoacetate Ethylene Ketal ***25c***

To freshly prepared aluminum amalgam (19) (from 6.9 g aluminum foil) in 100 ml ether was added solution of 29.5 g (85 mmol) of **23***c* in 600 ml of moist ether over 1 h. There was a mildly exothermic reaction and after the addition was complete, it was refluxed for 2 h. It was cooled, filtered through Celite, and extracted with 4 × 100 ml 10% hydrochloric acid. White crystals separated from the aqueous phase, were filtered, washed with cold water, and dried to give 29.0 g (93%) solid, mp 181–183 °C, recrystallized from ethanol–ether; mp 182–184 °C. The free base was obtained by suspending the hydrochloride in water and neutralizing with cold concentrated ammonium hydroxide.

Benzyl α-Amino-γ-benzyl Acetoacetate Ethylene Ketal ***25d***

To freshly prepared aluminum amalgam (19) (prepared from 27 g aluminum foil) covered with 300 ml moist ether was added with stirring a solution of 43 g (0.2 mol) of **23***d* in 300 ml ether. There was an exothermic reaction and after it subsided, the system was refluxed for 4 h. The inorganic material was filtered on Celite and the filtrate shaken well with 10% hydrochloric acid (100 ml). White crystals separated, were collected by filtration, washed with ether, and dried in a dessicator to give 54.0 g solid; mp 186–188 °C. The free base was obtained by suspending the solid in water, carefully neutralizing with cold concentrated ammonium hydroxide, and extracting with methylene chloride. After evaporation of the solvent, 27.91 g (69%) of a yellow oil was obtained.

Preparation of Schiff Bases ***26a–d***

The Schiff bases **26***a–d* were prepared from cinnamaldehyde and the appropriate amine **25***a–d* in quantitative yields according to our previously published method (1). The nmr spectra of **26***a–d* are listed in Table 1.

cis-N-(α-Carboethoxy-β,β-ethyleneketalpropyl)-3-azido-4-styryl-2-azetidinone ***27a***

From 197.2 g (0.65 mol) of **26***a*, 72 g (0.715 mol) triethylamine and 85.19 g (0.715 mol) azidoacetylchloride was prepared 245 g (98%) of crude **27***a* as a red oil according to our previously published method. A small sample crystallized from methanol to give a white solid, mp 81.5–82.5 °C.

cis-N-(α-Carbobenzoxy-β,β-ethyleneketalpropyl)-3-azido-4-styryl-2-azetidinone ***27b***

From ***27a***

To a solution of 64.31 g (0.168 mol) of **27***a* in 700 ml tetrahydrofuran was added 670 ml of 0.25 *N* sodium hydroxide solution (0.168 mol) at such a rate as to maintain the temperature at 25 °C. The addition took 1 h following which the solution was stirred an additional hour until thin layer chromatography indicated that no **27***a* remained in the mixture. The reaction mixture was carefully acidified to p*H* 3 with concentrated hydrochloric acid, saturated with salt, and extracted with methylene chloride (3 times). The methylene chloride extracts were washed with brine, dried over sodium sulfate, and evaporated at reduced pressure. The residue was dissolved in ether and extracted with 10% sodium bicarbonate solution until the extracts were colorless. The combined basic extracts were washed twice with ether, then carefully acidified to p*H* 3 with concentrated hydrochloric acid saturated with salt and extracted with methylene chloride. The extracts were washed with brine, dried over sodium sulfate, filtered, and evaporated to yield 51.86 g (86%) of the acid as a brown solid. Recrystallization from benzene gave pure **27***e*, mp 131–131.5 °C (dec.) (single isomer).

Treatment of **27***e* with triethylamine and benzyl chloroformate according to the procedure given for the conversion of **9***c* to **9***b* gave pure **27***b* in 99% yield, mp 65.5–66.5 °C after recrystallization from benzene – petroleum ether (30–60 °C) as a single isomer.

From ***25b***

Treatment of **26***b* with triethylamine and azidoacetyl chloride according to our previously published procedure (1) gave **27***b* in 94% yield as a mixture of diastereoisomers.

cis-N-(α-Carbobenzoxy-β,β-ethyleneketal-γ-phenylpropyl)-3-azido-4-styryl-2-azetidinone ***27c***

Treatment of **26***c* with triethyl amine and azidoacetyl chloride as in ref. 1 gave **27***c* as a mixture of diastereoisomers in quantitative yield. The crude oil was used as such in subsequent experiments.

cis-N-(α-Carbobenzoxy-β,β-ethyleneketal-γ-benzylpropyl)-3-azido-4-styryl-2-azetidinone ***27d***

Treatment of **26***d* with triethylamine and azidoacetyl chloride as in ref. 1 gave **27***d* as a red oil in quantitative yield and as a mixture of diastereoisomers. The crude oil was used as such in subsequent experiments.

cis-N-(α-Carbobenzoxy-β,β-ethyleneketalpropyl)-3-azido-4-formyl-2-azetidinone ***28a***

A solution of 117.5 g (0.262 mol) of **27***b* in 1 litre of methylene chloride was cooled to −50 to −60 °C in a dry ice – acetone bath, and ozonized until a faint blue-green color appeared. The solution was then flushed with nitrogen until the color faded. Methyl sulfide (100 ml) was added to the solution at −50 °C which was then allowed to slowly reach 25 °C as the cooling bath gradually melted. It was kept overnight at room temperature under nitrogen and then it was washed twice with 1% sodium bicarbonate solution and twice with brine, dried over anhydrous sodium sulfate, and evaporated to dryness. The resulting oil was triturated four times with 100 ml portions of petroleum ether (bp 30–60 °C) to remove benzaldehyde. The oil was then triturated carefully with diethyl ether whereupon it solidified. The solid was filtered off and dried to provide 75 g (71.5%) of aldehyde as a mixture of isomers diasteriomeric at the carbon α to the carbonyl of the benzyl ester.

In another experiment, 36.36 g (81.24 mmol) of a single isomer of **27***b* was ozonized at −78 °C in 300 ml

of methylene chloride. After work-up as above, there was obtained 32.92 g of an oil which crystallized on standing. This material was slurried with ether and filtered to provide 18.84 g (69%) off-white solid, mp 97–100 °C (corr). The analytical sample was recrystallized from ether; white crystals, mp 101–102 °C (corr.).

cis-N-(α-Carbobenzoxy-β,β-ethyleneketal-γ-phenylpropyl)-3-azido-4-formyl-2-azetidinone ***28b***

Ozonolysis of **27***c* according to the procedure described above for **28***a* gave **28***b* as an oil (95%). The nmr and ir spectra of **28***b* were compatible with the assigned structure and it was used as such in subsequent experiments.

cis-N-(α-Carbobenzoxy-β,β-ethyleneketal-γ-benzylpropyl)-3-azido-4-formyl-2-azetidinone ***28c***

Ozonolysis of **27***d* according to the procedure given for **28***a* to yield **28***c* as an oil. Chromatography of the oil (7.0 g) on silica gel (deactivated with 15% water) (250 g) using ether – petroleum ether (2:1) as eluent to remove the benzaldehyde followed by pure ether gave **28***c* in 45% yield. The oil was used as such in subsequent experiments.

cis-N-(α-Carbobenzoxy-β,β-ethyleneketalpropyl)-3-azido-4-mesyloxymethyl-2-azetidinone ***30a***

The aldehyde **28***a* (116.3 g; 0.31 mol) was dissolved in 600 ml of THF (reagent grade) and the solution was then cooled to −10 °C (ice–methanol bath). Sodium borohydride (5.88 g; 0.155 mol) was added and the reaction mixture was stirred 1 h. 10% aqueous hydrochloric acid was added until the mixture was slightly acidic, then 600 ml brine was added. The THF layer was separated and the aqueous phase was extracted twice with 250 ml portions of diethyl ether. The combined organic phases were washed twice with 400 ml portions of brine, dried over anhydrous sodium sulfate, and evaporated *in vacuo* to yield 117.3 g of crude alcohol **29***a* as an orange oil. This oil was used as such in the next reaction.

A solution of methanesulfonyl chloride (37.8 g; 0.34 mol) in 100 ml of methylene chloride was added dropwise at 0 °C (ice–water bath) to a stirring solution of alcohol **29***a* (105.6 g; 0.28 mol), triethylamine (56.6 g; 0.34 mol), and 1 litre of methylene chloride. Afterwards, the reaction was stirred for 30 h at 25 °C. It was then washed twice with brine (500 ml portions), dried over anhydrous sodium sulfate, and evaporated *in vacuo*. The resulting oil was dissolved in methylene chloride, treated with Norite, and then filtered over *ca.* 200 g of activity I silica gel. The silica gel was then washed with *ca.* 2 l of methylene chloride. The filtrate was evaporated to dryness and the resulting oil (116 g) was covered with diethyl ether. It crystallized on standing giving 87.2 g (80% from aldehyde **28***a*) of mesylate **30***a* as an off-white solid, mp 97–99 °C (corr.) after recrystallization from benzene–ether.

cis-N-(α-Carbobenzoxy-β,β-ethyleneketal-γ-phenylpropyl)-3-azido-4-mesyloxymethyl-2-azetidinone ***30b***

Reduction of **28***b* with sodium borohydride as in **28***a* gave **29***b* in 89% yield. The alcohol was mesylated as in the above example to yield **30***b* as an oil in 95% yield. This oil was used as such in subsequent reactions.

cis-N-(α-Carbobenzoxy-β,β-ethyleneketal-γ-benzylpropyl)-3-azido-4-mesyloxymethyl-2-azetidinone ***30c***

Reduction of **28***c* with sodium borohydride as in **28***a* gave **29***c* in 92% yield. The alcohol was mesylated as in the conversion of **29***a* to **30***a* to give **30***c* in 46% yield after chromatography on silica gel (deactivated with 15% water) (4.0 g substrate to 250 g silica gel) using ether – petroleum ether (3:1) as eluent. The oil was used as such in subsequent reactions.

Benzyl 7-β-Azido-3-methyl-Δ³-O-2-isocephem-4-carboxylate ***32a***

A mixture of mesylate **30***a* (3.19 g; 6.43 mmol) and 30 ml of 95% trifluoroacetic acid was stirred at 25 °C for 2 h. The mixture was diluted with 300 ml of brine and extracted three times with methylene chloride (100 ml portions). The combined extracts were washed three times with water (50 ml portions, until neutral), dried (anhydrous sodium sulfate), and evaporated to dryness *in vacuo* leaving 3.17 g of a brown oil. The nmr spectrum of this oil indicates the presence of > 90% enol **31***a*.

A solution of 12.02 g (29.4 mmol) of **31***a* and 2.95 g (29.5 mmol) triethylamine in 100 ml of methylene chloride was refluxed for 2 h. The solution was washed with 10% hydrochloric acid and brine, and dried over sodium sulfate. Evaporation gave 8.56 g of an oil which was filtered through 100 g silica gel in methylene chloride. Evaporation of the filtrate gave 6.58 g (80.5%) of **32***a*, mp 87–88 °C after recrystallization from ether.

Benzyl 7-Azido-3-benzyl-Δ³-O-2-isocephem-4-carboxylate ***32b***

The ketal mesylate **30***b* (1.36 g; 2.5 mmol) was dissolved in 95% trifluoroacetic acid (15 ml) and stirred at 50–55 °C for 2 h on an oil bath. It was poured into brine and extracted with CH_2Cl_2. After washing the organic extracts with water and drying over Na_2SO_4, the solvent was removed on the aspirator and left 1.20 g red oil, **31***b*. No further purification was attempted.

A mixture of crude enol mesylate **31***b* (5.4 g) and triethylamine (2 ml) in dry CH_2Cl_2 (100 ml) was refluxed for 5 h. It was cooled, washed with 10% HCl and water, dried over Na_2SO_4 and evaporated on the aspirator to give 4.24 g oil. This was purified by chromatography on 200 g of silica gel (deactivated with 15% water) eluting with ether – petroleum ether (2:1) to give 1.3 g (33%) of **32***b*, mp 117–118 °C, recrystallized from methanol.

Benzyl 7-Azido-3-phenethyl-Δ³-O-2-isocephem-4-carboxylate ***32c***

Ketal mesylate **30***c* (2.05 g; 3.7 mmol) was dissolved in 95% trifluoroacetic acid (200 ml) and stirred at 50–55 °C for 2 h on an oil bath. It was then poured into a mixture of crushed ice and brine and extracted with CH_2Cl_2. After washing the organic extracts with water, and drying over Na_2SO_4, the solvent was removed on the aspirator and left 1.73 g oil. No further purification was attempted.

A mixture of crude 'enol mesylate' **31***c* (1.71 g; 3.4 mmol) and triethylamine (0.48 ml; 3.4 mmol) in CH_2Cl_2 (50 ml) was refluxed for 5 h. It was cooled, washed with 10% HCl and water, dried over Na_2SO_4, and evaporated on the aspirator to give 1.35 g oil. This was purified by chromatography on 75 g silica gel (deactivated with 15% water) eluting with ether – petroleum ether (2:1) to yield 0.45 g (33%) pure **32***c*, mp 97–98 °C after recrystallization from methanol.

Ethyl 7-β-(Aminophenoxyacetoyl)-Δ³-O-2-isocephem-4-carboxylate ***34a***

A suspension of 242.5 mg (1.02 mmol) of **8***a* and

260 mg 10% Pd/C in 15 ml ethyl acetate was stirred under hydrogen at atmospheric pressure for 30 min. The suspension was filtered through diatomaceous earth and evaporated to yield 220 mg of an oil. The nmr and ir spectra of which were compatible with the amine **33***a*.

The oil was taken up in 15 ml methylene chloride and 101 mg (1 mmol) triethylamine was added. The solution was cooled to 0–5 °C and a solution of 170.5 mg (1 mmol) phenoxyacetyl chloride in 5 ml methylene chloride was added over 5 min. The solution was stirred 30 min at 25 °C and washed with water, 10% hydrochloric acid, and saturated sodium bicarbonate solution. The solution was dried over sodium sulfate and concentrated to yield 316 mg of an oil. The oil was chromatographed on 25 g silica gel with benzene–acetone as eluent (initially 100% benzene gradually changed to 1:1 5% every 50 ml). There was obtained 194 mg (56%) of **34***a*, mp 148–148.5 °C, recrystallized from benzene–ether.

Benzyl 7-β-(Aminophenoxyacetoyl)-Δ^3-O-2-isocephem-4-carboxylate **34***b*

Compound **8***b*, 500 mg (1.66 mmol) was dissolved in 20 ml of dry ethyl acetate. To this was added 450 mg of 10% Pd/C and the solution was stirred under hydrogen at atmospheric pressure and room temperature for 30 min. The solution was filtered through Celite and the filter cake washed thoroughly with methylene chloride. Evaporation of the filtrate yielded 500 mg of crude amine. The nmr and ir spectra of the compound were compatible with the assigned structure.

Compound **33***b* (500 mg) was dissolved in 10 ml of dry methylene chloride and cooled to 0–5 °C in an ice bath. To this was added 280 mg (2.8 mmol) of triethylamine and 346 mg (2.0 mmol) of phenoxyacetyl chloride was added slowly. After stirring for 1 h at 0–5 °C, the solution was washed with water (2 × 10 ml) and dried over Na_2SO_4. After evaporation, the residual oil was taken up in 50 ml of ether and filtered. The filtrate was evaporated and triturated with ether – petroleum ether (1:1). The solid thus obtained was filtered to yield 570 mg crude amide. The amide was chromatographed on a silica gel column (not deactivated) (25 g) with benzene–acetone (initially in a ratio 50:1, gradually changed to 1:1, 2% more acetone every 25 ml). The desired amide was obtained pure, 195 mg (29%), as a gum.

Benzyl 7-β-(Aminophenoxyacetoyl)-3-methyl-Δ^3-O-2-isocephem-4-carboxylate **34***c*

A suspension of 210 mg (0.64 mmol) of **32***a* and 100 mg PtO_2 in 35 ml absolute ethanol was hydrogenated at atmospheric pressure for 7 min. Filtration and evaporation of the filtrate gave 190 mg (100%) of **33***c*, mp 91–92 °C. The nmr and ir spectra of **33***c* were compatible with the assigned structure.

To a solution of 190 mg (0.64 mmol) of **33***c* in 20 ml methylene chloride was added 97.4 mg (0.64 mmol) of phenoxyacetic acid followed by 158 mg (0.64 mmol) EEDQ. The solution was let stand 1 h. It was washed with 1% sodium bicarbonate solution (2 × 10 ml), 10% hydrochloric acid (2 × 10 ml), and brine (50 ml), and dried over sodium sulfate. Evaporation of the solvent gave 180 mg (65%) of **34***c* which crystallized on trituration with ether, mp 133–135 °C (dec.).

Benzyl 7-β-(Aminophenoxyacetoyl)-3-benzyl-Δ^3-O-2-isocephem-4-carboxylate **34***d*

A mixture of compound **32***b* (0.49 g; 1.25 mmol) and triethylamine (0.9 ml; 6.5 mmol) in CH_2Cl_2 (50 ml) was cooled in an ice bath and while being stirred, was saturated with H_2S. The cooling bath was removed and there was gas evolution which subsided in 10 min. At this point, tlc showed no starting material remained. Attempts to extract the amine from the solution as its hydrochloride failed as it is more soluble in CH_2Cl_2 than in water. The CH_2Cl_2 solution of the free base was dried over Na_2SO_4 and evaporated on the aspirator to leave 0.49 g (87%) of **33***d* as a semisolid. It was used as such with no further purification.

A solution of **33***d* (0.46 g; 1.25 mmol), phenoxyacetic acid (0.19 g; 1.25 mmol), and EEDQ (0.31 g; 1.25 mmol) in CH_2Cl_2 (100 ml) was stirred at room temperature for 16 h. It was washed with 1% $NaHCO_3$ solution, then with brine, dried over Na_2SO_4, and evaporated on the aspirator to leave 0.56 g (89%) of a slightly yellow gum. It was used as such with no further purification.

Benzyl 7-β-(Aminophenoxyacetoyl)-3-phenethyl-Δ^3-O-2-isocephem-4-carboxylate **34***e*

A mixture of **32***c* (0.81 g; 2 mmol) and triethylamine (0.56 ml; 4 mmol) in methylene chloride (50 ml) was cooled in an ice bath and while being stirred, was saturated with H_2S. The cooling bath was removed and there was gas evolution. After stirring at room temperature for 1 h, the solution was evaporated at room temperature and partitioned between ether and 10% HCl. White crystals separated and were collected by filtration, washed with ether, and dried to give 1.12 g white solid, mp 120–123 °C. The free base was obtained by suspending the solid in water, alkalizing with cold concentrated ammonium hydroxide and extracting with methylene chloride. This was washed with brine, dried over sodium sulfate, and evaporated on the aspirator. There was obtained 0.68 g (90%) of **33***d* as an oil.

A solution of **33***e* (0.40 g; 1.05 mmol), phenoxyacetic acid (0.16 g; 1.05 mmol), and EEDQ (0.26 g; 1.05 mmol) in CH_2Cl_2 (50 ml) was stirred at room temperature for 2 h. It was washed with 1% $NaHCO_3$ solution, then with brine, dried over Na_2SO_4, and evaporated on the aspirator to leave 0.49 g (91%) white solid, mp 146–148 °C. This was used as such in the subsequent step.

7-β-(Aminophenoxyacetoyl)-Δ^3-O-2-isocephem-4-carboxylic acid **35***a*

Compound **34***b* 210 mg (0.514 mmol) was dissolved in 40 ml ethyl acetate and 1 ml glacial acetic acid was added. Using 610 mg (~20%) palladium hydroxide on charcoal as catalyst, the solution was hydrogenated at 58 psi for 50 min.

The reaction mixture was filtered through Celite (twice) and the catalyst was washed thoroughly with chloroform (20 ml). The filtrate was evaporated to dryness. It was evaporated 3 times with benzene in order to strip off the acetic acid. A very viscous oil was obtained which was washed with 10 ml benzene. The residual oil was scratched with 10 ml ether. The solid material formed was filtered out. Yield: 115 mg (70.5%). Compound **35***a* did not show a sharp melting point but decomposed in the range of 215–250 °C. The ir and nmr spectra of **35***a* were compatible with the assigned structure.

Compound **35***a* was converted to its potassium salt **35***b*.

To a solution of 30 mg, compound **35***a* in 3 ml methylisobutylketone was added one or two drops of 50% solution of potassium 2-ethylhexanoate in butanol. A

white crystalline material separated almost immediately which was filtered out and washed with methyl isobutylketone and dried over P_2O_5 for 48 h under high vacuum. There was obtained 18 mg (53.5%) of **35***b*. This compound slowly decomposed on heating 230–260 °C.

7-β-(Aminophenoxyacetoyl)-3-methyl-Δ³-O-2-isocephem-4-carboxylic Acid 35c

Benzyl ester **34***c* (100 mg; 0.237 mmol) was dissolved in a mixture of absolute ethanol (10 ml) and tetrahydrofuran (7 ml). 10% Pd–C (100 mg) was carefully added and the mixture was hydrogenated at atmospheric pressure. Hydrogen uptake was complete after *ca.* 7 min. The catalyst was filtered off and washed once with EtOH. The EtOH was removed *in vacuo* leaving 90 mg of partly crystalline residue. The residue was crystallized from acetone–ether to give **35***c*, mp 171–172 °C (dec.), 65 mg (84%).

7-β-(Aminophenoxyacetoyl)-3-benzyl-Δ³-O-2-isocephem-4-carboxylic Acid 35d

Compound **34***d* (0.49; 1 mmol) was dissolved in ethyl acetate (100 ml) and glacial acetic acid (10 ml), 20% $Pd(OH)_2$-on-carbon (0.50 g) was added, and the mixture was agitated on a Paar apparatus at 60 psi of H_2 for 2 h. The solid was filtered off on Celite and the filtrate evaporated to dryness. The residue was extracted with saturated $NaHCO_3$, the aqueous phase was acidified with 10% HCl, and extracted with CH_2Cl_2. This was then washed with water, dried over Na_2SO_4 and evaporated to dryness. The resulting solid was recrystallized from benzene and gave white crystals, mp 123–125 °C. There was obtained 0.08 g (20%) of **35***d*.

7-β-(Aminophenoxyacetoyl)-3-phenethyl-Δ³-O-2-isocephem-4-carboxylic Acid 35e

A solution of compound **34***e* (0.49 g; 0.9 mmol) in ethyl acetate (75 ml) was added to a prehydrogenated sample of 20% $Pd(OH)_2$-on-carbon (0.50 g) in ethyl acetate (25 ml). It was then stirred under hydrogen at atmospheric pressure and after 15 min, gas consumption had ceased. It was filtered through a Celite pad, washed well with ethyl acetate, and the solvent was removed on the aspirator to leave 0.40 g of an amorphous solid. This was suspended in ether and extracted with 2% $NaHCO_3$. The aqueous extract was acidified with 10% HCl and the white solid collected by suction filtration, washed with water, and dried to give a white solid, mp 160–162 °C. Recrystallized from $CHCl_3$–ether, mp 162–163 °C. There was obtained 0.35 g (92%) of **35***e*.

Acknowledgements

Partial financial support of this work by the National Research Council of Canada through its Industrial Research Assistance Program is gratefully acknowledged. We also thank Dr. V. DiTullio, Dr. Y. Lambert, Mr J. Chapuis, and Mr. J. Lajeunesse for technical assistance. Microbiological data were supplied by M. Misiek whom we also thank.

1. T. W. Doyle, B. Belleau, B. Y. Luh, C. F. Ferrari, and M. P. Cunningham. Can, J. Chem. This issue.
2. G. E. Gutowski, B. J. Foster, C. J. Daniels, L. D. Hatfield, and J. W. Fisher. Tetrahedron Lett. 3433 (1971).
3. V. E. Matthews and D. G. Kubler. J. Org. Chem. **25**, 266 (1960).
4. N. A. Tikhonova, K. K. Babievskii, and V. M. Belikov. Izv. Akad. Nauk. SSSR, Ser. Khim. 877–80 (1967); Chem. Abstr. **67**, 108117 (1967).
5. E. J. Corey, N. H. Andersen, R. M. Carlson, J. Paust, E. Vedejs, I. Vlatips, and R. Winter. J. Am. Chem. Soc. **90**, 3245 (1968).
6. R. Nagarajan and D. O. Spry. J. Am. Chem. Soc. **93**, 2310 (1971).
7. C. Djerassi, J. D. Gray, and F. A. Kinel. J. Org. Chem. **25**, 2174 (1960).
8. A. I. Scott. Interpretation of the ultraviolet spectra of natural products. Pergamon Press, Oxford, London, Edinburgh, N.Y., Paris, Frankfurt. 1964. p. 81.
9. E. H. Flynn (*Editor*). Cephalosporins and penicillins, chemistry and biology. Academic Press, New York and London. 1972.
10. H. Adkins and J. Reeve. J. Am. Chem. Soc. **60**, 1328 (1939).
11. W. G. Laver, A. Neuberger, and J. J. Scott. J. Chem. Soc. C, 1474 (1959).
12. D. J. Drinkwater and P. W. G. Smith. J. Chem. Soc. C, 1305 (1971).
13. B. Belleau and G. Malek. J. Am. Chem. Soc. **90**, 1651 (1968).
14. Y. G. Perron, W. F. Minor, C. T. Holdrege, W. J. Gottstein, J. C. Godfrey, L. B. Crast, R. B. Babel, and L. C. Cheney. J. Am. Chem. Soc. **82**, 3934 (1960).
15. J. C. Sheehan and K. R. Henry-Logan. J. Am. Chem. Soc. **81**, 3089 (1959).
16. G. R. Ames and W. Davey. J. Chem. Soc. 3480 (1957).
17. G. W. Anderson, I. F. Halverstadt, W. H. Miller, and R. O. Roblin, Jr. J. Am. Chem. Soc. **67**, 2197 (1945).
18. B. R. Baker, R. E. Schaub, M. V. Querry, and J. H. Williams. J. Org. Chem. **17**, 77 (1952).
19. A. I. Vogel. Practical organic chemistry. 3rd ed. Longmans Green and Co., London. 1957. p. 198.
20. T. A. Pursiano, M. Misiek, F. Leitner, and K. E. Price. Antimicrob. Agents Chemother. **3**, 33 (1973).

Electrophilic additions of bromonium nitrate to unsaturated substrates

J. WILLIAM LOWN AND ALUMMOOTTIL V. JOSHUA[1]

Department of Chemistry, University of Alberta, Edmonton, Alta., Canada T6G 2G2

Received August 12, 1976

J. WILLIAM LOWN and ALUMMOOTTIL V. JOSHUA. Can. J. Chem. **55**, 508 (1977).

Bromonium nitrate (generated *in situ* by the reaction of bromine with silver nitrate in chloroform–pyridine) reacts *trans*-stereospecifically and regiospecifically in electrophilic additions to a series of *Z*–*E* pairs of alkenes to give bromoalkyl nitrate esters and bromoalkyl pyridinium nitrates. Addition to the less hindered (*Z*)-[β-^{2}H]-styrene is also stereospecific, eliminating the possibility of restricted rotation during addition. Reaction with conjugated dienes gives rise to bipyridinium salts from 1,4-conjugate addition and displacement. The accompanying alkyl bromonitrate esters rearrange readily to the more stable 1,4-bromonitrates in the liquid phase. In contrast to the behavior of iodonium nitrate, bromonium nitrate reacts with 3,3,3-triphenylpropene to give an allylic pyridinium nitrate, which results from phenyl migration, the structure of which was proven by synthesis. Bromonium nitrate reacts with pent-4-en-1-ol to give 2-bromomethyltetrahydrofuran. Similar reaction with cyclohex-2-en-1-ol provides products corresponding to the addition of the bromonium ion both *cis* and *trans* to the hydroxyl group, unlike iodonium nitrate where specific interaction between the hydroxyl and the pyridine group leads exclusively to *cis* addition.

J. WILLIAM LOWN et ALUMMOOTTIL V. JOSHUA. Can. J. Chem. **55**, 508 (1977).

L'addition électrophile du nitrate de bromonium (produit *in situ* par réaction du brome sur le nitrate d'argent dans le chloroforme–pyridine) sur une série de paires *Z* et *E* d'alcènes se produit régiospécifiquement et d'une façon stéréospécifique *trans* pour conduire aux esters nitrates de bromoalkyles et aux sels pyridinium de nitrates de bromoalkyles. L'addition au site le moins empêché du (*Z*)-[β-^{2}H] styrène est aussi stéréospécifique; ce résultat élimine la possibilité d'une rotation empêchée durant l'addition. La réaction avec des diènes conjugués conduit aux sels de bipyridinium par une addition conjuguée de 1,4 suivie d'un déplacement. En phase liquide, les esters bromonitrates d'alkyles qui les accompagnent se réarrangent avec facilité pour donner les bromonitrates-1,4 plus stables. Par opposition au comportement du nitrate d'iodonium, le nitrate de bromonium réagit avec le triphényl-3,3,3 propène pour donner un nitrate de pyridinium allylique qui provient d'une migration du groupe phényle; la structure de ce composé a été prouvée par synthèse. Le nitrate de bromonium réagit avec le pentène-4 ol-1 pour fournir le bromométhyl-2 tétrahydrofuranne. Une réaction semblable avec le cyclohexène-2 ol-1 conduit à des produits correspondants à l'addition de l'ion bromonium à la fois *cis* et *trans* par rapport au groupe hydroxyle; ce résultat est en opposition avec ceux observés avec le nitrate d'iodonium où une interaction spécifique entre le groupe hydroxyle et le groupe pyridine conduit exclusivement à une addition *cis*.

[Traduit par le journal]

Introduction

In previous papers we discussed the reactions of iodonium nitrate with unsaturated substrates of various types and structures and also the effect of neighboring groups in the addition reaction (1–4). The stereochemical and regiochemical outcome in these reactions was explained by assuming the formation of an intermediate iodonium ion.

Hassner and co-workers (5–7) have compared the reactivities of iodine azide and bromine azide and found that the former reacted exclusively by an ionic pathway involving a bridged iodonium ion whereas the latter can react either by an ionic or free radical pathway depending upon the nature of the solvent and the presence of oxygen.

Since the electronegativity of bromine is greater than that of iodine (6), bromonium nitrate may be expected to react by both ionic and free radical pathways. But as in the case of iodonium nitrate in chloroform–pyridine, the bromine in bromonium nitrate is also complexed to two pyridine rings. So it was anticipated that bromonium nitrate will also behave like iodonium nitrate, although the higher electrophilicity of bromonium ion may be reflected in its relative reactivity towards unsaturated substrates. Ac-

[1]NRCC scholarship holder 1974–1975.

cordingly the reactions of bromonium nitrate with a wide variety of unsaturated substrates have been examined.

Bromonium nitrate is generated *in situ* by the reaction of bromine with silver nitrate in chloroform–pyridine. The silver bromide is removed by filtration and the clear light yellow solution can be used for additions to unsaturated substrates.

$$AgNO_3 + Br_2 \xrightarrow[\text{Pyridine}]{CHCl_3} [Br\cdot 2Py]^+NO_3^- + AgBr\downarrow$$

Results

Reactions with Acyclic Alkenes

Reaction of bromonium nitrate in chloroform–pyridine with simple alkenes gives products of the type shown in [1]. In contrast to the addition

[1] 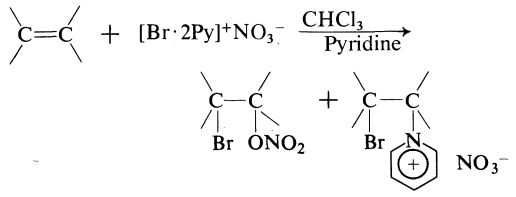

of iodonium nitrate to hex-1-ene, which gave only Markovnikov-type addition products, bromonium nitrate gave 1-bromohex-2-yl nitrate **1** and 2-bromohex-1-yl nitrate **2** in a combined yield of 49% and in a ratio of 67:33. The bromopyridinium salt produced in this reaction in 34% yield was a mixture of two isomers, **3** and **4**, in a ratio of *ca.* 60:40. Assignments of structures to

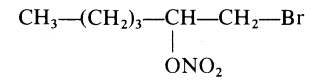

1

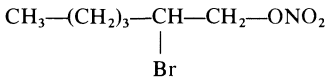

2

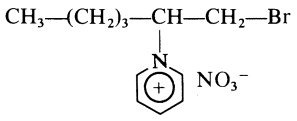

3

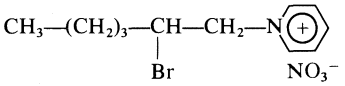

4

these and similar products and determinations of product ratios were performed by nmr spectroscopy. It was observed that methine protons α to an ONO_2 group absorb in the range 4.8–5.4 δ, whereas protons α to a bromo function absorb in the range 3.8–4.5 δ. The methylene protons α to a bromo function absorb at about 3.5 δ, whereas methylene protons α to a nitrate function absorb at 4.5–5 δ. The presence of a pyridine group in structures such as **3** deshields the methylene protons α to the bromine by about 0.7–0.9 ppm.

In the case of 3,3-dimethylbut-1-ene, the bromonitrate ester **5** and the bromopyridinium nitrate **6** with the nitrate group and pyridine respectively at the primary position are the products obtained as clearly demonstrated by the nmr spectra.

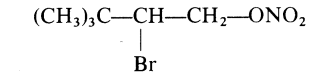

5

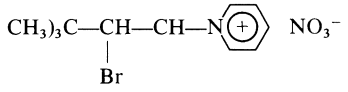

6

(*E*)-But-2-ene, on reaction with bromonium nitrate in chloroform–pyridine, afforded the *erythro*-bromonitrate ester **7** and the *erythro*-bromopyridinium nitrate **8** in 44 and 37% yields

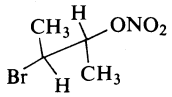

7

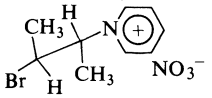

8

respectively. Similar addition to (*Z*)-but-2-ene produced the *threo*-bromonitrate ester **9** in 48% yield and the *threo*-bromopyridinium nitrate **10** in 29% yield.

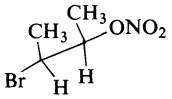

9

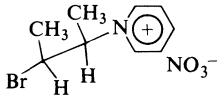

10

The addition of bromonium nitrate to (*Z*)- and (*E*)-4-methylpent-2-enes also gave stereoisomeric products as clearly shown by the nmr spectra. In the case of the (*Z*)-isomer the reaction was regiospecific and stereospecific in the forma-

tion of the *threo*-bromonitrate ester **11** and the *threo*-bromopyridinium nitrate **12**, whereas for the (*E*)-isomer, the reaction was stereospecific and regioselective. The *erythro*-bromonitrate esters **13** and **14** were produced in a ratio of

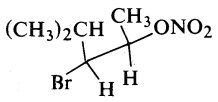

11

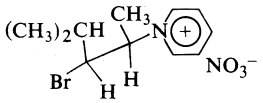

12

74:26. The ratio of the corresponding *erythro*-bromopyridinium salts **15** and **16** was also approximately the same as for the bromonitrate esters.

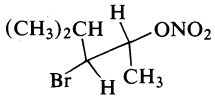

13

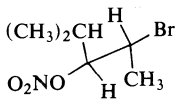

14

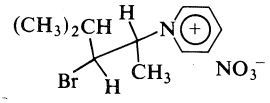

15

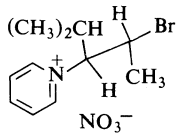

16

Reaction of bromonium nitrate in chloroform–pyridine with (*Z*)-pent-2-ene gave a mixture of *threo*-3-bromopent-2-yl and *threo*-2-bromopent-3-yl nitrates, **17** and **18**, in a ratio of 64:36, together with the isomeric *threo*-bromopyridinium nitrates, **19** and **20**, in a ratio of 70:30. For the pyridinium salts, the isomer ratio was

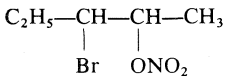

17

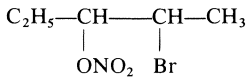

18

determined by comparing the nmr intensities of the methyl (italic portion of structures **19** and **20**) signals which appeared as triplets at δ 1.1 and 0.74 respectively.

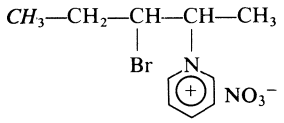

19

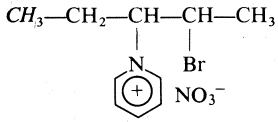

20

In the case of (*E*)-4,4-dimethylpent-2-ene, the greater bulk of the *tert*-butyl group ensures regiospecific addition of bromonium nitrate the sole product being the *erythro*-bromonitrate ester **21**, which was formed in 80% yield. No

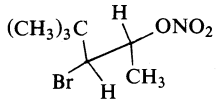

21

isolable yield of the corresponding bromopyridinium salt was obtained from this reaction. The reaction of bromonium nitrate with (*Z*)- and (*E*)-stilbenes was also stereospecific in the formation of the bromonitrate esters *threo* **22** and *erythro* **24** and the bromopyridinium salts *threo* **23** and *erythro* **25** respectively. **22** and **23** were produced in 52% and 32% yields respectively from the (*Z*)-isomer and **24** and **25** in 21 and 63.5% yields respectively from the (*E*)-isomer.

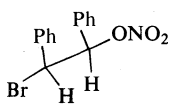

22

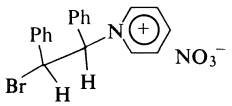

23

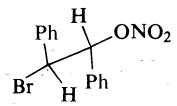

24

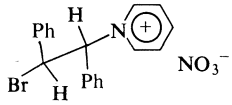

25

To eliminate the possibility that the observed stereospecificity in all the above reactions is due to restricted rotation in the intermediate bromocarbonium ions in the additions to (*Z*)- and (*E*)-alkenes and to establish conclusively the *trans* stereospecificity of addition, the reaction of bromonium nitrate with (*Z*)-β-deuterostyrene (>95% D) was performed. First it was shown that reaction of styrene with bromonium nitrate gave the bromonitrate ester **26** as the major product (49%). The pyridinium salt produced in this reaction was a mixture of **27** and **28** as shown by the nmr spectrum. The mixture was converted into **28** in an overall yield of 26.5% by treatment with potassium carbonate. In the analogous reaction with (*Z*)-β-deuterostyrene the bromonitrate ester **29** and the alkenyl pyridinium bromide **30** were isolated in 46% and 26.5% yields respectively. In the nmr spectrum of **29** the methine hydrogen absorbed as a doublet at $\delta_{TMS}(CDCl_3)$ 6.0 (J = 7.5 Hz) whereas for

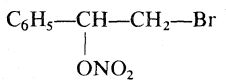

26

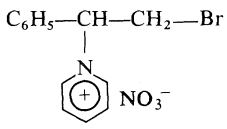

27

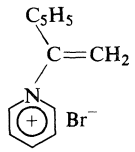

28

the protium analog **26**, it absorbed as a quartet at $\delta_{TMS}(CDCl_3)$ 6.0 (J = 6, 7.5 Hz). The methylene hydrogen in **29** appeared as a doublet further

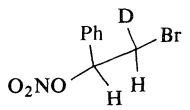

29

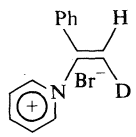

30

split by H–D coupling at $\delta_{TMS}(CDCl_3)$ 3.62 (J = 7.5 Hz) whereas for **26** the methylene hydrogens absorbed as a triplet at $\delta_{TMS}(CDCl_3)$ 3.62 (J = 6 and 7.5 Hz).

The nmr spectrum of **30** was identical to that of the salt formed in iodonium nitrate addition to (*Z*)-β-deuterostyrene.

2-Methylbut-2-ene with bromonium nitrate afforded the bromonitrate ester **31** as the major product together with a small yield of the corresponding bromopyridinium nitrate **32**. Ethyl

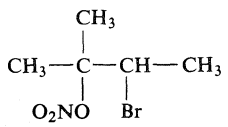

31

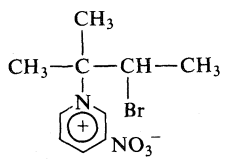

32

vinyl ether, an example in which the carbonium ion involved is considerably stabilized, gave only the bromopyridinium nitrate **33**.

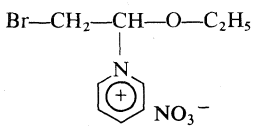

33

Reactions with Cyclic Monounsaturated Compounds

As in the case of iodonium nitrate additions, addition of bromonium nitrate to cyclic olefins allows a preliminary examination of the stereochemistry of the reaction (2). Cyclohexene gave the bromonitrate ester **34** in 52% yield which has a *trans*-diequatorial conformation as shown by the nmr spectrum. The corresponding bromopyridinium nitrate **35** was formed in 31.5% yield.

34

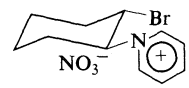

35

Norbornene gave nortricyclanyl bromide **36** in 50% yield and the expected bromonitrate ester **37** in 15% yield. They were readily separated by fractional distillation. No bromopyridinium nitrate was produced in this reaction, but a stoichiometric amount of pyridinium nitrate

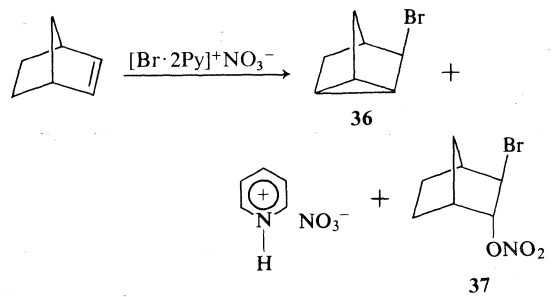

36 37

was formed. This reaction is analogous to that undergone by INO_3 (2) and plausibly involves participation across the ring aided by removal of the proton by solvent pyridine.

Reaction of 2,3-dihydropyran with bromonium nitrate in chloroform–pyridine afforded in 45% yield *trans*-equatorial *N*-(3-bromotetrahydropyranosyl)pyridinium nitrate **38**, the nmr spectrum of which compared well with that of the product obtained in the addition of iodonium nitrate to 2,3-dihydropyran (2). As in the case of ethyl vinyl ether no bromonitrate ester could be isolated in this reaction.

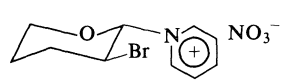

38

Reactions with Unconjugated Dienes

Unconjugated dienes, on reaction with 1 equiv of bromonium nitrate, gave only mono-addition products. Thus 1,4-cyclohexadiene gave 5-bromocyclohexen-4-yl nitrate **39** in 54% yield and *N*-[4-(5-bromocyclohexenyl)]pyridinium nitrate **40** in 25% yield. Reaction of bromonium nitrate

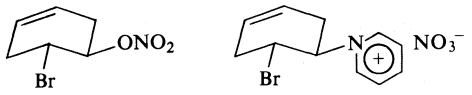

39 40

with 4-vinylcyclohexene gave the bromonitrate ester **41** in 35% yield and the bromopyridinium nitrate **42** in 40% yield corresponding exclusively to addition in the ring. The positions of bromine

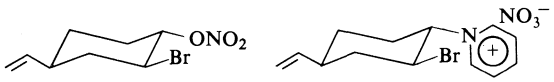

41 42

and nitrate groups in **41** and the bromine and pyridinium groups in **42** on the 1,2-cyclohexane bond could not be assigned unambiguously. As in iodonium nitrate additions the marked preference for electrophilic additions in this case to the cyclic olefinic bond may be ascribed to the greater stability of the resulting bromonium ion.

The addition of bromonium nitrate to norbornadiene shows a reduced propensity for neighboring π-bond participation than in iodonium nitrate additions. In the latter case, only products corresponding to cross-ring interactions were formed (2). On the other hand reaction of bromonium nitrate with norbornadiene produced two bromonitrate esters and one bromopyridinium nitrate. 3-Bromo-4-norbornen-2-yl nitrate **43** and tricyclo[2.2.1.$0^{2,6}$]-5-bromohept-3-yl nitrate **44** were produced in yields of 16 and 29% respectively. They were not separable by distillation. The structure of **43** was evident from the nmr spectrum of the mixture, which showed olefinic hydrogen signals at $\delta_{TMS}(CDCl_3)$ 6.3. The bromopyridinium salt formed in 12% yield

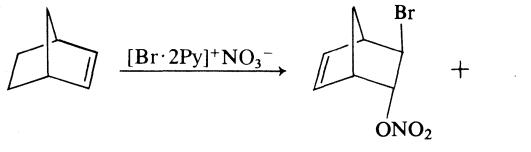

43

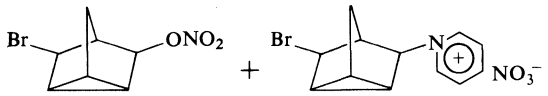

44 45

in this reaction was exclusively *N*-[3-(5-bromonortricyclanyl)]pyridinium nitrate **45**; corresponding to cross-ring interaction. The nmr spectrum of **45** compared well with that of the corresponding iodopyridinium nitrate.

Reactions with Conjugated Dienes

In contrast to the addition of iodonium nitrate to conjugated dienes, which gave only the iodopyridinium salts corresponding to 1,2-addition (2), the reaction of bromonium nitrate gave significant yields of bromonitrate esters (4).

Reaction of bromonium nitrate with 2,3-dimethyl-1,3-butadiene gave three products. The bromonitrate ester formed in 31% yield corresponded to the kinetically controlled 1,2-addition product **46**. This was evident from the nmr spectrum of the product soon after isolation (Fig. 1). The olefinic hydrogens absorbed as a

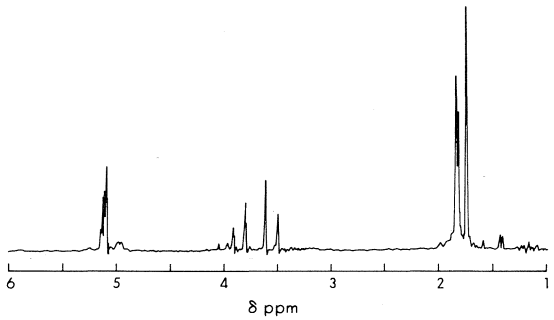

FIG. 1. Proton magnetic resonance spectrum at 100 MHz (500 Hz sweep width, 100 Hz offset) in $CDCl_3$ of 2,3-dimethyl-1,3-butadiene – bromonium nitrate adducts, **46**, 1 h after isolation. The signals at δ 3.97, 4.04, 4.95, and 4.98 correspond to the rearranged product **52**.

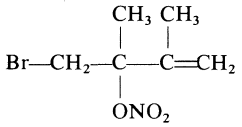

46

multiplet at $\delta_{TMS}(CDCl_3)$ 5.12, while the $-CH_2-Br$ group appeared as an AB quartet at δ 3.55 and 3.85 (J = 11 Hz). The methyl group attached to the olefinic carbon absorbed as a multiplet (allylic coupling) at δ 1.82, while the other methyl group appeared as a singlet at δ 1.73.

In addition, pyridinium salts were also formed which were readily separated by crystallization. The major product is assigned structure **47**, corresponding to 1,2-addition on the basis of the nmr spectrum, which was comparable with that of the product formed in iodonium nitrate addition. The other product was shown to be an approximately equimolar mixture of **48***a* and **48***b*.

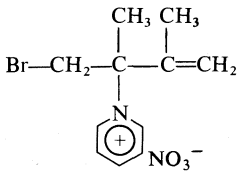

47

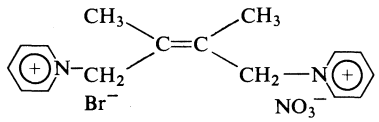

48*a*

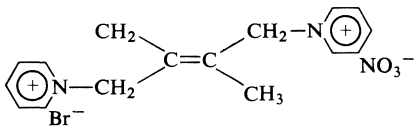

48*b*

trans,trans-2,4-Hexadiene behaved similarly. The bromonitrate ester, **49** was produced in 19% yield. In this case the two pyridinium salts **50** and **51** were not separable by crystallization.

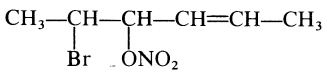

49

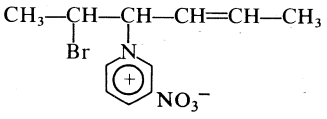

50

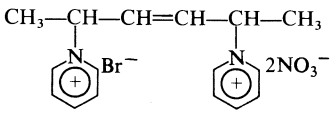

51

An interesting characteristic of these allyl nitrates is their tendency to rearrange to the thermodynamically more stable 1,4-bromonitrates. Thus both **46** and **49** rearrange either in the liquid phase or in solution to **52** and **53** respectively. The rearrangement can be followed by nmr spectroscopy. Figures 1–3 show the nmr spectra of the bromonitrate ester from 2,3-dimethyl-1,3-butadiene at different times after its isolation. In the case of **46** the rearranged product was a mixture of two isomers in approximately equal amounts as shown by high pressure

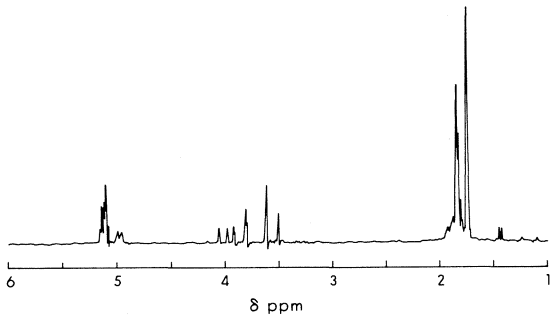

FIG. 2. Proton magnetic resonance spectrum at 100 MHz (500 Hz sweep width, 100 Hz offset) in $CDCl_3$ of 2,3-dimethyl-1,3-butadiene – bromonium nitrate adduct 3 h after isolation.

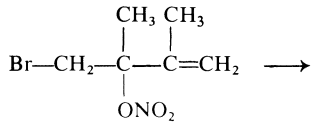

46

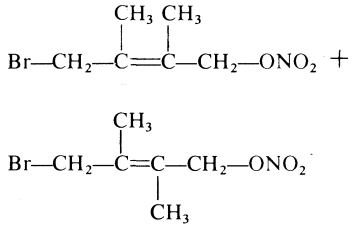

52*a*,*b*

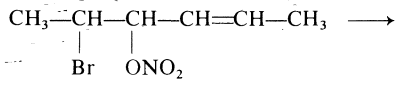

49

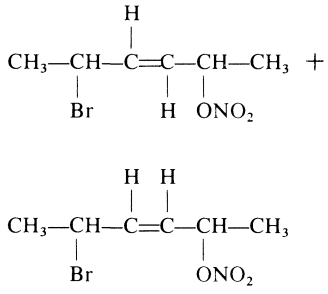

53*a*,*b*

liquid chromatography. Figure 3 shows the nmr spectrum of the rearranged product. The $-CH_2Br$ groups appear as two singlets at $\delta_{TMS}(CDCl_3)$ 3.97 and 4.04, while the $-CH_2-ONO_2$ groups absorb as two singlets at δ 4.95 and 4.98. On this basis structures **52***a* and **52***b* are assigned to the products. Moreover, treat-

ment of the mixture with pyridine in chloroform at room temperature gave **48** in almost quantitative yield. This proves that product **48** is a mixture of two geometrical isomers **48***a* and **48***b*.

The rearranged product from **49** was predominantly the *trans*-isomer **53***a* as shown by the nmr spectrum, although high pressure liquid chromatography showed the presence of a minor product, probably the *cis*-isomer **53***b*. The nmr spectrum of **53** showed $\delta_{TMS}(CDCl_3)$ 1.43 (d, 3H, CH_3—CH—ONO_2, J = 6.5 Hz), 1.78 (d, 3H, CH_3—CH—Br, J = 7 Hz), 4.65 (quint, 1H, —CH—Br, J = 7 Hz), 5.5 (m, 1H, —CH—ONO_2). The olefinic hydrogens appeared as an octet centered at δ 5.92 with $J_{CH=CH}$ = 14.5 Hz, from which follows the *trans*-stereochemistry about the olefinic bond.

Treatment of **53** with pyridine in chloroform gave **51** in quantitative yield. The nmr spectrum of **51** showed two identical methyl groups which absorbed as a doublet at $\delta_{TMS}((CD_3)_2SO)$ 1.80. The other signals were at δ 5.8 (m, 2H, 2—CH—$\overset{+}{N}$≤), 6.15–6.5 (m, 2H, olefinic hydrogens), 8.1–9.3 (m, 10H, pyridine hydrogens).

Reactions with Acetylenic Compounds

Like iodonium nitrate, bromonium nitrate was unreactive towards non-terminal acetylenes. With terminal acetylenes, alkynyl bromides were formed together with a stoichiometric quantity of pyridinium nitrate. Thus phenylacetylene gave a 63% yield of β-bromophenylacetylene, **54**.

Ph—C≡C—Br

54

Reaction with Olefinic Alcohols

Allyl alcohol on reaction with bromonium nitrate gave two isomeric bromonitrate esters.

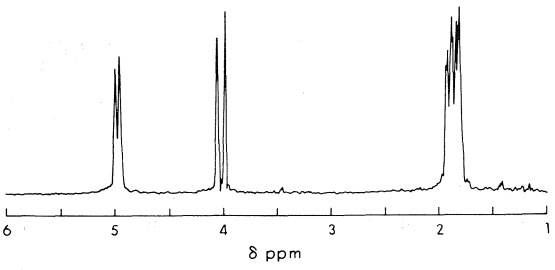

FIG. 3. Proton magnetic resonance spectrum at 100 MHz (500 Hz sweep width, 100 Hz offset) in $CDCl_3$ of 2,3-dimethyl-1,3-butadiene – bromonium nitrate adduct after complete rearrangement to **52**.

3-Hydroxyl-1-bromoprop-2-yl nitrate **55** and 3-hydroxy-2-bromoprop-1-yl nitrate **56** were formed in a combined yield of 31% and in a ratio of 69:31, as determined by nmr. The accompanying bromopyridinium salt was also a mixture of two regioisomers, **57** and **58**. The isomer

HO—CH_2—CH(—ONO_2)—CH_2—Br

55

HO—CH_2—CH(—Br)—CH_2—ONO_2

56

HO—CH_2—CH(—N$^+$ NO_3^-)—CH_2—Br

57

HO—CH_2—CH(—Br)—CH_2—N$^+$ NO_3^-

58

ratio could not be determined in this case by nmr because of overlapping signals.

But-3-en-1-ol also gave a comparable result. The bromonitrate esters, **59** and **60** were formed in 33% yield (isomer ratio 57:33). The pyridinium salt consisted of two isomers, **61** and **62**, in a ratio of 85:15.

HO—CH_2—CH_2—CH(—ONO_2)—CH_2—Br

59

HO—CH_2—CH_2—CH(—Br)—CH_2—ONO_2

60

HO—CH_2—CH_2—CH(—N$^+$ NO_3^-)—CH_2—Br

61

HO—CH_2—CH_2—CH(—Br)—CH_2—N$^+$ NO_3^-

62

The reaction of bromonium nitrate with pent-4-en-1-ol gives an opportunity to compare the extent of neighboring hydroxy group participation in this and iodonium nitrate additions. The major product in this case was a mixture of bromonitrate esters, **63** and **64**, formed in 29% yield and in a ratio of 67:33. The cyclic ether 2-bromoethyltetrahydrofuran, **65**, was produced in only 20% yield as compared to 60% in iodonium nitrate addition. In addition the isomeric bromopyridinium nitrates **66** and **67** were

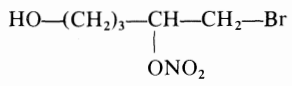

63

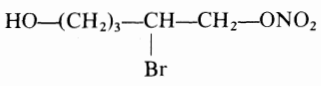

64

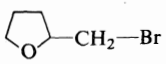

65

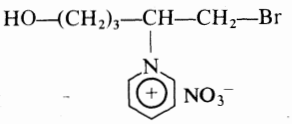

66

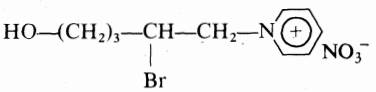

67

formed in approximately 20% yield (ratio 60:40).

Cyclohex-2-en-1-ol, on reaction with bromonium nitrate, gave a mixture of bromonitrate esters in 52% yield and bromopyridinium nitrates in 23.5% yield. Of the bromonitrates the major isomer was **68**, which is derived from a bromonium ion formed *cis* to the hydroxy group. Another isomer is assigned structure **69** which is derived from a bromonium ion formed *trans* to the hydroxy group. Compound **69** had the —CH—ONO_2 absorption in the nmr spectrum at δ 5.14 as a quartet superimposed on a multiplet.

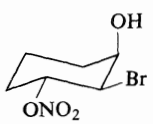

68

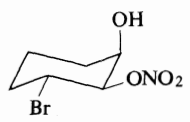

69

3,3,3-Triphenylpropene is unreactive towards iodonium nitrate (1). On the other hand it does react with bromonium nitrate. The product formed in 73% yield is assigned structure **70** on the basis of the nmr spectrum, elemental analysis, and synthesis from the allyl bromide, **71**. The allylic bromide, **71** is one of the products formed in the addition of bromine to 3,3,3-triphenylpropene (8).

In the nmr spectrum of **70**, one of the phenyl groups was different from the other two and absorbed at about 0.4 ppm downfield. The integration showed the presence of one pyridine per molecule. In addition there was a singlet at δ 5.72 integrating for two hydrogens. This is assigned to the methylene hydrogens.

Compound **71** may be envisaged as arising as a result of a phenyl migration as shown.

Discussion

The results show that bromonium nitrate can react with a wide variety of unsaturated substrates to form the two types of products that result from a competition of the two nucleophiles present, nitrate and pyridine, for the intermediate bromonium ion. As was found for iodonium nitrate (1), steric hindrance factors appear to play an important role directing the approach of the nucleophiles to the bromonium ion, exemplified by the regiospecific additions to 3,3-dimethylbut-1-ene to give **5** and **6** only, and similarly accounts for the formation of **7**, **8**, **9**, and **10** from the isomeric but-2-enes and of the products **11** to **21**. This steric hindrance factor resulting in regiospecificity or regioselectivity can, however, be overcome when a very stable cationic centre is generated as in the case of **31**, **32**, **33** (see below). Additions of bromonium nitrate to a series of (*Z*) and (*E*) pairs of alkenes is *trans*-stereospecific. Confirmatory evidence was obtained with (*Z*)-β-deuterostyrene that the observed stereospecificity does not arise because of restricted rotation in the intermediate bromocarbonium ions, *i.e.* that there is no equilibration of the cationic centre in the additions to olefins. In this respect $BrNO_3$ behaves like INO_3.

The stereochemical and regiochemical outcome in the additions of bromonium nitrate to unsaturated substrates can thus be explained by an ionic mechanism involving the formation of a three-membered ring bromonium ion intermediate **72**, which is opened up from the backside by nucleophilic attack by nitrate ion or pyridine.

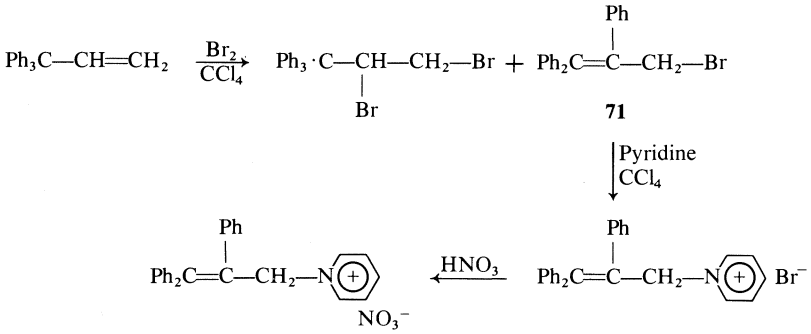

70

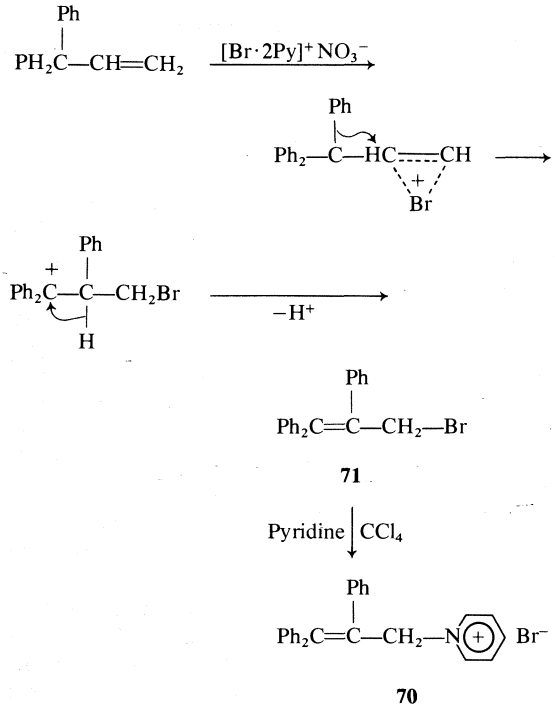

70

In the case of unsymmetrically substituted olefins, there can be substantial contribution from the unsymmetrically bridged form **73** and the open cationic form **74** to permit nucleophilic attack despite increased steric hindrance to permit neighboring hydroxyl group attack to form cyclic ethers. The intermediate can be sufficiently stabilized through the bridged form **73** to maintain its stereochemical integrity to lead to the observed stereospecificity in addition to alkenes. The open carbonium form **74** evidently makes a major contribution to the hybrid in those cases, *e.g.* **31**, **32**, and **33**, where a tertiary or oxonium stabilized cation is formed leading to preferential attack of the nucleophile at this centre despite the steric hindrance involved.

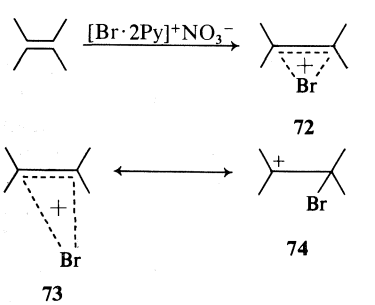

73 **74**

The observed stereospecificity in the additions to stilbenes and to (*Z*)-β-deuterostyrene and the regiospecificity in the addition to (*Z*)-β-deuterostyrene eliminate the possibility of any contribution from a free radical component under the conditions in which the above reactions were performed. Free radical contribution results in nonstereospecific addition and a reversal of the regiochemistry as is observed in bromine azide and chlorine azide additions (9). Bromonium nitrate also differs from iodonium nitrate in undergoing 1,4-conjugate additions to dienes, at least in the examples studied.

Compounds **48** and **51** corresponding to 1,4-addition may be envisaged as arising by two pathways (Scheme 1). (*a*) The initially formed bromonium ion intermediate **75** can undergo nucleophilic attack at the terminal carbon atom to give the thermodynamically more stable 1,4-addition product **76**. The allylic bromine can then be displaced by pyridine to give **48**. Alternatively, (*b*) the initially formed allyl nitrate **46** can rearrange to the thermodynamically more stable 1,4-bromonitrate **52**. Nucleophilic displacement of allylic bromine and nitrate in **52** by pyridine can lead to **48**.

To distinguish between these two possibilities,

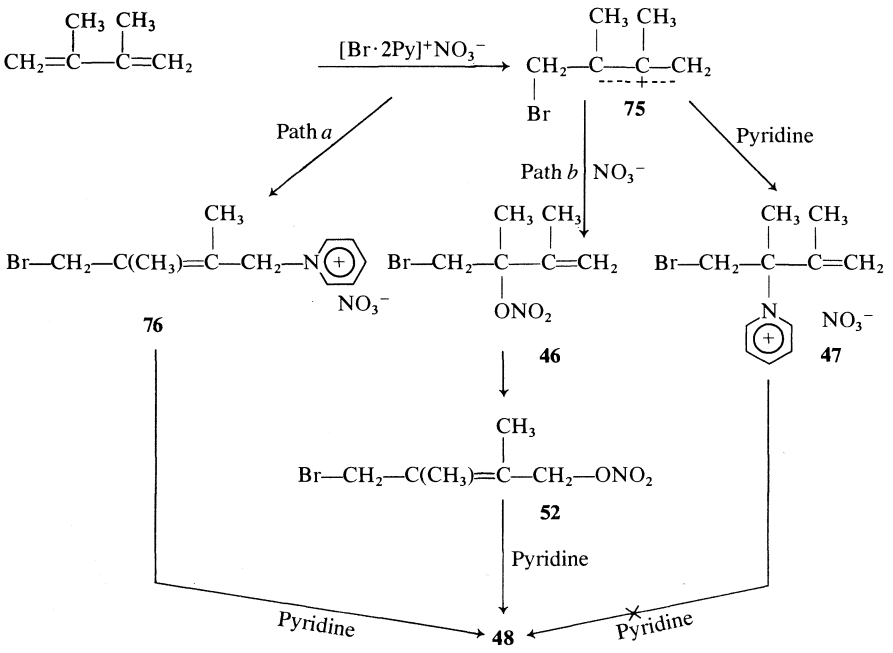

SCHEME 1

the reaction between bromonium nitrate and 2,3-dimethyl-1,3-butadiene was allowed to proceed for a longer time. The yield of 1,4-addition product was found to increase (*ca.* 8% after 3½ h, 16.5% after 12 h). Since the conversion of **46** to **48** is slow and since no equilibration of the benzylic center is observed in the addition of bromonium nitrate to (*Z*)-β-deuterostyrene it is reasonable to assume that products of the type **48** are formed by path *b*, although it is difficult to rule out path *a* entirely. A similar mechanism may be operating in the addition of iodonium nitrate to 2,3-dimethyl-1,3-butadiene (4).

As far as the mechanism of rearrangement of **46** to **52** and of **49** to **53** is concerned, one can visualize two possible pathways. First, the bromonitrate ester **46** can ionize to the allylic cation **75** and nitrate ion which can recombine to give the more stable 1,4-addition product. Alternatively, it can proceed by a concerted mechanism involving a six-membered cyclic transition state **77**.

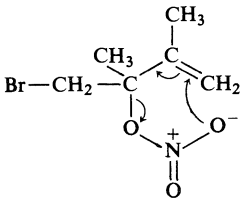

77

Such a concerted mechanism has been postulated by Hassner for the rearrangement of the allyl azide **78** to **79** (7). Although there is insufficient

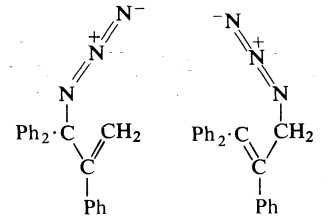

78 **79**

evidence to prove or disprove either mechanism, the concerted mechanism is more likely, since the rearrangement can proceed either in the liquid phase or in a weakly ionizing solvent like chloroform.

The reactions of iodonium nitrate and bromonium nitrate with olefins to give halonitrate esters and halopyridinium salts and with olefinic alcohols to give the corresponding addition products and/or cyclic ethers are quite general. The isolation of substantial quantities of haloalkyl nitrates in the reactions of these pseudohalogens with olefinic substrates in chloroform–pyridine is surprising in view of the reported relative nucleophilicities of pyridine and nitrate (20:1 for aqueous solutions) (10). However, since the reported heat of hydration of the nitrate ion

is -61 ± 2 kcal (g ion)$^{-1}$, (11) and therefore comparable with that of the iodide ion (12) (-68 kcal (g ion)$^{-1}$), then the nucleophilicity of this ion may be expected to be increased relative to that of the unchanged pyridine upon going to an aprotic solvent. No data are available for a more direct comparison.

In all these reactions the products isolated are formed under kinetic control. The primary products do not interconvert to any appreciable extent under the reaction conditions. This conclusion is consistent with the observed *trans* stereochemistry of addition.

Although iodonium nitrate and bromonium nitrate behave similarly towards unsaturated substrates, there is some apparent difference in reactivity between the two pseudohalogens. Thus, while iodonium nitrate is unreactive towards 3,3,3-triphenylpropene, bromonium nitrate did react with this olefin to give a pyridinium salt. While for iodonium nitrate this inertness may be attributed to steric hindrance in the olefin, the reactivity of bromonium nitrate may reflect its higher electrophilicity which is able to overcome the steric factors. For example in a competition reaction towards (*E*)-4,4-dimethylpent-2-ene the ratio of bromonitrate and iodonitrate esters was determined by nmr spectroscopy which was found to be approximately 4:1. This result suggests that bromonium nitrate is at least 4 times as reactive as iodonium nitrate.

Pent-4-en-1-ol reacts with both iodonium and bromonium nitrates to afford similar types of products. But with bromonium nitrate the proportion of the cyclized product is lower than with iodonium nitrate. This is consistent with the behaviour of pent-4-en-1-ol towards iodine and bromine, where iodine gave a much larger proportion of the cyclic ether (13).

A major difference between bromonium nitrate and iodonium nitrate is found in their reactions with phenyl, tri-alkyl, and tetra-alkyl substituted olefins. Bromonium nitrate gave substantial yields of the ester whereas iodonium nitrate gave only the pyridinium salts. With other olefinic systems too, the relative yields of pyridinium salts are in general lower in bromonium nitrate additions than in iodonium nitrate additions. If we assume that it is the thermodynamic stability of the intermediate halonium ions which allows solvent pyridine to compete successfully with the nitrate, then the above results give some indication of the relative stability of the three-membered ring iodonium ion *vs.* the three-membered ring bromonium ion. This again is consistent with the relative stabilities of iodonium and bromonium ions involved in halogen azide additions (5).

Bromonium nitrate differs from other positive bromine containing pseudohalogens, for example, bromine azide, in that with this pseudohalogen, even additions to aryl substituted olefins are stereospecifically *trans*. On the other hand addition of bromine azide to such olefinic systems under ionic conditions results in equilibration of benzylic centres suggesting involvement of an open bromocarbonium ion. This difference in behaviour may be attributed to complexation with pyridine in the case of bromonium nitrate.

Like the iodonium nitrate – pyridine complex, the bromonium nitrate – pyridine complex can also be isolated as a white solid. However, unlike the former which can be purified and shown to undergo stoichiometric addition to alkenes, attempts to purify the bromonium nitrate – pyridine complex by recrystallization were not successful. Attempted drying of the complex over anhydrous calcium sulfate in a desiccator resulted in a violent explosion.

Experimental

Melting points were determined on a Fisher–Johns apparatus and are uncorrected. The ir spectra were recorded on a Perkin–Elmer model 421 spectrophotometer, and only the principal, sharply defined peaks are reported. The nmr spectra were recorded on Varian A-60 and A-100 analytical spectrometers. The spectra were measured on approximately 10–15% (w/v) solutions in appropriate deuterated solvents with tetramethylsilane as standard. Line positions are reported in ppm from the reference. Mass spectra were determined on an Associated Electrical Industries MS-9 double focussing high resolution mass spectrometer. The ionization energy, in general, was 70 eV. Peak measurements were made by comparison with perfluorotributylamine at a resolving power of 15000. Kieselgel DF-5 (Camag, Switzerland) and Eastman Kodak precoated sheets were used for thin layer chromatography.

The gc analyses were performed with an Aerograph model A-700 gas chromatograph. The lc analyses were made with a Waters Associates model ALC-100 liquid chromatograph. Microanalyses were carried out by Mrs. D. Mahlow of this department.

General Procedure for the Addition of Bromonium Nitrate to Unsaturated Substrates

Silver nitrate (6.8 g, 0.04 mol) was dissolved in a mixture of 30 ml of chloroform and 15 ml of reagent grade pyridine. The solution was cooled in an ice-water bath and bromine (6.4 g, 0.04 mol), in 15 ml of chloroform, was added dropwise to the stirred solution. The silver bromide produced was collected and washed with a

mixture of 10 ml of chloroform and 10 ml of pyridine. To the clear light yellow filtrate at 0 °C 0.04 mol of the olefin was added all at once. The mixture was stirred at 0 °C for 3–4 h and then poured into an excess of ether and chilled. The resulting oil or precipitate was collected and the ether solution concentrated *in vacuo*. The residual oil was extracted with ether, washed with 50 ml of cold 5% hydrochloric acid, and then with 50 ml of water. Concentration of the solution, after drying ($MgSO_4$), *in vacuo* gave the bromonitrate ester, which was purified by distillation under reduced pressure.

The ether insoluble residue, after washing several times with ether, was extracted with ethanol and filtered. Crystallization was effected by the addition of ether. The product thus obtained is the bromopyridinium nitrate.

In a few instances, addition of the reaction mixture to ether did not give any oil or precipitate. In those cases, the solution was concentrated *in vacuo* and the resulting oil extracted several times with ether. After that, work-up was accomplished by the procedure described before.

1-Hexene gave an isomeric mixture of (*a*) 1-bromohex-2-yl nitrate and (*b*) 2-bromohex-1-yl nitrate in 49% yield; bp 57–58 °C/0.05 torr. *Anal.* calcd. for $C_6H_{12}NO_3Br$: C 31.85, H 5.31, N 6.19, Br 35.40; found: C 31.89, H 5.30, N 6.36, Br 35.99; nmr 5.2 (0.67H, quint, J = 5.5 Hz, $—CHONO_2$), 3.55 (1.34H, d, J = 5.5 Hz, $—CH_2Br$); (*b*) 4.15 (0.33H, m, —CHBr), 4.7 (0.66H, t, $—CH_2ONO_2$). In addition were formed the corresponding pyridinium nitrates in 34% yield as an oil: nmr (*a*) *N*-[2-(1-bromohexyl)]pyridinium nitrate 4.3 (1.3H, t, J = 6.8 Hz, —CHBr), (*b*) *N*-[1-(2-bromohexyl)]pyridinium nitrate 4.8–5.55 (1H, m, $—CH\overset{+}{N}<$), 4.8 (0.7H, m, $—CH_2—\overset{+}{N}<$).

3,3-Dimethylbut-1-ene gave 2-bromo-3,3-dimethylbutyl nitrate; bp 54–55 °C/0.05 torr; 51.5% yield. *Anal.* calcd. for $C_6H_{12}NO_3Br$: C 31.85, H 5.31, N 6.19, Br 35.40; found: C 31.87, H 5.33, N 6.10, Br 35.36; nmr 4.02 (1H, m, —CHBr), 4.7 (2H, m, $—CH_2ONO_2$), 1.3 (s, 9H, $(CH_3)_3C—$). In addition was found *N*-[1-(2-bromo-3,3-dimethylbutyl)]pyridinium nitrate; mp 126–127 °C; 30% yield. *Anal.* calcd. for $C_{11}H_{17}N_2O_3Br$: C 43.28, H 5.57, N 9.18, Br 26.23; found: C 43.28, H 5.62, N 9.09, Br 26.25; nmr 4.02 (1H, m, CHBr), 4.7 (2H, m, $—CH_2ONO_2$), 1.3 (s, 9H, $(CH_3)_3C$).

(Z)-Pentene gave an isomeric mixture of (*a*) *threo*-3-bromopent-2-yl nitrate and (*b*) *threo*-2-bromopent-3-yl nitrates; bp 32–33 °C/0.06 torr; 53% yield. *Anal.* calcd. for $C_5H_{10}NO_3Br$: C 28.31, H 4.72, N 6.6, Br 37.74; found: C 28.37, H 4.75, N 6.45. Br 37.72; nmr (*a*) 4.00 (0.64H, q, J = 4.5 Hz, —CHBr), 5.31 (0.64H, octet, J = 4.5, 6.5 Hz, $—CHONO_2$); (*b*) 4.25 (0.36H, octet, J = 4.5, 7 Hz, CHBr), 5.07 (0.36H, quint, J = 4.5 Hz, $CHONO_2$). In addition were formed the corresponding (*a*) *threo-N*-[2-(3-bromopentyl)]pyridinium nitrate and (*b*) *threo-N*-[3-(2-bromopentyl)]pyridinium nitrates as an oil in 27.5% yield.

(E)-4,4-Dimethylpent-2-ene gave *erythro*-3-bromo-4,4-dimethylpent-2-yl nitrate; bp 53 °C/0.02 torr; 80% yield. *Anal.* calcd. for $C_7H_{14}NO_3Br$: C 35.00, H 5.82, N 5.82, Br 33.34; found: C 35.02, H 5.74, N 5.74, Br 33.42; nmr 4.2 (1H, d, J = 2.5 Hz, CHBr), 5.37 (1H, octet, J = 2.5, 7.5 Hz, $CHONO_2$).

2-Methylbut-2-ene gave 3-bromo-2-methylbut-2-yl nitrate; bp 30 °C/0.3 torr; 35% yield. *Anal.* calcd. for $C_5H_{10}NO_3Br$: C 28.32, H 4.72, N 6.60; found: C 28.43, H 4.93, N 6.47; nmr 4.7 (1H, q, J = 7 Hz, CHBr). In addition was formed *N*-[2-(2-methyl-3-bromobutyl)]pyridinium nitrate; mp 117–118 °C in 20% yield. *Anal.* calcd. for $C_{10}H_{15}N_2O_3Br$: C 41.25, H 5.19, N 9.62; found: C 40.83, H 5.27, N 9.20; nmr 4.9 (1H, q, J = 7 Hz, CHBr).

Cyclohexene gave 2-bromocyclohexyl nitrate; bp 67 °C/0.05 torr; 52% yield. *Anal.* calcd. for $C_6H_{10}NO_3Br$: C 32.15, H 4.47, N 6.25, Br 35.72; found: C 32.36, H 4.56, N 6.14, Br 35.65; nmr 4.03 (1H, sextet, J = 9, 4.5 Hz, —CH—Br), 5.1 (1H, m, $—CHONO_2$). In addition was formed *N*-(2-bromocyclohexyl)pyridinium nitrate; mp 135–136 °C in 31.5% yield. *Anal.* calcd. for $C_{11}H_{15}N_2O_3Br$: C 43.57, H 4.95, N 9.24, Br 26.40; found: C 43.49; H 5.00, N 9.11, Br 26.23; nmr 4.6–5.4 (2H, m, —CHBr, $—CH—\overset{+}{N}<$).

Norbornene afforded 2-bromonorborn-3-yl nitrate; bp 73 °C/0.03 torr; 15% yield. *Anal.* calcd. for $C_7H_{10}NO_3Br$: C 35.59, H 4.24; found: C 35.32, H 4.29; nmr 3.93 (1H, m, —CHBr), 4.9 (1H, m, $—CHONO_2$). Tricyclanyl bromide was also produced in 50% yield.

Norbornadiene gave (*a*) tricyclo[2.2.1.$0^{2,6}$]-5-bromohept-3-yl nitrate and (*b*) 3-bromo-5-norbornen-2-yl nitrate; bp 57 °C/0.05 torr; 45% yield. *Anal.* calcd. for $C_7H_8NO_3Br$: C 35.90, H 3.42, N 5.98, Br 34.20; found: C 35.99, H 3.50, N 5.56, Br 34.28; nmr (*a*) 4.42 (0.64H, m, —CHBr), 4.95 (1H, m, $—CHONO_2$); (*b*) 4.1 (0.36H, m, —CHBr). In addition was formed *N*-[3-(5-bromonortricyclanyl)]pyridinium nitrate; mp 174–177 °C; 12% yield. *Anal.* calcd. for $C_{12}H_{13}N_2O_3Br$: C 46.02, H 4.15, N 8.99, Br 25.57; found: C 45.85, H 4.19, N 8.87, Br 25.30; nmr 4.05 (1H, s, CHBr), 5.12 (1H, s, $—CH—\overset{+}{N}<$).

1,4-Cyclohexadiene gave 5-bromocyclohexen-4-yl nitrate; bp 56 °C/0.05 torr, 54% yield. *Anal.* calcd. for $C_8H_8NO_3Br$: C 32.43, H 3.60, N 6.30; found: C 32.06, H 3.59, N 6.22; nmr 4.30 (1H, m, —CHBr), 5.4 (1H, m, $—CHONO_2$). In addition was formed *N*-[4-(5-bromocyclohexenyl)]pyridinium nitrate; mp 132–134 °C in 25% yield. *Anal.* calcd. for $C_{11}H_{13}N_2O_3Br$: C 43.85, H 4.32, N 9.30, Br 26.58; found: C 43.66, H 4.33, N 9.07, Br 26.58; nmr 4.9–5.6 (2H, m, —CHBr and $CH—\overset{+}{N}<$).

4-Vinylcyclohex-1-ene gave 2-bromo-4(5)-vinylcyclohexyl nitrate; bp 63 °C/0.05 torr; 35% yield. *Anal.* calcd. for $C_8H_{12}NO_3Br$: C 38.41, H 4.80, N 5.60, Br 32.00; found: C 38.50, H 4.79, N 5.31, Br 32.18; nmr 4.4 (1H, m, CHBr), 5.25 (1H, m, $—CHONO_2$). *N*-[1(2)-2(1)-Bromo-4-vinylcyclohexyl)]pyridinium nitrate was also formed as an oil in 40% yield; nmr 4.7–5.6 (5H, m, —CHBr, $CH—\overset{+}{N}<$ and vinyl protons).

2,4-trans-trans-Hexadiene gave 5-bromohex-3-en-2-yl nitrate; bp 58–59 °C/0.05 torr; 19% yield. *Anal.* calcd. for $C_6H_{10}NO_3Br$: C 32.15, H 4.47, N 6.25, Br 35.72; found: C 31.95, H 4.44, N 6.07, Br 36.11; nmr 4.65 (1H, quint, J = 7 Hz, CHBr), 5.5 (1H, m, $—CHONO_2$). In addition were formed (*a*) *N*-[4-(5-bromohex-2-enyl)]pyridinium nitrate and (*b*) *N,N'*-[2,5-(hex-3-enyl)]pyridinium nitrate, bromide as an oil in 70% yield; nmr (*a*) 5.00 (0.58, m, —CHBr), and (*b*) 5.85 (1.42H, m, $—CH—\overset{+}{N}<$).

2,3-Dimethyl-1,3-butadiane gave 4-bromo-2,3-dimethylbut-2-en-1-yl nitrate; bp 57–58 °C/0.05 torr; 31% yield.

Anal. calcd. for $C_6H_{10}NO_3Br$: C 32.15, H 4.47, N 6.25, Br 35.72; found: C 31.84, H 4.43, N 6.32, Br 35.72; nmr 3.55, 3.85 (2H, 2d, J = 11 Hz, $—CH_2Br$), 5.12 (m, 2H, vinyl protons). *N*-[2-(4-Bromo-2,3-dimethylbutenyl)]pyridinium nitrate was also found as an oil in 34% yield; nmr 4.7 (2H, q, J = 12 Hz, $—CH_2Br$).

Styrene gave 2-bromo-1-phenylethyl nitrate; bp 80 °C/0.03 torr; 49% yield. *Anal.* calcd. for $C_8H_8NO_3Br$: C 39.24, H 3.24, N 5.44, Br 32.93; found: C 39.03, H 3.25, N 5.69, Br 32.53; nmr 6.00 (1H, q, J = 6, 7.5 Hz, $—CHONO_2$), 3.62 (2H, t, J = 6, 7.5 Hz, $—CH_2Br$). *N*-[1-(1-Phenylethenyl)]pyridinium bromide was also formed; bp 80 °C, 26.5% yield.

(Z)-But-2-ene gave *threo*-3-bromobut-2-yl nitrate; bp 23 °C/0.05 torr; 48% yield. *Anal.* calcd. for $C_4H_8NO_3Br$: C 24.24, H 4.04, N 7.07, Br 40.40; found: C 23.98, H 3.98, N 6.78, Br 40.79; nmr 4.26 (1H, octet, J = 4.5, 7 Hz, —CHBr), 5.12 (1H, octet, J = 4.5, 6.5 Hz, $—CHONO_2$). *threo-N*-[2-(3-Bromobutyl)]pyridinium nitrate was also formed as an oil in 29% yield.

E-But-2-ene gave *erythro*-3-bromobut-2-yl nitrate; bp 25 °C/0.03 torr; 44% yield. *Anal.* calcd. for $C_4H_8NO_3Br$: C 24.24, H 4.04, N 7.07, Br 40.40; found: C 24.24, H 4.07, N 7.01, Br 40.33; nmr 4.25 (1H, octet, J = 4.5, 7 Hz, —CHBr), 5.1 (1H, octet, J = 4.5, 6.5 Hz, $—CHONO_2$). *erythro-N*-[2-(3-Bromobutyl)]pyridinium nitrate was also formed as an oil in 37% yield.

(Z)-4-Methylpent-2-ene gave *threo*-3-bromo-4-methylpent-2-yl nitrate; bp 30 °C/0.7 torr; 58% yield. *Anal.* calcd. for $C_6H_{12}NO_3Br$: C 31.85, H 5.31, N 6.19, Br 35.40; found: C 32.02, H 5.42, N 6.26, Br 35.77; nmr 3.89 (1H, q, J = 6.5, 5 Hz, —CHBr), 5.07 (1H, quint, J = 6.5 Hz, $—CHONO_2$).

(E)-4-Methylpent-2-ene gave a mixture of (*a*) *erythro*-3-bromo-4-methylpent-2-yl nitrate and (*b*) *erythro*-2-bromo-4-methylpent-3-yl nitrate; bp 27 °C/0.17 torr; 61% yield. *Anal.* calcd. for $C_6H_{12}NO_3Br$: C 31.85, H 5.31, N 6.19, Br 35.40; found: C 32.03, H 5.41, N 6.12, Br 36.22; nmr (*a*) 4.00 (0.74H, q, J = 6.5, 5 Hz, —CHBr); (*b*) 4.24 (0.26H, quint, J = 6.5 Hz, —CHBr); (*a*, *b*) 5.24 (1H, quint, J = 6 Hz, $—CHONO_2$). In addition was formed a mixture of *erythro-N*-[3-(2-bromo-4-methylpentyl)]pyridinium nitrate; mp 108–110 °C; 21% yield. *Anal.* calcd. for $C_{11}H_{17}N_2O_3Br$: C 43.28, H 5.57, N 9.18, Br 26.53; found: C 42.48, H 5.49, N 8.73, Br 26.79; nmr 4.2–5.6 (2H, m, —CHBr, $—CH—\overset{+}{N}\lessgtr$).

(Z)-Stilbene gave *threo*-2-bromo-1,2-diphenylethyl nitrate; mp 87–88 °C; 52% yield. *Anal.* calcd. for $C_{14}H_{12}NO_3Br$: C 52.17, H 3.73, N 4.35; found: C 51.63, H 3.74, N 4.37; nmr 5.11 (1H, d, J = 9.2 Hz, —CHBr), 6.21 (1H, d, J = 9.2 Hz, $—CHONO_2$). *threo-N*-[1-(2-Bromo-1,2-diphenylethyl)]pyridinium nitrate, mp 168–171 °C, was formed in 32% yield. *Anal.* calcd. for $C_{19}H_{17}N_2O_3Br$: C 56.85, H 4.24, N 6.98, Br 19.95; found: C 55.43, H 4.29, N 6.90, Br 19.49; nmr 7.02 (1H, d, J = 12 Hz, —CHBr).

E-Stilbene gave *erythro*-2-bromo-1,3-diphenylethyl nitrate; mp 144–145 °C; 21% yield. *Anal.* calcd. for $C_{14}H_{12}NO_3Br$: C 52.17, H 3.73, N 4.35, Br 24.83; found: C 52.21, H 3.78, N 4.12, Br 24.68; nmr 5.13 (1H, d, J = 8 Hz, —CHBr), 6.28 (1H, d, J = 8 Hz, $—CHONO_2$). *erythro-N*-[1-(2-Bromo-1,2-diphenylethyl)]pyridinium nitrate; mp 174–176 °C; 63.5% yield. *Anal.* calcd. for $C_{19}H_{17}N_2O_3Br$: C 56.85, H 4.24, N 6.98, Br 19.95; found: C 56.83, H 4.28, N 6.74, Br 19.98; nmr 7.02 (1H, d, J = 12 Hz, —CHBr).

Allyl alcohol gave an isomeric mixture of (*a*) 3-hydroxy-1-bromoprop-2-yl nitrate and (*b*) 3-hydroxy-2-bromoprop-1-yl nitrate as an oil in 33% yield. *Anal.* calcd. for $C_3H_6NO_3Br$: C 18.00, H 3.00, N 7.00, Br 40.00; found: C 18.50, H 3.06, N 6.53, Br 39.95; nmr (*a*) 5.30 (0.69H, quint, J = 6 Hz, $—CHONO_2$), 3.63 (1.38H, d, J = 6 Hz, $—CH_2Br$); (*b*) 4.3 (0.31H, m, —CHBr). The corresponding *N*-[2-(3-hydroxy-1-bromopropyl)]pyridinium nitrate and *N*-[2-(4-hydroxyl-1-bromopropyl)]pyridinium nitrate were formed as an oil in 37% yield; nmr 4.5–4.4 (3H, m, $—CH—\overset{+}{N}\lessgtr$, $—CH_2—\overset{+}{N}\lessgtr$).

Cyclohex-2-en-1-ol gave a mixture of (*a*) 3-hydroxy-2-bromocyclohexyl nitrate and (*b*) 6-hydroxy-2-bromocyclohexyl nitrate; bp 81–82 °C/0.02 torr; 52% yield. *Anal.* calcd. for $C_6H_{10}NO_4Br$: C 30.00, H 4.17, N 5.82, Br 39.34; found: C 29.85, H 4.14, N 5.26, Br 33.45; nmr (*a*) 4.2 (0.625H, q, $J_{a,e}$ = 3 Hz, $J_{a,a}$ = 8.5 Hz, —CHBr), 5.41 (0.625H, sextet, $J_{a,e}$ = 4 Hz, $J_{a,a}$ = 8.5 Hz, $—CHONO_2$), (*b*) 5.14 (0.37H, q, $J_{a,e}$ = 3 Hz, $J_{a,a}$ = 8.5 Hz, $—CHONO_2$). The corresponding pyridinium salt was formed; mp 172–177 °C; 23.5% yield. *Anal.* calcd. for $C_{11}H_{15}N_2O_4Br$: C 41.38, H 4.70, N 8.78, Br 25.1; found: C 41.20, H 4.78, N 8.61, Br 24.49.

Reaction of 4-Bromo-2,3-dimethylbut-2-en-1-yl Nitrate **52** *with Pyridine in Chloroform*

A mixture of 0.224 g (1 mmol) of 4-bromo-2,3-dimethylbut-2-en-1-yl nitrate, 2 ml of pyridine, and 10 ml of chloroform was set aside overnight. Ether was added to the reaction mixture and the resulting precipitate collected. Recrystallization from methanol–ether gave the dipyridinium salt **48** in almost quantitative yield.

Reaction of 5-Bromohex-3-en-2-yl Nitrate, **53** *with Pyridine in Chloroform*

The reaction was carried out by the procedure described above for **52**. Thus reaction of 0.224 g (1 mmol) of 5-bromohex-3-en-2-yl nitrate with 2 ml pyridine in 10 ml of chloroform gave the dipyridinium salt **51** as an oil in almost quantitative yield.

Procedure for the Reaction of Bromonium Nitrate with Phenylacetylene

The procedure was the same as that used for the reaction of iodonium nitrate with terminal alkynes. β-Bromophenylacetylene **54** was obtained in 63% yield; bp 30.5 °C/0.07 torr (lit. (14) bp 84–85 °C/10 torr).

Procedure for the Reaction of Bromonium Nitrate with Pent-4-en-1-ol in Chloroform–Pyridine

The reaction was performed by the general procedure described above. Separation of the cyclic ether and hydroxy-bromo-nitrate esters was accomplished by chromatography on Florisil and elution with petroleum ether – chloroform (9:1) and then with chloroform–methanol (9:1). Evaporation of the first fraction gave 0.65 g (20%) of *2-bromomethyltetrahydrofuran*, **65**.

The nmr spectrum $\delta_{TMS}(CDCl_3)$ 1.65–2.3 (m, 4H, $2—CH_2—$), 3.4 (t, 2H, $—CH_2Br$, J = 5 Hz, 6.5 Hz), 3.5–4.3 (m, 2H, $—CH_2—O$, —CH—O).

Evaporation of the second fraction gave a mixture of hydroxy-bromo-nitrate esters, **63** and **64**; yield 29%.

From the ether insoluble residue was isolated by the

usual procedure a mixture of bromopyridinium salts, **66** and **67**; yield 20%.

3,3,3-Triphenylpropene

This compound was prepared according to reported procedures (7, 15). mp 80–81 °C (lit. mp 80–81 °C).

Reaction of Bromonium Nitrate with 3,3,3-Triphenylpropene in Chloroform–Pyridine

The reaction was carried out by the general procedure described above. No bromonitrate ester was isolated. Crystallization of the ether insoluble residue from ethanol–ether gave a mixture of compound **70** and pyridinium bromide (yield 3.75 g). Purification was effected as follows. A mixture of 1 g of the crude reaction product, 1 g of potassium carbonate, and 25 ml of water was heated on a steam bath to about 50 °C whereupon dissolution occurred. On cooling a solid separated, which was collected. Recrystallization from methanol–ether gave 0.6 g of pure *N-[1-(2,3,3-triphenyl)prop-2-enyl]pyridinium nitrate*, **70**; mp 211–212 °C. *Anal.* calcd. for $C_{26}H_{22}N_2O_3$: C 76.1, H 5.37, N 6.83; found: C 75.71, H 5.40, N 6.75. The nmr spectrum $\delta_{TMS}((CD_3)_2SO)$ 5.72 (s, 2H, $—CH_2—$), 7–7.65 (m, 15H, 3Ph), 7.9–9.17 (m, 5H, pyridine hydrogens). The melting point and nmr spectrum were identical to those of an authentic sample synthesized as follows.

Synthesis of N-[1-(2,3,3-Triphenyl)prop-2-enyl]pyridinium Nitrate, 70

To a solution of 0.64 g (2.37 mmol) of 3,3,3-triphenylpropene in 15 ml of carbon tetrachloride was added a solution of 0.397 g (2.37 mmol) of bromine in 5 ml of carbon tetrachloride and the mixture allowed to stand for 48 h. The solvent was removed *in vacuo* and the residual solid taken up in 20 ml of carbon tetrachloride. To the solution 1 ml of pyridine was added and the mixture allowed to stand for 3 h. The precipitated solid was collected and taken up in 50 ml of hot water. Addition of a few drops of concentrated nitric acid and cooling gave a precipitate, which was collected. Recrystallization from methanol–ether gave 0.7 g (72%) of *N-[1-(2,3,3-triphenyl)prop-2-enyl]pyridinium nitrate*, **70**.

Addition of Bromonium Nitrate to (Z)-β-Deuterostyrene in Chloroform–Pyridine

The reaction was carried out by the general procedure discussed before. Thus reaction of 3.78 g (0.036 mol) of (*Z*)-β-deuterostyrene with bromonium nitrate (0.04 mol) in 60 ml of chloroform and 25 ml of pyridine at 0 °C for 3 h and work-up by the usual procedure gave 4.5 g (46%) of *threo-2-deutero-2-bromo-1-phenylethyl nitrate*, **29**. The nmr spectrum $\delta_{TMS}(CDCl_3)$ 3.62 (d, further split by H–D coupling, 1H, —CHD—Br, J_{CH-CHD} = 7.5 Hz), 6.0 (d, 1H, —CH—ONO_2, $J_{CH-CH-D}$ = 7.5 Hz), 7.37 (m, 5H, Ph). The ir spectrum ν_{max} (liquid film) 1630, 1275 cm^{-1} ($—ONO_2$).

From the ether insoluble residue and by the procedure described for the addition of iodonium nitrate to (*Z*)-β-deuterostyrene was isolated 2.5 g (26.5%) of *(Z)-N-[1-(2-deutero-1-phenyl)ethyl]pyridinium bromide*, **30**. The nmr spectrum $\delta_{TMS}((CD_3)_2SO)$ 6.43 (s, 1H, $=C<^{H}_{D}$), 7.45 (m, 5H, Ph), 8.17–9.27 (m, 5H, pyridine hydrogens).

Acknowledgments

This research was supported by the National Research Council of Canada and the Chemistry department of the University of Alberta.

1. J. W. Lown and A. V. Joshua. J. Chem. Soc. Perkin Trans. 1, 2680 (1973).
2. U. E. Diner and J. W. Lown. Can. J. Chem. **49**, 403 (1971).
3. U. E. Diner, M. Worsley, and J. W. Lown. J. Chem. Soc. C, 3131 (1971).
4. J. W. Lown and A. V. Joshua. Can. J. Chem. **55**, 122 (1977).
5. A. Hassner, F. P. Boerwinkle, and A. B. Levy. J. Am. Chem. Soc. **92**, 4879 (1970).
6. J. H. Hine. Physical organic chemistry. 2nd ed. McGraw-Hill, New York. 1962. p. 5.
7. A. Hassner and J. S. Teeter. J. Org. Chem. **35**, 3397 (1970).
8. R. O. C. Norman and C. B. Thomas. J. Chem. Soc. B, 598 (1967).
9. A. Hassner. Acc. Chem. Res. **4**, 9 (1971).
10. R. Breslow. Organic reaction mechanisms. 2nd ed. Benjamin, New York. 1969. (*a*) p. 85; (*b*) p. 125.
11. M. F. C. Ladd and W. H. Lee. J. Inorg. Nucl. Chem. **13**, 218 (1960).
12. J. D. Roberts and M. C. Caserio. Basic principles of organic chemistry. Benjamin, New York. 1965. p. 303.
13. D. L. H. Williams, E. Bienvenue-Goetz, and J. E. Dubois. J. Chem. Soc. B, 517 (1969).
14. C. J. Wilson and H. H. Wenzke. J. Am. Chem. Soc. **56**, 2026 (1934).
15. W. D. McPhee and E. G. Linstrom. J. Am. Chem. Soc. **65**, 2177 (1943).

Ab initio calculations on 4-substituted styrenes: a theoretical model for the separation and evaluation of field and resonance substituent parameters

WILLIAM F. REYNOLDS, PAUL G. MEZEY, AND GORDON K. HAMER[1]

Department of Chemistry, University of Toronto, Toronto, Ont., Canada M5S 1A1

Received June 8, 1976

WILLIAM F. REYNOLDS, PAUL G. MEZEY, and GORDON K. HAMER. Can. J. Chem. **55**, 522 (1977).

Ab initio (STO-3G minimal basis set) molecular orbital calculations on 4-substituted styrenes and CH_3X–C_2H_4 pairs indicate that Δq_H (the charge density difference between β-vinyl protons) provides a direct theoretical measure of the field effect of a polar substituent. $\Sigma q_C\pi$, the total substituent-induced π electron density change in styrene provides a theoretical measure of the resonance effect of the substituent. Δq_H and $\Sigma q_C\pi$ provide the basis of a theoretical dual substituent parameter scale, T_F and T_R^0. This scale compares very closely with experimental DSP scales, indicating the latter scales are fundamentally valid. The calculations also indicate that field effects and σ inductive effects do not show parallel trends. It is concluded that field effects are more important than σ inductive effects except at very close range. Individual carbon π electron densities reflect both resonances effects and polar π inductive effects.

WILLIAM F. REYNOLDS, PAUL G. MEZEY et GORDON K. HAMER. Can. J. Chem. **55**, 522 (1977).

Des calculs *ab initio* d'orbitales moléculaires (base minimale STO/3G) sur des styrènes substitués en position 4 et sur des paires CH_3X–C_2H_4 indiquent que le Δq_H (différence dans la densité de charge entre les protons vinyliques β) fournit une mesure théorique directe de l'effet de champ d'un substituant polaire. La valeur $\Sigma q_C\pi$, qui correspond au changement total dans la densité des électrons π qui est induit par les substituants du styrène, fournit une mesure théorique de l'effet de résonance du substituant. On utilise Δq_H et $\Sigma q_C\pi$ comme base d'une échelle théorique double pour les substituants impliquant deux paramètres, T_F et T_R^0. Cette échelle se compare très bien avec les échelles expérimentales de DSP indiquant que cette dernière échelle est valide sur une base fondamentale. Les calculs indiquent aussi que les effets de champs et les effets inductifs σ ne montrent pas des tendances parallèles. On en conclut que les effets de champs sont plus importants que les effets inductifs σ, excepté à une très courte distance. Les densités d'électrons π sur chacun des carbones individuelles sont un reflet des effets combinés de résonance et d'induction polaire des électrons π.

[Traduit par le journal]

Introduction

There are two main dual substituent parameter (DSP) scales which are claimed to divide Hammett σ constants into field/inductive and resonance substituent parameters; the σ_I–σ_R scale of Taft and co-workers (ref. 1 and references therein) and the *F*–*R* scale of Swain and Lupton (2). These DSP scales have been used to investigate substituent effects upon reaction rates, equilibrium constants, spectroscopic parameters, and calculated electron densities in aromatic molecules (3–6). While detailed statistical analyses have been presented to justify both the σ_I–σ_R scale (1) and the *F*–*R* scale (2), both DSP scales have been seriously criticized. The most important criticisms involve the criteria used for the separation of the field/inductive and resonance parameters. For example, *R* constants were evaluated assuming $R = 0$ for the $N(CH_3)_3^+$ group (2). Several groups have pointed out that this is not strictly valid (7–9). Similarly, the evaluation of σ_R values has been questioned on the grounds that it involved arbitrary (8) and possibly dubious (10) assumptions. Dewar *et al.* have particularly criticized the use of ^{19}F chemical shifts in fluorobenzenes in establishing the σ_I–σ_R scale (10). If valid, this criticism would cast particular doubt on the σ_R^0 scale which is largely based on ^{19}F chemical shifts (1). In addition, it has been claimed field parameters evaluated from aliphatic systems cannot be used in aromatic systems (11); a criticism which would cast considerable doubt on the validity of the *F* scale (2). Finally, σ_R values for individual substituents have been criticized (12).

4-Substituted styrenes have geometric charac-

[1]Present address: Department of Chemistry, McGill University, Montreal, P.Q.

teristics which allow separation of field and resonance effects (13). Consequently, we decided to carry out *ab initio* calculations on 4-substituted styrenes, using an STO/3G minimal basis set (14) and a standard geometry for the styrene system. The major purpose of this investigation was to provide a check on the validity of experimental DSP scales, based on what we hoped would prove to be an unambiguous theoretical separation of field and resonance effects. A secondary purpose was to derive a theoretical DSP scale which would apply to calculations at this level of approximation.

Since the styrene derivatives contained eight to twelve heavy atoms, the choices of minimal basis set and fixed geometries were both necessitated by cost considerations. However, we were confident that STO-3G calculations based upon fixed geometries would reproduce charge density differences with sufficient accuracy to satisfy the main purpose of the investigation. This view was supported by the fact that analogous calculations have reproduced substituent effects upon protonation energies (15) and chemical shifts (6) of aromatic derivatives with good accuracy.

Results and Discussion

Carbon and vinyl hydrogen charge densities for 4-substituted styrenes are listed in Table 1. Calculations were performed for planar and pyramidal NH_2 groups, OH, CHO, CH_3, F, CF_3, CN, and NO_2. These correspond to the minimal substituent set of Taft (1) with planar NH_2, OH, and CHO substituting for $N(CH_3)_2$, OCH_3, and $COCH_3$ for reasons of computational economy.

As a test of the accuracy of the calculated charge densities, the π charge densities for C(1) and C(β) were correlated with previously reported ^{13}C chemical shifts for these carbons (13)[2]

$$\delta_{C(1)} = 180 q_{C(1)}\pi \quad (r = 0.988)$$

$$\delta_{C(\beta)} = 193 q_{C(\beta)}\pi \quad (r = 0.987)$$

where r = correlation coefficient. Both the very good correlations and the fact that the scaling factors relating chemical shifts and charge densities are consistent with previously reported scaling factors of 160–200 ppm/π electron (17, 18) indicate that the calculations reproduce charge densities with sufficient accuracy for the purpose of the investigation as anticipated.

Since styrene is planar, electronic effects can be separated into σ and π contributions. The resonance effect of a substituent can be defined in terms of $\sum q_C\pi$, the extent of charge transfer between the substituent and the π electron system (19). Correlations of $\sum q_C\pi$ with σ_R^0 and R have been respectively reported for substituted benzenes (19, 6) and 4-substituted styrenes (13). The unique feature of the styrene system is that it also allows isolation of field effects. Through-bond effects should affect the two β vinyl hydrogen charge densities equally. However, there should be greater field-induced polarization of C(β)—H(C) than C(β)—H(B) due to the geometric arrangement of these bonds (Fig. 1). Therefore Δq_H ($\equiv q_{H(C)} - q_{H(B)}$) should in principle provide a direct measure of the electric field effect of the substituent.

There is one possible weakness in this argument. There are large π electron density changes in the phenyl group, primarily due to resonance effects. This could lead to a secondary field effect (similar to the mesomeric field effect of Dewar *et al.* (10)) which would affect $q_{H(B)}$ and $q_{H(C)}$ unequally. If so, then there would be a small resonance contribution to Δq_H and consequently an imperfect separation of field and resonance effects. To eliminate possible secondary field effects due to the phenyl group, calculations were performed for CH_3X–C_2H_4 pairs (isolated molecule or IM calculation), main-

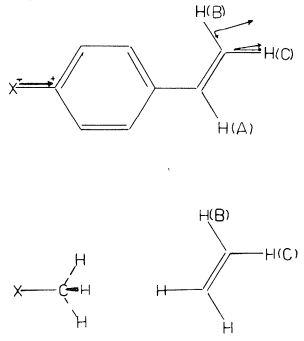

FIG. 1. 4-Substituted styrene and CH_3X–C_2H_4 pairs showing proton labelling. Arrows show electric field vectors and resolved components of field along C—H bonds.

[2] ^{13}C chemical shifts for aromatic carbons which are remote (*e.g.* 3 or more bonds removed) from a substituent are believed to accurately reflect changes in ground state carbon π electron density (see ref. 16 and references therein).

TABLE 1. Calculated charge densities ($\times 10^4$) for 4-substituted styrenes[a] relative to the unsubstituted derivative (negative sign corresponds to increased electron density)

	Value								
Parameter	NH_2(pl)[b]	NH_2(py)[c]	OH[d]	CH_3[e]	F	CHO[d]	CF_3[e]	CN	NO_2
$q_{C(4)\pi}$	+605	+476	+274	+288	−63	−189	−379	−599	−929
$q_{C(4)\sigma}$	+1478	+1336	+1737	+498	+2163	+579	+599	+1207	+1319
$q_{C(3)\pi}$	−868	−682	−677	−180	−419	+183	+143	+254	+358
$q_{C(3)\sigma}$	+545	+413	+364	+95	+164	−107	−72	−51	−173
$q_{C(2)\pi}$	+301	+245	+255	+70	+168	−35	−7	−25	−56
$q_{C(2)\sigma}$	−170	−132	−132	−48	−69	+29	+28	+45	+19
$q_{C(1)\pi}$	−561	−422	−380	−121	−192	+170	+170	+297	+415
$q_{C(1)\sigma}$	+330	+254	+229	+67	+122	−97	−90	−162	−226
$q_{C(\alpha)\pi}$	+88	+62	+43	+20	+6	−39	−51	−94	−134
$q_{C(\alpha)\sigma}$	−65	−46	−28	−30	+3	+32	+45	+77	+109
$q_{C(\beta)\pi}$	−226	−162	−124	−49	−36	+95	+110	+196	+279
$q_{C(\beta)\sigma}$	+134	+99	+75	+34	+22	−57	−66	−111	−155
$q_{H(A)}$	−35.6	−23.8	−14.1	−8.1	+1.8	+19.9	+24.5	+45.2	+65.1
$q_{H(B)}$	−51.3	−38.3	−31.2	−11.8	−12.6	+19.2	+20.0	+34.9	+48.3
$q_{H(C)}$	−51.8	−35.3	−20.1	−13.7	+3.6	+29.8	+36.6	+66.0	+93.8
$\Sigma q_C\pi$[f]	−1226	−920	−1033	−82	−787	+331	+120	+257	+234
Δq_H[g]	−0.5	+3.0	+11.1	−1.9	+16.2	+10.6	+16.6	+31.1	+45.5
Σq_σ[h]	+2231	+1925	+2480	+563	+2760	+617	+790	+1643	+2990

[a]Average for two planar conformations of vinyl group.
[b]Planar NH_2.
[c]Pyramidal NH_2. Experimental geometry from ref. 32.
[d]Average of planar *syn* and *anti* conformations.
[e]Conformation with one bond at right angles to the plane of the phenyl group.
[f]Sum of all π charge densities for styrene.
[g]Difference in charge densities for H(C) and H(B) ($\equiv q_{H(C)} - q_{H(B)}$).
[h]Total substituent-induced change in charge density for hydrogen 1*s* and carbon σ orbitals of styrene.

taining the same orientation for the C—X bond and ethylene as in styrene (Fig. 1). Results are summarized in Table 2.

There is an excellent linear relationship between values of Δq_H in the two systems:

[1] $\Delta q_H(\text{styrene}) = 1.54\Delta q_H(\text{IM}) \quad (r = 0.997)$

This demonstrates that Δq_H in styrene is insensitive to secondary field effects.[3] A linear relationship was also noted between Δq_H (styrene) and μ_X(IM), the dipole moment component along the C—X bond in the IM calculation ($r = 0.988$). An even better correlation coefficient ($r = 0.996$) was obtained for a correlation of Δq_H with $\mu_X(\text{IM})/r^3$ where r is the distance from the mid-point of the polar substituent bond to the mid-point of C(β)—H(C). This is exactly what would be expected for a dipolar electric field effect since the field varies as r^{-3} (20). These results confirm that Δq_H provides a direct measure of the dipolar electric field effect of the substituent. Therefore, Δq_H and $\sum q_C\pi$ are independent parameters which can be used to separate and estimate field and resonance effects of substituents in the styrene system.

Values of these parameters are listed in Table 1. To facilitate comparison of experimental and theoretical DSP scales, Δq_H and $\sum q_C\pi$ were scaled to produce a theoretical DSP scale labelled T_F and T_R^0.[4] Δq_H for OH was scaled to +0.27 and $\sum q_C\pi$ for OH to −0.45, corresponding to σ_I and σ_R^0 for OCH_3 (1). T_F and T_R^0 values are listed in Table 3, along with σ_I and σ_R^0 values.

In general, there is very good agreement between T_F and σ_I and particularly between T_R^0 and σ_R^0 (excluding T_F values for CN and NO_2, there is a standard deviation of less than 0.05σ units between theoretical and experimental DSP scales). The use of planar NH_2, OH, and CHO in place of $N(CH_3)_2$, OCH_3, and $COCH_3$ does not appear to introduce any significant error. A similar close parallel exists if Δq_H and $\sum q_C\pi$

[3]The slope of 1.54 reflects the enhancement of the field effect when transmitted through the cavity of the polarizable phenyl group (13).

[4]It is labelled a T_R^0 scale since the vinyl group is a neutral probe which is equally capable of the accepting or donating electrons (13). The scaling is justified since the absolute value of any substituent parameter scale is arbitrarily defined. OH was chosen to define the scale since it is a group with substantial field and resonance effects (1). F could have equally well been used for this purpose.

TABLE 2. Calculated charge densities ($\times 10^4$) for CH_3X–C_2H_4 pairs, expressed relative to calculation for CH_4–C_2H_4 (negative sign indicates increased electron density)

	Value									
Parameter	NH_2(pl)[a]	NH_2(py)	OH	CH_3	F	CHO	CF_3	CN	NO_2
q_{CH_3X}[b]	+1942	+1810	+2081	+860	+2257	+500	+363	+661	+1583
$q_{C(\alpha)}\pi$	+1.4	−4.0	−14.6	+2.2	−25.7	−17.2	−25.0	−44.4	−69.3
$q_{C(\beta)}\pi$	−1.4	+4.0	+14.6	−2.2	+25.7	+17.2	+25.0	+44.4	+69.3
$q_{H(A)}$	−0.2	+1.8	+5.9	+3.5	+10.1	+6.6	+9.6	+17.0	+26.7
$q_{H(B)}$	−0.4	+0.2	+1.8	−0.5	+4.0	+1.9	+2.9	+4.7	+9.2
$q_{H(C)}$	−0.9	+2.4	+8.2	−1.2	+13.7	+9.4	+14.4	+26.1	+38.2
Δq_H[c]	−0.5	+2.2	+6.4	−0.7	+9.7	+7.7	+11.5	+21.4	+29.0
μ_X[d]	−0.01	+0.13	+0.73	−0.01	+1.12	+1.09	+1.32	+3.09	+3.77

[a]See footnotes to Table 1 for descriptions of substituent conformations.
[b]Charge density relative to methane.
[c]$\Delta q_H = q_{H(C)} - q_{H(B)}$.
[d]Dipole moment component along C—X bond (in Debyes).

are scaled to allow comparison with F and R. We believe that the styrene calculations provide an unambiguous theoretical separation of field and resonance effects. While the procedures used to derive the σ_I–σ_R and F–R scales have been criticized (see Introduction), *the results in Table 3 demonstrate that these scales are fundamentally valid.*

While the calculations reproduce the general pattern of substituent effects for CN and NO_2 (strong electron-withdrawing field effect and weak electron-withdrawing resonance effect), they appear to over-estimate the field effects of these substituents. By contrast the field effect of F is slightly underestimated. One possible explanation is that the deviations were due to the use of non-optimized substituent geometries. This seemed improbable since the gross change in substituent geometry from planar to pyramidal NH_2 (involving a change of 0.4 Å in hydrogen atom coordinates) changes T_F for this group by only 0.08σ units. However, to check this point, full geometry optimization was performed for CH_3F and CH_3CN. When the fully optimized geometries were used in the IM calculations, Δq_H for F changed from $+9.7 \times 10^{-4}$ to $+10.6 \times 10^{-4}$ while Δq_H for the CN derivative changed from $+21.4 \times 10^{-4}$ to $+21.8 \times 10^{-4}$. This corresponds to slightly better agreement between T_F and σ_I for F but slightly worse for CN. Thus it appears that the deviations noted in Table 3 are not due to the use of incorrect substituent geometries. Rather, we believe that these discrepancies are due to the size limitation of the basis set. In particular, there are indications from previous *ab initio* studies with STO-3G basis sets that the nitrogen atom AO basis set is not matching in quality to those for other heavy atoms.[5] This could cause a lower degree of precision in calculating molecules with one or more nitrogen-heavy atom bonds (particularly with respect to bond polarities). However, it should be stressed again that the failure of the calculations to quantitatively predict the field effects of CN and NO_2 groups does not significantly detract from the overall pattern of good agreement noted in Table 3.

TABLE 3. Derived T_F and T_R^0 substituent parameters based on STO-3G charge densities for 4-substituted styrenes and σ_I–σ_R^0 values for corresponding substituents

Substituent	T_F[a]	T_R^0[b]	σ_I[c]	σ_R^0
NH_2(pl)	−0.01	−0.53	+0.06[d]	−0.52[d]
NH_2(py)	+0.07	−0.40	+0.12	−0.48
OH	+0.27	−0.45	+0.27[e]	−0.45[e]
CH_3	−0.05	−0.04	−0.04	−0.11
F	+0.39	−0.34	+0.50	−0.34
CHO	+0.26	+0.14	+0.28[f]	+0.16[f]
CF_3	+0.40	+0.05	+0.45	+0.08
CN	+0.76	+0.11	+0.56	+0.13
NO_2	+1.11	+0.10	+0.65	+0.15

[a]Estimated from Δq_H by scaling Δq_H for OH to +0.27.
[b]Estimated from $\Sigma q_C\pi$ by scaling $\Sigma q_C\pi$ for OH to −0.45.
[c]σ_I and σ_R^0 values from ref. 1.
[d]Experimental value for $N(CH_3)_2$. Dimethylaniline is believed to be planar (33).
[e]Experimental value for OCH_3. Reference 3 lists $\sigma_I = 0.27$ and $\sigma_R^0 = -0.44$ for OH. No values are given in the most recent compilation (1).
[f]Experimental value for $COCH_3$.

In addition to demonstrating the fundamental validity of experimental DSP scales, the data in Tables 1 and 2 provide further insight into the nature of polar substituent effects. First, since CH_3X is an aliphatic derivative eq. 1 suggests that the same polar substituent parameters can be used for aliphatic and aromatic compounds, contrary to the conclusions of Sjöström and Wold (11). Second, there appears to be little relation between the field effect and the σ inductive effect of the substituent. The field effect is measured by Δq_H (or T_F) while the σ inductive effect of the substituent can be estimated from $\sum q\sigma$ the substituent-induced change in σ electron density for the styrene system (Table 1). As noted previously (19, 24), the σ inductive effect primarily depends on the electronegativity of the directly bonded substituent atom, *e.g.* C < N < O < F, although other substituent atoms have some effect (particularly for CN and NO_2). By contrast, the field effect is proportional to the σ dipole moment of the substituent group as a whole (see Table 2), *e.g.* $NH_2 < OH < F \lesssim CF_3 < CN < NO_2$. As shown in Table 3, there is a close parallel between σ_I and the theoretically calculated field effect (T_F). Since polar substituent effects generally follow the σ_I order (1), this indicates that these polar effects are basically field effects rather than σ inductive effects, in agreement with previous conclusions (25). While the σ inductive effect induces large charge density changes, the calculations suggest that it

[5]According to the quality characterization of basis sets by their logarithmic energy gradients, $G_l = \partial E/\partial \log \alpha$ (where α is the orbital exponent) (21), the nitrogen STO/3G basis set appears to be off balance ($|G| = 1.52$). Convergence difficulties in the SCF procedure, that also possibly indicate lack of balance in the basis set system, have been observed with unusually high frequency for molecules containing nitrogen bonded to other heavy atoms (see *e.g.* refs. 22, 23).

is a localized effect which attenuates very rapidly with increasing number of bonds. The main inductive charge density changes in the styrene σ system occur at the directly bonded carbon C(4). At other carbons, $q_C\sigma$ appears to primarily mirror the π charge density change (see Table 1). CNDO/2 calculations for 4-substituted 1-fluorobicyclo[2.2.2]octanes have also indicated that the σ inductive effect is a localized phenomenon with very little effect beyond three carbons removed from the substituent (19).

In addition to field and σ inductive effects, polar substituent effects can also be transmitted via perturbation of the π electron system. Substituent effects which alter the π electron system without charge transfer to or from the π electron system are labelled π inductive effects (5, 26). Two types of polar π inductive effects are believed to be important. The first is field-induced polarization of the π electron system (π_F in the terminology of Topsom (5)), an effect which was previously shown to be present in both aromatic derivatives (13, 16, 27, 28) and vinyl groups (13). The IM calculations provide further evidence for the π_F effect since electron withdrawing groups polarize the ethylene π bond towards the substituent, decreasing π electron density at C(β). Changes in ethylene π electron density correlate with Δq_H or T_F:

$$q_{C(\beta)}\pi(\text{ethylene}) = 1.50\Delta q_H(\text{styrene}) \quad (r = 0.998)$$

This demonstrates that the same field substituent parameters can be used in investigations of through-space field effects and π polarization effects, π_F.

The second type of π inductive effect is the inductoelectromeric effect (29) (π_σ in the terminology of Topsom (5)). An electronegative group can withdraw electrons from the directly bonded phenyl carbon via the C—X σ bond, *i.e.* a σ inductive effect. This may induce a redistribution of the phenyl π electron system as represented by **1** (with a possible small increase in π electron

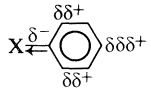

1

density at the *meta* carbons). By contrast with π_F, the π_σ effect should not be directly proportional to polar substituent constants such as σ_I, since field and σ inductive effects are not proportional to one another.

TABLE 4. Correlations of carbon charge densities for 4-substituted styrenes with T_F and T_R^0

Parameter	Value		
	ρ_F[a]	ρ_R[a]	r[b]
$q_{C(4)}\pi$	−0.089	−0.086	0.986
$q_{C(3)}\pi$	+0.023	+0.149	0.996
$q_{C(2)}\pi$	+0.002	−0.049	0.994
$q_{C(1)}\pi$	+0.033	+0.096	0.997
$q_{C(\alpha)}\pi$	−0.011	−0.017	0.998
$q_{C(\beta)}\pi$	+0.023	+0.039	0.998

[a]Weighting coefficients for equation $q_C\pi = \rho_F T_F + \rho_R T_R^0$.
[b]Correlation coefficient.

While $\sum q_C\pi$ provides a measure of the resonance effect of the substituent group, individual carbon charge densities should reflect both resonance effects and π inductive effects of the type discussed above. Correlations of individual π charge densities with T_F and T_R^0 confirm this (see Table 4).[6]

The ρ_R values for the various carbons show the expected alternation in sign and decrease in magnitude with increasing distance, *i.e.* C(4) > C(2) > C(α) and C(3) > C(1) > C(β). The pattern of ρ_F values is more complex. The expected pattern of π charge density changes associated with the π_σ effect has been illustrated schematically in **1**. When a polar substituent is separated from a phenyl group by either an aliphatic linkage (16) or a second phenyl group (29), it polarizes the entire phenyl π electron system towards the substituent (π_F effect) in a manner which can be represented schematically by **2**.

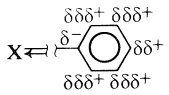

2

However, in the styrene system where the polar group is attached directly to the ring, the pattern of ρ_F values appears to be a composite of **1** and **2**. Inductive withdrawal of σ electron density from C(4) may cause a short-range perturbation of the π electron system, particularly at C(4) and C(3) (π_σ effect). This would account for the relatively poorer correlation at C(4) (since the π_σ effect is

[6]The sum of ρ_F values, $\Sigma\rho_F = 0.001$. This indicates that there is no π charge transfer component to the T_F scale (by contrast $\Sigma\rho_R = 0.232$). Therefore, the ρ_F values for individual carbons must reflect π inductive effects, *i.e.* effects which redistribute π electron density without π charge transfer to or from the substituent.

not linearly related to T_F). At longer ranges, the π_F effect seems to be dominant. It has already been shown that the vinyl ^{13}C chemical shifts in 4-substituted styrenes can be accounted for in terms of both through-space polarization of the vinyl group (as in the IM calculations, see Table 2) and polarization of the entire π electron system from phenyl to vinyl groups (13), resulting in a large field dependence for $\delta_{C(\beta)}$. This π_F effect also can account for the large ρ_F value for $q_{C(\beta)}\pi$ (Table 4).

In summary, STO-3G minimal basis set calculations for 4-substituted styrenes allow the separation and isolation of resonance effects and field effects of individual substituents. This has allowed estimation of theoretical field, T_F, and resonance, T_R^0, substituent parameters. Comparison with experimental DSP scales indicates that the latter are fundamentally valid. Individual carbon charge densities not only reflect resonance (or π charge transfer) effects but also effects by which polar substituents induce redistribution of π electron density without charge transfer to or from the substituent, *i.e.* π inductive effects. The calculations also demonstrate σ inductive effects and field effects are not parallel phenomena and that the former is important only at short range.

Details of Calculations

Throughout this study an STO–3G basis set as contracted to a minimal basis (14) was used. All *ab initio* SCF MO calculations were carried out on an IBM 370/165 computer using a version of the Gaussian 70 program (30).

Standard geometries were used for the styrene system (r_{C-H} = 1.08 Å, r_{C-C}(phenyl) = 1.40 Å, $r_{C(1)-C(\alpha)}$ = 1.46 Å, $r_{C(\alpha)-C(\beta)}$ = 1.35 Å, all angles = 120°) and for the IM calculations (r_{C-H} = 1.09 Å and tetrahedral angles for CH_3X). Substituent geometries were chosen to reproduce experimental geometries as accurately as possible. Full details of substituent geometries have been given elsewhere (31).

Acknowledgments

Financial support from the National Research Council of Canada is gratefully acknowledged. We thank Professor R. W. Taft and Professor R. D. Topsom for providing copies of manuscripts prior to publication and for helpful discussions.

1. R. T. C. Brownlee, S. Ehrenson, and R. W. Taft. *In* Progress in physical organic chemistry. Vol. 10. *Edited by* A. Streitwiser and R. W. Taft. John Wiley and Sons, New York. 1973.
2. C. G. Swain and E. C. Lupton. J. Am. Chem. Soc. **90**, 4328 (1968).
3. P. R. Wells, S. Ehrenson, and R. W. Taft. *In* Progress in physical organic chemistry. Vol. 6. *Edited by* A. Streitwieser and R. W. Taft. John Wiley and Sons, New York. 1968.
4. A. R. Katritzky and R. D. Topsom *In* Advances in linear free energy relationships. *Edited by* N. B. Chapman and J. Shorter. Plenum Press, New York. 1972.
5. R. D. Topsom. *In* Progress in physical organic chemistry. Vol. 12. *Edited by* A. Streitwieser and R. W. Taft. John Wiley and Sons, New York. 1976.
6. W. J. Hehre, R. W. Taft, and R. D. Topsom. *In* Progress in physical organic chemistry. Vol. 12. *Edited by* A. Streitwieser and R. W. Taft. John Wiley and Sons, New York. 1976.
7. (*a*) P. J. Q. English, A. R. Katritzky, T. T. Tidwell, and R. D. Topsom. J. Am. Chem. Soc. **89**, 1767 (1968). (*b*) N. C. Cutress, T. B. Grindley, A. R. Katritzky, M. V. Sinnot, and R. D. Topsom. J. Chem. Soc. Perkin II, 2255 (1972).
8. I. R. Ager, L. Phillips, T. J. Tewson, and V. Wray. J. Chem. Soc. Perkin II, 1979 (1972).
9. W. Adcock, J. Alste, S. Q. A. Rizvi, and M. Aurangzeb. J. Am. Chem. Soc. **98**, 1701 (1976).
10. M. J. S. Dewar, R. Golden, and J. M. Harris. J. Am. Chem. Soc. **93**, 4187 (1971).
11. M. Sjöström and S. W. Wold. Chem. Scripta, **6**, 114 (1974).
12. A. H. Hoefnagel and B. M. Wepster. J. Am. Chem. Soc. **95**, 5357 (1973).
13. G. K. Hamer, I. R. Peat, and W. F. Reynolds. Can. J. Chem. **51**, 897 (1973); **51**, 915 (1973).
14. W. J. Hehre, R. F. Stewart, and J. A. Pople. J. Chem. Phys. **51**, 2657 (1969).
15. J. M. McKelvey, S. Alexandratos, A. Streitwieser, J.-L. M. Abboud, and W. J. Hehre. J. Am. Chem. Soc. **98**, 244 (1976).
16. W. F. Reynolds, I. R. Peat, M. H. Freedman, and J. R. Lyerla. Can. J. Chem. **51**, 1857 (1973).
17. P. C. Lauterbur. J. Am. Chem. Soc. **83**, 1838 (1961).
18. H. Spiesecke and W. G. Schneider. Tetrahedron Lett. 468 (1961).
19. R. T. C. Brownlee and R. W. Taft. J. Am. Chem. Soc. **92**, 707 (1970).
20. C. J. F. Böttcher. Theory of electric polarization. Elsevier, Amsterdam. 1952.
21. R. E. Kari, P. G. Mezey, and I. G. Csizmadia. J. Chem. Phys. **63**, 581 (1975).
22. J. D. Goddard, P. G. Mezey, and I. G. Csizmadia. Theor. Chim. Acta, **39**, 1 (1975).
23. P. G. Mezey, A. J. Kresge, and I. G. Csizmadia. Can. J. Chem. **54**, 2526 (1976).
24. P. R. Wells. Progress in physical organic chemistry. Vol. 6. *Edited by* A. Streitwieser and R. W. Taft. John Wiley and Sons, New York. 1968.
25. L. M. Stock. J. Chem. Ed. **49**, 400 (1972).
26. A. R. Katritzky and R. D. Topsom. J. Chem. Ed. **48**, 427 (1971).

27. D. A. DAWSON and W. F. REYNOLDS. Can. J. Chem. **52**, 373 (1975).
28. W. F. REYNOLDS and G. K. HAMER. J. Am. Chem. Soc. **98**, 7296 (1976).
29. M. J. S. DEWAR and P. J. GRISDALE. J. Am. Chem. Soc. **84**, 3539 (1962).
30. W. J. HEHRE, W. A. LATHAN, R. DITCHFIELD, M. D. NEWTON, and J. A. POPLE. GAUSSIAN 70, Quantum Chemistry Program Exchange, Indiana University, Bloomington, Indiana.
31. G. K. HAMER. Ph.D. Thesis, University of Toronto, Toronto, Ont. 1973.
32. D. G. LISTER and K. TYLER. Chem. Commun. 152 (1966).
33. H. H. JAFFÉ and M. ORCHIN. Theory and applications of ultraviolet spectroscopy. John Wiley and Sons, New York. 1962. p. 409.

Substituent-induced ^{1}H chemical shifts for 4-substituted (2,2-dichlorocyclopropyl)benzenes: further evidence for intramolecular electric field effects on ^{1}H chemical shifts

ROBERT H. KOHLER AND WILLIAM F. REYNOLDS

Department of Chemistry, University of Toronto, Toronto, Ont., Canada M5S 1A1

Received June 8, 1976

ROBERT H. KOHLER and WILLIAM F. REYNOLDS. Can. J. Chem. **55**, 530 (1977).

Correlations of cyclopropyl proton chemical shifts for 4-substituted (2,2-dichlorocyclopropyl)-benzenes with σ_I and σ_R^0 provide evidence that these chemical shifts reflect direct field effects and weak phenyl–cyclopropyl conjugative interactions. Corrections for variable ring current effects due to substituent-induced changes in conformation improve the individual correlations but do not alter the basic pattern of results. Correlation of the β cyclopropyl ^{1}H chemical shift difference with σ_I, with calculated hydrogen electron densities, and with calculated electric field components provides further strong evidence for a field effect on ^{1}H chemical shifts.

ROBERT H. KOHLER et WILLIAM F. REYNOLDS. Can. J. Chem. **55**, 530 (1977).

Des corrélations entre les déplacements chimiques des protons du cyclopropyle de (dichloro-2,2 cyclopropyl-) benzènes substitués en position 4 avec σ_I et σ_R^0 suggèrent que ces déplacements chimiques sont un reflet d'effets directs de champs et d'interactions faibles de conjugaison du phényle avec le cyclopropyle. Des corrections pour les effets de courant de cycle qui varient à cause de changements, induits par les substituants, dans la conformation améliorent les corrélations individuelles mais n'altèrent pas les tendances de base des résultats. La corrélation des différences dans les déplacements chimiques du ^{1}H en β du cyclopropyle avec le σ_I, avec les densités électroniques calculées pour l'hydrogène et avec les composantes calculées pour les champs électriques suggèrent encore plus fortement l'influence d'effet de champ sur les déplacements chimiques de ^{1}H.

[Traduit par le journal]

Introduction

Substituent-induced ^{1}H chemical shifts in 4-substituted styrenes (1) and phenylacetylenes (2) can be accounted for in terms of through-space field effects, resonance effects, and π inductive (polarization) effects. In each case, the side chain is conjugated with the phenyl group. Investigations of 4-substituted α-alkylstyrenes showed that the transmission of resonance and π inductive effects to the side chain decreased as conjugation decreased (3). Consequently, it was decided to extend these investigations to systems in which side chain conjugation was weak, in an attempt to provide further evidence for the existence of through-space electric field effects on ^{1}H chemical shifts. The compounds chosen for this purpose were 4-substituted (2,2-dichlorocyclopropyl)benzenes. These seemed particularly useful compounds for investigation since, as in the case of styrenes (1), the two β hydrogens have different geometries with respect to the 4-X phenyl group, thus potentially allowing the isolation of through-space effects from through bond effects:

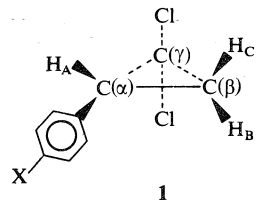

1

In addition, these compounds could easily be synthesized by dichlorocarbene addition to the corresponding styrenes (4). The ABC spectrum for the dichlorocyclopropyl group is also considerably easier to analyze than the ABB′CC′ spectrum which would be given by cyclopropylbenzene derivatives. Finally, very unusual substituent-induced ^{1}H chemical shifts had been reported for **1** (5), results which suggested to us that a more thorough investigation of this system was desirable.

Results and Discussion

^{1}H chemical shifts for 4-substituted derivatives of **1** are given in Table 1. Correlations of these shifts with the dual substituent parameters σ_I and σ_R^0 are also given in Table 1, along with correla-

TABLE 1. ^{1}H chemical shifts for cyclopropyl protons (in ppm relative to tetramethylsilane) of 4-substituted (2,2-cyclopropyl)benzene derivatives and correlations of these chemical shifts with $\sigma_I - \sigma_R^0$

Substituent	$\delta_{H(A)}$[a]	$\delta_{H(B)}$	$\delta_{H(C)}$	$(\delta_{H(C)} - \delta_{H(B)})$
H	2.7841	1.7136	1.8103	0.0967
$N(CH_3)_2$	2.6953	1.6182	1.7315	0.1133
OCH_3	2.7240	1.6412	1.7726	0.1314
OC_2H_5	2.7203	1.6349	1.7686	0.1339
CH_3	2.7453	1.6787	1.7829	0.1042
$C(CH_3)_3$	2.7452	1.6860	1.7942	0.1082
F	2.7495	1.6630	1.8246	0.1616
C_6H_5	2.7068	1.6890	1.8683	0.1193
CF_3	2.8210	1.7585	1.8969	0.1384
CN	2.8041	1.7594	1.9101	0.1507
NO_2	2.8511	1.8031	1.9497	0.1466

Family	Parameter	ρ_I[b]	ρ_R[b]	r[c]
1	$\delta_{H(A)}$	0.054	0.137	0.974
1	$\delta_{H(B)}$	0.068	0.202	0.985
1	$\delta_{H(C)}$	0.151	0.181	0.996
1	$\delta_{H(C)} - \delta_{H(B)}$[d]	0.077	—	0.934
1	$\delta_{H(C)} - \delta_{H(B)}$	0.083	−0.021	0.962
Styrene	$\delta_{H(A)}$[e]	0.081	0.204	0.979
	$\delta_{H(B)}$	0.148	0.457	0.995
Styrene	$\delta_{H(C)}$	0.266	0.475	0.996
	$\delta_{H(C)} - \delta_{H(B)}$	0.116	0.017	0.984

[a]For proton labelling see **1**.
[b]Weighting coefficients for equation $\delta = \rho_I\sigma_I + \rho_R\sigma_R^0 + \delta_0$.
[c]Correlation coefficient.
[d]Correlation for σ_I only.
[e]Correlations include some derivatives as **1** plus SCH_3, $COCH_3$. Data from ref. 1.

tions of the ^{1}H chemical shifts for 4-substituted styrenes, for comparison. σ_I should measure the polar (field/inductive) effect of the substituent while σ_R^0 measures the resonance (conjugative) effect of the substituent (6). Through-bond (resonance and inductive) effects should affect $\delta_{H(B)}$ and $\delta_{H(C)}$ equally since H(B) and H(C) are separated by the substituent by the same number of bonds. However, $\delta_{H(C)}$ should be more sensitive to through-space electric field effects since the substituent-induced electric field acts more directly along the C(β)—H(C) bond than along C(β)—H(B) (the field effect depends upon the magnitude of the electric field acting along a C—H bond (7)). This greater field effect for $\delta_{H(C)}$ should be reflected by a greater ρ_I value for $\delta_{H(C)}$ than $\delta_{H(B)}$ in the σ_I,σ_R correlations:

$$[1] \qquad \delta = \rho_I\sigma_I + \rho_R\sigma_R^0 + \delta_0$$

In fact ρ_I is greater for $\delta_{H(C)}$ than $\delta_{H(B)}$, indicating the presence of a significant electric field effect. By contrast ρ_R is similar for $\delta_{H(B)}$ and $\delta_{H(C)}$, as expected for a through-bond effect.

ρ_R values are slightly greater for $\delta_{H(B)}$ and $\delta_{H(C)}$ than for $\delta_{H(A)}$, as observed in a more pronounced manner for styrene. In the latter case, this reflects conjugative interactions which alter π electron density at C(β) (1). Therefore, it appears that there is weak phenyl–cyclopropyl conjugation in **1**, with the cyclopropyl C—C bonds having some π character.[1] This is consistent with previous evidence for phenyl–cyclopropyl conjugation (11–14), including the observation that the cyclopropyl group is a weaker transmitter of electronic effects than an alkene function (14).

In spite of the generally reasonable ρ_I and ρ_R values in the σ_I,σ_R^0 correlations, the correlation of $(\delta_{H(C)} - \delta_{H(B)})$ with both σ_I and σ_I,σ_R^0 is mediocre.

(2,2-Dichlorocyclopropyl)benzene is a conformationally mobile system. On the basis of Kerr constant and dipole moment measurements, Aroney *et al.* estimated that the equilibrium angle of twist, ϕ, of the phenyl group was 60° (15).

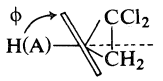

2

This represents a balance between conjugative effects which favor ϕ = 0° (as observed in electron diffraction studies of cyclopropylbenzene (11)) and steric interactions (particularly phenyl–Cl interactions). It was also concluded that *para* substituents could alter ϕ by as much as 7° (15), presumably by altering phenyl–cyclopropyl conjugation. Since variation in ϕ would significantly alter the ring current effect of the phenyl group at H(A), H(B), and H(C), it was felt that this might account for the poor correlations for $(\delta_{H(C)} - \delta_{H(B)})$. Consequently, we undertook CNDO/2 energy minimization calculations for **1**, varying ϕ from 45° to 75°. The calculations predict a shallow minimum about ϕ = 60° with the shape of the potential well being substituent-dependent. Typical results are presented in Fig. 1.[2] The apparent success of the calculation in predicting

[1]In the ^{1}H spectra of 4-substituted ethylbenzene the CH_3 protons are about 40% as sensitive to substituent effects as the CH_2 protons (8–10). This is presumably the pattern characteristic of non-conjugating alkyl groups.

[2]The complete set of calculated energy levels is available, at a nominal charge, from the Depository of Unpublished Data, CISTI, National Research Council of Canada, Ottawa, Canada K1A 0S2.

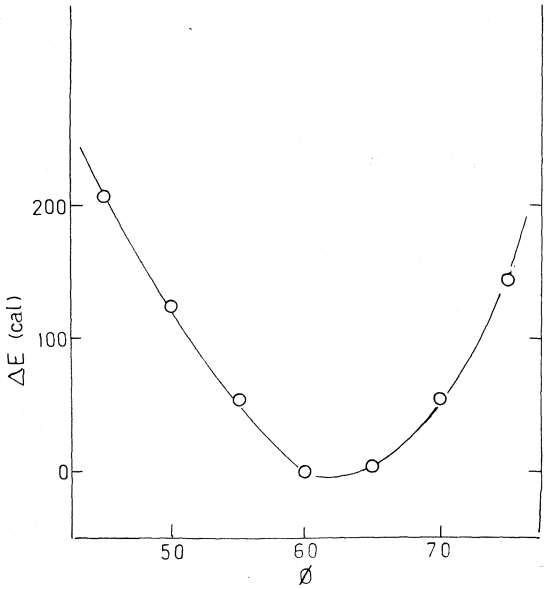

FIG. 1. Energy (cal/mol) for unsubstituted 2,2-(dichlorocyclopropyl)benzene as a function of the angle ϕ between C(α)—H and the plane of the phenyl group.

the energy minimum is in itself interesting since CNDO/2 calculations for conjugated molecules often fail to predict the most stable conformations (16). The calculations may be better in cases like this where steric interactions dominate.

A weight-averaged angle of twist, $\langle\phi\rangle$, was estimated for each derivative by first determining the relative population, N_ϕ, at each angle ϕ, using the Boltzmann expression

$$[2] \qquad N_\phi/N_0 = e^{-(E_\phi - E_0)/RT}$$

where E_0 and N_0 refer to the angle of minimum energy and T was taken as 300 K, corresponding to the probe temperature, then calculating $\langle\phi\rangle$ from

$$[3] \qquad \langle\phi\rangle = \sum^{n} N_\phi \cdot \phi \Big/ \sum^{n} N_\phi$$

Estimated values of $\langle\phi\rangle$ are given in Table 2. These are generally smaller for electron-withdrawing substituents, corresponding to increased phenyl–cyclopropyl conjugation (as expected since the cyclopropyl group is an electron donor group (14, 17)). Ring current corrections were estimated by Johnson–Bovey calculations (18), using a program written for that purpose (19). The ring current correction was estimated for the average angle $\langle\phi\rangle$. This may introduce a small error since the ring current correction varies in a non-linear fashion with angle. However, since the ring current calculations may not be quantitatively accurate (20), this approximation seemed justified. Corrected chemical shifts are given in Table 3. The correlations of $(\delta_{H(C)} - \delta_{H(B)})$ with σ_I and with $\sigma_I - \sigma_R^0$ are both improved by the ring current corrections (see Table 3). Comparison of the correlations in Tables 1 and 3 shows that substituent-induced changes in conformation introduce a spurious[3] resonance contribution to $\delta_{H(B)}$ which contributes to the poor correlation for $(\delta_{H(C)} - \delta_{H(B)})$. The corrected correlations indicate very similar field effects upon $(\delta_{H(C)} - \delta_{H(B)})$ as in the case of styrenes (Table 1). The significantly improved correlation coefficients suggests that the ring current corrections must be at least semi-quantitatively correct, in spite of the approximations noted above. This is supported by the equations given below. It is also important to note that the fundamental conclusions concerning greater field effects for $\delta_{H(C)}$ and greater resonance effects for β than α hydrogens are unaltered by corrections.

$(\delta_{H(C)} - \delta_{H(B)})$ primarily reflects field effects. The electric field effect due to a substituent can be estimated from the Buckingham equation (7):

$$[4] \qquad \Delta\delta_H = AE_z$$

where E_z is the field component acting along the C—H bond (7) and A is a constant with a value in the range $2.9–5.5 \times 10^{-12}$ (esu)$^{-1}$ (3). Conse-

TABLE 2. Table of weight-averaged angles, $\langle\phi\rangle$, for 4-substituted (2,2-dichlorocyclopropyl)benzene derivatives

Substituent	$\langle\phi\rangle^a$
H	60.4
$N(CH_3)_2$	61.2
OCH_3	61.0
OC_2H_5	61.0
CH_3	60.6
$C(CH_3)_3$	60.7
F	60.7
C_6H_5	60.4
CF_3	59.7
CN	60.0
NO_2	59.3

[a] $\langle\phi\rangle$ = average dihedral angle for C(α)—H bond relative to plane of phenyl group as determined by [2] and [3].

[3] Spurious in the sense that it arises from magnetic anisotropy effects rather than from changes in local electron density.

TABLE 3. Ring current corrections and corrected chemical shifts for cyclopropyl protons of **1**

Substituent	H(A) $\Delta\delta_{RC}$[a]	H(A) $\delta_{H(A)corr}$[b]	H(B) $\Delta\delta_{RC}$	H(B) $\delta_{H(B)corr}$	H(C) $\delta_{H(C)corr}$[c]	H(C)—H(B) $(\delta_{H(C)} - \delta_{H(B)})_{corr}$
H	—	2.784	—	1.714	1.810	0.097
$H(CH_3)_2$	+0.002	2.697	+0.017	1.635	1.732	0.097
OCH_3	+0.002	2.726	+0.014	1.655	1.773	0.118
OC_2H_5	+0.002	2.712	+0.014	1.649	1.769	0.120
CH_3	+0.001	2.746	+0.005	1.684	1.783	0.099
$C(CH_3)_3$	+0.001	2.746	+0.007	1.693	1.794	0.101
F	+0.001	2.750	+0.007	1.670	1.825	0.155
C_6H_5	0.000	2.761	0.000	1.689	1.808	0.119
CF_3	−0.002	2.819	−0.015	1.743	1.897	0.153
CN	−0.001	2.803	−0.009	1.751	1.910	0.159
NO_2	−0.003	2.841	−0.025	1.778	1.947	0.171

Parameter	ρ_I[d]	ρ_R[d]	r[e]
$\delta_{H(A)corr}$	0.083	0.132	0.975
$\delta_{H(B)corr}$	0.049	0.161	0.987
$\delta_{H(C)corr}$	0.151	0.181	0.996
$(\delta_{H(C)} - \delta_{H(B)})_{corr}$[f]	0.108	—	0.973
$(\delta_{H(C)} - \delta_{H(B)})_{corr}$	0.101	0.018	0.986

[a]Correction factor to compensate for ring current change (relative to unsubstituted derivative) due to angle change in Table 2. The correction factor is opposite in sign to the ring current change to remove the effect of this change, *e.g.* the decrease in $\langle\phi\rangle$ for the NO_2 derivative leads to a positive (lowfield) shift for $\delta_{H(B)}$. Therefore the correction factor is negative.
[b]^1H chemical shift including $\Delta\delta_{RC}$.
[c]Correction factors ranged from 0.0003 ppm for $N(CH_3)_2$ to −0.0004 ppm for NO_2.
[d]Weighting factors for correlation equation $\delta = \rho_I\sigma_I + \rho_R\sigma_R^0 + \delta_0$.
[e]Correlation coefficient.
[f]Correlation with σ_I only.

quently, $(\delta_{H(C)} - \delta_{H(B)})_{corr}$ was correlated with ΔE_z(H(C)—H(B)), the difference in substituent-induced electric fields acting along the two C(β)—H bonds. Field components were estimated using aliphatic σ bond moments (21) for the substituents[4] and using previously listed parameters (19). Values of ΔE_z(H(C)—H(B)) are given in Table 4. The following correlation was obtained:

$$[5]\quad (\delta_{H(C)} - \delta_{H(B)})_{corr} = 4.31 \times 10^{-12}\Delta E_z(H(C)—H(B)) \quad (r = 0.970)$$

Both the reasonable value of A and the good correlation coefficient indicate that $\delta_{H(C)} - \delta_{H(B)}$ reflects field effects. (A much worse correlation was obtained for the uncorrected shifts (r = 0.836).)

Hydrogen charge densities were also estimated by CNDO/2 molecular orbital calculations (see Table 4). Correlation of $(\delta_{H(C)} - \delta_{H(B)})_{corr}$ *vs.* $(q_{H(C)} - q_{H(B)})$ yielded:

$$[6]\quad (\delta_{H(C)} - \delta_{H(B)})_{corr} = 26.9\Delta(q_{H(C)} - q_{H(B)}) \quad (r = 0.976)$$

The scaling factor of 27 ppm/1*s* electron is in good agreement with previously reported values which range from 18 to 30 ppm/1*s* electron (23, 24). Since through-space field effects alter hydrogen charge density by polarizing C—H bonds (1), [6] provides further evidence for the presence of these effects. Thus correlations of $\delta_{H(C)} - \delta_{H(B)}$ (corrected for changes in ring current effects) with field/inductive substituent parameters, with calculated electric field components, and with hydrogen charge densities all indicate the presence of a through-space field effect. This provides further proof for the importance of intramolecular field effects on ^1H chemical shifts.

Both the corrected correlations for **1** (Table 3) and the styrene correlations (Table 1) show a slightly greater ρ_R value for $\delta_{H(C)}$ than for $\delta_{H(B)}$. This could be taken as an indication of a secondary field effect due to the large resonance-induced π electron density changes at C(1). Due to the bond geometries, $\delta_{H(C)}$ should be slightly more sensitive than $\delta_{H(B)}$ to a secondary field effect, thus possibly accounting the slight larger

[4]*Ab initio* calculations on 4-substituted styrenes demonstrate that the field effect of the substituent is directly proportional to (aliphatic) σ bond moment of the substituent (22).

TABLE 4. Calculated electric field components (in esu) due to polar substituents and calculated (CNDO/2) charge densities ($\times 10^4$) for 4-substituted (2,2-dichlorocyclopropyl)benzene derivatives

Substituent	ΔE_z(H(C)—H(B))[a] ($\times 10^4$)	$\Delta(q_{H(C)} - q_{H(B)})$[b]	$q_{C(1)}$[c]	$\Sigma\Delta E_z$(H(C)—H(B))[d] ($\times 10^4$)
$N(CH_3)_2$	+0.092	−1	−368	−0.409
OCH_3	+0.392	+5	−280	+0.009
OC_2H_5	+0.392	+5	−276	+0.015
CH_3	−0.162	−2	−100	−0.318
$C(CH_3)_3$	−0.243	−1	−140	−0.434
F	+0.937	+17	−175	+0.701
C_6H_5	+0.150	+3	−28	+0.122
CF_3	+0.996	+21	+151	+1.202
CN	+1.393	+13(+16)[e]	+ 39(+48)[e]	+1.458
NO_2	+1.598	+34(+27)	+215(+169)	+1.829

[a]Difference in electric field components (due to polar substituent) acting along C(β)—H(C) and C(β)—H(B).
[b]Charge density difference between H(C) and H(B), expressed relative to the charge density difference in the pattern compound.
[c]Charge density at C(1), relative to the parent compound (negative sign indicates increased electron density).
[d]Difference in electric field components due to both the polar substituent (dipolar field) and charge density change at C(1) (monopolar field).
[e]Charge densities scaled by ratio of experimental/calculated dipole moment in benzonitrile and nitrobenzene. Charge densities were scaled since CNDO/2 calculations respectively underestimate and overestimate electronic effects of CN and NO_2 groups (1, 2). Scaled charge densities were used in correlations.

ρ_R value for $\delta_{H(C)}$. A similar explanation has been advanced to account for the chemical shifts of $\delta_{H(A)}$ in styrene (1) and the methyl ^1H chemical shifts in trimethylanilinium ions (25, 26). On the other hand, *ab initio* calculations on styrene provide no evidence for the existence of a secondary field effect (22).

To investigate this point further, an attempt was made to calculate secondary field effects. Since field effects drop off rapidly with distance and since both resonance (1) and π polarization effects (27) cause much larger π electron density changes at C(1) than C(2,6), the secondary field effect was estimated assuming a point charge at C(1). Electron densities were estimated by CNDO/2 calculations (see Table 4). Values of $\sum \Delta E_z$(H(C)—H(B)), the sum of direct (dipolar) and secondary (monopolar) field components, are also given in Table 4. However, the correlation of this parameter with $(\delta_{H(C)} - \delta_{H(B)})_{corr}$ was worse than the correlation in [5] ($r = 0.952$ as compared to 0.970 for [5]). A similar observation was made when an attempt was made to estimate secondary field effects in styrene. This leads to the conclusion that secondary field effects are not important in these systems, in agreement with the results of *ab initio* calculations on styrene derivatives (22). However, there may be inductive transmission of the effects of electron density changes at C(1) to the side chain protons, since $q_{H(A)}$ (and $\delta_{H(A)}$) in styrene appear to reflect the electron density changes at C(1) (1). While field effects appear to dominate over inductive effects at long range (28, 29), calculations on aliphatic compounds suggest that inductive effects may be important at distances up to three bonds (29). The smaller shifts for CH_3 protons than CH_2 protons for ethylbenzenes (8–10) are consistent with inductive effects, possibly combined with weak hyperconjugative interactions of the alkyl and phenyl groups (25). The apparent resonance contribution to $\delta_{H(C)} - \delta_{H(B)}$ may be due to small substituent induced distortions of the side-chain group. The difference in ρ_R values for $\delta_{H(B)} - \delta_{H(C)}$ in each case corresponds to a resonance contribution of *ca.* 0.01 ppm. Due to the close proximity of H(B) to the phenyl group in each system, very minor substituent induced changes in bond length and/or bond angle could lead to this apparent resonance contribution.

As mentioned in the Introduction Mal'tsev *et al.* reported very unusual ^1H chemical shifts for derivatives of **1** (5). They found that $\delta_{H(A)}$, $\delta_{H(B)}$, and $\delta_{H(C)}$ for the unsubstituted derivative were to high field of the corresponding protons in both nitro and dimethylamino derivatives (5). Their data and ours are compared in Table 5. The $N(\cdot CH_3)_2$ and NO_2 derivatives show the expected low field shifts associated with the transfer of a polar solute from C_6D_{12} to CCl_4 (30) but the unsubstituted derivative shows an anomalous high field shift. However, Cox and Smith reported data for the unsubstituted derivative in CCl_4 (31) which are much more consistent with the other data. This suggests that there may be significant experimental errors in the data of Mal'tsev *et al.* (5). Certainly our ^1H chemical shift data show no similar anomalies.

TABLE 5. Comparison of ^1H chemical shifts of 4-substituted derivatives of **1** from this work and from ref. 5. Chemical shifts in ppm from tetramethylsilane

Substituent	Solvent	$\delta_{H(A)}$	$\delta_{H(B)}$	$\delta_{H(C)}$
$N(CH_3)_2$[a]	C_6D_{12}	2.695	1.618	1.732
H	C_6D_{12}	2.784	1.713	1.810
NO_2	C_6D_{12}	2.851	1.803	1.950
$N(CH_3)_2$[b]	CCl_4	2.79	1.66	1.80
H	CCl_4	2.60	1.53	1.59
NO_2	CCl_4	3.00	1.97	2.13
H[c]	CCl_4	2.824	1.772	1.888

[a]This work.
[b]Data from ref. 5.
[c]Data from ref. 31.

Experimental

Four-substituted (2,2-dichlorocyclopropyl)benzenes were synthesized by addition of dichlorocarbene to the corresponding 4-substituted styrene, using the method of Makoszka and Wawrzyniewiecz (4). The styrenes were either obtained commercially or were available from a previous investigation (1). The (2,2-dichlorocyclopropyl)-benzene derivatives were characterized by their nmr spectra which showed characteristic ABC multiplets for the cyclopropyl protons and AA'BB' spectra for the *para*-disubstituted benzene group.

^1H spectra were obtained using procedures identical to those previously reported (1). It is estimated that individual chemical shifts are accurate to 0.001 ppm. CNDO/2 calculations were carried out on an IBM 370/165 computer using a standard program (32) and standard geometries (33). The energy minimization calculations were carried out using previously reported geometries for cyclopropylbenzenes (11, 15).

Acknowledgement

Financial support from the National Research Council of Canada is gratefully acknowledged.

1. G. K. HAMER, I. R. PEAT, and W. F. REYNOLDS. Can. J. Chem. **51**, 897 (1973).
2. D. A. DAWSON and W. F. REYNOLDS. Can. J. Chem. **53**, 373 (1975).
3. G. K. HAMER, I. R. PEAT, and W. F. REYNOLDS. Can. J. Chem. **51**, 915 (1973).
4. M. MAKOSZKA and M. WAWRZYNIEWIECZ. Tetrahedron Lett. 4659 (1969).
5. A. K. MAL'TSEV, A. J. STEINSCHNEIDER, A. V. KESSENICK, and O. M. NEFEDOV. Teor. Eksp. Khim. **8**, 265 (1972).
6. S. EHRENSON, R. T. C. BROWNLEE, and R. W. TAFT. *In* Progress in physical organic chemistry. Vol. 10. *Edited by* A. Streitwieser and R. W. Taft. John Wiley and Sons, New York. 1973.
7. A. D. BUCKINGHAM. Can. J. Chem. **38**, 300 (1960).
8. K. L. WILLIAMSON, N. C. JACOBUS, and K. T. SOUCY. J. Am. Chem. Soc. **86**, 4021 (1964).
9. T. A. WITTSTRUCK and E. N. TRACHTENBERG. J. Am. Chem. Soc. **89**, 3803 (1967).
10. R. KOHLER and W. F. REYNOLDS. Unpublished results.
11. L. VILKOV and N. I. SADOVA. Dokl. Akad. Nauk SSSR, **162**, 565 (1965).
12. G. L. CLOSS and H. B. KLINGER. J. Am. Chem. Soc. **87**, 3265 (1965).
13. J. P. PETE. Bull. Soc. Chem. Fr. 357 (1967).
14. R. G. PEWS and N. D. OJHA. J. Am. Chem. Soc. **91**, 5769 (1969).
15. M. J. ARONEY, K. E. CALDERBANK, and H. J. STOOTMAN. J. Chem. Soc. Perkin Trans. II, 2060 (1973).
16. O. GROPEN and H. M. SEIP. Chem. Phys. Lett. **11**, 445 (1971).
17. Y. KUSUYAMA and Y. IKEDA. Bull. Chem. Soc. Fr. **46**, 204 (1973).
18. C. E. JOHNSON and F. A. BOVEY. J. Chem. Phys. **29**, 1012 (1958).
19. G. K. HAMER. Ph.D. Thesis, University of Toronto, Toronto, Ontario. 1973.
20. R. B. MALLION. *In* Nuclear magnetic resonance. Vol. 4. Chemical Society Specialist Report. *Edited by* R. K. Harris. London. 1975.
21. C. W. CUMPER. Tetrahedron, **25**, 3131 (1969).
22. W. F. REYNOLDS, P. G. MEZEY, and G. K. HAMER. Can. J. Chem. This issue.
23. J. A. POPLE, W. G. SCHNEIDER, and H. J. BERNSTEIN. High resolution nmr. McGraw-Hill, New York. 1959. Chapt. 7.
24. W. T. RAYNES. *In* Nuclear magnetic resonance. Vol. 2. The Chemical Society, London. 1973. p. 23.
25. D. A. DAWSON and W. F. REYNOLDS. Can. J. Chem. **52**, 39 (1974).
26. B. M. LYNCH. Org. Magn. Reson. **6**, 190 (1974).
27. W. F. REYNOLDS, I. R. PEAT, M. H. FREEDMAN, and J. R. LYERLA. Can. J. Chem. **51**, 1857 (1973).
28. L. M. STOCK. J. Chem. Educ. **49**, 400 (1972).
29. R. T. C. BROWNLEE and R. W. TAFT. J. Am. Chem. Soc. **92**, 7007 (1970).
30. I. O. KUNTZ and M. D. JOHNSTON. J. Am. Chem. Soc. **89**, 6008 (1967).
31. R. H. COX and S. H. SMITH. J. Mol. Spectrosc. **21**, 232 (1966).
32. Quantum Chemistry Program Exchange Program 141.
33. J. A. POPLE and D. L. BEVERIDGE. Approximate molecular orbital theory. McGraw-Hill, New York. 1970.

^{13}C Chemical shifts for 4-substituted phenylvinyl ethers, sulfides, and selenides: evidence concerning the relative abilities of O, S, and Se to transmit electronic effects

WILLIAM F. REYNOLDS AND ROBERT A. MCCLELLAND
Department of Chemistry, University of Toronto, Toronto, Ont., Canada M5S 1A1

Received June 8, 1976

WILLIAM F. REYNOLDS and ROBERT A. MCCLELLAND. Can. J. Chem. **55**, 536 (1977).

^{13}C chemical shifts for β carbons of 4-substituted phenylvinyl ethers, sulfides, and selenides plus previous data for styrenes indicate that the relative ability of link groups to transmit electronic effects between conjugative groups is S > Se ≈ — > O (where — refers to no link group, *i.e.* styrene). However, marked deviations from additivity are noted for C(1) chemical shifts which may indicate that O deactivates the ring to electronic substituent effects while S and Se activate the ring. If this explanation is valid then the actual ability of the link atom to transmit electronic effects is — > O > S > Se.

WILLIAM F. REYNOLDS et ROBERT A. MCCLELLAND. Can. J. Chem. **55**, 536 (1977).

Les déplacements chimiques du carbone-13 des carbones-β d'éthers sulfures et sélénures de vinyle et de phényles substitués en position 4, utilisés de concert avec des données antérieures pour les styrènes, indiquent que l'habilité relative des groupes liants à transmettre les effets électroniques entre les groupes conjugués est S > Se ≈ — > O (où — se réfère au cas ou il n'y a pas de groupe liant, *i.e.* le styrène). Toutefois on note des déviations importantes de l'addivité pour les déplacements chimiques du C(1); ces déviations peuvent indiquer que l'oxygène désactive le cycle par rapport aux effets électroniques des substituants alors que le S et le Se activent le cycle. Si cette explication est valide, l'habilité réelle des groupes liants à transmettre les effets électroniques serait — > O > S > Se.

[Traduit par le journal]

There has been considerable interest in the relative abilities of O, S and, to a lesser extent, Se to transmit electronic effects, particularly in the case where these atoms act as a link or bridge between two conjugative groups. The initial investigation was by Litvinenko who investigated the reactivity of the amino group to acylation in compounds of the type $X—C_6H_4—Y—C_6H_4NH_2$ where X is the variable substituent and Y = O, S, etc. (1). He concluded that the ability to transmit electronic substituent effects decreased in the order S > Se > O > —.[1] Subsequent investigations involving ^1H (2, 3), ^{19}F (4, 5), and ^{13}C (6) nmr spectroscopy supported the order S > O ≳ — in cases involving conjugative transmission of substituent effects. Perhaps the most striking feature of these investigations is the general conclusion that interposition of O or S between two conjugative groups apparently enhances the transmission of electronic effects relative to the case where the two groups are directly linked, a phenomenon which has been referred to as a positive bridge effect (1) or superconductivity (2).

The most recent investigation involved ^1H and ^{13}C chemical shifts measurements for phenylvinyl ethers and sulfides (6). However, measurements were carried out for a limited number of derivatives (including only three *para* derivatives in each case) and ^{13}C chemical shifts were measured for neat liquids. Since we had a large number of phenylvinyl ethers, sulfides, and selenides as part of another investigation (7), a further more careful ^{13}C nmr spectroscopic investigation of this system seemed desirable. It was hoped that this would provide further evidence concerning the relative position of Se on the transmission scale and possibly also help to elucidate the origin of the positive bridge effect. In fact, the investigation has shown that the previous order S > Se > O > — possibly does not reflect the ability of these linking groups to transmit substituent effects.

Results and Discussion

^{13}C chemical shifts for 4-substituted phenylvinyl ethers, sulfides, and selenides are listed

[1]Throughout this manuscript the symbol — refers to the case where the two conjugative groups are directly linked, *i.e.* biphenyl in this case.

TABLE 1. ^{13}C chemical shifts[a] for 4-substituted derivatives X—C_6H_4YCH=CH_2

Y	X	$\delta_{C(4)}$	$\delta_{C(3)}$	$\delta_{C(2)}$	$\delta_{C(1)}$	$\delta_{C(\alpha)}$	$\delta_{C(\beta)}$	$\Delta\delta_{C(1)}$[b]	$\Delta\delta_{C(\beta)}$[b]
O	H	122.74	129.23	117.00	156.69	147.95	94.64	—	—
O	NH_2	142.10	115.50	118.73	149.00	149.74	92.40	−7.69	−2.24
O	OCH_3	155.51	114.29	118.45	150.34	149.30	93.06	−6.35	−1.58
O	CH_3	131.77	129.71	117.05	154.62	148.46	93.87	−2.07	−0.78
O	F	158.54	115.89	118.53	152.57	148.50	94.49	−4.12	−0.15
O	Cl	128.24	129.37	118.24	155.17	147.60	95.41	−1.52	+0.77
O	Br	115.56	132.35	118.64	155.72	147.52	95.59	−0.97	+0.95
O	NO_2	147.95	125.52	116.06	160.98	145.82	98.59	+4.29	+3.95
S	H	126.72	128.74	130.54	134.26	132.18	114.58	—	—
S	NH_2	146.30	115.16	134.70	119.20	134.70	110.63	−15.06	−3.95
S	OCH_3	159.47	114.47	134.07	123.49	133.93	111.71	−10.77	−2.87
S	CH_3	136.58	129.28	131.37	129.50	133.00	113.27	−4.76	−1.31
S	F	162.24	116.04	133.88	128.76	132.59	113.87	−5.50	−0.71
S	Cl	133.26	129.03	131.66[c]	132.66	131.66[c]	115.47	−1.60	+0.89
S	Br	121.90	131.96[d]	131.72[d]	133.41	131.29	115.73	−0.85	+1.15
S	CF_3	128.88	125.66	128.68	140.20	129.73	118.48	+5.94	+3.40
S	NO_2	152.05	123.81	128.23	144.30	128.23	120.88	+10.04	+6.30
Se	H	127.14	128.92	133.15	129.16	127.98	118.53	—	—
Se	NH_2	146.34	115.44	136.40	114.81	129.85	115.59	−14.35	−2.94
Se	OCH_3	159.58	114.72	136.03	118.30	129.23	116.36	−10.86	−2.17
Se	CH_3	136.87	129.73	136.87	125.18	128.57	117.50	−3.98	−1.03
Se	F	162.54	116.29	135.73	123.20	128.14	118.10	−5.96	−0.43
Se	Cl	133.80	129.21	134.30	127.20	127.36	119.26	−1.96	+0.73
Se	Br	121.82	132.17	134.50	127.99	127.23	119.50	−1.17	+0.97
Se	CF_3	129.68	125.74	131.71	135.06	125.95	121.74	+5.90	+3.19
Se	NO_2	146.90	123.76	130.62	139.91	124.71	123.97	+10.75	+5.44

[a]In ppm to low field for tetramethylsilane.
[b]Chemical shift relative to unsubstituted derivative.
[c]Overlapping peaks.
[d]Assignments uncertain.

in Table 1. Based on both the maximum range of substituent effects upon β carbon ^{13}C chemical shifts (from NH_2 to NO_2 derivatives) and on correlations of β carbon chemical shifts against one another, the apparent order of transmission of substituent effects is S > Se ≈ — > O (see Table 2). This parallels the order of Litvinenko (1) and subsequent workers (2–6) with respect to O, S, and Se. However, the directly bonded system (styrene) appears to be more efficient at transmitting substituent effects than previously deduced from systems of the type X—C_6H_4—Y—C_6H_4Z (1, 3–6). It could be argued that the present system supplies a more reliable order since styrene (8) (and presumably the other derivatives) are planar while the systems X—C_6H_4—Y—C_6H_4Z undergo uncertain conformational changes as Y is varied (9).

However, inspection of the phenyl carbon chemical shifts indicates an additional complexity. The effect of substituents on C(1) chemical shifts varies markedly from system to system (Table 1). Taft and co-workers have recently reported similar marked deviations from additivity of ^{13}C chemical shifts in *para*-disubstituted benzenes (10). They suggested that σ electron-withdrawing groups deactivate the ring towards both π-inductive and resonance effects of substituents (10). The obvious corollary of this is that σ-donor groups should activate the phenyl group; a trend which is apparent in ^{13}C chemical shift data for 4-substituted trimethylsilylbenzenes (11). On this basis, it would appear from our results that —SCH=CH_2 and —SeCH=CH_2 groups both activate the phenyl groups (see $\delta\Delta_{C(1)}$). While S and Se are normally considered to have electronegativities similar to carbon (12), it is possible that the polarizabilities of these atoms contribute to their apparent activating effect.[2] By contrast —OCH=CH_2 appears to be a de-

[2]Lynch has collected data for a large number of *p*-disubstituted benzenes and has concluded that the deviations from additivity for the ^{13}C chemical shifts of the carbon *para* to the variable substituent depend upon the polarizability of the fixed substituent (13). The other ^{13}C chemical shifts show little deviation from additivity.

TABLE 2. Various parameters which measure the relative abilities of O, S, and Se to transmit electronic effects, relative to the case where the two conjugative groups are directly linked

Parameter	Values			
	—[d]	O	S	Se
$\Delta\Delta_{C(\beta)}$[a]	8.50	6.17	10.25	8.38
Slope[b]	1.00	0.75	1.25	1.01
$\Delta\Delta_{C(1)}$[a]	15.00	11.98	25.10	25.10
$\Delta\Delta_{C(\beta)}/\Delta\Delta_{C(1)}$	0.57	0.51	0.41	0.33
$\rho_R C(\beta)/\rho_R C(1)$[c]	0.44	0.39	0.36	0.29

[a]Chemical shift difference between NO_2 and NH_2 derivative.
[b]Slope of a correlation of C(β) chemical shifts *vs.* C(β) for 4-substituted styrenes.
[c]ρ_R values from Table 3.
[d]Data from ref. 18.

activating group (as observed for the σ-withdrawing OCH_3 group (10)) while $-CH{=}CH_2$ is essentially neutral (the total range of *para* carbon chemical shifts from NH_2 to NO_2 derivatives of benzene is 16.0 ppm (10) compared to 15.0 ppm for C(1) in styrene, see Table 2).

Taking our results in conjunction with those of Taft and co-workers (10), total range of substituent-induced *para* carbon chemical shifts (from NH_2 to NO_2) varies from 9.9 ppm in 4-substituted fluorobenzenes to 25.1 ppm in 4-substituted phenylvinyl sulfides and selenides. This raises the possibility that these deviations from non-additivity reflect variations in the sensitivity of ^{13}C chemical shifts to electron density changes rather than variations in electron density changes. Put in empirical terms, this would indicate that the scaling factor relating ^{13}C chemical shifts to π electron density changes is altered from the normal value of 160–200 ppm/π electron (14, 15) by the effect of the directly bonded atom. In support of this view, *ab initio* (STO/3G minimal basis set) calculations for 4-substituted fluorobenzenes and substituted benzenes indicate much smaller deviations from additivity than noted from the ^{13}C chemical shifts (16). However, these calculations assume a regular hexagonal structure for the benzene rings. Available structural data indicates that substituents can induce significant distortions of the benzene ring in poly-substituted benzenes (17) which might result in non-additive electronic effects not predicted by calculations based on idealized geometries. Obviously this is an area worthy of further investigation, although geometry-optimization calculations on poly-substituted benzenes would be prohibitively expensive.

If it is assumed that these non-additive effects on ^{13}C chemical shifts accurately reflect ground state electron density changes (previous investigations of ^{13}C chemical shifts in benzene derivatives support this view (18–21)), the phenyl carbon chemical shift data allow an alternative interpretation of transmission of electronic effects by O, S, and Se. The effect of the link group can be divided into two parts: (*1*) its ability to activate (or deactivate) the directly bonded carbon of phenyl group towards electronic substituent effects and (*2*) the ability to transmit these effects to the second conjugative group. On this basis, a better measure of the actual ability of the substituent group to transmit electronic effects should be the ratio of C(β) to C(1) chemical shifts. These ratios are given in Table 2. They indicate a much different order of transmission ability, *i.e.* — > O > S > Se. If this approach is correct, it indicates that the apparent 'superconducting' or 'positive bridge' effect of S and Se is not really a transmission effect but rather reflects the ability of these linking atoms to activate the phenyl group towards substituent effects. In many ways, this seems more satisfactory than an explanation involving positive bridge effects. It is also consistent with previous conclusions that O is more capable of conjugative interactions than S (22).

Assuming that the phenyl carbon shifts parallel electronic effects, a more detailed picture of these electronic effects can be obtained by correlating ^{13}C chemical shifts for C(1), C(α), and C(β) with Taft's σ_I and σ_R^0 substituent constants (23) (Table 3). These correlations indicate that C(β) and C(1) show different relative sensitivities to field/inductive and resonance effects. Considering the resonance

TABLE 3. Correlations of C(1), C(α), and C(β) chemical shifts with σ_I and σ_R^0

Y	C	ρ_I[b]	ρ_R[b]	λ[c]	r[d]
—[a]	C(1)	5.62	18.47	3.29	0.996
—	C(α)	−2.48	−0.12		0.988
—	C(β)	5.62	8.19	1.55	0.996
O	C(1)	3.67	16.09	4.39	0.995
O	C(α)	−2.31	−4.42	1.92	0.991
O	C(β)	4.38	6.31	1.44	0.997
S	C(1)	10.92	29.63	2.69	0.995
S	C(α)	−4.23	−6.73	1.59	0.997
S	C(β)	6.64	10.77	1.62	0.997
Se	C(1)	10.02	30.29	3.02	0.998
Se	C(α)	−3.54	−5.18	1.46	0.997
Se	C(β)	5.57	8.62	1.55	0.995

[a]Experimental data from ref. 18. Correlations were based on the same substituents as for phenylvinyl sulfide. Inclusion of other substituents gives slight different values (19).
[b]Weighting coefficients for equation $\delta = \rho_I\sigma_I + \rho_R\sigma_R^0 + \delta^0$.
[c]$\lambda \equiv \rho_R/\rho_I$.
[d]Correlation coefficient.

effects first, the ρ_R values indicate an enhancement of resonance effects at C(1) on going from phenylvinyl ether to the sulfide and selenide analogues. The correlations for the vinyl group indicate the alternation in sign and magnitude of ρ_R which seems typical of resonance effects. Since C(β) and C(1) have different sensitivities to field/inductive and resonance effects, $\rho_R C(\beta)/\rho_R C(1)$ should provide a better measure of the ability of the bridge group to transmit conjugative effects. These ratios are given in Table 2. While quantitatively different from $\Delta\Delta_{C(\beta)}/\Delta\Delta_{C(1)}$, they predict the same order.

There is an even greater variation of ρ_I values for C(1) since these vary by a factor of three. Taft and co-workers also noted greater variations in ρ_I than ρ_R (10). We have previously suggested that polar substituents can polarize the entire π electron system towards the substituent (20)

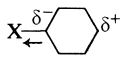

1

Taft *et al.* suggested that σ-withdrawing groups *para* to X would inhibit this polarization by making it more difficult to remove π electron density from the *para* carbon (while σ donor groups should enhance the polarization) (10). Our results are consistent with this explanation. In this regard, it may or may not[3] be significant that carbons *ortho* to the variable substituent show much smaller deviations from additivity (19, 20*b* and Table 1) than in the case of the *para* carbon. This is consistent with π polarization effects, **1**, as well as resonance effects, **2**, involving quininoid structures:

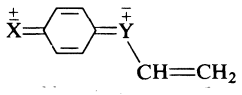

2

It is interesting to note that C(β) chemical shifts show a large sensitivity to field/inductive effects (in fact ρ_I is larger for C(β) than for C(1) in phenylvinyl ether). This indicates the present of polar π inductive effects, *i.e.* effects which can alter the π electron distribution without charge transfer to or from the substituent. We have previously shown that π polarization in styrene involves two components (1, 24); polarization of the entire conjugated system from vinyl to phenyl groups and through space polarization of the vinyl π bond towards the substituent. The latter effect can account for the relatively large sensitivity of C(β) to field/inductive effects. Although the vinyl group is further removed from the substituent in ethers, sulfides, and selenides than in styrene, it is aligned more directly with the C—X bond axis:

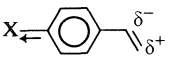

3

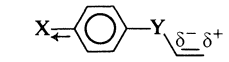

4

[3]It may not be significant because it could equally well be argued that this demonstrated that the deviations from additivity for the *para* carbon reflected different sensitivities of these carbons to electron density changes.

Since the field effect depends upon the field component acting along the C—C bond (25, 26), this more favorable alignment of the bond should compensate for the greater distance.

Conclusions

Results of ^{13}C chemical shift measurements for 4-substituted phenylvinyl ethers, sulfides, and selenides along with previous data for styrenes indicate that the order of transmission of substituent effects to the β carbon is S > Se ≈ — > O. However, the C(1) chemical shifts show marked deviations from additivity which can be interpreted as indicating that S and Se activate the phenyl group towards substituent effects while O deactivates this group, consistent with previous findings. If it is accepted that the phenyl carbon shifts accurately reflect ground state electron density changes (the evidence is indecisive on this point), then the actual ability of the link group to transmit conjugative effects is in the order — > O > S > Se. In any case, the very marked deviations from additivity noted in this and a previous investigation suggest that great care should be exercised in assigning ^{13}C chemical shifts in polysubstituted benzene derivatives on the basis of addivity.

Experimental

The phenylvinyl ethers, sulfides, and selenides were synthesized as part of another investigation. Details of the syntheses will be reported elsewhere (7). All compounds gave characteristic ^1H nmr spectra with an ABC vinyl spectrum and an A′A′BB′ aromatic spectrum.

^{13}C chemical shifts were measured at 25.16 MHz on a Varian XL-100 spectrometer, using 0.4 *M* solutions in CCl_4 with 8% C_6D_{12} as internal lock. All peak positions were measured relative to internal tetramethylsilane with an estimated maximum experimental error of 0.04 ppm. $\delta_{C(4)}$, $\delta_{(13)}$, and $\delta_{C(2)}$ were assigned on the basis of relative intensities, from off-resonance decoupling experiments and by assuming additivity of ^{13}C chemical shifts. These carbons show little deviation from additivity (10, 13, 19, 20*b*). The first two criteria were used to assign $\delta_{C(1)}$, $\delta_{C(\alpha)}$, and $\delta_{C(\beta)}$.

Acknowledgements

Financial support from the National Research Council of Canada is gratefully acknowledged. We thank Professor Taft for supplying a copy of ref. 10 prior to publication and Professor Lynch for supplying results prior to publication.

1. L. M. Litvinenko. Izv. Akad. Nauk SSSR, Otd. Khim. Nauk 1737 (1962) and references therein.
2. S. H. Marcus, W. F. Reynolds, and S. I. Miller. J. Org. Chem. **31**, 1872 (1966).
3. J. B. Hyne and J. W. Greidanus. Can. J. Chem. **47**, 803 (1969).
4. I. R. Ager, L. Phillips, and S. J. Robert. J. Chem. Soc. Perkin Trans. II, 1988 (1972).
5. S. K. Dayal and R. W. Taft. J. Am. Chem. Soc. **95**, 5595 (1973).
6. O. Kajamoto, M. Kobayashi, and T. Fueno. Bull. Chim. Soc. Jpn. **46**, 1422 (1973).
7. R. A. McClelland. Can. J. Chem. This issue.
8. L. A. Carriera and T. G. Towns. J. Chem. Phys. **63**, 5283 (1975).
9. R. J. W. LeFevre and J. O. Saxby. J. Chem. Soc. B, 1064 (1966).
10. J. Bromilow, R. T. C. Brownlee, R. D. Topsom, and R. W. Taft. J. Am. Chem. Soc. **98**, 2020 (1976).
11. C. D. Schaeffer, J. J. Zuckerman, and C. H. Yoder. J. Organomet. Chem. **80**, 29 (1974).
12. F. A. Cotton and G. Wilkinson. Basic inorganic chemistry. John Wiley and Sons, New York. 1976.
13. B. M. Lynch. Private communication.
14. P. C. Lauterbur. J. Am. Chem. Soc. **83**, 1838 (1961).
15. H. Spiesecke and W. G. Schneider. Tetrahedron Lett. 468 (1961).
16. W. J. Hehre, R. W. Taft, and R. D. Topsom. Progress in physical organic chemistry. Vol. 12. *Edited by* A. Streitwieser and R. W. Taft. John Wiley & Sons, New York. 1976.
17. A. Domenicano, P. Mazzeo, and A. Vaciago. Tetrahedron Lett. 1029 (1976).
18. G. L. Nelson, G. C. Levy, and J. D. Cargioli. J. Am. Chem. Soc. **94**, 3089 (1972).
19. G. K. Hamer, I. R. Peat, and W. F. Reynolds. Can. J. Chem. **51**, 897 (1973); **51**, 915 (1973).
20. (*a*) W. F. Reynolds, I. R. Peat, M. H. Freedman, and J. R. Lyerla. Can. J. Chem. **51**, 1857 (1973); (*b*) D. A. Dawson and W. F. Reynolds. Can. J. Chem. **53**, 373 (1975).
21. G. A. Olah, P. W. Westerman, and D. A. Forsyth. J. Am. Chem. Soc. **97**, 3419 (1975).
22. C. C. Price and S. Oae. Sulfur bonding. Ronald Press, New York. 1962.
23. R. T. C. Brownlee, S. Ehrenson, and R. W. Taft. Progress in physical organic chemistry. Vol. 12. *Edited by* A. Streitwieser and R. W. Taft. John Wiley & Sons, New York. 1973.
24. W. F. Reynolds, P. G. Mezey, and G. K. Hamer. Can. J. Chem. Submitted for publication.
25. A. D. Buckingham. Can. J. Chem. **38**, 300 (1960).
26. J. G. Batchelor. J. Am. Chem. Soc. **97**, 3410 (1975).

Proportionality relationships in the carbon-13 nuclear magnetic resonance spectra of *para*-disubstituted benzenes: a new interpretation of non-additive behavior

BRIAN MAURICE LYNCH

Department of Chemistry, Saint Francis Xavier University, Antigonish, N.S., Canada B2G 1C0

Received September 7, 1976

BRIAN MAURICE LYNCH. Can. J. Chem. **55**, 541 (1977).

The carbon-13 chemical shifts for 214 distinct sites (the 4-carbons) in 24 sets of 1-X,4-Y-disubstituted benzenes and for 270 distinct sites (the 1- and 2-carbons) in 16 of these sets are reproduced with excellent precision (correlation coefficients 0.99 or greater) either by linear proportionality relationships with the appropriate substituent chemical shift (scs) in a monosubstituted benzene (for the 4-carbons), or by simple additivity relationships with the scs (for the 1- and 2-carbons).

Inconsistencies are pointed out in a theoretical rationalization of 4-carbon shifts used in discussing the non-additivity of these shifts in terms of a DSP approach, whereas the above one-parameter approach yields sets of proportionality constants (slopes of scs relative to Y = H) following systematic trends which are interpreted as results of changes in the excitation energy term at carbon-4 dependent upon the ionization potential of the group Y. There is no significant association between the scs slopes and sets of calculated CNDO/2 electron densities for these *para*-disubstituted benzenes.

BRIAN MAURICE LYNCH. Can. J. Chem. **55**, 541 (1977).

On reproduit avec une excellente précision (coefficient de corrélation de 0.99 ou plus) les déplacements chimiques de ^{13}C de 214 sites distincts (les carbones-4) dans 24 groupes de benzènes disubstitutés 1-X, 4-Y et pour 270 sites distincts (des carbones-1 et -2) dans 16 de ces groupes; ces reproductions sont effectuées soit par des relations de proportionnalité linéaire avec des déplacements chimiques du substituants appropriées (dcs) dans les benzènes monosubstitués (pour les carbones-4) ou par des règles d'additivités simples avec les dcs (pour les carbones-1 et -2).

On met en relief des inconsistances dans la rationalisation théorique des déplacements chimiques des carbone-4 utilisée dans la discussion de la non-additivité de ces déplacements en termes d'une approche DSP alors que l'approche utilisant un paramètre qui est mentionnée plus haut conduit à des groupes de constantes de proportionnalité (pentes de dcs relatives à Y = H) qui suivent des tendances systématiques que l'on interprète comme résultant de changements dans le terme d'énergie d'excitation au niveau du carbone 4 en fonction du potentiel d'ionisation du groupe Y. Il n'y a aucune association importante entre les pentes des dcs et les groupes de densités électroniques calculées par la méthode CNDO/2 pour ces benzènes *para*-disubstitués.

[Traduit par le journal]

Introduction

Additivity parameters (substituent chemical shifts, scs) derived from the carbon-13 shifts of monosubstituted benzenes have been very useful in signal assignments in polysubstituted compounds (for examples, see refs. 1–5), but a cautionary note is sounded through a recent communication of Bromilow, Brownlee, Topsom, and Taft (6), reporting marked non-additivity in *para*-substituent ^{13}C shifts for the 4-carbon in compounds of type **1**

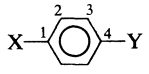

1

with Y a fixed substituent (NO_2, F, OMe, NH_2, CN) and X a minimum basis set of substituents (7) (X = NH_2, OMe, F, Me, H, CF_3, CN, NO_2 for each Y). Taft's group analysed the influence of the Y substituent on the *para*-scs through the dual substituent parameter (DSP) approach (7), and through a suggested parallelism between the influence of Y upon the ρ_I value and upon the STO-3G *ab initio* σ-electron density at the 4-carbon of the monosubstituted benzene (*i.e.* for X = H), their results were interpreted to indicate that the σ-charge density at the 4-carbon regulates the ease of π-polarization by the distant *para*-substituent X.

Their interpretation leads to the prediction that σ-donor Y groups will show amplified *para*-

scs by comparison with Y = H, with increased ρ_I and ρ_R values. Published data for a set of phenyltrimethylsilanes (8) support this prediction, but a limited data set for bromobenzenes (measured as neat liquids) (5) also show amplified *para*-scs, and it seems inconceivable to classify a halogen as a σ-donor. Furthermore, plots of the published 4-carbon shifts for the bromobenzenes against σ_R or σ_R^0 are linear, with σ_I influences apparently absent ($\rho_I \simeq 0$). The evident failure of the Y = Br set to fit the logic of the Taft model requires a more searching examination of the reported non-additivity patterns, through examination of additional Y groups, extension of the range of X substituents, and different modelling assumptions.

In this paper, I use an alternative single-parameter approach to explore non-additivity patterns in the scs for the 1-, 2-, and 4-carbons with an extended range of substituents Y, including the following (the number of X substituents in the data set follows the Y descriptor): Br, 10; I, 8; Cl, 10; CF_3, 9; Me, 10; Et, 9; $CH{:}CH_2$, 11; $CMe{:}CH_2$, 8; $C(CMe_3){:}CH_2$, 9; $C{\equiv}CH$, 11; C_6H_5, 8; CMe_3, 8; $SiMe_3$, 7; $GeMe_3$, 6; $SnMe_3$, 7; $CO.NH_2$, 7; $O.CH{:}CH_2$, 8; $S.CH{:}CH_2$, 9; $Se.CH{:}CH_2$, 9. The single-parameter approach analyses the scs patterns in terms of δ–δ relationships (*cf.* 4, 9) as in eq. 1:

$$\delta_1 = a_0 + b\delta_0 \quad [1]$$

where δ_1 is the carbon chemical shift for a given position and substituent X, a_0 the shift calculated for the parent species with X = H, and the δ_0 are the set of carbon scs for a given position for monosubstituted benzenes with Y = H; b is the slope parameter. Such an approach is equivalent to the use of the scs in monosubstituted benzenes as *substituent constants*. Equation 1 could reproduce experimental results through additivity relationships with $b = 1$, or through *proportionality relationships*, with $b < 1$ or $b > 1$.

Results and Discussion

Table 1 assembles the results of fitting the data of Taft's group and the extended data sets of Y substituents listed above to eq. 1 to the various 4-carbon scs, using the parent δ_0 values assembled in Table 2. Proportionality relationships of excellent precision are evident for all the sets, and the data of Taft's group are reproduced almost as precisely by eq. 1 as by the DSP treatment. Two instances with evidence of saturation of substituent effects (Y = X = NO_2, scs = 2.77 ppm and Y = CF_3, X = NO_2, scs 2.74 ppm) were omitted from the analyses. Data-fitting to eq. 1 was also made for the 1- and 2-carbons for all Y substituents except those cited in ref. 6, using the appropriate scs from Table 2. For these 16 substituents and 270 sites, additivity relationships prevail ($b = 1.00 \pm 0.05$) with excellent precision (minimum correlation coefficient, 0.993). Since the goodness of fit to eq. 1 is either comparable to that for the DSP analysis (for the 4-carbons) or superior to it (*ortho*-substituents (2-carbons) are very poorly correlated by the DSP analysis (6)), one must prefer the simpler treatment unless the DSP analysis has a superior theoretical basis. The cited data for bromobenzenes (5) indicate significant deficiencies in the approach separating σ_I and σ_R as applied to carbon-13 substituent chemical shifts.

Equation 1 is remarkably successful in organizing the shift data, and the systematic trends in relative slopes, including the orders

$$F < OMe < NH_2, NO_2 < H < Me$$

$$F < H < Cl < Br < I$$

$$CMe_3 < SiMe_3 < GeMe_3 < SnMe_3$$

suggest that dependences on physical quantities attributable to the key atom of the Y substituent, such as electronegativity or ionization potential will indicate an appropriate theoretical model accounting for these trends.

The most obvious proposal is that the differing electronegativities of the key atoms of the Y groups lead to differences in their abilities to modify the charge redistribution resulting from the presence of the X substituent; for example, the smaller slope for Y = F than for Y = H would then indicate a smaller range of variation in electron density at the 4-carbon for Y = F as compared with Y = H. Note that the validity of this proposal depends upon the unproved assumption of uniform response of the 4-carbon shift (in ppm/electron) throughout the data sets, while in fact, comparisons of *ab initio* calculations of electron densities for *para*-substituted fluorobenzenes and the corresponding monosubstituted benzenes (10) indicate that variations in the electron densities approximately parallel one another. This pattern of behavior is also observed with more approximate (CNDO/2)

TABLE 1. Proportionality relationships of the 4-carbon shifts in *para*-disubstituted benzenes to the shifts in monosubstituted benzenes[a]

Fixed substituent, Y	No. of data points, n	Chemical shift for X = H (ppm from TMS), a_0 Obs.	Calcd.	Slope, b	Uncertainty of slope,[b] $s_b(t)$	Correlation coefficient, r	Goodness of fit,[c] SD/RMS (%)	Reference
F	10	163.50	163.03	0.619	0.060	0.9930	11.65	6
OMe	10	160.10	160.15	0.714	0.062	0.9945	10.84	6
NH_2	10	146.70	146.97	0.825	0.085	0.9925	12.86	6
NO_2	10[d]	148.50	147.78	0.820	0.099	0.9893	12.75	6
CF_3	9[d]	131.10	131.00	1.049	0.070	0.9972	6.65	[e]
Me	10	137.60	138.13	1.103	0.062	0.9976	8.28	[e]
Cl	10	134.70	134.77	1.119	0.037	0.9992	4.27	[e]
CN	10	113.30	113.03	1.161	0.120	0.9921	12.73	6
$CH{:}CH_2$	11	137.40	137.42	0.918	0.043	0.9981	6.44	19[f]
$CMe{:}CH_2$	8	141.07	141.02	0.963	0.038	0.9992	3.84	20[f]
$C(CMe_3){:}CH_2$	9	143.08	143.08	0.990	0.049	0.9985	5.33	20[f]
C≡CH	11	122.52	122.39	1.034	0.050	0.9979	6.40	21[f]
Et	9	143.42	141.61	1.087	0.041	0.9991	4.68	[g]
C_6H_5	8	141.45	141.61	0.978	0.058	0.9982	6.71	22[h]
CMe_3	8	150.48	150.97	1.073	0.097	0.9960	9.40	8[i]
$SiMe_3$	7	139.70	140.00	1.251	0.103	0.9974	6.02	8[i]
$GeMe_3$	6	142.60	142.24	1.305	0.087	0.9998	3.82	8[i]
$SnMe_3$	7	141.53	141.99	1.345	0.128	0.9966	7.26	23[j]
$O.CH{:}CH_2$	8	156.69	156.40	0.765	0.066	0.9963	8.30	24
$S.CH{:}CH_2$	9	134.26	134.76	1.536	0.083	0.9982	6.47	24
$Se.CH{:}CH_2$	9	129.16	129.77	1.537	0.069	0.9988	6.78	24
$CO.NH_2$	7	134.37	134.25	0.988	0.140	0.9924	14.1	This work[k]
Br	10	122.48	122.58	1.241	0.063	0.9981	6.39	This work[k]
I	8	94.35	94.32	1.474	0.123	0.9965	9.12	This work[k]

[a]Unless specified otherwise, shifts were determined for dilute solutions (approximately 0.4 *M*) in $CDCl_3$. The basic set of 4-carbon shifts relative to benzene is taken from ref. 6, and is reproduced in Table 2. Secondary shifts for other substituents were used in analyses if some of these substituents were missing from the available data sets; these are also listed in Table 2.

[b]Product of the standard deviation of the slope, s_b, and the t distribution for the 95% confidence level for the n data points; for a discussion of this indication of goodness of fit, see ref. 18.

[c]Standard deviation ($s_{x,y}$) from linear relationship, divided by the root-mean-square value of the n data points.

[d]Data points for X = NO_2 were omitted from the analysis.

[e]Personal communication from Professor R. W. Taft.

[f]Data in CCl_4 solvent.

[g]G. K. Hamer and W. F. Reynolds, personal communication.

[h]Data in acetone solvent.

[i]Data for 50% (w/v or v/v) solutions in CCl_4.

[j]Data for pure liquids plus 10% (v/v) benzene.

[k]Data for the benzamides are for solutions in DMSO-d_6. Concentrations of the solutions were in the range 0.1–0.4 *M*.

calculations on these two series (11), and my own CNDO/2 calculations of electron densities for a variety of *para*-disubstituted benzenes (X = H, F, NH_2, Me, NO_2, OH, CN; Y = H, NH_2, NO_2, Me, C≡CH, OH, $CO.NH_2$) yield results for the 4-carbon electron densities approximately paralleling the set Y = H (see Table 3), but displaced in direction and magnitude as a function of the Y group. Since there is no significant association ($r = -0.50$, corresponding to a vector angle of 120°) between the ratios of electron density variations and the observed scs slopes of Table 1, I conclude tentatively that the differing slopes are not a consequence of differing ranges of ground-state variations in electron density. This conclusion requires reinforcement through geometry-optimized *ab initio* calculations for full confidence in the electron densities, but the electronegativity-controlled influence of which the above model is an example would require that groups Y with key atoms of similar electronegativities should exhibit similar amplifications of scs influences. This is not so: the electronegativities of carbon and of iodine are accepted generally (12) as closely similar, yet the scs slopes are: Me, 1.103; I, 1.474.

TABLE 2. Carbon-13 substituent chemical shift parameters for monosubstituted benzenes[a]

Substituent	Position		
	Ipso (1)	*ortho* (2)	*para* (4)
H	0.00	0.00	0.00
NMe_2	22.6[b]	−15.6[b]	−11.69[c]
NH_2	18.0	−13.3	−9.80
OMe	31.4	−14.4	−7.68
OH	26.9	−12.7	−7.30[d]
F	34.8	−12.9	−4.39
Cl	6.2	0.4	−1.36
Br	−6.02[e]	2.95[e]	−1.76[e]
CF_3	2.60[f]	−3.30[f]	3.41
CMe_3	20.5[g]	−3.30[g]	−2.80[g]
Et	14.92[h]	−0.99[h]	−3.12[h]
Me	8.9	0.7	−3.05
CN	−15.4	3.6	4.35
NO_2	20.0	−4.8	6.22
$COCH_3$	9.1	0.1	4.20[d]
CH:O	8.6	1.3	5.50[d]
CO_2H	2.40[i]	1.60[i]	4.80[i]

[a]Unless specified otherwise, all ipso and *ortho* shift parameters are taken from ref. 25 and all *para* shift parameters from ref. 6.
[b]From ref. 26.
[c]R. W. Taft, personal communication.
[d]From ref. 25.
[e]This work.
[f]C. D. Schaeffer, personal communication.
[g]From ref. 1 p. 97.
[h]W. F. Reynolds, personal communication.
[i]From ref. 27.

A more successful accounting of the slope trends is obtained by postulating changes in the excitation energy term ΔE of the paramagnetic shielding expression for carbon-13 shifts[1] (Karplus and Pople (13)). Since the deviations from scs additivity do not extend beyond the 4-carbon (that bearing the substituent Y) any such changes must be highly local (Karplus and Pople (13) suggest the possibility of localized excitations). I propose that the relative energies of the ground-state and excited-state configurations of carbon-4 are modified by interaction with the key atom of the substituent Y, and that the extent of this modification will be determined largely by the ionization potential of Y.

My proposal predicts that the scs slope will be a linear function of the reciprocal of the ionization potential of the key atom of Y, and for the sets Y = F, H, Cl, Br, I and Y = CMe_3, $SiMe_3$, $GeMe_3$, $SnMe_3$, linear associations of high quality are evident between these quantities (Table 4). Further, the scs slopes for a set of groups with varying ligand nature and number (Y = F, OMe, NH_2, NO_2, C:CH_2, Me) also follow the sequence of the reciprocals of the calculated valence-state ionization potentials (*cf.* Hinze and Jaffe (14)) although the precision of the linear relationship is less. Finally, the large amplifications noted for Y = S.CH:CH_2 and Y = Se.CH:CH_2 (Table 1) by comparison with Y = O.CH:CH_2 and Y = CH:CH_2 may be interpreted (in addition to the low ionization potentials of S and Se) by a model for these groups akin to a perturbed allyl anion substituent ($\bar{C}$H.CH:CH_2), in which low-lying (albeit unoccupied) orbitals of the substituents interact strongly with carbon-4.

Conclusions

The major features of the chemical shift patterns at the 4-carbon in *para*-disubstituted benzenes, and the trends in scs effects, are well explained by the proposed modification of the excitation energy term. A test of the proposed localized nature of the modification is that scs additivity would be predicted for the 1- and for the 2-carbons in the *para*-disubstituted series (as is observed, see above) and also for the 2-, 3-, 4-, and 6-carbons in 1-Y,3-X-disubstituted benzenes. The limited available data support this latter prediction, which I hope to test in the near future with a wider data base. At present, it appears that the small scs at the 3-position in 1-X,4-Y-disubstituted benzenes exhibit an insufficient range to allow development of statistically significant correlation models.

Experimental

Materials

The substituted benzamides were prepared by ammonolysis of the commercially available benzoyl chlorides,

[1]A referee comments that correlations of appropriate inverse ionization potentials with proton and with fluorine chemical shifts have been made previously by Schaefer *et al.* (17), but these do not relate directly to my approach. My quoted data sets are concerned with the effect of ipso-substituent (Y) variation in modifying the scs influence of *para*-substituents X on the ipso-carbon (4-carbon) shifts *relative* to the species where Y = H, rather than upon the influence of variation of Y upon the ipso chemical shift where X = H. A study of this latter influence would be directly analogous to the examples studied by Schaefer *et al.*; unfortunately, our preliminary work (B. M. Lynch and J. J. MacDonald, unpublished data) indicates that the influence of Y upon the ipso shift includes (at least) contributions from steric, electron-density, and excitation-energy terms.

TABLE 3. Relationships among CNDO/2 total electron densities at the 4-carbon in *para*-disubstituted benzenes

Varying substituents, X	Total electron densities for fixed substituent, Y						
	H	NH_2	NO_2	CH_3	C≡CH	OH	$CONH_2$
H	3.9926	3.8400	3.9660	3.9589	3.9316	3.8141	4.0340
F	4.0151	3.8548	3.9901	3.9808	3.9637	3.8303	4.0505
OH	4.0187	3.8624	3.9953	3.9954	3.9656	3.8380	4.0571
NH_2	4.0301	3.8737	4.0058	3.9954	3.9862	3.8624	4.0745
CH_3	4.0008	3.8458	3.9750	3.9661	3.9562	3.8210	4.0410
NO_2	3.9680	3.8307	3.9389	3.9310	3.9360	3.7810	4.0120
CN	3.9853	3.8307			3.9360		4.0260
Slope of linear plot of electron densities relative to Y = H	1.000	1.012	1.086	1.039	1.126	1.200	0.956
Correlation coefficient for linear plot	1.000	0.9907	0.9997	0.9992	0.9770	0.9800	0.9900

TABLE 4. Substituent chemical shift (scs) responses correlated with inverse ionization potentials of key atoms.[a] The least-squares linear relationship is $b = -0.6455 + 22.366/(IP)$; $r = 0.9970$; SD/RMS = 10%; uncertainty of slope = 3.19

(*a*) Benzene and halobenzenes

Key atom Y	Slope (*b*) of scs response		$(1/(IP)) \times 10^2$
	Observed	Calculated	
F	0.619	0.639	5.741
H	1.000	1.000	7.356
Cl	1.119	1.078	7.708
Br	1.243	1.244	8.446
I	1.474	1.494	9.566

(*b*) *t*-Butylbenzenes, phenyltrimethylsilanes, phenyltrimethylgermanes, and phenyltrimethylstannanes. The least-squares linear relationship is $b = 0.5577 + 5.778/(IP)$; $r = 0.9950$; SD/RMS = 14.2%; uncertainty of slope = 1.77

Key atom	Slope *b*		$(1/(IP)) \times 10^2$
	Observed	Calculated	
C	1.073	1.071	8.884
Si	1.251	1.267	12.271
Ge	1.305	1.291	12.690
Sn	1.345	1.345	13.624

[a]Atom ionization potentials are from ref. 28.

using a standard procedure (15); the substituted bromobenzenes and iodobenzenes were commercial samples. All were purified by crystallization or distillation where appropriate, to agreement with literature melting or boiling points. The pmr spectra of the compounds were fully consistent with the purported structures, and indicated purities were over 97%.

Carbon-13 Nuclear Magnetic Resonance Spectra

These were acquired in the Fourier Transform mode using full proton decoupling, with either a Varian CFT-20 spectrometer[2] or a Varian XL-100 spectrometer.[3] Shift data for the ring protons of the benzamides, bromobenzenes, and iodobenzenes, and parameters of the

[2]Courtesy of Dr. D. L. Hooper, Dalhousie University, Halifax, Nova Scotia.

[3]Courtesy of Drs. A. G. McInnes and J. A. Walter, Atlantic Regional Laboratory, NRCC.

additivity equations for the 1- and 2-carbon shifts for these compounds, appear in Table 5.

CNDO/2 Calculations

These were made on a Hewlett-Packard 3000 computer using a standard program (*cf.* 16); recommended standard bond lengths and bond angles were used in defining the input geometries.

TABLE 5. Ring carbon chemical shifts for substituted benzamides, bromobenzenes, and iodobenzenes (in ppm from internal tetramethylsilane)

(*a*) *para*-Substituted benzamides[a]

Substituent	Chemical shift C-1	C-2	C-3	C-4
H	131.24	128.23	127.54	134.37
OMe	160.84	112.51	128.56	125.64
Cl	136.04	128.23	129.36	133.07
F	163.99	115.05	130.16	130.81
Me	141.16	128.79	127.60	131.56
CN	113.68	132.33	128.28	138.38
NO_2	—	123.38	128.92	140.07

[a]Additivity equations $\delta_{C-1} = 130.32 + 0.987\ \delta_{0,C-1}$ ($r = 0.9978$; SD/RMS = 7.10%, $s_b(t) = 0.092$); $\delta_{C-2} = 128.22 + 1.050\ \delta_{0,C-2}$ ($r = 0.9988$; SD/RMS = 4.92%, $s_b(t) = 0.059$).

(*b*) *para*-Substituted bromobenzenes[a]

Substituent	Chemical shift C-1	C-2	C-3	C-4
H	126.74	129.92	131.45	122.48
NMe_2	149.47	114.06	131.62	108.45
NH_2	145.49	116.67	131.95	110.00
OH	154.20	117.28	132.58	113.32
OMe	160.88	115.88	130.20	112.58
CH:O	135.18	130.96	132.46	129.77
Me	136.57	130.72	131.21	119.09
Et	142.29	129.15	131.19	119.34
COMe	135.87	129.81	131.85	128.22
NO_2	146.82	125.29	132.80	129.37

[a]Additivity equations $\delta_{C-1} = 126.45 + 1.054\ \delta_{0,C-1}$ ($r = 0.9978$; SD/RMS = 3.72%, $s_b(t) = 0.057$); $\delta_{C-2} = 129.91 + 0.9945\ \delta_{0,C-2}$ ($r = 0.9996$; SD/RMS = 2.44%, $s_b(t) = 0.024$).

(*c*) *para*-Substituted iodobenzenes[a]

Substituent	Chemical shift C-1	C-2	C-3	C-4
H	127.24	130.03	137.24	94.35
NH_2	145.24	116.70	138.00	80.30
OMe	158.72	116.84	138.06	82.42
Me	137.31	131.10	137.20	90.21
Et	143.01	129.59	137.12	90.49
Cl	134.18	130.45	138.65	91.16
CO_2H	130.31	131.00	137.50	100.90
NO_2	147.30	124.80	138.65	104.13

[a]Additivity equations $\delta_{C-1} = 127.89 + 0.9840\ \delta_{0,C-1}$ ($r = 0.9991$; SD/RMS = 2.86%, $s_b(t) = 0.041$). $\delta_{C-2} = 130.00 + 0.9585\ \delta_{0,C-2}$ ($r = 0.9966$; SD/RMS = 8.02%, $s_b(t) = 0.079$).

Acknowledgments

I thank Professors R. W. Taft and W. F. Reynolds for their courtesy in supplying unpublished results and for clarifying discussions, Messrs. B. J. Cusack, B. A. Dawson, J. J. MacDonald, and R. A. Turle for computational and spectroscopic assistance, and Drs. Hooper, McInnes, and Walter for access to instrumentation. This research was supported by the National Research Council of Canada and by an allowance of computer time from the St. Francis Xavier University Council for Research.

1. J. B. STOTHERS. Carbon-13 nmr spectroscopy. Academic Press, New York. 1972.
2. S. GRONOWITZ, I. JOHNSON, A. MAHOLANYIOVA, S. TOMA, and E. SOLCANIOVA. Org. Magn. Reson. **7**, 732 (1975).
3. G. DANA, O. CONVERT, J.-P. GIRAULT, and E. MULLIEZ. Can. J. Chem. **54**, 1827 (1976).
4. G. J. RAY, R. J. KURLAND, and A. K. COLTER. Tetrahedron, **27**, 735 (1971).
5. J. F. HINTON and B. LAYTON. Org. Magn. Reson. **4**, 353 (1972).
6. J. BROMILOW, R. T. C. BROWNLEE, R. D. TOPSOM, and R. W. TAFT. J. Am. Chem. Soc. **98**, 2020 (1976).
7. R. T. C. BROWNLEE, S. EHRENSON, and R. W. TAFT. Prog. Phys. Org. Chem. **10**, 1 (1973).
8. C. D. SCHAEFFER, J. J. ZUCKERMAN, and C. H. YODER. J. Organomet. Chem. **80**, 29 (1974).
9. G. R. WILEY and S. I. MILLER. J. Org. Chem. **37**, 767 (1972).
10. W. J. HEHRE, R. W. TAFT, and R. D. TOPSOM. Prog. Phys. Org. Chem. In press.
11. R. T. C. BROWNLEE and R. W. TAFT. J. Am. Chem. Soc. **92**, 7007 (1970).
12. L. PAULING. Nature of the chemical bond. 3rd ed. Cornell University Press, Ithaca, New York. 1960. pp. 88*ff*.
13. M. KARPLUS and J. A. POPLE. J. Chem. Phys. **38**, 2803 (1963).
14. J. HINZE and H. H. JAFFE. J. Am. Chem. Soc. **84**, 540 (1962).
15. A. I. VOGEL. A textbook of practical organic chemistry. Longman, London. 1950. p. 755.
16. J. A. POPLE and D. L. BEVERIDGE. Approximate molecular orbital theory. McGraw-Hill, New York. 1970.
17. T. SCHAEFER, F. HRUSKA, and H. M. HUTTON. Can. J. Chem. **45**, 3143 (1967).
18. W. H. DAVIS and W. A. PRYOR. J. Chem. Educ. **53**, 285 (1976).
19. G. K. HAMER, I. R. PEAT, and W. F. REYNOLDS. Can. J. Chem. **51**, 897 (1973).
20. G. K. HAMER, I. R. PEAT, and W. F. REYNOLDS. Can. J. Chem. **51**, 915 (1973).

21. D. A. DAWSON and W. F. REYNOLDS. Can. J. Chem. **53**, 373 (1975).
22. E. M. SCHULMAN, K. A. CHRISTENSEN, D. M. GRANT, and C. WALLING. J. Org. Chem. **39**, 2686 (1974).
23. C. D. SCHAEFFER and J. J. ZUCKERMAN. J. Organomet. Chem. **55**, 97 (1973).
24. W. F. REYNOLDS and R. A. MCCLELLAND. Can. J. Chem. This issue.
25. G. L. NELSON, G. C. LEVY, and J. D. CARGIOLI. J. Am. Chem. Soc. **94**, 3089 (1972).
26. C. P. NASH and G. E. MACIEL. J. Phys. Chem. **68**, 832 (1964).
27. A. M. IHRIG and J. L. MARSHALL. J. Am. Chem. Soc. **94**, 1756 (1972).
28. National Bureau of Standards Circular 467, Atomic Energy Levels, Vols. I, II, and III.

Vinyl sulfide hydrolysis

ROBERT A. MCCLELLAND

Department of Chemistry, University of Toronto, Scarborough College, West Hill, Ont., Canada M1C 1A4

Received July 27, 1976

ROBERT A. MCCLELLAND. Can. J. Chem. **55**, 548 (1977).

The hydrolysis of vinyl sulfides in acid solutions is shown to proceed via a mechanism analogous to that of vinyl ethers, with slow proton transfer to the carbon–carbon double bond to produce a sulfur stabilized carbonium ion. Relative rates of hydrolysis of compounds $RXCH{=}CH_2$ are CH_3S—, 41; CH_3O—, 1500; C_6H_5S—, 1; and C_6H_5O—, 10.5. This order is compared with that of other systems which produce similar stabilized carbonium ions.

ROBERT A. MCCLELLAND. Can. J. Chem. **55**, 548 (1977).

On montre que l'hydrolyse des sulfures de vinyle en solutions acides se produit par un mécanisme semblable à celui des éthers vinyliques impliquant un transfert lent de proton vers la double liaison carbone–carbone afin de produire un carbocation stabilisé par le soufre. Les vitesses relatives d'hydrolyse des composés $RXCH{=}CH_2$ sont: CH_3S—, 41; CH_3O—, 1500; C_6H_5S—, 1 et C_6H_5O—, 10.5. On compare cet ordre avec celui observé avec d'autres systèmes qui produisent des carbocations stabilisés de la même manière.

[Traduit par le journal]

A recent study (1, 2) of acylal and thioacylal hydrolysis allowed a comparison of the effects of oxygen and sulfur in a reaction generating an adjacent carbonium ion centre (reaction 1, X = O, S; R = Me, Ar),

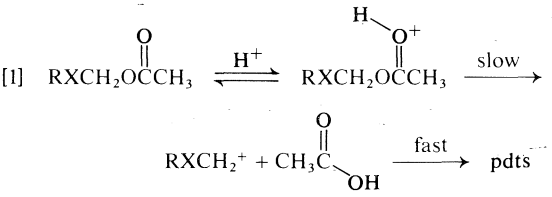

this system showing a much closer reactivity between oxygen- and sulfur-containing compounds than that anticipated on the basis of previous results, for example, on the solvolysis of chloromethyl ethers and chloromethyl sulfides (3). For further comparison, we have turned to the acid-catalyzed hydrolysis of vinyl ethers and vinyl sulfides. Vinyl ethers are now well established (4) to undergo such hydrolyses with rate-determining proton transfer to the carbon–carbon double bond giving the intermediate oxycarbonium ion. Although no mechanistic study appears to have been carried out with vinyl sulfides, they should behave similarly, as, in fact, we will first establish. In particular, this report focuses on the hydrolysis of methyl vinyl sulfide and a series of aryl vinyl sulfides, along with their vinyl ether analogs, and a comparison of their relative reactivities in the light of the acylal–thioacylal study.

Experimental

Materials

Methyl vinyl sulfide was commercially available. Aryl vinyl ethers were prepared using a method similar to that employed previously (5). In a typical procedure, phenol (0.1 mol), ethylene bromide (0.2 mol), and sodium hydroxide (0.1 mol) were refluxed overnight with 250 ml of water. The resultant phenetoles were separated from the aqueous layer and purified by fractional distillation. These were dehydrobrominated by adding to 25 ml of dimethyl sulfoxide containing a slight excess of potassium *tert*-butoxide. Water (200 ml) was added and the vinyl ether extracted with ether and purified by vacuum distillation.

Aryl vinyl sulfides were prepared as follows. The benzenethiol (0.1 mol) and sulfuryl chloride (0.12 mol) were refluxed in 100 ml of carbon tetrachloride for 1 h, and the solvent and excess chloride removed on the rotary evaporator to yield the arylsulfenyl chloride (6). Addition of this reagent to ethylene (6) was accomplished by passing an excess of the olefin through a solution in methylene chloride. The solvent was again removed and the adduct was dehydrochlorinated with potassium hydroxide (slight excess) in refluxing 95% ethanol (*ca.* 2 h). After removal of much of the solvent and addition of water the vinyl sulfide was obtained by ether extraction and vacuum distillation.

The identity and purity of all compounds were established using ^1H and ^{13}C nmr spectroscopy; analysis of the ^{13}C nmr spectra has been reported separately (7). Boiling points of known compounds agreed with literature values (5, 8). New compounds gave satisfactory analyses.

Kinetic Measurements

All rates were obtained using uv spectroscopy at a wavelength corresponding to the greatest spectral change on hydrolysis (for methyl vinyl sulfide, λ = 225 nm; aryl vinyl ethers, 230–240, except 3-NO_2—, 280; 4-NO_2—, 330; aryl vinyl sulfides, 260–270, except 4-NO_2—, 340).

The spectrometer (Cary 16) was thermostatted at 25.0 or 50.0 °C (±0.1 °C) and the kinetic runs were initiated by addition of a solution of the substrate in methanol (0.005 ml) directly to the aqueous solution (2.5 ml) in the uv cell, final concentrations in substrate ranging from 10^{-4} to 10^{-3} *M*. First-order rate constants were evaluated as slopes of plots of ln $(A_t - A_\infty)$ or ln $(A_\infty - A_t)$ *vs.* time. Rate constants were reproducible to ±2%. Stable infinity values were obtained in all cases, and the first order plots were linear over the entire course of the reaction.

Products

The compounds studied here are expected to give acetaldehyde and the phenol or thiol on hydrolysis. In all cases quantitative conversion to the latter was verified by comparison of the uv spectrum of the products with that of an authentic sample. With methyl vinyl sulfide and phenyl vinyl sulfide conversion to both products was established by nmr spectroscopy, the solvent in this case being 0.5 *N* DCl in 80% dimethyl sulfoxide-d^6: 20% D_2O.

Results

Products

The hydrolysis of the vinyl sulfides studied here produces the expected products (9), acetaldehyde and thiol

$$CH_2{=}CHSR + H_2O \xrightarrow{H^+} CH_3\overset{O}{\overset{\|}{C}}H + RSH$$

Buffer Catalysis

Rates of hydrolysis of methyl vinyl sulfide were obtained at 50 °C in a series of buffer solutions of four different carboxylic acids. Using solutions of constant buffer ratio but differing total buffer concentration,[1] catalysis by the acid component of the buffer was found, with strict adherence to the rate law of eq. 2,

$$[2] \qquad k_{obs} = k_{H^+}[H^+] + k_{HA}[HA]$$

The catalytic coefficients are listed in Table 1, while the Bronsted plot is shown in Fig. 1. Ignoring the point for the hydronium ion (which displays a similar negative deviation in Bronsted plots involving vinyl ethers (13)) a Bronsted α value of 0.73 is obtained.

Solvent Isotope Effect

Hydrolysis of methyl vinyl sulfide in H_2O and D_2O at 25 °C using dilute HCl and DCl (0.01–0.1 *M*) as catalyst acid gave rate constants of 0.0210 M^{-1} s^{-1} for H_3O^+ and 0.00742 M^{-1} s^{-1} for D_3O^+; their ratio $k_{H_3O^+}/k_{D_3O^+}$ is 2.83.

Aryl Vinyl Ethers and Aryl Vinyl Sulfides

Rates of hydrolysis of a series of these compounds in 1 *N* HCl are reported in Table 2;

[1]Suitable corrections were made in this treatment for "buffer failure" with the stronger acids (10).

TABLE 1. Catalytic rate constants for hydrolysis of methyl vinyl sulfide in aqueous solution at 50 °C

Catalyst	pK_a (50 °C)	$10^4 k_{HA}$ (M^{-1} s^{-1})
CH_3COOH	4.79[a]	0.834
$HOCH_2COOH$	3.85[a]	3.39
$MeOCH_2COOH$	3.65[b]	5.04
$ClCH_2COOH$	2.97[c]	18.0
H_3O^+	−1.74[d]	2060[e]

[a]Reference 11.
[b]Reference 12.
[c]Obtained by extrapolation of data in ref. 11.
[d]At 25 °C (12).
[e]In dilute HCl solutions. The average value obtained from the intercept of plots of k_{obs} *vs.* [HA] is 0.222 (±0.014) M^{-1} s^{-1}.

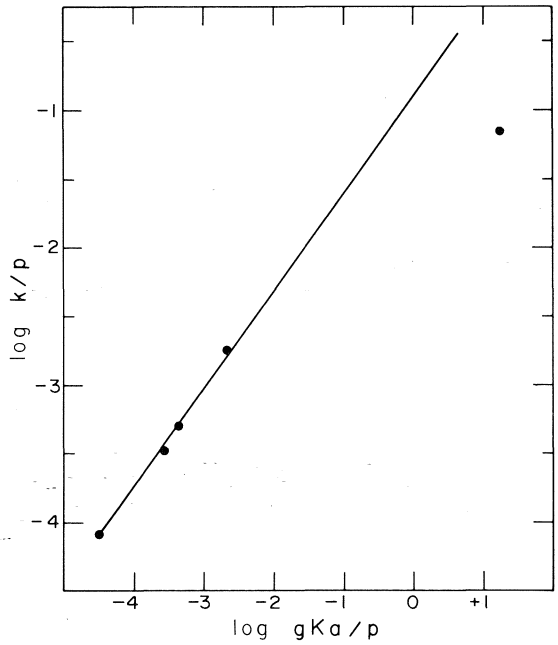

FIG. 1. Bronsted plot for the hydrolysis of methyl vinyl sulfide.

Fig. 2 depicts plots of log k_{obs} *vs.* the Hammett σ constant. The ρ values, ignoring the electron donating substituents, are −1.78 (sulfides) and −2.09 (ethers).

Discussion

Mechanism of Vinyl Sulfide Hydrolysis

All data are consistent with a mechanism of vinyl sulfide hydrolysis analogous to that of vinyl ethers (reaction 3)

$$[3] \quad RSCH{=}CH_2 \xrightarrow[\text{slow}]{H^+} RS\overset{+}{C}HCH_3 \xrightarrow[\text{fast}]{H_2O} \text{products}$$

Consistent with this are (*a*) the Hammett plot for the aryl vinyl sulfides (and its similarity to that of the aryl vinyl ethers (Fig. 2)), (*b*) the

TABLE 2. Rates of hydrolysis of aryl vinyl ethers and aryl vinyl sulfides in 1.00 *N* HCl at 25.0 °C

	$10^4 k_{obs}$ (s^{-1})	
Substituent	$ArSCH{=}CH_2$	$ArOCH{=}CH_2$
4-MeO	14.7	118
4-Me	9.05	89.6
3-Me	7.06	66.0
H	5.49	56.1
4-F	4.75	37.2
3-MeO	3.88	36.2
4-Cl	2.21	18.2
4-Br	2.31	17.9
3-Cl	1.22	9.63
$4\text{-}CF_3$	0.681	
$3\text{-}NO_2$		1.89
$4\text{-}NO_2$	0.230	1.26
$CH_3SCH{=}CH_2$	220	

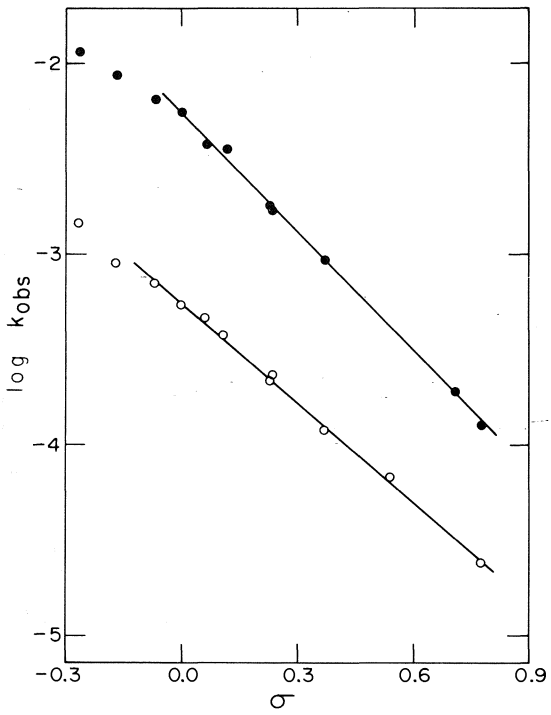

FIG. 2. Hammett plots for the hydrolysis of aryl vinyl ethers (●) and aryl vinyl sulfides (○) in 1 *N* HCl at 25 °C.

solvent isotope effect, and (*c*) the general acid catalysis; (*b*) and (*c*) pointing to a process with a slow proton transfer and (*a*) consistent with the intermediacy of a thiocarbonium ion, $ArS\overset{+}{C}HCH_3$.

For comparison purposes, the Bronsted α value for ethyl vinyl ether hydrolysis (at 25 °C) is 0.70 based on carboxylic acid catalysts (13); k_{H^+}/k_{D^+} for this compound is 2.95 (14). Taking the data of a number of vinyl ethers, Kresge and co-workers have pointed out that there are rough correlations between the values of α (10) or k_{H^+}/k_{D^+} (14) and the relative reactivity. Within such a framework the two pieces of data for methyl vinyl sulfide are seen to fit quite well, although they would be more appropriate if the compound were slightly more reactive.

Oxygen vs. Sulfur

Table 3 summarizes relative rates for vinyl ethers and sulfides, along with those of the acylals and thioacylals (reaction 1). The latter data are based on the step-wise comparison previously described (1); the former data are based on direct comparison in 1 *N* HCl (Table 2), the number for methyl vinyl ether being obtained by comparing its hydrolysis rate in more dilute acid ($k_{H^+} = 0.76\ M^{-1}\ s^{-1}$ (15)) with that of methyl vinyl sulfide.

In comparing the two sets of data we note initially that the reactivity differences between the CH_3S— and C_6H_5S compounds are approximately the same, while this is not true for the oxygen analogs. More importantly in considering oxygen *vs.* sulfur there is no correlation, the oxygen-containing molecules in the $RXCH{=}CH_2$ series being substantially more reactive than their sulfur analogs, in comparison to similar cases in $RXCH_2OAc$. In explaining these behaviours a number of factors come to mind, none of which, in our opinion, satisfactorily accounts for all aspects of Table 3.

(i) Ground State Differences: One major difference in the two classes is that in the vinylic series the heteroatom is conjugatively linked with the reacting centre in the ground state; in other words there may be differences in ground state energy levels due to relative conjugative stabilizing effects in $RXCH{=}CH_2$. This explanation requires for our data that sulfur be better conjugated with the adjacent C=C than oxygen, and although there appears to be no

TABLE 3. Relative rates of hydrolysis

	Relative rate	
RX	$RXCH{=}CH_2$[a]	$RXCH_2OAc$[b] (via $RXCH_2^+$)
CH_3S	41	49
CH_3O	1400	81
C_6H_5S	1.000	1.000
C_6H_5O	10.5	0.022
ρ(ArS)	−1.78	−2.6
ρ(ArO)	−2.09	−3.0

[a]In 1 *N* HCl.
[b]References 1 and 2.

evidence either for or against this idea, it seems unattractive since sulfur is generally regarded as a poorer π donor. Certainly the higher nmr upfield shifts of the β-carbon and β-hydrogens in the vinyl ethers (7) is more consistent with the opposite, a greater conjugation with oxygen.

(ii) Steric Effects: A recent theoretical calculation (16) has predicted that phenyl vinyl ether is not completely planar. With longer C—S bond lengths the corresponding sulfide may be more so, giving rise again to an increased reactivity in the former due to less conjugative stabilization in the ground state. This might explain why the rate differences between MeO and C_6H_5O compounds in the two series do not correlate, while those for sulfur do.

In addition, following the reasoning of Deslongchamp (17), the conformation responsible for reaction in the acylal–thioacylal compounds must have a heteroatom lone pair aligned antiperiplanar to the leaving carboxylic acid, as below.

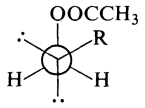

Front atom: O or S
R = methyl or aryl

With a *gauche* interaction between the methyl or aryl group and the carboxylate this is less stable than the conformer with these groups *anti*. The longer C—S bond lengths, however, make the *gauche* conformer more readily available in the thioacylals, and may then account for their enhanced reactivity.

(iii) Transition State Differences: Although similar cations are being formed in the two series, what is being measured here is not their stability but rather that of the transition state leading to them, so that the reactivity differences may be due to differences in detailed transition state structure. A pertinent observation here is that in general ethers are more basic than sulfides in dilute acid (18). This preference of oxygen molecules for the proton may be reflected in the vinylic rates, even though the proton is not being placed directly on the heteroatom. One can imagine perhaps that in the transition state the incoming solvated proton utilizes a heteroatom lone pair in its hydrogen bonding network, and oxygen is certainly more capable of this than sulfur (18).

In conclusion it is worth pointing out that although the differences in Table 2 appear large on a relative rate basis, on a free energy basis they are quite small, particularly when compared to the enormous rate variations observed in general for olefin hydration reactions (19) and $A_{A1}1$ acetate ester hydrolyses (1, 20).

Acknowledgement

Financial support from the National Research Council of Canada is gratefully acknowledged.

1. R. A. McCLELLAND. Can. J. Chem. **53**, 2763 (1975).
2. R. A. McCLELLAND. Can. J. Chem. **53**, 2772 (1975).
3. F. J. BORDWELL and P. J. BOUTON. J. Am. Chem. Soc. **78**, 854 (1956); H. BÖHME. Ber. **74**, 248 (1949); H. BÖHME, H. FISHER, and R. FRANK, Annalen, **573**, 54 (1949); T. C. JONES and F. R. THORNTON. J. Am. Chem. Soc. **89**, 4863 (1967).
4. A. J. KRESGE and Y. CHIANG. J. Chem. Soc. B, 58 (1967); M. M. KREEVOY and R. E. ELIASON. J. Phys. Chem. **72**, 1313 (1968); D. M. JONES and N. F. WOOD. J. Chem. Soc. 5400 (1974); P. SALOMAA, A. KANKAANPERÄ, and M. LAJUNEN. Acta Chem. Scand. **20**, 1790 (1966); T. H. FIFE. J. Am. Chem. Soc. **87**, 1084 (1965); T. OKUYAMA, T. FUENO, H. MAKATSUJI, and J. FURUKAWA. J. Am. Chem. Soc. **89**, 5826 (1967); A. J. KRESGE and H. CHEN. J. Am. Chem. Soc. **94**, 2819 (1972).
5. T. FUENO, I. MATSUMURA, T. OKUYAMA, and J. FURUKAWA. Bull. Chem. Soc. Jpn. **41**, 818 (1968).
6. G. H. SCHMID and D. G. GARRATT. Can. J. Chem. **51**, 2463 (1973), and references therein.
7. W. F. REYNOLDS and R. A. McCLELLAND. Can. J. Chem. In press.
8. T. FUENO, O. KAJIMOTO, K. IZAWA, and M. MASAGO. Bull. Chem. Soc. Jpn. **46**, 1418 (1973); H. MEERWEIN. Chem. Ber. **90**, 841 (1957).
9. T. MUKAIYAMA, S. FUKUYAMA, and T. KUMAMOTA. Tetrahedron Lett. 3787 (1968); G. A. RUSSELL and L. A. OCHRYMOWYCZ. J. Org. Chem. **35**, 764 (1970); E. J. COREY and J. I. SHULMAN. J. Org. Chem. **35**, 777 (1970); T. MUKAIYAMA, K. KAMIO, S. KOBAYASHI, and H. TAKEI. Bull. Chem. Soc. Jpn. **45**, 3723 (1972).
10. A. J. KRESGE, H. L. CHEN, Y. CHIANG, E. MURRILL, M. A. PAYNE, and D. S. SAGATYS. J. Am. Chem. Soc. **93**, 413 (1971).
11. G. KORTUM, W. VOGEL, and K. ANDRUSSOV. Pure Appl. Chem. **1**, 187 (1960).
12. E. J. KING. J. Am. Chem. Soc. **82**, 3575 (1960).
13. A. J. KRESGE and Y. CHIANG. J. Am. Chem. Soc. **95**, 803 (1973).
14. A. J. KRESGE, D. S. SAGATYS, and H. L. CHEN. J. Am. Chem. Soc. **90**, 4174 (1968).
15. A. J. KRESGE. Private communication.
16. R. H. DONNAY and F. GARNIER. J. Phys. Chem. **78**, 440 (1974).
17. P. DESLONGCHAMPS. Tetrahedron, **31**, 2463 (1975).
18. P. BONVICINI, A. LEVI, V. LUCCHINI, G. MODENA, and G. SCORRANO. J. Am. Chem. Soc. **95**, 5960 (1973).
19. K. OYAMA and T. T. TIDWELL. J. Am. Chem. Soc. **98**, 947 (1976).
20. R. A. McCLELLAND, T. A. MODRO, M. F. GOLDMAN, and K. YATES. J. Am. Chem. Soc. **97**, 5223 (1975).

The *para* substituent dependence of the internal rotational barrier in benzenethiol

TED SCHAEFER AND WILLIAM J. E. PARR[1]

Department of Chemistry, University of Manitoba, Winnipeg, Man., Canada R3T 2N2

Received August 19, 1976

TED SCHAEFER and WILLIAM J. E. PARR. Can. J. Chem. **55**, 552 (1977).

On the basis of the observed spin–spin coupling constants between the sulfhydryl and ring protons and a hindered rotor treatment of the twofold barrier to internal rotation in a series of *para* substituted benzenethiol derivatives, it is argued that V_2 is essentially zero in *p*-aminobenzenethiol and is 2.5 ± 0.2 kcal/mol in *p*-nitrobenzenethiol; having intermediate values for the methoxy, fluoro, methyl, and bromo derivatives in solution. The results are based on an assumed relationship between the four-bond and the fictitious six-bond couplings to the sulfhydryl proton. The conclusions are consistent with the observed magnitudes of the couplings over six and seven bonds, respectively, between the sulfhydryl proton and the fluorine nucleus and the methyl protons in the appropriate derivatives; as well as with the coupling between the sulfhydryl and methyl protons in 4-bromo-3-methylbenzenethiol. The experimental barriers are compared with *ab initio* molecular orbital calculations of their substituent dependence.

TED SCHAEFER et WILLIAM J. E. PARR. Can. J. Chem. **55**, 552 (1977).

En se basant sur les constantes de couplage spin–spin observées entre les protons sulfhydryles et les protons du cycle et en traitant comme un rotor empêché la barrière binaire à la rotation interne dans une série de benzènethiols substitués en *para*, on suggère que V_2 est pratiquement égal à zéro dans le *p*-aminobenzènethiol et à 2.5 ± 0.2 kcal/mol dans le *p*-nitrobenzènethiol; en solution, les valeurs sont intermédiaires pour les dérivés méthoxy-, fluoro-, méthyl- et bromo-. Ces résultats sont basés sur une relation hypothétique entre les couplages à travers quatre liaisons et sur les couplages fictifs à travers six liaisons pour le proton sulfhydryle. Les conclusions sont en accord avec les ordres de grandeur observés respectivement pour les couplages à travers six et sept liaisons entre le proton sulfhydryle et le noyau de fluor et les protons des méthyles dans des dérivés appropriés: ces conclusions sont aussi en accord avec le couplage entre les protons sulfhydryles et méthyles du bromo-4 méthyl-3 benzènethiol. On compare les barrières expérimentales avec les résultats de calculs *ab initio* d'orbitales moléculaires prédisant leur dépendance sur les substituants.

[Traduit par le journal]

Introduction

On the basis of the long-range spin–spin coupling constant over six bonds between the sulfhydryl proton and the ring proton in the *para* position, ${}^6J_p^{H,SH}$, of the analogy of its angular dependence to β-proton hyperfine interactions in radicals, and of the hyperconjugative overlap integrals involving C—H and S—H bonds, it was shown recently (1) that a maximum value of the barrier to internal rotation in benzenethiol in CCl_4 solution is 1.3 kcal/mol; although a final estimate of 1.1 ± 0.3 kcal/mol was suggested as covering most likely eventualities.

Now, in *p*-substituted phenol derivatives theory and experiment agree that substantial changes can occur in the internal rotational barrier of the phenol fragment (2), depending on the electron-withdrawing or donating characteristics of the *para* substituent. Because the internal barriers in both phenol and benzenethiol presumably arise from a partial loss of conjugation of the lone pair electrons with the π system of the ring, it is likely that *p*-substituted benzenethiol derivatives also display substituent dependent barriers to rotation of the sulfhydryl group.

Of course, ${}^6J_p^{H,SH}$ does not exist for these compounds. However, ${}^4J_o^{H,SH}$ is possibly roughly proportional to the nonexistent ${}^6J_p^{H,SH}$ so that the former may serve as an indicator of the internal barrier. Furthermore, in the *p*-fluoro and the *p*-methyl derivatives spin–spin coupling between the sulfhydryl proton, the ^{19}F nucleus, and the methyl protons constitutes a check on the deductions based on ${}^4J_o^{H,SH}$. This paper concerns itself with these questions.

Experimental

Five mole percent solutions in CCl_4 containing a little tetramethylsilane were degassed by the freeze–pump–thaw technique. For reasons of solubility or stability other

[1]Postdoctoral fellow, 1974–1976.

TABLE 1. Spectral parameters* for a 5 mol% solution in CCl_4 of 4-fluorobenzenethiol

Parameter	Value	Parameter	Value
ν_{SH}	324.584(3)‡	$^3J_o^{H,F}$	8.350(7)
$\nu_{2,6}$	722.225(4)	$^4J_m^{H,F}$	5.008(7)
$\nu_{3,5}$	688.982(4)	$^6J_p^{SH,F}$	1.000(5), 1.028(7)§
ν_F	1930.42†	$^4J_o^{SH,H}$	−0.531(4)
$^3J_o^{H,H}$	8.585(6)‡	$^5J_m^{SH,H}$	0.270(4)
$^4J_m^{H_2H_6}$	2.914(6)	rms error	0.0178
$^4J_m^{H_3H_5}$	2.474(6)	Peaks assigned	97
$^5J_p^{H,H}$	0.372(5)	Transitions calculated	128‖

*Proton chemical shifts in Hz to low field of internal tetramethylsilane at 100 MHz at 305 K.
†To high field of internal CF_3CCl_3 at 56.443 MHz at 302 K, in Hz.
‡The numbers in parentheses are the standard deviations in the last place.
§For the proton and fluorine spectra at 100 MHz and 56.443 MHz, respectively.
‖In the proton spectrum.

solvents were necessary for two compounds. Proton magnetic resonance spectra were calibrated in the frequency sweep mode on an HA-100 spectrometer at 305 K. Partial decoupling (3) and weak irradiation (4) experiments established the signs of coupling constants relative to $^3J_o^{H,F}$, $^3J_o^{H,H}$, and $^4J_o^{H,CH_3}$, known to be positive (5), positive (6), and negative (7), respectively. Intermolecular proton exchange was hindered by the presence of molecular sieve, although drying periods of a few weeks were sometimes necessary.

Ab initio molecular orbital calculations at the STO 3G level (8, 9) were performed on an IBM 370/158 computer system.

Results and Discussion

(1) Spectral Analyses

Spectral analyses using the program LAME (10, 11) were relatively straightforward. In Table 1 the full results of the analysis of the *p*-fluorobenzenethiol are given as an example. The standard deviations in the parameters suggest an accuracy of at least 0.02 Hz in the coupling constants of major interest in this paper. In Fig. 1 the spectrum of the sulfhydryl proton is displayed. Rather than tabulate the plethora of spectral parameters, we give in Table 2 the long-range coupling constants to sulfhydryl protons, methyl protons, and the ^{19}F nucleus for seven *p*-substituted benzenethiol derivatives. The chemical shifts of the sulfhydryl proton have been discussed for most of these compounds (12).

(2) Substituent Dependence of the Internal Barrier

(i) $^4J_o^{H,SH}$ and the Barriers

In previous work (1) it was argued that $^6J_p^{H,SH}$ in benzenethiol follows a $\sin^2\theta$ law as in [1],

$$[1] \qquad {}^6J_p^{H,SH} = {}^6J_{90}\sin^2\theta$$

where θ is the angle by which the S—H bond twists out of the aromatic plane. $^6J_{90}$ is the maxi-

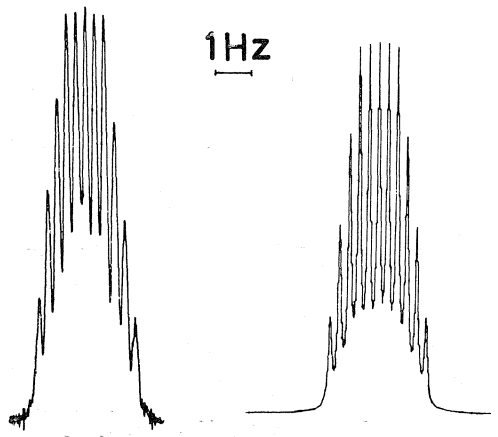

FIG. 1. The proton magnetic resonance spectrum at 100 MHz and 305 K of the sulfhydryl proton in a 5 mol% solution of *p*-fluorobenzenethiol in CCl_4. The calculated spectrum is based on the parameters in Table 1.

TABLE 2. Long-range coupling constants to the sulfhydryl proton in some *p*-substituted benzenethiol derivatives*

Substituent	$^4J_o^{H,SH}$	$^5J_m^{H,SH}$
H†	−0.380	0.250
NH_2‡	−0.697	0.294
OCH_3	−0.649	0.298
F§	−0.531	0.270
CH_3‖	−0.439	0.271
Br	−0.333	0.231
NO_2¶	−0.203	0.203

*For 5 mol% solutions in CCl_4 unless otherwise stated, to an accuracy of 0.02 Hz.
†$^6J_p^{H,SH} = -0.334$ Hz.
‡A 3 mol% solution in C_6D_6 gave $^4J_o = -0.713$ and $^5J_m = 0.296$ Hz; a 2 mol% solution in $CDCl_3$ gave $^4J_o = -0.682$ and $^5J_m = 0.293$ Hz.
§$^6J_p^{F,SH} = 1.01 \pm 0.02$ Hz.
‖$^7J_p^{SH,CH_3} = 0.40 \pm 0.02$ Hz, $^4J_o^{H,CH_3} = -0.71$ Hz, $^5J_m^{H,CH_3} = 0.33$ Hz.
¶For a 2 mol% solution in $CDCl_3$.

TABLE 3. The twofold barriers* to internal rotation in *p*-substituted derivatives of benzenethiol in solution

	$\langle\sin^2\theta\rangle$, $^4J^{H,SH} = 1.16J_p^{H,SH}$			
	1	**2**	V_2 (kcal/mol)	
Substituent	$^6J_{90} = -1.06$ Hz	$^6J_{90} = -1.24$ Hz	**1**	**2**
NO_2	0.165	0.141	2.4	2.7
Br	0.271	0.231	1.3	1.6
H	0.309	0.264	1.0	1.3
CH_3	0.357	0.305	0.7	1.1
F	0.432	0.369	0.3	0.7
OCH_3	0.527	0.451	−0.1	0.2
NH_2	0.567	0.485	−0.3	0.1

*Quoted to the nearest 0.1 kcal/mol.

mum value of $^6J_p^{H,SH}$ and the twofold potential hindering the internal barrier determines the average value of $\sin^2\theta$, which also depends on the reduced moment of inertia and the temperature. A value of $^6J_{90}$ of −1.06 Hz was preferred, a lower limit of −1.24 Hz being possible (1).

In the *para* derivatives in Table 2, $^6J_p^{H,SH}$ is not available. However, if it is assumed that $^4J_o^{H,SH}$ is dominated by a σ–π mechanism, this coupling may be used to estimate the barriers to internal rotation. In phenol (13), $|^6J_p^{H,OH}| \leq 0.03$ Hz and $|^4J_o^{H,OH}| \leq 0.07$ Hz, suggesting that $^4J_o^{H,OH}$ is nearly zero for the high barrier of 3.5 kcal/mol (14); the σ–π mechanism contributing little to the magnitude of the coupling. In toluene, for an effectively zero internal barrier (15), $^4J_o^{H,CH}/^6J_p^{H,CH} = 1.19$ (16), and if $^6J_p^{H,CH}$ is σ–π determined (17), it follows from the magnitudes of the coupling constants that the non σ–π component of $^4J_o^{H,CH}$ does not likely exceed −0.1 Hz.

In benzenethiol $^4J_o^{H,SH}$ is -0.38 ± 0.02 Hz and $^6J_p^{H,SH}$ is -0.33 ± 0.02 Hz. Therefore the ratio of the couplings lies between 1.29 and 1.03. The average is 1.16 and will be taken as holding for the compounds in Table 2. Either limit of this ratio shifts the ensuing barrier by 0.1 kcal/mol. $^6J_{90}$ is taken as −1.06 Hz and as −1.24 Hz, yielding two sets of average values of $\sin^2\theta$ in Table 3. These are related via the hindered rotor treatment (18) to the two sets of V_2, the twofold barrier to internal rotation, also given in Table 3.

(ii) Consistency of V_2 with $^7J_p^{SH,CH_3}$ and $^6J_p^{SH,CH_3}$ and $^6J_p^{F,SH}$

In toluene $^6J_p^{H,CH}$ is −0.62 Hz (16), while in *p*-xylene (19, 20) $^7J_p^{CH_3,CH_3}$ is +0.62 Hz. The sign reversal is expected for a σ–π mechanism. The magnitudes of the two numbers suggest that for the benzenethiol analogues, $^6J_p^{H,SH} = -^7J_p^{SH,CH_3}$ with the proviso, of course, that the methyl group changes the barrier. Therefore $^6J_p^{H,SH}$ here refers not to benzenethiol but to a fictitious $^6J_p^{H,SH}$ in *p*-methylbenzenethiol. In fact (Table 2), $^7J_p^{SH,CH_3}$ is 0.40 ± 0.02 Hz, whereas the assumed ratio of 1.16 for $^4J_o^{H,SH}/^6J_p^{H,SH}$ implies that the fictitious $^6J_p^{H,SH}$ is −0.38 Hz. In other words, the two V_2 values of 0.7 and 1.1 kcal/mol in Table 2 are consistent to within 0.1 kcal/mol with the magnitude of $^7J_p^{SH,CH_3}$ in *p*-methylbenzenethiol.

In *p*-fluorobenzenethiol, $^6J_p^{F,SH}$ is 1.01 ± 0.02 Hz. In *p*-fluorotoluene, $^6J_p^{F,CH_3}$ is 1.15 Hz (21). Assuming that the latter coupling determines the σ–π parameter for the C—F bond and that free methyl group rotation occurs (22), one has $\langle\sin^2\theta\rangle = 1.01/(2 \times 1.15) \times 1.06 = 0.414$; corresponding to a barrier of 0.5 kcal/mol, or a value of 0.3 kcal/mol if $^6J_{90} = -1.24$ kcal/mol. In other words, the values of 0.3 and 0.7 kcal/mol based on $^4J_o^{H,SH}$ in Table 3 are in agreement with the conclusions based on $^6J_p^{F,SH}$.

From our previous work (1) we prefer the lower values of V_2 in Table 3, although the mean values may well be as reliable. In any event, the error limits are probably near 0.2 kcal/mol.

(iii) Consistency of V_2 with $^6J_m^{SH,CH_3}$ in 4-Bromo-3-methylbenzenethiol

In *m*-xylene, $^6J_m^{CH_3,CH_3}$ is −0.21 Hz (19, 20). If this coupling is taken as the magnitude of the π electron contribution to $^5J_m^{H,CH_3}$ in toluene (19, 20), a test of the arguments concerning $^6J_{90}$

in the benzenethiol derivatives can be made as follows. In toluene and in *m*-xylene one has $\langle \sin^2 \theta \rangle$ as 0.5. In Table 3, $\langle \sin^2 \theta \rangle$ is 0.25 ± 0.02 for *p*-bromobenzenethiol, the limits being given by the extremes in $^6J_{90}$. Consequently $^6J_m^{SH,CH_3}$ in 4-bromo-3-methylbenzenethiol should be −0.21/2 or −0.11 ± 0.02 Hz. In fact, the analysis of the proton spectrum indicated a value of −0.13 ± 0.02 Hz.

Now, this compound is asymmetrical so that the internal barrier to rotation about the C—S bond may well contain a significant component which is not twofold in character. Furthermore, the presence of the methyl group may alter the magnitude of the barrier. However, if the barrier is sensitive to resonance interactions, the presence of the methyl group *meta* to the sulfhydryl group suggests a smaller perturbation than if it were placed *para* to the sulfhydryl moiety. Nevertheless the observed value of −0.13 ± 0.02 Hz for $^6J_p^{SH,CH_3}$ is consistent with the conclusions concerning the internal barrier in the *p*-substituted benzenethiol derivatives.

(iv) Comparison with p-Substituted Phenols

In Table 3, V_2 ranges from 2.5 kcal/mol for *p*-nitrobenzenethiol through 1.1 kcal/mol for benzenethiol to −0.2 kcal/mol for *p*-aminobenzenethiol, always with an accuracy of *ca.* 0.2 kcal/mol. Clearly, an electron-withdrawing group increases the barrier, presumably by increasing the conjugation[2] of the SH group with the aromatic nucleus in the planar form. Then the electron-donating groups lower the barrier by decreasing the double bond character of the C—S bond in the planar, ground state.

In the phenol analogue, the nitro group increases the internal barrier by 1 kcal/mol (2), the increase of 1.4 kcal/mol in *p*-nitrothiophenol being somewhat larger. In the phenol derivatives, the hydroxy, fluoro, and methyl groups decrease the barrier by 0.9, 0.6, and 0.3 kcal/mol, respectively, rather similar to the decreases of 1.0, 0.7, and 0.3 kcal/mol in the methoxy, fluoro, and methyl derivatives of benzenethiol. In view of the larger barrier in phenol, it appears that the sulfhydryl group is more susceptible than the hydroxyl group to substituent induced changes in conjugation with the aromatic π electrons (24).

(v) Comparison with Ab Initio MO Calculations

The STO3G calculations are rather expensive for benzenethiol derivatives, particularly when geometry optimization procedures are adopted. Optimization of the C—S—H geometry yielded C—S (S—H) bond lengths of 1.76_2 (1.34) Å and a CSH angle of 95.8° for the planar conformation of benzenethiol. These bond parameters then gave V_2 as 3.52 kcal/mol, *i.e.*, the conformation in which the S—H bond lies in a plane perpendicular to the aromatic plane had the higher energy. The apparent overestimate of about 2.4 kcal/mol is similar to the overestimate for phenol (2). When a standard geometry (25) was used, *i.e.*, C—S = 1.815 Å and ∠CSH = 109.5°, the barrier was calculated as 2.8 kcal/mol.

The optimized geometry of the CSH group above gave a barrier of 2.55 kcal/mol for *p*-aminobenzenethiol, a decrease of 0.97 kcal/mol relative to benzenethiol, close to the experimental value in Table 3. For *p*-fluorobenzenethiol the calculated decrease of 0.46 kcal/mol also compares favorably with the observed decrease of 0.6 ± 0.2 kcal/mol in Table 3. Unfortunately, no convergence in the calculations was obtained for the *p*-nitro derivative.

Apparently, the *ab initio* calculations overestimate substantially the barriers in both phenol and benzenethiol derivatives but predict substituent-induced changes in the barriers in reasonable agreement with experiment.

(vi) Correlations Involving $^4J_o^{H,SH}$ and $^5J_m^{H,SH}$

A plot of $^4J_o^{H,SH}$ against $^5J_m^{H,SH}$ is roughly linear; the former varying by 0.5 Hz, the latter by 0.1 Hz, over the range of *para* substituents in Table 2. In view of the preceding discussion, the increase in magnitude of both coupling constants reflects an increase in the σ–π contribution as the substituent varies from NO_2 to NH_2. In terms of simple MO theory, the smaller increase in $^5J_m^{H,SH}$ occurs because the two ring carbon atoms belong to the same starred (or unstarred) set and, to zero order, the mobile bond order between these carbons vanishes. Because $^5J_m^{H,SH}$ presumably contains a substantial σ component (compare corresponding couplings in phenol (13), benzaldehyde (26), aniline (23), for example), the rather small increase in $^5J_m^{H,SH}$ may reflect a compensating decrease in this component as the σ–π component grows with increasing $\langle \sin^2 \theta \rangle$.

[2]It might have been argued that an increased double bond character of the C—S bond would increase the magnitude of $^6J_p^{H,SH}$ if the coupling were transmitted via the conjugative π electrons. The opposite occurs, just as in phenol (13), and aniline (23), in agreement with the hyperconjugative ($\sin^2 \theta$) mechanism.

(vii) Intermolecular Association

The concentrations of the solutions in Table 2 are 0.5 *M* or less. At these concentrations chemical shift (27) and infrared (28) studies suggest that perhaps only about 1% of the solute molecules are associated. Of course, the solvent molecules are interacting with the solute molecules by dispersion forces, if in no other way. A gas-phase measurement of the coupling constants is desirable but their small magnitude may vitiate their determination to the needed accuracy.

Conclusions

It is very likely that *para* substituents alter the barrier to rotation about the C—S bond in benzenethiol derivatives and that the barrier ranges over as much as 2.5 kcal/mol. This conclusion, reached on the basis of long-range proton–proton spin–spin coupling constants, should be confirmed if possible by microwave or high resolution infrared or Raman measurements in the gas phase.

Acknowledgments

We are grateful to Mr. Kalvin Chum for some of the measurements and to the National Research Council of Canada for financial assistance.

1. T. SCHAEFER and W. J. E. PARR. J. Magn. Reson. In press (1977).
2. L. RADOM, W. J. HEHRE, J. A. POPLE, G. L. CARLSON, and W. G. FATELEY. J. Chem. Soc. Chem. Commun. 308 (1972).
3. J. P. MAHER and D. F. EVANS. Proc. Chem. Soc. 208 (1961).
4. R. FREEMAN and W. A. ANDERSON. J. Chem. Phys. **37**, 2053 (1962).
5. A. SAUPE. Z. Naturforsch. Teil A, **19**, 161 (1964); **20**, 572 (1965).
6. R. FREEMAN. J. Chem. Phys. **43**, 3087 (1965).
7. G. KOTOWYCZ and T. SCHAEFER. Can. J. Chem. **44**, 2743 (1966).
8. W. J. HEHRE, R. F. STEWART, and J. A. POPLE. J. Chem. Phys. **51**, 2657 (1969).
9. Program No. 236. Q.C.P.E. University of Indiana, Bloomington, Indiana.
10. S. CASTELLANO and A. A. BOTHNER-BY. J. Chem. Phys. **41**, 3863 (1964); LAOCN 3, Mellon Institute, Pittsburgh, Pa. 1966.
11. C. W. HAIGH and J. M. WILLIAMS. J. Mol. Spectrosc. **32**, 398 (1969).
12. S. H. MARCUS and S. I. MILLER. J. Phys. Chem. **68**, 331 (1964).
13. T. SCHAEFER, J. B. ROWBOTHAM, and K. CHUM. Can. J. Chem. **55**, 3666 (1976).
14. H. FOREST and B. P. DAILEY. J. Chem. Phys. **45**, 1736 (1966); T. PEDERSEN, N. W. LARSEN, and L. NYGAARD. J. Mol. Struct. **4**, 59 (1969); H. D. BIST and D. R. WILLIAMS. Bull. Am. Phys. Soc. **11**, 826 (1966).
15. H. D. RUDOLPH, H. DREIZLER, A. JAESCHKE, and P. WENDLING. Z. Naturforsch. Teil A, **22**, 940 (1967).
16. M. P. WILLIAMSON, R. J. KOSTELNIK, and S. M. CASTELLANO. J. Chem. Phys. **49**, 2218 (1968).
17. R. WASYLISHEN and T. SCHAEFER. Can. J. Chem. **50**, 1852 (1972).
18. T. SCHAEFER, J. B. ROWBOTHAM, W. J. E. PARR, K. MARAT, and A. F. JANZEN. Can. J. Chem. **54**, 1322 (1976).
19. C. J. MACDONALD and W. F. REYNOLDS. Can. J. Chem. **48**, 1002 (1970).
20. J. B. ROWBOTHAM and T. SCHAEFER. Can. J. Chem. **52**, 489 (1974).
21. R. WASYLISHEN and T. SCHAEFER. Can. J. Chem. **49**, 94 (1971).
22. H. D. RUDOLPH and H. SEILER. Z. Naturforsch. Teil A, **20**, 1682 (1965).
23. R. WASYLISHEN, J. B. ROWBOTHAM, L. ERNST, and T. SCHAEFER. Can. J. Chem. **50**, 2575 (1972).
24. S. H. MARCUS, W. F. REYNOLDS, and S. I. MILLER. J. Org. Chem. **31**, 1872 (1966).
25. J. A. POPLE and M. S. GORDON. J. Am. Chem. Soc. **89**, 4253 (1967).
26. R. J. KOSTELNIK, M. P. WILLIAMSON, D. E. WISNOSKY, and S. M. CASTELLANO. Can. J. Chem. **47**, 3313 (1969).
27. S. H. MARCUS and S. I. MILLER. J. Am. Chem. Soc. **88**, 3749 (1966).
28. J. G. DAVID and H. E. HALLAM. Spectrochim. Acta, **21**, 841 (1965).

A proton magnetic resonance determination of the small rotational barriers about the C—Si bond in phenyl derivatives of chloro and methyl silanes

WILLIAM J. E. PARR[1] AND TED SCHAEFER

Department of Chemistry, University of Manitoba, Winnipeg, Man., Canada R3T 2N2

Received August 31, 1976

WILLIAM J. E. PARR and TED SCHAEFER. Can. J. Chem. **55**, 557 (1977).

The long-range spin–spin coupling constants between protons bonded to silicon and ring protons in $C_6H_5SiH_3$, $C_6H_5SiH_2Cl$, $C_6H_5SiH_2CH_3$, $C_6H_5SiHCl_2$, and $C_6H_5SiH(CH_3)_2$ are determined from the proton magnetic resonance spectra of benzene solutions. A hindered rotor treatment of the barrier to internal rotation about the C—Si bond, in conjunction with the coupling constants over six bonds, allows the deduction of the low-energy conformations for $C_6H_5SiH(CH_3)_2$ and for $C_6H_5SiHCl_2$, as well as of barriers of 1.0 ± 0.2 kcal/mol. The approach becomes less reliable for $C_6H_5SiH_2CH_3$ and for $C_6H_5SiH_2Cl$ and, particularly for the latter compound, the derived barrier is very likely an upper limit only. *Ab initio* molecular orbital calculations of the conformational energies are reported for $C_6H_5SiH_3$, $C_6H_5SiH_2Cl$, and for $C_6H_5SiHCl_2$.

WILLIAM J. E. PARR et TED SCHAEFER. Can. J. Chem. **55**, 557 (1977).

On a déterminé les constantes de couplage spin–spin à longue distance entre les protons liés au silicium et les protons du cycle dans $C_6H_5SiH_3$, $C_6H_5SiH_2Cl$, $C_6H_5SiH_2CH_3$, $C_6H_5SiHCl_2$ et $C_6H_5SiH(CH_3)_2$; ces constantes ont été déterminées à partir des spectres de résonance magnétique nucléaire du proton en solutions benzéniques. Si l'on traite la barrière à rotation interne autour du lien C—Si sous forme de rotor empêché et que l'on utilise aussi les constantes de couplage à travers six liaisons, il est possible de déduire les conformations de basse énergie pour $C_6H_5SiH(CH_3)_2$ et pour $C_6H_5SiHCl_2$; on peut aussi en déduire que les barrières sont de l'ordre 1.0 ± 0.2 kcal/mol. Cette approche devient moins fiable pour $C_6H_5SiH_2CH_3$ et pour $C_6H_5SiH_2Cl$ et particulièrement dans le cas du dernier composé, la barrière qui est déduite est probablement uniquement une limite supérieure. On rapporte des calculs *ab initio* d'orbitales moléculaires des énergies conformationnelles pour $C_6H_5SiH_3$, $C_6H_5SiH_2Cl$ et $C_6H_5SiHCl_2$.

[Traduit par le journal]

Introduction

In toluene the coupling over six bonds between methyl protons and ring protons in the *para* position, $^6J_p^{H,CH}$ displays a $\sin^2\theta$ dependence,

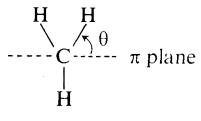

1

where θ is the angle in **1** (1, 2). For free rotation about the C—CH_3 bond (3) the average value of $\sin^2\theta$ is 0.5. If it is assumed that ^6J in α and α,α derivatives is also a function of $\sin^2\theta$, reasonable twofold barriers to rotation about the C—CH_2X and C—CHX_2 bonds can be derived on the basis of hindered rotor treatments (4, 5). These yield $\langle\sin^2\theta\rangle$ as a function of the hindering potentials and of the reduced moments of inertia (4).

[1]Postdoctoral fellow, 1974–1976.

The sixfold barrier to rotation about the C—Si bond in phenylsilane is 0.018 kcal/mol (6), very similar to the 0.014 kcal/mol in toluene (3). When one or two Si—H bonds are replaced by

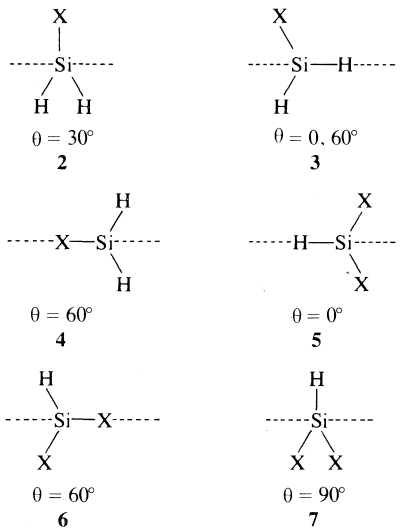

TABLE 1. Chemical shifts* and spin–spin coupling constants† for some phenylsilane derivatives in benzene-d_6 solution

Parameter	ϕCH_3‡	ϕSiH_3	ϕSiH_2CH_3§	ϕSiH_2Cl	$\phi SiH(CH_3)_2$§	$\phi SiHCl_2$
ν_α	—	421.60	445.66	508.09	459.26	575.0
$\nu_{2,6}$	697.30	738.54	744.09	737.45	745.19	742.29
$\nu_{3,5}$	708.51	707.50	714.20	705.08	718.18	702.08
ν_4	700.36	712.06	716.00	710.92	717.99	708.97
ν_{CH_3}	—	—	21.26	—	21.72	—
$^3J_{2,3}$	7.64	7.322(8)	7.383(6)	7.386(7)	7.367(9)	7.534(6)
$^3J_{3,4}$	7.52	7.576(6)	7.526(4)	7.584(6)	7.499(5)	7.570(4)
$^4J_{2,4}$	1.25	1.363(7)	1.350(5)	1.381(8)	1.417(8)	1.341(6)
$^4J_{2,6}$	1.87	1.363(7)	1.343(4)	1.344(8)	1.322(6)	1.455(5)
$^4J_{3,5}$	1.51	1.309(7)	1.275(4)	1.196(9)	1.251(6)	1.233(5)
$^5J_{2,5}$	0.60	0.694(8)	0.708(5)	0.737(7)	0.686(8)	0.716(6)
$^4J_o^{H,XH}$‖	−0.75	−0.142(5)	−0.183(4)	−0.061(11)	−0.197(7)	−0.036(8)
$^5J_m^{H,XH}$	0.36	0.204(6)	0.198(6)	0.218(6)	0.181(10)	0.291(7)
$^6J_p^{H,XH}$	−0.62	−0.343(8)	−0.293(9)	−0.231(8)	−0.221(15)	−0.177(11)
$^1J(^{29}Si, H)$	—	−200.0	−193.3	−236.0	−188.0	−289.1
rms error	—	0.028	0.019	0.017	0.023	0.015

*In Hz at 100 Mz to low field of internal tetramethylsilane for 10 mol% solutions at 305 K.
†In Hz, numbers in parentheses representing standard deviations in the analysis.
‡For a neat toluene sample, ref. 1.
§$^3J^{HSiCH}$ is 4.23 Hz for $C_6H_5SiH_2CH_3$ and is 3.77 Hz for $C_6H_5SiH(CH_3)_2$.
‖X stands for C or Si, as required.

Si—Cl and Si—CH_3 bonds it is reasonable to discuss the predominantly twofold barriers in terms of conformations **2** to **7**. In this paper the proton magnetic resonance spectra of phenylsilane derivatives where X = Cl and CH_3 are analyzed. $^6J_p^{H,SiH}$ is discussed in terms of the ground state conformations and of the magnitudes of the internal rotational barriers. Molecular orbital calculations at the *ab initio* STO-3G level are compared with results based on $^6J_p^{H,SiH}$.

Experimental

The only compound not of commercial origin was $C_6H_5SiH_2Cl$, which was prepared from phenylsilane using anhydrous stannic chloride (7). For reasons of spectral dispersion, samples were prepared as *ca.* 10 mol% solutions in C_6D_6 containing a small amount of internal tetramethylsilane. After degassing the samples by the freeze–pump–thaw technique, the proton magnetic resonance spectra were calibrated on an HA100 spectrometer in the frequency sweep mode at a probe temperature of 305 K.

Ab initio STO-3G molecular orbital calculations (8) were performed on an IBM 370/158 system and employed a standard geometry (9) for the phenyl group, tetrahedral angles about silicon and C—Si, Si—H, Si—Cl bond lengths of 1.843, 1.48, and 2.03 Å, respectively.

Results and Discussion

Spectral Analysis

Analysis of the spectra utilized the computer program LAME (10, 11). The chemical shift and spin–spin coupling parameters are arrayed in Table 1. The analyses showed that the signs of the long-range couplings were as given in Table 1, alternative sign combinations yielding clear disagreement with spectral patterns. The $^1J(^{29}Si,H)$ values were obtained from the satellite spectra arising from the 4.7% abundant ^{29}Si.

Ring Proton Chemical Shifts

The substituent dependence of the chemical shifts of the ring protons is partially masked by the aromatic solvent induced shifts, ASIS (12–15). However, the ASIS caused by toluene are very similar to those arising from benzene (14). The parameters given for toluene itself in Table 1 originate in a neat solution of toluene, so that a comparison of these parameters with those of phenylsilane and its derivatives is approximately valid. The chemical shift of the benzene protons in benzene solution is 7.07 ppm, very close to the shift of 7.08_5 ppm of the *meta* protons of toluene in toluene solution. The shift to high field of the *ortho* and *para* ring proton is consistent with a small increased π electron density at the *ortho* and *para* carbon atoms (16) and with a negative value for the σ constant for the methyl group.

Comparison of the *para* proton shifts in Table 1 suggests that the SiH_3 group is a weak π electron acceptor (17), although for the SiH_2Cl and $SiHCl_2$ groups the conclusions are clouded by the possibility of larger ASIS values for molecules containing appreciable polar bonds (15). For the most part, the large low-field shifts of the *ortho* protons in all the phenylsilane derivatives are

hardly due to electronegativity effects. It may be noted that these shifts may be another example of the so-called heavy-atom perturbations, for which numerous and probably related explanations have been advanced (18–20).

Coupling Constants within the Phenyl Group

In benzene, to within 0.04 Hz, the couplings $^3J_o^{H,H}$, $^4J_m^{H,H}$, and $^5J_p^{H,H}$ are 7.54, 1.37, and 0.69 Hz, respectively (21). $^3J_o^{H_2,H_3}$ in the phenylsilane derivatives is less than 7.54 Hz, although only by 0.2 Hz at most. This result implies (22) that the side chains are less electronegative than the methyl group and therefore that the low-field shifts of the *ortho* protons do not have their origin in a polarization of the intervening σ electron system.

The other couplings between the ring protons in Table 1, when compared with the benzene coupling parameters and with those for toluene, are consistent with a relatively weak perturbation of the electrons in the phenyl group. For example, in phenylsilane all these coupling constants equal those in benzene to within experimental error. This fact contrasts strongly with the data for other benzene derivatives and even with the data for toluene in Table 1.

$^1J(^{29}Si,H)$

The magnitudes of these coupling constants lie within 0.5 Hz of literature values (23, 24) and the usual arguments (25–29) concerning hybridization and substituent electronegativities apply to them. Of particular interest is the iterative hybridization method of Rastelli and Pozzoli (29) which reproduces the available experimental bond angles involving silicon for phenyl- and phenylmethylsilane derivatives. Their work suggests that the bond angles do not deviate by more than 1° from a tetrahedral geometry and that therefore the tetrahedral geometry assumed in the STO-3G calculations below is reasonable.

Long-range Proton–Proton Couplings to the Side Chain

$^6J_p^{H,SiH}$ in phenylsilane has approximately half the magnitude[2] of $^6J_p^{H,CH_3}$ in toluene (see Table 1), suggesting that the σ–π parameter for the SiH_3 group is very nearly half as large as for the CH_3 group. The smaller magnitude for the SiH_3 group is at least partially attributable to the greater length (1.843 Å) of the C—Si bond, as compared to the C—C bond length (1.52 Å) in toluene.

$^4J_o^{H,SiH}$ is markedly smaller in magnitude than is $^4J_o^{H,CH_3}$ in toluene, indicating that a positive σ electron contribution partially compensates the negative π electron contribution to $^4J_o^{H,SiH}$ in phenylsilane; expected to be of nearly the same magnitude as for $^6J_p^{H,SiH}$.

In toluene, $^5J_m^{H,CH_3}$ consists of a mixture of positive σ and π electron contributions (2, 30, 31). The smaller magnitude of the corresponding coupling constant in phenylsilane can once more be partially attributed to a smaller π electron transmission of spin state information. In any event, $^6J_p^{H,SiH}$ is of primary interest and is discussed below.

$^6J_p^{H,SiH}$ and the Barriers to Internal Rotation

In a manner analogous to the work on toluene derivatives (4, 5) it is assumed that $^6J_p^{H,SiH}$ obeys [1].

$$[1] \qquad {}^6J = {}^6J_{90} \sin^2 \theta$$

For phenylsilane $\langle \sin^2 \theta \rangle$, the value of $\sin^2 \theta$ averaged over the essentially free rotation about the C—Si bond, is 0.5.

In an α,α-disubstituted phenylsilane, $\langle \sin^2 \theta \rangle$ depends on which of **5**, **6**, or **7** is the ground state conformation, on the magnitude of the internal barrier to rotation, on the temperature, and on the reduced moment of inertia; being relatively insensitive to the latter quantity. For low barriers near 305 K, the temperature of measurement, a hindered rotor treatment is essential and has been performed (4), yielding $\langle \sin^2 \theta \rangle$ as a function of the two-fold barrier to internal rotation. If **5** is the conformation of lowest energy, $\langle \sin^2 \theta \rangle$ increases from zero for a large barrier to 0.5 for free rotation; whereas if **6** is of lowest energy, $\langle \sin^2 \theta \rangle$ decreases from 0.75 to 0.5 as the barrier decreases.

(i) $C_6H_5SiH(CH_3)_2$

In toluene, α substitution by methyl groups does not change $^6J_{90}^{H,CH}$ (5, 32). A similar assumption for phenylsilane gives $^6J_{90}^{H,SiH}$ as -0.68_6 Hz. For $C_6H_5SiH(CH_3)_2$, $\langle \sin^2 \theta \rangle$ is 0.221/0.686 or 0.32. It follows that **5**, and not **6** or **7**, is the stable conformation. A reduced moment of inertia of 0.8×10^{-38} g cm^2 then implies a barrier of 1.0 ± 0.2 kcal/mol, where the error depends on possible errors in the measured coupling constant. The percentage error is larger than in the barrier of 2.0 ± 0.2 kcal/mol

[2]An analysis of a CS_2 solution gave −0.312 Hz. We are grateful to Dr. C. J. MacDonald for this information, prior to publication.

TABLE 2. Barriers to internal rotation about C—Si and C—C bonds in phenylsilane and in toluene derivatives

Compound	Conformer* Low	Conformer* High	Barrier (kcal/mol) ^6J	Barrier (kcal/mol) STO-3G	Barrier (kcal/mol) Other	Reference
ϕSiH_3	**3**	**2**	—	0.001†	0.018‡	6
ϕCH_3	—	—	—	0.00	0.014‡	3
$\phi SiH(CH_3)_2$	**5**	**7**	1.0±0.3	—	—	—
3,5-diBr$\phi CH(CH_3)_2$	**5**	**7**	2.0±0.2	—	—	33
$\phi SiHCl_2$	**5**	**7**	1.0±0.3	0.50	—	—
$\phi CHCl_2$	**5**	**7**	2¶	—	—	—
ϕSiH_2CH_3	**2**	**4**	0.8±0.4	—	—	—
3,5-diBrϕCH_2CH_3	**2**	**4**	1.2±0.1	2.2§	1.3‖	35
ϕSiH_2Cl	**2**	**4**	1.7¶	0.39	—	—
3,5-di$Cl\phi CH_2Cl$	**2**	**4**	2.1±0.2	2.22§	—	34

*The conformer numbers refer to the diagrams in the text, and indicate low and high energy forms.
†Below level of significance.
‡Microwave, gas phase.
§Partial optimization of geometry.
‖Thermodynamic value, ref. 35.
¶Upper limit.

recently derived (33) by the same method for 3,5-dibromoisopropylbenzene in solution and reflects the smaller magnitudes of $^6J_p^{H,SiH}$, the error in measurement being of the same magnitude for $^6J_p^{H,SiH}$ and $^6J_p^{H,CH}$. However, there appears to be no doubt of the ground state conformation, **5**, for the groups $HSi(CH_3)_2$ and $HC(CH_3)_2$.

(ii) $C_6H_5SiHCl_2$

Determination of the barrier in $C_6H_5SiHCl_2$ involves an estimate of the change in $^6J_p^{H,SiH}$ caused by the electronegative chlorine substituents. For the CH_2Cl moiety it has been estimated that the magnitude of $^6J_{90}^{H,CH}$ decreases by 8% from its magnitude for a CH_3 group (34). Introduction of a second chlorine substituent would presumably cause a further decrease of no more than 8%. Assuming a similar pair of numbers for $SiHCl_2$ one arrives at $^6J_{90}$ for this group of 0.58 Hz, a $\langle \sin^2 \theta \rangle$ of 0.30_5, and a barrier of 1.0 ± 0.2 kcal/mol, the error including a situation where $^6J_{90}^{H,SiH}$ is the same as in the SiH_3 group.

(iii) $C_6H_5SiH_2CH_3$

The errors in the barriers for $C_6H_5SiH(CH_3)_2$ and $C_6H_5SiHCl_2$ are somewhat mitigated by the fact that **5** is the low energy conformation and that therefore $\langle \sin^2 \theta \rangle$ varies between 0 and 0.5 as a function of the barrier. In $C_6H_5SiH_2Cl$ and $C_6H_5SiH_2CH_3$, on the other hand, $\langle \sin^2 \theta \rangle$ changes at most by 0.25 in going from free rotation to a very large barrier on the assumption that one of **2**, **3**, or **4** is the stable conformer. This insensitivity of $\langle \sin^2 \theta \rangle$, combined with the small magnitudes of the $^6J_p^{H,SiH}$ numbers and with a constant error in measurement, entails even greater uncertainties in the deductions of the barriers and ground state conformations of these compounds.

For $C_6H_5SiH_2CH_3$, $\langle \sin^2 \theta \rangle$ is 0.43, eliminating **4** as the ground state conformation because $\langle \sin^2 \theta \rangle$ must lie between 0.75 and 0.5 for **4**. A rigid **3** implies $-0.69 \times \frac{3}{8}$ or -0.26 Hz for $^6J_p^{H,SiH}$ and is perhaps compatible with the observed -0.29 Hz. However, the analogous toluene derivative has a barrier of 1.2 kcal/mol and a stable form analogous to **2**. On the assumption that the stable form of $C_6H_5SiH_2CH_3$ is **2**, the barrier becomes 0.8 kcal/mol. The relative insensitivity of $\langle \sin^2 \theta \rangle$ to the barrier leads us to suggest a barrier of 0.8 ± 0.4 kcal/mol.

(iv) $C_6H_5SiH_2Cl$

If $^6J_{90}^{H,SiH}$ in $C_6H_5SiH_2Cl$ undergoes a similar reduction in magnitude from its value in $C_6H_5SiH_3$ as that estimated in the corresponding toluenes, *i.e.*, to -0.63 Hz, $\langle \sin^2 \theta \rangle$ becomes 0.36. The assumption of **2** as stable then yields a barrier of 1.7 ± 0.5 kcal/mol. This value seems unreasonably high and could presumably only be rationalized by a strong hyperconjugative interaction of the Si—Cl bond with the π electrons system of the phenyl group in conformation **2**. The barrier in benzyl chloride is only 2.1 kcal/mol (34).

Table 2 contains the barriers to internal rotation about the bond to the aromatic carbon atom for the phenylsilane derivatives and for the available, analogous toluene derivatives. In general,

the barriers are smaller for the phenylsilane than for the corresponding toluene derivatives; as expected on the basis of steric interactions, the C—Si and Si—X bonds being longer than the C—C and C—X bonds.

Molecular Orbital Calculations

The *ab initio* STO-3G results are also given in Table 2 for $C_6H_5SiH_3$, $C_6H_5SiH_2Cl$, and $C_6H_5SiHCl_2$. The calculations agree with the coupling constant data as to the low and the high energy forms of the chlorine derivatives. However, they suggest other than a twofold form for the hindering potential and also predict rather lower barriers than those based on the coupling constant data. For $C_6H_5SiHCl_2$ a twofold barrier implies that **6** has an energy of 0.25 kcal/mol relative to **5** *if*, as calculated, **7** has an energy of 0.5 kcal/mol higher than that of **5**. The MO calculations suggest an energy of 0.44 kcal/mol for **6**. The reverse situation holds for the calculation on $C_6H_5SiH_2Cl$, where **2**, **3**, and **4** have relative energies of 0.39, 0.07, and 0.00 kcal/mol, respectively. In our opinion, however, the minimal basis set calculations are not reliable enough to vitiate the assumption of a two-fold barrier as used in the discussion of the coupling constant data.

Conclusions

The assumed twofold barriers to rotation about the C—Si bond, as derived from long-range coupling constants, are probably accurate to 20% for $C_6H_5SiH(CH_3)_2$ and $C_6H_5SiHCl_2$. Molecular orbital calculations provide support for the low-energy conformations deduced from the coupling constants. For $C_6H_5SiH_2CH_3$ and $C_6H_5SiH_2Cl$ the barriers derived from the coupling data are very likely upper limits to the true values and, for the latter compound, the method may be unreliable. It would be interesting to have microwave values for these barriers. Measurements of the spin–lattice relaxation rates of ^{29}Si and of the *ortho* ^{13}C nuclei could possibly aid in assessing the magnitudes of the internal barriers.

Acknowledgment

We are grateful to the National Research Council of Canada for financial support.

1. M. P. Williamson, R. Kostelnik, and S. M. Castellano. J. Chem. Phys. **49**, 2218 (1968).
2. R. Wasylishen and T. Schaefer. Can. J. Chem. **50**, 1852 (1972).
3. H. Rudolph, H. Dreizler, A. Jaeschke, and P. Wendling. Z. Naturforsch. **22**a, 940 (1967).
4. T. Schaefer, J. B. Rowbotham, W. J. E. Parr, K. Marat, and A. F. Janzen. Can. J. Chem. **54**, 1322 (1976).
5. T. Schaefer, L. Kruczynski, and W. Niemczura. Chem. Phys. Lett. **38**, 498 (1976).
6. W. Caminati, G. Cazzoli, and A. M. Mirri. Chem. Phys. Lett. **35**, 475 (1975).
7. N. S. Nametkin, T. I. Chernysheva, and O. V. Kuz'min. Akad. Nauk. SSSR Bull. Chem. Sci. (Engl. Trans) 2043 (1967).
8. W. J. Hehre, R. F. Stewart, and J. A. Pople. J. Chem. Phys. **51**, 2657 (1969); program 236, Q.C.P.E. University of Indiana, Bloomington, Indiana.
9. J. A. Pople and M. S. Gordon. J. Am. Chem. Soc. **89**, 4254 (1967).
10. S. Castellano and A. A. Bothner-By. J. Chem. Phys. **41**, 3863 (1964).
11. C. W. Haigh and J. M. Williams. J. Mol. Spectrosc. **32**, 398 (1969).
12. A. A. Bothner-By and R. E. Glick. J. Chem. Phys. **26**, 1651 (1957).
13. J. Ronayne and D. H. Williams. Annu. Rev. NMR Spectrosc. **2**, 83 (1969).
14. P. Laszlo. Prog. Nucl. Magn. Reson. Spectrosc. **3**, 231 (1967).
15. R. Wasylishen, T. Schaefer, and R. Schwenk. Can. J. Chem. **48**, 2885 (1970).
16. W. J. Hehre, L. Radom, and J. A. Pople. J. Am. Chem. Soc. **94**, 1496 (1972).
17. Nguyen-Duc-Chuy, V. Chvalovsky, J. Schraml, M. Mägi, and E. Lippma. Coll. Czech. Chem. Commun. **40**, 875 (1975).
18. J. Feeney, L. H. Sutcliffe, and S. M. Walker. Mol. Phys. **11**, 117 (1966).
19. T. Schaefer, F. E. Hruska, and H. M. Hutton. Can. J. Chem. **45**, 3143 (1967).
20. I. Morishima, K. Endo, and T. Yonezawa. J. Chem. Phys. **59**, 3356 (1973).
21. J. M. Read and J. H. Goldstein. J. Mol. Spectrosc. **23**, 179 (1972).
22. A. D. Cohen and T. Schaefer. Mol. Phys. **10**, 209 (1966).
23. E. A. V. Ebsworth and J. J. Turner. J. Chem. Phys. **36**, 2628 (1962).
24. M. A. Jensen. J. Organomet. Chem. **11**, 423 (1968).
25. S. S. Danyluk. J. Am. Chem. Soc. **86**, 4505 (1964).
26. N. Muller and D. E. Pritchard. J. Chem. Phys. **31**, 768 (1959).
27. C. Juan and H. S. Gutowsky. J. Chem. Phys. **37**, 2198 (1962).
28. D. M. Grant and W. M. Litchman. J. Am. Chem. Soc. **87**, 3994 (1965).
29. A. Rastelli and S. A. Pozzoli. J. Mol. Struct. **18**, 463 (1973).
30. C. J. MacDonald and W. F. Reynolds. Can. J. Chem. **48**, 1002 (1970).
31. J. B. Rowbotham and T. Schaefer. Can. J. Chem. **52**, 481 (1974).
32. A. F. Janzen and T. Schaefer. Can. J. Chem. **49**, 1818 (1971).
33. T. Schaefer, W. J. E. Parr, and W. Danchura. J. Magn. Reson. In press.
34. T. Schaefer, L. J. Kruczynski, and W. J. E. Parr. Can. J. Chem. **54**, 3210 (1976).
35. F. G. Brickwedde, M. Moskow, and R. B. Scott. J. Chem. Phys. **13**, 547 (1945).

A stereospecific, total synthesis of thromboxane B_2

STEPHEN HANESSIAN AND PIERRE LAVALLEE[1]

Department of Chemistry, Université de Montréal, Montréal (Que.), Canada H3C 3V1

Received October 28, 1976

STEPHEN HANESSIAN and PIERRE LAVALLEE. Can. J. Chem. **55**, 562 (1977).

A stereospecific, total synthesis of crystalline thromboxane B_2 from D-glucose is described.

STEPHEN HANESSIAN et PIERRE LAVALLEE. Can. J. Chem. **55**, 562 (1977).

La synthèse stéréospécifique et totale de la thromboxane B_2 cristalline à partir du D-glucose est décrite.

The pioneering recent studies of Hamberg *et al.* (1) on the biosynthesis of prostaglandins has led to the discovery of a new class of compounds called the thromboxanes. It appears that in many cells, the normal transformation of endoperoxide intermediates into prostaglandins is altered in favor of the formation of thromboxane A_2, which, in turn, is rapidly transformed into thromboxane B_2 (2).

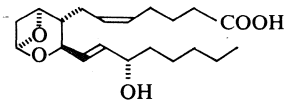

Thromboxane A_2

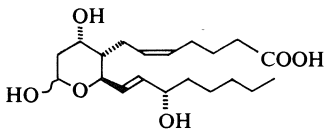

Thromboxane B_2

While the remarkable biological properties of the relatively unstable A_2 component (half-life in aqueous solution ~30 s) have been recognized, much less is known of the more stable B_2 component. In this paper, we describe a stereospecific total synthesis of crystalline thromboxane B_2, from D-glucose, based on the systematic and stereocontrolled introduction of functional groups.[2] Thromboxane B_2 can be considered as a 2,4,6-trideoxy-D-*ribo*-hexose, in which positions 4 and 6 are the sites of *C*-branching and chain extension, respectively. The plan for a practical synthesis of this substance was therefore based on the stereospecific introduction of the acid side chain at C-4, and appropriate chain extension at C-6 in a suitable carbohydrate derivative. Scheme 1 outlines the synthetic sequence leading to thromboxane B_2, and its C-15 epimer.[3]

The readily available methyl 4,6-*O*-benzylidene-2-deoxy-α-D-*ribo*-hexopyranoside **1** (4) was transformed into the corresponding 3-benzoate **2**, mp 100–101 °C, $[\alpha]_D^{25}$ +183° (*c* 1.18)[4] (89%), and the latter was sequentially hydrogenolyzed (20% $Pd(OH)_2/C$, H_2, quantitative), and silylated with *tert*-butyldiphenylsilyl chloride (5), to give the crystalline compound **3** (90%), mp 116–117 °C, $[\alpha]_D^{25}$ +90.2° (*c* 1.1). Oxidation of **3** in dimethyl sulfoxide and 1-ethyl-3-(3′-dimethylaminopropyl)carbodiimide hydrochloride (EDAC·HCl) (6) in the presence of pyridinium trifluoroacetate (25 °C, overnight), gave the highly crystalline 4-uloside derivative **4** (85%), mp 86–88 °C, $[\alpha]_D^{25}$ +148° (*c* 1.22). Lack of any detectable epimerization at C-3 was ascertained by nmr spectral data, and by subsequent transformation. Treatment of **4** with trimethylphosphonoacetate in the presence of potassium *tert*-butoxide gave a mixture of two compounds **5** and **6** that were

[1]NRCC predoctoral fellow, 1972–1976.

[2]While this manuscript was in preparation, a series of papers was published on the synthesis of thromboxane B_2 from prostaglandin $F_{2\alpha}$ and from a prostaglandin intermediate, see ref. 3).

[3]Prostaglandin numbering.

[4]Optical rotations were recorded in chloroform. Melting points are uncorrected. Crystalline compounds gave correct microanalyses. All compounds exhibited nmr spectra (60, 100 MHz) that were in accord with their structures.

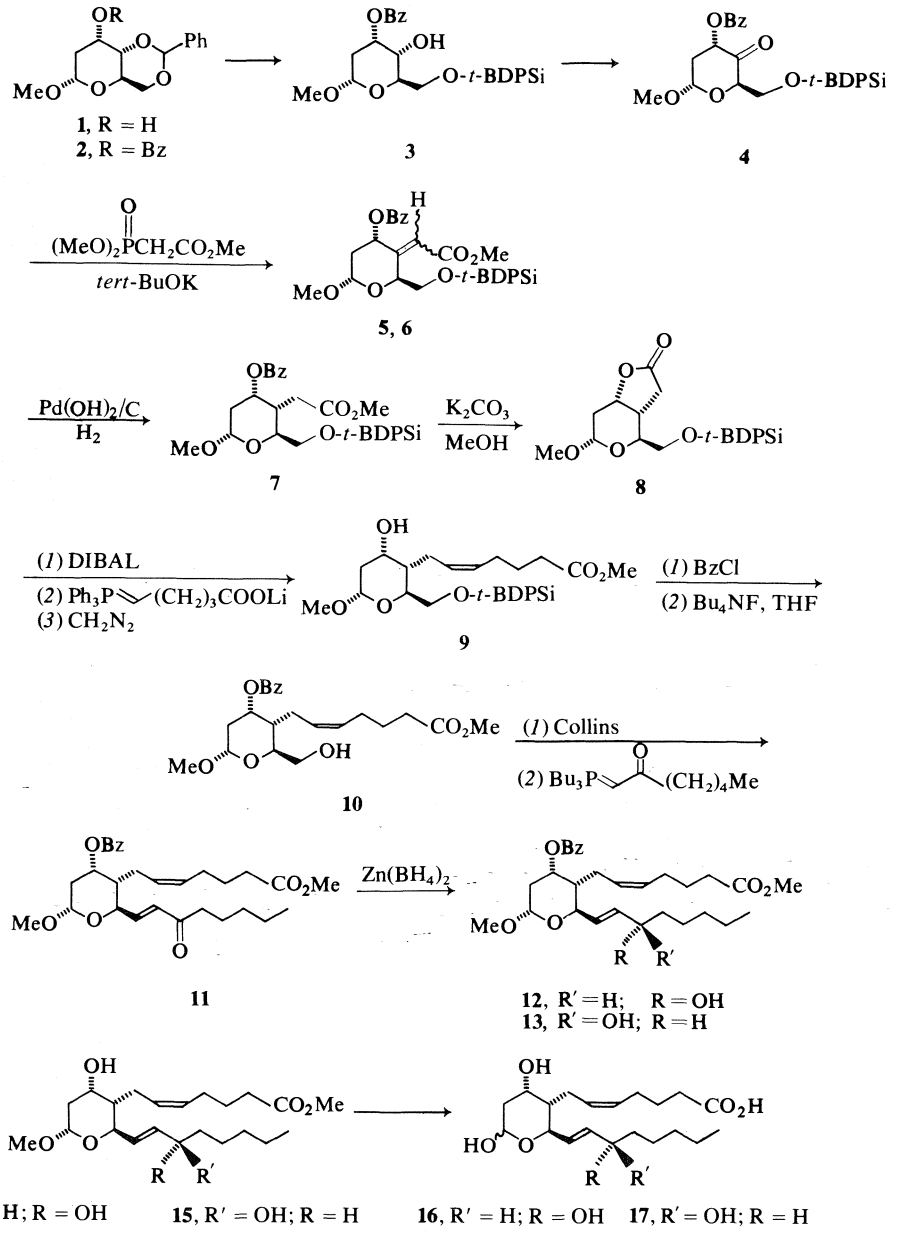

SCHEME 1

separated by chromatography and isolated as syrups (95%) in a ratio of 3:2.[5] For the more polar component, $[\alpha]_D$ +162.5° (*c* 1.0); for the less polar component, $[\alpha]_D$ +199.3° (*c* 1.2). Hydrogenation (20% $Pd(OH)_2/C$, H_2, overnight) of **5** and **6** individually, or as a mixture resulting from the above reaction, gave **7**, isolated as a syrup (95%); $[\alpha]_D^{25}$ +100° (*c* 1.1). Treatment of **7** with potassium carbonate in methanol (25 °C, 60 h, N_2) gave the highly crystalline lactone **8** (85%); mp 80.5–81.5 °C; $[\alpha]_D^{25}$ +41.8° (*c* 1.05); *m/e* 409 (*M* − 31), *m/e* 383 (*M* − 57). Reduction of **8** with diisobutylaluminium hydride (DIBAL) in

[5]Ozonolysis of **5** and **6** individually gave the crystalline 4-uloside derivative **4**.

toluene (quantitative), followed by treatment with 4-carboxybutyltriphenylphosphonium bromide in HMPT, in the presence of lithium bis(trimethylsilyl)amide 7, gave, after esterification with diazomethane and chromatography, the branched-chain derivative **9** as a syrup (67–71%); $[\alpha]_D^{25}$ +62° (*c* 1); *m/e* 483 (*M* − 57), *m/e* 465 (*M* − 57 − 18). Since hydrogenation of **5** and **6** was expected to occur by *cis*-addition, it was possible that the resulting products **7** and **8** could also have alternative configurations, *i.e.* epimeric at C-4. This possibility was dismissed by detailed nmr analysis of the products **7** and **8**, and by chemical means. Thus, oxidation of **9** with EDAC·HCl in DMSO, followed by attempted equilibration with K_2CO_3–MeOH, and finally reduction with sodium borohydride gave the starting compound **9**, in which the configurations at C-3 and C-4 were preserved. It is well known from work done in this laboratory and elsewhere, that axial substituents that are vicinal to carbonyl groups are prone to epimerization, leading to the thermodynamically more stable equatorial isomer. Thus, had the catalytic reduction led to a lactone of opposite configuration at C-4 (*i.e.* D-*xylo* configuration), the axially disposed C-branched unit at C-4 would have most assuredly undergone epimerization during the treatment of the corresponding 3-uloside with base, in contrast to experimental results.

Benzoylation of **9**, followed by treatment of the product with tetra *n*-butylammonium fluoride in THF (8), gave, after chromatographic purification, compound **10** as a syrup (90%); $[\alpha]_D^{25}$ +130° (*c* 1.02); *m/e* 374 (*M* − 32). Collins oxidation (quantitative), followed by a Wittig reaction in the usual manner (9), gave the expected product **11**, isolated as a syrup in 76–80% yield; $[\alpha]_D^{25}$ +153° (*c* 1.14); M^+ 500; *m/e* 468 (*M* − 32). Reduction of **11** with zinc borohydride in a mixture of DME and ether (25 °C, 4 h) gave a mixture of the epimeric products **12** and **13** (1:1) (73%). Chromatographic separation gave the 15 *S* isomer **12**, $[\alpha]_D^{25}$ +137.8° (*c* 1.19); M^+ 502, *m/e* 484 (*M* − 18), and the 15 *R* isomer **13**, $[\alpha]_D^{25}$ +132.0° (*c* 0.91), M^+ 502, etc., as colorless syrups. Treatment of **12** and **13** individually with potassium carbonate in methanol, effected smooth debenzoylation to give the respective epimeric alcohols, **14** (15 *S* isomer), $[\alpha]_D^{25}$ +95.8° (*c* 1.09); *Exact Mass* calcd. for a fragment, *M* − H_2O: 348.2249; measured: 348.2246, and **15** (15 *R* isomer), $[\alpha]_D^{25}$ +93.2° (*c* 1.1). The chromatographic properties of **14**, and the mass spectral fragmentation of the corresponding *O*-trimethylsilyl derivative were in accord with data recorded for the natural thromboxane B_2 derivatives (1). For the bis *O*-trimethylsilyl derivative, *Exact Mass* calcd. for a fragment, *M* − 32: 510.3197; measured: 510.3214.

Finally, sequential deesterification of **14** (aqueous NaOH, 1.2 equiv.), followed by treatment with excess Dowex-50 (H^+), gave thromboxane B_2 **16**, as a chromatographically homogeneous syrup (90%), which crystallized from a mixture of ethyl acetate, ether, and petroleum ether (30–60 °C); mp and mixture mp 91–93 °C.[6] Recrystallization from the same solvent mixture gave beautiful elongated plates, mp 95–96 °C; $[\alpha]_D^{25}$ +57.4° (*c* 0.26, EtOAc); ν_{max}(film) 1705 cm^{-1} (C=O), 3380 cm^{-1} (OH); *m/e* 335 (*M* − H_2O − OH) *m/e* 317 (*M* − $2H_2O$ − OH). The epimeric derivative **17**, was similarly prepared, and isolated as a syrup.

The synthesis of thromboxane B_2 by the sequence described in this paper encompasses the elements of practicality, efficacy, and versatility, and it also provides access to intermediates that could be useful in the preparation of analogs.[7] In addition, it further illustrates the utility of carbohydrates as chiral precursors in the total synthesis of natural products (11).

Acknowledgments

Financial assistance from the National Research Council of Canada and le Ministère de l'éducation du Québec is gratefully acknowledged. It is also a pleasure to acknowledge stimulating discussions with Dr. A. G. Pernet, Abbott Labs, Montreal.

1. M. HAMBERG, J. SVENSSON, and B. SAMUELSSON. Proc. Natl. Acad. Sci. U.S.A. **72**, 2994 (1975).
2. M. HAMBERG and B. SAMUELSSON. Proc. Natl. Acad. Sci. U.S.A. **71**, 3400 (1974); M. HAMBERG, J. SVENSSON, and B. SAMUELSSON. Proc. Natl. Acad. Sci. U.S.A. **71**, 3824 (1974).

[6]We thank Drs. N. A. Nelson, R. C. Kelly, and W. P. Schneider of the UpJohn Company for a sample of their synthetic material, which they reported to be identical to natural thromboxane B_2. Our preparation had chromatographic and ir spectral properties that were identical to those of the UpJohn sample.

[7]Since an optically active Wittig reagent corresponding to the C-15 side chain can be prepared from a readily available intermediate (see ref. 10), the synthesis of thromboxane B_2 can be considered as being entirely stereospecific.

3. N. A. NELSON and R. W. JACKSON. Tetrahedron Lett. 3275 (1976); R. C. KELLY, I. SCHLETTER, and S. J. STEIN. Tetrahedron Lett. 3279 (1976); W. P. SCHNEIDER and R. A. MORGE. Tetrahedron Lett. 3283 (1976).
4. A. ROSENTHAL and P. CATSOULACOS. Can. J. Chem. **46**, 2868 (1968); L. F. WIGGINS. Methods in Carbohydr. Chem. **2**, 188 (1963).
5. S. HANESSIAN and P. LAVALLEE. Can. J. Chem. **53**, 2975 (1975).
6. J. C. SHEEHAN, P. A. CRUICKSHANK, and G. L. BOSHART. J. Org. Chem. **26**, 2525 (1961); J. C. SHEEHAN and P. A. CRUICKSHANK. Org. Synth. **48**, 82 (1968).
7. P. ROSEN, G. W. HOLLAND, J. L. JERNOW, F. KIENZLE, and S. KWOH. Abstracts of Papers, 9th IUPAC Conference on Natural Products, Ottawa, June 24–28. 1974. p. 5A.
8. E. J. COREY and A. VENKATESWARLU. J. Am. Chem. Soc. **94**, 6190 (1972).
9. N. FINCH, L. DELLAVECCHIA, J. J. FITT, R. STEPHANI, and I. VLATTAS. J. Org. Chem. **38**, 4412 (1973).
10. E. J. COREY, H. SHIRAHAMA, H. YAMAMOTO, S. TERASHIMA, A. VENKATESWARLU, and T. K. SCHAAF. J. Am. Chem. Soc. **93**, 1490 (1971).
11. S. HANESSIAN and G. RANCOURT. Abstracts, Am. Chem. Soc. Meeting, April 5–9, New York. 1976. CARB 32.

Canadian Journal of Chemistry

Published by
THE NATIONAL RESEARCH COUNCIL OF CANADA

Journal canadien de chimie

Publié par
LE CONSEIL NATIONAL DE RECHERCHES DU CANADA

Volume 55 Number 4 February 15, 1977

Volume 55 numéro 4 15 février 1977

Carbon monoxide activation by bromorhodate complexes; a catalyzed reduction of iron(III)[1]

BRIAN R. JAMES AND GEORGE ROSENBERG

Department of Chemistry, University of British Columbia, Vancouver, B.C., Canada V6T 1W5

Received July 26, 1976

BRIAN R. JAMES and GEORGE ROSENBERG. Can. J. Chem. **55**, 567 (1977).

Kinetics have been studied for the decomposition of $Rh(CO)Br_5^{2-}$ to *cis*-$Rh(CO)_2Br_2^-$ in aqueous HBr solutions at 60 °C under a carbon monoxide atmosphere. A hydrolysis step leads to formation of rhodium(I) which is stabilized as the dicarbonyl; this dicarbonyl then reacts with $Rh(CO)Br_5^{2-}$ in an autocatalytic process to give more $Rh(CO)_2Br_2^-$ via a mixed valence [$Rh^I \ldots Br \ldots Rh^{III}$] bridged intermediate. Ferric ion may be reduced according to the net reaction:

$$2Fe^{III} + CO + H_2O \rightarrow 2Fe^{II} + CO_2 + 2H^+$$

using the bromorhodate(III or I) complexes as catalyst, and the kinetics of this process are also reported.

BRIAN R. JAMES et GEORGE ROSENBERG. Can. J. Chem. **55**, 567 (1977).

On a étudié la cinétique de la décomposition du $Rh(CO)Br_5^{2-}$ en $Rh(CO)_2Br_2^-$ *cis* dans des solutions aqueuses de HBr, à 60 °C et sous une atmosphère de monoxyde de carbone. Une étape d'hydrolyse conduit à la formation de rhodium(I) qui est stabilisé sous forme de dicarbonyle; ce dicarbonyle réagit alors avec $Rh(CO)Br_5^{2-}$ dans un processus autocatalytique pour conduire à d'autre $Rh(CO)_2Br_2^-$ grâce à un intermédiaire ponté de valence mixte [$Rh^I \ldots Br \ldots Rh^{III}$]. On peut réduire l'ion ferrique suivant la réaction globale suivante

$$2Fe^{III} + CO + H_2O \rightarrow 2Fe^{II} + CO_2 + 2H^+$$

en utilisant des complexes de bromorhodates(III ou I) et on rapporte aussi la cinétique de ce processus.

[Traduit par le journal]

Introduction

We recently reported (1) on the carbonylation of bromorhodate(III) species in aqueous solutions to give the *cis*-dibromodicarbonylrhodate(I) anion, $Rh(CO)_2Br_2^-$. One path in this reductive carbonylation process was considered to involve decomposition by water of an intermediate rhodium(III) carbonyl anion which was formed in a rate-determining step and thus not detected directly. This paper considers the decomposition in aqueous hydrobromic acid solution of one such anion, the pentabromocarbonylrhodate(III) complex, $Rh(CO)Br_5^{2-}$, and investigates the use of such a system under carbon monoxide for catalytic reduction of inorganic substrates. Kinetic studies show the role of rhodium(I) intermediates. The work stems from initial observations in this laboratory that indicated that $Rh(CO)_2Cl_2^-$ could catalyze the carbon monoxide-reduction of ferric ion (2); later work has considered the catalytic reduction of molecular dioxygen (3, 4), and nitric oxide (5).

[1]Taken from the Ph.D. thesis of G. Rosenberg, University of British Columbia, Vancouver, British Columbia, 1974.

Since solutions of rhodium(III) halide complexes also activate dihydrogen (1), the potential of such systems to promote Fischer-Tropsch type reactions (the H_2-reduction of CO to hydrocarbons) seems real. Thus, the detailed understanding of the gas activation processes is important and critical.

Experimental

The cesium salts of $Rh(CO)Br_5^{2-}$ and $Rh(CO)Cl_5^{2-}$ were prepared according to the method of Cleare and Griffith (6) from the corresponding rhodium(III) trihalides; tribromide was obtained as the dihydrate from Platinum Chemicals, and the trichloride as a trihydrate from Johnson Matthey Ltd. The synthesis of the bromo complex involves boiling the tribromide in air with a mixture of conc. HBr and formic acid for 15 min; during this time the initially red solution goes yellow, and finally orange which contains the $Rh(CO)Br_5^{2-}$ anion. Addition of $(n\text{-}C_4H_9)_4NBr$ to the yellow solution (stable in the absence of air) precipitates the $Rh(CO)_2Br_2^-$ salt (7, 8).

The precipitated $Rh(CO)X_5^{2-}$ anions decomposed readily when washed with distilled water, being reduced to metal, although there was no noticeable decomposition on treatment with the hydrohalic acid at room temperature (9) (see also points in the Results and Discussion). All other materials used, and the procedure used for following CO uptake at constant pressure, have been described previously (1, 2); the CO concentration in the aqueous HBr solutions was computed from solubility data of Seidell (10), assuming the solubility to be the same as in pure water.

Results

Carbonylation of $Rh(CO)X_5^{2-}$

The solid cesium salts of $Rh(CO)X_5^{2-}$ (X = Cl, Br) are quite stable in air, and the reflectance spectra show peaks at 398 and 502 nm for the chloride, and at 440 and 550 nm for the bromide. In aqueous solutions of the corresponding hydrohalic acids, the initially measured spectra are essentially the same: λ_{max} at 393 nm (ε 450 M^{-1} cm^{-1}) and 500 nm (ε 60) for the chloride, and at 435 nm (ε 1050) and 550 nm (ε 120) for the bromide. Upon standing in an inert atmosphere (N_2 or Ar), however, the solutions decompose with evolution of CO_2 (1 mole per mole Rh) and eventual precipitation of metal; the decomposition rate increases with temperature and decreasing acidity. The decomposition reactions can be studied directly by monitoring the gas evolution rate or changes in optical density, but the methods are somewhat impractical due to the deposition of rhodium metal which ruins permanently any glassware used.

The decomposition occurs via production of Rh(I) according to reaction 1 (1, 2, 11)

$$[1] \quad Rh^{III}(CO) + H_2O \rightarrow Rh^{I} + CO_2 + 2H^+$$

Metal is likely produced via the disproportionation reaction shown in [2] (2, 12, 13):

$$[2] \quad 2Rh^{I} \rightleftharpoons Rh^{0} + Rh^{II}$$

Metal formation can be avoided by efficient removal of the Rh(I) formed in [1]. A carbon monoxide atmosphere stabilizes the Rh(I) as $Rh(CO)_2X_2^-$ (1, 2), while reagents such as ferric or dioxygen oxidize the rhodium to the trivalent state and give halorhodate(III) species (2–4); the solution products in all cases are readily confirmed by the characteristic uv/vis spectra reported previously (1, 2).

Figure 1 shows gas-uptake plots for solutions of $Rh(CO)Br_5^{2-}$ in 0.5 *M* HBr at 60 °C under a CO atmosphere. The total net measurable uptake corresponded to an apparent 1:1 mole ratio of gas:Rh; experiments in the presence of a soda-lime tube (to absorb CO_2) resulted in a 2:1 uptake. The original orange solution became yellow (λ_{max} 330 nm, ε = 3300 M^{-1} cm^{-1}) indicating reduction to $Rh(CO)_2Br_2^-$ (1). The overall reaction is

$$[3] \quad Rh^{III}(CO) + H_2O + 2CO \rightarrow Rh^{I}(CO)_2 + CO_2 + 2H^+$$

The uptake plots are sigmoid in shape suggesting autocatalytic behaviour, and maximum rates were measured over a range of rhodium concentrations (0.009–0.021 *M*) and CO pressures up to 1 atm. The maximum rates were found at about 50% reaction and were proportional to the

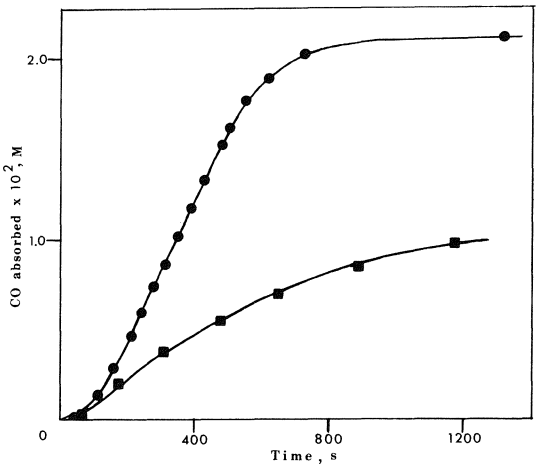

FIG. 1. Rate plot for decomposition of $Rh(CO)Br_5^{2-}$ in 0.5 *M* HBr at 60 °C under 615 mm CO; ●, 0.0207 *M* Rh; ■, 0.0086 *M* Rh.

product $[Rh^{III}][Rh^{I}]$ (Fig. 2); the same result has been found previously (1, 2) for corresponding carbonylation of $RhCl_5(H_2O)^{2-}$ and $RhBr_4(H_2O)_2^{-}$ (reaction 4):

[4] $Rh^{III} + 3CO + H_2O \rightarrow Rh^{I}(CO)_2 + CO_2 + 2H^+$

As for these systems (see ref. 2), there is a significant rate at zero $[Rh^{I}]$, as can be seen in Fig. 1 and from the non-zero intercept of Fig. 2. The rate law then for reaction 3 can be expressed as:

[5] $-d[CO]/dt = k_1'[Rh^{III}]^n + k_2'[Rh^{III}][Rh^{I}]$

where k_1' and k_2' contain all variables other than the dependence on rhodium. The slope of Fig. 2 gives a k_2' value of 0.32 M^{-1} s^{-1}. Information on the initial reaction (the k_1' term) was obtained from studies carried out in the presence of added ferric ion, which rapidly reoxidizes the Rh^{I} as it is formed and prevents the autocatalytic reaction.

In order to determine the CO dependence, maximum rate measurements were made for varying CO pressures at a constant $[Rh^{III}]$; the rate was essentially independent of CO pressure above 600 mm, but showed a first order dependence up to about 300 mm (Fig. 3). Thus at higher CO pressures k_2' is a true second order rate constant, and the second term of rate law [5] becomes $k_2[Rh^{III}][Rh^{I}]$. Integration of just this part of the rate law yields eq. 6:

[6] $\log [Rh^{I}] - \log [Rh^{III}] = k_2[Rh]_{total}\, t/2.3 + \text{constant}$

and plots of $(\log [Rh^{I}] - \log [Rh^{III}])$ *vs.* time for the data from plots such as Fig. 1 are shown in Fig. 4; as expected, the plots deviate from linearity during the first part of the reaction, but the slopes of the lines drawn give k_2 values of 0.35 and 0.39 M^{-1} s^{-1}, in reasonable agreement with the value determined from the slope of Fig. 2.

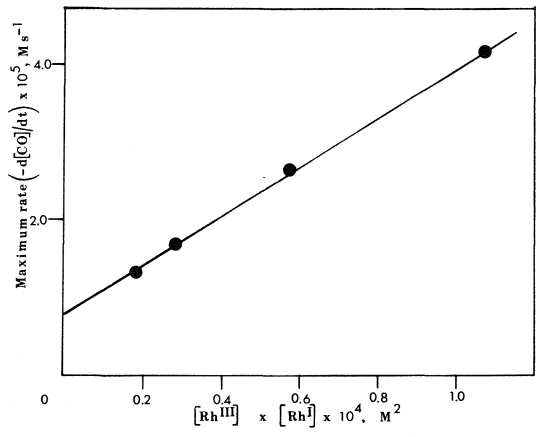

FIG. 2. Dependence of the maximum rate on $[Rh^{III}]$ $[Rh^{I}]$ at 60 °C, under 615 mm CO in 0.5 *M* HBr.

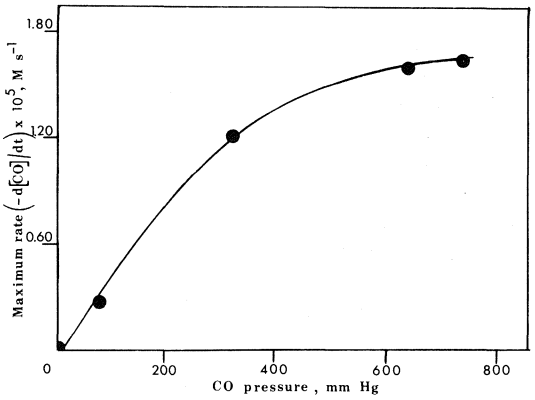

FIG. 3. Dependence of the maximum rate on CO pressure at 60 °C, 0.0105 *M* Rh in 0.5 *M* HBr.

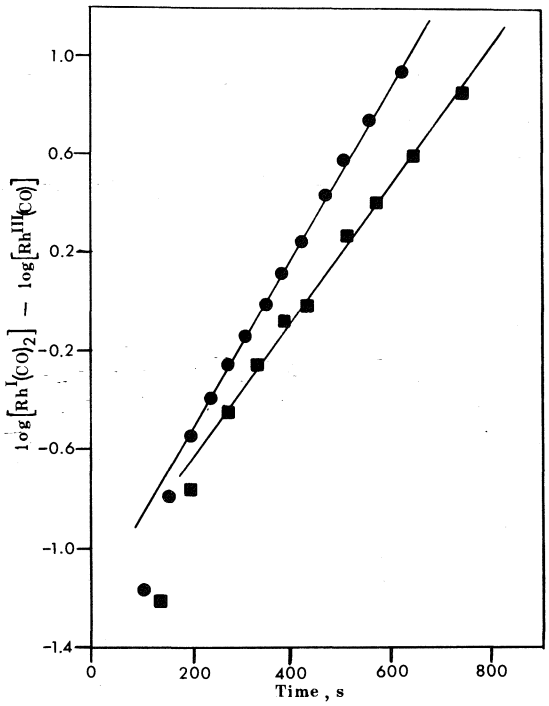

FIG. 4. Plots of log $[Rh(CO)_2Br_2^{-}]$ − log $[Rh(CO)Br_5^{2-}]$ *vs.* time (eq. 6), 60 °C, 615 mm CO in 0.5 *M* HBr; ●, 0.0207 *M* initial Rh; ■, 0.0152 *M* initial Rh.

The Initial Reaction and Catalytic Reduction of Iron(III)

The initial reaction was the decomposition of $Rh(CO)Br_5^{2-}$ by water to yield a Rh^I species (*cf.* reaction 1), and thus the presence of an oxidant such as Fe^{III} should lead to an overall catalytic process in which the Rh^I is oxidized to Rh^{III}, followed by absorption of CO to give $Rh^{III}(CO)$ (see refs. 1, 2), and resumption of the catalytic cycle. Such a cycle gives the net reaction 7 with no overall gas volume change,

$$[7] \quad 2Fe^{III} + CO \xrightarrow{H_2O} 2Fe^{II} + CO_2 + 2H^+$$

and so the reaction was monitored by measuring the CO uptake in the presence of sodalime. Reaction 7 does not occur at the conditions used in the absence of rhodium.

The uptake plots for mixtures of $Rh(CO)Br_5^{2-}$ and $Fe(ClO_4)_3 \cdot 6H_2O$ in 0.5 *M* HBr at 60 °C were unusual in shape (Fig. 5), but were reproducible. There was little measurable uptake till about 500 s, after which an essentially linear CO absorption first occurred followed by an enhanced rate of absorption, which then fell away to zero. The visible spectrum of the final solution was that of $Rh(CO)_2Br_2^-$; the Fe^{III} was completely reduced to Fe^{II} which was measured spectrophotometrically as the $Fe(phen)_3^{2+}$ complex (14), after first precipitating the Rh^I carbonyl species (7, 8) as $[(n\text{-}C_4H_9)_4N][Rh(CO)_2Br_2]$. It was readily shown that the linear region of the uptake plot was associated with the ferric reduction, and for the conditions of Fig. 5 at least up to the stage of 50% Fe^{III} reduction, the solution showed a λ_{max} at 550 nm ($\varepsilon = 100\ M^{-1}\ cm^{-1}$) indicating that the rhodium is probably still present mainly as $Rh(CO)Br_5^{2-}$ (see below). The subsequent part of the absorption involves production of $Rh(CO)_2Br_2^-$ from a bromorhodate(III) species, and the stoichiometry for this stage shows about a 3:1 mole ratio of CO:Rh, consistent with reaction 4. A number of experiments using varying $[Rh^{III}]$ and $[Fe^{III}]$, like those in Fig. 5, shows that at the end of the linear region the uptake corresponds to about $(x/2 - y)$ moles of CO per x moles of Fe^{III} and y moles of Rh^{III}.

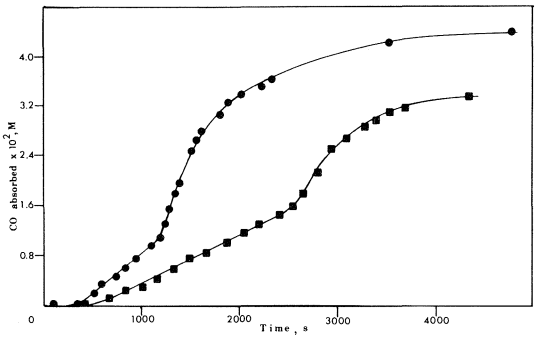

FIG. 5. Rate plot for the $Rh(CO)Br_5^{2-}$-catalyzed reduction of 0.046 *M* Fe^{III} in 0.5 *M* HBr at 60 °C under 615 mm CO, in the presence of sodalime; ●, 0.0105 *M* Rh; ■, 0.0052 *M* Rh.

Mixtures of $Rh(CO)Br_5^{2-}$ and iron(III) in 0.5 *M* HBr at 60 °C in the absence of CO (under N_2 or air) react with the stoichiometry of reaction 8

$$[8] \quad Rh^{III}(CO) + 2Fe^{III} \xrightarrow{H_2O} Rh^{III} + 2Fe^{II} + 2H^+ + CO_2$$

The final visible spectrum featured a maximum at 532 nm ($\varepsilon \approx 170$), characteristic of bromorhodate(III) species (1). More concentrated solutions of $Rh(CO)Br_5^{2-}$ (>0.02 *M*) reacted similarly, but eventually precipitated $Cs_3[Rh_2Br_9]$ as a green solid (the reflectance spectrum showed maxima at 485 and 583 nm. *Anal.* calcd: Rh 15.6, Br 54.3. Found: Rh 15.7, Br 54.2).

Reaction 8 represents the sum of reaction 1, plus the reduction of 2 equivalents of Fe^{III} by 1 equivalent of Rh^I. The coordinated CO is acting overall as a 2-equivalent reductant. The stoichiometry at the end of the linear region in uptake plots such as shown in Fig. 5 corresponds to the net reaction:

$$[9] \quad yRh^{III}(CO) + xFe^{III} + \left(\frac{x}{2} - y\right)CO \xrightarrow{\frac{x}{2}H_2O} yRh^{III} + xFe^{II} + \frac{x}{2}CO_2 + xH^+$$

The linear rates of the initial region (Fig. 5) were first-order in $[Rh^{III}]$ up to 10^{-2} *M*, and independent of the $[Fe^{III}]$. The CO dependence is first-order at lower pressures but then becomes less than one and approaches zero-order at pressures above 600 mm (Fig. 6*A*). The rate law at the higher pressure thus becomes

$$[10] \quad -d[CO]/dt = k_1[Rh^{III}]$$

with k_1 being about $0.14 \times 10^{-2}\ s^{-1}$ at 60 °C.

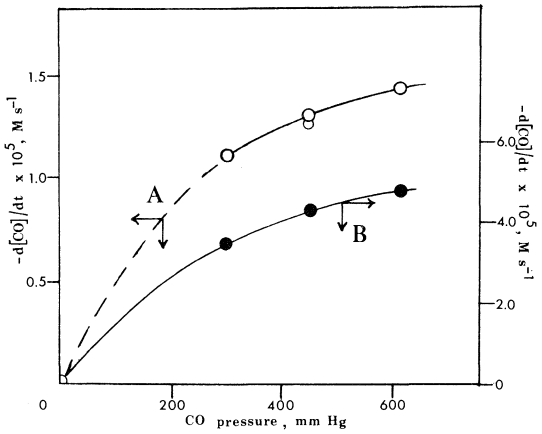

FIG. 6. (*A*) Effect of CO pressure on the reduction rate of 0.046 *M* Fe^{III} in 0.5 *M* HBr at 60 °C with 0.0105 *M* Rh. (*B*) Effect of CO pressure on the maximum rate of Rh^{III} decomposition following the catalytic Fe^{III} reduction; conditions as in *A*.

Following the linear region, the kinetics for the carbonylation of bromorhodate(III) species to give $Rh(CO)_2Br_2^-$ were determined by measuring the maximum rates after the inflexion points (Fig. 5). The rates were first-order in $[Rh^{III}]$ up to 10^{-2} *M*, and the CO dependence (Fig. 6*B*) was similar to that observed for the Fe^{III} reduction. At the higher CO pressures (>500 mm), the rate law for the second region of the uptake plots approximates to:

$$[11] \qquad -d[CO]/dt = k_3[Rh^{III}]$$

where $k_3 = (0.43 \pm 0.02) \times 10^{-2}\ s^{-1}$ at 60 °C.

Discussion

Carbon Monoxide Uptake in the Absence of Iron(III)

The autocatalytic production of $Rh(CO)_2Br_2^-$ from $Rh(CO)Br_5^{2-}$ in the absence of Fe^{III} (Fig. 1, reaction 3, rate law [5]) must proceed via a mechanism involving bridged $[Rh^{III} \ldots Br \ldots Rh^I]$ intermediates, as established previously for the reaction of CO with aquopentachloro- and bisaquotetrabromorhodate(III) complexes (1, 2).

The initial formation of $Rh(CO)_2Br_2^-$ proceeds via reactions 1 and 12

$$[1] \qquad Rh^{III}(CO) + H_2O \xrightarrow{k_1} Rh^I + CO_2 + 2H^+$$

$$[12] \qquad Rh^I + 2CO \longrightarrow Rh^I(CO)_2$$

Reaction 1 presumably gives rise to the first term in rate law [5], *i.e.* the $k_1'[Rh^{III}]^n$ term is identified as $k_1[Rh^{III}]$ and rate law [5] at higher CO pressures becomes $(k_1[Rh^{III}] + k_2[Rh^{III}][Rh^I])$. The maximum rates at approximately 50% reaction are then given by:

$$[13] \qquad -d[CO]/dt = \frac{k_1[Rh]_T}{2} + \frac{k_2[Rh]_T^2}{4}$$

where $[Rh]_T$ = total [Rh]. Substitution of the k_2 and k_1 values, estimated by the methods described, into expression [13] gives maximum rates in good agreement with those measured from plots such as those in Fig. 1.

The reductive carbonylation process of Rh(III) to Rh(I) has been discussed in detail previously (1, 2, 15) and is thought to involve a carboxylate intermediate:

$$[14] \qquad Rh^{III}(CO) \xrightarrow{OH^-(H_2O)} [Rh(CO_2H)] \rightarrow Rh^I + CO_2 + H^+ \quad (2)$$

Some data on decomposition of a $Rh^{III}(CO)$ complex in *N*,*N*-dimethylacetamide (11) indicate that decomposition proceeds via hydroxide. Since the acid strength was not varied in the present system, it is uncertain whether attack at the carbonyl involves water or hydroxide. Furthermore it is difficult to determine whether the hydroxide or water need be coordinated to the metal before migration to the carbonyl, *i.e.* by the 'insertion mechanism'. These problems were considered in our previous paper (1), and we tend to favour attack by coordinated water or hydroxide. This implies that k_1 ($1.4 \times 10^{-3}\ s^{-1}$ at 60 °C) refers to an aquation of $Rh(CO)Br_5^{2-}$ with loss of bromide. A corresponding aquation of $RhCl_5(H_2O)^{2-}$ in acid solution has a rate constant of *ca.* $4 \times 10^{-3}\ s^{-1}$ at 60 °C and is believed to occur via a dissociative process (16), but the similarity in rate constants is probably fortuitous; the π-bonding CO ligand could possibly promote associative-type hydrolysis (17). An initially formed *trans*-$Rh(CO)(H_2O)Br_4^-$ product seems probable, with rearrangement to a *cis* geometry being required for the subsequent insertion reaction and reductive carbonylation (18). Studies on the kinetics and equilibration of various aquobromorhodate(III) species are being pursued (19). The isolation of the $Cs_3[Rh_2Br_9]$ complex from the HBr solutions of Rh(III) is of interest in this respect. The compound has been prepared earlier by the addition of CsBr to aqueous solutions of rhodium tribromide (20).

By analogy with the previous papers on the autocatalytic production of Rh^I carbonyls (1, 2), the process giving rise to the $k_2[Rh^{III}][Rh^I]$ term of rate law [5] may be written:

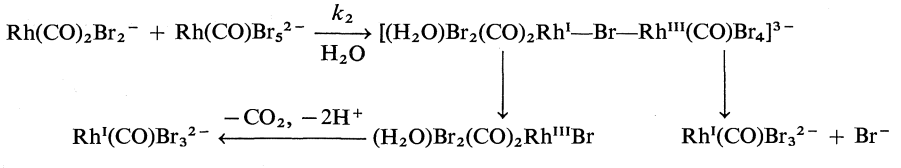

[15]

$$Rh(CO)_2Br_2^- + Rh(CO)Br_5^{2-} \xrightarrow[H_2O]{k_2} [(H_2O)Br_2(CO)_2Rh^{I}—Br—Rh^{III}(CO)Br_4]^{3-}$$

$$Rh^{I}(CO)Br_3^{2-} \xleftarrow{-CO_2,\ -2H^+} (H_2O)Br_2(CO)_2Rh^{III}Br \qquad Rh^{I}(CO)Br_3^{2-} + Br^-$$

[16] $$Rh^{I}(CO)Br_3^{2-} + CO \underset{k_{-4}}{\overset{k_4}{\rightleftharpoons}} Rh(CO)_2Br_2^- + Br^-$$

$$K_4 = k_4/k_{-4}$$

After a two-electron transfer within the bromide-bridged intermediate, decomposition via cleavage of the newly-formed labile Rh^{I}–bromide bond will lead to $Rh(CO)Br_3^{2-}$. This species must then react with CO to form the dicarbonyl species. Above CO pressures of *ca.* 600 mm, the k_2 step is rate-determining and this implies that reaction 16 is relatively fast.

The observed CO dependence at lower CO pressures (Fig. 3) could arise from reaction 16 becoming rate-determining, or from this reaction being a pre-equilibrium for formation of $Rh(CO)_2Br_2^-$ required for the k_2 step. At lower CO pressures, if [16] is a rapid equilibrium, the maximum rate expression [13] becomes

$$-d[CO]/dt = \frac{k_1K_4[Rh]_T[CO]}{(2K_4[CO] + [Br])} + \frac{k_2K_4^2[Rh]_T^2[CO]^2}{(2K_4[CO] + [Br])^2}$$

Using the determined values of k_1 and k_2, and the measured maximum rates gives a K_4 value of $\sim 2 \times 10^3$, which would account for the data of Fig. 3. However, at lower CO pressures, this implies that the product of the carbonylation reaction would be a rhodium(I) monocarbonyl, and yet the measured stoichiometry is still 2CO:Rh, in agreement with reaction 3. Thus, the alternative explanation of [16] becoming rate-determining is favoured. Such a suggestion for the related $Rh(CO)_2Cl_2^-/RhCl_5(H_2O)^{2-}$ system was made previously (2), and evidence for a $Rh(CO)Cl_3^{2-}$ species has been obtained also (21) by studying the reaction of $Rh(CO)_2Cl_2^-$ with $Rh(CO)Cl_5^{2-}$ under N_2 atmospheres (*cf.* the reactions in [15]). There is no kinetic evidence to suggest that a $Rh(CO)Br_3^{2-}$ species will react with $Rh(CO)Br_5^{2-}$ to give a bridged species, and such a reaction involving two double-negatively charged anions is likely to be unfavourable.

The k_2 value for the reaction of $Rh(CO)_2Br_2^-$ with $Rh(CO)Br_5^{2-}$ ([15]) is about twice that for reaction of the dicarbonyl with $RhBr_4(H_2O)_2^-$ under corresponding conditions (1). Considering the less favourable electrostatic factor for $Rh(CO)Br_5^{2-}$, the π-acceptor CO ligand likely plays an important role in facilitating electron transfer to the Rh^{III} centre in the bridged complex.

Carbon Monoxide Uptake in the Presence of Iron(III); the Catalytic Reduction of Fe^{III}

The kinetics and observations for the catalytic reduction of Fe^{III} at higher CO pressures (eq. 10) are consistent with the mechanism of reaction 1 followed by:

[17] $$Rh^{I} + 2Fe^{III} \xrightarrow{fast} Rh^{III} + 2Fe^{II}$$

[18] $$Rh^{III} + CO \xrightarrow{k} Rh^{III}(CO)$$

The spectral and kinetic data show that at least up to 50% Fe^{III} reduction the catalyst is mainly regenerated as the pentabromocarbonyl species at higher CO pressures, although the nature of the coordinated ligands on the intermediates in reactions 1, 17, and 18 is not known definitely. Since $(x/2 - 1)$ moles of CO are absorbed per mole of $Rh^{III}(CO)$ during the reduction of x moles of Fe^{III}, it appears that the Rh^{I} reductant contains no coordinated CO and also implies that at the completion of ferric reduction, the Rh^{III} complex present contains no carbonyl. Step [17] then appears faster than coordination of CO to Rh^{I}, which is also known to be fast (1, 2). The stoichiometry data then tend to rule out an alternative process such as:

[19] $$Rh^{I} + CO \xrightarrow{fast} Rh^{I}(CO)$$

[20] $$Rh^{I}(CO) + 2Fe^{III} \xrightarrow{Br^-} Rh^{III}(CO)Br_5^{2-} + 2Fe^{II}$$

The mechanism of reactions 1, 17, 18 also readily accounts for the CO dependence (Fig.

6*A*). Above CO pressures of about 600 mm, reaction 18 must occur more rapidly than reaction 1, but at lower pressures reaction 18 could become rate-determining. The slope of the linear region in Fig. 6*A* at lower CO pressures would then represent an estimate for the rate of reaction between CO and a bromorhodate(III) complex; the estimated rate constant k at 60 °C is 4.5 M^{-1} s^{-1}, and this is close to a value of 2.6 M^{-1} s^{-1} extrapolated from an Arrhenius plot for the direct carbonylation of $RhBr_4(H_2O)_2^-$ in the same media (1). It should be noted that at 600 mm CO, the rate of loss of the Rh^{III} in reaction 18 (*assuming* a CO solubility of 5.2 × 10^{-4} M at this pressure) is about 2.5 × 10^{-3} $[Rh^{III}]$ s^{-1}, while the rate-loss of $Rh(CO)Br_5^{2-}$ is about 1.4 × 10^{-3} $[Rh^{III}]$ s^{-1}. The rates of reactions 1 and 18 are clearly of the same order of magnitude over the pressure range studied, and the solutions in the linear regions of uptake plots will likely contain both bromocarbonyl- and bromo-rhodate(III) species, the relative amounts depending on the CO pressure. The somewhat similar visible spectra of the species in 0.5 M HBr makes this difficult to study quantitatively. The *equilibrated* solutions of bromorhodate(III) complexes in this media (mainly $RhBr_4(H_2O)_2^-$) show a maximum at 537 nm, ε 175 M^{-1} cm^{-1} (1), and the species resulting in [17] are not necessarily equilibrated.

To account for the CO dependence via the mechanism of [1], [19], and [20] requires [19] to become rate-determining at lower CO pressure, but this would lead to metal production via reaction 2. A mechanism analogous to [1], [19], and [20] has been demonstrated by Halpern and co-workers (15) for a formally related cobalt-catalyzed CO reduction of Fe^{III} (see below).

The net reduction of Fe^{III} (reaction 7) catalyzed by the rhodium system is of interest in that the essential mechanism of reactions 1, 17, and 18 shows that any reagent capable of oxidizing aqueous bromorhodate(I) systems to the Rh^{III} state can be catalytically reduced in the presence of CO under mild conditions. Electrode potential data for the rhodium couple ($Rh^{III} + 2e \rightleftharpoons Rh^{I}$) are not yet available. Higher CO pressures will offer no advantage since reaction 1 is rate-controlling. The corresponding rhodium chloride system also effects the catalysis (2), and solutions containing halorhodate(III), carbonylhalorhodate(III), or biscarbonyldihalorhodate(I) are all equally effective since they are interconvertible in the presence of CO and an oxidant. $(Rh(CO)_2X_2^-$ acts as a six-equivalent reductant toward Fe^{III} (2).)

The non-complementary electron transfer reaction between Rh^{I} and Fe^{III} could take place by a two-step mechanism involving a transient Rh^{II} species, or possibly by a one-step termolecular reaction. The latter mechanism has rarely been postulated for reactions involving only simple metal ion species and would likely be slow (22). The electron transfer could proceed by an inner sphere mechanism involving a bromide-bridged intermediate $[Rh^{I} \ldots Br \ldots Fe^{III}]$, or by an outer sphere mechanism. Such bridged intermediates involving cyanide have been established for the related cobalt(I)–iron(III) system outlined below (15):

[21]
$$Co^{I}(CO)L_4 + 2Fe^{III}(CN)_6^{3-} \xrightarrow[\text{fast}]{OH^-} [(CN)_5Fe^{II}(CN)Co^{III}L_4(COOH)] + Fe^{II}(CN)_6^{4-}$$

$(L_4 = (CN)_2(PEt_3)_2)$

$+ CO$

$\text{slow} \downarrow -CO_2, -H^+$

$-Fe^{II}(CN)_6^{4-}$

$[(CN)_5Fe^{II}(CN)Co^{I}L_4]$

As for our $Rh^{I}/2Fe^{III}$ system, the details of the initial $Co^{I}/2Fe^{III}$ interaction remain unclear. Formally analogous $[Rh^{I} \ldots Br \ldots Rh^{III}]$ intermediates also seem well-established (1, 2), and are almost certainly involved in the autocatalytic reaction observed in the absence of Fe^{III} (Fig. 1).

Following reduction of the ferric substrate, reduction of Rh^{III} species to $Rh(CO)_2Br_2^-$ occurs (Fig. 5); subsequent to the inflexion point, the CO uptake corresponds to about 3 moles CO per Rh, indicating that the reduced Rh^{III} species contains no carbonyl and the reaction occurs according to [4]. The reductive carbonylation process now appears to show no autocatalysis, although this could be masked near the inflexion region of the curves. However, the fact that the maximum rates developed show a first-order dependence on Rh confirm no autocatalysis, or at least a relative unimportance of such a process (*cf.* reaction 5), and rate law [11]

operates at higher pressures. The measured rate constant k_3, written in terms of CO uptake, is about three times that (k_1) estimated for decomposition of $Rh(CO)Br_5^{2-}$, and since the rate constant in terms of loss of Rh^{III} will be three or two times smaller (depending whether the reduction process corresponds to reaction 4 or 3, respectively), it seems that the rate-determining step is reaction 1. Furthermore, the CO dependence (Fig. 6*B*) gives at low CO pressures a second-order rate constant of $12.6\ M^{-1}\ s^{-1}$ which corresponds to 12.6/3, *i.e.* $4.2\ M^{-1}\ s^{-1}$ for loss of Rh^{III} and again this is essentially the same as that determined for reaction 18. Thus the reduction of the Rh(III) species after catalysis almost certainly occurs at higher pressures via reaction 1 (rate-determining) and 12, and at lower pressures via reactions 18 (rate-determining), 1, and 12. The stoichiometries at the inflexion points at the higher pressures (Fig. 5) should perhaps be treated with some caution since as mentioned earlier the rates of [1] and [18] are such that the solutions at this stage could contain both carbonyl-free and carbonyl-containing rhodium(III) species.

The lack of autocatalysis, which is being studied further, could be due to the presence of excess Fe(II) species preventing formation of the required $Rh^{III} \ldots Br \ldots Rh^{I}$ bridge; evidence has been presented for the existence of bridged Co^{I}—Fe^{II} species (15).

Acknowledgements

We thank the National Research Council of Canada for support of this research, and Johnson Matthey for the loan of $RhCl_3 \cdot 3H_2O$.

1. B. R. James and G. Rosenberg. Can. J. Chem. **54**, 313 (1976).
2. B. R. James and G. L. Rempel. J. Chem. Soc. A, 78 (1969).
3. J. A. Stanko, G. Petrov, and C. K. Thomas. Chem. Commun. 1100 (1969).
4. B. R. James and G. Rosenberg. Proc. XVIth Intern. Conf. on Coordin. Chem. Dublin, 1974, Abstract 4.33.
5. C. D. Meyer and R. Eisenberg. J. Am. Chem. Soc. **98**, 1364 (1976).
6. M. J. Cleare and W. P. Griffith. J. Chem. Soc. A, 2788 (1970); 372 (1969).
7. L. M. Vallarino. Inorg. Chem. **4**, 161 (1965).
8. D. Forster. Inorg. Chem. **8**, 2556 (1969).
9. D. Forster and G. R. Beck. Chem. Commun. 1072 (1971).
10. A. Seidell. Solubilities of inorganic and metal organic compounds. Vol. 1. 4th ed. Van Nostrand, New York. 1958. p. 453.
11. B. R. James, G. L. Rempel, and F. T. T. Ng. J. Chem. Soc. A, 2454 (1969).
12. K. Thomas, J. A. Osborn, A. R. Powell, and G. Wilkinson. J. Chem. Soc. A, 1801 (1968).
13. B. R. James and M. Kastner. Unpublished results.
14. A. I. Vogel. A textbook of quantitative inorganic analysis. 3rd ed. Longmans, Toronto. 1962. p. 787.
15. J. E. Bercaw, L. Y. Goh, and J. Halpern. J. Am. Chem. Soc. **94**, 6534 (1972).
16. D. Palmer and G. M. Harris. Inorg. Chem. **14**, 1316 (1975).
17. F. Basolo and R. G. Pearson. Mechanisms of inorganic reactions. 2nd ed. Wiley, New York. 1967. p. 170.
18. K. Noack and F. Calderazzo. J. Organomet. Chem. **10**, 101 (1967).
19. W. Robb and P. van Z. Bekker. Inorg. Chim. Acta, **7**, 626 (1973).
20. P. Poulenc. Ann. Chim. **4**, 567 (1935).
21. B. R. James and G. Rosenberg. To be published.
22. J. Halpern. Q. Rev. **15**, 207 (1961); J. O. Edwards. Inorganic reaction mechanisms. Benjamin, New York. 1965. p. 128.

High resolution ^1H nuclear magnetic resonance studies of a flavine and its product with $MoCl_4$ [1]

T. ROBERIE, N. S. BHACCA, AND J. SELBIN
Department of Chemistry, Louisiana State University, Baton Rouge, LA 70803

Received June 14, 1976

T. ROBERIE, N. S. BHACCA, and J. SELBIN. Can. J. Chem. **55**, 575 (1977).

The high resolution ^1H nmr spectra of the substituted flavine, 3-*N*-methyltetraacetylriboflavine (3-Me-TARF), and its non-aqueous solution complexes with $Gd(fod)_3$, $Eu(fod)_3$, $MoCl_4$, and $MoCl_4 \cdot 2CH_3(CH_2)_2CN$, were studied in order to try to discern the binding sites of the flavine as it attaches to the molybdenum. Evidence was found that all three metal atoms, Gd(III), Eu(III), and Mo(IV), are attached in solution not only by the primary binding (chelating) sites of the flavine, *viz.*, the O-4 and N-5 atoms, but also by an acetyl oxygen atom, at the C-4′ site of the ribityl side chain. 300 MHz spectra of the 3-Me-TARF have permitted the coupling constants for the side chain methine and methylene protons to be obtained.

T. ROBERIE, N. S. BHACCA et J. SELBIN. Can. J. Chem. **55**, 575 (1977).

On a étudié les spectres rmn du proton à haute résolution de la flavine substituée, *N*-méthyl-3 tétraacétylriboflavine (Me-3 TARF), et de ses complexes, en solutions non-aqueuses avec $Gd(fod)_3$, $Eu(fod)_3$, $MoCl_4$ et $MoCl_4 \cdot 2CH_3(CH_2)_2CN$; ces études ont été effectuées afin d'essayer de déterminer le site de complexation de la flavine lorsqu'elle s'attache avec le molybdène. On a obtenu des résultats indiquant qu'en solution, les trois métaux Gd(III), Eu(III) et Mo(IV) ne s'attachent pas uniquement par les sites de complexation primaire (chélation) des flavines, à savoir les atomes O-4 et N-5, mais aussi par un atome d'oxygène de l'acide acétyle au niveau du site C-4′ de la chaîne latérale ribityle. Les spectres à 300 MHz du Me-3 TARF ont permis d'obtenir les constantes de couplage pour les protons du méthine et du méthylène de la chaîne latérale.

[Traduit par le journal]

Introduction

Several studies have been reported of the interactions between flavines and flavocoenzymes with metal ions, and the extensive review by Hemmerich and Lauterwein (2) is a valuable background to much of this literature. Most of the studies have been carried out in solution, mainly by Hemmerich and co-workers; but more recently there have also been X-ray structural studies of solids, primarily by Fritchie and co-workers. The solution work, mainly in aqueous but more recently in non-aqueous media, has led to the recognition of at least three types of flavine–metal complexes (2). This work, but in particular solid state structural work (3), has also established certain structural features related to metal–ligand binding at the several potential binding sites of the flavines. Whereas X-ray structures clearly establish metal–ligand binding sites, these may only be inferred from solution data. It is far from certain that solution and crystalline state structures are necessarily the same when fluxional ligands such as flavines are involved. One means for obtaining structural information on species in solution is through high resolution nuclear magnetic resonance.

We have found relatively little proton nmr (^1H nmr) data in the literature on flavoquinones (**1**).

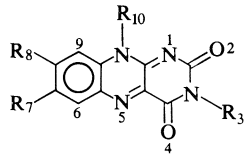

1

A brief report was made of the ^1H nmr spectra of FMN or riboflavin 5′-phosphate ($R_3 = H$; $R_7 = R_8 = CH_3$; $R_{10} = CH_2(CHOH)_3CH_2OPO_3H$), lumiflavin ($R_3 = H$; $R_7 = R_8 = R_{10} = CH_3$), and its 7-ethyl analogue in D_2O at pH = 6.8. The protons in positions 6 through 10 were again assigned for lumiflavin and its 9-bromo- and 9-deutero- and 6,9-dideutero-derivatives (4, 5). More thorough ^1H nmr studies of FMN and FAD (flavin adenine dinucleotide) confirmed *intra*molecular interaction between the adenine and the isoalloxazine rings in FAD and also suggested *inter*molecular interaction

[1]Presented at the First Chemical Congress of the North American Continent, Mexico City, December 4, 1975.

between isoalloxyazine rings of neighboring FAD molecules (6, 7). In 1972, a brief account of the ^1H nmr spectra was published of tetraacetylriboflavine ($R_3 = H$; $R_7 = R_8 = CH_3$; $R_{10} = CH_2(CHOCOCH_3)_3CH_2OCOCH_3$) and its complexes with Fe^{2+}, Co^{2+}, Ni^{2+}, and Cu^{2+} in acetone-d_6 (8). A full account of that work including additional information on the ^1H nmr of complexes of Cu^+, Ag^+, Zn^{2+}, Cd^{2+}, Mn^{2+}, Mg^{2+}, and Fe^{3+} has now been published (9, 10). ^1H nmr studies of hydroxyquinolinate complexes of Mo(VI, V) and V(V) have also been reported as models of molybdenum–flavine interactions (11).

Inasmuch as molybdenum and a flavine (FAD in particular) are essential co-factors in several enzyme systems (12), and since neither X-ray nor any kind of solution studies have established the ligand binding sites of flavines on molybdenum, we decided to undertake a detailed ^1H nmr study of solutions of a particular molybdenum–flavine system. From earlier studies it is not clear that biological molybdenum and FAD are even near each other (12), except possibly during a turnover of the enzyme molecule, and so we recognize that this study may or may not have any relevance to the biological systems. In any case the study has revealed some new and interesting chemistry of both molybdenum and of the derivative of riboflavin which we employed as a model of FAD.

We report here a study of the ^1H nmr spectra of 3-*N*-methyltetraacetylriboflavine (3-Me-TARF) (**2**)

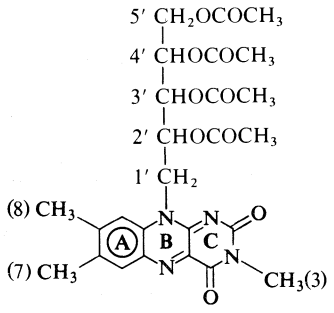

2

and its non-aqueous solution complexes with $Gd(fod)_3$, $Eu(fod)_3$ (fod = 1,1,1,2,2,3,3-heptafluoro-7,7,-dimethyl-4,6-octanedione), and $MoCl_4$.

Experimental

All solutions used in this study were prepared in an efficient nitrogen-filled dry box. $CDCl_3$ was used as the solvent for the nmr work involving $Eu(fod)_3$ and $Gd(fod)_3$. On the other hand, because of the very low solubility of $MoCl_4$ in $CDCl_3$, it was dissolved in a 99:1 $CDCl_3$–ethanol mixture. These 'reagent' solutions were stored in 8.0 ml septum vials capped with teflon 'mininert' valves (obtained from Precision Sampling Corp., Baton Rouge, Louisiana 70815, Cat. No. 614250). The vials were transferred then from the dry box to N_2-filled glove bags where continuous and easy sampling could be carried out. During a typical nmr determination, the nmr sample tube containing the flavine solution was placed in the glove bag and an incremental amount of 'reagent' solution was then added with a Hamilton microliter syringe. ^1H nmr spectra were obtained at 100 and 300 MHz on Varian HA-100 and HR-300 spectrometers. A small amount of tetramethylsilane was added to the sample solution, to act both as an internal reference as well as an internal lock signal.

3-*N*-Methyl-riboflavintetraacetate (14) (3-Me-TARF) and anhydrous $Gd(fod)_3$ (15) were synthesized according to known procedures. $MoCl_4$ was supplied in vacuum sealed vials by Climax Molybdenum Company. $Eu(fod)_3$ was purchased from Kary Laboratories, Somerville, N.J.

$CDCl_3$ was dried by refluxing it under N_2 with CaH_2 before distilling it under N_2. Absolute ethanol was refluxed with magnesium acetate overnight before being distilled under N_2.

After ^1H nmr data had been obtained on the $MoCl_4$ and 3-Me-TARF, it was found from esr studies of the $MoCl_4$ dissolved in the 99:1 $CDCl_3$–ethanol mixture that there was a small quantity of Mo(V) present in the sample. Efforts to wash out the Mo(V) species from the $MoCl_4$ sample using benzene were only partially successful but in any case when the $MoCl_4$ was redissolved in the mixed solvent some Mo(IV) was oxidized to Mo(V). We believe that it may be impossible to prevent some Mo(V) from forming whenever $MoCl_4$ is put into solution. Since the observed ^1H nmr resonance broadening in the 3-Me-TARF spectra upon addition of $MoCl_4$ might be due to the impurity levels of Mo(V), we prepared the compound, $MoCl_4 \cdot 2CH_3(CH_2)_2CN$ (17), to reexamine the Mo(IV) ^1H nmr studies. This Mo(IV) compound can be made nearly Mo(V)-free. It dissolves in $CDCl_3$ without the necessity of ethanol being present (which may be the cause of the Mo(V) forming) and without any increase in Mo(V) impurity. The latter was verified by means of esr measurements. The results of the ^1H nmr study using the butyronitrile complex of $MoCl_4$ in place of $MoCl_4$ itself gave the same order of broadening effects on 3-Me-TARF. Thus the conclusion we draw is that it is indeed Mo(IV) and not Mo(V) that is responsible for the proton broadenings on the ligand and that the ligand is indeed attached to Mo(IV).

Results and Discussion

The Flavine

In the 100 MHz spectrum of 3-Me-TARF (see bottom spectrum of Fig. 1) most of the resonances corresponding to the side chain protons are indecipherable and therefore 300 MHz spectra (in $CDCl_3$ and CD_3COCD_3 solutions) of the sample were obtained (see Fig. 1). The subsequent first order, as well as calculated, spectral

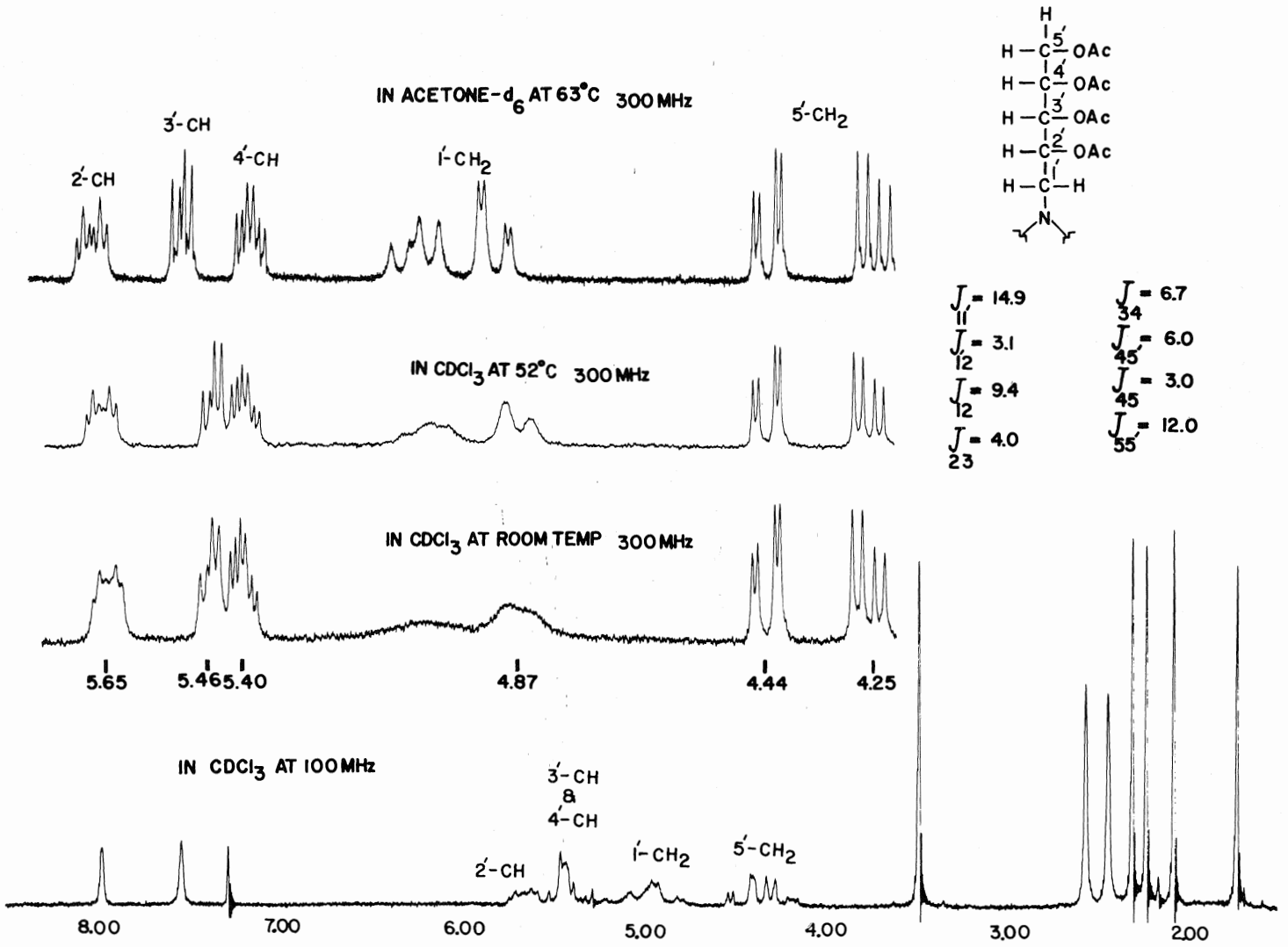

FIG. 1. 300 MHz spectra of the 4 to 6 δ region of 3-Me-TARF in acetone-d_6 at 63 °C (top spectrum) and in $CDCl_3$ at 52 °C and at ambient temperature (two middle spectra). The bottom spectrum is the complete 100 MHz spectrum run in $CDCl_3$, shown for reference. The C-2′ methylene proton resonances in $CDCl_3$ spectra are broader due to their spin–spin interaction with ^{14}N quadrupole.

analysis yields all the coupling constants related to the side chain protons. Finally from the direct comparison of these coupling constants with those of acyclic ribose and arabinose (as shown in Table 1) the ribose structure was assigned to the side chain. This conclusion is in harmony with the fact that the 3-Me-TARF had been prepared from riboflavin whose side chain possesses the *d*-ribose structure.

The Flavine and Eu(fod)$_3$

The addition of incremental amounts of Eu(fod)$_3$ to $CDCl_3$ solutions of 3-Me-TARF produced the shifts of the isoalloxazine protons as a function of concentration shown plotted in Fig. 2. The shifts fall in the order: H-6 ≫ N-3—CH_3 > H-9 ≫ C-8—CH_3 > C-7—CH_3. These data support 1:1 Eu(fod)$_3$:3-Me-TARF complexing. The H-6 proton signal is immediately severely broadened as well as shifted. The sequence of shifts confirms metal chelation at the primary binding site of the isoalloxazine, O-4 and N-5.

The shifting and broadening of methylene and methine side chain proton signals with increasing Eu(fod)$_3$ concentration were also examined and the shifts are plotted in Fig. 3. Again, 1:1 complexing is supported by the evidence shown in Fig. 3. The sequential order of shifts may be rationalized by certain side chain structural information. For example, the extreme high field position ($\delta = 1.75$) of the 2′-$OCOCH_3$ methyl peak (Fig. 1) strongly suggests that this methyl group is located in the shielding region of aromatic **A** ring and, as molecular models clearly reveal, that one of the two C-1′ methylene protons is the deshielding zone of the C-2′—carbonyl function. On the other hand, the H-2′ is

TABLE 1. Coupling constants for the side chain methine and methylene protons from 300 MHz spectra

Parameter	Value		
	3-Me-TARF	Ribose*	Arabinose*
$J_{11'}$	14.9	†	†
$J_{1'2}$	3.1	†	†
J_{12}	9.4	6.5	6.7
J_{23}	4.0	3.9	2.6
J_{34}	6.7	5.5	8.3
$J_{45'}$	6.0	6.3	5.1
J_{45}	3.0	2.5	2.9
$J_{55'}$	12.0	12.2	12.3

*Reference 16.
†C-1′ has two methoxy groups and only one H.

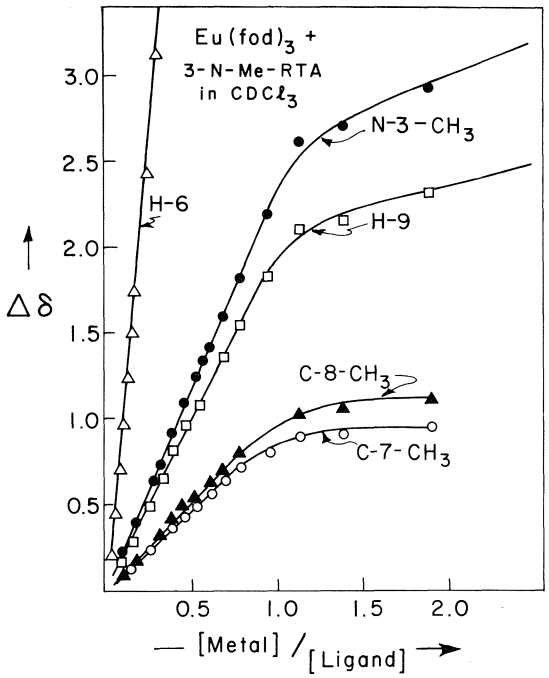

FIG. 2. Shifts in ppm of the isoalloxazine proton resonances with increasing Eu(fod)$_3$ to ligand mole ratios.

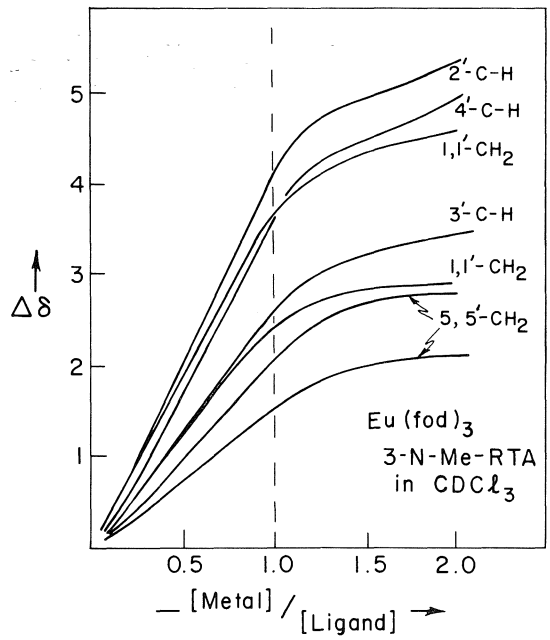

FIG. 3. Shifts in ppm of the methylene and methine side chain proton resonances with increasing Eu(fod)$_3$ to ligand mole ratios.

deshielded either by proximity to a carbonyl group or by proximity to the metal atom, depending upon which side of the fused ring system the ribityl side chain falls. This is the likely explanation for the large downfield shifts observed (Fig. 3) for the H-2′ resonance and for the signals of one of the two C-1′ methylene protons.

The comparatively large downfield shift of the H-4′ proton signal (Fig. 3) was not expected. We believe that this shift is caused by the proximity of the H-4′ to the Eu atom due to binding of the Eu atom by the carbonyl oxygen of C-4′—$OCOCH_3$ (*vide infra*).

The shifting of the methyl proton signals of the acetate groups with increasing $Eu(fod)_3$ concentration was examined and the results are plotted in Fig. 4. The 1:1 complexing is again evident from the latter figure as is the unexpected result that the C-4′—$OCOCH_3$ signal is shifted considerably more than the remaining three acetate signals. We interpret this result to mean that complexing of the flavine occurs not only through the primary binding site but via the 4′-acetate as well. Molecular models support this interpretation since they show that, with the 2′-acetate locked over the **A** ring (*vide infra*), only the acetate at C-5′ or C-4′ can come within reasonable bonding distance to a metal atom bound at the primary site. The choice between these two possibilities can then be made in the model by requiring the side chain configuration to conform to all other ^1H nmr shift results. From model studies and, in particular, on the basis of the ^1H nmr data for the 4′-methine and acetate protons, we propose that at least in solution there is strong evidence that the metal atom (here Eu) is bound by *three* ligand atoms, the primary binding pair, O-4 and N-5, and the carbonyl oxygen of the C-4′—acetate.

The Flavine and Gd(fod)$_3$

Gadolinium has an $^8S_{7/2}$ ground state and thus its complexes are magnetically isotropic and therefore do not exhibit dipolar shifts (13). However, the broadening of ^1H nmr lines caused by increasing concentrations of $Gd(fod)_3$ supplies very useful information since the *only* effect operating is a pseudocontact or through-space interaction. Although the signals due to the side chain methine and methylene protons are too weak and too rapidly broadened, meaningful results have been obtained for both the isoalloxazine protons and the acetate protons. The

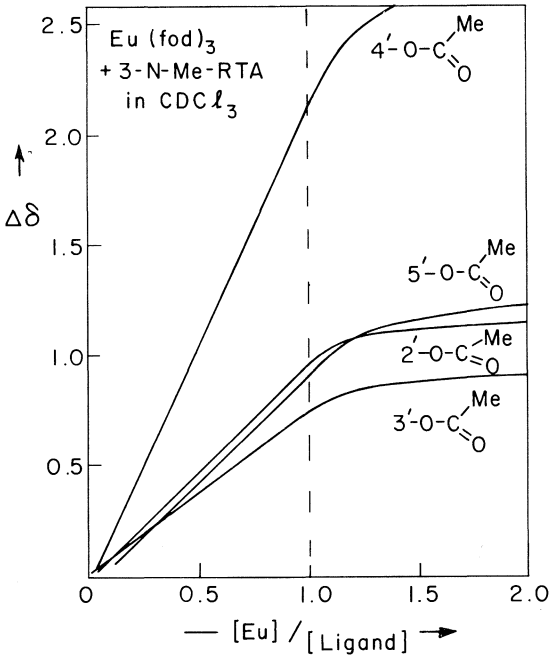

FIG. 4. Shifts in ppm of the side chain acetate methyl resonances with increasing $Eu(fod)_3$ to ligand mole ratios.

line width broadening as a function of $Gd(fod)_3$ concentration is plotted for these signals in Figs. 5 and 6, respectively. The broadening sequence (Fig. 5), H-6 ≫ N-3—CH_3 > C-7—CH_3 ≫ H-9 > C-8—CH_3, is just that expected from an isotropic magnet placed at the primary binding site between the N-5 and O-4 positions. Of much greater interest is the broadening sequence shown in Fig. 6 for the acetate methyl proton signals: C-4′ ≫ C-3′ > C-5′ > C-2′. Although these could only be followed out to a metal/ligand mole ratio of roughly 10^{-2}, it is clear that the C-4′—acetate must be much closer to the Gd atom than the other three acetate groups. Thus we again find evidence in support of attachment of the flavine to a metal atom via *three* sites.

The Flavine and $MoCl_4$

The addition of incremental amounts of $MoCl_4$ (or $MoCl_4 \cdot 2CH_3(CH_2)_2CN$, see Experimental section) to chloroform-*d* solutions of 3-Me-TARF produced the results shown in Fig. 7. The more pronounced effect is a broadening, but there is also a very slight shifting of signals. This is more evident in Fig. 8, where the broadening and slight shifting (in chloroform solutions) is shown for the several acetyl protons and the C-7 and C-8 methyl protons.

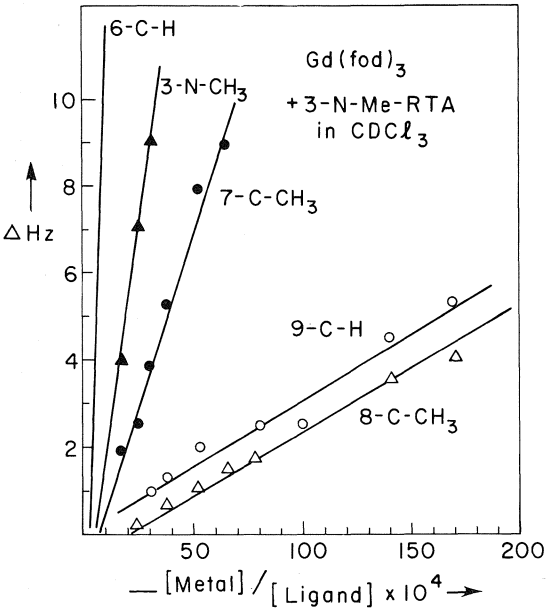

FIG. 5. Line width broadening of the isoalloxazine proton resonances plotted as a function of increasing $Gd(fod)_3$ to ligand mole ratios.

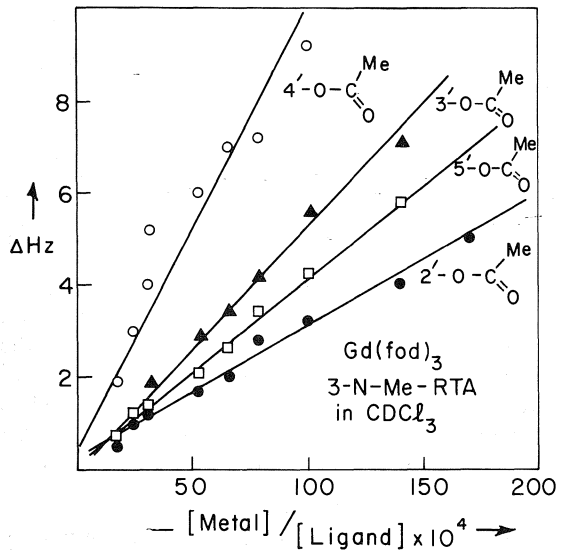

FIG. 6. Line width broadening of the side chain acetate methyl resonances plotted as a function of increasing $Gd(fod)_3$ to ligand mole ratios.

The broadening sequence in the isoalloxazine protons for the $MoCl_4$–3-Me-TARF interaction is (Fig. 9): H-9 ~ H-6 > C-8—CH_3 > *N*-3—CH_3 > C-7—CH_3. This sequence for the paramagnetic Mo(IV) species supports the binding of

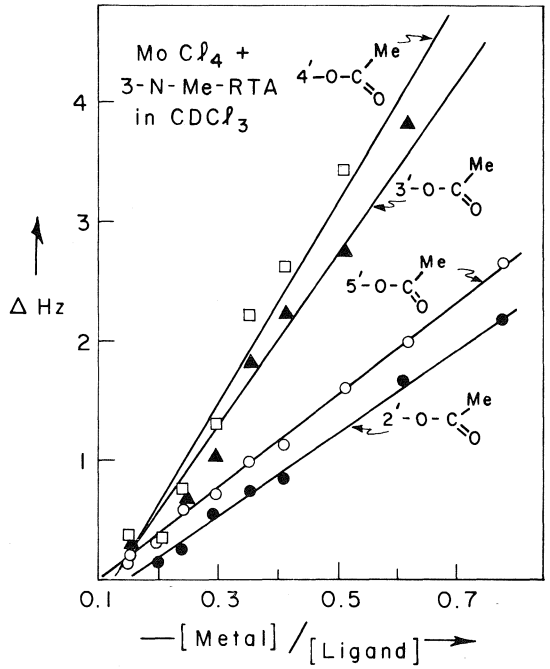

FIG. 7. Line width broadening of the side chain acetate methyl resonances plotted as a function of increasing $MoCl_4$ to ligand mole ratios.

the molybdenum atom by at least the primary binding site, O-4 and N-5. It is a sequence expected if a contact interaction is superimposed upon the pseudocontact interaction. Thus, the differences between this sequence for the gadolinium case (*vide supra*) where only pseudocontact interactions are operative, and the europium and molybdenum cases can be explained on the basis of expected increasing (Eu to Mo) contributions from contact interactions. For example, the relative positions of C-7—CH_3 and C-8—CH_3 in the Eu and Mo sequences compared to their positions in the Gd sequence bear out the increased importance of electron delocalization (*i.e.*, Fermi contact interaction) in the Mo complex. The C-7—CH_3 is spatially closer to a metal atom complexed at O-4 and N-5, but the π-electron spin density at position 7 is near 0.0 whereas it is near 0.15 at position 8 (1).

In addition to the molybdenum atom being bound by the primary site of the isoalloxazine system, it appears that it is further bound by the acetate oxygen of C-4′—$OCOCH_3$. Thus, both the broadening sequence (from Fig. 9) and the shifting sequence show the greatest effect is on the

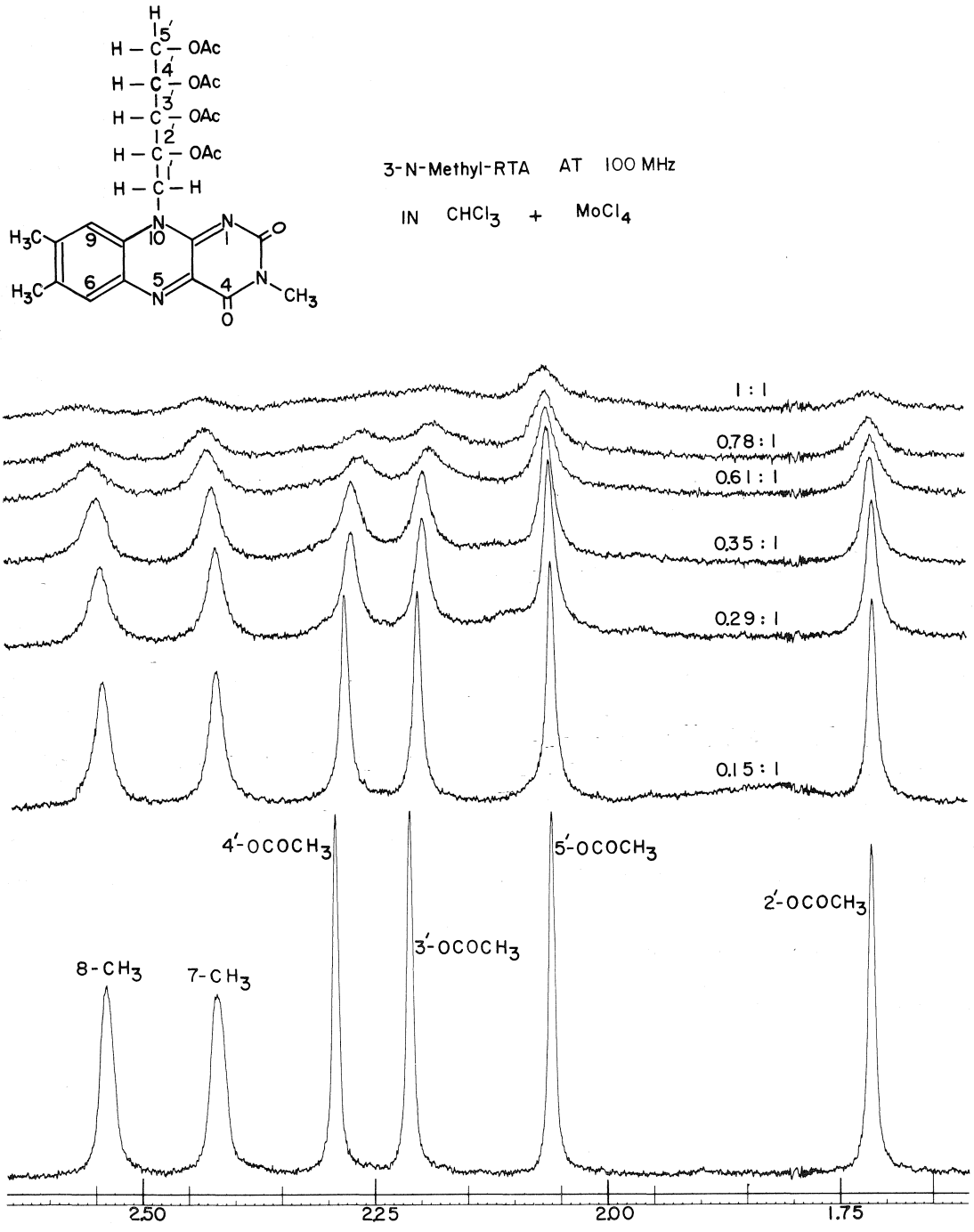

FIG. 8. 100 MHz spectrum of the 1.50 to 2.75 δ region of 3-Me-TARF at 100 sweep width and the resulting spectra obtained upon incremental additions of $MoCl_4$ solution in amounts giving mole ratios of 0:1, 0.15:1, 0.29:1, 0.35:1, 0.61:1, 0.78:1, and 1:1 as we go from bottom to top.

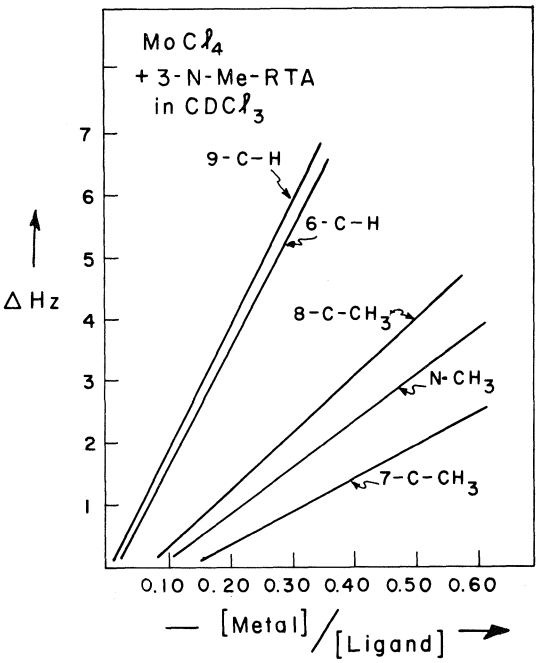

FIG. 9. Line width broadening of the isoalloxazine protons plotted as a function of increasing $MoCl_4$ to ligand mole ratios.

methyl proton of C-4′—$OCOCH_3$. This is in agreement with analogous results for both the Gd and Eu compounds.

On the basis of the foregoing results and their interpretation, it is tentatively suggested that molybdenum is bound to flavine molecules through the agency of at least two binding sites and very likely a third binding site present on the folded ribityl side chain. For the tetraacetylriboflavin compound studied here, that binding site is the C-4′—acetyl group.

Acknowledgement

The authors are grateful to the Climax Molybdenum Company for their generous donation of samples of Mo compounds. The authors are also grateful to Mr. Everett R. Santee of The University of Akron Institute of Polymer Science for his help in obtaining 300 MHz of 3-Me-TARF.

1. A. V. GUZZO and G. TOLLIN. Arch. Biochem. Biophys. **105**, 380 (1964).
2. P. HEMMERICH and J. LAUTERWEIN. *In* Inorganic biochemistry. *Edited by* G. Eichhorn. Elsevier, Amsterdam. 1973, pp. 1168–1190.
3. M. W. YU and C. J. FRITCHIE, JR. J. Chem. Soc. Dalton Trans. 377 (1975) and earlier papers by Fritchie and co-workers.
4. F. J. BULLOCK and O. JARDETZKY. J. Org. Chem. **30**, 2056 (1965).
5. D. B. MCCORMICK. J. Heterocyclic Chem. **4**, 629 (1967).
6. R. H. SARMA, P. DANNIES, and N. O. KAPLAN. Biochem. **7**, 4359 (1968).
7. G. KOTOWYCZ, N. TENG, M. P. KLEIN, and M. CALVIN. J. Bio. Chem. **244**, 5656 (1969).
8. J. LAUTERWEIN, P. HEMMERICH, and J. M. LHOSTE. Z. Naturforsch. **27***b*, 1047 (1972).
9. J. LAUTERWEIN, P. HEMMERICH, and J. M. LHOSTE. Inorg. Chem. **14**, 2152 (1975).
10. J. LAUTERWEIN, P. HEMMERICH, and J. M. LHOSTE. Inorg. Chem. **14**, 2161 (1975).
11. L. W. AMOS and D. T. SAWYER. Inorg. Chem. **13**, 78 (1974).
12. R. C. BRAY and J. C. SWANN. Struct. Bonding Berlin, **11**, 107 (1972); R. A. D. WENTWORTH. Coord. Chem. Rev. **18**, 1 (1976).
13. W. DEW. HORROCKS, JR. *In* Nmr of paramagnetic molecules. *Edited by* G. N. LaMar, W. DeW. Horrocks, Jr., and R. H. Holm. Academic Press, New York. 1973. p. 491.
14. P. HEMMERICH. Helv. Chim. Acta, **47**, 464 (1964).
15. C. S. SPRINGER, D. W. MEEK, and R. E. SIEVER. Inorg. Chem. **6**, 1105 (1967).
16. D. HORTON, M. MUESSER, D. GAGNAIRE, and J. DEFAYE. Carbohyd. Rev. **21**, 407 (1972).
17. E. A. ALLEN, B. J. BRISDON, and G. W. A. FOWLES. J. Chem. Soc. 4531 (1964).

Acetyl group relaxation in four aromatic ketones

C. K. McLellan and S. Walker

Department of Chemistry, Lakehead University, Thunder Bay, Ont., Canada P7B 5E1

Received August 5, 1976

C. K. McLellan and S. Walker. Can. J. Chem. **55,** 583 (1977).

Dielectric absorption studies have been made of group relaxation of acetophenone, 1,4-diacetylbenzene, 4-acetylbiphenyl, and 2-acetylfluorene in a polystyrene matrix, and two rigid molecules have also been examined. For acetyl group relaxation in acetophenone, $\Delta H_E = 29.6 \pm 0.6$ kJ mol^{-1} and $\Delta S_E = 26 \pm 3$ J K^{-1} mol^{-1} (95% confidence intervals). The energy barrier for acetyl group relaxation is of the same order as that obtained from nmr data. Our results for acetophenone differ appreciably from the values reported for the gaseous phase by the far-infrared approach and from those by the dielectric absorption of aromatic ketones in benzene solution. The enthalpies of activation for acetyl group relaxation in 1,4-diacetylbenzene, 4-acetylbiphenyl, and 2-acetylfluorene are 29, 30, and 32 kJ mol^{-1}, respectively, which values are identical within their experimental errors. These three substances have also been examined as pure solids, yielding enthalpies of activation for acetyl group relaxation of a similar magnitude.

C. K. McLellan et S. Walker. Can. J. Chem. **55,** 583 (1977).

On a effectué des études, dans des matrices de polystyrène, d'absorption diélectrique afin d'évaluer la relaxation du groupe de l'acétophénone, du diacétyl-1,4 benzène, de l'acétyl-4 biphényle et de l'acétyl-2 fluorène; on a aussi examiné deux molécules rigides. Pour la relaxation du groupe acétyle de l'acétophénone, $\Delta H_E = 29.6 \pm 0.6$ kJ mol^{-1} et $\Delta S_E = 26 \pm 3$ J K^{-1} mol^{-1} (avec des intervalles de confiance de 95%). La barrière d'énergie pour la relaxation du groupe acétyle est du même ordre que celle obtenue par des données de rmn. Nos résultats pour l'acétophénone diffèrent toutefois d'une façon appréciable des valeurs rapportées pour la phase gazeuse alors qu'une approche par infrarouge lointain ayant été utilisée ainsi que de celles obtenues à partir de l'absorption diélectrique de cétones aromatiques en solution dans le benzène. Les enthalpies d'activation pour la relaxation du groupe acétyle dans le diacétyl-1,4 benzène, l'acétyl-4 biphényle et l'acétyl-2 fluorène sont respectivement de 29, 30 et 32 kJ mol^{-1}; ces valeurs sont identiques à l'intérieur des erreurs expérimentales. On a aussi examiné ces trois substances à l'état de solides purs; on a pu en dériver des enthalpies d'activation pour la relaxation du groupe acétyle qui sont d'une grandeur sembable.

[Traduit par le journal]

Introduction

The energy barrier to acetyl group rotation, when the acetyl group is attached to an aromatic ring, has received some attention. A far-infrared study (1) of acetophenone in the gas phase gave a value of 13.0 kJ mol^{-1}. *Ab initio* calculations (2) yielded 18.4 kJ mol^{-1}. Fong and Smyth studied 2-acetylnaphthalene and 4-acetyl-*o*-terphenyl (3), 4-phenylacetophenone, and 1,4-diacetylbenzene (4) in benzene solution and obtained values of 4.2 to 6.3 kJ mol^{-1} for the activation enthalpy barrier (ΔH_E from Eyring theory) which the acetyl group encounters as it rotates. Grindley, Katritzky, and Topsom (5) have estimated from nmr data on *para*-substituted acetophenones that the rotation barrier for acetophenone itself is 26 kJ mol^{-1}. Thus, the energy barriers for acetyl group rotation estimated by these procedures differ considerably and merit further examination.

It seemed of interest to examine acetophenone and some related substances at low concentrations in a solid matrix where the means existed of directly separating the group relaxation contribution from the molecular relaxation. Such a procedure appeared more straightforward than studying the dielectric absorption of these solutes in an inert liquid solvent, since in this latter situation the molecular and group absorptions overlap, and the number of microwave frequencies available is usually fairly limited. In addition, in such work it is necessary to obtain the group relaxation time (τ_2), which has to be obtained at a few temperatures to estimate the enthalpy of activation for group relaxation; the deduction of τ_2 requires a Budó analysis which in a number of cases is now known to be unsatisfactory (6).

Experimental Results

The dielectric measurements have been made on a General Radio 1615A capacitance bridge in the frequency range 50 to 10^5 Hz. The mea-

suring cell was a three-terminal circular parallel plate capacitor mounted in a temperature-controlled chamber purged with dry nitrogen gas. The cell may be operated from liquid nitrogen temperature to about 400 K. For the polystyrene matrix sample of acetophenone only, additional measurements have been made using a Hewlett-Packard 4342A Q-meter with a temperature-controlled two-terminal cell in the range 2.5×10^4 to 1.5×10^7 Hz. The apparatus and measurement techniques have been described previously (7).

We have adopted the Davies and Swain (8) procedures both experimentally and in the evaluation of the relaxation time and distribution parameter by means of the Fuoss–Kirkwood equation and the enthalpy of activation from the Eyring equation. The polystyrene used here had a nominal $M_w = 230\,000$. The matrix solutions were prepared by dissolving weighed quantities of polystyrene and the desired solute in a third non-polar solvent, *trans*-1,2-dichloroethylene. This latter solvent was then removed by heating to 360 K followed by treatment in a heated vacuum oven. The resultant matrix mass was pressed (5 ton ram load) in a cylindrical die heated to 395 K to produce a sample disk 2.0 in. in diameter and approximately 0.065 in. in thickness. Prior to pressing, the matrix mass containing acetophenone was returned to the vacuum oven at 360 K for 24 h with no resultant weight loss, indicating that this preparation procedure did not produce any loss of solute from the matrix. The sample disks were allowed to relax possible strains from pressing for at least 24 h prior to measurements, and repeat measurements several months later on the same disk yielded comparable data. We have also taken the precautions which Davies and Swain (8) have pointed out are necessary for accurate measurements and have repeated their study on cyclohexyl chloride in polystyrene, obtaining an enthalpy of activation of 43 ± 7 kJ mol^{-1} for the intramolecular process, in good agreement with their value of 42 ± 2.5 kJ mol^{-1} and with the value of 43 ± 2 kJ mol^{-1} deduced from nmr studies on the pure liquid (9).

Acetophenone, 1,4-diacetylbenzene, 4-acetylbiphenyl, and 2-acetylfluorene have each been examined in a polystyrene matrix, and a sample plot of loss factor ($\varepsilon'' = \varepsilon''(\text{obs}) - \varepsilon''(\text{polystyrene})$) against log (frequency) is given in Fig. 1 for acetophenone. Similar dielectric measurements were carried out out on three of these as pure polycrystalline powders pressed into disks. The results of Eyring equation analyses of these data and of data for two other rigid molecules (4-bromotoluene and 4-nitrobiphenyl) are given in Table 1, along with relaxation times calculated from these analyses at three temperatures.

In the fitting of the data of relaxation time as a function of temperature to the Eyring equation, standard statistical techniques (10) have been employed to obtain the slope and intercept of the line and the variances of these two parameters. These data yielded values of the enthalpy (ΔH_E) and entropy (ΔS_E) of activation for the relaxation process along with confidence intervals for each of these two. The 95% confidence intervals on ΔH_E were typically $\pm 10\%$ of the nominal values, or less, in agreement with the work of Davies *et al.* (8, 11). For the ΔS_E term these confidence intervals were of the order of $\pm 50\%$ of the nominal values in some cases, since this term is often a small part of the intercept, (ln $(h/k) - \Delta S_E/R$), of the ln $(T\tau)$ *vs.* $(1/T)$ plot. For this reason an extensive study of the acetophenone/polystyrene matrix was undertaken to obtain a larger number of points on the Eyring plot extending to higher temperatures (smaller $1/T$ values). This procedure produced values of $\Delta H_E = 29.6 \pm 0.6$ kJ mol^{-1} and $\Delta S_E = 26 \pm 3$ J K^{-1} mol^{-1} (95% confidence intervals). For other samples the values have been quoted to two significant digits in line with the error estimates as outlined above.

Discussion

From good straight line plots of log $T\tau$ *vs.*

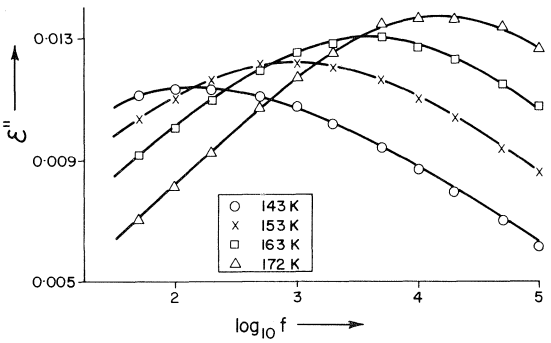

FIG. 1. Dielectric loss factor *vs.* $\log_{10} f$ for 0.265 *M* acetophenone in polystyrene at four temperatures as indicated. The solid lines result from computer analyses of the experimental points via the Fuoss–Kirkwood equation.

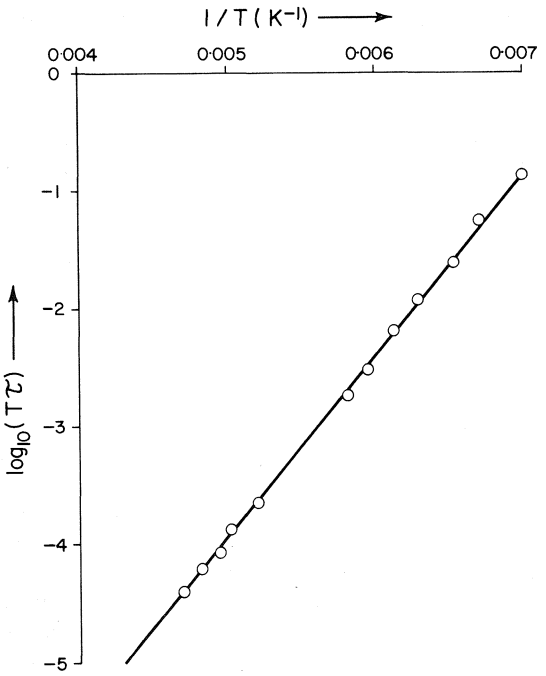

FIG. 2. Eyring plot of $\log_{10} T\tau$ *vs.* $(1/T)$ for 0.265 *M* acetophenone in polystyrene. The solid line represents the computer-generated best fit to the experimental points.

$1/T$ (for example, see Fig. 2), the corresponding enthalpies of activation were 29.6, 29, 30, and 32 kJ mol^{-1} for 3% (wt.) solutions of acetophenone, 1,4-diacetylbenzene, 4-acetylbiphenyl, and 2-acetylfluorene in polystyrene. Thus, all four ketones exhibited dielectric absorptions in similar ranges of temperature and frequency, yielding ΔH_E values in very good agreement, well within our estimate of experimental error.

If we take into account the studies of Davies and Swain (8) in polystyrene matrices at similar temperatures, the two possible sources of the dielectric absorptions in these aromatic ketones are molecular or group relaxation. For several flexible molecules examined by Davies and Swain (8), only intramolecular relaxation was observed; indeed, they noted that "molecular reorientation thus has been restricted to such low frequencies that it does not appear at all". It is to be noted that the ketones considered here differ appreciably in size, and that the enthalpy of activation for molecular relaxation tends to increase with size. For example, one may note the values in Table 1 for two rigid molecules chosen for the similarities of their sizes to those of the ketones

TABLE 1. Eyring analysis results for several molecules in polystyrene matrices (p.s.) or as compressed solids (solid)

Molecule	State	T (K)	Molarity	ΔH_E (kJ mol^{-1})	ΔS_E (J K^{-1} mol^{-1})	τ (s) 150 K	τ (s) 225 K	τ (s) 300 K
Acetophenone	p.s.	143–213	0.265	29.6	26	2.8×10^{-4}	6.9×10^{-8}	9.8×10^{-10}
1,4-Diacetylbenzene	p.s.	133–168	0.193	29	36	4.1×10^{-5}	1.3×10^{-8}	2.0×10^{-10}
	Solid	137–162	6.85	27	16	8.7×10^{-5}	4.7×10^{-8}	9.9×10^{-10}
4-Acetylbiphenyl	p.s.	146–172	0.162	30	35	1.3×10^{-4}	2.9×10^{-8}	4.0×10^{-10}
	p.s.	311–331	0.161	68	33	3.0×10^{9}	26	2.2×10^{-3}
	Solid	154–192	5.85	33	21	5.5×10^{-3}	6.1×10^{-7}	5.9×10^{-9}
2-Acetylfluorene	p.s.	158–177	0.154	32	28	1.9×10^{-3}	2.2×10^{-7}	2.3×10^{-9}
	p.s.	317–337	0.154	89	100	1.6×10^{13}	5.3×10^{2}	2.8×10^{-3}
	Solid	212–242	4.06	32	−24	1.1	1.2×10^{-4}	1.2×10^{-6}
4-Bromotoluene*	p.s.	174–264	0.245	30	−1	7.6×10^{-3}	1.8×10^{-6}	2.6×10^{-8}
4-Nitrobiphenyl	p.s.	294–312	0.538	86	106	5.7×10^{11}	45	3.7×10^{-4}

*Data provided through the courtesy of Mr. B. K. Morgan of this laboratory.

under investigation. Further, it may be seen from Table 1 that we have observed for the two larger ketones a second dielectric absorption process at higher temperatures although still below the glass transition temperatures (approximately 345 K) of the matrix samples. The ΔH_E and τ values for these absorptions are in good agreement with the corresponding values obtained from the data for the similarly-sized rigid molecule, 4-nitrobiphenyl.

Table 1 includes the results of dielectric measurements on crystalline solid samples of three of the ketones under discussion. In this state one may reasonably expect that molecular relaxation would be eliminated while group relaxation may still occur. It is apparent in this table that the ΔH_E values so obtained, being 27, 33, and 32 kJ mol^{-1} for 1,4-diacetylbenzene, 4-acetylbiphenyl, and 2-acetylfluorene, respectively, are in good agreement with the values derived from analyses of the low-temperature dielectric absorptions in the polystyrene matrix samples.

For the cases of 4-acetylbiphenyl and 2-acetylfluorene, then, we have observed two dielectric absorption processes in polystyrene matrix samples. In each case the Eyring activation parameters for the lower-temperature process is in agreement with that obtained from a crystalline sample. In addition, the parameters for the higher-temperature process are in reasonable agreement with the data for a polystyrene matrix sample of the rigid molecule 4-nitrobiphenyl. For the case of 1,4-diacetylbenzene a low-temperature absorption similarly has been observed in both the polystyrene matrix and crystalline samples. Further, for this substance the components of the substituent groups' dipole moments along the molecule's long axis cancel out one another. The possible relaxation candidates in this case then could be molecular relaxation of a rigid *cis* form of the molecule or acetyl group relaxation. A stable *cis* form would imply a high energy barrier opposing group relaxation, probably considerably higher than that obtained for acetyl group rotation by other methods. It may be noted also that the relaxation times for the slightly smaller 4-bromotoluene in polystyrene at 150, 225, and 300 K were approximately two orders of magnitude longer than those of 1,4-diacetylbenzene, which is just the opposite of what would have been expected if both molecules had exhibited molecular relaxation.

It would seem that the most likely interpretation of this information is that acetyl group relaxation has been observed in 1,4-diacetylbenzene, 4-acetylbiphenyl, and 2-acetylfluorene at temperatures near 150 K, and that molecular relaxation has also been observed in the latter two at temperatures near 320 K. One may note that in these two rod-shaped ketones the relaxation times for molecular and group processes at 300 K differed by a factor of approximately 10^6 in the polystyrene matrices, which factor is enormously larger than is usually found in liquid studies. From the existence of acetyl group relaxation in all three of these ketones one would anticipate that the same process should be found in acetophenone itself, and as Table 1 shows the ΔH_E, ΔS_E, and τ values for this molecule are entirely in accord with the values found for the lower-temperature process in the other three. The fact that the relaxation time values for acetophenone are approximately twice as long as those of the lower-temperature process in the much larger molecule 4-acetylbiphenyl is further indication that these processes could not both be molecular relaxation.

The possibility has to be considered that our matrix values do not correspond with those of an isolated molecule. Borisova and Chirkov (12) found that the energy barrier for molecular relaxation of small molecules in a polystyrene matrix was independent of concentration provided that these were below 5–7 mol%. Similarly, Davies and Swain (8) reported an anomalous dielectric absorption in one of their samples at 15% (wt.) which disappeared when solute concentration was reduced to 9%. These authors indicated that at concentrations less than 10% the solute was monomolecularly dispersed in the polystyrene matrix. Our results for each of the aromatic ketones was at a considerably lower concentration, approximately 3% (wt.). Further, it would be expected that group relaxation would be less sensitive to environment than molecular relaxation.

Conclusions

Altogether, the relaxation time and enthalpy data favour group relaxation in acetophenone, 1,4-diacetylbenzene, 4-acetylbiphenyl, and 2-acetylfluorene. Further, molecular relaxation appears to have been observed in the latter two of these completely separated from the group process.

It is interesting to compare our energy barrier

values for group relaxation in acetophenone in the polystyrene matrix with values from other procedures. A good correspondence is obtained with the estimated nmr value (5) of $\Delta G_E = 26$ kJ mol^{-1} for acetophenone in liquid solution. Our data yield $\Delta G_E = 26$ kJ mol^{-1} at 140 K, which is within the range of coalescence temperatures reported by Klinck *et al.* (13). It may be worth recollecting that the energy barrier for the intramolecular process of cyclohexyl chloride in the polystyrene matrix agreed precisely with the nmr value obtained from a study in the liquid state. The agreement with the *ab initio* calculated value of 18.4 kJ mol^{-1} is perhaps all that one can expect bearing in mind the difference in phase, the assumptions in such calculations, and the fact that they are not based on the rate theory as is the case in the Eyring treatment of both nmr and dielectric data.

Serious disagreement results between our value and that for (*a*) the one obtained from far-infrared data in the gas phase and, (*b*) the dielectric absorption of aromatic ketones in benzene solutions where in the latter case the values are about a factor of five less than our value.

It would seem that much further work is necessary in which the energy barriers are compared for group rotation in the different phases and by the different techniques. In particular, it would be interesting to compare more results from the direct techniques of dielectric absorption, ultrasonics, and nmr, and to examine further whether the energy barrier for group relaxation from dielectric absorption measurements by the matrix technique corresponds with that from nmr in the liquid phase. Certainly, significant differences have been noted for intramolecular energy barriers as determined on gases and pure liquids from far-infrared data for substituted benzaldehydes (1). It is difficult to understand why the barrier for acetyl group relaxation in benzene solution should be ~ 5 kJ mol^{-1} as determined from dielectric studies in the microwave region while the corresponding value in the matrix work is ~ 30 kJ mol^{-1}. Yet it is apparent that the matrix value is very similar to that estimated from the nmr approach in which toluene is used as the solvent. Very likely far more systems will have to be examined before an appreciation of the factors responsible is gained.

If accurate energy barrier values can be established, then these ought to be of considerable interest in relating their magnitude to conjugative, inductive, and steric effects in small aromatic molecules.

Acknowledgements

We are grateful to the National Research Council of Canada for support and to Mr. B. K. Morgan for invaluable technical help.

1. F. A. MILLER, W. G. FATELEY, and R. E. WITKOWSKI. Spectrochim. Acta, **23**A, 891 (1967).
2. W. J. HEHRE, L. RADOM, and J. A. POPLE. J. Am. Chem. Soc. **94**, 1496 (1972).
3. F. K. FONG and C. P. SMYTH. J. Am. Chem. Soc. **85**, 548 (1963).
4. F. K. FONG and C. P. SMYTH. J. Am. Chem. Soc. **85**, 1565 (1963).
5. T. B. GRINDLEY, A. R. KATRITZKY, and R. D. TOPSOM. Tetrahedron Lett. **26**, 2643 (1972).
6. J. CROSSLEY, S. P. TAY, and S. WALKER. Adv. Mol. Relax. Processes, **6**, 79 (1974).
7. S. P. TAY and S. WALKER. J. Chem. Phys. **64**, 1634 (1975).
8. M. DAVIES and J. SWAIN. Trans. Faraday Soc. **67**, 1637 (1971).
9. J. HEIJBOER. Koll. Z. **171**, 7 (1960).
10. B. OSTLE. Statistics in research. 2nd ed. Iowa State University Press, Ames, Iowa. 1963.
11. M. DAVIES and A. EDWARDS. Trans. Faraday Soc. **63**, 2163 (1967).
12. T. I. BORISOVA and V. N. CHIRKOV. Russ. J. Phys. Chem. **47**, 949 (1973).
13. R. E. KLINCK, D. H. MARR, and J. B. STOTHERS. Chem. Commun. 409 (1967).

Reactions of ozonides. XII. Ozonolysis of methylenecyclohexane

DUNDAPPA R. KERUR AND DENNIS G. M. DIAPER

Department of Chemistry, Royal Military College of Canada, Kingston, Ont., Canada K7L 2W3

Received June 22, 1976

DUNDAPPA R. KERUR and DENNIS G. M. DIAPER. Can. J. Chem. **55**, 588 (1977).

Ozonization of methylenecyclohexane in various solvents gives several peroxides and the ozonide in competing reactions. All products can be adequately explained by adaptation of the Criegee theory, without invoking a Baeyer–Villiger reaction of carbonyl solvents. Solvent effect on product proportions is not linked with dielectric constant or enol content, but appears to be a zwitterion solvation effect.

DUNDAPPA R. KERUR et DENNIS G. M. DIAPER. Can. J. Chem. **55**, 588 (1977).

L'ozonation du méthylènecyclohexane dans divers solvants conduit, par réactions concurrentes, a son ozonide ainsi qu'à plusieurs peroxydes. L'ensemble des produits peut être expliqué dans le cadre d'une modification de la théorie de Criegee, excluant l'intervention de solvants carbonyles par une réaction de Baeyer–Villiger. Cet effet est relié ni à la constante dieléctrique ni au contenu en énol du solvant, mais semble intervenir par une solvation des zwitterions.

The course of the ozonolysis of alkylidenecyclohexanes is modified by the use of very large proportions of certain carbonyl compounds as solvents (1–3). This observation led to a drastically modified general theory of ozonolysis mechanisms now largely discarded (4–7) following detailed re-investigations which showed that the products of carbonyl-modified ozonolysis were explicable by mechanism theories hitherto found adequate. There remain some unanswered questions about the observations on carbonyl-modified ozonolysis which led us to re-investigate the methylenecyclohexane reaction in detail. First it has been assumed that diminution of ozonide yields in carbonyl solvents has been due to chemical reaction of the carbonyl group. We now find that the partial suppression of ozonide formation with concomitant increase of peroxide products is not specifically a property of carbonyl solvents, but is a phenomenon shared by non-carbonyl solvents, which may even be more effective. Second, it has been assumed, but not proved, that 6-hexanolide is a secondary product from peroxides; we have now identified the peroxides and in some cases ascertained the yields.

Ozonation of methylenecyclohexane **1** in a number of solvents, carbonyl and non-carbonyl, has been found to give the products of Scheme 1 in agreement with previous reports (1–3) but we have encountered other products as well. We have also attempted to correlate the ability of a solvent to partially suppress ozonide **2** formation with its physical or chemical nature.

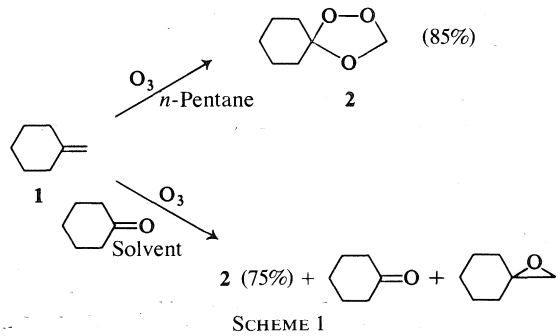

SCHEME 1

Experimental

The reference substances 1-hydroperoxy-1′-hydroxydicyclohexyl peroxide **3**, dicyclohexylidene diperoxide **4**, and bis(hydroxymethyl) peroxide **8** were prepared by standard procedures (8). Thin-layer chromatography was done on pre-coated silica gel on plastic (Merck) using butyl acetate solvent. For ozonides and hydroxyperoxides a 3% KI in 50% acetic acid visualizing spray was used and for the diperoxide **4**, concentrated sulphuric acid at 100 °C. R_f values were: **2**, 0.65; **3**, 0.74; **4**, 0.96; polymers, stationary. For nmr spectra, CCl_4 was used as solvent in all cases except the residue after reaction in pentane which was examined undiluted; residues from acetone, dichlorotetrafluoroacetone, and diisopropyl ketone experiments which were examined both undiluted and in CCl_4; the residue after ozonolysis in hexamethylacetone, was examined in CCl_4 and $(CMe_3)_2CO$ solvents. The nmr spectrum of bis(hydroxymethyl) peroxide **8** was obtained in D_2O with DSS marker. Infrared spectra of all liquid products were obtained from smears on NaCl plates and solids as KBr discs.

Methylenecyclohexane (Baker or Chemicals Procurement) in 0.2 *M* solution in the designated solvent (Table 1) was ozonized using an ozone–oxygen stream until absorption ceased. The residue after solvent removal was examined by thin layer chromatography, nmr and ir

spectroscopy, qualitative tests, and comparison with authentic samples. Wherever possible, crystalline products were recovered.

Thermal decomposition of 1-hydroxy-1′-hydroperoxydicyclohexyl peroxide **8** in boiling toluene gave after solvent removal cyclohexanone (25%), hexanoic acid (8%), adipic acid (4%), and dodecanedioic acid (trace). There was also an unidentified acidic brown gummy substance. This reaction will be discussed further (9).

Results

Product analyses are tabulated in Table 1.

Residues from methylenecyclohexane ozonized in most halogenated solvents showed the characteristic (10–12) ir ozonide absorption at 9.4–9.6 μm and nmr peaks at δ 5.08 ppm. Release of oxygen from lead tetraacetate in acetic acid indicated (13) hydroperoxide or oligomeric hydroperoxide (a weak result after ozonolysis in diisopropyl ketone). The presence of ketone peroxides was further demonstrated by a positive test with aqueous ferrous sulphate and ammonium thiocyanate (14). Infrared absorption at 2.9 (hydroxy) and 5.8–5.9 μm (carbonyl) was observed.

Even at slow flow rates, considerable entrainment losses of olefin and products were sustained in 1,4-dioxane which could not be cooled below its freezing point, 10 °C. Attempts to trap the mist were only partly successful. Small sample size in this solvent as in hexamethylacetone increased the seriousness of this product loss.

The nmr spectrum of the residue after ozonolysis in hexachloroacetone had no ozonide peak, but a multiplet at δ 1.62–1.80 ppm, three peaks in the 2.08–2.41 ppm region, four peaks between 3.45 and 4.20 ppm, a broad absorption centred at 5.20 ppm, and a singlet at 8.17 ppm. Extensive decomposition associated with production of hydrochloric acid from the solvent was suspected.

In trifluoroacetone, although no ozonide was produced, traces of adipic acid and cyclohexanone were detected as well as 18.5% of dicyclohexylidene peroxide **4** and 10% of bis(hydroxymethyl) peroxide **8**, mp 61–63 °C (dec.) (lit. (8) mp 62.5 °C). The latter, encountered now for the first time in methylenecyclohexane ozonolyses, was identified with an authentic sample (nmr δ 4.81 and 5.23 ppm, Na 2,2-dimethyl-2-silapentane-5-sulphonate marker). Decomposition products from authentic **8** and this sample were identical. Both **3** and **8** and oligomeric peroxides related to **8** were detected qualitatively but were not isolated in several experiments.

TABLE 1. Products from methylenecyclohexane ozonized in various solvents

Solvent	Temperature (°C)	Ozonide yield (%)	Hydroxy hydroperoxide, **3** (%)	Diperoxide, **4** (%)	Adipic acid, **5** (%)	Dodecane dioic acid, **6**	Cyclohexanone, **7**	Comments
n-Pentane	−78	89						*
Tetrahydrofuran	−45	74	11				Present	
1,4-Dioxane	10	37		2			Present	†
Cyclohexanone	−15	71		5	4		Present	
Acetone	−78	86		5	0.5		Present	
Pinacolone	−45	80			2	Present	Present	
Diisopropyl ketone	−78	77					Present	
Hexamethylacetone	−30	52					Present	
1,1,1-Trifluoroacetone	−78	0		18.5			Present	‡
Dichlorotetrafluoroacetone	−78	Trace					Present	
Hexachloroacetone	0	0			3		Present	

*The only other product detected was a white, partially gummy material, mp 51–56 °C.
†Major losses of olefin and products by entrainment as smoke.
‡A 10% yield of $HOCH_2—O—O—CH_2OH$ (8).

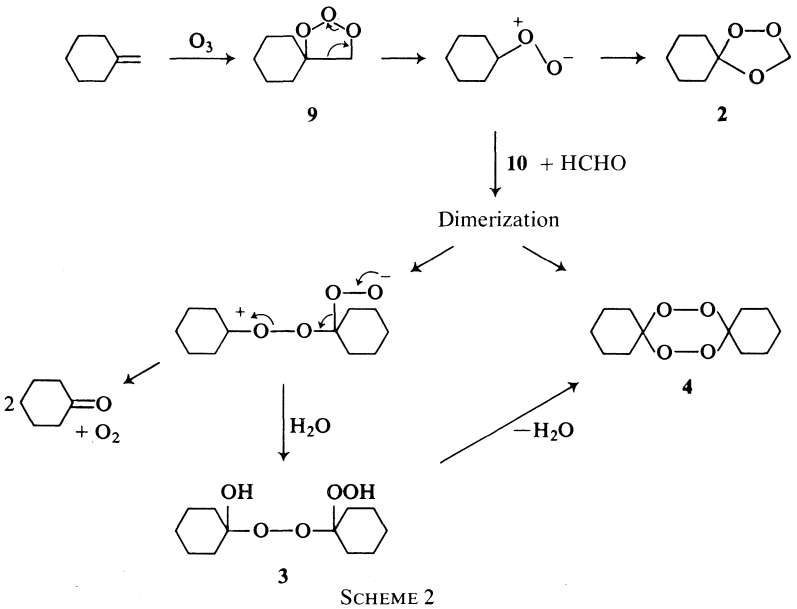

SCHEME 2

Discussion

It is remarkable that ozonide formation from alkenes is partly suppressed by carbonyl compounds but especially remarkable when that particular carbonyl compound used as solvent is one of the end products of the ozonolysis of that particular alkene and is one of the intermediates in accepted theories of the mechanism of the reaction. It is true that the initial alkene–ozone adduct here preferentially breaks up in the direction of Scheme 2 rather than Scheme 3 (15, 16), but identification of **8** shows that production of cyclohexanone is not negligible. If it is assumed that the ozonide **2** is formed solely from **10** and formaldehyde or from **11** and cyclohexanone, and that the solvent does not intervene in these or competing reactions, then ozonide yield should depend on the kinetics of these two reactions and competing zwitterion reactions. Increase of cyclohexanone concentrations should therefore increase ozonide yield, yet the result is opposite. More intermediate gives less product.

It is well known that participating solvents diminish ozonide yields in two ways at least: alcohols and acids by trapping the zwitterion giving alkoxy- or acyloxyhydroperoxides, and bases, such as pyridine, by catalysis of ozonide decomposition in a regenerative reaction. Neither appears to apply here; rather it is suggested that the role of the solvent is a complex balance of intermediate solvation effects. The most abundant polar intermediate zwitterion **10**, would seem to be the most important factor here, especially as it is the source of the relatively abundant side products **3** and **4** as well as polymers.

Story and co-workers (1–3) invoked Baeyer–Villiger oxidation of a ketone solvent as another possible mechanism for diminution of ozonide yield: we have used ^{14}C to demonstrate that cyclohexanone can function this way in ethylidenecyclohexane ozonolysis in no more than 0.02% yield (6). There is no clear relation between effectiveness of suppression of ozonide formation and dielectric constant of solvents of Table 1. The dioxane, $(Cl_3C)_2CO$, and CH_3COCH_3 results clearly show this.

Cyclohexanone and pinacolone were the ketones for which the effect was first reported, but they are in fact relatively feeble suppressants of ozonide formation. Both have a significant enol content; diisopropyl ketone, with less enol, falls between the two in suppression efficiency. Tetrahydrofuran and 1,4-dioxane, having neither enol nor ketone groups, are more powerful than either of the first two ketone solvents. The effect is not, therefore, an enol effect analogous to alcohol–zwitterion interaction. The products are completely explicable with Criegee zwitterions, provided that it is assumed that the kinetics of competing zwitterion reactions are affected by solvation. Zwitterions consumed by

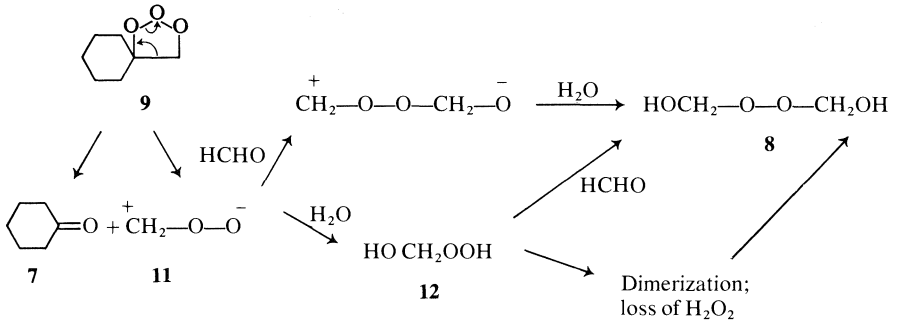

SCHEME 3

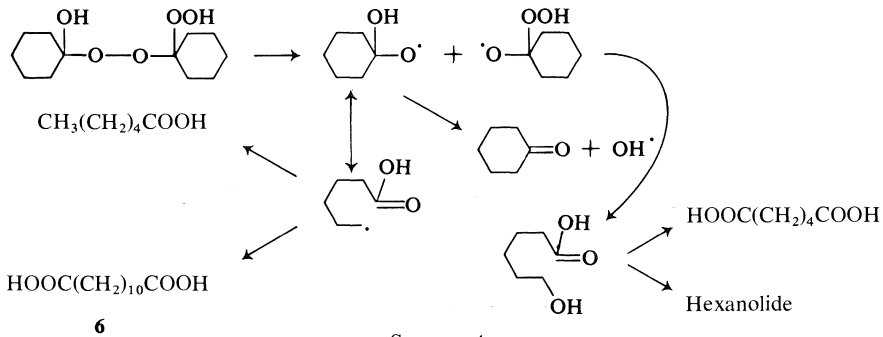

SCHEME 4

peroxide production are unavailable for production of ozonide **2**. Solvation probably extends zwitterion half-life, enhancing dimerization possibilities.

The experiment with hexamethylacetone, which cannot enolize, was inconclusive. The other non-enolizable ketones employed were fluoro and/or chloro ketones. They were strong ozonide suppressants as was the enolizable CF_3COCH_3. In all cases the products were explicable through the Criegee zwitterions of Scheme 2 and Scheme 3. Cyclohexanone as a product of bimolecular loss of oxygen from zwitterions is readily explained (17). Both directions of cleavage of the primary ozonide **9** are represented in the observed products: **8** comes from **11** in several possible ways. Traces of water necessary in Schemes 2 and 3 could come from concurrent elimination reactions or from atmospheric moisture during work-up. In another solvent system, methylenecyclohexane primary ozonide cleaved (15) to give **10** rather than **11** (96.8% and 3.2%); in trifluoroacetone 90% seems to be an upper limit because 10% of **8** was isolated.

Adipic acid **5** is attributable to the decomposition of hydroxyhydroperoxide **3** which was difficult to isolate from the reaction products because of its instability. Although it was isolated from only one solvent system, qualitative tests showed it present in most, if not all, experiments. An authentic sample of **3**, heated in toluene, gave **5**, cyclohexanone, and dodecane-1,12-dioic acid **6** but not **4**. The three products detected were also formed from **3** by dry pyrolysis (18) and under acid conditions (19). In the latter case, an ionic mechanism has been invoked, but here a radical process (18, 20) is considered more likely (Scheme 4). Peroxide by-products, frequently major products, always accompany ozonides (16, 21, 22). 6-Hexanolide from alkylidenecyclohexane ozonolysis is explicable (6) as a secondary decomposition product of peroxides. No Baeyer–Villiger reaction occurred in an acetylated cyclopentene ozonolysis (23). Ozonolysis of methylenecyclohexane in the solvents presently used gave no evidence of cross ozonide formation. This is probably due in part to low concentrations of zwitterion **11** as well as the use of ketones rather than aldehydes (except the formaldehyde from primary ozonide break-up).

Ozonide **2** yield is only one part of a jig-saw puzzle of concurrent reactions in these systems; it can come from the two zwitterions **10** and **11**

which can each form a range of other condensation and decomposition products. In the solvents used, kinetics determining product ratios are not only the kinetics of zwitterion reactions, but the kinetics of solvated species. The highly polar halogenated ketones, for example, may be expected to be more efficient solvating agents than cyclohexanone for zwitterions. Zwitterion solvation, rather than enol, dielectric, or Baeyer–Villiger participation of solvent, must be the key to results hitherto described as 'carbonyl-modified' ozonolysis.

Acknowledgment

Financial support of Defence Research Board of Canada under DRB Grant No. 9530-17 is gratefully acknowledged.

1. P. R. STORY, J. A. ALFORD, J. R. BURGESS, and W. C. RAY. J. Am. Chem. Soc. **93**, 3042 (1971).
2. P. R. STORY, J. A. ALFORD, W. C. RAY, and J. R. BURGESS. J. Am. Chem. Soc. **93**, 3044 (1971).
3. P. R. STORY, E. A. WHITED, and J. A. ALFORD. J. Am. Chem. Soc. **94**, 2143 (1972).
4. K. R. KOPECKY, P. A. LOCKWOOD, J. E. FILBY, and R. W. REID. Can. J. Chem. **51**, 468 (1973).
5. P. S. BAILEY, J. P. CARTER, JR., C. M. FISCHER, and J. A. THOMPSON. Can. J. Chem. **51**, 1278 (1973).
6. D. R. KERUR and D. G. M. DIAPER. Can. J. Chem. **51**, 3110 (1973).
7. P. R. STORY, R. W. MURRAY, and R. D. YOUSSEFYEH. J. Am. Chem. Soc. **88**, 3144 (1966).
8. M. S. KHARASCH and G. SOSNOVSKY. J. Org. Chem. **23**, 1322 (1958).
9. D. G. M. DIAPER and D. R. KERUR. To be published.
10. R. CRIEGEE, A. KERCHOW, and H. ZINKE. Chem. Ber. **88**, 1878 (1955).
11. E. BRINER and E. DALLWIGK. Helv. Chim. Acta, **39**, 1446 (1956).
12. E. BRINER and E. DALLWIGK. C. R. Acad. Sci. Paris, **243**, 630 (1956).
13. R. CRIEGEE. Fortschr. Chem. Forsch. **1**, 536 (1950).
14. R. ROBINSON and L. H. SMITH. J. Chem. Soc. 371 (1937).
15. S. FLISZAR and J. RENARD. Can. J. Chem. **48**, 3002 (1970).
16. D. G. M. DIAPER. Oxid. Combust. Rev. **6**, 145 (1973).
17. S. FLISZAR and J. B. CHYLINSKA. Can. J. Chem. **46**, 783 (1968).
18. W. COOPER. J. Chem. Soc. 1340 (1951).
19. M. S. KHARASCH and J. G. BURT. J. Org. Chem. **15**, 150 (1951).
20. P. GEORGE and A. D. WALSH. Trans. Faraday Soc. **42**, 94 (1946).
21. F. L. GREENWOOD and H. RUBINSTEIN. J. Org. Chem. **32**, 3369 (1967).
22. O. S. PRIVETT. Prog. Chem. Fats Other Lipids, **9**, 91 (1966).
23. R. CRIEGEE, A. BANCIU, and H. KEUL. Chem. Ber. **108**, 1642 (1975).

Studies on the condensation of lignins in alkaline media. Part II.[1] The formation of stilbene and arylcoumaran structures through neighbouring group participation reactions[2]

JOSEF GIERER AND INGEGERD PETTERSSON

Swedish Forest Products Research Laboratory, Chemistry Department, Box 5604, S-114 86 Stockholm, Sweden

Received September 28, 1976

JOSEF GIERER and INGEGERD PETTERSSON. Can. J. Chem. **55**, 593 (1977).

The alkaline condensation of *p*-hydroxyarylglycerol-β-aryl ether units in lignin with other phenolic structures and the subsequent reactions of the condensation products have been elucidated using appropriate model compounds. It is shown that the primary condensation of simple phenols (2,6-xylenol or resorcinol) into the α-position of phenolic compounds of the β-aryl ether type is followed by an aryl participation (A_1-3) reaction resulting in the cleavage of the β-aryl ether bond and formation of the corresponding stilbene derivative. When resorcinol is used as reaction partner, the condensation is also followed by the cleavage of the β-aryl ether linkage through another type of neighbouring group participation reaction involving the phenolate anion *ortho* to the site of condensation and giving rise to the corresponding arylcoumaran derivative.

The consequences of these findings for the course of alkaline delignification processes are briefly discussed.

JOSEF GIERER et INGEGERD PETTERSSON. Can. J. Chem. **55**, 593 (1977).

On a élucidé, utilisant des composés modèles appropriés, le mécanisme de la condensation alcaline d'unités d'éther *p*-hydroxyarylglycérol β-aryle de la lignine avec d'autres structures phénoliques et les réactions subséquentes des produits de condensation. On a montré que la condensation primaire de phénols simples (xylénol-2,6 ou résorcinol) en position α des composés phénoliques du type éther β-aryle est suivie par une réaction de participation du groupe aryle (A_1-3) qui conduit au bris du lien éther β-aryle et à la formation du dérivé stilbène correspondant. Quand on utilise le resorcinol comme partenaire de la réaction, la condensation est aussi suivie par une coupure du lien éther β-aryle par un autre type de réaction de participation de groupe voisin impliquant l'anion phénolate *ortho* par rapport au site de condensation et donnant lieu au dérivé arylcoumarane correspondant.

On discute des conséquences de ces résultats pour les processus de délignification alcaline.

[Traduit par le journal]

Numerous studies on the alkaline condensation of lignins have shown that the benzylic position in phenolic units constitutes the main site of reaction in this complex process (1–6). In most of these studies, model compounds of the *p*-hydroxybenzyl alcohol type were reacted with simple phenols and the resulting diarylmethanes were isolated. The condensation reaction was formulated as a nucleophilic addition of an *ortho*- or *para*-cyclohexadienone carbanion to the appropriate *para*-quinonemethide, followed by proton or side-chain elimination with rearomatization (7).

Results from studies using model compounds of the *p*-hydroxyaryl coumaran (8) and β-arylglycerol (9) types indicated that this conjugate addition reaction is not prevented by the presence of an aryl or an aroxy group in the adjacent β-position (*cf.* also condensations in acidic media (10)). Thus, carbanions formed from phenolic lignin structures compete, in fact, with the other nucleophiles present in the pulping liquor (SH^-, OH^- ions) for the various quinonemethide intermediates (7).

In the present work, the condensation between phenolic compounds of the β-aryl ether type and added phenols is investigated and the behaviour of the condensation products towards alkali under pulping conditions is studied.

Results and Discussion

The compounds and conditions used and the results obtained are summarized in Table 1.

[1]Part I, see ref. 18.

[2]The results of this work have been presented (by J.G.) at the Fifth Plenary Meeting of the International Academy of Wood Science, Copenhagen, Denmark, June 17–19, 1976, and at the 1976 Canadian Wood Chemistry Symposium at Mont Gabriel, Que., Canada, September 1–3, 1976.

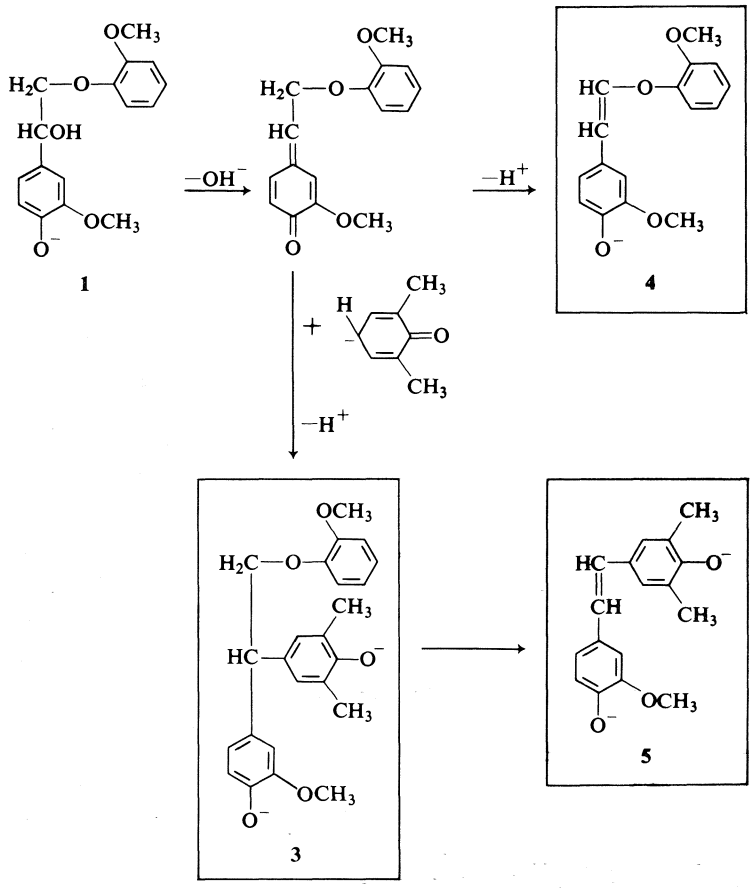

SCHEME 1

When compound **1** (Scheme 1) was reacted with 2,6-xylenol in 1 *N* sodium hydroxide at 150 °C for 1.5 h, an extensive condensation took place and the expected product **3** could be isolated in 60% yield. In a competing reaction, a proton is abstracted from the quinonemethide intermediate and the β-guaiacoxy styrene derivative **4** is formed (11). In a separate experiment it was shown that compound **4**, similarly treated with 2,6-xylenol, also gives compound **3** although in a lower yield (37%). Part of the compound **3** obtained from **1** could thus have been formed via compound **4** (*cf.* below however).

Among the remaining reaction products, the 4,4′-dihydroxystilbene **5** is of particular interest. The formation of this compound, in a small amount, is suggested to proceed via the product of condensation **3** and to involve elimination of the β-aroxy substituent through an aryl participation (A_1-3) reaction (Scheme 2). Hence, the elimination is brought about by an intramolecular nucleophilic attack of a carbanion **3***a* on the β-carbon atom resulting in the formation of a spiro cyclohexadienone intermediate. Rearrangement of this intermediate with participation of the aryloxide ion results in the opening of the three-membered ring and subsequent proton elimination yields the 4,4′-dihydroxystilbene derivative **5**.

The formation and the opening of the three-membered ring are reminiscent of the corresponding reaction steps in other eliminations of β-aroxy substituents involving neighbouring group participation such as the cleavage of β-aryl ether linkages by neighbouring mercaptide groups (12). The function of a spiro cyclohexadienone as a transient intermediate has been previously (13) proposed in order to interpret a related reaction, *i.e.* the alkaline solvolysis of 2-*p*-hydroxyphenylethyl bromide. Shortly after,

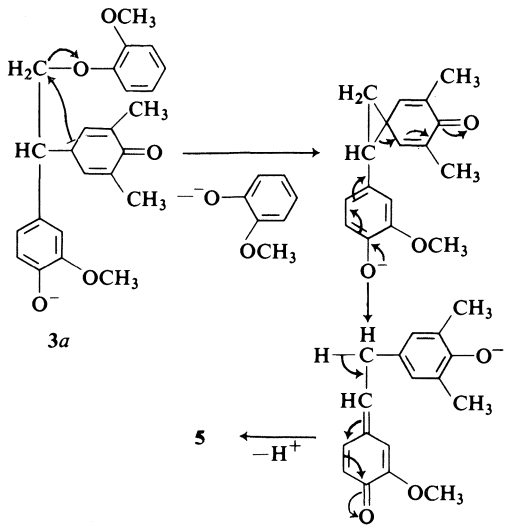

SCHEME 2

this intermediate was isolated and its behaviour under different reductive and solvolytic conditions was studied (14).

The intermediacy of the condensation product **3** in the formation of stilbene **5** was shown by treating compound **3** with 1 *N* sodium hydroxide at 170 °C for 2 h and isolating compound **5** and guaiacol in high yields (61 and 74%, respectively). Apparently, the aryl participation reaction requires a higher temperature (about 170 °C) than does the preceding condensation step.

It can be expected that the condensation of a phenol to compound **1** and the subsequent elimination of the β-guaiacoxy substituent through aryl participation will be enhanced by the presence of one or two additional phenolic hydroxyl groups in the *meta*-position(s) (resorcinol, phloroglucinol, and their derivatives). In these instances, all phenolic hydroxyl groups should contribute to the ease of formation of reactive carbanions in the *ortho*- and *para*-positions, thus facilitating both the condensation and the subsequent elimination step. In fact, treatment of compound **1** with resorcinol in 1 *N* sodium hydroxide at 150 °C for 1.5 h (Scheme 3) gave an almost quantitative yield (98%) of guaiacol, indicating an extensive condensation and elimination reaction. The reaction mixture contained, in addition to guaiacol and small amounts of unreacted resorcinol and stilbene **6** (2%), the expected stilbene **7** (11%), the bis-stilbene **8** (5%), and the arylcoumaran **9** (10.5%).

TABLE 1. Treatment of phenolic β-aryl ethers with 2,6-xylenol and resorcinol in alkaline media

Compounds (mg, mmol)	Conditions: 1 *N* NaOH (ml)	Temp. (°C)	Reaction time (h)	Yields (mg)*: Before acetyl.	After acetyl.	After separation	Products isolated as acetates after separation by column chromatography† (mg, % of theoretical)	Starting compound(s) recovered as acetate(s) (mg, mmol)
1(870, 3.0) + Xyl(439, 3.6)	15.0	150	1.5	1340	1940	1590	G(91, 18.3), **3**(857, 60.5), **4**(150, 16.0), **5**(75, 7.1)	Xyl(209, 1.27)
3-diacetate (143, 0.3)	1.5	170	2.0	120	170	160	G(37, 74.3), **5**(65, 61.2)	**3**(30, 0.06)
4(157, 0.5) + Xyl(74, 0.6)	2.5	150	1.5	230	300	220	G(6, 0.04), **3**(89, 37.2)	**4**(49, 0.15) + Xyl(58, 0.35)
1(580, 2.0) + Res(220, 2.0)	10.0	150	1.5	880	1510	880	G(325, 98.1), **6**(16, 2.3), **7**(85, 11.1) **8**(29, 5.1), **9**(72, 10.5)	Res (30, 0.15)
2(480, 1.5) + Res(330, 3.0)	8.0	150	1.5	920	1210	910	G(128, 51.5), **6**(14, 2.6), **7**(125, 21.7), **10**(51, 8.2)	Res(153, 0.79)

*Most of the yields of the crude mixtures are too high due to the content of solvents which were difficult to remove completely.
†G = guaiacol, Xyl = 2,6-xylenol, Res = resorcinol.

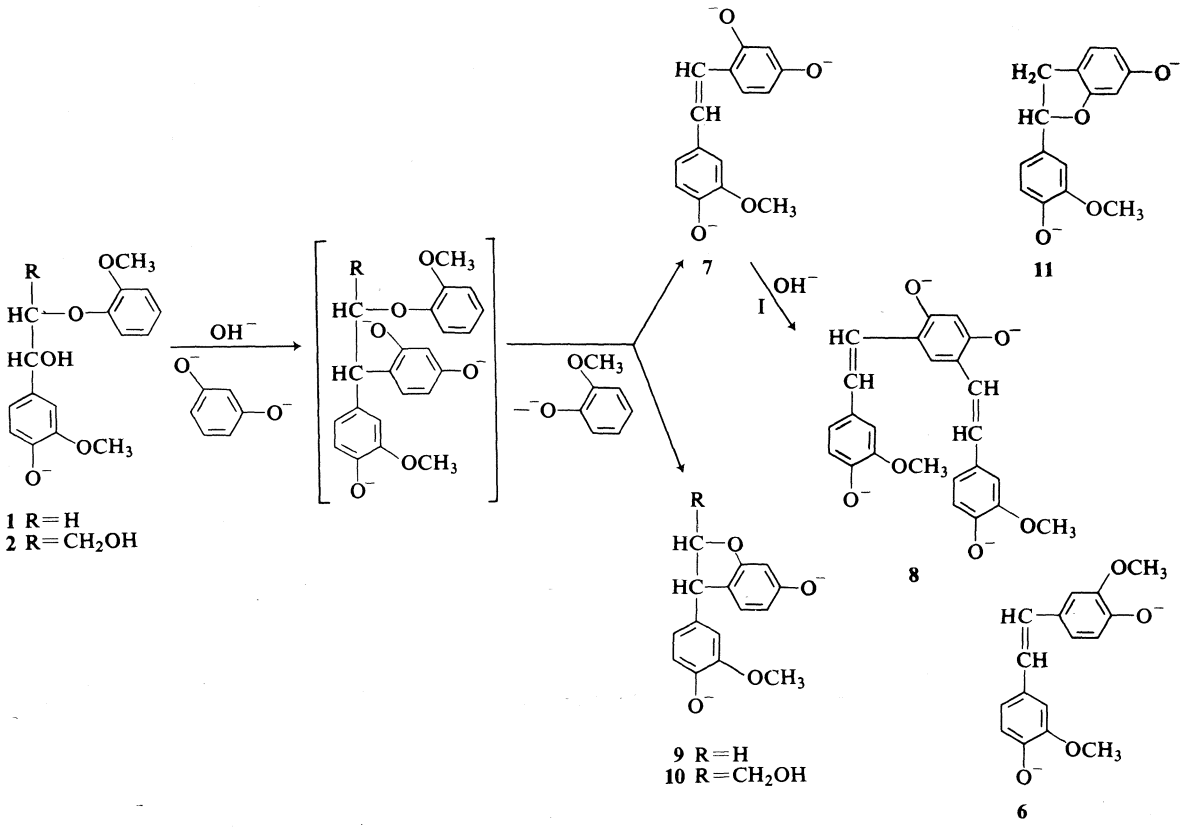

SCHEME 3

Undoubtedly, the formation of stilbene **7** follows a route analogous to that for stilbene **5** (Scheme 1). However, in the case of stilbene **7**, the precursor, *i.e.* the condensation product corresponding to compound **3** was not isolated. This is probably due to the high rate of the aryl participation reaction caused by the *ortho*- and *para*-hydroxyl groups of the resorcinol residue in the condensation product.

The high reactivity of resorcinol in this type of condensation with subsequent aryl ether cleavage through aryl participation is also reflected by the presence of the distilbene **8** in the reaction mixture. Obviously, this compound is formed by a repetition of the condensation and aryl participation reactions involving stilbene **7** and the starting compound **1** as reaction species.

Although the initial condensation product between resorcinol and compound **1** was not isolated, its intermediacy is revealed by the isolation of the 3-arylcoumaran **9**. It is obvious that this compound arises from the expected condensation product through another type of neighbouring group participation in which the *ortho*-phenolate ion nucleophilically attacks the β-carbon atom and eliminates the β-aroxy substituent. Thus, the formation of **9** competes with that of compound **7**, but both neighbouring group participation reactions result in the cleavage of the β-aryl ether linkage.

According to the nmr and mass spectroscopic data, the isolated coumaran could also be the 2-aryl-substituted isomer **11** which might be formed from stilbene **7** by a subsequent ring closure. However, this possibility was excluded by treating stilbene **7** with 1 *N* sodium hydroxide under the same conditions as were used for compound **1** and demonstrating the absence of the coumaran obtained from **1** in the resulting reaction mixture (thin-layer chromatography). This experiment also showed that a considerable part of the stilbene **7** was converted into other compounds unidentified so far. Conversely, a similar alkaline treatment of the isolated coumaran did not afford any detectable amount of the stilbene **7**. This result also supports the structure of a 3-

TABLE 2. Proton chemical shifts (τ values in ppm) of acetylated products from alkaline condensations of model compounds*

Acetate of compound	mp (°C)	Aromatic+ olefinic H	Aliphatic H	Methoxyl H	Acetyl H	Methyl H
3	132–134	2.88–3.22 (m, 9H)	5.45–5.64 (m, 3H)	6.25(s, 3H) 6.29(s, 3H)	7.73(s, 3H) 7.76(s, 3H)	7.90(s, 6H)
Cis-**4** (18)	102–103	2.42(d, 1H) 2.80–3.25 (m, 7H) 3.46(d, 1H) 4.48(d, 1H) $J = 7.0$		6.18(s, 6H)	7.72(s, 3H)	
5	155–156	2.84–3.12 (m, 7H)		6.17(s, 3H)	7.71(s, 3H) 7.74(s, 3H)	7.86(s, 6H)
6	227–229	2.87–3.17 (m, 8H)		6.17(s, 6H)	7.73(s, 6H)	
7	129–130	2.40(d, 1H) 2.88–3.13 (m, 7H)		6.16(s, 3H)	7.53–7.80 (os 9H)	
Dihydro-**7**	75–76	2.90–3.50 (m, 6H)	7.21(s, 4H)	6.28(s, 3H)	7.60–7.81 (os, 9H)	
8	191–193	2.16–2.51 (m, 2H) 2.82–3.10 (m, 10H)		6.15(s, 6H)	7.52–7.80 (os, 12H)	
9	143–145	2.90–3.70 (m, 6H)	4.98–5.70 (m, 3H)	6.26(s, 3H)	7.73–7.75(os, 9H)	
10	150–151	2.80–3.51 (m, 6H)	4.65–5.20 (m, 1H) 5.20–6.20 (m, 3H)	6.29(s, 3H)	7.75(s, 6H) 8.02(s, 3H)	

*s = singlet, d = doublet, m = multiplet, os = overlapping singlets.

arylcoumaran **9** since the 2-aryl isomer **11** on treatment with alkali would be expected to give an equilibrium mixture consisting of **7** and the starting compound.

Stilbene **6** is formed by a pathway analogous to the formation of **7** (and **8**), the eliminated guaiacol acting as condensation partner in competition with resorcinol.

The total yield of stilbenes **6–8** together with the arylcoumaran **9** is only about 30%. In view of the large amount of guaiacol obtained (98%), the low yields of the other reaction products may be ascribed to partial alkaline degradation of the stilbenes (see above) and/or to losses during the work-up and separation procedures (Table 1), rather than to incomplete conversion of the starting compound **1**.

The behaviour of compound **2** upon treatment with resorcinol in 1 *N* sodium hydroxide under similar conditions is analogous to that of compound **1**. Guaiacol was obtained in a large amount (51.5%) and the stilbenes **6** and **7** were isolated in 2.6 and 21.7% yields, respectively. Furthermore, the reaction mixture contained the arylcoumaran **10** (8.2%), corresponding to **9** obtained from **1**. The presence of **10** and the absence of **9** in the reaction mixture from **2** show that the initial condensation step involves the quinonemethide derived from **2**, rather than the β-guaiacoxystyrene derivative **4**. In other words, formaldehyde elimination most likely takes place after, rather than before, the condensation and aryl participation steps in the formation of **6**, **7**, and **8** (*cf.* also proton elimination from the quinonemethide in Scheme 2). The absence of **4** in the reaction mixtures obtained from the treatments of **1** or **2** with resorcinol further supports this view. Apparently, conjugate addition of the carbanion from resorcinol to the quinonemethide from **1** more effectively competes with proton

elimination than does the conjugate addition of the carbanion from 2,6-xylenol (Scheme 1). The formation of **4** during the treatment of compound **1** with 2,6-xylenol (see Scheme 1) should thus be considered as a side reaction rather than a step in the formation of stilbene **5**. Eliminated guaiacol and formaldehyde, together with the excess of resorcinol, may undergo alkaline condensation reactions yielding high molecular weight materials of the phenoplast type. Such condensations could be responsible for the lower yield of guaiacol obtained from compound **2** as compared to that obtained from **1**.

Conclusions

The results of the present work illustrate the behaviour of phenolic lignin units of the β-aryl ether type towards other phenolic structures upon heating in alkaline solution. The primary condensation, which gives the diarylmethane type of structures, is followed by the cleavage of the β-aryl ether bond through neighbouring group participation involving an aromatic nucleus (aryl participation) or, if present, a phenolate anion in the *ortho*-position to the condensation site. These reactions lead to the formation of stilbene and/or arylcoumaran types of structures. Thus, the increase in molecular size of lignin brought about by the initial condensation step involving phenolic β-aryl ether units may be counterbalanced by the subsequent fragmentation due to β-aryl ether cleavage through neighbouring group participation.

The stilbene structures found in alkali-treated lignins (15) may thus originate not only from native structures in which the carbon skeleton is preformed (aryl coumaran and 1,2-diarylpropane 1,3-diol structures) (15) (Scheme 3) but also from β-aryl ether structures which undergo condensation and subsequent aryl participation reactions.

The possible genesis of stilbene structures by this route has been recently[3] confirmed by heating wood powder (*picea abies*) with 2,6-xylenol in alkaline solution at 170 °C, demonstrating the presence of stilbene **5** as dominant component in the reaction mixture.

These findings suggest the advisability of conducting the alkaline delignification in the presence of a suitable (added) phenol. The latter, by condensing with reactive α-positions, should not only inhibit the self-condensation of lignin (16) but also facilitate its fragmentation through the neighbouring group participation reactions demonstrated in this work.

Experiments to explore this possibility are being currently carried out.

[3]J. Gierer and O. Lindeberg, unpublished results.

Experimental

Materials

The compounds used in this study were prepared as previously described: **1** (11) and **2** (17). Compound **4** was obtained as a sodium salt after treatment of **1** with 2 *N* sodium hydroxide (11).

TABLE 3. Mass spectral fragmentation of acetylated products from alkaline condensations of model compounds (all fragments having $m/e > 120$ and intensities > 10% of the base peak are listed)

Acetate of compound	M (m/e)	$M - n42$* (n = 1, 2, or 3)	Misc.
3	478(11)		355(7)† 313(80)‡ 299(20) 271(100)§ 257(45) 137(20) 122(25)
cis-**4** (18)	314(14)	272(100)	243(21) 211(78) 165(39) 149(15) 137(43)
5	354(16)	312(27) 270(100)	
6	356(10)	314(15) 272(100)	
7	384(10)	342(30) 300(40) 258(100)	
Dihydro-**7**	386(3)	344(25) 302(5) 260(3)	137(100)‖ 123(35)
8	574(10)	532(30) 490(50) 448(60) 406(100)	203(10) 151(10)
9	342(10)	300(30) 258(100)	241(15) 227(10)
10	414(15)	372(50) 330(30)	312(10) 270(100) 255(20) 147(20)

*m/e 42 corresponds to CH_2CO arising from aromatic acetyl groups.
†$M - 123$.
‡$M - 123 - 42$.
§$M - 123 - (2 \times 42)$.
‖Benzyl cation.

Methods

The treatments with 1 *N* sodium hydroxide were carried out in an atmosphere of nitrogen to avoid autoxidation reactions. The other reaction conditions (amount of model compound and alkali, temperature, and length of treatment) were chosen to simulate the conditions prevailing during alkaline pulping or, if necessary, to facilitate the isolation of the reaction products. These conditions and the results of the alkaline condensations are summarized in Table 1.

Work-up Procedure

After the alkaline treatment, the reaction mixture was neutralized by adding dry ice and extracted repeatedly with ethyl acetate. The combined extracts were evaporated under reduced pressure. The residue was acetylated with acetic anhydride – pyridine and the resulting mixture of acetylated reaction products was separated by column chromatography. The separation was followed by thin-layer chromatography.

Thin-layer (tlc) and Column Chromatography

The acetylated compounds were separated on an analytical scale by tlc using silica gel HF_{254} (E. Merck A. G. Darmstadt) as adsorbant and mixtures of petroleum ether – ethyl acetate in proportions between 2:1 to 4:1 as solvent systems. The spots were developed by spraying with a 1% solution of vanillin in concentrated sulphuric acid and heating at 120 °C for about 10 min. The preparative separations were carried out by column chromatography using silica gel 60 (120–230 mesh, ASTM, Merck) as adsorbant and the same mixtures of petroleum ether – ethyl acetate as those used in tlc.

The isolated compounds were identified by nmr and mass spectroscopic methods. Compound **7** was also characterized as the (acetylated) dihydro derivative.

Nuclear Magnetic Resonance Spectrometry

The nmr spectra ($CDCl_3$) were recorded with a Perkin–Elmer R-12 spectrometer. The nmr data are summarized in Table 2 which also contains the melting points of the isolated (acetylated) reaction products. Chemical shifts (τ values/ are given in ppm downfield from TMS.

Mass Spectrometry

Mass spectra were recorded on a Perkin–Elmer 270 instrument at 20 eV using the direct inlet system. Mass spectral data are summarized in Table 3.

1. A. ISHIZU, J. NAKANO, H. OYA, and N. MIGITA. J. Jpn. Wood Res. Soc. **4**, 176 (1958).
2. J. GIERER, S. SÖDERBERG, and S. THORÉN. Sven. Papperstidn. **66**, 990 (1963).
3. K. KRATZL, J. ZAUNER, and P. CLAUS. Holzforschung, **18**, 47 (1964).
4. J. M. HARKIN. Adv. Chem. Ser. **59**, 65 (1966).
5. K. KRATZL, I. WAGNER, and O. ETTINGSHAUSEN. Holzforsch. Holzverwert. **24**, 32 (1972).
6. K. KRATZL and I. WAGNER. Holzforsch. Holzverwert. **24**, 56 (1972).
7. J. GIERER. Svensk Papperstidn. **73**, 571 (1970).
8. J. GIERER, I. PETTERSSON, and L. Å. SMEDMAN. Acta Chem. Scand. **26**, 3366 (1972).
9. B. JOHANSSON and G. E. MIKSCHE. Acta Chem. Scand. **23**, 924 (1969).
10. H. NIMZ. Holzforschung, **18**, 47 (1964).
11. J. GIERER and I. NORÉN. Acta Chem. Scand. **16**, 1713 (1962).
12. J. GIERER and L. Å. SMEDMAN. Acta Chem. Scand. **19**, 1103 (1965).
13. S. WINSTEIN and R. BAIRD. J. Am. Chem. Soc. **79**, 756 (1957).
14. R. BAIRD and S. WINSTEIN. J. Am. Chem. Soc. **79**, 4238 (1957).
15. S. I. FALKEHAG, J. MARTON, and E. ADLER. Adv. Chem. Ser. **59**, 75 (1966).
16. M. YA. ZARUBIN and V. I. RYABYKH. Izv. Vissh. Uchebn. Zaved. Lesn. Zh. **9**, 116 (1966); Chem. Abstr. **66**, 11986 (1967).
17. K. KRATZL, W. KISSER, J. GRATZL, and H. SILBERNAGEL. Monatsh. Chem. **90**, 771 (1959).
18. J. GIERER, F. IMSGARD, and I. PETTERSSON. J. Appl. Polym. Sci. Appl. Polym. Symp. **28**, 1195 (1976).

The structure of isoflavipucine[1]

JOHN A. FINDLAY, JIRI KREPINSKY, AND ANITA SHUM
Chemistry Department, University of New Brunswick, Fredericton, N.B., Canada E3B 5A3

C. G. CASINOVI
Department of Biological Chemistry, Istituto Superiore di Sanita, Rome, Italy

AND

L. RADICS
NMR Laboratory, Central Research Institute for Chemistry, H-1525 Budapest, Hungary

Received August 9, 1976

JOHN A. FINDLAY, JIRI KREPINSKY, ANITA SHUM, C. G. CASINOVI, and L. RADICS. Can. J. Chem. **55**, 600 (1977).

The structure of isoflavipucine **2***a*, a remarkable rearrangement product of the antibiotic flavipucine **1**, is proposed on the basis of spectral data and chemical and mechanistic considerations.

JOHN A. FINDLAY, JIRI KREPINSKY, ANITA SHUM, C. G. CASINOVI et L. RADICS. Can. J. Chem. **55**, 600 (1977).

En se basant sur des données spectrales et sur des considérations chimiques et mécanistiques on propose la structure **2***a* pour l'isoflavipucine, un produit remarquable de réarrangement de l'antibiotique flavipucine **1**.

[Traduit par le journal]

Recently we reported (1) the structure **1** for flavipucine $C_{12}H_{15}NO_4$, an optically active metabolite of *Aspergillus flavipes* possessing antibiotic activity (2). In the course of isolating this substance, the co-occurrence of an isomeric compound in the culture filtrates was noted. Isoflavipucine (mp 166–171 °C) is apparently optically inactive, $[\alpha]_D^{21}$ 0° (*c* 1% 95% EtOH), and its nmr spectrum (see Table 1) is remarkably similar to that of flavipucine apart from the displacement of the signal at δ 3.80 for the C7-H to much lower field (δ 6.04) in the isomeric compound. The ultraviolet spectrum of isoflavipucine (λ_{max} (EtOH) 221 (ε 26 090), 307 (ε 10 260) nm) is substantially different from that of flavipucine indicating the presence of a new chromophore.

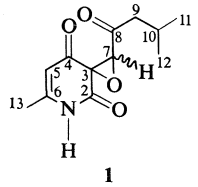

1

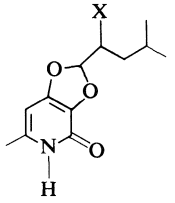

2*a* X = O=
2*b* X = O—H

We propose the structure **2***a* for isoflavipucine on the basis of spectral and chemical data. Nuclear magnetic resonance parameters (see Tables 1 and 2) and nuclear magnetic double resonance experiments are in excellent agreement with this structure. The infrared (KBr) spectrum displays a strong carbonyl absorption at 1670 cm^{-1} (conjugated amide) accompanied by a ketone band at 1730 cm^{-1} and bands assigned to conjugation at 1630 and 1610 cm^{-1}. The mass spectrum is practically indistinguishable from that of flavipucine and confirms the elemental composition while the base peak *m/e* 152 ($M - (CH_3)_2CHCH_2CO$) affirms the presence of the isobutyl ketone moiety. Microanalysis is in agreement with the elemental composition $C_{12}H_{15}NO_4$.

A useful confirmation of the isoflavipucine structure can be derived from a comparison of the ^{13}C nmr spectra of **1** and **2***a* (see Table 3). One notable difference is that isoflavipucine contains an additional sp^2 carbon (δ 143.5 ppm) at the expense of an sp^3 carbon (δ 60.0 ppm) present in flavipucine. Also, the signal at δ 68.8 ppm for C7 in flavipucine **1** is found at δ 107.6 ppm in isoflavipucine **2***a* consistent with the C7 change from mono- to dioxygen substitution. Thus the major difference between **1** and **2***a* concerning C3 and C7 is corroborated in

[1]Presented in part at the 9th International Symposium on the Chemistry of Natural Products, Ottawa, Canada (June 1974).

TABLE 1. Chemical shift data (δ_{TMS} ppm)

	5H	7H	8H	$9H_a$	$9H_b$	10H	11H	12H	13H	NH/OH	Solvent/temperature
2*a*	5.98	6.04	—	2.57*	2.57*	2.22*	0.96*	0.96*	2.39	13.3	$CDCl_3$/26 °C
2*b*	5.83	5.93	3.76*	1.26*	1.40*	1.81*	0.82	0.93	2.21	11.7/4.9	$CDCl_3$–DMSO-d_6/60 °C

*For these parameters iterative calculations were performed using the LAOCN3 program of Bothner-By and Castellano (5). Long range couplings were assumed to be zero and the spectra were approximated by the simplified spin systems indicated in Table 2. An IBM 7040 Computer was employed for these calculations and the estimated accuracy is of the order of 0.1 Hz.

detail. Of interest in comparing the signal assignments is compound **4**, a synthetic material, which we have prepared recently.

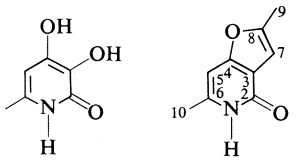

3 **4**

Chemical corroboration of the structural assignment **2***a* comes from the ready acid hydrolysis of isoflavipucine to give 3,4-dihydroxy-6-methyl-2-pyridone **3**. This structure was confirmed by independent synthesis by the method of Lapworth and Collie (3) who converted 2,4-dihydroxy-6-methyl pyridine to the 3-nitro derivative which was reduced to 3-amino-3,4-dihydroxy-6-picoline. Treatment of the latter amino dihydroxypicoline with Na_2CO_3 gave **3**. Attempts to prepare **3** by the procedure of Hess (4) were singularly unsuccessful. We formulate **3** as a pyridone rather than a trihydroxypicoline (3) since its infrared spectrum shows bands for a conjugated amide (1650, 1610 cm^{-1}).

Reduction of the ketone in **2***a* was readily achieved by hydrogenation in glacial acetic acid with Adams' catalyst. Dihydroisoflavipucine **2***b* (mp 204–206 °C) was obtained and shows spectral characteristics consistent with its formulation. Thus, while a strong amide carbonyl band at 1670 cm^{-1} is present in the infrared (KBr) spectrum, the absence of any ketone absorption near 1730 cm^{-1} is noted. In addition, the mass spectrum displays the appropriate molecular ion at *m/e* 239 as well as prominent ions at 196 ($M - (CH_3)_2CH$) and 152 ($M - (CH_3)_2CHCH_2CHOH$) and the ultraviolet spectrum (*vide infra*) resembles that of isoflavipucine.

We have now succeeded in transforming flavipucine (mp 130–131 °C) into isoflavipucine in 30% yield by heating the crystalline solid at 138–140 °C for 15 min. Heating **1** in boiling xylene (139 °C) did not effect any transformation and this suggests an ionic rather than a radical mechanism for the interconversion **1** to **2***a*. In addition, traces of isoflavipucine can be found in the reaction mixture resulting when flavipucine is treated with cold aqueous Na_2CO_3 solution (2%).

Scheme 1 contains mechanistic proposals to account for the transformation **1** to **2***a*. In pathway '*a*' the tautomer **5** is visualized as undergoing a rearrangement via a transition state involving a four-membered ring and requiring an external proton transfer agent (*e.g.*, another molecule of **1**). Route '*b*' proposes the initial generation of a five-membered lactol ring **6** which then undergoes rearrangement via the resonance stabilized zwitterion **7** to isoflavipucine **2***a*. Both pathways require the external assistance of proton transfer agents and are consistent with the finding that the pyrolytic conversion does not occur in boiling anhydrous xylene (139 °C) but occurs readily with molten flavipucine at the same temperature. Pathway '*b*' readily accommodates the observation that isoflavipucine is optically inactive; however, route '*a*' cannot be excluded on this basis alone since racemization of **2***a* after its formation is also feasible. The pathway '*b*' is favoured by us since it would ap-

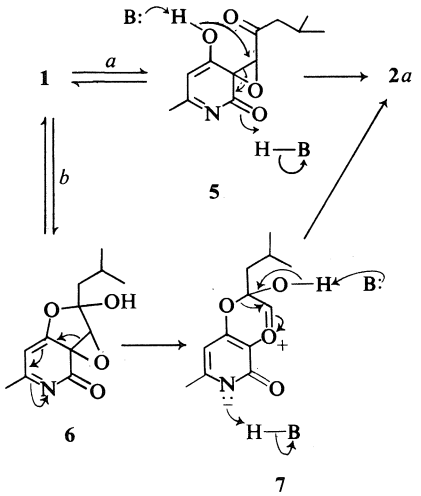

SCHEME 1

TABLE 2. Coupling constants (Hz)

	$J_{5,13}$	$J_{7,8}$	$J_{8,9A}$	$J_{8,9B}$	$J_{9A,9B}$	$J_{9A,10}$	$J_{9B,10}$	$J_{10,11}$	$J_{10,12}$	Spin system
2*a*	0.8	—	—	—	—	6.7*	6.7*	6.7*	6.7*	ABMXY
2*b*	0.8	3.8*	8.6*	5.0*	−13.5*	4.8*	9.0*	6.7*	6.7	ABMXY

*For these parameters iterative calculations were performed using the LAOCN3 program of Bothner-By and Castellano (5). Long range couplings were assumed to be zero and the spectra were approximated by the simplified spin systems indicated in Table 2. An IBM 7040 Computer was employed for these calculations and the estimated accuracy is of the order of 0.1 Hz.

TABLE 3. ^{13}C nmr chemical shift data (δ_{TMS} ppm)*

	C2	C3	C4	C5	C6	C7	C8	C9	C10	C11	C12	C13
2*a*	155.2	130.1	154.3	93.3	143.5	107.6	200.6	45.4	23.6	22.4	22.4	19.1
1	168.8	60.0	186.9	107.3	156.2	68.8	203.6	49.6	24.1	22.8	22.5	20.8
4	161.8†	114	161.3†	94.8	140.6	102.2	153.0	13.7	19.2	—	—	—

*Solvent = $CDCl_3$.
†Assignments may be interchanged. The assignments of ^{13}C resonances to the individual carbon atoms in the molecules are based on standard Fourier transform ^{13}C nmr techniques, selective ^{13}C–{^1H} decoupling experiments, spectral comparison, and known substituent effects.

pear to proceed via lower energy transition states than does route '*a*'. It, of course, requires a *cis* relationship of C4 and C8 with respect to the oxirane bridge.

Experimental

Melting points were determined on a Kofler hot stage apparatus and are uncorrected. Mass spectra were determined with a Consolidated Electrodynamics Corporation R6-1 instrument. A Varian HA-100 spectrometer was employed for recording nmr spectra. Ultraviolet spectra were obtained with a Perkin-Elmer Model 467 spectrophotometer and infrared spectra with a Perkin-Elmer Model 457 grating instrument. ^{13}C nmr spectra were obtained with a Varian XL-100-15 equipped with SL-124 Fourier transform accessory and 16K 620L computer.

Isolation of Isoflavipucine 2a

The crude chloroform extract of the acidified fermentation broth of strain F2091/7 of *Aspergillus flavipes* was chromatographed on silica gel. Initial benzene–ether (3:1) eluates yielded flavipucine (mp 130–131 °C) while later benzene ether fractions proved to be mixtures of flavipucine and isoflavipucine. Rechromatography of these fractions on silica gel columns or plates afforded pure isoflavipucine which was recrystallized from ether to give white crystals, mp 166–171 °C. *Anal.* calcd. for $C_{12}H_{15}NO_4$: C 60.75, H 6.37, N 5.90; found: C 60.41, H 6.39, N 5.75. The mass spectrum *m/e* 237 (M^+), 153, 152 (100%) (M − $(CH_3)_2CHCH_2CHO$), 126, 125, 96. The ir spectrum ν_{max} (KBr) 3440, 3110, 2960, 2870, 2800, 2750–2500, 1730, 1670 (broad v. strong), 1630, 1600, 1460, 1420, 1390, 1370, 1285, 1210, 1170, 1140, 1115, 1040, 990, 820, 740, 660, 640, 620 cm^{-1}. The uv spectrum λ_{max} (95% ethanol) 221 (ε 26 090), 307 (ε 10 260) nm. $[\alpha]_D^{21}$ 0° (*c* 1%, 95% ethanol).

Isoflavipucine 2a from Flavipucine 1

(a) By Pyrolysis

Flavipucine (200 mg) was heated in a stoppered round bottomed flask (above its melting point) at 138–140 °C for 15 min in an oil bath. Subsequent chromatography afforded isoflavipucine **2***a* (60 mg, 30% yield) identical in spectral characteristics and melting point (and mixture mp) with isoflavipucine isolated from acidified culture filtrates of *Aspergillus flavipes*.

(b) By Na_2CO_3 Treatment

Flavipucine (0.20 g) was dissolved in 2% aqueous Na_2CO_3 solution (250 ml) and the yellow solution was allowed to stand 15 min at room temperature before extraction with $CHCl_3$ which afforded after drying and evaporation an oil (0.15 g) which proved by preparative layer chromatography on silica gel to be a mixture of flavipucine and isoflavipucine (40:1). The identity of the isoflavipucine prepared in this way was confirmed by spectral data and mixture melting point with an authentic sample.

Dihydroisoflavipucine 2b

Flavipucine (0.50 g) in glacial acetic acid (20 ml) was hydrogenated over Adams' catalyst (0.10 g) for 22 h. Filtration and evaporation gave a crude product (0.49 g), essentially homogeneous on tlc, which was crystallized from ethanol yielding pure dihydroisoflavipucine (0.215 g), mp 204–206 °C. Mass spectrum *m/e* 239 (M^+), 196 (M − C_3H_7), 154, 153, 152 (100%), 141, 125, 124, 112, 109, 97, 96. The ir spectrum ν_{max} (KBr) 3300, 2960, 2900–2500, 1660 (broad, strong), 1615, 1595, 1560, 1480, 1450, 1425, 1390, 1380, 1368, 1340, 1330, 1310, 1295, 1260, 1212, 1170, 1140, 1120, 1110, 1090, 1080, 1040, 920, 858, 810, 780, 755, 740, 710, 660, 640, 590, 560, 510, 480 cm^{-1}. The uv spectrum (95% EtOH) λ_{max} 220 (ε 20 060), 308 (ε 6560) nm.

3,4-Dihydroxy-6-methyl-2-pyridone 3

(a) From Isoflavipucine

Isoflavipucine **2***a* (0.0542 g, 0.23 mmol) was added to a solution of 3.8% HCl in water–ethanol 1:1 (2 ml), and stirred at room temperature until completely dissolved. The solution was then heated at 80 °C for 14 h. The cooled aqueous solution was extracted with ether and then evaporated *in vacuo* at room temperature yielding

the white crystalline product **3** (0.0314 g, 96.5%), mp 212–226 °C. The mass spectrum *m/e* 141 (M^+). The ir spectrum ν_{max} (KBr) 3400–2300 cm^{-1} broad (NH, OH), 1650, 1600 (conjugated amide). The uv spectrum λ_{max} (H_2O) 302 (ε 3740); ($H_2O + H^+$) 300 (ε 3660); ($H_2O + OH^-$) 335 (ε 3280) nm. The nmr spectrum δ_{TMS} (D_2O), 2.3 (s, 3H, CH_3), 6.38 (s, 1H, aromatic CH).

(b) By Synthesis

3,4-Dihydroxy-6-methyl-2-pyridone prepared by the method of Lapworth and Collie (3) was identical with compound **3** obtained by hydrolysis of isoflavipucine as above.

Acknowledgments

The authors are grateful to the Italian Ministry of Health and the National Research Council of Canada for financial support. Thanks are also due to Professor G. Grandolini (University of Perugia) and Dr. F. W. Wehrli (Varian AG) for assistance in early phases of this work. Thanks are also due to D. G. Smith (Atlantic Regional Laboratory, Halifax, Nova Scotia) for providing the ^{13}C nmr spectrum, together with useful comments, for compound **4**.

1. (*a*) J. A. FINDLAY and L. RADICS. J. Chem. Soc. Perkin Trans. I, 2071 (1972); (*b*) J. A. FINDLAY and D. KWAN. J. Chem. Soc. Perkin Trans. I, 2963 (1972).
2. (*a*) C. G. CASINOVI, G. GRANDOLINI, R. MERCANTINI, N. ODDO, R. OLIVIERI, and A. TONOLO. Tetrahedron Lett. 3175 (1968); (*b*) C. G. CASINOVI, G. GRANDOLINI, R. MERCANTINI, N. ODDO, R. OLIVIERI, and A. TONOLO. Ann. Ist. Super. Sanita (Rome), **5**, 514 (1969).
3. A. LAPWORTH and J. N. COLLIE. J. Chem. Soc. **71**, 838 (1897).
4. A. HESS. Chem. Ber. **32**, 1985 (1899).
5. D. F. DETAR (*Editor*). Computer programs for chemistry. Benjamin. 1968. p. 10.

The stereochemical dependence of ^{13}C nuclear magnetic resonance chemical shifts and ^{13}C–^{31}P couplings in some dialkylphosphonocyclohexanes

GERALD W. BUCHANAN AND JOHN H. BOWEN[1]

Department of Chemistry, Carleton University, Ottawa, Ont., Canada K1S 5B6

Received September 14, 1976

GERALD W. BUCHANAN and JOHN H. BOWEN. Can. J. Chem. **55**, 604 (1977).

^{13}C chemical shifts and ^{13}C–^{31}P couplings are reported for 15 dialkylphosphonocyclohexanes. Data are compared to those for three related hydroxyphosphonates. Both direct and vicinal ^{13}C–^{31}P couplings are useful stereochemical probes. Materials with equatorial phosphorus exhibit one bond couplings larger by *ca.* 5 Hz than their axial counterparts. Vicinal couplings follow an approximate dihedral angle dependence but are attenuated by OH substitution. In addition to the expected *gauche*-γ shielding effects, pentavalent phosphorus substituents induce minor (*ca.* 1 ppm) upfield shifts at carbons to which they bear an *anti*-periplanar relation.

GERALD W. BUCHANAN et JOHN H. BOWEN. Can. J. Chem. **55**, 604 (1977).

On rapporte les déplacements chimiques du ^{13}C et les constantes de couplage ^{13}C–^{31}P de 15 dialkylphosphonocyclohexanes. On compare ces données avec celles de trois hydroxyphosphonates voisins. Les couplages directs et vicinaux ^{13}C–^{31}P sont tous les deux des sondes stéréochimiques utiles. Les composés avec un phosphore en position équatoriale présentent des couplages à travers une liaison qui sont plus grands par environ 5 Hz que leurs contreparties axiales. Il existe une dépendance approximative entre les couplages vicinaux et l'angle dièdre; ces couplages sont toutefois atténués par l'introduction d'un OH. En plus des effets de blindage γ *gauche* attendus, les phosphores pentavalents induisent au niveau des carbones par rapport auxquels ils ont une relation *anti*-périplanaire, des déplacements chimiques mineurs (environ 1 ppm) vers les hauts champs.

[Traduit par le journal]

Introduction

It has been a decade since the first report (1) of the utility of ^{13}C nmr as a technique for the stereochemical analysis of cyclohexyl compounds and the method is now well established (2, 3). An area of recent interest has been in the application of ^{13}C nmr to conformational effects among cyclohexyl phosphorus compounds containing tri- and tetravalent phosphorus atoms (4). Herein we report our findings for a series of substituted dimethyl-, diethyl-, and diisopropylphosphonocyclohexanes in which the influence of axial and equatorial pentavalent phosphorus atoms on the carbon shifts and ^{13}C–^{31}P couplings has been examined.

Results are compared with earlier data for *cis*- and *trans*-4-*tert*-butyl-1-hydroxy-1-dimethylphosphonocyclohexanes (5) to clarify the effects of OH substitution on the nmr parameters. Employing the isomeric 4-*tert*-butyl cyclohexyl compounds as models as well as the known influence of methyl stereochemistry on carbon shifts (6), the preferred geometries of some previously unknown 2-methyldialkylphosphonocyclohexanes have been deduced.

[1]Present address: Department of Biochemistry, Queen's University, Kingston, Ont., Canada K7L 3N6.

Results and Discussion

(a) Spectral Assignments

Routinely the ^{13}C spectra were recorded using complete ^{1}H noise decoupling. Subsequently the single frequency off-resonance decoupling procedure was employed to identify CH_3, CH_2, CH, and quaternary carbons. Selective ^{1}H decoupling was used occasionally as were lanthanide shift reagent studies (0.1 *M* equivalent $Pr(FOD)_3$) to distinguish between small chemical shift differences and ^{13}C–^{31}P coupling phenomena (7). Assignments were also facilitated by the knowledge of ^{13}C–^{31}P couplings found earlier (5) in related molecules of known geometry.

(b) Chemical Shifts

The ^{13}C shieldings for compounds **1**–**18** are presented in Table 1, with the corresponding structures and numbering scheme shown in Fig. 1. Comparing the epimeric 4-*tert*-butylcyclohexyl systems **1** and **2** the most notable differences appear at C-1 and C-3,5 which are

TABLE 1. ^{13}C chemical shifts for **1–18** (δ_C from TMS ± 0.1)[a]

	Position											
Compound	1	2	3	4	5	6	7	8	CH_3(ax)	CH_3(eq)	O—$\overset{*}{C}$	O—C—$\overset{*}{C}$
1	31.0	25.8	23.4	47.7	23.4	25.8	32.6	27.5			52.2	
2	35.4	26.3	26.5	47.5	26.5	26.3	32.5	27.4			52.6	
3	35.5	26.0	26.3	26.0	26.3	26.0					52.5	
4	72.3	32.4	23.5	46.8	23.5	32.4	32.3	27.6			53.4	
5	71.1	32.1	20.8	47.5	20.8	32.1	32.5	27.5			53.3	
6	71.6	31.7	20.1	25.4	20.1	31.7					53.5	
7	31.4	25.8	23.4	47.9	23.4	25.8	32.6	27.5			61.2	16.6
8	35.8	26.6	26.4	47.5	26.4	26.6	32.5	27.5			61.4	16.5
9	35.9	26.0	26.3	25.9	26.3	26.0					61.4	16.6
10	32.2	25.9	23.3	47.9	23.3	25.9	32.7	27.5			69.5	24.3
11	36.5	26.5	26.6	47.6	26.6	26.5	32.5	27.4			69.7	24.1
12	36.6	26.2	26.3	26.2	26.3	26.2					69.5	24.1
13	41.9	32.7	36.2	26.0	26.0	25.7				21.8	52.4	
											52.5	
14	39.1	28.4	33.3	20.6	26.2	21.3			15.1		52.3	
											52.4	
15	42.3	32.9	36.6	25.8	26.7	25.9				22.0	61.1	16.6
											61.2	16.7
16	39.5	28.2	33.6	20.6	26.3	21.2			15.0		61.2	16.6
											61.3	16.7
17	43.2	33.0	36.3	26.0	26.7	25.9				22.0	69.5	24.1
											69.6	24.2
18	40.2	28.2	33.7	20.4	26.5	20.9			14.8		69.5	24.1
											69.6	24.2

[a]0.2–0.3 *M* solutions in $CDCl_3$.

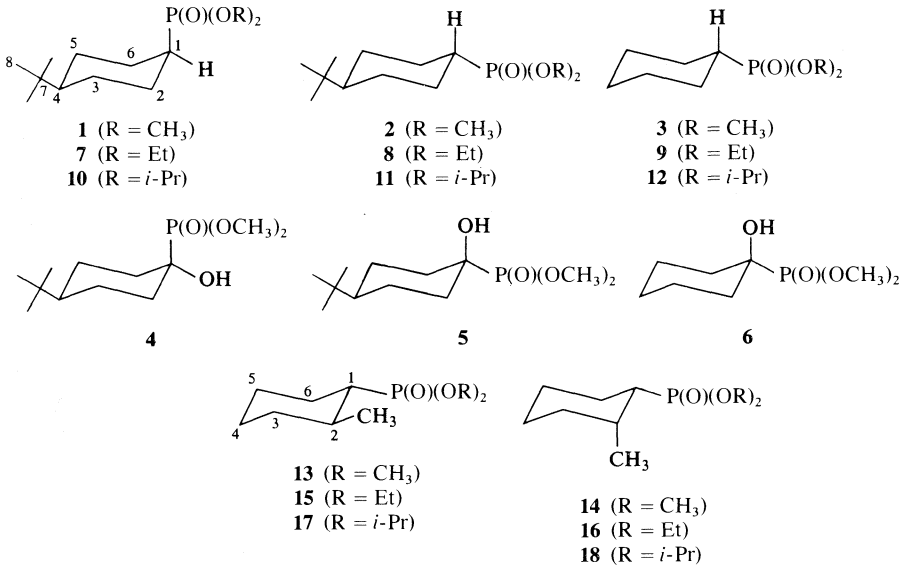

FIG. 1. Structures and numbering schemes for phosphonates.

shielded by 4.4 and 3.1 ppm, respectively, in the axial isomer **1**. The observation of increased shielding for the carbon bearing the axial substituent has ample precedent (1–3) but is not always predictable (8). The upfield shift at C-3,5 of **1** exemplifies the well known '*gauche*-γ' shielding effect (2, 3). Although it is clear that these γ shifts do not correlate with the steric bulk of the axial group (8) it is interesting to note that the *gauche* γ-effect for the pentavalent $-P(O)(OCH_3)_2$ function (3.1 ppm), is nearly identical to that for the trivalent $-P(OCH_3)_2$ moiety (4).

Comparison of the C-3,5 shifts for the *trans*-isomer **2** with C-2,6 of *tert*-butylcyclohexane (δ 27.7 for a 0.3 *M* solution in $CDCl_3$) indicates the presence of a 1.2 ppm shielding effect on these resonances due to the *anti*-periplanar phosphorus substituent on C-1. Germane to this observation are the recent results of Eliel *et al.* (9) who have pointed out the operation of shielding effects at γ carbons induced by second row elements held rigidly in *trans*-coplanar orientations. For third row elements such as S or Cl, however, Eliel *et al.* found no evidence of this *trans*-γ shielding effect and suggested that none would be expected for other third row elements. Thus our findings cast doubt on the model proposed by Eliel and indicate the N, O, and F do not, as was suggested (9), play a "unique role" in the *trans*-γ shift. It is interesting to note that for a series of trivalent phosphorus substituents both shielding and deshielding *trans*-γ shifts have been obtained (4).

Compound **3**, which lacks the 4-*tert*-butyl substituent, exhibits C-1 and C-3,5 chemical shifts nearly identical to **2** which suggests a strong preference for an equatorial disposition of the dimethylphosphono group. In the limiting low temperature spectrum of **3** (−120 °C in CD_2Cl_2) we have not detected any resonances characteristic of the axially substituted conformer. Given the high preference for equatorial $-P(O)(OCH_3)_2$ in **3**, it is interesting to compare the C-3,5 shift for **3** (δ 26.3) with cyclohexane itself (δ 27.2 for a 0.3 *M* solution in $CDCl_3$). Again the existence of a minor (*ca.* 1 ppm) upfield *trans*-γ effect is operative for the carbons to which the pentavalent phosphorus bears an *anti*-periplanar relationship.

For the series of *cis*-4-*tert*-butylcyclohexyl isomers **1**, **7**, and **10** and the *trans*-isomers **2**, **8**, and **11**, it is evident that further branching in the O-alkyl chain of the phosphono group has only minor perturbing effects on the carbon shifts. Comparing **1**, **7**, and **10**, there is a minor deshielding (*ca.* 1 ppm) effect at C-1 as the $(OR)_2$ group changes from R = CH_3 to R = Et and R = isopropyl. Similarly in the *trans*-isomers **2**, **8**, and **11** and in the simple cyclohexyl compounds **3**, **9**, and **12** C-1 becomes deshielded as the degree of O-alkylation increases. In each case, the additional substitution is at a position

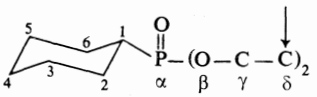

which bears a 'δ' relationship to C-1. The magnitudes of these 'δ' effects are reminiscent of those noted for linear and branched alkanes (10). Other ring carbon resonances are nearly identical in the above isomeric series. The trends for the shifts of the O-alkyl carbons are consistent with the well documented influences of alkyl substitution (2, 10).

In the context of the earlier discussion *re trans*-γ effects it is useful to compare the C-3,5 shifts for **1** and **4** shown below. Clearly the *anti*-periplanar OH in **4** has no effect on the ^{13}C shieldings of the *trans*-γ carbons. It appears therefore that even for second row elements the *trans*-γ shielding effect (9) is not completely

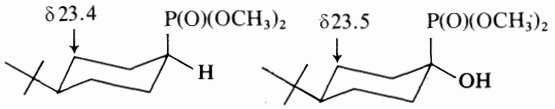

1 **4**

general. Recently some examples of marked *deshielding trans*-γ effects (up to 4 ppm) have been noted (11) in arrangements such as that depicted below, where both the α and the β carbons are quaternary.

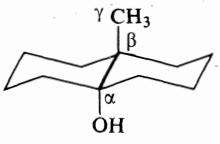

When group 4B substituents are present at the *anti*-periplanar positions (*i.e.* C, Si, Ge, and Sn) one also finds substantial downfield *trans*-γ shifts (12).

For the conformationally 'mobile' hydroxyphosphonate **6** the C-3,5 shifts are similar to those of **5**, again suggesting a high preference for the equatorial dialkylphosphono functions. It is notable, however, that the C-3,5 shift for **6** does not lie between the values for the 'model' compounds **4** and **5**.

With regard to the 2-methyl compounds **13**–**18**, resonance assignments were facilitated by the previous ^{13}C–^{31}P coupling results (5) and by the known effects of methyl stereochemistry on cyclohexyl carbon resonances (6, 13). In each case the large vicinal couplings to ^{31}P indicated that the dialkylphosphono group was equatorial. For **13**, the 2-CH_3 resonance is at δ 21.8 which is 6.7 ppm deshielded relative to the case where the 2-CH_3 is axial (compound **14**). This difference in methyl shieldings is comparable to that of other epimeric methyl substituted cyclohexanes (6, 13). Further support for the designation of an axial 2-CH_3 group in **14** comes from the *gauche*-γ shielding (*ca.* 5 ppm) found at C-4 and C-6 of **14** relative to **13**. There appears to be no measurable *trans*-γ effect of the equatorial CH_3 in **13** as evidenced by the close correspondence in the C-4 and C-6 shifts for **13** and **3**. At C-1 and C-3 of **13** to **18** there are appreciable shift differences between isomers. In all instances, compounds having the axial CH_3 exhibit *ca.* 3 ppm upfield β-effects at these centres. These constitute further examples of the coexistence of shielding β and *gauche*-γ effects although the β effects are normally smaller in magnitude (2).

In **13**–**18** the O—$\overset{*}{C}$ and O—C—$\overset{*}{C}$ positions become diastereotopic (14) and therefore minor (*ca.* 0.1 ppm) shift differences are observed.

(c) Coupling Constants

(i) One Bond Couplings

The direct ^{13}C–^{31}P couplings are shown in Table 2, and from earlier work (15) the sign is assumed to be positive. Couplings for the hydroxy phosphonates **4**, **5**, and **6** are considerably larger than those for the related phosphonates **1**,

TABLE 2. One bond ^{13}C–^{31}P couplings (±0.2 Hz)[a]

Compound	J(Hz)
1	138.0
2	144.0
3	143.2
4	156.8
5	164.6
6	165.5
7	137.9
8	143.1
9	143.0
10	139.2
11	144.3
12	144.2
13	137.7
14	139.8
15	137.7
16	139.8
17	139.7
18	141.9

[a]Sign assumed to be positive (15).

2, and **3**. These findings are in accord with those of Gray (16) who reported an increase of *ca.* 20 Hz in the ^{13}C–^{31}P coupling in phosphonates in which a hydrogen bonded to the carbon of interest is replaced by a methoxyl group.

For **1–12** it is important to note the stereospecificity of the one bond ^{13}C–^{31}P J's. In the phosphonates the coupling between C-1 and an equatorial pentavalent phosphorus is 5–6 Hz larger than when the phosphorus is axial. For

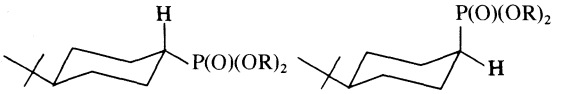

$^1J_{CP} \approx 144$ Hz $^1J_{CP} \approx 139$ Hz

the hydroxyphosphonates **4** and **5** the difference is larger (7.8 Hz). The present results parallel the values for $^1J_{CH}$ at the anomeric carbons of α- and β-D-glucose (169 and 160 Hz) respectively (17), although the mechanisms of ^{13}C–^{31}P and ^{13}C–H couplings are no doubt very different. For the pentavalent phosphine oxides depicted (18) the stereochemical trend in $^1J_{CP}$ is opposite to that in the phosphonates.

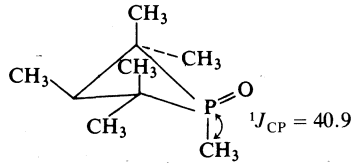

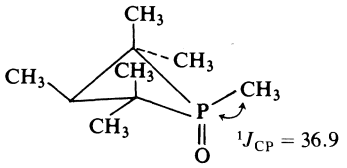

A further point of interest, although we can offer no rationale at present, is the difference in $^1J_{CP}$ for the isomeric pairs **13**,**14**, **15**,**16**, and **17**,**18**. In each case where the 2-CH_3 is axial the $^1J_{CP}$ value is larger by *ca.* 2 Hz than when the 2-CH_3 is equatorial.

(ii) Geminal Couplings

In Table 3 are presented the two bond ^{13}C–^{31}P couplings found for **1–18**. For the P–O–C J's, the range of 6.4–7.4 Hz is similar to that found in cyclic phosphates (19) and in acyclic phosphonates (16). Although absolute values only are depicted in Table 3, the sign is likely negative for these couplings by analogy with the findings for $(CH_3O)_2P(O)CH_3$ (15).

TABLE 3. Geminal ^{13}C–^{31}P couplings (±0.2 Hz)[a]

Compound	Path	$\|J\|$ (Hz)
1	$^{2,6}C$—^1C—P	3.0
	CH_3—O—P	7.0
2	$^{2,6}C$—^1C—P	2.8
	CH_3—O—P	6.8
3	$^{2,6}C$—^1C—P	2.9
	CH_3—O—P	6.8
4	$^{2,6}C$—^1C—P	1.5
	CH_3—O—P	7.4
5	$^{2,6}C$—^1C—P	3.1
	CH_3—O—P	7.4
6	$^{2,6}C$—^1C—P	2.8
	CH_3—O—P	7.4
7	$^{2,6}C$—^1C—P	2.6
	—CH_2—O—P	7.0
8	$^{2,6}C$—^1C—P	3.0
	—CH_2—O—P	6.4
9	$^{2,6}C$—^1C—P	3.1
	—CH_2—O—P	6.8
10	$^{2,6}C$—^1C—P	3.2
	CH—O—P	6.9
11	$^{2,6}C$—^1C—P	3.4
	>CH—O—P	7.0
12	$^{2,6}C$—^1C—P	3.1
	>CH—O—P	7.1
13	^2C—^1C—P	3.8
	^6C—^1C—P	3.4
14	^2C—^1C—P	3.1
	^6C—^1C—P	3.6
15	^2C—^1C—P	4.1
	^6C—^1C—P	3.6
16	^2C—^1C—P	3.1
	^6C—^1C—P	3.8
17	^2C—^1C—P	4.2
	^6C—^1C—P	3.8
18	^2C—^1C—P	3.3
	^6C—^1C—P	3.7

[a]For **13–18**, O—C carbons are diastereotopic and P—O—C J's undetermined due to spectral complexity.

With regard to the C–C–P couplings, again only absolute values are quoted since it has been noted (20) for trivalent phosphorus compounds at least, that the sign of these interactions can be positive or negative. The total range of J_{gem} values is small (1.5–4.2 Hz) and few clear trends are evident. It is notable that in the *cis*-dimethylphosphono compound **1**, J_{CCP} is 3.0 Hz whereas in the corresponding hydroxyphosphonate **4** J_{CCP} falls to 1.5 Hz. It is known for geminal

C–C–H couplings (21) that hydroxyl substituents can reduce the value of J_{gem}. In the case where the OH is axial, *i.e.* **5**, the OH group does not appreciably alter the coupling compared to **2**.

(iii) Vicinal Couplings

Data for the 3-bond couplings are collected in Table 4. For the *trans*-4-*tert*-butylcyclohexyl compounds **2**, **8**, and **11**, the couplings are nearly identical (*ca.* 16 Hz) and reflect a dihedral angle near 180° between P and C-3,5. The simple cyclohexyl systems **3**, **9**, and **12** show similar values again mirroring their high preference for equatorial phosphorus. It is instructive to recall that for the *exo*-2-norbornyl compound shown below the J_{CCCP} value is 18.4 Hz where θ again is near 180° (5). Thus these couplings tend to vary with the nature of the pathway even though the dihedral angles are essentially identical.

TABLE 4. Vicinal ^{13}C–^{31}P couplings (±0.2 Hz)

Compound	Path	J (Hz)[a]
1	^{3,5}C—C—C—P	N.R.[b]
2	^{3,5}C—C—C—P	16.2
3	^{3,5}C—C—C—P	16.2
4	^{3,5}C—C—C—P	N.R.
5	^{3,5}C—C—C—P	12.6
6	^{3,5}C—C—C—P	11.1
7	^{3,5}C—C—C—P	N.R.
	CH_3—C—O—P	6.0
8	^{3,5}C—C—C—P	16.1
	CH_3—C—O—P	5.7
9	^{3,5}C—C—C—P	16.2
	CH_3—C—O—P	5.6
10	^{3,5}C—C—C—P	N.R.
	CH_3—C—O—P	2.6
11	^{3,5}C—C—C—P	16.0
	CH_3—C—O—P	3.0
12	^{3,5}C—C—C—P	16.1
	CH_3—C—O—P	3.0
13	^{3}C—C—C—P	16.3
	^{5}C—C—C—P	14.9
	CH_3—C—C—P	1.3
14	^{3}C—C—C—P	15.0
	^{5}C—C—C—P	14.7
	CH_3—C—C—P	1.1
15	^{3}C—C—C—P	16.1
	^{5}C—C—C—F	15.8
	CH_3—C—C—P	1.1
16	^{3}C—C—C—P	14.9
	^{5}C—C—C—P	14.8
	CH_3—C—C—P	1.1
17	^{3}C—C—C—P	16.1
	^{5}C—C—C—P	15.6
	CH_3—C—C—P	1.2
18	^{3}C—C—C—P	15.7
	^{5}C—C—C—P	15.1
	CH_3—C—C—P	1.1

[a]Sign taken as positive (15).
[b]N.R. = non resolvable *i.e.* < 0.6 Hz.

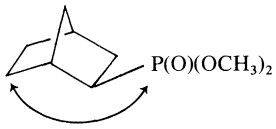

$^{3}J_{CCCP}$ = 18.4 Hz

When an OH is inserted at C-1 as in **5** and **6** the vicinal coupling is reduced by *ca.* 5 Hz. There have been similar phenomena noted for vicinal C–H couplings (21) and for vicinal H–H interactions (22, 23) although these influences tend to be maximal when the OH is *trans*-coplanar to a terminus of the coupling path.

For the 2-methyl compounds **13–18** the vicinal couplings of the equatorial phosphorus to positions 3 and 5 of the ring tend to be slightly less than in compounds where the 2 position is not substituted. It is plausible that *gauche*-interactions between the 2-CH_3 and the equatorial P cause minor ring deformations so that the θ values deviate from 180° and result in reduced J's.

When the dihedral angle between ^{31}P and a ring carbon is near 60° (compounds **1**, **4**, **7**, and **10**) no resolvable vicinal coupling is apparent. In the 2-methyl compounds, however, resolvable J's to the methyls are obtained but they are all rather small (*ca.* 1 Hz).

Combining the present findings with those noted earlier (5) it is evident that both direct and vicinal ^{13}C–^{31}P couplings are useful stereochemical probes in pentavalent phosphorus compounds. Care must be taken however in the strict application of a Karplus type relationship for J_{CCCP}. The influence of OH groups on vicinal couplings parallels results for ^{13}C–H and H–H interactions although a sufficient number of model compounds with a wide range of dihedral angles is still lacking.

Experimental

Spectra

^{13}C spectra were measured employing a Varian XL-100-12 nmr spectrometer, equipped with a Nicolet

TABLE 5. Properties of new materials

Compound	*m/e* (M^+)	n_D^{25}	Analysis (%) Calculated C	H	P	Found C	H	P
1	248	1.4598	58.05	10.15	12.47	57.99	10.20	12.39
2	248	1.4570	58.05	10.15	12.47	58.03	10.22	12.46
10	304	1.4580	63.13	10.93	10.18	63.25	10.88	10.25
11	304	1.4566	63.13	10.93	10.18	63.05	10.98	10.30
13	206	1.4560	52.42	9.28	15.02	52.25	9.40	15.10
14	206	1.4590	52.42	9.28	15.02	52.30	9.42	15.01
15	234	1.4525	56.40	9.89	13.22	56.41	9.72	13.19
16	234	1.4548	56.40	9.89	13.22	56.47	9.95	13.13
17	262	1.4493	59.52	10.37	11.81	59.60	10.47	11.72
18	262	1.4499	59.52	10.37	11.81	59.57	10.31	11.99

Technology Corporation TT-100 Fourier transform accessory, via techniques described previously (5).

Materials

Compounds **4** and **5** were available from previous work (5) and **6** was synthesized from cyclohexanone and dimethyl phosphite according to the published procedure (24).

The phosphonates **3**, **13**, and **14** were synthesized via the corresponding cyclohexane-1,1-dithiols (25) which were subsequently reacted with trimethyl phosphite and Raney nickel according to recently reported methods (26, 27). Similarly **9**, **15**, and **16** were prepared using triethyl phosphite and **12**, **17**, and **18** employing triisopropyl phosphite.

For the 4-*tert*-butylcyclohexyl compounds **1**, **2**, **7**, **8**, **10**, and **11** it was necessary to proceed from 4-*tert*-butylcyclohexanone to its morpholine enamine derivative which then was converted to 4-*tert*-butylcyclohexane-1,1-dithiol using the published method (28). Conversion of the *gem*-dithiol to the phosphonates was then accomplished in a manner similar to that for the simpler cyclohexane derivatives.

Separation of epimers was accomplished in all cases by preparative glc using a 5% Ucon on Chromosorb W.H.P. column of dimensions 6 ft by 6 mm inner diameter. Typical oven temperatures were near 200 °C, with the detector near 210 °C and injector at 310 °C. The N_2 flow rate on the Perkin-Elmer 990 gas chromatograph was typically 130 ml/min. Isomer ratios obtained (%) were as follows: **1**:**2**, 58:42; **7**:**8**, 68:32; **10**:**11**, 62:38. In each case the axial epimer was eluted first (retention time near 45 min) and the equatorial isomer retention times were near 55 min. For the 2-methyl compounds **13**–**18** the isomer ratios were nearly 50:50 with the isomers having the equatorial 2-methyl group exhibiting the shorter retention times (*ca.* 40 min).

Characterization of Products

Physical properties of **7** and **8** were in agreement with those reported previously (29) as were those of **3**, **9**, and **12** (26, 27). For the remaining new materials mass spectral parent ions, refractive indices, and analytical data are collected in Table 5.

Acknowledgments

We thank the National Research Council of Canada for financial assistance.

1. G. W. BUCHANAN, D. A. ROSS, and J. B. STOTHERS. J. Am. Chem. Soc. **88**, 4301 (1966).
2. J. B. STOTHERS. Carbon-13 NMR spectroscopy. Academic Press, New York, New York. 1972.
3. N. K. WILSON and J. B. STOTHERS. Top. Stereochem. **8**, 1 (1974).
4. M. D. GORDON and L. D. QUIN. J. Org. Chem. **41**, 1690 (1976).
5. G. W. BUCHANAN and C. BENEZRA. Can. J. Chem. **54**, 231 (1976).
6. F. A. L. ANET, C. H. BRADLEY, and G. W. BUCHANAN. J. Am. Chem. Soc. **93**, 258 (1971).
7. K. C. YEE and W. G. BENTRUDE. Tetrahedron Lett. 2775 (1971).
8. H.-J. SCHNEIDER and V. HOPPEN. Tetrahedron Lett. 579 (1974).
9. E. L. ELIEL, W. F. BAILEY, L. D. KOPP, R. L. WILLER, D. M. GRANT, R. BERTRAND, K. A. CHRISTENSEN, D. K. DALLING, M. W. DUCK, E. WENKERT, F. M. SCHELL, and D. W. COCHRAN. J. Am. Chem. Soc. **97**, 322 (1975).
10. D. M. GRANT and E. G. PAUL. J. Am. Chem. Soc. **86**, 2984 (1964).
11. W. A. AYER, L. M. BROWNE, S. FUNG, and J. B. STOTHERS. Can. J. Chem. **54**, 3272 (1976).
12. W. KITCHING, M. MARRIOTT, W. ADCOCK, and D. DODDRELL. J. Org. Chem. **41**, 1672 (1976).
13. D. K. DALLING and D. M. GRANT. J. Am. Chem. Soc. **89**, 6612 (1967).
14. K. MISLOW and M. RABAN. Top. Stereochem. **1**, 1 (1967); **2**, 199 (1967).
15. W. MCFARLANE. Proc. R. Soc. London, Ser. A. **306**, 185 (1968).
16. G. A. GRAY. J. Am. Chem. Soc. **93**, 2132 (1971).
17. A. S. PERLIN and B. CASU. Tetrahedron Lett. 2921 (1969).

18. G. A. GRAY and S. E. CREMER. J. Org. Chem. **37**, 3458 (1972).
19. A. A. BORISENKO, N. M. SERGEYEV, E. Y. NIFANTEV, and Y. A. USTYNYUK. Chem. Commun. 406 (1972).
20. S. SORENSEN, R. S. HANSEN, and H. J. JAKOBSEN. J. Am. Chem. Soc. **94**, 5900 (1972).
21. J. A. SCHWARCZ and A. S. PERLIN. Can. J. Chem. **50**, 3667 (1972).
22. D. H. WILLIAMS and N. S. BHACCA. J. Am. Chem. Soc. **86**, 2742 (1964).
23. H. BOOTH. Tetrahedron Lett. 411 (1965).
24. V. S. ABRAMOV. Dokl. Akad. Nauk. SSSR, **73**, 487 (1950); Chem. Abstr. **45**, 2855 (1951).
25. M. DEMUYNCK and J. VIALLE. Bull. Soc. Chim. Fr. **4**, 1213 (1967).
26. Z. YOSHIDA, S. YONEDA, and T. KAWASE. Chem. Lett. 279 (1975).
27. Z. YOSHIDA, T. KAWASE and S. YONEDA. Tetrahedron Lett. 235 (1975).
28. M. DEMUYNCK and J. VIALLE. Bull. Soc. Chim. Fr. 2126 (1962).
29. C. BENEZRA and J.-L. BRAVET. Can. J. Chem. **53**, 474 (1975).

Kinetic studies on the mechanism of the decomposition of a number of β-substituted *tert*-butyl α,α-dimethylperpropionates

DENNIS D. TANNER, H. YABUUCHI,[1] AND H. LUTZER
Department of Chemistry, University of Alberta, Edmonton, Alta., Canada T6G 2G2

Received September 14, 1976

DENNIS D. TANNER, H. YABUUCHI, and H. LUTZER. Can. J. Chem. **55**, 612 (1977).

A series of *tert*-butyl peresters having a general formula corresponding to I were synthesized.

$$Y—CH_2C(CH_3)_2CO_3C(CH_3)_3$$

I

(Y = H, C_2H_5, Cl, Br, I, C_6H_5S)

The thermally initiated rates of decomposition of these peresters were determined at several temperatures and the activation parameters for these thermolyses were calculated.

The rates of decomposition were relatively insensitive to the substituents and followed the order I > C_2H_5 > C_6H_5S > H > Br > Cl. The activation parameters and product studies were consistent with a simple two bond scission mechanism and no evidence could be found for neighboring group participation in these homolyses.

DENNIS D. TANNER, H. YABUUCHI et H. LUTZER. Can. J. Chem. **55**, 612 (1977).

On a synthétisé une série d'esters *tert*-butylés ayant une formule générale correspondant à I.

$$Y—CH_2C(CH_3)_2CO_3C(CH_3)_3$$

I

(Y = H, C_2H_5, Cl, Br, I, C_6H_5S)

On a déterminé les vitesses de décomposition, initiées thermiquement, de ces peresters à diverses températures et on a calculé des paramètres d'activation de ces thermolyses.

Les vitesses de décomposition sont relativement insensibles à la nature des substituants et l'ordre est le suivant I > C_2H_5 > C_6H_5S > H > Br > Cl. Les paramètres d'activation et les études de produits sont en accord avec un mécanisme de scission simple de deux liens et on ne trouve aucune indication pouvant supporter la participation d'un groupe voisin dans ces réactions homolytiques.

[Traduit par le journal]

Introduction

A large number of investigations of the mechanism of *tert*-butyl perester decompositions have been concerned with the relationship between the structure of the peroxide and its mode of decomposition (1). The thermal decompositions of the simple peresters have been proposed to proceed by two mechanistically distinct pathways, one-bond scission (reaction 1) and two-bond scission (reaction 2). Kinetic criteria for

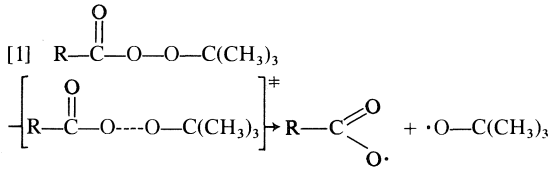

distinguishing between the two paths has been established by Bartlett and Hiatt by comparing the activation parameters of a series of peresters and by correlating these comparisons with the chemical information available for these systems (2). Although these criteria have been somewhat modified, the analysis of the problem has been well supported (1).

Another facet of the structure–reactivity relationship in perester decomposition has been the effect of neighboring groups on not only the mechanism of the decomposition, but on its

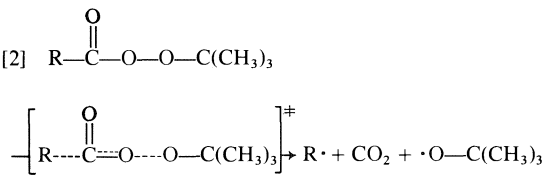

[1] Visiting scientist on leave from Sumitomo Chemical Co., Osaka, Japan.

absolute rate relative to the unsubstituted perester (ref. 1, pp. 137–143).

Substituted peresters have been shown to be subject to polar effects as well as effects attributed to anchimeric assistance during homolysis (3, 4).

A study of the decomposition of *tert*-butyl α,α-dimethylperpropionate **1** and its β-substituted analogues affords a method for the study of the substituent effect on the decomposition of a perester which has been considered as decomposing via the two-bond scission process [2] (2,5–8). Homolytic cleavage of the β-substituted peresters can in theory proceed through a variety of possible transition states (I–IV).

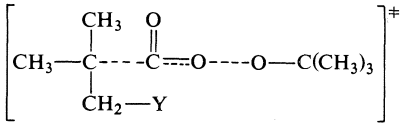

I

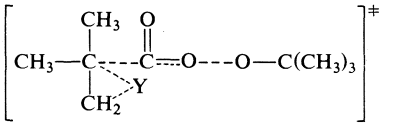

II

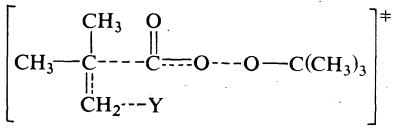

III

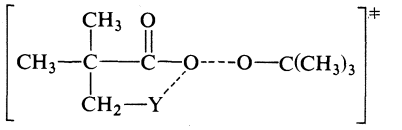

IV

Assisted homolysis of the (O—O) bond by the substituent Y should result in an increased rate for the decomposition of the substituted perester compared to its unsubstituted analogue (9–11). If the decomposition path proceeds via transition states II–IV one would expect the assistance to be reflected in the activation parameters, a smaller $\Delta H^{\ddagger}$ and a more negative $\Delta S^{\ddagger}$.

Polar effects on the decomposition of peresters proceeding via transition state I would predict, by inductive interaction with the polar structure **i**, that the order of the rates of decomposition of the substituted peresters would be the inductive order, $C_2H_5 > H > SCH_3 > I > Br > Cl$ (12). Unless the polar interactions were large, however, small changes in the steric requirements of the groups or upon the solvation of the transition state would easily mask the observation of a regular trend (1, 13, 14). The same polar order

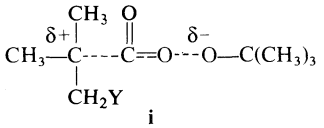

i

$SCH_3 > I > Br > Cl > F$ has been observed for the decomposition of a series of 3-substituted *tert*-butyl perpropionates. Peresters of this structure, presumably, proceed via one-bond scission, although it has been suggested that *tert*-butyl 3-methylthioperpropionate undergoes a concerted three-bond scission (15).

Results and Discussion

The rates for the thermal decomposition of the *tert*-butyl peroxides **1–6** were determined at several temperatures and the results are listed in Table 1.

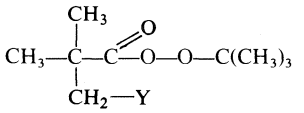

1 Y = H **4** Y = Cl
2 Y = C_2H_5 **5** Y = I
3 Y = Br **6** Y = C_6H_5S

The thermolyses of cyclohexane solutions of peresters **1** and **2** (0.04 *M*) gave 98 and 99% yields of the theoretically calculated amounts of CO_2 and followed steady first-order kinetics to >80% reaction. The rate of decomposition of **1** in cyclohexane agrees extremely well with that reported by Koenig and Wolf (5)[2] for its thermolysis in isooctane, and the activation parameters are, within the limits of the experimental error (which masks any solvent effect), comparable with those reported by Bartlett and Simons (8) or by Lorand *et al.* (6) for decompositions run in chlorobenzene and cumene. The rate constant observed for **2** in cyclohexane was approximately 60% lower than that reported by Fort and Franklin (7) when its decomposition was carried out in cumene. The decreased rate of decomposition observed in the less polar

[2]The rate constant at 73.88 °C was calculated for comparison using the activation parameters reported in this manuscript.

TABLE 1. Rate constants and activation parameters for the thermal decomposition of the *tert*-butyl 3-substituted 2,2,-dimethylperpropionates (X—CH_2—$C(CH_3)_2$—CO_3—$C(CH_3)_3$) at several temperatures, in cyclohexane

Substrate X	Temp. (°C)	Rate constant $k \times 10^5$ (s^{-1})	Relative rates	Activation parameters ΔH^* (kcal/mol)	Activation parameters ΔS^* (eu)
Cl[a]	55	0.355±0.014	0.345±0.007		
	65	1.48 ±0.04	0.368±0.005	30.7±1.4	10.0±4.3
	75	5.65 ±0.10	0.390±0.010		
Br[a]	55	0.950±0.028	0.922±0.10		
	65	3.58 ±0.19	0.890±0.016	28.2±1.4	4.0±3.3
	75	12.3 ±0.6	0.841±0.007		
H	55	1.03 ±0.02	1		
	65	4.02 ±0.16	1	29.3±1.4	7.8±4.1
	75	14.5 ±0.6	1		
C_6H_5S[a]	55	1.63 ±0.04	1.58 ±0.01		
C_6H_5S	65	1.61 ±0.04	1.56 ±0.01	27.9±0.7	3.8±0.7
C_6H_5S[a]	75	19.8 ±0.4	1.37 ±0.03		
C_2H_5	55	1.66 ±0.01	1.61 ±0.02		
	65	6.31 ±0.25	1.57 ±0.00	28.8±0.9	7.0±2.7
	75	22.3 ±0.4	1.54 ±0.04		
I[a]	55	2.91 ±0.08	2.83 ±0.03	27.9±0.3	5.7±1.4
	75	37.6 ±0.70	2.59 ±0.10		

[a]Iodine was added to exclude catalyzed decomposition (0.04 *M*).

solvent, cyclohexane, would be expected for this concerted homolytic process (16).

The decompositon of **3** and **4** in various solvents (chlorobenzene, cumene, and cyclohexane) did not show simple first-order kinetics and at higher percentage decomposition the calculated instantaneous first-order rate constants increased with time. When radical scavengers such as DPPH, galvinoxyl, or molecular iodine were added steady first-order kinetics were obtained. The induced decompositions without added scavengers are presumed to be due to a β-scission process which results in a heterolytic acid catalyzed decomposition of the peroxide. Associ-

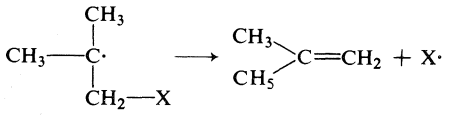

$$X\cdot + RH \longrightarrow HX + R\cdot$$

ated with the induced decompositon was a decreased yield of carbon dioxide and the accompanying production of the parent carboxylic acid. When the thermolyses were carried out in the presence of added molecular iodine first-order kinetics were obtained and quantitative

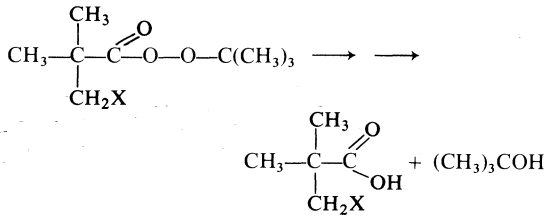

yields (100 ± 3%) of carbon dioxide were obtained. No carbonyl containing compounds could be detected by ir analyses.

Both compounds **5** and **6** (0.04 *M*) gave steady first-order kinetics in cyclohexane with added molecular iodine (0.04 *M*) and produced carbon dioxide in near quantitative yields (97 and 95%). When the thermolysis of **6** was carried out in the absence of molecular iodine the same first-order rate constant was determined (1.63×10^{-5} s^{-1}, 55 °C) and the yield of carbon dioxide (99%) was essentially the same as that obtained when the decomposition was carried out in the presence of a scavenger. It was anticipated that although the β-scission process would be quite favourable for thiyl radical elimination, the stability of the sulphur centered radical would lead almost exclusively to coupling products and

TABLE 2. Products of decomposition of *tert*-butyl 2,2-dimethyl-3-phenylthioperpropionate in cyclohexane at 75 °C

Product	Amount (mg)	Amount (mmol)	Mol/mol perester
Carbon dioxide	30.8	0.673	0.97
tert-Butyl alcohol	46.3	0.625	0.90
*Iso*butylene	33.8	0.603	0.84
β-Methylallylphenylsulphide	18.0	0.110	0.16
Cyclohexylphenylsulphide	64.1	0.334	0.47
Diphenyldisulphide	21.3	0.098	0.14

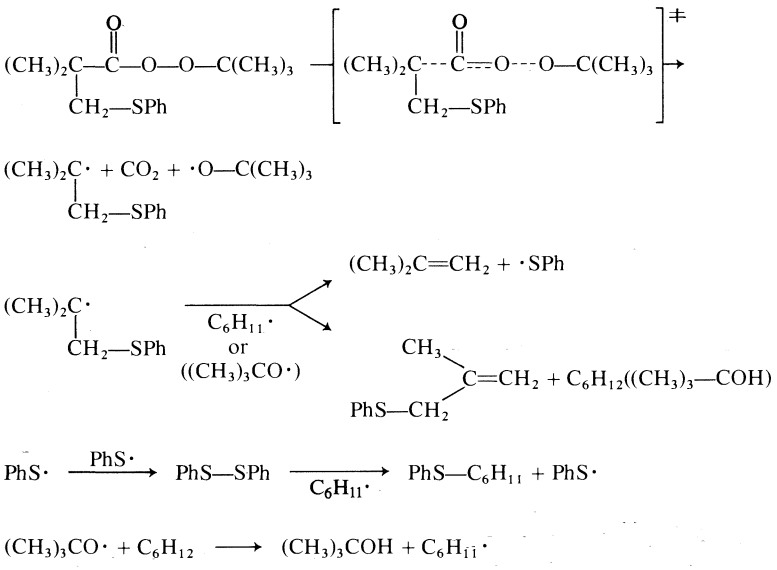

not products resulting from hydrogen abstraction. Since the acid (C_6H_5SH) catalyzed reaction would not be involved in the decomposition it was not surprising that the scavenged and unscavenged rates of decomposition were the same. A study of the decomposition products resulting from the thermolysis (75 °C) of **6**, *tert*-butyl 2,2-dimethyl-3-phenylthioperpropionate, confirmed these predictions (see Table 2), and allowed the suggestion for a decomposition mechanism which is consistent with the products of the reaction and the activation parameters that were obtained.

Mechanistic Conclusions

It has convincingly been argued that *tert*-butyl peroxypivalate decomposes by a concerted two-bond scission (1, 2, 5–7, 14). The criteria used, the magnitude of the activation parameters, and the high yields of carbon dioxide produced, have been taken with some modification (1, 4, 6) as indications of a concerted two-bond scission. The activation parameters obtained for the decomposition of peresters **1–6** vary from $\Delta H^{\ddagger}$ 30.7 ± 1.4 kcal/mol, $\Delta S^{\ddagger}$ 10.0 ± 4.3 eu (Y = Cl) to 27.9 ± 0.7 kcal/mol and 3.8 ± 0.7 eu (Y = PhS), and the interpretation of these differences must be considered mechanistically indistinguishable from *tert*-butyl peroxyperpivalate ($\Delta H^{\ddagger}$ 29.3 ± 1.4 kcal/mol and $\Delta S^{\ddagger}$ 7.8 ± 4.1 eu). The high yields of carbon dioxide obtained for all of the peresters confirm this mechanistic conclusion. The similarity in the activation parameters and the observed rate constants (a variation of less than 3 from the unsubstituted perester) are clearly indicative of the same mechanistic pathway for all of the decompositions, *i.e.* via transition state I. The minor

differences in energetics due to polar effects, steric or solvation interactions are too small to justify a detailed analysis.

Experimental

Materials

Cyclohexane and cumene (Phillips Research Grade) were purified by heating to reflux over sodium metal for several hours followed by fractional distillation. Chlorobenzene was fractionally distilled from phosphorous pentoxide. All solvents were found to be without detectable impurities by ir and glpc.

3-Bromo-2,2-dimethylpropionic acid was prepared by the reaction of fuming hydrobromic acid upon 3-hydroxy-2,2-dimethylpropionic acid. The acid was prepared by potassium permanganate oxidation of 2,2-dimethyl-1,3-propane diol according to the method of Testa *et al.* (17). The oxidation by this method netted a 36% yield of 3-hydroxy-2,2-dimethylpropionic acid, mp 122–126 °C (lit. (17) mp 123–125 °C). The hydroxycarboxylic acid was converted to 3-bromo-2,2-dimethylpropionic acid with hydrobromic acid according to a modification of a procedure described by Nerdel *et al.* (18). A mixture of 38.97 g (0.33 mol) of 3-hydroxy-2,2-dimethylpropionic acid and 218 ml (4.80 mol) of 48% hydrobromic acid was allowed to stir for 24 h at 95–100 °C while a constant flow of hydrogen bromide was bubbled through the solution. The acid was isolated by the given method (18) in a 98% yield and recrystallized from water, mp 51–52 °C (lit. (17) mp 52 °C).

3-Iodo-2,2-dimethylpropionic acid was prepared according to the method of Kohn and Schmitt (19), mp 48.5–49.5 °C (lit. (19) mp 54 °C). *Anal.* calcd. for $C_5H_9O_2I$: C 26.30, H 3.95; found: C 26.49, H 3.95.

2,2-Dimethyl-3-phenylthiopropionic acid was prepared according to the method used by Truce and Knospe (20) for the preparation of 2,2-dimethyl-3-methylthiopropionic acid. To a solution of absolute ethyl alcohol (130 ml) and sodium metal (9.7 g, 0.47 mol) was added the reaction mixture of absolute ethyl alcohol (130 ml), thiophenol (25 g, 0.52 mol), and sodium metal (11.3 g, 0.50 mol). The solution was allowed to stir for 2 h at 30 °C. The combined mixture was subsequently added dropwise into an ethyl alcohol solution of 3-chloro-2,2-dimethylpropionic acid (64 g, 0.47 mol). The reaction mixture was concentrated under vacuum and the solid residue was acidified with 10% aqueous hydrochloric acid. The aqueous solution was extracted several times with ether, and the combined ethereal extracts were dried over anhydrous magnesium sulphate. After distillation of the solvent 87 g (80%) of a white solid was isolated. The crude product was recrystallized from chloroform – carbon tetrachloride mp 115.5–116 °C (lit. (21) mp 115 °C). *Anal.* calcd. for $C_{11}H_{14}O_2S$: C 62.82, H 6.71, S 15.25; found: C 62.50, H 6.49, S 15.36.

3-Substituted 2,2-dimethylpropionyl chlorides were synthesized from their corresponding carboxylic acids (either synthesized as above or commercially available from Aldrich Chemicals Co.) by treatment with thionyl chloride (22).

2,2-Dimethyl-3-phenylthiopropionyl chloride was not prepared by the standard thionyl chloride method since reflux with thionyl chloride produced not only the desired acid chloride but also 1-thiocromanon. The acid chloride was prepared by the dropwise addition of a benzene solution of oxalyl chloride (112.5 g, 0.89 mol) to a benzene solution (100 ml) of 2,2-dimethyl-3-phenylthiopropionic acid (10.4 g, 0.05 mol). The mixture was stirred for 1 h at 30 °C. The volatile fraction of the mixture was distilled at reduced pressure (room temperature) leaving 11 g (97%) of a yellow liquid.

*tert-Butyl peresters (**1–5**)*: peresters **1–5** were prepared by the dropwise addition of (0.17 mol) of purified pyridine to a cooled, 0 °C, *n*-pentane (100 ml) solution of the acid chloride (0.15 mol) and *tert*-butyl hydroperoxide (0.25 mol). The temperature was always maintained below 5 °C. The reaction mixture was then allowed to stand at room temperature for 40 min. Subsequently the mixture was poured onto ice. The organic layer was separated and washed successively with cold 10% hydrochloric acid, 10% sodium bicarbonate solution, and distilled water, and finally dried over anhydrous sodium sulphate. After removal of the solvent, the remaining crude material (usually 80–90% yield) was purified either by recrystallization from *n*-pentane at −78 °C or by passing it through a column of Woelm neutral alumina at 0 °C, using ether as the eluant. The latter method was shown to be particularly effective to remove all traces of impurities. Peroxide contents as determined by the iodometric titration procedure developed by Silbert and Swern (23) were as previously reported (8, 24) not reliable (β-C_2H_5, 86.5%; β-H, 84.7%; β-Cl, 98.3%; β-Br, 98.2%). The purity of the peresters was therefore determined by their infrared and nmr spectra, kinetic behaviour, and elemental analysis. The refractive indices, carbonyl absorptions, microanalyses and the nmr spectra (CCl_4) of the peresters are listed in Tables 3 and 4.

*tert-Butyl 2,2-dimethyl-3-phenylthioperpropionate **6*** was synthesized in a different manner. An attempt to synthesize this perester from the corresponding acid chloride according to the procedure employed for the other peresters, led to an apparent spontaneous decomposition of the perester during the preparation. The perester **6** was consequently prepared by a simple modification of the procedure described for the other peresters. To a stirred cold (0 °C) *n*-pentane (10 ml) solution of *tert*-butyl hydroperoxide were slowly and simultaneously added two *n*-pentane solutions (10 ml each), one containing 2,2-dimethyl-3-phenylthiopropionyl chloride (3.07 g, 0.0135 mol) and the other pyridine (1.34 g, 0.0170 mol). After the addition was completed (20 min) the perester was isolated in the same manner as were the other peresters.

The nmr and ir spectra and elemental analyses of peresters **1–6** showed them to be without experimentally detectable impurities.

β-*Methylallylphenylsulphide* was prepared by the reaction of thiophenol with β-methylallyl chloride according to the procedure of Cope *et al.* (25); bp 83–84 °C/2.8 torr (lit. 89 °C/3.4 torr); the nmr spectrum (neat) was compatible with the one reported for this compound by Kwart and Evans (26). *Anal.* calcd. for $C_{10}H_{22}S$: C 73.11, H 7.36, S 19.52, found: C 73.27, H 7.46, S 19.64.

Cyclohexylphenylsulphide was prepared according to the method employed by Saville (27); bp 126–129 °C/2.8 torr (lit. 111 °C/0.1 torr); nmr (neat) 2.74–3.29 (m, 5H, aromatic), 6.80–7.51 (m, 1H, H_1 of cyclohexyl), and 8.00–9.65 (m, 10H, cyclohexyl). *Anal.* calcd for $C_{12}H_{16}S$: C 74.94, H 8.39, S 16.67; found: C 75.00, H 8.69, S 16.70.

TABLE 3. Refraction index, carbonyl absorption, and elemental analyses of various *tert*-butyl 3-substituted 2,2-dimethylperpropionates ($X—CH_2—C(CH_3)_2—CO_3—C(CH_3)_3$)

Substrate X	n_D^{25}	$\nu_C = 0$ (cm^{-1})	Analysis ($C_9H_{17}O_3X$) Calculated C	Calculated H	Found C	Found H
H	1.4100	1761	62.04	10.41	61.98	10.30
C_2H_5	1.4226	1765	65.31	10.96	65.15	11.14
Cl	1.4390	1765	51.80	8.21	51.56	8.40
Br	1.4569	1775	42.69	6.77	42.49	6.62
I	1.5198	1764	36.02	5.71	35.78	5.72
C_6H_5S	—	1760	63.79	7.85	63.59	7.97

TABLE 4. Nuclear magnetic resonance spectra of various *tert*-butyl 3-substituted 2,2-dimethylperpropionates ($X—CH_2—C(CH_3)_2—CO_3—C(CH_3)_3$)[a]

Substrate X	Chemical shift Methylene	*gem*-dimethyl	*tert*-Butyl (peroxy)	Other
H			8.76(s)	8.80 (s, *tert*-butyl)
C_2H_5	8.68(m)	8.84(s)	8.74(s)	9.08 (t, methyl)
Cl	6.40(s)	8.68(s)	8.73(s)	
Br	6.58(s)	8.69(s)	8.74(s)	
I	6.72(s)	8.69(s)	8.73(s)	
C_6H_5S	6.88(s)	8.72(s)		2.60–2.97 (m, aromatic)

[a]The nmr spectra were taken in carbon tetrachloride with TMS as internal standard.

Kinetic Studies

The rate of disappearance of the peresters was monitored by following the disappearance of the carbonyl stretching band of the peresters at 1760–1775 cm^{-1}. A Perkin-Elmer infrared spectrophotometer, Model 21 or 421, was employed throughout this study. Products from the decomposition of the peresters did not have any absorptions in this region of the infrared spectrum.

A cyclohexane solution of a perester (0.04 *M*) was initially prepared. In the case of the peresters, **4** (X = Cl), **3** (X = Br), and sometimes **5** (X = I) and **6** (X = C_6H_5S), iodine (0.04 *M*) was added in order to exclude anticipated induced decomposition of these peresters. Beer's Law was verified for this system, as evidenced by the straight lines obtained from a plot of log percentage transmittance *vs.* the known concentration of the perester, for a series of standard solutions. Aliquots (1.5 ml) of the solution were degassed by three cycles of the freeze–thaw method and sealed in Pyrex ampoules. The ampoules were then immersed in an oil bath, thermostated at the appropriate temperature within ±0.05° for 10 min, and after various subsequent reaction periods the tubes were removed from the bath, quenched in liquid nitrogen, and analyzed by ir spectroscopy. The initial and final concentrations of the peresters were obtained from the linear plots of perester concentration *vs.* ($\log T_\infty - \log T$), when T is the percentage transmittance for a known perester concentration. The errors for the rate constants reported in Table 1 are average deviations from the mean values obtained for the calculated instantaneous first-order rate constants. Duplicate experiments were carried out and the values obtained were within the experimental limits listed in Table 1.

Studies on the Perester Decomposition Products

The decompositions of 0.04 *M* solutions of peresters **1**–**6** were carried out in reaction vessels fitted with break-seals at 75 °C for 10 half-lives. The reaction vessels were opened to a vacuum line and the volatile gases were fractionated into three traps, the first two cooled to −122 °C and the third cooled to −198 °C. The content of the third trap was measured by means of a Toepler pump (see Table 5). After measurement the gas was identified by its glpc retention time (poly-pack 1, 4 ft × ¼ in. glass column, 0 °C) and was collected and submitted for mass spectral analysis. The cracking pattern, MS-9 high resolution mass spectrometer, confirmed that the gas collected was pure carbon dioxide. Infrared spectra of the residual product mixtures showed an absence of any detectable carbonyl absorption.

tert-Butyl 2,2-dimethyl-3-phenylthioperpropionate ***6*** was decomposed without added iodine and a 97% yield of carbon dioxide was collected, identified, and measured (see Table 5).

The residual reaction mixture was collected, a known amount of benzene was added as an internal standard, and the low boiling fraction of the mixture was analyzed by glpc (20 ft × ⅛ in. 4% FFAP on Chromosorb W A/W DMCS, 72 °C). Two products were detected; isobutylene (84%) and *tert*-butyl alcohol (90%). The reaction mixture was concentrated by distillation under vacuum, a known amount of dibenzyl was added as an internal standard,

TABLE 5. Measurement of carbon dioxide in the decomposition of *tert*-butyl 3-substituted 2,2-dimethylperpropionates[a,b]

Perester substrate	Perester (mmol)	Solvent	CO_2 (mmol)	Carbon dioxide (mol/mol perester)
1[c]	2.00	Cyclohexane	1.95	0.98
2[c]	2.00	Cyclohexane	1.97	0.99
4	2.00	Chlorobenzene	2.06	1.03
3	0.85	Cyclohexane	0.85	0.99
5	1.55	Cyclohexane	1.50	0.97
6	1.69	Cyclohexane	1.61	0.95
6[c]	0.72	Cyclohexane	0.71	0.97

[a]The decompositions were carried out with 0.04 *M* iodine added except where otherwise indicated.
[b]The peresters were decomposed to greater than 10 half-lives.
[c]No iodine was added.

the mixture was dissolved in ether, and analyzed by glpc (5 ft × ¼ in. 10% SE-30 on Chromosorb W A/W, 172 °C). The products found under these conditions were: β-methylallylphenylsulphide (15%), cyclohexylphenylsulphide (47%), and diphenyldisulphide (14%).

The products (see Table 2) were identified by a comparison of their glpc retention times and mass and ir spectra with those of the authentic materials.

Acknowledgements

The authors wish to thank the National Research Council of Canada and the University of Alberta for their generous support of this work. One of the authors (D.D.T.) is also grateful to the administration of the University of St. Andrews and the Faculty of the Department of Chemistry at St. Andrews for their hospitality during the period in which this manuscript was prepared.

1. T. KOENIG. *In* Free radicals. Vol. 1. *Edited by* J. K. Kochi. Wiley-Interscience, New York, N.Y. 1973. pp. 130–136.
2. P. D. BARTLETT and R. R. HIATT. J. Am. Chem. Soc. **80**, 1398 (1958).
3. P. D. BARTLETT and C. RÜCHARDT. J. Am. Chem. Soc. **82**, 1757 (1960).
4. W. A. PRYOR and K. SMITH. J. Am. Chem. Soc. **93**, 5403 (1970); **89**, 1741 (1967).
5. T. KOENIG and R. WOLF. J. Am. Chem. Soc. **91**, 2569 (1968); **89**, 2948 (1967).
6. J. P. LORAND, S. D. CHODROFF, and R. W. WALLACE. J. Am. Chem. Soc. **90**, 5266 (1968).
7. R. C. FORT and R. E. FRANKLIN. J. Am. Chem. Soc. **90**, 5267 (1968).
8. P. D. BARTLETT and D. SIMONS. J. Am. Chem. Soc. **82**, 1753 (1960).
9. T. H. FISCHER and J. C. MARTIN. J. Am. Chem. Soc. **88**, 3382 (1966).
10. M. M. MARTIN. J. Am. Chem. Soc. **84**, 1986 (1962).
11. W. G. BENTRUDE and J. C. MARTIN. J. Am. Chem. Soc. **84**, 1561 (1960).
12. E. M. KOSOWER. Physical organic chemistry. Wiley, New York, N.Y. 1968. pp. 48–49.
13. W. A. PRYOR and K. S. SMITH. Int. J. Chem. Kinet. III, 387 (1971).
14. C. RÜCHARDT. Angew Chem. Int. Ed. Engl. **9**, 830 (1970).
15. (*a*) L. K. MONTGOMERY and D. P. CORDS. Abstracts, 150th National Meeting of the American Chemical Society, Atlantic City, NJ, Sept. 1965. p. 52S; (*b*) J. P. STANLEY. Diss. Abstr. **30**, 140B (1969).
16. J. C. MARTIN. *In* Free radicals. Vol. 2. *Edited by* J. K. Kochi. Wiley-Interscience, New York, N.Y. 1973. pp. 502–507.
17. E. TESTA, L. FONTANELLA, G. CRISTIANI, and G. GALLO. J. Org. Chem. **24**, 1928 (1959).
18. F. NERDEL, P. WEYERSTAHL, and V. KZETZSCHMAN. Chem. Ber. **92**, 1329 (1959).
19. M. KOHN and A. SCHMITT. Monatsh. Chem. **28**, 1057 (1907).
20. W. E. TRUCE and R. H. KNOSPE. J. Am. Chem. Soc. **77**, 5063 (1963).
21. K. W. WUENSCH, K. H. STAHNKE, and A. ETHLERS. Chem. Ber. **103**, 2302 (1970).
22. A. I. VOGEL. Practical organic chemistry. 3rd ed. Longmans, London. 1956. pp. 792.
23. L. S. SILBERT and D. S. SWERN. Anal. Chem. **30**, 385 (1958).
24. T. KOENIG and R. WOLF. J. Am. Chem. Soc. **89**, 2948 (1967).
25. A. C. COPE, D. E. MORRISON, and L. FIELD. J. Am. Chem. Soc. **72**, 59 (1950).
26. H. KWART and E. R. EVANS. J. Org. Chem. **31**, 413 (1966).
27. R. W. SAVILLE. J. Chem. Soc. 2880 (1958).

Carbon-13, proton spin–spin coupling constants in some 4-substituted isothiazoles and related heterocyclics

RODERICK E. WASYLISHEN AND HAROLD M. HUTTON

Department of Chemistry, University of Winnipeg, Winnipeg, Man., Canada R3B 2E9

Received August 18, 1976

RODERICK E. WASYLISHEN and HAROLD M. HUTTON. Can. J. Chem. **55**, 619 (1977).

Carbon-13, proton nuclear spin–spin coupling constants have been measured for a number of 4-substituted isothiazoles. The observed values are compared with those measured in other heterocyclic systems and those calculated in the parent and related heterocyclics using finite perturbation theory and semi-empirical molecular orbital theory at the CNDO/2 and INDO levels of approximation.

RODERICK E. WASYLISHEN et HAROLD M. HUTTON. Can. J. Chem. **55**, 619 (1977).

On a mesuré les constantes de couplage spin–spin entre les noyaux de proton et de carbone-13 pour un certain nombre d'isothiazoles substitués en position 4. On a comparé les valeurs observées avec celles mesurées dans d'autres systèmes hétérocycliques et celles calculées pour le composé fondamental et pour des hétérocycles apparents; ces calculs ont été effectués, à des niveaux d'approximation CNDO/2 et INDO, à l'aide de la théorie des perturbations finies et la théorie semi-empirique des orbitales moléculaires.

[Traduit par le journal]

Introduction

Although $^{13}C,H$ coupling constants are available for a large variety of molecules (1–8), there have been few systematic studies of substituent effects on $^{n}J(^{13}C,H)$ where $n > 1$. A better understanding of substituent effects on these coupling constants should be helpful in the assignment of complex ^{13}C nmr spectra (9–11). As part of our continuing interest in the isothiazole ring system (12, 13) we report $^{n}J(^{13}C,H)$ values in a number of 4-substituted isothiazoles (**1**).

1

The observed coupling constants are compared with those observed in other heterocyclic systems. Those observed in the parent compound are also compared with coupling constants calculated using semi-empirical molecular orbital theory (4, 14–16).

Experimental

Compounds

The ester of isothiazole-4-carboxylic acid was prepared as described earlier (12). All the other isothiazoles were obtained from Raylo Chemical Company, Edmonton, Alberta. Isoxazole, and its methyl derivatives were obtained from Aldrich Chemical Company. 1-Methylpyrazole was obtained from ICN K & K Laboratories, Inc.

Carbon-13 Nuclear Magnetic Resonance Spectra

Natural abundance ^{13}C nmr spectra were measured in 10 mm sample tubes at 20 MHz using a Varian CFT-20 Fourier Transform nmr Spectrometer. Gated proton decoupling (decoupler on during the pulse delay) was used in order to retain nuclear Overhauser enhancements of the proton coupled spectra. Typically, flip angles of 30 to 40° were used with acquisition times >4 s and a pulse delay of 2–3 s. All coupling constants reported here are accurate to ±0.3 Hz or better unless otherwise indicated. All measurements were made at 33 ± 2 °C on approximately 3 *M* solutions of the 4-substituted isothiazoles in DMSO and on neat solutions of isoxazole, the methyl derivatives of isoxazole, and 1-methylpyrazole. Proton-coupled carbon-13 nmr spectra were also obtained at 55 MHz for neat solutions of isothiazole and its methyl derivatives as previously described (12).

Proton Nuclear Magnetic Resonance Spectra

^{1}H nmr spectra of the isothiazoles were obtained on a Varian A-60 nmr spectrometer. A Perkin Elmer R24 spectrometer was used to obtain approximate proton chemical shifts of neat isothiazole.

Molecular Orbital Calculations

Molecular orbital calculations at the CNDO/2 and INDO-MO-FPT levels of approximation (14, 15) were performed on an IBM 370/158 system. The following parameters were added to the MO program (14–16) so that INDO calculations on molecules containing sulfur were possible: G1(16) = 0.31302 and F2(16) = 0.21794 (17).

References to the geometries used for isothiazole and its derivatives are given on p. 599 of ref. 12. The structures of the isoxazole and pyrazole rings were taken from microwave studies (18, 19). Standard geometries (given on p. 110 of ref. 14) were used for the methyl substituents.

For isothiazole and its methyl derivatives the calculated coupling constants did not converge before the density

matrix rms error of 10^{-9} was reached. In these calculations this value was 0.7×10^{-5} or smaller, using a perturbation of 10^{-3}. Some of the coupling constants were still changing significantly with successive iterations when the calculations were terminated.

Results and Discussion

All $^{13}C,H$ coupling constants were extracted from the ^{13}C nmr spectra assuming that the spectra were essentially first order. This assumption was verified by simulating several of the ^{13}C nmr spectra using the computer program LAOCOON III. Proton nmr parameters were obtained for the same sample on which coupled ^{13}C nmr spectra were measured. Results for the 4-substituted isothiazoles and the neat solutions of isoxazole (**2**) and 1-methylpyrazole (**3**) are presented in Table 1.

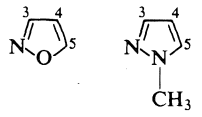

2 **3**

The various two and three bond $^{13}C,H$ coupling constants in isothiazole and isoxazole were assigned by comparing the spectra of the parent compounds with those obtained in neat solutions of their 3-methyl- and 5-methyl- derivatives. Results for these compounds also appear in Table 1.

Calculated values of the various $^{13}C,H$ coupling constants in isothiazole, isoxazole, and 1-methylpyrazole are given in Table 2.

$^1J(^{13}C,H)$

In isothiazole, $^1J(C_5,H)$ is approximately 3.6 Hz greater than $^1J(C_3,H)$. This trend is also observed in thiazole (20), where $^1J(C,H)$ for the carbon adjacent to the sulfur is 2.6 Hz greater than that observed for the carbon adjacent to the nitrogen. Similarly in thiophene $^1J(C_2,H)$ is 184.7 Hz (21), approximately 7.1 Hz greater than the value of 177.6 Hz observed for this coupling in pyridine (22).

In all 4-substituted isothiazoles $^1J(C_5,H) > {}^1J(C_3,H)$, although the difference is only about 1 Hz in the case of X = NO_2 and CN. $^1J(C_3,H)$ and $^1J(C_5,H)$ values increase by 15.6 and 13.0 Hz respectively from X = CH_3 to X = NO_2. These values are to be compared with corresponding increases of ~10 Hz and ~16 Hz for $^1J(C_4,H)$ and $^1J(C_2,H)$ in 3-substituted thiophenes (23), and 12.3 Hz in monosubstituted benzenes (24–27) (where X varies from CH_3 to NO_2).

The MO calculations are not successful in predicting $^1J(C_5,H) > {}^1J(C_3,H)$. $^1J(C,H)$ values have often been related to $P^2_{C(2s)H(1s)}$, where $P_{C(2s)H(1s)}$ is the carbon $2s$ – hydrogen s bond order (4, 15). Both the CNDO/2 and INDO calculations predict $P_{C(2s)H(1s)}$ to be greater for C_3—H_3 than for C_5—H_5. It is of interest to point out that *ab initio* calculations[1] also predict such behaviour but in this case the difference in bond orders is small (29).

In isoxazole, $^1J(C_5,H)$ is 203.5 Hz, similar to the value of 201.7 Hz observed in furan (30). The value of $^1J(C_3,H)$ is approximately 10.5 Hz greater than the analogous coupling constant in pyridine (22). Also, $^1J(C_4,H)$ in isoxazole is more than 9 Hz larger than $^1J(C_3,H)$ in furan (30), pyridine (22), or benzene (31). The MO calculations on isoxazole are successful in that they predict $^1J(C_5,H) > {}^1J(C_3,H)$ or $^1J(C_4,H)$.

For 1-methylpyrazole we find that the average of $^1J(C_3,H)$ and $^1J(C_5,H)$ is approximately 5 Hz less than the value observed in pyrazole (32) where C_3 and C_5 are equivalent because of tautomerism. $^1J(C_4,H)$ in **3** is about 2 Hz less than the corresponding value in pyrazole. The INDO calculations correctly predict $^1J(C_5,H) > {}^1J(C_3,H) > {}^1J(C_4,H)$.

$^2J(C,H)$

$^2J(C_{sp^2}$–$C_{sp^2}H)$ values can be of either sign (3, 5, 33). In the fragment (**4**) $^2J(C_2,H_1)$ increases with increasing electronegativity of a substituent

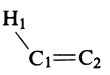

4

at C_1. For example, in 1-chloroethylene (34, 35), $^2J(C_2,H_1)$ is +6.9 Hz as opposed to −2.4 Hz in ethylene (36, 37). Monosubstitution at C_2 results in opposite trends which are dependent upon the orientation of the substituent (1, 3, 34). If the substituent is *trans* to H_1, then $^2J(C_2,H_1)$ increases as the electronegativity of the substituent increases. Thus very large $^2J(C,H)$ values are observed when two electronegative substituents are *cis* to one another. For example, in 1,3-dioxide (**5**), $^2J(C,H)$ is 20.0 Hz (38).

5

[1]STO-3G level *ab initio* calculations (28) were carried out using the geometry given in reference (12).

TABLE 1. $^{13}C,H$ spin–spin coupling constants in Hz in 4-substituted isothiazoles and related compounds

Compound	C_3			C_4			C_5			$^{13}C,H$ coupling constants with substituents
	H_3	H_4	H_5	H_3	H_4	H_5	H_3	H_4	H_5	
Isothiazole	183.5	8.2	11.3	14.2	173.3	5.4	6.2	8.0	187.1	
4-Nitroisothiazole	196.0		7.9	*		*	3.9		197.0	
4-Bromoisothiazole	192.2		9.0	12.6		1.5	4.8		194.8	
4-Cyanoisothiazole	193.8		9.5	13.9		3.9	4.7		195.1	$^3J(CN,H_5) = 2.7$; $^3J(CN,H_3) < 1.0$
4-Carboxylisothiazole	187.9		9.7	11.7		3.8	5.0		191.2	$^3J(COOH,H_5) = 2.2$; $^3J(COOH,H_3) < 1.0$
4-Methylisothiazole	180.4		10.4	13.0		4.6	5.3		184.0	$^3J(C_3,CH_3) = 4.3$; $^3J(C_5,CH_3) = 5.3$; $^2J(C_4,CH_3) = 6.5$ $^3J(CH_3,H_3) \approx 1 \pm 0.5$; $^3J(CH_3,H_5) \approx 2 \pm 0.5$
4-Benzylisothiazole	181.7		10.3	12.8		5.0	5.3		185.9	$^3J(C_3,CH_2) = 4.3$; $^3J(C_5,CH_2) = 5.3$ $^2J(C_4,CH_2) = 7.2$
4-Carboxymethylisothiazole	188.4		9.5	11.8		3.5	4.9		191.8	
5-Methylisothiazole	181.7	8.1		13.7	170.3		6.5	6.5		$^2J(C_5,CH_3) = 6.5$; $^3J(C_4,CH_3) = 4.3$
3-Methylisothiazole		7.3	11.0		170.7	5.0		8.1	185.7	$^2J(C_3,CH_3) = 6.5$; $^3J(C_4,CH_3) = 3.0$
Isoxazole	187.6	6.2	6.2	9.6	184.6	14.3	4.4	10.9	203.5	
3-Methylisoxazole		6.2	6.2		181.8	14.0		10.0	201.3	$^2J(C_3,CH_3) = 6.2$; $^3J(C_4,CH_3) = 2.7$
5-Methylisoxazole	185.3	6.0		9.3	181.8		4.5	10.2		$^2J(C_5,CH_3) = 6.9$; $^3J(C_4,CH_3) = 2.8$
1-Methylpyrazole	183.8	5.7 or 8.4	8.4 or 5.7	9.8	175.5	9.8	*	*	187±5	

*Coupling constants not available from spectrum.

TABLE 2. Calculated $^{13}C,H$ coupling constants in Hz

Compound	MO calculation	C_3			C_4			C_5		
		H_3	H_4	H_5	H_3	H_4	H_5	H_3	H_4	H_5
Isothiazole	CNDO/2*	139	1.4	11.6	2.5	125	−1.5	4.6	−3.3	96
	INDO*	164	−0.91	13.7	−0.34	146	−4.7	1.9	−13.6	123
Isoxazole	CNDO/2	131.1	2.12	7.46	3.41	140.5	4.60	5.78	4.31	143.3
	INDO	162.9	−2.43	10.90	0.31	165.7	3.11	7.94	0.12	171.9
1-Methylpyrazole	CNDO/2	131.7	2.42	7.18	4.14	134.7	3.03	5.72	4.79	142.9
	INDO	161.5	−1.87	11.11	2.15	158.5	0.44	8.76	1.15	168.5

*Density matrix rms error of 0.7×10^{-5}, or smaller (see text).

If the substituent at C_2 is *cis* to H_1, then $^2J(C_2,H_1)$ generally decreases as the electronegativity of the substituent increases. For example, in benzene, $^2J(C,H) = +1.0$ Hz while in chlorobenzene and nitrobenzene, $^2J(C_1,H_2) = -3.4$ and -3.5 Hz, respectively (24, 27, 31).

Some of the striking features of the data in Table 1 are the large values of $^2J(C_4,H_3)$. In contrast to monosubstituted benzenes (24–27), thiophenes (23, 32, 39, 40), and pyridines (22, 41–44) where $^3J(C,H)$ is generally larger than $^2J(C,H)$, we find several cases where the reverse is true.

For all the isothiazoles studied here, we observe that $^2J(C_4,H_3)$ is more than twice $^2J(C_4,H_5)$. This trend is in agreement with that predicted on the basis of the electronegativity arguments presented above since nitrogen is more electronegative than sulfur.

$^2J(C_4,H_5)$ becomes very small in the case of 4-bromoisothiazole.

In the case of isoxazole, $^2J(C_4,H_5) > {}^2J(C_4,H_3)$. In furan, $^2J(C_3,H_2) = 13.8$ Hz while $^2J(C_3,H_4)$ is only 4.05 Hz. Finally it is of interest to mention that in furan, $^2J(C_2,H_3) = 11.0$ Hz. In isoxazole the analogous coupling constant, $^2J(C_5,H_4)$ is 10.0 Hz.

$^2J(C_4,H_3) \simeq {}^2J(C_4,H_5) \simeq 9.8$ Hz in 1-methylpyrazole, very similar to the value of 9.5 Hz observed in pyrazole (32). One would expect $^3J(C_3,H_5)$ in 1-methylpyrazole to fall between 6.2 and 11.2 Hz, the values observed for this coupling constant in isoxazole and isothiazole (see Discussion below). Also, since $^3J(C_2,H_4) > 6.8$ Hz in both pyridine (22) and pyrole (45), we tentatively assign the splitting of 5.7 Hz in **3** to $^2J(C_3,H_4)$ instead of $^3J(C_3,H_5)$.

Previously (46), we have found that INDO calculates $^2J(C,H)$ values in unsaturated systems which are roughly 10 Hz too negative. In Table 3 we have added 10 Hz to the values calculated using INDO. For isothiazole the calculations predict $^2J(C_4,H_3)$ to be about 4.5 Hz greater than $^2J(C_4,H_5)$ in qualitative agreement with experiment. The value calculated for $^2J(C_5,H_4)$ is clearly erroneous. The experimental trends observed for $^2J(C,H)$ in isoxazole and 1-methylpyrazole seem to be reproduced reasonably well by the INDO calculations.

From plots of magnetic susceptibility anisotropy, $\Delta\chi$, *vs.* $^3J(H—C=C—H)$ Schaefer (47) has found two distinct relationships. Compounds which are generally considered aromatic including isoxazole fall on the one line, while nonaromatic compounds fall on the other line. Schaefer and co-workers (48) have also found that distinct correlations exist between $^2J(^{13}C=C—H)$ and $^3J(H—C=C—H)$ for aromatic and nonaromatic compounds. Averaging $^2J(C_4,H_5)$ and $^2J(C_5,H_4)$ and plotting this value against $^3J(C,H)$, we find that both isoxazole and isothiazole are aromatic according to the criteria discussed above.

$^3J(^{13}C,H)$

The various structural features which seem to be important in determining the magnitude of $^3J(C,H)$ in alkenes have recently been reviewed by Vögeli and von Philipsborn (49). They stated that in the $^{13}C_1—C_2=C_3—H$ fragment, an electronegative substituent at the C_1 position leads to an enhancement in $^3J(C_1,H)$, however, such a substituent at C_2 produces a decrease in $^3J(C_1,H)$. Similar observations have been made for monosubstituted benzenes (24–27). For example, in fluorobenzene, $^3J(C_1,H_3) = 11.1$ Hz and $^3J(C_2,H_6) = 5.0$ Hz (24). The value in benzene is 7.4 Hz (31).

In isothiazole and its 4-substituted derivatives, $^3J(C_3,H_5)$ is generally about twice as large as

TABLE 3. Observed and calculated $^2J(^{13}C,H)$*

Parameter	Isothiazole		Isoxazole		1-Methylpyrazole	
	Obs.	INDO	Obs.	INDO	Obs.	INDO
$^2J(C_3,H_4)$	8.2	9.1	6.2	7.6	5.7	8.1
$^2J(C_4,H_3)$	14.2	9.7	9.6	10.3	9.8	12.2
$^2J(C_4,H_5)$	5.4	5.3	14.3	13.1	9.8	10.4
$^2J(C_5,H_4)$	8.0	−3.6	10.9	10.1	—	11.2

*10 Hz has been added to all calculated values.

$^3J(C_5,H_3)$. This difference may be rationalized on the basis of electronegativity arguments since the nitrogen can be considered somewhat electronegative while the sulfur is somewhat electropositive.[2] However, it is difficult to account for the similarity of $^3J(C_2,H_4)$ and $^3J(C_4,H_2)$ in other heterocyclics. For example, in the case of thiophene, $^3J(C_2,H_4) = 10.0$ Hz, and $^3J(C_4,H_2) = 9.8$ Hz; in pyridine, $^3J(C_2,H_4) = 6.85$ Hz and $^3J(C_4,H_2) = 6.34$ Hz; in furan, $^3J(C_2,H_4) = 10.04$ Hz and $^3J(C_4,H_2) = 9.79$ Hz; in pyrrole, $^3J(C_2,H_4) = 7.46$ Hz and $^3J(C_4,H_2) = 7.31$ Hz. Notice that in every case $^3J(C_2,H_4)$ and $^3J(C_4,H_2)$ are similar.

In isoxazole we also observe $^3J(C_3,H_5) > {}^3J(C_5,H_3)$, however, in this case the difference is not as large as in the case of isothiazole.

It is interesting to note that the MO calculations correctly predict the observed trends in $^3J(^{13}C,H)$ for isothiazole and isoxazole.

In the 4-substituted isothiazoles both $^3J(C_3,H_5)$ and $^3J(C_5,H_3)$ decrease as the electronegativity of a substituent increases, however, factors other than electronegativity may be important.

Finally it is of interest to discuss the coupling constants which involve the substituent when X = CN, COOR, and CH_3. In all of the isothiazoles considered here we found that $^3J(C,H)$ coupling constants involving the carbon of the substituent were less than 2.7 Hz. These small values observed for these coupling constants are consistent with the empirical relationship, $^3J(C,H) \simeq 0.6\ ^3J(H,H)$ proposed by Vögeli and von Philipsborn (49). In isothiazole, $^3J(H_3,H_4) = 1.66$ Hz and $^3J(H_4,H_5) = 4.66$ Hz, thus one would not expect $^3J(C,H)$ to exceed 3.3 Hz.

In the methyl substituted isothiazoles we observe quite different values for $^3J(C,CH_3)$. For example, in 4-methylisothiazole $^3J(C_3,CH_3) = 4.3$ Hz while $^3J(C_5,CH_3) = 5.3$ Hz. The larger coupling constant to C_5 is probably due to the larger π-bond order for the C_4—C_5 bond as opposed to that of the C_4—C_3 bond (13, 16). Previously (13), we found $^4J(H_5,CH_3)$ much larger than $^4J(H_3,CH_3)$. As well as π-bond order, the orientation of the methyl group will also be important in determining the magnitude of $^3J(C,CH_3)$ (16). In contrast to toluene where the methyl group is essentially a free rotor (50), the barrier to methyl-group rotation in the heterocyclics studied here will probably be greater than kT (51–53).

It is interesting to notice that in the case of the 3- and 5-methyl-substituted isoxazoles, $^3J(C_4,CH_3)$ is the same within experimental error, 2.7 and 2.8 Hz, respectively.

[2]Although CNDO/2 calculations predict a slight positive charge on the sulfur (+0.0013e⁻), *ab initio* calculations (28, 29) predict a large positive charge on the sulfur (+0.443e⁻).

Acknowledgments

We would like to thank Dr. Bill Parr and Dr. Ted Schaefer for allowing us to use the MO program which has been parameterized to allow INDO calculations for 2nd row elements.

We thank the National Research Council of Canada for its support.

1. J. H. GOLDSTEIN, V. S. WATTS, and L. S. RATTET. Prog. Nucl. Magn. Reson. Spectrosc. **8**, 104 (1971).
2. J. B. STOTHERS. Carbon-13 NMR Spectroscopy. Academic Press, New York. 1972.
3. D. F. EWING. *In* Annual reports on nmr spectroscopy. Vol. 6A. *Edited by* E. F. Mooney. Academic Press, New York. 1975. p. 389.
4. P. D. ELLIS and R. DITCHFIELD. *In* Topics in carbon-13 nmr spectroscopy. Vol. 2. *Edited by* G. C. Levy. John Wiley and Sons, New York. 1976. p. 433.
5. J. L. MARSHALL, D. E. MIILLER, S. A. CONN, R. SEIWELL, and A. M. IHRIG. Acc. Chem. Res. **7**, 333 (1974).
6. R. GRINTER. *In* Specialist periodical reports. Vol. 4. *Edited by* R. K. Harris. The Chemical Society, London. 1975. p. 67.

7. R. H. Cox. Magn. Reson. Rev. **3**, 207 (1974).
8. J. R. Wasson and D. R. Lorenz. Anal. Chem. **48**, 246*R* (1976).
9. J. Feeney, P. Partington, and G. C. K. Roberts. J. Magn. Reson. **13**, 268 (1974).
10. H. Günther, H. Schmickler, and G. Jikeli. J. Magn. Reson. **11**, 344 (1973).
11. A. A. Chalmers, K. G. R. Pachler, and P. L. Wessels. Org. Magn. Reson. **6**, 445 (1974).
12. R. E. Wasylishen, T. R. Clem, and E. D. Becker. Can. J .Chem. **53**, 596 (1975).
13. R. E. Wasylishen, J. B. Rowbotham, and T. Schaefer. Can. J. Chem. **52**, 833 (1974).
14. J. A. Pople and D. L. Beveridge. Approximate molecular orbital theory. McGraw-Hill Book Co., New York. 1970.
15. G. E. Maciel, J. W. McIver, Jr., N. W. Ostlund, and J. A. Pople. J. Am. Chem. Soc. **92**, 1 (1970).
16. R. Wasylishen and T. Schaefer. Can. J. Chem. **51**, 961 (1973).
17. V. Galasso. Theor. Chim. Acta, **34**, 137 (1974).
18. J. R. Davidson, A. K. Burnham, B. Giegel, P. Beak, and W. H. Flygare. J. Am. Chem. Soc. **96**, 7394 (1974).
19. L. Nygaard, D. Christen, I. T. Nielsen, E. J. Pedersen, O. Snerling, E. Vestergaard, and G. O. Sorensen. J. Mol. Struct. **22**, 401 (1974).
20. I. N. Bojesen, J. H. Høg, J. T. Nielson, I. B. Petersen, and K. Schaumberg. Acta Chem. Scand. **25**, 2739 (1971).
21. T. N. Huckerby. J. Mol. Struct. **31**, 161 (1976).
22. M. Hansen and H. J. Jakobsen. J. Magn. Reson. **10**, 74 (1973).
23. S. Gronowitz, I. Johnson, and A.-B. Hörnfeldt. Chem. Scripta, **7**, 76 (1975).
24. A. R. Tarpley, Jr. and J. H. Goldstein. J. Phys. Chem. **76**, 515 (1972).
25. J. P. Jacobsen and K. Schaumburg. Mol. Phys. **28**, 1505 (1974).
26. M. Hansen and H. J. Jakobsen. J. Magn. Reson. **20**, 520 (1975).
27. L. Ernst, E. Lustig, and V. Wray. J. Magn. Reson. **22**, 459 (1976).
28. W. J. Hehre, R. F. Stewart, and J. A. Pople. J. Chem. Phys. **51**, 2657 (1969); Program #236 Q.C.P.E., Indiana University, Bloomington, Indiana.
29. R. Wasylishen. Unpublished results.
30. (*a*) M. Hansen, R. S. Hansen, and H. J. Jakobsen. J. Magn. Reson. **13**, 386 (1974). (*b*) J. Runsink, J. de Wit, and W. D. Weringa. Tetrahedron Lett. 55 (1974).
31. F. J. Weigert and J. D. Roberts. J. Am. Chem. Soc. **89**, 2967 (1967).
32. F. J. Weigert and J. D. Roberts. J. Am. Chem. Soc. **90**, 3543 (1968).
33. C. J. Jameson and M. C. Damasco. Mol. Phys. **18**, 491 (1970).
34. K. M. Crecely, R. W. Crecely, and J. H. Goldstein. J. Mol. Spectrosc. **37**, 252 (1971).
35. F. J. Weigert and J. D. Roberts. J. Phys. Chem. **73**, 449 (1969).
36. R. M. Lynden-Bell and N. Sheppard. Proc. R. Soc. A, **269**, 385 (1962).
37. D. M. Graham and C. E. Holloway. Can. J. Chem. **41**, 2114 (1963).
38. T. Schaefer, K. Chum, D. McKinnon, and M. S. Chauhan. Can. J. Chem. **53**, 2734 (1975).
39. K. Takahashi, T. Sone, and K. Fujieda. J. Phys. Chem. **74**, 2765 (1970).
40. T. Sone, K. Fujieda, and K. Takahashi. Org. Magn. Reson. **7**, 572 (1975).
41. Y. Takeuchi. Org. Magn. Reson. **7**, 181 (1975).
42. G. Miyazima, K. Takahashi, and H. Sugiyama. Org. Magn. Reson. **6**, 18 (1974).
43. Y. Takeuchi and N. Dennis. J. Am. Chem. Soc. **96**, 3657 (1974).
44. Y. Takeuchi and N. Dennis. Org. Magn. Reson. **7**, 244 (1975).
45. J. M. Briggs, E. Rahkamaa, and E. W. Randall. J. Magn. Reson. **12**, 40 (1973).
46. R. L. Lichter and R. E. Wasylishen. J. Am. Chem. Soc. **97**, 1808 (1975).
47. T. Schaefer. J. Magn. Reson. **20**, 182 (1975).
48. D. M. McKinnon and T. Schaefer. Can. J. Chem. **49**, 89 (1971).
49. U. Vögeli and W. von Philipsborn. Org. Magn. Reson. **7**, 617 (1975).
50. W. A. Kreiner, H. D. Rudolph, and B. T. Tan. J. Mol. Spectrosc. **48**, 86 (1973).
51. T. Ogata and K. Kozima. J. Mol. Spectrosc. **42**, 38 (1972).
52. W. G. Norris and L. C. Krisher. J. Chem. Phys. **51**, 403 (1969).
53. T. Ogata and K. Kozima. Bull. Chem. Soc. Jpn. **44**, 2344 (1971).

The photolysis of hexaaquoiron(III) perchlorate in the presence of ethylene glycol

JOHN H. CAREY, ERNEST G. COSGROVE, AND BARRY G. OLIVER

Water Chemistry Section, Process Research Division, Canada Centre for Inland Waters, Burlington, Ont., Canada

Received May 28, 1976

JOHN H. CAREY, ERNEST G. COSGROVE, and BARRY G. OLIVER. Can. J. Chem. **55**, 625 (1977).

Two types of reactions occur when hexaaquoiron(III) ion is irradiated at 254 nm in the presence of alcohols. Firstly, a charge transfer transition from a water centred orbital to an iron centred orbital produces OH· radicals which go on to abstract hydrogen from the alcohols. Secondly, the reaction with the charge transfer excited states of iron(III) species can lead to outer sphere oxidation of the alcohols. In this paper, these reactions have been studied in detail for the diol ethylene glycol in aqueous solutions. It has been found that the quantum yield of acetaldehyde, the major product of hydroxyl radical reactions with ethylene glycol, is 0.09 and the yield of formaldehyde, the major product of the direct charge transfer reaction, is 0.05 in 1 *M* ethylene glycol. The quantum yields for these major products, as well as minor products, such as glycolaldehyde and succinaldehyde, have been determined at several concentrations of ethylene glycol and iron. A detailed reaction scheme for the photolysis has been developed.

JOHN H. CAREY, ERNEST G. COSGROVE et BARRY G. OLIVER. Can. J. Chem. **55**, 625 (1977).

Il y a deux types de réaction qui se produisent lorsque l'ion hexaaquofer(III) est irradié à 254 nm en présence d'alcools. En premier lieu, il y a une transition de transfert de charge à partir d'une orbitale centrée au niveau de l'eau vers une orbitale centrée sur le fer qui produit des radicaux OH qui ensuite enlèvent de l'hydrogène des alcools. Deuxièmement il y a une réaction avec les états excités de transfert de charge des espèces du fer(III) qui peut conduire à des oxydations par les sphères extérieures de l'alcool. Dans la présente communication, on a étudié ces réactions en détail pour le diol éthylène glycol en solution aqueuse. On a trouvé que le rendement quantique d'acétaldéhyde, le produit majeur des réactions du radical hydroxyle avec l'éthylène glycol, est de 0.09 et le rendement de formaldéhyde, qui est le produit majeur de la réaction de transfert directe de charge, est de 0.05 dans l'éthylène glycol 1 *M*. On a déterminé les rendements quantiques de ces produits majeurs ainsi que des produits mineurs tel que le glycolaldéhyde et le succinaldéhyde à plusieurs concentrations d'éthylène glycol et de fer. On a développé un schéma réactionnel détaillé pour la photolyse.

[Traduit par le journal]

Introduction

Two types of reactions occur when hexaaquoiron(III) ion is irradiated at 254 nm in the presence of organic scavengers. Firstly, a charge transfer transition from a water centred orbital to an iron centred orbital produces OH· radicals which react with the organics via hydrogen abstraction (1). Secondly, the direct reaction of charge transfer excited states of iron(III) species can lead to outer sphere oxidation (2). Since either mechanism may prove to be a pathway for pollutant degradation in natural waters, particularly at sediment–water interfaces, it was decided to examine them in closer detail. The compound chosen for study was ethylene glycol which is used as a deicer and finds its way into the environment mainly in airport runoff (3).

Previous studies on the radiolysis of deaerated ethylene glycol (4) showed that high yields of acetaldehyde were produced in a chain reaction. Radiolysis of aqueous ethylene glycol in the presence of H_2O_2 (5) and far ultraviolet (185 nm) irradiation of 2 *M* aqueous ethylene glycol solutions (6) also showed acetaldehyde to be the major product. The proposed reaction mechanism was the abstraction of an α-hydrogen from ethylene glycol by OH· to produce the HO—$\dot{C}$H—CH_2OH radical which loses H_2O in an acid catalyzed reaction to produce O=CH—$\dot{C}H_2$. The O=CH—$\dot{C}H_2$ radical would then abstract hydrogen from another ethylene glycol to produce acetaldehyde. Both these radicals have been shown to be present by electron spin resonance spectroscopy (7, 8).

It was decided that a detailed look at the reactions and product yields in the aqueous iron system would shed more light on OH· radical reactions as well as reveal the extent of any direct excited state reactions in the system.

Experimental

Solutions to be irradiated were prepared from stock solutions of reagent grade chemicals to be 0.01 to 0.04 *M* ferric perchlorate, 2.0 *M* $HClO_4$, and various ethylene glycol concentrations. Irradiations were performed in a

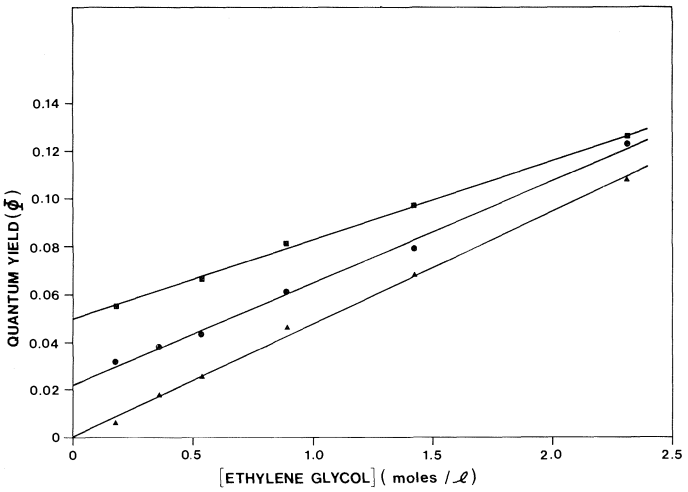

FIG. 1. The quantum yields of formaldehyde ▲, iron(II) ●, and acetaldehyde ■ as a function of ethylene glycol concentration. Concentration of ferric perchlorate: 0.02 *M*.

cylindrical quartz cell with an outer jacket through which distilled water was circulated to control the temperature to 35.0 ± 0.1 °C. Samples were deoxygenated by bubbling high purity nitrogen through them for 15 min prior to irradiation. The 254 nm light source was a photoreactor (Ultraviolet Products Inc., San Gabriel, California) containing four circular low pressure mercury lamps. A magnetic stirrer was used to agitate the solutions during photolysis. Light intensities were measured using ferrioxalate actinometry (9).

The Fe(II) yields were determined from the absorbance at 510 nm ($a = 1.09 \times 10^4$) using *o*-phenanthroline and a neutralization/dilution technique (1). All the organic analyses were performed on the supernatant after precipitation of the iron and perchlorate from the solutions by addition of known volumes of 2 *M* KOH. The presence of acetaldehyde, formaldehyde, and glycolaldehyde was demonstrated by thin layer chromatography of their 2,4-DNPH derivatives on alumina using cyclohexane–nitrobenzene (2:1) as solvent. Acetaldehyde was determined in cold H_2SO_4 with *p*-hydroxydiphenyl by measuring the absorbance at 568 nm ($a = 4.7 \times 10^4$) (10). Formaldehyde concentrations were evaluated colorimetrically ($a = 1.8 \times 10^4$ at 570 nm) using a modified chromatrophic acid technique (11). Glycolaldehyde was determined colorimetrically as the osazone (12) at 580 nm ($a = 1.76 \times 10^4$). Succinaldehyde was measured with *p*-dimethylaminobenzaldehyde (13) at 546 nm ($a = 7.1 \times 10^4$).

The solvation analysis were carried out on a Varian T-60 nuclear magnetic resonance spectrometer with probe temperature 35 °C. The treatment of the data was done using procedures described in refs. 2, 14, 15, and 16.

Results and Discussion

A preliminary study showed that the major photoproducts formed during the ultraviolet irradiation of degassed, strongly acidic, aqueous solutions of ferric perchlorate containing ethylene glycol were iron(II), acetaldehyde, and formaldehyde. Figure 1 shows that the quantum yields of these three products vary as a function of ethylene glycol concentration. In addition to these products, small yields of glycolaldehyde (0.010) and succinaldehyde (0.003) were observed. The yields of these two products were essentially independent of the ethylene glycol concentration.

Based on these results the following reaction scheme for the photolysis of aqueous iron(III) in the presence of ethylene glycol is proposed:

[1] $Fe^{3+}(aq) \underset{k_{-1}}{\overset{h\nu}{\rightleftharpoons}} Fe^{3+}(aq)^* \xrightarrow{k_1} Fe^{2+}(aq) + OH^{\cdot} + H^+$ **1**

[2] $OH^{\cdot} + HOCH_2CH_2OH \xrightarrow{k_2} HOCH_2\dot{C}HOH + H_2O$

[3] $HOCH_2\dot{C}HOH \xrightarrow[(H^+)]{k_3} \dot{C}H_2C(=O)H + H_2O$

[4] $\cdot CH_2C(=O)H + Fe^{2+}(aq) + H^+ \xrightarrow{k_4} CH_3C(=O)H + Fe^{3+}(aq)$ **2**

[5] $\cdot CH_2C(=O)H + HOCH_2CH_2OH \xrightarrow{k_5} CH_3C(=O)H + HOCH_2\dot{C}HOH$

[6] $HOCH_2\dot{C}HOH + Fe^{3+}(aq) \xrightarrow{k_6} HOCH_2\overset{O}{\overset{\|}{C}}—H + Fe^{2+}(aq) + H^+$

3 **1**

[7] $\cdot CH_2\overset{O}{\overset{\|}{C}}—H + \cdot CH_2\overset{O}{\overset{\|}{C}}—H \xrightarrow{k_7} H—\overset{O}{\overset{\|}{C}}—CH_2CH_2\overset{O}{\overset{\|}{C}}—H$

4

Reaction 1 represents the photoproduction of hydroxyl radicals by excitation of the water to iron charge transfer (CT) transition. At high scavenger concentration (>0.1 *M*) all the $OH^{\cdot}$ radicals react by abstraction of an α-hydrogen from ethylene glycol (reaction 2). The $HOCH_2\dot{C}HOH$ radical can then undergo acid catalyzed dehydration (7) to give the $\dot{C}H_2\overset{O}{\overset{\|}{C}}H$ radical via reaction 3. The major reaction of the $\dot{C}H_2\overset{O}{\overset{\|}{C}}H$ radical will be with Fe(II), which will be produced in close proximity to it, to give acetaldehyde, **2** (reaction 4). At higher ethylene glycol concentrations reaction 5, a chain propagating reaction, will begin to become important. This is evident from the positive slope, 0.033, of the acetaldehyde quantum yield as a function of glycol concentration in Fig. 1. Alternate fates of the $HOCH_2\dot{C}HOH$ and the $\dot{C}H_2\overset{O}{\overset{\|}{C}}H$ radicals are depicted in reactions 6 and 7 and result in formation of the two minor products glycolaldehyde, **3**, and succinaldehyde, **4**, respectively.

At low glycol concentration reaction 5 is unimportant and thus extrapolation of the acetaldehyde yield to zero glycol concentration will give a value for the quantum yield of acetaldehyde produced by reactions 1–4 (Φ^0 (acetaldehyde)). The primary yield of hydroxyl radicals in this system, based on the stoichiometry of reactions 1–7, is then equal to

$$\Phi(\text{hydroxyl radical}) = \Phi^0(\text{acetaldehyde}) + \Phi(\text{glycolaldehyde}) + 2\Phi(\text{succinaldehyde})$$

The limiting yields of acetaldehyde and the yields of glycolaldehyde and succinaldehyde are 0.050, 0.010, and 0.003, respectively, giving an hydroxyl radical yield of 0.066. This value is in excellent agreement with the primary hydroxyl radical yield 0.065 found by Langford and Carey (1) using *tert*-butyl alcohol as a scavenger.

Reactions 1–7 are essentially identical to those observed by Walling and Johnson (17) in the Fenton's reagent oxidation of ethylene glycol. However, several features of the present study cannot be explained by this reaction sequence. They are the appearance of formaldehyde as a photoproduct and the linear increase of quantum yields for formaldehyde and iron(II) with increasing ethylene glycol concentration. Based on reactions 1–7, the iron(II) yield should depend only on the iron(III) and the acid concentrations, and should be constant at high levels of scavenger. Some other photoprocess must be included to successfully account for all observed features.

If ethylene glycol molecules were present in the primary solvation sphere of Fe(III), a ligand-to-metal charge transfer (LMCT) transition between glycol and iron would arise. Excitation of such a transition would likely result in production of iron(II) and an electron deficient glycol. Should this glycol species react via C—C bond fission, the resulting products would be formaldehyde and a hydroxy-methyl radical. Since the latter radicals react with iron(III) to give formaldehyde and iron(II), the net products of the alcohol-to-iron CT photoreaction could be two molecules of formaldehyde and two molecules of iron(II). The C—C bond cleavage proposed is not without precedent. Cox and Kemp (18) have shown that C—C bond fission occurs upon irradiation of iron(III) species in neat alcohol glasses when tertiary alcohols are used as substrates. For primary and secondary alcohols however, the predominant process was C—H bond fission at the α-carbon.

A nuclear magnetic resonance technique for determining whether molecules are in the immediate paramagnetic environment of iron(III) has been described elsewhere (2, 14–16). Hydroxy proton linewidths measured for the ethylene glycol system were essentially identical to those obtained by Carey and Langford (2) for methyl, *tert*-butyl, and isopropyl alcohols. The linewidths are consistent with lack of entry of the scavenger into the coordination sphere and rule out the CT transition as the source of formaldehyde.

However, if ethylene glycol can react with an iron excited state prior to hydroxyl radical production, it is not necessary to propose excitation of a glycol-to-iron transition to explain reactions different from hydroxyl radical scavenging. The reactive excited state need not be long lived since

at the scavenger levels employed a significant number of glycol molecules will be present in the secondary solvation sphere of Fe(III) (*i.e.*, in encounter) at the time of excitation and thus the reaction will not be limited by diffusion of reactants. Such a reaction was recently proposed to explain scavenger dependent iron(II) yields in the photolysis of ferric perchlorate when methyl and isopropyl alcohols and formic acid were used as scavengers (2). The reaction scheme may be written as follows:

$$[8]\quad Fe(H_2O)_6^{3+} + HOCH_2CH_2OH \leftrightarrows Fe(H_2O)_6^{3+}, HOCH_2CH_2OH$$

$$[9]\quad Fe(H_2O)_6^{3+}, HOCH_2CH_2OH \xrightarrow{h\nu} Fe(H_2O)_6^{2+} + HOCH_2^{\cdot} + CH_2O + H^+$$

$$[10]\quad HOCH_2^{\cdot} + Fe(H_2O)_6^{3+} \rightarrow Fe(H_2O)_6^{2+} + CH_2O + H^+$$

The observed glycol dependence of the quantum yield is in agreement with formation of the reactive species via a reaction such as [8] while reactions 9 and 10 represent the formation of iron(II) and formaldehyde via the outer sphere oxidation and indicate that these two products should be formed in a 1:1 ratio. Thus, if the reaction via the outer sphere pathway did not affect the primary yield of hydroxyl radicals the slope of the formaldehyde and iron(II) yields (Fig. 1) should be the same. In fact, the Fe(II) slope is 0.043 l mol^{-1} while the formaldehyde slope is 0.047 l mol^{-1} and the ratio $\Phi_{Fe^{2+}}/\Phi_{CH_2O} = 0.91$. If the outer sphere reaction actually involves an excited state precursor to hydroxyl radicals, the Fe(II) slope must be corrected to account for those excited states which would have produced Fe(II) via the hydroxyl radical pathway but instead undergo prior reaction via the outer sphere pathway.

In order to calculate the magnitude of this correction, it is necessary to know the number of excited states reacting via the outer sphere pathway and the fraction of these which would have produced hydroxyl radicals. Previous studies on the outer sphere reaction suggested that it occurred with unit efficiency for those scavenger molecules in the reactive site at the time of excitation (2). Assuming this to be true for the ethylene glycol system, we find the number of excited states reacting with outer sphere scavenger at any glycol concentration would be $(\frac{1}{2})\Phi_{CH_2O}$ (recall each excited state reacting produces two formaldehyde). If we assume that the state reacting with unit efficiency is the primary excited state, then the fraction of these which would have produced hydroxyl radicals is simply the primary hydroxyl radical yield, 0.066. In this case the hydroxyl radical yield at any ethylene glycol concentration is given by the expression

$$\Phi_{OH^{\cdot}} = 0.066 - 0.066 \times \tfrac{1}{2} \times \Phi_{CH_2O}$$

and the iron(II) yield from the hydroxyl radical pathway is twice this value. Therefore in order to judge the magnitude of the outer sphere reaction from the iron(II) slope, this slope must be corrected according to corrected Fe(II) slope = observed Fe(II) slope + 2 × 0.066 × $\frac{1}{2}$ × formaldehyde slope. We calculate the corrected Fe(II) slope to be 0.046 l mol^{-1}, in good agreement with the observed formaldehyde slope.

We note that in the ethylene glycol case, the observed slope of the iron(II) yield is 0.043, somewhat higher than the 0.030 slopes previously observed for methyl and isopropyl alcohols and formic acid (2). For the latter three organics, the limiting reactivity with the excited state was thought to include a statistical factor which was related to the probability that the scavenger in encounter occupies a reactive site. A higher statistical factor might be anticipated for ethylene glycol since it has two reactive centres while methyl and isopropyl alcohols and formic acid have only one.

To provide additional support to the proposed reaction mechanisms, studies were done at three different Fe(III) concentrations. A plot of Fe(II) as a function of ethylene glycol concentration for three Fe(III) concentrations is shown in Fig. 2. It can be seen that there is very little difference between the slopes of the three lines but there is a significant change in the intercept. Even when radical–radical reaction [7] is omitted, the steady state method yields an extremely complex expression for the $\Phi_{Fe^{2+}}$. However, at zero glycol concentration, a fairly simple expression for $1/\Phi_{Fe^{2+}}{}^0$ is obtained.

$$[11]\quad \frac{1}{\Phi_{Fe^{2+}}{}^0} = \frac{V}{I}\frac{(k_1 + k_{-1})k_3}{2k_1k_6[Fe^{3+}]} + \frac{V}{I}\frac{(k_1 + k_{-1})}{2k_1}$$

where V represents volume, I light intensity in einsteins/s and $\Phi_{Fe^{2+}}{}^0$ the iron(II) yield obtained from extrapolation of the linear portion of Fig. 2 to zero glycol concentration. Since V and I are

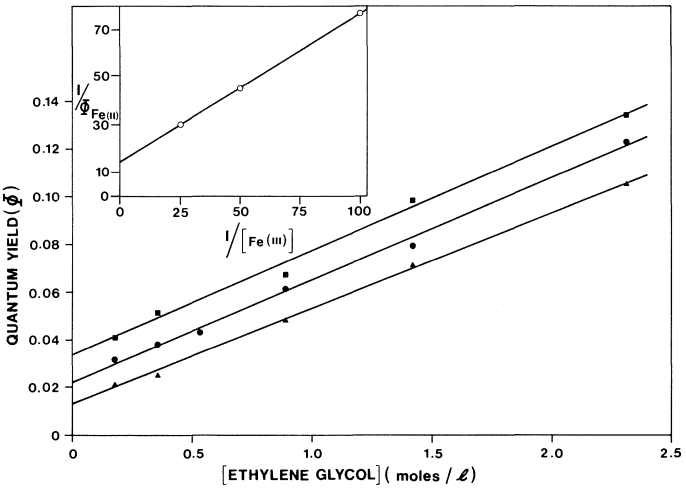

FIG. 2. The quantum yields of Fe(II) at Fe(III) concentrations of 0.01 *M*, ▲; 0.02 *M*, ●; and 0.04 *M*, ■, as a function of ethylene glycol concentration. Inset: Dependence of $1/\Phi^0$ Fe(II) on 1/Fe(III) at zero glycol concentration where Φ^0 Fe(II) is obtained by extrapolation of Fig. 2.

constant during the experiment, the expression simplifies to

$$[12] \qquad \frac{1}{\Phi_{Fe^{2+}}{}^0} = C_1 + \frac{C_2}{[Fe^{3+}]}$$

A plot of $1/\Phi_{Fe^{2+}}{}^0$ *vs.* $1/[Fe^{3+}]$ (inset Fig. 2) is seen to be linear. As the Fe(III) concentration is increased, the Fe(II) quantum yield at zero glycol (the intercept) is seen to increase as predicted by eq. 12. As the Fe(III) concentration is increased, the absolute yield of Fe(II) and glycolaldehyde increase and the yield of acetaldehyde decreases. This behaviour is consistent with the proposed reaction scheme.

The photolysis of aqueous iron solutions containing ethylene glycol proceeds by two major pathways. Reactions based on abstraction of α-hydrogens by hydroxyl radicals leads to production of acetaldehyde as the major product whereas the direct outer sphere oxidation of ethylene glycol by excited states of Fe(III) yields formaldehyde and Fe(II) as major products. The observation that different products are formed by the two different mechanisms of oxidation is of interest since it raises the possibility that scavenging with ethylene glycol/iron(III) can be used to elucidate mechanisms of photooxidation of other systems. We are presently investigating the use of this scavenger system to study reaction mechanisms during illumination of semi-conductor electrode surfaces (19) and sediment–water interfaces.

1. C. H. LANGFORD and J. H. CAREY. Can. J. Chem. **53**, 2430 (1975).
2. J. H. CAREY and C. H. LANGFORD. Can. J. Chem. **53**, 2436 (1975).
3. B. E. JANK, H. M. GUO, and V. W. CAIRNS. Environment Canada, Technology Development Report, EPS4-WP-73-6 (1973).
4. P. J. VENTER, H. J. VAN DER LINDE, and R. A. BASSON. Chem. Commun. 187 (1972).
5. C. E. BURCHILL and K. M. PERRON. Can. J. Chem. **49**, 2382 (1971).
6. H. J. VAN DER LINDE and C. V. SONNTAG. Photochem. Photobiol. **13**, 147 (1971).
7. A. L. BULEY, R. O. C. NORMAN, and R. J. PRITCHETT. J. Chem. Soc. B, 849 (1966).
8. B. C. GILBERT, J. P. LARKIN, and R. O. C. NORMAN. J. Chem. Soc. Perkin II, 794 (1972).
9. C. G. HATCHARD and A. C. PARKER. Proc. R. Soc. A, **235**, 518 (1956).
10. F. D. SNELL and C. T. SNELL. Colorimetric methods of analysis. Vol. III. Van Nostrand, New York. 1953. p. 263.
11. M. J. HOULE, D. E. LONG, and D. SMITHE. Anal. Lett. **3**, 401 (1970).
12. M. AHMAD, M. AWAN, and D. MOHAMMAD. J. Chem. Soc. B, 946 (1968).
13. E. SAWICKI and J. D. PFAFF. Chem. Anal. **55**, 6 (1966).
14. L. S. FRANKEL, T. R. STENGLE, and C. H. LANGFORD. Can. J. Chem. **46**, 3183 (1968).
15. L. S. FRANKEL, T. R. STENGLE, and C. H. LANGFORD. J. Phys. Chem. **74**, 1645 (1970).
16. V. S. SASTRI, R. W. HENWOOD, S. BEHRENDT, and C. H. LANGFORD. J. Am. Chem. Soc. **94**, 753 (1972).
17. C. WALLING and R. A. JOHNSON. J. Am. Chem. Soc. **97**, 2405 (1975).
18. A. COX and T. J. KEMP. J. Chem. Soc. Faraday I, **71**, 2490 (1975).
19. J. H. CAREY and B. G. OLIVER. Nature, **259**, 554 (1976).

A study of 3-hydroxy-1,2,3-benzotriazin-4-one and its *O*-methyl and *O*-acyl derivatives

T. PATRICK AHERN, THOMAS NAVRATIL, AND KEITH VAUGHAN[1]

Department of Chemistry, Saint Mary's University, Halifax, N.S., Canada B3H 3C3

Received August 4, 1976

T. PATRICK AHERN, THOMAS NAVRATIL, and KEITH VAUGHAN. Can. J. Chem. **55**, 630 (1977).

3-Hydroxy-1,2,3-benzotriazin-4-one, **1**, was prepared by diazotization of *o*-aminobenzhydroxamic acid, **2**. 3-Methoxy-1,2,3-benzotriazin-4-one, **5***a*, was obtained by reaction of **1** with dimethyl sulphate and was found to be stable to thermolysis. Acetylation and benzoylation of **1** yielded the *N*-acetoxy-**5***b* and benzoyloxy-**5***c* derivatives respectively. The *N*-benzoyloxy derivative **5***c* is converted into the acetate **5***b* by a novel 'acyl-exchange' reaction in acetic anhydride. Acid hydrolysis of **1** gives anthranilic acid, and thermolyses of **1** in amyl alcohol and aniline afford amyl anthranilate and *N*-phenylanthranilamide, respectively. The ketenimine **11** is postulated as an intermediate in the thermal breakdown of **1**, and this is confirmed by the isolation of the Diels–Alder adduct **12** from reaction of **1** with phenyl isocyanate. Thermolysis of **1** in inert solvents affords a novel compound, 3-(*o*-aminobenzoyloxy)-1,2,3-benzotriazin-4-one, **6**, which polymerizes when **1** is subjected to prolonged thermolysis in diglyme. **6** resisted methylation and acid hydrolysis, but underwent acyl-oxygen cleavage when diazotization of **6** was attempted and suffered 'acyl-exchange' when acylation was attempted. The formation of **6** from **1** also involves the ketenimine **11**. The importance of these observations to an understanding of previously reported reactions of benzotriazinones is discussed. The *o*-aminobenzoyloxy derivative **6** shows potential as an *o*-aminobenzoylating agent.

T. PATRICK AHERN, THOMAS NAVRATIL et KEITH VAUGHAN. Can. J. Chem. **55**, 630 (1977).

On a préparé l'hydroxy-3 benzotriazine-1,2,3 one-4, **1**, par diazotation de l'acide *o*-aminobenzhydroxamique, **2**. On a obtenu la méthoxy-3 benzotriazine-1,2,3 one-4, **5***a*, par réaction de **1** avec le sulfate de méthyle et on a trouvé qu'il est stable vis-à-vis la thermolyse. L'acétylation et la benzoylation de **1** conduisent respectivement aux dérivés *N*-acétoxy-**5***b* et benzoyloxy-**5***c*. Le dérivé *N*-benzoyloxy **5***c* peut être transformé en acétate **5***b* par une nouvelle réaction 'd'échange acyle' dans l'anhydride acétique. L'hydrolyse acide de **1** fournit l'acide anthranilique et les thermolyses de **1** dans l'alcool amylique et l'aniline conduisent respectivement à l'anthranilate d'amyle et au *N*-phénylanthranilamide. On fait l'hypothèse que la cétimine **11** est un intermédiaire dans la décomposition thermique de **1** et cette hypothèse est confirmée par le fait que l'on peut isoler l'adduit de Diels–Alder **12** à partir de la réaction de **1** en présence d'isocyanate de phényle. La thermolyse de **1** dans des solvants inertes conduit à un nouveau composé la (*o*-aminobenzoyloxy)-3 benzotriazine-1,2,3 one-4, **6**, qui se polymérise lorsque **1** est soumis à une thermolyse prolongée dans le diglyme. On ne peut ni méthyler ni hydrolyser le composé **6** en milieu acide; toutefois si l'on essaie d'effectuer une diazotation de **6**, il subit un clivage au niveau acyl-oxygène alors qu'il subit un échange d'acyle lorsque l'on essaie l'acylation. La formation de **6** à partir de **1** implique elle aussi la cétimine **11**. On discute de l'importance de ces observations pour la compréhension des réactions rapportées antérieurement pour les benzotriazinones. Il semble que le dérivé *o*-aminobenzoyloxy **6** montre des potentialités comme agent *o*-aminobenzoylant.

[Traduit par le journal]

Introduction

3-Hydroxy-1,2,3-benzotriazin-4-one, **1**, was first reported by Harrison and Smith (1) from diazotization of *o*-aminobenzhydroxamic acid, **2**. The cyclic hydroxamic acid structure was assigned to **1** because of the observed red colouration with ferric chloride and the alkaline degradation of **1** to *o*-azidobenzoic acid. The unique nature of **1**, being a combination of hydroxamic acid and triazine moieties in a single structure, presents the possibility of some interesting chemistry. A preliminary account of the thermolysis of **1** has been reported previously (2), and this paper reports some new reactions of **1** and its derivatives.

[1]Author to whom correspondence should be addressed (present address, until August 1977, Department of Pharmacy, University of Aston in Birmingham, Birmingham B4 7ET, England).

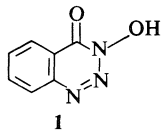
1

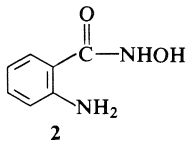
2

Discussion

o-Aminobenzhydroxamic acid, **2**, required for the synthesis of **1**, was prepared by the reaction of methyl anthranilate with hydroxylamine in alkaline solution as described by Scott and Wood (3). The reaction of isatoic anhydride **3** with hydroxylamine, a possible alternate route to **2**, was interpreted by Scott and Wood (3) as giving rise to the isomer of **2**, the *O*-acyl-hydroxylamine **4**.

Diazotization of *o*-aminobenzhydroxamic acid, **2**, afforded the same 3-hydroxy-1,2,3-benzotriazin-4-one, **1**, described by Harrison and Smith (1); the spectral characteristics of **1**, and the structure of the derivatives described below, confirm the assignment of the cyclic hydroxamic acid structure to the diazotization product. The ir spectrum of **1** displays a broad, hydrogen-bonded hydroxyl band at 2700 cm^{-1} and carbonyl absorption at 1660 cm^{-1}. Methylation of **1** with dimethyl sulphate under basic conditions affords a single *O*-methyl derivative **5***a*, which shows an *O*-methyl proton resonance at τ 5.72 in the nmr spectrum. The structure of **5***a* was confirmed by the mass spectrum, elemental analysis, and a narrow carbonyl absorption band at 1700 cm^{-1} in the ir spectrum. The broadness of the carbonyl band in **1**, and the shift to lower frequency compared with the carbonyl absorption in **5***a*, suggest the presence of intramolecular hydrogen bonding in **1**. Strong intramolecular hydrogen bonds have also been shown to exist in other cyclic hydroxamic acids, *e.g.* *N*-hydroxy-2-pyridone (4, 5).

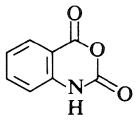
3

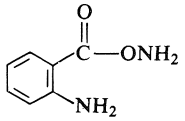
4

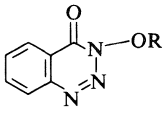
5 *a* R = CH_3
b R = $COCH_3$
c R = COPh

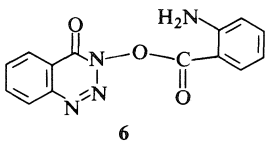
6

Acetylation of the *N*-hydroxytriazinone **1** with acetyl chloride or acetic anhydride afforded a single mono-acetyl derivative, characterized as the *N*-acetoxytriazinone **5***b* by the presence of a strong carbonyl band at 1805 cm^{-1} and acetyl-methyl proton resonance at τ 7.43. Reaction of the *N*-hydroxytriazinone **1** with benzoyl chloride similarly gave the *N*-benzoyloxy derivative **5***c*. The uv spectra of the *N*-hydroxytriazinone **1** and the methyl-**5***a*, acetyl-**5***b*, and benzoyl-**5***c* derivatives show distinct similarities, with common bands at 220–230 and 300–313 nm (Fig. 1). However, the band at 250–260 nm, common to **1**, **5***a*, and **5***b*, is absent in the spectrum of the benzoate **5***c*, whereas the band at 280–290 nm, common to the derivatives **5***a*, **5***b*, and **5***c*, is not observed in the spectrum of **1**. An additional band at 384 nm is observed only in the spectrum of **1**.

The mass spectral fragmentation patterns of the derivatives **5***a–c* show several common features, but also significant differences (Scheme 1). Two fragmentation pathways are evident for the *O*-methyl derivative **5***a*. The major pathway is ring cleavage (route *d*), apparently by direct loss of the fragment HNCO; *N*-alkoxy cleavage (route *a*), involving loss of CH_2O, is the lesser pathway. No fragments are observed in the mass spectrum of **5***a* corresponding to loss of N_2 (route *c*) or to *O*-alkyl cleavage (route *b*). Ring cleavage (route *d*) is also the principle fragmentation of the acetate **5***b*, but in this case *O*-acyl cleavage (route *b*) is more evident than *N*-acetoxy cleavage (route *a*); fragmentation by loss of N_2 (route *c*) is not observed. The mass spectrum of the benzoate **5***c* shows both *N*-acyloxy (route *a*) and *O*-acyl (route *b*) cleavages, but unlike the methyl and acetyl derivatives, **5***c* shows fragmentation by the loss of N_2 (route *c*) and, surprisingly, by loss of CO_2 (route *e*).

The properties and reactions of **1** described above are clearly consistent with the cyclic hydroxamic acid structure proposed previously (**1**) and no evidence has been found to suggest the existence of an *N*-oxide tautomer of **1**. In this respect, **1** is similar to many other *N*-hydroxy α-oxo compounds, which have been shown to prefer the oxo form over the *N*-oxide form (ref. 5, p. 407–408).

Thermolysis of the *N*-hydroxytriazinone **1** in anhydrous inert solvents, *e.g.* diglyme (1.3 h), *p*-xylene (2.5 h), toluene (20 h), or benzene (4–5 days), afforded in each case the same yellow solid,

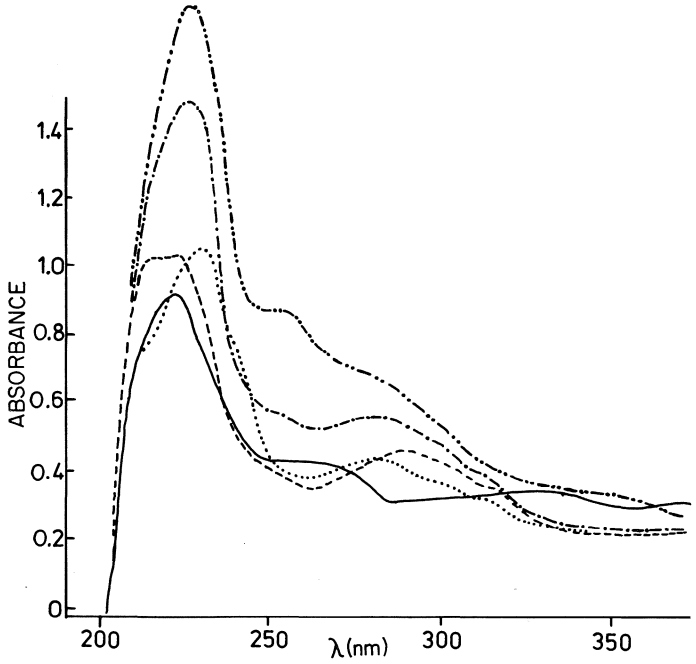

FIG. 1. Ultraviolet spectra, recorded in ethanol solution, of *I* (—) 3-hydroxy-1,2,3-benzotriazin-4-one **1**; *II* (---) 3-methoxy-1,2,3-benzotriazin-4-one **5***a*; *III* (·····) 3-acetoxy-1,2,3-benzotriazin-4-one **5***b*; *IV* (····) 3-benzoyloxy-1,2,3-benzotriazin-4-one **5***c*; and *V* (·····) 3-(*o*-aminobenzoyloxy)-1,2,3-benzotriazin-4-one **6**.

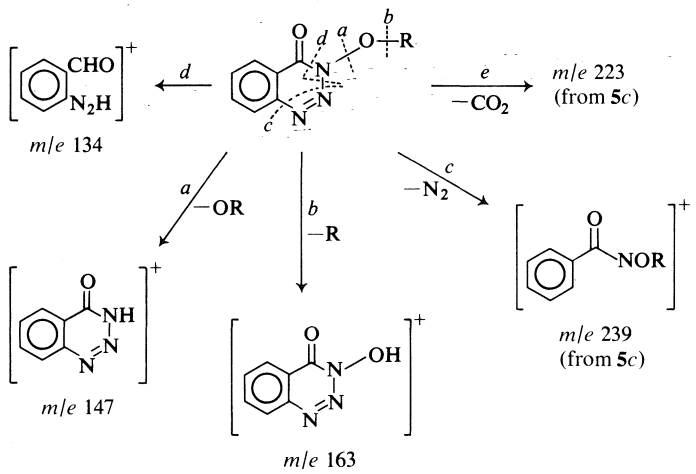

SCHEME 1

which was found by molecular ion mass measurement to have molecular formula $C_{14}H_{10}N_4O_3$. The yellow solid evidently arises from a dimerization of **1**, minus the elements of N_2O, and was identified as 3-(*o*-aminobenzoyloxy)-1,2,3-benzotriazin-4-one, **6**, on the basis of spectral data and degradation. The presence of NH_2 is indicated by bands at 3480 and 3365 cm^{-1} in the ir spectrum of **6**, which also displays bands for two carbonyl groups at 1740 and 1713 cm^{-1}. The mass spectrum of **6** exhibits fragments arising from *N*-acyloxy cleavage (route *a*), *O*-acyl cleavage (route *b*), and loss of CO_2 (route *e*), but not direct loss of N_2 (route *c*) (see Scheme 1). The uv spectrum of **6** shows close similarity to the acyl derivatives **5***b* and **5***c* (Fig. 1).

The *N*-benzoyloxy function in heterocyclic compounds is generally labile and susceptible to ready hydrolysis (6), whereas **6** was resistant to concentrated acid at room temperature and did not react with dimethyl sulphate under basic conditions. However, when diazotization of **6** was attempted in order to react the diazonium salt with hydroxylamine or azide ion, rapid cleavage of the acyloxy group resulted and the *N*-hydroxytriazinone **1** was isolated in high yield. These observations imply that the *o*-amino group in **6** renders the acyloxy group unreactive by its electron-donating resonance effect, but that this effect is reversed when the amino group is converted to a diazonium group.

Attempted acetylation of **6** with acetyl chloride or acetic anhydride also caused acyl-oxy cleavage, affording a mixture of the *N*-acetoxy derivative **5***b* and *N*-acetylanthranilic acid. Similarly, treatment of **6** in pyridine with benzoyl chloride resulted in immediate formation of the *N*-benzoyloxy derivative **5***c*. Acylation of the amino group in **6** would certainly lessen the deactivation of the acyloxy group and this may be a factor in facilitating these apparent cleavage reactions. However, a similar 'acyl-exchange' reaction was observed when 3-benzoyloxy-1,2,3-benzotriazin-4-one, **5***c*, was treated with acetic anhydride, even though specific precautions were taken to exclude water from the reaction mixture, resulting in formation of the acetoxy derivative **5***b*. Benzoic acid, an expected product of hydrolysis of **5***c*, was not observed as a by-product in the conversion **5***c* → **5***b*. Thus, the 'acyl-exchange' reaction does not require activation by a substituent in the aryl group, and apparently is not a result of hydrolysis and re-acylation. It is therefore likely that the conversions **6** → **5***b*, **6** → **5***c* and **5***c* → **5***b* occur by a common 'acyl-exchange' mechanism involving a cyclic, six-membered transition state (*e.g.* [1]).[2] This behaviour of the *N*-aroyloxy derivatives **6** and **5***c* is analogous to the property of 1-benzoyloxy-2-pyridone, which is a good benzoylating agent

[1]

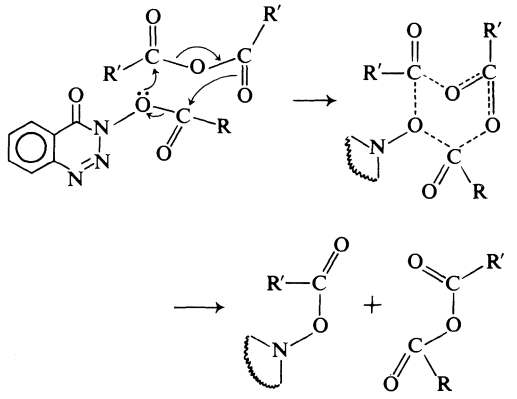

(6*a*). The *o*-aminobenzoyl derivative **6** may also have application as an *o*-aminobenzoylating (anthraniloylating) agent; indeed, benzylamine was converted into *N*-benzylanthranilamide by reaction with **6** in acetonitrile [2]. However,

[2]

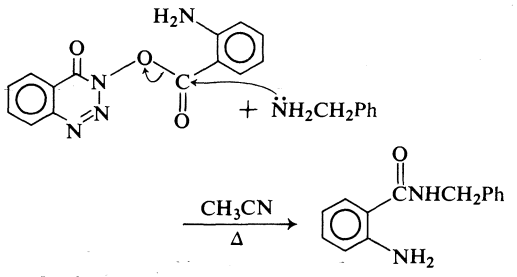

reaction of **6** with aqueous methylamine did not afford *N*-methylanthranilamide; the *N*-hydroxytriazinone **1** was recovered in the latter reaction. The synthetic potential of **6** as an *o*-aminobenzoylating agent is under further investigation.

The *N*-*o*-aminobenzoyloxy derivative **6** shows no tendency to form a diazoxepine by ring closure. Prolonged thermolysis of the *N*-hydroxytriazinone **1** in diglyme resulted in further reaction of **6**, but the preferred mode of reaction appears to be polymerization of **6**, and cyclodehydration of the polymer species. The diglyme reaction gave a low yield of a high melting solid, which exhibited mass spectral fragments as high as *m*/*e* 577. More significantly, the mass spectral fragments fall into several sequences, which are identical but for a common increment of 119 mass units (corresponding to the monomer unit —NH · C_6H_4 · CO—). This observation suggests the polymerization and cyclodehydration pathway shown in Scheme 2. Initially, the monomer **6** anthraniloylates itself by nucleo-

[2]The 'acyl-exchange' observed here is significantly different from previously observed 'acyl-transfer' reactions (20). Transacylation from benzoyl chloride has been observed in the conversion of *N*-acyl-5-aminopyrimidines to pyrimidino-isoxazoles (20*a*), whereas the transacylation of diacylanilines takes place only with carboxylic acids, or with anhydrides in the presence of a catalyst (20*b*). In the latter reactions, acylium ions are postulated as intermediates. Transacylation in anthracene di-*O*-acyl derivatives is also initiated by carboxylic acids (20*c*).

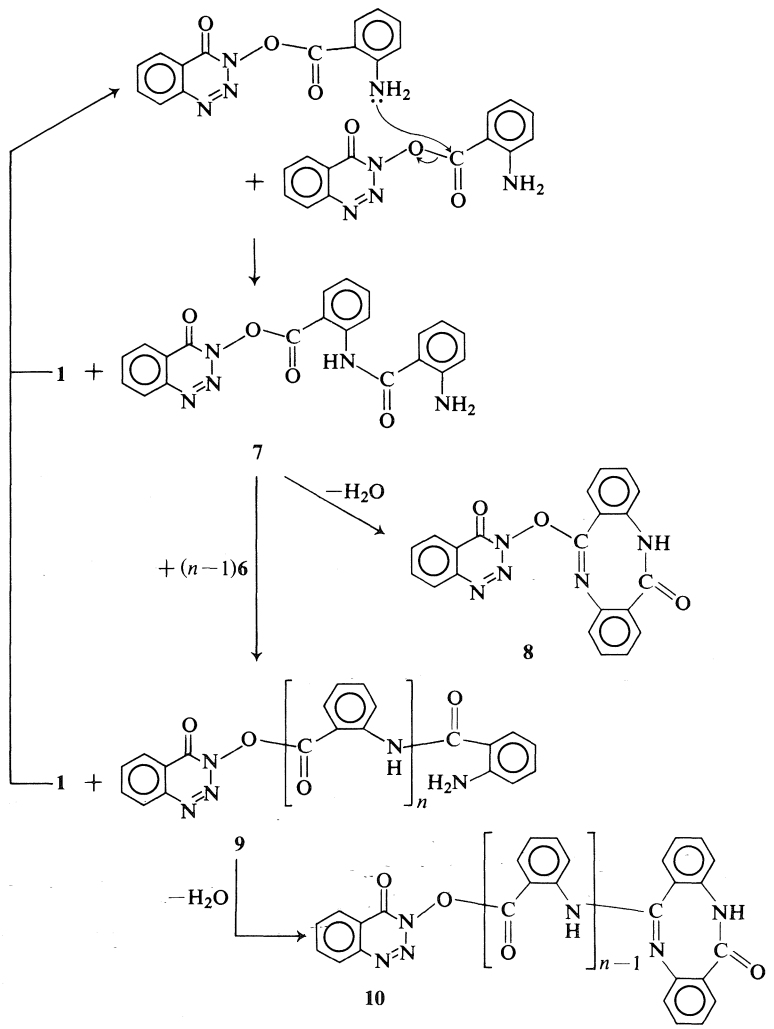

SCHEME 2

philic displacement of the *N*-oxytriazinone fragment, resulting in formation of the amide **7**, which can then readily cyclodehydrate to afford the diazocine **8**. The molecular ion of **8** (M^+ 383), and fragments at *m/e* 366, 357, 339, 322, 312, and 297 resulting from breakdown of **8**, are observed in the mass spectrum of the polymeric material from the diglyme reaction. Repeated reaction of **7** with **6** affords the polymeric amides **9** ($n = 2, 3, 4 \ldots$ etc) which can dehydrate in an analogous manner to give a series of diazocines **10**. The mass spectrum of the polymeric material shows clearly a fragment at *m/e* 502, corresponding to the molecular ion of the diazocine **10** ($n = 2$), and further fragments at *m/e* 485, 476, 458, 441, and 432. The fragments at *m/e* 577, 560, 551, and 533 correspond exactly to the breakdown predicted for the diazocine **10** ($n = 3$) on the basis of the fragmentations of **8** and **10** ($n = 2$). Thus, the mass spectrum of the polymeric material from the diglyme thermolysis of **1** is a conglomeration of the mass spectra of several diazocines of general formula **10**. Similar diazocine formation has been observed recently in the pyrolysis of an *o*-aminobenzoylimidazole (7).

The formation of **6** in the thermolysis of **1** has previously been accounted for (2) by the initial formation of the ketenimine **11**, followed by nucleophilic addition to the ketene by the hydroxylic function of a second molecule of **1** [3].

[3] 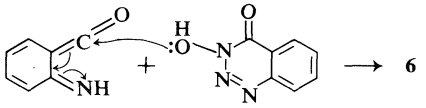 6

11

Further evidence for ketenimine formation is found in the solvolyses of **1** with nucleophilic solvents. Thermolysis of **1** in *n*-amyl alcohol affords *n*-amyl *o*-aminobenzoate and in aniline affords *N*-phenylanthranilamide, both products arising by addition of the nucleophile (ROH and $PhNH_2$ respectively) to the ketene. Addition of water to the ketene may also account for the formation of anthranilic acid in the acid hydrolysis of **1**, in contrast to the previously recorded (1) formation of *o*-azidobenzoic acid in the alkaline hydrolysis of **1**. The *N*-hydroxytriazinone **1** was recovered mainly unchanged from boiling water, but the formation of a small amount of anthranilic acid was evident. The formation of the Diels–Alder adduct, 3-phenylquinazolin-2,4(1*H*)-dione, **12**, from the reaction of **1** with phenyl isocyanate is clear evidence for the intermediate formation of **11** from **1** [4].

[4] 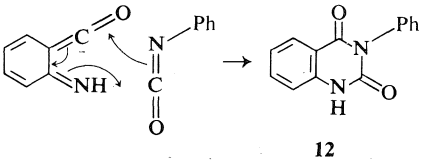

12

Ketenimines, valence tautomers of benzazetidones, have been postulated as intermediates in the thermolysis of 1,2,3-benzotriazin-4(3*H*)-one **13** (8, 9), isatoic anhydride (9), saccharin (10) and 3-phenyl-1,2,3-benzotriazin-4-one (11). Several modes of formation of the ketenimine **11** in

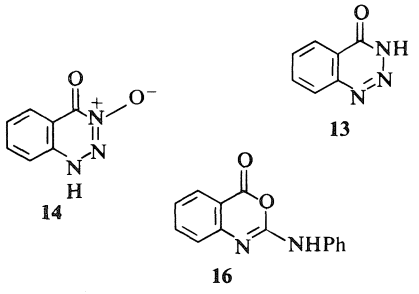

14 13 16

the thermolysis of **1** are possible. Direct loss of N_2O from the *N*-oxide tautomer **14** is a very attractive and simple mechanism, but the properties of **1** give no indication of the existence of an *N*-oxide tautomer and the involvement of **14** in the conversion **1** → **11** is unlikely. A further possibility is that fragmentation of **1** involves initial loss of N_2 by ring cleavage, as observed in the thermolysis of 3-phenyl-1,2,3-benzotriazin-4-one (11), in which case an analogous thermal breakdown of 3-methoxy-1,2,3-benzotriazin-4-one **5***a* would be expected. However, the *N*-methoxytriazinone was recovered quantitatively unchanged after prolonged refluxing in *p*-xylene.

Since the same ketenimine **11** has been postulated as an intermediate in the thermolysis of benzotriazinone **13** (8, 9), the possibility of an initial deoxygenation of **1** to give **13** as an intermediate was considered. Thermal deoxygenation of cyclic hydroxamic acids, although rare, has been reported previously (12). However, the conversion **1** → **6** takes place at temperatures much lower than those required to initiate reaction of benzotriazinone **13**, and benzotriazinone is not formed as a by-product of the thermolysis of **1**. Furthermore, benzotriazinone **13** was recovered almost quantitatively unchanged when an equimolar mixture of **1** and **13** was subjected to thermolysis in benzene. Only a small recovery of **13** was obtained when **1** and **13** were refluxed together in *p*-xylene and the only product in addition to **13** was the *N*-(*o*-aminobenzoyloxy)triazinone **6**, the yield of which was greater than could be accounted for on the basis of the amount of **1** used. Evidently, at least some of **6** arises by direct interaction of **1** and **13**, where the nucleophile **1** attacks the 4-oxo group in **13**, as observed previously in the reaction of benzotriazinone **13** with alcohols and other nucleophiles (13) [5].

[5] 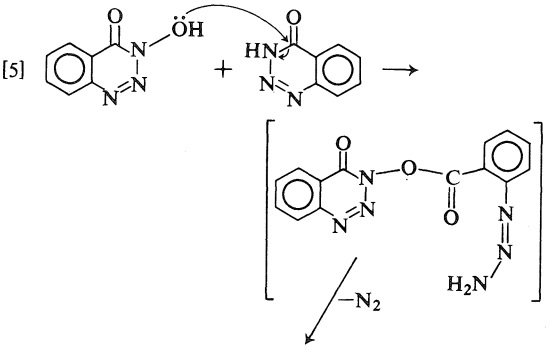

6

The alternative, and most likely, mechanism of formation of the ketenimine from **1** is a concerted process involving deoxygenation accom-

panied by fragmentation of the triazine ring. Such a deoxidative ring cleavage mechanism would give rise to the open-chain triazene intermediate **15**, which would be expected to undergo facile nitrogen elimination (14) directly to the ketenimine [6].

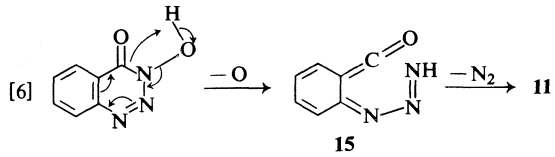

An analogous mechanism, also involving a triazene intermediate, has been postulated to account for the formation of acridone in the photolysis of 3-phenyl-1,2,3-benzotriazin-4-one (15).

The mode of thermal decomposition of the cyclic hydroxamic acid **1** is clearly different from that of benzotriazinone **13**. Thermolyses of the latter in diglyme (13), and in reactive methylene compounds (16), have been shown to be bimolecular, whereas Herlinger (8) and Crabtree *et al.* (9) have suggested that the ketenimine **11** is an intermediate in the thermolysis of benzotriazinone. Herlinger's hypothesis was based on the observation that thermolysis of **13** with phenyl isocyanate afforded the oxazinone **16**, which was explained as a Diels–Alder adduct of the ketenimine and the isocyanate. However, such a Diels–Alder reaction is contrary to the normal mode of cycloaddition of the isocyanate group (17), in which the C=N group, not C=O, is the dienophile. Crabtree *et al.* (9) also questioned the validity of the Diels–Alder mechanism for the formation of **16** from **13**, but on the basis of comparison of thermolysis temperatures; they proposed an alternative polar mechanism which was substantiated by isolation of an intermediate carbamoylbenzotriazinone. In the present work, no such intermediate was evident in the conversion **1** + PhN=C=O → **12**. The formation of **12** from the thermolysis of **1** with phenyl isocyanate is consistent with the normal mode of cycloaddition of the isocyanate, and is therefore clear evidence for the intermediate formation of the ketenimine **11** in the thermolysis of **1**.

Experimental

Melting points were recorded on a hot-stage apparatus (Reichert) and are uncorrected. Infrared spectra were recorded with Nujol suspensions on a Perkin-Elmer model 467 grating spectrophotometer; uv spectra were obtained for ethanolic solutions with a Perkin-Elmer model 402 spectrophotometer. Nuclear magnetic resonance spectra were measured on Varian A-60A or EM360 spectrometers using tetramethylsilane as internal standard. Mass spectra (medium resolution) were recorded with a Dupont/C.E.C. model 21-491 spectrometer using direct insertion, and high resolution molecular ion mass measurement was carried out by the peak-matching method, using electrical detection, with a Dupont/C.E.C. 21-110B spectrometer. Microanalyses were conducted by Chemalytics Inc., Tempe, Arizona.

o-Aminobenzhydroxamic Acid ***2***

Methyl anthranilate reacted with hydroxylamine in the presence of sodium hydroxide, according to the method of Scott and Wood (3), to yield *o*-aminobenzhydroxamic acid (43–51%); mp 144–146 °C (from ether) (lit. (3) mp 149 °C); ν_{max} 3400, 3300, 3150, 3300–2500 (broad), and 1640 cm^{-1}.

3-Hydroxy-1,2,3-benzotriazin-4-one ***1***

o-Aminobenzhydroxamic acid (32.2 g) in concentrated hydrochloric acid (56 ml), diluted with water (600 ml), was diazotized at 0–5 °C with sodium nitrite (16.0 g) in water (50 ml). The diazonium salt solution was then removed from the cold bath, stirred at room temperature for 0.75 h, and filtered to afford the *N*-hydroxytriazinone (19.2 g, 55%), mp 182–182.5 °C (dec.) (colourless needles from ethanol) (lit. (1) mp 180–181 °C), ν_{max} 2700 (broad OH), 1700 (sh), and 1660 cm^{-1}; λ_{max} 221, 260, 303, and 384 nm.

Methyl Derivative

The *N*-hydroxytriazinone **1** reacted with dimethyl sulphate in aqueous sodium hydroxide at room temperature to afford 3-methoxy-1,2,3-benzotriazin-4-one **5***a* (55% yield); mp 134–135 °C (white needles from ethanol); ν_{max} 1700 cm^{-1}; λ_{max} 220, 250(sh), 290, and 313 nm; δ($CDCl_3$) 7.3–8.5 (4H, m, aromatic), 4.28 (3H, s, —OMe); M^+ 177(22%), *m/e* 147(2%), 134(25%), 120(4%), 118(22%), 106(31%), 104(59%), 91(100%), 78(100%). *Anal.* calcd. for $C_8H_7N_3O_2$: C 54.20, H 3.98, N 23.70; found: C 53.77, H 4.03, N 23.61.

3-Acetoxy-1,2,3-benzotriazin-4-one ***5b***

(*a*) The *N*-hydroxytriazinone **1** (0.5 g) was refluxed in freshly distilled acetyl chloride (20 ml) for 1.0 h. The excess acetyl chloride was evaporated under vacuum, with care to avoid sublimation of the product, and the residue yielded the *N*-acetoxy derivative (0.26 g, 41%), mp 174–175 °C (colourless prisms from benzene), ν_{max} 1805 and 1700 cm^{-1}; λ_{max} 225, 250 (sh), 280, and 312 (w) nm; δ(DMSO-d_6) 8.5–7.9 (4H, m, aromatic) and 2.57 (3H, s, —CO·Me); M^+ 205(73%), *m/e* 163(10%), 147(5%), 135(95%), 104(50%), 91(27%) and 79(100%). *Anal.* calcd. for $C_9H_7N_3O_3$: C 52.70, H 3.41, N 20.50; found: C 52.46, H 3.54, N 20.41.

(*b*) The *N*-hydroxytriazinone **1** (0.5 g) was heated with acetic anhydride (4.0 ml) at 100 °C for 0.5 h. After standing at room temperature for 2 h, the mixture was treated with water to afford the same *N*-acetoxy derivative (0.4 g, 64%).

3-Benzoyloxy-1,2,3-benzotriazin-4-one ***5c***

The *N*-hydroxytriazinone **1** (0.5 g) was dissolved in

redistilled pyridine (3.0 ml) and freshly distilled benzoyl chloride (0.5 g) was added, whereupon a vigorous reaction ensued. The mixture was heated over a flame for 2 min and poured, with constant agitation, into cold water (15 ml). After vigorous mixing, the supernatant liquor was decanted and the residue was triturated with 1 *N* sodium carbonate (10 ml). Separation of the solid material afforded the benzoate **5***c* (0.65 g, 79%), mp 158–160 °C (pale yellow needles from ethanol), ν_{max} 1760 and 1700 cm^{-1}; λ_{max} 215 (sh), 230, 280, 300 (sh), and 313 nm; M^+ 267(53%), *m/e* 238(0.3%), 223(0.4%), 209(3%), 195(0.7%), 180(0.8%), 163(0.4%), 152(5%), 147(3%), 122(9%), 119(3%), 105(100%). *Anal.* calcd. for $C_{14}H_9N_3O_3$: C 62.90, H 3.37, N 15.70; found: C 62.68, H 3.47, N 15.68.

Reaction of the Benzoate 5c with Acetic Anhydride

3-Benzoyloxy-1,2,3-benzotriazin-4-one (0.1 g) was refluxed in anhydrous, freshly distilled acetic anhydride (0.5 ml) for 10 min and the resulting mixture was poured into cold water (10 ml). After boiling briefly to destroy acetic anhydride, the mixture was cooled and filtered to afford 3-acetoxy-1,2,3-benzotriazin-4-one **5***b* (44 mg, 62%), identical in all respects with a sample prepared above.

The aqueous mother liquor was extracted with ether, and the dried ($MgSO_4$) ether extract was evaporated to dryness. Trituration of the residue with petroleum ether afforded a small yield (less than 5%) of the *N*-hydroxytriazinone **1**. Evaporation of the petroleum ether washings gave an oily residue; tlc analysis of the residue showed that benzoic acid was not present.

3-(o-Aminobenzoyloxy)-1,2,3-benzotriazin-4-one 6

(*a*) 3-Hydroxy-1,2,3-benzotriazin-4-one (1.0 g) was refluxed in anhydrous diglyme (Na dried) (25 ml) for 1.3 h. The solution changes colour slowly from yellow to brown. Evaporation of the diglyme under vacuum left a brown oil, which solidified after 5 min. Trituration of the residue with benzene afforded 3-(*o*-aminobenzoyloxy)-1,2,3-benzotriazin-4-one **6** (0.92 g, 97%); mp 204–206 °C (dec.) (yellow prisms from toluene); ν_{max} 3480, 3365, 1740, and 1713 cm^{-1}; λ_{max} 226, 253, 276, 310, and 350 nm; M^+ found 282.0743(7%), calcd. for $C_{14}H_{10}N_4O_3$ 282.0753; *m/e* 238 (0.5%, $M - CO_2$), 163 (0.2%, $M - NHC_6H_4CO$), 147 (0.3%, $M - NHC_6H_4CO_2$), 137 (0.7%, $C_7H_7NO_2$), 120 (100%, $NH_2C_6H_4CO$).

(*b*) 3-Hydroxy-1,2,3-benzotriazin-4-one (0.5 g) was refluxed in anhydrous *p*-xylene (17.5 ml) for 2.5 h. The reaction mixture was cooled and the resulting crystalline mass was filtered to afford directly the *o*-aminobenzoyloxytriazinone **6** (0.34 g, 72%), identical with the product from (*a*) above.

(*c*) The *N*-hydroxytriazinone **1** (0.25 g) was refluxed in anhydrous toluene (20 ml) for 20 h. The yellow solution was evaporated to dryness and the residue was the *o*-aminobenzoyloxy compound **6** (quantitative yield), which was identical with the product from (*a*).

(*d*) *i*—**1** (0.25 g) was refluxed in anhydrous benzene (20 ml) for 48 h. Separation of the crystallized solid from the cooled reaction mixture afforded unchanged starting material (0.176 g, 70% recovery). Evaporation of the mother liquor under vacuum afforded the same *o*-aminobenzoyloxy compound **6** (0.065 g, 100% yield based on unrecovered starting material).

ii—**1** (0.25 g) was refluxed in anhydrous benzene (125 ml) for 112.5 h. The reaction was followed by tlc analysis until **1** did not appear on the chromatogram. Evaporation of the benzene under vacuum afforded a quantitative yield of **6**.

Prolonged Thermolysis of the N-Hydroxytriazinone 1 in Diglyme

1 (0.5 g) was refluxed in anhydrous diglyme (20 ml) for 24 h (tlc analysis of the reaction mixture showed the presence of several components after only 5 h of reflux). The reaction mixture was cooled and the precipitate was filtered to afford a solid material, yield 10.4 mg; mp > 300 °C. The mass spectrum of the high-melting solid exhibited the following fragments: *m/e* 577, 560, 551, 533, 514, 502, 485, 476, 458, 441, 432, 411, 383, 366, 357, 339, 322, 312, 297, 281, 265, 249, 238, 221, 210, 120 (base).

Evaporation of the diglyme mother liquor gave an intractable brown gum.

Thermolysis of 3-Hydroxy-1,2,3-benzotriazin-4-one 1 with 1,2,3-Benzotriazin-4-one 13

(*a*) 1,2,3-Benzotriazin-4-one (0.3 g, 0.002 mol) was dissolved in anhydrous *p*-xylene (40 ml) with 3-hydroxy-1,2,3-benzotriazin-4-one (0.66 g, 0.004 mol) and the mixture was refluxed for 2.5 h. The cooled reaction mixture produced a bright yellow precipitate; filtration afforded the *o*-aminobenzoyloxytriazinone **6** (0.55 g). Evaporation of the filtrate and trituration of the residue with benzene gave a solid which was extracted with aqueous NaOH and filtered to afford a second crop of the *o*-aminobenzoyloxytriazinone (total yield 0.58 g, 0.0021 mol). The sodium hydroxide washings were acidified with acetic acid and extracted with chloroform. Evaporation of the dried ($MgSO_4$) chloroform extract afforded unreacted benzotriazinone **13** (< 10 mg).

(*b*) **13** (0.226 g, 0.00153 mol) and **1** (0.250 g, 0.00153 mol) were mixed in anhydrous benzene (125 ml) and refluxed for 112.5 h. The solution was concentrated, under vacuum, to approximately 20 ml in volume and cooled to afford an orange precipitate, which was filtered. This solid (0.237 g) consisted almost entirely of unreacted benzotriazinone **13** (recovery > 95%), but did contain a small amount of the *o*-aminobenzoyloxytriazinone **6**.

Evaporation of the benzene filtrate afforded a pure sample of **6** (0.188 g, 87% based on **1**).

Reactions of 3-(o-Aminobenzoyloxy)-1,2,3-benzotriazin-4-one 6

(i) Acetylation

(*a*) **6** (0.2 g) was refluxed in freshly distilled acetyl chloride (10 ml) for 1 h. The solution was evaporated to dryness under vacuum and the brown, solid residue was recrystallized from benzene to afford *N*-acetylanthranilic acid (0.051 g, 40%), mp 175–176 °C, identical (mixture mp 175–176 °C and ir spectrum) with an authentic sample (Eastman). Evaporation of the benzene mother liquor gave 3-acetoxy-1,2,3-benzotriazin-4-one **5***b* (0.074 g, 51%).

(*b*) Similarly, heating **6** (0.25 g) in redistilled acetic anhydride (1.0 ml) for 10 min and treatment of the mixture with water afforded the same 3-acetoxy-1,2,3-benzotriazin-4-one (yield 70%).

(ii) Benzoylation

6 (0.25 g) was dissolved in warm, anhydrous pyridine (2 ml) and freshly distilled benzoyl chloride (0.252 g) was added in one portion. A precipitate formed quickly and was separated immediately. The solid was scrubbed with 1 *N* sodium carbonate (20 ml), filtered, and recrystallized from ethanol to afford 3-benzoyloxy-1,2,3-benzotriazin-4-one **5***c* (78% yield), identical with the product of benzoylation of **1**.

(iii) Diazotization

6 (0.25 g) was dissolved in concentrated HCl (5 ml), cooled to 0 °C and diazotized to starch–iodide end-point with sodium nitrite (0.0625 g). The diazonium salt solution was treated with hydroxylamine hydrochloride (0.1 g) in water (20 ml) and the mixture stirred for 20 min. Separation of the precipitate afforded the *N*-hydroxytriazinone **1** (0.118 g, 82%).

A similar result was observed when the diazonium salt solution was treated with sodium azide.

(iv) N-(o-Aminobenzoyl)benzylamine

3-(*o*-Aminobenzoyloxy)-1,2,3-benzotriazin-4-one **6** (0.5 g) was suspended in acetonitrile (30 ml) and benzylamine (0.2 g) was added. An immediate reaction was observed, with precipitation, and the mixture was refluxed for 0.25 h, whereupon a clear solution was obtained. The reaction mixture was cooled slowly to room temperature, and then to 0 °C, before filtration to remove a small amount of unidentified solid. Evaporation of the filtrate gave an orange residue, which was washed thoroughly with saturated $NaHCO_3$ solution and filtered to give *N*-(*o*-aminobenzoyl)-benzylamine (0.37 g, 90%), mp 120–123 °C (lit. (18) mp 123 °C), identical (ir spectrum) with an authentic sample, prepared by reaction of benzotriazinone **13** with benzylamine (13).

*(v) Reaction of **6** with Methylamine*

Aqueous methylamine (2.0 ml, 40%) was added dropwise to **6** (0.5 g), whereupon a clear solution was obtained. After standing at room temperature for 0.5 h, the solution was acidified with 2 *N* hydrochloric acid and the resulting precipitate filtered to afford the *N*-hydroxytriazinone **1** (0.2 g, 69%).

Acid Hydrolysis of 3-Hydroxy-1,2,3-benzotriazin-4-one

1 (0.7 g) was refluxed in 5 *N* hydrochloric acid (15 ml) for 0.5 h and left at room temperature for 3 h. The mixture was filtered, and the filtrate made almost neutral with solid sodium bicarbonate, which precipitated anthranilic acid (0.15 g, 25%), identical with an authentic sample.

*Thermolysis of **1** in n-Amyl Alcohol*

1 (0.5 g) was refluxed in *n*-amyl alcohol (15 ml) for 27.5 h. After cooling and standing for 2 h at room temperature, the excess alcohol was evaporated under vacuum and the oily residue was triturated with benzene. Filtration of the benzene solution and evaporation of the filtrate afforded *n*-amyl *o*-aminobenzoate (0.6 g, 94%), identical with an authentic sample (13).

*Thermolysis of **1** in Aniline*

1 (0.5 g) was refluxed in freshly distilled aniline (20 ml) for 0.5 h. The excess aniline was removed under vacuum and the brown, gummy residue was triturated with benzene – petroleum ether to give a pale yellow solid, which was recrystallized from benzene – petroleum ether to afford *N*-phenylanthranilamide (0.252 g, 35%), mp 120 °C, identical (ir spectrum) with an authentic sample (13). *Anal.* calcd. for $C_{13}H_{12}N_2O$: C 73.57, H 5.70, N 13.20; found: C 73.86, H 5.76, N 13.15.

*Reaction of **1** with Phenyl Isocyanate*

(*a*) **1** (0.25 g) and phenyl isocyanate (0.4 g) were mixed in anhydrous diglyme (10 ml) and refluxed for 1.5 h. The solution was evaporated under vacuum and the orange, gummy residue was triturated with benzene. Separation of the precipitate afforded 3-phenyl-2,4-quinazolinedione **12** (0.16 g, 45%), mp 282–284 °C (colourless needles from ethanol) (lit. (19) mp 276 °C), identical (ir spectrum) with an authentic sample prepared by base-catalyzed rearrangement of the oxazinone **16** (8). *Anal.* calcd. for $C_{14}H_{10}N_2O_2$: C 70.58, H 4.23, N 11.76; found: C 70.45, H 4.19, N 11.78.

(*b*) **1** (0.25 g) and phenyl isocyanate (0.4 g) were mixed in *p*-xylene (10 ml) and refluxed for 2.5 h. The solution was cooled in ice and the pale yellow precipitate was filtered to afford the same quinazolinedione (0.17 g, 48%). Evaporation of the *p*-xylene from the filtrate left an unidentified orange gum.

*Thermolysis of 3-Methoxy-1,2,3-benzotriazin-4-one **5***a*

5*a* (0.073 g) was refluxed in *p*-xylene (5 ml) for 22 h. Evaporation of the solution to dryness under vacuum afforded a quantitative recovery of unchanged starting material.

Acknowledgment

The financial support of the Saint Mary's University Senate Research Committee is gratefully acknowledged.

1. D. HARRISON and A. C. B. SMITH. J. Chem. Soc. 2157 (1960).
2. T. P. AHERN, T. NAVRATIL, and K. VAUGHAN. Tetrahedron Lett. 4547 (1973).
3. A. W. SCOTT and B. L. WOOD. J. Org. Chem. **7**, 508 (1942).
4. J. N. GARDNER and A. R. KATRITZKY. J. Chem. Soc. 4375 (1957).
5. A. R. KATRITZKY and J. M. LAGOWSKI. The chemistry of the heterocyclic *N*-oxides. Academic Press, 1971. pp. 152–153.
6. (*a*) J. K. SUTHERLAND and D. A. WIDDOWSON. J. Chem. Soc. 4561 (1964); (*b*) C. D. HURD, C. M. BUESS, and L. BAUER. J. Org. Chem. **19**, 1140 (1954).
7. J. C. CASS, A. R. KATRITZKY, R. L. HARLOW, and S. H. SIMONSEN. J. Chem. Soc. Chem. Commun. 48 (1976).
8. H. HERLINGER. Angew. Chem. Int. Ed. Engl. **3**, 378 (1964).
9. H. E. CRABTREE, R. K. SMALLEY, and H. SUSCHITZKY. J. Chem. Soc. C, 2730 (1968).
10. A. J. BARKER and R. K. SMALLEY. Tetrahedron Lett. 4629 (1971).
11. D. H. HEY, C. W. REES, and A. R. TODD. J. Chem. Soc. C. 1028 (1968).

12. G. DI MAIO and P. TARDELLA. Gazz. Chim. Ital. **94**, 590 (1964); G. TENNANT and K. VAUGHAN. J. Chem. Soc. C, 2287 (1966).
13. A. W. MURRAY and K. VAUGHAN. J. Chem. Soc. C, 2070 (1970).
14. P. A. S. SMITH. Open-chain nitrogen compounds. Vol. II. W. A. Benjamin. 1966. p. 366.
15. E. M. BURGESS and G. MILNE. Tetrahedron Lett. 93 (1966).
16. M. S. S. SIDDIQUI and M. F. G. STEVENS. J. Chem. Soc. Perkin Trans. I, 2482 (1974).
17. H. ULRICH. Cycloaddition reactions of heterocumulenes. Academic Press. 1967. p. 122.
18. R. ANET and S. SOMASEKHARA. Can. J. Chem. **38**, 746 (1960).
19. G. JACINI. Gazz. Chim. Ital. **73**, 85 (1943).
20. (*a*) T. NISHIWAKI. Nature, **211**, 737 (1966); (*b*) M. MICHMAN and M. FRENKEL. J. Chem. Soc. C, 3856 (1971); (*c*) M. L. BURSTALL. Chem. Commun. 15 (1965).

General base catalysis in acidic solutions. Acceleration of intramolecular phosphonate-assisted amide hydrolysis

RONALD KLUGER and C.-H. LAM

Department of Chemistry, University of Toronto, Toronto, Ont., Canada M5S 1A1

Received June 14, 1976

RONALD KLUGER and C.-H. LAM. Can. J. Chem. **55**, 640 (1977).

The hydrolysis of the amide linkage of 2′-phosphonobenzanilide, **1**, occurs with nucleophilic assistance from the adjacent phosphonic acid moiety. The basic component of buffers in acidic solutions provides additional rate acceleration. A Brønsted plot yields a straight line for buffers of phosphoric acid, cyanoacetic acid, chloroacetic acid, and dichloroacetic acid with $\beta \cong 1.0$. It is suggested that the second acidic group of the phosphonic acid of **1** dissociates upon formation of an addition intermediate, leading to a zwitterion ($T^{\pm}$). This zwitterionic intermediate decomposes in the rate-determining step, with added base or water removing a proton from a hydroxyl group of the intermediate. The product is a mixed phosphonic–carboxylic anhydride which hydrolyzes rapidly. It is concluded that a phosphoric acid derivative is a particularly good catalyst for this type of reaction since a stabilized intermediate can be internally generated along the reaction coordinate.

RONALD KLUGER et C.-H. LAM. Can. J. Chem. **55**, 640 (1977).

L'hydrolyse du lien amide du phosphono-2′ benzanilide **1** se produit avec l'aide de l'acide phosphonique adjacent agissant comme nucléophile. Le composant basique des tampons, en solutions acides, fournit une autre accélération de vitesse. Une courbe de Brønsted conduit à une ligne droite pour des tampons d'acide phosphorique, d'acide cyanoacétique, d'acide chloroacétique et d'acide dichloroacétique avec une valeur de $\beta \cong 1.0$. On suggère que le second groupe acide de l'acide phosphonique de **1** se dissocie lors de la formation d'un intermédiaire d'addition qui conduit à un zwitterion ($T^{\pm}$). Ce zwitterion intermédiaire se décompose dans l'étape déterminant la vitesse de la réaction alors que les bases ajoutées ou l'eau enlèvent un proton du groupe hydroxyle de l'intermédiaire. Le produit est un anhydride mixte phosphonique–carboxylique qui s'hydrolyse rapidement. On en conclut qu'un dérivé d'acide phosphorique est un catalyseur qui est particulièrement bon pour ce type de réaction puisqu'un intermédiaire stabilisé peut être généré d'une façon interne au cours de la réaction.

[Traduit par le journal]

Covalent interactions of amides and phosphates are of particular interest because of their potential significance in aggregates of proteins and nucleotides. We have been studying these interactions in model compounds containing the two functionalities in reactive proximity using hydrolysis rates as a probe (1–3). Evidence that a phosphate derivative can undergo addition to an amide includes our observation that a neighboring phosphonic acid markedly accelerates the hydrolysis of an amide (2). We have examined the mechanism of this catalytic interaction in detail in order to obtain an understanding of the stepwise processes involved. Although analogies can be drawn to situations in which carboxylic acids participate in the hydrolysis of amides, contrasts provide important information about the details of both types of interactions. In this report, we present evidence that external Brønsted bases facilitate the hydrolysis reaction promoted by a phosphonic acid in acidic solution. The function of the base can be contrasted to the requirement for Brønsted *acids* in cases involving participation by carboxylic acids (4, 5). The nature of the phosphonate–amide adduct uniquely accounts for the observed difference and suggests ways in which enzymic catalysis might be brought about.

Materials and Methods

Procedures were based on those we have used in related studies (4, 5). The substrate for these studies, 2′-phosphonobenzanilide **1**, was prepared and purified according to the procedure described by Kluger and Chan (2). Kinetic data were obtained by monitoring the decrease in absorbance at 270 nm as **1** was hydrolyzed to 2-phos-

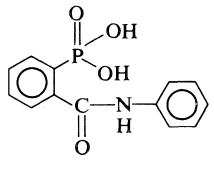

1

phonobenzoic acid and aniline. Products were identified in a large scale reaction by spectroscopic comparison with genuine samples. Ultraviolet absorbance was followed with a Unicam SP1800A spectrophotometer and rate constants were obtained from conventional first-order plots which gave straight line fits for at least four half lives and correlation coefficients greater than 0.95 on least-squares analysis. Dissociation constants were taken from published compilations (6) and corrected for temperature (7) and proton number (8). All acid strengths were confirmed by titration. Ionic strength of the reaction medium was maintained with potassium chloride. Substrate concentration (added in ~10 μl methanol to 3 ml solution) was approximately 10^{-4} *M*.

First-order rate constants observed (k_{obsd}) for hydrolysis of **1** at varying buffer concentrations, but at constant hydrogen ion concentration, were plotted as function of buffer concentration, using the data in Table 1. From the slopes of these plots (k_{app}) the observed net buffer catalysis rate constant (k_{corr}) was obtained after correction for dissociation of the substrate:

$$k_{corr} = (\Delta k_{obsd}/\Delta[B])/f = k_{app}/f$$

$$f = [AH_2]/([AH_2] + [AH^-])$$

where AH_2 is **1** and AH^- is its conjugate base ($pK_a' = 1.6$). The dependence of k_{corr} on the separate buffer components was determined by variation of buffer ratios (changing hydrogen ion concentration) and plotting the dependence of k_{corr} on the buffer ratio. These plots indicated that k_{corr} is entirely accounted for by reaction involving the basic component of the buffer, giving k_B, the specific rate constant for general base catalysis. For Brønsted plots the rate constant, k_B, is statistically corrected for the number of basic sites on the added catalyst (8).

Results

The hydrolysis of **1**, while several orders of magnitude greater in rate than that of its unsubstituted amide analog (2), is promoted further by addition of buffers to the reaction solution in the region below p*H* 4 (see Table 1). To analyze these results we first determined that it is the undissociated form of the substrate that is reactive, based on the p*H*–rate profile for hydrolysis (2). Therefore buffer effects were necessarily corrected to account for substrate in the undissociated form, as described under Materials and Methods. Then, the effect of total buffer concentration at a particular acidity was measured. A plot of total buffer concentration *vs.* observed first-order rate constant, corrected for substrate in undissociated form, for hydrolysis of **1** (data in Table 1) gave a significant slope (k_{corr}) for all buffers we studied. The intercepts of these plots gave the values of rate constants obtained earlier for the p*H*–rate profile. It was then necessary to determine which component of the buffer is responsible for the catalysis. In order to measure this, we plotted k_{corr} as a function of the fraction of buffer present as conjugate base. The plots for all buffers (see Fig. 1) revealed that only the basic component of the buffer is involved in catalysis. Therefore, the value for the true, net rate constant, k_B, is that due to purely the basic component of the buffer, obtained from the value of the intercept of the plot of buffer, fraction *vs.* k_{corr}.

Finally, with the values of k_B obtained for the reaction of **1** with added phosphate, cyanoacetate, chloracetate, and dichloracetate buffers, a value for the Brønsted coefficient, β, was determined. Since the buffers contained different numbers of dissociable protons, conventional statistical corrections were made for each k_B (8) in the Brønsted plot. The plot (Fig. 2) utilizes the pK_a of the conjugate acid of the buffer, so that the slope is equal to $-\beta$. We find then that $\beta \cong 1.0$ (least-squares analysis gives a correlation coefficient of 0.988 for a value of $\beta = 0.98$).

Discussion

The hydrolysis of the amide functionality of **1** in acidic solutions is rapid compared to that of similar amides without adjacent acidic substituent groups (2). Kinetic studies suggested that this is due to the availability of a pathway for hydrolysis of **1** in which the phosphonic acid moiety adds to the amide center to form an internal addition intermediate. This decomposes to yield a reactive mixed anhydride along with expulsion of aniline. We now have observed that

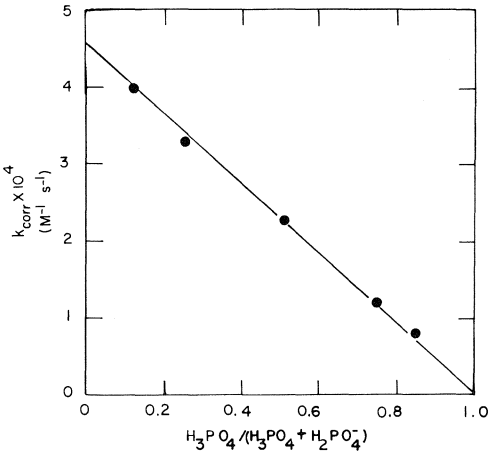

FIG. 1. Buffer fraction plot for phosphate buffer data in Table 1. Intercept value gives k_B.

TABLE 1. Observed rate constants and derived values

Buffer pH	Buffer M	10^5 k_{obsd} (s^{-1})	10^5 k_{app}[a] (M^{-1} s^{-1})	10^4 k_{corr}[b] (M^{-1} s^{-1})	f[c]	10^4 k_B[d] (M^{-1} s^{-1})	10^4 $k_B e/q$ (M^{-1} s^{-1})
Phosphate							
1.2	1.0	12.2					
	0.7	10.4					
	0.4	8.39					
	0.1	5.35					
			7.05	0.985	0.857		
1.5	1.0	12.1					
	0.7	10.2					
	0.4	8.38					
	0.1	5.68					
			7.03	1.29	0.750		
2.0	1.0	11.2					
	0.7	9.33					
	0.4	6.42					
	0.1	4.74					
			7.43	2.63	0.500		
2.5	0.7	5.43					
	0.5	4.66					
	0.3	3.95					
	0.1	3.14					
			3.37	3.08	0.250		
2.8	0.7	3.86					
	0.4	3.07					
	0.1	2.17					
			2.82	4.70	0.143		
						4.67	2.34
Cyanoacetate							
1.9	1.0	5.90					
	0.7	5.42					
	0.4	5.10					
	0.1	3.93					
			2.08	0.616	0.667		
2.3	1.0	5.13					
	0.7	4.48					
	0.4	3.78					
	0.1	2.72					
			2.64	1.52	0.500		
2.7	0.75	2.63					
	0.53	2.50					
	0.30	2.12					
	0.08	1.35					
			1.88	1.72	0.333		
						3.31	1.66
Chloroacetate							
2.5	1.0	5.09					
	0.7	4.36					
	0.4	3.41					
	0.1	2.42					
			2.99	2.71	0.667		
2.8	1.0	3.88					
	0.7	3.15					
	0.4	2.51					
	0.1	1.95					
			2.14	3.60	0.500		
3.1	0.75	2.67					
	0.53	2.16					
	0.30	1.61					
	0.08	1.34					
			2.02	6.06	0.333		
						10.0	5.00

TABLE 1 (*Concluded*)

Buffer pH	Buffer M	10^5 k_{obsd} (s^{-1})	10^5 k_{app}[a] (M^{-1} s^{-1})	10^4 k_{corr}[b] (M^{-1} s^{-1})	f[c]	10^4 k_B[d] (M^{-1} s^{-1})	10^4 k_B/q[e] (M^{-1} s^{-1})
Dichloroacetate							
1.3	1.0	7.23					
	0.7	6.97					
	0.4	6.50					
	0.1	6.44					
			0.947	0.135	0.500		
1.6	1.0	6.89					
	0.7	6.50					
	0.4	6.04					
	0.1	5.70					
			1.35	0.180	0.333		
						0.270	0.135

[a]Buffer rate constant (slope of [B] *vs.* k_{obsd}).
[b]k_{app} corrected for substrate in undissociated form ($pK_a' = 1.6$).
[c]Buffer fraction = [BH]/([BH] + [B^-]).
[d]Rate constant for general base catalysis.
[e]k_B statistically corrected for number of protonation sites.

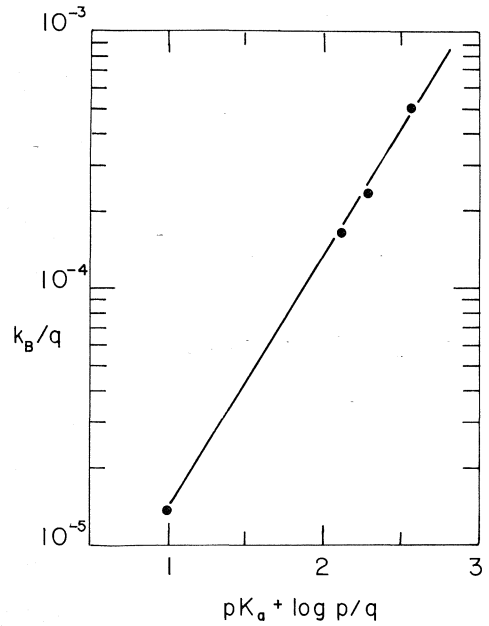

FIG. 2. Statistically corrected rate constant (k_B) *vs.* statistically corrected pK_a for buffer catalyzed hydrolysis of **1** (see Table 1). The values used for 'pK_a + log p/q' are: 0.99 (dichloroacetic acid), 2.13 (cyanoacetic acid), 2.30 (phosphoric acid), and 2.56 (chloroacetic acid).

this reaction is further promoted by the conjugate base component of acidic buffers. In the case of carboxylic acid participation in the hydrolysis of amides in acidic solutions, it has been observed that the reaction is further promoted by what is described kinetically as general acid catalysis (4, 5, 9, 10). In the carboxylic acid case, recent studies have indicated that the observed general acid catalysis is probably due to a mechanism involving sequentially specific acid – general base catalysis (5, 10). This gives the same empirical rate equation for buffer catalysis as general acid catalysis (5).

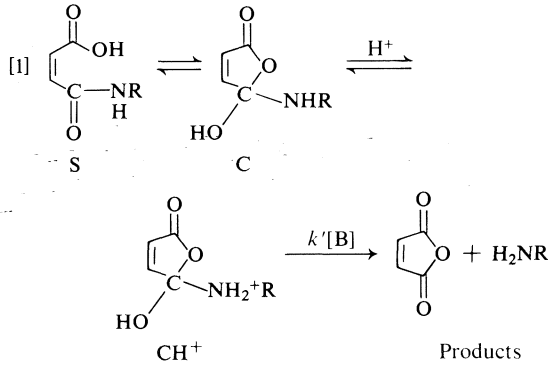

For the case of phosphonic acid participation, which we observe, a parallel mechanism utilizing a similar sequence of reactions should also apply. However, the observation that the phosphonic acid reaction is subject to general base catalysis requires an important modification. In reaction 2 we have proposed a mechanism for general base-assisted hydrolysis of **1**.

The major modification of the mechanism shown in reaction 1 that appears in reaction 2, is formation of a zwitterionic intermediate $T^{\pm}$. In the case of carboxylic acid participation, intermediate C of reaction 1 cannot decompose without formation of the cationic intermediate CH^+ which decomposes in the rate-determining step. The intermediate indicated in reaction 2, T,

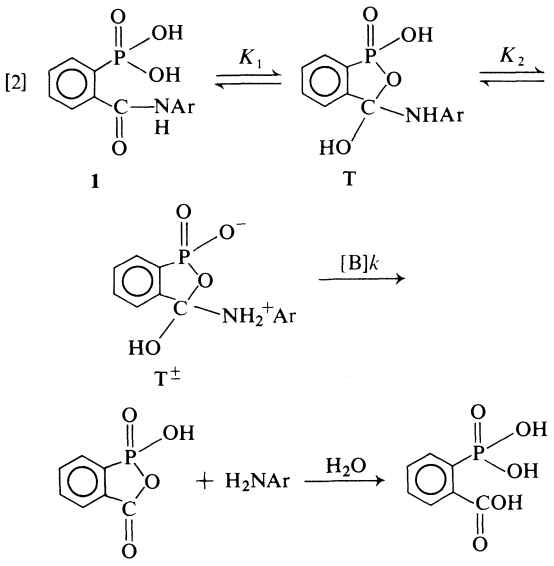

has an alternative means of arriving at a cationic nitrogen center (in order to develop a leaving group). Since the phosphonic acid moiety of **1** has two dissociable protons, formation of intermediate T only utilizes one of the acidic groups. The remaining group is a fairly strong acid (phosphonic acid monoesters typically have pK_a's near 2) and the zwitterion, $T^{\pm}$, should be present as a significant portion of the total of species T and $T^{\pm}$. The decomposition of $T^{\pm}$ requires only the Brønsted base, B, indicated in reaction 2. The rate expression for the buffer catalyzed hydrolysis of **1** according to reaction 2 is:

$$[3] \quad v = k[B][T^{\pm}] = k_B[B][\mathbf{1}] = kK_1K_2[B][\mathbf{1}]$$

$$[4] \quad k_B = K_1K_2k$$

We see from [4] that k_B depends on the stability of the intermediates relative to the starting material, the relative amount of zwitterion present, and the energy of the transition state associated with k. Since general acid catalysis was not observed, reaction proceeding via a cationic intermediate generated by protonation of T without dissociation of the phosphonic acid must not be significant. The contrast then with carboxylic acid participation [1] is that the phosphonic acid can proceed via a zwitterion, $T^{\pm}$, while the carboxylic acid cannot.

We can now analyze further the nature of the transition state associated with k by examining the results of the Brønsted plot (Fig. 2). The slope we observe of unity (or nearly that) requires that proton transfer in the rate determining step be nearly complete at the transition state (11). This suggests that transfer of the hydroxylic proton of $T^{\pm}$ to B is itself rate-determining, leading to the metastable intermediate T* which can decompose rapidly. Con-

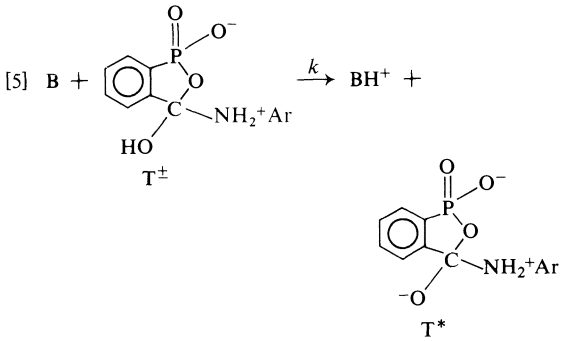

sistent with this view, we find that the rate constant for the 'uncatalyzed' reaction of **1** (2), corresponding to water acting as a general base when plotted relative to the pK_a of its conjugate acid, hydronium ion (as in the plot of Fig. 2), falls considerably above the extrapolated line. This is consistent with arguments that suggest that water is a relatively superior catalyst for proton transfer (11) and should deviate positively from that extrapolated from Brønsted plots ($pK_a = -1.75$, $k_{H_2O} = 1.6 \times 10^{-6}\ M^{-1}\ s^{-1}$; k (extrapolated) $= 3.0 \times 10^{-7}\ M^{-1}\ s^{-1}$).[1] The decomposition of $T^{\pm}$ by a stepwise process is consistent with Jencks's expectations for many elimination reactions which produce carbonyl groups (12, 13). Since aniline is a good leaving group, the endergonic proton–transfer leading to formation of T* may become rate-determining. The observation of buffer catalysis suggests that this interpretation is applicable here. If expulsion of aniline were rate-determining, there would be no likely role for the Brønsted base catalyst. Kirby and co-workers (9, 10) have presented their findings for other amides in which structural factors determine whether buffer catalysis may be observed and for which rate-limiting proton-transfer must be invoked. Since our results are based on a limited Brønsted plot, we must regard these results as suggestive of the proposed mechanism and await further data to test these hypotheses.

[1] k_{H_2O} is obtained from the appropriate value in ref. 2 divided by the water concentration to adjust for units.

Our results suggest that one means by which enzymatic cleavage of peptides might be assisted is through electrostatic stabilization of protonated intermediates by adjacent anions. The case we have studied indicates that the zwitterion derived from a phosphonic acid addition intermediate may be a good model for this type of environment.

Acknowledgements

We thank the National Research Council of Canada for support of this research. C.-H.L. is the holder of a scholarship from the Ontario Ministry of Colleges and Universities. R.K. is a fellow of the Alfred P. Sloan Foundation.

1. R. KLUGER and J. L. W. CHAN. J. Am. Chem. Soc. **95**, 2362 (1973).
2. R. KLUGER and J. L. W. CHAN. J. Am. Chem. Soc. **96**, 5637 (1974).
3. R. KLUGER and J. L. W. CHAN. J. Am. Chem. Soc. **98**, 4913 (1976).
4. R. KLUGER and C.-H. LAM. J. Am. Chem. Soc. **97**, 5536 (1975).
5. R. KLUGER and C.-H. LAM. J. Am. Chem. Soc. **98**, 4154 (1976).
6. W. P. JENCKS and J. REGENSTEIN. *In* Handbook of biochemistry. *Edited by* H. Sober. Chemical Rubber Co., Cleveland, Ohio. 1968. pp. J-150–J-189.
7. D. D. PERRIN. Aust. J. Chem. **17**, 484 (1964).
8. D. BISHOP and K. J. LAIDLER. J. Chem. Phys. **42**, 1688 (1965).
9. M. F. ALDERSLEY, A. J. KIRBY, and P. W. LANCASTER. J. Chem. Soc. Chem. Commun. 570 (1972).
10. M. F. ALDERSLEY, A. J. KIRBY, P. W. LANCASTER, R. S. MCDONALD, and C. R. SMITH. J. Chem. Soc. Perkin Trans. 2, 1488 (1974).
11. A. J. KRESGE. Chem. Soc. Rev. **2**, 475 (1973).
12. W. P. JENCKS. Chem. Rev. **72**, 705 (1972).
13. J. P. FOX, M. I. PAGE, A. SATTERTHWAIT, and W. P. JENCKS. J. Am. Chem. Soc. **94**, 4729 (1972).

Rules for the quantitative prediction of stereochemistry in the reduction of cyclohexanones by sodium borohydride

DONALD C. WIGFIELD

Department of Chemistry, Carleton University, Ottawa, Ont., Canada K1S 5B6

Received July 8, 1976

DONALD C. WIGFIELD. Can. J. Chem. **55**, 646 (1977).

A procedure is outlined which allows calculation of the stereoselectivity of reduction of cyclohexanones by sodium borohydride under normal conditions (room temperature, 2-propanol as solvent). The procedure rests on incremental enthalpy values of steric hindrance, coupled with known isokinetic relationships to obtain values of $\Delta\Delta G^{\ddagger}$; thus it delineates quantitatively the steric factors governing stereoselectivity in these reductions.

DONALD C. WIGFIELD. Can. J. Chem. **55**, 646 (1977).

On décrit un procédé qui permet de calculer la stéréosélectivité de la réduction de cyclohexanones par le borohydrure de sodium dans des conditions normales (température de la pièce; propanol-2 comme solvant). Ce procédé repose sur des valeurs additives d'enthalpie due à l'empêchement stérique qui sont couplées avec des rapports isocinétiques connus afin de déterminer les valeurs $\Delta\Delta G^{\ddagger}$; ce procédé délimite donc quantitativement les facteurs stériques qui gouvernent la stéréosélectivité de ces réductions.

[Traduit par le journal]

Sodium borohydride has been known for over 30 years and has been extensively used in organic chemistry for much of this period. Yet despite its central place, the reductions of cyclohexanones by sodium borohydride are still very puzzling from the point of view of mechanism and stereochemistry. The detailed mechanism of reduction, the origin of stereoselectivity, and even a practical, if empirical, formula for quantitatively predicting stereoselectivity, are all problems that remain inadequately resolved. This communication is directed at the last of these problems.

In 1953, it was recognized by Barton that "reduction (of cyclohexanones) with sodium borohydride or lithium aluminum hydride in general affords the equatorial epimer if the ketone group is not hindered, the polar (axial) epimer if it is hindered or very hindered" (1). In the 23 years that have passed since that statement was made its generality has been amply confirmed, but a *quantitative* prediction of stereochemistry has never been possible. Our recent measurements of specific activation parameters for axial and equatorial attack by sodium borohydride on a wide variety of cyclohexanones (2, 3) have indicated the reason why it is so difficult to make such predictions. The observed stereochemical product ratio must be a result of the difference in *free energy* ($\Delta\Delta G^{\ddagger}$) between the two transition states for axial and equatorial attack. Yet the reaction is *enthalpy* controlled (3), and the compensating entropy effects (isokinetic relationships) *differ* significantly depending on whether the ketone is unhindered or hindered and, to a lesser extent, whether axial or equatorial attack is being considered (3). Thus, a neat series of incremental free energy additions is not possible and efforts to find such increments must fail. Despite the fact that the origin of stereoselectivity in these reductions still remains unestablished, one line of attack worth pursuing is the reflection that, *if* changes in stereoselectivity from one ketone to another are simply the consequence of differential steric impedance between ketone and reducing agent, then it should be possible to devise a series of appropriate *enthalpy* increments for substituents in various locations around the cyclohexanone ring. By combining these increments with the appropriate isokinetic relationship, the entropy and thence the free energy increments may be obtained, leading to a calculated value of $\Delta\Delta G^{\ddagger}$, from which the derivation of stereochemical product ratio in a kinetically controlled reaction is trivial. We wish to report that this approach to predicting quantitatively the stereoselectivity successfully produces a workable tool, and details of the steps in such a calculation follow.

Step 1. Values of $\Delta H_{ax}{}^{\ddagger}$ and $\Delta H_{eq}{}^{\ddagger}$ (enthalpies of activation for axial and equatorial attack

TABLE 1. Increments in $\Delta H^{\ddagger}$ for methyl substitution on cyclohexanones

Substituent	$\Delta H^{\ddagger}$(kcal/mol) Axial attack (Base value 6.3 kcal/mol)	Equatorial attack (Base value 7.5 kcal/mol)
2-Equatorial	+1.1	+0.5
2-Axial	0.0	+2.0
3-Equatorial	+0.6	+0.7
3-Axial	+2.8	0.0
4-Equatorial	0.0	0.0
4-Axial	+0.2	+1.2

respectively) are calculated by addition of the appropriate incremental substituent effects to the base values of 6.3 kcal/mol for axial attack and 7.5 kcal/mol for equatorial attack.

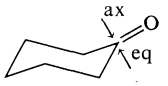

These incremental substituent effects, which follow from previously published activation parameter data (2, 3), are shown in Table 1.

Step 2. The cyclohexanone under consideration is classified as unhindered, hindered, or very hindered, and values of $\delta\Delta H_{ax}^{\ddagger}$ and $\delta\Delta H_{eq}^{\ddagger}$ (difference between calculated $\Delta H^{\ddagger}$ and 'standard'[1] value for that class of ketone) calculated by [1] and [2].

$$[1] \qquad \delta\Delta H_{ax}^{\ddagger} = \Delta H_{ax}^{\ddagger} - (\Delta H_{ax}^{\ddagger})_0$$

$$[2] \qquad \delta\Delta H_{eq}^{\ddagger} = \Delta H_{eq}^{\ddagger} - (\Delta H_{eq}^{\ddagger})_0$$

For this purpose, isokinetic plots (3) make it clear that *unhindered ketones* are those which contain only 3-equatorial and/or 4-substitution (axial and/or equatorial); *very hindered ketones* are those which contain two 3-axial substituents; *hindered ketones* are those with any other substituent pattern. The values of $(\Delta H_{ax}^{\ddagger})_0$ and $(\Delta H_{eq}^{\ddagger})_0$ are indicated in Table 2 and in the isokinetic plot sketches in Fig. 1.

Step 3. The values of $\delta\Delta H_{ax}^{\ddagger}$ and $\delta\Delta H_{eq}^{\ddagger}$ are converted to $\delta\Delta G_{ax}^{\ddagger}$ and $\delta\Delta G_{eq}^{\ddagger}$ respectively using the isokinetic relationship [3]

$$[3] \qquad \delta\Delta G^{\ddagger} = \delta\Delta H^{\ddagger}(1 - T/\beta)$$

where β is the appropriate isokinetic temperature.[2] Values of $(1 - T/\beta)$, calculated from published data, (3) are given in Table 2.

TABLE 2. Conversion factors for calculation of $\Delta\Delta G_{eq}^{\ddagger}$

Factor	Type of ketone: Unhindered	Hindered	Very hindered
$(\Delta H_{ax}^{\ddagger})_0$*	6.3	8.2	10.1
$(\Delta H_{eq}^{\ddagger})_0$*	7.5	8.7	9.9
$(1 - T/\beta)_{ax}$	0.21	0.32	0.41
$(1 - T/\beta)_{eq}$	0.25	0.36	0.44
$\Delta\Delta G_0^{\ddagger}$	+1.2	+0.5	−0.2

*See footnote 1.

Step 4. $\Delta\Delta G_{ea}^{\ddagger}(= \Delta G_{eq}^{\ddagger} - \Delta G_{ax}^{\ddagger})$ is calculated from [4]

$$[4] \qquad \Delta\Delta G_{ea}^{\ddagger} = \Delta\Delta G_0^{\ddagger} + \delta\Delta G_{eq}^{\ddagger} - \delta\Delta G_{ax}^{\ddagger}$$

where the appropriate values of $\Delta\Delta G_0^{\ddagger}$ are given in Table 2.

Step 5. $\Delta\Delta G_{ea}^{\ddagger}$ is converted to stereochemical product ratio (at 25 °C) using [5]

$$[5] \qquad \%\ \text{equatorial alcohol} = \frac{100}{1 + e^{-1.69\Delta\Delta G_{ea}^{\ddagger}}}$$

Despite the rather involved above description of the calculation procedure, it is, in practice, not unduly cumbersome, and a worked example follows to illustrate this point. All data required is contained in Tables 1 and 2.

[1]The subscript 0 and the term 'standard' do not imply physical significance and simply refer to an arbitrarily chosen point on the appropriate isokinetic line.

[2]Or, more correctly, the slope of the $\Delta H^{\ddagger}$ *vs.* $\Delta S^{\ddagger}$ plot since there is no evidence that an isokinetic temperature actually exists. Insufficient information is available on the characteristics (slope, position of line) of the isokinetic relationship for very hindered ketones. However, it appears that the shift in characteristics between the line for hindered ketones and that for very hindered ketones is approximately the same as the (known) shift between the lines for unhindered ketones and hindered ketones. We have assumed here that these two shifts are, in fact, equal, and this assumption appears to work satisfactorily for product ratio prediction.

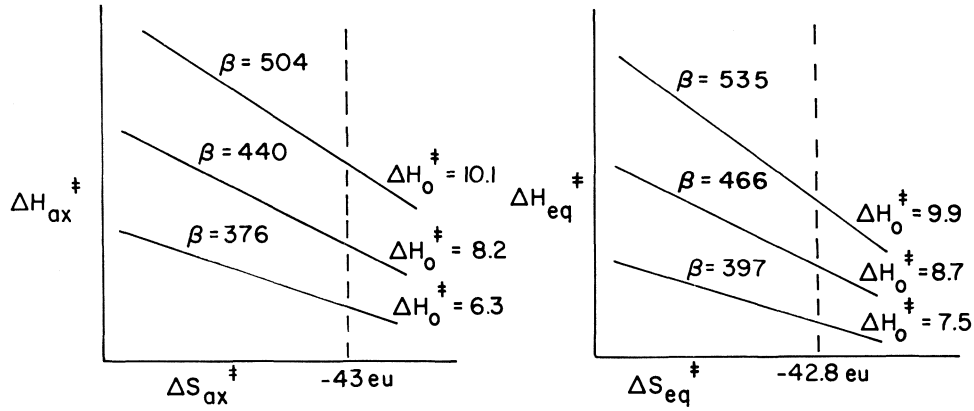

FIG. 1. Isokinetic relationships for reduction of unhindered (lower lines), hindered (centre lines), and very hindered (upper lines) ketones.

Calculation of Stereochemical Product Ratio for Reduction of 3,3,5-Trimethylcyclohexanone

Step 1. Ketone has two 3-equatorial and one 3-axial substituents.

$$\Delta H_{ax}^{\ddagger} = 6.3 + 2(0.6) + 2.8 = 10.3 \text{ kcal/mol}$$

$$\Delta H_{eq}^{\ddagger} = 7.5 + 2(0.7) + 0.0 = 8.9 \text{ kcal/mol}$$

Step 2. The ketone is classified as 'hindered'.

$$\delta\Delta H_{ax}^{\ddagger} = 10.3 - 8.2 = +2.1 \text{ kcal/mol}$$

$$\delta\Delta H_{eq}^{\ddagger} = 8.9 - 8.7 = +0.2 \text{ kcal/mol}$$

Step 3.

$$\delta\Delta G_{ax}^{\ddagger} = +2.1 \times 0.32 = +0.7 \text{ kcal/mol}$$

$$\delta\Delta G_{eq}^{\ddagger} = +0.2 \times 0.36 = +0.1 \text{ kcal/mol}$$

Step 4.

$$\Delta\Delta G_{ea}^{\ddagger} = +0.5 + 0.1 - 0.7 = -0.1 \text{ kcal/mol}$$

Step 5.

$$\% \text{ equatorial alcohol} = \frac{100}{1 + e^{-1.69(-0.1)}} = 46\% \text{ (experimental value 48\%)} \quad (3)$$

Calculated stereochemical product ratios of the reduction of a variety of cyclohexanones using this procedure, and comparisons with experimental observations are shown in Table 3.[3] Examination of Table 3 makes it clear that there is good agreement (within 4%) between calculation and experiment, which suggests that the method presented is a workable predictive tool, and also provides evidence that the original premise of differential stereoselectivity being a result of predictable incremental steric interactions may be correct. The method is clearly only valid for reductions performed under the conditions for which the activation parameters were measured (*i.e.* in 2-propanol at 25 °C), and, strictly speaking, valid only for the substituents being methyl groups. However, the calculation appears to work satisfactorily when the substituent is part of a methylene chain, either cyclic (see steroids **3**, **4**, **5**, **7**, **19** and particularly the comparison of **3** and **4**) or acyclic (entries **14**–**18**). Surprisingly, the agreement is apparently tolerable even with an isopropyl group substituent (entry **18**), but (not surprisingly) breaks down when a *tert*-butyl group is in a significantly

[3]For entries **4**, **8**, **9**, **13**, **15**, **16**, **19** of Table 3, the specific activation parameters for reduction are unknown, and thus these are pure predictions. For the other ketones (those whose specific activation parameters have been measured and from which the approach is derived) the approach is cyclic and thus deviations represent only deviations from idealized linearity. It should be emphasized, however, that because of the differing isokinetic relationships that exist, not even a cyclic prediction of stereochemistry covering a variety of ketone reductions has previously been successful. The data in Table 3 demonstrate that the approach is consistent and that it may be generally applied in a predictive way.

TABLE 3. Calculated and observed stereochemical product ratios from ketone reductions with $NaBH_4$

Ketone	% equatorial alcohol	
	Calculated	Observed*
(1) 4-Methylcyclohexanone	88	86,89 (4)
(2) 3-Methylcyclohexanone	89	86,87 (4)
(3) Cholestan-3-one	93	94
(4) Coprastone	93	93 (5)
(5) Androstan-3-one	93	91
(6) 2-Methylcyclohexanone	70	70
(7) Cholestan-2-one	42	46
(8) *cis*-3,5-Dimethylcyclohexanone	88	86 (4)
(9) *trans*-3,4-Dimethylcyclohexanone	89	88 (4)
(10) 2,2-Dimethyl-4-*tert*-butylcyclohexanone	90	92
(11) *cis*-2,6-Dimethylcyclohexanone	62	62
(12) 3,3,5-Trimethylcyclohexanone	46	48
(13) 2,4,4-Trimethylcyclohexanone	82	82
(14) 4-*tert*-Butylcyclohexanone	88	86
(15) 3-*tert*-Butylcyclohexanone	89	83 (4)
(16) 2-*tert*-Butylcyclohexanone	70	50 (2)
(17) 5-*n*-Butyl-3,3-dimethylcyclohexanone	46	45
(18) Menthone(*trans*-5-methyl-2-isopropyl-cyclohexanone)	73	69
(19) D-Homotestan-3α-ol-11,17a-dione acetate	90	94 (6)

*Product ratios are taken from ref. 3 unless otherwise noted.

hindering position (entry **16**). It is also doubtful that the relationship would be of any relevance to cyclohexanones with polar substituents. It is of interest to extend these calculations to very hindered ketones: 3,3,5,5-tetramethylcyclohexanone is a ketone for which clearly no product ratio is experimentally measurable and estimates of the ratio of axial:equatorial attack have ranged from 0.5 to 30% axial attack. (For a discussion of this point, see ref. 7.) The above calculation method gives 95.4% equatorial attack (*i.e.* 4.6% equatorial alcohol) in excellent agreement with the 95:5 product ratio recently determined on a 4-substituted derivative in our laboratory (8). Extension to the reduction of 11-ketosteroids gives an axial:equatorial product ratio of 97.2:2.8. While sodium borohydride does not reduce these highly hindered ketones, reductions of 11-ketosteroids with lithium aluminum hydride have been reported to give essentially only the axial alcohol[4] (ref. 9 and references cited therein).

In summary, the procedure outlined here appears to give a quantitative (±4%) estimate of the stereochemical product ratio in the reduction of cyclohexanones by sodium borohydride in 2-propanol. While the procedure was designed for methyl substitution, it appears to give reliable answers for cyclohexanones with a variety of nonpolar substituents, including steroids. The steric factors controlling stereoselectivity are thus delineated and the Barton generalization (1) converted to a quantitative tool.

[4]We are not aware of any efforts to detect small amounts (< 3%) of the equatorial alcohol.

1. D. H. R. BARTON. J. Chem. Soc. 1027 (1953).
2. D. C. WIGFIELD and D. J. PHELPS. J. Am. Chem. Soc. **96**, 543 (1974).
3. D. C. WIGFIELD and D. J. PHELPS. J. Org. Chem. **41**, 2396 (1976).
4. B. RICKBORN and M. T. WUESTHOFF. J. Am. Chem. Soc. **92**, 6894 (1970).
5. J. D. MORRISON and H. S. MOSHER. Asymmetric organic reactions. Prentice-Hall, Englewood Cliffs, New Jersey. 1971. pp. 121–126.
6. R. O. CLINTON, R. G. CHRISTIANSEN, H. C. NEUMANN, and S. C. LASKOWSKI. J. Am. Chem. Soc. **79**, 6475 (1957).
7. D. J. PHELPS. Ph.D. Thesis, Carleton University, Ottawa, Ontario. 1973.
8. D. C. WIGFIELD, G. W. BUCHANAN, C. M. ASHLEY, and S. FEINER. Can. J. Chem. **54**, 3536 (1976).
9. A. V. KAMERNITZKY and A. A. AKHREM. Tetrahedron, **18**, 705 (1962).

Synthesis of 6-substituted 5,6,7,12-tetrahydrodibenzo[*a*,*d*]cyclooctenes[1]

ROGER N. RENAUD AND JOHN W. BOVENKAMP

Division of Chemistry, National Research Council of Canada, Ottawa, Ont., Canada K1A 0R6

Received June 4, 1976

ROGER N. RENAUD and JOHN W. BOVENKAMP. Can. J. Chem. **55,** 650 (1977).

The eight-membered ring 6,6-dicyano-5,6,7,12-tetrahydrodibenzo[*a*,*d*]cyclooctene was prepared from 2,2′-bis(bromomethyl)diphenylmethane and sodiomalononitrile. From this dicyano derivative a series of mono- and disubstituted cyclooctenes was synthesized.

The corresponding 5,7,12-trihydro-6*H*-dibenzo[*a*,*d*]cycloocten-6-one was obtained by the ring enlargement of 5,10-dihydro-11*H*-dibenzo[*a*,*d*]cyclohepten-11-one with diazomethane. The parent compound and its dideuterio derivative were prepared from the eight-membered ring ketone. A Wittig reaction on the ketone gave the methylene derivative.

ROGER N. RENAUD et JOHN W. BOVENKAMP. Can. J. Chem. **55,** 650 (1977).

Le dicyano-6,6 tétrahydro-5,6,7,12 dibenzo[*a*,*d*]cyclooctène fut preparé à partir du bis-(bromométhyl)-2,2′ diphénylméthane en présence de sodiomalononitrile. Le groupement fonctionnel a servi à la synthèse de plusieurs composés substitués en position 6.

La trihydro-5,7,12 dibenzo-6*H*-[*a*,*d*]cyclooctènone-6 a été préparée par l'agrandissement de l'anneau cycloheptènone de la dihydro-5,10 dibenzo-11*H*-[*a*,*d*]cycloheptènone-11 en présence de diazométhane. Cette cétone fut soit réduite en cyclooctane normal et dideutérié ou transformée en dérivé méthylènique par la réaction de Wittig.

In earlier papers (1, 2), it has been shown that the eight-membered ring system, *N*-alkyl-5,6-dihydro-7*H*,12*H*-dibenzo[*c*,*f*]azocines, shows conformational behaviour in which the ring can be in a rigid and in a flexible conformation. These results were interesting enough to cause us to have a detailed look at the corresponding all-carbon ring system.[2] Thus it was necessary to have available a series of mono- and di-6-substituted 5,6,7,12-tetrahydrodibenzo[*a*,*d*]cyclooctenes **1** and this paper describes the synthesis of these compounds. The only other carbocyclic compounds reported in the literature having the skeleton of **1** are those with substitution at C-12 (3). These were prepared according to Scheme 1 where $R_1 = R_2 = H$. This approach could only have been used to synthesize some of the C-6 substituted compounds described in this paper since the first step is limited to just a few 1-substituted phenylbromoethanes. For instance, this procedure is certainly not suitable for the preparation of **1***b*, **1***d*, or **1***i*. Also, Winthrop *et al.* (3) found that the cyclization step was very sensitive to structural change in the reactants, and in some cases the desired cyclization product was not obtained.

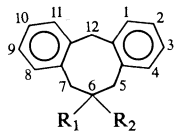

1

	R_1	R_2
a	COOEt	COOEt
b	CN	CN
c	COOH	H
d	$COOCH_3$	H
e	CH_2OH	H
f	CH_2OTs	H
g	CH_3	H
h	COOH	COOH
i	$COOCH_3$	$COOCH_3$
j	CH_2OH	CH_2OH
k	CH_2OTs	CH_2OTs
l	CH_3	CH_2OH
m	CH_3	CH_3
n	H	H
o	D	D

The reaction sequence chosen by us is shown in Scheme 2. The first reaction attempted was that between 2,2′-bis(bromomethyl)diphenylmethane and diethyl sodiomalonate. This reaction did not give any detectable monomeric compound **1***a* but did give a good yield of the 16-membered ring compound **3** along with some polymeric products (4). In direct contrast, the smaller sodiomalononitrile gives a good yield of eight-membered ring cyclization product. In

[1]NRCC No. 15670.

[2]A manuscript (R. R. Fraser, R. N. Renaud, and J. W. Bovenkamp) describing the conformational behaviour of this ring system is in preparation.

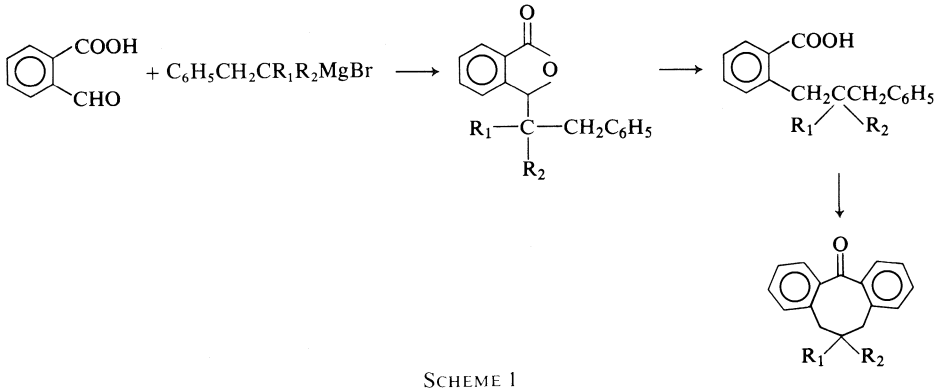

SCHEME 1

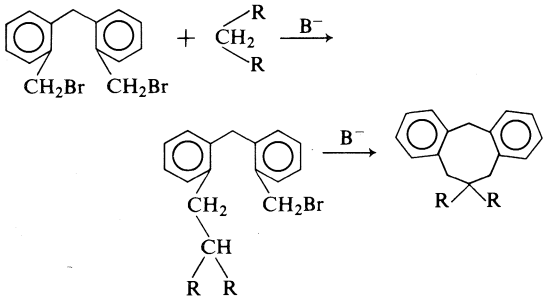

SCHEME 2

our view, the different results obtained with these disubstituted nucleophiles are due to the steric effect of the substituents during cyclization. An examination of the Dreiding models shows that the eight membered ring compound substituted at C-6 can exist in four interconvertible conformations,[3] namely two rigid boat-chair conformers (**a** and **b**) and two flexible boat-boat conformers (**c** and **d**).[4] The conformers **b** (R quasi-axial) and **c** (R inside) contain interactions which could be highly unfavourable with large groups. These are the interactions of R with the π electrons of the benzene rings in **b** or with one of the protons at C-12 in **c**. In contrast, the interactions in conformations **a** and **d** are expected to be much less severe. In the case of the *N*-alkyl-5,6-dihydro-7*H*,12*H*-dibenzo[*c*,*f*]-azocines (2), the eight-membered ring is formed readily from the dibromide and the corresponding amine even when the alkyl substituent is as large as *tert*-butyl. In these cases, cyclization to the two high energy conformations can be avoided. When two substituents are present at C-6, one of the substituents is always involved with one of the high energy interactions already mentioned. Thus, during cyclization with disubstituted nucleophiles, the development of these interactions as the transition state is approached may prevent the cyclization to the eight-membered ring. This appears to be the most plausible explanation for the bimolecular cyclization with the large diethyl sodiomalonate to give the 16-membered ring **3** (4) while with the smaller sodiomalononitrile intramolecular cyclization occurs to give the eight-membered ring **1***b*.

Starting from this dinitrile, a series of mono- and disubstituted benzocyclooctenes were synthesized (**1***c* to **1***m*). The dinitrile **1***b* could be converted to both monoacid **1***c* and diacid **1***h* under basic conditions. The hydrolysis with 5% sodium hydroxide in refluxing ethylene glycol gave only the monoacid **1***c* upon neutralization. The diacid **1***h* was obtained in good yield by refluxing the dinitrile in 25% aqueous sodium hydroxide solution for 36 h. Even after a 24 h reflux, sizeable amide peaks could be seen in the infrared spectrum.

From the monoacid were obtained the methyl ester **1***d*, the alcohol **1***e*, the tosylate **1***f*, and the hydrocarbon **1***g*. Trideuterated **1***g* (at C-6, C-12, and C-12) was obtained by carrying out the hydrolysis of **1***b* in ethylene glycol-d_2. It is of interest to note that, as has been observed in the case of fluorene (7), the protons at C-12 (*i.e.* the protons of the methylene group between the two

[3]The conformational interconversion has been discussed in the case of *N*-alkyl-5,6-dihydro-7*H*,12*H*-dibenzo[*c*,*f*]azocines (2, 5).

[4]The force field calculations of Allinger *et al.* (6) indicate that in 1,4-cyclooctadiene the boat–boat conformer does not twist to relieve the severe repulsion between the hydrogens at C-3 and C-7. In the case of *N*-alkyl-5,6-dihydro-7*H*,12*H*-dibenzo[*c*,*f*]azocines (2) and of **1** (see footnote 2), the dynamic nmr is best explained by two lower energy twist–boat enantiomers.

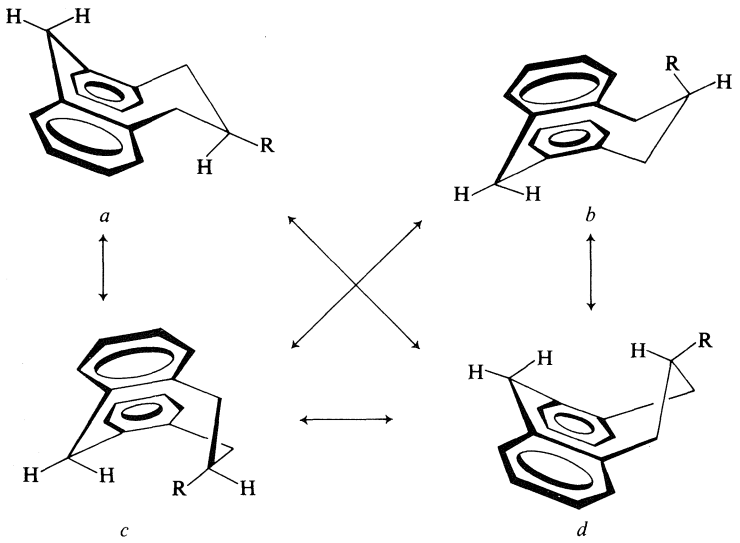

benzene rings) are readily exchanged under relatively mild basic conditions; however, according to nmr the methylene protons at C-5

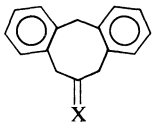

2

a X = O
b X = CH_2

and C-7, having only one adjacent benzene ring, are not exchanged. It is known that benzylic protons exchange in the presence of a very strong base (8). The diacid gave successively the diester **1***i*, the diol **1***j*, and the ditosylate **1***k*. The ditosylate upon reduction with lithium aluminum hydride gave both **1***l* and **1***m*. It was easier to obtain **1***l* pure when ether was used as the solvent while for **1***m* purification was simpler with the use of tetrahydrofuran.

The synthesis of the ketone **2***a* from 2,2′-bis(bromomethyl)diphenylmethane either by the Thorpe reaction (9) or by cyclization with ethyl ethylthiomethyl sulfoxide (10) led to very poor yields of **2***a* (2% and 6% respectively). The

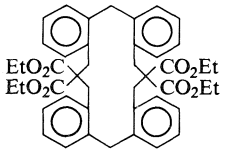

3

preparation of **2***a* by the ring enlargement of 5,10-dihydro-11*H*-dibenzo[*a*,*d*]cyclohepten-5-one with diazomethane by the method described by House *et al.* (11) gave a much improved yield.

The parent hydrocarbon **1***n* was easily obtained from **2***a* by the Wolff–Kishner reaction (12). However, the synthesis of the dideuterio compound **1***o* proved to be surprisingly difficult. The tosyl derivative of the monodeuterated alcohol, obtained from the reduction of **2***a* with lithium aluminum deuteride followed by tosylation, gave back the alcohol on reduction. The bromo analogue, synthesized from the alcohol by the method of Squires *et al.* (13), gave very impure product either when reacted with lithium aluminum deuteride or with zinc dust in refluxing acetic acid-*d* (14). It is well known that the conversion of unactivated aliphatic ketones into a dideuterio methylene group is difficult to achieve without deuterium scrambling (15). Sodium cyanoborohydride, has been used to reduce ketones to methylene groups (16). It was thought worthwhile to attempt to obtain **1***o* by the use of sodium cyanoborodeuteride; however, the use of this reagent led to a hydrocarbon with excessive scrambling. A suitable sample (85% d_2, 11% d_1 and 4.5% d_3) of **1***o* was finally obtained using the improved Clemmensen reaction described by Steiner (17*a*). Thus we have further demonstrated the usefulness of Steiner's method by achieving an acceptable level of scrambling in a compound where the ketone group is next to two benzylic methylenes.

The methylene derivative **2***b* was prepared according to the method of Corey and co-workers (18) using a 1:1 ratio of Wittig reagent and ketone. When a large excess of Wittig reagent was used an impurity appeared which could not be separated by column chromatography, recrystallization, or distillation. The same impurity was also formed when the reaction was carried out using *n*-butyllithium to form the Wittig reagent and the reaction carried out in boiling ether (19). In this latter case, a large amount of the methylene **2***b* rearranged to the conjugated olefin 6-methyl-7,12-dihydrodibenzo-[*a*,*d*]cyclooctane.

Experimental

All melting points are uncorrected. Infrared spectra were observed on a Perkin-Elmer model 267 spectrophotometer and only the characteristic bands are reported. ^{1}H nuclear magnetic resonance spectra were, unless otherwise noted, taken in deuterochloroform solution on a Varian Associates spectrometer model E.M. 360 and the chemical shifts are reported on the δ scale. Molecular weight determinations were carried out on a Mechrolab vapor pressure osmometer apparatus and/or on a Hitachi–Perkin–Elmer RMU-6D mass spectrometer.

Preparation of Compound ***1b***

The method described by Bloomfield (20) for the preparation of dialkylmalononitrile was followed. Malononitrile (0.73 g, 11 mmol) freshly distilled from phosphorus pentoxide was dissolved in dry dimethyl sulfoxide (3.5 ml). This solution was added over a period of 15 min to a stirred slurry of sodium hydride (0.6 g, 25.1 mmol) in dry dimethyl sulfoxide (5 ml) in a nitrogen atmosphere and the stirring was continued for an additional 15 min with occasional cooling. Then 2,2′-bis(bromomethyl)diphenylmethane (1) (3.46 g, 9.78 mmol) in dry dimethyl sulfoxide (14 ml) was added to the above mixture over a period of 20 min with occasional cooling. The reaction mixture, after being stirred at room temperature overnight, was poured into water (250 ml). The resultant precipitate was collected by filtration and washed with water. The solid was added to benzene and after filtering off the insoluble brownish powder, the yellow solution was treated with decolourizing carbon. The benzene was removed to leave 1.92 g of a pale yellow solid melting at 174–180 °C. On recrystallization from an absolute ethanol – benzene mixture, a colourless solid melting at 183–185 °C was obtained in 50% yield (1.25 g). An analytical sample (mp 185.5–186.5 °C) was prepared; nmr 7.38 (8H, s, aromatic), 3.02–4.68 (6H, m, methylene protons at C-5, C-7, and C-12); ir ($CHCl_3$) 2256 cm^{-1} (CN). *Mol. wt.* (benzene) calcd: 258; found: 263; ms *m*/*e* 258 (M^+). *Anal.* calcd. for $C_{18}H_{14}N_2$: C 83.69, H 5.46, N 10.85; found: C 83.89, H 5.59, N 10.68.

Preparation of Compound ***1d***

The dinitrile **1***b* (1.01 g, 3.88 mmol) was added to a solution of sodium hydroxide (1.5 g) in ethylene glycol (30 ml). The mixture was refluxed for 3 h and then allowed to come to room temperature. The resulting solution was diluted with water and filtered. The precipitate which was formed on neutralization of the filtrate with concentrated hydrochloric acid was filtered off and washed with water. The resultant white solid **1***c* (0.76 g, 3.01 mmol), mp 168–170 °C, was obtained in 78% yield.

The monoacid **1***c* (0.76 g) was methylated with an excess of diazomethane in ether to give 0.76 g (95%) of a white powder, mp 98–99.5 °C. An analytical sample was prepared by recrystallization from ethanol–water to give fine white needles melting at 101–102 °C; ms *m*/*e* 266 (M^+). *Anal.* calcd. for $C_{18}H_{18}O_2$: C 81.17, H 6.81; found: C 80.63, H 6.95.

Preparation of Compound ***1e***

The methyl ester **1***d* (0.73 g, 2.74 mmol) was reduced by subjecting it to a 20 h reflux in a suspension of lithium aluminum hydride (0.27 g, 7.11 mmol) in ether. The product was worked-up in the usual manner to give 0.62 g (95%) of a white solid melting at 123.5–125 °C. An analytical sample was prepared by recrystallization from benzene – petroleum ether (bp 60–80 °C) to give a white solid with a melting point of 126.5–127 °C; nmr 6.90–7.55 (8H, m, aromatic), 2.35–4.55 (7H, m, methylenes at C-5, C-7, and C-12, and methine at C-6), 1.53 (1H, s, OH, exchanges with D_2O); ir ($CHCl_3$) 3435 cm^{-1} (OH bonded), 3609 cm^{-1} (OH free). *Anal.* calcd. for $C_{17}H_{18}O$: C 85.67, H 7.61; found: C 85.48, H 7.35.

Preparation of Compound ***1f***

The alcohol **1***e* (0.62 g, 2.60 mmol) was dissolved in pyridine and the flask was then packed in ice. After the addition of the tosyl chloride (0.60 g, 3.2 mmol) the ice was allowed to melt and the solution was stirred overnight. The reaction mixture was added to cold dilute sulfuric acid and a red gummy precipitate was obtained which was filtered and washed with water. The material was added to chloroform and filtered. On removal of the chloroform a clear orange oil was obtained (1.06 g). Attempts to crystallize the oil were unsuccessful.

Preparation of Compound ***1g***

To a stirred suspension of lithium aluminum hydride (0.23 g, 5.9 mmol) in anhydrous ether (10 ml), cooled in ice, was added 1.05 g (2.7 mmol) of the tosylate **1***f* in anhydrous ether (10 ml). The suspension was refluxed for 24 h. After destroying the excess of lithium aluminum hydride with aqueous sodium hydroxide (5%), more ether was added and the precipitate was filtered off. The ether was removed to leave a clear colourless oil (0.57 g). The oil was purified by dissolving it in chloroform and passing it through a small column of silica gel. The first 20 ml of eluent were collected. After removal of the chloroform solvent, a bulb-to-bulb distillation was carried out at 100 °C/0.01 torr to give 0.406 g (68%) of a viscous colourless oil; nmr 6.88–7.60 (8H, m, aromatic), 2.30–4.67 (6H, m, methylenes at C-5, C-7, and C-12), 1.50–2.10 (1H, br m, methine), 0.35–1.45 (3H, two broad peaks, methyl); ms *m*/*e* 222 (M^+). *Anal.* calcd. for $C_{17}H_{18}$: C 91.84, H, 8.16; found: C 91.66, H 8.13.

Preparation of the 6,12,12-Trideuterio Derivative of Compound ***1g***

The same procedure as described for the preparation of **1***g* was followed. Positions 6 and 12 were deuterated by the hydrolysis of compound **1***b* with the sodium salt of

ethylene glycol in ethylene glycol-d_2 and by neutralization of the resultant basic solution with deuterium chloride (10 *N*). The trideuterio derivative of **1***g* analyzed 91% d_3 and 9% d_2 by mass spectrometry; nmr 6.87–7.58 (8H, m, aromatic), 2.35–3.75 (4H, m, methylenes at C-5 and C-7), 0.33–1.45 (3H, two br peaks, methyl). *Anal.* calcd. for $C_{17}H_{15}D_3$: C 90.61, H and D 9.39; found: C 90.39, H and D 9.04.

Preparation of Compound **1***h*

The dinitrile **1***b* (0.60 g, 2.32 mmol) was added to a solution of sodium hydroxide (9 g) in water (27 ml) and the mixture was refluxed for 36 h.[5] The mixture was cooled and the white precipitate was filtered off and washed with water. The filtrate and the water washings were then combined and neutralized with concentrated sulfuric acid while cooling the mixture in ice. The white solid obtained upon filtration (0.42 g, 61%) melted to a clear liquid at 159–161 °C with the production of bubbles (CO_2). A recrystallization from ethanol–water did not improve the melting point. Nmr 6.94–7.61 (8H, m, aromatic), 5.1–6.9 (2H, broad peak, carboxylic hydrogens, exchanges with D_2O), 2.94–4.61 (6H, m, methylenes at C-5, C-7, C-12); in (Nujol) 1688 cm^{-1} (acid C=O). *Anal.* calcd. for $C_{18}H_{16}O_4$: C 72.96, H 5.44; found: C 73.17, H 5.63.

Preparation of Compound **1***i*

The diacid **1***h* (0.38 g) was methylated with an excess of diazomethane in ether to give a quantitative yield of a viscous clear oil. An analytical sample was obtained by a Späth distillation on a portion of the diester (125 °C/0.002 torr); nmr 6.81–7.54 (8H, m, aromatic), 3.75 (6H, s, ester methyls), 2.87–4.54 (6H, m, methylenes at C-5, C-7, and C-12); ir ($CHCl_3$) 1729 cm^{-1} (ester C=O). *Anal.* calcd. for $C_{20}H_{20}O_4$: C 74.05, H 6.22; found: C 74.20, H 6.19.

Preparation of Compound **1***j*

The diester **1***i* (1.93 g, 0.0060 mol) in ether (10 ml) was added to a suspension of 1.50 g lithium aluminum hydride in 20 ml of ether. The mixture was refluxed for 24 h. The excess hydride was destroyed by the addition of 5% aqueous sodium hydroxide, the solid was removed by filtration, the ether solution was dried, and the ether removed to leave 1.52 g (95%) of a white solid (mp 135–146 °C). An analytical sample was obtained by twice recrystallizing a portion from benzene to give a sample with mp 165–166 °C; nmr 6.87–7.56 (8H, m, aromatic), 2.63–4.53 (10H, m, methylenes at C-5, C-7, C-12, and of the CH_2OH groups), 1.77 (2H, s, OH, exchanges with D_2O); ir ($CHCl_3$) 3435 (OH bonded), 3606 cm^{-1} (OH free). *Anal.* calcd. for $C_{18}H_{20}O_2$: C 80.56, H 7.51; found: C 80.39, H 7.35.

Preparation of Compound **1***k*

When the diol **1***j* was treated with tosyl chloride at room temperature as described for the preparation of the monotosylate **1***f*, an incomplete reaction was obtained. A good yield (84%) was obtained when the reaction mixture was subjected to a 3 h reflux. An analytical sample (mp 156–158 °C) was obtained by recrystallization from methanol–water. *Anal.* calcd. for $C_{32}H_{32}O_6S_2$: C 66.65, H 5.59; found: C 66.49, H 5.66.

Preparation of Compound **1***l*

A mixture of the ditosylate **1***k* (0.20 g, 0.34 mmol) and lithium aluminum hydride in dry diethyl ether (10 ml) was heated to reflux for 2.5 days. The resultant mixture was worked-up as described for the preparation of compound **1***m*. The oily material obtained was purified by fractionation on a silica gel column using firstly chloroform (to elute impure dimethyl derivative off the column) followed by methanol (to elute the required alcohol). The viscous oil obtained was distilled in a Späth bulb at 115–130 °C/0.005 torr to give a white solid melting at 109–111 °C (41 mg, 48% yield); nmr 6.87–7.56 (8H, m, aromatic), 2.34–4.60 (8H, m, methylenes at C-5, C-7, C-12, and of the CH_2OH group), 1.78 (1H, s, OH, exchanges with D_2O), 0.38 and 1.30 (3H, two s, methyl); ir ($CHCl_3$) 3432 (OH bonded), 3610 cm^{-1} (OH free). *Anal.* calcd. for $C_{18}H_{20}O$: C 85.67, H 7.99; found: C 85.39, H 7.86.

Preparation of Compound **1***m*

A mixture of the ditosylate **1***k* (0.25 g, 0.42 mmol) and lithium aluminum hydride (0.10 g, 2.63 mmol) in dry tetrahydrofuran (10 ml) was heated to reflux for 5 days. The excess hydride was destroyed with aqueous sodium hydroxide (5%) and the precipitate filtered off. The solution was dried and the organic solvent was removed to leave an oil which contained some THF decomposition products. The mixture was chromatographed through silica gel using chloroform as the eluent. The first fraction (44 mg) contained the expected dimethyl derivative. This fraction was distilled in a Späth bulb at 75–95 °C/0.005 torr. The oil obtained was filtered through an aluminum oxide column and again distilled under reduced pressure; nmr 6.90–7.47 (8H, m, aromatic), 2.37–4.54 (6H, m, methylenes at C-5, C-7, and C-12), 0.40–1.43 (6H, two s of equal intensity and a smaller peak, methyl peaks).[6] ms *m/e* 236 (M^+). *Anal.* calcd. for $C_{18}H_{20}$: C 91.47, H 8.53; found: C 91.58, H 8.37.

Preparation of Compound **2***a*

To a solution of 5,10-dihydro-11*H*-dibenzo[*a*,*d*]cycloheptene-11-one (5.0 g, 24.3 mmol) in absolute ether (150 ml) was added boron trifluoride etherate (3.4 g, 24.0 mmol) (6). The solution was cooled to 0 °C and 480 ml of an alcohol free ether solution of diazomethane (146 mmol) were added with stirring over a period of 0.5 h. The solution was then filtered, washed with water, and then dried with $MgSO_4$. On removal of the ether, a yellowish oil was obtained. The mixture was fractionated on a column of Woelm neutral aluminum oxide (the eluent used was benzene) until all the eight-membered ring ketone had come off the column. Then the seven-membered ring ketone was eluted off the column with chloroform. The middle fractions which contained both ketones were recombined and refractionated in the same way on a new column of aluminum oxide. In this manner 1.47 g of impure compound **2***a* were obtained. It was

[5]An amide peak is present in the ir spectrum when the mixture is refluxed for 24 h, while a lower yield of diacid was obtained when refluxing for 48 h.

[6]The low temperature nmr of **1***l* has been completely interpreted (see footnote 2); however, some smaller details of the low temperature nmr of **1***m* have resisted interpretation. Thus at this time a small amount of isomerization during the reduction cannot be ruled out.

twice recrystallized from 95% ethanol to give 0.83 g of the ketone **2***a* melting at 150.5–151.0 °C. The net yield was 29%; nmr 7.00–7.42 (8H, m, aromatic), 4.00 (2H, s, methylene at C-12), 3.83 (4H, s, methylenes at C-5 and C-7); ir ($CHCl_3$) 1708 cm^{-1} (C=O). *Anal.* calcd. for $C_{16}H_{14}O$: C 86.45, H 6.35; found: C 86.35, H 6.47.

Preparation of Compound **1***n*

The ketone **2***a* (0.15 g, 0.68 mmol) was reduced using the Huang-Minlon modification of the Wolff–Kishner reaction (12). The white precipitate obtained after the work up of the reaction mixture weighed 0.13 g (88%) (mp 81.5–83.5 °C). An analytical sample (mp 86–86.5 °C) was prepared by recrystallization from 95% ethanol; nmr 6.99–7.69 (8H, m, aromatic), 3.56–4.70 (2H, broad peak, methylene at C-12), 2.68–3.50 (4H, br peak, methylenes at C-5 and C-7), 1.10–2.60 (2H, br peak, methylene at C-6); ms *m/e* 208 (M^+). *Anal.* calcd. for $C_{16}H_{16}$: C 92.26, H 7.74; found: C 92.14, H 7.90.

Preparation of Compound **1***o*

The method described by Steiner was followed (17*a*). All operations were carried out over nitrogen. Freshly distilled trimethylchlorosilane (0.50 g, 4.61 mmol) was added by syringe with gentle agitation to deuterium oxide (0.07 g, 3.80 mmol) in dry tetrahydrofuran (3 ml) in a dropping funnel. After 5 min, the resulting deuterium chloride solution was added over a period of 20 min to a stirred, ice cooled, mixture of zinc dust (0.51 g) and the ketone **2***a* (0.20 g, 0.91 mmol) in dry tetrahydrofuran (5 ml). After 1 h, a further 200 mg of zinc dust were added and the mixture was allowed to stir at room temperature overnight.

After an addition of ether (40 ml), the mixture was filtered and then washed with ice water and aqueous sodium carbonate. The ether solution was dried and the solvent removed to leave a sticky solid. This solid was subjected to an aluminum oxide column purification. The first 20 ml of benzene eluent contained 0.137 g of a white solid melting at 62–70 °C. The impure solid was recrystallized three times from 95% ethanol to give a white solid (63 mg, 33%) melting at 86–86.5 °C; nmr 7.00–7.60 (8H, m, aromatic), 3.58–4.56 (2H, br peak, methylene at C-12), 3.08 (4H, br s, methylenes at C-5 and C-7); ms 11% d_1, 85% d_2 and 4.5% d_3.

Preparation of Compound **2***b*

Compound **2***b* was prepared according to the procedure of Corey and co-workers (18). Sodium hydride (0.35 g, freed from mineral oil with *n*-pentane) and dimethyl sulfoxide (20 ml) were heated at 80 °C for 1 h under nitrogen. With a syringe, 2 ml of this solution (1.45 mmol of methylsulfinyl carbanion) was placed in a flask filled with nitrogen. The solution was cooled in an ice-water bath and methyltriphenylphosphonium bromide (0.52 g, 1.45 mmol) in warm dimethyl sulfoxide (4 ml) was added. The resulting mixture was stirred at room temperature for 1 h and then the ketone (0.303 g, 1.36 mmol) was added. After being stirred overnight at room temperature, the solution was poured into water and the aqueous solution was extracted twice with *n*-pentane. The pentane extracts were washed with water and dried over anhydrous magnesium sulfate. Upon removal of the solvent, 0.20 g of a solid was obtained which was shown by nmr to consist of 50% starting material and 50% of the desired product. The olefin (0.097 g, mp 87–88 °C, net yield 49%) was obtained free of the ketone by dissolving the mixture in benzene and filtering through a column of alumina. The retained ketone can be eluted with chloroform. The analytical sample was obtained by recrystallization from 95% ethanol to give 79 mg of white needles (mp 89–89.5 °C); nmr 6.90–7.48 (8H, m, aromatic), 4.97 (2H, s, olefinic H), 4.07 (2H, s, methylene at C-12), 3.65 (4H, s, methylenes at C-5 and C-7); ir ($CHCl_3$) 1638, 894 cm^{-1} ($CR_2{=}CH_2$); ms *m/e* 220 (M^+). *Anal.* calcd. for $C_{17}H_{16}$: C 92.58, H 7.32; found: C 92.51, H 7.42.

Acknowledgments

We are grateful to Dr. R. R. Fraser of the University of Ottawa for helpful discussions and to Mr. H. Séguin for the elemental analyses and the mass spectral determinations.

1. R. N. Renaud, R. B. Layton, and R. R. Fraser. Can. J. Chem. **51**, 3380 (1973).
2. R. R. Fraser, M. A. Raza, R. N. Renaud, and R. B. Layton. Can. J. Chem. **53**, 167 (1975).
3. S. O. Winthrop, M. A. Davis, F. Herr, J. Stewart, and R. Gaudry. J. Med. Chem. **6**, 130 (1963).
4. R. N. Renaud and J. W. Bovenkamp. Can. J. Chem. **54**, 3548 (1976).
5. W. D. Ollis, J. F. Stoddart, I. O. Sutherland. Tetrahedron, **30**, 1903 (1974).
6. N. L. Allinger, J. F. Viskocil, Jr., U. Burkert, and Y. Yuh. Tetrahedron Lett. 33 (1976).
7. A. F. Thomas. Deuterium labelling in organic chemistry. Appleton-Century-Crofts, New York. 1971. p. 27.
8. T.-S. Chen, J. Wolinska-Mocydlarz, and L. C. Leitch. J. Labelled Comp. **7**, 285 (1970).
9. J. J. Bloomfield and P. V. Fennessey. Tetrahedron Lett. 2273 (1964).
10. G. Schill and P. R. Jones. Synthesis, 117 (1974); K. Ogura, M. Yamashita, M. Suzuki, and G. Tsuchihashi. Tetrahedron Lett. 3653 (1974).
11. H. O. House, E. J. Grubbs, and W. F. Gannon. J. Am. Chem. Soc. **82**, 4099 (1960).
12. Huang-Minlon. J. Am. Chem. Soc. **68**, 2487 (1946).
13. T. G. Squires, W. W. Schmidt, and C. S. McCandlish, Jr. J. Org. Chem. **40**, 134 (1975).
14. M. E. Isabelle and L. C. Leitch. Can. J. Chem. **36**, 440 (1958).
15. L. Tokis, G. Jones, and C. Djerassi. J. Am. Chem. Soc. **90**, 5465 (1968); M. St-Jacques, M. Bernard, and C. Vaziri. Can. J. Chem. **48**, 2386 (1970); C. R. Enzell. Tetrahedron Lett. 2135 (1966); C. R. Enzell and I. Wahlberg. Acta Chem. Scand. **23**, 871 (1969); J. Gloux and M. Guglielmi. Tetrahedron Lett. 2935 (1969).
16. R. O. Hutchins, R. A. Milewski, and B. E. Maryanoff. J. Am. Chem. Soc. **95**, 3662 (1973).
17. (*a*) R. P. Steiner. Ph.D. Thesis, University of Wisconsin, 1972; Diss. Abstr. **33**, 3563-B (1973); (*b*) E. Vedejs. Organic reactions. Vol. 22. John Wiley and Sons. Inc., N.Y. 1975. p. 415.
18. R. Greenwald, M. Chaykowski, and E. J. Corey. J. Org. Chem. **28**, 1128 (1963).
19. G. Wittig and U. Schoellkopf. Organic synthesis. Coll. Vol. 5. J. Wiley and Sons, N.Y. 1973. p. 751.
20. J. J. Bloomfield. J. Org. Chem. **26**, 4112 (1961).

Voltammetric studies of metal chlorides in $AlCl_3$–CsCl and $ZnCl_2$–CsCl melts using an oscillating solid microelectrode

H. S. RAY,[1] N. KH. TUMANOVA,[2] AND S. N. FLENGAS

Department of Metallurgy and Materials Science, University of Toronto, Toronto, Ont., Canada M5S 1A4

Received September 20, 1976

H. S. RAY, N. KH. TUMANOVA, and S. N. FLENGAS. Can. J. Chem. **55**, 656 (1977).

The oscillating planar solid microelectrode developed previously (1) has been used to investigate the reduction of the ions Co^{2+}, Ni^{2+}, Pb^{2+}, Cd^{2+}, Cu^{+}, Ag^{+}, as well as of the redox system Fe^{2+}/Fe^{3+} in solvent melts containing various amounts of CsCl and $AlCl_3$.

Similarly, the reductions of the ions Co^{2+}, Ni^{2+}, and Cd^{2+} as well as Zr^{4+} have been investigated in solvent melts containing various amounts of CsCl and $ZnCl_2$.

Well-defined limiting currents have been obtained in all systems. These were found to vary linearly with the concentration of the solute. From the slopes of E *vs.* $\log (i_L - i)$, or $\log i/(i_L - i)$, the electrode reactions were established in most cases. The analysis of the results for Zr^{4+} indicates a three step reduction process.

H. S. RAY, N. KH. TUMANOVA et S. N. FLENGAS. Can. J. Chem. **55**, 656 (1977).

On a utilisé la microélectrode solide, planaire et oscillante qui avait été développée antérieurement (1) pour étudier la réduction des ions Co^{2+}, Ni^{2+}, Pb^{2+}, Cd^{2+}, Cu^{+}, Ag^{+}, de même que le système redox Fe^{2+}/Fe^{3+}, dans des milieux fondus contenant diverses quantités de CsCl et de $AlCl_3$.

De la même manière on a étudié les réductions des ions Co^{2+}, Ni^{2+} et Cd^{2+} de même que Zr^{4+} dans des milieux fondus contenant diverses quantités de CsCl et de $ZnCl_2$.

On a pu obtenir des courants limites bien définis dans tous les systèmes. On a trouvé que ceux-ci varient d'une façon linéaire avec les concentrations du soluté. A partir des pentes de E en fonction de $\log (i_L - i)$ ou de $\log i/(i_L - i)$, on a pu établir les réactions d'électrode dans la plupart des cas. L'analyse des résultats obtenus avec Zr^{4+} indique que le processus de réduction se fait en trois étapes.

[Traduit par le journal]

Introduction

Previous work from this laboratory has resulted in the development of an oscillating planar solid microelectrode which was found to be suitable for voltammetric studies in aqueous and fused salt solutions (1).

This microelectrode consisted of a platinum or tungsten wire flame-sealed in a Pyrex capillary tube ground flat at the lower end. The electrodes were vibrated mechanically.

The limiting currents i_L obtained were well defined and reproducible and were found to be proportional to the surface area of the metal electrode disc A in cm^2, the frequency ν given as the number of oscillations per minute and the concentration of the electroreducible species i, X_i given as a mole fraction. The empirical equation relating these variables was given as

$$[1] \qquad i_L = (K_1 + K_2\nu)AX_i$$

where K_1 and K_2 are constants dependent upon temperature and the nature of the ionic species present in solution.

The electrode was used successfully at room temperature with aqueous solutions and in molten alkali nitrate electrolytes at temperatures up to 330 °C. With the molten alkali nitrate solvent, results were obtained for Ag^{+}, which is the only ion reduced at potentials below the decomposition potential of the supporting electrolyte, which is −0.5 V.

The technique was also applied to chloride melts containing AgCl dissolved in the equimolar mixture of KCl and NaCl at about 700 °C. It was found that the voltammetric curves were not well defined and exhibited unusually large residual currents. In addition, the limiting currents could not be measured with the automatically driven polarograph due to kinetic factors and had to be measured at fixed values

[1]Visiting Scientist. Present address: Department of Metallurgical Engineering, Indian Institute of Technology, Kanpur, 208016, India.

[2]Visiting Scientist. Present address: The Institute of General and Inorganic Chemistry, Ukrainian Academy of Sciences, Kiev, U.S.S.R.

TABLE 1. Composition of solvent melts

CsCl (mol %)	$AlCl_3$ (mol %)	$ZnCl_2$ (mol %)	Melting point (°C)	Comments	E_{dec}* (V)
54	46	—	344	Eutectic composition in the $CsCl$–$CsAlCl_4$ subsystem	−1.55
50	50	—	377	Congruently melting compound	−1.55
41.6	58.4	—	148	Eutectic composition in the $CsAlCl_4$–$AlCl_3$ subsystem	−1.55
37.74	—	52.26	285	Compound $CsZn_2Cl_5$ and excess CsCl	−1.35
33.33	—	66.67	294	Compound $CsZn_2Cl_5$	−1.20
30.21	—	69.79	290	Compound $CsZn_2Cl_5$ and excess $ZnCl_2$	−1.30

**Versus* the Pt–foil reference electrode. Decomposition potentials versus a graphite reference electrode are of the same order of magnitude if the graphite electrode is saturated with chlorine by pre-electrolysis. Otherwise its potentials are ill-defined.

of applied potentials after allowing sufficient time for equilibrium.

In the present work the technique has been applied to dilute solutions of a large number of metal chlorides dissolved in solvent melts containing CsCl with the covalently bonded $AlCl_3$ or $ZnCl_2$.

Pure $AlCl_3$ and $ZnCl_2$ in the solid and molten states are poor electrical conductors and highly volatile. The boiling points (2) for $AlCl_3$ and $ZnCl_2$ are, respectively, 187 and 732 °C. However, solutions of these salts in molten alkali chlorides are ionic conductors and show a pronounced thermal stability which increases as the size of the alkali metal cation increases from Li^+ to Cs^+. Particularly, the solutions of $AlCl_3$ and of $ZnCl_2$ in CsCl exhibit very low vapour pressures. The increased thermodynamic stability of solutions containing CsCl is related to the presence of congruently melting compounds which appear in the phase diagrams for the systems $AlCl_3$–CsCl (3) and $ZnCl_2$–CsCl (4). Thus, in the former, the phase diagram shows the congruent compound $CsAlCl_4$ melting at 377 °C and two adjacent compositions melting at 344 and 148 °C, respectively. Similarly, the $ZnCl_2$–CsCl phase diagram indicates, among others, the compound $CsZn_2Cl_5$, which melts at 284 °C and has two adjacent eutectic compositions melting at 268 and 263 °C, respectively.

The solvent melts which have been used as supporting electrolytes for the present study involve compositions rich in CsCl, the chemical compounds $CsAlCl_4$ and $CsZn_2Cl_5$, and compositions rich in $ZnCl_2$ or $AlCl_3$. These compositions were chosen in order to observe possible solvent effects on the reduction of metal chloride cations.

The metal chloride solutes investigated include $NiCl_2$, $CoCl_2$, $CdCl_2$, $PbCl_2$, AgCl, CuCl, and the redox systems containing $FeCl_2$ and $FeCl_3$, and $ZrCl_4$.

Experimental

The anhydrous compounds $PbCl_2$, $CdCl_2$, CuCl, AgCl, $ZnCl_2$, $FeCl_3$, $NiCl_2$ as well as CsCl were all of analytical reagent grade. $AlCl_3$, $CoCl_2$, and $FeCl_2$ were Puratex reagents of 99.9% purity.

All reagents were treated at 100 °C with anhydrous gaseous HCl, degassed under vacuum and stored in desiccators. $ZrCl_4$ was added as the compound Cs_2ZrCl_6 prepared in this laboratory (5).

The $AlCl_3$–CsCl and the $ZnCl_2$–CsCl mixtures were prepared in closed Pyrex tubes by mixing together the appropriate amounts of each component and were further purified by pre-electrolysis between tungsten electrodes at 1.2 V for about 1 h and/or by bubbling chlorine gas for 1 h through the melts. The exact compositions of the various solvent melts are given in Table 1.

Solutions of the various metal chlorides in these melts were made by adding the appropriate amounts to the molten solvent through a feeding tube attached to the cell.

The voltammetric cells were made out of Pyrex glass and were operated under an inert atmosphere of argon gas. The cell design is shown in Fig. 1. The oscillating indicator electrode consisted of a tungsten wire of 0.5 mm diameter flame-sealed in a Pyrex capillary tube having an outside diameter of 0.5 cm. The tip of this electrode was ground flat until its cross-section consisted of two concentric discs, *i.e.* the tungsten wire surrounded by ground Pyrex glass.

The reference electrode was a platinum foil with surface area of about 8 cm^2. A third auxillary electrode was also present in the cell and consisted of a second platinum foil. The function of the latter was to make possible the electrochemical removal of the metallic deposits from the indicator electrode after each run. To this end the indicator electrode was made anodic and all deposits could be transferred by electrolysis to the auxillary electrode acting as a cathode. For best results, however, it was found necessary to remove the indicator electrode and polish its surface prior to each experiment.

The mechanical oscillator consisted of an electrically driven cam and piston device capable of creating a harmonic motion having an amplitude of 1 cm at various

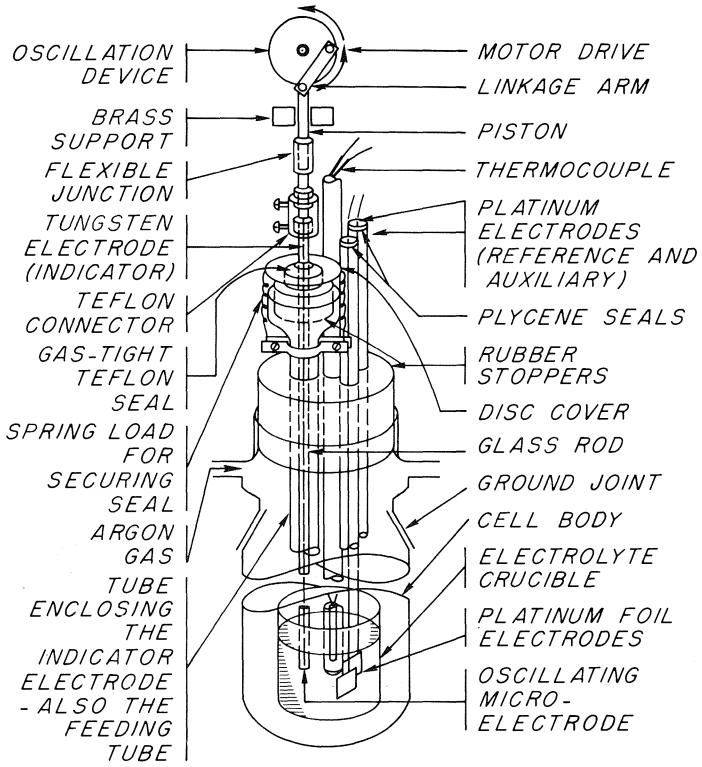

FIG. 1. Schematic diagram of the voltammetric cell.

frequencies between 30 and 200 opm. The experiments were conducted at 85 or 180 opm. As opposed to its behaviour in nitrate melts, the tungsten microelectrode did not react with chloride melts. The polarograph was a Fisher electropode, model 65, fitted with a recorder. The potential was applied at a rate of 200 mV per min.

All limiting currents were measured from the recorded voltammetric curves using the 'three tangents method'.

Results

Some typical voltammetric waves for the reduction of the cations of Ni^{2+}, Co^{2+}, Ag^{+}, Cu^{+}, and of the Fe^{2+}/Fe^{3+} redox system in the three solvent melts containing CsCl and $AlCl_3$, are given in Fig. 2.

These curves have been traced from the actual *i–v* curves recorded by the polarograph. It should be noted that for the purpose of presentation the reduction curves have been shifted arbitrarily along the current axis. The current scale indicated on the graph is common for all the metal cations and allows the exact calculation of the limiting currents for a given reduction process. However, the potential scale is exact. The order of these curves indicates the relative reducibility of the metal cations. It should also be noted that the mole fractions of the ions are all comparable and of the order of 10^{-3}, as shown.

The curves for the reduction of Ni^{2+}, Co^{2+}, Cu^{+}, Ag^{+}, and for the system Fe^{2+}/Fe^{3+} are smooth and indicate well defined limiting current plateaus. The corresponding curves for Pb^{2+} and Cd^{2+} indicate pronounced maxima. These are the only metals which at 400 °C deposit at the microelectrode in the molten state.

The concentration dependence of the limiting currents at a frequency of 85 opm is shown in Fig. 3. It is seen that all limiting currents are proportional to the mole fraction of the metal chloride in solution. For the redox system containing $FeCl_2$ and $FeCl_3$, only one reduction wave could be seen at about -1.05 V.

Figure 4 shows the shape of the reduction curves and the concentration dependence of the limiting current for Co^{2+} obtained at the much higher oscillation frequency of 180 opm. Some typical voltammetric curves obtained at the same higher frequency for the reduction of Ni^{2+}, Co^{2+}, and Cd^{2+} dissolved in the solvent melts containing CsCl and $ZnCl_2$ are given in Fig. 5.

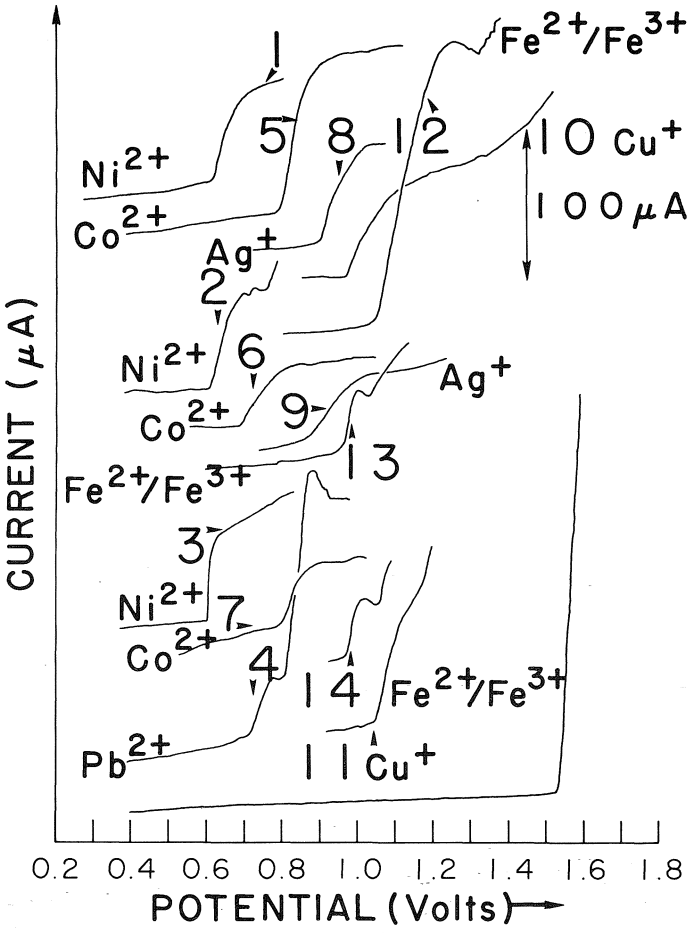

FIG. 2. Typical voltammetric waves for the reduction of metal cations dissolved in the $AlCl_3$–CsCl solvent melts. Curve (*1*) $NiCl_2$ dissolved in the CsCl–$CsAlCl_4$ melt at $X_{NiCl_2} = 5.25 \times 10^{-3}$, $t = 400$ °C. Curve (*2*) $NiCl_2$ dissolved in the $CsAlCl_4$ at $X_{NiCl_2} = 3.7 \times 10^{-3}$, $t = 400$ °C. Curve (*3*) $NiCl_2$ dissolved in the $CsAlCl_4$–$AlCl_3$ at $X_{NiCl_2} = 6 \times 10^{-3}$, $t = 200$ °C. Curve (*4*) $PbCl_2$ dissolved in CsCl–$CsAlCl_4$ melt at $X_{PbCl_2} = 6.07 \times 10^{-3}$, $t = 400$ °C. Curve (*5*) $CoCl_2$ dissolved in CsCl–$CsAlCl_4$ melt at $X_{CoCl_2} = 5.35 \times 10^{-3}$, $t = 400$ °C. Curve (*6*) $CoCl_2$ dissolved in the $CsAlCl_4$ melt at $X_{CoCl_2} = 2.8 \times 10^{-3}$, $t = 400$ °C. Curve (*7*) $CoCl_2$ dissolved in the $CsAlCl_4$–$AlCl_3$ melt at $X_{CoCl_2} = 2.8 \times 10^{-3}$, $t = 200$ °C. Curve (*8*) AgCl dissolved in the CsCl–$CsAlCl_4$ solvent melt at $X_{AgCl} = 7.3 \times 10^{-3}$, $t = 400$ °C. Curve (*9*) AgCl dissolved in the $CsAlCl_4$ solvent melt at $X_{AgCl} = 4.0 \times 10^{-3}$, $t = 400$ °C. Curve (*9*) AgCl dissolved in the $CsAlCl_4$ solvent melt at $X_{AgCl} = 4.0 \times 10^{-3}$, $t = 400$ °C. Curve (*10*) CuCl dissolved in the CsCl–$CsAlCl_4$ solvent melt at $X_{CuCl} = 8.6 \times 10^{-3}$, $t = 400$ °C. Curve (*11*) CuCl dissolved in $CsAlCl_4$–$AlCl_3$ solvent melt at $X_{CuCl} = 7.0 \times 10^{-3}$, $t = 200$ °C. Curve (*12*) $FeCl_2$ and $FeCl_3$ dissolved in the CsCl–$CsAlCl_4$ solvent melt at $X_{FeCl_2} = 5.2 \times 10^{-3}$ and $X_{FeCl_3} = 5.36 \times 10^{-3}$, $t = 400$ °C. Curve (*13*) $FeCl_2$ and $FeCl_3$ dissolved in the $CsAlCl_4$ solvent melt at $X_{FeCl_2} = 1.5 \times 10^{-3}$ and $X_{FeCl_3} = 1.5 \times 10^{-3}$, $t = 400$ °C. Curve (*14*) $FeCl_2$ and $FeCl_3$ dissolved in the $CsAlCl_4$–$AlCl_3$ solvent melt at $X_{FeCl_2} = 1.5 \times 10^{-3}$, $X_{FeCl_3} = 1.5 \times 10^{-3}$, $t = 200$ °C. Curve (*15*) Decomposition curve for the solvent melt CsCl–$CsAlCl_4$ after purification and pre-electrolysis, $t = 400$ °C. Current scale shown on diagram is common for all curves. Oscillation frequency was 85 opm. The reference electrode was a Pt foil.

These curves traced from the original automatic recordings of the polarograph also indicate well-defined limiting currents.

With regard to the behaviour of Cd^{2+} ions at low concentrations only one reduction wave could be recorded (curve *5*). However, with more concentrated solutions (curve *6*), a second reduction wave was evident. This second wave could not be seen at temperatures higher than 400 °C.

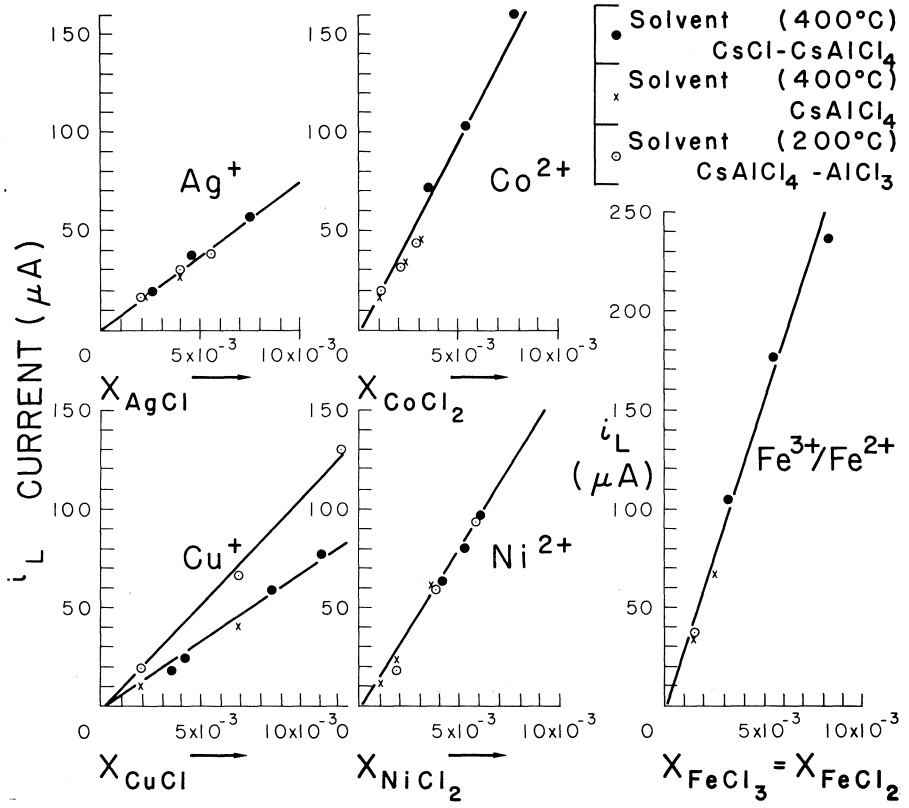

FIG. 3. Concentration dependence of the limiting currents for the reduction of various metal cations in the $AlCl_3$–CsCl solvent melts at an oscillation frequency of 85 opm.

The concentration dependence of the limiting currents at 350 °C is shown in Fig. 6.

In all cases the limiting currents are proportional to the mole fraction of the solute species. For the Cd^{2+} ions the plot is based on the limiting currents representing the first wave only.

The concentration dependence of the limiting currents, given in Fig. 3, shows that the slopes of the curves for the Ag^+ and Cu^+ ions are similar, except for Cu^+ dissolved in the $CsAlCl_4$–$AlCl_3$ solvent at 200 °C which indicates abnormally higher limiting currents. Similarly, Co^{2+} and Ni^{2+} show identical concentration dependence, the magnitude of a limiting current at a given concentration being almost double that for monovalent ions.

This relationship is to be expected since all mass transport expressions for limiting currents indicate, among others, a direct proportionality between the limiting current and the valence of the electroreducible species.

However, regarding the redox system Fe^{2+}/Fe^{3+}, the limiting current is very high, probably indicating a high diffusion rate for the small Fe^{3+} cation. It should be noted that for the redox reaction $Fe^{3+} \rightarrow Fe^{2+}$, the reaction represents a one electron electrode process and its limiting current is determined by the steady-state mass transport of Fe^{3+} from the bulk phase to the electrode-solution interface.

In Fig. 6, the slopes for the concentration dependence of the limiting currents for the reduction of divalent cations are also of similar magnitude.

The reduction of Zr^{4+} ions, added to a $ZnCl_2$–CsCl melt as the solid compound Cs_2ZrCl_6, has also been investigated. The system is of interest because zirconium has been reported to exist in four multiple oxidation states, namely, Zr^{4+}, Zr^{3+}, Zr^{2+}, and Zr^+ (6).

The reduction path of Zr^{4+} ions on a solid electrode is also related to the mechanism of electrodeposition of zirconium from fused chloride melts.

Figure 7*a* shows three voltammetric curves for the reduction of Zr^{4+} dissolved in the

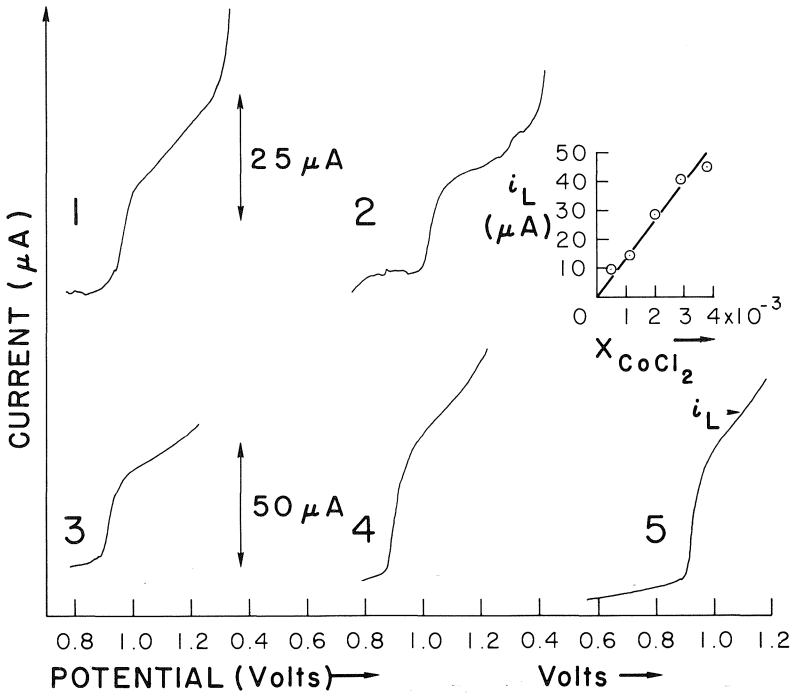

FIG. 4. Voltammetric waves for the reduction of Co^{2+}, dissolved in the CsCl–$CsAlCl_4$ solvent melt obtained at the higher oscillation frequency of 180 opm at 418 °C. Curve (*1*) Co^{2+} at $X_{CoCl_2} = 0.45 \times 10^{-3}$. Curve (*2*) Co^{2+} at $X_{CoCl_2} = 1.10 \times 10^{-3}$. Curve (*3*) Co^{2+} at $X_{CoCl_2} = 1.95 \times 10^{-3}$. Curve (*4*) Co^{2+} at $X_{CoCl_2} = 2.76 \times 10^{-3}$. Curve (*5*) Co^{2+} at $X_{CoCl_2} = 3.72 \times 10^{-3}$. Graph in upper right hand corner shows plots of i_L *vs.* X_{CoCl_2}. The reference electrode was a platinum foil.

$CsZn_2Cl_3$ melt. It should be noted that only one reduction wave appears before the breaking down of the supporting electrolyte. The reduction begins at about −1.02 V and the concentration dependence of the limiting current, shown in the upper left hand corner of the same figure, is linear.

A melt containing Zr^{4+} at a mole fraction, $X_{ZrCl_4} = 4.47 \times 10^{-3}$, after a period of about 70 h and repeated voltammetric runs began to indicate multiple reduction steps. This behaviour became more pronounced when the melt temperature was first increased to about 450 °C and then reduced to temperatures below 350 °C. The multiple reduction steps became even more evident when a run was repeated without polishing the indicator electrode surface. Figure 7*b* shows two typical voltammetric curves from among several similar recordings. They show three distinct reduction steps at about −0.85, −0.92, and −1.2 V.

The temperature dependence of the limiting current was also investigated in several cases. Figure 8 shows the temperature dependence of the limiting current obtained for a solution of $CdCl_2$ in $CsZn_2Cl_5$. The plot indicates that the dependence is exponential. The slope of the straight line represents an activation energy of about 9 kcal/mol which compares well with the activation energy for the diffusion of Cd^{2+} in some molten salts given by Delimarskii and Markov (7). It should be noted, however, that the limiting current observed in the present investigation is not necessarily controlled by diffusion alone and should also be influenced by viscosity variations with temperature.

Discussion

For metals depositing on tungsten at low temperatures, it is reasonable to assume that surface alloys do not form, and hence, the activity of the metal deposit should be unity.

For a cathodic reduction,

$$[2] \qquad M^{z+} + Ze^- \rightarrow M_{(a_M)}$$

where Z is the valence of the cation, the relationship between the applied potential and the corresponding voltammetric current on a solid

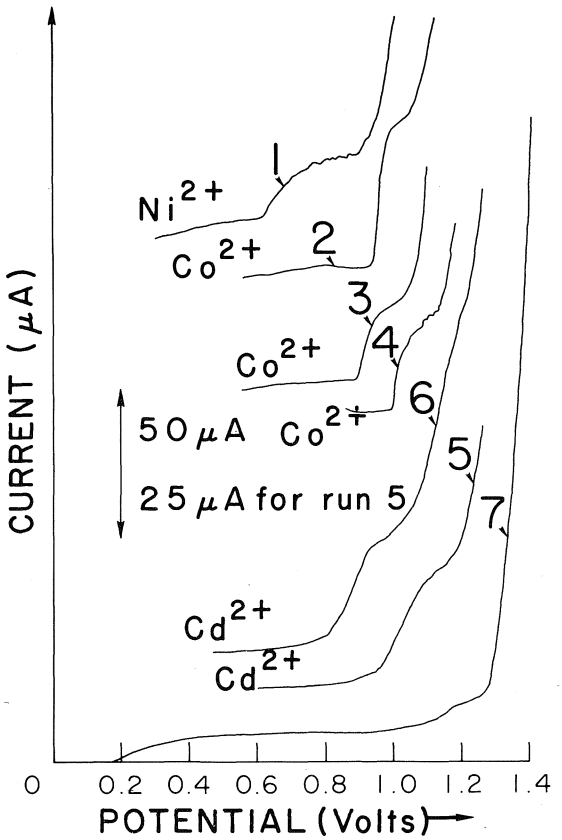

FIG. 5. Typical voltammetric curves for the reduction of metal cations dissolved in the CsCl–$ZnCl_2$ solvent melts at 350 °C and at an oscillation frequency of 180 opm. Curve (*1*) $NiCl_2$ dissolved in the $ZnCl_2$–$CsZn_2Cl_5$ melt at $X_{NiCl_2} = 3.5 \times 10^{-3}$. Curve (*2*) $CoCl_2$ dissolved in the $ZnCl_2$–$CsZn_2Cl_5$ melt at $X_{CoCl_2} = 2.0 \times 10^{-2}$. Curve (*3*) $CoCl_2$ dissolved in the CsCl–$CsZn_2Cl_5$ melt at $X_{CoCl_2} = 5.38 \times 10^{-3}$. Curve (*4*) $CoCl_2$ dissolved in the $CsZn_2Cl_5$ melt at $X_{CoCl_2} = 9.9 \times 10^{-3}$. Curve (*5*) $CdCl_2$ dissolved in the $CsZn_2Cl_5$ melt at $X_{CdCl_2} = 8.75 \times 10^{-2}$. Curve (*6*) $CdCl_2$ dissolved in the $CsZn_2Cl_5$ melt at $X_{CdCl_2} = 3.37 \times 10^{-2}$. Curve (*7*) Decomposition curve for solvent $CsZn_2Cl_5$–$ZnCl_2$. All curves except *5* were measured against the Pt foil reference electrode. Curve *5* was obtained against a graphite rod reference electrode saturated with chlorine by pre-electrolysis.

microelectrode should be similar to that derived by Kolthoff and Lingane (8) for the reduction of metal cations at the dropping mercury electrode, when the metal deposited is insoluble in mercury. Taking into account the expected difference in the value for the constant term, this expression is:

$$[3] \quad E_{applied} = \text{Constant} + \frac{RT}{ZF}\ln (i_L - i)$$

where i_L is the limiting current and i is the current along the rising part of the wave.

The derivation of this expression was based on the assumption that the electrode reaction is totally reversible and that the magnitude of the current is defined by the cathodic process at the microelectrode which is controlled by mass transfer only.

The so-called half-wave potential $E_{1/2}$ at the mid-point of the rising voltammetric curve is given as

$$[4] \quad E_{1/2} = \text{Constant} + \frac{RT}{ZF}\ln \frac{i_L}{2}$$

Since i_L is concentration dependent, $E_{1/2}$ also changes with the concentration of the electroreducible specie in solution. Therefore, $E_{1/2}$ is not as significant a quantity in the present case as in aqueous polarography.

Similarly, considering an electrode process which involves an intermediate reduction of a cationic species from one oxidation state to another, such as

$$[5] \quad M^{Z+} + ne^- \rightarrow M^{(Z-n)+}$$

the equation of the voltammetric wave would depend on whether or not any of the reduced form is originally present in the solution.

If none of the reduced form is originally present, then the equation for the wave derived by Kolthoff and Lingane (8) should also be applicable to a solid microelectrode. The equation is given as

$$[6] \quad E = \text{Constant} - \frac{RT}{ZF}\ln \frac{i}{i_L - i}$$

When the reduced form is originally present in solution, the equation for the wave becomes

$$[7] \quad E = \text{Constant} - \frac{RT}{ZF}\ln \frac{i - (i_L)_A}{(i_L)_C - i}$$

where $(i_L)_A$ and $(i_L)_C$ are, respectively, the anodic and cathodic components of the voltammetric curve.

When the free energy for the anodic reaction is sufficiently positive then the reduction curve does not contain an anodic component even at very low concentration ratios of X(red)/X(oxid). Thus $(i_L)_A = 0$, and eq. 7 reduces to eq. 6. Similar expressions for solid microelectrodes have been given by Delimarskii and Markov (7).

Figure 9 shows plots of E *vs.* log $(i_L - i)$ for the voltammetric curves shown in Fig. 2, except

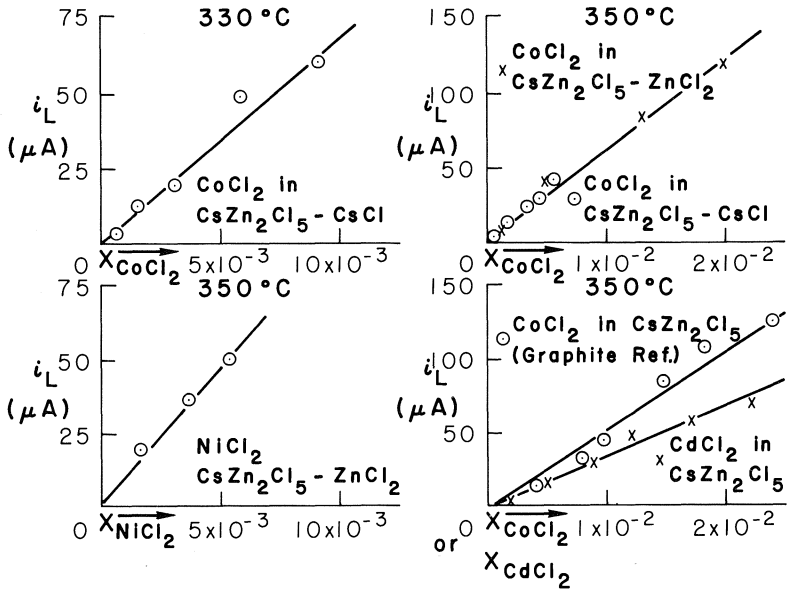

FIG. 6. Concentration dependence of limiting currents for Co^{2+}, Ni^{2+}, and Cd^{2+} ions dissolved in the CsCl–$ZnCl_2$ melts. Frequency of oscillations is common for all curves at 180 opm. Curves *1*, *2*, *3*, *4a* have been obtained against a Pt foil reference. Curve *4b* represents measurements against the graphite reference electrode.

for the reduction of Cd^{2+} and Pb^{2+} which exhibited maxima. It is evident that the linearity predicted by eq. 3 is followed in all cases. The graph also contains lines indicating theoretical slopes expected for one- and two-electron reduction processes, respectively.

It is seen that the reduction for Cu^+ and Ag^+ ions is clearly a one-electron process, while that for Co^{2+} is a two-electron process. The remaining curves indicate small deviations from the expected theoretical slopes, indicating possible irreversibility in the reduction process involved.

Similarly, Fig. 10 shows the E *vs.* log $(i_L - i)$ plots of three curves given in Fig. 5 for cations dissolved in the CsCl–$ZnCl_2$ melts.

Again, the reaction for Co^{2+} is distinctly a reversible two-electron reduction process. However, the reduction for Ni^{2+} is anomalous and shows a one-electron slope.

Figure 11 represents the analysis of multiple reduction waves obtained in the CsCl–$ZnCl_2$ solvent melt.

The corresponding voltammetric curves for the reduction of Cd^{2+} and Zr^{4+} are given in Figs. 5 and 7, and that for the redox system Fe^{3+}/Fe^{2+} is given in Fig. 2.

The graph contains plots of E *vs.* log $i/(i_L - i)$, as required by the Kolthoff–Lingane eq. 6 for reduction waves indicating multiple steps.

The redox system Fe^{3+}/Fe^{2+} showed one voltammetric curve and the plot of E *vs.* log $i/(i_L - i)$ is linear. The slope of the curve is that required for a reversible one-electron process and accordingly the reduction wave represents the reaction

$$[8] \qquad Fe^{3+} + e^- \rightarrow Fe^{2+}$$

For the first reduction wave seen in the Cd^{2+} voltammetric curve, the E *vs.* log $i/(i_L - i)$ is linear, but the slope is lower than that required for a one-electron process corresponding to a monovalent Cd^+. The second wave is not linear and cannot be defined.

For the multiple reduction steps seen in the reduction of Zr^{4+}, the first wave yields a well-defined linear plot with a two-electron slope, and the second wave indicates a one-electron slope. Accordingly, these waves represent the reduction processes

$$[9] \qquad Zr^{4+} + 2e^- \rightarrow Zr^{2+}$$

and

$$[10] \qquad Zr^{2+} + e^- \rightarrow Zr^+$$

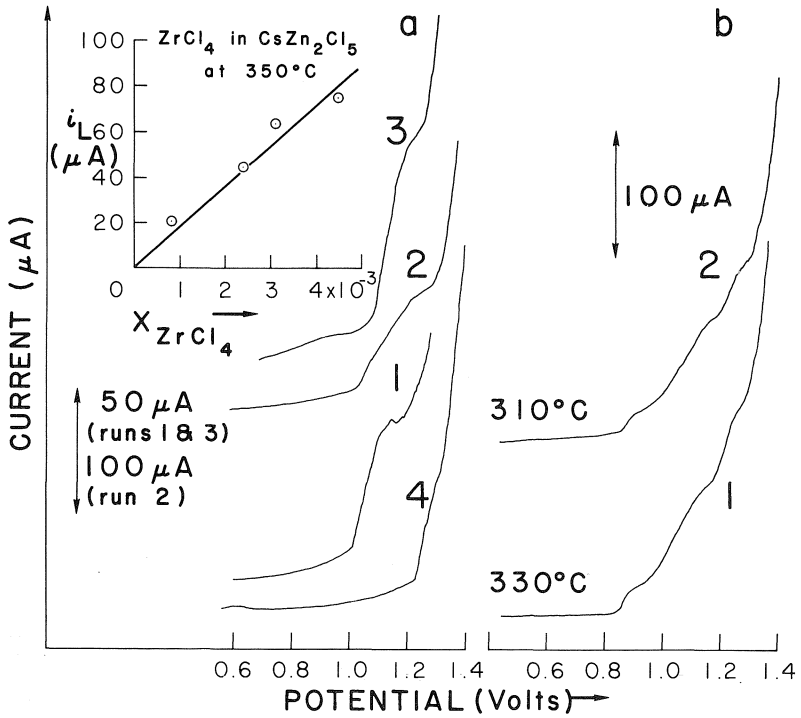

FIG. 7. Voltammetric curves for the reduction of Zr^{4+} added (as Cs_2ZrCl_6) in the $CsZn_2Cl_3$ solvent melt obtained at an oscillation frequency of 180 opm, $t = 350$ °C. Curve (*a1*) Zr^{4+} at $X_{ZrCl_4} = 2.44 \times 10^{-3}$. Curve (*a2*) Zr^{4+} at $X_{ZrCl_4} = 3.08 \times 10^{-3}$. Curve (*a3*) Zr^{4+} at $X_{ZrCl_4} = 4.47 \times 10^{-3}$. Curve (*a4*) Decomposition curve for solvent $CsZn_2Cl_3$. Plot in the upper left hand corner of Fig. 7*a* shows the concentration dependence of the limiting currents (voltammetric curve for first point not included in Fig. 7*a*). Curve (*b1*) Zr^{4+} at $X_{ZrCl_4} = 4.47 \times 10^{-3}$, $t = 330$ °C. Curve (*b2*) Zr^{4+} at $X_{ZrCl_4} = 4.47 \times 10^{-3}$, $t = 310$ °C. All measurements were against the Pt foil reference electrode at 180 opm.

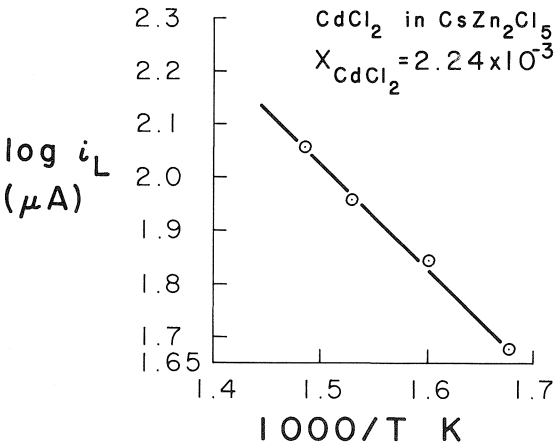

FIG. 8. Dependence of the limiting currents on temperature for a solution of $CdCl_2$ in $CsZn_2Cl_3$ melt at 180 opm. $X_{CdCl_2} = 2.24 \times 10^{-3}$.

The plot for the third wave shows slight deviations from linearity, and its average slope could be taken as representing a one-electron reduction process. Therefore, this wave could indicate the reduction to metal according to

$$[11] \qquad Zr^+ + e^- \rightarrow Zr$$

It should be noted that monovalent Zr^+ has been found in ZrCl (9) which is a chemically stable compound even at temperatures as high as 1000 °C.

These results seem to indicate that the intermediate reduction of Zr^{4+} to Zr^{3+} is not taking place in these melts. It has been shown by Copley and Shelton (10) that pure $ZrCl_3$ disproportionates to a lower valence state at temperatures above 310 °C.

It should be noted that the decomposition

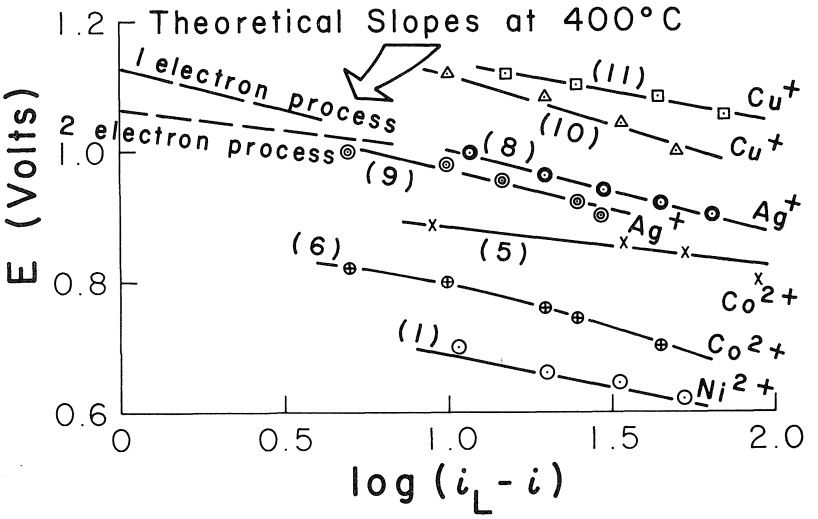

FIG. 9. Plots of E *vs.* log ($i_L - i$) for the reduction of metal cations dissolved in the CsCl–$AlCl_3$ solvent melts. Numbers on each curve correspond to voltammetric curves of the same number shown in Fig. 2. Theoretical slopes for one- and two-electron reduction processes are shown on the graph by dotted lines. (*1*) $NiCl_2$ dissolved in the CsCl–$CsAlCl_4$ melt at $X_{NiCl_2} = 5.25 \times 10^{-3}$, $t = 400$ °C. (*5*) $CoCl_2$ dissolved in CsCl–$CsAlCl_4$ melt at $X_{CoCl_2} = 5.35 \times 10^{-3}$, $t = 400$ °C. (*6*) $CoCl_2$ dissolved in the $CsAlCl_4$ melt at $X_{CoCl_2} = 2.8 \times 10^{-3}$, $t = 400$ °C. (*8*) AgCl dissolved in the CsCl–$CsAlCl_4$ melt at $X_{AgCl} = 7.3 \times 10^{-3}$, $t = 400$ °C. (*9*) AgCl dissolved in the $CsAlCl_4$ melt at $X_{AgCl} = 4.0 \times 10^{-3}$, $t = 400$ °C. (*10*) CuCl dissolved in the CsCl–$CsAlCl_4$ melt at $X_{CuCl} = 8.6 \times 10^{-3}$, $t = 400$ °C. (*11*) CuCl dissolved in $CsAlCl_4$–$AlCl_3$ melt at $X_{CuCl} = 7.0 \times 10^{-3}$, $t = 200$ °C.

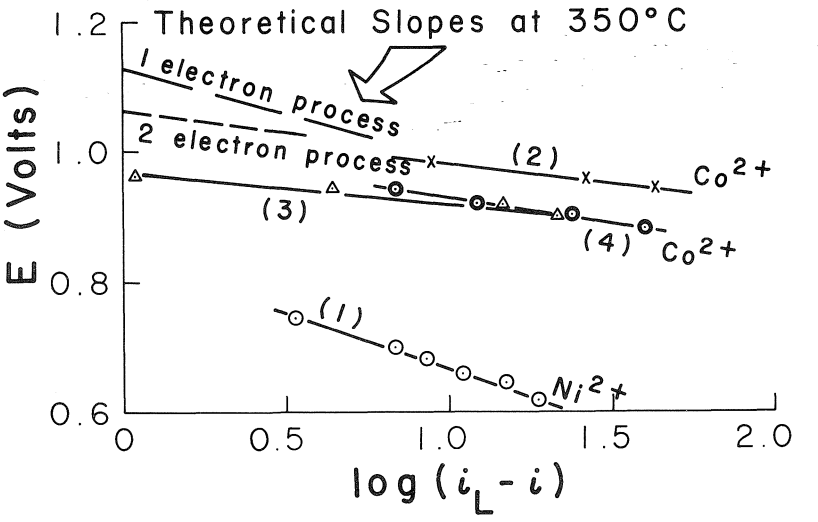

FIG. 10. Plots of E *vs.* log ($i_L - i$) for the reduction of metal cations dissolved in the CsCl–$ZnCl_2$ melts. Numbers on each curve correspond to voltammetric curves of the same number shown in Fig. 5. Theoretical slopes for one- and two-electron reduction processes are shown in the graph by dotted lines. (*1*) $NiCl_2$ dissolved in the $ZnCl_2$–$CsZn_2Cl_5$ melt at $X_{NiCl_2} = 3.50 \times 10^{-3}$, $t = 350$ °C. (*2*) $CoCl_2$ dissolved in the $ZnCl_2$–$CsZn_2Cl_3$ melt at $X_{CoCl_2} = 2.00 \times 10^{-2}$, $t = 350$ °C. (*3*) $CoCl_2$ dissolved in the CsCl–$CsZn_2Cl_5$ melt at $X_{CoCl_2} = 5.38 \times 10^{-3}$, $t = 350$ °C. (*4a*) $CoCl_2$ dissolved in the $CsZn_2Cl_5$ melt at $X_{CoCl_2} = 9.90 \times 10^{-3}$, $t = 350$ °C.

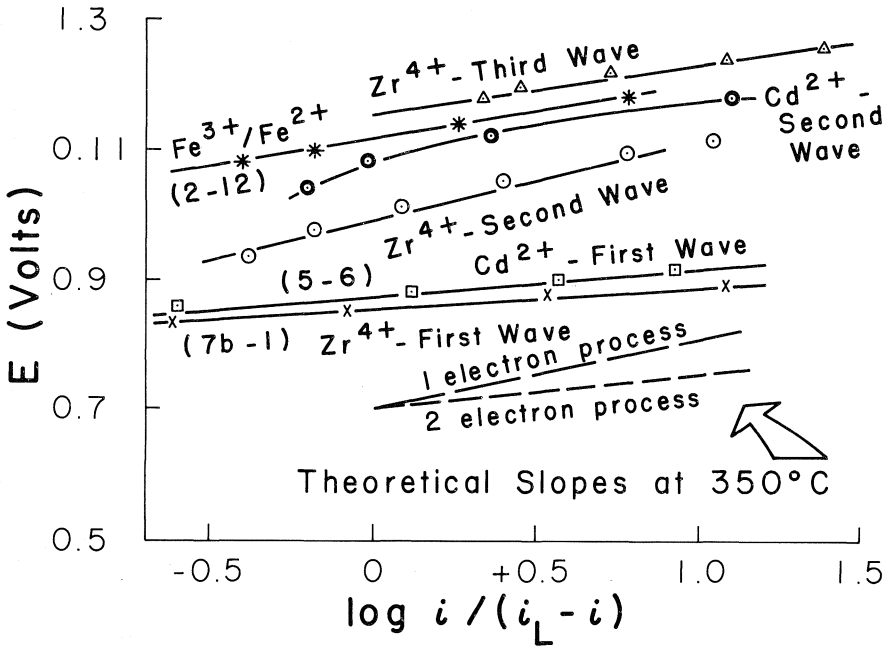

FIG. 11. Plots of E *vs.* log $i/(i_L - i)$ for multiple reduction waves. Numbers in each curve correspond to voltammetric curves of same number given in Figs. 2, 5, and 7, respectively. Theoretical slopes for one- and two-electron reduction processes are shown by dotted lines. (*7b-1*) $ZrCl_4$ dissolved in $CsZn_2Cl_5$ melt at $X_{ZrCl_4} = 4.47 \times 10^{-3}$, $t = 330$ °C. (*5-6*) $CdCl_2$ dissolved in $CsZn_2Cl_5$ melt at $X_{CdCl_2} = 3.37 \times 10^{-2}$, $t = 350$ °C. (*2-12*) $FeCl_2$ and $FeCl_3$ dissolved in $CsAlCl_4$ solvent melt at $X_{FeCl_2} = 5.20 \times 10^{-3}$ and $X_{FeCl_3} = 5.36 \times 10^{-3}$, $t = 400$ °C.

TABLE 2. Electroreduction characteristics of metal cations on the tungsten vibrating microelectrode ($X_{\text{metal chloride}} = 5 \times 10^{-3}$)

Overall reaction at the tungsten indicator electrode	$-E_{dep}$ (V)*		
	$CsCl$–$CsAlCl_4$ (400 °C)	$CsAlCl_4$ (400 °C)	$CsAlCl_4$–$AlCl_3$ (200 °C)
$Ni^{2+} + 2e^- = Ni$	0.65–0.66	0.60–0.62	0.6
$Pb^{2+} + 2e^- = Pb$	0.72	0.72	0.83
$Co^{2+} + 2e^- = Co$	0.80–0.83	0.70–0.72	0.80–0.82
$Cd^{2+} + 2e^- = Cd$	(*a*) 0.96; (*b*) 1.06	—	—
$Ag^+ + e^- = Ag$	0.90–0.93	0.80–0.86	0.84–0.88
$Cu^+ + e^- = Cu$	1.00–1.02	0.96–1.0	1.00–1.02
$Fe^{3+} + e^- = Fe^{2+}$	1.05	0.95–0.96	0.96–0.98

Reaction	E_{dep} (V)*		
	$CsCl$–$CsZn_2Cl_5$ (350 °C)	$CsZn_2Cl_5$ (350 °C)	$ZnCl_2$–$CsZn_2Cl_5$ (350 °C)
$Co^2 + 2e = Co$	0.90–0.91	—	0.92–0.94
$Ni^{2+} + 2e = Ni$	—	—	0.78–0.80
$Cd^{2+} + 2e = Cd$	—	(*a*) 0.83 and (*b*) 0.94	—
$Zr^{4+} + 4e = Zr$	—	(*a*) 0.85, (*b*) 0.94, and (*c*) 1.16	—

* (*a*), (*b*), and (*c*) indicate, respectively, first, second, and third waves.

voltages shown by the pure solvent electrolytes are different from those seen in voltammetric curves measured in the presence of solute metal cations. This variation may be attributed to the effect of coating the tungsten surface with minute amounts of the metal deposit during electrolysis.

The decomposition potentials for the pure solvent melts used in this study are given in Table 1.

Since half-wave potentials are not too significant in the present system and furthermore, since deposition on a solid microelectrode may proceed irreversibly, it is more meaningful to tabulate the initial deposition potentials for the electrode reactions investigated.

Table 2 shows the deposition potentials for cations in the various solvents investigated measured against the platinum reference electrode at solute mole fraction of 5×10^{-3}.

It should be noted that potential measurements taken against the graphite reference electrode saturated with chlorine did not indicate any appreciable differences from the values shown in Table 2.

Since the graphite electrode is definitely a chlorine electrode, it seems that the platinum reference electrode behaves like a chlorine electrode and that platinum dissolution does not take place. Accordingly, the possible anodic reaction at the platinum and the graphite reference electrodes should be written as

$$[12] \qquad Cl^- \rightarrow \tfrac{1}{2}Cl_2 + e^-$$

A comparison between the decomposition potentials in the various solvent melts at the common mole fraction for the solute ions of 5×10^{-3} shows that in the $AlCl_3$–CsCl solvent the lowest deposition potentials occur with the compound $CsAlCl_4$. With melts which contain $CsAlCl_4$ and an excess of either CsCl or $AlCl_3$ the potentials are slightly higher, indicating that the metal cations are at a lower activity level possibly due to complex formation. This effect, however, was not investigated in the $ZnCl_2$–CsCl melts.

Conclusions

This study has shown that the oscillating tungsten microelectrode is a very useful tool for investigating the electrochemical reduction of metal cations dissolved in chloride solvent melts in the temperature range 200 to 420 °C.

The voltammetric waves for Ag^+, Cu^+, Ni^{2+}, Co^{2+}, and for the redox system Fe^{2+}/Fe^{3+} consist of one well-defined reduction step. All the limiting currents are proportional to the mole fraction of the solute, indicating that the limiting currents are defined by steady-state mass transport.

For systems like Pb^{2+} and Cd^{2+} in solution in the CsCl–$AlCl_3$ melts, the voltammetric curves show two reduction waves with pronounced maxima. Cd^{2+} dissolved in a CsCl–$ZnCl_2$ melt also showed two waves but no maximum.

The reduction of Zr^{4+} ions at low concentrations shows one reduction wave only. However, at higher concentrations three well-defined waves are evident.

Regarding the choice of solvent melts used in this study, they are characterized mainly by CsCl as the common component and contained either $AlCl_3$ or $ZnCl_2$ in various proportions as the second component.

$AlCl_3$ and $ZnCl_2$ are useful in that they reduce the melting points of the solvent melts to temperatures as low as 200 °C. In addition they have a definite effect in reducing the residual currents which have been found to be very high in pure alkali chloride melts. The CsCl component in these melts has the additional advantage of reducing the escaping tendency of the volatile compounds $ZnCl_2$ and $AlCl_3$, due to strong chemical interactions in the liquid state. From among the various solvent melts investigated, those containing an excess of CsCl, like the CsCl–$CsAlCl_4$ and CsCl–$CsZn_2Cl_5$, appear to be the most stable supporting electrolytes.

It is of interest to note that the limiting currents in the CsCl–$AlCl_3$ and CsCl–$ZnCl_2$ solvent melts are of comparable magnitude for a given solute cation at the same concentration and temperature. A slight shift in the deposition potentials could be seen by comparing the voltammetric curves representing the various solvent melts for the reduction of a given cation, but the magnitude of the change is not sufficient to suggest the presence of different complex species in these melts. Thus, the deposition potentials of a given cation in the three melts having compositions corresponding to CsCl–$CsAlCl_4$, $CsAlCl_4$, and $CsAlCl_4$–$AlCl_3$, respectively, would be expected to be higher in the first melt containing an excess of CsCl, and hence an excess of 'free' chloride ions. Since this was not observed it should be concluded that the congruent compounds $CsAlCl_4$ and $CsZn_2Cl_5$ in the

molten state are sufficiently dissociated to provide an abundance of 'free' chloride ions in all these solvents.

Analysis of the shape of the voltammetric reduction curves following the Kolthoff and Lingane (8) relationships yielded linear plots.

The reduction of Ag^+, Cu^+, and Co^{2+} and of Fe^2/Fe^{3+} dissolved in the $CsCl$–$AlCl_3$ melts appears to be reversible, while the voltammetric curve for the reduction for Ni^{2+} indicates an abnormally high slope.

For Cd^{2+} and Pb^{2+} dissolved in the $CsCl$–$AlCl_3$ melts, the observed maxima did not allow an analysis of the shape of the voltammetric curves with any accuracy.

In the $CsCl$–$ZnCl_2$ melts the reduction of Cd^{2+} indicates the presence of an intermediated Cd^+ species.

From the analysis of the multiple reduction steps seen in the reduction of Zr^{4+}, it is concluded that the electron transfer takes place in the sequence $Zr^{4+} \rightarrow Zr^{2+} \rightarrow Zr^+$, followed by a possible final reduction step to metallic zirconium.

Acknowledgements

The authors are grateful to the National Research Council of Canada for providing senior visiting associateships to two of the authors (H.S.R. and N.Kh.T.).

The assistance of the Government of India and of the U.S.S.R. in this program is also gratefully acknowledged.

1. P. Pint and S. N. Flengas. J. Electrochem. Soc. **123**, 1042 (1976).
2. O. Kubaschewski, E. L. Evans, and C. B. Alcock. Metallurgical thermochemistry. 4th ed. Pergamon Press, Oxford. 1967.
3. I. S. Morozov and A. T. Simonich. Russ. J. Inorg. Chem. **2**, 311 (1957).
4. B. F. Markov, I. D. Panchenko, and T. G. Kostenko. Ukr. Khim. Zh. Russ. Ed. **22**, 287 (1956).
5. D. A. Asvestas, P. Pint, and S. N. Flengas. Can. J. Chem. In press.
6. B. Swaroop and S. N. Flengas. Can. J. Chem. **4**, 199 (1966).
7. Iu. K. Delimarskii and B. F. Markov. Electrochemistry of fused salts (English translation). The Sigma Press, Washington. 1961.
8. I. M. Kolthoff and J. J. Lingane. Polarography. 2nd ed. Vol. 1. Interscience Publishers, New York City. 1952.
9. R. S. Dean. U.S. Patent No. 2941931, June 21, 1960.
10. D. P. Copley and R. A. Shelton. J. Less-Common Met. **20**, 359 (1970).

The electronic structure of tetraphosphorus trisulphide

JOHN D. HEAD, KEITH A. R. MITCHELL, LOUIS NOODLEMAN, AND NORMAN L. PADDOCK[1]

Department of Chemistry, University of British Columbia, Vancouver, B.C., Canada V6T 1W5

Received July 27, 1976

JOHN D. HEAD, KEITH A. R. MITCHELL, LOUIS NOODLEMAN, and NORMAN L. PADDOCK. Can. J. Chem. **55**, 669 (1977).

The electronic structure of P_4S_3 has been investigated by the Xα scattered wave (XαSW) method as well as by the extended Hückel (EH) and complete neglect of differential overlap (CNDO) molecular orbital methods. The XαSW method gives a particularly good account of the ionization energies determined by HeI photoelectron spectroscopy. The valence shell levels fall into two groups. Those of lower energy are for the most part multicentre orbitals having high *s* character. The upper occupied levels are non-bonding or weakly bonding, and have a large *p* component. Contour plots of wave functions and charge distributions emphasize the importance of 'bent bonding' associated with electron density outside the framework of the cage structure, and of multicentre density inside the cage structure. These calculations provide a basis for understanding the relationship between the chemical properties of P_4S_3 and its electronic structure.

JOHN D. HEAD, KEITH A. R. MITCHELL, LOUIS NOODLEMAN et NORMAN L. PADDOCK. Can. J. Chem. **55**, 669 (1977).

On a étudié la structure électronique du P_4S_3 par la méthode des ondes diffusées de Xα (XαSW) de même que par des méthodes d'orbitales moléculaires de Hückel étendues (EH) et CNDO. La méthode XαSW fournit une bonne approximation des énergies d'ionisation qui ont été déterminées par spectroscopie photoélectronique HeI. Les niveaux des couches de valence se divisent en deux groupes. Les niveaux qui ont des énergies moins élevées sont pour la plupart des cas d'orbitales à plusieurs centres ayant un caractère *s* élevé. Les couches occupées de niveaux plus élevés ne lient pas ou ne lient que faiblement; de plus elles possèdent une composante *p* importante. Les tracés de contour des fonctions d'onde et des distributions de charge mettent en relief l'importance de la liaison déformée associée avec la densité électronique à l'extérieur du cadre de la structure en cage et de la densité à plusieurs centres à l'intérieur de la structure en cage. Ces calculs fournissent une base pour comprendre la relation entre les propriétés chimiques du P_4S_3 et sa structure électronique.

[Traduit par le journal]

Introduction

At the time of Stock's systematic investigation of the phosphorus sulphides (1), the compounds P_4S_3, P_4S_5, P_4S_7, and P_4S_{10} were known. More recently, the existence of P_4S_9 has been established (2, 3), and a new molecular form of P_4S_5 has been found (4). Although there is no detailed knowledge of the structures of the two latest additions to the series, P_4S_4 (3) and P_4S_2 (3, 5), thermochemical and spectroscopic evidence (6) suggests that these compounds, like those investigated earlier (4, 7–11), all have structures which are based on a P_4 tetrahedron. In P_4S_3, all the phosphorus atoms are tervalent, while one divalent sulphur atom is inserted in each of three coterminal edges of the phosphorus tetrahedron (Fig. 1). Similar cage structures are found for α- and β-As_4S_3 (12), P_4Se_3 (13), $As_3(CH_2)_3$-CMe (14), and the P_7^{3-} ion (15), isoelectronic with P_4S_3.

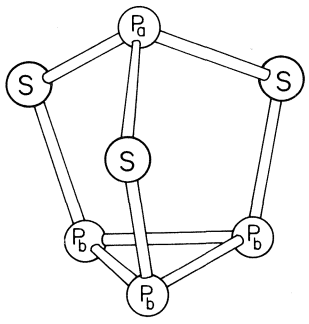

FIG. 1. The structure of P_4S_3 (7). Mean dimensions P_a—S, 2.090; P_b—S, 2.090; P_b—P_b, 2.235 Å; angles: S—P_a—S, 99.5°; P_a—S—P_b, 103.0°; S—P_b—P_b, 103.1°, P_b—P_b—P_b, 60°.

Tetraphosphorus trisulphide is the only phosphorus sulphide to retain its molecular structure in the solid, liquid, and vapour phases (16) and

[1]To whom all correspondence should be addressed.

in some chemical reactions. Although two electrons on each phosphorus atom and four on each sulphur atom are formally non-bonding, P_4S_3 is an effective donor only when the acceptor atom can release electrons to the ligand. Where structures of complexes with metal carbonyls (17, 18) are known, coordination occurs through the apical phosphorus atom, although the basal phosphorus atoms are involved in other reactions, for example with iodine (19, 20) and with elemental sulphur (21, 22). To provide a basis for assessing the chemical properties of P_4S_3 and its structural relationship to P_4 and the other molecules mentioned above, we report here a theoretical investigation of its electronic structure.

Calculational Methods

Calculations have been made with the Xα scattered wave (XαSW) (23), the extended Hückel (EH) (24), and the complete neglect of differential overlap (CNDO) (25) methods. The procedures and parameters for the EH calculations follow those used by Bartell *et al.* (26) except that *d* functions were not included. This seems reasonable since all atoms in P_4S_3 are in low oxidation states, although conventionally *d* orbitals are included in CNDO calculations for phosphorus and sulphur in all their compounds. The CNDO calculations were performed using the CNDO/2 version with the parameters specified by Pople and Beveridge (25). Convergence problems in the CNDO calculations were overcome in a way similar to those used by Bennett, McCarroll, and Messmer (27) and by Blyholder (28). This involves expressing the density matrix used as input for the *i*th iteration as

$$[1] \qquad P_i = (1 - A)P_{i-1}{}^{\text{new}} + AP_{i-1}$$

where P_{i-1} is the density matrix used as input for the $(i - 1)$th iteration and $P_{i-1}{}^{\text{new}}$ is the density matrix calculated in the $(i - 1)$th iteration. A was fixed at 0.7.

The XαSW method uses a self-consistent field approach, but does not use a basis of atomic orbital functions; the method relies instead on obtaining numerical radial functions which accurately solve a model Schrödinger equation. It is based on a statistical total energy expression in which the exchange-correlation energy $E_{XC}(\rho)$ is assumed to be a functional of the total electron density ρ (29). By using the variational principle, a set of orbitals μ_i and the corresponding one-electron eigenvalues ε_i are obtained from the one-electron Schrödinger equation

$$[2] \qquad [-\nabla^2 + V_C(r) + V_{X\alpha}(r)]\mu_i(r) = \varepsilon_i\mu_i(r)$$

This equation is given in Rydberg units (1 Ry = 13.605 eV). $V_C(r)$ is the classical Coulomb potential produced at r by the total electron density ρ and the nuclear charges, and

$$[3] \qquad X_{X\alpha}(r) = -6\alpha[(3/8\pi)\rho(r)]^{1/3}$$

is the exchange-correlation potential for the spin restricted case.

In practice, this method depends on partitioning the molecule into regions and choosing a suitable potential for each region. Each atom is surrounded by a sphere (centered at the nucleus), and the potential inside each atomic sphere is found by spherically averaging the one-electron potential $V_C(r) + V_{X\alpha}(r)$. The potential in the region between the atomic spheres (the intersphere region) is replaced by a constant volume-averaged potential, and in addition an isolated molecule is entirely surrounded by an extramolecular (outer sphere) region in which the potential is again spherically averaged. With this model potential [2] can be solved accurately by numerical methods. The wave functions are joined smoothly from one region to another, and, within the regions of spherically symmetric potentials, are expanded over spherical harmonics (the convergence in l is usually rapid). The foundations of the Xα theory and detailed descriptions of the method for solving the scattered wave equations have been discussed elsewhere (29, 30).

A recent development has been to allow the atomic spheres to overlap (31–33); the volume of the constant potential region is reduced, and the volumes over which the more accurate spherical averaging is performed are increased. Table 1 gives the atomic sphere radii and values of α (eq. 3) used here. The α values are those reported

TABLE 1. P_4S_3 sphere radii* and α parameters

Atom	Model 1‡	Model 2‡	α
P_a†	2.4900	2.2980	0.72620
P_b†	2.5800	2.3820	0.72620
S	2.5600	2.3630	0.72475
Outer sphere	6.5275	6.3300	0.72558§

*In units of the Bohr radius.
†P_a = apical; P_b = basal phosphorus atom.
‡See text.
§Same value used for intersphere region.

TABLE 2. One-electron energy eigenvalues (eV) from XαSW calculations

Core state	Model 1*	Model 2*	Valence shell orbital	Model 1*	Model 2*
$P_a(2p)$	−125.42	−126.78	$17e$	−5.64	−7.21
$(2s)$	−173.17	−174.54	$3a_2$	−6.23	−7.67
$(1s)$	−2076.90	−2078.19	$17a_1$	−6.70	−7.88
			$16e$	−7.31	−8.80
$P_b(2p)$	−124.72	−126.14	$15e$	−7.79	−9.10
$(2s)$	−172.45	−173.88	$16a_1$	−8.41	−9.70
$(1s)$	−2076.22	−2077.69	$15a_1$	−9.94	−11.03
			$14e$	−9.97	−11.20
$S(2p)$	−156.30	−157.69	$13e$	−13.34	−14.68
$(2s)$	−209.36	−210.76	$14a_1$	−14.09	−15.38
$(1s)$	−2395.30	−2396.66	$13a_1$	−17.96	−18.85
			$12e$	−18.61	−19.87
			$12a_1$	−21.39	−21.93

*See text.

by Schwarz (34). The ratios of the atomic sphere radii were fixed by a prescription given by Norman (32). This involved an initial calculation of a molecular charge distribution constructed from the superimposed charge densities of the free atoms, using the wave functions of Herman and Skillman (35). Preliminary sphere radii were chosen so that each sphere enclosed a total electron charge equal to the appropriate atomic number; the ratios of the atomic sphere radii for the XαSW calculations were then taken as equal to the appropriate ratios of the preliminary sphere radii. The two sets of absolute radii which have been used in this study (Table 1) are respectively 30% (Model 1) and 20% (Model 2) greater than required for contact of the spheres. For Model 1, the wave functions within the atomic spheres were expanded over a basis set involving spherical harmonics corresponding to $l = 0$ and $l = 1$; for Model 2, the basis was extended to include $l = 2$ functions.

Results

All calculations were made using the geometry of Fig. 1. Table 2 gives the one-electron eigenvalues obtained from the XαSW calculations for both the core and the valence shell levels. The one-electron ε_i are defined as

$$[4] \qquad \varepsilon_i = \frac{\partial \langle E_{X\alpha} \rangle}{\partial n_i}$$

where $\langle E_{X\alpha} \rangle$ is the expectation value of the total energy of the molecule, and n_i is the occupation number of the ith level. Ionization energies were calculated by transition state theory (27), which includes first order corrections for relaxation. For the semi-empirical methods, the ionization energies were taken to be the negatives of the calculated one-electron energies. The ionization energies calculated by all the methods are given in Table 3, together with the values measured by photoelectron spectroscopy.[2] The individual molecular orbitals from the XαSW method (Model 2) are analysed in Table 4, and the charge distributions for all the methods in Table 5. The total atomic valence-shell electron populations are given in Table 6. Table 7 gives the low lying dipole allowed excitation energies from spin restricted transition state calculations for the XαSW method (Model 1), and from differences in orbital energy for the EH and CNDO methods.

Discussion

Orbital Energies and Charge Distribution

The HeI photoelectron spectrum of P_4S_3 is shown in Fig. 2, with the ionization energies calculated by the XαSW method (Model 2) superimposed upon it. This calculation accounts particularly well for the relative positions of the energy levels (Table 3). The range covered by the first eight ionization energies is similar for Model 1 (4.45 eV) and Model 2 (4.09 eV), and close to the observed range (4.27 eV). The corresponding ranges calculated by the EH and CNDO methods, using Koopmans' theorem, are less satisfactory, being 3.38 and 6.83 eV, respectively.

The spacings in the ionization energies calculated by the XαSW method are changed slightly, but significantly, by the inclusion in Model 2 of d waves, to the extent of about 0.2–0.3 d electron

[2]The spectrum (HeI) was determined by Dr. J. N. A. Ridyard of Perkin–Elmer, using a PS-18 photoelectron spectrometer.

TABLE 3. Calculated and observed ionization energies (eV)

Orbital	XαSW (Model 1)	XαSW (Model 2)	Band No.	Obs.	EH	CNDO
$17e$	8.10	9.59	1	9.09	9.80	11.18
$3a_2$	8.75	10.05	2	9.29	10.15	11.86
$17a_1$	9.20	10.32	3	9.66	10.87	11.38
$16e$	9.75	11.19	4	10.70	10.71	12.52
			5	10.85		
$15e$	10.20	11.51	6	11.06	11.12	13.89
$16a_1$	10.90	12.12	7	11.72	11.36	14.34
$15a_1$	12.46	13.52	8	13.36	12.43	19.87
$14e$	12.55	13.68			13.18	18.01
$13e$					16.35	19.96
$14a_1$					16.22	20.80
$13a_1$					23.83	27.90
$12e$					24.54	28.38
$12a_1$					29.11	36.40

TABLE 4. Partial wave decomposition*

Orbital		P_a	S	P_b	%	Orbital		P_a	S	P_b	%
	s	0	0.002	0.005	2.5		s	0	0.011	0.018	10.2
$17e$	p	0.014	0.078	0.148	92.2	$14e$	p	0.174	0.132	0.049	84.7
	d	0.009	0.004	0.006	5.3		d	0.010	0.005	0.006	5.1
	s	0	0	0	0		s	0	0.026	0.164	62.4
$3a_2$	p	0	0.234	0.015	98.0	$13e$	p	0.064	0.063	0.016	32.8
	d	0	0.001	0.004	2.0		d	0.010	0.007	0.004	4.8
	s	0.030	0.000	0.003	5.1		s	0.277	0.083	0.011	59.9
$17a_1$	p	0.271	0.033	0.111	91.4	$14a_1$	p	0.000	0.055	0.055	35.2
	d	0.002	0.005	0.004	3.5		d	0.000	0.007	0.008	4.8
	s	0	0.002	0.009	4.4		s	0.160	0.009	0.190	80.1
$16e$	p	0.047	0.159	0.060	90.7	$13a_1$	p	0.003	0.025	0.026	16.3
	d	0.017	0.004	0.003	4.9		d	0.001	0.007	0.004	3.6
	s	0	0.002	0.018	7.3		s	0	0.240	0.035	85.9
$15e$	p	0.003	0.159	0.082	87.8	$12e$	p	0.040	0.006	0.015	10.7
	d	0.009	0.002	0.009	4.8		d	0.013	0.002	0.005	3.4
	s	0.082	0.007	0.016	19.0		s	0.199	0.162	0.049	88.6
$16a_1$	p	0.127	0.022	0.137	75.8	$12a_1$	p	0.021	0.015	0.010	10.2
	d	0.000	0.009	0.005	5.2		d	0.000	0.002	0.001	1.2
	s	0.002	0.021	0.001	8.7						
$15a_1$	p	0.044	0.149	0.078	86.7						
	d	0.007	0.003	0.007	4.7						
Total						Total					
for all	s	1.498	1.698	1.532		for all		1.272	1.571	1.296	
valence	p	2.298	3.451	2.342		levels		0.463	0.462	0.305	
levels†	d	0.289	0.157	0.203		$12a_1$–$13e$‡		0.093	0.067	0.065	

*From XαSW calculations on Model 2. The outer sphere contributions are excluded from individual orbital summations.
†Outer sphere populations: s, 0.074; p, 0.274; d, 0.196; f, 0.274; g, 0.129.
‡Outer sphere populations: s, 0.007; p, 0.024; d, 0.060; f, 0.029; g, 0.008.

on each atom. Model 2 gives the slightly better description, in that the preferential stabilization of the e levels by the (small) d-wave component separates the levels clearly into the groups of 3, 3, and 2 found in the spectrum. The chief differences between the absolute values of the ionization energies calculated for Models 1 and 2 are caused by the different choices of sphere overlap.

Norman (32) has suggested that the virial theorem be used as a criterion for establishing the absolute value of the sphere overlap. For

TABLE 5. Percentage charge distribution by atom type*

	Apical P (1)			Sulphur (3)			Basal P (3)				
State	XαSW	EH	CNDO	XαSW	EH	CNDO	XαSW	EH	CNDO	Int.	Out
$17e$	2	0	6	25	89	29	48	11	68	22	3
$3a_2$	0	0	0	70	91	89	6	9	11	21	3
$17a_1$	30	62	43	11	18	21	35	20	36	17	6
$16e$	6	12	8	50	56	65	21	32	25	19	3
$15e$	1	1	11	49	41	46	33	58	43	13	4
$16a_1$	21	8	14	11	54	30	48	38	56	16	3
$15a_1$	5	14	25	52	22	32	26	64	42	13	4
$14e$	18	13	15	44	35	62	22	52	23	14	2
$13e$	7	11	7	29	24	33	55	65	60	7	1
$14a_1$	28	29	19	43	37	59	22	34	22	5	2
$13a_1$	16	22	18	12	15	23	66	62	58	5	0
$12e$	5	5	9	74	71	68	16	23	23	3	1
$12a_1$	22	19	17	54	47	42	18	34	42	5	0

*For each molecular orbital, charge densities are given for the apical phosphorus atom, the three sulphur atoms, and the three basal phosphorus atoms. For each type of atom, the successive columns refer to (*1*) total sphere charges (XαSW Model 2), (*2*) the gross atomic population from a Mulliken population analysis of the EH wave functions, (*3*) the diagonal terms of the density matrix (CNDO). The last two columns of the table refer to the intersphere and outer sphere charges calculated by the XαSW method.

TABLE 6. Valence shell electronic populations on individual atoms

Atom	XαSW*	EH	CNDO
P_a	4.82	4.74	4.95
S	6.26	6.10	6.04
P_b	4.81	4.99	4.98

*Results for Model 2. The charge in the intersphere and outer sphere regions has been reallocated to the atomic sphere charges in the ratio of the actual valence atomic sphere charges.

TABLE 7. Calculated optical transitions in P_4S_3

	Excitation energy (eV)		
Transition	XαSW*	EH	CNDO
$17e \rightarrow 4a_2$	5.16	5.42	11.47
$17e \rightarrow 18e$	5.52	10.78	10.31
$17e \rightarrow 18a_1$	5.65	12.94	8.55
$17e \rightarrow 19a_1$	5.70	38.13	11.12
$3a_2 \rightarrow 4a_2$	6.10	5.78	12.15
$17e \rightarrow 19e$	6.19	15.07	10.75

*Model 1. Averaged over singlet–singlet and singlet–triplet transitions.

Models 1 and 2, $-2T/V = 1.000204$ and 1.000627 respectively. Although the deviation from unity is slightly greater in Model 2, this model is nevertheless preferable both because it avoids the unphysical negative intersphere charge (-4% to -13%) found for the four lowest valence orbitals in the calculations on Model 1 and because it gives the closer account of the measured ionization energies. If a constant 0.55 eV is subtracted from the ionization energies of Table 3 (Model 2), the mean deviation of the individual calculated and observed values is 0.16 eV.

The semi-empirical methods perform less well. Both follow the XαSW method in giving $17e$ as the highest occupied level, but, among the higher levels, the EH method interchanges $16e$ and $17a_1$, and CNDO interchanges $17a_1$ and $3a_2$. The ordering of levels derived from the XαSW calculations is supported by the interpretations of the photoelectron spectra of other molecules. The $3a_2$ orbital is an almost pure nonbonding combination of sulphur $3p$ (tangential) orbitals with only weak involvement of $3p$ orbitals on the basal phosphorus atoms. This is the case for all the methods (see Tables 4 and 5). The assignment of this level to the energy of the second band (9.29 eV) in Fig. 3 is consistent with the set of lone pair ionization energies of S_8, the highest being 9.23 (36) or 9.40 eV (37). The energy of the apical lone pair (defined here as the highest occupied a_1 orbital) in phosphines is lowered (relative to sulphur) by electronegative substituents, *cf.* H_2S, 10.47 (38); PH_3, 10.59 (39); $(CF_3)_2S$, 11.11 (40); $(CF_3)_3P$, 11.70 eV (41), and the corresponding assignment of the third band to $17a_1$, shown below to have this type of electron distribution, is a natural one. The equal intensities of bands 4 and 5 in the experimental spectrum suggest that this structure could correspond to a degenerate level ($16e$)

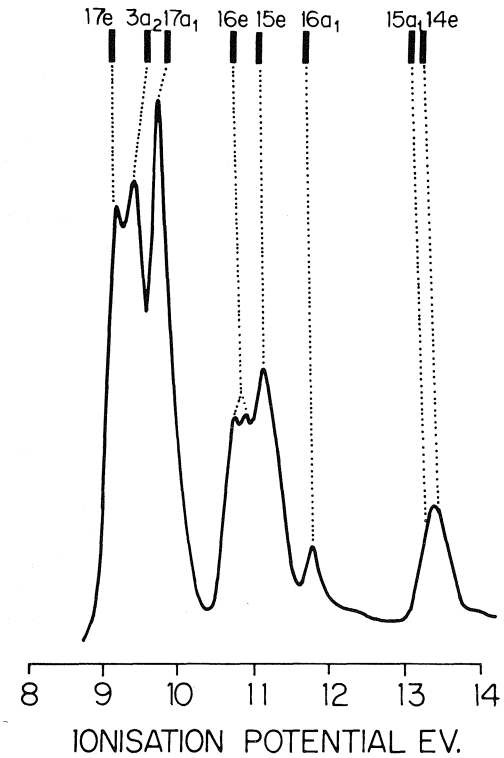

FIG. 2. The photoelectron spectrum (HeI) of P_4S_3. The ionization energies calculated by the XαSW method (Model 2), uniformly decreased by 0.55 eV from those given in Table 3 (see text) are shown at the top.

split by the Jahn–Teller effect. The eighth band seems broad enough to include both the $15a_1$ and $14e$ levels calculated to be in this region.

The ultraviolet spectrum[3] of P_4S_3 shows a single dipole-allowed band, with a transition energy of 6.0 eV ($\varepsilon = 13\,800$ l cm^{-1} mol^{-1}), near the instrumental limit of 6.2 eV. The XαSW method, through transition state theory, predicts several bands in the observable spectral region (Table 7), while the EH method predicts two bands ($17e \rightarrow 4a_2$ and $3a_2 \rightarrow 4a_2$) and the CNDO method none.

The XαSW partial wave decompositions in Table 4 show a substantial contrast between the upper occupied levels $14e$ to $17e$ and the lower valence levels $12a_1$ to $13e$. The former predominantly involve p functions (76 to 98% p), and the latter involve primarily s functions (60 to 89% s), although orbitals $13e$ and $14a_1$ have an appreciable p-content (33 and 35% respectively) which reduces their antibonding character.

[3]M. R. LeGeyt. Private communication.

The intersphere and outer sphere contributions in Table 5 also show that the upper occupied orbitals are more spatially diffuse than the lower valence orbitals. The involvement of d waves is small throughout, averaging about 5% (Table 4). From Table 2 (XαSW, Model 2) an energy gap of about 3.48 eV between the s-type and p-type states is expected. Measurements by X-ray photoelectron spectroscopy[4] show a peak, here assigned to the $13e$ state, at an energy $\sim$3.6 eV higher than the ionization energy of the deepest level ($14e$) found by HeI photoelectron spectroscopy. The separation calculated by the EH method is 3.17 eV. No direct comparison is possible with the CNDO method, because the order of the levels is different in this region, but there is no clear separation between the s- and p-type orbitals.

Orbital Compositions in the Extended Hückel and CNDO Methods

The CNDO orbitals have a larger d character (11% average) and a greater degree of s/p mixing than the XαSW orbitals. However, the components of s and p functions in the individual molecular orbitals are broadly similar to those from the XαSW method, as are the charge distributions on the various atoms (Table 5), the largest discrepancy being for the $15a_1$ state. The CNDO method indicates the states $14e$ to $17e$ to be composed primarily of p orbitals (58–86% p), while the lower states involve greater proportions of s orbitals (48–77% s).

An essentially similar situation holds in the EH calculations, although here the s/p mixing is less than from the XαSW calculations. According to the EH method, the states $14e$ to $17e$ are composed of more than 90% p functions (in an s,p basis only), and similarly $12a_1$ to $13a_1$ involve predominantly s orbitals (89 to 100% s). In common with the XαSW and CNDO methods EH indicates significant s/p mixing in the $13e$ and $14a_1$ orbitals. EH is the only method in which the amount of p character in these two orbitals (56 and 66% respectively) exceeds that of s. The EH charge distributions on the different atoms (Table 5) are similar to those from XαSW for the lower valence levels $12a_1$ to $13e$, but there are marked differences in the higher valence levels $14e$–$17e$. Figure 3 shows how the EH energy levels of the P_3 and PS_3 fragments change on

[4]M. S. Banna, D. C. Frost, C. A. McDowell, and B. Wallbank. Unpublished results.

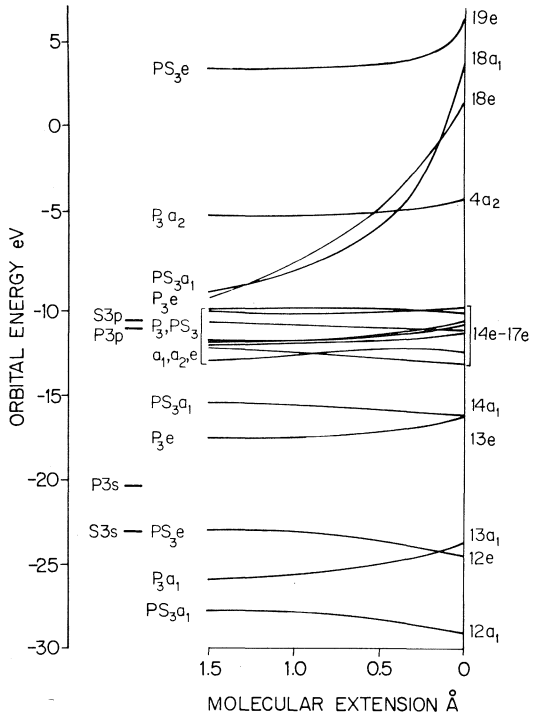

FIG. 3. Energies (EH) of the orbitals of P_3 and PS_3 approaching (C_{3v} symmetry) to form P_4S_3. The last 1.5 Å of the idealized process is shown.

bringing them together to the distance which separates them in P_4S_3. It highlights the existence of both bonding interactions between the P_3 and PS_3 fragments in the states $12a_1$, $12e$, and $14a_1$, and antibonding interactions in the states $13a_1$ and $13e$. These results are interesting in view of the similarity of the lower valence levels as determined by the EH and XαSW methods.

Contour Plots of the XαSW Orbitals and Electronic Charge Distributions

The XαSW method provides no numerical measure of bonding character corresponding to the concept of bond order in molecular orbital theory. Contour plots of wave functions and electronic charge distribution[5] are more detailed and informative, and are presented in this section for some of the more important orbitals. Wave function contour diagrams[6] for some of the higher lying levels of P_4S_3 are given in Fig. 4. Sections of a wave function belonging to $17e$ (Fig. 4 *a*, *b*) show that electron density is concentrated on the sulfur atoms in non-interacting *p* orbitals, and that there are weak interactions within the basal phosphorus ring. The apical atom barely contributes to $17e$. The $17a_1$ state, and to a lesser extent the $16a_1$ state, should be expected from consideration of symmetry, energy, and charge distribution to constitute the apical phosphorus lone pair, although the total charge on P_a from the $17a_1$ and $16a_1$ orbitals is only 1.02 electrons. Of the total electronic charge in $17a_1$, 30% is found on P_a, as compared with about 50% on P for the highest occupied a_1 orbital in PH_3 (32). The plots of $17a_1$ in Fig. 4 *c*, *d* illustrate that the electron density arises mainly from phosphorus *p* orbitals oriented towards the centre of the molecule. The $16e$, $15e$, and $15a_1$ levels are weakly bonding orbitals delocalized over both the P and S rings, but (Table 5) with little charge on P_a. Sections of a wave function belonging to $14e$, the deepest found by HeI photoelectron spectroscopy, are shown in Fig. 4*e* and *f*. Both show 'bent bonds'; in one, the bonding electrons are predominantly outside the phosphorus triangle, in the other they are concentrated somewhat outside the P_a—S internuclear axis.

Further contour plots are shown in Fig. 5 for wave functions corresponding to the lower valence levels $12a_1$ to $13e$. Figures 5*a* and *b* show that although $13e$ is antibonding with respect to atomic *s* functions for both P_b—P_b and P_b—S bonds, the appreciable mixing in of *p* waves results in net P_a—S bonding. In $14a_1$ (Fig. 5*c*) the high concentration of charge in the P_a *s*-orbital is antibonding with respect to the sulphur orbitals, and there is also appreciable bonding density in the middle of the P_3 face. The dominant feature of $13a_1$ (Fig. 5 *d*, *e*) is the multicentre nature of the bonding within the P_3 subunit; Fig. 5*d* also shows an antibonding interaction between the P_3 and PS_3 subunits. The two lowest valence orbitals, $12e$ and $12a_1$, are both strongly bonding. The former (Fig. 5*f*) corresponds to polar σ-bonding between S and P_b, and the latter (Fig. 5 *g*, *h*) has considerable multicentre character within the PS_3 subunit. The participation of *p* functions in these predominantly *s* states reduces significantly the antibonding character of the $13e$ and $14a_1$ orbitals, and slightly increases the bonding character of $13a_1$, $12e$, and $12a_1$.

[5]R. P. Messmer, S. K. Knudson, and K. H. Johnson. Unpublished data.

[6]From Model 1 calculations. Small differences in detail are to be expected from plots of the Model 2 wave functions, but the fundamental characteristics of the orbitals will be unchanged.

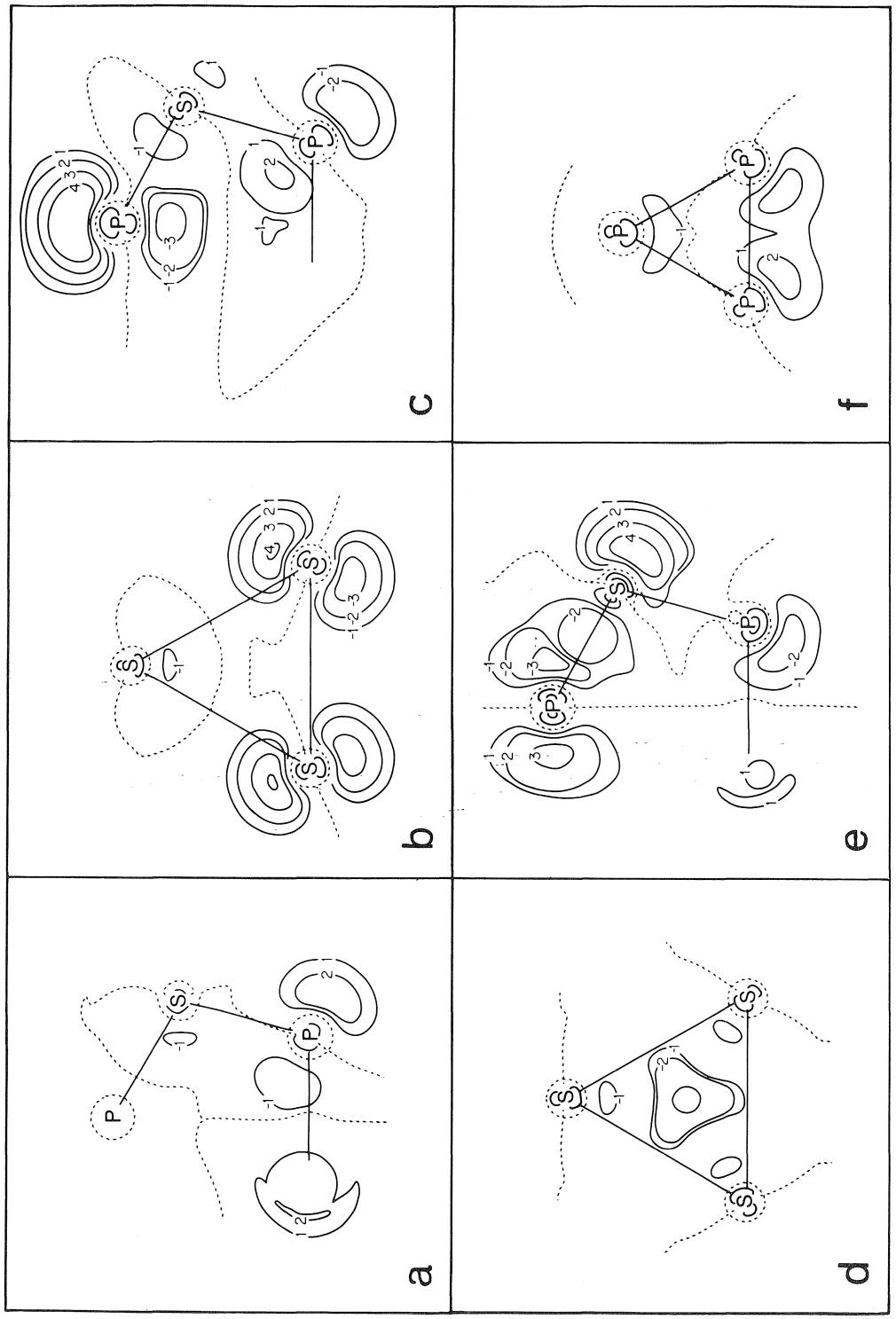

FIG. 4. Wave function contour diagrams for (*a*) and (*b*) 17*e*; (*c*) and (*d*) $17a_1$; (*e*) and (*f*) 14*e*. Contour specification: 1 = 0.05, 2 = 0.07, 3 = 0.10, 4 = 0.13 in units of (probability)$^{1/2}a_0^{-3}$. The dashed lines represent nodal surfaces.

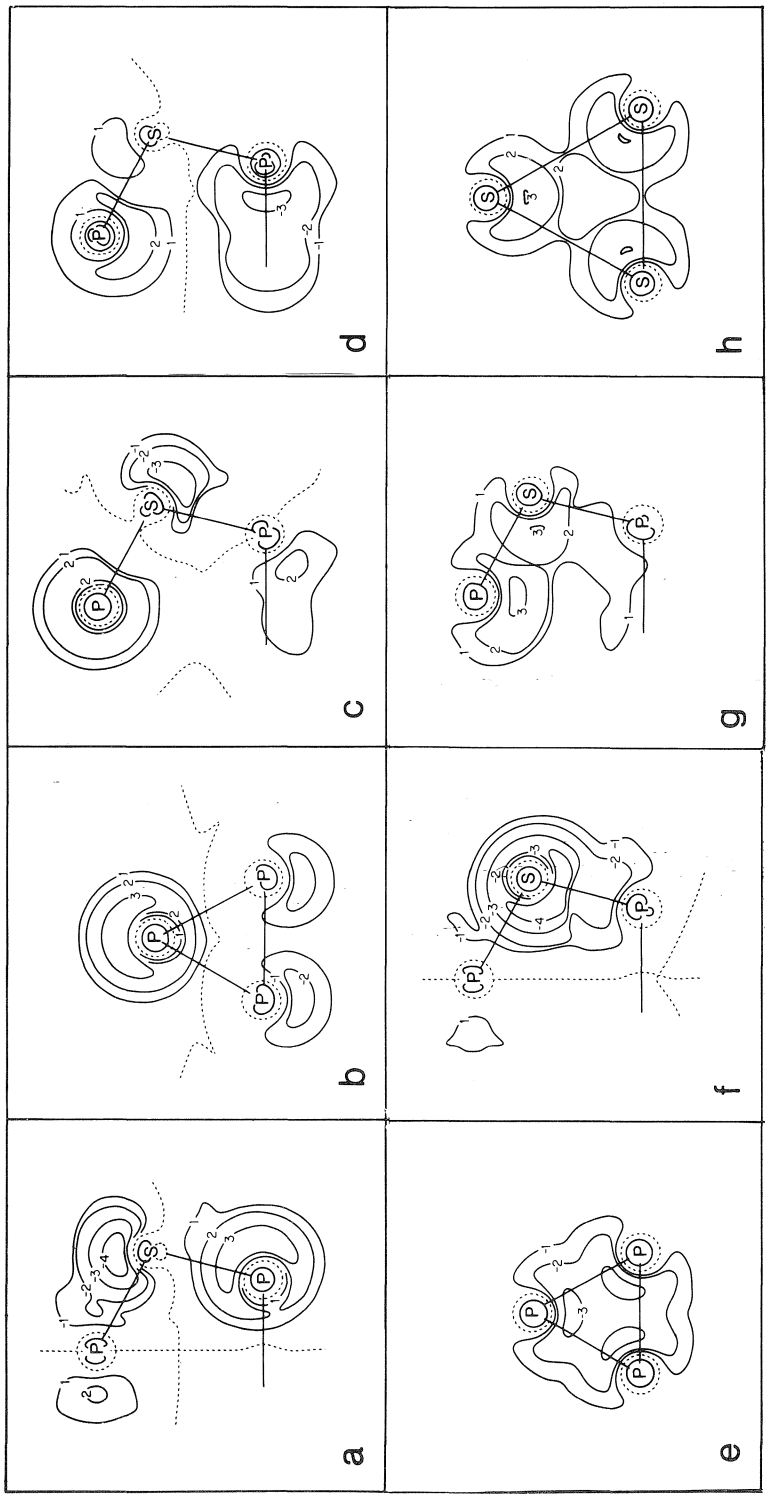

FIG. 5. Wave function contour diagrams for (*a*) and (*b*) $13e$; (*c*) $14a_1$; (*d*) and (*e*) $13a_1$; (*f*) $12e$; (*g*) and (*h*) $12a_1$. For contour specification, see Fig. 4.

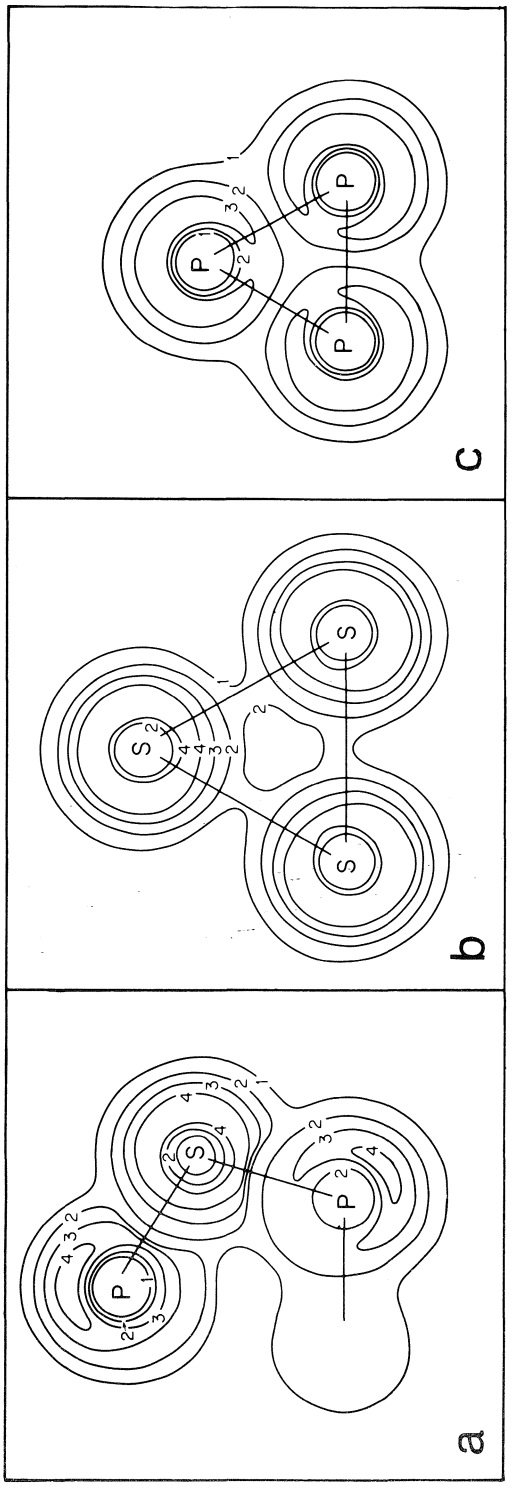

FIG. 6. Total valence charge distribution in three planes of P_4S_3. Contour specification: 1 = 0.023, 2 = 0.053, 3 = 0.084, 4 = 0.122 electrons/a_0^3.

The total electronic charge distributions (Fig. 6) show a number of features of chemical interest. Distributions characteristic of directed lone pairs at both P_a and P_b are evident in Fig. 6*a*. The symmetrical nature of the charge distribution round each sulphur atom (Fig. 6*b*) shows that direct S—S bonding is unimportant, though there is some indirect S—S bonding mediated by P_a (Fig. 6 *a*, *b*). Figure 6*c* displays both lone pair density and 'bent bonding' density in the basal phosphorus ring. The individual contour diagrams show the division into *s* type and *p* type, 13*e* and $14a_1$ being intermediate in this respect. The *s* type orbitals have appreciable electron density within the molecule, to give multicentre bonding, whereas some of the higher *p* type orbitals have electron density outside the internuclear axes, forming 'bent bonds'. Brundle and co-workers (42) have suggested that multicentre bonding density ('omnidirectional' in their terminology) may be important to the stability of P_4. According to the present analysis, such bonding may account for the frequent appearance of the P_4 structural unit in the phosphorus sulphides; it is probably significant that the ion P_3S^+, isoelectronic with P_4, is abundant in the mass spectrum of P_4S_3 (43).

Chemical Properties

Various properties of P_4S_3 depend on the fact that the higher occupied levels are essentially nonbonding, so that small perturbations can have a large effect on charge distribution. Accordingly, the ^{31}P chemical shifts of P_4 (44) and the basal phosphorus atoms of P_4S_3 (45) are both very sensitive to the solvent, the apical phosphorus atom being somewhat less so (45). The sensitivity can be attributed to the high polarizability of the occupied orbitals, especially 17*e* in P_4S_3 and 2*e* and $6t_2$ in P_4 (42, 46). It is also interesting that an investigation of the dynamic polarization of the ^{31}P nucleus (47) showed a higher scalar enhancement, and hence a greater *s* character, in the P_a than in the P_b lone pair. This result is consistent with the XαSW calculations (Table 4), which show that the *s* density in both the 'lone pair' orbitals $17a_1$, $16a_1$ is greater on P_a. Most of the chemistry of P_4S_3 involves donor–acceptor interactions. The highest occupied orbital in a symmetrical phosphine is normally of a_1 symmetry, and P_4S_3 is unusual in having its highest a_1 orbital below a degenerate orbital which has its major electron density on phosphorus spread among the basal atoms. Both types of phosphorus atom can be expected to act as donors, and we can now discuss in more detail the complexes referred to in the Introduction.

The ionization energy of $17a_1$ is 9.66 eV, comparable to that of the highest *a'* level of $MePH_2$ (9.72, 9.6 eV (48, 49)). This compound is a very weak base, and, consistently, P_4S_3 is not protonated by normally available methods. Tetraphosphorus trisulphide does, however, form the complexes *cis*-$(P_4S_3)_2M(CO)_4$ (M = Cr, Mo, W), *cis*-$(P_4S_3)_3M(CO)_3$ (M = Cr, Mo), and $Ni(P_4S_3)_4$, in which, on the basis of their ^{31}P nmr spectra, coordination takes place through P_a (17). A crystallographic analysis (18) of a further complex $P_4S_3Mo(CO)_5$ shows that a strong P_a—Mo bond is formed at the expense of all the P—S bonds in the ligand, not merely those from P_a itself. The P_a—Mo bond can be explained in terms of σ-donation from $17a_1$ (Fig. 4*c*) accompanied by π donor and acceptor interactions involving 14*e* (Fig. 4*e*), 17*e* (Fig. 4*a*), excited states of P_4S_3, and *d* and *s* orbitals of molybdenum.

In these reactions, P_4S_3 does not differ greatly from such tertiary phosphines as Ph_3P, as shown by the corresponding CO stretching frequencies in $P_4S_3Mo(CO)_5$ (18) and (in parentheses) $Ph_3PMo(CO)_5$ (50): A_1, 2075 (2075); B_1, 1985 (1989); A_1, 1965 (1945); *E*, 1940 (1950) cm^{-1}. However, P_4S_3 forms another complex[7] P_4S_3-$Mo(CO)_3$ with two strong bands (1999, 1940 cm^{-1}) in the CO stretching region, similar to the $(A + E)$ bands of $C_6H_6Mo(CO)_3$ (1991, 1919 cm^{-1}) (51) and $(PhPCl_2)_3Mo(CO)_3$ (2016, 1943 cm^{-1}) (52). The complex evidently has trigonal symmetry, and it seems most likely[7] that coordination takes place through the basal phosphorus atoms, though confirmation of coordination by a P_3 triangle by X-ray methods is not yet available, either for this compound or the rhodium complexes of P_4 (53).

An example of a different type of interaction at the basal atoms of P_4S_3 is given by its reaction with iodine. The first product that can be isolated is β-$P_4S_3I_2$ (19, 20) (Fig. 7*a*), whose formation is presumably a result of the high electron density at P_b in 17*e*. Its subsequent rearrange-

[7]W. Willingham and A. W. Cordes, private communication; W. Willingham, Ph.D. thesis, University of Arkansas, 1972.

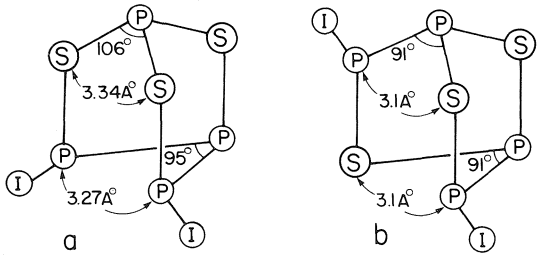

FIG. 7. Structures of (*a*) β-$P_4S_3I_2$ (19, 20) and (*b*) α-$P_4S_3I_2$ (54).

ment to give the more stable α-$P_4S_3I_2$ (54) (Fig. 7*b*) is accompanied by a reduction of the separation of the formally nonbonded P and S atoms to 3.1 Å, well below the sum of the van der Waals radii (3.5 Å). The skeletal mobility of $P_4S_3I_2$ and the occurrence of such indirect bonding are both compatible with the concept of multicentre bonding indicated by the XαSW calculations.

Concluding Remarks

Calculation of the electronic structure of P_4S_3 by the XαSW method gives a good account of the ionization energies determined by photoelectron spectroscopy. A small *d*-component is fairly evenly spread among all the orbitals, and, although it is unlikely to have a major effect on molecular geometry, it is important in determining the detailed spacing of the levels. Of the two semi-empirical methods used, EH gives a better account of the measured ionization energies, but the CNDO charge distributions are closer to those found by the XαSW method. An important feature of the XαSW calculations is that, although there are some significant effects of *s–p* mixing, there is a distinct energetic division between the lower states based mainly on 3*s* orbitals and the higher, 3*p* type. Their bonding characteristics are different, the former providing the main cohesive energy of the molecule through multicentre bonding within the P_3 and PS_3 subunits, (and perhaps accounting for the prevalence of the P_4 unit in the phosphorus sulphides) the latter being more directed, and having a high electron density both in the conventional lone pair directions, and, in some cases, outside the conventional bond axes ('bent bonds'). All these characteristics can be seen in the contour diagrams.

Chemically, P_4S_3 can be expected to act as a donor at both the apical and basal sites, as found, there being no clear theoretical preference. The donor properties of P_a are similar to those of other tertiary phosphines, and the formation of complexes with metal carbonyls can be understood in terms of the calculated molecular orbitals. The basal P_3 atoms behave like P_4, and further experimental investigations of coordination in this region would be valuable. Multicentre bonding is likely to be important here, and in such reactions as the structure transformation of β-$P_4S_3I_2$.

Acknowledgements

We are grateful to Dr. L. S. Bartell and to Dr. K. H. Johnson, respectively, for the EH and XαSW programs, to Dr. R. P. Messmer and Dr. J. G. Norman for the plotting programs, to Dr. J. N. A. Ridyard and Dr. D. C. Frost, respectively, for the HeI and X-ray photoelectron spectra, to Dr. A. W. Cordes for unpublished information, and to the National Research Council of Canada for financial support.

1. A. STOCK. Chem. Ber. **43**, 150 (1910); **43**, 414 (1910); **43**, 1223 (1910).
2. M. MEISEL and H. GRUNZE. Z. Anorg. Chem. **366**, 152 (1969).
3. H. VINCENT. Bull. Soc. Chim. Fr. 4517 (1972).
4. A. M. GRIFFIN and G. M. SHELDRICK. Acta Crystallogr. Sect. B, **31**, 2738 (1975).
5. R. FORTHMANN and A. SCHNEIDER. Z. Phys. Chem. (N.F.), **49**, 22 (1966).
6. H. VINCENT and C. VINCENT-FORAT. Bull. Soc. Chim. Fr. 499 (1973).
7. Y. C. LEUNG, J. WASER, S. VAN HOUTEN, A. VOS, G. A. WIEGERS, and E. H. WIEBENGA. Acta Crystallogr. **10**, 574 (1957).
8. S. VAN HOUTEN and E. H. WIEBENGA. Acta Crystallogr. **10**, 156 (1957).
9. A. VOS and E. H. WIEBENGA. Acta Crystallogr. **8**, 217 (1955).
10. A. VOS and E. H. WIEBENGA. Acta Crystallogr. **9**, 92 (1956).
11. H. HILMER. Acta Crystallogr. Sect. B, **25**, 1229 (1969).
12. H. G. WHITFIELD. J. Chem. Soc. A, 1800 (1970); J. Chem. Soc. Dalton Trans. 1737 (1973).
13. E. KEULEN and A. VOS. Acta Crystallogr. **12**, 323 (1959).
14. J. ELLERMANN and H. SCHOSSNER. Angew. Chem. Int. Ed. Engl. **13**, 601 (1974).
15. W. DAHLMANN and H.-G. VON SCHNERING. Naturwissenschaften, **59**, 420 (1972).
16. M. GARDNER. J. Chem. Soc. Dalton Trans. 691 (1973).
17. R. JEFFERSON, H. F. KLEIN, and J. F. NIXON. Chem. Commun. 536 (1969).
18. A. W. CORDES, R. D. JOYNER, R. D. SHORES, and E. D. DILL. Inorg. Chem. **13**, 132 (1974).
19. G. W. HUNT and A. W. CORDES. Inorg. Chem. **10**, 1935 (1971).

20. G. J. PENNEY and G. M. SHELDRICK. J. Chem. Soc. A, 1100 (1971).
21. R. BOULOCH. C. R. Acad. Sci. **138**, 364 (1904).
22. W. D. TREADWELL and C. BEELI. Helv. Chim. Acta, **18**, 1161 (1935).
23. J. C. SLATER and K. H. JOHNSON. Phys. Rev. B, **5**, 844 (1972).
24. R. HOFFMANN. J. Chem. Phys. **39**, 1397 (1963).
25. J. A. POPLE and D. L. BEVERIDGE. Approximate molecular orbital theory. McGraw-Hill, New York. 1970.
26. L. S. BARTELL, L. S. SU, and H. YOW. Inorg. Chem. **9**, 1903 (1970).
27. A. J. BENNETT, B. MCCARROLL, and R. P. MESSMER. Phys. Rev. B, **3**, 1397 (1971).
28. G. BLYHOLDER. J. Res. Inst. Catal. Hokkaido Univ. **21**, 92 (1973).
29. J. C. SLATER. Adv. Quantum Chem. **6**, 1 (1972).
30. K. H. JOHNSON. Adv. Quantum Chem. **7**, 143 (1973).
31. N. ROSCH, W. G. KLEMPERER, and K. H. JOHNSON. Chem. Phys. Lett. **23**, 149 (1973).
32. J. G. NORMAN. J. Chem. Phys. **61**, 4630 (1974).
33. F. HERMAN, A. R. WILLIAMS, and K. H. JOHNSON. J. Chem. Phys. **61**, 3508 (1974).
34. K. SCHWARZ. Phys. Rev. B, **5**, 2466 (1972).
35. F. HERMAN and S. SKILLMAN. Atomic structure calculations, Prentice-Hall, New York. 1963.
36. R. BOSCHI and W. SCHMIDT. Inorg. Nucl. Chem. Lett. **9**, 643 (1973).
37. N. V. RICHARDSON and P. WEINBERGER. J. Electron Spectrosc. **6**, 109 (1975).
38. W. C. PRICE. Chem. Rev. **41**, 257 (1947).
39. G. R. BRANTON, D. C. FROST, C. A. MCDOWELL, and I. A. STENHOUSE. Chem. Phys. Lett. **5**, 1 (1970).
40. W. R. CULLEN, D. C. FROST, and D. A. VROOM. Inorg. Chem. **8**, 1803 (1969).
41. A. H. COWLEY, M. J. S. DEWAR, and D. W. GOODMAN. J. Am. Chem. Soc. **97**, 3653 (1975).
42. C. R. BRUNDLE, N. A. KUEBLER, M. B. ROBIN, and H. BASCH. Inorg. Chem. **11**, 20 (1972).
43. G. J. PENNEY and G. M. SHELDRICK. J. Chem. Soc. A, 243 (1971).
44. G. HECKMANN and E. FLUCK. Z. Naturforsch. **26**b, 282 (1971).
45. G. HECKMANN and E. FLUCK. Z. Naturforsch. **26**b, 982 (1971).
46. S. EVANS, P. J. JOACHIM, A. F. ORCHARD, and D. W. TURNER. Int. J. Mass Spectrom. **9**, 41 (1972).
47. R. A. DWEK, R. E. RICHARDS, D. TAYLOR, G. J. PENNEY, and G. M. SHELDRICK. J. Chem. Soc. A, 935 (1969); J. A. POTENZA, E. H. POINDEXTER, P. J. CAPLAN, and R. A. DWEK. J. Am. Chem. Soc. **91**, 4356 (1969).
48. M. F. LAPPERT, J. B. PEDLEY, B. T. WILKINS, O. STELZER, and E. UNGER. J. Chem. Soc. Dalton Trans. 1207 (1975).
49. S. CRADOCK, E. A. V. EBSWORTH, W. J. SAVAGE, and R. A. WHITEFORD. J. Chem. Soc. Faraday Trans. II, 934 (1972).
50. D. J. DARENSBOURG and T. L. BROWN. Inorg. Chem. **7**, 959 (1967).
51. R. D. FISCHER. Chem. Ber. **93**, 165 (1960).
52. E. W. ABEL, M. A. BENNETT, and G. WILKINSON. J. Chem. Soc. 2323 (1959).
53. A. P. GINSBERG and W. E. LINDSELL. J. Am. Chem. Soc. **93**, 2082 (1971).
54. D. A. WRIGHT and B. R. PENFOLD. Acta Crystallogr. **12**, 455 (1959).

Use of the scaled-particle theory for the determination of single ion standard free energy of transfer between solvents

CLAUDE TREINER

Laboratoire d'Electrochimie, Université P. et M. Curie, 4, Place Jussieu—Bât. F—75230 Paris Cedex 05-ERA 310

Received September 27, 1976

CLAUDE TREINER. Can. J. Chem. **55**, 682 (1977).

The tetraphenylboron extrathermodynamic assumption is one of the methods most often used for the evaluation of single ion standard thermodynamic functions of transfer between two solvents. We show in this article that the scaled-particle theory may be useful for discriminating among those solvents for which this extrathermodynamic assumption may be questionable because of strong solute–solvent interactions. Although no general rule is proposed, the tetraphenylboron assumption seems valid in the case of the free energy of transfer between water and solvents like methanol, ethanol, acetonitrile, and formamide; it should not be used in the case of the transfer to solvents like propylene carbonate, dimethylsulfoxide or sulfolane. The scaled-particle theory may also be used to predict within 20% the standard free energy of transfer of the tetraphenylboron ion between water and aqueous mixed solvents; examples are given for water–methanol and water–ethanol mixtures.

CLAUDE TREINER. Can. J. Chem. **55**, 682 (1977).

L'hypothèse de l'équisolvatation des ions tetraphénylborure et tetraphénylarsénium est une des méthodes extrathermodynamiques les plus utilisées pour la détermination des fonctions thermodynamiques de transfert d'ions individuel entre deux solvants. Nous montrons ici que la théorie des sphères rigides peut être utilisée pour désigner les solvants pour lesquels dues à de fortes interactions soluté–solvant, cette méthode extrathermodynamique est peu sure. Aucune règle générale n'est proposée; toutefois il semble que la méthode soit valable dans le cas du transfert de l'eau à des solvants tels que le méthanol, l'éthanol, l'acétonitrile et le formamide. Elle semble devoir être rejetée dans le cas du transfert de l'eau à des solvants dont les molécules sont plus complexes tels que le carbonate de propylène, le diméthylsulfoxide et le sulfolane. La théorie des sphères rigides peut également être utilisée pour prédire à 20% près l'énergie libre standard de transfert de l'ion tétraphénylborure entre l'eau et des mélanges hydroorganiques: on donne les exemples des mélanges eau–méthanol et eau–éthanol.

Introduction

The evaluation of single ion thermodynamic properties has been the subject of many discussions. A wide variety of extrathermodynamic assumptions have been proposed (1) and have been critically reviewed in recent years (2–5); none of them has gained so much popularity as the tetraphenylboron (TϕB) assumption first proposed by Grunwald *et al.* (6) in 1960. According to this extrathermodynamic approach, the tetraphenylboron ion (ϕ_4B^-) and the tetraphenylphosphonium ion (ϕ_4P^+) are taken as identical in size and weakly solvated to the same extent. The replacement of ϕ_4P^+ with ϕ_4As^+ (7) does not change the basic assumptions of this approach. Some warnings may be found in the literature against the TϕB assumption based mostly on spectroscopic studies (8, 9); unfortunately, comparison between chemical shifts and thermodynamic quantities is not straightforward, and a theoretical approach was felt necessary.

We have shown recently (10), that the scaled-particle theory (SPT) can account for the main part of the standard free energy of transfer of a large ion like tetrabutylammonium from water to water–acetone and to water–acetonitrile mixtures. It was thus felt interesting to investigate the possibility of using the SPT to discriminate between the solvents for which the TϕB assumption could be useful for the evaluation of reliable single ion free energies of transfer between two solvents, and those for which this assumption should not be used.

Theory

According to the SPT, the standard free energy associated with the dissolution of a hard sphere in a solvent can be represented by the following relationship (11):

$$[1] \quad \Delta G^0 = \Delta G^0(\text{cav}) + \Delta G^0(\text{int}) + RT \log RT/V$$

TABLE 1. Characteristic constant* for the calculation of ΔG_t^0 for the tetraphenylarsenium ion from water to some pure organic solvents at 298.15 K using the scaled-particle theory (11)

Solvent	d	a (Å)	$10^{-3}\ \Delta G^0$† (kJ mol^{-1})	$-\Delta G_t^0$ (kJ mol^{-1}) Calcd	Expt
Water	0.9971	2.76	97.54	0.0	0.0
Methanol	0.7868	3.59	59.22	38.3	25.5
Ethanol	0.7851	4.36	67.58	30.0	23.0
Acetonitrile	0.7768	4.12	64.12	33.4	35.1
Formamide	1.1292	3.63	64.64	32.9	25.9
Dimethylformamide	0.9443	4.98	73.45	24.1	41.8
Dimethylsulfoxide	1.0961	5.05	105.11	−7.6	40.2
Sulfolane‡	1.262	5.76	125.65	−28.1	39.7
Propylene carbonate	1.192	5.40	99.13	−1.6	39.3
N-Methyl 2-pyrrolidone	1.0279	5.69	103.82	−6.3	43.9

*ΔG_t° is expressed in the mole fraction scale.
†Equation 1, $\Delta G^\circ(\text{int}) = 0$.
‡Value at 30 °C.

where ΔG^0(cav) is the free energy for creating a cavity in the solvent and ΔG^0(int) is the free energy of interaction of the solute particle in the cavity with the solvent molecules; V is the molar volume of the solvent. In the case of the standard free energy of transfer of the solute between a reference solvent (here water) and a given solvent s, one may write:

$$[2]\quad \Delta G_t^0 = \Delta G_t^0(\text{cav}) + \Delta G_t^0(\text{int}) + RT \ln (V_w/V_s)$$

with

$$\Delta G_t^0(\text{cav}) = \Delta G_s^0(\text{cav}) - \Delta G_w^0(\text{cav})$$

and

$$\Delta G_t^0(\text{int}) = \Delta G_s^0(\text{int}) - \Delta G_w^0(\text{int})$$

ΔG_t^0(int) is not known for the chemical systems we want to study; Masterton *et al.* (12) have pointed out that when dealing with aromatic molecules, the scaled-particle theory is relatively inaccurate presumably because of uncertainties in the interaction energy term. Thus we shall assume that $\Delta G_t^0(\text{int}) \cong 0$ which corresponds to the basic hypothesis of the TϕB assumption (see Discussion section).

The only constants necessary for the calculation of ΔG_t^0(cav) are the diameter of the solute and solvent molecules considered as hard spheres and the density of the solvents. The diameter of ϕ_4As^+ was assumed equal to that of ϕ_4B^-: Grunwald's value of 8.4 Å was adopted (6). The hard sphere diameter a of the solvent molecules was calculated using the de Ligny and van der Veen (13) method based on Bondi's (14) estimates of van der Waals volumes. The a values thus obtained may be in error by some unknown amounts especially for molecules like *N*-methylpyrrolidone, but they represent a consistent set of values based on the same calculation method. The density d of the solvents were taken from the literature (15).

Results and Discussion

(*A*) *Free Energy of Transfer of* ϕ_4As^+ *from Water to Pure Solvents*

In Table 1 we present the results obtained on the mole fraction scale together with the experimental ΔG_t^0 values taken from a review article by Cox *et al.* (16) and expressed on the same concentration scale. ΔG_t^0(calcd) should of course be corrected by a coulombic term as the SPT is only concerned with uncharged particles; however, if we assume that the Born equation gives a good estimate of the electrostatic effect one can easily show that for the large ion we are dealing with ΔG_t^0(coul) is at most equal to 4.6 kJ mol^{-1} (in the case of the transfer from water to ethanol which has the lowest dielectric constant value of the solvent listed).

Most often for the solvents considered here ΔG_t^0(coul) is of the order of 2.5 kJ mol^{-1} and may therefore be neglected.

The data listed in Table 1 show that ΔG_t^0(exp) is negative from water to all the solvents studied: the comparison between calculated (eq. 2 with $\Delta G_t^0(\text{int}) = 0$) and experimental values indicates surprisingly good agreement for the transfer to methanol, ethanol, acetonitrile, and formamide. This may be taken as evidence that ΔG_t^0(int)

which has been assumed to be zero in our calculation is indeed small and may be neglected in these cases, *i.e.* the interaction between ϕ_4As^+ and the solvents is small (or similar in water and in these organic solvents).

The agreement is not good in the case of dimethylformamide and is obviously bad for sulfolane, *N*-methylpyrrolidone, dimethylsulfoxide, and propylene carbonate: even the sign of ΔG_t^0 is not predicted by the SPT. This means that in these cases we are not allowed to neglect ΔG_t^0(int) and that this term is large for some of the solvents listed (for example of the order of -67.8 kJ mol^{-1} from water to sulfolane).[1] It implies that strong solute–solvent interactions take place which are different in water and in those organic solvents. We should note however that this conclusion rests to some extent on the (reasonable) assumption that ϕ_4As^+ or ϕ_4B^- are more strongly solvated in the organic solvents than in water; it follows that ΔG_t^0(int) is negative from water to the organic solvents. This assumption is in agreement with the observations of Coetzee and Sharpe (9). It then follows that the stronger the solute–solvent interactions, the larger can be the difference between the solvation of the cation and the anion (that such a difference may exist has been indeed pointed out by Grunwald when the TϕB assumption was first proposed). The obvious conclusion is that the TϕB assumption should not be used in the cases just discussed and the following procedure can be proposed.

If ΔG_t^0(exp) $\cong \Delta G_t^0$(cav) within, say, 30% then single ion values as obtained through the TϕB assumption can be considered reliable. In other cases, the TϕB assumption should not be used.

(*B*) *Free Energy of Transfer of* ϕ_4As^+ *from Water to Mixed Solvents*

It is also interesting to compare calculated and experimental ΔG_t^0 values in the case of mixed aqueous solvents. ΔG_t^0(calcd) is obtained using equations published previously (10, 17).

ΔG_t^0(exp) from water to water–ethanol mixtures had been obtained from solubility measurements (18), and from water to water–methanol mixtures from vapor pressure measurements (19).

The density of the solvent mixtures were taken from ref. 15. Figures 1 and 2 present the results obtained with ΔG_t^0(int) = 0. The agreement between experimental and calculated ΔG_t^0 values is good, being of the order of 20%. If the Born effect is also considered the agreement is even better. It seems then, that in the cases for which ΔG_t^0 for ϕ_4As^+ may be predicted by the SPT from water to a pure solvent, the calculation may be extended to the mixture of the two solvents. However, complications may arise from strong solvent–solvent interactions as in the case of water + acetonitrile mixtures (10).

Conclusion

The tetraphenylboron assumption should be used with great care. Our study confirms previous warnings against its use, but it also shows that in the cases of the standard free energy of transfer between water and organic solvents it may be used with some confidence after comparison between experimental and calculated ΔG_t^0 data using the simple SPT equations.

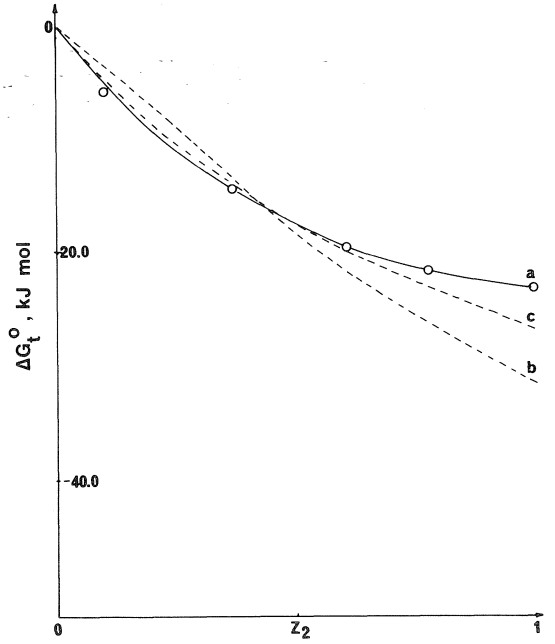

FIG. 1. ΔG_t^0 for $As\phi_4^+$ from water to water–ethanol mixtures: (*a*) "experimental", (*b*) calculated by SPT without the Born term, (*c*) calculated with the Born term ($r^+ = 4.2$ Å) (mole fraction scale).

[1]One of the referees pointed out to us the work of Neff and McQuarrie who try to introduce the influence of the solute on the solvent–solvent interactions in their solubility calculations. (Note that the discrepancies between experimental and calculated ΔG_t^0 values are usually larger when the density of the organic solvent is higher than of water.) However the system they study (neon in argon) is so different from ours that it seems difficult to apply their ideas to the present problem.

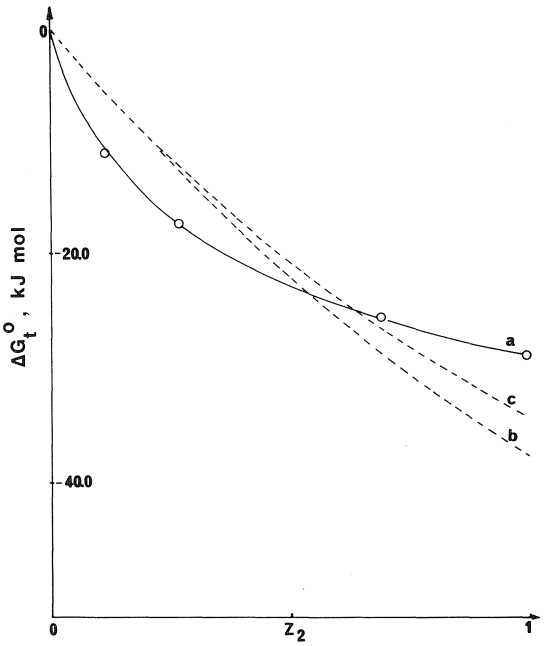

FIG. 2. ΔG_t^0 for $As\phi_4^+$ from water to water–methanol mixtures. Same notation as for Fig. 1.

It seems clear, however, that the safest way of using extrathermodynamic assumptions is to apply several different approaches to the same chemical system (23). In this respect mention should be made of the work of Parsons and Rubin (20) who have suggested that the extrathermodynamic approach of Alexander *et al.* (21), *i.e.* assuming no liquid junction potential in an emf cell, might be the "best" method available at the present time for predicting single ion standard free energy of transfer between two solvents.

1. A. J. PARKER and R. ALEXANDER. J. Am. Chem. Soc. **90**, 3313 (1968).
2. O. POPOVYCH. Crit. Rev. Anal. Chem. **1**, 73 (1970).
3. H. STREHLOV. *In* The chemistry of aqueous solutions. *Edited by* J. J. Lagowski. Academic Press. 1966.
4. R. G. BATES. *In* Hydrogen-bonded solvent systems. *Edited by* A. K. Covington and P. Jones. Taylor and Francis. 1968.
5. J. PADOVA. *In* Modern aspects of electrochemistry. Vol. 7. *Edited by* B. E. Conway and J. O'M. Bockris. Butterworths. 1972.
6. E. GRUNWALD, G. BAUGHAM, and G. KOHNSTAM. J. Am. Chem. Soc. **82**, 5801 (1960).
7. E. M. ARNETT and D. R. MCKELVEY. Record Chem. Prog. **26**, 185 (1965).
8. E. M. ARNETT, H. C. KO, and R. J. MINACZ. J. Phys. Chem. **75**, 2474 (1972).
9. J. F. COETZEE and W. R. SHARPE. J. Phys. Chem. **75**, 3141 (1971).
10. C. TREINER, P. TZIAS, M. CHEMLA, and G. N. POLTORATSKI. J. Chem. Soc. Faraday Trans. I, **72**, 2007 (1976).
11. R. A. PIEROTTI. J. Phys. Chem. **69**, 281 (1965).
12. W. L. MASTERTON, D. BOLOCOFSKI, and T. P. LEE. J. Phys. Chem. **75**, 2809 (1971).
13. C. L. DE LIGNY and N. G. VAN DER VEEN. Rec. Trav. Chim. **90**, 964 (1971).
14. A. BONDI. J. Phys. Chem. **68**, 441 (1964).
15. G. J. JANZ and R. P. T. TOMKINS. Nonaqueous solelectrolytes handbook. Vol. 1. Academic Press. 1972.
16. B. G. COX, G. R. HEDWIG, A. J. PARKER, and D. W. WATTS. Aust. J. Chem. **27**, 477 (1968).
17. M. LUCAS and A. FEILLOLLAY. Bull. Soc. Chim. Fr. 1267 (1970).
18. O. POPOVYCH, A. GIBOVSKY, and D. H. BERNE. Anal. Chem. **44**, 811 (1972).
19. S. VILLERMAUX and J. J. DELPUECH. Bull. Chem. Soc. Fr. 2534 (1974).
20. R. PARSONS and B. T. RUBIN. J. Chem. Soc. Faraday Trans. I, 1636 (1974).
21. R. ALEXANDER, A. J. PARKER, J. H. SHARP, and W. E. WAGHORNE. J. Am. Chem. Soc. **94**, 1148 (1972).
22. NEEF and MCQUARRIE. J. Phys. Chem. **77**, 413 (1973).
23. C. TREINER and P. FINAS. J. Chem. Phys. **71**, 67 (1974).

Studies in solvolysis. Part VIII. An entropy correlation related to the reaction of various nucleophiles with malachite green

STEPHEN HARVEY MORRIS, JOHN MARSHALL WILLIAM SCOTT,[1] AND FREDERICK STEELE

Chemistry Department, Memorial University of Newfoundland, St. John's, Nfld., Canada A1C 5S7

Received July 5, 1976

STEPHEN HARVEY MORRIS, JOHN MARSHALL WILLIAM SCOTT, and FREDERICK STEELE. Can. J. Chem. **55**, 686 (1977).

The entropies of activation related to the reactions of aqueous malachite green with the nucleophiles water, hydroxide, hydrazine, ammonia, hypochlorite, and sulphite have been calculated from the temperature dependence of the rate constants appropriate to these reactions. The entropies of the transition states for these reactions have been characterized and the transition states shown to be 'reactant like'. A similar correlation, based on data for a series of nucleophiles attacking methyl iodide, suggests that the transition states for the S_N2 displacement reactions are also 'reactant like' with respect to the attacking nucleophile. A relationship between two distinct parameters each of which is related to the position of transition states along the reaction coordinate is considered.

STEPHEN HARVEY MORRIS, JOHN MARSHALL WILLIAM SCOTT et FREDERICK STEELE. Can. J. Chem. **55**, 686 (1977).

On a calculé les entropies d'activation reliées aux réactions du vert de malachite aqueux avec les nucléophiles eau, hydroxyde, hydrazine, ammoniac, hypochlorite et sulphite; ces calculs ont été effectués à partir de la dépendance qui existe entre la température et les constantes de vitesses appropriées de ces réactions. On a caractérisé les entropies des états de transition de ces réactions et on a démontré que les états de transitions ressemblent aux réactifs. Une corrélation semblable, basée sur des données pour une série de nucléophiles attaquant l'iodure de méthyle, suggère que, par rapport au nucléophile qui attaque, les états de transition des réactions de déplacement S_N2 ressemblent aussi au réactif. On considère une relation entre deux paramètres distincts chacun desquels est relié à la position de l'état de transition le long des coordonnées de la réaction.

[Traduit par le journal]

Introduction

The thermodynamic parameters $\Delta H^{\ddagger}$ and $\Delta S^{\ddagger}$ which characterize the reactions of charged and neutral nucleophiles with triaryl carbonium ions

[1] $$Ar_3C^+ + N^{n-} \rightarrow Ar_3CN^{(n-1)-}$$

where $n = 0$, 1, and 2, have been measured frequently (1–6). The previous use of these quantities has been to extrapolate or interpolate measured rates for correlations based on relative rates (free energies of activation, $\Delta G^{\ddagger}$). Moreover, little attention has been directed to the precision with which these quantities have been measured. Reported values for the entropies of activation show considerable variation. For instance when Ar_3C^+ = malachite green and $N^{n-} = OH^-$, $\Delta S^{\ddagger}$ has been reported as -19 (4), -14 (6), -10.4 (1), and -7 (3) cal mol^{-1} K^{-1} and no systematic entropy data for these reactions exist to offer further insight into the details of the activation process.

Conclusions concerning the nature of the activated state can often be deduced from entropies of activation in conjunction with the appropriate initial state data. Correlations of this type have been used by Robertson *et al.* (7–10) for the methyl (7, 9), allyl (7), and isopropyl halides (7, 8). The correlations take the form,

[2] $$S^{\ddagger}(RX) = \alpha S(X^-) + \text{constant}$$

where R = methyl, allyl, and *s*-propyl, $S^{\ddagger}$ is the entropy of the transition state, and $S(X^-)$ is the standard entropy of the completely formed solvated aqueous anionic leaving group. The quantity α is best considered as a reaction coordinate parameter, which in this case measures the degree of resemblance of the activated state to the products, *i.e.* the fully formed ions. The quantity $S^{\ddagger}(RX)$ is calculated from the equation

[3] $$S^{\ddagger}(RX) = S_g(RX) + \delta_s S(RX) + \Delta S^{\ddagger}$$

where the symbols on the right hand side are the gas phase entropy of RX, the entropy of

[1]To whom all correspondence should be addressed.

solution of RX, and the entropy of activation respectively.

The intention of the present paper is twofold. Firstly, to provide a careful study of the temperature dependence of the rates of attack of several nucleophiles on malachite green, from which the entropies of activation can be calculated. Secondly, to combine these entropies with the appropriate initial state data so that the transition state entropies for the malachite green – nucleophile reaction series can be characterized and to use the transition state entropies as a means of investigating the details of the activation process.

Experimental

Materials

Malachite green perchlorate was prepared and purified as described elsewhere in this series. The nucleophilic reagents were the best quality grade commercially available and were used without further purification.

All solutions were prepared with freshly distilled water.

Sodium hydroxide, hypochlorite, and sulphite solutions were prepared immediately prior to use. The sulphite solutions were stabilized with quinol (*ca.* 1×10^{-5} mol dm^{-3}) which had no effect on the measured rates (18).

The ammonia solutions were buffered to $pH = 9.25$.

A stock solution of malachite green was prepared by dissolving the perchlorate in acetone (1 cm^3) and diluting to 1 dm^3 with water. The final concentration of malachite green in the reaction cells was *ca.* 5×10^{-6} mol dm^{-3}.

Kinetic Measurements

Reactions involving hydroxide and ammonia were carried out using a Unicam SP500 spectrophotometer. Solutions were contained in 10 mm stoppered silica cells and the kinetics of the pseudo first order reactions were measured by recording the decrease of the absorption at 615 nm for at least three half-lives using a Varian A25 chart recorder.

Water flowing around the cell housing was maintained at the required temperature by means of a large thermostat regulated by a Tronac PTC-1000 precision controller described in more detail in an earlier paper of the present series. Temperature control was better than ± 0.01 K.

The reactions with hypochlorite and sulphite as nucleophiles were followed by stopped-flow spectroscopy. The custom-built apparatus used for these measurements will be described elsewhere. The temperature for this system was also maintained as described above.

Analysis of Rate Constants

Kinetic data from both the above systems were analysed using a three parameter nonlinear curve fit computer program (Basic for PDP-11) based on a method given by Moore (11). Best fit values of k_0, P_0, and P_∞ related to the equation

$$[4] \quad \ln [(P_\infty - P)/(P_\infty - P_0)] = -k_0 t = -(k_1 + k_{-1})t = -(k_2[N] + k_{-1})t$$

were computed together with their respective standard deviations. The quantity k_0 is the observed pseudo first order rate constant, P_0 and P_∞ are the dye absorbances at $t = 0$ and $t = \infty$ respectively, and P is the absorbance at $t = t$. When the reaction goes to equilibrium k_0 becomes the sum of the forward (k_1) and back (k_{-1}) rate constants and k_2 the second order rate constant for the attack of the nucleophile. Using a three parameter fit in this manner P_∞ becomes a disposable parameter and correct values of k_2 may be obtained irrespective of whether the reaction goes to equilibrium or completion. Second order rate constants (k_2) were obtained subsequently from a weighted least squares slope of the linear dependence of the pseudo first order rate constant on the concentration of nucleophile. The intercept from such an analysis of the hydroxide kinetic runs also yielded the pseudo first order rate constants for the water reaction, *i.e.*

$$[5] \quad k_0 = k_2[OH^-] + k_w$$

where k_2 is the second order rate constant for the hydroxide reaction k_w the pseudo first order rate constant for the concurrent reaction with water. The k_w constants were converted to second order constants in the usual way.

Temperature Dependence of the Rate Constants

A two parameter nonlinear least squares program was used to evaluate $\Delta H^\ddagger$ and $\Delta S^\ddagger$ from the Eyring equation

$$[6] \quad \ln k_2 = \ln \left(\frac{kT}{h}\right) + \frac{\Delta S^\ddagger}{R} - \frac{\Delta H^\ddagger}{RT}$$

Values of the second order rate constants and their corresponding temperatures were introduced into the program and best fit values of $\Delta S^\ddagger$ and $\Delta H^\ddagger$ together with their respective standard deviations were calculated via an iterative procedure.

Results

Some preliminary experiments showed that the pseudo first order rate constants, measured as described above, were relatively insensitive to ionic strength effects. Ritchie *et al.* (12) observed that the addition of inert electrolytes ($< 1 \times 10^{-2}$ mol dm^{-3}), had no detectable effect on the rate of attack of hydroxide on malachite green. Consequently even though the rates are all measured at variable ionic strength in the present study, concentrations were such that ionic strength influences on the reaction rates are negligible.

The second order rate constants for the attack of each nucleophile on malachite green at various temperatures are reported in Table 1. A typical plot representing (*a*) the dependence of pseudo first order rate constants on the concentration of a particular nucleophile (ammonia) and (*b*) the influence of temperature on this correlation is shown in Fig. 1.

TABLE 1. Second order rate constants for the reaction of malachite green with a series of nucleophiles at various temperatures

Nucleophile	T/K	k_2/mol^{-1} dm^3 s^{-1}	n^a
SO_3^{2-}	288.40	2285 ± 77	6
	292.15	2735 ± 132	6
	298.35	3557 ± 111	6
	304.15	4476 ± 116	6
	308.05	5422 ± 360	6
OH^-	294.89	1.33 ± 0.08	6
	298.14	1.65 ± 0.01	6
	303.80	2.37 ± 0.12	6
	309.12	3.38 ± 0.02	6
ClO^-	286.19	549.2 ± 11	11
	298.15	1020.0 ± 31	11
	302.89	1279.7 ± 17	11
	309.59	1637.1 ± 28	10
H_2O^b	294.89	$5.92 \times 10^{-6} \pm 1.00 \times 10^{-6}$	
	298.14	$8.63 \times 10^{-6} \pm 1.30 \times 10^{-6}$	
	303.80	$1.85 \times 10^{-5} \pm 0.63 \times 10^{-5}$	
	309.12	$2.79 \times 10^{-5} \pm 0.50 \times 10^{-5}$	
NH_3	240.36	0.141 ± 0.002	7
	293.93	0.184 ± 0.002	6
	296.98	0.225 ± 0.003	6
	300.12	0.274 ± 0.060	6
	303.31	0.349 ± 0.002	6
	306.98	0.436 ± 0.004	6

[a]Number of kinetic runs.
[b]Calculated from intercept of the second order hydroxide plot.

A comparison of the new rate measurements with those reported previously is made in Table 2. The differences in both ionic strength (see above) and temperature related to the previous measurements make meaningful comparisons with the present data difficult. The rate of attack of hydroxide on malachite green reported in this communication is in good agreement with that measured by Taft (reported in ref. 12). The water rate is slighly higher than those previously reported, but since this rate is derived from the intercept of the second order plot when hydroxide ion is the nucleophile, some uncertainty in the derived water rates is inevitable. The second order rate constants associated with the reactions of sulphite and hypochlorite as nucleophiles are also in reasonable agreement with those given by Ritchie and Virtanen (17). Dixon and Bruice (15) report rate constants which are considerably smaller. Ritchie and Virtanen rationalize the difference between their measurements and those of Dixon and Bruice on the basis of ionic strength differences. For the sulphite reaction the observed rate constant is 'corrected' from 2.8×10^2 mol^{-1} dm^3 s^{-1} ($I = 1.0$) to 3×10^3 mol^{-1} dm^3 s^{-1} ($I = 0$) using the Debye–Hückel Limiting Law (DHLL). The corrected value is still low considering the temperature (303.16 K) at which the rates were measured. The use of the DHLL for large ionic strength corrections must be considered suspect.

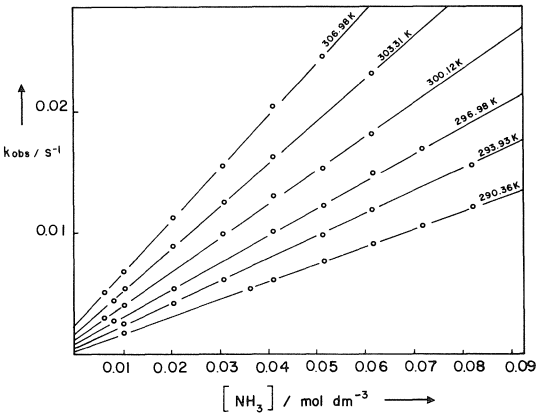

FIG. 1. The dependence of the pseudo first order rate constant on the concentration of ammonia for the reaction with malachite green at various temperatures.

The thermodynamic parameters calculated from the temperature–rate data are collected in Table 3, together with values of the standard entropies of the attacking nucleophile measured in aqueous solution at 298.16 K. These latter values collected by Latimer (13) are the most recent compilation of entropy data available, incorporating selected values by the U.S. National Bureau of Standards (14).

The entropies of activation derived from the kinetic data are negative for all the nucleophiles ranging from $-15 \rightarrow -24$ cal mol^{-1} deg^{-1}. The entropy of activation for the hydroxide ion reaction (-19.7 cal mol^{-1} K^{-1}) is in excellent agreement with that reported by Taft and coworkers (4) (-19 cal mol^{-1} K^{-1}) and is in fair agreement with the value reported by Ritchie *et al.* (6) (-14 cal mol^{-1} K^{-1}). The value of $\Delta S^{\ddagger}$ for the water reaction is more positive than previously reported values, -31.7 cal mol^{-1} K^{-1} (4) and -28.9 cal mol^{-1} K^{-1} (6), however the large differences in $\Delta S^{\ddagger}$ for this nucleophile are not surprising in view of the relatively large errors which must characterize the individual rate measurements (see above). The values of $\Delta H^{\ddagger}$ and $\Delta S^{\ddagger}$ reported here for the reactions of ammonia, hypochlorite, and sulphite with malachite green are new. The thermodynamic parameters of activation which characterize the hy-

TABLE 2. A comparison of previously reported second order rate constants for the reaction of malachite green with various nucleophiles

Nucleophile	k_2/mol^{-1} dm^3 s^{-1}	T/K	I	Reference
OH^-	1.65[a]	298.16	$<10^{-2}$	
	1.59	298.16		12
	1.36	298.16		16
	2.18	298.16	Variable	12
	1.23	303.16	1.0	15
H_2O	8.63×10^{-6}[a]	298.16	$<10^{-2}$	
	3.93×10^{-6}	298.16		12
	6.84×10^{-6}	298.16		16
	3.80×10^{-6}	298.16	Variable	12
	6.84×10^{-6}	303.16	1.0	15
SO_3^{2-}	3259[a,b]	296.16	$<10^{-2}$	
	4000	296.16	1×10^{-3}	17
	283	303.16	1.0	15
ClO^-	905[a,b]	296.16	$<10^{-2}$	
	1000	296.16	5×10^{-4}	17
	50	303.16	1.0	15

[a]Data reported in this paper.
[b]Calculated value using activation parameters.

TABLE 3. Enthalpies and entropies of activation and related thermodynamic data characterizing the reaction of a series of nucleophiles with malachite green

Nucleophile	$\Delta H^{\ddagger}$/kcal mol^{-1}	$\Delta S^{\ddagger}$/cal mol^{-1} K^{-1}	S(N)/cal mol^{-1} K^{-1}	$S^{\ddagger}$(CINAC) − S(CI) /cal mol^{-1} K^{-1}
SO_3^{2-}	7.02±0.15	−18.72±0.50	−7.0	−25.72±0.5
OH^-	11.26±0.17	−19.73±0.55	−2.52	−22.25±0.55
ClO^-	7.72±0.32	−18.90±1.5	10.0	−8.90±1.5
H_2O	19.63±1.4	−15.75±4.8	16.72	+0.97±4.8
NH_3	11.42±0.15	−23.00±0.48	26.3	+3.3 ±0.48
N_2H_4[a]	7.93±0.48	−24.37±1.64	33	+8.63±1.64

[a]Data obtained from ref. 5.

drazine reaction, are based on the rate–temperature data reported by Dixon and Bruice (5) which were reprocessed using our computer program in order to maintain uniformity of calculation. Values of $\Delta H^{\ddagger}$ and $\Delta S^{\ddagger}$ obtained for this nucleophile are also reported in Table 3.

The entropy of activation for any given nucleophile attacking malachite green is given by

[7] $$\Delta S^{\ddagger} = S^{\ddagger}(\text{CINAC}) - S(\text{N}) - S(\text{CI})$$

where $S^{\ddagger}$(CINAC) is the entropy of the carbonium ion – nucleophile activated complex, S(N) is the entropy of the nucleophile, and S(CI) is the entropy of the carbonium ion. Hence

[8] $$S^{\ddagger}(\text{CINAC}) - S(\text{CI}) = \Delta S^{\ddagger} + S(\text{N})$$

Since S(CI) is constant for all the nucleophiles, the experimental quantities on the right hand side of [8] give a *relative* characterization of $S^{\ddagger}$(CINAC) as the structure of N is altered. Such a relative characterization of $S^{\ddagger}$(CINAC) is sufficient for the purposes of this communication. Values of $S^{\ddagger}$(CINAC) for the various nucleophiles attacking malachite green are recorded in Table 3.

Discussion

The second order rate constants related to the various nucleophiles in the present study show a wide range of reactivity (*ca.* 10^9) and these reagents may be classified tentatively in several ways. For instance water, at various times, has been postulated to react via a general-base catalysis mechanism (6), although the evidence for this is neither conclusive nor compelling. Sulphite, hypochlorite, and hydrazine are classified as α-effect nucleophiles and show enhanced reactivity when related to the pK_a of their con-

jugate acids. Hydroxide and ammonia might be described as 'normal' nucleophiles but may react as general bases (see above). The entropies of activation show no obvious correlation with the nucleophile classifications elaborated above, but tend to more negative values as the entropy of the aqueous nucleophile becomes more positive (see Table 3). The α-effect nucleophiles show no marked differences on the basis of their entropies of activation and this is unexpected, since the electronic nature of the α-effect suggests that a considerable degree of desolvation should be necessary before the effect is evident.

Whilst the entropies of activation themselves provide little indication of the details of the activation process, the entropy of the transition state is more useful. Ritchie's (18) extensive study suggests a 'reactant like' transition state, hence a correlation between $S^{\neq}$(CINAC) and the entropy of the initial state (S_i) is anticipated. The quantity S_i is given by

[9] $S_i = S(\mathrm{N}) + S(\mathrm{CI}) = S(\mathrm{N}) + \text{constant}$

hence for a 'reactant like' transition state the correlation anticipated is

[10] $S^{\neq}(\mathrm{CINAC}) = \lambda S(\mathrm{N}) + \text{constant}$

where λ is a constant. The relationship between $S^{\neq}$(CINAC) and S(N) is shown in Fig. 2, and a weighted linear least-squares treatment of the data gives $\lambda = 0.88 \pm 0.02$, *i.e.* confirming the 'reactant like' description of the transition states. This particular correlation has a further novel feature. The absolute entropies of individual ions are not known with any certainty since all entropy measurements of ions must involve two or more ions with some arbitrary division of the total entropy change between the ions involved. Although ions in chemical processes are always present in pairs, trios, quartets, etc., kinetic situations are possible where a *single ion* is the effective reagent. This is true in the present case where the hydroxide, sulphite, and hypochlorite ions are the attacking reagents. The fact that *both* the neutral and charged nucleophiles are embraced by a *single* line (Fig. 2) suggests that the approximation $S(\mathrm{H}^+) = 0$ is correct within the error of our correlation (*ca.* ±1.0 cal mol^{-1} K^{-1}). Thus the correlation between $S^{\neq}$(CINAC) and S(N) provides indirect confirmation of the scale currently used to represent single ion entropies.

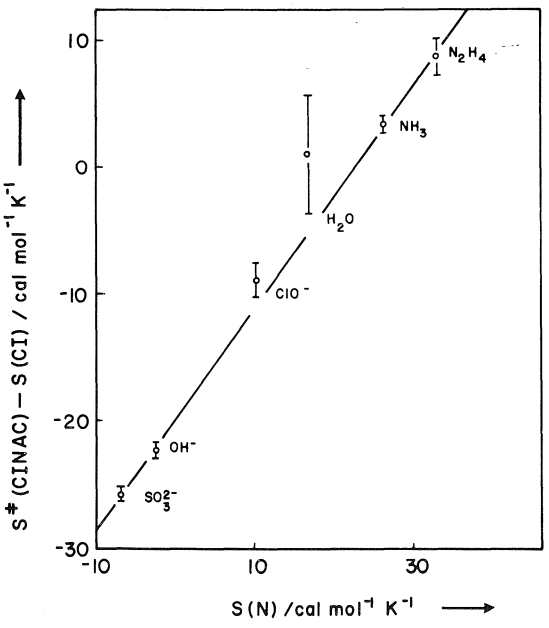

FIG. 2. An entropy correlation related to the reactions of various nucleophiles with malachite green.

Whilst there is no problem in specifying the relative values of the entropy of the initial state for the reactions representing *e.g.*, [1], the present reaction series, the possibility of specifying the entropy of the final state (S_f) as the nucleophile is varied is more problematical. However the products of the reactions for the water and hydroxide as nucleophiles differ only by a proton and hence $S_f(\mathrm{OH}^-) = S_f(\mathrm{H_2O})$, since $S(\mathrm{H}^+) = 0$. The data in Table 4 show that $\delta_N S_f \neq \delta_N S^{\neq}$ for H_2O and OH^- irrespective as to whether or not one or two water molecules are used to define the initial state for the carbonium ion reaction with water.[2] Since the quantity $S^{\neq}$(CINAC) shows no correlation with S_f for hydroxide and water we extrapolate this result to the remaining nucleophiles and retain the notion that the correlation of $S^{\neq}$(CINAC) with S(N) is the more meaningful relationship. Finally, if the appropriate kinetic data are available [10] provides a rough method of determining the standard state entropy of anions if such thermodynamic data are otherwise unavailable. The significance of the quantity λ in [10] has been discussed elsewhere by Robertson *et al.* (7–9). Constants such as λ or α (see above) are best considered as 'reaction coordinate parameters' and will be discussed more fully below.

[2] δ_N is an operator denoting changes in the structure of the nucleophile.

TABLE 4. Entropies of activation and related thermodynamic data characterizing the reaction of a series of nucleophiles with methyl iodide

Nucleophile	Reference	$\Delta S^{\ddagger}$ /cal mol^{-1} K^{-1}	S(N) /cal mol^{-1} K^{-1}	$S^{\ddagger} - S(CH_3I)$ /cal mol^{-1} K^{-1}
OH^-	25	−5.14±0.39	−2.52	−7.66±0.39
N_2H_4	24	−6.37±0.47	33	26.63±0.47
$S_2O_3^{2-}$	25	−2.93±0.82	8.0	5.07±0.82
H_2O	8	−7.40	16.72	9.32
N_3^-	22	0.88±0.93	32	31.12±0.93
SO_3^{2-}	26	0.56±1.2	−7	−6.44±1.2

It is of some interest to examine the correlation between $S^{\ddagger}$ and S(N) for a system other than a triaryl carbonium ion. The reaction between methyl iodide and a similar series of nucleophiles provides a useful system for comparison. In a recent communication by Robertson, Annesa, and Scott (9), it was suggested that the mechanism for these reactions involved prior activation of the methyl halide to an intimate or tight ion pair followed by nucleophilic attack on this intermediate with *very little bond making*. This leads to the prediction that the $S^{\ddagger}(CH_3I)$ *vs.* S(N) correlation would give a slope very close to unity and this is indeed the case. The data for this correlation are displayed in Fig. 3 and tabulated in Table 4. The weighted linear least squares slope of the line is 0.94 ± 0.09 which agrees with previous proposals (9) in all respects, and perhaps represents the most important rebuttal of the usual S_N2 mechanism. The old S_N2 description of the methyl iodide displacements emphasizes the synchronous motion of the new and old bonding pairs related to the reacting carbon. The entropy correlation (Fig. 4) provides additional evidence which suggests that the old picture of these processes should be abandoned (see references given in ref. 9).

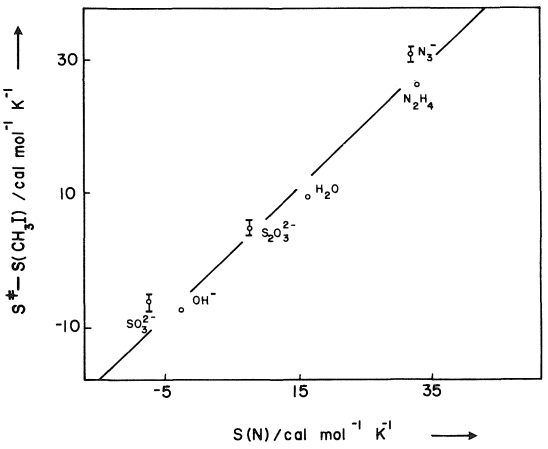

FIG. 3. An entropy correlation related to the reactions of various nucleophiles with methyl iodide.

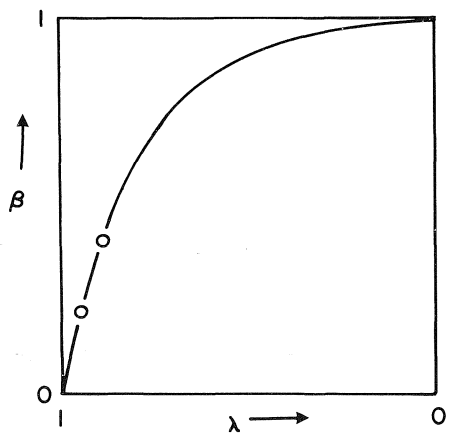

FIG. 4. The relationship between the Brønsted exponent (β) and the entropy quantity (λ).

Returning to the triaryl carbonium ion reactions we recall that Ritchie (18) has used the equation

$$[11] \qquad \log (k_n/k_0) = N_+$$

to accommodate the reaction of a range of carbonium ions and nucleophiles. The N_+ scale is defined by *p*-nitromalachite green as the standard carbonium ion and water as the standard nucleophile. Equation 11 indirectly demands that the selectivity of all nucleophiles with carbonium ions be identical. This conclusion is rather unusual and is in contradiction with data already in the literature (19). We note some thoughtful comments by Pross (20) on this matter and we hope to deal with the problem in some detail in later papers of the present series. The correlations between N_+ and the rates of attack of the nucleophiles on various carbonium ions appear adequate, but these reactions do not show any rate–equilibrium or equilibrium–equilibrium re-

lationships. This situation has prompted Ritchie (18) to postulate transition states which are somewhere between the solvent separated ($R^+//X^-$) and the intimate ion pair (R^+X^-) of the reversed Winstein scheme (21)

[12] $$R^+ + X^- \rightleftharpoons R^+//X^- \rightleftharpoons R^+X^- \rightleftharpoons RX$$

for all the nucleophiles studied. Whilst the extent of bond making does not emerge from correlations related to the N_+ scale, Dixon and Bruice (5) have shown that the Brønsted exponent (β) for a series of amines attacking malachite green is 0.4. Assuming the range of the Brønsted exponent is from zero to unity,[3] requires the conclusion that there is considerable bond making in the transition state between the amine and the carbonium ion. This conclusion is both at variance with Ritchie's views and contrasts with the entropy correlation (Fig. 2) presented here. The point is further illustrated by a comparison with the observed β values (0.22) for the reaction of similar amines with methyl iodide (22). Thus the β values and the λ parameters from the entropy correlations show a common trend for both substrates but the λ values suggest a much more 'reactant-like' transition state than the Brønsted exponents. The question then arises as to whether β or λ is the more significant measure of the position of the transition state along the reaction coordinate. Since $\beta = 0$ when $\lambda = 1$ and intuitively $\lambda = 0$ when $\beta \simeq 1$ (see footnote 3 and above) we can sketch the curve relating these two parameters, including the two experimentally observed points (Fig. 4). If Ritchie's conclusions concerning the 'reactant-like' nature of the transition state are valid then λ is the better measure of the transition state along the reaction coordinate. However the relationship between β and λ is clearly complex since the linear free energy quantity (β) may include factors to which the entropy quantity (λ) is either more or less insensitive. The correlation between β and λ does however suggest that β may be a nonlinear function of the reaction coordinate and therefore a deduction of the position of the transition state along the reaction coordinate using the Brønsted exponent is fraught with uncertainty particularly for reactions which are not proton transfers.

[3]For reactions which do not involve proton transfers as the rate determining step this proposal is arbitrary. Dixon and Bruice (5) are aware of this fact.

Acknowledgements

The authors wish to thank the National Research Council of Canada for partial support of these studies. Thanks are also due to the technical services unit for their continued cooperation. We would also like to thank Dr. Peter Golding for some thoughtful comments on this paper.

1. J. C. Turgeon and V. K. LaMer. J. Am. Chem. Soc. **74**, 5988 (1952).
2. D. T. Chen and K. J. Laidler. Can. J. Chem. **37**, 599 (1959).
3. V. V. Sinev. Zh. Org. Khim. **9**, 1921 (1973).
4. R. A. Diffenbach, K. Sano, and R. W. Taft. J. Am. Chem. Soc. **88**, 4747 (1966).
5. J. E. Dixon and T. C. Bruice. J. Am. Chem. Soc. **93**, 3248 (1971).
6. C. D. Ritchie, D. J. Wright, Der-Shing Huang, and A. A. Kamego. J. Am. Chem. Soc. **97**, 1163 (1975).
7. R. E. Robertson and J. M. W. Scott. J. Chem. Soc. 1596 (1961).
8. R. E. Robertson, R. L. Heppolette, and J. M. W. Scott. Can. J. Chem. **37**, 803 (1959).
9. R. E. Robertson, A. Annesa, and J. M. W. Scott. Can. J. Chem. **53**, 3106 (1975).
10. R. E. Robertson and J. M. W. Scott. Can. J. Chem. **50**, 167 (1972).
11. P. Moore. J. Chem. Soc. Faraday Trans. I, **68**, 1890 (1972).
12. C. D. Ritchie, G. A. Skinner, and V. G. Badding. J. Am. Chem. Soc. **89**, 2063 (1967).
13. W. M. Latimer. Oxidation potentials. 2nd ed. Prentice-Hall Inc., New York. 1952.
14. U.S. National Bureau of Standards, Circular 500. 1952.
15. J. E. Dixon and T. C. Bruice. J. Am. Chem. Soc. **93**, 6592 (1971).
16. E. F. J. Dunystee and E. Grunwald. J. Am. Chem. Soc. **81**, 4524 (1959).
17. C. D. Ritchie and P. O. I. Virtanen. J. Am. Chem. Soc. **95**, 1882 (1973).
18. C. D. Ritchie. Acc. Chem. Res. **5**, 348 (1972).
19. J. M. W. Scott. Can. J. Chem. **48**, 3807 (1970).
20. A. Pross. J. Am. Chem. Soc. **98**, 776 (1976).
21. S. Winstein, P. E. Klinedinst, Jr., and G. C. Robinson. J. Am. Chem. Soc. **83**, 885 (1961).
22. M. J. Gregory and T. C. Bruice. J. Am. Chem. Soc. **89**, 4400 (1967).
23. Chang Min Won and A. V. Willi. J. Phys. Chem. **76**, 427 (1972).
24. R. Hasty. J. Phys. Chem. **73**, 317 (1969).
25. E. A. Moelwyn-Hughes. Proc. R. Soc. Ser. A, **196**, 540 (1949).
26. R. Hasty and S. Sutter. Can. J. Chem. **47**, 4537 (1969).

The rearrangement of 4-chloromethyl-1,4-dihydropyridine derivatives to pyrrolo[1,2-*c*]pyrimidines

ERIC BULLOCK, BRIAN GREGORY, AND M. THOMAS THOMAS

Department of Chemistry, Memorial University of Newfoundland, St. John's, Nfld., Canada A1C 5S7

Received August 10, 1976

ERIC BULLOCK, BRIAN GREGORY, and M. THOMAS THOMAS. Can. J. Chem. **55**, 693 (1977).

When refluxed with urea in ethanol, certain 4-chloromethyl-1,4-dihydropyridines undergo rearrangement to give 1,2,5,9-tetrahydro-1-oxopyrrolo[1,2-*c*]pyrimidines in good yield. The structures of the products are established by spectroscopic properties and by dehydrogenation, hydrolysis, and decarboxylation to a 1,2-dihydro-1-oxopyrrolo[1,2-*c*]pyrimidine. In contrast, the reaction between thiourea and the 4-chloromethyl-1,4-dihydropyridines occurs without rearrangement and gives isothiouronium salts which were isolated as the picrates.

ERIC BULLOCK, BRIAN GREGORY et M. THOMAS THOMAS. Can. J. Chem. **55**, 693 (1977).

Lorsque l'on porte certaines chlorométhyl-4 dihydro-1,4 pyridines au reflux avec de l'urée dans l'éthanol, il se produit un réarrangement qui conduit aux tétrahydro-1,2,5,9 oxo-1 pyrrolo[1,2-*c*]pyrimidines avec de bon rendement. On a établi les structures des produits par des méthodes spectroscopiques et par déshydrogénation, hydrolyse et décarboxylation pour conduire à la dihydro-1,2 oxo-1 pyrrolo[1,2-*c*]pyrimidine. Par opposition, la réaction entre la thiourée et les chlorométhyl-4 dihydro-1,4 pyridines se produit sans réarrangement et donne des sels d'isothiouronium qui ont pu être isolés sous forme de picrates.

[Traduit par le journal]

4-Chloromethyl-1,4-dihydropyridines having electron-withdrawing substituents such as ethoxycarbonyl (1), acetyl (2), and cyano (3) groups at C_3 and C_5 were first synthesized by Benary who also reported some of their reactions with nucleophilic reagents. A reinvestigation of the action of cyanide ion on the diester **1***c* revealed that ring expansion had taken place leading to a 4,5-dihydro-1*H*-azepine (4), and this was extended to the dicyano (5) and diacetyl compounds (6). Subsequent work has shown that the chloromethyl compounds may be used in the synthesis of azepines (7), pyrroles (4–7), fulvenes (8), 2,3-dihydrofurans (6), 2-aza-8-thiabicyclo-[3.2.1]oct-3-enes (9), and furo[2,3-*b*]pyridines (10). We now report that the reaction of urea on the 4-chloromethyl compounds leads to pyrrolo[1,2-*c*]pyrimidine derivatives in adequate yield.

When the chloromethyl compound **1***c* was refluxed with urea in ethanol, the ultraviolet maxima at 231 and 349 nm (4) of the dihydropyridine chromophore were replaced, over the course of a few hours, by bands at 263 and 310 nm. Addition of water at this stage caused precipitation of a compound $C_{15}H_{20}N_2O_5$, M^+ 308 whose ultraviolet spectrum was incompatible with the presence of dihydropyridine, tetrahydropyridine, dihydroazepine, and pyrrole chromophores. The infrared spectrum revealed the presence of NH (ν_{max} 3415 cm^{-1}) and ester group(s) (ν_{max} 1707 cm^{-1}), while the mass spectrum was indicative of the presence of two ester groups (see below). The nmr spectrum showed signals due to methyl groups at δ 2.68 (t,[1] $J \sim 1$ Hz) and 2.28 (d, $J \sim 1$ Hz), which exhibit homollylic coupling to two and one protons respectively. The appearance of 1:1:1:1 quartets at δ

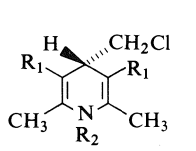

1

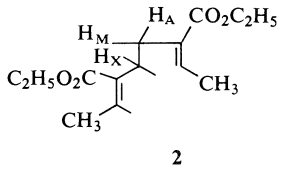

2

a $R_1 = COCH_3$ $R_2 = H$
b $R_1 = CO_2CH_3$ $R_2 = H$
c $R_1 = CO_2C_2H_5$ $R_2 = H$
d $R_1 = CN$ $R_2 = H$
e $R_1 = CO_2CH_3$ $R_2 = CH_3$

4.68 (H_X) and 3.22 (H_M) leaves no doubt that the protons responsible for homoallylic splitting of the methyl groups are attached to adjacent carbons (the signal due to H_A at approximately

[1]We cannot rule out the possibility that this signal consists of overlapping doublets due to the small coupling constant.

δ 2.64 is partly obscured by the methyl resonance at δ 2.68). A consideration of the origin of the compound, the above splitting pattern, and the infrared spectrum suggest the presence of the diethyl octa-2,6-diene-3,6-dicarboxylate (part structure **2**), while the low-field position of H_X suggests the attachment of a nitrogen function at this point. Since deuteration caused no change in the H_X signal the adjacent nitrogen atom is devoid of protons. In addition the nmr spectrum confirms the presence of two ethyl ester groups and a proton attached to nitrogen. These data are accommodated by the pyrrolo[1,2-*c*]pyrimidine structure **3***c*. In the presence of the paramagnetic shift reagent $Eu(fod)_3$ the H_A signal is revealed as a triplet which, like the signals due to H_M and H_X, is broadened by homoallylic coupling. The mass spectrum is in good agreement with structure **3***c*, and is dominated by fragmentation pathways involving the ethoxycarbonyl and ring methyl groups which are situated *ortho* to each other. One important pathway involves loss of ethyl group from the molecular ion to give an

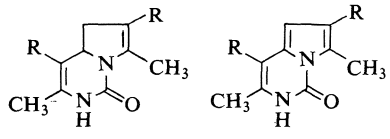

3 **4**

a R = $COCH_3$
b R = CO_2CH_3
c R = $CO_2C_2H_5$
d R = H

ion *m/e* 279 (98.5%) which subsequently loses ethanol to give an ion *m/e* 233 (81%) while sequential loss of ethoxyl and ethyl radicals from the molecular ion gives rise to the base peak at *m/e* 234. The ions at *m/e* 183, 155, and 137 are reminiscent of the 1,2,3,4-tetrahydro-2-oxopyrimidines (11) and may arise by scission between C_5 and C_9 (see Scheme 1) followed by loss of the side chain from nitrogen with concomitant hydrogen transfer to give the 2-oxopyrimidinium ion (*m/e* 183). This ion may lose ethylene from the ethyl ester by McLafferty rearrangement to give an ion at *m/e* 155 or lose ethanol to give an ion *m/e* 137.[2]

[2]In support of this interpretation, the corresponding dimethyl ester (see below) gives rise to expected ions at *m/e* 169 and 137 but no fragment analogous to the *m/e* 155 ion.

The structure **3***c* was confirmed, as outlined below, by dehydrogenation to give a compound showing an aromatic proton, and subsequent removal of ethoxycarbonyl groups to give a compound having three aromatic protons, two of which are attached to adjacent carbon atoms.

The pyrrolo[1,2-*c*]pyrimidine **3***c* was dehydrogenated by 10% palladium-on-carbon in boiling mesitylene, or, less efficiently, by heating with sulfur, to a compound $C_{15}H_{18}N_2O_5$, M^+ 306 whose nmr spectrum reveals the presence of non-equivalent ethyl esters, methyl singlets at δ 2.97 and 2.42, and a one proton singlet at δ 6.79. The low-field shift of the methyl resonances and the chemical shift of the one-proton singlet, typical of pyrrole β protons, are consistent with structure **4***c* for this product.

When **4***c* was refluxed with 50% aqueous sulfuric acid, hydrolysis and decarboxylation occurred to give **4***d*, $C_9H_{10}N_2O$, in which the functionality of the oxygen is indicated by the presence of a carbonyl stretching absorption at 1701 cm^{-1} in the infrared spectrum. The nmr of **4***d* exhibited a pair of doublets (an AB system due to adjacent aromatic protons) in addition to two methyl singlets, a broad NH singlet and a singlet due to a further uncoupled aromatic proton. The mass spectrum showed intense M and $M - 1$ ions.

When refluxed with urea in ethanol, the dihydropyridines **1***a* and **1***b* gave the corresponding pyrrolopyrimidine derivatives **3***a* and **3***b* whose structures are supported by their spectroscopic properties. Under similar reaction conditions the dicyano compound **1***d* was unchanged.

The rearrangement of the dihydropyridines **1***a–c* to the pyrrolopyrimidines **3***a–c* is believed to proceed via alkylation of urea on nitrogen (12), with simultaneous ring expansion. to give the 4-ureido-4,5-dihydro-1*H*-azepine derivative **5** followed by hydrolytic ring-opening to give the acyclic compound **6** and subsequent cyclization. (see Scheme 2). An alternative is possible which involves intramolecular Michael addition (*cf.* ref. 13) forming **7** followed by ring-opening to give **8** and cyclization. In an attempt to isolate intermediates, several by-products including ethyl acetoacetate, ethyl 2-methylpyrrole-3-carboxylate, ethyl carbamate, and ethyl 3-ureidocrotonate were isolated from the reaction of urea with **1***c*. It is well-known that urea decomposes in boiling ethanol to give ethyl carbamate and

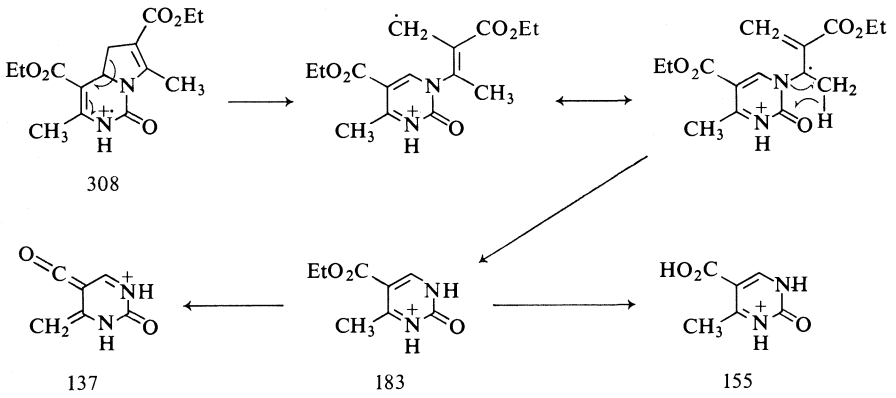

Et = C_2H_5

SCHEME 1

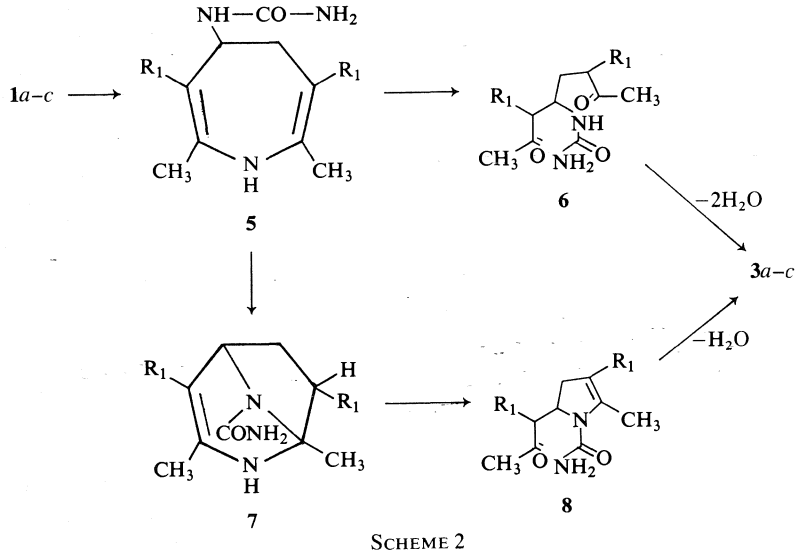

SCHEME 2

ammonia (14). Anderson and Johnson have shown that **1***c* reacts with ammonium hydroxide in alcohol to give ethyl 2-methylpyrrole-3-carboxylate and ethyl acetoacetate (7). In view of the suggested mechanisms (above) it is interesting that ethyl 3-ureidocrotonate may be isolated. This is formed from ethyl acetoacetate and urea (15) and demonstrates that the cyclization of a ureido function onto the carbonyl group of a β-ketoester moiety is possible under these reaction conditions. In addition, it is unlikely that dimethyl 2,7-dimethyl-4*H*-azepine-3,6-dicarboxylate, which has been shown to be an intermediate in the cyanide catalyzed ring expansion of **1***b* (16), is an intermediate in this reaction, since no pyrrolopyrimidine is formed when the azepine is refluxed in ethanol with urea alone or

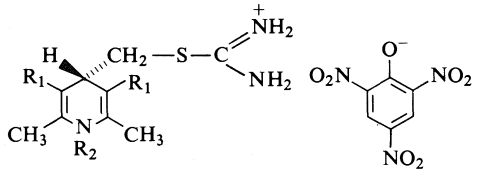

a $R_1 = COCH_3$ $R_2 = H$
b $R_1 = CO_2CH_3$ $R_2 = H$
c $R_1 = CO_2CH_3$ $R_2 = CH_3$
d $R_1 = CO_2C_2H_5$ $R_2 = H$

in the presence of ammonium acetate or ammonium chloride.

The above mechanisms each suggest that the nitrogen of the dihydropyridine is eliminated during the reaction and, in support of this, it has been shown that the *N*-methyl compound **1***e* gives the pyrrolopyrimidine **3***b* when refluxed with urea.

Although the report of the degradation of the paralytic shellfish toxin saxitoxin to a pyrrolo-[1,2-*c*]pyrimidine (17) stimulated work on this ring system, there are still few synthetic routes available (18). Pyrrolo[1,2-*c*]pyrimidine derivatives have been prepared from pyrrol-2-aldehyde (19), aminoethylpyrrolidines (20), 3-(4-pyrimidyl)-1-propanol (21), and pyrimidine quaternary salts (22–24). The preparation from 4-chloromethyl-1,4-dihydropyridines represents a convenient entry into this ring system and its scope is presently under investigation.

In contrast to the rearrangement which occurs on reaction with urea, the reaction of **1***a–c,e* with thiourea has been shown to give *S*-alkylisothiouronium salts. When the 4-chloromethyl-1,4-dihydropyridines **1***a–c,e* were refluxed with thiourea in ethanol until tlc revealed absence of the chloromethyl compound, it was found that the solution still showed ultraviolet absorption typical of the 1,4-dihydropyridine (λ_{max} 231 and 350 nm) rather than the dihydroazepine (4) or pyrrolopyrimidine chromophores. Addition of picric acid to the solution allowed crystallization of the isothiouronium picrates **9***a–d*. The nmr spectra of these compounds were in agreement with the assigned structures. Again the 3,5-dicyano compound **1***d* failed to react.

The pyrrolopyrimidine **3***c* was screened for pharmacological activity, and found to have no *in vitro* antibiotic, antiparasitic, enzyme inhibitory, contraceptive, or antihypertensive activity.

Experimental

Melting points were determined using a Fisher-Johns melting point apparatus. Infrared spectra were obtained in chloroform solution using a Perkin-Elmer 237B grating infrared spectrometer. Ultraviolet spectra were measured on Unicam SP 800D or Perkin Elmer 202 spectrophotometers using solutions in 95% ethanol. Spectra were calibrated using the bands at 2850.7 and 1601.4 cm^{-1} of polystyrene (ir) or at 279.4 and 360.9 nm of a holmium oxide filter (uv). The ^1H nmr spectra were obtained on Varian HA 100 or EM 360 spectrometers using deuterochloroform as solvent unless specified otherwise. All chemical shifts are expressed in parts per million downfield from internal tetramethylsilane. The sample of Sievers Eu(fod)$_3$ shift reagent was obtained from Norell Chemical Company, Inc., Landing, New Jersey, 07850. Mass spectra were determined at 70 eV ionizing energy using a Hitachi–Perkin-Elmer RMU 6E mass spectrometer. Only the most intense peaks are listed; normalized intensities are given in parentheses. Initial and final total ion current values differed by $< 5\%$. New compounds were homogeneous by tlc and were analyzed for C, H, N, S by Alfred Bernhardt, West Germany. The identity of known compounds was established by mp, mixture mp, and comparison of ir, nmr, and ms with those of authentic specimens.

Diethyl 1,2,5,9-Tetrahydro-3,7-dimethyl-1-oxopyrrolo[1,2-c]pyrimidine-4,6-dicarboxylate, 3c

The chloromethyl compound **1***c* (5.03 g) and urea (3.35 g) were heated under reflux in ethanol (100 ml) for 7 h and then concentrated to about 40 ml. Water (200 ml) was added and, on standing, a precipitate was formed which was filtered, washed with water, and recrystallized from cyclohexane to give the product **3***c* (4.07 g, 79%), mp 132–133 °C. *Anal.* calcd. for $C_{15}H_{20}N_2O_5$: C 58.43, H 6.54, N 9.09; found: C 58.38, H 6.61, N 9.11. Spectral data: ir 3415 (NH, free), 3217 (NH, bonded), 1707 (unsaturated ester), 1670 (amide), 1640 cm^{-1} (C=C); uv 263 (ε 26 200) 310 nm (ε 7150); ^1H nmr δ 1.29 and 1.31 (two t, J = 7.0 Hz, 6H, methyls of ethyl esters), 2.28 (d, $J_{homoallylic}$ ~1 Hz, CH_3 at C_3), 2.64 approx (m, partly obscured by methyl resonance at δ 2.68, H_A at C_5), 2.68 (t, $J_{homoallylic}$ ~ 1 Hz, 4H,[3] CH_3 at C_7), 3.22 (two q, J_{AM} 14.5 Hz, J_{MX} = 9.5 Hz, $J_{homoallylic}$ ~ 1 Hz, 1H, H_M at C_5), 4.24 and 4.20 (overlapping q, J = 7.0 Hz, 4H, CH_2 of ethyl esters), 4.68 (q broadened by homoallylic coupling, J_{AX} = 13 Hz, J_{MX} = 9.5 Hz, 1H, H_x at C_9), 9.01 (s, 1H, NH). Compound **3***c* (3.1×10^{-4} mol) and the shift reagent Eu(III)(fod)$_3$ (4.8×10^{-5} mol) in $CDCl_3$ (0.6 ml) showed δ 1.40 and 1.43 (two t, J = 7.0 Hz, 6H methyls of ethyl esters), 2.39 (s, 3H, CH_3 at C_3), 3.11 (br t, J_{AM} = 14.5 Hz, J_{AX} = 13 Hz, 1H, H_A at C_5), 3.62 (q, J_{AM} = 14.5 Hz, J_{MX} = 9.5 Hz, 1H, H_M at C_5), 4.23 (s, 3H, CH_3 at C_7), 4.40 (q, J = 7 Hz, 4H, CH_2 of ethyl esters), 5.38 (q, broadened, J_{AX} = 13 Hz, J_{MX} = 9.5 Hz, 1H, H_M at C_9), 9.95 (s, 1H, NH); ms *m/e* 308(51, M^+), 279(98), 263(40), 261(28), 235(43), 234(100), 233(81), 207(53), 206(63), 205(26), 189(69), 183(15), 163(27), 162(55), 161(33), 155(18), and 137(23).

The filtrate was concentrated to remove ethanol, acidified with hydrochloric acid, and extracted with ether. The ether was washed with water, dried ($MgSO_4$), filtered, and evaporated to give a pleasant smelling oil which contained ethyl acetoacetate. On standing, crystals were obtained, which were filtered off, recrystallized from aqueous ethanol and then sublimed to give ethyl 2-methylpyrrole-3-carboxylate mp 76–77 °C (lit. (1, 7) 78–79 °C) and had ir and ms identical with those of an authentic specimen.

In a separate experiment, after concentration and addition of water the reaction mixture was extracted using ether. Evaporation of the ether and chromatography on silica gel afforded ethyl acetoacetate, ethyl 2-methylpyrrole-3-carboxylate, diethyl 1,2,5,9-tetrahydro-3,7-dimethyl-1-oxopyrrolo[1,2-*c*]pyrimidine-4,6-dicarboxylate,

[3]The integration includes that of the signal due to H_A.

TABLE 1. Isothiouronium picrates of 4-chloromethyl-1,4-dihydropyridines, **9***a–d*

Compound	Reaction time (h)	Yield (%)	Melting point (°C)	Molecular formula	Analysis (%) Calculated C	H	N	S	Found C	H	N	S
9*a*	2.5	77	222–224(dec.)	$C_{19}H_{22}N_6O_9S$	44.70	4.35	16.47	6.28	44.85	4.55	16.27	6.40
9*b*	3	67	218–220	$C_{19}H_{22}N_6O_{11}S$	42.06	4.09	15.49	5.91	42.23	4.17	15.42	6.10
9*c*	8.5	72	195–197(dec.)	$C_{20}H_{24}N_6O_{11}S$	43.16	4.35	15.10	5.76	43.30	4.42	15.03	5.65
9*d*	3	89	204–205	$C_{21}H_{26}N_6O_{11}S$	44.21	4.59	14.73	5.62	44.40	4.71	14.70	5.81

TABLE 2. Nuclear magnetic resonance spectra of isothiouronium picrates of 4-chloromethyl-1,4-dihydropyridines, **9***a–d*, in DMSO-d_6

Compound	NH	NH_2	N—CH_3	Aromatic H of picrate anion	C_4—H	CH_2—S	CH_3 at $C_{2,6}$	$COCH_3$	CO_2CH_3	$CO_2C_2H_5$ CH_2	CH_3
9*a*	9.28	8.98	—	8.69	4.27(t, J=6.5 Hz)	2.90(d, J=6.5 Hz)	2.33[a]	2.33[a]			
9*b*	9.14	8.92	—	8.68	4.22(t, J=5.5 Hz)	3.08(d, J=5.5 Hz)	2.28		3.71		
9*c*	—	8.94	3.39	8.68	4.23(t, J=6.5 Hz)	2.94(d, J=6.5 Hz)	2.46		3.71		
9*d*	9.13	8.94	—	8.70	4.35(t, —)[a]	3.07(d, J=5.5 Hz)	2.28			4.20(q, J=7 Hz)[a]	1.33(t, J=7 Hz)

[a]Denotes signals overlap or superimpose.

ethyl carbamate, and ethyl 3-ureidocrotonate. When the *N*-methyl compound **1***e* was refluxed with urea in ethanol, the pyrrolopyrimidine **3***c* was produced.

*Dimethyl 1,2,5,9-Tetrahydro-3,7-dimethyl-1-oxopyrrolo-[1,2-c]pyrimidine-4,6-dicarboxylate, **3b***

The chloromethyl compound **1***b* (1.368 g) was refluxed with urea (0.9 g) in ethanol (20 ml) as above and recrystallized from ethanol to give the dimethyl ester **3***b* (0.836 g, 60%) mp 210–212 °C. *Anal.* calcd. for $C_{13}H_{16}N_2O_5$: C 55.71, H 5.75, N 10.00; found: C 55.79, H 6.07, N 10.22. Spectral data: ir 3410, 1709, 1683, 1637 cm^{-1}; uv 262 (ε 25 000), 310 nm (ε 7000); ^1H nmr δ 2.40 (d, $J \sim 1$ Hz, 3H, CH_3 at C_3), 2.75 (br t obscured by methyl resonances, $J_{AM} \sim 14$ Hz, H_A at C_5), 2.93 (distorted d, $J \sim 1$ Hz, 3H, CH_3 at C_7), 3.32 (q, $J_{AM} = 14$ Hz, $J_{MX} = 9$ Hz, 1H, H_M at C_5) 3.63 (s, 3H, methyl ester), 3.67 (s 3H, methyl ester), 4.69 (q, $J_{MX} = 9$ Hz, $J_{AX} \sim 12$ Hz, 1H, H_X at C_9), 10.59 (br s, 1H, NH); ms *m/e* 280 (70, M^+) 265(100), 249(45), 247(89), 233(66), 221(42), 220(90), 189(37), 169(19), 162(30), 161(24), 137(19).

*4,6-Diacetyl-1,2,5,9-tetrahydro-3,7-dimethyl-1-oxopyrrolo-[1,2-c]pyrimidine, **3a***

The chloromethyl compound **1***a* (1 g) was refluxed with urea (1 g) in ethanol as above and after recrystallization from aqueous ethanol gave the product **3***a* (0.42 g, 41%), mp 215–216 °C. *Anal.* calcd. for $C_{13}H_{16}N_2O_3$: C 62.88, H 6.50, N 11.29; found: C 62.78, H 6.49, N 11.37. Spectral data: ir 3405, 1700, 1622 cm^{-1}; uv 283 (ε 24 270) 330 nm (ε 8700); ^1H nmr δ (pyridine-d_5) 2.15 (s, 3H, acetyl), 2.27 (d, approx. 3H, $J_{homoallylic} = 1.5$ Hz, CH_3 at C_3), 2.30 (s, 3H, acetyl), 2.91 (br t, partly obscured by methyl resonances, $J_{homoallylic} = 1.5$ Hz, $J_{AM} = 15.5$ Hz, $J_{AX} = 13.8$ Hz, H_A at C_5), 2.91 (t, $J_{homoallylic} = 1.5$ Hz, 3H, CH_3 at C_7), 3.40 (broadened dd, $J_{homoallylic} = 1$–5 Hz, $J_{AM} = 15.5$ Hz, $J_{MX} = 9.6$ Hz, 1H, H_M at C_5), 4.75 (two d d (8 lines), $J_{homoallylic} = 1.5$ Hz, $J_{AX} = 13.8$ Hz, $J_{MX} = 9.6$ Hz, 1H, H_X at C_5), 10.66 (br s, 1H, NH); ms *m/e* 248 (60, M^+), 246(26), 205(48), 191(26), 186(100), 153(19), 121(97), 107(31), 66(27), 65(33), 56(46), 43(44).

*Dimethyl 1,2-Dihydro-3,7-dimethyl-1-oxopyrrolo[1,2-c]-pyrimidine-4,6-dicarboxylate, **4b***

The dimethyl ester **3***b* (115 mg) and 10% palladium-on-charcoal (55 mg) in dry mesitylene (20 ml) were refluxed for 3 h, cooled, and diluted with ethanol (150 ml). Filtration through a pad of Celite followed by evaporation gave colorless needles which were recrystallized from aqueous methanol to give the product **4***b* (83 mg, 73%) mp 283–284.5 °C. *Anal.* calcd. for $C_{13}H_{14}N_2O_5$: C 56.11, H 5.07, N 10.07; found: C 56.14, H 5.10, N 10.05. Spectral data: ir 3390, 1728, and 1706 cm^{-1}; uv 222 (ε 37 400), 252 (sh, ε 7220), 292 (ε 4820), 303 (ε 5100) 328 nm (ε 5240); ^1H nmr δ (DMSO-d_6) 11.13 (br s, 1H, NH), 6.68 (s, 1H, C_5—H), 3.79 (s, 3H, CH_3O_2C), 3.77 (s, 3H, CH_3O_2C), 2.9 (s, 3H, C_7—CH_3), 2.34 (s, 3H, C_3—CH_3); ms *m/e* 278 (100, M^+), 263(52), 247(23), 246(7), 231(23) 218(25).

*Diethyl 1,2-Dihydro-3,7-dimethyl-1-oxopyrrolo[1,2-c]-pyrimidine-4,6-dicarboxylate, **4c***

The diethyl ester **3***c* (1.008 g) and 10% palladium-on-charcoal (522 mg) in dry mesitylene (175 ml) were treated as above to yield the product **4***c* (0.73 g, 73%), mp 219–220 °C. *Anal.* calcd. for $C_{15}H_{18}N_2O_5$: C 58.82, H 5.92, N 9.15; found: C 58.81, H 6.04, N 9.10. Spectral data: ir 3406, 3225, 1726, 1703, 1621 cm^{-1}; uv 221 (ε 41 900), 293 (ε 4900), 303 (ε 5200), 340 nm (ε 4900); ^1H nmr δ (DMSO-d_6, HA 100) 6.79 (s, 1H, C_5—H), 5.76 and 5.71 (overlapping q, $J = 7$ Hz, 4H, CH_2 of ethyl), 2.97 (s, 3H, C_7—CH_3), 2.42 (s, 3H, C_3—CH_3), 1.35 and 1.37 (overlapping t, $J = 7$ Hz, 6H, CH_3 of ethyl); ms *m/e* 306 (80, M^+), 277(100), 261(27), 249(80), 232(20), 231(21).

*1,2-Dihydro-3,7-dimethyl-1-oxopyrrolo[1,2-c]pyrimidine, **4d***

The diethyl ester **4***c* (1.367 g) in 50% sulfuric acid (100 ml) was refluxed with stirring for 3 h. The resulting red solution was cooled, diluted with water (100 ml), and neutralized by addition of solid sodium carbonate. Extraction using ether afforded a crude product which was purified by sublimation at 80 °C/0.01 torr to give the pure product **4***d* (0.45 g, 62%) mp 183–185 °C (dec.). *Anal.* calcd. for $C_9H_{10}N_2O$: C 66.65, H 6.22, N 17.27; found: C 66.61, H 6.36, N 17.00. Spectral data: ir 3407 (NH, free) 1701 (strong, C=O), 1664 cm^{-1} (medium, amide II); uv max 205 (ε 14 960), 278 (sh, ε 12 870), 284 nm (ε 13 060); ^1H nmr δ 9.88 (br s, 1H, NH) 6.17 (d, $J = 3.6$ Hz, 1H), 5.99 (s, 1H, H at C_4), 5.97 (d, $J = 3.6$ Hz, 1H), 2.75 (s, 3H), 2.16 (s, 3H); ms *m/e* 162 (93, M^+) 161(100).

*Preparation of Isothiouronium Picrates of 4-Chloromethyl-1,4-dihydropyridines, **9a–d***

The chloromethyl compound (1.5 g) and thiourea (1.5 g) were heated under reflux in ethanol (25 ml). After addition of picric acid (1.5 g), the solution was cooled when the isothiouronium salt crystallized. Recrystallization from ethanol afforded the pure product.

The time required for reaction, yield, melting point, and elemental analysis are shown in Table 1 and ^1H nmr spectra are reported in Table 2.

Acknowledgements

The authors wish to thank the National Research Council of Canada and Memorial University of Newfoundland for financial support and Memorial University for the award of a demonstratorship to one of us (M.T.T.). In addition we are deeply indebted to Dr. M.A. Davis and Ayerst Research Laboratories, Montreal for the pharmacological evaluation of compound **3***c*.

1. E. Benary. Ber. **44**, 489 (1911).
2. E. Benary. Ber. **51**, 567 (1918).
3. E. Benary and G. Lowenthal. Ber. **55**, 3429 (1922).
4. P. J. Brignell, E. Bullock, U. Eisner, B. Gregory, A. W. Johnson, and H. Williams. J. Chem. Soc. 4819 (1963).
5. E. Bullock and B. Gregory. Can. J. Chem. **43**, 332 (1965).
6. R. C. Allgrove, L. A. Cort, U. Eisner, and J. A. Elvidge. J. Chem. Soc. C, 434 (1971).
7. M. Anderson and A. W. Johnson. J. Chem. Soc. 2411 (1965).
8. R. F. Childs, R. Grigg, and A. W. Johnson. J. Chem. Soc. C, 201 (1967); M. Mahendran and A. W. Johnson. J. Chem. Soc. C, 1237 (1971).

9. U. EISNER, J. FLIPPEN, M. Z. HAQ, and I. KARLE. J. Chem. Soc. Perkin Trans. I, 357 (1972).
10. E. BULLOCK, B. GREGORY, and A. W. JOHNSON. J. Chem. Soc. 1632 (1964).
11. E. BULLOCK, R. A. CARTER, B. GREGORY, and D. S. SHIELDS. Chem. Commun. 97 (1972).
12. S. GABRIEL and R. STELZNER. Ber. **28**, 2937 (1895); J. P. PICARD and A. F. MCKAY. Can. J. Chem. **31**, 896 (1953); G. R. PETTIT, D. S. BLONDA, and R. A. UPHAM. Can. J. Chem. **43**, 1798 (1965).
13. J. ASHBY, L. A. CORT, J. A. ELVIDGE, and U. EISNER. J. Chem. Soc. C, 2311 (1968).
14. A. W. HOFMANN. Ber. **4**, 262 (1871).
15. R. BEHREND. Ann. **229**, 1 (1885).
16. P. J. BRIGNELL, U. EISNER, and H. WILLIAMS. J. Chem. Soc. 4226 (1965).
17. W. SCHUETT and H. RAPOPORT. J. Am. Chem. Soc. **84**, 2266 (1962).
18. V. AMARNATH and R. MADHAV. Synthesis, 837 (1974).
19. W. HERZ. J. Am. Chem. Soc. **71**, 3982 (1949).
20. R. R. IRINO. Sci. Aerosp. Rep. **3**, 2499 (1965).
21. J. L. WONG, M. S. BROWN, and H. RAPOPORT. J. Org. Chem. **30**, 2398 (1965).
22. V. BOEKELHEIDE and S. S. KERTELJ. J. Org. Chem. **28**, 3212 (1963).
23. J. TAYLOR and D. G. WIBBERLEY. J. Chem. Soc. C, 2693 (1968).
24. T. MELTON, J. TAYLOR, and D. G. WIBBERLEY. Chem. Commun. 151 (1965).

The chromous chloride promoted addition of *N*-haloamides to olefins. III.[1] Scope and limitations for the synthesis of *N*-(2-haloalkyl)amides[2]

HUGHES DRIGUEZ,[3] JOHN M. PATON,[4] AND JEAN LESSARD[5]

Département de chimie, Université de Sherbrooke, Sherbrooke (Qué.), Canada J1K 2R1

Received July 29, 1976

HUGHES DRIGUEZ, JOHN M. PATON, and JEAN LESSARD. Can. J. Chem. **55**, 700 (1977).

A study of the chromous chloride promoted addition of various *N*-chloro- and *N*-bromoamides (ZCONHX) to a variety of olefins shows that two types of addition products can be obtained, namely *N*-(2-haloalkyl)amides (1,2-adducts) which generally predominate and *N*-alkylamides (1,H-adducts). The total yield of addition products, the relative proportion of *N*-(2-haloalkyl)amide(s) and *N*-alkylamide, and the stereochemistry of 1,2-addition to cyclic olefins vary with the *N*-haloamide, that is with both Z and X, and also with the olefin. The best yields of 1,2-adducts were obtained with *N*-chlorocarbamates (Z = *O*-alkyl) and the proper choice of Z (*e.g.*, 2,2,2-trichloroethoxy, benzyloxy) shows the potential of this method for the synthesis of N-protected β-chloro primary amines where the amino group is attached to the less substituted carbon atom. The use of an excess of *N*-haloamide results in high yields (> 90%) of 1,2-addition based on the olefin, the excess of *N*-haloamide being simply reduced to the corresponding amide. *N*-Chloro-*N*-alkylamides (ZCONRCl) do not add to cyclohexene and are simply reduced to the corresponding amides.

HUGHES DRIGUEZ, JOHN M. PATON et JEAN LESSARD. Can. J. Chem. **55**, 700 (1977).

Une étude de l'addition, catalysée par le chlorure chromeux, de divers *N*-chloro- et *N*-bromoamides (ZCONHX) à des oléfines variées montre que deux types de produits d'addition sont possibles, soit des *N*-(halo-2 alkyl)amides (adduits-1,2) qui généralement prédominent, et des *N*-alkylamides (adduits-1,H). Le rendement total en addition, la proportion relative de *N*-(halo-2 alkyl)amide(s) et de *N*-alkylamide, et la stéréochimie d'addition-1,2 aux oléfines cycliques varient avec le N-haloamide selon la nature de Z et X, et avec l'oléfine. De façon générale, les *N*-chlorocarbamates (Z = *O*-alkyle) donnent les meilleurs rendements en addition-1,2 et avec un choix approprié de Z (par exemple un groupement trichloro-2,2,2 éthoxy ou benzyloxy), peuvent servir à la synthèse de β-chloroamines primaires N-protégées dont le groupement amino est fixé à l'atome de carbone le moins substitué. Et utilisant un excès de *N*-haloamide, il est possible d'obtenir d'excellents rendements (> 90%) en addition-1,2 par rapport à l'oléfine car le *N*-haloamide en excès est tout simplement réduit en amide correspondant. Les *N*-chloro-*N*-alkylamides (ZCONRCl) ne s'additionnent pas au cyclohexene et sont simplement réduits en amides correspondants.

Introduction

In the photochemically induced reaction of *N*-haloamides with olefins, the halogen atom can compete with the amido radical. Thus the failure of certain *N*-haloamides (*e.g.* *N*-bromo- and *N*-chloro-*N*-methylacetamide) to add to olefins (3, 4)[6] could be due to the greater reactivity of the halogen atom and not necessarily to the fact that the amido radical would abstract hydrogen in preference to adding to the double bond as proposed by Neale *et al.* (3). This hypothesis led us to study the one-electron reduction of *N*-haloamides by low-valent transition metal salts as a way of producing amido radicals without the concomitant formation of halogen atoms, and to develop a simple and efficient method for adding *N*-haloamides to olefins using chromous chloride. This paper reports a study of the scope and limitations of the method for the synthesis of *N*-(2-haloalkyl)-amides and *N*-protected β-haloamines (Scheme 1). The standard reaction conditions are very mild and the reaction procedure quite simple (see the Experimental). As will be seen, this reaction constitutes a useful alternative and complement to other methods of addition of

[1]References 1 and 2 are to be considered as parts I and II respectively in this series.

[2]Taken in part from the Ph.D. thesis of H. Driguez, Faculté des Sciences, Université de Sherbrooke, 1971.

[3]Arts Council of Canada Predoctorate Fellow, 1969–1971. Present address: Centre de Recherches sur les Macromolécules Végétales. C.N.R.S. B.P. 53. 38041 Grenoble (France).

[4]NRCC Postdoctorate Fellow, 1968–1970.

[5]Author to whom correspondence should be addressed.

[6]D. Touchard and J. Lessard, unpublished results.

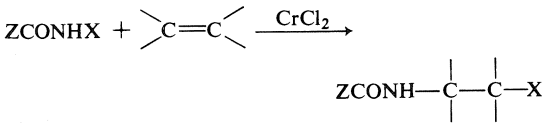

Z = *O*-alkyl, alkyl
X = Cl, Br

SCHEME 1

N-haloamides to olefins (5); namely, the thermal addition of *N*,*N*-dichlorourethane (6–8*b*, 8*c*), the photochemical addition of *N*-chlorourethane (8) and of *N*-chloro- and *N*-bromocarboxamides (4). This reaction constitutes also a novel use for the chromous ion (9, 10).

Additions

Addition of N-Chlorourethane 1a to Cyclohexene (Scheme 2: Z = CH_3CH_2O, X = Cl)

Since it is known that the photochemical addition of *N*-chlorourethane (NCU, **1***a*) to cyclohexene proceeds with a good yield (8*a*), we chose the NCU–cyclohexene system to study the possibility of using a low-valent transition metal salt to initiate the addition of *N*-haloamides to olefins. A cursory investigation of the reduction of NCU by various metal salts in aqueous methanol at *ca.* 0 °C and under an oxygen-free atmosphere (nitrogen or carbon dioxide) showed that Fe(II), Cu(I), and Ti(III)salts were ineffective whereas V(II), Cr(II), and Ti(II) chlorides did reduce NCU as evidenced by changes in color and the complete disappearance of active chlorine. The reduction of NCU by the latter three salts was then carried out under the same conditions but in the presence of cyclohexene (3 mol per mol of NCU). No β-chlorocarbamate was formed with V(II) chloride,[7] a 10% yield of β-chlorocarbamates **2***a* and **3***a* (*cis*:*trans* = 2) was obtained with Ti(II) chloride, and a 42% yield (*cis*:*trans* = 1.9) with Cr(II) chloride. This led us to investigate further the chromous chloride promoted addition of NCU **1***a* to cyclohexene.

The results of this investigation are summarized in Table 1. Besides the *cis* and *trans* β-chlorocarbamates **2***a* and **3***a* (1,2-adducts), the carbamate **4***a* (1,H-adduct)[8] was isolated in small amounts. In the presence of chloroform, which was necessary at −78 °C to maintain an homogeneous solution, higher yields of 1,2-adducts and larger *cis*–*trans* ratios were obtained (compare entries 1 and 3, 2 and 4). The yield of 1,2-adducts and, in the presence of chloroform, the proportion of the *cis* isomer **2***a*, were also increased by lowering the temperature (see entries 1 and 2, and entries 3, 4, and 5). A slow rate of addition of chromous chloride (a lower effective concentration of chromous ions) resulted in a noticeable increase in the yield of **2***a* and **3***a* (compare entries 5 and 6). A fourfold dilution of the reaction mixture and a decrease in the chloroform–methanol voluminal ratio had little effect (compare entries 6 and 7). All the NCU which did not add to cyclohexene was recovered as urethane as seen from the material balance. Bicyclohexenyl was formed in small amounts, but none of the chlorinated products (dichlorocyclohexane, 3-chlorocyclohexene, 4-chlorocyclohexene) which could be expected if chlorine atoms were involved,[9] were detected. The reaction is thus very clean and a very high yield of 1,2-adducts **2***a* and **3***a* (99% based on cyclohexene) was obtained when using an excess of NCU even though the reaction was carried out at −40 °C, in the absence of chloroform, and with a fast rate of addition of chromous chloride (entry 8).

The investigation was extended to include the addition of various *N*-haloamides **1** to cyclohexene (Tables 2 and 3) and then to a variety of olefins (Tables 4 to 8). The reaction conditions were similar to those referred to in Table 1, entry 6, except for the total amount of solvent and relative proportions of chloroform and methanol (see the Experimental).

Addition of N-Chloroamides (1, X = Cl) to Cyclohexene (Scheme 2)

The results of a comparative study of the addition of various *N*-chloroamides to cyclohexene are reported in Table 2. The total yield of addition (**2** + **3** + **4**), the ratio of 1,2-addition (**2** + **3**) to 1,H-addition (**4**), and the *cis* (**2**) – *trans* (**3**) ratio vary with the structure of **Z**: increase of the total yield of addition in the order

[7]In chloroform–methanol at −20 °C, 1.5% of β-chlorocarbamates **2***a* and **3***a* (*cis*:*trans* = 1) was formed according to vapor phase chromatographic (vpc) analysis.

[8]Throughout the paper, the addition products having a hydrogen instead of the halogen at position β will be referred to as the 1,H-adducts. They do not result from reduction of the 1,2-adducts as will be seen.

[9]Dichlorocyclohexane and, in smaller amounts, bicyclohexenyl, 3-chlorocyclohexene, and 4-chlorocyclohexene, are formed in the photochemical decomposition of *N*-chlorocarboxamides and *N*-chlorosuccinimide in the presence of cyclohexene (4*a*,*c*).

TABLE 1. Addition of *N*-chlorourethane **1***a* to cyclohexene (Scheme 2: Z = CH_3CH_2O, X = Cl)

	Reaction conditions					Yield[a] of products					
				Addition of $CrCl_2$[d]							
Entry	**1***a*/olefin (mmol)	$CHCl_3/CH_3OH$ (ml)[b]	T[c] (°C)	(mmol)	(min)	**2***a*+**3***a* (%)	**2***a*/**3***a*	**4***a* (%)	Urethane (%)	Material balance (%)	Bicyclohexenyl (%)
1	2.5/5	0/3.5	0	2.5	5	34	2.0	4	64	102	8[e]
2	2.5/5	0/3	−40	2.5	10	50	1.9	5	45	100	4
3	2.5/5	2.5/1	0	2.5	5	47	3.7	5	42	94	6
4	2.5/5	2.5/1	−40	2.5	10	55	4.9	5	41	101	4
5	2.5/5	2.5/1	−78	2.5	5	63	6.0	7	32	102	2.5
6	5/10	5/1	−78	4.5	70	87	6.7	6	6.5	99.5	<1
7	10/20	25/15	−78	10	90	83	7.8	4	17	104	<1
8	10/5	0/6	−40	9.5	15	99	1.9	2		101	<1

[a]Based on *N*-chlorourethane except in entry 7 where it refers to cyclohexene. Of chromatographically pure products for the 1,2-adducts **2***a* and **3***a*. By vpc for the 1,H-adduct **4***a*, urethane, and bicyclohexenyl.
[b]Amount of solvent before adding the solution of chromous chloride.
[c]Temperature of the cooling bath.
[d]1 *M* methanolic solution. The addition was stopped when all the NCU was consumed (negative starch–iodide paper test).
[e]Small amounts of electrophilic chlorination products were also formed: 2-chloro-1-methoxycyclohexane (3%) and 2-chlorocyclohexanol (1.5%) (yields determined by vpc).

TABLE 2. Addition of *N*-chloroamides (**1**, X = Cl) to cyclohexene (Scheme 2)[a]

	Yield of addition products		
N-Chloroamide	**2**+**3** (%)	**2**/**3**	**4** (%)
$CH_3CH_2OCONHCl$ **1***a*[b]	87	6.7	6[c]
$ClCH_2CH_2OCONHCl$ **1***b*	80	6.5	[d]
$CCl_3CH_2OCONHCl$ **1***c*	85	4.5	[d]
$C_6H_5CH_2OCONHCl$ **1***d*	87	6.5	[d]
$CH_3CONHCl$ **1***e*	34	2.1	36
$ClCH_2CONHCl$ **1***f*	75	2.0	13
$CCl_3CONHCl$ **1***g*	56	1.6	≥2
$CF_3CONHCl$ **1***h*	78	1.5	2.5[c]
$NH_2CONHCl$ **1***i*[e]	57	[f]	[d]

[a]In this and the following tables, unless specified otherwise, the reactions were carried out at −78 °C (cooling bath temperature), 2 mol of olefin per mol of *N*-haloamide were used, the yields are based on the *N*-haloamide and represent yields of isolated chromatographically pure products. The yield of amide was determined in many cases and the balance of material (addition products plus amide) was greater than 95% except when the amide was very soluble in water.
[b]From Table 1, entry 6.
[c]By vpc.
[d]No attempt was made to detect or isolate the 1,H-adduct **4**.
[e]Cooling bath temperature of −55 °C. *N*-Chlorourea **1***i* was insoluble at −78 °C.
[f]The *cis* and *trans* isomers could not be separated completely. The *cis* adduct **2***i* was obtained pure by recrystallization.

$CCl_3 < CH_3 < CF_3 < ClCH_2 <$ *O*-alkyl; increase of the 1,2-adducts – 1,H-adduct ratio in the order $CH_3 < CH_2Cl < OC_2H_5 < CCl_3 \leq CF_3$; and variation of the *cis–trans* ratio in the order $CF_3 \simeq CCl_3 \leq CH_3 \simeq CH_2Cl <$ *O*-alkyl. Thus the best yields of 1,2-adducts **2** and **3** and the highest *cis* (**2**) – *trans* (**3**) ratios were obtained with the *N*-chlorocarbamates **1***a* to **1***d*. The addition of *N*-chloro-2,2,2-trichloroethylcarbamate **1***c* and *N*-chlorobenzylcarbamate **1***d* illustrates the potential of this reaction for the synthesis of

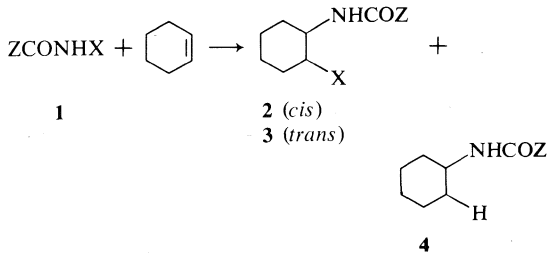

SCHEME 2

N-protected β-chloro primary amines. Treatment of the β-chlorocarbamates **2***c* and **3***c* with zinc dust in acetic acid at 0 °C afforded the pure β-chlorocyclohexylamines *cis* (**5**) and *trans* (**6**), respectively, which were characterized as their *N*-acetyl derivatives **2***c* (11) and **3***c* (12) (90 and 88% yield, respectively). Hydrogenolysis of the β-chlorocarbamate **2***d* followed by acetylation gave the *N*-acetyl derivative **2***c* in a 98% yield.

*Addition of N-Bromoamides (**1**, X = Br) to Cyclohexene (Scheme 2)*

The results are recorded in Table 3. The influence of the structure of Z on the yield of addition products, on the ratio of 1,2-adducts – 1,H-adduct, and on the *cis–trans* ratio is much less important than with the *N*-chloroamides. The *N*-bromoamides gave lower *cis–trans* ratios[10] and a much smaller proportion of 1,H-adduct **4** than the corresponding *N*-chloroamides. Since alkyl bromides should be reduced more easily

[10]Lower *cis–trans* ratios with the *N*-bromoamides as compared to the *N*-chloroamides have also been observed in the photochemical additions to cyclohexene (4*a*).

TABLE 3. Addition of *N*-bromoamides (**1**, X = Br) to cyclohexene (Scheme 2)

N-Bromoamide	Yield of addition products			
	2+**3** (%)	**2**/**3**	**4** (%)	Electrophilic bromination (%)[a]
$CH_3CH_2OCONHBr$ **1***j*	71	1.5	<0.5[b]	26
$ClCH_2CH_2OCONHBr$ **1***k*	77	1.3	[c]	[d]
$CCl_3CH_2OCONHBr$ **1***l*	70	1.4	[c]	20
	85[e]	1.6	[c]	12
$C_6H_5CH_2OCONHBr$ **1***m*	61	1.7	[c]	35
$CH_3CONHBr$ **1***n*	67	1.1	9	2
$ClCH_2CONHBr$ **1***o*	74	1.3	~4[f]	[d]
$CCl_3CONHBr$ **1***p*	66	1.0	[c]	[d]
$CH_3(CH_2)_3CONHBr$ **1***q*	66	1.4	[c]	2

[a]The yields of 2-bromomethoxycyclohexane and 2-bromocyclohexanol were determined by vpc: respectively, 15% and 11% for **1***j*, 2% and 8% with **1***l*, 19% and 16% with **1***m*. No 2-bromocyclohexanol was detected with **1***n* and **1***q*.
[b]By vpc.
[c]Not detected in the chromatographic fractions.
[d]Not determined.
[e]The *N*-bromocarbamate **1***l* was recrystallized from methylene chloride – pentane at *ca.* −40 °C immediately before the reaction. Five moles of cyclohexene per mol of **1***l* were used.
[f]By nmr in a mixture of **4***o* and 2-chloroacetamide.

than alkyl chlorides, the smaller amount of 1,H-adduct **4** with the *N*-bromoamides strongly suggests that this addition product does not arise from reduction of the 1,2-adducts **2** and **3**. Indeed, each of the 1,2-adducts **2***a*, **3***a*, **2***j*, and **3***j* was recovered unchanged after treatment with chromous chloride under the standard reaction conditions. These experiments also show that no *cis–trans* isomerization occurred during the addition reaction. The 1,H-adduct **4** most probably results from Cr(II) reduction of the intermediate β-amidocyclohexyl radical followed by protonolysis of the organochromium derivative. A faster halogen-atom transfer to the radical in the case of the *N*-bromoamides would then account for the smaller proportion of 1,H-addition.[11]

Due to electrophilic bromination, the *N*-bromocarbamates **1***j* to **1***m* gave lower yields of addition than the corresponding *N*-chlorocarbamates **1***a* to **1***d*. This competing ionic process limits the synthetic value of the *N*-bromocarbamates for the preparation of N-protected β-bromo primary amines. When the *N*-bromocarbamate was recrystallized at low temperature (< −40 °C) then dissolved in the cold and the solution used immediately, electrophilic bromination was less important (see **1***l*). We believe the electrophilic brominating species to be the *N*,*N*-dibromocarbamate which would then be partly removed by low temperature recrystallization. *N*-Bromocarbamates have been shown to be in equilibrium with their disproportionation products, [1], ($K \simeq 0.1$ near room temperature) (13). With the *N*-bromocarboxamides which have much less tendency to dismutate (13), electrophilic bromination was almost negligible

[1] $2ROCONHBr \rightleftarrows ROCONBr_2 + ROCONH_2$

and the yields of addition (**2** + **3** + **4**) were more or less comparable to those obtained with the corresponding *N*-chlorocarboxamides.

The addition of *N*-bromopentanoamide **1***q* was studied in order to see if intramolecular hydrogen abstraction in the amido radical could compete significantly with the intermolecular attack on the double bond.[12] It did not since the yield of addition was quite similar to that obtained with *N*-bromoacetamide **1***n*. Furthermore we could not obtain any evidence of the formation of 4-bromopentanoamide. When *N*-bromopentanoamide **1***q* was treated with chromous chloride under the same conditions but in the absence of an olefin, pentanoamide was isolated in a 95% yield. A microanalytical determination of bromine indicated that about 2% of 4-bromopentanoamide could have been formed. Thus

[11]See the accompanying paper for a discussion of the mechanistic aspects.

[12]*N*-Halocarboxamides are known to photochemically rearrange to the 4-halo isomers through a free-radical chain reaction involving an intramolecular hydrogen-atom transfer to the amido radical (3, 14). For example, *N*-bromopentanoamide was reported to yield 37% of 4-bromopentanoamide (3).

intermolecular addition of the pentanoamido radical to cyclohexene is faster than intramolecular hydrogen abstraction which appears to be slower than its chromium(II) reduction.

Additions to 1-Octene, 1-Methylcyclohexene, and Norbornene

The additions to 1-octene (Scheme 3 and Table 4) and to 1-methylcyclohexene (Scheme 4 and Table 5) illustrate the regiospecificity of the reaction. The amido group becomes attached to the less substituted carbon atom as expected if an amido radical is the attacking species. Small amounts of the 1,2-adducts **11** and **12** resulting from the attack on the more substituted carbon atom of 1-methylcyclohexene were isolated in the case of NCU **1***a* and *N*-bromoacetamide **1***n*. They were probably formed also with the other *N*-haloamides but were not isolated. The additions to norbornene (Scheme 5 and Table 6) gave exclusively products having the amido group *exo* in agreement again with the initial attack of an amido radical. Indeed, in free radical additions to norbornene, the initial addition generally occurs from the less hindered *exo* side (8*b*, 15); very few examples of a partial attack from the *endo* side have been reported (16).

With 1-octene (Table 4) and 1-methylcyclohexene (Table 5), the yields of addition products (1,2-addition plus 1,H-addition) were similar to those obtained with cyclohexene and generally somewhat lower than with norbornene (Table 6). In the case of 1-methylcyclohexene, no 1,H-adduct was isolated even with *N*-chloroacetamide **1***e* which gave the highest proportion of 1,H-addition with the other olefins whereas, with

TABLE 4. Addition of *N*-haloamides **1** to 1-octene (Scheme 3)

N-Haloamide	Yield of addition products (%) 7	8
$CH_3CH_2OCONHCl$ **1***a*	85	[a]
$CH_3CONHCl$ **1***e*	28	47[b]
$ClCH_2CONHCl$ **1***f*	64	13
$NH_2CONHCl$ **1***i*[c]	53	[a]
$CH_3CH_2OCONHBr$ **1***j*[d]	81	[a]
$CH_3CONHBr$ **1***n*	62[e]	[a]
$ClCH_2CONHBr$ **1***o*	80	[a]

[a]Not detected by preparative layer chromatography.
[b]By vpc.
[c]Cooling bath temperature of −55 °C. *N*-Chlorourea **1***i* was insoluble at −78 °C.
[d]The *N*-bromourethane **1***j* was recrystallized from methylene chloride – pentane at −60 to −50 °C immediately before the reaction.
[e]Based on the conversion into the oxazoline **38**. The 1,2-adduct **7***n* underwent partial decomposition upon chromatography on silica gel.

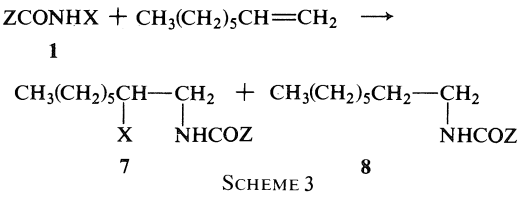

SCHEME 3

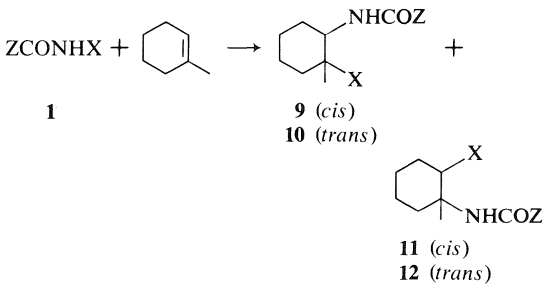

SCHEME 4

TABLE 5. Addition of *N*-haloamides **1** to 1-methylcyclohexene (Scheme 4)

	Yield of addition products 9+10 (%)	9/10	11+12 (%)	11/12
$CH_3CH_2OCONHCl$ **1***a*	80	25	7	3.4[a]
$CH_3CONHCl$ **1***e*	74	6.4	[b]	
$ClCH_2CONHCl$ **1***f*	77	5.5	[b]	
$CH_3CH_2OCONHBr$ **1***j*	75	2.0	[b]	
$CH_3CONHBr$ **1***n*	60	2.0	<5[c]	
$ClCH_2CONHBr$ **1***o*	77	2.5	[b]	

[a]The ratio was determined by vpc. The *trans* isomer **12***a* was not isolated as such (see section entitled Structure of the addition products).
[b]The addition products **11** and **12** could not be isolated by preparative layer chromatography but they were probably formed according to the tlc of the crude reaction product.
[c]A chromatographic fraction contained at least one of the isomers according to the ^1H nmr and mass spectra.

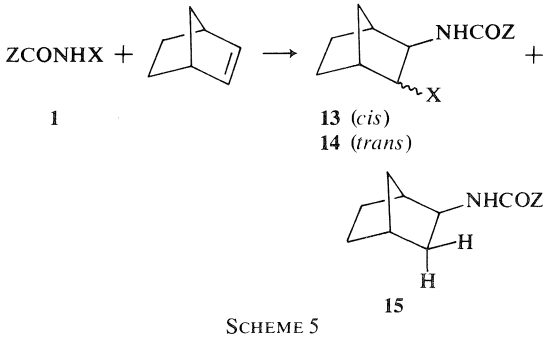

SCHEME 5

1-octene and norbornene, the ratio of 1,2-addition – 1,H-addition did increase with Z in the order $CH_3 < CH_2Cl < OC_2H_5$ as found with cyclohexene. However, norbornene is unique among the mono-olefins studied in leading

TABLE 6. Addition of *N*-haloamides **1** to norbornene (Scheme 5)

N-Haloamide	Yield of addition products: **13+14** (%)	**13/14**	**15** (%)
$CH_3CH_2OCONHCl$ **1***a*	41[a]	5.8	54[a]
$CH_3CONHCl$ **1***e*	1.6	[b]	93
$ClCH_2CONHCl$ **1***f*	33	2.8	55
$CH_3CH_2OCONHBr$ **1***j*	76	1.9	2
$CH_3CONHBr$ **1***n*	91	1.0	4
$ClCH_2CONHBr$ **1***o*	88	1.8	2.5

[a]By vpc.
[b]Only the *cis* isomer **13***e* could be isolated from the chromatographic fractions.

predominantly to 1,H-addition with *N*-chloroamides whereas with *N*-bromoamides, the amount of 1,H-addition was more or less comparable to that obtained with cyclohexene. For instance, *N*-chloroacetamide **1***e* gave 98% of 1,H-addition whereas *N*-bromoacetamide **1***n* gave 4% of 1,H-addition (Table 6). The highest yields of 1,2-addition to 1-octene and 1-methylcyclohexene were obtained with a *N*-chlorocarbamate as was the case in the additions to cyclohexene. Finally, for the 1,2-addition to 1-methylcyclohexene and to norbornene, the *cis–trans* ratios (respectively **9**:**10** and **13**:**14**) were found to vary with Z in the order $CH_3 < CH_2Cl < OC_2H_5$ and to be larger for X = Cl than for X = Br as for the 1,2-addition to cyclohexene. With a given *N*-haloamide, 1-methylcyclohexene led to a larger *cis–trans* ratio than cyclohexene whereas norbornene led to a similar *cis–trans* ratio.

Addition of NCU 1a and N-Bromo-2-chloroacetamide 1o to Conjugated Dienes

The products and yields of addition of these two *N*-haloamides to butadiene and 1,3-cyclohexadiene are given in Table 7. With NCU, no chlorinated products (1,2- or 1,4-adducts) could be detected. The adducts **16***a* and **17***a* from butadiene and **18***a* from cyclohexadiene were most probably formed *via* chromous ion trapping of the corresponding intermediate α-ethoxycarbonylamino allylic radicals. They did not arise from reduction of the allylic chlorides resulting from a 1,2- or a 1,4-addition since 3-chlorocyclohexene was not reduced to a significant extent by excess chromous chloride under similar reaction conditions. Trapping of the 4-ethoxycarbonylaminobutenyl radical occurred with equal ease at both positions 1 and 3 whereas trapping of the 4-ethoxycarbonylaminocyclohexenyl radical occurred predominantly at position 3.

The addition of *N*-bromo-2-chloroacetamide **1***o* to the above conjugated dienes did not give any brominated products. Since bromine-atom transfers are usually faster than chlorine-atom transfers, 1,2- and/or 1,4-adducts could have been expected. However, the exclusive isolation of adducts **16***o* and **17***o* from butadiene, and of adducts **18***o* and **19***o* from cyclohexadiene, does not exclude the formation first of 1,2- and/or 1,4-adducts (allylic bromides). Indeed 3-bromocyclohexene was readily reduced by chromous chloride under the reaction conditions. The formation of a relatively large proportion of **19***o* is noteworthy since the corresponding adduct **19***a* was not isolated.

Addition of N-Chlorocarbamates (1: Z = OR, X = Cl) to Various Mono-olefins

We have seen that among the *N*-haloamides studied, the *N*-chlorocarbamates were the most efficient for the 1,2-addition to simple mono-olefins like cyclohexene, 1-octene, and 1-methylcyclohexene (norbornene being an exception because of the predominant 1,H-addition of *N*-chloroamides). Furthermore, with the proper choice of the carbamate alkyl group (*e.g.* **1***c* R = CH_2CCl_3, and **1***d* R = $CH_2C_6H_5$), a method for synthesizing N-protected β-chloro primary amines, with the amino group attached to the less substituted carbon atom, becomes available. We have thus extended the chromous chloride promoted additions of *N*-chlorocarbamates to a variety of mono-olefins using NCU **1***a* as a representative *N*-chlorocarbamate. The results together with the reaction conditions are recorded in Table 8.

Cyclopentene gave a lower yield of addition (64%), a smaller *cis–trans* ratio (**20**:**21** = 1.56), and a higher proportion of 1,H-addition (**22**) than cyclohexene. Thus with NCU, the 1,2-addition – 1,H-addition ratio decreases in the order cyclohexene (14.5) > cyclopentene (2.6) > norbornene (0.76), which is also the order of increasing ring strain.

The addition to tetramethylethylene is noteworthy since upon photochemical initiation, *N*-chloroamides do not add to tetrasubstituted olefins (4*c*). Dehydrohalogenation of the 1,2-adduct **23** did occur to a small extent during the

TABLE 7. Addition of NCU **1***a* and *N*-bromo-α-chloroacetamide **1***o* to conjugated dienes

		Addition products			
	Diene	Product	Yield (%)	Product	Yield (%)
$C_2H_5OCONHCl$ **1***a*	Butadiene	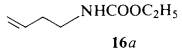 **16***a*	37[a]	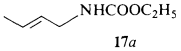 **17***a*	37[a]
	1,3-Cyclohexadiene	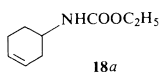 **18***a*	78	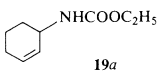 **19***a*	—[b]
$ClCH_2CONHBr$ **1***o*	Butadiene	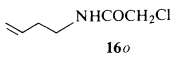 **16***o*	29[a]	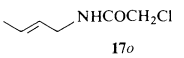 **17***o*	30[a]
	1,3-Cyclohexadiene	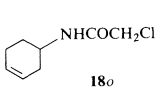 **18***o*	17	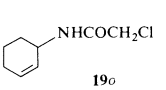 **19***o*	11

[a]By vpc.
[b]Not detected in the chromatographic fractions.

work-up and/or during the chromatographic separation leading to the olefinic derivative **24**.

With styrene, no 1,2-adduct nor 1,H-adduct could be isolated. A complex mixture was obtained consisting most probably of telomers and/or polymers and was not investigated further. The addition of the intermediate β-ethoxycarbonylamino radical (C_6H_5—$\dot{C}H$—CH_2—$NHCOOC_2H_5$) to another styrene molecule was thus faster than its chromous ion reduction and/or its trapping by chlorine-atom transfer.

The additions to pregnenolone acetate illustrate the possibility of obtaining high yields of 1,2-adducts to a more complex and somewhat hindered olefin. The addition is completely regiospecific, the amido group being attached to the less substituted carbon atom (C-6) in both 1,2-adducts **25** and **26**. No 1,H-adduct was detected in the chromatographic fractions. The A and B rings' fusion is *trans* in both adducts indicating that the transfer of chlorine onto the intermediate radical at C-5 occurred from the α-side in order to give the more stable A/B *trans* junction. The predominant formation of the adduct **25** where a 1,3-diaxial interaction exists between the β-amido group at C-6 and the methyl group at C-10, shows the strong preference for the axial attack of the 5,6-double bond by the amido radical. Ponsold and Ihn (17) have studied the photochemical addition of NCU to cholesteryl acetate and to androst-5-en-3β-ol-17-one acetate and have isolated only the corresponding 5α-chloro-6β-ethoxycarbonylamino derivatives (axial attack) in 34% and 9% yield respectively.

Attempts to add NCU to 1-(*N*-piperidino)-cyclohexene were unsuccessful due to rapid electrophilic chlorination. Indeed, the active chlorine disappeared quickly (≤30 s) when NCU was mixed with this enamine in chloroform–methanol at −78 °C and 2-chlorocyclohexanone (34%) was obtained after acid hydrolysis. However, the addition of NCU to the less electron rich 1-methoxycyclohexene, followed by acid hydrolysis, led to a high yield (85%) of the α-ethoxycarbonylamino ketone **27**; no 2-chlorocyclohexanone was detected by vpc. With 1-acetoxycyclohexene, the yield of addition was much lower (43% of ketone **27**). The addition to 1-chlorocyclohexene was still less efficient (27%) giving the 1,2-adduct **28** and the 1,H-adducts **2***a* and **3***a*. The orientation of these additions is again in agreement with the attack of the olefinic system by an amido radical.

The addition of NCU to methyl acrylate and to methyl vinyl ketone gave, in low yields, respectively, the β-ethoxycarbonylamino ester **29** and the β-ethoxycarbonylamino ketone **30** via the more stable carbonyl substituted intermediate radical. No chlorinated products (1,2-adducts) were isolated. Since α-chlorocyclohexanone was not reduced to a significant extent by excess chromous chloride under similar re-

TABLE 8. Addition of *N*-chlorocarbamates (**1**, Z = OR, X = Cl) to various mono-olefins

Olefin	Addition products: Product		Yield (%)	Product		Yield (%)
Cyclopentene		**20** (*cis*)	28[a]		**22**	18[a]
		21 (*trans*)	18[a]			
Tetramethylethylene	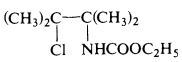	**23**	71	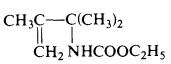	**24**	7
Styrene	[h]					
Pregnenolone acetate[b]	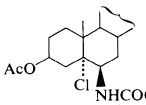	**25***a* (R = C_2H_5)	79	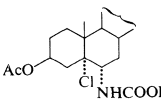	**26***a* (R = C_2H_5)	21
		25*d* (R = $CH_2C_6H_5$)	61		**26***d* (R = $CH_2C_6H_5$)	13
1-(*N*-Piperidino)cyclohexene[c]	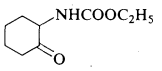	**27**	$2^{a,d}$			
1-Methoxycyclohexene[c]	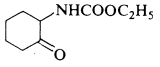	**27**	85 (90)[a]			
1-Acetoxycyclohexene[c]	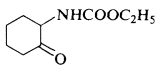	**27**	43 (47)[a]			
1-Chlorocyclohexene	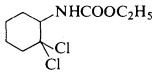	**28**	20[a]	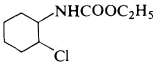	**2***a* (*cis*)	5[a]
					3*a* (*trans*)	4[a]
Methylacrylate	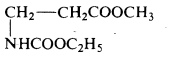	**29**	38[e]			
Methyl vinyl ketone	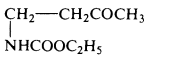	**30**	14[e]	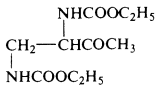	**31**	4[e]
			24[e,f]			24[e,f]
Progesterone[g]	[i]					
1-Octyne	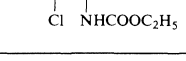	**33**	28	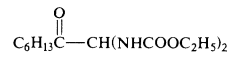	**34**	Traces
			9			13

[a] By vpc.
[b] An excess of *N*-chlorocarbamate was used (2 mol per mol of olefin) and the yields are based on the olefin.
[c] After the addition of $CrCl_2$, dilute H_2SO_4 was added and the reaction mixture was stirred at room temperature for 4 h.
[d] The major product was 2-chlorocyclohexanone (34% by vpc) resulting from electrophilic chlorination.
[e] This represents a minimum yield since the compound underwent partial decomposition upon chromatography on silica gel.
[f] These yields refer to a reaction carried out with an excess of NCU **1***a* (2 mol per mol of methyl vinyl ketone) and are based on the olefin.
[g] Three moles of NCU **1***a* per mol of progesterone were used.
[h] Mixture of telomers and polymers.
[i] No addition product was isolated.

action conditions, the adducts **29** and **30** most probably result from chromous ion reduction of the intermediate carbonyl-substituted radical (1,H-addition). The addition to methyl vinyl ketone led, in addition to the 1,H-adduct **30**, to a small amount of the β-diethoxycarbonylamino ketone **31**. When the reaction was carried out with an excess of NCU, the proportion of compound **31** was increased noticeably. This compound was not formed via the adduct **30** (for

instance by addition on the enol form of **30**) since the latter did not react with an excess of NCU under the conditions used for the additions. One possible route for the formation of **31** would be the radical addition of NCU to the organochromium intermediate **32**, the assumed precursor of **31**. With a more hindered α,β

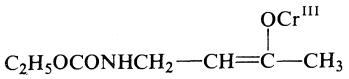

32

unsaturated ketone like progesterone, no addition product could be isolated even if an excess of NCU was used; 90% of unreacted progesterone was recovered.

The addition of NCU to 1-octyne gave a complex mixture from which the 1,2-adduct **33** and the α,α-diethoxycarbonylamino ketone **34** (resulting from the hydrolysis of a two-to-one adduct) were isolated, but in quite different proportions from two different experiments.

Miscellaneous Additions to Cyclohexene

As mentioned in the introduction, *N*-halo-*N*-alkyl amides fail to add to olefins upon photochemical decomposition (3, 4). In order to see if they could be added using the present method, we studied the addition of *N*-chloro-*N*-methyl-2,2,2-trichloroethyl carbamate and *N*-chloro-*N*-methylacetamide to cyclohexene. As indicated in Table 9, no 1,2-adduct nor 1,H-adduct was isolated or even detected; the corresponding amide was isolated in high yields and small amounts (~5%) of bicyclohexenyl were detected.

We investigated also the addition of *N*-chloro- and *N*-bromosuccinimide to cyclohexene; the corresponding *trans* 1,2-adducts **35** and **36** were isolated in low yields (Table 9). These *trans* additions to cyclohexene contrast with the predominance of *cis* addition of the *N*-haloamides **1** (ZCONHX); the bulkiness of the succinimidyl group could be responsible for this preference for *trans* addition.

Finally, the addition of *N*-fluorourethane to cyclohexene gave *N*-cyclohexylurethane (1,H-adduct **4***a*) as the sole addition product albeit in a low yield, the other reaction product being urethane according to vpc analysis (Table 9).

Structure and Stereochemistry of the Addition Products

All the addition products had ir and ^{1}H nmr spectra, an elemental analysis and/or a mass spectrum, consistent with their structure. The protons on the carbons bearing the amido groups are easily identified in the ^{1}H nmr spectra by the narrowing of the signal after N-deuteration; in many cases, the multiplicity of the N—H signal is resolved. The interpretation and analysis of the ^{1}H nmr and ir spectra are quite straightforward and will not be discussed further here. Chemical proofs of structure and stereochemistry are described below.

Whenever possible, known compounds were identified by comparison with samples prepared according to procedures described in the literature. For instance, the 1,H-adducts resulting from the addition to cyclohexene, 1-octene, norbornene, and cyclopentene were prepared from the corresponding amines; the *trans* 1,2-adduct **3***a* was prepared by the addition of *N*,*N*-dichlorourethane to cyclohexene (7); the *cis* and *trans* 1,2-adducts **13** and **14** were obtained from the photochemical addition of NCU **1***a* to norbornene according to the procedure published by Schrage (8*b*) who rigorously established their structure and stereochemistry.

We have already mentioned the following conversions (see section entitled Addition of *N*-chloroamides to cyclohexene): **2***c* (Z = OCH_2CCl_3) to **2***e* (Z = CH_3), **3***c* to **3***e*, **2***d* (Z = $OCH_2C_6H_5$) to **2***e*. The *cis*-β-chlorocarbamate **2***b* (Z = OCH_2CH_2Cl) and the *cis*-β-bromocarbamate **2***l* (Z = OCH_2CCl_3) were converted respectively to **2***e* (74% yield) and **2***n* (41% yield) (Z = CH_3) by zinc dust reduction followed by acetylation: **2***b*, reduction in 80% aqueous acetic acid at *ca.* 80 °C in the presence of excess potassium iodide; **2***l*, reduction in glacial acetic acid at room temperature. The compounds **2***e* (11), **3***e* (12), and **2***n* (11) have been described in the literature.

Pyrolysis of the 2-halo-*N*-ethoxycarbonyl-1-octylamines **7***a* (X = Cl) and **7***j* (X = Br) gave the oxazolidone **37**. The 1,2-adduct **7***e* (Z = CH_3, X = Cl) was converted to the oxazoline **38** by sodium methoxide. Attempts to purify the

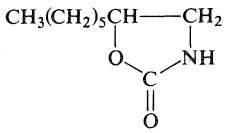

37

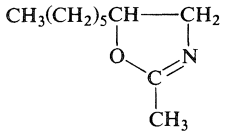

38

1,2-adduct **7***n* (Z = CH_3, X = Br) by microdistillation at 140 °C yielded the hydrobromide of the oxazoline **38**.

TABLE 9. Miscellaneous additions to cyclohexene

	Reaction conditions				Reaction products			
			Addition of $CrCl_2$					
N-Haloamide	>NX/>=< (mmol)	$CHCl_3/CH_3OH/CH_3CN$ (ml)	mmol	h	Addition product	Yield (%)	Recovered amide	Yield (%)
N-Chloro-*N*-methyl-2,2,2-trichloroethyl-carbamate	2.5/10	5/1/0	5	4	None		$CCl_3CH_2OCONHCH_3$	90[a]
N-Chloro-*N*-methyl acetamide	8/20	10/2/0	16	6	None		$CH_3CONHCH_3$	88[a]
N-Chloro-succinimide	5/10	5/2/15[b]	10	2.5	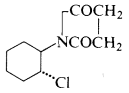 **35**	18	$\overline{CH_2CH_2CONHCO}$	40[c]
N-Bromo-succinimide	5/10	5/2/15[b]	10	2	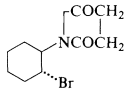 **36**	15	$\overline{CH_2CH_2CONHCO}$	30[c]
N-Fluorourethane	8.9/20	10/2/0	15	5	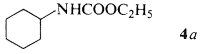 **4***a*	20	$C_2H_5OCONH_2$	[d]

[a]Bicyclohexenyl was also detected (~2 to 5% by vpc).
[b]Bath temperature of −40 °C.
[c]The high solubility of succinimide in water prevented its complete recovery.
[d]Not determined.

The stereochemistry of the *trans* 1,2-adducts **10***a* (X = Cl) and **10***j* (X = Br) (addition to 1-methylcyclohexene) was established by their conversion to the *N*-ethoxycarbonylaziridine **39** with alcoholic potassium hydroxide. Under the same conditions, the *cis* isomers **9***a* and **9***j* were recovered unchanged. With silica gel or silicic acid, the aziridine **39** was converted to the *trans*-β-hydroxycarbamate **40**. The stereochemistry of the other 1,2-adducts **9** and **10** follows from a comparison of their ^{1}H nmr spectra with those of **9***a*, **9***j*, **10***a*, and **10***j*.

39

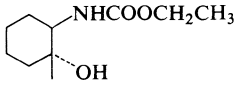

40

In the addition of NCU to 1-methylcyclohexene (Table 5), small amounts of 1,2-adducts **11***a* and **12***a* were isolated as a mixture of both isomers which were not separated as such but were treated with alcoholic potassium hydroxide to afford a mixture of **11***a* and the *N*-ethoxycarbonylaziridine **39**. On silica gel, it gave a mixture of **11***a* and the *trans*-β-hydroxycarbamate **40** which were then easily separated.

The stereochemistry of the *trans* 1,2-adduct **14***j* (Z = OCH_2CH_3, X = Br) (addition to norbornene) was confirmed by its conversion to the oxazolidone **41** (8*b*) upon pyrolysis at 180 °C. The *cis* isomer **13***j* was recovered unchanged under the same conditions.

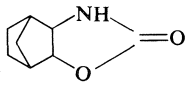

41

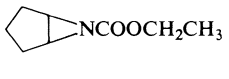

42

The stereochemistry of the 1,2-adducts **20** and **21** (addition to cyclopentene) was established by their treatment with alcoholic potassium hydroxide. The *trans* isomer **21** was converted to the aziridine **42** while the *cis* isomer was recovered unchanged.

The *E* configuration was tentatively assigned to the 1-amido-2-butenes **17** (addition to butadiene, Table 7) on the basis of a strong band at 960–962 cm^{-1} in the ir spectrum (18). The two olefinic protons have nearly the same chemical shifts at 60 MHz.

In the 1,2-adducts **25** and **26** obtained from the addition of *N*-chlorocarbamates to pregnenolone acetate (Table 8), the A/B ring fusion is *trans* (chlorine α at C-5) and the carbamate group at C-6 is respectively β (axial) and α (equatorial) according to ^{1}H and ^{13}C nmr spectroscopy (see the Experimental for the assignment of the ^{13}C chemical shifts). The structural conclusions derived from nmr spectroscopy are confirmed by the chemical transformations summarized in Scheme 6. The aziridine **43***a* was readily formed from **25***a* whereas, under the same reaction conditions, no aziridine was formed from **26***a*. The 3β-alcohol **44** obtained from the adduct **25***a* was oxidized by Jones' reagent under carefully controlled conditions, The 3-ketone **45** was quite labile and was characterized by its ^{1}H nmr spectrum only. Silica gel impregnated with hydrochloric acid, when added to the nmr tube, caused elimination of hydrochloric acid from **45** followed by isomerization of α,β-unsaturated ketone **46** into the more stable epimer **47**: the AB quartet centered at 3.23 ppm ($\Delta\nu_{AB}$ = 21.4 Hz, J_{AB} = 16.5 Hz) due to the protons at C-4 of ketone **45** disappeared gradually while a narrow singlet appeared at 6.10 ppm (no allylic coupling between H-4 and equatorial H-6 in **46**) which then gradually changed to a doublet (J = 1.8 Hz) at 5.99 ppm (allylic coupling between H-4 and H-6 axial in **47**). The oxidation of alcohol **48** (obtained by saponification of the 1,2-adduct **26***a*) again under carefully controlled conditions, gave the labile ketone **49** which was characterized by its ^{1}H nmr spectrum only. Elimination of HCl monitored by nmr in the same conditions as above led directly to the 6α-ethoxycarbonylamino-Δ^4-3-ketone **47**. The latter, when treated with concentrated hydrochloric acid in benzene, gave 5α-pregnane-3,5,20-trione **50** (19).

Summary and Conclusions

The present work shows that two types of adducts can be formed in the chromous chloride promoted addition of *N*-haloamides (ZCONHX) to olefins: *N*-(2-haloalkyl)amides (1,2-adducts) and *N*-alkylamides (1,H-adducts). Their relative proportion depends on the olefin, on the halogen, and on the nature of Z. For instance no 1,H-adduct was isolated from the additions to trisubstituted olefins (1-methylcyclohexene, pregnenolone acetate) whereas with conjugated olefins (methyl acrylate, conjugated dienes) it was the sole addition product(s) obtained: the conjugated dienes led to a mixture of *N*-(2-alkenyl)- and *N*-(3-alkenyl)amides. The additions of *N*-bromoamides to simple mono-olefins usually gave less than 5% of 1,H-adduct but with

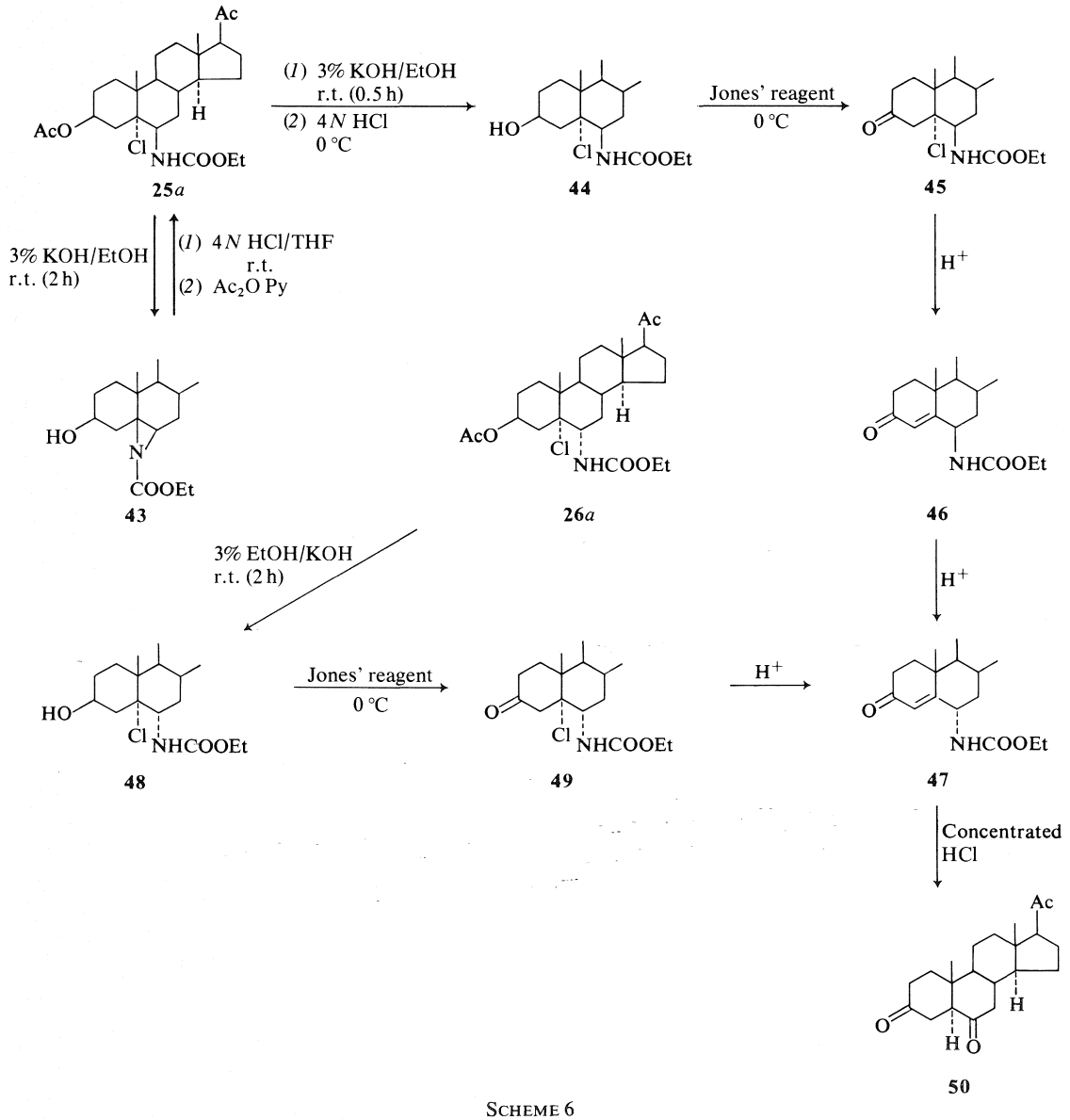

SCHEME 6

certain *N*-chloroamides (*e.g.* *N*-chloroacetamide **1***c*) and olefins, it was the predominant adduct (*e.g.* 64% with 1-octene, 98% with norbornene). On the other hand, the proportion of 1,H-adduct was usually much lower with *N*-chlorocarbamates (Z = *O*-alkyl) than with *N*-chlorocarboxamides (Z = alkyl).

The best yields of 1,2-addition to a variety of olefins were obtained with *N*-chlorocarbamates. The addition of NCU **1***a* to a tetrasubstituted olefin, tetramethylethylene, is noteworthy since no addition was observed upon photochemical initiation.[6] The addition of *N*-chlorocarbamates **1***c* ($Z = OCH_2CCl_3$) and **1***d* ($Z = OCH_2C_6H_5$) shows the potential of the chromous chloride promoted additions for the preparation of N-protected β-chloro primary amines in which the amino group is attached to the less substituted carbon atom of the olefin; the regiospecificity of the additions to unsymmetrical olefins was greater than 90%. With the corresponding *N*-bromocarbamates **1***l* and **1***m*, electrophilic bromination competed with the radical addition to the extent of 20 to 35%, which severely limits

their synthetic value for the preparation of N-protected β-bromo primary amines. *N*-Bromo-2-chloroacetamide **1***o* might be useful for that purpose since the *N*-chloroacetyl group has been reported to be cleaved by thioureas in neutral medium (20). However we did not study its removal in any of the *N*-(2-bromoalkyl)-2-chloroacetamides obtained. *N*-Chlorotrifluoroacetamide could probably be used also for the synthesis of N-protected β-chloro primary amines since its yield of addition to cyclohexene was quite good and the proportion of 1,H-addition small (see Table 2).

We would like to emphasize the fact that, in these additions, all the *N*-haloamide which does not react with the olefin is simply reduced to the amide. Therefore, in the cases where electrophilic halogenation is not a competing process, high yields of addition based on the olefin can be obtained by using an excess of *N*-haloamide and the amide can be recovered (see for instance entry 7 of Table 1 and the addition to pregnenolone acetate in Table 8).

The addition of NCU to electron-poor olefins (*e.g.* 1-chlorocyclohexene, α,β-unsaturated carbonyl compounds) and to 1-octyne was inefficient. With olefins being very rich in electrons (*e.g.* enamines), electrophilic chlorination was faster than the addition. However the addition of NCU to 1-methoxycyclohexene was quite efficient (>85%) and the scope and limitations of the chromous chloride promoted addition of *N*-chloroamides to enol ethers as a method for synthesizing N-protected α-amino acetals (ketones and aldehydes) will be evaluated in a forthcoming paper.

N-Chloro-*N*-alkylamides which do not add to olefins upon photochemical initiation (3, 4) also failed to add to cyclohexene with the present method, but most probably for different reasons. In the photochemical decomposition, the halogen atom might be more reactive than the *N*-alkylamido radical, whereas, with chromous chloride, the reduction of the *N*-alkylamido radical might be faster than its addition to the olefin.

Mechanistic aspects of these chromous chloride initiated reactions are discussed in the accompanying paper in the light of the results presented in this paper, trying the rationalization of them, and in the light of additional experimental facts. We would like to point out here that the reduction of the amido radical competes with its addition to the olefin and that the reduction of the intermediate adduct-radical (leading to 1,H-addition) competes with the chain-propagation step (leading to 1,2-addition). Therefore, the slower the addition of the chromous chloride solution (the smaller the amount of chromous chloride added at a time) the better the yield of 1,2-addition as we have seen (Table 1, entries 5 and 6). However we did not try to optimize the yields of 1,2-addition by allowing the addition of very minute amounts of chromous chloride at a time.

The additions to cyclic olefins have shown that the stereochemistry of 1,2-addition does vary with the halogen, the nature of Z, and the olefin. However, discussion of the stereochemical aspects of these additions must await further investigation and we are currently studying the stereochemistry of the radical addition of *N*-haloamides to cyclic (rigid and non-rigid) as well as acyclic (*E* and *Z*) olefins, comparing chromous chloride promoted additions with photochemically initiated additions.

Experimental[13]

Melting points were determined on a Buchi apparatus and are uncorrected. Infrared spectra were taken on a Perkin-Elmer 257 spectrometer. ^{1}H nmr spectra were recorded on a Varian A-60 spectrometer using TMS as internal reference. ^{13}C nmr spectra were recorded on a Bruker HX-90 spectrometer equipped with a Nicolet 1083 computer for Fourier transform spectroscopy. Mass spectra were taken on a Hitachi RMU-6E spectrometer. Optical rotations were determined on a Perkin-Elmer 141 digital polarimeter at 589 nm. Column chromatography was done using Davison's silica gel No. 923 or 950. Merck silica gel GF_{254} was used for thin and preparative layer chromatography. Vapor phase chromatographic analyses were performed on a Hewlett Packard chromatograph model 5750 equipped with both thermal conductivity and flame ionization detectors; an OS-138 column (15% polyphenyl ether on dimethylsilylated Chromosorb W) with o.d. 0.25 in. and length 6 ft was used unless specified otherwise. Preparative separations were done on a similar column with o.d. 0.375 in. and length 6 ft. Organic phases from extractions were dried over anhydrous sodium sulfate.

N-Haloamides

With the exception of *N*-chlorourea **1***i*, *N*-bromoacetamide **1***n* (commercially available), and *N*-bromo-2,2,2-trichloroacetamide **1***p*, the *N*-haloamides were prepared by the sodium hypohalite method (13).

[13]A few addition products are fully described in the Experimental. For the others, the melting points together with the microanalytical and/or mass spectral data and the ir and ^{1}H nmr characteristic absorptions are available, at a nominal charge, from the Depository of Unpublished Data, CISTI, National Research Council of Canada, Ottawa, K1A 0S2.

N-Chlorourea **1***i* was prepared according to the method described by Chalsty and Israelstam (21). We found that the bath temperature had to be maintained at 0 °C while evaporating the solvent (rotating evaporator) to prevent decomposition. However, when crystalline and dry, *N*-chlorourea **1***a* was stable at room temperature. The crude product (98% active chlorine, 98% yield), mp 74–76 °C (dec.), was used without purification.

N-Bromo-2,2,2-trichloroacetamide **1***p* was prepared according to the method of Park *et al.* (22) and recrystallized from methylene chloride, mp 124–125 °C (100% active bromine, 80% yield).

N-Chloro-*N*-methyl-2,2,2-trichloroethylcarbamate was prepared by treatment of the corresponding carbamate (obtained from methylamine and 2,2,2-trichloroethyl chloroformate and having mp 72–73 °C) in methylene chloride with 5% aqueous sodium hypochlorite at *ca.* 0 °C, followed by extraction with methylene chloride. The crude product contained 96% active chlorine (90% yield) and was used without purification.

N-Chloro-*N*-methylacetamide was prepared by treatment of an aqueous solution of the corresponding amide containing sodium bicarbonate with chlorine followed by extraction with methylene chloride and distillation under reduced pressure: bp 45–46 °C/16 torr (95% active chlorine, 73% yield).

Fluorination of urethane was carried out as described in the literature (23) and was followed by ^{1}H nmr spectroscopy. The reaction was stopped when the ratio of *N*-fluorourethane–urethane did not increase any more and the ratio of *N*-fluorourethane–ethanol reached a maximum. The crude product (90% active fluorine, 40% yield) was used without purification.

General Procedure for the Chromous Chloride Promoted Additions of N-Haloamides to Olefins

The additions were carried out in the apparatus illustrated in Fig. 1 under a stream of dry carbon dioxide or nitrogen. At temperatures below −70 °C, an appreciable amount of carbon dioxide dissolved in the reaction mixture which then became more viscous. A more efficient stirring could be achieved by using nitrogen but most reactions were carried out using carbon dioxide.

From 25 to 75 ml of a 1 *M* methanolic chromic chloride solution (0.2 *N* in HCl, 6.3 *M* in H_2O) (266.5 g of $CrCl_3 \cdot 6H_2O$, 16 ml of concentrated HCl, and absolute methanol[14] in a 1 ℓ volumetric flask) was reduced in flask A by stirring with freshly prepared and dry amalgamated zinc (7 g of zinc dust and 2.6 g of $HgCl_2$). The reduction took 10 to 30 min then the needed amount of the clear blue chromous chloride solution was transferred into the dropping funnel C (containing a small amount of amalgamated zinc) by closing **a** and forcing the inert gas through **b**.

The *N*-haloamide (alternatively the olefin) was dissolved in a chloroform – absolute methanol[14] mixture and the solution was cooled to the desired temperature, usually −78 °C (methanol – dry ice bath), in the reaction vessel B. The olefin (alternatively the *N*-haloamide) in solution in the same solvent was added slowly. In the case

[14]When using ordinary methanol, we could not obtain homogeneous reaction mixtures at −78 °C throughout the addition of the chromous chloride solution with olefins like cyclohexene, 1-octene, norbornene, etc.

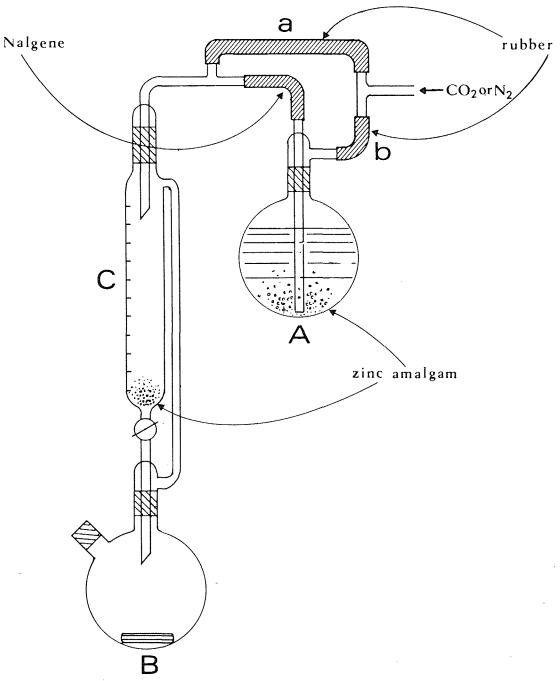

FIG. 1. Apparatus for the chromous chloride promoted addition of *N*-haloamides to olefins.

of the addition of NCU to 1-methoxycyclohexene and for the additions of *N*-bromoamides, the two solutions were cooled to −78 °C before being mixed in order to minimize the extent of electrophilic halogenation. The total amount of solvent as well as the relative proportions of chloroform and methanol had to be varied according to the solubility of the *N*-haloamide and/or the olefin in order to obtain an homogeneous solution at −78 °C; the concentration of the starting solutions varied from 0.3 to 0.9 *M* in *N*-haloamide and the chloroform–methanol voluminal ratio varied from 1.5 to 5. Such variations had little effect on the addition of NCU to cyclohexene (compare entries 6 and 7 of Table 1). The insolubility of *N*-chlorourea **1***i* precluded the use of the general conditions: the reactions were carried out at −55 °C (CCl_4–CH_2Cl_2 – dry ice bath) in chloroform–methanol 1:1.6, the starting solution being 0.1 *M* in **1***i*.

The chromous chloride solution was then added dropwise, at a slow rate (time of addition: 1.5–4 h), with vigorous stirring of the reaction mixture. The addition was stopped either immediately after no more *N*-haloamide was present in the reaction mixture (negative starch–iodide paper test) or, as in most cases, after adding an additional 10% of the chromous chloride solution. The total amount of chromous chloride added varied from 0.9–2.2 mol per mol of *N*-haloamide depending on whether the yield of 1,2-addition (based on the *N*-haloamide) was high (> 85%) or low (< 20%) respectively.

Work-up A

This work up allowed a separation of the 1,2-adduct(s) from the amide and 1,H-adduct. The reaction mixture was poured into a mixture of ice and water (five to ten

times the final volume of methanol) then extracted rapidly with ether in the presence of ice. The organic phases were washed, usually once or twice, with cold water to remove all the chromic salts then dried. The organochromium derivatives which are the precursors of the 1,H-adduct and of the amide (see the accompanying paper) were not extensively hydrolyzed and remained in the aqueous layers. The ether layer contained almost exclusively the 1,2-adduct(s). The 1,H-adduct and the amide were then obtained by continuous extraction of the combined aqueous phases for 24–48 h with methylene chloride.

Work-up B

The reaction vessel B was removed from the apparatus (to allow air to oxidize the chromous ions in excess) and the reaction mixture was allowed to warm up to room temperature after adding water, and kept at room temperature for 30–60 min. It was then thoroughly extracted with methylene chloride or chloroform. The organic layers were washed with water, combined, and dried. The organic phase contained the 1,2-adduct(s), the 1,H-adduct, and the amide. In some cases complete recovery of the amide necessitated a continuous extraction with methylene chloride.

In the case of the addition of NCU to 1-methoxycyclohexene and 1-acetoxycyclohexene (Table 8), the reaction mixture was allowed to warm up to room temperature, dilute H_2SO_4 (1 *N*) was added, and the mixture stirred for 4 h before being extracted with methylene chloride.

The addition products were isolated by preparative layer chromatography, using ether–hexane mixtures, when working on a 5–10 mmol scale as in most cases. Some reactions were carried out on a 25–50 mmol scale and column chromatography followed by preparative layer chromatography was used. The yields of addition products (Tables 1 to 9) represent yields of isolated products homogeneous by tlc. In a few cases the yields were determined by vpc using an authentic sample as standard. The chromatographic fractions were purified by recrystallization or microdistillation for complete characterization.[13] It is noteworthy that in the additions to cyclic olefins, the *cis* 1,2-adduct was always less polar than the *trans* isomer. The 1,2-adducts **11** and **12** (additions to 1-methylcyclohexene, Table 5) were slightly less polar than the *cis* 1,2-adduct **9** and, although their presence could be inferred from the tlc of the crude reaction product, they have been successfully isolated in one instance only: addition of NCU. In the case of the addition of *N*-bromoacetamide **1***n*, a chromatographic fraction less polar than the one containing the *cis* 1,2-adduct **9***n* probably contained, along with some other products, one of the isomeric 1,2-adducts **11***n* or **12***n* according to its ^{1}H nmr and mass spectrum: δ ($CDCl_3$) 1.52 (s, CH_3), 2.02 (s, $COCH_3$), 4.38 (m, CH—Br), 5.57 ppm (br s, NH); *m/e* 233, 235 (relative intensity 1:1, M^+); it was not investigated further.

The yields of amide were determined by vpc or preparative tlc. The material balance, addition products plus amide, was usually quite good (95–102%). The yields of bicyclohexenyl, of 2-halo-1-methoxycyclohexanes, of 2-halocyclohexanols, and of 2-chlorocyclohexanone were determined by vpc using authentic samples as standards. These authentic samples were either available commercially or prepared according to the literature. These compounds were isolated from the crude reaction product by preparative vpc for their complete identification (ir and ^{1}H nmr).

Typical Procedures for the Chromous Chloride Promoted Addition of N-Haloamides to Olefins

(a) Addition of NCU ***1a*** *to Cyclohexene (Excess of Olefin)*

In the reaction vessel B (Fig. 1), NCU (644 mg, 96% active chlorine, 5 mmol) was dissolved in chloroform (3 ml) and absolute methanol (1 ml) and the solution was cooled to *ca.* −78 °C. Cyclohexene (1 ml, ∼10 mmol) in chloroform (2 ml) was added slowly. The 1 *M* chromous chloride solution was then added dropwise until the starch–iodide paper test was negative: 4.5 ml (4.5 mmol) added over 70 min. The reaction mixture was poured into a mixture of ice and water (50 ml) and rapidly extracted with ether (3 × 100 ml) in the presence of ice (work-up A). The ether layer was washed once with cold water (25 ml) then dried. The solution was concentrated and analyzed by vpc: urethane, ∼0.5%; bicyclohexenyl, ∼0.8%; *N*-ethoxycarbonylcyclohexylamine **4***a* ∼0.5%; *cis* adduct **2***a*, 77%; *trans* adduct **3***a*, 11%. The solvent was removed *in vacuo* and the crude product (964 mg) separated by preparative layer chromatography (ether–hexane 1:3) to afford two main fractions. The less polar fraction consisted of *cis-2-chloro-N-ethoxycarbonylcyclohexylamine* **2***a*, mp 52–54 °C (782 mg, 76%). Two recrystallizations from pentane afforded the analytical sample, mp 57.5–58 °C (lit. (8*a*) 58 °C); ν_{max} (CCl_4) 3458 and 3350 (free and bonded NH), 1721 (C=O), 1505 (NH), 1220 and 1050 (C—O—C), 688 cm^{-1} (C—Cl axial (24)); δ ($CDCl_3$) 1.21 (t, J = 7 Hz, OCH_2CH_3), 3.81 (m, $\Delta\nu_{1/2}$ = 22 Hz, $\Delta\nu_{1/2}$ = 14 Hz after exchange with D_2O, H_1), 4.48 (q, J = 2.6 Hz, H_2), 4.11 (q, J = 7 Hz, OCH_2CH_3), 4.95 ppm (br d, J = 8 Hz, NH); *m/e* 205, 207 (3:1 ,M^+). *Anal.* calcd. for $C_9H_{16}ClNO_2$: C 52.55, H 7.84, Cl 17.24; found: C 52.35, H 7.73, Cl 17.12.

The other fraction (117 mg, 11%) consisted of *trans-2-chloro-N-ethoxycarbonylcyclohexylamine* **3***a*, mp 91–92 °C. It was recrystallized from ether–hexane for analysis, mp 93.5–94 °C (lit. (7) 96 °C); ν_{max} (CCl_4) 3460 and 3355 (free and bonded NH), 1722 (C=O), 1505 (NH), 1225, 1045, 1055 cm^{-1}; ν_{max} (CS_2) 737 cm^{-1} (C—Cl equatorial (24)); δ ($CDCl_3$) 1.25 (t, J = 7 Hz, OCH_2CH_3), 3.70 (m, $\Delta\nu_{1/2}$ ∼ 30 Hz, H_1 and H_2), 4.13 (q, J = 7 Hz, OCH_2CH_3), 4.95 (br, NH). *Anal.* calcd. for $C_9H_{16}ClNO_2$: Cl 17.24; found: Cl 17.19. It proved identical (ir, ^{1}H nmr) to an authentic sample prepared by addition of *N,N*-dichlorourethane to cyclohexene (7).

The aqueous phases from the ether extraction were combined and extracted with methylene chloride for 48 h. The organic phase was dried. The solution was concentrated and analyzed by vpc: urethane, 6%; *N-ethoxycarbonylcyclohexylamine* **4***a*, 5.5%. The products were then separated by preparative layer chromatography (ether–hexane 1:1) and proved identical (mixture mp, ir) with authentic specimens (**4***a* was prepared from cyclohexylamine and ethyl chloroformate): **4***a*, mp 53–54 °C (lit. (25) 55–56 °C); ν_{max} ($CHCl_3$) 3450 (NH), 1715 (C=O), 1515 (NH), 1230, 1060 cm^{-1} (doublet).

(b) Addition of NCU ***1a*** *to Pregnenolone Acetate (Excess of Amide)*

In the reaction vessel B (Fig. 1), a solution of pregnenolone acetate (8.96 g, 25 mmol) in chloroform

(35 ml) and absolute methanol (20 ml) was cooled to *ca.* −78 °C. A solution of NCU (8.4 g, 88% active chlorine, 60 mmol) in chloroform (15 ml) was added slowly. The 1 *M* chromous chloride solution was added dropwise until a negative starch–iodide paper test: 100 ml (100 mmol) added over 4 h (the product began to precipitate after about 60 ml of the $CrCl_2$ solution was added). The reaction mixture was allowed to warm up to room temperature while adding water (500 ml) then extracted with chloroform (5 × 100 ml) (work-up B). The organic phases were washed once with water, then collected and dried. The crude product was recrystallized from chloroform–ether to yield 8.77 g (73%) of *3β-acetoxy-5α-chloro-6β-ethoxycarbonylamino-pregnane-20-one* **25***a*, mp 200–202 °C. Recrystallization from ethanol afforded the analytical sample, mp 201–203 °C; $[\alpha]_D^{20}$ −20° (*c* 1.0, $CHCl_3$); ν_{max} ($CHCl_3$) 3455 (NH), 1726 (carbamate and ester), 1704 (ketone), 1505 (carbamate), 1250 and 1034 cm^{-1} (carbamate and ester); ^1H nmr ($CDCl_3$) 0.65 (s, 18-CH_3), 1.23 (s, 19-CH_3), 1.25 (t, J = 7 Hz, OCH_2CH_3), 2.02 (s, 20-CH_3), 2.10 (s, $OCOCH_3$), 4.13 (q, J = 7 Hz, OCH_2CH_3), 4.20 (m, $\Delta\nu_{1/2}$ < 20 Hz, H-6 equatorial), 4.90 (br d, J = 10 Hz, NH), 5.33 ppm (m, $\Delta\nu_{1/2}$ = 30 Hz, H-3 axial); ^{13}C nmr ($CDCl_3$) 13.7 (C-18) 14.6 (OCH_2CH_3), 18.9 (C-19), 21.3 (C-11 and $OCOCH_3$), 22.9 (C-15), 24.3 (C-16), 26.5 (C-2), 31.1 (C-8), 31.5 (C-21), 32.2 (C-7), 34.2 (C-1), 37.8 (C-4), 38.8 (C-12), 40.2 (C-10), 44.3 (C-13), 45.9 (C-9), 55.8 (C-6 and C-14), 61.3 (OCH_2CH_3), 63.6 (C-17), 70.6 (C-3), 83.5 (C-5), 156.1 ($-\overset{O}{\overset{\|}{C}}OCH_2CH_3$), 170.1 ppm ($O\overset{O}{\overset{\|}{C}}CH_3$) downfield TMS.[15] *Anal.* calcd. for $C_{26}H_{40}O_5NCl$: C 64.78, H 8.36, Cl 7.36; found: C 64.60, H 8.25, Cl 7.31.

The mother liquors were evaporated to dryness (4 g) and separated by column chromatography on silica gel and then preparative layer chromatography to yield, in order of decreasing polarity, 0.75 g of urethane, an additional 0.73 g (total, 9.50 g, 79%) of *1,2-adduct* **25***a*, mp 196–198 °C, and 2.55 g (21%) of *3β-acetoxy-5α-chloro-6α-ethoxycarbonylamino-pregnane-20-one* **26***a*, mp 112–115 °C. The analytical sample was obtained after two recrystallizations from ether–hexane, mp 117–119 °C; $[\alpha]_D^{20}$ + 34.6° (*c* 0.3, $CHCl_3$); ν_{max} ($CHCl_3$) 3440 (NH), 1720 (carbamate and ester), 1704 (ketone), 1250 and 1046 cm^{-1} (carbamate and ester); ^1H nmr ($CDCl_3$) 0.62 (s, 18-CH_3) 1.18 (s, 19-CH_3), 1.23 (t, J = 7 Hz, OCH_2CH_3), 2.02 (s, $COCH_3$), 2.10 (s, $OCOCH_3$), 4.05 (m, $\Delta\nu_{1/2}$ = 30 Hz, H-6 axial), 4.11 (q, J = 7 Hz, OCH_2CH_3) 4.88 (br d, J = 10 Hz, NH), 5.23 (m, $\Delta\nu_{1/2}$ = 32 Hz, H-3 axial); ^{13}C nmr ($CDCl_3$) 13.5 (C-18), 14.6 (OCH_2CH_3), 16.4 (C-19), 21.3 (C-11 and $OCOCH_3$), 22.9 (C-15), 24.1 (C-16), 26.2 (C-2), 31.6 (C-7 and C-21), 34.0 (C-1 and C-8), 36.6 (C-4), 38.7 (C-12), 41.5 (C-10), 44.1 (C-13), 45.5 (C-9), 52.4 (C-6), 55.8 (C-14), 61.0 (OCH_2CH_3), 63.4 (C-17), 70.0 (C-3), 87.8 (C-5), 156.1 ($COOCH_2CH_3$), 170.2 ppm ($OCOCH_3$) downfield from TMS.[15] *Anal.* calcd. for $C_{26}H_{40}O_5NCl$: C 64.78, H 8.36, Cl 7.36; found: C 64.67, H 8.57, Cl 7.26.

Chromous Chloride Reduction of N-Bromopentanoamide ***1q***

To a solution of *N*-bromopentanoamide (1.45 g, 90% active bromine, 7.27 mmol) in chloroform (5 ml) and absolute methanol (1 ml) cooled in a dry ice – methanol bath (*ca.* −78 °C) (see Fig. 1), the 1 *M* chromous chloride solution was added slowly: 18 mmol added over 5 h. Work-up B gave pentanoamide (862 mg, 95% by taking into account the 145 mg present in the starting material), mp 100–102 °C, identified by comparison to an authentic sample by ir and ^1H nmr spectroscopy. The crystals were ground in a mortar then dried under vacuum. A microanalytical determination of bromine gave 1.18% which could be due to the presence of some (< 2%) 4-bromopentanoamide.

Chromous Chloride Reduction of 3-Chloro- and 3-Bromocyclohexene, and 2-Chlorocyclohexanone

3-Chlorocyclohexene

A solution of 3-chlorocyclohexene (820 mg, 8.4 mmol) in chloroform (8 ml) and absolute methanol (3 ml) was cooled to *ca.* −78 °C in the reaction vessel B (Fig. 1). The 1 *M* chromous chloride solution was added slowly: 10 mmol added over 70 min. The reaction mixture remained blue during most of the addition; it turned slightly green (turquoise) towards the end of the addition indicating that no extensive reduction of 3-chlorocyclohexene had occurred. The reaction vessel was removed from the apparatus and the reaction mixture allowed to warm up to room temperature during which it became dark green. Water (50 ml) was added and the mixture was stirred at room temperature overnight. It was extracted with ether and analyzed by vpc on a SE-30 column (10% on dimethylsilylated Chromosorb W) for the dosage of cyclohexene (22%) and on the OS-138 column for the dosage of 3-methoxycyclohexene (16%), 3-chlorocyclohexene (42%), and 3-hydroxycyclohexene (25%). The products were isolated by preparative vpc for complete identification (ir and ^1H nmr).

3-Bromocyclohexene

The reaction was carried out as above except that the mixture was stirred at room temperature for 90 min after adding water. The chromous chloride solution turned green as soon as it touched the reaction mixture indicating that 3-bromocyclohexene was reduced at *ca.* −78 °C. Analysis of the crude product by vpc (SE-30 and OS-138 columns) showed that no 3-bromocyclohexene was left. However the yield of cyclohexene was 67% only, which could probably be explained by the fact that hydrolysis of the organochromium derivative was not complete after 90 min.

2-Chlorocyclohexanone

The reaction was carried out as described for 3-chlorocyclohexene except that the mixture was stirred at room temperature for 45 min after the addition of water. The reaction mixture remained blue throughout the addition indicating that no extensive reduction had occurred at *ca.* −78 °C. It turned dark green when allowed to warm up to room temperature. The product was analyzed by vpc (OS-138 column): 73% of 2-chlorocyclohexanone and 24% of cyclohexanone.

The formation of cyclohexene (22%) with 3-chlorocyclohexene and of cyclohexanone (24%) with 2-chloro-

[15]We thank Professor J. K. Saunders for the interpretation of the ^{13}C nmr spectra. The chemical shifts of ring A and B carbons, and in particular of C-3, C-5, C-6, C-8, and C-19, are in complete agreement with the structure and stereochemistry of the isomeric 1,2-adducts **25***a* and **26***a*.

cyclohexanone indicate that some reduction did occur despite the fact that the reaction mixture remained blue. The reduction probably occurred during the warming up of the reaction mixture· the diffusion of air into the reaction mixture being slow enough to allow chromous ions to be present at higher temperatures.

Removal of the Trichloroethoxycarbonyl Group

cis-β-Chlorocarbamate 2c

The adduct **2***c* (309 mg, 1 mmol) was treated with freshly activated zinc dust (300 mg) in glacial acetic acid (5 ml) at room temperature for 60 min. The reaction mixture was made strongly alkaline with an ice-cold 4 *N* NaOH solution then extracted with ether. The ether layer was dried and the solvent removed on a rotating evaporator to yield *cis-2-chlorocyclohexylamine* **5** (132 mg) as a liquid: ν_{max} ($CHCl_3$) 3400 and 3330 cm^{-1} (NH_2); δ ($CHCl_3$) 2.90 (m, $\Delta\nu_{1/2} \simeq 26$ Hz, H_1 axial) and 4.35 ppm (m, $\Delta\nu_{1/2} = 11$ Hz, H_2 equatorial). It was acetylated in the usual way, Ac_2O (0.5 ml) in pyridine (1 ml), to give *cis-2-chloro-N-acetylcyclohexylamine* **2***e* (158 mg, 90%), mp 95–96 °C (lit. (17) 88 °C). It proved identical (ir, ^1H nmr) to the *cis* 1,2-adduct **2***e* obtained from *N*-chloroacetamide **1***e* and cyclohexene.

trans-β-Chlorocarbamate 3c

The reduction (216 mg, 0.7 mmol) carried out as above gave, after acetylation of the crude β-chloroamine **6** (88 mg), *trans-2-chloro-N-acetylcyclohexylamine* **3***e* (108 mg, 88%) mp 128–130 °C (lit. (12) mp 129–130 °C) which proved identical (ir, ^1H nmr) to the *trans* 1,2-adduct **3***e* obtained from *N*-chloroacetamide **1***e* and cyclohexene.

cis-β-Bromocarbamate 2l

The reduction (291 mg, 0.8 mmol) as above gave, after acetylation of the crude amine (103 mg) followed by preparative layer chromatography (ether–hexane 4:1), *cis-2-bromo-N-acetylcyclohexylamine* **2***n* (73 mg 41%), mp 97.5–99 °C (lit. (11) 103–104 °C). It proved identical (ir, ^1H nmr) with the *cis* 1,2-adduct **2***n* obtained from *N*-bromoacetamide **1***n* and cyclohexene.

Reduction of the cis-β-Chlorocarbamate 2b (Z = OCH_2CH_2Cl)

The β-chlorocarbamate **2***b* (480 mg, 2 mmol) was treated with freshly activated zinc dust (1.2 g, added in portions of 200 mg every 2 h) and potassium iodide (1.33 g, 8 mmol) in 80% aqueous acetic acid (16 ml) at 80 °C for 16 h. The reaction mixture was cooled to 0 °C then made strongly alkaline with 4 *N* NaOH. It was extracted with methylene chloride. The organic phase was dried and the solvent removed at the rotating evaporator. The crude product was acetylated in the usual way to give, after recrystallization of the residue (345 mg), *cis-2-chloro-N-acetylcyclohexylamine* **2***e* (211 mg), mp 95–96.5 °C, which proved identical (ir, ^1H nmr) with an authentic sample.

The mother liquors (130 mg) were separated by preparative layer chromatography to yield an additional amount (63 mg) of the *cis-β-chloroamide* **2***e*, mp 96.5–97.5 °C (total amount 274 mg, 78% yield). A more polar oily fraction (15 mg) contained *cis-2-chloro-N-(2-acetoxyethoxycarbonyl)cyclohexylamine* according to the following spectral data: ν_{max} (CCl_4) 3440 and 3360 (free and bonded NH), 1735 (br and vs, ester and carbamate), 1505 (carbamate), 1240 (vs) and 1060 (ester and carbamate), 685 cm^{-1} (C-Cl ax. (24)); δ (CCl_4) 2.00 (s, $COCH_3$), 3.67 (m, $\Delta\nu_{1/2} = 18$ Hz, H_1 ax.), 4.15 (s, OCH_2CH_2O), 4.43 (q, $J = 3$ Hz, H_2 eq.), 5.07 (br d, $J = 8$ Hz, NH).

Hydrogenolysis of cis-2-Chloro-N-benzyloxycarbonylcyclohexylamine 2d

A solution of the *cis*-β-chlorocarbamate **2***d* (321 mg, 1.2 mmol) in 95% ethanol (90 ml) was hydrogenated over 30% palladium-on-charcoal at atmospheric pressure until no more carbon dioxide was produced (3 h). The catalyst was filtered and the solvent was evaporated to yield *cis-2-chlorocyclohexylamine* **5** (165 mg, quantitative) identified by ir and ^1H nmr spectroscopy. Acetylation in the usual way led to *cis-2-chloro-N-acetylcyclohexylamine* **2***e* (206 mg, 98%), mp 96–97 °C, identical (ir and ^1H nmr) to an authentic specimen.

5-(1-Hexyl)-2-oxazolidone 37

Pyrolysis of 2-Chloro-N-ethoxycarbonyl-1-octylamine 7a

The β-chlorocarbamate **7***a* (670 mg, 2.84 mmol) was heated at 185 °C under nitrogen for 3 h to give the *oxazolidone* **37**, mp 87–88 °C (486 mg, quantitative). The analytical sample (recrystallization from ether) had mp 88 °C; ν_{max} ($CHCl_3$) 3480 (NH), 1750 (C=O), 1240 and 1075 cm^{-1} (C—O—C); δ ($CDCl_3$) 3.20 and 3.70 (two t, $J = 8$ Hz, H-4), 4.58 (q, $J = 8$ Hz, H-5), 6.90 (s, NH); *m/e* 171 (M^+). *Anal.* calcd. for $C_9H_{17}NO_2$: C 63.15, H 10.01, N 8.19; found: C 62.90, H 9.98, N 8.19.

Pyrolysis of 2-Bromo-N-ethoxycarbonyl-1-octylamine 7j

The β-bromocarbamate **7***j* (400 mg, 1.43 mmol) was heated at 185 °C under nitrogen for 2 h to give, after treatment of the black residue with activated charcoal, the *oxazolidone* **37**, mp 87–88 °C (171 mg, 70%) identical (ir, ^1H nmr) with the above sample.

5-(1-Hexyl)-2-methyl-2-oxazoline 38

From 2-Chloro-N-acetyl-1-octylamine 7e

The β-chloroamide **7***e* (170 mg, 0.83 mmol) was treated with sodium methoxide in absolute methanol (18 mg of sodium and 2 ml of methanol) at 60 °C for 10 h. The reaction mixture was evaporated to dryness. The residue was dissolved in methylene chloride and washed with brine. The organic phase was dried and the solvent evaporated to give the *oxazoline* **38** as a liquid (137 mg, 97%), ν_{max} (CCl_4) 1725 (C=N), 1438 (CH_2—N), and 1230 cm^{-1} (C—O—C); δ (CCl_4) 1.81 (t, $J = 1.3$ Hz, CH_3), 3.50 (m, H-4), and 4.40 ppm (H-5); *m/e* 169 (M^+). It was further characterized as the hydrobromide derivative, mp 71–72 °C (ether); ν_{max} ($CHCl_3$) 2400–3000 cm^{-1} (very broad); δ ($CDCl_3$) 2.62 (m, CH_3), 3.95 and 4.50 (respectively d of d, $J \sim 8$ and 9 Hz, and t, $J \sim 9$ Hz, H-4), 5.40 ppm (m, H-5). *Anal.* calcd. for $C_{10}H_{20}BrNO$: C 48.00, H 8.05, Br 31.94, N 5.60; found: C 48.02, H 7.86, Br 32.70, N 5.56.

From 2-Bromo-N-acetyl-1-octylamine 7n

Attempts to purify the β-bromoamide **7***n* by microdistillation at 140 °C/0.01 torr resulted in its conversion to the *hydrobromide of the oxazoline* **38**, mp 69–70 °C, identical (ir, ^1H nmr) to the sample obtained above.

Alternatively the crude product from the addition of *N*-bromoacetamide **1***n* (8.7 mmol) to 1-octene (20 mmol), work-up A, was treated with sodium methoxide as described above to yield the *oxazoline* **38** (913 mg, 62%) identical (ir, ^1H nmr) to the sample obtained above. The

yield of **38** was taken as the yield of 1,2-adduct **7***n* assuming that its conversion to the oxazoline was quantitative.

1-Methyl-7-aza-7-ethoxycarbonylbicyclo[4.1.0]heptane ***39***

From trans-2-Chloro-2-methyl-N-ethoxycarbonylcyclohexylamine ***10a***

A solution of the *trans*-β-chlorocarbamate **10***a* (180 mg, 0.82 mmol) and potassium hydroxide (69 mg, 1.2 mmol) in 95% ethanol (10 ml) was heated to reflux for 1 h, then poured into cold water (25 ml) and extracted with ether (3 × 25 ml). After drying and evaporating the solvent, the residue was filtered on activity III neutral alumina to yield the *N-ethoxycarbonyl aziridine* **39** as a liquid (113 mg, 75%). The analytical sample was obtained by microdistillation at 64–65 °C/2.4 torr; ν_{max} (CCl_4) 1725 (C=O), 1260, 1100, 1035 cm^{-1}; δ ($CDCl_3$) 1.26 (superimposed s and t with J = 7.0 Hz, C—CH_3 and OCH_2CH_3), 2.50(t, J = 3.5 Hz, H-2), 4.20 ppm (q, J = 7.0 Hz, OCH_2CH_3). *Anal.* calcd. for $C_{10}H_{17}NO_2$: C 65.54, H 9.35, N 7.64; found: C 65.75, H 9.46, N 7.93.

The filtration on alumina removed the free aziridine (NH) resulting from partial cleavage of the *N*-ethoxycarbonyl group of **39**. The free aziridine was not recovered.

From trans-2-Bromo-2-methyl-N-ethoxycarbonylcyclohexylamine ***10j***

The *trans*-β-bromocarbamate **10***j* (150 mg, 0.56 mmol) was treated with alcoholic potassium hydroxide (1.7 mmol in 10 ml) at 50 °C for 45 min. Work-up as above gave the *aziridine* **39** (85 mg, 82%) identical (ir, ^1H nmr) to the sample obtained above. Again partial cleavage of the *N*-ethoxycarbonyl group of **39** occurred.

trans-2-Hydroxy-2-methyl-N-ethoxycarbonylcyclohexylamine ***40***

The aziridine **39** (85 mg, 0.46 mmol) in ether (10 ml) was stirred with silicic acid (1 g) for 16 h at room temperature. The mixture was filtered and the solids washed with ether–methanol 9:1. Evaporation to dryness gave the *trans-β-hydroxycarbamate* **40**, mp 109–111 °C (114 mg, quantitative). Recrystallization from methylene chloride–ether gave the analytical sample, mp 110–111 °C; ν_{max} ($CHCl_3$) 3590 (free OH), 3450 (free NH), 3430 (broad, bonded OH and NH), 1703 (bonded C=O), 1510 cm^{-1} (NH); δ ($CDCl_3$) 1.14 (s, CH_3), 1.24 (t, J = 7 Hz, OCH_2CH_3), 3.46 (br s, OH), 3.58 (m, $\Delta\nu_{1/2} \sim 25$ Hz, H-1), 4.20 (q, J = 7 Hz, OCH_2CH_3) 5.10 ppm (br d, J = 7.5 Hz, NH).

*Treatment of a Mixture of cis- and trans-2-Chloro-1-methyl-N-ethoxycarbonylcyclohexylamines (**11a** and **12a**) with Alcoholic Potassium Hydroxide*

The mixture of *cis*- and *trans*-β-chlorocarbamates **11***a* and **12***a* (386 mg, 1.75 mmol) was obtained from the chromatographic separation of the crude product from the addition of NCU (25 mmol) to 1-methylcyclohexene (50 mmol), the **11***a*–**12***a* ratio being 3.4 according to vpc analysis (see Table 5). A solution of this mixture and potassium hydroxide (202 mg, 3.6 mmol) in 95% ethanol (40 ml) was heated to reflux for 20 min. The usual work up gave a mixture of the *cis*-β-chlorocarbamate **11***a* and the aziridine **39** according to vpc analysis. It was put on a silica gel plate (1.5 mm thick) and kept at room temperature for 22 h. Elution with ether–hexane 1:2 gave two main fractions. The less polar fraction consisted of *cis-2-chloro-1-methyl-N-ethoxycarbonylcyclohexylamine* **11***a*, liquid (289 mg, 1.32 mmol). The analytical sample was obtained by microdistillation at 75 °C/0.12 torr; ν_{max} (CCl_4) 3420 (free NH), 1730 (C=O), 1505 (NH), 1230 and 1100 (C—O—C), 729 cm^{-1} (C—Cl ax. (24)); δ ($CDCl_3$) 1.28 (t, J = 7.0 Hz, OCH_2CH_3), 1.51 (s, CH_3), 4.17 (m which narrowed on D_2O exchange, H-2), 4.21 (q, J = 7.0 Hz, OCH_2CH_3), 5.03 ppm (br s, NH). *Anal.* calcd. for $C_{10}H_{18}ClNO_2$: C 54.67, H 8.26, Cl 16.14, N 6.38; found: C 54.89, H 8.09, Cl 16.32, N 6.57.

The more polar fraction was identical (mixture mp, ir, ^1H nmr) to the *trans*-β-hydroxycarbamate **40**, mp 109–110 °C (60 mg, 0.30 mmol).

The free aziridine resulting from the cleavage of the *N*-ethoxycarbonyl group was not recovered.

Oxazolidone ***41***

The *trans*-β-bromocarbamate **14***j* (70 mg, 2.3 mmol) was heated at 180 °C for 3 h under nitrogen. The brown residue was treated with activated charcoal to yield the *oxazolidone* **41** (26 mg, 63%), mp 133–134 °C (lit. (8*b*) 136–137 °C); ν_{max} ($CHCl_3$) 3470 and 3260 (free and bonded NH), 1750 (C=O), 1240 and 1050 cm^{-1} (C—O—C); δ ($CDCl_3$) 2.22 and 2.47 (m's bridgehead protons), 3.66 (d, J = 7 Hz, H-2), 4.48 (d, J = 7 Hz, H-3) 5.75 (br s, NH).

Under the same conditions, the *cis* isomer **13***j* was recovered unchanged.

N-Ethoxycarbonyl Aziridine ***42***

A solution of *trans*-2-chloro-*N*-ethoxycarbonylcyclopentylamine **21** (192 mg, 1 mmol) and potassium hydroxide (180 mg, 3 mmol) in 95% ethanol (20 ml) was heated to reflux for 10 min then poured into cold water and extracted with ether. The ether layer was dried then distilled. The residue was passed through a small column of activity III alumina with ether–hexane 1:1 to remove the free aziridine resulting from the cleavage of the *N*-ethoxycarbonyl group. The *N-ethoxycarbonyl aziridine* **42** (74 mg, 51%) was purified further by microdistillation at 83–85 °C/21 torr; ν_{max} (CCl_4) 1725 (C=O), 1275, 1190, 1105 cm^{-1}; δ ($CDCl_3$) 1.27 (t, J = 7.0 Hz, OCH_2CH_3), 2.91 (narrow m, $\Delta\nu_{1/2}$ = 3 Hz, H-1 and H-2), 4.10 (q, J = 7.0 Hz, OCH_2CH_3). *Anal.* calcd. for $C_8H_{13}NO_2$: C 61.93, H 8.38, N 9.03; found: C 61.75, H 8.38, N 9.21.

Under these conditions, the *cis* isomer **20** was recovered unchanged.

Steroidal Aziridine ***43a***

The *trans* 1,2-adduct **25***a* (1.0 g, 2.1 mmol) was suspended in a solution of potassium hydroxide (1.5 g) in ethanol (20 ml) and water (30 ml). After 2 h at room temperature, all the starting material had reacted (tlc). The reaction mixture was poured into water (200 ml) and extracted with methylene chloride. The organic layer was dried and the solvent evaporated to give the *aziridine* **43***a* (800 mg, 94%), mp 166–168 °C, homogeneous according to tlc. A recrystallization from chloroform–ether afforded the analytical sample, mp 171–172 °C, $[\alpha]_D^{20}$ +53.5° (*c* 1.0 in $CHCl_3$); ν_{max} (CS_2) 3600 and 3440 (free and bonded OH), 1715 (C=O), 1265, 1065 cm^{-1}; δ ($CDCl_3$) 0.61 (s, 18-CH_3), 1.07 (s, 19-CH_3), 1.28 (t, J = 7 Hz, OCH_2CH_3), 2.13 (s, 20-CH_3), 2.60 (m, OH), 2.83 (m, $\Delta\nu_{1/2}$ = 7 Hz, H-6), 3.80 (m, $\Delta\nu_{1/2} \sim 20$ Hz, H-3) 4.18 ppm (q, J = 7 Hz, OCH_2CH_3). *Anal.* calcd.

for $C_{24}H_{37}NO_4$: C 71.43, H 9.24, N 3.47; found: C 71.25, H 9.07, N 3.74.

5α-Chloro-6β-ethoxycarbonylamino-pregnan-3β-ol-20-one ***44***

The *trans* 1,2-adduct **25***a* (1.92 g, 4 mmol) was suspended in a solution of potassium hydroxide (3 g) in ethanol (80 ml) and water at room temperature. When all the steroid was dissolved (30 min), the solution was cooled to *ca.* 0 °C, acidified with 4 *N* HCl, then diluted with water (200 ml), and extracted with methylene chloride. The residue (1 g) after evaporation of the solvent was purified by preparative layer chromatography on silica gel (benzene–ether 1:2) to yield the pure *alcohol* **44** (0.80 g, 46%), mp 148–150 °C, which was recrystallized from ether for analysis: mp 150–151 °C; $[\alpha]_D^{20}$ −13.5° (*c* 1.0 in $CHCl_3$); ν_{max} ($CHCl_3$) 3600 (free OH), 3460 (free NH and bonded OH), 1715 (C=O), 1510 (NH), 1240 and 1040 (C—O—C), 910 cm^{-1} (str); δ ($CDCl_3$) 0.65 (s, 18-CH_3), 1.23 (s, 19-CH_3), 1.27 (t, J = 7 Hz, OCH_2CH_3), 2.15 (s, 20-CH_3), 2.48 (m, OH), 4.16 (q, J = 7 Hz, OCH_2CH_3), ~4.2 (m, H-3 and H-6), 5.00 ppm (br d, J = 10 Hz, NH). *Anal.* calcd. for $C_{24}H_{38}ClNO_4$: C 65.51, H 8.71, Cl 8.06; found: C 65.43, H 9.04, Cl 8.16.

Opening of Aziridine ***43a***

The aziridine **43***a* (200 mg, 0.5 mmol) in tetrahydrofuran (15 ml) was treated with 4 *N* HCl (5 ml) at room temperature for 16 h. The mixture was poured into water (100 ml), extracted with methylene chloride, dried, and evaporated. The residue was acetylated in the usual way and the crude product separated on a silica gel plate (benzene–ether 2:1) to yield the *trans* 1,2-adduct **25***a* (108 mg, 45%) mp 195–197 °C. It proved identical (ir, nmr) with an authentic sample.

Oxidation of Alcohol ***44***

Jones' reagent (2.7 *M* in CrO_3) was added slowly with a syringe to a cold solution (*ca.* 0 °C) of the alcohol **44** (320 mg, 0.73 mmol) in acetone (30 ml). The reaction was followed by tlc and the addition (~0.1 ml) was stopped when some starting alcohol could still be detected on the plates. The reaction mixture was poured into cold water and extracted with chloroform. The residue (284 mg) contained mainly (≥90%) the *3-ketone* **45** according to the ^1H nmr spectrum: δ ($CDCl_3$) 0.70 (s, 18-CH_3), 1.28 (t, J = 7 Hz, OCH_2CH_3), 1.42 (s, 19-CH_3), 2.20 (s, 20-CH_3), 3.23 (AB quartet: $\Delta\nu_{AB}$ = 21.3 Hz, J_{AB} = 16.5 Hz; protons at C-4), ~4.2 (m, H-6), 4.25 (q, J = 7 Hz, OCH_2CH_3), 5.28 ppm (m, NH). An attempt to purify an aliquot (80 mg) of this residue by preparative tlc on silica gel with ether resulted in partial loss of HCl and gave a mixture of ketone **45**, 6β-ethoxycarbonylamino α,β-unsaturated ketone **46**, and the 6α-isomer **47** according to the ^1H nmr spectrum.

Separation of another aliquot (120 mg) on activity III alumina with ether containing methanol (1%) gave *6α-ethoxycarbonylamino-4-pregnene-3,20-dione* **47** (104 mg, 84% from alcohol **44**) mp 162–164 °C. One recrystallization from ether gave the analytical sample, mp 164–166 °C; $[\alpha]_D^{20}$ +100° (*c* 0.43 in $CHCl_3$); λ_{max} (EtOH) 238 nm (ε 12 400); ν_{max} ($CHCl_3$) 3440 (NH), 1705 (C=O, carbamate and 20-ketone), 1670 (3-keto group), 1620 (C=C), 1230, 1110 cm^{-1}; δ ($CDCl_3$) 0.68 (s, 18-CH_3), 1.23 (t, J = 7 Hz, OCH_2CH_3), 1.28 (s, 19-CH_3), 2.15 (s, 20-CH_3), 4.15 (q, J = 7 Hz, OCH_2CH_3), 4.53 (m, $\Delta\nu_{1/2}$ = 25 Hz, H-6 axial), 5.03 (br d, J = 10 Hz, NH), 5.99 ppm (d, J = 1.8 Hz, H-4). *Anal.* calcd. for $C_{24}H_{35}NO_4$: C 71.80, H 8.79, N 3.49; found: C 71.63, H 8.62, N 3.49. Hence, on alumina, the ketone **45** lost HCl readily and the α,β-unsaturated ketone **46** was isomerized to the more stable α,β-unsaturated ketone **47**.

A third aliquot (75 mg) of the residue from oxidation of **44** was placed in an nmr tube in $CDCl_3$ with silica gel impregnated with concentrated HCl. ^1H nmr spectra were run repeatedly. First the absorptions due to ketone **45** disappeared gradually while the absorptions of *ketone* **46** appeared: δ 0.73 (s, 18-CH_3), 1.23 (t, J = 7 Hz, OCH_2CH_3), 1.33 (s, 19-CH_3), 2.16 (s, 20-CH_3), 4.18 (q, J = 7 Hz, OCH_2CH_3), 4.39 (m, H-6), 5.35 (m, NH), 6.10 ppm (narrow s, H-4). When the AB quartet at 3.23 ppm due to ketone **45** had completely disappeared, a doublet at 5.99 ppm due to α,β-unsaturated ketone **47** began to appear next to the narrow singlet at 6.10 ppm due to the 6β-isomer **46**. After 1 h, the isomerization of **46** into **47** was complete. The solution was filtered and the solvent evaporated. The residue was purified by preparative tlc on silica gel to afford pure *6α-ethoxycarbonylamino-α,β-unsaturated ketone* **47** (67 mg, 86% from **44**), mp 163–165 °C, identical (ir, nmr) to the sample obtained above.

5α-Chloro-6α-ethoxycarbonylamino-pregnan-3β-ol-20-one ***48***

The *cis* 1,2-adduct **26***a* (500 mg, 1.04 mmol) was suspended in a solution of potassium hydroxide (0.15 g) in ethanol (15 ml) and water (15 ml) and stirred at room temperature for 2 h. The mixture was poured into water (200 ml) and extracted with chloroform to yield, after evaporation of the solvent, the pure *alcohol* **48** (384 mg, 84%), mp 123–125 °C. One recrystallization from ether gave the analytical sample, mp 127–128 °C; $[\alpha]_D^{20}$ +48.3° (*c* 1.0 in $CHCl_3$); δ ($CDCl_3$) 0.62 (s, 18-CH_3), 1.20 (s, 19-CH_3), 1.28 (t, J = 7 Hz, OCH_2CH_3), 2.15 (s, 20-CH_3), ~4.2 (m, H-3 and H-6), 4.23 (q, J = 7 Hz, OCH_2CH_3), 5.08 ppm (br d, J = 10 Hz, NH). *Anal.* calcd. for $C_{24}H_{38}ClNO_4$: C 65.51, H 8.71, Cl 8.06; found: C 65.19, H 8.80, Cl 8.19.

Oxidation of Alcohol ***48***

To a cold (*ca.* 0 °C) solution of the alcohol **48** (140 mg, 0.32 mmol) in acetone (10 ml) was added slowly, with a syringe, 0.075 ml of Jones' reagent (2.7 *M* in CrO_3). Work-up as above (oxidation of **44**) gave the *3-ketone* **49** (142 mg) which was characterized by its ^1H nmr spectrum only: δ ($CDCl_3$) 0.65 (s, 18-CH_3), 1.25 (t, J = 7 Hz, OCH_2CH_3) 1.35 (s, 19-CH_3), 2.13 (s, 20-CH_3), 2.85 (s, 2H, protons at C-4), ~4.1 (m, H-6), 4.15 (q, J = 7 Hz, OCH_2CH_3), 4.95 ppm (br d, J = 10 Hz, NH).

Attempts to purify an aliquot (70 mg) by preparative tlc on silica gel gave the *6α-ethoxycarbonylamino α,β-unsaturated ketone* **47** (56 mg, 88% from **48**), mp 163–165 °C, which proved identical (ir ^1H nmr) to an authentic sample. Another aliquot (65 mg) in $CDCl_3$ was treated with silica gel impregnated with HCl in an nmr tube. ^1H nmr spectra were run repeatedly. The elimination of HCl led directly to the *6α-ethoxycarbonylamino α,β-unsaturated ketone* **47** as shown by the appearance of a doublet (J = 1.8 Hz) at 5.99 ppm while the singlet at 2.85 ppm gradually disappeared. The ketone **47** (54 mg, 92% from **48**), mp 162–164 °C, was isolated and identified by comparison with an authentic sample.

5α-Pregnane-3,6,20-trione ***50***

A mixture of α,β-unsaturated ketone **47** (100 mg, 0.2 mmol) and concentrated HCl (0.5 ml) in benzene (10 ml) was stirred at room temperature for 20 h. The crude product was separated on a thin layer silica gel plate (benzene–ether 4:1) to afford *5α-pregnane-3,6,20-trione* **50** (49 mg, 62%), mp 220–225 °C. It was recrystallized from benzene–ether to afford the analytical sample, mp 225–230 °C: $[\alpha]_D^{25}$ +63° (*c* 0.6 in $CHCl_3$) (lit. (19*a*) 232.5–233 °C, $[\alpha]_D$ +61° (*c* 1.0 in $CHCl_3$); (19*b*) 226–230 °C, $[\alpha]_D$ +59°); ν_{max} ($CHCl_3$) 1710 cm^{-1} (C=O); δ ($CDCl_3$) 0.68 (18-CH_3), 0.98 (19-CH_3) and 2.20 ppm (20-CH_3). *Anal.* calcd. for $C_{21}H_{30}O_3$: C 46.34, H 9.15; found: C 46.23, H 8.97.

Acknowledgements

We are grateful to the 'Ministère de l'Education du Québec' and the National Research Council of Canada for financial assistance. We wish to acknowledge the helpful assistance of J. P. Vermes, M. Mondon, J. Langlois, R. Lapalme, and C. Bachand who carried out some of the reactions.

1. J. Lessard and J. M. Paton. Tetrahedron Lett. 4883 (1970).
2. J. Lessard, H. Driguez, and J. P. Vermes. Tetrahedron Lett. 4887 (1970).
3. R. S. Neale, N. L. Marcus, and R. G. Schepers. J. Am. Chem. Soc. **88**, 3051 (1966).
4. (*a*) D. Touchard and J. Lessard. Tetrahedron Lett. 4425 (1971); (*b*) 3827 (1971).
5. R. S. Neale. Synthesis, 1 (1971).
6. P. Chabrier. Ann. Chim. **17**, 353 (1942).
7. T. A. Foglia and D. Swern. J. Org. Chem. **31**, 3625 (1966).
8. (*a*) K. Schrage. Tetrahedron Lett. 5795 (1966); (*b*) Tetrahedron, **27**, 3033 (1967); (*c*) **27**, 3039 (1967).
9. J. R. Hanson and E. Premuzic. Angew. Chem. Int. Ed. Engl. **7**, 247 (1968); J. R. Hanson. Synthesis, 1 (1974).
10. L. F. Fieser and M. Fieser. Reagents for organic synthesis. John Wiley and Sons, Inc., New York. Vol. I. 1967. pp. 147–151; Vol. II. 1969. pp. 75–78; Vol. III. 1972. pp. 57–62.
11. A. E. Osterberg and E. C. Kendall. J. Am. Chem. Soc. **42**, 2616 (1970).
12. T. L. Cairns and P. J. Graham. J. Org. Chem. **17**, 751 (1952).
13. C. Bachand, H. Driguez, J. M. Paton, D. Touchard, and J. Lessard. J. Org. Chem. **39**, 3136 (1974).
14. D. H. R. Barton, A. L. J. Beckwith, and A. Goosen. J. Chem. Soc. 181 (1965); A. L. J. Beckwith and J. E. Goodrich. Aust. J. Chem. **18**, 747 (1965); Y. L. Chow and T. C. Joseph. Chem. Commun. 490 (1969).
15. (*a*) P. A. Bohm and P. I. Abell. Chem. Rev. **62**, 599 (1962); (*b*) D. I. Davies and S. J. Cristol. *In* Advances in free-radical chemistry. Vol. 1. *Edited by* G. H. Williams. Logos Press Ltd., London. 1965. pp. 155 ff; (*c*) C. L. Osborn, T. V. Van Auken, and D. J. Trecker. J. Am. Chem. Soc. **90**, 5806 (1968), and references cited therein.
16. N. A. Lebel. J. Am. Chem. Soc. **82**, 623 (1960); N. A. Lebel, P. D. Beirne, E. R. Karger, J. C. Powers, and P. M. Subramanian. J. Am. Chem. Soc. **85**, 3199 (1963); K. Kwart and J. L. Nyce. J. Am. Chem. Soc. **86**, 2601 (1964).
17. Von K. Ponsold and W. Ihn. J. Prakt. Chem. **313**, 811 (1971).
18. K. Nakanishi. Infrared absorption spectroscopy. Holden-Day Inc., San Francisco. 1962. p. 25.
19. (*a*) C. P. Balant and M. E. Ehrenstein. J. Org. Chem. **17**, 1587 (1952); (*b*) J. F. Bagli, P. F. Morand, and R. Gaudry. J. Org. Chem. **27**, 2938 (1962).
20. M. Masaki, T. Kitahara, H. Kurita, and M. Ohta. J. Am. Chem. Soc. **90**, 4508 (1968); A. Fontana and E. Scoffone. Gazz. Chim. Ital. **98**, 1261 (1968); W. Steglich and H. G. Batz. Angew. Chem. Int. Ed. Engl. **10**, 75 (1971).
21. J. S. Chalsty and S. S. Israelstam. Chem. Ind. 1452 (1954).
22. J. D. Park, H. J. Gerjovich, W. R. Lycan, and J. R. Lacher. J. Am. Chem. Soc. **74**, 2189 (1952).
23. R. E. Banks, R. N. Haszeldine, and J. P. Lalu. J. Chem. Soc. C, 1514 (1966).
24. C. Altona. Tetrahedron Lett. 2325 (1968).
25. M. Barker, L. Hunter, and N. G. Reynolds. J. Chem. Soc. 874 (1948).

The chromous chloride promoted addition of *N*-haloamides to olefins. IV.[1] Mechanistic aspects[2]

HUGHES DRIGUEZ[3] AND JEAN LESSARD

Département de chimie, Université de Sherbrooke, Sherbrooke (Qué.), Canada J1K 2R1

Received July 29, 1976

HUGHES DRIGUEZ and JEAN LESSARD. Can. J. Chem. **55**, 720 (1977).

A discussion on the mechanism of the chromous chloride promoted addition of *N*-haloamides to olefins is presented on the basis of the results already reported and some additional evidence. The mechanism proposed involves a radical chain addition in which the *N*-haloamide acts as the transfer agent, the termination steps being chromium(II) reduction of the amido radical and chromium(II) reduction of the intermediate adduct radical. The addition of *N*-chloro- and *N*-bromoacetamide to norbornadiene is described. The use of chromous chloride to initiate the reaction of *N*-chloropiperidine with ethyl vinyl ether and cyclohexene led to low yields of addition.

HUGHES DRIGUEZ et JEAN LESSARD. Can. J. Chem. **55**, 720 (1977).

Le mécanisme de l'addition, catalysée par le chlorure chromeux, de *N*-haloamides aux oléfines est discuté en regard des résultats déjà rapportés et de quelques expériences additionnelles. Le mécanisme proposé fait intervenir une addition radicalaire en chaîne où l'amide *N*-halogéné agit comme agent de transfert. Les étapes de terminaison sont la réduction du radical amido et de l'adduit radicalaire intermédiaire par l'ion chromeux. On décrit l'addition du *N*-chloro- et *N*-bromoacétamide au norbornadiène. La réaction, initiée par le chlorure chromeux, de la *N*-chloropiperidine avec l'éthyl vinyl éther et avec le cyclohexène a donné de faibles rendements en addition.

In the preceding paper (1), we described the chromous chloride promoted addition of various *N*-haloamides to a variety of olefins in order to try to delineate the scope and limitations of the method for the synthesis of *N*-(2-haloalkyl)amides. We will now discuss a working hypothesis concerning the mechanism in the light of the facts reported and some additional experimental evidence described in this paper. This working hypothesis is summarized by reactions 1 to 7.[4] Some allylic hydrogen abstraction does occur as evidenced by the detection of bicyclohexenyl ($\leq 5\%$ under the usual reaction conditions) in the reaction of *N*-chlorourethane and *N*-chloro-*N*-methylacetamide with cyclohexene (1).[5]

Discussion and Results

Amido Radical Formation

Mechanistic studies on the chromium(II) reduction of alkyl halides (2–6) and of hydroxylamine and amine oxides (7–9)[6] have indicated that the first step involves the formation of a radical species. The following observations support the contention that the first step of the reaction of chromium(II) with a *N*-haloamide also involves the formation of an amido radical [1]: the orientation of the addition to unsymmetrically substituted olefins (the amide moiety is attached to the less substituted carbon atom (1))

[1]For part III of this series, see ref. 1.

[2]Abbreviated in part from the Ph.D. thesis of H. Driguez, Université de Sherbrooke, 1971.

[3]Arts Council of Canada Predoctorate Fellow, 1969–1971. Present address: Centre de Recherches sur les Macromolécules Végétales, C.N.R.S., B.P. 53, 38041 Grenoble (France).

[4]We have established in the preceding paper (1) that *N*-alkylamides (1,H-adducts) do not arise from chromium(II) reduction of *N*-(2-haloalkyl)amides (1,2-adducts) under the reaction conditions.

[5]The amount of bicyclohexenyl formed is probably less than the extent of allylic hydrogen abstraction since some of the cyclohexenyl radicals formed might have been converted to cyclohexene by chromium(II) reduction followed by protonolysis. 3-Chlorocyclohexene has never been detected even at *ca.* -78 °C where it was not reduced to a significant extent by excess chromous chloride (1).

[6]For reviews on the reduction of organic compounds by chromous salts, see ref. 10.

[1] $ZCONHX + Cr^{II} \rightarrow ZCO\dot{N}H + XCr^{III}$

[2] $ZCO\dot{N}H + >C=C< \rightarrow ZCONH-\overset{|}{\underset{|}{C}}-\overset{|}{\underset{|}{C}}\cdot$

[3] $ZCONH-\overset{|}{\underset{|}{C}}-\overset{|}{\underset{|}{C}}\cdot + ZCONHX \rightarrow ZCONH-\overset{|}{\underset{|}{C}}-\overset{|}{\underset{|}{C}}-X + ZCO\dot{N}H$

1,2-adduct

[4] $ZCONH-\overset{|}{\underset{|}{C}}-\overset{|}{\underset{|}{C}}\cdot + Cr^{II} \rightarrow ZCONH-\overset{|}{\underset{|}{C}}-\overset{|}{\underset{|}{C}}-Cr^{III}$

[5] $ZCONH-\overset{|}{\underset{|}{C}}-\overset{|}{\underset{|}{C}}-Cr^{III} + H^+ \rightarrow ZCONH-\overset{|}{\underset{|}{C}}-\overset{|}{\underset{|}{C}}-H + Cr^{III}$

1,H-adduct

[6] $ZCO\dot{N}H + Cr^{II} \rightarrow ZCONH-Cr^{III}$

[7] $ZCONH-Cr^{III} + H^+ \rightarrow ZCONH_2 + Cr^{III}$

and to norbornene (the amido group is *exo*[7] (1)), the formation of nortricyclenyl derivatives in the additions to norbornadiene (see below), and the formation of formaldehyde when the reduction is carried out in methanol and in the absence of an olefin (see below). By analogy with the reduction of alkyl halides, hydroxylamine, and amine oxides, the formation of the amido radical is assumed to occur via an inner-sphere or bridged activated complex as shown in [1*a*] or in [1*b*]:[8] the *N*-haloamide could act as a bidentate ligand in the formation of the activated complex, which would lead to an amido radical bonded to the chromic ion. Even if the amido radical is not directly bonded to the chromic ion as depicted in [1*b*], it could still be associated with it since association complexes between radicals and transition metal ions have been postulated (14).

[1*a*] $ZCONHX + Cr^{II}L_6 \longrightarrow [ZCONH\cdots X\cdots CrL_5]^{\ddagger} \longrightarrow ZCO\dot{N}H + XCr^{III}L_5$

[1*b*] $ZCONHX + Cr^{II}L_6 \longrightarrow$ 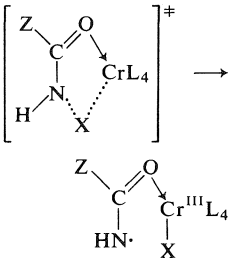 $\longrightarrow$

Stoichiometric Studies

If the above mechanism is correct, the generation of the amide ([1], [6], and [7]) and the formation of the 1,H-adduct ([1], [2], [4], and [5]) should require 2 mol of chromium(II) per mol of *N*-haloamide whereas the 1,2-addition process ([1], [2], and [3]) should require only a catalytic amount of chromium(II). This was confirmed by a study of the stoichiometry of these three processes.

The stoichiometry of amide formation was studied with *N*-chlorourethane and *N*-chloroacetamide, in methanol and in chloroform–methanol, and in the absence of an olefin[9]. The results are reported in Table 1. In methanol (entries 1 to 3), 1 mol of chromium(II) per mol of *N*-chloroamide was consumed and some formaldehyde was produced, which could be accounted for in the following way. The amide is formed by hydrogen abstraction from the solvent [8] and the resulting hydroxymethylene radical undergoes disproportionation to give formaldehyde [9] and most probably also coupling to give

[7]Radical attack on norbornene shows a strong preference for the less hindered *exo* face (11, 12).

[8]Since ligands on chromium(II) are readily interchanged (13) and methanol as solvent is present in large excess, the coordination sphere most probably contained methanol molecules (L = CH_3OH).

[9]*N*-Chlorourethane and *N*-chloroacetamide do not react with methanol in the absence of chromous chloride at 0 °C (no loss of active chlorine after 1 h).

ethylene glycol [10].[10] However, in chloroform–

[8] $ZCO\dot{N}H + CH_3OH \rightarrow ZCONH_2 + \cdot CH_2OH$

[9] $2 \cdot CH_2OH \rightarrow CH_2O + CH_3OH$

[10] $2 \cdot CH_2OH \rightarrow (CH_2OH)_2$

methanol (the solvent used for the additions to olefins), 2 mol of chromium(II) per mol of *N*-chloroamide were used and formaldehyde could not be detected. Thus chromium(II) reduction of the amido radical [6] appears to be faster than hydrogen abstraction from methanol, which could be due to a preferential solvation of the amido radical by chloroform;[11] protonolysis of the nitrogen–chromium bond [7] would then afford the amide.[12] If the amido radical is complexed with the halochromic ion formed in [1] (such complexation could be favored in the presence of chloroform), its reduction could occur through bridging with the halide ion of the complex (see [6*a*]) as has been suggested for the chromium(II) reduction of alkyl halides to alkanes (10).

[6*a*] $[ZCO\dot{N}H\ Cr^{III}X] + Cr^{II} \rightarrow ZCONHCr^{III} + XCr^{III}$

To study the stoichiometry of *N*-alkylamide formation (1,H-addition), we chose the addition of *N*-chloroacetamide to norbornene which was shown to lead almost exclusively to 1,H-addition (1). The results reported in Table 2 show that the formation of 1 mol of *N*-acetylnorbornylamine **1** requires nearly 2 mol of chromium(II) as in the postulated mechanism.

[10]The hydroxymethylene radical generated by radiolysis of methanol was reported to give ethylene glycol and formaldehyde; metal ions were found to increase the proportion of formaldehyde and an association complex $[M^{n+} \cdot CH_2OH]$ was suggested to be responsible for this (14*a*). We made no attempt to see if ethylene glycol was formed or not.

[11]The C—H bond of chloroform is less reactive than a C_α—H bond of an alcohol or an ether towards electrophilic radicals (15). Chromium(II) reduction of the amido radical could then be faster than hydrogen abstraction from chloroform.

[12]For the reduction of hydroxylamine and amine oxides in aqueous acidic medium, Taube and his co-workers (9) have suggested that the aminium radicals might react with chromium(II) by abstracting a hydrogen atom from the water molecules of the coordination sphere to explain the fact that they could not obtain evidence for the formation of a $Cr^{III}NR_3$ intermediate. The amido radical could react with chromium(II) in a similar fashion but the proposed mechanism ([6] and [7]) is similar to the accepted mechanism of chromium(II) reduction of alkyl halides (2–5, 16) and appears more probable to us.

Finally, studies on the stoichiometry of the addition of *N*-chlorourethane to cyclohexene (Table 2) have confirmed that the 1,2-addition process occurs by a chain mechanism. Indeed, the amount of urethane and *N*-cyclohexylurethane **4** formed (0.92 mmol all together) should have required about 1.8 mmol of chromous chloride; since 1.75 mmol was consumed, no chromous chloride was effectively used for the formation of the 1,2-adducts **2** and **3** (Scheme 1). Alternatively, when 1.0 mmol of chromous chloride was added to a tenfold excess of *N*-chlorourethane and a twentyfold excess of cyclohexene under the standard reaction conditions and the reaction mixture stirred at −78 °C for 24

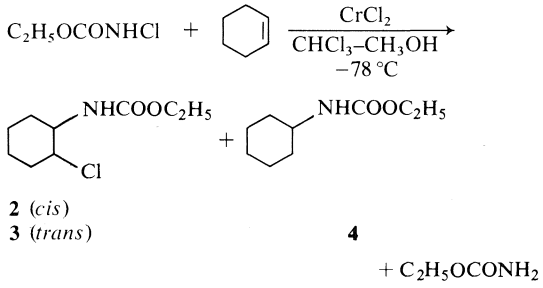

2 (*cis*)
3 (*trans*)
4

SCHEME 1

h, 5.0 mmol of 1,2-adducts **2** and **3** were obtained together with 0.3 mmol of 1,H-adduct **4** and about 0.3 mmol of urethane; again the amount of urethane and 1,H-adduct **4** (~0.6 mmol) accounts for all the chromous chloride consumed and therefore none was used for the 1,2-addition process.

β-*Amido-alkylchromium Intermediate*

In order to obtain further evidence for the formation of a β-amido-alkylchromium intermediate, *N*-chloro-*N*-deuteroacetamide was added to norbornene, all the acidic hydrogens of the medium being replaced by deuterium (Scheme 2). In a first experiment, the reaction mixture was allowed to warm to *ca.* 0 °C then worked-up in water: no deuterium was incorporated in *N*-acetylnorbornylamine **1**. In a second experiment, heavy water was added immediately after removing the cooling bath: the isolated *N*-acetylnorbornylamine (**1**-d_2) had two deuteriums according to its nmr spectrum. The N-deuterium was exchanged readily with water, the other being at position 3 as required by the formation and protonolysis of a β-amido-alkylchromium intermediate ([4] and [5]); the

TABLE 1. Stoichiometry of the reduction of ZCONHCl in the absence of an olefin

	Reaction conditions							Yield[d] of products (%)	
Z	ZCONHCl (mmol)	Solvent	Volume (ml)	T (°C)	Cr(II) added[a] (mmol)	Cr(II) used[b] (mmol)	Stoichiometry Cr(II)/>NCl[c]	$ZCONH_2$	$CH_2(NHCOZ)_2$
1 C_2H_5O	2.50	CH_3OH	3.5	0	5.05	2.47	0.99	80	17[e]
2 CH_3	2.50	CH_3OH	3.5	0	5.05	2.61	1.04	77	[f]
3 C_2H_5O	2.50	CH_3OH	3.5	−78	5.05	2.47	1.24	92	[g]
4 C_2H_5O	2.45	$CHCl_3/CH_3OH$	2.5/1	0	5.05	4.80	1.97	93	[g,h]
5 C_2H_5O	2.50	$CHCl_3/CH_3OH$	2.5/1	−78	5.05	4.87	1.95	96	[g]
6 CH_3	4.00	$CHCl_3/CH_3OH$	4/1	−78	9.10	7.90	1.98	95	[g]

[a]The 1.01 ± 0.01 *M* methanolic solution of $CrCl_2$ was added rapidly (5 to 10 min).
[b]The amount of unreacted chromium(II) was determined by titration using sodium triiodide and sodium thiosulfate (see the Experimental).
[c]Molar ratio.
[d]By vpc.
[e]Formaldehyde was also trapped with dimedone in a separate experiment.
[f]No attempt was made to see if diacetylaminomethane was formed or not. Formaldehyde was trapped with dimedone.
[g]Not detected.
[h]Formaldehyde could not be detected with dimedone.

TABLE 2. Stoichiometry of the 1,H-addition and 1,2-addition processes[a]

				Yield[c] (mmol)			Stoichiometry		
Olefin	*N*-Chloroamide	Cr(II) added (mmol)	Cr(II) used[b] (mmol)	Amide	1,H-add'n.	1,2-add'n.	Cr(II)/>NCl	Cr(II)/1-H add'n.	Cr(II)/1,2-add'n.
Norbornene (5 mmol)	$CH_3CONHCl$ (2.50 mmol)	5.05	4.75	0.57	1.80	—[d]	1.90	1.96	—
Cyclohexene (5 mmol)	$C_2H_5OCONHCl$ (2.50 mmol)	5.05	1.75	0.80	0.12	1.55	0.70	(2.0)	0[e]

[a]The reactions were carried out in the usual conditions, that is at a bath temperature of −78 °C and in chloroform (2.5 ml) – methanol (1 ml) but the chromous chloride methanolic solution (1.0 ± 0.02 *M*) was added rapidly (5 to 10 min) which explains why the yields of addition are lower than those given in the foregoing paper (1).
[b]From tritration of unreacted chromium(II) (see Table 1, footnote *b*).
[c]By vpc.
[d]Not detected.
[e]The Cr(II)/1,H-addition and the Cr(II)/amide molar ratios were taken as 2 for the calculation of Cr(II)/1,2-addition ratio.

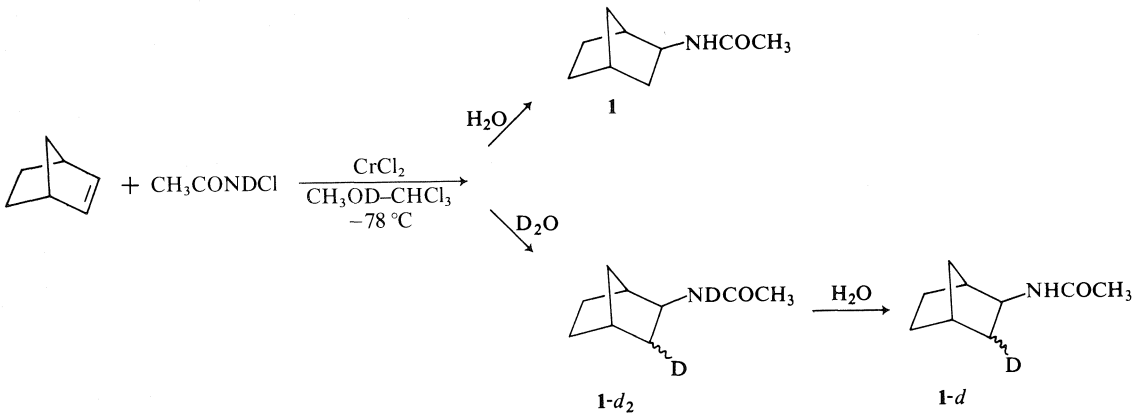

SCHEME 2

proton and carbon nmr spectra showed that the deuterium was distributed between the *exo* and *endo* positions (see the Experimental). The first experiment indicates that protonolysis of the β-amido-alkylchromium intermediate does not occur readily in the reaction medium at temperatures up to 0 °C. The proposed mechanism for the 1,H-addition process is in agreement with a number of studies on chromium(II) reduction of alkyl halides indicating that alkylchromium ions are formed when alkyl radicals are captured by chromous ions (3*a*, 5*a*, 5*c*, 9, 16) and that the corresponding alkanes result from protonolysis (3*a*, 5*c*, 16*a*, 16*d*).

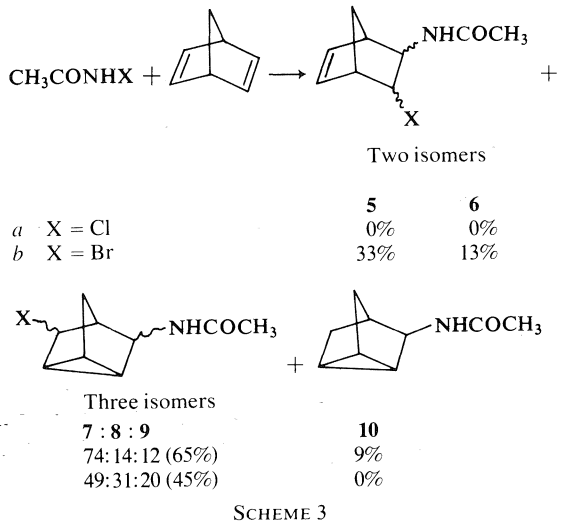

SCHEME 3

Chain-transfer Step

The radical nature of the chromous chloride promoted addition of *N*-haloamides to olefins was further confirmed by the addition of *N*-chloro- and *N*-bromoacetamide to norbornadiene (Scheme 3). Indeed radical additions to norbornadiene can give 5,6-disubstituted norbornenes via 1,2-addition and/or 3,5-disubstituted nortricyclenes via 1,5-homoconjugative addition (17). *N*-Chloroacetamide led exclusively to nortricyclene products (**7***a*, **8***a*, **9***a*, and **10**) (no olefinic proton absorption could be detected in the nmr spectrum of the crude product and of the chromatographic fractions) whereas with *N*-bromoacetamide, the ratio of norbornene derivatives **5***b* and **6***b* to nortricyclene derivatives **7***b*, **8***b*, and **9***b* was approximately one-to-one.[13] The chain-transfer step is thus faster with *N*-bromoacetamide. This agrees with the proposed mechanism in which the *N*-haloamide acts as the transfer agent (see [3]), a bromine-atom transfer being faster than a chlorine-atom transfer. But it would also agree with a transfer step (see [11]) involving a ligand transfer from the halochromium(III) produced in [1] since a bromide is transferred more readily than a chloride.[14] A number of free radical 1,2-additions of organic halides to olefins have been initiated

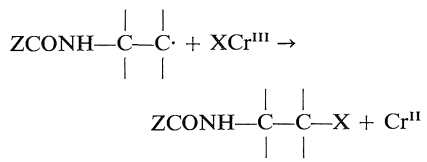

by various low-valent transition metal salts and a redox-transfer chain mechanism has been sug-

[13]The stereochemistry of the products of addition of various *N*-haloamides to norbornadiene is under study and will be reported later.

[14]The analogy between oxidation of an alkyl radical by ligand transfer and atom transfer to an alkyl radical has been discussed by Kochi (18).

gested for these reactions (19–21). However the metal salts participating in the ligand-transfer step (*e.g.* Cu(II) chloride, Fe(III) chloride) have a much higher redox potential than the chromic ion and we believe that the ligand transfer illustrated in reaction 11 is not very probable.[15,16] Nevertheless the following experiments were carried out in an attempt to distinguish between [11] and [3].

First we carried out a chromous bromide initiated addition of *N*-chlorourethane to cyclohexene in the presence of a slight excess of chromic bromide. We could not detect any β-bromocarbamate, the β-chlorocarbamates **2** and **3**, cyclohexylurethane **4**, and urethane accounting for all the starting *N*-chlorourethane (Scheme 4); this is in agreement with the chain-transfer step [3]. The yield of addition (47%) was much

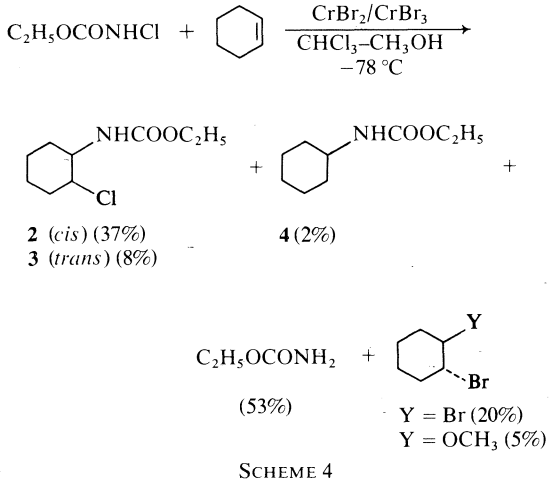

SCHEME 4

lower than in the chromous chloride promoted addition (93%) (1), probably as a result of the reduction of *N*-chlorourethane by bromide ions; part of the molecular bromine thus formed was trapped by cyclohexene to give *trans*-dibromocyclohexane and *trans*-bromomethoxycyclohexane, the other part being most probably reduced by the chromous ions. We then compared the chromous chloride promoted simultaneous addition of *N*-chlorourethane and *N*-bromo-α-chloroacetamide to 1-octene with the photochemical simultaneous addition in methylene chloride at −70 °C. An excess of *N*-chlorourethane over the *N*-bromo-α-chloroacetamide was used to compensate for the fact that both the initiation step and the chain-transfer step should be faster with the *N*-bromo derivative in the chromous chloride as well as in the photochemically induced reaction. The results are summarized in Scheme 5. The proportions of crossed 1,2-adducts **12** and **14** (respectively 6–7% and 3–5%) are similar whether the addition was initiated by chromous chloride or by irradiation. The formation of crossed 1,2-adducts is therefore also in agreement with the chain-transfer step [3].[17,18]

Chain-termination Steps

According to the proposed mechanism, the two main chain-termination steps are chromium(II) reduction of the amido radical [6] and chromium(II) reduction of the intermediate adduct radical [4]. The first one competes with the addition of the amido radical to the olefin [2] and leads to the amide through [7]; the

[15]Reaction 11 would be the microscopic reverse of the first step of the chromium(II) reduction of alkyl halides (2–6).

[16]Recently Surzur and Stella (22) suggested that in the radical cyclization of olefinic *N*-chloroamines catalyzed by Ti(III) chloride, oxidation of the intermediate radical does not occur by ligand transfer of chlorine from Ti(IV) chloride but rather by chlorine-atom transfer from a molecule of *N*-chloroamine. Minisci *et al.* (23) had previously shown that ligand transfer of chlorine from Ti(IV) chloride was much less efficient than from Fe(III) chloride. The redox potential of titanium(IV), although much lower than that of iron(III), is still appreciably higher than that of chromium(III).

[17]The photochemical addition of *N*-haloamides to olefins has been shown to proceed by a chain mechanism (D. Touchard, Ph.D. Thesis, Université de Sherbrooke, 1974).

[18]The two crossed experiments reported in this paragraph do not constitute fool-proof experimental evidence against the ligand-transfer step [11]. In the second experiment, some halogen exchange could have occurred between *N*-chlorourethane and *N*-bromo-α-chloroacetamide before completion of the reaction. In the first experiment, all the steps leading to a 1,2-adduct could involve radical–halochromium(III) complexes in which the halide ion would come originally from the *N*-haloamide:

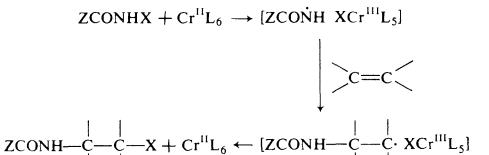

Chromium(III) being substitution inert (13), the halide ion in the complex would not be exchanged readily with an halide ion in solution. Furthermore the radical–halochromium(III) complexes could react before the occurrence of any exchange between the halochromic ion in the complex and the halochromic ions in solution.

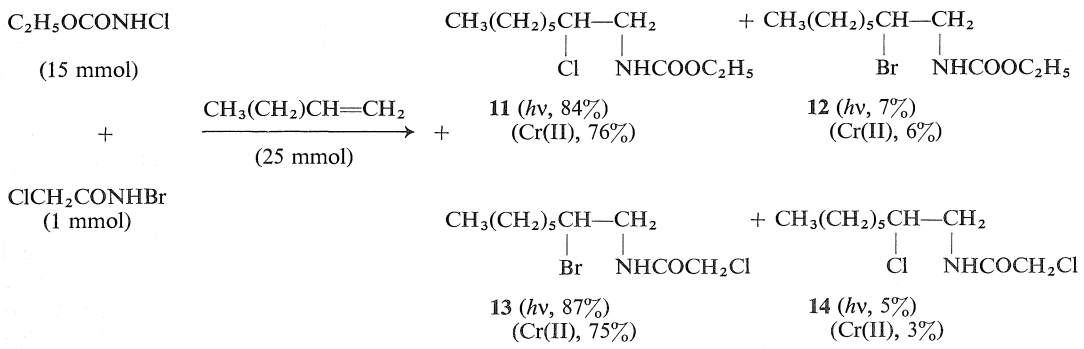

SCHEME 5

second one competes with the halogen-atom transfer [3] and leads to the 1,H-adduct through [5]. The yield of addition and the 1,2-addition – 1,H-addition ratio should then be higher when lowering the concentration of chromous chloride. Indeed in the reaction of *N*-chlorourethane with cyclohexene, the yield of addition and the 1,2-addition – 1,H-addition ratio were higher (respectively, 93% and 14.5) when the chromous chloride solution was added slowly (*e.g.* over 70 min) (lower effective concentration of chromous ions) than when it was added rapidly (*e.g.* over 10 min) (respectively, 70% and 9) (1). Similarly a very slow rate of addition of chromous chloride (3 h) led to a 94% yield of addition of *N*-chloroacetamide to norbornene (1) whereas a fast rate (5 min) led to a 43% yield of addition (Table 2); in this case the amount of 1,2-addition was too small to measure a meaningful variation of the 1,2-addition – 1,H-addition ratio.

The competition between addition of the amido radical to the olefin [2] and its chromium(II) reduction [6] should also depend on the relative reactivity of the amido radical in these two processes. The reactivity of $ZCO\dot{N}H$ towards addition to simple olefins would be expected to increase with the electrophilic character of the radical,[19] that is with the electron-withdrawing ability of the ZCO moiety. On the other hand the ease of chromium(II) reduction of $ZCO\dot{N}H$ should also increase with the ability of ZCO to accept electrons (anionic character of the organochromium derivative) but not necessarily to the same extent. The variation with Z of the ratio of addition–chromium(II) reduction of $ZCO\dot{N}H$ is indicated in Table 3 for the addition of ZCONHX to cyclohexene and indeed it shows no definite trend.[20] The ratio is the highest with the ethoxycarbonylamino radical ($Z = OC_2H_5$) which is probably more electrophilic than the acetylamino radical ($Z = CH_3$) because of the inductive effect of the ethoxy group but would be reduced less readily by chromium(II) than the latter because the carboethoxy group would be less efficient than the acetyl group to accommodate the electrons of the organochromium derivative.[21] An *N*-methylamido radical ($ZCO\dot{N}CH_3$) should be less reactive than $ZCO\dot{N}H$ towards addition to olefins because of greater spin delocalization but mainly because of a steric effect. On the other hand, the steric effect would be expected to be less important for the chromium(II) reduction. As a result, the chromium(II) reduction of $ZCO\dot{N}CH_3$ could be faster than its addition to cyclohexene which would explain that no addition products to cyclohexene were detected with *N*-chloro-*N*-methylacetamide and *N*-chloro-*N*-methyl-2,2,2-trichloroethylcarbamate (Table 3). Finally the succinimidyl radical should be more readily re-

[19]The amido radical is most probably electrophilic which implies the contribution of polar resonance forms (indicating some electron transfer from the olefin to the radical) to the stabilization of the transition state for the addition (24).

[20]It is noteworthy here that in the photochemical addition of ZCONHX (X = Cl, Br) to cyclohexene where the addition of the amido radical competes with the reactions of the halogen atom, the yield of addition increases with the electron-withdrawing power of Z (25).

[21]The acidity of the protons on nitrogen of *N*-chlorourethane ($pK_a = 8.02$) is lower than that of *N*-chloroacetamide ($pK_a = 7.22$) (F. Comtois, J. Lessard, H. Ménard, and M. Paquette, unpublished results) and the pK_a of an acetate (~25) is higher than that of acetone (~20).

TABLE 3. Ratio of addition–chromium(II) reduction of ZCONR in the addition of ZCONRX to cyclohexene

ZCONRX	Addition/chromium(II) reduction[a] (X = Cl)	(X = Br)
CCl_3CONHX	1.3	2.1
CH_3CONHX	2.3	3.5
CF_3CONHX	4.1	
$ClCH_2CONHX$	7.3	3.9
$C_2H_5OCONHX$	14.3	23
$CH_3CON(CH_3)X$	0	
$CCl_3CH_2OCON(CH_3)X$	0	
CH_2——CO | | CH_2CONX	0.22	0.18

[a]These ratios were calculated from the additions reported in ref. 1. In the cases where the yield of amide was not determined, we assumed that all the *N*-haloamide which did not add to cyclohexene and did not lead to electrophilic halogenation was converted to the amide by reduction ([4] and [5]) as in other cases: percentage of chromium(II) reduction = 100 − (yield of addition + yield of electrophilic halogenation).

duced by chromium(II) than ZCONH because of a greater stabilization of the ionic transition state (partial negative charge on the organic group). On the other hand even if it could be more electrophilic than ZCONH, it is bulkier. The low addition – chromium(II) reduction ratios in the reaction of *N*-chlorosuccinimide and *N*-bromosuccinimide with cyclohexene (Table 3) are therefore not unexpected.

For a given amido radical, the competition between addition to the olefin [2] and chromium(II) reduction [6] should depend also on the reactivity of the olefin. Indeed, in the additions of *N*-chlorourethane to 1-substituted cyclohexenes, the yield of addition increases in the order 1-chlorocyclohexene (29%) < 1-acetoxycyclohexene (47%) < 1-methylcyclohexene (87%) ≤ 1-methoxycyclohexene (90%) (1), in agreement with both the relative ability of the substituents to delocalize an unpaired electron and their relative electron-releasing power.[22] Norbornene is known to be more reactive than cyclohexene towards electrophilic radicals (27) and effectively the yields of addition of the various *N*-haloamides studied were generally higher with norbornene (1). With monosubstituted olefins the yield of addition of *N*-chlorourethane increases in the following order: methyl vinyl ketone (18%) < methyl acrylate (38%) < 1-octene (85%) (1). This is again in agreement with a competition between step [2] and step [6] and with the electrophilic character of the urethane radical.

We have seen that the competition between the halogen-atom transfer [3] and chromium(II) reduction of the intermediate adduct radical [4] does depend on the chromous ion concentration. It should also depend on other factors affecting the relative rates of [3] and [4]. One of these factors is the reactivity of the *N*-haloamide as a halogen-atom transfer agent. The additions to norbornadiene have established that an *N*-bromoamide is more reactive than an *N*-chloroamide and indeed the 1,2-addition – 1,H-addition ratio, for a given olefin, is larger with *N*-bromoamides than with the corresponding *N*-chloroamides (see Table 4). It is interesting to note in Table 4 the increase in the 1,2-addition – 1,H-addition ratio with Z in the order CH_3 < $ClCH_2$ < C_2H_5O ≤ CCl_3 < CF_3. We hypothesize that the reactivity of the *N*-haloamide in the chain-transfer step [3] increases with the electron-withdrawing power of the ZCO moiety as a result of increasing contribution of a polar resonance form to the stabilization of the transition state. Work is in progress to verify this hypothesis.

Two other factors affecting the relative rates of steps [3] and [4] and hence the 1,2-addition – 1,H-addition ratio would be, for a given *N*-haloamide, the reactivity of the intermediate adduct radical and the stability of the alkylchromium derived from it. For instance, the more stable the radical, the slower the transfer step [3]; the more stable the alkylchromium, the faster the

TABLE 4. Ratio of 1,2-addition – 1,H-addition in the addition of ZCONHX to cyclohexene

ZCONHX	1,2-addition/1,H-addition[a] (X = Cl)	(X = Br)
CH_3CONHX	0.94	7.4
$ClCH_2CONHX$	5.8	18.5
$C_2H_5OCONHX$	14.5	~140
CCl_3CONHX	≥28[b]	>33[b]
CF_3CONHX	31	

[a]Ratios calculated from the results reported in ref. 1.
[b]The 1,H-adduct was not detected in the chromatographic fractions and we assume that we would have been able to detect 2% of it.

[22]The reactivity of the olefin towards an electrophilic radical should depend not only on steric factors and on the ability of the substituents to delocalize an unpaired electron but also on their ability to donate electrons (polar effect).

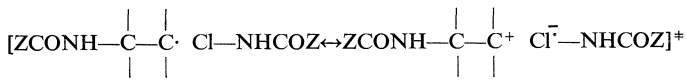

reduction of the radical [4]. We have seen that, for the additions of *N*-chloroacetamide for example, the 1,2-addition – 1,H-addition ratio is much smaller with 1-octene (0.57) and cyclohexene (0.94) than with 1-methylcyclohexene (≥ 37, no 1,H-adduct was isolated) (1). The determining factor in this case is probably the stability of the alkylchromium derivative. Indeed a secondary radical is less stable than a tertiary radical but a secondary alkylchromium should be more stable than a tertiary alkylchromium (carbanion character). In the additions to conjugated systems, both spin delocalization in the adduct radical (allylic radical, radical α to a carbonyl group) and the charge delocalization in the alkylchromium derived from it should favor the reduction step [4] over the transfer step [3] in agreement with the experimental facts reported in the preceding paper (1): the sole addition products isolated from the addition of *N*-chlorourethane to butadiene, cyclohexadiene, methyl acrylate, and methyl vinyl ketone, are derived from the reduction of the adduct radical [4]. Finally we have observed that the 1,2-addition – 1,H-addition ratio (*e.g.* addition of *N*-chlorourethane) decreases in the order cyclohexene (14.5) > cyclopentene (2.6) > norbornene (0.76), which is the order of increasing ring strain and could be the order of increasing stability of the intermediate adduct radical. But we do not know if this is due to an influence on the rate of step [3] or on the rate of step [4], or on both rates.

Conclusion

The discussion and experimental facts presented in this paper do not provide an answer to all the questions concerning the mechanism of the chromous chloride promoted addition of *N*-haloamides to olefins but we hope it will be useful to potential users of the reaction and might foster a more thorough mechanistic investigation. One puzzling fact is the following. Stoichiometric studies have shown that virtually no chromium(II) is used for the 1,2-addition process; however in the reactions where the yield of 1,2-addition to an excess of olefin is high (>85%), at least 0.9 mol of chromous chloride has to be added to consume all the *N*-haloamide (1).

To the best of our knowledge, no example of a radical 1,2-addition to olefins initiated by chromium(II) was known until the appearance of our preliminary reports on the chromous chloride promoted addition of *N*-chlorocarbamates to olefins (26). It would be interesting to see if chromium(II) could be used to initiate other 1,2-additions. As a first step in that direction, we studied the chromous chloride promoted addition of *N*-chloropiperidine to ethyl vinyl ether hoping that electrophilic halogenation might not compete with the radical reactions at −78 °C.[23] We did obtain the expected adduct **15** but in a very low yield (14%), the other products being the α-chloroacetal **16** (24%) resulting from electrophilic chlorination, and piperidine. The yield of 1,2-addition (**17** and **18**) to cyclohexene was also quite low (14%, **17**/**18** = 2.5), piperidine being the sole other product isolated; no chloromethoxycyclohexane (electrophilic chlorination) was detected. Thus it appears that chromium(II) reduction of the piperidino radical would be faster than its addition to either ethyl vinyl ether or cyclohexene.[24]

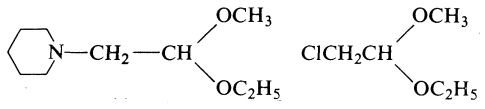

15 **16**

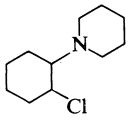

17 *cis*
18 *trans*

Experimental

The pertinent general information and a description of the apparatus used for the chromous chloride promoted reactions have been given in the preceding paper (1).

[23]According to Minisci *et al.* (21), in methanol at 0 °C and in the presence of Fe(II), Cu(I), and Ti(III) salts, electrophilic chlorination of enol ethers was faster than reduction of the *N*-chlorodialkylamine.

[24]With a milder reducing salt, the yields of 1,2-addition are much better. Minisci *et al.* (21) reported an 80% yield and a large predominance of the *cis*-adduct **17** for the addition catalyzed by the ferrous sulfate – ferric chloride couple in methanol at 0 °C; in our hands, however, the yield of 1,2-addition was 67% (**17**/**18** = 2). Using titanous chloride in methanol at −15 °C, L. Stella (Thèse de Doctorat ès-Sciences physiques, Université de Provence, 1972) obtained a 66% yield of 1,2-addition; using the same conditions, we obtained a 75% yield, (**17**/**18** = 2).

General Procedure for Stoichiometry Determinations

A known volume (5 or 10 ml) of the chromous chloride solution measured as accurately as possible in dropping funnel C was added drop-wise over 5 to 10 min into flask B containing the *N*-haloamide (and the olefin) in methanol or in chloroform–methanol and cooled in an ice bath or a dry ice – methanol bath. An excess of chromous chloride, generally 2 mol per mol of *N*-haloamide, was added rapidly (5 to 10 min). Then a standard 0.2 *N* sodium triiodide solution (10 or 25 ml) was added with a volumetric pipet. The mixture was allowed to warm to room temperature and titrated with a 0.1 *N* standard sodium thiosulfate solution using the coloration of the chloroform layer to determine the end point. The organic products were separated from the inorganic salts by continuous extraction with methylene chloride for 24–48 h. The solvent was partly removed by distillation and the resulting mixture transferred into a volumetric flask. The yields were determined by vpc using authentic samples as standards. For each of the results reported in Table 1 and Table 2, at least two determinations (sometimes three) were made. The titration values were always within 2% of one another and the yields were within 5%. The mean values are given in Tables 1 and 2.

An aliquot of the crude product was separated by preparative tlc on silica gel for complete identification of the products. Diethoxycarbonylaminomethane (Table 1, entry 1), mp 130–131 °C, proved identical (mixture mp ir, ^{1}H nmr) to an authentic sample prepared from urethane and formaldehyde (27).

The chromous chloride solution was titrated in the same apparatus, using a chloroform layer to determine the end point, and the different values were within 1% of one another.

Trapping of Formaldehyde with Dimedone in the Chromous Chloride Reduction of N-Chlorourethane and N-Chloroacetamide

The reactions were carried out under the same conditions as those used for the stoichiometry determination (see Table 1) except that no excess chromous chloride was used: the addition of the chromous chloride solution was stopped when the starch–iodide paper test was negative. The reaction flask was then heated to reflux under a stream of nitrogen and the exit gases were allowed to pass through a saturated aqueous solution of dimedone. The precipitate was collected and dried, mp 185–187 °C (lit. (28) 189 °C). In the experiments corresponding to the conditions of entries 1 and 2 of Table 1, the following quantities of precipitate were obtained: 86 mg and 115 mg respectively. In the experiment corresponding to the conditions of entry 4, no precipitate was formed.

Addition of N-Chloro-N-deuteroacetamide to Norbornene in a Deuterated Medium

Chromous Chloride Solution

To $CrCl_3 \cdot 6H_2O$ (5.3 g, 20 mmol), freshly distilled thionyl chloride was added dropwise and the mixture heated to reflux for 4 h. The excess thionyl chloride was distilled off and the violet powder was dried overnight under vacuum (29). The anhydrous $CrCl_3$ thus obtained was dissolved in CH_3OD (20 ml) containing D_2O (2 ml) and DCl (0.3 ml of a 38% solution in D_2O). The resulting green solution was reduced over zinc amalgam (prepared in D_2O acidified with DCl).

Addition

The chromous chloride solution (7 ml) was added dropwise to a solution, cooled in a dry ice – methanol bath, of *N*-chloro-*N*-deuteroacetamide (240 mg, 2.5 mmol) and norbornene (470 mg, 5 mmol) in $CHCl_3$ (2 ml) and CH_3OD (1 ml). The addition took 3 h and the reaction mixture was allowed to warm to 0 °C then poured into water (50 ml). Continuous extraction with methylene chloride for 48 h and separation of the residue by preparative layer chromatography gave *N*-acetylnorbornylamine **1**, mp 133–135 °C, (290 mg, 77%) identical (^{1}H nmr, mass spectrum) to an authentic sample.

The reaction was repeated in exactly the same conditions except for the work-up procedure. Deuterated water (20 ml) was added before the reaction mixture was allowed to warm up to room temperature. Continuous extraction followed by chromatography as above gave *N*-acetyl-*N*,3-dideutero-norbornylamine **1**-d_2, mp 132–134 °C (315 mg, 84%); δ ($CDCl_3$) 3.65 ppm (br d, $J \sim 4$ Hz, $\Delta\nu_{1/2} = 10$ Hz, H-3). Exchange with water gave *N*-acetyl-3-deutero-norbornylamine **1**-*d*; *m/e* 154 (M^+); ^{1}H nmr δ ($CDCl_3$) 3.65 ppm (br t, $J \sim 6$ Hz, $\Delta\nu_{1/2} = 14$ Hz, H-3); ^{13}C nmr δ ($CDCl_3$) 23.28 ($CO\mathit{CH}_3$), 26.47 (C-6), 28.09 (C-5), 35.44 (C-7), 35.53 (C-4), 39.80 (C-3, t, $J_{C-D} = 20.5$ Hz), 42.28 (C-1), 52.77 ppm (C-2). The signal of C-5 at 28.09 ppm is broader ($\Delta\nu_{1/2} = 2.5$ Hz) than the signal of C-6 at 26.47 ppm ($\Delta\nu_{1/2} \simeq 1$ Hz) due to coupling between C-5 and the deuterium at position 3. Since the vicinal $^3J_{C,D}$ should be about 1 Hz with the deuterium *exo* (dihedral angle of 180°) and about 0.3 Hz with the deuterium *endo* (dihedral angle of 60°), the deuterium must be distributed between the *exo* and *endo* positions.[25] The same conclusion is reached by considering the half band width of the signal of H-3 in the ^{1}H nmr spectrum of N-deuterated *N*-acetylnorbornylamine **1**-ND and of the *N*,3-dideuterated derivative **1**-d_2. The difference $\Delta(\Delta\nu_{1/2})$ between **1**-ND and **1**-d_2 is 5 Hz and should be about 7–8 Hz if the deuterium at C-3 was *exo* and about 2–3 Hz if it was *endo*.

Addition of N-Chlorourethane to Cyclohexene with a Catalytic Amount of Chromous Chloride.

Chromous chloride (10 ml of a 0.1 *M* methanolic solution, 1 mmol), was added to a solution of *N*-chlorourethane (1.29 g, 96% active chlorine, 10 mmol) and cyclohexene (2 ml, 20 mmol) in chloroform (10 ml) and absolute methanol (2 ml) cooled in a dry ice – methanol bath (−78 °C). The mixture was kept at *ca.* −78 °C under a carbon dioxide atmosphere for 24 h. A saturated sodium bisulfite aqueous solution was added to reduce the unreacted *N*-chlorourethane and the mixture was allowed to warm up to *ca.* 0 °C then extracted with ether (4 × 100 ml). The residue was separated on silica gel plates (ether–hexane 1:4) to give *cis-N-(2-chlorocyclohexyl)urethane* **2**, mp 56–58 °C (0.85 g) and *trans-N-(2-chlorocyclohexyl)urethane* **3**, mp 92–94 °C (0.18 g) (total yield of 1,2-addition: 1.03 g, 5 mmol, 50%).

The aqueous phases were combined, saturated with sodium chloride, and extracted continuously with methylene chloride for 2 days. Vapor phase chromatographic analysis of the crystalline residue, mp 46–48 °C (0.620 g), showed that it contained 0.052 g (0.3 mmol, 3%) of *N*-cyclohexylurethane **4**, the rest being urethane only.

---

[25]We thank professor J. K. Saunders for the interpretation of the ^{13}C nmr spectrum.

Additions to Norbornadiene

N-Chloroacetamide

The chromous chloride solution (20 ml, 20 mmol) was added over 5 h to a solution of *N*-chloroacetamide (940 mg, 10 mmol) and norbornadiene (1843 mg, 20 mmol) in chloroform (10 ml) – methanol (4 ml) at *ca.* −78 °C. The reaction mixture was poured into cold water and extracted rapidly with ether (4 × 200 ml), work-up A (ref. 1). The ^{1}H nmr spectrum of the residue (1310 mg) did not show any absorption in the olefinic proton region. An aliquot (570 mg) was separated on silica gel plates (ether–pentane 2:1) to give one main fraction (499 mg) showing no olefinic absorption in the nmr. The other fractions (20 mg or less) did not have any olefinic protons according to their nmr spectrum. Further separation of the main fraction (ether–pentane 1:1) followed by recrystallizations of the various fractions from ether or ether – methylene chloride allowed the complete separation of two isomeric *3-acetylamino-5-chlorononortricyclenes*, **7***a* and **8***a*. Isomer **7***a*: mp 136 °C; ν_{max} ($CHCl_3$) 3440 and 3320 (free and bonded NH), 1675 (C=O), 1520 (NH), 818 cm^{-1} (nortricyclene (30)); δ ($CDCl_3$) 2.00 (s, CH_3), 3.95 (d of t, J = 7 and 1.5 Hz, H-3), 4.05 (t, J = 1.5 Hz, H-5), 6.25 ppm (m, NH). *Anal.* calcd. for $C_9H_{12}ClNO$: C 58.22, H 6.51, N 7.54; found: C 58.42, H 6.56, N 7.32. Isomer **8***a*: mp 115 °C; ν_{max} ($CHCl_3$) 3450 and 3330 (free and bonded NH), 1675 (C=O), 1520 (NH), 815 cm^{-1} (nortricyclene (30)); δ ($CDCl_3$) 2.02 (s, CH_3), 4.05 (t, J = 1.5 Hz, H-5), 4.62 (d of t, J = 7 and 1.5 Hz, H-3), 6.32 ppm (m, NH); molecular weight by osmometry in $CHCl_3$, 187 (calcd. 185.65). *Anal.* calcd. for $C_9H_{12}ClNO$: C 58.22, H 6.51, N 7.54; found: C 58.07, H 6.56, N 7.25. A crystalline fraction containing a third isomer of *3-acetylamino-5-chlorononortricyclene*, **9***a*, was obtained but this isomer could not be isolated free from contamination by isomer **7***a*. The ir spectrum showed the characteristic absorptions of the acetylamino group and of the nortricyclene skeleton (815 cm^{-1}). In the nmr spectrum, after the exchange of NH with D_2O, H-3 appears as a triplet at 3.82 ppm with J = 1.5 Hz (beside the triplet of the H-3 proton of isomer **7***a* at 3.95 ppm) and H-5 absorbs at 4.42 ppm (m, $\Delta\nu_{1/2}$ = 4 Hz). From the nmr spectrum of the crude product, after exchange of the NH protons with D_2O, it was possible to determine the relative proportion of **7***a*, **8***a*, and **9***a* as 74:14:12.

Continuous extraction with methylene chloride of the aqueous layer from the ether extraction of the reaction mixture gave a residue (460 mg) which afforded three main fractions after chromatographic separation on silica gel plates (ether–pentane 2:1): acetamide (153 mg, 21%) identified by its mp, ir, and ^{1}H nmr spectra. A mixture of **7***a*, **8***a*, and **9***a* (60 mg, altogether 1206 mg, 65%); and *3-acetylaminonortricyclene* **10**, mp 100–102 °C (136 mg, 9%). A recrystallization from ether afforded a sample melting at 104–105 °C; ν_{max} ($CHCl_3$) 3440 (free NH), 1670 (C=O), 1510 (NH), 815 cm^{-1} (nortricyclene (30)); δ ($CDCl_3$) 2.00 (s, CH_3), 3.83 (d of t, J = 1.5 Hz), ~5.7 ppm (very broad, NH); *m/e* 151 (M^+), 91 (base peak).

N-Bromoacetamide

The reaction was carried out as above on 1.380 g (9.8 mmol) of *N*-bromoacetamide and 1.843 g (20 mmol) of norbornadiene to give, after the usual work-up, 2.134 g of crude product which was separated by preparative layer chromatography on silica gel (ether–pentane 3:1) to afford three main fractions.

(*a*) *5-Acetylamino-6-bromonorbornene* **5***b*, mp 120–123 °C (0.284 g, 13%). One recrystallization from ether gave the analytical sample, mp 126 °C; ν_{max} ($CHCl_3$) 3420 (NH), 1670 (C=O), 1505 cm^{-1} (NH); δ($CDCl_3$) 2.00 (s, CH_3), 2.80 and 3.16 (two m, H-1 and H-4), 4.00 (octet, J = 7.5, 7, and 2 Hz, H-5), 4.28 (d of d, J = 7 and 2 Hz, H-6), 6.18 and 6.38 (m, olefinic protons), 6.20 ppm (m, NH). *Anal.* calcd. for $C_9H_{12}BrNO$: C 46.97, H 5.26, Br 34.72, N 6.09; found: C 46.87, H 5.41, Br 34.70, N 5.90.

(*b*) *5-Acetylamino-6-bromonorbornene* **6***b*, mp 130–134 °C (0.734 g, 33%). One recrystallization from methylene chloride – ether gave the analytical sample, mp 134–135 °C; ν_{max} ($CHCl_3$) 3420 and 3340 (free and bonded NH), 1670 (C=O), 1500 cm^{-1} (NH); δ($CDCl_3$) 2.00 (s, CH_3), 3.16 (m, H-1 and H-4), 3.45 (t, J ~ 2.6 Hz, H-6), 4.80 (octet, J = 9, 4 and 2.6 Hz, H-5), 6.00 (m, NH), 6.38 (m, olefinic protons). *Anal.* calcd. for $C_9H_{12}BrNO$: C 46.97, H 5.26, Br 34.72, N 6.09; found: C 47.15, H 5.25, Br 34.92, N 5.87.

(*c*) A mixture of isomeric *3-acetylamino-5-bromonortricyclenes* **7***b*, **8***b*, and **9***b* in the ratio 49:31:20 by ^{1}H nmr. Chromatographic separation on silica gel plates (ether–pentane 3:1) followed by recrystallizations of the various fractions from ether gave the pure isomers **7***b* and **8***b* but the isomer **9***b* could not be isolated free from contamination by isomer **7***b*. Isomer **7***b*: mp 121–123 °C; ν_{max} ($CHCl_3$) 3440 and 3330 (free and bonded NH), 1675 (C=O), 1510 (NH), 815 cm^{-1} (nortricyclene (30)); δ ($CDCl_3$) 2.00 (s, CH_3), 3.92 (d of t, J = 7 and 1.5 Hz, H-3), 4.08 (t, J = 1.5 Hz, H-5), 6.00 ppm (m, NH). *Anal.* calcd. for $C_9H_{12}BrNO$: C 46.97, H 5.26, N 6.09; found: C 46.79, H 5.09, N 6.11. Isomer **8***b*: 125–126 °C; ν_{max} ($CHCl_3$) 3445 and 3320 (free and bonded NH), 1670 (C=O), 1515 (NH), 815 cm^{-1} (nortricyclene (30)); δ ($CDCl_3$) 2.02 (s, CH_3), 4.10 (t, J = 1.5 Hz, H-5), 4.68 (d of ill-defined t with J = 7 Hz and $\Delta\nu_{1/2}$ ~ 4 Hz, H-3), 6.45 ppm (m, NH); osmometric molecular weight determination ($CHCl_3$), 233 (calcd. 230.1). *Anal.* calcd. for $C_9H_{12}BrNO$: C 46.97, H 5.26, Br 34.72, N 6.09; found: C 46.85, H 5.51, Br 34.69, N 6.19. Mixture of **9***b* and **7***b* in a 8:21 ratio: ν_{max} ($CHCl_3$), 3440 and 3330 (free and bonded NH), 1675 (C=O), 1510 (NH), 815 cm^{-1} (nortricyclene); δ ($CDCl_3$) 2.00 (s, CH_3 of **9***b* and **7***b*), 3.92 (d of t, J = 7 and 1.5 Hz, H-3 of **7***b* masking H-3 of **9***b*), 4.08 (t, J = 1.5 Hz, H-5 of **7***b*), 4.31 (m, $\Delta\nu_{1/2}$ = 3.5 Hz, H-5 of **9***b*), 6.00 and 6.32 ppm (NH of **9***b* and **7***b*).

Chromous Bromide Promoted Addition of N-Chlorourethane to Cyclohexene.

The chromic bromide solution (5.933 g of $CrBr_3$, 3.3 ml of concentrated HCl, and absolute methanol in a 100 ml volumetric flask) was reduced over zinc amalgam as usual (1). The resulting clear blue chromous bromide solution (33 ml, 6.6 mmol) was added slowly (over 10 h) to a solution of *N*-chlorourethane (0.635 g, 97% active chlorine, 5 mmol), cyclohexene (10 ml, ~10 mmol), and chromic bromide (1.600 g, 5.5 mmol) in chloroform (6 ml) – methanol (4 ml) cooled to *ca.* −78 °C (methanol – dry ice bath). The mixture was then poured into water (100 ml) and continuously extracted with methylene chloride for 24 h. The solvent was partly removed by distillation and the resulting solution was transferred into a 25 ml volumetric flask. Analysis by vpc using authentic samples as standards gave the following results: urethane, 51%; *trans*-bromomethoxycyclohexane, 5%; bicyclo-

hexenyl, ~1%; *trans*-dibromocyclohexane, 20%; *N*-cyclohexylurethane **4**, 2%; *cis*-*N*-(2-chlorocyclohexyl)urethane **2**, 39%; *trans*-*N*-(2-chlorocyclohexyl)urethane **3**, 9%. No trace of *cis*- or *trans*-*N*-(2-bromocyclohexyl)urethane could be detected by vpc or tlc. The bromomethoxycyclohexane and dibromocyclohexane were isolated from an aliquot by preparative vpc for complete identification (ir, ^{1}H nmr). Another aliquot (12 ml) was separated by preparative tlc on silica gel (ether–hexane 1:2) to afford the *cis*-β-chlorocarbamate **2**, mp 55–57 °C (0.184 g, 37%), the *trans*-β-chlorocarbamate **3**, mp 94–96 °C (0.039 g, 8%), and urethane, mp 44–46 °C (0.113 g, 53%).

Simultaneous Addition of N-Chlorourethane and N-Bromo-α-chloroacetamide to Cyclohexene

Photochemical Addition

N-Chlorourethane (1.950 g, 95% active chlorine, 15 mmol), *N*-bromo-α-chloroacetamide (0.173 g, 1 mmol), 1-octene (2.5 ml, ~25 mmol) in methylene chloride (75 ml), and absolute methanol (2 ml) in a Vycor cell were irradiated at −70 °C at 254 nm in a Rayonnet RPR 100 reactor for 6 h. The solvent was evaporated in a rotating evaporator and the residue (3.72 g) separated by column chromatography and preparative tlc (ether–hexane 1:2) into two main fractions. The less polar fraction (3.265 g) was an oil and had ir and ^{1}H nmr practically identical to those of *N*-(2-chlorooctyl)urethane **11**. It was dried carefully and submitted to microanalysis: C 55.07%, H 9.14%, Cl 13.68%, Br 2.57%. Assuming that the fraction contained only *N*-(2-chlorooctyl)urethane **11** and *N*-(2-bromooctyl)urethane **12**, the halogen analysis would correspond to 92.3% of **11** (84% yield) and 7.7% of **12** (7% yield).

The more polar fraction, mp 43–44 °C (0.260 g), had ir and ^{1}H nmr spectra very similar to those of *N*-(2-bromooctyl)-α-chloroacetamide **13**. The crystals were ground in a mortar, dried under vacuum, and submitted to bromine and chlorine microanalysis: Br 26.78%, Cl 13.24%. Again assuming that this fraction contained only *N*-(2-bromooctyl)-α-chloroacetamide **13** and *N*-(2-chlorooctyl)-α-chloroacetamide **14**, the analysis would correspond to 94.6% of **13** (87% yield) and 5.4% of **14** (5% yield).

Chromous Chloride Promoted Addition

The reaction was carried out under the usual conditions: chromous chloride solution (18 ml, 18 mmol) added over 2 h, *N*-chlorourethane (1.954 g, 95% active chlorine, 15 mmol), *N*-bromo-α-chloroacetamide (1.175 g, 1 mmol), 1-octene (2.5 ml, ~25 mmol), chloroform (15 ml), absolute methanol (5 ml), dry ice – methanol bath. The mixture was poured into ice and water (10 ml) and rapidly extracted with ether (4 × 200 ml), work-up A (1). The residue (3.25 g) was separated into two fractions as above, each of them being submitted to bromine and chlorine analysis. The oily fraction (2.934 g) had Br 2.44% and Cl 13.75%, which would correspond to 92.7% of β-chlorocarbamate **11** (76% yield) and 7.3% of β-bromocarbamate **12** (6% yield). The crystalline fraction, mp 41–43 °C (0.222 g), had Br 27.19% and Cl 12.99%, which would correspond to 96.3% of β-bromoamide **13** (75% yield) and 3.7% of β-chloroamide **14** (3% yield).

Addition of N-Chloropiperidine to Cyclohexene

Ferrous Sulfate – Ferric Chloride Promoted Addition

The reaction was carried out at 0 °C, under nitrogen, according to the method described by Minisci *et al.* (21) with the following quantities: *N*-chloropiperidine (6.50 g, 92% active chlorine, 50 mmol), ferric chloride (7 g), ferrous sulfate (14 g), and cyclohexene (100 ml, 100 mmol). The reaction mixture was poured into cold water (500 ml), acidified with 4 *N* HCl (10 ml), and extracted with ether. The aqueous phase was made basic by adding 4 *N* NaOH (60 ml) then extracted with methylene chloride (4 × 200 ml). Molecular distillation of the residue (7.4 g) at 70 °C/0.1 torr gave a mixture (6.8 g, 67%) of *cis- and trans-N-(2-chlorocyclohexyl)piperidine* **17** and **18** in a 2:1 ratio according to the ^{1}H nmr spectrum. The two isomers were separated by preparative layer chromatography on silica gel (ethyl acetate – hexane 1:2). *cis* Isomer **17**: ν_{max} (CS_2) 680 cm^{-1} (C-Cl axial (31)); δ (CS_2) 1.0–2.1 (14H), 2.2–2.7 (5H, H-3 + 4H of the piperidine ring), 4.43 ppm (m, $\Delta\nu_{1/2}$ = 6.5 Hz, H-2 equatorial). The picrate melted at 140–141 °C (lit. (21) 146–147 °C). *trans* Isomer **18**: ν_{max} (CS_2) 730 cm^{-1} (C-Cl equatorial (31)); δ (CS_2) 1.0–2.1 (14H), 2.1–2.7 (5H, H-1 + 4H of the piperidine ring), 3.72 (m, $\Delta\nu_{1/2}$ = 25 Hz, H-2 axial). The picrate melted at 153–154 °C (lit. (21) 153–154 °C).

Titanous Chloride Promoted Addition

The addition was carried out under nitrogen as described by Stella[26] at −15 °C (CCl_4 – dry ice bath) with 60 g (100% active chlorine, 50 mmol) of *N*-chloropiperidine and 100 ml (100 mmol) of cyclohexene in 50 ml of methanol. Titanous chloride (6 ml of a 26% commercial solution, 10 mmol) was added dropwise and the mixture stirred at −15 °C for an additional 30 min. The reaction mixture was made strongly alkaline by adding 10 *N* sodium hydroxide. The precipitate was filtered on Celite and washed many times with ether. The ether layer was decanted and dried. The residue was distilled at 64 °C/0.01 torr to afford 7.4 g (75%) of a mixture of *cis- and trans-N-(2-chlorocyclohexyl)piperidine* **17** and **18** in a 2:1 ratio according to the ^{1}H nmr spectrum; ν_{max} (CS_2) 680 (C-Cl axial) and 730 cm^{-1} (C-Cl equatorial).

Chromous Chloride Promoted Addition

The reaction was carried out under the usual conditions: *N*-chloropiperidine (4.77 g, 100% active chlorine, 40 mmol), cyclohexene (8 ml, 80 mmol), chloroform (100 ml), absolute methanol (20 ml), dry ice – methanol bath (−78 °C). The chromous chloride solution (80 ml, 80 mmol) was added over 5 h. The reaction mixture was allowed to warm up to *ca.* 0 °C then acidified and extracted with ether. The aqueous phase was made strongly alkaline with a 10 *N* sodium hydroxide solution in methanol–water (1:1). The precipitate was filtered on Celite and washed many times with ether. The ether layer was washed with water then dried. The solvent was removed in the rotating evaporator. The piperidine was removed *in vacuo* to give 1.12 g (14%) of a mixture of **17** and **18** in a 2.5:1 ratio according to the ^{1}H nmr spectrum; ν_{max} (CS_2) 680 and 730 cm^{-1}; *m/e* 201, 203 (3:1, M^+).

Chromous Chloride Promoted Addition of N-Chloropiperidine to Ethyl Vinyl Ether

A solution of *N*-chloropiperidine (6.0 g, 50 mmol) in absolute methanol (50 ml) was cooled in a dry ice – methanol bath (−78 °C). Freshly distilled ethyl vinyl ether (7.2 g, 100 mmol) cooled to −78 °C was added. The chromous chloride solution (80 ml, 80 mmol) was

[26]L. Stella, Thèse de Doctorat ès-Sciences physiques, Université de Provence, 1972.

added over 30 min. Then sodium methoxide (50 ml of a ~1 *M* solution) was added. The mixture was allowed to warm up to 0 °C and made strongly alkaline with 10 *N* sodium hydroxide. The residue obtained after the usual work-up was distilled to give two compounds: (*a*) The *α-chloroacetal* **16**, bp 34 °C/15 torr (1.68 g, 24%); ν_{max} (CCl_4) 1060 and 1030 (acetal), 720 cm^{-1} (C-Cl); δ (CCl_4) 1.23 (t, J = 7 Hz, OCH_2CH_3), 3.36 (s, OCH_3), 3.45 (d, J = 5.5 Hz, $ClCH_2CH$), 3.65 and 3.68 (two q of equal intensity, J = 7 Hz, OCH_2CH_3), 4.58 ppm (t, J = 6 Hz, CH_2CH(O)(O)); *m/e* 107, 109 (5:2, $M^+ - OCH_3$). (*b*) The *adduct* **15**, bp 85–90 °C/15 torr (1.27 g, 15%); ν_{max} (CCl_4) 1060 and 1130 (acetal), 1300 cm^{-1} (C—N); δ ($CDCl_3$) 1.22 (t, J = 7 Hz, OCH_2CH_3), 1.4–1.8 (6H, piperidine ring), 2.5 (4H, piperidine ring), 2.53 (d, J = 5 Hz, NCH_2CH), 3.40 (s, OCH_3), 3.67 and 3.70 (two q, J = 7 Hz, OCH_2CH_3), 4.67 ppm (t, J = 5 Hz, CH_2CH(O)(O)); *m/e* 187 (M^+). *Anal.* calcd. for $C_{10}H_{21}O_2N$: C 64.13, H 11.30; found: C 63.74, H 11.28.

Acknowledgements

We are grateful to the "Ministère de l'Education du Québec" and the National Research Council of Canada for financial assistance. We thank P. Mackiewicz who carried out the additions of *N*-chloropiperidine.

1. H. Driguez, J. M. Paton, and J. Lessard. Can. J. Chem. This issue.
2. F. A. L. Anet and E. Leblanc. J. Am. Chem. Soc. **79**, 2649 (1957); F. A. L. Anet. Can. J. Chem. **37**, 58 (1959).
3. (*a*) C. E. Castro and W. C. Kray, Jr. J. Am. Chem. Soc. **85**, 2768 (1963); (*b*) W. C. Kray, Jr. and C. E. Castro. J. Am. Chem. Soc. **86**, 4603 (1964).
4. L. H. Slaugh and J. H. Raley. Tetrahedron, **20**, 1005 (1964).
5. (*a*) J. K. Kochi and D. D. Davis. J. Am. Chem. Soc. **86**, 5264 (1964); (*b*) D. M. Singleton and J. K. Kochi. J. Am. Chem. Soc. **89**, 6547 (1967); (*c*) J. K. Kochi and J. W. Powers. J. Am. Chem. Soc. **92**, 137 (1970).
6. D. H. R. Barton and N. K. Basu. Tetrahedron Lett. 3151 (1964); D. H. R. Barton, N. K. Basu, R. H. Hesse, F. S. Morehouse, and M. M. Pechet. J. Am. Chem. Soc. **88**, 3016 (1966).
7. P. Davis, M. G. Evans, and W. C. E. Higginson. J. Chem. Soc. 2563 (1951).
8. C. F. Wells and M. A. Salam. Chem. Ind. 2079 (1967).
9. W. Schmidt, J. M. Swinehart, and H. Taube. Inorg. Chem. **7**, 1984 (1968).
10. J. R. Hanson and E. Premuzic. Angew. Chem. Int. Ed. Engl. **7**, 247 (1968); J. R. Hanson. Synthesis, 1 (1974).
11. P. A. Bohm and P. I. Abell. Chem. Rev. **62**, 599 (1962); D. I. Davies and S. J. Cristol. *In* Advances in free-radical chemistry. Vol. 1. *Edited by* G. H. Williams. Logos Press Ltd. London. 1965. pp. 155 ff; K. Shrage. Tetrahedron, **27**, 3033 (1967); C. L. Osborn, T. V. Van Auken, and D. J. Trecker. J. Am. Chem. Soc. **90**, 5806 (1968) and references cited therein.
12. N. A. Lebel. J. Am. Chem. Soc. **82**, 623 (1960); N. A. Lebel, P. D. Beirne, E. R. Karger, J. C. Powers, and P. Subramanian. J. Am. Chem. Soc. **85**, 3199 (1963); K. Kwart and J. L. Nyce. J. Am. Chem. Soc. **86**, 2601 (1964).
13. H. Taube and H. Myers. J. Am. Chem. Soc. **76**, 2103 (1954); A. G. Sykes. Chem. Br. **6**, 159 (1970) and references cited therein.
14. (*a*) W. Backman, F. Van de Craats, and P. J. Smit. Recl. Trav. Chim. Pays Bas, **83**, 1253 (1954); (*b*) J. K. Kochi. *In* Free radicals. Vol. 1. *Edited by* J. K. Kochi. John Wiley and Sons Inc. New York. 1973. pp. 626 and 627.
15. M. Anbar and P. Neta. Int. J. Appl. Radiat. Isot. **18**, 493 (1967); C. Walling. Bull. Soc. Chim. Fr. 1069 (1968).
16. (*a*) J. K. Kochi and D. Buchanan. J. Am. Chem. Soc. **87**, 853 (1965); (*b*) R. P. A. Sneeden and H. P. Throndsen. Chem. Commun. 509 (1965); (*c*) R. G. Coombes, M. D. Johnson, and N. Winterton. J. Chem. Soc. 7029 (1965); (*d*) W. Schmidt, J. H. Swinehart, and H. Taube. J. Am. Chem. Soc. **93**, 1117 (1971); (*e*) H. Cohen and D. Meyerstein. J. Chem. Soc. Chem. Commun. 320 (1972).
17. D. J. Trecker and J. P. Henry. J. Am. Chem. Soc. **85**, 3204 (1963); S. J. Cristol and D. I. Davies. J. Org. Chem. **29**, 1282 (1964).
18. J. K. Kochi. Science, **155**, 415 (1967).
19. M. Asscher and D. Vofsi. J. Chem. Soc. B, 947 (1968); J. Chem. Soc. 4962 (1964); J. Chem. Soc. 3921 (1963); J. Chem. Soc. 1887 (1963).
20. H. Matsumoto, T. Nakano, and Y. Nagai. Tetrahedron Lett. 5147 (1973) and literature cited therein.
21. F. Minisci, R. Galli, and G. Pollina. Chim. Ind. (Milan), **47**, 736 (1965) and references cited therein.
22. J. M. Surzur and L. Stella. Tetrahedron Lett. 2191 (1974).
23. F. Minisci, R. Galli, and M. Cecere. Chim. Ind. (Milan), **48**, 132 (1966); F. Minisci. Chem. Ind. (Milan), **49**, 705 (1967).
24. C. Walling, E. R. Briggs, K. B. Wolfstirn, and F. R. Mayo. J. Am. Chem. Soc. **70**, 1537 (1948); C. Walling, D. Seymour, and K. B. Wolfstirn. J. Am. Chem. Soc. **70**, 2559 (1948); P. I. Abell. *In* Free radicals. Vol. 2. *Edited by* J. K. Kochi. John Wiley and Sons Inc. New York. 1973. p. 86.
25. D. Touchard and J. Lessard. Tetrahedron Lett. 4425 (1971).
26. J. Lessard and J. M. Paton. Tetrahedron Lett. 4883 (1970); J. Lessard, H. Driguez, and J. P. Vermes. Tetrahedron Lett. 4887 (1970).
27. M. Conrad and H. Hock. Ber. Dtsch. Chem. Ges. **36**, 2206 (1903); Beilstein, **3**, 24 (1921).
28. A. I. Vogel. Practical organic chemistry. Longmans. London. 1956. p. 334.
29. A. R. Pray. Inorganic synthesis. McGraw-Hill, New York. 1957. p. 153.
30. J. D. Roberts, E. R. Turnbull Jr., W. Bennett, and R. Armstrong. J. Am. Chem. Soc. **73**, 3116 (1950); E. R. Lippincott. J. Am. Chem. Soc. **73**, 2001 (1951); G. E. Pollard. Spectrochim. Acta, **18**, 837 (1962).
31. C. Altona. Tetrahedron Lett. 2325 (1968).

Oxidation with chromium(VI) oxide – pyridine complex. A study of reaction parameters using cholesterol as substrate[1]

EDWARD PIERS AND PAUL M. WORSTER

Department of Chemistry, University of British Columbia, 2075 Wesbrook Place, Vancouver, B.C., Canada V6T 1W5

Received September 27, 1976

EDWARD PIERS and PAUL M. WORSTER. Can. J. Chem. **55**, 733 (1977).

Oxidation of cholesterol with chromium(VI) oxide – pyridine complex under various conditions produced cholest-5-en-3-one accompanied by varying amounts of cholest-4-ene-3,6-dione. The efficiency of the oxidation and the product distribution were found to be dependent on the atmosphere, temperature, molar ratio of oxidant to substrate, molar ratio of pyridine to chromium trioxide, the heterocyclic amine used, and the proton source employed. The yield of cholest-5-en-3-one was optimized by oxidation of cholesterol with a ten-fold excess of the monopyridine – chromium(VI) oxide complex in dichloromethane under a nitrogen atmosphere at 0°C.

EDWARD PIERS et PAUL M. WORSTER. Can. J. Chem. **55**, 733 (1977).

L'oxydation du cholesterol par le complexe d'oxyde de chrome(VI) – pyridine sous diverses conditions conduit à la cholestène-5 one-3 accompagnée par des quantités variables de cholestène- 4 dione-3,6. On a trouvé que l'efficacité de l'oxydation et la distribution des produits dépendent de l'atmosphère, de la température, du rapport molaire d'oxydant–substrat, du rapport molaire de pyridine – trioxyde de chrome, de l'amine hétérocyclique et de la source de proton utilisée. On a pu optimiser le rendement de la cholestène-5 one-3 par oxydation du cholesterol avec un excès de dix fois de complexe d'oxyde de chrome(VI) – monopyridine dans le dichlorométhane, sous atmosphère d'azote, à 0°C.

[Traduit par le journal]

The oxidation of alcohols to ketones or aldehydes with chromium(VI) reagents in non-acidic media has found extensive application in organic synthesis. However, even though a significant number of technically advantageous modifications on the original work of Sarett (1) have been reported (2–7), little detail concerning the effect of various reaction parameters on oxidations with chromium(VI) oxide – pyridine complexes has as yet become available.[2] Furthermore, it is well known that chromium(VI) oxidation of homoallylic alcohols to the corresponding β,γ-unsaturated ketones fails in acidic media (9) and is troublesome in non-acidic media (10). In order to provide fundamental information regarding both of these problems, we have studied the effect of several reaction parameters on the outcome of the chromium(VI) oxide – pyridine oxidation of cholesterol (**1**) in dichloromethane.

Oxidation of **1** under a variety of conditions afforded, in each case, the expected product cholest-5-en-3-one (**2**) accompanied by varying amounts of cholest-4-ene-3,6-dione (**3**) and trace amounts of 6β-hydroxycholest-4-en-3-one (**4**).[3] In addition, varying quantities of starting material **1** were recovered. Some of our initial results are summarized in Table 1.

As expected (3, 5), complete oxidation of cholesterol (**1**) required 6 mol equiv. of oxidant (run 3), while use of lesser quantities of oxidizing agent resulted in recovery of appreciable

[1]Support for this work from the National Research Council of Canada and an NRCC scholarship (to P.M.W.) are gratefully acknowledged.

[2]Collins (3) has shown that a six-fold molar excess of $CrO_3 \cdot 2C_5H_5N$ complex was required to oxidize primary and secondary aliphatic alcohols, while Holum (8) found that pyridine solutions of allylic or benzylic alcohols usually require only a three-fold excess of CrO_3 for complete oxidation.

[3]The allylic alcohol **4** is oxidized much faster than the homoallylic alcohol **1**. For the purpose of product analysis, compound **4** could be ignored since the ratio of **3**:**4** was >5:1. Oxalic acid catalyzed isomerization of the product mixture afforded compounds **5** and **3** along with trace amounts of **6**.

TABLE 1. $CrO_3 \cdot 2C_5H_5N$ oxidations of cholesterol (**1**) in CH_2Cl_2

Run[a]	Changes	Oxidant/alcohol molar ratio[b]	Percentage mass recovery[c]	Average product ratio[d] **2**:**3** (%**1**)
1	Standard	2	96	89:11 (51)
2	Standard	4	94	85:15 (16)
3	Standard	6	88	85:15 ($\leq$3)
4	N_2 atmosphere	4	89	91:9 (37)
5	N_2 atmosphere	6	86	93:7 (9)
6	Temp 0°C	4	89	94:6 (29)
7	Temp 0°C	6	85	92:8 (9)
8	Standard + H_2O[e]	4	87	84:16 (79)
9	Standard + H_2O[e] + P_2O_5[f]	4	91	91:9 (41)

[a]All experiments were done at least in duplicate with the standard reaction being done in air at 23 ± 1°C for 30 min; cholesterol (**1**) (1 mmol), CrO_3 (2, 4, or 6 mmol), pyridine (12 mmol), CH_2Cl_2 (50 ml).
[b]This indicates the molar ratio of CrO_3 to cholesterol.
[c]Non-acidic material recovered after crude oxidation product was isomerized with aqueous oxalic acid.
[d]A measure of cholesterol (**1**) recovered and the ratio of cholest-5-en-3-one (**2**) to cholest-4-ene-3,6-dione (**3**) as determined by ^{1}Hmr integration of the olefinic protons of compounds **1**, **5**, and **3**, respectively.
[e]2 mmol of H_2O added.
[f]6 mmol of P_2O_5 added.

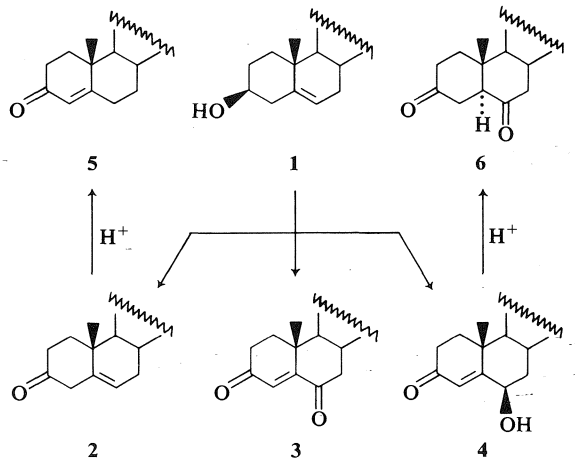

amounts of **1** (runs 1, 2). The drop in oxidation efficiency, along with an increase in the ratio of products **2**:**3**, caused by replacing the air atmosphere with nitrogen (runs 4, 5) was from a synthetic viewpoint a significant observation and was presumably due to the known (11) uptake of oxygen in chromate oxidations and the susceptibility of **2** to autoxidation. Furthermore, in contrast to Collins' (3) conclusion, a lower reaction temperature appeared to decrease oxidation efficiency (at least within a specified reaction time), but also produced a synthetically more pleasing ratio of **2**:**3** (runs 6, 7). Finally, addition of water (run 8) had the expected effect, since it is known (3) that the $CrO_3 \cdot 2C_5H_5N$ complex readily hydrates to give an insoluble, unreactive species $C_{10}H_{12}Cr_2N_2O_7$. Addition of the dehydrating agent P_2O_5 (run 9) failed to restore full oxidation efficiency.[4]

Table 2 summarizes results of experiments aimed at determining the effect of adding varying amounts of pyridine in the *in situ* oxidation of **1** with CrO_3–pyridine in dichloromethane. These results clearly show that, although pyridine is necessary for oxidation (run 5), there is no justification for the current practice (5) of employing a 2:1 molar ratio of pyridine to CrO_3 for the *in situ* generation of Sisler's complex (12). Thus, use of a 1:1 CrO_3–pyridine ratio gave oxidation results essentially identical with those obtained by employing the two substances in a 1:2 ratio (runs 2,3 and 7,8). Furthermore, filtering the solutions containing either the 2:1 or the 1:1 pyridine–CrO_3 complex before addition of the sterol left the subsequent oxidation results unchanged (footnote *e*, Table 2), even though CrO_3 itself is completely insoluble in dichloromethane. Mechanistically, therefore, our results are at least consistent with the postulate that oxidation takes place via the intermediate monopyridine complex **7**, rather than via the dipyridine complex **8** usually postulated.

Results obtained from oxidation of cholesterol (**1**) (1 mmol) with CrO_3 (6 mmol) in the presence of several different heterocyclic amines (6 mmol) in dichloromethane for 30 min are summarized in Table 3. Of those studied, pyridine appeared

[4]We feel that the most important aspect of adding P_2O_5 is the addition of a good proton source, as phosphoric acid, rather than the use of P_2O_5 as a dehydrating agent.

TABLE 2. Oxidation of cholesterol (**1**) with CrO_3 in CH_2Cl_2 in the presence of varying amounts of pyridine

Run[a]	Oxidant/alcohol molar ratio[b]	Pyridine/oxidant molar ratio	Percentage mass recovery[c]	Average product ratio[d] **2**:**3** (%**1**)
1	6	6	90	82:18 (6)
2[e]	6	2	91	86:14 (2)
3[e]	6	1	93	89:11 (4)
4[e]	6	0.5	89	91:9 (14)
5	6	0	92	— (100)
6	4	3	89	87:13 (15)
7	4	2	90	91:9 (15)
8	4	1	93	92:8 (17)

[a]All experiments were done at least in duplicate in air at 23 ± 1°C for 30 min; cholesterol (**1**) (1 mmol), CrO_3 (4 or 6 mmol), pyridine (0–36 mmol), CH_2Cl_2 (50 ml).
[b]As in footnote *b*, Table 1.
[c]As in footnote *c*, Table 1.
[d]As in footnote *d*, Table 1.
[e]Filtering the solution containing either the 2:1 or the 1:1 pyridine–CrO_3 complex before addition of the sterol **1** left the oxidation results unchanged but filtering the 1:2 reagent complex (run 4) increased substantially the recovered cholesterol (to > 30%).

TABLE 3. Oxidation of cholesterol (**1**) with CrO_3 in CH_2Cl_2 in the presence of different pyridine analogs

Run[a]	Amine (pK_{BH^+})	Percentage mass recovery[b]	Average product ratio[c] **2**:**3** (%**1**)
1	Quinoline (5.00)	97	85:15 (34)
2	Pyridine (5.25)	91	89:11 (4)
3	4-Methylpyridine (6.02)	95	75:25 (2)
4	2,4-Dimethylpyridine (6.99)	84	79:21 (3)
5	2,4,6-Trimethylpyridine (7.43)	79	80:20 (31)

[a]All experiments were done at least in duplicate in air at 23 ± 1°C for 30 min; cholesterol (**1**) (1 mmol), CrO_3 (6 mmol), amine (6 mmol), CH_2Cl_2 (50 ml).
[b]As in footnote *c*, Table 1.
[c]As in footnote *d*, Table 1.

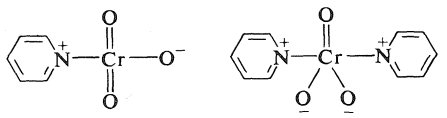

7 **8**

to be the most favorable amine for the purpose of minimizing the formation of enedione product **3**. Unexpectedly, it was found that virtually no oxidation occurred when aryl amines such as *N*,*N*-dimethylaniline (13) (pK_{BH^+} = 5.15) were used. Similarly, little if any cholesterol was oxidized when 2,2-dipyridyl, 4,4-dipyridyl, or picolinic acid were employed. Recently, the latter compound was shown (14) to exert a strong rate accelerating effect on chromium(VI) oxidation of alcohols in aqueous acidic media. Finally, it was found that introduction of amines such as triethylamine (pK_{BH^+} = 11.0) to a solution of the active oxidizing complex (**7** or **8**) resulted in a dramatic increase in the amount of cholesterol that was recovered.[5]

Other studies showed that enone **5** is not produced directly in the oxidizing media employed and that **5** is stable under the oxidation conditions. Therefore, it is probable that **3** is produced from **2**, probably via enolization followed by further oxidation. However, the above results demonstrate the futility of trying to avoid the formation of **3** by simply buffering the reaction media with an amine. Nevertheless, from a synthetic point of view, it is important to note that the favorable parameter changes outlined in Tables 1, 2, and 3 can be advantageously combined. That is, it was found that oxidation of cholesterol (**1**) with a ten-fold excess of the monopyridine – chromium(VI) oxide com-

[5]The proton dependence of oxidations with CrO_3–amine reagents will be the subject of a future publication.

plex in dichloromethane at 0°C under a nitrogen atmosphere produced, in very high yield, practically pure cholest-5-en-3-one (**2**).[6]

1. G. I. Poos, G. E. Arth, R. E. Beyler, and L. H. Sarett. J. Am. Chem. Soc. **75**, 425 (1953).
2. K-E. Stensio and C. A. Wachtmeister. Acta Chem. Scand. **18**, 1013 (1964); K-E. Stensio. Acta Chem. Scand. **25**, 1125 (1971).
3. J. C. Collins, W. W. Hess, and F. J. Frank. Tetrahedron Lett. 3363 (1968); J. C. Collins and W. W. Hess. Org. Synth. **52**, 5 (1972).
4. W. M. Coates and J. R. Corrigan. Chem. Ind. 1594 (1969).
5. R. Ratcliffe and R. Rodehorst. J. Org. Chem. **35**, 4000 (1970); R. Ratcliffe. Org. Synth. **55**, 84 (1975).
6. E. J. Corey and J. W. Suggs. Tetrahedron Lett. 2647 (1975).
7. K. B. Sharpless and K. Akashi. J. Am. Chem. Soc. **97**, 5927 (1975).
8. J. R. Holum. J. Org. Chem. **26**, 4814 (1961).
9. L. F. Fieser. J. Am. Chem. Soc. **75**, 4377 (1953).
10. J. B. Jones and K. D. Gordon. Can. J. Chem. **50**, 2712 (1972), and references cited therein.
11. K. B. Wiberg and T. Mill. J. Am. Chem. Soc. **80**, 3022 (1958).
12. H. H. Sisler, J. D. Bush, and O. E. Accountius. J. Am. Chem. Soc. **70**, 3827 (1948).
13. F. Holloway, M. Cohen, and F. H. Westheimer. J. Am. Chem. Soc. **73**, 65 (1951).
14. T-Y. Peng and J. Roček. J. Am. Chem. Soc. **98**, 1026 (1976).

[6]Analogous results were obtained when 3β-hydroxyandrost-5-ene was substituted for cholesterol in this and other experiments described in this communication. In addition, the results obtained from the oxidation of primary (*e.g.*, 1-octadecanol), secondary (*e.g.*, 4-*tert*-butylcyclohexanol), and benzylic (*e.g.*, $C_6H_5CH_2OH$) alcohols with either the dipyridine or the monopyridine complex of CrO_3 were indistinguishable.

Canadian Journal of Chemistry

Published by
THE NATIONAL RESEARCH COUNCIL OF CANADA

Journal canadien de chimie

Publié par
LE CONSEIL NATIONAL DE RECHERCHES DU CANADA

Volume 55 Number 5 March 1, 1977

Volume 55 numéro 5 1 mars 1977

Information theory and bulk rotational or vibrational relaxation processes

ANDREW W. YAU AND HUW O. PRITCHARD

Centre for Research in Experimental Space Science, York University, Downsview, Ont., Canada M3J 1P3

Received July 14, 1976

ANDREW W. YAU and HUW O. PRITCHARD. Can. J. Chem. **55**, 737 (1977)

The possible occurrence in bulk relaxation of pure-exponential, near-exponential, and non-exponential decay of the total energy is examined in terms of the normal-mode and information-theoretic approaches. Experimental tests are suggested for the identification of pure-exponential decay caused by adherence to the 'sum rule', and of near-exponential decay. In the case of near-exponential decay (as opposed to pure-exponential decay), it is not possible to derive reliable state-to-state rate constants by invoking approximate adherence to the sum rule.

ANDREW W. YAU et HUW O. PRITCHARD. Can. J. Chem. **55**, 737 (1977).

On examine la possibilité de l'existence, dans la relaxation globale, de décompositions exponentielles pures, pratiquement exponentielle et non-exponentielle de l'énergie totale en termes des approches du mode normal et de l'information théorique. On suggère des essais expérimentaux permettant d'identifier une décomposition exponentielle pure par une adhésion à la "règle des sommes" ainsi qu'une décomposition pratiquement exponentielle. Dans le cas d'une décomposition pratiquement exponentielle (par opposition à une décomposition exponentielle pure), il n'est pas possible d'obtenir des constantes de vitesse d'état à état qui soient certaines en invoquant l'adhésion approximative à la "règle des sommes".

[Traduit par le journal]

Two recent papers from this laboratory have examined the bulk relaxation behaviour of a model diatomic molecule, infinitely diluted in an inert-gas bath, in terms of normal modes of relaxation (1, 2). An alternative treatment of simple bulk relaxation processes, in terms of an information-theoretic approach (3), has also been developed recently by Procaccia and Levine (4–6). On the surface, it appears that these two treatments are not always consistent with each other: in particular, markedly non-exponential decay of the total energy would seem to be a distinct possibility, given the right kind of experiment (2), whereas accepting pure-exponential decay as a constraint, the information-theoretic treatment provides an attractive and elegant framework within which to describe such bulk relaxation processes. Since both approaches to the problem are based on the application of the master equation, we will begin by restating the relevant useful equations.

The isothermal relaxation of a diatomic gas, with N rotation–vibration levels, diluted in a heat bath is governed by the transition matrix **A** where (1)

$$[1] \quad A_{ij} = [\mathrm{M}]Z\left\{(1-\delta_{ij})P_{ji} - \delta_{ij}\times\sum_{k=0}^{N-1}(1-\delta_{ik})P_{ki}\right\}$$

In [1], P_{ji} is the probability per collision for a transition *from* state i *to* state j, [M] is the concentration of buffer gas, and Z is the collision number. As a consequence of detailed balancing

$$[2] \quad A_{ij}\,\tilde{n}_i = A_{ji}\,\tilde{n}_j$$

where $\tilde{n}_i$ is the population of the ith level at equilibrium, **A** may be symmetrized to **B** by the

transformation

$$[3] \qquad \mathbf{B} = \mathbf{N}^{1/2}\,\mathbf{A}\,\mathbf{N}^{-1/2}$$

where

$$[3a] \qquad N_{ij} = \delta_{ij}\,\tilde{n}_i$$

The matrix **B** therefore has real eigenvalues, λ_j, which may be found using the transformation matrix **S**, *i.e.*

$$[4] \qquad \mathbf{B}\,\mathbf{S} = \mathbf{S}\,\mathbf{\Lambda}$$

The final attainment of Boltzmann equilibrium is guaranteed by the fact that one eigenvalue, λ_{N-1}, is zero, with a corresponding eigenvector

$$[4a] \qquad S_{i,N-1} = \tilde{n}_i^{1/2}$$

and all of the other eigenvalues are negative. The time evolution of the total internal energy of the system, $E(t)$, is

$$[5] \quad E(t) = \sum_{i=0}^{N-1} \varepsilon_i n_i(t) = \sum_{j=0}^{N-1} e^{\lambda_j t} \sum_{i=0}^{N-1} \tilde{n}_i^{1/2} \varepsilon_i S_{ij} \times \sum_{k=0}^{N-1} S_{kj} \tilde{n}_k^{-1/2} n_k(0)$$

where $n_i(t)$ is the population of the ith level at time t, and ε_i is the energy of that level. An alternative way of writing [5] is (1)

$$[5a] \qquad E(t) = \sum_{j=0}^{N-1} \xi_j\, e^{\lambda_j t}$$

where ξ_j, the amount of energy which decays with characteristic time constant λ_j, is given by

$$[6] \quad \xi_j = \sum_{i=0}^{N-1} \tilde{n}_i^{1/2} \varepsilon_i S_{ij} \sum_{k=0}^{N-1} S_{kj} \tilde{n}_k^{-1/2} n_k(0)$$

Inspection of [5] or [5*a*] shows that, in general, the energy must decay in a non-exponential manner: pure-exponential decay will occur under rather special circumstances. Nevertheless, these model calculations (1, 2) have shown that, often, very few of the normal modes may have associated with them a significant value of ξ_j, and in these cases the relaxation behaviour would be very difficult indeed to distinguish from a pure-exponential decay under normal experimental conditions; other examples are given by Cukier and Hynes (7).

Pure-exponential decay can occur in two ways. First, in a trivial way, when all the non-zero eigenvalues are degenerate: the necessary and sufficient condition for this to occur (8) is that the transition rate matrix should have the form

$$[7] \quad A_{ij} = \alpha \left\{ (1 - \delta_{ij})\tilde{n}_j - \delta_{ij} \times \sum_{k=0}^{N-1} (1 - \delta_{ik})\tilde{n}_k \right\}$$

where α is a constant.[1] Second, a much less restrictive and well-known condition (4–13), that the transition rates obey the 'sum rule'

$$[8] \qquad \sum_j \varepsilon_j A_{ij} = \mu(E(\infty) - \varepsilon_i)$$

for all i, where μ is a positive constant, whence

$$[8a] \qquad \frac{dE(t)}{dt} = \mu[E(\infty) - E(t)]$$

Equation 7 is, in fact, a special case of [8]. In conventional terms, we have $0 = \lambda_{N-1} > -\mu = \lambda_{N-2} \geq \lambda_{N-3} \geq \ldots \lambda_0$; adapting the formula of van Kampen (13), the vector of the symmetrized form of [8] corresponding to the eigenvalue $-\mu$ is

$$[9] \qquad S_{i,N-2} = \frac{\tilde{n}_i^{1/2}(E(\infty) - \varepsilon_i)}{\{E^2(\infty) - (E(\infty))^2\}^{1/2}}$$

Using this, together with [4*a*], it is then a simple matter (8) to show that all the other modes of relaxation are passive in the sense that all ξ_j, $j < (N-2)$ are zero: hence each of these $(N-2)$ modes only shuffles the populations without changing the total energy of the assembly of molecules.

The occurrence of pure-exponential decay requires certain relationships between the transition rates. To begin with, we may classify possible transition-probability patterns into three distinct classes.

(*i*) Those which conform to eq. 7, whence both the energy and all the individual populations decay exponentially: we do not know whether there exist any examples of such behaviour in molecular relaxation.

(*ii*) Those which conform to the sum rule, eq. 8, whence the energy will decay exponentially, but the populations will not. Several examples of such conformity are known (7), most notably the Landau–Teller transition probabilities for harmonic-oscillator transitions. It appears also

[1]Since this paper was submitted, we have learnt that this condition has been proved also by Procaccia *et al.* (9).

that certain classically computed V–T transition probabilities (14) for

$$H + HBr(v) \rightleftarrows H + HBr(v')$$

$$Cl + Cl_2(v) \rightleftarrows Cl + Cl_2(v')$$

conform approximately to the sum rule (5). On the other hand, some transition probabilities derived from quantum calculations, in the breathing-sphere approximation (15), on

$$He + CO(v) \rightleftarrows He + CO(v')$$

do not conform, in the sense that the energy evolution derived from these probabilities is not exponential for some initial population distributions.

Adherence to the sum rule is verifiable, in principle at least, by experiment since at long time, after all the initial transients have died out, the evolution of the populations depends on the initial energy but is independent of the fine structure of the initial distribution of that energy. Thus (8)

$$[10] \quad \underset{(t \gg -\lambda_{N-3}^{-1})}{n_i(t)} \rightarrow \tilde{n}_i + n_i(N-2, t)$$

$$= \tilde{n}_i + \tilde{n}_i\, e^{-\mu t} \frac{[E(\infty) - \varepsilon_i][E(\infty) - E(0)]}{\{E^2(\infty) - (E(\infty))^2\}}$$

(*iii*) Those which conform to neither [7] nor [8], in which case neither the energy nor the populations decay in a strictly exponential fashion. Again, we may subdivide into three classes: (*a*) those probabilities which conform to linear surprisal,[2] in which case, as is shown below, the range of eigenvalues can be very small; (*b*) those which conform to more complex surprisal forms (9, 16), a development which arose after we had completed this analysis, and which we will not discuss further; (*c*) arbitrary transition probabilities, such as those used in our own previous model calculations (1, 2), where the range of the eigenvalues can be very large indeed, *cf.* also ref. 17, Fig. 3.

The 'linear surprisal' form of the rate constant is

$$[11] \quad k_{i\rightarrow j} = k^0_{i\rightarrow j} \exp(-\theta|\varepsilon_j - \varepsilon_i|/kT) \equiv ZP_{ji}$$

where $k^0_{i\rightarrow j}$ is the 'prior rate constant' (the rate constant in the absence of any dynamical constraint) and θ is the 'surprisal' (a measure of the effect of the energy defect for transition from state i to state j). For a system with an array of rotation–vibration levels at temperature T (18)

$$[12] \quad k^0_{vJ\rightarrow v'J'} = \text{constant} \times T^{1/2} g_{J'} \times \exp(\Delta) \cdot \Delta \cdot K_1(\Delta)$$

where $g_{J'} = 2J' + 1$, Δ = 'reduced energy transfer' = $(\varepsilon_{vJ} - \varepsilon_{v'J'})/2kT$, and $K_1(\Delta)$ = modified Bessel function of the first order. Since $K_1(\Delta)$ is odd with respect to Δ, eq. 12 satisfies the principle of detailed balancing. This implies that the surprisal θ in eq. 11 is symmetric with respect to the initial and final states, and the rate constant then takes the form

$$[13] \quad k_{vJ\rightarrow v'J'} = \text{constant} \times (2J' + 1) \times \exp(\Delta) \cdot \Delta \cdot K_1(\Delta) \cdot \exp(-2\theta|\Delta|)$$

As examples of V–T transfer, the experimental rates of

$$Li_2^*(v) + M \rightleftarrows Li_2^*(v') + M$$

$$CO^*(v) + M \rightleftarrows CO^*(v') + M$$

have been shown to conform to a linear surprisal form (4). Among the theoretically calculated rates (14)

$$Cl + Cl_2(v) \rightleftarrows Cl + Cl_2(v')$$

$$I + I_2(v) \rightleftarrows I + I_2(v')$$

$$Br + HBr(v) \rightleftarrows Br + HBr(v')$$

have been shown to obey (approximately) the linear surprisal form, although the last reaction does not obey the sum rule (5, 6); more recently (9, 16) the $Cl + Cl_2$ case has been re-analysed, giving a functional (v, v') dependence on the surprisal. No quantal V–T data have yet, to our knowledge, been analysed in this way, but we have shown (8) that the impulsive limit of the first-order distorted-wave approximation for nearest-neighbour transitions has the same temperature dependence as the linear surprisal form. For R–T collisions, the quantal data of Green (19) on

$$He + HD(J) \rightleftarrows He + HD(J')$$

have been analysed by Procaccia and Levine (20): there is (semiquantitative) agreement in respect of the temperature coefficients, and the fit to the linear surprisal form is accurate to about $\pm 20\%$.

Given that many transition probabilities appear to obey the linear surprisal form, it is a simple matter to show that, at least for V–T and

[2]Linear surprisal forms may or may not obey the sum rule.

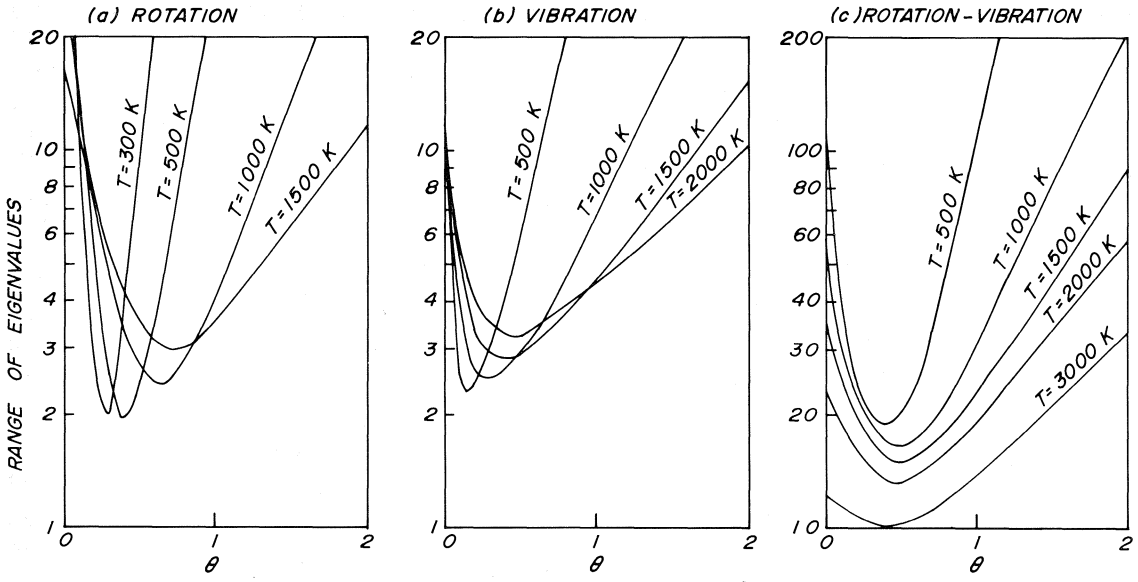

FIG. 1. Comparison of the range of eigenvalues λ_0/λ_{N-2} for the information-theoretic descriptions of three model molecules (see text) for a series of temperatures and surprisal values: (*a*) pure rotational relaxation; (*b*) pure vibrational relaxation; (*c*) mixed rotation–vibration relaxation.

R–T processes, one would expect to find *almost* pure-exponential decay of the energy, *even if* the sum rule is not obeyed. Since in eq. 13, the 'reduced energy transfer' is representative for all diatomic molecules in either pure vibrational or pure rotational relaxation if a reduced temperature scale is used, *viz.* $\beta_v = hc\omega_e/kT$ or $\beta_R = hcB_e/kT$, we can continue to use our previous model molecule, *ortho*-H_2, in this illustration. Figure 1 shows plots of the ratio λ_0/λ_{N-2} (*i.e.* the spread of the eigenvalues) for a range of values of θ, for three kinds of processes: (*a*) pure rotational relaxation involving the lowest 8 rotational states of *ortho*-H_2; (*b*) pure vibrational relaxation involving the lowest 8 vibrational states of $J=1$ H_2;[3] (*c*) mixed vibration–rotation relaxation involving the lowest 20 levels of *ortho*-H_2. Over a wide range of reduced temperature, the minimum spread in eigenvalues occurs near $\theta = 0.5$, compared with values of θ of the order of unity found in many analyses reported in the literature (20). The fact that the spread of eigenvalues is indeed modest means that these *distinct* relaxation times will be hard to resolve experimentally (1, 2) and the bulk relaxation will *appear* to be very close to a pure-exponential decay, because, in fact, we have an approximation to the $(N-1)$-fold degenerate case, eq. 7.

However, as is well known (1, 7), near-exponential decay (we may define near-exponential decay to mean that it would be difficult to detect experimentally any non-exponential behaviour) can occur when the eigenvalues are well separated, and this is shown by two pairs of calculations illustrated in Fig. 2. In these calculations, we compare the bulk relaxation behaviour for (*a*) rotation and (*b*) vibration, for a temperature change from 700 to 500 K, using transition probabilities *either* of the functional form of [13] *and* having the minimum spread of eigenvalues (see Fig. 1) *or* the empirical set of transition probabilities used previously (1, 2). The lower curve shows that the behaviour is hardly distinguishable[4] for bulk vibrational relaxation, despite the fact that in one case the spread of eigenvalues λ_0/λ_{N-2} is 2.3, whereas in the other case it is 120; in normal-mode terms, this is because the succession of normal modes of longest time constant (see *e.g.* Fig. 3 of ref. 2) are relatively close together, with the last one carrying most of the traffic (*i.e.* ξ_{N-2} dominates).

[3]In the usual formulation, each vibrational state is averaged over its rotational manifold, assuming rotational equilibrium (5). However, there is some difficulty with detailed balancing in such a formulation, and since we are interested at the present time in only a model calculation, we consider only one rotational state.

[4]Of course, drawn out on a much larger scale, both lines are slightly curved.

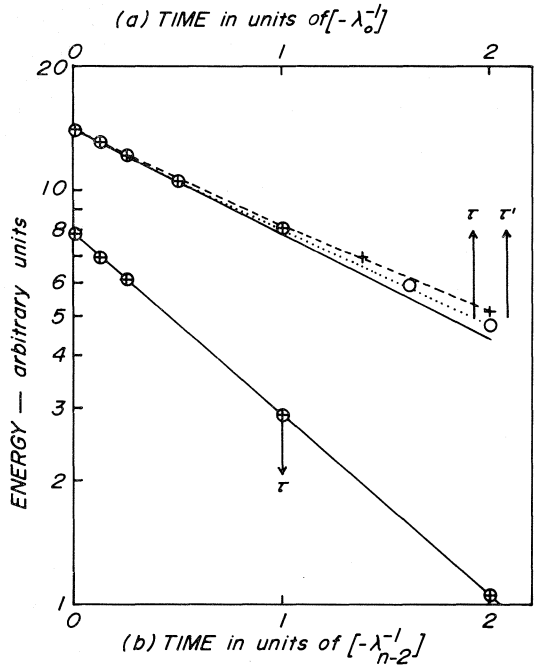

FIG. 2. Logarithmic plots of the total energy *vs.* time for (*a*) pure rotational relaxation and (*b*) pure vibrational relaxation. Open circles represent points calculated using information-theoretic rate constants of *minimum eigenvalue spread*, and crosses represent points calculated with an empirical set of transition rates (1). The solid lines represent exact exponential decay, and the vertical arrows marked τ represent the points at which $1/e$ of the total energy remains: this occurs very close to $-\lambda_{N-2}{}^{-1}$ in the vibrational cases, but near $-2\lambda_0{}^{-1}$ in the rotational cases. The eigenvalue ranges (*i.e.* λ_0/λ_{N-2}) in these calculations were (*a*) rotation 1.9 and 75, (*b*) vibration 2.3 and 120 for the information-theoretic and the empirical rates respectively.

Non-exponential decay of vibrational energy will always be difficult to detect unless the molecule is very anharmonic (which will cause a wider spacing of the eigenvalues) *and* the relative populations of high-v and low-v states change appreciably in the relaxation process.

The upper part of Fig. 2 shows the rotational relaxation behaviour using probabilities which have an eigenvalue range λ_0/λ_{N-2} of 1.9 and 75 respectively. Here the plots are just about distinguishable from each other, and they are both slightly curved. The curvature is of course more severe for the case where the range of eigenvalues is larger, and it is interesting to note that, in this case, the time it takes the energy to relax is closely related to the *fastest* time constant, not the slowest as is usually assumed: Cukier and Hynes (7) also give a numerical example of this kind, and the reasons for this behaviour are easily understood in terms of our previous discussion of rotational sound dispersion (1). For these reasons also, non-exponentiality should be much easier to detect in rotational than in vibrational relaxation, and a relatively simple experiment based on our earlier calculations (2) should suffice to settle the issue one way or the other: all that is necessary is to measure the shock-wave rotational relaxation time for hydrogen from a series of different starting temperatures to a single fixed final temperature; if a monotonically increasing progression of relaxation times is found, converging to the ultrasonic relaxation time for the final temperature in question, then the decay is non-exponential and the treatment depicted in Fig. 1 of ref. 2 would be essentially correct. In the case of T–VR processes, we can expect, as discussed previously (2), a complete spectrum of behaviour from that in which the rotational and vibrational relaxations separate completely to that where they are completely inseparable: in the former case, the considerations we have just discussed would apply, whereas in the latter case, noting (*a*) the larger spread of eigenvalues shown in Fig. 1*c* and (*b*) the apparent failure of Alexander's calculations (21) for T–VR processes in hydrogen to conform to the linear surprisal form, it would seem that non-exponential decay will be the rule rather than the exception. Thus, in fact, we see no real and irreconcilable differences between the normal-mode and the information-theoretic descriptions of bulk relaxation processes.

However, there is one aspect of the information-theoretic approach where we feel that some caution is appropriate. Procaccia and Levine (4–6) have claimed that if the observed decay is exponential, then it is possible to deduce microscopic state-to-state transition rates from the observed *bulk relaxation* time constant. If the sum rule holds, this may well be true, although some doubts have been expressed[5] about this possibility unless the relaxing system behaves in a canonically invariant manner. But it seems that adherence to the sum rule, from the evidence cited above, is unlikely to be the general behaviour, in which case the claim can have, at best, only limited validity. There are two difficulties,

[5]K. E. Shuler and R. I. Cukier, personal communications.

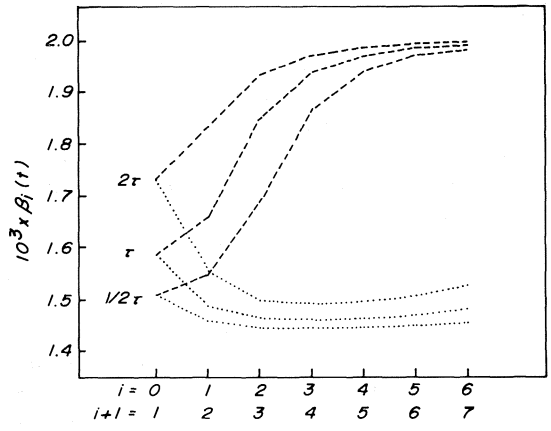

FIG. 3. Comparison of vibrational temperatures at various levels for a sudden cooling process from 700 to 500 K. The temperature is defined as $\beta_i = k \ln [n_i(t)/n_{i+1}(t)]/(\varepsilon_{i+1} - \varepsilon_i)$, and the plots are shown for $t = \frac{1}{2}\tau$, τ, and 2τ where $\tau = -\lambda_{N-2}{}^{-1}$. Dashed line = empirical probabilities (1); dotted line = information-theoretic probabilities of *minimum eigenvalue spread.*

in our view. First, a relaxation may appear to be exponential, or very nearly so, but this in no way implies that the sum rule holds, unless the long-time behaviour of the populations is shown to conform to eq. 10. Second, as can be seen from Fig. 2 (especially in the vibrational case), the bulk relaxation behaviour is extremely insensitive to the transition probabilities assumed: hence, as Carrington (22) recognized, it is a very ill-conditioned problem to work back from the observed bulk relaxation behaviour to the detailed rate constants. As an example of this, we show in Fig. 3 the behaviour of the vibrational population distributions at $\frac{1}{2}\tau$, τ, and 2τ for the two relaxations which are energetically indistinguishable in Fig. 2. Although the bulk relaxation behaviours are only imperceptibly different, the populations show diametrically different evolution behaviours, and it is evident that the ill-conditioned nature of the problem is quite severe: we can do no more than reiterate Carrington's conclusion of 15 years ago, that the present precision of relaxation experiments does not allow a meaningful deduction of transition rate constants from observed bulk relaxation rates. Nevertheless, in the absence of other sources of information, the information-theoretic approach (9) still provides the least-biased guess at a set of transition rates which will reproduce the known behaviour.

Acknowledgments

This work was supported by the National Research Council of Canada. We would also like to thank Drs. T. Carrington, K. E. Shuler, and two referees for helpful remarks on the original version of this paper.

1. H. O. PRITCHARD and N. I. LABIB. Can. J. Chem. **54**, 329 (1976).
2. H. O. PRITCHARD. Can. J. Chem. **54**, 2372 (1976).
3. E. T. JAYNES. Phys. Rev. **106**, 620 (1957); **108**, 171 (1957).
4. I. PROCACCIA and R. D. LEVINE. J. Chem. Phys. **63**, 4261 (1975).
5. I. PROCACCIA and R. D. LEVINE. Chem. Phys. Lett. **33**, 5 (1975).
6. I. PROCACCIA and R. D. LEVINE. J. Chem. Phys. **62**, 2496 (1975).
7. R. I. CUKIER and J. T. HYNES. J. Chem. Phys. **64**, 2674 (1976).
8. A. W. YAU. Thesis, York University, Downsview. To be submitted.
9. I. PROCACCIA, Y. SHIMONI, and R. D. LEVINE. J. Chem. Phys. **65**, 3302 (1976).
10. K. E. SHULER, G. H. WEISS, and K. ANDERSEN. J. Math. Phys. **3**, 550 (1962).
11. H. C. ANDERSEN, I. OPPENHEIM, K. E. SHULER, and G. H. WEISS. J. Math. Phys. **5**, 522 (1964).
12. I. OPPENHEIM, K. E. SHULER, and G. H. WEISS. Adv. Mol. Relaxation Processes, **1**, 13 (1967).
13. N. G. VAN KAMPEN. Adv. Chem. Phys. **15**, 65 (1969).
14. D. L. THOMPSON. J. Chem. Phys. **60**, 4557 (1974); J. M. WHITE and D. L. THOMPSON. J. Chem. Phys. **61**, 719 (1974).
15. M. R. VERTER and H. RABITZ. J. Chem. Phys. **64**, 2939 (1976).
16. H. KAPLAN, R. D. LEVINE, and J. MANZ. Mol. Phys. **31**, 1765 (1976).
17. H. RABITZ and G. ZARUR. J. Chem. Phys. **62**, 1425 (1975).
18. M. RUBINSON and J. I. STEINFELD. Chem. Phys. **4**, 467 (1974).
19. S. GREEN. Physica, **76**, 609 (1974).
20. I. PROCACCIA and R. D. LEVINE. Physica, **82A**, 623 (1976).
21. M. H. ALEXANDER. Chem. Phys. Lett. **40**, 101 (1976); **40**, 267 (1976).
22. T. CARRINGTON. J. Chem. Phys. **35**, 807 (1961).

The preparation and characterisation of $Sb_3Cl_{11}F_4$

JACK G. BALLARD, THOMAS BIRCHALL,[1] AND DAVID R. SLIM
Department of Chemistry, McMaster University, Hamilton, Ont., Canada L8S 4M1

Received September 14, 1976

JACK G. BALLARD, THOMAS BIRCHALL, and DAVID R. SLIM. Can. J. Chem. **55**, 743 (1977).

The title compound has been prepared by the reaction of SbF_5 and $SbCl_5$ in liquid SO_2. Raman and Mössbauer spectra have been recorded and its crystal structure determined by three-dimensional X-ray counter measurements. Crystals are monoclinic with a = 12.359(6) Å, b = 16.480(10) Å, c = 9.387(3) Å, β = 103.96(5)°. The structure has been refined in the space group $P2_1/n$ to a final agreement index R_2 of 0.113 for 2415 independent reflections. The structure consists of a *cis* fluorine-bridged trimer with one of the chlorine atoms 25% substituted by fluorine.

JACK G. BALLARD, THOMAS BIRCHALL et DAVID R. SLIM. Can. J. Chem. **55**, 743 (1977).

On a préparé le composé mentionné dans le titre par la réaction du SbF_5 et du $SbCl_5$ dans le SO_2 liquide. On en a enregistré les spectres Raman et de Mössbauer et on a déterminé sa structure cristalline par des mesures de diffraction de rayon-X en trois dimensions. Les cristaux sont monocliniques avec a = 12.359(6) Å, b = 16.480(10) Å, c = 9.387(3) Å, β = 103.96(5)°. On a affiné la structure dans le groupe d'espace $P2_1/n$ jusqu'à un indice final de R_2 de 0.113 pour 2415 réflexions indépendantes. La structure consiste en un trimère ponté contenant un fluor *cis* avec un atome de chlore substitué à 25% par le fluor.

[Traduit par le journal]

Introduction

The $SbCl_{5-x}F_x$ system has been investigated by numerous workers since the early work of Swarts (1). All of these compounds behave as powerful Lewis acid catalysts and are excellent halogenating and oxidizing agents. From a stereochemical point of view they are of interest, since the antimony atom rarely remains five coordinate. Indeed only for $SbCl_5$ has five-coordination been established (2). However, a phase change is thought to occur at low temperatures, resulting in a different structure. Although a number of structures have been postulated (3–5), Mössbauer evidence at 4 K suggests a trigonal bipyramidal arrangement of chlorine atoms around antimony (6). SbF_5 (7), $SbCl_4F$ (8), and $SbCl_3F_2$ (9) have all been shown by X-ray crystallography to exist as *cis* fluorine-bridged tetramers. Two other chlorofluorides, $SbCl_2F_3$ (10) and $Sb_3Cl_4F_{11}$ (11) have been shown to contain the $[SbCl_4^+]$ cation and $[Sb_2Cl_2F_9^-]$ and $[Sb_2F_{11}^-]$ anions, respectively.

We now report the preparation and characterisation of $Sb_3Cl_{10.7}F_{4.3}$ which has a previously unreported trimeric structure.

Experimental

An amount of 6.73 g of doubly distilled (142–143 °C) SbF_5 was added to one side of a dry reaction vessel. Freshly distilled $SbCl_5$ (6 ml) were added to the other side of the same reaction vessel, but separated by a glass frit. All additions were made in a dry N_2 glove box. SO_2 was condensed onto the SbF_5 at −196 °C and, when allowed to warm, the SbF_5 dissolved completely. The SbF_5 in SO_2 solution was slowly added to the $SbCl_5$ and the mixture was stirred overnight. A white precipitate, partially soluble in SO_2, was produced and was washed with liquid SO_2. The SO_2 was pumped away and the dry white powder was vacuum sublimed at 20 °C. Single crystals were obtained by subliming the material in a quartz capillary tube. The sample melted at 64–69 °C.

Analysis was carried out by the Mikroanalytisches Laboratorium (Found: Sb 45.71, Cl 41.11, F 11.57. *Anal.* calcd. for $Sb_3Cl_{11}F_4$: Sb 43.91, Cl 46.95, F 9.14; $Sb_3Cl_{10}F_4$: Sb 44.80, Cl 43.55, F 11.65). The Mössbauer spectrum was recorded and analyzed by procedures already described (12, 13). Raman spectra were recorded on a Spectro Physics He/Ne (6328 Å) or an Ar ion laser (5145 Å) with a Spex 1400 Spectrophotometer system. The spectra recorded for the single crystal were the same as for the bulk material. The following crystal data were obtained.

$Sb_3Cl_{10.7}F_{4.3}$ fw = 827.5
Monoclinic, a = 12.359(6), b = 16.480(10), c = 9.387(3), β = 103.96(5), V = 1856 Å^3, Z = 4, D_c = 2.96 g cm^{-3}, F(0,0,0) = 1496, λ(Mo Kᾱ) = 0.71069 and μ(Mo Kᾱ) = 53.0 cm^{-1}.

The unit cell parameters were obtained from a least-squares refinement of 15 reflections within the range 20° < 2θ < 25°. Weissenberg and precession photographs indicated that reflections were absent for $0k0$ when $k = 2n+1$ and $h0l$ when $h+l = 2n+1$, characteristic of the non-standard space group $P2_1/n$ which is alternative setting for $P2_1/c$ (No. 14) (14). The equivalent positions of this space group are x,y,z; $-x,-y,-z$; $\frac{1}{2}-x,\frac{1}{2}+y,\frac{1}{2}-z$; $\frac{1}{2}+x,\frac{1}{2}-y,\frac{1}{2}+z$.

[1]To whom all correspondence should be addressed.

X-ray Intensity Measurements

The crystal, which was an irregular block of approximate dimensions 0.20 × 0.20 × 0.16 mm, was sealed in a quartz capillary and mounted on a syntex $P\bar{1}$ diffractometer with the 0.16 edge, which was perpendicular to the (0,0,1) face, almost coincident with the ϕ axis of the diffractometer. Intensities were measured with graphite monochromated radiation, using a θ–2θ scan, with a scan rate varying from 8.0 to 24.0°/min in 2θ, so that the weaker reflections were examined more slowly to minimize counting errors. Stationary background counts, with a time equal to half the scan time for each reflection, were made at each end of the scan range. One standard reflection was regularly checked to monitor the stability of the crystal and its alignment, but no significant variation was observed. A total of 3055 reflections within a unique quadrant with $2\theta < 50°$ were measured. Subsequent averaging resulted in a total of 2415 independent reflections, of which 1934 had intensities greater than three times their standard error, based on counting statistics. Lorentz, polarisation, and absorption corrections were applied to the observed intensities.

Solution and Refinement of the Structure

The positions of three independent antimony atoms were located from the three-dimensional Patterson function. The real and imaginary parts of the anomalous dispersion correction were applied to the scattering factors for neutral antimony (15). Full-matrix least-square refinement of positional and isotropic thermal parameters yielded an R_1 index of 0.32. The positions of 15 light atoms were located from a three-dimensional electron density map, 11 of which were assumed to be chlorine as they were about 2.2 Å from an antimony atom and the remaining 4 were assumed to be fluorine. Four cycles of least-squares refinement gave an R_1 index of 0.15. Anisotropic temperature factors were introduced for the antimony atoms and further refinement reduced R_1 to 0.11. Examination of the molecular geometry around Sb(2) indicated that the Sb(2)—Cl(11) bond was much shorter than the other Sb—Cl bond lengths. This suggested that Cl(11) was partially substituted by a fluorine atom. The occupation parameters of this site were varied and refinement terminated when the site contained 75% chlorine and 25% fluorine. Anisotropic temperature factors were introduced for the chlorine and fluorine atoms but the drop in R_1 index to 0.102 was insignificant based on Hamilton's significance tests (16). The final R_1 index was 0.106 and the final R_2 index with unit weight was 0.114.[2] The maximum shift was 0.1 of the estimated standard deviation in the final cycle and a difference electron density map showed no significant peaks. A list of structure factors is available on request.[3]

Discussion

The final parameters, and a list of the interatomic bond lengths and bond angles, are given in Tables 1 and 2 respectively. The trimeric unit is shown in Fig. 1 and the projection of the unit cell down the *c* axis is shown in Fig. 2.

In the atomic arrangement, each antimony atom has a distorted octahedral coordination of chlorine and fluorine. One antimony has one terminal fluorine atom and two fluorine atoms in *cis* positions, bridging to the other two antimony atoms which in turn are linked through a bridging fluorine atom. One of these antimony atoms has four terminal chlorine atoms while the other has three chlorines in a *cis* arrangement and a fourth site which consists of 75% chlorine and 25% fluorine.

In the trimer the mean Sb—Cl distance is 2.26 Å. This is comparable to the corresponding values found in $SbCl_4F$ (8), $SbCl_3F_2$ (9), $Sb_3Cl_9F_4O$ (17), and $[SbCl_4^+][Sb_2F_{11}^-]$ (11) respectively, *i.e.*, 2.29 Å, 2.25 Å, 2.26 Å, and 2.23 Å. All of these mean bond lengths are longer than that found in $[SbCl_4^+][Sb_2Cl_2F_9^-]$ (10), 2.18 Å. One might have expected that the Sb—Cl bond length in the cation would be shorter than that in the anion. Even more surprising is the 2.23 Å value found in the $[Sb_2F_{11}^-]$ salt, although it must be pointed out that this structure has never been refined satisfactorily. The *cis* Cl—Sb—Cl′ angles, which vary from 94.2° to 102.4°, are intermediate between the 90° angle expected for octahedral coordination and the tetrahedral angle achieved in the $[SbCl_4^+]$ cation. Presumably the greater repulsive effect of the chlorine atoms compared to fluorine would cause the Cl—Sb—Cl′ angles to open up from 90°.

The Sb—F (terminal) bond length, 1.87 Å, is somewhat shorter than those found in $SbCl_3F_2$ (9) and in $SbCl_9F_4O$ (17), 1.92 Å and 1.94 Å respectively. In the $[Sb_2Cl_2F_9^-]$ ion (10) the Sb—F (terminal) distances vary over rather a wide range, 1.83–1.99 Å and although the errors are rather high, this variation may be the result of cation–anion interaction which is discussed later.

The bridges between Sb(1) and Sb(2), and Sb(2) and Sb(3) are both symmetric (mean Sb—F = 2.08 Å) whereas that between Sb(1) and Sb(3) is asymmetric (Sb(1)—F = 2.04 Å, Sb(3)—F = 2.12 Å, mean = 2.08 Å). These bridging fluorine atoms complete the distorted octahedral coordination about each antimony. The mean bridge distance is comparable to the corresponding means in $Sb_3Cl_9F_4O$ (17), $SbCl_3$-

[2] R_2 is given by the expression $R_2 = [\sum w(|F_o|^2 - |F_c|^2)\sum wF_o^2]^{-1}$.

[3] Photocopies are available at a nominal charge, upon request, from the Depository of Unpublished Data, CISTI, National Research Council of Canada, Ottawa, Canada K1A 0S2.

TABLE 1. Positional and thermal parameters* ($\times 10^4$) for $Sb_3Cl_{10.7}F_{4.3}$

Atom	x/a	y/b	z/c	$u(1,1)$	$u(2,2)$	$u(3,3)$	$u(1,2)$	$u(1,3)$	$u(2,3)$
Sb(1)	2985(2)	1857(1)	4989(2)	486(12)	284(9)	498(12)	55(9)	183(10)	60(9)
Sb(2)	2294(2)	4284(1)	5035(2)	619(14)	328(10)	398(11)	60(10)	103(10)	−31(9)
Sb(3)	3729(2)	3339(1)	1871(3)	578(14)	346(10)	580(13)	−86(10)	311(11)	−25(10)
				u(Å^2)					
Cl(1)	3852(9)	696(7)	4539(11)	745(26)					
Cl(2)	1290(8)	1654(6)	3405(10)	602(22)					
Cl(3)	2497(10)	1506(7)	7072(13)	836(31)					
Cl(4)	2311(9)	5626(7)	4465(13)	847(31)					
Cl(5)	686(9)	4044(7)	3420(12)	784(29)					
Cl(6)	4026(12)	4277(11)	6345(16)	1061(62)					
Cl(7)	1547(9)	4293(7)	7028(13)	860(31)					
Cl(8)	4491(10)	2402(7)	632(13)	842(31)					
Cl(9)	1957(9)	3120(6)	627(12)	742(27)					
Cl(10)	4016(9)	4497(7)	707(13)	834(31)					
ClF	5291(12)	3465(9)	3636(16)	961(62)					
F(1)	3384(14)	2401(10)	3237(17)	442(40)					
F(2)	4328(17)	2332(13)	5997(22)	702(57)					
F(3)	2388(14)	3009(10)	5174(18)	461(41)					
F(4)	3011(15)	4004(10)	3283(19)	508(43)					

*The anisotropic temperature factors are given by the expression $\exp[-2\pi^2(a^{*2}h^2u(1,1) + b^{*2}k^2u(2,2) + c^{*2}l^2u(3,3) + 2a^*b^*hku(1,2) + 2a^*c^*hlu(1,3) + 2b^*c^*klu(2,3))]$.

TABLE 2

(*a*) Bond lengths in $Sb_3Cl_{10.7}F_{4.3}$

Bond	Length (Å)	Bond	Length (Å)	Bond	Length (Å)
Sb(1)—Cl(1)	2.28(1)	Sb(2)—Cl(4)	2.28(1)	Sb(3)—Cl(8)	2.27(1)
—Cl(2)	2.28(1)	—Cl(5)	2.24(1)	—Cl(9)	2.25(1)
—Cl(3)	2.26(1)	—Cl(6)	2.20(1)	—Cl(10)	2.27(1)
—F(1)	2.04(2)	—Cl(7)	2.28(1)	—ClF	2.12(1)
—F(2)	1.87(2)	—F(3)	2.11(2)	—F(1)	2.12(2)
—F(3)	2.06(2)	—F(4)	2.10(2)	—F(4)	2.08(2)

(*b*) Bond angles in $Sb_3Cl_{10.7}F_{4.3}$

Bonds	Angle (deg)	Bonds	Angle (deg)	Bonds	Angle (deg)
Cl(1)—Sb(1)—Cl(2)	98.9(3)	Cl(4)—Sb(2)—Cl(5)	95.6(4)	Cl(8)—Sb(3)—Cl(9)	95.6(4)
—Cl(3)	100.4(4)	—Cl(6)	94.2(5)	—Cl(10)	101.1(5)
—F(1)	90.2(6)	—Cl(7)	102.4(5)	—ClF	94.9(5)
—F(2)	92.6(7)	—F(3)	168.5(6)	—F(1)	89.0(6)
—F(3)	169.3(6)	—F(4)	90.0(6)	—F(4)	168.5(6)
Cl(2)—Sb(1)—F(3)	97.6(6)	Cl(5)—Sb(2)—Cl(6)	164.7(5)	Cl(9)—Sb(3)—Cl(10)	97.5(4)
—F(1)	84.4(5)	—Cl(7)	95.1(4)	—Cl	161.7(5)
—F(2)	162.4(7)	—F(3)	82.2(5)	—F(1)	83.4(5)
—F(3)	84.2(5)	—F(4)	84.1(6)	—F(4)	84.5(5)
Cl(3)—Sb(1)—F(1)	168.8(6)	Cl(6)—Sb(2)—Cl(7)	94.2(5)	Cl(10)—Sb(3)—ClF	95.2(5)
—F(2)	93.4(8)	—F(3)	85.9(6)	—F(1)	169.7(6)
—F(3)	89.3(6)	—F(4)	84.2(6)	—F(4)	90.3(6)
F(1)—Sb(1)—F(2)	82.3(8)	Cl(7)—Sb(2)—F(3)	89.1(6)	ClF—Sb(3)—F(1)	81.8(6)
—F(3)	79.9(7)	—F(4)	167.6(6)	—F(4)	82.3(6)
F(2)—Sb(1)—F(3)	82.2(8)	F(3)—Sb(2)—F(4)	78.6(7)	F(1)—Sb(3)—F(4)	79.6(7)
Sb(1)—F(1)—Sb(3)	159.1(9)	Sb(1)—F(3)—Sb(2)	158.4(1.0)	Sb(2)—F(4)—Sb(3)	160.4(9)

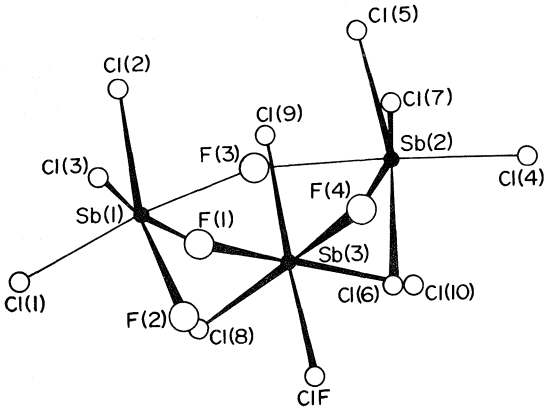

FIG. 1. View of the $Sb_3Cl_{10.7}F_{4.3}$ structure.

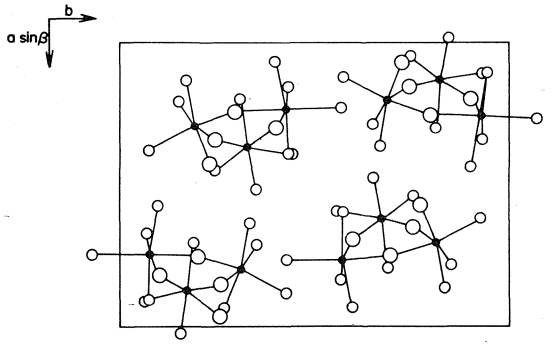

FIG. 2. Projection of the unit cell of $Sb_3Cl_{10.7}F_{4.3}$ down the *c* axis (circles of increasing size represent Sb, Cl, and F respectively).

F_2 (9), and $SbCl_4F$ (8), of 2.07 Å, 2.07(2) Å, and 2.12 Å respectively, all of which are longer than the bridging distances in $[ClO_2^+][Sb_2F_{11}^-]$ (18) and $[Sb_2Cl_2F_9^-]$, that is 2.01 Å and 2.00 Å, respectively.

The Cl—F disorder has already been discussed in the section concerning the refinement of the structure. The Sb—Cl(F) bond length, 2.12 Å, is approximately the value expected for a site consisting of 75% chlorine and 25% fluorine. We conclude that the composition of the crystal and the bulk material is a 3:1 mixture of $Sb_3Cl_{11}F_4$ and $Sb_3Cl_{10}F_5$. One site has four chlorines and two *cis* bridging fluorines as in $SbCl_4F$ (8), while the other site has three chlorines, one terminal fluorine, and two *cis* bridging fluorines, as in $SbCl_3F_2$. Two of the former and one of the latter units constitute the trimer $Sb_3Cl_{11}F_4$, while the converse is true for $Sb_3Cl_{10}F_5$. It should be noted that the relative orientation of the terminal fluorines in $Sb_3Cl_{10}F_5$ is the same as those in $SbCl_3F_2$. We have made repeated attempts to isolate pure components of the mixture by varying the sublimation conditions but with no success. However, it must be noted that the unit cell dimensions for the two compounds would be expected to be very similar.

The Sb_3F_3 unit is considerably distorted, with mean F—Sb—F′ and Sb—F—Sb′ angles of 79.4° and 158.2° respectively. These are in sharp contrast to the corresponding O—Sb—O′ and Sb—O—Sb′ angles in the trimeric anion $[Sb_3O_3F_{12}^{3-}]$ of 101° and 130° respectively (19). Presumably $Sb_3Cl_{10.7}F_{4.3}$ forms a less efficiently packed entity and the large chlorine atoms would tend to close down the F—Sb—F′ angles and hence open up the Sb—F—Sb′ angles. It is interesting to compare these angles with the corresponding angles in $SbCl_4F$ and $SbCl_3F_2$, 82.7° and 173°, and 78° and 164° respectively. Again, packing considerations are probably dominant since in these compounds there is an attempt to form an approximate cubic close packed array. However, it must be admitted that possible constraints can be expected in going from a trimer to a tetramer.

At first sight the existence of the compound as a cyclic trimer seems surprising since the only other reported antimony V chlorofluorides are cyclic tetramers, or ionic structures. An ionic structure for $Sb_3Cl_{10}F_5$ or $Sb_3Cl_{11}F_4$, similar to those already established (10, 11), that is $[SbCl_4^+]$ salts, would probably be unstable, since the basicity of the anion would be significantly reduced by the increased number of chlorines. For the compound to be a tetramer there would probably be substantial disorder as opposed to the minor disorder observed for the trimer.

Closer examination of the data for $[SbCl_4^+][Sb_2Cl_2F_9^-]$ reported by Preiss (10) reveals that there are four weak contacts from fluorine atoms of the anion to the antimony atom of the cation. These contacts, which are in the range 2.95 Å to 3.25 Å, are probably involved to some extent in the bonding. Such interaction may be the cause of the large variation in the terminal Sb—F bond lengths alluded to earlier. Each of the four weak contacts are perpendicular to a face of the $[SbCl_4^+]$ tetrahedron giving three F—Sb—Cl angles of 71° and one of 180°, as shown in Fig. 3. Mössbauer data recorded for $[SbCl_4^+][Sb_2Cl_2F_9^-]$ have been interpreted in these terms, and in addition, similar data for $[SbCl_4^+][Sb_2F_{11}^-]$ also suggest substantial cation–anion inter-

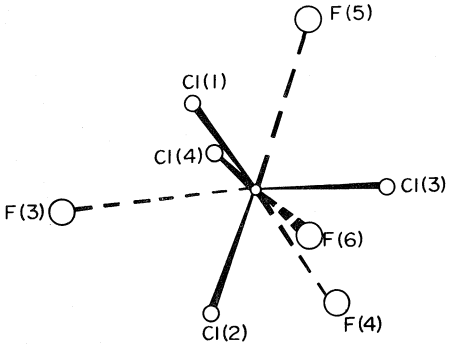

FIG. 3. A view of the antimony environment in the cation of $[SbCl_4^+][Sb_2Cl_2F_9^-]$. (The F numbering refers to the anion.)

actions (19). Furthermore the cation in $[SbCl_4^+][Sb_2Cl_2F_9^-]$ is situated in such a way, relative to the anion, so as to form the triangular arrangement of antimony atoms, which is shown in Fig. 4. The trimeric nature of the $Sb_3Cl_{10.7}F_{4.3}$ is then, perhaps, not so surprising.

Mössbauer Spectrum

The ^{121}Sb Mössbauer spectrum consisted of a resonance which could not be fitted to a single antimony site. A good fit was obtained only when two antimony sites were considered. The isomer shift and quadrupole coupling constants obtained for the two sites are, I.S. = 5.3 and 7.7 mm/s; e^2qQ_g = 8.9 and 2.7 mm/s. These values have been discussed elsewhere in more detail (20). It was concluded, on the basis of the isomer shift values, that one site would have four chlorines and two bridging fluorines while the other site would have one chlorine replaced by a terminal fluorine. Mössbauer data were unable to establish with any certainty the amounts of each site present since the recoil free fractions for the individual sites will not be the same.

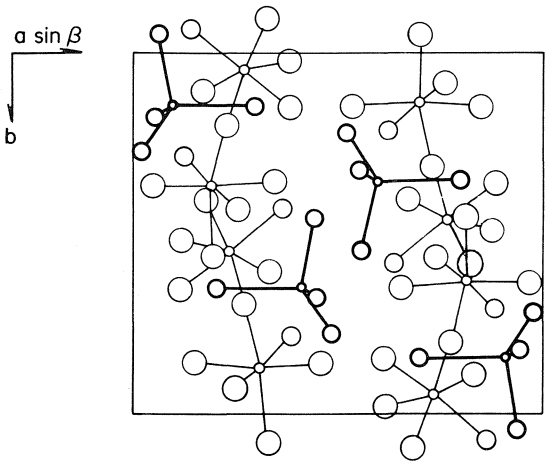

FIG. 4. Projection of the unit cell of $[SbCl_4^+][Sb_2Cl_2F_9^-]$ down the *c* axis (circles of increasing size represent Sb, Cl, and F respectively).

Raman Spectrum

The Raman spectra of the solid and liquid phases of $Sb_3Cl_{10.7}F_{4.3}$ are given in Table 3. The spectra are not easily assigned since both trimers, $Sb_3Cl_{10}F_5$ and $Sb_3Cl_{11}F_4$ have C_s symmetry. The spectra of the solid and liquid phases contain 16 and 10 bands respectively. When the solid melts some of the bands coalesce into a broad band. This is probably due to some halogen exchange occurring in the liquid form. Some of the weak bands observed for the solid were not observed for the melt. The polarization data recorded for the melt indicated that the bands at 659 cm^{-1}, 380 cm^{-1}, and 351 cm^{-1} are almost totally polarized. The band at 659 cm^{-1} can be assigned to the symmetric Sb—F stretch while those at 380 cm^{-1} and 351 cm^{-1} can be assigned to the symmetric Sb—Cl equatorial and axial stretches respectively. This agrees with the assignments made by Beattie *et al.* (21) for the *cis* fluorine-bridged tetramer $SbCl_4F$. It is reasonable to attribute the very weak band at 431 cm^{-1} to the Sb—F—Sb bridging mode,

TABLE 3. Raman spectra (cm^{-1}) of solid and liquid $Sb_3Cl_{10.7}F_{4.3}$

Solid[b]	Liquid[c]	Assignments
654(5)br[a]	659(4)p[a]	ν Sb—F
624(2)[d]		
	431(6)p	ν (Sb...F...Sb) bridge
413(5)sh[a]		
401(48)sh		
393(67)sh		
380(100)	380(100)br p	ν Sb—Cl equatorial
346(42)	351(51)p	ν Sb—Cl axial
	301(2)	
237(3)br		
221(5)br		
175(11)	176(8)sh	
162(34)	162(17)dp[d]	Deformation modes
148(42)	149(19)dp	
137(21)sh		
121(39)	122(13)dp	
110(22)sh		Lattice modes
104(13)sh		

[a]Abbreviations: br, broad peak; sh, shoulder; p, polarized; dp, depolarized.
[b]Solid 20 °C.
[c]Melt at 70 °C.
[d]Values in parentheses denote intensity relative to largest band.

which is consistent with the analogous assignment for that vibration (446 cm^{-1}) in $SbCl_4F$ (21). The lower frequency may be a consequence of the smaller Sb—F—Sb bridge angle, 158° as opposed to 173° for $SbCl_4F$. The bands at 121 to 175 cm^{-1} are depolarized and can be assigned to the deformation modes. The polarization data are not available for some of these bands because of their very weak intensity.

Acknowledgement

The National Research Council of Canada is thanked for financial support.

1. F. SWARTS. Bull. Acad. R. Belg. **29**, 874 (1895).
2. S. M. OHLBERG. J. Am. Chem. Soc. **81**, 811 (1959).
3. W. BUES, F. DERNIRAY, and W. BROCKNER. Spectrochim. Acta, **30**A, 1709 (1974).
4. R. F. SCHNEIDER and J. V. DILORENZO. J. Chem. Phys. **47**, 2343 (1967).
5. J. G. STEVENS and L. H. BOWEN. Mössbauer effect methodology. Vol. 5. Plenum Press, N.Y. 1970. p. 27.
6. J. G. BALLARD and T. BIRCHALL. J. Chem. Soc. Dalton Trans. 1859 (1976).
7. A. J. EDWARDS and P. TAYLOR. Chem. Commun. 1376 (1971).
8. H. PREISS. Z. Chem. **6**, 350 (1960).
9. J. G. BALLARD, T. BIRCHALL, and D. R. SLIM. J. Chem. Soc. Chem. Commun. 653 (1976).
10. H. PREISS. Z. Anorg. Chem. **389**, 254 (1972).
11. H. B. MILLER, H. W. BAIRD, C. L. BRAMLETT, and W. K. TEMPLETON. Chem. Commun. 262 (1972).
12. T. BIRCHALL and A. F. REID. J. Solid State Chem. **13**, 351 (1975).
13. J. G. BALLARD, T. BIRCHALL, R. FOURCADE, and G. M. MASHERPA. J. Chem. Soc. Dalton Trans. 2409 (1976).
14. International tables for X-ray crystallography. Vol. 1. Kynoch Press, Birmingham, U.K. 1965.
15. International tables for X-ray crystallography. Vol. IV. Kynoch Press, Birmingham, U. K. 1975.
16. W. C. HAMILTON. Acta Crystallogr. **18**, 502 (1975).
17. A. J. EDWARDS and G. R. JONES. Private communication.
18. A. J. EDWARDS and R. J. C. SILLS. J. Chem. Soc. Dalton Trans. 1726 (1974).
19. W. HAASE. Acta Crystallogr. B**30**, 2465 (1974).
20. J. G. BALLARD and T. BIRCHALL. J. Phys. In press.
21. I. R. BEATTIE, K. M. S. LIVINGSTON, G. A. OZIN, and D. J. REYNOLDS. J. Chem. Soc. A, 958 (1969).

Recombination of iodine atoms by flash photolysis over a wide temperature range. VIII. I_2 in O_2[1]

R. E. ANTRIM,[2] GEORGE BURNS,[3] AND J. K. K. IP

Lash Miller Chemical Laboratories, Department of Chemistry, University of Toronto, Toronto, Ont., Canada M5S 1A1

Received May 19, 1976

R. E. ANTRIM, GEORGE BURNS, and J. K. K. IP. Can. J. Chem. **55**, 749 (1977).

Flash photolysis of I_2 in a large excess of O_2 was studied between 300 and 1173 K. Between 573 and 1173 K the rate of atomic recombination $2I(^2P_{3/2}) + O_2(^3\Sigma_g^-) \rightleftharpoons I_2(^1\Sigma_g^+) + O_2(^3\Sigma_g^-)$ was measured without interference of side reactions. Its rate constant was found to be $\log k_r^{O_2}(T) = 9.000 - 0.71 \log (T/573)$. Between 573 and 873 K there is an induction period lasting several hundred microseconds during which only a small net change in the iodine molecule concentration takes place. This induction period is consistent with the reaction $O_2(^1\Delta_g) + I_2 = O_2(^3\Sigma_g^-) + 2I$. Beow 573 K, the overall recombination rate constant has a temperature dependent negative temperature coefficient and is enhanced when the flash includes radiation in the neighborhood of 200 nm. Evidently this occurs because the flash photolysis of O_2 creates new efficient third bodies, such as O_3 and $O_2(^1\Delta_g)$, which accelerate the recombination reaction either directly or via an IO intermediate. The mechanism for the formation of IO during the flash photolysis of I_2 in an excess of O_2 was studied. It was shown that the reactions $O(^3P)$ or $O_3^* + I_2 \rightleftharpoons IO + I + (O_2)$, where O_3^* refers to an electronically or vibrationally excited state of O_3, account for the formation of IO under our experimental conditions. IO may also possibly be formed via the reaction $O_3^* + I \rightleftharpoons IO + O_2$. On the other hand, reactions between excited or ground state I atoms and O_2 suggested by earlier workers do not occur. Thus, all experimental complications observed are traceable to the presence of O_2 photolysis products and to the reaction of $I(^2P_{1/2})$ with $O_2(^3\Sigma_g^-)$.

R. E. ANTRIM, GEORGE BURNS et J. K. K. IP. Can. J. Chem. **55**, 749 (1977).

On a étudié, entre 300 et 1173 K, la photolyse éclair de I_2 dans un grand excès de O_2. Entre 573 et 1173 K, la vitesse de recombinaison atomique $2I(^2P_{3/2}) + O_2(^3\Sigma_g^-) \rightleftharpoons I_2(^1\Sigma_g^+) + O_2(^3\Sigma_g^-)$ a été mesurée sans interférence des réactions secondaires. On a trouvé que sa vitesse de réaction est égale à $\log K_r^{O_2}(T) = 9.000 - 0.71 \log (T/573)$. Entre 573 et 873 K, il y a une période d'induction qui dure plusieurs centaines de microsecondes durant laquelle il n'y a qu'un très faible changement net dans la concentration des molécules d'iode. Cette période d'induction est en accord avec la réaction $O_2(^1\Delta_g) + I_2 \rightleftharpoons O_2(^3\Sigma_g^-) + 2I$. En dessous de 573 K, la constante de vitesse globale de recombinaison possède un coefficient de température négatif qui dépend de la température et qui augmente quand l'éclair inclut des radiations aux environs de 200 nm. Evidemment ceci se produit parce que la photolyse éclair de O_2 crée de nouveaux troisième corps efficaces, tels que O_3 et $O_2(^1\Delta_g)$, qui accélèrent la réaction de combinaison soit directement ou par l'intermédiaire de IO. On a étudié le mécanisme de formation de IO durant la photolyse éclair de I_2 dans un excès de O_2. On a montré que les réactions $O(^3P)$ ou $O_3^* + I_2 = IO + I + (O_2)$, où O_3^* se réfère à un état excité électroniquement ou vibrationnellement de O_3, expliquent la formation de IO dans nos conditions expérimentales. Il est aussi possible que IO puisse se former par l'intermédiaire de la réaction $O_3^* + I \rightleftharpoons IO + O_2$. Par ailleurs, il ne semble pas que la réaction entre l'état excité ou fondamental des atomes d'iode et de O_2, qui avait été suggérée antérieurement par des chercheurs, se produit. Donc toutes les complications expérimentales qui ont été observées peuvent être attribuées à la présence de produits de photolyse de O_2 et à la réaction de $I(^2P_{1/2})$ avec $O_2(^3\Sigma_g^-)$.

[Traduit par le journal]

Introduction

One of the reactions which affects the efficiency of the iodine gas phase laser at 1315 nm is the reaction

[1] $I(^2P_{1/2}) + O_2(^3\Sigma_g^-) \rightarrow I(^2P_{3/2}) + O_2(a^1\Delta_g)$

because it is known (1) to be very fast. If laser

[1]Research sponsored, in part, by the Air Force Office of Scientific Research, Air Force Systems Command, USAF, under grant no. AFOSR-A75-2856. The United States Government is entitled to reproduce and distribute reprints for Government purposes notwithstanding any copyright notation hereon.

[2]Present address: Richard Bland College, Petersburg, VA 23803.

[3]The final portion of this work was done at the Université de Bordeaux I, Unité de Chimie, Laboratoire de Chimie Physique A, 351, cours de la Libération, 33405 Talence, France.

action is generated by flash photolysis, reaction 1 decreases the concentration of electronically excited iodine atoms, and this lowers the efficiency of the iodine laser. On the other hand, it was suggested (2) that the reverse of the reaction 1 can be used to increase the concentration of $I(^2P_{1/2})$ in an electric discharge, and thus to improve the efficiency of the iodine laser.

For these reasons, it seemed appropriate to study the iodine–oxygen reaction under the simplest possible experimental conditions. Specifically, in flash photolysis atomic recombination studies (3–13), one generates a minimum number of reactive species, making detailed elucidation of reaction mechanisms often possible.

In the present work, recombination of iodine atoms in oxygen is investigated using the flash photolysis technique over a wide temperature range, and the results are compared to earlier recombination studies.

Experimental

One spectrophotometric and one spectroscopic flash photolysis apparatus were used for the present study. The spectrophotometric apparatus, experimental and purification techniques, and methods of data analysis have been described previously (7, 8). To ensure a sufficient iodine vapour pressure in the reaction cell at high temperatures, an auxiliary oven was used (8) to prepare iodine–oxygen mixtures at elevated temperatures. Cylinder oxygen (Canox) was used without purification; in several experiments, Ultra High Purity oxygen (Matheson, minimum purity 99.95%) was used. The experiments were conducted in a double-walled quartz reaction vessel, with an outer jacket available for gas filters, which eliminate flash radiation of undesirable wavelengths. The Pyrex glass filter used in some experiments consisted of a 1.5 mm wall thickness cylindrical sleeve fitted over the quartz vessel. As in previous studies (5, 7–10), the experimental observable, from which the recombination rate constant was obtained, was the rate of change of the optical absorption at 487 nm, a wavelength close to the peak of the iodine absorption spectrum (14). The concentration of I_2 was, typically, 1 to 3×10^{-5} mol/l, while that of O_2 was 1 to 4×10^{-2} mol/l.

The kinetic spectroscopy apparatus, which was described previously (15), was equipped with a Jarrell–Ash *f*/6.3 grating spectrograph. Eastman Kodak 103F plates were used. These plates were photometered on a Joyce–Loebl microdensitometer, model Mk. IIIC.

Results

In spectrophotometric studies, the time dependent I_2 absorption was studied between 300 and 1173 K. In experiments conducted between 300 and 573 K and between 873 and 1173 K the absorption traces were similar to those observed in earlier investigations of halogen atom recombination (3). This suggests that, within the temperature specified above, the predominant reaction was the recombination of iodine atoms in the presence of chemically inert O_2:

$$[2] \qquad 2I + O_2 \rightarrow I_2 + O_2$$

In addition, I_2 should contribute to the reaction:

$$[3] \qquad 2I + I_2 \rightarrow 2I_2$$

The traces yield apparent recombination rate constants, k_r^{app}, defined by

$$[4] \quad d[I_2]/dt = k_r^{app}[I]^2[O_2] = \sum_M k_r^M[I]^2[M]$$

where M refers to O_2, I_2, and to all possible other third bodies in the reacting mixture.

Between 723 and 873 K all traces display a 'hump', *i.e.*, a slight dip and a rise before decaying smoothly with time (Fig. 1). Since the 'hump' is shallow, the optical absorption appears to be nearly in a steady state for a few hundred microseconds following initiation of the reaction. Rate constants were obtained from such anomalous traces by discarding the raw data from the first 2 ms. All apparent recombination rate constants obtained in this work are plotted in Fig. 2.

In an attempt to isolate the excitation energy from the flash lamp responsible for the anomalous 'hump', ammonia (0.5 to 1.5 atm), chlorine (1 atm), bromine (0.2 atm), and a Pyrex glass sleeve were used, in various combinations, as filters around the reaction vessel. The absorption spectra of all these filters are published elsewhere (16). No apparent change in the shape of the trace was observed in such experiments. In some runs, Ultra High Purity oxygen was used as the diluent but that did not affect the 'hump' either. When argon was substituted for oxygen as the diluent, the 'hump' disappeared, and the rate constant, k_r^{Ar}, (Fig. 2) agreed well with previous values which were determined using the same apparatus (8). The rate constants obtained from individual runs at 723 K, where the 'hump' appeared to be most noticeable, indicate that no matter what filter was used, the rate constant at this temperature did not change outside of experimental error, which is between 10 and 15%.

Between 300 and 573 K, k_r^{app}, obtained with ammonia gas or Pyrex glass filters, are in agreement with each other, within experimental error. However, they are invariably smaller than rate constants obtained without the use of filters around the reaction vessel. The apparent rate

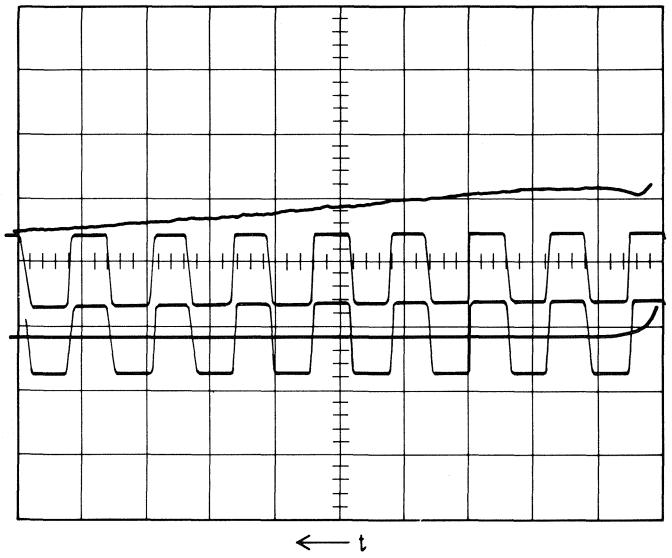

FIG. 1. Oscilloscope trace for I atom recombination in $[O_2]$ at 723 K. $[I_2] = 1.3 \times 10^{-5}$ mol/l and $[O_2] = 8.1 \times 10^{-3}$ mol l^{-1}. Flash energy 1200 J. Flash traces, ordinate 0.05 V/cm, abscissa 0.5 ms/cm. Square wave ordinate 1 V/cm.

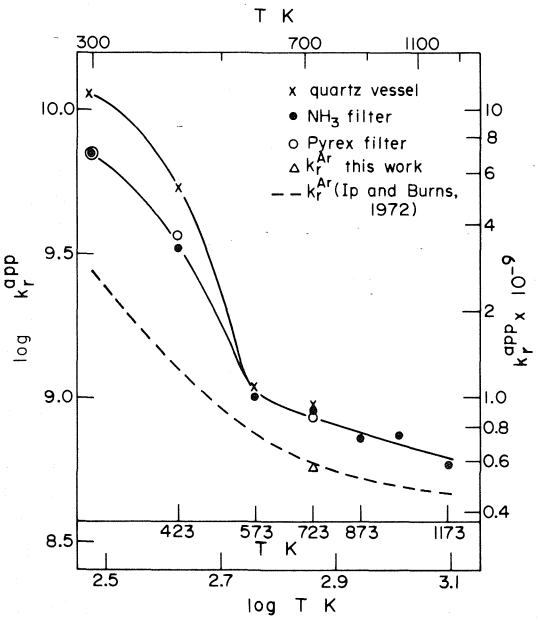

FIG. 2. Temperature dependence of k_r^{app}, the apparent iodine atom recombination rate constant in oxygen, and of k_r^{Ar} in l^2 mol^{-2} s^{-1}.

constants, determined at room temperature from mixtures with various compositions of iodine and oxygen, yield values of $k_r^{I_2}$ (reaction 3) equal to $(1.3 \pm 1.0) \times 10^{12}$ (result from experiments with quartz vessel alone) and $(1.5 \pm 0.7) \times 10^{12}$ l^2 mol^{-2} s^{-1} (combined result from experiments with ammonia and Pyrex filters), in agreement with a more accurate value of $k_r^{I_2} = 1.3 \times 10^{12}$ l^2 mol^{-2} s^{-1} reported previously (8).

In order to further study reaction generated by flash photolysis of $I_2 + O_2$ mixtures, the kinetic spectroscopy apparatus was used. In these experiments the IO spectrum was observed. The IO spectrum rose to its maximum at the time the main flash reached its peak intensity (10–15 μs). The half-life for IO decay was about 80 μs. These results are in agreement with earlier data (17). A typical IO spectrum obtained in the present work is shown in Fig. 3. This spectrum was observed previously (17) in the photolysis of iodine–oxygen mixtures in an all-quartz reaction vessel; our results confirm this finding. However, in the present work, we found that the IO spectrum was absent if a Pyrex sleeve was installed around the reaction cell (Fig. 3).

Discussion

Earlier systematic studies of halogen atom recombination reactions, over a wide temperature range, and in the presence of a large excess of various third bodies (3–13), revealed some consistent trends. In agreement with a previous investigation (11), it was invariably found (3–10) that heavier and more complex non-reacting molecules were more efficient third bodies.

The experimental recombination reaction rate

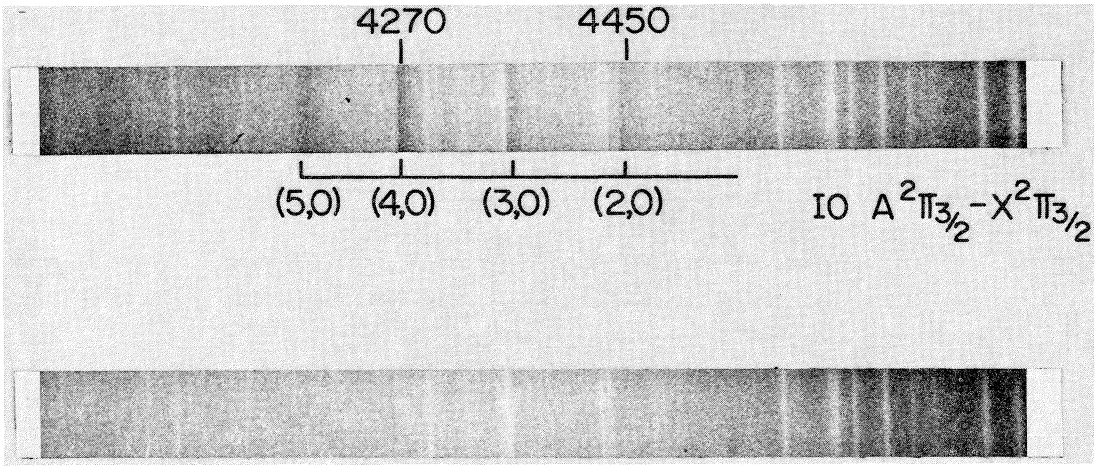

FIG. 3. Spectrum of IO produced by flash photolysis of I_2–O_2 mixtures: 2 torr I_2, 620 torr O_2, T = 350 K. Top, 25 μs delay without filter; bottom, 25 μs delay with Pyrex filter. Flash energy 1125 J.

constants could normally be expressed via the relationship

$$[5] \quad \log k_r = \log k_r^{300\,K} - n \log (T/300) + m \log (T/300)^2$$

Furthermore, the higher the efficiency of the third body, the higher was the negative temperature coefficient at room temperature, *i.e. n*. When data over a sufficiently wide temperature were accumulated (3–8), it became apparent that *m*, eq. 5, was either positive or zero, and generally increased with molecular weight and complexity of the third body as well as with chemical reactivity between the third body and recombining atom. As was shown recently (18–25), these empirical findings have a theoretical basis.

Present results on the $I_2 + O_2$ system do not fit well into these established trends (3–13). Specifically, three experimental results need to be examined: (*a*) formation of IO during flash photolysis; (*b*) the discrepancy between k_r^{app} obtained in experiments with filters around the reaction vessel and those without filters, and k_r^{app} temperature dependence; and (*c*) presence of the 'hump' between 723 and 873 K. These experimental findings are discussed below.

(a) Mechanism of the Formation of Iodine Monoxide

Under our experimental conditions, flash light may produce the following primary photolysis products: $I(^2P_{3/2})$, $I(^2P_{1/2})$, and $O(^3P)$.

Consequently, IO can be formed, in principle, via reactions 6–9:

$$[6] \quad I(^2P_{1/2}) + I(^2P_{1/2}) + O_2(^3\Sigma_g^-) \rightleftharpoons 2IO$$

$$[7] \quad I(^2P_{1/2}) + I(^2P_{3/2}) + O_2(^3\Sigma_g^-) \rightleftharpoons 2IO$$

$$[8] \quad I(^2P_{3/2}) + I(^2P_{3/2}) + O_2(^3\Sigma_g^-) \rightleftharpoons 2IO$$

$$[9] \quad I_2(^1\Sigma_g^+) + O(^3P) \rightleftharpoons IO + I(^2P_{3/2})$$

Of these reactions, the reaction 8 involves the least energetic species, is endothermic by 34 kcal/mol, and therefore should be the slowest and the least important. Furthermore, present results indicate that the mechanism involving reactions 6 and 7, proposed previously (16), plays no role in IO formation. This is because flash photolysis of $I_2 + O_2$ mixture in a reaction vessel with a Pyrex sleeve, which yields $I(^2P_{1/2})$ and $I(^2P_{3/2})$, does not produce IO. This finding is in agreement with predictions made earlier (16).

Thus, the only primary flash photolysis product, which can yield IO under our experimental conditions, is $O(^3P)$ (reaction 9). Oxygen atoms can be produced (16) by direct flash photolysis of O_2 between 180 and 200 nm. Although the absorption of short wavelengths at about 200 nm produces O_2 in a $^3\Sigma_u^+$ attractive state, these molecules should predissociate, producing $O(^3P)$ atoms. The reverse process, *i.e.* inverse predissociation leading to the formation of O_2 in $^3\Sigma_u^+$ state has been observed in shock waves (26).

Secondary photolysis products, which can yield IO, may be produced in reactions involving $O(^3P)$ atoms. Recent investigators (27) have shown that during flash photolysis of O_2 in

quartz vessels, $O(^3P)$ atoms react via:

[10] $$O(^3P) + 2O_2(^3\Sigma_g^-) \rightleftharpoons O_3^* \text{ (or } O_3) + O_2$$

where O_3^* is ozone in an electronically or vibrationally excited state. The prevailing literature (28–32) value of k_{10} is 2×10^8 l^2 mol^{-2} s^{-1} while its most recent measurement yields (27) 1×10^8 l^2 mol^{-2} s^{-1}. Therefore, the reaction half-life, τ_{10}, is of the order of 5 μs, and is about equal to τ_9, if reaction 9 were to occur on every tenth collision. Although k_9 has not been measured, the reaction

[11] $$Br_2 + O \rightarrow BrO + Br$$

occurs (33), approximately, on every ten collisions at 300 K. We conclude, therefore, that the most likely fate of the $O(^3P)$ atom in our experiments is reactions 9 and 10. Consequently, we are unable to exclude the possibility that

$$O_3^* + I_2 \rightleftharpoons IO + I + O_2$$

also contributes to the formation IO.

The formation of ozone increases the number of plausible reactions which can make interpretation of our experimental data ambiguous. This is because O_3 itself can be photolyzed (27) producing $O(^1D)$, $O_2(^1\Delta_g)$, $O_2(^1\Sigma_g^+)$, and vibrationally excited $O_2(^3\Sigma_g^-)$. Fortunately for us, this ambiguity resolved itself because in our experiment O_3 is rapidly depleted via the reaction

[12] $$I + O_3 \rightleftharpoons IO + O_2$$

The rate constant for this reaction, measured (34) by the flow discharge technique, is 5×10^{14} l mol^{-1} s^{-1}, which is about as fast as k_{11} (7×10^{14} l mol^{-1} s^{-1}). However, except in initial stages of photolysis, *i.e.* during first 30 μs or so, reaction 12 cannot be the main cause for the IO observed in our experiments. This is because IO is produced within about 15 μs after flash initiation and essentially disappears within 200 μs, while I atoms exist for milliseconds.

The mechanism of the formation of BrO in flash photolysis of Br_2 and O_2 mixtures was studied earlier (16). It was found that BrO is formed predominantly via reactions with $O(^3P)$, ozone, or excited O_2. Thus, the mechanisms of the formation of IO and BrO are essentially identical, within the limitations of the present experiments, as was suggested earlier (16).

The temperature dependence of IO formation was studied here qualitatively only up to 600 K, and it was found that the concentration of IO decreases with temperature. This is due in part to the decreased transparency of quartz at an elevated temperature, and, possibly, to the thermal decomposition of O_3^*. Similar temperature dependence for BrO formation was reported earlier (15).

(b) A Comparison of k_r^{app} Obtained with and without Filters, and its Temperature Dependence

It follows from the above discussion (*a*) that the reaction mixture in early stages of photolysis, *i.e.* first 10 to 30 μs after the flash initiation, consists of several reacting species, some of which exist in excited electronic and/or vibrational states. However, about 200–300 μs after the flash initiation, *i.e.* at the earliest time at which our spectrophotometric measurements can be made, all these species have decayed, and the reaction mixture consists of $I(^2P_{3/2})$, I_2, $O_2(^3\Sigma_g^-)$, $O_2(^1\Delta_g)$, and O_3. The $I(^2P_{1/2})$ atoms, which constitute about 20% of all iodine atoms produced by the flash, also disappear via reaction 1. The rate constant for this reaction (1) at 300 K is $1.6 \pm 0.2 \times 10^{10}$ l mol^{-1} s^{-1}, which means that, under our experimental conditions, the half-life of $I(^2P_{1/2})$ (10^{-8} to 10^{-9} s) is much shorter than the duration of the flash.

The $O_2(^1\Delta_g)$ molecules, produced via reaction 1 and by photolysis of ozone

[13] $$O_3 + h\nu \rightleftharpoons O_2(^1\Delta_g) + O$$

are quenched via

[14] $$O_2(^1\Delta_g) + O_2(^3\Sigma_g^-) \rightleftharpoons 2O_2(^3\Sigma_g^-)$$

and

[15] $$O_2(^1\Delta_g) + I(^2P_{3/2}) \rightleftharpoons O_2(^3\Sigma_g^-) + I(^2P_{3/2})$$

of which [14] should be predominant. At 300 K, k_{14} was found (35) to be equal to 1.3×10^3 l mol^{-1} s^{-1}. This means (35, 36) that under our experimental conditions, at 300 K the lifetime of $O_2(^1\Delta_g)$ is about 35 times longer than the lifetime of $I(^2P_{3/2})$, which disappears via reactions 2 and 3.

Since at 300 K the values of k_r^{app} obtained with ammonia and Pyrex glass filters are in agreement with each other, the flash photolytic reactions in these two cases appear to be indistinguishable. This conclusion is also reasonable because it was shown above that in our experiments no photochemical reactions are generated by radiation between 2000 and 2900 Å. The

difference between k_r^{app} (filter) and k_r^{app} (no filter) is due primarily to the presence of O_3, which is absent in experiments with filters, and O_3 photolysis products, of which only $O_2(^1\Delta_g)$ has a long enough lifetime to interfere with recombination reaction (27).

Therefore, in order to account for a difference in k_r^{app} (filter) and k_r^{app} (no filter) we must assume that in experiments with no filter additional recombination occurs via

[16] $$2I + O_3 \rightleftharpoons I_2 + O_3$$

[17] $$2I + O_2(^1\Delta_g) \rightleftharpoons I_2 + O_2(^1\Delta_g)$$

as well as via reaction 12 which is followed by rapid

[18] $$2IO + O_2 \rightleftharpoons I_2 + 2O_2$$

As the temperature of the reaction vessel is increased, contributions from the reactions 16, 17, 12, and 18 should decrease because the concentration of intermediate complexes, such as I—O_3, would drop with the temperature rise. Furthermore, O_3 itself is unstable with respect to O_2. For these reasons, the difference between k_r^{app} (filter) and k_r^{app} (no filter) decreases with temperature, and above 500 K, k_r^{app} (filter) = k_r^{app} (no filter) (Fig. 2). The absolute values of k_r^{app} suggest that at room temperature, the magnitude of $k_r^{O_2}$ is determined primarily by the RMC (18) mechanism. However, at highest temperatures, the ET mechanism (19) predominates. Between 573 and 1173 K the atomic recombination $2I(^2P_{3/2}) + O_2(^3\Sigma_g^-) \rightleftharpoons I_2(^1\Sigma_g^+) + O_2(^3\Sigma_g^-)$ can be measured without interference of side reactions. Its rate constant was found to be $\log k_r^{O_2} = 9.000 - 0.71 \log (T/573)$.

(c) An Induction Period in I Atom Recombination between 723 and 873 K

Production of oxygen atoms, O_3, and IO cannot explain the anomalous 'hump' in recombination traces observed between 723 and 873 K (Fig. 1). This is because the anomaly is present whether or not filters are used, even though IO, O_3, and O atoms cannot be formed in the absence of unfiltered radiation. Neither can we explain the 'hump' by impurities, because it is present even if Ultra Pure O_2 is used.

The 'hump' can be explained either by the presence of molecules, other than I_2, which absorb at 487 nm, and which are destroyed in some chemical reactions, or by a reaction which destroys stable I_2 molecules. Only the IO spectrum may, conceivably, overlap with I_2 spectrum at 487 nm; oxygen is transparent at this wavelength. However, the IO absorption could not explain the anomalous 'hump', because again it is present in experiments in which filters were used. Therefore, the only reasonable alternative is a reaction which destroys stable I_2. It is possible to calculate from the available experimental data, such as Fig. 1, that such a reaction would yield an additional decomposition of 2 to 3% of the initial iodine concentration. This can be done by extrapolating the absorption curve (Fig. 1) from $t > 2$ ms to $t = 0$ using the known k_r^{app} (Fig. 2) at 723 K.

As discussed above, the only excited species present at this temperature are $O_2(^1\Delta_g)$. It appears that at 723 K, a new reaction becomes significant.

[19] $$I_2(^1\Sigma_g^+) + O_2(^1\Delta_g) \rightarrow 2I(^2P_{3/2}) + O_2(^3\Sigma_g^-)$$

A value of k_{19} at 723 K may be estimated from the iodine molecule concentration which remains approximately constant during the induction period for about 0.5 ms after the initiation of the reaction. The steady state approximation for I_2 molecules yields

[20] $$k_{19} = \frac{(k_r^{O_2}[O_2] + k_r^{I_2}[I_2])([I(^2P_{3/2})]_{fl} + [I(^2P_{3/2})]_{eq})^2}{[I_2][O_2(a^1\Delta_g)]}$$

where $[I(^2P_{3/2})]_{eq}$ is the equilibrium concentration of iodine atoms prior to the photolysis. Typical concentrations at 723 K are $[O_2] = 1.5 \times 10^{-2}$ mol l^{-1}, and $[I_2] = 1.5 \times 10^{-5}$ mol l^{-1} and typically 20% of I_2 is decomposed by the flash. At 723 K, the concentration of iodine atoms in equilibrium with 1.5×10^{-5} mol l^{-1} iodine is 8.2×10^{-7} mol l^{-1}. From the percentage decomposition, $[I(^2P_{3/2})]_{fl} = 6 \times 10^{-6}$ mol l^{-1} and $[I_2] = 1.2 \times 10^{-5}$ mol 'immediately' after the flash. The concentration of singlet oxygen, $O_2(^1\Delta_g)$, will be $0.2[I(^2P_{3/2})]_{fl}$, because

essentially all of the excited iodine atoms form $O_2(^1\Delta_g)$ via reaction 1. Thus, $k_{19} \simeq 4 \times 10^7$ l mol^{-1} s^{-1} at 723 K.

Comparison of this value with the value obtained from the simple collision theory, using a steric factor of unity and molecular diameters of 5.0 Å for iodine and 3.4 Å for oxygen, results in an activation energy of 12 kcal/mol. This calculated activation energy is in reasonable agreement with the endothermicity of reaction 19, which is 13.1 kcal/mol.

It is possible that reaction 19 proceeds via electronically excited attractive states of iodine, which dissociate to two $I(^2P_{3/2})$ atoms. Of these states, one $(A^3\Pi_{1u})$ has dissociation energy of 1.8 kcal/mol. Two others have not been observed spectroscopically.

Because reaction 19 has an appreciable activation energy, the 'hump' can be observed only over a relatively narrow temperature range. At 573 K and below, the reaction is too slow to be observed and $O_2(^1\Delta_g)$ atoms participate in three-body recombination of iodine atoms. On the other hand, above 873 K, the reaction is essentially completed within the duration of the flash.

An alternative explanation of the 'hump' would be the reaction of two $O_2(^1\Delta_g)$ with I_2,

$$[21] \quad 2O_2(^1\Delta_g) + I_2(^1\Sigma_g^+) \rightarrow 2I(^2P_{3/2}) + 2O_2(^3\Sigma_g^-)$$

A steady state treatment similar to that involving reaction 19 predicts that $k_{21} = 3.7 \times 10^{13}$ l^2 mol^{-1} s^{-1} at 723 K. This would be an unusually fast rate constant for a termolecular reaction involving molecular species. Furthermore, it is not likely that the reaction 21 could be important because Derwent and Thrush (37) did not find the proper pressure dependence to justify the occurrence of reaction 21 in their I_2–O_2 discharge system.

These results are in essential agreement with a previous study of bromine recombination in oxygen (4), in which the recombination rate constants decrease smoothly with temperature. In contrast with excited iodine atoms, excited bromine atoms, $Br(^2P_{1/2})$ do not possess sufficient energy to excite oxygen to the $O_2(a^1\Delta_g)$ state. Therefore no 'hump' was observed in $Br_2 + O_2$ system. On the other hand, the rate constants for bromine atom recombination in a quartz cell were about 20% higher than in a Vycor reaction cell (4), which should be due to the production of O_3 in the quartz reaction vessel.

Acknowledgements

We would like to acknowledge the support of the Air Force Office of Scientific Research, U.S.A., and the National Research Council of Canada. One of us (G.B.) wishes to acknowledge the kind hospitality of Professor J. Joussot-Dubien who created an atmosphere at the University of Bordeaux that made completion of this work possible.

1. J. J. Deakin and D. Husain. J. Chem. Soc. Faraday Trans. II, **68**, 1603 (1972).
2. V. Yu. Zalessky. Zh. Eksp. Teor. Fiz. **67**, 30 (1974).
3. J. K. K. Ip and George Burns. Discuss. Faraday Soc. **44**, 241 (1967); **44**, 278 (1967).
4. J. K. K. Ip and George Burns. J. Chem. Phys. **41**, 3414 (1969).
5. J. Brown and George Burns. Can. J. Chem. **48**, 2133 (1970).
6. S. K. Chang, A. G. Clarke, and George Burns. J. Chem. Phys. **54**, 1835 (1971).
7. J. A. Blake and George Burns. J. Chem. Phys. **54**, 1480 (1971).
8. J. K. K. Ip and George Burns. J. Chem. Phys. **56**, 3155 (1972).
9. H. W. Chang and George Burns. J. Chem. Phys. **59**, 1053 (1973).
10. H. W. Chang and George Burns. Can. J. Chem. **51**, 3394 (1973).
11. K. E. Russell and J. Simons. Proc. R. Soc. London Ser. A, **217**, 271 (1953).
12. H. W. Chang and George Burns. J. Chem. Phys. 349 (1976).
13. R. L. Strong, J. C. W. Chien, P. E. Graf, and J. E. Willard. J. Chem. Phys. **26**, 1287 (1957).
14. P. Sulzer and K. Wieland. Helv. Phys. Acta, **25**, 653 (1952).
15. J. Brown and George Burns. Can. J. Chem. **48**, 3487 (1970).
16. George Burns and R. G. W. Norrish. Proc. R. Soc. London Ser. A, **271**, 289 (1963).
17. R. A. Durie and D. A. Ramsay. Can. J. Phys. **36**, 35 (1958).
18. A. G. Clarke and George Burns. J. Chem. Phys. **55**, 4717 (1971).
19. A. G. Clarke and George Burns. J. Chem. Phys. **56**, 4636 (1972).
20. W. H. Wong and George Burns. J. Chem. Phys. **58**, 4459 (1973).
21. W. H. Wong and George Burns. J. Chem. Phys. **59**, 2974 (1973).
22. W. H. Wong and George Burns. Can. J. Chem. **52**, 1988 (1974).
23. W. H. Wong and George Burns. Proc. R. Soc. London Ser. A, **341**, 105 (1974).
24. V. H. Shui, J. P. Appleton, and J. C. Keck. Symp. Combust., 13th, Utah, 1970 (1971). p. 21.

25. D. T. CHANG and GEORGE BURNS. Can. J. Chem. **54**, 1535 (1976).
26. B. F. MYERS and E. R. BARTLE. J. Chem. Phys. **48**, 3935 (1968).
27. C. W. VAN ROSENBERG, JR. and DANIEL W. TRAINOR. J. Chem. Phys. **61**, 2442 (1974).
28. S. W. BENSON and A. E. AXWORTHY. J. Chem. Phys. **42**, 2614 (1965).
29. F. KAUFMAN and J. R. KESLO. J. Chem. Phys. **46**, 4541 (1967).
30. M. F. R. MULCAHY and D. J. WILLIAMS. Trans. Faraday Soc. **64**, 59 (1968).
31. P. D. FRANCIS. Br. J. Appl. Phys. **20**, 1717 (1969).
32. F. STUHL and H. NIKI. J. Chem. Phys. **55**, 3948 (1971).
33. M. A. A. CLYNE and R. T. WATSON. J. Chem. Soc. Faraday Trans. I, **71**, 336 (1975).
34. M. A. A. CLYNE and H. W. CRUSE. Trans. Faraday Soc. **66**, 2227 (1970).
35. I. D. CLARK and R. P. WAYNE. Chem. Phys. Lett. **3**, 93 (1969); R. P. WAYNE. Adv. Photochem. **7**, 311 (1969).
36. R. P. STEER, R. A. ACKERMAN, and J. N. PITTS, JR. J. Chem. Phys. **51**, 843 (1969).
37. R. G. DERWENT and B. A. THRUSH. J. Chem. Soc. Faraday Trans. II, **68**, 720 (1972).

Cyclopropanediols. VI. Obtention de dérivés du cyclopropanediol

RAYMOND LE GOALLER ET JEAN-LOUIS PIERRE

Laboratoire de Chimie Organique, Université Scientifique et Médicale de Grenoble, B.P. 53, Centre de tri, 38041 Grenoble Cedex, France

Reçu le 22 juillet 1976

RAYMOND LE GOALLER et JEAN-LOUIS PIERRE. Can. J. Chem. **55**, 757 (1977).

Le texte décrit deux méthodes d'obtention de dérivés cyclopropanedioliques: la réduction des β-dicétones et le pontage des bissiloxy-1,2 alcènes dont certains sont obtenus par une nouvelle méthode.

RAYMOND LE GOALLER and JEAN-LOUIS PIERRE. Can. J. Chem. **55**, 757 (1977).

Two methods are described for the preparation of substituted cyclopropanediols: reduction of β-diketones, and bridging of 1,2-bissiloxyalkenes; a number of the latter compounds were prepared by a new method.

[Journal translation]

Introduction

Ce travail s'intègre à une étude générale des voies d'accès aux cyclopropanediols (réf. 1. et les références qui y sont citées). Il avait fait l'objet de deux communications préliminaires (2, 3).

Depuis que Staschewski (4) proposa pour la réduction de Clemmensen de la diméthyl-5,5 cyclohexanedione-1,3 un mécanisme faisant intervenir un cyclopropanediol, divers auteurs ont repris l'étude de cette réaction sur de nombreux substrats (réfs 5 et 6 et les références qui y sont citées), ces différents travaux vérifiant d'ailleurs l'hypothèse alors avancée.

A notre connaissance, hormis (1), aucune étude permettant de rendre accessible la structure cyclopropanediolique n'a encore été réalisée, bien qu'en fait quelques composés de ce type aient déjà été obtenus: (*i*) par réduction des β-dicétones: dès 1969, trois équipes isolent les premiers dérivés de cyclopropanediols (2, 7, 8) et plus tard, quelques diols libres ont pu être obtenus (9–11); (*ii*) par pontage des doubles liaisons: ce sont essentiellement l'action du diazométhane sur les carbonates de vinylène (12) et des dihalogénocarbènes sur les diéthers éthyléniques (13).

Pour notre part, après avoir montré que la réduction de la diméthyl-3,3 pentanedione-2,4 par le sodium dans l'éther en présence de triméthylchlorosilane (TMCS), fournissait les deux composés cyclopropaniques attendus (2), nous avons entrepris de mettre au point des méthodes d'obtention des dérivés de cyclopropanediols et nous exposons ici les résultats obtenus: (*i*) d'une part en généralisant la réduction des composés β-dicarbonylés, (*ii*) d'autre part en appliquant la réaction de Simmons et Smith aux bissiloxyalcènes, préparés pour la première fois en 1960 par Ruhlmann par une méthode qui consiste à piéger la forme ènediolique obtenue au cours de la réaction acyloïne par du TMCS (14).

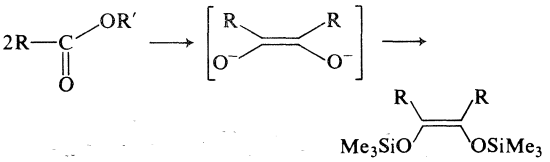

Afin d'obtenir des bis(trimethylsiloxy-1,2) alcènes dissymétriques, nous avons appliqué cette même réaction aux α-dicétones.

Résultats et discussion

A. Réduction des composés β-dicarbonylés

Afin d'éviter les complications dues à l'énolisation, nous avons utilisé des substrats non énolisés. Nous avons opéré avec du sodium dispersé et avec le mélange Na–K plus facile à mettre en œuvre et qui donne de meilleurs résultats, dans l'éther et en présence de triméthylchlorosilane (TMCS). Nous avons étudié les substrats suivants:

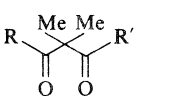

	R	R′		R	R′
1	Me	Me	**5**	Ph	H
2	Et	Et	**6**	Me	H
3	Et	Me	**7**	Me	OEt
4	Ph	Ph	**8**	EtO	OEt

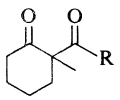

9 R = H
10 R = Me

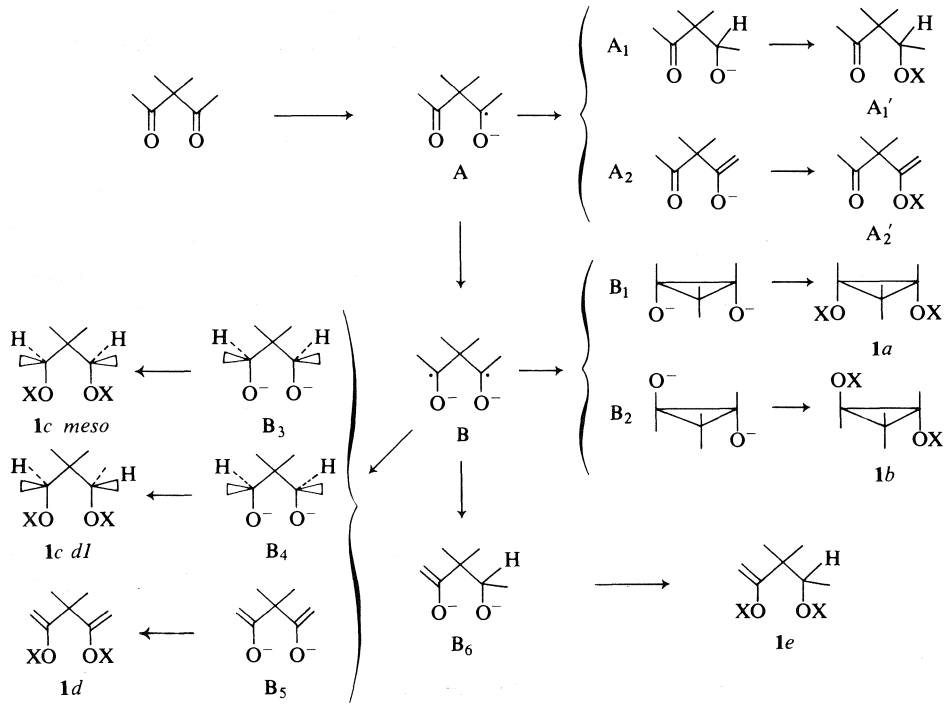

SCHÉMA 1. $X = SiMe_3$

Les résultats obtenus avec **1** ont été décrits dans notre communication préliminaire (2). Ils peuvent s'expliquer par le mécanisme généralement invoqué pour la réduction des cétones par les métaux (15) et sont résumés dans le schéma 1. Avec une quantité équivalente de sodium, on obtient deux fractions A et B. Les proportions relatives de la fraction B étant: **1***a* 20%; **1***b* 10%; **1***c meso* 15%; **1***c dl* 5%; **1***d* 20%; **1***e* 30%. Si on opère avec un excès de sodium, seule la fraction B est obtenue.

Les produits A_1' et **1***c* ont été d'autre part obtenus par action du TMCS en présence de triéthylamine sur les composés hydroxylés correspondants. Nous avons vérifié que A_2' et **1***d* donnent par hydrolyse la dicétone de départ, tandis que A_1' et **1***e* donnent le cétol attendu. L'hydrolyse de **1***a* en milieu neutre conduit à la dicétone de départ alors qu'en milieu acide concentré, nous obtenons un produit non encore identifié, mais différent du cétol obtenu par réduction de Clemmensen de la diméthyl-3,3 pentanedione-2,4 (16).

La stéréochimie de **1***a* et **1***b* a été déterminée par rmn de même que celle des isomères de **1***c* et cette étude a fait l'objet d'une communication séparée (17).

Il est à remarquer nous avons obtenu une fraction importante de transfert d'H sur les cétyles. Ce phénomène avait également été observé lors de la réduction de la cyclohexanone dans les mêmes conditions (15).

Nous avons vérifié le comportement de la dicétone initiale en milieu basique: une coupure normale est observée conduisant à l'acétate et à la méthyl-3 butanone-2. La cétone transposée de Brohmann et Pinder et de Inamoto *et al.* n'est pas observée (18). La présence de TMCS ne semble pas avoir d'effet sur la marche de la réaction puisque les résultats sont inchangés en opérant son addition avant, pendant ou après la réduction de la dicétone.

Les autres dicétones ou cétoaldéhydes étudiés ont un comportement absolument identique qui peut se résumer de la façon suivante (schéma 2).

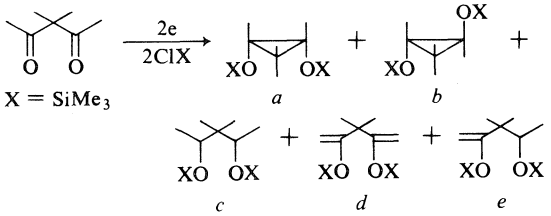

SCHÉMA 2

TABLEAU 1. Les résultats de la réduction des composés β-dicarbonylés

Produit	Rendement*(%) $a + b$	Rapport a/b	Rendement (%) $c + d + e$
1	30	2	70
2	30	2	70
3	30	2	70
4	90	*a* seul	0
5	40	3	0
6	90	1.5	0
9	30	3	60
10	50	3	50

*Il s'agit de rendements moyens établis sur plusieurs réactions, évalués par rapport au produit de départ. Dans certains cas, on obtient un peu de polymérisation.

Les résultats, obtenus en utilisant un gros excès de réducteur, ce qui permet de supprimer la fraction A et de consommer entièrement les produits de départ, sont résumés dans le tableau 1.

Pour **4** on obtient exclusivement le composé *Z*. Les produits analogues à **1***d* et **1***e* qui représentaient 50% des produits de la réaction ne peuvent intervenir. L'absence des analogues de **1***c* implique que le cétyle ne capte pas d'hydrogène ce qui semble indiquer pour **1**, les H provenaient de la dismutation du cétyle lui-même (schéma 3).

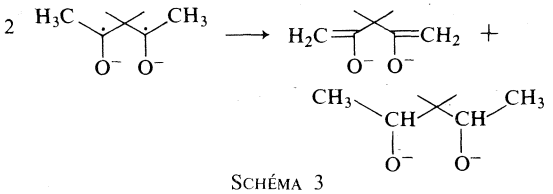

SCHÉMA 3

Le cétoaldéhyde **5** conduit aux dérivés cyclopropaniques avec un rendement de l'ordre de 40% accompagnés de nombreux sous-produits non analysables alors que **6** fournit le cyclopropane à 90%.

A titre de comparaison, nous avons effectué la réduction de **6** par le sodium dans l'ammoniac liquide, en captant ensuite les énolates formés par le TMCS. Aucun cyclopropane n'est obtenu sans doute à cause du caractère donneur de H du solvant (schéma 4).

Le β-cétoester **7** conduit également avec un excellent rendement (>80%) à un dérivé cyclopropanique **7***a* qui semble être unique mais dont nous n'avons pu préciser la structure, accompagné de 20% du composé ouvert **7***c*. (schéma 5).

La réduction de **7** dans NH_3–Et_2O–TMCS ne fournit aucun produit cyclopropanique et

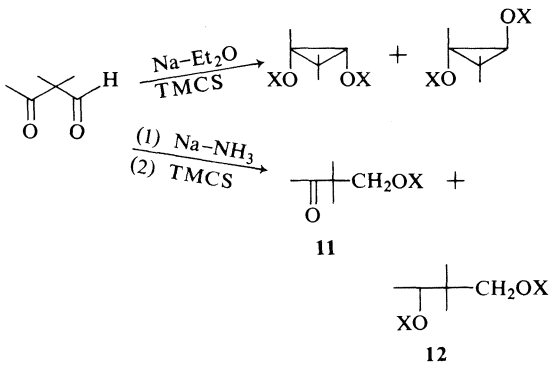

SCHÉMA 4

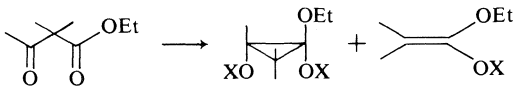

SCHÉMA 5

nous avons obtenu quantitativement les produits de la réduction normale **11** et **12**.

Enfin le diester **8** qui aurait pu selon le schéma de la réduction acyloïne conduire à un dérivé disiloxylé du cyclopropène, nous a en réalité fourni le composé ouvert **8***c* avec un rendement supérieur à 90%. Un résultat analogue au nôtre a été observé par réf. 19 et expliqué par réf. 20.

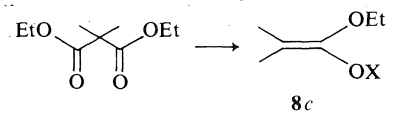

Les attributions de configuration ont été faites de façon certaine pour **1***a* et **1***b*, **2***a* et **2***b*, et **4***a* sur la base de l'équivalence des méthyles en 3 pour les composés *E* et de leur inéquivalence pour les composés *Z* (17). On constate que dans tous ces cas le composé *Z* est majoritaire, ce qui nous a conduit à admettre cette structure pour le composé majoritaire obtenu dans les autres cas.

Discussion

Sur le plan théorique, le résultat est clairement interprété, deux voies pouvant être envisagées (schéma 6).

L'étude électrochimique de Curphey *et al.* (7), suivie en rpe, a permis de montrer qu'il se formait un radical donnant une simple absorption large, l'absence de structure fine empêchant toute interprétation. D'autre part, Curphey

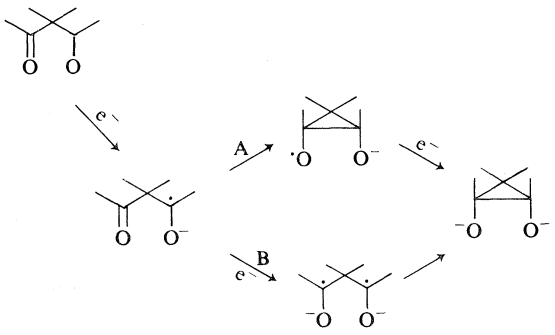

SCHÉMA 6

indique qu'il est impossible d'ajouter plus d'un électron aux dicétones, par voie électrochimique, et conclut à l'existence d'un seul radical anion. Ceci pose le problème des composés obtenus par dismutation, composés qui ne sont jamais hydroxylés ainsi que pourrait le suggérer l'intermédiaire cyclopropanique de la voie A.

B. Pontage des bis(trimethylsiloxy)-1,2 alcenes

La réaction de Ruhlmann, à laquelle nous avons apporté une petite modification en utilisant, comme agent réducteur, l'alliage sodium–potassium qui donne de meilleurs résultats que le sodium dispersé, nous a permis d'atteindre les siloxyalcènes du tableau 2. Ces produits ont été caractérisés par leurs données spectroscopiques.

La réduction des α-dicétones dissymétriques dans les mêmes conditions a conduit aux bissiloxyalcènes du tableau 3 qui ont été également caractérisés pas spectroscopie ir et rmn, à côté d'autres produits résultant de la dismutation des radicaux anions intermédiaires (21).

Pontage des bis(triméthylsiloxy)-1,2 alcènes

Nous avons examiné divers réactifs carbéniques.

(*i*) *Le diazométhane* peut donner le méthylène (CH_2:) et conduire aux cyclopropanes par addition aux oléfines (22). Ce réactif avait été utilisé avec succès par Breitbeil *et al.* (12) avec les carbonates de vinylène, mais il s'est avéré inerte sur nos composés.

(*ii*) *Le phényl carbène* (Ph—CH:) peut entre autres méthodes (22) être préparé par la décomposition catalytique de tosylhydrazones (réaction de Bamford–Stevens). *Le phényl carbène ainsi préparé, ajouté au siloxy alcènes précédents, n'a conduit à aucun phényl cyclopropane.* Les substrats sont récupérés accompagnés de goudrons.

(*iii*) L'addition thermocatalysée (Cu, 80° C) du *diazoacétate d'éthyle* (donc du carboéthoxycarbène) au bis(triméthylsiloxy)-1,2 butène-2, *Z*, a conduit, à côté du produit de duplication du carbène, à l'ester cyclopropanique correspondant avec un rendement de 60% (schéma 7).

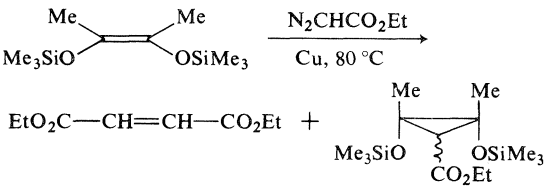

SCHÉMA 7

Le cyclopropane obtenu est caractérisé par spectroscopie. La relation *cis* des méthyles est démontrée par l'observation de leur équivalence magnétique (17). Par contre, nous n'avons pas de critère de la configuration relative du groupement ester. Il est important de remarquer que la réaction n'a conduit à aucun produit d'ouverture du cyclopropane, contrairement à la réaction d'addition du même réactif aux monosiloxyalcène (23).

Bien qu'elle soit positive, nous n'avons pas étendu cette réaction aux autres dissiloxyalcènes, notre but n'étant pas de préparer des cyclopropanes trifonctionnalisés. L'hydrolyse de **24** par H_2O–MeOH–C_6H_6 conduit à

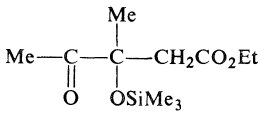

(*iv*) *La réaction de Simmons et Smith.* Cette réaction, souvent apparentée aux réactions carbénoïdes (24), conduit à un cyclopropane en traitant une oléfine par de l'iodure de méthylène en présence du couple zinc/cuivre.

Nous l'avons appliquée aux siloxyalcènes des tableaux 2 et 3 et obtenu dans tous les cas les composés cyclopropaniques attendus avec de bons rendements (tableau 4).

En utilisant la technique habituelle (hydrolyse puis précipitation des sels de zinc solubles dans l'éther par du carbonate de sodium), il se forme des produits d'ouverture du cyclopropane obtenu. Le rendement est nettement amélioré si, avant hydrolyse, on remplace l'éther par du pentane dans lequel les sels de zinc sont insolubles. L'extraction est ensuite effectuée au pentane

TABLEAU 2. Les siloxyalcènes obtenus par la réaction de Ruhlmann

Produit de départ	Bis(triméthylsiloxy)-1,2 alcène		Rendement après purification (%) Na	Na–K
H—CO_2Et	Me_3SiO—CH=CH—$OSiMe_3$	**(13)***	10	12
H—CO_2-*i*-Pr			2	10
Me—CO_2Et	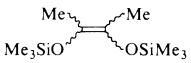	**(14)***	25	80
Me—CO_2Bu			40	80
Et—CO_2Me	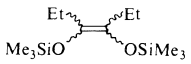	**(15)***	40	85
i-Pr—CO_2Et	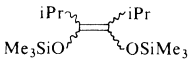	**(16)***	50	70
Pr—CO_2Et	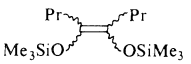	**(17)***	50	75
Adipate de Me	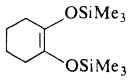	**(18)**	60	70
Adipate de Et			40	70
Glutarate d'Et	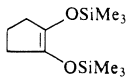	**(19)**	65	70

*Mélange *Z–E*.

TABLEAU 3. Les produits de la réaction de Simmons et Smith

Produit de départ	Bis(triméthylsiloxy)-1,2 alcène		Rendement (%)
Ph—C(=O)—C(=O)—H	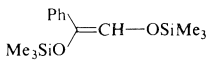	**(20)**	40
tert-Bu—C(=O)—C(=O)—H	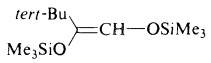	**(21)**	50
Et—C(=O)—C(=O)—Me	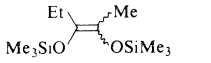	**(22)**	50
Pr—C(=O)—C(=O)—Me	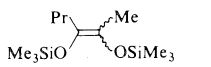	**(23)**	40

et les sels de zinc précipités sous forme d'hydroxydes par addition d'eau.

La structure des produits obtenus a été caractérisée par leurs spectres ir et rmn et leurs analyses centésimales. Les isomères *cis–trans* ont pu être séparés par cpv préparative et la stéréochimie caractérisée par rmn (17). Dans tous les cas, l'isomère *Z* est très prépondérant dans le rapport 9/1 vis-à-vis de l'isomère *E*.

Les bis(triméthylsiloxy)-1,2 cyclopropanes sont des liquides incolores stables à l'air et à la chaleur, jusqu'à 200 °C environ. Ils peuvent

TABLEAU 4. Bis(triméthylsiloxy)-1,2 cyclopropanes obtenus par réaction de Simmons et Smith

Composé		Rendement (%) Méthode classique	Méthode modifiée
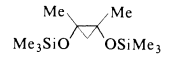	**25** *Z*	25	65
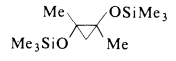	**25** *E*		
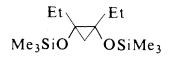	**26** *Z*	45	70
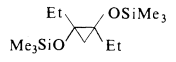	**26** *E*		
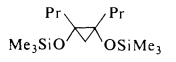	**27** *Z*	55	70
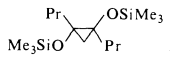	**27** *E*		
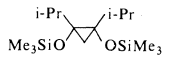	**28** *Z*	25	70
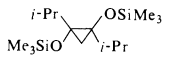	**28** *E*		
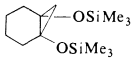	**29**	50	70
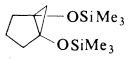	**30**	40	60
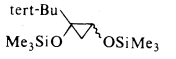	**31**	25	60
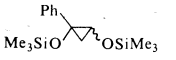	**32**	8	10
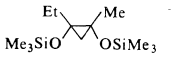	**33** *Z*	45	70
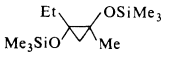	**33** *E*		
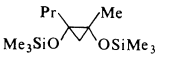	**34** *Z*	40	60
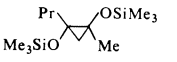	**34** *E*		

être quantitativement transformés en acétates par l'action du bromure d'acétyle. Leurs réactions avec divers autres réactifs (H_2O, ROH, HX, RLi, etc...) ont été étudiées et seront publiées prochainement (25).

Conclusions

Il est vérifié que les β-dicétones et les β-cétoesters non énolisables fournissent sous l'action du sodium dispersé ou de l'alliage Na–K dans l'éther des dérivés cyclopropanedioliques à côté d'autres produits issus des radicaux-anions intermédiaires qui limitent l'intérêt pratique de cette méthode du fait de la difficulté de séparation des produits.

Par contre, la réaction de Simmons et Smith appliquée aux bis(triméthylsiloxy)-1,2 alcènes s'est avérée être une bonne voie d'accès à ce type de composés et constitue sans doute actuellement, la méthode de choix pour préparer les dérivés de cyclopropanediols.

Partie Expérimentale

Les spectres rmn ont été enregistrés dans CCl_4 sur appareil fonctionnant à 60 MHz. Tous les déplacements chimiques sont donnés en $\delta \times 10^6$, sauf précision contraire. Les spectres ir sur Perkin-Elmer 227.

Substrats

1, **2**, **3**, **4**, **7** et **8** ont été obtenus par diméthylation des dicétones énolisables selon réf. 26; **5**, **6** et **10** à partir des èneamines selon réf. 27; **9**, selon réf. 28 suivi de méthylation.

*Réduction par $Na–Et_2O$ ou $Na–K–Et_2O$ (mode opératoire type: cas de **1**)*

Na–K est obtenu en chauffant un mélange 1:1 en poids de Na et de K. Dans un tricol équipé d'un réfrigérant, d'un agitateur et d'une ampoule à brome, maintenu sous azote sec et exempt d'oxygène, on introduit 0.5 mol de sodium dispersé dans 300 ml d'éther anhydre. A reflux d'éther on ajoute goutte à goutte un mélange de 0.5 mol de TMCS et de 0.25 mol de dicétone. On maintient ensuite l'agitation pendant 5 h à température ordinaire, on filtre rapidement et distille après évaporation de l'éther.

De nombreux essais ont été effectués. Dans tous les cas, le composé dicarbonylé est totalement consommé au bout de quelques heures.

Dans le cas **1**, la distillation conduit à deux fractions A et B (A n'est pas obtenue si on opère avec un excès de sodium).

Fraction A (54–58 °C/4 torr)

Deux produits sont séparés par cpv et identifiés.

A_1' Me—C(=O)—$C(Me)_2$—$CH(OSiMe_3)$—Me: ir 1700, 1250, 830 cm^{-1}; rmn 0.05 (s, 9H, $SiMe_3$), 0.98 (d, 3H, J = 6 Hz, CH_3—CH), 3.87 (q, 1H, J = 6 Hz, CH—CH_3), 2.00 (s, 3H, CH_3—CO), 1.00 (s, 6H, Me_2). *Anal.* calc.: C 59.40, H 10.89, Si 13.86; trouvé: C 61.60, H 10.02, Si 13.49.

A_2': Me—C(=O)—$C(Me)_2$—$C(OSiMe_3)$=CH_2: ir 3125, 1720, 1625, 1250 et 850 cm^{-1}; rmn 0.19 (s, 9H, $SiMe_3$), 1.12 (Me_2C), 2.00 (CH_3CO), 252 et 245 Hz (J = 2 Hz, CH_2=). *Anal.* calc.: C 60, H 10, Si 14; trouvé: C 60.14, H 10.34, Si 13.74.

Fraction B (65–70 °C/2 torr)

La cpv permet de distinguer six produits qui sont séparés par cpv préparative en plusieurs temps (Apiezon 20 pieds).

1*a*: 20%; ir 1250 cm^{-1}; rmn *cf* réf. 18.

1*b*: 10%; ir et nmr (voir **1***a*). *Anal.* calc.: C 56.93, H 10.94, Si 20.43; trouvé: C 57.30, H 10.90, Si 20.08.

Diacétate *E*: rmn 1.09 (s, Me_2C), 1.39 (s, *Me*-CO(CH_3)—), 1.95 (s, Me—CO—).

Spectre de masse (réalisé par M. Pechiney au laboratoire de Chimie Structurale Organique d'Orsay): faible pic à 114 (PM); pic important à *m/e* 171 (214 − 43, correspondant à la perte de CH_3CO^+); pic important à *m/e* 154 (fragmentation de MacLafferty: perte de CH_3CO_2H); pic important à *m/e* 139 (perte d'un CH_3); pics importants à *m/e* 129, 112, 97, 87 et 69 (interprétables par pertes de cétènes et de méthyle).

1*c meso*: 15%; ir 1250 cm^{-1}; rmn *cf.* réf. 18. *Anal.* calc.: C 56.52, H 11.59, Si 20.28; trouvé: C 56.77, H 11.67, Si 20.36.

1*c dl*: 5%; ir 1250 cm^{-1}; rmn *cf.* réf. 18.

1*d*: ir 1255, 1610, 3115 cm^{-1}; rmn 0.2 ($SiMe_3$), 1.15 (Me_2C), 242.5 et 237.5 (J = 1.5 Hz, H_2C). *Anal.* calc.: C 57.35, H 10.29, Si 20.58; trouvé: C 58.10, H 9.90, Si 19.87.

1*e*: ir 3100, 1610, 1250, 830 cm^{-1}; rmn 0.12 et 0.25 ($SiMe_3$), 0.91 et 1.01 (Me_2C), 1.00 (*Me*—CH, J = 6.5 Hz), 3.91 (*CH*—Me, J = 6.5 Hz), 244.5 et 235.5 Hz (=CH_2), J = 1.6 Hz. *Anal.* calc.: C 56.93, H 10.94, Si 20.43; trouvé: C 57.65, H 11.03, Si 20.18.

Nous ne détaillerons pas les résultats obtenus avec **2** et **3** qui sont en tous points identiques à ceux obtenus à partir de **1** et qui ne souffrent d'aucune ambiguïté.

Le dérivé cyclopropanique obtenu à partir de **4** est aisément identifié: **4***a*: ir 1250 cm^{-1}; rmn 0.05 ($SiMe_3$), 1.09 et 1.4 (Me, Me>C non équivalents, d'où la configuration *cis*, *cf.* réf. 18), 7.35 (massif phényl).

Réduction de **5**: Les deux isomères **5***a* et **5***b* sont séparés. Ils sont dans des proportions 75:25 et présentent les mêmes caractéristiques ir; rmn du produit majoritaire 0.05 et 0.03 ($SiMe_3$), 0.64 et 1.10 (Me_2C), 3.10 (H), 7.2 à 7.4 (Ph); rmn du produit minoritaire 0.05 et 0.30 ($SiMe_3$), 0.81 et 1.30 (Me_2C), 3.28 (H), 7.1 à 7.6 (Ph).

Là encore nous n'avons pas de critère sûr de configuration. Un raisonnement basé sur les déplacements chimiques (effet d'un Ph β-*cis* sur un proton cyclopropanique, effet d'un $OSiMe_3$) milite en faveur de la configuration *cis* pour le composé majoritaire.

Réduction de **6**: nous n'avons pas pu séparer les deux isomères **6***a* et **6***b*. Cependant la rmn du mélange permet à partir des pics du proton H d'évaluer les proportions à 60:40; rmn du mélange 0.05 ($SiMe_3$), 0.90 et 0.95 (Me_2C), 1.25 (Me), 2.45 et 2.82 (H de chaque isomère).

11: ir 1700, 1250, 1160, 830 cm^{-1}; rmn 0.05 ($SiMe_3$), 1.00 (Me_2C), 2.00 (MeCO), 3.4 (CH_2).

12: ir 1250, 1185 et 830 cm^{-1}, rmn 0.04 ($OEtMe_3$), 0.70 (Me_2C), 0.97 (*Me*—CH, d, J = 6.6 Hz), 3.65 (q, H), 3.62 (spectres AB, —CH_2—).

Réduction de **7**: nous n'avons pu séparer les deux isomères **7***a* et **7***b* dont le mélange présente en ir 1250 et 850 cm^{-1}; rmn 0.13 ($SiMe_3$), 0.85 et 0.90 (Me_2C), 1.2 (Me), 3.6 (CH_2), 1.05 (CH_3CH_2).

7*c*: ir 1700, 1250, 830 cm^{-1}; rmn 0.15 ($SiMe_3$), 1.2 (CH_3CH_2), 1.50 et 1.59 (Me, Me>=), 3.8 (CH_2).

Réduction de **9**: les deux isomères sont séparés par cpv préparative. Ils sont dans les proportions 80:20 et présentent les mêmes caractéristiques ir; rmn du produit majoritaire 0.05 ($SiMe_3$), 0.90 (Me), 1.1 à 1.9 (cycle), 2.7 (H); rmn du produit minoritaire 0.05 ($SiMe_3$), 1.00 (Me), 1.4 à 1.8 (cycle), 2.8 (H).

Réduction de **10**: la cpv sur colonne Apiezon montre quatre produits. Les produits cyclopropaniques **10***a* et **10***b* sont séparés sur DEGS 5 pied à 90 °C. *Anal.* calc.: C 60, H 10.66, Si 18.66; trouvé: C 59.63, H 11.28, Si 18.54; rmn du produit majoritaire 0.05 ($SiMe_3$), 0.82 (Me ang.), 1.16 (MeCO), 1.2 à 2 (cycle); rmn du produit minoritaire 0.05 ($SiMe_3$), 0.85 (Me ang.), 0.98 (MeCO), 1.2 à 2.2 (cycle).

Tous les produits siloxylés non cyclopropaniques obtenus ont été hydrolysés et les diols, cétones ou

dicétones obtenus comparés à des échantillons authentiques.

Les bissiloxyalcènes symétriques sont préparés par réduction des esters selon réf. 14 en utilisant comme agent réduction du sodium dispersé ou Na–K.

13: p éb 45–55 °C/12 torr; ir 3050, 1660, 1250, 840 cm^{-1}; rmn 0.05 (s, 9H), 5.5 (s, 1H).

14: p éb 65–72 °C/10 torr; ir 1660, 1250, 840 cm^{-1}; rmn 0.08 (s, 18H), 1.7 (s, 6H).

15: p éb 85–88 °C/12 torr; ir 1682, 1250, 830 cm^{-1}; rmn 0.1 (s, 18H), 0.95 (t, 6H), 1.95 (q, 4H).

16: p éb 88–89 °C/12 torr; ir 1255, 835 cm^{-1}; rmn 0.08 (s, 18H), 0.95 (d, 12H), 1.90 (H, 2H).

18: p éb 92 °C/6 torr; ir 1690, 1250, 830 cm^{-1}; rmn 0.1 (s), massifs entre 1.55 et 2.

19: p éb 90 °C/8 torr; ir 1680, 1240, 840 cm^{-1}; rmn 0.12 (s, 18H), massifs entre 1.6 et 2.2 (6H).

17: p éb 90–92 °C/9 torr; ir 1672, 1250, 830 cm^{-1}; rmn 0.1 (s, 18H), massifs à 1.5 et 2.

Les bissiloxyalcènes dissymétriques sont obtenus par la même méthode à partir des α-dicétones.

20: p éb 80–82 °C/3 torr; ir 3100, 3000, 1640, 1600, 1250, 835 cm^{-1}; rmn 0.02 (s, 9H), 0.22 (s, 9H), 6.5 (s, 1H), 7–7.4 (s, 5H).

21: p éb 80–84 °C/16 torr; ir 3090, 1670, 1250, 845 cm^{-1}; rmn 0.005 (s, 18H), 0.98 (s, 9H), 5.6 (s, 1H).

22: p éb 86–88 °C/11 torr; ir 1680, 1250–1255, 830–840 cm^{-1}; rmn 0.07 (s, 18H), 0.9 (3H), 1.6 (3H), 1.9 (2H).

23: p éb 85–89 °C/5 torr; ir 0.1 (s, 18H), 0.95, 1.5, et 1.95.

Les α-dicétones ont été obtenues par la méthode de Riley.

Carbéthoxy-1 bissiloxy-1,2 cyclopropane **24**: à 15 g de **14** (0.067 mol), additionné d'1 g de cuivre en poudre contenu dans un ballon tricol maintenu sous courant d'azote, muni d'un réfrigérant, d'une ampoule à brome et d'un agitateur magnétique, on ajoute lentement 7.6 g de diazoacétate d'éthyle dilué dans 8 g de cyclohexane. Le ballon est maintenu à 80 °C. Après filtration, la distillation permet de récupérer 11 g de produit; p éb 93–100 °C/0.7 torr (60%). La séparation en cpv (Apiezon 10 pieds) fournit 2 isomères de **24** présentant le même spectre infrarouge: 3010 (ép.) 1725, 1255, 830 cm^{-1}; rmn de **24***A* (55%) à 0.05 (s, 18H), 1.2 (t, 3H), 1.5 (s, 6H), 1.75 (s, 1H), 4.1 (q, 2H); rmn de **24***B* (45%) 0.1 (s, 18H), 1.2 (t, 3H), 1.75 (s, 6H), 2.3 (s, 1H), 4.1 (q, 2H).

L'hydrolyse de ce composé dans le mélange H_2O–MeOH–C_6H_6, fournit essentiellement (par séparation cpv Apiezon L 15%) un produit présentant en ir des bandes à 1740–1710, 1250 et 830 cm^{-1}; en rmn 0.1 (s, 9H), 1.2 (t, 3H), 1.27 (s, 3H), 2.1 (s, 3H), 2.6 (AB, J_{AB} = 16 Hz, δ_A = 90 Hz, δ_B = 114.7 Hz), 4.4 (q, 2H); en accord avec la formule proposée dans le texte.

Réaction de Simmons et Smith

A 17 g de couple Zn–Cu préparé selon Simmons–Smith (24) ou de couple Zn–Ag selon Conia et ses collegues (29) dans 80 ml d'éther anhydre, on ajoute suffisamment de CH_2I_2 pour faire démarrer le couple maintenu sous courant d'azote. On ajoute ensuite 0.1 mol de bissiloxyalcène, puis l'iodure de méthylène de façon à maintenir un bon reflux. On maintient ensuite ce reflux pendant 18 h. On élimine la majeure quantité d'éther et on ajoute 100 ml de pentane. Puis on ajoute goutte à goutte 10 ml d'eau, on filtre et on extrait au pentane. La phase organique est ensuite lavée à l'eau, jusqu'à ce que l'hydroxyde de zinc ne précipite plus. Après sèchage au sulfate de sodium, on élimine le solvant et on distille.

25: p éb 69–72 °C/5 torr; n_D^{20} 1.4182. *Anal.* calc.: C 53.66, H 10.57, Si 22.75; trouvé: C 52.89, H 10.28, Si 22.28. **25***Z*: ir 3088, 1255, 1025, 840 cm^{-1}; rmn 0.05 (s, 18H), 1.25 (6H); spectres AB δ_A = 14.7 Hz, δ_B = 45.3 Hz, J_{AB} = 6 Hz. **25***E*: ir 3075, 1255, 1025, 840 cm^{-1}; rmn 0.07 (s, 18H), 0.85 (3H), 1.15 (3H), 0.5 (2H).

26: p éb 80 °C/2 torr; n_D^{20} 1.4334. *Anal.* calc.: C 56.91, H 10.95, Si 20.42; trouvé: C 56.32, H 10.48, Si 20.16; ir 3075, 1255, 1020, 830 cm^{-1}; rmn (*i*) *Z* 0.1 (s, 18H), 0.95 (3H), 1.45 (2H), J_{AB} = 6.6 Hz, δ_A = 20 Hz, δ_B = 35.2 Hz; (*ii*) *E* 0.1 (s), 0.95 (3H), 1.45 (2H) δ_{A_2} = 0.4 Hz.

27: p éb 97 °C/5 torr; n_D^{20} 1.4346 *Anal.* calc.: C 59.6, H 11.26, Si 18.71; trouvé: C 61.18, H 11.26, Si 17.89; ir 3075, 1255, 1010, 830–835 cm^{-1}; rmn (*i*) *Z* 0.1 (18H), 0.9 (6H), 1.3–1.6 (8H), δ_A = 18.5 Hz, δ_B = 44.2 Hz, J_{AB} = 6.1 Hz; (*ii*) *E* spectre A_2 δ_A = 0.6 Hz (2H), reste identique à *Z*.

28: p éb 89–91 °C/4 torr; n_D^{20} 1.4428; ir 3081, 1250, 1010, 850 cm^{-1}; rmn 0.1 (18H), 0.9 (6H), 1.4–1.6 (2H), δ_A = 18 Hz, δ_B = 44.2 Hz, J_{AB} = 6 Hz.

29: p éb 63 °C/0.2 torr; n_D^{20} 1.4459; *Anal.* calc.: C 57.35, H 10.33, Si 19.85; trouvé: C 58.18, H 10.41, Si 19.48; ir 3070, 1250, 1010, 840 cm^{-1}; rmn 0.1 (18H), 1.05–1.45 (4H), 1.75–2.15 (4H), δ_A = 27.4 Hz, δ_B = 44.6 Hz, J_{AB} = 6 Hz.

30: p éb 78 °C/5 torr; n_D^{20} 1.4523. *Anal.* calc.: C 58.12, H 10.50, Si 22.58; trouvé: C 57.84, H 10.22, Si 22.12; ir 3080, 1250, 1005, 835 cm^{-1}; rmn 0.1 (18H), 1.05–1.95 (6H), δ_A = 16 Hz, δ_B = 41.3 Hz, J_{AB} = 6 Hz.

31: p éb 96 °C/8 torr; n_D^{20} 1.4488; ir 3065, 1255, 1020, 830 cm^{-1}; rmn 0.15 (18H), 1.05 (9H), 0.4 (2H), 2.9 (1H).

32: p éb 125–130 °C/0.25 torr; n_D^{20} 1.4365; ir 3000, 3080, 1600, 1250, 838 cm^{-1}; rmn (2 isomères) 0.05 (9H) et 0.3 (9H), massif entre 0.7 et 1.3 (2H), 1.8 (1H), 7.1–7.5 (5H).

33: p éb 75 °C/2 torr; n_D^{20} 1.4285. *Anal.* calc.: C 53.75, H 10.00, Si 21.58; trouvé: C 53.15, H 9.81, Si 20.94; rmn (*i*) *Z* 0.08 (18H), 1.05 (6H), 1.5 (2H), δ_A = 18 Hz, δ_B = 48 Hz, J_{AB} = 6.5 Hz; (*ii*) *E* 0.05 (18H), 1.2 (6H), 1.7 (2H), 0.55 (2H).

34: p éb 95 °C/3 torr; n_D^{20} 1.4352; ir 3075, 1255, 1010 et 835 cm^{-1}; rmn 0.09 (18H), 1.05 (6H), 1.25 (2H), 1.45 (2H), 0.4 (2H).

1. R. Le Goaller et J. L. Pierre. C.R. Acad. Sci. Ser. C, **279**, 785 (1974).
2. R. Le Goaller, M. Rougier, C. Zimero et P. Arnaud. Tetrahedron Lett. 4193 (1969).
3. M. Audibrand, R. Le Goaller et P. Arnaud. C.R. Acad. Sci. Ser. C, **268**, 2322 (1969).
4. D. Staschewski. Angew. Chem. **71**, 726 (1959).
5. J. G. Buchanan et P. D. Woodgate. Q. Rev. 522 (1969).
6. D. H. Gibson et C. H. Depuy. Chem. Rev. **6**, 805 (1974).
7. T. J. Curphey, C. W. Amelotti, T. P. Layloff, R. L. McCarthwey et J. H. Williams. J. Am. Chem. Soc. **91**, 2817 (1969).
8. W. Reusch et D. B. Priddy. J. Am. Chem. Soc. **91**, 3677 (1969).
9. T. J. Curphey et R. L. McCarthwey. Tetrahedron Lett. 5295 (1969).

10. F. CHEN et C. AINSWORTH. J. Am. Chem. Soc. **94**, 4037 (1972).
11. J. ARMAND et L. BOULARES. Can. J. Chem. **54**, 1197 (1976).
12. F. W. BREITBEIL, D. T. DENNERLEIN, A. E. FIEBIG et R. E. KUZNICKI. J. Org. Chem. **33**, 3389 (1968).
13. A. J. BIRCH et R. KEETON. Aust. J. Chem. **24**, 331 (1971).
14. J. SCHRAPLER et K. RUHLMANN. Chem. Ber. 1833 (1964) et réf. cit.
15. K. RUHLMANN, A. SITZKI et C. MICHAEL. Chem. Ber. **101**, 285 (1968).
16. N. S. CUSACK et B. R. DAVIS. J. Org. Chem. **30**, 2062 (1965).
17. R. LE GOALLER, J. L. PIERRE et P. ARNAUD. Org. Magn. Reson. **1**, 337 (1969).
18. I. INAMOTO, N. IWATA et O. SINAMURA. Chem. Ind. 47 (1959); N. H. BROMHAN et A. R. PINDER. J. Chem. Soc. 2688 (1959).
19. Y. N. KUO, F. CHEN, C. AINSWORTH et J. J. BLOOMFIELD. Chem. Commun. 136 (1971).
20. J. J. BLOOMFIELD, D. C. OSLEY, C. AINSWORTH et R. E. ROBERTSON. J. Org. Chem. **40**, 393 (1975).
21. K. RUHLMANN, B. GICHTE, T. KIAIAKIDIS, C. MICHAEL et G. MICHAEL, J. Organometal. Chem. **34**, 41 (1972).
22. W. KIRMSE. Carbene chemistry. Academic Press. 1971.
23. R. LE GOALLER et J. L. PIERRE. C.R. Acad. Sci. Ser. C, **276**, 193 (1973).
24. H. E. SIMMONS, T. L. CAIRNS, S. A. VLADUCHICK et C. M. HOINESS. Organic reactions. Vol. XX. J. Wiley. 1973. p. 1.
25. R. LE GOALLER et J. L. PIERRE. A paraître.
26. J. J. BLOOMFIELD. J. Org. Chem. **26**, 4112 (1961).
27. T. INUKAÏ et R. YOSHIZAWA. J. Org. Chem. **32**, 404 (1967).
28. C. AINSWORTH. Org. Synth. **4**, 536 (1963).
29. J. M. DENIS, G. GIRARD et J. M. CONIA. Synthesis, 549 (1972).

Redox properties of 2,3,7,8-tetramethoxyselenanthrene: a charge-transfer donor

A. W. ADDISON, T. H. LI, AND L. WEILER

Chemistry Department, University of British Columbia, Vancouver, B.C., Canada V6T 1W5

Received September 2, 1976

A. W. ADDISON, T. H. LI, and L. WEILER. Can. J. Chem. **55**, 766 (1977).

The redox properties of 2,3,7,8-tetramethoxyselenanthrene and 2,3,7,8-tetramethoxythianthrene have been studied in solution in order to compare their potential applicability as charge-transfer donors. The selenium compound is the weaker reductant, yielding a stable radical cation and a reactive dication, the former dimerizing in solution. Electron spin resonance and visible absorption spectra of the stable species were obtained. The 1:1 charge-transfer complexes of the above donors with tetracyanoquinodimethane are found to be insulators.

A. W. ADDISON, T. H. LI et L. WEILER. Can. J. Chem. **55**, 766 (1977).

On a étudié les propriétés rédox du tétraméthoxy-2,3,7,8 sélénanthrène et du tétraméthoxy-2,3,7,8 thianthrène; ces études ont été effectuées en solution de façon à comparer les possibilités d'application de ces composés comme donneurs de transfert de charge. Le composé contenant le sélénium est un réducteur plus faible conduisant à un cation radical stable et un dication réactif; le premier se dimérise en solution. On a obtenu les spectres rpe et d'absorption dans le visible des espèces stables. On a trouvé que les complexes de transfert de charge 1:1 des donneurs mentionnés plus haut avec le tétracyanoquinodiméthane peuvent agir comme des isolants.

[Traduit par le journal]

Introduction

Intensive current interest (1) in the field of organic conductors and in the chemistry of their component donor and acceptor species has led to the development of selenium analogs (2–4) of an as yet limited number of previously known organosulfur donors. The availability of HOMO electrons for donation is reflected by the oxidizability of a molecule, and consequently the redox properties of the sulfur and selenium-based donors (5–7), as well as of acceptors (5, 8), is receiving considerable attention, not only because of the relationships (5) between redox potentials and CT complex conductivity, but also because electrosynthesis has proved convenient in these systems (9). Our laboratories are engaged in the redox chemistry of both mononuclear and binuclear metal and pseudometal centres. We report here aspects of the redox, solution, and solid-state chemistry of 2,3,7,8-tetramethoxyselenanthrene **1**, the selenium analogue of the thianthrene **2**.

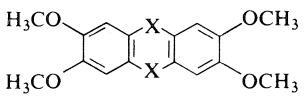

1 X = Se
2 X = S

Experimental[1]

Ultraviolet, visible, and near-ir spectra were obtained on a Cary-14 spectrophotometer, and esr spectra on a Varian E3 spectrometer, operating in the *X*-band, and calibrated with a ^{1}H nmr probe and DPPH.[1]

Electrochemistry was performed with a PAR-173 potentiostat, incorporating a PAR-176 *i*/*E* converter. A platinum sphere electrode (*ca.* 0.5 mm radius) and a Beckman rpe[1] were used as working electrodes in the three-electrode cell. The nonaqueous reference electrodes used were Ag(s)/$AgClO_4$ (0.01 *M*), TEAP[1] (0.1 *M*), CH_3CN or Ag(s)/$AgClO_4$ (0.01 *M*), TEAP (0.1 *M*), CH_3NO_2 half cells, their potentials being positive of the sce at 25 °C by 0.30 V and 0.74 V respectively.

All potentials reported herein are referred to the sce. All polarography, voltammetry, and coulometry was performed under nitrogen, in nitromethane (distilled off 4 Å molecular sieves under nitrogen), or in acetonitrile (distilled off phosphorus(V) oxide under nitrogen) and, except where noted, at 25.0 ± 0.2 °C. Supporting electrolyte was TEAP (from Eastman Kodak, recrystallized from H_2O, or from G. F. Smith) or tetraethylammonium trifluoromethanesulfonate,[1] prepared according to Rousseau *et al.* (10), both being dried *in vacuo* over phosphorus(V) oxide. Trifluoroacetic anhydride (Matheson, Coleman and Bell) was used as received.

[1]Abbreviations: DPPH, diphenylpicrylhydrazyl radical; TEAP, tetraethylammonium perchlorate; TEFS, tetraethylammonium trifluoromethanesulfonate; TFAA, trifluoroacetic anhydride; TPFS, tetra(*n*-propyl) ammonium trifluoromethanesulfonate; rpe, rotating platinum electrode; sce, saturated calomel electrode; TCNQ ,7,7,8,8-tetracyanoquinodimethane.

For simultaneous spectrophotometry and electrochemistry, a simple dual cell was constructed, incorporating a 4 cm optical path connected to an approximately 50 ml electrochemical cell by all-pyrex tubing. The solution was circulated throughout the cell by the action of a teflon-coated magnetic stirring bar.

The electrical resistivity of single crystals was measured using a two-probe technique (11). 2,3,7,8-Tetramethoxyselenanthrene **1** was prepared according to the method of Weiss *et al.* (12), and the 2,3,7,8-tetramethoxythianthrene **2** was prepared according to the method of Fries *et al.* (13). TCNQ[1] was prepared by the method of Acker and Hertler (14). All compounds were vacuum sublimed before use and gave acceptable elemental analyses. The lustrous dark blue complexes of **1** and **2** with TCNQ were prepared by adding hot concentrated solutions of the donor in acetonitrile to a hot concentrated solution of TCNQ. The complexes crystallized on cooling and they could be recrystallized from acetonitrile. The 1:1 nature of the complexes was corroborated by uv and esr spectra of acetonitrile solutions of the complexes and the chemical analyses. *Anal.* calcd. for $C_{28}H_{20}N_4O_4Se_2$ (**1**–TCNQ): C 52.99, H 3.15, N 8.83; found: C 53.12, H 3.00, N 8.60. *Anal.* calcd. for $C_{28}H_{20}N_4O_4S_4$ (**2**–TCNQ): C 62.20, H 3.73, N 10.36; found: C 62.02, H 3.46, N 10.20.

Results and Discussion

Compound **2** is known (15) to undergo two one-electron oxidation processes in solution, in a fashion similar to its unsubstituted analogue (16), and a third oxidation process has also been observed (15). Indeed, under our experimental conditions, polarography of **2** (rpe) at 1–3 $\times 10^{-4}$ *M* in acetonitrile containing *ca.* 1% TFAA (10, 17) and 0.1 *m* TEFS[1] as supporting electrolyte yielded two oxidation waves of equal height, with $E_{1/2}$-values of +0.53 and +0.88 V *vs.* sce. These two oxidation steps have been shown previously (17) in the case of **2** to be electrochemically reversible, one-electron processes, yielding the dithianthrene cation radical $\dot{\mathbf{2}}^+$ and the dication $\mathbf{2}^{2+}$, successively. Under the same conditions, polarography of the selenium compound **1** at the rpe, also yielded two well-defined oxidation waves of essentially equal height with half-height potentials of +0.90 and +1.21 V *vs.* sce.

This contrasts with a recent report (4) on the redox properties of the selenanthrene **1**, in which a single irreversible oxidation at +0.90 V was observed. No definite reason for the discrepancy can be given, as the paper by Wheland and Gillson (4) gives no details as to experimental conditions under which voltammetry was performed. However, we suspect that the species formed by the oxidation process at +0.90 V reacted rapidly with a nucleophile in their solutions, and the likelihood of the reactant's being trace water will emerge from the discussion below. It is to be noted also that a third oxidation wave was observed for neither compound **1** nor **2** in the nitromethane/TFAA solvent system below +1.2 V. A third oxidation step was observed for the selenanthrene **1** in acetonitrile/TEFS/TFAA only at a rotating gold disc electrode. Its potential (*ca.* +1.5 V) was not reproducible, although it was of the same height as the other two waves.

Diffusion control of the limiting oxidative current at the rpe for the first two oxidation steps of both the sulfur and selenium heterocycles was evidenced by excellent linearity (18) of the *i vs.* $\omega^{1/2}$ plot from 400 to 3000 rpm and leads to a value of $n = 1$ for each step, consistent with diffusion coefficients, calculated from the first wave, which are essentially the same as one another, at $D = 2.0\ (\pm 0.8) \times 10^{-5}$ cm^2 s^{-1}.

Cyclic voltammetry (platinum bead electrode) of the selenanthrene in CH_3NO_2 showed that the first two oxidation waves had peak-to-peak potential separations of 60 mV at a scan rate of 0.1 V s^{-1}, consistent with one-electron Nernstian processes (19). At scan rates of this order, the peak current ratio, i_c/i_a, was essentially unity for the first oxidation process, as expected for a chemically reversible system. However, the second oxidation process had $i_c/i_a < 0.95$ at 1.0 V s^{-1}, and the ratio decreased with decreasing scan rate, indicating decay of the expected dication product in solution. Thus, attempts to electrosynthesize this two-electron oxidation product resulted in its complete decomposition on the time scale of the electrolysis (several minutes) and bleaching of the solution.

The third oxidation process could be observed more readily in the absence of TFAA, and was irreversible at scan rates up to 4 V s^{-1} under all conditions.

In the case of the thianthrene **2**, one-electron oxidative coulometry at a platinum gauze anode (in nitromethane/TEFS) gave the green solution of the previously reported (15) radical cation $\dot{\mathbf{2}}^+$ (Table 2). Further oxidation at 150 mV positive of the second $E_{1/2}$ resulted in the consumption of another 0.93 Faraday per mol, yielding a bright blue solution of the dication $\mathbf{2}^{2+}$. The absorbance (Table 2) decreased gradually in time.

TABLE 1. Redox properties of the anthrenes

Heteroatoms	Concentration ($M \times 10^{-4}$)	Solvent[b]	Supporting electrolyte	E_1[a]	E_2[a]
S	1	CH_3CN	TEFS	+0.83	+1.17
S	1	CH_3NO_2	TEFS	+0.83	+1.18
Se	1	CH_3CN	TEAP	+0.89	+1.20
Se	1	CH_3CN	TEFS	+0.89	+1.21
Se	0.1	CH_3CN	TEFS	+0.91	+1.19
Se	1	CH_3NO_2	TEFS	+0.90	+1.21

[a]In volts (V) measured *vs.* nonaqueous reference electrodes (Ag/Ag^+) and quoted *vs.* sce. Values (± 10 mV) from voltammetry and rpe polarography.
[b]1–2% TFAA.

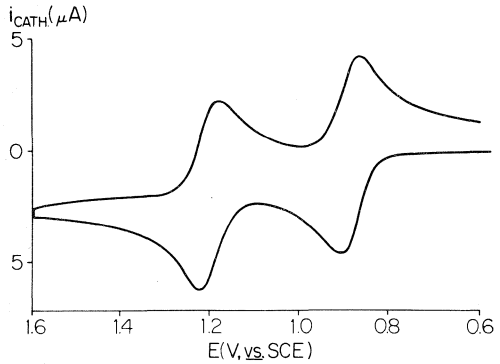

FIG. 1. Cyclic voltammagram of 2,3,7,8-tetramethoxyselenanthrene (0.18 m*M*) in acetonitrile/TFAA/TEFS, at platinum sphere electrode, scan rate 100 mV s^{-1}.

TABLE 2. Absorption spectra

Heteroatoms	Species	λ (nm)	Log ε
Se	**1**	295[a]	2.74
		254	3.37
		238	3.36
Se	$\dot{\mathbf{1}}^+$	820[b]	4.04
S	**2**	297	2.72
		244	3.58
S	$\dot{\mathbf{2}}^+$	840	4.00
S	$\mathbf{2}^{2+}$	710	4.15

[a]Shoulder; neutral molecules in acetonitrile.
[b]Cations in nitromethane, TEFS.

Controlled potential oxidation of a 1.0 × 10^{-4} *M* solution of the selenanthrene **1** in acetonitrile/TEFS at 160 mV positive of $E_{1/2}$ for the first oxidation wave caused the solution to become bright blue. After 5 half-lives, 0.96 Faraday per mol had been consumed in production of the cation radical $\dot{\mathbf{1}}^+$ and the solution yielded an esr signal, with $g = 2.0246$ and $a_{Se} = 20.7$ G. The spectrum of the radical $\dot{\mathbf{2}}^+$ is a complex pattern at $g = 2.0073$ (20). The *g*-values are similar to those of the analogous radical cations of tetrathiofulvalene **3** (21) and its selenium counterpart **4**, the latter having $g = 2.027$ (22).

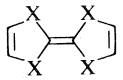

3 X = S
4 X = Se

As expected, the effect of methoxyl substituents is to delocalize the spin density on $\dot{\mathbf{1}}^+$, and lower (23) its reduction potential by *ca.* 0.24 V (16) relative to the unsubstituted radical cation ($g = 2.0315$) (24).

The solution's electronic absorption spectrum exhibited two overlapping bands of approximately equal intensity, at 690 and 820 nm (Table 2). This observation was reminiscent of the aggregation observed for the unsubstituted analog of $\dot{\mathbf{2}}^+$ in solution (25). Accordingly, simultaneous electrochemistry and spectrophotometry were carried out. The absorption spectra of increasing concentrations of $\dot{\mathbf{1}}^+$ (acetonitrile, 2% TFAA, 0.1 *M* TPFS, 27 °C), prepared by *in situ* electrooxidation of aliquots of **1** in solution at +785 mV, were obtained. The absorption band at 820 nm was dominant in the 1–20 μ*M* region, but limiting spectra (*i.e.* of the 680 nm or 820 nm species) could not be obtained directly, the former because of solubility limitations (even though the trifluoromethanesulfonate salt is appreciably more soluble than the perchlorate), the latter because of the strong association. Thus, in the above concentration range, where the absorbance of the aggregated

species may, to a first approximation, be considered negligible at 820 nm, the apparent molar absorptivity at 820 nm decreased linearly with concentration, evidencing a dimerization process. If this is written to be comparable with the case of $\dot{\mathbf{2}}^+$, then the equilibrium constant for the process

$$2\dot{\mathbf{1}}^+ + 2CF_3SO_3^- \rightleftharpoons (\mathbf{1}\cdot CF_3SO_3)_2$$

is computed to be approximately 2×10^6, for ε 11 000 at 820 nm for $\dot{\mathbf{1}}^+$. Further aggregation may also occur. This equilibrium is reflected also in a concentration dependence of the $E_{1/2}$ values (Table 1), and presumably contributes to the dependence of the $E_{1/2}$-values on solvent and supporting electrolytes.

All solutions of the radical cation $\dot{\mathbf{1}}^+$ reacted with water, being bleached immediately water was added, whereas the sulfur radical $\dot{\mathbf{2}}^+$ had a half-life of a few minutes. It is not surprising that the use of TFAA as a dehydrating agent (17) is important for preparation of $\dot{\mathbf{1}}^+$ and $\mathbf{2}^{2+}$ when they are in the 10^{-4} *M* range. It is also expected, therefore, that $\mathbf{1}^{2+}$ and $\mathbf{2}^{2+}$ will be even more susceptible to nucleophilic attack than the monocations, and thus decay more rapidly in solution. It is noteworthy that TFAA addition readily extends the potential range of reagent nitromethane/TEAP for anodic electrochemistry (to *ca.* +2.0 *vs.* sce).

The relationship between the electrochemical properties of **1** and **2** closely parallels that (6) between the fulvalenes **3** and **4**, in that selenium monocation is a stronger oxidant in solution than the sulfur analogue. The differences between the two oxidation potentials of the selenium compounds are less than for their sulfur analogues. Thus, the tendency of $\dot{\mathbf{1}}^+$ to redox disproportionate in solution is slightly greater than that of $\dot{\mathbf{2}}^+$, and a product of the process will be the relatively unstable dication.

The single crystal resistivity value (11) for the TCNQ complex of the selenanthrene **1** is $1.3 \pm 0.3 \times 10^8$ ohm cm, and for the thianthrene–TCNQ adduct, $1.1 \pm 0.3 \times 10^8$ ohm cm. Both materials are therefore insulators. It is possible that the packing geometry in the complexes is unfavourable for electron transfer. This could be contributed to by steric interactions of the methoxyl groups, if bent out of the rings' planes, or by the bent (domed) nature of the heterocyclic rings. In addition, we have been unable to detect an esr signal in either of the solid complexes of **1** or **2** with TCNQ, indicating very few unpaired spins, and hence very little net electron transfer in the ground state of the CT interactions.

The effect of methoxyl substitution appears to be greater (0.34 V) for the sulfur heterocycle than for the selenium system (0.24 V), to the extent that the relative reduction potentials of the sulfur and selenium cation radicals are reversed by methoxylation. This increased sensitivity of the sulfur compound may relate to more effective participation of the relatively lower energy orbitals of the sulfur in the ring conjugation.

Acknowledgements

We are indebted to Drs. R. S. Glass and E. M. Engler for providing results prior to publication. We thank N. Mayr and Ms. J. Lee for technical assistance, and gratefully acknowledge research support from the National Research Council of Canada and the U.B.C. Committee on Research.

1. A. F. Garito and A. J. Heeger. Acc. Chem. Res. **7**, 232 (1974).
2. T. E. Phillips, T. J. Kistenmacher, A. N. Block, and D. O. Cowan. J. Chem. Soc. Chem. Commun. 334 (1976).
3. E. M. Engler, R. A. Craven, Y. Tomkiewicz, B. A. Scott, K. Bechgaard, and J. R. Andersen. J. Chem. Soc. Chem. Commun. 337 (1976).
4. R. C. Wheland and J. L. Gillson. J. Am. Chem. Soc. **98**, 3916 (1976).
5. R. C. Wheland. J. Am. Chem. Soc. **98**, 3926 (1976).
6. E. M. Engler, F. B. Kaufman, D. C. Green, C. E. Klots, and R. N. Compton. J. Am. Chem. Soc. **97**, 2921 (1975).
7. B. A. Scott, F. B. Kaufman, and E. M. Engler. J. Am. Chem. Soc. **98**, 4342 (1976).
8. D. L. Jeanmaire and R. P. van Duyne. J. Am. Chem. Soc. **98**, 4029 (1976).
9. E. M. Engler, D. C. Green, and J. Q. Chambers. J. Chem. Soc. Chem. Commun. 148 (1976).
10. K. Rousseau, G. Farrington, and D. Dolphin. J. Org. Chem. **37**, 3968 (1972).
11. H. Meier. Organic semiconductors. Verlag Chemie, Weinheim, Germany. 1974. p. 84.
12. T. Weiss, W. Nitsche, F. Bohnke, and G. Klar. Justus Liebigs Ann. Chem. 1418 (1973).
13. K. Fries, H. Koch, and H. Stukenbrock. Justus Liebigs Ann. Chem. **478**, 162 (1929).
14. D. S. Acker and W. R. Hertler. J. Am. Chem. Soc. **84**, 3370 (1962).
15. R. S. Glass, W. J. Britt, W. N. Miller, and G. S. Wilson. J. Am. Chem. Soc. **95**, 2375 (1973).
16. C. Barry, G. Cauquis, and M. Maurey. Bull. Soc. Chim. Fr. 2510 (1966).

17. O. HAMMERICH and V. D. PARKER. Electrochim. Acta, **18**, 537 (1973).
18. J. ALBERY. Electrode kinetics. Clarendon Press, Oxford. 1975. p. 57.
19. R. S. NICHOLSON and I. SHAIN. Anal. Chem. **36**, 706 (1974).
20. I. B. GOLDBERG, H. R. CROWE, G. S. WILSON, and R. S. GLASS. J. Phys. Chem. **80**, 988 (1976).
21. F. WUDL, G. M. SMITH, and E. J. HUFNAGEL. J. Chem. Soc. Chem. Commun. 1453 (1970).
22. Y. TOMKIEWICZ, E. M. ENGLER, and T. D. SCHULTZ. Phys. Rev. Lett. **35**, 456 (1975).
23. A. RONLÁN, J. COLEMAN, O. HAMMERICH, and V. D. PARKER. J. Am. Chem. Soc. **96**, 845 (1974).
24. B. LAMOTTE and B. BERTHIER. J. Chim. Phys. **63**, 369 (1966).
25. M. DE SORGO, B. WASSERMAN, and M. SZWARC. J. Phys. Chem. **76**, 3468 (1972).

Conformational and configurational analysis of hydrocarbon chains based on time-averaged carbon-13 chemical shifts

HELMUT BEIERBECK AND JOHN K. SAUNDERS
Département de Chimie, Université de Sherbrooke, Sherbrooke (Qué.), Canada J1K 2R1

Received August 30, 1976

HELMUT BEIERBECK and JOHN K. SAUNDERS. Can. J. Chem. **55**, 771 (1977).

The conformations of saturated hydrocarbon chains are analysed by a least-squares fit of calculated to observed time-averaged carbon-13 chemical shifts. The calculated resonances are the sums of products of conformer resonances and conformer probabilities. The conformer shieldings are derived with predictive parameters developed earlier for conformationally well defined systems. The conformer probabilities are taken to be products of rotamer probabilities. The rotamer probabilities are variables in the analysis.

HELMUT BEIERBECK et JOHN K. SAUNDERS. Can. J. Chem. **55**, 771 (1977).

On a analysé les conformations de chaînes hydrocarbonées saturées par un ajustement, par la méthode des moindres carrés, des valeurs calculées et observées pour les déplacements chimiques du carbone-13 moyennés dans le temps. Les résonances calculées sont les sommes des produits des résonances d'un conformère et des probabilités de ce conformère. On peut obtenir les blindages d'un conformère à partir des paramètres qui permettent de les prédire et qui ont été développés antérieurement pour des systèmes qui sont conformationnellement bien définis. On fait l'hypothèse que les probabilités des conformères sont les produits des probabilités des rotamères. Les probabilités des rotamères sont des variables dans cette analyse.
[Traduit par le journal]

The carbon-13 resonances of saturated hydrocarbon chains at ambient temperatures are the sums of the chemical shifts in all molecular conformations, weighted by the probability of occurrence of each conformation. If the conformer resonances may be measured, or calculated to a good approximation, the conformer populations may be derived by fitting calculated to observed time-averaged carbon-13 resonances. Since conformational analysis is a prerequisite for the determination of the configurations of mobile systems, the derivation of the conformational probabilities from time-averaged carbon-13 resonances also allows the determination of configuration in asymmetric hydrocarbon chains.

Results

The method was developed and tested with the hydrocarbon resonances of Lindeman and Adams (1). Conformer resonances and probabilities were derived in the following way.

Conformer Chemical Shifts

The conformer resonances were derived with a set of substituent parameters described previously (2, 3). The numerical values for the parameters were treated as variables in the analysis. The derivation of the resonances for primary, secondary, tertiary, and quaternary carbons is based on four separate reference values, since α-carbon substituent effects are nonadditive. The resonances of the primary, secondary, tertiary, and quaternary carbons in ethane, propane, isobutane, and neopentane, respectively, served as starting estimates for these references. Two substituent parameters, HC and CC, account for the deshielding effect of β-carbons. A shift increment HC is associated with every 1,3-diaxial hydrogen–hydrogen interaction introduced by a β-carbon. An increment CC is associated with every carbon–carbon *gauche* interaction. Previously derived parameter values (2, 3) served as starting estimates for HC and CC. No γ-carbon parameter is required. An incoming *anti* γ-carbon does not cause any significant displacement and the upfield shift associated with the introduction of a *gauche* γ-carbon is due to the disappearance of the 1,3-diaxial hydrogen interaction, *i.e.* the elimination of an HC increment (3). The only δ-parameter which is required is a deshielding increment δ(C) associated with *syn*-axial δ-carbon interactions (4, 5). Its starting estimate was derived from methyl resonances in terpenoids. The definitions and optimized values of the structural parameters are found in Table 1.

The derivation of the carbon resonances for one of the *d,l*-3,4-dimethylhexane conforma-

tions may serve to illustrate the application of these parameters. The conformer is superimposed onto cyclohexane and the hydrogens are labelled axial and equatorial. The hydrogens and carbons are engaged in the following interactions.

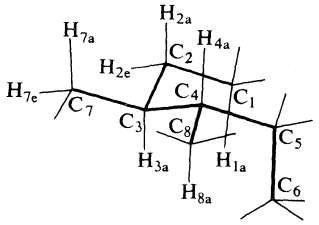

HC Interactions

C(1) → H(1a)—H(3a)
C(2) → H(2a)—H(4a), H(2a)—H(7a), H(2e)—H(7e)
C(3) ← H(3a)—H(1a)
→ H(3a)—H(8a)
C(7) ← H(7a)—H(2a), H(7e)—H(2e)
→ H(7a)—H(4a)

CC Interactions

C(1) —
C(2) → C(1)—C(4)
C(3) ← C(4)—C(1)
→ C(2)—C(5), C(7)—C(8)
C(7) —

δ(C) Interactions

C(1) → C(1)—C(5)
C(2) —
C(3) —
C(7) —

Only C(1), C(2), C(3), and C(7) need to be considered for reasons of symmetry. The interactions have been divided into two groups, backward and forward along the chain, for reasons which will be explained in the section defining conformer probabilities.

Rotamer Populations

The contributions of any given conformation to the time-averaged carbon resonances are proportional to the fraction of the time that the molecule adopts that conformation. These conformer probabilities are taken to be products of rotamer probabilities. It is assumed that the energies of the rotational states about a given bond are solely a function of the atoms directly attached to the terminal carbons of that bond. If one of these carbons is primary, all three rotational states are obviously equivalent. If one of the terminal carbons of the bond is quaternary, the three rotamer populations are again assumed to be equal, whether there is a threefold axis of symmetry (*tert*-butyl group) or whether the three carbons are nonequivalent (as in 3,3-dimethylhexane). Three possibilities remain: (*1*) Both carbons are secondary. (*2*) One carbon is secondary and the other is tertiary. (*3*) Both carbons are tertiary.

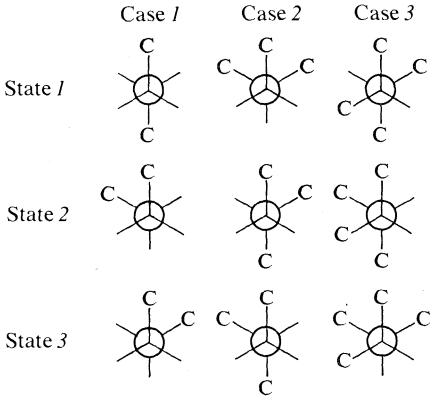

The populations of the three unique rotamers (state *1*) are designated p_{11}, p_{21}, and p_{31}. Since it is assumed that only the directly bonded atoms affect the energies of the rotational states, we have

$$p_{i2} = p_{i3}$$

and

$$p_{i2} = (1 - p_{i1})/2$$

The populations of the three unique rotamers, p_{11}, p_{21}, and p_{31}, are the three remaining variables in the analysis, for which starting estimates of 1/3 were used. The optimized values are included in Table 1.

Conformer Populations

The probability of finding a molecule or molecular segment in a given conformation is taken to be the product of the probabilities of finding the individual carbon–carbon bonds in their corresponding rotational states. There are two ways to derive all conformer contributions. For short hydrocarbon chains one may simply generate all molecular conformations and derive all carbon resonances in each conformation. For longer chains one needs to deal only with the molecular segment containing the carbon in question, because only the rotational states of the closest bonds affect the carbon resonances.

TABLE 1. Definition of the structural parameters on which the present analysis is based, and their numerical values[a]

Parameter definitions	Comparison			This work		
	1	*2*	*3*	*4*	*5*	*6*
Reference chemical shifts						
Primary	5.9	6.39	7.44	5.63	5.71	0.38
Secondary	16.1	17.62	17.62	16.25	16.48	0.48
Tertiary	25.2	24.99	24.17	23.00	23.18	0.47
Quaternary	27.9	29.73	26.53	27.82	27.84	0.53
Structural parameters						
HC 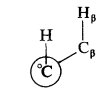		4.45	4.55	4.57	4.57	0.04
CC 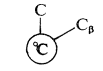		1.27	1.85	1.24	1.23	0.08
δ(C) 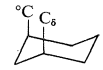			2.56	3.57	3.55	0.33
Rotamer populations						
p_{11} 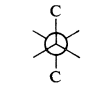				0.763	0.745	0.067
p_{21} 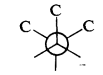				−0.063	0.000	0.051
p_{31} 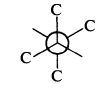				0.588	0.581	0.087

[a]The reference chemical shifts are given in ppm from TMS and the substituent parameters in ppm. The resonances in column *1* and the parameter values in columns *2* and *3*, derived from carbon resonances in rigid systems, were included for comparison. Column *1*, Observed resonances in ethane, propane, isobutane, and neopentane (9). Column *2*, Parameter values derived from resonances in decalin derivatives found in the literature (10). Column *3*, Parameter values derived from resonances in steroids and terpenoids (to be published). Column *4*, Parameter values derived from the data in Table 4, without restraints on population variables. Column *5*, Parameter values derived from the data in Table 4, and the restraint $0 \leq p_{ij} \leq 1$. Column *6*, Standard errors for the parameters in column *5*.

The conformations of the molecular segments along the four tetrahedral directions are assumed to be independent. Only unsubstituted and methylated chains are considered here. Therefore, only the conformations of molecular segments in at most two directions, backward and forward along the chain, are required.

In order to establish the presence or absence of a δ-carbon in a *syn*-axial position it is necessary to define the rotational states of at least the three closest bonds. A definition of the rotational state of the fourth bond would also be required in order to establish whether a δ-hydrogen points toward °C, *i.e.* to distinguish δ-interactions from unrealistic ε-interactions. However, the combination of rotational states leading to such an ε-arrangement is usually so improbable that the definition of the three-bond segment seemed sufficient. We will return to this point in the Discussion section.

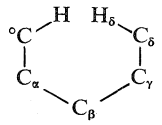

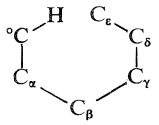

Summation over Conformer Contributions

The summation over the conformer contributions to the carbon resonances in the 3,4-dimethylhexane isomers may serve as illustration. For these six-carbon chains it would have been simpler to generate all molecular

TABLE 2. Calculation of HC, CC, and δ(C) conformer contributions to the averaged C-13 resonances of C(1), C(2), C(3), and C(7) of *d,l*-3,4-dimethylhexane[a]

	[HC + CC + δ(C)]		×	Conformer population	=	Conformer contribution
C(1)	→	(4.57+0.00+3.55)	×	(0.500×0.581)	=	2.359
C(2)	→	(13.71+1.23+0.00)	×	(0.500×0.581×0.000)	=	0.000
C(3)	←	(4.57+1.23+0.00)	×	(0.500)	=	2.900
	→	(4.57+2.46+0.00)	×	(0.581×0.000)	=	0.000
C(7)	←	(9.14+0.00+0.00)	×	(0.500)	=	4.570
	→	(4.57+0.00+0.00)	×	(0.581×0.000)	=	0.000

[a]The conformation is defined by the figure in the text. The reference values are added after summation over HC, CC, and δ(C) contributions of all conformations. The reference values and calculated resonance averages are in ppm from TMS.

conformations and count the interactions in each conformer. However, this example will be used to demonstrate the general procedure of dealing only with three-bond segments. Only bonds C(2)—C(3), C(3)—C(4), and C(4)—C(5) give rise to nonequivalent rotational states. The conformations of the following molecular segments have to be defined.

Segment	Probability
C(1) → C(1)—C(4)	$p_{22} \times p_{31}$
C(2) → C(2)—C(5)	$p_{22} \times p_{31} \times p_{21}$
C(3) ← C(1)—C(3)	p_{22}
→ C(3)—C(6)	$p_{31} \times p_{21}$
C(7) ← C(1)—C(7)	p_{22}
→ C(7)—C(5)	$p_{31} \times p_{21}$

The resonance of C(1) receives contributions from 3 × 3 conformations, since bonds C(2)—C(3) and C(3)—C(4) occur in segment C(1)—C(4). In the conformation defined at the beginning of the Results section bond C(2)—C(3), type *2*, is in rotational state *2* and bond C(3)—C(4), type *3*, is in state *1*. This conformation of segment C(1)—C(4) therefore occurs with probability $p_{22} \times p_{31}$. The combination of the rotational states of the three bonds in segment C(2)—C(5) gives rise to 3 × 3 × 3 conformational contributions to the C(2) resonance. Bond C(4)—C(5), type *2*, is in state *1* and this conformation of segment C(2)—C(5) therefore occurs with probability $p_{22} \times p_{31} \times p_{21}$. Both C(3) and C(7) receive contributions from 3 conformations in the first part of the chain, and from 3 × 3 conformations in the second part. In the example above the probabilities of occurrence are p_{22} and $p_{31} \times p_{21}$, respectively. These products of rotamer populations are listed above with the corresponding chain segments. The derivation of the numerical values for the β- and δ-contributions to the C(1), C(2), C(3), and C(7) resonances in the same *d,l*-3,4-dimethylhexane conformation is shown in Table 2. The reference shifts are added after the derivation of the total β- and δ-shift contributions from all conformations.

Table 3 gives the substituent interactions for all carbons and segmental conformations of *meso* and *d,l*-3,4-dimethylhexane. For each segmental conformer four types of interactions are listed, namely the number of 1,3-diaxial hydrogen interactions HC, the number of carbon–carbon *gauche* interactions CC, the number of *gauche* γ-carbons γ(C), and the number of *syn*-axial δ-carbons δ(C). No substituent parameter for *gauche* γ-carbons is required. The number of γ-carbons was included simply because the sum of these four types of interactions is constant for a given chain segment, regardless of the conformation of that segment. For example, C(2) is always engaged in a total of four such interactions along C(2)—C(5). In the first conformation $n_{HC} = 1$, $n_{CC} = 2$, $n_{\gamma(C)} = 1$, and $n_{\delta(C)} = 0$, etc.

The segmental conformations are generated and listed in the tables in the following sequence. In the starting conformation all bonds are in their unique rotational state. In the direction from the lowest to the highest numbered carbon in the segment the last bond is rotated clockwise by 120° and 240°, then the second and finally the first bond. This convention is used whether the carbon under observation is at the beginning or end of the segment. For example, the conformation of segment C(2)—C(5) in the *d,l*-3,4-dimethylhexane example would be the tenth

TABLE 3. Structural parameters for all conformations of *meso* and *d,l*-3,4-dimethylhexane[a,b]

				meso-3,4-Dimethylhexane				
C(1) →								
0020	0011	0011	1001	1001	1010	1010	1010	1010
C(2) →								
1210	1210	1210	1201	1210	1210	2200	2200	2200
3100	3100	3100	*2110*	2110	2110	2110	2110	*2101*
2110	*2110*	2110	1111	1120	1120	2110	2110	*2101*
C(3) ←								
0200	1100	1100						
→								
1210	2200	2200	1300	1300	0310	1300	1300	1300
C(7) ←								
1010	2000	1010						
→								
1010	1010	*1001*	1010	*1010*	1010	0011	0020	0020
				d,l-3,4-Dimethylhexane				
C(1) →								
0020	0011	0011	1001	1001	1010	1010	1010	1010
C(2) →								
1210	1201	1210	1210	1210	1210	2200	2200	2200
3100	3100	3100	*2101*	2110	2110	2110	2110	*2110*
2110	*2101*	2110	1111	1120	1120	2110	2110	*2110*
C(3) ←								
0200	1100	1100						
→								
1210	2200	2200	1300	1300	1300	1300	0310	1300
C(7) ←								
1010	2000	1010						
→								
1010	1010	*1010*	1010	*1001*	1010	0011	0020	0020

[a]For each segmental conformer four types of interactions are listed, namely the number of 1,3-diaxial hydrogen interactions HC, the number of carbon–carbon *gauche* interactions CC, the number of *gauche* γ-carbons γ(C), and the number of *syn*-axial δ-carbons δ(C). The segmental conformations are generated and listed in the following sequence. In the starting conformation all bonds are in their unique rotational states.

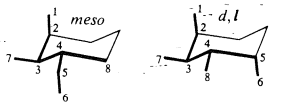

In the direction from the lowest to the highest numbered carbon in the segment the last bond is rotated clockwise by 120° and 240°, then the second, and finally the first bond.

[b]Interactions which lead to shift differences in *meso* and *d,l*-isomers are set in italics. For example, the set *1001* for C(7) occurs with probability $p_{31} \times p_{22}$ in the *meso* isomers (item 3 in row C(7)→) but with probability $p_{32} \times p_{22}$ in the *d,l*-isomers (item 5 in row C(7)→).

conformer generated,

$$9 \times (j - 1) + 3 \times (k - 1) + l$$
$$= 9 \times (2 - 1) + 3 \times (1 - 1) + 1 = 10$$

since the first bond C(2)—C(3) is in state $j = 2$, the second bond C(3)—C(4) in state $k = 1$, and the last bond C(4)—C(5) in state $l = 1$. Therefore the set 3100 of three HC interactions and one CC interaction of C(2) along direction C(2)→C(5) is found in position 10 in row C(2) → of Table 3.

The references, substituent parameters, and rotamer populations in Table 1 were derived with the data set in Table 4. If no constraints were placed on the rotamer parameters, p_{21} was found to be negative. The deviation of p_{21} from the smallest possible value of zero is slightly larger than the standard error for that parameter. The value of p_{21} was set equal to zero and the remaining parameters were redetermined. Both parameter sets are shown in Table 1. Table 4 also contains quaternary carbon resonances, even though the resonances of quaternary carbons are taken to be independent of conformation for reasons of symmetry and because they are only engaged in carbon–carbon *gauche* interactions. The quaternary carbon resonances were included in the analysis because substituent parameters and reference shifts were also optimized. The results of analyses of heptane and

TABLE 4. Observed (1) and differences ($\delta_{obs} - \delta_{calc}$) between observed and calculated time-averaged C-13 resonances for a series of butane, pentane, and hexane derivatives[d]

Substrate	C(1)	C(2)	C(3)	C(4)	C(5)	C(6)	C(7)	C(8)	C(9)
Butane derivatives									
2-Me	21.9	29.9	31.6	11.5					
	0.2	0.9	0.2	1.2					
2,2-diMe	28.7	30.3	36.5	8.5					
	−1.4	0.0	−0.7	2.8					
2,3-diMe	19.2	34.0							
	0.7	0.6							
2,2,3-triMe	27.0	32.7	37.9	17.7					
	0.0	−0.1	0.7	2.9					
2,2,3,3-tetraMe	25.6	35.0							
	1.6	−0.2							
Pentane derivatives									
Nil	13.5	22.2	34.1						
	−0.3	−1.6	1.0						
2-Me	22.7	27.9	41.9	20.8	14.3				
	0.8	−0.5	2.2	0.0	0.2				
3-Me	11.4	29.4	36.8			18.7			
	0.2	−0.9	2.0			−0.7			
2,2-diMe	29.5	30.6	47.3	18.1	15.1				
	−0.9	0.3	1.8	1.3	0.5				
2,3-diMe[a]	20.0	31.9	40.6	26.8	11.6	17.7	14.5		
	0.5	−1.0	1.4	−0.9	−0.1	−1.1	−1.7		
2,4-diMe	22.7	25.7	49.0						
	0.1	−1.0	2.6						
3,3-diMe	7.7	33.4	32.3			25.6			
	1.2	−1.8	−0.5			−1.4			
2,2,3-triMe	27.1	33.0	45.4	24.4	13.0			13.3	
	−0.5	0.2	2.4	−0.2	1.0			0.7	
2,2,4-triMe	29.9	30.9	53.3	25.3	24.7				
	−1.4	0.6	1.1	0.9	1.2				
2,3,3-triMe	17.1	35.1	34.9	32.6	7.9		23.3		
	1.5	−1.1	−0.3	−0.6	0.6		−0.7		
2,3,4-triMe[a]	21.4	29.8	45.3			18.1	10.4		
	1.0	−1.7	1.7			−1.3	−2.5		
2,2,3,3-tetraMe	25.6	36.0	37.3	28.8	9.0			20.6	
	0.8	0.8	−0.4	−2.3	0.9			−0.3	
2,2,3,4-tetraMe[a]	28.2	34.0	47.9	27.4	24.5			11.6	17.3
	−0.3	1.2	0.5	−2.4	3.2			2.3	−2.7
2,2,4,4-tetraMe	31.8	32.4	56.5						
	−0.7	2.1	−1.5						
2,3,3,4-tetraMe	17.2	37.1	33.6				18.9		
	0.8	1.9	−4.1				−2.0		
Hexane derivatives									
Nil	13.7	22.7	31.7						
	−0.1	−1.2	−0.3						
2-Me	22.4	28.1	38.9	29.7	23.0	13.6			
	0.5	−0.4	0.2	0.6	−1.2	−0.2			
3-Me	10.9	29.5	34.3	39.0	20.2	13.9	18.8		
	−0.3	−0.9	0.1	0.4	−1.4	−0.2	−0.9		
2,2-diMe	29.2	30.1	44.1	27.0	23.7	13.9			
	−1.2	−0.2	−0.4	1.9	−0.8	0.1			
2,3-diMe[a]	20.0	32.8	38.5	36.7	20.7	14.0	17.8	15.1	
	0.5	−0.2	−0.1	0.7	−1.3	−0.1	−1.0	−1.3	
2,4-diMe[b]	22.2	25.4	46.6	32.1	29.9	11.0	23.2	19.0	
	−0.4	−1.7	1.4	−0.4	−0.8	−0.2	0.6	−1.3	
2,5-diMe	22.4	28.4	36.9						
	0.5	−0.2	1.2						
3,3-diMe	8.1	34.3	32.8	44.3	17.3	14.8	26.5		
	1.6	−1.1	0.0	0.8	−0.2	0.2	−0.8		

TABLE 4 *(Concluded)*

Substrate	C(1)	C(2)	C(3)	C(4)	C(5)	C(6)	C(7)	C(8)	C(9)
3,4-diMe *meso*[c]	11.8	25.8	39.5				15.8		
	0.1	−2.3	0.8				−1.4		
3,4-diMe *d,l*[c]	11.8	27.6	38.5				13.8		
	0.1	−0.6	−0.2				−2.6		
2,2,4-triMe	29.9	31.0	51.0	31.9	31.0	11.2			21.9
	−1.4	0.7	0.0	1.7	−0.2	0.0			0.7
2,2,5-triMe	29.3	30.1	42.0	33.9	28.9	22.5			
	−1.1	−0.2	0.5	2.2	0.1	0.6			
2,3,3-triMe	17.1	35.0	35.5	43.1	17.0	14.8		23.8	
	1.1	−0.9	0.3	0.6	−1.9	0.2		−1.2	
2,3,5-triMe[a,b]	20.0	32.4	36.2	43.9	25.7	21.9	17.8	15.3	23.5
	0.5	−0.7	−0.7	1.3	−1.7	−0.7	−1.0	−1.8	0.9

[a]Numbering system (n = chain length)

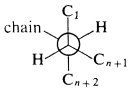

[b]Numbering system (n = chain length)

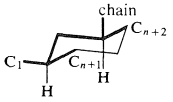

[c]Not included in the data set which was used for the derivation of the parameters in Table 1.
[d]Root-mean-squares deviation between calculated and observed resonances was 1.24 ppm.

octane derivatives and of nonane are shown in Table 5.

Discussion

The present analysis is based on the assumption of independent rotational potentials, *i.e.* the rotational energy of any given bond is taken to be independent of the rotational states of the adjacent bonds. This model of independent rotational potentials is generally believed to be inadequate for the analysis of hydrocarbon chain conformations (6), since it does not take into account long range effects such as *syn*-axial δ-interactions. For example, the energy of the $g_{\pm}\, g_{\mp}$ combination of *gauche* rotational states is believed to be considerably higher than the sum of the energy increments associated with the two *trans*→*gauche* transitions (6).

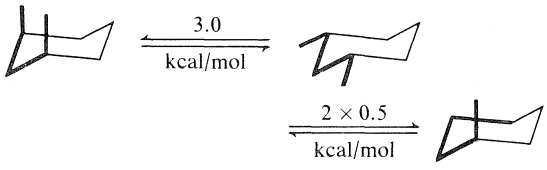

It was decided nevertheless to test this simplest model first, and from our results it appears that the assumption of independent rotational potentials leads to a satisfactory interpretation of the conformational dependence of time-averaged C-13 chemical shifts. The parameter set in Table 1 represents a minimum set and no attempt was made to improve the fit between calculation and experiment by the addition of corrective parameters. The reference shifts are in satisfactory agreement with the corresponding resonances in ethane etc., and also with references derived with carbon resonances in conformationally well defined substrates (Table 1). The values for the structural parameters also compare favorably with parameters for rigid systems. The population parameters favor the expected rotational states. Finally, the root-mean-squares deviation between calculated and observed time-averaged carbon resonances is of the same order of magnitude as error estimates for the prediction of carbon resonances in rigid molecules. Thus there is no indication that conformations with *syn*-axial δ-interactions require special considerations, and $g_{\pm}g_{\mp}$ and $g_{\pm}g_{\pm}$ states are taken to be equally probable. For example, the following probabilities are predicted for the molecular conformations of pentane and 2-methylpentane.

$1 \times 0.745 \times 0.745 = 0.555$

$2 \times 0.500 \times 0.745 = 0.745$

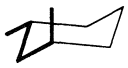

$4 \times 0.745 \times 0.128 = 0.380$

$2 \times 0.500 \times 0.128 = 0.128$

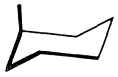

$2 \times 0.128 \times 0.128 = 0.033$

$2 \times 0.500 \times 0.128 = 0.128$

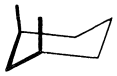

$2 \times 0.128 \times 0.128 = 0.033$

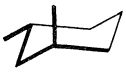

$1 \times 0.000 \times 0.745 = 0.000$

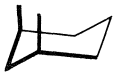

$2 \times 0.000 \times 0.128 = 0.000$

It is also quite evident that predictive schemes like Lindeman and Adam's (1) or Grant and Paul's (7), which do not explicitly take into account conformational interconversions, are successful because the average conformation of a molecular segment remains constant as additional substituents are added to the chain.

An analysis based on rotational probabilities and three-dimensional parameters automatically accounts for the effects of asymmetry, and therefore permits the assignment of resonances to nonequivalent carbons and the distinction of diastereoisomers. The assignment of the resonances for C(1) and C(6) in 2,3-dimethylpentane may serve to illustrate how molecular asymmetry leads to different resonances at nonequivalent carbons. Structural information is carried by two sets of parameters, namely the set of interactions in a given conformation and the combination of rotational states which define the probability of occurrence of that conformation. C(1) and C(6) are engaged in the same number of interactions in an equal number of conformations, since rotation about C(2)—C(3) brings C(6) into the position previously occupied by C(1). However, these same interactions occur with unequal probability. For example, the C(1) parameter set 3001 in conformation **2** occurs with probability $p_{31} \times p_{22}$, whereas C(6) experiences the same interactions with probability $p_{32} \times p_{22}$. In other words, asymmetry is not carried by the structural parameters in this

Conformation		Probability	C(1)	C(6)
1	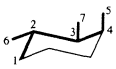	$p_{31} \times p_{21}$	3010	3010
2	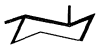	$p_{31} \times p_{22}$	3001	3010
3	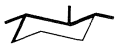	$p_{31} \times p_{23}$	3010	3010
4		$p_{32} \times p_{21}$	2011	3010
5		$p_{32} \times p_{22}$	2020	3001
6	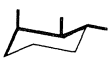	$p_{32} \times p_{23}$	2020	3010
7	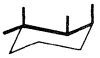	$p_{33} \times p_{21}$	3010	2011
8	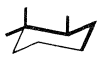	$p_{33} \times p_{22}$	3010	2020
9		$p_{33} \times p_{23}$	3010	2020

analysis, but rather by the population parameters. Conformers do not give rise to nonequivalent contributions if both carbons are in equivalent structural surroundings in that conformer, or if there is an equally probable conformation in which the two carbons interchange interactions. Thus, the parameter sets 3010 cancel each other in conformations **1** and **3**. The effects of the C(1) interactions 2011 in **4**, 2020 in **5** and **6**, and 3010 in **7** and **9** are offset by the corresponding C(6) interactions in **7**, **8**, and **9**, and **4** and **6**, since $p_{22} = p_{23}$ and $p_{32} = p_{33}$, and conformations **4** and **7**, as well as conformations **5**, **6**, **8**, and **9** are equally probable. This leaves the transfer of 3001 from C(1) in conformation **2** to C(6) in conformation **5**, and of 3010 from C(1) in conformation **8** to C(6) in conformation **2**. The three HC interactions cancel again and only the γ(C)—δ(C) exchange makes unequal contributions to the C(1) and C(6) resonances. The probability $p_{31} \times p_{22}$ that C(1) is engaged in a δ-interaction is higher than

TABLE 5. Observed (1) and differences ($\delta_{obs} - \delta_{calc}$) between observed and calculated time-averaged C-13 resonances for a series of heptane and octane derivatives and for nonane[c]

Substrate	C(1)	C(2)	C(3)	C(4)	C(5)	C(6)	C(7)	C(8)	C(9)
Heptane derivatives									
Nil	13.7	22.6	32.0	29.0					
	−0.1	−1.3	−0.1	−2.0					
2-Me	22.4	28.1	39.3	27.2	32.4	22.8	13.8		
	0.5	−0.4	0.5	−0.9	0.0	−1.1	0.0		
3-Me	11.3	29.7	34.7	36.5	29.7	23.3	14.1	19.3	
	0.1	−0.7	0.4	−1.1	−0.1	−0.9	0.3	−0.4	
4-Me	14.1	20.2	39.5	32.3				19.3	
	0.0	−1.4	0.8	−1.3				−0.6	
2,2-diMe	29.2	30.2	44.4	24.4	33.0	22.8	13.8		
	−1.2	−0.1	−0.2	0.3	0.2	−1.1	0.0		
2,3-diMe[a]	20.1	32.2	38.8	34.0	30.0	23.1	13.8	17.9	15.2
	0.6	−0.8	0.1	−1.0	−0.3	−1.1	0.0	−0.9	−1.2
2,4-diMe[a]	23.1	25.3	47.0	30.2	39.9	19.9	14.0	22.1	19.4
	0.5	−1.8	1.7	−1.7	0.9	−1.7	−0.1	−0.5	−1.1
2,5-diMe[a]	22.5	28.4	36.5	34.4	34.8	29.5	11.0	22.3	19.0
	0.6	−0.2	0.0	−0.2	0.4	−0.9	−0.2	0.4	−0.7
2,6-diMe	22.4	28.1	39.5	25.2					
	0.5	−0.4	0.4	0.1					
3,3-diMe	8.0	34.2	32.5	41.3	26.4	23.7	13.7	26.4	
	1.5	−1.2	−0.3	−1.2	0.6	−0.8	−0.1	−0.9	
3,4-diMe *meso*	11.9	27.6	39.8	37.2	37.5	20.8	14.2	15.8	16.3
	0.2	−0.5	1.0	−0.9	1.1	−1.2	0.1	−1.4	−1.1
3,4-diMe *d,l*	11.9	25.8	38.9	36.3	35.5	20.8	14.2	13.9	14.2
	0.1	−2.4	0.1	−1.8	−1.0	−1.2	0.1	−2.6	−2.5
3,5-diMe *meso*[b]	10.9	29.5	31.9	44.3				18.9	
	−0.2	−1.2	−1.0	0.2				−1.4	
3,5-diMe *d,l*[b]	11.1	30.5	32.0	44.5				19.6	
	−0.1	−0.2	−0.9	0.4				−0.7	
4,4-diMe	14.9	17.3	44.8	32.8				27.0	
	0.3	−0.2	1.1	0.0				−0.6	
Octane derivatives									
Nil	13.6	22.7	32.1	29.4					
	−0.2	−1.2	0.0	−1.7					
2-Me	22.3	28.0	39.2	27.4	29.7	32.0	22.7	13.6	
	0.4	−0.5	0.4	−0.8	−1.7	−0.1	−1.2	−0.2	
3-Me	11.1	29.7	34.6	36.7	26.9	32.4	22.7	13.8	19.0
	−0.1	−0.7	0.3	−1.0	0.0	−1.2	−1.2	0.0	−0.7
4-Me	14.0	19.4	39.6	32.6	36.8	29.3	23.0	13.7	20.2
	−0.1	−2.2	0.9	−1.1	−0.9	−0.5	−1.2	−0.1	0.3
Nonane derivatives									
Nil	13.8	22.7	32.0	29.4	29.6				
	0.0	−1.2	−0.1	−1.7	−1.6				

[a]For definition of C(1) and C(8) see footnotes, Table 4.
[b]The present method does not distinguish these *meso* and *d,l* isomers, and no assignment is implied in this case.
[c]The root-mean-squares deviation between calculated and observed resonances was 0.91 ppm.

the probability $p_{32} \times p_{22}$ for C(6), and the downfield signal is therefore assigned to C(1). This assignment would appear to be quite certain, since there is little doubt that $p_{31} > p_{32}$, and that *syn*-axial δ-interactions cause rather large downfield shifts. However, the assumption that the remaining conformer resonances do not contribute to the nonequivalence of C(1) and C(6) is not rigorously true. There is no molecular symmetry operation with interchanges C(1) and C(6) and therefore $p_{31} \times p_{22}$ and $p_{31} \times p_{23}$ are not exactly equal, etc. Furthermore, deviations between calculated and actual conformer resonances will not affect C(1) and C(6) equally and may therefore also contribute to the nonequivalence of C(1) and C(6).

The 3,4-dimethylhexanes are the only examples of diastereoisomers in Table 4. Since only the spectrum of the mixture of diastereoisomers is available, they do not provide a test for the assignment of configuration. The derivation of the resonances for both isomers may nevertheless serve as an example. Table 3 lists the structural parameters in all conformations. C(1) is predicted to have the same resonances in both isomers, because the substituents on the second asymmetric carbon are beyond the three-bond segment C(1)—C(4) (v.i.). A small shift difference between *meso* and *d,l* isomers is predicted at C(2). Elimination of all interactions which occur in equally probable conformations in the *meso* and *d,l* isomers leaves two sets of parameters (set in italics in Table 3).

Conformation	*meso*		*d,l*		Probability
13	2110	↓	2101	↑	$p_{22} \times p_{32} \times p_{21}$
18	2101		2110		$p_{22} \times p_{33} \times p_{23}$
20	2110	↓	2101	↑	$p_{23} \times p_{31} \times p_{22}$
27	2101		2110		$p_{23} \times p_{33} \times p_{23}$

Since conformation **13** is less probable than **18**, the **13**/**18** interchange of the δ-interactions causes a differential downfield shift at C(2) in the *meso* isomer. This is partially offset by the **20**/**27** interchange of δ-interactions, since conformation **20** is more likely than **27**. C(3) is predicted to have the same resonance values in both isomers. The C(7) signal shows the largest observed and predicted isomeric shift. In this case the 1001 set of interactions occurs in conformation **3** in the *meso* isomer, but in conformer **5** in the *d,l* isomer. Since $p_{31} \times p_{22} > p_{32} \times p_{22}$, the low field signal is assigned to the *meso* isomer.

The further the asymmetric center is from a given carbon, the larger the number of rotational states which have to be defined in order to transmit the effect of asymmetry. The present three-bond treatment only allows the distinction of diastereoisomers with adjacent asymmetric

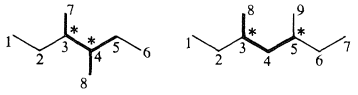

centers. The definition of the rotational states of the three closest bonds, together with the substituents of the δ-carbon, only specify the presence or absence of a *syn*-axial δ-interaction. It does not indicate whether a δ-hydrogen (δ-interactions) or an ε-carbon (ε-interactions) point toward the carbon in question. Thus, in the 3,4-dimethylhexanes the probabilities of δ-interactions of C(7) along the two C_β—C_γ bonds differ, since δ-interactions are only possible along C(4)—C(5), but not along C(4)—C(8). In the 3,5-dimethylheptanes, on the other hand, the δ-interactions of C(8) with C(6) and C(9) are taken to be equally probable, since the distinguishing feature, C(7), occurs beyond the three-bond segment and therefore is not recognized. In this case a definition of the rotational state of the fourth bond would be required to distinguish the two diastereoisomers.

The 2,4-dimethylhexanes may serve as examples. Table 6 lists the δ- and ε-interactions for the nonequivalent carbons C(1) and C(7) in all molecular conformations. If all rotational states in the four-bond segments C(1)—C(5), C(1)—C(8), C(7)—C(5), and C(7)—C(8) are defined, the nonequivalence of C(1) and C(7) is traced to the fact that ε-interactions with C(6) occur with probabilities $p_{21} \times p_{21} \times p_{21}$ and $p_{23} \times p_{22} \times p_{23}$ for C(1), but only with probabilities $p_{21} \times p_{22} \times p_{23}$ and $p_{22} \times p_{21} \times p_{21}$ for C(7). Since the occurrence of unrealistic ε-interactions, *i.e.* the loss of δ-interactions, is more probable for C(1), its signal is expected to be upfield from the C(7) resonance.

The asymmetry effect is still relatively large if the two asymmetric centers are only separated by a methylene group, but becomes quite small as they move apart. For example, the C(1)—C(8) differences in 2,3-, 2,4-, and 2,5-dimethylheptane are 2.2 ppm, 1.0 ppm, and 0.2 ppm, respectively (Table 5). The four-bond treatment might there-

TABLE 6. δ- and ε-interactions of C(1) and C(7) in 2,4-dimethylhexane[a,b]

ijk	C(1)	C(7)	*ijk*	C(1)	C(7)	*ijk*	C(1)	C(7)
111	ε6	δ8	211	—	ε6	311	δ8	—
112	δ5	δ8	212	—	δ5	312	δ8	—
113	δ5	δ8	213	—	δ5	313	δ8	—
121	—	δ5	221	—	—	321	δ5	—
122	—	δ5	222	—	—	322	δ5	—
123	—	ε6	223	—	—	323	ε6	—
131	δ8	—	231	—	δ8	331	—	—
132	δ8	—	232	—	δ8	332	—	—
133	δ8	—	233	—	δ8	333	—	—

[a]Conformer probabilities: $ijk = p_{2i} \times p_{2j} \times p_{2k}$; δ8 = δ-interaction with C(8); ε6 = ε-interaction with C(6), etc.
[b]Starting conformation:

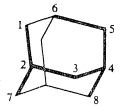

fore seem a useful general procedure. However, the need to eliminate ε-conformations, rather than introduce ε-parameters, creates complications. The elimination of such a conformation contradicts the assumption of independent rotational potentials, if that conformation would have a substantial probability of occurring. Returning to the example in Table 6, conformer **1** is taken to occur with probability $p_{21} \times p_{21} \times p_{21} = 0$ and its elimination would not pose any problem. However, conformation **24** occurs with nonzero probability $p_{23} \times p_{22} \times p_{23}$ and its elimination would contradict the assumption $p_{21} + p_{22} + p_{23} = 1$. One therefore has a choice between two approximate treatments of long range asymmetry effects. Either a four-bond treatment is adopted and conformations with ε-interactions are eliminated, even though this procedure would contradict the assumption of independent rotation potentials. Alternatively, the three-bond method is retained and long range asymmetry effects are considered separately. The assignment of the C(1) and C(7) resonances in 2,4-dimethylhexane illustrated in Table 6 was an example. Since the structural and population parameters in Table 1 seem reasonable, the three-bond treatment is retained. It would seem more appropriate to improve the prediction of conformer resonances before going to a more elaborate scheme of weighing these conformer resonances.

Finally, this method of conformational analysis is easily adopted to the description of heterosubstituted chains, since the derivation of carbon resonances in heterosubstituted substrates is entirely analogous to the predictive scheme used here (8).

Acknowledgment

We thank the National Research Council of Canada for their generous financial support.

1. L. P. LINDEMAN and J. Q. ADAMS. Anal. Chem. **43**, 1245 (1971).
2. H. BEIERBECK and J. K. SAUNDERS. Can. J. Chem. **53**, 1307 (1975).
3. H. BEIERBECK and J. K. SAUNDERS. Can. J. Chem. **54**, 2985 (1976).
4. S. H. GROVER, J. P. GUTHRIE, J. B. STOTHERS, and C. T. TAN. J. Magn. Res. **10**, 227 (1973).
5. J. G. BATCHELOR. J. Magn. Res. **18**, 212 (1975).
6. P. J. FLORY. Statistical mechanics of chain molecules. Wiley, New York. 1969.
7. D. M. GRANT and E. G. PAUL. J. Am. Chem. Soc. **86**, 2984 (1964).
8. H. BEIERBECK and J. K. SAUNDERS. Can. J. Chem. **54**, 632 (1976).
9. J. B. STOTHERS. Carbon-13 nmr spectroscopy. Academic Press, New York. 1972.
10. D. K. DALLING, D. M. GRANT, and E. G. PAUL. J. Am. Chem. Soc. **95**, 3718 (1973).

Synthesis of 4,4′-bis(dicyanomethylene)bicyclohexylidine

LARRY D. PEDERSEN AND LARRY WEILER[1]

Department of Chemistry, University of British Columbia, Vancouver, B.C., Canada V6T 1W5

Received August 25, 1976

LARRY D. PEDERSEN and LARRY WEILER. Can. J. Chem. **55**, 782 (1977).

4,4′-Bis(dicyanomethylene)bicyclohexylidine and its dihydro derivative, 4,4′-bis(dicyanomethylene)bicyclohexyl were prepared from the condensation of malononitrile with the corresponding diketone. Bicyclohexylidene-4,4′-dione was synthesized from the monoketal of cyclohexanedione via the symmetric azosulfide.

The uv spectra of the 4,4′-bis(dicyanomethylene)bicyclohexylidine and related model compounds indicate the presence of a long range interaction between the dicyanomethylene groups of the title compound.

LARRY D. PEDERSEN et LARRY WEILER. Can. J. Chem. **55**, 782 (1977).

On a préparé la bis(dicyanométhylène)-4,4′ bicyclohexylidine et son dérivé dihydro bis-(dicyanométhylène)-4,4′ bicyclohexyle par condensation du malononitrile avec la dicétone correspondante. On a synthétisé la bicyclohexylidènedione-4,4′ à partir du monoacétal de la cyclohexanedione par l'intermédiaire d'un azosulfure symétrique.

Le spectre uv du bis(dicyanométhylène)-4,4′ bicyclohexylidine et des composés modèles voisins indiquent la présence d'une interaction à longue distance entre les groupes dicyanométhylènes du composé mentionné dans le titre.

[Traduit par le journal]

Many cyano-substituted olefins form a variety of charge-transfer complexes with electron donors (1). We became interested in studying potential complexes of an acceptor in which there were two symmetrically disposed sites in the same molecule, not directly conjugated with each other. 1,4-Bis(dicyanomethylene)cyclohexane **1** (2) and 4,4′-bis(dicyanomethylene)bicyclohexylidine **2** are two examples of such molecules. We now wish to report the synthesis of **2** and its dihydro derivative **3**. Catalytic reduction

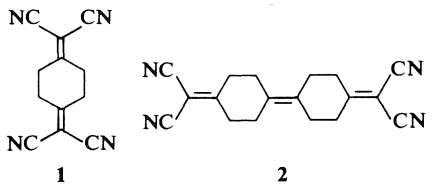

1 **2**

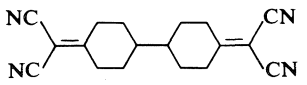

3

of *p,p′*-biphenol and subsequent oxidation gave bicyclohexyl-4,4′-dione (3). Condensation of this diketone with malononitrile catalyzed by β-alanine (2) gave **3** in 38% yield from the dione. All attempts to partially reduce the *p,p′*-biphenol to **9** (Scheme 1) or the corresponding diols by various catalysts and solvent systems gave either monoaromatic products or fully reduced bicyclohexyl-4,4′-diol.

Thus we turned to an investigation of the reductive dimerization of the monoketal of cyclohexane-1,4-dione **4** (4) using the azosulfide

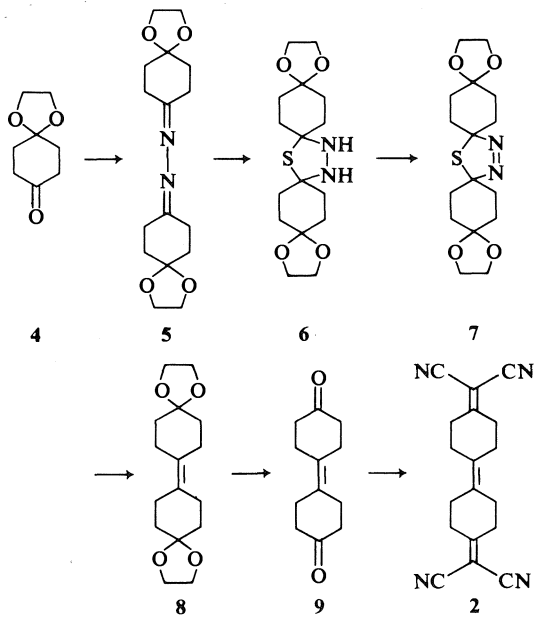

4 **5** **6** **7** **8** **9** **2**

SCHEME 1

[1]Author to whom correspondence should be addressed.

method recently developed by Barton and Willis (5*a*) and by Kellogg and Wassenaar (5*b*) (Scheme 1). Treatment of **4** with hydrazine in ethanol (or methanol) gave the azine **5** which was converted into the tetrahydrothiadiazole **6** with H_2S in water. Isolation of **5** and subsequent conversion to **6** usually resulted in lower yields of **6** than the one pot reaction (5*a*). The tetrahydrothiadiazole **6** was oxidized with lead tetraacetate in methylene chloride to give the azosulfide **7** in 95% yield. Treatment of **7** with triphenylphosphine neat at 120 °C for 2 h produced a smooth elimination of nitrogen and sulfur, and the bisketal **8** was isolated in quantitative yield. Hence this symmetric reductive dimerization of a ketone is compatible with a ketal protecting group. The ketal group was removed by treating **8** with 5% aqueous hydrochloric acid in tetrahydrofuran to give bicyclohexylidene-4,4′-dione **9** in quantitative yield. Finally **9** was condensed with malononitrile with β-alanine as catalyst to give 4,4′-bis(dicyanomethylene)bicyclohexylidene **2** in 45% yield.

The infrared spectrum of the dione **9** has a strong band at 1710 cm^{-1} ($CHCl_3$) which can be compared to the reported value of 1728 cm^{-1} (CCl_4) for 1,4-cyclohexanedione (6) and 1715 cm^{-1} ($CHCl_3$) for bicyclohexyl-4,4′-dione. Also, the Raman spectrum of a powder sample of dione **9** has medium bands at 1661 cm^{-1} and 1708 cm^{-1} due to the carbon–carbon double bond and the carbon–oxygen double bond respectively. 1,4-Cyclohexanedione shows only a weak band at 1702 cm^{-1} in the Raman spectrum (7). The enhancement of the intensity of the carbonyl stretch in the Raman spectrum of **9** may be due to some coupling with the 1661 cm^{-1} band or to different solid state conformations of **9** and 1,4-cyclohexanedione.

The uv spectra of **1**–**3** and **10** are given in Table 1. The bathochromic shift from **10** to **1** is

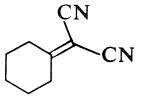

10

consistent with a long range interaction between the dicyanomethylene groups in **1**. Similarly, a comparison of the longest wavelength absorption of **2** and **3** indicate a long range interaction through the central double bond of **2**. A similar bathochromic shift has been reported in the uv spectra of 4-methylene cyclohexanones (8). We have not been able to obtain any well defined charge transfer spectra for these dicyanomethylene derivatives in the presence of an electron donor.

TABLE 1. Ultraviolet absorption of dicyanomethylene compounds[a]

Compound	λ_{max} (nm)
Dicyanomethylenecyclohexane **10**	239 (ε 13 600)
1,4-Bis(dicyanomethylene)cyclohexane **1**	248 (ε 34 500)
4,4′-Bis(dicyanomethylene)bicyclohexyl **3**	239 (ε 35 000)
4,4′-Bis(dicyanomethylene)bicyclohexylidene **2**	235 (ε 29 400) 268 (sh, ε 12 000)

[a]All uv spectra were obtained in methylene chloride solutions.

Experimental

All melting points are uncorrected. The ir spectra were recorded on a Perkin-Elmer Model 700 or Model 421 spectrophotometer. Raman spectra were recorded on a Cary 81 spectrometer. Nuclear magnetic resonance spectra were recorded on a Varian T60 or XL-100 spectrometer and chemical shifts are reported in δ units from internal TMS. Mass spectra were recorded on an AEI-MS9 spectrometer. Microanalyses were performed by Mr. Peter Borda, University of British Columbia.

Bicyclohexyl-4,4′-dione

Bicyclohexyl-4,4′-dione was prepared in 90% yield from *p,p′*-biphenol by catalytic reduction in ethanol ethyl acetate – acetic acid (10:10:6) using 5% Rh on alumina as catalyst at 50 psi and subsequent oxidation of the diol with Jones' reagent (9); mp 111.5–114.5 °C (lit. (3) mp 114–115 °C).

4,4′-Bis(dicyanomethylene)bicyclohexyl 3

A mixture of 5.4 g of bicyclohexyl-4,4′-dione and 3.8 g of malononitrile was melted on a steam bath. To the melt was added 1.0 ml of an aqueous β-alanine solution (0.125 g/25 ml of H_2O) and heating continued for 1 h. After cooling, the reaction mixture was washed with water and ether and the solid recrystallized from 250 ml of acetone to give 3.0 g (37.5% yield) of **3**; mp 227–228 °C; ir (CH_2Cl_2) 2250, 1600 cm^{-1}; nmr ($CDCl_3$) δ 1.45 (m, 6H), 2.25 (m, 8H), 3.04 (br d, J = 15 Hz, 4H). *Anal.* calcd. for $C_{18}H_{18}N_4$: C 74.48, H 6.21, N 19.31; found: C 74.40, H 6.06, N 19.49.

1,4-Dioxaspiro[4.5]decan-8-one Azine 5

To a stirred solution of 1.0 g of 1,4-cyclohexanedione monoketal (4) in 10 ml of methanol was added 5.8 ml of 25% hydrazine hydrate over a period of 5 min. The reaction mixture was allowed to stir for an additional 30 min. After removing the methanol by rotary evaporation, the residue was diluted with 10 ml of water and extracted with 30 ml of ether. The ether solution was dried (Na_2SO_4) and evaporated to dryness, affording 300 mg of crude product. Recrystallization from hexanes afforded 75 mg of white crystals; mp 118–120 °C; ir (CH_2Cl_2) 1645 cm^{-1}; nmr ($CDCl_3$) δ 1.68–2,0 (m, 8H), 2.44–2.66 (m, 8H), 3.96 (s, 8H); ms (70 eV) *m/e* (relative intensity):

308(81), 222(15), 207(16), 170(33), 154(100), 99(49), 86(19), 82(25), 44(47), 40(59). *Anal.* calcd. for $C_{18}H_{24}N_2O_4$: C 62.31, H 7.84, N 9.09; found: C 61.58, H 7.56, N 8.91.

Bisethylene Ketal of Cyclohexan-4-onespiro-2′-1′,3′,4′-thiadiazolidine-5′-spirocyclohexan-4-one **6**

To a stirred solution of 13.5 g of 1,4-cyclohexanedione monoketal (4) in 125 ml of ethanol was added 78 ml of 25% hydrazine hydrate over a period of 1 h. An initially formed white precipitate dissolved upon continued addition of the hydrazine hydrate. After stirring for an additional 10 min, the ethanol was removed by rotary evaporation. The residue was diluted to 150 ml with water. A stream of hydrogen sulfide was passed through this stirred aqueous solution for 2 h. The white precipitate was collected by filtration, washed with water, and air dried to give 12.8 g (86.4% yield) of crude tetrahydrothiadiazole **6**. A small amount was recrystallized from hexanes; mp 135–138 °C; ir (CH_2Cl_2) 3250, 1140 cm^{-1}; nmr ($CDCl_3$) δ 1.64–1.92 (m, 8H), 1.92–2.1 (m, 8H), 3.94 (s, 8H). *Anal.* calcd. for $C_{16}H_{26}N_2O_4S$: C 56.11, H 7.65, N 8.18, S 9.36, found: C 55.90, H 7.50, N 8.19, S 9.65.

Bisethylene Ketal of Cyclohexan-4-onespiro-2′-1′,3′,4′-thiadiazoline-5′-spirocyclohexan-4-one 7

A solution of 10.5 g of **6** in 85 ml of methylene chloride was added to a stirred solution of 15.4 g of lead tetraacetate in 50 ml of methylene chloride under nitrogen and cooled to 0 °C over a period of 45 min. The reaction mixture was allowed to warm to room temperature with stirring over a period of 1 h and was then diluted to 300 ml with methylene chloride. This mixture was washed with 200 ml of saturated sodium bicarbonate, filtered, washed with an additional 50 ml of saturated sodium bicarbonate and 50 ml of water, and dried (Na_2SO_4). Evaporation to dryness gave 9.9 g (95% yield) of thiadiazoline **7**. A small amount of **7** was recrystallized from hexanes to give clear crystals which clouded on heating at *ca.* 118 °C and decomposed with gas evolution to a white powder at 130 °C. The resulting white powder melts at 233–234 °C; ir (CH_2Cl_2) 1580 cm^{-1}; nmr ($CDCl_3$) δ 1.64–2.10 (m, 12H), 2.48–2.86 (m, 4H), 4.0 (s, 8H). *Anal.* calcd. for $C_{16}H_{24}N_2O_4S$: C 56.44, H 7.11, N 8.23; found: C 56.20, H 7.22, N 8.44.

Bisethylene Ketal of Bicyclohexylidene-4,4′-dione **8**

A mixture of 8.5 g of triphenylphosphine and 9.6 g of **7** was heated at 120 °C for 2 h. Rapid gas evolution was observed at the beginning of the reaction. After cooling, the solid reaction mixture was taken up in chloroform and chromatographed on a silica gel column (31 × 3.5 cm) eluting with chloroform. Triphenylphosphine sulfide came off first, followed by 8.0 g of the bisketal **8** (quantitative yield); mp 114–117 °C; nmr ($CDCl_3$) δ 1.50–1.84 (m, 8H), 2.20–2.50 (m, 8H), 4.00 (s, 8H). *Anal.* calcd. for $C_{16}H_{24}O_4$: C 68.54, H 8.63; found: C 68.57, H 8.46.

Bicyclohexylidene-4,4′-dione **9**

A solution of 7.9 g of bisketal **8** in 150 ml of 5% hydrochloric acid and 150 ml of tetrahydrofuran was refluxed for 1 h. After cooling, the tetrahydrofuran was removed by rotary evaporation. The resultant aqueous solution was extracted with chloroform (2 × 100 ml). The combined chloroform extracts were washed with 50 ml of saturated sodium bicarbonate and 50 ml of water, dried ($MgSO_4$), and evaporated to dryness. Thus 5.5 g (quantitative yield) of bisketone **9** was obtained. A small amount was recrystallized from hexanes; mp 117–118 °C; ir ($CHCl_3$) 1710 cm^{-1}; nmr ($CDCl_3$) δ 2.34–2.76 (m). *Anal.* calcd. for $C_{12}H_{16}O_2$: C 74.96, H 8.39; found: C 74.90, H 8.40.

4,4′-Bis(dicyanomethylene)bicyclohexylidene **2**

A mixture of 1.0 g of bisketone **9** and 1.0 g of malononitrile was melted on a steam bath. To the melt was added 5 drops of an aqueous β-alanine solution (0.125 g/25 ml of H_2O). The reaction flask was stoppered and heating continued for 30 min. The resulting light green solid reaction mixture was washed with water and ether, and recrystallized from 150 ml of ethyl acetate to give 0.685 g (45% yield) of light yellow needles; mp 223–224 °C; ir (CH_2Cl_2) 2255, 1600 cm^{-1}; nmr ($CDCl_3$) δ 2.20–3.00 (m). *Anal.* calcd. for $C_{18}H_{16}N_4$: C 74.97, H 5.59, N 19.43; found: C 74.85, H 5.73, N 19.33.

Acknowledgements

We are grateful to the National Research Council of Canada and the University of British Columbia for financial support of this work.

1. L. R. Melby. *In* The chemistry of the cyano group. *Edited by* Z. Rappoport. Interscience Publishers, New York, N.Y. 1970. Chapt. 10.
2. D. S. Acker and W. R. Hertler. J. Am. Chem. Soc. **84**, 3370 (1962).
3. (*a*) A. L. Wilds, C. H. Shunk, and C. H. Hoffman. J. Am. Chem. Soc. **76**, 1733 (1954); (*b*) W. Kern, W. Gruber, and H. O. Wirth. Makromol. Chem. **37**, 198 (1960).
4. M. Haslanger and R. G. Lawton. Synthetic Commun. **4**, 155 (1974).
5. (*a*) D. H. R. Barton and B. J. Willis. J. Chem. Soc. Perkin Trans. I. 305 (1972); (*b*) R. M. Kellogg and S. Wassenaar. Tetrahedron Lett. 1987 (1970).
6. D. Döpp and H. Musso. Spectrochim. Acta, **22**, 1813 (1966).
7. (*a*) N. L. Allinger, H. M. Blatter, L. A. Freeberg, and F. M. Karkowski. J. Am. Chem. Soc. **88**, 2999 (1966); (*b*) M. V. Bhatt, G. Srinivasan, and P. Neelakantan. Tetrahedron, **21**, 291 (1965).
8. S. Winstein, L. de Vries, and R. Orloski. J. Am. Chem. Soc. **83**, 2020 (1961).
9. A. Bowers, T. G. Halsall, E. R. H. Jones, and A. J. Lemin. J. Chem. Soc. 2548 (1953).

A synthetic approach to resistomycin

JOHN F. KINGSTON AND LARRY WEILER

Department of Chemistry, University of British Columbia, Vancouver, B.C., Canada V6T 1W5

Received September 3, 1976

JOHN F. KINGSTON and LARRY WEILER. Can. J. Chem. **55**, 785 (1977).

An outline of a synthetic route to the antibiotic resistomycin is presented. We report the successful construction of an intermediate containing all of the carbon atoms in resistomycin with requisite functionalities. The key steps involved an aldol type condensation of the dianion from 2,4,6-trimethoxybenzoylacetone and a suitable acetophenone. This was followed by a novel acid-catalyzed cyclization–condensation to form the naphthalene intermediate required in our scheme.

JOHN F. KINGSTON et LARRY WEILER. Can. J. Chem. **55**, 785 (1977).

On présente une ébauche d'une voie de synthèse conduisant à l'antibiotique résistomycine. On a construit avec succès un intermédiaire contenant tous les atomes de carbone de la résistomycine ainsi que les fonctions requises. Les étapes clés impliquent une condensation de type aldolique du dianion de la triméthoxy-2,4,6 benzoylacétone et d'une acétophénone appropriée. Cette réaction est suivie d'une nouvelle réaction de cyclisation–condensation catalysée par les acides conduisant au naphtalène intermédiaire requis dans notre schéma.

[Traduit par le journal]

Recently structure **1** was proposed for resistomycin (1, 2), an antibiotic first isolated from *Streptomyces resistomycificus* (3). The compound was resistant, hence its name, to decomposition in hot normal potassium hydroxide or hot concentrated sulfuric acid. Resistomycin is the only

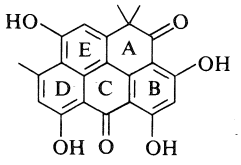

1

known example of a natural product with this pentacyclic skeleton. Its oxygenation pattern suggests that its biosynthesis involves the condensation of ten acetate units which can fold in two possible modes, **2** (1*a*) or **3** (2), to produce resistomycin. Rings B, C, D in resistomycin **1**

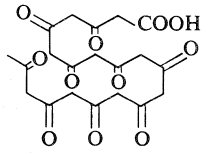

2

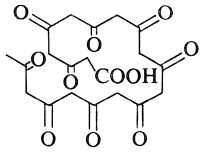

3

have distinct similarities to the tetracycline antibiotics (4) and the anthracycline family (5) of antitumor agents. In addition rings C, D, E in resistomycin **1** are quite similar to the natural phenalones and their dimers (6). This invited the hope that the methodology developed in the synthesis of resistomycin might be of widespread synthetic utility in the field of aromatic acetogenins (7).

Our general synthetic approach to resistomycin involved using a molecule containing ring E as the cornerstone on which is constructed ring D. Subsequent introduction of ring B and cyclizing to form rings C and A would generate the desired carbon skeleton as shown schematically in [1]. A suitable ring E precursor would

[1] 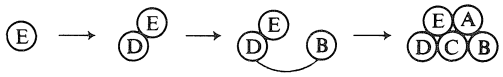

be the keto nitrile **7**. This material was prepared from 3,5-dimethoxybenzoic acid **4** as shown in Scheme 1. The acid **4** was reduced with lithium aluminum hydride to the corresponding alcohol which was converted via the chloride to the nitrile **5** (8) in 67% yield. The nitrile **5** was alkylated in 80% yield with sodium hydride and methyl iodide in refluxing 1,2-dimethoxyethane to give **6**. Finally, acylation of **6** gave **7** in 79% yield. The symmetry of the proton and carbon nmr spectra of this product were consistent with structure **7** rather than the possible isomeric structure with the acetyl group *ortho* to the 2-methylpropionitrile group.

Reaction of acetophenone **7** with an excess of the dianion of methyl acetoacetate (9) gave the δ-hydroxy-β-keto ester **8** (10) which was charac-

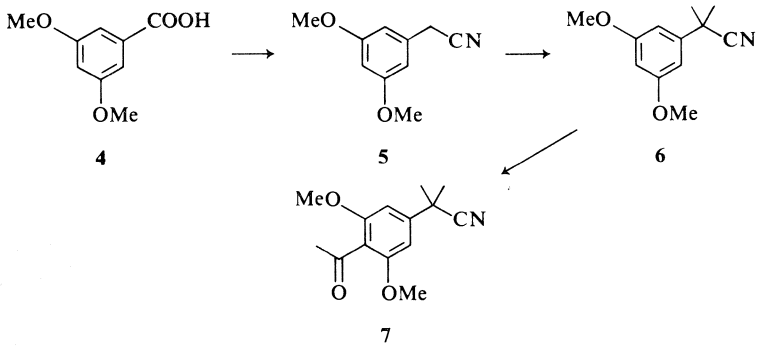

SCHEME 1. Synthesis of 2-(4-acetyl-3,5-dimethoxyphenyl)-2-methylpropionitrile **7**.

terized as its trimethylsilyl ether (11). The alcohol **8** was smoothly dehydrated to an *E,Z*-mixture of olefins **9** in greater than 85% yield from **7**. All attempts to cyclize **9** to the naphthalene **10** with acids, bases (for related base-catalyzed cyclizations, see ref. 12), or photolysis (for related photochemical cyclizations, see ref. 13) were unsuccessful. In addition attempted

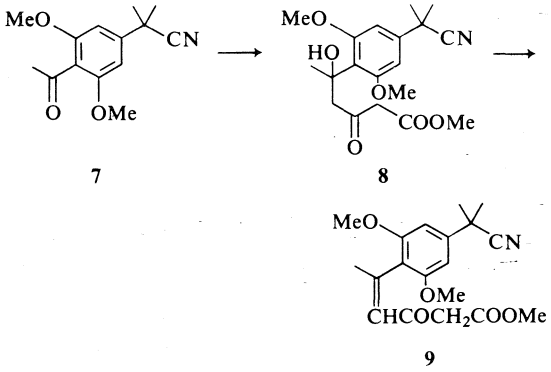

cyclizations via thermolysis or photolysis of the corresponding enol acetate of **9** were not successful.

In our proposed route to resistomycin we had intended to use **10** in an acylation reaction with 1,3,5-trimethoxybenzene to give **11**. However,

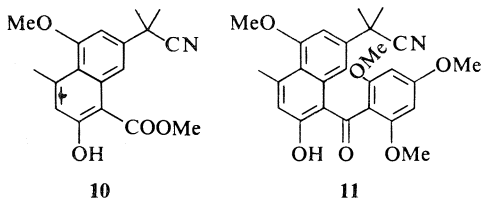

our failure to cyclize **9** to **10**, suggested that a more convergent route to **11** might fare better. In particular, we have consistently found that the α-carbon in a β-keto ester is significantly less reactive than the corresponding carbon in a β-diketone in acid- and base-catalyzed alkylation reactions. The feasibility of utilizing this fact was suggested by the following observation. An excess of the dianion of benzoylacetone (for a review of the generation and reactions of dianions from β-diketones, see ref. 14) was added to 2,4,6-trimethoxyacetophenone to produce the aldol product **12**. This material was

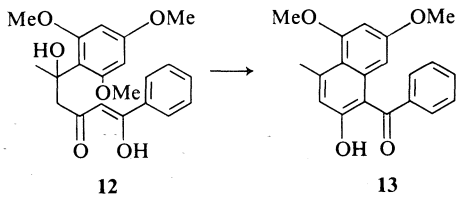

dehydrated with HCl in chloroform to a mixture of the corresponding *E* and *Z* alkenes. If the above dehydration reaction mixture was allowed to stand for about 5 h a new product was produced in over 50% yield from 2,4,6-trimethoxyacetophene. The structure of this new product was readily shown to be **13**.

Similarly, the aldol product **14** was obtained in quantitative yield from the condensation of the dianion of 2,4,6-trimethoxybenzoylacetone with the acetophenone **7**. Attempts to dehydrate this material with HCl in chloroform gave a complex mixture of products; however, we found that boron trifluoride etherate in ether smoothly

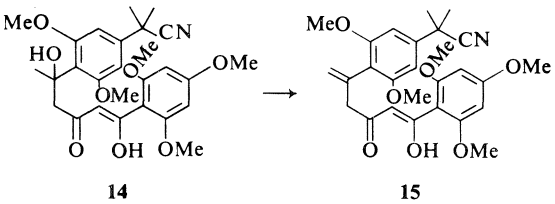

effected the dehydration of **14**. But the major dehydration product was the unconjugated alkene **15** plus small amounts of the *E* and *Z* conjugated isomers of **15**. No attempt was made to separate the isomers at this stage. But this mixture of isomers, containing mainly **15**, was treated first with HCl in benzene to isomerize the double bond into conjugation and subsequently with stannic chloride (15) to produce the cyclized ketone **11** in *ca.* 50% yield.

At present we have very little evidence as to the mechanism of this novel cyclization to yield the naphthalenes **11** and **13**, but we suggest the following possibility. It has been shown that methoxybenzene derivatives are readily protonated on a ring carbon in strong acid (16). A similar protonation in the above cyclizations would produce **16**. Attack of the resulting elec-

[2]

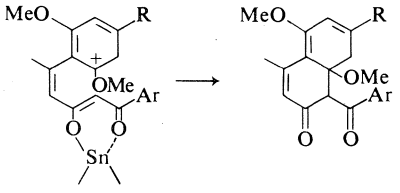

16 **17**

trophilic ring carbon on the tin enolate would give **17** [2] which, on loss of methanol and enolization, yields the cyclized products **11** and **13**. In this reaction the roles of electrophile and nucleophile have been reversed from those normally encountered in aromatic substitutions. The stannic chloride is essential for the cyclization and we can attribute two possible advantageous properties to this Lewis acid. First, the chelating properties of the tin may be important in holding intermediate **16** in the appropriate conformation for cyclization. In addition, the high ionic character of the tin–oxygen bond may enhance the nucleophilic character of the enol carbon and hence assist the cyclization. A similar type of mechanism may also be involved in the stannic chloride-catalyzed cyclization of the β-keto ester **18** shown in [3] (17).

[3]

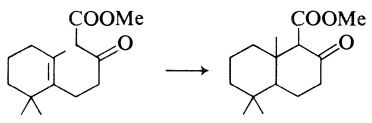

18

This completes the synthesis of a resistomycin intermediate containing all of the carbon atoms of resistomycin and rings B, C, and E. The remaining steps involve a cyclization and loss of methanol to produce ring C, and an internal acylation, perhaps of the Hoesch type (18) to form ring A. In light of the above successful cyclizations [2] which we suggest are initiated by ring protonation, we undertook a study of the acid cyclizations of **11**. Indeed, treatment of **11** with a variety of strong acids gave a product in high yield which had undergone a cyclization and loss of methanol. Unfortunately this product was shown to be the xanthone **19** from its spectral properties. It would appear that protonation of

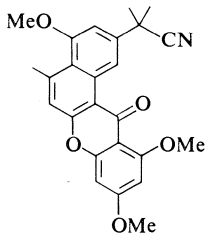

19

the ketone or trimethoxybenzene ring was occurring, as hoped, but the oxygen of the ring D hydroxyl was a more efficient nucleophile than ring E. We are currently involved in the preparation of suitable derivatives of **11** and in their subsequent cyclization.

Experimental

Infrared (ir) spectra were taken in chloroform solution (unless otherwise noted). They were recorded on a Perkin-Elmer model 700 spectrophotometer and were calibrated with the 1601 cm^{-1} band of polystyrene. Nuclear magnetic resonance (nmr) spectra were taken in deuterochloroform (unless otherwise noted) and were recorded on a Varian model T-60 spectrometer. Tetramethylsilane was used as an internal standard except where indicated. Chemical shifts are reported using the δ scale. The following abbreviations are used regarding the multiplicity of peaks: s singlet, d doublet, t triplet, q quartet, m multiplet. Coupling constants are denoted by *J* and are quoted in cycles per second (Hz). The multiplicity, coupling constants, integrated peak areas, and proton assignments are listed in parentheses after each signal. Ultraviolet–visible (uv–vis) spectra were recorded on either a Unicam model SP 800 or a Perkin-Elmer model 202 spectrophotometer. Unless otherwise noted the spectra were taken in methanol. The molar extinction coefficients of the main bands are listed in parentheses after the absorptions. The mass spectra were obtained using an Atlas CH-4b mass spectrometer. High resolution measurements were made on an AEI MS-9 mass spectrometer. Each mass (*m/e*) has its relative intensity listed in parentheses after it. Both instruments were operated at an ionizing potential of 70 V.

Melting points (mp) were determined on a Kofler hot

stage microscope and are uncorrected. Elemental microanalyses were performed by Mr. Peter Borda, University of British Columbia.

3,5-Dimethoxybenzyl Alcohol

A 1000 ml three-necked flask was fitted with a dropping funnel, a condenser with a calcium sulphate drying tube, and a magnetic stirrer. It was charged with a suspension of lithium aluminum hydride (4.80 g, 126 mmol) in THF (200 ml). A solution of 3,5-dimethoxybenzoic acid **4** (10.0 g, 55.0 mmol) in dry THF (200 ml) was added dropwise at a rate that maintained gentle reflux. After the addition was complete (1 h) the mixture was allowed to stir for an additional ½ h. This was followed by the dropwise addition of ether (250 ml) saturated with water and the dropwise addition of 6 *N* sulphuric acid (180 ml). The aqueous and organic phases were separated and the aqueous phase was extracted with ether (2 × 100 ml). The combined organic phases were washed with water (3 × 50 ml), dried over sodium sulphate, and evaporated under reduced pressure to yield 3,5-dimethoxybenzyl alcohol (9.17 g, 99%); ir 3400, 1600 cm^{-1}; nmr δ 2.16 (s, 1, hydroxyl proton, exchangeable in D_2O), 3.70 (s, 6, methoxy group protons), 4.47 (s, 2, methylene protons), 6.25 (m, 3, aromatic protons).

3,5-Dimethoxybenzyl Chloride

A 1000 ml three-necked flask was fitted with a dropping funnel, a condenser, and a magnetic stirrer. It was charged with a solution of 3,5-dimethoxybenzyl alcohol (28.4 g, 169 mmol) and pyridine (3 ml) in anhydrous ether (300 ml). A solution of thionyl chloride (50.0 g, 324 mmol) in anhydrous ether (250 ml) was added dropwise over a period of 1 h. The solution was then allowed to stir an additional 1 h before water (60 ml) was added, carefully, through the dropping funnel. The aqueous and organic phases were separated and the organic phase was washed with water (2 × 100 ml) and dried over magnesium sulphate. The solvents were removed under reduced pressure to yield 3,5-dimethoxybenzyl chloride (28.6 g, 90%) as a yellowish oil which crystallized on standing; mp 42–44 °C (lit. (8) mp 46 °C).

3,5-Dimethoxybenzyl Cyanide

A mixture of 3,5-dimethoxybenzyl chloride (33.0 g, 187 mmol), sodium cyanide (60.0 g, 1.23 mol), ethanol (600 ml), and water (150 ml) was refluxed for 4 h. The solution was poured onto 1000 g of ice. The precipitate formed was collected on a filter and dissolved in ether. This solution was dried over magnesium sulphate and the solvents were removed under reduced pressure to yield **5** (23.7 g, 75%); mp 50–51 °C (lit, (8) mp 53 °C); ir 2260 cm^{-1}; nmr δ 3.55 (s, 2, methylene protons), 3.71 (s, 6, methoxy group protons), 6.25 (m, 3, aromatic protons).

2-(3,5-Dimethoxyphenyl)-2-methylpropionitrile ***6***

A 500 ml three-necked flask was fitted with a dropping funnel, a condenser, and gas inlet and outlet tubes. It was charged with sodium hydride as a 57% dispersion in mineral oil (12.0 g, 289 mmol) and the mineral oil was removed by washing with petroleum ether (2 × 20 ml). Dry DME (150 ml) was added and the flask was flushed with nitrogen. A solution of 3,5-dimethoxybenzyl cyanide **5** (12.0 g, 67.8 mmol) in dry DME (100 ml) was added dropwise over a period of ½ h. The mixture was allowed to stir for 15 min and then methyl iodide (41.0 g, 288 mmol) was added dropwise over a period of 20 min. The mixture was refluxed for 24 h and then cooled to room temperature. Water (100 ml) and ether (150 ml) were added and the phases separated. The aqueous phase was extracted with ether (2 × 150 ml) and the combined organics were washed with water (2 × 150 ml), dried over magnesium sulphate, and the solvents were removed by evaporation under reduced pressure. The crude oil obtained was distilled *in vacuo* to afford **6** (11.1 g, 80%); bp 97 °C/2 torr (lit. (8) bp 147–150 °C/760 torr); nmr δ 1.67 (s, 6, *gem*-dimethyl group protons), 3.75 (s, 6, methoxy group protons), 6.45 (m, 3, aromatic protons).

2-(4-Acetyl-3,5-dimethoxyphenyl)-2-methylpropionitrile ***7***

A solution of **6** (511 mg, 2.50 mmol) and acetic anhydride (600 mg, 5.88 mmol) in methylene chloride (50 ml) was added to a 50 ml three-necked flask fitted with nitrogen inlet and outlet syringe needles and a magnetic stirrer. The flask was flushed with nitrogen and cooled to −10 °C in an ice–salt bath. Aluminum chloride (2.0 g, 15.0 mmol) was added, a portion at a time, with stirring, over a period of ½ h. The mixture was allowed to stir at 0 °C for an additional 1½ h after the addition of the aluminum chloride was complete. Water (15 ml) was added with vigorous shaking. The phases were separated and the aqueous phase was extracted with methylene chloride (2 × 15 ml). The combined organics were washed with water (2 × 15 ml) and dried over magnesium sulphate. The solvents were removed under reduced pressure to yield crude brown crystals which were recrystallized twice from ligroin – carbon tetrachloride to afford **22** (491 mg, 79%) as fine tan coloured crystals; mp 120–121 °C; ir 2250, 1700, 1610, 1580, 1250 cm^{-1}; nmr δ 1.78 (s, 6, *gem*-dimethyl group protons), 2.50 (s, 3, acetyl methyl group protons), 3.89 (s, 6, methoxy group protons), 6.71 (s, 2, aromatic protons); uv 262 nm (3240); ms *m/e* 247(23), 233(15), 232(100), 216(11), 175(5), 165(5), 121(3), 119(5), 116(5), 115(5), 91(8), 83(6), 57(3), 56(3), 55(5); *Anal.* calcd. for $C_{14}H_{17}O_3N$: C 68.00, H 6.93, N 5.66; found: C 67.73, H 7.05, N 5.38.

Methyl-5(4-1′-Cyano-1′-methylethyl-2,6-dimethoxyphenyl)-5-hydroxy-3-oxohexanoate ***8***

Sodium hydride as a 57% dispersion on mineral oil (175 mg, 4.17 mmol) was weighed into a 50 ml flask equipped with a magnetic stirrer. The mineral oil was removed by washing with dry THF (5 ml) and a further 10 ml of dry THF was added as solvent. The flask was stoppered with a serum cap, fitted with nitrogen inlet and outlet syringe needles, flushed with nitrogen, and cooled to 0 °C in an ice bath. Methyl acetoacetate (464 mg, 4.00 mmol) was added dropwise to the stirred mixture at a rate which maintained a vigorous but not excessive evolution of hydrogen. The reaction was allowed to stir for 10 min after the addition was complete. Next, a solution of *n*-butyllithium (165 ml, 2.50 *M*, 4.12 mmol) was added dropwise to the reaction mixture over a period of 1 min. After a further 10 min of stirring, a solution of ketone **7** (100 mg, 0.405 mmol) in dry THF (10 ml) was added to the reaction mixture, still at 0 °C. The reaction was allowed to stir at this temperature for a further 10 min and then 1 *N* hydrochloric acid (10 ml) was added in one portion. The mixture was poured into ether (100 ml) and the phases were separated. The organic phase was washed with water (5 × 15 ml) and dried over magnesium sulphate. The solvents were removed under reduced pressure and the oil obtained was separated into its components by preparative tlc on silica gel using a mixture of carbon tetrachloride and ether (2:1 v/v) as devel-

oping solvent. The band lying in the region R_f 0.1–0.2 was removed and extracted with chloroform. The solvent was removed under reduced pressure to yield **8** (129 mg, 88%); ir 3500, 2250, 1745, 1710, 1610, 1575 cm^{-1}; nmr δ 1.60 (s, 3, carbinol carbon methyl group protons), 1.70 (*gem*-dimethyl group protons), 2.95 (d, $J = 16$ Hz, 1, proton on methylene group α to carbinol carbon), 3.52 (d, $J = 16$ Hz, 1, proton on methylene group α to carbinol carbon), 3.47 (s, 2, methylene protons on carbon α to ester), 3.68 (s, 3, ester methoxy group protons), 3.90 (s, 6, ether methoxy group protons), 6.72 (s, 2, aromatic protons); uv 276 nm (1670), 283 (shoulder); ms (*a*) low resolution *m/e* 345(2), 332(8), 314(13), 249(21), 248(100), 233(11), 232(65), 230(27), 217(12), 162(25), 129(21), 101(10), 85(12), 59(14), 57(15), 55(10); (*b*) high resolution calcd. for $C_{19}H_{23}O_5N$ (P-18) (amu): 345.158; found (*m/e*): 345.162.

Methyl 5-(4-1′-Cyano-1′-methylethyl-2,6-dimethoxyphenyl)-3-oxo-5-trimethylsiloxyhexanoate

Methyl 5-(4-1′-cyano-1′-methylethyl-2,6-dimethoxyphenyl)-5-hydroxy-3-oxohexanoate **8** (95 mg, 0.26 mmol), trimethylsilylchloride (30 mg, 0.28 mmol), and hexamethyldisiliazane (24 mg, 0.15 mmol) were dissolved in dry pyridine (5 ml) and the solution was stirred at room temperature for ½ h. The fine, white precipitate formed was filtered off and washed with anhydrous ether (5 ml). The washing was combined with the filtrate and the solvents were removed under reduced pressure. The oil obtained was purified by preparative tlc on silica gel using an ether – carbon tetrachloride mixture (1:2 v/v) as developing solvent. The band at R_f 0.3–0.4 was removed and extracted with chloroform. The solvent was removed under reduced pressure to yield the TMS derivative of **8**; (52 mg, 46%); ir 2250, 1745, 1710, 1610, 1575 cm^{-1}; nmr δ −0.04 (s, 9, silyl methyl group protons), 1.66 (s, 6, *gem*-dimethyl group protons), 1.80 (s, 3, protons on methyl group α to silyl ether carbon), 2.95 (d, 1, proton on methylene group α to silyl ether carbon), 3.30 (d, 1, proton on methylene group α to silyl ether carbon), 3.55 (s, 2, methylene protons on carbon α to ester), 3.66 (s, 3, ester methoxy group protons), 3.76 (s, 6, ether methoxy group protons), 6.60 (s, 2, aromatic protons); uv 283 nm (1640); ms (*a*) low resolution *m/e* 436(3), 421(3), 406(3), 345(17), 321(10), 315(21), 314(100), 272(17), 248(28), 232(14), 230(10), 162(11), 101(10), 75(14), 59(11); (*b*) high resolution calcd. for $C_{22}H_{33}O_6NSi$ (amu): 435.207; found (*m/e*): 435.200.

Methyl 5-(4-1′-Cyano-1′-methylethyl-2,6-dimethoxyphenyl)-3-oxohex-4-enoate ***9***

Chloroform (25 ml) was saturated with hydrogen chloride by bubbling the anhydrous gas directly through the solvent for 20 min. Methyl 5-(4-1′-cyano-1′-methylethyl-2,6-dimethoxyphenyl)-5-hydroxy-3-oxohexanoate **8** (135 mg, 0.372 mmol) was added and the solution was allowed to stir at room temperature for 2 h. It was then washed with saturated aqueous sodium hydrogen carbonate solution (3 × 10 ml) and water (3 × 10 ml), and dried over magnesium sulphate. The solvent was removed under reduced pressure to afford **9** (125 mg, 98%) as an *E,Z* mixture; ir 2250, 1740, 1680, 1610, 1575 cm^{-1}; nmr δ 1.75 (s, 6, *gem*-dimethyl group protons), 2.09, 2.32 (2d, $J = 2$ Hz, 3 total, vinyl methyl groups in *E* and *Z* isomers respectively), 3.24, 3.53 (2s, 2 total, methylene protons on carbon α to ester in *E* and *Z* isomers respectively), 3.65, 3.75 (2s, 3 total, ester methoxy group protons for *E* and *Z* isomers respectively), 3.87 (s, 6, ester methoxy group protons), 6.16, 6.32 (2q, $J = 2$ Hz, 1 total, vinyl protons in *Z* and *E* isomers respectively), 6.70 (s, 2, aromatic protons); uv 285 nm (6400); ms (*a*) low resolution *m/e* 345(2), 315(11), 314(70), 272(13), 257(21), 256(100), 214(13), 176(11), 162(12), 161(10), 101(12), 59(12), 51(36); (*b*) high resolution calcd. for $C_{19}H_{23}O_5N$ (amu): 345.158; found (*m/e*): 345.158.

5-Hydroxy-1-phenyl-5-(2,4,6-trimethoxyphenyl)hexane-1,3-dione ***12***

A 50 ml flask containing isopropylcyclohexylamine (1.150 g, 8.16 mmol) and dry THF (20 ml) was equipped with a magnetic stirrer, stoppered with a serum cap, fitted with nitrogen inlet and outlet syringe needles, and flushed with nitrogen. A solution of *n*-butyllithium in hexane (3.30 ml, 2.50 *M*, 8.25 mmol) was added and the reaction was stirred at room temperature for 10 min. After this time, a solution of benzoylacetone (648 mg, 4.00 mmol) in dry THF (5 ml) was added and the reaction was stirred at room temperature for ½ h before being cooled to 0 °C. A solution of 2,4,6-trimethoxyacetophenone (168 mg, 0.800 mmol) in dry THF (2 ml) was added and the reaction mixture was stirred at 0 °C for 10 min before being quenched by the addition of 1 *N* hydrochloric acid (15 ml). The contents of the flask were poured into ether (75 ml) and the organic phase was washed with water (5 × 10 ml) and dried over magnesium sulphate. Evaporation of the solvents under reduced pressure yielded a mixture of compounds composed primarily of benzoylacetone and **12** (by tlc). Isolation of the product was accomplished by preparative tlc on silica gel using a carbon tetrachloride – ether mixture (2:1 v/v) as developing solvent. The band lying at R_f 0.3–0.4 was removed and extracted with chloroform. Evaporation of the chloroform under reduced pressure afforded **12** (303 mg, 100%) as a light yellow oil; ir 3550–3500, 1650–1550 cm^{-1}; nmr (assignment simplified by ignoring the keto tautomer present in minor amount) δ 1.75 (s, 3, carbinol carbon methyl group protons), 2.89 (d, $J = 14$ Hz, 1, proton on methylene group α to carbinol carbon), 3.24 (d, $J = 14$ Hz, 1, proton on methylene group α to carbinol carbon), 3.75 (2s, 9, methoxy group protons), 6.15 (s, 1, vinyl proton of enol), 6.18 (s, 2, protons on trimethoxyphenyl ring), 7.2–7.8 (m, 5, protons on phenyl ring); uv 338 nm (10,200); ms (*a*) low resolution *m/e* 354(50), 338(10), 324(17), 323(76), 322(17), 249(12), 221(17), 219(14), 194(14), 193(43), 177(12), 168(26), 147(45), 106(10), 105(100), 91(14), 77(48), 68(52); (*b*) high resolution calcd. for $C_{21}H_{22}O_5$ (P-18) (amu): 354.147; found (*m/e*): 354.151.

1-Phenyl-5-(2,4,6-trimethoxyphenyl)hex-4-ene-1,3-dione

Chloroform (40 ml) was saturated with hydrogen chloride by bubbling the anhydrous gas through the solvent for ¼ h. A solution of 5-hydroxy-1-phenyl-5-(2,4,6-trimethoxyphenyl)hexane-1,3-dione **12** (149 mg, 0.412 mmol) in chloroform (2 ml) was added and the solution was stirred for 1½ h before being washed with water (5 × 10 ml) and dried over magnesium sulphate. Evaporation of the solvent under reduced pressure afforded the dehydrated products (138 mg, 97%) as a crude orange oil; ir 1650–1550 cm^{-1}; nmr δ 2.15, 2.49 (2d, $J = 2$ Hz, 3 total, vinyl methyl group protons in *E* and *Z* isomers), 4.75–4.85 (several s, 9 total, methoxy group protons), 5.90–6.40 (m, vinyl proton, vinyl proton

of enol, trimethoxyphenyl ring protons), 7.30–8.20 (m, 5, phenyl ring protons).

5,7-Dimethoxy-2-hydroxy-4-methyl-1-naphthyl Phenyl Ketone ***13***

A 50 ml flask containing diisopropylamine (1.05 g, 10.4 mmol) and THF (20 ml) was equipped with a magnetic stirrer, stoppered with a serum cap, fitted with nitrogen inlet and outlet syringe needles, and flushed with nitrogen. A solution of *n*-butyllithium in hexane (4.60 ml, 2.20 *M*, 10.1 mmol) was added and the mixture was stirred for 5 min before a solution of benzoylacetone (0.810 g, 5.00 mmol) in dry THF (5 ml) was added. The reaction was refluxed under nitrogen for 2 h and then cooled to room temperature. A solution of 2,4,6-trimethoxyacetophenone (0.108 g, 0.515 mmol) in dry THF (5 ml) was added and the solution was stirred at room temperature for 2 h. After this time, the contents of the flask were transferred via a stainless steel cannula to a rapidly stirred mixture of 1 *N* hydrochloric acid (50 ml) and ether (250 ml). The organic phase was washed with water (3 × 50 ml) and dried over magnesium sulphate. The mixture of compounds obtained after evaporation of the solvents under reduced pressure was dissolved in chloroform (100 ml) saturated with anhydrous hydrogen chloride gas. This solution was stirred for 5 h and then washed with water (20 ml) and extracted with 1 *N* sodium hydroxide (5 × 20 ml). The base insoluble portion was washed with water (3 × 20 ml) and dried over magnesium sulphate. The solvents were evaporated under reduced pressure to yield a mixture of compounds which was separated into two components by preparative tlc on silica gel. A mixture of carbon tetrachloride and ether (2:1 v/v) was used to develop the plates. The band lying at R_f 0.6–0.7 was removed and extracted with chloroform. Evaporation of the chloroform under reduced pressure afforded 1-phenyl-5-(2,4,6-trimethoxyphenyl)hex-4-ene-1,3-dione (46 mg, 25%); spectral data as described under synthesis of this compound above. Extraction of the band lying at R_f 0.3–0.4 on the plates afforded **13** (88 mg, 53%). A sample of this yellow crystalline compound was sublimed for analysis; mp 135–137 °C; ir 1640, 1600, 1575 cm^{-1}; nmr δ 2.49 (s, 3, methyl group protons), 3.85 (2s, 6, methoxy group protons), 6.10–6.40 (m, 3, naphthyl ring protons), 7.30–8.40 (m, 5, phenyl ring protons); uv–vis 240 (34 300), 260 (shoulder), 285 (shoulder), 415 (shoulder), 435 nm (51 500); ms *m/e* 322(79), 305(39), 246(16), 245(100), 230(18), 188(10), 147(10), 105(12), 77(29). *Anal.* calcd. for $C_{20}H_{18}O_4$: C 74.52, H 5.63; found: C 74.40, H 5.60.

1-(2,4,6-Trimethoxyphenyl)butane-1,3-dione

A 250 ml flask containing a solution of 2,4,6-trimethoxyacetophenone (1.976 g, 9.41 mmol) in dry THF (175 ml) was equipped with a magnetic stirrer, stoppered with a serum cap, fitted with nitrogen inlet and outlet syringe needles, and flushed with nitrogen. A solution of trityl-potassium in DME (~0.5 *M*) was added dropwise until a permanent red colour appeared in the reaction mixture. During this addition a flocculent white precipitate was formed. Methyl acetate (10.0 ml, 132 mmol) was added and the reaction mixture was stirred at room temperature for 16 h, during which time the precipitate dissolved. Next, the contents of the flask were transferred via a stainless steel cannula to a rapidly stirred mixture of 1 *N* hydrochloric acid (100 ml) and ether (500 ml). The aqueous phase was extracted with ether (2 × 50 ml) and the combined organics were washed with water (100 ml) and extracted with 1 *N* sodium hydroxide (3 × 75 ml). The combined base extracts were acidified by the addition of concentrated hydrochloric acid and reextracted with ether (3 × 75 ml). The combined ether extracts were washed with water (3 × 50 ml) and dried over magnesium sulphate. The product obtained after evaporation of the solvents under reduced pressure was recrystallized from ethanol–ligroin to afford 1-(2,4,6-trimethoxyphenyl)-butane-1,3-dione (0.876 g, 37%); mp 102–104 °C; ir 1650–1560 cm^{-1}; nmr δ 2.11 (s, 2, terminal methyl group in enol tautomer), 2.26 (s, 1, terminal methyl group in keto tautomer), 3.8 (m, ~10, methoxy group protons and methylene protons of keto tautomer), 5.74 (s, 0.66, vinyl proton of enol tautomer), 6.15 (2s, 2 total, aromatic protons in keto and enol tautomers); uv 295 nm (15 200); ms *m/e* 252(15), 221(40), 196(13), 195(100), 168(19), 167(15), 165(15), 153(10), 137(10), 70(12), 61(12). *Anal.* calcd. for $C_{13}H_{16}O_5$: C 61.90, H 6.39; found: C 61.79, H 6.40.

The base insoluble portion of the product mixture from the above reaction (still in ether) was washed with water (3 × 50 ml) and dried over magnesium sulphate. The mixture obtained after the solvents were removed under reduced pressure was recycled twice following the same procedure as outlined above. This resulted in an overall yield of 55% from the original 2,4,6-trimethoxyacetophenone.

2-(3,5-Dimethoxy-4-(4,6-dioxo-2-hydroxy-6-2′,4′,6′-trimethoxyphenylhex-2-yl)phenyl)-2-methylpropionitrile ***14***

This compound was prepared following the procedure employed in the preparation of 5-hydroxyl-1-phenyl-5-(2,4,6-trimethoxyphenyl)hexane-1,3-dione **12**. The following reagents were used: isopropylcyclohexylamine (720 mg, 5.11 mmol), *n*-butyllithium in hexane (2.15 ml, 2.50 *M*, 5.36 mmol), 1-(2,4,6-trimethoxyphenyl)butane-1,3-dione (630 mg, 2.50 mmol) and 2-(4-acetyl-3,5-dimethoxyphenyl)-2-methylpropionitrile **7** (124 mg, 0.502 mmol) in dry THF (30 ml total volume). The product was separated from unreacted dione by preparative tlc on silica gel. The plates were developed with a mixture of carbon tetrachloride and ether (1:1 v/v). The band lying at R_f 0.4–0.6 was removed and extracted with chloroform. Evaporation of the solvent under reduced pressure afforded unreacted dione (395 mg, 78% of theoretical excess). No unreacted **7** was observed on the plates. Extraction of the band lying at R_f 0.1–0.2 afforded **14** (252 mg, 100%) as a clear oil; ir 3550, 2255, 1650–1560 cm^{-1}; nmr δ 1.55, 1.77, 1.70 (3s, 9 total, carbinol carbon methyl group protons in enol and keto tautomers and *gem*-dimethyl group protons respectively), 2.6–3.4 (m, 2, protons on methylene group α to carbinol carbon in enol and keto tautomers), 4.8 (several s, 15 total, methoxy group protons), 5.72 (s, <1, vinyl proton of enol tautomer), 6.15 (s, 2, protons on trimethoxyphenyl ring), 6.71 (s, 2, protons on dimethoxyphenyl ring); uv 285–310 nm (broad) (8650); ms (*a*) low resolution *m/e* 499(2), 481(4), 468(5), 252(45), 248(32), 232(32), 221(48), 197(10), 196(15), 195(100), 168(15), 161(9); (*b*) high resolution calcd. for $C_{27}H_{33}O_8N$ (amu): 499.220; found (*m/e*): 499.220.

2-(3,5-Dimethoxy-4-(4,6-dioxo-6-2′,4′,6′-trimethoxyphenylhex-1-en-2-yl)phenyl)-2-methylpropionitrile ***15***

Boron trifluoride etherate (~1 ml) was added to a stirred solution of **14** (232 mg, 0.465 mmol) in anhydrous

ether (20 ml). A precipitate which formed during the addition dissolved in 2 min. After 20 min the solution was washed with water and dried over magnesium sulphate. Evaporation of the solvents under reduced pressure afforded a crude mixture of **15** and the conjugated isomers (223 mg, 100%) as a bright orange foam; ir 2255, 1650, 1580, 1530 cm^{-1}; nmr δ 1.72 (s, 6, *gem*-dimethyl group protons), 2.23, 2.55 (2d, $J = 2$ Hz, vinyl methyl group protons in *E* and *Z* isomers), 3.3–3.9 (methylene group protons in **15** and methoxy group protons), 6.10 (s, 2, protons on trimethoxyphenyl ring), 6.66 (2s, 2, protons on dimethoxyphenyl ring), 6.0–6.7 (m, vinyl proton of **29** and vinyl proton of various enol tautomers).

2-(7-Hydroxy-5-methyl-4-methoxy-8-2′,4′,6′-trimethoxybenzoyl-2-naphthyl)-2-methylpropionitrile ***11***

A sample of the mixture of **15** and conjugated isomers (212 mg, 0.440 mmol) was dissolved in dry benzene (50 ml) and anhydrous hydrogen chloride was bubbled through the solution for 1½ h. After this time, stannic chloride (2 ml) and water (2 drops) were added and the resulting mixture was stirred at room temperature for 16 h before being poured into water (20 ml). A precipitate which had formed in the reaction flask was dissolved in chloroform (100 ml) and added to the benzene–water mixture. The organic phase was washed with water (4 × 20 ml) and dried over magnesium sulphate. Evaporation of the solvents under reduced pressure afforded 187 mg of crude product which was recrystallized from ethanol–ligroin to yield **11** (90 mg, 46%) as bright yellow crystals mp 218–220 °C. A sample was sublimed for analysis (180 °C/0.04 torr); ir 2255, 1640, 1600, 1540 cm^{-1}; nmr δ 2.70 (s, 6, *gem*-dimethyl group protons), 2.51 (s, 3, aromatic methyl group protons), 4.8 (several s, 12 total, methoxy group protons), 5.8–8.0 (several s, 5 total, aromatic protons); uv 295 (shoulder), 304 (18 000), 398 (54 400), 420 nm (shoulder); ms *m/e* 449(24), 432(28), 282(12), 267(13), 266(10), 256(23), 255(100), 242(25), 240(23), 211(12), 195(49), 180(11), 168(11), 167(10), 165(11), 152(13), 149(13), 139(16), 137(14), 115(12), 109(13), 95(13), 91(17), 85(14), 83(11), 81(17), 79(13), 77(18), 71(18), 70(11), 69(26), 67(15), 63(10), 57(52), 56(23), 55(61), 53(17), 51(16), 50(13). *Anal.* calcd. for $C_{26}H_{27}O_6N$: C 69.47, H 6.05, N 3.12; found: C 69.42, H 6.15, N 3.00.

Cyclization of ***11*** *to the Xanthone* ***19***

A 15 mg sample of **11** was dissolved in 10 ml of cold (0 °C) acetic acid containing anhydrous HCl. This reaction mixture was allowed to warm to room temperature and stirred for ½ h. The reaction mixture was poured into saturated aqueous $NaHCO_3$ and extracted with chloroform (5 × 20 ml). The extracts were combined, washed with water (2 × 10 ml), and dried over magnesium sulphate. The solvents were removed under reduced pressure to afford 13 mg of crude product which was purified by tlc on silica gel using chloroform–ether (1:1) as developing solvent. The band at R_f 0.3–0.5 was removed and extracted with chloroform to yield 8 mg of xanthone **19** as a yellow semi-solid; ir 2255, 1650, 1600 cm^{-1}; nmr δ 2.68 (s, 6, *gem*-dimethyl group protons), 2.46 (s, 3, aromatic methyl group protons), *ca.* 4.8 (three s, 9, methoxy group protons), 6–8 (several s, 5, aromatic protons); ms (*a*) low resolution *m/e* 417(65), 402(10), 349(17), 334(10), 265(27), 237(12), 180(35), 152(22), 91(20); (*b*) high resolution calcd. for $C_{25}H_{23}O_5N$ (amu): 417.1576; found (*m/e*): 417.1589.

Acknowledgment

We are grateful to the National Research Council of Canada and the University of British Columbia for financial support and to B. M. Joyce and S. Fung for experimental assistance.

1. (*a*) H. Brockmann, E. Meyer, K. Schrempp, F. Reiners, and T. Reschke. Chem. Ber. **102**, 1224 (1968); (*b*) W. Rosenbrook. J. Org. Chem. **32**, 2924 (1967).
2. N. A. Bailey, C. P. Falshaw, W. D. Ollis, M. Watanabe, M. M. Dhar, A. W. Khan, and C. V. Vara. Chem. Commun. 374 (1968).
3. H. Brockmann and G. Schmidt-Kastner. Naturwissenschaften, **38**, 479 (1951).
4. D. L. J. Clive. Q. Rev. **22**, 435 (1968).
5. A. S. Kende, Y. Tsay, and J. E. Mills. J. Am. Chem. Soc. **98**, 1967 (1976); T. M. Smith, A. N. Fujiwara, D. W. Henry, and W. W. Lee. J. Am. Chem. Soc. **98**, 1969 (1976).
6. I. C. Paul and G. A. Sim. J. Chem. Soc. 1097 (1965).
7. J. H. Richards and J. B. Hendrickson. Biosynthesis of steroids, terpenes and acetogenins. W. A. Benjamin, Inc., New York, N.Y. 1964.
8. R. Adams, S. MacKenzie, Jr., and S. Loewe. J. Am. Chem. Soc. **70**, 664 (1948).
9. (*a*) L. Weiler. J. Am. Chem. Soc. **92**, 6702 (1970); (*b*) S. N. Huckin and L. Weiler. J. Am. Chem. Soc. **96**, 1082 (1974).
10. (*a*) S. N. Huckin and L. Weiler. Tetrahedron Lett. 4835 (1971); (*b*) S. N. Huckin and L. Weiler. Can. J. Chem. **52**, 2157 (1974).
11. C. C. Sweeley, R. Bentley, M. Makita, and W. W. Wells. J. Am. Chem. Soc. **85**, 2497 (1963).
12. (*a*) J. S. Davies, V. M. Davies, and C. H. Hassall. J. Chem. Soc. C, 1873 (1969); (*b*) C. H. Hassall and B. A. Morgan. Chem. Commun. 1345 (1970); (*c*) G. M. Holmwood and J. C. Roberts. Tetrahedron Lett. 833 (1971); (*d*) C. H. Hassall and B. A. Morgan. J. Chem. Soc. Perkin Trans. I, 2853 (1973).
13. (*a*) C. S. Wood and F. B. Mallory. J. Org. Chem. **29**, 3373 (1964); (*b*) N. C. Yang, L. C. Lin, A. Shani, and S. S. Yang. J. Org. Chem. **34**, 1845 (1969); (*c*) Y. Tamura, S. Fukumori, S. Kato, and Y. Kita. Chem. Commun. 285 (1974); (*d*) M. Tada, H. Saiki, K. Miura, and H. Shinozaki. Chem. Commun. 55 (1975).
14. T. M. Harris and C. M. Harris. Org. React. **17**, 155 (1969).
15. G. Stork and M. Gregson. J. Am. Chem. Soc. **91**, 2373 (1969).
16. A. J. Kresge, S. G. Mylonakis, Y. Sato, and V. P. Vitullo. J. Am. Chem. Soc. **93**, 6181 (1971), and references therein; G. A. Olah, S. Kobayashi, and Y. K. Mo. J. Org. Chem. **38**, 4056 (1973), and references therein.
17. R. W. Skllan, G. L. Trammell, and J. D. White. Tetrahedron Lett. 525 (1976).
18. P. O. Spoerie and A. S. DuBois. Org. React. **5**, 387 (1949).

Studies on the iodide–triiodide equilibrium

ROBERT L. BENOIT, MICHAEL F. WILSON, AND SING-YEUNG LAM
Département de chimie, Université de Montréal, C.P. 6210, Montréal (Qué.), Canada H3C 3V1

Received May 25, 1976

ROBERT L. BENOIT, MICHAEL F. WILSON, and SING-YEUNG LAM. Can. J. Chem. **55,** 792 (1977).

The solvent effect on the iodide–triiodide equilibrium has been investigated by means of calorimetric and potentiometric measurements. The aprotic solvents studied were nitromethane, nitrobenzene, sulfolane, acetonitrile, propylene carbonate, acetophenone, dimethylformamide, dimethylsulfoxide, and *o*-dichlorobenzene. The resulting enthalpy and free energy changes imply that the variations of the enthalpies and free energies of transfer of the iodide and triiodide ions probably are small and that there is an important non-coulombic contribution to these transfer parameters. Values were obtained for the enthalpy of formation of two solid triiodides, which together with values for other triiodides, cast doubt on reported calculated lattice enthalpies of triiodides and formation enthalpy of I_3^- ion in the gas phase. This latter formation enthalpy is found to be, from our solution data, more negative than -22 kcal mol^{-1}.

ROBERT L. BENOIT, MICHAEL F. WILSON et SING-YEUNG LAM. Can. J. Chem. **55,** 792 (1977).

On a étudié l'effet de solvant sur l'équilibre iodure–triiodure au moyen de déterminations calorimétriques et potentiométriques. Les solvants aprotoniques considérés incluent le nitrométhane, le nitrobenzène, le sulfolane, l'acétonitrile, le carbonate de propylène, l'acétophénone, le diméthylformamide, le diméthylsulfoxyde et l'*o*-dichlorobenzène. Les changements d'enthalpie et d'énergie libre observés impliquent des variations vraisemblablement faibles pour les enthalpies et énergies libres de transfert des ions iodures et triiodures et une composante non-coulombienne importante pour ces grandeurs de transfert. On a obtenu des valeurs de l'enthalpie de la réaction de formation de deux triiodures solides et ces valeurs jointes à celles d'autres triiodures mettent en question des valeurs publiées de l'énergie de réseau des triiodures et de l'enthalpie de formation de l'ion I_3^- en phase gazeuse. Cette dernière enthalpie de formation est, d'après nos résultats, plus négative que -22 kcal mol^{-1}.

We have recently reported thermodynamic data for an anion–molecule reaction, $Cl^-(s) + HR(s) \rightleftharpoons ClHR^-(s)$, involving hydrogen-bonding between Cl^-, a halide ion, and a series of Brønsted acids HR (1). A comparison of the enthalpy data obtained in sulfolane with gas-phase data allowed us to make a complete analysis of the solvent effect on that reaction. Another type of anion–molecule reaction of general interest is that where the molecule is an uncharged Lewis acid. We have now completed a study of such a reaction, namely

$$[1] \qquad I^-(s) + I_2(s) \rightleftharpoons I_3^-(s)$$

in a series of dipolar aprotic (dpa) solvents (s).

Association constants K for [1] have been reported for many solvents of different classes (refs. 2, 3 and references cited therein). It is generally found that K is larger for aprotic solvents than for protic solvents. These differences are qualitatively accounted for in terms of strong hydrogen-bonding interactions between I^- and the protic solvents and strong dipolar interactions between I_3^- and the dpa solvents. Values of K also vary significantly within the group of dpa solvents but apparently for another reason, *i.e.* the more basic the solvent, the stronger the interaction of the Lewis acid I_2 with the solvent and the lower the value of K.

In the present work we have tried to assess more completely the solvent effect on the iodide–triiodide equilibrium by determining first the enthalpy change $\Delta H(s, c)$[1] for

$$[2] \qquad I^-(s) + I_2(c) \rightleftharpoons I_3^-(s)$$

The solvents studied include the dpa solvents, nitromethane (NM), nitrobenzene (NB), sulfolane (TMS), acetonitrile (AN), propylene carbonate (PC), acetophenone (AP), dimethylformamide (DMF), dimethylsulfoxide (DMSO), and also *o*-dichlorobenzene (DCB). An attempt was made to estimate for some of these solvents, the free energy of transfer[1] for the single ions I^- and I_3^-, from potentiometric measurements on the redox system I^-/I_3^-, together with the

[1]The thermodynamic functions can be approximated to ΔH^0 and ΔG^0 considering the dilute solutions used and the nature of the reaction.

aid of some extrathermodynamic assumptions. Calorimetric measurements were also carried out to evaluate, through thermodynamic cycles, the enthalpy changes ΔH(c) for

[3] $$MI(c) + I_2(c) \rightleftharpoons MI_3(c)$$

(where M^+ is tetramethyl and tetrabutylammonium ions) and ΔH(g) for the gas phase reaction

[4] $$I^-(g) + I_2(g) \rightleftharpoons I_3^-(g)$$

These enthalpy changes were then compared with values calculated from emf measurements of solid-state galvanic cells (4).

Experimental

Materials

Sulfolane (Shell) was purified according to a method given earlier (1). Spectroanalytical grade DMSO (Fisher) and reagent grade DMF (Anachemia) were treated with 4A molecular sieves heated to 200 °C, decanted, and then distilled. PC (Aldrich) was doubly distilled at a temperature below 100 °C and a pressure less than 10 mm Hg; only the middle portion of the distillate was collected. AP (Matheson, Coleman, and Bell) was crystallised twice by freezing, followed by distillation under vacuum. Baker analysed NB and spectrochemical grade NM (M, C, and B) were dried with 4A molecular sieves. Reagent grade AN and DCB (Eastman) were used as received. Residual water[2] in the solvents was found to be between 0.002 and 0.02 *M* as determined by Karl Fischer titration.

Tetramethylammonium and tetrabutylammonium iodides (Me_4NI and Bu_4NI) were obtained from Eastman. The corresponding triiodide salts were synthesized by equilibrating stoichiometric amounts of the appropriate iodide and iodine under vacuum for 3 days at 70 and 40 °C for the tetramethylammonium and tetrabutylammonium salts respectively; the method was according to Topol (4). Baker analytical reagent iodine was used as purchased. Tetraethylammonium picrate (Et_4NPic) was prepared according to the method of Coetzee and Padmanabhan (5).

Calorimetry

The apparatus and calorimetric procedure used have been described in an earlier publication (6). The heats of solution of various amounts of solid iodine in 27 ml of 0.05 *M* Bu_4NI solution in the solvents (0.01 *M* Me_4NI solution in DMF) were determined at 25 °C (30 °C in the case of TMS as solvent). Molar concentration ratios of I_2 to I^- were between 0.1 and 0.9. Measurements of the heats of solution of Bu_4NI in DMF and Bu_4NI_3 in DMF and DMSO were also carried out at salt concentrations between 0.001 and 0.01 *M*. In all cases, at least three determinations were made for each reaction. Dissolving solid iodine in the solvents containing R_4NI took usually less than 10 min except in the case of TMS and NM (30 min).

Potentiometric Measurements

Electromotive force measurements were carried out using the following cell

[5]

−						+
	Bu_4NI (10^{-2} *M*)		Et_4NPic (10^{-1} *M*)	Bu_4NI (10^{-2} *M*)		
Pt	Bu_4NI_3 (10^{-2} *M*)	‖	in PC	Bu_4NI_3 (10^{-2} *M*)		Pt
	in PC			in solvent s		

The assembly was contained in a water jacketted glass vessel thermostated at 25.0 °C (30.0 °C in the case of TMS). The potentiometric measurements were made with a Tacussel-Aries 10000 potentiometer with digital readout. The Et_4NPic bridge was selected in order to eliminate the liquid junction potential (7). Measurements, made after 10 min to allow the system to equilibrate, were reproducible within 3 mV or less. Readings drifted 1–3 mV over a subsequent 15 min period. The effect of light catalyzed oxidation of I^- was assumed to be minimal in these 'redox buffered' solutions under our experimental conditions.

Results

Calorimetry

The heats of solution of solid iodine ΔH(s,c) in the dpa solvents containing 0.05 *M* Bu_4NI, as represented by [2], are listed in Table 1; the mean experimental value for each reaction is given. The completeness of [2] under our experimental conditions results from the values of $K \geq 10^5$ (3) and is evidenced for each solvent by the constancy within 0.1–0.2 kcal mol^{-1} of the heats of solution per mole of I_2 added. The results of Hepler and co-workers (8) for the same reaction in water are also included in Table 1.

The heats of solution determined for Me_4NI_3, Bu_4NI, and Bu_4NI_3 in DMF, and Bu_4NI_3 in DMSO together with literature values are given in Table 2. These heats of solution were combined with our values of ΔH(s,c) both in DMF and DMSO to yield, by means of a simple thermodynamic cycle, the ΔH(c) values for [3]

[2]On the basis of our results on the hydration of anions in dpa solvents (22) the hydration of the large ions I^- and I_3^- and hence the effect of residual water on [1] are assumed to be negligible considering the relative concentrations involved.

TABLE 1. Enthalpy changes (kcal mol^{-1}) at 25 °C for reactions and ion transfers in aprotic solvents and water

Reaction	Enthalpy change	Solvent									
		PC	DMSO	AN	DMF	TMS*	NB	NM	AP	DCB	H_2O†
$I^-(s) + I_2(c) \rightleftarrows I_3^-(s)$	ΔH(s,c)	−7.05	−6.0	−5.1	−7.25	−7.55	−7.1	−4.4	−8.5	−7.3	+1.35
$I_3^-(PC) + I^-(s) \rightleftarrows I_3^-(s) + I^-(PC)$	$\Delta\Delta H$(s,c)	0	+1.05	+1.95	−0.2	−0.5	−0.05	+2.6	−1.5	−0.25	+8.4
$I^-(PC) \rightleftarrows I^-(s)$	ΔH(PC→ s) (I^-) ‡	0	−3.0	−1.5	−3.1	−1.9					
	§	0	+0.7		−0.6	+0.4					
	‖	0	−2.0	+0.4	−3.3	−2.4					
$I_3^-(PC) \rightleftarrows I_3^-(s)$	ΔH(PC→ s) (I_3^-)§	0	+0.5		−0.4	+0.3					

*30 °C.
†Reference 8.
‡Calculated from ref. 10.
§Calculated from values of ΔH derived from Born equation (see text) with $r_{I^-} = 2.2$ Å and $r_{I_3^-} = 3.0$ Å.
‖Calculated from ΔH(PC→ s) (I^-) and ΔH(s,c).

listed in Table 2. A ΔH(c) value obtained by Topol (4) from emf measurements on a solid-state cell is also included.

Electromotive Force Measurements

The redox system to be considered in order to calculate the emf of the cell represented by [5] is

[6] $$I_3^- + 2e \rightleftarrows 3I^-$$

Since the concentrations of iodide and triiodide are the same at both electrodes, the overall emf of the cell, ΔE, is given as

[7] $$\Delta E = E_j + 0.0296 \log {}^{PC}\gamma^s_{I_3^-} - 0.0888 \log {}^{PC}\gamma^s_{I^-}$$

where E_j is the liquid junction potential and $\log {}^{PC}\gamma_i^s$ the medium effect for the transfer of the single ionic species i from PC to solvent s. $\Delta G(i)$ and $\log \gamma_i$ are related by

[8] $$\Delta G(PC \rightarrow s)(i) = RT \ln {}^{PC}\gamma_i^s$$

Table 3 presents our observed emf values ΔE which are related to free energies of transfer of I_3^- and I^- through eqs. 7 and 8 if E_j is known.

Discussion

First we will discuss the solvent effect on the iodide–triiodide equilibrium as deduced from our calorimetric results. The data in Table 1 show that while ΔH(s,c) is endothermic in water, it is, as expected, exothermic in the aprotic solvents, but the variations between the dpa solvents are relatively small. We also note that for three out of the four solvents NB, NM, AP, and DCB where ion-pair formation is either partial or extensive, ΔH(s,c) is not very different from the values for the more dissociating aprotic solvents. The enthalpy change ΔH(s) for reaction 1 could be deduced from our ΔH(s,c) values by subtracting the generally endothermic heat of solution of solid iodine in the solvents (9). However, by comparing our values of ΔH(s,c) for reaction 2, rather than ΔH(s), we simplify the interpretation of the solvent effect on the I^-–I_3^- equilibrium by eliminating the basicity-related solvent influence on I_2 (9). This becomes apparent when we calculate $\Delta\Delta H$(s,c), the difference between the values of ΔH(s,c) for the solvent s and for PC taken as reference solvent:

[9] $$\Delta\Delta H(s,c) = \Delta H(s,c) - \Delta H(PC,c) = \Delta H(PC \rightarrow s)\,(I_3^-) - \Delta H(PC \rightarrow s)\,(I^-)$$

TABLE 2. Enthalpy changes (kcal mol^{-1}) at 25 °C for reaction $R_4NI(c) + I_2(c) \rightleftharpoons R_4NI_3(c)$

Reaction	Phase	Enthalpy change
$Me_4NI_3(c) \rightleftharpoons Me_4N^+(s) + I_3^-(s)$	DMF	$\Delta H_s = -2.27$
$Me_4NI(c) \rightleftharpoons Me_4N^+(s) + I^-(s)$	DMF	$\Delta H_s = +4.0$*
$Me_4NI(c) + I_2(c) \rightleftharpoons Me_4NI_3(c)$	Solid	$\Delta H(c) = -1.0$
		$\Delta H(c) = -1.7$†
$Bu_4NI_3(c) \rightleftharpoons Bu_4N^+(s) + I_3^-(s)$	DMF	$\Delta H_s = +9.2$
$Bu_4NI(c) \rightleftharpoons Bu_4N^+(s) + I^-(s)$	DMF	$\Delta H_s = +3.9$
$Bu_4NI(c) + I_2(c) \rightleftharpoons Bu_4NI_3(c)$	Solid	$\Delta H(c) = -12.5$
$Bu_4NI_3(c) \rightleftharpoons Bu_4N^+(s) + I_3^-(s)$	DMSO	$\Delta H_s = +12.8$
$Bu_4NI(c) \rightleftharpoons Bu_4N^+(s) + I^-(s)$	DMSO	$\Delta H_s = +7.3$‡
$Bu_4NI(c) + I_2(c) \rightleftharpoons Bu_4NI_3(c)$	Solid	$\Delta H(c) = -11.6$

*Reference 20.
†Reference 4.
‡Reference 21.

TABLE 3. Electromotive force values (V) for cell [5] and free energies of transfer for I^- and I_3^- (kcal mol^{-1}) at 25 °C

		$\Delta G(PC \rightarrow s)(I^-)$		$\Delta G(PC \rightarrow s)(I_3^-)$	
Solvents	ΔE*	Ref. 10†	Born equation‡	Equation 7§	Born equation‡
DMSO	−0.034	−2.0	+0.4	−7.6	+0.3
DMF	−0.074	+0.3	+0.9	−2.5	+0.7
TMS‖	−0.029	+0.7	+0.7	+0.8	+0.5
AN	−0.002	+0.3	+0.8	+0.8	+0.6
NM	+0.030				
NB	−0.064				
AP	−0.112				

*Cell [5].
†Calculated from ref. 10.
‡Calculated from values of ΔG derived from Born equation (see text) with $r_{I^-} = 2.2$ Å and $r_{I_3^-} = 3.0$ Å.
§Calculated from $\Delta G(PC \rightarrow s)(I^-)$ and eq. 7 with $E_j = 0$.
‖30 °C.

where $\Delta H(PC \rightarrow s)(i)$ is the enthalpy of transfer of the species i from PC to s.

Now when we compare these latter $\Delta\Delta H(s,c)$ values in Table 1 we face the difficult problem of assessing ionic solvation effects from data on a pair of ions, in our case on two anions I^-, I_3^-. The problem is not unlike that met when trying to separate heats of solution of salts M^+A^- into cationic and anionic contributions. The relatively small variations (less than 2.5 kcal mol^{-1}) of $\Delta\Delta H(s,c)$, *i.e.* the difference between the enthalpies of transfer of I_3^- and I^- is most simply accounted for by assuming that the single anions enthalpies of transfer are also small, at least for the solvents PC, DMSO, AN, DMF, and TMS. This point of view is supported by similarly small changes for the enthalpies of transfer of two more anion pairs, Cl^-,$SbCl_6^-$ (13) and Cl^-,$ClHR^-$ (7), pairs whose components are quite dissimilar. Some single anion enthalpies of transfer obtained by using the tetraphenylarsoniumtetraphenylborate (tatb) extrathermodynamic assumption (10) and given in Table 1 indicate somewhat larger variations (up to 3.3 kcal mol^{-1}). However, such single ion enthalpies of transfer carry appreciable errors coming from the many experimental steps involved in their calculation. For example from different but carefully obtained experimental data, Arnett and McKelvey (11) and Parker and co-workers (10) calculated $\Delta H(H_2O \rightarrow DMSO)$ (I^-) values to be, respectively, −2.52 and −3.23 kcal mol^{-1}. Our values for $\Delta H(PC \rightarrow s)$ (I_3^-) − $\Delta H(PC \rightarrow s)$ (I^-) are on the contrary obtained in one experimental step. We can next show that these values are not governed by coulombic interactions. An expression can be derived, from the Born equation, giving values for $\Delta H(PC \rightarrow s)$

(*i*), the enthalpy of transfer of ion *i* from PC to solvent s (12). We have given in Table 1 (line §) the ΔH(PC → s) values calculated for I^- and I_3^-. The differences deduced for ΔH(PC → s)(I_3^-) − ΔH(PC → s)(I^-) can then be shown to be at variance with our experimental values, the sign of the difference being even opposite for transfers to DMSO and DMF. A similar state of affair prevails for the enthalpies of transfer of another anion pair Cl^-,$SbCl_6^-$ (13). It would therefore seem that the non-coulombic contribution to the anionic enthalpies of transfer between dpa solvents plays an important part.

Next, we consider briefly the solvent effect on the iodide–triiodide equilibrium as deduced from our emf determinations. The interpretation of the ΔE values for cell [5], reported in Table 3, in terms of free energies of transfer by means of eqs. 7 and 8 is more difficult than in the case of the calorimetric data. First, eq. 7 shows that there are different coefficients affecting the transfer of I^- and I_3^-. Second, there is the problem of estimating E_j. Parker (*7b*) in his studies on ionic solvation in dpa solvents found good agreement between six quite different sets of extrathermodynamic assumptions and recommended the assumption that there was negligible liquid junction potential in a cell composed of silver electrodes in two dissimilar solvents linked by a 0.1 *M* Et_4NPic bridge in either solvent. With this assumption $E_j = 0$ in eq. 7, we have deduced ΔG(PC → s)(I_3^-) using eq. 7 and values of ΔG(PC → s)(I^-) calculated from the data of Parker and co-workers (10). These free energies of transfer listed in Table 3 can be compared with values calculated from an expression, derived from the Born equation, giving values for ΔG(PC → s)(*i*) (11). Just as was the case for the ionic enthalpies of transfer, the agreement is poor between the Born derived values and the experimental values. A further interpretation of transfer parameters would require the knowledge of the corresponding parameter for an uncharged analog of I^- and I_3^-, since the non-coulombic contribution to the transfer energy must be important. This latter point can be clearly seen by comparing the significant differences between ΔG or ΔE values for DMF and AN, two solvents selected for their nearly identical dielectric constant 36.7 and 38.8, respectively.

Our enthalpy data can be used to calculate enthalpy changes ΔH(c) and ΔH(g) for the formation of triiodides, respectively in the solid phase [3] and gas phase [4]. These ΔH(c) and ΔH(g) values are then compared with previously reported data. First, our calculated ΔH(c) for $M^+ = Me_4N^+$ in Table 2, is in fair agreement with a value determined from variations with temperature of emf of solid-state cells (4). Our values for $M^+ = Bu_4N^+$ calculated respectively from measurements in DMF and DMSO are reasonably close considering the many steps involved. We can then combine our values of ΔH(c) for [3] with those of Topol (4, 14) to consider the influence on ΔH(c) of the radius r_+(Å) of the cation M^+. The ΔH(c) values (kcal mol^{-1}) for MI(c) + I_2(c) ⇌ MI_3(c) are as follows: −2.1, NH_4^+ (r_+ = 1.43); −3.1, Rb^+ (r_+ = 1.48); −3.7, Cs^+ (r_+ = 1.68); −1.0, Me_4N^+ (r_+ = 3.0); and −12.0, Bu_4N^+ (r_+ = 5.0). It is clear that the exothermicity of ΔH(c) does not increase smoothly with r_+ which is contrary to what is expected from the Kapustinskii equation (15). The use of this equation by others (4, 16), in the calculation of $U(MI_3)$ (and possibly U(MI) when M is an alkylammonium ion) is then open to criticism.

We can at this point discuss the values of the enthalpy change ΔH(g) for [4] estimated (4) from values of ΔH(c) and lattice energies of MI and MI_3 calculated from a form of the Kapustinskii equation. By using his ΔH(c) values for $M^+ = Rb^+$ and Cs^+ with r_{I^-} = 2.25 Å, Topol calculated an effective radius $r_{I_3^-}$ = 2.45 Å and the lattice energies $U(RbI_3)$ and $U(CsI_3)$. From these latter values, U(RbI), U(CsI), and the experimental values of ΔH(c), Topol obtained an enthalpy change of −9.1 kcal mol^{-1} for I^-(g) + I_2(c) ⇌ I_3(g) and finally ΔH(g) = −24.0 kcal mol^{-1}. However, the lattice enthalpy $U(CsI_3)$ = 137.7 kcal mol^{-1} used by Topol differs from an older value $U(CsI_3)$ = 118 calculated by Halliwell and Nyburg (16) from the Kapustinskii equation but this time with $r_{I_3^-}$ = 3.0 Å. It is surprising that both previous authors note a good agreement between their different values for $r_{I_3^-}$ and the same set of crystallographic data (17). The latter value of $U(CsI_3)$ leads to ΔH(g) = −44 kcal mol^{-1}, *i.e.* a value 20 kcal mol^{-1} more exothermic than Topol's value. It would thus seem that such values of ΔH(g) involving the use of the Kapustinskii equation are not reliable. We have therefore calculated a limit for ΔH(g) from our enthalpies of reaction ΔH(s,c). Taking from Table 1, ΔH(s,c) = −7.5 kcal mol^{-1} for the

solvent TMS, we obtain a ΔH(s,g) value of $-7.5 - 14.9 = -22.4$ kcal mol^{-1} for the reaction $I^-(s) + I_2(g) \rightleftharpoons I_3^-(s)$. This value represents a limit for ΔH(g) since the enthalpy of solvation of I_3^- is likely to be less exothermic than that of I^-. The real value of ΔH(g) may, however, be considerably more exothermic than -22.4 kcal mol^{-1}. Such a situation has been discussed previously (6) for a similar reaction leading to the formation of hydrogen dichloride ion. Another way of estimating ΔH(g) would be to use an argument similar to that advanced by McDaniel and Vallee (18), *i.e.* that ΔH(c) for [3] should tend towards ΔH(g) in eq. 10 when r_+ is large, because $U(MI) - U(MI_3)$ then tends towards 0. Although this argument is open to criticism, since we have seen that ΔH(c) does not vary smoothly with r_+, using $\Delta H(c) = -12.0$ kcal mol^{-1} for Bu_4N^+ would lead to a limiting value for $\Delta H(g) = -12.0 - 14.9 = -26.9$ kcal mol^{-1}. Finally, a theoretical value has also been calculated for ΔH(g) using a modified Hückel procedure (19). The formation energy thus found for I_3^- with respect to the reactants in free state is 2.1 kcal mol^{-1}, a value which is at odds with the limits set above.

Acknowledgement

The financial assistance of the National Research Council of Canada is gratefully acknowledged.

1. S. Y. Lam, C. Louis, and R. L. Benoit. J. Am. Chem. Soc. **98**, 1156 (1976).
2. A. I. Popov. *In* Halogen chemistry. Vol. I. *Edited by* V. Gutmann. Academic Press, New York, N.Y. 1967.
3. (*a*) R. L. Benoit. Inorg. Nucl. Chem. Lett. **4**, 723 (1968); (*b*) R. L. Benoit and C. Louis. Inorg. Nucl. Chem. Lett. **6**, 817 (1970).
4. L. E. Topol. Inorg. Chem. **10**, 736 (1971).
5. J. F. Coetzee and G. R. Padmanabhan. J. Phys. Chem. **66**, 1708 (1962).
6. R. L. Benoit, M. Rinfret, and R. Domain. Inorg. Chem. **11**, 2603 (1972).
7. (*a*) B. G. Cox, A. J. Parker, and W. E. Waghorne. J. Am. Chem. Soc. **95**, 1010 (1973); (*b*) R. Alexander, A. J. Parker, J. H. Sharp, and W. E. Waghorne. J. Am. Chem. Soc. **94**, 1148 (1972).
8. C. S. Wu, M. M. Birky, and L. G. Hepler. J. Phys. Chem. **67**, 1202 (1963).
9. R. L. Benoit and C. Louis. *In* The chemistry of non-aqueous solvents. Vol. V. *Edited by* J. J. Lagowski. Academic Press, New York, N.Y. In press.
10. B. G. Cox, G. R. Hedwig, A. J. Parker, and D. W. Watts. Aust. J. Chem. **27**, 477 (1974).
11. E. M. Arnett and D. R. McKelvey. J. Am. Chem. Soc. **88**, 2598 (1966).
12. G. Choux and R. L. Benoit. J. Am. Chem. Soc. **91**, 6221 (1969).
13. R. Domain, M. Rinfret, and R. L. Benoit. Can. J. Chem. **54**, 2101 (1976).
14. L. E. Topol. Inorg. Chem. **7**, 451 (1968).
15. D. A. Johnson. Some thermodynamic aspects of inorganic chemistry. Cambridge University Press, Cambridge. 1968.
16. (*a*) H. F. Halliwell and S. C. Nyburg. Trans. Faraday Soc. **59**, 1126 (1963); (*b*) H. F. Halliwell and S. C. Nyburg. J. Chem. Soc. 4603 (1960).
17. H. A. Tasman and K. H. Boswijk. Acta Crystallogr. **8**, 59 (1955).
18. D. H. McDaniel and R. E. Vallee. Inorg. Chem. **2**, 996 (1963).
19. E. H. Wiebenga and D. Kracht. Inorg. Chem. **8**, 738 (1969).
20. O. N. Bhatnagar and C. M. Criss. J. Phys. Chem. **73**, 174 (1969).
21. C. V. Krishnan and H. L. Friedman. J. Phys. Chem. **73**, 3934 (1969).
22. R. L. Benoit and S. Y. Lam. J. Am. Chem. Soc. **96**, 7385 (1974).

Comment: A problem in extracting structure information from the temperature of maximum density for aqueous solutions

JAMES R. KUPPERS

Department of Chemistry, The University of North Carolina at Charlotte, Charlotte, NC 28223

Received September 26, 1976

JAMES R. KUPPERS. Can. J. Chem. **55**, 798 (1977).

The shift in the temperature of maximum density for aqueous solutions customarily has been dissected into an *ideal* and a *structural* contribution. This analysis demonstrates that the dissection leads to the formulation of an *ideal* state which is attained by a fortuitous superposition of temperature dependent properties of pure components and, hence, cannot serve as a reliable reference state for comparing the influence of different solutes upon solution structure.

JAMES R. KUPPERS. Can. J. Chem. **55**, 798 (1977).

Le déplacement dans la température de densité maximum de solutions aqueuses est généralement disséqué en termes de contributions idéale et structurale. Cette analyse démontre que cette dissection conduit à la formulation d'un état idéal qui peut être obtenu par une superposition fortuite de propriétés des composants purs qui dépendent de la température et qu'ainsi il ne peut pas servir comme état de référence adéquat pour comparer l'influence de différents solutés sur la structure de la solution.

[Traduit par le journal]

The shift in the temperature of maximum density, TMD, of a water solution relative to that of pure water is given by the relation of Wada and Umeda (1)

$$[1] \quad \Delta\theta = -1/(1-x)2\beta V_1^*[x\alpha V_2^0 + \partial\Delta V^M/\partial T]$$

where x is the mole fraction of solute, α is the thermal coefficient of expansion of pure solute (assumed to be constant over the temperature range considered), β is the coefficient in the parabolic relation to temperature of the molar volume of water in the vicinity of 3.98 °C, V_2^0 is the molar volume of pure solute at 0 °C, V_1^* is the molar volume of water at 3.98 °C, and ΔV^M is the excess volume of mixing.

It has been assumed (1–4) that $\Delta\theta$ could be decomposed into an 'ideal' term and a 'structural' term such that $\Delta\theta = \Delta\theta_I + \Delta\theta_{st}$, where

$$[2] \quad \Delta\theta_I = -x\alpha V_2^0/(1-x)2\beta V_1^*$$

and

$$[3] \quad \Delta\theta_{st} = -(\partial\Delta V^M/\partial T)/(1-x)2\beta V_1^*$$

The 'ideal' state inferred by this decomposition is one in which ΔV^M is not necessarily zero but one in which it remains constant over some finite temperature range. In order that a solution satisfy the proposed criterion for 'ideality' it is not sufficient that $\partial\Delta V^M/\partial T$ be zero at just one specified temperature. To do so would be analogous to identifying conditions under which the compressibility factor of an imperfect gas is unity.

To further clarify this issue let us examine in detail the necessary consequences of assuming that $\Delta\theta_{st} = 0$ signifies that the solute has no influence upon the structure of water near its TMD, and then determine whether or not these consequences are consistent with our special concepts of 'ideality' of mixing. Suppose that $\Delta\theta_{st} = 0$ for a particular solute over a small finite range of concentration. This implies that $\partial\Delta V^M/\partial T$ must be zero at any concentration within this range. Now recall that

$$[4] \quad \Delta V^M = V - xV_2 - (1-x)V_1$$

where V_1, V_2, and V are the molar volumes of pure solute, pure solvent, and solution, all at some specified temperature. Furthermore

$$[5] \quad \partial\Delta V^M/\partial T = \partial V/\partial T - (1-x)(\partial V_1/\partial T) - x(\partial V_2/\partial T)$$

If we now apply eq. 5 at the TMD, then $\partial V/\partial T = 0$, and it is immediately revealed that $\partial\Delta V^M/\partial T$ at the TMD is uniquely determined by $\partial V_1/\partial T$ and $\partial V_2/\partial T$, which are properties of the pure components. However, the values to be assigned these quantities will depend upon the TMD. Note that $\partial V_1/\partial T$ and $\partial V_2/\partial T$, both functions

of temperature, were made implicit functions of concentration when $\partial V/\partial T$ was set equal to zero, *i.e.* for a given concentration of a particular solute there is a unique temperature at which the solution possesses its maximum density. Moreover, if we require that eq. 5 be set equal to zero then

$$[6] \qquad (1 - x)(\partial V_1/\partial T) = -x(\partial V_2/\partial T)$$

and if eq. 6 is required to hold over any finite range of concentration it demands a most unusual thermal expansibility for the pure solute.

This result is sufficient grounds for rejecting $\Delta\theta_{st}$ as a completely reliable indicator of solution structuring.

Having demonstrated that $\partial\Delta V^M/\partial T$ at the TMD can be calculated from the properties of the pure components, it follows immediately that, if β is sufficiently insensitive to temperature, $\Delta\theta_{st}$ can be also. Of course, this is not the method used previously for computing $\Delta\theta_{st}$. Instead, $\Delta\theta_I$ was calculated, with the assumption that α and β were constant, then subtracted from the measured $\Delta\theta$ to give $\Delta\theta_{st}$. By this artifact a $\Delta\theta_{st}$ was obtained which could be correlated with other indices to nonideality of mixing. Although $\Delta\theta_{st}$ undoubtedly contains information regarding solution structure, it cannot tell us more than $\Delta\theta$ itself.

There is still no reason to question the validity of eq. 1 provided the possible temperature dependence of α and β are recognized. Furthermore, it provides a means for calculating a fundamental thermodynamic property of the solute, $\partial\phi/\partial T$, the apparent molal expansibility of the solute at the TMD.

$$[7] \qquad \Delta\theta = -x/(1 - x)2\beta V_1^*(\partial\phi/\partial T)$$

Also, by extrapolating measured values of $\Delta\theta/x$ to infinite dilution, one may obtain a value of the partial molal expansibility of the solute at 3.98 °C, a potentially meaningful indicator of solution structural properties (5). The apparent molal expansibility of solutes in aqueous solution was used earlier as an index of the structural interaction of solutes with water (6).

1. G. WADA and S. UMEDA. Bull. Chem. Soc. Jpn. **35**, 646 (1962); **35**, 1797 (1962).
2. F. FRANKS and B. WATSON. Trans. Faraday Soc. **63**, 329 (1967).
3. A. J. DARNELL and J. GRAYSON. J. Phys. Chem. **72**, 3021 (1968).
4. D. D. MACDONALD and J. B. HYNE. Can. J. Chem. **54**, 3073 (1976).
5. J. R. KUPPERS. J. Phys. Chem. **78**, 1041 (1974); **79**, 2105 (1975).
6. J. L. NEAL and D. A. I. GORING. J. Phys. Chem. **74**, 658 (1970).

Reply to comment: "A problem in extracting structure information from the temperature of maximum density for aqueous solutions"

DIGBY D. MACDONALD

Department of Chemistry, University of Calgary, Calgary, Alta., Canada T2N 1N4

Received November 23, 1976

DIGBY D. MACDONALD. Can. J. Chem. **55**, 800 (1977).

The arguments presented by Kuppers in the preceding paper on the use of the temperature of maximum density parameters $\Delta\theta$ and $\Delta\theta_{st}$ for the analysis of the effect of solutes on the structure of water are critically examined. The validity of these arguments is challenged on both theoretical and experimental grounds. In particular, the proper choice of the standard state is stressed, and it is demonstrated that $\Delta\theta_{st}$ contains structural information which cannot be extracted from $\Delta\theta$ directly.

DIGBY D. MACDONALD. Can. J. Chem. **55**, 800 (1977).

On examine d'une façon critique les arguments présentés par Kuppers, dans la publication précédente, sur l'utilisation des paramètres de température de densité maximum $\Delta\theta$ et $\Delta\theta_{st}$ pour l'analyse de l'effet des solutés sur la structure de l'eau. Utilisant une base théorique et expérimentale on met en doute la validité de ces argumentations. En particulier, on met en relief l'importance de faire le choix approprié de l'état de référence et on démontre que $\Delta\theta_{st}$ contient une information structurale qui ne peut pas être obtenue directement à partir de $\Delta\theta$.

[Traduit par le journal]

In the preceding paper Kuppers (1) presents an analysis of the effect of solutes on the temperature of maximum density (TMD) of aqueous solutions, and claims that the structural component of the shift in the TMD of a real system, $\Delta\theta_{st}$, cannot yield more information as to the influence of solutes on the structure of water than can the observed shift, $\Delta\theta$, itself. The purpose of this communication is to present a critical examination of Kuppers' arguments, and to emphasise our previous claim (2) that the structure-selective parameter, $\Delta\theta_{st}$, *does* yield structural information which cannot be obtained directly from the undissected parameters, $\Delta\theta$.

Kuppers states that "it has been assumed that $\Delta\theta$ could be decomposed into an 'ideal' term and a 'structural' term such that $\Delta\theta = \Delta\theta_I + \Delta\theta_{st}$, . . .". Furthermore, he states that "the ideal state inferred by this decomposition is one in which ΔV^M is not necessarily zero but one in which it remains constant over some finite temperature range" (see eq. 1, preceding paper). However, by definition a thermodynamically ideal mixture is characterised by a zero ΔV^M at all temperatures, *i.e.* $(\partial\Delta V^M/\partial T) = 0$, in which case $\Delta\theta = \Delta\theta_I$. Therefore, the thermodynamically ideal system satisfies the criteria for the standard state as dictated by eq. 1 of the preceding paper. It is important to note that this definition of the standard state is independent of the composition of the system, *i.e.* both ΔV^M and its temperature dependence are *zero at all solute concentrations.* According to Kuppers, a system which is characterised by $(\partial\Delta V^M/\partial T) = 0$, but $\Delta V^M \neq 0$, is also an acceptable standard state. However, this would be analogous to stating that an acceptable standard state for aqueous HCl at 25 °C is a 1.2 *M* solution because the activity (not the activity coefficient) is equal to one at this concentration. If this were so, then each solute would be characterised by a unique standard state! Accordingly, the limited criteria suggested by Kuppers are not acceptable for defining the standard state of a liquid mixture. Interestingly enough, many structure making solutes do exhibit $\Delta\theta_{st} = 0$ at some (unique) concentration (3, 4); a behaviour which parallels that of the activity of aqueous HCl alluded to above.

The crux of Kuppers' arguments is contained in eq. 6 of the preceding paper which, he claims, "demands a most unusual thermal expansibility for the pure solute". However, this equation is better written as

$$[1] \quad (\partial V_1^0/\partial T)_{TMD} = -[x/(1-x)] \times (\partial V_2^0/\partial T)_{TMD}$$

where x is the mole fraction of solute (subscript

1) and $1 - x$ is the mole fraction of the solvent (subscript 2). The subscript TMD has been included to emphasise that the temperature to which eq. 1 above refers is the temperature of maximum density for the ideal system for a given composition (note that the TMD is a function of concentration). Work to date (3, 4) indicates that those solutes which form near ideal mixtures with water depress the temperature of maximum density (*i.e.* TMD $< 3.98\,^{\circ}C$). In this region of temperature $(\partial V_2^0/\partial T)$ is negative, and it is this unusual behaviour of the solvent (water) which is responsible for the maximum in density in the first place. Accordingly, $(\partial V_1^0/\partial T)$ is positive; a result which this author does not find "most unusual" as claimed by Kuppers.

Finally, Kuppers offers no experimental evidence to support his contention that $\Delta\theta_{st}$ cannot tell us more about the structural properties of aqueous solutions than can $\Delta\theta$ itself. On the other hand, a considerable amount of data exists which shows that those solutes which are normally regarded as water-structure makers (*e.g.* alcohols) exhibit positive $\Delta\theta_{st}$ values (as expected) even though $\Delta\theta$ may be positive or negative. Likewise, structure breakers exhibit negative $\Delta\theta_{st}$ values. This clearly demonstrates that the indexing of solutes as "structure makers" of "structure breakers" using TMD data can only be made upon the basis of $\Delta\theta_{st}$ and not upon the basis of the undissected parameter $\Delta\theta$, *i.e.* $\Delta\theta_{st}$ contains information which cannot be extracted from $\Delta\theta$ directly. The experimental evidence for the utility of $\Delta\theta_{st}$ *vs.* $\Delta\theta$ as an index of the effect of solutes on the structure of water has been examined recently by Macdonald and Hyne (2) and the reader is referred to this paper for a more detailed discussion of this subject.

1. J. R. KUPPERS. Can. J. Chem. This issue.
2. D. D. MACDONALD and J. B. HYNE. Can. J. Chem. **54**, 3073 (1976).
3. G. WADA and S. UMEDA. Bull. Chem. Soc. Jpn. **35**, 646 (1962).
4. G. WADA and S. UMEDA. Bull. Chem. Soc. Jpn. **35**, 1797 (1962).

The linear mixture formula in non-equilibrium chemical kinetics

ROBERT K. BOYD

Department of Chemistry, University College, Swansea, U.K.
and
Guelph-Waterloo Centre for Graduate Work in Chemistry, Guelph Campus, Guelph, Ont., Canada N1G 2W1

Received June 25, 1976

ROBERT K. BOYD. Can. J. Chem. **55**, 802 (1977).

The recent extensions of the 'eigenvalue approximation' of non-equilibrium kinetics proposed by Bartis and Widom to explain in a direct qualitative sense some general features of phenomenological chemical kinetics in ideal gas systems, have been used to investigate the problem of the 'linear mixture formula' applied to non-equilibrium kinetics of reactions proceeding in mixtures. For isomerization reactions in mixtures dilute in reactant, the model of Bartis and Widom, without further embellishment, has been shown to justify such an equation. Extrapolation of this result to account for recent empirical successes of a linear mixture formula in dissociation–recombination reactions of diatomic molecules X_2 is not straightforward; the physical implications of the mathematical approximations employed are examined, and the non-linear recombination term is accounted for in the present purely qualitative context by an appropriate linearization. However, the appreciable contributions from X_2–X_2 collisions, under the conditions of the experiments cited, introduce inescapable non-linearities if vibration–vibration exchange, for example, is important. Problems associated with the role of the free atom X as a collision partner seem likely to be less important.

ROBERT K. BOYD. Can. J. Chem. **55**, 802 (1977).

On a utilisé les extensions récentes de l'approximation des valeurs de eigen pour des cinétiques de systèmes qui ne sont pas en équilibre et qui ont été proposées par Bartis et Widom pour expliquer d'une manière qualitative directe quelques caractéristiques générales de la cinétique chimique phénoménologique dans des systèmes gazeux idéaux pour étudier le problème de la "formule de mélange linéaire" appliquée à des cinétiques qui ne sont pas en équilibre de réactions se produisant dans des mélanges. Pour des réactions d'isomérisation dans des mélanges dilués en réactif, on a montré que le modèle de Bartis et Widom sans autres embellissements justifie une telle équation. L'extrapolation de ces résultats pour tenir compte de succès empiriques récents de la "formule de mélange linéaire" dans des réactions de dissociation et de recombinaison de molécules diatomiques X_2 n'est pas directe; on a examiné les implications physiques des approximations mathématiques qui ont été utilisées et on tient compte des termes de combinaisons non-linéaires dans le contexte purement qualitatif actuel par une linéarisation appropriée. Toutefois les contributions importantes des collisions X_2–X_2 dans les conditions de réactions citées introduisent des non-linéarités qui ne peuvent être empêchées si, par exemple, l'échange vibration–vibration est important. Les problèmes associés avec le rôle de l'atome X libre agissant comme un partenaire de collision semblent vraisemblablement moins importants.

[Traduit par le journal]

I. Introduction

The empirical relations of the phenomenological chemical kinetics of thermal systems have long been intuitively understood, in a qualitative way, on the basis of what may be conveniently termed 'local-equilibrium' theories. In general, a common basic assumption of such theories is that the internal (physical) modes of the reacting (chemical) species are equilibrated amongst themselves. This postulate greatly simplifies the theoretical treatments, as in transition state theory (1), for example; the justification for the 'local-equilibrium' assumption concerns the much shorter timescale associated with internal relaxation than with chemical reaction, under most conditions. In such cases, local-equilibrium theories offer qualitative understanding, as well as quantitative or semi-quantitative accounts, of such relations as the phenomenological rate equations, the temperature dependence of rate constants, the principle of detailed balance, etc.

However, in experiments where the rates of internal relaxation and chemical reaction are not well-separated, the local-equilibrium postulate breaks down, and in such cases it is not immediately obvious that the empirical relationships of 'normal' chemical kinetics should apply. Theoretical understanding, in a qualitative sense at least, of non-equilibrium chemical kinetics in ideal gas systems has been made possible in re-

cent years through the work of Widom and collaborators (2–4); this work represents a development of an idea first proposed by Zwolinski and Eyring (5), and subsequently extended by a number of authors (6–9). This approach will here be termed the 'eigenvalue approximation', for convenience, and is discussed at some length below. The general thrust of the present work may be divided into three main sections:

(*a*) An analysis is attempted of some of the physical implications of mathematical approximations made in the more recent developments of the eigenvalue approximation due to Widom and co-worker (3, 4).

(*b*) The simple eigenvalue theory (2–9) refers only to first-order, or pseudo-first-order, reactions. In view of the present slant towards dissociation–recombination reactions of diatomic molecules, an attempt is made to provide a justification for extending the insights and understanding offered by Widom's treatment (3, 4) to such cases.

(*c*) Recently (10–16), the laser–schlieren technique, used to follow diatomic dissociation rates in shock-tubes, has yielded rate data of high precision over a wide range of reactant composition. This development has permitted a meaningful test of the linear mixture formula for non-equilibrium chemical kinetics, *viz.*;

$$[1]\quad -\mathrm{d}[\mathrm{X}_2]/\mathrm{d}t = [\mathrm{X}_2]\sum_i k_\mathrm{d}{}^i[\mathrm{M}_i] - [\mathrm{X}]^2\sum_i k_\mathrm{r}{}^i[\mathrm{M}_i]$$

where $[\mathrm{X}_2]$ is the concentration of diatomic molecules, [X] that of the free atom, and the M_i represent the heat-bath collision partners, including both X_2 and X as well as added inert species such as argon. The first serious question as to the applicability of such a simple linear combination of separable rates, in cases where non-equilibrium effects seemed likely to be important, appears to have been raised by Byron (17). In the present work, this problem is discussed in the spirit of Widom's development (3, 4) of the eigenvalue approximation.

II. Physical Implications of Widom's Extension of Eigenvalue Approximation

In this section, the discussion will centre upon a simple isomerization reaction, proceeding via the agency of collisions with an inert heat-bath species M, assumed present in large excess:

$$[2]\quad \mathrm{A} + \mathrm{M} \underset{k_\mathrm{r}}{\overset{k_\mathrm{f}}{\rightleftharpoons}} \mathrm{B} + \mathrm{M}$$

The phenomenological rate equation for this reaction would then take the form:

$$[3]\quad -\mathrm{d}[\mathrm{A}]/\mathrm{d}t = k_\mathrm{f}[\mathrm{A}] - k_\mathrm{r}[\mathrm{B}]$$

where the concentration of M has conveniently been included in the pseudo-first-order rate constants k_f and k_r. Consideration of just *two* isomers A and B avoids the complications due to chemical mechanisms with closed loops (4, 9), and also provides a linear analogue for the dissociation–recombination reactions of homonuclear diatomic molecules.

In common with earlier work on such problems (2–9), it is assumed from the outset that the microscopic description is given by an appropriate master equation:

$$[4]\quad -(\mathrm{d}/\mathrm{d}t)|\alpha\rangle = \boldsymbol{K}^\mathrm{M}|\alpha\rangle$$

where $|\alpha\rangle$ is a column vector, whose ith component α_i ($1 \leq i \leq \mathrm{n}$) is the population per unit volume of the isomerizing molecule in state i; $\boldsymbol{K}^\mathrm{M}$ is the transport matrix for changes of state via collisions with M, such that

$$K_{ii}{}^\mathrm{M} = \sum_{i=1}^{n} k_{ij}$$

($k_{ii}{}^\mathrm{M} = 0$), and $K_{ij}{}^\mathrm{M} = -k_{ji}{}^\mathrm{M}$ for $i \neq j$. The $k_{ij}{}^\mathrm{M}$ include the concentration of M, and are thus pseudo-first-order rate constants for $i \rightarrow j$ transitions. An exact solution to this equation is known:

$$[5]\quad \alpha_i(t) = \alpha_i{}^* + \sum_{r=2}^{n} c_r{}^0\phi_r{}^\mathrm{M}(i)\exp(-\lambda_r{}^\mathrm{M}t)$$

where $\alpha_i{}^*$ is the equilibrium ($t \rightarrow \infty$) limit of α_i, the $c_r{}^0$ are constants dependent on the initial ($t = 0$) distribution function $|\alpha(0)\rangle$, $\phi_r{}^\mathrm{M}(i)$ is the ith component of the rth eigenvector of $\boldsymbol{K}^\mathrm{M}$ and $\lambda_r{}^\mathrm{M}$ is the corresponding eigenvalue. In order to contract this purely physical description to a chemical one, it is necessary to ascribe some of the states (say 1 to $m - 1$, inclusive) to isomer A, and the remainder to B, thus:

$$[6]\quad [\mathrm{A}] = \sum_{i=1}^{m-1}\alpha_i;\quad [\mathrm{B}] = \sum_{i=m}^{n}\alpha_i$$

The conditions under which the phenomenological rate equation [3] is an *exact* consequence of the microscopic description, as given

by [5] and [6], are known (9) to be impossibly stringent, and approximate solutions must be sought. The traditional 'local-equilibrium' approximation identifies the rate constants with the following theoretical constructs;

$$[7]\quad {}^{E}k_f^{M} = \sum_{i=1}^{m-1} (\alpha_i^*/[A^*]) \sum_{j=m}^{n} k_{ij}^{M}$$
$$[7]\quad {}^{E}k_r^{M} = \sum_{j=m}^{n} (\alpha_j^*/[B^*]) \sum_{i=1}^{m-1} k_{ji}^{M}$$

As discussed in the Introduction, however, this approximation is not expected to be universally valid, and in such cases a very general non-equilibrium theory may be delineated (5) by considering that the eigenvalue spectrum of $\boldsymbol{K}^{M}$ has the form:

$$[8]\quad 0 = \lambda_1^{M} \approx \lambda_2^{M} \gg \lambda_3^{M} > \ldots > \lambda_n^{M}$$

The smallest eigenvalue λ_1^{M} is identically zero for reactions in closed systems.

The exact solution [5] may, after an incubation time $\sim(1/\lambda_3^{M})$, be approximated by omitting all terms with $r \geq 3$; then by requiring that the rate constants be independent of time and of initial conditions, the following theoretical constructs are derived (2–9) as the 'eigenvalue approximations' to the rate constants:

$$[9]\quad ({}^{\lambda}k_f^{M} + {}^{\lambda}k_r^{M}) = \lambda_2^{M}$$
$$[9]\quad ({}^{\lambda}k_f^{M}/{}^{\lambda}k_r^{M}) = K^* = [B^*]/[A^*]$$

The number of almost-degenerate eigenvalues (two in the present case) must be the same as the number of chemical species. Previously, this property of the eigenvalue spectrum [8] was assumed; however, by making further assumptions whose range of validity is discussed below, Widom (3, 4) was able to derive a special case of the eigenvalue approximation for which [8] was a readily understandable result. Further, this same special case (3, 4) also led to a crucial 'orthogonality relation' for the eigenvectors of $\boldsymbol{K}^{M}$, which simultaneously guarantees detailed balance for non-trivial cases (9) (chemical mechanisms *with* closed loops), and also permits a demonstration (9) that the eigenvalue approximation is quite generally a better approximation to the 'exact' solution, as given by [5] plus [6], than is the local equilibrium approximation given by [7]. In view of these successes of the extended version (3, 4) of the eigenvalue approximation, it seemed important to investigate the special additional assumptions involved, with a view to establishing their probable range of validity with respect to the experimental systems of interest. In this model (3, 4), the discrete states labelled by the integer variables i,j are replaced by a continuum of states, labelled by x,y; the ranges of x and of y are assumed to be $-\infty \leq x(y) \leq +\infty$. Then, under various assumptions whose physical significance is discussed below, the relevant eigenvalue equation reduced (3) to:

$$[10]\quad (M_2^{M}/2)\{-[\psi_r^{M}(x)]'' + ([f(x)^{1/2}]''/[f(x)^{1/2}])\psi_r^{M}(x)\} = \lambda_r^{M}\psi_r^{M}(x)$$

where the sign of the left side of [10] has been changed from that in the original (3), in order to permit positive eigenvalues λ_r as in the discrete model. In [10], $f(x)$ is the equilibrium (Boltzmann) distribution function of the molecule (and thus independent of the nature of M), and prime denotes differentiation with respect to x; $\psi_r^{M}(x)$ is the rth eigenvector of the *symmetrized* transition kernel, and may be converted to the analogue of $|\phi_r^{M}\rangle$ in the discrete case by a simple transformation involving only $f(x)$. The quantity M_2^{M} is the second moment of the symmetrized transition probability function:

$$[11]\quad w_s^{M}(x, y) = [f(x)/f(y)]^{1/2} w^{M}(x, y) = w_s^{M}(y, x)$$

where $w^{M}(x, y)\,dy$ is the probability per unit time, in heat-bath composed of M, that a molecule in state x will undergo a transition to a state in the range y to $y + dy$, (*cf.* k_{ij} in the discrete model, Section II). Then M_2^{M} is defined by:

$$[12]\quad M_2^{M} = \int_{-\infty}^{+\infty} w_s^{M}(y, x)\cdot(y - x)^2\,dy$$

The crucial approximation in reducing the general case to the special eigenvalue equation [10] involves the assumption (3, 4) that the values of $w_s(x, y)$ be significant only for $y \approx x$; then, moments higher than the second moment M_2 may be discarded. In fact, such an assumption may be justified physically if the state label x is defined such as to be a smoothly varying function of internal energy, since energy transfers from internal modes to translational energy of a structureless atom like argon are known to be fairly small; the Landau–Teller transition probabilities for a harmonic oscillator undergoing

near-adiabatic transitions offer a possibly extreme example of this point. Thus, the above restriction (3, 4) on $w_s(x, y)$ is physically reasonable, provided the label x is a smooth function (not necessarily monotonic) of the internal energy.

Nonetheless, the state label x cannot be identified precisely with the state energy, since a specified energy may correspond to more than one state, which in turn may be ascribed to different chemical species; thus the state label x carries a more detailed description than that provided by only the state energy.

In addition, under this same assumption concerning $w_s(x, y)$, M_1 should also be small since:

$$[13]\quad \frac{w_s(x,x+\delta x)}{w_s(x,x-\delta x)} = \left[\frac{f(x-\delta x)}{f(x+\delta x)}\right]^{1/2} \times \left[\frac{w(x,\, x+\delta x)}{w(x,\, x-\delta x)}\right] \approx [e^{2\delta\varepsilon/kT}]^{1/2}[e^{-\delta\varepsilon/kT}] \approx 1.0$$

where $\delta\varepsilon$ is the internal energy difference associated with both $\pm\delta x$, (δx and $\delta\varepsilon$ small), and deexcitation processes are assumed to involve negligible activation energy. Thus, M_1 should be approximately zero, since $w_s(x,y)$ is invariant to a change of sign of y; thus, only M_2 remains in [10].

The remaining approximation concerns the functional dependence of $M_2{}^{M}$ upon the state label x, *i.e.* effectively upon the internal energy; in order for [10] to be useful, it is necessary that this functional dependence be weak, relative to that of the other factor on the left side of [10]. In turn, this implies that the functional dependence of this latter factor should be approximately that of the eigenfunction $\psi_r{}^{M}(x)$. It does not seem possible, at present, to make any useful generalization here; however, if the Landau–Teller probabilities for a harmonic oscillator are again invoked as a rather special simple case, $M_2{}^{M}$ clearly increases approximately linearly with the vibrational quantum number, since $k_{v+1,v} = (v+1)k_{10}$. The eigenvectors may be expressed (6) in terms of Gottlieb polynomials, for which the variation of the eigenvector elements is a complex function of the index μ:

$$[14]\quad l_r(\mu) = \exp(-r\theta) \times \sum_{\nu=0}^{n} [1-\exp\theta]^{\nu} \binom{r}{\nu}\binom{\mu}{\nu}$$

where θ is the vibrational spacing and n the number of levels considered. It is clear that the dependence of $l_r(\mu)$ upon μ is considerably greater than the linear dependence of $M_2{}^{M}$, discussed above, and to this extent the approximation (3, 4) of constant $M_2{}^{M}$ is reasonable in this rather special case.

It is well-known (6) that the simple harmonic oscillator model is inadequate insofar as a quantitative account of dissociation–recombination reactions of diatomic molecules is concerned. However, the results of interest here are very general conclusions regarding the transition kernel; by assuming that these results are at least approximately valid in general, Widom (3, 4) has shown that the all-important property [8] of the eigenvalue spectrum, together with the chemical principle of detailed balance, follows immediately. The present section has demonstrated that the necessary assumptions (3, 4) are consistent with the known properties of a model which is physically meaningful, even if not quantitatively valid (6).

Quite apart from these residual uncertainties just outlined, which refer to reactions proceeding via collisions with inert, structureless heat-bath molecules such as argon, additional difficulties arise when dissociation–recombination reactions of diatomic molecules are considered. These difficulties are associated with the fact that the diatomic X_2 and free atom X are usually present in significant concentration, and are clearly not inert, structureless collision partners. Discussion of these additional problems is best deferred to Section V below.

III. Dissociation–Recombination Reactions

The simple linear model used thus far is not applicable to dissociation–recombination reactions, since the recombination terms are nonlinear. The approach adopted in the present work is to devise an approximate linearization procedure, valid close to complete equilibrium, whereby the truly non-linear master equation may be re-expressed in a linear form analogous to that discussed above. The qualitative conclusions derived previously (2–9) for the linear isomerization model reaction, as well as those derived below, may then be applied to dissociation–recombination reactions. In order for this extrapolation to be valid, it is necessary that the experimental rate constants, obtained in shock-tube experiments as the ratio of a dissociation

rate to a concentration, are indeed true rate constants, independent of time and of composition; it is this crucial assumption which permits the identification of the appropriate theoretical constructs for the rate constants within the 'eigenvalue approximation', and implies that the measurements were made well after the incubation time.

While preparing this work for publication, it was realised that the results of this linearization procedure had been given previously by Nikitin (18). However, the method of derivation and limits of validity of this result are not readily available, and these are included here as an Appendix for the sake of completeness.

Then, within the limits of this approximate linearization (see Appendix), the eigenvalue approximation expressions for the rate constants are:

$$[15] \qquad \begin{aligned} (k_d^{\lambda}/k_r^{\lambda}) &= [A^*]^2/[A_2^*] = K^* \\ \lambda_2 &= (k_d^{\lambda} + 4[A^*]k_r^{\lambda}) \end{aligned}$$

This result is analogous to [9], which applies to the strictly linear isomerization model; note that, according to [15], the rate constants are true constants only if λ_2 varies with [A*] as $(1 + 4[A^*]/K^*)$. While it is true that λ_2 must increase with [A*], it does not seem possible to prove that this particular functional dependence is necessary; however, it seems likely that this apparent prediction of a composition dependence of k_d^{λ} and k_r^{λ} is an artefact of the force-fit of the true master equation into the linearized form.

In other words, in view of the somewhat artificial linearization required, it is *not* the eigenvalue which should here be regarded as the more fundamental quantity, but rather the rate constants themselves.

It is not claimed that the present linearization procedure offers a good model for quantitative treatments; rather, it was intended to provide a justification for extending to dissociation–recombination reactions the qualitative conclusions reached for isomerization reactions (2–9).

IV. Linear Mixture Formula

The experimental findings which prompted the present work involve dissociation–recombination reactions of diatomic molecules, for which [1] gives the appropriate form of the linear mixture formula. However, the discussion of the theoretical implications of such a formula is most easily given for the linear isomerization model described in Section II; extension of the qualitative conclusions thus reached to the systems of interest is then justified by the considerations of Section III.

Now, the reaction described by [2] is assumed to proceed via collisions with inert, structureless heat-bath molecules M and N, such that F_M and $F_N = (1 - F_M)$ are the mole fractions of M and N respectively in the heat-bath. Then, in view of the present restriction to ideal gas systems, the microscopic description of the rate, assumed again to be given by a master equation analogous to [4], becomes:

$$[16] \qquad -(\mathrm{d}/\mathrm{d}t)|\alpha\rangle = (F_M\boldsymbol{K}^M + F_N\boldsymbol{K}^N)|\alpha\rangle = \boldsymbol{K}|\alpha\rangle$$

This 'linear mixture formula' for the *microscopic* description is simply a consequence of the additivity and independence of collision rates in ideal gases. The present problem is to justify the contraction of [16], via the definition of chemical species [6], to the phenomenological linear mixture formula [17] relevant to our model reaction:

$$[17] \qquad \begin{aligned} -\mathrm{d}[A]/\mathrm{d}t = {} & (F_M k_f^M + F_N k_f^N)[A] \\ & - (F_M k_r^M + F_N k_r^N)[B] \end{aligned}$$

In the local equilibrium approximation, the theoretical constructs [7] for the rate constants become:

$$[18] \qquad \begin{aligned} {}^{E}k_f &= \sum_{i=1}^{m-1} \Big\{(\alpha_i^*/[A^*]) \\ &\qquad \times \sum_{j=m}^{n} (F_M k_{ij}^M + F_N k_{ij}^N) \\ &= (F_M{}^{E}k_f^M + F_N{}^{E}k_r^N) \end{aligned}$$

and similarly for ${}^{E}k_r$. Such definitions are entirely consistent with the linear mixture formula [17], as is intuitively obvious (19).

Again, however, in the non-equilibrium eigenvalue approximation (2–9), the result is non-trivial; the definitions of theoretical expressions for the rate constants analogous to [9] are derived from [16] in the usual way, and are valid whatever the composition of the heat-bath:

$$[19] \qquad {}^{\lambda}k_f + {}^{\lambda}k_r = \lambda_2; \quad {}^{\lambda}k_f/{}^{\lambda}k_r = K^*$$

In [19], λ_2 is the smallest non-zero eigenvalue of $\boldsymbol{K}$ (see [16]), and is thus a function of F_M and $F_N(= 1 - F_M)$, as well as of *all* the micro-

scopic rate constants k_{ij}^{M} and k_{ij}^{N}. If ${}^{\lambda}k_f$ and ${}^{\lambda}k_r$ are to satisfy [17], it is clearly necessary and sufficient that this functional dependence be of the following form:

$$[20] \qquad \lambda_2 = F_M\lambda_2{}^{M} + F_N\lambda_2{}^{N}$$

since K^* is not a function of the nature of M and N. ($\lambda_2{}^{M}$ is a function of the k_{ij}^{M} only, and $\lambda_2{}^{N}$ of the k_{ij}^{N}.)

A sufficient condition for [20] to be valid is that $\boldsymbol{K}^{M}$ and $\boldsymbol{K}^{N}$ shall commute; in such a case $\boldsymbol{K}^{M}$, $\boldsymbol{K}^{N}$, and $\boldsymbol{K}$ (see [16]) share common eigenvectors, so that [20] and thus [17] follow directly. This commutation condition is not necessary, since it is required only that the first two eigenvectors $|\phi_1\rangle$ and $|\phi_2\rangle$, corresponding to λ_1 and λ_2 be shared, in the present two-species model reaction; $|\phi_1\rangle = |\alpha^*\rangle$ is shared, in any event.

The question of the commutation of $\boldsymbol{K}^{M}$ and $\boldsymbol{K}^{N}$ was investigated by considering the vector $\boldsymbol{K}^{M}(\boldsymbol{K}^{N}|\alpha\rangle)$, and attempting to reduce it to a form symmetrical with respect to interchange of M and N; in the trivial two-level case ($n = 2$) it is possible to do so, using the microscopic reversibility relations $(k_{ij}^{M}/k_{ji}^{M}) = (\alpha_j{}^*/\alpha_i{}^*) = (k_{ij}^{N}/k_{ji}^{N})$. However, for $n > 2$ this is not possible, in principle, as is readily seen from writing out the matrix product explicitly; thus, $\boldsymbol{K}^{M}$ and $\boldsymbol{K}^{N}$ do not commute, in general.

However, as mentioned above, this commutation requirement is too strong; furthermore, it is not necessary that the relation [20] be obeyed *exactly*, since the experimental relation [1] may be confirmed in shock-tubes only to within an appreciable experimental scatter, even in the more recent investigations (10–16). In the spirit of the latter comment, it is instructive to consider the further approximations introduced by Bartis and Widom (4), discussed in Section II above.

The crucial eigenvalue equation [10] yields invaluable insights (3, 4) if $M_2{}^{M}$, as defined by [12], is effectively constant, *i.e.* has a much weaker dependence on the state label x than do the eigenfunctions $\psi_r{}^{M}(x)$. Under this *same* approximation (3, 4), it is clear that [10] implies that the $\psi_r{}^{M}(x)$ are independent of the nature of M, and the corresponding eigenvalues scale linearly with $M_2{}^{M}$. In fact, it is only necessary to assume that $M_2{}^{M}$ is approximately independent of x, relative to the dependence of $\psi_r{}^{M}(x)$, for $r < \hat{n}$, where $\hat{n}$ is the number of chemical species involved (9) (two in the present case).

Thus, the same approximations as used previously by Widom and co-worker (3, 4), culminating in the relation [10] plus the above assumption regarding $M_2{}^{M}$, lead immediately to [20], and thus to the linear mixture formula given by [17]. An earlier investigation (20) of this same problem concluded that the linear mixture formula was valid under local-equilibrium conditions, but was unable to justify the formula for non-equilibrium kinetics.

V. Empirical Tests of Linear Mixture Formula

A direct test of the preceding discussion, for dissociation–recombination reactions, would require data obtained using highly dilute mixtures of X_2 in mixtures of inert gases (*e.g.*, neon plus argon); no systematic investigations of this type are known to the present author. The nearest approach to this experiment was achieved by Breshears *et al.* (11) for the shock dissociation of O_2; also relevant is the elegant investigation of the relaxation of hydrogen by Dove and collaborators (21, 22). In both cases, in order to obtain good shocks into mixtures containing helium, it was necessary (11, 21, 22) to add a proportion of a diluent (Kr) heavier than He. The linear mixture formula (23, 24) appropriate to the relaxation experiment was found (21, 22) to account for the data quite satisfactorily. This observation is, at least, perfectly understandable in the context of the simple harmonic oscillator approximation; this is most readily seen in terms of the treatment due to Montroll and Shuler (25). If the factor κ (eq. (1.7) of ref. 25) is identified as $(k_{10}{}^{M}F_M + k_{10}{}^{N}F_N)$, in line with the additivity of collision rates, then it is a simple exercise to show that the original analysis (25) is not sensibly altered, and the simple Bethe–Teller expression for the energy relaxation is still obtained, modified according to the linear mixture formula (23, 24). However, in view of the finding (22) that the rotational mode is probably involved in the observed relaxation, this simple demonstration is clearly not the last word on this subject. The case of the O_2 dissociation experiments (11) is discussed more fully below.

In the case of those dissociation experiments (11–16) for which a truly meaningful test of the linear mixture rate equation [1] was possible, the heat-bath collision partners involved have been an inert gas (typically argon), the diatomic molecule X_2 itself, and the dissociated atom X.

Before discussing the added theoretical complications arising from this fact, it is appropriate to comment on the degree to which the linear mixture equation has been tested in this work (11–16), and on its success or otherwise.

It appears that the most impressive successes of [1] are in the experimental investigations with $X_2 = H_2$ (13) and $X_2 = Br_2$ (15, 16). In both cases, the experiments suggested that k_d^M, $k_d^{X_2}$, and k_d^X are all true rate constants, independent of the particular reaction mixture used. Thus, for example, the value of $k_d^{H_2}$ extracted using [1] was independent (13) of the nature of M; also, the very precise values of k_d^{Ar} obtained (13) for H_2 using the laser–schlieren technique are in excellent agreement with the equally precise results of Myerson and Watt (26), obtained in very dilute mixtures using an atomic resonance absorption technique to follow the rate of H atom production. In the case of $X_2 = Br_2$, each of k_d^{Ar}, k_d^{Kr}, $k_d^{Br_2}$, and k_r^{Br} is a true rate constant, in that values obtained from high-temperature flash photolysis (27), laser–schlieren, molecular absorption spectroscopy, or atomic two-body emission in shock waves (15, 16, 35) are all in agreement to within experimental uncertainty.

In the case of $X_2 = O_2$, the laser–schlieren results (11) are again a satisfyingly self-consistent set of data when treated in terms of the linear mixture formula [1]. However, values so obtained (11) for k_d^{Ar} are about a factor of three higher than the comparable results of Watt and Myerson (28) using atomic resonance absorption spectroscopy, which are in good agreement with direct high-temperature measurements (29) of k_r^{Ar}; this discrepancy is far outside the combined experimental scatter, and seems significant in the light of the excellent agreement, cited above, for $X_2 = H_2$. The reasons for this disagreement are not clear.

In the cases (12, 14) of $X_2 = HCl$ and $X_2 = F_2$, the linear mixture formula [1] was found to be perfectly adequate, but these experiments (12, 14) were less extensive, and do not provide as severe a test of [1] as do the first two cases discussed. Nevertheless, these findings (12, 14) provide a significant contribution to confidence in the linear mixture formula as applied to this class of reactions; on the whole, it seems to be a fair conclusion that the recent shock-tube data (11–16) are well described by the linear mixture formula [1], with only one ($X_2 = O_2$) reservation.

However, this empirical success of the linear mixture formula [1] cannot be accounted for simply and directly in terms of the considerations of Sections II, III, and IV above, since the collision partners X_2 and X are very special, not at all covered by the assumption in the theoretical treatment of inert, structureless heat-bath molecules. The case of the dissociated atom X seems marginally simpler, and will be dealt with first.

The extraordinary efficiency of free atoms X in relaxation and dissociation of X_2 is well documented, and has frequently been cited as evidence of a 'chemical' interaction. From the present point of view, this need not necessarily nullify the present theoretical treatment, provided that this extra efficiency still retains the characteristics that $M_2 \gg M_3$, M_4, etc., and that M_2 has a relatively weak functional dependence on x, (see Sections II and IV above). That is to say, relatively small energy transfers in $X–X_2$ collisions must still be appreciably more probable than larger energy transfers; as emphasized recently (30), there is a great need for further theoretical studies of this problem. The most relevant study is that due to Thompson (31), who carried out a classical dynamical study of vibrational relaxation and atom-exchange in the systems $Cl + Cl_2$ and $I + I_2$. As can be seen readily from Figs. 10 and 11 of ref. 31 the distributions over v' for the process

$$X + X_2(v) \rightarrow X_2(v') + X$$

are sharply peaked around $v = v'$, for $v = 14$ at 1100 K; this distribution is particularly narrow for $X \equiv I$, and less so for $X \equiv Cl$. Although these results (31) are invaluable, they are unfortunately inadequate to permit a quantitative evaluation of the validity of Widom's contraction of the Taylor-series expansion (3, 4), of the transition kernel, which led to [10]; this is because no information is available on the eigenvectors and their derivatives. However, the evidence available (31) is clearly consistent with the free atom X meeting the requirements of Widom's qualitative model (3, 4). In addition, of course, it must be assumed that the translational and electronic modes of the atom X are fully relaxed at all times under shock-tube conditions; then X may be regarded effectively as a structureless collision partner, and may be represented as a single state n in [A1] (see Appendix). Under these conditions, it appears that there should be no breakdown of [1] due to the special

nature of the dissociated atom X as collision partner.

No such accommodation in the present theory is possible for the case of X_2 as a collision partner, since it is the disequilibrium of the internal states of X_2 during dissociation which is the object of the present exercise. Thus, significant contributions of X_2–X_2 collisions in which *both* molecules change their internal states introduce non-linearities which are inescapable. The only escape for the present theoretical approach, in this case, would require a demonstration that in X_2–X_2 collisions, translational–vibrational exchange, for example, is much more probable than vibrational–vibrational (V–V) exchange, possibly due to non-matching of the anharmonic vibrational levels. The fitting of vibrational relaxation times of pure X_2 into semi-empirical correlation schemes (32), based upon simple theory of translational–vibrational relaxation, offers some heavily circumstantial evidence to sustain this hope, but clearly more work is necessary here also. The phenomenological success of [1] in including $k_d^{X_2}$ is thus not properly accounted for by the present approach.

An alternative theoretical approach, which has yielded useful information on this question, involves numerical (computer) experiments. In a study of a model system designed to resemble H_2 dissociation in He, McElwain and Pritchard (33) showed that the linear mixture formula would hold in mixtures containing appreciable H_2 provided that the V–V coupling was not too strong, but would break down badly if such processes were efficient, in broad agreement with present conclusions. The problem remains to ascertain the efficiency of V–V exchange for H_2 in He, under experimental shock dissociation conditions, and thus to determine into which regime (33) the real system should fall; the experimental evidence, for H_2 in Ar (13, 26), clearly indicates the linear mixture formula is valid, suggesting (33) that V–V coupling is *not* efficient in this latter system.

Similar work due to Kiefer (34), on a model system designed to simulate O_2, seems to confirm the conclusion that when V–V exchange is significant the linear mixture rate law is not valid. One explicitly stated conclusion (34), that significant deviations from the linear mixture formula seem to be largely confined to the effect of the self-atom, would appear to be an inevitable consequence of the method used (34) to reduce the 'experimental' (*i.e.* computational) data. Rate constants $k_d^{X_2}$ and k_d^{M}, where M is Ar for example, were obtained using [1] for mixtures of closely similar compositions *not* containing any X; then the rate data for a mixture of M, X_2, and X were reduced (34) through [1], using these same values of k_d^{M} and $k_d^{X_2}$. That is, *all* deviations from [1], whatever their cause, were automatically assigned (34) to the k_d^{X} so calculated. Thus, the conclusion stated elsewhere in (34) that breakdown of [1] is generally a consequence of significant V–V exchange would appear to be the appropriate one.

Such computational 'experiments' are invaluable in that they afford the opportunity of providing quantitative insights which the present analytic approach cannot provide; on the other hand, the numerical approach *alone* has not offered qualitative physical understanding. For example, the question, treated above, as to *why*, in the absence of significant V–V coupling, the linear mixture formula should be valid for non-equilibrium kinetics, was not broached in either of the studies cited (33, 34). Thus the two approaches should be considered as complementary to one another. The most pressing problem now would seem to be to account for the empirical success (11–16, 35) of the linear mixture formula in a range of systems, including *pure* diatomic X_2, for which V–V coupling and other exchanges of internal energy might be expected to be significant.

Acknowledgements

This work was carried out while the author was on sabbatical leave from the University of Guelph, enjoying the hospitality of Prof. J. H. Beynon at University College, Swansea. The author would also like to acknowledge the interest of Prof. G. Burns in this work.

1. S. Glasstone, K. Laidler, and H. Eyring. The theory of rate processes. McGraw-Hill, New York. 1941.
2. B. Widom. Science, **148**, 1555 (1965).
3. B. Widom. J. Chem. Phys. **55**, 44 (1971).
4. J. T. Bartis and B. Widom. J. Chem. Phys. **60**, 3474 (1974).
5. B. J. Zwolinski and H. Eyring. J. Am. Chem. Soc. **62**, 2702 (1947).
6. E. W. Montroll and K. E. Shuler. Adv. Chem. Phys. **1**, 361 (1958).
7. J. Wei and C. D. Prater. Adv. Catal. **13**, 203 (1962).
8. N. S. Snider. J. Chem. Phys. **42**, 548 (1965).
9. R. K. Boyd. J. Chem. Phys. **60**, 1214 (1974); **61**, 5474 (1974).
10. J. H. Kiefer and R. W. Lutz. J. Chem. Phys. **44**, 658 (1966).

11. W. D. BRESHEARS, P. F. BIRD, and J. H. KIEFER. J. Chem. Phys. **55**, 4017 (1971).
12. W. D. BRESHEARS and P. F. BIRD. J. Chem. Phys. **56**, 5347 (1972).
13. W. D. BRESHEARS and P. F. BIRD. 14th Symposium (International) on Combustion. Combustion Institute, Pittsburgh. 1973. p. 211.
14. W. D. BRESHEARS and P. F. BIRD. J. Chem. Phys. **58**, 5176 (1973).
15. R. K. BOYD, G. BURNS, R. G. MACDONALD, and W. H. WONG. 15th Symposium (International) on Combustion, 1975. p. 731.
16. R. K. BOYD, G. BURNS, and R. G. MACDONALD. Modern developments in shock tube research. *In* Proc. Tenth Internat. Shock Tube Symposium. *Edited by* G. Kamimoto. 1975. p. 552.
17. S. BYRON. J. Chem. Phys. **44**, 1378 (1966).
18. E. E. NIKITIN. Theory of thermally induced gas phase reactions. Indiana University Press, Bloomington, Indiana. 1966. p. 123.
19. K. G. DENBIGH. Principles of chemical equilibrium. Cambridge University Press, London. 1966. p. 440.
20. E. W. SCHLAG and W. G. VALANCE. J. Chem. Phys. **49**, 605 (1968).
21. J. E. DOVE and H. TEITELBAUM. Chem. Phys. **6**, 431 (1974).
22. J. E. DOVE, D. G. JONES, and H. TEITELBAUM. Proc. 14th Symposium (International) on Combustion, The Combustion Institute, Pittsburgh. 1973. p. 177.
23. K. F. HARZFELD and T. A. LITOVITZ. The absorption and dispersion of ultrasonic waves. Academic Press, New York. 1959. p. 206.
24. F. D. SHIELDS. J. Acoust. Soc. Am. **47**, 1262 (1970).
25. E. W. MONTROLL and K. E. SHULER. J. Chem. Phys. **26**, 454 (1957).
26. A. L. MYERSON and W. S. WATT. J. Chem. Phys. **49**, 425 (1968).
27. J. K. K. IP and G. BURNS. J. Chem. Phys. **51**, 3414 (1969).
28. W. S. WATT and A. L. MYERSON. J. Chem. Phys. **51**, 1638 (1969).
29. K. L. WRAY. J. Chem. Phys. **38**, 1518 (1963).
30. R. E. CENTER. J. Chem. Phys. **58**, 5230 (1973).
31. D. L. THOMPSON. J. Chem. Phys. **60**, 4557 (1974).
32. R. C. MILLIKAN and D. R. WHITE. J. Chem. Phys. **39**, 3209 (1963).
33. D. L. S. MCELWAIN and H. O. PRITCHARD. J. Am. Chem. Soc. **92**, 5027 (1970).
34. J. H. KIEFER. J. Chem. Phys. **57**, 1938 (1972).
35. R. G. MACDONALD, G. BURNS, and R. K. BOYD. J. Chem. Phys. In press.

Appendix: Linearization of Dissociation–Recombination Master Equation

For convenience, in the following derivation the superscript M is dropped from the rate constants, which are again pseudo-first-order, or pseudo-second-order in the case of recombination steps. Denoting by β_n the concentration of free dissociated atoms, the relevant master equation is:

$$[A1] \quad (-d/dt)\begin{pmatrix} \alpha_1 \\ \alpha_2 \\ \cdot \\ \cdot \\ \alpha_{n-1} \\ \beta_n \end{pmatrix} = \begin{pmatrix} \left(\sum_i k_{1i}\right) & -k_{21} & \cdots & \cdots & -k_{n,1} \\ \cdot & & & & \cdot \\ \cdot & & & & \cdot \\ \cdot & & & & \cdot \\ -k_{1,n-1} & -k_{2,n-1} & \cdots & \left(\sum_i k_{n-1,i}\right) & -k_{n,n-1} \\ -2k_{1,n} & -2k_{2,n} & \cdots & -2k_{n-1,n} & \left(2\sum_i k_{n,i}\right) \end{pmatrix} \begin{pmatrix} \alpha_1 \\ \alpha_2 \\ \cdot \\ \cdot \\ \alpha_{n-1} \\ \beta_n^2 \end{pmatrix}$$

The problem with [A1] is that the two composition vectors are not identical; the aim is to approximate [A1] in such a way as to render the two vectors identical, while still retaining all the appropriate properties (2–9) of the transport matrix. This may be achieved by defining:

$$[A2] \qquad \alpha_n \equiv (\beta_n^*/2) + \Delta \quad \text{where } \Delta \equiv (\beta_n - \beta_n^*)$$

Thus, $\beta_n^2 \approx 2\beta_n^*\alpha_n$, provided $(\Delta/\beta_n^*)^2 \ll 1$; also: $(d\alpha_n/dt) = (d\beta_n/dt)$. Then, to within this approximation, [A1] may be written:

$$[A3] \qquad -(d/dt)|\alpha\rangle = \boldsymbol{L}|\alpha\rangle$$

where $L_{i,n} = -2\beta_n^* k_{n,i}$, for $1 \leq i < n$, and

$$L_{nn} = 4\beta_n^* \sum_i k_{ni}$$

all other elements of $\mathbf{L}$ are unchanged from those of the matrix in [A1]. The determinant $|\mathbf{L}|$ is zero, and thus $\mathbf{L}$ has one zero eigenvalue, λ_1 say, with the corresponding eigenvector given by $|\phi_1\rangle = |\alpha^*\rangle$, as required (2–9).

The analysis now proceeds as usual (2–9); the matrix **L** may be diagonalized by a similarity transform ($\mathbf{A}^{-1/2}\mathbf{L}\,\mathbf{A}^{+1/2}$), where **A** is a diagonal matrix with $A_{ii} = \alpha_i^*$, for $1 \leq i < n$, and $A_{nn} = 2\alpha_n^* = \beta_n^*$; the solution given as [5] then applies. The chemical classification of the states is now:

$$[A4] \qquad [A_2] = \sum_{i=1}^{n-1} \alpha_i; \quad [A] = \beta_n$$

and insertion of [5] into [A4] gives the appropriate theoretical predictions of the chemical composition as a function of time. However, the mass conservation condition upon the eigenvectors $|\phi_r\rangle$ must be reinvestigated; this is best done by deriving two expressions for β_n, one directly from α_n, and the other from the expression for $[A_2]$ plus mass balance. Thus:

$$[A5] \qquad \beta_n = \alpha_n + \tfrac{1}{2}\beta_n^* = \beta_n^* + \sum_{r=2}^{n} c_r^0 \exp(-\lambda_r t)\phi_r(n)$$

The mass balance condition is:

$$[A6] \qquad [A_2] + \tfrac{1}{2}[A] = \sum_{i=1}^{n-1} \alpha_i + \tfrac{1}{2}\beta_n = \sum_{i=1}^{n-1} \alpha_i^* + \tfrac{1}{2}\beta_n^* = \sum_{i=1}^{n} \alpha_i^*$$

From [5], we have:

$$[A7] \qquad \sum_{i=1}^{n} \alpha_i = \sum_{i=1}^{n} \alpha_i^* + \sum_{r=2}^{n} c_r^0 \exp(-\lambda_r t) \left(\sum_{i=1}^{n} \phi_r(i) \right)$$

From [A2], [A6], and [A7] is derived:

$$[A8] \qquad \beta_n = \beta_n^* + 2 \sum_{r=1}^{n} c_r^0 \exp(-\lambda_r t) \cdot \left(\sum_{i=1}^{n} \phi_r(i) \right)$$

Then, since the c_r^0 are arbitrary, it is true, for $2 \leq r \leq n$, that

$$[A9] \qquad \phi_r(n) = -2 \sum_{i=1}^{n-1} \phi_r(i) \equiv -2u_r$$

and this is the mass conservation condition upon the eigenvectors. Now, ignoring all terms with $r > 2$, yields for the eigenvalue approximation:

$$[A10] \qquad [A_2] = \sum_{i=1}^{n-1} \alpha_i = [A_2^*] + c_2^0 u_2 \exp(-\lambda_2 t)$$

$$[A11] \qquad (-\mathrm{d}/\mathrm{d}t)[A_2] = c_2^0 u_2 \lambda_2 \exp(-\lambda_2 t)$$

$$[A12] \qquad [A]^2 = \beta_n^2 \approx 2\beta_n^* \alpha_n = 2\beta_n^* \alpha_n^* + 2\beta_n^* c_2^0 \exp(-\lambda_2 t)\phi_2(n) = [A^*]^2 - 4[A^*]c_2^0 u_2 \exp(-\lambda_2 t)$$

Equations A10–A12 are consistent with the phenomenological description of the rate, provided that the rate constants correspond to the eigenvalue approximation expressions, given by [15].

An acidity function based on thiocarbonyl indicators

JOHN T. EDWARD, IVAN LANTOS, GARY D. DERDALL, AND SIN CHEONG WONG

Department of Chemistry, McGill University, Montreal, P.Q., Canada H3C 3G1

Received July 5, 1976

JOHN T. EDWARD, IVAN LANTOS, GARY D. DERDALL, and SIN CHEONG WONG. Can. J. Chem. **55**, 812 (1977).

The ionization of 16 thiocarbonyl indicators of overlapping range has been used to establish an acidity function H_T for 10–90% sulfuric acid. Agreement with an earlier H_T scale of Tissier and Tissier using different thiocarbonyl indicators is good. Protonation constants pK_{TH^+} derived by the classic Hammett–Deyrup approach are in good agreement with those derived by the Bunnett–Olsen relations, but in less satisfactory agreement with those derived by the Marziano–Cimino–Passerini relations.

JOHN T. EDWARD, IVAN LANTOS, GARY D. DERDALL et SIN CHEONG WONG. Can. J. Chem. **55**, 812 (1977).

On a utilisé l'ionisation de 16 indicateurs thiocarbonyles ayant des écarts qui se recoupent pour établir une fonction d'acidité H_T pour l'acide sulfurique de 10–90%. L'accord avec une échelle antérieure H_T de Tissier et Tissier utilisant différents indicateurs thiocarbonyles est bon. Les constantes de protonation pK_{TH^+}, obtenues par une approche classique de Hammett–Deyrup, sont en bon accord avec celles obtenues par des relations de Bunnett–Olsen mais ne sont pas en aussi bon accord avec celles dérivées de relations Marziano–Cimino–Passerini.

[Traduit par le journal]

Introduction

The extent to which thioamides and related compounds (T) are converted into their conjugate acid forms (TH^+) in aqueous sulfuric acid is governed by an acidity function H_T (1), defined by

$$[1] \quad H_T = -\log (a_{H^+} f_T / f_{TH^+}) = pK_{TH^+} - \log ([TH^+]/[T])$$

where the symbols have their customary definitions (1, 2). This acidity function proves to be very close to H_0''' (2), which governs the protonation of tertiary anilines, in its dependence on acid concentration (3–5). Our need to interpret results on the kinetics of the acid-catalyzed hydrolysis of thioamides and thionesters (1) has led us to establish the H_T scale for 10–90% aqueous sulfuric acid, using 16 thiocarbonyl indicators of varying structures (1) and the overlap procedure of Hammett and Deyrup (6), and we report these results in this paper.

Since Hammett and Deyrup's classic paper, two new approaches for establishing an acidity function scale, and hence for obtaining thermodynamic ionization constants of weak bases, have been reported in the literature. The first approach is based on the linear free energy relationship of Bunnett and Olsen (7):

$$[2] \quad \log ([TH^+]/[T]) + H_0 = \phi(H_0 + \log [H^+]) + pK_{TH^+}$$

The ϕ parameters, which characterize the changing activity coefficient behaviour of bases with changing acidity (7–9), can be calculated from ionization ratio data for a set of indicators. The H_T scale may then be derived from the average ϕ value and the H_0 function (6, 10) by

$$[3] \quad H_T = H_0 - \phi(H_0 + \log [H^+])$$

(obtained by rearranging [2]). Tissier and Tissier (11) have applied this method and established H_T for 10–80% aqueous sulfuric acid using 11 indicators, all of them different from ours, with an average ϕ value of 0.36.

The second approach is based on another empirical linear relationship, this one discovered by Marziano, Cimino, and Passerini (M.C.P.) (12). They found that for a series of overlapping indicators A, B, C ..., at any given acid concentration the following relationship holds:

$$[4] \quad \log \frac{[H^+][B]}{[BH^+]} + pK_{BH^+} = n_B \left(\log \frac{[H^+][A]}{[AH^+]} + pK_{AH^+} \right)$$

$$\log \frac{[H^+][C]}{[CH^+]} + pK_{CH^+} = n_C \left(\log \frac{[H^+][B]}{[BH^+]} + pK_{BH^+} \right)$$

etc.

$$[4a]\quad \log\frac{[H^+][B]}{[BH^+]} = n_B \log\frac{[H^+][A]}{[AH^+]} + (n_B pK_{AH^+} - pK_{BH^+})$$

$$\log\frac{[H^+][C]}{[CH^+]} = n_C \log\frac{[H^+][B]}{[BH^+]} + (n_C pK_{BH^+} - pK_{CH^+})$$

etc. A plot of log ($[H^+][B]/[BH^+]$) for the indicator B against the corresponding function for A at the same acid concentrations should give the parameter n_B as the slope, and the protonation constant pK_{BH^+} of the second indicator can be calculated from the intercept and from n_B if pK_{AH^+} is known.

In this way, starting from an 'anchor' compound A whose protonation constant is known in dilute aqueous solution, the protonation constants of the weaker bases B, C ... may be established by a stepwise procedure which does not depend on any acidity function. Furthermore, from the same data one may derive a new activity coefficient function M_C, based on a single reference base A. Equation 4 may be rewritten as

$$[5]\quad \log\frac{f_{H^+}f_B}{f_{BH^+}} = n_B \log\frac{f_{H^+}f_A}{f_{AH^+}}$$

$$\log\frac{f_{H^+}f_C}{f_{CH^+}} = n_C \log\frac{f_{H^+}f_B}{f_{BH^+}}$$

etc. M_C is defined by

$$[6]\quad M_C = -\log\frac{f_{H^+}f_A}{f_{AH^+}} = -\frac{1}{n_B}\log\frac{f_{H^+}f_B}{f_{BH^+}} = -\frac{1}{n_C^*}\log\frac{f_{H^+}f_C}{f_{CH^+}} = -\frac{1}{n_D^*}\log\frac{f_{H^+}f_D}{f_{DH^+}} = \ldots$$

where $n_X^* = n_B n_C \ldots n_X$. This equation may be rewritten as

$$[7]\quad M_C = -\log\frac{f_{H^+}f_A}{f_{AH^+}} = \frac{1}{n_B}\left(\log\frac{[B]}{[BH^+]} + \log[H^+] + pK_{BH^+}\right)$$

$$= \frac{1}{n_C^*}\left(\log\frac{[C]}{[CH^+]} + \log[H^+] + pK_{CH^+}\right) = \ldots$$

Since thermodynamic parameters for the anchor compound A are known, M_C may be established by measurement of the ionization ratios of indicators B, C ... at higher acid concentrations, using the values of n_B, n_C ... and pK_{BH^+}, pK_{CH^+} ... already established.

The pK_{TH^+} values obtained by the M.C.P. procedure should be free from errors caused by the cumulative effects of deviations from parallelism in plots of log $[BH^+]/[B]$ against acid concentration in the classic Hammett–Deyrup procedure, and from errors inherent in the long extrapolation to dilute aqueous solution involved in the Bunnett–Olsen approach. Furthermore, the M_C function, referring to a single reference base A, should in theory eliminate the need for a multiplicity of acidity functions H_0, H_0''', H_A, H_R, etc., the differing behaviour of different types of base being reflected in different values of n.

In the present paper we apply these two new approaches also to data for the ionization of the 16 thiocarbonyl indicators, and compare the pK_{TH^+} values thus obtained with those yielded by the traditional overlap procedure of Hammett and Deyrup.

Experimental

Materials

1,3-Diethylthiourea was a gift of Professor W. Cocker, and 1,3-di-*tert*-butylthiourea was a commercial product. 4,5-dimethyl-4-imidazoline-2-thione was prepared by reaction of 3-aminobutanone hydrochloride and ammonium thiocyanate in water (13). All three compounds were purified by crystallization from ethanol and had melting points close to those reported.

Thiobenzamide (mp 117–118°C, lit. (14) mp 116°C), 4-methoxythiobenzamide (mp 151–152°C, lit. (14) mp 148.5–149.5 °C), and 4-chlorothiobenzamide (mp 131–132°C, lit. (14) mp 124°C) were prepared by reactions of the appropriate nitriles with hydrogen sulfide in the presence of triethylamine (14) and crystallized from ethanol.

Thioheptanamide was prepared by reaction of heptanamide with phosphorus pentasulfide in refluxing pyridine (*cf.* ref. 15), and melted at 63–65°C after crystallization from ethanol. *Anal.* calcd. for $C_7H_{15}NS$: C 57.9, H 10.4, N 9.6, S 22.1; found: C 58.0, H 10.2, N 9.8, S 22.0.

4-Nitrothioacetanilide was similarly prepared (mp 173.5–175°C, lit. (16) mp 175°C). The reaction mixture was quenched in water after only 10 min of reflux to prevent decomposition.

The 1,2-dithiole-3-thiones (17) were gifts of E. Klingsberg.

Ethyl thionbenzoate was prepared from benzonitrile according to the procedure of Renson and Bidaine (18), and was separated from a small amount of ethyl benzoate by chromatography of a hexane solution over alumina. The other thionesters were prepared in similar fashion. Ethyl 3-bromothionbenzoate, bp 98–99.5°C/3 torr, was a new compound: λ_{max} (EtOH) 416, 285, 251 nm (ε 119, 11500, 7350). *Anal.* calcd. for C_9H_9BrOS: C 44.1, H 3.7; found: C 44.0, H 3.9.

Thiobenzamidonium pentacyanopropenide was prepared by adding 10 mol excess of pyridinium pentacyanopropenide (19) to a solution of thiobenzamide in 70% sulfuric acid at 30–35°C (*cf.* ref. 20). Because of the hygroscopic nature of the salt it was not submitted for elemental analysis, but was analyzed by measurement of the ultraviolet absorption spectrum of a solution in sulfuric acid. The absorbances at different wavelengths were those expected for a 1:1 salt (at 275 nm, ε found 13 600; ε calcd. 13 900). 1,3-Diethylthiouronium pentacyanopropenide was prepared in similar fashion. Its spectrum established it also as a 1:1 salt (at 210 nm, ε found 23 800; ε calcd. 23 400).

Spectral Measurements

Measurements were made with a Unicam SP800 spectrophotometer having a cell compartment thermostatted at 25.0 ± 0.2°C, following general procedures already described (3–5). In general, good isosbestic points were observed for most families of spectra. When an isosbestic point was not evident (as in the case of curves for the substituted thioureas), extinction coefficients of the unprotonated (ε_T) and of the protonated bases (ε_{TH^+}) were taken as the extinction coefficients three H_0 units before and after half-ionization, determined by a preliminary plot according to Stewart and Granger (21).

Thionesters were stable in dilute or very concentrated sulfuric acid; ε_T and ε_{TH^+} could be determined with relative ease. In moderately concentrated acid, however, these compounds hydrolyzed fairly rapidly and their extinction coefficients were obtained by extrapolation to the time of preparing the solutions.

The ionization ratios I ($\equiv [TH^+]/[T]$) were then obtained from the extinction coefficients according to the equation

$$[8] \qquad \log I = \log [(\varepsilon - \varepsilon_T)/(\varepsilon_{TH^+} - \varepsilon)]$$

In an attempt to minimize errors (*cf.* Kresge and Chen (22)) most measurements were kept within the range: $\log I = \pm 0.6$.

Solubility Measurements

A suspension of an excess of solid in about 2 ml of sulfuric acid of known concentration, contained in a 10 ml flask immersed in a water-bath maintained at 25.0 ± 0.4°C, was shaken with a mechanical shaker. Saturation of neutral bases required 12–15 h; of pentacyanopropenide salts, 2–4 h. The suspension was filtered through a sintered glass funnel and the ultraviolet absorbance of the filtrate (diluted, if necessary, with acid of the same strength) was measured. Following Boyd (23), solubilities were expressed as absorbance (A) at a designated wavelength in a 1.0 cm cell without dilution.

Measurements of solubilities of thiobenzamide (Table 3) were carried out in solutions of increasing acidity, up to concentrations sufficient for 50% protonation, and corrections were made for solubility due to protonation of base by use of the equation

$$[9] \qquad A_T = A / (1 + I\varepsilon_{TH^+}/\varepsilon_T)$$

where A is the measured absorbance at 287 nm (due to T and TH^+), A_T is the absorbance due to unprotonated base, and I, ε_{TH^+} and ε_T are from results of the preceding section.

Solubilities of salts were followed by the changing absorbance of the 412 nm band of the pentacyanopropenide anion. Results are given in Table 4.

Results and Discussion

Site of Protonation of Thiocarbonyl Compounds

The 16 indicators used to establish our H_T scale are shown in Table 1 with their identifying numerals, and include several different types of thiocarbonyl compounds: thioureas (numbers 1–3), thioamides (numbers 4–8), 1,2-dithiole-3-thiones (**1**; X=S) (numbers 9, 10, and 12), a 2,4-dithiohydantoin (**2**) (number 11), and thionesters (numbers 13–16).

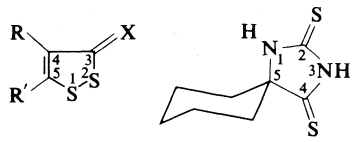

1 **2**

There is now general consensus that thioureas (24), thioamides (24), and thionesters (25) are protonated on the thiocarbonyl sulfur in strongly acidic solution, and ultraviolet spectral changes indicate 2,4-dithiohydantoins to be protonated on the sulfur at the 2-position (4). Protonation of the thiocarbonyl sulfur of 1,2-dithiole-3-thiones is suggested by the fact that their protonation follows the same acidity function as the other thiocarbonyl compounds, as shown by the parallelism of the curves of Fig. 1. On the other hand, the protonation of 5-phenyl-1,2-dithiole-3-one (**1**; R = H, R′ = Ph, X = O) follows H_A (26) ($pK = -3.26$), as would be expected if protonation takes place on the carbonyl oxygen.

Ionization Constant of the 'Anchor' Base

The pK_{TH^+} of the strongest base of Table 1, 1,3-di-*tert*-butylthiourea, has been determined by an extrapolation procedure due to Paul (27). Equation 1 may be rewritten as

$$[10] \qquad pK_{TH^+} = \log I - \log [H^+] + \log (f_{TH^+}/f_T f_{H^+})$$

TABLE 1. Protonation constants (pK_{TH+}) of indicators used to establish H_T scales

Indicators	Hammett approach		Bunnett–Olsen approach			M.C.P. approach		
	$\Delta \log I$	pK_{TH+}	ϕ	pK_{TH+}	σ_y[a]	n	pK_{TH+}	σ_y[a]
1. 1,3-Di-*tert*-butylthiourea		(−1.32)[b]	−0.30	−1.05	0.007		(−1.32)[b]	
2. 4,5-Dimethyl-4-imidazoline-2-thione	0.10±0.01	−1.42	−0.27	−1.15	0.012	1.019	−1.42	0.011
3. 1,3-Diethylthiourea	0.28±0.01	−1.70	−0.26	−1.42	0.010	1.086	−1.81	0.009
4. Thiocaprolactam[c]	0.54±0.02	−2.24	−0.42	−2.07	0.011	1.260	−2.70	0.002
5. Thioheptanamide	0.31±0.02	−2.55	−0.45	−2.44	0.011	1.042	−3.11	0.013
6. 4-Methoxythiobenzamide	0.41±0.01	−2.96	−0.49	−2.89	0.011	1.006	−3.53	0.005
7. 4-Chlorothiobenzamide	0.71±0.03	−3.67	−0.35	−3.39	0.008	0.916	−4.00	0.015
8. 4-Nitrothioacetanilide	0.35±0.03	−4.02	−0.26	−3.60	0.013	0.943	−4.17	0.010
9. 5-Phenyl-1,2-dithiole-3-thione (**1**; R=H, R′=Ph, X=S)	0.90±0.01	−4.92	−0.53	−5.18	0.014	0.975	−4.96	0.008
10. 4-Phenyl-1,2-dithiole-3-thione (**1**; R=Ph, R′=H, X=S)	0.32±0.01	−5.24	−0.53	−5.50	0.022	0.954	−5.09	0.016
11. 5,5-Pentamethylene-2,4-dithiohydantoin (**2**)[d]	0.97±0.03	−6.21	−0.41	−6.09	0.007	0.814	−5.24	0.009
12. 4,5-Benzo-1,2-dithiole-3-thione (**1**; RR′=C_6H_4, X=S)	0.39±0.03	−6.60	−0.48	−6.80	0.010	1.062	−5.94	0.005
13. Ethyl 4-methoxy-thionbenzoate	1.03±0.02	−7.63	−0.44	−7.61	0.005	0.991	−6.90	0.008
14. Ethyl thionbenzoate	0.92±0.02	−8.55	−0.48	−8.72	0.033	0.987	−7.74	0.016
15. Ethyl 3-bromothion-benzoate	1.08±0.03	−9.63	−0.42	−9.49	0.022	0.981	−8.68	0.018
16. Ethyl 4-nitrothion-benzoate	0.92±0.04	−10.55	−0.37	−10.07	0.023	0.977	−9.42	0.031

[a] σ_y is the standard deviation of points from the linear regression line in the y-direction.
[b] 'Anchor' base: pK_{TH+} derived from Fig. 2.
[c] Experimental data given in ref. 3.
[d] Experimental data given in ref. 4.

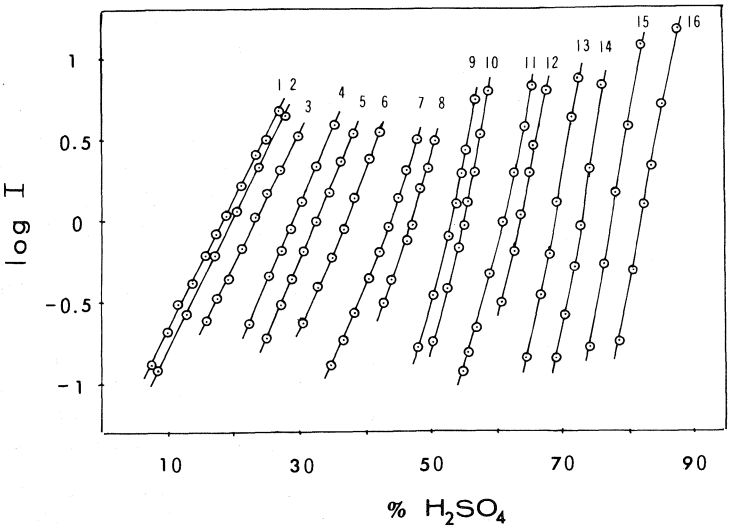

FIG. 1. Effect of acid concentration on ionization of thiocarbonyl indicators (identified by numbers in Table 1).

In dilute acid solution, as $[H^+] \rightarrow 0$, $\log (f_{TH^+}/f_T f_{H^+}) \rightarrow 0$, so that

$$[11] \quad pK_{TH^+} = \lim_{[H^+]\rightarrow 0} (\log I - \log [H^+])$$

In dilute sulfuric acid $[H^+]$ is uncertain because of the incomplete dissociation of the weak acid HSO_4^-, but perchloric acid is completely dissociated (27), so that $[H^+]$ may be determined by titration. In Fig. 2 is shown a plot of ($\log I - \log [H^+]$) against concentration of perchloric acid ($\sim$0.7–1.7 *M*). Extrapolation of the plot gives a pK_{TH^+} of -1.32 for 1,3-di-*tert*-butylthiourea.

H_T Function from the Hammett Procedure

Using the 'anchored' pK_{TH^+} value of -1.32 for 1,3-di-*tert*-butylthiourea and the experimental difference of 0.10 in the logarithm of the ionization ratio ($\Delta \log I$) between this compound and the next strongest base, 1,3-vinylenethiourea, for a given acid concentration (Fig. 1), the pK_{TH^+} of the latter in aqueous sulfuric acid was calculated to be -1.42. This is in excellent agreement with the value of -1.43 obtained from Fig. 2.

This stepwise procedure (6) was repeated for the other 14 indicators. Their pK_{TH^+} values are given in Table 1, column 3, along with the data used in calculating them (column 2). From these pK_{TH^+} values, values for H_T were calculated by application of [1] to the experimental values of I ($\equiv [TH^+]/[T]$) in different strengths of acid. Values obtained from a smoothed-out curve are given in Table 2, column 2.

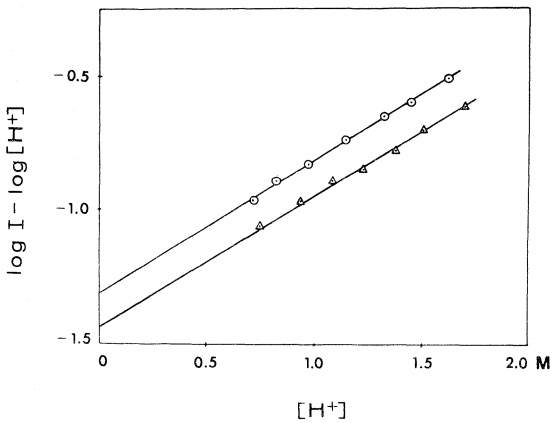

FIG. 2. Extrapolation of the ionization of 1,3-di-*tert*-butylthiourea (○) and ~~1,3-vinylenethiourea~~ (△) in perchloric acid to infinite dilution.

4,5-dimethyl-4-imidazoline-2-thione

H_T Function from the Bunnett–Olsen Approach

From [2], it is evident that a plot of ($\log I + H_0$) against ($H_0 + \log [H^+]$) for any thiocarbonyl base should give a straight line with the hydration parameter ϕ as the slope and the ionization constant pK_{TH^+} as the intercept.

This alternative to the stepwise overlap procedure of analyzing experimental ionization data has been applied to our 16 indicators, and the results are given in Table 1, columns 4–6. H_0 values were interpolated from the data of Paul and Long (28) and Jorgenson and Hartter (10) $[H^+]$ ($\equiv [H_3O^+]$) values[1] were interpolated from the data of Robertson and Dunford (29).

The pK_{TH^+} values of the 16 bases studied are mostly within 0.3 unit of those obtained by the preceding method. The ϕ values are scattered from -0.26 for 1,3-diethylthiourea and 5,5-pentamethylene-2,4-dithiohydantoin (**2**) to -0.53 for 5-phenyl (**1**; R = H, R′ = Ph, X = S) and 4-phenyl (**1**; R = Ph, R′ = H, X = S) 1,2-dithiole-3-thiones. The average ϕ value is -0.40, but only six compounds have ϕ values within the range -0.35 to -0.45. Tissier and Tissier (11) have reported less scatter in their set of ϕ values: eight of their eleven indicators had ϕ values between -0.32 and -0.38, the remaining three had values of -0.25, -0.48, and -0.52; and their average was -0.36. However, the H_T scale constructed by application of [3] shows that the average ϕ value of -0.40 gives results which are in good agreement with results of the traditional Hammett approach, especially in concentrated aqueous sulfuric acid. (Compare columns 3 and 4 with column 2 of Table 2.)

The justification for the Bunnett–Olsen approach has been empirical, and various theoretical objections to it have been raised (30–32). Accordingly, the closeness of the H_T scales established by the Bunnett–Olsen approach to that established by the traditional approach indicates the practical equivalence of the two approaches.

M_C Function for Thiocarbonyl Compounds

As another approach, the M.C.P. procedure was applied to the data of our 16 indicators, with 1,3-di-*tert*-butylthiourea again being the 'anchor'

[1]Bunnett and Olsen (7), in applying [2] to data on ionizations in sulfuric acid, took $[H^+]$ to be equal to the stoichiometric concentration of acid. Because of the small but finite dissociation of HSO_4^- in strong acid, this practice introduces a small error into the results.

TABLE 2. H_T scales derived by different methods compared with H_0''' and H_A

H_2SO_4 (%)	$-H_T$[a]	$-H_T$[b]	$-H_T$[c]	$-M_C$	$-H_T$[d]	$-H_0'''$	$-H_A$
10	0.62	0.38	0.37	0.43	0.65	0.53	0.29
15	1.02	0.79	0.78	0.69	1.15	0.99	0.70
20	1.42	1.22	1.20	0.94	1.58	1.47	1.00
25	1.84	1.68	1.65	1.21	2.01	1.96	1.25
30	2.27	2.13	2.09	1.49	2.41	2.44	1.50
35	2.76	2.58	2.53	1.75	2.79	2.93	1.74
40	3.24	3.04	2.98	2.04	3.20	3.46	2.00
45	3.76	3.63	3.55	2.40	3.67	4.01	2.24
50	4.43	4.35	4.25	2.84	4.23	4.54	2.51
55	5.19	5.07	4.97	3.46	5.00	5.11	2.77
60	5.99	5.83	5.70	4.21	5.90	5.91	3.10
65	6.84	6.69	6.53	5.00	6.84	6.73	3.38
70	7.83	7.68	7.50	6.01	8.04	7.65	3.74
75	9.01	8.73	8.52	7.12	9.35	8.53	4.15
80	10.07	9.82	9.59	8.26	10.68	9.44	4.62
85	11.20	10.97	—	9.45	11.98	10.30	5.02
90	12.25	12.10	—	10.63	13.24	11.14	5.57

[a]Hammett approach.
[b]Bunnett–Olsen approach.
[c]Tissier and Tissier (11).
[d]$n^*M_C - \log [H^+]$.

compound. In all cases, linear relations were found for a plot of log ($[H^+][T]/[TH^+]$) against the corresponding value of the succeeding indicator of Table 1, generally with very high correlation coefficients (>0.998 or 0.999). The results are given in Table 1, columns 7–9.

While most indicators have n values in the range of 1.0 ± 0.1, two compounds, thiocaprolactam ($n = 1.260$) and 5,5-pentamethylene-2,4-dithiohydantoin ($n = 0.814$), have n values that are appreciably different. However, this difference is no worse than many reported by Marziano *et al.* (12) for other types of bases, n values less than 0.8 or greater than 1.2 being not uncommon. Most pK_{TH^+} values differ appreciably from those calculated by the previous two methods (some by as much as one logarithmic unit). In a similar comparison, differences of these magnitudes or greater were encountered also by Marziano *et al.* (12).

From pK_{TH^+} and n values, M_C values for thiocarbonyl compounds were calculated from ionization ratios by application of [7]. They are reported in Table 2, column 5.

The M_C function for a base of type X in general is related to the appropriate acidity function H_X by:

$$[12] \qquad n^*M_C = H_X + \log [H^+]$$

n^* (1.156) being the average of n_B^*, n_C^* ... for our 16 indicators. The H_T scale thus derived from the M_C function for the thiocarbonyl compounds and from $[H^+]$ values of Robertson and Dunford (29) agrees fairly well with the H_T scales derived by the previous two methods (compare column 6 with columns 2 and 3 of Table 2), except in the most concentrated acid.

We are faced with the choice of a set of pK_{XH^+} values to accept. Marziano *et al.* (12) give various reasons for considering values derived by their approach to be more reliable: the order of pK_{XH^+} is occasionally altered to one which seems more plausible on intuitive grounds; a better linear relationship is observed between pK_{XH^+} and partial molal heats of transfer of primary nitroanilines to fluorosulfonic acid (33); etc. However, none of these arguments can be considered conclusive. It seems likely that no choice between the alternative approaches can be made without a refinement of techniques which allows measurement of very low or very high ionization ratios, $[BH^+]/[B]$, $[CH^+]/[C]$..., and hence experimental discrimination between the various extra-thermodynamic assumptions on which the different approaches are based. For the traditional Hammett–Deyrup approach, the assumption is made that for *all* acid concentrations

$$[13] \qquad \log \frac{f_B}{f_{BH^+}} = \log \frac{f_C}{f_{CH^+}} = \ldots = \log \frac{f_Z}{f_{ZH^+}}$$

For any two indicators of overlapping range, this assumption can be tested by noting whether the vertical separation between the two curves for log I (Fig. 1) at different acid concentrations remains constant (the criterion of 'parallelism' (28)). However, present experimental techniques make it possible to observe this parallelism between neighbouring curves only over a small range of acid concentrations. Arnett (34) has given reasons to believe that outside this observable range the parallelism *may* break down for certain bases, but at the moment this point cannot be established experimentally.

On the other hand, the M.C.P. approach makes the assumption that for all acid concentrations

$$[14] \quad \log \frac{f_C}{f_{CH^+}} + \log f_{H^+} = \log \left(\frac{f_B}{f_{BH^+}}\right)^{n_C} + \log (f_{H^+})^{n_C}$$

etc. This assumption is supported to the extent that plots of log ([B][H$^+$]/[BH$^+$]) against log ([C][H$^+$]/[CH$^+$]) give straight lines; again, such linear relationships can in fact be observed, because of experimental limitations, over only a limited range of acid concentrations.[2] To the extent that n_B, n_C ... approach unity, [14] reduces to [13]; however, n values frequently deviate strongly from unity.

It would seem, then, that at the moment there are no decisive grounds to preferring the M.C.P. to the Hammett–Deyrup approach, and the matter must be regarded as *sub judice*. However, the M.C.P. and Bunnett–Olsen approaches share a great practical advantage over the Hammett–Deyrup approach, in that they can be applied to compounds for which an appropriate acidity scale has not yet been, or cannot be, developed.

[2]By expressing H_T and H_0 in terms of activity coefficients, [3] becomes

$$[i] \quad \log (f_T/f_{TH^+}) + \log f_{H^+} = \log (f_B/f_{BH^+})^{1-\phi} + \log (f_{H^+})^{1-\phi}$$

(B in this case being a Hammett H_0 base.) Comparison of [i] and [14] shows that the Bunnett–Olsen and M.C.P. approaches are theoretically equivalent, and that the different results for the more concentrated acid solutions obtained by each approach come from the different ways in which extrapolation to the standard state of dilute aqueous solution is carried out.

*The Activity Coefficients f_T and f_{TH^+}**

The discussion above emphasizes the importance of direct measurements of f_X and f_{XH^+} in acidity function studies (23, 35).

The activity coefficient of a neutral Bronsted base in an acid solution is given by the ratio of its solubility in water (S_0) to its solubility in the acid under consideration (S)

$$[15] \quad f = S_0/S$$

when these solubilities are sufficiently low.

The activity coefficients of thiobenzamide in 0–40% sulfuric acid, calculated from the solubility data of Table 3, are shown in Fig. 3 along with those of 2,4-dinitrobenzamide (20) and *N*,*N*-dimethyl-3,4-dinitroaniline (36).

Following Boyd (23), activity coefficients of conjugate acids are referred to a standard ion, tetraethylammonium ion (TEA$^+$). By definition

TABLE 3. Solubilities (S) and activity coefficients (f) of thiobenzamide in various concentrations of sulfuric acid

H_2SO_4 (%)	$S \times 10^{-2}$	$S' \times 10^{-2}$[a]	log f[b]
0	1.09 (S_0)	1.09	0
8.3	0.866	0.866	0.10
16.1	0.726	0.726	0.18
24.1	0.568	0.553	0.30
33.8	0.500	0.410	0.42
39.7	0.703	0.391	0.45

[a]S' is the solubility of free base corrected for protonation.
[b]$f = S_0/S'$.

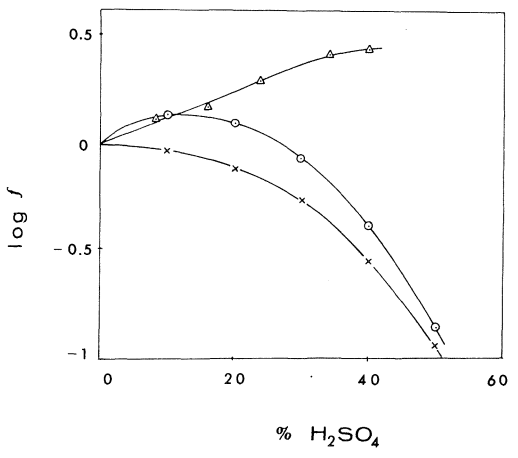

FIG. 3. Activity coefficients (f) of neutral bases: △ Thiobenzamide (T); × 2,4-Dinitrobenzamide (A); ○ *N*, *N*-Dimethyl-3,4-dinitroaniline (B$''$).

[16] $$f_{TH^+}^* = f_{TH^+}/f_{TEA^+}$$

It is impossible to measure single-ion activity coefficients, but the mean ionic activity coefficients $f_\pm$ of a sparingly soluble 1:1 salt may be determined by solubility measurements:

[17] $$f_\pm = (f_+f_-)^{1/2} = S_0/S$$

where f_+ and f_- are individual ionic activity coefficients. Boyd (23) found that the salts of many organic bases with the strong acid, pentacyanopropene (H^+PCP^-) had conveniently low solubilities. Thus, for each concentration of acid, the relative activity coefficient of the ion TH^+ is given by:

[18] $$f_{TH^+}^* = (f_{TH^+}f_{PCP^-})/(f_{TEA^+}f_{PCP^-}) = [(f_\pm(TH^+PCP^-)/f_\pm(TEA^+PCP^-)]^2$$

We have determined the solubility of the PCP salt of protonated 1,3-diethylthiourea in 37.8–69.1% sulfuric acid and of protonated thiobenzamide in 53.5–71.0% sulfuric acid (Table 3). These salts are hydrolyzed in more dilute acid solutions, and so the change in their activity coefficients in dilute acid cannot be determined directly. Yates and Sweeting (20) have described a method of anchoring these relative activity coefficients to dilute aqueous solution as standard states; the following method is simpler but basically equivalent.

Since in a given concentration of acid a_{H^+} should not be affected by the nature of base present in the vanishingly small amount necessary for spectrophotometric determination of I, the difference between H_T and any acidity function H_X is given by:

[19] $$H_T - H_X = \log(f_{TH^+}f_X/f_Tf_{XH^+})$$

so that

[20] $$\log f_{TH^+}^* = \log f_T - \log f_X + \log f_{XH^+}^* + (H_T - H_X)$$

The values of $f_{TH^+}^*$ for 1,3-diethylthiouronium ion in 0–37.8% sulfuric acid were calculated from this equation using the data of thiobenzamide for $\log f_T$; 2,4-dinitroaniline (23) for $\log f_X$, anilinium ion (23) for $\log f_{XH^+}^*$ and H_0 for H_X. (Calculations based on H_0''' (2) give essentially the same results.) The values for thiobenzamidonium ion were calculated by interpolating the first reference point (57.5% H_2SO_4) from the data of 1,3-diethylthiouronium ion. The results are shown in Fig. 4 along with those for benzamidonium ion (20) and *N,N*-dimethylanilinium ion (23).

Difference between H_T and H_A

In spite of the close similarity of amides and thioamides, there is a large difference between the protonating power of sulfuric acid when measured by thiocarbonyl indicators (T) (including thioamides) and when measured by amide indicators (A). The reasons for this difference can be understood by considering [20]. Below 40% acid, $\log f_{TH^+}^* \simeq \log f_{AH^+}^*$, and most of the difference between H_T and H_A arises from the variation in $\log f_T/f_A$. (In 30% acid, for instance, $H_A - H_T \simeq 0.8$, $\log f_T/f_A \simeq 0.7$; in 40% acid, $H_A - H_T \simeq 1.2$, $\log f_T/f_A \simeq 1.0$.) Thiobenzamide is increasingly salted-out as the concentration of acid goes up, while 2,4-dinitrobenzamide is salted-in. A part of this difference can be attributed to the specific effect of nitro groups, which cause a compound to be salted-in in sulfuric acid (35), but most of the difference comes from the different behaviour of amide and thioamide groups. Thioamides are probably more polar, and so more strongly hydrated than amides (3). Consequently, it is to be expected that they will be salted-out in acid solution as the water activity of the solution decreases.

Above 40% sulfuric acid, while $\log f_T/f_A$ still remains important, the contribution of the term

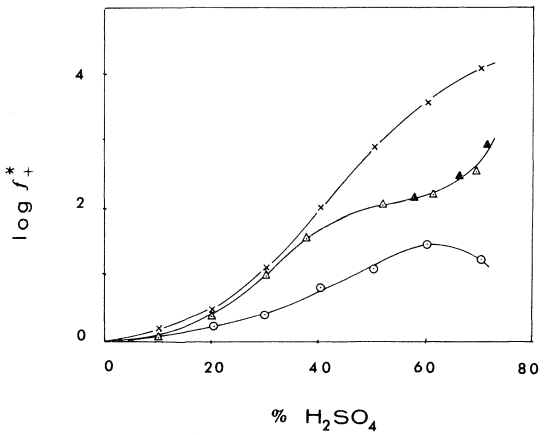

FIG. 4. Activity coefficients (f_+^*) of conjugate acids: △ 1,3-Diethylthiouronium ion (TH^+); ▲ Thiobenzamidonium ion (TH^+); × Benzamidonium ion (AH^+); ○ *N,N*-Dimethylanilinium ion ($B'''H^+$).

TABLE 4. Solubilities (S) and activity coefficients (f_+*) of thiobenzamidonium pentacyanopropenide (A) and of 1,3-diethylthiouronium pentacyanopropenide (B)

Compound	H_2SO_4 (%)	$S \times 10^{-2}$	log $f_\pm$[a]	log f_+*[b]
A	57.5	5.08 (S_0)	0	2.15
	65.8	9.15	−0.255	2.50
	71.0	17.40	−0.534	2.96
B	37.8	4.55 (S_0)	0	1.54
	52.1	9.12	−0.302	2.04
	60.9	16.7	−0.566	2.18
	69.1	37.4	−0.917	2.54

[a] $f_\pm = S_0/S$.
[b] f_+* $= [f_\pm/f_\pm$ (TEA$^+$PCP$^-$)]^2 and were anchored to infinite dilution.

log f_{TH^+}/f_{AH^+} to the difference between H_T and H_A becomes quite significant. (In 60% acid, for instance, $H_A - H_T \simeq 3$, log $f_{AH^+}/f_{TH^+} \simeq 1.4$.) Amidonium ions are salted-out to a much greater extent than thioamidonium ions, suggesting the latter is less hydrated than the former. This order is not unexpected since a protonated sulfur base, by virtue of its larger size and consequently lower charge density, would be expected to have lower hydration requirements.

Several classes of thio bases (thioureas, thioamides, 1,2-dithiole-3-thiones, and thionesters) have been used to construct a single H_T acidity function, indicating that structural variations have little effect on the protonation behaviour of thiocarbonyl compounds. This is probably the most striking difference between thiocarbonyl compounds and carbonyl compounds. The latter are known to exhibit a diversified acidity function behaviour, aldehydes, ketones, esters, amides, and acids following slightly different acidity functions (1, 9, 37).

Difference between H_T and H_0'''

The apparent closeness of the acidity function scales derived from thiocarbonyl (T) and tertiary aniline (B''') indicators in 10–75% aqueous sulfuric acid does not necessarily imply that the two classes of compounds have identical activity coefficient behaviour. On the contrary, available data indicate that the variation of f_T and f_{TH^+} with acid concentration is quite different from that of $f_{B'''}$ and $f_{B'''H^+}$. However, the difference $H_T - H_0'''$, which equals log $(f_{TH^+}f_{B'''}/f_Tf_{B'''H^+})$, remains small. In 30% acid, log $f_T/f_{B'''} \simeq 0.5$, log $f_{TH^+}/f_{B'''H^+} \simeq 0.6$ and in 40% acid, log $f_T/f_{B'''} \simeq 0.8$, log $f_{TH^+}/f_{B'''H^+} \simeq 0.9$, so that in both cases, log $(f_{TH^+}f_{B'''}/f_Tf_{B'''H^+}) \simeq 0.1$. Thus thioamides are hydrated to a greater extent than tertiary anilines, again probably because of the highly polar nature of the former. But this is compensated for by thioamidonium ions also being hydrated to a greater extent than tertiary anilinium ions, presumably because of the greater number of acid hydrogen atoms available for hydrogen bonding to water molecules.

Acknowledgments

Grateful acknowledgment is made to Dr. G. Welch for discussion about experimental techniques, and to the National Research Council of Canada for financial support.

1. I. LANTOS. Ph.D. Thesis, McGill University, Montreal, P.Q. 1967; G. D. DERDALL. Ph.D. Thesis, McGill University, Montreal, P.Q. 1971; S. C. WONG. Ph.D. Thesis, McGill University, Montreal, P.Q. 1974.
2. E. M. ARNETT and G. W. MACH. J. Am. Chem. Soc. **86**, 2671 (1964); **88**, 1177 (1966).
3. J. T. EDWARD and H. STOLLAR. Can. J. Chem. **41**, 721 (1963).
4. J. T. EDWARD and J. K. LIU. Can. J. Chem. **47**, 1117 (1969); **47**, 1123 (1969).
5. W. I. CONGDON and J. T. EDWARD. J. Am. Chem. Soc. **94**, 6096 (1972).
6. L. P. HAMMETT and A. J. DEYRUP. J. Am. Chem. Soc. **54**, 2721 (1932); **55**, 1901 (1933).
7. J. F. BUNNETT and F. P. OLSEN. Can. J. Chem. **44**, 1899 (1966).
8. L. P. HAMMETT. Physical organic chemistry. 2nd. ed. McGraw Hill, New York. 1970. p. 275.
9. P. BONVICINI, A. LEVI, V. LUCCHINI, G. MODENA, and G. SCORRANO. J. Am. Chem. Soc. **95**, 5960 (1973); A. LEVI, G. MODENA, and G. SCORRANO. J. Am. Chem. Soc. **96**, 6585 (1974).
10. M. J. JORGENSON and D. R. HARTTER. J. Am. Chem. Soc. **85**, 878 (1963).
11. C. TISSIER and M. TISSIER. Bull. Soc. Chim. Fr. 2109 (1972).

12. N. C. MARZIANO, G. M. CIMINO, and R. C. PASSERINI. J. Chem. Soc. Perkin Trans. II, 1915 (1973).
13. H. KUNNE. Ber. **28**, 2036 (1895).
14. J. L. CAVE and D. A. PEAK. J. Chem. Soc. 742 (1952).
15. W. WALTER and K. BODE. Angew. Chem. Int. Ed. Engl. **5**, 447 (1966).
16. G. HOPTKINS and L. HUNTER. J. Chem. Soc. 638 (1942).
17. E. K. KLINGSBERG. J. Org. Chem. **31**, 3489 (1963).
18. M. RENSON and J. BIDAINE. Bull. Soc. Chim. Belg. **70**, 517 (1961).
19. W. J. MIDDLETON, E. L. LITTLE, D. D. COFFMAN, and V. A. ENGELHARDT. J. Am. Chem. Soc. **80**, 2795 (1958).
20. L. M. SWEETING and K. YATES. Can. J. Chem. **44**, 2395 (1966).
21. R. STEWART and M. R. GRANGER. Can. J. Chem. **39**, 2508 (1961).
22. A. J. KRESGE and H. J. CHEN. Anal. Chem. **41**, 74 (1969).
23. R. H. BOYD. J. Am. Chem. Soc. **85**, 1555 (1963).
24. T. BIRCHALL and R. J. GILLESPIE. Can. J. Chem. **41**, 2642 (1963).
25. G. A. OLAH and A. T. KU. J. Org. Chem. **35**, 331 (1970).
26. K. YATES, J. B. STEVENS, and A. R. KATRITZKY. Can. J. Chem. **42**, 1957 (1964).
27. M. A. PAUL. J. Am. Chem. Soc. **76**, 3236 (1954).
28. M. A. PAUL and F. A. LONG. Chem. Rev. **57**, 1 (1957).
29. E. B. ROBERTSON and H. B. DUNFORD. J. Am. Chem. Soc. **86**, 5080 (1964).
30. C. C. GREIG and C. D. JOHNSON. J. Am. Chem. Soc. **90**, 6453 (1968).
31. A. J. KRESGE, H. J. CHEN, and Y. CHIANG. J. Chem. Soc. Chem. Commun. 969 (1972).
32. H. WAI. Ph.D. Thesis, University of Toronto, Toronto, Ont. 1968.
33. E. M. ARNETT, R. P. QUIRK, and J. J. BURKE. J. Am. Chem. Soc. **92**, 1260 (1970).
34. E. M. ARNETT. Progress in physical organic chemistry. Vol. I. *Edited by* S. G. Cohen, A. Streitwieser, and R. W. Taft. Interscience, New York. 1963. p. 223.
35. K. YATES and R. A. MCCLELLAND. Progress in physical organic chemistry. Vol. II. *Edited by* A. Streitwieser and R. W. Taft. John Wiley, New York. 1974. p. 323.
36. G. WELCH. Ph.D. Thesis, University of Toronto, Toronto, Ont. 1969.
37. R. A. MCCLELLAND and W. F. REYNOLDS. Can. J. Chem. **54**, 718 (1976).

Synthetic application of cyclobutanes V.[1] α-Carbalkoxymethylation of α,β-unsaturated ketones

HSING-JANG LIU AND PATRICK CHI-LIN YAO

Department of Chemistry, University of Alberta, Edmonton, Alta., Canada T6G 2G2

Received August 23, 1976

HSING-JANG LIU and PATRICK CHI-LIN YAO. Can. J. Chem. **55**, 822 (1977).

Two general methods for α-carbalkoxymethylation of both enolizable and nonenolizable (towards the γ-position) α,β-unsaturated ketones have been developed. Method A involves three synthetic steps: photocycloaddition of the starting enone to 1,1-dimethoxyethylene, hydrolysis–oxidation of the adduct with acetic acid and 30% hydrogen peroxide, and *O*-alkylation of the resulting mixture of lactone and acid using anhydrous potassium carbonate and an alkyl iodide, *e.g.*, **13** → **17** → **21** + **22** → **23**. Method B differs from method A in the means of securing the required cyclobutanone intermediate. Thus, photocycloaddition of **13** to vinyl acetate followed by hydrolysis of the adduct gave two epimeric keto alcohols **39** whose oxidation with dimethyl sulfoxide and acetic anhydride afforded diketone **40**. Baeyer–Villiger oxidation of **40** followed by methylation of the products **21** and **22** completed the overall α-carbomethoxymethylation process to give keto ester **23**.

HSING-JANG LIU et PATRICK CHI-LIN YAO. Can. J. Chem. **55**, 822 (1977).

On a développé deux méthodes générales pour effectuer l'α-carbalkoxyméthylation de cétones α,β-nonsaturées énolisables ainsi que nonénolisables (vers la position γ). La méthode A implique trois étapes de synthèse: une photocycloaddition de l'énone de départ avec le diméthoxy-1,1 méthylène, une hydrolyse avec oxydation de l'adduit par l'acide acétique en présence de peroxyde hydrogène à 30%, et finalement une *O*-alkylation du mélange de lactone et d'acide qui en résulte faisant appel à du carbonate de potassium anhydre et un iodure d'alkyle, par exemple **13** → **17** → **21** + **22** → **23**. La méthode B diffère de la méthode A par les moyens utilisés pour obtenir la cyclobutanone requise comme intermédiaire. Ainsi la photocycloaddition de **13** sur de l'acétate de vinyle suivie par une hydrloyse de l'adduit conduit à deux cétoalcools épimères **39** qui par oxydation avec le diméthyle sulfoxyde et anhydride acétique fournissent la dicétone **40**. Une oxydation de Baeyer–Villiger de **40** suivie par une méthylation des produits **21** et **22** obtenus complète le processus global d'α-carbométhoxyméthylation conduisant au cétoester **23**.

[Traduit par le journal]

Introduction

The utilization of the photocycloaddition reaction as a potential method for the introduction of a single alkyl chain specifically to the α-carbon of an α,β-unsaturated ketone was first demonstrated in the total synthesis of the *Ormosia* skeleton (5). The crucial step of alkylation of the nonenolizable enone **1** in the synthesis was achieved via a suitably substituted cyclobutane intermediate **2** using a three-step sequence (Scheme 1). This procedure was, however, later shown to be limited to α,β-unsaturated ketones in which the enolization of the ketone group towards the α′-carbon was not possible due to either substitution or strain; the preferential incorporation of a leaving group into the desirable α-position which was required for a Grob fragmentation (**3** → **4**) (6) was found difficult in cases in which the α′-carbon was also reactive (7). Using a photocycloaddition reaction as a general entry, two additional methods were subsequently developed. Valenta and coworkers (7) showed that the photoadducts of 2-cyclohexen-1-ones and enol acetates after hydrolysis underwent oxidative cleavage of the cyclobutane ring upon treatment with a variety of oxidants, in particular, ceric ammonium nitrate, to give products of type **5** (Scheme 2). More recently photoadducts of conjugated enones and vinylene carbonate were found to undergo fragmentation with alkali to yield compounds of type **6** (Scheme 3) (8). These α-monoalkylation procedures are synthetically attractive. In addition to providing useful 1,4-dicarbonyl compounds of broad synthetic interest,[2] by virtue of the mode of the initial photocycloaddition

[1]For parts I–IV of this series, see refs. 1–4 respectively.

[2]For a relevant discussion see ref. 7.

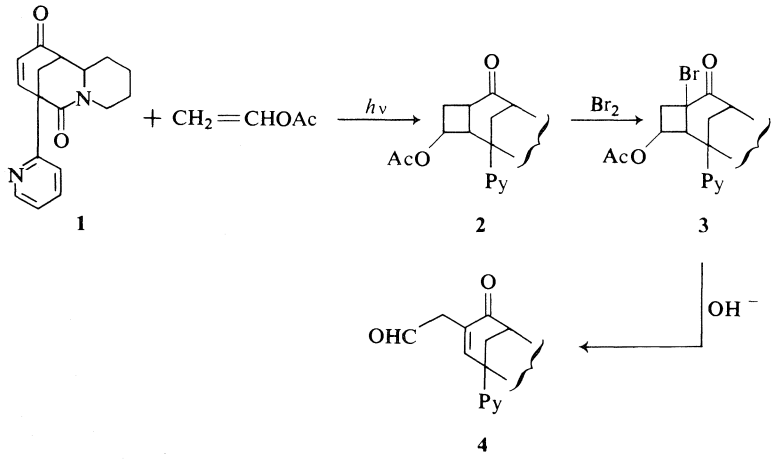

SCHEME 1

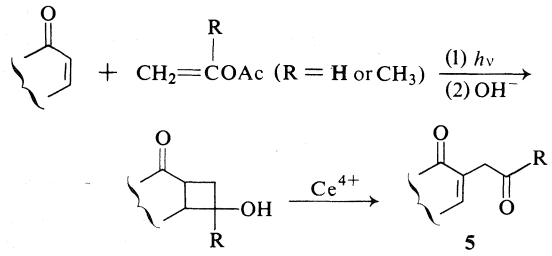

SCHEME 2

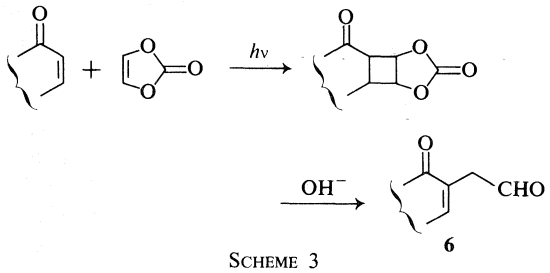

SCHEME 3

reaction, they have the following outstanding features in comparison with the conventional alkylation methods (9). (*i*) An enolizable γ-hydrogen atom is not required to effect the alkylation.[3] (*ii*) The position of the double bond in the starting enone fully determines the site of the addition. (*iii*) The introduction of a single activated alkyl chain can be readily controlled.

[3]Though no specific examples were given, the method cited in ref. 8 is apparently applicable to α,β-unsaturated ketones without an enolizable γ-hydrogen atom. This method has recently been extended to uracil (10) and its nucleoside (11).

Although the above procedures differ from each other in principle, they all furnish 1,4-dicarbonyl compounds of the type **5**, in which, of the three possible sites for nucleophilic attack, the side chain carbonyl has been shown to be usually more reactive (5, 12). Consequently, in cases in which the transformation of the enone system, *e.g.*, addition of Grignard reagent, is subsequently desired, it is necessary to modify the side chain in advance (12). In order to circumvent this deficiency, complementary methods allowing the direct incorporation of a less reactive functionality into the side chain are needed. We wish to report two new photochemical routes which facilitate the α-monocarbalkoxymethylation of both enolizable α,β-unsaturated ketones and those in which enolization toward the γ-position is blocked.[4]

Results and Discussion

Conceptually, the α-alkylation of both enolizable and nonenolizable α,β-unsaturated ketones can be achieved by concomitant Michael type addition and cyclization, using a reagent which possesses both a nucleophilic center and a leaving group, followed by β-elimination as illustrated schematically in Scheme 4. In practice, such a scheme poses obvious problems; the reagent chosen may easily undergo polymerization or internal cyclization. It is conceivable, however, to achieve a similar transformation by the use of a cycloaddition reaction,

[4]A part of this work has been reported in preliminary form (4). A number of reactions have since been improved.

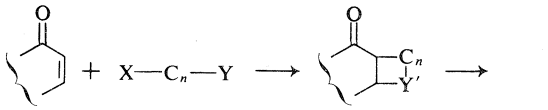

X = Leaving group
Y = Nucleophile

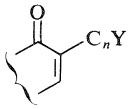

SCHEME 4

e.g., Diels–Alder reaction or photocycloaddition, to form two carbon–carbon bonds to give compounds of type **7** (as shown in Scheme 5)

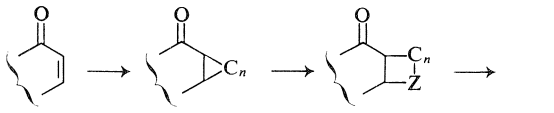

7 **8**

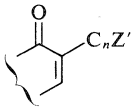

SCHEME 5

followed by selective introduction of a leaving group at the β-position as shown in **8**. The present studies followed this principle and the photochemical route has been used as the initial cycloaddition.

In order to facilitate the incorporation of the desired leaving group, it is necessary to activate the cyclobutane ring resulting from the photochemical process. In the first approach (method A) 1,1-dimethoxyethylene was selected for this purpose since it has been well established that its addition to conjugated enones proceeds in a head-to-tail fashion to give adducts of type **9** (13). The hydrolysis of **9** was expected to provide **10** which in principle could undergo selective Baeyer–Villiger oxidation under controlled reaction conditions to give desirable intermediates such as **11** for the regeneration of the initial double bond in the starting enone and thus completing an overall α-alkylation of a conjugated enone.

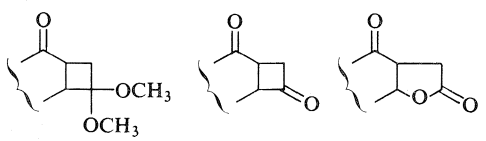

9 **10** **11**

In order to test the feasibility and generality of this alkylation procedure, four representative enones **12**–**15** were examined. The results of their photocycloaddition to 1,1-dimethoxyethylene are compiled in Table 1.

The photocycloadditions proceeded with a high degree of regioselectivity. The relative orientation of the functionalities of the photoadduct in each case follows unambiguously from further transformations. Photoadducts **16** and **17** were obtained as a mixture of *cis* and *trans* isomers. The mixture nature of these products was revealed by their nuclear magnetic resonance (nmr) spectra. Four singlets at τ 8.93, 8.89, 8.86, and 8.74 were observed for the *gem*-dimethyl group of **16** in its nmr spectrum, whereas compound **17** showed in the nmr spectrum a total of six singlets at τ 9.04, 8.98, 8.93, 8.88, 8.78, and 8.69 for the three methyl substituents. Since the two chiral centers presented in these molecules would be subsequently destroyed, no attempts were made to separate the two isomers.

Photoadduct **18** was thought to be a single stereoisomer since gas–liquid chromatography (glc) analysis showed a single peak for the distilled compound and its nmr spectrum displayed a singlet for the acetyl group at τ 8.10 and two singlets at τ 7.05 and 6.92 for the methoxy groups. The data available, however, do not permit unambiguous definition of its stereochemistry.

Photocycloaddition of enone **15** to 1,1-dimethoxyethlyene gave a mixture of two isomers, one of which crystallized readily from Skelly B. The mother liquor enriched in the other isomer was subsequently boiled with aqueous sodium hydroxide in methanol to epimerize it and to provide an additional crop of the first isomer. The ring junction of the crystalline compound thus obtained could readily be assigned as *cis*, since it has been established that in the bicyclo-[4.2.0]octan-2-one systems, the *trans* ring junction is readily epimerized upon treatment with base to give the thermodynamically more stable *cis* form (13). The nmr spectrum of the isolated crystalline photoadduct was in full agreement with its assigned stereochemistry. The two singlets for the methoxy groups appeared at τ 6.73 and 7.07. The appearance of one methoxy group at abnormally high field could be attributed to the shielding effect of the benzene

TABLE 1. Photocycloaddition of conjugated enones to 1,1-dimethoxyethylene

Enone	Photoadduct obtained	Isolated yield (%)
 12	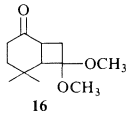 16	78
 13	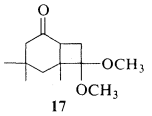 17	71
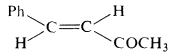 14	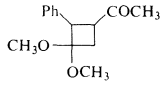 18	37
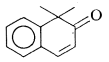 15	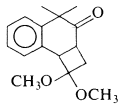 19	81

ring and suggested that the ring junction of the compound was *cis*, since inspection of Drieding models revealed that the methoxy group could be shielded by the benzene ring only when the rings were so fused.

The subsequent two-step transformation of the photoadducts **16**–**19** into compounds of type **20**, illustrated in Scheme 6 for the conversion of photoadduct **17** to keto ester **23**, completed the

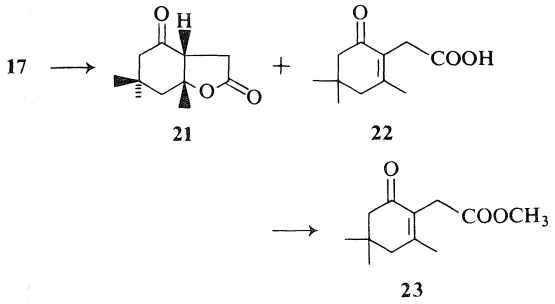

SCHEME 6

overall α-carbalkoxyalkylation of a conjugated enone. Treatment of **17** with a solution of 30% hydrogen peroxide in glacial acetic acid, 1:1, furnished a mixture of keto lactone **21** and acid **22** as a result of concomitant deketalization, selective Baeyer–Villiger oxidation, and partial lactone ring cleavage. For the purpose of identification, the crystalline lactone **21**[5] could be isolated by extensive chromatography of the crude mixture. Attempts to purify the acid **22** were futile, due to its rapid conversion to the lactone **21**. For further conversion, the mixture of **21** and **22** was boiled with fivefold excess of anhydrous potassium carbonate and a large excess of methyl iodide in acetone. After 2 days, keto ester **23** was isolated in 42% yield based on **17**. Similarly, photoadduct **16** was transformed into **24** via intermediates lactone **25** and acid **26** in 41% overall yield.

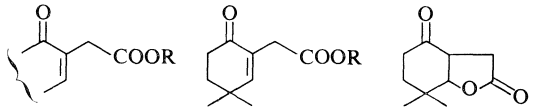

20 **24** R = CH_3 **25**
26 R = H

In the case of photoadduct **19**, the hydrolysis–oxidation proceeded abnormally. In addition to

[5]Its stereochemistry follows from the fact that Baeyer–Villiger oxidation (which is known to proceed with retention of configuration (14)) of **40** with *m*-chloroperbenzoic acid gave the same lactone as the only product.

the expected products, lactone **27** and acid **28** (a total yield of 51%), a 24% yield of ester **29** was also obtained. When the mixture of **27**, **28**, and **29** was subjected to alkylation under the conditions described previously, another mixture was obtained. Though it was found to be homogeneous on thin-layer chromatography (tlc), glc analysis showed two partially overlapped peaks. Besides the expected peak at 244, the mass spectrum showed an additional peak of approximately equal intensity at 258. Exact mass measurements of these two peaks indicated a difference of a methylene unit. Although there were insufficient data to permit conclusive assignments of the identities of the two components, it was logical to deduce from the mode of the reaction that the mixture consisted of the desired ester **29** and the dialkylated compound **30**.

As a consequence of this finding, methyl iodide was replaced by a less reactive alkylating agent, namely, isopropyl iodide, in the alkylation step. As anticipated, this modification circumvented the dialkylation problem and a mixture of esters **29** and **31** was obtained. Separation of these two compounds was achieved by extensive column chromatography on silica gel. The yields of the pure substances were low, due to the loss of material incurred during the purification. It was found more convenient to separate ester **29** from lactone **27** and acid **28** prior to the alkylation reaction. Subsequent treatment of **27** and **28** with isopropyl iodide and potassium carbonate in acetone resulted in the formation of ester **31** in 71% yield. Accordingly, from photoadduct **19**, methyl ester **29** and isopropyl ester **31** were obtained in a ratio of 1:1.5 and in a total yield of 60%.

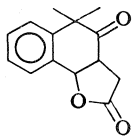

27

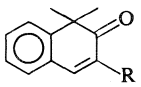

28 R = CH_2COOH
29 R = CH_2COOCH_3
30 R = $CH(CH_3)COOCH_3$
31 R = $CH_2COOCH(CH_3)_2$

Upon hydrolysis–oxidation and subsequent alkylation under the same conditions which effected the transformation of **17** → **23**, photoadduct **18** gave rise to a 58% yield of a mixture of **32**, **33**, and **34** in the ratio of *ca.* 4:1:1 via intermediates **35** and **36**. The major product could be separated by column chromatography and its structure readily assigned as **32** on the basis of the spectral data. The minor components were obtained as a mixture of **33** and **34** as indicated by the mass spectrum showing two molecular ion peaks at 232 and 218. The two singlets at τ 8.10 and 8.07 in the nmr spectrum confirmed the presence of two acetyl groups while a high field doublet at τ 8.47 could be accounted for by the extra methyl group introduced during the alkylation. The stereochemistry of **33** and **34** was assigned as shown because of the shielding on the acetyl groups with respect to *trans*-benzalacetone as observed in the nmr spectrum. The shielding effect indicated that the acetyl group, in each case, was in the proximity of the phenyl group, which required that these two groups be *cis*. The major ester, the acetyl singlet of which appeared in the nmr spectrum at τ 7.60, was consequently assigned the *trans* structure **32**.

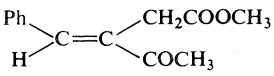

32

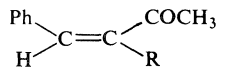

33 R = CH_2COOCH_3
34 R = $CH(CH_3)COOCH_3$

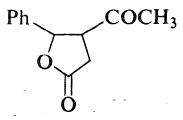

35

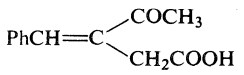

36

The second method (method B) is based on the same principle as that previously described for method A but differs from it in the means of securing the required cyclobutanone intermediate, *e.g.* **39**. Whereas in method A the cyclobutanone moiety was incorporated directly in the ketal form in the initial photochemical process and later generated *in situ*, it was produced in method B by oxidation of the corresponding alcohol which, in turn, was prepared in two steps from the starting enone and vinyl acetate. Thus, irradiation of a benzene solution of isophorone **13** and vinyl acetate afforded an 85% yield of a mixture consisting of at least two diastereomers of **37**. Hydrolysis of **37** with aqueous potassium carbonate in methanol gave a 98% yield of two epimeric alcohols **38** (1). Subsequent oxidation of **38** using dimethyl sulfoxide and acetic anhydride (15) at 5 °C resulted in the formation of diketone **39** in 91% yield. Transformation of **39** to **23** (67%) com-

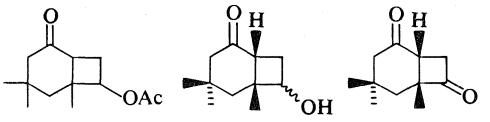

37 38 39

pleted the overall α-carbomethoxymethylation process in two steps under reaction conditions similar to those used for **17** → **23**. This procedure was shown to be equally applicable to α,β-unsaturated ketones in which enolization toward the γ-position is blocked. By the same reaction sequence, the conversion of **12** into **24** was achieved in an overall yield of 45% by the route outlined in Scheme 7.

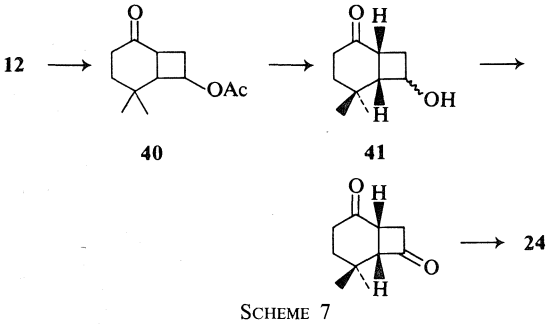

SCHEME 7

Both methods provide comparable overall yields for the conversion. Where the starting enone is easily obtainable, method B would be preferable because of the availability of the reagent required, *i.e.*, vinyl acetate. Method A however has the advantage of having relatively few steps and is more suitable in cases where the starting enone is not as easily obtained.

Experimental

General

Melting points were determined on a Kofler hot stage apparatus and are uncorrected. Mass spectra were recorded on AEI MS-50, MS-9, and MS-2 spectrometers. Infrared spectra were obtained by using Perkin-Elmer model 457 and 337 spectrophotometers. Nuclear magnetic resonance spectra were recorded on Varian A-60, 90 MHz Perkin-Elmer 32 and HR-100 spectrometers. Unless otherwise stated, carbon tetrachloride was employed as the solvent and tetramethylsilane as internal standard. The following abbreviations are used in the text: s singlet, d doublet, t triplet, q quartet, and m multiplet. Elemental analyses were performed by the microanalytical laboratory of this department. Gas chromatographic analyses were performed using an Aerograph A-90-P-3 with a column of 15% SE 30 on Chromosorb W.

Materials

The commercially available isophorone **13** and *trans*-benzalacetone **14** were freshly distilled under reduced pressure before use. 4,4-Dimethyl-2-cyclo-hexene-1-one **12** (16) and 1,1-dimethyl-2-oxo-1,2-dihydronaphthalene **15** (17) were synthesized according to the described procedures. 1,1-Dimethoxyethylene was obtained from dehydrobromination (13) of bromoacetaldehyde dimethylacetal which was prepared according to the reported procedure (18) with the modification of using methanol instead of ethanol as a solvent.

General Procedure for Photocycloaddition Reactions

The enone used was dissolved in *ca.* 15 mol excess of 1,1-dimethoxyethylene or 20 mol excess of vinyl acetate. The solution was then diluted with benzene to four or five times its original volume. A constant and moderate flow of dry and oxygen-free nitrogen was maintained to agitate the solution throughout the reaction period. The solution was irradiated using a 450 W Hanovia high-pressure quartz mercury-vapor lamp and a Pyrex filter at ~0 °C (ice bath) for 6–20 h. The progress of the reaction was monitored by checking the ir of an aliquot of the reaction mixture. Concentration of the resulting solution gave the crude adduct.

7,7-Dimethoxy-5,5-dimethylbicyclo[4.2.0]octan-2-one ***16***

4,4-Dimethyl-2-cyclohexen-1-one **12** (3.589 g, 28.94 mmol) and 1,1-dimethoxyethylene (40 g, 0.45 mol) were dissolved in benzene (~120 ml). The solution was irradiated for 15 h. The solvent and the unreacted olefin were distilled off at atmospheric pressure and the residue was subjected to bulb-to-bulb distillation at 108–112 °C/3 torr to give **16** (4.767 g, 78%): nmr τ 8.93, 8.89, 8.86, and 8.74 (all s, total 6H, *gem*-dimethyl), 6.82 (s, 6H, 2 OCH_3); ir (film) 1735 cm^{-1} (ketone); ms M^+ 212.1419 (calcd. for $C_{12}H_{20}O_3$: 212.1413).

7,7-Dimethoxy-4,4,6-trimethylbicyclo[4.2.0]octan-2-one ***17***

Irradiation (16 h) of isophorone **13** (4.272 g, 30.96 mmol) and 1,1-dimethoxyethylene furnished after distilling the crude product from bulb-to-bulb at 107–112 °C/1.7 torr, photoadduct **17** (4.969 g, 71%): nmr τ 9.04, 8.98, 8.93, 8.88, 8.78, and 8.69 (all s, total 9H, 3 CH_3), 6.88 and 6.84 (both s, 3H each, 2 OCH_3); ir (film) 1720 cm^{-1} (ketone); ms M^+ 226.1214 (calcd. for $C_{13}H_{22}O_3$: 226.1205).

3-Acetyl-1,1-dimethoxy-2-phenylcyclobutane ***18***

Irradiation (20 h) of *trans*-benzalacetone **14** (15.08 g, 0.103 mol) and 1,1-dimethoxyethylene gave rise to, after bulb-to-bulb distillation of the crude product at 82–125 °C/0.8–3.1 torr, **18** (8.850 g, 37%): nmr τ 8.10 (s, 3H, $COCH_3$), 7.05 (s, 3H, OCH_3), and 6.92 (s, 3H, OCH_3); ir (film) 1710 cm^{-1} (ketone); ms M^+ 234.1259 (calcd. for $C_{14}H_{18}O_3$: 234.1256).

cis-6,6-Dimethoxy-2,2-dimethyltricyclo[6.4.0.0^{4,7}]dodecan-1,9,11-triene-3-one ***19***

The crude product obtained from the photocycloaddition of 1,1-dimethyl-2-oxo-1,2-dihydronaphthalene **15** (8.256 g, 48 mmol) to 1,1-dimethoxyethylene (irradiated for 9 h) was dissolved in Skelly B. Upon standing at 0 °C, crystalline material **19**, mp 104.5–106 °C, was obtained. The mother liquor was concentrated and dissolved in 10 ml of methanol. One drop of 2.5 *N* aqueous sodium hydroxide was added and the resulting solution

was refluxed under nitrogen for 4 h. The reaction mixture was diluted with water and extracted with ether. The product obtained after the usual work-up of the organic solution was dissolved in Skelly B. After standing at 0 °C, it afforded an additional crop of **19**. The total amount of **19** thus obtained was 11.76 g (81%). Compound **19** exhibited the following spectral data: nmr ($CDCl_3$) τ 8.65 (s, 3H, CH_3), 8.45 (s, 3H, CH_3), 7.07 (s, 3H, OCH_3), 6.73 (s, 3H, OCH_3), and 2.60–2.82 (m, 4H, aromatic); ir ($CHCl_3$) 1710 cm^{-1} (ketone); ms M^+ 260.1408 (calcd. for $C_{16}H_{20}O_3$: 260.1413). *Anal.* calcd. for $C_{16}H_{20}O_3$: C 73.82, H 7.74; found: C 73.55; H 7.92.

7-Acetoxy-4,4,6-trimethylbicyclo[4.2.0]octan-2-one **37**

A solution of isophorone **13** (20 g, 0.145 mol) and vinyl acetate (250 g, 2.9 mol) in benzene was irradiated for 6 h. Column chromatography of the crude product on silica gel using a solution of 5% ether in benzene as eluent gave 27.6 g (85%) of **37**: ir (film) 1740 (ester) and 1705 cm^{-1} (ketone); nmr τ 4.67–5.53 (complex, total 1H, CHOAc), 7.98, 8.01 (both s, total 3H, $OCOCH_3$), and 8.81–9.08 (8 s, total 9H, 3 CH_3); ms M^+ 224.1413 (calcd. for $C_{13}H_{20}O_3$: 224.1413). *Anal.* calcd. for $C_{13}H_{20}O_3$: C 69.61, H 8.99; found: C 69.69, H 9.10.

7-Acetoxy-5,5-dimethylbicyclo[4.2.0]octan-2-one **40**

The crude product obtained after irradiating enone **12** (3.49 g, 28.15 mmol) and vinyl acetate (50 g, 0.58 mol) for 16 h was subjected to short-path distillation to give a mixture of four diastereomers of **40** (4.66 g, 79%): bp 89–94 °C/0.1 torr; nmr τ 4.67–5.38 (complex, total 1H, CHOAc), 7.96, 8.00, 8.02, 8.04 (all s, total 3H, $OCOCH_3$), and 8.81–9.09 (7 s, total 6 H, 2 CH_3); ir (film) 1730 (ester) and 1705 cm^{-1} (ketone); ms M^+ 210.12518 (calcd. for $C_{12}H_{18}O_3$: 210.12560). *Anal.* calcd. for $C_{12}H_{18}O_3$: C 68.55, H 8.63; found: C 68.17, H 8.72.

General Procedure for the Hydrolysis–Oxidation of the Photoadducts ***16–19***

The reaction was carried out in such a manner that 1 g of the photoadduct was dissolved in 10 ml of acetic acid – 30% hydrogen peroxide (1:1) solution and the resulting solution was stirred at room temperature. The progress of the reaction was monitored by tlc. At the end of the reaction (6–7 h for photoadducts **16–18** and 3 h for **19**), the solution was diluted with water and extracted with chloroform. The chloroform solution was washed with aqueous sodium bisulfite and saturated sodium chloride solutions. Drying ($MgSO_4$), filtration, and concentration gave the crude product.

cis-4,4,6-Trimethyl-7-oxabicyclo[4.3.0]nonane-2,8-dione ***21*** *and 2-Carboxymethyl-3,5,5-trimethyl-2-cyclohexene-1-one* ***22***

From photoadduct **17** (1.352 g, 6 mmol) a mixture of lactone **21** and acid **22** (700 mg, ~60%) was obtained. The crude mixture was used without purification for further transformation (see below). An analytical sample of **21** was obtained by column chromatography of the crude reaction product on silica gel with 30% benzene in Skelly B elution, followed by crystallization (petroleum ether – ether): mp 116–117 °C; nmr τ 6.45–7.40 (m, 3H, CH_2 and CH), 7.68 (s, 2H, CH_2), 8.49 (s, 3H, CH_3), 8.90 (s, 3H, CH_3), and 9.10 (s, 3H, CH_3); ir ($CHCl_3$) 1770 (lactone) and 1712 cm^{-1} (ketone); ms M^+ 196.1104 (calcd. for $C_{11}H_{16}O_3$: 196.1101). *Anal.* calcd. for $C_{11}H_{16}O_3$: C 67.32, H 8.22; found: C 67.56, H 8.26.

Acid **22** was found to undergo rapid lactonization to give **21** and was not obtained in pure form.

5,5-Dimethyl-7-oxabicyclo[4.3.0]nonane-2,8-dione ***25*** *and 2-Carboxymethyl-4,4-dimethyl-2-cyclohexene-1-one* ***26***

Photoadduct **16** (962 mg, 4.54 mmol) was treated with acetic acid – 30% hydrogen peroxide according to the general procedure to give a mixture of lactone **25** and acid **26** (668 mg, ~81%): ir (film) 2700–3450 (acid), 1768 (lactone), 1715 (ketone and acid) and 1665 cm^{-1} (ketone). Attempts made to separate these two compounds were unsuccessful due to their rapid interconversion and the mixture was used for the subsequent alkylation reaction.

2,2-Dimethyl-7-oxatricyclo[7.4.0.0^{4,8}]trideca-1,10,12-triene-3,6-dione ***27****, 3-Carboxymethyl-2,2-dimethyl-2-oxo-1,2-dihydronaphthalene* ***28****, and 3-Carbomethoxymethyl-2,2-dimethyl-2-oxo-1,2-dihydronaphthalene* ***29***

Hydrolysis–oxidation of photoadduct **19** (2.04 g, 7.85 mmol) under the described conditions gave 1.623 g of the crude product. A portion of this material (1.258 g) was purified by column chromatography on silica gel. Elution with a solution of 30% benzene in Skelly B gave 96 mg (7%) of lactone **27**. Further elution with the same solvent, gave 301 mg (24%) of ester **29**. Final elution with a solution of 10% methanol in ether afforded acid **28** (620 mg, 45%).

Compound **27** was crystallized from chloroform to give a constant mp of 109–110 °C and showed the following spectral data: nmr (CD_3OD) τ 2.55–2.82 (m, 4H, aromatic), 5.05 (t of d, J = 10 Hz, J' = 1.5 Hz, 1H, CO_2CH), 6.18–6.77 (m, 3H, CHCO, and CH_2CO_2), 8.45 (s, 3H, CH_3), and 8.55 (s, 3H, CH_3); ir ($CHCl_3$) 1785 (lactone), 1715 cm^{-1} (ketone); ms M^+ 230.

An analytical sample of **29** was obtained by bulb-to-bulb distillation at 127–131 °C (oven temperature)/0.2 torr and showed the following spectral data: nmr τ 2.66–2.88 (m, 5H, aromatic and vinylic), 6.33 (s, 3H, CO_2CH_3), 6.67 (s, 2H, $CH_2CO_2CH_3$), and 8.57 (s, 6H, *gem*-dimethyl); ir (film) 1735 (ester) and 1660 cm^{-1} (ketone); ms M^+ 244.1099 (calcd. for $C_{15}H_{16}O_3$: 244.1086). *Anal.* calcd. for $C_{15}H_{16}O_3$: C 73.75, H 6.60; found: C 73.69, H 6.59.

Acid **28** was crystallized from chloroform to a constant mp of 144–145 °C and displayed the following spectral data: nmr ($CDCl_3$) τ 2.50–2.82 (m, 5H, aromatic and vinylic), 6.55 (s, 2H, CH_2CO_2H), and 8.53 (s, 6H, *gem*-dimethyl); ir ($CHCl_3$) 2700–3500 (acid), 1720 (acid) and 1660 cm^{-1} (ketone); ms M^+ 230.0943 (calcd. for $C_{14}H_{14}O_3$: 230.0933).

3-Acetyl-5-oxo-2-phenylcycloxapentane ***35*** *and 3-Benzilidene-4-oxopentanoic Acid* ***36***

Photoadduct **18** (3.128 g, 13.4 mmol) was subjected to acetic acid – 30% hydrogen peroxide treatment to give a mixture of **35** and **36** (2.599 g, 95%) which was used without purification for the subsequent transformation.

General Procedure for Methylation of Hydrolysis–Oxidation Products of Photoadducts ***16–19***

The crude mixture obtained from the hydrolysis–oxidation of the photoadduct was dissolved in acetone (0.1 g/ml). Anhydrous potassium carbonate (~5 mol equiv.) and methyl iodide (~2 ml/1 g of reactant) were

added. The resulting mixture was refluxed under a nitrogen atmosphere for 1–4 days. After cooling to room temperature, the mixture was diluted with water and extracted with chloroform. The organic solution was washed with water, dried with $MgSO_4$, filtered, and concentrated. The crude product thus obtained was purified by column chromatography on silica gel using a solution of 10% ether in benzene as eluent.

2-Carbomethoxylmethyl-3,5,5-trimethyl-2-cyclohexene-1-one ***23***

The crude mixture of **21** and **22** (0.458 g) obtained directly from **17** was subjected to methylation conditions for 2 days according to the general procedure resulting in the formation of **23** (326 mg, 42% based on **17**): nmr τ 8.95 (s, 6H, *gem*-dimethyl group), 8.10 (s, 3H, CH_3), 7.82 (s, 2H, CH_2), 7.72 (s, 2H, CH_2), 6.73 (s, 2H, $CH_2CO_2CH_3$), and 6.38 (s, 3H, CO_2CH_3); ir (film) 1665 (ketone), and 1740 cm^{-1} (ester); ms M^+ 210.1263 (calcd. for $C_{12}H_{20}O_3$: 210.1256). *Anal.* calcd. for $C_{12}H_{20}O_3$: C 68.28, H 8.89; found: C 68.54, H 8.63.

2-Carbomethoxymethyl-4,4-dimethyl-2-cyclohexene-1-one ***24***

The crude mixture of **25** and **26** (688 mg) directly obtained from photoadduct **16**, was treated under the described reaction conditions for 2 days to give **24** (362 mg, 41% based on **16**): nmr τ 3.54 (s, 1H, vinylic), 6.34 (s, 3H, CO_2CH_3), and 6.96 (s, 2H, $CH_2CO_2CH_3$); ir (film) 1740 (ester), and 1665 cm^{-1} (ketone); ms M^+ 196.1101 (calcd. for $C_{11}H_{16}O_3$: 196.1099). *Anal.* calcd. for $C_{11}H_{16}O_3$: C 67.32, H 8.22; found: C 67.52, H 8.16.

3-(1′-Carbomethoxyethyl)-1,1-dimethyl-2-oxo-1,2-dihydronaphthalene ***30*** *and 3-Carbomethoxymethyl-1,1-dimethyl-2-oxo-1,2-dihydronaphthalene* ***29***

Attempted monomethylation of a mixture of **27**, **28**, and **29** (800 mg) in crude form with methyl iodide and potassium carbonate under the usual conditions for 3 days gave 640 mg of a mixture consisting of **30** and **29**: ir (film) 1740 (esters) and 1660 cm^{-1} (ketones); ms M^+ 258.1246 (calcd. for $C_{16}H_{18}O_3$: 258.1256) and 244.1094 (calcd. for $C_{15}H_{16}O_3$: 244.1099).

(E)-Methyl-3-benzilidene-4-oxopentanoate ***32****, (Z)-Methyl-3-benzilidene-4-oxopentanoate* ***33****, and (Z)-Methyl-3-benzilidene-2-methyl-4-oxopentanoate* ***34***

The crude mixture (279 mg) obtained from the hydrolysis–oxidation reaction of photoadduct **18** was methylated according to the general procedure for 1 day. After purification, the major product **32** (127 mg, 40% based on **18**; slower moving) was obtained in pure form and **33** and **34** as a 1:1 (nmr) mixture (58 mg, 18% based on **18**). The major product showed the following spectral data: nmr τ 2.42 (s, 1H, vinylic), 2.58–2.85 (m, 5H, aromatic), 6.65 (s, 2H, $CH_2CO_2CH_3$), 6.35 (s, 3H, CO_2CH_3), and 7.60 (s, 3H, $COCH_3$); ir (film) 1740 (ester) and 1660 cm^{-1} (ketone); ms M^+ 218.0947 (calcd. for $C_{13}H_{14}O_3$: 218.0943).

The mixture showed the two parent molecular ion peaks in the mass spectrum at 218 and 232. The nmr spectrum showed signals at τ 8.07 (s, $COCH_3$), 8.10 (s, $COCH_3$), and 8.58 (d, J = 7 Hz, CH_3) in 1:1:1 ratio.

Isopropylation of ***27*** *and* ***28***

Lactone **27** (96 mg) and acid **28** (483 mg) were dissolved in acetone (20 ml). Anhydrous potassium carbonate (1.7 g) and isopropyl iodide (1 g) were added. The resulting mixture was refluxed under nitrogen for 20 h. After the usual work-up, the oily product was purified by column chromatography on silica gel. Elution with a solution of 10% ether in benzene afforded 3-carbisopropoxymethyl-1,1-dimethyl-2-oxo-1,2-dihydronaphthalene **31** (320 mg, 71% based on consumed starting material (see below)): nmr τ 2.55–2.80 (m, 5H, aromatic and vinylic), 8.53 (s, 6H, *gem*-dimethyl), 8.78 (d, 6H, J = 6 Hz, $CO_2CH(CH_3)_2$); ir (film) 1740 (ester) and 1660 cm^{-1} (ketone); ms M^+ 272.1412 (calcd. for $C_{17}H_{20}O_3$: 272.1413). Further elution with a solution of 10% methanol in ether afforded 210 mg of the starting acid **28**.

7-Hydroxy-4,4,6-trimethylbicyclo[4.2.0]octan-2-one ***38***

To a solution of **37** (1.805 g, 8.06 mmol) in methanol (20 ml), was added saturated aqueous potassium carbonate solution (20 ml). The reaction mixture was refluxed under an atmosphere of nitrogen for 3 h. After cooling to room temperature, the reaction mixture was poured into water and extracted with chloroform. Drying ($MgSO_4$), filtration, and concentration gave an oil which was chromatographed on silica gel. Elution with a solution of 20% ether in benzene gave **38** (1.438 g, 98%): ir (film) 3400 (alcohol) and 1690 cm^{-1} (ketone); nmr τ 5.56–6.40 (complex, 2H, CHOH), 8.76, 8.79, 8.90, 8.99, 9.02, and 9.11 (all s, total 9H, 3 CH_3); ms M^+ 182.1305 (calcd. for $C_{11}H_{18}O_2$: 182.1306). *Anal.* calcd. for $C_{11}H_{18}O_2$: C 72.49, H 9.95; found: C 72.69, H 10.25.

4,4,6-Trimethylbicyclo[4.2.0]octane-2,7-dione ***39***

A solution of **38** (1.438 g, 7.9 mmol) in dimethyl sulfoxide (15 ml) and acetic anhydride (10 ml) was kept at 5 °C for 4 days. Water (30 ml) was added and the resulting solution, after stirring at room temperature for 2 h, was extracted with chloroform. The chloroform solution was washed with saturated aqueous sodium carbonate and water, dried ($MgSO_4$), filtered, and concentrated. The crude product was chromatographed on silica gel with a solution of 5% ether in benzene as eluent to give **39** (1.294 g, 91%): ir (film) 1778 (ketone) and 1700 cm^{-1} (ketone); nmr τ 6.53 (dd, 1H, J = 18, J' = 10 Hz, $COCH_2CH$), 6.93 (dd, 1H, J = 18, J' = 5 Hz, $COCH_2CH$), 7.42 (dd, 1H, J = 10, J' = 5 Hz, COCH), 8.68 (s, 3H, CH_3), 8.98 (s, 3H, CH_3), and 9.17 (s, 3H, CH_3); ms M^+ 180.1148 (calcd. for $C_{11}H_{16}O_2$: 180.1150).

Keto Ester ***23*** *from* ***39***

Diketone **39** (1.156 g, 6.42 mmol) was dissolved in glacial acetic acid (15 ml) and 30% hydrogen peroxide (15 ml) was slowly added. The reaction mixture was stirred at room temperature for 16 h. Water (50 ml) was added and the resulting solution extracted with chloroform. The extracts were washed with aqueous sodium bisulfite solution and water. Drying ($MgSO_4$), filtration, and concentration gave a mixture of **21** and **22** (1.07 g, ~85%) which, without purification, was dissolved in acetone (15 ml) and anhydrous potassium carbonate (3.8 g) and methyl iodide (2 ml) were added. The reaction mixture was refluxed under a nitrogen atmosphere for 2 days. After cooling to room temperature, the mixture was poured into water and extracted with chloroform. The organic solution, after the usual work-up gave an oily product which was purified by column

chromatography on silica gel. Elution with a solution of 10% ether in benzene afforded **23** (903 mg, 67% from **39**).

7-Hydroxy-5,5-dimethylbicyclo[4.2.0]octan-2-one ***41***

Saturated aqueous sodium carbonate solution (10 ml) was added to a solution of **40** (449 mg, 2.14 mmol) in methanol (10 ml). The reaction mixture was stirred at room temperature under a nitrogen atmosphere for 16 h. Work-up in the usual manner followed by column chromatography of the oily product on silica gel using a solution of 20% ether in benzene as eluent gave **41** (348 mg, 97%): ir (film) 3420 (alcohol) and 1700 cm^{-1} (ketone); nmr τ 5.42–6.44 (complex, 2H, CHOH), 8.90, 8.92, 8.98, and 9.02 (all s, total 6H, *gem*-dimethyl); ms M^+ 168.1154 (calcd. for $C_{10}H_{16}O_2$: 168.1150). *Anal.* calcd. for $C_{10}H_{16}O_2$: C 71.39, H 9.59; found: C 71.64, H 9.44.

5,5-Dimethylbicyclo[4.2.0]octane-2,7-dione ***42***

Under the same conditions described previously for the oxidation of **38** to **39**, keto alcohol **41** (252 mg, 1.5 mmol) was treated with dimethyl sulfoxide (3 ml) and acetic anhydride (2 ml). Chromatography of the crude product on silica gel with benzene elution gave **42** (214 mg, 86%): ir (film) 1780 (ketone) and 1705 cm^{-1} (ketone); nmr τ 8.87 and 8.98 (both s, 3H each, *gem*-dimethyl); ms M^+ 166.0998 (calcd. for $C_{10}H_{14}O_2$: 166.0993).

Keto Ester ***24*** *from* ***42***

The transformation was carried out by the use of the same reaction sequence and conditions described for **39** → **23**. Oxidation of **42** (1.351 g, 8.14 mmol) with 30% hydrogen peroxide (20 ml) and acetic acid (20 ml) gave a mixture of **25** and **26** (1.362 g, ~92%) which was methylated with potassium carbonate (5 g) and methyl iodide (3 ml) in acetone (15 ml) to give, after bulb-to-bulb distillation of the crude product at 110 °C (oven temperature)/0.2 torr, **24** (1.082 g, 68% from **42**).

Acknowledgment

We wish to thank the National Research Council of Canada and the University of Alberta for financial support.

1. H. J. Liu and T. Ogino. Tetrahedron Lett. 4937 (1973).
2. H. J. Liu. Synth. Commun. **3**, 441 (1973).
3. H. J. Liu. Synth. Commun. **4**, 237 (1974).
4. H. J. Liu and P. C. L. Yao. Synth. Commun. **5**, 161 (1975).
5. H. J. Liu, Z. Valenta, J. S. Wilson, and T. T. J. Yu. Can. J. Chem. **47**, 509 (1969).
6. C. A. Grob. Angew. Chem. Int. Ed. Engl. **8**, 535 (1969).
7. N. R. Hunter, G. A. MacAlpine, H. J. Liu, and Z. Valenta. Can. J. Chem. **48**, 1436 (1970).
8. P. T. Ho, S. F. Lee, D. Chang, and K. Wiesner. Experientia, **27**, 1377 (1971).
9. H. O. House. Modern synthetic reactions. 2nd ed. W. A. Benjamin Inc., Menlo Park, Calif. 1972, Chapt. 9.
10. D. E. Bergstrom and W. C. Agosta. Tetrahedron Lett. 1087 (1974).
11. J. L. Charlton and H. K. Lai. Can. J. Chem. **54**, 1445 (1976).
12. H. F. Koo. M.Sc. Thesis, the University of Alberta, Edmonton. 1975.
13. E. J. Corey, J. D. Bass, R. LeMahieu, and R. B. Mitra. J. Am. Chem. Soc. **86**, 5570 (1964).
14. R. B. Turner. J. Am. Chem. Soc. **72**, 878 (1950).
15. J. D. Albright and L. Goldman. J. Am. Chem. Soc. **89**, 2416 (1967).
16. R. L. N. Harris, F. Komitsky, Jr., and C. Djerassi. J. Am. Chem. Soc. **89**, 4765 (1967).
17. E. N. Marvell and J. L. Stephenson. J. Am. Chem. Soc. **77**, 5177 (1955).
18. S. M. McElvain and D. Kundiger. Org. Synth. Col. Vol. III. *Edited by* E. C. Horning. John Wiley and Sons Inc., New York, NY. 1955. p. 123.

Triazolopyridine nucleosides. II. Glycosylations of 3-oxo-*s*-triazolo[4,3-*a*]pyridines with accompanying conversions into 2-oxo-*s*-triazolo[1,5-*a*]pyridine nucleosides[1]

BRIAN MAURICE LYNCH[2] AND SURESH CHANDRA SHARMA[3]

Department of Chemistry, Saint Francis Xavier University, Antigonish, N.S., Canada B2G 1C0

Received September 13, 1976

BRIAN MAURICE LYNCH and SURESH CHANDRA SHARMA. Can. J. Chem. **55**, 831 (1977).

3-Oxo-*s*-triazolo[4,3-*a*]pyridine and various *C*-methyl derivatives (general structure **1**) have been converted into the 2-β-D-ribofuranosyl species **2** and thence **4** via Friedel–Crafts catalyzed reaction with tetra-*O*-acetyl-β-D-ribofuranose, followed by deblocking. During the course of these reactions, rearrangements into the isomeric 3-β-D-ribofuranosyl-2-oxo-*s*-triazolo[1,5-*a*]-pyridines occur through ring-opening of the pyridine rings yielding species **3** and **5**. The proportion of rearrangement products is dependent upon the position and number of the *C*-methyl substituents.

Structural assignments for these compounds are based upon comparisons of spectroscopic properties (^{1}H nmr, ^{13}C nmr, uv) with model compounds from each isomeric series; structural assignments for these models are based on unequivocal mass-spectral fragmentation patterns. Unlike related triazolopyridine nucleosides with the ribose moiety attached to a pyridine nitrogen (Lynch and Sharma (1976)), there are no unusual aspects in the conformations of the nucleosides of types **4** and **5**.

BRIAN MAURICE LYNCH et SURESH CHANDRA SHARMA. Can. J. Chem. **55**, 831 (1977).

On a transformé l'oxo-3 *s*-triazolo[4,3-*a*]pyridine et ses divers dérivés *C*-méthylés (structure générale **1**) en espèces β-D-ribofurannosyl-2 **2** et de là en composés du type **4** par l'intermédiaire d'une réaction catalysée de Friedel–Crafts avec le tétra-*O*-acétyl-β-D-ribofurannose suivie d'un déblocage du produit. Au cours de ces réactions, il se produit des réarrangements, par une ouverture du cycle de la pyridine, qui conduisent aux β-D-ribofurannosyl-3 oxo-2 *s*-triazolo-[1,5-*a*]pyridines isomères **3** et **5**. La proportion de produits de réarrangement dépend de la position et du nombre de substituants *C*-méthyle.

Les attributions de structure de ces composés sont, dans chaque série, basées sur des comparaisons de propriétés spectroscopiques (rmn ^{1}H, rmn ^{13}C, uv) avec des composés modèles; les attributions de structures pour ces modèles sont basées sur des types non-équivoques de fragmentations de spectres de masse. Par opposition avec les triazolopyridines nucléosides voisins ayant une portion ribose attachée à l'azote de la pyridine (Lynch et Sharma (1976)) il n'y a pas d'aspects inusités dans les conformations des nucléosides des types **4** et **5**.

[Traduit par le journal]

Introduction

In this paper, we report further exploration of synthetic routes to nucleosides of triazolopyridines (for the initial paper, see ref. 1), focussing attention on representatives of two isomeric ring systems possessing bridgehead nitrogen atoms. As noted previously (1), the objective of this synthetic program is to obtain positionally isomeric nucleosides expected to possess differing constraints on preferred sugar–base torsional angles.

As starting heterocyclic components, we used a series of 3-oxo-*s*-triazolo[4,3-*a*]pyridines of general structure **1**. These compounds were prepared by reactions of the appropriately substituted 2-hydrazinopyridines with urea or ethyl chloroformate (2, 3) and were converted into the trimethylsilyl derivatives, and then subjected to Lewis-acid catalyzed glycosylation using 1,2,3,5-tetra-*O*-acetyl-β-D-ribofuranose and tin(IV) chloride. This method provides triacetylribofuranosides of β-configuration (4, *cf.* 5), readily deblocked to the corresponding nucleosides, and avoids the epimerizations sometimes observed (6, 7) using the fusion method.

Results and Discussion

The glycosylations of compounds of general structure **1** would be expected to give 2-substituted derivatives, but reactions with the

[1]For Part I see ref. 1. Research assisted by grants-in-aid from the National Research Council of Canada. Presented in part at the Canadian Chemical Conference of the Chemical Institute of Canada, London, Ontario, June 1976.

[2]Author to whom all correspondence should be addressed.

[3]Professional Research Associate.

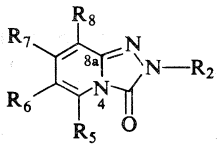

1, 2, and **4**
(also **6** and **9**)

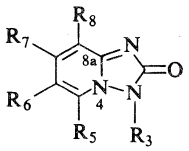

3 and **5**
(also **7** and **10**)

All R functions not indicated imply a hydrogen substituent
X is β-D-(2,3,5-triacetyl)ribofuranosyl
Y is β-D-ribofuranosyl

1

a $R_2 = H$
b $R_2 = CH_3$
c $R_5 = CH_3$
d $R_6 = CH_3$
e $R_7 = CH_3$
f $R_8 = CH_3$
g $R_5 = R_7 = CH_3$

2

a $R_2 = X$
b —
c $R_5 = CH_3, R_2 = X$
d $R_6 = CH_3, R_2 = X$
e $R_7 = CH_3, R_2 = X$
f $R_8 = CH_3, R_2 = X$
g $R_5 = R_7 = CH_3, R_2 = X$

3

a —
b $R_3 = CH_3$
c $R_5 = CH_3, R_3 = X$
d $R_6 = CH_3, R_3 = X$
e $R_7 = CH_3, R_3 = X$
f $R_8 = CH_3, R_3 = X$
g $R_5 = R_7 = CH_3, R_3 = X$

4

a $R_2 = Y$
b —
c $R_5 = CH_3, R_2 = Y$
d $R_6 = CH_3, R_2 = Y$
e $R_7 = CH_3, R_2 = Y$
f $R_8 = CH_3, R_2 = Y$
g $R_5 = R_7 = CH_3, R_2 = Y$

5

a —
b —
c $R_5 = CH_3, R_3 = Y$
d $R_6 = CH_3, R_3 = Y$
e $R_7 = CH_3, R_3 = Y$
f $R_8 = CH_3, R_3 = Y$
g $R_5 = R_7 = CH_3, R_3 = Y$

6

$R_2 = R_6 = CH_3$

7

$R_3 = R_6 = CH_3$

9

$R_2 = COCH_3, R_6 = NO_2$

10

$R_3 = H, R_6 = NO_2$

methyl-substituted species **1***d*, **1***e*, and **1***f* provided *mixtures of comparable amounts of two isomeric triacetylnucleosides* from each starting material. These were separable into the individual species by preparative thin-layer chromatography. Each triacetylnucleoside species was deblocked readily to the corresponding nucleoside (or mixture of nucleosides in some cases) by methanolic sodium methoxide. The compounds **1***a* and **1***c* yielded single triacetylnucleosides,[4] and the dimethyl compound **1***g* provided one major product and a trace of a second triacetylnucleoside; again, deblocking was effected readily.

Accompanying *O*- and *N*-glycosylation might explain the formation of two products from a single starting heterocycle, but the conditions used for glycosylation are those standard for *O*- to *N*-rearrangement (8) of glycosides. We suggest that the isolations of two isomeric species from a single starting material result from rearrangement of the 3-oxo-*s*-triazolo[4,3-*a*]-pyridine nuclei to 2-oxo-*s*-triazolo[1,5-*a*]pyridine nuclei during the reaction sequence. There is equivocal support in the literature for this suggestion. Potts *et al.* (9) have observed rearrangements of certain 3-substituted-*s*-triazolo-[4,3-*a*]pyridines into 2-substituted-*s*-triazolo[1,5-*a*]pyridines, but they specifically exclude the 3-oxo species, noting that it is degraded into 'pyridine derivatives', without rearrangement. However, closer examination of some of their reported experimental results shows that they are consistent with our proposed rearrangement. Thus, methylation of the parent oxo compound **1***a* by dimethyl sulfate in alkali was reported to yield two products: one assigned as 2-methyl-3-oxo-*s*-triazolo[4,3-*a*]pyridine **1***b*, mp 112–113 °C, and a second minor species of 'unknown constitution' (9), mp 217–219 °C with decomposition, assigned the formula $C_{14}H_{16}N_6O_3$. We noted that the reported analytical data are consistent with a hemihydrate species ($(C_7H_7N_3O)_2 \cdot H_2O$), and repetition of the methylation experiments in our laboratory provided the two products with the physical properties cited by

[4]A referee has pointed out that the assignment of anomeric configuration is readily verifiable by preparation of the 2′,3′-*O*-isopropylidene derivative, and use of the differences in proton chemical shifts of the methyl groups to diagnose configuration (a difference greater than 0.18 ppm characterizing a β configuration (14)); indeed, this approach was employed in Part I (1). Preparation of this derivative from the parent **1***a* using the standard procedure furnished an oil after preparative thin-layer chromatography, which showed *C*-methyl proton signals at δ 1.36 and 1.60, thus confirming the β assignment.

Potts' group (separations were effected by preparative thin-layer chromatography), and the ^{1}H nmr spectra of thoroughly dried samples showed *N*-methyl and aromatic ring proton signals in the ratio 3:4. We therefore assign the second product as 3-methyl-2-oxo-*s*-triazolo-[1,5-*a*]pyridine, **3***b*. The unrearranged 2-methyl-3-oxo compound **1***b* shows a pattern of aromatic ring proton shifts closely similar to one set of the triacetylribosylation and ribosylation products (see Table 1*a*), *i.e.* a one-proton signal in the range δ 5.9–6.6, assigned as proton 6 of species **1**, **2**, and **4**; two protons of closely similar chemical shifts between δ 6.7–7.4, assigned to protons 7 and 8, and a low-field one-proton signal showing a well-resolved *ortho*-coupling of *ca.* 7 Hz and falling in the range δ 7.4–7.8, assigned to the 5-proton. These shifts, and the *C*-methyl proton shifts, closely resemble those reported for correspondingly substituted simple *s*-triazolo[4,3-*a*]pyridines by Potts *et al.* (10).

In contrast, the ^{1}H nmr spectrum of the minor methylation product, assigned above as the 3-methyl-2-oxo species **3***b*, shows aromatic ring proton shifts fitting the pattern of the second set of triacetylribosylation and ribosylation products (Table 1*b*), *i.e.* a one-proton signal between δ 6.6–7.1, assigned to the 6-proton in type **3** or **5** species; two one-proton signals between δ 7.47–7.87, assigned to the 8- and the 7-protons, and a low-field one-proton signal at δ 7.9–8.25 from the 5-proton.

The matching of patterns to those of **1***b* and **3***b* is strongly suggestive of rearrangements from the [4,3-*a*] to the [1,5-*a*] series in the glycosylation processes, but since the glycosylation of the [4,3-*a*] compound **1***a* yields a single triacetylnucleoside, and deblocking yields a single nucleoside, each one of which shows ^{1}H nmr patterns (Table 1) indicative of retention of the *s*-triazolo[4,3-*a*]pyridine structure; more decisive evidence would be marshalled through comparison of species where rearrangements occurred in both the methylation and the glycosylation processes, together with unequivocal structure proofs of the methylation products.

This evidence was provided by a methylation study of 6-methyl-3-oxo-*s*-triazolo[4,3-*a*]pyridine **1***d*, which on glycosylation yields a mixture of two products. The major methylation product (mp 135 °C, 71% yield) gave a ^{13}C nmr spectrum closely similar to that of the parent compound **1***d*, and also to one of the triacetylnucleosides obtained from **1***d* (see Table 2), and is therefore assigned as the 2,6-dimethyl-3-oxo-*s*-triazolo-[4,3-*a*]pyridine **6**. The ^{1}H nmr spectrum of this product closely resembled that of the compound assigned as **1***b*. The second methylation product (mp 234 °C, 10% yield) is expected to have structure **7** (3,6-dimethyl-2-oxo-*s*-triazolo[1,5-*a*]-pyridine), and the isomeric nature and the structures of the two methylation products were proved by their mass spectra and fragmentation patterns. Each compound gave a molecular ion peak at *m/e* 163, and the species of mp 135 °C showed successive losses of N—CH_3 ($M^+ - 29$) and CO (($M^+ - 29$) − 28) moieties, while the compound of mp 234 °C fragmented successively with the loss of N—C—O ($M^+ - 42$), N—CH_3 (($M^+ - 42$) − 29), and HCN (($M^+ - 71$) − 27). The fragmentation sequences are indicated on the proposed structures **6** and **7**, and these sequences are in full agreement with expectation.

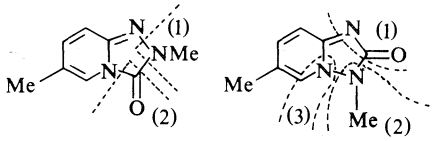

6 **7**

We therefore conclude that the two sets of triacetylribosylation products, and the corresponding sets of deblocked nucleosides, represent 2-glycosylated *s*-triazolo[4,3-*a*]pyridines and 3-glycosylated *s*-triazolo[1,5-*a*]pyridines respectively. The electronic absorption spectra of the two series of compounds (Table 3) (general structures **1**, **2**, **4**, and **6** for one series, and general structures **3**, **5**, and **7** for the other) show significant differences: five distinct absorption maxima for the [4,3-*a*] series, and three for the [1,5-*a*] series. These differences are useful in monitoring the separations of isomer mixtures by thin-layer chromatography.

Rearrangements in basic media analogous to those occurring during the methylations of compounds **1***a* and **1***d* are well documented (9, 11, 12), and acid-catalyzed reactions have been reported for *s*-triazolo[4,3-*a*]pyrimidine/*s*-triazolo[1,5-*a*]pyrimidine and *s*-triazolo[4,3-*c*]-quinazoline/*s*-triazolo[1,5-*c*]quinazoline conversions (11, 12). These reactions may be generalized as variations of a Dimroth rearrangement, as illustrated in Scheme 1.

Under basic conditions, following Novinson

TABLE 1. Proton magnetic resonance spectra of oxotriazolopyridines and their glycosylation and methylation products
(*a*) 3-Oxo-1-substituted *s*-triazolo[4,3-*a*]pyridines

Compound	Solvent	Proton shifts					Coupling constants (Hz)				
		H-2	H-5	H-6	H-7	H-8	$J_{5,6}$	$J_{6,7}$	$J_{7,8}$	$J_{5,7}$	$J_{6,8}$
1*a*	DMSO-d_6	11.80	7.79	6.54	7.15	7.15	7.0	3.2	nr	nr	nr*
1*b*	DMSO-d_6	3.60†	7.93	6.71	7.33	7.33	6.5	3.0	nr	nr	nr
2*a*	$CDCl_3$	6.16	7.73	6.50	7.11	7.11	7.0	3.4	nr	nr	nr
		($J_{1'2'}$ = 3.1 Hz)									
4*a*	DMSO-d_6	5.75	7.86	6.60	7.27	7.27	7.0	3.6	nr	nr	nr
		($J_{1'2'}$ = 4.3 Hz)									
1*c*	$CDCl_3$	11.28	2.82‡	6.12	6.91	6.91	—	4.0	nr	—	1.0
6	DMSO-d_6	3.54†	7.61	2.16‡	7.09	7.09		—	—	—	—
1*d*	DMSO-d_6	12.33	7.66	2.38‡	7.15	7.15	—	—	nr	1.5	—
2*d*	$CDCl_3$	6.00(s)	7.42	2.10‡	6.98	6.98	—	—	nr	—	—
4*d*	DMSO-d_6	5.85	7.77	2.10‡	7.27	7.27	—	—	nr	—	—
		($J_{1'2'}$ = 3.8 Hz)									
1*e*	$CDCl_3$	10.75	7.71	6.36	2.31‡	6.90	7.4	—	—	—	1.0
2*e*	$CDCl_3$	6.71	7.57	6.30	2.26‡	6.76	7.0	—	—	—	nr
		($J_{1'2'}$ = 2.8 Hz)									
4*e*	D_2O	5.86	7.76	6.43	2.24‡	7.44	7.2	—	—	—	nr
		($J_{1'2'}$ = 4.3 Hz)									
1*f*	DMSO-d_6	12.42	7.73	6.54	7.01	2.26‡	6.6	6.6	—	1.1	—
2*f*	DMSO-d_6	6.34	7.76	6.57	7.04	2.37‡	6.8	6.8	—	nr	—
		($J_{1'2'}$ = 3.2 Hz)									
4*f*	D_2O	5.95	7.61	6.61	7.06	2.26‡	6.6	6.6	—	nr	—
		($J_{1'2'}$ = 4.5 Hz)									
1*g*	$CDCl_3$	11.27	2.77‡	5.88	2.18‡	6.67					
4*g*	$CDCl_3$	5.89	2.63‡	6.00	2.12‡	6.68					
		($J_{1'2'}$ = 4.5 Hz)									

TABLE 1 (*Concluded*)

(*b*) 2-Oxo-3-substituted *s*-triazolo[1,5-*a*]pyridines

Compound	Solvent	Proton shift					Coupling constants (Hz)				
		H-3	H-8	H-7	H-6	H-5	$J_{7,8}$	$J_{6,7}$	$J_{6,5}$	$J_{6,8}$	$J_{5,7}$
3*b*	DMSO-d_6	3.80†	7.68	or 7.76	7.01	8.15	nr	nr	7.0	nr	nr
7	DMSO-d_6	3.80†	7.58	7.58	2.28‡	7.92	nr	—	—	—	2.0
3*c*	$CDCl_3$	6.16	7.49	7.49	6.67	3.05	6.5	6.5	—	—	—
		($J_{1'2'}$ = 2.0 Hz)									
5*c*	DMSO-d_6	5.88	7.55	7.55	6.67	2.86‡	6.0	6.0	—	—	—
		($J_{1'2'}$ = 3.4 Hz)									
3*d*	$CDCl_3$	6.16(s)	7.57	7.57	2.40‡	8.00	nr	—	—	—	nr
5*d*	DMSO-d_6	5.96	7.73	7.87	2.32‡	8.08	6.3	—	—	—	nr
		($J_{1'2'}$ = 3.4 Hz)									
3*e*	DMSO-d_6	6.45(s)	7.90	2.48‡	7.08	8.25	—	—	7.0	1.0	—
5*e*	DMSO-d_6	5.98	7.82	2.45‡	7.00	8.15	—	—	6.8	0.6	—
		($J_{1'2'}$ = 3.8 Hz)									
3*g*	DMSO-d_6	6.38	7.65	2.37‡	6.70	2.88‡					
		($J_{1'2'}$ = 1.7 Hz)									
5*g*	DMSO-d_6	5.89	7.52	2.32‡	6.57	2.93‡					
		($J_{1'2'}$ = 3.2 Hz)									

NOTE: Proton chemical shifts, and coupling constants for the anomeric proton of the triacetylnucleosides and nucleosides are listed under H-2 or H-3 as appropriate.
*Small apparent coupling, not resolvable.
†*N*-Methyl protons.
‡*C*-Methyl protons.

TABLE 2. ^{13}C nmr spectra of oxotriazolopyridine derivatives and their glycosylation products

	Compound				
	1*d*	**6**	**2***d*	**3***d*	Tetra-O-acetyl-β-D-ribofuranose
^{13}C signals					
Aromatic carbons 2-				153.5	
3-	149.7	148.0	147.9		
5-	133.5	136.6	135.4	140.0	
6-	119.6	119.9	120.5	125.8	
7-	120.0	120.0	120.2	122.8	
8-	114.9	114.2	114.5	109.2	
8a-	141.9	140.2	141.6	140.2	
C-Methyl	17.07	17.07	17.01	17.56	
N-Methyl		32.40			
Ribosyl carbons					
Acetyl carbonyls			169.9, 169.4	171.1, 170.4	168.6, 169.1, 169.3, 170.0
C-1′			85.3	87.9	98.2
C-2′			70.4	70.8	70.6
C-3′			72.5	73.7	74.2
C-4′			78.9	79.7	79.4
C-5′			62.9	63.3	63.6
Acetyl methyls			20.4, 20.2	20.9, 20.8	20.9, 20.55 20.33, 20.31

TABLE 3. Electronic spectra of oxotriazolopyridine derivatives and their glycosylation products

(*a*) *s*-Triazolo[4,3-*a*]pyridines

Species	λ_{max} (nm)					log ε_{max}				
1*a*	221	258	265	275	328	3.85	3.45	3.48	3.31	3.34
4*a*	219	259	265	275	328	4.10	3.38	3.42	3.28	3.44
1*c*	223	259	268	279	327	3.72	3.47	3.51	3.35	3.49
1*d*	225	258	268	279	326	3.84	3.15	3.20	3.03	3.27
2*d*	224	258	268	279	328	4.11	3.35	3.40	3.37	3.49
4*d*	227	261	268	279	327	3.87	3.27	3.29	3.20	3.37
6	227	263	269	280	328	3.96	3.10	3.16	3.05	3.36
1*e*	222	257	266	276	322	3.77	3.65	3.71	3.57	3.47
2*e*	221	257	265	276	323	4.05	3.74	3.79	3.66	3.63
4*e*	222	259	266	277	325	4.02	3.52	3.60	3.46	3.50
1*f*	223	259	265	275	318	3.77	3.51	3.56	3.43	3.54
2*f*	223	258	265	275	319	3.91	3.37	3.44	3.30	3.58
4*f*	222	259	265	276	319	3.93	3.05	3.22	3.05	3.52
1*g*	222	261	270	280	322	3.70	3.52	3.58	3.47	3.44
2*g*	222	261	270	280	322	4.23	3.89	3.95	3.83	3.71
4*g*	222	260	269	280	321	3.92	3.28	3.37	3.24	3.43

(*b*) *s*-Triazolo[1,5-*a*]pyridines

Species	λ_{max} (nm)			log ε_{max}		
3*c*	241	288	342	3.92	3.34	3.68
5*c*	240	286	342	4.01	3.47	3.75
3*d*	241	286	338	4.04	3.45	3.85
5*d*	241	285	340	4.11	3.48	3.76
7	240	282	341	3.97	3.26	3.45
3*e*	235	289	332	3.79	3.42	3.47
5*e*	236	285	331	4.00	3.64	3.69
3*f*	238	292	333	3.99	3.58	3.81
5*f*	238	290	333	4.01	3.59	3.79
3*g*	239	291	338	4.08	3.60	3.81
5*g*	237	287	338	3.86	3.34	3.61

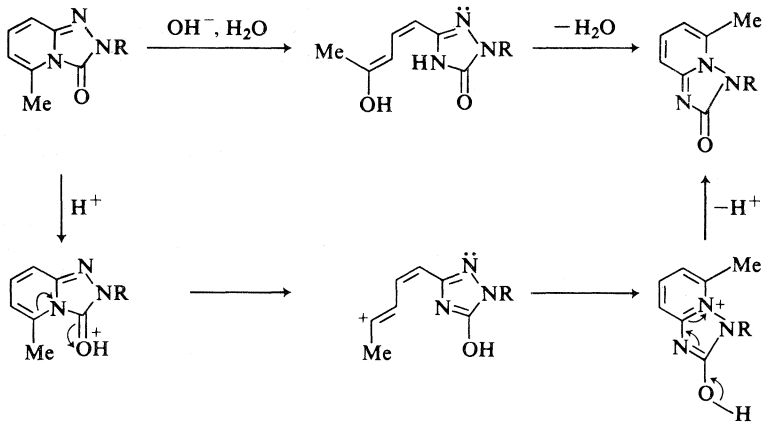

SCHEME 1. Proposed rearrangement pathways for conversions of *s*-triazolo[4,3-*a*]pyridines into *s*-triazolo[1,5-*a*]pyridines.

and co-workers (11) we postulate nucleophilic attack at the carbon adjacent to the bridgehead nitrogen to yield a triazole intermediate, then recyclizing to the isomeric species. The acid-catalyzed process is suggested to involve initial protonation (or Lewis acid conjugation) followed by ring-opening to generate a carbonium-ion intermediate, again recyclizing as indicated. The extent of rearrangement during triacetylribosylation appears to be determined by the extent of stabilization of the proposed carbonium ion; thus, complete rearrangement occurs on triacetylribosylation of 5-methyl-3-oxo-*s*-triazolo-[4,3-*a*]pyridine **1***c* to yield **3***c* (in **1***c*, the methyl group would stabilize the carbonium ion most effectively), and virtually complete rearrangement with 5,7-dimethyl-3-oxo-*s*-triazolo[4,3-*a*]-pyridine **1***g*; the other methyl-substituted species give mixtures of both isomeric triacetylnucleosides in comparable amounts, and with the parent species **1***a*, no rearrangement occurs.

Rearrangements were also found to accompany attempted syntheses and substitution reactions of derivatives of the parent compound **1***a*. Thus, nitration of **1***a* using nitric acid – acetic anhydride reagent afforded a product $C_8H_6N_4O_4$, mp 218–220 °C, assigned as 2-acetyl-6-nitro-3-oxo-*s*-triazolo[4,3-*a*] pyridine **9**. Sublimation of a crude sample of **9** yielded a deacetylated product $C_6H_4N_4O_3$, mp 299–301 °C, with a ^{1}H nmr spectrum differing significantly from that of **9** in the aromatic region. Since the remote 2-acetyl substituent would be expected to have little effect on the aromatic ring shifts, we suggest that the product of mp 299–301 °C is 6-nitro-2-oxo-*s*-triazolo[1,5-*a*]pyridine **10**; the differences in the ^{1}H nmr spectra of the two products (see Experimental) resemble those for the isomeric series assembled in Table 1. An attempted synthesis of the 6-nitro-3-oxo-*s*-triazolo[4,3-*a*]pyridine by ring closure of 2-ethoxycarbonylhydrazino-5-nitropyridine with *N*-sodium hydroxide at 80 °C failed, since the product of mp 299–301 °C was obtained, probably through base-catalyzed rearrangements of the [4,3-*a*] compound.

The Conformations of Triazolopyridine Nucleosides

In marked contrast to the related compound 4-β-D-ribofuranosyl-*vic*-triazolo[4,5-*b*]pyrid-5-one, **8**, which shows marked deshielding of H-1′ by comparison with monocyclic precursors, and a large 1′–2′ proton coupling (6.50 Hz) (*cf.* ref. 1), the nucleosides of series **4** and **5**

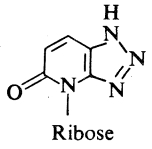

8

exhibit normal H-1′ shielding (δ 5.8–6.0) and 1′–2′ couplings (series **4**, 3.8–4.5 Hz, series **5**, 3.4–3.8 Hz). The severe conformational constraints proposed to account for the ^{1}H nmr patterns of **8** are thus absent in the series **5**, although in each type of compound the sugar–base link is positioned between an amide carbonyl and a conjoined ring.

The differing behavior is interpreted in terms of the greater separation between the amide oxygen (at C-2) and the ribose carbon C-1′ in

TABLE 4. Glycosylations of 3-oxo-*s*-triazolo[4,3-*a*]pyridines with tetra-*O*-acetyl-β-D-ribofuranose

Starting species	Reaction product	Reactants: Triazolo-pyridine (g)	Reactants: Tetra-acetyl-ribose (g)	Reactants: $SnCl_4$ (ml)	Reflux time (h)	Yield(s) of product(s): g	Yield(s) of product(s): %
1*a*	**2***a*	2.97	6.36	1.5	2*	7.61	96
1*c*	**3***c*	1.64	3.05	1.5	10	2.98	73
1*d*	**2***d*	1.64	3.18	1.5	8	0.84	21
	3*d*					1.98	50
1*e*	**2***e*	1.64	3.18	1.0	8	1.51	37
	3*e*					1.02	25
1*f*	**2***f*	1.36	2.51	1.0	10	1.61	48
	3*f*					1.60	47
1*g*	**2***g*	1.80	3.18	1.0	8	0.05	2
	3*g*					1.64 (0.57 g recovered starting material)	57

Product species	Melting point (°C)	Crystalliz. solvent	Molecular formula	Analysis: Calculated C	Calculated H	Calculated N	Found C	Found H	Found N
2*a*	135–136	EtOH:Et_2O	$C_{17}H_{19}N_3O_8$	51.90	4.87	10.68	51.96	4.86	10.49
3*c*	188–192	MeOH	$C_{18}H_{21}N_3O_8$	53.08	5.20	10.32	53.24	5.19	10.44
2*d*	46–49	MeOH					52.83	5.25	9.92
3*d*	65–67	MeOH					53.44	5.46	10.44
2*e*	113–115	MeOH					52.66	5.46	10.08
3*e*	210–212	MeOH					52.90	5.37	9.90
2*f*	Viscous oil						52.66	5.25	9.86
3*f*	129–131	MeOH					52.66	5.61	10.08
3*g*	98–99	MeOH	$C_{19}H_{23}N_3O_8$	54.15	5.50	9.97	54.00	5.48	10.26

*Reflux time of 8 h did not give any isomeric *s*-triazolo[1,5-*a*]pyridine nucleoside, **3***a*.

type **5** compounds in contrast to **8**, allowing the type **5** compounds greater rotational freedom and conformational flexibility; thus models using 120° bond angles for the six-membered ring moiety of **8**, and 108° internal angles for **5**, together with standard bond lengths (13), indicate that the O—C-1′ separation in **8** is 0.27 nm, and in **5** is 0.30 nm.

Experimental

General

Melting points were determined using a Fisher-Johns apparatus and are uncorrected. The ^1H nmr spectra were recorded with a Varian A-60D instrument, and the ^{13}C nmr spectra using a Varian CFT-20. All chemical shifts are expressed in parts per million from tetramethylsilane, present as internal reference. Electronic absorption (uv) spectra were measured for solutions in methanol, with a Beckman Acta III spectrophotometer. Specimens for elemental analyses were dried at 65 °C/0.2 torr for at least 6 h and were analyzed using a Hewlett-Packard model 185 analyser. Mass spectra were obtained using a DuPont CEC 21-491 instrument. Thin-layer chromatography was performed using Fluka Kieselgel GF 254. All extracts were dried over anhydrous sodium sulfate and evaporations were effected below 35 °C under reduced pressure. Known compounds referred to in details of experiments had physical properties according with literature values.

Standard Procedure for Reactions of 3-Oxo-s-triazolo-[4,3-a]pyridines with Tetra-O-acetylribofuranose

For details of scale and duration of reactions, see Table 4. The appropriate 3-oxo-*s*-triazolo[4,3-*a*]pyridine was heated under reflux in excess of hexamethyldisilazane in the presence of a catalytic amount of ammonium sulfate for 6 h, with precautions for exclusion of moisture. Hexamethyldisilazane was removed under reduced pressure, and the crude trimethylsilyl derivative of the triazolopyridine was dissolved in 1,2-dichloroethane. A

solution of tetra-*O*-acetyl-β-D-ribofuranose in dichloroethane was added, followed by tin(IV) chloride. The mixture was heated under reflux for the indicated time, washed with saturated aqueous sodium hydrogen carbonate, and the organic layer was separated and dried. Concentration of the reaction mixture yielded the crude triacetylnucleosides. For the examples where single products were obtained (species **2***a*, **3***c*), the crude materials were purified by crystallization from the indicated solvent. The mixtures containing both *s*-triazolo[4,3-*a*]pyridine and *s*-triazolo[1,5-*a*]pyridine triacetylnucleosides (**2***d*, **3***d*; **2***e*, **3***e*; **2***f*, **3***f*; **2***g*, **3***g*) were separated by preparative thin-layer chromatography on silica gel, using a benzene:ethyl acetate:methanol (30:75:5 v/v) solvent system in development. The separated species were purified by crystallization as indicated.

Deblocking of the Triacetylnucleosides

The triacetylnucleoside was treated with an excess of freshly prepared 1% (w/v) sodium methoxide in methanol at room temperature for 18 h. The reaction mixture was passed through an Amberlite IRC-50(H) column and eluted with methanol. Concentration under reduced pressure, followed by crystallization from methanol, provided the deblocked nucleosides listed in Table 5. Deblocking of the triacetylnucleosides in the *s*-triazolo-[4,3-*a*]pyridine series led to some isomerization, as the mother liquors contained proportions of the *s*-triazolo-[1,5-*a*]pyridine nucleosides detectable by ^{1}H nmr spectroscopy.

Methylation of 3-Oxo-6-methyl-s-triazolo[4,3-a]pyridine, 1d

3-Oxo-6-methyl-*S*-triazolo[4,3-*a*]pyridine **1***d* (1.50 g) was dissolved in methanol (60 ml) and treated with methyl iodide (1.0 ml) and anhydrous potassium carbonate (1.40 g). The reaction mixture was stirred at room temperature for 18 h and concentrated under reduced pressure. Preparative thin-layer chromatography on silica gel with development in an ethyl acetate:methanol (93:7 v/v) solvent system provided 2,6-dimethyl-3-oxo-*s*-triazolo[4,3-*a*]pyridine **6** (1.16 g, 71%), mp 135 °C; *m/e* 163 (100%, M^+), 134 (20%, $M^+ - NCH_3$), 106 (30%, $M^+ - NCH_3 - CO$), after evaporation and crystallization from methanol, together with 3,6-dimethyl-2-oxo-*s*-triazolo[1,5-*a*]pyridine **7** (0.17 g, 10%), mp 234 °C; *m/e* 163 (100%, M^+), 121 (100%, $M^+ - CNO$); 92 (60%, $M^+ - CNO - NCH_3$), 65 (100%, $M^+ - CNO - NCH_3 - HCN$) after similar recrystallization.

Methylation of 3-Oxo-s-triazolo[4,3-a]pyridine, 1a

This was effected according to Potts *et al.* (9), providing a 3:1 mixture ^{1}H nmr spectroscopic examination from *N*-methyl signal intensities) of the 2-methyl species **1***b* and the 1-methyl species **3***b*, with melting points coincident with those reported (9).

Nitro Compounds and Rearrangements

(a) Nitration of 3-Oxo-s-triazolo[4,3-a]pyridine, 1a

To **1***a* (2.00 g) in acetic anhydride (40 ml) was added (dropwise) a solution of nitric acid (90%, 4 ml) in acetic anhydride (6.0 ml) at 5 °C. After completion of addition the reaction mixture was kept below 10 °C for 30 min and poured onto ice (200 g). Filtration afforded a

TABLE 5. β-D-Ribofuranosyl-oxo-*s*-triazolopyridines obtained by deblocking of triacetyl precursors

Conversion effected	Quantity of precursor (g)	NaOMe (ml)*	Yield		Melting point (°C)	Molecular formula	Analysis					
			g	%			Calculated			Found		
							C	H	N	C	H	N
2*a* → **4***a*	1.0	†	0.58	86	203	$C_{11}H_{13}N_3O_5$	49.44	4.90	15.72	49.65	4.90	15.88
2*d* → **4***d*	0.31	18	0.19	87	Glassy foam	$C_{12}H_{15}N_3O_5$	51.24	5.38	14.92	50.92	5.46	14.54
2*e* → **4***e*	0.40	20	0.27	97	161					51.21	5.32	14.82
2*f* → **4***f*	0.40	20	0.26	96	177					51.21	5.44	14.73
3*c* → **5***c*	2.39	65	1.58	96	238					50.93	5.46	14.58
3*d* → **5***d*	1.14	33	0.76	96	216					51.50	5.16	14.94
3*e* → **5***e*	0.66	30	0.41	90	224–226					51.13	5.73	14.76
3*f* → **5***f*	1.16	42	0.74	92	189					51.24	5.38	14.94
3*g* → **5***g*	1.41	60	0.84	85	218	$C_{13}H_{17}N_3O_5$	52.87	5.80	14.23	52.65	5.86	14.55

*1% (w/v) of sodium in methanol.
†Saturated methanolic ammonia (50 ml) solution.

product (0.63 g), mp 218–220 °C. *Anal.* calcd. for $C_8H_6N_4O_4$: C 43.25, H 2.72, N 25.22; found: C 43.16, H 3.10, N 25.12; *m/e* 222 (3.7%, M^+), 180 (100%, $M^+ -$ NCO); ^{1}H nmr spectrum (DMSO-d_6) δ 2.68 (s, 3H, N—$COCH_3$), 7.50 (d, 1H, J = 10.0 Hz, H-8), 8.07 (dd, 1H, J = 1.50 and 10.0 Hz, H-7), 8.95 (d, 1H, J = 1.50 Hz, H-5), assigned as 2-acetyl-6-nitro-3-oxo-*s*-triazolo[4,3-*a*]-pyridine, **9**. Sublimation of the crude material provided 0.40 g, mp 299–301 °C. *Anal.* calcd. for $C_6H_4N_4O_3$: C 40.00, H 2.24, N 31.11; found: C 39.61, H 2.35, N 31.44; *m/e* 180 (100%, M^+); ^{1}H nmr spectrum (DMSO-d_6) δ 7.72 (d, 1H, J = 9.5 Hz, H-4), 8.42 (dd, 1H, J = 2.50 and 9.5 Hz, H-5), 9.88 (d, 1H, J = 2.50 Hz, H-7), assigned as 6-nitro-2-oxo-*s*-triazolo[1,5-*a*]pyridine, **10**.

(b) Synthesis and Ring Closure of 2-Ethoxycarbonylhydrazino-5-nitropyridine

Synthesis—2-Hydrazino-5-nitropyridine (2.20 g) was heated at 100 °C with ethyl chloroformate (20 ml) for 1 h; excess ethyl chloroformate was removed under reduced pressure, and the residue was washed with saturated aqueous sodium hydrogen carbonate, dried, evaporated, and crystallized from aqueous ethanol, providing 2-ethoxycarbonylhydrazino-5-nitropyridine (2.86 g), mp 161–162 °C.

Ring Closure—The above compound (2.50 g) was heated at 80 °C in 1 *N* aqueous sodium hydroxide for 15 min; after cooling to room temperature, the reaction mixture was neutralized with dilute sulfuric acid and the precipitated solid was collected. Crystallization from ethanol gave 6-nitro-2-oxo-*s*-triazolo[1,5-*a*]pyridine **10**, (1.43 g), mp and mixture mp 299–301 °C, identical to the material obtained in (*a*) above.

Acknowledgments

We thank the National Research Council of Canada for support through an Operating Grant and its Regional Development Program, and the Saint Francis Xavier University Council for Research for partial support. Dr. W. D. Jamieson (Atlantic Regional Laboratory, National Research Council, Halifax) is thanked for the mass-spectrometric data, and Dr. D. L. Hooper (Dalhousie University) for the ^{13}C nmr spectra.

1. B. M. Lynch and S. C. Sharma. Can. J. Chem. **54**, 1029 (1976).
2. K. T. Potts and H. R. Burton. J. Org. Chem. **31**, 251 (1966).
3. O. Siho and S. Tagami. J. Am. Chem. Soc. **82**, 4044 (1960).
4. L. Y. Foo and B. M. Lynch. Efficient syntheses of ribosides. Abstracts, 54th Annual Meeting Canadian Chemical Conference of the Chemical Institute of Canada, Halifax, N.S. 1971.
5. U. Niedballa and H. Vorbruggen. J. Org. Chem. **39**, 3654 (1974).
6. J. A. Montgomery, K. Hewson, A. G. Laseter, and M. C. Thorpe. J. Am. Chem. Soc. **94**, 7176 (1972).
7. J. L. Barascut, C. Tamby, and J. L. Imbach. J. Carbohydr. Nucleosides, Nucleotides, **1**, 77 (1974).
8. D. Thacker and T. L. V. Ulbricht. Chem. Commun. 122 (1967).
9. K. T. Potts, H. R. Burton, and S. K. Roy. J. Org. Chem. **31**, 265 (1966).
10. K. T. Potts, H. R. Burton, T. H. Crawford, and S. W. Thomas. J. Org. Chem. **31**, 3522 (1966).
11. T. Novinson, T. Okabe, R. K. Robins, and P. Dea. J. Heterocycl. Chem. **12**, 1187 (1975).
12. K. T. Potts and E. G. Brugel. J. Org. Chem. **35**, 3448 (1970).
13. J. A. Pople and D. L. Beveridge. Approximate molecular-orbital theory. McGraw-Hill, New York. 1970. p. 111.
14. J. M. Imbach, J. L. Barascut, B. L. Kam, B. Rayner, C. Tamby, and C. Tapiero. J. Heterocycl. Chem. **10**, 1069 (1973).

^{13}C nuclear magnetic resonance studies. 64.[1] The ^{13}C spectra of a variety of bicyclo[3.2.1]octanols

J. B. STOTHERS AND C. T. TAN[2]

Department of Chemistry, University of Western Ontario, London, Ont., Canada N6A 5B7

Received September 10, 1976

J. B. STOTHERS and C. T. TAN. Can. J. Chem. **55**, 841 (1977).

The ^{13}C nmr spectra of a series of 20 bicyclo[3.2.1]octanols and -octenols have been determined to examine the shielding effects of the hydroxyl group on the skeletal carbons in this ring system. For comparison, the previously unreported data for a few closely related alcohols in the [2.1.1], [2.2.1], and [3.2.2] systems were also collected. The utility of these substituent effects for configurational and conformational assignments is discussed.

J. B. STOTHERS et C. T. TAN. Can. J. Chem. **55**, 841 (1977).

On a déterminé les spectres rmn du ^{13}C d'une série de 20 bicyclo[3.2.1]octanols et -octénols afin d'examiner les effets de blindage du groupe hydroxyle sur le squelette carboné de ce système cyclique. Pour fins de comparaisons, on a aussi rassemblé des valeurs, qui n'avaient pas été rapportées antérieurement, pour quelques alcools voisins dans les systèmes [2.1.1], [2.2.1] et [3.2.2]. On discute de l'utilité de ces effets de substituants pour des attributions de configuration et de conformation.

[Traduit par le journal]

As part of our continuing examination of the effects of molecular geometry on ^{13}C shieldings we have obtained the spectra of a series of bicyclo[3.2.1]octanols and -octenols to compare the effects of the hydroxyl group on the skeletal shieldings in this ring system with the results for other bicyclic systems (1). The prime reason for investigating these series is that the well-defined carbon skeleton allows one to study the shielding variations as a function of molecular geometry. The [3.2.1] saturated examples have the additional feature of a flexible six-membered ring permitting an examination of this factor on the shielding trends. In general, the shifts produced by the substituent at carbons within four bonds are of particular interest as potential probes for stereochemical analysis. A possible deficiency in the use of bicyclic systems as models for these perturbations is the contribution of 'strain' to the observed shieldings, a factor which is difficult to assess. However, the influence of strain could be revealed in a comparison of the corresponding interactions in a variety of systems differing in strain energy. For this reason, the bicyclo[3.2.1]octane skeleton was selected as a model system for comparison with the results for the bicyclo[2.2.1]heptane and bicyclo[2.2.2]octane skeletons which are more highly strained and of similar strain, respectively. According to molecular mechanics the calculated strain energies for the parent hydrocarbons are 17.1, 13.0, and 12.1 kcal/mol for the [2.2.1], [2.2.2], and [3.2.1] systems, respectively (2). Another reference point is, of course, provided by the cyclohexanol system for which the data for a variety of derivatives are available (3) as are the results for several decalols (4) and sterols (5). While it is well established that ^{13}C shieldings for compounds in closely related series are correlated very well by additivity of substituent effects, the origins of these effects are not well understood (6) but empirical analysis of the data on carefully selected systems, in combination with the continuing development of shielding theory, may gain the ultimate goal of understanding. In any event, the results may be applied directly to problems involving the skeletons for which data are available. A few of the compounds included in this study have been reported previously (7); these have been reexamined, however, to obtain data for the entire series under closely similar conditions, 5–15% solutions in deuteriochloroform, for internal consistency and for meaningful comparison with previous results.

Experimental

Materials

The compounds examined in this study have been

[1]For part 63 see ref. 18; part 62 see ref. 1*c*.

[2]Present address: Department of Pharmacology, University of Toronto, Toronto, Ont., Canada.

TABLE 1. ^{13}C shieldings[a] of several bicyclo[3.2.1]octanols and -octenols

Compound	Substitution[b]	C-1	C-2	C-3	C-4	C-5	C-6	C-7	C-8
1[c]	Nil	35.2	32.8	19.1	32.8	35.2	28.9	28.9	39.7
2	*exo*-2-OH	41.7	71.3	[26.9]	[26.5]	34.3	28.4	[26.8]	32.1
		(−3.0)	(+2.7)	(−3.1)	(+0.6)	(−0.2)	(+0.5)	(0.0)	(+0.8)
3	*endo*-2-OH	42.7	72.5	[28.3]	30.7	33.7	[28.5]	23.3	37.3
		(−3.0)	(+2.7)	(−3.6)	(−0.1)	(+0.2)	(−0.1)	(+0.9)	(−0.1)
4	*exo*-3-OH	34.9	42.3	66.2	42.3	34.9	29.1	29.1	39.1
		(−0.2)	(−4.2)	(+3.2)	(−4.2)	(−0.2)	(−0.5)	(−0.5)	(−0.2)
5	*endo*-3-OH	33.9	40.9	66.7	40.9	33.9	28.8	28.8	38.6
		(−0.2)	(−3.2)	(+2.7)	(−3.2)	(−0.2)	(−0.3)	(−0.3)	(−0.1)
6	*exo*-6-OH	35.8	31.4	19.5	29.8	44.6	76.0	41.2	36.2
7	*endo*-6-OH	34.2	32.6	19.4	26.8	39.3	74.8	37.8	37.8
8	*exo*-8-OH	42.2	31.3	17.1	31.3	42.2	26.2	26.2	82.2
		(−2.5)	(−0.1)	(0.0)	(−0.1)	(−2.5)	(+0.4)	(+0.4)	(+2.8)
9	*endo*-8-OH	37.8	25.4	17.8	25.4	37.8	24.6	24.6	74.7
10[c]	Δ^6	39.5	25.2	18.7	25.2	39.5	132.1	132.1	45.1
11	Δ^6-*exo*-2-OH	46.4	66.1	27.4	21.9	39.2	134.8	132.9	37.3
12	Δ^6-*endo*-2-OH	46.8	68.5	28.5	23.3	38.4	134.3	130.1	42.5
13	Δ^6-*exo*-3-OH	39.1	35.2	67.1	35.2	39.1	132.6	132.6	44.9
14	Δ^6-*endo*-3-OH	38.1	36.8	67.4	36.8	38.1	138.3	138.3	44.7
15[c,d]	'Δ^3'	33.6	37.5	123.8	134.7	35.6	35.5	30.6	35.5
16	Δ^3-*exo*-2-OH	40.5	72.1	125.2	137.9	35.6	[31.0]	24.8	[30.8]
17	Δ^3-*endo*-2-OH	41.8	73.7	127.1	135.9	35.2	32.5	21.3	37.5
18	Δ^3-*exo*-6-OH	33.3	36.4	125.9	130.2	44.0	78.0	42.7	31.4
19	Δ^3-*endo*-6-OH	32.7	37.9	128.1	129.4	40.0	80.5	40.8	32.7
20[d]	'Δ^3-*exo*-8-OH'	40.7	37.5	124.2	132.6	42.3	32.6	28.3	78.1
21[d]	'Δ^3-*endo*-8-OH'	35.7	32.2	126.6	129.9	39.8	31.5	28.4	73.5

[a]In ppm from internal TMS for $CDCl_3$ solutions; values in square brackets may be interchanged. Values in parentheses are the shifts produced upon acetylation, *i.e.*, for a given carbon $\delta_C^{ROAC} - \delta_C^{ROH}$. For the acetates the carbonyl signals appeared in the range 170.1 ± 0.2 ppm and the methyl carbons absorbed at δ_C 21.2 ± 0.1.
[b]Substituent orientations (*exo*/*endo*) are given with respect to the larger of the two unsubstituted bridges.
[c]Data taken from ref. 8.
[d]For ease of comparisons within this table, **15**, **20**, and **21** are numbered in an unconventional manner and the substitutions are listed in quotation marks.

described in the literature and samples with the appropriate physical data were prepared from the published procedures. Infrared and proton spectra of each alcohol were recorded to ensure their identities. The parent ketone of each alcohol was available from earlier studies in this laboratory (8, 9) and **2**, **6**, **16**, and **18** had been prepared as intermediates in these ketone syntheses. The remaining examples were, with two exceptions, obtained by reduction of the appropriate ketone; **3**, **7**, **9**, **17**, **19**, **21**, **23**, **25**, **28**, and **30** were isolated as the sole products of metal hydride reduction using $LiAlH_4$, $NaBH_4$, or $LiAlH(OMe)_3$. Mixtures of **4**/**5**, **11**/**12**, **13**/**14**, and **20**/**21** were obtained in approximately 1:3 ratios by reduction and the relative intensities of the two sets of signals in their ^{13}C spectra readily permitted assignments to the individual isomers. A sample of **12** was also available from Li–NH_3 reduction of bicyclo[3.2.1]octa-3,6-dien-2-one. Ketone reduction failed to provide samples of **8** and **26** thereby requiring a different approach. Thus **8** was prepared from **9** via the tosylate, acetolysis, and hydrolysis (**10**) while **26** was generated from norbornene as described by Baird (11).

^{13}C Spectra

A Varian XL-100-15 system operating in the Fourier transform mode at 25.2 MHz was employed for the ^{13}C spectra. Carbon types were distinguished by off-resonance decoupling. All compounds were examined as $CDCl_3$ solutions (5–15%, w/v) containing TMS as an internal standard.

Results

The ^{13}C shieldings for the series of bicyclo-[3.2.1]octanols, their unsaturated analogs, and the corresponding hydrocarbons are listed in Table 1; our data for these hydrocarbons were reported previously (8). For each alcohol, the carbinyl signal was readily assigned from its characteristic position, δ_C 66–82. The bridgehead carbon signals were distinguished by off-resonance decoupling and, thus, directly assigned for the 3- and 8-alcohols with the exception of **20** and **21** for which the allylic centres were taken to be at lower field as in the olefin. For the 2- and 6-alcohols, that at lower field was assigned to the bridgehead carbon α to the carbinyl centre. The olefinic signal assignments were made by comparison of the observed shieldings with those for the corresponding olefin. Reversal of the present assignments for **16**–**21** would require that the hydroxyl group exerts markedly

TABLE 2. ^{13}C shieldings[a] of some bicyclic compounds

Skeleton	Compd.	Substitution	C-1	C-2	C-3	C-4	C-5	C-6	C-7	C-8	C-9
[2.2.1]	**22**[b]	Nil	36.3	29.6	29.6	36.3	29.6	29.6	38.3		
	23	7-OH	40.4	26.8[c]	26.8[c]	40.4	27.0[d]	27.0[d]	79.7		
	24[b]	Δ^2	41.8	135.2	135.2	41.8	24.6	24.6	48.5		
	25	Δ^2-*anti*-OH	45.6	134.3	134.3	45.6	21.4	21.4	82.0		
	26	Δ^2-*syn*-OH	47.4	131.9	131.9	47.4	22.2	22.2	86.9		
[3.2.2]	**27**	Nil	29.0	35.7	22.4	35.7	29.0	25.9	25.9	25.9	25.9
	28	*endo*-6-OH	30.2	36.7	21.8	26.6	36.8	70.0	38.3	24.4	23.7
[2.1.1]	**29**	Nil	39.7	26.4	26.4	39.7	39.1	39.1			
	30	2-OH	46.2	72.0	39.2	38.8	34.9[c]	38.2[d]			

[a]In ppm from internal TMS for $CDCl_3$ solutions.
[b]Data from ref. 13.
[c]*Syn* with respect to the hydroxyl group.
[d]*Anti* with respect to the hydroxyl group.

larger substituent effects in this ring system than in bicyclo[2.2.2]octenols (1*a*) and bicyclo[2.2.1]-heptenols (1*b*) and that these effects are directionally opposite in **18**–**21** from those found for the corresponding analogs in these other bicyclic systems. Such drastic alterations in substituent effects are unprecedented. For **11** and **12**, the assignments listed in Table 1 seem the more consistent with the findings for the norborn-5-en-2-ols (1*b*) and the bicyclo[2.2.2]oct-5-en-2-ols, particularly the upfield shift for C-7 in **12** and the small downfield shift for C-7 in **11**. For **13** and **14**, there is no difficulty completing the assignments because of their symmetry.

The methylene assignments for the remaining unsaturated alcohols were made on the basis of the appearance of the pattern in the off-resonance decoupled spectrum and by consideration of the shifts caused by the hydroxyl substitution relative to those found for analogous substitutions in other bicyclic systems. For example, the off-resonance pattern for C-2 in **20** and **21** was a clean triplet while C-6 and C-7 gave rise to more complex multiplets owing to the fact that the protons bonded thereto form a closely coupled system. Grutzner (12) has discussed the basis for such assignments. The C-6 and C-7 signals in **20** and **21** were assigned as listed since it was expected that the 8-hydroxyl group shields both carbons; reversal of the assignments would mean that C-6 is shielded by ~7 ppm while C-7 is deshielded by 1–2 ppm, a very strange pattern. Both were expected to be shielded since the methylene carbons in 7-norbornanol (**23**) are shielded relative to those in norbornane (see Table 2). Although a recent paper (7) reports that the methylene carbons in **23** are equivalent, in an unspecified medium, we find C-2,C-3 (*syn* to the hydroxyl) 0.2 ppm upfield from C-5,C-6. Reduction of **25** with deuterium over PtO_2 furnished **23**-*5,6-d*$_2$ whose spectrum permitted unequivocal methylene assignments. The off-resonance decoupled spectra of **11**, **12**, **16**, and **17** readily identified the C-8 methylene signal and C-3 and C-4 were distinguished for **11** and **12** by the expected 8–10 ppm downfield shift (the β effect) exhibited by C-3. For **16** and **17**, the C-6 and C-7 signals were distinguished from the expected upfield shift for C-7 arising from the γ effect of the hydroxyl group. Finally, the three methylene signals for **18** and **19** were assigned by comparison with the shifts produced by the hydroxyl group in the 2-norbornanols (1*b*). It could be anticipated that the hydroxyl substituent effects at C-7 and C-8 in **18** and **19** should be closely similar to those for C-3 and C-7 in the corresponding norbornanols while the shift for C-2 (**18**, **19**) may resemble those for C-5 in the norbornanols. In fact with the present assignments the shifts at these centres in **18** are 12.1, −4.1, and −1.1 ppm, respectively, while the corresponding shifts for *exo*-2-norbornanol are 12.6, −3.9, and −1.5 ppm.

The methylene signals in the spectra of bicyclooctanols **2**–**9** were assigned in a similar fashion; those for **4** and **5** were particularly straightforward. The less intense methylene signals arose from C-8 while C-6,C-7 were distinguished from C-2,C-4 by their patterns in the off-resonance decoupled spectra. For **6** and **7**, the C-7 and C-8 signals were identified by the off-resonance spectra and, as in the case of **18** and **19**, these were distinguished in **6** by the marked downfield shift, 12.3 ppm, expected for C-7. The highest field signal, ~19 ppm, was ascribed to C-3 for **6** and **7** while C-4 was identified by the

upfield shifts arising from the γ effect of the hydroxyl group. For **8** and **9**, the C-3 signal was readily identified by its upfield position and lower relative intensity. The absorption positions appear to distinguish C-2,C-4 from C-6,C-7 for **8** but the relatively small difference of 0.8 ppm for these shieldings in **9** renders our assignment equivocal. The off-resonance spectra served to identify the C-8 signal for **2** and **3** showing that the hydroxyl shields this centre in **2** by −7.6 ppm; this tends to support our assignment for **9** in which C-2,C-4 are shielded by −7.5 ppm. In **2**, C-6 can be expected to be least affected by the hydroxyl group leading to its assignment as 28.4 ppm, while the remaining methylene signals cannot be definitively assigned since all are very similar, 26.5–26.9 ppm. Similarly, the assignments for C-3 and C-6 in **3** may be interchanged but those for C-4 and C-7 seem most appropriate. The present assignments for **2**–**5** agree with those reported recently by Lippmaa *et al.* (7) although the individual shieldings in the two sets of data differ by 0–0.9 ppm presumably because of the difference in solvent but the medium is unspecified for the earlier data (7). The shifts produced upon acetylation of **2**–**5** and **8** are included in Table 1 and these are unexceptional (1*b*, 7).

The data for a few previously unreported model compounds are collected in Table 2. The assignments for **23** were discussed above and those for **25** and **26** presented no problems. For **28**, the assignments are by no means established but seem the most reasonable; a similar situation obtains for **30**.

Discussion

The bicyclo[3.2.1]octane skeleton (**31**) contains a cyclohexane ring with two axial substituents, the 6,7-ethano bridge, which form a unit analogous to the norbornane skeleton. Comparisons can be made to both parent systems to gain a better understanding of hydroxyl substituent effects. The six-membered ring of **1** exists predominantly in the chair conformation **31***a* with the *endo*-2 and *exo*-3 C—H bonds essentially equatorial. The 6,7 bridge tends to pinch together the axial bonds at C-1,5 (**31***b*) such that the axial bonds at C-2,4 are splayed relative to their arrangement in a 'strainless' cyclohexane or decalin (**32**). Thus, this ring is flattened at C-2,3,4 and this should be accentuated in the Δ^6 derivatives because of the shorter

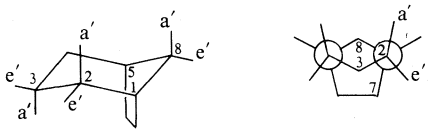

a **31** *b*

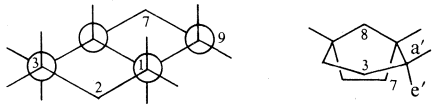

32 **33**

6,7 bond (**33**). Introduction of a 3,4 double bond renders this portion of the molecule planar. In the saturated skeleton, *endo*-3 and *endo*-6 substitution could introduce nonbonded interactions of sufficient magnitude to alter the conformation of the six-membered ring. It is of interest, therefore, to examine the shielding changes produced by hydroxyl substitution to check for shifts which differ appreciably from those expected from the data for cyclohexanols and norbornanols. For this purpose, the differences $\delta_C^{ROH} - \delta_C^{RH}$, from Tables 1 and 2 are collected in Table 3. Some caution is necessary since some assignments were based in part on the anticipated hydroxyl effects but, in most cases, there was other evidence to support the assignments, as discussed above, and often the alternative assignments would require remarkable variations in the substituent effects. Table 3 includes data for some model cyclohexanols, decalols, and norbornanols. Considerable effort has been directed toward the study of substituted cyclohexanols (3–5) and a recent discussion of hydroxyl substituent effects in cyclohexanols, decalols, and sterols (5) can serve as a basis for examination of the present data.

A priori it is reasonable to expect the effects of *exo*-3-hydroxyl substitution to resemble those for an unhindered equatorial hydroxyl group in the cyclohexanol and decalol systems (items 1, 2: Table 3) but items 3 and 4 show marked differences with all carbons less shielded by the OH group. It is particularly interesting that the bridgehead carbons fail to exhibit appreciable γ *anti* shifts although in sterols analogous methine carbons tend to show larger upfield shifts than methylene carbons (5). The enhanced α effect (~4 ppm) may be a result of the smaller dihedral angle between the hydroxyl and the *exo*-2 and -4 protons caused by ring flattening. Some support for this notion is given by the

TABLE 3. Substituent effects[a] of the hydroxyl group on the skeletal sp^3 carbon shieldings of various cyclic systems

Item	Skeleton	Compd.	Substitution	α	β		γ		δ	
					CH	CH_2				
1	Cyclohexane		Equatorial OH[b]	43.7		8.5	−2.8		−1.8	
2	*trans*-Decalin		Equat-2-OH[c]	43.3		8.7	−2.4		−1.2	
3	Bicyclo[3.2.1]octane	**4**	*exo*-3-OH	47.1		9.5	−0.3		−0.6(C-8)	0.2(C-6,7)
4		**13**	Δ[6]-*exo*-3-OH	48.0		10.0	−0.4		−0.2(C-8)	
5	*trans*-Decalin		Equat-1-OH[c]	40.3	6.7	8.9	−2.8(C-3)	−5.2(C-9)	−0.8(C-4)	−0.6(C-6)
							−2.5(C-5)			−0.7(C-8)
6	Bicyclo[3.2.1]octane	**3**	*endo*-2-OH	39.7	7.5	9.2	−2.1(C-4)	−5.6(C-7)	−1.5(C-5)	−0.4(C-6)
							−2.4(C-8)			
7		**12**	Δ[6]-*endo*-2-OH	43.3	7.8	9.8	−1.9(C-4)		−1.1(C-5)	
							−2.6(C-8)			
8		**17**	Δ[3]-*endo*-2-OH	36.2	8.2		+2.0(C-8)	−9.3(C-7)	−0.4(C-5)	−3.0(C-6)
9	Cyclohexane		Axial OH[b]	38.9		5.6	−7.5		−0.9	
10	*trans*-Decalin		Axial-2-OH[c]	39.7		6.1,7.0	−6.7(C-4)		−0.5(C-5)	
							−7.3(C-10)		−1.4(C-9)	
11	Bicyclo[3.2.1]octane	**5**	*endo*-3-OH	47.6		8.1	−1.3		−1.1(C-8)	−0.1(C-6,7)
12		**14**	Δ[6]-*endo*-3-OH	48.3		11.6	−1.4		−0.4(C-8)	
13	*trans*-Decalin		Axial-1-OH[c]	36.1	3.7	7.4	−6.9(C-3)		−0.4(C-4)	−0.4(C-6)
							−8.1(C-5)			−0.5(C-8)
							−4.7(C-9)			
14	Bicyclo[3.2.1]octane	**2**	*exo*-2-OH	38.5	6.5	7.7	−5.9(C-4)	−2.4(C-7)	−0.9(C-5)	−0.5(C-6)
							−7.6(C-8)			
15		**11**	Δ[6]-*exo*-2-OH	40.9	6.9	8.7	−3.3(C-4)		−0.3(C-5)	
							−7.8(C-8)			
16		**16**	Δ[3]-*exo*-2-OH	34.6	6.8		−4.7(C-8)	−5.8(C-7)	0.0(C-5)	4.5(C-6)
17		**9**	*endo*-8-OH	34.7	2.5		−8.2(C-2,4)	−3.6(C-6,7)	−1.3(C-3)	
18		**21**	Δ[3]-*endo*-8-OH	38.0	2.1(C-1)		−6.0(C-2)	−3.3(C-6)		
					4.2(C-5)			−2.2(C-7)		
19	Bicyclo[2.2.1]heptane	**23**	7-OH	41.4	4.1		−2.8(C-2,3)	−2.6(C-5,6)		
20		**25**	Δ[2]-*anti*-7-OH	33.5	3.8		−3.2(C-5,6)			
21		**26**	Δ[2]-*syn*-7-OH	38.4	5.6			−2.4(C-5,6)		
22	Bicyclo[3.2.1]octane	**8**	*exo*-8-OH	42.4	7.0		−2.7(C-6,7)	−1.5(C-2,4)		
23		**20**	Δ[3]-*exo*-8-OH	42.6	7.1		−2.9(C-6)	0.0(C-2)		
							−2.3(C-7)			
24		**6**	*exo*-6-OH	47.1	9.4	12.3	−3.5(C-8)	−3.0(C-4)	−1.4(C-2)	0.4(C-3)
								0.6(C-1)		

TABLE 3 (*Concluded*)

Item	Skeleton	Compd.	Substitution	α	β		γ	δ
					CH	CH_2		
25		**18**	Δ^3-*exo*-6-OH	42.5	8.4	12.1	−4.1(C-8)	−0.3(C-1) −1.1(C-2)
26	Bicyclo[2.2.1]heptane		*exo*-2-OH[d]	45.1	7.9	12.6	−3.9(C-7)	−5.2(C-6) −1.5(C-5) −0.9(C-4)
27	Bicyclo[2.1.1]hexane	**30**	2-OH	45.6	6.5	12.8	−4.2(C-5)	−0.9(C-4) −0.9(C-6)
28	Bicyclo[2.2.1]heptane		*endo*-2-OH[d]	43.3	6.2	9.8	−9.6(C-6)	−0.7(C-7) 0.3(C-5) 0.9(C-4)
29	Bicyclo[3.2.1]octane	**7**	*endo*-6-OH	45.9	4.1	8.9	−6.0(C-4)	−1.9(C-8) −0.2(C-2) 0.3(C-3) −1.0(C-1)
30		**19**	Δ^3-*endo*-6-OH	45.0	4.4	10.2		−2.8(C-8) 0.4(C-2) −0.9(C-1)

[a] $\Delta\delta^{OH} = \delta_c^{ROH} - \delta_c^{RH}$ where RH = hydrocarbon (in ppm); positive values indicate downfield shifts.
[b] These substituent effects were obtained by comparison of the shieldings for the 3- and 4-*tert*-butylcyclohexanols with those for *tert*-butylcyclohexane in $CDCl_3$ (C. T. Tan, Ph.D. thesis, University of Western Ontario, 1976).
[c] Data from ref. 4.
[d] Data from ref. 1*b*.

50 ppm α effect observed for 16α-hydroxyl substitution in androstane (5) relative to the ~45 ppm shift found for 2α and 3β substitution. An equatorial hydroxyl group at C-2 in the [3.2.1] system, however, exerts effects which are very similar to those in the corresponding decalol (*cf.* items 5 and 6). The smaller α effect can be ascribed to a γ interaction with a neighboring methylene proton on C-7 (C-9 in the decalol). Although suggestions to the contrary have been made (14), it seems generally true that γ *gauche* carbons must bear a hydrogen atom closely neighboring the hydroxyl group to produce an upfield γ *gauche* effect. Introduction of the Δ^6 double bond produces a larger α effect (item 7), as expected, since the olefinic proton at C-7 is well separated from the hydroxyl group, whereas the Δ^3 double bond decreases the α effect (item 8) by enhancing the γ interaction with C-7 through ring flattening at C-2. In accord with this interpretation, a larger upfield shift is found for C-7. However, a puzzling feature emerges from the shifts for items 6–8. While the γ *anti* effects at C-4 and C-8 are similar for **3** and **12** (−2 ppm) there is a downfield shift of 2 ppm for C-8 in **17**. The C-8 assignment for **17** was confirmed by the off-resonance spectrum and the lowest field methylene carbon in olefin **15** was proved to be C-2 by deuteration (15). A larger downfield shift (4 ppm) occurs for the corresponding interaction in *exo*-2-bicyclo[3.2.1]-octa-3,6-dienol (8). Upfield γ *anti* effects are common (16) but with fully substituted intervening carbons these are downfield (1*c*).

Items 9–18 include compounds bearing axial hydroxyl groups and the 3-hydroxy [3.2.1] derivatives exhibit marked differences from axial alicyclic alcohols having two β methylene groups (items 9, 10). In the former, pronounced ring-flattening at C-3 can be anticipated through the *syn*-axial δ interaction of the hydroxyl group with C-6 and C-7, an arrangement known to cause deshielding (1*a*, 1*b*, 17). The shifts for the *endo*- and *exo*-3 derivatives (items 3, 4, 11, and 12) are remarkably similar indicating ^{13}C spectra could not be used for stereochemical assignments in closely related cases. In contrast, the *exo*-2-hydroxyl derivatives seem well behaved with the somewhat flattened ring of **2** leading to slightly stronger α and β effects and reduced γ effects relative to those found for the decalol (items 13 and 14), trends which are accentuated upon introduction of the 6,7- double bond

TABLE 4. Shielding effects[a] of the hydroxyl group on sp^2 carbons in bicyclic systems

Skeleton	Compd.	Substitution	γ		δ
			$Q \sim 180°$	$Q > 90°$	
[3.2.1]	**11**	Δ^6-*exo*-2-OH	0.8		2.7
	12	Δ^6-*endo*-2-OH		−2.0	2.2
	13	Δ^6-*exo*-3-OH			0.5
	14	Δ^6-*endo*-3-OH			6.2
[2.2.1]		Δ^5-*exo*-2-OH[b]	−1.7		5.0
		Δ^5-*endo*-2-OH[b]		−4.1	4.8
	25	Δ^5-*anti*-7-OH	−0.9		
	26	Δ^5-*syn*-7-OH		−3.3	
[3.2.1]	**20**	Δ^3-*exo*-8-OH	−2.3		0.2
	21	Δ^3-*endo*-8-OH		−5.0	2.7
	18	Δ^3-*exo*-6-OH	−4.5		2.1
	19	Δ^3-*endo*-6-OH		−5.3	4.3
[2.2.2]		Δ^5-*exo*-2-OH[c]	−2.1		1.1
		Δ^5-*endo*-2-OH[c]		−5.1	1.8

[a] $\Delta\delta_C = \delta_C^{ROH} - \delta_C^{RH}$ (in ppm) where RH is the appropriate olefin. Negative values are upfield shifts.
[b] Data taken from ref. 1*b*.
[c] Data taken from ref. 1*c*.

(item 15). As above, the allylic alcohol **16** exhibits an attenuated α effect and a smaller upfield shift for C-8. In **16**, C-7 is strikingly shielded, a γ *anti* effect in the expected direction but more than twice as large as that found for the saturated analog **2**. This would suggest that the dihedral angle relating the hydroxyl group and the *anti* γ carbon is a critical factor governing these effects.

An *endo*-8 hydroxyl group is axial with respect to the six-membered ring (see **31***a*) and the substituent effects for **9** are similar for the model decalol (item 13). The Δ^3 function produces the trends expected from ring flattening and the removal of one γ *gauche* interaction. Similar upfield γ *anti* effects occur in the [3.2.1] and [2.2.1] systems (items, 17–19 and 21) for which the geometries must be similar. The smaller γ *gauche* effects in the [2.2.1] cases (items 19 and 20) are ascribed to the increased separation of the hydroxyl group from the *exo*-protons. An *exo*-8-hydroxyl group exerts comparable γ *gauche* shifts (items 22 and 23) while its effects at the carbons of the six-membered ring are similar to those for the equatorial models (items 1, 2, and 5).

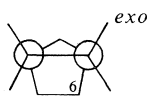

34

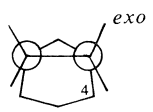

35

The effects of an *exo*-6-hydroxyl group in the [3.2.1] skeleton resemble those for an *exo*-2-OH group in the norbornane system (items 24–26) with curious differences in the α effects and the β effects at the bridgehead carbons. The attenuation of the γ *anti* effect in the [3.2.1] case relative to that in the [2.2.1] system may reflect the change in dihedral angle. Representations **34** and **35** illustrate the relative orientations of the bonds in this portion of the two bicyclic systems. Differences for an *endo*-6-hydroxyl group are also apparent from **34** and **35** and there is a significant difference in the γ *gauche* effects at C-6 and C-4, respectively (items 27 and 28).

An *endo* γ C—H bond is more nearly aligned with the C—O bond in the [2.2.1] skeleton indicating that the transmission of the γ *gauche* effect is more effective when the hydroxyl and a hydrogen are closer. It is also interesting that the γ *anti* effects at C-7 (C-8) (items 28–30) are more shielding in the [3.2.1] examples. Any interchanges of the methylene assignments for **19** lead to an even stronger set of shifts. As noted above, the angular dependence of the γ *anti* effects seems quite striking.

To compare the hydroxyl substituent effects in a variety of bicyclic systems the results for the [2.1.1], [2.2.1], [2.2.2], and [3.2.2] skeletons are shown in **36**–**39**; those for the [2.2.1] and [2.2.2] were reported earlier (1*a*, 1*b*). The effects are very similar indicating the absence of significant perturbations due to strain.

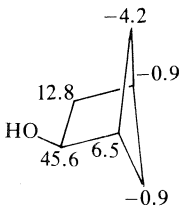

36

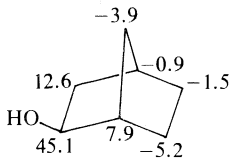

37

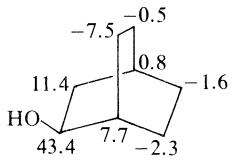

38

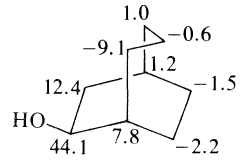

39

The hydroxyl substituents effects on the sp^2 carbons of the unsaturated alcohols are listed in Table 4. The general trends are similar to those discussed above with γ *gauche* interactions producing larger upfield shifts than γ *anti* effects. The δ effects are larger than those in Table 3 with maximum deshielding effects occurring in the compounds in which the hydroxyl group closely approaches the double bond. These resemble *syn*-axial perturbations in saturated systems (1*a*, 1*b*, 17). In the two allylic alcohols, both olefinic carbons appear to be deshielded by the hydroxyl group, behavior which is analogous to acyclic allylic alcohols.

In summary, the most puzzling trends are associated with γ *anti* effects for which the angular dependence may be a critical factor. It has been established that the degree of substitution of the intervening carbons in the γ fragment also has a major influence on the magnitude and direction of these shifts (1*c*). Thus their use for diagnostic purposes must be approached cautiously. Interestingly, there seems to be no obvious trend associated with the different strain energies of these various bicyclic systems. In general the relative orientations of the hydroxyl and a γ C—H bond tend to govern the magnitude of the upfield shift. The present data confirm earlier conclusions on this point (5) although contrary proposals have appeared (14).

Acknowledgements

We are grateful for the financial support of the National Research Council of Canada for this study and we thank Ms. Lucille Gough, Cornelia Ferriera, and Inara Grikis for technical assistance. We thank Dr. A. K. Cheng who kindly provided us with a sample of bicyclo[2.1.1]-hexane by Wolff–Kishner reduction of the ketone which was generously given to us by Prof. J. L. Charlton.

1. (*a*) J. B. Stothers and C. T. Tan. Can. J. Chem. **54**, 917 (1976); (*b*) J. B. Stothers, C. T. Tan, and K. C. Teo. Can. J. Chem. **54**, 1211 (1976); (*c*) W. A. Ayer, L. M. Browne, S. Fung, and J. B. Stothers. Can. J. Chem. **54**, 3272 (1976).
2. E. M. Engler, J. D. Andose, and P. von R. Schleyer. J. Am. Chem. Soc. **95**, 8005 (1973).
3. J. D. Roberts, F. J. Weigert, J. I. Kroschwitz, and H. J. Reich. J. Am. Chem. Soc. **92**, 1338 (1970); T. Pehk, H. Kooskora, and E. Lippmaa. Org. Magn. Reson. **8**, 5 (1976).
4. S. H. Grover and J. B. Stothers. Can. J. Chem. **52**, 870 (1974).
5. H. Eggert, C. L. Vanantwerp, N. S. Bhacca, and C. Djerassi. J. Org. Chem. **41**, 71 (1976).
6. G. E. Maciel. *In* Topics in carbon-13 nmr spectroscopy. *Edited by* G. C. Levy. Wiley-Interscience, New York. 1974. pp. 53–77.
7. E. Lippmaa, T. Pehk, N. A. Belikova, A. A. Bobyleva, A. N. Kalinichenko, M. D. Ordubadi, and A. F. Platé. Org. Magn. Reson. **8**, 74 (1976).
8. J. B. Stothers, J. R. Swenson, and C. T. Tan. Can. J. Chem. **53**, 581 (1975).
9. S. H. Grover, D. H. Marr, J. B. Stothers, and C. T. Tan. Can. J. Chem. **53**, 1351 (1975).
10. C. S. Foote and R. B. Woodward. Tetrahedron, **20**, 687 (1964).
11. W. C. Baird. J. Org. Chem. **31**, 2411 (1966).
12. J. B. Grutzner. J. Chem. Soc. Chem. Commun. 64 (1974).
13. J. B. Stothers, C. T. Tan, and K. C. Teo. Can. J. Chem. **51**, 2893 (1973).
14. E. Lippmaa, T. Pehk, and J. Passivirta. Org. Magn. Reson. **5**, 277 (1973).
15. A. K. Cheng and J. B. Stothers. Can. J. Chem. **55**, 50 (1977).
16. E. L. Eliel, W. F. Bailey, L. D. Kopp, R. L. Willer, D. M. Grant, R. Bertrand, K. A. Christenson, D. K. Dalling, M. W. Duch, E. Wenkert, F. M. Schell, and D. W. Cochran. J. Am. Chem. Soc. **97**, 322 (1975).
17. J. B. Stothers, C. T. Tan, and K. C. Teo. J. Magn. Reson. **20**, 570 (1975).
18. A. Stoessl, E. W. B. Ward, and J. B. Stothers. Tetrahedron Lett. 3271 (1976).

The crystal and molecular structure of lead(II)bromide-bis-dimethylsulphoxide, $PbBr_2 \cdot 2[(CH_3)_2SO]$

ANTHONY D. BARANYI AND MARIO ONYSZCHUK
Department of Chemistry, McGill University, Montreal, P.Q., Canada H3C 3G1
AND
YVON LE PAGE AND GABRIELLE DONNAY
Crystallographic Laboratory, McGill University, Montreal, P.Q., Canada H3C 3G1

Received July 13, 1976

ANTHONY D. BARANYI, MARIO ONYSZCHUK, YVON LE PAGE, and GABRIELLE DONNAY. Can. J. Chem. **55**, 849 (1977).

The title compound has two $PbBr_2 \cdot 2[(CH_3)_2SO]$ units, $Z = 2$, in a cell with $a = 11.093(2)$, $b = 12.382(3)$, $c = 4.540(1)$ Å, belonging to space group *Pmmn*. The structure was solved by Patterson functions and was refined by full-matrix least-squares calculations to a final R of 0.054 for 348 observed diffractometer intensities. Passing through the unit cell are two antiparallel, infinite polar chains, each with symmetry *mm*2, extending along z and interacting with each other by weak van der Waals forces. Lead(II) is six-coordinate with a close, covalent hemisphere consisting of two bromine atoms [Pb—Br^{I},Br^{II} 2.93(1) Å], and two oxygen atoms [Pb—O,O′ 2.50(3) Å] which subtend an angle of 157.9(9)° at lead, located at the intersection of the O—Pb—O′ and Br^{I}—Pb—Br^{II} perpendicular mirror planes. The other hemisphere consists of bridging bromine atoms from the neighboring $PbBr_2 \cdot 2$dmso unit [Pb—Br^{III},Br^{IV} 3.24(1) Å], resulting in a rectangle of bromine atoms around lead [Br^{I}—Pb—Br^{II} 90.5(1)°, Br^{III}—Pb—Br^{IV} 80.2(1)°]. The distortion of the octahedral coordination sphere around lead is discussed in terms of (*a*) a repulsive effect of the Pb(II) valence lone electron-pair, (*b*) weak Br—S bonding, and (*c*) crystal packing forces.

ANTHONY D. BARANYI, MARIO ONYSZCHUK, YVON LE PAGE et GABRIELLE DONNAY. Can. J. Chem. **55**, 849 (1977).

Le composé mentionné dans le titre a deux unités de $PbBr_2 \cdot 2[(CH_3)_2SO]$ et $Z = 2$ par maille de dimensions $a = 11.093(2)$, $b = 12.382(3)$, $c = 4.540(1)$ Å et appartenant au groupe d'espace *Pmmn*. On a résolu la structure par les fonctions de Patterson et on l'a affinée par méthode des moindres carrés (matrice complète) jusqu'à une valeur finale de R de 0.054 pour 348 intensités observées par diffractométrie. Passant par la maille, il y a deux chaînes polaires infinies et antiparallèles qui possèdent chacune une symétrie *mm*2 s'étendant le long de l'axe z et qui interagissent l'une avec l'autre par des forces de Van der Waals faibles. Le plomb(II) est hexacoordonné avec un hémisphère covalent fermé consistant de deux atomes de brome [Pb—Br^{I},Br^{II} 2.93(1) Å] et deux atomes d'oxygène [Pb—O,O′ 2.50(3) Å] qui soutendent un angle de 157.9(9)° au niveau du plomb, situé à l'intersection des plans miroirs perpendiculaires de O—Pb—O′ et Br^{I}—Pb—Br^{II}. L'autre hémisphère consiste d'atomes de brome qui forment un pont et qui proviennent de l'unité $PbBr_2 \cdot 2$dmso voisine [Pb—Br^{III},Br^{IV} 3.24(1) Å]; ces arrangements conduisent à l'existence d'un rectangle d'atomes de brome autour de l'atome de plomb [Br^{I}—Pb—Br^{II} 90.5(1)°, Br^{III}—Pb—Br^{IV} 80.2(1)°] .On discute de la distorsion de la coordination octaédrique de la sphère autour du plomb en termes: (*a*) d'un effet répulsif de la paire d'électrons libres de valence du Pb(II), (*b*) de liaisons Br—S faibles et (*c*) de forces d'entassement du cristal.

[Traduit par le journal]

Introduction

Crystal and molecular structures of coordination compounds of lead(II) halides and pseudohalides are known only for lead(II) chloride-bis-thiourea (1), $PbCl_2 \cdot 2$tu, and di-isothiocyanato lead(II)-bis-dimethylsulphoxide (2), $Pb(NCS)_2 \cdot 2$dmso. In the first structure, lead is seven coordinate due to bonding with four sulphur and two chlorine atoms, all at the corners of a distorted trigonal prism, and a third chlorine atom near the center of a prism face. Sulphur atoms and apical chlorine atoms bridge to neighbouring lead atoms forming a polymeric chain. Polymeric chains are also present in crystalline $Pb(NCS)_2 \cdot 2$dmso, the lead atom of which is six-coordinate in a distorted octahedral arrangement of two nitrogen atoms and two bridging sulphur atoms approximately coplanar, with one oxygen atom above and another below the plane (2).

Adducts of lead(II) bromide with a variety of O-, S-, and N-donor ligands have been prepared and characterized (3), but few conclusions were made about structure on the basis of the measured vibrational spectra. Of the available complexes, $PbBr_2 \cdot 2dmso$ was chosen for an X-ray diffraction study because it offered the possibility of a direct comparison with the structure of $Pb(NCS)_2 \cdot 2dmso$ (2). Structures of dimethylsulphoxide complexes are also of particular interest because of the ambidentate coordinating ability of this ligand. Dimethylsulphoxide is sulphur-bonded in $Ir(C_{15}H_{13}O)Cl_2 \cdot 2dmso$ (4), $PdCl_2 \cdot 2dmso$ (5), $Pd(NO_3)_2 \cdot 2dmso$ (6), and $[Ru(dmso)(NH_3)_5][PF_6]_2$ (7); oxygen-bonded in $[FeCl_2(dmso)_4][FeCl_4]$ (8), $CuCl_2 \cdot 2dmso$ (9), $(CH_3)_2SnCl_2 \cdot 2dmso$ (10), $SnCl_4 \cdot 2dmso$ (11), $Pb(NCS)_2 \cdot 2dmso$ (2), and $La(NO_3)_3 \cdot 4dmso$ (12); and oxygen-bridge-bonded in $3HgCl_2 \cdot 2dmso$ (13).

Experimental

Lead(II) bromide-bis-dimethylsulphoxide, $PbBr_2 \cdot 2dmso$ (3)

Small white needles were obtained after $PbBr_2$ (3.7 g, 10 mmol) was dissolved in dimethylsulphoxide (50 ml) at 40 °C, and the solution was allowed to stand for several days until crystallization took place. Crystals were separated by filtration and dried with suction in a nitrogen-filled dry-box. The complex decomposed rapidly to a white powder on exposure to moist air, and at approximately 100 °C in a capillary tube filled and sealed under nitrogen. *Anal.* calcd. for $PbBr_2 \cdot 2[(CH_3)_2SO]$: C 9.2, H 2.3, Pb 39.6; found: C 9.3, H 2.3, Pb 38.5.

Data Collection

The crystal selected for study was held in a Lindeman glass capillary tube by a thin film of silicone grease, sealed under nitrogen, and mounted with the longest dimension of the crystal, *c*, approximately parallel with the rotation axis of the Eulerian cradle to minimize absorption. The dimensions of the crystal were *ca.* 0.01 × 0.01 × 0.30 mm.

The diffraction aspect *P**n* was determined from rotation, Weissenberg, and precession films using Ni-filtered CuK_α radiation, and two possible space-groups were indicated: *Pmmn* and $P2_1mn$. Measurements of the independent reflections with the diffractometer confirmed the systematic extinction *hk*0 for $h + k = 2n + 1$. The unit-cell parameters were refined by least-squares fit of χ,ϕ,ω and 2θ values for 12 general reflections with $2\theta > 35°$ measured on a diffractometer with MoKα radiation. Crystal data are:

$PbBr_2 \cdot 2[(CH_3)_2SO]$ fw = 523.3
Orthorhombic, $a = 11.093(2)$, $b = 12.382(3)$, $c = 4.540(1)$ Å, $u = 623.6$ Å^3, $Z = 2$, $\rho_c = 2.79$, Space group *Pmmn*, (D_{2h}^{13}), MoKα, $\lambda = 0.70926$ Å, μ(MoKα) = 202.6 cm^{-1}, $T = 20$ °C.

Intensities were measured on a Picker four-circle automated diffractometer using graphite monochromated MoKα radiation. Reflections were collected using the θ–2θ scan method, scanning from 0.6° below α_1 to 0.6° above α_2 at $\frac{1}{2}°$ 2θ min^{-1}, with 20 s background counts being measured at each end of the scan. The intensities of three standard reflections, measured after every 10 reflections, showed only the deviations from the mean predicted from counting statistics. A total of 883 symmetry independent reflections were measured in the range $5° \leq 2\theta \leq 60°$, 348 of which had $I > 2\sigma(I)$ and were classed observed. Intensities were corrected for Lorentz and polarization factors by means of the DATRDN program of X-Ray 70 (14). No absorption corrections were made because the width of the crystal is only 0.01 mm, which is considerably smaller than the calculated optimum size, $t_{opt} = 0.33$ mm (15). The transmission factor was in the range 0.82 to 0.87, and the error due to absorption was estimated to be ±5% on intensities. Atomic scattering factors were taken from Hanson *et al.* (16) and corrections were made for anomalous dispersion of lead, bromine, and sulfur (17).

Structure Determination and Refinement

A study of the Patterson function provided a unique spatial distribution of the heaviest atoms, Pb, Br, and S, giving a pseudo-body-centered Bravais lattice which had not been noticed from photographic measurements. The mean of $h + k + l$ odd intensities was only 14% of the mean of $h + k + l$ even intensities. A partial Patterson synthesis of $h + k + l$ odd terms indicated that the difference between the true structure and the body-centered pseudo-structure was not due to the light atoms, but mainly to a displacement of the lead atom from the center of the rectangle of bromine atoms (18). A model of two parallel chains along [001], probably in space group *Pmm*2, pseudo-*Imm*2, was indicated. The systematic extinctions in this space group become structural absences. The difference from a model of antiparallel chains, rejected by the partial Patterson synthesis, lay only in the *z* coordinate of one oxygen atom. Since *Pmm*2 is a subgroup of *Pmmn*, both models were first refined and compared in that space group.

The *n* glide-plane systematic extinctions were included in the observed data. The model of parallel chains refined to a residual *R* of 0.090 using isotropic temperature factors for the five atoms Pb, Br, S, O, and C. In the least-squares calculation all atoms were accepted except one oxygen atom whose temperature factor became unacceptably large during refinement.

The difference Fourier synthesis showed a wide peak at the position where an oxygen atom was expected in the model of antiparallel chains. By introducing the oxygen atom in this position, the residual *R* decreased to 0.055, using anisotropic thermal parameters for Pb, Br, and S.

An analysis of this model showed that it was compatible with space group *Pmmn*, the largest difference being 4σ in the *z* position of bromine. After removing the systematic extinctions of the *n* glide-plane from the data, the structure was further refined in the *Pmmn* space group by full-matrix least-squares methods using anisotropic temperature factors for all atoms. Three cycles were required for final convergence. The function minimized was $\Sigma\omega(|F_o| - |F_c|)^2$ where $\omega = 1$. The refinement terminated with an unweighted residual *R* of 0.054 for all atoms except hydrogen which could not be located from

TABLE 1. Final positional parameters with estimated standard deviations in parentheses; space group *Pmmn*, origin at center*

Atom	Position	x	y	z
Pb	2(*a*)	1/4	1/4	0.2115(4)
Br	4(*f*)	0.5622(3)	3/4	0.2435(8)
O	4(*e*)	1/4	0.4479(24)	0.1063(58)
S	4(*e*)	1/4	0.4801(8)	0.7681(19)
C	8(*g*)	0.8719(26)	0.0750(26)	0.2646(61)

*Coordinates of general position: $\pm(x,y,z;\ \frac{1}{2}-x,y,z;\ x,\frac{1}{2}-y,z;\ \frac{1}{2}-x,\frac{1}{2}-y,z)$.

TABLE 2. Final anisotropic thermal parameters ($U_{ij} \times 100$ Å^2) and their estimated standard deviations*

Atom	U_{11}	U_{22}	U_{33}	U_{12}	U_{13}	U_{23}
Pb	4.86(13)	4.84(11)	2.67(8)	0.0	0.0	0.0
Br	3.95(22)	5.85(23)	5.03(24)	0.0	0.21(16)	0.0
O	13.9(26)	6.9(20)	5.1(15)	0.0	0.0	3.1(15)
S	6.9(66)	4.95(51)	4.00(46)	0.0	0.0	0.36(43)
C	7.8(21)	10.1(22)	6.4(17)	−4.8(19)	−0.1(16)	−1.2(17)

*The form of the thermal ellipsoid is: $\exp(-2\pi^2 \sum_{i=1}^{3}\sum_{j=1}^{3} h_i h_j a_i^* a_j^* U_{ij})$.

the final difference-Fourier map. When the refinement was repeated with a statistical weighting of the data, $\omega = 1/\sigma^2$, an R value of 0.055 was obtained: the refined parameters and estimated standard deviations were unchanged within the error limits. The refinement displayed a large U_{11} thermal parameter for the oxygen atoms. This thermal motion had smeared out the Pb—O peak in the partial Patterson synthesis to such an extent that this peak was absent and led to the initial assumption of space group *Pmm*2. The final residual R of 0.054 corresponds to a partial residual of 0.044 on 214 observed $h + k + l = 2n$ structure factors and 0.086 on 134 odd ones. The larger residual for the odd terms indicates that they contribute less to the sum of the structure factors than even terms rather than forming a large contribution to the sum of the errors.

Results and Discussion

Atomic co-ordinates are listed in Table 1, anisotropic temperature factors in Table 2, and bond distances and angles in Table 3. Observed and calculated structure factors have been placed in the Depository of Unpublished Data.[1]

The crystal structure consists of two antiparallel chains of symmetry *mm*2 extending along the z direction, corresponding to one another by an n glide-plane perpendicular to c. The chains consist of $PbBr_2 \cdot 2dmso$ units bridged through bromine atoms (Fig. 1). Lead has a coordination number of six and sits at the intersection of the two mirror planes. Four bromine atoms form a rectangle in a mirror plane with two short Pb—Br bonds (2.93(1) Å) and two longer bridging Pb—Br interactions (3.24(1) Å). The Br—Pb—Br angles range from 80 to 95°. The two oxygen atoms of the dimethylsulphoxide groups complete the coordination sphere of lead and subtend an angle of 157.9(9)° at lead. The dmso units point toward the region of short Pb—Br distances (Fig. 2).

The directions of the largest thermal motions of Br and O are perpendicular to the plane of their bonds. The maximum vibration of sulfur is in the same direction as oxygen, while the carbon atoms vibrate in the xy plane, indicating a probable oscillation of the dmso group around the S—O bond. The lead atom has an oblate thermal motion ellipsoid along the z axis, corresponding to transverse vibrations of chains rather than to independent movements of individual lead atoms.

The coordination sphere of lead has changed drastically from the parent $PbBr_2$ in which lead is bound to nine bromine atoms, six at the apices of a trigonal prism and three beyond the centers of the three prism faces (19). The lead–bromine distances in $PbBr_2$ range from 3.0 to 3.88 Å. In $PbBr_2 \cdot 2dmso$ lead is six-coordinate and there are two distinct coordination hemispheres (Fig. 2). There is a close-packed, covalently bound region consisting of two oxygen atoms, O and O′, and two bromine atoms, Br^I and Br^{II}. The Pb—Br^I and Pb—Br^{II} distances,

[1]The structure factor table is available, at a nominal charge, from the Depository of Unpublished Data, CISTI, National Research Council of Canada, Ottawa, Canada K1A 0S2.

TABLE 3. Bond lengths (Å), interatomic distances (Å), and bond angles (deg), with estimated standard deviations in parentheses

Bond	Length	Bonds	Angle
Pb—Br^{I},Br^{II}	2.93(1)	Br^{I}—Pb—Br^{II}	90.5(1)
Pb—Br^{II},Br^{IV}	3.24(1)	Br^{III}—Pb—Br^{IV}	80.2(1)
Pb—O	2.50(3)	Br^{I}—Pb—Br^{III}	94.7(1)
S—O	1.59(3)	$Br^{I,II}$—Pb—O	82.3(4)
S—C	1.80(3)	$Br^{III,IV}$—Pb—O	98.4(5)
		O—Pb—O′	157.9(9)
		Pb—O—S	115.6(15)
		C—S—C	97.6(15)
		O—S—C	104.2(12)

Non-bonding approaches	Observed	van der Waals radii sums (25)	Covalent radii sums (25)
(*i*) Within each unit* of a chain			
Br^{I}. . .Br^{II}	4.17(1)	3.6–4.0	2.28
Br^{III}. . .Br^{IV}	4.540(1)	3.6–4.0	2.28
O. . .$Br^{I,II}$	3.59(2)	3.3–3.5	1.87
O. . .$Br^{III,IV}$	4.37(2)	3.3–3.5	1.87
S. . .$Br^{I,II}$	3.53(1)	3.6–3.8	2.16
CH_3. . .$Br^{I,II}$	4.10(2)	3.8–4.0	1.91
(*ii*) Between neighbouring units in the same chain			
Pb. . .S	3.81(1)	3.8	2.60
S. . .O	3.03(3)	3.3	1.75
CH_3. . .CH_3	4.540(1)	4.0	1.54
CH_3. . .Br	4.10(2)	3.8–4.0	1.91
(*iii*) Between units in neighbouring chains			
CH_3. . .CH_3	4.02(4)	4.0	1.54
	4.32(4)	4.0	1.54
CH_3. . .Br	3.76(2)	3.8–4.0	1.91
	3.80(2)	3.8–4.0	1.91
CH_3. . .O	4.27(4)	3.5	1.10
CH_3. . .S	4.83(4)	3.8	1.79

*Unit refers to the $PbBr_2$·2dmso cluster.

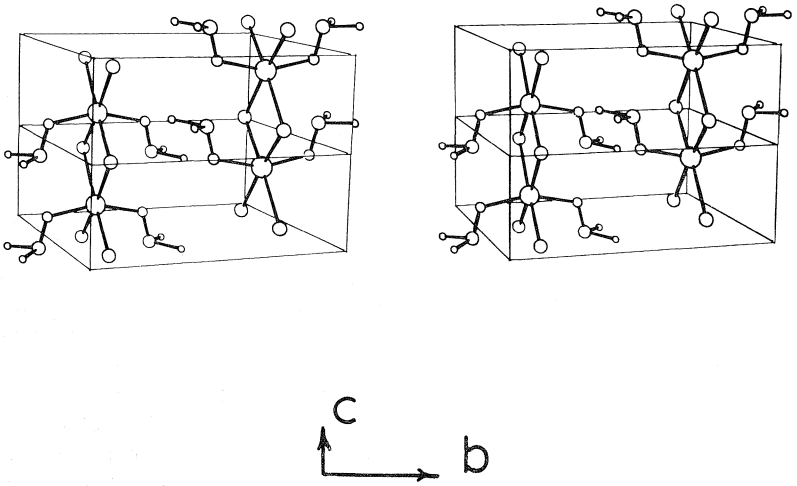

FIG. 1. ORTEP diagram (26) showing stereoscopically the packing in two unit cells along *c*.

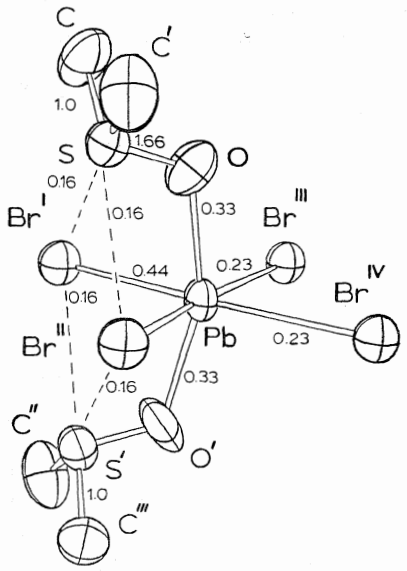

FIG. 2. ORTEP plot (26) of the molecular structure (including Br^{III} and Br^{IV} from the next unit) showing equatorial plane, atomic labelling, and bond valences in valence units (vu).

2.93(1) Å, are only slightly longer than the sums of corresponding covalent radii (2.7 Å) and appreciably shorter than the sums of corresponding van der Waals radii (3.9 Å), indicating that Pb—Br^{I} and Pb—Br^{II} bonds are predominantly covalent. Lead–oxygen distances, 2.50(3) Å, also show appreciable covalent character, being much closer to the covalent radii sum, 2.31 Å, than to the van der Waals radii sum, 3.5 Å. In the same region $Br^{I,II}$—O, $Br^{I,II}$—O′, and Br^{I}—Br^{II} interatomic approaches are equal to or greater than the sums of their respective van der Waals radii (Table 3). On the opposite side of the lead atom, *i.e.*, in the second hemisphere, there are two bridging bromine atoms from the neighboring $PbBr_2$·2dmso unit (Fig. 2). The Pb—Br^{III} and Pb—Br^{IV} distances, 3.24 Å, are greater than the sums of their ionic radii, 3.13 Å (25) but less than the sums of their van der Waals radii, 3.9 Å. The other interatomic approaches, O. . .$Br^{III,IV}$ and Pb. . .S, are equal to, or greater than the sums of the respective van der Waals radii (Table 3).

Three possibilities are suggested for the distortions of the octahedral configuration around Pb(II): (*a*) a repulsive effect of the Pb(II) valence lone electron-pair, (*b*) weak Br. . .S bonding, and (*c*) crystal packing forces.[2] Each of these possibilities will now be discussed in detail.

(*a*) The two dmso molecules of each octahedral cluster are bent away from 180°, O—Pb—O′ 157.9(9)°, toward the nearest bromine atoms, Br^{I} and Br^{II}, rather than towards the more distant bromine atoms, Br^{III} and Br^{IV}, a region one might have expected more sterically able to accommodate dmso molecules. A similar distortion of the O—Pb—O angle (160.1(8)°) in crystalline $Pb(NCS)_2$·2dmso was attributed to the repulsive effect of the unshared electron-pair of Pb(II) occupying a coordination site between two bridging thiocyanate groups (2). In $PbBr_2$·2dmso, none of the angles in the $PbBr_4$ rectangle is large enough to suggest the presence of a directed lone electron-pair. However, the unsymmetrical arrangement of bromine atoms and the 22° departure of the O—Pb—O′ angle from linearity suggest the existence of a repulsive effect which might be due to the distribution of the unshared electron-pair of Pb(II) being asymmetric rather than spherically symmetric. Similar examples of coordination spheres containing short and long bonds as well as angular distortions have been reported for As(III), Sb(III), and Bi(III) compounds and attributed to asymmetric lone electron-pairs (20).

(*b*) Thc fact that Br. . .S and S. . .O nonbonding distances are slightly less than the corresponding van der Waals radii sums (Table 3) prompts us to suggest that the observed distortions of the Pb(II) octahedral coordination sphere might be due to weak Br. . .S and S. . .O bonding within chains. When this possibility is examined in terms of the bond valence analysis of Donnay and Allman (21), or Brown (22), Pb(II) emerges with two strong, two medium, and two weak bonds, corresponding to Brown's configuration A. Bond valence units (vu) around Pb(II) were calculated from bond distances in the usual way (21, 22) and are given in Fig. 2. Lead(II) is assigned a bond valence sum of 2.0 and the proportions among the six bonds are similar to those of SnO in which Sn(II) is six-coordinate in a distorted octahedral geometry (22). Although the long Pb—Br bonds have only half the bond valence of the short Pb—Br

[2]These were suggested and preferred by one of the referees.

TABLE 4. Data for dimethylsulphoxide compounds

	Compound	M—S distance (Å)	M—O distance (Å)	M—O—S angle (deg)	S—O distance (Å)	Reference
S-bonded:	$Ir(C_{15}H_{13}O)Cl_2 \cdot 2dmso$	2.24			1.44, 1.46	4
	$PdCl_2 \cdot 2dmso$	2.29			1.47	5
	$Pd(NO_3)_2 \cdot 2dmso$	2.23, 2.25			1.46	6
	$[Ru(dmso)(NH_3)_5](PF_6)_2$	2.19			1.53	7
O-bridged:	$3HgCl_2 \cdot 2dmso$		2.52, 2.56	121.9, 130.2	1.54	13
O-bonded:	$[FeCl_2(dmso)_4][FeCl_4]$		2.0	124.5	1.54	8
	$CuCl_2 \cdot 2dmso$		1.96	118.2	1.53	9
	$Me_2SnCl_2 \cdot 2dmso$		2.32, 2.38	122	1.51, 1.61	10
	$SnCl_4 \cdot 2dmso$		1.51, 1.54			11
	$La(NO_3)_3 \cdot 4dmso$		2.47, 2.48		1.48, 1.52	12
	$Pb(NCS)_2 \cdot 2dmso$		2.45, 2.50	123.7, 128.2	1.50, 1.53	2
	$PbBr_2 \cdot 2dmso$		2.50	115.6	1.59	

bonds, their bond valence is large enough to indicate that Br^{III} and Br^{IV} are within the primary coordination sphere of Pb(II). The fact that the bond valence sum at each Br atom is 0.67 rather than 1.0 vu suggests that Br atoms are involved in additional bonding interactions, most likely with nearby S atoms of coordinated dmso molecules. Unfortunately, bond valences around sulfur cannot be calculated directly because the required sulfur radii are not yet available; however, bond valences surrounding sulfur can be obtained indirectly as follows. Since the total bond valence of oxygen is 2.0 vu and 0.33 vu of this is attributed to the Pb—O bond, 1.66 vu remain for the S—O bond. Sulfur is also covalently bound to two methyl groups, each bond accounting for 1.0 vu. Therefore, the bond valence sum at sulfur is 3.66 vu instead of 4.0 vu required by its oxidation number. If the difference of 0.34 vu is attributed to a weak interaction of the sulfur atom with two neighbouring Br atoms, *i.e.*, 0.17 vu per bond, the total bond valence of each Br atom becomes 1.0 as shown in Fig. 2. This proposal is supported by the good agreement between the observed Br. . .S distance of 3.53(1) Å and the calculated distance of 3.2 to 3.6 Å obtained from the bond valence equation (22). Additional evidence of a Br. . .S interaction is provided by the Pb—O—S angle of 115.6(15)° being the smallest reported in crystal structures of dmso complexes (Table 4). Since the S. . .O distance between neighbouring $PbBr_2 \cdot 2dmso$ units in the same chain is about 10% less than the van der Waals radii sums, the possibility of weak S. . .O bonding cannot be excluded. The S=O bond length (1.59(3) Å) in $PbBr_2 \cdot 2dmso$ is one of the longest found in dmso complexes (Table 4). The S—C bond length is unchanged from that in solid dmso (1.80 Å) (23).

(*c*) Crystal packing forces are usually proposed to account for differences in structure observed between the gaseous and crystalline phases of a substance. Unfortunately, such a comparison is not possible with $PbBr_2 \cdot 2dmso$ because it does not exist in the gaseous phase. Nevertheless, the fact that so many non-bonding approaches (Table 3) are approximately equal to van der Waals radii sums might suggest that deviations from a Pb(II) octahedral configuration are due primarily to inter- and intra-chain van der Waals forces arising from dipole–dipole, dipole – induced dipole, and London dispersion forces among neighbouring molecules and atoms (24). Thus the small interatomic Br. . .S and S. . .O distances with the consequent deviation of the O—Pb—O′ angle from 180° may not be due to weak bonding interactions, as previously suggested, but merely the result of the need for the crystal to achieve the most efficient packing arrangement possible both within each chain and between the chains.

Acknowledgments

We are grateful to the National Research Council of Canada and to le Gouvernement du Québec, Ministère de l'Education, for financial support. Professor P. H. Bird of Concordia University kindly provided some of the computer programs.

1. M. NARDELLI and G. FAVA. Acta Crystallogr. **12**, 727 (1959).
2. A. D. BARANYI, M. ONYSZCHUK, S. FORTIER, and G. DONNAY. J. Chem. Soc. Dalton. Trans. 2301 (1976).

3. I. WHARF, T. GRAMSTAD, R. MAKHIJA, and M. ONYSZCHUK. Can. J. Chem. **54**, 3430 (1976).
4. M. MCPARTLIN and R. MASON. J. Chem. Soc. A, 2206 (1970).
5. M. J. BENNETT, F. A. COTTON, and D. L. WEAVER. Acta Crystallogr. **23**, 788 (1967).
6. D. A. LANGS, C. R. HARE, and R. G. LITTLE. Chem. Commun. 366 (1974).
7. F. C. MARCH and G. FERGUSON. Can. J. Chem. **49**, 3590 (1971).
8. M. J. BENNETT, F. A. COTTON, and D. L. WEAVER. Acta Crystallogr. **23**, 581 (1967).
9. R. D. WILLET and K. CHANG. Inorg. Chim. Acta, **4**, 447 (1970).
10. N. W. ISAACS and C. H. L. KENNARD. J. Chem. Soc. A, 1257 (1967).
11. I. LINDQUIST. Inorganic adduct molecules of oxo-compounds. Academic Press, New York. 1963. p. 71.
12. K. K. BHANDARY and H. MANOHAR. Acta Crystallogr. **28B**, 1093 (1973).
13. P. BISCARINI, L. FUSINA, G. D. NIVELLINI, A. MANGIA, and G. PELIZZI. J. Chem. Soc. Dalton, 1846 (1974).
14. J. M. STEWART, F. A. KUNDELL, and J. C. BALDWIN. The X-ray 70 system. University of Maryland, College Park, Md. 1970.
15. G. H. STOUT and L. H. JENSON. X-Ray structure determination. MacMillan Co., New York. 1968. p. 68.
16. H. P. HANSON, L. HERMAN, J. D. LEA, and S. SKILMAN. Acta Crystallogr. **17**, 1040 (1964).
17. International tables of X-ray crystallography. Vol. III. Kynoch Press, Birmingham. 1962. p. 215.
18. Y. TAKEUCHI. Z. Krist. **135**, 130 (1972).
19. R. W. G. WYKOFF. Crystal structures. Vol. I. Interscience Publishers, New York. 1963. p. 298.
20. S. L. LAWTON, C. J. FUHRMEISTER, R. G. HAAS, C. S. JARMAN, JR., and F. G. LOHMEYER. Inorg. Chem. **13**, 135 (1974).
21. G. DONNAY and R. ALLMAN. Am. Mineral. **55**, 1003 (1970).
22. I. D. BROWN. J. Solid State Chem. **11**, 214 (1974).
23. M. A. VISWAMITRA and K. K. KANNAN. Nature, **21**, 1016 (1966).
24. A. K. BARNARD. Theoretical basis of inorganic chemistry. McGraw-Hill Publishing Co. Ltd., New York. 1965. p. 97.
25. J. E. HUHEEY. Inorganic chemistry. Harper and Row, New York. 1972. p. 184.
26. C. K. JOHNSON. ORTEP, Oak Ridge National Laboratory Report ORNL-3794, 1965.

The heat capacities, volumes, and expansibilities of *tert*-butyl alcohol – water mixtures from 6 to 65 °C

CEES DE VISSER,[1] GERALD PERRON, AND JACQUES E. DESNOYERS[2]

Department of Chemistry, Université de Sherbrooke, Sherbrooke (Qué.), Canada J1K 2R1

Received September 9, 1976

CEES DE VISSER, GERALD PERRON, and JACQUES E. DESNOYERS. Can. J. Chem. **55**, 856 (1977).

The densities and specific heat capacities of mixtures of *tert*-butyl alcohol (TBA) and water (W) have been measured at 6, 10, 25, 40, 55, and 65 °C. From these data the apparent molal volumes (ϕ_V), heat capacities (ϕ_C), and expansibilities (ϕ_E) were evaluated. Generally, the temperature dependence of these quantities is rather characteristic of hydrophobic solutes in water. At high concentrations ϕ_C and ϕ_V resemble those of surfactants, suggesting the existence of some microphase separation. At low temperatures ϕ_C show a significant hump as a function of concentration, which is probably not due to the presence of the —OH group on the TBA molecule. A similar behaviour is observed for ϕ_E. The ϕ_V and ϕ_C of water in TBA have also been calculated; $\phi_{V,W}$ is in the TBA-rich region 2 to 2.5 $cm^3\ mol^{-1}$ smaller than the molar volume of water, but $\phi_{C,W}$ is of the same order of magnitude as the molar heat capacity of water.

CEES DE VISSER, GERALD PERRON et JACQUES E. DESNOYERS. Can. J. Chem. **55**, 856 (1977).

Les masses volumiques et capacités calorifiques des mélanges du *tert*-butanol (TBA) et de l'eau (W) ont été mesurées à 6, 10, 25, 40, 55 et 65 °C. Les volumes (ϕ_V), capacités calorifiques (ϕ_C) et expansibilités (ϕ_E) molaires apparents ont été calculés sûr tout le domaine de concentration. En général la dépendance sur la température de ces quantités est assez typique du comportement des solutés hydrophobes dans l'eau. Aux fortes concentration ϕ_C et ϕ_V ressemblent à ceux des détergents suggérant l'existence d'une fonction de microphases. Aux basses températures ϕ_C augmente d'une façon non-linéaire avec la concentration avant de diminuer rapidement vers sa valeur molaire aux plus fortes concentrations. L'existence de cette bosse en fonction de la concentration ne semble pas reliée à la présence du groupement OH. Un comportement similaire est observé pour ϕ_E. Les volumes et capacités calorifiques molaires apparents de W dans le TBA ont aussi été calculés; $\phi_{V,W}$ dans la région riche en TBA est de 2 à 2.5 $cm^3\ mol^{-1}$ plus petit que le volume molaire de W mais $\phi_{C,W}$ est du même ordre de grandeur que la capacité calorifique molaire de W.

Introduction

The numerous studies on mixtures of alcohols and water have been very well reviewed by Franks and co-workers (1–3). Most of the alcoholic systems fall in a class of solutions which are generally classified as typically aqueous (3–5); the excess free energy G^E is positive, $|TS^E| > |H^E|$ (entropy-controlled mixing), the solution tends to unmix at high temperatures and the concentration dependence of the thermodynamic properties show characteristic trends. The hydrophobic character of the cosolvent seems to be responsible for the general behaviour of these solutions.

tert-Butyl alcohol (TBA) is of particular interest since, although it is quite hydrophobic, it is still miscible in all proportions with water. Most properties of this binary system, especially in the water-rich region, have been well investigated (1–14). However, precise heat capacity data over the whole concentration range and at many temperatures are still scarce: previous studies were often limited to the water-rich region and to 25 °C (14, 15). Only Kenttamaa *et al.* (6) reported mean molar heat capacities over the whole mole fraction range. Unfortunately, they reported their data "at about 30–33 and 50–53 °C". Moreover, as will be shown in this paper, mean molar heat capacities do not give much information on specific (structural) effects on dissolution. Also the heat capacities of pure TBA are not known accurately enough above 25 °C (16).

Heat capacity data are of interest since they are known to be very sensitive to structural changes in solutions. We therefore felt it would be useful to measure this property for mixtures of TBA and water over a wide temperature range

[1]On leave of absence from Department of Chemistry, the Free University of Amsterdam, Amsterdam, The Netherlands.

[2]To whom correspondence should be addressed.

and whenever possible over the complete mole fraction range. Under similar conditions the volumes were also evaluated because the flow microcalorimetric technique used for the measurements of the differences in heat capacities requires the knowledge of precise densities. In addition, the apparent molal expansibilities can then be calculated from the temperature dependence of the apparent molal volumes.

Finally, it should be mentioned that precise data of the binary TBA–W system are required for a systematic study of ternary systems involving the TBA–W mixtures, which we have investigated (17).

Experimental

All solutions were prepared by weight with deionized (Continental Deionised Water System) distilled water, and TBA (Baker Analyzed Reagent) was used as such (14).

The solution densities (d) and heat capacities per unit volume (σ) were measured with a flow densimeter (18) and a Picker flow microcalorimeter (19, 20). At 25 °C, the detection limits, in differential measurements, were respectively $\pm 3 \times 10^{-6}$ g cm^{-3} and $\pm 7 \times 10^{-5}$ J K^{-1} cm^{-3}. The experimental techniques, the uncertainties at other temperatures, and the general procedures have been described elsewhere (18–21). In the present study, using a flow rate of 0.6 cm^{-3} min^{-1} and a heating power of 21 mW, the temperature increment during the heat capacity measurements was ~0.5 °C. All data are expressed relative to NaCl solutions (20). The absolute temperature of the measurements was measured to 0.01 K with a Hewlett-Packard Quartz Thermometer.

Results

The apparent molal volume, ϕ_V, and heat capacity, ϕ_C, of TBA in the mixtures were calculated from the data using the following equations:

$$[1] \qquad \phi_V = \frac{M}{d} - \frac{1000(d - d_0)}{mdd_0}$$

and

$$[2] \qquad \phi_C = Mc_p + \frac{1000(c_p - c_{p0})}{m}$$

where M is the solute molecular weight, m the molality, and c_p the specific heat capacity. The density d_0 and specific heat capacity c_{p0} of pure water are taken respectively from Kell (22) and Stimson (23). The difference in specific heat capacity can be derived from the measured difference in heat capacity per unit volume by the relation:

$$[3] \qquad c_p - c_{p0} = c_{p0}\left\{\frac{\sigma - \sigma_0}{\sigma_0} + 1\right\} d_0/d - c_{p0}$$

where σ_0 is given by $c_{p0}d_0$. By reversing TBA and W, it is of course also possible using eqs. 1 to 3 to calculate the corresponding functions for water.

The original data and derived ϕ_V and ϕ_C values at 6, 10, 25, 40, 55, and 65 °C are given elsewhere.[3] Except for ϕ_C at 65 °C, at least 10 measurements were made below $m_{TBA} = 1$ at each temperature and both ϕ_V and ϕ_C were fitted by least-squares methods to equations of the form:

$$[4] \qquad \phi = \phi^\theta + Am$$

The resulting coefficients at different temperatures are collected in Table 1. At 10 °C two different sets of measurements yielded slightly different ϕ_C^θ (486.3 and 482.9 J K^{-1} mol^{-1}) values. Since we do not know which one is the best, we used them both in order to calculate $\phi_C - \phi_C^\theta$. In Table 1 the mean value for ϕ_C^θ has been reported. The value of ϕ_V^θ at 25 °C is in good agreement with that (87.95 cm^3 mol^{-1}) reported by Franks and Smith (7) obtained from precise density measurements at very low concentrations. The agreement with the data of Avédikian *et al.* (14) is also within the experimental error. The value of 87.73 cm^3 mol^{-1} reported by Jolicoeur and Lacroix (24) is slightly lower but they obtained ϕ_V^θ by extrapolating against molarity with a lowest concentration of 0.27 mol l^{-1}. Kenttamaa *et al.* (6) reported partial molal volumes at 15, 25, 40, and 50 °C covering the complete mole fraction range. Their infinite dilution data ($\bar{V}^\theta = \phi_V^\theta$) deviate generally by about 2 cm^3 mol^{-1} from the present results. However, calculation of ϕ_V for the complete mole fraction range using their density data shows that only below $X_{TBA} = 0.05$ do important differences exist; above $X_{TBA} = 0.05$ the agreement with the present data is generally within 0.1 cm^3 mol^{-1}, both at 25 and 40 °C. Their values for the molar volume of pure TBA at 25 °C (supercooled liquid) of 94.96 cm^3 mol^{-1} and at 40 °C of 96.88 cm^3 mol^{-1} are in excellent agreement with the present results of 94.97 and 96.86 cm^3 mol^{-1}, respectively, given in Table 1. Finally, Nakanishi *et al.* (25) reported on excess and partial molal volumes of TBA–W systems at 25 °C. Calcula-

[3]Complete set of tabular data is available, at a nominal charge, from the Depository of Unpublished Data, CISTI, National Research Council of Canada, Ottawa Canada K1A 0S2.

TABLE 1. Standard apparent molal volumes (ϕ_V^θ), heat capacities (ϕ_C^θ), and expansibilities (ϕ_E^θ) and molar volumes (V^0) heat capacities (C_p^0), and expansibilities (E^0) of *tert*-butyl alcohol in water at different temperatures and the corresponding coefficients of eq. 4

T (°C)	ϕ_V^θ (cm³ mol⁻¹)	A_V (cm³ mol⁻² kg)	Max. mol. (mol kg⁻¹)	V^0 (cm³ mol⁻¹)	ϕ_C^θ (J K⁻¹ mol⁻¹)	A_C (J K⁻¹ mol⁻² kg)	Max. mol. (mol kg⁻¹)	C_p^0 (J K⁻¹ mol⁻¹)	T (°C)	ϕ_E^θ (cm³ mol⁻¹ K⁻¹)	E^0 (cm³ mol⁻¹ K⁻¹)
6	87.85	−3.04	0.4		497	−5.5	1.1				
10	87.88	−3.03	0.4		484.6	−0.6	1.2		8	0.007_5	
25	87.76	−1.89	0.4	94.95	463.6	7.91	1.2	210	17.5	−0.001	
40	88.43	-1.10_5	0.8	96.86	451.0	11.46	0.8	232	32.5	0.038	
55	89.59	−0.89	0.8	99.00	440.9	16.55	0.8	246	47.5	0.077	0.127
65	90.30	−0.23	1.0		442				60	0.071	0.143

tions of the ϕ_V from their densities yield very close results to the present ones below $X_{TBA} = 0.3$ while at higher X_{TBA} their values are slightly lower, the difference increasing to 0.2 cm³ mol⁻¹ for the molar volume of pure TBA.

Our ϕ_C^θ at 25 °C is in excellent agreement with that, 464.0 J K⁻¹ mol⁻¹, reported by Jolicoeur and Lacroix (24) and with the corrected value (20) of 462.8 J K⁻¹ mol⁻¹ given by Avédikian *et al.* (14). It is also possible to obtain ϕ_C^θ ($= \bar{C}_p^\theta$) from the integral heat of solution method as carried out by Alexander and Hill (12). At 25 °C, a value for $\bar{C}_p^\theta$ of 475 ± 20 J K⁻¹ mol⁻¹ can be derived from their data, which is, although less accurate, in agreement with the present results.

The molar heat capacities of pure TBA C_p^0 above room temperature are, as mentioned before, rather scarce. Only Oetting (26) seems to have reported heat capacities and entropies of TBA from 15 to 330 K. His (interpolated) heat capacities at 25, 40, and 55 °C are 220, 233, and 244 J K⁻¹ mol⁻¹ respectively. These data are, especially at higher temperatures, in very good agreement with our results given in Table 1. Precise data for ϕ_C in the TBA–W mixture are also scarce in the literature. Kenttamaa *et al.* (6) reported mean molar heat capacities C_p at temperatures around 31.5 and 51.5 °C. From the present results it is also possible to calculate mean molar heat capacities using the following equation:

$$[5] \qquad C_p = \sigma(X_W M_W + X_{TBA} M_{TBA})/d$$

Values obtained using eq. 5 at 25, 40, and 55 °C show the same trends as those given by Kenttamaa *et al.* (6). Arnaud *et al.* (15) reported also mean molar heat capacities up to $X_{TBA} = 0.27$. The difference from the present results is within 1 J K⁻¹ mol⁻¹ in most cases. We can therefore say that the present data are in good agreement with existing literature values where available and give us confidence that they are close to the true values.

Discussion

Thermodynamic properties of binary solvent mixtures are often discussed in terms of excess molar thermodynamic functions. With the exception of free energies and entropies these are defined by

$$[6] \qquad Y^E = Y - X_1 Y_1^0 - X_2 Y_2^0$$

where Y is the mean molar quantity and Y_1^0 and Y_2^0 are the standard molar quantities of the two pure components. The excess volumes and heat capacities of the TBA–W mixtures at 25, 40, and 55 °C are shown in Fig. 1. On this kind of graph the TBA–W mixtures do not seem too anomalous. With the exception of the pronounced asymmetry with C_p^E, this system does not appear too different from other liquid mixtures, and shows little dependence on temperature. On the other hand, if the apparent molal volumes and heat capacities are plotted against the mole fraction of TBA, then the particularities of this hydrophobic solute are more evident as seen from Figs. 2 and 3. The ϕ_V goes through a characteristic minimum in the water-rich region and this minimum is more pronounced and shifted to higher concentrations the lower the temperature. In the TBA-rich region ϕ_V tends to the molar volume of TBA as expected. The general trends of ϕ_C are again typical of hydrophobic solutes; ϕ_C first increases with concentration and then rapidly falls to its molar value. These transitions are even sharper if partial molal quantities are plotted instead of apparent molal ones. For example $\bar{C}_p$ nearly reaches its molar value at concentrations as low as 0.1 mole fraction. Qualitatively speaking, ϕ_V and ϕ_C of TBA in W are quite similar to those of surfactants (27, 28) which also show characteristic maxima and minima but of course at much lower concentration (10^{-3} to 10^{-1} mol kg^{-1}). Still, the similarity between the present system and surfactants suggests that the relatively sharp increase in volume and decrease in heat capacity corresponds to some kind of microphase transition as in the case of micellization. Above 0.1 to 0.2 mole fraction, the hydrophobic part of TBA is seeing only other TBA molecules. The system can probably be considered to be a micro emulsion although the present data do not give us information on the size and structure of the aggregates.

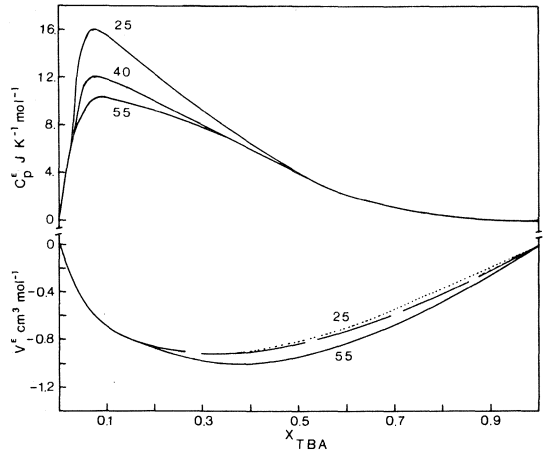

FIG. 1. Excess molar volumes and heat capacities of *tert*-butyl alcohol and water at 25, 40, and 55 °C.

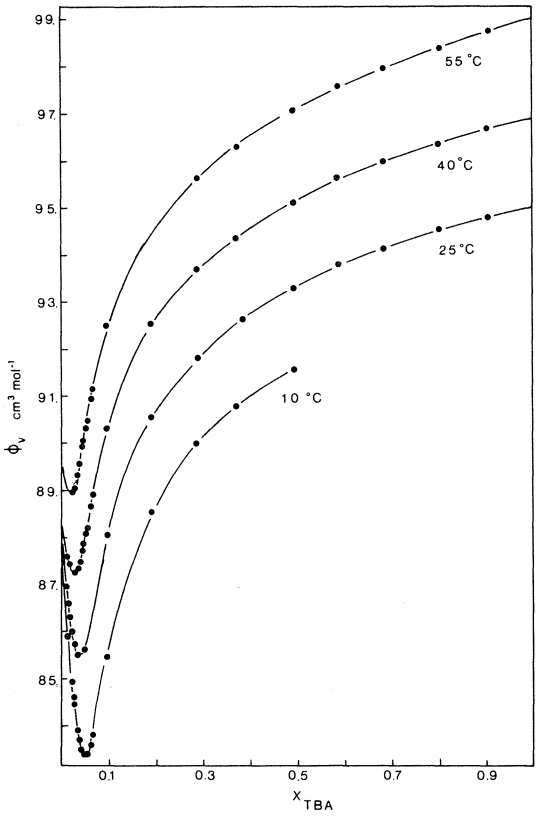

FIG. 2. Apparent molal volumes of *tert*-butyl alcohol in water at different temperatures.

The concentration dependence of the apparent molal quantities, $\phi_Y - \phi_Y^\theta$, are plotted for the water-rich region in Figs. 4 and 5. Here the volumes are showing the normal trends of hydrophobic solutes: the negative slopes, increasing in magnitude as the temperature is lowered, are also observed with hydrophobic electrolytes (21). On the other hand, the concentration and temperature dependences of $\phi_C - \phi_C^\theta$ show significant differences with normal hydrophobic electrolytes. For example, tetrapentylammonium bromide (21) and nonyltrimethylammonium bromide (28) have negative

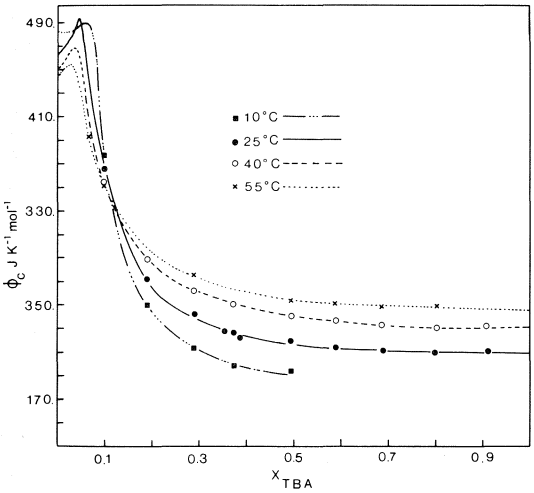

FIG. 3. Apparent molal heat capacities of *tert*-butyl alcohol in water at different temperatures.

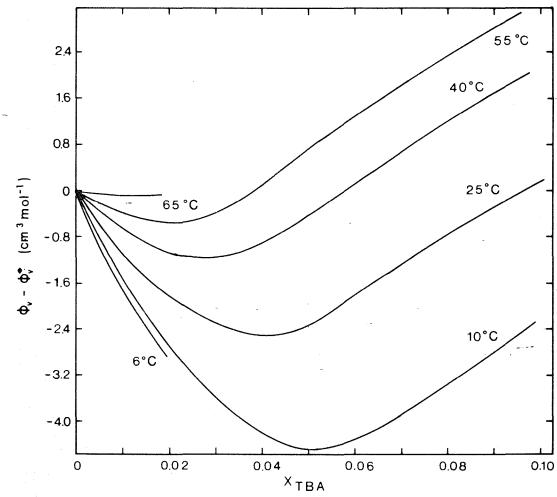

FIG. 4. Excess apparent molal volumes of *tert*-butyl alcohol in the water-rich region at different temperatures.

initial slopes at high temperatures and positive ones at low temperatures. With TBA, the initial slope changes little with temperature from 25 °C upwards while $\phi_C - \phi_C^0$ is nearly independent of concentration at low temperatures in the water-rich region. There is also a significant hump in $\phi_C - \phi_C^0$ at 25 and 10 °C at higher concentrations. A somewhat similar observation was made with tetrabutyloctanoate in water (29).

Recently Savage and Wood (30) have suggested that the interaction of the polar group (*e.g.* the —OH group) of one molecule with the alkyl chain of another may be just as important

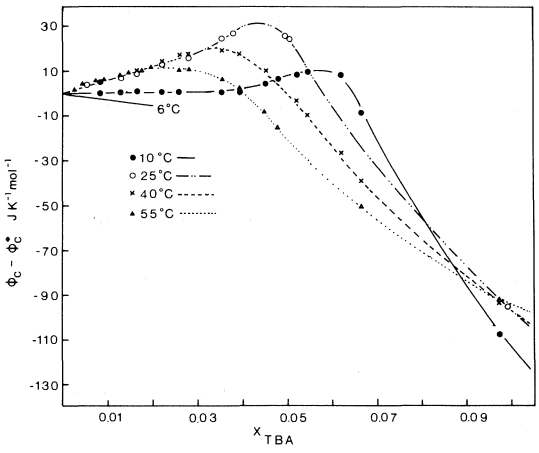

FIG. 5. Excess apparent molal heat capacities of *tert*-butyl alcohol in the water-rich region at different temperatures.

as the hydrophobic–hydrophobic interactions in predicting the signs and magnitudes of pair interaction functions. As a check that the peculiar behaviour of $\phi_C - \phi_C^0$ of TBA was not due to the presence of the —OH group we have also begun a study of ϕ_C of triethylamine in water (31). At 15 °C this liquid is completely miscible with water. As with TBA, $\phi_C - \phi_C^0$ changes little with concentration at rather low concentrations, rises to over 150 J K^{-1} mol^{-1} at about 1 mol kg^{-1}, and then decreases sharply to about -400 J K^{-1} mol^{-1}. The hump in $\phi_C - \phi_C^0$ is therefore related to hydrophobic interactions and suggests that there are structural changes which occur in these solutions at certain concentrations which resemble a microphase separation or higher order transition in the liquid phase. The sharp decrease in $\phi_C - \phi_C^0$ can well be accounted for in terms of contact pairing: the hydrophobic solutes lose part of their cospheres on contact association. The hump in $\phi_C - \phi_C^0$ probably corresponds to a much weaker transition since it is not seen with excess volumes and enthalpies. One such possibility would be a solvent-shared association complex which could occur in a cooperative way (32).

At present we cannot offer any reasonable explanation for the peculiar temperature dependence of $\phi_C - \phi_C^0$ at low concentration. Studies are under way now with other non-electrolyte–water systems to clarify this behaviour.

The apparent molal expansibilities ϕ_E can be calculated from the temperature dependence of

ϕ_V. At low concentration ϕ_E can be shown to be in excellent agreement witn the direct measurements of Desrosiers and Desnoyers (33). The concentration dependence of ϕ_E is shown for three temperatures on Fig. 6; ϕ_E initially increases sharply, goes through a maximum and finally tends to the molar expansibility E^0 of pure TBA, the maximum being more pronounced at low temperatures. The negative sign of $\phi_E^\theta - E^0$ is consistent with the models of hydrophobic hydration (34, 35); since there is less free space in the cosphere of an hydrophobic solute ($\phi_V^\theta - V^0 < 0$) there will be less expansion during a rise in temperature. The maximum in ϕ_E is obviously related to the minimum in ϕ_V. It is also related to the maximum in ϕ_C. This follows from Eley's theory (36) and from the scaled-particle theory (37) which both show that there is a relation between the heat capacity of cavity formation and the change in expansibility of the medium with temperature. It is therefore not surprising that interactions giving rise to an extremum with ϕ_C should also influence ϕ_E.

The temperature dependences of ϕ_C^θ, ϕ_V^θ, and ϕ_E^θ are compared with the corresponding molar values of pure TBA in Fig. 7. These data are all fairly typical of hydrophobic solutes and are consistent with the models that suggest that these solutes promote water structure at low concentrations; the positive value of $\phi_C^\theta - C_p^0$ and negative values of $\phi_V^\theta - V^0$ and $\phi_E^\theta - E^0$ all decrease in magnitude as the temperature increases. The positive sign of $T\,\partial\phi_E^\theta/\partial T$ ($= -\partial\phi_C/\partial P$) also seems characteristic of hydrophobic solutes (38).

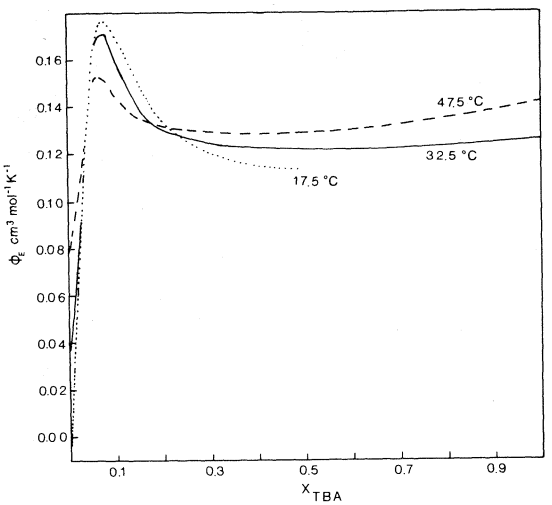

FIG. 6. Apparent molal expansibilities of *tert*-butyl alcohol in water.

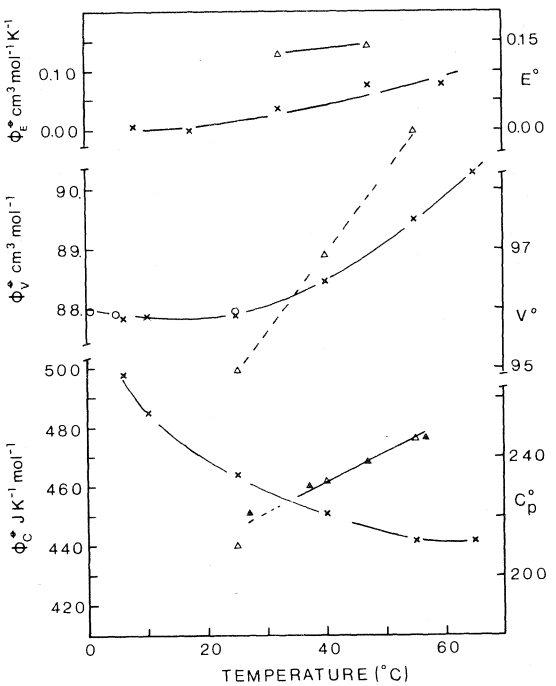

FIG. 7. Standard apparent molal volumes, heat capacities, and expansibilities and the corresponding molar quantities as a function of temperature. Standard apparent molal quantities: ×: present results; ○: ref. 7. Molar quantities: △: present results; ▲: ref. 26.

Finally, since we have volume and heat capacity data over the whole concentration range, except at low temperatures, it is also possible to calculate the apparent molal volumes

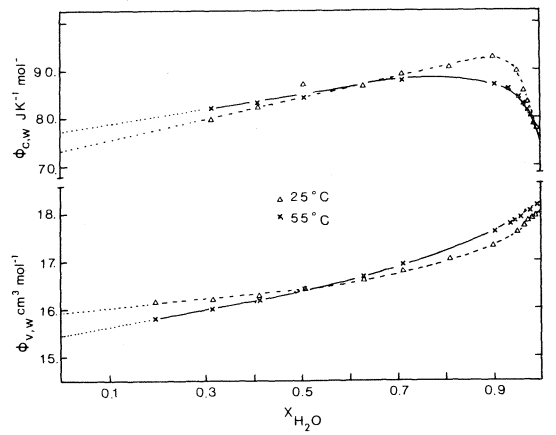

FIG. 8. Apparent molal volumes and heat capacities of water in *tert*-butyl alcohol at 25 and 55 °C.

and heat capacities of W in TBA–W mixtures. These are shown in Fig. 8. The $\phi_{V,W}^0$ in TBA is lower than its molar volume V_W^0 by about 2 to 2.5 $cm^3\ mol^{-1}$ as we would expect from a closer packing of the TBA molecules around the water molecule compared with the more open structure of pure water. On the other hand, as with water in dimethylformamide (39), $\phi_{C,W}^0$ remains comparable with $C_{p,W}^0$ and the difference hardly changes with temperature. Further work is under way to find the origin of this apparently anomalous value of $\phi_{C,W}^0$.

NOTE ADDED IN PROOF: Work presently under way in this laboratory indicates that ϕ_C of many apparently hydrophobic nonelectrolytes (ethers, esters, ketones, and amides) in water show a large initial decrease with concentration at 25 °C in contrast to alcohols, carboxylic acids, and amines. Alcohols may therefore not be typical of hydrophobic solutes as far as heat capacities are concerned.

Acknowledgements

The financial support of the National Research Council of Canada and of the Quebec Ministry of Education is gratefully acknowledged. One of us (C. de V.) is greatly indebted to the Canada Council for the award of a scholarship during the academic year 1975–1976.

1. F. FRANKS and D. J. G. IVES. Q. Rev. **20**, 1 (1966).
2. F. FRANKS. Physico-chemical processes in mixed aqueous solvents. Heineman Education Books, London. 1967.
3. F. FRANKS and D. S. REID. Water, a comprehensive treatise. Vol. 2. *Edited by* F. Franks. Plenum Press, New York. 1973. p. 323.
4. M. J. BLANDAMER and J. BURGESS. Chem. Soc. Rev. **4**, 55 (1975).
5. F. FRANKS. *In* Hydrogen-bonded solvent systems. *Edited by* A. Covington and P. Jones. Taylor and Francis, London. 1968. p. 31.
6. J. KENTTAMAA, E. TOMMILA, and M. MASTTI. Ann. Acad. Sci. Fenn. Ser. A2, **93**, 3 (1959).
7. F. FRANKS and H. T. SMITH. J. Chem. Eng. Data, **13**, 538 (1968).
8. M. J. BLANDAMER and O. J. WADDINGTON. J. Phys. Chem. **74**, 2569 (1970).
9. R. G. ANDERSON and M. C. R. SYMONS. Trans. Faraday Soc. **65**, 2550 (1969).
10. M. C. R. SYMONS and M. J. BLANDAMER. *In* Hydrogen-bonded solvent systems. *Edited by* A. Covington and P. Jones. Taylor and Francis, London. 1968. p. 211.
11. H. ENDO and O. NOMOTO. Bull. Chem. Soc. Jpn. **46**, 3004 (1973).
12. D. M. ALEXANDER and D. J. T. HILL. Aust. J. Chem. **22**, 347 (1969).
13. G. WADA and S. UMEDA. Bull. Chem. Soc. Jpn. **35**, 646 (1962).
14. L. AVÉDIKIAN, G. PERRON, and J. E. DESNOYERS. J. Solution Chem. **4**, 331 (1975).
15. R. ARNAUD, L. AVÉDIKIAN, and J.-P. MOREL. J. Chim. Phys. **69**, 45 (1972).
16. R. C. WILHOIT and B. J. ZWOLINSKI. J. Phys. Chem. Ref. Data, **2**(1), 113 (1973).
17. C. DE VISSER, G. PERRON, and J. E. DESNOYERS. In preparation.
18. P. PICKER, E. TREMBLAY, and C. JOLICOEUR. J. Solution Chem. **3**, 377 (1974).
19. P. PICKER, P.-A. LEDUC, P. R. Philip, and J. E. DESNOYERS. J. Chem. Thermodyn. **3**, 631 (1971).
20. J. E. DESNOYERS, C. DE VISSER, G. PERRON, and P. PICKER. J. Solution Chem. In press.
21. G. PERRON, N. DESROSIERS, and J. E. DESNOYERS. Can. J. Chem. **54**, 2163 (1976).
22. G. S. KELL. J. Chem. Eng. Data, **12**, 66 (1967).
23. H. F. STIMSON. Am. J. Phys. **23**, 614 (1955).
24. C. JOLICOEUR and G. LACROIX. Can. J. Chem. **54**, 624 (1976).
25. K. NAKANISHI, N. KATO, and M. MARUYAMA. J. Phys. Chem. **71**, 814 (1967).
26. F. L. OETTING. J. Phys. Chem. **67**, 2757 (1963).
27. G. M. MUSBALLY, G. PERRON, and J. E. DESNOYERS. J. Coll. I. Sci. **48**, 494 (1974).
28. G. M. MUSBALLY, G. PERRON, and J. E. DESNOYERS. J. Coll. I. Sci. **54**, 80 (1976).
29. P.-A. LEDUC and J. E. DESNOYERS. Can. J. Chem. **51**, 2993 (1973).
30. J. J. SAVAGE and R. H. WOOD. J. Solution Chem. **5**, 733 (1976).
31. G. PERRON, C. DE VISSER, and J. E. DESNOYERS. In preparation.
32. S. ABLETT, M. D. BARRATT, F. FRANKS, M. D. PEDLEY, and D. S. REID. L'eau et les systèmes biologiques. *Edited by* A. Alfsen and A. J. Berteaud. CNRS, Paris. 1976. p. 105.
33. N. DESROSIERS and J. E. DESNOYERS. Can. J. Chem. **54**, 3800 (1976).
34. J. L. NEAL and D. A. I. GORING. J. Phys. Chem. **74**, 658 (1970).
35. D. D. MACDONALD and J. B. HYNE. Can. J. Chem. **54**, 3073 (1976).
36. D. D. ELEY. Trans. Faraday Soc. **35**, 1281, 1421 (1938).
37. M. LUCAS. J. Phys. Chem. **77**, 2479 (1973).
38. L. G. HEPLER. Can. J. Chem. **47**, 4613 (1969).
39. C. DE VISSER, G. PERRON, J. E. DESNOYERS, W. J. W. HEUVELSLAND, and G. SOMSEN. J. Chem. Eng. Data. In press.

The structure and energetics of low-lying states of RCO and RNN free radicals[1]

N. Colin Baird and Harish B. Kathpal

Department of Chemistry, University of Western Ontario, London, Ont., Canada N6A 5B7

Received September 15, 1976

N. Colin Baird and Harish B. Kathpal. Can. J. Chem. **55**, 863 (1977).

The important geometrical variables in the structures of the lowest $^2A'$ and $^2A''$ states of the free radicals HCO, CH_3CO, NH_2CO, HNN, and CH_3NN have been determined by *ab initio* MO calculations using the STO-3G basis set. The energy differences between the states, and the energies of the radicals relative to their decomposition products and relative to their hydrogen atom addition products, are reported using both STO-3G and 4-31G basis sets in the restricted open-shell calculations. The trends in these results and their relation to available experimental data are discussed.

N. Colin Baird et Harish B. Kathpal. Can. J. Chem. **55**, 863 (1977).

Utilisant des calculs d'orbitales moléculaires *ab initio* faisant appel à une base STO-3G, on a déterminé des variables géométriques importantes dans les structures des états $^2A'$ et $^2A''$ les plus bas des radicaux libres HCO, CH_3CO, NH_2CO, HNN et CH_3NN. On rapporte les différences d'énergie entre ces états et les énergies des radicaux, relatives à leurs produits de décomposition et relatives à leurs produits d'addition d'atome d'hydrogène, en faisant appel à des bases STO-3G et 4-31G dans des calculs restreints de couches ouvertes. On discute des tendances dans ces résultats et de leur relation avec des données expérimentales disponibles.

[Traduit par le journal]

Introduction

Free radicals of the type R—Ċ=O and R—N=N· are often encountered as transient intermediates in photochemical reactions. Although the parent system HCO has been the subject of both spectral studies (1, 2) and sophisticated *ab initio* calculations (3, 4), rather little information is available for its derivatives (*e.g.*, CH_3CO, NH_2CO, PhCO). For the dinitrogen radicals, the parent HNN has received some theoretical attention (4–6) although neither it nor its simple derivatives (*e.g.*, CH_3NN) have been characterized experimentally as yet.

We wish to report here the results of our *ab initio* molecular orbital calculations for the ground and lowest-lying excited state of the parent and methyl derivative of both the RCO and RNN series, and also for NH_2CO, a radical which is isomeric with the *N*-formamido radical NHCHO which we discussed previously (7).

Method of Calculation

All results reported herein are based upon Roothaan restricted open-shell SCFMO calculations (8); to improve convergence, half-electron method wavefunctions were used as initial guesses to the open-shell eigenvectors (9). The basis sets used were the minimal STO-3G and the extended 4-31G sets, with the usual molecular scale factors, of Pople and co-workers (10, 11). All geometry optimizations are believed accurate to 0.01 Å and to 1°. The calculations were performed on the CDC Cyber 73 computer at the University of Western Ontario, using programs described previously (9).

In CH_3CO and CH_3NN, carbon–hydrogen bond lengths of 1.090 Å and tetrahedral H—C—H bond angles were assumed. For NH_2CO, nitrogen–hydrogen distances of 1.013 Å and H—N—H and H—N—C bond angles of 120°, and a completely coplanar arrangement of atoms, were assumed.

Results and Discussion

Geometric Structure of the Radicals

Optimum geometries calculated using the STO-3G basis set for the lowest pair of electronic states of each of the five radicals are given in Table 1. For HNN and HCO, the results of optimizations using the 4-31G basis are also given (in parentheses).

The restricted open-shell results for both the ground $^2A'$ state and the low-lying $^2A''$ state of HCO agree very well with the latest experimental values (2) given in square brackets in Table 1.

[1]Research supported by the National Research Council of Canada.

TABLE 1. Geometries of XCO and XNN radicals[a]

Radical	State	R_{CO} or R_{NN} (Å)	R_{CX} or R_{NX} (Å)	∠OCX or ∠NNX
HCO	$^2A'$	1.19	1.11	126°
		(1.18)	(1.09)	(129°)
		[1.175]	[1.125]	[125.0°]
	$^2A''(C_{\infty v})$	1.20	1.07	180° ass.
		(1.19)	(1.05)	(180° ass.)
		[1.186]	[1.064]	180°
CH_3CO	$^2A'$	1.19	1.54	128°
	$^2A''(C_{3v})$	1.20	1.48	180° ass.
NH_2CO	$^2A'$	1.21	1.38	128°
	$^2A''(C_{2v})$	1.22	1.41	180° ass.
HNN	$^2A'$	1.23	1.06	111°
		(1.18)	(1.02)	(118°)
	$^2A''(C_{\infty v})$	1.20	1.01	180° ass.
		(1.17)	(0.98)	(180° ass.)
CH_3NN	$^2A'$	1.23	1.52	116°
	$^2A''(C_{3v})$	1.20	1.44	180° ass.

[a]Values in parentheses refer to the 4-31G basis; those in square brackets are experimental values from ref. 2. See also the values quoted in ref. 20.

Both basis sets reproduce the small increase in the carbon–oxygen length, and the larger decrease in the carbon–hydrogen length, which occur upon excitation and linearization. The agreement between the STO-3G and the experimental H—C—O angle in the ground state is particularly good. Similar restricted and unrestricted SCF results using larger basis sets have been reported by Bruna, Buenker, and Peyerimhoff (*3a*) and by Botschwina (*3b*) respectively. Unrestricted STO-3G open-shell results give too long a carbon–oxygen distance in the $^2A'$ state due to contamination of the wavefunction by quartet character (4).

In fact the structure for the $^2A'$ state of the formyl radical HCO is quite similar to that of formaldehyde H_2CO. Removal of one hydrogen atom from the latter yields a radical with an HCO angle increased by 3° and a CO bond length decreased by 0.03 Å according both to experiment and to STO-3G calculations. Similar trends are evident when one compares the structure of the HNN radical to that of *trans*-diimide HNNH.[2] Upon hydrogen abstraction from the latter,[2] the HNN bond angle is calculated to increase by 6° and the NN distance to decrease by 0.04 Å. Thus the rather different HXY bond angles in the ground states of the isoelectronic radicals HNN and HCO are inherited from the HNNH and H_2CO systems.

As in HCO, excitation and linearization in the HNN system leads to a significant shortening of the bond to hydrogen (see Table 1). However the NN bond length decreases upon excitation of HNN compared to the slight increase which occurs in HCO.

The structures calculated for the methyl derivatives are very similar to those found for the parent radicals. Thus the CO length in CH_3CO and the NN lengths in CH_3NN are equal to those for HCO and HNN respectively in both ground and excited states, and the bond angles in the ground states are only a few degrees larger for the methyl systems (see Table 1). The C—C and C—N length in the linear excited state are significantly shorter than in the bent ground state, in analogy with the H—C and H—N contraction mentioned above for the parent systems.

The carbon–oxygen bond lengths calculated for the $^2A'$ and $^2A''$ states of the carbamyl free radical, NH_2CO, are slightly longer than those in HCO and CH_3CO, although the bond angles about the central heavy atom are identical to those in CH_3CO. The carbon–nitrogen distance in the $^2A'$ state of 1.38 Å is shorter than that *calculated* by the same method for any of the low-lying states of either formamide, NH_2CHO, or the *N*-formamido radical, NHCHO (7, 12). The CN length in the excited A'' state is larger,

[2]See ref. 4 for the calculated STO-3G structures of H_2CO and HNNH, and the experimental structure of the former.

TABLE 2. Ground state energetics for RCO and RNN radicals

Radical	Total energies (au)		Energies[a] of H atom addition (kcal mol^{-1})		C—X or N—X bond dissociation energies[b] (kcal mol^{-1})	
	STO-3G	4-31G	STO-3G	4-31G	STO-3G	4-31G
HCO	−111.7301	−113.0666	80.0	79.1	+6.1	+9.9
CH_3CO	−150.3242	−152.0612	78.2	78.0	+17.0	+5.5
NH_2CO	−166.0690	−168.0193	70.3	99.8	+6.6	−2.1
HNN	−107.9894	−109.2320	38.1	50.0	−3.9	−8.9
CH_3NN	−146.5749	−148.2086	41.8	50.5	+1.6	−24.5

[a]Energies for H addition products refer to standard geometries and are from ref. 13. The energies for atomic hydrogen use optimum atomic exponents (13). Use of optimum STO-3G geometries for the product decreases the 4-31G energy of addition by 3.6 kcal mol^{-1} for HNN and by 0.2 kcal mol^{-1} for HCO.

[b]Negative dissociation energies indicate that the products are more stable than is the reactant radical. The HNH angle in NH_2 was taken to be the STO-3G optimum value of 101° (7). The CH_3 radical was assumed to be planar with 120° bond angles.

and is close to that established for these other systems (7, 12).

Ground-state Energies

The total energies, calculated both by the STO-3G and by the 4-31G bases, for the ground states of the five radicals are listed in Table 2, along with the calculated energies of hydrogen atom addition to yield formaldehyde, acetaldehyde, formamide, *trans*-diimide, and *trans*-methyldiimide. (Total energies for these products and for atomic hydrogen were taken from the compilations by Pople and co-workers (13), and refer to 'standard' rather than optimized geometries.) Also given in Table 2 are the energy differences between the radicals and the ground states of the dissociation products formed by X—C or X—N fission.

The hydrogen addition energies of 78 kcal mol^{-1} for the acetyl radical, CH_3CO, agree fairly well with the value of 88 which is obtained using the most recent experimental heats of formation for CH_3CO (14) and acetaldehyde and hydrogen (15). Closer agreement is not expected, given the significant change in correlation energy that probably accompanies such reactions. For the same reason, too much faith should not be placed in the calculated values for diimide and methyldiimide (Table 2).

Although the hydrogen addition energies calculated for the methyl derivatives are almost identical to those of HCO and HNN, the values for NH_2CO are quite different than those for HCO (see Table 2). In particular the STO-3G basis set predicts the hydrogen atom affinity of NH_2CO to be 9.3 kcal mol^{-1} *less* than that for HCO whereas the more reliable 4-31G basis predicts the result for NH_2CO is 20.7 kcal mol^{-1} *greater* than for HCO. Much of this discrepancy is due probably to a significant underestimation by the STO-3G method of the substantial stabilizing interaction between the $—NH_2$ group and the carbonyl double bond in the formamide molecule itself (13*c*). Apparently this stabilizing interaction is much less important in the radical, with the result (by 4-31G) that the C—H bond dissociation energy in formamide is significantly greater than those in formaldehyde and acetaldehyde. Interestingly, the effect of conjugation between a p_π lone pair on nitrogen with the carbonyl group was also found to be smaller in the Σ_N state of the *N*-formamido radical, $\cdot NH—C(H)=O$, than in formamide (7).

The carbon–carbon bond dissociation energies calculated for the CH_3CO free radical bracket the latest experimental value of +11 kcal mol^{-1} for this process (14). According to both basis sets, the dissociation energy for NH_2CO to give CO and the ground π state of NH_2 is somewhat less than that for CH_3CO. At first glance this prediction would appear to be in conflict with the fact that NH_2CO is stable to decomposition at much higher temperatures than is CH_3CO (16*a*). However, resistance to decomposition refers to the *kinetic* stability of the radicals whereas the dissociation energies relate to *thermodynamic* stability. The NH_2CO radical appears more stable since its activation energy for decomposition is larger than is that for CH_3CO (14, 16*b*). This is so presumably because of the presence of two avoided crossings in the decomposition of the former as compared to only one for CH_3CO and HCO. (Decomposition of *linear* HCO to ground state H and CO

TABLE 3. $^2A' \rightarrow {}^2A''$ excitation energies (in kcal mol^{-1})

	Geometry used		ΔE	
Radical	$^2A'$ state	$^2A''$ state	STO-3G[a]	4-31G[b]
HCO	$^2A'$	$^2A'$	58.2	52.5
	$^2A'$	$^2A''$	29.1	23.9
				(23.9)
CH_3CO	$^2A'$	$^2A'$	58.3	54.2
	$^2A'$	$^2A''$	29.0	
NH_2CO	$^2A'$	$^2A'$	92.8	
	$^2A'$	$^2A''$	62.3	67.0
	$^2A''$	$^2A''$	25.1	28.3
HNN	$^2A'$	$^2A'$	51.4	44.5
	$^2A'$	$^2A''$	36.5	20.0
				(22.4)
CH_3NN	$^2A'$	$^2A'$	50.2	
	$^2A'$	$^2A''$	33.0	

[a]See Table 1 for numerical values used (STO-3G results).
[b]Values in parentheses are 4-31G energies using optimum 4-31G geometries (see Table 1).

requires excitation of one π electron to the σ system, whereas dissociation of planar NH_2CO with a linear N—C—O arrangement to ground state NH_2 and CO requires the excitation of both a b_1 and a b_2 electron into an a_1 orbital. In the *bent* geometries of the radicals the crossings are avoided and no actual excitations need occur; however, their 'memory' gives rise to activation barriers for decomposition in excess of the bond energy, and to activation energies for recombination of the reaction products (17).) Similarly, the activation energy for recombination of the NH_2 and CO radicals should be greater than that of 6.0 kcal mol^{-1} found for CH_3 + CO (14). For this reason we feel that the value of 89 kcal mol^{-1} given by Back and Boden for the C—H bond dissociation energy of formamide must be too low since it is based upon the assumption that the activation energies for recombination in the two reactions are identical (16*b*). We are currently engaged in a study of the potential surfaces for RCO decomposition reactions to clarify further this point.

The *total* energy calculated by the 4-31G basis for the ground state of the carbon-centered radical NH_2—$\dot{C}$=O is virtually identical to that computed for the (planar) π_N ground state of the isomeric nitrogen-centered radical $\dot{N}$H—C(H)=O by the same method (see Table 2 and ref. 7). Since the 4-31G basis underestimates the N—H bond energy in methylamine by about 7 kcal mol^{-1} more than it does the C—H bond in acetaldehyde, it is probable that in reality the N—H and C—H bond energies in formamide are not equal but rather that the value for C—H is 5–10 kcal mol^{-1} less than for N—H. Experimentally, free radical abstraction of hydrogen from formamide occurs preferentially, if not exclusively, at the carbon atom (16), suggesting that the carbon-centered radical is indeed the more stable species (assuming that no activation energy in addition to the reaction enthalpy is required for abstraction from the closed-shell species).

The A'' Excited States of the Radicals

It is well-known that, in its linear geometry, the $^2A'$ ground state and the lowest-lying $^2A''$ state of HCO become the two degenerate components of the $^2\pi$ state (18, 19). The same situation should arise also for HNN, CH_3CO, and CH_3NN although the designation of linear geometries (of the heavy atoms) for the latter two is ^2E rather than $^2\pi$. The $^2A'$ and $^2A''$ states of NH_2CO are *not* degenerate for a linear N—C—O geometry, however, as discussed below.

The *relative* energies of the $^2A'$ and $^2A''$ states of the five radicals are given in Table 3. In each case we report both the *vertical* excitation energy (*i.e.*, that computed using the optimum $^2A'$ geometry for both states) and the *adiabatic* energy (*i.e.* that computed using optimum geometries appropriate to each state). The working hypothesis is that the vertical energy can be

associated with highest-intensity band in the electronic spectrum, and the adiabatic energy with the O—O band.

The only experimental spectral data available for these systems are those for HCO (18, 19). The adiabatic energy difference of 23.9 kcal mol^{-1} calculated by 4-31G is in excellent agreement[3] with the difference in electronic energies of 24.8 observed by Johns, Priddle, and Ramsay (18). The strongest sharp bands in the absorption spectrum occur in the 46–51 kcal mol^{-1} region, in very good agreement with the 4-31G vertical excitation energy of 52.5 kcal mol^{-1}. The corresponding STO-3G energies are about 5 kcal mol^{-1} higher than are the 4-31G results (see Table 3). The calculated excitation energies for CH_3CO are virtually identical to those for HCO (Table 3), and thus the positions of the intensity maximum band and the O—O band in the spectra should be very similar.

Both the STO-3G and 4-31G calculations predict that vertical excitation from the $^2A'$ ground state to the $^2A''$ excited state of both HNN and CH_3NN should require less energy than for the RCO free radicals (see Table 3). The 4-31G basis set results predict the maximum intensity bands in HNN should occur about 1000 Å to the red of those for HCO. The two basis set predictions disagree as to the relative adiabatic excitation energies of HCO and HNN. (The STO-3G basis predicts larger adiabatic energy gaps for HNN and CH_3NN than for HCO and CH_3CO, whereas the 4-31G basis predicts a slightly smaller gap for HNN than for HCO (see Table 3).) Recalculation of the latter results using optimum 4-31G geometries (see results in parentheses in Table 3) does not alter these conclusions.

The excitation energies for the NH_2CO free radical given in Table 3 are much greater than those for the related HCO and CH_3CO radicals. In addition, the NH_2CO radical is unusual in that the $^2A'$ and $^2A''$ states are still widely split in energy even for a linear N—C—O geometry. The difference in electronic structure of the linear states is illustrated in Fig. 1. In the $^2A'$ state, the π electron system (perpendicular to the five-atom plane) contains four electrons and corresponds essentially to a p_π lone pair on nitrogen

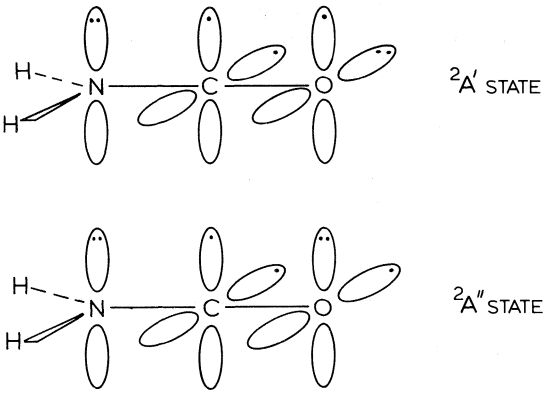

FIG. 1. Electron configurations in the $^2A'$ and $^2A''$ states of NH_2CO.

conjugated to a two-electron carbonyl π bond. The in-plane p orbitals perpendicular to the N—C—O line contain three electrons essentially localized as shown in Fig. 1 with one at carbon and two at oxygen. In the $^2A''$ state, however, the π system contains five electrons and corresponds essentially to lone p_π pairs on nitrogen and oxygen and a single p_π electron on carbon (see Fig. 1). The in-plane p orbitals, however, now form a strong two-electron carbon–oxygen 'π' bond. The five-electron N—C—O π network is very similar to that in the lowest $^3n\pi^*$ state of formamide (12). In both cases there appears to be no stabilization associated with conjugation of the nitrogen lone pair with the three-electron π network of the CO unit. In fact the optimum geometry about the nitrogen in the $^2A''$ state of NH_2CO is probably pyramidal as it is in the $^3n\pi^*$ state (12) and the ground state of formamide; however, we have not investigated this point in these calculations.

As a consequence of the conjugative stabilization of the $^2A'$ state but not the $^2A''$ state, the energy gap between the states amounts to 28.3 kcal mol^{-1} (by 4-31G) at the optimum linear geometry for the $^2A''$ state (see Table 3). The predicted O—O band energy (by 4-31G) is 67.0 kcal mol^{-1}, some 43.1 kcal mol^{-1} greater than that predicted for HCO. Similarly the vertical excitation energy calculated for NH_2CO is much greater than that for HCO.

[3]Since both states involved originate from the same degenerate state in the linear geometry, there should be no large difference in correlation energy between the two states; thus calculations even without CI should give good excitation energy predictions.

1. J. W. C. JOHNS, S. H. PRIDDLE, and D. A. RAMSAY. Discuss. Faraday Soc. **35**, 90 (1963) and references therein.
2. J. M. BROWN and D. A. RAMSAY. Can. J. Phys. **53**, 2232 (1975).
3. (*a*) P. J. BRUNA, R. J. BUENKER, and S. D.

PEYERIMHOFF. J. Mol. Struct. **32**, 217 (1976) and references therein; (*b*) P. BOTSCHWINA. Chem. Phys. Lett. **29**, 98 (1974).
4. W. A. LATHAN, L. A. CURTISS, W. J. HEHRE, J. B. LISLE, and J. A. POPLE. Prog. Phys. Org. Chem. **11**, 175 (1974).
5. K. VASUDEVAN, S. D. PEYERIMHOFF, and R. J. BUENKER. J. Mol. Struct. **29**, 285 (1975).
6. N. C. BAIRD. J. Chem. Phys. **62**, 300 (1975).
7. N. C. BAIRD and H. B. KATHPAL. J. Am. Chem. Soc. **98**, 7532 (1976).
8. C. C. J. ROOTHAAN. Rev. Mod. Phys. **32**, 179 (1960).
9. N. C. BAIRD and R. F. BARR. Theoret. Chim. Acta, **36**, 125 (1974).
10. W. J. HEHRE, R. F. STEWART, and J. A. POPLE. J. Chem. Phys. **51**, 2657 (1969).
11. R. DITCHFIELD, W. J. HEHRE, and J. A. POPLE. J. Chem. Phys. **54**, 724 (1971).
12. N. C. BAIRD and H. B. KATHPAL. Chem. Phys. Lett. **43**, 315 (1976).
13. (*a*) L. RADOM, W. J. HEHRE, and J. A. POPLE. J. Chem. Soc. A, 2299 (1971); (*b*) J. Am. Chem. Soc. **93**, 289 (1971); (*c*) W. J. HEHRE, R. DITCHFIELD, L. RADOM, and J. A. POPLE. J. Am. Chem. Soc. **92**, 4796 (1970).
14. K. W. WATKINS and W. W. WORD. Intl. J. Chem. Kinet. **6**, 855 (1974).
15. J. D. COX and G. PILCHER. Thermochemistry of organic and organometallic compounds. Academic Press, London. 1970.
16. (*a*) J. C. BODEN and R. A. BACK. Trans. Faraday Soc. **66**, 175 (1970); (*b*) R. A. BACK and J. C. BODEN. Trans. Faraday Soc. **67**, 88 (1971); (*c*) S. R. BOSCO, A. CIRILLO, and R. B. TIMMONS. J. Am. Chem. Soc. **91**, 3140 (1969).
17. N. C. BAIRD. J. Chem. Phys. **62**, 300 (1975) and references therein.
18. J. W. C. JOHNS, S. H. PRIDDLE, and D. A. RAMSAY. Discuss. Faraday Soc. **35**, 90 (1963).
19. G. HERZBERG. Molecular spectra and molecular structure. Vol. III. Van Nostrand, Princeton, NJ. 1967. pp. 468, 495, 496.
20. J. F. OGILVIE. J. Mol. Struct. **31**, 407 (1976).

The reactivity of tungsten halides with organic sulfides. Part II.[1] Desulfurization of tetrahydrothiophene

P. MICHAEL BOORMAN,[2] TRISTRAM CHIVERS, AND KALABEERAPPA N. MAHADEV

Department of Chemistry, University of Calgary, Calgary, Alta., Canada T2N 1N4

Received August 13, 1976

P. MICHAEL BOORMAN, TRISTRAM CHIVERS, and KALABEERAPPA N. MAHADEV. Can. J. Chem. **55**, 869 (1977).

WCl_6 reacts with tetrahydrothiophene (tht) to yield initially $[C_4H_8SC_4H_8Cl]_2$ $[W_2S_2Cl_6(tht)_2]$. The sulfonium ion is slowly degraded at 120 °C in tht and a green, neutral complex $[W_2S_2Cl_4(tht)_4]$ is produced. The formation of $[C_4H_8SC_4H_8Cl]^+$ occurs through the desulfurization of tht by WCl_6 to form $Cl(CH_2)_4Cl$, which in turn alkylates a tht molecule. The identity of most of the organic by-products of these reactions has been determined, and on this basis it is suggested that *S*-chlorination of tht occurs to give $[C_4H_8SCl]$ Cl. The degradation of this species by various possible pathways may account for the formation of some of the diverse products.

P. MICHAEL BOORMAN, TRISTRAM CHIVERS et KALABEERAPPA N. MAHADEV. Can. J. Chem. **55**, 869 (1977).

WCl_6 réagit avec le tétrahydrothiophène (tht) pour conduire initialement au $[C_4H_8SC_4H_8Cl]_2$ $[W_2S_2Cl_6(tht)_2]$. L'ion sulfonium se dégrade lentement à 120 °C dans le tht et un complexe vert, neutre $[W_2S_2Cl_4(tht)_4]$ se produit. Il y a formation du $[C_4H_8SC_4H_8Cl]^+$ par une désulfurisation du tht par WCl_6 conduisant au $Cl(CH_2)_4Cl$ qui, à son tour, vient alkylé une molécule de tht. On a déterminé l'identité de la plupart des sous-produits de ces réactions et sur cette base on suggère qu'une *S*-chloration du tht se produit pour donner le $[C_4H_8SCl]Cl$. La dégradation de cette espèce par divers mécanismes possibles permet d'expliquer la formation de quelques-uns des divers produits finals.

[Traduit par le journal]

Introduction

In an earlier publication (1) we showed that tungsten hexachloride reacts with alkyl sulfides to give $(R_3S)_2[WCl_6]$. The reactions involve *S*-dealkylation followed by reductive elimination of R_2S_2. Alkylation of R_2S by RCl probably occurs at the tungsten site through the intermediacy of $WCl_4(R_2S)_2$. Clearly there could not be a completely analogous reaction between WCl_6 and a cyclic sulfide and it was therefore of interest to study such a case.

Frequent references have been made recently to the incorporation of WCl_6 into organometallic catalytic systems, such as for olefin metathesis (2), and yet few comprehensive studies of systems involving WCl_6 and relatively simple organic molecules have been reported. The ability of WCl_6 to react with Lewis bases to form adducts, with or without reduction of tungsten, has been well documented (3). Fowles and co-workers have also reported on the reactivity of various tungsten halides with potential donors in which organic molecules underwent an unexpected reaction, rather than forming the predicted adduct (4, 5). Reactivity of this kind with potential sulfur donors is of particular interest in that it may possibly be relevant to proposed mechanisms for hydrodesulfurization processes on molybdenum or tungsten-containing heterogeneous catalysts (6).

In this paper we discuss the direct reaction of WCl_6 (and WCl_5) with tetrahydrothiophene (tht) from which we have obtained two new dimeric tungsten species. Of particular interest was the ability of the tungsten halide to desulfurize the cyclic sulfide and the nature of the organic by-products which arise.

Experimental

General Procedures

All handling procedures were carried out in a dry nitrogen atmosphere. Tetrahydrothiophene (Aldrich 93% Technical Grade) was dried by refluxing over CaH_2, triple-distilled under nitrogen, and degassed before use. The purity was checked by gas chromatography. Tungsten hexachloride was obtained from Alfa Inorganics and was resublimed *in vacuo* before use; WCl_5 was obtained as previously described (1). Tungsten was analyzed by ignition to the oxide and other elements were determined by Alfred Bernhardt Laboratories. Infrared spectra were recorded as Nujol mulls between CsI plates using a

[1]For Part I, see ref. 1.

[2]Author to whom correspondence should be addressed.

TABLE 1. Analytical data for compounds **1** and **2**

Product from	W	Cl	C	H	S
WCl_6 + tht reaction (green)	40.2	20.7	20.7	3.50	15.8
WCl_5 + tht reaction (green)	39.7	20.7	20.5	3.30	15.6
Calculated for $[WSCl_2(tht)_2]_2$	39.7	20.8	20.8	3.48	15.3
WCl_6 + tht reaction (brown)	31.2	24.3	24.7	3.80	16.3
WCl_5 + tht reaction (brown)	31.0	24.2	24.2	4.21	—
Calculated for $\left[\text{C}_4\text{H}_8\text{S}\text{—}(CH_2)_4\text{—}Cl\right]_2[W_2S_2Cl_6(tht)_2]$	31.2	24.0	24.4	4.10	16.3
(also for $\left[\text{C}_4\text{H}_8\text{S}\text{—}(CH_2)_4\text{—}\text{S}\text{C}_4\text{H}_8\right][W_2S_2Cl_8]$ and $WCl_4(tht)_3$)					

Beckman IR 20-A spectrometer; far infrared spectra were recorded as Nujol mulls between polyethylene plates using a Digilab FTS-16 spectrometer. Magnetic data were obtained using a standard Gouy technique at 22 °C. The susceptibilities were corrected for the diamagnetism of the ligands using Pascal's constants. The nmr spectra were recorded using a Varian HA-100 spectrometer and mass spectra using a Varian MAT CH5 Series 1 Mass Spectrometer. Conductivity data were obtained in dry $PhNO_2$ solutions by standard methods. Molecular weight determinations were made by cryoscopy in $PhNO_2$.

Volatile by-products from the various reactions were separated on Reoplex 400 columns, and fed directly into the mass spectrometer from the Varian Aerograph Series 1200 gas chromatograph.

Reactions of WCl_6 and WCl_5 with tht

The reactions were carried out in evacuated sealed Pyrex tubes at 120 °C for 72 h. In a typical experiment 4–5 g of WCl_6 were loaded into a tube in the glovebox, and tht (*ca.* 10 ml) was added, whereupon a vigorous exothermic reaction occurred. Attempts to isolate solid products at this stage resulted in the formation of oils. After 72 h of refluxing at 120 °C, a brown solid product was produced, with a green supernatant liquid. Upon addition of hexane to the filtered green solution a green precipitate was formed, which was washed with hexane and dried *in vacuo*. The brown compound which was earlier removed by filtration from the mother liquor was washed with CH_2Cl_2 and hexane and dried. Yields were typically:

Green compound, **1**, $W_2Cl_4S_6C_{16}H_{32}$, 16%.
Brown compound, **2**, $W_2Cl_8S_6C_{24}H_{48}$, 73%.

Some green product was lost during the CH_2Cl_2 washing of the brown product. Identification of the products as $\left[\text{C}_4\text{H}_8\text{S}\text{—}(CH_2)_4Cl\right]_2[W_2S_2Cl_6(tht)_2]$ brown and $[W_2S_2Cl_4(tht)_4]$ (green) is discussed later. Analytical data are presented in Table 1.

The reaction system was modified for the purpose of collecting and identifying volatile by-products, so that an H-shaped tube was used which was loaded with reactants in one vertical arm. After reaction under sealed evacuated conditions the volatiles were cold distilled into the second arm and sealed off.

The mixture was fractionated, and from ^1H nmr spectra it was found to contain large quantities of HCl in the first two of five fractions. The large amount of tht in the heavier fractions precluded identification of all of the compounds, but in the fifth (heaviest) fraction 2-chlorotetrahydrothiophene was suggested on the basis of a characteristic multiplet centered at δ 5.68. Subsequently this was confirmed by running each fraction through a gas chromatographic column (Reoplex 400) directly into the mass spectrometer. Complete separation was achieved, and the components identified are shown in Table 2. Apart from confirming the presence of 2-chlorotetrahydrothiophene in fraction 5, the other components of interest were ethylene and a dihydrothiophene. This was identified as 2,3-dihydrothiophene by addition of a *bona fide* sample of this species to a gas chromatographic sample.

*Reaction of **1** with Pyridine*

Approximately 0.5 g of **1** was dissolved in *ca.* 5 ml of pyridine (py) and after stirring for 3 h at room temperature, hexane was added. The green precipitate so formed was filtered, washed with hexane, and dried in vacuum. The product **3** was identified as $[W_2Cl_4S_2(py)_4]$ (calcd.: W 41.8, Cl 15.9, C 27.0, H 2.26; found: W 41.9, Cl 16.9, C 28.2, H 2.62).

*Reaction of **1** with Et_4NCl*

0.5 g of **1** was reacted in CH_2Cl_2 (~20 ml) with an approximately 5 *M* excess of Et_4NCl, also dissolved in CH_2Cl_2 (~15 ml). A tarry green precipitate was formed which was converted to a dark green powder by stirring with fresh CH_2Cl_2. After washing with hexane and drying, the compound was found by infrared spectroscopy to contain Et_4N^+ cations and no coordinated tht. Analysis indicated that this product was $(Et_4N)_2$ $[W_2S_2Cl_6]$, **4**, which requires: W 40.6, Cl 23.5, S 7.09, N 3.10, C 21.3, H 4.45; found: W 40.7, Cl 23.2, S 7.30, N 2.86, C 21.1, H 4.35.

Preparation of $\left[\text{C}_4\text{H}_8\text{S}\text{—}(CH_2)_4Cl\right]^+Cl^-$ *(**5**)*

This compound was prepared by reaction of tht with 1,4-dichlorobutane in a 1:1 ratio in a sealed tube containing a catalytic quantity of HCl. Both **5** and

TABLE 2. Volatile products from the reaction of WCl_6 with tht

Compound	Approximate percentage of total organic by-products*	Major peaks in the mass spectrum†
Ethylene	7	28, 27, 26
Propanethiol	3	76, 47, 43, 42, 27
Butene	4	41, 56, 39, 27, 28
Thiophene	4	84, 58, 57, 45, 39
2,3-Dihydrothiophene	3	86, 60, 58, 57, 45
Chlorobutene	45	55, 90, 75, 62, 39
2-Chlorotetrahydrothiophene	31	122, 87, 60, 35, 45
Unidentified components	3	—

*Based on peak areas in gc trace.
†Given in order of decreasing intensity; identified from 'CRC Atlas of Spectral Data'.

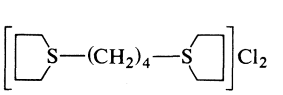

were formed but after repeated recrystallization **5** could be isolated in a pure state. The spectral properties of **5** are shown in Table 3 and in the Fig. 1*c* (nmr).

Preparation of 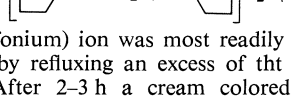 *(6)*

The bis(sulfonium) ion was most readily prepared as compound **6** by refluxing an excess of tht with 1,4-diiodobutane. After 2–3 h a cream colored precipitate formed which was filtered, washed with hexane, and dried at 80 °C under vacuum. Spectral data are given in Table 2 and in Fig. 1*b*. (Calcd. for 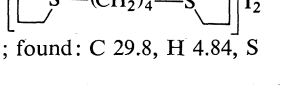 C 29.6, H 4.98, S 13.2, I 52.2; found: C 29.8, H 4.84, S 13.3, I 52.5%.)

Reaction of 1 with **5**

$[W_2S_2Cl_4(tht)_4]$ (0.5 g) was dissolved in CH_2Cl_2 and a 3*M* quantity of 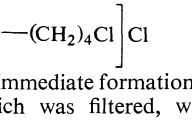 was added also in CH_2Cl_2 solution. Immediate formation of a brown precipitate occurred which was filtered, washed with CH_2Cl_2, hexane, and dried in vacuum. Analysis and infrared spectra showed that this product was identical with **2**. (Calcd. for 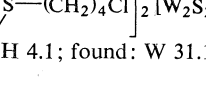 $[W_2S_2Cl_6(tht)_2]$: W 31.2, Cl 24.0, C 24.4, H 4.1; found: W 31.1, Cl 23.9, C 24.3, H 4.29.)

Results and Discussion

Characterization of the Green Compound 1 as $[W_2S_2Cl_4(tht)_4]$

The soluble green compound obtained from the direct reaction of WCl_6 or WCl_5 with tht was shown by analysis to have the empirical formula $[WSCl_2(tht)_2]_n$ (Table 1). The compound hydrolyzes rapidly in moist air with liberation of both HCl and H_2S, suggesting the presence of both coordinated chloride and sulfide ions. The solubility of **1** in polar organic solvents enabled solution data to be obtained. Solutions in nitrobenzene were non-conducting and the cryoscopically determined molecular weight in this solvent was 870 ± 50, consistent with the formulation of **1** as the dimer $[WSCl_2(tht)_2]_2$ (calculated molecular weight 926). The magnetic susceptibility of **1**, χ_m, calculated for a formula $WSCl_2(tht)_2$ was $+41 \times 10^{-6}$ cgs units, giving a relatively low magnetic moment of 0.32 BM per tungsten atom, at 21 °C. This formally tungsten (IV) (d^2) compound might have been expected to possess a larger degree of paramagnetism, if it were not a bridged binuclear species, since even relatively low symmetry mononuclear tungsten (IV) species tend to have μ values in the range 1.5–2.0 BM (7). Nevertheless the paramagnetism was found to be sufficiently large to prevent the observation of an nmr spectrum of **1** in the non-coordinating solvent CH_2Cl_2.

In dmso (d_6) the spectrum of free tht was observed, presumably due to displacement of this weak sulfur donor by the strongly donating solvent. The infrared spectrum of **1** is typical of coordinated tht. The free ligand possesses a band at 685 cm^{-1} which has been assigned to C—S stretching (8), which usually is lowered upon coordination. Such is the case in the spectrum of **1** where the ν(C—S) band occurs at 665 cm^{-1}. No band is observed in the 500 cm^{-1} region of the spectrum which could be assigned to a terminal W=S group, suggesting that the compound therefore contains bridging sulfide groups. Two strong bands at 312 cm^{-1} and 275 cm^{-1} (shoulder) can probably be assigned to W—Cl stretching vibrations.

These observations are consistent with a

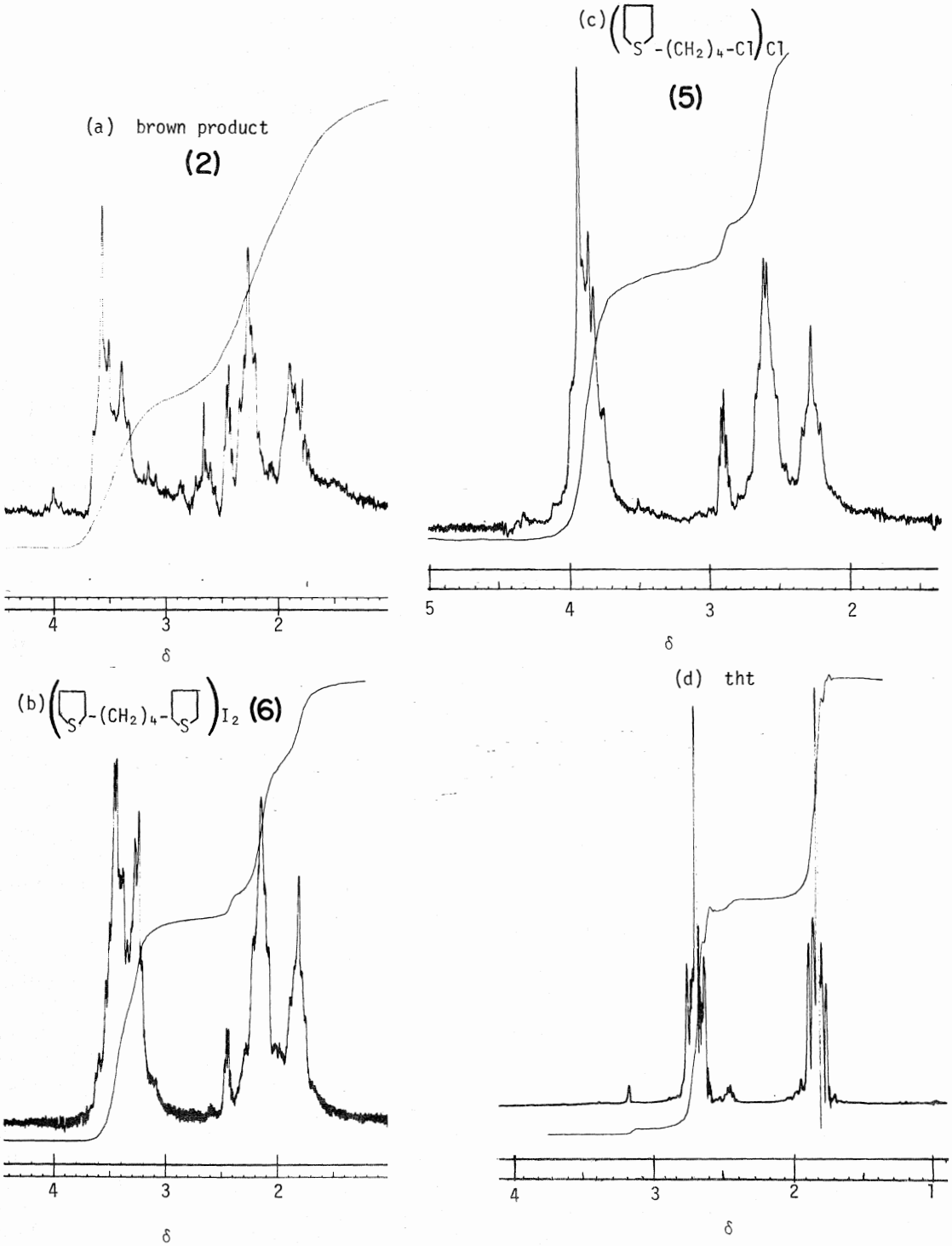

FIG. 1. Nuclear magnetic resonance spectra of (*a*) **2**, (*b*) **6**, (*c*) **5**, and (*d*) tht.

TABLE 3. Mass spectral data for red liquid obtained from thermal decomposition of **2**, and for compounds **4** and **5**

Compound	*m/e**	Relative abundance	Assignment
Red liquid	214	18	$\left[\left(\bigcirc\!\!\!\!\bigcirc S—(CH_2)_4—Cl\right)Cl\right]^+$
	179	16	$\left[\bigcirc\!\!\!\!\bigcirc S—(CH_2)_4—Cl\right]^+$
	137	100	$\left[\bigcirc\!\!\!\!\bigcirc S—CH_2Cl\right]^+$
	123	10	$\left[\bigcirc\!\!\!\!\bigcirc S—Cl\right]^+$
	91	46	$((CH_2)_4Cl)^+$
	88	61	$\left[\bigcirc\!\!\!\!\bigcirc S\right]^+$
	60	83	$[S(CH_2)_2]^+$
$\left[\bigcirc\!\!\!\!\bigcirc S—(CH_2)_4—Cl\right]Cl$	214	21	$\left[\left(\bigcirc\!\!\!\!\bigcirc S—(CH_2)_4Cl\right)Cl\right]^+$
	179	20	$\left[\bigcirc\!\!\!\!\bigcirc S—(CH_2)_4Cl\right]^+$
	137	100	$\left[\bigcirc\!\!\!\!\bigcirc S—(CH_2)Cl\right]^+$
	123	8	$\left[\bigcirc\!\!\!\!\bigcirc S—Cl\right]^+$
	91	48	$[(CH_2)_4Cl]^+$
	88	61	$\left[\bigcirc\!\!\!\!\bigcirc S\right]^+$
	60	83	$[S(CH_2)_2]^+$
$\left[\bigcirc\!\!\!\!\bigcirc S—(CH_2)_4—S\bigcirc\!\!\!\!\bigcirc\right]I_2$	398	2	$\left[\left(\bigcirc\!\!\!\!\bigcirc S—(CH_2)_4I\right)I\right]^+$
(compound **5**)	310	2	$(I(CH_2)_4I)^+$
	271	8	$\left(\bigcirc\!\!\!\!\bigcirc S—(CH_2)_4I\right)^+$
	229	6	$\left(\bigcirc\!\!\!\!\bigcirc S—(CH_2)I\right)^+$
	183	73	$((CH_2)_4I)^+$
	155	13	$((CH_2)_2I)^+$
	141	5	$(CH_2I)^+$
			$(I)^+$
	88	100	$\left(\bigcirc\!\!\!\!\bigcirc S\right)^+$

*Based on ^{35}Cl, ^{127}I.

structure of **1** which involves a sulfur-bridged dimer as shown below, or one of its geometric isomers:

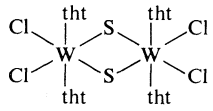

Further evidence in favor of such a structure was obtained by reaction of **1** with pyridine, which enabled the compound **3**, $W_2S_2Cl_4(py)_4$, to be isolated as a green solid. The infrared spectrum of **3** showed the presence of coordinated pyridine, the absence of terminal W=S groups, and bands at 312 cm^{-1} (vs) and ~275 cm^{-1} (shoulder) which we assign to W—Cl stretching. The latter region of the spectrum is very similar to that of the spectrum of **1**, as expected if pyridine has displaced tht from a common $W_2S_2Cl_4$ structural unit. The solution properties of **3** support this conclusion, since in nitrobenzene as solvent it is an essentially non-conducting dimeric species, although some slight dissociation probably occurs (observed molecular weight 740 ± 50; calculated for $W_2S_2Cl_4(py)_4$, 890).

Characterization of the Brown Compound, **2**, *as* 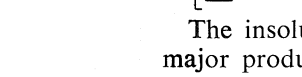

The insoluble brown compound, **2**, was the major product from the reaction of WCl_6 (or WCl_5) with tht. Its characterization presented some problems due to its insolubility. Analysis (Table 1) was consistent with a simple formulation as $WCl_4(tht)_3$ but such a formulation was inconsistent with the following facts. Firstly, $WCl_4(tht)_2$ is a known compound (7) which exhibits no tendency to take up further tht. Secondly, upon hydrolysis of **2**, H_2S is liberated (in addition to HCl) suggesting the presence of inorganic sulfide. Furthermore, the infrared and nmr spectral properties were not consistent with this suggestion.

Thermal decomposition of **2** in a sealed, evacuated tube gave rise to two volatile products. One of these was readily identified as tht, while the other was a red oil with a mass spectrum suggesting the formulation 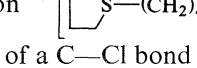 , **5**. However, the presence of a C—Cl bond in the structure of **2** could not be unequivocally identified from the infrared spectrum, and so both **5** and the corresponding disulfonium cation derived from tht and $Cl(CH_2)_4Cl$ were synthesized. The mass spectrum of

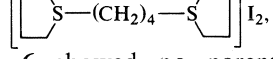

6 showed no parent ion peak (Table 3) and thus this technique was unable to prove conclusively which cation occurs in the compound **2**.

The two plausible structures of **2** involving such sulfonium ions derived from tht and $Cl(CH_2)_4Cl$ are:

(*A*) 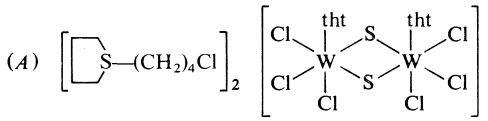

(*B*) 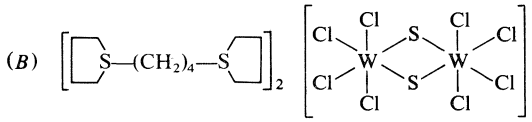

Analysis cannot distinguish between (*A*), (*B*), and $WCl_4(tht)_3$, but strong support for (*A*) was derived from the ^1H nmr spectrum of **2** in dmso (d_6). (This was the only solvent in which **2** showed appreciable solubility.) The spectra of **2**, **5**, and **6** are shown in Fig. 1, and it can readily be seen that the δ 2.0–4.0 region of the spectrum suggests that structure (*A*) involving a monosulfonium cation is correct. The displacement of tht by dmso (d_6) is also implied by the spectrum of **2**.

Confirmation of structure (*A*) was obtained by synthesis of **2** from the green compound **1**, and the sulfonium chloride **5**, in CH_2Cl_2 solution:

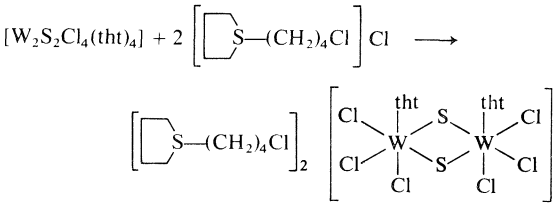

The corresponding compound $(Et_4N)_2[W_2S_2Cl_6(tht)_2]$ was not obtained from the reaction of Et_4NCl with **1**, but instead the compound **4**, $(Et_4N)_2[W_2S_2Cl_6]$ was obtained, from which the sixth ligand, neutral tht, had been lost. **4** showed no tendency to take up further chloride ion to yield the anion of structure (*B*).

The other properties of **2** are consistent with

formulation as (*A*). Its infrared spectrum shows bands typical of coordinated tht, in addition to bands found for compound **5**, although the C—Cl stretching vibration found as a strong band at 644 cm^{-1} in the spectrum of **5** is relatively weak in the spectrum of **2**. The presence of both the sulfonium cation and coordinated tht makes a complete assignment of the spectrum of **2** impossible. The magnetic moment of **2** was found to be 1.05 BM per tungsten atom, rather higher than that of **1**. Nevertheless the relationship between **1** and **2** is proven by the synthesis of **2** from **1** and **5**. The reverse reaction, conversion of **2** into **1** is readily achieved by heating **2** in a sealed tube with tht and HCl (catalytic quantity). After 72 h at 120 °C a good yield of **1** can be obtained, together with products of decomposition of the sulfonium cation which are discussed later.

These reactions all confirm the relationship between **1** and **2** in which a common binuclear tungsten species $[W_2S_2Cl_4]$ is involved. It seems likely that more examples of such sulfur-bridged species will be discovered in the chemistry of tungsten with sulfur donors, since we have already found other examples of this phenomenon (9, 10) and Fowles and co-workers have suggested polymeric sulfur-bridged structures for $WSCl_2$ and $WSCl_3$ (11).

Mechanism of Reaction Between WCl_6 and tht

The predominant product from the reaction between WCl_6 and tht has been shown to be **2**, and the origin of this product is a matter of some interest, since the WCl_6 has abstracted sulfur from the ring system and has been reduced to W(IV). The secondary product, **1**, has been shown to arise from the degradation of **2** in the presence of excess tht, and HCl.

The postulated pathway for desulfurization of tht by WCl_6 is shown in Scheme 1. Such a pathway is consistent with the presence of the sulfonium cation, and inorganic sulfide in the product.

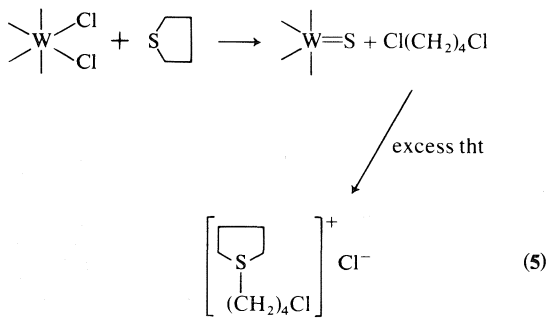

SCHEME 1

The reaction is very similar to that between $MoCl_5$ and tetrahydrofuran (thf) reported by Kepert and Mandyczewsky (12) which yields $MoOCl_3(thf)_2$ with 1,4-dichlorobutane as the by-product. The present reaction is more complex, however, due to the concomitant reduction of tungsten (VI) to tungsten (IV). This leaves more room for conjecture and it was at first expected that a reductive elimination of organic disulfide would be involved as in the case of simple alkyl sulfides (1). This is shown in Scheme 2.

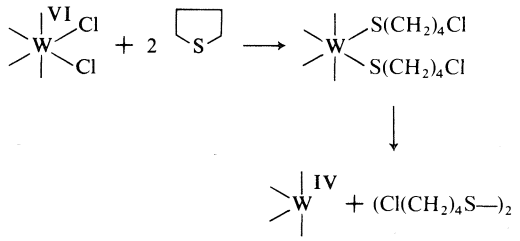

SCHEME 2

However an analysis of the volatile by-products from the reaction failed to show any sign of disulfides (Table 2). Instead, a major product, which begins to be formed very early in the reaction, is HCl. A more likely mechanism therefore would seem to be an *S*-chlorination reaction with subsequent reactions of the chlorosulfonium ion, as studied extensively by Wilson and co-workers (13, 14). Such a reaction can follow two pathways, involving either the elimination of HCl (Pummerer Reaction) or C—S bond cleavage to yield a sulfenyl chloride (13). For the present system these alternatives are shown in Scheme 3.

The superposition of Schemes 1 and 3 would account for the desulfurization of tht to yield the cation in **2**, the presence of inorganic sulfide in **2**, the reduction of W(VI) to W(IV), and the nature of several of the by-products. The sequence of the reduction and desulfurization reactions is uncertain, and indeed they may well occur simultaneously. The immediate formation of large quantities of HCl upon reaction of WCl_6 with tht suggests that the reduction reaction begins at an early stage.

Scheme 3 is able to account for the formation of at least two of the important by-products. Both 2-chlorotetrahydrothiophene and 2,3-dihydrothiophene were confirmed as being prod-

TABLE 4. Products obtained from degradation of

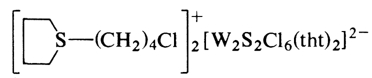 in tht

Compound	Approximate percentage of total organic by-products	Major peaks in the mass spectrum
Ethylene	15	28, 27, 26
CH_3—CH_2—C≡C—SH	9	86, 71, 57, 56, 41
CH_2=CH—C≡C—SH	9	84, 57, 56, 55, 27
Thiophene	2	84, 58, 57, 45, 39
Chlorobutene	65	55, 90, 75, 62, 39

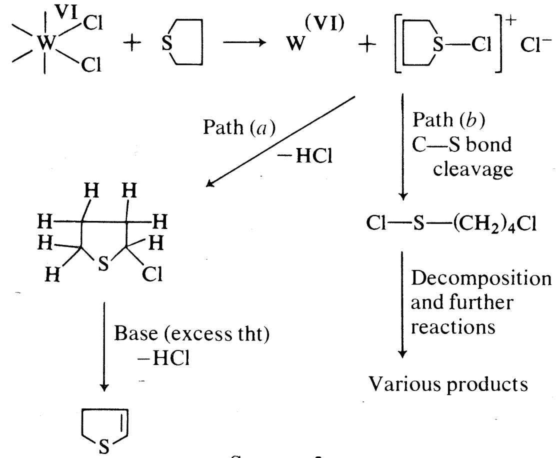

SCHEME 3

ucts. This is consistent with the *S*-chlorination of tht and subsequent reactions described by Wilson and co-worker (14), who showed that direct reaction of Cl_2 with tht in various solvents yields 2-chlorotetrahydrothiophene and under some circumstances 2,3-dichlorotetrahydrothiophene. However, we found no evidence for the presence of the latter compound. Loss of HCl from 2-chlorotetrahydrothiophene is presumably responsible for formation of 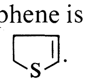 .

The alternative pathway for the degradation of 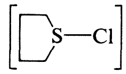 Cl, which has been previously established for chlorination reactions of thioethers is via C—S bond cleavage to produce a sulfenyl chloride. In the case of tht this would imply the formation of $Cl(CH_2)_4SCl$. It is well known that sulfenyl halides are highly reactive species and even the simplest of such compounds, CH_3SCl, has been shown to decompose spontaneously to yield at least seven different products (15). It is therefore conceivable that some of the products listed in Table 3 arise in this way, but in view of the lack of information in the literature on the reactivity of this particular sulfenyl chloride, we can only speculate upon the mechanisms involved.

A second source of volatile organic by-products lies in the degradation of

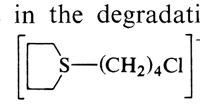

ions, in the conversion of **2** to **1**. To identify those species which might arise in this way, compound **2** was subjected to controlled thermal decomposition. The volatiles from the direct dry decomposition were only tht and **5**, which were readily identified by mass spectroscopy, and the residue was $WSCl_2$. However, upon heating **2** to 120 °C in excess tht and in the presence of HCl, decomposition of the cation occurred with the production of **1**. The volatiles were collected and analyzed by gc/ms as shown in Table 4. In the case of chlorobutene there is some uncertainty as to the isomer produced, and thus the description given is a general one. It may be noted that thiophene is produced and thus may arise via this route to produce the small amounts found in the products from the WCl_6/tht reaction. The presence of acetylenic thiols implies that the degradation of

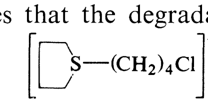

involves rupture of the tht ring, as well as of the side chain. Clearly this is a complex reaction and there is little point in speculating about the pathways involved. It is of interest, however, that the reaction of WCl_6 with tht is capable of desulfurization of the ring, and yields a number of alkenic by-products, including

ethylene. Apart from the information that may be useful in studies of heterogeneous catalytic hydrodesulfurization, it is possible that direct desulfurization of organosulfur constituents of hydrocarbon fuels may be a viable proposition, particularly in view of the alkenic by-products formed.

Acknowledgements

The financial support of the National Research Council of Canada is gratefully acknowledged. We wish to thank Drs. Tavares and Yamdagni for helpful discussions and Miss M. Sisley for experimental assistance in part of the work.

1. P. M. BOORMAN, T. CHIVERS, and K. N. MAHADEV. Can. J. Chem. **53**, 383 (1975).
2. R. J. HAINES and G. J. LEIGH. Chem. Soc. Rev. **4**, 155 (1975).
3. D. L. KEPERT. The early transition metals. Academic Press. 1972.
4. B. J. BRISDON, G. W. A. FOWLES, and B. P. OSBORNE. J. Chem. Soc. 1330 (1962).
5. D. BRITNELL, M. G. B. DREW, G. W. A. FOWLES, and D. A. RICE. Inorg. Nucl. Chem. Lett. **9**, 415 (1973).
6. C. H. AMBERG. Proceedings of the First International Conference on the Chemistry and Uses of Molybdenum, 180 (1973).
7. M. A. SCHAEFER KING and R. E. MCCARLEY. Inorg. Chem. **12**, 1972 (1973).
8. J. A. ALKINS and P. J. HENDRA. Spectrochim. Acta, **22**, 2075 (1966).
9. P. M. BOORMAN and K. J. REIMER. Can. J. Chem. **49**, 2926 (1971).
10. P. M. BOORMAN, T. CHIVERS, K. N. MAHADEV, and B. D. O'DELL. Inorg. Chim. Acta, **19**, L35 (1976).
11. D. BRITNELL, G. W. A. FOWLES, and D. A. RICE. J. Chem. Soc. Dalton, 2191 (1974).
12. D. L. KEPERT and R. MANDYCZEWSKY. J. Chem. Soc. A, 530 (1968).
13. G. E. WILSON, JR. and M. G. HUANG. J. Org. Chem. **35**, 3002 (1970).
14. G. E. WILSON, JR. and R. ALBERT. J. Org. Chem. **38**, 2156 (1973).
15. I. B. DOUGLASS. Int. J. Sulfur Chem. **6**, 177 (1971).

Cobalt(II) and zinc(II) complexes of the 'tripod' ligand tris(2-benzimidazylmethyl)amine. Some five-coordinate derivatives and some with mixed stereochemistries[1]

LAURENCE K. THOMPSON,[2] BARATHAM S. RAMASWAMY, AND ELIZABETH A. SEYMOUR

Department of Chemistry, Memorial University of Newfoundland, St. John's, Nfld., Canada A1C 5S7

Received August 10, 1976

LAURENCE K. THOMPSON, BARATHAM S. RAMASWAMY, and ELIZABETH A. SEYMOUR. Can. J. Chem. **55,** 878 (1977).

A series of cobalt(II) and zinc(II) complexes of the title ligand are reported which contain mixed stereochemistries, *e.g.*, five-coordinate trigonal bipyramidal cations $[M(ligand)X]^+$, and four-coordinate anions, $[MX_4]^{2-}$ (M = Co, Zn; X = Cl, Br, NCS). The blue cobalt complexes, $[Co(ligand)X]_2[CoX_4]$, are readily converted to purple five-coordinate complexes, [Co(ligand)X]X, by recrystallisation from a solvent containing water, *e.g.* acetone. Other five-coordinate cobalt and zinc derivatives were also prepared, [Co(ligand)X]X (X = NO_3, ClO_4), $[Co(ligand)X]BPh_4$ (X = Cl, Br, NCS, NO_3, ClO_4), $[Zn(ligand)X]BPh_4$ (X = Cl, Br, I, NCS). Nuclear magnetic resonance data for all the zinc complexes indicate a significant deshielding of one benzene ring proton on each coordinated benzimidazole group. Conductance data suggest the possibility of cationic association through pseudo-hydrogen bonding in both the cobalt and zinc derivatives involving Cl, Br, NCS anions.

LAURENCE K. THOMPSON, BARATHAM S. RAMASWAMY et ELIZABETH A. SEYMOUR. Can. J. Chem. **55,** 878 (1977).

On rapporte la préparation d'une série de complexes du cobalt(II) et du zinc(II) contenant le ligand mentionné dans le titre et qui contiennent des stéréochimies mixtes; par exemple des cations bipyramidaux trigonaux pentacoordonnés $[M(ligand)X]^+$ et des anions tétracoordonnés $[MX_4]^{2-}$ (M = Co, Zn; X = Cl, Br, NCS). Les complexes bleus du cobalt, $[Co(ligand)X]_2[CoX_4]$, se transforment facilement en complexes pentacoordonnés violets [Co(ligand)X]X, par recristallisation à partir d'un solvant contenant de l'eau, par exemple l'acétone. D'autres dérivés pentacoordonnés du cobalt et du cuivre ont aussi été préparés: [Co(ligand)X]X (X = NO_3, ClO_4), $[Co(ligand)X]BPh_4$ (X = Cl, Br, NCS, NO_3, ClO_4) et $[Zn(ligand)X]BPh_4$ (X = Cl, Br, I, NCS). Les données de rmn pour tous les complexes du zinc indiquent qu'il y a un déblindage important d'un proton du noyau benzénique de chacun des groupes benzimidazole qui a été coordonné. Les données de conductivité suggèrent la possibilité d'une association cationique, par l'intermédiaire d'un pseudo pont hydrogène dans les dérivés du cobalt ainsi que du zinc, qui impliquerait les anions Cl, Br, NCS.

[Traduit par le journal]

Introduction

The coordinating ability of a number of monodentate benzimidazole derivatives has been reported in the literature (1–6). However, examples of polyfunctional benzimidazole derivatives and their complexes appear to be lacking. We report here the synthesis and characterization of a trisbenzimidazole derivative, tris(2-benzimidazylmethyl)amine, which contains four potential donor sites (Fig. 1, ligand abbreviated NTB) and a number of its cobalt and zinc complexes. The ligand has been synthesized by two independent routes, one involving condensation of *o*-phenylenediamine with nitrilotriacetonitrile and the other by condensation of the diamine with nitrilotriacetic acid (Fig. 1).

Reaction of the ligand with cobalt and zinc salts, MX_2 (M = Co, Zn; X = Cl, Br, NCS) in ethyl alcohol led to the formation of ionic derivatives, $[M(NTB)X]_2[MX_4]$, containing five-coordinate pseudo-trigonal bipyramidal cations and a four-coordinate tetrahedral anion. The blue cobalt complexes appear to be stable in fairly dry non-aqueous solvents but on recrystallization from aqueous acetone a series of purple five-coordinate derivatives, [Co(NTB)X]X (X = Cl, Br, NCS) were formed. These trigonal bipyramidal cations could also be stabilized as their tetraphenylborate salts by direct synthesis from alcoholic solution. Other

[1]Presented in part at the 56th Canadian Chemical Conference of the Chemical Institute of Canada, Montreal, June 1973.

[2]To whom correspondence should be addressed.

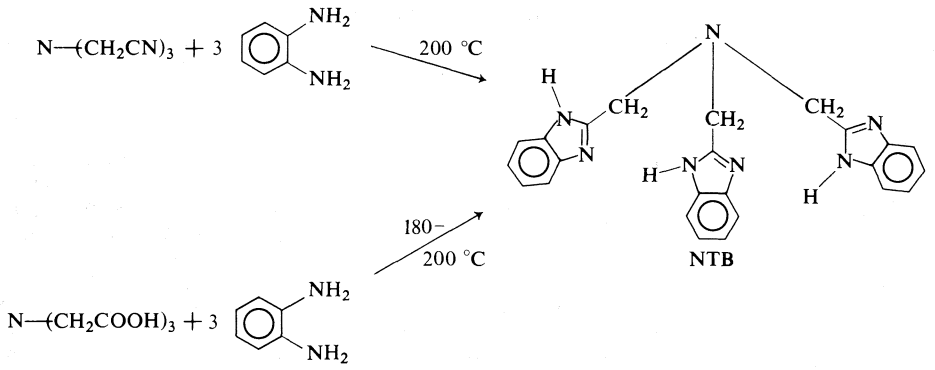

FIG. 1. Synthesis of tris(2-benzimidazylmethyl)amine.

five-coordinate derivatives include pink cobalt nitrate and perchlorate derivatives, [Co(NTB)X]X, [Co(NTB)X]BPh_4 (X = NO_3, ClO_4) and a series of white zinc complexes, [Zn(NTB)X]BPh_4 (X = Cl, Br, I, NCS). Structural assignments have been justified by electronic, vibrational, and nmr spectra and by conductance and magnetic data.

Experimental

Nuclear magnetic resonance data were obtained in deuterated DMSO with Varian Associates A60 and EM360 Spectrometers using $SiMe_4$ as internal calibrant. Electronic spectra were recorded using Beckman DK2A and Cary 17 Spectrometers and infrared data using Perkin-Elmer models 457 and 283. Magnetic susceptibilities were obtained by the Faraday method at room temperature using a Cahn model #7600 coupled to a Cahn gram electrobalance and conductivity data were obtained using a General Radio Company bridge with impedance comparator and a constant temperature bath adjusted to 25 °C. Microanalyses were carried out by the Beller laboratories, Göttingen, W. Germany and by Chemalytics, Tempe, Arizona. Metal analyses were determined by Atomic Absorption using a Varian Techtron AA-5, after prior digestion of the samples in concentrated HCl or ternary solution (HNO_3, H_2SO_4, $HClO_4$ in a ratio of 10:1:4 respectively).

Tris(2-benzimidazylmethyl)amine (NTB)

Method A

Nitrilotriacetonitrile (5.0 g, 0.037 mol) and *o*-phenylenediamine (12.0 g, 0.11 mol) were finely ground, mixed, and heated together using an oil bath at 200–210 °C. When evolution of ammonia was essentially complete (approx. 24 h) the cooled solid was crushed to a fine powder, washed with ether, and extracted into methanol and refluxed with decolourizing charcoal. After filtration the methanol solution was reduced in volume to give a creamy crystalline product (10.0 g, 66% yield) which was recrystallized from methanol and dried thoroughly under vacuum (mp 271 °C). Vacuum drying of the product appears to be essential since nmr data indicate the presence of solvate molecules (*e.g.*, methanol, ethanol) in the undried product, in a ratio of 1:3, (ligand(solvent)$_3$). These solvate molecules are probably hydrogen bonded, one to each imidazole ring.

Method B

Nitrilotriacetic acid (15.3 g, 0.0800 mol) and *o*-phenylenediamine (27.0 g, 0.250 mol) were finely ground and heated together at 190–200 °C for 1 h using an oil bath. The reaction mixture was cooled and crushed, and refluxed in methanol containing decolourizing charcoal. The solution was filtered hot and its volume reduced until on cooling pinkish white crystals were obtained (17.5 g, 54% yield). Recrystallization was effected using methanol and the product dried under vacuum (mp 270 °C). *Anal.* calcd. for $C_{24}H_{21}N_7$: C 70.8, H 5.16, N 24.1; found: C 70.5, H 5.21, N 23.5. Infrared spectrum (Nujol mull) 3140 (νNH), 1622, 1588 (νCN) cm^{-1}; nmr (DMSO-d_6) (σ(relative intensity)) 12.1(8.5) (broad singlet, NH), 7.60(17), 7.19(17) (*AA'BB'* multiplet, aromatic CH), 4.12(17) (CH_2); mass spectrum, major mass peaks (*m/e*(relative intensities)) 407(3) P, 277(15), 276(80), 248(8), 146(57), 133(10), 132(96), 131(100), 119(24), 104(22), 92(9), 77(24).

Metal Complexes of NTB

Complexes of Mixed Stereochemistry [M(NTB)X]$_2$-[MX_4]

Stoichiometric amounts of the metal salt, MX_2 (hydrated or anhydrous) (M = Co, Zn; X = Cl, Br, NCS) and NTB were dissolved separately in hot absolute ethanol and the hot solutions mixed with stirring for about 1/2 h. In some cases the products crystallized from the hot solution while in others reduction in volume followed by cooling was necessary to induce crystallization. The products were recrystallized from absolute ethanol and dried under vacuum at 90 °C.

Five-coordinate Complexes

[Co(NTB)X]X (X = Cl, Br, NCS)

The blue cobalt complexes of mixed stereochemistry were found to be hydrolytically unstable in aqueous solvents and on recrystallization from aqueous acetone (approx. 10% H_2O) purple complexes of formula [Co(NTB)X]X were produced. The compounds were dried under vacuum at 90 °C.

[Co(NTB)X]BPh_4 (X = Cl, Br, NCS, NO_3, ClO_4)

A hot ethanolic solution of the ligand and a slight

TABLE 1. Analytical and other data

Compound	Colour	% yield	Found C	Found H	Found N	Calcd C	Calcd H	Calcd N	M Found	M Calcd
$[Co(NTB)Cl]_2[CoCl_4]$	Blue	95	47.1	3.95	15.8	47.8	3.49	16.3	13.9	14.7
$[Co(NTB)Br]_2[CoBr_4]$	Blue	97	39.1	3.13	13.4	39.2	2.86	13.3	11.4	12.0
$[Co(NTB)(NCS)]_2[Co(NCS)_4]$	Blue	95	48.7	3.89	20.7	48.5	3.14	20.9	12.8	13.2
$[Co(NTB)Cl]Cl.H_2O$	Purple	71	50.4	4.18	17.4	50.3	4.35	17.1	9.9	10.6
[Co(NTB)Br]Br	Purple	51	45.4	3.78	15.5	46.0	3.35	15.7	9.00	9.41
$[Co(NTB)(NCS)]NCS.H_2O$	Purple	73	52.0	3.76	20.8	52.0	3.84	21.0	9.20	9.82
$[Co(NTB)Cl]BPh_4.2H_2O$	Purple	91	66.3	5.34	11.8	66.6	5.20	11.5	7.25	7.01
$[Co(NTB)Br]BPh_4$	Purple	46	66.0	4.94	11.8	66.0	4.75	11.3	6.93	6.82
$[Co(NTB)(NCS)]BPh_4$	Purple	98	69.0	4.78	13.1	69.6	4.86	13.3	6.60	6.98
$[Co(NTB)(NO_3)]NO_3$	Pink	95	49.0	4.12	21.0	48.9	3.56	21.4	9.60	9.98
$[Co(NTB)(NO_3)]BPh_4$	Pink	78	67.8	4.91	13.0	68.0	4.84	13.2	6.25	6.95
$[Co(NTB)(ClO_4)]ClO_4$	Pink	80	43.0	3.37	14.8	43.4	3.16	14.7	7.80	8.86
$[Co(NTB)(ClO_4)]BPh_4.2EtOH$	Pink	75	63.6	5.19	10.0	63.9	5.42	10.0	5.96	6.03
$[Zn(NTB)Cl]_2[ZnCl_4]$	White	98	47.4	4.14	16.1	47.3	3.45	16.1	14.9	15.6
$[Zn(NTB)Br]_2[ZnBr_4]$	White	64	40.0	3.76	13.1	38.8	2.83	13.2	11.9	12.8
$[Zn(NTB)(NCS)]_2[Zn(NCS)_4]$	White	66	47.1	3.44	19.7	47.9	3.11	20.7	13.5	14.1
$[Zn(NTB)Cl]BPh_4.H_2O$	White	92	67.6	4.53	11.8	68.3	5.20	11.6	7.97	7.53
$[Zn(NTB)Br]BPh_4.H_2O$	White	93	64.8	4.76	10.9	64.8	4.84	11.0	7.50	7.30
$[Zn(NTB)I]BPh_4$	White	87	62.1	4.57	10.3	62.6	4.46	10.7	6.98	7.11
$[Zn(NTB)(NCS)]BPh_4$	White	78	68.9	5.03	13.0	69.4	4.84	13.2	7.10	7.50

excess of sodium tetraphenylborate was added with stirring to a hot ethanolic solution of a stoichiometric amount of the cobalt salt. On cooling purple (X = Cl, Br, NCS) and pink (X = NO_3, ClO_4) products were obtained which were recrystallized from ethanol and dried under vacuum at 90 °C.

The chloro-, bromo-, and isothiocyanato compounds were also synthesized by adding ethanolic $NaBPh_4$ to an ethanolic solution of [Co(NTB)X]X.

[Zn(NTB)X]BPh₄ (X = Cl, Br, I, NCS)

These complexes were prepared in a similar fashion to the analogous cobalt derivatives.

[Co(NTB)X]X (X = NO_3, ClO_4)

Stoichiometric amounts of the cobalt salt and NTB were mixed in hot ethanol to give pink solutions from which pink crystalline solids were obtained. The products were recrystallized from acetone and dried under vacuum at 90 °C.

Analytical and other data for these systems are given in Table 1.

Results and Discussion

Characterization of the Ligand

Our interest in this ligand, which to our knowledge has not been previously reported in the literature, stemmed in part from our earlier involvement with ligands containing imidazoline rings (7) which were obtained by simple condensation of dinitriles with diamines, *e.g.*, ethylenediamine. A simple extension of this reaction to the trinitrile, nitrilotriacetonitrile, led to the title ligand which appeared to have the right geometrical features to be a stereochemically selective 'tripod' ligand capable of forcing metal ions to adopt predominantly one stereochemistry, *i.e.*, a distorted trigonal bipyramid.

2-Substituted benzimidazoles have been prepared in good yield by the reaction of *o*-phenylenediamine with monobasic acids (*e.g.* formic, propionic, acetic, etc.) under reflux in dilute hydrochloric acid. Extension of this reaction to dibasic acids, *e.g.* oxalic and malonic, did not lead to 2-substituted benzimidazoles, but with succinic acid both mono and bis-2-benzimidazole derivatives were produced (8, 9). Hein and co-workers (10) prepared 2-alkyl and -aryl benzimidazole derivatives by the high temperature (250 °C) condensation of acids, esters, amides, or nitriles with an appropriate diamine in the presence of polyphosphoric acid which acts both as a catalyst and a solvent. Both of these methods were tried for the preparation of NTB but with little success. A much better method proved to be the direct fusion of nitrilotriacetonitrile or nitrilotriacetic acid with *o*-phenylenediamine at high temperatures, followed by recrystallization from methanol (Fig. 1). The products obtained by both synthetic routes were identical in all respects as indicated by analysis, melting point, infrared, nmr, and mass spectros-

copy. An attempted degradation of NTB using conc. HCl was carried out under reflux. NTB did not degrade but simply formed its hydrochloride salt from which NTB was regenerated on treatment with base.

In the nmr spectrum of the ligand the methylene protons are all equivalent, appearing as a singlet shifted downfield slightly in comparison with nitrilotriacetonitrile, while the aromatic protons appear as a symmetrical set of peaks typical of the *AA'BB'* spectrum observed for symmetrically *ortho*-disubstituted benzene rings, *e.g.*, *o*-phenylenediamine, naphthalene, benzimidazole, etc. (Table 5). The symmetrical nature of this set of peaks indicates a plane of symmetry bisecting each benzimidazole unit and passing through the 2-carbon atom. This suggests that the imidazole ring proton is delocalized equally along the N—C—N framework. This proton appears as a very broad resonance at 12.1 σ. As will be shown later, the symmetry or lack of symmetry associated with this set of nmr peaks indicates whether or not the benzimidazole rings are coordinated.

The infrared spectrum of NTB is similar to that of benzimidazole itself.

Characterization of the Complexes

Complexes of the general formula $[M(NTB)X]_2[MX_4]$ (M = Co, Zn; X = Cl, Br, NCS), $[M(NTB)X]X$ (M = Co; X = Cl, Br, NCS, NO_3, ClO_4), and $[M(NTB)X]BPh_4$ (M = Co; X = Cl, Br, NCS, NO_3, ClO_4; M = Zn; X = Cl, Br, I, NCS) were obtained. These complexes bear some resemblance to previously reported systems involving tetradentate tripod ligands. Sacconi and co-workers (11–13) have recently reported five-coordinate cobalt and nickel complexes of potentially tetradentate tripod ligands based on triethylamine with a β position on each ethyl group replaced by a donor group, *e.g.*, N, O, P, As. The bulkiness of the coordinating groups appeared to be a factor in directing the stereochemistry of the resulting complexes, *e.g.*, with decreasing bulkiness of the donor groups a trend towards six-coordination was observed. In addition complexes were cited where the ligand behaved as a bidentate or terdentate. In terms of the chromophoric environment of the ligand, NTB, it bears more resemblance to trenMe (tris(2-dimethylaminoethyl)amine) which acts as a tetradentate tripod ligand, forming pseudo-trigonal bipyramidal systems (14). NTB appears to be the first example of a tetradentate tripod ligand involving three coordinating benzimidazole groups.

Cobalt Complexes

The tetraphenylborate ion is a good noncoordinating anion which has been used effectively to stabilize five-coordinate cations. Reaction of NTB with cobalt salts in ethanol, in the presence of one equivalent of sodium tetraphenylborate, produces a series of complexes $[Co(NTB)X]BPh_4$ (X = Cl, Br, NCS, NO_3, ClO_4) (Table 1). Electronic spectral data for these salts are given in Table 2. The solid mull transmittance and acetone solution spectra are very similar indicating a similar metal ion stereochemistry both in the solid state and in solution. The spectral band positions and their intensities are not typical of either octahedral or tetrahedral cobalt(II) but they bear a close resemblance to previously reported spectra for pseudo-trigonal bipyramidal cobalt derivatives containing tetradentate tripod ligands (Figs. 2, 3) (11–14).

Recent studies by Bertini and co-workers (15) have attempted to simulate observed spectra of some pseudo-trigonal bipyramidal cobalt(II) complexes using both the crystal field and angular overlap approach. Using a C_{3v} field good agreement was obtained between calculated and observed transition energies for the chromophores $CoNN_3Br$ (NN_3 = trenMe), $CoNS_3Br$ (NS_3 = tris(2-*tert*-butylthioethyl)amine) and $CoNP_3Br$ (NP_3 = tris(2-diphenylphosphinoethyl)amine). Four major transitions are observed in these systems assigned from the $^4A_2$ ground state in C_{3v} symmetry. A low energy band around 5–6 kK, assigned to $^4E \leftarrow {}^4A_2$, appears to be largely unaffected by structural variations whereas tetrahedral distortion tends to shift the other $^4E \leftarrow {}^4A_2$ and the P ← F transitions to lower energy. The main features of the spectra include four bands: $^4E \leftarrow {}^4A_2$ (5–6 kK), $^4E \leftarrow {}^4A_2$ (10–12 kK), $^4A_2(P) \leftarrow {}^4A_2$ (14–16 kK), $^4E(P) \leftarrow {}^4A_2$ (17.5–19.5 kK).

The spectra of the tetraphenylborate NTB derivatives exhibit absorptions in three main areas; 5.2–6.8 kK, 10.5–13.3 kK, 16.7–20.5 kK. The lower energy band shows little fine structure in solution but in the solid state splitting of the band is observed in some cases, which is en-

TABLE 2. Electronic spectra (cm^{-1})*

(*a*) $[Co(NTB)X]^+$

Compound	$^4E \longleftarrow {}^4A_2$		$^4E \longleftarrow {}^4A_2$	$^4E(P) \longleftarrow {}^4A_2$†	
$[Co(NTB)Cl]Cl.H_2O$	*a* 6100(41)	6800(38)	10900(41)	17000(215)	18200(231)
	b 5800	6700	10200	[17800]	18900
$[Co(NTB)Cl]BPh_4.2H_2O$	*a* 6100(42)	6800(45)	10600(40)	16700(240)	18200(248)
	b 6000	6800	10900	17500	[18500]
$[Co(NTB)Cl]_2[CoCl_4]$	*a* 6100(145)	6700(136)	10800(81)	16750(726)	[18400](535) 18150 (560)
	b	6300	10800	17200	18100[19000]
$[Co(NTB)Br]Br$	*a*	6650(56)	10900(40)	17100(320)	[17800](300)
	b 5700	6500	10500	17500	
$[Co(NTB)Br]BPh_4$	*a*	6450(64)	11100(42)	17100(330)	[17700](292)
	b 6000	6500	11200	17400	[18200]
$[Co(NTB)Br]_2[CoBr_4]$	*a* 5600(150)	6250(167)	10700(75)	17100(755)	[17700](665)
	b 5800	[6300]	10900	17900	
$[Co(NTB)(NCS)]NCS.H_2O$	*a*	6600(104)	12500(42)	17400(469)	[18600](266)
	b 5200	6450	12900	17900	[19100]
$[Co(NTB)(NCS)]BPh_4$	*a*	6600(81)	12500(32)	17300(364)	[18600](200)
	b 5200	6500	12400	17500	[19100]
$[Co(NTB)(NCS)]_2[Co(NCS)_4]$	*a*	6950(403)	12400(83)	17100(1920)	[18800](512)
	b 5200		12400	16700	
$[Co(NTB)(NO_3)]NO_3$	*a*	6700(39)	[10900](29)13300(38)	18900(228)	
	b 5100	6900	[11400] 13700	19100	
$[Co(NTB)(NO_3)]BPh_4$	*a*	6700(28)	[10900](20)13300(31)	19100(208)	
	b 5250	6700	[10500] 12900	18900	
$[Co(NTB)(ClO_4)]ClO_4$	*a*	6200(43)	12900(27)	18900(166)	[20400](52)
	b[5850]	6400	12800	18900	[20400]
	c	6620	14100	19120	[21000]
$[Co(NTB)(ClO_4)]BPh_4$	*a*	6300(43)	12900(26)	18900(148)	[20500](81)
	b[5850]	6500	12900	18500	[20300]
	c	6600	13900	19050	[20800]

(*b*) $[CoX_4]^{2-}$

Compound	$^4T_1(F) \longleftarrow {}^4A_2$ (ν_2)			$^4T_1(P) \longleftarrow {}^4A_2$ (ν_3)			
$[Co(NTB)Cl]_2[CoCl_4]$	*a* 6100(145)		6700(136)	14500(480)	15200(480)	16000(363)	16750(726)
	b 5200	5600	6300	14600		[16000]	17200
$[Co(NTB)Br]_2[CoBr_4]$	*a* 5600(150)			14300(775)	15000(467)	15700(300)	
	b 5200	5800		14300			
$[Co(NTB)(NCS)]_2[Co(NCS)_4]$	*a* 6950(403)		8300(260)	16150(1980)	16600(1910)	17100(1920)	
	b 6900	7500	8500		16700		

*Labels mean the following: *a*, solution in acetone; *b*, mull transmittance spectrum (room temperature); *c*, solution in nitromethane. [ ] shoulder, ( ) molar extinction coefficient. Some bands have been assigned twice, *i.e.* to both five-coordinate and tetrahedral cobalt(II). These bands probably contain overlapping components associated with both stereochemistries.

†The $^4A_2(P) \leftarrow {}^4A_2$ transition appears to be missing in almost all the spectra with the exception of [Co(NTB)Cl]Cl and $[Co(NTB)Cl]BPh_4$ where a weak shoulder at 16000 cm^{-1} can possibly be assigned to this transition.

hanced at low temperature (77 K). The high energy band is split into two components in most cases, especially in solution. The splitting of this band has been observed in some other trigonal bipyramidal systems and can possibly be associated with spin–orbit effects or deviations from C_{3v} symmetry. In the NTB complex ions the ligand is assumed to be acting as a tetradentate in an approximately C_{3v} symmetry environment (Fig. 4) and the observed spectral bands are tentatively assigned as follows: $^4E \leftarrow {}^4A_2$ (5.2–6.8 kK), $^4E \leftarrow {}^4A_2$ (10.5–13.3 kK), and $^4E(P) \leftarrow {}^4A_2$ (two components 16.7–20.5 kK) (Table 2). (The $^4A_2(P) \leftarrow {}^4A_2$ transition is probably hidden beneath the band envelope associated with $^4E(P) \leftarrow {}^4A_2$; see footnote †, Table 2.)

Magnetic data (Table 3) indicate that these complexes are high spin, typical of systems of this type with hard donor atoms (16). The

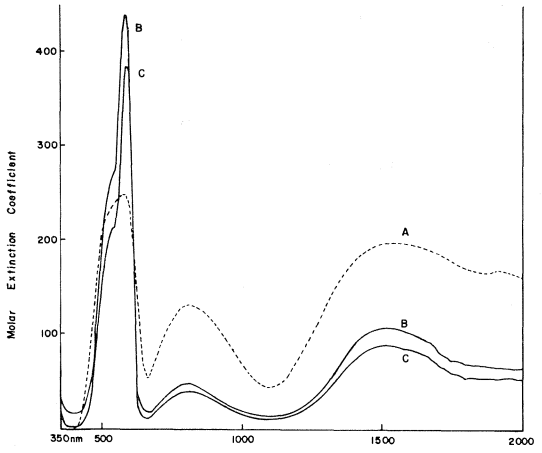

FIG. 2. Electronic spectra of some NTB complexes. *A*. Mull transmittance spectrum of [Co(NTB)(NCS)]BPh_4 (arbitrary absorbance). *B*, *C*. [Co(NTB)(NCS)]NCS and [Co(NTB)(NCS)]BPh_4, respectively, in acetone.

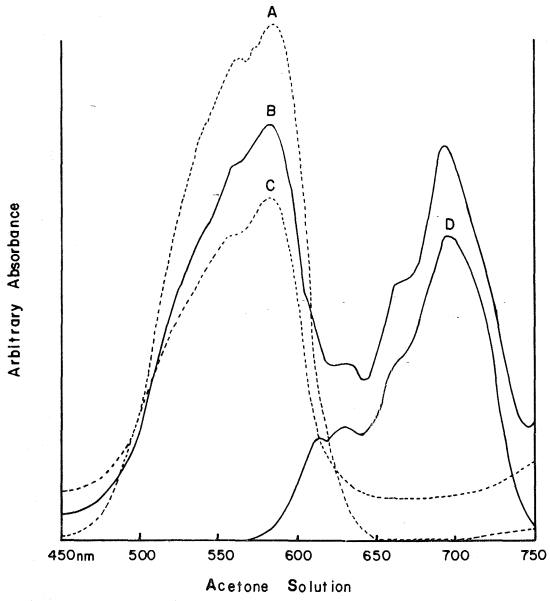

FIG. 3. Acetone solution spectra to illustrate the presence of $[CoBr_4]^{2-}$ and $[Co(NTB)Br]^+$ in the cobalt bromide complex of mixed stereochemistry. The chloro- and isothiocyanato analogues exhibit similar spectra which indicate the presence of four-coordinate anions and five-coordinate cations. *A*, [Co(NTB)Br]Br; *B*, $[Co(NTB)Br]_2[CoBr_4]$; *C*, [Co(NTB)Br]BPh_4; *D*, $[nBu_4N]_2[CoBr_4]$.

'nucleophilic reactivity constant' established by Sacconi (16) for the donor set N_4X (X = Cl, Br, NCS) lies in the range 15.4–19.1, typical of high spin systems. The magnetic moments for

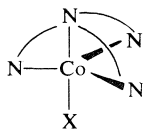

FIG. 4. Stereochemistry of NTB complex.

the five-coordinate tetraphenylborate derivatives fall in the range 4.3–4.7 BM. Moments for typical trigonal bipyramidal systems with tripod ligands containing N, O, S, P donor atoms fall in the range 4.4–4.7 BM (11, 13, 14).

The tetraphenylborate complexes (X = Cl, Br, NCS) exhibit conductances (Table 3) which are somewhat lower than would be expected for 1:1 electrolyte species (17). These data are rather difficult to rationalize in the light of the proposed nature of these species, which are assumed to exist as five-coordinate cations stabilized by the tetraphenylborate anion. However cationic association leading to large bulky ions with low ion mobility and the low ion mobility associated with BPh_4^- itself could lead to significantly lower molar conductances than would be expected. Cobalt complexes of tren-(2,2′,2′′-triaminotriethylamine) of formula $[Co_2(tren)_2X_2](BPh_4)_2$ (X = OCN^-, SCN^-, Cl^-, N_3^-) have recently been shown to contain five-coordinate, outer sphere bridged cations, in which the bridging association is thought to occur via a hydrogen bond, Co—X----HN—Co (18). This association leads to weak antiferromagnetic exchange between the cobalt centres. Outer sphere association of this type could possibly exist in the NTB complexes via the imidazole ring hydrogen, which is likely to reside on the non-coordinating ring nitrogen atom.

A concentration dependence of the molar conductance of [Co(NTB)Br]BPh_4 in nitromethane was studied in the range 10^{-3}–10^{-5} *M* at 25 °C (Table 3). Λ_0 was found to be 75.9 and the slope of the Kohlrausch plot ($\Lambda_0 - \Lambda_e$ *vs.* $\sqrt{c}$) was found to be 960. A typical slope for a 1:1 electrolyte is around 200 (slope for $NaBPh_4$ in $MeNO_2$ = 216 (19)) and it is evident that cationic association is occurring in solution. One possible associative mechanism could involve pseudo-hydrogen bonding, as suggested previously, of an axial halogen (or pseudo-halogen) on one ion with one of the three imidazole hydrogen atoms on another to form a species of the type $\{[Co(NTB)Br]_n\}^{n+}$. It

TABLE 3. Magnetic moment and conductance data

Compound	Λ_M* (mho mol^{-1} cm^2)	μ (BM) Solid†	μ (BM) Solution‡
$[Co(NTB)Cl]_2[CoCl_4]$	61.0	4.17 (24.0)	
$[Co(NTB)Br]_2[CoBr_4]$	90.0	4.18 (23.5)	
$[Co(NTB)(NCS)]_2[Co(NCS)_4]$	131	4.19 (23.4)	4.22 (25.0)
$[Co(NTB)Cl]Cl.H_2O$	21.0	4.21 (22.5)	
[Co(NTB)Br]Br	35.9	4.28 (22.5)	4.12 (25.0)
$[Co(NTB)(NCS)]NCS.H_2O$	45.5	4.23 (22.5)	4.28 (25.0)
$[Co(NTB)Cl]BPh_4.2H_2O$	45.9	4.66 (24.2)	
$[Co(NTB)Br]BPh_4$	49.9	4.74 (23.8)	4.55 (25.0)
$[Co(NTB)(NCS)]BPh_4$	47.8	4.41 (24.1)	
$[Co(NTB)(NO_3)]NO_3$	65.7	4.41 (23.0)	
$[Co(NTB)(NO_3)]BPh_4$	64.6		4.34 (25.0)
$[Co(NTB)(ClO_4)]ClO_4$	170	4.42 (22.7)	
$[Co(NTB)(ClO_4)]BPh_4.2EtOH$	92.0		4.42 (25.0)
$[Zn(NTB)Cl]_2[ZnCl_4]$	58.1		
$[Zn(NTB)Br]_2[ZnBr_4]$	92.5		
$[Zn(NTB)(NCS)]_2[Zn(NCS)_4]$	123		
$[Zn(NTB)Cl]BPh_4.H_2O$	59.6		
$[Zn(NTB)Br]BPh_4.H_2O$	57.3		
$[Zn(NTB)I]BPh_4$	62.4		
$[Zn(NTB)(NCS)]BPh_4$	56.7		

*Solvent nitromethane at approx. 10^{-3} *M* (25 °C).
†Magnetic moment per metal measured in solid state by Faraday method.
‡Magnetic moment measured in $CHCl_3/(CH_3)_2CO$(4% $CHCl_3$) by nmr method (22 and references therein).

seems likely that the other cobalt halide and thiocyanate derivatives would behave similarly in nitromethane. Further studies on the concentration dependence of the conductivity of these systems are being carried out. However, additional support for an associative interaction of this type is apparent when one considers the molar conductance values which follow the order NCS > Br > Cl, in keeping with the electronegativities associated with these coordinated anions. Also the strong association that exists between NTB and alcohols (a 1:3 solvate is formed on recrystallization from, *e.g.*, methanol or ethanol which required prolonged drying under vacuum to desolvate) lends support to an associative effect of a hydrogen bonding type in the NTB complexes.

The purple complexes [Co(NTB)X]X (X = Cl, Br, NCS) have magnetic moments (Table 3) typical of high spin systems and electronic spectra which are identical to their tetraphenylborate analogues both in solution and in the solid state (Fig. 2). This indicates that these species contain pseudo-trigonal bipyramidal cations, apparently stabilized by a negative ion capable of coordination. Spectral assignments for these five-coordinate cations are assumed to be the same as those for the tetraphenylborate analogues (Table 2).

Conductivity data in nitromethane (Table 3) indicate species with some ionic character and low values again suggest the possibility of cationic association involving N—H---X bridges. This is supported by the conductance values which follow the order NCS > Br > Cl. An alternative explanation for the low conductance values for these systems results from a consideration of solution equilibria involving the formation of *e.g.* neutral four- or six-coordinate species:

$$[Co[NTB]X]X \rightleftharpoons [Co(NTB)X_2] \ (T_d \text{ or } O_h)$$

In the octahedral case NTB would act as a tetradentate, while in the tetrahedral case it would presumably act as a bidentate ligand. Electronic spectra of nitromethane solutions of these complexes do not show the presence of bands attributable to tetrahedral or octahedral species but are the same as the spectra obtained in acetone.

The pink nitrate and perchlorate complexes, [Co(NTB)X]X (X = NO_3, ClO_4), have electronic spectra (Table 2) which are almost identical to their tetraphenylborate analogues,

their three main absorption bands occurring at slightly higher energies than the corresponding chloro, bromo, and isothiocyanato derivatives. It seems reasonable to suppose that these compounds contain trigonal bipyramidal cations each with one coordinated nitrate and perchlorate group. Magnetic data for these systems also appear to be consistent with five-coordinate, trigonal bipyramidal cobalt(II).

Conductivity data for the nitrato derivatives in nitromethane (Table 3) suggest the presence of 1:1 electrolytes. The bisperchlorato derivative appears to be a 1:2 electrolyte, which is rather surprising since it implies displacement of a coordinated perchlorate group by a nitromethane molecule. The tetraphenylborate analogue exhibits a lower molar conductance which could possibly be associated with a 1:2 electrolyte in the presence of a large bulky ion like BPh_4^-. The electronic spectra of nitromethane solutions of $[Co(NTB)(ClO_4)]ClO_4$ and $[Co(NTB)(ClO_4)]BPh_4$ are almost identical, but differ somewhat in terms of transition energies (Table 2) from their corresponding acetone spectra, suggesting possible axial involvement of a solvent molecule.

The deep blue complexes $[Co(NTB)X]_2[CoX_4]$ (X = Cl, Br, NCS) exhibit electronic spectra (Fig. 3) (Table 2) which show unequivocally the presence of tetrahedral $[CoX_4]^{2-}$ anions and five-coordinate cations identical to those present in the purple complexes [Co(NTB)X]X and $[Co(NTB)X]BPh_4$. In each case a 1:1 correspondence is observed between the peaks associated with the $[CoX_4]^{2-}$ anions in the blue complexes and the salts $[n\text{-}Bu_4N][CoX_4]$ run in the same solvent. Magnetic data (Table 3) indicate high spin systems but the moments are slightly lower than would be expected. The observed moment should represent an average for the three metal centres in the complex and an average moment based on two five-coordinate cations (Table 3) and *e.g.* $CoCl_4^{2-}$, should be around 4.4 BM. The low observed moments could indicate the presence of cationic association in the solid state, *e.g.* of the hydrogen bonding type (18), leading to weak antiferromagnetic exchange.

The thiocyanate complex exhibits a molar conductance close to the range expected for a 1:2 electrolyte, while the lower values of the chloride and bromide complexes are perhaps more typical of 1:1 electrolytes. Again the conductance order follows the sequence NCS > Br > Cl suggesting a hydrogen bonding association between cations. These conductivity data are paralleled by the analogous zinc complexes $[Zn(NTB)X]_2[ZnX_4]$. A comparison of the solution (CH_3NO_2, $(CH_3)_2CO$) and solid electronic spectra of these mixed stereochemistry systems suggests that the same species exist both in the solid state and in solution.

Zinc Complexes

Two series of zinc complexes were obtained: $[Zn(NTB)X]_2[ZnX_4]$ (X = Cl, Br, NCS) and $[Zn(NTB)X]BPh_4$ (X = Cl, Br, I, NCS). The former are thought to be analogous to the cobalt complexes of mixed stereochemistry, containing two five-coordinate cations and a four-coordinate, tetrahedral anion. The tetraphenylborate salts are assumed to contain trigonal bipyramidal cations. Conductivity data in nitromethane (Table 3) indicate ionic species, but again low values suggest the possible existence of associative effects.

Nuclear magnetic resonance data obtained in DMSO-d_6 (Table 5) indicate that the ligand is acting as a quadridentate and lies on a threefold axis of symmetry within each complex cation. The methylene proton resonance occurs as a singlet in each case, indicating equivalent methylene protons, which are shifted downfield slightly (12–18 Hz) with respect to the free ligand. NTB exhibits a very symmetrical set of aromatic proton resonances (*AA'BB'*) indicative of a plane of symmetry within each benzimidazole group. In all the complexes the aromatic proton resonances are observed in two groups of lines (Fig. 5). Three protons remain at essentially the same chemical shift observed for the free ligand, while one proton of the lower field pair is shifted downfield considerably. It is assumed that the benzene ring protons nearest to the imidazole ring are the more deshielded and would be observed at lower field, corresponding to the lower field half of the aromatic proton resonances observed for NTB. On coordination one of these protons, which is still coupled to the other ring protons, is shifted downfield by some 70–80 Hz. This significant downfield shift corresponds to a marked deshielding of one ring proton with respect to the others.

One obvious conclusion to draw from the lack of symmetry of the benzene ring proton reson-

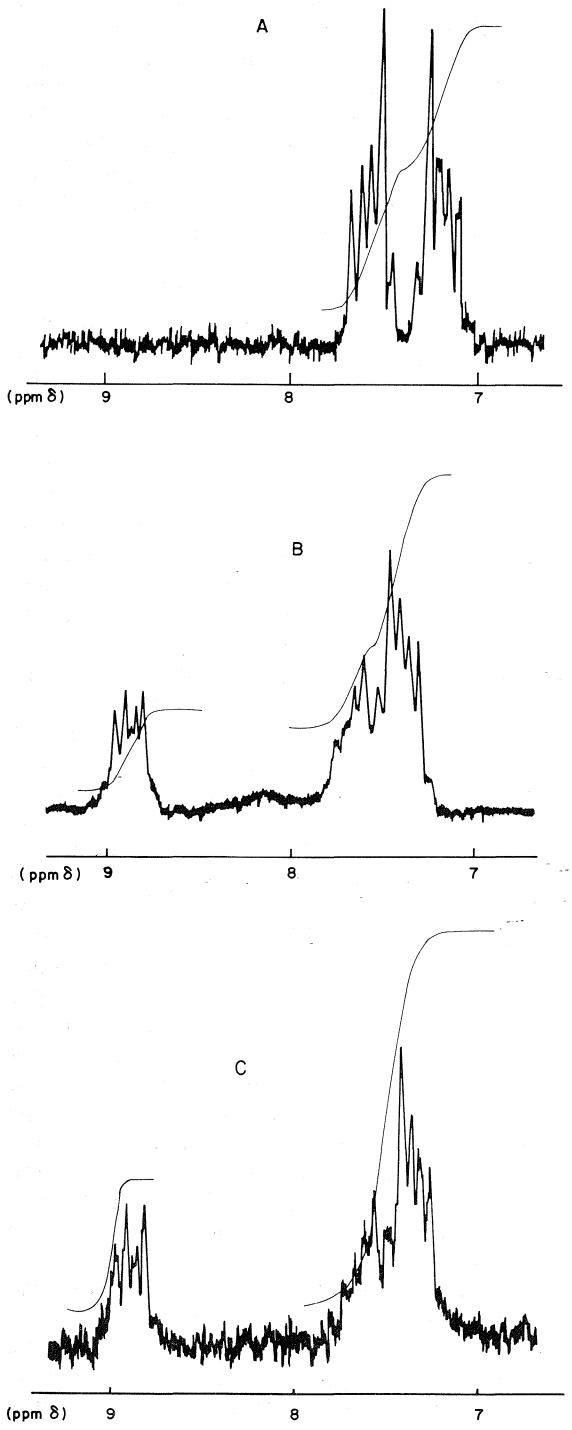

FIG. 5. Nuclear magnetic resonance spectra in DMSO-d_6. *A*, NTB; *B*, [Zn(NTB)Br]BF_4 (the tetrafluoroborate complex was used because of interfering peaks associated with the corresponding tetraphenylborate complex); *C*, [Zn(NTB)Br]$_2$[$ZnBr_4$].

ances would be the coordination of one imidazole nitrogen to a zinc ion. In addition, since only one set of benzimidazole proton resonances appear in the spectrum, it is assumed that all three benzimidazole groups are involved in coordination to the same metal. The slight downfield shift associated with the methylene protons suggests coordination of the apical nitrogen also.

Models suggest that an essentially strain free way for the ligand to coordinate to a metal ion would be as a tripod ligand, with the apical nitrogen occupying an axial site and a nitrogen atom from each benzimidazole group occupying a trigonal equatorial site in a pseudo-trigonal bipyramidal structure. In this configuration one α proton in each benzene ring lies close to the other axial site which contains an electronegative group, *e.g.* Cl, Br, NCS. The close proximity of this electronegative group to the α ring proton could be responsible for a through space electronic interaction leading to a deshielding effect and a downfield shift of the α proton. Alternative, but perhaps less likely, explanations would be an electron withdrawing effect, transmitted from the axial anionic group via the metal through five bonds or from a neighbouring hydrogen bonded ion in an associated structure, if such association exists in highly polar dimethylsulfoxide.

Infrared Data

The infrared spectra of the NTB complexes studied were in general fairly complex and did not provide very much structurally useful information. This was especially true in the far infrared where interfering bands associated with the ligand itself prevented any definitive structural assignments.

Infrared spectra of the nitrate derivatives contain bands that can be assigned to ionic and monodentate nitrate groups. The bisnitrato derivative exhibits bands at 846, 1390, and 700 cm^{-1} (Table 4) which can be associated with an ionic nitrate, and are absent in the tetraphenylborate analogue. Both compounds exhibit bands around 980 and 1310 cm^{-1} assigned to A_1 modes associated with a monodentate nitrate group (20). In the case of the perchlorate derivatives it is possible to pick out a strong doublet (1050, 1130 cm^{-1} for [Co(NTB)(ClO_4)]ClO_4; 1050, 1140 cm^{-1} for [Co(NTB)(ClO_4)]BPh_4) due to the $\nu_3(T_2)$ vibration in a tetrahedral species like ClO_4^- which is split into $A_1 + E$ on lowering the symmetry from T_d to C_{3v}. This suggests the

TABLE 4. Infrared data (cm^{-1})

(*a*) Thiocyanato derivatives

Compound	ν(CN)[NCS]
$[Co(NTB)(NCS)]_2[Co(NCS)_4]$	2070(sh),2047
$[Co(NTB)(NCS)]NCS.H_2O$	2063,2038*
$[Co(NTB)(NCS)]BPh_4$	2060*
$[Zn(NTB)(NCS)]_2[Zn(NCS)_4]$	2097,2076
$[Zn(NTB)(NCS)]BPh_4$	2075*

(*b*) Nitrato derivatives

	NO_3^-			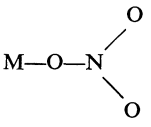	
Compound	$\nu_2(A_2'')$	$\nu_3(E')$	$\nu_4(E')$	A_1	A_1
$[Co(NTB)(NO_3)]NO_3$	846	1390	700	980	1311
$[Co(NTB)(NO_3)]BPh_4$				981	1310

(*c*) Perchlorato derivatives

	ClO_4^-	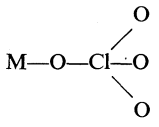	
Compound	$\nu_3(T_2)$	E	A_1
$[Co(NTB)(ClO_4)]ClO_4$	1110	1130	1050
$[Co(NTB)(ClO_4)]BPh_4$	—	1140	1050

*KBr disc spectra. All other data obtained using mulls in either Nujol or hexachlorobutadiene.

TABLE 5. Nuclear magnetic resonance data (ppm in DMSO-d_6)*

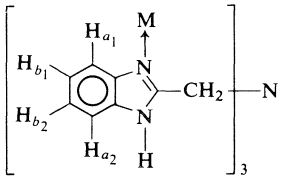

Compound	δH_{a_1} (m)	δH_{a_2} (m)	δH_b (m)	δCH_2 (s)	δNH (bs)
NTB	7.60	7.60	7.19	4.12	12.1
$[Zn(NTB)Cl]_2[ZnCl_4]$	8.79	7.66	7.37	4.66	nd
$[Zn(NTB)Br]_2[ZnBr_4]$	8.89	7.65	7.33	4.60	nd
$[Zn(NTB)(NCS)]_2[Zn(NCS)_4]$	8.69	7.68	7.39	4.68	nd
$[Zn(NTB)Cl]BPh_4.H_2O$	8.67	7.60	7.30	4.57	nd
$[Zn(NTB)Br]BPh_4.H_2O$	8.70	7.49	7.20	4.45	nd
$[Zn(NTB)I]BPh_4$	8.76	7.55	7.26	4.50	nd
$[Zn(NTB)(NCS)]BPh_4$	8.12	7.56	7.28	4.53	nd
$[Zn(NTB)Cl]BF_4$	8.64	7.55	7.26	4.59	nd
$[Zn(NTB)Br]BF_4$	8.77	7.56	7.26	4.58	nd

*m = multiplet, s = singlet, bs = broad singlet, nd = not detected. The H_a and H_b protons appear as asymmetric complex multiplets which appear to contain five major components, one of which has relatively low intensity. In estimating the chemical shifts associated with these protons the centre of gravity of the four higher intensity components was determined in each case.

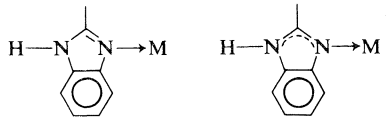

FIG. 6. *a*, Localized ring structure; *b*, delocalized ring structure.

presence of a coordinated perchlorate group in both cases. The bisperchlorato derivative exhibits a strong singlet at 1110 cm^{-1}, which is assigned to the $\nu_3(T_2)$ stretching vibration in an ionic perchlorate group (20).

The thiocyanate complexes exhibit bands associated with CN stretch in the range 2039–2097 cm^{-1} (Table 4). For the complexes $[M(NTB)(NCS)]_2[M(NCS)_4]$ (M = Co, Zn) the higher energy band is assigned to N-bonded thiocyanate in the complex cation, while the lower energy band is associated with N-bonded thiocyanate in the anion $[M(NCS)_4]^{2-}$ (M = Co, Zn). The tetraphenylborate complexes exhibit a single CN stretch which is associated with N-bonded thiocyanate, while for the complex $[Co(NTB)(NCS)]NCS\cdot H_2O$ the higher energy band is assigned to N-bonded thiocyanate and the lower energy band to ionic thiocyanate (21).

NTB exhibits two absorptions at 1622 and 1588 cm^{-1} which are assumed to be due to CN stretch in the imidazole ring. The complexes all exhibit the same two bands; the lower energy band falling in the range 1590–1607 cm^{-1}, while the higher energy band falls in the range 1610–1632 cm^{-1}. In most cases, with the exception of the nitrate and perchlorate complexes, the higher energy band lies below its counterpart in the free ligand, while the lower energy band occurs above 1588 cm^{-1} in all cases. The close similarity of all the complexes in this spectral region suggests a similar coordination environment around the metal in all cases and the behaviour of the ligand as a tetradentate.

A previous study on the cobalt and nickel complexes of some bidentate imidazoline ligands (7) related the CN stretching frequency in the imidazoline rings to the state of localization along the NCN ring framework. As expected, X-ray data confirmed the coordination of the imidazoline ring via the tertiary nitrogen, but also suggested two possible structural types based on CN bond lengths. A CN frequency below that of the free ligand indicated a delocalized imidazoline ring, with essentially equal CN bond lengths while frequencies higher than the free ligand suggested a more localized ring structure in which the CN bond lengths were different. By analogy with the imidazoline complexes the nitrato and perchlorato derivatives possibly have more localized ring structures (Fig. 6*a*) while the other complexes possibly have more delocalized ring structures (Fig. 6*b*). Also it is assumed that in the NTB complexes the imidazole ring is coordinated to the metal via the tertiary ring nitrogen atom (Fig. 6).

Acknowledgements

We are indebted to the National Research Council of Canada for financial support for this work and in particular for the purchase of the Cary 17 Spectrometer. Also we wish to express our gratitude to Greg Mawhinney of this department for obtaining a large proportion of the conductance data.

1. D. M. L. GOODGAME, M. GOODGAME, and G. W. RAYNER CANHAM. Inorg. Chim. Acta, **6**(2), 245 (1972).
2. M. V. ARTEMENKO and E. A. CHISTGAKOVA. Ukr. Khim. Zh. **37**, 978 (1971).
3. S. P. GHOSH and A. MISHRA. J. Inorg. Nucl. Chem. **33**, 4199 (1971).
4. M. V. ARTEMENKO, K. F. SLYUSARENKO, and D. A. STAKHOV. Ukr. Khim. Zh. **38**, 227 (1972).
5. M. V. ARTEMENKO, K. F. SLYUSARENKO, and D. A. STAKHOV. Zh. Neorg. Khim. **17**(1), 164 (1972).
6. M. J. M. CAMPBELL, D. W. CARD, R. GRZESKOWIAK, and M. GOLDSTEIN. J. Chem. Soc. Dalton, 1687 (1972).
7. A. B. P. LEVER, B. S. RAMASWAMY, S. H. SIMONSEN, and L. K. THOMPSON. Can. J. Chem. **48**, 3076 (1970).
8. M. A. PHILLIPS. J. Chem. Soc. 172 (1928).
9. M. A. PHILLIPS. J. Chem. Soc. 2393 (1928).
10. D. W. HEIN, R. J. ALHEIM, and J. J. LEAVITT. J. Am. Chem. Soc. **79**, 427 (1957).
11. L. SACCONI and R. MORASSI. J. Chem. Soc. A, 575 (1970).
12. R. MORASSI and L. SACCONI. J. Chem. Soc. A, 492 (1971).
13. R. MORASSI and L. SACCONI. J. Chem. Soc. A, 1487 (1971).
14. M. CIAMPOLINI and N. NARDI. Inorg. Chem. **5**, 41 (1966).
15. I. BERTINI, D. GATTESCHI, and A. SCOZZAFAVA. Inorg. Chem. **14**, 812 (1975).
16. L. SACCONI. J. Chem. Soc. A, 248 (1970).
17. W. J. GEARY. Coord. Chem. Rev. **7**, 81 (1971).
18. D. MICHAEL DUGGAN and DAVID N. HENDRICKSON. Inorg. Chem. **14**, 1944 (1975).
19. R. D. FELTHAM and R. G. HAYTER. J. Chem. Soc. 4587 (1964).
20. KAZUO NAKAMOTO. Infrared spectra of inorganic and coordination compounds. 2nd ed. Wiley-Interscience, New York. 1970.
21. E. KONIG and K. MADGEJA. Inorg. Chem. **6**, 48 (1967).
22. J. LÖLIGER and R. SCHEFFOLD. J. Chem. Ed. **9**, 646 (1972); DAVID OSTFELD and IRWIN A. COHEN. J. Chem. Ed. **12**, 829 (1972).

The kinetics of the solid state transformation of racemic to optically active 1,1′-binaphthyl

KEITH R. WILSON AND RICHARD E. PINCOCK

The Department of Chemistry, University of British Columbia, Vancouver, B.C., Canada V6T 1W5

Received August 24, 1976

KEITH R. WILSON and RICHARD E. PINCOCK. Can. J. Chem. **55**, 889 (1977).

Rates of the solid state reaction which thermally converts racemic to optically active 1,1′-binaphthyl (mp 158 °C) have been determined at temperatures between 105 and 135 °C using polycrystalline samples. The presence of a sufficiently uniform distribution of enantiomorphic seed crystals results in a smooth conversion of the racemate to the eutectic crystal forms of binaphthyl. Although it is possible to force the resolution reaction almost to completion at higher temperatures (150 °C) where the melt phase is an intermediate, lower final specific rotations are obtained when only solid phases are involved (below 145 °C) because of the independent nucleation of racemic material from the reacting crystals. Both spontaneous nucleation and reaction rates in the solid state were increased by grinding the initially prepared samples and were decreased by the storage of samples. The Arrhenius activation energy of this phase transformation giving optically active product is *ca.* 60 kcal/mol in a variety of different samples. This is consistent with a mechanism in which a molecule of 1,1′-binaphthyl attains considerable freedom from the racemic solid in order to interconvert to its enantiomer and add to the growing optically active phase.

KEITH R. WILSON et RICHARD E. PINCOCK. Can. J. Chem. **55**, 889 (1977).

On a déterminé, à des températures allant de 105 à 135 °C et faisant appel à des échantillons polycristallins, les vitesses de réactions à l'état solide, qui permettent de transformer d'une façon thermique du binaphthyl-1,1′ (pf 158 °C) racémique en produit optiquement actif. La présence d'une distribution suffisamment uniforme de cristaux permettant d'ensemencer un énantiomorphe conduit à la conversion facile du racémique en une forme cristalline eutectique du binaphtyl. Il est possible de forcer la réaction de façon à obtenir une résolution pratiquement complète à des températures plus élevées (150 °C) alors que la phase fondue est un intermédiaire; toutefois on obtient des rotations spécifiques finales qui sont plus basses quand il n'y a que des phases solides d'impliquées (en dessus de 145 °C) et ce résultat est dû à la nucléation indépendante du composé racémique à partir des cristaux qui réagissent. La nucléation spontanée et les vitesses de réaction à l'état solide sont toutes les deux augmentées lorsque l'on broie les échantillons préparés initialement; toutefois elles sont diminuées lorsque l'on garde les échantillons d'une façon prolongée. L'énergie d'activation d'Arrhénius de cette transformation de phase conduisant à un produit optiquement actif est d'environ 60 kcal/mol dans une grande quantité d'échantillons différents. Cette valeur est en accord avec un mécanisme dans lequel une molécule de binaphtyl-1,1′ devient très libre du solide racémique de façon à se convertir dans son énantiomère et à s'additionner à la phase optiquement active qui est en croissance.

[Traduit par le journal]

The transformation of optically inactive into optically active 1,1′-binaphthyl may occur simply by heating a sample below its melting point (1). This is possible because the racemate form (mp 145 °C) of this compound is unstable relative to a mixture of separate *R*(−) and *S*(+) enantiomeric crystals (mp 158 °C). At temperatures of *ca.* 76 to 145 °C a solid state reaction of racemate occurs and optically active product (*i.e.* an unequal mixture of *R* and *S* crystals) may result. This reaction shows the typically complex aspects of solid state transformations (2–4); it appears to be sensitive to any previous treatment which influences the size of crystals and the presence of lattice imperfections. It is well known in general that these factors greatly determine the ability to nucleate and grow new interfaces between the reactant and product. In the case of the solid state resolution of binaphthyl such factors may determine the extent of optical resolution as well as the rate of development of optical activity. When ordinarily recrystallized racemic binaphthyl is used these complex and variable factors result in widely scattered and erratic values for the final optical activity even in polycrystalline samples taken from a single preparation (see Fig. 2 of ref. 1).

However, the recrystallization of binaphthyl

which is slightly optically active gives samples which show a smooth and consistent development of optical activity and allows a more thorough investigation of this solid state reaction. We report here our observations on the kinetic aspects of the transformation of several of these samples of 1,1′-binaphthyl into optically active product. Relatively few solid → solid reactions, especially organic reactions, have been kinetically studied (2). In this case the reacting system is very simple in that the product is at least molecularly the same as the reactant. The availability of smoothly resolving samples presents an opportunity to study the rate of production of enantiomorphic crystals and obtain information on the specific mechanism of the solid state resolution of 1,1′-binaphthyl. Also, as discussed below, the system lends itself in a unique way to the study of factors affecting the spontaneous nucleation of a new phase in an organic crystal.

Experimental

Samples of 1,1′-binaphthyl used in these kinetic studies were prepared from racemic binaphthyl by admixture of small amounts of optically active binaphthyl according to procedure B of ref. 1. The designation of the individual batch, the total weight, and the specific rotation in benzene are, respectively; *S*-1, 3.0 g, +1.4°; *S*-2, 4.0 g, +11.8°; *S*-3, 5.7 g, +1.8°; and *R*-1, 3.8 g, −11.0°. As indicated by the notations *R* and *S*, three samples gave predominately *S*(+) and one gave *R*(−) binaphthyl when heated at temperatures of 105 to 150 °C.

The resolution reaction of each batch was followed by heating individually sealed ampules containing a carefully weighed amount (15–20 mg) of the polycrystalline binaphthyl at a given temperature for various lengths of time. Samples were dissolved in benzene and optical rotations measured as previously described on a Bendix type 143A automatic polarimeter at the sodium D line (5890 Å). Since the kinetic characteristics of individual batches changed after storage (*e.g.*, see Fig. 1 for a comparison of samples before and after storage at 25°C for 6 weeks) all samples were stored at 0 °C and runs reported here were performed within 5 weeks.

All batches resolved to final rotations greater than $[\alpha]_D \pm 200°$ when heated at 150 °C, but with a half-life too short at this temperature for an accurate kinetic description. (Optically pure 1,1′-binaphthyl has $[\alpha]_D \pm 245°$ (1).) The final rotation in several runs at temperatures in the range 105 to 135 °C was considerably less than ±200° (see Table 1 of ref. 1).

An assessment of how closely the relatively easily measured optical rotations of a sample reflected the actual extent of phase transformation of racemate to eutectic forms of binaphthyl was carried out using quantitative X-ray powder diffraction (5) (with a Debye–Scherrer powder camera, Philips PW 1024/10). By choosing one line in the diffraction pattern of the racemate

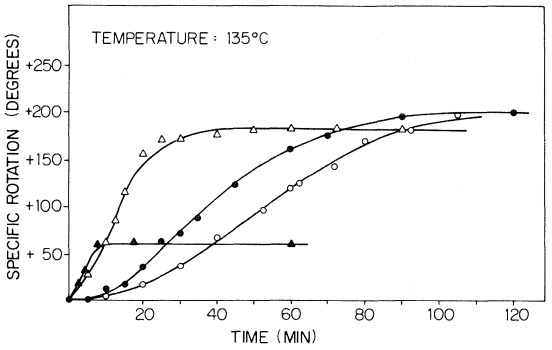

FIG. 1. Kinetic data for the solid state resolution of neat, polycrystalline 1,1′-binaphthyl, *S*-1 kinetic batch at 135 °C. Effect of grinding and of storage at 25 °C for 6 weeks: ● original kinetic run; ○ run performed after 6 weeks' storage at 25 °C; △ run using ground samples; ▲ run using more highly ground samples.

(d = 10.1 Å) and one in the pattern of the eutectic form (d = 6.4 Å) which is distinct in a mixture of the two forms, the disappearance of racemate and the appearance of eutectic could be quantitatively followed. A standard procedure for exposure and development of powder photographs, followed by analysis on a microdensitometer (Joyce double beam recording instrument MKIIIc) and calibration with known mixtures of eutectic and racemate forms resulted in reproducible analyses which agreed within 2% (6). Application of this method to the analysis of the phase transformation of the *S*-2 kinetic batch at 125 °C, and comparison to the independently obtained optical rotations, showed that the ratio $[\alpha]_t/[\alpha]_{final}$ was closely equivalent to the extent of phase transformation, *i.e.* to the mole fraction of the eutectic form present. As this is the case even in this batch of binaphthyl which resolved only to a relatively low rotation ($[\alpha]_{final}$ 136° at 125 °C) then the fraction of final rotation achieved at any time is a good measure of the actual fraction of eutectic form present at that time, *i.e.* $y = [\alpha]_t/[\alpha]_{final}$, where y is the mole fraction of eutectic form. The mole fraction of product phase, y, is thereby made accessible from readily measured optical activity data alone; it is a direct measure of the fraction of reaction and therefore suitable for further kinetic analysis.

Results and Discussion

The thermal production of optical activity in specially seeded samples of 1,1′-binaphthyl shows a very prominent difference from that in ordinary racemic samples; the resolution reaction in any small portion of the sample is remarkably smooth and consistent. This is shown, for example, in some representative specific rotation *vs.* time plots for the various kinetic batches in Figs. 1, 2, and 3. The specially prepared batches apparently have a highly refined and uniform dispersion of seed crystals which enable a smooth development of optical activity even in small polycrystalline samples.

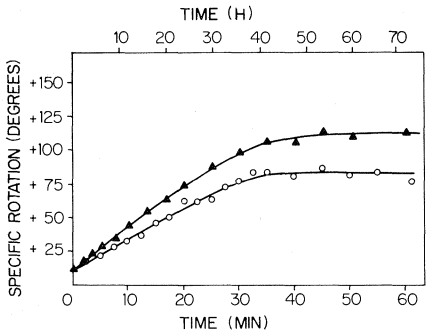

FIG. 2. Kinetic data for the solid state resolution of neat, polycrystalline 1,1′-binaphthyl, *S*-2 kinetic batch, at 115 °C (upper time scale ▲) and at 135 °C (lower time scale ●).

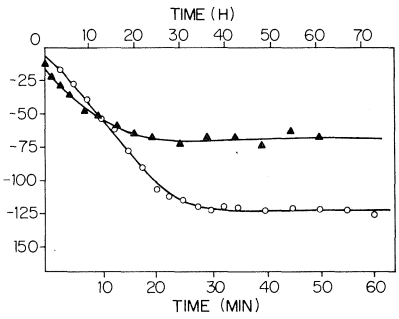

FIG. 3. Kinetic data for the solid state resolution of neat, polycrystalline 1,1′-binaphthyl, *R*-1 kinetic batch, at 115 °C (upper time scale ▲) and at 135 °C (lower time scale ●).

Although the activity of samples develops smoothly, there appears to be no characteristic shape to the curves. Some are sigmoid (although none have prolonged induction periods), while others appear to increase linearly with time or even show an initial rate maximum. The extent of resolution also varies in different batches and in the same batch at different temperatures. Generally lower resolutions were obtained at lower temperatures. As discussed below a low final rotation indicates nucleation and growth during a run of the enantiomer opposite from that seeded into the sample.

As shown in Fig. 1 the results of kinetic runs were sensitive to grinding of the crystals and such disruption of the initial crystals always caused a faster resolution to a lower specific rotation. Storage of samples resulted in the opposite results; a higher final rotation was obtained from samples stored at 0 °C for 4 months (see Fig. 3 of ref. 1) and a somewhat slower rate of resolution occurred in a sample stored at 25 °C for 6 weeks (see Fig. 1). These effects of storage and of grinding, as well as the relationship of temperature to extent of resolution may all be explained in a qualitative manner after consideration of the mechanism of the resolution reaction.

An ideal seeded sample, *i.e.* suitable for the production of optically pure binaphthyl, consists of a slight excess of one enantiomer (*e.g.*, the *R* enantiomer in its 'eutectic' crystal form) and *all* the rest of the sample would be in the *R,S*-racemate form (1). When such a sample is heated, and provided that no nucleation of the other enantiomer (*e.g.*, the *S* eutectic form) occurs, the growth of only *R* enantiomeric crystals proceeds at the expense of *R,S*-racemate and the entire sample is converted to optically pure *R* crystals. In practice such an ideal sample is probably impossible to obtain and, in addition, nucleation during a run can be an important factor in obtaining a high optical resolution.

When nucleation occurs in a racemic 1,1′-binaphthyl reactant phase, which could be a racemic crystal below 145 °C or a melt below 158 °C, it is just as likely to involve *R* molecules as *S* molecules (7). In other words, nucleation (which is independent of crystal growth) is expected to create *R* and *S* crystallites with equal probability. The growth of these new nucleites produces separate *R* and *S* eutectic crystals and leads to low overall resolutions. Low values of the final rotation therefore may result from the presence of initial seed crystallites of undesired enantiomer in the material before heating and/or from the nucleation of racemic material during the reaction.

All of the specially seeded samples appear to be sufficiently free from unwanted enantiomeric 'seeds' so that high rotations (greater than 200° or 82% optically pure) resulted when samples were heated at 150 °C. At this temperature, the reaction involves a conversion of racemate through the melt to optically active solid (1). Since a binaphthyl melt will remain supercooled indefinitely at 150 °C, nucleation in a melted phase does not occur at this temperature. The situation in the seeded samples at 150 °C therefore approaches the ideal for production of optically pure product as mentioned above. In this way, advantage can be taken of the phase relationships in the 1,1′-binaphthyl system in order to obtain, reproducibly, excellent resolutions in either direction in a single heating step (1).

In the solid → solid conversion (not involving

melt), which occurs below 145 °C, nucleation in some samples definitely occurs as is shown by the lower final specific rotations. The inability to control or even reproduce the nucleation of new product sites (and the resulting autocatalytic growth of product) is the major reason why solid state reactions are so dependent on the past history of samples. Mild disruption of the binaphthyl crystals by grinding produces a greater reactant–product interface and causes a more rapid reaction. In addition there are stresses, dislocations, and other imperfections produced by grinding and these act as sites for the nucleation of racemic material. The result is the observation of higher rates of reaction but to a lower degree of resolution (shown in Fig. 1). On the other hand, storage of samples apparently allows for slow annealing out of such nucleation sites and gives material that resolves slower but to a greater extent. In samples prone to nucleation (*e.g.*, *R*-1 as in Fig. 3), lower temperatures and therefore longer reaction times gave lower final rotations possibly because the nucleation of racemic material has a greater dependency on time and temperature than does the rate of phase transfer.

Although some features of this solid state reaction may therefore be qualitatively understood, the above examples of the variations present in different batches and the effects of grinding and storage all provide a good illustration of the complex sensitivity of a solid state reaction to the previous treatment of a sample. Samples of binaphthyl that resolve to high optical purity are available (1) but our results here show that reproducible preparations of samples which give essentially the same extent and rate of resolution below 140 °C would be very difficult.

Kinetic Analysis

As already indicated by the varied qualitative results discussed above, the solid state resolution of various samples of 1,1′-binaphthyl is too complex to fit any single general kinetic scheme. Nevertheless there are few kinetic studies of simple solid → solid organic transformations and the ease of measurement of optical rotations with binaphthyl presents an opportunity to obtain data which might fit (at least in an individual preparation) some empirical kinetic equation for solid state reactions. However, the relationship of measured specific rotations to the actual extent of phase transformation must first be considered.

In an ideal solid state resolution, *i.e.* one giving a completely resolved product (a situation approached by batches *S*-1 and *S*-3), the extent of phase transformation (y) at any time must equal the ratio of measured specific rotation to the final specific rotation ($y = [\alpha]_t/[\alpha]_{final}$). For a batch of binaphthyl that finally resolves only to a restricted extent (batches *S*-2 and *R*-1) the phase transformation may not necessarily run parallel to the specific rotation. However, the relationship of measured rotations to extent of phase transformation given above was experimentally established by quantitative X-ray analysis of partially reacted samples (6). Therefore for a comparison of various rate equations, the use of measured rotations as an expression of the fraction of phase transformation is justified.

Of the rate equations for solid state reactions that have been developed two seem most widely used (2, 3). The first of these, the Avrami–Erofeev equation may be expressed by the relationship $-\log(1 - y) = (kt)^n$ and a plot of log [log (1/(1-y))] against log (t) results in a line with the slope equal to n. Such a plot was made for all four kinetic batches, two of which are illustrated in Figs. 4 and 5. With the *S*-1 batch the results fit a straight line (with n near two) rather well (Fig. 4). Less perfect fits are found with the other batches where the plots are better described at a given temperature as two straight lines. The most obvious bend occurs with the *S*-2 kinetic batch (Fig. 5) which gives limiting slopes of 0.65 and 1.9 at all four temperatures.

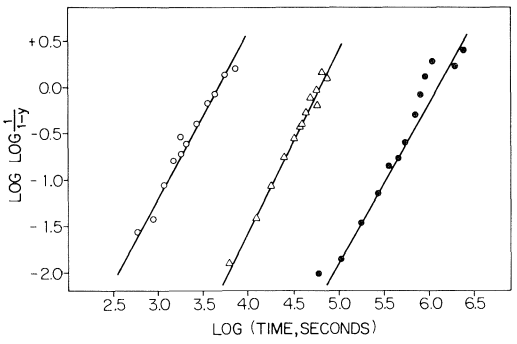

FIG. 4. Avrami–Erofeev plots for the solid state resolution of neat, polycrystalline 1,1′-binaphthyl, *S*-1 kinetic batch at 135 °C ○, and 105 °C ●. The results from the sample stored 6 weeks at 25 °C are plotted against [log (time) + 1] and given by ▲ from a run at 135 °C.

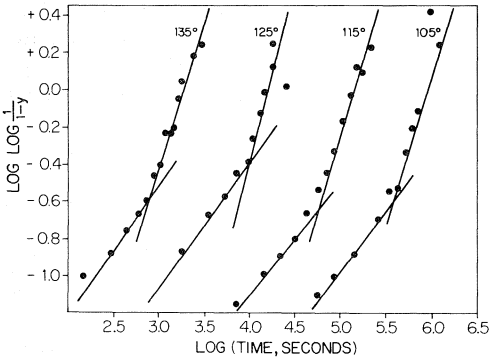

FIG. 5. Avrami–Erofeev plots for the solid state resolution of neat, polycrystalline 1,1′-binaphthyl, *S*-2 kinetic batch at 135, 125, 115, and 105 °C.

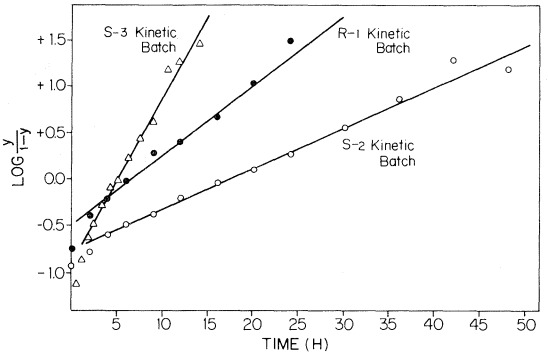

FIG. 6. Prout–Tompkins plots for the solid state resolution of neat polycrystalline 1,1′-binaphthyl, *S*-2, *S*-3, and *R*-1 kinetic batches at 115 °C.

Any mechanistic implications from the fit of data from the *S*-1 batch to the Avrami–Erofeev equation are not altogether certain. One common interpretation of the exponent n is that it is composed of two quantities, namely $n = \beta + \gamma$ (2, 8). The β component refers to the number of steps required to form a nucleus and is revealed in a power law of the type $N = kt^{\beta}$ where N is the number of nuclei formed in time t. In the case of the *S*-1 and *S*-3 kinetic batches the high resolutions finally attained indicate that nucleation (which gives racemic product) is not important, *i.e.* $\beta = 0$. The observed value of $n = 2$ is then equivalent to γ, the number of dimensions in which growth of existing crystallites occur. At least in the case of the *S*-1 batch of Fig. 4 the implication is that the growing product crystallites spread in two dimensions along, for example preferred lattice planes or boundaries between racemate crystallites.

The other commonly used rate law is the Prout–Tompkins equation: $\log (y/(1-y)) = kt$ + constant. Plots of $\log (y/(1-y))$ against time often show two straight lines (2); in the case of 1,1′-binaphthyl the plots show linearity beyond $y \simeq 0.3$ for all the kinetic batches (see representative runs in Fig. 6). Since a rate constant k is derived from the slopes of such plots the Prout–Tompkins treatment leads to a determination of an activation energy for the reaction, at least in this part of its overall reaction progress. This is shown in Fig. 7, where Arrhenius activation energies, calculated from $2.30R$ (slope of line) are 57.7, 62.4, 59.4, and 67.0 kcal mol^{-1} for the *S*-1, *S*-2, *S*-3, and *R*-1 batches, respectively. This large activation energy for a conversion of racemate to eutectic crystals may be contrasted with

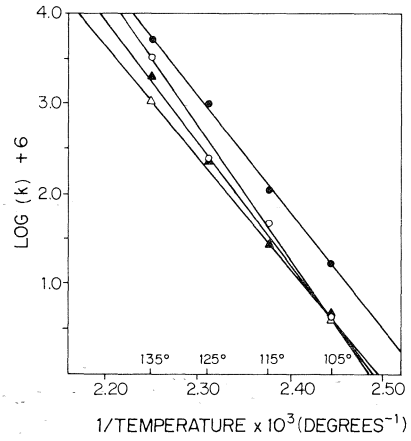

FIG. 7. Relation of log k (from Prout–Tompkins plots) to reciprocal temperature for the solid state resolution of neat, polycrystalline 1,1′-binaphthyl, kinetic batches *S*-3 ●, *R*-1 ○, *S*-2 ▲, and *S*-1 △.

the relatively small enthalpy value of approximately 7 kcal mol^{-1} required to melt the racemate (6). This contrast shows that the resolution is certainly not analogous simply to the release of molecules from the racemate to an interface resembling the melt. Even if an activation energy expected for interconversion of enantiomers in solution (*ca.* 22 kcal/mol in *n*-heptane) (9) is added to the energy required to melt the racemate the figure obtained is still far from the observed *ca.* 60 kcal/mol activation energy.

The observed energy may be more closely related to the energy increment associated with the removal of a single molecule from inside a crystal to the vapour state. This is twice the energy needed to vaporize the complete crystal (*i.e.* the heat of sublimation which is about 22

kcal/mol^{-1}). The energy required for this process of breaking the van der Waals forces in the racemate crystal is then approximately 44 kcal mol^{-1} and if the molecule interconverts to its enantiomer in addition to effectively vaporizing, an activation energy estimate could be as high as 44 + 22 = 66 kcal mol^{-1}.

The fact that 1,1′-binaphthyl has an activation energy of the order of 60 kcal mol^{-1} means that for the resolution reaction to be observable at all at the moderate temperatures used, the high activation energy must be compensated by a high entropy of activation. The high activation energy and entropy are consistent with a picture in which a molecule of 1,1′-binaphthyl attains a great deal of freedom from the solid, similar to that obtained by transfer to a gas phase, in order to interconvert to enantiomer and grow the optically active solid phase.

Acknowledgments

Financial support of this research by the National Research Council of Canada and fellowship assistance to K.R.W. from the H. R. MacMillan Family Fund and the Graduate Student Fellowship Fund of the University of British Columbia are gratefully acknowledged.

1. K. R. Wilson and R. E. Pincock. J. Am. Chem. Soc. **97**, 1474 (1975).
2. A. K. Galwey. Chemistry of solids. Chapman and Hall, Ltd., London. 1967. pp. 163–184.
3. P. W. M. Jacobs. *In* Reactivity of solids. *Edited by* J. W. Mitchell, R. C. DeVries, R. W. Roberts, and P. Cannon. Wiley-Interscience, New York. 1969. p. 207.
4. I. C. Paul and D. Y. Curtin. Acc. Chem. Res. **6**, 217 (1973).
5. B. D. Cullity. Elements of X-ray diffraction. Addison-Wesley, London. 1956. Chapt. 14.
6. K. R. Wilson. Ph.D. Thesis. University of British Columbia, Vancouver, B.C. 1972.
7. R. E. Pincock, R. R. Perkins, A. S. Ma, and K. R. Wilson. Science, **174**, 1018 (1971).
8. L. G. Harrison. *In* Chemical kinetics. Vol. II. *Edited by* C. H. Bamford and C. F. H. Tipper. Elsevier, Amsterdam. 1969. p. 377.
9. A. K. Colter and L. M. Clemens. J. Phys. Chem. **68**, 651 (1964); A. S. Cooke and M. M. Harris, J. Chem. Soc. 2365 (1963).

The synthesis of 1,3-diazepine derivatives by the ring expansion of alkyl 4-chloromethyl-1,2,3,4-tetrahydro-6-methyl-2-oxopyrimidine-5-carboxylates

ERIC BULLOCK, ROGER A. CARTER, REGINA M. COCHRANE, BRIAN GREGORY, AND DOUGLAS C. SHIELDS

Department of Chemistry, Memorial University of Newfoundland, St. John's, Nfld, Canada A1C 5S7

Received August 16, 1976

ERIC BULLOCK, ROGER A. CARTER, REGINA M. COCHRANE, BRIAN GREGORY, and DOUGLAS C. SHIELDS. Can. J. Chem. **55**, 895 (1977).

Alkyl 4-chloromethyl-1,2,3,4-tetrahydro-6-methyl-2-oxopyrimidine-5-carboxylates are obtained from the reaction of 1,2-dichloroethyl ethyl ether with alkyl 3-ureidocrotonates. Reaction of the chloromethyl compounds with basic nucleophilic reagents causes ring expansion and leads, in high yield, to 7-substituted 2,3,6,7-tetrahydro-2-oxo-1*H*-1,3-diazepine derivatives. In the case of sulfhydryl ion, intramolecular Michael addition follows ring expansion and gives derivatives of 3-oxo-8-thia-2,4-diazabicyclo[3.2.1]octane, whose structures are established by spectroscopic examination and chemical degradation. The alkyl 7-alkoxy-2,3,6,7-tetrahydro-2-oxo-1*H*-1,3-diazepine-5-carboxylates react rapidly with acid to give alkyl 1-carbamoyl-2-methylpyrrole-3-carboxylates. Mechanisms are suggested for these rearrangement reactions.

ERIC BULLOCK, ROGER A. CARTER, REGINA M. COCHRANE, BRIAN GREGORY et DOUGLAS C. SHIELDS. Can. J. Chem. **55**, 895 (1977).

On obtient les chlorométhyl-4 tétrahydro-1,2,3,4 méthyl-6 oxo-2 pyrimidinecarboxylates-5 d'alkyle par réaction du dichloro-1,2 éthoxyéthane avec des uréidocrotonates-3 d'alkyle. La réaction des composés chlorométhylés avec des réactifs nucléophiles basiques produit une extension de cycle et conduit, avec de bons rendements, aux dérivés tétrahydro-2,3,6,7 oxo-2 1*H* diazépines-1,3 substitués en position 7. Dans le cas de l'ion sulfhydryle, l'addition intramoléculaire de Michael suit l'extension de cycle et conduit aux dérivés oxo-3 thia-8 diaza-2,4 bicyclo-[3.2.1]octanes dont les structures ont pu être déterminées par des méthodes spectroscopiques et une dégradation chimique. Les alkoxy-7 tétrahydro-2,3,6,7 oxo-2 1*H* diazépine-1,3 carboxylates-5 d'alkyle réagissent rapidement avec les acides pour conduire au carbamoyl-1 méthyl-2 pyrrolecarboxylates-3 d'alkyle. On suggère des mécanismes pour ces réactions de réarrangement.

[Traduit par le journal]

Lack of suitable synthetic methods has limited studies of monocyclic 1,3-diazepines to derivatives of tetramethylene urea, 4,5,6,7-tetrahydro-1*H*-1,3-diazepine, and hexahydro-1,3-diazepine (1, 2). 1,3-Diazepines of higher oxidation level have recently been prepared from 2-amino-1-methylimidazole (3), 3,5,6-triphenyltriazine,[1] and 1,3-disubstituted uracil-carbene adducts (5) while the dihydro-1,3-diazepine-2,4-dione squamolone has been isolated from *Anona squamosa* (6). We have recently (7) reported the ring expansion of 4-chloromethyl-1,2,3,4-tetrahydro-2-oxopyrimidine derivatives to derivatives of 1*H*-1,3-diazepine and now present an account of this work in full.

Earlier, we have shown (8) that dialkyl 4-chloromethyl-1,4-dihydrolutidine-3,5-dicarboxylates (9) will undergo ring expansion reactions when treated with basic nucleophilic reagents. In the case of cyanide ion, evidence has been presented which supports a mechanism involving loss of proton from the ring nitrogen, followed by rapid elimination of halide ion with concomitant ring expansion and conjugate addition of hydrogen cyanide (10). Other evidence has been obtained, however, which suggests that under certain conditions, such chloromethyl compounds behave as typically homoallylic systems and reactions may proceed via an homoallyl carbonium ion which is stabilized by electron release from the ring nitrogen,[2] reminiscent of the behaviour of 3,5-dimethoxy-1,4-dihydrobenzyl tosylate (11).

By analogy with these results, it was antici-

[1]A. Hassner and D. J. Anderson, unpublished results quoted in ref. 4.

[2]E. Bullock, T. S. Chen, and B. Gregory, unpublished results.

pated that 4-chloromethyl-1,2,3,4-tetrahydro-2-oxopyrimidines (*e.g.*, **1***a*) would undergo ring expansion. 1,2,3,4-Tetrahydro-2-oxopyrimidines are readily available by the Biginelli reaction (12, 13) between urea, a β-ketoester, and an aldehyde, or by the Folkers and Johnson modification using ethyl 3-ureidocrotonate and an aldehyde in the presence of acid (14). The nmr spectrum of ethyl and methyl 3-ureidocrotonate, prepared by the method of Donleavy and Kise (15), showed the presence of only one tautomer and one geometrical isomer. The appearance of the NH resonance at low field (δ ~ 10–15 ppm) (16–18) and its relative insensitivity to changes in solvent polarity and concentration (19) are characteristic of chelation in vinylogous amides, imides, and urethanes. Accordingly the chelated *Z*-configuration **2** is assigned to these 3-ureidocrotonates. Since the condensation of 1,2-dichloroethyl ethyl ether

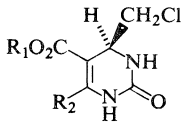

1

a $R_1 = R_2 = CH_3$
b $R_1 = CH_3$, $R_2 = CHBr_2$
c $R_1 = C_2H_5$, $R_2 = CH_3$

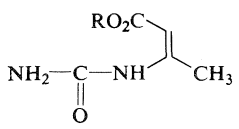

2

a $R = CH_3$
b $R = C_2H_5$

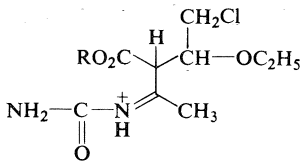

3

with an alkyl ureidocrotonate is expected to involve **3**, in which free rotation is permitted about C_2—C_3, the use of the less-preferred *Z*-isomer offers little disadvantage (*cf.* ref. 20).

Condensation of the dichloroether with ethyl 3-ureidocrotonate[3] in the absence of solvent

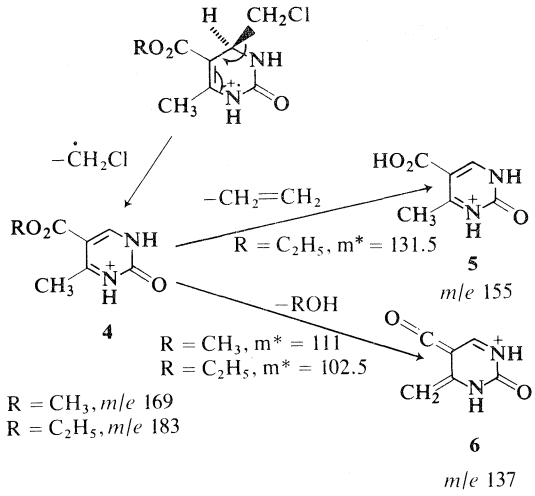

a $R = CH_3$, *m/e* 169
b $R = C_2H_5$, *m/e* 183

4

$R = C_2H_5$, m* = 131.5

5

m/e 155

$R = CH_3$, m* = 111
$R = C_2H_5$, m* = 102.5

6

m/e 137

SCHEME 1

afforded in good yield, a compound $C_9H_{13}ClN_2O_3$ (7), the spectroscopic properties of which were in full accord with the assigned structure **1***c*. Thus the mass spectrum was dominated by peaks at *m/e* 183, 155, and 137, which arise through loss of a chloromethyl radical to give the resonance stabilized ion **4***b*, followed by loss of ethylene[4] by a McLafferty rearrangement to give ion **5**, or loss of ethanol to give ion **6** (see Scheme 1). A number of ethyl 4-alkyl-1,2,3,4-tetrahydro-2-oxopyrimidine-5-carboxylates have been prepared and undergo similar fragmentations[5] (see Experimental). At high inlet temperatures, thermal elimination of HCl from **1***c* takes place. The nmr spectrum showed two broad NH absorptions, one of which is a doublet and is coupled to a proton attached to an adjacent carbon which appeared as a multiplet at δ 4.45. Deuteration resulted in the disappearance of both NH signals, while the CH signal at δ 4.45 collapsed to a triplet thus demonstrating the presence of the NH—CH—CH_2 moiety and eliminating the 2-imino-1,3-oxazine structure **7***a*. The methylene group appeared as a doublet, showing that, although the CH—CH_2 should, in principle, be an ABX system (C_4 is asym-

[3]It is well-known that 1,2-dichloroethyl ethyl ether reacts with ethyl acetoacetate in the presence of ammonium hydroxide to give a furan (21) and a pyrrole (21) and with urea to give 2-aminooxazole (22), while dialkylureas react with ethyl acetoacetate to give 1,3-oxazines (23). To reduce the number of possible products we decided to use the Folkers–Johnson approach. Subsequently, Ashby and Griffiths (24) have shown that a product identical with ours is formed from 1,2-dichloroethyl ethyl ether, ethyl acetoacetate, and urea, although in considerably lower yield.

[4]In the case of the methyl ester **1***a*, which has been prepared in a similar manner, and other 4,6-dialkyl-1,2,3,4-tetrahydropyrimidines, the loss of the 4-alkyl substituent gives an ion *m/e* 169 which loses methanol to give ion **6**. As expected, no ion corresponding to **5** is observed.

[5]The fragmentation of various aryl 1,2,3,4-tetrahydro-2-oxo-pyrimidines lacking electron-withdrawing substituents at C-5 is dominated by loss of aryl radicals (25).

metric), the methylene hydrogens are equivalent and free rotation is permitted about C_4—C_4'. The chemical shift values were in good agreement with those of authentic 1,2,3,4-tetrahydro-2-oxopyrimidines. The 2-oxo tautomeric structure was supported by the similarity between the ultraviolet spectra of **1***c*, ethyl 3-aminocrotonate, and ethyl 3-ureidocrotonate. In order to unequivocally eliminate[6] the 2-imino-1,3-oxazine structure **7***b*, compound **1***c* was reduced to the known ethyl 4,6-dimethyl-1,2,3,4-tetrahydro-2-oxopyrimidine-5-carboxylate using tri-*n*-butyltin hydride (cf. ref. 26) in the presence of azobisisobutyronitrile, thus confirming the structure **1***c*. Reduction of **1***b* using sodium borohydride in acetonitrile gave an isomeric product whose spectroscopic properties were in agreement with the 1,3-diazepine structure **8***e* resulting from ring expansion. None of this product was detected in the tributyltin hydride reduction.

The action of bromine (2 mol) in chloroform on the methyl ester **1***a* gave the 6-dibromomethyl compound **1***b*, whose nmr spectrum showed a 1H singlet at δ 8.03 and lacked the 3H singlet due to the C_6 methyl group. A similar compound was obtained by bromination of methyl 1,2,3,4-tetrahydro-4,6-dimethyl-2-oxopyrimidine-5-carboxylate (cf. ref. 27). We have been unable to effect hydrolysis of the 6-dibromomethyl compounds to the 6-aldehydes.

Treatment of the chloromethyl compound **1***a* in methanol with dilute aqueous potassium hydroxide, followed by acidification, resulted in formation of a small amount of methyl 2-methylpyrrole-3-carboxylate **9***a* and a major product $C_8H_{10}N_2O_3$ whose mass spectrum showed a molecular ion at *m/e* 182 and fragments at *m/e* 139, 124, 108, and 107 due to loss of HNCO followed by loss of methyl or methoxyl radicals and methanol respectively (cf. ref. 28). The nmr spectrum showed signals due to an NH_2 group, a pair of adjacent aromatic protons, a methyl group attached to an aromatic ring, and a methyl of methoxycarbonyl group. The nmr and ms are consistent with the *N*-carbamoylpyrrole structure **9***c*. The structure was confirmed when **9***c* was shown to give the pyrrole **9***a* when treated with base. Potassium fluoride in acetonitrile converted **1***a* directly to **9***a* in good yield. The ethyl ester **1***c* yielded a similar

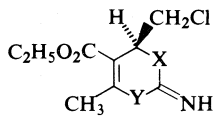

7

a X = O, Y = NH
b X = NH, Y = O

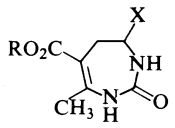

8

a R = CH_3, X = CN
b R = CH_3, X = OCH_3

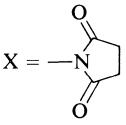

c R = CH_3, X = —N(CO)$_2$CH$_2$CH$_2$

d R = CH_3, X = $CH(CO_2C_2H_5)_2$
e R = C_2H_5, X = H
f R = C_2H_5, X = CN
g R = C_2H_5, X = OCH_3
h R = C_2H_5, X = OC_2H_5

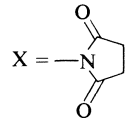

i R = C_2H_5, X = —N(CO)$_2$CH$_2$CH$_2$

j R = C_2H_5, X = $CH(CO_2C_2H_5)_2$

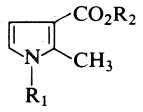

9

a R_1 = H, R_2 = CH_3
b R_1 = H, R_2 = C_2H_5
c R_1 = $CONH_2$, R_2 = CH_3
d R_1 = $CONH_2$, R_2 = C_2H_5
e R_1 = CO_2CH_3, R_2 = C_2H_5

N-carbamoylpyrrole **9***d* with potassium hydroxide in ethanol. Several unsuccessful attempts were made to synthesize **9***d* by a rational route. For example, ethyl 2-methylpyrrole-3-carboxylate **9***b* was converted to the corresponding pyrrolylmagnesium bromide which reacted with methyl chloroformate[7] to yield ethyl 1-methoxycarbonyl-2-methylpyrrole-3-carboxylate, **9***e*. However, reaction of **9***e* with ammonia gas in methanol resulted only in removal of the methoxycarbonyl group to regenerate **9***b*. Con-

[6]Additional support was obtained when compound **1***c* was converted to ethyl 1-carbamoyl-2-methylpyrrole-3-carboxylate.

[7]The methyl ester was used in order to facilitate the interpretation of the reaction of the product, a 1-methoxycarbonyl-3-ethoxycarbonylpyrrole, with ammonia.

densation of α-chloroacrylonitrile (cf. ref. 29) with ethyl 3-ureidocrotonate did not yield **9***d*.

When the chloromethyl compound **1***a* was reacted with sodium methoxide in methanol, a major product $C_9H_{14}N_2O_4$ was obtained and was assigned the 7-methoxy-1,3-diazepine structure **8***b*. The nmr spectrum showed singlets due to methoxyl and methoxycarbonyl groups and a doublet which was due to a C-methyl group which exhibited homoallylic coupling. In addition, the spectrum showed two NH absorptions, one of which was coupled to H_X of an AMX system. The H_X proton appeared at δ 4.76 as a multiplet which was changed to a 1:1:1:1 quartet on exchange of the labile NH protons for deuterium. A consideration of this and the chemical shift of proton H_X suggests the presence of the —CH_2—CH(OCH_3)—NH— moiety. In spin decoupling experiments, irradiation on the proton H_X at δ 4.76 caused the quartet at δ 3.70 due to H_M to collapse to a doublet (J = 14.5 Hz) but no change in the H_A signal (broadened d at δ 2.67) while irradiation at δ 2.67 caused the quartet of H_M at δ 3.70 to collapse to a doublet (J = 6.5 Hz). The homoallylic coupling of the proton H_A to the C-methyl group and the above nmr data provide strong support for the structure **8***b*.

When treated with methanolic hydrogen chloride or other acidic reagents at room temperature the methoxy-1,3-diazepine **8***b* was very rapidly and quantitatively converted to the 1-carbamoylpyrrole **9***c*. In the absence of water, we believe this reaction occurs via protonation at N-1 followed by methoxyl-assisted cleavage, in a manner reminiscent of acetal hydrolysis, to give a carbonium ion (see Scheme 2). Cyclization

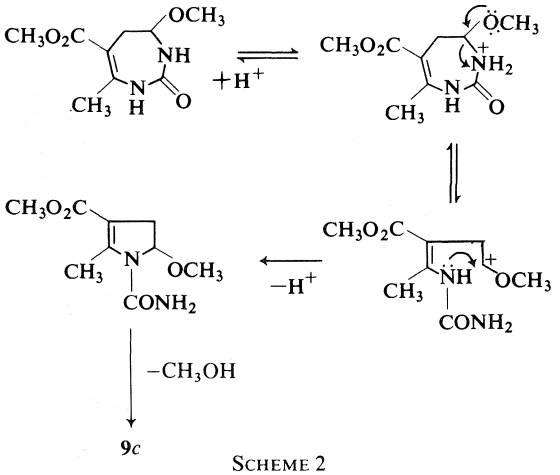

SCHEME 2

by nucleophilic attack of N-3, and acid-catalyzed loss of methanol would then yield **9***c*. An alternative mechanism, which cannot be excluded, involves protonation of the methoxyl group, transannular displacement to give the 1,6-diazabicyclo[3.2.0]heptanone **10**, and subsequent acid-catalyzed ring opening to **9***c*. In the presence of water, a third mechanism is possible which involves hydrolytic ring-opening of the vinylogous urethane to give the ketoester **11**. Subsequent cyclization and loss of methanol would

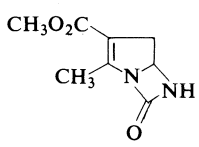

10

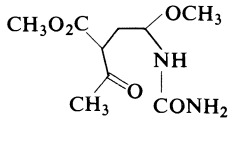

11

yield **9***c*. In the formation of **9***c* or **9***d* directly[8] from the chloromethyl compounds **1***a* and **1***c* respectively, the pathway appears to depend on the solvent used. The reaction proceeds via the 7-alkoxy-1,3-diazepine in high alcohol:water ratios and requires acid to complete the transformation to the pyrrole. Carbinolamines *e.g.* **12**, **13** appear to be formed competitively in aqueous ethanol or aqueous tetrahydrofuran.

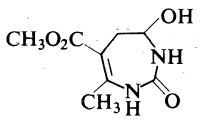

12

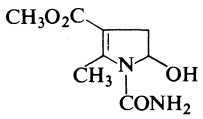

13

Other 7-substituted 1,3-diazepines have been prepared from **1***a* and **1***c* using nucleophilic reagents. Thus the 7-ethoxy compound **8***h* was prepared by the action of potassium cyanate in dry ethanol on **1***c*, while tetramethylammonium hydroxide and **1***c* in methanol gave the 7-methoxy compound **8***g* without ester exchange. The reaction of the chloromethyl compounds **1***a* and **1***c* with potassium cyanide, potassium succinimide, or diethyl sodiomalonate gave the 7-cyano-1,3-diazepines **8***a* and **8***f* (7),[9] 7-succinimino-1,3-diazepines **8***c* and **8***i*, and 7-diethoxycarbonylmethyl-1,3-diazepines **8***d* and **8***j* respectively. The spectroscopic properties of the compounds **8***a*–**8***j* were in good agreement

[8]For the ring contraction of a pyrimidine to a pyrrole under reductive/acidic conditions see ref. 30.

[9]Some of our results reported earlier (7) have recently been confirmed by Ashby and Griffiths (24).

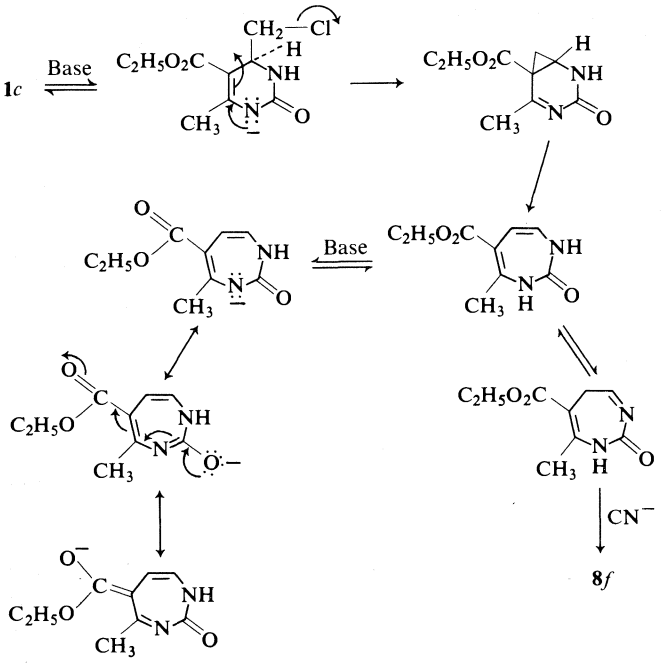

SCHEME 3

with the proposed structures. Thus, the ultraviolet absorption maxima which invariably appeared about 265 nm (ε 13 000 approximately) are about 15 nm to shorter wavelength than those of typical 4,6-dialkyl-1,2,3,4-tetrahydro-2-oxopyrimidine-5-carboxylates and may reflect a decrease in planarity of the cyclic ureidocrotonate chromophore. In the case of the 7-succinimino- and 7-(diethoxycarbonylmethyl)-1,3-diazepines, the base peaks in the mass spectrum were formed by a McLafferty rearrangement which resulted in loss of succinimide or diethyl malonate respectively.

Although, in principle, ring expansion of **1***a* and **1***c* may take place by participation of either N-3 or the aminocrotonate system, the former would result in attachment of the nucleophile at C-6 rather than C-7 as found. It has been observed that the reaction of **1***a* and **1***c* in dipolar aprotic solvents, *e.g.* dimethyl sulfoxide or dimethylformamide, with bases such as cyanide, *tert*-butoxide, methoxide, or succinimide anions or 1,5-diazabicyclo[4.3.0]non-5-ene causes the production of an intensely violet-colored solution. This violet color gradually fades over 30–60 min to give a yellow-brown solution and work-up by addition of water at this point results in isolation of ring-expanded product in high yield. The violet-colored species is formed by reaction of **1***c* with cyanide anion in aprotic solvents such as pyridine, tetrahydrofuran, or acetonitrile only on addition of a crown ether such as dicyclohexyl-18-crown-6 and is not observed at all in hydroxylic solvents. Alkyl 4,6-dimethyl-1,2,3,4-tetrahydro-2-oxopyrimidine-5-carboxylates and the 1,3-diazepines **8***a*–**8***j* do not give violet-colored solutions with bases in dimethyl sulfoxide and dimethylformamide. These results are accommodated by a mechanism shown in Scheme 3. In the absence of kinetic measurements we are not able to eliminate the possibility that ring expansion takes place by a mechanism involving a homoallylic carbonium ion.

Recently, Ashby and Griffiths have reported (24) the reaction of potassium hydrosulfide in ethanol with **1***c* to give the 8-thia-2,4-diazabicyclo[3.2.1]octane derivatives **14***a* and **14***c*. We have studied[10] the reaction of compounds **1***a* and **1***c* with sulfhydryl ion and have similarly observed the formation of compounds **14***a*–**14***c*, whose structures follow from the lack of ultraviolet maxima above 210 nm, the presence of saturated acid or ester and unsaturated ester carbonyl frequencies in the infrared spectra, and

[10]Taken in part from B.Sc Hons. Thesis of Miss R. M. Cochrane, Memorial University of Newfoundland, Nfld., May 1974.

TABLE 1. Ultraviolet absorption data

Compound	Solvent*	λ_{max} (nm) and intensity
Ethyl 3-aminocrotonate†	A	274 (ε 20 400)
2*a*	E	270.5 (ε 14 100)
2*b*	E	272.5 (ε 17 900)
1*a*	E	281 (ε 10 500)
1*b*	E	232 (ε 5050)
		297.5 (ε 7850)
1*c*	E	282 (ε 10 500)
8*a*	E	265 (ε 13 300)
8*b*	E	264 (ε 13 200)
8*c*	E	264.5 (ε 11 600)
8*d*	E	268.5 (ε 12 400)
8*e*	E	270 (ε 12 550)
8*f*	E	264.5 (ε 12 900)
8*g*	E	264 (ε 12 500)
8*h*	E	264.5 (ε 13 250)
8*i*	E	264.5 (ε 11 450)
8*j*	E	268.5 (ε 12 800)
9*c*	M	212.5 (ε 23 800)
		233.5 (ε 9900)
		248 (sh, ε 5800)
9*d*	M	212.5 (ε 24 500)
		234.5 (ε 11 300)
		249 (sh, ε 6800)
9*e*‡	M	232 (ε 10 700)
		267 (sh, ε 5100)

*Solvent: A is absolute alcohol; E is 95% ethanol; M is methanol.
†Reference 37.
‡Reference 35.

the formation of the ion **15** at *m/e* 130 by loss of acrylic acid or its esters in the mass spectra. The nmr spectra are in agreement with those reported (24). In addition, we have obtained chemical confirmation for this structure. Thus carboxylic acid **14***a* eliminated urea on treatment with acid to yield the known 2-methyl-3-thenoic acid and desulfurization of **14***c* with Raney nickel gave the hexahydro-2-oxo-1,3-diazepine **16**.

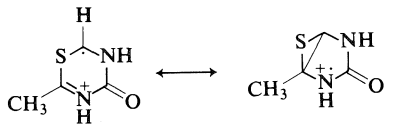

15

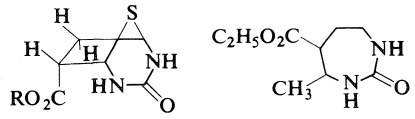

14

16

a R = H
b R = CH_3
c R = C_2H_5

Compounds **1***c*, **8***f*, and **9***d* were screened for pharmacological activity, and found to have no *in vitro* antibiotic, antiparasitic, enzyme inhibitory, contraceptive, and antihypertensive activity.

Experimental

Melting points were determined using a Fisher–Johns melting point apparatus. Infrared spectra were obtained in chloroform solution using a Perkin-Elmer 237B grating infrared spectrometer. Ultraviolet spectra were measured on Unicam SP 800D or Perkin-Elmer 202 spectrophotometers using solutions in 95% ethanol. Spectra were calibrated using the bands at 2850.7 and 1601.4 cm^{-1} of polystyrene (ir) or at 279.4 and 360.9 nm of a holmium oxide filter (uv). The pmr spectra were obtained on Varian HA 100 or EM 360 spectrometers using deuterochloroform as solvent unless specified otherwise. All chemical shifts are expressed in parts per million downfield from internal tetramethylsilane. Mass spectra were determined at 70 eV ionizing energy using a Hitachi–Perkin-Elmer RMU 6E mass spectrometer. Only the most intense peaks are listed; normalized intensities are given in parentheses. Initial and final total ion current values differed by $< 5\%$. New compounds were homogeneous by tlc and elemental analyses were performed by Alfred Bernhardt, West Germany. The identity of known compounds was established by mp, mixture mp, and comparison of ir, pmr, and ms with those of authentic specimens.

Ethyl 3-ureidocrotonate was prepared by the method of Donleavy and Kise (15). The product, after two recrystallizations had mp 169.5–170.5 °C (lit. (15) mp 170 °C). Methyl 3-ureidocrotonate was prepared in a similar manner and had mp 186–186.5 °C (lit. (31) mp 180–181 °C); pmr (DMSO-d_6) δ 2.28 (s, CH_3 at C_3), 3.63 (s, methyl ester), 4.82 (d, $J \sim 1$ Hz, olefinic H), 6.83 (br s, NH_2), 10.2 (br s, NH).

Methyl 4-Chloromethyl-1,2,3,4-tetrahydro-6-methyl-2-oxopyrimidine-5-carboxylate, ***1a***

Methyl 3-ureidocrotonate **2***a* (15.8 g) was stirred to a stiff paste with 1,2-dichloroethyl ethyl ether (15.7 g) and heated slowly to 95 °C. At this temperature the reaction mixture existed as two liquid phases and on mixing, a vigorous reaction occurred in which hydrogen chloride and ethanol vapour were evolved. After a few minutes the melt solidified and was then cooled, triturated with absolute methanol (15 ml), and filtered. The solid was suspended in absolute methanol and heated under reflux for 6 h, during which time a slow stream of dry hydrogen chloride was passed through the solution.[11] The resulting solution was then concentrated, cooled, and the crude product obtained by filtration. Recrystallization once from methanol and twice from dry acetone yielded the pure product (11.2 g, 51%), mp 196 °C. *Anal.* calcd. for $C_8H_{11}ClN_2O_3$: C 43.92, H 5.07, Cl 16.20, N 12.80; found: C 44.09, H 4.91, Cl 16.15, N 12.67.

[11]Elimination of ethanol in the presence of hydrogen chloride in the early stages of the reaction caused some ester exchange.

The ir 3420, 1705, 1685, 1640 cm^{-1}; pmr δ (DMSO-d_6) 2.22 (s, 3H, CH_3 at C_6), 3.59 (d, J = 3.8 Hz, 2H, —CH_2-Cl), 3.66 (s, 3H, —CO_2CH_3), 4.43 (doublet t approximating to a q, J = 3.8 Hz and 7.5 Hz, 1H, H at C_4), 7.49 (br d, $J \sim 3$ Hz, 1H, N_1-H), 9.25 (br s, N_3-H): on addition of D_2O, the NH absorptions at δ 7.49 and 9.25 disappeared and the signal at δ 4.43 simplified to a triplet, J = 3.8 Hz; mass spectrum *m/e* 218(0.5, M^+, ^{35}Cl), 169(100) 137(53), 42(15).

Ethyl 4-Chloromethyl-1,2,3,4-tetrahydro-6-methyl-2-oxopyrimidine-5-carboxylate, **1***c*

The crude material obtained from the reaction of ethyl 3-ureidocrotonate (**2***b*, 8.6 g) with 1,2-dichloroethyl ethyl ether (7.9 g) was recrystallized twice from acetone to give the pure product **1***c* (7.56 g, 65%) as colorless needles, mp 176.5–177 °C. *Anal.* calcd. for $C_9H_{13}ClN_2O_3$: C 46.42, H 5.59, Cl 15.27, N 12.03; found: C 46.28, H 5.74, Cl 15.13, N 11.94. The ir 3420, 1705, 1682, 1645 cm^{-1}; pmr δ (DMSO-d_6) 1.27 (t, J = 7 Hz, 3H, CH_3 of ethyl), 2.22 (s, 3H, CH_3 at C_6), 3.62 (d, J = 4.5 Hz, 2H, CH_2Cl), 4.12 (q, J = 7 Hz, 2H, CH_2 of ethyl), 4.45 (m, 1H, H at C_4) 7.5 (br d, 1H, N_1-H) 9.2 (br s, 1H, N_3-H): on addition of D_2O the NH absorptions at δ 7.5 and 9.2 disappeared and the multiplet at δ 4.45 collapsed to a triplet (J = 4.5 Hz); ms, *m/e* 232(1, M^+, ^{35}Cl), 189(3), 187(9), 183(100), 155(34), 137(35), 110(5), 86(5), 84(4), 42(14).

The chloromethyl compound **1***c* (20 mg), tri-*n*-butyltin hydride (213 mg), and azobisisobutyronitrile (2 mg) in dry xylene (1.5 ml) were heated at 90 °C for 24 h. After evaporation of the xylene at reduced pressure, the crude material was separated by preparative tlc using silica gel GF_{254} and 4:1 benzene–acetone as eluting solvent. Further purification by sublimation at 80 °C/0.01 torr, gave the product, ethyl 1,2,3,4-tetrahydro-4,6-dimethyl-2-oxopyrimidine-5-carboxylate (8 mg, 47%); mp 193–194 °C (lit. (32) mp 192.5–193.5 °C), mixture mp 193.5–194 °C, which had identical ms to that of authentic material and in particular had major ions at *m/e* 198, 183, 155, 137.

Ethyl 2,3,6,7-Tetrahydro-4-methyl-2-oxo-1H-1,3-diazepine-5-carboxylate, **8***e*

Sodium borohydride (0.25 g) was added over 10 min to a stirred solution of the chloromethyl compound **1***c* (0.50 g) at 75 °C. After stirring for a further 1½ h, the acetonitrile was evaporated and water (10 ml) added to the residue. Extraction with chloroform (4 × 10 ml) gave the almost pure product (0.40 g). Purification by sublimation at 80 °C/0.01 torr or recrystallization from ethanol gave pure ethyl 2,3,6,7-tetrahydro-4-methyl-2-oxo-1*H*-1,3-diazepine-5-carboxylate (0.37 g, 87%); mp 194–195 °C (lit. (24) mp 192–193 °C). *Anal.* calcd. for $C_9H_{14}N_2O_3$: C 54.53, H 7.12, N 14.13; found: C 54.58, H 7.06, N 14.04. The ir 3425, 3396, 3216, 1692, 1645; the pmr (pyridine-d_5) δ 1.08 (t, J = 7.0 Hz, CH_3 of ethyl ester), 2.42 (s, CH_3 at C_4), 2.68 (m, 6-CH_2), 3.27 (m, 7-CH_2), 4.07 (q, J = 7.0 Hz, CH_2 of ethyl ester), 8.27 (br s, N_1-H) 9.08 (N_3-H).

Methyl 6-Dibromomethyl-1,2,3,4-tetrahydro-4-methyl-2-oxopyrimidine-5-carboxylate

A solution of bromine (17.6 g) in chloroform (100 ml) was added, over a period of 15 min to a suspension of methyl 1,2,3,4-tetrahydro-4,6-dimethyl-2-oxopyrimidine-5-carboxylate (9.2 g) in chloroform (100 ml). The solid rapidly dissolved after approximately 10 ml of the bromine solution had reacted. Considerable heat was evolved as the reaction proceeded, accompanied by brisk evolution of hydrogen bromide. After briefly refluxing on a stream bath, the chloroform solution was cooled, washed with saturated sodium bicarbonate solution (3 × 5 ml) and water (2 × 50 ml), and dried ($MgSO_4$). Removal of the solvent on the rotary evaporator yielded an orange gum which crystallized on treatment with methanol. The crude material (16.2 g) was recrystallized twice from methanol–benzene (1:5, v/v) to give the pure product (14.1 g, 82%) as colorless needles mp 162–162.5 °C. *Anal.* calcd. for $C_8H_{10}Br_2N_2O_3$: C 28.07, H 2.92, Br 46.75, N 8.18; found: C 28.11, H 3.05, Br 46.94, N 8.32. The ir 3422, 1720, 1705, 1645 cm^{-1}; pmr (DMSO-d_6) 1.16 (d, J = 6.5 Hz, CH_3 at C_4), 3.77 (s, CH_3 of ester), 4.23 (m, a double q, approximating to a 1:1:1:1 q, J = 6.5 Hz and 3 Hz H at C_4), 7.5 (br s, N_3-H), 8.0 (s, $CHBr_2$), 9.47 (br s, 1H, N_1-H); exchange of the NH protons using D_2O simplified the signal at δ 4.23 to a quartet (J = 6.5 Hz); ms 340(2, M^+, ^{79}Br isotopes), 329(47), 327(91), 325(47), 167(100).

Methyl 6-Dibromomethyl-4-chloromethyl-1,2,3,4-tetrahydro-2-oxopyrimidine-5-carboxylate, **1***b*

Following the procedure used in the previous preparation, bromine (8.8 g) in chloroform (75 ml) was reacted with the chloromethyl compound **1***a* (5.4 g) in chloroform (75 ml). The reaction mixture was washed with 5% sodium acetate solution (3 × 50 ml), water (2 × 50 ml), and worked-up in the manner indicated. The crude product was recrystallized from methanol to give colorless crystals of **1***b* (8.1 g, 87%); mp 186–187 °C. *Anal.* calcd. for $C_8H_9Br_2ClN_2O_3$: C 25.47, H 2.39, Br 42.50, Cl 9.41, N 7.43; found: C 25.56, H 2.52, Br 42.37, Cl 9.49, N 7.61. The ir 3405, 1720, 1710, 1640 cm^{-1}; the pmr (DMSO-d_6): δ 3.7 (d, $J \sim 4$ Hz, 2H, CH_2Cl), 3.77 (s, 3H, CH_3O_2C), 4.53 (double t approximating to q, $J \sim 4$ Hz and 3 Hz, 1H, H at C_4), 7.6 (br, 1H, N_3-H), 8.03 (s, 1H, $CHBr_2$), 9.65 (br s, 1H, N_1-H). Deuterium exchange simplified the signal at δ 4.53 to a t $J \sim 4$ Hz.

Methyl 1-Carbamoyl-2-methylpyrrole-3-carboxylate, **9***c*

(*a*) To a solution of the chloromethyl compound **1***a* (2.2 g) in methanol (100 ml) was added potassium hydroxide (0.84 g) in water (15 ml). After stirring overnight at room temperature, water (50 ml) was added and the solution was concentrated to approximately 70 ml on a rotary evaporator. The aqueous solution was extracted with ether (3 × 50 ml) and then acidified with hydrochloric acid (3 ml, 6 *N*). The aqueous solution was cooled in ice for 3 h and then filtered to yield the 1-carbamoylpyrrole **9***c* as almost colorless needles. Recrystallization from aqueous methanol and sublimation at 125 °C/0.05 torr yielded the pure product (1.32 g, 72%); mp 210–211 °C. *Anal.* calcd. for $C_8H_{10}N_2O_3$: C 52.74, H 5.53, N 15.38, found: C 52.66, H 5.36, N 15.26. The ir 3512, 3405, 1738, 1707, 1588, 1570, 1440, 1375, 1320 cm^{-1}; the pmr (DMSO-d_6): δ 2.73 (s, CH_3 at C-2), 3.78 (s, CH_3 of methyl ester), 6.53 (d, J = 3.5 Hz,

4-H), 7.25 (d, J = 3.5 Hz, 5-H), 7.79 (br s, 2H, NH_2); the ms m/e 182(51, M^+), 139(76), 124(32), 108(100), 107(42), 106(20).

Evaporation of the dried ($MgSO_4$) ether extract yielded a low-melting solid identified, after sublimation at 55 °C/0.1 torr, as methyl 2-methylpyrrole-3-carboxylate **9***a*; mp 64 °C (lit. (33) mp 63–64 °C, (34) mp 67–68 °C) and whose spectral properties were consistent with those reported for this compound.

The 1-carbamoyl pyrrole **9***c* was also formed from the chloromethyl compound by the action of sodium bicarbonate in dimethyl sulfoxide.

(*b*) A solution of the methoxydiazepine **8***b* (1.05 g) in absolute methanol (50 ml) was treated with a slow stream of dry hydrogen chloride. The solution became very warm and after a few minutes developed a bright green color which almost immediately faded. At this point, the gas flow was halted and the solution allowed to cool. The solvent was removed under reduced pressure and the residue purified by recrystallization from aqueous methanol and sublimation at 125 °C/0.05 torr to give the product **9***c* (0.85 g, 95%); mp 210–211 °C undepressed on admixture with the product from (*a*) and having identical spectral properties.

*Ethyl 1-Carbamoyl-2-methylpyrrole-3-carboxylate, **9d***

Finely ground chloromethyl compound **1***c* (2.3 g) was added, in portions of approximately 0.25 g, to a stirred mixture of aqueous potassium hydroxide (15 ml, 1 *M*) and ethanol (10 ml). Stirring was continued for 12 h at room temperature, when hydrochloric acid was added (3 ml, 6 *M*). After cooling in ice, the crude product was filtered off and recrystallized from aqueous ethanol. Sublimation at 110–115 °C/0.05 torr yielded the pure product **9***d* (1.4 g, 71%); mp 186–187 °C. *Anal.* calcd. for $C_9H_{12}N_2O_3$: C 55.09, H 6.17, N 14.28; found: C 55.01, H 6.04, N 14.12. The ir 3510, 3400, 1740, 1702, 1585, 1570 cm^{-1}; pmr (DMSO-d_6) δ 1.27 (t, J = 7 Hz, CH_3 of ethyl), 2.7 (s, CH_3 at C-2), 4.23 (q, J = 7 Hz, 2H, CH_2 of ethyl), 6.49 (d, J = 3.5 Hz, H at C-4), 7.2 (d, J = 3.5 Hz, H at C-5), 7.75 (br s, 2H, NH_2); the broad singlet at δ 7.75 disappeared in the presence of D_2O; ms m/e 196(38, M^+), 153(54), 124(93), 108(100), 107(28), 106(21), 80(24), 53(29).

*The Reaction of the Chloromethylpyrimidine **1a** with Anhydrous Potassium Fluoride*

The chloromethyl compound **1***a*, (218 mg) and anhydrous potassium fluoride (580 mg) in dried acetonitrile (30 ml) were heated under reflux for 4 days and then evaporated to dryness. The solid residue was washed with water (2 × 5 ml), and the residue extracted with benzene (3 × 10 ml). The benzene solution was dried ($MgSO_4$), filtered, and evaporated to give a colorless solid (119 mg) which afforded, after sublimation at 40–50 °C/0.01 torr, colorless crystals (84 mg, 60%), identified as methyl 2-methylpyrrole-3-carboxylate; mp 64 °C (lit. (33) mp 63–64 °C, (34) 67–68 °C) having spectral properties identical with an authentic specimen.

*3-Ethoxycarbonyl-1-methoxycarbonyl-2-methylpyrrole **9e** and Reaction with Ammonia*

A solution of ethyl 2-methylpyrrole-3-carboxylate (1.5 g) in dry ether (25 ml) was added to the Grignard solution prepared from the reaction of ethyl iodide (1.5 g) and magnesium (0.25 g) in dry ether (25 ml). To the well-stirred solution, under nitrogen, dimethyl carbonate (1.9 g) in ether (10 ml) was added. The resulting mixture was stirred at room temperature for 2 h and then refluxed for 12 h. The reaction mixture was treated with 10% ammonium chloride and then extracted with ether (3 × 20 ml). Evaporation of the ether extract yielded an orange oil which was chromatographed on neutral alumina (Fluka type 507C neutral) using benzene as eluant. The first fractions were evaporated and purified by sublimation at 35 °C/0.01 torr to give the product as colorless crystals; mp 40 °C (lit. (35) mp 39.5–41 °C) ms, m/e 211(82, M^+), 182(100), 166(70), 165(30), 138(31), 122(25), 106(26), 59(45), 42(26); the ir, uv, and pmr were identical with those reported by Biellmann and Goeldner (35).

The above pyrrole diester (50 mg) was dissolved in anhydrous methanol (5 ml) and the solution saturated with dry ammonia gas. After standing overnight at room temperature, the solution was evaporated and the residue purified by sublimation at 40 °C/0.01 torr when crystals (31 mg, 85%) of ethyl 2-methylpyrrole-3-carboxylate **9***b* were obtained. No traces of ethyl 1-carbamoyl-2-methylpyrrole-3-carboxylate **9***d* were found on examination of the crude product by both tlc and mass spectrometry.

*Methyl 7-Methoxy-2,3,6,7-tetrahydro-4-methyl-2-oxo-1H-1,3-diazepine-5-carboxylate, **8b***

(*a*) A solution of the chloromethyl compound **1***a* (4.4 g) and sodium methoxide (6.1 g) in absolute methanol (250 ml) was stirred at room temperature for 24 h, then distilled until 120 ml of methanol had been collected. To the concentrate, water was added and after cooling in ice for 2 h the crude product was obtained by filtration. Recrystallization from absolute methanol yielded the pure product **8***b* (3.1 g, 70%); mp 199–200 °C. *Anal.* calcd. for $C_9H_{14}N_2O_4$: C 50.46, H 6.59, N 13.08; found: C 50.33, H 6.44, N 12.98. The ir 3415, 3395, 1700, 1685, 1680, 1640 cm^{-1}; pmr (pyridine-d_5, HA 100) δ 2.51 (d, $J_{homoallylic}$ = 1 Hz, CH_3 at C_4), 2.67 (br d, J_{AM} = 14.5 Hz, H_A at C_6), 3.35 (s, CH_3O—), 3.70 (q, J_{AM} = 14.5 Hz, J_{MX} = 6.5 Hz, H_M at C_6), 3.67 (s, CH_3 of ester) 4.76 (m, J_{MX} = 6.5 Hz, J_{AX} = 2 Hz, H_X at C_7), 9.13 (br d, H at N_1), 9.66 (br s, H at N_3). Irradiation at δ 4.76 caused the q at δ 3.70 to collapse to a d, J = 14.5 Hz but no change in the d at δ 2.67; irradiation at δ 2.67 caused the q at δ 3.70 to change to a d, J = 6.5 Hz; addition of D_2O to the solution resulted in disappearance of the signals δ 9.13 and 9.66 while the resonance at δ 4.76 changed to a q; ms m/e 214(5, M^+), 182(54), 151(22), 140(43), 123(21), 108(49), 96(17), 60(100), 42(41).

(*b*) The chloromethyl compound (4.4 g) was reacted with a solution of potassium hydroxide (1.2 g) in methanol (170 ml) by the above procedure and yielded the product (2.7 g, 61%) identical in all respects with that obtained in (*a*) above.

*Ethyl 7-Methoxy-2,3,6,7-tetrahydro-4-methyl-2-oxo-1H-1,3-diazepine-5-carboxylate, **8e***

A solution of the chloromethyl compound **1***c* (2.3 g) and tetramethylammonium hydroxide (2 ml, 0.2 *M* aqueous) in methanol (100 ml) was stirred at room temperature for 24 h and then concentrated by distilla-

tion to about 30 ml. Addition of water (30 ml) afforded a crystalline material which recrystallized from methanol to give the pure methoxydiazepine **8***e* (1.8 g, 78%) as small, colorless prisms; mp 195–196 °C. *Anal.* calcd. for $C_{10}H_{16}N_2O_4$: C 52.60, H 7.02, N 12.28; found: C 52.42, H 7.04, N 12.19. The ir 3412, 3395, 1698, 1685, 1675, 1640 cm^{-1}; pmr (DMSO-d_6) δ 1.2 (t, J = 7 Hz, CH_3 of ethyl), 2.17 (s, CH_3 at C_4), 2.5 approximately (d of H_A, partly obscured by DMSO), 2.97 (one half of the H_B quartet, J_{BX} = 5 Hz approximately), 3.18 (s, CH_3O at C_7, conceals one half of H_B quartet), 4.07 (q, J = 7 Hz, CH_2 of ethyl ester) 4.43 (m, overlaps with q at δ 4.07, H_X at C_7), 7.95 (br, N_1-H), 8.5 (br, N_3-H), ms *m/e* 228(4, M^+), 196(33), 151(21), 60(100), 42(24).

Methyl 7-Cyano-2,3,6,7-tetrahydro-4-methyl-2-oxo-1H-1,3-diazepine-5-carboxylate, 8a

When sodium cyanide (2.5 g) was added to a stirred solution of the chloromethyl compound **1***a* (4.4 g) in dimethyl sulfoxide (35 ml), an intense violet color was immediately developed, which faded over 0.5 h to give a yellow solution. Stirring was continued for 12 h at room temperature, when sodium chloride was precipitated. Ice water (500 ml) was then added and the precipitated product was collected and washed with water, methanol (25 ml), and ether (25 ml). Recrystallization from aqueous methanol yielded the colorless crystalline product (3.3 g, 78%); mp 238–239 °C (dec.). *Anal.* calcd. for $C_9H_{11}N_3O_3$: C 51.67, H 5.30, N 20.09; found: C 51.87, H 5.30, N 20.02. The ir (KBr) 3320, 3225, 3100, 2240, 1695–1670 (broad), 1620 cm^{-1}; pmr (DMSO-d_6) δ 2.27 (s, 3H, CH_3 at C_4), 2.63 (br d partially obscured by DMSO signal, J_{AM} ~ 16 Hz, H_M at C_6), 3.28 (q, 1H, J_{AM} = 15.5 Hz, J_{AX} = 6 Hz, H_A at C_6), 3.68 (s, 3H, CH_3O_2C), 4.73 (m, 1H, H_X of AMX coupled to N_1-H), 7.95 (br d, 1H, J ~ 6.5 Hz N_1-H), 8.77 (br s, 1H, N_3-H); the CH_XCN multiplet, which is symmetrical since the coupling constants to H_A and N_1-H are almost the same, is simplified to a double doublet J_{AX} = 6 Hz, J_{MX} ~ 2.5 Hz on addition of D_2O; ms *m/e* 209(69, M^+) 182(57), 178(29), 177(14), 150(27), 128(41), 123(24), 122(23), 108(24), 96(100), 68(22), 55(53), 53(25), 42(67).

Ethyl 7-Cyano-2,3,6,7-tetrahydro-4-methyl-2-oxo-1H-1,3-diazepine-5-carboxylate, 8f

Reaction of the chloromethyl compound **1***c* (5.0 g) and sodium cyanide (2.5 g) in dimethyl sulfoxide (30 ml) in a similar manner to the above yielded, after recrystallization from aqueous ethanol, the pure product (4.1 g, 84%); mp 236–237 °C (dec.). *Anal.* calcd. for $C_{10}H_{13}N_3O_3$: C 53.80, H 5.87, N 18.83; found: C 53.62, H 5.69, N 18.95. The ir (KBr) 3322, 3225, 2243, 1695–1670 (broad) 1622 cm^{-1}; the pmr (DMSO-d_6) δ 1.22 (t, J = 7 Hz, 3H, CH_3 of ethyl), 2.25 (s, 3H, CH_3 at C_4), 2.62 (d, partially obscured by DMSO signal, J_{AM} ~ 15.5 Hz, H_M), 3.23 (q, 1H, J_{AM} = 16 Hz, J_{AX} ~ 5.5 Hz, H_A), 4.13 (q, J = 7 Hz, 2H, CH_2 of ethyl), 4.72 (m, 1H, CH_XCN coupled to N_1-H), 7.9 (br m, 1H, N_1-H), 8.73 (br s, 1H, N_3-H); deuteration caused the H_X signal to collapse to a double doublet, J_{AX} = 5 Hz, J_{MX} ~ 2 Hz; ms *m/e* 223(36, M^+), 196(34), 178(30), 150(23), 142(26), 123(23), 122(20), 96(100), 42(61).

Ethyl 7-Ethoxy-2,3,6,7-tetrahydro-4-methyl-2-oxo-1H-1,3-diazepine-5-carboxylate, 8h

The chloromethyl compound **1***c* (4 g) and potassium cyanate (4 g) were refluxed in dry ethanol (300 ml) for 15 h. The ethanol solution was then decanted from inorganic material, evaporated, water (20 ml) added, and the resulting suspension extracted with chloroform (4 × 25 ml). The chloroform extract was washed with water (2 × 10 ml), dried ($MgSO_4$), filtered, and evaporated. Crystallization of the residue from aqueous ethanol yield the product as pale yellow crystals (3.47 g, 83%); mp 171–172 °C (lit. (24) mp 164–166 °C).

Methyl 2,3,6,7-Tetrahydro-4-methyl-2-oxo-7-(1-succinimino)-1H-1,3-diazepine-5-carboxylate, 8c

The chloromethyl compound **1***a* (1 g) and potassium succinimide (0.756 g) in dimethylformamide (10 ml) were stirred for 24 h at room temperature. Water (80 ml) was added and after cooling for 4 h at 0 °C, the precipitated solid was obtained by filtration and recrystallized from methanol to give the succiniminodiazepine **8***c* (0.637 g, 53%) mp 216–217.5 °C (dec). *Anal.* calcd. for $C_{12}H_{15}N_3O_5$: C 51.24, H 5.38, N 14.94; found: C 51.36, H 5.32, N 14.96. The ir (KCl) 3336, 3196, 1711, 1681, 1636 cm^{-1}; pmr (DMSO-d_6) δ 2.14 (s, CH_3 at C_4), 2.53 (s, CH_2—CH_2 of succinimino group), 2.60–3.40 (m, H's at C_6), 3.60 (s, CH_3 of ester), 5.09 (dd, H at C_7), 7.10 (br s, N_1-H), 8.52 (br s, N_3-H); ms *m/e* 281(2, M^+), 182(100), 151(27), 140(69), 123(31), 108(63), 99(82), 96(30), 56(78), 55(31), 42(60).

Ethyl 2,3,6,7-Tetrahydro-4-methyl-2-oxo-7-(1-succinimino)-1H-1,3-diazepine-5-carboxylate, 8i

The chloromethyl compound **1***c* (4.31 g) and potassium succinimide (3.738 g) in dry dimethylformamide (20 ml) were stirred at room temperature for 20 h. The dimethylformamide was removed at 50 °C/0.01 torr and the residue triturated with water (30 ml) and cooled in the refrigerator to give, after filtration, the almost pure product **8***i* (4.295 g, 78%). The pure succinimino compound, mp 202–205 °C, was obtained by recrystallization from ethanol. *Anal.* calcd. for $C_{13}H_{17}N_3O_5$: C 52.88, H 5.80, N 14.23; found: C 52.84, H 5.74, N 14.23. The ir 3490, 3233, 1718 (sh), 1710, 1641 cm^{-1}; pmr (pyridine-d_5) δ 1.02 (t, J = 7.0 Hz, CH_3 of ethyl ester), 2.39 (s, CH_3 at C_4 and —CH_2CH_2— of succinimino group), 3.03 (dd, J_{AM} = 14 Hz, J_{AX} = 2.5 Hz, H_A at C_6), 3.72 (br t, overlaps with signal at δ 4.02, J_{AM} = 14 Hz, J_{MX} = 10 Hz, H_M at C_6), 4.02 (q, J = 7.0 Hz, CH_2 of ethyl ester), 5.76 (dd, J_{AX} = 2.5 Hz, J_{MX} = 10 Hz, H_X at C_7), 8.38 (br s, N_1-H), 9.68 (br s, N_3-H); ms *m/e* 295(0.7, M^+), 250(1.5), 196(100), 155(20), 151(39), 150(45), 124(32), 123(27), 108(27), 99(77), 56(47), 42(21).

Ethyl 7-Diethoxycarbonylmethyl-2,3,6,7-tetrahydro-4-methyl-2-oxo-1H-1,3-diazepine-5-carboxylate, 8j

Sodium hydride in paraffin (1.5 g, approximately 1:1) was washed with dry petroleum ether (4 ml) and anhydrous tetrahydrofuran (2 × 4 ml). The remaining solid was suspended in anhydrous tetrahydrofuran (4 ml) and diethyl malonate (1.93 g) was added. After stirring for 0.5 h, the chloromethyl compound **1***c* (2.32 g) was added and stirring continued for 3 days. After addition of water (25 ml) the crystals (2.53 g, 71%) thus obtained were filtered off and shown to be homogeneous by tlc. Recrystallization from 95% ethanol gave the product as colorless needles; mp 157–159 °C. *Anal.* calcd. for $C_{16}H_{24}N_2O_7$: C 53.93, H 6.79, N 7.86; found: C 53.74, H 6.71, N 8.02. The ir (KCl) 3321 and 3206 (NH str.),

1749 (malonate ester), 1693 (unsaturated ester), 1676 (urea C=O), and 1614 (C=C) cm^{-1}; pmr δ 1.25 (t, J = 7.0 Hz, 9H, CH_3's of ethyl esters), 2.25 (s, CH_3 at C_4), 2.4–3.4 (m, 2H, 6-CH_2), 3.49 (d, J = 9.0 Hz, CH of malonate), 4.19 (m, CH_2's of ethyl esters and H at C_7), 6.15 (s, N_1-H), 7.95 (s, N_3-H); ms *m/e* 356(1, M^+), 311(9), 196(100), 151(17), 142(59), 133(25), 115(36), 96(31), 43(34), 42(22).

Methyl 7-Diethoxycarbonylmethyl-2,3,6,7-tetrahydro-4-methyl-2-oxo-1H-1,3-diazepine-5-carboxylate, ***8d***

Reaction of the chloromethyl compound **1***a* (0.438 g) with sodiodiethylmalonate in an analogous manner yielded the product **8***d* (0.336 g, 49%) as colorless needles, mp 161–162 °C. *Anal.* calcd. for $C_{15}H_{22}N_2O_7$: C 52.63, H 6.48, N 8.18; found: C 52.95, H 6.41, N 8.27. The ir (KCl) 3329 and 3209 (N—H str.), 1741 (ester of malonate), 1698 (unsaturated ester), 1676 (urea C=O), and 1616 (C=C) cm^{-1}; pmr δ 1.25 (t, 6H, CH_3 of ethyl esters), 2.86 (m, 2H, 6-CH_2), 3.47 (d, J = 9.0 Hz, 1H, CH of malonate), 3.67 (s, 3H, methyl ester), 4.19 (overlapping q and unresolved m, 5H, CH_2's of ethyl ester and H at C_7), 6.05 (br d, N_1-H), 7.73 (br s, N_3-H); ms *m/e* 342(3, M^+), 182(100), 151(13), 140(18), 133(24), 128(60), 115(31), 96(29), 43(28), 42(22).

Methyl 1-Methyl-3-oxo-8-thia-2,4-diazabicyclo[3.2.1]-octane-7-carboxylate, ***14b***

To a solution of the chloromethylpyrimidine **1***a* (4.38 g) in anhydrous methanol (150 ml) was added potassium hydrosulfide solution (8 ml of 6.3 × 10^{-3} M), and the mixture stirred at 50–60 °C for 2 h. After concentrating to approximately 30 ml, the mixture was cooled, diluted with ether (100 ml), and allowed to stand at 0 °C overnight. The solid (3.42 g) which deposited was crystallized twice from aqueous methanol to yield the product (2.09 g, 48%) as colorless cubic crystals which decomposed at 200 °C. *Anal.* calcd. for $C_8H_{12}N_2O_3S$: C 44.44, H 5.56, N 12.95, S 14.80; found: C 44.32, H 5.51, N 12.79, S 14.70. The ir (KBr) 3575, 3515, 3315, 3205, 1745, 1730, 1677, 1643 cm^{-1}; pmr (DMSO-d_6) δ 1.83 (s, 3H, CH_3 at C-1), 2.1–3.45 (complex signals partly obscured by DMSO signal, approximately 3H), 3.68 (s, 3H, methyl of ester), 5.03 (m, approximately t, 1H, H at C-5), 7.35–7.75 (two overlapping resonances, total 2H, N_2-H and N_4-H). Deuteration caused disappearance of signals at δ 7.35–7.75 and conversion of the δ 5.03 signal to a double d (J = 3.5, 1 Hz approximately); ms *m/e* 216(22, M^+) 183(21), 130(100), 84(22), 59(21), 42(37).

Ethyl 1-Methyl-3-oxo-8-thia-2,4-diazabicyclo[3.2.1]-octane-7-carboxylate, ***14c***

Reaction of the chloromethyl compound **1***c* with sodium hydrosulfide in a manner similar to that of Ashby and Griffiths yielded, after recrystallization three times from ethanol and once from water, the product; mp 203–205 °C (lit. (24) mp 200–202 °C).

Acid-catalyzed Hydrolysis of 1-Methyl-3-oxo-8-thia-2,4-diazabicyclo[3.2.1]octane-7-carboxylic Acid ***14a*** *to 2-Methyl-3-thenoic acid*

The sulfur compound **14***a* (24) (0.200 g) was refluxed with concentrated hydrochloric acid (30 ml) for 4.5 h, cooled, and extracted with chloroform (3 × 30 ml). The bulked chloroform extract was evaporated and the brown tarry residue extracted with water (8 ml) over a steam bath for 0.5 h. The aqueous solution was then decanted and cooled when 2-methyl-3-thenoic acid (0.01 g, 7%) was obtained as brownish yellow crystals; mp 114–116 °C (lit. (36) mp 115–117 °C). The product has identical ir, uv, nmr, and ms to material prepared by the method of Gaertner (36).

Ethyl 2,3,4,5,6,7-Hexahydro-4-methyl-2-oxo-1H-1,3-diazepine-5-carboxylate, ***16***

The sulfur compound **14***c* (0.245 g) and Raney nickel W2 (approximately 3 g) in 90% ethanol (100 ml) were refluxed with stirring for 4 h. The reaction mixture was then cooled, filtered through a pad of Celite, and evaporated to give a colorless residue (202 mg, 95%); mp 140.5–142 °C. *Anal.* calcd. for $C_9H_{16}N_2O_3$: C 53.99, H 8.05, N 13.99; found: C 54.01, H 8.09, N 13.99. The ir 3420, 1727, 1666 cm^{-1}; the nmr δ 1.24 (t, J = 7.0 Hz, CH_3 of ethyl ester), 1.25 (d, J = 7.0 Hz, CH_3 at C_4), 2.0 (m, 2H, 6-CH_2), 2.69 (m, 1H, H at C_5), 3.17 (m, 2H, 7-CH_2), 3.80 (m, 1H, H at C_4), 4.13 (q, 2H, J = 7.0 Hz, CH_2 of ethyl ester), 5.60 (br s, NH), 5.98 (br s, NH); after exchange with D_2O, the m at δ 3.80 changed to two q, J = 7.0 Hz and 3.2 Hz; ms *m/e* 200(6, M^+), 101(8), 86(8), 73(10), 55(8), 44(100).

Acknowledgements

The authors wish to thank the National Research Council of Canada and Memorial University of Newfoundland for financial support and Memorial University for the award of a fellowship to one of us (R.A.C.). In addition the authors wish to express their gratitude to Dr. M. A. Davis and Ayerst Research Laboratories, Montreal, for the pharmacological testing.

1. F. D. Popp and A. C. Noble. *In* Advances in heterocyclic chemistry. Vol. 8. *Edited by* A. R. Katritzky and A. J. Boulton. Academic Press, New York and London. 1967. pp. 21–27.
2. G. Homyak, K. Lempert, and G. Simig. Kem. Kozl. **33**, 81 (1970).
3. F. Troxler, H. P. Weber, A. Jaunin, and H. R. Loosli. Helv. Chim. Acta, **57**, 750 (1974).
4. A. Hassner and D. J. Anderson. Synthesis, 483 (1975).
5. H. P. M. Thiellier, G. J. Koomen, and U. K. Pandit. Heterocycles, **3**, 707 (1975).
6. T. H. Yang and C. M. Chen. J. Chin. Chem. Soc. (Taipei), **19**, 149 (1972).
7. E. Bullock, R. A. Carter, B. Gregory, and D. C. Shields. Chem. Commun. 97 (1972).
8. P. J. Brignell, E. Bullock, U. Eisner, B. Gregory, A. W. Johnson, and H. Williams. J. Chem. Soc. 4819 (1963).
9. E. Benary. Ber. **44**, 489 (1911).
10. P. J. Brignell, U. Eisner, and H. Williams. J. Chem. Soc. 4226 (1965).
11. O. L. Chapman and P. Fitton. J. Am. Chem. Soc. **85**, 41 (1963).
12. P. Biginelli. Gazz. Chim. Ital. **23**, 360 (1893).

13. D. J. BROWN. The pyrimidines. Wiley, New York. 1962. pp. 440.
14. K. FOLKERS and T. B. JOHNSON. J. Am. Chem. Soc. **55**, 3784 (1933).
15. J. J. DONLEAVY and M. A. KISE. Org. Synth. **17**, 63 (1937).
16. D. L. OSTERCAMP. J. Org. Chem. **30**, 1169 (1965).
17. G. O. DUDEK and R. H. HOLM. J. Am. Chem. Soc. **84**, 2691 (1962).
18. G. J. MARTIN and M. J. MARTIN. *In* Progress in N.m.r. spectroscopy. Vol. 8. *Edited by* J. W. Emsley, J. Feeney, and L. H. Sutcliffe. Pergamon, London. 1972.
19. G. O. DUDEK. J. Org. Chem. **30**, 548 (1965).
20. G. DESTEVENS, B. SMOLINSKY, and L. DORFMAN. J. Org. Chem. **29**, 1115 (1964).
21. E. BENARY. Ber. **44**, 493 (1911).
22. G. W. ANDERSON, H. E. FAITH, H. W. MARSON, P. S. WINNEK, and R. O. ROBIN, JR. J. Am. Chem. Soc. **64**, 2902 (1942).
23. S. AHMED, R. LOFTHOUSE, and G. SHAW. Chem. Commun. 959 (1974).
24. J. ASHBY and D. GRIFFITHS. J. Chem. Soc. Perkin Trans. I, 657 (1975).
25. L. Y. IVANOVSKAYA, V. F. SEDOVA, M. I. GORFINKEL, and V. P. MAMAEV. Izv. Sib. Otd. Akad, Nauk. SSSR, Ser. Khim. Nauk. 123 (1969).
26. C. R. WARNER, R. J. STRUNK, and H. G. KUIVILA. J. Org. Chem. **31**, 3381 (1966).
27. G. ZIGEUNER, H. HAMBERGER, H. BLASCHKE, and H. STERK. Monatsh. Chem. **97**, 1408 (1966).
28. H. BUDZIKIEWICZ, C. DJERASSI, A. H. JACKSON, G. W. KENNER, D. J. NEWMAN, and J. M. WILSON. J. Chem. Soc. 1949 (1964).
29. J. O. MADSEN and S. O. LAWESSON. Tetrahedron, **24**, 3369 (1968).
30. J. L. LONGRIDGE and T. W. THOMPSON. J. Chem. Soc. C, 1658 (1970).
31. R. HARADA. Nippon Kagaku Zasshi, **90**, 1044 (1969).
32. K. FOLKERS and T. B. JOHNSON. J. Am. Chem. Soc. **55**, 1140 (1933).
33. M. ANDERSON and A. W. JOHNSON. J. Chem. Soc. 2411 (1965).
34. H. RAPOPORT and C. D. WILLSON. J. Org. Chem. **26**, 1102 (1961).
35. J. F. BIELLMANN and M. P. GOELDNER. Tetrahedron, **27**, 2957 (1971).
36. R. GAERTNER. J. Am. Chem. Soc. **73**, 3934 (1951).
37. S. A. GLICKMAN and A. C. COPE. J. Am. Chem. Soc., **67**, 1017 (1945).

N-Methylamino acids in peptide synthesis. V. The synthesis of *N*-*tert*-butyloxycarbonyl,*N*-methylamino acids by *N*-methylation[1]

S. T. CHEUNG AND N. LEO BENOITON

Department of Biochemistry, University of Ottawa, Ottawa, Ont., Canada K1N 9A9

Received August 23, 1976

S. T. CHEUNG and N. LEO BENOITON. Can. J. Chem. **55**, 906 (1977).

The preparation of enantiomerically pure *N*-*tert*-butyloxycarbonyl,*N*-methylamino acids by *N*-methylation of the parent amino acid derivatives using sodium hydride and methyl iodide in tetrahydrofuran at room temperature is described for neutral amino acids including *O*-benzyl-protected threonine and tyrosine. Methylation of the *O*-benzylserine derivative under these conditions gives the *N*-methyldehydroalanine derivative. The β-elimination is completely suppressed, giving the corresponding *N*-methylserine derivative when the reaction is carried out at 5 °C. Other related data on *N*-methylation and *N*-methylamino acid derivatives are presented.

S. T. CHEUNG et N. LEO BENOITON. Can. J. Chem. **55**, 906 (1977).

On décrit la préparation des *N*-méthylamino-acides *N*-*tert*-butyloxycarbonylés optiquement purs par la *N*-méthylation, à l'aide d'hydrure de sodium et d'iodure de méthyle dans le tétrahydrofuranne à la température de la pièce, de dérivés des acides aminés correspondants; cette méthode a été appliquée aux acides aminés neutres, y compris la thréonine et la tyrosine protégées par un groupe *O*-benzyle. La méthylation du dérivé de la *O*-benzylsérine, dans de telles conditions, conduit au dérivé de la *N*-méthyldéhydroalanine. Lorsque l'on effectue la réaction à 5 °C, l'élimination β est complètement supprimée et l'on obtient le dérivé *N*-méthylsérine correspondant. On présente d'autres données sur la *N*-méthylation et les dérivés d'acides *N*-méthylaminés.

[Traduit par le journal]

Easy access to derivatives of *N*-methylamino acids which can be used in peptide synthesis is desirable for anyone wishing to incorporate an *N*-methylamino acid into peptides. We have previously described a method of preparing *N*-benzyloxycarbonyl derivatives of *N*-methylamino acids by *N*-methylation of the *N*-benzyloxycarbonylamino acid using sodium hydride – methyl iodide in THF containing DMF at 80 °C (2),[2] and subsequently in neat THF at room temperature (4).[3] The latter method is preferable since the former also esterifies the carboxyl group, and removal of the ester group by saponification is accompanied by some racemization (6). We now report the preparation of enantiomerically pure *N*-*tert*-butyloxycarbonyl,*N*-methylamino acids by this simple procedure, a small modification which allows the preparation of derivatives of serine as well, and other data related to *N*-alkylations. In the accompanying papers, we describe a general method for determining the enantiomeric purity of *N*-methylamino acids and their derivatives (7), and report that all of the other methods except one[4] which have been used to prepare optically active *N*-methylamino acids and their derivatives do not give optically pure products (8), a fact which adds considerably to the value of our method of synthesis.

The *N*-*tert*-butyloxycarbonyl,*N*-methylamino acids which we have prepared by reaction of the parent amino acid derivative with sodium hydride (3 mol) and methyl iodide (8 mol) in THF at room temperature are described in Table 1. All

[1]Supported by a grant from the Medical Research Council of Canada. N.L.B. is an Associate of the MRCC. Presented in part at the First Chemical Congress of the North American Continent, Mexico City, Mexico, Dec. 1975. For part IV of this series, see ref. 1.

[2]The abbreviations for the amino-acid derivatives are those recommended by the IUPAC–IUB Commission on Biochemical Nomenclature (3). The amino-acid symbols represent the L-isomer. Other abbreviations used: Boc, *tert*-butyloxycarbonyl; Bz, benzoyl; Bzl, benzyl; Z, benzyloxycarbonyl; THF, tetrahydrofuran; DMF, *N*,*N*-dimethylformamide; ΔAla, didehydroalanine.

[3]Pioneering work on urethane methylation using sodium hydride – methyl iodide was done by Dannley and Lukin (5).

[4]Only the synthesis of an *N*-*p*-toluenesulfonyl,*N*-methylamino acid followed by cleavage with sodium in liquid ammonia gives an optically pure product (8).

$$(CH_3)_3COCO—NHCHR—COOH \xrightarrow[THF,\ 23\ °C]{NaH,\ CH_3I} (CH_3)_3COCO—\underset{\displaystyle CH_3}{\underset{|}{N}}CHR—COOH$$

compounds were shown to contain <0.1% of unmethylated derivative, and <0.1% of contaminating enantiomer (8), except for the *O*-benzyl derivatives whose optical purities were not established. Boc-MeVal-OH has been crystallized for the first time, albeit with difficulty. The melting points for Boc-MeAla-OH and the dicyclohexylammonium salt of Boc-MeVal-OH are higher than those recorded in the literature (see below). Higher melting points for the *N*-benzyloxycarbonyl derivatives of these two *N*-methylamino acids are also reported. These data are in line with our findings (8) that these derivatives are not optically pure when prepared by most of the other methods.[4]

The *O*-benzyl groups of Boc-Thr(Bzl)-OH and Boc-Tyr(Bzl)-OH were found to be stable to the reaction conditions, allowing preparation of the appropriate *N*-methyl derivatives. These are oils which do not precipitate out in the presence of dicyclohexylamine in light petroleum. In contrast, Boc-Ser(Bzl)-OH underwent β-elimination simultaneously with the *N*-methylation to give an excellent yield of Boc-MeΔAla-OH.[5] Similar β-eliminations have been reported for analogous reactions (11, 14). Since we had not in our previous work (4) attempted the methylation of Z-Ser(Bu^t)-OH, which should be less susceptible to β-elimination, we did the experiment and obtained a mixture containing about 75% of the desired Z-MeSer(Bu^t)-OH and 25% of Z-MeΔAla-OH.[6] The latter could be removed easily by crystallizing it out as the dicyclohexylammonium salt thus allowing a practical synthesis (60% yield) of the pure desired compound.[7] At this stage, the temperature of the reaction was lowered to see if β-elimination might be suppressed completely. At 5 °C it was,

TABLE 1. Properties of *N*-*tert*-butyloxycarbonyl,*N*-methylamino acids

Amino acid	Yield (%)	mp (°C)	$[\alpha]_D^{26}$[g] (deg)	^{1}H nmr data (ppm) $\delta_{N\text{-}CH_3}$	δ_{Bu^t}	Formula	Analysis: Calculated C	H	N	Found C	H	N
Ala	83	93–94[b,c]	−30.4[e]	2.84	1.40	$C_9H_{17}NO_4$	53.2	8.4	6.9	53.4	8.6	7.1
Leu	83	56–57[d]	−24.6[d]	2.80	1.40	$C_{12}H_{23}NO_4$	59.75	9.45	5.7	59.7	9.5	5.55
Val		58–59[e]	−90.0	2.84	1.50	$C_{11}H_{21}NO_4$	57.1	9.2	6.1	57.3	9.4	6.2
Val	80[f]	113–114[g]	−49.3[g]	2.84	1.50	$C_{23}H_{44}N_2O_4$	66.95	10.75	6.8	66.75	10.6	6.8
Ile	90[f,h]	117	−45.6	2.85	1.50	$C_{24}H_{26}N_2O_4$	67.6	10.9	6.6	67.8	11.0	6.6
D-aIle	90[f,i]	94	+42.8	2.85	1.50	$C_{24}H_{26}N_2O_4$	67.6	10.9	6.6	67.7	11.0	6.7
Phe	90[f,j]	176[k]	−25.5[k]	3.00	1.50	$C_{27}H_{44}N_2O_4$	70.4	9.6	6.1	70.1	9.5	5.9
Thr(Bzl)	75	Oil		3.00	1.50							
Tyr(Bzl)	70	Oil		2.73	1.37							
ΔAla[l]	86	80[b]		3.18[l]	1.50	$C_9H_{15}NO_4$	53.7	7.5	6.95	53.85	7.5	6.7
D,L-Phe	85	136[b]		3.00	1.50							
Ser(Bzl)[m]	80	Oil		2.90	1.40							

[a] *c* 0.5 in ethanol for acids; methanol for *N*,*N*-dicyclohexylammonium salts. [b]Crystallized from ethyl acetate – light petroleum. [c]Literature mp 90–91 °C (9); mp 89 °C, $[\alpha]_D$ +30° (*c* 0.7 in ethanol) for the D-isomer (10); mp 89–91 °C, $[\alpha]_D^{26}$ −29° (*c* 1 in ethanol) (11); mp 91–92 °C, $[\alpha]_D^{20}$ −31.8° (*c* 2 in ethyl acetate) (12). [d]Crystallized from water; lit. mp 57–58 °C, $[\alpha]_D^{23}$ −25.3° (*c* 1 in DMF) (13); oil (14). [e]Crystals were obtained after 2 years. Crystallization is normal when a seed crystal is used; lit. oil (15). [f]Oil. Physical data, except for nmr data are for the dicyclohexylammonium salt. [g]Crystallized after 30 days; lit. mp 107–110 °C, $[\alpha]_D^{20}$ −54.1° (*c* 1 in methanol) (15); mp 109–110 °C, $[\alpha]_D^{15}$ −51.9° (*c* 1 in ethanol) (14). [h]Literature: oil (16). [i]Literature; oil for L-isomer (17). [j]Literature: oil (18, 19). [k]Literature: mp 165–170 °C, $[\alpha]_D$ −25° (*c* 1 in methanol (20); lit. mp 174 °C, $[\alpha]_D^{15}$ −28.1° (*c* 1 in ethanol) (14). [l]Dehydroalanine, from the methylation of Boc-Ser(Bzl)-OH. $\delta_{\beta\text{-}H}$, 5.42; $\delta_{\alpha\text{-}H}$, 6.00 ppm. [m]Methylation at 5 °C for 72 h.

[5]This derivative would be accessible also by methylation of Boc-ΔAla-OMe using methyl iodide and potassium carbonate in DMF (21).

[6]It follows that this compound could best be prepared from Z-Ser(Bzl)-OH.

[7]The rule seems to be that the Boc- and Z-methylamino acids protected on the side chain by a benzyl or *tert*-butyl group (*i.e.* for Ser, Thr, Tyr, Asp, Glu) do not form insoluble dicyclohexylammonium salts, while other derivatives exemplified by Boc-MeSer(Me)-OH, Z-MeVal-OH, Z-Ser(Bu^t)-OH, and Z-MeΔAla-OH do.

and the *N*-methylation still occurred, albeit more slowly. In fact, this allowed the preparation of not only Z-MeSer(Bu^t)-OH, but Boc-MeSer-(Bzl)-OH in 80% yield as well! It should be noted that this also provides two routes to optically pure *N*-methylserine which is not readily accessible.[8]

Several of the compounds described in Table 1 were obtained from the Boc-amino acids prepared in our own laboratory. Considerable difficulty was encountered when the Boc-amino acids (Boc-Val-OH and Boc-Phe-OH in particular) were purchased from commercial suppliers. The reactions did not go to completion, or else they went to completion only when carried out on a small scale (see below). Fortunately, we were able to resolve this dilemma, after most of this work had been carried out. It was found that there were no difficulties with the methylations when starting materials (Boc-Val-OH and Boc-Phe-OH) were left overnight *in vacuo* at 56 °C before they were used.[9]

In view of the more sluggish reaction at 5 °C, we compared the extents of *N*-methylation for the two types of derivatives and found that Z-Ala-OH had undergone 91% methylation, and Boc-Ala-OH 56% methylation, after 15 h. Hence the methylation of a Z-derivative proceeds more quickly.

In the previous paper (4), we had reported that methylations of Z-Glu-OH and Z-Asp-OH did not go to completion, probably due to precipitation during the reaction. Since other methylations have been carried out in acetonitrile (22), we investigated this solvent as an alternative to THF in case it might prove advantageous.[10] Excellent yields of Z-MeAla-OH and Z-MeLeu-OH were obtained, but no success was achieved with the dicarboxylic amino acids. Methylation of Z-Phe-OH was incomplete, but Z-MePhe-ONa precipitated from the aqueous solution during work-up, and regeneration of this gave pure Z-MePhe-OH (32%), mp 68–69 °C (lit. (11) mp 65–70 °C; (23) mp 69–71 °C). Acetonitrile, therefore, can be used as solvent for the methylations, but it does not offer any obvious advantage.

In order to see if *N*-acyl,*N*-methylamino acids could also be prepared by our method, a few *N*-acylamino acids were methylated. The results, as well as others obtained using the methylation procedure of Olsen (silver oxide and methyl iodide in DMF) (11), are given in Table 2. All these methylations were incomplete, except that of Bz-Leu-OH using our procedure. Moreover, the Bz-MeIle-OH obtained was shown to be partially epimerized. The reaction can be made to go to completion if carried out at 80 °C in the presence of DMF (2), however, these conditions also esterify the carboxyl group. Z-Ala-OH also was nearly completely esterified when a reaction was carried out at 80 °C in the absence of DMF. Since the ester group would normally be removed by saponification, and basic conditions are known to partially racemize fully protected *N*-methylamino acids (6), it would seem that this approach for the preparation of optically active *N*-acyl,*N*-methylamino acids is likely not to give products which are enantiomerically pure.

N-tert-Butyloxycarbonylamino acids are useful in peptide synthesis because the Boc-group satisfies the requirements of a selectively removable protecting group. Since *N*-methylamino acids and their derivatives often behave differently than the corresponding unmethylated compounds under various reaction conditions, it was thought useful to compare the rates of cleavage of the Boc-group from an *N*-methylamino and an amino acid under the same conditions. The amounts of amino acid and *N*-methylamino acid released during specified time periods from four derivatives left in a solution of trifluoroacetic acid (2%) in dichloromethane were determined with an amino-acid analyzer. This dilution was

TABLE 2. Extent of *N*-methylation[a]

Substrate	Percentage methylated[b]
For-Leu-OH	33
Ac-Leu-OH	66[c]
Bz-Leu-OH[d]	99.8[e]
Bz-Val-OH	87
Bz-Ile-OH	95[f]

[a]Using sodium hydride/methyl iodide in THF at 23 °C.
[b]Assuming methylated + unmethylated derivative = 100%.
[c]22% using methylation procedure of Olsen (11).
[d]Gave 60% yield of Bz-MeLeu-OH.
[e]54% using procedure of Olsen (11).
[f]Partial epimerization occurred.

[8]The methylation of serine derivatives will form the subject of a subsequent communication.

[9]We thank Dr. N. Chaturvedi, of Chemical Dynamics, for the gifts of Boc-Val-OH and Boc-Phe-OH, and for the valuable suggestion that our difficulties might be due to the presence of hydrazoic acid, which could be removed by using reduced pressure.

[10]These experiments were carried out by Mr. K. Kuroda.

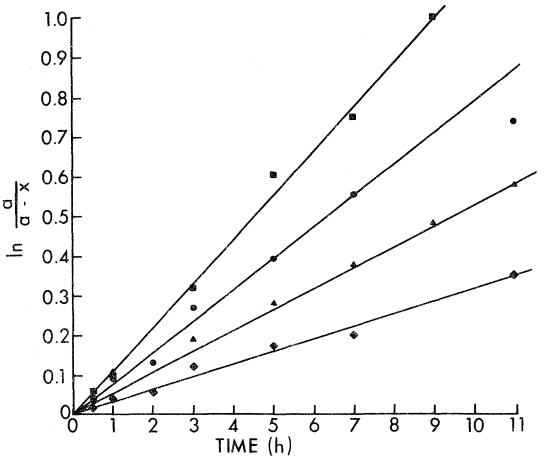

FIG. 1. Calculated least-squares lines of best fit for the apparent first-order cleavage of Boc-derivatives by 2% trifluoroacetic acid in dichloromethane at 23 °C. k = apparent first-order rate constant determined from the slope of the line: (■) Boc-MeAla-OH, $k = 30.9 \times 10^{-6}$; (●) Boc-MeLeu-OH, $k = 22.1 \times 10^{-6}$; (▲) Boc-Ala-OH, $k = 14.7 \times 10^{-6}$; (◆) Boc-Leu-OH, $k = 8.9 \times 10^{-6}$.

used because it was found to give rates slow enough to measure. The results are given in Fig. 1 in the form of a first-order reaction plot. It is seen that for both amino acids tested (alanine and leucine), the Boc-group was cleaved from the *N*-methylamino acid at least twice as fast (2.5 and 2.1 ×) as from the corresponding amino acid. This result is in agreement with the theory that acidolytic cleavage of urethane protecting groups is initiated by protonation of the oxygen atom of the urethane carbonyl group (see ref. 24 for a discussion) which would be favored by the positive inductive effect of the *N*-methyl group, but it is also compatible with protonation being at the nitrogen atom.

Experimental

Materials and Methods

Sodium hydride was obtained from Ventron Corporation, Berverly, Massachusetts, and J. T. Baker Chemical Company, Phillipsburg, New Jersey as a 57–60% dispersion in oil, which contained 1.6–3.7% by weight of NaOH (25). Methyl iodide, silver oxide, acetonitrile, THF, and DMF were products from Fisher Scientific Company, Fair Lawn, New Jersey. THF was refluxed over $LiAlH_4$ for 24 h, and distilled directly into the reaction vessel. This is a change from our previous method of purifying THF which we recommend. Acetonitrile was distilled from P_2O_5. DMF was distilled from CaO immediately before use. Light petroleum refers to the 30–60 °C fraction, from Fisher.

Boc-Ala-OH and Boc-Leu-OH·H_2O were purchased from Beckman Instruments, Palo Alto, California; Boc-Ser(Bzl)-OH, Boc-Thr(Bzl)-OH and Boc-Tyr(Bzl)-OH from Bachem Feinchemickalien, Marine Del Ray, Calif.; and Z-Ser(Bu^t)-OH dicyclohexylammonium salt from Fluka AG, Buchs, Switzerland. The latter was converted to the free acid using aqueous citric acid. Other *N-tert*-butyloxycarbonylamino acids were synthesized by the method of Schwyzer *et al.* (26). Water of hydration was removed by drying a solution of the compound in chloroform (10 ml/mmol) over $MgSO_4$ for ½ h, and evaporating. Final traces of chloroform were removed by reevaporating after having added THF, twice.

Proton nmr (Varian T-60) and amino-acid analyses after deprotection (70% aqueous trifluoroacetic acid for the Boc group, hydrogenation for the benzyl group, and acid hydrolysis for acyl groups) were used routinely for monitoring reactions and characterizing products. Amino-acid analyses were carried out with a Beckman model 120B amino-acid analyzer with the eluting buffer at half-normal flow rate to allow determination of the *N*-methylamino acids (27). Proton chemical shifts are for solutions in deuterochloroform and are given in ppm relative to tetramethylsilane as internal standard. Optical rotations were measured with a Perkin-Elmer model 141 polarimeter using a 1-dm tube. Melting points were taken by the capillary method, and are uncorrected. Elemental analyses were done by Organic Microanalyses, Montreal, on the compounds dried *in vacuo* over P_2O_5.

N-tert-Butyloxycarbonyl,N-methylamino Acids

N-tert-Butyloxycarbonylamino acid (10 mmol) and methyl iodide (5 ml, 80 mmol) were dissolved in purified THF (30 ml), and sodium hydride dispersion (1.32 g, 30 mmol) was added cautiously with gentle stirring to the solution at 0 °C. The suspension, protected from the atmosphere by a drying tube, was stirred at room temperature for 24 h, and the *N-tert*-butyloxycarbonyl,*N*-methylamino acid was isolated and purified as previously described for the *N*-benzyloxycarbonyl derivatives (4), using 5% aqueous citric acid for acidification. For methylations at lower temperature, the reaction vessel was kept in an ice-bath for 15 min after addition of sodium hydride, and then left at 5 °C.[11] Dicyclohexylammonium salts were prepared by adding excess amine to the product dissolved in ether, followed by the addition of light petroleum and storage at 4 °C. Recrystallization from the same solvent mixture gave yields of 65–75%.

The methylation of Boc-Val-OH is extremely sensitive to the quality of the THF used. The methylation of Boc-Ala-OH requires twice the volume of THF, otherwise the reaction is incomplete due to precipitation during the reaction, but it proceeds even if undistilled THF is used. Methylations of Boc-Thr(Bzl)-OH and Boc-Tyr(Bzl)-OH were incomplete when carried out on a 2 mmol scale, but complete on a 1 mmol scale. We were unable to achieve complete methylation (30–50% unmethylated) of samples of Boc-Val-OH (Chemical Dynamics, South Plainfield, N.J.; and Beckman, recrystallized), Boc-Ile-OH·½H_2O (Beckman, dehydrated) and Boc-Phe-OH (Chemical Dynamics; Peninsula, San Carlos, Calif.; Beckman, recrystallized). A 50:50 mixture of the latter and Boc-Phe-OH synthesized by us gave the same in-

[11]It is imperative that the temperature not be allowed to exceed 5 °C. Erratic results were obtained when a cold-room constantly used by others was used.

complete reaction despite the fact that an experiment with the synthetic Boc-Phe-OH alone run in parallel was successful. Methylations of Boc-Ser(Bzl)-OH and Z-Ser (Bu^t)-OH at 5 °C were complete when carried out on a 5 mmol scale but incomplete on a 10 mmol scale. It was then found that the problem could be eliminated by subjecting the starting materials to reduced pressure.[9]

N-Benzyloxycarbonyl,N-methylamino Acids[10]

Methylation conditions and work-up were as described above, with compounds being crystallized from ethyl acetate – light petroleum. Z-Ala-OH (10 mmol) in acetonitrile gave Z-MeAla-OH (84%); mp 67–68 °C; $[\alpha]_D^{26}$ −25.8° (*c* 1 in ethanol), −31.0° (*c* 2 in acetic acid) (lit. mp 58–59 °C, $[\alpha]_D^{20}$ −39.2° (*c* 1 in ethanol) (28); mp 64.5–66 °C, $[\alpha]_D^{28}$ −33.1° (*c* 2 in acetic acid) (29); mp 65–66 °C, $[\alpha]_D^{25}$ −29.2° (*c* 2 in DMF) (2); mp 62–64 °C, $[\alpha]_D^{28}$ −31.0° (*c* 2 in acetic acid) (11); mp 61–62 °C, $[\alpha]_D$ −31 °C (*c* 2 in acetic acid) (30)). Z-Leu-OH (5 mmol) in acetonitrile gave Z-MeLeu-OH (72%), mp 74–75 °C (lit. mp 73–74 °C (2, 4)). Z-Val-OH (10 mmol) in THF gave Z-MeVal-OH (87%), mp 70–71 °C, $[\alpha]_D^{26}$ −86.3° (*c* 2 in ethanol) (lit. mp 69–70 °C, $[\alpha]_D^{24}$ −85.8 °C (*c* 1 in ethanol) (31); mp 68–69 °C, $[\alpha]_D^{27}$ −84.8 °C (*c* 1 in ethanol) (4); mp 70 °C, $[\alpha]_D^{20}$ −82.6° (*c* 1 in ethanol) (14); mp 68.5–69 °C $[\alpha]_D^{20}$ +90 (*c* 0.5 in ethanol) for the D-isomer (32).

Kinetic Cleavage Experiments

A solution of Boc-derivative (0.5–2.0 mmol) in 2% trifluoroacetic acid in dichloromethane (5 ml) was divided into 0.5 ml portions which were kept at 23 ± 1 °C in screw-capped vials. At selected time periods, a tube was freed of solvent by passing a stream of nitrogen into the open vial. The residue was dissolved in citrate buffer, p*H* 7.0, and the mixture was kept frozen until analyzed. Liberated amino acids were determined with the amino-acid analyzer using a 1 × 15 cm column of Aminex A-5 resin eluted with 0.2 *N* sodium citrate buffer at 23 °C at half-normal flow rate (34 ml/h). Ninhydrin color constants were determined for each compound. The data are as follows: p*H* 4.25 buffer: MeLeu, elution time 78.5 min, constant 7.5; Leu, 87.5 and 42.7. p*H* 3.28 buffer: MeAla, 28 and 2.65; Ala, 40 and 38.3. Boc-derivatives are partially cleaved by these buffers if elution is carried out at 57 °C.

1. J. R. McDermott and N. L. Benoiton. Can. J. Chem. **51**, 2562 (1973).
2. J. R. Coggins and N. L. Benoiton. Can. J. Chem. **49**, 1968 (1971).
3. IUPAC-IUB Commission on Biochemical Nomenclature. J. Biol. Chem. **247**, 977 (1972).
4. J. R. McDermott and N. L. Benoiton. Can. J. Chem. **51**, 1915 (1973).
5. R. L. Dannley and M. Lukin. J. Org. Chem. **22**, 268 (1957).
6. J. R. McDermott and N. L. Benoiton. Can. J. Chem. **51**, 2555 (1973).
7. S. T. Cheung and N. L. Benoiton. Can. J. Chem. 55, 911 (1977).
8. S. T. Cheung and N. L. Benoiton. Can. J. Chem. **55**, 916 (1977).
9. W. Broadbent, J. S. Morley, and B. F. Stone. J. Chem. Soc. C, 2632 (1967).
10. S. L. Portnova, V. F. Bystrov, V. I. Tsetlin, V. T. Ivanov, and Yu. A. Ovchinnikov. J. Gen. Chem. USSR. **38**, 428 (1968).
11. R. K. Olsen. J. Org. Chem. **35**, 1912 (1970).
12. R. H. Andreatta and H. A. Scheraga. J. Med. Chem. **14**, 489 (1971).
13. N. Ling and W. Vale. Biochem. Biophys. Res. Commun. **63**, 801 (1975).
14. K. Okamoto, H. Abe, K. Kuromizu, and N. Izumiya. Mem. Fac. Sci. Kyushu Univ. Ser. C, **9**, 131 (1974).
15. J. Meienhofer and R. P. Patel. Int. J. Protein Res. **3**, 347 (1971).
16. M. C. Khosla, M. M. Hall, R. R. Smeby, and F. M. Bumpus. J. Med. Chem. **17**, 431 (1974).
17. M. C. Khosla, M. M. Hall, R. R. Smeby, and F. M. Bumpus. J. Med. Chem. **17**, 1156 (1974).
18. M. C. Khosla, R. R. Smeby, and F. M. Bumpus. J. Am. Chem. Soc. **94**, 4721 (1972).
19. C. Peña, J. M. Stewart, and T. C. Goodfriend. Life Sci. **14**, 1331 (1974).
20. J. Blake and C. H. Li. Int. J. Peptide Protein Res. **4**, 343 (1972).
21. D. H. Rich, J. Tam, P. Mathiaparanam, and J. Grant. Synthesis, 402 (1975).
22. G. Marino, L. Valente, R. A. W. Johnstone, F. Mohammedi-Tabrizi, and G. C. Sodini. J. Chem. Soc. Chem. Commun. 357 (1972).
23. H. Gregory, D. S. Jones, and J. S. Morley. J. Chem. Soc. C, 531 (1968).
24. K. Blaha and J. Rudinger. Coll. Czech Chem. Commun. **30**, 585 (1965).
25. J. R. McDermott and N. L. Benoiton. Chem. Ind. (London) 169 (1972).
26. R. Schwyzer, P. Sieber, and H. Kappeler. Helv. Chim. Acta, **42**, 2622 (1959).
27. J. R. Coggins and N. L. Benoiton. J. Chromatogr. **52**, 251 (1970).
28. G. Losse and H. Raue. Tetrahedron, **25**, 2677 (1969).
29. S. Gerchakov and H. P. Schultz. J. Med. Chem. **12**, 141 (1969).
30. M. Goodman, F. Chen, and F. R. Prince. Biopolymers, **12**, 2549 (1973).
31. P. A. Plattner, K. Vogler, R. O. Studer, P. Quitt, and W. Keller-Schierlein. Helv. Chim. Acta, **46**, 927 (1963).
32. Yu. A. Ovchinnikov, V. T. Ivanov, and A. A. Kiryuskin. Izv. Akad. Nauk. SSSR Otd. Khim. Nauk. 2046 (1962).

N-Methylamino acids in peptide synthesis. VI. A method for determining the enantiomeric purity of *N*-methylamino acids and their derivatives by ion-exchange chromatography as their C-terminal lysyl dipeptides[1]

S. T. CHEUNG AND N. LEO BENOITON

Department of Biochemistry, University of Ottawa, Ottawa, Ont., Canada K1N 9A9

Received August 23, 1976

S. T. CHEUNG and N. LEO BENOITON. Can. J. Chem. **55**, 911 (1977).

A method capable of detecting one part in one thousand of the other isomer is described for determining the enantiomeric purity of *N*-methylamino acids and their cleavable derivatives. The method consists in converting the *N*-methylamino acid to its *N*-benzyloxycarbonyl derivative, and/or coupling the derivative with benzyl N^{ε}-benzyloxycarbonyl-L-lysinate using *N,N'*-dicyclohexylcarbodiimide, followed by removal of protecting groups by catalytic hydrogenation or other cleavage methods not affecting the chirality of the product. The resulting diastereomeric lysyl peptides are analyzed by ion-exchange chromatography on a 15 cm column of Aminex A-5 resin using an amino-acid analyzer. The method is applicable to samples contaminated by the corresponding unmethylated amino acid or derivative, and in effect, provides a new method for determining the enantiomeric purity of amino acids and their derivatives as well.

Examples are given where, in some cases, optical purity verification or configurational assignment for *N*-methylamino acids can be achieved by inspection of the nmr spectra of related lysyl dipeptide derivatives.

S. T. CHEUNG et N. LEO BENOITON. Can. J. Chem. **55**, 911 (1977).

On décrit une méthode de détermination de la pureté énantiomérique d'acides *N*-méthylaminés et de leurs dérivés pouvant être clivés qui permet de détecter une partie dans mille de l'autre isomère. Cette méthode est basée sur la conversion de l'acide *N*-méthylaminé en dérivé *N*-benzyloxycarbonylé et/ou le couplage, à l'aide de la *N,N'*-dicyclohexylcarbodiimide, du dérivé avec le N^{ε}-benzyloxycarbonyl L-lysinate de benzyle; on enlève ensuite les groupements protecteurs par une hydrogénation catalytique ou par d'autres méthodes de clivage n'affectant pas la chiralité du produit. On analyse les peptides diastéréoisomères contenant de la lysine qui en résultent par chromatographie d'échange ionique sur une colonne de 15 cm de résine Aminex A-5 utilisant un analyseur d'acide aminé. La méthode peut être appliquée à des échantillons contaminées par les acides aminés non-méthylés correspondants ou leurs dérivés et fournit en effet une nouvelle méthode pour déterminer la pureté énantiomérique d'acides aminés ainsi que celle de leurs dérivés.

On donne quelques exemples où la vérification de la pureté optique ou l'attribution de configuration des acides *N*-méthylaminés a pu être effectuer par un examen des spectres rmn des dérivés de dipeptides connexes contenant de la lysine.

[Traduit par le journal]

Despite the many methods available for determining the optical purity of amino acids (see ref. 2) there is no general method available for determining the optical purity of *N*-methylamino acids or their derivatives. N-Protected *N*-methylamino acids are used in peptide synthesis, and these are accessible by methylation of the corresponding N-protected amino acids, so a method applicable to the derivatives as well as the free *N*-methylamino acids, would be valuable. This paper describes such a method. The method consists in coupling the N-protected *N*-methylamino acid, or an *N*-methylamino acid which has been converted to its *N*-benzyloxycarbonyl derivative, with an N^{ε}-protected L-lysine ester, followed by deprotection and analysis for the diastereomeric lysyl dipeptides with an amino-acid analyzer. There are conflicting reports in the literature on the application to *N*-methylamino acids of the method of Manning and Moore (2) for determining amino-acid enantiomers. We have reexamined this question. Some data on the analysis of related protected diastereomeric peptides by nmr spectroscopy are also given. Results on the application of the chromatographic method to *N*-methylamino acids and their derivatives pre-

[1]Supported by a grant from the Medical Research Council of Canada. N.L.B. is an Associate of the MRCC. Presented in part at the First Chemical Congress of the North American Continent, Mexico City, Mexico, Dec. 1975. For part V of this series, see ref. 1.

pared by various methods appear in the accompanying paper (3).

In 1968, Manning and Moore described a simple and elegant chromatographic method for the determination of amino acid enantiomers (2). The method consists of reacting the amino acid with, in most cases, L-leucine *N*-carboxyanhydride, followed by analysis for the leucyl-amino acid dipeptide with an amino-acid analyzer. Choice of the appropriate chromatographic system allows complete separation of the diastereomeric L-L- and L-D-dipeptides. We attempted to apply this method to *N*-methylamino acids, using L-alanine *N*-carboxyanhydride instead of L-leucine *N*-carboxyanhydride because our *N*-methylation experiments had been carried out with leucine derivatives. We reported that the reaction was sluggish, that more by-products were formed, but that it worked (4). Reexamination of this, however, led us to retract this conclusion (5). It was found that the peptide H-Ala-MeLeu-OH[2] had an unusually low ninhydrin color-yield, and that the peaks had been misassigned. Since then, three reports on the use of this method for configurational assignments for MeAla and MePhe (7) and optical purity determinations for MeLeu (8) and MeAla[3] have come to our attention. We have therefore again reexamined this question. The reaction was carried out as described (4), and the peptides were analyzed as previously described (5) but also by pumping the eluting buffer at half-normal flow-rate, which allows definite distinction between *N*-methylamino acids and amino acids or peptides.[4] D,L-Alanine and D,L-leucine were used as controls. We found that L-alanine *N*-carboxyanhydride did not couple with D,L-MeAla, D,L-MeLeu, and D,L-MeVal; and that D,L-leucine *N*-carboxyanhydride did not couple with D,L-MeVal and D,L-MeLeu; but that D,L-leucine *N*-carboxyanhydride did couple with D,L-MeAla. These results are in agreement with the two reports for MeAla (7),[3] and also our previous conclusion for MeLeu (5). There is no obvious explanation for the different behavior of MeAla towards leucine *N*-carboxyanhydride and alanine *N*-carboxyanhydride. We suggest extreme caution in interpreting results if this method is used.

Having resigned ourselves several years ago to the impossibility of using the method of Manning and Moore, we were nevertheless able to establish the optical purity of one of our synthetic derivatives, Z-MeLeu-OH. This was accomplished by incorporating the *N*-methylamino acid, through the intermediate benzyl ester, into the dipeptide H-Ala-MeLeu-OH, whose diastereomers could be separated with the amino-acid analyzer (10). In the process, we established that this peptide had an unusually low ninhydrin color-yield (6% of that for H-Ala-Leu-OH) (10), and that the color-yield of its retro-isomer H-MeLeu-Ala-OH was negligible (10). It occurred to us that a lysyl residue should impart a normal color-yield to a dipeptide containing an *N*-methylamino acid regardless of its position in the peptide, and that the diastereomeric peptides might be separable on a short column of the analyzer which is used to separate basic amino acids. This proved to be the case, and we were able to couple our synthetic Boc- and Z-methylamino acids directly with a lysine derivative to achieve our objective.

The reactions are described in [1]. For the lysine derivative, we chose the H-Lys(Z)-OBzl whose protecting groups are then removed by catalytic hydrogenation, which also deprotects the Z-methylamino acid.[5] Boc-derivatives are deprotected by an additional treatment, with trifluoroacetic acid.[6] For determination of the optical purity of a free *N*-methylamino acid, it is converted to its Z-derivative which is obtained as an oil and used as such. The coupling is carried out on a 0.2 mmol scale. For the coupling reagent, we examined the use of *N*-ethoxycarbonyl-2-ethoxy-1,2-dihydroquinoline (13), and *N,N'*-dicyclohexylcarbodiimide

[2]The abbreviations for the amino-acid and peptide derivatives are those recommended by the IUPAC–IUB Commission on Biochemical Nomenclature (6). When not indicated, the amino-acid symbols represent the L-isomer. Other abbreviations used: Boc, *tert*-butyloxycarbonyl; Bzl, benzyl; Tos, *p*-toluenesulfonyl; Z, benzyloxycarbonyl.

[3]D. H. Rich, personal communication.

[4]The color-yield increases by more than twice if the compound is not an ordinary amino acid or peptide (4).

[5]H-Lys(Z)-OMe, with saponification of the dipeptide before hydrogenation, can be used to prepare the diastereomeric mixture for reference, but not for the analysis of optical purity because saponification would partially racemize the peptide (11).

[6]The purity of a Tos-methylamino acid prepared by the method of Fischer and Lipschitz (12) can be established similarly, if sodium in liquid ammonia is used for deprotection (3).

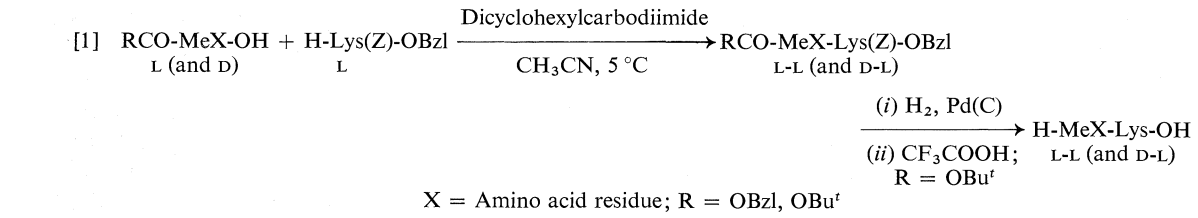

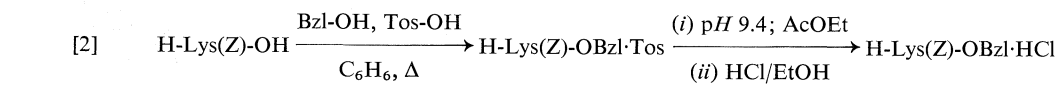

with *N*-hydroxysuccinimide as additive (14), which seemingly might have offered advantages (10), but we obtained the cleanest products using *N*,*N*′-dicyclohexylcarbodiimide alone (15). Acetonitrile was chosen as solvent to minimize acyl-urea formation (16). The yields obtained are not high (30–40% ?), but adequate for the purpose. The H-Lys(Z)-OBzl was prepared as the hydrochloride by the azeotropic method as shown in [2] followed by purification by extraction from a solution at p*H* 9.4 as had been done for the methyl ester (17), followed by crystallization. Without the purification (18), the *p*-toluenesulfonyl salt always contained some H-Lys(Z)-OH and/or H-Lys-OBzl. We found that the same compound prepared from Z-Lys(Z)-OH using phosphorus pentachloride and benzyl alcohol had a wide melting range several degrees lower than that reported (19).

The analysis of amino acids with a Beckman analyzer according to Spackman *et al.* (20) is based on the separation of the acidic and neutral amino acids on a long (62 cm) column of AA-15 resin, eluted with p*H* 3.25 and 4.25 buffers, and the basic amino acids on a short (7 cm) column of PA-35 resin, eluted with p*H* 5.28 buffer. Chromatography of the diastereomeric peptide pairs for H-MeAla-Lys-OH and H-MeVal-Lys-OH on the short column using p*H* 5.28 buffer as eluent gave single broad peaks at 55–60 min, and buffers of higher p*H* gave peaks emerging sooner which were sharper. However, good separation was achieved on the intermediate length (15 cm) column of Aminex A-5 resin, using p*H* 6.50 as eluting buffer. This additional column has been part of our instrument for nearly a decade, and has proven useful on several other occasions (10, 21). The chromatographic data for these and other dipeptides appear in Table 1. The data were obtained by chromatography of the products obtained by coupling the *N*-protected amino acids with H-D,L-Lys(Z)-OBzl.[7] The identities of the peaks were established by synthesis and chromatography of the L-L-peptides. Integration of the peaks gave the relative ninhydrin color-yields for each pair of diastereomers. Higher color-yields were observed for an L-D-peptide than for its L-L-isomer. This contrasts with the lower color yields for L-D-peptides not containing *N*-methylamino acids (2). These color-yield ratios are correct provided the mixtures from which they were obtained were 50:50 mixtures. Evidence for this is presented below. All the diastereomers are completely separated by the systems described, allowing detection of as little as one part in one thousand of one isomer in a diastereomeric mixture. This was confirmed by analyzing mixtures containing decreasing amounts of an L-D-peptide, prepared by the

TABLE 1. Chromatographic data for analysis of H-MeX-Lys-OH diastereomers[a]

X	Elution time (min)[b] L-L	Elution time (min)[b] D-L	Ninhydrin color-yield ratio D-L/L-L
Ala	31	36	1.18
Val	31	46	1.38
Leu	39	63	1.44
Phe[c]	32	80	1.10

[a]Beckman model 120B amino-acid analyzer, Aminex A-5 (0.9 × 15 cm) resin, eluted with 0.35 *N* sodium citrate buffer, p*H* 6.50, at 57 °C at 68 ml/h.
[b]Other elution times: lysine, 38; ammonia, 50; *N*,*N*′-dicyclohexylurea, 53.
[c]p*H* 7.50 eluting buffer.

[7]An alternative would be to couple the racemic *N*-methylamino-acid derivative with the optically active ester. The D-L-peptide obtained would then be the enantiomorph of the L-D-peptide obtained above.

addition of a 50:50 diastereomeric mixture to a solution of the L-L-peptide. The feasibility of this experiment implies that L-L-peptide gave a single peak with the analyzer. All our synthetic L-L-peptides did so (3). This proves that none of the reactions ([1] and [2]) involved in the method cause racemization, and establishes the validity of its use for demonstrating that an *N*-methylamino acid or its derivative is enantiomerically pure. The accuracy of the method was verified by analyzing samples of Z-MeAla-OH containing 2.5 and 10% of D-isomer, prepared by adding racemate to the enantiomer. The results were within 12% of the theoretical values.[8]

A noteworthy and valuable feature of the method is that it can be applied to a compound in the presence of some of the corresponding unmethylated compound. This is because the unmethylated peptide emerges from the column shortly before the corresponding methylated peptide for the eight peptides listed in Table 1. Moreover, each unmethylated diastereomeric peptide pair emerges separated, which provides, in effect, a new, general method for the determination of the enantiomeric purity of amino acids and their derivatives, which we are using routinely in preference to the method of Manning and Moore (2).

Recent additions to the methods allowing distinction between dipeptide diastereomers include nmr spectroscopy. Weinstein and Pritchard have reported different chemical shifts for the alanine methyl group in some *N*-protected alanyl dipeptide methyl esters (22), and Davies *et al.* have reported different chemical shifts for the methoxy methyl group in the *N*-benzoyl dipeptide methyl esters containing alanine and valine (23). Examination of the nmr spectra (100 MHz) of a few protected lysyl dipeptides containing an *N*-methylamino acid revealed that the diastereomers of Z-MeLeu-Lys(Z)-OMe and Z-MeVal-Lys(Z)-OMe could be readily distinguished by virtue of the different chemical shifts of the methoxy methyl singlets. These are at 371 (L-L) and 368 (D-L) Hz for the leucyl derivative (*N*-methyl, 283), and 371.5 (L-L) and 366.5 (D-L) Hz for the valyl derivative (*N*-methyl, 287). Integration of the pertinent peaks allowed the demonstration that the products formed by coupling equimolar amounts of Z-D,L-MeVal-OH or Z-D,L-MeLeu-OH with H-Lys(Z)-OMe were 50:50 mixtures of L-L- and D-L-isomers. When these protected racemic *N*-methylamino acids were coupled with 0.1 mol. equiv. of ester, the products contained the peptides in the L-L:D-L ratios of 57:43 and 58:42, respectively. It thus transpires that some kinetic resolution obtains, the L-L-isomer being favored, but not when there is enough ester present to react with all of the *N*-methylamino acid derivative. We therefore consider the color-yield ratios described above (Table 1) as true values.

Use of nmr as described above, in effect, provides a second method, albeit a less sensitive one, for determining the enantiomeric purity of MeLeu and MeVal, and their derivatives, or for establishing the configuration of samples of these *N*-methylamino acids. The method cannot be used for MeAla, since the methoxy methyl singlets of Z-D,L-MeAla-Lys(Z)-OMe coincide. Boc-D,L-MeLeu-Lys(Z)-OMe also did not give separated methoxy methyl peaks. However, another derivative of this same peptide, namely Z-D,L-MeLeu-Lys(Z)-OH, gave separated *N*-methyl singlets, at 282 and 278 Hz.

Experimental

Materials and Methods

The Boc- and Z-methylamino acids were prepared as described in (1). L-Alanine *N*-carboxyanhydride, mp 92 °C, and D,L-leucine *N*-carboxyanhydride mp 49–50 °C, were prepared from the Z-amino acid using thionyl chloride by standard procedures (24). Acetonitrile was distilled from P_2O_5. The amino-acid analyzer was a standard model 120B Beckman instrument. Aminex A-5 resin was purchased from Bio-Rad Laboratories, Richmond, California. The resin compresses more during an analysis than do the AA-15 and PA-35 resins, and give more variable elution times. The eluting buffers were prepared by adding 50% NaOH to the standard p*H* 5.28 buffer.

Synthesis of H-Lys(Z)-OBzl·HCl

A mixture of H-Lys(Z)-OH (5.60 g, 20 mmol), *p*-toluenesulfonic acid·H_2O (4.56 g, 25 mmol), benzyl alcohol (25 ml), and benzene (35 ml) was heated (oil bath) under reflux for 7 h, the water formed being collected in a Dean–Stark receiver. Ether (100 ml) and light petroleum (100 ml) were added with shaking to the cooled mixture. The precipitate was collected and washed well with light petroleum. Four grams of the air-dried product (10.4 g) were suspended in water (100 ml), the p*H* of the solution was adjusted to 9.0,[9] and the ester was extracted into ethyl acetate (50 ml). The aqueous layer was washed with ethyl acetate (25 ml), the combined extracts were dried ($MgSO_4$), and the solvent was

[8]Higher accuracy could likely be obtained, but we did not explore this further.

[9]A few drops of ethyl acetate solubilize the ester.

evaporated off. Evaporation was repeated after the addition of ethanol (10 ml), and ethanolic HCl (20 ml) was added. After cooling overnight, the crystals were collected and washed by trituration in ether. Yield: 1.5–1.6 g (45–50%), mp 140–141 °C, $[\alpha]_D^{27}$ − 12.4° (*c* 0.5 in 0.1 *N* HCl) (lit. mp 139 °C, $[\alpha]_D$ − 9.9° (19) and mp 138–140 °C, $[\alpha]_D$ − 7.0° (9)). Thin-layer chromatography on silica gel GF_{254} in 1-butanol – acetic acid – water (4:1:1) gave R_f 0.80; H-Lys(Z)-OH, 0.60; H-Lys-OBzl, 0.23. Melting point for H-D,L-Lys(Z)-OBzl·HCl, 135–135.5 °C. Substantial amounts of H-Lys-OBzl were formed when the reaction was carried out for a longer period of time.

Derivatization of the N-Methylamino Acid

The *N*-methylamino acid is converted to its *N*-benzyloxycarbonyl derivative by the usual procedure. The crystals or residue (≃1 mmol; we have occasionally used 0.5 mmol) remaining after evaporation of a solution are dissolved in 3 ml of 4 *N* NaOH, 0.2 ml of benzyl chloroformate is added, and the mixture is stirred vigorously at 5 °C for 4 h. The solution is extracted with ether (5 ml), acidified to Congo Red with 5 *N* HCl while still cold, and the product is extracted into ethyl acetate (10 ml × 2). The combined extracts are washed with water (× 2), dried ($MgSO_4$), and evaporated to give an oil, which is used as such to avoid fractionation. The yield for MeVal is lower than for MeAla or MeLeu.

Dipeptide Synthesis

To the Boc- or Z-methylamino acid (0.2 mmol) in 2 ml of acetonitrile at 5 °C are added H-Lys(Z)-OBzl·HCl (81.4 mg, 0.2 mmol) and triethylamine (20.3 mg, 0.2 mmol). The mixture is stirred for 15 min, *N,N'*-dicyclohexylcarbodiimide (41.2 mg, 0.2 mmol) is added, and the mixture is stirred at 5 °C for 18 h. One drop of acetic acid is added, followed by acetone (5 ml), and the mixture is filtered after cooling for 1 h. The solvents are evaporated off, the residue is taken up in chloroform (35 ml), and the solution is washed successively with 10% aqueous citric acid (× 2), water, aqueous $NaHCO_3$ (× 2), and water, dried, and the solvent is evaporated off. The protected peptides which were analyzed by nmr were prepared in the same manner using H-Lys(Z)-OMe·HCl (17). One of these was then saponified.[5]

The residue is taken up in 80% aqueous acetic acid and the solution is hydrogenated over 10% palladium-on-charcoal catalyst (100 mg) for 18 h after filtration through Celite. The catalyst is removed by filtration, the solution is evaporated to dryness, and the residue is left for 1 h in 70% aqueous trifluoroacetic acid if a Boc-group is present. After evaporation, 10 ml of water are added, and the last traces of *N,N'*-dicyclohexylurea are allowed to crystallize by leaving the solution at 5 °C for several hours.

Analysis of Diastereoisomers

A 1-ml aliquot of the above solution which has been filtered through Celite is diluted to 5 ml with 0.2 *N* sodium citrate, p*H* 2.2, and 0.5 ml of this is analyzed using the conditions described in Table 1. The relative amounts of the two isomers in the sample are obtained by comparison of the surface areas of the two peaks after having divided the surface area of the D,L-peak by the color-yield ratio given in Table 1. These ratios can be obtained by couplings in which either one or both of the components are racemic.

NOTE ADDED IN PROOF

We have found in studies on couplings that if 1-hydroxybenzotriazole (W. König and R. Geiger. *Chem. Ber.* **103**, 788 (1970)) is added to the *N,N*-dicyclohexylcarbodiimide-mediated coupling of a Z-methylamino acid, the acylurea normally formed does not appear, and the yields are very good (F.M.F. Chen and N.L.B.).

1. S. T. CHEUNG and N. L. BENOITON. Can. J. Chem. **55**, 906 (1977).
2. J. M. MANNING and S. MOORE. J. Biol. Chem. **243**, 5591 (1968).
3. S. T. CHEUNG and N. L. BENOITON. Can. J. Chem. **55**, 916 (1977).
4. J. R. COGGINS and N. L. BENOITON. J. Chromatogr. **52**, 251 (1970).
5. J. R. MCDERMOTT and N. L. BENOITON. Can. J. Chem. **51**, 1915 (1973).
6. IUPAC–IUB Commission on Biochemical Nomenclature. J. Biol. Chem. **247**, 977 (1972).
7. W. L. MEYER, L. F. KUYPER, R. B. LEWIS, G. E. TEMPLETON, and S. H. WOODHEAD. Biochem. Biophys. Res. Commun. **56**, 234 (1974).
8. N. LING and W. VALE. Biochem. Biophys. Res. Commun. **63**, 801 (1975).
9. E. WÜNSCH, H-G. HEIDRICH, and W. GRASSMANN. Chem. Ber. **97**, 1818 (1964).
10. J. R. MCDERMOTT and N. L. BENOITON. Can. J. Chem. **51**, 2562 (1973).
11. J. R. MCDERMOTT and N. L. BENOITON. Can. J. Chem. **51**, 2555 (1973).
12. E. FISCHER and W. LIPSCHITZ. Ber. **48**, 360 (1915).
13. B. BELLEAU and G. MALEK. J. Am. Chem. Soc. **90**, 1651 (1968).
14. F. WEYGAND, D. HOFFMANN, and E. WÜNSCH. Z. Naturforsch. Teil B, **21**, 426 (1966).
15. J. C. SHEEHAN and G. P. HESS. J. Am. Chem. Soc. **77**, 1067 (1955).
16. ST. GUTTMANN and R. A. BOISSONNAS. Helv. Chim. Acta, **41**, 1852 (1958).
17. J. COGGINS, R. DEMAYO, and N. L. BENOITON. Can. J. Chem. **48**, 385 (1970).
18. O. ABE, H. TAKIGUCHI, M. OHNO, S. MAKISUMI, and N. IZUMIYA. Bull. Chem. Soc. Jpn. **40**, 1945 (1967).
19. B. F. ERLANGER and E. BRAND. J. Am. Chem. Soc. **73**, 4025 (1951).
20. D. H. SPACKMAN, W. H. STEIN, and S. MOORE. Anal. Chem. **30**, 1190 (1958).
21. J. H. SEELY, R. EDATTEL, and N. L. BENOITON. J. Chromatogr. **44**, 618 (1969).
22. B. WEINSTEIN and A. E. PRITCHARD. J. Chem. Soc. Perkin Trans. I, 1015 (1972).
23. J. S. DAVIES, R. J. THOMAS, and M. K. WILLIAMS. J. Chem. Soc. Chem. Commun. 76 (1975).
24. H. LEUCHS. Ber. **39**, 857 (1906).

N-Methylamino acids in peptide synthesis. VII. Studies on the enantiomeric purity of *N*-methylamino acids prepared by various procedures[1]

S. T. CHEUNG AND N. LEO BENOITON

Department of Biochemistry, University of Ottawa, Ottawa, Ont., Canada K1N 9A9

Received August 23, 1976

S. T. CHEUNG and N. LEO BENOITON. Can. J. Chem. **55**, 916 (1977).

The enantiomeric purity of *N*-methylamino acids and their derivatives obtained by various procedures has been examined by analysis with an amino-acid analyzer of the diastereomeric lysyl dipeptides formed by coupling them with a lysyl derivative. *N*-Benzyloxycarbonyl, and *N*-*tert*-butyloxycarbonyl,*N*-methylamino acids obtained by methylation of the parent derivative using sodium hydride and methyl iodide, and *N*-methylamino acids obtained by methylation of the *p*-toluenesulfonylamino acid followed by treatment with sodium in liquid ammonia, are optically pure. Compounds obtained by other procedures which include reductive alkylations or the use of silver oxide – methyl iodide are generally not optically pure.

S. T. CHEUNG et N. LEO BENOITON. Can. J. Chem. **55**, 916 (1977).

On a examiné la pureté énantiomérique d'acides *N*-méthylaminés et de leurs dérivés qui avaient été obtenus par divers procédés; ces études ont été effectuées en examinant à l'aide d'un analyseur d'acide aminé des dipeptides diastéréoisomères contenant de la lysine et qui ont été formés par couplage de ces acides aminés avec un dérivé contenant de la lysine. Les acides *N*-méthylaminés portant aussi des groupes *N*-benzyloxycarbonyle ou *N*-*tert*-butyloxycarbonyle, obtenus par méthylation du composé de base à l'aide d'hydrure de sodium et d'iodure de méthyle, ainsi que les acides *N*-méthylaminés obtenus par une méthylation de l'acide *p*-toluènesulfonylaminé correspondant suivie par un traitement avec le sodium dans l'ammoniac liquide, sont optiquement purs. Les composés obtenus par d'autres méthodes, y compris les alkylations réductives et l'utilisation de l'oxyde d'argent et l'iodure de méthyle, ne sont généralement pas optiquement purs.

[Traduit par le journal]

N-Methylamino acids are frequently encountered, or incorporated into peptides for various studies of a biological or physical nature. A method for their preparation has been available since the time of Fischer [1],[2] and a second, more commonly used one [2] was introduced by Quitt *et al.* (4) in 1963. Others [3]–[5] have made their appearance more recently. It has generally been accepted that these methods give optically pure products, however, the only criterion of purity available has been specific rotation measurements. No unequivocal method of establishing the enantiomeric purity of *N*-methylamino acids has been available. In the accompanying paper (1), we describe a method for doing this. In this paper, we report the results of enantiomeric purity determinations on *N*-methylamino acid products prepared by most of the general methods available for their synthesis. Also included are results on the optical purity of *N*-benzylamino acids prepared by reductive alkylation using various reducing agents.

Methylation of p-Toluenesulfonyl Derivatives

This method involves methylation of the Tos-amino acid in basic solution with methyl iodide at 65 °C (2), followed by cleavage of the Tos-amido group by one of various procedures [1].[4] The results appear in Table 1. All cleavage methods using acid led to significant racemization. Only sodium in liquid ammonia (3) gave pure products. The original acid hydrolysis method of Fischer and Lipschitz (2) gave less racemization than did acidolytic cleavage by hydrogen bromide in acetic acid (11), which gave about the same results whether carried out at room temperature or at 70 °C. The fact that at least one of these methods gave optically pure products proves that the inversion occurs

[1]Supported by a grant from the Medical Research Council of Canada. N.L.B. is an Associate of the MRCC. Presented in part at the First Chemical Congress of the North American Continent, Mexico City, Mexico, Dec. 1975. For part VI of this series, see ref. 1.

[2]Abbreviations used: Bzl, benzyl; Boc, *tert*-butyloxycarbonyl; Tos, *p*-toluenesulfonyl; Z, benzyloxycarbonyl; DMF, dimethylformamide; THF, tetrahydrofuran; MeLeu, *N*-methylleucine, etc.

[1] $Ph(CH_3)SO_2NH—CHR'—COOH \xrightarrow[65\ °C,\ 20–60\ min]{2\ N\ NaOH,\ CH_3I} Ph(CH_3)SO_2N(CH_3)—CHR'—COOH$

$\xrightarrow[(c)\ 5.6\ N\ HBr/AcOH\ 70\ °C,\ 2\ h\quad (d)\ 2\ N\ HBr/AcOH,\ 24\ h]{(a)\ 12\ N\ HCl,\ 100\ °C,\ 8\ h\quad (b)\ Na/NH_3} HN(CH_3)—CHR'—COOH$

(*a*) Method of Fischer and Lipschitz, 1915 (2)
(*b*) Method of du Vigneaud and Behrens, 1937 (3)

[2] $NH_2—CHR'—COOH \xrightarrow[(a)\ OH^-,\ NaBH_4\quad (b)\ OH^-,\ H_2\text{–}Pd(C)\quad (c)\ pH\ 6.5,\ NaCNBH_3]{Aqueous\ PhCHO} PhCH_2NH—CHR'—COOH \xrightarrow[HCOOH,\ \Delta]{Aqueous\ HCHO}$

$PhCH_2N(CH_3)—CHR'—COOH \xrightarrow[Pd(C)]{H_2} HN(CH_3)—CHR'—COOH$

(*a*, *b*) Method of Quitt *et al.*, 1963 (4)

[3] $RCONH—CHR'—COOH \xrightarrow[DMF,\ 23\ or\ 45\ °C]{Ag_2O,\ CH_3I} RCON(CH_3)—CHR'—COOCH_3 \xrightarrow{N\ NaOH\text{–}EtOH(1:3)} RCON(CH_3)—CHR'—COOH$

$R = OCH_2Ph$

Method of Olsen, 1970 (5)[3]

[4] $RCONH—CHR'—COOH \xrightarrow[THF\text{–}DMF\ (10:1),\ 80\ °C]{NaH,\ CH_3I} RCON(CH_3)—CHR'—COOCH_3$

$\xrightarrow{(a)\ 2\ N\ NaOH\text{–}MeOH,\ 35\ °C;\ R = OCH_2Ph} RCON(CH_3)—CHR'—COOH$

$\xrightarrow[5.6\ N\ HBr/AcOH;\ R = OCH_2Ph]{(b)\ N\ NaOH\text{–}THF;\ R = Ph,\ CH_3} HN(CH_3)—CHR'—COOCH_3$

Method of Coggins and Benoiton, 1971 (7)

[5] $RCONH—CHR'—COOH \xrightarrow[THF,\ 23\ °C]{NaH,\ CH_3I} RCON(CH_3)—CHR'—COOH$

$R = OCH_2Ph,\ OBu^t;\ 5\ °C\ for\ R' = CH_2OBzl,\ CH_2OBu^t$

Method of Benoiton and co-workers, 1973, 1976 (8–10)

during cleavage, and not during the methylation.[5] The inversion observed for acidolytic cleavage agrees with our previous demonstration that hydrogen bromide in acetic acid racemizes N-substituted *N*-methylamino acids (12). The inversion observed for cleavage by acid hydrolysis is probably higher than that which would occur for the corresponding unmethylated derivative, but this was not verified.

Methylation of Urethane Derivatives using Silver Oxide

This method involves methylation of the Boc- or Z-derivative in DMF using silver oxide and methyl iodide, sometimes aided by heating, followed by saponification of the methyl ester which is formed [3] (5, 6). The results appear in Table 2. It is seen that all products contained either about 1% or else substantially more of the D-isomer. Generally, except for *N*-methylalanine which was higher, all Boc-derivatives were about 2% racemized. Boc-MeLeu-OH

[3]Similar work, presented at a meeting in 1970, was published by Okamoto *et al.* in 1974 (6).

[4]Fischer and Lipschitz also used phosphonium iodide in hydriodic acid for Tos-amido cleavage (2).

[5]The methylation of Tos-Phe-OH may be an exception to this because in their work, Fischer and Lipschitz isolated two fractions of Tos-MePhe-OH, one with a specific rotation 15% lower than that of the other (2).

TABLE 1. Enantiomeric purity of *N*-methylamino acids prepared from the *N*-*p*-toluenesulfonyl derivative [1][a]

Method of detosylation	MeAla	MeVal
(*a*) 12 *N* HCl, 100 °C, 8 h	4.4	2.3
(*b*) Na/NH_3	<0.1	<0.1
(*c*) 5.6 *N* HBr/AcOH, 70 °C, 2 h	13.6	5.1
(*d*) 2 *N* HBr/AcOH, 24 h	11.3	

[a]Percentage D-isomer.

TABLE 2. Enantiomeric purity of *N*-methylamino acids prepared by methylation of the urethane derivative[a]

Amino acid	Reagents and derivatives employed			
	$NaH/CH_3I/THF/23$ °C [5]		$Ag_2O/CH_3I/DMF$[b] [3]	
	Boc	Z	Boc	Z
MeAla	<0.1	<0.1	6.3	8.7
MeLeu	<0.1	<0.1		0.9
MeVal	<0.1	<0.1	0.9	4.5 8.7[c]
MePhe	<0.1	<0.1	0.85	4.1
MeIle	<0.1	0.9	1.2[d]	6.0[e] 14.2[c]
Me*a*lle	<0.1			

[a]Percentage D-isomer.
[b]At 23 °C for Z, and 45 °C for Boc, followed by saponification (1 h).
[c]After the 4 h required to complete the saponification.
[d]25% of the ester remained.
[e]55% of the ester remained.

might be purer, but it was not examined. Except for *N*-methylleucine, the Z-derivatives were 8–28% racemized, the higher figures being for those which had been more difficult to saponify. These results confirm our previous demonstration that fully protected *N*-methylamino acids are racemized by base (12). The Boc-derivatives were more easy to saponify than the Z-derivatives, and we attribute the higher degree of optical purity of products to this fact. The amino-acid side chain also had no effect on the results for the Boc-derivatives, which contrasts with the pronounced effect it had on the results for the Z-derivatives. It would seem that the method of methylating itself does not cause racemization. The results for *N*-methylalanine derivatives seem anomalous in several respects.

Methylation of Urethane Derivatives using Sodium Hydride

The more recent version of this method involves the methylation of the Boc- or Z-derivative in THF using sodium hydride and methyl iodide at room temperature to give directly the N-protected *N*-methylamino acid [5] (8–10). The results appear in Table 2. All the derivatives tested were optically pure, except for Z-MeIle-OH, which contained 0.9% of diastereomer. Since procedures are available for deprotecting these derivatives without affecting their chirality, this method provides a source for optically pure *N*-methylamino acids.

The earlier version of this method included some DMF as well as THF as solvent, with heating [4] (7). The product is the corresponding methyl ester. The protected *N*-methylamino acid is then obtained by saponification. But we have also shown that fully protected *N*-methylamino acids can undergo some inversion in aqueous base (12). Therefore, products obtained in this manner are suspect, and in view of our success with the recent version of this method, none were examined. It should be noted, nevertheless, that *N*-methylamino acid derivatives with a free methylamino group are not racemized by base, therefore optically pure *N*-methylamino acids are still accessible through this procedure as well as via [3] if the saponification is carried out after removal of the N-protecting group. Removal of N-protecting groups occurs without change in chirality, unless hydrogen bromide in anhydrous acetic acid is used on a

TABLE 3. Enantiomeric purity of *N*-alkylamino acids prepared by reductive alkylation using various reducing agents [2][a]

Amino acid	*N*-Methylamino acid	*N*-Benzylamino acid		
	$NaBH_4$[b]	$NaBH_4$	H_2, Pd(C)	$NaCNBH_3$
Ala	2.7, 4.3	2.6, 2.3	4.5	<0.1[c]
Leu	0.3, 0.3	0		
Val	13.9	6.0, 5.1	5.1	[d]
Phe	3.1	1.6, 1.6		
Ile	12.0			
D-Ala	5.2			

[a]Percentage D-isomer. Each value represents a different experiment.
[b]Followed by reductive alkylation of the *N*-benzylamino acid using HCHO/HCOOH.
[c]A sample showed 5.5% D-isomer after methylation using HCHO/HCOOH.
[d]Could not be prepared due to insolubility of valine at p*H* 6.5.

derivative containing a free carboxyl group (12). Finally, we have not shown definitely that methylation according to this earlier version gives optically pure products, but we have no reason to believe otherwise.

Methylation by Successive Reductive Alkylations

This method involves reductive alkylation of the amino acid using benzaldehyde and either of two reducing agents, sodium borohydride, or hydrogen and palladium-on-charcoal catalyst, to give the *N*-benzylamino acid, followed by methylation by the procedure of Clarke–Eschweiler (13, 14) using aqueous formaldehyde in hot formic acid [2] (4). The first alkylation is carried out on the sodium salt of the amino acid. This promotes Schiff base formation by deprotonating the amino group, and also solubilizes the amino acid. The benzyl group is finally removed by catalytic hydrogenation. The results are given in Table 3. The products prepared using sodium borohydride all contained between 2.7–13.9% of D-isomer, except for *N*-methylleucine which contained 0.3% of D-isomer. Particularly striking are the results for the two 'hindered' compounds, *N*-methylvaline and *N*-methylisoleucine, which had undergone ~25% inversion.

In order to identify the origin of the racemization, *N*-benzylamino acids were prepared by both procedures, and examined for optical purity. All of the products, except Bzl-Leu-OH, were found to be racemized, but generally to an extent less than had been found for the corresponding *N*-methylamino acids. This suggested that racemization might also be occuring during the second step of the synthesis, namely, the methylation. This was proven definitely, at least for alanine, after an optically pure sample of Bzl-Ala-OH was synthesized by another procedure. Methylation of this by the Clarke–Eschweiler method gave a product containing 5.5% of the D-isomer.

The reductive alkylation of an amino acid to the benzylamino acid involves the reduction of the Schiff base in the presence of base. It is known that tautomerism of a Schiff base can occur under these conditions, (see ref. 15 for references and a discussion), and this would be promoted by the adjacent carboxylate anion. The partial racemization observed for the *N*-benzylamino acids[6] (Table 3) can therefore be accounted for on this basis, as in [6].

[6] $PhCH{=}N{-}CHR{-}COO^- \rightleftarrows PhCH_2{-}N{=}CR{-}COO^-$

The mechanism of the Clarke–Eschweiler reaction has been investigated in several laboratories (17, 18). A common by-product of the reaction is the carbonyl compound, attributed to hydrolysis of the isomerized Schiff base, exemplified as in [7] for a primary amine. The methylation of a few chiral primary amines

[7] $RCH_2{-}N{=}CH_2 \rightarrow RCH{=}N{-}CH_3 \xrightarrow{H_2O} RCHO + CH_3NH_2$

including a benzylamine has been examined (18, 19) and despite formation of some carbonyl product, no evidence for epimerization was obtained, leading to the conclusion that

[6]These results should be taken into account if *N*-benzylamino-acid derivatives are used for purposes, for example, such as the synthesis of optically active α-hydrazino acids (16).

the Clarke–Eschweiler reaction proceeds without epimerization (18, 19), and to the postulate that any isomerized Schiff base is neither further methylated nor reisomerized, but converted completely to the carbonyl compound (18). However, benzylamino acids incorporate an additional factor besides the benzyl group, the carboxyl group, which would also favor migration of unsaturation. The latter is substantiated by the nature (methylamine and carbon dioxide) and extent of by-product formation during the methylation of amino acids (14). The combination of these two groups must be sufficient to cause a small but significant reversal of the isomerization, as in [8]. This seems to be the first report of an epimerization occuring during methylation by the Clarke–Eschweiler procedure.

[8] $PhCH_2—\overset{+}{N}(=CH_2)—CHR—COOH \rightleftarrows PhCH_2—\overset{+}{N}(CH_3)=CR—COOH$

Reductive Alkylations at Acidic pH

Having demonstrated that reductive alkylations carried out at alkaline p*H* give partially racemized Bzl-amino acids (Table 3), the use of cyanoborohydrides as reducing agent was examined. These reagents of Borcht and Hassid (20) are stable down to p*H* 3, and effective at acidic p*H*. Indeed, it was found that by carrying out the reduction of L-alanine at p*H* 6.5, optically pure Bzl-Ala-OH was obtained in good yield (Table 3). However, success was not achieved until a p*H*-stat was used. Addition of sodium cyanoborohydride to an aqueous amino acid solution causes an immediate rise in p*H* of about 3–4 units, and a sample of Bzl-Ala-OH containing as much as 20% D-isomer was once obtained. This served to demonstrate dramatically the effect of p*H* on the optical integrity of an amino acid which is undergoing reductive alkylation, and confirmed our suspicions that benzylamino acids prepared by the methods of Quitt *et al.* (4) are not optically pure because base is added to the reaction mixture. However, it is sometimes necessary for practical reasons, to keep the amino acid in solution. We were unable to prepare Bzl-Val-OH using sodium cyanoborohydride at p*H* 6.5 because valine is not soluble enough at this p*H*.

In view of the demonstration that racemization had also occurred during the methylation of Bzl-Ala-OH by the Clarke–Eschweiler procedure, attempts were made to use sodium cyanoborohydride instead of formic acid as reducing agent for the reductive methylation of Bzl-Ala-OH. The same, but even worse, solubility problem arose. A few mixed solvents were examined, but without success. The question was abandoned, without exhaustive consideration.

General

The results, obtained with difunctional amino acids, can be summarized as follows: optically pure *N*-methylamino acids can be obtained using methods [1](b) and [5]. For the latter, Z-groups can be cleaved off by catalytic hydrogenation or hydrogen bromide in aqueous acetic acid (12), and Boc-groups, by any acidolytic reagent other than hydrogen bromide in anhydrous acetic acid (12). Though it has not been proven definitely, methods [3] and [4] probably give optically pure *N*-methylamino acids provided that saponification is not used before N-deprotection to obtain the final product. The two alternatives are saponification subsequent to N-deprotection, or O-deprotection by acid hydrolysis. Optically pure N-protected *N*-methylamino acids can be obtained by methylation of the corresponding amino acid derivative using method [5] for Boc- and Z-derivatives, and [1] for Tos-derivatives. *N*-Methylleucine is exceptional in that, in addition to the above, essentially optically pure products are obtainable also using methods [2] and [3] (the Boc-derivative).

With respect to the relative sensitivities to inversion of the different amino acids under synthetic conditions, the side-chain of leucine consistently allowed the least amount of inversion. The side-chains of valine and isoleucine allowed surprizingly high amounts of inversion during reductive alkylations (Table 3), and caused more racemization than others during saponifications (Table 2) because their derivatives are more difficult to saponify. When all methods are taken into consideration, alanine is the most sensitive to inversion, since even both products obtained by method [3] (Table 2) were substantially racemized. *N*-Methylalanine also racemized more than did *N*-methylvaline during tosyl removal by acid (Table 1). The demonstration that inversion occurred in many of the cases examined provides an explanation for the discrepancies in physical data (melting

points and specific rotations) which are recorded in the literature, particularly for *N*-methylalanine and *N*-methylvaline and their derivatives, for the same compounds prepared by various methods (see ref. 10 for examples). *N*-Methylamino acids other than those considered here have been prepared over the years by the methods described. The results presented in this paper as well as recognition of the individuality of the amino acids should be borne in mind when attempting to assess the likelihood that these were optically pure.

It is interesting to note that the classical synthetic method of Fischer–du Vigneaud [1](b) gives optically pure products, while variations of this and some other methods do not, and that the introduction of this method (3), a synthesis of N^{α}-methylhistidine by methylation of Tos-His(Bzl)-OH and subsequent deprotection, represented the introduction of the use of sodium in liquid ammonia for the removal of these *N*-protecting groups in amino acid and peptide chemistry.

Experimental

The Z- and Boc-methylamino acids prepared using sodium hydride [5] (Table 2) were those described in (10). The same derivatives obtained using silver oxide [3] (Table 2) were prepared as described by Olsen (5). The *N*-alkylamino acids recorded in Table 3 were prepared as described by Quitt *et al.* [2] (4), except for the Bzl-Ala-OH obtained using $NaCNBH_3$. The *N*-benzylamino acids were cleaved by catalytic hydrogenation in 80% aqueous acetic acid. Silver oxide and sodium borohydride were products from Fisher Scientific Company, Fair Lawn, New Jersey; sodium cyanoborohydride, from Sigma Chemical Company, St. Louis, Missouri.

For synthesis from the Tos-derivatives [1], synthetic Tos-Ala-OH and Tos-Val-OH (2) were methylated with heating for 1 h according to Fischer and Lipschitz (2) to give Tos-MeAla-OH, mp 128–130 °C, and Tos-MeVal-OH, mp 87 °C, upon acidification of the solutions. Half-gram quantities were treated with the reagents described in Table 1. The acid hydrolysis was carried out in a sealed tube. Samples treated with HBr/AcOH were evaporated to an oil, and the *N*-methylamino acid was isolated by adsorption onto Dowex 50 (H^+) followed by elution with aqueous ammonia.

Solutions containing *N*-methylamino acid or amino acid were evaporated to dryness. Residual compounds and Boc- and Z-derivatives were examined for enantiomeric purity as described in the accompanying paper (1). The values recorded in the tables are considered to be accurate to within about ±10%.

Optically Pure Bzl-Ala-OH

A mixture containing L-alanine (8.9 g, 0.1 mol), 10 ml of benzaldehyde and 50 ml of water was stirred until it became homogeneous (30 min). A p*H*-stat charged with *N* HCl was connected to the solution and the p*H* was adjusted to 6.5 and kept at that p*H*. Sodium cyanoborohydride (1.89 g, 0.03 mol) was added, and after stirring for 2 h, the additions of aldehyde and reducing agent were repeated. Stirring was continued until HCl consumption had ceased (24 h). The copious precipitate was brought into solution by adjusting the p*H* to 8.5, excess benzaldehyde was removed by extraction with ether, and the product was crystallized by bringing the p*H* back to 6.5. The air-dried product, after washing with ether (yield, 90%), was recrystallized from water–ethanol. The compound had the expected nmr spectrum, and was shown to contain <0.1% of the D-isomer.

1. S. T. CHEUNG and N. L. BENOITON. Can. J. Chem. **55**, 911 (1977).
2. E. FISCHER and W. LIPSCHITZ. Ber. **48**, 360 (1915).
3. V. DU VIGNEAUD and O. K. BEHRENS. J. Biol. Chem. **117**, 27 (1937).
4. P. QUITT, J. HELLERBACH, and K. VOGLER. Helv. Chim. Acta, **46**, 327 (1963).
5. R. K. OLSEN. J. Org. Chem. **35**, 1912 (1970).
6. K. OKAMOTO, H. ABE, K. KUROMIZU, and N. IZUMIYA. Mem. Fac. Sc. Kyushu Univ. Ser. C, **9**, 131 (1974).
7. J. R. COGGINS and N. L. BENOITON. Can. J. Chem. **49**, 1968 (1971).
8. B. A. STOOCHNOFF and N. L. BENOITON. Tetrahedron Lett. 21 (1973).
9. J. R. MCDERMOTT and N. L. BENOITON. Can. J. Chem. **51**, 1915 (1973).
10. S. T. CHEUNG and N. L. BENOITON. Can. J. Chem. **55**, 906 (1977).
11. D. I. WEISBLAT, B. J. MAGERLEIN, and D. R. MYERS. J. Am. Chem. Soc. **75**, 3630 (1953).
12. J. R. MCDERMOTT and N. L. BENOITON. Can. J. Chem. **51**, 2555 (1973).
13. W. ESCHWEILER. Ber. **38**, 880 (1905).
14. H. T. CLARKE, H. B. GILLESPIE, and S. Z. WEISSHAUS. J. Am. Chem. Soc. **55**, 4571 (1933).
15. P. Y. SOLLENBERGER and R. B. MARTIN. *In* The chemistry of the amino group. *Edited by* S. Patai. Interscience Publishers, London. 1968. p. 349.
16. K. ACHIWA and S. YAMADA. Tetrahedron Lett. 2701 (1975).
17. A. C. COPE, E. CIGANEK, L. J. FLECKENSTEIN, and M. A. P. MEISINGER. J. Am. Chem. Soc. **82**, 4651 (1960).
18. S. H. PINE and B. L. SANCHEZ. J. Org. Chem. **36**, 829 (1971).
19. J. MCKENNA and J. B. SLINGER. J. Chem. Soc. 2759 (1958).
20. R. F. BORCH and A. I. HASSID. J. Org. Chem. **37**, 1673 (1972).

3,4-Methylenedioxyphthalide-α-carboxylic acid; its use in the total synthesis of isoquinoline alkaloids

BALA C. NALLIAH AND DAVID B. MACLEAN
Department of Chemistry, McMaster University, Hamilton, Ont., Canada L8S 4M1
AND
RUSSELL G. A. RODRIGO AND RICHARD H. F. MANSKE
Department of Chemistry, University of Waterloo, Waterloo, Ont., Canada N2L 3G1

Received December 10, 1976

BALA C. NALLIAH, DAVID B. MACLEAN, RUSSELL G. A. RODRIGO, and RICHARD H. F. MANSKE. Can. J. Chem. **55**, 922 (1977).

3,4-Methylenedioxyphthalide-α-carboxylic acid has been synthesized in four steps from piperonal. From it and phenylethylamines ten phthalideisoquinoline and spirobenzylisoquinoline alkaloids have been synthesized.

BALA C. NALLIAH, DAVID B. MACLEAN, RUSSELL G. A. RODRIGO et RICHARD H. F. MANSKE. Can. J. Chem. **55**, 922 (1977).

Utilisant le pipéronal comme produit de départ, on a synthétisé, en quatre étapes, l'acide méthylènedioxy-3,4 phtalide α carboxylique. Utilisant cet acide ainsi que des phényléthylamines, on a synthétisé dix alcaloïdes des séries phtalideisoquinoléine et spirobenzylisoquinoléine.

[Traduit par le journal]

We report a simple and efficient synthesis of 3,4-methylenedioxyphthalide-α-carboxylic acid **1** and illustrate its use in the total synthesis of six spirobenzylisoquinoline (1) and four phthalideisoquinoline (1) alkaloids.

Piperonal was carboxylated (2) to provide piperonal-2-carboxylic acid (63%) which was treated successively with aqueous potassium cyanide and 15% hydrochloric acid to yield 3,4-methylenedioxyphthalide-α-carboxamide **2** (71%) (mp 239–240°C; ν_{max}(Nujol) 3460, 3220, 1770, and 1650 cm^{-1}).[1] The amide was hydrolyzed by brief treatment with hot concentrated hydrochloric acid to the acid **1** (70%) (mp 210°C; ν_{max}(Nujol) 1790 and 1733 cm^{-1}). The acid **1** now obtained in 31% overall yield from piperonal (four steps) is the methylenedioxy analogue of meconine-α-carboxylic acid **3** employed by Haworth and Pinder (3) in their synthesis of the phthalideisoquinoline alkaloid, hydrastine. This route to the phthalideisoquinolines has since been virtually ignored presumably because of the inaccessibility of the hitherto unknown **1** and of **3**.

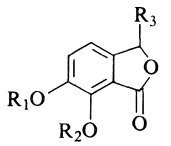

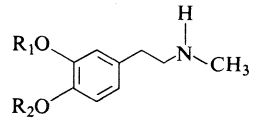

1 $R_1 + R_2 = CH_2$, $R_3 = CO_2H$
2 $R_1 + R_2 = CH_2$, $R_3 = CONH_2$
3 $R_1 = R_2 = Me$, $R_3 = CO_2H$
4 $R_1 + R_2 = CH_2$
5 $R_1 = R_2 = CH_3$

When **1** was converted to its acid chloride (oxalyl chloride, tetrahydrofuran, reflux) and condensed with *N*-methylhomopiperonylamine **4** it provided the amide **6** (61%) (mp 155°C, $\nu_{max}(CHCl_3)$ 1665 and 1780 cm^{-1}). This amide underwent Bischler–Napieralski cyclization with phosphorus oxychloride in acetonitrile to yield the dehydrophthalideisoquinoline **8** (72%) (mp 259°C; $\nu_{max}(CHCl_3)$ 1760 cm^{-1}). Contrary to an earlier suggestion (4) this compound has been shown to have the *E* configuration because of a strong nuclear Overhauser enhancement at the

[1]The full range of spectral data (consistent with the assigned structures) will be reported in detail in the full communication.

proton at C-10 when the N-Me group is irradiated. The dehydrophthalide **9** (**9**, mp 218°C; $\nu_{max}(CHCl_3)$ 1765 cm^{-1}) was similarly obtained from **5** through the amide **7** (**7**, mp 145–146°C; $\nu_{max}(CHCl_3)$ 1660, 1780 cm^{-1}).

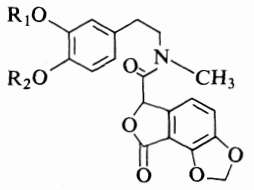

6 $R_1 + R_2 = CH_2$
7 $R_1 = R_2 = CH_3$

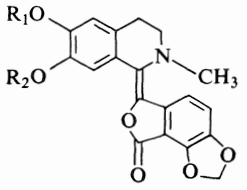

8 $R_1 + R_2 = CH_2$
9 $R_1 = R_2 = CH_3$

Catalytic hydrogenation of **8** (H_2/Pt/acetic acid) provided (±)-adlumidine **10** (mp 199°C) (31%) ((−)-adlumidine is also known as capnoidine) and (±)-bicuculline **11** (mp 216°C) (34%) separable by chromatography (tlc) on silica gel. Similarly, (±)-adlumine **12** (mp 191°C) (32%) and (±)-corlumine **13** (mp 174°C) (35%) were obtained by the hydrogenation of **9**.[2]

All the known spirobenzylisoquinoline alkaloids (1) possess methylenedioxy substitution in ring D and several carry two different oxygen substituents in ring C (*e.g.*, **14**–**17**). The latter type is not easily obtainable by the usual indanetrione approach and to date only one synthesis, that of yenhusomidine **16** has been reported (5).

The synthetic value of **1** is enhanced by an earlier observation (6) that a dehydrophthalide-isoquinoline similar to **8** (and **9**) was smoothly rearranged to products like **14**–**17**. In the present instance **8** upon treatment with diisobutylaluminum hydride in dry tetrahydrofuran at 0°C under nitrogen for 1 h provided (±)-corydaine (7) **14** (26%) and (±)-sibiricine (8) **15** (41%) while similar treatment of **9** yielded (±)-yenhusomidine (9) **16** (42%) and (±)-raddeanone (10) **17** (27%).

We have observed that in these reactions the sibiricine/corydaine (or raddeanone/yenhusomidine) ratio in the product is highest when the reaction mixture is worked-up immediately. Conversely, when the hydride is decomposed by methanol at completion of the reaction as

[2]All synthetic alkaloids reported here were chromatographically pure (tlc on at least two solvent systems) and were found to be identical with natural samples (where available) in their chromatographic and spectroscopic properties.

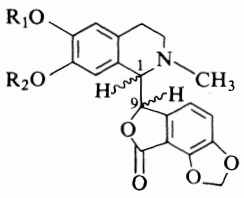

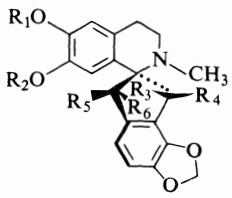

10 $R_1 + R_2 = CH_2$ (1*S*,9*S* and 1*R*,9*R*)
11 $R_1 + R_2 = CH_2$ (1*S*,9*R* and 1*R*,9*S*)
12 $R_1 = R_2 = CH_3$ (1*S*,9*S* and 1*R*,9*R*)
13 $R_1 = R_2 = CH_3$ (1*S*,9*R* and 1*R*,9*S*)
14 $R_1 + R_2 = CH_2$, $R_3 = H$, $R_4 = OH$, $R_5 + R_6 = O$
15 $R_1 + R_2 = CH_2$, $R_3 = OH$, $R_4 = H$, $R_5 + R_6 = O$
16 $R_1 = R_2 = CH_3$, $R_3 = H$, $R_4 = OH$, $R_5 + R_6 = O$
17 $R_1 = R_2 = CH_3$, $R_3 = OH$, $R_4 = H$, $R_5 + R_6 = O$
18 $R_1 + R_2 = CH_2$, $R_3 = H$, $R_4 = OH$, $R_5 = OH$, $R_6 = H$
19 $R_1 = R_2 = CH_3$, $R_3 = H$, $R_4 = OH$, $R_5 = OH$, $R_6 = H$

before but the mixture is then left stirring overnight at room temperature, the corydaine (or yenhusomidine) content now predominates. Furthermore, sibiricine may be transformed to corydaine (potassium hydroxide, methanol, reflux) although we have not yet been successful in effecting 100% conversions. These observations imply that aldol (6) and retro-aldol reactions occurring at the β-hydroxyketone system in ring C transform the sibiricine (raddeanone) configurations, initially produced, into the more stable corydaine (yenhusomidine) arrangements where intramolecular hydrogen bonding of the hydroxyl group to the nitrogen atom has been shown to prevail (7, 9). This process racemizes two chiral centres; its operation is probably responsible for the fact that those alkaloids for which rotations are reported have been found in an optically inactive form and it also raises the possibility that corydaine and yenhusomidine may be artefacts produced from sibiricine and raddeanone respectively by exposure to base during isolation. Further investigations in this area are in progress.

The preferential formation of sibiricine or raddeanone may be accounted for if one assumes that, after reduction, both oxygens of the original lactone remain coordinated with aluminum until ring closure occurs.

Sodium borohydride reduction (methanol, 24 h, room temperature) of (±)-corydaine **14** and (±)-yenhusomidine **16** yielded (±)-ochrobirine (11) **18** (80%) and (±)-yenhusomine (9) **19** (78%), respectively. The diastereomic *cis*-

diols were not formed in detectable amounts (tlc).[3]

Further applications of **1** in isoquinoline alkaloid synthesis are under investigation.

Acknowledgements

We thank the National Research Council of Canada for financial support. We are grateful to Professor S. McLean, University of Toronto, for informing us of his synthetic route to these alkaloids.

1. M. SHAMMA. The isoquinoline alkaloids. Academic Press, New York, NY. 1972.
2. F. E. ZIEGLER and K. W. FOWLER. J. Org. Chem. **41**, 1564 (1976).
3. R. D. HAWORTH and A. R. PINDER. J. Chem. Soc. 1776 (1950).
4. T. KAMETANI, S. HIRATA, M. IHARA, and K. FUKUMOTO. Heterocycles, **3**, 405 (1975).
5. H. IRIE, A. KITAGAWA, A. KUNO, J. TANAKA, and N. YOKOTANI. Heterocycles, **4**, 1083 (1976).
6. D. B. MACLEAN, H. L. HOLLAND, R. RODRIGO, and R. H. F. MANSKE. Tetrahedron Lett. 4323 (1975).
7. KL. SL. BAISHEVA, D. A. FESENKO, B. K. ROSTOTSKII, and M. E. PERELSON. Khim. Prir. Soedin. **6**, 456 (1970); Chem. Abstr. **74**, 10343f (1971); D. A. FESENKO and M. E. PERELSON. Khim. Prir. Soedin. **7**, 166 (1971); Chem. Abstr. **75**, 49381n (1971).
8. R. H. F. MANSKE, R. RODRIGO, D. B. MACLEAN, D. E. F. GRACEY, and J. K. SAUNDERS. Can. J. Chem. **47**, 3585 (1969).
9. S-T. LU, T-L. SU, T. KAMETANI, and M. IHARA. Heterocycles, **3**, 301 (1975).
10. T. KAMETANI, M. TAKEMURA, M. IHARA, and K. FUKUMOTO. Heterocycles, **4**, 723 (1976).
11. R. H. F. MANSKE, R. RODRIGO, D. B. MACLEAN, D. E. F. GRACEY, and J. K. SAUNDERS. Can. J. Chem. **47**, 3589 (1969).

[3]The structures of all new compounds synthesized in this work are supported by acceptable elemental analyses or high resolution mass analysis or both. Samples of natural corydaine, raddeanone, yenhusomidine, and yenhusomine, were not available for comparison at the time of writing but their published spectral data are identical with those of our synthetic samples within experimental error. Our sample of corydaine has been compared with a sample synthesized by a different route in the laboratory of Professor S. McLean at the University of Toronto. In several cases the melting points of our synthetic compounds do not agree with published values suggesting that the compounds may exist in more than one crystalline form.

Total synthesis of spirobenzylisoquinoline alkaloids. Part IV

STEWART MCLEAN AND DAVID DIME

Department of Chemistry, University of Toronto, Toronto, Ont., Canada M5S 1A1

Received December 10, 1976

STEWART MCLEAN and DAVID DIME. Can. J. Chem. **55,** 924 (1977).

The stereoselective synthesis of the racemic forms of the spirobenzylisoquinoline alkaloids corydaine and yenhusomidine is reported.

STEWART MCLEAN et DAVID DIME. Can. J. Chem. **55,** 924 (1977).

On décrit la synthèse stéréosélective des formes racémiques de deux alcaloïdes spirobenzylisoquinoléine, à savoir la corydaine et la yenhusomidine.

[Traduit par le journal]

Our original synthesis (1) of ochotensimine, using a Pictet–Spengler reaction of an indanedione to construct the spirobenzylisoquinoline skeleton, was subsequently modified (2) by using a bromoindanedione to afford eventual access to those alkaloids having two oxygen functions on the five-membered ring. In principle, this strategy provides for control of both functionality and stereochemistry, permitting the synthesis of any of the alkaloids of this class. In practice, although the intermediate **1***a* was synthesized, apparently with complete stereoselectivity, and required only *N*-methylation to be converted to the alkaloid **2***a* having different oxidation levels at C-9 and C-14, the Eschweiler–Clarke reaction failed, and an alternative pro-

diols were not formed in detectable amounts (tlc).[3]

Further applications of **1** in isoquinoline alkaloid synthesis are under investigation.

Acknowledgements

We thank the National Research Council of Canada for financial support. We are grateful to Professor S. McLean, University of Toronto, for informing us of his synthetic route to these alkaloids.

[3]The structures of all new compounds synthesized in this work are supported by acceptable elemental analyses or high resolution mass analysis or both. Samples of natural corydaine, raddeanone, yenhusomidine, and yenhusomine, were not available for comparison at the time of writing but their published spectral data are identical with those of our synthetic samples within experimental error. Our sample of corydaine has been compared with a sample synthesized by a different route in the laboratory of Professor S. McLean at the University of Toronto. In several cases the melting points of our synthetic compounds do not agree with published values suggesting that the compounds may exist in more than one crystalline form.

1. M. SHAMMA. The isoquinoline alkaloids. Academic Press, New York, NY. 1972.
2. F. E. ZIEGLER and K. W. FOWLER. J. Org. Chem. **41**, 1564 (1976).
3. R. D. HAWORTH and A. R. PINDER. J. Chem. Soc. 1776 (1950).
4. T. KAMETANI, S. HIRATA, M. IHARA, and K. FUKUMOTO. Heterocycles, **3**, 405 (1975).
5. H. IRIE, A. KITAGAWA, A. KUNO, J. TANAKA, and N. YOKOTANI. Heterocycles, **4**, 1083 (1976).
6. D. B. MACLEAN, H. L. HOLLAND, R. RODRIGO, and R. H. F. MANSKE. Tetrahedron Lett. 4323 (1975).
7. KL. SL. BAISHEVA, D. A. FESENKO, B. K. ROSTOTSKII, and M. E. PERELSON. Khim. Prir. Soedin. **6**, 456 (1970); Chem. Abstr. **74**, 10343f (1971); D. A. FESENKO and M. E. PERELSON. Khim. Prir. Soedin. **7**, 166 (1971); Chem. Abstr. **75**, 49381n (1971).
8. R. H. F. MANSKE, R. RODRIGO, D. B. MACLEAN, D. E. F. GRACEY, and J. K. SAUNDERS. Can. J. Chem. **47**, 3585 (1969).
9. S-T. LU, T-L. SU, T. KAMETANI, and M. IHARA. Heterocycles, **3**, 301 (1975).
10. T. KAMETANI, M. TAKEMURA, M. IHARA, and K. FUKUMOTO. Heterocycles, **4**, 723 (1976).
11. R. H. F. MANSKE, R. RODRIGO, D. B. MACLEAN, D. E. F. GRACEY, and J. K. SAUNDERS. Can. J. Chem. **47**, 3589 (1969).

Total synthesis of spirobenzylisoquinoline alkaloids. Part IV

STEWART MCLEAN AND DAVID DIME

Department of Chemistry, University of Toronto, Toronto, Ont., Canada M5S 1A1

Received December 10, 1976

STEWART MCLEAN and DAVID DIME. Can. J. Chem. **55,** 924 (1977).

The stereoselective synthesis of the racemic forms of the spirobenzylisoquinoline alkaloids corydaine and yenhusomidine is reported.

STEWART MCLEAN et DAVID DIME. Can. J. Chem. **55,** 924 (1977).

On décrit la synthèse stéréosélective des formes racémiques de deux alcaloïdes spirobenzylisoquinoléine, à savoir la corydaine et la yenhusomidine.

[Traduit par le journal]

Our original synthesis (1) of ochotensimine, using a Pictet–Spengler reaction of an indanedione to construct the spirobenzylisoquinoline skeleton, was subsequently modified (2) by using a bromoindanedione to afford eventual access to those alkaloids having two oxygen functions on the five-membered ring. In principle, this strategy provides for control of both functionality and stereochemistry, permitting the synthesis of any of the alkaloids of this class. In practice, although the intermediate **1***a* was synthesized, apparently with complete stereoselectivity, and required only *N*-methylation to be converted to the alkaloid **2***a* having different oxidation levels at C-9 and C-14, the Eschweiler–Clarke reaction failed, and an alternative pro-

cedure led to ochrobirine, in which the C-9 carbonyl is also reduced.

The hydroxyl groups at C-14 appeared to be implicated in the failure of the Eschweiler–Clarke reaction, and a modified reductive methylation sequence has now been developed that takes this feature into account. The procedure was first investigated in a model series with an analog lacking the ring D methylenedioxy group. A solution of **3***a* (16 mg) and

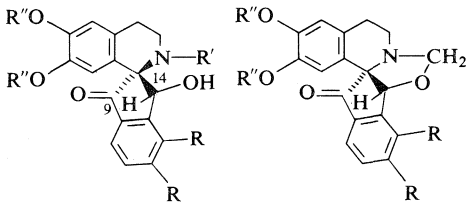

1 R + R = —OCH_2O—, R′ = H
a R″ + R″ = —CH_2—
b R″ = CH_3
2 R + R = —OCH_2O—, R′ = CH_3
a R″ + R″ = —CH_2—
b R″ = CH_3
3 R = H, R″ = CH_3
a R′ = H
b R′ = CH_3
4 R = H, R″ = CH_3

formaldehyde (37% aqueous, 0.1 ml) in 5 ml of acetonitrile was stirred at room temperature under nitrogen for 2 h. Evaporation under reduced pressure afforded a residue which was dissolved in methylene chloride and washed with water; the material obtained from the organic layer was recrystallized and the product, mp 160–163°C, had the spectroscopic characteristics (ir, nmr, ms) expected for the oxazolidine **4**. A solution of **4** (20 mg) and sodium cyanoborohydride (3.3 mg) in 3 ml of methanol containing sufficient dilute hydrochloric acid to bring it to p*H* 3 was stirred at room temperature under nitrogen for 1 h. Dilution with water and extraction into methylene chloride afforded a product (12 mg) which showed the spectroscopic characteristics (ir, nmr, ms) expected for **3***b*.

The intermediate **1***a* (2) was then converted by the same reaction sequence to **2***a*, mp 127–128°C, the structure assigned to the alkaloid corydaine (3). Despite the difference in melting points, the spectroscopic and tlc characteristics of the synthetic product were identical in all significant respects with those of the optically active natural material.

The corresponding sequence of reactions converted the intermediate **1***b* to its *N*-methyl derivative **2***b*, mp 239–241°C, the structure assigned to the alkaloid yenhusomidine (4). The spectroscopic data for natural and synthetic samples confirm their identity. The synthesis of racemic yenhusomidine by a different route was announced recently (5).

Our reductive methylation sequence appeared to lead unequivocally to the configuration at C-14 shown in the products and to provide chemical proof for this assignment in the alkaloids. However, we have now become aware of the work of Nalliah *et al.* (6) who have synthesized these alkaloids by a different route; comparison of samples and spectra confirms the identities of their products with ours. One outcome of their work has been the demonstration of the facile isomerization of these alkaloids, and that **2***a* and **2***b* are thermodynamically the more stable epimers. Our route remains stereoselective, but since we have not proven that equilibration could not have taken place during the isolation of the products, it falls short of providing the intended *proof* of configuration.

Acknowledgements

We are grateful to Drs. M. E. Perel'son and N. Margvelashvily for spectra of corydaine and a generous sample of the alkaloid. We thank Professor T. Kametani for kindly supplying copies of the original spectra of yenhusomidine. We very much appreciate the friendly cooperation of Professor D. B. MacLean, especially after it became apparent that our synthetic efforts were approaching the same goal at the same time. The financial support of the National Research Council of Canada is gratefully acknowledged.

1. S. McLean, M.-S. Lin, and J. Whelan. Tetrahedron Lett. 2425 (1968); Can. J. Chem. **48**, 948 (1970).
2. S. McLean and J. Whelan. Can. J. Chem. **51**, 2457 (1973).
3. K. S. Baisheva, D. A. Fesenko, B. K. Rostotskii, and M. E. Perel'son. Khim. Prir. Soedin. **6**, 456 (1970). D. A. Fesenko and M. E. Perel'son. Khim. Prir. Soedin. **7**, 166 (1971).
4. S.-T. Lu, T.-L. Su, T. Kametani, and M. Ihara. Heterocycles, **3**, 301 (1975).
5. H. Irie, A. Kitagawa, A. Kuno, J. Tanaka, and N. Yokotani. Heterocycles, **4**, 1083 (1976).
6. B. C. Nalliah, D. B. MacLean, R. G. A. Rodrigo, and R. H. F. Manske. Can. J. Chem. This issue.

Canadian Journal of Chemistry

Published by
THE NATIONAL RESEARCH COUNCIL OF CANADA

Volume 55 Number 6 March 15, 1977

Journal canadien de chimie

Publié par
LE CONSEIL NATIONAL DE RECHERCHES DU CANADA

Volume 55 numéro 6 15 mars 1977

High resolution ^{119}Sn nuclear magnetic resonance studies by pulse Fourier transform

C. R. Lassigne and E. J. Wells

Department of Chemistry, Simon Fraser University, Burnaby 2, B.C., Canada V5A 1S6

Received November 8, 1976

C. R. Lassigne and E. J. Wells. Can. J. Chem. **55**, 927 (1977).

The T_1's, linewidths (T_2's), and chemical shifts of ^{119}Sn nuclei in a variety of tin compounds have been surveyed using pulse Fourier transform techniques. The results span the very large chemical shift range for tin-119 (~2000 ppm), and indicate rather short T_1 values with widely varied T_2 relaxation times. Possible mechanisms are discussed for both T_1 and T_2 relaxation times. Our results show an approximate correlation between T_1 (^{119}Sn) and the paramagnetic contribution to the observed shielding of the ^{119}Sn nucleus, indicating that apart from a large scalar contribution in Sn(IV) iodides and bromides, the dominant ^{119}Sn T_1 mechanism is spin rotation interaction.

C. R. Lassigne et E. J. Wells. Can. J. Chem. **55**, 927 (1977).

On a examiné les T_1, les largeurs des lignes (T_2) et les déplacements chimiques du noyau ^{119}Sn dans une grande variété de composé de l'étain; ces études ont été effectuées en utilisant les techniques de transformation de Fourier pulsées. Les résultats recouvrent une très grande variété de déplacements chimiques pour l'étain-119 (~2000 ppm) et indiquent que les valeurs de T_1 sont relativement courtes même avec des temps de relaxation T_2 qui varient beaucoup. On discute des mécanismes possibles pour les temps de relaxation T_1 ainsi que T_2. Nos résultats montrent qu'il existe une corrélation approximative entre les T_1 de ^{119}Sn et la contribution paramagnétique au blindage observé au niveau du noyau de ^{119}Sn; cette corrélation indiquerait, en plus d'une grande contribution scalaire dans les bromures et les iodures du Sn(IV), que le mécanisme prédominant dans le T_1 du ^{119}Sn est une interaction spin rotation.

[Traduit par le journal]

I. Introduction

The ^{119}Sn isotope ($I = 1/2$) is the most abundant isotope of tin and the one most frequently studied in nmr investigations. Previous measurements of ^{119}Sn chemical shifts have been done under rapid passage dispersion mode (1) and also absorption mode signals involving proton decoupling (2). However now that Fourier transform is readily available a number of heavy nuclei may be studied with greater ease. We report the results of some signal-averaged pulse Fourier transform experiments on ^{119}Sn in a variety of tin compounds.

II. Experimental

All spectra were obtained on natural abundance (8.68%) ^{119}Sn samples in 12 mm tubes at 15.05 MHz, using a modified NMR-Specialties spectrometer with a home built crossed-coil, external water-lock probe.[1] The sample was not spun. Fourier transformation of the free induction decay (FID) was accomplished using a Nicolet 1082 FT system. Spin–lattice relaxation times were obtained by the usual 180°–τ–90° pulse sequence. All chemical shifts are given relative to the reference $Sn(CH_3)_4$.

All tin compounds were obtained commercially except for $SnCl_2$, $SnBr_2$, $SnCl_4 \cdot 2CH_3OH$, and $SnCl_4 \cdot 2CH_3CN$. Both stannous chloride and bromide were prepared by

[1] T. P. Higgs, A. Brooke, and E. J. Wells. Unpublished results.

TABLE 1. ^{119}Sn chemical shifts, T_1's and T_2's

Compound	δ (ppm)[a]	$J_{H-^{119}Sn}$ (Hz)	T_2 (ms)	T_1 (s)[b]
SnI_4 (2 *M* in CS_2)	1698.6	940[c]	10	$T_1^{SC} \simeq 0.38$ $T_1^{SR} \simeq 10$
$SnCl_4 \cdot 2CH_3CN$ (satd. in CH_3CN)	775.0	—	4	[g]
$SnBr_4$ (3 *M* in CS_2)	631.6	920[d]	3	$T_1^{SC} \simeq 1.8$ $T_1^{SR} \simeq 7$
$SnCl_4 \cdot 2MeOH$ (satd. in MeOH)	602.1	—	8	7.3
$Na_2Sn(OH)_6$ (aq)	591.0	—	64	[h]
$SnCl_2$ (satd. in 12 *M* HCl)	388.1	—	80	4.2
$SnBr_2$ (satd. in 9 *M* HBr)	385.0	—	21	3.8
$SnCl_4$ (neat)	147.8	470[e]	1.5	1.6
$Sn(CH_3)_4$ (neat)	(0)	54.0[f]	106	0.6
$Sn(CH_3)(Cl)_3$ (5 *M* in CCl_4)	−15.2	99.7[f]	3	2.0
$Sn(CH_3)_2Cl_2$ (acetone)	−19.6	86.2[f]	21	1.0
$Sn(CH_3)_2Cl_2$ (satd. in CCl_4)	−141.2	71.0[f]	11	[g]
$Sn(CH_3)_3Cl$ (5 *M* in CCl_4)	−160.0	59.9[f]	40	0.66

[a]Precision ± 0.1 ppm. Instrumental linewidth 3 Hz. All spectra recorded at 301 K.
[b]T_1 ± 10%.
[c]$J_{^{119}Sn-I}$ (5).
[d]$J_{^{119}Sn-Br}$ (6).
[e]$J_{^{119}Sn-Cl}$ (5).
[f]Measured also on a Varian A56/60 high resolution nmr spectrometer by observing proton spectrum.
[g]Not measured owing to weakness of signal.
[h]Not measured.

reacting stannous oxide with concentrated HCl and HBr respectively. Both stannic chloride adducts were prepared by reacting methanol and acetonitrile with cold $SnCl_4$ (anhydrous) producing immediately a white precipitate of $SnCl_4 \cdot 2CH_3OH$ and $SnCl_4 \cdot 2CH_3CN$. The melting points of these adducts are in agreement with those reported in the literature (3).

III. Results and Discussion

1. Chemical Shifts

The large range of chemical shifts observed (Table 1) shows that the major contributory term to the shielding of the tin-119 nucleus is the paramagnetic term. This has been shown to be the case for ^{13}C chemical shifts (4) and also ^{119}Sn (5)[2]. The diamagnetic contribution to the total shielding constant remains essentially constant and it is the changes in the paramagnetic term which cause the changes in observed chemical shift for a particular nucleus. The chemical shift data are tabulated in Table 1.

The variation in chemical shift for the series $(CH_3)_nSnCl_{4-n}$ is the same as that observed for $(n\text{-butyl})_n$ $SnCl_{4-n}$ (1, 2) and similarly suggests that there are two important factors opposing each other in the shielding of the tin nuclei of this series: (*a*) an inductive effect resulting in the increased shielding by the addition of alkyl groups and (*b*) an opposite effect due to $(p \rightarrow d)\pi$ bonding between Sn and Cl. The tin chemical shifts and coupling constants J_{Sn-C-H} are very dependent on the concentration and type of solvent used, in agreement with the results of Hunter and Reeves (2), and suggesting specific solvation effects. A typical high resolution ^{119}Sn spectrum is shown in Fig. 1.

In Me_4Sn we have measured $J_{^{119}Sn-^{13}C}$ to be 338 Hz while in Me_3SnCl the coupling constant is measured to be 387 Hz (Fig. 1). The increase in $J_{^{119}Sn-^{13}C}$ in going from Me_4Sn to Me_3SnCl is due to the slight increase in '*s*' character at the

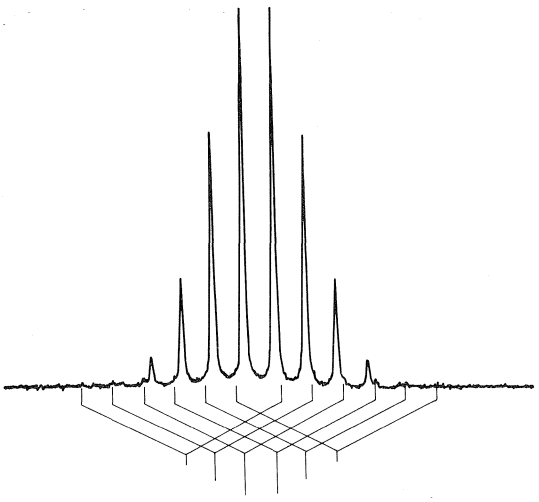

FIG. 1. Natural abundance ^{119}Sn FT spectrum of $Sn(CH_3)_3Cl$, 5 *M* in CCl_4 solvent. The eight inner members of the expected proton coupled decet are clearly visible with separation 59.9 Hz. Additional splitting due to ^{13}C (in natural abundance) is visible (387 Hz) and indicated below (8000 scans, 1.1 s delay).

[2]C. R. Lassigne and E. J. Wells. Unpublished results.

tin atom by the substitution of a Cl for a Me group.

2. Linewidths and T_2 Relaxation

The linewidth is indicative of the various possible spin–spin relaxation mechanisms contributing to the transverse relaxation time T_2. The possible mechanisms are: (*a*) experimental, *i.e.* magnet inhomogeneity, (*b*) scalar relaxation, and (*c*) exchange, which can be determined from the temperature dependence. The T_2 values measured for the various ^{119}Sn compounds are listed in Table 1.

$SnCl_4$, $SnBr_4$, and SnI_4 (5, 6) all have a T_2 dominated by scalar relaxation of the second kind (7) to the geminal halogen nuclei assumed to be relaxing independently,

$$[1]\quad R_2^{SC} = \frac{1}{T_2} = \frac{4\pi^2 J^2 S(S+1)}{3} \times \left\{ T_{1Q} + \frac{T_{2Q}}{1 + (\omega_I - \omega_S)^2 T_{2Q}^2} \right\} N_s$$

where J is the scalar coupling constant between nuclei I and S; S is the spin of the quadrupolar nucleus, usually $T_{1Q} = T_{2Q}$ for liquids and N_s is the number of quadrupolar nuclei involved. The large scalar coupling constants (5, 6) in all three compounds along with the fairly short T_{1Q} of the quadrupolar halogens produce a relatively efficient transverse relaxation in ^{119}Sn.

The series of methyltin chlorides shows decreasing linewidths as the number N_s of chlorines is decreased. Again this is consistent with the scalar contribution to T_2 by the rapidly relaxing chlorines according to [1].

The two adducts of stannic chloride ($SnCl_4 \cdot 2CH_3OH$ and $SnCl_4 \cdot 2CH_3CN$) have a smaller linewidth than the anhydrous $SnCl_4$. This may be a reflection of the decrease in *s* character of the tin nucleus in going from a tetrahedral (sp^3) geometry to a *cis*-octahedral (sp^3d^2) geometry (8, 9). This decrease in *s* character of the nucleus would cause the $J_{^{119}Sn-Cl}$ to be smaller than the 470 Hz reported by Sharp, and therefore would make a smaller contribution to T_2^{SC} (see eq. 1) making the tin-119 linewidth smaller. Also the change to the octahedral species increases the moment of inertia, lowering the angular velocity correlation time τ_ω and raising the angular orientation correlation time τ_θ, assuming rotational equipartition of energy and rotational diffusion. This effect shortens T_{1Q} and thus decreases the scalar T_2 at the Sn in the fast relaxation limit of quadrupolar spin *S*.

3. Spin–Lattice Relaxation Times (T_1)

The wide range of T_1's shows that a number of spin–lattice mechanisms may be operative. The possible mechanisms are: (*a*) dipole–dipole, (*b*) scalar relaxation, (*c*) spin–rotation, and in some cases (*d*) chemical shift anisotropy. The last case would only be found in the compounds which do not have T_d or O_h symmetry and thus may contain an anisotropic shielding for the central tin-119 nucleus. However, for the near-symmetrical structures studied here, this contribution is expected to be very small and is neglected hereafter. In principle, this contribution can be isolated by variable temperature, variable field T_1 studies.

For tetramethyl tin, we have shown[2] that T_1 is strictly dominated by the spin–rotation interaction. The T_1 of $SnCl_4$ is also dominated by spin–rotation as has been demonstrated by Sharp (5). However in $SnBr_4$ (6) and SnI_4 (5) the spin–lattice relaxation rate is a mixture of both spin–rotation and scalar relaxation. For neat $SnBr_4$, Sharp (5) has decomposed the T_1 mechanisms, obtaining $T_1^{SR} \simeq 7$ s, $T_1^{SC} \simeq 1.8$ s at 300 K. For the neat SnI_4 case, Sharp (5) obtained data at 477 K and extrapolation of his data back to 300 K yields $T_1^{SR} \simeq 10$ s and $T_1^{SC} \simeq 0.38$ s. Our T_1 solution data for the various Sn(IV) halides are in agreement with Sharp's (5, 6) reported values on the neat liquids. We were only able to measure the T_1 of one $SnCl_4$ adduct ($SnCl_4 \cdot 2CH_3OH$) because the signal of the acetonitrile adduct was very weak. The $SnCl_4 \cdot 2CH_3OH$ adduct most probably relaxes by spin–rotation; its T_1 (7.3 s) is much longer than $SnCl_4$ (T_1 = 1.6 s). We interpret this as due to a smaller angular correlation time (τ_ω) due to increased moment of inertia, along with a smaller spin–rotation constant (C_0) related to the smaller paramagnetic shielding (10). All of the T_1's of methyl tin chlorides here most probably are also dominated by the spin–rotation interaction, with the dipole–dipole relaxation being negligible because of the r^{-6} dependence. Both Sn(II) dihalides in their respective acids have similar T_1 values (4 s). Aqueous solutions of Sn(II) halides exhibit concentration dependent ^{119}Sn spectra which resolve at low temperature (11). ^{119}Sn spectra of Sn(II) halides are concentration dependent, but to date we have been unable to

resolve individual species resonances. Sn(II) halide solutions thus cannot be identified from Sn(IV) halide solutions by either ^{119}Sn shifts or T_1 values.

From the data in Table 1 there is a trend showing that with increasing paramagnetic chemical shift there is also an increase in the T_1^{SR}. The reason for this is that the trace of the paramagnetic term of the shielding tensor becomes smaller with the upfield shift in going from $Sn(CH_3)_4$ to SnI_4 and thus the spin–rotation constant becomes smaller (10); also the value of τ_ω decreases with increasing moment of inertia causing overall a less effective spin–rotation interaction and therefore the T_1^{SR} values become longer.

The total nuclear shielding constant has been related to the spin–rotation constant (12, 13);

$$\sigma_{av} = \frac{e^2}{3mc^2}\left\{\left\langle 0\left|\sum_k \frac{1}{r_k}\right|0\right\rangle - \sum_j \frac{Z_j}{R_{ij}}\right\} + \left\{\frac{2\pi}{\hbar g_I}\cdot\frac{M_p}{m_e}\cdot IC_0\right\} = \sigma_d' + \sigma_p' \quad [2]$$

Deverell (10) has argued that the first term σ_d' associated with a given nucleus i is constant from molecule to molecule, and that the paramagnetic shielding σ_p' given by the second bracketed term is responsible for the shift differences observed. Thus, σ_p' is directly related to the spin–rotation constant C_0 (Hz) and the molecular moment of inertia I. The spin–rotation relaxation rate R_1^{SR} for the central nucleus of a spherical top molecule is given by Hubbard (14) and McClung (15) as:

$$R_1^{SR} = T_{1,SR}^{-1} = \frac{2IkT}{\hbar^2}(2\pi C_0)^2\tau_\omega \quad [3]$$

where τ_ω is the correlation time for reorientation of the angular momentum vector. In the rotational diffusion limit τ_ω is related to the reorientational correlation time $\tau_{\theta,2}$.

$$\tau_{\theta,2}^*\tau_\omega^* = \tfrac{1}{6} \quad [4]$$

where the reduced correlation times τ_ω^*, $\tau_{\theta,2}^*$ are

$$\tau_\omega^* = \left(\frac{kT}{I}\right)^{1/2}\tau_\omega$$

$$\tau_{\theta,2}^* = \left(\frac{kT}{I}\right)^{1/2}\tau_{\theta,2} \quad [5]$$

Combination of [3] with σ_p' of [2] and τ_ω of [5] yields

$$R_1^{SR} = 2g_I^2\left(\frac{m_e}{M_p}\right)^2(kT)^{1/2}\tau_\omega^*\frac{(\sigma_p')^2}{I^{1/2}} \propto \tau_\omega^*\frac{(\sigma_p')^2}{I^{1/2}} \quad [6]$$

In general τ_ω^* can only be obtained from detailed relaxation studies. τ_ω^* values for those compounds that have been investigated are remarkably constant, at the same temperature in different media. Thus we have found $\tau_\omega^* = 0.054$ for neat $Sn(CH_3)_4$ at 300 K;[2] Sharp (5) finds $\tau_\omega^* = 0.048$ for neat $SnCl_4$ at 298 K, and 0.108 and 0.134 at 423 K for neat $SnCl_4$ and neat SnI_4 respectively. This suggests that τ_ω^* can be approximated as a constant in [6].

The validity of [6] across the present data may then be tested quantitatively from an absolute chemical shift scale which evaluated the σ_p'. We have determined such a scale for ^{119}Sn by temperature dependent relaxation studies of neat liquid $Sn(CH_3)_4$ and its isotopic modifications (16), which yielded a value of (17.7 ± 2) kHz for the spin–rotation interaction constant C_0 of ^{119}Sn. Use of this value in [2] sets σ_p' ($Sn(CH_3)_4$) as −3200 ppm. The measured ^{119}Sn shifts, spin–rotation relaxation rates, and calculated molecular constants for some of the other molecular species are displayed in Table 2, and these data are plotted according to [6] in Fig. 2.

Although the dependence is not exact, and is not expected to be because of the approximations made (isotropic motion, rotational diffusion limit, τ_ω independent of medium) we see that [6] does indeed correlate the measured relaxation behaviour with the measured shifts to first order. This verifies our interpretation of the relaxation as due predominantly to the spin–rotation mechanism, and also validates Deverell's relation between the spin–rotation constant and the paramagnetic shielding term for ^{119}Sn in a variety of compounds.

Comparison of the measured slope of Fig. 2 with the numerical coefficient of [6] yields an average value of τ_ω^* for these molecules in the liquid phase at 304 K of 0.055. The smallness of this value compared to unity confirms that molecules on or near the best fit line are in the rotational diffusion limit. $SnBr_4$ and $Sn(CH_3)Cl_3$ are apparently anomalous in this series. The anomaly of $SnBr_4$ has been noticed previously (6), and this molecule alone of the tin tetrahalides is thought to be in intermediate motion between rotational diffusion and inertial rotation.

TABLE 2. ^{119}Sn values for σ_p'; I and R_1^{SR}

	σ_p' (ppm)	I ($\times 10^{40}$) (g cm^2)	$(\sigma_p'^2\sqrt{I})$ ($g^{-1/2}cm^{-1} \times 10^{-12}$)	T_1^{SR}(obs) (s)	R_1^{SR}(obs) (s^{-1})
SnI_4	−1500	4270[b]	3.4	10	0.10
$SnBr_4$	−2568	2140[c]	14.3	7	0.14
$SnCl_4$	−3040	854[d]	31.6	1.6	0.63
$Sn(CH_3)_4$	(−3200)[a]	344[e]	55.2	0.6	1.67
$Sn(CH_3)_2Cl_2$	−3220	602[e]	42.2	1.0	1.0
$Sn(CH_3)Cl_3$	−3215	720[e]	38.5	2.0	0.5
$Sn(CH_3)_3Cl$	−3341	503[e]	49.8	0.66	1.51

[a]Independently obtained value for σ_p' (see ref. 16). All other σ_p' values obtained from differences between experimental σ_p' ($Sn(CH_3)_4$) and measured chemical shift differences relative to $^{119}Sn(CH_3)_4$.
[b]Reference 17.
[c]Reference 18.
[d]Reference 19.
[e]Obtained assuming all bond angles 109.5° and bond distances r_{C-H} = 1.09 Å; r_{C-Sn} = 2.18 Å; and r_{Sn-Cl} = 2.28 Å.

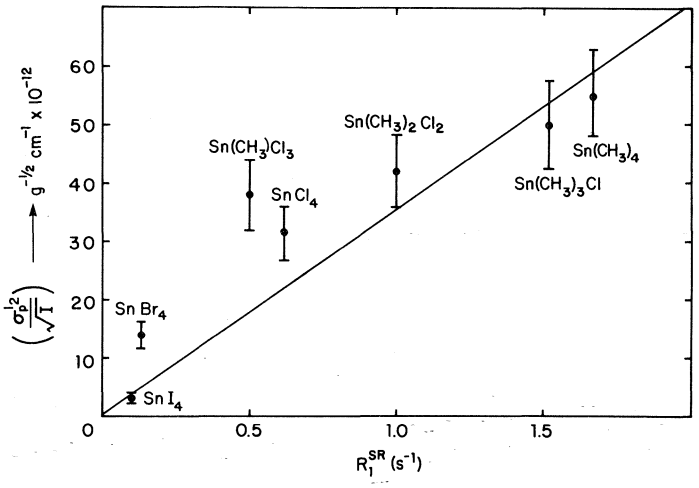

FIG. 2. ^{119}Sn relaxation and shift data from Table 2 plotted according to [6].

Generally, we conclude that the rather short spin–lattice relaxation times of ^{119}Sn make it a useful nucleus for further high resolution FT nmr studies.

Acknowledgements

We thank the Canadian Donner Foundation for initial funding toward purchase of the spectrometer, and the National Research Council of Canada for support of this work through operating grants to E.J.W.

1. J. J. BURKE and P. C. LAUTERBUR. J. Am. Chem. Soc. **83**, 326 (1961).
2. B. K. HUNTER and L. W. REEVES. Can. J. Chem. **46**, 1399 (1968).
3. S. ICHIBA, M. MISHIMA, H. SAKAI, and H. NEGITA. Bull. Chem. Soc. Jpn. **41**, 49 (1968).
4. C. R. LASSIGNE and E. J. WELLS. Can. J. Chem. In press.
5. R. R. SHARP. J. Chem. Phys. **57**, 5321 (1972).
6. R. R. SHARP. 14th ENC Conference, Boulder, Colorado. 1973.
7. A. ABRAGAM. Principles of nuclear magnetism. Oxford, London. 1961.
8. M. WEBSTER and H. E. BLAYDEN. J. Chem. Soc. A, 2443 (1969).
9. D. CUNNINGHAM, M. J. FRAZER, and J. D. DONALDSON. J. Chem. Soc. Dalton Trans. 1647 (1972).
10. C. DEVERELL. Mol. Phys. **18**, 319 (1970).
11. C. LASSIGNE, D. LOWELL, and E. J. WELLS. To be published.
12. N. F. RAMSEY. Phys. Rev. **78**, 699 (1950).
13. W. H. FLYGARE. J. Chem. Phys. **41**, 793 (1964).
14. P. S. HUBBARD. Phys. Rev. **131**, 1155 (1963).
15. R. E. D. MCCLUNG. J. Chem. Phys. **51**, 3842 (1969).
16. C. LASSIGNE. Ph.D. Thesis, Simon Fraser University, Burnaby, B.C. 1975.
17. F. MELLER and I. FANKUCHEN. Acta Crystallogr. **8**, 343 (1955).
18. P. BRAND and H. SACKMANN. Acta Crystallogr. **16**, 446 (1963).
19. H. FUGII and K. MASAO. Bull. Chem. Soc. Jpn. **43**, 2933 (1970).

Effect of nitric oxide on hydrogen formation in irradiated HCl[1]

NEIL M. BALLASH, SURJIT S. NAGRA, AND DAVID A. ARMSTRONG
Department of Chemistry, The University of Calgary, Calgary, Alta., Canada T2N 1N4

Received June 28, 1976

NEIL M. BALLASH, SURJIT S. NAGRA, and DAVID A. ARMSTRONG. Can. J. Chem. **55**, 932 (1977).

Nitric oxide reduces the production of hydrogen in irradiated HCl and leads to ClNO formation. The results can be interpreted on the basis of a competition between HCl and NO for H atoms and $(HCl)_x^-$ negative ion intermediates. The yield of $(HCl)_x^- = 2.4 \pm 0.3$ per 100 eV is similar to that found from experiments with chlorine, as was the total yield of scavengable H atoms plus electrons, $g_e + g_H$. From analyses of the competition kinetics for experiments both with and without added SF_6, the ratio of the termolecular rate constant for reaction of H with NO in the presence of HCl as third body to that for reaction of H with HCl was estimated to be $6.3 \pm 0.8 \times 10^{-19}$ cm^3 molecule^{-1} at 298 K.

NEIL M. BALLASH, SURJIT S. NAGRA et DAVID A. ARMSTRONG. Can. J. Chem. **55**, 932 (1977).

L'oxyde nitrique réduit la production d'hydrogène dans du HCl irradié et conduit à la formation de ClNO. On peut interpréter les résultats en se basant sur une compétition entre HCl et NO pour les atomes d'hydrogène et les intermédiaires ioniques négatifs $(HCl)_x^-$. Le rendement de $(HCl)_x^- = 2.4 \pm 0.3$ par 100 eV est semblable à celui trouver pour des expériences avec le chlore; il en avait été aussi de même pour le rendement total: atomes d'hydrogène piégeables plus électrons, $g_e + g_H$. A partir de l'analyse de la cinétique de compétition pour des expériences effectuées avec et sans SF_6 ajouté, le rapport de la constante de vitesse termoléculaire de la réaction de H avec NO en présence de HCl comme troisième corps et de celle de la réaction de H avec HCl peut être estimé à $6.3 \pm 0.8 \times 10^{-19}$ cm^3 molecule^{-1} à 298 K.
[Traduit par le journal]

Introduction

The mechanism of hydrogen formation in irradiated HCl has previously been investigated with the electron scavengers SF_6, CCl_4, and C_7F_{14} (1, 2), and with chlorine and bromine, which consume hydrogen atoms as well as negative ion species (1, 3). In the work reported here nitric oxide was used as a scavenger of intermediates. Like chlorine and bromine this molecule reacts with hydrogen atoms (4–6) as well as electrons (7). However, reaction 1 differs from

[1] $$H + NO + M \rightarrow HNO + M$$

the hydrogen atom reactions of the halogens (reaction 2) in that it requires the presence of a

[2] $$H + X_2 \rightarrow HX + X \quad (X = Cl \text{ or } Br)$$

third body for stabilization of the HNO molecule. Since the stabilization probability should decrease with increased translational energy of H, [1] is likely to be more specific for thermal H atoms than [2]. Thus, the use of nitric oxide provides a further and more definitive means of confirming the presence of this species. In addition the results discussed here support earlier evidence for the formation of an $(HCl)_x^-$ negative ion intermediate.

Experimental

Materials

Matheson 'electronic grade' HCl was purified by preirradiation and sublimation as already described (8). The nitric oxide and sulfur hexafluoride were also from the Matheson Company and of research grade. The sulfur hexafluoride was degassed before storage. The nitric oxide was separated from NO_2 and other trace impurities by sublimation. All gases were stored in liquid nitrogen traps attached to the mercury free vacuum line used for filling the radiation cells.

Apparatus and Procedure

Irradiations were performed at 298 K with an AECL ^{60}Co gamma cell 220 which accommodated the 350 cm^3 cylindrical pyrex cells. After irradiation these were reattached to the preparation line and the HCl and NO were condensed in a small side arm immersed in liquid nitrogen. For samples with large NO concentrations the side arm was immersed in a solid nitrogen slurry. The hydrogen was pumped through a trap to remove nitric oxide and into another vacuum line for analysis as already described (8).

The dose rate was determined regularly wth HCl, for which $G(H_2)$ in the absence of scavengers is 8.0 ± 0.2

[1]Research supported by NRCC A3571.

TABLE 1. Hydrogen yields from HCl–NO mixtures at 298 K

HCl (10^{18} molecules cm^{-3})	NO (10^{18} molecules cm^{-3})	$G(H_2)$ (molecules per 100 eV)	A^a	g_eB^b
9.7_2	0	8.00	1.00	4.00
9.7_2	0.049	7.26	0.972	3.41
9.7_2	0.194	6.20	0.898	2.65
9.7_2	0.389	5.29	0.814	2.00
9.7_2	0.486	5.00	0.778	1.80
9.7_2	1.264	4.40	0.574	2.03
19.4_4	0	8.00	1.00	4.00
19.4_4	0.194	6.64	0.898	3.14
19.4_4	0.486	5.54	0.778	2.49
19.4_4	0.972	4.47	0.636	1.77
19.4_4	1.75	4.15	0.493	2.16
19.4_4	2.53	3.71	0.402	1.96
19.4_4	3.50	3.39	0.327	1.84
38.8_8	0	8.00	1.00	4.00
38.8_8	0.194	7.00	0.898	3.55
38.8_8	0	8.00	0.814	2.98
38.8_8	0.718	4.88	0.703	2.01
38.8_8	1.94	4.06	0.467	2.18
38.8_8	5.05	3.07	0.252	1.65

[a]Fraction of H atoms reacting with HCl assuming $k_9k_1^{-1} = 1.7 \times 10^{18}$ molecules cm^{-3}.
[b]Yield per 100 eV of electrons forming H atoms (see text).

molecules per 100 eV (3). The average dose rate over the duration of the study was 5×10^{16} eV g^{-1} min^{-1}. Other details of technique and procedure may be found in earlier references (8, 9).

Results

From other work (see, for example, ref. 10) it can be shown that reaction 3 will compete with reaction 4 under the conditions employed here.

[3] $$Cl + NO + HCl \rightarrow ClNO + HCl$$

[4] $$Cl + Cl + HCl \rightarrow Cl_2 + HCl$$

By transferring a small aliquot of the irradiated mixture to a 1 cm path length spectroscopic cell and scanning the absorption in the 180 to 260 nm range the production of ClNO was confirmed from its strong absorption at 197 nm (11). However, the yields of this product were not examined in detail.

Hydrogen yields were normally measured in the dose range 0 to 4.6×10^{18} eV g^{-1} and hydrogen concentration *vs.* dose plots were linear to much larger doses, which showed that reactions of H atoms or other intermediates with products were unimportant. Table 1 summarizes the 100 eV yields obtained with various amounts of nitric oxide added to HCl at three different concentrations. Average deviations of replicate experiments were normally ≤ 0.15 molecules per 100 eV.

Previous studies (1–3, 12) have led to the conclusion that primary processes in HCl produce HCl^+, electrons, thermal hydrogen atoms (H), and hot hydrogen atoms (H) with the following yields per 100 eV: $g_{HCl^+} = g_e = 4.0$, $g_H = 1.8$, and $g_H = 2.2$. Electrons are captured in reactions 5 through 7 and hydrogen formation occurs through reactions 9 and 10.

[5] $$e + 2HCl \rightleftarrows (HCl)_2^{-*}$$

[6] $$(HCl)_2^{-*} + HCl \rightarrow H + Cl^-.2HCl$$

[7] $$(HCl)_2^{-*} + HCl \rightarrow (HCl)_2^- + HCl$$

[8] $$(HCl)_x^- + HCl \rightarrow H + Cl^-.xHCl$$

[9] $$H + HCl \rightarrow H_2 + Cl$$

[10] $$H + HCl \rightarrow H_2 + Cl$$

As stated earlier chlorine formation in [4] will be suppressed by [3] but this would not influence hydrogen production. Also, reaction 10 is rapid (13) and [1] cannot compete with it. However, interpretation of the hydrogen yields is complicated by the possibility that nitric oxide may compete for electrons and/or $(HCl)_x^-$, as well as for H atoms. For that reason the effect of nitric oxide on hydrogen yields from HCl containing 1 to 1.25 mol% SF_6 was also investigated. This scavenger suppresses all reactions of electrons (*i.e.* [5] through [8]) and should make it possible to study the competition between NO and HCl

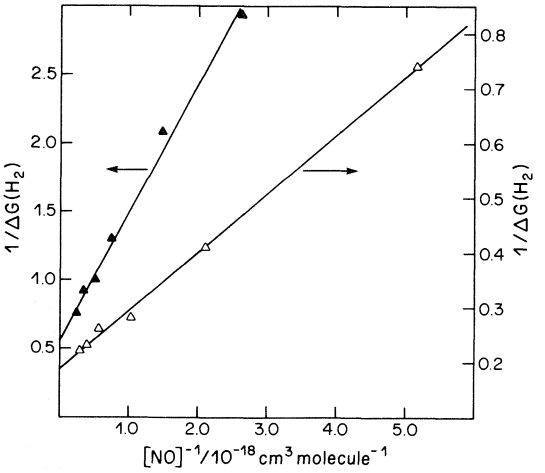

FIG. 1. Reciprocal plots of the change in $G(H_2)$ against $[NO]^{-1}$. Filled points, 1 to 1.25 mol% SF_6 present; open points, no SF_6 present; [HCl] = 19.4×10^{18} molecules cm^{-3}.

for thermal hydrogen atoms alone (*cf.* ref. 14). Under these circumstances the competition between reactions 1 and 9 should be described by expression 11, where y_H is equal to g_H.

$$[11] \quad \{\Delta G(H_2)\}^{-1} = y_H^{-1}\{1 + k_9/k_1[NO]\}$$

The solid points in Fig. 1 are values of $\{\Delta G(H_2)\}^{-1}$ from experiments with varying [NO] in $19.4_4 \times 10^{18}$ molecules cm^{-3} of HCl containing 1 mol% SF_6. The intercept of the linear plot gives $y_H = 1.8 \pm 0.1$ molecules per 100 eV. The slope divided by intercept leads to $k_9k_1^{-1} = 1.7 \pm 0.2 \times 10^{18}$ molecules cm^{-3}. The results of similar experiments with $38.8_8 \times 10^{18}$ molecules cm^{-3} of HCl are reported in Fig. 3 and discussed later.

Discussion

The magnitude of y_H from the experiments described in the preceding paragraph is in excellent agreement with g_H from other experiments (see above). Also, taking k_9 at 298 K = $1.1 \pm 0.1 \times 10^{-13}$ cm^3 $molecule^{-1}$ s^{-1} from a number of experimental studies (15, 16) one finds from $k_9k_1^{-1} = 1.7 \pm 0.2 \times 10^{18}$ molecule cm^{-3}, $k_1 = 6.6 \pm 1.0 \times 10^{-32}$ cm^6 $molecule^{-2}$ s^{-1} for HCl as third body. This is somewhat larger than $\sim 3 \times 10^{-32}$ cm^6 $molecule^{-2}$ s^{-1} for argon as third body (4–6), which seems entirely reasonable, and closer to $6.0 \pm 0.2 \times 10^{-32}$ cm^6 $molecule^{-1}$ s^{-1} for hydrogen as third body. Further justification for the magnitude of $k_9k_1^{-1}$ and for the termolecular character of reaction 1 in HCl is given later. However, the values of y_H and $k_9k_1^{-1}$ from the system with SF_6 present are seen to be in reasonable accord with expectations for the scavenging of thermal H atoms, and we turn now to the interpretation of experiments with NO alone as scavenger.

Reactions 6 and 7 are fast and NO should not compete with them. This is also true for the clustering of $(HCl)_2^-$ to form $(HCl)_x^-$, which is not explicitly shown. To allow for the possible scavenging of e and/or $(HCl)_x^-$ one can use the term B to represent the fraction of electrons proceeding through reactions 5 to 8 to form H atoms. The total hydrogen yield is then given by

$$[12] \quad G(H_2) = g_H + A\{g_H + Bg_e\}$$

where A, the fraction of H atoms undergoing [9], is equal to $\{1 + k_1[NO]/k_9\}^{-1}$. Both A and B must go to unity as $[NO] \rightarrow 0$, and the decrease in $G(H_2)$ for $[NO] \neq 0$ is given by [13].

$$[13] \quad \Delta G(H_2) = g_H + g_e - A\{g_H + Bg_e\}$$

In the event that NO did not react with e or $(HCl)_x^-$ B would always be unity and [13] could be reduced to the same reciprocal form as [11] with y_H now equal to $(g_e + g_H)$. This expression was tested for the results in Table 1 by making plots of $\{\Delta G(H_2)\}^{-1}$ *vs.* $[NO]^{-1}$. The open points in Fig. 1 illustrate this for the $19.4_4 \times 10^{18}$ molecule cm^{-3} HCl concentration. From the magnitudes of the slope/(intercept) apparent values of $k_9 \times k_1^{-1}$ equal to 0.8×10^{18}, 0.5×10^{18}, and 0.2×10^{18} molecules cm^{-3} were found for [HCl] = 38.9×10^{18}, 19.4×10^{18}, and 9.7×10^{18} molecules cm^{-3}, respectively. The fact that these decrease progressively with [HCl] and are all smaller than the value of $k_9k_1^{-1}$ from the experiments with SF_6 present demonstrates that a simple competition for H atoms alone does not hold. This was also shown by the fact that $(g_e + g_H)$ from the intercepts $(= y_H^{-1})$ varied from 5.9 to 5.2 to 4.3 respectively for the three HCl concentrations.

For the purpose of investigating the scavenging of e and $(HCl)_x^-$ by NO, expression 13 was rearranged to [14].

$$[14] \quad \{g_H + g_e - \Delta G(H_2) - Ag_H\}A^{-1} = g_eB$$

Assuming $k_9k_1^{-1} = 1.7 \times 10^{18}$ molecules cm^{-3} from above, we calculated the values of A in column four of Table 1 for the experimental conditions listed in columns one and two, and used

them to evaluate the quantity on the left-hand side of expression 14. This was used as a measure of g_eB and is given in column five of Table 1. Also the dependence of g_eB on [NO]/[HCl] is shown in Fig. 2*a*, where it is interesting to note that: (*a*) the points for the three HCl concentrations fall on a single curve; and (*b*) this is flat at ~2 molecules/100 eV for [NO]/[HCl] $\geq$ 0.04. Since $g_e = 4.0$ the latter feature suggests that NO cannot compete with reaction 5, but does scavenge $(HCl)_x^-$ in reaction 15 (also see below).

[15] $(HCl)_x^- + NO \rightarrow$ *No* H *or* H_2

Likely products for this reaction are HNO and $Cl^-.(x - 1)HCl$.

Figure 2*b* presents a plot of $\{g_e(1 - B)\}^{-1}$ *vs.* [HCl]/[NO], which conforms to expression 16.

[16] $$\{g_e(1 - B)\}^{-1} = (g_{(HCl)_x^-})^{-1}\left\{1 + \frac{k_8[HCl]}{k_{15}[NO]}\right\}$$

The intercept leads to $g_{(HCl)_x^-} = 2.4 \pm 0.3$ molecules per 100 eV and the (slope/intercept) to $k_8/k_{15} = 1.4 \pm 0.3 \times 10^{-2}$. Thus, the quantity B can now be set equal to $[(1 - \alpha) + \alpha\{1 + k_{15}[NO]/k_8[HCl]\}^{-1}]$, where $\alpha = k_7/(k_6 + k_7) = (g_{(HCl)_x^-}/g_e) = 0.60$. This formula has the correct form to explain Fig. 2*a* and leads also to expression 16.

To determine whether the values of the parameters above are consistent with the best value of $k_9k_1^{-1}$ the following approach was employed.

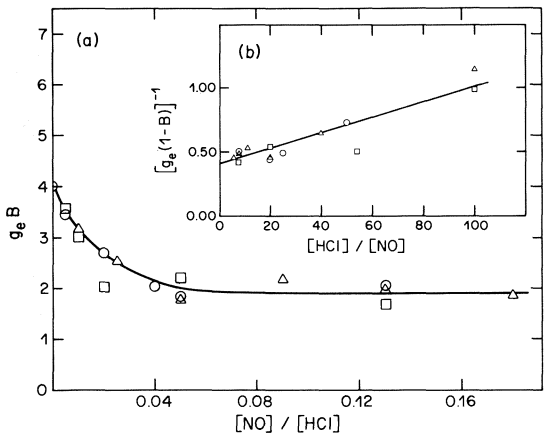

FIG. 2. Effect of NO on hydrogen atom formation by electrons. (*a*) Plot of number of electrons forming H atoms per 100 eV, g_eB, *vs.* [NO]/[HCl]. (*b*) Plot of $\{g_e(1 - B)\}^{-1}$ *vs.* [HCl]/[NO]. ○, [HCl] = 9.7 × 10^{18}; △, 19.4 × 10^{18}; □, 38.9 × 10^{18} molecules cm^{-3}.

Substituting the explicit formula for B into expression 13 and rearranging it, one obtains

[17] $$A = \frac{[g_H + g_e - \Delta G(H_2)]}{g_H + g_e\left[(1 - \alpha) + \alpha\left\{1 + \frac{k_{15}[NO]}{k_8[HCl]}\right\}^{-1}\right]}$$

Using the magnitudes of α and $k_{15}k_8^{-1}$ determined above the fraction A of H atoms undergoing [9] was recalculated. It is plotted as a function of the nitric oxide pressure in Fig. 3. The scatter of points is greater for experiments with SF_6 present because the fractional change in $G(H_2)$ for a given [NO] is much smaller. However, the results for the different HCl concentrations both with and without SF_6 fall on a single line. The slope of this gave $k_9k_1^{-1} = 1.6 \pm 0.2 \times 10^{18}$, whence using k_9 from above we find $k_1 = 6.9 \pm 1.0 \times 10^{-32}$ cm^6 $molecule^{-2}$ s^{-1}. These values are within experimental error the same as those found from the experiments with SF_6 present in the Results section, and a more elaborate determination of α, $k_{15}k_8^{-1}$, and $k_9k_1^{-1}$ by successive approximation is not required.

The observed value of $g_{(HCl)_x^-} = 2.4 \pm 0.3$ is very similar to $g_{(HCl)_x^-} = 2.4 \pm 0.3$ at 274 K and 2.5 ± 0.1 molecules per 100 eV at 196 K estimated by Davidow and Armstrong (1) using chlorine as a scavenger. Also the magnitude of $k_8/k_{15} = 1.2 \times 10^{-2}$ is to be compared with $k_8/k_{18} = 3.3 \times 10^{-3}$ calculated for 298 K from the earlier results.

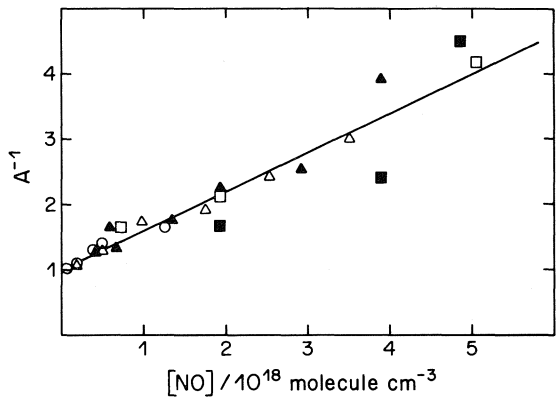

FIG. 3. Reciprocal of the fraction A of H atoms reacting with HCl. Plotted as a function of NO concentration. HCl concentrations shown by points as in Fig. 2; filled points, 1 to 1.25 mol% SF_6 present; open points, without SF_6.

[18] $(HCl)_x^- + Cl_2 \rightarrow$ *No* H *or* H_2

Although the interpretation of the present results is relatively complex these comparisons strongly support the view that NO is scavenging the same species $(HCl)_x^-$ as was previously postulated to explain the chlorine results. The absence of a competition for free electrons is not entirely unexpected, since electron capture by nitric oxide is much slower than by the common electron scavengers SF_6 and CCl_4. The electron capture mechanism in pure NO is considered to involve reactions 19, 20, and 21 (7).

[19]/[20] $e + NO + NO \rightleftharpoons NO^- + NO$

[21] $NO^- + 2NO \rightarrow$ Stable ions

The magnitude of k_{19}, which determines the rate when every NO^- undergoes [21],[2] is $8 \pm 4 \times 10^{-31}$ cm^6 $molecule^{-2}$ s^{-1}. Assuming reaction 22 occurs with a rate constant similar to reaction 19

[22] $e + NO + HCl \rightarrow NO^- + HCl$

the maximum rate of capture in HCl for a given set of [HCl] and [NO] would be 8×10^{-31} [NO][HCl]. With this and a rate of electron capture by HCl $= 10.4 \pm 0.7 \times 10^{-50}$ $[HCl]^3$ from (12) we find that 13% nitric oxide in HCl will capture electrons at one tenth, one twentieth, and one fortieth the rate by HCl at concentrations of 9.7×10^{18}, 19.4×10^{18}, and 38.9×10^{18} molecules cm^{-3} respectively.

The fate of HNO in the HCl system is obviously of particular interest. In contrast to the analogous process in HI (17), reaction 23

[23] $HNO + HCl \rightarrow H_2 + ClNO$

is found from data in ref. 18 to be endothermic by 10 kcal per mole and can be excluded. Some HNO may disappear in reaction 24 (19–21) and by reaction with NO (19).

[24] $HNO + HNO \rightarrow H_2O + N_2O$

However, an important factor here is the presence of Cl_2 and ClNO, which may remove NO through reactions 25 and 26.

[25] $Cl_2 + HNO \rightarrow HCl + ClNO$

[26] $ClNO + HNO \rightarrow HCl + 2NO$

These reactions are exothermic and seem likely in the present circumstances.

[2]In HCl NO^- should undergo the reaction $NO^- + HCl \rightarrow Cl^- + HNO$ which has a second order rate constant of 1.6×10^{-9} cm^3 s^{-1} (22).

1. R. S. Davidow and D. A. Armstrong. J. Chem. Phys. **48**, 1235 (1968).
2. G. R. A. Johnson and J. L. Redpath. Trans. Faraday Soc. **66**, 861 (1970).
3. D. E. Wilson and D. A. Armstrong. Radiat. Res. Rev. **2**, 297 (1970).
4. T. Hikida, J. A. Eyre, and L. M. Dorfman. J. Chem. Phys. **54**, 3422 (1971).
5. J. J. Ahumada, J. V. Michael, and D. T. Osborne. J. Chem. Phys. **57**, 3736 (1972).
6. R. Atkinson and R. J. Cvetanović. Can. J. Chem. **51**, 370 (1973).
7. G. E. Caledonia. Chem. Rev. **75**, 333 (1975).
8. D. A. Armstrong. Can. J. Chem. **40**, 1385 (1962); R. C. Rumfeldt and D. A. Armstrong. Can. J. Chem. **41**, 1104 (1963).
9. S. S. Nagra and D. A. Armstrong. Can. J. Chem. **53**, 3305 (1975).
10. R. B. Timmons and B. de B. Darwent. J. Phys. Chem. **73**, 2208 (1969).
11. N. M. Ballash and D. A. Armstrong. Spectrochim. Acta, **30A**, 941 (1974).
12. S. S. Nagra and D. A. Armstrong. Can. J. Chem. **54**, 3580 (1976).
13. D. K. Jardine, N. M. Ballash, and D. A. Armstrong. Can. J. Chem. **51**, 656 (1973).
14. R. S. Davidow, R. A. Lee, and D. A. Armstrong. J. Chem. Phys. **45**, 3364 (1966).
15. M. A. A. Clyne and D. H. Stedman. Trans. Faraday Soc. **61**, 2164 (1966).
16. A. A. Westenberg and N. deHaas. J. Chem. Phys. **48**, 4405 (1968).
17. J. L. Holmes and E. V. Sundaram. Trans. Faraday Soc. **62**, 1 (1966); **62**, 523 (1966).
18. United States Department of Commerce. JANA Thermochemical Tables, 2nd Edition, NSRDS-NBS 37. U.S. Printing Office, Washington. 1971.
19. O. P. Strausz and H. E. Gunning. Trans. Faraday Soc. **60**, 347 (1964).
20. F. C. Kohout and F. W. Lampe. J. Chem. Phys. **46**, 4075 (1967).
21. A. B. Callear and R. W. Carr. J. Chem. Soc. Faraday Trans. II, **71**, 1603 (1975).
22. E. E. Ferguson, D. B. Dunkin, and F. C. Fehsenfeld. J. Chem. Phys. **57**, 1459 (1972).

Synthetic routes to nucleoside analogs of *N*-substituted 1-oxa-4-azacyclohexanes and 1-thia-4-azacyclohexanes. ^{13}C nuclear magnetic resonance spectra of six-membered, cyclic amides

B. MARIO PINTO, DOLATRAI M. VYAS, AND WALTER A. SZAREK[1]

Department of Chemistry, Queen's University, Kingston, Ont., Canada K7L 3N6

Received September 7, 1976

B. MARIO PINTO, DOLATRAI M. VYAS, and WALTER A. SZAREK. Can. J. Chem. **55**, 937 (1977).

Nucleoside analogs, namely 6-chloro-9-(4-benzoyl-1-oxa-4-azacyclohexan-2-yl)-9*H*-purine **6** and 6-chloro-9-(4-benzoyl-1-thia-4-azacyclohexan-2-yl)-9*H*-purine **7**, were obtained by treatment of 4-benzoyl-2-hydroxy-1-oxa-4-azacyclohexane **13** and 4-benzoyl-2-hydroxy-1-thia-4-azacyclohexane **18**, respectively, with 6-chloropurine, methyldiphenylphosphine, and diethyl azodicarboxylate in refluxing tetrahydrofuran. Compounds **13** and **18** were obtained by *O*-deacetylation of the corresponding 2-acetoxy derivatives **11** and **16** with a catalytic amount of sodium methoxide in chloroform. 2-Acetoxy-4-benzoyl-1-oxa-4-azacyclohexane **11** was obtained from 4-benzoyl-1-oxa-4-azacyclohexane **10** by treatment with *tert*-butyl peracetate, cuprous chloride, and benzene, whereas 2-acetoxy-4-benzoyl-1-thia-4-azacyclohexane **16** was prepared by a Pummerer reaction with 4-benzoyl-1-thia-4-azacyclohexane 1-oxide **15**. The ^{13}C nmr spectra of all the compounds are reported; the spectra provided unambiguous proof of structure.

B. MARIO PINTO, DOLATRIA M. VYAS et WALTER A. SZAREK. Can. J. Chem. **55**, 937 (1977).

On a obtenu des analogues nucléosides à savoir la chloro-6 (benzoyl-4 oxa-1 aza-4 cyclohexanyl-2)-9 9*H*-purine **6** et chloro-6 (benzoyl-4 thia-1 aza-4 cyclohexanyl-2)-9 9*H*-purine **7** par les réactions respectives du benzoyl-4 hydroxy-2 oxa-1 aza-4 cyclohexane **13** et du benzoyl-4 hydroxy-2 thia-1 aza-4 cyclohexane **18** avec la chloro-6 purine, la méthyldiphénylphosphine et l'azodicarboxylate de diéthyle dans le tétrahydrofuranne au reflux. On a obtenu les composés **13** et **18** par une *O*-déacylation des dérivés acétoxy-2 correspondants (**11** et **16**) avec des quantités catalytiques de méthylate de sodium dans le chloroforme. On a obtenu l'acétoxy-2 benzoyl-4 oxa-1 aza-4 cyclohexane **11** à partir du benzoyl-4 oxa-1 aza-4 cyclohexane **10** par réaction avec le peracétate de *tert*-butyle, le chlorure cuivreux et le benzène alors qu'on a préparé l'acétoxy-2 benzoyl-4 thia-1 aza-4 cyclohexane **16** par une réaction de Pummerer avec le benzoyl-4 thia-1 aza-4 cyclohexane oxyde-1 **15**. On rapporte les spectres rmn du ^{13}C de tous les composés; les spectres fournissent une preuve non-ambigue des structures.

[Traduit par le journal]

Introduction

In the quest for potent anticancer agents for chemotherapeutic use, an active area of research in this laboratory is the synthesis of novel nucleoside analogs containing more than one hetero-atom in the carbohydrate ring. A stimulus for this aspect of nucleoside chemistry was provided by the fact that *N*-[2-(9-adenyl)-3,5-dihydroxy-6-(hydroxymethyl)morpholino]iso-nicotinamide **1**, obtained by condensation of periodate-oxidized adenosine with isonicotinic acid hydrazide, is a substituted morpholine structure and possesses both antitumor and immunosuppressive properties (1). The reduction of the adduct of periodate-oxidized adenosine 5′-phosphate and methylamine has also afforded a nucleotide analog of an *N*-methylmorpholine derivative (2*a*), and a uridine-base derivative of a morpholine derivative has been synthesized by Jones and Walker (2*b*) by reacting "uridine-dialdehyde" with benzoylhydrazine. As part of this program, the synthesis (3) and conformational analysis (4) of nucleoside-base derivatives of 1,4-oxathiane (**2** and **3**), 1,4-dithiane **4**, and 1,4-dioxane **5** have been reported; some of these compounds have exhibited anticancer activity.[2]

As a further extension, in this paper we report the synthesis of 6-chloro-9-(4-benzoyl-1-oxa-4-azacyclohexan-2-yl)-9*H*-purine **6** and 6-chloro-9-(4-benzoyl-1-thia-4-azacyclohexan-2-yl)-9*H*-purine **7** from the readily available, non-carbohydrate precursors, 1-oxa-4-azacyclohexane **8** and 1-thia-4-azacyclohexane **9**, respectively. In earlier studies (6, 7), suitably protected

[1]Author to whom inquiries should be addressed.

[2]W. A. Szarek, D. M. Vyas, and A. Bloch, unpublished results.

carbohydrates have been converted into derivatives of 1-oxa-4-azacyclohexanes. Interestingly, several guanidine derivatives of 1-thia-4-azacyclohexane and 1-thia-4-azacycloheptane have also been studied (8) for their potential antihypertensive properties. ^{13}C magnetic resonance (^{13}Cmr) and proton magnetic resonance (^{1}Hmr) spectroscopic data of all intermediates, side-products, and product nucleosides are also reported in this paper; these data have been employed for proof of structure and examination of conformational behaviour.

In contrast to our earlier study (4) on ^{13}Cmr spectra of 1,4-oxathiane derivatives in which the assignment of chemical shifts was straightforward, in the case of the present series of

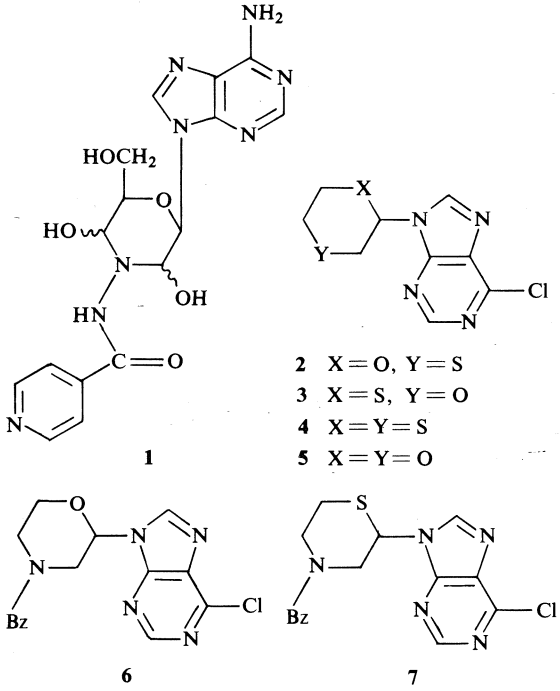

1

2 X = O, Y = S
3 X = S, Y = O
4 X = Y = S
5 X = Y = O

6 7

compounds, namely the *N*-acylated nitrogen heterocycles, the assignment of signals in their ^{13}Cmr spectra obtained at ambient temperature was complicated because of broadening of certain signals owing to restricted rotation about the amide bond (9). Hirsch *et al.* (10) have recently reported barriers to amide rotation in a series of substituted, six-membered nitrogen heterocycles, including 4-benzoyl-1-oxa-4-azacyclohexane **10**, as studied by ^{13}C dnmr. In the present study, spectra obtained at various temperatures were employed to distinctly assign the signals of all of the carbons in the six-membered rings. Details of a ^{1}H dnmr study of the effects of substitution on nitrogen on barriers to rotation of cyclic amides have been published (11).

Results and Discussion

Commercially available 1-oxa-4-azacyclohexane **8** was readily converted into 4-benzoyl-1-oxa-4-azacyclohexane **10** (see Scheme 1) by treatment with benzoyl chloride and pyridine in chloroform. Treatment of **10** with *tert*-butyl peracetate in refluxing benzene in the presence of cuprous chloride for 5.5 h by the procedure of Sosnovsky and Lawesson (12) afforded chromatographically separable 2-acetoxy-4-benzoyl-1-oxa-4-azacyclohexane **11** and *trans*-2,3-diacetoxy-4-benzoyl-1-oxa-4-azacyclohexane **12** in a ratio of approximately 4:1, respectively; prolonged heating resulted in the formation of a greater proportion of **12**.

The regioselectivity of the acetoxylation reaction to give the 2-acetoxy derivative **11** was readily confirmed by ^{13}Cmr spectroscopy. The ^{13}C chemical shifts for the 1-oxa-4-azacyclohexane derivatives **8** and **10**–**13** are given in Table 1. In the case of compounds **11** and **13**, the spectral data are reported at temperatures at which the rates of rotation about the amide bond are slow, intermediate, and fast on the nmr time-scale; in the case of 4-benzoyl-1-oxa-4-azacyclohexane **10**, the two temperatures given are those representing slow and intermediate rates. The data given for the diacetate **12** are those for the slow-exchange rate. The

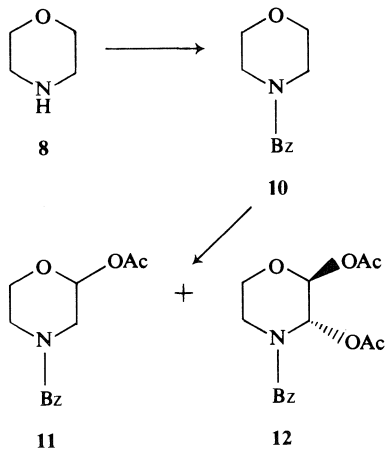

8 10 11 12

SCHEME 1

TABLE 1. ^{13}C chemical-shift data[a] of 1-oxa-4-azacyclohexane derivatives

Compound	Temperature (K)	Carbon 2	3	5	6	$OCOCH_3$	$OCOCH_3$	NCOPh	NCO*Ph*
 **8**	305	68.2	46.9	46.9	68.2	—	—	—	—
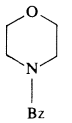 **10**	270	66.9	48.2	42.5	66.9	—	—	170.3	127.0, 128.6 129.9, 135.1
	295	66.9	(40.2–52.0)[b]		66.9	—	—	170.3	127.0, 128.5 129.8, 135.3
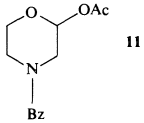 **11**	260[c]	88.7	46.8(1.0) 49.9(3.1)	41.5(2.4) 44.2(1.0)	60.9	21.0	[d]	[d]	127.0, 128.5, 130.1 133.8, 134.5
	305	89.2	(35.0–53.8)[b]		61.3	20.9	169.1	171.0	127.2, 128.6 130.1, 134.9
	330	89.6	48.2	43.8	61.5	20.8	[d]	[d]	127.2, 128.6 130.1, 134.9
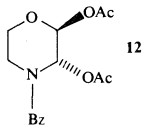 **12**	305	88.3	76.9	38.2	60.0	20.7	[d]	[d]	127.4, 128.5 130.8
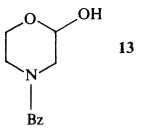 **13**	260	90.3	47.2	41.7	60.8	—	—	171.3	127.4, 128.5 130.1, 134.5
	309	90.8	(38.4–48.5)[b]		61.3	—	—	[d]	127.3, 128.5 130.0
	330	91.0	(41.5–46.5)[b]		61.4	—	—	[d]	127.4, 128.5 130.0

[a]In ppm downfield from internal tetramethylsilane (TMS) in chloroform-*d*.
[b]Values represent extremities of a broad band.
[c]Values in parentheses are peak heights standardized on the basis of each carbon of the minor isomer having a peak height of 1.0.
[d]Signal not observed.

presence of the acetoxy group at C-2 in 2-acetoxy-4-benzoyl-1-oxa-4-azacyclohexane **11** causes a large downfield shift (~22 ppm) of the C-2 signal relative to that in the spectrum of 4-benzoyl-1-oxa-4-azacyclohexane **10** and only slight changes in the chemical shifts of the C-3 and C-5 signals. It is noteworthy that the C-6 signal in the spectrum of **11** (recorded at the slow-exchange limit) is shifted upfield by 6.0 ppm relative to the corresponding signal in the spectrum of **10**. This result is consistent with the preponderant conformation of compound **11** having the acetoxy group in the axial orientation, since there then would be a γ steric interaction (4, 13) between this group and the axial hydrogen at C-6. The assignment of the axial orientation for the acetoxy group is in accordance with the anomeric effect (14), and was corroborated by the observation, in the ^{1}Hmr spectrum of **11**, of the H-2 signal as a broad singlet at τ 3.82 ($J_{2,3} + J_{2,3'} \simeq 5$ Hz); the value of 5 Hz includes the long-range coupling across oxygen.

The constitution and stereochemistry of the diacetoxy derivative, *trans*-2,3-diacetoxy-4-benzoyl-1-oxa-4-azacyclohexane **12**, were also established by nmr spectroscopy. The observation that the C-6 signal in the ^{13}Cmr spectrum of the diacetate **12** is shifted upfield by 1.3 ppm relative to that in the spectrum of the monoacetate **11** (recorded at 305 K) is only consistent with the second acetoxy group being at C-3 in compound **12**; the presence of this group at C-6 or C-5 would be expected to cause a downfield shift of the C-6 signal in **12** (relative to **11**) as a consequence of the α or β effect (4, 15), respectively. In the ^{1}Hmr spectrum of **12** the H-2 and H-3 signals appeared as broad singlets having half-height widths of 3 and 4 Hz,[3] respectively, an observation which suggests that the acetoxy groups at C-2 and C-3 in the preferred conformation of **12** are *trans*-diaxially disposed. This stereochemistry is also manifested by the upfield shifts (4.3 and 6.9 ppm) of the C-5 and C-6 signals, respectively, in the ^{13}Cmr spectrum of **12** relative to the corresponding signals in the spectrum of 4-benzoyl-1-oxa-4-azacyclohexane **10** (recorded at 270 K) attributable to the γ steric interactions between the axial acetoxy groups and the axial hydrogens at C-5 and C-6.

Another interesting aspect of the ^{13}Cmr-spectral study of compounds **10** and **11** is the effect of restricted rotation about the amide bond on ^{13}C chemical shifts. In the spectrum of **10** at 295 K the C-3 and C-5 resonances appear as a broad band; however, at 270 K distinct signals are observed at 48.2 and 42.5 ppm indicating a slow rate of rotation about the amide bond on the nmr time-scale. Previous workers have shown (17) that the carbon *syn* to the carbonyl oxygen of an amide is shielded relative to the corresponding carbon in the *anti* conformer. Thus, the signals at 48.2 and 42.5 ppm are assigned to the carbons which are *anti* and *syn*, respectively, to the carbonyl oxygen. In the case of the 2-acetoxy derivative **11**, the C-3 and C-5 resonances, which appear as a broad band at 305 K (see Fig. 1*b*), are resolved into two sharp peaks at 48.2 and 43.8 ppm at the fast-exchange limit (see Fig. 1*a*); the signal at 48.2 ppm is assigned to C-3 on the basis of an expected β effect of a neighboring acetoxy group. At the slow-exchange limit, signals for the two ring carbons α to the nitrogen for the two rotational isomers are clearly revealed (see Fig. 1*c*); the signals for the *syn* and *anti* isomers were assigned on the basis of the approach outlined above.

Treatment of compound **11** with a catalytic amount of sodium methoxide afforded 4-benzoyl-2-hydroxy-1-oxa-4-azacyclohexane **13** (see Scheme 2) as a colorless syrup. The ^{13}C

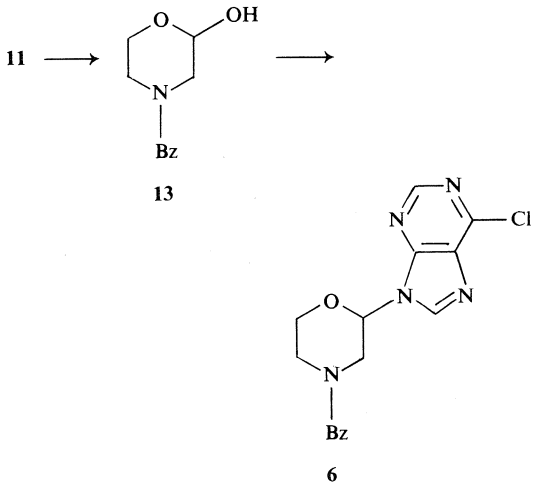

SCHEME 2

[3]These values presumably include long-range couplings across the two heteroatoms in the ring (compare refs. 4 and 16).

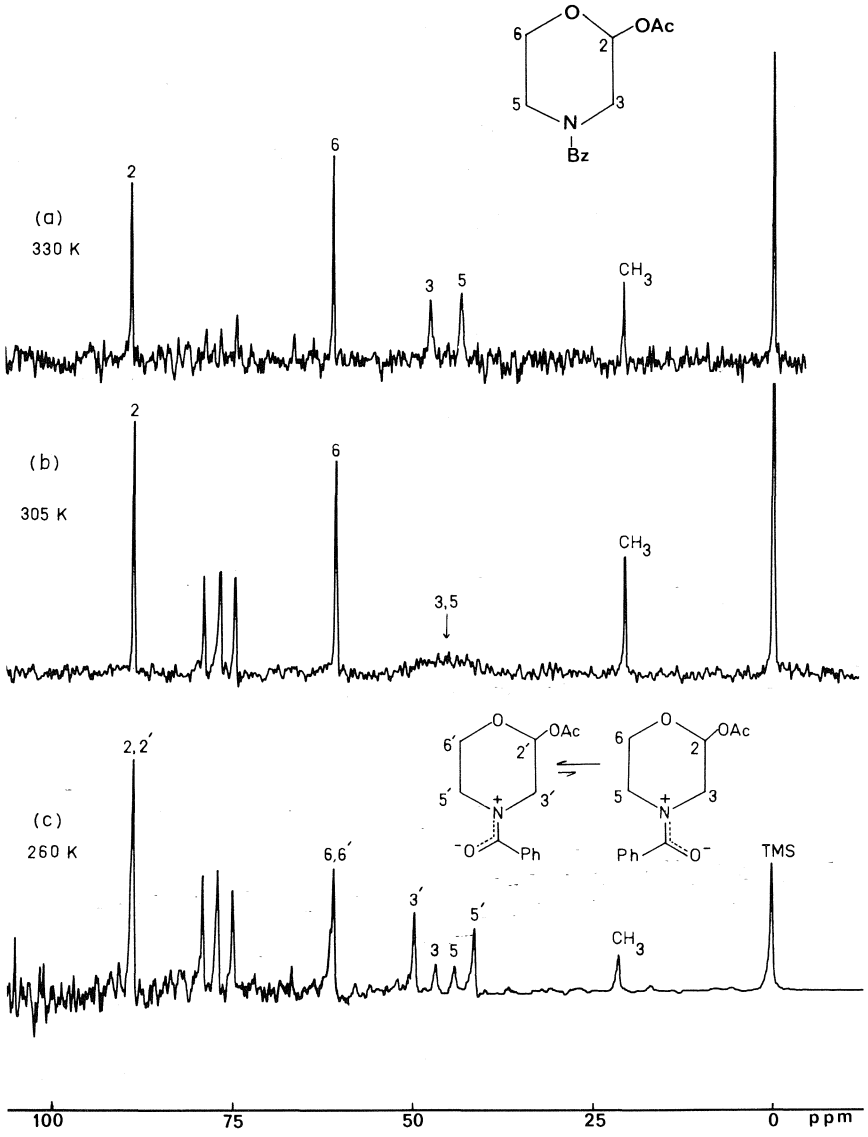

FIG. 1. ^{13}Cmr spectra of 2-acetoxy-4-benzoyl-1-oxa-4-azacyclohexane **11** at (*a*) 330 K, (*b*) 305 K, and (*c*) 260 K.

chemical shift assignments for the 2-hydroxy derivative **13** were relatively straightforward and are documented in Table 1. Compound **13** was converted into the nucleoside analog **6** in 50% yield by treatment (18) with 6-chloropurine, methyldiphenylphosphine, and diethyl azodicarboxylate in refluxing tetrahydrofuran. The maximal uv absorption for **6** at 264 nm in neutral, acid, or basic solution is in agreement (19) with a 9-substituted purine. The value (12 Hz) obtained for $J_{2',3'} + J_{2',3''}$ from the ^{1}Hmr spectrum of **6** is indicative of a preponderance in chloroform-*d* of the conformer having the purine moiety in an equatorial orientation. This conformational preference is further indicated by the observation that the C-6′ signal in the ^{13}Cmr spectrum of nucleoside **6** (recorded at 330 K) is shifted upfield by only 0.8 ppm (see Table 2) with respect to the C-6 signal in the spectrum of **10**; a preference for the conformer having the purine moiety in an axial orientation would have been expected to be

TABLE 2. ^{13}C chemical-shift data[a] for nucleoside analogs

Compound	Temperature (K)	Carbon 2′	3′	5′	6′	NCO*Ph*	Purine
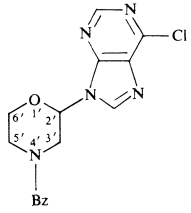 6	305	79.7	47.5[b]	44.2[b]	66.1	127.3, 128.8 130.6	142.9, 152.2
	330	79.9	47.7	44.9	66.1	127.3, 128.8 130.6	143.0, 152.3
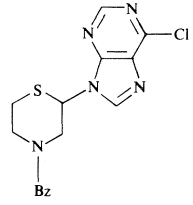 7	305	52.2	[c]	[c]	25.8	126.5, 128.4 130.2	143.7, 151.8
	330	52.3	51.1	45.7	25.9	126.6, 128.5 130.3	143.8, 151.8

[a]In ppm downfield from internal TMS in chloroform-*d*.
[b]Slightly broadened peak.
[c]Signal not observed.

manifested by a significantly larger upfield shift of the C-6′ signal owing to a γ steric interaction between the purine ring and the axial hydrogen at C-6′.

1-Thia-4-azacyclohexane **9**, prepared from diethanolamine by the method of Cymerman-Craig *et al.* (20), was converted into 4-benzoyl-1-thia-4-azacyclohexane **14** (see Scheme 3) by treatment with benzoyl chloride and pyridine in chloroform. The sulfoxide **15** was obtained from **14** by oxidation with sodium metaperiodate by the method of Leonard and Johnson (21). Treatment of **15** with 2.4 equiv. of acetic anhydride in benzene containing a trace of *p*-toluenesulfonic acid monohydrate at 60 °C for 3.5 h afforded the chromatographically separable Pummerer-reaction product **16**, as a colorless syrup, and a small proportion of 4-benzoyl-1-thia-4-azacyclohex-2-ene **17**; treatment of **15** with these reagents at 80 °C for 1 h afforded a 1:1 mixture of the Pummerer-reaction product **16** and the elimination product **17**.

The ^{13}C chemical shift assignments in the spectrum of 4-benzoyl-1-thia-4-azacyclohexane **14** (see Table 3) were made in analogy to those made in the spectrum of 4-benzoyl-1-oxa-4-azacyclohexane **10**; however, in the case of **14**, the C-2 and C-6 signals were observed to have slightly different chemical shifts. The assignment of the C-2 and C-6 signals was made by an extension of the approach employed for the C-3 and C-5 signals.

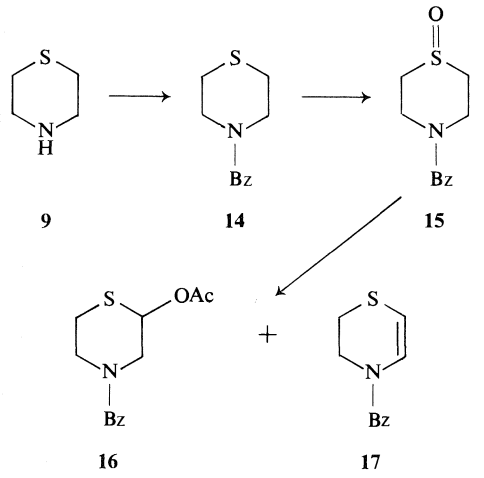

9 **14** **15** **16** **17**

SCHEME 3

In Fig. 2 are shown the ^{13}Cmr spectra of the sulfide **14** and the sulfoxide **15**. The relative shifts observed for corresponding signals parallel the trends described previously (4) for 1,4-oxathiane and 1,4-oxathiane 1-oxide.

The ^{13}Cmr spectrum of the Pummerer product **16** was analyzed in a manner analogous to that employed in the case of 2-acetoxy-4-benzoyl-1-oxa-4-azacyclohexane **11**. A salient feature again is the 4.1 ppm upfield shift of the C-6 signal in the spectrum of **16** (recorded at the slow-exchange limit) relative to the corresponding signal in the spectrum of 4-benzoyl-1-thia-4-azacyclohexane **14** indicating that the preponderant conformation of compound **16** has the acetoxy group at C-2 in the axial orientation; the value (~8 Hz) obtained for $J_{2,3} + J_{2,3'}$ from the ^{1}Hmr spectrum of **16** could also be considered to be in agreement with this assignment, provided that it is noted that the value presumably includes the long-range coupling across sulfur. Moreover, the assignment is in accordance with previous examples (22) of the anomeric effect in sulfur heterocycles. Finally, the ^{13}Cmr spectra of **16** recorded at both fast- and slow-exchange limits exhibit nearly identical features to those described above for the spectra of 2-acetoxy-4-benzoyl-1-oxa-4-azacyclohexane **11**.

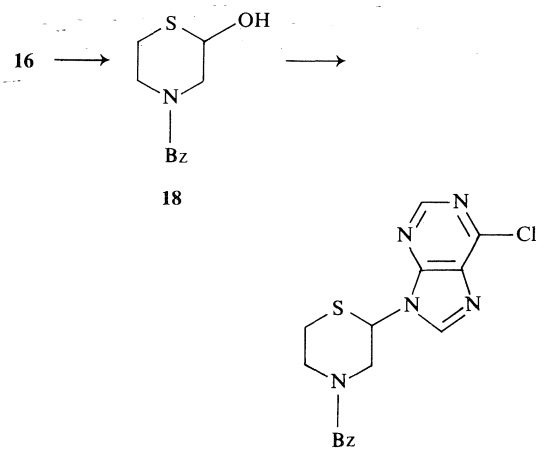

SCHEME 4

Treatment of compound **16** with a catalytic amount of sodium methoxide afforded 4-benzoyl-2-hydroxy-1-thia-4-azacyclohexane **18** (see Scheme 4) as a colorless syrup. Compound

TABLE 3. ^{13}C chemical-shift data[a] for 1-thia-4-azacyclohexane derivatives

Compound	Temperature (K)	Carbon 2	3	5	6	$OCOCH_3$	$OCOCH_3$	NCOPh	NCO*Ph*
 **9**	305	28.3	47.9	47.9	28.3	—	—	—	—
 **14**	250	27.9	50.0	44.2	27.3	—	—	170.6	126.5, 128 6 129.7, 136.1
	305	27.8	(38.8–55.1)[b]		27.8	—	—	170.9	126.8, 128.6 129.7, 136.3
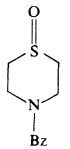 **15**	250	45.2	38.4	32.8	44.7	—	—	170.7	126.7, 128.8 130.3, 134.2
	305	45.4	(29.7–41.7)[b]		45.4	—	—	170.5	126.8, 128.7 130.1, 134.8
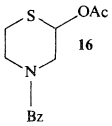 **16**	260[c]	68.7	53.1(2.4) 48.8(1.0)	47.4(1.0) 43.8(4.2)	23.2	21.2	[d]	[d]	127.0, 128.5 130.0, 135.5
	305	69.0	52.9[e]	44.5[e]	23.6	21.1	169.1	171.6	127.0, 128.5 129.9, 135.5
	330	69.3	51.3	45.6	23.8	21.0	[d]	[d]	127.1, 128.5 129.9, 135.5
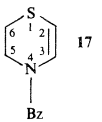 **17**	243[c]	104.5(1.0) 101.2(2.2)	124.5(2.8) 121.5(1.0)	47.5(1.0) 40.8(2.3)	25.9	—	—	169.0	128.5, 129.2, 129.4 131.5, 135.6
	305	101.4	123.2	41.3[e]	25.9	—	—	169.0	128.2, 128.5 130.5, 134.6
	346	101.9	123.3	43.1	25.9	—	—	169.0	128.2, 128.9 130.7, 134.5
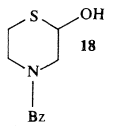 **18**	305	69.3	(38.0–56.0)[b]		23.4	—	—	[d]	127.4, 128.4 129.8
	330	69.4	53.3	46.7	23.6	—	—	[d]	127.6, 128.5 129.9

[a]In ppm downfield from internal TMS in chloroform-*d*. [b]Values represent extremities of a broad band. [c]Values in parentheses are peak heights standardized on the basis of each carbon of the minor isomer having a peak height of 1.0. [d]Signal not observed. [e]Slightly broadened peak.

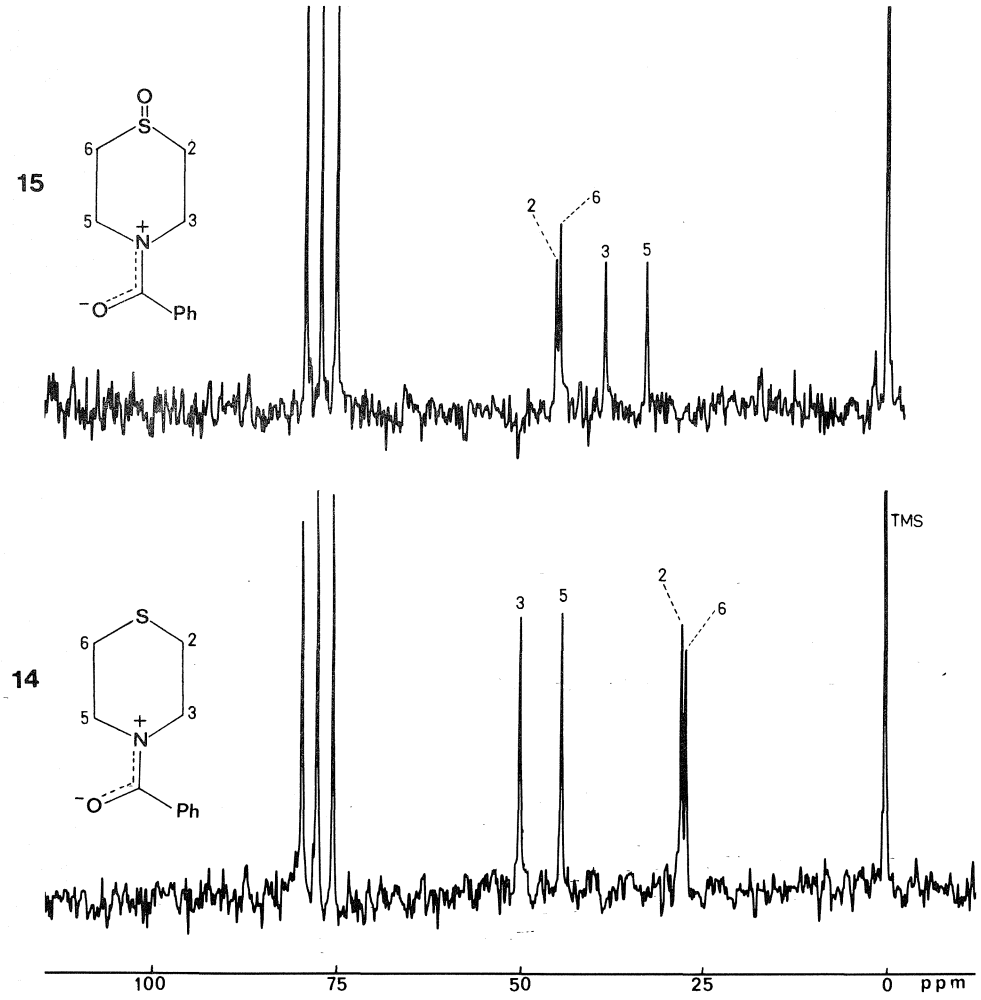

FIG. 2. ^{13}Cmr spectra of 4-benzoyl-1-thia-4-azacyclohexane **14** and 4-benzoyl-1-thia-4-azacyclohexane 1-oxide **15** recorded at 250 K.

18 was then converted into the nucleoside analog **7** in 35% yield by the same coupling procedure as described for **6**. The maximal uv absorption for **7** at 264–266 nm in neutral, acid, or basic solution is in agreement with a 9-substituted purine. The ^{13}C chemical-shift data for **7** are given in Table 2. As in the case of 2-acetoxy-4-benzoyl-1-thia-4-azacyclohexane **16**, the ^{13}Cmr and ^{1}Hmr data suggested that the preponderant conformation of the nucleoside analog **7** has the substituent at C-2 in the axial orientation; however, the C-6 signal in the spectrum of **7** (recorded at 330 K) is shifted upfield by only 1.4 ppm relative to the C-6 signal in the spectrum of **14**.

Experimental

Melting points were determined with a Fisher-Johns melting point apparatus and are uncorrected. The ir spectra were recorded on a Perkin-Elmer 180 spectrophotometer. Ultraviolet (uv) spectra were recorded on a Beckman ACTA MIV spectrophotometer. Proton magnetic resonance (^{1}Hmr) spectra were recorded at 60 MHz on a Varian EM-360 or Bruker HX-60 spectrometer in chloroform-*d* with tetramethylsilane (TMS, $\tau = 10.00$) as the internal standard. ^{13}Cmr spectra were recorded in chloroform-*d* solution on a Bruker HX-60 spectrometer equipped with a FT60M Fourier transform accessory at 15.09 MHz; chemical shifts are given in ppm downfield from TMS. Thin-layer chromatography was performed with silica gel G as the adsorbent in the following solvent systems (v/v): (*A*) benzene – ethyl acetate, 1:1; (*B*) 4:1; (*C*) 1:2; (*D*) petroleum ether (bp 60–80 °C) – ethyl acetate – methanol, 3:3:1. The

developed plates were air dried, and exposed to uv light and/or sprayed with a solution of cerium sulfate (1.0%) and molybdic acid (1.5%) in 10% aqueous sulfuric acid, and heated at ~150 °C. Column chromatography was performed on Brinkmann silica gel (70–325 mesh). Solvents were evaporated under reduced pressure below 50 °C.

4-Benzoyl-1-oxa-4-azacyclohexane ***10***

To a solution of 1-oxa-4-azacyclohexane **8** (10 g, 0.115 mol) in chloroform (100 ml) containing pyridine (18.9 g) at 0 °C was added benzoyl chloride (16.3 g, 0.116 mol) in chloroform (20 ml) over a period of 1.5 h. The mixture was stirred at room temperature for 8 h and then poured onto ice. The layers were separated, and the organic layer was washed successively with 6 *N* hydrochloric acid, aqueous sodium hydrogen carbonate solution (3 × 30 ml), aqueous copper sulfate solution (30 ml), and water (30 ml). The organic layer was dried over anhydrous magnesium sulfate, and the solvent evaporated to afford a syrup (20 g) which crystallized upon cooling *in vacuo*. The sample was recrystallized from ether–hexane to give **10** as white crystals (16.8 g, 76%); mp 69–70 °C; ^{1}Hmr data: τ 2.62 (s, 5H, Ph), 6.38 (br s, 8H, 2H-2′s, 2H-3′s, 2H-5′s, 2H-6′s).

2-Acetoxy-4-benzoyl-1-oxa-4-azacyclohexane ***11***

To a stirred solution of 4-benzoyl-1-oxa-4-azacyclohexane **10** (0.75 g, 3.9 mmol) in benzene (50 ml) containing cuprous chloride (40 mg), under an atmosphere of nitrogen at 81 °C, was added *tert*-butyl peracetate (0.56 g of a 75% solution in Mineral Spirits, 3.2 mmol) in benzene (15 ml) over a period of 2 h. The mixture was stirred at 81 °C for 3.5 h. Thin-layer chromatography indicated the presence of three new components having R_F values of 0.5, 0.4, and 0.3 together with unreacted starting material **10** (R_F 0.2). The mixture was cooled, diluted with benzene (50 ml), washed successively with aqueous sodium hydrogen carbonate solution (2 × 25 ml) and water (25 ml), and dried over anhydrous sodium sulfate. Evaporation of the solvent afforded a syrup which was chromatographed on silica gel, with solvent *A* as eluant, to give components having R_F values of 0.5, 0.4, 0.3, and 0.2. The component having an R_F value of 0.5 was obtained from ethanol as white crystals (28 mg), mp 146–147 °C, and was identified as being *trans*-2,3-diacetoxy-4-benzoyl-1-oxa-4-azacyclohexane **12**; ^{1}Hmr data: τ 2.5 (s, 5H, Ph), 3.82, 4.02 (two-1H br s, $W_{1/2}$ = 3 and 4 Hz, respectively, H-2 or H-3), 5.50–7.00 (m, 4H, 2H-5′s, 2H-6′s), 7.82 (s, 3H, OAc), 7.90 (s, 3H, OAc). *Anal.* calcd. for $C_{15}H_{17}NO_6$: C 58.62, H 5.58, N 4.56; found: C 58.61, H 5.66, N 4.48.

The component having an R_F value of 0.4 was isolated as a syrup (12 mg) and was not identified. The component having an R_F value of 0.3 was isolated as a syrup and was identified as being 2-acetoxy-4-benzoyl-1-oxa-4-azacyclohexane **11** (82 mg, 44%); ^{1}Hmr data: τ 2.5 (s, 5H, Ph), 4.0 (br s, 1H, H-2), 5.6–7.1 (6H, 2H-3′s, $|J_{2,3} + J_{2,3'}| \simeq 5$ Hz, 2H-5′s, 2H-6′s), 7.9 (s, 3H, OAc). The component having R_F value of 0.2 was isolated as a white solid and was identified as being unreacted starting material **9** (0.60 g).

4-Benzoyl-2-hydroxy-1-oxa-4-azacyclohexane ***13***

To a stirred solution of 2-acetoxy-4-benzoyl-1-oxa-4-azacyclohexane **11** (0.29 g, 1.16 mmol) in chloroform (20 ml) at 0 °C was added sodium methoxide (~0.1 *M*) in methanol (1 ml); stirring was continued at 0 °C for 5 h. Thin-layer chromatography (solvent *A*) indicated the presence of a new component having an R_F value of 0.1. The solution was washed with an aqueous sodium hydrogen carbonate solution (2 × 7 ml) and then with water (7 ml), and dried over anhydrous magnesium sulfate. Evaporation of the solvent afforded a syrup which was identified as being 4-benzoyl-2-hydroxy-1-oxa-4-azacyclohexane **13** (0.24 g, 98%); ^{1}Hmr data: τ 2.58 (s, 5H, Ph), 5.17 (br s, 1H, after deuteriation of OH, H-2) 5.67–6.92 (br signals, 6H, 2H-3′s, 2H-5′s, 2H-6′s).

6-Chloro-9-(4-benzoyl-1-oxa-4-azacyclohexan-2-yl)-9H-purine ***6***

A mixture of 6-chloropurine (0.179 g, 1.16 mmol), methyldiphenylphosphine (0.232 g, 1.16 mmol), and diethyl azodicarboxylate (0.202 g, 1.16 mmol) in dry tetrahydrofuran (20 ml) was added to 4-benzoyl-2-hydroxy-1-oxa-4-azacyclohexane **13** (0.235 g, 1.14 mmol) in dry tetrahydrofuran (20 ml) with stirring; stirring was continued for 20 h at room temperature. The reaction mixture was brought to reflux, and each of the reagents (0.5 equiv.) was added; refluxing was continued for 12 h. The reaction mixture was concentrated, and the residue was chromatographed on silica gel, with solvent *C* as eluant, to give a component having an R_F value of 0.1 in solvent *A* and 0.2 in solvent *C*. The sample was obtained as a white foam and was identified as being 6-chloro-9-(4-benzoyl-1-oxa-4-azacyclohexan-2-yl)-9*H*-purine **6** (0.20 g, 50%); mp 61 °C (sintered at 55 °C); ir (chloroform): 1578, 1550, and 1480 (purine ring), 1625 (C=O) cm^{-1}; uv λ_{max} (ethanol): 264 (ε 3492) (purine ring), 248 (ε 3257) (benzamide), 210 nm (ε 7039) (purine ring); λ_{max} (ethanol containing a trace of hydrochloric acid): 264 (ε 3603), 248 (ε 3408), 209 nm (ε 6536); λ_{max} (ethanol containing a trace of sodium hydroxide): 264 (ε 3743) shoulder, 246 (ε 5251), 217 nm (ε 16 480); ^{1}Hmr data: τ 1.28, 1.63 (2s, 1H each, H-2, H-8), 2.55 (s, 5H, Ph), 4.05 (d of d, 1H, $|J_{2',3'} + J_{2',3''}| = 12$ Hz, H-2′), 5.1–6.9 (6H, H-3′, H-3″, H-5′, H-5″, H-6′, H-6″). *Anal.* calcd. for $C_{16}H_{14}N_5O_2Cl$: C 55.90, H 4.10, N 20.37, Cl 10.32; found: C 55.87, H 4.23, N 20.21, Cl 10.52.

4-Benzoyl-1-thia-4-azacyclohexane ***14***

Crude 1-thia-4-azacyclohexane **9**, prepared from diethanolamine (16.8 g, 0.16 mol) by the method of Cymerman-Craig *et al.* (20), was dissolved in chloroform (250 ml) and pyridine (16 g) was added to the solution. The mixture was cooled to 0 °C, and benzoyl chloride (27.3 g, 0.19 mol) was then added dropwise with stirring over a period of 1 h; stirring was continued at room temperature for 12 h. The mixture was stirred vigorously with 2 *N* hydrochloric acid, and the layers were separated. The organic layer was washed successively with aqueous sodium hydrogen carbonate solution (4 × 150 ml), aqueous copper sulfate solution (100 ml), and water (2 × 100 ml), and dried over anhydrous magnesium sulfate. Evaporation of the solvent afforded a brown syrup which was chromatographed on silica gel, with solvent *A* as eluant, to yield a syrup (15 g) having an R_F value of 0.5. Compound **14** was obtained from ether

as a white, crystalline solid (45% based on diethanolamine); mp 68 °C; ^{1}Hmr data: τ 2.65 (s, 5H, Ph), 6.23 (m, 4H, 2H-3′s, 2H-5′s), 7.41 (m, 4H, 2H-2′s, 2H-6′s). For compound **14**, mp 63 °C has been reported (5). *Anal.* calcd. for $C_{11}H_{13}NOS$: C 63.80, H 6.28, N 6.76, S 15.48; found: C 63.90, H 6.53, N 6.61, S 15.38.

4-Benzoyl-1-thia-4-azacyclohexane 1-Oxide ***15***

To a solution of 4-benzoyl-1-thia-4-azacyclohexane **14** (3.63 g, 17.5 mmol) in methanol (25 ml) at 5 °C was added sodium metaperiodate (3.74 g, 17.5 mmol) in 1:1 (v/v) methanol–water (50 ml) with stirring; stirring was continued at 5 °C for 24 h. The mixture was evaporated to dryness, and the residue was extracted with chloroform (150 ml). The extracts were washed with aqueous sodium thiosulfate solution (25 ml) and then with water (25 ml), and dried over anhydrous magnesium sulfate. Evaporation of the solvent afforded a yellow solid (3.44 g) which was revealed by tlc (solvent *D*) to consist of two components having R_F values of 0.6 and 0.2; fractionation on silica gel, with solvent *D* as eluant, yielded the two components. The faster-moving component (0.94 g) was identified as being unreacted starting material **14**. The slower-moving component was recrystallized from ethyl acetate to give **15** as white crystals (2.50 g, 86%); mp 113–114 °C; ir (KBr): 1048 (S=O) cm^{-1}; ^{1}Hmr data: τ 2.57 (s, 5H, Ph), 5.90 (m, 4H, 2H-3′s, 2H-5′s), 7.20 (m, 4H, 2H-2′s, 2H-6′s). *Anal.* calcd. for $C_{11}H_{13}NO_2S$: C 59.22, H 5.83, N 6.28, S 14.37; found: C 59.14, H 5.91, N 6.21, S 14.21.

Pummerer Reaction with 4-Benzoyl-1-thia-4-azacyclohexane 1-Oxide ***15***

A solution of the sulfoxide **15** (0.85 g, 3.8 mmol) in benzene (40 ml) containing acetic anhydride (1 ml) and *p*-toluenesulfonic acid monohydrate (~10 mg) was heated at 60 °C for 3.5 h. Thin-layer chromatography (solvent *B*) showed the presence of two new components having R_F values of 0.6 and 0.3 together with unreacted sulfoxide **15** (R_F 0.05). The reaction mixture was stirred vigorously with aqueous sodium hydrogen carbonate solution (50 ml) for 2 h, and the layers were separated; the organic layer was washed with aqueous sodium hydrogen carbonate (2 × 15 ml) and then with water (20 ml), and dried over anhydrous magnesium sulfate. Evaporation of the solvent afforded a partially crystalline syrup which was chromatographed on silica gel, with, initially, solvent *B* and, finally, ethanol as eluants. The faster-moving component (R_F 0.6) was recrystallized from ether to give **17** (66 mg, 20%); mp 89–90 °C; ^{1}Hmr data: τ 2.57 (s, 5H, Ph), 3.34 (br d, 1H, H-3), 4.70 (br d, 1H, H-2) 5.86 (m, 2H, 2H-5′s), 6.89 (m, 2H, 2H-6′s). *Anal.* calcd. for $C_{11}H_{11}NOS$: C 64.42, H 5.36, N 6.83, S 15.64; found: C 64.64, H 5.32, N 6.64, S 15.41.

The slower-moving component (R_F 0.3) was isolated as a syrup (0.33 g, 80%) and was identified as being 2-acetoxy-4-benzoyl-1-thia-4-azacyclohexane **16**; ^{1}Hmr data: τ 2.59 (s, 5H, Ph), 4.32 (br s, 1H, $|J_{2,3} + J_{2,3'}| \simeq$ 8 Hz, H-2), 5.67–7.67 (br signals, 6H, 2H-3′s, 2H-5′s, 2H-6′s), 7.93 (s, 3H, OAc). *Anal.* calcd. for $C_{13}H_{15}NO_3S$: C 58.90, H 5.66, N 5.28, S 12.10; found: C 59.01, H 5.63, N 5.14, S 11.94.

The unreacted sulfoxide **15** (0.49 g, 2.2 mmol) was isolated as a white, crystalline solid.

When the reaction was performed at 80 °C, most of the starting sulfoxide **15** was consumed in 1 h, and compounds **16** and **17** were produced in a ratio of ~1:1.

4-Benzoyl-2-hydroxy-1-thia-4-azacyclohexane ***18***

To a stirred solution of 2-acetoxy-4-benzoyl-1-thia-4-azacyclohexane **16** (0.30 g, 1.15 mmol) in chloroform (20 ml) at 0 °C was added sodium methoxide (0.1 *M*) in methanol (1 ml); stirring was continued at 0 °C for 2 h. The solution was washed with aqueous sodium hydrogen carbonate solution (2 × 7 ml) and then with water (10 ml), and dried over anhydrous magnesium sulfate. Evaporation of the solvent afforded a syrup (0.25 g, 98%) which was homogeneous in tlc (solvent *A*, R_F = 0.4) and was identified as being 4-benzoyl-2-hydroxy-1-thia-4-azacyclohexane **18**; ^{1}Hmr data: τ 2.58 (s, 5H, Ph), 5.17 (br signal, 1H, H-2), 5.50–7.83 (br signals, 7H, 2H-3′s, 2H-5′s, 2H-6′s, OH).

6-Chloro-9-(4-benzoyl-1-thia-4-azacyclohexan-2-yl)-9H-purine 7

A mixture of 6-chloropurine (0.172 g, 1.11 mmol), methyldiphenylphosphine (0.223 g, 1.11 mmol), and diethyl azodicarboxylate (0.194 g, 1.11 mmol) in dry tetrahydrofuran (20 ml) was added to a solution of 4-benzoyl-2-hydroxy-1-thia-4-azacyclohexane **18** (0.249 g, 1.11 mmol) in tetrahydrofuran (20 ml) with stirring; stirring was continued for 12 h at room temperature. Thin-layer chromatography (solvent *A*) indicated the presence of starting material **18**. The mixture was heated at reflux temperature for 2 h, and each of the reagents (1 equiv.) was added. Thin-layer chromatography (solvent *A*) indicated that most of **18** (R_F 0.4) had been consumed, and revealed the presence of a new component having an R_F value of 0.2. The reaction mixture was evaporated to dryness, and the orange residue was chromatographed on silica gel, with solvent *A* as eluant, to yield the 2 compounds **18** and **7**. Compound **7** was obtained from ethyl acetate as a white, crystalline solid (121 mg, 35%); mp 174–175 °C; ir (KBr): 1588, 1565 and 1478 (purine ring), 1625 (C=O) cm^{-1}; uv λ_{max} (ethanol): 265 (ε 7475), 215 nm (ε 10 918) (purine ring); λ_{max} (ethanol containing a trace of hydrochloric acid): 265 (ε 7628), 215 nm (ε 10 204); λ_{max} (ethanol containing a trace of sodium hydroxide): 261 (ε 7653) shoulder (purine ring), 245 (ε 9260) (benzamide), 217 nm (ε 11 531) (purine ring); ^{1}Hmr data: τ 1.53, 1.60 (2s, 1H each, H-2, H-8), 2.33–2.67 (m, 5H, Ph), 4.33–4.67 (br signal, 1H, $|J_{2',3'} + J_{2',3''}| = 8$ Hz, H-2′), 4.92–6.13 (2H, H-3′, H-3′′), 6.30–8.17 (4H, H-5′, H-5′′, H-6′, H-6′′). *Anal.* calcd. for $C_{16}H_{14}N_5OSCl$: C 53.44, H 3.89, N 19.47, S 8.92, Cl 9.86; found: C 53.39, H 4.04, N 19.31, S 8.78, Cl 9.92.

The unreacted starting material **18** was obtained as a syrup (24 mg).

Acknowledgment

The authors are grateful to the National Research Council of Canada for financial support of this research.

1. W. Dvonch and H. E. Alburn. Abstr. Papers Am. Chem. Soc. Meeting, **155**, C56 (1968); Chem. Eng. News, **46**, 41 (1968); U.S. Patent No. 3,542,776, (November, 1970); Chem. Abstr. **74**, 31,760 (1971).
2. (*a*) J. X. Khym. Biochemistry, **2**, 344 (1963); D. M.

BROWN and A. P. READ. J. Chem. Soc. 5072 (1965); (*b*) A. S. JONES and R. T. WALKER. Carbohydr. Res. **26**, 255 (1973).
3. W. A. SZAREK, D. M. VYAS, and B. ACHMATOWICZ. J. Heterocycl. Chem. **12**, 123 (1975).
4. W. A. SZAREK, D. M. VYAS, A.-M. SEPULCHRE, S. D. GERO, and G. LUKACS. Can. J. Chem. **52**, 2041 (1974); W. A. SZAREK, D. M. VYAS, and B. ACHMATOWICZ. Tetrahedron Lett. 1553 (1975).
5. C. J. M. STIRLING. J. Chem. Soc. 3676 (1962).
6. K. W. BUCK, F. A. FAHIM, A. B. FOSTER, A. R. PERRY, M. H. QADIR, and J. M. WEBBER. Carbohydr. Res. **2**, 14 (1966).
7. J. M. J. TRONCHET, F. RACHIDZADEH, and J. TRONCHET. Helv. Chim. Acta, **57**, 65 (1974).
8. L. D. WISE. G. C. MORRISON, K. EGAN, M. A. COMMRATO, G. KOPIA, and E. C. LATTIME. J. Med. Chem. **17**, 1232 (1974).
9. W. E. STEWART and T. H. SIDDALL III. Chem. Rev. **70**, 517 (1976); L. M. JACKMAN and F. A. COTTON. Dynamic nuclear magnetic resonance spectroscopy. Academic Press, New York, N.Y. 1975.
10. J. A. HIRSCH, R. L. AUGUSTINE, G. KOLETAR, and H. G. WOLF. J. Org. Chem. **40**, 3547 (1975).
11. T. B. GRINDLEY, B. M. PINTO, and W. A. SZAREK. Can. J. Chem. This issue.
12. G. SOSNOVSKY and S.-O. LAWESSON. Angew. Chem. Int. Ed. Engl. **3**, 269 (1964).
13. D. M. GRANT and B. V. CHENEY. J. Am. Chem. Soc. **89**, 5315 (1967).
14. R. U. LEMIEUX. *In* Molecular rearrangements. Part 2. *Edited by* P. de Mayo. John Wiley and Sons, Inc., New York. 1964. p. 709; E. L. ELIEL. Angew. Chem. Int. Ed. Engl. **11**, 739 (1972).
15. J. B. STOTHERS. Carbon-13 NMR spectroscopy. Academic Press, New York. 1972.
16. H. PAULSEN and K. TODT. Chem. Ber. **100**, 3397 (1967).
17. D. A. TORCHIA, J. R. LYERLA, JR., and C. M. DEBER. J. Am. Chem. Soc. **96**, 5009 (1974); W. MCFARLANE. Chem. Commun. 418 (1970); G. C. LEVY and G. L. NELSON. J. Am. Chem. Soc. **94**, 4897 (1972).
18. W. A. SZAREK, C. DEPEW, H. C. JARRELL, and J. K. N. JONES. Chem. Commun. 648 (1975).
19. E. E. LEUTZINGER, W. A. BOWLES, R. K. ROBINS, and L. B. TOWNSEND. J. Am. Chem. Soc. **90**, 127 (1968); L. B. TOWNSEND, R. K. ROBINS, R. N. LOEPPKY, and N. J. LEONARD. J. Am. Chem. Soc. **86**, 5320 (1964).
20. J. CYMERMAN-CRAIG, W. P. ROGERS, and M. E. TATE. Aust. J. Chem. **9**, 397 (1956).
21. N. J. LEONARD and C. R. JOHNSON. J. Org. Chem. **27**, 283 (1962).
22. N. S. ZEFIROV and I. V. KAZIMIRCHIK. Russ. Chem. Rev. **43**, 107 (1974); M. OKI, T. SUGAWARA, and H. IWAMURA. Bull. Chem. Soc. Jpn. **47**, 2457 (1974).

Effects of substitution on nitrogen on barriers to rotation of cyclic amides. Part I. Investigation of the rotational barrier in 4-benzoyl-1-thia-4-azacyclohex-2-ene by ^{1}H dynamic nuclear magnetic resonance spectroscopy

T. Bruce Grindley

Department of Chemistry, Dalhousie University, Halifax, N.S., Canada B3H 4J3

AND

B. Mario Pinto and Walter A. Szarek

Department of Chemistry, Queen's University, Kingston, Ont., Canada K7L 3N6

Received August 30, 1976

T. Bruce Grindley, B. Mario Pinto, and Walter A. Szarek. Can. J. Chem. **55**, 949 (1977).

The rotational barrier in 4-benzoyl-1-thia-4-azacyclohex-2-ene has been investigated by total line-shape analysis of variable temperature ^{1}H nmr spectra in acetonitrile-d_3. Separate treatment of the vinyl and methylene signals yielded sets of values for activation parameters which were in excellent agreement. Assignment of the major and minor rotational isomers was made from chemical-shift data derived from the ^{13}C nmr spectrum at 243 K in acetonitrile-d_3.

T. Bruce Grindley, B. Mario Pinto et Walter A. Szarek. Can. J. Chem. **55**, 949 (1977).

On a étudié la barrière à la rotation dans le benzoyl-4 thia-1 aza-4 cyclohexène-2 par une analyse globale de la forme des raies des spectres rmn du proton, à température variable, dans l'acétonitrile-d_3. Des traitements séparés des signaux des groupes vinyles et méthylènes ont conduit à des ensembles de valeurs pour les paramètres d'activation qui sont en très bon accord. L'attribution des isomères majeurs et mineurs de rotation a été effectuée à partir de données de déplacements chimiques dérivées de spectres rmn ^{13}C à 243 K dans l'acétonitrile-d_3.
[Traduit par le journal]

Introduction

A large number of studies of rotational barriers in amides has been performed (1, 2). Nevertheless, there have been few systematic studies (3, 4) of the effects of substitution on nitrogen on these rotational barriers and no study in which it is possible to clearly separate resonance, steric, and bond angle effects. A useful technique for investigating such intramolecular rate processes is the total line-shape analysis of variable temperature, nuclear magnetic resonance (nmr) spectra. The validity and reliability of the careful application of this technique to appropriate systems has been confirmed by comparison of the results obtained by the line-shape method with those obtained by direct thermal equilibration (for example, see refs. 5 and 6). However, to obtain accurate values of the enthalpies and entropies of activation, it is necessary to perform the line-shape analysis over as large a temperature range as possible, and to have systems of sufficient complexity (7) to facilitate band-shape matching over this range. In the present article the rotational barrier in 4-benzoyl-1-thia-4-azacyclohex-2-ene **1** has been investigated by total line-shape analysis of variable temperature ^{1}H nmr spectra in acetonitrile-d_3. Compound **1**,

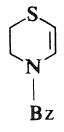

1

an interesting candidate for heterocyclic conformational analysis, was obtained during the course of a synthesis of some novel nucleoside analogs (8).

Experimental

Acetonitrile-d_3 was obtained from Stohler Isotope Chemicals. ^{1}H nmr spectra at 220 MHz were measured on a Varian HR-220 spectrometer at the Canadian 220 MHz NMR Centre; the solution was 0.8 *M* in acetonitrile-d_3. Spectra required for simulation were recorded using a 500-Hz sweep width. Temperatures were obtained by measuring peak separations in standard Varian samples of methanol and ethylene glycol and converting these into temperature values using the quadratic equation (9) of Van Geet for methanol and the linear equation (10) for ethylene glycol. Temperature gradients within the sample region of the HR-220 spectrometer

are considered to be negligible because of the large distance between the heating unit and the probe; temperatures are believed to be accurate to ±1 °C. Coupling constants and chemical shifts were obtained by analysis of the spectra (500-Hz sweep width) recorded at 245.9, 255.0, and 267.0 K using a modified version of the iterative program NMR-LAOCN-4A (11); coupling constants were assumed to be temperature invariant. Chemical shifts in the exchange-broadened region were derived by a linear extrapolation of the values obtained at the three lowest temperatures; this procedure resulted in excellent matching of the experimental and calculated chemical shifts of the vinyl signals, but the chemical shifts of the methylene signals required adjustment. Similarly, linear extrapolation of the population values obtained at the three lowest temperatures afforded values for the exchange-broadened region. Line widths were found to be unchanged at the slow and fast exchange limits and were assumed to be temperature invariant. Calculation of simulated line shapes was performed by use of a slightly modified version of the DNMR3 program (12) on a CDC-6400 computer equipped with a CALCOMP plotter. Rate constants were obtained by visual comparison of the experimental spectra with those calculated for various rates; the errors were considered to be the ranges in rates over which it was impossible to distinguish between the experimental and calculated spectra.

Activation parameters and errors were calculated by the use of a weighted, linear least-squares program (RATES)[1] which employed equations described by Wolberg (13); this program weights the data in accordance with their estimated errors and specifically treats errors in both temperatures and rate constants.

^{13}C nmr spectra were recorded in a 0.4 *M* acetonitrile-d_3 solution on a Bruker HX-60 spectrometer equipped with a FT60M Fourier transform accessory at 15.1 MHz, with tetramethylsilane (TMS) as the internal standard; chemical shifts are given in parts per million downfield from TMS. A 90° pulse was employed. The probe thermocouple was used for temperature calibration (error ±1 °C).

Results and Discussion

The conformational analysis of 4-benzoyl-1-thia-4-azacyclohex-2-ene **1** is potentially complex because of the occurrence of two dynamic processes, namely, ring inversion and restricted rotation about the amide bond, as illustrated in Fig. 1. In the present work it has been found to be possible to study the latter process without interference from the former; this situation is not surprising, since the magnitude of the inversion barrier would be expected to be significantly lower than that for amide rotation. Thus, for example, in the case of 4-benzoyl-1-oxa-4-azacyclohexane the free energies of activation for the inversion (14) and rotation (3) processes have been determined to be 7.4 and 14.4 kcal/mol, respectively. The remainder of this section, therefore, will be concerned with the conformational equilibrium of the two amide isomers **1***a* and **1***b*.

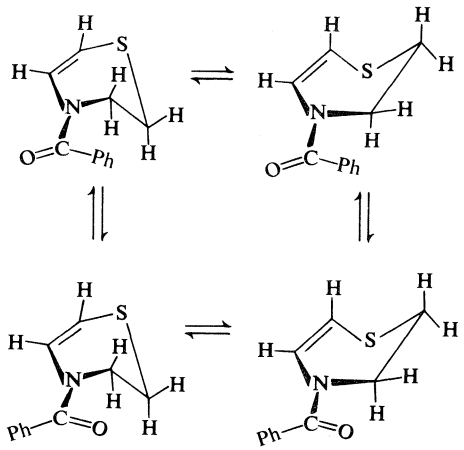

FIG. 1. Conformational processes in 4-benzoyl-1-thia-4-azacyclohex-2-ene **1**.

The determination of the conformational preference in the case of several tertiary amides has frequently been a difficult task by ^1H nmr spectroscopy (15). In the present work the assignment of the major and minor rotational isomers was readily made from chemical-shift data derived from the ^{13}C nmr spectrum at 243 K in acetonitrile-d_3. Previous workers have shown (16) that the carbon *syn* to the carbonyl oxygen of an amide is shielded relative to the corresponding carbon in the *anti* conformer. In Table 1 are documented ^{13}C chemical-shift data for the rotational isomers **1***a* and **1***b*. On the basis of this data, isomer **1***b* was deemed to be the major contributor to the rotational equilibrium. Thus, in the case of isomer **1***b*, the C-5 signal is shifted upfield by 6.7 ppm relative to the corresponding signal in the spectrum of **1***a*, whereas the C-3

TABLE 1. ^{13}C chemical-shift data[a] of rotational isomers

Isomer	Temperature (K)	Carbon 2	3	5	6
1*a*	243	104.5 (1.0)	121.5 (1.0)	47.5 (1.0)	25.9
1*b*	243	101.2 (2.2)	124.5 (2.8)	40.8 (2.3)	25.9

[a]In ppm downfield from internal tetramethylsilane (TMS) in acetonitrile-d_3. Values in parentheses are peak heights standardized on the basis of each carbon of the minor isomer **1***a* having a peak height of 1.0.

[1]Copies of the RATES program may be obtained from T.B.G.

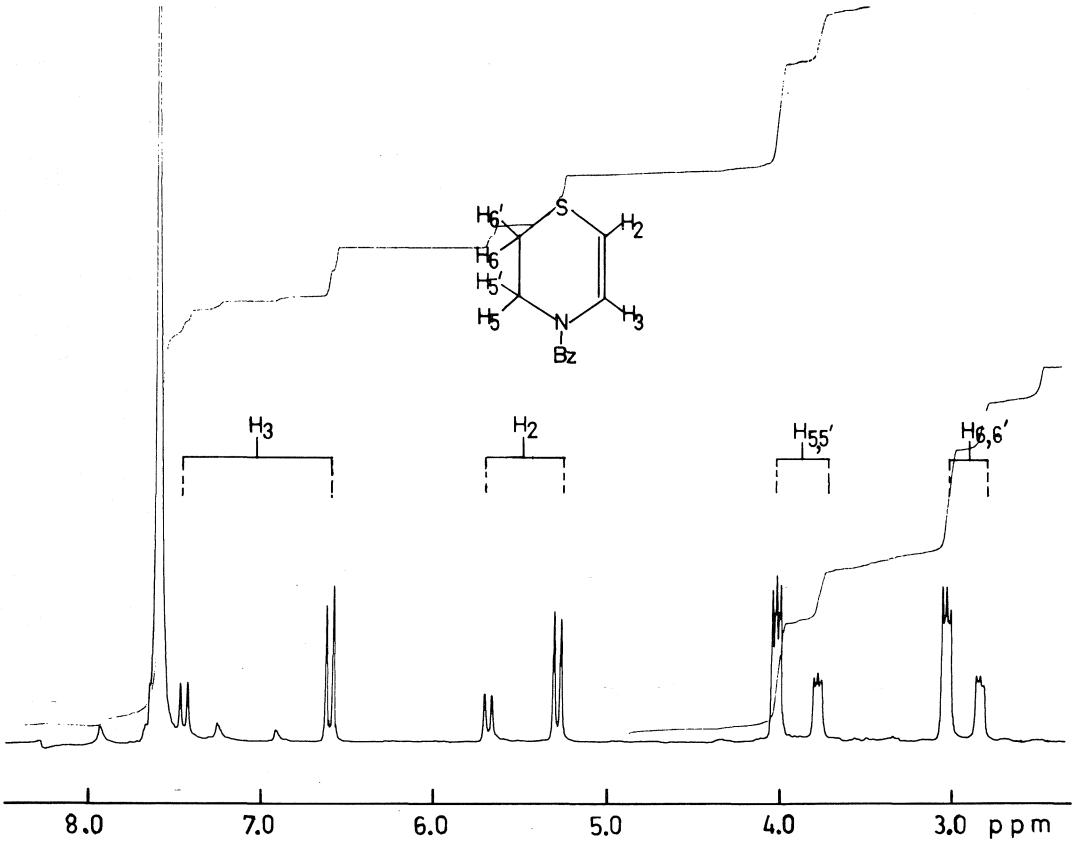

FIG. 2. ^{1}H nmr spectrum at 220 MHz of 4-benzoyl-1-thia-4-azacyclohex-2-ene **1** (0.8 *M* in acetonitrile-d_3) at 255.0 K.

signal is shifted downfield by 3.0 ppm. It is interesting to note that the signals for the C-2 carbons in the two isomers are also distinct, whereas those for the C-6 carbons are not. Moreover, C-2 in the major isomer **1***b* is shielded relative to the corresponding carbon in the minor isomer **1***a*.

The ^{1}H nmr spectrum at 220 MHz of 4-benzoyl-1-thia-4-azacyclohex-2-ene **1** (0.8 *M* in acetonitrile-d_3) at 255.0 K is shown in Fig. 2. The signal assignments were readily made on the basis of published (17) chemical-shift data. Integration of the spectrum showed that isomers **1***a* and **1***b* were present in the ratio 1:2.1, respectively. An interesting feature of the spectrum is the observation that the sequence of signals for the individual isomers **1***a* and **1***b* in the case of each of the vinyl protons is the reverse of that in the case of the protons of each of the methylene groups. Moreover, the sequence of signals for H-3 and H-5,5′ in the

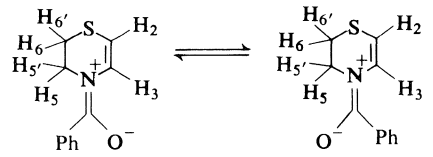

1*a* **1***b*

^{1}H nmr spectrum is the reverse of that for C-3 and C-5 in the ^{13}C nmr spectrum.

The static parameters obtained from the LAOCN-4A analysis of the two ABCC′DD′ systems, corresponding to the vinyl and methylene protons in **1***a* and **1***b*, in the 220 MHz spectrum recorded at 255.0 K are given in Tables 2 and 3. The values of the long-range coupling constants were estimated from line widths, and are in agreement with those reported for ^4J across sulfur (18) and amide nitrogen (19).

The experimental and calculated dnmr spectra of the vinyl and methylene protons in compound

TABLE 2. Calculated chemical shifts[a] for nmr signals of vinyl and methylene protons in **1**

	Signal			
Isomer	H-2	H-3	H-5,5′	H-6,6′
1*a*	5.65	7.37	3.84	2.95
1*b*	5.27	6.52	4.08	3.14

[a]In ppm from tetramethylsilane at 220 MHz and 255.0 K.

TABLE 3. Calculated coupling constants (Hz) for vinyl and methylene protons in **1**

Parameter	Value	Parameter	Value
$J_{2,3}$	8.4	$J_{5,5'} = J_{6,6'}$	−11.0
$J_{2,6} = J_{2,6'}$	~0.6	$J_{5,6} = J_{5',6'}$	7.8
$J_{3,5} = J_{3,5'}$	~1.1	$J_{5,6'} = J_{5',6}$	2.8

1 are illustrated in Figs. 3–5. The total line-shape analysis was performed by independently treating the exchange processes for the vinyl and methylene protons as AB ⇌ CD and AA′BB′ ⇌ CC′DD′, respectively. The effects of the long-range couplings were incorporated by adjusting the appropriate line-width parameter. The two-spin system was simulated by analysis of the process going from the more populated conformer to the less populated conformer (**1***b* → **1***a*), whereas the four-spin system was simulated by analysis of the process going from the less populated conformer to the more populated conformer (**1***a* → **1***b*); this approach was adopted in order to eliminate any possible bias in the analysis, since the rate constants for the processes in the two directions were expected to be significantly different. The rate constants derived from this treatment are documented in Table 4.

Activation parameters for the restricted rotation about the amide bond in 4-benzoyl-1-thia-4-azacyclohex-2-ene **1** were calculated as described in the Experimental section. The results are presented in Table 5. In addition to the careful execution of the present analysis, the reliability of the values of the derived parameters may be attributed to the fact that, in the case of compound **1**, each spin system is comprised of two components each of which has a significantly different chemical-shift difference between the corresponding signals of the two isomers, a situation which permits the observation of maximum broadening of the individual segments at different temperatures. A further outstanding feature of the data is the very close agreement between the sets of parameters obtained by independent analysis of the two-spin system and the four-spin system.

The magnitude of the barrier to rotation determined for amide **1** ($\Delta G^{\ddagger}$ 14.79 or 14.37 kcal/mol at 300 K) is essentially the same as those of the barriers in some related amides, for example, 1-benzoylpiperidine (14.82 kcal/mol at 292 K) and 1-benzoyl-4-piperidone (14.32 kcal/mol at 303 K). However, in the case of acyclic amides, the magnitude of the rotational barrier is decreased by the introduction of unsaturation into one of the substituents attached to nitrogen (see Table 6); Jackman (2)

TABLE 4. Rate constants (k, s^{-1}) derived from line-shape analysis

Temperature (K)	AB ⇌ CD[a]		AA′BB′ ⇌ CC′DD′[b]	
	k	Error	k	Error
267.0	—	—	10	1
285.0	58	2	30	1
289.5	80	3	45	2
292.0	110	5	57	2
295.0	140	5	77	3
298.0	177	7	95	5
303.5	280	15	155	10
306.0	310	15	175	10
313.0	510	30	295	15
323.0	1300	100	600	50
337.0	3500	300	1500	500
351.5	8000	1000	—	—

[a]Data for process **1***b* → **1***a*.
[b]Data for process **1***a* → **1***b*.

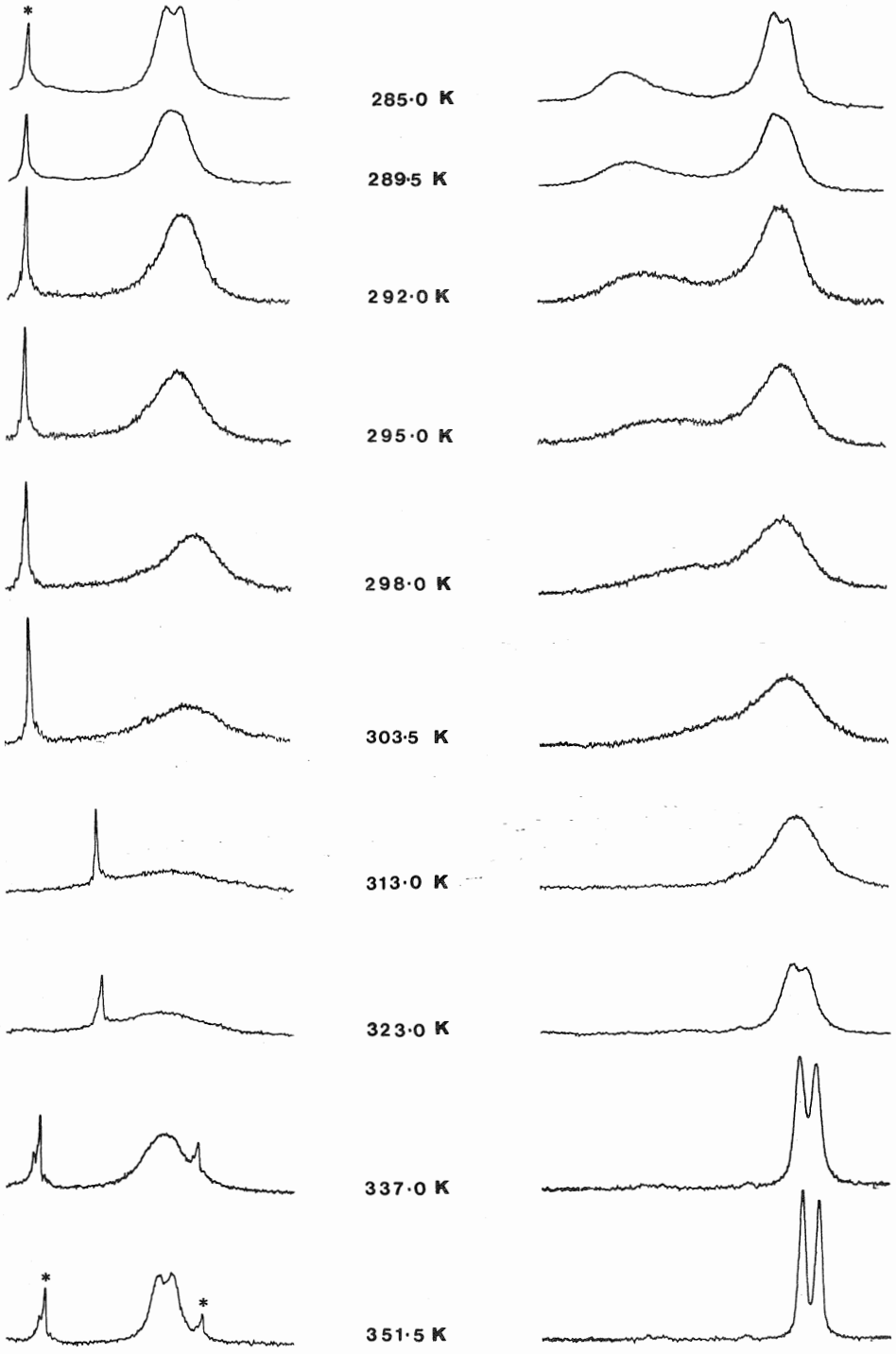

FIG. 3. Experimental dnmr spectra of vinyl protons in **1**. Peaks marked with * are spinning sidebands. The H-3 signal for isomer **1***a* was obscured by the phenyl resonances.

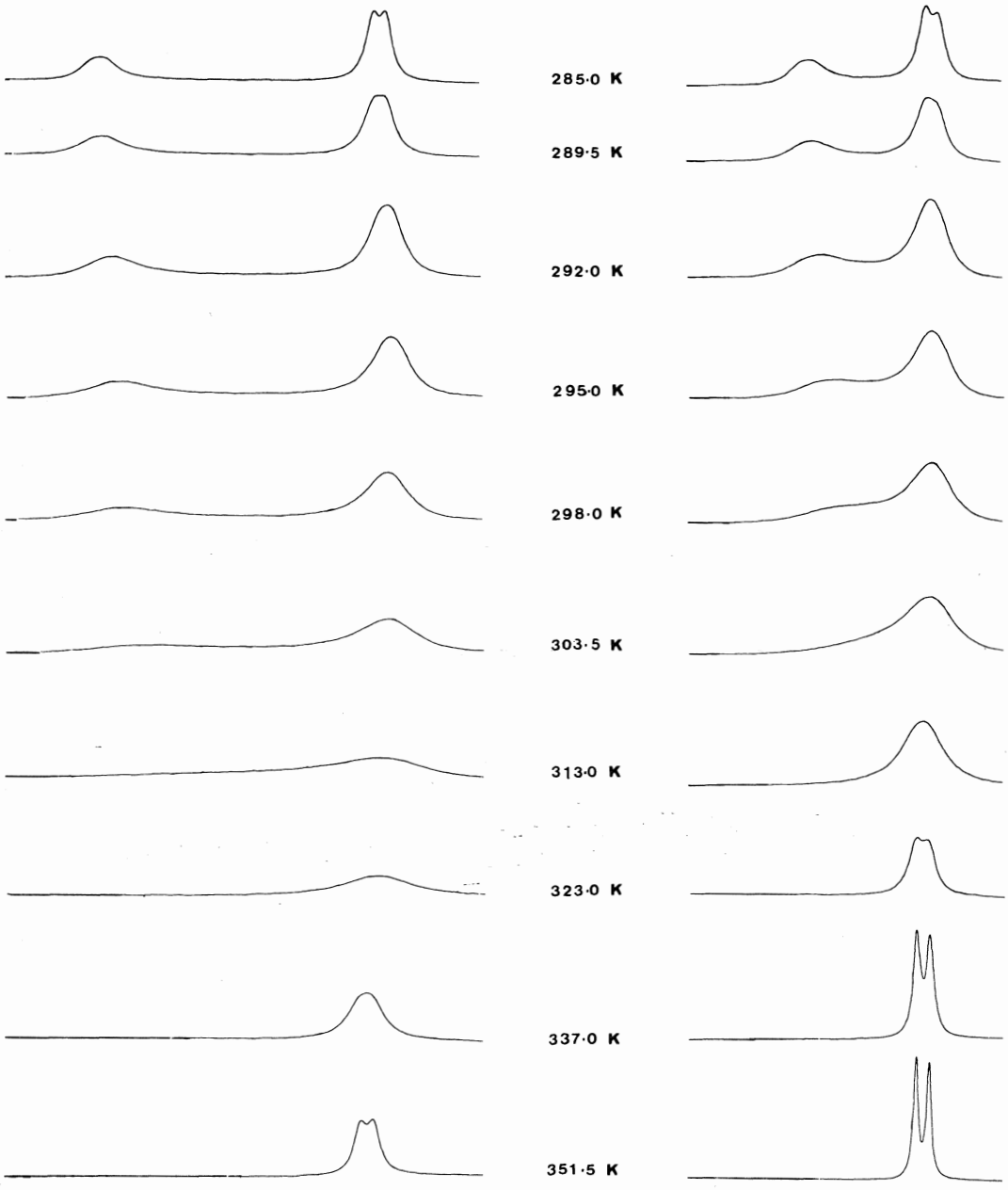

FIG. 4. Calculated dnmr spectra of vinyl protons in **1**.

has suggested that resonance stabilization of the transition state is a key factor in causing this decrease in the free energy of activation. On the basis of the results obtained in the present work, namely that the magnitude of the rotational barrier in amide **1** does not differ substantially from those in corresponding saturated amides, it would appear that other factors may also be of significance. A detailed investigation of the barriers in appropriate cyclic amides is

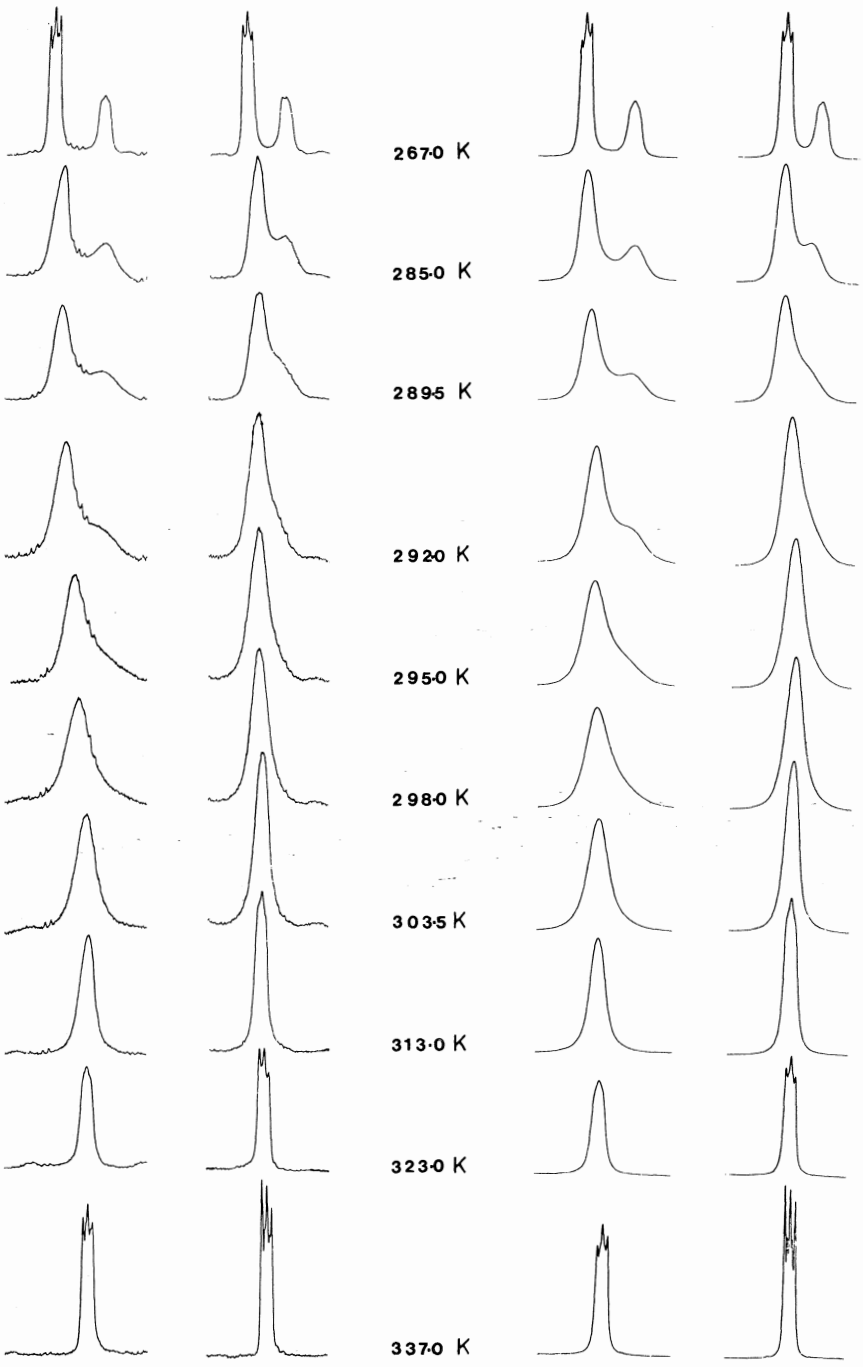

FIG. 5. Experimental (left) and calculated (right) dnmr spectra of methylene protons in **1**.

TABLE 5. Activation parameters for the restricted rotation about the amide bond in **1**

Parameter	AB ⇌ CD	AA'BB' ⇌ CC'DD'	Mean value
	(*a*) Data for process **1***a* → **1***b*		
E_a (kcal/mol)	14.9 ±0.2	14.6 ±0.2	14.8 ±0.2
Log A	12.9 ±0.2	12.7 ±0.2	12.8 ±0.2
$\Delta H^{\ddagger}$ (kcal/mol)	14.1 ±0.2	14.0 ±0.2	14.1 ±0.2
$\Delta S^{\ddagger}$ (eu)	−1.7 ±0.8	−2.6 ±0.8	−2.2 ±0.8
$\Delta G^{\ddagger}$ (kcal/mol)[a]	14.8_2 ±0.1	14.7_6 ±0.1	14.7_9 ±0.1
	(*b*) Data for process **1***b* → **1***a*		
E_a (kcal/mol)	14.8 ±0.3	14.4 ±0.2	14.6 ±0.3
Log A	13.1 ±0.2	12.9 ±0.2	13.0 ±0.2
$\Delta H^{\ddagger}$ (kcal/mol)	14.2 ±0.3	13.8 ±0.2	14.0 ±0.3
$\Delta S^{\ddagger}$ (eu)	−0.8 ±0.9	−1.6 ±0.8	−1.2 ±0.9
$\Delta G^{\ddagger}$ (kcal/mol)[a]	14.3_9 ±0.1	14.3_4 ±0.1	14.3_7 ±0.1

[a]Values for $\Delta G^{\ddagger}$ were calculated at 300 K; the errors in these values were obtained by the use of the following formula (20) for the linearized relative statistical error in $\Delta G^{\ddagger}$:

$$(\sigma_{\Delta G^{\ddagger}}/\Delta G^{\ddagger})^2 = [\ln (k_B T/hk)]^{-2}(\sigma_k/k)^2 + [1 + \{\ln (k_B T/hk)\}^{-1}]^2(\sigma_T/T)^2$$

TABLE 6. Barriers to rotation in some acyclic amides[a]

Compound	$\Delta G^{\ddagger}$ (kcal/mol)	Temperature (K)	Reference
$(CH_3)_2NCHO$	20.9	392	21
$(CH_3CH_2)_2NCHO$	20.4	298	4
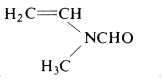	18.3	372	22
$(CH_3)_2NCOCH_3$	17.3	298	23
$(CH_3CH_2)_2NCOCH_3$	16.9	298	4
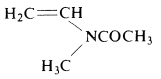	13.4	298	4

[a]Values were obtained using neat liquids, except in the case of *N,N*-dimethylacetamide in which carbon tetrachloride was the solvent.

in progress, in an effort to assess the relative importance of resonance, steric, and bond angle effects.

Acknowledgments

The authors are grateful to the National Research Council of Canada for grants (to T.B.G. and W.A.S.). They also thank the Canadian 220 MHz NMR Centre for providing facilities for the recording of spectra, and Dr. C. H. Warren for helpful discussions on the statistical treatment of data.

1. W. E. STEWART and T. H. SIDDALL III. Chem. Rev. **70**, 517 (1970).
2. L. M. JACKMAN. *In* Dynamic nuclear magnetic resonance spectroscopy. *Edited by* L. M. Jackman and F. A. Cotton. Academic Press, Inc., New York. 1975. Chapt. 7.
3. J. A. HIRSCH, R. L. AUGUSTINE, G. KOLETAR, and H. G. WOLF. J. Org. Chem. **40**, 3547 (1975).
4. R. M. HAMMAKER and B. A. GUGLER. J. Mol. Spectrosc. **17**, 356 (1965).
5. H. S. GUTOWSKY, J. JONAS, and T. H. SIDDALL III. J. Am. Chem. Soc. **89**, 4300 (1967).
6. C. H. BUSHWELLER, J. W. O'NEIL, M. H. HALFORD, and F. H. BISSETT. J. Am. Chem. Soc. **93**, 1471 (1971).

7. D. A. KLEIER, G. BINSCH, A. STEIGEL, and J. SAUER. J. Am. Chem. Soc. **92**, 3787 (1970).
8. B. M. PINTO, D. M. VYAS, and W. A. SZAREK. Can. J. Chem. This issue.
9. A. L. VAN GEET. Anal. Chem. **42**, 679 (1970).
10. A. L. VAN GEET. Anal. Chem. **40**, 2227 (1968).
11. J. A. MUSSO. Nuclear magnetic resonance spectra analysis by least squares with magnetic equivalence factoring, self-assignment, and plots. Program 232, Quantum Chemistry Program Exchange, Indiana University. 1973.
12. D. A. KLEIER and G. BINSCH. DNMR3: A computer program for the calculation of complex exchange-broadened NMR spectra. Modified version for spin systems exhibiting magnetic equivalence or symmetry. Program 165, Quantum Chemistry Program Exchange, Indiana University. 1970.
13. J. R. WOLBERG. Prediction analysis. Van Nostrand, New York. 1967. Chapt. 3.
14. P. LE CAM and J. SANDSTRÖM. Chem. Scripta, **1**, 65 (1971).
15. A. H. LEWIN and M. FRUCHT. Org. Magn. Reson. **7**, 206 (1975).
16. D. A. TORCHIA, J. R. LYERLA, JR., and C. M. DEBER. J. Am. Chem. Soc. **96**, 5009 (1974); W. MCFARLANE. Chem. Commun. 418 (1970); G. C. LEVY and G. L. NELSON. J. Am. Chem. Soc. **94**, 4897 (1972).
17. L. M. JACKMAN and S. STERNHELL. Applications of nuclear magnetic resonance spectroscopy in organic chemistry. 2nd ed. Pergamon Press, New York. 1969. Chapt. 3–5.
18. R. F. C. BROWN and I. D. RAE. Aust. J. Chem. **18**, 1071 (1965).
19. H. PAULSEN and K. TODT. Chem. Ber. **100**, 3397 (1967).
20. G. BINSCH. *In* Dynamic nuclear magnetic resonance spectroscopy. *Edited by* L. M. Jackman and F. A. Cotton. Academic Press, Inc., New York. 1975. Chapt. 3.
21. M. RABINOVITZ and A. PINES. J. Am. Chem. Soc. **93**, 685 (1971).
22. D. G. GEHRING, W. A. MOSHER, and G. S. REDDY. J. Org. Chem. **31**, 3436 (1966).
23. L. W. REEVES, R. C. SHADDICK, and K. N. SHAW. Can. J. Chem. **49**, 3683 (1971).

Crystal and molecular structure of L-prolinatodiphenylboron

STEVEN J. RETTIG AND JAMES TROTTER

Department of Chemistry, University of British Columbia, 2075 Wesbrook Place, Vancouver, B.C., Canada V6T 1W5

Received September 13, 1976

STEVEN J. RETTIG and JAMES TROTTER. Can. J. Chem. **55**, 958 (1977).

Crystals of L-prolinatodiphenylboron are monoclinic, $a = 5.9427(5)$, $b = 14.4633(7)$, $c = 8.9654(4)$ Å, $\beta = 98.423(8)°$, $Z = 2$, space group $P2_1$. The structure was solved by direct methods and was refined by full-matrix least-squares procedures to a final R of 0.037 and R_w of 0.053 for 1477 reflections with $I \geq 3\sigma(I)$. The proline ring exhibits conformational disorder. The crystal structure consists of discrete molecules linked by N—H...O hydrogen bonds (N...O = 2.893(3) Å) along the short a axis. Intramolecular N—B coordination occurs to form a system of two fused five-membered rings. Bond lengths (corrected for libration) are: N—B, 1.630(3), O—B, 1.529(3), O—C, 1.219(3) and 1.300(3), N—C, 1.506(3) and 1.507(3), C(sp^3)—C(sp^3), 1.525(4), C(sp^2)—C(sp^3), 1.517(3), and mean C—C(phenyl), 1.394 Å.

STEVEN J. RETTIG et JAMES TROTTER. Can. J. Chem. **55**, 958 (1977).

Les cristaux du L-prolinatodiphénylbore sont monocliniques, $a = 5.9427(5)$, $b = 14.4633(7)$, $c = 8.9654(4)$ Å, $\beta = 98.423(8)°$, $Z = 2$, groupe d'espace $P2_1$. On a résolu la structure par les méthodes directes et on l'a affinée par la méthode des moindres carrés (matrice complète) jusqu'à une valeur finale de R de 0.037 et de R_w de 0.053 pour 1477 réflexions avec $I \geq 3\sigma(I)$. Le cycle de proline présente du désordre conformationnel. La structure cristalline consiste de molécules individuelles liées par les ponts hydrogène N—H...O (N...O = 2.893(3) Å) le long de l'axe a qui est court. La coordination N—B intramoléculaire se produit de façon à former un système de deux cycles à cinq chaînons qui sont reliés. Les longueurs des liaisons (corrigées pour les librations) sont: N—B, 1.630(3), O—B, 1.529(3), O—C, 1.219(3) et 1.300(3), N—C, 1.506(3) et 1.507(3), C(sp^3)—C(sp^3), 1.525(4), C(sp^2)—C(sp^3), 1.517(3) et la valeur moyenne de C—C(phényle) 1.394 Å.

[Traduit par le journal]

Introduction

The crystal structures of a number of ethanolamine esters of the boron acids (**1–3**) have

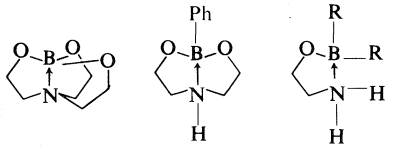

1 **2** **3**

a, R = C_6H_5
b, R = *p*-FC_6H_4
c, R = *p*-$CH_3C_6H_4$

recently been determined (1–6). The unusual hydrolytic and oxidative stability (7) of these compounds is attributed to intramolecular N—B coordination. The mixed anhydrides of diphenylborinic acid and amino acids form a closely related class of compounds which exhibit similar hydrolytic stability (8–10) and are also believed to feature intramolecular N—B coordination. We now report the crystal structure of a member of this class of compounds, namely L-prolinatodiphenylboron **4**.

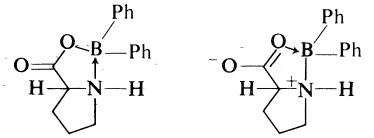

4*a* **4***b*

Experimental

A solution of L-proline (0.67 g, 5.8 mmol) in 75 ml of 1:1 ethanol/water was added to a solution of diphenyl borinic acid (from acid hydrolysis of 1.30 g, 5.8 mmol of 2-aminoethyldiphenylborinate) in 75 ml of ethanol/diethylether. Precipitation of a fine white powder commenced almost immediately. The reaction mixture was refluxed for 1 h, allowed to cool, and filtered. The precipitate was washed with water, then with ethanol, and dried to yield 1.40 g (5.0 mmol, 87% yield) of L-prolinatodiphenylboron. *Anal.* calcd. for $C_{17}H_{18}BNO_2$: C 73.16, H 6.50, N 5.02; found: C 73.13, H 6.41, N 5.11. Melting point (decomp) 263–265 °C.

Crystals suitable for X-ray analysis were obtained by recrystallization from 2-butanone. The crystal chosen for study was mounted with a^* parallel to the goniostat axis and had dimensions of *ca.* 0.40 × 0.25 × 0.40 mm. Unit-cell and space group data were obtained from film and diffractometer measurements. The unit-cell parameters were refined by a least-squares treatment of $\sin^2\theta$ values for 20 reflections measured on a diffractometer with Cu K_α

radiation (λ = 1.5418 Å). Crystal data (at 22 °C) are:

$C_{17}H_{18}BNO_2$ fw = 279.1

Monoclinic, a = 5.9427(5), b = 14.4633(7), c = 8.9654(4) Å, β = 98.423(8)°, V = 762.26(9) Å^3, ρ_m = 1.20 (flotation in aqueous KI), Z = 2, ρ_c = 1.2161(1) g cm^{-3}, $F(000)$ = 296, $\mu(CuK_\alpha)$ = 6.3 cm^{-1}. Absent reflections: $0k0$, $k \neq 2n$, space group $P2_1$ (C_2^2, No. 4).

Intensities were measured with nickel-filtered Cu K_α radiation on a Datex-automated General Electric XRD-6 diffractometer. A θ–2θ scan at 2° min^{-1} over a range of (1.80 + 0.86 tan θ) degrees in 2θ was employed. Background counts (10 s) were measured at each end of the scan. Data were measured to 2θ = 146° (minimum interplanar spacing 0.81 Å). The intensity of the check reflection, measured every 40 reflections throughout the data collection, remained constant to within ±3%. Lorentz and polarization corrections and check reflection scaling were applied, and the structure amplitudes were derived. No absorption correction was made in view of the low value of μ. Of the 1590 independent reflections measured, 1482 had intensities greater than $3\sigma(I)$ above background where $\sigma^2(I) = S + B + (0.06S)^2$ with S = scan count and B = time averaged background count. These reflections were used in the solution and refinement of the structure.

The systematic absences allow space groups $P2_1$ or $P2_1/m$, the centrosymmetric space group $P2_1/m$ being ruled out by the presence of the chiral L-proline moiety. The structure was solved by direct methods, 210 reflections with $|E| \geq 1.40$ being used in the symbolic addition procedure for noncentrosymmetric crystals (11). Four sets of phases were generated by a computer program which determines phases using the tangent formula (12).[1] There were two nearly identical sets of phases with R_k of 0.16 and all 210 phases determined. The highest 20 peaks on E-maps calculated from both sets of phases accounted for all of the nonhydrogen atoms except C(4). The difference between the two E-maps was in the location of the C(4) peak, which had an electron density which was about 50% of that observed for the other carbon atoms. One of the two possible C(4) locations was chosen on the basis of slightly higher electron density and more reasonable geometry.

Two cycles of isotropic, followed by two cycles of anisotropic full-matrix least-squares refinement of the nonhydrogen atoms, gave R = 0.073. Examination of the thermal parameters of C(3), C(4), and C(5) (especially C(4)) indicated conformational disordering of the proline ring where C(4) is either folded away from or toward O(1). A difference map calculated at this point gave positions for 14 of the 18 hydrogen atoms; of those associated with C(3)—C(5) only two were found. C(4) was then refined as a split atom, initially with site occupancies fixed at 0.5 and later allowed to vary, reducing R to 0.045. A difference map then gave positions for the remaining hydrogen atoms associated with C(3), C(4), and C(5). The atom H(4a) is shared by both C(4) and C(4′) and thus has a site occupancy of 1.0. The second hydrogen atom associated with C(4′) was not located and has been left out of the refinement. The site occupancy of H(4b) was not refined but was kept equal to that of C(4). The atoms C(3), C(5), and their respective hydrogen atoms could not be successfully refined as split atoms and the disorder manifests itself as relatively large thermal parameters for these atoms. The entire structure was refined for three more cycles giving a final R of 0.037 and R_w of 0.053 for 1477 reflections with $I \geq 3\sigma(I)$ (5 reflections which had $|F_o| - |F_c| > 3\sigma(F)$ were removed from the data set in the final stages of refinement).

The least-squares refinement was based on the minimization of $\Sigma w[|F_o| - |F_c|/(1 + gI)|]^2$ where g is the extinction parameter and I the uncorrected intensity. The final value of g was 5.3 × 10^{-8}. The scattering factors of ref. 14 were used for the non-hydrogen atoms and those of ref. 15 for the hydrogen atoms. Anomalous scattering factors from ref. 16 were used for the nonhydrogen atoms. The anisotropic thermal parameters employed in the refinement are U_{ij} in the expression:

TABLE 1. Final positional parameters (fractional × 10^4, H × 10^3) with estimated standard deviations in parentheses

Atom	x	y	z
O(1)	6317(3)	7652	3717(2)
O(2)	7861(3)	8487(2)	2048(2)
N	2570(4)	8287(2)	3385(2)
C(1)	6231(4)	8252(2)	2634(3)
C(2)	3863(4)	8637(2)	2179(3)
C(3)	3733(7)	9687(3)	2216(6)
C(4)*	2087(21)	9908(5)	3439(10)
C(4′)*	3587(89)	9891(7)	3576(22)
C(5)	2441(7)	9095(2)	4423(3)
C(6)	3102(4)	6486(2)	3032(2)
C(7)	4643(6)	5792(2)	2797(3)
C(8)	4002(7)	5005(2)	1967(4)
C(9)	1778(7)	4889(3)	1320(4)
C(10)	203(7)	5561(3)	1521(5)
C(11)	863(5)	6342(3)	2372(4)
C(12)	3978(4)	7240(2)	5824(2)
C(13)	2100(6)	6876(3)	6378(3)
C(14)	2097(7)	6742(3)	7907(4)
C(15)	3957(7)	6946(3)	8915(3)
C(16)	5866(7)	7310(3)	8410(3)
C(17)	5854(5)	7458(2)	6880(3)
B	3965(4)	7372(2)	4042(3)
H(N)	133(6)	819(2)	296(4)
H(2)	313(5)	837(2)	121(4)
H(3a)	530(18)	994(8)	229(10)
H(3b)	300(12)	992(6)	125(8)
H(4a)	296(11)	1038(6)	384(7)
H(4b)	52(11)	989(4)	296(7)
H(5a)	372(9)	908(4)	519(6)
H(5b)	124(12)	906(6)	487(8)
H(7)	616(7)	590(3)	323(4)
H(8)	512(9)	456(4)	180(6)
H(9)	131(8)	440(4)	59(5)
H(10)	−155(11)	545(5)	97(7)
H(11)	−33(7)	685(3)	245(5)
H(13)	96(6)	666(3)	569(4)
H(14)	73(9)	649(4)	818(5)
H(15)	396(6)	685(3)	997(5)
H(16)	702(8)	757(4)	912(6)
H(17)	714(5)	769(2)	651(3)

*Final site occupancies are 0.59(4) for C(4) and 0.42(5) for C(4′).

[1]Also M. G. B. Drew. Private communication. See, for example, ref. 13.

TABLE 2. Final thermal parameters and their estimated standard deviations

(*a*) Anisotropic thermal parameters ($U_{ij} \times 10^3$ Å^2)

Atom	U_{11}	U_{22}	U_{33}	U_{12}	U_{13}	U_{23}
O(1)	41(1)	47(1)	48(1)	3(1)	5(1)	7(1)
O(2)	45(1)	80(1)	72(1)	−7(1)	13(1)	24(1)
N	42(1)	39(1)	43(1)	1(1)	2(1)	−2(1)
C(1)	40(1)	49(1)	49(1)	−4(1)	1(1)	5(1)
C(2)	44(1)	54(1)	51(1)	−1(1)	2(1)	13(1)
C(3)	78(2)	54(2)	115(3)	6(2)	14(2)	31(2)
C(4)	68(7)	42(3)	82(4)	12(2)	−12(3)	−4(2)
C(4′)	197(40)	33(5)	109(10)	−9(8)	41(14)	−4(4)
C(5)	93(2)	48(1)	60(1)	17(1)	4(2)	−12(1)
C(6)	56(1)	41(1)	38(1)	0(1)	12(1)	0(1)
C(7)	68(2)	48(1)	51(1)	10(1)	6(1)	3(1)
C(8)	98(2)	47(1)	68(2)	14(1)	18(2)	−8(1)
C(9)	96(2)	60(2)	80(2)	−10(2)	18(2)	−30(2)
C(10)	72(2)	82(2)	103(3)	−14(2)	12(2)	−44(2)
C(11)	52(2)	65(2)	82(2)	−5(1)	12(1)	−29(2)
C(12)	58(1)	40(1)	39(1)	7(1)	9(1)	0(1)
C(13)	65(2)	81(2)	54(1)	−7(1)	15(1)	2(1)
C(14)	88(2)	87(2)	61(2)	−5(2)	29(2)	7(2)
C(15)	123(3)	63(2)	40(1)	11(2)	20(2)	4(1)
C(16)	103(2)	67(2)	44(1)	3(2)	−8(1)	−4(1)
C(17)	70(2)	55(1)	44(1)	−3(1)	2(1)	1(1)
B	43(1)	39(1)	40(1)	4(1)	7(1)	2(1)

(*b*) Isotropic thermal parameters ($U \times 10^3$)

Atom	U (Å^2)	Atom	U (Å^2)	Atom	U (Å^2)
H(N)	51(8)	H(5a)	112(15)	H(11)	92(12)
H(2)	52(7)	H(5b)	156(25)	H(13)	69(9)
H(3a)	198(35)	H(7)	75(11)	H(14)	96(13)
H(3b)	138(21)	H(8)	107(14)	H(15)	89(12)
H(4a)	117(17)	H(9)	105(14)	H(16)	97(13)
H(4b)	56(14)	H(10)	132(19)	H(17)	51(7)

$$f = f^0 \exp[-2\pi^2(U_{11}h^2a^{*2} + U_{22}k^2b^{*2} + U_{33}l^2c^{*2} + 2U_{12}hka^*b^* + 2U_{13}hla^*c^* + 2U_{23}klb^*c^*)]$$

where f^0 is the tabulated scattering factor and f is that corrected for thermal motion. The weighting scheme: $w = 1/\sigma^2(F)$ where $\sigma^2(F)$ is derived from the previously defined $\sigma^2(I)$ gave uniform average values of $w(|F_o| - |F_c|)^2$ over ranges of $|F_o|$ and was employed in the final stages of refinement.

The absolute configuration of the molecule was determined from that known for the L-proline moiety. On the final cycle of refinement the mean parameter shift was 0.05σ and no parameter shift was greater than 0.55σ. The mean error in an observation of unit weight was 1.448. A final electron density difference map showed maximum fluctuations of ± 0.20 e Å^{-3}. The final positional and thermal parameters appear in Tables 1 and 2 respectively. Measured and calculated structure factors have been placed in the Depository of Unpublished Data.[2]

[2]The structure factor table is available, at a nominal charge, from the Depository of Unpublished Data, CISTI, National Research Council of Canada, Ottawa, Canada K1A 0S2.

The ellipsoids of thermal motion for the non-hydrogen atoms are shown in Fig. 1. The thermal motion has been analysed in terms of the rigid-body modes of translation (T), libration (L), and screw (S) motion (17) using the computer program MGTLS. The rms standard error in the temperature factors σU_{ij} (derived from the least-squares analysis) is (excluding the C(4) atoms) 0.0018 Å^2. Analyses were successful for the two phenyl groups C(6)—C(11), B and C(12)—C(17), B (rms $\Delta U_{ij} = 0.0017$ and 0.0028 Å^2 respectively), and for the eight atom group O(1), O(2), N, C(1), C(2), B, C(6), and C(12) (rms $\Delta U_{ij} = 0.0023$ Å^2).

The appropriate bond distances have been corrected for libration (18, 19), using shape parameters q^2 of 0.08 for all atoms involved. Corrected bond lengths appear in Table 3 along with the uncorrected values.

Results and Discussion

Figure 1 shows a general view of the molecule and the crystallographic numbering scheme and Fig. 2 shows a general view of the packing arrangement. Bond angles are given in Table 4 and intra-annular torsion angles in Table 5.

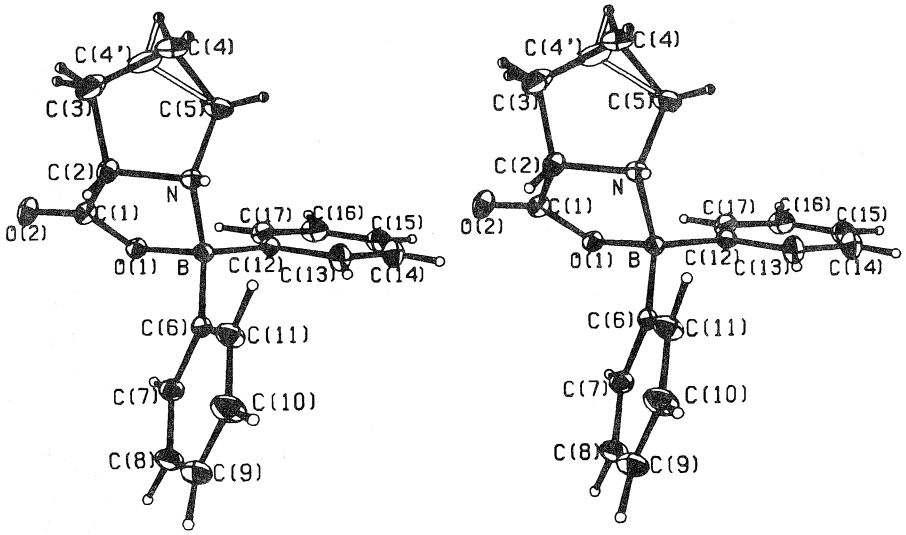

FIG. 1. A stereo view of the L-prolinatodiphenylboron molecule. 50% ellipsoids are shown for the nonhydrogen atoms. Hydrogen atoms have been given artificially small temperature factors for clarity.

TABLE 3. Bond lengths (Å) with estimated standard deviations in parentheses

(*a*) Nonhydrogen atoms

Bond	Uncorr.	Corr.	Bond	Uncorr.	Corr.
O(1)—C(1)	1.297(3)	1.300	C(6)—C(11)	1.390(4)	1.403
O(1)—B	1.524(3)	1.529	C(6)—B	1.609(3)	1.614
O(2)—C(1)	1.216(3)	1.219	C(7)—C(8)	1.383(4)	1.388
N—C(2)	1.503(3)	1.507	C(8)—C(9)	1.374(6)	1.387
N—C(5)	1.503(3)	1.506	C(9)—C(10)	1.378(6)	1.388
N—B	1.626(3)	1.630	C(10)—C(11)	1.388(4)	1.393
C(1)—C(2)	1.513(3)	1.517	C(12)—C(13)	1.390(4)	1.401
C(2)—C(3)	1.521(4)	1.525	C(12)—C(17)	1.389(4)	1.401
C(3)—C(4)	1.605(14)		C(12)—B	1.608(3)	1.612
C(3)—C(4′)	1.270(15)		C(13)—C(14)	1.385(4)	1.389
C(4)—C(5)	1.467(8)		C(14)—C(15)	1.354(6)	1.366
C(4′)—C(5)	1.587(19)		C(15)—C(16)	1.385(6)	1.396
C(6)—C(7)	1.396(4)	1.406	C(16)—C(17)	1.388(4)	1.392

(*b*) Bonds involving hydrogen atoms

Bond	Distance	Bond	Distance
N—H(N)	0.79(4)	C(8)—H(8)	0.96(6)
C(2)—H(2)	0.99(3)	C(9)—H(9)	0.97(5)
C(3)—H(3a)	0.99(11)	C(10)—H(10)	1.10(6)
C(3)—H(3b)	0.97(8)	C(11)—H(11)	1.03(5)
C(4)—H(4a)	0.90(8)	C(13)—H(13)	0.91(4)
C(4)—H(4b)	0.97(7)	C(14)—H(14)	0.95(5)
C(4′)—H(4a)	0.85(8)	C(15)—H(15)	0.95(4)
C(5)—H(5a)	0.94(5)	C(16)—H(16)	0.94(5)
C(5)—H(5b)	0.87(7)	C(17)—H(17)	0.94(3)
C(7)—H(7)	0.94(4)		

TABLE 4. Bond angles (deg) with estimated standard deviations in parentheses

(*a*) Nonhydrogen atoms

Bonds	Angle (deg)	Bonds	Angle (deg)
C(1)—O(1)—B	112.6(2)	C(6)—C(7)—C(8)	122.6(3)
C(2)—N—C(5)	105.2(2)	C(7)—C(8)—C(9)	120.0(3)
C(2)—N—B	103.4(2)	C(8)—C(9)—C(10)	119.3(3)
C(5)—N—B	118.6(2)	C(9)—C(10)—C(11)	120.2(3)
O(1)—C(1)—O(2)	124.3(2)	C(6)—C(11)—C(10)	122.2(3)
O(1)—C(1)—C(2)	112.4(2)	B—C(12)—C(13)	120.9(2)
O(2)—C(1)—C(2)	123.3(2)	B—C(12)—C(17)	122.4(2)
N—C(2)—C(1)	103.6(2)	C(13)—C(12)—C(17)	116.7(2)
N—C(2)—C(3)	106.7(3)	C(12)—C(13)—C(14)	121.6(3)
C(1)—C(2)—C(3)	114.2(2)	C(13)—C(14)—C(15)	120.7(3)
C(2)—C(3)—C(4)	104.6(4)	C(14)—C(15)—C(16)	119.5(3)
C(2)—C(3)—C(4′)	105.3(6)	C(15)—C(16)—C(17)	119.7(3)
C(3)—C(4)—C(5)	101.7(5)	C(12)—C(17)—C(16)	121.7(3)
C(3)—C(4′)—C(5)	112.7(13)	O(1)—B—N	98.5(2)
N—C(5)—C(4)	105.4(4)	O(1)—B—C(6)	109.2(2)
N—C(5)—C(4′)	101.7(5)	O(1)—B—C(12)	110.5(2)
B—C(6)—C(7)	119.7(2)	N—B—C(6)	109.9(2)
B—C(6)—C(11)	124.4(2)	N—B—C(12)	112.6(2)
C(7)—C(6)—C(11)	115.8(2)	C(6)—B—C(12)	114.8(2)

(*b*) Angles involving hydrogen atoms

Bonds	Angle (deg)	Bonds	Angle (deg)
C(2)—N—H(N)	105(2)	C(4′)—C(5)—H(5a)	91(4)
C(5)—N—H(N)	108(2)	C(4′)—C(5)—H(5b)	134(6)
B—N—H(N)	115(2)	H(5a)—C(5)—H(5b)	107(6)
N—C(2)—H(2)	107(2)	C(6)—C(7)—H(7)	115(3)
C(1)—C(2)—H(2)	111(2)	C(8)—C(7)—H(7)	122(3)
C(3)—C(2)—H(2)	113(2)	C(7)—C(8)—H(8)	120(3)
C(2)—C(3)—H(3a)	108(7)	C(9)—C(8)—H(8)	120(3)
C(2)—C(3)—H(3b)	110(5)	C(8)—C(9)—H(9)	122(3)
C(4)—C(3)—H(3a)	123(5)	C(10)—C(9)—H(9)	118(3)
C(4)—C(3)—H(3b)	107(4)	C(9)—C(10)—H(10)	117(3)
C(4′)—C(3)—H(3a)	93(6)	C(11)—C(10)—H(10)	123(4)
C(4′)—C(3)—H(3b)	133(5)	C(6)—C(11)—H(11)	119(3)
H(3a)—C(3)—H(3b)	103(7)	C(10)—C(11)—H(11)	118(3)
C(3)—C(4)—H(4a)	93(4)	C(12)—C(13)—H(13)	117(2)
C(3)—C(4)—H(4b)	110(3)	C(14)—C(13)—H(13)	121(2)
C(5)—C(4)—H(4a)	110(4)	C(13)—C(14)—H(14)	115(3)
C(5)—C(4)—H(4b)	107(4)	C(15)—C(14)—H(14)	124(3)
H(4a)—C(4)—H(4b)	131(6)	C(14)—C(15)—H(15)	120(2)
C(3)—C(4′)—H(4a)	124(5)	C(16)—C(15)—H(15)	120(2)
C(5)—C(4′)—H(4a)	103(5)	C(15)—C(16)—H(16)	119(3)
N—C(5)—H(5a)	109(4)	C(17)—C(16)—H(16)	120(3)
N—C(5)—H(5b)	111(5)	C(12)—C(17)—H(17)	117(2)
C(4)—C(5)—H(5a)	119(4)	C(16)—C(17)—H(17)	121(2)
C(4)—C(5)—H(5b)	105(5)		

Table 6 lists nonbonded distances and details of the hydrogen-bonding scheme.

The expected intramolecular N—B coordination occurs to form a system of two fused five-membered rings, both of which are puckered (see Table 5). The coordination of the boron atom is tetrahedral, slightly distorted by the 98.5(2)° O(1)—B—N angle. The disordering of C(4) results in two conformations for the proline ring, that containing C(4) being folded away from O(1) while that containing C(4′) is folded toward O(1) (see Fig. 1).

The C(6)—C(11) phenyl ring is rigorously planar within experimental error while the

TABLE 5. Intra-annular torsion angles (deg)

BOCCN ring		Proline ring		
			Value	
Bond	Value	Bond	With C(4)	With C(4′)
B—O(1)	−24.0(2)	N—C(2)	−19.4(3)	−19.4(3)
O(1)—C(1)	10.3(2)	C(2)—C(3)	−4.7(4)	30(2)
C(1)—C(2)	10.0(2)	C(3)—C(4/4′)	27.3(5)	−28(2)
C(2)—N	−24.0(2)	C(4/4′)—C(5)	−39.9(5)	15(2)
N—B	28.3(2)	C(5)—N	38.4(4)	4(1)

TABLE 6
(*a*) Selected intra- and intermolecular contacts

Intramolecular		Intermolecular*	
Atoms	Distance	Atoms	Distance
C(4)...C(4′)	0.88(4)	O(1)...H(11)[1]	2.70(4)
C(1)...C(4′)	3.03(3)	H(3b)...H(10)[2]	2.19(10)
C(5)...C(12)	3.046(4)		
C(11)...N	3.083(4)		
N...H(4b)	2.62(6)		
C(1)...H(3a)	2.51(11)		
C(4)...H(N)	2.55(3)		
C(6)...H(N)	2.68(3)		
B...H(5a)	2.68(6)		
H(11)...H(N)	2.20(6)		

(*b*) Hydrogen-bond data* (distances in Å and angles in deg)

D—H...A	H...A	D...A	∠DHA	∠XAH
N—H(N)...O(2)[3]	2.15(4)	2.893(3)	157(3)	124.1(8)
	C—H...O interactions			
C(7)—H(7)...O(1)	2.57(4)	2.944(3)	104(3)	122(1), 76(1)
C(17)—H(17)...O(1)	2.48(3)	2.902(3)	107(2)	136(1), 82(1)
C(3)—H(3a)...O(2)	2.62(11)	3.027(4)	105(8)	71(2)
C(4)—H(4b)...O(2)[3]	2.62(7)	3.34(1)	131(5)	124(1)
C(11)—H(11)...O(2)[3]	2.61(5)	3.570(3)	156(3)	91.4(9)

NOTE: Other angles at O(1) and O(2) are: H(7) ... O(1) ... H(17), 101(1), H(N) ... O(2) ... H(3a), 132(2), H(N) ... O(2) ... H(4b), 62(2), H(N) ... O(2) ... H(11), 54(1), H(3a) ... O(2) ... H(4b), 72(3), H(3a) ... O(2) ... H(11), 162(2), and H(4b) ... O(2) ... H(11), 116(2)°.
*Superscripts refer to atoms at positions noted below.
[1] $1 + x, y, z$.
[2] $-x, \frac{1}{2} + y, -z$.
[3] $x - 1, y, z$.

C(12)—C(17) ring is not, although all atoms of the ring lie within ±0.01 Å of the mean plane. The boron atom is significantly displaced from both phenyl mean planes, by −0.023 Å from the C(6)—C(11) plane and by 0.045 Å from the C(12)—C(17) plane. The dihedral angles defining the orientation of the phenyl rings are: O(1)[B—C(6)]C(7), 38.5(2), N[B—C(6)]C(11), −35.7(3), O(1)[B—C(12)]C(17), 6.4(3), and N[B—C(12)]C(13), 78.9(3)°. The dihedral angle between normals to the mean planes is 104.1°.

The BOCCN ring in **4** may be regarded as a keto derivative of those in **1**–**3** and **5** (20). The C(1) carbonyl group in **4** significantly alters the electron distribution around the BOCCN ring when compared to **1**–**3**, an effect also noted for the substituted ring in **5**. The O—B, O—C, C—C, C—N, and N—B bond lengths are 1.529(3),

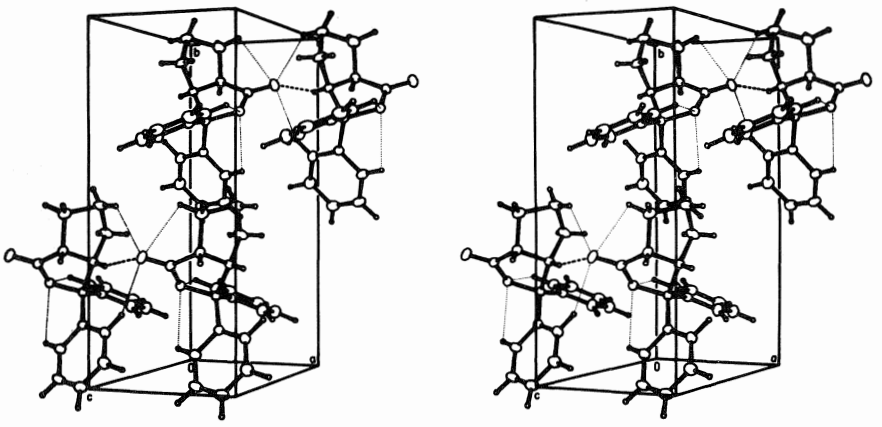

FIG. 2. A stereo view of the packing arrangement. Broken lines represent hydrogen bonds and dotted lines C—H...O interactions.

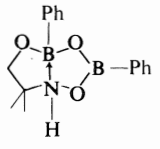

5

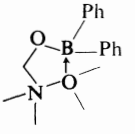

6

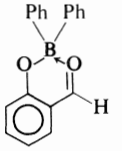

7

1.300(3), 1.517(3), 1.507(3), and 1.630(3) Å in the present structure compared to values[3] of 1.43(1), 1.43(1), 1.52(1), 1.49(1), and 1.647(9) Å for **1** (1, 2); 1.467(7), 1.415(4), 1.519(5), 1.486(1), and 1.666(3) Å for **2** (3); 1.477(5), 1.412(4), 1.503(5), 1.488(2), and 1.654(2) Å for **3** (4–6); and 1.452(2), 1.426(2), 1.530(2), 1.513(2), and 1.692(2) Å for **5** (20). The most important influence of the carbonyl group on the electron distribution in the BOCCN ring is contribution to the overall structure by resonance forms such as **4***b*. This is evidenced by increases in the B—O and C—N bond lengths and decreases in the B—N and C—O bond lengths in **4** when compared to those in **2** and **3**. The C—C bond in **4** at 1.517(3) Å corresponds to a normal C(sp^2)—C(sp^3) single bond whereas the ring C—C bonds in **2** and **3** are significantly shorter than normal C(sp^3)—C(sp^3) single bonds.

The B—C distances of 1.612(3) and 1.614(3) Å are near the weighted mean B—C distance of 1.615(9) Å for compounds **2**, **3**, **5**, and related diphenylboron chelates **6** (21) and **7** (22). The individual B—C distances in these compounds range from 1.599(2) Å in **5** to 1.639(8) Å in **6**. The mean phenyl C—C distance is 1.394(10) Å and as in other B-substituted phenyl rings (6, 23) the C—C distances decrease with greater distance from the boron substituent, the mean values being 1.401(2), 1.391(2), and 1.384(12) Å. The substituent-induced angular variations are also as expected (6, 23); the mean angles in the phenyl rings at carbon atoms bonded to boron and at the *ortho*, *meta*, and *para* positions relative to the boron substituent are 116.2(5), 122.0(6), 120.2(4), and 119.4(1)°.

The mean C(sp^3)—H and C(ar)—H distances of 0.94(5) and 0.96(5) Å are as expected for X-ray data. Both of the N—C bonds are significantly longer than the usual distance of 1.485 Å. All other bonds not involving the disordered C(4) atom are normal.

The crystal structure consists of discrete molecules of L-prolinatodiphenylboron linked together by N—H...O hydrogen bonds (N...O = 2.893(3) Å) along the short *a* axis. There are a number of weak C—H...O interactions which may have some influence on the structure, both in the orientation of the phenyl rings and also the greater occupation of the C(4) site since the partially occupied site H(4b) is involved in one of these interactions.

[3]Weighted mean values are given where appropriate. Here and elsewhere in this paper when mean values are quoted, numbers in parentheses refer to rms deviations from the mean.

Acknowledgements

We thank the National Research Council of Canada for financial support and the University of British Columbia Computing Centre for assistance.

1. Z. TAIRA and K. OSAKI. Inorg. Nucl. Chem. Lett. **7**, 509 (1971).
2. (*a*) R. MATTES, D. FENSKE, and K. F. TEBBE. Chem. Ber. **105**, 2089 (1972); (*b*) H. FOLLNER. Mh. Chem. **104**, 477 (1973).
3. S. J. RETTIG and J. TROTTER. Can. J. Chem. **53**, 1393 (1975).
4. S. J. RETTIG and J. TROTTER. Can. J. Chem. **51**, 1288 (1973).
5. S. J. RETTIG and J. TROTTER. Acta Crystallogr. Sect. B, **30**, 2139 (1974).
6. S. J. RETTIG and J. TROTTER. Can. J. Chem. **54**, 3130 (1976).
7. H. C. BROWN and E. A. FLETCHER. J. Am. Chem. Soc. **73**, 2808 (1951).
8. K. LANG, K. NUTZEL, and F. SCHUBERT. German Patent 1130445. 1962.
9. (*a*) S.-H. TUNG, K.-M. CHANG, S.-L. TAH, C.-C. LIU, and S.-L. CHANG. K'o Hsueh T'ung Pao, **17**, 414 (1966); Chem. Abstr. **66**, 37990*m* (1967); (*b*) I. H. SKOOG. J. Org. Chem. **29**, 492 (1964).
10. G. BAUM. J. Organomet. Chem. **22**, 269 (1970).
11. J. KARLE and I. L. KARLE. Acta Crystallogr. **21**, 849 (1966).
12. J. KARLE and H. HAUPTMAN. Acta Crystallogr. **9**, 635 (1956).
13. M. G. B. DREW, D. H. TEMPLETON, and A. ZALKIN. Acta Crystallogr. Sect. B, **25**, 261 (1969).
14. D. T. CROMER and J. B. MANN. Acta Crystallogr. Sect. A, **24**, 321 (1968).
15. R. F. STEWART, E. R. DAVIDSON, and W. T. SIMPSON. J. Chem. Phys. **42**, 3175 (1965).
16. D. T. CROMER and D. LIBERMAN. J. Chem. Phys. **53**, 1891 (1970).
17. V. SCHOMAKER and K. N. TRUEBLOOD. Acta Crystallogr. Sect. B, **24**, 63 (1968).
18. D. W. J. CRUICKSHANK. Acta Crystallogr. **9**, 747 (1956); **9**, 754 (1956).
19. D. W. J. CRUICKSHANK. Acta Crystallogr. **14**, 896 (1961).
20. S. J. RETTIG, J. TROTTER, W. KLIEGEL, and H. BECKER. Can. J. Chem. **54**, 3142 (1976).
21. S. J. RETTIG, J. TROTTER, and W. KLIEGEL. Can. J. Chem. **52**, 2531 (1974).
22. S. J. RETTIG and J. TROTTER. Can. J. Chem. **54**, 1168 (1976).
23. A. DOMENICANO, A. VACIAGO, and C. A. COULSON. Acta Crystallogr. Sect. B, **31**, 231 (1975); **31**, 1630 (1975).

Flash thermolysis of formal oxirene–arene adducts. Rearrangement to cycloheptatriene carboxaldehydes and the question of the formation of oxirene[1]

E. G. LEWARS AND G. MORRISON

Department of Chemistry, Trent University, Peterborough, Ont., Canada K9J 7B8

Received September 16, 1976

E. G. LEWARS and G. MORRISON. Can. J. Chem. **55**, 966 (1977).

Flash thermolysis of 11,12-epoxy-9,10-dihydro-9,10-ethanoanthracene (dibenzobarrellene oxide) (**2**) gave 5*H*-dibenzo[*a*,*d*]cycloheptene-5-carboxaldehyde (**3**). At higher temperatures the products included 5*H*-dibenzo[*a*,*d*]cycloheptene-10-carboxaldehyde (**4**), 5*H*-dibenzo[*a*,*d*]cycloheptene (**5**), and fluorene (**6**). Flash thermolysis of dimethyl 3-oxatricyclo[3.2.2.0^{2,4}]nona-6,8-diene-6,7-dicarboxylate (the oxide of barrellene-2,3-dicarboxylic acid dimethyl ester) (**16**) gave a compound considered to be either dimethyl 3-methanoyl-1,3,5-cycloheptatriene-1,2-dicarboxylate (**17**) or dimethyl 1-methanoyl-1,3,5-cycloheptatriene-2,3-dicarboxylate (**18**), while at higher temperatures dimethyl 1-methanoyl-1,3,5-cycloheptatriene-6,7-dicarboxylate (**19**) was obtained. **16** also yielded small amounts of ketene, which was detected by low-temperature infrared spectroscopy. The mechanistic significance of these results is discussed.

E. G. LEWARS et G. MORRISON. Can. J. Chem. **55**, 966 (1977).

La thermolyse éclair de l'époxy-11,12 dihydro-9,10 éthano-9,10 anthracène (oxyde du dibenzobarrèllène) (**2**) conduit au 5*H*-dibenzo[*a*,*d*]cycloheptènecarboxaldéhyde-5 (**3**). A des températures plus élevées, les produits obtenus comprennent le 5*H*-dibenzo[*a*,*d*]cycloheptènecarboxaldéhyde-10 (**4**), le 5*H*-dibenzo[*a*,*d*]cycloheptène (**5**) et le fluorène (**6**). La thermolyse éclair de l'oxa-3 tricyclo[3.2.2.0^{2,4}]nonadiène-6,8 dicarboxylate-6,7 de diméthyle (l'ester diméthylique de l'oxyde de l'acide barrèllènedicarboxylique-2,3) (**16**) conduit à un composé que l'on considère être soit le méthanoyl-3 cycloheptatriène-1,3,5 dicarboxylate-1,2 de diméthyle (**17**) ou le méthanoyl-1 cycloheptatriène-1,3,5 dicarboxylate-2,3 de diméthyle (**18**) alors qu'à des températures plus élevées, on obtient le méthanoyl-1 cycloheptatriène-1,3,5 dicarboxylate-6,7 de diméthyle (**19**). **16** conduit aussi à des petites quantités de cétène qui peut être détecté par spectroscopie infrarouge à basse température. On discute des implications mécanistiques de ces résultats.

[Traduit par le journal]

Oxirene (**1**) is a molecule of considerable interest (2) which has, however, never been isolated. The molecule represents both an experimental and a theoretical challenge: there is evidence that oxirene, if formed, rapidly rearranges to ketene (2*a*), and while the involvement in the photochemical Wolff rearrangement of a species with the symmetry of oxirene has been elegantly demonstrated (2*b*), it is by no means clear if this species is a true intermediate or merely a transition state (2*c*). The reverse Diels–Alder reaction has been widely used for generating highly reactive alkenes (3), and its application to the synthesis of oxirene appeared to us a possibility worthy of investigation. To this end, a promising precursor would appear to be a (formal!) adduct of oxirene and an arene, since the activation energy of the reaction will be lowered insofar as the transition state resembles the products, owing to the thermodynamic stability of the incipient arene. Indeed, an apprehension of the putative utility of such oxirene–arene adducts for the generation of the elusive heterocycle is implicit in a paper by Vogel and coworkers (4) where passing reference is made to the possibility of effecting cleavage of adduct **16** to "acetylene oxide" and dimethyl phthalate. We were intrigued by this possibility, as well as the question of the pathway that would be followed should **16** decline to be so obliging.

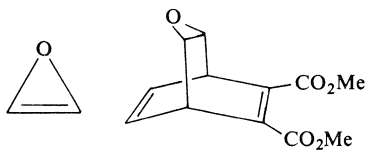

1 **16**

For our purpose, the ideal technique for effecting the reverse Diels–Alder reaction ap-

[1]A preliminary communication of some of this work has been published (1).

peared to be flash thermolysis (flash vacuum thermolysis/pyrolysis). In this technique (5), the compound in the vapor phase at low pressure contacts a hot surface for a duration of the order of a few ms; the resulting thermolysate is then deposited on a cold surface for chemical or spectroscopic investigation. With these facts in mind, we subjected to flash thermolysis with observation of the low-temperature infrared spectrum (*5a*) compound **2** (6), a formal oxirene–anthracene adduct, and the above-mentioned compound **16** (a formal oxirene – dimethyl phthalate adduct). Although thermolysis of **16** gave some evidence for the formation of **1**, the main pathways taken by **2** and **16** were more complex.

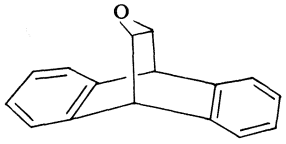

2

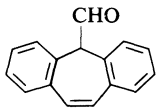

3

Thermolysis of **2** gave a mixture, the composition of which varied considerably with the thermolysis temperature. The identity of the components was established by chromatographic isolation and direct comparison with authentic samples, and the composition was calculated from the integrated ^{1}H nmr spectra. The results are summarized in Table 1.

The formation of **3** may be rationalized by epoxide cleavage to **7** and a Wagner–Meerwein shift to give **8**, followed by carbon–carbon bond cleavage (**8**, arrow *1*),[2] while the alternative cleavage (**8**, arrows *2*) would give the *o*-xylylene

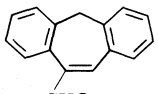

4

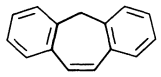

5

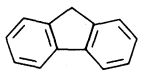

6

9 which could be converted to **4** by a 1,5-sigmatropic suprafacial shift of a hydrogen atom (7). Thermolysis of **3** at 500 °C gives only a small (*ca.* 5%) yield of **4**, showing that most of the aldehyde **4** formed under these conditions arises from **2** without the intermediacy of **3**. Intermediate **8** may also be involved in the transformation of **3** to **4**, since electrophilic attack of the aldehyde group of **3** on the transannular

[2]*Cf.* ref. 6.

TABLE 1. The products of the thermolysis of **2**

Temperature (°C)	Thermolysate composition (mol%)					
	2	**3**	**4**	**5**	**6**	Others*
400	20	75	5	0	0	0
500	0	10	90	0	0	0
650	0	0	25	65	0	10
800	0	0	0	0	25	75

*Compounds showing mainly only aromatic H's in the ^{1}H nmr spectrum; the presence of 8 aromatic H's was assumed.

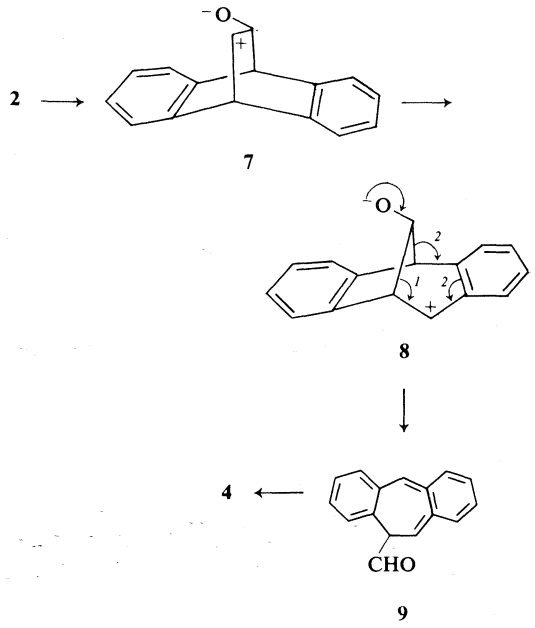

double bond would generate **8**. Transannular reactions are not prominent in seven-membered rings, but one need rationalize only a low yield of **4**. We wish to point out that the invoking of an ionic mechanism here does not necessarily imply that we regard it as being more likely than a free radical one. Since explicit mechanistic studies were not conducted, a detailed discussion of reaction mechanisms seems pointless here. The dibenzocycloheptatriene **5** is presumably a decarbonylation product of **4**, and fluorene (**6**) probably results from loss of ethyne from **5** (**5** → **10** → **11** → **6**), which seems more likely (8) than concerted extrusion, which would require an antiaromatic transition state (9).

That these thermolysis products had the structures which have been assigned them was suggested by their infrared and ^{1}H nmr spectra and their molecular weights (mass spectra)

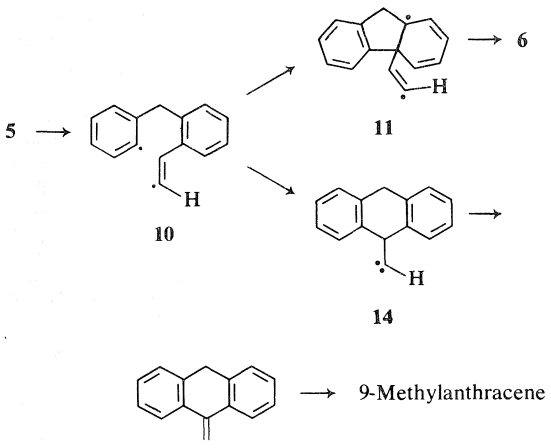

15

and confirmed by direct comparison with authentic samples. An authentic sample of **3** was made by isomerizing **2** with acidic alumina, as described by Cristol and Bly (6). A surprising feature of the nmr spectrum of **3** is that the aldehyde proton and the proton on the adjacent carbon give sharp singlets, rather than the expected doublets. Space-filling molecular models suggest that the proximal *ortho* hydrogens of the lateral benzene rings constrain the CHO group to take up a conformation such that the dihedral angle between the C—H bonds of the CHO group and the hydrogen on the adjacent carbon is *ca.* 90°, making any coupling small (<1 Hz) (10).

Authentic samples of **4** and **5** were synthesized from the commercially available (Aldrich 10-bromo-5*H*-dibenzo[*a*,*d*]-5-cycloheptenone by reduction and metallation followed by carbonylation with dimethylformamide, giving **4**, or protonation with water, giving **5**.[3]

Besides fluorene, 9-methylanthracene seems to be a major component (*ca.* 20%) of the 800 °C thermolysate. The presence of this was not rigorously demonstrated, but is rendered likely by two facts: the ^{1}H nmr spectrum of the thermolysate mixture showed, besides a singlet at δ 3.77 for fluorene, a sharp singlet at δ 3.00, the position of the methyl group of 9-methylanthracene (these were the only peaks in the nonaromatic region of the spectrum). Furthermore, the mass spectrum of an impure sample of the non-fluorene material, collected from a partially resolved vpc peak, gave a molecular ion of *m*/*e* 192, consistent with a methylanthracene. This probable component could arise by the kind of mechanism suggested by Srinivasan and co-workers for the photorearrangement of **12** to **13** (12). However, the fact that thermolysis of the aldehyde **4** at 700 °C gave **5** and the putative 9-methylanthracene (molar ratio 1.5;1 by ^{1}H nmr) suggests the pathway **5** → **10** → **14** → **15** → 9-methylanthracene.

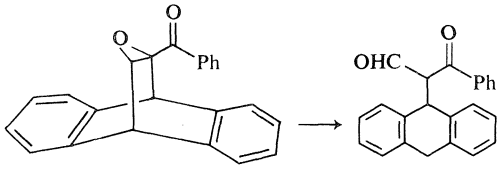

12 13

When the thermolysate was trapped at −140 °C on the sodium chloride disc of an infrared cryostat, at none of the thermolysis temperatures tried (see Table 1) was there any indication of ketene[4] or of a species which gave ketene or was otherwise unstable, and vpc examination of the 650 and 800 °C thermolysates (the only ones containing unidentified components) showed that anthracene, if present, was only a minor (not more than *ca.* 5%) component. Clearly, if reverse Diels–Alder cleavage of **2** to **1** and anthracene occurred under our conditions, it represented only a minor pathway.

The flash thermolytic behavior of **16** was somewhat analogous to that of **2**. At 300 °C there was obtained a 62% yield of an aldehyde, mp 105–106 °C, as well as 4% yield of another aldehyde, mp 108–110 °C, and 24% of recovered **16**. The aldehyde of mp 105–106 °C was assigned structure **17** or **18** on the basis of its

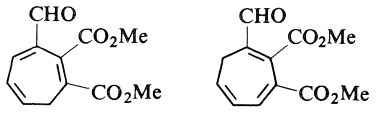

17 18

formula, $C_{12}H_{12}O_5$, spectra, and transformation to the other aldehyde (see below). The ^{1}H nmr spectrum showed an AMX pattern (δ_A 7.50, δ_M 6.52, δ_X 5.97, J_{AM} = 5.5 Hz, J_{MX} =

[3] **5** has been made by other methods, see *e.g.* ref. 6; a patent describes the preparation of **4** from the corresponding methyl compound (11).

[4] *Cf.* ref. 2*a*.

9 Hz) with H_X also coupled to a CH_2 group at δ 2.67 (J = 7 Hz), revealing a $C{=}CH_A{-}CH_M{=}CH_X{-}CH_2$ grouping with H_A strongly deshielded. In addition, the spectrum displayed a CHO peak (δ 9.48, s) and two CO_2Me methyls (δ 3.77, 6H, giving way to two 3H singlets on addition of Eu(fod)$_3$-d_{27} shift reagent). This spectrum is very similar to that of a compound reported by King *et al.* (13) which differs from **17**/**18** only in having a phenyl group in place of a CHO, and is almost uniquely compatible with structure **17**/**18**. Consonant with this structure, the ultraviolet spectrum revealed extensive unsaturation, λ_{max}(MeOH) 242 (ε 15 600), 285 nm (ε 5000), and the infrared spectrum showed λ_{max}(KBr) 5.80 (conjugated ester) and 5.93 μm (conjugated aldehyde). We believe a choice between **17** and **18** cannot be made with the information at hand.

Thermolysis of **17**/**18** or of **16** at 400 °C gave, in addition to a 23% yield of the aldehyde discussed above, a 58% yield of the aldehyde of mp 108–110 °C. This compound was assigned structure **19** on the basis of its formula, $C_{12}H_{12}O_5$, spectra, and formation from **16** by treatment with acidic alumina. The ^{1}H nmr spectrum displayed, besides a CHO peak (δ 9.43, s) and two CO_2Me methyls (δ 3.77, s and 3.45, s), an olefinic ABCD system (δ 7.50–7.27, m, 1H; 7.13–6.93, m, 1H; 6.93–6.67, m, 2H) and a peak at 5.63 (s, 1H). Structure **19** is strongly supported by the infrared spectrum, λ_{max}(KBr) 5.76 (saturated ester), 5.86 (conjugated ester), 5.94 μm (conjugated aldehyde), and the ultraviolet spectrum λ_{max}(MeOH) 228 (ε 34 000), 313 nm (ε 6500), which is quite similar to the uv spectra reported by Eschenmoser and co-workers (14) and Vogel *et al.* (15) for **20** and **21** respectively. Aside from its electronically isolated central carbomethoxy group, our aldehyde is a half-way house between **20** and **21**. The significantly shorter wavelength absorption of the conjugated ester groups in the infrared spectrum of **17**/**18** (5.80 μm) as compared to that of the conjugated ester group of **19** (5.86 μm) probably reflects close juxtaposition of the central carbomethoxy group to its neighbours.[5] In **19**, on the other hand, the central carbomethoxy group is attached to an sp^3-hybridized carbon and can lie out of the planes defined by the carbon–carbon double bonds bearing the other carbonyl groups. The fact that the carbomethoxy groups of **20** absorb at 5.85 μm is consistent with this suggestion. Further support for a bis(carbomethoxy)cycloheptatriene carboxaldehyde structure for this aldehyde was provided by the fact that treatment of **16** with acidic alumina gave the aldehyde in 50% yield; this rearrangement finds precedence in the alumina-promoted isomerization of **2** to **3** (6).

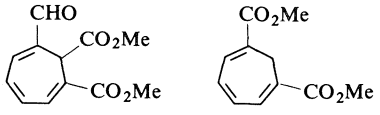

19

20

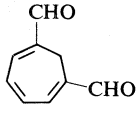

21

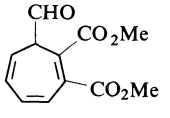

22

The formation of the aldehydes **17** or **18**, and **19**, can be rationalized by C—O bond cleavage (*cf.* **7**; heterolytic, as shown here, when promoted by alumina, possibly homolytic under flash thermolysis conditions) and Wagner–Meerwein-type rearrangement to give a bicyclo[3.2.1] system, analogous to **8**, which undergoes another Wagner–Meerwein-type shift, yielding **22**; this could be transformed into **17** or **18**, or into **19**, by sequential 1,5-sigmatropic hydrogen atom shifts (on thermolysis) (17) or by alumina-catalyzed double bond isomerization.

When the thermolysate from runs in the temperature range 600–800 °C was trapped at −140 °C on the sodium chloride disc of an infrared cryostat, a band at 4.63 μm, growing weaker as the cryostat was allowed to warm up, and attributable to ketene, was seen. The simplest interpretation of this is that oxirene was extruded from **16** and isomerized to ketene, but isomerization of **16** to the bicyclo[2.2.2]-octadienone followed by extrusion of ketene cannot be ruled out. Based on the strength of the ketene band from a known amount of **16** we estimate the yield of ketene to be roughly

[5]Propinquity of a polar group to a carbonyl group can shift the infrared absorption of the carbonyl to shorter wavelength (see, *e.g.* ref. 16).

5% at the optimum temperature of 700 °C, and vpc examination of the crude thermolysate showed a peak with the same retention time as dimethyl phthalate, again roughly 5% of the mixture. The ^{1}H nmr spectrum of the crude 700 °C thermolysate showed three carbomethoxy methyls, but could not be used to estimate the yield of dimethyl phthalate since the signals of one of the products of this high-temperature thermolysis, 7-carbomethoxyisocoumarin (22), obscure those of dimethyl phthalate.

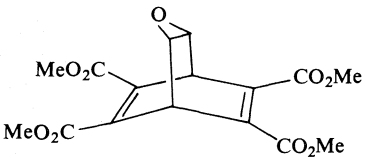

23

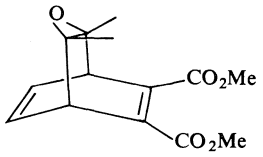

24

A few flash thermolysis experiments were also conducted with the barrellene oxides **23** (18) and **24** (19) using the infrared cryostat. Compound **23** gave a band at 4.63 μm (optimum temperature 600 °C) suggesting that ketene was formed to the extent of roughly 10%, and the vpc trace showed that material of the same retention time as tetramethyl benzene-1,2,4,5-tetracarboxylate constituted about 10–20% of the crude thermolysate. Compound **24**, too, gave a band at 4.63 μm, ascribed to dimethylketene (optimum temperature 500 °C), indicating that the ketene was formed in a yield of roughly 5%, and vpc examination of the crude thermolysate showed a peak with the same retention time as dimethyl phthalate, representing *ca.* 2–5% of the mixture. These results, which, we are fully aware, are only suggestive, lend credence to the hypothesis that some barrellene oxides thermolytically extrude an oxirene, which quickly rearranges to a ketene. We are investigating the possibility that appropriate substitution of the barrellene oxide system might make extrusion of oxirene the main reaction.[6]

[6]See ref. 13 for a discussion of a case where small substituent changes showed a large effect on the propensity toward reverse Diels–Alder fragmentation of a thiabarrellene derivative.

Summary

The question as to whether **16** (4) or **2** undergo thermal reverse Diels–Alder cleavage to oxirene (**1**) and the corresponding arene has been essentially answered. The main reaction pathway is isomerization to cycloheptatriene carboxaldehydes, although **16** (as well as **23** and **24**) do give small amounts of ketene (or dimethylketene, from **24**), which could be interpreted as evidence for the extrusion of oxirene.

Experimental

All melting points were determined on a Fisher-Johns melting point hot stage and are uncorrected.

Unless stated otherwise, all infrared spectra (ir) were recorded as carbon tetrachloride solutions on a Unicam SP-200 spectrophotometer. The spectra were calibrated with the 6.24 μm band of polystyrene film.

Ultraviolet spectra (uv) were recorded in methanol solutions, unless stated otherwise, with a Unicam SP-800A spectrophotometer using 1 cm pathlength cells.

^{1}H nuclear magnetic resonance spectra (nmr) were recorded in deuteriochloroform solution unless stated otherwise, with a Jeol C-60 HL spectrometer. Chemical shifts are reported in parts per million downfield from tetramethylsilane as internal references (δ scale). The following abbreviations apply: s = singlet, d = doublet, t = triplet, dd = doublet of doublets, m = an unresolved multiplet.

Mass spectra were obtained with an A.E.I. MS 12 spectrometer at an electron beam energy of 70 eV. High resolution mass spectra were taken on a Varian MAT 311A mass spectrometer.

Gas chromatography was carried out with a Pye series 104 gas chromatograph equipped with a flame ionization detector. The instrument was fitted with both a $\frac{3}{8}$ in. × 7 ft, 10% silicon grease on Chromosorb W glass preparative column, and a $\frac{1}{4}$ in. × 5 ft, 5% SE-30 on Chromosorb W glass analytical column. Helium was employed as the carrier gas.

Unless otherwise stated, all R_f values refer to analytical thin layer chromatography (tlc) using commercially available aluminum sheets precoated with silica gel 60F-254, layer thickness 0.2 mm (Brinkmann Instruments, Rexdale, Ontario). Preparative tlc was performed on 20 × 20 cm glass plates coated with Fluka silica gel HF-254. Each plate contained approximately 20 g of silica gel to which a maximum of 200 mg of material was applied. The bands were visualized with a Mineralight UVS-12 ultraviolet lamp and extracted with a methanol–dichloromethane (1:10) solution.

Unless otherwise stated, anhydrous magnesium sulphate was used for drying of solutions. Solvents were removed with a Büchi Rotovapor in conjunction with a water aspirator.

The gas phase thermolyses were carried out by subliming a known amount of material, typically 50 mg, under high vacuum (10^{-4}–10^{-3} torr) through a hot quartz tube. The product mixture was then frozen out on either a liquid-nitrogen-cooled cold finger or the sodium chloride disc of the cryostat (Fig. 1). Sublimation of

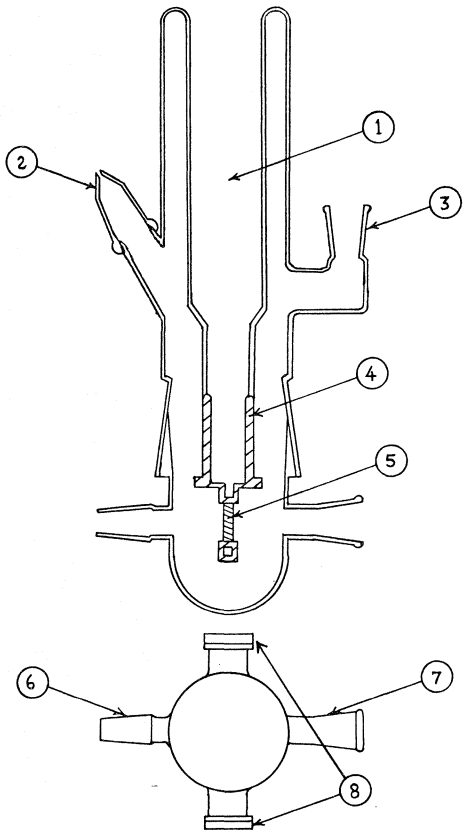

FIG. 1. Infrared cryostat (*ca.* one-quarter actual size): *1.* liquid nitrogen reservoir, *2.* head carrying thermocouple wires (wires sealed at orifice with epoxy resin), *3.* joint for receiving Pirani gauge, *4.* metal collar (attached to reservoir through glass-to-metal seal), *5.* NaCl disc, *6.* to vacuum system, *7.* to thermolysis tube (51 × 1 cm), *8.* optical windows. Silicone grease was used on all ground-glass joints.

the substrate was facilitated by the use of a preheater set at 100 °C. A post-heater, situated immediately after the oven, was utilized at a temperature of 175 °C to eliminate any condensation of the thermolysate prior to its impingement onto the liquid-nitrogen-cooled surface. When all the material had been thermolyzed and the products frozen out, the infrared spectrum could be taken, or, alternatively, the vacuum broken and the products rinsed off for analysis.

The quartz tube inserted through the oven was capped at one end by a B14 ground glass socket and joined to the cryostat via another B14 ground glass joint. The furnace unit enveloping the quartz tube was a Lindberg Type 550 35A oven, capable of maintaining temperature (±5 °C) up to 1000 °C. The preheater and post-heater were 2.5 × 10 cm pieces of Pyrex tubing wrapped with asbestos strips, 30-gauge Nichrome wire, and glass wool, and connected to variable transformers.

The cryostat consisted of two sections. The upper section contained a 270 ml liquid nitrogen reservoir. The sodium chloride disc was held in a hollow brass frame which formed part of the reservoir enabling liquid nitrogen to circulate within the frame. The temperature of the disc was measured with a chromel–alumel thermocouple inserted into a small hole in the disc. The lower section of the cryostat was fitted with two B14 ground glass joints connecting the cryostat to the vacuum system and to the quartz tube, and also contained two sodium chloride windows directly opposite one another and at right angles to the other joints. The upper and lower sections were joined by a B60 ground glass joint which enabled the sodium chloride plate to be turned 90° while still under vacuum to a position in line with the two optical windows for the recording of spectra. The vacuum system utilized a Speedivac E.D. 35 mechanical pump and a two-stage oil diffusion pump, and was connected to the thermolysis unit through a liquid-nitrogen-cooled trap. The pressure at the cryostat and at the trap were monitored with an Edwards Pirani G9 gauge and an Edwards No. 6 Penning gauge, respectively. Contact times are thought to have been a few ms (*5c*).

Thermolysis of **2**

400 °C

Thermolysis of **2** (40 mg) gave 36 mg of thermolysate (yellow oil). The nmr spectrum of the crude thermolysate showed it to be a mixture of unchanged **2**, as well as **3** and **4** in the molar ratio 4:15:1. The material was subjected to preparative tlc (methanol – light petroleum, 1:20) to give **2** (8 mg), **3** (25 mg), and **4** (2.5 mg). The aldehyde **3**, R_f = 0.25, was crystallized from ether; mp 110–112 °C (lit. (6) mp 112–114 °C) and readily formed a yellow 2,4-dinitrophenylhydrazone derivative (2,4-DNP), mp 215–217 °C (lit. (6) mp 221–223 °C). The aldehyde showed ir λ_{max} 5.77 μm; uv λ_{max} (hexane) 224, 290 nm; nmr (CCl_4) δ 4.33 (1H, s), 6.70 (2H, s), 7.15 (8H, m), 9.40 (1H, s); *m/e* 220(M^+).

500 °C

Compound **2** (47 mg) gave 42 mg of an oily thermolysate which was shown by nmr to contain **3** and **4** in the molar ratio 1:9. Preparative tlc (methanol – light petroleum, 1:20) gave a band (R_f = 0.56) which gave 34 mg of **4**. The product crystallized from ether to give a colourless solid mp 133–134 °C (lit. (11) mp 133–135 °C); 2,4-DNP (red) mp 235–237 °C; ir λ_{max} 5.88 μm, uv λ_{max} (hexane) 228, 303 nm; nmr δ 3.58 (2H, s), 7.20 (8H, m), 7.62 (1H, s), 9.68 (1H, s); *m/e* 220 (M^+). *Exact Mass* calcd. for $C_{16}H_{12}O$: 220.08826; found: 220.08835.

650 °C

Compound **2** (54 mg) afforded on thermolysis an oil (49 mg) which was shown by nmr to contain **4** and **5** in a molar ratio 5:13. Preparative tlc gave **4** (13 mg) and **5** (25 mg). Compound **5** (R_f = 0.74) was recrystallized from methanol to give a white solid, mp 123–126 °C (lit. (6) mp 132–134 °C); ir λ_{max} 6.65, 6.88 μm; uv λ_{max} (hexane) 223, 289 nm; nmr δ 3.66 (2H, s), 6.90 (2H, s) 7.15 (8H, m); *m/e* 192 (M^+).

800 °C

The 800 °C thermolysate of **2** was shown by nmr to contain **6** (25 mol %). Preparative gas chromatography of the thermolysate (column temperature = 190 °C) gave a 3 mg sample of **6**, mp 109–112 °C. Mixture melting

point was 109–113 °C with an authentic sample of mp 109–111 °C. The two samples were indistinguishable by their ultraviolet, infrared, and mass spectra as well as their retention times on gas chromatography.

Thermolysis of ***16***

300 °C

Compound **16** (40 mg) gave 34 mg of an oil which was shown by nmr to contain unchanged **16**, **17** (or **18**), and **19** in the molar ratio 4:15:1. The thermolysates from three runs were combined (190 mg) and subjected to preparative tlc (ether–hexane, 1:1). Extraction of the bands gave **16** (47 mg), **17**/**18** (118 mg), and **19** (8 mg). Compound **17**/**18** (R_f = 0.20) crystallized from ether, mp 105–106 °C, and formed a red 2,4-DNP, mp 208–210 °C. The aldehyde possessed the following characteristics: ir λ_{max} (KBr) 5.80, 5.93 μm; uv λ_{max} 242 (ε 15 600), 285 nm (ε 5000); nmr δ 2.67 (2H, d, J = 7 Hz), 3.77 (6H, s), 5.97 (1H, m, J = 9, 7 Hz), 6.52 (1H, dd, J = 9, 5.5 Hz), 7.50 (1H, d, J = 5.5 Hz), 9.48 (1H, s) *m*/*e* 236 (M^+). *Exact Mass* calcd. for $C_{12}H_{12}O_5$: 236.06792; found: 236.06791.

400 °C

Compound **16** (56 mg) on thermolysis at 400 °C gave 49 mg of a yellow oil. Analysis by nmr showed **17** (or **18**) and **19** in a molar ratio of *ca.* 1:3. Preparative tlc (ether–hexane 1:1) of two thermolysates combined (119 mg) gave **17**/**18** (28 mg) and **19** (70 mg). Compound **19** (R_f = 0.55) was crystallized from ether to give a solid, mp 108–110 °C 2,4-DNP (red) mp 227–228 °C; ir λ_{max} (KBr) 5.76, 5.86, 5.94 μm; uv λ_{max} 228 (ε 34 000), 313 nm (ε 65 000); nmr δ 3.45 (3H, s), 3.77 (3H, s), 5.63 (1H, s), 6.67–6.93 (2H, m), 6.93–7.13 (1H, m), 7.27–7.50 (1H, m); *m*/*e* 236 (M^+). *Exact Mass* calcd. for $C_{12}H_{12}O_5$: 236.06792; found: 236.06860.

Infrared Cryostat Experiments with ***2***, ***16***, ***23***, *and* ***24***

All analytical thermolyses for the low temperature infrared studies were conducted with *ca.* 7 mg of substrate. The thermolysate was condensed on the liquid-nitrogen-cooled sodium chloride disc of the cryostat and the spectrum recorded. Gas chromatographic analysis of the thermolysates was done by rinsing the product mixture from the sodium chloride disc with hot carbon tetrachloride.

Thermolyses of **2** at temperatures from 300 to 900 °C resulted in infrared spectra with no absorption due to ketene, although at 700, 800, and 900 °C the gas chromatograph trace (analytical column, temperature = 180 °C) showed five main peaks, one of these (not more than *ca.* 5% of the mixture) possessing the same retention time as anthracene.

Thermolysis of **16** at 600, 700, and 800 °C resulted in infrared spectra having a weak to medium absorption at 4.63 μm due to ketene. Gas chromatography (analytical column, temperature = 183 °C) revealed a complex mixture with five main products. A minor product (*ca.* 5% of the mixture) had a retention time identical to that of dimethyl phthalate.

The 600 °C thermolysate of **23** had an infrared spectrum with a weak to medium absorption band at 4.63 μm, ascribed to ketene. Gas chromatography (analytical column, temperature = 200 °C) showed three main products, one of which constituted *ca.* 20% of the mixture and had the same retention time as tetramethyl benzene-1,2,4,5-tetracarboxylate.

The infrared spectra of the 400, 500, 600, and 800 °C thermolysates of **24** all showed absorption at 4.65 μm attributable to dimethyl ketene. The optimum temperature for dimethyl ketene formation was 500 °C. Gas chromatography (analytical column temperature = 150 °C) showed that a product with the same retention time as dimethyl phthalate was obtained in all these thermolyses as a minor product (*ca.* 3% of the mixture). An authentic infrared spectrum of dimethyl ketene was obtained by flash thermolysis of dimethyl ketene dimer (2,2,3,3-tetramethylcyclobutane-1,3-dione)[7] at 700 °C and 0.10 torr.

Except for the disappearance of a ketene band with compounds **16**, **23**, and **24**, no change occurred in any of the infrared spectra when the product mixtures were allowed to warm to room temperature.

*11,12-Epoxy-9,10-dihydro-9,10-ethanoanthracene (****2****)*

The following modifications of the literature (6) procedure were made.

11,12-Dichloro-9,10-dihydro-9,10-ethanoanthracene (6.0 g, 22 mmol) and Zn–Cu couple (20) (6.0 g 92 mmol) were refluxed under a $CaCl_2$ drying tube with anhydrous ethanol (800 ml) for 1 week. Filtration and evaporation gave a solid which was taken up in dichloromethane and washed with 3 × 50 ml of water, dried, and evaporated to give 9,10-dihydro-9,10-ethenoanthracene (4.42 g, 95%), mp 106–112 °C (lit. (6) mp 118–119 °C).

Epoxidation of the ethenoanthracene to afford **2** was effected with *m*-chloroperbenzoic acid, essentially as described (6) for reaction with perbenzoic acid. Recrystallization from ether gave a 75% yield of **2**, mp 158–160 °C (lit. (6) mp 154–165 °C).

*Authentic 5H-Dibenzo[a,d]cycloheptene-5-carboxaldehyde (****3****)*

An authentic sample of **3** was prepared according to the procedure outlined by Cristol and Bly (6). The epoxide **2** was eluted through a column of acidic alumina (previously washed with 5% trifluoroacetic acid in CCl_4, then with CCl_4) with carbon tetrachloride as reported. The sample obtained gave a melting point of 111–113 °C (lit. (6) mp 112–114 °C) and formed a 2,4-DNP derivative, mp 214–217 °C (lit. (6) mp 221–223 °C). The mixture melting point of the authentic and thermolytic samples of **3** (mp 110–112 °C) was 110–113 °C. The two samples were indistinguishable by ir, uv, and nmr spectrometry.

*Authentic 5H-Dibenzo[a,d]cycloheptene-3-carboxaldehyde (****4****)*

Reduction of the ketone function of the commercially available (Aldrich) 10-bromo-5*H*-dibenzo[*a*,*d*]cycloheptene-5-one was accomplished by the method of Toda *et al.* (21). The bromo ketone (1.00 g) afforded the bromo compound (0.950 g, 91%) as a solid foam which decomposes slowly on standing, mp (crude solid) 67–78 °C; ir λ_{max} 6.69 μm; uv λ_{max} (hexane) 288 nm; nmr δ 3.58 (2H, s), 7.00 (8H, m), 7.43 (1H, s); *m*/*e* 270 (M^+). *Exact Mass* calcd. for $C_{15}H_{11}{}^{79}Br$: 270.00446; found: 270.00311.

[7]Kindly donated by Professor A. H. Rees of this department.

This bromide (50 mg, 0.18 mmol) was placed in a round bottom flask flushed with nitrogen gas, and sealed with a wired-on septum. Anhydrous ether (1 ml) was syringed in and swirled to dissolve the bromide. Over 10 s, 2 *M* *n*-butyllithium (0.10 ml, 0.20 mmol) was injected with slight agitation of the flask; the brown lithium salt sometimes precipitated. After 4 min, dimethylformamide (5 ml, distilled from calcium hydride) was added and the mixture magnetically stirred 1 h. The mixture was then diluted with 10 ml of ether and washed successively with 10 ml of 1 *M* hydrochloric acid, 10 ml of water, and 5 ml of a saturated sodium bicarbonate solution. The ether solution was dried, concentrated, and the residue subjected to preparative tlc (dichloromethane, run 2×). A band of $R_f = 0.51$ on extraction gave **4** (13 mg, 32%), mp 132–134 °C (lit. (11) mp 133–135 °C); mixture melting point with the thermolytic sample (mp 133–134 °C), 133–134 °C; 2,4-DNP mp 236–237 °C. The authentic and thermolytic samples gave very similar infrared spectra; their nmr and uv spectra were indistinguishable, and the infrared spectra of their 2,4-DNP derivatives were identical.

*Authentic 5H-Dibenzo[a,d]cycloheptene (**5**)*

Treatment of the lithium derivative of the bromo compound (see above) with water instead of dimethylformamide, followed by the work-up described for the synthesis of **3**, gave **5** (98%) as a cream-colored solid, mp 124–127 °C (lit. (6) mp 132–134 °C). The mixture melting point with thermolytic **5** of mp 123–126 °C was 123–126 °C, and the authentic and thermolytic samples were indistinguishable by ir, uv, and nmr spectrometry.

*Dimethyl 3-Oxatricyclo[3.2.2.0^{2,4}]nona-6,8-diene-6,7-dicarboxylate (**16**)*

Compound **16** was prepared essentially as described by Vogel and coworkers (4) but with the following modifications.

Pyridinium tribromide ("pyridinium hydrobromide perbromide") (0.85 g, 2.6 mmol), 1,4-cyclohexadiene (0.213 g, 2.6 mmol), and hexane (10 ml) in a stoppered round bottom flask were magnetically stirred for 4 h (until the orange pyridinium tribromide had been converted to the white pyridinium bromide). Filtration and concentration gave dibromocyclohexene (0.556 g, 90%).

This material (556 mg, 2.30 mmol) and *m*-chloroperbenzoic acid (575 mg of 85% peracid, 2.84 mmol) in chloroform (10 ml) were allowed to stand in a stoppered flask at room temperature for 4 days. The precipitated *m*-chlorobenzoic acid was filtered off and the filtrate washed successively with 4 ml of a saturated sodium bisulfite solution (2×), 4 ml of a saturated sodium bicarbonate solution (2×), and 4 ml of a brine solution (1×). The organic layer was dried and concentrated to afford 1,2-epoxy-4,5-dibromocyclohexane (412 mg, 70%). Sodium metal (0.16 g, 6.9 mmol) was added in small pieces to dry methanol (4 ml). When all the sodium had dissolved, the excess methanol was distilled off to give a thick slurry of methanol – sodium methoxide. Anhydrous ether (4 ml) was added, then a solution of the 1,2-epoxy-4,5-dibromocyclohexane (0.36 g, 1.4 mmol) in anhydrous ether (2 ml). The bright yellow solution was then refluxed 1 h. Work-up of the reaction mixture as outlined in the literature (4) gave oxepin (0.134 g, 70%).

Dimethyl acetylene dicarboxylate (0.96 g, 6.7 mmol) and oxepin (0.63 g, 6.7 mmol) were dissolved in ether (2 ml) and allowed to stand in a stoppered flask at room temperature for 1 week. Concentration and crystallization from ether gave **16** (1.48 g, 93%), mp 55.5–56 °C (lit. (4) mp 56 °C). The nmr spectrum was identical to that previously reported (4).

*Dimethyl 1-Methanoyl-1,3,5-cycloheptatriene-6,7-dicarboxylate (**19**)*

Isomerization of **16** to **19** was effected by column chromatography. A 2.0 cm × 10 cm column containing 20 g of Fisher alumina (neutral, activity I) was washed with 20 ml of trifluoroacetic acid – carbon tetrachloride (1:20), and then with 100 ml of carbon tetrachloride. Compound **16** (50 mg) in carbon tetrachloride was passed through the column, eluting with carbon tetrachloride. After 1 h a faint brown band was observed moving down the column. Preceding this band was another product, $R_f = 0.22$ (tlc with dichloromethane) which was collected. Evaporation of the eluate gave a colourless oil (30 mg, 60%) which was shown by ir, uv, and nmr spectrometry to be identical with the thermolytic sample **19**.

Acknowledgements

We thank the National Research Council of Canada and the Trent Committee on Research for financial support, Professor J. F. King of the University of Western Ontario for arranging to have the high-resolution mass spectra taken, and Mr. John Fulford for the preparation of compound **2**. G.M. acknowledges the award of an Ontario Graduate Fellowship.

1. E. Lewars, G. Morrison, and J. Fulford. Chem. Ind. 488 (1976).
2. (*a*) I. Haller and G. C. Pimental. J. Am. Chem. Soc. **84**, 2855 (1964); R. N. McDonald and P. A. Schwab. J. Am. Chem. Soc. **86**, 4866 (1964); J. K. Stille and D. D. Whitehurt. J. Am. Chem. Soc. **86**, 4871 (1964); A. Padwa, D. Crumrine, R. Hartman, and R. Layton. J. Am. Chem. Soc. **89**, 4435 (1967); (*b*) S. A. Mathu and P. G. Sammes. Chem. Commun. 11 (1972); J. Fenwick, G. Frater, K. Ogi, and O. P. Strausz. J. Am. Chem. Soc. **95**, 124 (1973); (*c*) M. J. S. Dwar and C. A. Ramsden. J. Chem. Soc. Chem. Commun. 688 (1973); O. P. Strausz, R. K. Gosavi, A. S. Denes, and I. G. Csizmadia. J. Am. Chem. Soc. **98**, 4784 (1976).
3. H. Kwart and K. King. Chem. Rev. **68**, 415 (1968).
4. E. Vogel, W. A. Böll, and H. Günther. Tetrahedron Lett. 609 (1965).
5. (*a*) J. F. King, R. A. Marty, P. de Mayo, and D. L. Verdun. J. Am. Chem. Soc. **93**, 6304 (1971); R. Bloch, R. A. Marty, and P. de Mayo. Bull. Soc. Chim. Fr. 2031 (1972); P. de Mayo. Endeavour, **31**, 135 (1972); (*b*) E. Hedaya. J. Am. Chem. Soc. **89**, 4213 (1967); **89**, 4214 (1967); E. Hedaya, D. W. McNeil, P. Schissel, and D. J. McAdoo. J. Am. Chem. Soc. **90**, 5284 (1968); J. F. King, P. de Mayo, and D. J. Verdun. Can. J. Chem. **47**, 4509 (1969); (*c*) J. F. King, P. de Mayo, C. L. McIntosh, K. Piers,

and D. J. H. SMITH. Can. J. Chem. **48**, 3704 (1970); H. HAGEMAN and U. WIERSUM. Chem. Br. 206 (1973).
6. S. J. CRISTOL and R. L. BLY. J. Am. Chem. Soc. **82**, 6155 (1960).
7. R. B. WOODWARD and R. HOFFMANN. The conservation of orbital symmetry. Academic Press, New York. 1970.
8. L. M. STEPHENSON and T. A. GIBSON. J. Am. Chem. Soc. **96**, 5624 (1974).
9. M. J. S. DEWAR. *In* Aromaticity. Chem. Soc. Spec. Publ. No. 21, London. 1967; H. E. ZIMMERMAN. Acc. Chem. Res. **4**, 272 (1971).
10. E. D. BECKER. High resolution nmr. Academic Press, New York. 1969.
11. J. R. GEIGY A.-G. Neth. Appl. Patent No. 6,611,324 (February 1967); Chem. Abstr. **67**, 90,587g (1967).
12. P. S. VENKATARAMANI, N. SAXENA, R. SRINIVASAN, and J. ORS. J. Org. Chem. **41**, 2784 (1976).
13. J. F. KING, R. M. ENANOZA, and E. G. LEWARS. Can. J. Chem. **52**, 2409 (1974).
14. R. DARMS, T. THREFALL, M. PESARO, and A. ESCHENMOSER. Helv. Chim. Acta, **46**, 2893 (1963).
15. E. VOGEL, R. FELDMANN, and H. DÜWEL. Tetrahedron Lett. 1941 (1970).
16. R. M. SILVERSTEIN and G. C. BASSLER. Spectrometric identification of organic compounds. 2nd ed. Wiley, New York. 1967. p. 88.
17. (*a*) A. P. TER BORG, H. KLOOSTERZIEL, and N. VAN MEURS. Proc. Chem. Soc. 359 (1962); Recl. Trav. Chim. **82**, 717 (1963); (*b*) G. BÜCHI and E. M. BURGESS. J. Am. Chem. Soc. **84**, 3104 (1962); E. WETH and S. A. DREIDING. Proc. Chem. Soc. 59 (1964).
18. H. PRINZBACH, M. ARGUËLLES, and E. DRUCKREY. Angew. Chem. Int. Ed. Engl. **5**, 1039 (1966).
19. E. VOGEL, R. SCHUBART, and W. A. BÖLL. Angew. Chem. Int. Ed. Engl. **3**, 510 (1964); Org. Synth. Coll. Vol. 5. 1973. p. 467.
20. R. D. SMITH and H. E. SIMMONS. Org. Synth. **41**, 72 (1961).
21. M. TODA, Y. HIRATA, and Y. SHOSUKE. Chem. Commun. 419 (1969).
22. E. G. LEWARS and G. MORRISON. Can. J. Chem. This issue.

Rearrangement of a barrellene oxide to an isocoumarin under flash thermolysis conditions. An apparent series of sigmatropic shifts

E. G. LEWARS AND G. MORRISON

Department of Chemistry, Trent University, Peterborough, Ont., Canada K9J 7B8

Received September 16, 1976

E. G. LEWARS and G. MORRISON. Can. J. Chem. **55**, 975 (1977).

Flash thermolysis of dimethyl 3-oxatricyclo[3.2.2.0^{2,4}]nona-6,8-diene-6,7-dicarboxylate (the oxide of barrellene-2,3-dicarboxylic acid dimethyl ester) (**2**) at 700 °C gave methyl isocoumarin-7-carboxylate (**3**) as a major component of the thermolysate. The rearrangement is discussed in terms of sigmatropic shifts in cycloheptatrienes and their norcaradiene tautomers.

E. G. LEWARS et G. MORRISON. Can. J. Chem. **55**, 975 (1977).

La thermolyse éclair de l'oxa-3 tricyclo[3.2.2.0^{2,4}]nonadiène-6,8 dicarboxylate-6,7 de diméthyle (l'oxyde du barrèllènedicarboxylate-2,3 de diméthyle) (**2**) à 700 °C conduit à l'isocoumarinecarboxylate-7 de méthyle (**3**) comme produit majeur de la thermolyse. On discute du réarrangement en termes d'un déplacement sigmatropique dans les cycloheptatriènes et leurs tautomères norcaradiènes.

[Traduit par le journal]

Our interest in oxirene (**1**) led us to study the flash thermolysis of the barrellene oxide **2** in the hope of effecting reverse Diels–Alder cleavage to **1** and dimethyl phthalate (1). At temperatures in the range 300–600 °C, the main reaction was rearrangement to cycloheptatriene

1

carboxaldehydes, although the formation of a small amount of ketene, detected by low-temperature infrared spectrometry, could be interpreted as indicating that the desired fragmentation had occurred to a minor extent. Here, we wish to report that flash thermolysis of **2** at 700 °C gave methyl isocoumarin-7-carboxylate (**3**).

When **2** was subjected to flash thermolysis (1) at 700 °C, a complex thermolysate (10 spots on thin layer chromatography) was obtained from which only one pure compound was isolated. This compound, a colorless, microcrystalline solid, was shown by mass spectrometry to have the formula $C_{11}H_8O_4$, corresponding to the loss of methanol from **2**. Its origin and ^{1}H nmr spectrum [δ ($CDCl_3$) 3.90 (s, 3H), 6.40 (d, J = 6 Hz, 1H), 7.20 (d, J = 6 Hz, 1H), 7.32 (d, J = 8 Hz, 1H), 8.15 (d of d, J = 8 and 2 Hz, 1H), 8.72 (d, J = 2 Hz, 1H)] suggested that it might be a benzene-ring-substituted isocoumarin, and its infrared [λ_{max} (KBr) 5.81 μm] and ultraviolet [λ_{max} (MeOH) 225 (ε 24 000), 242 (ε 17 000), 250 (ε 16 000), 285 nm (ε 16 000)] spectra were consistent with this view. The isocoumarin structure received strong support when the compound absorbed one and only one molar equivalent of hydrogen at atmospheric pressure in the presence of palladium–charcoal, giving a dihydro derivative, δ ($CDCl_3$) 3.05 (t, J = 6 Hz, 2H), 3.88 (s, 3H), 4.47 (t, J = 6 Hz, 2H), 7.23 (d, J = 8 Hz, 1H), 8.05 (d of d, J = 8 and 2 Hz, 1H), 8.58 (d, J = 2 Hz, 1H), λ_{max} (KBr) 5.82 μm, λ_{max} (MeOH) 214 (ε 38 000), 236 nm (sh, ε 11 400). The nmr spectra pointed strongly to a 1,2,4-substituted benzene ring, and the low-field position of the isolated (weakly coupled, J = 2 Hz) proton in both compounds indicated that it was located between the carbons bearing carbonyl groups,[1] thus suggesting structure **3** for the thermolysis product, and structure **4** for its dihydro derivative.

That structures **3** and **4** were correct was shown by an unambiguous synthesis of **4** starting with 4-nitrohomophthalic acid **5** (3), the structure of which has been rigorously established (4). Compound **5**, made by treating homophthalic acid with fuming nitric acid, was converted into the carbomethoxy diol **11** by standard

[1] *Cf.* the analogous proton in 3-toluic acid (δ 7.4 or 7.8) and in benzene-1,3-dicarboxylic acid (δ 8.7) (2).

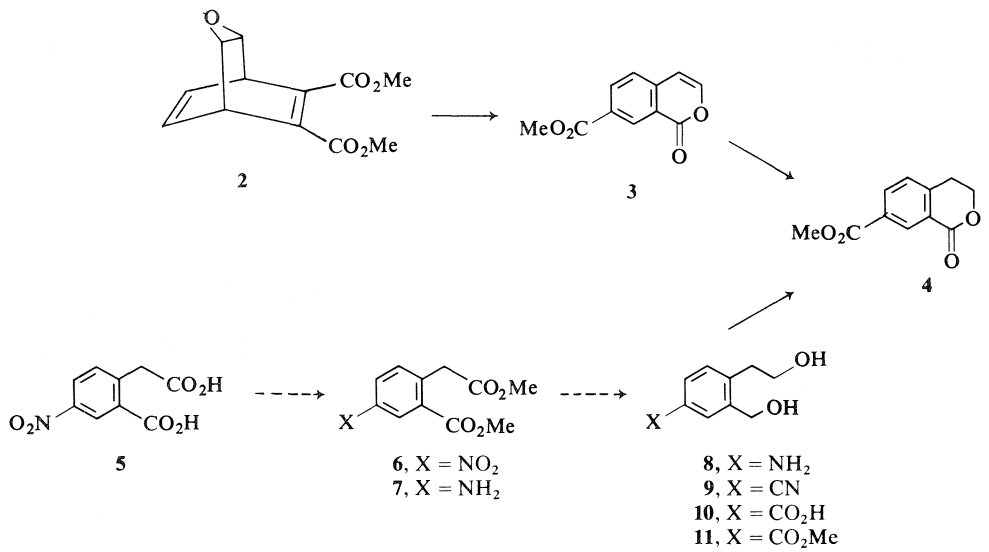

procedures. The oxidation of **11** to the dihydroisocoumarin **4**, effected by activated manganese dioxide (5) in good yield (73%), is noteworthy; although the oxidation of 2-(2-hydroxymethylphenyl)ethanols to dihydroisocoumarins by chromium trioxide has been reported (6), the yield was very low (*ca.* 10%). We believe that this oxidation, as effected by activated manganese dioxide, proceeds by oxidation of the benzylic hydroxyl (7) to an aldehyde group which is attacked by the remaining hydroxyl group; the resulting hemiketal is again a benzylic alcohol, and is oxidized to **4**.

The barrellene oxide **2** has been shown (1) to rearrange at 400 °C to the cycloheptatriene carboxyaldehyde **12**. The observation that **12** gave the isocoumarin **3** under the same conditions as those under which **2** rearranged to **3** enables us to propose a likely mechanism for the genesis of **3**. Two consecutive sigmatropic shifts of hydrogen could convert **12** into **13**, the norcaradiene tautomer of which, **14**, could undergo a 1,5-sigmatropic shift of carbon giving **15**, the norcaradiene tautomer of **16**; another 1,5-hydrogen shift (to give **17**) followed by tautomerization leads to **18**, which could reasonably be expected to isomerize to **19**. The isomerization of cycloheptatrienes by sigmatropic shifts of hydrogen and of carbon is well known (8), and the conversion of cycloheptatriene and its derivatives to toluene or substituted toluenes (**19** is a toluene substituted in the benzene nucleus and on the side chain) is well established (ref. 9, and especially refs. 11–16 therein). The cyclization of **19** to the isocoumarin **3**, possibly by way of the enol form of **19**, appears reasonable.

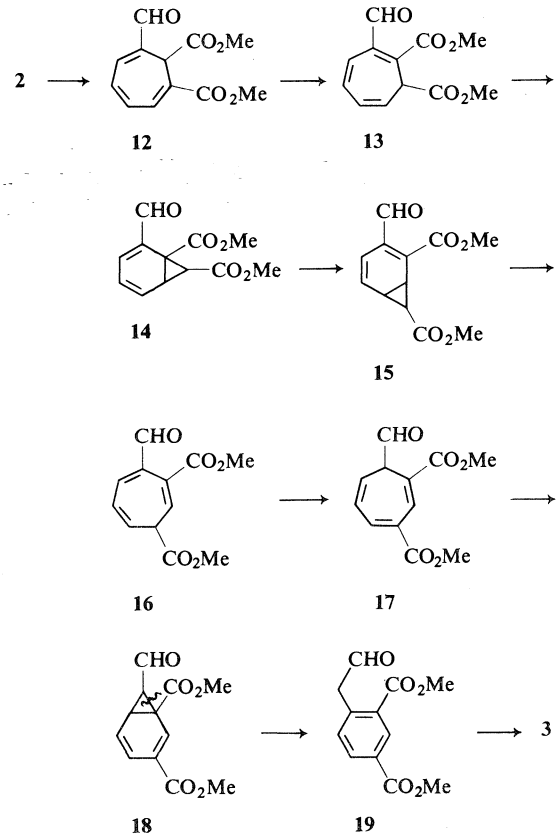

The mechanism of the rearrangement of **2** to **12** can thus be plausibly rationalized (1), and the subsequent transformation[2] of **12** into **3** is interpretable in terms of amply documented processes.

Experimental

General experimental techniques, including a description of thermolysis procedures and the apparatus used, are given in our earlier paper (1). Homophthalic acid, for the preparation of **5**, was purchased from the Aldrich Chemical Company.

Thermolysis of 2 at 700 °C; Methyl Isocoumarin-7-carboxylate (3)

Compound **2** (203 mg) gave 150 mg of thermolysate as a sticky solid. The ^{1}H nmr spectrum of the crude mixture showed it to be composed of *ca.* 25 mol % isocoumarin **3**. Preparative tlc (chloroform, run 3×) gave a band of $R_f = 0.36$ which on extraction gave a white powder, 23 mg. Recrystallization from carbon tetrachloride gave colorless microneedles, 17 mg, mp 178–179 °C; *m/e* 204 (M^+). *Exact Mass* calcd. for $C_{11}H_8O_4$: 204.04170; found: 204.04320.

Methyl Dihydroisocoumarin-7-carboxylate (4)

A thermolytic sample of **3** (12.1 mg, 0.059 mmol) in ethyl acetate (2 ml) was hydrogenated at 1 atm with 5% Pd/charcoal (*ca.* 50 mg). Approximately 1 mol. equiv. of hydrogen was absorbed over 30 min. Filtration and concentration gave 11.9 mg of the dihydro derivative **4** (97%). Recrystallization from carbon tetrachloride gave microcrystals, mp 108–109 °C; *m/e* 206 (M^+). *Exact Mass* calcd. for $C_{11}H_{10}O_4$: 206.05735; found: 206.05774.

Thermolysis of 12

Aldehyde **12** (80 mg) was thermolyzed at 700 °C and the crude thermolyzate was subjected to preparative tlc (chloroform, run 3×). The band of $R_f = 0.36$ was extracted and the material was crystallized from carbon tetrachloride to give 7 mg of a white powder, mp 177–178 °C; the mixture mp with isocoumarin **3**, from epoxide thermolysis, of mp 178–179 °C was 177–179 °C, and the two materials had identical ir, uv, and mass spectra.

Authentic Methyl Isocoumarin-7-carboxylate (4)

Diester 6

4-Nitrohomophthalic acid (**5**) (3) (400 mg, 1.7 mmol) was dissolved in methanol (20 ml) and a slight excess of standardized diazomethane solution was added. Evaporation gave 386 mg (87%) of 4-nitrohomophthalic acid dimethyl ester. Recrystallization from methanol gave white plates, mp 87–88 °C; ir λ_{max} 5.75, 7.39 μm; uv λ_{max} 219, 262 nm; nmr δ 3.67 (3H, s), 388 (3H, s), 4.08 (2H, s), 4.40 (1H, d, $J = 8$ Hz), 4.90 (1H, dd, $J = 8$, 2 Hz), 8.68 (1H, d, $J = 2$ Hz); *m/e* 253 (M^+).

Amino Diester 7

Compound **6** (420 mg, 1.6 mmol) in ethyl acetate (15 ml) was hydrogenated at 1 atm with 5% Pd–charcoal (100 mg). Over 2 h, *ca.* 3 mol. equiv. of hydrogen were absorbed. Filtration and concentration gave 333 mg (90%) of 4-aminohomophthalic acid dimethyl ester, mp 93–98 °C; ir λ_{max} 5.79 μm; uv λ_{max} 221, 248, 320 nm; nmr δ 3.62 (3H, s), 3.75 (3H, s), 3.78 (2H, s), 6.59 (1H, dd, $J = 8$, 2 Hz), 688 (1H, d, $J = 8$ Hz), 7.15 (1H, d, $J = 2$ Hz); *m/e* 223 (M^+). *Exact Mass* calcd. for $C_{11}H_{11}NO_4$: 223.08445; found: 223.08429.

Amino Diol 8

Vitride reducing agent (sodium bis(2-methoxyethoxy)-aluminum hydride in benzene) (6.0 ml of a 70% solution, 22 mmol) in tetrahydrofuran (130 ml, distilled from calcium hydride) was brought to reflux under a nitrogen atmosphere. 4-Aminohomophthalic acid dimethyl ester (1.30 g, 5.0 mmol) was added over 1.5 h. After refluxing an additional 6 h, the mixture was carefully poured into ice water (100 ml) and continuously extracted with dichloromethane overnight. Drying and concentration of the organic layer gave 0.91 g (93%) of an oil which showed mainly one spot on analytical thin layer chromatography (methanol–dichloromethane, 1:20); $R_f = 0.20$, ir λ_{max} (CH_2Cl_2) 6.15 μm; uv λ_{max} 240, 290 nm, shifting to shorter wavelength on addition of acid; nmr (DMSO-d_6) δ 2.63 (2H, t, $J = 6$ Hz), 3.50 (2H, m), 4.40 (2H, s), 6.37 (1H, dd, $J = 8$, 2 Hz), 6.56 (1H, d, $J = 2$ Hz), 6.77 (1H, d, $J = 8$ Hz); *m/e* 167 (M^+). *Exact Mass* calcd. for $C_9H_{13}NO_2$: 167.09407; found: 167.09473.

Cyano Diol 9

Amino diol **8** (826 mg, 4.9 mmol) was dissolved in a solution of concentrated sulfuric acid (5 ml) and water (7 ml). When solution was complete, another 20 ml of water was added and the solution was cooled to 0 °C. To the cooled solution was added sodium nitrite (355 mg, 5.1 mmol), at such a rate as to keep the temperature of the solution below 5 °C. After addition, the solution was stirred at 0 °C for 30 min, and carefully neutralized with sodium carbonate. A solution of cuprous cyanide (0.50 g, 5.6 mmol) and sodium cyanide (0.60 g, 12.2 mmol) in water (20 ml) was added, and stirred at room temperature for 1 h. The solution was then continuously extracted with dichloromethane overnight and the organic layer dried and concentrated to afford 353 mg (40%) of **9** as an oil. Analytical tlc (methanol–dichloromethane, 1:20) showed one spot, $R_f = 0.26$; uv λ_{max} 235 nm, no change on addition of acid, showing no amine was present; *m/e* 177 (M^+).

Carboxy Diol 10

The crude cyano diol (**9**) (353 mg, 2.0 mmol) was refluxed with 10% sodium hydroxide (20 ml) for 2 h. The solution was extracted with ether to remove non-basic impurities and the aqueous layer was acidified with concentrated hydrochloric acid. The acidified solution was continuously extracted with ether overnight and the ether layer dried and evaporated to give 193 mg (49%) of **10**, mp 153–157 °C; ir λ_{max} (KBr) 5.90 μm; uv λ_{max} 238 nm; nmr (DMSO-d_6/$CDCl_3$) δ 2.83 (2H, t, $J = 6$ Hz), 3.65 (2H, t, $J = 6$ Hz), 4.55 (2H, s), 7.15 (1H, d, $J = 8$ Hz), 7.70 (1H, d, $J = 8$ Hz), 7.87 (1H, s); *m/e* 196 (M^+). *Exact Mass* calcd. for $C_{10}H_{12}O_4$: 196.07300; found: 196.07270.

Carbomethoxy Diol 11

An ethereal solution of diazomethane was added to a solution of the acid-diol **10** (90 mg, 0.46 mmol) in

[2]It is of course possible that a pathway exists for the transformation of **2** into **3** without the intermediacy of **12**; we choose, however, to invoke Occam's razor.

methanol (3 ml) until a yellow color persisted. The solution was then evaporated to give 81 mg (84%) of the ester **11** as an oil; ir λ_{max} 5.80 μm; uv λ_{max} 239 nm, nmr δ 2.86 (2H, t, J = 6 Hz), 3.73 (2H, t, J = 6 Hz), 3.80 (3H, s), 4.50 (2H, s), 7.10 (1H, d, J = 6 Hz), 7.70 (1H, dd, J = 6, 2 Hz), 7.77 (1H, d, J = 2 Hz); m/e 210 (M^+).

*Methyl Dihydroisocoumarin-7-carboxylate (**4**)*

The diol **11** (81 mg, 0.39 mmol) was refluxed with activated manganese dioxide (5) (0.80 g) in ether (15 ml) for 12 h. The mixture was filtered, dried, and concentrated to give 58 mg (73%) of a solid that showed one spot (R_f = 0.30) on tlc (dichloromethane). The compound was crystallized from carbon tetrachloride to give microcrystals, mp 106–107 °C. The mixture melting point with the compound (mp 108–109 °C) obtained from hydrogenation of thermolytic methyl isocoumarin-7-carboxylate was 106–108 °C. The two samples were indistinguishable by ir, uv, and nmr spectrometry, and by tlc.

Acknowledgements

We thank the National Research Council of Canada and the Trent Committee on Research for support of this work. G.M. acknowledges the receipt of an Ontario Graduate Fellowship. We thank Professor J. K. King of the University of Western Ontario for arranging to have the high resolution mass spectra taken.

1. E. Lewars and G. Morrison. Can. J. Chem. This issue.
2. Aldrich library of nmr spectra. Vol. 6. Aldrich Chemical Co., Inc., Milwaukee, WI. Spectra 146A and 153C.
3. H. E. Ungnade, D. V. Nightingale, and H. E. French. J. Org. Chem. **10**, 533 (1945).
4. C. K. Ingold and H. A. Piggott. J. Chem. Soc. **123**, 1469 (1923).
5. I. M. Goldman. J. Org. Chem. **34**, 1979 (1969).
6. T. Kobuta, Y. Tomita, and K. Suzuki. Tetrahedron Lett. 223 (1961); Y. Tomita. Nippon Kagaku Zasshi, **82**, 505 (1961); Chem. Abstr. **57**, 16,541 (1962).
7. L. F. Fieser and M. Fieser. Reagents for organic synthesis. Vol. I. Wiley, New York. 1967. p. 637.
8. J. A. Berson. Acc. Chem. Res. **1**, 152 (1968), and references therein. C. W. Spangler. Chem. Rev. **76**, 187 (1976), and references therein.
9. J. A. Berson and M. R. Willcott III. J. Am. Chem. Soc. **88**, 2494 (1966).

An optically active cyclopropene as a mechanistic probe in cyclopropene photochemistry

JAMES A. PINCOCK AND ALEXIOS A. MOUTSOKAPAS
Department of Chemistry, Dalhousie University, Halifax, N.S., Canada B3H 4J3

Received September 27, 1976

JAMES A. PINCOCK and ALEXIOS A. MOUTSOKAPAS. Can. J. Chem. **55**, 979 (1977).

The photochemistry of methyl 1-methyl-2-phenylcyclopropene-3-carboxylate has been examined in both the racemic and optically active forms. In the excited singlet the cyclopropene is converted to 2-methoxy-5-methyl-4-phenylfuran whereas the triplet state dimerizes to a tricyclohexane derivative. Experiments with optically active cyclopropene ester demonstrate that photochemical racemization occurs about 2.5 times as fast as conversion to the furan product indicating that there is an intermediate vinyl carbene on the singlet surface. No racemization is observed in the triplet state.

JAMES A. PINCOCK et ALEXIOS A. MOUTSOKAPAS. Can. J. Chem. **55**, 979 (1977).

On a examiné la photochimie du méthyl-1 phényl-2 cyclopropènecarboxylate-3 de méthyle dans ses formes racémique et optiquement active. Dans l'état singulet excité, le cyclopropène est transformé en méthoxy-2 méthyl-5 phényl-4 furanne alors que l'état triplet se dimérise en un dérivé tricyclohexane. Des expériences avec l'ester de cyclopropène optiquement actif permettent de démontrer que la racémisation photochimique se produit environ 2.5 fois plus rapidement que sa conversion en dérivé de furanne; ces résultats indiquent qu'il y a un intermédiaire vinyle carbène à la surface du singulet. Il n'y a aucune racémisation d'observé à l'état triplet.
[Traduit par le journal]

Introduction

The photochemistry of cyclopropene derivatives has been shown to be remarkably dependent on the multiplicity of the excited state involved. Singlet states react by σ-bond cleavage to give products which are explained in terms of the chemistry of vinyl carbenes; an example is shown in reaction 1 for the direct irradiation of 3,3-dimethyl-1,2-diphenylcyclopropene, **1**, to a mixture of *cis*- and *trans*-1,2-diphenyl-3-methylbutadiene, **3** and **4**, with a quantum yield for the conversion of 0.045 (1). In contrast, triplet states generated by

[1] 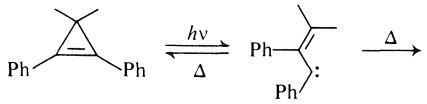

1 **2**

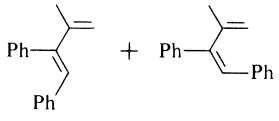

3 **4**

sensitization techniques give high yields of cyclopropene dimers; for example, [2], photolysis of methyl 1,2-diphenylcyclopropene-3-carboxylate, **5**, in the presence of a variety of sensitizers gives the tricyclic dimer **6** with quantum yields as high as 0.8 (2).

[2] 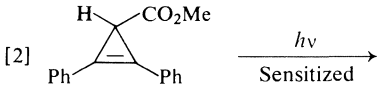

5

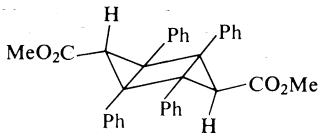

6

The surprising feature of these results is that, despite the extra energy introduced by electronic excitation, in neither case is there efficient ring cleavage to relieve the strain energy (~54 kcal/mol (3) in the ground state) of the cyclopropene ring. The triplet reacts with high quantum yield but retains the three-membered ring; the singlet reacts by ring cleavage but with very low efficiency. This low efficiency for singlet state reactivity has been explained by thermal return of the carbene intermediate (*i.e.* **2** in [1]) to the cyclopropene (1). Such thermal behaviour of vinyl carbenes is well known and is in fact the basis of a synthetic procedure for the preparation of cyclopropenes (1, 4). More quantitative information is available from a study (5) of the thermal racemization of 1,3-diethylcyclopropene where return of the carbene intermediate to starting

material is favoured over rearrangement to products by a factor of 9. Thus the possibility exists that the low efficiency of cyclopropene excited singlet reactions is a result of favourable return and not of inherent unreactivity of the cyclopropene ring.

In order to test this possibility and also to gain a better understanding of vinyl carbene intermediates generated from excited states we have examined the photochemistry of both racemic and optically active methyl 1-methyl-2-phenylcyclopropene-3-carboxylate, **7**, by direct and sensitized irradiations.

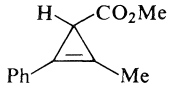

7

Results and Discussion

(1) Synthesis of Methyl 1-Methyl-2-phenylcyclopropene-3-carboxylate

In a series of papers D'yakonov and coworkers (6, 7) have reported that the reaction of ethyl diazoacetate with 1-phenylpropyne gives two products, the cyclopropene ester **8**, and the 2-ethoxyfuran **9**, as in [3]. This carbenoid reaction was said to be catalyzed by copper sulfate with the ratio of **9**/**8** increasing with increased amounts of catalyst and temperature and is quoted in standard texts (8) as an example of copper catalysis affecting the ratio of carbene to 1,3-dipolar addition in ketocarbenes. As an obvious precursor to the methyl ester **7**[1] we have examined this procedure for the preparation of **8** in some detail. By ^{1}H nmr analysis of the crude reaction mixtures immediately after these rapid (~10 min) reactions were completed the ratio of **9**/**8** could be easily determined. Under a variety of conditions no **9** could be detected. However, on distillation of the reaction mixtures (P = 0.3 torr, T = 125 °C)[2] when copper sulfate was present, considerable amounts of an ethoxyfuran presumed to be **9** were observed. The amount was dependent on the temperature and duration of the distillation and in fact heating the reaction for 3 h at 120 °C and then distilling gave only the furan. In contrast the ester **8** could be cleanly distilled when copper sulfate was absent. The conversion of **8** to **9** is therefore not a simple thermal reaction but is metal catalyzed. Since the presence of copper sulfate as a catalyst improved the yield of the addition reaction and only interfered with the isolation procedure, this difficulty is best avoided by saponification of the crude reaction mixture and purification of the cyclopropene as the free acid. The acid was then cleanly converted to **7** by 3-methyl-1-*p*-tolyltriazene (9).

[3] $N_2CH—CO_2Et + PhC{\equiv}CMe \xrightarrow[90\text{–}120\ ^\circ C]{CuSO_4}$

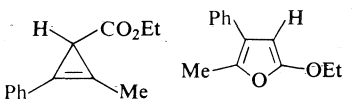

8 **9**

(2) Direct Photolysis of Methyl 1-Methyl-2-phenylcyclopropene-3-carboxylate

The cyclopropene ester **7** was irradiated in acetonitrile solution using a 200 W medium pressure Hanovia lamp and a Vycor filter. Analysis by ^{1}H nmr of the crude photolysate indicated one major component (estimated at ~75% yield based on reacted cyclopropene), 2-methoxy-5-methyl-4-phenylfuran, **10** [4]. Isolation of this furan proved to be extremely difficult since it was sensitive to air oxidation. Pure samples could be obtained by column chromatography but the recoveries were always low. The gross structure of **10** was suggested by several key spectral features; lack of a carbonyl band in the infrared and a vinyl singlet in the ^{1}H nmr at 5.25 δ. This high field signal is characteristic of the 3H in 2-alkoxyfuran derivatives; compare, for example, 5.10 δ for 2-methoxyfuran (10). The remaining question then was the substitution pattern of the phenyl and methyl groups. Advantage was taken of the ready oxidation of alkoxy furans to derivatives of esters of 4-keto-2-butenoic acids (6, 7, 11). There are two possibilities as shown in [5] and [6]. Compound **13** is known (12) and its ^{1}H nmr gives the expected allylic coupling (J = 2 Hz) of a

[4]

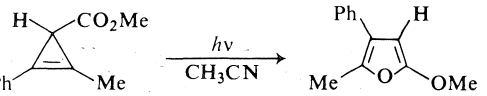

7

[1]The methyl ester was preferred for the photochemical study because the methoxy singlet makes monitoring by nmr easier, particularly when using chiral shift reagents.

[2]Temperatures of the flask in a bulb-to-bulb distillation.

[5] 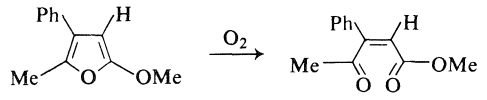

10 11

[6] 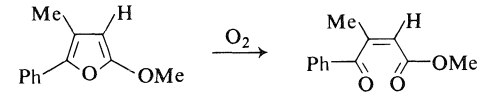

12 13

methyl doublet and a vinyl quartet. As well, the ir bands in the carbonyl region are at 1680 and 1731 cm^{-1}. Oxidation of **10**, however, did not give **13** but rather, as the only product, **11**; ^1H nmr δ: 2.40 (s, 3H), 3.73 (s, 3H), 6.28 (s, 1H) and 7.35–7.40 (s, 5H). Moreover the carbonyl bands in the infrared are at 1728 and 1760 cm^{-1}. The observation of the sharp singlets for the methyl and vinyl protons and the different ir bands rule out **13** as an oxidation product. Therefore the furan from the photolysis of the cyclopropene ester **7** must be the 5-methyl-4-phenyl derivative **10**.

D'yakonov (6, 7) has reported that this is the same furan substitution pattern obtained by addition of ethyl diazoacetate to 1-phenylpropyne; note **9** in [3]. As shown above this furan is actually formed in a catalyzed thermal process by rearrangement of the cyclopropene ester **8**. The ^1H nmr spectrum of **9** showed methyl (2.20 δ) and vinyl (5.10 δ) singlets which seemed sufficiently different from those of **10**, methyl (2.36 δ) and vinyl (5.25 δ), to be surprising when the only change should be from a 2-ethoxy group in **9** to a 2-methoxy group in **10**. Similar differences also occurred in the carbon spectra: for **9**, 86.1 (C-2 of ring) and 14.5 δ (CH_3); for **10**, 90.9 and 12.6 δ. This discrepancy was easily clarified by air oxidation of **9**. Although the ethyl ester corresponding to **11** should have been formed, the product actually obtained was the ethyl ester of **13**; by ^1H nmr the allylic coupling was obvious and the ir bands were at 1728 and 1687 cm^{-1}.[3] Therefore D'yakonov's **9** is actually **14**.

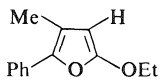

14

[3]D'yakonov does not report an nmr spectrum but does give ir bands of 5.78 (1718 cm^{-1}) and 5.96 μm (1678 cm^{-1}).

Two factors concerning the direct photolysis of **7** are noteworthy. First of all the product obtained, 2-methoxy-5-methyl-4-phenylfuran **10**, is a result of σ-bond cleavage of the cyclopropene ring as expected. This must reflect the reactivity of the excited singlet state since intersystem crossing efficiencies for phenyl substituted cyclopropenes are known to be low (2). Moreover generation of the triplet state by sensitization (see below) does not give the furan product. The second feature of this photolysis is that the product obtained results from cleavage of the cyclopropene single bond which is methyl rather than phenyl substituted. This seems surprising since one might have expected the alternate cleavage to be preferred. At the moment we have no explanation for this behaviour except to note that similar effects seem to be present in the ground state thermal chemistry of cyclopropenes, *i.e.* substitution that should normally stabilize radical centers and make bond cleavage easier raises the activation barrier (5).

(3) Sensitized Photolysis of Methyl 1-Methyl-2-phenylcyclopropene-3-carboxylate, 7

Photolysis of **7** in either acetone as solvent or in acetonitrile with benzophenone gave very clean conversions to a dimeric product **15**, mp 33–34 °C, mass spectrum parent ion, 376. (Note [7].)

[7] 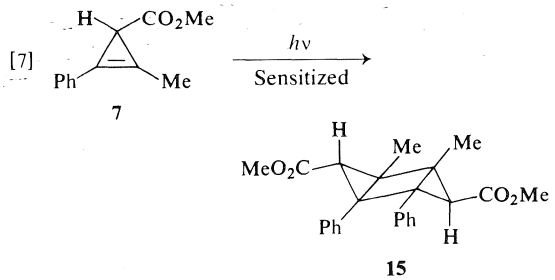

7 15

This conversion could be nicely followed by ^1H nmr spectra taken during photolysis in deuterated acetone. Although there are six possible *anti*-structures for a tricyclic hexane formed from dimerization of **7** the simplicity of the ^1H nmr spectrum (δ 1.63 (s, 3H), 2.85 (s, 1H), 3.41 (s, 3H), 7.20 (m, 5H)) requires that the structure have either both carbomethoxy groups *endo* or both *exo*. The structure of an analogous dimer (**6** in [2]) has been confirmed by X-ray crystallography (13) and both groups are *exo*. Therefore the photoproduct from **7** is either **15** or the isomeric **16**. Evidence for the proposed

structure **15** is available from photolysis of optically active **7** as described below.

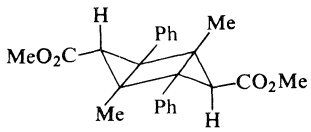

16

(4) Optically Active Methyl 1-Methyl-2-phenylcyclopropene-3-carboxylate; Determination of Optical Purity

The resolution of 1-methyl-2-phenylcyclopropene-3-carboxylic acid by formation of the diastereomeric salts with *l*-ephedrene has been reported previously (14) although without experimental details. The resolved acid was then converted to the methyl ester with 1-methyl-3-*p*-tolyltriazine (9) as for the racemic acid.

Rather than use optical rotation measurements to determine optical purity of the cyclopropene ester **7** we have found that the chiral lanthanide shift reagent, tris(3-heptafluorobutyryl-*d*-camphorato)europium III, [Eu(hfbc)$_3$], is preferable (15). This ^{1}H nmr method has the obvious advantage that, provided resolution of the enantiomeric signals can be attained, the percentage composition can be determined even in the presence of other compounds which would interfere with rotation measurements. Shown in Fig. 1 is a spectrum of optically active **7**, $[\alpha]_D^{25}$ 76.1° (*c* 1.34, CH_3CN) with added Eu(hfbc)$_3$. The enantiomeric signals are obviously well resolved. No detailed studies were made to attempt to maximize the chemical shift differences; rather the shift reagent was added until reliable resolution was obtained (molar ratio of Eu(hfbc)$_3$:**7** of about 0.1). Peak areas were measured by at least five integrator scans and then the values averaged. From the spectrum in Fig. 1 the following values are obtained; —OMe signal, ratio high field/low field 1:3.12; methine H, 1:3.13; —CMe, 3.19:1. Therefore the sample contains 76 ± 1% (+) enantiomer.

(5) Direct Photolysis of Optically Active Methyl 1-Methyl-2-phenylcyclopropene-3-carboxylate, 7

With a convenient method available for monitoring racemization of **7** during photolysis a study for the intervention of vinyl carbene intermediates in the conversion of cyclopropene **7** to the furan **10** is now possible. This is outlined in [8]. If **17** is an intermediate in the photolysis, *i.e.*

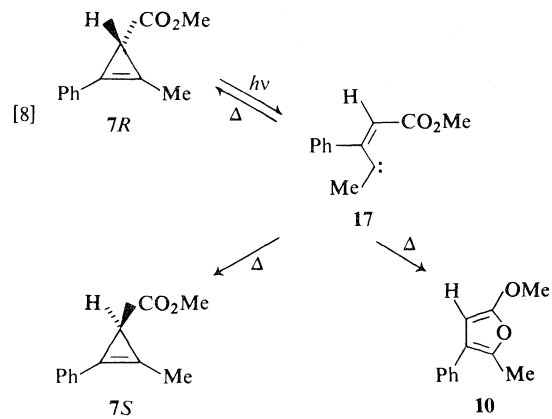

the end point of the excited state chemistry, and if thermal return of **17** to **7***R* (or **7***S*)[4] competes with conversion to the furan **10** then photochemical racemization of the cyclopropene should occur faster than its rate of disappearance. This results because **17** as drawn is flat and return to either of the two enantiomers is equally probable.

The results for the photolysis of optically active **7** are shown in Table 1. The cyclopropene

TABLE 1. Photoracemization of **7** as a function of conversion to **10**

Conversion (%)	Racemization of **7** (%)
10	29 ± 2
16	39 ± 4
25	56 ± 8

was photolyzed and its disappearance monitored by gas chromatography. At the conversions given the cyclopropene was reisolated by thin layer chromatography and the enantiomeric composition determined. Clearly from the results photochemical racemization is occurring about 2.5 times as fast as conversion.

(6) Sensitized Photolysis of Optically Active Methyl 1-Methyl-2-phenylcyclopropene-3-carboxylate, 7

Photolysis of optically active **7** in acetone gave no indication of photochemical racemization. For example, a sample of 65 ± 2% (+)-enriched **7** was photolyzed until 50% conversion to the dimer **15**. Reisolation of **7** and measurement of the enantiomeric composition indicated 67 ± 3%

[4]Note that the absolute configurations of the cyclopropenes are unknown but are unnecessary for this study.

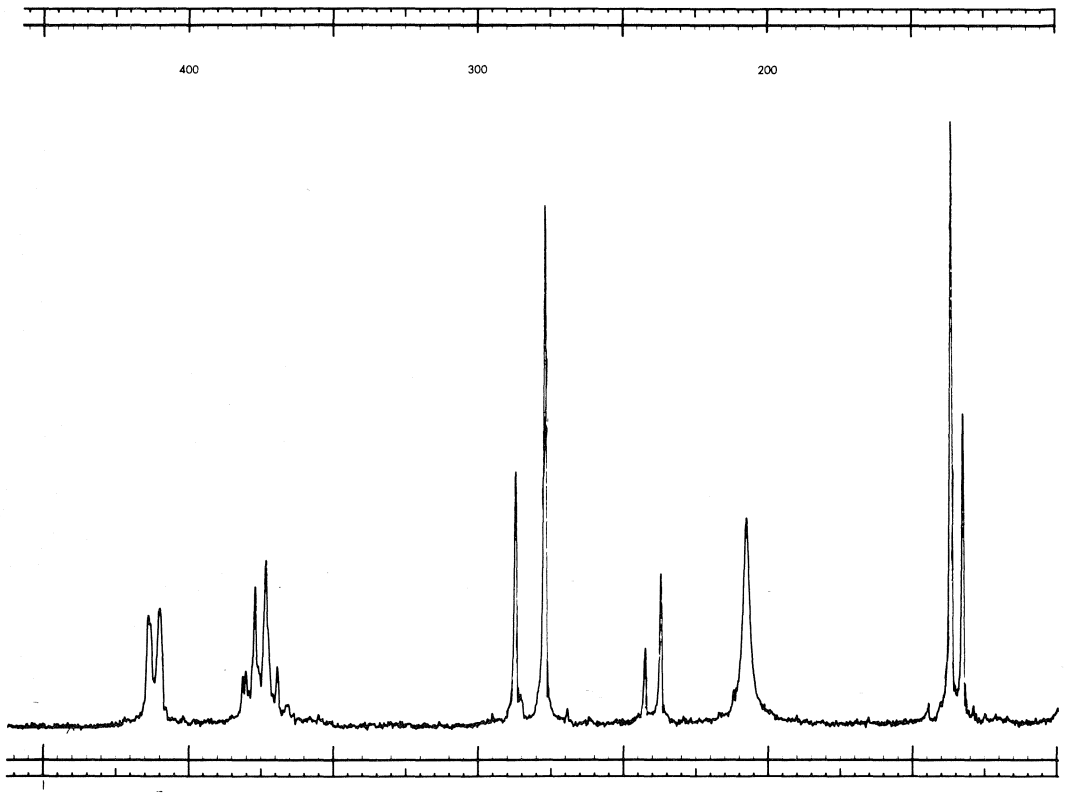

FIG. 1. Nuclear magnetic resonance spectrum of (+)-enriched **7** with $Eu(hfbc)_3$.

(+)-enriched. Similar results were observed at lower conversions. These observations demonstrate that the triplet state does exhibit only π-bond reactivity to form the dimer with no indication of σ-bond cleavage.

Moreover, this result is only consistent with structure **15** as the correct one for this dimeric product. As shown in [9] and [10] the two possible dimers **15** and **16** would be formed by two possible orientations of cyclopropene rings. However dimer **16** can only be formed by reaction of two cyclopropenes of opposite configuration, **7***R* + **7***S*. Therefore each time a dimer of structure **16** was formed a *d*/*l* pair of **7** would have reacted and the residual cyclopropene would have increased in optical purity. On the other hand, formation of **15** only occurs by reaction of cyclopropenes of the same configuration, **7***R* + **7***R* as shown or **7***S* + **7***S*. Since the rate constants for the *R* + *R* and the *S* + *S* reactions will be the same, the rates will only be dependent on the concentrations of *R* and *S*.

[9] 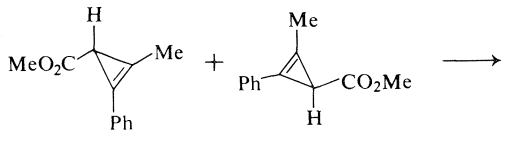

7*R* **7***R*

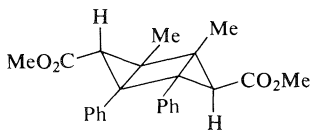

15

[10] 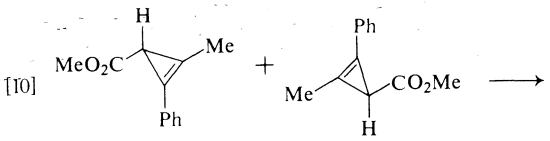

7*R* **7***S*

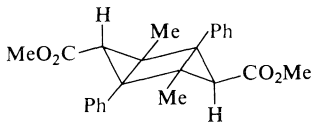

16

Therefore the rates of disappearance of *R* and *S* will be the same as the ratio of their concentrations and the *R*/*S* ratio in the unreacted cyclopropene will remain constant. Since this is the observed behaviour for the photolysis of optically active **7**, the structure of the dimeric product must be **15**.

The triplet state photochemistry of cyclopropene ester **7** is then as shown in [7]. Interestingly enough the dimer obtained probably has worse steric interactions than the alternate possibility assuming that a phenyl–phenyl interaction is worse than a phenyl–methyl one. However, this observation is nicely explained by the suggestion (2) that the primary photochemical product of these triplet state reactions is actually a diradical, *i.e.*, **17**. The formation of **15** then results because **17** allows maximum delocalization of the radical centers in the intermediate.

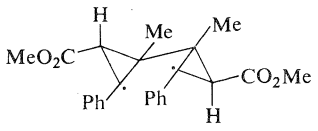

17

(7) General Conclusions on Cyclopropene Photochemistry

The results of this study confirm previous observations on cyclopropene excited state reactivity; singlet states react only by σ-bond cleavage and triplet states by dimerization. The low quantum yield for singlet reactivity (1) is at least in part explained by photochemical racemization of the cyclopropene. At the moment there is not an example where both quantum yield of racemization and reactivity have been measured so the overall efficiency of ring opening is unknown. It would not be surprising if this efficiency were high considering the highly exothermic nature of this process.

The reactivity of triplet cyclopropenes is more puzzling. In a recent publication of *ab initio* calculations of the cyclopropene – vinyl carbene surface (16) the exothermic nature of the triplet cyclopropene to triplet vinyl carbene conversion is clearly shown. Why then does the cyclopropene remain intact long enough to react with another molecule in the ground state? The answer must be that there is a barrier on the cyclopropene – vinyl carbene triplet surface which does not exist on the singlet surface. Preliminary results by MINDO-3 calculations[5] suggest that this indeed may be the correct explanation.

Experimental

1-Methyl-2-phenylcyclopropene-3-carboxylic Acid

A variation of the reported procedure was followed (6, 7). To 23.7 g (0.204 mol) of 1-phenylpropyne and 20 mg (0.126 mmol) of copper sulfate heated to 120 °C in an oil bath was added 13.5 g (0.118 mol) of ethyl diazoacetate (16) over a 15 min period. The reaction mixture was then cooled and added to a solution of 20 g KOH in 360 ml of 95% ethanol. After stirring at room temperature for 48 h 800 ml of water was added and the mixture extracted with 2 × 200 ml ether to recover the unreacted acetylene. The aqueous phase was then acidified with 10% HCl and extracted with 2 × 200 ml ether. The extract was washed with 2 × 200 ml saturated NaCl, dried over $MgSO_4$, and concentrated to give 7.27 g of dark brown solid. This solid was chromatographed on 110 g of silica gel using $CHCl_3$ as eluant. The volume from 200–800 ml contained 6.03 g of crude acid which could be recrystallized to give 4.05 g (0.0232 mol, 20% yield) of pure 1-methyl-2-phenylcyclopropene-3-carboxylic acid; mp 139–140 °C (lit. (6) 137.2–137.9); ^{1}H nmr ($CDCl_3$) δ 2.37 (s, 3H), 2.48 (s, 1H), 7.4–7.6 (m, 5H), 9.8 (br s, 1H).

Methyl 2-Methyl-2-phenylcyclopropene-3-carboxylate

To 0.250 g (1.44 mmol) of the acid in 10 ml of ether was added 0.500 g (3.3 mmol) of 1-methyl-3-(*p*-tolyl)triazene (9) dissolved in 10 ml of ether. The reaction mixture was stirred for 20 h at room temperature. The solution was then washed with 4 × 10 ml of 10% HCl, 15 ml of 10% $NaHCO_3$, and finally with 2 × 15 ml water. The ether solution was dried over $MgSO_4$ and concentrated to give 0.244 g (1.31 mmol, 91%) of the known (17) ester: ^{1}H nmr ($CDCl_3$) δ 2.33 (s, 3H), 2.45 (s, 1H), 4.18 (s, 3H), 7.2–7.3 (s, 5H); ir (film) 1730, 1895 cm^{-1}; uv (CH_3CN) 257 nm (ε 17 700).

Photolysis of Methyl 1-Methyl-2-phenylcyclopropene-3-carboxylate

In a typical experiment 1.00 g of the ester was dissolved in 300 ml of CH_3CN (distilled from P_2O_5) and irradiated for 2.5 h in a nitrogen atmosphere with a 250 W Hanovia medium pressure lamp and a Vycor filter. Evaporation of the solvent gave 1.14 g of material which by nmr analysis contained ~75% of 2-methoxy-5-methyl-4-phenylfuran. This furan could be purified in low yield by column chromatography; 240 mg of the crude photolysate on 13 g of basic alumina eluted with 25% ether in petroleum ether gave 38.1 mg (16% yield based on initial cyclopropene) of pure furan: ^{1}H nmr ($CDCl_3$), δ 2.36 (s, 3H), 3.87 (s, 3H), 5.25 (s, H), 7.3–7.5 (s, 5H); ^{13}C nmr ($CDCl_3$) δ 12.57 (q), 57.82 (q), 80.89 (d); ir (film) 1612 cm^{-1}; ms 188(100), 173(100), 145(26), 131(22), 102(40). Elemental analysis on this compound was not attempted because of its ready oxidation by air.

Air Oxidation of 2-Methoxy-5-methyl-4-phenylfuran

A solution of 30 mg (0.16 mmol) of the furan in 2 ml of $CHCl_3$ was saturated with air for 1 h. Evaporation of the

[5]R. J. Boyd and J. A. Pincock, to be published.

solvent gave a quantitative yield of methyl 4-keto-3-phenyl-2-butenoic acid as a pale yellow oil; ^{1}H nmr ($CDCl_3$) δ 2.43 (s, 3H), 3.78 (s, 3H), 6.17 (s, H), 7.4–7.5 (m, 5H); ir (film) 1728, 1760 cm^{-1}. *Anal.* calcd. for $C_{12}H_{12}O_3$: C 70.57, H 5.92; found: C 70.82, H 5.68.

2-Ethoxy-4-methyl-5-phenylfuran

According to the procedure of D'yakonov (6, 7) 5.8 g (0.050 mol) of 1-phenylpropyne and 29 mg of $CuSO_4$ at 120 °C were reacted with 2.85 g (0.025 mol) of ethyldiazoacetate over 15 min. The ^{1}H nmr of the crude reaction mixture indicated no furan but only ethyl 1-methyl-2-phenylcyclopropene-3-carboxylate, diethyl fumarate, and 1-phenylpropyne. The reaction mixture was then maintained at 120 °C under nitrogen for 3 h, at which point ^{1}H nmr analysis indicated the cyclopropene ester had completely disappeared. Bulb-to-bulb distillation then gave two fractions: fraction 1, 70–90 °C/10 torr, consisting of 1-phenylpropyne and diethyl fumarate; fraction 2, 125–130 °C/0.2 torr, 2-ethoxy-4-methyl-5-phenylfuran, 620 mg (3.2×10^{-3} mol, 13%); ^{1}H nmr ($CDCl_3$) δ 1.38 (t, 3H), 2.20 (s, 3H), 4.05 (q, 2H), 5.10 (s, 1H), 7.0–7.5 (m, 5H); ^{13}C nmr ($CDCl_3$) δ 12.2 (q), 14.5 (q), 66.58 (t), 86.19 (d).

Air Oxidation of 2-Ethoxy-4-methyl-5-phenylfuran (6)

A solution of 60 mg (0.29 mmol) of the furan in 2 ml of $CHCl_3$ was saturated with oxygen for 1 h. Removal of the solvent gave a quantitative yield of ethyl 3-benzoyl-2-butenoate: ^{1}H nmr δ 1.02 (t, J = 7 Hz, 3H), 2.10 (d, J = 2 Hz, 3H), 3.95 (q, J = 7 Hz, 2H), 5.98 (q, J = 2 Hz, 1H), 7.0–7.3 (m, 3H), 7.7–8.0 (m, 2H); ir (film) 1685, 1728 cm^{-1}.

Sensitized Photolysis of Methyl 1-Methyl-2-phenylcyclopropene-3-carboxylate

A solution of 200 mg (1.06 mmol) of the ester in 5 ml of acetone was irradiated for 22 h in a Pyrex container using a 200 W Hanovia medium pressure lamp. After evaporation of the acetone and recrystallization of the residue from benzene there was obtained 102 mg (51%) of the bicyclic dimer: mp 32–34 °C; ^{1}H nmr ($CDCl_3$) δ 1.63 (s, 3H), 2.85 (s, 1H), 3.41 (s, 3H), 7.20 (m, 5H); ir (film) 1745 cm^{-1}; ms 376(3), 344(7), 316(22), 284(100), 258(25), 256(22), 129(20), 115(20), 105(26), 91(25). *Anal.* calcd. for $C_{24}H_{24}O_4$: C 76.56, H 6.43; found: C 76.43, H 6.49.

Resolution of 1-Methyl-2-phenylcyclopropene-3-carboxylic Acid

The resolution of this acid has been described (14) but no experimental details were given. In a typical resolution experiment a mixture of 0.765 g (4.42 mmol) of the acid and 0.730 g (4.42 mmol) of *l*-ephedrene was dissolved in 20 ml of benzene and heated to 50 °C for 10 min. The salt solution was cooled and 70–90 °C petroleum ether was added until a slight cloudiness appeared. The mixture was then left to crystallize. The precipitated salt was crystallized four times in this way to give 0.420 g (28.1% yield). The salt was then dissolved in 30 ml of 2% KOH in 30% methanol–water solution and stirred for 24 h at room temperature. The ephedrene was extracted with ether and then the aqueous layer was acidified to pH 2 with 10% H_2SO_4. The acid was extracted with ether and the ether layer dried over $MgSO_4$ and concentrated *in vacuo* to give 0.168 g (78% based on the salt) of the acid. The acid was transformed to the ester as described above. Measurement of the optical rotation gave $[\alpha]_D^{25}$ +76.1° (c 1.340, CH_3CN). The enantiomeric purity of this sample was measured at 76 ± 1% (+) as shown by the ^{1}H nmr spectrum, Fig. 1, in the presence of Eu(hfbc)$_3$ (15).

Acknowledgements

The financial support of the National Research Council of Canada and the Dalhousie University Faculty of Graduate Studies is gratefully acknowledged.

1. J. A. Pincock, R. Morchat, and D. R. Arnold. J. Am. Chem. Soc. **95**, 7536 (1973).
2. C. D. DeBoer, D. H. Wadsworth, and W. C. Perkin. J. Am. Chem. Soc. **95**, 861 (1973).
3. S. W. Benson. Thermochemical kinetics. Wiley, New York, N.Y. 1968. p. 179.
4. G. L. Closs, L. E. Closs, and W. A. Boll. J. Am. Chem. Soc. **85**, 3796 (1963).
5. E. J. York, W. Dittmar, J. R. Stevenson, and R. G. Bergman. J. Am. Chem. Soc. **95**, 5680 (1973).
6. I. A. D'yakonov and M. I. Komendantov. J. Gen. Chem. USSR (Engl. Transl.) **31**, 3618 (1961).
7. I. A. D'yakonov, M. I. Komendantov, and S. P. Korshunov. J. Gen. Chem. USSR (Eng. Transl.) **32**, 912 (1962).
8. W. Kirmse. Carbene chemistry. Academic Press, New York. 1964. p. 100.
9. E. H. White, A. A. Baum, and D. E. Eitel. Org. Synth. **48**, 102 (1968).
10. C. J. Pouchert and J. R. Campbell. The Aldrich library of NMR spectra. Vol. VIII. Aldrich Chemical Co., Milwaukee, WI. 1974. p. 5A.
11. R. Scarpati, M. L. Graziano, and R. A. Nicolaus. Gazz. Chim. Ital. **97**, 1317 (1967).
12. K. Bowden and M. P. Henry. J. Chem. Soc. B, 156 (1971).
13. M. J. Bennett, J. T. Purdham, S. Takada, and S. Masamune. J. Am. Chem. Soc. **93**, 4063 (1971).
14. I. N. Domnin, I. A. D'yakonov, and M. I. Komendantov. J. Org. Chem. USSR (Engl. Transl.) **3**, 2076 (1967).
15. H. L. Goering, H. N. Eikenberry, G. S. Koermer, and C. J. Lattimer. J. Am. Chem. Soc. **96**, 1493 (1974).
16. J. H. Davis, W. A. Goddard III, and R. G. Bergman. J. Am. Chem. Soc. **98**, 4015 (1976).

The balance between electronic and nuclear energy in conformational change

IMRE G. CSIZMADIA AND GIANNOULA THEODORAKOPOULOS
Department of Chemistry, University of Toronto, Toronto, Ont., Canada M5S 1A1
AND
H. BERNHARD SCHLEGEL, MYUNG-HWAN WHANGBO, AND SAUL WOLFE
Department of Chemistry, Queen's University, Kingston, Ont., Canada K7L 3N6
Received May 26, 1976

IMRE G. CSIZMADIA, GIANNOULA THEODORAKOPOULOS, H. BERNHARD SCHLEGEL, MYUNG-HWAN WHANGBO, and SAUL WOLFE. Can. J. Chem. **55**, 986 (1977).

The relative contributions of nuclear repulsion and electronic attraction to conformational rotational potentials have been analysed for several types of systems. It is shown that decomposition of a computed total energy into these two components provides a diagnostic tool for the evaluation of the reliability of such computations. It is also pointed out that Hartree–Fock theory is sufficient to reproduce experimental stereochemical observations, provided that one is aware of the accuracy needed to compute the molecular electronic wavefunction. This accuracy is predetermined by the nuclear or electronic dominance of the process.

IMRE G. CSIZMADIA, GIANNOULA THEODORAKOPOULOS, H. BERNHARD SCHLEGEL, MYUNG-HWAN WHANGBO et SAUL WOLFE. Can. J. Chem. **55**, 986 (1977).

On a analysé les contributions relatives de la répulsion nucléaire et de l'attraction électronique par rapport au potentiel rotationnel conformationnel de plusieurs types de systèmes. On a montré que la décomposition, dans ces deux composantes, de l'énergie totale calculée fournit un outil diagnostique pour l'évaluation de la certitude de tels calculs. On met aussi en relief que la théorie de Hartree–Fock est suffisante pour reproduire des observations stéréochimiques expérimentales à condition que l'on soit conscient de la précision nécessaire pour calculer les fonctions d'onde électroniques moléculaires. Cette précision est prédéterminée par la dominance nucléaire ou électronique du processus.

[Traduit par le journal]

Introduction

With the advent and availability of computer programmes for the computation of the total energies and stable geometries of molecules, theoretical stereochemistry has entered an extremely productive era (1). Accumulated experience in this field seems to indicate that there are two classes of problems. In the first, it is found that SCF-MO computations performed at almost any level of accuracy afford fairly good agreement with experiment; but in the second, very extensive computations combined with careful geometry optimization are required to yield such agreement.

The classical example of the first type is rotation in ethane (2), and for the second type, the classical examples are rotation in hydrogen peroxide (3) and pyramidal inversion in ammonia (4). Thus, even the simplest semi-empirical computations are able to reproduce the *ca.* 3 kcal/mol barrier of ethane, but to reproduce the *trans* barrier to rotation in hydrogen peroxide (*ca.* 1 kcal/mol), it has been necessary to go almost to the Hartree–Fock limit using *d*-orbitals on oxygen and *p*-orbitals on hydrogen, in conjunction with geometry optimization at each torsional angle (3*a*).

It might be tempting to suggest that the difficulty lies in the relatively low barrier that is being computed. However, the rotational barrier in methanol is also about 1 kcal/mol, and it can be reproduced without great difficulty (5) (*i.e.*, methanol is a member of the first class of molecules). Consequently, it is clear that, for the class of compounds exemplified by H_2O_2, one has to use a much more accurate wavefunction than for the class of compounds exemplified by ethane.

Why it is necessary to approach the Hartree–Fock limit more closely in one case than in another does not appear to have been discussed previously, and the purpose of the present work is to attempt an analysis of this problem. In terms of this analysis it becomes possible, in

principle, to estimate the quality of computation that will be necessary to reproduce a particular observation.

Theory

In the Born–Oppenheimer approximation, the total energy (E_{tot}) of a molecular system is the sum of electronic attraction ($E_{elec} = T + V_{ne} + V_{ee}$, where T, V_{ne}, and V_{ee} are the kinetic energy, electron–nuclear attraction, and electron–electron repulsion terms, respectively), a negative quantity and nuclear repulsion (E_{nucl}), a positive quantity (eq. 1).

$$[1] \qquad E_{tot} = E_{elec} + E_{nucl}$$

The nuclear repulsion component can be computed without difficulty, according to classical electrostatics, from the nuclear charges (Z_I, Z_J, etc.) and their interatomic distances (R_{IJ}) (eq. 2)

$$[2] \qquad E_{nucl} = \sum_{I=1} \sum_{J>I} \frac{Z_I Z_J}{R_{IJ}}$$

In contrast, computation of the electronic component requires solution of the Schröedinger equation through the variation theorem (eq. 3).

$$[3] \qquad E_{elec} = \frac{\langle \psi_{elec} | H_{elec} | \psi_{elec} \rangle}{\langle \psi_{elec} | \psi_{elec} \rangle}$$

Clearly, the effort required to evaluate eq. 2 is insignificant in comparison to what is needed for eq. 3.

It is therefore useful to be aware of the equality shown in eq. 1, because it means (1*a*) that a semi-quantitative understanding of E_{tot} based on experimental observations (*e.g.*, observations of conformational equilibria) can be combined with a computation of E_{nucl} to provide a semi-quantitative understanding of E_{elec} and, in particular, its phase.[1]

Our chemical experience is that molecules have stability with respect to separated atoms. This requires that E_{nucl} and E_{elec} always have opposite phase (see Fig. 1*b*). Were this not the case, our chemical experience would consist either of a collapsing universe (Fig. 1*a*) in which only a single giant atom exists, or a dissociating universe (Fig. 1*c*), in which only separated atoms exist. These alternatives are illustrated schematically for the general case of a diatomic molecule in Fig. 1, and they allow the formulation of a rule:

"*The nuclear and electronic components of a molecular conformational potential curve always have opposite phase*".

We may now note that, in any region of a potential curve corresponding to that cross-section of a conformational hypersurface which describes the conformational change, the total energy is in phase either with the electronic component or with the nuclear component. Employing the example of the stretching potential shown in Fig. 1*b*, it can be seen that at a large internuclear separation ($r_e < r < \infty$) the total energy is in phase with the electronic component (and may be said to be electronic dominant) and, at a shorter bond length ($0 < r < r_e$), the total energy is in phase with the nuclear component (and may be said to be nuclear dominant). This observation permits the formulation of a second rule:

"*In any region of a potential curve, the variation of the total energy of a molecular system during conformational change is in phase either with the nuclear repulsion (nuclear dominant) or with the electronic attraction (electronic dominant)*".

As a consequence of this second rule, we should recognize that the total energy may be in phase with one of these components *throughout* the conformational charge, as in the case of rigid rotation in ethane in which the total

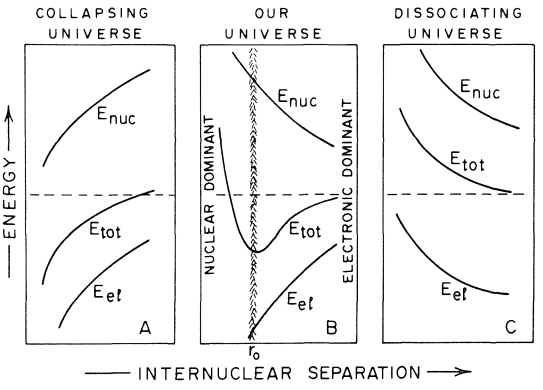

FIG. 1. Alternatives of nuclear and electronic components of the total energy. (*A*) Collapsing universe, where E_{nucl} and E_{elec} are in phase. (*B*) Our universe, where E_{nucl} and E_{elec} are in opposite phase. (*C*) Dissociating universe, where E_{nucl} and E_{elec} are in phase.

[1]By phase we mean the direction of change, *i.e.* the sign of the derivative with respect to a geometrical parameter of the molecule.

energy is in phase with the nuclear repulsion (see below), or there may be a cross-over from electronic dominance to nuclear dominance at some point. This cross-over represents a balance between the attractive electronic forces and the repulsive nuclear forces. These considerations permit the formulation of a third rule:

"*Whenever there is a change from nuclear dominance to electronic dominance in a conformational process, this change will be found at an energy extremum*".

Discussion

The preceding considerations have been derived by inductive reasoning, and we may now consider their application to the problems of torsion and pyramidal inversion.

(a) Rotation (Torsion)

In the general molecule **1**, nuclear repulsion is a maximum and electronic attraction is a minimum in the most crowded conformation **1***a* if we allow rigid rotation only. The opposite is true for the less crowded conformation **1***b*.

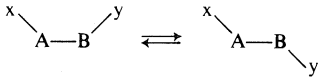

1*a* **1***b*

Whether the actual structure adopted by **1** is closer to **1***a* or to **1***b* will then depend on the relative importance of nuclear repulsion and electronic attraction. For example, $^{-}CH_2OH$ (6) displays two energy minima corresponding to the W and Y conformations **2***a* and **2***b*.

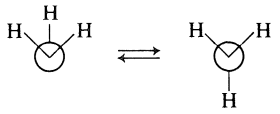

2*a* **2***b*

As shown in Fig. 2, (*i*) the nuclear and electronic components have opposite phase; (*ii*) the total energy is in phase either with the nuclear repulsion or the electronic attraction; (*iii*) the more stable Y conformation is dominated by nuclear repulsion, and the less stable W conformation is dominated by electronic attraction; a balance between the two components is achieved at the transition state which connects the two minima. Thus, the rotational behaviour of $^{-}CH_2OH$ illustrates the operation of all three rules.

A second example is given in Fig. 3 for

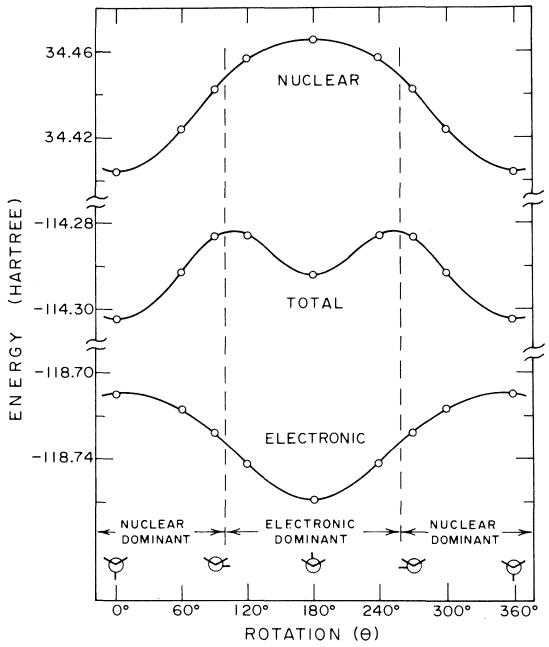

FIG. 2. The variation of total energy as well as its nuclear and electronic components of $^{-}:CH_2—OH$ with the rotational (dihedral) angle along the C—O bond.

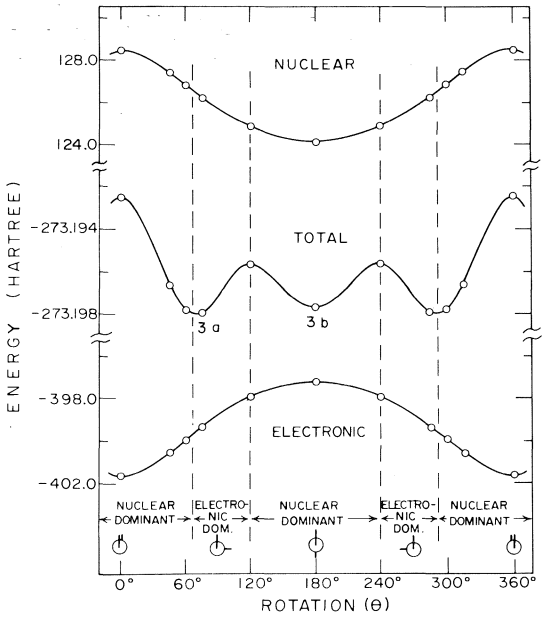

FIG. 3. The variation of total energy as well as its nuclear and electronic components of $FCH_2—CH_2F$ with the rotational (dihedral) angle along the C—C bond.

1,2-difluoroethane as obtained by a minimal (STO-3G (7)) basis set calculation. In this case, the higher minimum (**3***b*) is fully dominated by nuclear repulsion, and the change in dominance between the opposing nuclear and electronic components occurs in the *gauche* conformation (**3***a*).

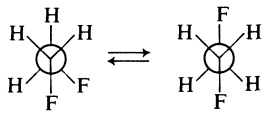

3*a* **3***b*

Consequently, both the position and the energy of the lower minimum (**3***a*) depend upon the accuracy of the computation of the electronic component. The situation is analogous to that of hydrogen peroxide (*cf.* Fig. 4*B*) but different from that of ethane (*cf.* Fig. 5). In the latter case, the total energy is in phase with only one of the components. However, it should be noted that the behavior changes from nuclear dominance to electronic dominance as one changes from rigid rotation (*cf.* Fig. 5*A*) to relaxed rotation (*cf.* Fig. 5*B*) on the conformational hypersurface (8, 9). Because one of the components is always dominant the total barrier is always relatively easy to obtain even though the component barrier heights differ significantly in the two modes shown in Fig. 5 *A* and *B*.

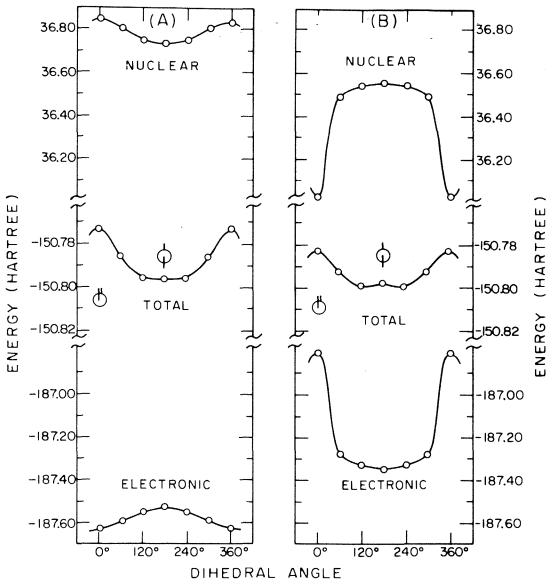

FIG. 4. The variation of nuclear repulsion, total and electronic energy of HOOH with angle of (*A*) rigid rotation and (*B*) relaxed rotation about the O—O bond.

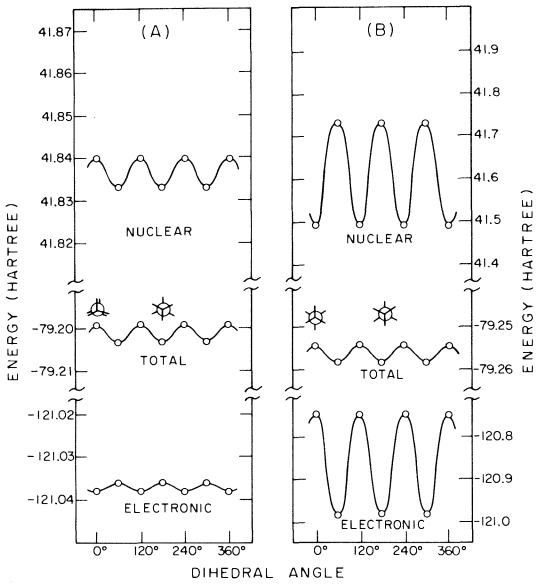

FIG. 5. The variation of nuclear repulsion, total and electronic energy of CH_3CH_3 with angle of (*A*) rigid rotation and (*B*) relaxed rotation about the C—C bond.

The situation is much more complicated in the case of H_2O_2 because there is a change from exclusive nuclear dominance to balanced dominance as one goes from Fig. 4*A* to Fig. 4*B*. Consequently, both geometry optimization (*i.e.*, relaxation) and the inclusion of polarization functions in the basis set are required to obtain the small *trans* barrier (Fig. 4*B*) (10).

(b) Inversion

In a pyramidal molecule **4**,

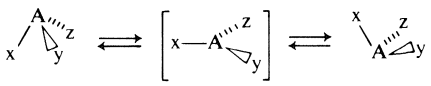

4*a* **4***b* **4***c*

nuclear repulsion is greater in the pyramidal conformations **4***a* and **4***c* than in the planar conformation **4***b* when rigid inversion (*i.e.*, inversion with fixed bond lengths) is considered. For relaxed inversion (*i.e.*, inversion with variable bond lengths) the opposite may be true. However, the barrier to pyramidal inversion is always dominated by one of the components and the minimum is always characterized by a change in dominance. Therefore, the computation of the barrier to inversion will depend upon the accuracy of the electronic component. The pyramidal inversion of NH_3 exemplifies this mode of motion (11).

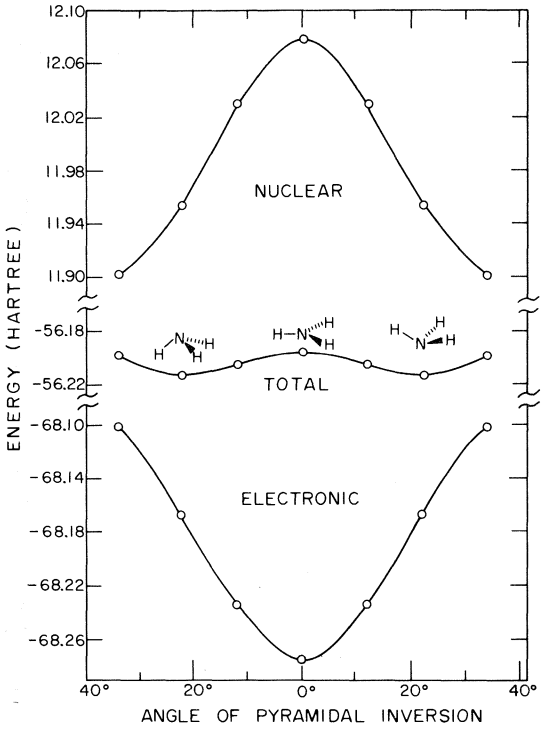

FIG. 6. The variation of nuclear repulsion, total and electronic energy of NH_3 with angle of relaxed pyramidal inversion.

Figure 6 shows relaxed pyramidal inversion of NH_3. The total energy is nuclear dominant between the two minima, including the planar transition state. The minima are characterized by a change from nuclear to electronic dominance. The calculated barrier is thus very sensitive to the accuracy of the calculation.

(c) Rotation–Inversion

The conformational surface $E = E(\theta,\phi)$ associated with two independent modes of motion such as pyramidal inversion (ϕ) and rotation (θ) may be calculated for any molecule (*e.g.*, **5**) that has these internal modes of motion available by virtue of its molecular structure

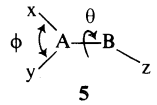

5

Two systems of interest are $^{-}CH_2NO_2$ (**6**) and NH_2PH_2 (**7**)

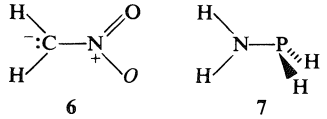

6 **7**

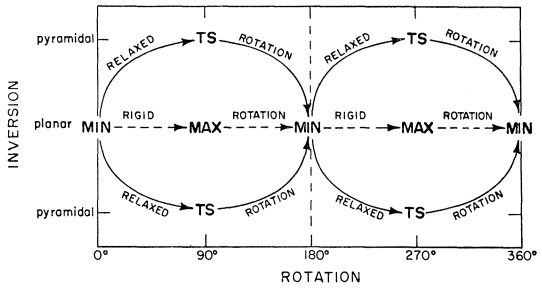

FIG. 7. The topological features of a general rotation–inversion surface.

The rotation–inversion surfaces of **6** (12) and **7** (13) are to be published elsewhere. However, Fig. 7 summarizes the topological features of both surfaces.

Rigid and relaxed rotational cross-sections of the surfaces of **6** and **7** are shown in Figs. 8 and 9 respectively. In the case of **6** the components are well behaved, and there is no change in dominance on going from rigid rotation to relaxed rotation. However, the situation with H_2NPH_2 is different. For the rigid rotation, the nuclear and electronic components are in phase *with each other and with the total energy*! This represents an exception to the three rules proposed above. However, when the geometry is relaxed to permit rotation and nitrogen inversion to occur simultaneously, the apparent

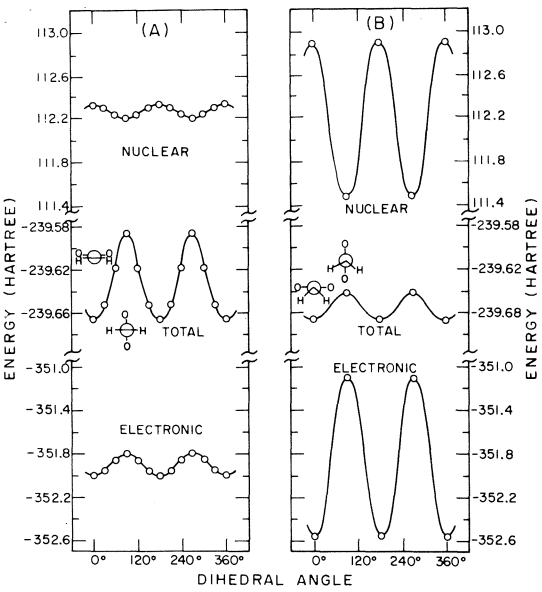

FIG. 8. The variation of nuclear repulsion, total and electronic energy of $^{-}CH_2NO_2$ with angle of (*A*) rigid rotation and (*B*) relaxed rotation about the C—N bond.

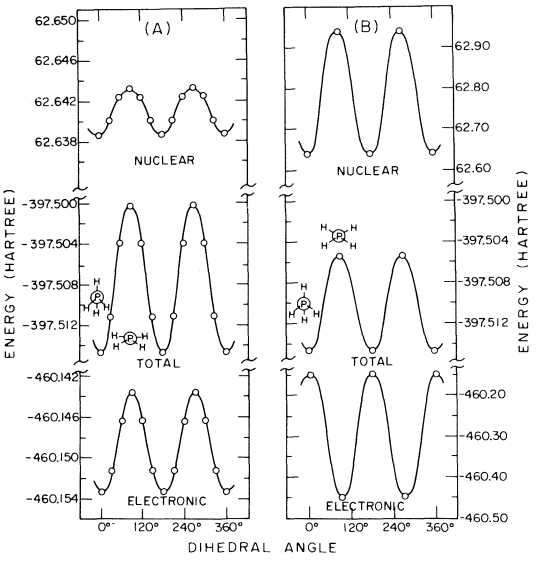

FIG. 9. The variation of nuclear repulsion, total and electronic energy of H_2PNH_2 with angle of (*A*) rigid rotation and (*B*) relaxed rotation about the P—N bond.

discrepancy disappears. This leads to the conclusion that the three rules are strictly valid along the "reaction coordinates". The rules may not be operative along an unstable cross-section, because the system will "roll down" from the side of the surface to the nearest minimum path.

Conclusion

In conclusion, it appears that when there is exclusive dominance of one component (either electronic or nuclear) it is relatively easy to reproduce the experimental stabilities (thermodynamic or kinetic) by theoretical calculations. However, when there is a change in dominance along a given mode of motion the accuracy of the calculations required to reproduce the corresponding experimental stabilities is very high.

Finally, it appears that the anti-parallelism of the phases of the nuclear and electronic components may be valid throughout the hypersurface or for only certain regions of it: the latter type of surface is the more intriguing. In this case, one of the two components may be in phase with the total energy in one region of the hypersurface, and the other component may be in phase with the total energy in another region of the hypersurface, as in the case of rigid and relaxed rotation. On going from one region of the hypersurface to the other, both the nuclear and the electronic components must change phase.

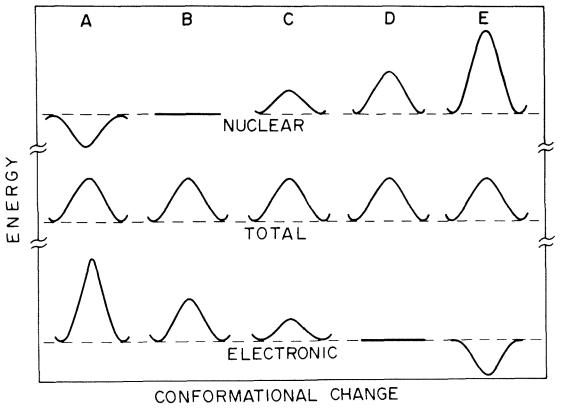

FIG. 10. The variation of the nuclear repulsion, total and electronic energy of a molecule with conformational change showing in five stages (*A* to *E*) the change in the phase of the two components but no change in the phase of the total energy.

Such a simultaneous change would require the existence of an intermediate region in which both components are in phase with the total energy. This is illustrated schematically in Fig. 10. Clearly, the situation is more complicated when there is a change of dominance during the conformational change, as in HO—OH, $^-CH_2$-OH, FCH_2—CH_2F, and NH_3.

1. (*a*) J. P. LOWE. Progr. Phys. Org. Chem. **6**, 1 (1968); (*b*) J. M. LEHN. Top. Curr. Chem. **15**, 311 (1970); (*c*) A. RAUK, L. C. ALLEN, and K. MISLOW. Angew. Chem. Int. Ed. Engl. **9**, 400 (1970); (*d*) S. WOLFE. Acc. Chem. Res. **5**, 102 (1972).
2. (*a*) J. P. LOWE. Science, **179**, 527 (1973); (*b*) J. P. LOWE. J. Am. Chem. Soc. **96**, 3759 (1974).
3. (*a*) A. VEILLARD. Chem. Phys. Lett. **4**, 51 (1969); (*b*) R. B. DAVIDSON and L. C. ALLEN. J. Chem. Phys. **55**, 519 (1971).
4. (*a*) A. RAUK, L. C. ALLEN, and E. CLEMENTI. J. Chem. Phys. **52**, 4133 (1970); (*b*) R. M. STEVENS. J. Chem. Phys. **55**, 1725 (1971); (*c*) R. E. KARI and I. G. CSIZMADIA. J. Chem. Phys. **56**, 4337 (1972).
5. L. M. TEL, S. WOLFE, and I. G. CSIZMADIA. J. Chem. Phys. **59**, 4047 (1973).
6. S. WOLFE, L. M. TEL, and I. G. CSIZMADIA. Can. J. Chem. **51**, 2423 (1973).
7. L. RADOM, W. A. LATHAN, W. J. HEHRE, and J. A. POPLE. J. Am. Chem. Soc. **95**, 693 (1973).
8. E. CLEMENTI and H. POPKIE. J. Chem. Phys. **57**, 4870 (1972).
9. J. P. COLPA, H. B. SCHLEGEL, and S. WOLFE. Can. J. Chem. In press.
10. A. VEILLARD. Theoret. Chim. Acta, **18**, 21 (1970).
11. R. E. KARI and I. G. CSIZMADIA. J. Chem. Phys. **56**, 4337 (1972).
12. P. G. MEZEY, A. J. KRESGE, and I. G. CSIZMADIA. Can. J. Chem. **54**, 2526 (1976).
13. A. H. COWLEY, I. G. CSIZMADIA, M. W. TAYLOR, M. H. WHANGBO, and S. WOLFE. To be published.

Density of states and the steepest descent method: a non-iterative procedure

ANDREW W. YAU AND HUW O. PRITCHARD

Centre for Research in Experimental Space Science, York University, Downsview, Ont., Canada M3J 1P3

Received September 13, 1976

ANDREW W. YAU and HUW O. PRITCHARD. Can. J. Chem. **55**, 992 (1977).

A non-iterative approximation to the method of steepest descent is given for the evaluation of state density in a molecular system. Test calculations on 'large' and 'small' model molecules consisting of harmonic oscillators and rigid rotors show excellent agreement with the 'exact' first-order steepest-descent solutions, but are almost an order of magnitude faster in computing times.

ANDREW W. YAU et HUW O. PRITCHARD. Can. J. Chem. **55**, 992 (1977).

On présente une approximation non-itérative pour la méthode de descente la plus rapide pour l'évaluation de la densité d'états d'un système moléculaire. Des essais de calcul sur des molécules modèles "grande" et "petite" consistant d'oscillateurs harmoniques et de rotors rigides montrent un accord excellent avec les solutions "exactes" de descente la plus rapide du premier ordre, mais sont presque un ordre de grandeur plus rapide en temps de calcul.

[Traduit par le journal]

The density of states $N(E)$ of a model molecule at energy E is an important quantity in statistical rate theories (1, 2). Several approximate methods of calculation have been proposed in recent years, and extensive comparisons between them have been made by Forst and Prášil (3). Among various 'quantal' methods, the method of steepest descent (3–5) proves most attractive since it yields excellent approximations to the exact count, whilst requiring less computation than the method using Cauchy's residue theorem (6, 7).

The method of solution of the (first-order) steepest-descent approximation (4) has been derived independently by Forst and Prášil (3) and by Hoare and Ruijgrok (5): $N(E)$, formally the inverse Laplace Transform of the partition function, is related analytically to the saddle point of the integrand of the inversion integral; in this procedure, several iterations (10 to 15 for the first energy and typically 5 thereafter) are required to determine the saddle point. In the present paper, we report an alternative procedure which does not require such an accurate determination of the saddle point: a sufficiently accurate value for the saddle point can be constructed without iteration, with a consequent saving in computing time of a factor of between 5 and 10 in the calculation of $N(E)$. Since in unimolecular rate calculations $N(E)$ is required at some hundreds of values of the energy, the time saving can become appreciable.

The density of states $N_{vr}(E)$ for a system with v independent vibrators and r free rotors[1] is formally the inverse Laplace Transform of the partition function $Z(\beta)$ (3–5), *i.e.*

$$[1] \quad N_{vr}(E) = \mathscr{L}^{-1}\{Z(\beta)\} = (2\pi i)^{-1} \times \int_{c-i\infty}^{c+i\infty} Z(\beta) \exp(\beta E)\, d\beta \equiv I$$

where $\beta = 1/kT$ is the transform parameter; the sum of states $G_{vr}(E)$ is readily related to $N_{v,r+2}(E)$ (1).

To evaluate I, one defines

$$[2] \quad \phi(\beta) = \ln [Z(\beta)] + \beta E$$

and the first-order steepest-descent method gives (3)

$$[3] \quad I \simeq \exp [\phi(\beta^*)][2\pi\phi''(\beta^*)]^{-1/2}$$

where β^* is the *saddle point*. Since

$$[4] \quad \phi'(\beta^*) = 0$$

$$[4a] \quad \left.\frac{-\partial \ln Z(\beta)}{\partial \beta}\right|_{\beta^*} = E$$

identifying β^* as the (inverse) temperature at which the average energy of the system is E (8). In the Forst–Prášil formulation (3), eq. 4 is transformed to an algebraic equation via $\theta = \exp(-\beta)$. The transformation, although mathematically convenient, makes subsequent

[1]We follow the definition of Forst and Prášil (1, 3): a two-dimensional rotor is counted as two one-dimensional rotors.

computations more difficult. This is because, whereas β^* is between 0 and 10^{-3}, θ^* is between 0.999 and unity; thus, whilst a precision of 10^{-4} suffices for β^*, a precision of 10^{-10} is needed for θ^* (3). And it is precisely this less stringent requirement on the precision in β^*, together with the thermodynamic relation [4*a*], that permits a 'one-shot' approximation which yields accurate $N_{vr}(E)$. Note that using eq. 4*a*, one obtains

$$[5]\quad I \simeq Z(\beta^*)\exp(\beta^* E)\left[-2\pi\left.\frac{\partial E(\beta)}{\partial\beta}\right|_{\beta^*}\right]^{-1/2}$$

The 'one-shot' approximation is achieved by relating β^* explicitly to β_0, a first approximation, via the Taylor expansion of E, using [4*a*], *viz.*

$$[6a]\quad E(\beta^*) = E(\beta_0) + \Delta\beta\frac{\partial E}{\partial\beta} + \tfrac{1}{2}(\Delta\beta)^2\frac{\partial^2 E}{\partial\beta^2} + O[(\Delta\beta)^3]$$

$$[6b]\quad = \frac{-\partial \ln Z}{\partial\beta} - \Delta\beta\frac{\partial^2 \ln Z}{\partial\beta^2} - \tfrac{1}{2}(\Delta\beta)^2\frac{\partial^3 \ln Z}{\partial\beta^3} - O[(\Delta\beta)^3]$$

where $\Delta\beta = \beta^* - \beta_0$ and all derivatives are evaluated at β_0. Now substituting the first-order approximation

$$[7]\quad \Delta\beta \simeq \Delta E\left(\frac{\partial E}{\partial\beta}\right)^{-1}$$

where $\Delta E = E(\beta^*) - E(\beta_0)$, back into the $(\Delta\beta)^2$ term of eq. 6*a*, one obtains

$$[8]\quad \beta^* \simeq \beta_0 + \Delta E\left(\frac{\partial E}{\partial\beta}\right)^{-1} \times\left[1 - \tfrac{1}{2}\Delta E\left(\frac{\partial E}{\partial\beta}\right)^{-2}\left(\frac{\partial^2 E}{\partial\beta^2}\right)\right]$$

$$[8a]\quad \equiv \beta_0 - \Delta E\left(\frac{\partial^2 \ln Z}{\partial\beta^2}\right)^{-1} \times\left[1 + \tfrac{1}{2}\Delta E\left(\frac{\partial^2 \ln Z}{\partial\beta^2}\right)^{-2}\left(\frac{\partial^3 \ln Z}{\partial\beta^3}\right)\right]$$

It might be thought that values of I thus computed might be grossly in error since [8] is only a second-order approximation to β^*, and the truncation error in β^* would be magnified by the exponential in eq. 5. However, since $\phi'(\beta^*) = 0$, a simple error analysis gives

$$[9]\quad \delta[\exp(\phi)] \simeq \exp(\phi)\phi'\delta\beta + O(\delta\beta)^2 \simeq O(\delta\beta)^2$$

which is necessarily small *near* β^*. This insensitivity arises because $\exp(\beta E)$ increases with β whereas $Z(\beta)$ decreases. In test calculations, I computed using [5] and [8] agrees with the exact steepest-descent solution to better than 1% even when β_0 differs from β^* by as much as 20%, except for very large r at low E (since then $Z(\beta) \propto \beta^{-r/2}$). Thus, the ultimate performance of this approximation hinges upon the initial choice of β_0. In practice, however, where $N_{vr}(E)$ is computed at hundreds of energies, typically only 50–100 cm^{-1} apart, β^* for two neighbouring energies are not very different. Thus, except for the first cycle, we may take β_0 to be the β^* value corresponding to the preceding energy, *fully exploiting the fact that in* [8], β_0, ΔE *and* $(\partial E/\partial\beta)|_{\beta_0}$ *are all known quantities*: β^* is readily determined by explicit evaluation of $(\partial^2 E/\partial\beta^2)|_{\beta_0}$; no iteration is needed. This leaves only the choice of the initial value of β_0 at the starting energy, and for r rigid rotors and n groups of harmonic oscillators of degeneracies g_i and frequencies ν_i ($\nu_1 < \nu_2 < \ldots < \nu_n$ and $\sum_i^n g_i = v$), the following empirical relation is convenient[2]

$$[10]\quad \beta_0 = \frac{r}{2E} + \frac{m}{S_m}\ln\left(1 + \frac{S_m}{E}\right)$$

where

$$S_m = \sum_{i=1}^{m} g_i\nu_i$$

with

$$m = 1 \quad \text{if} \quad g_1\nu_1 \geqslant E$$

or

$$m = n \quad \text{if} \quad S_n \leqslant E$$

and

$$S_m \leqslant E < S_{m+1}$$

otherwise.

To test the performance of the method, we have computed $N_{vr}(E)$ for two model molecules for which both exact direct counts and exact steepest-descent solutions are available (3): they are model *A*, representing a typical 'small' molecule and model *B* representing a typical 'large' molecule, both with varying numbers of rotors. Tables 1 and 2 compare these previous calculations with those using eqs. 10, 8, and 5;

[2]Because of the insensitivity of I to β_0 (see text above), any empirical relation which gives a good approximation to β^* will suffice: the choice of [10] is based on the realisation that β_0 is exactly β^* for a system of r rotors or v degenerate oscillators.

TABLE 1. Reduced density $N_{vr}'(E)$ for model A*

r	E (cm^{-1})	Exact count (ref. 3)	Steepest descent: Exact (ref. 3)	Steepest descent: This work
2	2 000	5	5.41	5.42
	5 000	35	37.70	37.72
	10 000	291	298.0	298.2
	20 000	3730	3801	3800
4	2 000	4624	4703	4717
	5 000	5.500×10^4	5.725×10^4	5.739×10^4
	10 000	7.102×10^5	7.266×10^5	7.279×10^5
	20 000	1.557×10^7	1.582×10^7	1.583×10^7

*The frequency pattern is (3): 880, 1296, 1440, 3774, 3788 cm^{-1}.

TABLE 2. Reduced density $N_{vr}'(E)$ for model B*

r	E (cm^{-1})	Exact count (ref. 3)	Steepest descent: Exact (ref. 3)	Steepest descent: This work
2	2 000	2.0×10^1	1.616×10^1	1.612×10^1
	5 000	6.2×10^2	5.747×10^2	5.750×10^2
	10 000	3.677×10^4	3.729×10^4	3.722×10^4
	20 000	1.052×10^7	1.066×10^7	1.067×10^7
4	2 000	8.753×10^3	9.576×10^3	9.598×10^3
	5 000	5.009×10^5	5.180×10^5	5.182×10^5
	10 000	4.783×10^7	4.869×10^7	4.867×10^7
	20 000	2.124×10^{10}	2.145×10^{10}	2.147×10^{10}
12	2 000	3.052×10^{14}	3.144×10^{14}	3.252×10^{14}
	5 000	1.383×10^{17}	1.409×10^{17}	1.445×10^{17}
	10 000	6.815×10^{19}	6.917×10^{19}	6.930×10^{19}
	20 000	1.855×10^{23}	1.873×10^{23}	1.879×10^{23}

*The frequency pattern is (3): 983(4), 1415(4), 2000(1), 3034(6) cm^{-1}.

following Forst and Prášil (3), the tabulated quantities are *reduced* state densities, *i.e.*

$$[11] \qquad N_{vr}'(E) = N_{vr}(E)/Q_r'$$

where Q_r' is the classical partition function for r rotors with the factor $(kT)^{r/2}$ deleted. Note that in practice, one would not use eq. 10 to estimate β_0 at each value of the energy, as we have done in this test, but one would use the value of β^* calculated at the preceding value of the energy; this will be a better approximation than [10], so that the method will actually perform better than is shown in Tables 1 and 2 in any practical application.

We conclude by noting that since the desired accuracy of $N_{vr}(E)$ in unimolecular rate calculations is of the order of a few percent, this method should prove efficient and useful in the entire range where the standard steepest-descent method is applicable: at low energy, direct counts, for which efficient algorithms exist (9, 10), may be used. We note also that the accuracy of the approximation improves as E increases, making it attractive for calculations in the very high energy range, such as are needed in mass-spectral applications.[3] Finally, generalisation to more

[3]An annotated FORTRAN program listing (including test cases and specimen output) is available upon request, at a nominal charge, from The Depository of Unpublished Data, CISTI, National Research Council of Canada, Ottawa, Canada K1A 0S2.

realistic systems, *e.g.* Morse oscillators, is straightforward.

Acknowledgment

This research was supported by the National Research Council of Canada.

1. W. FORST. Theory of unimolecular reactions. Academic Press, New York. 1973. p. 182; W. FORST. Chem. Rev. **71**, 339 (1971).
2. P. J. ROBINSON and K. A. HOLBROOK. Unimolecular reactions. John Wiley, London. 1972. p. 109.
3. W. FORST and Z. PRÁŠIL. J. Chem. Phys. **51**, 3006 (1969).
4. R. KUBO. Statistical mechanics. North-Holland, Amsterdam. 1971. p. 102.
5. M. R. HOARE and TH. W. RUIJGROK. J. Chem. Phys. **52**, 113 (1970).
6. P. C. HAARHOFF. Mol. Phys. **6**, 337 (1963); **7**, 101 (1963).
7. W. FORST, Z. PRÁŠIL, and P. ST. LAURENT. J. Chem. Phys. **46**, 3736 (1967); **48**, 1431 (1968).
8. F. REIF. Fundamentals of statistical and thermal physics. McGraw Hill, New York. 1965. p. 213.
9. T. BEYER and D. F. SWINEHART. Comm. A.C.M. **16**, 379 (1973).
10. S. E. STEIN and B. S. RABINOVITCH. J. Chem. Phys. **58**, 2438 (1973).

Ring formation via β-keto ester dianions

PHAIK-ENG SUM AND LARRY WEILER[1]

Department of Chemistry, University of British Columbia, Vancouver, B.C., Canada V6T 1W5

Received October 4, 1976

PHAIK-ENG SUM and LARRY WEILER. Can. J. Chem. **55**, 996 (1977).

The reaction of α,ω-dihalides with the dianion of methyl acetoacetate gives a mixture of mono- and bisalkylated products. The monoalkylated products can be cyclized via the monoanion to cyclic β-keto esters with a seven- or eight-membered ring. Alternatively these monoalkylated products can be cyclized via the dianion to γ-cyclopentyl- or γ-cyclohexyl-β-keto esters.

PHAIK-ENG SUM et LARRY WEILER. Can. J. Chem. **55**, 996 (1977).

La réaction de dérivés dihalogénés α,ω avec le dianion de l'acétoacétate de méthyle conduit à un mélange de produits mono- et bisalkylés. Les produits monoalkylés peuvent être cyclisés, par l'intermédiaire du monoanion, en esters β cétoniques cycliques possédant un cycle à sept ou huit membres. D'une manière alternative, ces produits monoalkylés peuvent être cyclisés, par l'intermédiaire du dianion, en esters β-céto γ-cyclopentyl ou γ-cyclohexyl.

[Traduit par le journal]

Previously, cyclic β-keto esters were prepared by two different routes. The first route involves carboxylation of the corresponding cyclic ketone with diethyl carbonate and base (1). Alternatively, they have been prepared by the route shown in reaction 1 (2–4). In this case, the ketone is first converted into the corresponding enamine and this is treated with methyl propiolate to yield the enamine **1** in which two carbons have been inserted into the original ring. Hydrolysis of **1** and reduction yields the cyclic β-keto ester with two more carbons than the starting

[1]

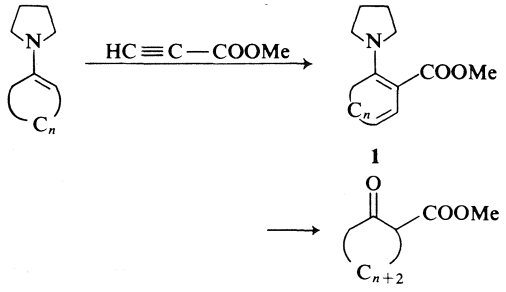

cyclic ketone. Neither of these routes offers any regioselective control over the position of carboxylation, except in the case of an α-alkylated starting ketone. We would like to report a new synthesis of cyclic β-keto esters.

On treating the dianion of methyl acetoacetate (**2**) (5) with 1 equiv. of an α,ω-dihaloalkane, a mixture of products containing approximately equal amounts of the monohalo β-keto ester **3** and the bis β-keto ester **4** is

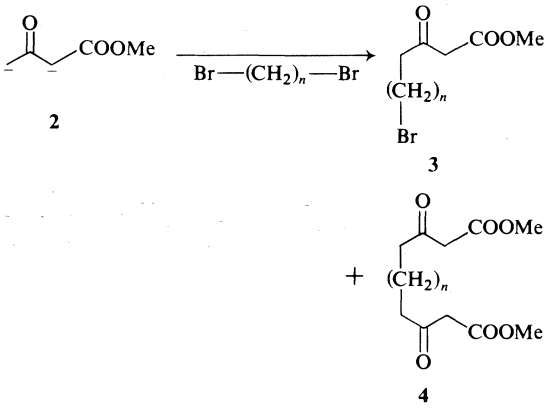

obtained (see ref. 5 also). Except in the case of $n = 3$ (5), no cyclic β-keto ester could be detected in these reactions. Even if the purified monohalo compound **3** ($n = 4$, 5, or 10) was allowed to reflux with 1 equiv. of sodium hydride in tetrahydrofuran (THF) for several hours, no sign of C-alkylation at the α-carbon was observed. This correlates with the previously observed lack of reactivity of the α-carbanion of β-keto esters in THF (refs. 5–7 and references therein) and the fact that no dialkylation was observed in this alkylation or in the original dianion alkylations (5). However, treating the monohalo compounds **3** ($n = 4$ or 5) with 1 equiv. of sodium methoxide in refluxing methanol lead to cyclization at the α-carbon to

[1]Author to whom correspondence may be addressed.

yield the corresponding cyclic β-keto esters in good yield. In addition, we have found that the crude mixture of **3** and **4** could also be subjected to these cyclization conditions to produce the cyclic β-keto esters **5** (n = 4 or 5) in reasonable yield. These cyclic β-keto esters could be

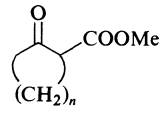

5

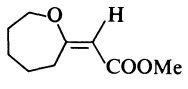

6

readily separated from the bisalkylated product **4** and hence this provides a simple two-step synthesis of **5** from acyclic precursors.

We were intrigued by the lack of cyclization of the monoanion of **3** in THF and investigated this further for n = 4. Cyclization of **3** (n = 4) in THF could eventually be induced by treating the bromo compound **3** with sodium hydride in a mixture of THF and hexamethylphosphoramide (HMP). But the cyclization proceeded exclusively via O-alkylation to yield **6**. This is consistent with the observed intermolecular O-alkylation of β-keto esters in dipolar aprotic solvents (8). The O-alkylation product appeared to be exclusively the *E* isomer shown. This was determined by comparing the nmr spectra of **6** with the corresponding *E,Z* isomers of the cyclic furylidene **7** (9).[2] The formation of **6** probably

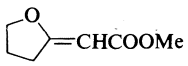

7

involves cyclization of the ω-shaped conformation (10) of the monoanion from **3**. This is expected to be the most stable conformation, in which dipole–dipole repulsions are minimized, of the *free* monoanion formed in HMP (11).

We have also found that the dianion **2** from methyl acetoacetate reacts with *cis*-1,4-dichloro-2-butene to yield the mono-alkylated product **8** and the bis β-keto ester **9** in approximately equal amounts. The geometry about the double bond of both products is thought to remain *cis*. In the case of **8**, the nmr spectrum of the olefinic protons shows a 12 Hz coupling which is consistent with a *cis* geometry. The ir spectra of **8** and **9** are consistent with the proposed *cis* geometry. Cyclization of the monochloro product **8** with sodium methoxide in methanol gave the seven-membered ring compound **10** as the

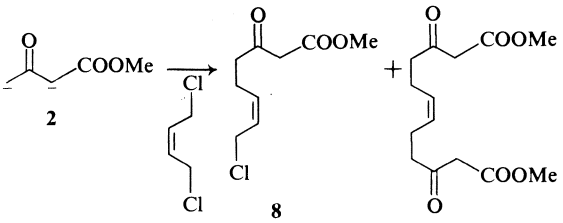

2 **8** **9**

only detectable product in mediocre yield. The fact that only **10** was observed was interesting because one might expect formation of the five-membered ring product **11** as well.[3] An

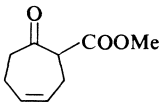

10

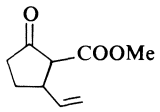

11

examination of molecular models of the carbanion from **8** indicates that the transition state to the seven-membered ring is quite favourable. The presence of the four sp^2-hybridized ring carbons in the transition state leading to **10** no doubt reflects the ease of the formation of the seven-membered ring in this case. If the geometry of the double bond in **8** were *trans*, then direct cyclization to **10** would be impossible and one would probably observe production of the five-membered ring product **11**.[3]

The stability of the monoanions of the halides **3** in THF has led to another useful facet in the chemistry of β-keto ester dianions. Treatment of the monoanions of **3** in THF with 1 equiv. of lithium diisopropyl amide generated the dianion **12** which, in the case of n = 4 and 5, underwent an internal cyclization to provide the β-keto esters **13** along with some bisalkylated product **4** which could be readily separated by

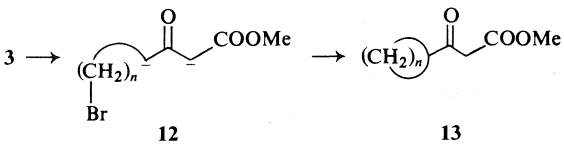

12 **13**

thin layer chromatography. This route to **13** is quite convenient when compared to the previously reported multistep route to these compounds (12).

[2]P.E. Sum and L. Weiler, unpublished results.

[3]Professor Borch (University of Minnesota) has informed us that reaction of dianion **2** with 1,4-dichloro-2-butene of unknown stereochemistry followed by cyclization does lead to a mixture of **10** and **11**.

Experimental

Melting points, which were determined on a Kofler hot stage microscope, and boiling points are uncorrected. All ir spectra were recorded in $CHCl_3$ solution using a Perkin-Elmer Model 700 spectrophotometer, and were calibrated with the 1601 cm^{-1} band of polystyrene. The ^1H-nmr spectra were recorded in $CDCl_3$ solution on either a Varian model T-60 or HA-100 spectrometer. The signal positions are reported using the δ scale with tetramethylsilane as internal standard. The multiplicity, coupling constants, and integrated peak areas are indicated in parentheses after each signal. The mass spectra were obtained using an Atlas CH-4B mass spectrometer, and high resolution determinations were obtained using an AEI MS-9 or MS-50 mass spectrometer. Both instruments were operated at an ionizing potential of 70 eV. Elemental microanalyses were performed by Mr. Peter Borda, University of British Columbia. The silica gel used was obtained from E. Merck and that used for thin layer chromatography (tlc) was the grade PF_{254}, whilst that used for column chromatography was the grade finer than 200 mesh ASTM.

Alkylation of the Dianion of β-Keto Esters with Dihaloalkanes

Reactions of 1,4-Dibromobutane with Dianion 2

Sodium hydride, as a 57% mineral oil dispersion (1.0896 g, 0.02 mol) was weighed into an oven-dried 100 ml flask, and tetrahydrofuran (50 ml) was distilled from lithium aluminum hydride, directly into this flask. The flask was fitted with a magnetic stirrer and septum cap, cooled in ice to 0 °C, and flushed with nitrogen. Methyl acetoacetate (2.32 g, 0.02 mol) was added dropwise, and the reaction mixture was stirred for 10 min after the addition was complete. *n*-Butyllithium, as a 2.2 *M* solution in hexane, (9 ml, 0.02 mol) was added dropwise to the reaction which was allowed to stir for a further 10 min before the addition of 1,4-dibromobutane (4.3186 g, 0.02 mol) in one portion. The reaction mixture was allowed to stir for an additional 1 h at 0 °C. It was then quenched with dilute hydrochloric acid, extracted with ethyl ether (2 × 50 ml), washed with saturated sodium bicarbonate (2 × 50 ml) and saturated sodium chloride solution (50 ml), dried over magnesium sulfate, and filtered. The solvents were removed by evaporation under reduced pressure to give 3.2729 g of crude products. Purification of these products was achieved by tlc using silica plates and a mixture of carbon tetrachloride and ethyl ether (7:3 v/v) as eluent. Two components were isolated from this chromatography, and these were, in order of elution, methyl 8-bromo-3-oxooctanoate (**3**, $n = 4$) (26%) and dimethyl 3,10-dioxododecanedioate (**4**, $n = 4$) (15%).

Methyl 8-bromo-3-oxooctanoate (**3**, $n = 4$) was characterized by: ir 1745 and 1720 cm^{-1}; nmr δ 1.25–2.0 (m, 6H), 2.56 (t, $J = 7.0$ Hz, 2H), 3.5 (s, 2H), 3.42 (t, $J = 6.2$ Hz, 2H), and 3.75 ppm (s, 3H); ms *m/e* (relative intensity) 40(44), 41(16), 43(57), 44(100), 55(9), 59(6), 69(16), 73(1), 101(8), 113(11), 116(20), 129(2), 171(11), 177(5), 179(4), 250(1), and 252(1). *Anal.* calcd. for $C_9H_{15}BrO_3$: C 43.05, H 6.02, Br 31.82; found: C 42.96, H 5.93, Br 31.98.

Dimethyl 3,10-dioxododecanedioate (**4**, $n = 4$) was characterized by: ir 1745, 1720 cm^{-1}; nmr δ 1.1–1.8 (m, 8H), 2.52 (t, $J = 6.20$ Hz, 4H), 3.42 (s, 4H), and 3.75 ppm (s, 6H); ms *m/e* (relative intensity) 41(20), 43(20), 55(29), 58(20), 59(33), 69(22), 74(13), 83(17), 97(45), 101(37), 111(22), 116(68), 129(24), 139(27), 153(12), 171(100), 172(10), 181(13), 213(8), 255(8), 268(11), and 286(1). *Anal.* calcd. for $C_{14}H_{22}O_6$: C 58.73, H 7.74; found: C 58.67, H 7.66.

Reaction of 1,5-Dibromopentane with Dianion 2

The procedure used in this reaction was the same as that employed in the reaction of 1,4-dibromobutane with dianion **2**. The reagents used were: sodium hydride, as a 57% mineral oil dispersion (1.0896 g, 0.02 mol), methyl acetoacetate (2.32 g, 0.02 mol), *n*-butyllithium, as a 2.2 *M* solution in hexane (9 ml, 0.02 mol), and 1,5-dibromopentane (4.6 g, 0.02 mol) which gave 4.16 g of a mixture of crude products. Purification of these products was achieved by tlc using a mixture of carbon tetrachloride and ethyl ether (7:3 v/v) as eluent. Two components were isolated from this chromatography, and these were, in order of elution, methyl 9-bromo-3-oxononaoate (**3**, $n = 5$) (25%) and dimethyl 3,11-dioxotridecanedioate (**4**, $n = 5$) (16%).

Methyl 9-bromo-3-oxononaoate (**3**, $n = 5$) was characterized by: ir 1745 and 1720 cm^{-1}, nmr δ 1.2–2.0 (m, 8H), 2.55 (t, $J = 7.0$ Hz, 2H), 3.42 (t, $J = 6.5$ Hz, 2H), 3.45 (s, 2H), and 3.72 ppm (s, 3H); ms *m/e* (relative intensity) 43(72), 44(75), 55(36), 58(40), 59(21), 69(12), 74(17), 83(25), 84(16), 101(25), 111(11), 116(100), 117(15), 127(9), 129(8), 185(25), 191(15), 193(13), 264(0.1), and 266(0.1). *Anal.* calcd. for $C_{10}H_{17}BrO_3$: C 45.30, H 6.46, Br 30.14; found: C 45.47, H 6.27, Br 29.90.

Dimethyl 3,11-dioxotridecanedioate (**4**, $n = 5$) was characterized by: ir 1745 and 1720 cm^{-1}; nmr δ 1.2–1.8 (m, 10H), 2.5 (t, $J = 7.0$ Hz, 4H), 3.45 (s, 4H), and 3.75 ppm (s, 6H); ms *m/e* (relative intensity) 43(35), 55(58), 59(48), 69(28), 81(10), 84(22), 97(20), 101(47), 111(43), 116(79), 125(23), 129(29), 153(25), 167(76), 185(100), 195(20), 227(18), 267(16), 268(16) and 300(7). *Anal.* calcd. for $C_{15}H_{14}O_6$: C 59.98, H 8.05; found: C 59.87, H 8.05.

Reaction of 1,10-Dibromodecane with Dianion 2

The procedure used in this reaction was the same as that employed in the reaction of 1,4-dibromobutane with dianion **2**. The reagents used were: sodium hydride, as a 57% mineral oil dispersion (1.0896 g, 0.02 mol), methyl acetoacetate (2.32 g, 0.02 mol), *n*-butyllithium as a 2.2 *M* solution in hexane (9 ml, 0.02 mol), and 1,10-dibromodecane (5.996 g, 0.02 mol), which gave 7.03 g of a mixture of crude products. Purification of the products was achieved by tlc using a mixture of carbon tetrachloride and ethyl ether (7:3 v/v) as eluent. Two components were isolated from this chromatography, and these were, in order of elution, methyl 14-bromo-3-oxotetradecanoate (**3**, $n = 10$) (39%) and dimethyl 3,16-dioxooctadecanedioate (**4**, $n = 10$) (22%) which was identified by comparison of its ir and nmr spectra with those of the authentic compound.

Methyl 14-bromo-3-oxotetradecanoate (**3**, $n = 10$) was characterized by: ir 1745 and 1720 cm^{-1}; nmr δ 1.0–1.6 (m, 18H), 2.5 (t, $J = 7.0$ Hz, 2H), 3.42 (s, 2H), 3.42 (t, $J = 6.5$ Hz, 2H), and 3.7 ppm (s, 3H); ms (*a*) high resolution calculated for $C_{15}H_{27}BrO_3$: 334.1144 amu;

found (*m/e*): 334.1120; (*b*) low resolution *m/e* (relative intensity) 55(82), 58(89), 59(45), 69(45), 71(40), 74(33), 81(29), 83(31), 85(33), 97(23), 101(26), 116(100), 129(41), 130(16), 138(14), 149(11), 159(9), 162(16), 163(9), 179(10), 181(11), 183(11), 193(6), 195(8), 236(5), 252(3), and 254(6).

*Methyl 2-Cycloheptanone Carboxylate (**5**, n = 4)*

An oven-dried 100 ml 3-neck flask was fitted with a condenser and calcium chloride tube, and a 10 ml dropping funnel. Fifty millilitres of dry methanol was added gradually to the flask containing sodium (0.23 g, 0.01 mol). When the sodium had dissolved, a crude mixture of compound **4** ($n = 4$) and 3.5 g of methyl 8-bromo-3-oxooctanoate (**3**, $n = 4$) in 2 ml of methanol was added dropwise to the sodium methoxide solution. The reaction mixture was then heated to gentle boiling and refluxed for 13 h. It was then allowed to cool and the methanol was removed under reduced pressure. Water (25 ml) was added to dissolve the solid, and the product was extracted with ethyl ether (2 × 25 ml). The organic layer was then washed with water until it was neutral to litmus, dried over magnesium sulfate, and the solvent removed under reduced pressure to give 1.9254 g of crude product which was chromatographed on silica plates using a mixture of carbon tetrachloride and ethyl ether (7:3 v/v) as eluent. The top fraction isolated from this chromatography was methyl 2-cycloheptanone carboxylate (**5**, $n = 4$) (73% based on bromo-compound **3**, $n = 4$) which was characterized by: ir 1735 and 1700 cm^{-1}; nmr δ 1.2–2.0 (m, 8H), 2.5 (m, 2H), 3.5 (m, 1H), and 3.7 ppm (s, 3H); ms (*a*) high resolution calculated for $C_9H_{14}O_3$: 170.0943 amu; found (*m/e*): 170.0944; (*b*) low resolution *m/e* (relative intensity) 41(33), 55(73), 68(23), 69(20), 74(31), 82(31), 87(25), 110(37), 111(6), 113(27), 128(15), 138(100), 139(45), 142(43), and 170(60).

*Methyl 2-Cyclooctanone Carboxylate (**5**, n = 5)*

This compound was prepared by the same procedure as that employed in the preparation of compound **5** ($n = 4$). The reagents used were: sodium (0.23 g, 0.01 mol), dry methanol (50 ml), and 4.2 g of a crude mixture of compound **4** ($n = 5$) and methyl 9-bromo-3-oxononaoate (**3**, $n = 5$). The crude product was chromatographed as above to give 73% (based on compound **3**) of methyl 2-cyclooctanone carboxylate (**5**, $n = 5$) which was characterized by: ir 1735 and 1700 cm^{-1}; nmr δ 1.0–2.0 (m, 1.0H), 2.4 (m, 2H), 3.38 (m, 1H), and 3.65 ppm (s, 3H); ms (*a*) high resolution calculated for $C_{14}H_{16}O_3$: 184.1099 amu; found (*m/e*): 184.1098; (*b*) low resolution *m/e* (relative intensity) 41(52), 43(32), 45(27), 55(92), 59(19), 68(36), 68(36), 69(44), 74(100), 83(23), 84(34), 86(18), 87(31), 96(27), 98(23), 109(23), 124(27), 125(4), 152(63), 153(31), 156(36), and 184(67).

*Methyl 2-Oxacycloheptaethylidene Carboxylate (**6**)*

Hexamethylphosphoramide (15 ml) was added to an oven-dried 25 ml flask containing 0.027 g of sodium hydride (as a 57% mineral oil dispersion). The flask was fitted with a magnetic stirrer and a septum cap and was flushed with nitrogen. Methyl 8-bromo-3-oxooctanoate (**3**, $n = 4$) (0.125 g, 0.0005 mol) in 1 ml of tetrahydrofuran was added dropwise to the solution. The reaction mixture was allowed to stir for 1½ h. It was then diluted with pentane, washed with water, and dried over magnesium sulfate. The solvents were removed by evaporation under reduced pressure. Purification was achieved by tlc to give 0.0502 g (59%) of compound **6** which was characterized by: ir 1700, 1630, and 840 cm^{-1}; nmr δ 1.2–1.9 (m, 6H), 3.2 (m, 2H), 3.7 (s, 3H), 4.2 (m, 2H), and 5.25 ppm (s, 1H); ms: (*a*) high resolution calculated for $C_9H_{14}O_3$: 170.0943 amu; found (*m/e*): 170.0944; (*b*) low resolution *m/e* (relative intensity) 41(73), 43(36), 44(82), 56(100), 60(28), 69(30), 70(86), 75(34), 83(32), 85(86), 87(51), 98(32), 102(28), 111(41), 129(30), 134(45), 139(77), 140(61), 143(42), and 170(66).

*Reaction of Sodio Lithio Methyl Acetoacetate (**2**) with Dihaloalkene*

Preparation of cis-1,4-Dichloro-2-butene

N-Chlorosuccinimide (11.74 g, 0.088 mol) was dissolved in 400 ml of anhydrous methylene chloride. The flask was fitted with a septum cap and magnetic stirrer, cooled in ice, and flushed with nitrogen. Methyl sulfide (5.456 g, 0.088 mol) was added dropwise over a few minutes. A heavy white precipitate was observed. The reaction mixture was then cooled to −20 °C (carbon tetrachloride, plus dry ice) and *cis*-2-butene-1,4-diol (3.520 g, 0.040 mol) in 5 ml of methylene chloride was added over 10 min. The resulting solution was then warmed to 0 °C and stirred for 50 min. The white precipitate disappeared, leaving a clear colorless solution. The mixture was stirred for an additional 70 min, diluted with pentane, and poured into 400 ml of ice-cold brine. The aqueous phase was extracted with pentane (2 × 200 ml) and the organic layers were combined. It was then washed with cold brine (2 × 400 ml) and dried over magnesium sulfate. The solvents were removed under reduced pressure and the resulting crude product was then distilled to give 3.6104 g (72%) of *cis*-1,4-dichloro-2-butene, bp 128 °C/760 torr (lit. (13) bp 83–85 °C/80 torr).

*Alkylation of Sodio Lithio Methyl Acetoacetate (**2**) with cis-1,4-Dichloro-2-butene*

The procedure used in this reaction was the same as that employed in the reaction of 1,4-dibromobutane with dianion **2**. The reagents in this preparation were: sodium hydride, as a 57% mineral oil dispersion (1.0896 g, 0.02 mol), methyl acetoacetate (2.32 g, 0.02 mol), *n*-butyllithium, as a 2.2 *M* solution in hexane (9 ml, 0.02 mol) and *cis*-1,4-dichloro-2-butene (2.5 g, 0.02 mol) which gave 3.00 g of crude product. Purification of the products was achieved by tlc on silica using a mixture of carbon tetrachloride and ethyl ether (7:3 v/v) as eluent. Two components were isolated from this chromatography, and these were, in order of elution, methyl 3-oxo-8-chloro-6-octenoate (**8**) (18%) and dimethyl 3,10-dioxo-6-dodecenedioate (**9**) (18%). Methyl 3-oxo-8-chloro-6-octenoate (**8**) was characterized by: ir 1745, 1720, and 1660 cm^{-1}; nmr δ 2.2–2.8 (m, 4H), 3.45 (s, 2H), 3.75 (s, 3H), 4.08 (d, $J = 6.5$ Hz, 2H), and 5.5–5.8 ppm (m, 2H); ms: (*a*) high resolution calculated for $C_9H_{13}ClO_3$: 204.0553 amu; found (*m/e*): 204.0540; (*b*) low resolution *m/e* (relative intensity) 53(20), 55(16), 59(20), 67(42), 69(100), 81(14), 94(13), 95(13), 101(79), 109(13), 127(13), 136(25), 137(34), 168(37), 169(10), and 204(1).

Dimethyl 3,10-dioxo-6-dodecenedioate (**9**) was characterized by: ir 1740, 1718, and 1660 cm^{-1}; nmr δ 2.18–2.8 (m, 8H), 3.45 (s, 4H), 3.75 (s, 3H), and 5.4 ppm (t, $J = 4.0$ Hz, 2H); ms (*a*) high resolution calculated for $C_{14}H_{20}O_6$: 284.1259 amu; found (*m/e*): 284.1305; (*b*)

low resolution *m/e* (relative intensity) 43(33), 57(10), 59(12), 71(25), 85(19), 91(16), 94(29), 95(33), 101(61), 109(13), 113(12), 116(20), 127(19), 129(13), 136(12), 137(45), 150(12), 155(18), 159(12), 168(48), 169(100), 179(11), 221(16), 252(11), and 284(4).

*Methyl 2-Oxo-5-cycloheptene Carboxylate (**10**)*

This compound was prepared by the same procedure as that employed in the preparation of compound **5**. The reagents used were: sodium (0.1570 g, 0.0068 mol), dry methanol (10 ml), and pure methyl 3-oxo-8-chloro-6-octenoate (**8**) (0.1383 g, 0.0068 mol) which gave 0.0460 g (40%) of methyl 2-oxo-5-cycloheptene carboxylate (**10**) characterized by: ir 1735, 1700, and 1660 cm^{-1}; nmr δ 2.0–2.8 (m, 4H), 3.65 (m, 1H), 3.72 (s, 3H), and 5.78 ppm (t, J = 4.0 Hz, 2H); ms (*a*) high resolution calculated for $C_9H_{12}O_3$: 168.0787 amu; found (*m/e*): 168.0779; (*b*) low resolution *m/e* (relative intensity) 32(100), 39(38), 42(47), 44(28), 53(22), 55(20), 59(23), 66(22), 67(68), 68(38), 79(24), 80(31), 81(46), 84(34), 101(21), 108(23), 109(21), 110(21), 136(95), 137(43), and 168(60).

Internal Dialkylation at the γ-Carbon of the Dianion of Methyl Acetoacetate

*Methyl 3-Oxo-3-cyclopentyl Propanoate (**13**, n = 4)*

Sodium hydride, as a 57% mineral oil dispersion, (1.0896 g, 0.02 mol) was weighed into an oven-dried 100 ml flask, and tetrahydrofuran (50 ml) was distilled, from lithium aluminum hydride, directly into the flask. The flask was fitted with a magnetic stirrer and a septum cap, cooled in ice to 0 °C, and flushed with nitrogen. Methyl acetoacetate (2.32 g, 0.02 mol) was added dropwise, and the reaction mixture was stirred for 10 min after the addition was complete. *n*-Butyllithium as a 2.2 *M* solution in hexane (9.6 ml, 0.021 mol) was added dropwise to the reaction which was allowed to stir for a further 10 min before the addition of 1,4-dibromobutane (4.3186 g, 0.02 mol). The reaction was then stirred for 1 h and lithium diisopropylamide (made by stirring 3.08 ml of diisopropylamine with 9.9 ml of *n*-butyllithium at 0 °C for ½ h) was added dropwise. The reaction mixture was stirred for an additional 30 min. It was then quenched with dilute hydrochloric acid, extracted with ethyl ether (2 × 50 ml), washed with saturated sodium bicarbonate and water, and dried over magnesium sulfate. The solvents were removed under reduced pressure to give 3.29 g of crude products. Purification was achieved by tlc on silica using a mixture of carbon tetrachloride and ethyl ether (7:3 v/v) as eluent to give methyl 3-oxo-3-cyclopentyl propanoate (**13**, n = 4) in 26% yield based on methyl acetoacetate or in approximately quantitative yield based on the amount of monohalide intermediate produced. Compound **13** (n = 4) was characterized by: ir 1740 and 1710 cm^{-1}; nmr δ 1.05–2.0 (m, 8H), 3.0 (m, 1H), 3.5 (s, 2H), and 3.75 ppm (s, 3H); ms *m/e* (relative intensity) 41(64), 43(50), 44(19), 57(7), 59(60), 69(62), 74(19), 96(40), 97(100), 101(73), 129(86), 139(7), and 170(51). *Anal.* calcd. for $C_9H_{14}O_3$: C 63.51, H 8.29; found: C 63.68, H 8.16.

*Methyl 3-Oxo-3-cyclohexylpropanoate (**13**, n = 5)*

This compound was prepared by the same procedure as that employed in the preparation of methyl 3-oxo-3-cyclopentylpropanoate (**13**, n = 4). The reagents used were: sodium hydride, as a 57% mineral oil dispersion (0.545 g, 0.01 mol), methyl acetoacetate (1.16 g, 0.01 mol), *n*-butyllithium (4.8 ml, 0.01 mol), 1,5-dibromopentane (2.30 g, 0.01 mol), and lithium diisopropylamide (made by stirring 1.67 g, 0.016 mol of diisopropylamine with 7.5 ml of *n*-butyllithium at 0 °C for ½ h), which gave 1.79 g of crude products. This crude material was chromatographed to give methyl 3-oxo-3-cyclohexylpropanoate (**13**, n = 5) in 32% yield based on methyl acetoacetate. This compound was characterized by: ir 1740 and 1710 cm^{-1}; nmr δ 1.8–2.0 (m, 10H), 2.3–2.6 (m, 1H), 3.45 (s, 2H), and 3.72 ppm (s, 3H); ms *m/e* (relative intensity) 41(64), 43(29), 44(50), 55(76), 59(26), 69(48), 74(22), 83(100), 100(25), 101(35), 106(20), 129(33), 143(8), and 184(29). *Anal.* calcd. for $C_{10}H_{16}O_3$: C 65.19, H 8.75; found: C 65.19, H 8.70.

Acknowledgements

We are grateful to the National Research Council of Canada and the University of British Columbia for financial support of this work.

1. (*a*) S. J. Rhoads, J. C. Gilbert, A. W. Decora, T. R. Garland, R. J. Spangler, and M. J. Urbigkit. Tetrahedron, **19**, 1625 (1963); (*b*) L. Ruest, G. Blouin, and P. Deslongchamps. Synth. Commun. **6**, 169 (1976).
2. G. A. Berchtold and J. F. Uhlig. J. Org. Chem. **28**, 1459 (1963).
3. R. Burpitt and J. Thweatt. Org. Synth. **48**, 56 (1965).
4. J. A. Hirsch and F. J. Cross. J. Org. Chem. **36**, 955 (1971).
5. S. N. Huckin and L. Weiler. J. Am. Chem. Soc. **96**, 1082 (1974).
6. S. N. Huckin and L. Weiler. Can. J. Chem. **52**, 1343 (1974).
7. S. N. Huckin and L. Weiler. Can. J. Chem. **52**, 2157 (1974).
8. H. House. *In* Modern synthetic reactions. 2nd ed. W. A. Benjamin, Menlo Park, California. 1972. p. 521 ff.
9. T. A. Bryson. J. Org. Chem. **38**, 3428 (1973).
10. H. E. Zaugg and A. D. Schaefer. J. Am. Chem. Soc. **87**, 1857 (1965).
11. B. Miller, H. Margulies, T. Drabb, Jr., and R. Wayne. Tetrahedron Lett. 3801 (1970); 3805 (1970).
12. R. Jacquier, C. Petrus, F. Petrus, and J. Verducci. Bull. Soc. Chim. Fr. **10**, 3694 (1969).
13. J. M. Bobbitt, L. H. Amundsen, and R. I. Steiner. J. Org. Chem. **25**, 2230 (1960).

Products and stereochemistry of thermolysis of some diazenes containing the 2-phenyl-2-butyl group[1]

KARL R. KOPECKY, THOMAS W. MOJELSKY, THOMAS GILLAN,[2] JAMES A. BARRY, AND JUAN A. LOPEZ SASTRE

Department of Chemistry, University of Alberta, Edmonton, Alta., Canada T6G 2G2

Received October 7, 1976

KARL R. KOPECKY, THOMAS W. MOJELSKY, THOMAS GILLAN, JAMES A. BARRY, and JUAN A. LOPEZ SASTRE. Can. J. Chem. **55**, 1001 (1977).

Thermolysis of (−)-(*R*)-1-benzyl-2-(2-phenyl-2-butyl)diazene, (−)-*R*-**4**, produces (+)-(*S*)-2-methyl-1,2-diphenylbutane with 12% net retention of configuration at 110 °C in benzene or pentane containing 1 *M* butanethiol. The ratio of the rate constant for coupling of the initial radical pair to that of rotation of the 2-phenyl-2-butyl radical, k_c/k_r, is calculated to be ~0.04–0.08. Thermolysis of (+)-(*S*)-1-(2-phenyl-2-butyl)-2-(2-propyl)diazene at 100 °C in benzene containing 1 *M* butanethiol produces 2,3-dimethyl-3-phenylpentane with no observable rotation. The product must be less than 15% optically pure. The reaction produces (−)-(*R*)-2-phenylbutane, (−)-(*R*)-**16**, with 0.6–1.3% retention of configuration. The ratio of the rate constant for disproportionation to (−)-(*R*)-**16** to k_r is calculated to be 0.02–0.04. Thermolysis of (−)-(*R*)-1-(4-nitrophenyl)-2-(2-phenyl-2-butyl-diazene, (−)-(*R*)-**12**, at 175 °C in diphenylether produced no 2-(4-nitrophenyl)-2-phenylbutane. This product was produced on photolysis of (+)-(*S*)-**12** in hexadecane at 15 °C but had no rotation. Neither (+)-(*S*)-**7** nor (−)-(*R*)-**12** was racemized during thermolysis and (+)-(*S*)-**12** was not racemized during photolysis. Activation parameters for thermolysis of (±)-**4** are $\Delta H^{\ddagger}$ = 33 kcal/mol, $\Delta S^{\ddagger}$ = 15 eu and for (±)-**12**, $\Delta H^{\ddagger}$ = 37.3 kcal/mol, $\Delta S^{\ddagger}$ = 5.5 eu.

KARL R. KOPECKY, THOMAS W. MOJELSKY, THOMAS GILLAN, JAMES A. BARRY et JUAN A. LOPEZ SASTRE. Can. J. Chem. **55**, 1001 (1977).

La thermolyse du (−)-(*R*) benzyl-1 (phényl-2 butyl-2)-2 diazène, (−)-*R*-**4**, conduit au (+)-(*S*) méthyl-2 diphényl-1,2 butane avec une rétention nette de 12% de la configuration à 110 °C dans du benzène ou dans du pentane contenant 1 *M* de butanethiol. Le rapport des constantes de vitesse du couplage de la paire de radicaux initiaux et de la rotation du radical phényl-2 butyle-2, k_c/k_r, est d'environ 0.04–0.08. La thermolyse du (±)-(*S*) (phényl-2 butyl-2)-1 (propyl-2)-2 diazène à 100 °C dans du benzène contenant 1 *M* de butanethiol conduit au diméthyl-2,3 phényl-3 pentane pratiquement sans rotation. Le produit doit être moins que 15% optiquement pur. La réaction fournit du (−)-(*R*) phényl-2 butane, (−)-(*R*)-**16**, avec une rétention de configuration de 0.6–1.3%. On a calculé que le rapport de la constante de vitesse de disproportionation en (−)-(*R*)-**16** sur k_r est de 0.02–0.04. La thermolyse du (−)-(*R*) (nitro-4 phényl)-1 (phényl-2 butyl-2)-2 diazène, (−)-(*R*)-**12**, à 175 °C dans l'éther diphénylé ne conduit pas au (nitro-4 phényl)-2 phényl-2 butane. Ce composé est obtenu par photolyse du (+)-(*S*)-**12** dans l'hexadécane à 15 °C mais il n'y a pas de rotation. Il n'y a pas de racémisation lors de la thermolyse du (+)-(*S*)-**7** ou du (−)-(*R*)-**12** et le (+)-(*S*)-**12** n'est pas racémisé durant sa photolyse. Les paramètres d'activation pour la thermolyse de (±)-**4** sont $\Delta H^{\ddagger}$ = 33 kcal/mol, $\Delta S^{\ddagger}$ = 15 ue et pour (±)-**12** $\Delta H^{\ddagger}$ = 37.3 kcal/mol, $\Delta S^{\ddagger}$ = 5.5 ue.

[Traduit par le journal]

The results of the earlier studies of the thermolysis of the chiral diazenes **1** (1) and **2** (2) are consistent with the assumption that in these compounds both C—N bonds are breaking simultaneously in the rate determining step, [1].

[1] $\mathrm{R{-}N{=}N{-}R' \longrightarrow R\cdot N_2\cdot R'}$

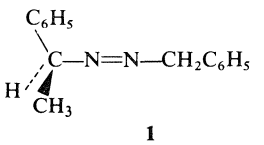

1

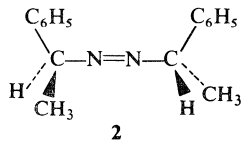

2

There has already been evidence, which is still accumulating, that such a concerted cleavage occurs on thermolysis of a number of acyclic (3) and cyclic (4) diazenes. In most of these compounds R· and R′· are radicals of similar stability.

[1]This research was supported by the National Research Council of Canada.

[2]Holder of a National Research Council of Canada Studentship 1966–1968, a Province of Alberta Scholarship, 1966–1967, and a University of Alberta Dissertation Fellowship 1968–1969.

At the time that we initiated studies in this area we began also to examine diazenes that might provide stereochemical evidence for one-bond cleavage (5) as indicated by racemization of optically active starting material, [2], in which R·

[2] (+)-R—N=N—R′ ⇄ R· ·N=N—R′ ⇄ (−)-R—N=N—R′

is a much more stable radical than is R′·.

Since our work began, stereochemical evidence for one-bond cleavage during thermolysis of several optically active diazenes has appeared (6). Other evidence for one-bond cleavage has been obtained from kinetic (7), pressure (8), and nmr (9) studies of, and the observation of isomerization (10) in, the thermolysis of diazenes.

In this paper the thermolyses of (−)-(*R*)-1-benzyl-2-(2-phenyl-2-butyl)diazene (−)-(*R*)-**4**, (+)-(*S*)-1-(-2-phenyl-2-butyl)-2-(2-propyl)diazene (+)-(*S*)-**7**, and (−)-(*R*)-1-(4-nitrophenyl)-2-(2-phenyl-2-butyl)diazene (−)-(*R*)-**12** are described. The diazenes each contain a 2-phenyl-2-butyl group, chosen because it cannot undergo racemization by reversible hydrogen atom abstraction, and constitute a series in which the other substituent is varied from benzyl to 2-propyl to 4-nitrophenyl. This is in order of decreasing radical stability. It was expected that (−)-(*R*)-**4** would undergo concerted two-bond cleavage and produce a coupling product with retention of configuration (1, 2), whereas (−)-(*R*)-**12** would decompose by a one-bond cleavage reaction [2] and thus might racemize during thermolysis. The mechanism of thermolysis of (+)-(*S*)-**7** is not so easy to predict and a comparison of the stereochemistry of the product of coupling with that from (−)-(*R*)-**4** might be informative. In fact, indirect evidence indicates that the coupling product from (+)-(*S*)-**7** was formed with a somewhat smaller amount of retention of configuration than that from (−)-(*R*)-**4**, that (+)-(*S*)-**7** was not racemized during thermolysis, and that (−)-(*R*)-**12** was not racemized during either thermolysis or photolysis.

Syntheses of Optically Active Diazenes and Coupling Products

The syntheses of the optically active diazenes and of the coupling products expected from (−)-(*R*)-**4** and (+)-(*S*)-**7** are outlined in Schemes 1 to 3. Rotations given are those calculated for optically pure compounds. The maximum rotations and absolute configurations of (+)-(*R*)-(2-phenyl-2-butyl)diazane (+)-(*R*)-**3** (11),[3] (−)-(*R*)-1,2-diphenyl-2-methyl-2-butanone (−)-(*R*)-**5** (12), and (−)-(*R*)-2-methyl-2-phenylbutanoic acid (−)-(*R*)-**9** (13) have been determined. Thus, the absolute configurations and maximum rotations of (−)-(*R*)-**4**, (+)-(*S*)-1,2-diphenyl-2-methylbutane (+)-(*S*)-**6**, (+)-(*S*)-2,3-dimethyl-3-phenyl-1-pentene (+)-(*S*)-**10**, (−)-(*S*)-2,3-dimethyl-3-phenylpentane (−)-(*S*)-**11**, and (−)-(*R*)-**12** are established. The absolute configuration and maximum rotation of (+)-(*S*)-**7** were determined by hydrogenolysis to (−)-(*S*)-2-phenyl-2-butylamine (−)-(*S*)-**8**, of known configuration (11). This amine was also prepared again in this work from (+)-(*S*)-2-methyl-2-phenylbutanoic acid (+)-(*S*)-**9** to check the magnitude of its rotation.

The magnitude of the rotation of the optically pure coupling product (−)-(*S*)-**11** expected from thermolysis of optically active **7** is smaller than expected. It was prepared from (−)-(*R*)-**9** by reactions that do not affect the chiral center and the immediate precursor (+)-(*S*)-**10** has a significant rotation. Values of $[M]_D$ −19.2 or −4.4° for the rotation of (−)-(*S*)-**11** were calculated using Brewster's empirical rules (14). By estimating the density of (−)-(*S*)-**11** to be 0.87 values of α_D −9.5 or −2.2° (neat, *l* 1 dm) were obtained. The larger values were obtained using the higher polarizability of the phenyl group which has been found to give the more accurate estimate of rotation for many compounds. However, it is known that empirical rules for calculating optical rotation give erroneous results for compounds with 2-propyl groups attached to the chiral center (15), presumably because of steric crowding. The rotation of (−)-(*S*)-**11** did not vary greatly with wavelength down to 300 nm, the shortest wavelength utilizable. The maximum rotation at the position of a low intensity peak was $[\alpha]_{310}^{23}$ = −33° (*c* 1.05, CH_3OH).

Results

Rates and Products of Thermolysis

The rates of thermolysis of (±)-**4**, (±)-**7**, and (±)-**12** are presented in Table 1. The rate of thermolysis of (±)-**4** is about 17 times that of **1** (1). This is about the effect to be expected on replacing a hydrogen atom of **1** by an alkyl group (16). The rate of thermolysis of (±)-**7** is nearly

[3]A much more convenient method of resolution of (±)-**3** has been found, see Experimental.

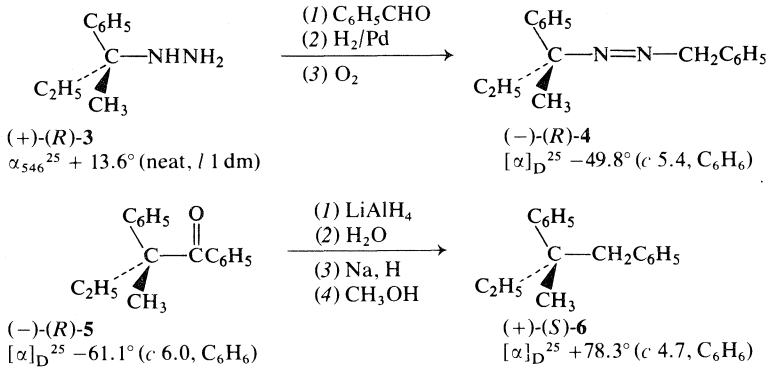

SCHEME 1

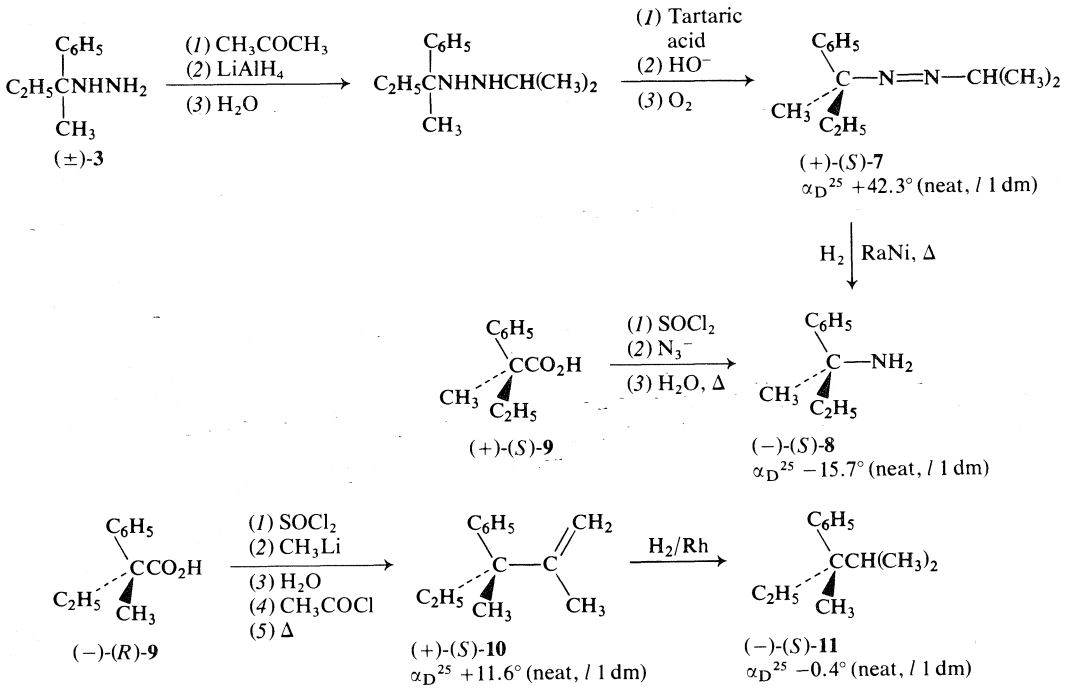

SCHEME 2

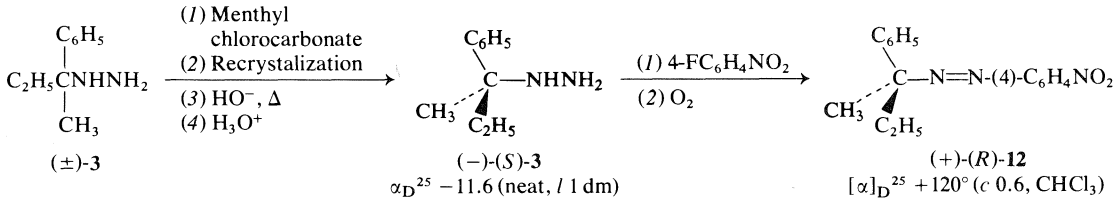

SCHEME 3

TABLE 1. Rates of thermolysis of diazenes (±)-**4**, (±)-**7**, and (±)-**12**

Diazene	Solvent	Concentration (M)	Temperature (°C)	Moles N_2[a]	$k \times 10^4$ (s^{-1})
(±)-**4**	Cumene	0.16	86.6	0.85	0.131[b]
(±)-**4**	Cumene	0.16	103.7	0.89±0.04[c]	1.18±0.05[c]
(±)-**7**	Cumene	0.25	122.5	0.85±0.01[c,d]	1.46±0.02[c]
(±)-**12**	Diphenyl ether	0.35	160.5	0.88±0.01[c]	0.213±0.007[c,e]
(±)-**12**	Diphenyl ether	0.35	187.0	0.90±0.02[c]	2.77±0.03[c]

[a]Mol N_2 per mol of diazene.
[b]At 103.7 °C $\Delta H^{\ddagger}$ = 33 kcal/mol, $\Delta S^{\ddagger}$ = 15 eu.
[c]Average of two runs.
[d]Based on 2 mol of gas (N_2 + propane or propene) per mol of 7.
[e]At 160.5 °C $\Delta H^{\ddagger}$ = 37.3 ± 0.6 kcal/mol, $\Delta S^{\ddagger}$ = 5.5 ± 1.5 eu.

identical to that of 1-(2-phenyl-2-propyl)-2-(2-propyl)diazene **13** (17). Thus, replacement of a methyl group in **13** by an ethyl group has little effect on the rate of thermolysis.

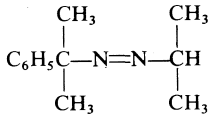

13

The rate of thermolysis of (±)-**12** is very much slower than that of either (±)-**4** or (±)-**7**. This might suggest that (±)-**12** thermolyzes by a mechanism different from that of the other two compounds, but the main factor contributing to the rate difference between (±)-**7** and (±)-**12** is the difference in the entropies of activation, about 8 eu (reported for **13** (17) $\Delta H^{\ddagger}$ = 36.0 kcal/mol, $\Delta S^{\ddagger}$ = 14 eu), assuming that the activation parameters of (±)-**7** and **13** are nearly the same. A larger difference in the enthalpies of activation than the observed 1.7 kcal/mol might have been expected if **13** were decomposing according to [1] and (±)-**12** according to [2].

Thermolysis of a 10^{-2} M solution of (±)-**4** in benzene at 110 °C produced toluene, (±)-**6**, 3,4-dimethyl-3,4-diphenylhexane **14**, and 1,2-diphenylethane **15** in a 12:53:22:13 molar ratio in 50% total yield [3]. About a 10% yield of a mixture, only partially resolved under the gc conditions used, of 2-phenylbutane (±)-**16**, 2-phenyl-1-butene **17**, Z- and possibly E-2-phenyl-2-butene Z- and E-**18** was also formed, as was about a 20% yield of several unidentified compounds. Very similar results were obtained when pentane was used as solvent.

Thermolysis of (±)-**4** in the presence of 1 M butanethiol or benzenethiol resulted in greatly increased yields, relative to those of (±)-**6**, toluene, and (±)-**16**, Table **2**. No symmetrical

[3] (±)-**4** $\xrightarrow{\Delta}$ $C_6H_5CH_3$ + (±)-**6** + 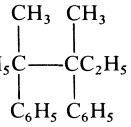 **14**

+ $C_6H_5CH_2CH_2C_6H_5$ + 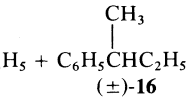 + 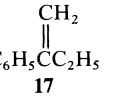

15 (±)-**16** **17**

+ 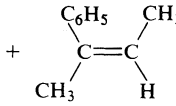 + 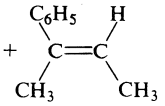

Z-**18** *E*-**18**

coupling products were formed. Toluene and (±)-**16** are formed outside the initial solvent cage from benzyl and 2-phenyl-2-butyl radicals by abstraction of hydrogen atoms from the thiols. An additional source of toluene could be from disproportionation of the two radicals in the initial solvent cage. Since the yield of toluene is only slightly higher than that of (±)-**16** only ~2% of the radicals undergo disproportionation in the cage. Such a high ratio of coupling to disproportionation is common to benzylic radical pairs (1, 18).

TABLE 2. Relative yields (%) of products from thermolysis of (±)-**4** at 110 °C in the presence of scavengers

Solvent	[Thiol] M	Toluene	(±)-**16**	(±)-**6**
Pentane–benzenethiol	1.2	46	46	8
Benzene–benzenethiol	0.97		77	23
Benzene–butanethiol	0.84		28[a]	15[a]
Butanethiol	9.7		74	26

[a]Absolute % yields.

Numerous other products, most of which were eluted between (±)-**16** and (±)-**6** under the gc conditions used, were also formed in the presence of the thiols. About half the amount of these products, relative to (±)-**6**, was formed in the presence of benzenethiol as was formed in the presence of butanethiol. Only one of these compounds was identified and it was shown to be *E*-1,2-diphenylethene *E*-**19**, formed in ~5% yield in the presence of butanethiol. No *E*-**19** was formed in the absence of thiol. The formation of *E*-**19** in low yield has been observed on thermolysis of 1,2-dibenzyldiazene in the absence of scavenger (19). Its origin in these reactions is not clear. It cannot be formed under the present conditions by dehydrogenation of **15** because none of the latter compound is formed. A possible route to the formation of *E*-**19** is shown in Scheme 4. Thermolysis of diazenes in the presence of thiols produces appreciable amounts of bis(methylene)diazanes (azines) (20). Presumably this occurs by successive hydrogen atom abstractions from the diazene by thiyl

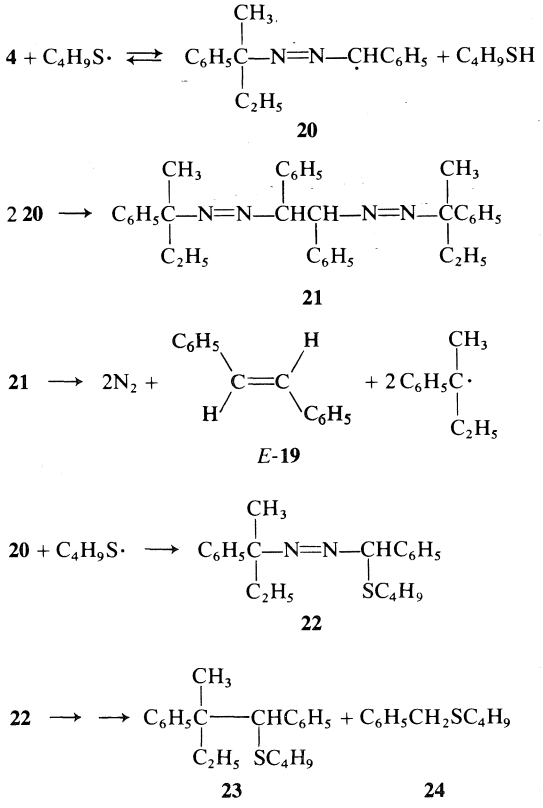

SCHEME 4

[4] 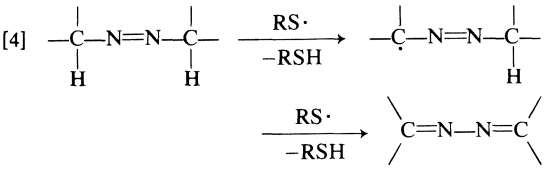

radicals [4] (20). This would mean that the radical generated upon abstraction of the first hydrogen atom must have enough stability so that it can survive sufficiently long in the presence of thiol to undergo a second hydrogen atom abstraction. The radical **20** generated in this way from **4** cannot undergo a second hydrogen atom abstraction.

Dimerization of two such radicals would give the bis-diazene **21** and subsequent thermolysis of this compound could produce *E*-**19**. The radical **21** also could couple with a thiyl radical to form the diazene **22** which would give rise to at least two other products **23** and **24** on thermolysis. A search for these compounds was not made.

Thermolysis of 0.5 *M* (±)-**7** in benzene at 100 °C produced (±)-**16**, **17**, *Z*-**18**, (±)-**11**, and **14** in a 23:2:2:59:14 molar ratio in 51% total yield. Very similar results were obtained at 125 °C. No *E*-**18** was detected. No attempt was made to detect other products of the 2-propyl radical. In the presence of 1 *M* butanethiol a 64:36 molar ratio of (±)-**16**:(±)-**11** was formed in 57% total yield. No symmetrical coupling product **14** was detected. A number of unidentified other products that eluted near (±)-**11** under the gc conditions used were formed in both the presence and absence of thiol. Under both conditions considerable amounts of hydrazone were formed. A significantly larger yield, 30%, of (±)-**11** was formed in the absence of butanethiol than in its presence, 21%. This indicates that a considerable amount of coupling between 2-phenyl-2-butyl and 2-propyl radicals must occur outside the initial solvent cage in benzene. Similar behavior was observed recently for 2-butyl and diphenylmethyl radicals (21).

Products of thermolysis of 0.3 *M* (±)-**12** under nitrogen in diphenyl ether at 175 °C that were identified are shown in [5]. Nitrobenzene and 1-phenyl-1-propanone were eluted together under the gc conditions used. The identified products accounted for ~50% of the 2-phenyl-2-butyl radicals. Unexpectedly, neither (±)-**16** nor the coupling product **14** could be detected. The coupling product **14** was shown to survive heat-

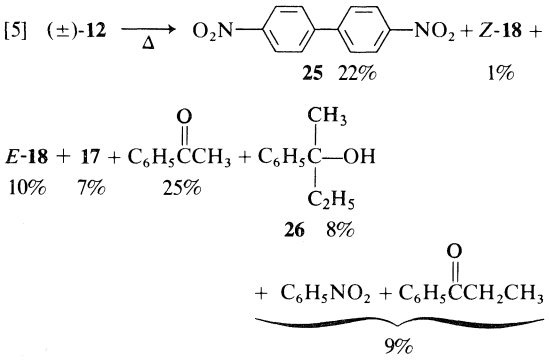

ing at 175 °C in diphenyl ether for a time equal to several half-lives of decomposition of (±)-**12**. None of the unsymmetrical coupling product 2-(4-nitrophenyl)-2-phenylbutane **27** was detected either. As in the thermolysis of (±)-**7**, *E*-**18** predominates greatly over *Z*-**18**.

Possible routes to some of the products are given in Scheme 5. The presence of the ketones among the products is good evidence that 2-phenyl-2-butoxy radicals are formed which then undergo β-sission. The alkoxy radicals must result from the reaction between 2-phenyl-2-butyl radicals and a nitro group. The alkenes **17** and *Z*- and *E*-**18** are not likely to be formed by disproportionation between two 2-phenyl-2-butyl radicals since neither the alkane (±)-**16**, which would be the other product of disproportionation, nor the coupling product **14** is formed. The absence of **14** is good evidence that the radicals never encounter each other since coupling is an important result of such encounters as shown by thermolysis of (±)-**4** and (±)-**7** at lower temperatures. The higher temperature in the thermolysis of (±)-**12** should not be the reason for lack of formation of **14** since in thermolysis of (±)-**7** a slightly higher relative yield of **14** was formed at 125 °C than at 100 °C. The alkenes may be formed by disproportionation of 2-phenyl-2-butyl and 4-nitrophenyldiazenyl radicals in the initial solvent cage.

Since 2-phenyl-2-butyl radicals do not couple under these reaction conditions it is unlikely that 4-nitrophenyl radicals would couple, hence the suggested route to **25** in Scheme 5. The formation of **25** in 79% yield on thermolysis of neat (±)-**12** at 175 °C is consistent with the proposed route. Higher concentrations of the diazene would favor the addition of the nitrophenyl radical to the diazene. Only ~15% total yield of the products of the 2-phenyl-2-butyl radical were detected. The reaction was not done in a sealed tube and these products may have evaporated.

Thermolysis of Optically Active Diazenes

Thermolysis of (−)-(*R*)-**4** in benzene at 110 °C produced (+)-(*S*)-**6** with 6% net retention of configuration, Table 3. In the presence of 0.9 *M* butanethiol (+)-(*S*)-**6** is formed with ~12% net retention of configuration in either benzene or

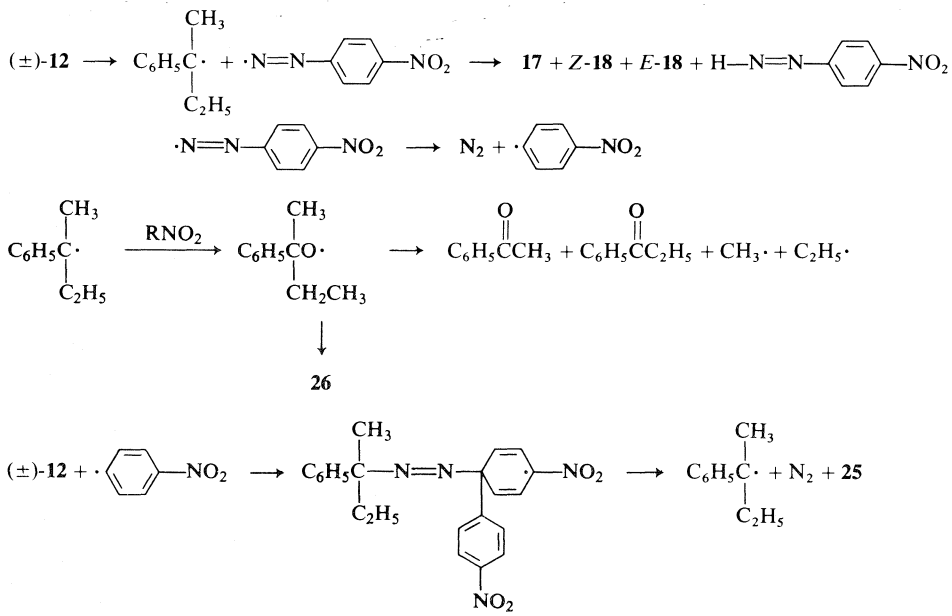

SCHEME 5

TABLE 3. Stereochemistry of (+)-(*S*)-**6** from thermolysis of (−)-(*R*)-**4**[a] at 110 °C

Solvent	(−)-(*R*)-**4** (mg)	Concentration (*M*)	Butanethiol, (*M*)	(+)-(*S*)-**6**[b] (mg)	$[\alpha]_{436}^{25}$ (deg)[c]	Retention[d] (%)
Benzene	360	0.1	0	39	+2.67	5.8
Benzene	460	0.04	0.9	40	+5.88	12.8
Pentane	450	0.04	0.9	23	+5.07	11.0
Butanethiol	1170	0.09	9.7	70	+5.54	12.1

[a]$[\alpha]_D^{25}$ − 12.8° (*c* 2.95, C_6H_6), 25.7% optically pure.
[b]Product dissolved in benzene to make up 1.0 ml solution.
[c]Net retentions calculated from specific rotation at 589 and 546 nm were all within 0.6% (absolute) of the values given.
[d]Optically pure (+)-(*S*)-**6** has $[\alpha]_D$ 178° (*c* 4.7, C_6H_6).

TABLE 4. Stereochemistry of thermolysis of (+)-(*S*)-**7** at 100 °C in benzene

(+)-(*S*)-**7** (mg)	Concentration (*M*)	Butanethiol, (*M*)	(−)-(*R*)-**16** mg	(−)-(*R*)-**16** Rotation	(−)-(*R*)-**16** Retention (%)	**11** mg	**11** α_{310}^{22}[a]
1840[b]	0.5	1.0	192	α_D^{25} −0.28°[c]	1.3	41	<0.05°
1650[d]	0.13	1.0	82	$[\alpha]_{436}^{22}$ −0.12°[b]	0.7	130	<0.05°
1400[e]	0.03	0				24	<0.05°

[a](*c* 2.2–2.7, CH_3OH).
[b]α_D^{25} + 35.5° (neat, *l* 1 dm), 84% optically pure.
[c]Optically pure material has α_D^{25} − 24.3° (neat, *l* 1 dm) (22*a*) and $[\alpha]_{436}^{23}$ − 55.5 (22*b*).
[d]α_D^{22} + 14.0° (neat, *l* 1 dm), 33% optically pure.
[e](−)-(*R*)-**7** was actually used, $[\alpha]_{436}^{22}$ − 82.9° (*c* 0.567, CCl_4). The material was heated for 22 h, 700 mg recovered material had $[\alpha]_{436}^{22}$ − 81.4° (*c* 0.631, CCl_4).

pentane. In neat butanethiol the degree of retention is also ~12%. These results are very similar to those obtained on thermolysis of **1** and **2**. There is a higher degree of retention in the presence of butanethiol because no racemic coupling product is formed outside the initial solvent cage as in unscavenged runs.

The stereochemistry of the coupling product obtained from thermolysis of (+)-(*S*)-**7** could not be determined. Even the isolated product from scavenged runs had no observable rotation at 310 nm, the position of the peak in the ord curve of optically pure (−)-(*S*)-**11**. At the maximum concentration of coupling product that could be used without overloading the photomultiplier, product with an optical purity of 15% would have given a reading on the ord instrument of ~0.05°. This is similar in magnitude to the baseline noise of the instrument. Thus, the optical purity of the coupling product is less than 15%.

Fortunately, the 2-phenyl-2-butyl radical produced in the reaction is also converted to another product with a chiral center, (−)-(*R*)-**16**, which has an observable rotation. Only in the presence of scavenger was enough (−)-(*R*)-**16** produced to be isolated. The optical activity of this product is due entirely to that fraction of the product that was formed by disproportionation in the original solvent cage. Since scavenging of the 2-phenyl-2-butyl radicals that escape from the original solvent cage must produce (±)-**16** the amount of retention of (−)-(*R*)-**16** formed in the cage must be greater than that indicated in Table 4. The relative amounts of material formed inside and outside the solvent cage were not determined but a reasonable estimate can probably be made. For the 2-phenyl-2-propyl–cyclohexyl radical pair the ratio of the rate of disproportionation to 2-phenylbutane and cyclohexene to the rate of coupling is estimated to be 0.24 (23). This ratio for the 2-phenyl-2-butyl–2-propyl radical pair should be quite similar. From the relative yields of (±)-**16** (64%) and (±)-**11** (36%) formed in the presence of butanethiol it can be reckoned that ~0.24 × 36/64 = ~$\frac{1}{7}$ of the total (±)-**16** was formed in the original solvent cage. Thus, the (−)-(*R*)-**16** that was formed from (+)-(*S*)-**7** in the original solvent cage was produced with ~5–9% net retention of configuration.[4]

Recovery of (−)-(*R*)-**7** after heating at 100 °C in benzene for one half-life of decomposition gave product with 1.8% lower rotation than that of starting material. Since the experimental error

[4]A radical disproportionation giving product with a high degree of retention has been observed already. Cage disproportionation during thermolysis of an optically active diacyl peroxide produced product with 31–37% net retention of configuration (24).

must be of nearly the same magnitude there is no evidence that (−)-(*R*)-**7** racemizes during thermolysis.

Thermolysis of (±)-**12** produced no coupling product, 2-(4-nitrophenyl)-2-phenylbutane **27** so the only stereochemical result sought was whether (−)-(*R*)-**12** racemized during thermolysis. Recovered (−)-(*R*)-**12** showed no loss of optical activity after heating at 175 °C for 3.5 half-lives of decomposition in cumene. After this experiment had been performed it was reported that optically active **28** racemized during photolysis (6*c*,*d*). The photolysis of (+)-(*S*)-**12** was then carried out. Starting material was recovered after 40% decomposition in hexane or 60% decomposition in hexadecane at 15 °C with no loss of optical activity. In hexadecane a 3% yield of coupling product **27** was formed which showed no optical activity. No attempt was made to isolate the *Z*-isomer of (+)-(*R*)-**12**.

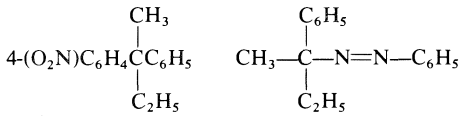

27 **28**

Discussion

The main purpose of this study was to determine whether **7** and **12** underwent thermolysis by a concerted two-bond [1] or a stepwise one-bond [2] cleavage process. The lack of racemization of the optically active isomers during thermolysis provides no support for the stepwise process. Stereochemical evidence obtained recently indicates that thermolysis of (−)-(*S*)-**29** proceeds by a one-bond cleavage process to give, initially, the diphenylmethyl–2-butyldiazenyl radical pair (21). Viewed in this light thermolysis of **12** also would be expected to proceed in a stepwise manner. The aryl–N bond of **12** is much stronger than the 2-butyl–N bond of (−)-(*S*)-**29** and the difference in the strengths of these two bonds probably is greater than the difference in the strengths of the other two C—N bonds of the two diazenes. Evidence in support of one-bond cleavage in the thermolysis of **12** is the observation that no coupling product **27** was formed. Had the 2-phenyl-2-butyl–4-nitro-phenyl radical pair been formed in the solvent cage some cage recombination very likely would have occurred as cage recombination appears to be a reaction common to all but the most bulky (25) of caged radical pairs. The observation that the *Z*-isomers of **28** and **30** decompose thermolytically by a one-bond cleavage mechanism (6*c*, 6*d*, 9) also lends support to a one-bond cleavage process for thermolysis of **12**.

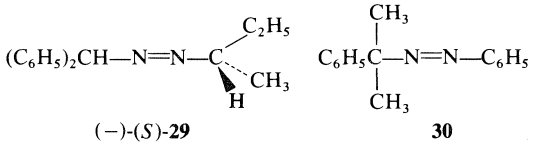

(−)-(*S*)-**29** **30**

It is more difficult to determine from circumstantial evidence whether **7** undergoes thermolysis by a one- or two-bond cleavage process. The enthalpy of activation for thermolysis of the structurally analogous compound **13**, 36 kcal/mol (17), is within experimental error of that for **12**. Thus, breaking of the 2-propyl–N bond of **7** does not appear to be important in the rate determining step. Cage coupling product still could be formed as a result of a one-bond cleavage process if the 2-propyldiazenyl radical has a very short lifetime. It appears that the 2-butyldiazenyl radical decomposes within the original solvent cage (21). Most of the chemistry of **7** can be accounted for in terms of either a one- or a two-bond cleavage process. Only the enthalpy of activation seems to be in favor of a one-bond cleavage process although arguments in favor of a concerted cleavage for **13** have been made (17).

The lack of racemization of (+)-(*S*)-**7** and, especially, of (−)-(*R*)-**12** during thermolysis contrasts with the reported racemization of optically active **31** (6*a*) and **32** (6*b*). It is clear that racemization does not necessarily occur during thermolysis of optically active diazenes that cleave by a one-bond mechanism.

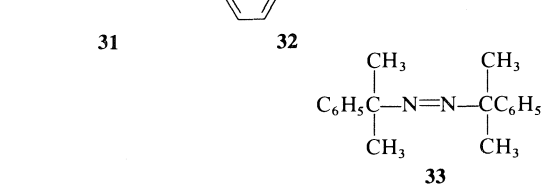

31 **32**

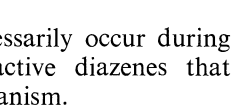

33

The lack of racemization of (+)-(*S*)-**12** during photolysis was also surprising in view of the

racemization of optically active **28** under essentially identical conditions. The latter compound is isomerized on photolysis to the thermally labile *Z*-isomer which then decomposes thermally by a one-bond cleavage process. Recombination of the 2-phenyl-2-butyl radical pair leads to partially racemized starting material (*6d*). The reason for the difference in behavior of (+)-(*S*)-**12** is not clear and a discussion of the possible factors involved would be premature before the *Z*-isomer is isolated and studied.

The ratio of the rate constant for coupling (or disproportionation) of the caged radical pair to that for rotation of the 2-phenyl-2-butyl radical with respect to its caged partner, k_c/k_r, can be estimated for the radicals derived from (−)-(*R*)-**4** and (+)-(*S*)-**7** [6] (1),

$$[6] \qquad k_c/k_r = F(1-f)\left(\frac{\text{retention}}{\text{inversion}} - 1\right)_{\text{cage}}$$

where F is the fraction of radicals which are consumed by coupling and disproportionation before diffusion from the original solvent cage and f is the fraction of radicals consumed in this way that undergo disproportionation. Accurate determinations of the cage effects were not carried out but reasonable estimates for the range of cage effects can be made. For (−)-(*R*)-**4** the minimum value is 15%, the absolute yield of **6** formed in the presence of scavenger. There is very little disproportionation. This value is lower than the values of the cage effect found for **1**, 25–30% at 110 °C (1), **2**, 28% at 105 °C (2, 26), and **33**, 21%, extrapolated to 110 °C (27). The actual cage effect is thus in the range 15–30%. For (+)-(*S*)-**7** the minimum value is 21%, the absolute yield of **11** formed in the presence of scavenger. However, a large amount of disproportionation must also take place. By analogy to the 2-phenyl-2-propyl–cyclohexyl radical pair (23) about 1.5 times as much disproportionation as coupling occurs and the actual cage effect for (+)-(*S*)-**7** must be ~50%. For the radical pair derived from (−)-(*R*)-**4**, k_c/k_r is in the range 0.04–0.08 at 110 °C in benzene and for the radical pair derived from (+)-(*S*)-**7**, k_c/k_r is 0.02–0.04 at 100 °C in benzene. In the latter case k_c actually represents the rate constant for disproportionation to (−)-(*R*)-**16** and propene. These values for k_c/k_r are similar in magnitude to those, ~0.06–0.10, found for the radical pairs derived from **1** and **2**.

Experimental

Boiling points and melting points are uncorrected. Infrared spectra were recorded on Perkin-Elmer model 421 or model 337 recording infrared spectrophotometers. Ultraviolet spectra were measured on a Bausch and Lomb Spectronic 600 spectrophotometer. Nuclear magnetic resonance spectra were recorded on Varian analytical spectrometers, models A-60 and A-56/60. Tetramethylsilane was used as internal reference. Neat optical rotations were taken with a Rudolph polarimeter model 80 and solution optical rotations were taken with a Perkin-Elmer 141 polarimeter. Optical rotatory dispersion curves were taken on a Japan Spectroscopic Company spectropolarimeter model ORD/UV-5. Gas chromatography was carried out on Aerograph 202 and A90-P3 fractometers with a 6 ft × ¼ in. stainless steel column packed with 20% SF96 on 60/80 Chromosorb P, column A, or with 10% Carbowax 20 M on 60/80 Chromosorb P, column B.

Chlorobenzene and bromobenzene were purified by successive shaking with three portions of sulfuric acid, two of water, and two of sodium bicarbonate. The materials were dried over magnesium sulfate and distilled from phosphorus pentoxide through a 4 ft Podbielniak column or a 24 in. Nester–Faust annular Teflon spinning band column. Middle fractions were collected and stored over molecular sieves. Aliquots were distilled from the stored solutions just before use. Benzene, cumene, and cyclohexane were purified and stored in the same manner except that they were distilled from sodium wire. Diphenyl ether was recrystallized twice from pentane.

(±)-1-(1-Methylethylidene)-2-(2-phenyl-2-butyl)diazane

A mixture made from 20 g (2-phenyl-2-butyl)diazane (28), bp 90 °C/1.4 torr, n_D^{25} 1.5365 (lit. (28) bp 81–84 °C/0.4 torr, n_D^{25} 1.5354), 7.5 g magnesium sulfate, and 133 ml acetone was stirred under nitrogen at 45 °C for 2 h and then at 23 °C for 12 h. The reaction mixture was filtered, concentrated, and distilled to yield 21 g (84%) of a light yellow oil bp 82 °C/0.6 torr; n_D^{27} 1.5219; nmr (CCl_4) τ 2.75 (m, 5.0H), 5.5 (br, 0.7H), 8.15 (q, J = 7.5 Hz, 2H), 8.17 (s, 3H), 8.34 (s, 3H), 8.65 (s, 3.1H) and 9.35 (t, J = 7.5 Hz, 3.0H).

(±)-1-(2-Phenyl-2-butyl)-2-(2-propyl)diazene, (±)-7

A solution of 2.0 g (0.01 mol) of the above hydrazone in 20 ml ether was added over 3 h to 0.50 g (0.013 mol) of lithium aluminum hydride in 100 ml ether. The reaction mixture was stirred under nitrogen at reflux for 3 days and then hydrolyzed by successive addition of 0.5 ml water, 1.0 ml 10% potassium hydroxide, and 0.5 ml water. The mixture was filtered and the filtrate was stirred in an unstoppered flask for 8 h, then washed with water, dried over sodium carbonate, and concentrated. The residue was adsorbed on a 30 × 1.5 cm column of neutral alumina. A green band was eluted with 50 ml pentane. Solvent was removed and the residue kept under vacuum as a thin film for several hours to leave 1.1 g (55%) of a green oil, n_D^{25} 1.4932; ir (CCl_4) 1580 cm^{-1} (N=N, weak); λ_{max} (ether) 368 nm, log ε 1.46; nmr (CCl_4) τ 2.62 (m, 5.0H), 6.25 (septet, J = 6.5 Hz, 1.0H) 8.04 (q, J = 7.5 Hz, 2.2H), 8.62 (s, 3.3H), 8.75 (d, J = 6.5 Hz, 6.1H), and 9.34 (t, J = 7.5 Hz, 3.1H).

(+)-(S)-1-(2-Phenyl-2-butyl)-2-(2-propyl)diazene, (+)-(S)-7

Reduction of 30 g of (±)-1-(1-methylethylidene)-2-(2-phenyl-2-butyl)diazane was carried out as described above except that the reaction mixture (1500 ml), after hydrolysis, was filtered into a 2 ℓ flask which contained a cold solution of 45 g dibenzoyl tartaric acid (29); mp 89–90 °C; $[\alpha]_D^{25}$ −115.3° (*c* 1.03, methanol) (lit. (29) mp 89–91 °C; $[\alpha]_D^{25}$ −112.5° (30)). Eight grams of precipitate formed immediately. The remainder of the solution was allowed to stand at 5 °C for 48 h to give 20 g of crystals. The two crops were recrystallized separately twice from 2:1 ethanol–water, 10 ml/g of crystals, to give 1.3 g and 7 g of white, slender needles. Both batches had mp 109–110 °C; $[\alpha]_D^{25}$ −65.2° (*c* 1, chloroform). Further recrystallization did not change the rotation of the salt or that of the diazene prepared from it. *Anal.* calcd. for $C_{31}H_{36}N_2O_8$: C 65.94, H 6.43, N 4.96; found: C 65.65, H 6.23, N 5.08.

The dibenzoyltartrate salt (3 g) was treated with 20 ml 10% potassium hydroxide solution and the hydrazine was extracted into ether (2 × 20 ml). The combined ether extracts were washed with water, dried, and the hydrazine oxidized to the azo compound, which was isolated as described for the preparation of (±)-**7**, to give 0.65 g oil; n_D^{25} 1.4934; α_D^{25} +35.5° (neat, *l* 1 dm); ord (*c* 0.25, cyclohexane) $[\Phi]_{700}$ +98°, $[\Phi]_{589}$ +130°, $[\Phi]_{500}$ +230°, $[\Phi]_{450}$ +408°, $[\Phi]_{410}$ +980°, $[\Phi]_{398}$ +1110°, $[\Phi]_{380}$ +506°, $[\Phi]_{374}$ 0°, $[\Phi]_{360}$ −945°, $[\Phi]_{346}$ −127°, $[\Phi]_{310}$ −620°. *Anal.* calcd. for $C_{13}H_{20}N_2$: C 76.42, H 9.87, N 13.71; found: C 76.12, H 9.86, N 13.86.

(±)-2-Acetoxy-2,3-dimethyl-3-phenylpentane

A solution of 13 g (0.066 mol) of 2-methyl-2-phenylbutanoyl chloride (31) in 90 ml ether was added to a rapidly stirred solution of methyllithium, made from 3.7 g (0.53 mol) lithium and 37.5 g (0.264 mol) methyl iodide in 200 ml ether, at −60 °C. The reaction mixture was allowed to warm to 0 °C, 100 ml saturated ammonium chloride solution was added, and the aqueous solution was extracted with ether. The combined ether solutions were successively washed with solutions of sodium bisulfite and sodium bicarbonate, water, and then dried. The ir spectrum of the oil obtained on concentration of a portion of the ether solution showed moderate carbonyl absorption (1710 cm^{-1}) so the entire solution was treated with excess methyllithium and the reaction mixture worked-up as described above. The ether was removed to give 12 g of an oil which was acetylated (32) with acetyl chloride to give 8.5 g (55%) of product, bp 88–89 °C/0.4 torr; n_D^{25} 1.5034; nmr (CCl_4) τ 2.8 (m, 5.1H), 7.75 (m, 2H), 8.14 (s, 3H), 8.55 (s, 3H), 8.66 (s, 6H), and 9.33 (t, *J* = 7.5 Hz, 3H). *Anal.* calcd. for $C_{15}H_{22}O_2$: C 76.88, H 9.46; found: C 77.06, H 9.17.

(±)-2,3-Dimethyl-3-phenyl-1-pentene, (±)-10

A solution of 1.9 g of the above acetate in 10 ml methanol was pyrolyzed by dropwise addition (33) into a heated 1 in diameter glass tube filled to 12 in with glass helices. The optimum conditions were determined by pyrolyzing small quantities of the solution and analyzing the pyrolysate by gc. An equal volume of water was added to the pyrolysate and the resulting mixture shaken with ether (2 × 20 ml). The combined ether extracts were shaken with sodium bicarbonate solution, dried, and concentrated. The residue was distilled through a microdistillation apparatus to yield 0.9 g (61%) of a colorless oil, bp 107–110 °C/23 torr; n_D^{25} 1.5103; ir (CCl_4) 1635 and 895 cm^{-1} (=CH_2); nmr (CCl_4) τ 2.8 (s, 5.1H), 5.05 (s, 1.9H), 8.12 (q, *J* = 7 Hz, 2.1H), 8.52 (s, 3.1H), 8.66 (s, 3.1H), and 9.21 (t, *J* = 7 Hz, 3.0H). *Anal.* calcd. for $C_{13}H_{18}$: C 89.58, H 10.41; found: C 89.80, H 10.60.

(+)-(S)-2,3-Dimethyl-3-phenyl-1-pentene, (+)-(S)-10

A sample of (−)-(*R*)-2-methyl-2-phenylbutanoic acid (31) of $[\alpha]_D^{25}$ −29.06° (*c* 4.8, benzene) (lit. (31) $[\alpha]_D^{25}$ −30.0° for optically pure material) was converted to the crude 2-acetoxy-2,3-dimethyl-3-phenylpentane as described above. This acetate, which was prepared from ketone free alcohol, was pyrolyzed as described above to give the product bp 105–109 °C/21 torr; n_D^{29} 1.5101; α_D^{25} +11.3° (neat, *l* 1 dm) whose ir and nmr spectra were identical to those of the racemic material.

(±)-2,3-Dimethyl-3-phenylpentane, (±)-11

A mixture of 1 g (±)-**10** in 20 ml ethanol and 0.1 g 5% rhodium on alumina was stirred under hydrogen in a microhydrogenation apparatus for 24 h. The theoretical amount of hydrogen was consumed after 1 h and no more was taken up. The catalyst was filtered, the solvent removed, and the residue distilled through a microdistillation apparatus to give a colorless oil, bp 105–107 °C/21 torr; n_D^{27} 1.5012; nmr (CCl_4) τ 2.86 (s, 5H), 7.9–8.7 (m, 3H), 8.83 (s, 3H), 9.10 (d, *J* = 6.5 Hz, 3H), 9.35 (d, *J* = 6.5 Hz, 3H), and 9.31 (t, *J* = 7 Hz, 3H). *Anal.* calcd. for $C_{13}H_{20}$: C 88.57, H 11.43; found: C 88.89, H 11.48.

(−)-(S)-2,3-Dimethyl-3-phenyl-1-pentane, (−)-(S)-11

Hydrogenation of (+)-(*S*)-**10**, α_D^{25} +11.3°, as described above afforded (−)-(*S*)-**11**, bp 108–111 °C/23 torr; n_D^{26} 1.5012; α_D^{25} −0.4° (neat, *l* 1 dm); ord (*c* 1.05, methanol) $[\Phi]_{350}$ −13°, $[\Phi]_{325}$ −34°, $[\Phi]_{310}$ −58°, $[\Phi]_{300}$ −42°, $[\Phi]_{293}$ 0°. Analysis by gc showed that the compound was >98% pure and contained no starting alkene.

Hydrogenolysis of (+)-(S)-7 to (−)-2-Phenyl-2-butylamine, (−)-(S)-8

A solution of 1.0 g (+)-(*S*)-**7**, α_D^{25} +35.5° (neat, *l* 1 dm), in 100 ml methanol was stirred over 4.5 g of W-2 Raney nickel under a hydrogen atmosphere at 22 °C. After 4 h hydrogen uptake ceased when nearly 1 equiv. was taken up. The contents of the flask were then held under reflux for 11 h. The catalyst was filtered, the methanol removed, and the residue taken up in ether. The ether solution was extracted with hydrochloric acid and the acid layer made basic with potassium hydroxide solution. The resulting mixture was shaken with ether and the ether layer dried over potassium carbonate and concentrated. The product was collected from the effluent of the gas chromatograph to give 200 mg of (−)-(*S*)-**8**; n_D^{25} 1.5146; α_D^{25} −14.0° (neat, *l* 1 dm) (lit. (29) n_D^{25} 1.5148; α_{546}^{25} −18.2° (neat, *l* 1 dm)).

(−)-(S)-2-Phenyl-2-butylamine, (−)-(S)-8

Using the reported procedure (28) (+)-(*S*)-2-methyl-2-phenylbutanoic acid $[\alpha]_D^{25}$ +6.60° (*c* 4.8, benzene) 22% optically pure was converted to (−)-(*S*)-**8**, α_D^{25} −3.42° (neat, *l* 1 dm). On this basis optically pure (−)-(*S*)-**8** would have α_D^{25} −15.7° (neat, *l* 1 dm) (lit. (34) α_D^{25} +16.8° (neat, *l* 1 dm) for (+)-(*R*)-**8** obtained by resolution of the maleate salt).

(±)-1-Benzyl-2-(2-phenyl-2-butyl)diazane

A mixture of 2.5 g (0.015 mol) (2-phenyl-2-butyl)diazane (28), 0.6 g (0.015 mol) benzaldehyde, 2 g magnesium sulfate, and 20 ml anhydrous ether was stirred for 4 h and then filtered. The filtrate was hydrogenated under 1 atm over 0.4 g 5% palladium-on-charcoal until 1 equiv. of hydrogen had been taken up. The mixture was filtered under nitrogen and the residue, after removal of solvent, was distilled to give 2.7 g (67%) of a colorless viscous oil, bp 130–132 °C/0.2 torr; n_D^{25} 1.5582; nmr (CCl_4) τ 2.6–2.9 (m, 10.1H), 6.20 (s, 1.8H), 6.77 (br s, 2.0H, NH), 8.3 (q, $J = 7.5$ Hz) and 8.56 (s) (total 5.2H) and 9.32 (t, $J = 7.5$ Hz, 3.1H). This material was readily oxidized by air and a satisfactory analysis was not obtained.

*(±)-1-Benzyl-2-(2-phenyl-2-butyl)diazene, (±)-**4***

A solution of 0.6 g of the above diazane in 50 ml ether was allowed to stand under an atmosphere of oxygen for 20 h, then washed with water and dried over potassium carbonate. Removal of the ether under reduced pressure left 0.45 g of a yellow oil, n_D^{25} 1.5538; nmr ($CDCl_3$) τ 2.66 (s, 10.0H), 4.97 (s, 2H), 7.98 (q, $J = 7.5$ Hz, 2.1H), 8.57 (s, 3.1H), 9.30 (t, $J = 7.5$ Hz, 3.0H). *Anal.* calcd. for $C_{17}H_{20}N_2$: C 80.91, H 7.99, N 11.10; found: C 80.46, 80.66, H 7.67, 7.68, N 11.06.

*(−)-(R)-1-Benzyl-2-(2-phenyl-2-butyl)diazene,(−)-(R)-**4***

This material was prepared as described for the racemic compound from (+)-(*R*)-**3** (28), α_{546}^{25} 3.52° (neat, *l* 1 dm), 26% optically pure (28). The product, n_D^{25} 1.5528, had an nmr spectrum identical with that of (±)-**4**; $[\alpha]_D^{25}$ −12.88°, $[\alpha]_{546}^{25}$ −16.60°, $[\alpha]_{436}^{25}$ −66.80° (*c* 2.95, C_6H_6); ord (*c* 32.8, C_6H_6) $[\Phi]_{550}$ −165°, $[\Phi]_{500}$ −230°, $[\Phi]_{450}$ −460°, $[\Phi]_{400}$ −1280°, $[\Phi]_{375}$ 0°, $[\Phi]_{350}$ 1680°, $[\Phi]_{300}$ 755°.

*(+)-(S)-**4***

The mother liquor from the first crystallization of the dibenzoyl tartrate salt of (±)-**3** (28) was evaporated and from the residue was isolated (−)-(*S*)-**3**, α_{546}^{25} −2.04° (neat, *l* 1 dm), 15% optically pure. This product was converted to the benzyl derivative, as described above, which was dissolved in a saturated solution of oxalic acid in ethanol. After several days at 5 °C crystals of the oxalate salt were filtered, treated with aqueous potassium hydroxide, and the hydrazine taken up in ether. Oxidation of the hydrazine with oxygen produced (+)-(*S*)-**4**, $[\alpha]_D^{25}$ +28.0° (*c* 1.25, C_6H_6), 56% optically pure. A further batch of the oxalate salt was obtained after concentration of the mother liquor and converted to the diazene, $[\alpha]_D^{25}$ 0.00 (*c* 1.50, C_6H_6). Thus, the oxalate salt had undergone spontaneous resolution.

*(−)-(S)-(2-Phenyl-2-butyl)diazane, (−)-(S)-**3***

A solution of 36.0 g (0.166 mol) menthyl chlorocarbonate (35) in 100 ml ether was added simultaneously with a separate solution of 19.2 g (0.19 mol) triethylamine to a stirred solution of 27.3 g (0.166 mol) (±)-**3** (28) in 150 ml ether under nitrogen. The reaction mixture was stirred overnight and filtered. The filter cake was washed with ether and the combined ether solutions were evaporated to give 58 g of a viscous oil. Five crystallizations at 0 °C from methanol, containing a little water gave material of constant rotation $[\alpha]_{436}^{25}$ −220° (*c* 1.03, CCl_4). Filtration was carried out at 0 °C and the crystals were quickly pressed dry. The crystals melted at ~15 °C. At 0 °C they turned to syrup after a few minutes exposure to air. A satisfactory analysis was not obtained.

A solution of 20 g of this resolved product and 20 g potassium hydroxide in 100 ml methanol was heated under reflux for 4 h and then evaporated to one half its volume. The residue was acidified with dilute hydrochloric acid and the resulting mixture extracted with ether. The aqueous layer was made basic with dilute sodium hydroxide and extracted with ether. The ether layer was dried under nitrogen with sodium sulfate and concentrated to an oil. The oil was distilled to give 3.2 g product, bp 68–69 °C/0.2 torr; n_D^{25} 1.5350; α_D^{25} −11.56° (neat, *l* 1 dm) (lit. (28) for (+)-(*R*)-**3**, α_{546}^{25} +11.8° (neat, *l* 1 dm) for material 80% optically pure).

*(+)-(S)-1,2-Diphenyl-2-methylbutane, (+)-(S)-**6***

A sample of (−)-(*R*)-2-methyl-2-phenylbutanoic acid (31), $[\alpha]_D^{25}$ −29.6° (*c* 4.8, C_6H_6), 98% optically pure, was converted (13) to (−)-(*R*)-1,2-diphenyl-2-methyl-1-butanone, n_D^{25} 1.5705; $[\alpha]_D^{25}$ −61.1° (*c* 6, benzene) (lit. (13) n_D^{25} 1.5700, α_D^{25} −63.7° (neat, *l* 1 dm)). The ketone was reduced to the alcohol with lithium aluminum hydride (13). A mixture of 2.0 g (0.009 mol) of the crude product, 2.5 g (0.017 mol) iodomethane in 100 ml dimethoxyethane, and 0.3 g (0.014 mol) sodium hydride was stirred for 4 h and then heated for 3 h under reflux. Water was added to the cooled reaction mixture and the resulting mixture was extracted with ether. The ether layer was washed several times with water and dried over potassium carbonate. The crude methyl ether left after removal of the ether was stirred with 2 ml sodium potassium alloy in 100 ml ether under nitrogen for 24 h at 21 °C. The red solution was then cooled to 0 °C and a methanol–ether mixture was added slowly until all the alloy was decomposed. The reaction mixture was shaken with water and the ether layer dried over potassium carbonate and concentrated. The product was isolated from the effluent of the gc (column A); $n_D^{26.5}$ 1.5584; $[\alpha]_D^{25}$ +78.3°; $[\alpha]_{546}^{25}$ +94.7°, $[\alpha]_{436}^{25}$ +178° (*c* 4.7, C_6H_6) (lit. (12) n_D^{25} 1.5550; α_D^{25} +67° (neat, *l* 1 dm)); ord (*c* 4.7, C_6H_6)$[\Phi]_{600}$ 118°, $[\Phi]_{550}$ +167°, $[\Phi]_{500}$ +224°, $[\Phi]_{450}$ +326°, $[\Phi]_{400}$ +500°, $[\Phi]_{350}$ +880°, $[\Phi]_{300}$ +1835°.

*(±)-1-(4-Nitrophenyl)-2-(2-phenyl-2-butyl)diazene, (±)-**12***

A mixture of 1.64 g (0.01 mol) (±)-**3**, 1.4 g (0.01 mol) 4-fluoronitrobenzene, and 1.68 g (0.02 mol) sodium bicarbonate in 6 ml dimethyl sulfoxide was stirred under nitrogen at 50 °C for 36 h. The mixture was then cooled and filtered. The filtrate was stirred under air for 12 h and then diluted with 20 ml ether. The resulting mixture was shaken several times with water and the ether layer dried and concentrated. The residue was chromatographed on a 1.5 × 15 cm column of neutral alumina. Elution with 50 ml ether followed by concentration of the eluate under vacuum yielded 1.8 g (65%) of a red oil, n_D^{25} 1.5830; nmr (CCl_4) τ 1.71 (d, $J = 8.8$ Hz, 2H), 2.21 (d, $J = 8.8$ Hz, 2H), 2.63 (m, 5H), 7.86 (m, 2H), 8.42 (s, 3H), 9.22 (t, $J = 7.0$ Hz, 3H). *Anal.* calcd. for $C_{16}H_{17}N_3O_2$: C 67.84, H 6.01, N 14.84; found: C 67.74, H 6.12, N 14.87.

*(−)-(R)-1-(4-Nitrophenyl)-2-(2-phenyl-2-butyl)diazene, (−)-(R)-**12***

The procedure used was identical to that for the pre-

paration of the racemic compound except that (+)-(*R*)-**3** (28), $[\alpha]_D^{25}$ +11.6° (*c* 1.04, $CHCl_3$) was used. The product had n_D^{25} 1.5910; $[\alpha]_D^{25}$ −109° (*c* 1.09, $CHCl_3$).

*(+)-(S)-1-(4-Nitrophenyl)-2-(2-phenyl-2-butyl)diazene, (+)-(S)-**12***

This material was prepared from (−)-(*S*)-**3**, α_D^{22} −11.6° (neat, *l* 1 dm) and had n_D^{26} 1.5910; $[\alpha]_D^{25}$ +120° (*c* 0.582, $CHCl_3$).

*(±)-2-(4-Nitrophenyl)-2-phenylbutane, (±)-**27***

A mixture of 1.0 ml concentrated nitric acid, 1.2 ml concentrated sulfuric acid and 2.0 g 2,2-diphenylbutane (36) was stirred at 60 °C for 20 min. The mixture was poured into 200 ml water. The water was extracted twice with hexane, the combined hexane layers dried and concentrated, and the residual oil chromatographed on a 1.5 × 10 cm column of activity 2 alumina using 1:1 hexane–benzene as eluent. The first 30 ml of eluent contained 700 mg starting material; the second 30 ml contained 250 mg of product contaminated (gc) by ~10% starting material; the third 30 ml afforded 650 mg of pure (gc) product on evaporation; n_D^{29} 1.5819; nmr (CCl_4) τ 1.96 (d, *J* = 8.5 Hz, 2H), 2.71 (d, *J* = 8.5 Hz, 2H), 2.87 (m, 5H), 7.85 (m, 2H), 8.40 (s, 3H), 9.28 (t, *J* = 7 Hz). *Anal.* calcd. for $C_{16}H_{17}NO_2$: C 75.29, H 6.67, N 5.49; found: C 74.97, H 6.67, N 5.69.

*Hydrogenolysis of (+)-(S)-1-(2-Phenyl-2-butyl)-2-(2-propyl)diazene, (+)-S-**12***

A solution of 1.0 g (+)-(*S*)-**12**, α_D^{25} +35.5° (neat, *l* 1 dm) in 100 ml methanol was hydrogenated using 4.5 g Raney nickel at 25 °C under 1 atm. Nearly 1 equiv. of hydrogen was consumed in 4 h when hydrogen uptake ceased. The mixture was then heated under reflux for 11 h, cooled, filtered, and the filtrate concentrated to an oil. The oil was taken up in ether and the resulting solution shaken with hydrochloric acid. The aqueous layer was made basic and then extracted with ether. The ether layer was dried over potassium carbonate, concentrated to an oil, and the product isolated from the effluent of the gc (column A) to give 200 mg (−)-(*S*)-**8**, n_D^{25} 1.5146; α_D^{25} −14.0° (neat, *l* 1 dm). Based on the calculated rotation of α_D^{25} −15.7° (neat, *l* 1 dm) for optically pure material as described above the product was 89% optically pure.

*Interrupted Thermolysis of (−)-(R)-**7***

A solution of 1.4 g (−)-(*R*)-**7**, n_D^{22} 1.4947, in 300 ml benzene was divided equally among three 150 ml pressure bottles. The solutions were boiled for several minutes and the bottles closed and kept at 100 °C for 22 h. The solutions were combined and concentrated through a 4 ft Podbielniak column to ~20 ml volume. The residue was taken up in pentane. Most of the benzene was removed by a series of crystallizations from this solution at −78 °C, concentrating the solution after each crystallization. The final residue was chromatographed on 30 g silica gel at −30 °C. The hydrocarbon products were eluted with pentane, and 2% ether in pentane removed pure (tlc, nmr) (−)-(*R*)-**7**, 0.70 g, n_D^{22} 1.4958. The coupling product **11** was isolated from the concentrated pentane eluent by gc, column A at 170 °C and 150 ml/min He flow. Rotations are given in Table 4.

*Interrupted Thermolysis of (−)-(R)-**12***

Nitrogen was bubbled for 10 min through a solution of 500 mg (−)-(*R*)-**12** (n_D^{25} 1.5910; $[\alpha]_D^{25}$ −108.8° (*c* 1.09, $CHCl_3$)) in 30 ml cumene in a stainless steel bomb which was then sealed and heated at 175 °C for 5 h. Cumene was distilled under reduced pressure and the residue was repeatedly chromatographed on activity I alumina using benzene–hexane as eluent until pure (tlc, nmr) (−)-(*R*)-**12**, 31 mg, was eluted, n_D^{25} 1.5898; $[\alpha]_D^{25}$ −111.7° (*c* 1.02, $CHCl_3$).

*Photolysis of (+)-(S)-**12***

A solution of 400 mg (+)-(*S*)-**12** (n_D^{25} 1.5902; $[\alpha]_D^{25}$ +110.2° (*c* 0.448, $CHCl_3$)) in 50 ml hexadecane was photolyzed at 15 °C under nitrogen in an immersion apparatus fitted with a Pyrex filter using a medium pressure 200 W Hanovia lamp until 60% of the theoretical amount of nitrogen had been evolved. The reaction mixture was concentrated under vacuum and the residue was chromatographed on 75 g activated alumina which had been heated over the full heat of a Bunsen burner for 4 h. The column was washed with 1.2 ℓ pentane and then with pentane containing increasing amounts of benzene. Benzene–pentane, 1:1, removed pure (tlc, nmr) (+)-(*S*)-**12**, 60 mg, n_D^{25} 1.5895; $[\alpha]_D^{25}$ +111° (*c* 0.130, $CHCl_3$).

In a similar way 236 mg (+)-(*S*)-**12**, $[\alpha]_D^{25}$ +120° (*c* 0.400, $CHCl_3$), was recovered from photolysis of 900 mg of the diazene, $[\alpha]_D^{25}$ +119° (*c* 0.590, $CHCl_3$), in hexane for 9 h until 40% of the theoretical amount of nitrogen had been evolved.

The recovered diazenes were combined with fractions from the chromatographies containing impure diazene and the resulting mixture photolyzed in hexadecane until no more diazene remained (tlc). It was necessary twice to remove a brown precipitate when nitrogen evolution ceased before the photolysis was complete. The photolysate was concentrated and the residue chromatographed on a 100 × 1.2 cm column of silica gel using pentane as eluent. A sample, 44 mg (3%), of pure (tlc) **27** was isolated, $[\alpha]_{365}^{25}$ 0.00(*c* 0.18, CCl_4).

*Thermolysis of (+)-(S)-**4** and (−)-(R)-**4***

A solution of 0.97 g of (+)-(*S*)-**4**, $[\alpha]_D^{25}$ +28.0° (*c* 1.25, C_6H_6), and 4.7 g butanethiol in 50 ml benzene in a stainless steel bomb was flushed with nitrogen. The bomb was closed and heated at 102 °C for 30 h, then cooled, and the contents evaporated under reduced pressure. The residue was fractionated by gc using column A. Material which eluted at the retention time of (±)-**6** was collected and found to consist of a liquid and a white solid. This mixture was refractionated using column B to two separate compounds, a small amount of *E*-**19**, identified by its nmr spectrum and gc retention time on both columns, and (−)-(*R*)-**6**, $[\alpha]_D^{25}$ −4.6° (*c* 1.8, C_6H_6), which was formed with 10.7% retention of configuration.

The same procedure was used for the thermolysis of (−)-(*S*)-**4**. The concentrated reaction mixtures were fractionated directly with column B. The results are presented in Table 3.

*Thermolysis of (+)-(S)-**7***

Benzene solutions of (+)-(*S*)-**7** were heated under nitrogen in a stainless steel bomb as described above. After 10 half-lives of decomposition the solvent was distilled slowly through a Vigreaux column. Traces of alkene were removed by heating the residual oil in a solution of 10 ml acetic acid containing 2 ml trichloro-

methylsulfenyl chloride at 85 °C for 60 min. The reaction mixture was taken up in 100 ml pentane and the pentane layer shaken 7 times with water, dried, and concentrated by distillation through a Vigreaux column. The residue was chromatographed on 200 g of activated basic alumina at 0 °C using pentane as eluent. The hydrocarbons **11** and (−)-(*R*)-**16** were isolated from the effluent of the gc using column A. The results are presented in Table 4.

Product Studies

Solutions of ~35 mg (±)-**7** in 0.4 ml benzene or 1 *M* butanethiol in benzene were placed in glass tubes and degassed by three freeze–thaw cycles under 10^{-4} torr. The tubes were sealed and heated at 100 °C for 130 h or at 125 °C for 14 h. The reaction mixtures were then adsorbed on 5 g of neutral activity I alumina and the alumina was washed with 15 ml pentane. Further elution with pentane removed another material, presumably hydrazone, which interfered with subsequent analysis. The eluent was concentrated by distillation through a Vigreaux column, a known amount of bromobenzene was added to the residue which was then analyzed by gc using column A (temperature programmed; initial temperature 90 °C, rate of increase 1.5°C/min, initial He 90 ml/min). Calibrations were made using mixtures of known concentration in benzene. The products were identified on the basis of their retention times. Authentic samples of **17**, *Z*- and *E*-**18** were prepared (37) as were *meso*- and *dl*-**14** (38), which were not separated under the gc conditions used. In the decompositions at 125 °C the relative yield of (±)-**16** was 2% lower and that of **14** was 3% higher than in the decompositions at 100 °C. The relative yields of the other products were the same at the two temperatures.

Solutions of (±)-**4** in the various solvents were placed in a stainless steel bomb and flushed for several minutes with nitrogen. The bomb was closed and heated at 110 °C for 20 h. The reaction mixtures were analyzed directly by gc using column B (temperature programmed; initial temperature 100 °C, rate of increase 3 °C/min, initial He 85 ml/min). The compounds were identified on the basis of their retention times. In one case a known amount of bromobenzene was added just before analysis. Calibrations were made using mixtures of known concentration in benzene.

A solution of 700 mg (±)-**12** in 7 g diphenylether was heated under nitrogen in a stainless steel bomb at 175 °C for 18 h. A known amount of dimethylaniline was added to the reaction mixture and this was analyzed by gc using column B (120 °C, He 50 ml/min). Calibrations were made using mixtures of known concentration in benzene. The volatile compounds were identified by mass spectral analysis as they emerged from the gc. The mass spectral cracking patterns were compared to those of the authentic compounds. The amount of **25** formed was found by adding an aliquot of the reaction mixture to hexane, collecting, and comparing (mp, ir) the precipitate with an authentic sample of **25**.

A 2 g sample of (±)-**12** was heated at 175 °C for 18 h under nitrogen in a 5 ml flask fitted with a condenser. After cooling the residue was stirred several times with small amounts of hexane. The insoluble material, 0.67 g (79%) was nearly pure **25**. Dimethylaniline was added to the combined hexane washings and the solution analyzed by gc.

Kinetic Studies

Rates of evolution of nitrogen from solutions of the diazenes were measured using an apparatus and a procedure similar to that described (39). Rate constants were determined from the slopes of plots of log $(V_\infty - V_0/V_\infty - V_t)$. The results are presented in Table 1.

1. K. R. KOPECKY and T. GILLAN. Can. J. Chem. **47**, 2371 (1969).
2. F. D. GREENE, M. A. BERWICK, and J. C. STOWELL. J. Am. Chem. Soc. **92**, 867 (1970).
3. (*a*) H. C. RAMSPERGER. J. Am. Chem. Soc. **51**, 2134 (1929); (*b*) S. G. COHEN and C. H. WANG. J. Am. Chem. Soc. **77**, 3628 (1955); (*c*) C. G. OVERBERGER and A. V. DIGUILIO. J. Am. Chem. Soc. **81**, 2154 (1959); (*d*) S. SELTZER. J. Am. Chem. Soc. **83**, 2625 (1961); (*e*) S. SELTZER. J. Am. Chem. Soc. **85**, 15 (1963); (*f*) S. SELTZER and S. G. MYLONAKIS. J. Am. Chem. Soc. **89**, 6584 (1967); (*g*) J. HINZ, R. OBERLINNER, and C. RÜCHARDT. Tetrahedron Lett. 1975 (1973); (*h*) T. R. LYNCH, F. N. MACLACHLAN, and J. L. SUSCHITZKY. Can. J. Chem. **51**, 1378 (1973).
4. (*a*) R. J. CRAWFORD and R. MISHRA. J. Am. Chem. Soc. **87**, 3768 (1965); (*b*) R. J. CRAWFORD and D. M. CAMERON. Can. J. Chem. **45**, 691 (1967); (*c*) B. H. AL-SADER and R. J. CRAWFORD. Can. J. Chem. **46**, 3301 (1968); (*d*) K. R. KOPECKY and J. SOLER. Can. J. Chem. **52**, 2111 (1974).
5. S. SELTZER and F. T. DUNNE. J. Am. Chem. Soc. **87**, 2628 (1965).
6. (*a*) A. TSOLIS, S. MYLONAKIS, M. NIEH, and S. SELTZER. J. Am. Chem. Soc. **94**, 829 (1972); (*b*) R. A. JOHNSON and S. SELTZER. J. Am. Chem. Soc. **95**, 938 (1973); (*c*) N. A. PORTER, M. E. LANDIS, and L. J. MARNETT. J. Am. Chem. Soc. **93**, 795 (1971); (*d*) N. A. PORTER and L. J. MARNETT. J. Am. Chem. Soc. **95**, 4361 (1973).
7. (*a*) W. A. PRYOR and K. SMITH. J. Am. Chem. Soc. **92**, 5403 (1973); (*b*) K. TAKAGI and R. J. CRAWFORD. J. Am. Chem. Soc. **94**, 7406 (1972); (*c*) A. W. GARNER, J. W. TIMBERLAKE, P. S. ENGEL, and R. A. MELAUGH. J. Am. Chem. Soc. **97**, 7377 (1975).
8. R. C. NEUMAN, JR., G. D. LOCKYER, JR., and M. J. AMRICH. Tetrahedron Lett. 1221 (1972).
9. (*a*) N. A. PORTER, L. J. MARNETT, C. H. LOCKMÜLLER, G. L. CLOSS, and M. SHOBATAKI. J. Am. Chem. Soc. **94**, 3664 (1972); (*b*) N. PORTER, J. G. GREEN, and G. R. DUBAY. Tetrahedron Lett. 3363 (1975).
10. N. A. PORTER and M. O. FUNK. Chem. Commun. 263 (1973).
11. D. J. CRAM and J. S. BRADSHAW. J. Am. Chem. Soc. **85**, 1108 (1963).
12. D. J. CRAM and J. ALLINGER. J. Am. Chem. Soc. **79**, 2858 (1957).
13. D. J. CRAM and J. ALLINGER. J. Am. Chem. Soc. **76**, 4516 (1954).
14. J. H. BREWSTER. J. Am. Chem. Soc. **81**, 5475 (1954).
15. T. R. THOMPSON. J. Am. Chem. Soc. **75**, 6070 (1953).
16. P. S. ENGEL and D. J. BISHOP. J. Am. Chem. Soc. **97**, 6754 (1975).
17. C. G. OVERBERGER and A. V. DIGUILIO. J. Am. Chem. Soc. **81**, 2154 (1959).
18. (*a*) S. F. NELSON and P. D. BARTLETT. J. Am. Chem.

Soc. **88**, 137 (1966); (*b*) R. C. NEUMAN, JR. and E. S. ALHADEFF. J. Org. Chem. **35**, 3401 (1970).
19. (*a*) A. F. BICKEL and W. A. WATERS. Recl. Trav. Chim. Pays-Bas **69**, 312 (1950); (*b*) B. K. BANDLISH, A. W. GARNER, M. L. HODGES, and J. W. TIMBERLAKE. J. Am. Chem. Soc. **97**, 5856 (1975).
20. A. F. BICKEL and E. C. KOOYMAN. Nature, **170**, 211 (1952).
21. K. R. KOPECKY, P. M. POPE, and J. A. LOPEZ SASTRE. Can. J. Chem. **54**, 2639 (1976).
22. (*a*) D. J. CRAM. J. Am. Chem. Soc. **74**, 2149 (1952); (*b*) J. KENYON, H. PHILLIPS, and V. P. PITTMAN. J. Chem. Soc. 1072 (1935).
23. R. C. NEUMAN, JR. and E. S. ALHADEFF. J. Org. Chem. **35**, 3401 (1970).
24. H. M. WALBORSKY and C.-J. CHEN. J. Am. Chem. Soc. **89**, 5499 (1967).
25. P. D. BARTLETT and J. D. MCBRIDE. Pure Appl. Chem. **15**, 89 (1967).
26. S. SELTZER and E. J. HAMILTON, JR. J. Am. Chem. Soc. **88**, 3775 (1966).
27. S. F. NELSON and P. D. BARTLETT. J. Am. Chem. Soc. **88**, 143 (1966).
28. D. J. CRAM and J. S. BRADSHAW. J. Am. Chem. Soc. **85**, 1108 (1962).
29. C. L. BUTLER and L. H. CRETCHER. J. Am. Chem. Soc. **55**, 2605 (1933).
30. G. LOSSE. Chem. Ber. **87**, 1279 (1954).
31. D. J. CRAM and J. D. KNIGHT. J. Am. Chem. Soc. **74**, 5835 (1952).
32. T. D. NEVITT and G. S. HAMMOND. J. Am. Chem. Soc. **76**, 4124 (1954).
33. C. H. DEPUY and R. W. KING. Chem. Rev. **60**, 431 (1960).
34. E. M. KOSSOWER and D. J. SEVERN. Tetrahedron Lett. 3125 (1966).
35. R. H. PICKARD and W. O. LITTLEBURY. J. Chem. Soc. 109 (1912).
36. T. WEINSTOCK and S. N. LEWIS. J. Am. Chem. Soc. **79**, 6243 (1957).
37. D. J. CRAM. J. Am. Chem. Soc. **71**, 3883 (1949).
38. R. L. HUANG and L. KUM-TALT. J. Chem. Soc. 2570 (1954).
39. R. C. PETERSEN, J. H. MARKGRAF, and S. D. ROSS. J. Am. Chem. Soc. **83**, 3819 (1961).

Conformational analysis of 2-substituted methylenecyclohexanes and 3-substituted cyclohexenes and the anomeric effect[1]

JEAN LESSARD, PHAN VIET MINH TAN,[2] ROBERT MARTINO,[3] AND JOHN K. SAUNDERS

Département de Chimie, Université de Sherbrooke, Sherbrooke (Qué.), Canada J1K 2R1

Received September 7, 1976

JEAN LESSARD, PHAN VIET MINH TAN, ROBERT MARTINO, and JOHN K. SAUNDERS. Can. J. Chem. **55**, 1015 (1977).

The analysis of the ^{13}C and ^{1}H nuclear magnetic resonance data of 2-substituted methylenecyclohexanes and 3-substituted cyclohexenes demonstrates that a double bond stabilizes the axial conformer for an electronegative substituent. Introduction of a methoxy group on the double bond further increases the relative stability of the axial conformer. These results are interpreted in terms of the 'double bond – no bond' resonance.

JEAN LESSARD, PHAN VIET MINH TAN, ROBERT MARTINO et JOHN K. SAUNDERS. Can. J. Chem. **55**, 1015 (1977).

L'analyse des spectres de résonance magnétique nucléaire du ^{13}C et du ^{1}H de méthylenecyclohexanes substitués à la position 2 et de cyclohexènes substitués à la position 3 démontre qu'une double liaison stabilise le conformère axial lorsque le substituant est électronégatif. L'introduction d'un groupement méthoxy sur la double liaison augmente d'avantage la stabilité relative du conformère axial. Les résultats sont interprétés en termes de résonance 'double bond – no bond'.

The effect that causes electronegative groups to occupy sterically unfavoured conformations when attached to a carbon bearing an electronegative atom is known as the anomeric effect (1). A number of hypotheses have been advanced in order to explain this effect. These include the dipole–dipole interaction (2) which would favour the axial conformation relative to the equatorial since in the former the two dipoles are virtually

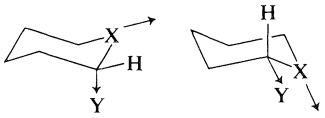

perpendicular, whereas in the latter the two dipoles have the same direction and are in much closer proximity. A second explanation (3), labelled the rabbit-ear effect, states that the interaction lone pair – lone pair is significantly larger than either the interactions lone pair – bonding pair or bonding pair – bonding pair. In the example where both X and Y are oxygens, a conformation can be defined for the axial conformer in which there is no lone pair – lone pair interaction whereas when Y is equatorial all possible conformations have at least one such interaction. Thus again, the conformation in which Y is equatorial is destabilized. A third possible explanation is known as double bond – no bond resonance (4). In this hypothesis, charged resonance forms such as

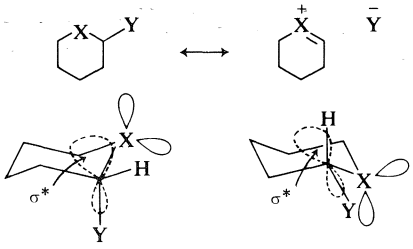

contribute. This can also be interpreted in term of an overlap between the lone-pair electrons on X and the σ antibonding orbital of the C—Y bond. This should be a maximum when the lone pair on X and the C—Y bond are antiperiplanar and thus this theory predicts that the form with Y axial would be stabilized.

In an attempt to obtain experimental evidence, other than crystallographic data (5), of the importance of the latter postulate, we have studied a number of 2-substituted methylenecyclohexanes and 3-substituted cyclohexenes. If the double bond – no bond resonance makes a significant contribution to the anomeric effect

[1]Based on the M.Sc. dissertation of Phan Viet Minh Tan, Université de Sherbrooke, 1976.

[2]NRCC Predoctorate Fellow 1974–1975.

[3]Permanent address: Université Paul Sabatier, U.E.R. de Chimie Organique, Toulouse, France.

TABLE 1. ^{13}C Chemical shift[a] data for cyclohexene derivatives

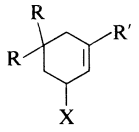

Compound	Substituents X	R	R′	Chemical shifts C-1	C-2	C-3	C-4	C-5	C-6	R_{eq}	R_{ax}	R′	X
1[b]	H	H	H	127.4	127.4	25.2	23.3	23.3	25.2				
2[b]	CH_3	H	H	126.8	134.1	32.7	30.8	22.2	25.8				22.2
3[c]	H	CH_3	CH_3	134.3	120.0	24.7	34.7	29.2	43.5	31.7	25.1	23.0	
4[b]	OCH_3	H	H			73.8	27.2	18.8	24.7				54.9
5[b]	$OCOCH_3$	H	H	126.0	132.8	68.1	28.4	19.0	25.0				170.2; 21.1
6	OH	CH_3	CH_3	136.0	124.5	66.4	44.3	31.1	45.1	31.5	26.2	23.6	
7	OCH_3	CH_3	CH_3	134.9	121.0	75.5	41.1	30.9	44.4	31.2	26.5	23.7	55.5
8[d]	$OCOCH_3$	CH_3	CH_3	136.7	119.8	68.8	40.4	30.1	43.8	30.1	26.7	23.2	168.7; 20.6

[a]Relative to TMS; approximately 7% in CF_2Br_2–CD_2Cl_2 75:25; 270 K.
[b]$CDCl_3$.
[c]125 K.
[d]CCl_4 – 10% CD_3COCD_3.

then a double bond should stabilize the axial conformer when the substituents are electronegative. The results of this study, presented in this paper, do in fact demonstrate that this postulate is important.

Results

The ^{13}C nuclear magnetic resonance (^{13}Cmr) chemical shift data for a number of cyclohexene derivatives is given in Table 1. The spectral assignments were made using the literature values for **1** (6) and (**2**) (7), and normal substituent effects. The spectrum of each compound as a function of temperature was then studied. However, **3** was the only compound to show marked spectral changes with temperature. At room temperatures the two methyl groups appeared as a single peak at 28.4 ppm. As the temperature approached 145 K, this peak broadened and at temperatures below 145 K, the resonances corresponding to each methyl group were observed. The coalescence temperature was estimated to be 145 K and since $\Delta\nu$ is 6.6 ppm (at 22.63 MHz), $\Delta G^{\ddagger}$ was calculated to be 6.5 ± 0.5 kcal/mol using the Eyring equation (8). This value is within experimental error of published values determined for other cyclohexene derivatives (9). The spectra of the other compounds exhibited small chemical shift changes with temperature but since the CF_2Br_2 resonances varied relative to the deuterium signal of CD_2Cl_2, no information could be gleaned from these variations. However, no evidence of coalescence behaviour was observed. This could be due to three factors: (*i*) chemical shift difference too small, (*ii*) decrease in the barrier of interconversion, or (*iii*) essentially one conformer being present. The first possibility can be neglected at least for **2**, **4**, and **5** since the difference at C-5 in these compounds between X pseudo axial or pseudo equatorial would be at least 5 ppm. The introduction of one of these substituents in cyclohexenes (9) and methylenecyclohexanes (10, 11) does not appear to cause a significant variation in the value of $\Delta G^{\ddagger}$ and thus it appears unlikely that the barrier to interconversion in **2**, **4**–**8** is significantly less than that observed in **3** and hence it appears that the second possibility is extremely unlikely. Thus it is reasonable to assume that the lack of observation of coalescence behaviour is due to essentially one isomer being present.

It is of interest to compare the chemical shifts of carbon 5 in compounds **1**, **2**, **4**, and **5**. In compound **2**, this carbon has virtually the same chemical shift as in **1**, whereas in **4** and **5** it is shielded by 4.5 and 4.3 ppm respectively. This is a consequence of the well known γ effect in ^{13}Cmr spectroscopy which causes an upfield shift when the group X and the proton on the γ carbon are 1,3 diaxial. Thus, it appears that in **2** the conformer with the CH_3 group equatorial is preferred, whereas for **2**, **4**, and **5**, it is the conformer with the OR group axial which is predominant. In order to verify these facts, the ^{1}Hmr of these compounds together with several other

TABLE 2. Linewidth at half height of H-3 in cyclohexene derivatives

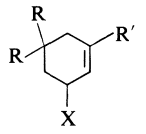

Compound	X	R	R′	Solvent	$\Delta\nu_{1/2}$[a]
4	OCH_3	H	H	CCl_4	9.6
5	$OCOCH_3$	H	H	CCl_4	8.9
				$CDCl_3$	8.6
6	OH	CH_3	CH_3	CCl_4	16.5
7	OCH_3	CH_3	CH_3	CCl_4	16.4
8	$OCOCH_3$	CH_3	CH_3	CCl_4	16.0
9	Br	H	H	CCl_4	7.5
10	OH	H	H	CCl_4	8.7
11	Br	CH_3	CH_3	CCl_4	17.0
12	OH	H	OCH_3	CCl_4	7.6
13	OCH_3	H	OCH_3	CCl_4	7.4
14	OCH_3	CH_3	OCH_3	CCl_4	15.5

[a]Linewidth at half height ±0.5 Hz.

derivatives were studied. In Table 2, the width at half height ($\Delta\nu_{1/2}$) for the 3 proton is given. The observed linewidth will be the sum of $^3J_{3,4a} + {}^3J_{3,4e} + {}^3J_{3,2} + {}^4J_{3,1} + {}^5J_{3,6}$. Using published values of J and dihedral angles (12), these values are for H-3 pseudo axial: $^3J_{3,4a} = 11.0$ Hz, $^3J_{3,4e} = 1.5$ Hz, $^3J_{3,2} = 1.5$ Hz, $^4J_{3,1} = 1.0$ Hz, and $^5J_{3,6} = 1.5$ Hz. For H-3 pseudo equatorial: $^3J_{3,4a} = 1.5$ Hz, $^3J_{3,4e} = 1.0$ Hz, $^3J_{3,2} = 4.0$ Hz, and $^4J_{3,1} + {}^5J_{3,6} < 0.5$ Hz. In the compounds where R′ = CH_3, the CH_3 appeared as a doublet of doublets with coupling constants of 1.5 Hz and 1.4 Hz with the latter corresponding to J_{2,CH_3}. The values of $\Delta\nu_{1/2}$ were then estimated to be 17.0 Hz (R′ = H) and 17.5 Hz (R′ = CH_3) for the group X pseudo equatorial and 6.5 Hz (R′ = H) and 8.0 Hz (R′ = CH_3) for X pseudo axial. Inspection of the data in Table 2 indicates that **6**, **7**, **8**, **11**, and **14** exist predominately, if not almost exclusively, with X in the pseudo equatorial conformation whereas the predominant conformation of **4**, **5**, **9**, **10**, **12**, and **13** is that in which the X group is pseudo axial. It is of interest to note that $\Delta\nu_{1/2}$ in **9** is less than that observed in **4**, **5**, and **10** indicating that the pseudo axial conformer is more highly populated when X = Br then when X is an oxygenated substituent. Also, comparison of **12** and **13** with **10** and **4** demonstrates that the replacement of H at C-1 by an OCH_3 group increases the proportion of X pseudo axial.

The ^{13}Cmr spectral data for the substituted methylenecyclohexanes are given in Table 3. Assignments were made with the aid of single frequency off-resonance decoupled spectra and the published chemical shift data for **15** (13) and **16**[4]. The compounds were then studied as a function of temperature. For **17**, the signals at 26.3 and 36.0 ppm become significantly broadened as the temperature approached 195 K as did the signal at 104.2 ppm. At 170 K, the signals for the two conformers were observed. The Overhauser effect should be the same in both conformers and thus integration of the respective signals can be used to determine the population in each conformation at this temperature. The average equatorial/axial ratio was determined to be 95:5, which leads to a ΔG_0 (axial–equatorial) of 1.0 ± 0.2 kcal/mol. The various absorptions exhibited coalescence temperatures between 185 and 198 K depending on the respective chemical shift difference. The average value for $\Delta G^{\ddagger}$ was found to be 9 ± 0.6 kcal/mol which is slightly higher than that found in dimethyl methylenecyclohexanes (10). Compound **18** also showed coalescence behaviour as can be seen in Fig. 1 in which the spectra recorded at 193 and 163 K are illustrated. The most intense absorption in the spectrum at 193 K is due to CF_2Br_2. At 193 K, the absorptions corresponding to C-4 and C-6 are extremely broad, that corresponding to the OCH_3 is reasonably broad, whereas the absorptions for C-1, C-2, and C-3 are relatively narrow.

[4]G. Caron, Ph.D. Thesis, Université de Sherbrooke, 1976.

TABLE 3. ^{13}C Chemical shifts[a] of methylenecyclohexane derivatives

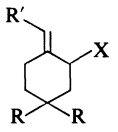

Compound	X	R	R′	C-1	C-2	C-3	C-4	C-5	C-6	C-7	R_{eq}	R_{ax}	R′	X
15[b]	H	H	H	149.7	36.2	28.9	26.9	28.9	36.7	107.1				
16[c]	H	H	OCH_3	118.4	30.6	28.9	27.1	27.1	25.6	138.8			59.1	
17	CH_3(eq)	H	H	155.7	37.5	36.7	26.5	28.4	36.7	104.0				18.6
	CH_3(ax)	H	H		35.9	35.4	20.7		31.2	107.8				18.0
18	OCH_3(eq)	H	H	149.3	81.6	35.2	25.1	27.9	34.9	104.2				57.1
	OCH_3(ax)	H	H	147.3	80.8	33.3	20.4	27.6	30.3	111.8				55.2
19[d]	OCH_3	H	OCH_3	116.6	77.8	33.6	21.4	26.4	21.4	141.0			58.7	54.3
20	OCH_3	CH_3	H	149.6	78.7	47.0	31.6	40.5	31.6	104.4	32.6	25.2		57.3
21	H	CH_3	OCH_3	117.4	26.1	38.6	30.9	39.8	21.5	138.1	32.9	23.4	58.0	

[a]Relative to TMS; approximately 7% in CF_2Br_2–CD_2Cl_2 75:25; 163 K.
[b]Reference 13.
[c]G. Caron, Ph.D. Thesis, Université de Sherbrooke, 1976.
[d]$CDCl_3$, ~305 K.

In the spectrum at 163 K, the absorption for the two conformers can be clearly observed and careful integration of several spectra at this temperature gave an axial/equatorial ratio of 3.5 ± 0.3. Thus, the conformer with the OCH_3 group axial is 0.4 ± 0.04 kcal/mol more stable than that in which the OCH_3 is equatorial. From the coalescence temperatures and respective chemical shift difference, $\Delta G^{\neq}$ could be calculated for the coalescence of each pair of resonances and an average value of 9 ± 0.6 kcal/mol was obtained.

In Fig. 2, the spectrum of **19** at 163 K is compared to that of **18** at the same temperature. The spectrum of **19** corresponds to only one conformation being present and the spectrum obtained at 130 K is essentially identical with that shown. In order to verify that the barrier to interconversion had not been drastically lowered by the introduction of the OCH_3 group at C-7, compound **21** was studied as a function of temperature. The coalescence temperature for the signals of the methyl groups is 198 K and since $\Delta\nu = 9.5$ ppm, $\Delta G^{\neq} = 9.0 \pm 0.6$ kcal/mol. Since the barriers to interconversion of compounds **17**, **18**, and **21** have all been calculated to be 9.0 ± 0.6 kcal/mol and since $\Delta\nu$ (axial–equatorial) for C-4 in **19** should be of the order of −4.5 ppm, it is reasonable to conclude that the axial/equatorial ratio at 163 K is at least 17. The predominant conformer present is readily assigned as the axial due to the chemical shifts of C-4 and C-6. Thus ΔG_0 (axial–equatorial) is at least −1.0 kcal/mol.

In order to destabilize the axial conformations, compound **20** and the 4,4-dimethyl analog of **19** were prepared. At low temperatures, only one conformer of **20**, namely the equatorial, was observed. Unfortunately, the dimethyl analog of **19** could not be obtained in a pure state (see Experimental).

Discussion

In cyclohexane derivatives, the A value of a group is a measure of the energy difference between an axial and equatorial orientation for the group in question. For methylenecyclohexanes substituted in the 2 position, we have introduced an interaction between the group X and the hydrogen of the double bond. This interaction is known as the allylic tension $A^{(1,3)}$. Thus, the observed free energy difference for 2-substituted methylenecyclohexanes will be $A - A^{(1,3)}$ provided only steric interactions are involved. The A value of a CH_3 group is 1.7 kcal/mol (14). As seen in the previous section, the free energy difference for 2-methylmethylenecyclohexane (**17**) is 1.0 kcal/mol and since the A value for **17** should be almost identical with that in cyclohexane the allylic interaction $A^{(1,3)}$ is of the order of 0.7 kcal/mol. This value is significantly less than that estimated by ^{1}Hmr spectroscopy (15) although St-Jacques[5] did not observe the axial conformer in the ^{1}Hmr spectrum at low temperatures. The value of 0.7

[5]M. St-Jacques, private communication.

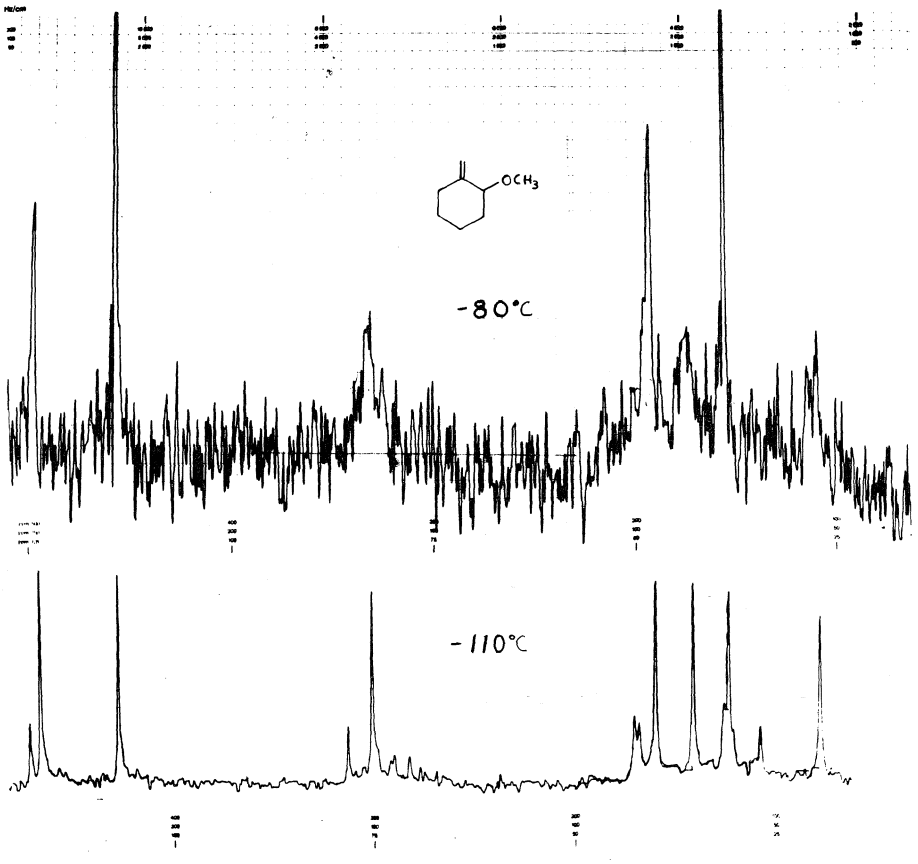

FIG. 1. ^{13}Cmr spectra of **18** at 193 and 163 K.

kcal/mol is reasonably close to the value observed for a 1,3 diaxial CH_3–hydrogen interaction.

The *A* value for an OCH_3 group is 0.8 kcal/mol (14). Thus, if we assume that the $A^{(1,3)}$ interaction for a OCH_3 is of the same order as for a CH_3 group, *i.e.* half the *A* value, then we would predict ΔG_0 (axial–equatorial) = 0.4 kcal/mol for 2-methoxymethylenecyclohexane (**18**). However, experimentally it is −0.4 kcal/mol and thus the conformation in which the OCH_3 is axial is stabilized by approximately 0.8 kcal/mol. Similarly, for **19**, where ΔG_0 (axial–equatorial) > −1.0 kcal/mol, the axial conformer is stabilized by at least 1.4 kcal/mol (0.6 kcal/mol relative to **18**). The difference in energy between that predicted and observed for **18** could be due to either double bond – no bond resonance or an electrostatic interaction between the C—O and C=C bonds. This interaction is either dipole–dipole or dipole–quadrupole in nature. The latter interaction has been proposed (11) in order to explain the conformational equilibrium observed for 3-substituted methylenecyclohexanes. We have carried out simple electrostatic calculations, similar to those performed by Lambert and Clikeman (11), using the standard dipole–dipole and dipole–quadrupole interaction equations (16–18) and have found that the two interactions stabilize the axial conformation of **18** relative to the equatorial conformation with the dipole–quadrupole interaction being more important. Introduction of the oxygen at C-7 will decrease the dipole moment and should also decrease the quadrupole moment (18) of the double bond. Hence, it appears that the difference in conformer population of **19** relative to **18** is not due to an increase in the electrostatic interaction between the C_2—O bond and the C—C double bond. In compound **19**, we have a situation which resembles that of 2-methoxytetrahydropyran. However, the influence of the oxygen–oxygen dipole–dipole interaction on the relative stability of the two conformations is calculated as being negligible

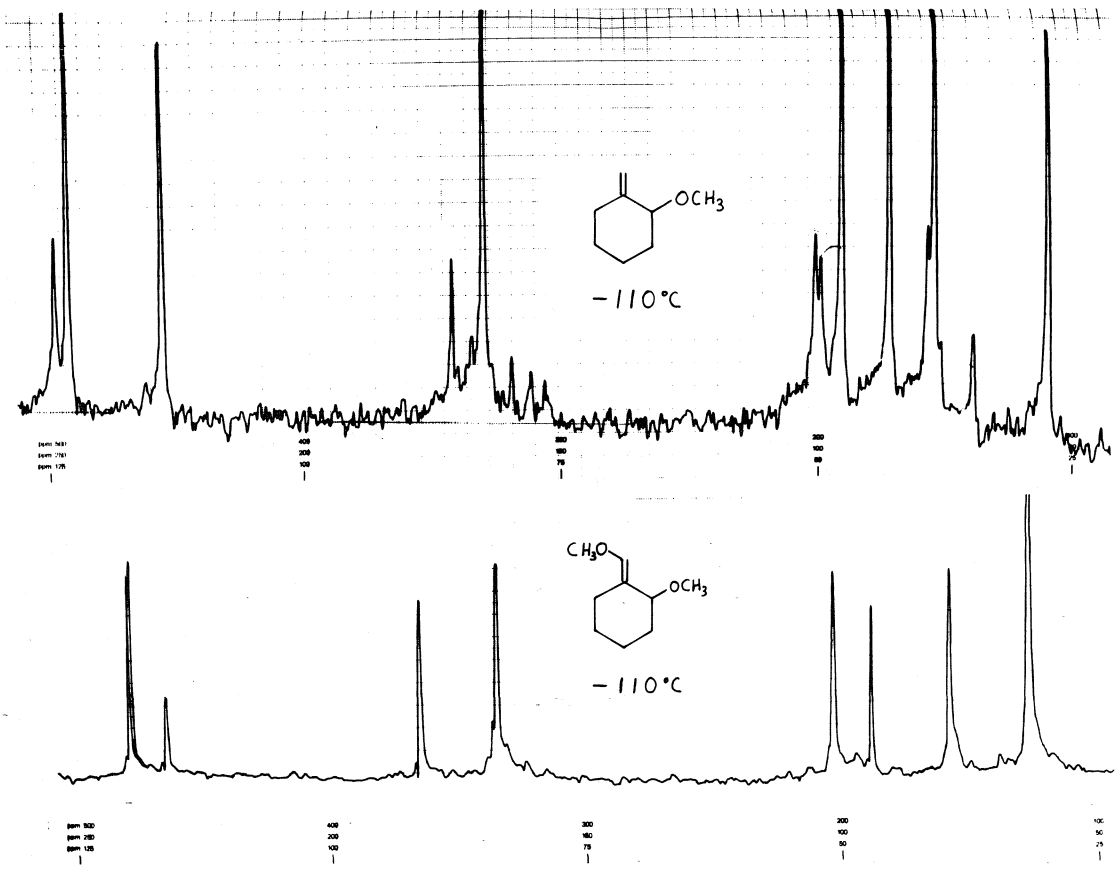

FIG. 2. ^{13}Cmr spectra of **18** and **19** at 163 K.

and the rabbit-ear effect can no longer be invoked. Hence we are left with the double bond – no bond resonance since the introduction of an OCH_3 group on the double bond increases its electron density. In order for an overlap to occur between the π molecular orbital of the double bond and the σ^* orbital of the C—O bond, the OCH_3 group must be axial and therefore the axial conformer '**19** ax' is stabilized by double bond – no bond resonance.

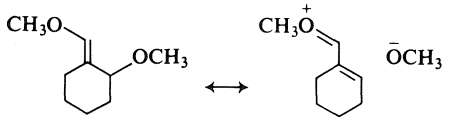

19 ax

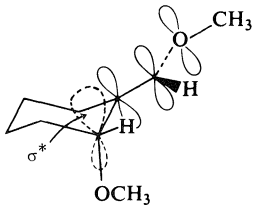

For 3 substituted cyclohexenes, the results are not quantitative. However, the compounds in which X is an electronegative group and R an hydrogen all have a preponderance of the conformation where X is pseudo axial, whereas when X is a CH_3 group, the preferred conformation is that with X pseudo equatorial. Again, as in the 2-substituted methylenecyclohexanes, the stabilization of the axial conformer by the double bond is adequately explained either in terms of double bond – no bond resonance or the dipole–quadrupole interaction between the C—X and the C=C bonds. Also the extra stabilization afforded by the introduction of the OCH_3 group is interpreted in terms of the former since the dipole–dipole interactions and the rabbit ear effect cannot be invoked and since the introduction of the OCH_3 group on the double bond should decrease its quadrupole moment.

Conclusion

The results obtained for the substituted

methylenecyclohexanes and cyclohexenes demonstrate that the double bond stabilizes the conformer with the electronegative group axial at the allylic position (C-2 and C-3 respectively). Introduction of an OCH_3 group on the double bond at either C-1 (cyclohexene) or C-7 (methylenecyclohexane) further stabilizes the axial conformer. The stabilization by the double bond is evaluated at 0.8 kcal/mol and the introduction of the OCH_3 results in an added stabilization of at least 0.6 kcal/mol. The stabilization by the double bond is interpreted as being due to either double bond – no bond resonance or an electrostatic interaction between the C—X and C=C bonds (predominantly the dipole–quadrupole interaction). However, it has been calculated (17) that when the two entities are in close proximity, the electrostatic interaction is less important which would tend to suggest that the principal factor causing the stabilization is the double bond – no bond resonance. The extra stabilization afforded by the introduction of the OCH_3 group on the double bond is interpreted in terms of double bond – no bond resonance. We would thus expect that in 2-methoxytetrahydropyran, for example, the overlap between the non bonding electron of oxygen and the σ antibonding orbital of the C—O bond to be important.

Experimental

Vapor phase chromatographic analyses and separations were performed on a Hewlett Packard chromatograph model 5750 equipped with both thermal conductivity and flame ionization detectors: an OS-138 column (15% polyphenyl ether on dimethylsilylated Chromosorb W) or an SE-30 column (10% on dimethylsilylated Chromosorb W) with o.d. 0.25 in. (analytical) or 0.375 in. (preparative) and length 6 ft were used. Infrared spectra were taken on a Perkin-Elmer 257 spectrophotometer. Mass spectra were recorded on a Hitachi RMU-6E spectrometer.

Nuclear Magnetic Resonance Spectra

Proton spectra were obtained using either a Varian A-60 spectrometer or a Bruker HX-90 spectrometer. ^{13}C spectra were obtained on a Bruker HX-90 system equipped with a Nicolet 1083 computer operating in the Fourier transform mode. The data were determined for $CDCl_3$ solutions (approximately 0.4 *M*) or in a mixture of 75% CF_2Br_2 – 25% CD_2Cl_2 (approximately 7%). The temperatures were monitored using a calibrated copper–constantin thermocouple and are accurate to ± 3 K.

Materials

Compounds not commercially available were prepared either as described in the literature or by standard procedures. All compounds were pure (> 98%) according to vpc analyses and had ir and ^{1}Hmr spectra consistent with their structure. The methods of preparation together with characteristic ^{1}Hmr absorptions are given below.

*1,5,5-Trimethylcyclohexene (**3**)*—Prepared from isophorone according to the method described by Sneen and Martheny (19). The 1,5,5 isomer was separated from the 3,5,5, isomer by preparative vpc at 80 °C (SE-30 column): δ (CCl_4) 0.90 (s, CH_3 at C-5), 1.65 (m, CH_3 at C-1), 5.40 ppm (m, H-2).

*3-Hydroxycyclohexene (**10**)*—Prepared by treating 3-bromocyclohexene (**9**) with 15% aqueous NaOH at room temperature overnight and also by $LiAlH_4$ reduction of 2-cyclohexenone in ether: bp 68 °C/13 torr (lit. (20) bp 85 °C/25 torr); δ ($CDCl_3$) 4.25 (m, H-3), 5.86 ppm (m, H-1 and H-2).

*3-Methoxycyclohexene (**4**)*—Prepared by treating 3-bromocyclohexene (**9**) with an equimolar quantity of sodium methoxide in refluxing methanol for 5 h and also by methylation of the sodium salt of 3-hydroxycyclohexene (**10**) (reaction with sodium metal in ether) with methyl iodide in ether at room temperature for 30 h: bp 45–50 °C/30 torr. It proved identical (vpc, ir, ^{1}Hmr) to a commercial sample (Pfatz and Bauer); δ ($CDCl_3$) 3.41 (s, OCH_3), 3.83 (m, H-3), 5.93 ppm (m, H-1 and H-2).

*3-Acetoxycyclohexene (**5**)*—Prepared by acetylation (acetic anhydride – sodium acetate) of alcohol **10**: bp 85–87 °C/50 torr (lit. (21) bp 83–84 °C/40 torr); δ ($CDCl_3$) 2.05 (s, $OCOCH_3$), 5.38 (m, H-3), 5.92 ppm (m, H-1 and H-2).

*3-Hydroxy-1,5,5-trimethylcyclohexene (**6**)*—Prepared by $LiAlH_4$ reduction of isophorone (equimolar quantities of reagents) in ether (92% yield); bp 89–90 °C/15 torr; δ ($CDCl_3$) 0.90 and 1.00 (two s, CH_3 at C-5), 1.71 (m, CH_3 at C-1), 4.32 (m, H-3), 5.60 ppm (m, H-2); *m/e* 140 (M^+).

*3-Methoxy-1,5,5-trimethylcyclohexene (**7**)*—Prepared by methylation (CH_3I) of the sodium salt of **6** in ether (80% yield): bp 63–64 °C/22 torr; δ ($CDCl_3$) 0.91 and 1.01 (two s, CH_3 at C-5), 1.72 (m, CH_3 at C-1), 3.42 (s, OCH_3), 3.89 (m, H-3), 5.62 ppm (m, H-2); *m/e* 154 (M^+).

*3-Acetoxy-1,5,5-trimethylcyclohexene (**8**)*—Prepared by acetylation of **6** (acetic anhydride – sodium acetate) (92% yield): bp 88 °C/15 torr; δ ($CDCl_3$) 0.96 and 1.01 (two s, CH_3 at C-5), 1.72 (m, CH_3 at C-1), 2.06 (s, $OCOCH_3$), 5.45 (m, H-3), 5.53 ppm (m, H-2); *m/e* 182 (M^+).

*3-Bromo-1,5,5-trimethylcyclohexene (**11**)*—Prepared from alcohol **6** and phosphorus tribromide (0.35 mol per mol of **6**) at room temperature overnight. The product was isolated from the reaction mixture by distillation. It was purified further by distillation: bp 53–55 °C/2 torr (lit. (22) bp 46–47 °C/1 torr); δ (CCl_4) 0.90 and 1.05 (two s, CH_3 at C-5), 1.75 (m, CH_3 at C-1), 4.80 (m, H-3), 5.72 ppm (m, H-2).

3-Methoxy-2-cyclohexenone—Prepared in a 71% yield from 1,3-cyclohexanedione and methanol following the procedure described for the preparation of 3-ethoxy-2-cyclohexenone (23): bp 114 °C/14 torr; δ ($CDCl_3$) 1.8–2.2 (6H), 3.79 (s, OCH_3), 5.50 ppm (s, H-2).

*3-Hydroxy-1-methoxycyclohexene (**12**)*—Prepared by $LiAlH_4$ reduction of 3-methoxy-2-cyclohexenone (equimolar quantities of reagents) in ether. A complex mixture was obtained from which compound **12** was obtained by repeated fractional distillations: bp 84 °C/1.5 torr; δ ($CDCl_3$) 3.60 (s, OCH_3), 4.32 (m, H-3), 4.90 ppm (d, J = 4.5 Hz, H-2); *m/e* 128 (M^+).

*1,3-Dimethoxycyclohexene (**13**)*—Prepared by methylation of the sodium salt of alcohol **12** with CH_3I in ether (65% yield): bp 67 °C/15 torr; δ ($CDCl_3$) 3.40 and 3.60

(two s, OCH_3 at C-3 and C-1), 3.89 (m, H-3), 4.90 ppm (d, J = 4.5 Hz, H-2); *m/e* 142 (M^+).

3-Methoxy-5,5-dimethyl-2-cyclohexenone—Prepared (98% yield) from 5,5-dimethyl-cyclohexane-1,3-dione and methanol following the procedure described by Gannon and House (23) for the preparation of 3-ethoxy-2-cyclohexenone: bp 124–125 °C/1.5 torr; δ ($CDCl_3$) 1.05 (s, CH_3), 2.22 and 2.32 (two s, H-6 and H-4), 3.78 (s, OCH_3), 5.47 ppm (s, H-2).

3-Hydroxy-1-methoxy-5,5-dimethylcyclohexene—Prepared by $LiAlH_4$ reduction of 3-methoxy-5,5-dimethyl-2-cyclohexenone (equimolar quantities) in ether and obtained pure after repeated fractional distillations: bp 108–112 °C/1.5 torr; δ ($CDCl_3$) 0.95 and 1.05 (two s, CH_3 at C-5), 3.62 (s, OCH_3), 4.46 (m, H-3), 4.83 (m, H-2); *m/e* 156 (M^+).

*1,3-Dimethoxy-5,5-dimethylcyclohexene (**14**)*—Prepared by methylation (CH_3I) of the sodium salt of 3-hydroxy-1-methoxy-5,5-dimethylcyclohexene in ether: bp 84 °C/15 torr; δ ($CDCl_3$) 0.95 and 1.04 (two s, CH_3 at C-5), 3.42 (s, OCH_3), 3.62 (s, OCH_3), 4.10 (m, H-3), 4.85 ppm (m, H-2); *m/e* 170 (M^+).

*2-Methylmethylenecyclohexane (**17**)*—Prepared by a Wittig reaction on 2-methylcyclohexanone (triphenylmethyl phosphonium bromide in ether–benzene (3:7) at −10 °C using phenyllithium) (37% yield): bp 120–122 °C (lit. (24) bp 120 °C); δ ($CDCl_3$) 1.05 (d, J = 6.4 Hz, CH_3), 4.70 ppm (m, 2 olefinic H).

2-Hydroxymethylenecyclohexane—Prepared by $LiAlH_4$ reduction of 2-carbomethoxycyclohexanone (25) as described by Dreiding and Hartman (26): bp 78–80 °C/25 torr (lit. (26) bp 78.5–80 °C/23 torr); δ ($CDCl_3$) 4.13 (m, H-2), 4.80 and 4.97 ppm (two m, olefinic H).

*2-Methoxymethylenecyclohexane (**18**)*—Prepared by methylation (CH_3I) of the sodium salt of 2-hydroxymethylenecyclohexane in ether: bp 66 °C/25 torr (lit. (27) bp 58–59 °C/43 torr); δ ($CDCl_3$) 3.40 (s, OCH_3) 3.80 (m, H-2), 4.95 ppm (m, 2 olefinic H).

2-Hydroxycyclohexanone—Prepared from 2-chlorocyclohexanone and aqueous potassium carbonate at room temperature for 20 h. A solid melting at 83.5 °C was obtained from which 2-hydroxycyclohexanone was distilled: bp 72 °C/15 torr (lit. (28) bp 55–60 °C/0.4 torr); δ ($CDCl_3$) 4.20 ppm (m, H-2).

2-Methoxycyclohexanone—Prepared from 2-hydroxycyclohexanone by the method described by Bergman and Gierth (29): bp 65 °C/15 torr (lit. (30) bp 72–75 °C/14 torr); δ ($CDCl_3$) 3.47 (s, OCH_3), 3.80 ppm (m, H-2); *m/e* 128 (M^+).

*2-Methoxy(methoxymethylene)cyclohexane (**19**)*—Prepared by a Wittig reaction on 2-methoxycyclohexanone (methoxymethyl triphenylphosphonium chloride in ether–benzene (3:7) at −10 °C using phenyllithium) (45% yield): bp 94 °C/44 torr; δ ($CDCl_3$) 3.25 (s, OCH_3), 3.56 (m, H-2), 3.66 (s, OCH_3), 6.07 ppm (olefinic H); *m/e* 156 (M^+).

2-Methoxy-4,4-dimethylcyclohexanone—Prepared by hydrogenation of 2-methoxy-4,4-dimethyl-2-cyclohexenone (30) in ethanol over 5% Pd/charcoal in a Parr apparatus at 20–40 psi (94% yield): bp 64–65 °C/0.5 torr; δ (CCl_4) 1.09 and 1.22 (two s, CH_3 at C-4), 3.40 (s, OCH_3), 3.74 ppm (d of d, ΣJ = 18 Hz, H-2); *m/e* 156 (M^+).

*2-Methoxy-4,4-dimethylmethylenecyclohexane (**20**)*—Prepared by a Wittig reaction on 2-methoxy-4,4-dimethylcyclohexanone (methyl triphenylphosphonium bromide and phenyllithium in ether). The crude product was separated by preparative vpc (OS-138 column): δ ($CDCl_3$) 0.99 and 1.00 (two s, CH_3 at C-4), 3.40 (s, OCH_3), 3.73 (m, H-2), 4.95 ppm (2 olefinic H); *m/e* 154 (M^+).

*4,4-Dimethyl(methoxymethylene)cyclohexane (**21**)*—Prepared by a Wittig reaction on 4,4-dimethylcyclohexanone (31) (methoxymethyl triphenylphosphonium chloride and phenyllithium in ether). The crude product was separated by preparative vpc (OS-138); δ (CCl_4) 0.92 (s, CH_3 at C-4), 1.8–2.4 (4 allylic H), 3.53 (s, OCH_3), 5.77 ppm (m, olefinic H); *m/e* 154 (M^+).

2-Methoxy-4,4-dimethyl(methoxymethylene)cyclohexane—Prepared by a Wittig reaction on 2-methoxy-4,4-dimethylcyclohexanone (methoxymethyl triphenylphosphonium chloride and phenyllithium in ether). The compound could not be obtained pure even after repeated distillation through a spinning band column. The sample thus obtained contained about 80% of the desired product according to vpc and spectral analyses: bp 63 °C/0.3 torr; δ ($CDCl_3$) 0.91 and 1.06 (two s, CH_3 at C-4), 3.30 (s, OCH_3 at C-2), 3.60 (m, H-2), 3.68 (s, OCH_3), 6.11 ppm (olefinic H); *m/e* 184 (M^+).

Acknowledgements

We are grateful to the National Research Council of Canada for financial assistance and to the 'Coopération franco-québécoise' for a fellowship to R. Martino. Helpful discussions with Professor A. D. Bandrauk are also gratefully acknowledged.

1. (*a*) O. Hassel and B. Ottar. Acta Chem. Scand. **1**, 927 (1947); (*b*) R. U. Lemieux. Adv. Carbohydr. Chem. **9**, 1 (1954); (*c*) L. J. Haynes and F. N. Newth. Adv. Carbohydr. Chem. **10**, 207 (1955); (*d*) R. U. Lemieux and N. S. Chu. Abstracts of papers. Am. Chem. Soc. **133**, 31N (1958); (*e*) N. J. Chu. Ph.D. Thesis, University of Ottawa, Ottawa, Ont. 1959.
2. (*a*) J. T. Edward. Chem. Ind. 1102 (1952); (*b*) C. B. Anderson and D. T. Sepp. Tetrahedron, **24**, 1707 (1968); (*c*) J. Org. Chem. **32**, 607 (1967).
3. (*a*) R. U. Lemieux. *In* Molecular rearrangements. *Edited by* Paul de Mayo. Interscience, New York. 1965. p. 45; (*b*) M. A. Kabayama and O. Patterson. Can. J. Chem. **46**, 1543 (1968); (*c*) R. O. Hutchin, L. O. Kopp, and E. L. Eliel. J. Am. Chem. Soc. **90**, 7174 (1968).
4. (*a*) L. Radom, W. J. Hehre, and J. A. Pople. J. Am. Chem. Soc. **93**, 289 (1971); (*b*) **94**, 2371 (1972); (*c*) C. Altona. Ph.D. Thesis. University of Leiden. 1964; (*d*) C. Romers, C. Altona, H. R. Buys, and E. Havinga. Top. Stereochem. **4**, 39 (1969); (*e*) S. David, O. Eisenstein, W. J. Hehre, L. Salem, and R. Hoffman. J. Am. Chem. Soc. **95**, 3806 (1973); (*f*) C. Baddeley. Tetrahedron Lett. 1645 (1973).
5. L. O. Brockway. J. Phys. Chem. **41**, 185 (1937); N. de Wolf, C. Romers, and C. Altona. Acta Crystallogr. **22**, 715 (1967) and references cited therein.
6. R. G. Parker and J. D. Roberts. J. Am. Chem. Soc. **92**, 743 (1970).
7. T. Pehk, S. Rang, O. Eisen, and E. Lippmaa. Eesti, NSV Tead. Akad. Toin. Keem. Ceol. **17**, 296 (1968).
8. S. Glasstone, K. J. Laidler, and H. Eyring. The

theory of rate processes. McGraw Hill, New York. 1941.
9. (*a*) F. R. JENSEN and C. H. BUSHWELLER. J. Am. Chem. Soc. **91**, 5774 (1969); (*b*) M. BERNARD and M. ST-JACQUES. Tetrahedron, **29**, 2539 (1973).
10. M. BERNARD, L. CANUEL, and M. ST-JACQUES. J. Am. Chem. Soc. **96**, 2929 (1974).
11. J. B. LAMBERT and R. R. CLIKEMAN. J. Am. Chem. Soc. **98**, 4203 (1976).
12. (*a*) E. W. GARBISH. J. Org. Chem. **27**, 4249 (1962); (*b*) Y. SENDA, S. IMAIZUMI, S. OCHIAI, and K. FUJITA. Tetrahedron, **30**, 539 (1974); (*c*) L. D. HALL. J. Org. Chem. **29**, 297 (1964); (*d*) G. V. SMITH and H. KRILOFF. J. Am. Chem. Soc. **85**, 2016 (1963).
13. S. H. GROVER and J. B. STOTHERS. Can. J. Chem. **53**, 589 (1975).
14. E. L. ELIEL, N. L. ALLINGER, S. J. ANGYAL, and G. A. MORRISON. Conformational analysis. John Wiley and Sons, New York, NY. 1965.
15. A. SEVIN and J. M. CENSE. Bull. Soc. Chim. Fr. 3552 (1970).
16. A. D. BUCKINGHAM. Discuss. Faraday Soc. **40**, 238 (1965).
17. H. MARGENAU and N. R. KESTNER. Theory of intermolecular forces. Pergamon Press, Oxford, U.K. 1969.
18. A. D. BUCKINGHAM, R. L. DISCH, and D. A. DUNMUR. J. Am. Chem. Soc. **90**, 3104 (1968).
19. R. A. SNEEN and N. P. MARTHENY. J. Am. Chem. Soc. **86**, 5503 (1964).
20. P. D. BARTLETT and G. F. WOODS. J. Am. Chem. Soc. **62**, 2933 (1940).
21. A. BERLANDE. Bull. Soc. Chim. Fr. **9**, 644 (1942).
22. YAU-TANGLIN and TUNG BIN LO. Essays and papers in memory of late president Fu Ssu-Nien. 1952. p. 215; Chem. Abstr. **49**, 255f (1955).
23. W. F. GANNON and H. O. HOUSE. Org. Synth. **40**, 41 (1960).
24. A. SEVIN and J. M. CENSE. Bull. Soc. Chim. Fr. 963 (1974).
25. L. RUEST, G. BLOUIN, and P. DESLONGCHAMPS. Synth. Commun. **6**, 169 (1976).
26. A. S. DREIDING and J. A. HARTMAN. J. Am. Chem. Soc. **75**, 939 (1953).
27. L. E. GRUENWALD and D. C. JOHNSON. J. Org. Chem. **32**, 318 (1967).
28. H. W. DÜRBECK, C. G. B. FRISHKORN, and K. HILPERT. Tetrahedron, **27**, 2927 (1971).
29. M. BERGMAN and M. GIERTH. Ann. **448**, 48 (1926).
30. E. WENKERT, N. F. GOLOB, S. S. SATHE, and R. A. SMITH. Synth. Commun. **3**, 205 (1973).
31. F. G. BORDWELL and K. M. WELLMAN. J. Org. Chem. **28**, 1347 (1963).

Secondary α-ferrocenyl substituted carbocations from tertiary carbinols

CHOI CHUCK LEE, SHI-CHOW CHEN, W. JACK PANNEKOEK, AND RONALD G. SUTHERLAND

Department of Chemistry and Chemical Engineering, University of Saskatchewan, Saskatoon, Sask., Canada S7N 0W0

Received September 3, 1976

CHOI CHUCK LEE, SHI-CHOW CHEN, W. JACK PANNEKOEK, and RONALD G. SUTHERLAND. Can. J. Chem. **55**, 1024 (1977).

The same secondary ferrocenylisopropylcarbenium ion was formed from treatment with concentrated H_2SO_4 at 10°C of either ferrocenylisopropylcarbinol or ferrocenylmethyldimethylcarbinol and the same secondary ferrocenyldiphenylmethylcarbenium ion was obtained when either ferrocenyldiphenylmethylcarbinol or ferrocenylmethyldiphenylcarbinol was treated with CF_3COOH at 5°C. The results indicate the occurrence of 1,2-hydride shifts converting tertiary to secondary carbocations.

CHOI CHUCK LEE, SHI-CHOW CHEN, W. JACK PANNEKOEK et RONALD G. SUTHERLAND. Can. J. Chem. **55**, 1024 (1977).

On forme le même ion ferrocénylisopropylcarbénium secondaire en traitant soit le ferrocénylisopropylcarbinol ou le ferrocénylméthyldiméthylcarbinol avec de l'acide sulfurique concentré à 10°C. On obtient aussi le même ion ferrocényldiphénylméthylcarbénium secondaire en traitant soit le ferrocényldiphénylméthylcarbinol ou le ferrocénylméthyldiphénylcarbinol avec de l'acide trifluoroacétique à 5°C. Les résultats indiquent l'intervention d'une migration-1,2 d'hydrure convertissant le carbocation tertiaire en carbocation secondaire.

[Traduit par le journal]

It is well known that carbocations can undergo rearrangements to give more stable cations and thus, usually, primary or secondary carbocations rearrange to give the more stable tertiary cations (1, 2). In a demonstration of the extraordinary stability of α-ferrocenyl substituted carbocations,[1] Larsen and Ashkenazi (3) have recently presented calorimetric data to show that primary and secondary α-ferrocenylcarbenium ions are more stable than tertiary cations such as the triphenylmethyl cation. Such findings led to the present work, in which attempts are made to effect rearrangements of tertiary carbocations to more stable secondary α-ferrocenylcarbenium ions, so as to provide some examples of rearrangement of tertiary to secondary cations, a reversal of the usually observed behaviour.

^{13}C nmr studies on a number of α-ferrocenylcarbenium ions generated from treatment of the corresponding alcohols with cold H_2SO_4 have been reported by Olah and Liang (4). A similar technique is utilized in the present work. It was found that the same secondary ferrocenylisopropylcarbenium ion (**1***a*) was obtained when either the secondary ferrocenylisopropylcarbinol (**2***a*) or the tertiary ferrocenylmethyldimethylcarbinol (**3***a*) was treated with concentrated H_2SO_4 at 10°C. The chemical shifts from the ^1H-decoupled ^{13}C nmr spectra of carbinols **2***a* and **3***a*, and carbenium ion **1***a*, are summarized in Table 1.

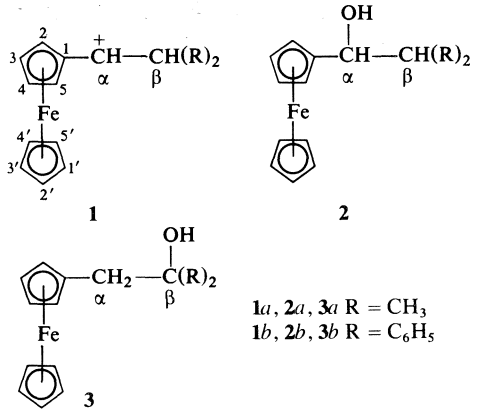

Braun *et al.* (5) have recently reported the ^{13}C nmr spectrum of **1***a* generated from **2***a* in CF_3COOD. The present data for **1***a* and **2***a* (Table 1) are essentially identical to those observed by these workers (5). It has been pointed out that the asymmetric center at C-α in **2***a* renders the C-2,5 and C-3,4 pairs of carbons diastereotopic, thus giving rise to five signals for the substituted cyclopentadienyl ring

[1]For further discussions on the stability of α-ferrocenylcarbenium ions, see literature cited in ref. 3.

TABLE 1. Data from the ^{1}H-decoupled ^{13}C nmr spectra of ferrocenylisopropylcarbinol (**2***a*), ferrocenylmethyldimethylcarbinol (**3***a*), and the ferrocenylisopropylcarbenium ion (**1***a*)

	Chemical shifts (ppm)*			
	2*a* (Acetone-d_6)	**2***a*† ($CDCl_3$)	**3***a* (Acetone-d_6)	**1***a*† (H_2SO_4)
C-1	93.7	93.4	85.4	104.7
C-2,5	66.1,68.3	64.9,68.9	68.0	81.4,82.1
C-3,4	67.7	67.6,67.9	70.8	95.1,95.6
C-1′–C-5′	69.1	68.3	69.1	82.1
C-α	75.2	75.1	45.7	133.4
C-β	36.3	34.9	—	35.5
CH_3	18.2,19.0	18.6,18.8	29.4	22.5,28.7

*Chemical shifts were measured from external TMS in a capillary tube which also contained some CD_3NO_2 as a locking compound in studies with **1***a*.
†Essentially identical results were reported in ref. 5 for **2***a* in $CDCl_3$ and **1***a* in CF_3COOD.

TABLE 2. Data from the ^{1}H-decoupled ^{13}C nmr spectra of ferrocenyldiphenylmethylcarbinol (**2***b*), ferrocenylmethyldiphenylcarbinol (**3***b*), and the ferrocenyldiphenylmethylcarbenium ion (**1***b*)

	Chemical shifts (ppm)*		
	2*b* (Acetone-d_6)	**3***b* (Acetone-d_6)	**1***b* (CF_3COOH)
C-1	94.5	83.6	104.9
C-2,5	66.3,68.6	67.8	79.9,81.2
C-3,4	67.7	71.3	94.5,94.7
C-1′–C-5′	69.1	69.1	81.7
C-α	72.9	43.8	140.3
C-β	61.5	78.9	56.0†
Aromatic	126.8,128.7 129.7,130.1	127.0,128.3	124.3,127.8,128.2 129.5,130.0,130.5
Aromatic quaternary	143.7,144.3	148.7	—

*Chemical shifts were measured from external TMS in a capillary tube which also contained some CD_3NO_2 as a locking compound in studies with **1***b*.
†Becomes a doublet in off resonance studies, indicating the presence of 1H at C-β.

of **2***a* (5). Similarly, the nonequivalence of the CH_3 groups of **2***a* is also due to the presence of the asymmetric center, a finding that was first observed for asymmetric isopropylcarbinols by Roberts and co-workers (6). The C-2,5 and C-3,4 pairs of carbons and the CH_3 groups are also nonequivalent in the carbenium ion **1***a*, and the origin of this nonequivalence has been attributed to a restricted rotation about the C-1—C-α bond in the α-ferrocenyl substituted carbocation (4, 5). The fact that tertiary carbinol **3***a* also gave rise to **1***a* indicates the occurrence of a 1,2-hydride shift, converting the tertiary ferrocenylmethyldimethylcarbenium ion to the more stable α-ferrocenyl substituted secondary carbocation **1***a*.

In analogous studies with the secondary ferrocenyldiphenylmethylcarbinol (**2***b*) and the tertiary ferrocenylmethyldiphenylcarbinol (**3***b*), it was found that treatment of either of these alcohols with cold concentrated H_2SO_4 gave rise to extensive decomposition. The ferrocenyldiphenylmethylcarbenium ion (**1***b*), however, was obtained by dissolving **2***b* in CF_3COOH at 5°C. When the tertiary carbinol **3***b* was treated with neat CF_3COOH, decomposition also occurred. Ion **1***b* was generated from **3***b* when CF_3-COOH (about 10%) was added to a solution of **3***b* in $CDCl_3$ at 5°C and the ^{13}C nmr spectrum was recorded after a relatively short contact time (about 4000 scans) in order to minimize decomposition. The chemical shifts from the ^{1}H-decoupled ^{13}C nmr spectra of carbinols **2***b* and **3***b*, and carbenium ion **1***b* are given in Table 2,

and the spectra of ions **1***a* and **1***b* are shown in Fig. 1. The identification of **1***b* as the secondary ferrocenyldiphenylmethylcarbenium ion is based on the general similarity of its ^{13}C nmr spectrum with that of **1***a*, the nonequivalence of the C-2,5 and C-3,4 pairs of carbon atoms, and the fact that off resonance gave a doublet for the C-β absorption showing the presence of one H on this carbon. The formation of **1***b* from **3***b* again indicates the occurrence of a 1,2-hydride shift converting the tertiary ferrocenylmethyldiphenylcarbenium ion to the secondary ferrocenyldiphenylmethylcarbenium ion.

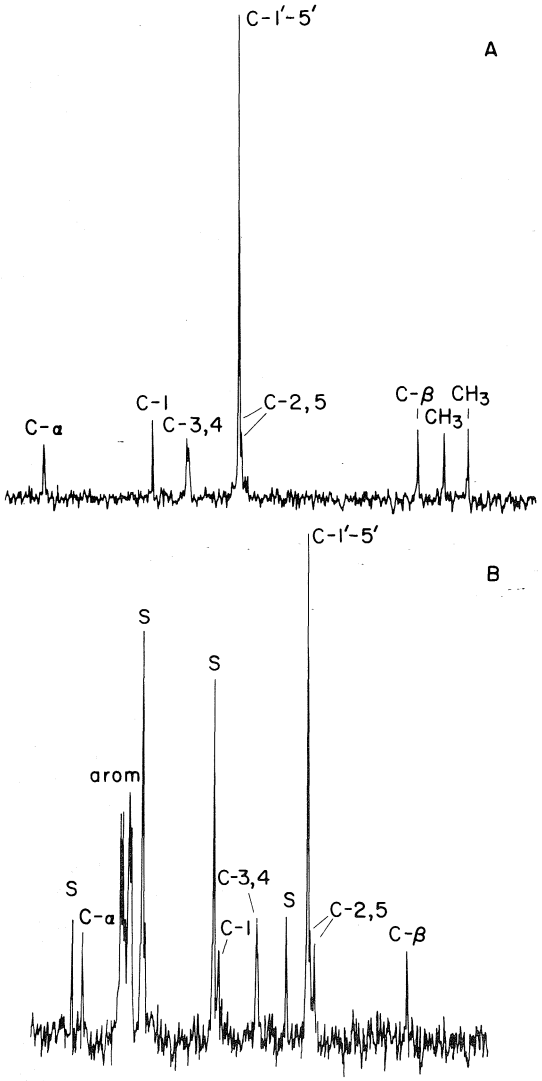

FIG. 1. ^1H-decoupled ^{13}C nmr spectra of the ferrocenylisopropylcarbenium ion (A) and the ferrocenyldiphenylmethylcarbenium ion (B) (the quartet marked S in (B) is due to CF_3 of the CF_3COOH solvent).

Experimental

Ferrocenyl Isopropyl Ketone (4)

To a solution of 2.02 g (19 mmol) of isobutyryl chloride and 3.52 g (19 mmol) of ferrocene in 70 ml of methylene chloride was added, with stirring and under nitrogen, 2.80 g (21 mmol) of aluminum chloride. The deep purple reaction mixture was stirred under nitrogen and at room temperature for 2 h and then heated under reflux for an additional 1 h. After cooling, 50 ml of water was added, the organic layer was separated, and the aqueous layer was extracted with methylene chloride (3 × 30 ml). The combined organic solution was washed with saturated sodium bicarbonate solution and then with water. After drying over Na_2SO_4, removal of the solvent gave 4.3 g of an oily product which was purified by column chromatography through neutral alumina (20 g) Unreacted ferrocene was first removed by elution with *n*-hexane. Subsequent elution with 1:1 (vol.) *n*-hexane–chloroform gave 4.1 g (85%) of the brownish red ketone **4**; ^1H nmr (CCl_4) δ 1.17 (d, J = 6.5 Hz, 6H, CH_3), 3.00 (sept. J = 6.5 Hz, 1H, CH) 4.10 (s, 5H, C_5H_5), 4.40 (t, J = 1.5 Hz, 2H, part of C_5H_4), 4.75 (t, J = 1.5 Hz, 2H, part of C_5H_4). *Anal.* calcd. for $C_{14}H_{10}OFe$: C 65.65, H 6.30; found: C 65.26, H 6.27.

Ferrocenylisopropylcarbinol (2a)

To a solution of 760 mg (20 mmol) of $LiAlH_4$ in 80 ml of anhydrous ether was added a solution of 4.0 g (16 mmol) of **4** in 20 ml of anhydrous ether. The resulting mixture was heated under reflux over N_2 for 4 h, cooled, and then treated with a few ml of H_2O. The ether layer was separated and dried over $MgSO_4$. Removal of the ether gave 3.8 g (94%) of product. Purification through an alumina column with elution by *n*-hexane gave the pure alcohol **2***a* as an orange liquid; ^1H nmr ($CDCl_3$) δ 0.75 (d, J = 7 Hz, 3H, CH_3), 0.93 (d, J = 7 Hz, 3H, CH_3), 1.75 (m, 1H, CH), 2.1 (s, 1H, OH), 4.06 (d, J = 6.5 Hz, 1H, CH), 4.15 (m, 2H, part of C_5H_4), 4.20 (s, 7H, C_5H_5 and part of C_5H_4). *Anal.* calcd. for $C_{14}H_{18}OFe$: C 65.14, H 7.03; found: C 65.26, H 7.01.

Ferrocenyldiphenylmethylcarbinol (2b)

Analogous to the synthesis of ketone **4**, acylation of ferrocene with diphenylacetyl chloride gave a 90% yield of ferrocenyl diphenylmethyl ketone (**5**) as an orange solid, which was recrystallized from tetrahydrofuran–pentane, mp 180–182°C; ^1H nmr ($CDCl_3$) δ 4.30 (s, 5H, C_5H_5), 4.70 (t, J = 2 Hz, 2H, part of C_5H_4), 5.00 (t, J = 2 Hz, 2H, part of C_5H_4) 5.75 (s, 1H, CH), 7.5 (m, 10H, aromatic). *Anal.* calcd. for $C_{24}H_{20}OFe$: C 75.80, H 5.30; found: C 76.11, H 5.24.

Similar to the reduction of **4** to **2***a*, ketone **5** was reduced with $LiA1H_4$ in anhydrous tetrahydrofuran to give 89% yield of carbinol **2***b* as a yellow solid, which was crystallized from chloroform–pentane, mp 125–127°C; ^1H nmr ($CDCl_3$) δ 2.25 (s, 1H, OH), 3.85 (d, J = 8.0 Hz, 1H, CH), 4.0–4.1 (m, 9H, C_5H_5 and C_5H_4), 5.00 (d, J = 8.0 Hz, 1H, CH), 7.15 (s, 5H, aromatic), 7.3 (m, 5H, aromatic). *Anal* calcd. for $C_{24}H_{22}OFe$: C 75.40, H 5.80; found: C 75.46, H 5.57.

Ferrocenylmethyldimethylcarbinol (3a)

Ferrocenylacetic acid (7) was esterified with diazomethane in ether to give methyl ferrocenylacetate (**6**); ^{1}H nmr ($CDCl_3$) δ 3.35 (s, 3H, CH_3), 3.70 (s, 2H, CH_2), 4.10 (s, 9H, C_5H_5 and C_5H_4).

A solution of 1.82 g (70 mmol) of **6** in 30 ml of ether was added dropwise, under N_2, to 2 mol equiv. of CH_3MgI in 50 ml of ether. The resulting mixture was heated under reflux for 2 h. After decomposition with a saturated aqueous solution of NH_4Cl, the ether layer was separated, dried over $MgSO_4$, and evaporated to give 1.72 g (89%) of carbinol **3***a*. Recrystallized from ether, it melted at 51–53°C; ^{1}H nmr ($CDCl_3$) δ 1.15 (s, 6H, CH_3), 1.70 (s, 1H, OH) 2.50 (s, 2H, CH_2), 4.10 (s, 9H, C_5H_5 and C_5H_4). *Anal.* calcd. for $C_{14}H_{13}OFe$: C 65.14, H 7.03; found: C 65.26, H 6.99.

Ferrocenylmethyldiphenylcarbinol (3b)

Carbinol **3***b* was prepared from reaction of **6** with PhMgBr in the same way as in the preparation of **3***a*. A 93% yield of the crude product was obtained as an orange oil. Purification by passage through a salicic acid column, with elution by $CHCl_3$, followed by trituration with *n*-hexane gave the crystalline product, mp103–104°C; ^{1}H nmr (CCl_4) δ 2.65 (s, 1H, OH), 3.33 (s, 2H, CH_2), 3.90 (t, J = 2 Hz, 2H, part of C_5H_4), 4.00 (t, J = 2 Hz, 2H, part of C_5H_4), 4.10 (s, 5H, C_5H_5), 7.1–7.4 (m, 10H, aromatic). *Anal.* calcd. for $C_{24}H_{22}OFe$: C 75.40, H 5.80; found: C 75.66, H 5.57.

Nuclear Magnetic Resonance Spectra

The ^{1}H nmr spectra were taken with a Varian T-60 or HA-100 spectrometer, and the ^{13}C nmr spectra were obtained with a Bruker WP-60 spectrometer with 8K memory. When ion **1***a* was generated from carbinol **2***a* or **3***a* in H_2SO_4 at 10°C, attempts at trapping the ion by pouring the reaction mixture into cold CH_3OH gave only the olefin, 1-ferrocenyl-2-methylpropene, mp (after sublimation) 35–36°C; ^{1}H nmr (CCl_4) δ 1.72 (s, 3H, CH_3), 1.75 (s, 3H, CH_3), 3.90 (s, 5H, C_5H_5), 3.95, 4.05 (m, 4H, C_5H_4), 5.85 (m, 1H, CH). *Anal.* calcd. for $C_{14}H_{16}Fe$: C 70.02, H 6.72; found: C 70.33, H 6.98. No attempts were made to trap ion **1***b* from studies with carbinol **2***b* or **3***b*.

Acknowledgment

The financial support given by the National Research Council of Canada is gratefully acknowledged.

1. J. HINE. Physical organic chemistry. 2nd ed. McGraw-Hill Book Co., New York, NY. 1962. Chapt. 14.
2. R. T. MORRISON and R. N. BOYD. Organic chemistry. 3rd ed. Allyn and Bacon Inc., Boston, Mass. 1973. pp. 171–174.
3. J. W. LARSEN and P. ASHKENAZI. J. Am. Chem. Soc. **97**, 2140 (1975).
4. G. A. OLAH and G. LIANG. J. Org. Chem. **40**, 1849 (1975).
5. S. BRAUN, T. S. ABRAM, and W. E. WATTS. J. Organomet. Chem. **97**, 429 (1975).
6. J. I. KROSCHWITZ, M. WINOKUR, H. J. REICH, and J. D. ROBERTS. J. Am. Chem. Soc. **91**, 5927 (1969).
7. D. LEDNICER, J. K. LINDSAY, and C. R. HAUSER. J. Org. Chem. **23**, 653 (1958).

A kinetic investigation of the effects of molecular complexing on the acidities of some π donor carboxylic acids

ALLAN K. COLTER[1] AND R. JAMES KERSTING

Department of Chemistry, Carnegie–Mellon University, Pittsburgh, PA, U.S.A. 15213, and Guelph–Waterloo Centre for Graduate Work in Chemistry, University of Guelph, Guelph, Ont., Canada N1G 2W1

Received August 6, 1976

ALLAN K. COLTER and R. JAMES KERSTING. Can. J. Chem. **55**, 1028 (1977).

Rates of reaction of the five π donor acids indole-3-acrylic acid (IAA), indole-5-carboxylic acid (ICA), 3,4,5-trimethoxybenzoic acid (TMBA), 2,4-dihydroxybenzoic acid (DHBA), and 3,4,5-trihydroxybenzoic acid (THBA) with 4-chlorodiphenyldiazomethane (4-ClDDM) in ethanol at 30 °C were measured in the presence of the π acceptors 1,3,5-trinitrobenzene (TNB), benzotrifuroxan (BTF), and 1,2,4,5-tetracyanobenzene (TCNB) and in the absence of acceptor. For 12 of the 13 combinations studied, added acceptor produced rate enhancements. The rate data were combined with independently-determined 1:1 acceptor – donor acid association constants to obtain second-order rate constants for reaction of the 1:1 acceptor – donor acid complexes. From the increase in the rate constant resulting from complexation, estimates of the increase in $K_a(H_2O, 25\,°C)$ produced by complexation were obtained for 13 acceptor – donor acid combinations. Second-order rate constants for reaction of 4-ClDDM with 10 other carboxylic acids and *p*-toluenesulfonic acid in ethanol at 30 °C were also measured and the pattern of reactivity shown to parallel very closely that of diphenyldiazomethane.

ALLAN K. COLTER et R. JAMES KERSTING. Can. J. Chem. **55**, 1028 (1977).

On a mesuré les vitesses de réaction de cinq acides donneur π l'acide indole acrylique-3, (IAA), l'acide indole carboxylique-5 (ICA) l'acide triméthoxy-3,4,5 benzoïque (TMBA) l'acide dihydroxy-2,4 benzoïque (DHBA) et l'acide trihydroxy-3,4,5 benzoïque (THBA) avec le chloro-4 diphényldiazométhane (4-ClDDM) dans l'éthanol à 30 °C en présence d'accepteurs π comme le trinitro-1,3,5 benzène (TNB), le benzotrifuroxanne (BTF) et le tétracyano-1,2,4,5 benzène (TCNB) ainsi qu'en l'absence d'accepteur. Dans les cas de 12 des 13 combinaisons étudiées, l'addition d'accepteur conduit à des augmentations de vitesse. On a combiné les données concernant les vitesses avec les constantes d'association acide donneur – accepteur 1:1 déterminé d'une façon indépendante de façon à obtenir les constantes de vitesses du deuxième ordre pour la réaction des complexes acide donneur – accepteur 1:1. A partir des augmentations dans la constante de vitesse par complexation, on a pu estimer l'augmentation dans $K_a(H_2O, 25\,°C)$, produite par une complexation, pour 13 des combinaisons acide donneur – accepteur. On a aussi mesuré les constantes de vitesse du deuxième ordre pour la réaction du 4-ClDDM avec 10 autres acides carboxyliques et l'acide *p*-toluènesulfonique dans l'éthanol à 30 °C; on a montré que les tendances dans la réactivité sont très parallèles avec celles du diphényldiazométhane.

[Traduit par le journal]

Our interest in the chemical effects of molecular complexing (ref. 1 and previous papers in this series) has led us to investigate the influence of molecular complexing on acid–base properties. The previous paper in the series (2) describes an approach to the problem involving potentiometric measurements in aqueous solution. While the potentiometric method is relatively direct, its application is limited in practice to investigations of electrically charged complexing agents, where the total effect of complexation is a result of contributions from both charge-transfer and direct electrostatic interactions.

An objective of the present work was to obtain a measure of the influence of charge-transfer interaction on acid–base properties in weak complexes. How, for example, is the acidity of a benzoic acid affected by complexation with trinitrobenzene? Information of this kind is of interest in relation to recurring questions (3) concerning the contribution of charge-transfer forces to the enthalpy of formation of weak donor – acceptor complexes and the extent of charge transfer in such complexes.

We describe here an indirect approach to the estimation of the effects of complexation on

[1]Present address: Department of Chemistry, University of Guelph, Guelph, Ontario.

acidity which is based on the effect of complexing on the rate of a general acid-catalyzed reaction.

Method

For a series of structurally related acids the catalytic constants k are frequently related to their acidity constants K_a by means of a Brönsted catalysis law expression [1] (4). For a reaction

$$[1] \qquad \log k = \alpha \log K_a + c$$

mixture containing a donor acid, HD, and an acceptor, A, which forms a 1:1 complex with the acid, the reaction will be catalyzed by both complexed and uncomplexed acid. Provided that the acceptor does not interact with the substrate and does not significantly affect the catalytic constant for the uncomplexed donor acid, the observed rate constant in such a mixture is given by [2]

$$[2] \quad \begin{aligned} k_{obs} &= k[HD] + k_c[HD{\cdot}A] \\ &= k\{c_{HD} - [HD{\cdot}A]\} + k_c[HD{\cdot}A] \\ &= kc_{HD} + (k_c - k)[HD{\cdot}A] \end{aligned}$$

where k_c is the catalytic constant for the 1:1 complex, [HD] and [HD·A] are actual concentrations of uncomplexed and complexed donor acid, respectively, and c_{HD} is the stoichiometric concentration of donor acid. Rearrangement of [2] leads to an expression [3] for the catalytic constant of the 1:1 complex. From

$$[3] \qquad k_c = k + \frac{k_{obs} - kc_{HD}}{[HD{\cdot}A]}$$

the equilibrium condition for 1:1 complexation [4] one can obtain an explicit expression for

$$[4] \quad \begin{aligned} K &= \frac{[HD{\cdot}A]}{[HD][A]} \\ &= \frac{[HD{\cdot}A]}{\{c_{HD} - [HD{\cdot}A]\}\{c_A - [HD{\cdot}A]\}} \end{aligned}$$

[HD·A] in terms of K, c_{HD}, and the stoichiometric acceptor concentration c_A. By substitution into [3] one could then obtain an equation containing only two unknowns, k_c and K. In theory, then, measurement of k_{obs} at two or more acceptor concentrations could lead to both k_c and K. However, the success of such an approach requires significant rate effects by added acceptor over a range of acceptor concentrations corresponding to a substantial variation in the fraction of the acid which is complexed (1, 5).

In the present work it was found necessary to determine K spectrophotometrically. Having K, c_{HD}, and c_A for a particular kinetic experiment, [HD·A] can then be calculated. From k_{obs}, k (the rate constant measured in the absence of acceptor), and c_{HD}, the catalytic constant for the 1:1 complex can then be calculated from [3]. Finally, assuming that k_c obeys the Brönsted relation [1], the acidity constant for the 1:1 complex, K_a^c, can be estimated by means of [5].

$$[5] \qquad \log (k_c/k) = \alpha \log (K_a^c/K_a)$$

The reaction chosen for the present investigation was the reaction of diphenyldiazomethane (DDM), or one of its derivatives, with carboxylic acids in ethanol solvent. In addition to its convenience, this reaction has several desirable features for our purposes. It is one of the most extensively studied of all organic reactions with respect to structural influences on the rate (6), it has been thoroughly studied from a mechanistic standpoint (7), and there is strong evidence that the rate determining step involves transfer of a proton from the acid to the DDM. General acid catalysis has been established, and for selected groups of closely related carboxylic acids at least, the rates are well correlated by means of a Brönsted relation (see later discussion, however).

Results

Since the method requires that the reactivity of the substrate be unchanged by the presence of acceptor we first examined mixtures of DDM and 1,3,5-trinitrobenzene (TNB) by uv–visible spectroscopy. The spectrum of a solution containing 0.003 M DDM and 0.051 M TNB shows some enhancement of absorption over the sum of the spectra of solutions of DDM and TNB alone. The DDM absorption band at 520 nm was enhanced and broadened by addition of TNB, indicating a weak interaction between the two compounds. With the hope of reducing the interaction by steric hindrance we synthesized 4,4′-di-*tert*-butyldiphenyldiazomethane and examined its spectrum with an without added TNB. Addition of TNB resulted in an even greater enhancement of the long wavelength absorption of the diazo compound (λ_{max} = 535 nm). In addition, a discrete new absorption band appeared at 465 nm. The failure of the two *tert*-butyl groups to hinder complexing suggests that the interaction must involve

TABLE 1. Rate of reaction of 4-ClDDM with acids in ethanol at 30 °C

Acid	[Acid] (M)	k (ℓ mol^{-1} min^{-1})[a]	pK_a (H_2O, 25 °C)[b]
Benzoic	0.030, 0.050, 0.070	0.517 ± 0.006(12)	4.20
o-Chlorobenzoic	0.035, 0.040, 0.050	2.42 ± 0.03(11)	2.92
p-Chlorobenzoic	0.040, 0.060, 0.080	0.862 ± 0.005(12)	3.98
trans-Cinnamic	0.030, 0.050, 0.070	0.502 ± 0.008(12)	4.44
p-Methoxy-*trans*-cinnamic	0.030	0.398 ± 0.005(3)	4.54
2-Furoic	0.035, 0.050, 0.070	2.58 ± 0.02(11)	3.16
o-Methoxybenzoic	0.030, 0.050, 0.070	0.691 ± 0.009(12)	4.09
1-Naphthoic	0.035, 0.050, 0.075	0.788 ± 0.012(13)	3.69
p-Nitrobenzoic	0.035, 0.050	2.32 ± 0.01(8)	3.43
Acetic	0.026, 0.050	0.274 ± 0.007(9)	4.75
p-Toluenesulfonic	(5.26, 6.57, 9.20, 10.51) × 10^{-4}	138 ± 7(12)	—
Indole-3-acrylic	0.035, 0.050, 0.080	0.211 ± 0.012(9)	—
Indole-5-carboxylic	0.035, 0.050, 0.080	0.202 ± 0.009(9)	4.83 (30 °C)[c]
3,4,5-Trimethoxybenzoic	0.035, 0.050, 0.080	0.646 ± 0.016(11)	4.03 (30 °C)[c]
2,4-Dihydroxybenzoic	0.035, 0.050, 0.080	1.62 ± 0.05(11)	3.22 (30 °C)
3,4,5-Trihydroxybenzoic	0.040, 0.050, 0.080	0.216 ± 0.009(11)	4.33

[a]Average of indicated numbers of runs (in parentheses), with average deviations.
[b]Taken from ref. 12 except where noted.
[c]D. Buben, unpublished work.

the diazo group. Interestingly, the thermal stability of 4,4′-di-*tert*-butyldiphenyldiazomethane in ethanol appears to be markedly increased by TNB. Because of the sensitivity of the interaction to substitution, 4-chlorodiphenyldiazomethane (4-ClDDM) was examined. Ultraviolet–visible spectra of mixtures of 4-ClDDM and TNB and of 4-ClDDM and benzotrifuroxan (BTF) showed no evidence of complexing.

Earlier kinetic studies of the reaction of 4-ClDDM with acids (8) have been limited to toluene solvent. We therefore examined the kinetics of reaction of 4-ClDDM with 14 carboxylic acids and *p*-toluenesulfonic acid in ethanol at 30 °C. Rate measurements were carried out under pseudo first-order conditions using an excess of acid and following the disappearance of 4-ClDDM spectrophotometrically. By analogy with the DDM reaction (7) we expect about 0.60 mol of carboxylic acid to be consumed per mol of 4-ClDDM reacting, with the formation of ester and ether in the ratio of about 3:2. In approximate agreement with expectations, reaction of 4-ClDDM with indole-3-acrylic acid was determined by titration to consume 0.54 mol of acid per mol of 4-ClDDM. No curvature in first-order rate plots could be detected under the conditions of our measurements. Second-order rate constants (Table 1), calculated by dividing observed pseudo first-order rate constants by the concentration of acid, showed no significant dependence on acid concentration over the concentration ranges studied. The second-order rate constants for 4-ClDDM can be compared to literature values for DDM (9) under identical conditions for nine of the carboxylic acids in Table 1 (all except *p*-methoxy-*trans*-cinnamic acid and the five donor acids chosen for the present study). For these nine acids k (DDM)/k (4-ClDDM) = 2.09 ± 0.17. Excluding 2-furoic acid (9*c*) (ratio = 2.65) and 2-methoxybenzoic acid (9*e*) (ratio = 1.79) the average ratio is 2.05 ± 0.08. For comparison, Hancock *et al.* (8*a*) found DDM to be 2.07 times as reactive as 4-ClDDM in reaction with benzoic acid in toluene at 25 °C. The very close correspondence in the reactivities of DDM and 4-ClDDM means that we can use the extensive literature data for the former to define the Brönsted relation [1] needed to estimate the influence of complexation on the acidity constant.

Using the reported K_a for benzoic acid in ethanol at 25 °C (6.3×10^{-11}) (10) and the measured catalytic constant for *p*-toluenesulfonic acid, we calculate that less than 1% of the reaction of 4-ClDDM with 0.05 M benzoic acid is due to oxonium ion catalysis. A similar conclusion was reached by Roberts *et al.* (11) for the reaction of benzoic acid with DDM under the same conditions.

Five donor acids were chosen for investigation of the influence of molecular complexing on acidity. These were indole-3-acrylic acid (IAA),

indole-5-carboxylic acid (ICA), 3,4,5-trimethoxybenzoic acid (TMBA), 2,4-dihydroxybenzoic acid (DHBA), and 3,4,5-trihydroxybenzoic acid (THBA). Benzoic acid itself, because of the electron-withdrawing nature of the carboxyl group, is expected to have only very weak π donor properties. It was anticipated that two or three hydroxy or methoxy groups or a fused pyrrole ring would more than neutralize the effect of the carboxyl group providing acids with pronounced π donor properties. In fact, all five donor acids gave visible color enhancement with TNB in ethanol solution. In contrast, *p*-methoxybenzoic, cinnamic, *p*-methoxycinnamic and 2-furoic acids gave no visible evidence for complexing with TNB. In addition to the pronounced π donor properties of the indole ring (13) the choice of IAA and ICA was based on a second consideration. If the donor–acceptor interaction is centred on the pyrrole ring, the substantial separation between the site of complexation and the carboxyl group should reduce the likelihood of steric hindrance by the acceptor in the transition state for reaction of the complexed acid. All five of the donor acids have conveniently measurable second-order rate constants (Table 1).

The acidity of a phenol is expected to be influenced to a greater extent by complexation than the acidity of a substituted benzoic acid since the charge on the phenoxide ion is delocalized onto the aromatic ring. Unfortunately, the π donor phenols are too weakly acidic to study in the 4-ClDDM reaction. For example, the rate of disappearance of 4-ClDDM in the presence of 0.3 *M* 2,6-dimethylphenol in ethanol at 65 °C was identical, within experimental uncertainty to the rate in the absence of phenol.

For the purposes of the present study the π acceptor must have reasonable solubility in ethanol and must be stable in ethanol at least for the time required for the kinetic measurements. Few of the stronger π acceptors meet both criteria. For example, 2,4,7-trinitrofluorenone and chloranil have insufficient solubility in ethanol; tetracyanoethylene and pyromellitic dianhydride solvolyze in ethanol to yield acidic solutions. The acceptors TNB, benzotrifuroxan (BTF) (14), and 1,2,4,5-tetracyanobenzene (TCNB) (15) were chosen for closer scrutiny. As measured by charge-transfer maxima (16), the acceptor strengths of the three acceptors lie in the order TCNB > TNB $\approx$ BTF. The few comparisons which have been made indicate that BTF (14) and TCNB (17) form complexes with aromatic π donors of comparable or greater stability than the corresponding TNB complexes.

In order to distinguish effects due to complexation of donor acid from other medium effects of added acceptor, two kinds of control experiments were carried out. The influence of added acceptor was examined in the reaction of 4-ClDDM with the non-donor acid acetic acid and in the thermal decomposition of 4-ClDDM at 30 °C in the absence of acids. A portion of the results are summarized in Table 2. The results clearly show that any increase in the rate of the acetic acid reaction produced by 0.070 *M* TNB is well within the experimental error. The effect of BTF varied from sample to sample. One sample (Table 2) produced a rate increase of about 12.5% at a concentration of 0.030 *M*. A rate measurement using the same concentration of this sample of BTF alone showed that the increase could be attributed entirely to catalytic activity of the BTF and was therefore not due to an interaction between the acetic acid and the BTF. This catalytic activity is apparently due to an acidic impurity in the BTF, though repeated crystallization from acetic acid and benzene failed to alter its catalytic activity. A second independently prepared sample gave approximately the same rate increase, while a third sample exhibited no effect whatever on the rate of decomposition of 4-ClDDM. This sample was used in the rate runs reported in Table 3. Finally, TCNB at saturation (approximately 0.010 *M*) had no measurable effect on the rate of decomposition of 4-ClDDM.

Tables 3 and 4 summarize the results of rate measurements involving the five donor acids with and without added TNB, BTF, and TCNB. The rate enhancements produced by 0.050 and 0.070 *M* TNB ranged from 12 to 22%, well outside the experimental uncertainty with all five donor acids (Table 3). Also included in Table 3 are the results of some experiments with *p*-methoxy-*trans*-cinnamic acid, an acid expected to have weak π donor properties but which gives no visible evidence for complexing with TNB in ethanol (above). Significantly, the rate increase (5%) was much smaller than that obtained with the other five donor acids, just marginally outside the combined experi-

TABLE 2. Rates of reaction of 4-ClDDM with acetic acid in ethanol at 30 °C, with and without added TNB and BTF

[Acetic acid] (M)	Acceptor	[Acceptor] (M)	10^2k_{obs} (min^{-1})[a]
0.026	none	—	0.716±0.022(3)
0.026	TNB	0.050	0.730±0.004(3)
0.026	TNB	0.070	0.718±0.006(3)
0.050	none	—	1.37±0.03(6)
0.050	TNB	0.050	1.38±0.04(6)
0.050	TNB	0.070	1.41±0.03(6)
0.142	none	—	4.15±0.04(3)
0.142	BTF	0.030	4.67±0.04(3)
0	BTF	0.030	0.58(1)

[a]Averages of indicated numbers of runs (in parentheses), with average deviations.

TABLE 3. Rates of reaction of 4-ClDDM with donor acids in ethanol at 30 °C, with and without added TNB[a]

Acid[b]	[Acid] (M)	10^2k_{obs} (without TNB)[c]	10^2k_{obs} (0.070 M TNB)[c]
IAA	0.035	0.793±0.028(3)	0.950±0.015(3)
	0.050	0.941±0.030(3)	1.11±0.04(3)
ICA	0.035	0.690±0.023(3)	0.785±0.023(3)
	0.050	1.07±0.01(3)	1.21±0.00(3)
	0.080	1.53±0.02(3)	1.76±0.08(3)
TMBA	0.035	2.17±0.02(4)	2.43±0.04(4)
	0.050	3.27±0.07(3)	3.74±0.05(3)
	0.080	5.27±0.01(5)	5.96±0.05(5)
DHBA	0.035	5.38±0.05(4)	6.54±0.08(4)
	0.050	7.83±0.14(4)	9.34±0.16(4)
	0.080	12.8±0.1(3)	15.4±0.0(3)
THBA	0.040	0.809±0.044(4)	0.963±0.034(4)
	0.050	1.08±0.02(4)	1.28±0.00(4)
	0.050	1.07±0.02(3)	1.20±0.01(3)[d]
	0.080	1.83±0.04(3)	2.15±0.05(3)
p-Methoxy-*trans*-cinnamic acid	0.035	1.39±0.02(3)	1.46±0.02(3)

[a]0.070 M unless otherwise specified.
[b]See text for abbreviations.
[c]Averages of indicated numbers of runs (in parentheses) with average deviations.
[d]Concentration of TNB is 0.050 M.

mental uncertainties of the two rate constants. Even at 0.010 and 0.015 M concentrations of BTF, rate increases well outside the experimental uncertainty (approximately 22, 11, and 13%, respectively) were observed with IAA, ICA, and DHBA. The difficulty in obtaining samples of BTF showing negligible catalysis in the absence of acid limited the scope of our study with this acceptor. For unknown reasons, the kinetics of the reaction of THBA with 4-ClDDM in the presence of BTF were not reproducible. The solubility of TCNB in ethanol in the presence of the donor acids is around 0.010 M. At this low concentration observed rate enhancements were just barely outside the combined experimental uncertainties of the rate constants with and without added acceptor with TMBA, DHBA, and THBA. With ICA a rate increase comparable to the experimental uncertainty was observed, while with IAA, 0.010 M TCNB gave a very small rate decrease, which, however, is well within the limits of the experimental uncertainty.

In addition to the studies with the three uncharged acceptors some preliminary investigations were carried out with one cationic acceptor, *N*-methylquinolinium chloride (NMQ^+Cl^-). In our potentiometric studies of the effects of

TABLE 4. Rates of reaction of 4-ClDDM with donor acids in ethanol at 30 °C with and without added BTF and TCNB

Acid[a]	[Acid] (M)	Acceptor[a]	[Acceptor] (M)	$10^2 k_{obs}$ (without acceptor)[b]	$10^2 k_{obs}$ (added acceptor)[b]
IAA	0.060	BTF	0.010	1.26±0.02(3)	1.44±0.02(3)
		BTF	0.015		1.53±0.03(3)
		TCNB	0.010		1.23±0.02(3)
ICA	0.045	BTF	0.010	0.818±0.011(3)	0.863±0.002(3)
		BTF	0.015		0.905±0.014(3)
		TCNB	0.010		0.835±0.014(3)
TMBA	0.050	TCNB	0.010	3.40±0.06(3)	3.57±0.04(3)
DHBA	0.050	BTF	0.010	8.32±0.14(3)	8.80±0.19(3)
		BTF	0.015		9.42±0.11(3)
		TCNB	0.010		8.64±0.08(3)
THBA	0.050	TCNB	0.010	1.07±0.02	1.11±0.00(3)

[a]See text for abbreviations.
[b]Averages of indicated numbers of runs (in parentheses) with average deviations.

TABLE 5. Equilibrium constants (K) ($\ell\,mol^{-1}$) for molecular complex formation in ethanol at 30 °C[a]

	Acceptor[b]		
Donor acid[b]	TNB	BTF	TCNB
IAA	2.45±0.16(2)	2.23±0.14(3)	1.93±0.06(2)
ICA	4.63±0.09(2)	4.36±0.28(3)	3.75±0.24(2)
TMBA	1.10(1)	—	3.52±0.08(3)
DHBA	1.56±0.65(2)	4.44±0.16(3)	0.67±0.14(3)
THBA	2.18(1)	4.76±0.02(2)	1.72±0.23(3)

[a]Averages of determinations at indicated numbers of wavelengths (in parentheses) with average deviations. See Experimental section for details.
[b]See text for abbreviations.

molecular complexing on acid–base equilibria (2) it was found that electrostatic effects are generally more important than effects due to charge-transfer interaction in weak complexes involving anionic acceptors. Addition of NMQ^+Cl^- to ethanolic solutions of IAA or THBA produces a visible color change. However, the rates of reaction of 0.040 M acetic acid, 0.040 M IAA, and 0.050 M THBA with 4-ClDDM in the presence of 0.050 M NMQ^+Cl^- were identical within experimental error to the rates of the same reactions in the presence of 0.050 M tetraethylammonium chloride (TEA^+Cl^-), a non-acceptor salt. Furthermore, second-order rate constants for the three acids in the presence of either salt were within 5% of those in the absence of salt. In contrast, Roberts *et al.* found that 0.05 M $LiClO_4$ produced rate increases of around 10–12% in the reaction of DDM with benzoic (11) and acetic (18) acids. It is possible that the NMQ^+ – donor acid complexes do not show the expected catalytic activity because of steric hindrance. However, there is no obvious reason why the NMQ^+ and TNB complexes should be any different in this respect, and no attempt was made to answer this question.

In order to estimate the catalytic constants for the acceptor – donor acid complexes for which kinetic data are available, it is necessary to have an estimate of the concentrations of complexed and uncomplexed acid under the conditions of a particular rate measurement. For this reason, 1:1 association constants for all donor acid – acceptor pairs were measured spectrophotometrically. The results are summarized in Table 5. The determinations were carried out using a modification of the procedure of de Maine and Seawright (19) (Experimental). Where possible, measurements were usually made at three wavelengths. With some systems overlap of the charge-transfer absorption with the acceptor absorption was so severe that measurements were only practical at one or

TABLE 6. Catalytic constants k_c (ℓ mol^{-1} min^{-1}) for reaction of acceptor–donor acid complexes with 4-ClDDM in ethanol at 30 °C

Acid[a]	[Acid] (M)	Acceptor[a]	[Acceptor] (M)	$10^2 k_c$ (ℓ mol^{-1} min^{-1})[b]	k_c/k[b]
IAA	0.035	TNB	0.070	0.55(0.46–0.66)	2.4(1.9–3.0)
	0.050	TNB	0.070	0.44(0.34–0.55)	2.3(1.7–3.0)
ICA	0.035	TNB	0.070	0.32(0.26–0.37)	1.6(1.3–2.0)
	0.050	TNB	0.070	0.35(0.33–0.37)	1.6(1.5–1.7)
	0.080	TNB	0.070	0.34(0.28–0.40)	1.8(1.4–2.1)
TMBA	0.035	TNB	0.070	1.7(1.4–2.1)	2.8(2.2–3.4)
	0.050	TNB	0.070	2.0(1.6–2.5)	3.1(2.4–3.9)
	0.080	TNB	0.070	1.9(1.8–2.2)	2.9(2.7–3.3)
DHBA	0.035	TNB	0.070	5.1(3.9–7.9)	3.3(2.5–5.2)
	0.050	TNB	0.070	4.8(3.6–7.8)	3.1(2.2–5.1)
	0.080	TNB	0.070	5.3(4.2–7.8)	3.3(2.6–4.9)
THBA	0.040	TNB	0.070	0.51(0.36–0.70)	2.5(1.7–3.7)
	0.050	TNB	0.070	0.54(0.49–0.61)	2.5(2.2–2.7)
	0.050	TNB	0.050	0.49(0.42–0.60)	2.3(1.9–2.8)
	0.080	TNB	0.070	0.57(0.46–0.70)	2.5(2.0–3.1)
IAA	0.060	BTF	0.010	1.8(1.4–2.2)	8.5(6.4–10.8)
	0.060	BTF	0.015	1.8(1.5–2.2)	8.5(6.9–10.5)
	0.060	TCNB	0.010	0(0–0.31)	0(0–1.5)
ICA	0.045	BTF	0.010	0.47(0.38–0.56)	2.6(2.0–3.1)
	0.045	BTF	0.015	0.55(0.44–0.68)	3.0(2.4–3.8)
DHBA	0.050	BTF	0.010	4.4(2.5–6.4)	2.6(1.5–3.9)
	0.050	BTF	0.015	5.9(4.9–7.0)	3.5(2.9–4.3)
ICA	0.045	TCNB	0.010	0.30(0.13–0.50)	1.7(0.7–2.8)
TMBA	0.050	TCNB	0.010	1.8(1.2–2.5)	2.7(1.7–3.7)
DHBA	0.050	TCNB	0.010	12(4–22)	6.9(2.5–13.6)
THBA	0.050	TCNB	0.010	0.69(0.33–1.08)	3.2(1.5–5.1)

[a]See text for abbreviations.
[b]Minimum and maximum values, estimated as described in text, given in parentheses.

two wavelengths. For all except three combinations (DHBA–TNB, DHBA–TCNB, and THBA–TCNB) where measurements were carried out at more than one wavelength, average deviations were ±6.5% or less. A more realistic estimate of the uncertainty in K is likely around 10 to 20%, except where average deviations are larger (20).

The 1:1 association constants were then combined with the results of the kinetic studies to calculate the catalytic constant k_c for the 1:1 acceptor – donor acid complex for each combination studied. The results are listed in Table 6 for each set of rate comparisons in Tables 3 and 4. Also listed are values of k_c/k, the factor by which the catalytic constant of the donor acid is increased by complexing. The first step in the calculation of k_c is calculation of the concentration of the 1:1 acceptor – donor acid complex, [HD·A], under the conditions of the rate measurements, from c_{HD}, c_A, and K. The calculated value of [HD·A] is then combined with pseudo first-order rate constants in the presence and absence of acceptor (where k_{obs} in the absence of acceptor $= kc_{HD}$) to calculate k_c by means of [3]. Rate measurements in the presence and absence of acceptor at the same acid concentration were carried out simultaneously and values of k_c/k were calculated from the value of k_{obs} in the absence of acceptor (Tables 3 and 4).

For purposes of comparison of k_c/k ratios it is important to have an estimate of experimental uncertainty, particularly for numbers calculated from small rate enhancements. Such estimates were obtained in the following way. Uncertainties in individual pseudo first-order rate constants were taken as the average deviations for three or four duplicate measurements (Tables 3 and 4), and used to calculate maximum and minimum values for the difference (k_{obs} –

TABLE 7. Estimates of the effect of complexing on the acidity, $K_a^c/K_a(H_2O, 25\ °C)$[a]

	Acceptor[b]		
Donor acid[b]	TNB	BTF	TCNB
IAA	2.6±0.1	10.5±0.1	0
ICA	1.8±0.1	3.1±0.3	1.8
TMBA	3.3±0.1	—	3.0
DHBA	3.6±0.1	3.4±0.6	8.4
THBA	2.7±0.1	—	3.6

[a]Averages of average K_a^c/K_a values from separate rate comparisons, with average deviations.
[b]See text for abbreviations.

kc_{HD}). Using the average deviation in K as a measure of its experimental uncertainty, minimum and maximum values of [HD·A] were calculated for the conditions of each rate comparison. Where a K was measured at a single wavelength its uncertainty was taken arbitrarily as ±10%. Minimum and maximum values of k_c were then calculated from minimum and maximum values of $(k_{obs} - kc_{HD})$ and maximum and minimum values of [HD·A], respectively. Although uncertainties in K may be underestimated in some cases by this procedure, the calculated uncertainties in k_c and k_c/k reflect mainly uncertainties in the rate increases and are influenced only slightly by a 10% uncertainty in K. We believe, therefore, that our estimates of the uncertainties in k_c and k_c/k are maximum uncertainties. Values of k_c and k_c/k obtained from rate comparisons at different acid and/or acceptor concentrations are generally in good agreement and the ranges of k_c and k_c/k overlap without exception.

Finally, it remains to estimate the effects of molecular complexing on the acidity constant by means of [5]. For this purpose α is the slope of a plot of log k for reaction of 4-ClDDM with carboxylic acids at 30 °C *vs.* log K_a in H_2O at 25 °C. For the 14 carboxylic acids in Table 1 for which the K_a's have been measured, α = 0.59 (standard deviation 0.06). However, since the relative reactivities of 4-ClDDM and DDM are essentially independent of the acid (above) we may use the much more extensive data for the latter to choose an appropriate value of α. Unfortunately, though good correlations are obtained for small groups of closely related carboxylic acids, there is considerable variation of α from one group to another. For example, for selected groups of *meta*- and *para*-substituted benzoic acids α (equal to the Hammett ρ in the case) is 0.93–0.95 (21–24), for phenylacetic acids, 0.72 (23) β-phenylpropionic acids 0.92 (23), phenoxyacetic acids 0.72 (23), *trans*-cinnamic acids 1.0 (23), 3-substituted acrylic acids 0.72–0.74 (24), *ortho*-substituted benzoic acids 0.79 (24), substituted acetic, and propionic acids 0.62 (9*f*). Values of both log k (DDM, ethanol, 30 °C) and K_a (thermodynamic, H_2O, 25 °C) have now been reported in the literature for 19 *meta*- and *para*-substituted benzoic acids. For this group α = 0.91 (standard deviation 0.02, corr. coeff. 0.995) and we have used this value to obtain the estimates of K_a^c/K_a listed in Table 7.

Discussion

The most important result of this work is the demonstration that with a single exception (IAA + TCNB) addition of the π acceptors TNB, BTF, and TCNB to the reactions of five π donor carboxylic acids with 4-ClDDM in ethanol produces measurable rate enhancements. We have interpreted these rate enhancements as resulting from formation of a 1:1 acceptor – donor acid complex which is a stronger acid than the uncomplexed acid. By combining the rate data with independently-determined 1:1 association constants we have calculated the factors, k_c/k, by which the catalytic constants of the acids are increased by complexation, and from these have estimated the factors, K_a^c/K_a, by which the acidity constant is increased by complexation.

Before considering the significance of the derived results in Tables 6 and 7, it is important to review the evidence supporting our interpretation of the rate enhancements. With 0.070 *M* TNB and 0.015 *M* BTF, rate enhancements well outside experimental error were observed with every acid showing visible evidence for

complexing, while the rate of reaction of *p*-methoxy-*trans*-cinnamic acid, a very weak π donor showing no visible evidence for complexing with TNB, was increased only 5 ± 3% by 0.07 *M* TNB. The rate of reaction of the non-donor acid acetic acid was unchanged by 0.070 *M* TNB. The rate of decomposition of 4-ClDDM in ethanol was unaffected by the presence of the three acceptors at concentrations used in the rate enhancement measurements. Finally, values of k_c/k calculated from rate comparisons at different concentrations of TNB or BTF and/or different donor acid concentrations are in good agreement.

The most striking feature of the k_c/k values in Table 6 is their similarity. Average k_c/k values for 8 of the 13 combinations studied lie in the range 2.0 to 3.5 and only 2 values, those for IAA–BTF (8.5) and IAA–TCNB (0) lie outside this range by more than the experimental uncertainty.

Complexing could produce an increase in acidity by means of at least two kinds of electronic effects. The most likely interaction mechanism of general importance is π electron charge-transfer from donor to acceptor, in accordance with the Mulliken description of donor–acceptor complexes (25). The extent of charge-transfer should increase with decreasing donor ionization energy and increasing acceptor electron affinity, however it is likely to be small and reasonably constant for the weak complexes studied in this work. Complexing could also influence acidity through direct electrostatic interaction between polar groups (*e.g.*, NO_2) in the acceptor and the donor carboxyl group. Such field effects could facilitate or impede loss of a proton, depending on the preferred relative orientation of the complexed donor and acceptor, and are more likely to vary from one donor–acceptor combination to another. Changes in equilibrium acidity resulting from complexing could be partly obscured by unfavorable steric effects in the proton transfer transition state. Again, steric effects should vary widely from one donor–acceptor combination to another.

The close similarity of the k_c/k values strongly suggests that steric effects are generally unimportant. On the other hand, steric hindrance appears to be the most plausible explanation for the lack of reactivity of the IAA–TCNB complex. This result is reminiscent of the work of Menger and Bender (26) who found complexes of *N*-(indole-3-acryloyl)imidazole and *p*-nitrophenyl 3-indoleacrylate with 3,5-dinitrobenzoate to be inert in basic hydrolysis. A similar, though somewhat weaker argument can be made for the general unimportance of dipolar field effects, though such effects could be important in either or both of the systems whose k_c/k values lie outside the 2.0–3.5 range. We consider, therefore, that the results of this investigation provide clear evidence for significant charge-transfer in weak donor–acceptor complexes.

Experimental uncertainties in k_c/k make comparisons between donors risky, particularly outside of the TNB results. No clear order of donor or acceptor strengths is discernible from the k_c/k values, nor does any constant pattern of donor or acceptor strengths emerge from the equilibrium studies. As was found in the catalysis of acetolysis of 2,4,7-trinitro-9-fluorenyl *p*-toluenesulfonate by aromatic hydrocarbon donors (1) and by methoxynaphthalene donors (27) there is little relationship between the stability of the complex (as measured by K) and the chemical effect of complexing (k_c/k).

Finally, it is interesting to compare the effects of complexing on acidity with the effects of electron-withdrawing substituents on the acidities of benzoic acids. Log (K_a^c/K_a) values from this work vary over the ranges 0.26–0.56 (TNB), 0.5–1.0 (BTF), and 0.2–0.9 (TCNB). These (presumed) electron-withdrawing effects are therefore similar to those of substituents in the benzoic acids (log K/K_0, or σ), *e.g.*, *p*-Cl (0.26), *m*-CN (0.56), *p*-CN (0.78). These effects are also comparable to the electronic effects of complexing by aromatic donors in acetolysis of 2,4,7-trinitro-9-fluorenyl *p*-toluenesulfonate where, for example, complexation with phenanthrene has about the same effect as removal of the 2-nitro group. The much smaller rate enhancements in the present work are due mostly to the much lower sensitivity of the K_a of benzoic and related acids to electron withdrawal from the benzene ring.

Experimental

Reagents

4-Chlorodiphenyldiazomethane, prepared as described by Schroeder and Katz (28), was purified by crystallizing twice from dry methanol; mp 34.5–35.5 °C, uv λ_{max} (ethanol) = 520 nm. 4,4′-Di-*tert*-butyldiphenyldiazomethane, was prepared by silver oxide oxidation (28)

TABLE 8. Experimental conditions for the determination of association constants

Donor–acceptor	λ (nm)	No. of solutions	[Donor] range (*M*)	[Acceptor] range (*M*)	O.D. range	1:1 Association constant
IAA–TNB	480	12	0.040–0.004	0.040–0.004	2.051–0.035	2.61
	520	13	0.060–0.015	0.060–0.015	1.367–0.110	2.30
ICA–TNB	430	11	0.040–0.008	0.040–0.008	1.812–0.113	4.72
	460	19	0.080–0.014	0.080–0.014	2.849–0.146	4.54
TMBA–TNB	418	14	0.090–0.020	0.090–0.020	1.179–0.112	1.10
DHBA–TNB	400	9	0.055–0.010	0.055–0.010	1.595–0.203	2.21
	414	18	0.100–0.015	0.100–0.0515	1.472–0.098	0.91
THBA–TNB	480	11	0.090–0.020	0.090–0.020	1.228–0.079	2.18
IAA–BTF	460	12	0.120–0.030	0.010–0.005	0.665–0.113	2.02
	470	12	0.120–0.030	0.010–0.005	0.486–0.086	2.44
	480	12	0.120–0.030	0.010–0.005	0.348–0.063	2.23
ICA–BTF	450	12	0.090–0.015	0.015–0.008	0.393–0.097	4.13
	460	10	0.090–0.020	0.015–0.008	0.316–0.077	4.79
	470	10	0.090–0.020	0.015–0.008	0.270–0.065	4.17
DHBA–BTF	365	12	0.200–0.080	0.010–0.005	1.429–0.536	4.45
	370	12	0.200–0.080	0.010–0.005	1.174–0.435	4.19
	375	12	0.200–0.080	0.010–0.005	0.969–0.360	4.66
THBA–BTF	410	12	0.100–0.020	0.015–0.008	1.240–0.264	4.78
	420	12	0.100–0.020	0.015–0.008	0.896–0.187	4.75
IAA–TCNB	460	12	0.080–0.016	0.007–0.003	0.644–0.061	1.86
	480	12	0.080–0.016	0.007–0.003	0.541–0.051	1.99
ICA–TCNB	420	12	0.090–0.020	0.010–0.004	1.070–0.154	3.52
	430	12	0.090–0.020	0.010–0.004	0.941–0.138	3.99
TMBA–TCNB	350	11	0.120–0.024	0.010–0.004	1.052–0.122	3.64
	360	11	0.120–0.024	0.010–0.004	0.950–0.107	3.44
	370	11	0.120–0.024	0.010–0.004	0.822–0.091	3.47
DHBA–TCNB	360	10	0.200–0.040	0.010–0.004	0.943–0.089	0.55
	370	10	0.200–0.040	0.010–0.004	0.793–0.073	0.58
	380	10	0.200–0.040	0.010–0.004	0.655–0.063	0.88
THBA–TCNB	390	11	0.120–0.024	0.010–0.004	1.095–0.108	1.44
	410	11	0.120–0.024	0.010–0.004	0.945–0.093	1.66
	430	11	0.120–0.024	0.010–0.004	0.738–0.074	2.07

of the corresponding hydrazone, obtained from 4,4′-di-*tert*-butylbenzophenone (29) by the method of Szmant and McGinnis (30). After crystallization from hexane the diazo compound had mp 95–98 °C, uv λ_{max} (ethanol) = 535 nm.

1,2,4,5-Tetracyanobenzene was prepared by the procedure of Bailey *et al.* (17*a*), mp 265–266 °C (lit. (17*a*) mp 270–272 °C), infrared spectrum identical to published spectrum (17*a*).

Benzotrifuroxan was prepared by the method of Bailey and Case (14), mp 193–195 °C (lit. (14) mp 194–195 °C), infrared spectrum identical to published spectrum.

1,3,5-Trinitrobenzene, all of the carboxylic acids, *p*-toluenesulfonic acid, *N*-methylquinolinium chloride, and tetraethylammonium chloride were obtained from commercial sources and, where necessary, purified by crystallization until their melting points agreed with published (31) values.

Kinetic Measurements

The progress of the reaction was followed by the usual spectrophotometric method (11, 32). Optical density measurements utilized a Guilford model 200 spectrophotometer equipped with a thermostatted cell compartment maintained at 30.00 ± 0.05 °C by circulation of water. The disappearance of 4-ClDDM was generally followed at 530 nm but when a molecular complex had significant absorption at this wavelength a longer wavelength was used. Measurements were carried out under pseudo first-order conditions using an excess of acid and following the reaction through at least two half-lives. Pseudo first-order rate constants were determined both graphically and by computer.

Determination of Association Constants

The association constants were determined spectrophotometrically using a Guilford model 200 spectrophotometer (above). The experimental data were analyzed

by computer using an adaptation of the iterative method of de Maine and Seawright (19), described by Dewar and Thompson (3*a*). The experimental conditions are summarized in Table 8 for each donor–acceptor pair studied.

Acknowledgments

This research was supported by the U.S. Department of Health, Education and Welfare (Grant GM 11967-03).

The authors are grateful to Dr. M. R. J. Dack for carrying out several product analyses.

1. A. K. COLTER, A. L. MCKENNA III, and M. A. KASEM. Can. J. Chem. **52**, 3748 (1974).
2. A. K. COLTER and D. BUBEN. Can. J. Chem. **54**, 2141 (1976).
3. (*a*) M. J. S. DEWAR and C. C. THOMPSON, JR. Tetrahedron Suppl. **7**, 97 (1966); (*b*) R. S. MULLIKEN and W. B. PERSON. Molecular complexes: a lecture and reprint volume. Wiley-Interscience, New York. 1969. p. 301; (*c*) M. W. HANNA and J. L. LIPPERT. *In* Molecular complexes. Vol. 1. Elek Science, London. 1973. Chapt. 1; (*d*) R. FOSTER. J. Chem. Soc. Perkin Trans. II, 507 (1975).
4. (*a*) R. P. BELL. The proton in chemistry. Cornell University Press, Ithaca. 1959. Chapt. 10; (*b*) A. J. KRESGE. Chem. Soc. Rev. **2**, 475 (1973).
5. W. B. PERSON. J. Am. Chem. Soc. **87**, 167 (1965).
6. M. R. J. DACK. J. Chem. Educ. **49**, 600 (1972), and references cited therein.
7. R. A. MORE O'FERRALL. *In* Advances in physical organic chemistry. Vol. 5. *Edited by* V. Gold. Academic Press, London and New York. 1967. p. 331, and references cited therein.
8. (*a*) C. K. HANCOCK, R. F. GILBY, JR., and J. S. WESTMORELAND. J. Am. Chem. Soc. **79**, 1917 (1957); (*b*) C. K. HANCOCK and J. S. WESTMORELAND. J. Am. Chem. Soc. **80**, 545 (1958); (*c*) C. K. HANCOCK and E. FOLDVARY. J. Org. Chem. **30**, 1180 (1965).
9. (*a*) N. B. CHAPMAN, J. SHORTER, and J. H. P. UTLEY. J. Chem. Soc. 1825 (1962); (*b*) A. BUCKLEY, N. B. CHAPMAN, and J. SHORTER. J. Chem. Soc. 178 (1963); (*c*) W. K. KWOK, R. A. MORE O'FERRALL, and S. I. MILLER. Tetrahedron, **20**, 1913 (1964); (*d*) K. BOWDEN, N. B. CHAPMAN, and J. SHORTER. Can. J. Chem. **42**, 1980 (1964); (*e*) K. BOWDEN, A. BUCKLEY, N. B. CHAPMAN, and J. SHORTER. J. Chem. Soc. 3380 (1964); (*f*) K. BOWDEN, M. HARDY, and D. C. PARKIN. Can. J. Chem. **46**, 2929 (1968); (*g*) K. BOWDEN and D. C. PARKIN. Can. J. Chem. **47**, 185 (1969).
10. L. D. GOODHUE and R. M. HIXON. J. Am. Chem. Soc. **57**, 1688 (1935).
11. J. D. ROBERTS, W. WATANABE, and R. E. MCMAHON. J. Am. Chem. Soc. **73**, 760 (1951).
12. (*a*) G. KORTÜM, W. VOGEL, and K. ANDRUSSOW. Dissociation constants of organic acids in aqueous solution. Butterworths, London. 1961; (*b*) A. ALBERT and E. P. SERJEANT. Ionization constants of acids and bases. Methuen and Co., London. 1962.
13. R. FOSTER and P. HANSON. Tetrahedron, **21**, 255 (1965).
14. A. S. BAILEY and R. J. CASE. Tetrahedron, **3**, 113 (1958).
15. R. E. MERRIFIELD and W. D. PHILLIPS. J. Am. Chem. Soc. **80**, 2778 (1958).
16. (*a*) M. J. S. DEWAR and A. R. LEPLEY. J. Am. Chem. Soc. **83**, 4560 (1961); (*b*) A. ZWEIG, J. E. LEHNSON, W. G. HODGSON, and W. H. JURA. J. Am. Chem. Soc. **85**, 3937 (1963); (*c*) A. S. BAILEY, R. J. P. WILLIAMS, and J. D. WRIGHT. J. Chem. Soc. 2579 (1965).
17. (*a*) A. S. BAILEY, B. R. HENN, and J. M. LANGDON. Tetrahedron, **19**, 161 (1963); (*b*) R. FOSTER and C. A. FYFE. Trans. Faraday Soc. **62**, 1400 (1966).
18. J. D. ROBERTS and C. M. REGAN. J. Am. Chem. Soc. **74**, 3695 (1952).
19. P. A. D. DEMAINE and R. D. SEAWRIGHT. Digital computer programs for physical chemistry. Vol. 1. MacMillan, New York. 1962. Chapt. IV.
20. (*a*) R. FOSTER. Organic charge-transfer complexes. Academic Press, London. 1969. Chapts. 6 and 7; (*b*) R. FOSTER. *In* Molecular complexes. Vol. 2. *Edited by* R. Foster. Crane, Russak and Co., New York. 1974. Chapt. 3.
21. J. D. ROBERTS, E. A. MCELHILL, and R. ARMSTRONG. J. Am. Chem. Soc. **71**, 2923 (1949).
22. R. A. BENKESER, C. E. DEBOER, R. E. ROBINSON, and D. M. SAUVE. J. Am. Chem. Soc. **78**, 682 (1956).
23. K. BOWDEN. Can. J. Chem. **41**, 2781 (1963).
24. K. BOWDEN. Can. J. Chem. **43**, 3354 (1965).
25. R. S. MULLIKEN and W. B. PERSON. Molecular complexes: a lecture and reprint volume. Wiley-Interscience, New York. 1969.
26. F. M. MENGER and M. L. BENDER. J. Am. Chem. Soc. **88**, 131 (1966).
27. A. K. COLTER and S. HUI. J. Org. Chem. **33**, 1935 (1968).
28. W. SCHROEDER and L. KATZ. J. Org. Chem. **19**, 718 (1954).
29. B. W. LARNER and A. T. PETERS. J. Chem. Soc. 680 (1952).
30. H. SZMANT and C. MCGINNIS. J. Am. Chem. Soc. **72**, 2890 (1950).
31. J. R. A. POLLOCK and R. STEVENS. Dictionary of organic compounds. 4th ed. Oxford, New York. 1965.
32. J. HINE and W. C. BAILEY, JR. J. Am. Chem. Soc. **81**, 2075 (1959).

Total synthesis of ylango sesquiterpenoids: (+)-*cis*- and (+)-*trans*-sativenediol, (+)-helminthosporal, (+)-helminthosporol, prehelminthosporal, prehelminthosporal diethyl acetal, (+)-victoxinine, (+)-isosativenediol

EDWARD PIERS AND HANS-PETER ISENRING

Department of Chemistry, University of British Columbia, 2075 Wesbrook Place, Vancouver, B.C., Canada V6T 1W5

Received October 19, 1976

EDWARD PIERS and HANS-PETER ISENRING. Can. J. Chem. **55**, 1039 (1977).

Oxidation of the previously prepared olefinic alcohol **26** with chromium trioxide – pyridine in dichloromethane containing trifluoroacetic acid gave the tricyclic ketone **29** as the major product. Hydroxylation of the latter, followed by reduction of the resulting α-hydroxy ketone **31**, afforded a 1:1 mixture of (+)-*cis*- (**22**) and (+)-*trans*-sativenediol (**23**). In view of earlier synthetic transformations reported by a number of different researchers, the present work also constitutes formal total syntheses of the enantiomers of the following sesquiterpenoids: (−)-helminthosporal (**1**), (−)-helminthosporol (**2**), prehelminthosporal (**3**), prehelminthosporal diethyl acetal (**4**), (−)-victoxinine (**8**), and (−)-isosativenediol (**19**).

EDWARD PIERS et HANS-PETER ISENRING. Can. J. Chem. **55**, 1039 (1977).

L'oxydation de l'alcool oléfinique **26**, préparé antérieurement, par le complexe oxyde de chrome – pyridine dans le dichlorométhane contenant de l'acide trifluoroacétique conduit à la cétone tricyclique **29** comme produit majeur. L'hydroxylation de ce dernier, suivie par une réduction de l'α-hydroxy cétone **31** qui en résulte, conduit à un mélange 1:1 des sativènediols (+)-*cis* (**22**) et (+)-*trans* (**23**). Si l'on tient compte des transformations synthétiques rapportées antérieurement par un certain nombre de chercheurs différents, le travail actuel constitue aussi une synthèse totale formelle des énantiomères des sesquiterpènes suivants: le (−) helminthosporal (**1**), le (−) helminthosporol (**2**), le préhelminthosporal (**3**), le diéthylacétal de préhelminthosporal (**4**), le (−) victoxinine (**8**) et le (−) isosativènediol (**19**).

[Traduit par le journal]

During the past 15 years, *Helminthosporium sativum*, a fungus which is responsible for assorted deleterious effects on a variety of cereal crops and grasses (1), has been the object of a series of chemical investigations carried out by a number of different research groups. The combined results of this work have shown that the fungus produces a fairly large number of structurally related sesquiterpenoids,[1] some of which have subsequently been obtained by partial or total synthesis.[4] Interestingly, some of these natural products exhibit significant biological activity, particularly as related to regulation of plant growth (4, 5, 9).

The recent isolation and structural elucidation of (−)-*cis*-sativenediol (**11**) was independently reported by two research groups (8, 9). This natural product, isolated from two different fungi (*Helminthosporium sativum* (8, 9) and *Cochliobolus setariae* IFO 6635 (9)) was shown to be a plant growth promotor with gibberellin-like activity (9). At the same time, both groups isolated an isomeric substance, also levorotatory, to which was initially assigned the *trans*-sativenediol structure **21** (8, 9). However, more recently, Dorn and Arigoni have clearly shown (13) that the isomeric compound actually

[1](−)-Helminthosporal (**1**) (1–3),[2] (−)-helminthosporol (**2**) (4, 5),[2] prehelminthosporal (**3**)[3] (6), (−)-prehelminthosporol (**5**) (6–9), (−)-sativene (**6**) (10), 9-hydroxyprehelminthosporol (**7**) (7), (−)-victoxinine (**8**) (11), (−)-longifolene (**9**) and a secolongifolane derivative (**10**) (12), (−)-*cis*-sativenediol (**11**) (8, 9) and related metabolites (**12**–**18**, excluding compound **15***a*) (8), (−)-isosativenediol (**19**) and the related triol (**20**) (13).

[2]It was subsequently reported (6) that **1** and **2** did not actually occur as such in crude extracts of the fungus. They were therefore believed to be artifacts of the isolation procedure.

[3]Prehelminthosporal (**3**) was isolated as the corresponding diethyl acetal **4** (6).

[4](−)-Helminthosporal (**1**) (14), (+)-, (±)-, or (−)-sativene (**6**) (10, 15–20), (−)-victoxinine (**8**) (11), (±)-longifolene (**9**) (21–23).

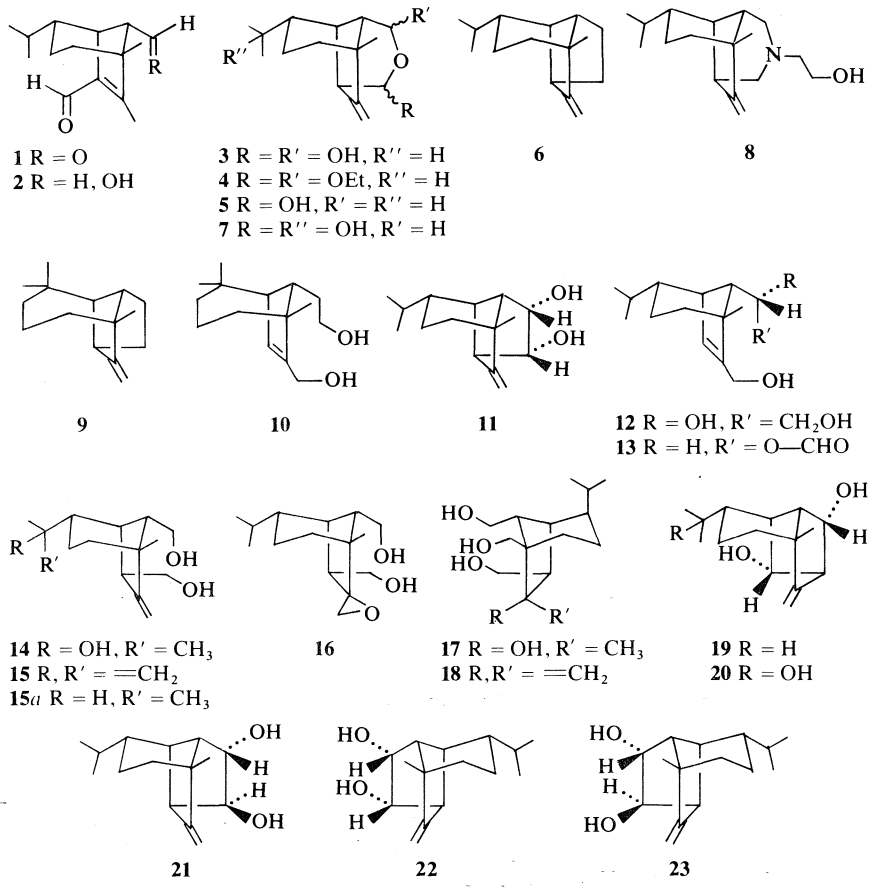

1 R = O
2 R = H, OH

3 R = R′ = OH, R″ = H
4 R = R′ = OEt, R″ = H
5 R = OH, R′ = R″ = H
7 R = R″ = OH, R′ = H

6

8

9

10

11

12 R = OH, R′ = CH_2OH
13 R = H, R′ = O—CHO

14 R = OH, R′ = CH_3
15 R, R′ = $=CH_2$
15*a* R = H, R′ = CH_3

16

17 R = OH, R′ = CH_3
18 R, R′ = $=CH_2$

19 R = H
20 R = OH

21

22

23

possesses the isosativenediol structure **19**.[5] We report herein the total synthesis of both (+)-*cis*- and (+)-*trans*-sativenediol (**22** and **23**, respectively).[6,7] Our work fully confirms the structural assignment made with respect to **11**, and also shows that the original assignments (**21**) (8, 9) made in the case of the isomeric compound were indeed incorrect.

It is pertinent to note that the following conversions have previously been accomplished: (*a*) (−)-*cis*-sativenediol (**11**) into prehelminthosporal (**3**) (9), prehelminthosporal diethyl acetal (**4**) (9), and (−)-isosativenediol (**19**) (13); (*b*) compound **4** into (−)-helminthosporal (**1**) (6); (*c*) (−)-helminthosporal (**1**) into (−)-helminthosporol (**2**) (5); (*d*) (−)-prehelminthosporol (**5**) into (−)-victoxinine (**8**) via the diol **15***a* (11), which has also been derived from (−)-*cis*-sativenediol (**11**) (13). In view of these transformations, our work also constitutes the completion of formal total syntheses of the enantiomers of the sesquiterpenoids **1**–**4**, **8**, and **19**.

In connection with earlier work concerning the total synthesis of ylango-type[8] sesquiterpenoids, we have already described (18, 19) the preparation of the diene **25** and its conversion into the olefinic alcohol **26**. Since these compounds were synthetically derived from (−)-carvone (**24**), their absolute stereochemistry was firmly established. Although oxidation of **26** with Collins' reagent (27, 28) under carefully controlled conditions produced the corresponding

[5]We are very grateful to Professors Arigoni and Marumo for personal communications regarding this point. We also thank Professor Arigoni for full experimental details regarding the work which he and his co-workers have done in this area.

[6]For a preliminary communication regarding this work, see ref. 24.

[7]McMurry and Silvestri (25) have recently completed a very elegant total synthesis of racemic *cis*-sativenediol via a sequence entirely different from that used in our work. We are grateful to Professor McMurry for a preprint regarding their synthesis.

[8]For an explanation regarding the origin of the term 'ylango', see ref. 26.

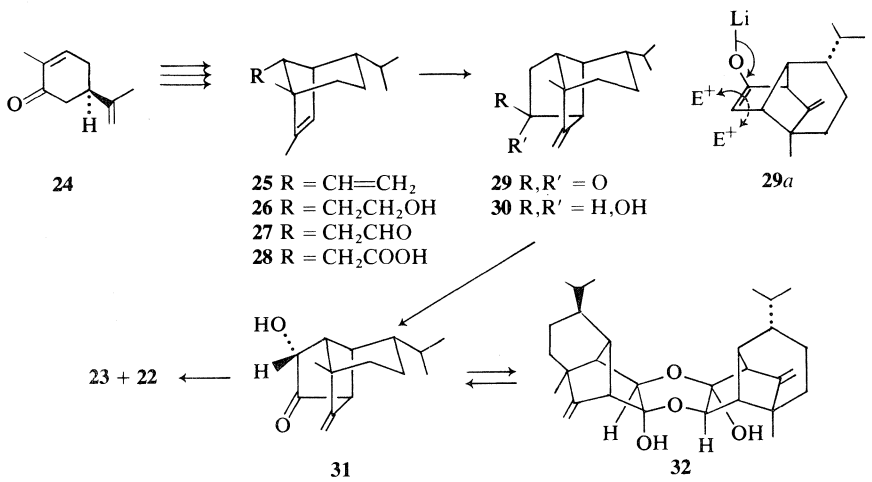

aldehyde **27** in good yield, the latter compound was invariably accompanied by a small amount (~5–8%) of another previously unidentified product (19). This minor product was isolated by preparative glc and was subjected to spectral analysis. The ir spectrum showed a strong absorption at 1741 cm^{-1}, indicating the presence of a cyclopentanone-type carbonyl group. Other particularly instructive bands were found at 1651 and 883 cm^{-1}, indicative of an exocyclic methylene functionality. The presence of the latter functional group was confirmed by the ^1H nmr spectrum in which signals due to the two olefinic protons appeared as singlets at τ 4.83 and 5.17. In addition, a one-proton signal at τ 6.83 could readily be attributed to an allylic proton. On the basis of these data, the structure of the minor product obtained from oxidation of **26** could be assigned the tricyclic structure **29**. Clearly, under the conditions of the oxidation reaction, the initially formed olefinic aldehyde **27** was, at least to a small extent, undergoing intramolecular cyclization (internal Prins reaction (29, 30)) to afford the alcohol **30**, which was then further oxidized to the corresponding ketone **29**. Since the latter compound appeared to be an ideal synthetic precursor for (+)-*cis*- (**22**) and (+)-*trans*-sativenediol (**23**), a study was undertaken with the aim of finding conditions for the oxidation of **26** which would give **29** as a major product.

After considerable investigation of various alternatives and reaction conditions, it was found that the overall conversion of **26** into **29** could be carried out in a fairly efficient manner as follows. When the olefinic alcohol **26** was treated with 8 mol equiv. of Collins' reagent (27, 28) in dichloromethane at room temperature, it was found that essentially all of **26** had been converted into the corresponding aldehyde **27** in ~20 min. Since the Prins reaction is known to be acid-catalyzed (29, 30), the reaction mixture was treated with a catalytic amount of trifluoroacetic acid, along with a further 8 equiv. of oxidizing agent. Work-up after an additional reaction time of 4.5 h gave a crude mixture of products which, upon subjection to column chromatography, yielded 30% of the desired tricyclic ketone **29**, 19% of the aldehyde **27**, and a crude oil that contained the olefinic acid **28**. Resubjection of **27** to the oxidizing conditions ($CrO_3 \cdot 2C_5H_5N$, CF_3COOH, CH_2Cl_2) gave a further 10% of **30**. Finally, two successive treatments of the crude acid **28** with oxalyl chloride in benzene, followed by appropriate purification by column chromatography afforded an additional 15% of the desired material **29**. Thus, the latter compound was obtained in 55% overall yield from the diene **25**.

Interestingly, alternative oxidation procedures for the direct conversion of **26** into **29** proved less satisfactory. For example, it is pertinent to note that pyridinium chlorochromate, a reagent recently employed to cyclize citronellol oxidatively to pulegone (31, 32) produced in our case an excellent yield of the aldehyde **27**, even in the presence of excess reagent.

Clearly, the conversion of the tricyclic ketone **29** into the two sativenediols **22** and **23** required only hydroxylation of **29** at the position adjacent to the carbonyl group, followed by reduction of the resulting hydroxy ketone.

Although there are now a number of apparently efficient methods available for effecting α-hydroxylation of a ketone, we chose the neat, experimentally convenient procedure recently introduced by Vedejs (33). Thus, conversion of **29** into the corresponding lithium enolate (lithium diisopropylamide, THF, −70 °C), followed by treatment of the resultant solution with the molybdenum peroxide MoO_5·Py·HMPA (33), afforded, stereoselectively, in 74% yield, the hydroxy ketone **31**. The stereochemistry of the latter compound, predicted to be as shown (approach of the electrophilic reagent from the less hindered side of the enolate anion, *cf.* **29***a*), was fully corroborated by the ^{1}H nmr spectrum. In particular, the carbinol proton in **31** appeared as a sharp singlet at τ 6.06, clearly showing that there was little or no coupling between this proton and the one on the adjacent carbon atom. A molecular model of **31** indicated that the dihedral angle between these two protons was very close to 90° and therefore little or no coupling would be expected (34). On the other hand, the corresponding dihedral angle in the epimeric compound would have been approximately 40–45° and coupling (~3–5 Hz) would have been expected.

It is interesting to note that during purification by column chromatography, or upon standing in solution, compound **31** slowly dimerized. The resultant substance (probably **32**) was only slightly soluble in ether, gave gas–liquid chromatographic retention times identical with those of **31** and, upon distillation, was smoothly transformed into the monomeric hydroxy ketone **31**. The reversible dimerization of α-hydroxy ketones is a well-known phenomenon and these observations therefore deserve no further comment.

Reduction of the hydroxy ketone **31** with lithium aluminum hydride in ether at 0 °C produced, in 90% yield, a 1:1 mixture of (+)-*cis*- (**22**) and (+)-*trans*-sativenediol (**23**). These compounds were cleanly separated by column chromatography on silica gel. The *cis*-diol **22** exhibited ir and ^{1}H nmr spectra identical with those of the naturally occurring enantiomer **11**.[9] The spectra (ir and ^{1}H nmr) obtained from the *trans*-diol **23** were similar to, but clearly distinguishable from, those of (−)-isosativenediol (**19**) and of the *cis*-diol **22**.

[9]We are very grateful to Professor Marumo for copies of the ir and ^{1}H nmr spectra of (−)-*cis*-sativenediol (**11**) and of (−)-isosativenediol (**19**).

Experimental

General

Melting points, which were determined on a Kofler block, and boiling points are uncorrected. Optical rotations were obtained at the sodium D line, using a Perkin-Elmer model 141 automatic polarimeter. Routine ir spectra were recorded on a Perkin-Elmer model 710 spectrophotometer, while comparison spectra were recorded on a Perkin-Elmer model 457 spectrophotometer. Proton magnetic resonance spectra were taken in deuteriochloroform solution on Varian Associates spectrometers, models T-60, HA-100 and/or XL-100. Signal positions are given in the Tiers τ scale, with tetramethylsilane as an internal standard. The multiplicity, integrated peak areas, and proton assignments are indicated in parentheses. Mass spectrometric measurements were carried out on an AEI type MS-9 mass spectrometer. Gas–liquid chromatographic analyses were carried out on a Hewlett-Packard model 5832A gas chromatograph. A variety of stainless steel columns (6 ft × 1/8 in., packed with 5% OV-1, 5% OV-17, 5% OV-210 or 5% SP-1000 on 80-100 mesh Chromosorb W) were employed and a carrier gas (helium) flow rate of 30 ml/min was used in all analyses. Microanalyses were performed by Mr. P. Borda, Microanalytical Laboratory, University of British Columbia, Vancouver, B.C.

Preparation of the Tricyclic Ketone 29

To a solution of freshly distilled 2-methyl-2-butene (2.3 ml, 21.6 mmol) in 35 ml of dry tetrahydrofuran at 0 °C was added 865 μl (9.1 mmol) of borane – methyl sulfide complex, and the resulting solution was stirred under an atmosphere of nitrogen for 30 min. A solution of the diene **25** (880 mg, 4.3 mmol) in 17.5 ml of dry tetrahydrofuran was added, the cooling bath was removed, and the reaction mixture was stirred at room temperature for 2.5 h. The solution was cooled to 0 °C, 9.1 ml of 10% aqueous sodium hydroxide and 7.7 ml of 30% aqueous hydrogen peroxide were carefully added, and the resulting mixture was stirred at room temperature for 1 h. After having been diluted with brine, the reaction mixture was thoroughly extracted with 2:1 petroleum ether (bp 30–60 °C) – ether. The combined extracts were washed with brine and dried over anhydrous magnesium sulfate. Removal of the solvent afforded 950 mg of a nearly colorless oil. Gas–liquid chromatographic analysis of this material showed the absence of starting material **25** and indicated that the product, olefinic alcohol **26**, was >98% pure.

A solution of this material in 9.5 ml of dry dichloromethane was added to a solution of chromium trioxide – dipyridine complex (34.5 mmol) in 86 ml of the same solvent. Examination (glc) of an aliquot indicated that all of the alcohol **26** had been converted into the aldehyde **27** after about 20 min. At this time, pyridine (69 mmol) and chromium trioxide (34.5 mmol) were added, followed after 15 min by 260 μl of trifluoroacetic acid. After 4.5 h, the dark reaction mixture was diluted with brine and the products were extracted with ether. The combined extracts were washed with brine, dried over anhydrous magnesium sulfate, and evaporated under reduced pressure. The residual oil was subjected to chromatog-

raphy on 50 g of silica gel. Elution with 5% ether in petroleum ether (bp 60–110 °C) afforded 180 mg of the olefinic aldehyde **27** and 280 mg (30%) of the tricyclic ketone **29**. Elution with pure ether afforded a crude oil which contained the olefinic acid **28**.

Subjection of the aldehyde **27** to the oxidation conditions described above (13 mmol chromium trioxide – dipyridine complex, 45 μl trifluoroacetic acid, 20 ml dichloromethane, reaction time 1.25 h), followed by chromatography of the crude product afforded an additional 95 mg (10%) of the desired ketone **29**.

The crude oil (~550 mg) containing the olefinic acid **28** (see above) was dissolved in 20 ml of dry benzene. The resulting solution was treated with 1.0 ml of oxalyl chloride and was then stirred at room temperature for 30 min. Removal of the benzene, followed by chromatography (silica gel) of the residual material gave pure cyclic ketone **29**, and a crude mixture containing some acid chloride (corresponding to **28**). Hydrolysis of the latter, followed by resubjection of the resultant crude material to reaction with oxalyl chloride in benzene afforded additional amounts of cyclic ketone. In this way, 140 mg (15%) of the desired material **29** was obtained.

The total yield (based on diene **25**) of the tricyclic ketone **29** was 515 mg (55%). This material exhibited bp 75 °C/0.3 torr; $[\alpha]_D^{22}$ +188° (*c* 1.35 in $CHCl_3$); ir (film) ν_{max} 1741, 1651, 883 cm^{-1}; ^1H nmr τ 4.83, 5.17 (s, s, 2H, olefinic protons), 6.83 (br s, 1H, allylic proton, $w_{1/2}$ = 4.0 Hz), 8.85 (s, 3H, tertiary methyl), 9.09, 9.12 (d, d, 6H, isopropyl methyls, J = 6 Hz). *Mol. Wt.* calcd. for $C_{15}H_{22}O$: 218.1670; found (high resolution mass spectrometry): 218.1701.

*Preparation of the Hydroxy Ketone **31***

To a cold (0 °C) solution of diisopropylamine (1.95 mmol) in 2.0 ml of dry tetrahydrofuran was added 0.72 ml of a solution of *n*-butyllithium in hexane (2.72 *M*). The resultant mixture was cooled to −70 °C, and a solution of the cyclic ketone **29** (327 mg, 1.5 mmol) in 8 ml of dry tetrahydrofuran was added slowly. The reaction mixture was stirred at −70 °C for 30 min, after which time 846 mg (1.95 mmol) of the molybdenum peroxide MoO_5·Py·HMPA (33) was added in one portion. Stirring was continued for 1 h at −70 to −65 °C, the cooling bath was removed, and the reaction mixture was allowed to warm slowly to 0 °C, at which temperature it became homogeneous. Brine was added and the resultant mixture was thoroughly extracted with ether. The combined ether extracts were washed once with 5% aqueous sodium carbonate, once with 5% hydrochloric acid, and then dried over anhydrous magnesium sulfate. Removal of the solvent yielded an oil which was subjected to chromatography on silica gel (16 g). Elution with 92:8 petroleum ether – ether gave 60 mg (18%) of starting material **29**. Elution with 1:1 petroleum ether – ether gave 230 mg of crystalline material. On the basis of the physical characteristics of the latter, it was clear that this material was a mixture of two compounds. One of them (the dimer **32**) was only slightly soluble in ether, while the other gave spectral data in accord with the desired monomeric hydroxy ketone **31**. Both compounds gave the same retention times on glc thus clearly showing that upon subjection to heat, the dimer reverted to the monomer. Distillation of the mixture (bath temperature up to 210 °C) at 0.3 torr afforded 212 mg (74%, based on unrecovered starting material) of pure hydroxy ketone **31**, mp 55 °C; $[\alpha]_D^{22}$ +194° (*c* 1.85 in $CHCl_3$); ir ($CHCl_3$) ν_{max} 3410 (br), 3075, 1750, 1655, 1059, 890 cm^{-1}; ^1H nmr τ 4.90, 5.22 (s, s, 2H, olefinic protons), 6.06 (s, 1H, carbinol proton), 6.83 (br s, 1H, allylic proton, $w_{1/2}$ = 4.0 Hz), 7.35 (br s, 1H, $w_{1/2}$ = 5.0 Hz), 8.86 (s, 3H, tertiary methyl), 9.10, 9.13 (d, d, 6H, isopropyl methyls, J = 6 Hz). *Mol. Wt.* calcd for $C_{15}H_{22}O_2$: 234.1619; found (high resolution mass spectrometry): 234.1644.

*(+)-cis- (**22**) and (+)-trans-Sativenediol (**23**)*

To a cold (0 °C) solution of the hydroxy ketone **31** (142 mg, 0.61 mmol) in 6 ml of dry ether was added 25 mg of lithium aluminum hydride and the mixture was stirred at 0 °C for 10 min. Saturated aqueous ammonium chloride (5 ml) was added carefully and the resulting mixture was stirred for another 5 min. The mixture was diluted with brine and thoroughly extracted with ether. The combined extracts were dried over anhydrous magnesium sulfate. Removal of the solvent yielded an oil which was subjected to chromatography on silica gel (30 g). The column was eluted with petroleum ether – ether (85:15 to 10:90, respectively), yielding *cis*-sativenediol (**22**) (62 mg, 43%), a mixture of **22** and **23** (5 mg), and *trans*-sativenediol (**23**) (63 mg, 44%).

Distillation (air-bath temperature 130 °C/0.3 torr) of *cis*-sativenediol (**22**) gave an oil: $[\alpha]_D^{24}$ +124° (*c* 0.98 in $CHCl_3$); ir (film) ν_{max} 3350 (br), 3065, 1660, 1055, 884 cm^{-1}; ^1H nmr τ 5.10, 5.42 (s, s, 2H, olefinic protons), 6.00 (d, 1H, carbinol proton, J = 6 Hz), 6.39 (d, 1H, carbinol proton, J = 6 Hz), 6.7 (br, 2H, —OH), 7.36 (br s, 1H, $w_{1/2}$ = 5 Hz), 7.59 (br s, 1H, $w_{1/2}$ = 4 Hz), 8.96 (s, 3H, tertiary methyl), 9.06, 9.19 (d, d, 6H, isopropyl methyls, J = 6 Hz). *Anal.* calcd. for $C_{15}H_{24}O_2$: C 76.22, H 10.26; found: C 75.82, H 10.24.

trans-Sativenediol (**23**) (air-bath temperature 135 °C/0.3 torr) was also an oil: $[\alpha]_D^{24}$ +64° (*c* 1.32 in $CHCl_3$); ir (film) ν_{max} 3380 (br), 3065, 1655, 1090, 1073, 1035, 889 cm^{-1}; ^1H nmr τ 5.11, 5.19 (s, s, 2H, olefinic protons), 6.24 (m, 1H, carbinol proton), 6.45 (d, 1H, carbinol proton, J = 2 Hz), 7.3 (br, 2H, —OH), 7.34 (br, 1H, $w_{1/2}$ = 8 Hz), 7.62 (br s, 1H, $w_{1/2}$ = 4 Hz), 8.96 (s, 3H, tertiary methyl), 9.10, 9.16 (d, d, 6H, isopropyl methyls, J = 6 Hz). *Anal.* calcd. for $C_{15}H_{24}O_2$: C 76.22, H 10.26; found: C 76.40, H 10.40.

Acknowledgments

Financial support from the National Research Council of Canada is gratefully acknowledged.

1. P. DE MAYO, E. Y. SPENCER, and R. W. WHITE. Can. J. Chem. **39**, 1608 (1961), and references cited therein.
2. P. DE MAYO, E. Y. SPENCER, and R. W. WHITE. J. Am. Chem. Soc. **84**, 494 (1962).
3. P. DE MAYO, E. Y. SPENCER, and R. W. WHITE. Can. J. Chem. **41**, 2996 (1963).
4. S. TAMURA, A. SAKURAI, K. KAINUMA, and M. TAKAI. Agr. Biol. Chem. Tokyo, **27**, 738 (1963).
5. S. TAMURA, A. SAKURAI, K. KAINUMA, and M. TAKAI. Agr. Biol. Chem. Tokyo, **29**, 216 (1965).
6. P. DE MAYO, R. E. WILLIAMS, and E. Y. SPENCER. Can. J. Chem. **43**, 1357 (1965).
7. D. C. ALDRIDGE and W. B. TURNER. J. Chem. Soc. C, 686 (1970).

8. F. DORN, P. BERNASCONI, and D. ARIGONI. Chimia, 29 (1975).
9. M. NUKINA, H. HATTORI, and S. MARUMO. J. Am. Chem. Soc. **97**, 2542 (1975).
10. P. DE MAYO and R. E. WILLIAMS. J. Am. Chem. Soc. **87**, 3275 (1965).
11. F. DORN and D. ARIGONI. J. Chem. Soc. Chem. Commun. 1342 (1972).
12. F. DORN and D. ARIGONI. Experientia, **30**, 851 (1974).
13. F. DORN and D. ARIGONI. Experientia, **31**, 753 (1975).
14. E. J. COREY and S. NOZOE. J. Am. Chem. Soc. **85**, 3527 (1963); **87**, 5728 (1965).
15. J. E. MCMURRY. J. Am. Chem. Soc. **90**, 6821 (1968).
16. G. L. HODGSON, D. F. MACSWEENEY, and T. MONEY. J. Chem. Soc. Perkin Trans. 1, 2113 (1973).
17. C. R. ECK, G. L. HODGSON, D. F. MACSWEENEY, R. W. MILLS, and T. MONEY. J. Chem. Soc. Perkin Trans. 1, 1938 (1974).
18. E. PIERS, M. B. GERAGHTY, and M. SOUCY. Synth. Commun. **3**, 401 (1973).
19. E. PIERS, M. B. GERAGHTY, R. D. SMILLIE, and M. SOUCY. Can. J. Chem. **53**, 2849 (1975).
20. H. HAGIWARA, M. MIYASHITA, H. UDA, and A. YOSHIKOSHI. Bull. Chem. Soc. Jpn. **48**, 3723 (1975).
21. E. J. COREY, M. OHNO, R. B. MITRA, and P. A. VATAKENCHERRY. J. Am. Chem. Soc. **86**, 478 (1964).
22. J. E. MCMURRY and S. J. ISSER. J. Am. Chem. Soc. **94**, 7132 (1972).
23. R. A. VOLKMANN, G. C. ANDREWS, and W. S. JOHNSON. J. Am. Chem. Soc. **97**, 4777 (1975).
24. E. PIERS and H.-P. ISENRING. Synth. Commun. **6**, 221 (1976).
25. J. E. MCMURRY and M. G. SILVESTRI. J. Org. Chem. **41**, 3953 (1976).
26. E. PIERS, R. W. BRITTON, M. B. GERAGHTY, R. J. KEZIERE, and R. D. SMILLIE. Can. J. Chem. **53**, 2827 (1975).
27. J. C. COLLINS, W. W. HESS, and F. J. FRANK. Tetrahedron Lett. 3363 (1968).
28. R. RATCLIFFE and R. RODEHORST. J. Org. Chem. **35**, 4000 (1970).
29. E. ARUNDALE and L. A. MIKESKA. Chem. Rev. **51**, 505 (1972).
30. C. W. ROBERTS. *In* Friedel–Crafts and related reactions. Vol. II, Part 2. *Edited by* G. A. Olah. Interscience Publishers, Inc., New York, NY. 1963. pp. 1175–1210.
31. E. J. COREY and J. W. SUGGS. Tetrahedron Lett. 2647 (1975).
32. E. J. COREY, H. E. ENSLEY, and J. W. SUGGS. J. Org. Chem. **41**, 380 (1976).
33. E. VEDEJS. J. Am. Chem. Soc. **96**, 5944 (1974).
34. M. KARPLUS. J. Am. Chem. Soc. **85**, 2870 (1963).

Selective, homonuclear pulse experiments in the Fourier transform mode: a study of 2′,3′-*O*-isopropylidene uridine[1]

KLAUS BOCK,[2] ROLAND BURTON, AND LAURANCE D. HALL

Department of Chemistry, The University of British Columbia, Vancouver, B.C., Canada V6T 1W5

Received September 17, 1976

KLAUS BOCK, ROLAND BURTON, and LAURANCE D. HALL. Can. J. Chem. **55**, 1045 (1977).

A simple modification of a conventional Fourier transform nmr spectrometer (Varian XL-100) makes it feasible to apply selective, radiofrequency pulses at the resonance frequency of one, or more, proton resonances and to monitor the effects of those perturbations in the usual F.t. fashion. Experiments with 2′,3′-*O*-isopropylidene uridine are used to illustrate the utility of this technique in measurements of selective spin-lattice relaxation rates, to eliminate unwanted resonances by selective saturation or by selective partial relaxation, and to perform the pulse equivalent of a ^1H–^1H INDOR experiment.

KLAUS BOCK, ROLAND BURTON et LAURANCE D. HALL. Can. J. Chem. **55**, 1045 (1977).

Une modification simple d'un spectromètre rmn à transformation de Fourier conventionnel (Varian XL-100) permet d'appliquer des pulsations de fréquences radiosélectives à la fréquence d'une ou de plusieurs résonances du proton et d'évaluer l'effet de ces perturbations dans un mode usuel de transformation de Fourier. On a utilisé des expériences avec la 2′,3′-*O*-isopropylidène uridine pour illustrer les utilités de cette technique dans les mesures de vitesses sélectives de relaxation spin réseau pour éliminer des résonances non-désirées par saturation sélective ou par relaxation partielle sélective, et pour effectuer l'équivalent pulsée d'une expérience INDOR H^1–H^1.

[Traduit par le journal]

Introduction

Two, closely related concepts are fundamental to the design of any pulse Fourier transform (F.t.) nmr experiment, that of the 'flip angle' and that of the 'pulse selectivity'.

The *flip angle* (α) is that angle through which the magnetization vector of a nucleus is turned by a pulse of radiofrequency power of the appropriate frequency. The magnitude of this angle is given by the product of the 'pulse duration' and the 'pulse intensity' and, in principle, an infinite number of combinations of these two variables can be used to provide any chosen value for α. In normal practice the experimental options are restricted somewhat by the desire to sample as wide a spectral region as possible, with a power distribution which is as homogeneous as possible, an experiment hereafter referred to as a *non-selective* pulse F.t. experiment.

Since the effective bandwidth (Δ) in the *frequency domain*, of a 360° flip angle pulse of duration t_{360}-s in the *time domain*, is given by the relationship,

$$\Delta = \gamma H_1/2\pi = 1/t_{360}$$

the *non-selective* pulse F.t. experiment makes use of rather intense pulses (100–200 W), of rather short duration (commonly 20–50 μs for a 90° pulse). Such pulses have a total bandwidth of 5–12 kHz but in common practice a flat, power-frequency distribution is experienced by only a few kHz on either side of the carrier frequency.

With a few notable exceptions, little attention has been directed towards nmr experiments in which highly selective pulses are applied to one, or a few, regions of a spectrum. We refer to these as a *selective-pulse* experiment. It is clear that the pulses for such an experiment should be rather weak, and of very long duration. This approach was first pioneered by Freeman and Wittekoek (2) with their 'audio-modulation' pulse technique; but, as we found to our cost when we used that approach (3), it suffered from the disadvantage that the effects of a perturbation also had to be monitored in a selective fashion, and this was extremely time consuming for multiple-spin nmr spectra. The obvious solution to this problem is to use the audio-modulation technique to provide

[1]Part 10 of a series, "Applications of pulsed nuclear magnetic resonance spectroscopy"; for part 9, see ref. 1. A full account of this study was given at the Canadian Chemical Conference of the Chemical Institute of Canada, Toronto, May 25–28, 1975.

[2]Visiting Associate Professor at U.B.C., 1974–1975. Permanent address, Institute for Organic Chemistry, The Technical University of Denmark, Lyngby, Denmark.

a long, weak, and therefore highly selective perturbation pulse, but to monitor its effect on the remainder of the nmr spectrum using a short, intense, non-selective monitoring pulse available from a conventional pulse F.t. nmr spectrometer. And as we shall see in the following discussion this solution is both simple and effective. However, it is appropriate to mention at this juncture that the 'tailored excitation' technique developed by Hill and Tomlinson (4) is likely to provide an even more effective solution in the future.[3]

It proved convenient for several reasons to use 2′,3′-*O*-isopropylidene uridine (**1**) as a model compound for an evaluation of the utility of various selective-pulse F.t. experiments. The ^1H nmr spectrum of **1** in dimethyl sulphoxide-d_6 at 100 MHz, is reasonably well dispersed. Equally important, the proton spin-lattice relaxation rates for **1** are sufficiently rapid to provide a stringent test of certain relaxation measurements and **1** is related to compounds which are of considerable interest to us in another context.

Results and Discussion

The basic pulse sequence used for all the experiments described here, is summarized in Fig. 1*A*. The selective, *perturbation pulse* is derived either directly, or via one of several different classes of audio-modulation, from the homonuclear decoupler of the spectrometer. The non-selective, *monitoring pulse* and the remainder of the detection system is generally derived from the usual pulse F.t. section of the spectrometer. Both pulses are computer controlled, either via the gates provided with the instrument or via a separate gate controlled by a flag specifically derived from the computer. Minor modifications may be required to obtain appropriately long pulses from the decoupler channel. In our laboratory we also have extensive options available for data storage and subsequent data manipulation, but these are not fundamental to the success of the experiments.

The objective of the first series of experiments, which are illustrated in Figs. 2–4, was to demonstrate experimentally the range of frequency selectivities which could be obtained by varying the pulse duration. In each instance the perturbation corresponded to a 180° pulse, and its effect

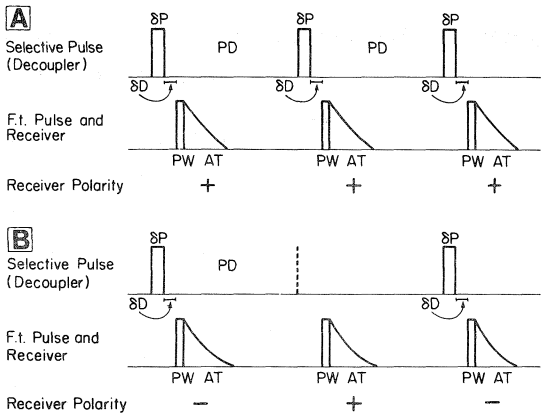

FIG. 1. Diagrammatic representation of the pulse sequences used for most of the experiments described in this paper: δP = width of selective pulse; δD = delay between selective pulse and F.t. pulse; PW = width of F.t. (monitoring) pulse; AT = acquisition time for F.I.D.; PD = pulse delay (four times T_1 value).

was monitored by a non-selective 90° pulse in the usual fashion.[4]

The effects of a 180° pulse applied to the high field component of the H-6 doublet are illustrated in Fig. 2. A pulse of 100 ms provides a reasonable degree of frequency selectivity and any decrease in its duration is accompanied by a rapid decrease in that selectivity. For example the 10 ms pulse applies a 180° flip angle to both components of the H-6 doublet. This is a pity because the shorter pulse clearly tips the H-6 magnetization more effectively than the longer pulse; this is simply because the latter is now sufficiently long for appreciable magnetization to be lost during the duration of the pulse itself. Clearly then, the selective relaxation rate[5] of the transition, or resonance of interest constitutes an effective upper limit for the pulse duration and hence for the frequency selectivity for that particular sample.

The spectra shown in Figs. 3 and 4 indicate the

[3]Since this manuscript was submitted Freeman and co-workers (20) have reported an alternative method for generating 'tailored excitation' sequences that seems to have considerable generality.

[4]A referee prompted us to draw the readers' attention to the work of Ernst and co-workers (21) (and also that of Meakin and Jesson (22)) which discusses the importance of the flip angle of the monitoring pulse used to sample the magnetization of a strongly coupled spin system that has previously been subjected to a selective perturbation. For large flip angles the observed line intensities do not always directly reflect population differences between just two energy levels. A brief discussion of this phenomenon in relation to the homonuclear pulse INDOR experiments is given in ref. 1.

[5]The *selective* relaxation rate of H-6 is 1063 ms^{-1}. Note that this value differs from the *non-selective* R_1-value (5).

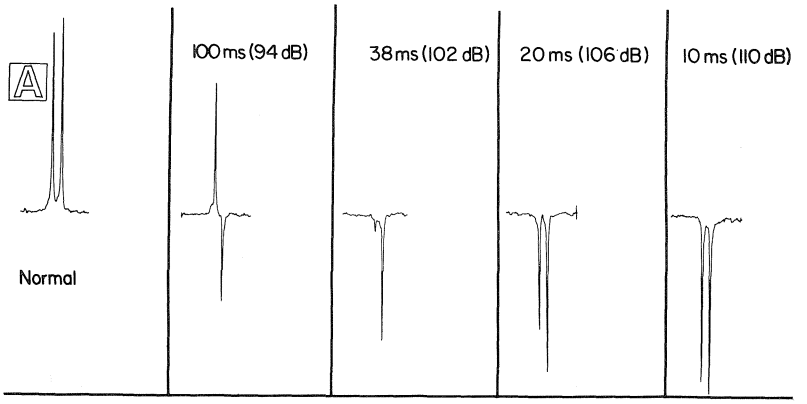

FIG. 2. Inset A shows the normal H-6 resonance of **1** measured with *PW* 75 μs, *PD* 5 s, *AT* 4 s, *NT* 10, and sensitivity enhancement 1.5. The remaining spectra were measured using identical conditions but with prior application, to the upfield transition, of a 180° pulse, the duration and intensity of which are indicated immediately above each resonance. Note that the 10 ms pulse flips *both* the H-6 transitions through 180°.

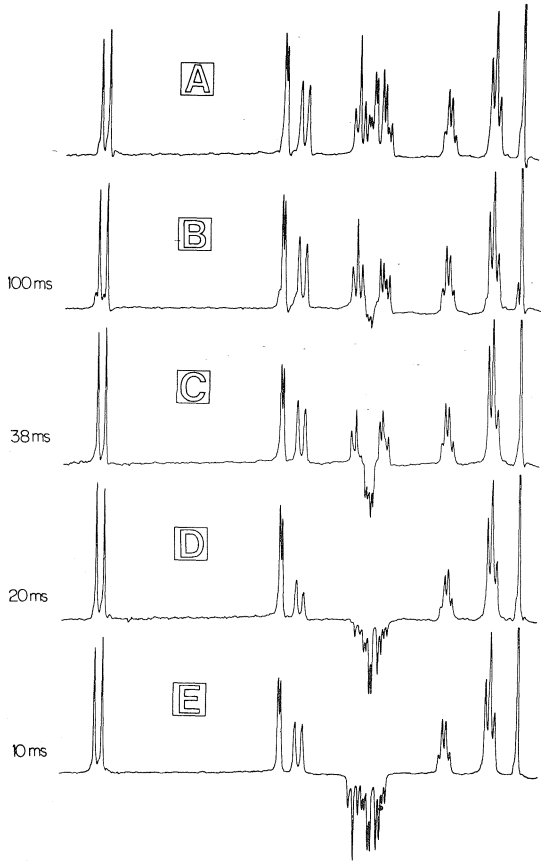

FIG. 3. Spectra showing the effects of changing the duration of a selective 180° pulse applied at the centre of a multiplet resonance (the δP values are listed at the side). The normal ^{1}H spectrum is shown in A. Note that even a 10 ms pulse has no significant effect on the H-5 and H-4′ resonances (the spectra were monitored as for Fig. 2).

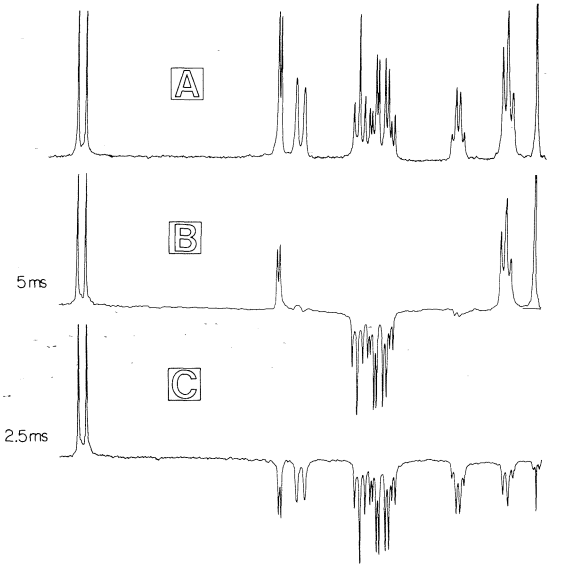

FIG. 4. These spectra show that it is feasible to invert the resonances of a substantial spectral region by applying a suitably short pulse. See Fig. 2 for monitoring conditions.

intermediate ranges of frequency selectivity which are possible; in each instance the decoupler frequency was set at the centre of the H-2′, H-3′, OH′ region. Note that even the 10 ms pulse has little effect on the H-5 and H-4′ resonances which is in accord with expectation since the *total* bandwidth of this pulse should only be 50 Hz.

The final set of spectra, shown in Fig. 4 illustrate that a pulse of 2–5 ms duration can be used to invert a substantial region of a ^{1}H spectrum, but still leave some spectral regions unper-

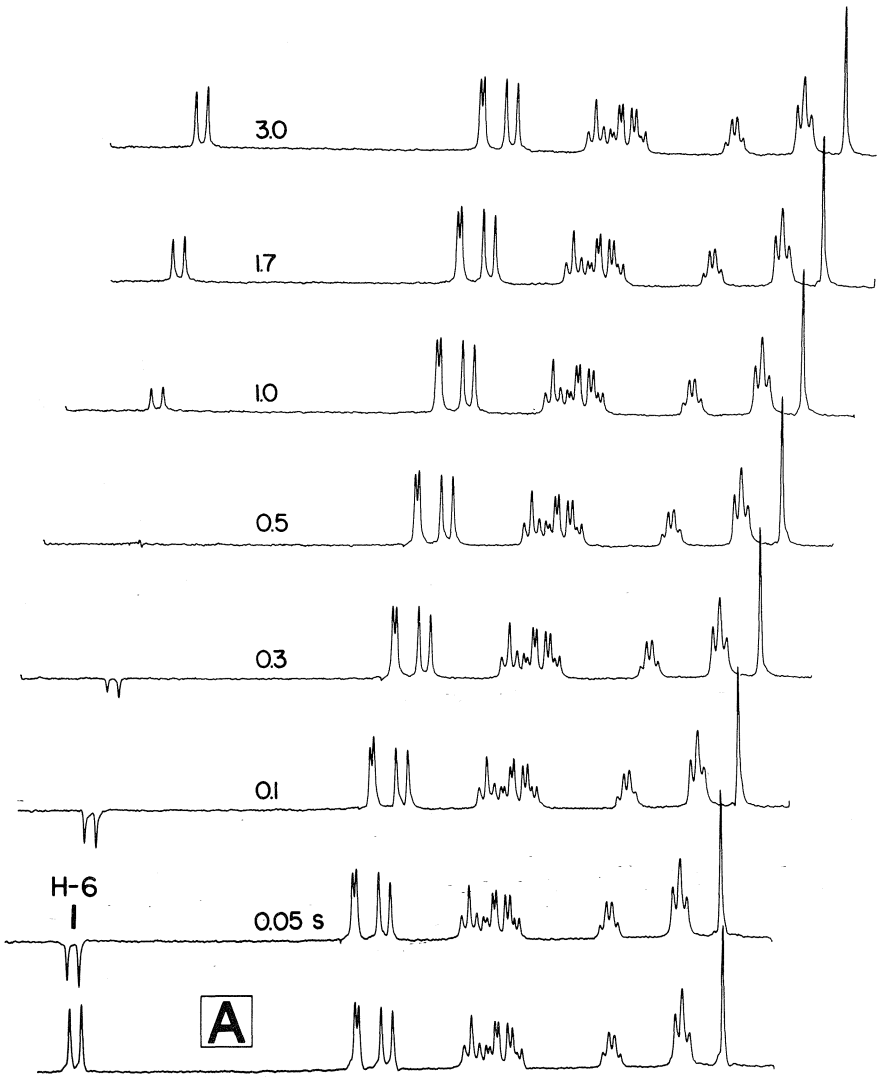

FIG. 5. The inversion-recovery determination of the selective relaxation rate for the H-6 resonances of **1**. A, shows part of the normal F.t. nmr spectrum (*NT* 5, *PW* 75 s, *AT* 4 s, *SE* 1.5). The other spectra were obtained by inverting the spin-states of H-6 with a selective 180° pulse (38 ms, 100 dB) and monitoring the magnetization using the parameters listed above: the pulse delay times are listed against the corresponding spectrum. Note the nearly complete cancellation of the H-6 resonance for the 0.5 s spectrum. The value for $R_1^6(6)$ calculated from these data is 1053 ms^{-1}.

turbed; in this case the H-6 resonance. Note that the 5 ms pulse has an off-resonance field equivalent to a 90° pulse for the H-5 and H-4′ resonances. The possibility of using the decoupler as a convenient source of perturbation pulse of intermediate frequency-bandwidth has many potentially useful applications, particularly in the area of heteronuclear nmr studies.

Selective Measurements of Spin-lattice Relation Rates

The *non-selective*, two-pulse, inversion-recovery sequence used for measuring spin-lattice relaxation rates is now well known (6). All the spins of one nuclear species are simultaneously inverted with a non-selective, 180° pulse and the amount of residual magnetization remaining

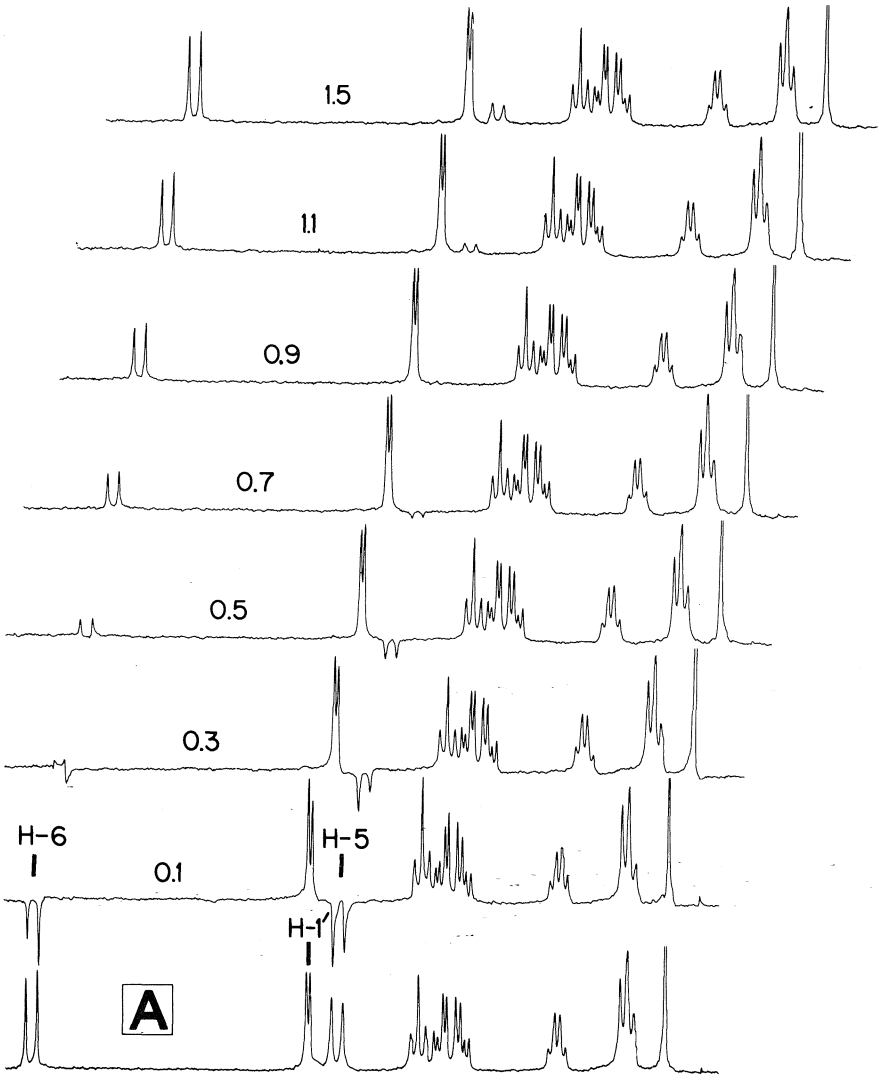

FIG. 6. Spectra showing the determination of the double-selective spin-lattice relaxation rate for the H-6 and H-5 resonances of **1**. The normal spectrum is shown in A (*NT* 5, *PW* 75 s, *AT* 4 s, *SE* 1.5). The remaining spectra show the inversion–recovery sequence following selective inversion of both the H-6 and H-5 resonances with a 180°-pulse (38 ms, 103 dB); these are plotted for delay times for 0.1 to 1.5 s. Note the more rapid relaxation of H-6 and the fact that the H-1′ resonance is not significantly affected by the 180° pulse applied to H-5. Processing these data gave $R_1^6(5,6)$ 1282 ms^{-1} and $R_1^5(5,6)$ 562 ms^{-1}.

after a known delay time (*PD*) is monitored with a non-selective, 90° pulse. The selective measurement merely involves the substitution of a selective 180° pulse from the decoupler for the non-selective pulse from the radiofrequency transmitter. The spectra shown in Fig. 5 illustrate the determination of the selective R_1-value of the H-6 resonance of **1**. The normal spectrum monitored with a non-selective 90° pulse is shown in A, Fig. 5. The partially-relaxed spectra, each accompanied by the appropriate delay time, are displayed in the form of a stack plot even though they were originally stored on a magnetic tape and were separately plotted.

An example of a double-selective, inversion-recovery experiment is given in Fig. 6. In this

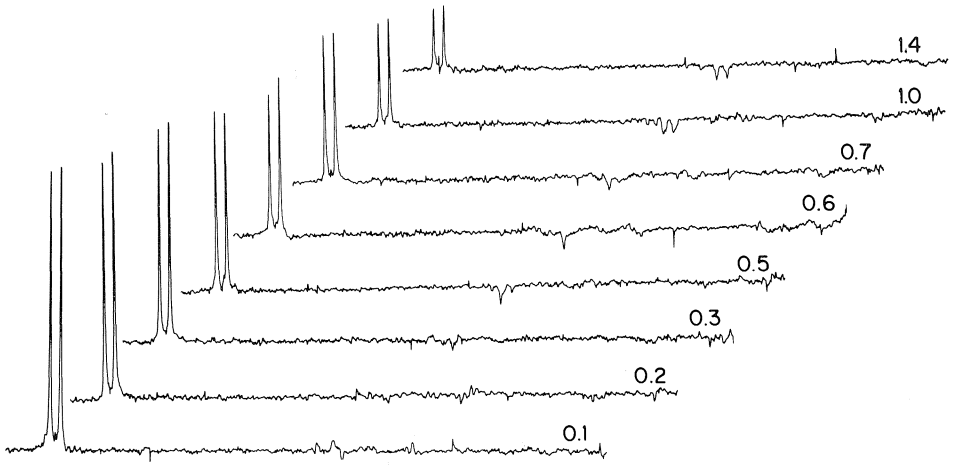

FIG. 7. Illustration of the selective, three-pulse sequences applied to the measurement of the R_1-value of the H-6 resonance of **1**.

case the frequency of the decoupler was set precisely between the H-6 and H-5 resonances and then an audio-modulation frequency, of precisely one half the chemical shift difference between the H-6 and H-5 resonances, was applied to the decoupler. This positioned the first audio-modulation side-bands precisely on the H-6 and H-5 resonances. Simultaneous timing of the audio-modulation pulse derived from both these side bands could be effected by gating either the decoupler or the audio-oscillator, or both. The selectivity of the applied 180° pulse is attested to by the minimal perturbation of the H-1′ resonance by the pulse. And the constancy of the intensity of the other resonances not directly involved in the experiment show that spurious, off-resonance effects are also commendably small.

Clearly there are many alternative procedures for effecting double-, triple-, quadruple-, etc., selective inversion experiments. In this present instance, addition of a second audio-modulation frequency would have produced *four* selective pulses; but these, like those used in the above experiment, would by definition have to have the *same* duration and intensity. For experiments which require several pulses, each of *differing intensity*, an alternate protocol is necessary. Now the decoupler frequency is offset to one side of the entire spectrum and then two, or more, audio-modulation frequencies are applied, each producing a side-band the intensity of which is proportional to the audio-modulation index. With a suitable choice of offset frequency for the decoupler- and audio-frequencies it is generally possible to ensure that only one set of side bands impinges on the entire spectral region. It must be noted, however, that the organization of such experiments is rather more complex than for the experiment summarized in Fig. 6.

It is a trivial matter to extend the above audio-modulation approach to encompass all of the other methods for measuring spin-lattice relaxation times, including the saturation recovery (7) and progressive saturation (8) methods. Although we do not illustrate these experiments here, Fig. 7 shows the efficiency with which a selective, three-pulse inversion-recovery experiment (9) can be performed; that is the sequence $[180°(\text{selective})\text{–}t\text{–}90°\text{–}5T_1\text{–}90°\text{–}5T_1]_n$. Note the efficiency with which this sequence results in the cancellation of the resonance not subjected to the selective, 180° pulse; this point will be discussed again in the next section.

A Pulse Equivalent of the INDOR Experiment

A useful variant on the experiments described in the previous section involves selective irradiation of a single transition of a spin-coupled multiplet. This pulse perturbs the populations of the spin states associated with the irradiated transition and this in turn induces changes in the transition probabilities, and hence transition intensities, of all the spectral components having an energy level in common with those which have been perturbed. This is illustrated diagrammatically for an AX-system in Fig. 8. Application of a 180° pulse to transition A-1 inverts the popula-

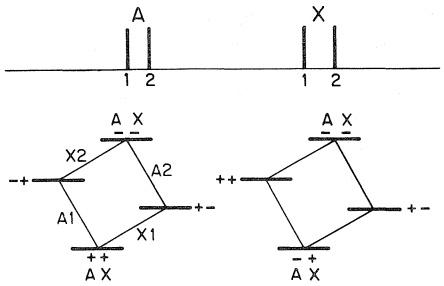

FIG. 8. Diagrammatic representation of the effect of 180° pulse applied to transition A-1 of an AX-spectrum.

tions of the two energy levels and this in turn increases the transition probabilities for X-1 and decreases the probability for X-2. This experiment is formally analogous to the continuous wave INDOR experiment (10) measured under power levels sufficient to cause spin-pumping but too low to cause spin-tickling. Heteronuclear, selective pulse experiments have previously been described by Pachler and Wessels (11) and Jakobsen and co-workers (12) and since we have previously given (1) an extensive discussion of the ^1H–^1H experiment only a brief account will be given here.

The spectra shown in Fig. 9 show the pulse INDOR experiment involving the H-5 and H-6 resonances of **1**. In this case the two transitions of H-5 whose intensities are altered by the perturbation, are both clearly resolved from the rest of the spectrum, and the spectra obtained by using the repetitive pulse sequency given in Fig. 1A can be easily interpreted. However, this direct mode of observation is totally unsuited to the detection of transitions which are obscured by the fortuitous overlap of other nuclear resonances, as is the case in the 'hidden resonance' problem. Now it is necessary to use a differential mode of display which can be obtained by the pulse sequence summarized in Fig. 1B; in essence this display mode subtracts those resonances whose intensities remain unperturbed by the selective pulse, and an example is given in Fig. 9. Note that the subtraction of the normal spectrum is by no means perfect, but there is no ambiguity between the 'residues' and the INDOR-like responses. This pulse experiment has a number of important advantages over c.w. INDOR measurements, not the least being the ease with which the experiments can be effected.

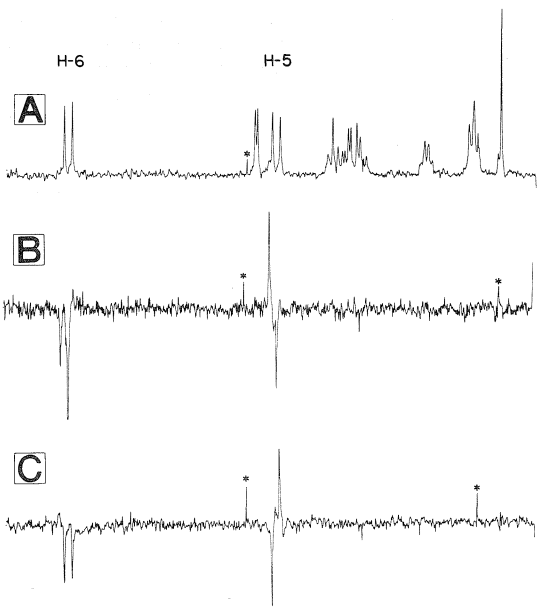

FIG. 9. These spectra illustrate the selective-pulse equivalent of an INDOR experiment, displayed in the difference mode. A shows the normal F.t. spectrum of **1**. B shows the effect of selectively irradiating the low field transition of H-6 with a selective 180° pulse (0.12 s, 93 dB) and monitoring the spectrum in the usual fashion, followed by subtraction of the normal F.t. spectrum measured with the decoupler off. All the resonances unaffected by the selective pulse are removed leaving the H-5 transitions displayed in the familiar, INDOR mode. C shows the effect of a similar experiment involving the high field transition of H-6. The sharp spikes marked * are due to pick up of the line frequency by the spectrometer.

Gated Nuclear Overhauser Experiments

Measurements of nuclear Overhauser enhancements (n.O.e.) factors (13, 14) using a continuous-wave spectrometer are often laborious and time consuming. One of the principal difficulties is that the irradiating field often causes spin decoupling which makes it necessary to measure intensity changes in the integral mode. In an F.t. mode of operation the irradiating field can be gated off during the acquisition of the nmr spectrum, thereby eliminating any spin-decoupling and allowing a direct intercomparison of 'normal' and 'enhanced' spectra by measurement of peak heights (15). The correct choice of pulse-timing is important, for example the acquisition time must be shorter than the relaxation time of the polarized nuclei, but this represents no problem. An example of this class of experiment is given, *inter alia*, in Fig. 10D and

TABLE 1. Nuclear Overhauser enhancement factors (I/I_0 ±5%) for **1**, obtained by gated ^1H–^1H decoupling. A saturation pulse was applied at a chosen frequency for 8 s (110 dB), gated off, and the spectrum sampled with a 90°-monitoring pulse

Nucleus irradiated	Nucleus observed					
	H-1′	H-2′,H-3′,OH′	H-4′	H-5′	H-5	H-6
H-4′	5	5	—	0	0	0
H-5′	0	10	10	—	0	5
H-6	25	5	0	0	45	—

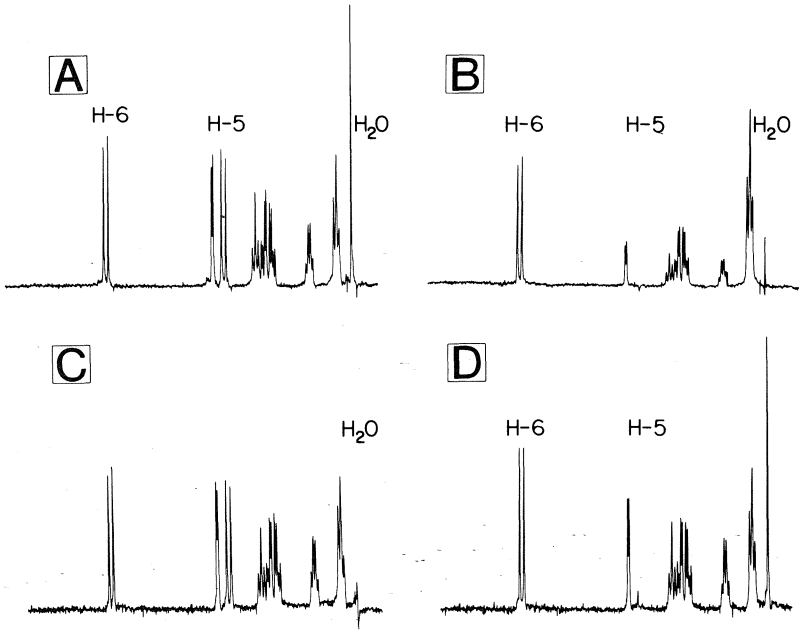

FIG. 10. Illustration of different methods for eliminating the resonance of the water impurity peak from the spectrum of **1** in dimethyl sulphoxide-d_6. The normal F.t. nmr spectrum is shown in A. The spectrum in B was measured using a *non-selective* two-pulse sequence (180°–t–90°) with t = 1.2 s; note that the H-5 resonance, which has approximately the same R_1-value, is also removed and that the relative intensities of the other peaks are perturbed from their normal values. The spectrum in C illustrates the effects of selectively saturating the H_2O resonance with a weak field which was gated off immediately prior to the monitoring pulse. A similar experiment in which the H-5 resonance was irradiated is shown in D; note the enhancement in the intensity of the H-6 resonance due the nuclear Overhauser enhancement.

the data obtained from a series of such experiments is summarized in Table 1.

Selected Removal of Unwanted Resonances

Although measurements of relaxation times are undoubtedly the most important applications of the manipulation of magnetization, the selective removal of unwanted resonances is also particularly useful. Two approaches have been used previously. The first depends on the fact that after application of a 180° pulse, the magnetization of a nucleus must pass through zero intensity; the rate at which different resonances reach their nul point depends on their spin-lattice relaxation times. Patt and Sykes (16) and Feeney and co-workers (17) demonstrated that this approach could be used to eliminate water resonances and Hall and co-workers (18) subsequently showed that overlapping resonances from the *same* molecule could be separately distinguished in the same way.

Powerful as it is, this approach has some important limitations. Principally the relative

intensities of the resonances which are detected depend on the relative values of their spin-lattice relaxation times, which makes interpretation of the spectra rather difficult: this is illustrated in Fig. 10B.

An alternative approach simply requires that the single resonance to be removed be saturated with a suitably powerful radiofrequency field. The principal difficulty here is that this technique indiscriminately eliminates all resonances from the region being irradiated and hence has none of the differential capability of the partial relaxation method. Nevertheless it is effective, as is illustrated in Figs. 10C and 10D. The latter show that the approach can result in a build up of a nuclear Overhauser enhancement of intensity in some instances; fortunately it is a trivial matter to suppress this by only gating the decoupler on during the acquisition time and by allowing a sufficiently long delay between successive pulses for complete relaxation to occur.

Fortunately a selective inversion-recovery experiment combines the best of both the above experiments. A 180° pulse is applied selectively to a particular spectral region and, after a suitable delay time, the spectrum is monitored with a non-selective 90° pulse. The spectra shown in Fig. 11 illustrate that this approach can lead to particularly efficient removal of resonances, and with an absolutely minimal perturbation of nearby resonances; all that is required is sufficient patience in selection of the *PD* value!

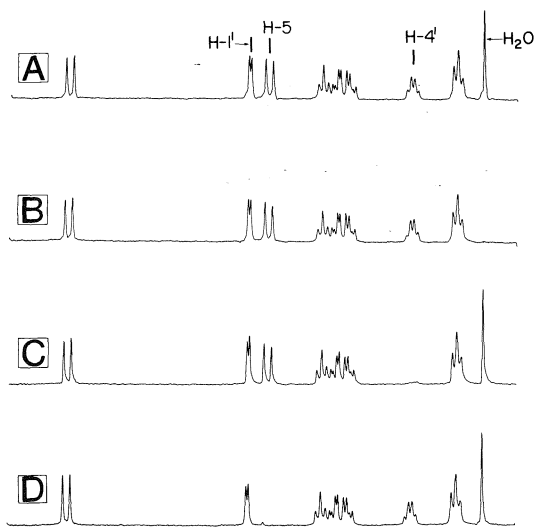

FIG. 11. Illustration of the use of the selective, inversion-recovery method for eliminating specific resonances: all spectra were monitored with a non-selective 90° pulse applied at a suitable time after application of a selective 180° pulse to the appropriate resonance. A, shows part of the F.t. nmr spectrum of **1**. In spectrum B the selective 180° pulse was applied to the H_2O resonance followed, 0.82 s later, by the 90°-pulse. In C, the H-4′ resonance was selectively inverted and the delay time was 0.90 s. In D, the H-5 resonance was irradiated and the delay time was 1.5 s; note that the off-resonance effect on the H-1′ resonance is rather small.

Conclusions

In the above discussion we have illustrated several types of proton nmr experiments in which the spectral responses of principal interest are associated with the prior perturbation of certain spectral transitions by a highly selective 180° pulse. These experiments can all be routinely performed and appear to have appreciable potential in chemical studies.

Several instrumental developments suggest that interest in the experiments described here is likely to increase in the future. Notable amongst these is the development of the elegant 'tailored excitation' method of Tomlinson and Hill (4), which provides a general method for applying perturbing pulses to many regions of an nmr spectrum with unprecedented ease. At a more prosaic level, the development of nmr instruments which only operate in the pulse F.t. mode seems likely to become a dominant one for many reasons and, if this be so, then the further development of pulse equivalents for other c.w. experiments will be imperative.

We have previously illustrated (19) the use of tailored excitation for selective relaxation and nuclear Overhauser enhancement measurements.

Experimental Section

All nmr measurements were made using a Varian Associated XL-100 (15) spectrometer fitted with a Varian 620L(16K) computer and Linc Tape Unit (model C0600).

An otherwise standard Varian programme (994100-D X-2) was modified so that the Gyrocode spin decoupler could be gated to provide the weak pulse required for selective manipulation. Several different modifications have now been used; full details will be given elsewhere.[6] Most of the single-selective experiments described here can be performed with the Varian Gyrocode decoupler working in the gated mode, using the gate provided by Varian. In like fashion double-selective experiments can be performed simply by connecting an audio-oscillator to the external modulation jack on the rear panel of the Gyrocode decoupler.

[6]K. Bock, L. D. Hall, T. Markus, and J. Sallos, to be published.

Acknowledgments

It is a great pleasure to acknowledge many helpful discussions with Dr. Howard D. W. Hill of Varian Associates. This study was supported by grants to L.D.H. from the National Research Council of Canada (A 1905) and the Alfred P. Sloan Foundation. K.B. wishes to thank N.A.T.O., The University of British Columbia, and the Otto Moensted Foundation for financial support.

1. K. Bock, R. Burton, and L. D. Hall. Can. J. Chem. **54**, 3526 (1977).
2. R. Freeman and S. Wittekoek. J. Magn. Reson. **1**, 238 (1969).
3. R. Burton, C. W. M. Grant, and L. D. Hall. Can. J. Chem. **40**, 497 (1972).
4. H. D. W. Hill and B. L. Tomlinson. J. Chem. Phys. **59**, 1775 (1973).
5. L. D. Hall and H. D. W. Hill. J. Am. Chem. Soc. **98**, 1269 (1976).
6. R. L. Vold, J. S. Waugh, M. P. Klein, and D. E. Phelps. J. Chem. Phys. **48**, 4831 (1968).
7. J. L. Markley, W. J. Hoisley, and M. P. Klein. J. Chem. Phys. **55**, 3604 (1971); G. G. McDonald and J. S. Leigh. J. Magn. Reson. **9**, 358 (1973).
8. R. Freeman and H. D. W. Hill. J. Chem. Phys. **54**, 3357 (1971); R. Freeman, H. D. W. Hill, and R. Kaptein. J. Magn. Reson. **7**, 82 (1972).
9. R. Freeman and H. D. W. Hill. J. Chem. Phys. **54**, 3367 (1971).
10. E. B. Baker. J. Chem. Phys. **37**, 911 (1962).
11. K. G. R. Pachler and P. L. Wessels. J. Magn. Reson. **12**, 337 (1973).
12. S. Sorensen, R. S. Hansen, and H. J. Jakobsen. J. Magn. Reson. **14**, 243 (1974).
13. F. A. L. Anet and A. J. R. Bourn. J. Am. Chem. Soc. **87**, 5250 (1965).
14. J. Noggle and R. E. Schirmer. The nuclear Overhauser effect. Academic Press, NY. 1971.
15. R. Freeman, H. D. W. Hill, and R. Kaptein. J. Magn. Reson. **7**, 327 (1972).
16. S. L. Patt and B. D. Sykes. J. Chem. Phys. **56**, 3182 (1972).
17. F. W. Benz, J. Feeney, and G. C. K. Roberts. J. Magn. Reson. **8**, 114 (1972).
18. L. D. Hall and C. M. Preston. Carbohydr. Res. **27**, 286 (1973); C. W. M. Grant, L. D. Hall, and C. M. Preston. J. Am. Chem. Soc. **95**, 7742 (1973); L. D. Hall, C. M. Preston, and J. D. Stevens. Carbohydr. Res. **41**, 41 (1975).
19. R. Freeman, H. D. W. Hill, B. L. Tomlinson, and L. D. Hall. J. Chem. Phys. **61**, 4466 (1974).
20. G. Bodenhausen, R. Freeman, and G. A. Morris. J. Magn. Reson. **23**, 171 (1976).
21. S. Schaublin, A. Hohener, and R. R. Ernst. J. Magn. Reson. **13**, 196 (1974).
22. P. Meakin and J. P. Jesson. J. Magn. Reson. **11**, 182 (1973); **13**, 354 (1974).

Velocity separation of isotopic mixtures in underexpanded supersonic beams

A. E. REDPATH AND M. MENZINGER

Department of Chemistry, University of Toronto, Toronto, Ont., Canada M5S 1A1

Received October 4, 1976

A. E. REDPATH and M. MENZINGER. Can. J. Chem. **55**, 1055 (1977).

The velocity distributions of the heavy components in $CD_4/CH_4/He(H_2)$ supersonic beams were measured by time-of-flight and the slippage with respect to the seeding gas was investigated as a function of nozzle pressure and temperature. The isotopic species attain different velocity distributions. Following a proposal by Anderson and Davidovits, isotope separation factors are calculated both for the present system and, by analogy, for $^{235}UF_6/^{238}UF_6/Ar(He,Xe)$.

A. E. REDPATH et M. MENZINGER. Can. J. Chem. **55**, 1055 (1977).

Utilisant le temps de vol, on a mesuré les distributions de vitesse des composants lourds dans les rayons supersoniques de $CD_4/CH_4/He(H_2)$; de plus on a étudié le décalage par rapport aux gaz d'ensemencement en fonction de la pression du jet et de la température. Les diverses espèces isotopiques atteignent une distribution différente de vitesses. En accord avec une proposition de Anderson et Davidovits on a pu calculé des facteurs de séparation isotopique à la fois pour le système actuel et, par analogie, pour $^{235}UF_6/^{238}UF_6/Ar(He,Xe)$.

[Traduit par le journal]

I. Introduction

Partial separation of isotopic mixtures can be achieved by utilizing a number of interrelated gas dynamic phenomena accompanying the free expansion of gas mixtures. The well known spatial enrichment of the heavier components in the beam core, through the more rapid pressure diffusion of the light components out of the beam, forms the basis of the supersonic jet (1, 2) and curved jet (3) methods developed by Becker and co-workers. Apart from this spatial separation, Anderson and Davidovits (4) (AD) have recently pointed out that isotopic components of a seeded beam can be differentially accelerated and attain different final velocities. This separation in velocity space can be utilized for a physical separation via velocity selection which could, according to AD, exceed the spatial effect. Literature data on velocity distributions of a single heavy component in seeded beams, in particular H_2 seeded Xe beams (5), were used (4) together with estimates of the *expected* mass dependent differential acceleration to predict the magnitude of the $^{238}UF_6/^{235}UF_6$ separation factors. The separation of isotopes in velocity space has *de facto* not been proven.

To provide an experimental test of this effect we chose He (and H_2) seeded CH_4/CD_4 mixtures as prototype systems. The velocity distribution of both isotopic components were measured by time-of-flight (TOF) for a range of experimental conditions (*i.e.* mass of the seeding gas, seeding ratio X, nozzle pressure, nozzle temperature). The goal of this work was (*1*) to present data on the properties of underexpanded seeded molecular beams, (*2*) to test Anderson and Davidovits' model for isotope separation, and (*3*) to arrive at new predictions of the separation effects in systems of technical interest.

The velocity separation factor α' (defined in eq. 7) computed from the measured CH_4/CD_4 velocity distributions attains a peak value of 1.4, demonstrating the feasibility of AD's separation scheme.

To obtain projections for the technically interesting $^{235}UF_6/^{238}UF_6$ system, *ad hoc* assumptions were made about the direct transferability of measured velocity distributions to systems of greatly disparate mass. The separation factors estimated thus fall somewhat short of AD's predictions, but they still exceed those of current gas dynamical (2, 3) and gaseous diffusion processes. While the CH_4/CD_4 measurements clearly demonstrate the feasibility of the proposed separation scheme, the assumptions in connection with UF_6 could be questioned, and it is conceivable that the extrapolation to UF_6 employed here actually underestimates the experimentally achievable separation. Detailed gas dynamic calculations (14) support this possibility. Mea-

surements on the real system (or, at least, on model systems SF_6, MoF_6, WF_6/He, Ar) will have to decide this point.

II. Experimental

A supersonic beam (from a He(H_2) seeded CH_4/CD_4 (50:50) mixture) is formed from a 0.01 cm diameter stainless steel converging nozzle and a 0.05 cm diameter conical skimmer, with the nozzle–skimmer separation held fixed at 1.0 cm. The nozzle can be resistively heated and its temperature is measured on a chromel–alumel thermocouple. A high speed chopper (250 Hz, opening time 16 μs every 2 ms, 5 cm downstream from the skimmer) pulses the beam which is ionized after a drift space of 37.2 cm and mass analyzed in a small magnetic 90° sector instrument. Detection is by an electron multiplier (EMI 9643/3B) followed by a high speed amplifier and the repetitive signal is averaged on a PAR TDH-9 wave form eductor. Important dimensions and experimental conditions are given (16) in Table 1.

The time calibration of the TOF measurement was checked with pure supersonic Ar and He beams of known bulk flow velocity. Time-of-flight spectra were recorded for two different mixtures of CH_4:CD_4:He (2:2:96 and 5:5:90) over a range of nozzle pressure (20–400 torr) for two different nozzle temperatures (281 K and 573 K). Some experiments were also performed using H_2 as the seeding gas. In addition, pure He, pure H_2, and pure CH_4 were run under the same conditions. Only 50:50 mixtures of the isotopic components were employed since at the low seeding ratios used here interaction of the heavy components is expected to be small. Measurements were made on both p (parent mass) and p − 1 mass peaks for CH_4 (p and p − 2 for CD_4) and no differences in the TOF spectra were observed.

Typical TOF spectra for the CH_4 and CD_4 components of the seeded beam are shown in Fig. 1*a*. They are characterized by two parameters: t_{max}, the position of the maximum, and $\Delta t_{1/2}$, the full width at half maximum. Rather than inverting the TOF spectra directly (6) and neglecting the apparatus resolution function,[1] the finite resolution was accounted for by the following empirical technique: The (number density) velocity distribution function appropriate to a supersonic beam is traditionally described by (6)

$$[1] \qquad f(v)\,dv = C(v/v_s)^2 \exp -[(v - v_s)S/v_s]^2\,dv$$

in terms of the streaming (= bulk flow) velocity v_s and the speed ratio S which measures the width of the distribution. S is defined as the ratio of bulk flow to the most probable velocity by

$$[2] \qquad S = v_s/(2kT_s/m)^{1/2}$$

where T_s is the (parallel) streaming temperature appropriate to the width of the distribution A number of assumed velocity distributions $f(v; v_s, S)$ were convoluted with the appropriate TOF resolution function[1] and the results were inverted to simulate TOF spectra. Two calibration plots were obtained, one relating the observed

[1]The resolution function accounts for finite chopper opening time, ionizer length, mass spectrometer transit time, and response time of the electronics.

TABLE 1. Apparatus dimensions and operating conditions

Chamber	Parameter	Value
Nozzle	Diameter	0.01 cm
Skimmer	Diameter	0.05 cm
	Inner angle	35°
	Outer angle	40°
	Height	0.3 cm
	Nozzle–skimmer separation	1.0 cm
	TOF flight path	37.2 cm

Chamber	Pump	Typical operating pressures (torr)
Nozzle	VHS-6 (Varian) (unbaffled) 2300 1/s	5×10^{-4}
Main	VHS-6 (Varian) (baffled) 1000 1/s	2×10^{-6}
Mass Spec.	EO-2 (Edwards)	1×10^{-6}

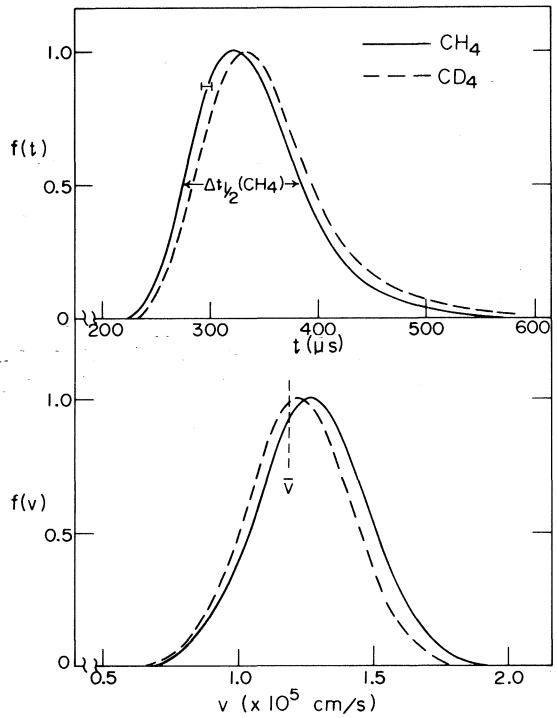

FIG. 1 (*a*) TOF spectra for both isotopic components of a CH_4/CD_4/He (2:2:96) mixture. Source pressure was 60 torr, source temperature 281 K. Signals were normalized at t_{max}. The FWHM, $\Delta t_{1/2}$ is indicated. The experimental uncertainty (one standard deviation) of flight time is typically ±4.5 μs for this data set and it decreases to ±2 μs at higher nozzle pressures ($p_0 > 150$ torr). (*b*) Velocity distributions of CH_4, CD_4 derived from Fig. 1*a* (eq. 1). $\bar{v}$, the separation velocity used is taken as the arithmetic mean of the v_s values. Full curve: CH_4 ($S = 4.21$, $v_s = 1.21 \times 10^5$ cm/s); dashed curve: CD_4 ($S = 4.23$, $v_s = 1.17 \times 10^5$ cm/s).

($t_{max}/\Delta t_{1/2}$) to S, and the other relating t_{max} to v_s for a given S. Given experimental t_{max}, $\Delta t_{1/2}$ values, S and v_s could be directly read off. Typical velocity distributions, derived from the spectra, Fig. 1*a*, are drawn in Fig. 1*b*.

III. Velocity Distributions

The properties of supersonic molecular beams depend markedly upon the source conditions, in particular upon the source number density, the nozzle diameter d, source temperature T_0, and on the skimmer geometry, and pressure in the nozzle and main chambers. The source Knudsen number, $Kn = \lambda/d$, the ratio of mean free path λ to nozzle diameter d, is a convenient characteristic parameter of the nozzle conditions. This representation has the advantage of compacting the experimental variables of P_0, T_0, and d onto one scale. Anderson and Fenn (6) have shown that for pure beams the terminal speed ratio is a linear function of $Kn^{-0.4}$:

$$[3] \qquad S = 2.05(\gamma/2)^{1/2}\varepsilon^{0.4}Kn^{-0.4}$$

where $\varepsilon \leq 1$ is a measure of the 'collision effectiveness' or average logarithmic energy loss per collision (7), that is assumed to be energy independent for a given gas.

The streaming velocity[2] v_S also depends upon the Knudsen number in the following fashion: For high values of the inverse source Knudsen number ($P_0 \sim Kn^{-1} \geq 1000$) the beam expansion is practically complete and both light and heavy components achieve the same isoentropic streaming velocity given by:

$$[4] \qquad v_{iso} = (2\bar{c}_p T_0/\overline{m})^{1/2}$$

where $\bar{c}_p$ and $\overline{m}$ are the mole fraction weighted average heat capacity and mass and T_0 is the source temperature. As the source pressure ($\sim Kn^{-1}$) decreases, fewer collisions take place during the expansion and velocity equilibration is no longer attained: the heavy component lags behind the light seeding gas. This velocity slip phenomenon, expressed in terms of the ratio of streaming velocity to maximum (ideal) isoentropic velocity, v_S/v_{iso}, is conveniently correlated with the mass-weighted slip Knudsen number (8), defined by

$$[5] \qquad Kn_{slip}^{-1} = \sqrt{2}\, n_0 \sigma_{HL} d \left(\frac{\overline{m}}{m_H - m_L}\right) = Kn^{-1}\left(\frac{\overline{m}}{m_H - m_L}\right)$$

Here σ_{HL} is the effective cross section (9) for collisions between heavy and light beam molecules, n_0 the source number density, and $\overline{m}$ the mole fraction weighted mass of the mixture with masses m_H (heavy) and m_L (light = seeding gas).

Under the same source conditions, two heavy isotopic components with masses m_{H1} and m_{H2} have different Kn_{slip}^{-1} due to the mass factor $[\overline{m}/(m_{Hi} - m_L)]$. In the slippage-dominated low P_0 regime the v_S/v_{iso} ratio is a sensitive function of Kn_{slip}^{-1} and two isotopic components reach different streaming velocities v_{S1} and v_{S2}.

According to eqs. 3, 4, and 5, S and (v_S/v_{iso}) were plotted as functions of $Kn^{-0.4}$ and $Kn_{slip}^{-0.4}$ respectively as shown in Figs. 2 and 3. Included in these graphs are data from the literature as explained in the captions.

The speed ratio *vs.* $Kn^{-0.4}$ plot (Fig. 2) shows that for $Kn^{-0.4} \leq 17$ the linear relationship (4) is indeed valid, but the slopes of the various data sets differ appreciably. The question arises to what extent these differences are characteristic of the systems studied (*e.g.*, He; CH_4/CD_4/He; H_2; Xe/H_2) and to what extent they arise from the experimental conditions (*i.e.* the different beam machines having different nozzle–skimmer assemblies, pump speeds, etc.). While Haberland's data (5) (Fig. 2) demonstrate a pronounced dependence on nozzle temperature, the different qualities of supersonic beams achieved in different laboratories (5, 8, 10–12) show that experimental design plays an important role, and that the data sets from different laboratories are not directly comparable. For instance, speed ratios in the range of $S > 50$ have recently been obtained for H_2 and He beams (10, 11).

Velocity distributions of the light components were also measured and were found to agree closely with those of pure beams of seeding gas and it was confirmed (12, 13) that the heavy component was characterized by substantially higher T_S than the seeding gas.

The data of Fig. 3 illustrate the increasing slippage (or decreasing v_S/v_{iso}) with falling source pressure ($P_0^{0.4} \sim Kn_{slip}^{-0.4}$). The lowest velocities measured are only ~40% of the ideal isoentropic expansion value. Figure 4 shows the relative

[2]The velocity v_{max} of the maximum in the distribution, is somewhat greater than v_S:

$$2v_{max} = v_S(1 + \sqrt{1 + 4/S^2})$$

However, for $S > 4$ the difference between the two is <6% and one can use v_S to approximate v_{max}.

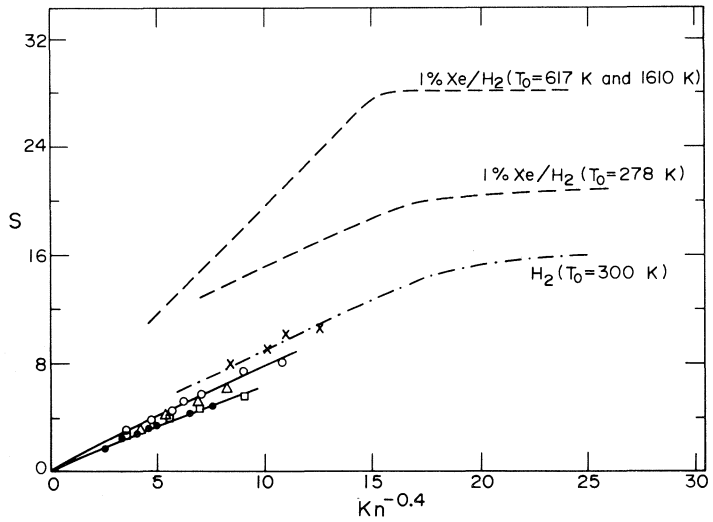

FIG. 2. Speed ratios *vs.* $Kn^{-0.4}$ for pure H_2, He, CH_4 beams and for CH_4/CD_4 and CH_4/CD_4/He mixtures. Also shown are the results for pure H_2 beams (17) and for Xe in Xe/H_2 beams (5). The values plotted for the CH_4/CD_4/He mixtures are the average values of the two components. For (2:2:96) mixtures, S is *ca.* 5% higher than for (5:5:90) mixtures, and CH_4 speed ratios exceed those for CD_4 by a few %. The estimated error of S is 6%. Symbols: × H_2; △ pure He; □ pure CH_4; ○ CH_4/CD_4 in (CH_4/CD_4/He) mixtures, all at T_0 = 281 K. ● CH_4/CD_4 in (CH_4/CD_4/He) mixtures at T_0 = 573 K.

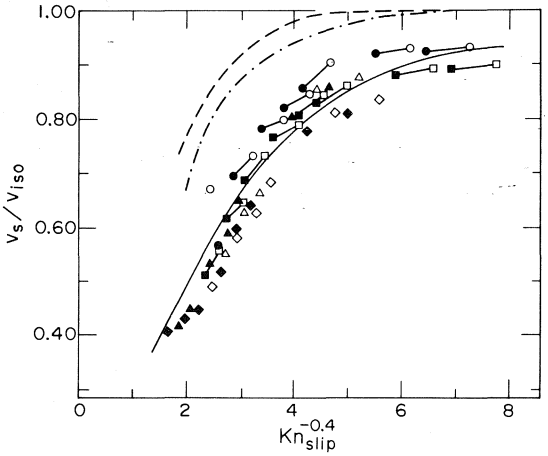

FIG. 3. (v_s/v_{iso}) *vs.* $Kn_{slip}^{-0.4}$ for CH_4/CD_4/He mixtures. Also shown are data from refs. 5 (dashed curve Xe/H_2 beams) and 8,12 (dash–dot curve, several He-seeded gases). The tie lines connect (v_s/v_{iso}) values for the two isotopic components of a given mixture at identical source conditions (shown for T_0 = 281 K only for clarity). The full line represents the fit to eq. 6. Symbols: (CH_4/CD_4/He = 2:2:96; CH_4 data): ○ T_0 = 281 K, △ T_0 = 573 K; (CH_4/CD_4/He = 2:2:96, CD_4 data): ● T_0 = 281 K, ▲ T_0 = 573 K; (CH_4/CD_4/He = 5:5:90; □ T_0 = 281 K, ◇ T_0 = 573 K); (CH_4/CD_4/He = 5:5:90; □ T_0 = 291 K, ◆ T_0 = 573 K).

difference in velocities of the two isotopic heavy components $\Delta v_s/\bar{v}$ plotted as a function of $Kn_{slip}^{-0.4}$. This method of plotting collapses data for different source conditions (T_0, P_0, seeding ratio, etc.) into one band of points. The solid curves represent a visual 'best' fit to the data of Fig. 3 of the form:

$$[6] \qquad (v/v_{iso}) = a[1 - \exp(-bx^c)]$$

with $a = 0.93$, $b = 0.3$, $c = 1.3$, and $x = Kn_{slip}^{-0.4}$. This fit optimally reproduces both the (v/v_{iso}) and ($\Delta v/v$) data of Figs. 3 and 4, the latter essentially being a measure of the slope of Fig. 3.

Systematic deviations from this average curve show, however, that this data compaction is only approximate: the tie lines in Fig. 3 join data points for the CH_4 and CD_4 components of a given mixture, run under a particular set of source conditions. For pairs of data points the difference in velocity of the two components ($\Delta v/v_{iso} = v_{S1}/v_{iso} - v_{S2}/v_{iso}$) is generally slightly smaller than that represented by the solid curve. It is possible that the assumption of independent expansions of the two heavy components at these low seeding ratios is not completely valid and/or

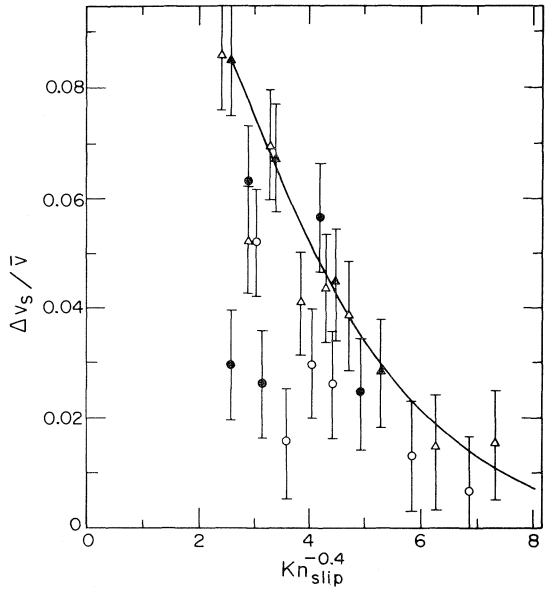

FIG. 4. Relative slippage $\Delta v_s/\bar{v}$ of the isotopic components in CH_4/CD_4/He mixtures (2:2:96 and 5:5:90). Δv_s is the difference in streaming velocities and $\bar{v}$ is their arithmetic mean. The solid curve corresponds to eq. 6. Symbols same as Fig. 3.

that collisions with background gas also diminishes the separation effect.[3] The shift of our results to lower (v/v_{iso}) values compared to literature curves (Xe/H_2 and H_2) demonstrates again the influence of the beam machine.

IV. Isotope Separation Factors

The results of the preceding section are used to calculate the efficiency of the isotope separation effect possible by velocity selection. This efficiency is normally given by the separation factor, α', defined in our case as (1, 3, 4):

$$[7] \qquad \alpha' = \frac{n_{1L}}{n_{1R}} \cdot \frac{n_{2R}}{n_{2L}}$$

where n_{1L} is the number of molecules of mass m_1 having velocities below (*i.e.* to the left of) the separating velocity $\bar{v}$ in Fig. 1*b*,[2] etc. For our calculations $\bar{v}$ was taken as the arithmetic mean of v_{S1} and v_{S2}. A different choice of $\bar{v}$ would, of course, result in a different value for α'. It has been pointed out (15) that for Maxwellian distributions α' can be made very large if the separating velocity is in the region of the high velocity tails, at the expense of a drastically reduced mass throughput. Our choice of $\bar{v}$ would allow close to maximum collection efficiency at the expense of a lower α'.

Anderson and Davidovits give the approximate analytic expression for α' for beams with high speed ratios where $f(v)$ can be approximated by a Gaussian. Their simple formula:

$$[8] \qquad \alpha' \simeq 1 + 4\pi^{-1/2} S \Delta v_S / v$$

shows more clearly than the following analytical expressions the basic dependence on the variables S and $\Delta v_S/\bar{v}$ of the separation effect: α' is a (linear) function of both speed ratio and the relative velocity difference. For the low speed ratios at which $S\Delta v_S/\bar{v}$ is maximized the expansion [8], that has been truncated after the linear term, is no longer valid: instead an exact calculation of n_{1L} etc. yields:

$$[9a] \quad n_{1L} = \int_0^{\bar{v}} n_1 f(v)\, dv = \int_0^{\bar{v}} n_1 N (v/v_{S1})^2 \times \exp -S_1^2 (v/v_{S1} - 1)^2\, dv$$

$$[9b] \quad n_{1R} = \int_{\bar{v}}^{\infty} n_1 N (v/v_{S1})^2 \times \exp -S_1^2 (v/v_{S1} - 1)^2\, dv$$

etc. Evaluation of the integrals leads to:

$$[10a] \quad n_{1L} = n_1 N [(1/2S_1) \exp(-S_1^2) - (a_1/2S_1^2 + 1/S_1) \exp(-a_1^2) + (3\sqrt{\pi}/4)(\operatorname{erf} a_1 + \operatorname{erf} S_1)]$$

$$[10b] \quad n_{1R} = 1 - n_{1L}$$

with

$$a_1 = (\Delta v / v_{S1})(S_1/2)$$

$$N = [(1/2S_1) \exp(-S_1^2) + (3\sqrt{\pi}/4)(1 + \operatorname{erf} S_1)]^{-1}$$

(v_{S1} and S_1 referring to the CH_4 component).

For a given mixture of CH_4:CD_4:He, $Kn_{slip}^{-0.4}$ values for the two heavy components are calculated, and S and v_S values are then derived from Figs. 3 and 4. Equations 10*a*, 10*b*, and 7 are then used to calculate α'. The results are presented in Fig. 5 as $(\alpha' - 1)$ *vs.* $Kn_{slip}^{-0.4}$. With decreasing $Kn_{slip}^{-0.4}$ the curve goes through a maximum at $Kn_{slip}^{-0.4} \sim 3.25$ and appears to drop off for lower $Kn_{slip}^{-0.4}$ values. The actual behaviour of

[3]P. Davidovits, private communication.

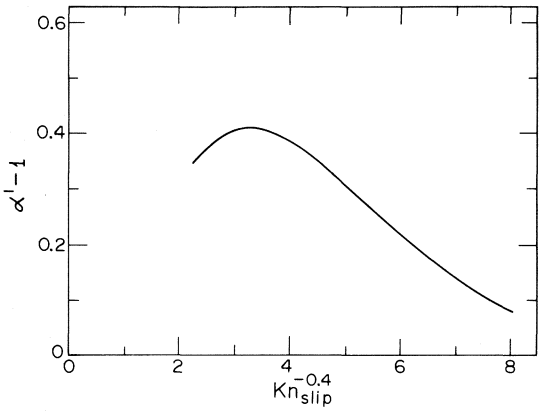

FIG. 5. Separation factor ($\alpha' - 1$) *vs.* $Kn_{slip}^{-0.4}$ calculated for CH_4/CD_4/He mixtures. For classical effusive CH_4/CD_4 beams,[4] $\alpha' - 1 = 0.6$, while for effusive 'garden hose' separation (15) $\alpha' - 1 = 0.46$.

($\alpha' - 1$) in the region of low $Kn_{slip}^{-0.5}$ is, however, uncertain. The isentropic beam expansion model fails in this region where the flow becomes effusive. A gas dynamic calculation by Anderson[4] of $\alpha' = 1.29$ at $Kn^{-0.4} = 5.04$ agrees well with our measurements and lends support to the calculations (14)[4] on heavier systems. The separation factor for classical effusive beams[4] and for 'garden hose' effusive beams (15) are ($\alpha'_{effusive} - 1$) = 0.6 and 0.46 respectively, if one assumes $\bar{v}$ equal to the average of the most probable velocities. The nozzle beam results ought to extrapolate to this value; how they do is not certain. It would appear that effusive beams provide as good, if not better, velocity separation than seeded supersonic beams. Although this is the case for the mass combinations of our system it is not clear at present whether this can be generalized to $^{235}UF_6/^{238}UF_6$.

V. Discussion

Applying the present results and those from the literature (5, 8) to systems of such substantially different mass and molecular structure as UF_6/He calls for a number of assumptions: (*1*) The slippage v/v_{iso} and $\Delta v/\bar{v}$, under identical experimental conditions and $Kn_{slip}^{-0.4}$, is taken to be the same for $^{235}UF_6/^{238}UF_6$ mixtures seeded by He, Ar, Xe as for He-seeded CH_4/CD_4. While the approximate agreement of slippage data for different beam gases (dash–dotted curve of Figs. 3 and 9 of ref. 8) supports this view, a closer examination of Fig. 9 exposes, not unexpectedly, an increased slippage for heavier beams. (*2*) Speed ratio for UF_6 in He were assumed to be given by the CH_4/CD_4/He measurements (Fig. 4), while for Ar- and Xe-seeded SF_6 speed ratios for pure Ar beams (8, 12) were substituted since He beams are known (12, 16) to yield, under comparable source conditions, lower speed ratios than pure H_2 or Ar beams.

Separation factors ($\alpha' - 1$) were calculated from eqs. 7, 10 for He-, Ar-, Xe-seeded (99:1) UF_6 mixtures as a function of Kn_{slip}^{-1} and results are presented in Fig. 6. The predicted maxima ($\alpha' - 1$) lie below the value ($\alpha'_{effusive} - 1$) = 0.018 for 'classical' effusive beams[4] and, with the exception of Xe-seeding also below ($\alpha'_{garden\ hose} - 1$) = 0.015 for 'garden hose' effusive beams (15). Our calculation predicts that α_{max}' increases with the mass of seeding gas, although the position of the maximum does not change. This is a direct consequence of assumption (*1*) that the slippage data (eq. 6) are independent of seeding gas: anything that increases the difference in $Kn_{slip}^{-0.4}$ values will increase α_{max}'. The $Kn_{slip}^{-0.4}$ values for the isotopic components are related by

$$Kn_{slip}^{-0.4}(^{235}UF_6) = Kn_{slip}^{-0.4}(^{238}UF_6)\left(\frac{m_{^{238}UF_6} - m_X}{m_{^{236}UF_6} - m_X}\right)$$

where m_X is the mass of the seeding gas. The bracketted term increases with m_X, predicting enhanced $\Delta Kn_{slip}^{-0.4}$ and α'. This approach leads

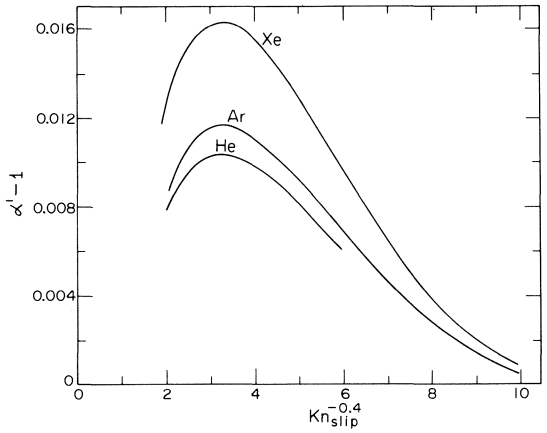

FIG. 6. Separation factor ($\alpha' - 1$) *vs.* $Kn_{slip}^{-0.4}$ predicted for $^{235}UF_6/^{238}UF_6$/X mixtures, where X = He, Ar, Xe, as described in the text. Gas dynamic calculations (14) predict an inverse effect: a decrease of α' with increasing m_X. For classical effusive $^{235}UF_6/^{238}UF_6$ beams[4] $\alpha' - 1 = 0.018$, while 'garden hose separation' (15) yields $\alpha' - 1 = 0.0146$.

[4]J. B. Anderson, private communication.

however to the wrong asymptotic limit $m_X \rightarrow m_{UF_6}$, a fact that strongly suggests an experimental test of assumption (*1*). Gas dynamic calculations (14)[4] indicate a reverse trend, while experiments using $CH_4/CD_4/H_2$ mixtures show indeed a lower α_{max}' for H_2 than for He.

The present calculation predicts α_{max}' values substantially lower than those of AD's original proposal (4) ($\alpha_{max}' = 0.01 - 0.016$ *vs.* 0.1). The major source of this discrepancy lies in the different speed ratios used; ours are *ca.* six times lower than the value $S \sim 24$ taken (4) by AD from the data (5) on Xe/H_2 mixtures. The critical, and most controversial, assumption of our analysis is thus number *2*.

For an estimate of the full potential of the beam separation, the spatial separation factor is estimated from Becker's values (1) extrapolated for pure $^{235}UF_6/^{238}UF_6$ mixtures, α (space) $\sim$ 1.008. An improvement of (α(space) $-$ 1) by 1.7 is predicted (*2b*) for seeding with a gas of a mass 1/10 of the beam gas (*e.g.*, Ar or N_2) .With this the overall separation factor for $^{235}UF_6/^{238}UF_6$/Ar mixtures is predicted to be α(total) = α(space) $\times$ α'(velocity) = 1.025. This value still lies below AD's original prediction (4) of 1.1 and below their more recent values $\alpha' = 1.05 - 1.09$ obtained from detailed gas dynamical calculations (14). However, it exceeds the separation factors of currently attainable gas dynamic and gaseous diffusion methods. Only experiments on UF_6 or on closely related model systems (SF_6, MoF_6, WF_6.../He, Ar...), employing a velocity selector similar to the one proposed (4, 14) (*i.e.* of the slotted disk type) will give an unambiguous assessment of the complicated and interrelated gas dynamic effects involved in the separation of isotopic mixtures.

Acknowledgments

It is a pleasure to acknowledge valuable discussions with Professors J. B. Anderson and R. Davidovits and to thank them for making their manuscript (14) and the calculations[4] available to us prior to publication. This work is supported by the National Research Council of Canada.

1. E. W. Becker, K. Bier, and H. Burghoff. Z. Naturforsch. **10**a, 565 (1955).
2. (*a*) E. W. Becker, W. Beyrich, K. Bier, H. Burghoff, and F. Zigan. Z. Naturforsch. **12**a, 609 (1957). (*b*). E. W. Becker, K. Bier, and W. Bier. Z. Naturforsch. **17**a, 778 (1962).
3. E. W. Becker, K. Bier, W. Bier, R. Schütte, and D. Seidel. Angew. Chem. Int. Ed. Engl. **6**, 507 (1967).
4. J. B. Anderson and P. Davidovits. Science, **187**, 644 (1974).
5. H. Haberland, F. P. Tully, and Y. T. Lee. *In* Rarefied gas dynamics. 8th Symposium. *Edited by* K. Karamatchi. Academic Press, New York. 1974.
6. J. B. Anderson and J. B. Fenn. Phys. Fluids, **8**, 780 (1965).
7. R. Wolfgang. J. Chem. Phys. **39**, 2983 (1963).
8. N. Abuaf, J. B. Anderson, R. P. Andres, J. B. Fenn, and D. R. Miller. *In* Rarefied gas dynamics. 5th Symposium. *Edited by* C. L. Brundin. Academic Press, New York. 1967. p. 1317.
9. J. O. Hirshfelder, C. F. Curtiss, and R. B. Bird. Molecular theory of gases and liquids. J. Wiley, New York. 1954.
10. U. Buck, M. Düker, H. Pauly, and D. Pust. 4th Int. Sympos. on Molecular Beams. Cannes. 1973.
11. R. Campargue and A. Lebehot. *In* Rarefied gas dynamics. 9th Symposium. *Edited by* M. Becker and M. Fiebig. DFVLR Press, Linderhoehe. 1974.
12. J. B. Anderson. Entropie, **18**, 33 (1967).
13. A. L. Cooper and G. K. Bienkowsky. *In* Rarefied gas dynamics. 5th Symposium. *Edited by* C. L. Brundin. Academic Press. New York. 1967. p. 381.
14. P. Raghuraman, P. Davidovits, and J. B. Anderson. *In* Rarefied gas dynamics. 10th Symposium. Aspen, CO. July 1976. To be published.
15. C. G. Wang. Nature, **253**, 260 (1975).
16. A. E. Redpath. Ph.D. Thesis, University of Toronto, Toronto, Ont. 1976.
17. N. Abuaf. Ph.D. Thesis, Princeton University, Princeton, New Jersey. 1966.

The viscosity of concentrated electrolyte solutions. I. Concentration dependence at fixed temperature

DOUGLAS E. GOLDSACK AND RAYMOND FRANCHETTO

Department of Chemistry, Laurentian University, Sudbury, Ont., Canada P3E 2C6

Received October 5, 1976

DOUGLAS E. GOLDSACK and RAYMOND FRANCHETTO. Can. J. Chem. **55**, 1062 (1977).

The absolute rate theory of viscosity for simple fluids has been extended to account for the concentration dependence of the viscosity of concentrated single electrolyte solutions (1–10 *m* region). Graphical and computer techniques for obtaining the two parameters (volume and free energy of activation) which control the concentration dependence of the viscosity of single salt solutions at fixed temperatures are described. The additivity of these parameters for single ions are discussed with reference to the alkali and ammonium halides at 25 °C and the *B* coefficients of the Jones–Dole equation.

DOUGLAS E. GOLDSACK et RAYMOND FRANCHETTO. Can. J. Chem. **55**, 1062 (1977).

Afin de rendre compte de la dépendance qui existe entre la concentration et la viscosité de solutions concentrées (région de 1–10 *m*) d'électrolytes simples, on a étendu la théorie des vitesses absolues de la viscosité à des fluides simples. On décrit des techniques graphiques et par ordinateur qui permettent d'obtenir les deux paramètres (volume et énergie libre d'activation) qui contrôlent la dépendance existant, à température fixe, entre la concentration et la viscosité de solution de sels simples. On discute de l'additivité de ces paramètres pour des ions uniques par référence aux halogénures alcalins et d'ammonium à 25 °C et aux coefficients *B* de l'équation de Jones–Dole.

[Traduit par le journal]

Introduction

Phenomenological Description of the Viscosity of Aqueous Electrolyte Solutions

The viscosity of aqueous electrolyte solutions has been studied in detail continuously since Arrhenius began his investigations of the properties of electrolyte solutions in the 1880's. Three major reviews of the subject have been written (1–3). Aside from the many empirical relations which have been explored for single and mixed electrolyte solutions, the major theoretical thrust for understanding the viscosity of electrolyte solutions has been in the dilute solution region (less than 0.1 *M*).

Einstein (1), in 1906, deduced from the classical principles of hydrodynamics that if the solute were composed of spherical incompressible uncharged particles which were large in comparison to the water molecules, then the viscosity of the solution could be expressed as

$$[1] \qquad \eta = \eta_1(1 + 2.5\theta)$$

where θ denotes the volume fraction of the solute particles, η_1 is the viscosity of the pure solvent, and η is the viscosity of the solution. This equation proved valid only at low concentrations.

Later, Falkenhagen and Dole (1) attacked the problem of the viscosity of electrolyte solutions in terms of the interionic forces in the adjacent layers of an electrolyte solution. They proposed that the electrical forces between ions in the solution tend to establish and maintain a preferred rearrangement and thus to "stiffen" the solution, *i.e.* to increase its viscosity. The mathematical treatment of this effect resulted in the following limiting law for very low concentrations of electrolytes (<0.01 *M*).

$$[2] \qquad \frac{\eta}{\eta_1} = \eta_{rel} = 1 + A\sqrt{c}$$

where the always positive constant A is a function of solvent properties, ionic charges, mobilities and temperature (1). Numerically, A is fairly small (0.005 for KI, 0.0167 for Li_2SO_4 at 25 °C).

Practically, the Falkenhagen equation was of little use in calculating viscosities since the square root term is swamped by a much larger linear term expressed in the empirical equation of Jones and Dole (1)

$$[3] \qquad \eta_{rel} = 1 + A\sqrt{c} + Bc$$

where A is again Falkenhagen's theoretical coefficient while the empirical parameter B

supposedly represents ion–solvent interaction. The B coefficient is found to be greater or less than zero depending on the salt and to be highly specific for both the electrolyte and temperature (*e.g.*, -0.014 for KCl and $+0.567$ for $LaCl_3$ at 25 °C) (1). The B coefficients are fairly accurately additive properties of the constituent ions based on the assumed equal values of -0.007 for K^+ and Cl^- at 25 °C. Negative values for B are found for ions which exert a 'structure-breaking' effect on the solution (*i.e.* they contribute to a considerable increase in the disorder of water when dissolved) such as Rb^+, Cs^+, I^-, ClO_3^-, and NO_3^-. Usually, however, the B values are fairly large and positive and correspond to ions which are strongly hydrated (structure makers) such as Na^+, Li^+, Mg^{2+}, and La^{3+}. The Jones–Dole equation is generally valid up to a few tenths molar concentration. Recently the Jones–Dole equation has also been extended to include higher terms in a power series in M (4, 5). However, no new interpretive information has been revealed by this approach.

In the concentrated solution region (0.1 to 10 M), several features of the viscosity of electrolyte solutions have been noted. For some salts a plot of the viscosity *vs.* the molality at a fixed temperature yields a roughly exponentially increasing function (Figs. 1 and 2). However, for other salts a pronounced minimum in this plot occurs (Figs. 3 and 4). These latter salts fall into the category of structure breakers mentioned previously.

Thus, any equation which proposes to describe the variation of viscosity with concentration in this region must account for both of these phenomena in a quantitative manner.

The effect of concentration on the viscosity of salt solutions in the more concentrated region, and at fixed temperature, has been approached empirically in various ways. Vand (7), for example, extended Einstein's limiting theory to higher concentrations giving

$$[4] \qquad \ln \eta_{rel} = \frac{2.5\theta}{1 - Q\theta}$$

where Q is proposed to be an interaction parameter dealing with the mutual interference between the spheres. Several other equations have been advanced in this direction:

Thomas (8):

$$[5] \qquad \eta_{rel} = 1 + 2.5\theta + 10.05\theta^2$$

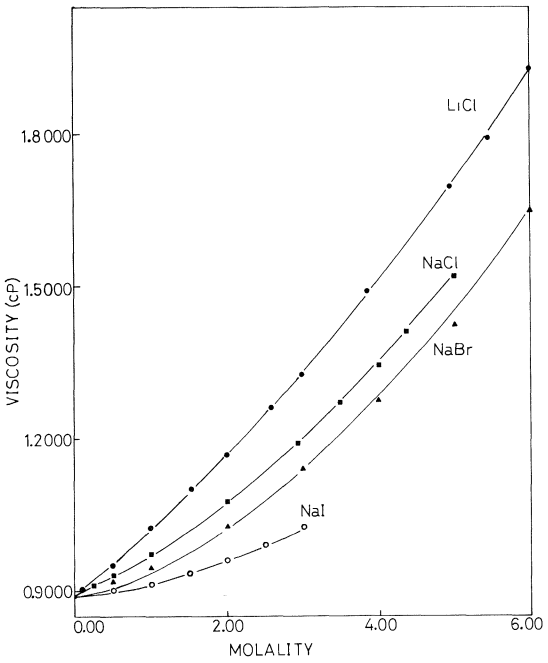

FIG. 1. Observed and calculated viscosities for LiCl, NaCl, NaBr, and NaI. The solid curves are calculated with eq. 20 and the parameters given in Table 3.

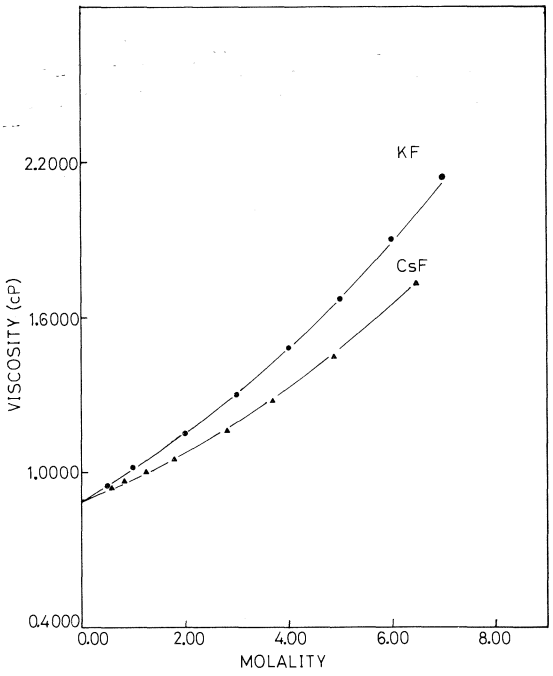

FIG. 2. Observed and calculated viscosities for KF and CsF. Solid curves as in Fig. 1.

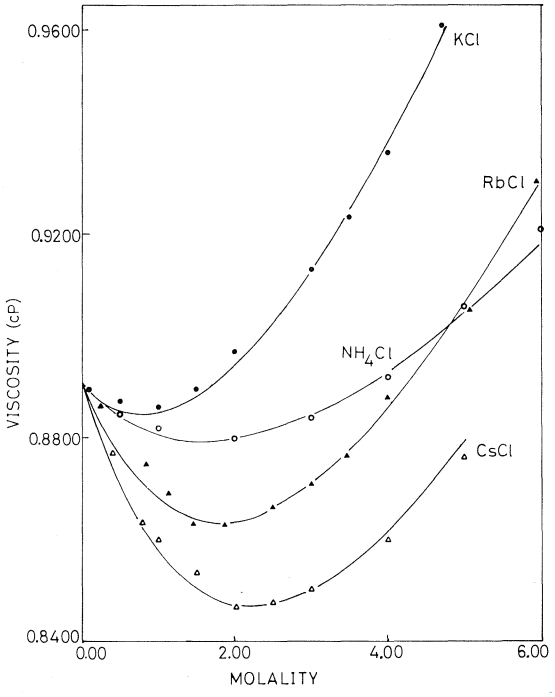

FIG. 3. Observed and calculated viscosities for KCl, RbCl, CsCl, and NH_4Cl. Solid curves as in Fig. 1.

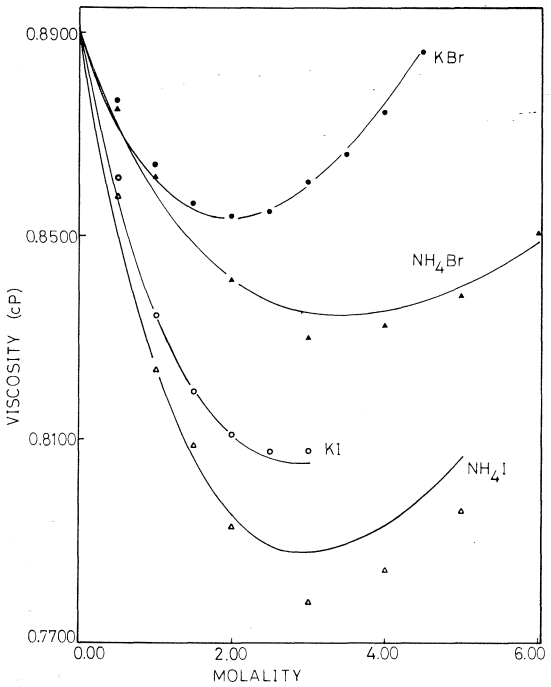

FIG. 4. Observed and calculated viscosities for KBr, KI, NH_4Br, and NH_4I. Solid lines as in Fig. 1.

Moulik (9):

$$[6] \qquad (\eta_{rel})^2 = M + kc^2$$

where M and k are constants.

Bingham (10), by an entirely empirical approach, proposed that the fluidities of one molar electrolyte solutions were composed of additive fluidity constituents of the solvent and ions. That is

$$[7] \qquad \phi = \phi_w + \phi_a + \phi_c$$

where ϕ is the fluidity of the solution, ϕ_w the fluidity of the solvent, ϕ_a the fluidity derived from the anions, and ϕ_c the fluidity derived from the cations. Since the fluidity of water is almost as large as that of the solution at the concentrations (up to 1 N) dealt with by Bingham, he regarded the fluidities of the ions as corrections to the fluidity of water. Equation 7 can then be written as

$$[8] \qquad \Delta_m = \phi - \phi_w = \Delta_a + \Delta_c$$

where Δ_c is the elevation or depression produced in the fluidity of the solution by the presence of one equivalent weight of cations and Δ_a is the corresponding elevation or depression for the anions. Bingham tabulated these ionic parameters at 25 °C assuming the Δ value for the potassium ion was equal to that of the chloride ion as a basis for determining the single ionic Δ parameters. Excellent agreement between calculated and experimental solution fluidities resulted when these values were used to calculate fluidities for a large number of salts at concentrations of 1 N and 0.5 N. While legitimate empirically, this approach lacked a sound molecular and theoretical basis.

Suryanarayana and Venkatesan (11) have observed that the equation

$$[9] \qquad \eta_p = A'' \exp(B''C_p)$$

adequately describes the variation of electrolyte viscosity throughout the high concentration range. Here η_p represents the ratio of the viscosity of the solution at a given concentration relative to that at saturation at the same temperature and C_p the ratio of the mole fraction of the solute at a given concentration to that at saturation at the same temperature. A'' and B'' are experimentally determined constants. However, no theoretical basis was found for this equation.

Another property of these solutions which has been studied in the high concentration region is

the temperature dependence of the viscosity at fixed composition. For pure liquids, the temperature dependence has been accounted for empirically by an equation attributed originally to Andrade (6):

$$[10] \qquad \eta = A' \, e^{B'/T}$$

where A' and B' are constants and T is the absolute temperature. Fixed composition electrolyte solutions of high concentration have also been found to follow this equation.

As a starting point for a molecular interpretation of the viscosity of electrolyte solutions, the approach of Eyring *et al.* has been used by several investigators (1, 12). However, an explanation of both the concentration effects observed in Fig. 1 through Fig. 4 at fixed temperatures or the temperature variation of these effects has not yet appeared. The following section outlines such an approach based on the absolute rate theory of viscosity.

Extension of the Absolute Rate Theory of the Viscosity of Liquids to Concentrated Single Electrolyte Solutions

The basic equation for the viscosity of a fluid from the absolute rate theory approach has been shown to be (14):

$$[11] \qquad \eta = \frac{hN}{V} e^{\Delta G^*/RT}$$

where η is the viscosity of the fluid, h is Planck's constant, N Avogadro's constant, R the gas constant, V the molar volume of the hole in the liquid, and ΔG^* the molar free energy of activation for creating this hole in the liquid by the particle moving in the fluid.

It has also been shown that the viscosity of electrolyte solutions at high fixed concentrations follows the simple temperature dependence of this equation (13). We assume this basic equation can be used therefore to represent the viscosity of an electrolyte solution. It must be kept in mind that, in such a solution, there will be solvent particles as well as anion and cation particles which will contribute to the total viscosity of the medium. Furthermore there are two parameters in this equation which characterize the viscosity of the medium: the volume of the hole in the liquid V, and the free energy of activation involved in forming the hole, ΔG^*. For a mixture of particles, we assume that these parameters are average parameters and that the volume and free energy parameters include solvent, anion, and cation components. We will outline the derivation of the equation first for a solution of a 1:1 salt.

The simplest relation between the average parameters and their sub-components involves the mole fraction of each component. We therefore assume the volume and free energy components are given as

$$[12] \qquad V_T = X_1 V_1 + X_c V_c + X_a V_a$$

$$[13] \qquad \Delta G^* = X_1 \Delta G_1^* + X_c \Delta G_c^* + X_a \Delta G_a^*$$

where X_1 = mole fraction of solvent, X_a = mole fraction of the anion, X_c = mole fraction of the cation, V_1 = molar volume of the solvent molecule hole, V_a = molar volume of the anion hole, V_c = molar volume of the cation hole, ΔG_1^* = free energy of activation for viscous flow per mole of solvent, ΔG_a^* = free energy of activation for viscous flow per mole of anion, and ΔG_c^* = free energy of activation for viscous flow per mole of cation.

Now the mole fraction must take into account all distinct particles in the medium and is therefore, for the mole fraction of cations, given by the equation (14)

$$[14] \qquad X_c = \frac{m_c}{55.51 + 2m}$$

This equation applies to an aqueous solution on the molal scale since there are 55.51 moles of water per kg of water and $2m$ moles of salt particles (anion plus cation) for an m molal solution of a 1:1 salt such as NaCl. For other solvents the appropriate number of moles per kg must be used. Now for a 1:1 salt the following relations are valid:

$$X_c = X_a$$

and

$$X_1 + X_c + X_a = 1$$

Thus,

$$[15] \qquad X_1 = 1 - 2X_c$$

Substitution of eq. 15 into eq. 12 gives

$$[16] \qquad \begin{aligned} V_T &= X_1 V_1 + X_c(V_c + V_a) \\ &= V_1 + X_c(V_c + V_a - 2V_1) \\ &= V_1 + \left[1 + X_c\left(\frac{V_c + V_a}{V_1} - 2\right)\right] \end{aligned}$$

Similarly

$$[17] \qquad \Delta G^* = \Delta G_1^* + X_c(\Delta G_c^* + \Delta G_a^* - 2\Delta G_1^*)$$

Substitution of eqs. 16 and 17 into eq. 11 yields

TABLE 1. Equations to express viscosity of single salt solutions[a]

Salt type	X	F	V
1:1	X_c	$\Delta G_c^* + \Delta G_a^* - 2\Delta G_1^*$	$\frac{V_c + V_a}{V_1} - 2$
1:2	X_c	$\Delta G_c^* + 2\Delta G_a^* - 3\Delta G_1^*$	$\frac{V_c + 2V_a}{V_1} - 3$
2:1	X_a	$2\Delta G_c^* + \Delta G_a^* - 3\Delta G_1^*$	$\frac{2V_c + V_a}{V_1} - 3$
1:3	X_c	$\Delta G_c^* + 3\Delta G_a^* - 4\Delta G_1^*$	$\frac{V_c + 3V_a}{V_1} - 4$
3:1	X_a	$3\Delta G_c^* + \Delta G_a^* - 4\Delta G_1^*$	$\frac{3V_c + V_a}{V_1} - 4$

[a]Basic equation: $\eta = \eta_1 e^{XF/RT}/(1 + XV)$.

the following relation for the viscosity of the solution η.

$$[18] \qquad \eta = hN \frac{\exp\{\Delta G_1^*/RT + X_c[(\Delta G_c^* + \Delta G_a^* - 2\Delta G_1^*)/RT]\}}{V_1\left[1 + X_c\left(\frac{V_c + V_a}{V_1} - 2\right)\right]}$$

For the pure solvent we assume eq. 11 is valid:

$$\eta_1 = \frac{hN}{V_1} e^{\Delta G_1^*/RT}$$

and therefore

$$[19] \qquad \eta = \eta_1 \frac{\exp\{X_c[(\Delta G_c^* + \Delta G_a^* - 2\Delta G_1^*)/RT]\}}{1 + \left[X_c\left(\frac{V_c + V_a}{V_1} - 2\right)\right]}$$

or in simplified form

$$[20] \qquad \eta = \frac{\eta_1 e^{XE}}{1 + XV}$$

where

$$E = (\Delta G_c^* + \Delta G_a^* - 2\Delta G_1^*)/RT$$

$$V = \frac{V_c + V_a}{V_1} - 2$$

$$X = X_c$$

This final equation for the viscosity of an electrolyte solution is in essence a two-parameter equation just as the equation for the viscosity of a pure liquid is a two-parameter equation. Furthermore, all salt types (1:1, 1:2, 1:3, 2:1, 3:1) yield equations of the same form involving two adjustable parameters. The appropriate definitions of the E and V parameters for all salt types are given in Table 1.

The purpose of this paper is to show how this extension of the basic absolute rate theory for the viscosity of fluids accounts quantitatively for the phenomena observed with the viscosities of concentrated electrolyte solutions of single 1:1 salts. The various empirical equations previously discussed which have been observed to account for some of the behaviour of the viscosity of concentrated electrolyte solutions, will be shown to be compatible with these new theoretical equations. Application of these equations to other salt types as well as a discussion of the temperature dependence of these parameters will be left to further papers in this series.

Experimental

The viscosities of concentrated solutions of NaF, KF, NaBr, KBr, NH_4Br, NaI, and KI were measured and are given in Table 2. All salts were certified ACS and were dried for at least 24 h at 110 to 120 °C prior to use. They were then temporarily stored in a glass desiccator over P_2O_5. In the case of the solutions of KF with molalities greater than 2.0, addition of a very slight amount of HF was necessary to adjust the pH of the solutions to within the pH range 6.5 to 7.5. The required amounts of salts

TABLE 2. Experimental and calculated viscosities of single salt solutions at 25 °C

m	η_{exp}	η_{calc}	m	η_{exp}	η_{calc}	m	η_{exp}	η_{calc}	m	η_{exp}	η_{calc}
	NaF			KF			NaBr			KBr	
0.100	0.9082	0.9080	0.500	0.9518	0.9468	0.500	0.9171	0.9050	0.500	0.8771	0.8716
0.200	0.9270	0.9269	1.000	1.020	1.008	1.000	0.9445	0.9333	1.000	0.8641	0.8604
0.300	0.9466	0.9472	2.000	1.148	1.146	2.000	1.025	1.020	1.500	0.8564	0.8548
0.400	0.9690	0.9688	3.000	1.303	1.303	3.000	1.139	1.139	2.000	0.8541	0.8536
0.500	0.9917	0.9917	4.000	1.479	1.479	4.000	1.273	1.284	2.500	0.8549	0.8558
0.600	1.015	1.016	5.000	1.672	1.674	5.000	1.421	1.455	3.000	0.8607	0.8607
0.700	1.039	1.041	6.000	1.900	1.889	6.000	1.646	1.651	3.500	0.8662	0.8679
0.800	1.070	1.068	7.000	2.144	2.120	7.000	1.947	1.871	4.000	0.8745	0.8769
									4.500	0.8865	0.8875
									5.000	0.9129	0.8995
	NH_4Br			NaI			KI				
0.500	0.8751	0.8717	0.500	0.9042	0.8984	0.500	0.8615	0.8570			
1.000	0.8618	0.8580	1.000	0.9138	0.9133	1.000	0.8345	0.8346			
2.000	0.8416	0.8416	1.250	0.9211	0.9230	1.250	0.8257	0.8264			
3.000	0.8300	0.8352	1.500	0.9327	0.9338	1.500	0.8194	0.8199			
4.000	0.8325	0.8355	1.750	0.9445	0.9459	1.750	0.8146	0.8149			
5.000	0.8385	0.8406	2.000	0.9585	0.9589	2.000	0.8111	0.8111			
6.000	0.8509	0.8492	2.250	0.9729	0.9729	2.250	0.8093	0.8084			
7.000	0.8662	0.8602	2.500	0.9891	0.9878	2.500	0.8079	0.8066			
			2.750	1.006	1.004	2.750	0.8075	0.8058			
			3.000	1.025	1.020	3.000	0.8078	0.8057			

were all weighed on a 5 place balance to yield the exact molality as indicated in Table 2.

For each of these solutions, densities and viscosities were determined at 25.00 ± 0.02 °C in a Cannon constant temperature bath (Model M-1). Density measurements were obtained using 25 ml pycnometers which had been previously calibrated with distilled water at 25 °C. A buoyancy correction (15) was applied in obtaining these densities. Viscosities were determined using Ostwald microviscometers (size 50) which were calibrated with 1.0 ml of distilled water which had been equilibrated to the bath temperature. The solution fall times were obtained with stopwatches accurate to ±0.1 s and in no cases were times less than 100 s. Measurements were repeated until three consecutive readings varying only by ±0.2 s were obtained. Each viscosity measurement on each viscometer was followed by at least five washings with distilled water and three with acetone. The viscometers were frequently cleansed with alcoholic KOH and chromic acid.

Absolute viscosities were calculated in centipoise using the formula:

$$\eta = \frac{\eta_1 dt}{d_1 t_1}$$

where $\eta_1 = 0.8904$ cP for water at 25.00 °C (16), d_1 is the density of water at 25.00 °C, t_1 the fall time for water, d the density of the salt solution, and t the fall time for the salt solution.

The data for other salts were obtained from a variety of sources as indicated in Table 3. Only data with four significant figures were accepted for analysis. Computations and tests of the data were carried out on an IBM 360 computer as indicated in the treatment of data section.

Treatment of Data

Two main approaches were used to obtain the values of the E and V parameters from the viscosities of the salt solutions as a function of concentration. Equation 20 can be rearranged as follows:

$$[21] \quad Y = \ln\left[\frac{\eta}{\eta_1}(1 + XV)\right] = XE$$

If the correct value of V were used to calculate values of $(\eta/\eta_1)(1 + XV)$, then a plot of the natural logarithm of this function *vs.* the mole fraction of cation, X, should give a straight line of slope E and an intercept of zero. To test this equation, a computer program was devised to calculate for each salt the function Y with a fixed value of V for all concentrations corresponding to the measured viscosities. The value of V was varied from 0 to 50 in increments of 0.01. For each value of V, a least-squares plot was performed on the values of the function Y and the values of X to generate a value of E from the slope of this plot. Theoretical values of the viscosities were computed using this fixed value of V and the least-squares value of E in eq. 20. The sum of the differences between the observed and calculated viscosities were then computed. The best value of V and the resultant best E parameter were picked when the minimum sum of deviations between observed and calculated viscosities resulted.

Examples of the plots of the best fit functions Y *vs.* X are given in Figs. 5 and 6 and the best fit parameters E and V for all salts are given in Table 3. Correlation coefficients calculated for the best fit plots of Y *vs.* X exceeded 0.9999 for all salts and all intercepts on this plot were zero within the error of the measurements. Calcu-

TABLE 3. Volume, free energy, and difference parameters at 25 °C

Salt	$\left(\frac{V_c + V_a}{V_1}\right)$	E	$\left[\left(\frac{V_c + V_a}{V_1} - 2\right) - E\right]$	Data reference
NaF	22.45	30.97	−10.52	4, this work
KF	9.51	14.21	−6.70	4, 22, this work
RbF	9.67	13.85	−6.18	4, 22
CsF	11.74	13.91	−4.17	4, 22
LiCl	8.03	13.51	−7.48	4, 22, 23, 24, 25
NaCl	13.36	15.21	−3.85	22, 23, 25, 26, 30
KCl	10.85	7.87	+0.98	22, 23, 25, 29
NH_4Cl	8.19	5.27	+0.92	23, 27
RbCl	11.74	7.51	+2.23	22, 23, 25
CsCl	12.62	7.61	+3.01	22, 25
NaBr	18.21	16.98	−1.23	This work
KBr	13.08	8.16	+2.92	This work
NH_4Br	10.50	5.80	+2.70	This work
LiI	7.24	10.73	−5.49	21
NaI	13.35	11.82	−1.53	This work
KI	15.10	8.08	+5.02	This work
NH_4I	16.54	8.48	+6.06	23, 21
RbI	15.56	7.61	+5.95	4, 21
CsI	14.83	6.34	+6.49	4, 28

lated viscosities for various salts using these best fit parameters are tabulated in Table 2 and graphically shown in Figs. 1 through 4.

Figures 3 and 4 reveal that certain salts yield minimum values on a viscosity *vs.* concentration scale plot. This fact led to the second approach to obtaining the parameters V and E from the minimum values of the viscosity η_{min} and the mole fraction value at this minimum X_{min} on a viscosity mole fraction plot. Equation 20 shows that for a minimum in this plot to occur, the first derivative $\partial\eta/\partial X$ must be zero.

$$[22] \quad \frac{\partial \eta}{\partial X} = \frac{\eta_1 E e^{EX}}{1 + XV} - \frac{\eta_1 V e^{EX}}{(1 + XV)^2} = 0$$

Hence

$$E - \frac{V}{1 + XV} = 0$$

$$[23] \quad X_{min} = \frac{V - E}{VE}$$

Equations 23 and 20 then yield for η_{min} the relation

$$[24] \quad \eta_{min} = \eta_1 \left(\frac{E}{V}\right) e^{(1-(E/V))}$$

From the known values of X_{min} and η_{min} obtained from the curve, distinct values of E and V can be obtained via relations 23 and 24. Theoretical values of the viscosity can then be calculated as a function of concentration to be compared with the observed values. Since in many cases the minimum in the curve of η *vs.* X is a broad minimum, some error occurs in picking the value of X_{min}. The values of E and V obtained in this way can be used however as first estimates of the best E and V values to be used in the computer iteration method previously discussed. It is found that the values of the parameters E and V obtained in this manner agree with those obtained by the least-squares analyses of the function Y *vs.* mole fraction plots.

Discussion

It is apparent from Table 2 and from Figs. 1 through 4 that the two-parameter eq. 20 can reproduce the observed viscosities within experimental error over the high concentration region for all the alkali and ammonium halide salts. Furthermore, eqs. 18 through 20 are of the same form as the empirical equations found to reproduce viscosity data in the high concentration region (11).

Since we are concerned with the concentration dependence of the viscosity of concentrated electrolyte solutions at fixed temperature, we shall leave the discussion of the temperature dependence of these effects to another paper. However, as indicated previously it has been found that eq. 10 accounts for the concentration dependence of the viscosity of electrolyte solutions at high concentrations. Equation 20 is compatible with eq. 10 and indeed indicates that eq. 10 is only an approximation to the real concentration dependence of the viscosity of electrolyte solutions. It has been observed that when log η is plotted *vs.* C_p (the ratio of the mole fraction of the salt at a given concentration relative to that at saturation), a straight line is obtained in the high concentration region but that curvature

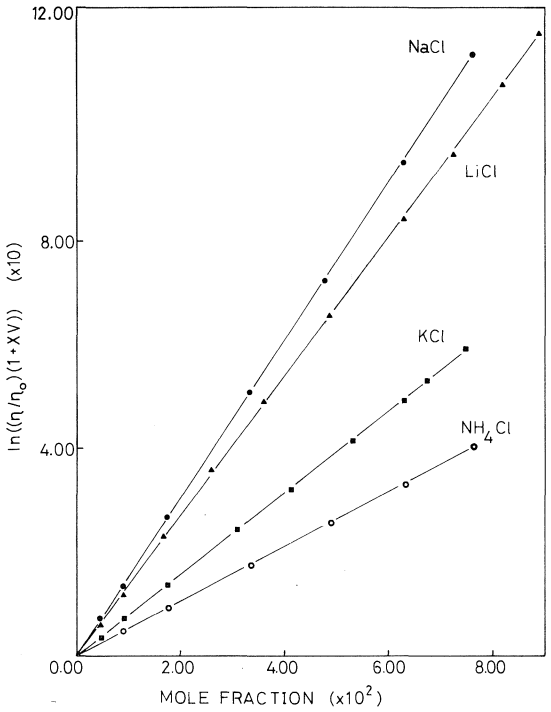

FIG. 5. Test of linearity of eq. 21 for LiCl, NaCl, KCl, and NH_4Cl.

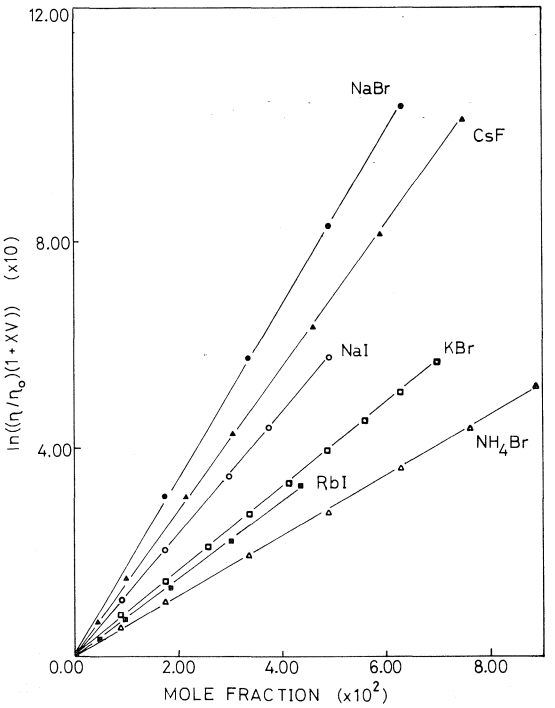

FIG. 6. Test of linearity of eq. 21 for NaBr, NaI, KBr, NH_4Br, and CsF.

in the low concentration region also occurs (11). This is just what would be predicted according to eq. 20. If X_{sat} is the mole fraction of the salt in the solution at saturation, then X/X_{sat} equals C_p and eq. 20 can be re-written as:

$$[25] \qquad \eta = \eta_1 \frac{\exp(X_{sat}EC_p)}{1 + X_{sat}VC_p}$$

If the term $\log \eta$ were plotted against C_p we could not expect a straight line relation from eq. 25 but rather a curve depending on the size of the parameter $X_{sat}V$ for any salt. If $X_{sat}V$ is small enough, then to a first approximation, a straight line relation would be observed at high concentrations, with deviations occurring at low concentrations. In these cases the high concentration slope would be equal to $X_{sat}E/2.303$ and the intercept of the straight portion of the curve at C_p equal to zero would be given by $\log \eta_1$.

If eq. 20 is valid over the whole range of electrolyte concentration, it should account quantitatively for both the high concentration as well as the low concentration viscosity effects. In the low concentration region, the Jones–Dole equation (eq. 3) has been used to describe the viscosity of electrolyte solutions in the region below 0.1 *M*. If we ignore the Falkenhagen term ($A\sqrt{c}$) in this expression and assume that the *B* coefficient is such that it will swamp out and encompass the long range electrostatic effects which are explained by the $A\sqrt{c}$ term, and noting that at concentrations <0.1 the molarity is almost equal to the molality, then we can write the Jones–Dole equation in terms of the molality as:

$$[26] \qquad \frac{\eta}{\eta_1} = 1 + B_c m$$

Here B_c is the corrected *B* coefficient of the Jones–Dole equation. Equation 20 can now be expanded as follows since the mole fraction *X* will be $\ll 1$ in the region of concentration $<0.1\,m$.

$$\frac{\eta}{\eta_1} = \frac{e^{XE}}{1 + XV}$$

$$\frac{\eta}{\eta_1} = \left(1 + XE + \frac{X^2E^2}{2}\right)(1 - XV + X^2V^2)$$

Ignoring terms in X^2 since $X \ll 1$, then

$$[27] \qquad \frac{\eta}{\eta_1} \simeq 1 + (E - V)X$$

Since the molality, *m*, is small, then *X* can be approximated as:

TABLE 4. Comparison between parameters obtained from various viscosity equations for electrolytes at 25 °C

Salt	B'	$\left(\frac{E-V}{55.51}\right)$	$(\Delta_a + \Delta_c)^a$	$1.953\,(V-E)$	$\left(\frac{\Delta_a + \Delta_c}{B}\right)$
NaF	+0.221[b]	+0.1895	−23.2	−20.5	−105
KF	+0.127[b]	+0.1207	−13.3	−13.1	−105
RbF	+0.109[b]	+0.1113	−11.7	−12.2	−107
CsF	+0.092[b]	+0.0751	−11.0	−8.1	−120
LiCl	+0.1425	+0.1348	−13.7	−14.6	−96
NaCl	+0.0793	+0.0694	−9.32	−7.52	−118
KCl	−0.0140	−0.0177	+0.56	+1.91	−40(−136)
NH_4Cl	−0.0144	−0.0166	+0.72	+1.80	−50(−125)
RbCl	−0.039	−0.0402	+2.14	+4.36	−55(−112)
CsCl	−0.052	−0.0542	+2.87	+5.88	−55(−113)
NaBr	+0.0543	+0.0222	−6.50	−2.40	−120
KBr	−0.0390	−0.0526	+2.81	+5.70	−72
NH_4Br	−0.0394	−0.0486	+3.53	+5.27	−90
LiI	+0.0810	+0.0989	−6.40	−10.72	−79
NaI	+0.0178	+0.0276	−2.02	−2.99	−113
KI	−0.0775	−0.0904	+7.86	+9.80	−101
NH_4I	−0.0759	−0.1092	+8.02	+11.83	−106
RbI	−0.110	−0.1072	+9.44	+11.62	−86
CsI	−0.1135	−0.1169	+10.17	+12.67	−90

[a]Reference 10.
[b]Reference 4.

$$X = \frac{m}{55.51 + 2m} \simeq \frac{m}{55.51}$$

and therefore

$$[28] \qquad \frac{\eta}{\eta_1} = 1 + \frac{(E - V)}{55.51} m$$

Comparing eqs. 26 and 28 shows that the B coefficient of the Jones–Dole expression should be approximately equal to $(E - V)/55.51$. Table 4 shows the good agreement between the observed B coefficients and the $(E - V)/55.51$ parameters for the salts studied in this paper. Because the B coefficients were obtained with either the full Jones–Dole expression or with an expanded Jones–Dole equation, exact agreement between these two parameters should not be expected.

Equation 20 can also be used to account for the Δ parameters of Bingham (10) which are additive up to 1 m. If we define $(\phi - \phi_1)/m$ as the molal fluidity increment or decrement, depending on the sign of the Δ parameters, then

$$\frac{\phi - \phi_1}{m} = \Delta_a + \Delta_c$$

In terms of viscosities this can be written as

$$[29] \qquad \frac{\frac{1}{\eta} - \frac{1}{\eta_1}}{m} = \frac{\frac{\eta_1}{\eta} - 1}{\eta_1 m} = \Delta_a + \Delta_c$$

Equation 20 can be rearranged and expanded as:

$$\frac{\eta_1}{\eta} = (1 + XV)\, e^{-EX}$$
$$= (1 + XV)\left(1 - EX + \frac{E^2X^2}{2} - \ldots\right)$$

Up to 1 m, the term $EX < 1$, and terms in E^2X^2 can be ignored. Hence

$$[30] \qquad \frac{\eta_1}{\eta} \simeq 1 + (V - E)X$$

If we consider a 1 m solution only to determine the Δ values then:

$$X = \frac{m}{55.51 + 2}$$

and

$$\left(\frac{\eta_1}{\eta} - 1\right) = \frac{(V - E)}{57.51} m$$

or

$$[31] \qquad \frac{\left(\frac{\eta_1}{\eta} - 1\right)}{\eta_1 m} = \frac{(V - E)}{57.51\eta_1}$$

Since η_1 for water at 25 °C is 0.008904 poise, then equating [29] and [31] we obtain for a 1 molal solution:

$$[32] \qquad \Delta_a + \Delta_c = 1.953(V - E)$$

Table 4 lists values of $\Delta_a + \Delta_c$ observed and those calculated using eq. 32.

Furthermore, according to eqs. 32 and 28 the ratio of the $(\Delta_a + \Delta_c)$ parameter to the B parameter for all salts should be a constant.

$$[33] \quad \frac{(\Delta_a + \Delta_c)}{B} = \frac{-55.51}{57.51\eta_1} = -108.4$$

Calculated values of this ratio are given in Table 4 and show good agreement with this prediction. Large differences in these values appear only for KCl, NH_4Cl, RbCl, CsCl. Since there does not appear to be any systematic error in these numbers, then the only possible source of this large error is in the prime data of Bingham (10). Shown in brackets beside these numbers in Table 4 are values calculated using $1.953(V - E)/B$.

It should be noted, in Table 4, in comparing the B values to the $(\Delta_a + \Delta_c)$ parameters of Bingham, that the signs of these parameters for each salt are opposite, *i.e.* if the B coefficient is positive then $(\Delta_a + \Delta_c)$ is negative and vice-versa. This follows from the fact that in the low concentration region, if a salt increases the viscosity relative to that of water at that temperature, such as NaCl, this results in a positive B value. However, since fluidity is the inverse of viscosity, then if the viscosity increases, the fluidity decreases and thus a negative value of $(\Delta_a + \Delta_c)$ results. Similarly if a salt initially decreases the viscosity from that of water, such as KCl, then a negative B value results. However, the fluidity would initially increase and thus yield a positive $(\Delta_a + \Delta_c)$ value.

It is also interesting to note that as the temperature is raised, negative B values found in 'structure-breaking' salts become less negative and eventually become positive. This is due to the fact that as the temperature increases, the initial decrease in viscosity shown in Figs. 3 and 4 is gradually lost until the exponentially increasing function of Figs. 1 and 2 is achieved.

The additivity of the B and $(\Delta_a + \Delta_c)$ parameters has been commented on, mulled over, and dissected in detail over the past 20 years (1, 17–20). Excellent discussions of the various possible component contributions to these parameters are available in these references. The V and E parameters of eq. 20, however, give another insight into the values of the B and Δ parameters. It can be seen from Table 3 that the individual E and V parameters do not show systematic trends or seem to have additive characteristics. However, the difference parameter $(E - V)$ reflects systematic trends and since it is directly proportional to the additive parameters B and Δ, it too must be made of additive components. The definitions of E and V given in eq. 20 and Table 1 for other salt types in fact indicate that the $(E - V)$ parameter should be additive. Thus, for 1:1 salts

$$(E - V) = \frac{\Delta G_c^*}{RT} + \frac{\Delta G_a^*}{RT} - 2\left(\frac{\Delta G_1^*}{RT}\right) - \left(\frac{V_c + V_a}{V_1}\right) - 2$$

$$[34] \quad (E - V) = \left(\frac{\Delta G_c^*}{RT} - \frac{V_c}{V_1}\right) + \left(\frac{\Delta G_a^*}{RT} - \frac{V_a}{V_1}\right) - 2\left(\frac{\Delta G_1^*}{RT} - \frac{V_1}{V_1}\right)$$

Thus, the thrust of any argument over the significance of the B and Δ parameters according to eq. 34 should concern itself with the free energy of activation of viscous flow for the anions, cations, and solvent molecules as well as the volume ratios of the holes created in the liquid structure by these particles during viscous flow.

However, the free energy parameters can only be properly understood in terms of the enthalpy and entropy of activation components according to eq. 35

$$[35] \quad \Delta G^* = \Delta H^* - T\Delta S^*$$

Furthermore, ionic B values show a linear relationship with the partial molar ionic entropies (1), and since the $(E - V)$ parameter is related to these B values, then the $(E - V)$ parameter should also show some kind of relationship to the entropy. Therefore a detailed discussion of the significance of the $(E - V)$ parameters for various salts should be properly deferred until the determination of the temperature dependence of the $(E - V)$ parameters has been carried out.

Conclusions

A simple extension of the transition state theory of viscosity for fluids has led to a two-parameter equation which quantitatively accounts for the viscosity of concentrated solutions of electrolytes. Comparison of this equation with several empirical equations in the high and low concentration regions shows that this new equa-

tion also successfully links the B parameters of the Jones–Dole equation and the Δ parameter of Bingham's equation with the free energy of activation and volume ratio parameters of this new equation.

Acknowledgement

We would like to thank the National Research Council of Canada for a scholarship for one of us (R.F.) and the International Business Machine Company (IBM) of Canada for funds in aid of this project.

1. R. H. STOKES and R. MILLS. Viscosity of electrolytes and related properties. Pergamon Press, New York. 1971.
2. J. R. PARTINGTON. Treatise of physical chemistry. Vol. 2. Longmans, Green and Co., New York. 1951.
3. B. S. HARRAP and E. HEYMANN. Chem. Rev. **48**, 46 (1951).
4. J. E. DESNOYERS and G. PERRON. J. Solution Chem. **1**, 199 (1972).
5. S. P. MOULIK and A. K. RAKSHIT. J. Indian Chem. Soc. **12**, 450 (1975).
6. E. N. ANDRADE. Nature, **125**, 309 (1930).
7. V. J. VAND. J. Phys. Chem. **52**, 277 (1948).
8. D. G. THOMAS. J. Colloid. Chem. **20**, 267 (1965).
9. S. P. MOULIK. J. Phys. Chem. **72**, 4689 (1968).
10. E. C. BINGHAM. J. Phys. Chem. **45**, 885 (1941).
11. C. V. SURYANARAYANA and V. K. VENKATESAN. Acta Chim. Hung. **16**, 149 (1958); **16**, 338 (1958).
12. W. GOOD. Electrochim. Acta, **9**, 203 (1964); **10**, 1 (1965); **11**, 759 (1966); **11**, 767 (1966); **12**, 1031 (1967).
13. C. V. SURYANARAYANA and V. K. VENKATESAN. Acta Chim. Hung. **16**, 451 (1958).
14. S. GLASSTONE, K. LAIDLER, and E. EYRING. The theory of rate processes. McGraw-Hill, New York. 1941.
15. F. DANIELS, J. W. WILLIAMS, P. BENDER, R. A. ALBERTY, and C. D. CORNWELL. Experimental physical chemistry. McGraw-Hill, New York. 1962.
16. R. C. WEAST (*Editor*). Handbook of physics and chemistry. 48th Ed. Chemical Rubber Co., Cleveland, Ohio. 1967.
17. R. GURNEY. Ionic processes in solution. McGraw-Hill, New York. 1953.
18. D. BURNS. Electrochim. Acta. **10**, 985 (1965).
19. T. ISONO and R. TAMAMUSHI. Electrochim. Acta, **12**, 1479 (1967).
20. P. K. MANDAL, B. K. SEAL, and A. S. BASU. J. Phys. Chem. **87**, 295 (1973).
21. J. D'ANS, J. BARTELS, P. TEN BRUGGENCATE, A. EUCKEN, G. JOOS, and W. A. ROTH (*Editors*). Landolt-Bornstein II Band, 5 Teil, Springer-Verlag. 1969.
22. S. LENGYEL, J. TAMAS, J. GIBER, and J. HOLDERITH. Acta Chim. Hung. **40**, 125 (1964).
23. International Critical Tables. Vol. V. McGraw-Hill, New York. 1933.
24. J. TIMMERMANS. The physico-chemical constants of binary systems in concentrated solutions. Vol. 3. Interscience, New York. 1959.
25. A. G. OSTROFF *et al.* J. Phys. Chem. 73(8), 2784 (1969).
26. G. JONES and S. M. CHRISTIAN. J. Am. Chem. Soc. **59**, 484 (1937).
27. G. JONES and S. K. TALLEY. J. Am. Chem. Soc. **55**, 624 (1933).
28. G. JONES and H. J. FORNWATT. J. Am. Chem. Soc. **58**, 619 (1936).
29. M. TANAKA. Nippon Kagaku Zasshi, **82**, 147 (1961).
30. M. TANAKA. Nippon Kagaku Zasshi, **83**, 639 (1962).

Studies in the usnic acid series. IV.[1] The base catalyzed usnic acid – isousnic acid rearrangement. Part II. An improved synthesis of (+)-isousnic acid

JAMES P. KUTNEY, IGNACIO H. SANCHEZ, AND TREVOR YEE

Department of Chemistry, University of British Columbia, 2075 Wesbrook Place, Vancouver, B.C., Canada V6T 1W5

Received September 30, 1976

JAMES P. KUTNEY, IGNACIO H. SANCHEZ, and TREVOR YEE. Can. J. Chem. **55**, 1073 (1977).

Investigations concerning the alkaline cleavage of (+)-2*H*-[1,2]oxazocinousnic acid (**3**) are described. These studies provide an interesting rearrangement from the 'normal' (usnic acid) to the 'iso' (isousnic) series and, in turn, a high yielding sequence for the synthesis of (+)-isousnic acid (**1**).

JAMES P. KUTNEY, IGNACIO H. SANCHEZ et TREVOR YEE. Can. J. Chem. **55**, 1073 (1977).

On décrit des études concernant les coupures alcalines de l'acide (+)-2*H*-[1,2]oxazocinousnique (**3**). Ces études fournissent un réarrangement intéressant de la série 'normale' (acide usnique) en série 'iso' (acide isousnique) aussi qu'une méthode pour effectuer la synthèse de l'acide (+)-isousnique (**1**) par une séquence impliquant dé bons rendements.

[Traduit par le journal]

During our continued studies on nitrogen containing usnic acid derivatives (1, 2) as useful synthetic intermediates for the preparation of the several biodegradation products isolated in our laboratories,[2] we have recognized an interesting base-catalyzed usnic acid – isousnic acid rearrangement (3).

The following studies confirm its generality and synthetic usefulness, as seen by the greatly improved preparation of the naturally occurring lichen substance (+)-isousnic acid (**1**) (4–6).

Thus, the alkaline treatment of (+)-2*H*-[1,2]oxazocinousnic acid (**3**) (2) follows a very similar course to that previously observed (3) for the isomeric isoxazole **2** (2) producing **5** as the main component, (Fig. 1) the latter belonging to the isousnic acid series (the 'iso' series). The structural assignment followed from the examination of the relevant spectroscopic properties. For example, in the ^{1}Hmr spectrum one notes the characteristic (3) two-proton AB quartet centered at δ 3.10 ppm (J = 18 Hz) corresponding to the C_4-methylene group of the *cis* B/C ring fused series (C_{4a}-αOH) as shown in **5** and the one-proton singlet at δ 6.08 ppm assigned to the C_8-aromatic proton. Further support for this assignment was derived from its cd spectrum which showed absorption maxima and Cotton effects (see Experimental) comparable in sign and magnitude to those observed for the oxazocine **7** also belonging to the iso series (3).

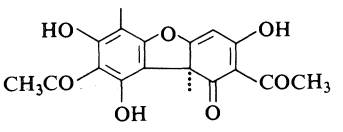

1

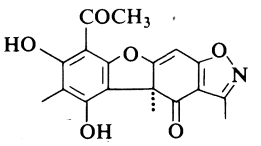

2

The minor components obtained from the basic treatment of **3** result from both Michael addition of water (solvent) to the C_4—C_{4a} double bond and alkali cleavage of the non-enolizable C_1 carbonyl group producing the C_{4a}-hydroxylated derivative **4** and the unsaturated acid **6** respectively (Fig. 1).

Dehydration of compound **5** by means of 0.5% concentrated sulfuric acid in acetic anhydride produced, in 80% yield, the desired olefin **7**. The latter substance shows the olefinic and aromatic protons as sharp singlets at δ 6.02 and 6.76 ppm, respectively, in its ^{1}Hmr spectrum.

Two other minor components were isolated and characterized from the dehydration reaction mixture. One of these (6% yield) revealed a molecular formula, $C_{22}H_{19}O_8N$ and was clearly the result of *C*-acylation of the aromatic ring (**8**, Fig. 2), as evidenced by new absorptions

[1]For part III see ref. 3.

[2]J. P. Kutney, I. H. Sanchez, T. Yee, and P. J. Salisbury, manuscript in preparation.

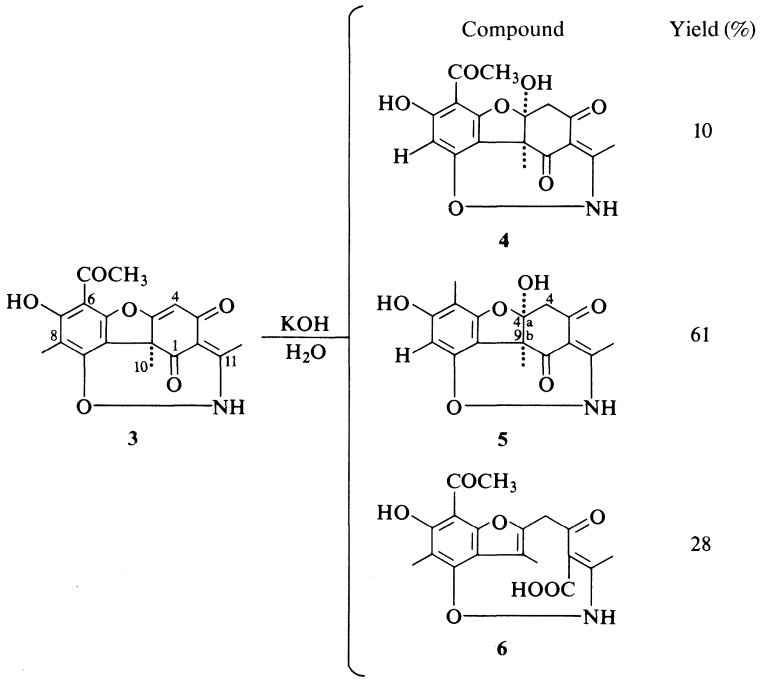

FIG. 1. The base cleavage of (+)-2*H*-[1,2]oxazocinousnic acid (**3**).

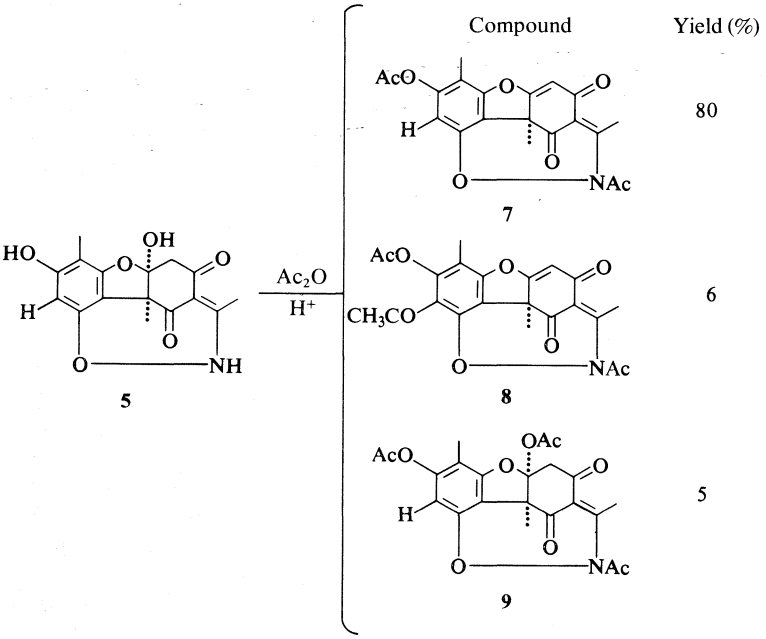

FIG. 2. The acid-catalyzed dehydration of (+)-α-hydroxydesacetyl-2*H*-[1,2]oxazocinoisousnic acid (**5**).

in its infrared spectrum at 1775 (phenolic acetate) and 1690 cm^{-1} (aromatic acetyl group). Its ^{1}Hmr spectrum showed three-proton singlets at δ 2.33, 2.45, and 2.50 ppm, representative of the C_7-phenolic acetate, the aromatic methyl ketone, and the *N*-acetyl group, respectively, with the one-proton singlet at δ 5.90 ppm being assigned to the olefinic proton.

The final component proved to be the acetoxy derivative **9**, for which the C_{4a}-α-configuration (*i.e. cis*-B/C ring junction) could be cleanly derived from the chemical shifts of both the C_4-methylene group protons, observed as an AB quartet centered at δ 3.65 ppm (J = 18 Hz), and the aromatic proton, seen at δ 6.70 ppm. These values are in full agreement with previous ^{1}Hmr data obtained for the isomeric isoxazole series (3).

Alkaline hydrolysis (0.8% aqueous sodium hydroxide in tetrahydrofuran) of the *O*,*N*-diacetate **8** furnished the first 'iso'-series intermediate available for direct comparison with the 'normal' series studied earlier. Thus compound **10** obtained as colorless prisms, mp 170–172°C, $[\alpha]_D^{26}$ +357° (CH_3CN), was shown not to be identical with the known (+)-2*H*-[1,2]oxazocinousnic acid (**3**) (2). Table 1 shows a comparison of the relevant ^{1}Hmr characteristics of these two materials.

Being certain at this point that we were involved with compounds of the iso series, we proceeded to complete the synthesis of (+)-isousnic acid (**1**) (Fig. 3) by performing the hydrogenolytic O—N bond cleavage (2) of

TABLE 1. Proton magnetic resonance data of (+)-2*H*-[1,2]oxazocinousnic acid (**3**) and (+)-2*H*-[1,2]oxazocinoisousnic acid (**10**)

	δ (ppm)	
Functionality	**3**	**10**
C_{9b}-CH_3	1.87	1.82
C_6-CH_3	—	2.15
C_8-CH_3	2.12	—
C_{11}-CH_3	2.48	2.58
C_6-$COCH_3$	2.74	—
C_8-$COCH_3$	—	2.75
C_4-H	6.13	6.01
N-H	4.38	7.45
C_7-OH	13.61	13.63

oxazocine **7** followed by immediate alkaline (1 *N* sodium hydroxide in tetrahydrofuran) regeneration of the ring C β-triketone system. In this manner, it was possible to obtain (+)-8-desacetylisousnic acid (**11**), in overall 80% yield. The latter substance was shown to be identical with the product obtained from similar treatment of the [4,5-*b*]isoxazole series in a previous study (3). Since **11** has been successfully converted into (+)-isousnic acid (**1**) by an aluminum-trichloride-catalyzed Fries rearrangement of its corresponding di-*O*-acetyl derivative (3), this sequence represents a much improved synthesis of **1** from the normal usnic acid series.

This base catalyzed interconversion from the normal to the iso series (**3** → **5**) obviously involves fission of the C—O bond in ring B of **3** and recyclization with the aromatic C_9 oxygen as the

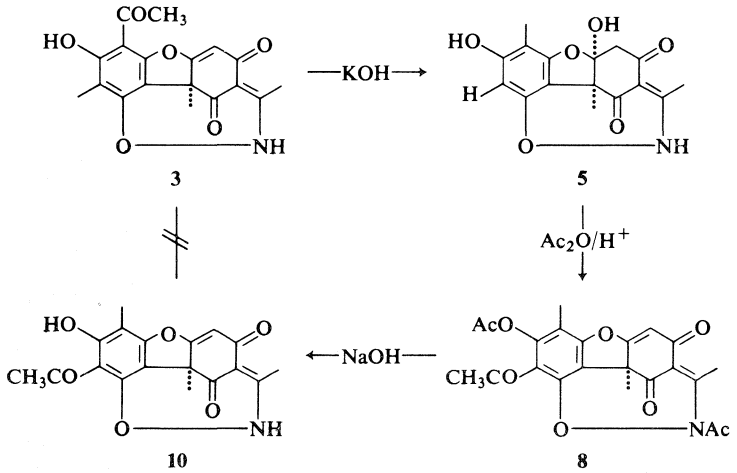

3 **5** **10** **8**

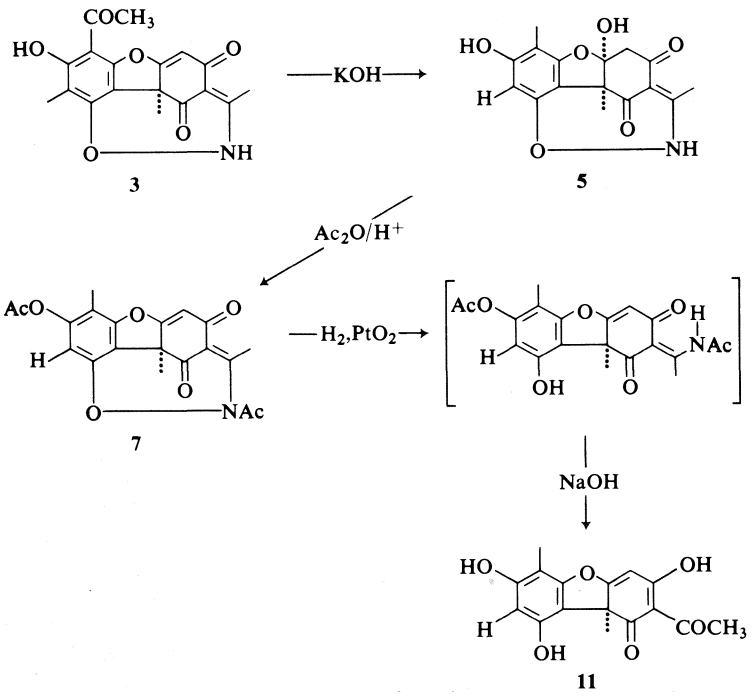

FIG. 3. The preparation of (+)-8-desacetylisousnic acid (**11**) from (+)-2*H*-[1,2]oxazocinousnic acid (**3**).

ring B hetero atom in the final product. Clearly such a rearrangement is made possible only if the O—N bond of the oxazocine ring is cleaved under the basic conditions to the corresponding phenolic hydroxylamine derivative, as shown.

It is our hope that the present work will also add some information to the sparse knowledge of oxazocine ring chemistry. Perhaps this interesting protecting group can be employed in other areas of organic synthesis.

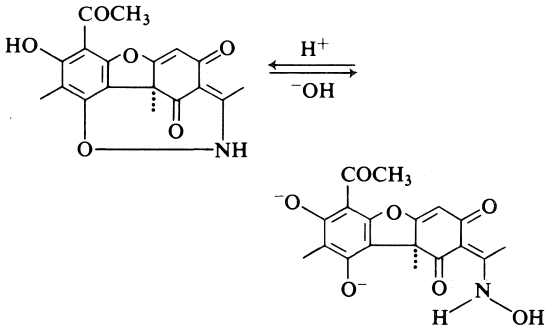

Experimental

Melting points were determined on a Kofler block and are uncorrected.

Ultraviolet (uv) spectra were recorded on a Cary 15 spectrophotometer in methanol solution (unless otherwise noted). The wavelength of the absorption maxima are reported in nanometres (nm).

Infrared (ir) spectra were measured routinely on a Perkin-Elmer model 710 spectrophotometer. Analytical or comparison spectra were recorded on a Perkin-Elmer model 457 spectrophotometer using matched cells with a cell path of 0.2 mm in chloroform solution. Calibration was achieved using the 1601 cm^{-1} absorption band of polystyrene. The absorption maxima are quoted in wave numbers (cm^{-1}).

Proton magnetic resonance (^{1}Hmr) spectra were measured in deuterochloroform ($CDCl_3$) solution (unless otherwise indicated) at room temperature. Routine spectra were recorded at 60 MHz on a Varian T-60 spectrometer, and analytical or comparison spectra at 100 MHz on either a Varian HA-100 or a Varian XL-100 spectrometer. All ^{1}Hmr spectra obtained via the Fourier transform (F.t.) technique are so noted and were recorded on a Varian X1-100 spectrometer. Line positions are given in the δ (ppm) scale using tetramethylsilane (TMS) as internal standard. The integrated peak areas, multiplicity, and proton assignments are indicated in parentheses.

Low resolution mass (ms) spectra were determined on either an AEI-902 or an Atlas CH-4B mass spectrometer, with high resolution mass spectra being recorded exclusively on an AEI-MS-902 mass spectrometer.

Circular dichroism (cd) spectra were obtained on a Jasco model J-20 spectropolarimeter in methanol solution (unless otherwise indicated). The wavelength of the absorption maxima is reported in nanometres (nm). The differential molar extinction coefficient ($\Delta\varepsilon$) and the sign of the observed Cotton effect are indicated in parentheses.

Optical rotations ($[\alpha]_D$) were measured on a Perkin-

Elmer model 141 polarimeter at the sodium D line in chloroform solution (unless otherwise noted) using cells with a 0.1 dm path.

Microanalyses were performed by Mr. P. Borda of the Microanalytical Laboratory, University of British Columbia.

Merck silica gel G (acc. to Stahl) impregnated with oxalic acid (2%) and with 2% fluorescent indicator added, was used as adsorbent for thin layer chromatography (tlc), unless otherwise noted. The tlc plates were activated in an oven at 90°C for 4 h before use. For qualitative chromatography layers of 0.3 mm thickness were used and the spots were visualized by viewing under ultraviolet (uv) light or spraying with a 1% ethanolic ferric chloride solution. For preparative (plc) chromatography large (20 × 20 and 20 × 60 cm) plates with a thicker layer (0.7 mm) were used. The developing systems were *A*, petroleum ether (30–60°C) – acetone (4:1), and *B*, chloroform – ethyl acetate (3:2), unless otherwise indicated.

Column chromatography was performed on either Mackerey-Nagel (0.2–0.5 mm grain size) or Merck 60 (0.063–0.2 mm grain size) silica gel.

The usnic acid utilized throughout the course of this study was obtained from Koch-Light Laboratories, England, as the optically active dextrorotatory isomer, (+)-usnic acid, isolated from lichen sources (*Usnea barbata*).

In order to present in a coherent manner the characteristic spectroscopic data for those compounds that are formally derived from usnic acid and retain its basic skeletal features, we have decided to maintain through the course of this work the numbering system recommended for the parent molecule, that is, the approved dibenzofuran numbering (7) instead of using those arising from the corresponding systematic names. In all other instances the latter numbering systems will be used.

*Base Cleavage of (+)-2H-[1,2]Oxazocinousnic Acid (**3**)*

A solution of (+)-2*H*-[1,2]oxazocinousnic acid (**3**) (3.973 g, 11.651 mmol) in freshly prepared 20% aqueous potassium hydroxide (200 ml) was stirred at room temperature under a nitrogen atmosphere for 1.5 h. The dark brown reaction mixture was diluted with cold distilled water (200 ml), acidified with 1 *N* hydrochloric acid, and extracted with ethyl acetate (3 × 120 ml). The combined extracts were washed with water, dried over anhydrous sodium sulfate, and evaporated under reduced pressure to afford a pale yellow foam (4.508 g). Purification by column chromatography on Macherey-Nagel silica gel (160 g) yielded the following pure components.

*Fraction I. (+)-α-Hydroxy-2H-[1,2]oxazocinousnic acid (**4**) (7-Acetyl-5aα,8-dihydroxy-3a,4,10b,11-tetrahydro-3,9,10bα-trimethyl-4,11-dioxo-2H-4,5-dihydro[1,2]-oxazocino[4,5,6,7,8-a,n,l,k]dibenzofuran)*

Colorless prisms from acetone–chloroform (0.423 g, 1.178 mmol; 10%), mp 211.5–212.5°C; $[\alpha]_D^{26}$ (CH_3CN) +158° (*c* 0.1195); uv: λ_{max} (log ε) 330 (3.44), 285 (3.85), 223 (3.92); ir (Nujol): ν_{max} 3500–3100 (OH, chelated), 1685 (C=O, enone system), 1620 (C=O, chelated aromatic acetyl), 1600 (C=C); ^{1}Hmr ($CDCl_3$–DMSO-d_6): δ 1.91 (3H, s, C_{9b}-CH_3), 2.01 (3H, s, C_8-CH_3), 2.37 (3H, s, C_{11}-CH_3), 2.53 (3H, s, C_6-$COCH_3$), 3.10 (1H, br, N-H), 3.12 (2H, AB q, J = 18 Hz, C_4-H_2), 9.36 (1H, br, C_{4a}-αOH), 13.43 ppm (1H, s, C_7-OH); ms: *m/e* 359 (M^+), 236, 234, 128, 118, 85, 83 (base peak), 43. *Anal.* calcd. for $C_{18}H_{17}O_7N$ (0.85 $CHCl_3$): C 49.13, H 3.91, N 3.04, Cl 19.62; found: C 49.14, H 3.92, N 2.97, Cl 19.54. High resolution molecular weight determination calcd. for $C_{18}H_{17}O_7N$: 359.100; found: 359.099; cd: λ_{max} (Δε) 276 (+3.02), 250 (+3.45), 226 (−7.32).

*Fraction II. (+)-α-Hydroxydesacetyl-2H-[1,2]oxazocinoisousnic Acid (**5**) (5aα,8-Dihydroxy-3a,4,5,5a,10b,11-hexahydro-3,7,10bα-trimethyl-4,11-dioxo-2H-4,5-dihydro[1,2]oxazocino[4,5,6,7,8-a,m,l,k]dibenzofuran)*

Colorless prisms from acetone–chloroform (2.250 g, 7.097 mmol; 61%), mp 227–229°C; $[\alpha]_D^{26}$ (CH_3CN) +284° (*c* 0.0845); uv: λ_{max} (log ε) 287 (3.11), 263 (3.26), 217 (3.86); ir (Nujol): ν_{max} 3550, 3500–3100 (OH, NH), 1700, 1630 (C=O), 1600 (C=C); ^{1}Hmr ($CDCl_3$–DMSO-d_6): δ 1.90 (3H, s, C_{9b}-CH_3), 2.16 (3H, s, C_6-CH_3), 2.40 (3H, s, C_{11}-CH_3), 3.10 (2H, AB q, J = 18 Hz, C_4-H_2), 6.08 (1H, s, C_8-H), 6.76 (1H, s, C_{4a}-αOH), 8.16 (1H, br, C_{11}-N—H), 8.56 ppm (1H, s, C_7-OH); ms: *m/e* 317 (M^+, base peak), 302, 289, 275, 260, 230, 219, 178. *Anal.* calcd. for $C_{16}H_{15}O_6N$: C 60.57, H 4.77, N 4.41; found: C 60.25, H 4.71, N 4.12. High resolution molecular weight determination: calcd.: 317.090; found: 317.088; cd: λ_{max} (Δε) 300 (+4.54), 268 (+10.26), 239 (−3.50), 218 (−6.01).

*Fraction III. 8-Acetyl-4-carboxy-9-hydroxy-3,10,12-trimethyl-5-oxo-2H-5,6-dihydro[1,2]oxazocino[7,8,9,10-b,c,d]dibenzofuran (**6**)*

Fluffy pale yellow needles from methanol (1.190 g, 3.314 mmol; 28%), mp 210–212°C; $[\alpha]_D^{26}$ (CH_3OH) 0° (*c* 0.1235); uv: λ_{max} (log ε) 356 (3.07), 287 (3.83), 237 (3.84); ir (Nujol): ν_{max} 3500–2400 (OH, NH), 1685 (C=O, carboxylic acid dimer), 1640 (C=O, chelated aromatic acetyl), 1620 (C=O, enone system), 1590 (C=C); ^{1}Hmr ($CDCl_3$–DMSO-d_6): δ 2.11 (3H, s, C_{10}-CH_3), 2.33 (3H, s, C_{12}-CH_3), 2.46 (3H, s, C_3-CH_3), 2.73 (3H, s, C_8-$COCH_3$), 4.28 (2H, s, C_6-H_2), 6.36 (2H, br, C_4-COOH and C_3-NH), 13.71 ppm (1H, s, C_9-OH); ms: *m/e* 359 (M^+), 317 233, 215, 84, 44 (base peak), 43. *Anal.* calcd. for $C_{18}H_{17}O_7N \cdot \frac{1}{4}H_2O$: C 59.43, H 4.85, N 3.85; found: C 59.56, H 4.72, N 3.69. High resolution molecular weight determination calcd.: for $C_{18}H_{17}O_7N$: 359.100; found: 359.098.

*Dehydration of (+)-α-Hydroxydesacetyl-2H-[1,2]oxazocinoisousnic Acid (**5**)*

A solution of (+)-α-hydroxydesacetyl-2*H*-[1,2]oxazocinoisousnic acid (**5**) (970 mg, 3.059 mmol) in 0.5% concentrated sulfuric acid in acetic anhydride (10 ml) was heated at 55°C (oil bath temperature) under a nitrogen atmosphere for 1 h. The reaction mixture was poured onto crushed ice (20 g), extracted with ethyl acetate (3 × 10 ml), and the combined extracts were washed with water, dried over anhydrous sodium sulfate, and evaporated under reduced pressure to produce a colorless foam (1.174 g), which upon purification by preparative chromatography afforded the following components.

Fraction I. (+)-N-Acetyldesacetyl-2H-[1,2]oxazocinoisousnic Acid Acetate (7) (N-Acetyl-8-acetoxy-3a,4,10b,11-tetrahydro-3,7,10bα-trimethyl-4,11-dioxo-4,5-dihydro[1,2]-oxazocino[4,5,6,7,8-a,m,l,k]dibenzofuran)

Colorless prisms from ethyl alcohol (934.3 mg, 2.439 mmol; 78%), mp 154–155°C; $[\alpha]_D^{26}$ (CH_3CN) +205° (*c* 0.20); uv: λ_{max} (log ε) 300 (3.40), 243 (3.75), 216 (4.20); ir (Nujol): ν_{max} 1760 (C=O, acetate), 1675 (C=O, enone system), 1660 (C=O, tertiary unsaturated amide), 1620, 1610 (C=O); ^{1}Hmr: δ 1.83 (3H, s, C_{9b}-CH_3), 2.16 (3H, s, C_6-CH_3), 2.32 (3H, s, C_7-$OCOCH_3$), 2.50 (3H, s, C_{11}-

N—$COCH_3$), 2.54 (3H, s, C_{11}-CH_3), 6.02 (1H, s, C_4-H), 6.76 ppm (1H, s, C_8-H); ms: *m/e* 383 (M^+), 341, 299, 284 (base peak), 260, 256, 218, 190, 44, 43. *Anal.* calcd. for $C_{20}H_{17}O_7N$: C 62.66, H 4.47, N 3.65; found: C 62.46, H 4.60, N 3.61. High resolution molecular weight determination calcd.: 383.100; found: 383.098; cd: λ_{max} ($\Delta\varepsilon$) 328 (+17.02), 265 (−7.10), 225 (−16.41).

*Fraction II. (+)-N-Acetyl[1,2]oxazocinoisousnic Acid Acetate (**8**) (N-Acetyl-8-acetoxy-9-acetyl-3a,4,10b,11-tetrahydro-3,7,10bα-trimethyl-4,11-dioxo-4,5-dihydro[1,2]-oxazocino[4,5,6,7,8-a,m,l,k]dibenzofuran)*

Colorless foam that could not be induced to crystallize (83.2 mg, 0.195 mmol; 6%); $[\alpha]_D^{26}$ (CH_3CN) +235° (*c* 0.051); uv: λ_{max} (log ε) 385 (3.18), 310 (3.79), 277 (3.68), 241 (4.13), 227 (4.20); ir: ν_{max} 1775 (C=O, acetate), 1690 (C=O, aromatic acetyl), 1670 (C=O, enone system), 1660 (C=O, tertiary amide), 1610, 1600 (C=C); ^{1}Hmr: δ 1.85 (3H, s, C_{9b}-CH_3), 2.16 (3H, s, C_6-CH_3), 2.33 (3H, s, C_7-$OCOCH_3$), 2.45 (3H, s, C_8-$COCH_3$), 2.50 (3H, s, C_{11}-N—$COCH_3$), 2.55 (3H, s, C_{11}-CH_3), 5.90 ppm (1H, s, C_4-H); ms: *m/e* 425 (M^+), 383, 341, 326 (base peak), 308, 298, 284, 259, 217. *Anal.* calcd. for $C_{22}H_{19}O_8N \cdot H_2O$: C 59.59, H 4.77, N 3.16; found: C 60.00, H 4.39, N 3.00. High resolution molecular weight determination calcd. for $C_{22}H_{19}O_8N$: 425.111; found: 425.103.

*Fraction III. (+)-N-Acetyl-α-acetoxydesacetyl[1,2]-oxazocinoisousnic Acid Acetate (**9**) (N-Acetyl-5aα,8-diacetoxy-3a,4,5,5a,10b,11-hexahydro-3,7,10bα-trimethyl-4,11-dioxo-4,5-dihydro[1,2]oxazocino[4,5,6,7,8-a,m,l,k]-dibenzofuran)*

Colorless prismatic needles from methanol (67 mg, 0.151 mmol; 4.9%, mp 182–183°C; $[\alpha]_D^{26}$ (CH_3CN) +112° (*c* 0.08); uv: λ_{max} (log ε) 280 (3.42), 238 (4.02), 223 (4.28); ir: ν_{max} 1761 (C=O, acetates), 1695 (C=O, enone system), 1630 (C=C); ^{1}Hmr: 1.90 (3H, s, C_{9b}-CH_3), 1.95 (3H, s, C_6-CH_3), 2.04 (3H, s, C_{4a}-α$OCOCH_3$), 2.24 (3H, s, C_7-$OCOCH_3$), 2.38 (3H, s, C_{11}-N—$COCH_3$), 2.41 (3H, s, C_{11}-CH_3), 3.65 (2H, AB q, J = 18 Hz, C_4-H_2), 6.70 ppm (1H, s, C_8-H); ms: *m/e* 443 (M^+), 401, 359, 317 (base peak), 299, 284, 43. *Anal.* calcd. for $C_{22}H_{21}O_9N$: C 59.59, H 4.77, N 3.16; found: C 59.75, H 4.64, N 2.99. High resolution molecular weight determination calcd.: 443.129; found: 443.129.

*Base Hydrolysis of (+)-N-Acetyl-[1,2]oxazocinoisousnic Acid Acetate (7). Formation of (+)-2H-[1,2]Oxazocino-isousnic acid (**10**) (9-Acetyl-8-hydroxy-3a,4,10b,11-tetrahydro-3,7,10bα-trimethyl-4,11-dioxo-2H-4,5-dihydro[1,2]-oxazocino[4,5,6,7,8-a,m,l,k]dibenzofuran)*

A solution of (+)-*N*-acetyl-[1,2]oxazocinoisousnic acid acetate (**7**) (50 mg, 0.118 mmol) in tetrahydrofuran (2 ml) was treated with freshly prepared 0.8% aqueous sodium hydroxide (10 ml) and stirred at room temperature under a nitrogen atmosphere for 40 min. The cold reaction was acidified with 1 *N* hydrochloric acid, extracted with ethyl acetate (2 × 15 ml), and the combined extracts washed with water, dried over anhydrous sodium sulfate, and evaporated under reduced pressure to afford a colorless glass (42.2 mg). Purification by preparative chromatography (silica gel – oxalic acid, solvent system *A*) produced colorless crystals from ethyl acetate of (+)-2*H*-[1,2]oxazocinoisousnic acid (**10**) (6.7 mg, 0.0196 mmol; 17%), mp 170–172°C; mixture mp with (+)-2*H*-[1,2]oxazocinousnic acid (**3**), 125–157°C; $[\alpha]_D^{26}$ (CH_3CN) +357° (*c* 0.014); uv: λ_{max} (log ε) 325 (3.50), 281 (4.24), 233 (4.43); ir (Nujol): ν_{max} 3200–2900 (OH, chelated), 1655 (C=O, diketoenamine system), 1625 (C=O, chelated aromatic acetyl grouping; C=C, enol ether, aromatic ring); ^{1}Hmr δ 1.82 (3H, s, C_{9b}-CH_3), 2.15 (3H, s, C_6-CH_3), 2.58 (3H, s, C_{11}-CH_3), 2.75 (3H, s, C_8-$COCH_3$), 6.01 (1H, s, C_4-H), 7.45 (1H, br, C_{11}-N—H), 13.63 ppm (1H, s, C_7-OH); ms: *m/e* 341 (M^+), 326 (M − 15, base peak), 308, 298, 280, 260, 232, 217. *Anal.* calcd. for $C_{18}H_{15}O_6N$: C 63.34, H 4.43, N 4.10; found: C 63.37, H 4.39, N 3.90. High resolution molecular weight determination: calcd.: 341.090; found: 341.088.

*Reductive Ring Opening and Base Hydrolysis of (+)-N-Acetyldesacetyl-[1,2]oxazocinoisousnic Acid Acetate (7). Preparation of (+)-8-Desacetylisousnic acid (**11**)*

A solution of (+)-*N*-acetyl-[1,2]oxazocinoisousnic acid acetate (**7**) (325 mg, 0.848 mmol) in absolute ethyl alcohol (50 ml) was hydrogenated over platinum oxide (50 mg) at room temperature and atmospheric pressure. After the absorption of 1 mol equiv. of hydrogen (20.7 ml at 25°C) the reaction mixture was filtered through Celite to eliminate the catalyst and the solvent evaporated under reduced pressure. The residue was dissolved in tetrahydrofuran (2 ml), treated with freshly prepared 1 *N* sodium hydroxide (20 ml), and stirred at room temperature under a nitrogen atmosphere for 1 h. The resulting deep green solution was cooled in an ice bath, acidified with 1 *N* hydrochloric acid, and extracted with ethyl acetate (3 × 20 ml). The combined extracts were washed with water, dried over anhydrous sodium sulfate, and evaporated under reduced pressure to produce a yellow foam (245.8 mg), which upon purification by column chromatography on Macherey-Nagel silica gel (20 g) afforded pure (+)-8-desacetylisousnic acid (**11**) (205 mg, 0.678 mmol; 80%), bright yellow small needles from chloroform – petroleum ether (30–60°C), mp 208–209°C (melts partially at 181–183°C and resolidifies as long prismatic needles); mixture mp with authentic (+)-8-desacetylisousnic acid, 208–210°C. All other spectroscopic and chromatographic properties confirmed the identity of the two samples.

Acknowledgements

Financial aid from the National Research Council of Canada is gratefully acknowledged. One of us (I.H.S.) wishes to thank NRCC for a scholarship during the period of this study. We would also like to acknowledge the efforts of Ms. I. B. Krizsan in preparing the illustrations.

1. J. P. KUTNEY and I. H. SANCHEZ. Can. J. Chem. **54**, 2795 (1976).
2. J. P. KUTNEY, I. H. SANCHEZ, and T. YEE. Can. J. Chem. **54**, 3713 (1976).
3. J. P. KUTNEY, I. H. SANCHEZ, and T. YEE. Can. J. Chem. **54**, 3721 (1976).
4. Y. ASAHINA and S. SHIBATA. Chemistry of lichen substances. Japan Society for the Promotion of Science, Tokyo, Japan. 1954. p. 171.
5. C. F. CULBERSON. Chemical and botanical guide to lichen products. The University of North Carolina Press, Chapel Hill, NC. 1969. p. 171.
6. C. F. CULBERSON. The Bryologist, **73**, 201 (1970).
7. A. M. PATTERSON, L. T. CAPELL, and D. F. WALKER. The ring index. 2nd ed. American Chemical Society, Washington, DC. 1960. p. 388.

Studies in the usnic acid series. V.[1] The base catalyzed usnic acid – isousnic acid rearrangement. Part III. (−)-Usnic acid isomethoxide monoacetate

JAMES P. KUTNEY AND IGNACIO H. SANCHEZ

Department of Chemistry, University of British Columbia, 2075 Wesbrook Place, Vancouver, B.C., Canada V6T 1W5

Received September 30, 1976

JAMES P. KUTNEY and IGNACIO H. SANCHEZ. Can. J. Chem. **55**, 1079 (1977).

Further studies on the base catalyzed usnic acid – isousnic acid rearrangement process clarify the situation concerning (−)-usnic acid isomethoxide monoacetate (**7**). This substance is now shown to be a mixture of the two possible C_{4a} epimers. These and previous data allow a mechanism to be proposed for this interesting rearrangement.

JAMES P. KUTNEY et IGNACIO H. SANCHEZ. Can. J. Chem. **55**, 1079 (1977).

De nouvelles études sur les réarrangements, catalysés par les bases, de l'acide usnique en acide isousnique clarifient la situation concernant le monoacétate de l'isométhylate d'acide (−) usnique. On démontre maintenant que cette substance est un mélange des deux épimères possibles en C_{4a}. Ces données et d'autres publiées antérieurement permettent de proposer un mécanisme pour ce réarrangement intéressant.

[Traduit par le journal]

During the course of our synthetic studies in the usnic acid area (1, 9), we have recognized a novel base catalyzed rearrangement which allows an attractive synthetic pathway from the 'normal', or usnic acid series to the 'iso' or isousnic family of compounds. These studies could then be applied to our initial objective, an efficient synthesis of the naturally occurring lichen substance (+)-isousnic acid (**1**) (2, 3). The present work provides a further understanding of this rearrangement and, in particular, illustrates the effect of substitution at the C_{4a} position on the outcome of this base-catalyzed transformation.

Bearing in mind that the ring C β-triketone system characteristic of usnic acid requires protection against alkaline treatment, an ideally suited starting material for the present study is the isoxazole **2** (4). When this material was treated with 20% methanolic potassium hydroxide at 50°C, a mixture of the epimeric C_{4a}-β- and α-methoxy derivatives **3** and **4** was isolated in approximately 60% yield (relative ratio of **3**:**4** is 1:4). Table 1 shows a comparison of the ^{1}Hmr spectra of both compounds.

However, due to the relatively low yield obtained (4) in the preparation of the isoxazole **2**, it was decided to investigate other synthetic routes leading to C_{4a}-methoxy epimers such as **3** and **4**. In 1953, Takahashi (5) was able to prepare (−)-usnic acid isomethoxide monoacetate (**6**) by an acid-catalyzed methanol addition onto the C_4—C_{4a} double bond of (+)-usnic acid diacetate (**5**) (6) and further converted it into *N*-phenylpyrazole derivatives already possessing the desired substitution. Although the same workers (7) proposed that the splitting observed in the ^{1}Hmr spectrum of **6** was due to the exis-

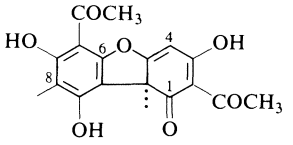

1

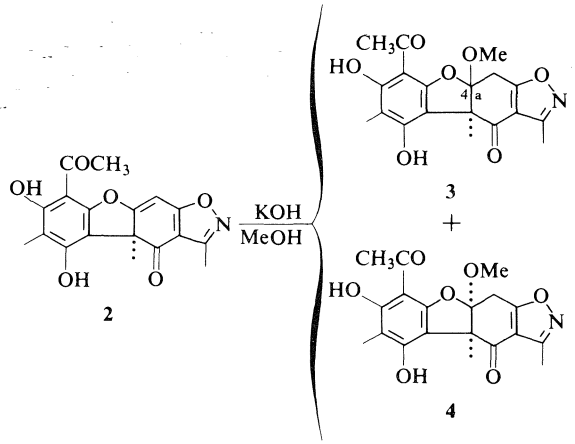

2 **3** **4**

[1]For part IV, see ref. 9.

TABLE 1. Proton magnetic resonance spectra of (+)-β-methoxyisoxazolo[4,5-*b*]usnic acid (**3**) and (+)-α-methoxyisoxazolo[4,5-*b*]usnic acid (**4**)

	δ (ppm)	
Functionality	**3**	**4**
C_{9b}-CH_3	1.75	1.75
C_8-CH_3	2.06	2.06
C_{11}-CH_3	2.46	2.45
C_6-$COCH_3$	2.60	2.63
C_4-H_2	3.66 (J = 18 Hz)	3.18 (J = 18 Hz)
C_{4a}-αOCH_3	—	3.50
C_{4a}-βOCH_3	3.55	—
C_9-OH	8.61	6.61
C_7-OH	13.33	13.45

tence in solution of ring C keto-enol tautomers, we have now demonstrated that it is indeed caused by epimeric substitution at the C_{4a}-position. In fact, when its ^{1}Hmr spectrum (Table 2) is analyzed according to our present results, a 2:3 epimeric ratio results with the α-methoxy derivative (*i.e. cis*-B/C ring junction) being predominant.

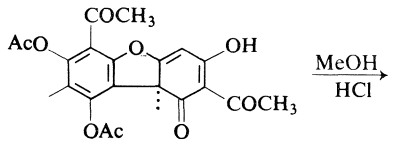

5

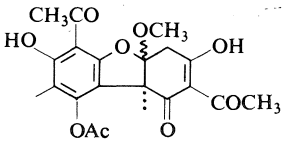

6

By means of the following transformations such an epimeric ratio was then shown to remain constant and to be due exclusively to the configuration about the C_{4a}-position. The methoxy monoacetate **6**, whose preparation was greatly improved by carefully controlling the amount of acid present during the reaction, was first treated with hydroxylamine hydrochloride in dry pyridine followed by thermal cyclization of the oxime intermediate in methanolic solution to produce, in 98% yield, an isoxazole generally represented by structure **7**, mp 190–191°C. This material showed infrared absorptions at 1780 (phenolic acetate), 1700 (C_1-carbonyl group),

TABLE 2. Proton magnetic resonance spectrum of (−)-usnic acid isomethoxide monoacetate (**6**)

	δ (ppm)	
Functionality	α-OCH_3	β-OCH_3
C_{9b}-CH_3	1.68	1.79
C_8-CH_3	1.91	1.94
C_9-$OCOCH_3$	2.36	2.40
C_2-$COCH_3$	2.44	2.58
C_6-$COCH_3$	2.64	2.64
C_4-H_2	3.16 (J = 16 Hz)	3.09 (J = 16 Hz)
C_{4a}-OCH_3	3.47	3.42
C_7-OH	13.22	13.25
C_3-OH	17.64	18.25

and 1640 cm^{-1} (chelated aromatic methyl ketone) while its ^{1}Hmr spectrum, unexpectedly, consisted of only one set of signals with the C_{4a}-methoxyl appearing at δ 3.50 and the C_4-methylene group protons as an AB quartet centered at δ 3.63 ppm (J = 18 Hz). Moreover, upon alkaline hydrolysis it produced a mixture which after purification provided the pure C_{4a}-β- and α-methoxyisoxazoles **3** and **4**, identical by all standard comparison techniques with the materials isolated directly from isoxazole **2** (*vide supra*). It was now clear that **7** in spite of its sharp melting point and spectroscopic characteristics was a mixture of the two possible C_{4a} epimers.

Surprisingly, strong alkaline treatment (KOH, 65°C) of **7** produced not only the expected aromatic deacylation but substitution of the angular methoxyl groups by hydroxyl with concomitant rearrangement. The reaction product, compound **8**, isolated in 86% yield, was shown to be identical with the C_{4a}-α-hydroxylated 'iso' series derivative previously isolated from the direct base treatment of isoxazole **2** (1). Conclusive evidence for the proposed rearrangement was obtained by dehydration (0.5% concentrated sulfuric acid in acetic anhydride) to the known (1) desacetyl diacetate **9**.

It is pertinent to note that alkaline cleavage of the present series does not lead to the formation of carboxylic acids via attack at the non-enolizable C_1 carbonyl group (1 ,9) indicating the competitive and mutually excluding nature of the rearrangement and normal cleavage processes. Thus based on all the information obtained thus far, it is possible to postulate a mechanism for the base-catalyzed usnic acid –

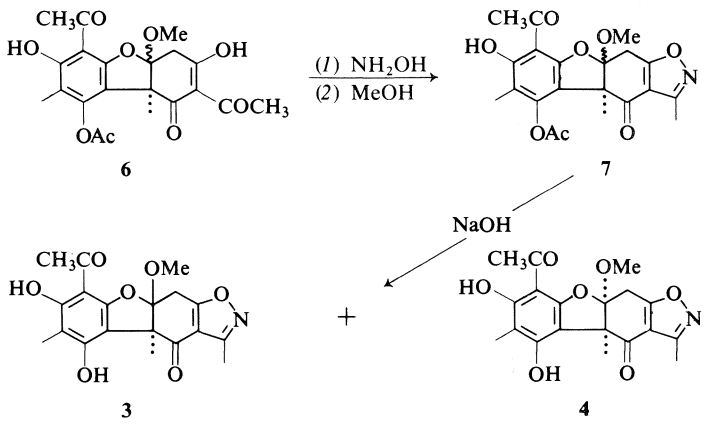

Relative ratio: 40:60

isousnic acid rearrangement, as exemplified for the isoxazole **2**.

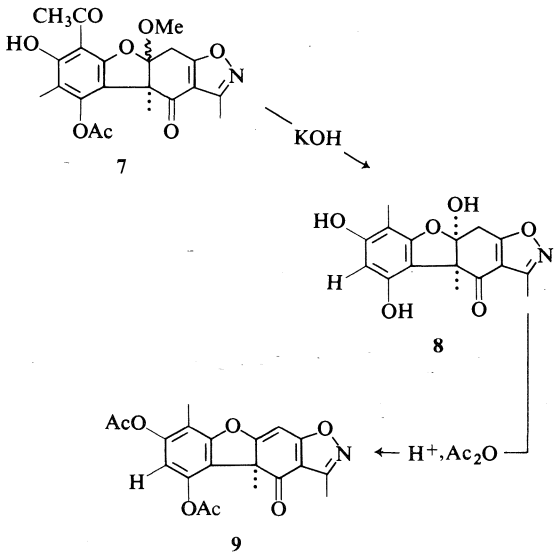

Experimental

All details concerning spectral measurements, chromatographic separations, etc., are provided in the accompanying publication (9). The numbering system employed is that approved for the dibenzofuran series (8).

Methanolic Base Treatment of (+)-Isoxazolo[4,5-b]usnic Acid (2)

A suspension of (+)-isoxazolo[4,5-*b*]usnic acid (**2**) (100 mg, 0.293 mmol) in a solution of potassium hydroxide (1 g) in dry methanol (5 ml) was heated at 50°C (oil bath temperature) under a nitrogen atmosphere for 0.5 h. The reaction mixture was diluted with cold water (30 ml), acidified with 1 *N* hydrochloric acid, and extracted with ethyl acetate (3 × 10 ml). The combined extracts were washed with water, dried over anhydrous sodium sulfate, and evaporated under reduced pressure to afford a brown glass (102.8 mg) which upon purification by preparative layer chromatography (silica gel – oxalic acid plates, solvent *A*) produced the following pure products.

Fraction I. (+)-β-Methoxyisoxazolo[4,5-b]usnic Acid (3) (10-Acetyl-7,9-dihydroxy-1aβ-methoxy-1a,2,6,6a-tetrahydro-5,6aα,8-trimethyl-6-oxoisoxazolo[4,5-b]-dibenzofuran)

Colorless prisms from chloroform – petroleum ether (30–60°C) (12.5 mg, 0.033 mmol; 11%), mp 152–154°C; $[\alpha]_D^{26}$ (CH_3CN) +120° (*c* 0.0415); uv: λ_{max} (log ε) 333 (3.26), 283 (3.86), 228 (3.93); ir: ν_{max} 3500–3200 (OH, chelated), 1660 (C=O, enone system), 1620 (C=O, chelated aromatic acetyl; C=C); ^{1}Hmr: δ 1.75 (3H, s, C_{9b}-CH_3), 2.06 (3H, s, C_8-CH_3), 2.46 (3H, s, C_{11}-CH_3), 2.60 (3H, s, C_6-$COCH_3$), 3.55 (3H, s, C_{4a}-βOCH_3), 3.66 (2H, AB q, J = 18 Hz, C_4-H_2), 8.61 (1H, s, C_9-OH), 13.33 ppm (1H, s, C_7-OH); ms: *m/e* 373 (M^+, base peak), 313, 298, 285, 273, 263, 250, 235, 233, 232, 217, 161. *Anal.* Calcd. for $C_{19}H_{19}O_7N$: C 61.12, H 5.12, N 3.75. Found: C 61.25, H 5.20, N 3.71. High resolution molecular weight determination calcd.: 373.116; found: 373.117.

Fraction II. (+)-α-Methoxyisoxazolo[4,5-b]usnic Acid (4) (10-Acetyl-7,9-dihydroxy-1aα-methoxy-1a,2,6,6a-tetrahydro-5,6aα,8-trimethyl-6-oxoisoxazolo[4,5-b]dibenzofuran)

Colorless prisms from chloroform – petroleum ether (30–60°C) (51.7 mg, 0.138 mmol; 47%), mp 222–224°C; $[\alpha]_D^{26}$ (CH_3CN) +188° (*c* 0.03175); uv: λ_{max} (log ε) 328 (3.33), 283 (3.64), 228 (3.74); ir: ν_{max} 3640, 3500–3200 (OH), 1690 (C=O, enone system), 1620 (C=O chelated aromatic acetyl; C=C); ^{1}Hmr: δ 1.75 (3H, s, C_{9b}-CH_3), 2.06 (3H, s, C_8-CH_3), 2.45 (3H, s, C_{11}-CH_3), 2.63 (3H, s, C_6-$COCH_3$), 3.18 (2H, AB q, J = 18 Hz, C_4-H_2), 3.50 (3H, s, C_{4a}-αOCH_3), 6.61 (1H, b, C_9-OH), 13.45 ppm (1H, s, C_7-OH); ms: *m/e* 373 (M^+, base peak), 358, 140, 43. *Anal.* calcd. for $C_{19}H_{19}O_7N$: C 61.12, H 5.12, N 3.75; found: C 61.17, H 5.09, N 3.81. High resolution molecular weight determination calcd.: 373.116; found: 373.112. Relative ratio α-OCH_3:β-OCH_3 (4:1).

Preparation of (+)-Usnic Acid Diacetate (5) (7,9-Diacetoxy-2,6-diacetyl-1,9b-dihydro-8,9bα-dimethyl-3-hydroxy-1-oxodibenzofuran)

A solution of (+)-usnic acid (5.0 g, 14.534 mmol) in a

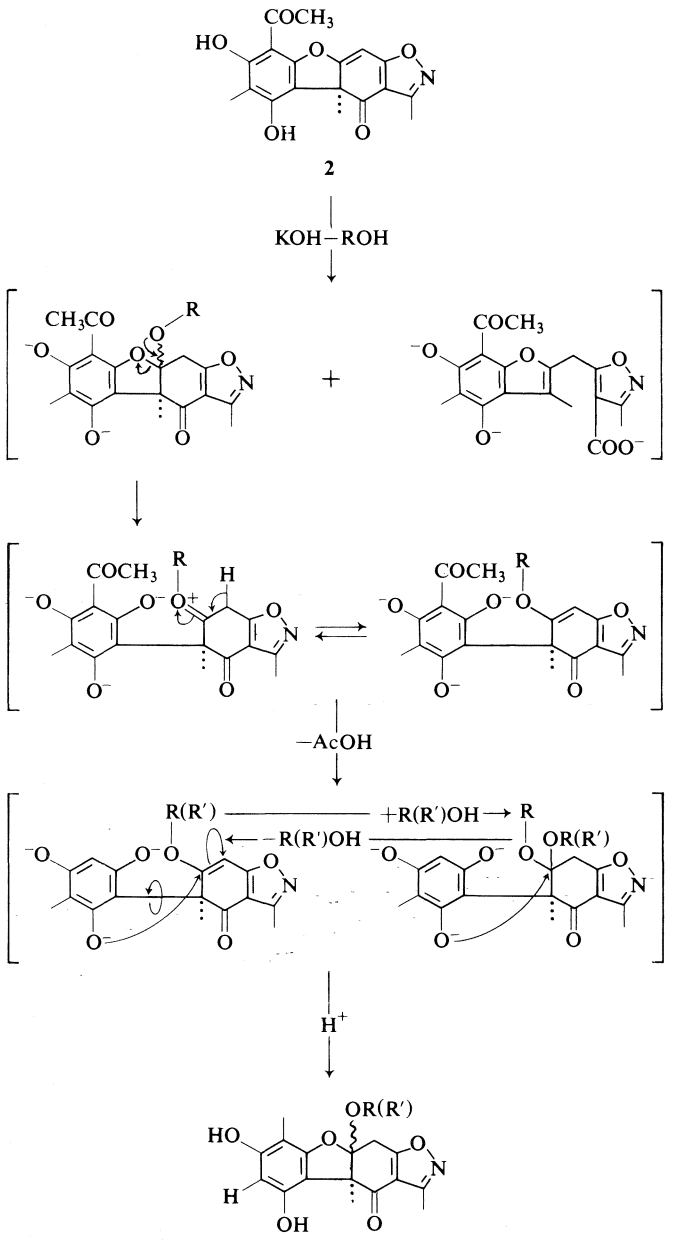

FIG. 1. Proposed mechanism for the base cleavage of (+)-isoxazolo[4,5-*b*]usnic acid (**2**).

mixture of 0.5% concentrated sulfuric acid in acetic anhydride (20 ml) was allowed to stand at room temperature overnight. The resulting dark red solution was poured onto crushed ice (50 g) and extracted with ethyl acetate (3 × 20 ml). The combined extracts were thoroughly washed with water, dried over anhydrous sodium sulfate, and evaporated under reduced pressure. The residue (6.32 g) was crystallized directly from ethyl alcohol–water to produce pure (+)-usnic acid diacetate (**5**) (6.10 g, 14.232 mmol; 98%), fine yellow needles, mp 202–204°C; $[\alpha]_D^{25}$ +250° (*c* 0.1095); uv: λ_{max} (log ε) 305 (3.95), 248 (4.23), 224 (4.41); ir: ν_{max} 3000–2500 (OH, chelated), 1770 (C=O, acetates), 1695 (C=O, enone system), 1660 (C=C), 1540 (C=O, chelated triketone system); ^{1}Hmr: δ 1.83 (3H, s, C_{9b}-CH_3), 2.00 (3H, s, C_8-CH_3), 2.35 (3H, s, C_9-$OCOCH_3$), 2.49 (3H, s, C_7-$OCOCH_3$), 2.56 (3H, s, C_6-$COCH_3$), 2.64 (3H, s, C_2-$COCH_3$), 5.95 (1H, s, C_4-H), 18.45 ppm (1H, s, C_3-OH); ms: *m/e* 428 (M^+), 386 (M − 42), 344, 329, 302, 275, 260, 223 (base peak), 217. *Anal.* calcd. for $C_{22}H_{20}O_9$:

C 61.67, H 4.70; found: C 61.55, H 4.73. High resolution molecular weight determination calcd.: 428.111; found: 428.110.

*Modified Preparation of (−)-Usnic Acid Isomethoxide Monoacetate (**6**) (9-Acetoxy-2,6-diacetyl-3,7-dihydroxy-8,9bα-dimethyl-4a-methoxy-9b,1,4,4a-tetrahydro-1-oxodibenzofuran)*

A suspension of (+)-usnic acid diacetate (**5**) (1.90 g, 4.439 mmol) in 10% methanolic hydrogen chloride (40 ml, prepared by reaction of acetyl chloride and anhydrous methanol) was heated to reflux under a nitrogen atmosphere for 1.5 h. The resulting deep red solution was concentrated under reduced pressure to approximately 10 ml, and after thorough cooling (ice-water bath) the sand-colored crystalline precipitate was removed by suction filtration. Two recrystallizations from methanol produced the pure (−)-usnic acid isomethoxide monoacetate (6) (1.532 g, 3.665 mmol; 82.5%), thin yellow plates, mp 167–168°C (lit. (5) mp 167–168°C); $[\alpha]_D^{25}$ (CH_3CN) −54° (*c* 0.0555) (lit. (5) $[\alpha]_D^{10}$ ($CHCl_3$) −83°); uv: λ_{max} (log ε) 346 (3.31), 267 (4.14); ir: ν_{max} 3200–2400 (OH, chelated), 1760 (C═O, acetate), 1670 (C═O, enone system), 1630 (C═O), 1620 (C═C), 1560 (C═O, chelated triketone system); ^{1}Hmr: α-OCH_3 isomer: δ 1.68 (3H, s, C_{9b}-CH_3), 1.91 (3H, s, C_8-CH_3), 2.36 (3H, s, C_9-$OCOCH_3$), 2.44 (3H, s, C_2-$COCH_3$), 2.64 (3H, s C_6-$COCH_3$), 3.16 (2H, AB q, J = 16 Hz, C_4-H_2), 3.47 (3H, s, C_{4a}-αOCH_3), 13.22 (1H, s, C_7-OH), 17.64 ppm (1H, s, C_3-OH); β-OCH_3 isomer: δ 1.79 (3H, s, C_{9b}-CH_3), 1.94 (3H, s, C_8-CH_3), 2.40 (3H, s, C_9-$OCOCH_3$), 2.58 (3H, s, C_2-$COCH_3$), 2.64 (3H, s, C_6-$COCH_3$), 3.09 (2H, AB q, J = 16 Hz, C_4-H_2), 3.42 (3H, s, C_{4a}-βOCH_3), 13.25 (1H, s, C_7-OH), 18.25 ppm (1H, s, C_3-OH); relative ratio α-OCH_3:β-OCH_3 3:2; ms: *m/e* 418 (M^+), 292 (base peak), 276, 250, 235, 234, 143, 43. *Anal.* calcd. for $C_{21}H_{22}O_9$: C 60.28, H 5.30; found: C 60.30, H 5.31. High resolution molecular weight determination calcd.: 418.126; found: 418.118.

*The reaction of (−)-Usnic Acid Isomethoxide Monoacetate (**6**) with Hydroxylamine Hydrochloride. Formation of (+)-Methoxyisoxazolo[4,5-b]usnic Acid Monoacetate (**7**) (9-Acetoxy-10-acetyl-7-hydroxy-1a-methoxy-1a,2,6,6a-tetrahydro-5,6aα,8-trimethyl-6-oxoisoxazolo[4,5-b]dibenzofuran)*

A solution of (−)-usnic acid isomethoxide monoacetate (**6**) (100 mg, 0.240 mmol) and hydroxylamine hydrochloride (25 mg, 0.360 mmol) in anhydrous pyridine (2 ml) was stirred at room temperature under a nitrogen atmosphere for 0.5 h. The reaction mixture was then diluted with cold water (10 ml), acidified with 1 *N* hydrochloric acid, and extracted with ethyl acetate (2 × 5 ml). The combined extracts were washed with water, dried over anhydrous sodium sulfate, and evaporated under reduced pressure. The residue (123 mg) was dissolved in dry methanol (5 ml) and heated to reflux under a nitrogen atmosphere for 0.75 h. Evaporation of the solvent under reduced pressure produced a pale yellow glass (111.4 mg) which upon purification by preparative chromatography (silica gel – oxalic acid plates, solvent system *A*) afforded (+)-methoxyisoxazolo[4,5-*b*]usnic acid monoacetate (**7**) (97.7 mg, 0.235 mmol; 98%), pale yellow prisms from methanol, mp 190–191°C; $[\alpha]_D^{26}$ (CH_3CN) +105° (*c* 0.05675), uv: λ_{max} (log ε) 346 (3.37), 266 (3.89); ir: ν_{max} 3400–2700 (OH, chelated), 1780 (C═O, acetate), 1700 (C═O, enone system), 1640 (C═O, chelated aromatic acetyl); ^{1}Hmr: δ 1.68 (3H, s, C_{9b}-CH_3), 2.3 (3H, s, C_8-CH_3), 2.43 (3H, s, C_{11}-CH_3), 2.61 (3H, s, C_6-$COCH_3$), 3.50 (3H, s, C_{4a}-OCH_3), 3.63 (2H, AB q, J = 18 Hz, C_4-H_2), 13.16 ppm (1H, s, C_7-OH); ms: *m/e* 415 (M^+, base peak), 373, 341, 313, 292, 285, 251, 236, 217, 43. *Anal.* calcd. for $C_{21}H_{21}O_8N$: C 60.71, H 5.09, N 3.37; found: C 60.91, H 5.11, N 3.30; High resolution molecular weight determination calcd.: 415.127; found: 415.130.

*Base Hydrolysis of (+)-Methoxyisoxazolo[4,5-b]usnic Acid Monoacetate (**7**)*

A solution of the (+)-methoxyisoxazolo compound (**7**) (95 mg, 0.229 mmol) in tetrahydrofuran (0.5 ml) was treated with freshly prepared 1 *N* sodium hydroxide (4 ml) and stirred at room temperature under a nitrogen atmosphere for 1 h. The cold reaction mixture was acidified with 1 *N* hydrochloric acid, extracted with ethyl acetate (2 × 2 ml), and the combined extracts washed with water, dried over anhydrous sodium sulfate, and evaporated under reduced pressure. Purification of the residue (85 mg) by preparative chromatography (silica gel – oxalic acid plates, solvent *A*) afforded three main components.

*Fraction I. (+)-β-Methoxyisoxazolo[4,5-b]usnic Acid (**3**)*

Colorless prisms from chloroform – petroleum ether (30–60°C) (14.0 mg, 0.037 mmol; 22.5%), mp 151–153°C; mixture mp with sample from previous experiments, 151–153°C. The other chromatographic and spectroscopic properties confirmed the identity of both products.

*Fraction II. (+)-Methoxyisoxazolo[4,5-b]usnic Acid Monoacetate (**7**)*

Pale yellow prisms from methanol–water (27.0 mg, 0.065 mmol; 28%), mp 190–192°C; mixture mp with the starting material, 190–192°C. Identity was shown as well by all other spectroscopic properties.

*Fraction III. (+)-α-Methoxyisoxazolo[4,5-b]usnic Acid (**4**)*

Colorless prisms from chloroform – petroleum ether (24.6 mg, 0.0662 mmol; 40%), mp 221–222°C; mixture mp with authentic material from a previous reaction, 220–222°C. Identical spectroscopic characteristics were shown by both samples.

*Base Cleavage of (+)-Methoxyisoxazolo[4,5-b]usnic Acid Monoacetate (**7**)*

To a suspension of (+)-methoxyisoxazolo[4,5-*b*]usnic acid monoacetate (**7**) (100 mg, 0.241 mmol) in methanol (0.5 ml) and water (1.5 ml) was added a solution of potassium hydroxide (1 g) in water (3 ml) and the resulting mixture heated at 65–67°C (oil bath temperature) under a nitrogen atmosphere for 40 min. The reaction mixture was diluted with cold distilled water (10 ml), acidified with 1 *N* hydrochloric acid, and extracted with ethyl acetate (3 × 10 ml). The combined extracts were washed with water, dried over anhydrous sodium sulfate, and evaporated under reduced pressure to produce a pale yellow glass (81 mg). Purification by preparative chromatography (silica gel – oxalic acid plates, petroleum ether – acetone (3:2)) yielded one main component.

*Fraction I. (+)-α-Hydroxydesacetylisoxazolo[4,5-b]-isousnic Acid (**8**)*

Colorless microcrystals from chloroform (65.8 mg,

0.207 mmol; 86%) mp 223–225°C; mixture mp with authentic (+)-α-Hydroxydesacetylisoxazolo[4,5-*b*]-isousnic acid from previous experiments, 222–224°C; $[\alpha]_D^{26}$ (CH_3CN) +304° (*c* 0.1295); uv: λ_{max} (log ε) 286 (2.98), 262 (3.18), 218 (3.90); ir: ν_{max} 3600–3100 (OH, chelated), 1690 (C=O, enone system), 1640, 1600 (C=C); ^{1}Hmr: ($CDCl_3$–DMSO-d_6): δ 1.93 (6H, s, C_{9b}-CH_3 and C_6-CH_3), 2.40 (3H, s, C_{11}-CH_3), 3.08 (2H, AB q, J = 18 Hz, C_4-H_2), 6.09 (1H, s, C_8-H), 6.67 (1H, br, C_{4a}-αOH), 8.28 (1H, br, C_7-OH), 8.50 ppm (1H, br, C_9-OH); ms: *m/e* 317 (M^+, base peak), 275, 260, 246, 219, 194, 178. *Anal.* calcd. for $C_{16}H_{15}O_6N$: C 60.56, H 4.77, N 4.41; found: C 60.59, H 4.75, N 4.39. High resolution molecular weight determination calcd.: 317.090; found: 317.088.

*Acid-catalyzed Dehydration of (+)-α-Hydroxydesacetylisoxazolo[4,5-b]isousnic Acid (**8**)*

A solution of the (+)-α-hydroxy derivative (**8**) (20 mg, 0.0631 mmol) in 0.5% concentrated sulfuric acid in acetic anhydride (1 ml) was heated at 55°C (oil bath temperature) under a nitrogen atmosphere for 1 h. The reaction mixture was then poured onto crushed ice (5 g), extracted with ethyl acetate (2 × 3 ml), and the combined extracts washed with water, dried over anhydrous sodium sulfate, and evaporated under reduced pressure. The residue was purified by preparative layer chromatography (silica gel plates, solvent *B*) to produce (+)-desacetylisoxazolo-[4,5-*b*]isousnic acid diacetate (**9**) (12 mg, 0.0319 mmol; 50.5%) colorless prisms from chloroform–methanol, mp 148–150°C; mixture mp with authentic (+)-desacetylisoxazolo[4,5-*b*]isousnic acid diacetate, 147–149°C; $[\alpha]_D^{26}$ (CH_3CN) +252° (*c* 0.0325); uv: λ_{max} (log ε) 297 (3.34), 246 (3.70), 216 (4.19); ir: ν_{max} 1775 (C=O, acetates), 1670 (C=O, enone system), 1620, 1600 (C=C); ^{1}Hmr: δ 1.83 (3H, s, C_{9b}-CH_3), 2.17 (3H, s, C_6-CH_3), 2.32 (3H, s, C_7-$OCOCH_3$), 2.50 (3H, s, C_9-$OCOCH_3$), 2.55 (3H, s, C_{11}-CH_3), 6.03 (1H, s, C_4-H), 6.78 ppm (1H, s, C_8-H); ms: *m/e* 383 (M^+), 341, 325, 299, 284 (base peak), 256, 220, 190, 43. High resolution molecular weight determination: Calcd. for $C_{20}H_{17}O_7N$: 383.100; found: 383.104.

Acknowledgement

Financial aid from the National Research Council of Canada is gratefully acknowledged. One of us (I.H.S.) wishes to thank NRCC for a scholarship during the period of this study. We would also like to acknowledge the efforts of Ms. I. B. Krizsan in preparing the illustrations.

1. J. P. KUTNEY, I. H. SANCHEZ, and T. YEE. Can. J. Chem. **54**, 3721 (1976).
2. C. F. CULBERSON. Chemical and botanical guide to lichen products. The University of North Carolina Press, Chapel Hill, NC. 1969. p. 171.
3. C. F. CULBERSON. The Bryologist, **73**, 201 (1970).
4. J. P. KUTNEY, I. H. SANCHEZ, and T. YEE. Can. J. Chem. **54**, 3713 (1976).
5. K. TAKAHASHI. Chem. Pharm. Bull. Jpn. **1**, 36 (1953).
6. Y. ASAHINA and S. SHIBATA. Chemistry of lichen substances. Japan Society for the Promotion of Science, Tokyo, Japan. 1954. p. 171.
7. K. TAKAHASHI, Y. HONDA, and S. MIYASHITA. Chem. Pharm. Bull. Jpn. **11**, 1229 (1963).
8. A. M. PATTERSON, L. T. CAPELL, and D. F. WALKER. The ring index. 2nd ed. American Chemical Society, Washington, DC. 1960. p. 388.
9. J. P. KUTNEY, I. H. SANCHEZ, and T. YEE. Can. J. Chem. This issue.

Studies in the usnic acid series. VI.[1] The preparation of some ether derivatives of (+)-usnic acid

JAMES P. KUTNEY AND IGNACIO H. SANCHEZ

Department of Chemistry, University of British Columbia, 2075 Wesbrook Place, Vancouver, B.C., Canada V6T 1W5

Received October 7, 1976

JAMES P. KUTNEY and IGNACIO H. SANCHEZ. Can. J. Chem. **55**, 1085 (1977).

Studies involving the selective *O*-alkylation of (+)-usnic acid (**1**) have provided high yielding methods for the preparation of mono- and diether derivatives of **1**. With appropriate selection of conditions, either 7- or 9-*O*-alkyl derivatives can be prepared.

JAMES P. KUTNEY et IGNACIO H. SANCHEZ. Can. J. Chem. **55**, 1085 (1977).

Des études impliquant une *O*-alkylation sélective de l'acide (+)-usnique (**1**) fournissent des méthodes, avec de bons rendements, permettant de préparer des dérivés mono- et diéther de **1**. Utilisant des conditions expérimentales appropriées, on peut préparer soit les dérivés 7- ou 9-*O*-alkylés.

[Traduit par le journal]

During investigations (1–5) leading to the synthesis of various biodegradation products of (+)-usnic acid (**1**),[2] it became essential to prepare a series of deacylated derivatives of the 'normal' usnic acid family. The extremely facile rearrangement of the usnic (normal) to the isousnic ('iso') series under a variety of experimental conditions prompted us to study the preparation of suitable ether derivatives which hopefully would prevent such transformations.

An examination of previous work in this area (6–8) showed that the observed products obtained in alkylation studies arise from predominant *C*-alkylation on the aromatic ring A, and Takahashi and co-workers (9–13) were able to demonstrate the generality of the reaction by preparing, under similar conditions, a variety of *C*-alkylated derivatives including (+)-methylusnic acid (**2**) and (+)-methyldihydrousnic acid (**3**). However, it was Bertilsson and Wachtmeister (14) who first prepared, in very low yield, the ether derivative, (+)-7-*O*-methylusnic acid (**4**), by prolonged treatment with excess methyl iodide and potassium carbonate in refluxing acetone. Although the same workers were unable to prepare the corresponding diether derivative, they showed (15) that reaction of **1** with ethereal diazomethane produces, instead, the tetracyclic furan derivative **5** in low yield.

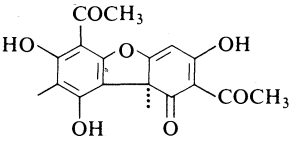

1

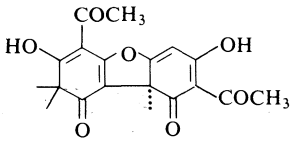

2

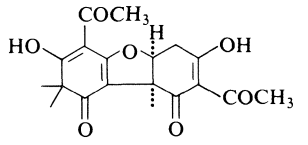

3

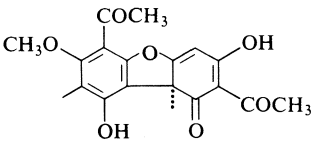

4

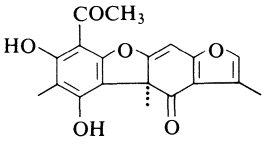

5

[1]For part V see ref. 5.

[2]J. P. Kutney, I. H. Sanchez, T. Yee, and J. D. Leman, manuscript in preparation.

TABLE 1. Proton magnetic resonance data of several ether derivatives of (+)-usnic acid (**1**)

Functionality	δ (ppm)					
	4	**6**	**7**	**8**	**9**	**10**
C_{9b}-CH_3	1.88	1.76	1.82	1.78	1.83	1.86
C_8-CH_3	2.20	2.18	2.32	2.18	2.25	2.24
C_6-$COCH_3$	2.62	2.55	2.50	2.56	2.54	2.74
C_2-$COCH_3$	2.66	2.64	2.58	2.66	2.54	2.56
C_7-OCH_3	3.80	—	—	—	—	—
C_9-OCH_3	—	—	—	—	4.06	4.14
C_7-$OCH_2C_6H_5$(*p*-Br)	—	4.86	4.94	4.86 (*p*-Br)	4.89	—
C_9-$OCH_2C_6H_5$	—	— (J = 10 Hz)	5.36	—	—	—
C_4-H	5.99	5.95	5.86	5.99	5.83	5.91
C_7-OH	10.80	—	—	—	—	13.22
C_9-OH	—	10.78	—	10.81	—	—
C_3-OH	18.80	18.80	17.99	18.82	18.15	18.00

However, in the light of the present knowledge (16–19) on the alkylation of ambident anions, we decided to investigate new high yielding methods, suitable for large scale, of preparing mono- and diether derivatives of usnic acid. Thus, compound **1** was treated with tetramethylammonium hydroxide pentahydrate (20) in dry hexamethylphosphoramide (HMPA) (21, 22) at 0° C, and the resulting phenoxide ion alkylated with benzyl bromide to produce the crystalline (+)-7-*O*-benzylusnic acid (**6**) in 75% yield. The presence of the benzyl group was readily evident from the ^{1}Hmr spectrum (singlet at δ 4.86 ppm). A minor component, isolated in 19% yield, (overall 94% yield of *O*-alkylated products), proved to be the racemic (±)-7,9-di-*O*-benzylusnic acid (**7**), yellow crystals, mp 145–146° C, which in its ^{1}Hmr spectrum showed the methylene groups of the C_7- and C_9-ethers at δ 4.94 (s) and 5.36 ppm (AB q, J = 10 Hz), respectively. This last result is in complete agreement with previous observations on the relative ease of racemization of 7,9-disubstituted usnic acid derivatives (14, 23). Moreover, the determination of the site of alkylation can be easily deduced from the characteristic chemical shift of the remaining functions in the molecule (*i.e.* aromatic acetyl, phenolic and/or enolic hydroxyls, etc.). Table 1 presents a summary of the observed chemical shifts for the various ether derivatives prepared.

The further application of our experimental procedure was evaluated by the alkylation of (+)-usnic acid (**1**) with *p*-bromobenzyl bromide. Thus, (+)-7-*O*-*p*-bromobenzylusnic acid (**8**), mp 122–123° C, was isolated in 82% yield, and there appears little doubt that under the reaction conditions developed ($(CH_3)_4\overset{+}{N}\overset{-}{O}H$, HMPA), predominant *mono-O*-alkylation at the 7-position can be easily achieved.

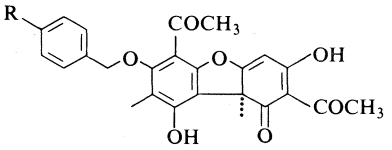

6 R = H
8 R = Br

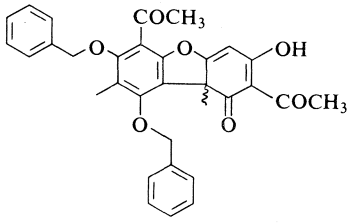

7

Although only low yields of diether derivatives have been achieved directly with the above method, we found that somewhat more vigorous conditions (*i.e.* sodium hydride in dry tetrahydrofuran at 60° C) produce good yields of di-*O*-alkylated materials. A combination of these procedures provides an excellent approach for the preparation of 'mixed' derivatives. Thus when the monobenzyl ether **6** was alkylated under the latter conditions with dimethyl sulfate, a 72% yield of (±)-7-*O*-benzyl-9-*O*-methylusnic acid (**9**) was obtained. This compound showed the methylene protons of the benzyl group at δ 4.89

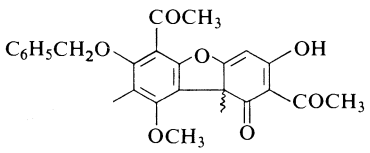

9

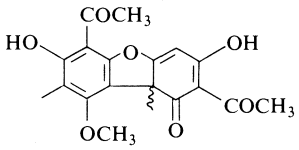

10

ppm (s) and the C_9-methoxyl as a sharp signal at δ 4.06 ppm in the ^{1}Hmr spectrum.

Moreover, pure 9-*O*-alkyl derivatives can be easily prepared from the corresponding 'mixed' diether derivative by selective debenzylation employing an excess of trifluoroacetic acid (TFA) in dichloromethane at room temperature (24, 25). In this manner, a yield of over 90% of (±)-9-*O*-methylusnic acid (**10**) was obtained.

An interesting relationship was also observed from the corresponding ultraviolet spectra, which show absorption maxima characteristic for each series regardless of the nature of the alkyl residue (Table 2).

On the other hand, *O*-alkylation of ring C protected usnic acid derivatives (*i.e.* isoxazoles) presents difficulties due to the higher base sensitivity of the isoxazole system (2–5). However, as a satisfactory complement to our previous methods, we have found that predominant *O*-alkylation of isoxazole derivatives can be achieved by the use of methyl iodide – silver oxide in chloroform (26, 27). In this way the isoxazole **11** was converted in 71% yield into the oily dimethyl ether **12** with complete retention of optical activity. These *O*-methyl substituents were observed as sharp singlets at δ 3.74 and 4.02 ppm, respectively, for the 7- and 9-positions. A minor product, isolated in 16% yield, resulted from di-*C*-alkylation on the aromatic ring A, and on the basis of spectroscopic evidence has been assigned structure **13**. Similar di-*C*-alkylated systems have been obtained (28, 29) by the nuclear methylation of phloroacetophenone under similar conditions. In conclusion we must indicate that the latter method is not directly applicable to (+)-usnic acid (**1**) itself. However, since all three methods seem to complement each other very adequately, the solutions to obtaining the required *O*-alkylated derivatives in the usnic acid series are now available.

TABLE 2. The ultraviolet absorption maxima for ether derivatives of (+)-usnic acid (**1**): λ_{max} (CH_3OH) and log ε in parentheses

6	8	7	9	10
346(2.99)	—	368(3.19)	370(3.03)	345(3.56)
266(4.03)	266(4.19)	325(3.56)	320(3.51)	274(4.13)
239(4.01)	229(4.36)	259(4.08)	259(4.02)	228(4.24)
		226(4.29)	226(4.23)	

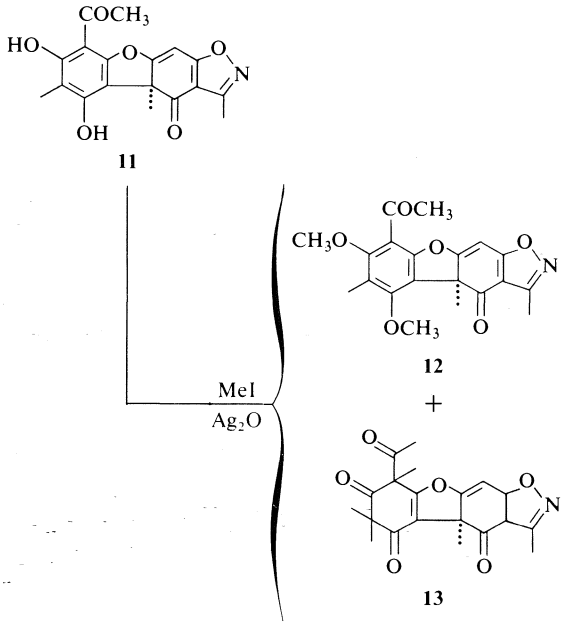

11

12

+

13

Experimental

Melting points were determined on a Kofler block and are uncorrected.

Ultraviolet (uv) spectra were recorded on a Cary 15 spectrophotometer in methanol solution (unless otherwise noted). The wavelength of the absorption maxima are reported in nanometres (nm).

Infrared (ir) spectra were measured routinely on a Perkin-Elmer model 710 spectrophotometer. Analytical or comparison spectra were recorded on a Perkin-Elmer model 457 spectrophotometer using matched cells with a cell path of 0.2 mm in chloroform solution. Calibration was achieved using the 1601 cm^{-1} absorption band of polystyrene. The absorption maxima are quoted in wave numbers (cm^{-1}).

Proton magnetic resonance (^{1}Hmr) spectra were measured in deuterochloroform ($CDCl_3$) solution (unless otherwise indicated) at room temperature. Routine spectra were recorded at 60 MHz on a Varian T-60 spectrometer, and analytical or comparison spectra at 100 MHz on either a Varian HA-100 or a Varian XL-100 spectrometer. Line positions are given in the δ (ppm) scale using

tetramethylsilane (TMS) as internal standard. The integrated peak areas, multiplicity, and proton assignments are indicated in parentheses.

Low resolution mass (ms) spectra were determined on either an AEI-MS-902 or an Atlas CH-4B mass spectrometer, with high resolution mass spectra being recorded exclusively on an AEI-MS-902 mass spectrometer.

Circular dichroism (cd) spectra were obtained on a Jasco model J-20 spectropolarimeter in methanol solution (unless otherwise indicated). The wavelength of the absorption maxima is reported in nanometres (nm). The differential molar extinction coefficient ($\Delta\varepsilon$) and the sign of the observed Cotton effect are indicated in parentheses.

Optical rotations ($[\alpha]_D$) were measured on a Perkin-Elmer model 141 polarimeter at the sodium D line in chloroform solution (unless otherwise noted) using cells with a 0.1 dm path.

Microanalyses were performed by Mr. P. Borda of the Microanalytical Laboratory, University of British Columbia.

Merck silica gel G (acc. to Stahl) impregnated with oxalic acid (2%) and with 2% fluorescent indicator added, was used as adsorbent for thin layer chromatography (tlc), unless otherwise noted. The tlc plates were activated in an oven at 90°C for 4 h before use. For qualitative chromatography layers of 0.3 mm thickness were used and the spots were visualized by viewing under ultraviolet (uv) light or spraying with a 1% ethanolic ferric chloride solution. For preparative (plc) chromatography large (20 × 20 and 20 × 60 cm) plates with a thicker layer (0.7 mm) were used. The developing systems were *A*, petroleum ether (30–60°C) – acetone (4:1), and *B*, chloroform – ethyl acetate (3:2), unless otherwise indicated.

Column chromatography was performed on either Mackerey-Nagel (0.2–0.5 mm grain size) or Merck 60 (0.063–0.2 mm grain size) silica gel.

The usnic acid utilized throughout the course of this study was obtained from Koch-Light Laboratories, England, as the optically active dextrorotatory isomer, (+)-usnic acid, isolated from lichen sources *Usnea barbata*).

The numbering system employed is that approved for the dibenzofuran series (30).

*Reaction of (+)-Usnic Acid (**1**) with Benzyl Bromide in Hexamethylphosphoramide (HMPA)*

A suspension of (+)-usnic acid (**1**) (2.0 g, 5.813 mmol) and tetramethylammonium hydroxide pentahydrate (3.46 g, 19.116 mmol) in dry hexamethylphosphoramide (60 ml, freshly distilled from lithium aluminum hydride) was stirred at 0°C under a nitrogen atmosphere for 1 h. The dark green solution was then treated with benzyl bromide (3.14 g, 18.362 mmol) and stirring continued at 0°C for 2 h. The resulting suspension was carefully poured into cold distilled water (200 ml) and extracted once with light petroleum ether (50 ml) to eliminate the excess alkylating agent. The aqueous phase was acidified with 1 *N* hydrochloric acid, extracted with ethyl acetate (4 × 100 ml), and the combined extracts were washed thoroughly with water (5 × 50 ml), dried over anhydrous sodium sulfate, and evaporated under reduced pressure to produce a yellow foam (2.748 g). Purification by column chromatography on Macherey-Nagel silica gel (200 g) afforded the following products.

*Fraction I. Recovered (+)-Usnic Acid (**1**)*

Yellow needles from chloroform (218.4 mg, 0.634 mmol; 10%), mp 202–203°C; mixture mp with (+)-usnic acid, 202–204°C. The sample showed superimposable ^{1}Hmr, ir, and uv spectra with those of the starting material.

*Fraction II. (+)-7-O-Benzylusnic Acid (**6**) (7-Benzyloxy-2,6-diacetyl-1,9b-dihydro-3,9-dihydroxy-8,9bα-dimethyl-1-oxodibenzofuran)*

Yellow prisms from acetone–methanol (1.6815 g, 3.874 mmol; 74%), mp 131–133°C; $[\alpha]_D^{26}$ (CH_3CN) +208° (*c* 0.0767); uv: λ_{max} (log ε) 346 (2.99), 266 (4.03), 239 (4.01); ir: ν_{max} 3400–2500 (OH, chelated), 1672 (C=O, aromatic acetyl, enone system), 1600 (C=C), 1540 (C=O, chelated triketone system); ^{1}Hmr: δ 1.76 (3H, s, C_{9b}-CH_3), 2.18 (3H, s, C_8-CH_3), 2.55 (3H, s, C_6-$COCH_3$), 2.64 (3H, s, C_2-$COCH_3$), 4.86 (2H, s, C_7-O—CH_2—C_6H_5), 5.95 (1H, s, C_4-H), 7.41 (5H, s, C_6H_5), 10.78 (1H, s, C_9-OH), 18.80 ppm (1H, s, C_3-OH); ms: *m/e* 434 (M^+), 416, 392, 343, 323, 308, 301, 281, 273, 260, 259, 241, 233, 215, 203, 90 (base peak). *Anal.* calcd. for $C_{25}H_{22}O_7$: C 69.12, H 5.10; found: C 69.08, H 5.06. High resolution molecular weight determination calcd.: 434.136; found: 434.132.

*Fraction III. (±)-7,9-Di-O-benzylusnic Acid (**7**) (2,6-Diacetyl-7,9-dibenzyloxy-1,9b-dihydro-8,9b-dimethyl-3-hydroxy-1-oxodibenzofuran)*

Yellow prisms from acetone – ethyl alcohol (0.505 g, 0.964 mmol; 18%), mp 145–146°C; $[\alpha]_D^{26}$ (CH_3CN) 0° (*c* 0.0272); uv: λ_{max} (log ε) 368 (3.19), 325 (3.56), 259 (4.08), 226 (4.29); ir: ν_{max} 2800–2400 (OH, chelated), 1680 (C=O, aromatic acetyl, enone system), 1610, 1590 (C=C, aromatic rings), 1560 (C=O, chelated triketone system); ^{1}Hmr: δ 1.82 (3H, s, C_{9b}-CH_3), 2.27 (3H, s, C_8-CH_3), 2.50 (3H, s, C_6-$COCH_3$), 2.58 (3H, s, C_2-$COCH_3$), 4.94 (2H, s, C_7-O—CH_2—C_6H_5), 5.36 (2H, AB q, J = 10 Hz, C_9-O—CH_2—C_6H_5), 5.86 (1H, s, C_4-H), 7.20–7.60 (10H, br, 2 × C_6H_5), 17.99 ppm (1H, s, C_3-OH); ms: *m/e* 524 (M^+), 480, 433 (base peak), 432, 390, 350, 343, 341, 323, 307, 259, 233, 231, 181, 90. *Anal.* calcd. for $C_{32}H_{28}O_7$: C 73.27, H 5.38; found: C 73.06, H 5.52, High resolution molecular weight determination calcd.: 524.183; found: 524.183.

*Preparation of (+)-7-O-p-Bromobenzylusnic Acid (**8**) (7-p-Bromobenzyloxy-2,6-diacetyl-1,9b-dihydro-3,9-dihydroxy-8,9bα-dimethyl-1-oxodibenzofuran)*

A suspension of (+)-usnic acid (**1**) (200 mg, 0.582 mmol) and tetramethylammonium hydroxide pentahydrate (346 mg, 1.911 mmol) in dry hexamethylphosphoramide (10 ml) was stirred at room temperature under a nitrogen atmosphere for 0.5 h. To the resulting dark green suspension was added crystalline *p*-bromobenzyl bromide (160 mg, 0.640 mmol) and the reaction allowed to proceed at room temperature under nitrogen for 2 h. The reaction mixture was diluted with cold distilled water (40 ml), acidified with 1 *N* hydrochloric acid, and extracted with ethyl acetate (3 × 20 ml). The combined extracts were washed with water, dried over anhydrous sodium sulfate, and evaporated under reduced pressure. The resulting dark yellow residue (314 mg) was purified by column chromatography on Macherey-Nagel silica gel (30 g) to afford pure (+)-7-*O*-*p*-bromobenzylusnic acid (**8**) (245 mg, 0.476 mmol; 81%), pale yellow-green

plates from ethyl alcohol, mp 122–123°C; $[\alpha]_D^{26}$ (CH_3CN) +245° (*c* 0.061); uv: λ_{max} (log ε) 266 (4.19), 229 (4.36); ir: ν_{max} 3400–2500 (OH, chelated), 1670 (C═O, aromatic acetyl, enone system), 1620, 1600 (C═C), 1530 (C═O, chelated triketone system); ^{1}Hmr: δ 1.78 (3H, s, C_{9b}-CH_3), 2.18 (3H, s, C_8-CH_3), 2.56 (3H, s, C_6-$COCH_3$), 2.66 (3H, s, C_2-$COCH_3$), 4.86 (2H, s, C_7-O—CH_2—C_6H_4—Br), 5.99 (1H, s, C_4-H), 7.45 (4H, AB q, J = 8 Hz, —CH_2—C_6H_4—Br), 10.81 (1H, s, C_9-OH), 18.82 ppm (1H, s, C_3-OH); ms: *m/e* 514 (M^+), 512, 496, 494, 472, 470, 403, 401, 389, 387, 344, 343 (base peak), 301, 260, 259, 233, 231, 171, 159, 90, 43. *Anal.* calcd. for $C_{25}H_{21}O_7Br$: C 58.48, H 4.12, Br 15.56; found: C 58.42, H 4.18, Br 15.47. High resolution molecular weight determination calcd. for $C_{25}H_{21}O_7{}^{79}Br$: 512.052; calcd. for $C_{25}H_{21}O_7{}^{81}Br$: 514.045; found: 512.047, 514.045.

*Preparation of (±)-7-O-Benzyl-9-O-methylusnic acid (**9**) (7-Benzyloxy-2,6-diacetyl-1,9b-dihydro-8,9bα-dimethyl-3-hydroxy-9-methoxy-1-oxodibenzofuran)*

Sodium hydride emulsion (55%, 4.0 g, 91.666 mmol) was washed twice with distilled light petroleum ether (2 × 10 ml) and suspended in dry tetrahydrofuran (600 ml, freshly distilled from lithium aluminum hydride). Under a stream of nitrogen (±)-7-*O*-benzylusnic acid (**6**) (15.0 g, 34.562 mmol) in dry tetrahydrofuran (200 ml) was added dropwise over 45 min and the reaction mixture stirred at room temperature for 1 h. Dimethyl sulfate (8.70 g, 69.00 mmol) in dry tetrahydrofuran (20 ml) was added dropwise and the reaction mixture heated at 60–62°C under a nitrogen atmosphere for 2.75 h. The resulting dark brown solution was slowly poured into an ice–water mixture (2:1), acidified with 1 *N* hydrochloric acid, and extracted with ethyl acetate (3 × 500 ml). The combined extracts were washed with water, dried over anhydrous sodium sulfate, and evaporated under reduced pressure to produce a dark yellow foam (16.892 g), which upon purification on Merck silica gel (600 g), afforded pure (±)-7-*O*-benzyl-9-*O*-methylusnic acid (**9**) (11.22 g, 25.048 mmol; 72%), bright yellow prisms from acetone – ethyl alcohol, mp 112–113°C; $[\alpha]_D^{26}$ (CH_3CN) 0° (*c* 0.065); uv: λ_{max} (log ε) 370 (3.03), 320 (3.57), 259 (4.02), 226 (4.23); ir: ν_{max} 2500–2400 (OH, chelated), 1680 (C═O, aromatic acetyl), 1670 (C═O, enone system), 1600, 1580 (C═C), 1540 (C═O, chelated triketone system); ^{1}Hmr: δ 1.83 (3H, s, C_{9b}-CH_3), 2.25 (3H, s, C_8-CH_3), 2.54 (6H, s, C_2-$COCH_3$ and C_6-$COCH_3$), 4.06 (3H, s, C_9-OCH_3), 4.89 (2H, s, C_7-O—CH_2—C_6H_5), 5.83 (1H, s, C_4-*H*), 7.39 (5H, s, C_6H_5), 18.15 ppm (1H, s, C_3-O*H*); ms: *m/e* 448 (M^+), 406, 391, 387 (base peak), 322, 315, 295, 287, 273, 247, 231, 230, 215, 91. *Anal.* calcd. for $C_{26}H_{24}O_7$: C 69.63, H 5.39; found: C 69.87, H 5.58. High resolution molecular weight determination calcd.: 448.152, found: 448.152.

*The Debenzylation of (±)-7-O-Benzyl-9-O-methylusnic Acid (**9**). Isolation of (±)-9-O-Methylusnic Acid (**10**) (2,6-Diacetyl-1,9b-dihydro-3,7-dihydroxy-8,9bα-dimethyl-9-methoxy-1-oxodibenzofuran) — Experiment I*

A solution of (±)-7-*O*-benzyl-9-*O*-methylusnic acid (**9**) (50 mg, 0.111 mmol) in trifluoroacetic acid (0.5 ml) was stirred at room temperature under a nitrogen atmosphere for 20 min. Excess trifluoroacetic acid was evaporated under reduced pressure (water-bath temperature 40°C). The residue was redissolved in dry benzene (2 ml) and the solvent once more evaporated under reduced pressure to produce a glassy residue which was dissolved in ethyl acetate (10 ml), and the solution thoroughly washed with cold distilled water, dried over anhydrous sodium sulfate, and evaporated under reduced pressure to afford a bright yellow crystalline residue (61.7 mg). Purification by preparative layer chromatography (silica gel – oxalic acid plates, solvent *A*) yielded pure (±)-9-*O*-methylusnic acid (**10**) (37.0 mg, 0.103 mmol; 92%), thick bright yellow prisms from acetone–hexane, mp 195–196°C (dec.); $[\alpha]_D^{26}$ (CH_3CN) 0° (*c* 0.103); uv: λ_{max} (log ε) 345 (3.56), 274 (4.13), 228 (4.24); ir: ν_{max} 3200–2700 (OH, chelated), 1680 (C═O, enone system), 1625 (C═O, chelated aromatic acetyl grouping), 1590 (C═C), 1560 (C═O, chelated triketone system); ^{1}Hmr: δ 1.86 (3H, s, C_{9b}-CH_3), 2.24 (3H, s, C_8-CH_3), 2.56 (3H, s, C_2-$COCH_3$), 2.74 (3H, s, C_6-$COCH_3$), 4.14 (3H, s, C_9-OCH_3), 5.91 (1H, s, C_4-*H*), 13.22 (1H, s, C_7-O*H*), 18.00 ppm (1H, s, C_3-O*H*); ms: *m/e* 358 (M^+), 343 (M − 15), 274, 247 (base peak), 246, 229. *Anal.* calcd. for $C_{19}H_{18}O_7$: C 63.68, H 5.06; found: C 63.65, H 5.06. High resolution molecular weight determination calcd.: 358.105. found: 358.104.

*The Debenzylation of (±)-7-O-Benzyl-9-O-methylusnic Acid (**9**) — Experiment II*

A solution of (±)-7-*O*-benzyl-9-*O*-methylusnic acid (**9**) (50 mg, 0.111 mmol) in dry dichloromethane (4 ml) was treated at room temperature under a nitrogen atmosphere with trifluoroacetic acid (128 mg, 1.122 mmol) and the reaction allowed to proceed with stirring for 3 h. The reaction mixture was then transferred to a separatory funnel, diluted with dichloromethane (4 ml), washed thoroughly with water, dried over anhydrous sodium sulfate, and evaporated under reduced pressure to produce a yellow glass, which upon direct crystallization from acetone–hexane produced pure (±)-9-*O*-methylusnic acid (**10**) (38.5 mg, 0.1075 mmol; 96%), mp 195–197°C; mixture mp with authentic material from previous experiments, 195–197°C. Chromatographic and spectroscopic characteristics were identical for both samples.

*Synthesis of (+)-7,9-Di-O-methylisoxazolo[4,5-b]usnic Acid (**12**) (10-Acetyl-6,6a-dihydro-7,9-dimethoxy-5,6aα,8-trimethyl-6-oxoisoxazolo[4,5-b]dibenzofuran)*

A solution of (+)-isoxazolo[4,5-*b*]usnic acid (**11**) (3.0 g, 8.797 mmol) in dry chloroform (150 ml) was treated with silver oxide (30 g, 129.6 mmol) and iodomethane (10 g, 70.422 mmol), and with mechanical stirring heated at 54–55°C (oil bath temperature) under a nitrogen atmosphere for 20 h. The solid material (salts) was removed by filtration through Celite, and the Celite cake washed with chloroform (2 × 25 ml). The combined filtrates were evaporated under reduced pressure to produce an orange foam (3.721 g). Purification by column chromatography on silica gel Merck (200 g) using 5% acetone in benzene produced the following pure compounds.

*Fraction I. (+)-7,9-Di-O-methylisoxazolo[4,5-b]usnic Acid (**12**)*

Yellow foam that could not be induced to crystallize (2.30 g, 6.233 mmol; 70%); $[\alpha]_D^{26}$ (CH_3CN) (*c* 0.05075);

uv: λ_{max} (log ε) 360 (3.10), 305 (3.35), 250 (3.85), 205 (4.37); ir: ν_{max} 2940 (C—H, aromatic —OCH_3), 2850 (C—H, aromatic —OCH_3), 1690 (C=O, aromatic acetyl), 1660 (C=O, enone system), 1600, 1590 (C=C); ^{1}Hmr: δ 1.82 (3H, s, C_{9b}-CH_3), 2.22 (3H, s, C_8-CH_3), 2.44 (3H, s, C_{11}-CH_3), 2.57 (3H, s, C_6-$COCH_3$), 3.74 (3H, s, C_7-OCH_3), 4.02 (3H, s, C_9-OCH_3), 6.22 ppm (1H, s, C_4-*H*); ms: *m/e* 369 (M^+, base peak), 354, 341, 326, 301, 285, 245, 43. *Anal.* calcd. for $C_{20}H_{19}O_6N$: C 65.03, H 5.18, N 3.79; found: C 65.30, H 5.40, N 3.50. High resolution molecular weight determination calcd.: 369.121; found: 369.124.

*Fraction II. (+)-10-β-Acetyl-6,6a,7,8,9,10-hexahydro-5,6aα,8,8,10α-pentamethyl-6,7,9-trioxoisoxazolo[4,5-b]dibenzofuran (**13**)*

Thick colorless prismatic needles from chloroform – petroleum ether (30–60°C) (525 mg, 1.422 mmol; 16%), mp 185–187°C; $[\alpha]_D^{26}$ (CH_3CN) +354° (*c* 0.13825); uv: λ_{max} (log ε) 318 (3.79), 264 (3.79), 220 (4.13), 214 (4.17); ir: ν_{max} 1730, 1690, 1675 (C=O), 1620 (C=C); ^{1}Hmr ($CDCl_3$–C_6D_6): δ 1.49 (3H, s, C_8-βCH_3), 1.64 (3H, s, C_8-αCH_3), 1.78 (3H, s, C_{9b}-CH_3), 2.43 (3H, s, C_{10}-β$COCH_3$), 2.45 (3H, s, C_{11}-CH_3), 6.62 ppm (1H, s, C_2-*H*); ms: *m/e* 369 (M^+, base peak), 326, 312, 298, 284, 257, 242, 231, 229, 219, 191, 153, 91, 77, 69, 43, 42, 41. *Anal.* calcd. for $C_{20}H_{19}O_6N$: C 65.03, H 5.18, N 3.79, found: C 65.07, H 5.41, N 3.45. High resolution molecular weight determination calcd.: 369.121; found: 369.119.

Acknowledgement

Financial aid from the National Research Council of Canada is gratefully acknowledged. One of us (I.H.S.) wishes to thank NRCC for a scholarship during the period of this study. We would also like to acknowledge the efforts of Ms. I. B. Krizsan in preparing the illustrations.

1. J. P. Kutney and I. H. Sanchez. Can. J. Chem. **54**, 2795 (1976).
2. J. P. Kutney, I. H. Sanchez, and T. Yee. Can. J. Chem. **54**, 3713 (1976).
3. J. P. Kutney, I. H. Sanchez, and T. Yee. Can. J. Chem. **54**, 3721 (1976).
4. J. P. Kutney, I. H. Sanchez, and T. Yee. Can. J. Chem. This issue.
5. J. P. Kutney and I. H. Sanchez. Can. J. Chem. This issue.
6. F. M. Dean, P. Halewood, S. Mongkolsuk, A. Robertson, and W. B. Whalley. J. Chem. Soc. 1250 (1953).
7. R. K. Sharma. Diss. Abstr. **24**, 4417 (1964).
8. K. Takahashi, A. Arai, K. Oshima, Y. Ueda, and S. Miyashita. Chem. Pharm. Bull. Jpn. **10**, 607 (1962).
9. K. Takahashi and S. Miyashita. Chem. Pharm. Bull. Jpn. **10**, 603 (1962); **11**, 209 (1963).
10. K. Takahashi, S. Miyashita, and Y. Ueda. Chem. Pharm. Bull. Jpn. **11**, 473 (1963).
11. K. Takahashi and S. Miyashita. Chem. Pharm. Bull. Jpn. **16**, 988 (1968).
12. K. Takahashi and M. Takani. Chem. Pharm. Bull. Jpn. **18**, 1831 (1970).
13. K. Takahashi, M. Takani, and A. Fukumoto. Chem. Pharm. Bull. Jpn. **22**, 115 (1974).
14. L. Bertilsson and C. A. Wachtmeister. Acta Chem. Scand. **22**, 1791 (1968).
15. L. Bertilsson and C. A. Wachtmeister. Acta Chem. Scand. **22**, 3081 (1968).
16. N. Kornblum, R. A. Smiley, R. K. Blackwood, and D. C. Iffland. J. Am. Chem. Soc. **85**, 1148 (1963).
17. N. Kornblum and A. P. Laurie. J. Am. Chem. Soc. **81**, 2705 (1959).
18. A. L. Kurz, J. P. Betefskaya, A. Macias, and O. A. Reutov. Tetrahedron Lett. 3679 (1968).
19. W. J. LeNoble. Synthesis, 1 (1970).
20. J. Dockx. Synthesis, 441 (1973).
21. H. Normant. Angew. Chem. Int. Ed. Engl. **6**, 1046 (1967).
22. W. J. LeNoble and H. F. Morris. J. Org. Chem. **34**, 1969 (1969).
23. S. MacKenzie. J. Am. Chem. Soc. **77**, 2214 (1955).
24. J. P. Marsh, Jr., and L. Goodman. J. Org. Chem. **30**, 2491 (1965).
25. N. Kornblum and A. Scott. J. Am. Chem. Soc. **96**, 590 (1974).
26. T. Purdie and J. C. Irvine. J. Chem. Soc. Trans. **83**, 1021 (1903).
27. J. F. Garden and R. H. Thomson. J. Chem. Soc. 2483 (1957).
28. W. Riedl and K. H. Riesse. Ann. **585**, 209 (1954).
29. G. Nowy, W. Riedl, and H. Simon. Chem. Ber. **99**, 2075 (1966).
30. A. M. Patterson, L. T. Capell, and D. F. Walker. The ring index. 2nd ed. American Chemical Society, Washington, D.C. 1960. p. 388.

On the construction of the C,D ring system of chasmanine by the photochemical method

K. WIESNER, I. H. SANCHEZ, K. S. ATWAL, AND S. F. LEE

Natural Products Research Center, University of New Brunswick, P.O. Box 4400, Fredericton, N.B., Canada E3B 5A3

Received October 20, 1976

K. WIESNER, I. H. SANCHEZ, K. S. ATWAL, and S. F. LEE. Can. J. Chem. **55**, 1091 (1977).

Two highly stereoselective syntheses of the methoxy ketal **18**, which had been previously transformed to the chasmanine model compound **IV** are described. Both these processes avoid the equilibration step **VII** ⇄ **VIII** which failed (with compounds **IX** ⇄ **X**) in the actual chasmanine synthesis. There is reason to believe that the second of these routes, remarkable by its brevity, will be applicable in the full chasmanine system.

K. WIESNER, I. H. SANCHEZ, K. S. ATWAL et S. F. LEE. Can. J. Chem. **55**, 1091 (1977).

On décrit deux synthèses hautement stéréosélectives du méthoxy acétal **18** qui a été transformé antérieurement dans le composé **IV**, modèle de la chasmanine. Les deux procédés évitent l'étape d'équilibration **VII** ⇄ **VIII** qui n'avait pas fonctionné (avec les composés **IX** ⇄ **X**) dans la synthèse réelle de la chasmanine. Il y a des raisons de croire que la deuxième de ces routes, remarquable par sa brièveté, pourra être applicable dans le système complet de la chasmanine.

[Traduit par le journal]

Introduction

Some time ago we have described a stereospecific conversion of the model compound **I** to the bromo derivative **II**. This material was then rearranged to **III** and functionalized to the ketone **IV** the structure of which was corroborated by X-ray crystallography (1). Recently we have finally reported (2) the total synthesis of the compound **V** which we hoped to transform by the above technique to the alkaloid chasmanine **VI**.

There was however in the sequence **I** → **II** a step which while perfectly satisfactory in the model series gave rise to some misgivings in the anticipated synthesis proper. It was the equilibration and separation of the epimeric α,β-unsaturated ketones **VII** and **VIII**.

It did not take long to ascertain that this operation in fact causes trouble with the fully functionalized system. Birch reduction, acetylation and acid treatment of the aromatic intermediate **V** yielded the anticipated compound **IX** without difficulty. However, the equilibration of this epimer with the desired epimer **X** could not be performed without some destruction of material and the separation of the two compounds turned out to be exceedingly difficult.

As soon as we realized that the step **IX** → **X** is bound to develop into an unacceptable bottleneck, it became clear that it was necessary to go 'back to the model'. It was our intention to set up the desired configuration (marked with arrow in formula **X**) by a series of irreversible stereospecific steps and thus to avoid the equilibration **IX** → **X**.

It is perhaps remarkable that both variants of this *detour* which we have worked out are *shorter* than the original route (1). This is primarily due to the operation of our photochemical addition rule (3) which requires that the diastereoisomers **IX** and **X** add photochemically olefins to the β and α face of the molecule respectively. More importantly, this development illustrates the process of refining the synthesis of polysubstituted polybridged compounds to the simplest possible variant by systematic switching between model work and synthesis proper.

Discussion

The starting point of the 'variant A' of our new process was the β,γ-unsaturated ketone **2** (Scheme 2) prepared by Birch reduction and mild acid treatment of the aromatic model compound **1** (1).[1]

Reduction of **2** with sodium borohydride

[1]All spectral data of all compounds are in agreement with the structures assigned and are recorded in the 'Experimental'. Only specially relevant data are presented also in the 'Discussion'.

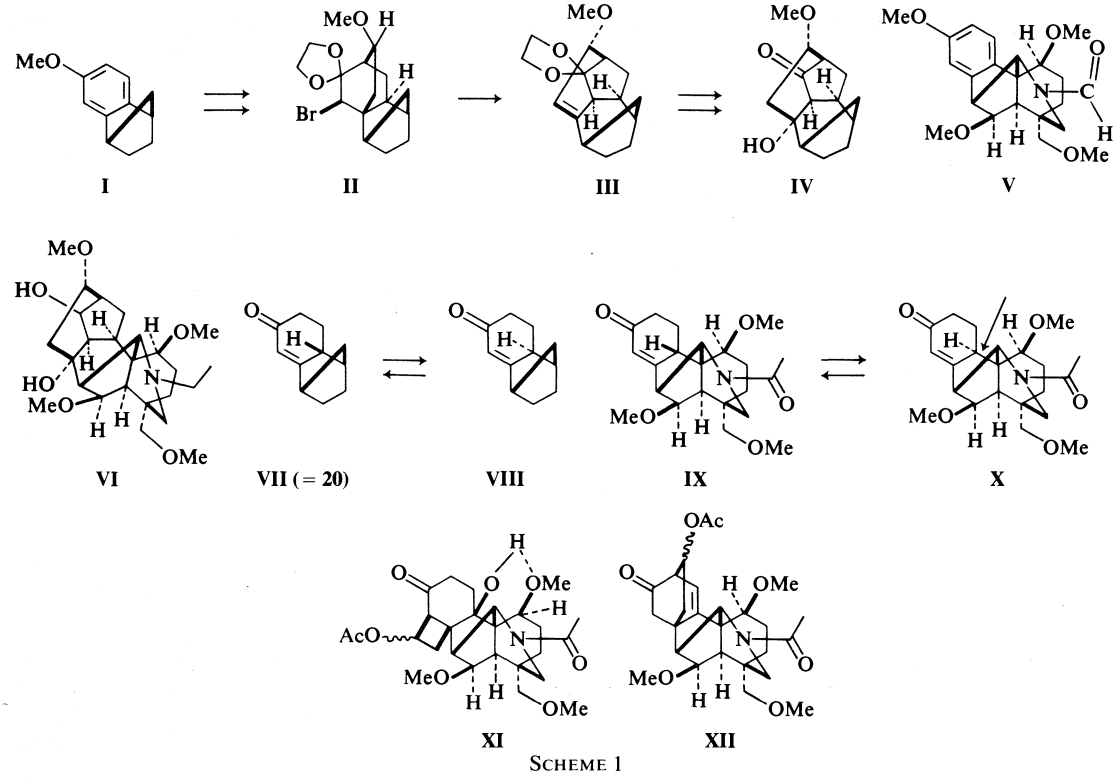

SCHEME 1

yielded the unsaturated alcohol **3**. The overall yield of the oily material **3** from **1** was approximately 90%. Compound **3** was now transformed to the crystalline hydroxy α,β-unsaturated ketone **4** in a yield of 81% as follows (4). The unsaturated alcohol **3** was first transformed into an *exo*-epoxide by treatment with *m*-chloroperbenzoic acid in dichloromethane. This material was immediately oxidized to the corresponding ketone by the addition of tetramethyl piperidine hydrochloride and more *m*-chloroperbenzoic acid in the same solvent. The conversion to **4** was finally completed by treatment of the epoxy ketone with methanolic sodium methoxide.

The photoaddition of allene to compound **4** gave the crystalline adduct **5** in a yield of 87%. The configuration of this adduct, predictable by the addition rule (3), was confirmed by further transformations to the hemiacetal **8** and finally to the methoxy ketal **18**, an intermediate of our original synthesis (1).

Compound **5** was now converted quantitatively into the dimethyl ketal **6** and this material gave on ozonolysis, borohydride reduction, and acetylation the crystalline acetoxy ketone **7** in an overall yield of 72%. In this sequence the dimethyl ketal function was lost during the work-up of the final acetylation step. In this manner the unstable keto-cyclobutanol functionality which undergoes spontaneous retro aldol cleavage was never completely unmasked. If the acetylation step is omitted and the product of the ozonolysis and borohydride reduction is chromatographed on silica gel the extremely stable crystalline hemiacetal **8** which is useless for further elaboration is obtained in a yield of 84%.

Dehydration of the tertiary alcohol **7** with thionyl chloride and pyridine yielded the oily β,γ-unsaturated ketone **9** in a yield of 71%. A small amount (10%) of the crystalline chloro ketone **10** was also isolated. Compound **9** showed in the infrared (ir) spectrum peaks at 1755, 1715, and 1676 cm^{-1} for the acetate carbonyl, the six-membered ketone, and the double bond. The nuclear magnetic resonance spectrum (nmr) showed a quadruplet centered at $\tau = 4.43$ ppm which corresponded to the vinylic hydrogen.

Treatment of the unsaturated keto acetate **9**

with dilute methanolic potassium hydroxide caused hydrolysis of the acetate group, retro aldol cleavage of the unmasked keto-cyclobutanol functionality, and immediate aldol ring closure of the resulting unsaturated keto-aldehyde to the mixture of epimeric alcohols **11***a,b*. This spontaneous aldol condensation of the enolate ion ***b*** to the aldols **11***a,b* was surprising since we have previously noted (1) that the saturated enolate ***a*** does not aldolize and the aldol condensation of the saturated keto-aldehyde has to be driven by boron trifluoride and acetic anhydride. It may be that the double bond in **11***a,b* diminishes the twist of the condensed system, which is considerable in the saturated skeleton **13** or **14**. In any event, the discovery of this spontaneous ring closure is a great advantage in the anticipated use of the method with polymethoxylated derivatives in the synthesis proper.

Benzoylation of the aldols **11***a,b* yielded the crystalline mixture of benzoates **12***a* and **12***b* and the major isomer **12***a* was purified by crystallization. Compound **12***a* showed in the ir spectrum peaks at 1720 and 1670 cm^{-1} for the benzoate carbonyl and ketone and for the double bond; the nmr spectrum displayed a doublet at $\tau = 4.40$ ppm for the vinylic proton.

Hydrogenation of the epimeric mixture **12***a,b* in methanol with rhodium on alumina yielded the two readily separable crystalline hexahydrobenzoates **13** and **14** in a ratio 3.2:1. The configuration of **13** followed from its conversion to the known compound **18** (Scheme 2) which required an inversion of the alcohol function. Compound **18**, it will be recalled, was an intermediate of our first synthesis (1) and it was transformed to the ketone **IV** (Scheme 1) the structure of which was verified by X-ray crystallography. The configuration of compound **14** differs from that of compound **13** at the ring junction since it could not be transformed to **18** by the appropriate manipulation of the functional groups. Specifically, while compound **13** yielded the keto-ketal **17**, compound **14** was converted by an analogous manipulation of functional groups into a diastereoisomer of **17**.

Compounds **12***a* and **12***b* are difficult to separate and thus we have only investigated the hydrogenation of the mixture. Since it is clear that compound **13** results from the hydrogenation of **12***a* it is reasonable to assume that compound **14** is the hydrogenation product of **12***b* and that the shielding by the benzoate group controls the stereochemistry of the double bond hydrogenation. This assumption is thus the reason for the assignment of the complete configuration to the diastereoisomer **14**. (Only the complete configuration of **13** is rigorously proved by its conversion to the final product **18**.)

The keto-ester **13** was now converted into the crystalline ketal **15** and this material was saponified to the unstable alcohol **16***b* which was immediately oxidized to the oily but homogeneous keto ketal **17**.

Reduction of this last compound with sodium borohydride proceeded stereospecifically and quantitatively to yield the crystalline alcohol **16***a*. Finally methylation of **16***a* gave the known methoxy ketal **18** which was an intermediate in our first synthesis (1).

Thus we have reached our objective and devised a route which avoided the equilibration step **VII** → **VIII** and was in fact two steps shorter than the original synthesis. All steps were stereospecific except for **12***a,b* → **13** which was highly stereoselective (3.2:1).

We were in fact so pleased by this method that we have committed an error. We have overlooked that in compound **XI** (Scheme 1), the full fledged analogue of the model intermediate **7**, there is a very serious nonbonded interaction between the tertiary hydroxyl and the ring A methoxy group which might lead to a considerable change in reactivity.

Instead of proceeding with caution Dr. S. F. Lee who was in charge of the synthesis proper converted at the instigation of the senior author almost our entire supply of the aromatic compound **V** into the intermediate **XI**. The transformation **V** → **XI** proceeded exactly as in the model series in excellent yield. Compound **XI**, however, displayed a very sharp singlet at $\tau = 3.5$ ppm for the hydroxyl hydrogen (identified by deuteration) and it was completely resistant to dehydration although all the methods found in the literature were tried. For the second time this meant 'back to the model'.

Our objective now was not to find new methods for dehydrating the tertiary alcohol **7** (practically all methods worked with this model compound) but to discover an entirely new variant which would completely avoid the dehydration step.

Thus, we have discovered 'variant B' which is even simpler than the 'variant A' and most

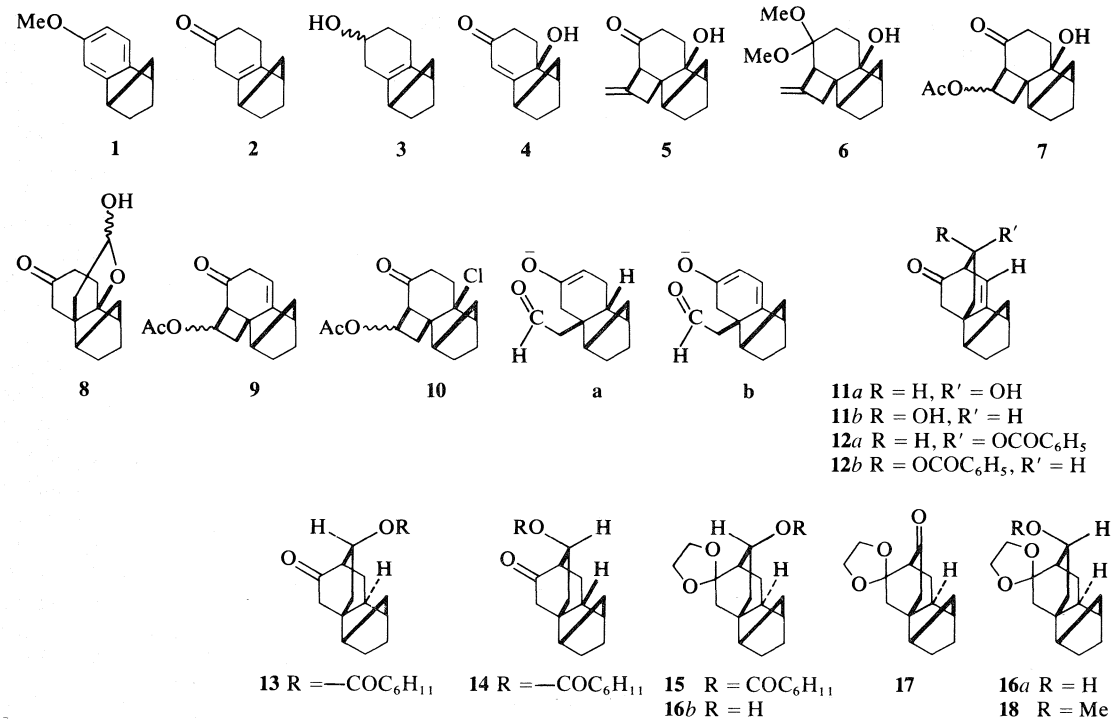

SCHEME 2

important, it works in the real system. On previous occasions it has not been our custom to discuss the ups and downs of synthetic work in publications. In the present instance the lesson to be drawn from the switches between model and real system seems to justify an exception.

The basis of the second 'variant B' was the α,β-unsaturated ketone **19***a* (Scheme 3). We have first obtained this compound by treatment of the β,γ-unsaturated isomer **9** with hydrochloric acid in chloroform. The ir spectrum of **19***a* showed maxima at 1749 (acetate carbonyl), 1675 (conjugated ketone), and 1652 cm^{-1} (double bond). The nmr spectrum showed a quadruplet centered at $\tau = 3.27$ ppm for the vinylic hydrogen in the β-position and a doublet of narrow doublets at $\tau = 3.92$ ppm for the vinylic hydrogen α to the ketone. The maximum absorption in the ultraviolet (uv) of compound **19***a* was at 235 nm ($\log \varepsilon = 4.16$). It is clear that the conjugated ketone **19***a* and the β,γ-unsaturated ketone **9** should by saponification, dealdolization, and conjugate enolate ion formation give rise to the same species ***b*** (Scheme 2). If this species is indeed an intermediate in the conversion **9** → **11***a*,*b* the reaction **19***a* → **11***a*,*b* should proceed equally well. In fact compound **19***a* gave the same aldols **11***a*,*b* and benzoates **12***a*,*b* in a similar yield as compound **9**.

There is now a very facile way to obtain **19***a* from the readily available (1) compound **20**.[2] Photoaddition of vinyl acetate to the α,β-unsaturated ketone **20** gave a 91% yield of a mixture consisting of approximately equal quantities of the isomers **21***a* and **21***b*. The pure isomer **21***a* was obtained by crystallization of the oily mixture.

It is of course also possible to prepare **21***a* regiospecifically from the allene adduct of **20**. The vinyl acetate addition saves five steps as compared to this allene route and thus would be only moderately inferior in yield; we chose it in this model study because of its brevity. Bromination of **21***a* gave a quantitative yield of the crystalline monobromide **22***a*. Dehydrobromination of **22***a* in anhydrous dimethylformamide with lithium bromide and lithium carbonate (5) gave compound **19***a* in an 82% yield.

We have also carried out a direct conversion of the vinyl acetate adduct mixture **21***a*,*b* to

[2]Compound **20** is obtained by further mild acid treatment of compound **2**.

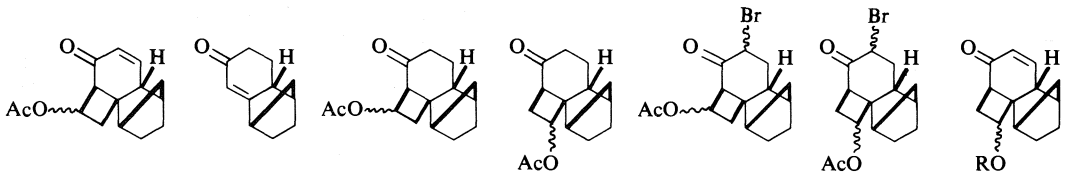

19*a* **20** **21***a* **21***b* **22***a* **22***b* **19***b* R = Ac; **23** R = H; **24** R = COC_6H_5

SCHEME 3

the pure compound **17**, an intermediate in the 'variant A' synthesis. The overall yield from the α,β-unsaturated ketone **20** to the keto ketal **17** was 13.7%. The details of this process are described in the Experimental. The reaction sequence proceeded via the mixtures **22***a,b* and **19***a,b*. Base treatment of **19***a,b* followed by benzoylation yielded the benzoates **12***a,b* and **24** which were separated by chromatography. Finally the conversion of **12***a,b* to **17** was performed as described above.

We had just enough of the α,β-unsaturated ketone **IX** at this point to subject it to this abbreviated vinyl acetate sequence. The entire operation was uneventful as in the model 'variant B' and the acetate **XII** was reached in a quantity just sufficient to be characterized. (Acetylation was used instead of the benzoylation employed in the model system.) The success of 'variant B' in the full system in which the 'variant A' failed is clearly due to the fact that in the course of the entire sequence no intermediate was needed which would have a serious nonbonded interaction absent from the model series.

We believe that one can derive from these findings an important lesson on how to evaluate critically the chances of a model study to succeed in the full system. Based on this lesson we believe that the chances of compound **XII** in the remaining steps are excellent.

We shall report in detail on the application of this study to the total synthesis of chasmanine and other aconite alkaloids as soon as we reach the corresponding natural products.

Experimental

Preparation of the β,γ-Unsaturated Ketone 2

A solution of compound **1** (1) (13.4 g) in anhydrous tetrahydrofuran (78 ml) and *tert*-butyl alcohol (78 ml) was added dropwise over a period of 45 min to a stirred solution of lithium metal (5.41 g) in distilled liquid ammonia (290 ml). The mixture was stirred at acetone – dry ice temperature for 2½ h. Absolute methanol was added until the blue colour disappeared and the reaction mixture was allowed to stand to evaporate the excess ammonia. The resulting white residue was dissolved in water (200 ml) and extracted thoroughly with ether (4 × 50 ml). The extracts were washed with water and dried over anhydrous potassium carbonate. Evaporation afforded a colorless oil (13.0 g) which was immediately dissolved in cold absolute methanol (250 ml) and treated with aqueous oxalic acid (1 *M* solution, 80 ml). After 45 min at 0°C (ice-bath) the reaction mixture was neutralized by dropwise addition of saturated sodium bicarbonate solution. Work-up by the standard procedure produced the unstable β,γ-unsaturated ketone **2** (11.72 g, 94%) as a colorless oil homogeneous by tlc in several solvent systems. *Mol. Wt.* calcd. for $C_{11}H_{14}O$: 162; found (ms): 162. Infrared (CCl_4): 1715 (six-membered ketone), 1670 cm^{-1} (tetrasubstituted double bond).

Preparation of the β,γ-Unsaturated Alcohol 3

The β,γ-unsaturated ketone **2** (4.60 g) was dissolved in absolute methanol (100 ml) and sodium borohydride (0.57 g) was added portion-wise at 0°C. After an additional ½ h at this temperature the reaction mixture was worked-up by the usual procedure. The resulting oily residue (4.72 g) was purified by chromatography on silica gel. Elution with ether–hexane (1:1, v/v) afforded the pure alcohol **3** (4.21 g, 91%) as a colorless oil homogeneous by tlc in various solvent systems. *Mol. Wt.* calcd. for $C_{11}H_{16}O$: 164; found (ms): 164. Infrared (CCl_4): 3625, 3400 (hydroxyl), 1665 cm^{-1} (double bond); nmr (CCl_4): τ 6.30 ppm (m, 1H, proton unshielded by hydroxyl).

Preparation of the α,β-Unsaturated Ketone 4

To a solution of the alcohol **3** (245 mg) in dry dichloromethane (10 ml) was added dropwise a solution of *m*-chloroperbenzoic acid (325 mg) in the same solvent (15 ml) at 0°C under a nitrogen atmosphere. After an additional hour at this temperature the reaction mixture was treated with freshly prepared 0.2 *M* solution of tetramethyl piperidine hydrochloride (4) (TMP·HCl) in dry dichloromethane (0.3 ml) followed by the dropwise addition of a solution of *m*-chloroperbenzoic acid (350 mg) in the same solvent (15 ml). The reaction was allowed to proceed with stirring for 8 h at room temperature. The resulting pale yellow solution was transferred into a separatory funnel and thoroughly washed with 5% aqueous sodium carbonate and water. The extract was dried over anhydrous magnesium sulfate and evaporated to dryness under reduced pressure to afford a yellowish oil (265 mg) which was taken up in absolute methanol

(5 ml) and treated with a 4 *M* methanolic sodium methoxide solution (0.4 ml) at 0°C for ½ h. The mixture was neutralized with dilute hydrochloric acid, diluted with saturated aqueous sodium chloride (15 ml), and thoroughly extracted with ether (4 × 10 ml). The combined extracts were washed with water, dried over anhydrous magnesium sulfate, and evaporated to dryness. The residue (247 mg) was purified by preparative tlc on silica gel using ether–hexane (2:1, v/v) to yield the pure α,β-unsaturated ketone **4** (215 mg, 81%) as colorless prisms mp 100–101°C from carbon tetrachloride – hexane. *Anal.* calcd. for $C_{11}H_{14}O_2$: C 74.13, H 7.92; found: C 73.89, H 7.89. *Mol. Wt.* calcd.: 178; found (ms): 178. Infrared (CCl_4): 3620, 3410 (hydroxyl), 1665 cm^{-1} (conjugated six-membered ketone); nmr (CCl_4): τ 4.33 (s, 1H, vinylic proton), 6.17 ppm (br, 1H, hydroxyl proton); uv: λ_{max} (MeOH) 237.5 nm (log ε 4.07).

Photoaddition of Allene to Compound 4

A mixture of the α,β-unsaturated ketone **4** (1.0 g) and excess allene (15 g) in anhydrous tetrahydrofuran (25 ml) was irradiated at −78°C with a 200 W Hanovia mercury lamp through a Pyrex filter for 8 h under a stream of nitrogen. Excess allene and solvent were removed by evaporation under reduced pressure and the resulting oily residue was purified by chromatography on silica gel using ether–hexane (2:1, v/v). The photoadduct **5** (1.07 g, 87%) was obtained as thin colorless plates mp 83–85°C from ether–hexane. *Anal.* calcd. for $C_{14}H_{18}O_2$: C 77.03, H 8.31; found: C 76.95, H 8.41. *Mol. Wt.* calcd.: 218; found (ms): 218. Infrared (CCl_4): 3625, 3485 (hydroxyl), 1718 (six-membered ketone), 1675, 875 cm^{-1} (terminal methylene); nmr (CCl_4): τ 5.05 and 5.18 (q, J = 3 and 6 Hz, 1H each, vinylic protons), 7.58 ppm (s, 1H, hydroxyl proton).

Preparation of Dimethyl Acetal 6

The allene photoadduct **5** (100 mg) was dissolved in absolute methanol (10 ml) and to this solution was added dry Rexyn 101-(H) R-204 (10 mg) and trimethylorthoformate (0.2 ml). After 1½ h stirring under nitrogen a second (0.2 ml) portion of orthoformate was added. The reaction mixture was stirred at room temperature for a further 1½ h. The resin was filtered off and the filtrate evaporated under reduced pressure in presence of triethyl amine (3 drops). The yield of the oily acetal **6** is quantitative. *Mol. Wt.* calcd. for $C_{16}H_{24}O_3$: 264; found (ms): 264. Infrared (CCl_4): 3625, 3475 (hydroxyl), 1670, 875 cm^{-1} (terminal methylene); nmr (CCl_4): τ 5.07 (q, J = 3 and 6 Hz, 1H, vinylic proton), 5.25 (q, J = 3 and 6 Hz, 1H, vinylic proton), 6.80, 6.87 ppm (s, 3H each, acetal methyl groups).

Preparation of Keto Acetate 7

The hydroxy acetal **6** (115 mg) was dissolved in absolute methanol (15 ml) and cooled to −70°C. A stream of ozonized oxygen was slowly passed through the solution until it acquired a permanent blue color. After removing excess ozone with a stream of nitrogen the reaction mixture was allowed to warm up to 0°C. Sodium borohydride (400 mg) was then added in portions and the resulting mixture stirred for an additional 1 h at 0°C. The solvent was evaporated under reduced pressure and the residue thoroughly extracted with ether. The combined extracts were washed with brine, dried over anhydrous potassium carbonate, and evaporated to dryness. The oily residue (125 mg) was dissolved in a mixture of pyridine – acetic anhydride (2:1, 3 ml) and allowed to stand at room temperature overnight. The reaction mixture upon acidic work-up (HCl) produced the desired keto acetate **7** (83.03 mg, 72%) as colorless prisms mp 134–135°C from carbon tetrachloride – hexane. *Anal.* calcd. for $C_{15}H_{20}O_4$: C 68.16, H 7.63; found: C 67.89, H 7.70. *Mol. Wt.* calcd.: 264; found (ms): 264. Infrared (CCl_4): 3620, 3500 (hydroxyl), 1750 (acetate), 1710 cm^{-1} (six-membered ketone); nmr ($CDCl_3$): τ 4.83 (q, J = 9 Hz, 1H, proton unshielded by acetoxyl), 7.97 ppm (s, 3H, acetoxy methyl).

Preparation of the Hemiacetal 8

The hydroxy acetal **6** (60 mg) was dissolved in absolute methanol (10 ml) and ozonized at −70°C until a pale blue color persisted. Excess ozone was removed by means of a stream of nitrogen and the cold (0°C) solution was treated with sodium borohydride (150 mg) in small portions with additional stirring at 0°C for 1 h. The solution was then concentrated under reduced pressure, diluted with water (10 ml), and extracted with ether. The combined (wet) ether extracts were treated with anhydrous magnesium sulfate (400 mg) with stirring at room temperature for 1 h. After evaporation of the solvent the residue was purified by preparative tlc on silica gel using ether–hexane (2:1, v/v) to produce the crystalline hemiacetal **8** (42.38 mg, 84%) as a colorless microcrystalline material, mp 125–126°C from ether–hexane, which consists (nmr) of a 3.5:1 mixture of epimers at the hemiacetal carbon. *Anal.* calcd. for $C_{13}H_{18}O_3$: C 70.23, H 8.17; found: C 70.23, H 8.20. *Mol. Wt.* calcd.: 222; found (ms): 222. Infrared (CCl_4): 3630, 3425 (hydroxyl), 1710 cm^{-1} (six-membered ketone); nmr (CCl_4): τ 4.53 (br, 1H, proton unshielded by the hemiacetal oxygen), 5.15 ppm (br, 1H, hemiacetal hydroxyl); nmr ($CDCl_3$): τ 4.49 (m, 1H, proton unshielded by the hemiacetal oxygen), 6.20 and 6.42 ppm (d, J = 4 Hz, 1H, minor and major epimers respectively, hemiacetal hydroxyl).

Preparation of the β,γ-Unsaturated Ketone 9

A solution of the keto acetate **7** (200 mg) in dry pyridine (6 ml) was cooled to 0°C (ice-salt bath) and treated with thionyl chloride (15 drops). After 10 min the pale yellow reaction mixture was poured into cold water (20 ml) and extracted with ether (3 × 10 ml). The combined extracts were washed with dilute hydrochloric acid and water, dried over anhydrous magnesium sulfate, and evaporated to dryness. The residue was purified by preparative tlc on silica gel using ether–hexane (1:1, v/v) to produce the oily β,γ-unsaturated ketone (133 mg, 71%). *Mol. Wt.* calcd. for $C_{15}H_{18}O_3$: 246; found (ms): 246. Infrared (CCl_4): 1755 (acetate), 1715 (six-membered ketone), 1676 cm^{-1} (double bond); nmr (CCl_4): τ 4.43 (dd, J = 2 and 6 Hz, 1H, vinylic proton), 4.80 (q, J = 9 Hz, 1H, proton unshielded by acetoxyl), 8.03 ppm (s, 3H, acetoxy methyl).

From the preparative tlc was also obtained the crystalline chloro ketone **10** (22.0 mg, 10%) mp 162–163°C from carbon tetrachloride – hexane. *Anal.* calcd. for $C_{15}H_{19}O_3Cl \cdot \frac{1}{5}CCl_4$: C 58.22, H 6.11; found: C 58.78, H 6.25. *Mol. Wt.* calcd. for $C_{15}H_{19}O_3Cl$: 282; found (ms): 282. Infrared ($CHCl_3$): 1745 (acetate), 1715 cm^{-1} (six-

membered ketone); nmr ($CDCl_3$): τ 4.90 (q, J = 9 Hz, 1H, proton unshielded by acetoxyl), 7.90 ppm (s, 3H, acetoxy methyl).

Base Treatment of Keto Acetate ***9***

Compound **9** (133 mg) was dissolved in 1% methanolic potassium hydroxide (2 ml) and stirred under nitrogen at room temperature for 20 min. The reaction mixture was diluted with cold water (10 ml) and the methanol evaporated under reduced pressure. The residue was thoroughly extracted with ether (4 × 5 ml) and the combined extracts were washed with brine, dried over anhydrous sodium sulfate, and evaporated to dryness. The residue was purified by preparative tlc on silica gel using ether–hexane (2:1, v/v) to afford the pure aldol mixture **11***a,b* (100 mg, 91%) as a colorless glass. *Mol. Wt.* calcd. for $C_{13}H_{16}O_2$: 204; found (ms): 204. Infrared ($CHCl_3$): 3620, 3420 (hydroxyl), 1735, 1725 (six-membered ring ketone), 1675 cm^{-1} (double bond); nmr (CCl_4): τ 4.50 (d, J = 6 Hz, 1H, vinylic proton), 6.00 (m, 2H, hydroxyl and proton unshielded by hydroxyl), 6.87 ppm (dd, J = 2 and 6 Hz, proton at the ring junction adjacent to the carbonyl grouping).

Benzoylation of Aldol ***11****a,b*

A solution of the mixture **11***a,b* (100 mg) in dry pyridine (2 ml) was cooled to 0°C and treated with freshly distilled benzoyl chloride (103 mg). The reaction was allowed to proceed at the same temperature for 1 h and it was then diluted with cold water (10 ml), neutralized with dilute hydrochloric acid, and extracted with ether (3 × 10 ml). The combined extracts were washed with water, dried over anhydrous magnesium sulfate, and evaporated to dryness. Purification of the residue by preparative tlc on silica gel using ether–hexane (1:2, v/v) produced the crystalline benzoate mixture **12***a,b* (120 mg, 79%), colorless prisms mp 116–123°C from carbon tetrachloride – hexane. *Mol. Wt.* calcd. for $C_{20}H_{20}O_3$: 308; found (ms): 308. Infrared (CCl_4): 1735 (benzoate), 1720 (six-membered ketone), 1670 cm^{-1} (double bond); nmr (CCl_4): τ 1.73 and 2.57 (m, 2 and 3H respectively, aromatic protons), 4.37 (d, J = 6.5 Hz, 1H, vinylic proton), 4.93 (m, 1H, proton unshielded by benzoate), 6.67 ppm (dd, J = 2 and 6 Hz, 1H, proton at the ring junction adjacent to the carbonyl grouping).

For analytical purposes, this epimeric mixture was fractionally recrystallized from carbon tetrachloride – hexane to produce the major benzoate **12***a* as colorless prisms mp 121–122°C. *Anal.* calcd. for $C_{20}H_{20}O_3$: C 77.90, H 6.54; found: C 77.73, H 6.55. *Mol. Wt.* calcd.: 308; found (ms): 308. Infrared ($CHCl_3$): 1720 (benzoate and six-membered ketone), 1670 cm^{-1} (double bond); nmr ($CDCl_3$): τ 1.91 and 2.47 (m, 2 and 3H respectively, aromatic protons), 4.40 (d, J = 6.5 Hz, 1H, vinylic proton), 4.80 (m, 1H, proton unshielded by benzoate), 6.57 ppm (dd, J = 4 and 6.5 Hz, 1H, proton at the ring junction).

Hydrogenation of the Benzoate Mixture ***12****a,b*

A mixture of the epimeric benzoates **12***a,b* (80 mg) and 5% rhodium on alumina catalyst (80 mg) in absolute methanol (4 ml) was hydrogenated at 94 psi for 32 h at room temperature. The resulting suspension was filtered through Celite and the filtering pad washed thoroughly with methanol (20 ml). The combined filtrates were evaporated to dryness and the oily residue was dissolved in dry dichloromethane (3 ml) and added in one portion to a stirred solution of the chromium trioxide – dipyridine complex (430 mg) in the same solvent (15 ml). The reaction was allowed to proceed at room temperature for 1 h, quenched with wet ether (20 ml), and filtered through a neutral alumina–Celite pad (1:1, w/w). The colorless filtrate was evaporated to dryness and purified by preparative tlc on silica gel using ether–hexane (2:3, v/v) to yield the dihydro derivatives **13** and **14** (70 mg, 88%). These compounds were isolated in a 3.2:1 ratio.

Compound ***13***

Colorless prisms mp 88–89°C from *n*-hexane (51 mg). *Anal.* calcd. for $C_{20}H_{28}O_3$: C 75.91, H 8.92; found: C 75.74, H 8.98. *Mol. Wt.* calcd.: 316; found (ms): 316. Infrared (CCl_4): 1740 (ester), 1735 cm^{-1} (six-membered ketone); nmr (CCl_4): τ 5.00 ppm (dd, J = 5 and 8 Hz, 1H, proton unshielded by the ester grouping).

Compound ***14***

Colorless prisms mp 96–97°C from *n*-hexane (16 mg). *Anal.* calcd. for $C_{20}H_{28}O_3$: C 75.91, H 8.92; found: C 75.83, H 9.02. *Mol. Wt.* calcd.: 316; found (ms): 316. Infrared (CCl_4): 1735 cm^{-1} (ester and six-membered ketone); nmr (CCl_4): τ 4.73 ppm (multiplet, 1H, proton unshielded by ester grouping).

Preparation of Ketal ***15***

A solution of the ketoester **13** (325 mg) and *p*-toluenesulfonic acid monohydrate (40 mg) in anhydrous benzene (75 ml) containing dry ethylene glycol (0.93 ml) was heated under reflux with a water separator for 5 h. Work-up by the usual procedure afforded ketal **15** (358 mg, 97%) as colorless prisms mp 105–106°C from methanol. *Anal.* calcd. for $C_{22}H_{32}O_4 \cdot \frac{1}{3}H_2O$: C 72.15, H 8.99; found: C 72.15, H 8.91. *Mol. Wt.* calcd. for $C_{22}H_{32}O_4$: 360; found (ms): 360. Infrared ($CHCl_3$): 1720 cm^{-1} (ester); nmr ($CDCl_3$): τ 5.23 (m, 1H, proton unshielded by ester), 6.17 ppm (br s, 4H, dioxolane protons).

Preparation of Ketone ***17***

Compound **15** (350 mg) was dissolved in 4% methanolic potassium hydroxide (40 ml) and heated to 60°C under nitrogen for 12 h. The resulting colorless solution was diluted with cold water (40 ml) and most of the methanol was evaporated under reduced pressure. The residue was thoroughly extracted with ether (4 × 10 ml). The combined extracts were washed with water, dried over anhydrous sodium sulfate, and evaporated to dryness. The unstable hydroxy ketal **16***b* (211 mg) was taken up in dry dichloromethane (3 ml) and added in one portion to a stirred solution of the chromium trioxide – dipyridine complex (1400 mg) in the same solvent (50 ml). The reaction mixture was stirred at room temperature for 1 h. Quenching with wet ether (50 ml) and filtration of the crude oxidation mixture through a neutral alumina–Celite pad (1:1, w/w) afforded a colorless filtrate which was evaporated to dryness. Purification of the residue by preparative tlc on silica gel using ether–hexane (1:1, v/v) yielded the oily ketal **17** (197 mg, 82%) as a colorless oil homogeneous by tlc in several solvent systems. *Mol. Wt.* calcd. for $C_{15}H_{20}O_3$: 248; found (ms): 248. Infrared (CCl_4): 1740 cm^{-1} (six-membered ketone); nmr (CCl_4): τ 6.10 ppm (s, 4H, dioxolane protons).

Preparation of Alcohol ***16a***

The ketone **17** (120 mg) was dissolved in absolute methanol (5 ml) and reduced at 0°C (ice bath) with excess sodium borohydride. Usual work-up afforded the crystalline alcohol **16***a* in quantitative yield as colorless prisms mp 98–99°C from *n*-hexane. *Anal.* calcd. for $C_{15}H_{22}O_3$: C 71.97, H 8.86; found: C 71.42, H 8.77. *Mol. Wt.* calcd.: 250; found (ms): 250. Infrared (CCl_4): 3540 cm^{-1} (hydroxyl); nmr (CCl_4): τ 6.13 (s, 4H, dioxolane protons), 6.60 ppm (br s, 1H, hydroxyl proton).

Preparation of Methoxy Ketal ***18***

A mixture of the hydroxy ketal **16***a* (80 mg), sodium hydride (15 mg, prewashed with petroleum ether), and excess methyl iodide (0.5 ml) in anhydrous dioxane (3 ml) was heated at 55°C under nitrogen for 12 h. The cold reaction mixture was quenched with absolute methanol (5 drops), diluted with brine (10 ml), and thoroughly extracted with ether (5 × 5 ml). The combined extracts were washed with water, dried over anhydrous sodium sulfate, and evaporated to dryness. Purification of the residue by preparative tlc on silica gel using ether–hexane (1:1, v/v) afforded the crystalline methoxy ketal **18** (75 mg, 89%) as colorless prisms mp 116–117°C from *n*-hexane, identical by all standard techniques (mixture mp, tlc, infrared, nmr, ms) with a sample previously prepared in our laboratories (1).

Preparation of the α,β*-Unsaturated Ketone* ***19a***

A solution of keto acetate **9** (100 mg) in dry chloroform (10 ml) was treated with concentrated hydrochloric acid (2 drops) and stirred at room temperature under nitrogen for 2 h. The reaction mixture was transferred into a separatory funnel and washed with a saturated sodium bicarbonate solution and water. Drying over anhydrous magnesium sulfate and evaporation gave a quantitative yield of the α,β-unsaturated ketone **19***a* as a colorless oil homogeneous by tlc in several solvent systems. *Mol. Wt.* calcd. for $C_{15}H_{18}O_3$: 246; found (ms): 246. Infrared (CCl_4): 1749 (acetate), 1675 (six-membered unsaturated ketone), 1652 cm^{-1} (double bond); nmr (CCl_4): τ 3.27 (dd, J = 2 and 10 Hz, 1H, vinylic proton at the β-position of the enone), 3.92 (dd, J = 1 and 10 Hz, 1H, vinylic proton at the α-position of the enone), 4.73 (m, 1H, proton unshielded by acetoxyl), 8.03 ppm (s, 3H, acetoxy methyl); uv λ_{max} (MeOH): 213 (sh) (log ε 4.02) and 235 nm (log ε 4.16).

Base Treatment of the α,β*-Unsaturated Ketone* ***19a***

Compound **19***a* (185 mg) was stirred in 1% methanolic potassium hydroxide (5 ml) at room temperature under nitrogen for 15 min. The pale yellow reaction mixture was diluted with cold water (10 ml) and most of the methanol evaporated under reduced pressure. The residue was extracted with ether and the combined extracts washed with water, dried over anhydrous sodium sulfate, and evaporated to dryness. The resulting material was purified by preparative tlc on silica gel using ether–hexane (3:2, v/v) to afford the pure aldol mixture **11***a,b* (145 mg, 95%) as a colorless oil homogeneous by tlc in several solvent systems. By all standard comparison techniques (nmr, ir, tlc, ms) this material was identical with that obtained from the base treatment on the β,γ-unsaturated ketone **9**.

Treatment of this material with benzoyl chloride in pyridine at 0°C (*vide supra*) gave 91% of a benzoate mixture which crystallized from carbon tetrachloride – hexane as colorless prisms mp 116–123°C. This sample showed spectroscopic and chromatographic properties identical to those of **12***a,b* obtained from the enone **9**.

Photoaddition of Vinyl Acetate to the α,β*-Unsaturated Ketone* ***20***

A solution of compound **20** (1) (2 g) and vinyl acetate (40 ml) in freshly distilled dry tetrahydrofuran (50 ml) was cooled to −78°C and irradiated through a Pyrex filter with a 200 W Hanovia mercury lamp for 6 h under nitrogen. The solvent and excess vinyl acetate were evaporated under reduced pressure and the residue was purified by chromatography on silica gel. Elution with ether–hexane (1:1, v/v) afforded the pure photoadduct (2.8 g, 91%) as a thick colorless oil consisting of approximately equal amounts of the isomers **21***a* and **21***b*. *Mol. Wt.* calcd. for $C_{15}H_{20}O_3$: 248; found (ms): 248. Infrared (CCl_4): 1748, 1740 (acetate), 1715, 1710 cm^{-1} (six-membered ketone); nmr ($CDCl_3$): τ 4.85 and 5.08 (q, J = 8 Hz, 1H, proton unshielded by acetoxyl), 7.92 and 8.00 ppm (s, 3H, acetoxy methyl).

The acetate mixture **21***a,b* was crystallized using carbon tetrachloride – hexane to afford the pure isomer **21***a* as colorless prisms, mp 96–98°C. *Anal.* calcd. for $C_{15}H_{20}O_3$: C 72.55, H 8.12; found: C 72.11, H 8.11. *Mol. Wt.* calcd.: 248; found (ms): 248. Infrared (CCl_4): 1740 (acetate), 1710 cm^{-1} (six-membered ketone); nmr ($CDCl_3$): τ 4.82 (q, J = 8 Hz, 1H, proton unshielded by acetoxyl), 7.98 ppm (s, 3H, acetoxy methyl).

Bromination of Keto Acetate ***21a***

A solution of the keto acetate **21***a* (60 mg) in dry tetrahydrofuran (5 ml) was treated in one portion with pyridinium hydrobromide perbromide (92.9 mg) and the resulting mixture stirred at room temperature under nitrogen for ½ h. The colorless reaction mixture was poured into cold saturated aqueous sodium bicarbonate (10 ml), diluted with brine (10 ml), and thoroughly extracted with ether (5 × 10 ml). The combined extracts were washed with dilute hydrochloric acid and water, dried over anhydrous sodium sulfate, and evaporated to dryness to afford the crystalline keto bromide **22***a* as colorless prisms mp 147–149°C from ether–hexane in quantitative yield. *Anal.* calcd. for $C_{15}H_{19}O_3Br$: C 55.06, H 5.85; found: C 54.93, H 5.91. *Mol. Wt.* calcd.: 327; found (ms): 327. Infrared (CCl_4): 1752 (acetate), 1718 cm^{-1} (six-membered ketone); nmr (CCl_4): τ 4.97 (br q, J = 8 Hz, 1H, proton unshielded by acetoxyl), 5.63 (t, J = 2 Hz, 1H, proton unshielded by the bromine atom), 8.02 ppm (s, 3H, acetoxy methyl).

Dehydrobromination of Bromo Ketone ***22a***

A recrystallized sample of the α-bromo ketone **22***a* (60 mg) was added in one portion to a stirred suspension of anhydrous lithium bromide (24.9 mg) and lithium carbonate (33.13 mg) in anhydrous *N,N*-dimethylformamide (2 ml) (5). The resulting mixture was heated to 145°C (oil-bath temperature) under nitrogen for 1 h. The cold reaction mixture was carefully poured into dilute acetic acid (15 ml) and extracted with ether (6 × 10 ml). The organic extracts were washed with water (6 × 10 ml), the aqueous washings back extracted with ether (2 × 10 ml), and the combined extracts

dried over anhydrous magnesium sulfate and evaporated to dryness under reduced pressure. The resulting pale yellow glass (42.2 mg) was purified by preparative tlc on silica gel using ether–hexane (2:1, v/v) to afford the pure α,β-unsaturated ketone **19***a* (36.7 mg, 82%) as a colorless oil. This material proved to be identical with the compound obtained by acid treatment of the β,γ-unsaturated ketone **9** by all standard comparison techniques.

Bromination–Dehydrobromination of the Keto Acetate Mixture ***21****a,b*

The mixture **21***a,b* (140 mg) was brominated in dry tetrahydrofuran (15 ml) with pyridinium hydrobromide perbromide (217 mg) as described for the keto acetate **21***a*. Identical work-up gave the oily bromo ketone mixture **22***a,b* in quantitative yield. *Mol. Wt.* calcd. for $C_{15}H_{19}O_3Br$: 327; found (ms): 327. Infrared (CCl_4): 1748, 1735 (sh) (acetates), 1718 cm^{-1} (six-membered ketone); nmr ($CDCl_3$): τ 4.67 and 5.00 (br q's, $J = 8$ and 9 Hz respectively, 1H, proton unshielded by acetoxyl), 5.57 (m, 1H, proton unshielded by the bromine atom), 7.93 and 7.97 ppm (s, 3H, acetoxy methyl).

The bromo ketone mixture **22***a,b* (91 mg) was dehydrobrominated at 145°C in anhydrous *N,N*-dimethylformamide (3 ml) with anhydrous lithium bromide (37.8 mg) and lithium carbonate (50.2 mg). The reaction was worked-up as before (*vide supra*) and the residue was purified by preparative tlc on silica gel using ether–hexane (2:1, v/v) to yield the mixture of α,β-unsaturated ketones **19***a,b* (55.4 mg, 81%) as a colorless oil.

For analytical purposes the mixture **19***a,b* can be easily separated by preparative tlc on silica gel using ether–hexane (2:3, v/v; run twice) to yield the pure α,β-unsaturated ketones **19***a* and **19***b*.

Compound ***19a***

This sample proved to be identical by all usual comparison standards with the material obtained from the β,γ-unsaturated keto acetate **9** and from the pure keto acetate **21***a*.

Compound ***19b***

Mol. Wt. calcd. for $C_{15}H_{18}O_3$: 246; found (ms): 246. Infrared (CCl_4): 1745 (acetate), 1670 cm^{-1} (six-membered unsaturated ketone); nmr ($CDCl_3$): τ 3.20 (m, 1H, vinylic proton at the β-position of the enone), 3.90 (dd, $J = 2$ and 12 Hz, 1H, vinylic proton at the α-position of the enone), 5.13 (m, 1H, proton unshielded by acetoxyl), 7.90 ppm (s, 3H, acetoxy methyl); uv λ_{max} (MeOH): 213 (sh) (log ε 4.07) and 235 nm (log ε 4.16).

Base Treatment of the Mixture ***19a,b***

The α,β-unsaturated ketone mixture **19***a,b* (1.5 g) was dissolved in 1% methanolic potassium hydroxide (20 ml) and stirred at room temperature under nitrogen for ½ h. Usual work-up and purification of the residue by column chromatography on silica gel using ether–hexane (1:2, v/v) gave a thick colorless oil (1.05 g, 84%) which consisted of a mixture of the aldols **11***a,b* and the α,β-unsaturated ketone **23**. This material was dissolved in dry pyridine (20 ml) and allowed to react at 0°C with freshly distilled benzoyl chloride (1.03 g) for 1 h. Work-up by the standard procedure furnished a crystalline substance (1.491 g) which could be separated by careful chromatography on silica gel using ether–hexane (1:3, v/v) into its two components, the less polar benzoates **12***a,b* (520.3 mg) and the ketoester **24** (754.5 mg).

The benzoates **12***a,b* were obtained as colorless prisms mp 116–123°C from carbon tetrachloride – hexane and presented chromatographic and spectroscopic characteristics identical to those previously recorded for the material prepared via the β,γ-unsaturated ketone **9**.

Benzoate **24** was obtained as colorless prisms mp 89–91°C from carbon tetrachloride – hexane. *Anal.* calcd. for $C_{20}H_{20}O_3$: C 77.90, H 6.54; found: C 77.83, H 6.59. *Mol. Wt.* calcd.: 308; found (ms): 308. Infrared (CCl_4): 1720 (benzoate), 1672 (six-membered unsaturated ketone), 1650 cm^{-1} (double bond); nmr ($CDCl_3$): τ 1.92 and 2.48 (m, 2 and 3H respectively, aromatic protons), 3.18 (dd, $J = 3$ and 11 Hz, 1H, vinylic proton at the β-position of the enone), 3.85 (dd, $J = 1$ and 11 Hz, 1H, vinylic proton at the α-position of the enone), 4.93 ppm (t, $J = 6$ Hz, 1H, proton unshielded by benzoate); uv λ_{max} (MeOH): 214 (log ε 3.64) and 231.5 nm (log ε 4.05).

Conversion of the Benzoates ***12a,b*** *into the Ketal* ***17***

The benzoates **12***a,b* (obtained from the mixture **19***a,b*) were converted to the ketone **17** exactly as described in the case of the same material originating from pure **9** or **19***a*. The homogeneous keto ketal **17** was obtained in an overall yield 13.7% from the α,β-unsaturated ketone **20**. Its identity with the previously prepared material was ascertained by tlc, ir, nmr, and ms.

Acknowledgments

We wish to thank the National Research Council of Canada, Ottawa, and the Hoffmann-La Roche Company, Vaudreuil, Quebec, for the steady support of our systematic synthetic studies over many years.

1. K. WIESNER, P. T. HO, W. C. LIU, and M. N. SHANBHAG. Can. J. Chem. **53**, 2140 (1975).
2. S. F. LEE, G. M. SATHE, W. W. SY, P. T. HO, and K. WIESNER. Can. J. Chem. **54**, 1039 (1976).
3. K. WIESNER. Tetrahedron, **31**, 1655 (1975).
4. J. A. CELLA, J. A. KELLY, and E. F. KENEHAN. J. Org. Chem. **40**, 1860 (1975); G. CHAPELET-LETOURNEUX, H. LEMAIRE, and A. RASSAT. Bull. Soc. Chim. Fr. 3283 (1965).
5. R. JOLY, J. WARNANT, G. NOMINÉ, and D. BERTIN. Bull. Soc. Chim. Fr. 366 (1958).

The synthesis of D-angolosamine

HANS H. BAER AND FAWZY F. Z. GEORGES
Department of Chemistry, University of Ottawa, Ottawa, Ont., Canada K1N 6N5

Received October 20, 1976

HANS H. BAER and FAWZY F. Z. GEORGES. Can. J. Chem. **55**, 1100 (1977).

The synthesis of 2,3,6-trideoxy-3-dimethylamino-D-*arabino*-hexose hydrochloride (**10**) (D-angolosamine, a constituent of the antibiotic, angolamycin) is described. First, a simplified procedure for the preparation of methyl 6-deoxy-α-D-glucopyranoside from methyl α-D-glucopyranoside is recorded. The deoxy derivative served as the starting point for sequential preparation of methyl 3,6-dideoxy-3-nitro-α-D-glucopyranoside (**1**), its 2,4-diacetate (**2**), its 4-monoacetate (**3**), its 2-*O*-mesyl-4-acetate (**4**), its 2-mesylate (**5**), and methyl 2,3,6-trideoxy-3-nitro-α-D-*erythro*-hex-2-enopyranoside (**6**) essentially according to procedures previously established (in part, in the L-series). Treatment of **5** or **6** with sodium borohydride produced methyl 2,3,6-trideoxy-3-nitro-α-D-*arabino*-hexopyranoside (**7**). Catalytic hydrogenation of **7** gave the corresponding 3-amino glycoside hydrochloride (**8**) which was hydrolyzed to furnish 3-amino-2,3,6-trideoxy-D-*arabino*-hexose hydrochloride (**9**) (D-acosamine, the enantiomer of a component of the antibiotic, actinoidin). *N,N*-Dimethylation of **8** followed by hydrolysis afforded the crystalline title compound (**10**).

HANS H. BAER et FAWZY F. Z. GEORGES. Can. J. Chem. **55**, 1100 (1977).

La synthèse de l'hydrochlorure de 2,3,6-tridésoxy-3-diméthylamino-D-*arabino*-hexose (**10**) (D-angolosamine, un constituant de l'antibiotique, angolamycine) est décrite. Tout d'abord, une méthode simplifiée de préparation du methyle 6-désoxy-α-D-glucopyranoside à partir du méthyle α-D-glucopyranoside est présentée. Le dérivé désoxy a servi comme produit de départ pour les préparations séquentielles du méthyle 3,6-didésoxy-3-nitro-α-D-glucopyranoside (**1**), de son 2,4-diacétate (**2**), de son 4-monoacétate (**3**), de son 2-*O*-mésyle-4-acétate (**4**), de son 2-mésylate (**5**) et du méthyle 2,3,6-tridésoxy-3-nitro-α-D-*érythro*-hex-2-énopyranoside (**6**) en suivant essentiellement des méthodes existantes (en partie, pour la série L). Le traitement de **5** ou **6** avec du borohydrure de sodium a produit le méthyle 2,3,6-tridésoxy-3-nitro-α-D-*arabino*-hexopyranoside (**7**). Par hydrogénation catalytique de **7** on a obtenue l'hydrochlorure du 3-amino glycoside correspondant (**8**) qui par hydrolyse a donné l'hydrochlorure de 3-amino-2,3,6-tridésoxy-D-*arabino*-hexose (**9**) (D-acosamine, l'énantiomère d'un composant de l'antibiotique actinoidine). Une *N,N*-diméthylation de **8** suivie d'une hydrolyse a fourni le produit désiré (**10**) sous forme crystalline.

The macrolide antibiotic angolamycin, isolated by Swiss workers (1) from *Streptomyces eurythermus*, was shown (2) to contain two neutral sugar moieties (L-mycarose and D-mycinose) together with a previously unknown amino sugar component (angolosamine) which proved to be 2,3,6-trideoxy-3-dimethylamino-D-*arabino*-hexose (**10**). A structure for the complete antibiotic was proposed (3) in 1972, at which time it was also found that angolamycin and a similar product, shincomycin A (4), appear in fact identical according to mass spectral analysis.

We now report the synthesis of **10**. The synthetic route led through another amino sugar of potential biological interest, namely, 3-amino-2,3,6-trideoxy-D-*arabino*-hexose (**9**). This compound had previously been synthesized by a different approach and characterized as its hydrochloride salt and *N*-acetyl derivative (5); some glycosidic derivatives had also been prepared (5, 6). More recently, the L-enantiomer of **9** was discovered (7) to occur in nature as a constituent of an antibiotic, actinoidin. It has been named acosamine and synthesized (8) along with several glycosidic derivatives (8, 9), but no reference to the known D-enantiomer was made. Synthetically modified analogs of daunorubicin and adriamycin containing L-acosamine in place of daunosamine (the L-*lyxo* isomer) were reported (10) to show interesting biological properties.

Methyl 3,6-dideoxy-3-nitro-α-D-glucopyranoside (**1**) was prepared from methyl 6-deoxy-α-D-glucopyranoside[1] by the nitromethane method as described (11) for its L-enantiomer. Acetylation of **1** to provide the 2,4-diacetate **2**, and selective

[1]The preparation of this starting compound was simplified by use of a procedure which avoids the need of tedious chromatographic purification of its precursor, the corresponding 6-chloro-6-deoxy derivative; see Experimental.

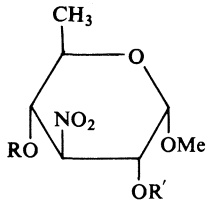

1 R = R′ = H
2 R = R′ = Ac
3 R = Ac, R′ = H
4 R = Ac, R′ = Ms
5 R = H, R′ = Ms

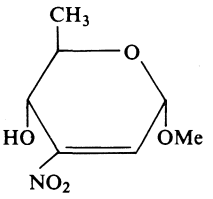

6

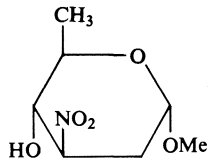

7

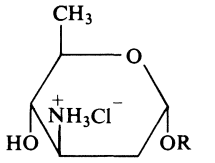

8 R = Me
9 R = H

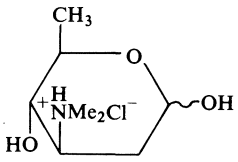

10

de-*O*-acetylation of **2** by means of acid-catalyzed methanolysis giving the 4-acetate **3** were likewise performed as reported (12) for the L-series. Methanesulfonylation of **3** followed by de-*O*-acetylation gave (13) methyl 3,6-dideoxy-2-*O*-methylsulfonyl-3-nitro-α-D-glucopyranoside (**5**) via the mixed ester **4**. All the products **1**–**5** were crystalline and the overall yield based on **1** was *ca.* 38%. The next key intermediate required was methyl 2,3,6-trideoxy-3-nitro-α-D-*arabino*-hexopyranoside (**7**). It was produced in good yield by sodium borohydride reduction of the crystalline nitro olefin **6**, methyl 2,3,6-trideoxy-3-nitro-α-D-*erythro*-hex-2-enopyranoside, which had been obtained before (13) by action of sodium hydrogen carbonate upon **5**. However, it was found unnecessary to prepare first the olefin **6** for this purpose. Direct application of sodium borohydride to the mesylate **5** resulted in a smooth replacement of the 2-mesyloxy group by a hydrogen atom, presumably by way of a reductive elimination proceeding through intermediary **6**. This shorter procedure appears to hold promise for similar syntheses in this area.[2] Unfortunately, the material designated as **7**, which was obtained in either way in about 75% yield, was a non-crystallizable syrup despite chromatographic purification. It did not give wholly correct microanalytical data and displayed some features in its nmr spectrum which may cast doubt on its homogeneity.[3] Nevertheless, the next preparative operation performed with the product confirmed that **7** must have been its chief component. Hydrogenation with Adams catalyst in methanol in the presence of 1 equiv. of anhydrous hydrogen chloride gave a 68% yield of crystalline methyl 3-amino-2,3,6-trideoxy-α-D-*arabino*-hexopyranoside hydrochloride (**8**) which agreed well in its melting point and $[\alpha]_D$-value (with opposite sign) with the known (9), synthetic L-enantiomer (methyl α-L-acosaminide hydrochloride). Acid hydrolysis of **8** afforded D-acosamine hydrochloride (**9**), which crystallized in the downward mutarotating α-form. *N*,*N*-Dimethylation of **8** by the Eschweiler–Clarke procedure (14) and hydrolysis of the product gave 2,3,6-trideoxy-3-dimethylamino-D-*arabino*-hexose that was isolated as a crystalline hydrochloride (**10**). It proved identical with D-angolosamine hydrochloride from angolamycin according to melting point, optical rotation, and an infrared spectrum (in KBr) which showed every detail of the published (2), somewhat less well resolved spectrum of the natural product.

Experimental

Optical rotations were recorded at room temperature in a Perkin-Elmer 141 automatic polarimeter. The nmr data refer to 100-MHz spectra of solutions in $CDCl_3$, internally standardized with tetramethylsilane. Infrared spectra were taken from Nujol mulls unless otherwise indicated. Thin layer chromatography (tlc) was performed on plates coated with silica gel G (E. Merck AG); unless otherwise specified, the developing phase was 5% methanol in chloroform (solvent *A*) or 1:2 ethyl acetate – petroleum ether, bp 30–60°C (solvent *B*).

[2]In the same manner we have converted methyl 3,6-dideoxy-4-*O*-methylsulfonyl-3-nitro-α-D-glucopyranoside (mp 93–94.5°C, $[\alpha]_D$ +96.6° in chloroform) into methyl 3,4,6-trideoxy-3-nitro-α-D-*xylo*-hexopyranoside (mp 55–56°C, $[\alpha]_D$ +197° in chloroform), a convenient intermediate for a new synthesis of D-desosamine (H. H. Baer and F. F. Z. Georges, unpublished results).

[3]The nmr spectrum of the material in chloroform-*d* or pyridine showed the substituent resonances expected of **7**, namely, a 3-proton doublet at high field for C-CH_3 and a 3-proton singlet at lower field for O-CH_3, with a 2-proton multiplet assignable to the C-2 methylene group in the intermediate region. The remaining ring protons, however, gave partially overlapping signals that could not be analyzed satisfactorily. It is possible that the spectra were affected by remnants of boric acid, or that other foreign matter was present, or that the compound displays a conformational behavior not yet understood. In the latter connection it is interesting to note that the specific rotation was positive (+23°) in water but negative (−34.5°) in chloroform solution.

Methyl 2,3,4-Tri-O-acetyl-6-chloro-6-deoxy-α-D-glucopyranoside

Methyl α-D-glucopyranoside was chlorinated to give methyl 6-chloro-6-deoxy-α-D-glucopyranoside essentially as described in the literature (15), but the crude product was converted without prior chromatographic isolation into its 2,3,4-triacetate, as follows. Methanesulfonyl chloride (37.5 ml, 0.5 mol) was added to a stirred solution of the glucoside (19.4 g, 0.1 mol) in *N,N*-dimethylformamide (200 ml) under external cooling (18°C). The cooling bath was removed and the temperature allowed to rise to 70 ± 5°C, at which the reaction mixture was kept for 16 h. Then 1-propanol (80 ml) and water (20 ml) were added, and stirring was continued for another 3 h at the same temperature. The reaction mixture was evaporated to near dryness (50°C bath, water aspirator), and added 1-propanol (50 ml) was evaporated from the residue. The dry solid material was acetylated by stirring it overnight with acetic anhydride (50 ml) in dry pyridine (100 ml), at 25°C. Excess anhydride was thereafter destroyed by the addition of methanol (50 ml) followed, after 1 h, by 1-propanol (50 ml). Coevaporation of the mixture with several additional portions of propanol gave a residue which was then dissolved in chloroform (50 ml). The solution was washed with water (3 × 20 ml), dried over Na_2SO_4, and evaporated to give the crystalline title compound (28 g, 83%), mp 96–97°C after recrystallization from methanol, $[\alpha]_D$ +175.7° (*c* 1, $CHCl_3$) (lit. (15) mp 96–97°C, $[\alpha]_D$ +178°).

The above triacetate (7 g) was reduced (and simultaneously deacetylated) to furnish methyl 6-deoxy-α-D-glucopyranoside as reported (15) for the non-acetylated chloro compound except that 5 + 2 g (instead of 3 + 2 g) of lithium aluminum hydride was employed.

*Methyl 3,6-Dideoxy-3-nitro-α-D-glucopyranoside (**1**)*

Methyl 6-deoxy-α-D-glucopyranoside was oxidized on a 20-g scale with sodium metaperiodate, and the product was cyclized with nitromethane in the presence of sodium methoxide, exactly as detailed for the preparation (11) of the L-enantiomer of **1** from methyl α-L-rhamnopyranoside except that a reaction time of 3 h (instead of 40 min) was allowed for the cyclization. The extended time was chosen in consideration of studies (16) indicating that this will favor formation of **1** over its *manno* isomer. Compound **1** was obtained in 35% yield by direct crystallization from the mixture of products, and processing of the mother liquor by column chromatography (11*a*) was dispensed with; mp 140–142°C, $[\alpha]_D$ +163.2° (*c* 1, water) (lit. (11*a*) for L-**1**, mp 141–143°C, $[\alpha]_D$ −164.3° (water)). The ir spectra of the enantiomers were superimposable.

*Methyl 2,4-Di-O-acetyl-3,6-dideoxy-3-nitro-α-D-glucopyranoside (**2**)*

Compound **2** was obtained in 94–99% yield by boron trifluoride-catalyzed acetylation of **1** with acetic anhydride as described (12) for the L-enantiomer; mp 110–112°C, $[\alpha]_D$ +156° (*c* 1, $CHCl_3$) (lit. (12) for L-**2**: mp 113–113.5°C, $[\alpha]_D$ −155.3° ($CHCl_3$) and (17) mp 109–110°C, $[\alpha]_D$ −154° ($CHCl_3$).

*Methyl 4-O-Acetyl-3,6-dideoxy-3-nitro-α-D-glucopyranoside (**3**)*

The procedure of partial methanolysis reported (12) for the L-series was slightly modified. The diacetate **2** (2.0 g) was dissolved in methanol (20 ml, dried over and distilled from magnesium) and acetone (2 ml, dried over molecular sieves type 4-A). Acetyl chloride (1 ml) was added, and the solution was agitated at 40°C under exclusion of moisture. Progress of the reaction was monitored by tlc (solvent *A*) which indicated complete disappearance of **2** after 3 h and appearance of two slower spots of similar strength (**3** and **1**). The reaction mixture was then evaporated to give a syrup which was chromatographed (solvent *A*) on a column of silica gel (50 g). The faster moving component (**3**) was obtained from the column in pure form (0.85 g, 50%) and crystallized on standing overnight after solvent evaporation; mp 110–111°C, $[\alpha]_D$ +176.5° (*c* 1, $CHCl_3$) (lit. (12) for L-**3**: mp 112–113°C, $[\alpha]_D$ −178.5° ($CHCl_3$)). The ir and nmr data of the two enantiomers were identical.

*Compounds **4**, **5**, and **6***

Mesylation of **3** to give its 2-*O*-methylsulfonyl derivative **4** (80% yield), de-*O*-acetylation of **4** to afford methyl 3,6-dideoxy-2-*O*-methylsulfonyl-3-nitro-α-D-glucopyranoside (**5**) in 98% yield, and conversion of **5** into methyl 2,3,6-trideoxy-3-nitro-α-D-*erythro*-hex-2-enopyranoside (**6**) by treatment with sodium bicarbonate in refluxing benzene (92% yield) have been described (13).

*Methyl 2,3,6-Trideoxy-3-nitro-α-D-arabino-hexopyranoside (**7**)*

*(a) From the Nitro Olefin **6***

Sodium borohydride (0.33 g) was added to a solution of **6** (500 mg) in 99% ethanol (13 ml), which was stirred at room temperature. Examination by tlc (solvent *B*) revealed that the reaction was complete after 10 min. Methanol (3 ml) was added and stirring was continued for another 15 min. The solvent was then evaporated to near dryness of the residue, and the latter was taken up in chloroform (10 ml). The suspension was filtered through a layer of Celite and the filtrate evaporated. The resulting syrup was dissolved in a small amount (1.5 ml) of fresh chloroform, and a voluminous precipitate which formed upon addition of acetone (8 ml) was removed and discarded. The filtrate was evaporated and several portions of methanol were successively evaporated from the remaining residue which was finally passed through a column of silica gel (8 g) by means of chloroform. A fast-moving impurity that had been seen in tlc was thus removed. The chromatographically homogeneous fractions containing the main product yielded a syrup (377 mg, 75%) believed to consist chiefly of **7**. Attempts at crystallization were unsuccessful. The material showed $[\alpha]_D$ +23° (*c* 0.6, water), −34.5° (*c* 0.6, $CHCl_3$); ν_{max} (neat) 3200 (br, OH) and 1550 cm^{-1} (NO_2). The nmr data: 4.50 (2H, unresolved m), 3.83 (1H, m, H-5), 3.5 region (unresolved m), 3.41 (3H, s, O-CH_3), 2.33 (2H, q, H-2,2′), 1.14 (3H, d, J = 6.5 Hz, C-CH_3). *Anal.* calcd. for $C_7H_{13}NO_5$ (191.2): C 43.97, H 6.85, N 7.32; found: C 43.11, H 7.65, N 6.68.

*(b) From the 2-Mesylate **5***

Sodium borohydride (0.66 g) was added in small portions to a stirred solution of **5** (1.65 g) in 99% ethanol (25 ml), with cooling in a cold water bath. The further course of operations was as described under (*a*). There was obtained 829 mg (75%) of a syrup which was identical with the previous preparation according to ir and nmr spectra.

Methyl 3-Amino-2,3,6-trideoxy-α-D-arabino-hexopyranoside Hydrochloride (8)

The syrupy nitro glycoside **7** (150 mg, approximately 0.8 mmol) was dissolved in absolute methanol (15 ml) to which exactly 0.055 ml (0.78 mmol) of acetyl chloride had been previously added to generate hydrogen chloride. The solution was introduced in a high-pressure hydrogenation flask containing platinum catalyst (150 mg of PtO_2 prereduced in a few millilitres of methanol) and shaken for 3 h under hydrogen at 40 psi and room temperature. The filtered solution gave upon evaporation a dry residue which was dissolved in 99% ethanol (1.5 ml). Dropwise addition of ether at 0°C caused crystallization of **8** which was isolated after 3 h. The yield was 105 mg (68%); mp 193–195°C (dec.), $[\alpha]_D$ +112.7° (*c* 0.5, methanol) (lit. (9*a*) for L-**8**: mp 196–198°C (dec.), $[\alpha]_D$ −115.5° (methanol)).

3-Amino-2,3,6-trideoxy-D-arabino-hexose Hydrochloride (9) (D-Acosamine Hydrochloride)

The amino glycoside **8** (50 mg) was hydrolyzed in 0.1 *M* hydrochloric acid (3 ml) for 1 h at 90°C. The hydrolyzate was evaporated to a brownish syrup with the addition of several portions of 40% aqueous ethanol. The product was finally dissolved in ethanol, decolorized with activated charcoal, and recovered by evaporation to near dryness. Trituration of the residue with a few drops of ethyl acetate gave crystalline **9**, $[\alpha]_D$ +31° (initial) → +22° (final, 3 h; *c* 0.7, water) (lit. (8) for L-**9**: $[\alpha]_D$ −18.3° at equilibrium (*c* 0.43, water)). We had previously obtained **9** in a crystalline form (presumably the α-anomer) showing $[\alpha]_D$ +81.7° (in water) without mutarotation (5). We have now hydrolyzed (1 h at 100°C in 0.5 *M* hydrochloric acid) a sample of the *N*-acetyl derivative of **9** that was still available from the previous work (5) and found $[\alpha]_D$ +18° for the product in the hydrolysis solution. The reason for the apparent lack of mutarotation of the earlier sample of **9** is not clear.

2,3,6-Trideoxy-3-dimethylamino-D-arabino-hexose Hydrochloride (10) (D-Angolosamine Hydrochloride)

A solution of the amino glycoside hydrochloride **8** (55 mg) in 37% aqueous formaldehyde (1.5 ml) was slightly basified with a few drops of 0.1 *N* sodium hydroxide solution, and 90% formic acid (3.5 ml) was then added. The mixture was heated to reflux for 5 h and then evaporated and coevaporated with added portions of ethanol. The resultant material was taken up in cold ethanol (1 ml) and kept at 0°C for 30 min, after which time an undissolved residue was filtered off and the filtrate evaporated to dryness. The product was hydrolyzed in 0.1 *M* hydrochloric acid (2 ml) for 1 h at 90°C. Removal of the acid by coevaporation with 40% aqueous ethanol gave a semicrystalline, brownish mass which was decolorized in ethanolic solution with activated charcoal. Concentration of the filtrate, ice cooling, and dropwise addition of absolute ether readily gave crystalline **10** (19 mg, 32%) which was washed repeatedly with cold ether; mp 170–173.5°C, $[\alpha]_D$ +5.5° (equilibrium; *c* 1, water) (lit. (2), mp 172–174°C, $[\alpha]_D$ +4.6° (water)). The infrared spectrum of **10** (in KBr) showed excellent agreement with the depicted (2) spectrum of the natural product.

Acknowledgment

The National Research Council of Canada is thanked for financial support of this work.

1. R. Corbaz, L. Ettlinger, E. Gäumann, W. Keller-Schierlein, L. Neipp, V. Prelog, P. Reusser, and H. Zähner. Helv. Chim. Acta, **38**, 1202 (1955).
2. M. Brufani and W. Keller-Schierlein. Helv. Chim. Acta, **49**, 1962 (1966).
3. A. Kinumaki and M. Suzuki. J. Antibiot. **25**, 480 (1972).
4. N. Nishimura, K. Kumagai, N. Ishida, K. Saito, F. Kato, and M. Azumi. J. Antibiot. Ser. A, **18**, 251 (1965).
5. H. H. Baer, K. Čapek, and M. C. Cook. Can. J. Chem. **47**, 89 (1969).
6. A. C. Richardson. Carbohydr. Res. **4**, 422 (1967).
7. N. N. Lomakina, I. A. Spiridonova, I. Yu. N. Sheinker, and T. F. Vlasova. Khim. Prir. Soedin. **9**, 101 (1973); Chem. Abstr. **78**, 148170m (1973).
8. W. W. Lee, H. Y. Wu, J. E. Christensen, L. Goodman, and D. W. Henry. J. Med. Chem. **18**, 768 (1975).
9. (*a*) S. K. Gupta. Carbohydr. Res. **37**, 381 (1974); (*b*) K. Heyns, M. Lim, and J. I. Park. Tetrahedron Lett. 1477 (1976).
10. F. Arcamone, S. Penco, A. Vigevani, S. Redaelli, G. Franchi, A. DiMarco, A. M. Casazza, T. Dasdia, F. Formelli, A. Necco, and C. Soranzo. J. Med. Chem. **18**, 703 (1975).
11. (*a*) H. H. Baer and K. Čapek. Can. J. Chem. **47**, 99 (1969); (*b*) A. C. Richardson and K. A. McLauchlan. J. Chem. Soc. 2499 (1962).
12. H. H. Baer and C. W. Chiu. Can. J. Chem. **52**, 111 (1974).
13. H. H. Baer and F. F. Z. Georges. J. Org. Chem. **41**, 3474 (1976).
14. H. T. Clarke, H. B. Gillespie, and S. S. Weisshaus. J. Am. Chem. Soc. **55**, 4571 (1933).
15. M. E. Evans and F. W. Parrish. Methods Carbohydr. Chem. **6**, 177 (1972); **6**, 193 (1972).
16. J. Kovář, K. Čapek, and H. H. Baer. Can. J. Chem. **49**, 3960 (1971).
17. F. W. Lichtenthaler, J. Breunig, and W. Fischer. Tetrahedron Lett. 2825 (1971).

Molecular structures of dichloro(dimethyl)germane and trichloro(methyl)germane determined by vapour phase electron diffraction

JOHN E. DRAKE, J. LAWRENCE HENCHER,[1] AND QUANG SHEN

Department of Chemistry, University of Windsor, Windsor, Ont., Canada N9B 3P4

Received June 4, 1976

JOHN E. DRAKE, J. LAWRENCE HENCHER, and QUANG SHEN. Can. J. Chem. **55**, 1104 (1977).

The molecular structures of dichloro(dimethyl)germane and trichloro(methyl)germane have been determined in the vapour phase by electron diffraction. The principal geometrical parameters for $(CH_3)_2GeCl_2$ are r_g(Ge—Cl) = 2.143 ± 0.004 Å, r_g(Ge—C) = 1.928 ± 0.006 Å, ∠(ClGeCl) = 105 ± 2°, ∠(CGeCl) = 108 ± 2°, and ∠(CGeC) = 121 ± 4°. In the analysis of CH_3GeGl_3 recently reported values of the rotational constants were combined with the electron diffraction data to give r_g(Ge—Cl) = 2.132 ± 0.003 Å, r_g(Ge—C) = 1.893 ± 0.010 Å, ∠(CGeCl) = 112.3 ± 0.9°, and ∠(ClGeCl) = 106.4 ± 0.7°. In both cases the methylgermane geometry was assumed for the methyl group (r_g(C—H) = 1.103 Å and ∠(GeCH) = 110.5°) which was fixed in the staggered configuration with respect to the C_2GeCl_2 and $CGeCl_3$ frames respectively. Both random and systematic errors were included in the uncertainty estimates, which are believed to be approximately at the 95% confidence level. In the case of $(CH_3)_2GeCl_2$ the uncertainties in ∠(ClGeCl), ∠(CGeCl), and ∠(CGeC) were enlarged to four times the least-squares values in order to reflect the difficulty of resolving the Cl...Cl, C...Cl, and C...C distances in the analysis.

JOHN E. DRAKE, J. LAWRENCE HENCHER et QUANG SHEN. Can. J. Chem. **55**, 1104 (1977).

On a déterminé les structures moléculaires du dichloro(diméthyle)germane et du trichloro-(méthyle)germane en phase gazeuse en faisant appel à la diffraction des électrons. Les principaux paramètres géométriques du $(CH_3)_2GeCl_2$ sont r_g(Ge—Cl) = 2.143 ± 0.004 Å, r_g(Ge—C) = 1.928 ± 0.006 Å, ∠(ClGeCl) = 105 ± 2°, ∠(CGeCl) = 108 ± 2° et ∠(CGeC) = 121 ± 4°. Dans l'analyse du CH_3GeCl_3, les valeurs des constantes de rotation, qui ont été rapportées récemment, ont été combinées avec des données de diffractions d'électrons pour conduire aux valeurs r_g(Ge—Cl) = 2.132 ± 0.003 Å, r_g(Ge—C) = 1.893 ± 0.010 Å, ∠(CGeCl) = 112.3 ± 0.9°, et ∠(ClGeCl) = 106.4 ± 0.7°. Dans les deux cas on a fait l'hypothèse que la géométrie du méthyle du méthylgermane est (r_g(C—H) = 1.103 Å et ∠(GeCH) = 110.5°) et on a fixé ce groupe dans une configuration décalée par rapport respectivement aux dispositions des C_2GeCl_2 et $CGeCl_3$. On a inclu les erreurs systématiques ainsi que celles dues au hasard dans les estimés des incertitudes que l'on croit être approximativement au niveau de confiance de 95%. Dans le cas du $(CH_3)_2GeCl_2$, les incertitudes dans les angles ∠(ClGeCl), ∠CGeCl) et ∠(CGeC) sont agrandies jusqu'à un niveau de quatre fois les valeurs des moindres carrés de façon à refléter les difficultés qu'il y a de résoudre les distances Cl...Cl, C...Cl, et C...C dans l'analyse.

[Traduit par le journal]

Introduction

In the recently determined structures of Me_4Ge (1), Me_2GeF_2 and $MeGeF_3$ (2), and Me_2GeBr_2 and $MeGeBr_3$ (3), large variations in the bond lengths and valence angles were observed to depend on the number of halogen atoms. We now report the structures of Me_2GeCl_2 and $MeGeCl_3$ as part of a continuing study of this group of compounds.

Experimental

The samples of both compounds were obtained from Alfa Inorganics Inc. The nmr spectra revealed no known impurities after simple vacuum distillation.

Sectored electron diffraction patterns were recorded on Kodak Electron Image Plates, which were developed and microphotometered as previously described (1, 4). A summary of the experimental conditions is given in Table 1. The s scale ($s = (4\pi/\lambda)\sin(\theta/2)$, λ = electron wavelength) for the diffraction angle, θ, was determined from CS_2 diffraction patterns using the structure suggested by Kuchitsu (5).

The procedure used to extract the experimental molecular intensity, $sI_m^x(s)$, and the details of the corresponding theoretical expression were the same as previously described (1, 2). In the least-squares analysis a set of independent bond lengths and angles, based on the r_g interatomic distances (6), and the root-mean-square amplitudes, l_{ij}, were the parameters. A diagonal weight matrix was employed.

The parameter uncertainties were estimated as $2(\sigma_{1s}^2 + \sigma_{sys}^2)^{1/2}$. The σ_{1s}^2 were obtained from the diagonal elements of the zeroth order, error matrix, M_x^0 as M_x =

[1]To whom all correspondence should be addressed.

TABLE 1. Experimental conditions

Compound	Sample pressure[a] (torr)	Camera length (mm)	Exposure time (s)	Optical density range	Number of plates	Useful range of s values ($Å^{-1}$)	Resolution factor[b]
Me_2GeCl_2	8	296.68	15	0.1–0.3	3	3–16	1.303 (10)
	8	95.24	60, 65, 70	0.3–0.8	3	15–33	1.226 (13)
$MeGeCl_3$	8	296.79	15, 25, 30	0.2–0.4	3	3–16	1.260 (15)
	8	95.22	50, 60, 70	0.3–1.0	3	15–35	1.229 (20)

[a]High voltage 58 kV stabilized to $< 1 \times 10^{-4}$; beam current 1×10^{-7} A; background pressure during exposures, $1–3 \times 10^{-5}$ torr; nozzle temperature, 21°C.
[b]Resolution factor $= \sum(|sI_m(s)|)_{calc} / (|sI_m{}^x(s)|)$. Reference numbers in parentheses.

$R_{aa}M_x{}^0$ where $R_{aa} = 2\gamma/[\Delta s(\gamma^2 + r^2)]$, (6, 7). With $\Delta s = (\pi/10)$ $Å^{-1}$, $\gamma = 1$ Å and r, the bond length, 2 Å (Ge—Cl or Ge—C for example), $R_{aa} \approx 1.3$. The overall systematic error, σ_{sys} due to the s scale uncertainty was estimated to be ± 0.002 Å for an interatomic distance. The factor, 2, estimates the 95% confidence level, assuming that the errors are randomly distributed (7).

Tables of the reduced intensities, backgrounds, and $sI_m(s)$ are available from the Depository of Unpublished Data.[2]

Analyses

Analysis of $MeGeCl_3$

The independent geometrical parameters were r(C—H), r(Ge—C), r(Ge—Cl), ∠(CGeCl), and τ(HCGeCl) (the angle of rotation of the methyl group about the Ge—C bond, relative to the eclipsed configuration). All parameters involving hydrogen were given assumed values and fixed in the least-squares analysis.[3] Simultaneous refinement of the remaining geometrical parameters was only possible when l(C...Cl) and l(Ge—C) were fixed, and led to an uncertain value of r(Ge—C) but good results were obtained for r(Ge—Cl), (2.132 ± 0.003 Å) and ∠(CGeCl) (112 ± 1°). The angle was consistent with the values of ∠(CGeX) in $MeGeF_3$ (2) and $MeGeBr_3$ (3) which were also larger than tetrahedral.

In the course of this work, a partial r_s structure was reported (8), based on rotational constants obtained by microwave spectroscopy. The bond length r_s(Ge—Cl) = 2.135 ± 0.006 Å agreed with our result, barring the difference between the r_s and r_g distance formalisms; however, ∠(CGeCl) was reported to be 106.0 ± 0.7° which is smaller by 6° than our electron diffraction result. Also, the value of r_s(Ge—C) = 1.945 assumed by the authors in their analysis was several hundredths of an Angstrom longer than we have found for $MeGeF_3$ (1.904 ± 0.009 Å) and $MeGeBr_3$ (1.89 ± 0.03 Å). Although there were difficulties in the electron diffraction analysis, as noted above, the angle was thought to be well determined (±1°). There was no evidence of large amplitude vibrational effects such as unusual broadness of the r(Cl...Cl)/r(C...Cl) peak in the radial distribution curve, and the experimental l(Cl...Cl) agreed well with the value calculated from the harmonic force field (8). Moreover, this angle is *predicted to be greater* than 109.5° by both the rehybridization and VSEPR theories, on the basis of the electronegativity arguments (see Discussion below). The reason for the discrepancy is probably the large value assumed for r(Ge—C) in the spectroscopic treatment. In a preliminary analysis of the rotational constants we found that with r(Ge—C) = 1.90 Å fixed, ∠(CGeCl) approached the electron diffraction result.

It was apparent that neither technique could determine all the parameters simultaneously; however, if the electron diffraction results were assumed for r(Ge—Cl) and ∠(CGeCl) and the methyl group geometry (r(C—H), ∠(GeCH), and τ(HCGeCl)) was transferred from methylgermane, only r(Ge—C) would remain to be determined from the rotational constants.

In the combined analysis of the spectroscopic and electron diffraction data, the structural parameters were referred to the distances between the mean atomic positions, $r_\alpha{}^0$ (0 K, electron diffraction) and equivalently r_z (ground vibrational state, spectroscopic) obtained by

[2]Photocopies may be obtained at a nominal charge, upon request, from the Depository of Unpublished Data, CISTI, National Research Council of Canada, Ottawa, Canada K1A 0S2.

[3]The scattering components due to r(C—H), r(Ge...H), etc. were very weak compared to r(Ge—Cl) and r(Cl...Cl) and were not well enough resolved to determine these parameters.

TABLE 2. r_z[a] structure of $MeGeCl_3$ and calculated rotational constants

Compound	B_0 (expt) (MHz)	B_z (MHz) Expt.[b]	B_z (MHz) Calcd.[c]
$Me^{70}Ge^{35}Cl_3$	1602.19±0.1	1601.38	1601.14
$Me^{72}Ge^{35}Cl_3$	1601.42±0.1	1600.62	1600.31
$Me^{74}Ge^{35}Cl_3$	1600.71±0.1	1599.91	1599.50
$Me^{70}Ge^{37}Cl_3$	1537.84±0.5	1537.04	1537.42
$Me^{72}Ge^{37}Cl_3$	1537.10±0.5	1536.32	1536.57
$Me^{74}Ge^{37}Cl_3$	1536.36±0.5	1535.56	1535.73

Compound	Parameter	Value	Parameter	Value Expt.	Value Calcd.
$Me^{72}Ge^{37}Cl^{35}Cl_2$	A_0	1597.96±0.5	A_z	1597.15	1598.15
	B_0	1559.31±0.5	B_z	1558.52	1560.35
	C_0	1203	C_z	1203	1205
$Me^{74}Ge^{37}Cl^{35}Cl_2$	A_0	1597.17±0.5	A_z	1596.36	1597.33
	B_0	1558.59±0.5	B_z	1557.79	1559.55
	C_0	1207	C_z	1207	1205

Parameter	Value
r_z(Ge—C)[d]	1.889(6) Å
r_z(Ge—Cl)	2.129 Å (assumed)
∠(CGeCl)[d]	112±1°
r_z(C—H)	1.083 Å
∠(GeCH)[e]	110.5°

[a] $r_z \approx r_\alpha^0$, see text.
[b] The rotational constant corrected for harmonic vibrational motion.
[c] The rotational constant calculated from the r_z geometrical parameters.
[d] See text for discussion of error limits.
[e] Taken from the methylgermane structure, see ref. 8.

making corrections for the effects of vibrational averaging on the interatomic distances and rotational constants respectively. The r_α^0 (9) were obtained from

$$[1] \quad r_\alpha^0 = r_g - \tfrac{3}{2}a[(l_{ij}^T)^2 - (l_{ij}^0)^2] - K_{ij}^0$$

where the Morse anharmonicity constants, a, were obtained from the estimated quadratic and cubic force constants (10) as 1.6 $Å^{-1}$ for Ge—Cl and 1.7 $Å^{-1}$ for Ge—C. The l_{ij}^T (T K = sample temperature), l_{ij}^0 (0 K) and K_{ij}^0 (0 K) (the vibrational correction due to the vibrational motion perpendicular to the bond), calculated from the known force field (8) by the methods of Stølevik *et al.* (11), are given in Table 3. The r_z were obtained from the $B_z^{(\alpha)}$ ($\alpha = a$, b, or c axis) (12) which were given by

$$[2] \quad B_z^{(\alpha)} = B_0^{(\alpha)} - \sum_{p=1}^{3N-6} \frac{B^2}{\omega_s}\left[3A_{ss}^{(\alpha\alpha)}\, 4 \sum_{\substack{s' \neq s \\ \omega_{s'} \neq \omega_s}} (\zeta_{ss'}^{(\alpha)})^2 \omega_{s'}^2/(\omega_s^2 - \omega_{s'}^2) - 3 \sum_{s'=s} (\zeta_{ss'}^{(\alpha)})\right]$$

where

$$A_{ss}^{(\alpha\alpha)} = 1 - \sum_i (l_{is}^{(\alpha)})^2$$

$$\zeta_{ss'}^{(\alpha)} = \sum_i (l_{is}^{(\beta)}\, l_{is'}^{(\gamma)} - l_{is}^{(\gamma)} l_{is'}^{(\beta)})$$

and $l_{is}^{(\alpha)}$ is the component of the ith atom in the sth normal mode for axis α. In all cases the x, y, and z axes were transformed to coincide with the inertial axes a, b, and c. The $\zeta_{ss'}^{(\alpha)}$ are the Coriolis coupling constants for normal modes s and s'.[4] A small correction for centrifugal distortion was ignored. As a test, the computer program successfully reproduced the previously reported

[4] Equation 2 differs from the reference in the notation used for the sums. Here, $\omega_{s'} = \omega_s$ indicates degenerate modes.

TABLE 3. The molecular structures (r_g) of Me_2GeCl_2 and $MeGeCl_3$[a]

	Value					
			$MeGeCl_3$			
	Me_2GeCl_2			l_{ij}[c]		K_{ij}[c]
Parameter	r_g	l_{ij}[c] (expt)	r_g	298 K	0 K	(0 K)
r(C—H)	1.103	0.078	1.103[b]	0.078	0.078	0.0200
r(Ge—C)	1.928(6)	0.050	1.893(10)[b]	0.049	0.047	0.0041
r(Ge—Cl)	2.143(4)	0.046	2.132(4)	0.047	0.041	0.0013
∠(ClGeCl)	105(2)		106.4(7)			
∠(CGeCl)	108(2)		112.3(9)			
∠(CGeC)	121(4)		—			
∠(CGeH)	110.5		110.5			
τ(ClGeCH)	360 (staggered)		60 (staggered)			
Cl...Cl	3.394	0.110	3.416(18)	0.104	0.066	0.0006
C...Cl	3.289	0.116	3.346(15)	0.13	0.081	0.0017
C...C	3.348	0.100	—			
Ge...H	2.546	0.117	2.51	0.118	0.116	0.0191
k_L	1.303(10)		1.260(15)			
k_S	1.226(13)		1.229(20)			
R	0.064		0.096[d]			

[a]Distances in Å and angles in degrees are based on the r_g distances and least-squares parameters given in Tables 4 and 5. The quoted uncertainties reflect both random and systematic errors discussed in the text.
[b]r_g values calculated from the r_z distances given in Table 2.
[c]All rms amplitudes calculated from the molecular force fields.
[d]$R = \{\Sigma_s[sM_{expt}(s) - sM_{theor}(s)]^2/\Sigma_s[sM_{expt}(s)]^2\}^{1/2}$.

vibrational parameters and rotational constants for H_2O (13), COF_2 (13), CH_3CN (14), and B_2H_6 (9). The observed and calculated rotational constants and the r_z structural parameters are presented in Table 2.

The differences between the observed and calculated $B_z^{(\alpha)}$'s for the symmetrically substituted species correspond to a ±0.002 Å variation in r_z(Ge—C) if all other parameters are considered exact. The agreement in the $MeGe^{37}Cl^{35}Cl_2$ cases is somewhat worse and may be a reflection of the severe constraints which were adopted. It was found that ±1° variation in ∠(GeCH) resulted in a further ±0.006 variation in r_z(Ge—C). Taking these factors into account it appeared that r_z(Ge—C) = 1.889 ± 0.010 Å was a reasonable estimate.

The r_g(Ge—C) parameter was obtained from r_z(Ge—C) using eq. 1 and fixed in a subsequent least-squares analysis of the electron diffraction data alone. The resulting r_g structure is presented in Table 3 and the matrix of correlation coefficients is given in Table 4. The molecular intensity is presented in Fig. 1.

Analysis of Me_2GeCl_2

The independent geometric parameters selected for Me_2GeCl_2 were r(C—H), r(Ge—C), r(Ge—Cl), ½∠(ClGeCl), ∠(ZGeCl) (π − ½∠(CGeC)), ∠(HCGe), and τ(HCGeCl) (the angle of rotation of the C—H bond about Ge—C relative to Ge—Cl). As in the case of $MeGeCl_3$ all parameters involving hydrogen atoms were given fixed values.[3]

TABLE 4. Correlation matrix for refined parameters of $MeGeCl_3$ (electron diffraction data only)

	r(Ge—Cl)	∠(CGeCl)	k_L[b]	k_S[b]
σ_{1s}[a]	0.0009	0.28	0.015	0.021
	1.000	0.227	0.038	−0.030
		1.000	−0.097	−0.097
			1.000	−0.388
				1.000

[a]Least-squares uncertainties representing only random errors in the present electron diffraction data.
[b]k_L, k_S are resolution factors for long and short camera lengths respectively.

In the least-squares analysis it was found that ½∠(ClGeCl), ∠(ZGeC), l(Ge—C), l(Cl...Cl), l(C...Cl), and l(C...C) could not be refined simultaneously because the scattering components due to r(Cl...Cl), r(C...Cl), and r(C...C) could not be resolved. This difficulty was partly overcome by fixing the l_{ij}'s at values calculated from the molecular force field (15). The correlation coefficients of the least-squares parameters are given in Table 5. The molecular

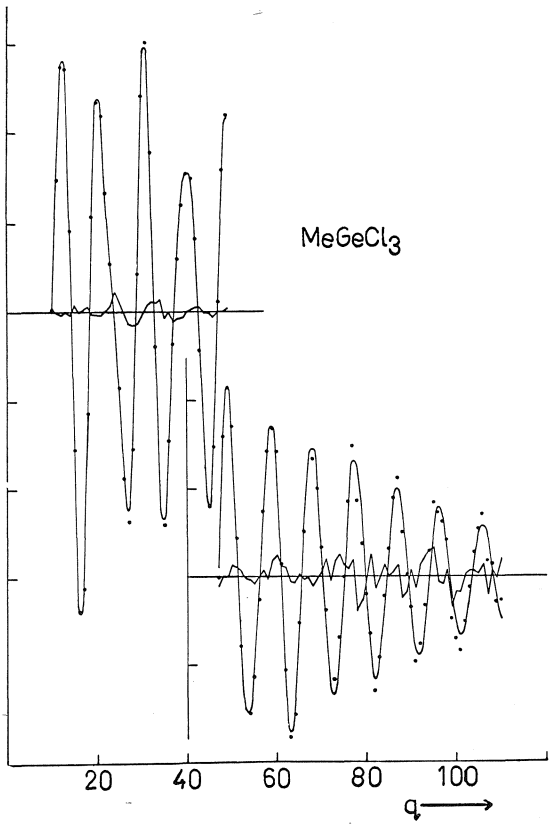

FIG. 1. The molecular intensity of $MeGeCl_3$. (*A*) Experimental (dots), theoretical (solid), and difference curves for the long distance camera. (*B*) Experimental (dots), theoretical (solid), and different curves for the short distance camera. The theoretical curves were calculated from the final structural parameters.

structure, based on these parameters, is given in Table 3. The molecular intensity $sI_m(s)$ is given in Fig. 2.

The difficulty of determining the two angle parameters is clear from the values of the Cl...Cl, C...Cl, and C...C distances given in Table 3, which are within less than a mean square amplitude of each other. Even with r(Ge—Cl) and r(Ge—C) well determined, and with independently obtained l_{ij}'s, these distances cannot be resolved mainly because the weakest component, due to C...C is comparable with the random intensity errors. Moreover, the effects of systematic intensity errors (16) were not evaluated in the present analysis. As a consequence, the uncertainties in the angles were much larger than indicated by the least-squares analysis. As a rough estimate, based on the comparison of trends in these angles within Me_2GeF_2 and Me_2GeBr_2, which were previously determined, the uncertainties in the angles were taken as four times the least-squares estimates.

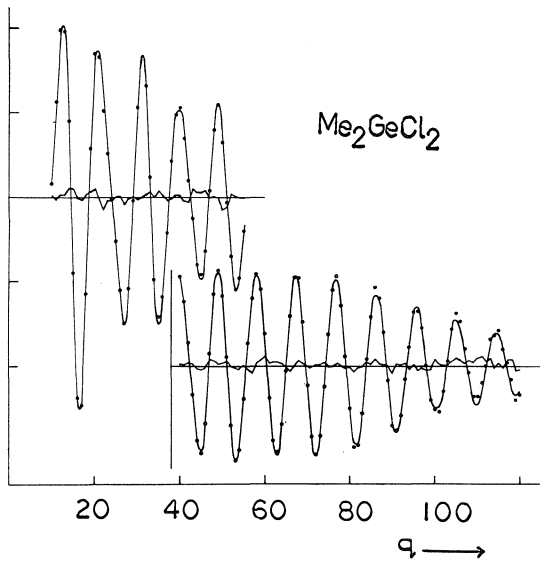

FIG. 2. The molecular intensity of Me_2GeCl_2. (*A*) Experimental (dots), theoretical (solid), and difference curves for the long distance camera. (*B*) Experimental (dots), theoretical (solid), and difference curves for the short distance camera. The theoretical curves were calculated from the final structural parameters.

Discussion

The structures of Me_3GeCl (16), Me_2GeCl_2, $MeGeCl_3$ (see Table 6) follow the same trends as the corresponding fluorides (2) and bromides (3). When successive chlorines are substituted for methyl groups, both the Ge—C and Ge—Cl bonds become shorter, and the angles deviate from the tetrahedron in the way predicted by the valence shell electron pair repulsion model (VSEPR) (18) as discussed previously (2). The observed trends in Ge—C bond length suggest that the change does not depend much on the species of halogen atom. In the trihalides, $MeGeX_3$, r(Ge—C) = 1.89(3) (Br), 1.893(10) (Cl), and 1.904(9) (F), while in the dihalides, Me_2GeX_2, r(Ge—C) = 1.91(1) (Br), 1.924(6) (Cl), and 1.928(3) (F). The overall large variation in bond length depends on the number of halogen atoms, not whether they are F, Cl, or Br. This trend is borne out by the similarities in the angles: XGeX angles ~ 105°, CGeX ~ 107° in the dihalides; and XGeX ~ 106° and CGeX ~ 112° in the trihalides.

TABLE 5. Correlation matrix for Me_2GeCl_2[a]

	r(Ge—Cl)	$\frac{1}{2}\angle$(ClGeCl)	r(Ge—C)	$\angle$(ZGeC)	k_L	k_S
σ	0.0005	0.2133	0.0021	0.6612	0.0104	0.0127
	1.000	−0.145	0.310	−0.138	−0.014	0.065
		1.000	−0.234	0.089	0.197	0.165
			1.000	−0.225	−0.417	0.387
				1.000	−0.035	−0.079
					1.000	−0.466
						1.000

[a]See footnotes of Table 4.

TABLE 6. Comparison of bond lengths and formal charges

Compound	r(Ge—Cl)	r(Ge—C)	δ_{Ge}	δ_{Cl}	δ_C	δ_H
$GeCl_4$[a]	2.112(1)	—	0.136	−0.034	—	—
CH_3GeCl_3[b]	2.132(4)	1.893(10)	0.028	−0.099	0.020	0.083
$(CH_3)_2GeCl_2$[b]	2.143(4)	1.928(6)	−0.031	−0.134	−0.010	0.053
$(CH_3)_3GeCl$[c]	2.170(1)	1.940(1)	−0.067	−0.156	−0.028	0.034
$(CH_3)_4Ge$[d]	—	1.945(3)	−0.092	—	−0.041	0.021
$HGeCl_3$[e]	2.118(1)	—	0.081	−0.067	—	—
H_2GeCl_2[f]	2.130(3)	—	0.028	−0.099	—	—
H_3GeCl[g]	2.148(3)	—	−0.029	−0.134	—	—
$FGeCl_3$[h]	2.067(5)	—	0.297	−0.063	—	—
Cl_3CGeCl_3[i]	2.111(1)	1.98(1)	0.134	−0.035	0.076	—

[a]Reference 18.
[b]Present work.
[c]Reference 17.
[d]Reference 1.
[e]Reference 22. The Ge—Cl bond length (r_0 = 2.114(1)) was corrected to r_g for the present comparison.
[f]Reference 23.
[g]Reference 24.
[h]Reference 25.
[i]Reference 21.

The major changes in geometry are strongly correlated with changes in charge distribution. In Table 6, formal atomic charges estimated by equalizing electronegativities (20) are compared with the r(Ge—Cl) and r(Ge—C) of several molecules. The effect of successive halogen substitution in the methyl series is to make *all* the atoms more positive and to increase the difference in charges between germanium and the ligand. The angles between negatively charged ligands tend to be smallest, while those between positively charged ligands tend to be largest (see Table 2) which is consistent with the VSEPR model.

Acknowledgments

The authors wish to thank Dr. L. S. Bartell for very helpful discussions, particularly concerning the error analysis. The financial support of the National Research Council of Canada is also gratefully acknowledged.

1. J. L. HENCHER and F. J. MUSTOE. Can. J. Chem. **53**, 3542 (1975).
2. J. E. DRAKE, R. T. HEMMINGS, J. L. HENCHER, F. J. MUSTOE, and Q. SHEN. J. Chem. Soc. Dalton, 394 (1976).
3. J. E. DRAKE, R. T. HEMMINGS, J. L. HENCHER, F. J. MUSTOE, and Q. SHEN. J. Chem. Soc. Dalton, In press.
4. G. BARBE, J. L. HENCHER, Q. SHEN, and D. G. TUCK. Can. J. Chem. **52**, 3936 (1974).
5. K. KUCHITSU. Molecular vibrations and structure studies. *Edited by* S. J. Cyvin. Elsevier, Amsterdam. 1972. Chapt. 10.
6. L. S. BARTELL. Physical methods in chemistry. Vol. 1. 4th ed. *Edited by* A. Weissberger and B. W. Rossiter. Interscience, New York. 1971.
7. L. S. BARTELL and M. G. ANASHKIN. J. Mol. Struct. **17**, 193 (1973).
8. J. R. DURIG, P. J. COOPER, Y. S. LI. J. Mol. Spectrosc. **57**, 169 (1975).
9. K. KUCHITSU. J. Chem. Phys. **49**, 4456 (1968).
10. D. R. HERSCHBACH and V. W. LAURIE. J. Chem. Phys. **35**, 458 (1961).
11. R. STØLEVIK, H. M. SEIP, and S. J. CYVIN. Chem. Phys. Lett. **15**, 263 (1972).

12. K. KUCHITSU, T. FUKUYAMA, and Y. MORINO. J. Mol. Struct. **4**, 41 (1969).
13. S. J. CYVIN. Molecular vibrations and mean square amplitudes. Elsevier, Amsterdam. 1968.
14. T. FUKUYAMA and K. KUCHITSU. J. Mol. Struct. **5**, 131, (1970).
15. J. E. DRAKE, J. L. HENCHER, and Q. SHEN. In preparation.
16. L. S. BARTELL and H. YOW. J. Mol. Struct. **15**, 173 (1973).
17. Y. S. LI and J. R. DURIG. Inorg. Chem. **12**, 306 (1973).
18. Y. MORINO, Y. NAKAMURA, and T. IIJIMA. J. Chem. Phys. **32**, 643 (1960).
19. R. J. GILLESPIE. Molecular geometry. Van Nostrand Reinhold, London. 1972.
20. J. E. HUHEEY. J. Phys. Chem. **69**, 3284 (1965).
21. I. HARGITTAI, E. VAJOLA, A. K. MALTSEV, and O. M. NEFEDOV. J. Mol. Struct. **23**, 417 (1974).
22. P. VENKATESWARLU, R. MOCHLER, and W. GORDY. J. Chem. Phys. **21**, 1713 (1953).
23. B. BEAGLEY, P. BROWN, and J. M. FREEMAN. J. Mol. Struct. **18**, 335 (1973).
24. R. C. LORD and C. M. STEESE. J. Am. Chem. Soc. **76**, 542 (1954).
25. W. E. ANDERSON, J. SHERIDAN, and W. GORDY. Phys. Rev. **81**, 819 (1951).

Carbohydrates as chiral intermediates in organic synthesis. Two functionalized chemical precursors comprising eight of the ten chiral centers of erythronolide A[1]

STEPHEN HANESSIAN AND GEORGES RANCOURT[2]

Department of Chemistry, University of Montreal, Montreal, P.Q., Canada H3C 3V1

Received December 29, 1976

STEPHEN HANESSIAN and GEORGES RANCOURT. Can. J. Chem. **55**, 1111 (1977).

Two appropriately functionalized branched-chain sugars have been synthesized as potentially useful chemical precursors to erythronolide A, encompassing its C-1–C-6 and C-9–C-15 segments respectively.

STEPHEN HANESSIAN et GEORGES RANCOURT. Can. J. Chem. **55**, 1111 (1977).

La synthèse de deux sucres ramifiés et fonctionnalisés, qui seraient potentiellement utiles comme précurseurs chimiques de l'érythronolide A, et correspondant à ses segments C-1–C-6 et C-9–C-15 respectivement est décrite.

In connection with a long-standing program designed to utilize carbohydrates as chiral intermediates in organic synthesis, we now report the synthesis of two, fully functionalized precursors to erythronolide A, **1**, encompassing its C-1–C-6 and C-9–C-15 segments, respectively. Efforts directed toward the total synthesis of macrolide antibiotics (1) have been recently highlighted by the ingenious development of macrolactonization procedures (2–4), and the first total synthesis of a macrolide antibiotic, methymycin (4), and a partial synthesis of tylonolide hemiacetal (5). The pursuit of equally formidable synthetic objectives will undoubtedly be immensely facilitated in the immediate future, by the availability of appropriately substituted, chiral precursors, in preparatively significant quantities.

The task of overcoming the functional and stereochemical complexities present in erythronolide A, **1**,[3] can be considerably simplified with the recognition of the sequence of chiral centers as two functionalized, acyclic, carbohydrate-derived chains (6). This can be best illustrated in **2**, where C-1–C-6, and C-9–C-15 can be configurationally related to two precursors, I and II, having the L-*ido* and D-*gluco* stereochemistry, respectively. Our synthetic plan for the elabora-

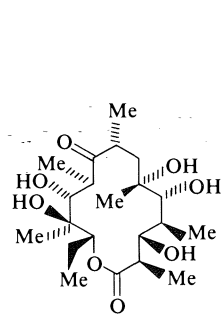

1

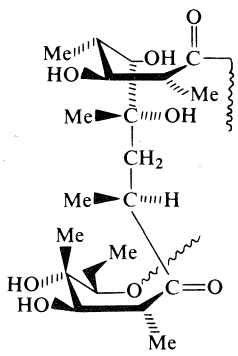

2

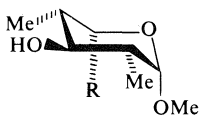

Precursor I
R = COOMe, COMe

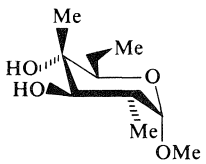

Precursor II

[1]Portions of this work were disclosed at a symposium on Modern research related to asymmetry in carbohydrates, Centennial meeting, Am. Chem. Soc., New York, NY, 1976; see ref. 6.

[2]NRCC predoctoral fellow.

[3]Because of the phenomenon of pseudorotation, the various groups in **1** tend to adopt orientations that depend on the arbitrary choice of conformation (see for example, ref. 7).

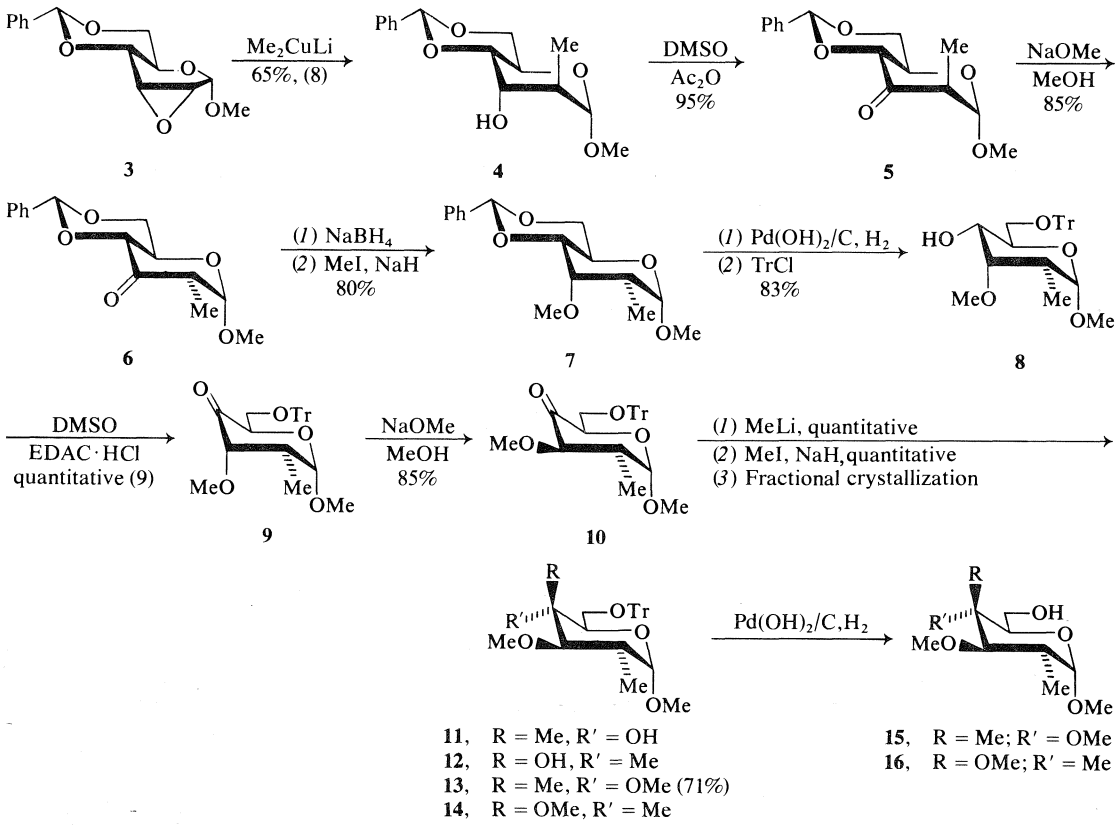

SCHEME 1. **4**, mp 111.5–112.5°C, $[\alpha]_D$ +118.1°; **5**, mp 125.5–127°C, $[\alpha]_D$ +75.2°; **6**, mp 199–201°C, $[\alpha]_D$ +143.6°C; **7**, mp 140–141°C, $[\alpha]_D$ +115.4°; **8**, mp 135–137°C, $[\alpha]_D$ +79.8°C; **10**, mp 137.5–139.5°C, $[\alpha]_D$ +130.1°C; **11**, syrup, $[\alpha]_D$ +53.1°C; **12**, mp 133–135°C; **13**, mp 155–157°C, $[\alpha]_D$ +72.9°; **15**, syrup, $[\alpha]_D$ +167°.

tion of these two precursors starts with D-glucose, and is based on the systematic and stereocontrolled introduction of appropriate functional groups as illustrated in Schemes 1 and 2.[4]

Precursor I

Detritylation of the mother liquors resulting from the crystallization of **13**, gave a mixture of **15** and **16**, which was oxidized (10) to the 6-*aldehydo* derivatives **17** (Scheme 2). Treatment of **17** with aqueous calcium hydroxide afforded **18** as a syrup (85–90%); $[\alpha]_D$ +227°, which was converted in high yield to **19** (syrup), $[\alpha]_D$ +184.5° by a known procedure (11). Catalytic hydrogenation of **19**, gave, almost exclusively, the expected product **20**, as a syrup (85–90%); $[\alpha]_D$ +97.3°.[5] Alternatively, treatment of the mixture of **17** with methyllithium, and oxidation (12) of the resulting mixture of epimeric alcohols to the ketones **21**, followed by base-catalyzed elimination (NaOMe), gave **22** as a syrup (64%); $[\alpha]_D$ +193.6°. Catalytic hydrogenation gave the expected product **23** (syrup), $[\alpha]_D$ +157.3°.[5,6]

Precursor II

Detritylation of the crystalline isomer **13** gave **15**, which was oxidized (10) to **24** (90–95%), and the latter was transformed via a Wittig reaction into **25** (syrup), $[\alpha]_D$ +190.2°. Catalytic hydro-

[4]New crystalline compounds gave correct microanalyses. All compounds had ^{1}Hmr and mass spectral features that were in accord with their structures. Yields are not optimized and melting points are uncorrected. Optical rotations were measured at 25°C in chloroform, at concentrations of 0.5–1.5%.

[5]A *CI* conformation is indicated from ^{1}Hmr data.

[6]Treatment of **23** with base (NaOMe) effected virtually complete epimerization at C-5.

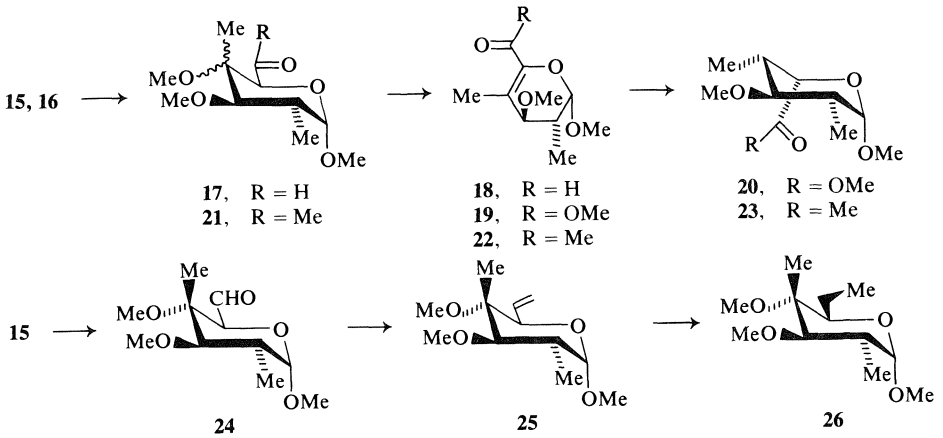

SCHEME 2

genation gave the desired product **26** as a syrup (85%), $[\alpha]_D$ +169.3°.

It is pertinent to note that the easily obtainable **13**, and the mother liquors resulting from its crystallization, are individually used in the preparation of precursors II and I, respectively, thus rendering the entire sequence highly efficient.

Compounds **20** (or **23**) and **26** are suitably protected derivatives of precursors I and II that can be obtained in gram quantities via a synthetic scheme involving crystalline intermediates, without recourse to chromatographic separation. These compounds comprise eight of the ten chiral centers and all but a two-carbon segment bearing a *C*-methyl group present in erythronolide A. The chiral and functional relationships between these compounds and the C-1–C-6 and C-9–C-15 segments of erythronolide A are depicted in Scheme 3.

The particular attributes of this seldom exploited carbohydrate precursor approach to total synthesis, as exemplified in this paper, are its conceptual simplicity, versatility, and practicality.[7] It is also evident that the total synthesis of other macrolide aglycones could be based on a similar approach, involving carbohydrate-derived precursors such as I and II that can be further manipulated and incorporated into the structural framework of these complex molecules.

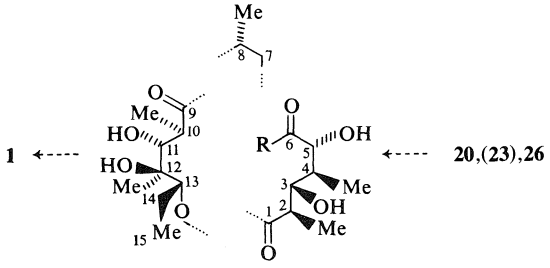

SCHEME 3

[7]A basically similar approach has been alluded to (13), and has led to a study of chain-branching reactions at C-2 and C-4 in sugar derivatives.

Acknowledgments

We thank the National Research Council of Canada and Le Ministère de l'éducation du Québec for financial support and for fellowships to G.R. It is also a pleasure to acknowledge the technical assistance of C. Bacquet, A. Côté, and C. Dufresne.

1. W. D. Celmer. Pure Appl. Chem. **28**, 413 (1971).
2. E. J. Corey and K. C. Nicolaou. J. Am. Chem. Soc. **96**, 5614 (1974).
3. E. J. Corey, K. C. Nicolaou, and L. S. Melvin, Jr. J. Am. Chem. Soc. **97**, 654 (1975).
4. S. Masamune, H. Yamamoto, S. Kamata, and A. Fukugawa. J. Am. Chem. Soc. **97**, 3513 (1975).
5. S. Masamune, Y. Hayase, W. K. Chan, and R. L. Sobczak. J. Am. Chem. Soc. **98**, 7874 (1976).
6. S. Hanessian and G. Rancourt. Abstracts papers, Centennial meeting, Am. Chem. Soc., CARB 32, April 1976, New York, NY.
7. T. J. Perun and R. S. Egan. Tetrahedron Lett. 387 (1969).
8. D. R. Hicks and B. Fraser-Reid. Can. J. Chem. **53**, 2017 (1975); S. Hanessian and G. Rancourt. Unpublished results.
9. J. C. Sheehan and P. A. Cruickshank. Org. Synth. **48**, 83 (1968).
10. J. C. Collins, W. W. Hess, and F. J. Frank. Tetrahedron Lett. 3303 (1968).
11. E. J. Corey, N. W. Gilman, and B. E. Ganem. J. Am. Chem. Soc. **90**, 5616 (1968).
12. E. J. Corey and J. W. Suggs. Tetrahedron Lett. 2647 (1975).
13. M. Miljkovic and D. Glisin. J. Org. Chem. **40**, 3357 (1975); M. Miljkovic, M. Gligorijevic, T. Satoh, and D. Miljkovic. J. Org. Chem. **39**, 1379 (1974).

Canadian Journal of Chemistry

Journal canadien de chimie

Published by
THE NATIONAL RESEARCH COUNCIL OF CANADA

Publié par
LE CONSEIL NATIONAL DE RECHERCHES DU CANADA

Volume 55 Number 7 April 1, 1977

Volume 55 numéro 7 1 avril 1977

Synthesis and crystal structure of diiodotetraethylthiuramdisulfidemercury(II)

CHUNG CHIEH

Guelph–Waterloo Centre for Graduate Work in Chemistry, Waterloo Campus, University of Waterloo, Waterloo, Ont., Canada N2L 3G1

Received October 18, 1976

CHUNG CHIEH. Can. J. Chem. **55**, 1115 (1977).

Reaction of mercury(II) iodide with tetraethylthiuramdisulfide in chloroform and ethanol mixed solvent produced bis(iodo-*N*,*N*-diethyldithiocarbamatomercury(II)) and diiodotetraethylthiuramdisulfidemercury(II), HgI_2.TETD. The crystal of HgI_2.TETD is orthorhombic with $a = 13.101(9)$, $b = 13.999(9)$, $c = 22.742(15)$ Å; space group *Pbca*. The structure was solved with 1960 observed reflections measured by a G.E. XRD-6 diffractometer. The final R factor was 0.064. The mercury atom is four-coordinated with two identical Hg—I distances of 2.668(1) Å and two Hg—S distances of 2.670(7) and 2.737(7) Å. The coordination is tetrahedral.

CHUNG CHIEH. Can. J. Chem. **55**, 1115 (1977).

La réaction de l'iodure mercurique(II) avec le tétraéthylthiuramdisulfure dans un solvant mixte de chloroforme et d'éthanol conduit au bis(iodo-*N*,*N*-diéthyldithiocarbamatomercure(II)) et au diiodotétraéthylthiuramdisulfure mercure(II), HgI_2.TETD. Le cristal de HgI_2.TETD est orthorhombique avec $a = 13.101(9)$, $b = 13.999(9)$, $c = 22.742(15)$ Å; groupe d'espace *Pbca*. On a résolu la structure à partir des 1960 réflexions observées par des mesures avec un diffractomètre G.E. XRD-6. Le facteur final de R est de 0.064. L'atome de mercure est tétracoordonné avec deux distances Hg—I identiques de 2.668(1) Å et deux distances Hg—S de 2.670(7) et 2.737(7) Å. La coordination est tétraédrique.

[Traduit par le journal]

Introduction

Chelating agents furnish the basis for medical treatment of many kinds of heavy metal poisoning. For example 2,3-dimercapto-1-propanol or BAL (British Anti-Lewisite) was used as an antidote for arsenic poisoning (1), and it was also found to be effective in the treatment of mercury poisoning. The affinity between mercury and the —SH group led to the use of unithiol, D-penicillamine, and *N*-acetyl-D-penicillamine as therapeutic agents for mercury poisoning but not without problems (2, 3). For a compound to be effective in removing heavy metals from a biological system, it or its metabolic products should form a stable complex and facilitate subsequent excretion. A cautious approach must be taken in the use of chelating agents, for complexation may enhance the toxicity of metal ions (4). Chelating agents containing —SH groups have been used in medicine, but no consideration has been given to compounds containing C=S groups as possible therapeutic agents (1). Thiourea (tu, $SC(NH_2)_2$) forms a series of complexes with mercury(II) chloride of stoichiometry $HgCl_2(tu)n$ ($n = 1$–4) (5, 6). In view of the complicated coordination chemistry between mercury and sulfur, the interaction of mercurials and tetraethylthioperoxydicarbonic diamide, which is better known as tetraethylthiuram disulfide (TETD), was studied. Some of the results have been published (7, 8). The reaction of mercury(II) iodide with TETD

in ethanol–chloroform solution (1:1 by volume) produced diiodotetraethylthiuramdisulfidemercury(II) in addition to bis(iodo-*N*,*N*-diethyldithiocarbamatomercury(II)) (8).

Although the existence of a HgI_2.TETD complex was mentioned by Brinkhoff *et al.* in their nmr studies (9), the formation of $(Et_2NCS_2HgI)_2$ was not mentioned. Both compounds were obtained in the same reaction; however their crystals were different in shape. Crystals of $(Et_2NCS_2HgI)_2$ were hexagonal prisms or sometimes irregular in shape whereas HgI_2.TETD crystals were square plates. The crystal structure of the latter is described in this paper.

Experimental

The red form of mercury(II) iodide was purchased from Fisher Scientific Co. and tetraethylthiuram disulfide from Sigma Chemical Company, St. Louis, MO. Reagent grade chloroform and absolute ethanol were used.

To 50 ml solution of TETD (0.21 g) in chloroform–ethanol (1:1 by volume), red crystalline mercury(II) iodide (0.32 g) was added. At room temperature (25 ± 3°C) the reaction proceeded rather quickly. In about 10 min, yellow square plates were seen under a 30× microscope. Both the red mercury(II) iodide and square plate crystals dissolved slowly resulting in a pale yellow solution in a few hours. The solution was then partially covered to allow slow evaporation. When the solution was reduced to 1 ml, both square plates and hexagonal prisms were obtained after filtration. Due to the fact that both crystals were of the same color, it was a difficult task to obtain enough sample for elemental analysis by separation under the microscope. With mixture, elemental analysis would have been meaningless. However, single crystals suitable for X-ray diffraction studies were easily chosen.

Raman spectra of solids were obtained on a Jarrel-Ash 25-100 spectrometer with argon ion laser excitation.

Cell constants and space groups were determined from photographic measurements; however, the former were refined by least-squares methods based on the 2θ (MoKα, Zr-filtered radiation) values of 17 reflections measured on a G.E. XRD-6 diffractometer.

Crystal Data

$C_{10}H_{20}HgI_2N_2S_4$ fw = 750.9

Orthorhombic, a = 13.101(9), b = 13.999(9), c = 22.742(15) Å, V = 4170.9 Å^3; ρ_m = 2.40(1) (by floatation), Z = 8, ρ_c = 2.391, (25°C, Mo–Kα, λ = 0.7107 Å); mp = 136°C; μ(MoKα) = 109.0 cm^{-1}. Space group *Pbca* (from systematic absences $0kl$, $k = 2n + 1$, $h0l$, $l = 2n + 1$; $hk0$, $h = 2n + 1$).

The crystal used for intensity measurements was approximately a sphere of diameter 0.13 mm cut from a square plate. The crystal was mounted with [111] along the φ axis of the goniostat of a G.E. XRD-6 card-controlled automatic diffractometer, which was equipped with a scintillation counter, pulse height analyzer, and Hewlett-Packard Scaler-Timer (Model 5201L). Intensities of 6044 reflections with 2θ ≤ 60 (Zr-filtered MoKα radiation) were measured using the stationary-crystal stationary-counter method. The scan method was not suitable because of the long c-axis. Four standard reflections (020, 112, 200, and 220) were repeatedly measured after each 100 reflections and showed a fluctuation of ±3% in their intensities throughout the data collection period. An averaged background curve as a function of 2θ was obtained from measurements with the crystal in several orientations. Integrated intensities were calculated by subtracting the corresponding backgrounds from the 30-second-counts for all reflections. Standard deviations $\sigma(I)$ were estimated according to counting statistics. A set of 1960 reflections for which $I > 3\sigma(I)$ was considered as observed and used in the structure determination. Many of the high-angle (2θ ≥ 45°) reflections were unobserved. No absorption correction was made (μ_R = 0.71). Lorentz and polarization correction were applied to derive the structure amplitudes.

The structure was solved by heavy atom methods. The initial x-coordinate for Hg atom was zero, and the Fourier map obtained from the phase of Hg only had false symmetry. When the two iodine atoms were included to calculate the phase, the Fourier map revealed the four sulfur atoms. Other non-hydrogen atoms were located in subsequent Fourier maps. With 19 atoms of Table 1 having isotropic thermal parameters, full-matrix least-squares refinement led to a $R = (\Sigma||F_o| - |F_c||)/\Sigma|F_o| = 0.13$. The revised program written by Doedens and Ibers was used. The atomic scattering factors from Cromer and Waber (10) were used with anomalous dispersion coefficients for Hg and I atoms from Cromer (11). With anisotropic thermal parameters for all atoms and a weighting scheme of $w^{-1} = (90.0 - F_o + 0.001F_o^2)$, the refinements gave $R = 0.064$ and $R_w = (\Sigma w^2(||F_o| - |F_c||)^2/\Sigma w^2|F_o|^2)^{1/2} = 0.083$. The weighting scheme gave uniform errors, $\Sigma w^2(|F_o| - |F_c|)^2/(m - n)$, in all ranges of F_o. In the final refinement, the maximum shift for all the parameters were less than 0.2σ. The final positional and thermal parameters are given in Table 1.[1]

Results and Discussion

The mercury atom forms a four-coordinate complex in HgI_2.TETD. The bond distances and angles are given in Fig. 1. The two Hg—I distances of 2.668(1) Å (twice) are significantly longer than that (2.641(1) Å) of $(Et_2NCS_2HgI)_2$. The Raman spectra of HgI_2.TETD and $(Et_2NCS_2HgI)_2$ in the region 50–1500 cm^{-1} are similar, and ν(Hg—I) are 132 and 139 cm^{-1} respectively. The Hg—S distances of 2.670(7) and 2.737(7) Å are also longer than those (2.422(4) and 2.644(4) Å) of $(Et_2NCS_2HgI)_2$ (8). These differences agree with the fact that the Hg atom is 4-coordinate in HgI_2.TETD and is three-coordinated in $(Et_2NCS_2HgI)_2$. Diiodotetramethylthiuramdisulfidemercury(II) (HgI_2.TMTD),

[1]The structure factor table is available, at a nominal charge, from the Depository of Unpublished Data, CISTI, National Research Council of Canada, Ottawa, Canada K1A 0S2.

TABLE 1. Final atomic parameters (e.s.d's) × 10^4 ± |x,y,z; $\frac{1}{2}+x,\frac{1}{2}-y,z$; $\bar{x},\frac{1}{2}+y,\frac{1}{2}-z$; $\frac{1}{2}-x,\bar{y},\frac{1}{2}+z$|
T.F. = exp {$-2\pi^2(a^{*2}h^2U_{11}$ + ... + $2a^*b^*hkU_{12}$ + ...) × 10^4 for Hg, I, S and × 10^3 for C, N}

Atom	x	y	z	U_{11}	U_{22}	U_{33}	U_{12}	U_{13}	U_{23}
HG	0081.2(9)	2244.2(7)	1379.1(5)	803(8)	601(6)	605(5)	−20(6)	61(6)	−39(5)
I(1)	−0887 (2)	2070 (1)	2405 (1)	971(15)	820(13)	686(10)	39(12)	166(10)	98(9)
I(2)	0690 (2)	1006 (1)	0559 (1)	842(12)	677(11)	690(10)	26(11)	3(10)	−142(9)
S(1)	−0987 (5)	3582 (5)	0753 (3)	726(44)	681(42)	597(37)	0(38)	−108(32)	−104(33)
S(2)	0196 (5)	5143 (5)	1375 (3)	570(40)	615(38)	906(49)	−6(31)	42(37)	−161(37)
S(3)	1081 (6)	4797 (5)	0694 (3)	742(45)	647(44)	853(49)	65(39)	178(39)	104(37)
S(4)	1666 (5)	3367 (5)	1639 (3)	643(42)	782(46)	586(39)	−100(39)	−61(31)	24(34)
N(1)	−1670 (15)	4598 (16)	1663 (10)	54(12)	76(15)	87(15)	−13(12)	13(12)	−8(12)
N(2)	2467 (16)	3421 (14)	0556 (8)	63(11)	66(12)	62(11)	12(12)	2(12)	−1(10)
C(1)	−0897 (18)	4449 (18)	1278 (11)	48(14)	70(16)	72(15)	−16(13)	−11(12)	−6(13)
C(2)	−2564 (21)	4033 (20)	1689 (14)	62(17)	75(19)	124(24)	−14(17)	12(18)	5(18)
C(3)	−3433 (21)	4464 (28)	1316 (17)	48(17)	140(30)	123(31)	0(20)	−25(18)	37(26)
C(4)	−1558 (23)	5394 (23)	2101 (13)	94(24)	102(24)	79(20)	−16(20)	14(16)	−40(18)
C(5)	−1121 (26)	4958 (27)	2700 (14)	116(24)	151(32)	78(21)	−85(16)	16(18)	−13(21)
C(6)	1820 (19)	3777 (18)	0941 (11)	61(15)	63(15)	68(16)	−17(14)	−9(13)	12(13)
C(7)	2586 (21)	3865 (22)	−0038 (10)	70(16)	137(25)	48(12)	6(19)	22(14)	32(14)
C(8)	1815 (26)	3366 (24)	−0471 (12)	123(26)	109(25)	67(18)	0(24)	−36(18)	−17(18)
C(9)	3141 (21)	2619 (18)	0715 (12)	83(18)	60(15)	81(17)	42(16)	−57(15)	−6(13)
C(10)	4175 (22)	2983 (22)	0935 (14)	63(18)	105(23)	105(23)	0(18)	−18(15)	7(18)

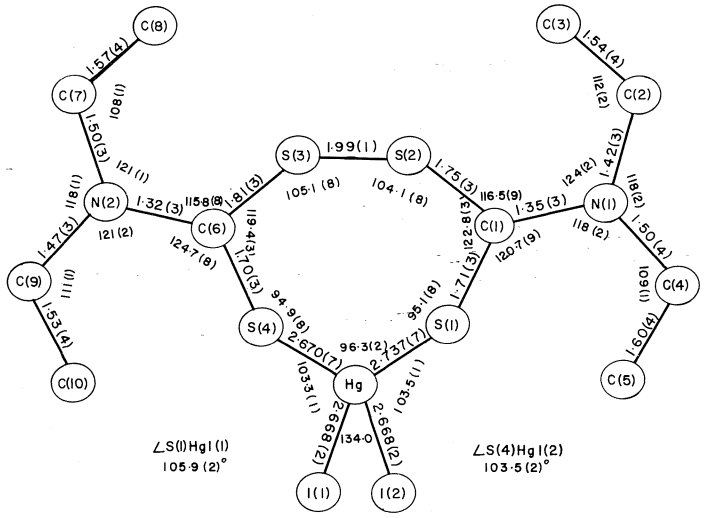

FIG. 1. Bond lengths and angles.

is a similar complex, in which the Hg—I distances are not significantly different (2.661(2), 2.654(2) Å); however, the difference (0.231 Å) in the two Hg—S bond lengths (2.651(7) and 2.882(7) Å) in HgI_2.TMTD, (12) is larger than that (0.067 Å) of HgI_2.TETD, Fig. 1. No simple *ad hoc* explanation can be offered at this time. In both compounds, the Hg—S distances are significantly different due to an unknown reason. Despite the large, I—Hg—I = 134.0(1)°, and small, S—Hg—S = 96.3(2)°, angles (see Fig. 1) the arrangement of the two iodine and the two sulfur atoms around the Hg is approximately tetrahedral. The plane containing HgS_2 is almost perpendicular to the plane containing HgI_2 with an angle of 92.4.

The bond lengths of the ligand, TETD, are essentially the same as those of the free TETD molecule (13) except the C=S bonds. The average C=S distance is 1.65(2) Å in the free molecule and is 1.71(3) Å in the HgI_2.TETD complex. The lengthening is expected as the bonding

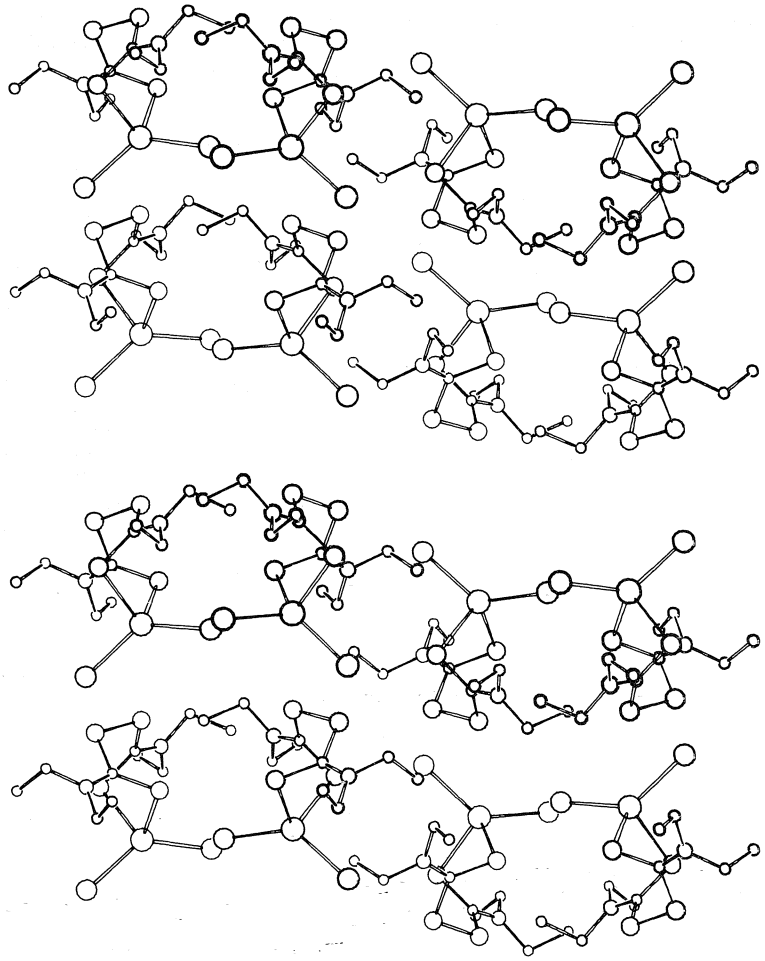

FIG. 2. Stereoview of the packing diagram.

of Hg to the sulfur atoms weakens the double bond character of C=S groups. The configuration of the ligand TETD molecule is not altered either. The shape of each individual molecule can be seen from the packing diagram, Fig. 2. Except for the terminal methyl groups, the ligand

S C
| |

consists of two planar S—C—N—C groups which are nearly perpendicular to each other. The equation of the least-squares plane for $S_2C(1)N(1)C_2$ is $-0.4059X + 0.6556Y - 0.6368Z = 2.685$ and for $S_2C(6)N(2)C_2$ is $0.7032X + 0.6265Y + 0.3362Z = 5.727$ where X, Y, and Z are coordinates in Å in a, b, and c directions. The maximum deviations of atoms for the two planes are 0.07 and 0.03 Å respectively. These deviations are similar to those of the free TETD molecules, and the difference in maximum displacements cannot be regarded as significant. The angle between these planes is 95.1°. The planarity and short N—C distances can be explained by the existence of partial double bond between N and C atoms (13). In diiodotetramethylthiuram-disulfidemercury(II). the corresponding angle is 86.6° (12), whereas in the free TETD molecule, it is 96.4° (13). The mercury atom is approximately at equal distances from the two planes 2.67 and 2.63 Å respectively). The dihedral C—S—S—C angle for HgI_2.TETD, HgI_2.TMTD, and free TETD are 88.5, 89.2, and 90.2° correspondingly. The rigidity of the ligand may restrict the S—Hg—S angle to be small.

In both the methyl and ethyl analogues, the S—S distances remain the same as those of the

free ligands and the average value is 2.00 Å, which is slightly shorter than the S—S distances of S_6 (rhombohedral) or S_8 (orthorhombic α), 2.06 Å (14). In organic disulfides, for example $PhCHCHCH_2S—SCH_2CHCHPh$, the S—S distance is 2.020(2) Å which is a typical value for this type of bonding (15).

A stereo-packing diagram is shown in Fig. 2. It is a molecular crystal with only van der Waals intermolecular attractions. The mercury atom is shielded rather well by the two iodine atoms and the TETD ligand to prevent any further secondary interactions. Atoms C(1) and C(6) are forced by the chelating group to be close to the Hg atom (3.35 and 3.28 Å respectively; see Fig. 1). No other atom is at a distance less than 3.4 Å from the mercury atom.

The formation of both HgI_2.TETD and $(Et_2NCS_2HgI)_2$ by reaction of HgI_2 and TETD demonstrates the complexity of mercuric ion coordination chemistry. It also indicates the flexibility of coordination between mercuric ion and sulfur groups. The existance of HgI_2.TETD provides additional evidence for the postulated mechanism for reducing TETD to thiocarbamate ions leading to the formation of $MeHg(S_2CNEt_2)$ (7). The formation of HgI_2.TETD or $(Et_2NCS_2HgI)_2$ seems to be dependent on the solvent used. The solvent chloroform favored the formation of the latter whereas in absolute or 95% ethanol, pure HgI_2.TETD can be obtained; however, the color of the crystals produced this way is only pale yellow. Recrystallization of HgI_2.TETD from mixed chloroform–ethanol solvent also gave a mixture of HgI_2.TETD and $(Et_2NCS_2HgI)_2$. These phenomena were observed very recently and the solvent dependence of these reactions will be reported in a separate publication. A compound $HgBr_2$.TETD was obtained from $HgBr_2$ and TETD in reaction conditions similar to those given for mercury(II) iodide and TETD. The compound $HgBr_2$.TETD is isostructural with HgI_2.TETD. Cell constants are $a = 13.050(5)$, $b = 13.593(7)$, and $c = 22.373(12)$ Å. The structure is being refined at present and will be published elsewhere. These studies have shown that the Antabuse drug, TETD, may become a chelating agent for mercurials in many ways.

Acknowledgements

I thank the National Research Council of Canada for financial support and Dr. S. Y. Tang for obtaining the Raman spectrum.

1. R. A. PETERS. Rec. Chem. Prog. **28**, 197 (1967).
2. M. M. JONES and T. H. PRATT. J. Chem. Educ. **53**, 342 (1976).
3. Y. S. WONG, A. J. CARTY, and C. CHIEH. J. Chem. Soc. Dalton, In press.
4. S. A. GUNN, T. C. GOULD, and W. A. D. ANDERSON. J. Pathol. Bacteriol. **96**, 89 (1968).
5. I. AUCKEN. Inorg. Synth. **6**, 27 (1960).
6. P. D. BROTHERTON, P. C. HEALY, C. L. RASTON, and A. H. WHITH. J. Chem. Soc. Dalton, 334 (1973).
7. C. CHIEH and L. P. C. LEUNG. Can. J. Chem. **54**, 3077 (1976).
8. C. CHIEH. Can. J. Chem. **55**, 65 (1977).
9. H. C. BRINKHOFF, A. M. GROTENS, and J. J. STEGGERDA. Rec. Trav. Chim. **89**, 11 (1970).
10. D. T. CROMER and J. T. WABER. Acta Crystallogr. **18**, 104 (1965).
11. D. T. CROMER. Acta Crystallogr. **18**, 17 (1965).
12. P. T. BEURSKENS, J. A. CRAS, J. H. NOORDIK, and A. M. SPRUIJT. J. Cryst. Mol. Struct. **1**, 93 (1971).
13. I. L. KARLE, J. A. ESTLIN, and K. BRITTS. Acta Crystallogr. **22**, 273 (1967).
14. J. DONOHUE. The structure of the elements. Wiley Interscience, New York. 1974.
15. J. DONOHUE and J. P. CHESICK. Acta Crystallogr. B, **31**, 986 (1975).

Crystal structure of Sb_2Tl_7

ROLF STOKHUYZEN, CHUNG CHIEH, AND WILLIAM B. PEARSON
Faculty of Science, University of Waterloo, Waterloo, Ont., Canada N2L 3G1

Received November 9, 1976

ROLF STOKHUYZEN, CHUNG CHIEH, and WILLIAM B. PEARSON. Can. J. Chem. **55**, 1120 (1977).

The single-crystal study of Sb_2Tl_7 confirms the work of Morral and Westgren. The crystal is cubic with $a = 11.618(6)$ Å and space group of *Im3m*. There are 54 atoms per unit cell. It is the only known example of this structure type which can be considered as a true superlattice of CsCl. The structure was determined using 106 observed reflections measured on a G.E. XRD-6 diffractometer. The final R and R_w were 0.097 and 0.060, respectively. The Tl–Tl distances range from 3.21 to 3.55 Å and the mean Sb–Tl distance is 3.27 Å. There is no Sb–Sb contact in the structure.

ROLF STOKHUYZEN, CHUNG CHIEH et WILLIAM B. PEARSON. Can. J. Chem. **55**, 1120 (1977).

L'étude d'un mono cristal de Sb_2Tl_7 confirme le travail de Morral et Westgren. Le cristal est cubique avec $a = 11.618(6)$ Å et le groupe d'espace est *Im3m*. Il y a 54 atoms par maille. C'est le seul exemple connu possédant ce type de structure qui peut être considéré comme une surstructure de CsCl. La structure a été déterminée en utilisant 106 reflexions observées mesurées sur un diffractiomètre G.E. XRD-6. Les facteurs d'accord R et R_w sont 0.097 et 0.060 respectivement. Les distances Tl–Tl varient de 3.21 à 3.55 Å et la distance moyenne Sb–Tl est de 3.27 Å. Il n'y a pas de contact Sb–Sb dans cette structure.

[Traduit par le journal]

Introduction

A phase of composition Sb_2Tl_7 was first reported by Persson and Westgren (1), and from powder photographs its structure was shown by Morral and Westgren (2) to be a superstructure composed of 27 CsCl type cells: cubic, *Im3m*, $a = 11.59$, $Z = 6$. Because of our interest in the γ-brass structure which has also been described as a superstructure composed of 27 CsCl type cells with the corner and centre atoms removed (the atom positions, however, are considerably adjusted from those of a stack of 27 CsCl type cells), we have re-examined the structure of Sb_2Tl_7 using single-crystal methods. Our results confirm the earlier work and Sb_2Tl_7 cannot be regarded as a filled up γ-brass; rather it is a true superlattice of CsCl. It is the only known example of this structure type.

Experimental

Since thallium reacts with oxygen and moisture at room temperature (25°C), an argon-filled box was used to weigh and mix 0.9925 g of Sb and 5.8321 g of Tl into a Pyrex tube. Both metal samples are 99.99% pure from A. D. Mackay Inc. The Pyrex tube was then evacuated to 2×10^{-6} torr and the mixture was left at molten state (300°C) for 3 h, with agitation from time to time, in the hope of obtaining homogeneity in the sample. The ingot was then annealed for 428 h at 200°C, followed by quenching in an ice–water bath. The alloy was cut into thin rods of 0.5 mm diameter using a spark cutter. The rods were cut into small pieces with a blade under a microscope. Small fragments were etched and then annealed again for 792 h at 213°C. Some small spherical crystals suitable for X-ray diffraction study were obtained. Weissenberg and precession methods were used to determine the cell constant and space group. The 2θ (Zr-filtered Mo-Kα) values of 6 reflections measured on the G.E. XRD-6 diffractometer were used in the least-squares refinement of a. Crystal data are as follows.

Sb_2Tl_7 fw = 1673.5
Cubic, $a = 11.618(6)$ Å, $V = 1568.1$ Å^3, $D_m = 10.67(9)$, $Z = 6$, $D_c = 10.635$ g cm^{-3}. Systematic absence, $h + k + l = 2n + 1$, space group *Im3m*. (Mo-Kα) = 0.7107 Å, μ(Mo-Kα) = 1131 cm^{-1}.

The crystal used for intensity measurement was an ellipsoid with maximum and minimum radii of 0.026 and 0.028 mm, respectively. It was mounted with [110] along the φ axis. The stationary-crystal stationary-counter method was used because of the small size of the crystal. The counting time was 150 s. Four strong reflections were repeatedly measured after each 100 reflections to monitor the stability of the instrument. Fluctuations in these intensities were less than 7%. The average background curve as a function of 2θ was obtained also by stationary

TABLE 1. Atomic parameters for γ-Sb_2Tl_7 (000, 1/2 1/2 1/2) ± (*xxz* $x\bar{x}\bar{z}$ $\bar{x}x\bar{z}$ $\bar{x}\bar{x}z$, *zxx* $z\bar{x}\bar{x}$ $\bar{z}x\bar{x}$ $\bar{z}\bar{x}x$, *xzx* $x\bar{z}\bar{x}$ $\bar{x}z\bar{x}$ $\bar{x}\bar{z}x$)

Atom	Point set	x	z	B (Å^2)
Tl(ce)	2*a* 000			2.6(5)
Tl(cub)	16*f* *xxx*	0.1704(5)		2.0(1)
Sb(oh)	12*e* 00*z*		0.3138(18)	3.2(4)
Tl(co)	24*h* *xx*0	0.3497(4)		1.6(1)

TABLE 2. Comparison of coordinates with similar structures

Symmetry	Point set	Sb_2Tl_7 x	Sb_2Tl_7 z	Cu_5Zn_8 (γ-brass) x	Cu_5Zn_8 (γ-brass) z	3 × 3 × 3 CsCl cells equiv. coordinates x	3 × 3 × 3 CsCl cells equiv. coordinates z	Ir_3Ge_7 x	Ir_3Ge_7 z
Center	000	0	0	—	—	0	0	—	—
Cube IT*	*xxx*	0.170		0.109		0.167		0.157	
Cube OT*	*xxx*	0.170		−0.172		0.167		0.157	
Octahedron	*x*00	0.314		0.356		0.333		0.342	
Cubooctahedron	*xxz*	0.350	0	0.313	0.037	0.333	0	Truncated octahedral mesh	

*IT and OT stand for inner and outer tetrahedral sites of γ-brass.

counting with the crystal in several orientations. A total of 1094 reflections were measured. Some reflections having intensities less than or equal to zero were discarded. The equivalent reflections were averaged. Among 292 reflections with $2\theta < 60°$ (Mo-Kα) measured 106 had net intensity greater than $3\sigma(I)$ and were considered observed and used throughout the structure analyses. The superlattice type structure resulted in many unobserved reflections. The spherical approximation (mean r = 0.027 mm) was assumed for absorption correction, μ_R = 3.0. Lorentz and polarization corrections were applied to derive the structure amplitudes.

Although the structure was reported to be of space group *Im3m*, refinement was carried out with the assumption of other space groups such as $I\bar{4}3m$. The refinement based on *Im3m* gave the best results. The three positional parameters suggested by Morral and Westgren (2) and the overall temperature factor of 1.3 obtained from a Wilson plot were used initially in the full-matrix least-squares refinement. The function minimized was $\Sigma w(|F_o| - |F_c|)^2$ with $w^{-1} = (305.0 - |F_o| + 0.00083|F_o|^2)$. The atomic scattering factors from International Tables for X-ray Crystallography (3) were used with anomalous scattering corrections from the same source. Programs used in the structure analysis have been described elsewhere (4). The final R $(= \Sigma(|F_o| - |F_c|)/\Sigma|F_o|)$ and R_w $(= (\Sigma w^2(|F_o| - |F_c|)^2/\Sigma w^2|F_o|^2)^{1/2})$ are 0.097 and 0.060 respectively. The atomic parameters are given in Table 1.[1]

Results and Discussion

The present single-crystal study confirms the work of Morral and Westgren and attests to the accuracy of their powder diffraction determination carried out 42 years ago.

For convenience in describing the structure of Sb_2Tl_7, the cluster concept for γ-brasses is used (4). It is only an identity for easy reference and bears no resemblance to a molecule. Each unit cell contains two identical clusters centred at 000 and 1/2 1/2 1/2. The atom Tl(ce) at the centre of the cluster is surrounded by 8 Tl(cub) atoms forming a cube. On each face of the cube is a Sb(oh) atom forming an octahedron, followed by a regular cubooctahedron with one Tl(co) atom outside each edge of the cube. The clusters so formed have *m3m* point symmetry and stack along the threefold axis which is the [111] direction of the cubic cell. This arrangement differs from that of the γ-brass structure which has no atom at 000 and 1/2 1/2 1/2 and has two tetrahedra (IT and OT) instead of the cube of atoms. Table 2 shows comparative atomic coordinates for Sb_2Tl_7, a typical γ-brass structure, a stack of 27 CsCl type cells, and the Ir_3Ge_7 structure (5). The latter also resembles the Sb_2Tl_7 structure in having clusters of atoms (cube surrounded by octahedron centred about 000 and 1/2 1/2 1/2) and these clusters are surrounded by truncated octahedra of atoms which form a space filling mesh running throughout the structure, instead of by separate regular cubooctahedra as in Sb_2Tl_7.

The interatomic distances are given in Table 3. The coordination number (CN) for most of the atoms is 8 except for Tl(cub) where it is 10. This also indicates that the relative distortion from stacking of 27 CsCl type cells is small. The Tl–Tl distances range from 3.21 to 3.55 Å and appear to be normal with respect to the size (CN8) of thallium, 3.34 Å (5). In β-Tl, which has a body centred cubic structure (262°C), the Tl–Tl distance is 3.362 Å (6). There is no Sb–Sb contact

[1]Photocopies of the structure factor table are available, at a nominal charge, from the Depository of Unpublished Data, CISTI, National Research Council of Canada, Ottawa, Ont., Canada K1A 0S2.

TABLE 3. Interatomic distances (standard deviations = 0.01 Å)

From atom	To No. atom(s)	Distance (Å)
Tl(ce)	8 Tl(cub)	3.43
Tl(cub)	1 Tl(ce)	3.43
	3 Sb(oh)	3.26
	3 Tl(cub)	3.21
	3 Tl(co)	3.55
Sb(oh)	4 Tl(cub)	3.26
	4 Tl(co)	3.28
Tl(co)	2 Sb(oh)	3.28
	2 Tl(co)	3.49
	4 Tl(co)	3.39

and the mean Sb–Tl distance of 3.27 Å is also comparable with the sum of metallic (CN8) radii of Sb and Tl, 3.23 Å.

Acknowledgements

We are grateful to the National Research Council of Canada for financial support and Mr. V. Fronz for help in the preparation of the sample.

1. E. PERSSON and A. WESTGREN. Z. Phys. Chem. **136**, 208 (1928).
2. F. R. MORRAL and A. WESTGREN. Svensk Kem. Tidskr. **46**, 153 (1934).
3. International Tables for X-ray Crystallography. Vol. III. Kynoch Press, Birmingham. 1962.
4. J. K. BRANDON, R. Y. BRIZARD, P. C. CHIEH, R. K. MCMILLAN, and W. B. PEARSON. Acta Crystallogr. B**30**, 1412 (1974).
5. W. B. PEARSON. The crystal chemistry and physics of metals and alloys. Wiley–Interscience. 1972.
6. H. LIPSON and A. R. STOKES. Nature, **148**, 437 (1941).

The reactions of isothiazolium salts with selected nucleophilic reagents. The preparation of thieno[2,3-*c*]isothiazolium salts

DAVID M. MCKINNON, MOHAMMED E. R. HASSAN, AND MOHINDER CHAUHAN

Department of Chemistry, University of Manitoba, Winnipeg, Man., Canada R3T 2N2

Received October 14, 1976

DAVID M. MCKINNON, MOHAMMED E. R. HASSAN, and MOHINDER CHAUHAN. Can. J. Chem. **55**, 1123 (1977).

Isothiazolium salts react with a number of carbanions by attack on sulfur. Thiophene derivatives, formed by ring opening and recyclization, are often products but with cyclopentadiene, pseudoazulene products are obtained. 3-Amino-2-acylthiophenes, prepared by suitable nucleophilic attack, are synthetic precursors of thieno[2,3-*c*]isothiazolium salts.

DAVID M. MCKINNON, MOHAMMED E. R. HASSAN et MOHINDER CHAUHAN. Can. J. Chem. **55**, 1123 (1977).

Les sels d'isothiazolium réagissent avec un nombre de carbanions par attaque au niveau du soufre. Les produits comprennent souvent des dérivés du thiophène, qui sont formés par une ouverture de cycle et une recyclisation; avec le cyclopentadiène, ont obtient toutefois des produits pseudoazulènes. Les amino-3 acyl-2 thiophènes, préparés par une attaque nucléophilique appropriée, sont des précurseurs de synthèse des sels de thiéno[2,3-*c*]isothiazolium.

[Traduit par le journal]

In the isothiazolium system **1**, attack by a carbanion on the ring sulfur atom has been demonstrated (1), although attack by nucleophiles at other ring positions has also been postulated (2–5). To provide further information on the positions of attack, and to examine the synthetic utility of these salts, some of which are readily accessible, we have examined their reaction with selected carbanions. In previous work (1) it was found that attack at ring sulfur was followed by ring opening of the isothiazole, then recyclization by condensation of an active methylene group with an imine function (Scheme 1). Thiophene derivatives were the final products. Using this scheme as a rationale, we have used other carbanions capable of similar reactions. Isothiazolium salts used in these reactions were synthesized according to previous work or procedures (1, 6).

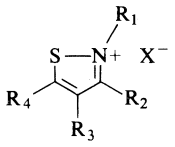

1

a, $R_1 = Me, R_2 = SMe, R_3 = R_4 = Ph, X = I$
b, $R_1 = R_3 = Ph, R_2 = R_4 = H, X = ClO_4$
c, $R_1 = R_3 = Ph, R_4 = SMe, R_2 = H, X = ClO_4$
d, $R_1 = R_4 = Ph, R_2 = R_3 = H, X = ClO_4$
e, $R_1 = R_4 = Ph, R_2 = SMe, R_3 = H, X = ClO_4$
f, $R_1 = Me_5, R_2 = R_3 = R_4 = H, X = ClO_4$
g, $R_1 = Me, R_2 = SMe, R_3,R_4 = —(CH{=}CH)_2—, X = ClO_4$

2-Methyl-3-methylthio-4,5-diphenylisothiazolium iodide (**1***a*), prepared by treatment of 2-methyl-4,5-diphenylisothiazoline-3-thione with methyl iodide, reacted with the anion of diethyl malonate in ethanol to form diethyl 3,4-diphenyl-3-methylimino-2,3-dihydrothiophene-2,2-dicarboxylate (**2**) and methanethiol. This reaction likely follows the above scheme except that aromatization to a thiophene is impossible and an exocyclic double bond is formed. Thus, in this case a dihydrothiophene is the final product. In this case compound **2** appears to exist as two

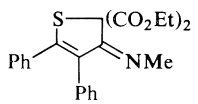

2

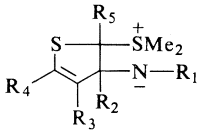

3

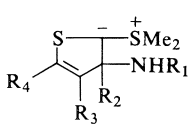

4

a, $R_1 = R_3 = Ph, R_2 = R_4 = R_5 = H$
b, $R_1 = R_3 = Ph, R_2 = R_5 = H, R_4 = SMe$
c, $R_1 = R_3 = Ph, R_2 = R_4 = H, R_5 = p\text{-}NO_2C_6H_4$

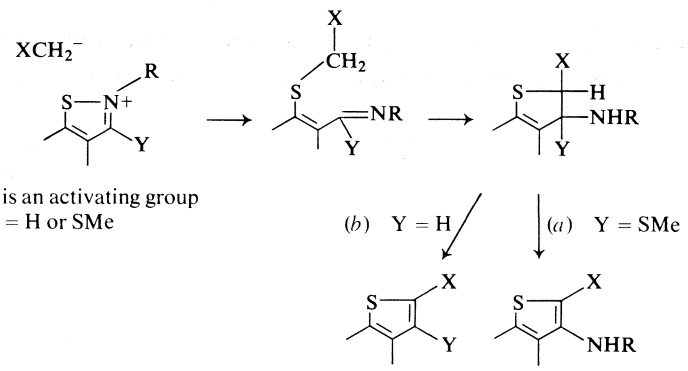

SCHEME 1

geometrical isomers with respect to the exocyclic imine function.

We then examined the reaction of the salts **1** with various stable ylides. 2,4-Diphenylisothiazolium perchlorate (**1***b*) was treated with the anion of diethyl benzylphosphonate in dimethylformamide. It was expected that the reaction would proceed according to the scheme shown, (Scheme 2) with the phosphonate grouping so enhancing the acidity of the Ph—CH-group in the intermediate sulfide as to allow cyclization to the dihydrothiophene. Aromatization in this case would probably occur through the typical four-centered intermediates of Wittig reactions and elimination of an aminophosphorus species. The reaction in fact afforded 2,4-diphenylthiophene, although in low yield.

It was of interest then to examine the effects of various sulfonium ylides on the salts **1**, where such four-centered reactions would be unlikely in view of the different reactions of phosphorus and sulfur ylides (7). In fact, treatment of **1**b and **1***c* with dimethylmethylene sulfurane afforded the thiophenes **5***a* and **5***b*, respectively, which contained methylthio substituents, obviously derived from the original sulfurane. These compounds are probably formed via reaction intermediates of type **3** by isomerism to the more stable ylide **4**, then oxidation followed by demethylation. Although the reactions were performed under nitrogen, it is not unlikely that traces of oxygen were present. Alternatively oxidation by unreacted isothiazolium salt could have occurred. Certainly the structurally and electronically related 1,2-dithiolium salts have this property (8, 9).

When *p*-nitrobenzylidenedimethyl sulfurane was allowed to react with **1***b*, a product was obtained whose analyses and properties were consistent with 2-*p*-nitrophenyl-4-phenylthiophene (**5***c*). While this reaction must have an intermediate **3***c* like the above reactions, oxidation of this is unlikely and the dimethylsulfonio group

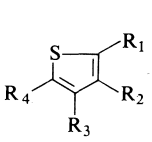

5

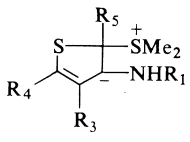

6

a, R_1 = SMe, R_2 = NHPh, R_3 = Ph, R_4 = H
b, R_1 = R_4 = SMe, R_2 = NHPh, R_3 = Ph
c, R_1 = *p*-$NO_2C_6H_4$, R_2 = NHPh, R_4 = H, R_3 = Ph
d, R_1 = PhCO, R_2 = NHPh, R_3 = H, R_4 = Ph
e, R_1 = PhCS, R_2 = NHPh, R_3 = H, R_4 = Ph
f, R_1 = PhCO, R_2 = NHMe, R_3,R_4 = $(CH{=}CH)_2$
g, R_1 = PhCO, R_2 = NHPh, R_3 = Ph, R_4 = H
h, R_1 = PhCO, R_2 = NHMe, R_3 = R_4 = H
i, R_1 = CH_3CO, R_2 = NHPh, R_3 = H, R_4 = Ph

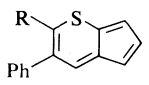

7

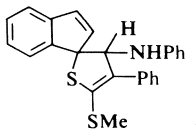

8

a, R = H
b, R = SMe

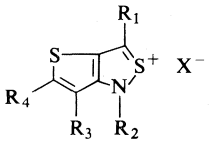

9

a, R_1 = R_2 = R_4 = Ph, R_3 = H X = ClO_4
b, R_1 = R_2 = R_3 = Ph, R_4 = H X = ClO_4
c, R_1 = Ph, R_2 = Me, R_3 = R_4 = H X = ClO_4
d, R_1 = Me, R_2 = R_4 = Ph, R_3 = H X = ClO_4
e, R_1 = **Ph**, R_2 = Me, R_3,R_4 = $(CH{=}CH)_2$, X = I_3

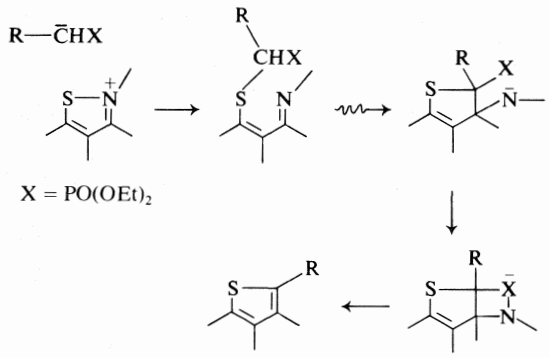

SCHEME 2

is lost, forming **5***c*. The exact mechanistic pathway from **3***c* to **5***c* is not known with certainty, but displacement by the nitrogen anion of dimethyl sulfide leading to a thienoaziridine, with rearrangement to **5***c* is a possibility. Alternatively **3***c* may rearrange to an intermediate **6**, with subsequent loss of dimethyl sulfide.

The reaction of phenacylidenedimethylsulfurane with **1***d* afforded 2-benzoyl-3-anilino-5-phenylthiophene (**5***d*), identical to a sample prepared by reaction of sodium benzoylacetate with 2,5-diphenyl-3-methylthioisothiazolium perchlorate (**1***e*) according to known procedures (1). This approach, where aromatization of the dihydrothiophene intermediate occurs by loss of a group originally on the attacking nucleophile, rather than the isothiazolium salt, is thus a method of making 2-acyl-3-aminothiophenes without using 3-alkylthioisothiazolium salts for which synthetic methods, in contrast to 3-unsubstituted isothiazolium salts, are sometimes unsatisfactory. These 2-acyl-3-aminothiophenes have synthetic potential for the preparation of thieno[3,2-*c*]isothiazolium salts, and further products of this type were made as intermediates (see below).

Treatment of 2,4-diphenylisothiazolium perchlorate (**1***b*) or 5-methylthio-2,4-diphenylisothiazolium perchlorate (**1***c*) with the cyclopentadienyl anion in ether gave dark blue products. The analyses and other data for these were consistent with the pseudoazulene structures **7***a* and **7***b* respectively, formed as above by initial nucleophilic attack on sulfur, with ring opening of the isothiazolium salt. Related pseudoazulenes have been prepared by alternate syntheses (10–12). Two modes of reaction of the initially formed cyclopentadienylthioether are possible, *i.e.* attack on the imine function either by a carbanion on the 1-position of the cyclopentadiene ring, leading to a cyclopentadienospirothiophene, or from a carbanion at position 2, leading to a pseudoazulene (Scheme 3). While anion formation at the 1-position would be favored owing to extra stabilization of the anion by the adjacent sulfur, it is obvious that the alternative reaction is relatively effective. Nevertheless, attack of the indenyl anion on **1***c* failed to give any crystalline product. In this case, an attacking anion (at the 2-position of the cyclopentadiene ring) would be unfavored due to the presence of an *o*-quinonoid structure. The properties of the crude product obtained appear to correspond to the spiran structure **8** formed by alternate cyclization from an attacking anion at the 1-position of the cyclopentadiene ring. These reactions have many analogies with the preparation of azulenes from pyridinium or pyrylium salts (13).

Since isothiazolium salts **1** may be synthesized from β-aminopropeneone derivatives by thionation, then oxidation (9, 14), it was of interest to find if the 2-acyl-3-aminothiophenes synthesized above could be likewise converted to the thieno-[3,2-*c*]isothiazolium system (**9**). Accordingly the compound **5***d* prepared as above was treated with phosphorus pentasulfide in benzene. The crude thione product **5***e* treated with iodine in ethanol afforded the 1,3,5-triphenyl[3,2-*c*]isothiazolium cation (**9***a*), isolated as its perchlorate. Likewise the 1,3,4-triphenyl system (**9***b*), and the 3-methyl-3-phenyl system (**9***c*) were made from 2,4-diphenylisothiazolium perchlorate (**1***b*) and 2-methylisothiazolium perchlorate (**1***f*), respectively. The preparation may also be extended to other sulfonium ylides, and treatment of acetonylidenedimethylsulfurane with **1***d* followed by thionation and oxidation gave the 2,5-diphenyl-

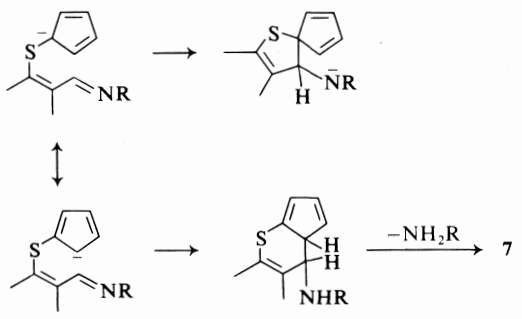

SCHEME 3

3-methylthieno[3,2-*c*]isothiazolium system (**9***d*), isolated as its perchlorate.

Finally, the readily accessible 2-methyl-3-methylthio-4,5-benzisothiazolium perchlorate (**1***g*) reacted with sodium benzoylacetate to give 2-benzoyl-3-methylaminobenzo[*b*]thiophene (**5***f*), which, on thionation followed by oxidation, afforded the benzothienoisothiazolium salt (**9***e*) as its triiodide.

Thus, in the cases described, the products isolated are compatible with initial nucleophilic attack on the sulfur atom of the isothiazolium ring. While attack at the carbon adjacent to nitrogen is favored on coulombic grounds (3), it is difficult to explain the formation of the products above by mechanisms based on such attack.

Experimental

The nmr spectra were obtained on a Varian model 56/60A spectrometer in deuterochloroform using tetramethylsilane as an internal standard. Mass spectra were obtained on a Finnegan 1015 quadrupole mass spectrometer. Chromatography (tlc) was performed on Camag silica gel type D.S.F. 5 supplied by Terochem, Laboratories. Elution, unless otherwise stated, was by benzene with increasing proportions of chloroform. Melting points (mp) were obtained on a precalibrated Thermopan apparatus. Analyses were performed by A. E. Bernhardt. Unless otherwise stated, solutions were dried over anhydrous magnesium sulfate.

*Preparation of 4,5-Diphenyl-2-methyl-3-methylthioisothiazolium Iodide (**1a**)*

The thione (1 g) (1) was dissolved in methyl iodide (10 ml) at room temperature and allowed to stand. After 1 h the pale yellow product was collected by filtration (95%). The product was recrystallized from methyl iodide as pale yellow prisms mp 138–40°C. *Anal.* calcd. for $C_{17}H_{16}NS_2I$: C 48.00, H 3.76, N 3.29, S 15.00; found: C 48.18, H 3.52, N 3.33, S 15.21.

*Reaction of 4,5-Diphenyl-2-methyl-3-methylthioisothiazolium Iodide (**1a**) with Diethyl Malonate*

To a solution of sodium ethoxide, prepared by dissolving sodium (25.3 mg, 1.2 mmol) in ethanol (5 ml), was added diethyl malonate (0.19 g, 1.2 mmol). To this solution with stirring was added **1***a* (0.51 g, 1.2 mmol). The solution became red, then gradually turned yellow, with the evolution of methanethiol. After 10 min the solution was diluted with water and extracted with benzene. The dried extract on evaporation gave a yellow oil which on dissolving in toluene and standing at 0°C afforded **2** as yellow prisms, mp 97°C (39%). *Anal.* calcd. for $C_{23}H_{23}NSO_4$: C 67.48, H 5.62, N 3.42, S 7.82; found: C 67.47, H 5.44, N 3.15, S 7.84. The nmr spectrum: τ 9.1–8.8 (2 superimposed t, methyl), 6.4–6.2 (2q, methylene; 2s, *N*-methyl), 2.91–2.62 (5H, aromatic).

*Reaction of 2,4-Diphenylisothiazolium Perchlorate (**1b**) with Diethyl Benzylphosphonate*

Diethyl benzylphosphonate, prepared by refluxing benzyl chloride (0.316 g, 2.5 mmol) with triethylphosphite (0.415 g, 2.5 mmol) for 1 h was treated in dimethylformamide (5 ml) with sodium methoxide (0.011 g, 2.5 mmol). To the mixture was added 2,4-diphenylisothiazolium perchlorate (**1***b*) (0.84 g, 2.5 mmol) (6). The solution was heated at 60°C for 5 min, then poured into ice water and the orange precipitate collected. Chromatography indicated a number of products but the first yellow band eluted was rechromatographed using 25% benzene in petroleum ether as an eluent and afforded a colorless solid with a blue fluorescence in ultraviolet light; mp 121°C (lit. (14) mp 121°C) (18%). The ms M^+ calcd.: 236; found 236.

*Reaction of Dimethylmethylenesulfurane with 2,4-Diphenylisothiazolium Perchlorate (**1b**)*

To a stirred suspension of trimethylsulfonium iodide (0.24 g, 1.2 mmol) in tetrahydrofuran (4 ml) at 0°C under nitrogen was added 1.2 ml of molar methyllithium in ether (Ventron). After stirring 5 min the isothiazolium salt (0.404 g, 1.2 mmol) was added and stirring maintained for 30 min at 0°C, then for a further 1 h at 25°C. After dilution of the solution with water, the benzene extract was dried, evaporated, and the resulting oil chromatographed. The most rapidly eluting band gave an orange oil which crystallized on trituration with methanol. It was recrystallized from methanol as orange prisms, mp 204°C (30%). The nmr spectrum for **5***a*: τ 7.21 (3H, s, methyl), 3.10–2.69 (11H, aromatic and heterocyclic), 1.83 (1H, s, amino). The ms M^+ calcd.: 297; found: 297. *Anal.* calcd. for $C_{17}H_{15}NS_2$: C 68.68, H 5.05, N 4.72, S 21.55; found: C 68.56, H 5.41, N 4.67, S 21.76.

*Reaction of Dimethylmethylenesulfurane with 2,4-Diphenyl-5-methylthioisothiazolium Perchlorate (**1c**)*

The reaction was performed as above. 3-Anilino-2,5-bismethylthiothiophene (**5***b*) was obtained as orange prisms mp 198°C (28%). The nmr spectrum for **5***b*: τ 7.25, 7.02 (3H, 2s, methyl), 3.05–2.63 (10H, aromatic), 1.85 (1H, s, amino). The ms M^+ calcd.: 243; found: 243. *Anal.* calcd. for $C_{18}H_{17}NS_3$: C 63.00, H 4.95, N 4.08, S 27.97; found: C 62.71, H 4.81, N 3.86, S 28.25.

*Reaction of p-Nitrobenzylidenedimethylsulfurane with 2,4-Diphenylisothiazolium Perchlorate (**1b**)*

p-Nitrobenzyldimethylsulfonium bromide (0.278 g), (16) 1.2 mmol in dry ethanol was treated with sodium ethoxide (1.0 mmol). A slight excess of the isothiazolium salt (0.404 g, 1.2 mmol) was then added, and the mixture stirred 15 min. Dilution with water and ether extraction gave an oil which was purified by chromatography. The main orange band on extraction and recrystallization from ethanol afforded **5***c* as yellow-orange prisms mp 158°C (42%). The ms M^+ calcd.: 372; found: 372. *Anal.* calcd. for $C_{22}H_{16}NSO_2$: C 70.96, H 4.30, N 7.52, S 8.60; found: C 70.71, H 4.70, N 7.52, S 9.10.

*Reaction of Phenacylidene Dimethylsulfurane with 2,5-Diphenylisothiazolium Perchlorate (**1d**)*

Phenacyldimethylsulfonium bromide (0.25 g, 1 mmol) in dry ethanol (10 ml) was treated with sodium ethoxide (1 mmol). After stirring 5 min, the perchlorate **1***d* (336 g, 1 mmol) (14) was added, and the solution stirred 15 min. The mixture was diluted with water (20 ml) and the ether extract dried and evaporated to yield a yellow oil. Purifi-

cation by chromatography yielded **5***d* as yellow needles mp 180°C (55%). The ms M^+ calcd.: 355; found: 355. *Anal.* calcd. for $C_{23}H_{17}NSO$: C 77.74, H 4.79, N 3.95, S 9.02, found: C 77.81, H 4.85, N 3.62, S 9.21.

*Reaction of Sodium Benzoylacetate with 2,5-Diphenyl-3-methylthioisothiazolium Iodide (**1***e) to Form **5***d*

This reaction was performed according to a known procedure (1). The salt (1 mmol) (17) was treated with sodium benzoylacetate (~1.5 mmol) in ethanol. Work-up afforded **5***d* (61%) identical to that above (mixture mp, ms, and ir).

*Preparation of 2-Methyl-3-methylthio-4,5-benzisothiazolium Perchlorate (**1***g)*

2-Methylbenzisothiazoline-3-thione (1.81 g, 10 mmol) (18) was heated with dimethyl sulfate (2 ml) for 5 min at 100°C. The mixture was diluted with ether and the ether phase decanted off the oily product. This was converted to its perchlorate in acetic acid. Pale yellow needles, mp 173–175°C were obtained (82%). *Anal.* calcd. for $C_9H_{10}NS_2ClO_4$: C 36.54, H 3.38, N 4.73, S 21.69, Cl 12.05; found: C 36.62, H 3.42, N 4.61, S 21.61, Cl 12.21.

*Reaction of 2-Methyl-3-methylthio-4,5-benzisothiazolium Perchlorate (**1***g) with Sodium Benzoylacetate. 2-Benzoyl-3-methylaminobenzothiophene (**5***f)*

This reaction was performed according to standard procedures (1). Work-up and crystallization from petroleum ether, bp 60–80°C, afforded yellow prisms mp 88–89°C (31%). The ms M^+ calcd.: 267; found: 267. The nmr spectrum: τ 6.52 (3H, s, methyl), 1.60–2.76 (9H, aromatic), −0.2 (1H, br s, NH). *Anal.* calcd. for $C_{16}H_{13}NSO$: C 71.91, H 4.87, N 5.24, S 11.98; found: C 71.77, H 4.80, N 5.16, S 11.65.

*Preparation of Thieno[2,3-c]isothiazolium Salts (**9**)*

Procedure a

The appropriate benzoylaminothiophene **5***c* or **5***f* was treated with an approximately equal weight of phosphorus pentasulfide in benzene and the mixture refluxed 4 h. The solvent was filtered off any solid and washed with sodium bicarbonate solution and dried. Evaporation gave the corresponding crude thiones as red oils. These were dissolved in ethanol and titrated with a saturated solution of iodine in ethanol until precipitation was complete. The crude triiodide salts were separated by filtration and in most cases, converted to the corresponding perchlorates in acetic acid or recrystallized from nitromethane. The results are summarized in Table 1.

Procedure b

The starting isothiazolium salts were treated with the appropriate sulfur ylides to afford the appropriate acylaminothiophenes. Thus **1***b* and phenacylidene dimethylsulfurane afforded the benzoylanilinothiophene **5***g*, 2-methylisothiazolium perchlorate **1***f* afforded 2-benzoyl-3-methylaminothiophene **5***h*, and **1***d* with acetonylidenedimethylsulfurane afforded 2-acetyl-3-anilino-5-phenylthiophene **5***i*. None of these were purified but were thionated by the above procedure to give the isothiazolium salts **9***b*, **9***c*, and **9***d* respectively. The results are summarized in Table 1.

In some cases it was difficult to remove all iodine from the perchlorates. This was best achieved by prolonged boiling in an open flask to allow acetic acid fumes to

TABLE 1. Preparation of thienoisothiazolium salts

Salt **9**	Procedure	Yield (%)*	mp (°C)	Formula	Analysis (%) Calculated C	H	N	S	Cl	I	Found C	H	N	S	Cl	I
9*a*	*a*	38	241	$C_{23}H_{16}NS_2ClO_4$	57.78	3.40	2.98	13.63	7.56	—	58.85	3.34	2.62	13.24	7.70	—
9*b*	*b*	41	222	$C_{23}H_{10}NS_2ClO_4$	57.78	3.40	2.98	13.63	7.56	—	58.67	3.55	2.58	13.80	7.80	—
9*c*	*b*	30	204	$C_{12}H_{10}NS_2ClO_4$	43.43	3.01	4.22	19.31	10.70	—	43.35	3.36	3.88	19.46	10.64	—
9*d*	*b*	35	237	$C_{18}H_{14}NS_2ClO_4$	53.00	3.43	3.43	15.71	8.71	—	52.79	3.63	3.21	15.64	8.74	—
9*e*	*a*	32	169–173	$C_{10}H_{12}NS_2I_3$	28.93	1.81	2.12	9.65	—	57.49	29.07	1.88	2.01	10.02	—	57.21

*Based on crude acylaminothiophenes.

remove iodine vapor. Care was necessary in this case to avoid over concentration of the perchloric acid – acetic acid mixture.

*Reaction of the Cyclopentadienyl Anion with 2,4-Diphenyl-5-methylthioisothiazolium Perchlorate (**1c**)*

Cyclopentadiene was obtained from its dimer according to the method described (19). To a solution of methyllithium (1 mmol) in anhydrous ether was added the cyclopentadiene (66 mg, 1 mmol) under a nitrogen atmosphere. The solution was cooled to −70°C by means of an acetone – dry ice bath and after stirring 5 min, the perchlorate salt **1***c* (383.5 mg, 1 mmol) was added. Stirring was maintained for 30 min and the mixture allowed to reach room temperature. After dilution of the mixture with water, the ether layer was separated, dried, and evaporated to give a dark oil which was examined by chromatography. A fast running dark blue band was removed by chloroform extraction and evaporation yielded **7***b* as a crystalline product mp 278°C (61%). *Anal.* calcd. for $C_{15}H_{12}S_2$: C 70.31, H 4.68, S 25.00; found: C 70.9, H 4.80, S 24.67. The nmr spectrum: τ 7.47 (3H, s, *S*-methyl), 2.87–2.41 (9H, aromatic). The ms M^+ calcd.: 256; found: 256.

Reaction of the Cyclopentadienyl Anion with 2,4-Diphenylisothiazolium Perchlorate

The reaction was performed as above. **7***a* was obtained as grey plates mp 250°C (55%). *Anal.* calcd. for $C_{14}H_{10}S$: C 80.00, H 4.76, S 15.23; found: C 79.80, H 4.97, S 14.91. The nmr spectrum: τ 2.91–2.45 (10H). The ms M^+ calcd.: 210; found: 210.

Reaction of the Indenyl Anion with 2,4-Diphenyl-5-methylthioisothiazolium Perchlorate

The reaction was performed as above. Chromatography indicated a major pink band which on elution and evaporation gave a dark pink oil (20%). This could not be crystallized and was not analyzed. The nmr spectrum: τ 7.65 (1H, s, the single dihydrothiophene proton) τ 7.48 (3H, s, *S*-methyl), 3.21–2.52 (16H, aromatic and amino). The ir spectrum: 3410 cm^{-1} (the NH str). The ms M^+ calcd.: 399; found: 399.

Acknowledgements

We are grateful to Mr. D. Buksak and Mr. W. Buchannon for the preparation of spectra, and to the National Research Council of Canada for financial support.

1. D. M. McKinnon and M. E. Hassan. Can. J. Chem. **51**, 3081 (1973).
2. K. R. H. Wooldridge. *In* Advances in heterocyclic chemistry. Vol. 14. Academic Press, New York, NY. 1972.
3. J. M. Landesberg and R. A. Olofson. Tetrahedron, **22**, 2135 (1966).
4. F. T. Lee and G. P. Volpp. J. Heterocycl. Chem. **7**, 415 (1970).
5. P. Sykes and H. Ullah. J. Chem. Soc. Perkin Trans. **1**, 2305 (1972).
6. G. E. Bachers, D. M. McKinnon, and J. M. Buchshriber. Can. J. Chem. **50**, 2568 (1972).
7. A. W. Johnson. Ylid chemistry. Academic Press, New York, NY. 1966.
8. E. Klingsberg and A. Schreiber. J. Am. Chem. Soc. **84**, 2941 (1962).
9. D. Leaver, D. M. McKinnon, and W. A. H. Robertson. J. Chem. Soc. 32 (1965).
10. A. G. Anderson, W. F. Harrison, R. G. Anderson, and A. G. Osborne. J. Am. Chem. Soc. **81**, 1255 (1959).
11. R. Mayer and H. Russ. Chem. Ber. **95**, 1311 (1962).
12. D. Leaver, J. Smolicz, and W. H. Stafford. J. Chem. Soc. 740 (1962).
13. K. Hafner and H. Kaiser. Justus Liebigs Ann. Chem. **618**, 140 (1958) and references therein.
14. D. M. McKinnon and E. A. Robak. Can. J.Chem. **46**, 1855 (1968).
15. E. Campaigne. J. Am. Chem. Soc. **66**, 684 (1944).
16. P. Mamalis. J. Chem. Soc. 4747 (1960).
17. F. Boberg and W. Von Gentzkow. Justus Liebigs Ann. Chem. **256** (1973).
18. J. L. Charlton, S. M. Loosmore, and D. M. McKinnon. Can. J. Chem. **52**, 3021 (1974).
19. R. B. Moffet. Organic Synth. Coll. Vol. IV, 238 (1963).

The isolation and identification of makisterone A from the yew, *Taxus cuspidata*

BRENTON GARTH BURNS AND MICHAEL WILSON GILGAN

Environment Canada, Fisheries and Marine Service, 1707 Lower Water Street, P. O. Box 429, Halifax, N.S., Canada B3J 2R3

Received July 6, 1976

BRENTON GARTH BURNS and MICHAEL WILSON GILGAN. Can. J. Chem. **55**, 1129 (1977).

The ecdysteroids were extracted from yew, *Taxus cuspidata*, needles and twigs and recovered from the aqueous extract by reversed phase adsorption. Purification of the ecdysteroids was achieved by a single solvent partition and a dry column chromatogram followed by fractionation on an adsorptive Porasil A (60) column. Makisterone A was a minor component identified by melting point, liquid chromatography, gas chromatography of the trimethylsilyl ether, mass spectrometry, and nuclear magnetic resonance spectrometry. A second minor component was isolated but not identified.

BRENTON GARTH BURNS et MICHAEL WILSON GILGAN. Can. J. Chem. **55**, 1129 (1977).

On a extrait des ecdystéroïdes à partir des aiguilles et des brindilles du yew, *Taxus cuspidata*, et on les a récupérées par une extraction aqueuse par une adsorption de phase renversée. On a effectué la purification des ecdystéroïdes par une partition unique de solvant et une chromatographie sur colonne sèche suivie par un fractionnement sur une colonne d'adsorption de Porasil A (60). On a pu identifier que la makistérone A est un composant mineur; cette identification a été effectuée par point de fusion, chromatographie liquide, chromatographie en phase gazeuse de l'éther triméthylsilyle, par spectrométrie de masse et par spectroscopie de résonance magnétique nucléaire. On a pu isoler un deuxième composant mineur mais il n'a pas été identifié.

[Traduit par le journal]

Introduction

At about the same time as a report by one of the authors (1), T. Takemoto *et al.* (2) reported insect molt hormone activity associated with extracts of yew (*Taxus cuspidata*, 1; *Taxus* sp. 2) leaves. The major components were reported to be an insect molt hormone, ecdysterone **2**, and a closely related compound, ponasterone A **3** (3). Ecdysterone was also reported as a constituent of *Taxus baccata* (4). Except to examine the activity present in *Taxaceans* in surveys (5, 6), the yews have attracted little subsequent interest.

Our purpose in isolating the ecdysteroids from the yew was to make them available for attempted forced molting in lobster (*e.g.*, ref. 7). One of the most important hormones, and the first to have its structure completely determined (8), α-ecdysone **1**, has been isolated from fern extracts (9). We have found it difficult to isolate from this source. Examination of yew extracts, fractionated by adsorptive liquid chromatography, with an insect assay (10), showed that a minor peak conforming approximately with the retention time of α-ecdysone was present in addition to the usual major ecdysterone and ponasterone A peaks. Since we wished to use α-ecdysone in our tests we completed the isolation of this compound. Unfortunately this proved to be makisterone A **4** (11) accompanied by what appears to be makisterone C (lemmasterone, **5**) or D **6** (11, 12). Nevertheless, makisterone A is of con-

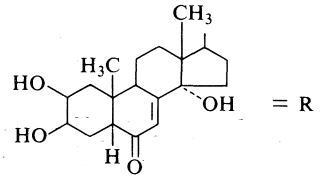

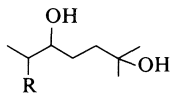

1 α-Ecdysone

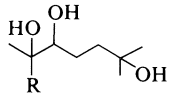

2 Ecdysterone

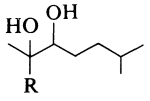

3 Ponasterone A

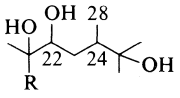

4 Makisterone A

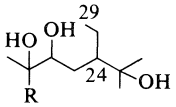

5 Lemmasterone (Makisterone C)

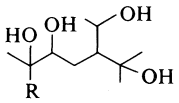

6 Makisterone D

siderable biological interest since it has been reported as a crustacean (13) and insect (14) constituent. The following is a report of the isolation and identification of makisterone A from the yew *Taxus cuspidata*.

Experimental

Extraction

Chopped yew (*Taxus cuspidata*, 2 kg fresh weight, 0.8 kg dry weight, obtained locally September 1973 and stored at −30°C) needles and twigs were stirred overnight in 8 ℓ of distilled water. The solids were removed by filtration through cheese cloth, resuspended as above for 4 h, and the mixture refiltered. The combined water extracts were filtered through Celite 545 (Johns Manville) to give a clear, dark brown solution.

Reversed Phase Adsorption

Amberlite XAD-2 (BDH Chemicals, Ltd.) was slurried and packed into a glass column (38 × 5 cm i.d.) and held in place by stainless steel screens (40 × 40 mesh, Newark Wire Cloth Co., Newark, N.J.) at both ends. The column was washed in a procedure like that of Hori (15).

The combined aqueous yew extracts were passed slowly through the column ($\frac{1}{20}$ bed volume (B.V.) per min) trapping most of the brown material, and the column was then eluted with water, 10% isopropanol – water, 70% isopropanol – water, and isopropanol ($1\frac{1}{2}$ B.V. each). The column was washed with water and the aqueous yew extract passed through the column a second time and the column eluted.

Solvent Fractionation

Water was added to the combined 70% isopropanol eluates, which contained the bulk of the ecdysteroids, to make the isopropanol to water proportion 2:1. The fat soluble materials were then removed by hexane extraction ($\frac{1}{20}$ vol.). The ecdysteroids were extracted with chloroform (proportions: chloroform–isopropanol–water, 2:2:1) and the extraction repeated once. The combined chloroform extracts were washed with *N* NaOH ($\frac{1}{20}$ vol.) and then repeatedly with water ($\frac{1}{20}$ vol.) until the wash was neutral. The alkali and water washes did not contain significant amounts of ecdysteroids as detected by thin-layer chromatography (tlc).

Dry Column Fractionation

Alumina (300 g, ICN, Pharmaceuticals, Inc.) was packed into a 50 mm wide nylon film tube (ICN Pharmaceuticals, Inc., 16). A layer (1 cm) of Celite 545 was packed on the top. A sample (5.0 g) of the dry residue from the combined chloroform extracts was dissolved in ethanol (10 ml), added to 5 g Celite 545, and the ethanol evaporated. The dry sample was then packed on the top of the alumina column and another thin layer of Celite 545 superimposed. The column was developed with ethyl acetate – ethanol (95%) 35:15 (200 ml). Bands were detected with u.v. light (254 nm), cut from the column, and the ecdysteroids eluted from each with chloroform–ethanol 1:1 (200 ml) by filtration. Fine alumina particles were removed by filtration through fine glass-frit funnels.

Thin-layer Chromatography (tlc)

The ecdysteroid composition of interesting bands was checked by tlc (silica gel F, E. Merck; CH_2Cl_2–Methanol 21:4). After observing the uv (254 nm) absorbing zones the plates were sprayed with sulfuric acid – ethanol (1:2) and heated (2–5 min, 120°C). Sulfuric acid treated plates were checked for fluorescence in uv (360 nm) light.

High Pressure Liquid Chromatography (lc)

Preparative

Selected dry column bands were chromatographed with a Waters ALC 100 chromatograph on a Porasil A (60) (Waters Associates, Inc.) column (188 cm × 7.7 mm diameter) with chloroform–ethanol (95%) 4:1 flowing at 2.7 ml/min. Samples (400 mg) were dissolved in chloroform–ethanol (95%) 1:1 and injected via a 0.5 ml loop. The column effluent stream was usually divided by passing it through a tee equipped with a variable resistance on one leg provided by a micrometer valve (Nupro Co., Cleveland, Ohio) to provide stream splitting (*ca.* $\frac{1}{25}$). The minor stream was monitored at 254 nm (Chromatronix photometer, model 200) and the main stream collected with a fraction collector. Each run required *ca.* 130 min.

Final purification of yew V and Va (see Fig. 1) was achieved by recycling the samples through a Porasil A column (180 mm × 4.7 mm diameter) in chloroform–isopropanol 70:30 at 2.0 ml/min. Tailing and resultant sample loss were minimized by adding 1% water. The eluted materials were monitored and collected as above.

Analytical

Normal Phase — Corasil II (Waters Associates, Inc., 37 μm) was packed (17) into a precision bore stainless steel tube (92 cm × 4.7 mm diameter) with fittings (Swagelock) modified to minimize dead volume and containing stainless steel frits (MOTT Metallurgical Corp., Framington, Ma., 5 μm). The column was developed with chloroform–ethanol (95%) 6:1 with a solvent flow of 1.0 ml/min at a nominal pressure of 500 psi. Samples were injected, as ethanol solutions, directly onto the head of the column through a valved injection port (Pierce Chemical Co.). The column effluent was monitored as with the preparative column but without stream splitting.

Reversed Phase — A Bondapak phenyl/Corasil column (Waters Associates Inc., 37–50 μm, 50 cm × 1.0 mm diameter) was prepared, samples injected, and separations monitored as above. Ecdysteroids were eluted with ethanol–water (1:20). The retention times of unknown samples were directly compared with those of known standards.

Gas–Liquid Chromatography (glc)

All glc separations, similar to those of others, (*cf.* refs. 18–20) were conducted with a Hewlett-Packard, model 402 equipped with a flame ionization detector. The silylized glass column (120 cm × 4 mm i.d.) was packed with 3% OV-101 on 80/100 mesh Chromosorb W HP (Pierce Chemical Co.). Separations were conducted at 320°C with a helium flow of 40 ml/min.

All samples (*ca.* 10 μg) were dried over Drierite *in vacuo* and silylized in a 1:1 solution of pyridine–TMSI (*N*-trimethylsilylimidazole, Pierce Chemical Co.) at 50°C for 20 min. Retention times were compared directly with known standards.

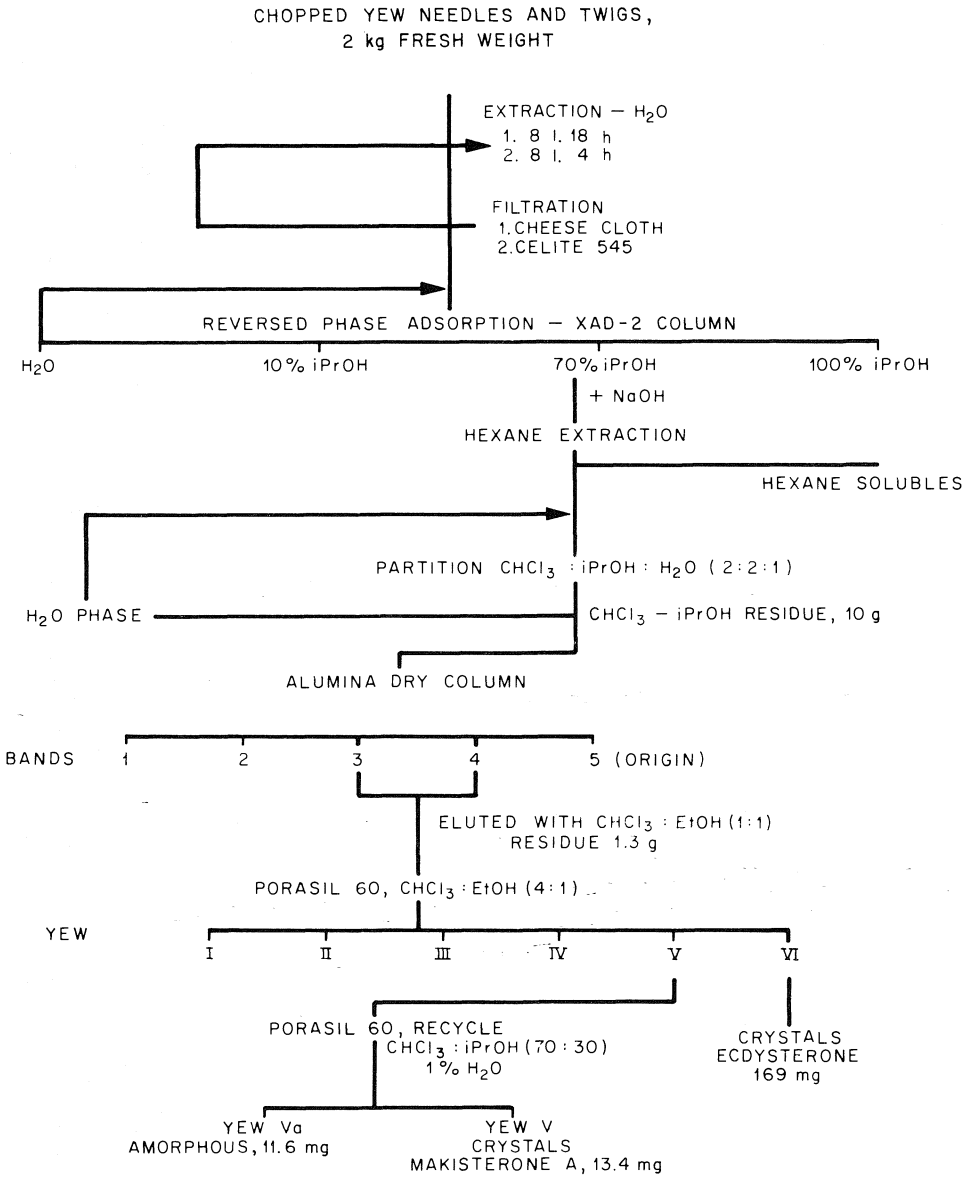

FIG. 1. Flow diagram for the isolation of makisterone A and ecdysterone from yew needles and twigs.

Physical Data

Melting points were determined with an air-bath, melting point apparatus (Gallenkamp). Mass spectra (ms) were determined by electron impact at a beam voltage of 70 eV and direct probe at 240°C with a DuPont/C.E.C., model 21-110 spectrometer). Nuclear magnetic resonance (nmr) spectra were determined with a Varian HA-100 in pyridine-d_5 with TMS as an internal reference. Melting points and spectra were compared with authentic ecdysterone (Schwarz/Mann).

Results and Discussion

An outline of the isolation procedure, detailed in the Experimental, is summarized in the flow diagram (Fig. 1). The coarseness of the yew twigs and needles (chopped rather than ground) permitted ready removal of the bulk of the debris but necessitated the long soaking. Filtration of the liquor through a Celite 545 bed prevented

TABLE 1. Retention times of standard and yew ecdysteroids on liquid chromatograph columns, Porasil A, Corasil II, and Bondapak phenyl/Corasil

Sample	Retention time (min)		
	Porasil A	Corasil II	Bondapak phenyl/Corasil
Ponasterone A		10.33	19.21
α-Ecdysone		16.00	13.00
Makisterone A		18.19	7.98
Ecdysterone		23.92	4.31
Yew I	42	10.33	18.91
Yew II	56	11.23,12.47	13.59
Yew III	66	13.89	3.84,7.39,15.96
Yew IV	74	15.84	4.73
Yew V	88	18.20	7.98
Yew VI	110	23.94	4.31

clogging of the XAD-2 column. The substitution of stainless steel screens for the usual column fritted disks greatly simplified and speeded the column operation. Removal of the dark brown (presumably tannins) color from the liquor by the XAD-2 column proved to be a useful monitoring device since these pigments behave similarly to the ecdysteroids on the column. They also largely eluted with the ecdysteroids in 70% isopropanol–water but could be conveniently removed by the alkaline wash during chloroform–isopropanol extraction. Back-washing the water washes proved to be unnecessary since no ecdysteroid was detected in the washes by tlc.

The alumina dry column proved valuable since it irreversibly adsorbed colored materials difficult to remove with Porasil A chromatography alone. The dry column technique was limited as we found it difficult to obtain clean separations.

Liquid chromatography of the crude ecdysteroids on Porasil A permitted the nearly complete separation of the major components as indicated by normal and reversed-phase analytical lc (Table 1). While tlc was routinely used for monitoring the separations it was most useful for crude samples, which do not resolve well in the analytical lc, and least useful for the purer fractions since the tlc R_f's (Table 2) are less stable and precise than the lc retention times (Table 1). After separation on Porasil A ecdysteroid fractions were also examined by glc as the TMS ethers (Table 3). This showed that yew V, which appeared to be pure by the other methods, contained a considerable contaminant. This fraction was therefore subjected to recycle chromatography on Porasil A with a modified solvent mixture which separated the two components after three passes through the column. Examination of the fractions by glc indicated they were essentially pure. Yew V and VI were subsequently crystallized from methanol–water and acetone–hexane, respectively. Yew Va remained amorphous. The melting points (V, mp 263.5–265.5°C (dec.); VI, mp 239–240°C (dec.)) were compared directly with that of

TABLE 2. R_f's of standard and yew ecdysteroids on silica gel F tlc plates

Compound	R_f
Ponasterone A	0.517
α-Ecdysone	0.309
Makisterone A	0.283
Ecdysterone	0.256
Yew I	0.520
Yew II	0.420
Yew III	0.330
Yew IV	0.300
Yew V	0.280
Yew Va	0.280
Yew VI	0.256

TABLE 3. Retention times of TMS-ethers of standard and yew ecdysteroids on an OV-101 column

Sample	Retention time (min)[a]	
Makisterone A	5.23	6.02
Ecdysterone	2.05	2.25
Yew V	5.25	6.04
Yew Va	4.62	5.02
Yew VI	2.05	2.25

[a]Each compound yielded a major and minor TMS-ether peak.

authentic ecdysterone (mp 239–240°C (dec.)). The melting (decomposition) point of yew V agrees with that published for makisterone A (11).

A comparison of the nmr and ms of yew V with those published for makisterone A **4** indicate essential agreement for the methyl chemical shifts and mass fragmentation. The nmr methyl chemical shifts of yew V (1.23, 1.09, 1.57, 1.32/1.29, 1.05) were like those of ecdysterone (1.19, 1.07, 1.57, 1.35 (6H) for C_{18}, C_{19}, C_{21}, $C_{26/27}$) with the one extra peak at 1.05 ppm like the C_{28} methyl of makisterone A **4** (11). The characteristic ms peaks corresponded to the extensive dehydration (allowing no parent peak at *M/e* 494) and the side chain cleavages expected for makisterone A (*M/e* 363, $P - 131$ (6.3%) of base peak at *M/e* 43; 345, $P - 131 - 18$ (14%) and 301, $P - 175 - 18$ (11%) respectively for cleavages at C_{20}—C_{22} and C_{17}—C_{20} with dehydration) with the expected side chain fragments (cleavage at: C_{20}—C_{22}, *M/e* 131 (25%); C_{20}—C_{22} —H_2O, *M/e* 113 (42%) and C_{20}—C_{22} $-2H_2O$, *M/e* 95 (43%)) as interpreted by Imai *et al.* (11). The nmr of yew Va indicated that this compound was closely related to yew V. The ms shows strong peaks at *M/e* 145, 127, and 109 which are 14 units heavier than the corresponding ones for yew V. These could be accounted for by the addition of an extra CH_2-group giving a molecular weight of 508 equivalent to makisterone (lemmasterone, **5**) C or D **6** (12).

The method reported above is similar to that reported by Schooley *et al.* (21) derived from the reverse phase separation work of Hori (15). The high water solubility (for a steroid) of the ecdysteroids allows the bulk of this material to be extracted with water and then concentrated on XAD-2 while many potential contaminants are not extracted or are not adsorbed by the resin. Some purification was also achieved by the selective nature of the extraction with XAD-2 and the subsequent alkali-solvent partition. To ensure complete ecdysteroid recovery, particularly since the XAD-2 columns tend to channel and the column was heavily loaded, the aqueous yew extract was passed through the column a second time and the trapped solutes eluted. After solvent extraction only a minimum volume of solvent had to be evaporated, the readily removed isopropanol and chloroform. The alumina 'dry column' was not suitable for ecdysteroid separation, however, as despite repeated trials the bands could not be sufficiently resolved. After removal of the 'resinous' material with the alumina column the lc fractionation presented no unusual difficulties. The final purification of yew V was most readily achieved by recycle chromatography. This mode of separation seems either to degrade the compound when the solvents are anhydrous or else produces pronounced smearing of the peaks not obvious from the peak uv absorption record because the peak intensities declined markedly with each recycle. We found that the inclusion of a small percentage of water in the solvent largely prevented this decline.

We have concluded that yew V was makisterone A. The crystalline yew V yielded nmr, uv, and ms data and a melting point which agree with the published data (11, 12) for makisterone A. In addition yew V shows the same retention times as authentic makisterone A in two lc systems (Table 1) and as the TMS ether by glc (Table 3).

The identification of makisterone A as a constituent of both insects (14) and crustaceans (13) has increased its significance to endocrinologists. The identification of this compound as a constituent of the common decorative shrub, *Taxus cuspidata*, should make it more readily available for research.

Acknowledgements

The authors thank Prof. K. Nakaniski for a gift of authentic makisterone A. Nuclear magnetic resonance spectra were ably recorded by Dr. A. G. McInnis and D. G. Smith and mass spectra by Dr. D. W. Jamieson and D. Embree of the National Research Council of Canada, Atlantic Regional Laboratory.

1. M. W. Gilgan and M. E. Retallack. J. Fish. Res. Board Can. **24**, 2497 (1967).
2. T. Takemoto, S. Ogawa, N. Nishimoto, and H. Hoffmeister. Z. Naturforsch. Teil B, **22**, 681 (1967).
3. S. Imai, S. Fujioka, K. Nakanishi, M. Koreeda, and T. Kurokawa. Steroids, **10**, 557 (1967).
4. H. Hoffmeister, G. Heinrich, G. B. Staal, and W. J. Van Der Burg. Naturwissenschaften, **54**, 471 (1967).
5. G. B. Staal. Proc. K. Ned. Akad. Wet. Ser. C, **70**, 409 (1967).
6. S. Imai, T. Toyosato, M. Sakai, Y. Sato, S. Fujioka, E. Murata, and M. Goto. Chem. Pharm. Bull. Jpn. **17**, 335 (1969).
7. M. W. Gilgan and M. E. Zinck. Comp. Biochem. Physiol. **52**, 261 (1975).
8. R. Huber and W. Hoppe. Chem. Ber. **98**, 2403 (1965).

9. J. N. KAPLANIS, M. J. THOMPSON, W. E. ROBBINS, and B. M. BRYCE. Science, **157**, 1436 (1967).
10. J. N. KAPLANIS, L. A. TABOR, M. J. THOMPSON, W. E. ROBBINS, and J. J. SHORTINO. Steroids, **8**, 625 (1966).
11. S. IMAI, M. HORI, S. FUJIOKA, E. MURATA, M. GOTO, and K. NAKANISHI. Tetrahedron Lett. 3883 (1968).
12. S. IMAI, S. FUJIOKA, E. MURATA, Y. SASAKAWA, and K. NAKANISHI. Tetrahedron Lett. 3887 (1968).
13. A. FAUX, D. H. S. HORN, E. J. MIDDLETON, H. M. FALES, and M. E. LOWE. Chem. Commun. 175 (1969).
14. J. N. KAPLANIS, S. R. DUTKY, W. E. ROBBINS, M. J. THOMPSON, E. L. LINQUIST, D. H. S. HORN, and M. N. GALBRAITH. Science, **190**, 681 (1975).
15. M. HORI. Steroids, **14**, 33 (1969).
16. B. LOEV and M. N. GOODMAN. Intra-Science chemistry report 4. 1970. p. 203.
17. R. A. HENRY. *In* Modern practice of liquid chromatography. *Edited by* J. Kirkland. Wiley-Interscience, New York, NY. 1971. pp. 72 ff.
18. H. MIYAZAKI, M. ISHIBASHI, C. MORI, and N. IKEKAWA. Anal. Chem. **45**, 1164 (1973).
19. C. F. POOLE, E. D. MORGAN, and P. M. BEBBINGTON. J. Chromatogr. **104**, 172 (1975).
20. D. W. BORST and J. D. O'CONNOR. Steroids, **24**, 637 (1974).
21. D. A. SCHOOLEY, G. WEISS and K. NAKANISHI. Steroids, **19**, 377 (1972).

Deuterium isotope effects and assignment of ^{13}C chemical shifts in spectra of methyl octadecanoate and the sixteen isomeric oxooctadecanoates[1]

A. P. TULLOCH

Prairie Regional Laboratory, National Research Council of Canada, Saskatoon, Sask., Canada S7N 0W9

Received July 5, 1976

A. P. TULLOCH. Can. J. Chem. **55**, 1135 (1977).

^{13}C nmr spectra of the 16 isomeric *gem*-dideuterooctadecanoates were measured and second and third atom deuterium isotope effects calculated for most of the affected carbons of 12 of the isomers. The average value for the second atom effect was -0.20 ppm and for the third atom effect was -0.05 ppm. From these effects and the changes in spectra caused by introduction of two deuterons at positions along the fatty acid chain, chemical shifts were determined for all carbons of methyl octadecanoate. Spectra of seven dideuterooxooctadecanoates, with both deuterons attached to a carbon γ to the oxo group, were measured, and using isotope effects, unambiguous assignments of chemical shift were made. Chemical shifts were thus assigned to all carbons in the 16 isomeric oxooctadecanoates and these show the effect of the carbonyl group at different positions in the chain. The results indicate that, in addition to large effects on carbons α and β to the oxo group, the γ to θ carbons are all shielded with displacements: γ -0.46, δ -0.30, ε -0.27, ζ -0.13, η -0.09, and θ -0.06 ppm. The effects of the oxo and ester carbonyls extend over seven methylene groups, but shielding due to ester carbonyl is a little smaller. Spectra of 2- to 9-oxo esters showed that interaction between the two carbonyl groups causes relatively greater shielding of carbons situated between the groups.

A. P. TULLOCH. Can. J. Chem. **55**, 1135 (1977).

On a mesuré des spectres rmn du ^{13}C de 16 *gem*-dideutérooctadécanoates isomères; les effets isotopiques du deuterium pour les deuxième et troisième atomes ont pu être calculés pour la plupart des carbones affectés de 12 des isomères. La valeur moyenne de l'effet du deuxième atome est de -0.20 ppm et celle du troisième atome est de -0.05 ppm. A partir de ces effets et des changements dans les spectres obtenus par l'introduction de deux atomes de deutérium à des positions le long de la chaîne d'acides gras, on a déterminé les déplacements chimiques de tous les atomes de carbone de l'octadécanoate de méthyle. On a mesuré les spectres de sept dideutéro-oxooctadécanoates avec deux deuterium attachés à un carbone γ par rapport au groupe oxo et faisant appel aux effets isotopiques, des attributions nonambiguës des déplacements chimiques ont pu être faites. Des déplacements chimiques ont pu être attribués à tous les atomes de carbone des 16 oxooctadécanoates isomères et ces déplacements chimiques montrent l'effet d'un groupement carbonyle à diverses positions de la chaîne. Les résultats indiquent qu'en plus de larges effets sur les carbones α et β par rapport au groupement oxo, les carbones γ jusqu'à θ sont blindés avec les déplacements décroissants: γ -0.46, δ -0.30, ε -0.27, ζ -0.13, η -0.09 et θ -0.06 ppm. Les effets des groupements carbonyles oxo et ester se font sentir sur sept groupes méthylènes mais le blindage dû au groupement carbonyle de l'ester est un peu plus petit. Les spectres des esters oxo-2 jusqu'à 9 montrent que l'interaction entre les deux groupements carbonyles cause des blindages relativement plus grands des carbones situés entre les groupes.

[Traduit par le journal]

Introduction

Application of second and third atom deuterium isotope effects to the assignment of ^{13}C signals in spectra of long chain methyl esters was reported previously (1). Several esters, with a CD_2 group in the chain near the terminal methyl group, and 2-D_2 hexadecanoate showed second atom effects of -0.12 to -0.28 ppm and third atom effects of about -0.04 ppm. Also, line widths of affected signals were increased approximately threefold due probably to ^{13}C–D coupling. Signal broadening facilitated identification of affected signals even when upfield displacements were relatively small. A preliminary application of this method to saturated and unsaturated C_{18} esters resulted in assignment of signals due to C-4, C-5, C-6, and C-15 in the spectrum of methyl octadecanoate (2) but shifts of C-8 to C-14 were not assigned.

Spectra have now been measured for all 16 isomers with D_2 groups at positions along the chain from positions 2 to 17, so that isotope

[1]NRCC No. 15765.

effects could be determined for a much larger number of compounds. The esters examined earlier (1) had the CD_2 group near the ends of the molecule and, for this reason, the effects might have been unusual. From these spectra, chemical shifts have been assigned to all the carbons in methyl octadecanoate.

Preliminary results have indicated the value of ^{13}C nmr spectra in determining structures of oxygenated esters (2). Spectra of seven dideuterooxooctadecanoates have also been used to assign chemical shifts in spectra of all 16 isomeric oxooctadecanoates. It has thus been possible to determine the effect, on the ^{13}C spectrum, of introducing an oxo group at different positions along the fatty acid chain.

Results and Discussion

To obtain chemical shifts for all carbons in methyl octadecanoate, signals in spectra of D_2 esters were assigned either from upfield displacement and broadening of an already visible signal or by the appearance of spectra after several overlapping signals had been removed as a result of deuteration. The spectral changes are illustrated in Fig. 1. The spectrum of octadecanoate shows 5 signals due to C-4, C-5, C-15, C-6, and C-7 and a composite signal due to C-8 to C-14. In the spectrum of 3-D_2 octadecanoate signals due to C-4 and C-5 are displaced and broadened and in the spectrum of 5-D_2 octadecanoate signals due to C-4, C-6, and C-7 are displaced. Signals for the D_2 carbons were not seen in these spectra or in those of any of the other isomers; signals due to dideuterated carbons are not usually observed (1, 3, 4) probably because of excessive signal splitting and increased relaxation times.

In the spectrum of 8-D_2 octadecanoate, signals due to C-6, C-7, and C-9 have been displaced and the signal now assigned to C-14 appears as a single peak at δ 29.66 ppm. The C-14 signal was previously obscured by the C-8, C-9, and C-10 signals which have disappeared or moved upfield. C-11, C-12, and C-13 all have almost the same chemical shift at δ 29.71 ppm. The signal due to C-14 can also be seen in spectra of 7-D_2, 9-D_2, and 10-D_2 esters. In the same way signals due to C-8 and C-9 appear in spectra of 12-D_2 and 13-D_2 esters and the C-12 and C-13 signals in the spectrum of 9-D_2 ester. C-10 and C-11 signals were not clearly observed in any of the spectra.

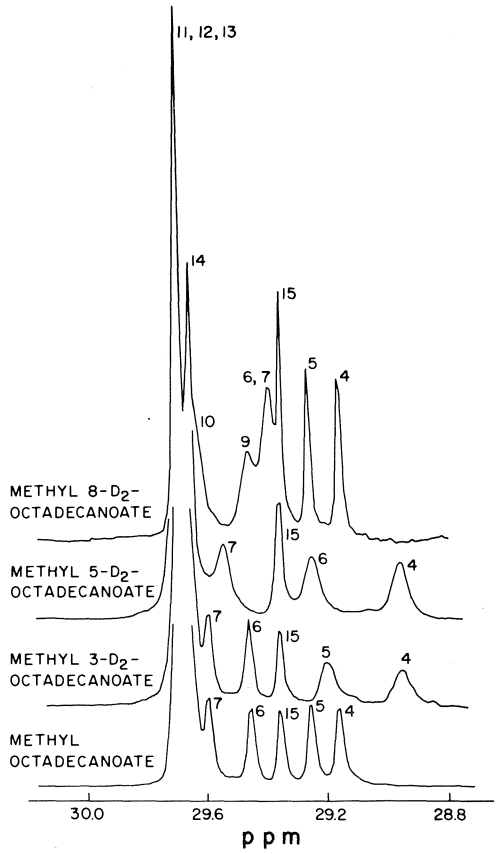

FIG. 1. 28.8 to 30.0 ppm region of ^{13}C nmr spectra of methyl octadecanoate and of methyl 3-D_2, 5-D_2, and 8-D_2 octadecanoates; spectra obtained with spectral width 1 kHz and horizontally expanded 10 times.

Average values of second and third atom effects of the CD_2 group obtained from unobscured and unambiguously assignable signals, which are listed in Table 1, were then used to confirm assignments made as above. Displacements of C-3 and C-4 in the 2-D_2 spectrum, of C-2 and of C-2 and C-3 in spectra of 3-D_2 and 4-D_2 esters, respectively, were lower than the rest, presumably due to their proximity to the ester group, and were excluded from calculation. Signals due to ester carbonyl carbon were observed in spectra of 2-D_2 and 3-D_2 esters, but the intensity was reduced, especially in the 2-D_2 spectrum (*cf.* spectra of D_2 steroid ketones (3)). Isotope effects were not, however, observed for the carbonyl carbons; electronegative substituents have previously been found to reduce isotope effects (1, 5) but the C-2 signal in the spectrum of acetone-d_6 showed an appreciable positive (downfield) isotope effect (6). In spectra

TABLE 1. Deuterium isotope effects in ^{13}C spectra of *gem*-dideuterooctadecanoates[a]

CD_2 position	Carbons affected	Respective isotope effects[b]
2	3, 4	−0.14, −0.05
3	2, 4, 5	−0.18, −0.20, −0.06
4	2, 3, 5, 6	−0.05, −0.15, −0.21, −0.06
5	3, 4, 6, 7	−0.04, −0.19, −0.20, −0.05
6	4, 5, 7	−0.04, −0.19, −0.20
7	5, 6	−0.05, −0.20
8	6, 7	−0.05, −0.19
13	15	−0.06
14	15, 16	−0.21, −0.06
15	16, 17	−0.21, −0.06
16	15, 17, 18	−0.20, −0.21, −0.06
17	15, 16, 18	−0.06, −0.20, −0.23

[a]Only clearly measurable effects have been tabulated.
[b]Upfield displacements are negative.

of amino acids with α-ND_2 groups and COOD carboxyl, the carbonyl carbon showed an upfield displacement of about 0.3 ppm (7).

The 14 second atom effects in Table 1 had an average value of −0.20 ppm and the 12 third atom effects an average value of −0.05 ppm. Thus the C-8 signal appears at higher field in spectra of 7-D_2 and 9-D_2 and its approximate value in octadecanoate can be calculated by addition of 0.2 ppm. Similarly C-9 appears in the spectrum of 8-D_2 (see Fig. 1) and (partly obscured) in the spectrum of 10-D_2, C-10 in spectra of 9-D_2 and 11-D_2, C-11 in spectra of 10-D_2 (partly obscured) and 12-D_2, C-12 in spectra of 11-D_2 and 13-D_2 (both partly obscured by other signals), C-13 in spectra of 12-D_2 and 14-D_2 and C-14 in spectra of 13-D_2 and 15-D_2 esters.

Further evidence that the C-11, C-12, and C-13 signals are together at the lowest field part of the large composite peak (see Fig. 1) was obtained from spectra of 11-D_2, 12-D_2, and 13-D_2 esters in which this low field portion was displaced to higher field. The change in the spectrum of 11-D_2 also confirms that C-14 is at higher field than C-11 to C-13. The spectrum of 15-D_2, in which the lower field portion of the composite peak is unchanged, also indicates the relatively high field position of the C-14 signal.

In this way signals in the D_2 isomers were assigned and hence chemical shifts of the seven overlapping signals in the spectrum of octadecanoate were calculated giving the results listed in Table 2. Shifts of C-7 to C-14 were not previously measured but those of C-4 to C-6 and of C-15 are in agreement with previous assignments (1, 2, 8). The shift of C-14 at δ 29.66 ppm, at higher field than the shifts of C-11 to C-13 at δ 29.71 ppm is of interest since the ε effect due to methyl substitution, which appears not to have been previously estimated, can be calculated. The shifts of C-11 to C-18 of octadecanoate (Table 2) show that the effects of methyl substitution are as follows: α effect +8.61, β effect +9.23, γ effect −2.56, δ effect +0.30 and ε effect −0.05 ppm. Since shifts of C-12 and C-11 are the same as that of C-13, and ζ and η effects are zero. The α to δ effects are similar to those of Batchelor *et al.* (8).

The effects of the ester group were also calculated by comparison with a C_{18} alkane (*cf.* ref. 8): C-1 +159.85, C-2 +11.39, C-3 −6.95, C-4 −0.20, C-5 −0.45, C-6 −0.20, C-7 −0.12, C-8 −0.07 and C-9 −0.04. Effects for carbons 4 to 7 are larger than those observed before (8) and those for C-8 and C-9 were not measured before. Thus, the ester group has a small shielding effect on the more distant carbons, detectable as far as C-9, and only C-11 to C-13 are completely unaffected by the ends of the chain.

Spectra of Oxooctadecanoates

There have been only a few previous investigations of the effect of a carbonyl group on spectra of alkanes (9). Chemical shifts were reported for some C_4 to C_{13} ketones (10); comparison of shifts of $RCOR^1$ with RH showed the usual appreciable deshielding of the α carbon and downfield displacement of about 1 ppm of signals of the other carbons (except the γ carbon)

TABLE 2. ^{13}C chemical shifts of methyl octadecanoate and dideuterooctadecanoates (in ppm from TMS)[a]

Carbon	Octadecanoate	Position of D_2 group															
		2	3	4	5	6	7	8	9	10	11	12	13	14	15	16	17
2	34.08	—	33.90	34.03	34.09	34.09	34.09	34.10	34.10	34.08	34.09	34.07	34.09	34.08	34.06	34.08	34.10
3	24.97	24.83	—	24.77	24.93	24.99	24.97	24.98	24.98	24.96	24.97	24.96	24.97	24.96	24.95	24.97	24.98
4	29.16	29.11	28.96	—	28.97	29.12	29.16	29.17	29.17	29.16	29.16	29.16	29.17	29.15	29.15	29.16	29.17
5	29.26	29.25	29.20	29.05	—	29.07	29.21	29.27	29.26	29.25	29.25	29.25	29.25	29.24	29.25	29.26	29.25
6	29.45	29.44	29.45	29.39	29.25	—	29.25	29.40	29.47[b]	29.45	29.45	29.44	29.45	29.44	29.45	29.45	29.45
7	29.59	29.59	29.59	29.59	29.54	29.39	—	29.40	29.55	29.59	29.59	29.58	29.59	29.58	29.59	29.60	29.59
8	29.64					29.60	29.44	—	29.47[b]	29.59[b]	29.65[b]	29.63	29.64				
9	29.67							29.47	—	29.45[b]	29.60[b]	29.67	29.66	29.65	29.64	29.64	29.64
		29.64	29.64	29.64	29.64	29.64	29.60	29.64	29.47[b]	—	29.48[b]	29.63[b]	to	to	to	to	to
10	29.68	to	to	to	to	to	to	to	29.64	29.45[b]	—	29.48[b]	29.68	29.66[b]	29.72	29.72	29.72
11	29.71								29.66	29.65[b]	29.65[b]	—	29.66[b]	29.71			
12	29.71								29.71	29.70	29.70	29.65[b]	29.45[b]				
13	29.71	29.72	29.72	29.72	29.72	29.72	29.72	29.72	29.71	29.65	29.65	29.65[b]	—	29.48	29.45		
14	29.66						29.66	29.66	29.66	29.65	29.65	29.63[b]	29.45[b]	—			
15	29.36	29.35	29.35	29.35	29.36	29.36	29.36	29.36	29.36	29.35	29.35	29.35	29.30	29.15		29.16	29.30
16	31.92	31.92	31.92	31.94	31.92	31.93	31.91	31.93	31.93	31.91	31.92	31.91	31.93	31.86	31.71	—	31.72
17	22.69	22.68	22.68	22.68	22.69	22.69	22.68	22.70	22.70	22.68	22.68	22.68	22.69	22.69	22.63	22.48	—
18	14.08	14.07	14.07	14.07	14.08	14.09	14.07	14.10	14.10	14.07	14.07	14.06	14.08	14.08	14.07	14.02	13.85

[a]In octadecanoate C-1 was at 174.00 ppm, in 2-D_2 at 174.04 ppm, and in 3-D_2 at 173.95 ppm; separate signals were not observed in spectra of mixtures.
[b]Composite peak, chemical shift not accurate for each component.

up to those separated from the carbonyl by 5 methylene groups. However, the measurements were not accurate enough to decide if the smaller deshielding effects were real (9).

Spectra of all 16 oxoesters, 2-oxo to 17-oxo, were measured. Signals due to carbons α and β to the oxo group could be clearly recognized in the spectrum but in many cases could not be unambiguously assigned to a particular α or β carbon. Also signals of γ, δ, ε, etc., carbons could not be easily assigned in spectra of esters where the oxo group was near the centre of the chain.

Spectra of specifically dideuterated oxo esters, 10-D_2-7-oxo, 5-D_2-8-oxo, 11-D_2-8-oxo, 8-D_2-11-oxo, 14-D_2-11-oxo, 9-D_2-12-oxo, and 16-D_2-13-oxo octadecanoates, were then examined. In each ester the CD_2 group is γ to the oxo group so that second and third atom isotope effects make possible assignment of signals of the two pairs of carbons α and β to the CD_2 group. Isotope effects were measured for signals of all affected carbons except for those of C-6 and C-7 of 8-D_2-11-oxo and C-7 and C-8 of 9-D_2-12-oxo which were obscured by signals of other carbons. Averages were calculated separately (from six values in each case) for isotope effects on carbons between the CD_2 and CO groups and on carbons the other side of the CD_2 group. In each case the average second atom effect was −0.20 and the average third atom effect was −0.05. Again affected signals were broadened approximately threefold. Thus, the isotope effects are the same as in the D_2 octadecanoates and are apparently not affected by the oxo group in contrast to the effect of the ester group on isotope displacement in the 2-D_2, 3-D_2, and 4-D_2 esters.

Using the effects, all signals in spectra of 7-, 8-, 11-, 12- and 13-oxo esters were assigned except for those of C-4 to C-10 in 13-oxo ester. Signals of carbons near the ends of the molecule could also be unambiguously assigned when the oxo group was at positions 2- to 5- and 14- to 17-. Average values for the effect of the oxo group on γ to θ carbons (comparing oxo ester to octadecanoate) were calculated from chemical shifts of carbons in the above esters. Chemical shifts could then be assigned to all carbons in all the oxo esters giving the results in Table 3. Effects of the oxygen on the oxygenated carbon and on carbons on the methyl ester side of the group are listed in Table 4 and effects on α to θ carbons on the terminal methyl side are in Table 5.

Effects on Carbonyl Carbon

Stothers and Lauterbur (11) examined carbonyl shifts in α, β, and γ oxo esters and observed shielding of both CO carbons particularly those in 2-oxo ester. The results in Table 4 for 2-, 3-, and 4-oxo esters are quite similar to these; however, neither CO group reaches a constant shift until 9-oxo ester (in which the ester carbonyl shift is almost the same as that for unsubstituted octadecanoate). It therefore appears that there is a small, and diminishing, but definite shielding effect of one CO group on the other which extends across 7 methylene groups. Thus, comparing 4-oxo with 9-oxo ester, the shifts of ester and ketonic carbonyl carbons of the former are upfield of those of the latter by 0.9 and 2.5 ppm, respectively.

Effects on α and β Carbons

These effects, which are considerably larger than those on more distant carbons, are conveniently considered separately. Unambiguous assignments obtained from spectra of D_2 oxo esters showed that those carbons which have signals at higher field in octadecanoate are also at higher field in the oxo esters. Thus in the spectrum of 13-oxo ester the signal due to C-14 is at higher field than the signal to C-12 by 0.04 ppm, in agreement with the shifts of C-14 and C-12 in the spectrum of octadecanoate (see Tables 2 and 3).

If the effect of the CO group were exactly additive then the differences between chemical shifts of the pairs of α carbons, and the pairs of β carbons, in the oxo esters should be the same as the differences between the corresponding pairs of shifts in the octadecanoate spectrum. Table 6 shows how these differences vary with position of the oxo group.

When the oxo group is at positions 10-, 11-, 12-, or 13-, close to the center of the chain, agreement between observed and calculated values is good. This is presumably because carbons α or β to these positions are little affected by the ester group; as was shown above, the influence of this group extends as far as C-9 but is quite small for C-8 and C-9. When the oxo group replaces one of the last four methylene groups differences between observed and calculated values appear, particularly when the terminal methyl is an α or β group suggesting that the oxo group affects a methyl group more than a methylene group.

TABLE 3. ^{13}C chemical shifts of methyl oxooctadecanoates (in ppm from TMS)[a]

Carbon	Position of oxo group																
	2[b]	3	4	5	6	7[b]	8[b]	9	10[b]	11[b]	12[b]	13[b]	14[b]	15[b]	16	17[b]
1	161.45	167.38	173.02	173.21	173.53	173.61	173.81	173.93	173.93	173.93	173.93	173.94	173.94	173.94	173.93	173.91
2	193.99	48.93	27.78	33.06	33.81	33.78	33.92	34.01	34.05	34.04	34.04	34.02	34.03	34.02	34.05	34.07
3	39.37	202.30	37.02	18.97	24.48	24.66	24.72	24.88	24.91	24.91	24.92	24.91	24.92	24.91	24.92	24.95
4	23.02	42.98	208.65	41.39	23.25	28.66	28.87	28.93	29.05	29.07	29.09	29.09	29.10	29.09	29.13	29.13
5	28.97	23.49	42.78	209.84	42.18	23.35	28.83	29.01	29.05	29.14	29.14	29.22	29.18	29.19	29.21	29.22
6	29.29	29.01	23.85	42.82	210.32	42.34	23.59	29.05	29.18	29.21	29.30	29.35	29.36	29.37	29.40	29.43
7	29.41	29.33	29.21	23.85	42.82	210.63	42.54	23.77	29.18	29.30	29.30	29.45	29.49	29.52	29.52	29.56
8	29.56	29.40	29.37	29.25	23.89	42.78	210.91	42.66	23.83	29.21	29.30	29.35	29.49	29.52	to	29.60
9		29.56	29.44	29.37	29.25	23.84	42.72	211.03	42.71	23.83	29.18	29.35	29.39	29.52	29.60	29.60
10				29.44	29.36	29.22	23.87	42.78	211.03	42.71	23.84	29.18	29.36	29.40		29.60
11	29.64		29.64		29.45	29.37	29.24	23.89	42.78	211.03	42.74	23.85	29.23	29.37	29.44	29.56
12	to		to	29.56	29.56	29.42	29.38	29.27	23.91	42.75	210.91	42.70	23.86	29.22	29.40	29.41
13	29.72		29.72	to	to	29.57	29.44	29.40	29.27	23.88	42.74	211.03	42.72	23.82	29.25	29.37
14				29.64	29.64	29.57	29.53	29.40	29.35	29.21	23.84	42.66	211.04	42.74	23.93	29.17
15		29.34	29.33	29.29	29.29	29.28	29.26	29.25	29.11	29.04	28.91	23.53	42.41	210.95	42.34	23.88
16		31.94	31.90	31.87	31.87	31.86	31.84	31.80	31.80	31.64	31.58	31.43	25.97	44.60	211.31	43.74
17		22.70	22.66	22.66	22.66	22.64	22.62	22.62	22.62	22.57	22.46	22.42	22.34	17.27	35.75	208.53
18		14.09	14.05	14.05	14.05	14.06	14.05	14.05	14.05	14.02	13.98	13.85	13.79	13.72	7.82	29.74
OCH_3		52.70	52.12	51.59	51.35	51.39	51.31	51.31	51.31	51.19	51.27	51.24	51.24	51.24	51.23	51.29

[a]Italicized figures were obtained using the oxo group effects calculated from spectra of D_2 oxo esters.
[b]Shifts are accurate to ±0.01 ppm; other shifts are accurate to ±0.03 ppm.

TABLE 4. Effect of oxygen atom on ^{13}C chemical shifts of carbonyl carbon and on carbons on the methyl ester side of the CO group in spectra of methyl oxooctadecanoates[a,b]

Position of CO group	Oxo carbon	Affected carbons α	β	γ	δ	ε	ζ	η	θ
2	+159.91	−12.55							
3	+177.33	+14.85	−6.32						
4	+179.49	+12.05	−6.30	−0.98					
5	+180.58	+12.23	−6.00	−1.02	−0.79				
6	+180.87	+12.92	−5.91	−0.49	−0.27	−0.47			
7	+181.04	+12.89	−5.91	−0.50	−0.31	−0.30	−0.39		
8	+181.27	+12.95	−5.86	−0.43	−0.29	−0.25	−0.16	−0.19	
9	+181.36	+13.02	−5.82	*−0.40*	*−0.25*	*−0.23*	−0.09	−0.07	
10	+181.35	+13.04	−5.81	*−0.41*	*−0.27*	*−0.21*	*−0.09*	−0.06	−0.03
11	+181.32	+13.03	−5.84	−0.43	−0.29	−0.24	−0.12	−0.09	−0.07
12	+181.20	+13.03	−5.84	−0.49	−0.34	−0.29	−0.15	−0.12	−0.07
13	+181.32	+12.99	−5.86	*−0.50*	*−0.32*	*−0.29*	*−0.14*	*−0.10*	*−0.04*
14	+181.38	+13.01	−5.85	*−0.48*	*−0.32*	*−0.28*	*−0.15*	*−0.10*	*−0.09*
15	+181.59	+13.08	−5.89	*−0.49*	*−0.34*	*−0.28*	*−0.15*	*−0.12*	*−0.07*
16	+179.39	+12.98	−5.73	*−0.46*	*−0.31*	*−0.27*	?	?	?
17	+185.84	+11.82	−5.48	*−0.49*	*−0.34*	*−0.30*	*−0.15*	*−0.08*	*−0.07*
Average values[c]				−0.46	−0.30	−0.27	−0.13	−0.09	−0.06

[a]In ppm calculated by comparison with methyl octadecanoate. Unitalicized figures were obtained from unambiguous assignments and were used to make the assignments which gave the italicized values.
[b]Effects on the OCH_3 carbon were: 2-oxo, +1.39; 3-oxo, +0.81; 4-oxo, +0.28.
[c]Average of unambiguous assignments only but excluding effects on the ester carbonyl carbon.

TABLE 5. Effect of oxo group on ^{13}C chemical shift of carbons on the terminal methyl side of the oxo group in spectra of methyl oxooctadecanoates[a]

Position of CO group	α	β	γ	δ	ε	ζ	η	θ
2	+14.40	−6.14	*−0.29*	*−0.16*	*−0.13*	*−0.08*	?	?
3	+13.82	−5.77	*−0.44*	*−0.26*	*−0.24*	*−0.11*	?	?
4	+13.52	−5.60	*−0.38*	*−0.27*	*−0.23*	?	?	?
5	+13.37	−5.74	*−0.39*	*−0.30*	*−0.24*	?	?	?
6	+13.23	−5.75	*−0.42*	*−0.32*	*−0.26*	?	?	?
7	+13.14	−5.83	−0.46	−0.34	−0.29	−0.14	−0.09	−0.08
8	+13.05	−5.81	−0.47	−0.33	−0.27	−0.13	−0.10	−0.06
9	+13.10	−5.82	*−0.50*	*−0.31*	*−0.26*	*−0.11*	−0.08	−0.07
10	+13.07	−5.80	*−0.44*	*−0.31*	*−0.25*	−0.12	−0.07	−0.03
11	+13.04	−5.83	−0.45	−0.32	−0.28	−0.12	−0.06	—
12	+13.03	−5.82	−0.45	−0.34	−0.23	−0.10	—	—
13	+13.00	−5.83	−0.49	−0.27	−0.23	—	—	—
14	+13.05	−5.95	−0.35	−0.29	—	—	—	—
15	+12.68	−5.42	−0.36	—	—	—	—	—
16	+13.06	−6.26	—	—	—	—	—	—
17	+15.66	—	—	—	—	—	—	—
Average values[b]			−0.47	−0.32	−0.26	−0.12	−0.08	−0.06

[a]In ppm calculated by comparison with methyl octadecanoate. Unitalicized figures were obtained from unambiguous assignments and were used to make the assignments which gave the italicized values.
[b]Average calculated from values for 7-, 8-, 11-, 12-, and 13-oxo esters.

There is an increasing divergence between observed and calculated values when the oxo group is at positions 9- to 4-; Tables 4 and 5 show that this is mainly because α and β carbons on the ester side of the CO group are at higher field than corresponding carbons on the terminal methyl side. The α displacement for 9-oxo ester is +13.02 on the ester side and +13.10 on the methyl side, but for 5-oxo ester the corresponding values are +12.23 and +13.37. Apparently interaction between the two CO groups results in a relative shielding of carbons between the groups and the shielding increases with decrease in separation of the groups. It

TABLE 6. Observed and calculated differences between ^{13}C chemical shifts of pairs of α carbons and pairs of β carbons in spectra of methyl oxooctadecanoates[a]

	Differences in α carbons		Differences in β carbons	
Position of oxo group	Observed	Calculated	Observed	Calculated
2	122.08	149.03	—	—
3	5.95	4.92	143.89	144.74
4	5.76	4.29	3.93	4.63
5	1.43	0.29	4.88	4.62
6	0.64	0.33	0.64	0.48
7	0.44	0.19	0.49	0.41
8	0.18	0.08	0.28	0.23
9	0.12	0.04	0.12	0.12
10	0.07	0.04	0.08	0.07
11	0.04	0.03	0.05	0.04
12	—	—	—	0.02
13	0.04	0.05	0.32	0.35
14	0.31	0.35	2.11	2.21
15	1.86	2.26	6.55	7.02
16	6.59	6.67	16.11	15.58
17	14.00	17.84	—	—

[a]In ppm, calculated values obtained from shifts of corresponding carbons in spectrum of methyl octadecanoate.

also appears from spectra of 2-oxo to 6-oxo esters that α carbons on the methyl side of the oxo group are shielded to some extent, but, except for the β-carbon of 2-oxo ester, β carbons are not affected.

Effects on γ to θ Carbons

The average values in Tables 4 and 5 were calculated from shifts of carbons on both sides of the oxo group in spectra of 7-, 8-, 11- and 12-oxo esters and from shifts of carbons on the methyl side only in 13-oxo ester (these signals were assigned using the D_2 oxo esters). Then, from assignments made to signals in spectra of other oxo esters (Table 3) effects of the oxo group in these isomers were calculated and are shown in Table 4 and 5 in italics. It is clear that, for most positions of the oxo group, values are quite close to the average. In 2-oxo ester (Table 5) the oxo group has a smaller than average shielding effect on γ to ε carbons. Table 4 also shows that, in the case of 4- to 7-oxo esters, when the carbon under consideration is the ester carbonyl (or C-2 of 5-oxo ester), then the effect is appreciably larger than average.

Effects on carbons on both sides of the oxo group have almost the same average values. They do not decrease regularly since there is a drop of 0.16 ppm from the γ to δ effect, the ε effect is only a little lower and there is a drop of 0.13 ppm to the ζ effect followed by a gradual decline to the θ effect. The results in Tables 4 and 5 show that the longer range effects of ketonic carbonyl are consistently slightly larger than those of ester carbonyl. They also show that effects previously reported for tridecan-7-one (9, 10) were too large and in the wrong direction. Since the average γ to θ effects given in Tables 4 and 5 were calculated from accurately determined and unambiguously assigned chemical shifts they differ slightly from previously reported values (2).

It was concluded by Batchelor *et al.* (12) that an electric field effect of the CO_2CH_3 group could affect the signals of double bond carbons in the spectrum of methyl oleate and it was also thought that this effect could explain the long range influence of the ester group on saturated carbons (8). Whatever the explanation of long range effects, it is clear that the carbonyl group can affect chemical shifts of carbons separated by seven methylene groups. Also the present results obtained for the oxooctadecanoates enable the effects of the oxo group to be related to its position in a long chain molecule and so could be used to determine carbonyl position in long chain natural products.

Experimental

A Varian XL-100-15 spectrometer in the Fourier transform mode at 25.2 MHz, with proton noise decoupling, was used to obtain natural abundance ^{13}C nmr spectra. All deuterated compounds were examined using a data

length of 8192 points, sweep width was 1 kHz and acquisition time 4 s (0.25 Hz/point), the 28.8 to 30.0 ppm region was also observed after 10-fold horizontal expansion; chemical shifts so obtained were accurate to ± 0.01 ppm. A data length of only 4096 points was used with some of the oxo esters and these shifts were accurate to ± 0.03 ppm. To determine shifts of carbonyl carbons, spectral widths of 5 kHz and acquisition times of 0.8 s (1.25 Hz/point) were used; 2-oxooctadecanoate and 3-D_2 octadecanoate also required pulse delays of 1 s and 2-D_2 octadecanoate required a pulse delay of 3 s. Off-resonance proton decoupling was used to assign the signal due to C-18 in the spectrum of methyl 17-oxooctadecanoate. All spectra were measured as 15% solutions in $CDCl_3$ and the solvent also provided the internal deuterium lock. All chemical shifts are downfield from TMS. The oxo esters were synthesized previously (13) and synthesis of the deuterated esters is being reported elsewhere.

Acknowledgement

The author is indebted to Mr. M. Mazurek for ^{13}C nmr measurements.

1. A. P. Tulloch and M. Mazurek. J. Chem. Soc. Chem. Commun. 692 (1973).
2. A. P. Tulloch and M. Mazurek. Lipids, **11**, 228 (1976).
3. H. Eggert and C. Djerassi. J. Org. Chem. **38**, 3788 (1973).
4. G. W. Gribble, R. B. Nelson, J. L. Johnson, and G. C. Levy. J. Org. Chem. **40**, 3720 (1975).
5. P. A. J. Gorin. Can. J. Chem. **52**, 458 (1974).
6. G. E. Maciel, P. D. Ellis, and D. C. Hofer. J. Phys. Chem. **71**, 2160 (1967).
7. H. K. Ladner, J. J. Led, and D. M. Grant. J. Magn. Reson. **20**, 530 (1975).
8. J. G. Batchelor, R. J. Cushley, and J. H. Prestegard. J. Org. Chem. **39**, 1698 (1974).
9. J. B. Stothers. Carbon-13 NMR spectroscopy. Academic Press, New York, NY. 1972. p. 144.
10. E. Lippmaa and T. Pehk. Eesti NSV Tead. Akad. Toim. Keem. Geol. **17**, 210 (1968).
11. J. B. Stothers and P. C. Lauterbur. Can. J. Chem. **42**, 1563 (1964).
12. J. G. Batchelor, J. H. Prestegard, R. J. Cushley, and S. R. Lipsky. J. Am. Chem. Soc. **95**, 6358 (1973).
13. A. P. Tulloch. J. Am. Oil Chem. Soc. **41**, 833 (1964).

The use of polymer supports in organic synthesis. VIII.[1] Solid phase syntheses of insect sex attractants[2]

CLIFFORD C. LEZNOFF[3] AND THOMAS M. FYLES[4]

Department of Chemistry, York University, Downsview, Ont., Canada M3J 1P3

AND

J. WEATHERSTON

The Insect Pathology Research Institute, Sault St. Marie, Ont., Canada P6A 5M7

Received October 14, 1976

CLIFFORD C. LEZNOFF, THOMAS M. FYLES, and J. WEATHERSTON. Can. J. Chem. **55**, 1143 (1977).

A 2% cross-linked divinylbenzene–styrene copolymer, incorporating trityl chloride groups, (**1**), was used in the synthesis of insect sex attractants of Lepidoptera by two independent routes. Polymer **1** reacted with the symmetrical diols 1,6-hexanediol, 1,8-octanediol, and 1,10-decanediol to give the monoblocked polymer-bound diols **5–7**, respectively. Mesylation of **5–7** gave the polymer-bound monomesylates **8–10**, which on coupling with 1-lithio-1-hexyne or 1-lithio-1-butyne gave the polymer-bound alkyne trityl ethers **18–20**. Alkynols, obtained by hydrolysis from polymers **18–20**, were selectively reduced and acetylated to give *cis*-7-dodecen-1-ol acetate (**28**), *cis*-9-tetradecen-1-ol acetate (**29**), and *cis*-11-tetradecen-1-ol acetate (**30**), the sex attractants of *Trichoplusia ni* (Hübner), *Spodoptera frugiperda* (J. E. Smith), and *Argyrotaenia velutinana* (Walker), respectively. Alternatively, polymer-bound 1,7-heptanediol (**33**), polymer-bound 1,9-nonanediol (**34**), and **7** were oxidized with the Sharpless reagent (CrO_2Cl_2/*tert*-butyl alcohol/pyridine) to give polymer-bound aldehydes **35–37**, which on reaction with Wittig reagents and subsequent hydrolysis and acetylation gave **28**, **29**, and 10-tetradecen-1-ol acetate (**47**), the sex attractant of *Archips semiferanus* (Walker). A 'reverse' Wittig synthesis of **47** was achieved by the reaction of polymer **10** with molten triphenylphosphine followed by base and treatment with butyraldehyde. Subsequent cleavage and acetylation gave **47** in high yield and stereoselectivity containing greater than 91% of the *cis* isomer.

CLIFFORD C. LEZNOFF, THOMAS M. FYLES et J. WEATHERSTON. Can. J. Chem. **55**, 1143 (1977).

On a utilisé un copolymère à 2% divinylbenzène–styrène réticulé, et incorporant des groupes chlorure de trityle (**1**) pour la synthèse, par deux routes indépendantes, d'attirants sexuels d'insectes de Lepidoptera. Le polymère **1** réagit avec les diols symétriques hexanediol-1,6 octanediol-1,8 et décanediol-1,10 pour conduire respectivement aux diols **5–7** possédant un lien covalent avec le polymère. La mésylation de **5–7** conduit aux monomésylates **8–10** liés au polymère; par couplage avec le lithio-1 hexyne-1 ou le lithio-1 butyne-1 ils fournissent les éthers tritylés acétyléniques liés au polymère (**18–20**). Les alkynols obtenus par hydrolyse des polymères **18–20** ont pu être réduits sélectivement et acétylés pour conduire aux acétates des dodécèn-7 ol-1 *cis* (**28**), tétradécèn-9 ol-1 *cis* (**29**) et tétradécèn-11 ol-1 *cis* (**30**) qui sont respectivement les attirants sexuels des *Trichoplusia ni* (Hübner), *Spodoptera frugiperda* (J. E. Smith) et *Argyrotaenia velutinana* (Walker). D'une manière alternative, l'heptanediol-1,7 et le nonanediol-1,9 liés au polymère (**33** et **34**) et **7** ont pu être oxydés par le réactif de Sharpless (CrO_2Cl_2/*tert*-butanol/pyridine) pour conduire aux aldéhydes liés au polymère **35–37** qui par réaction avec des réactifs de Wittig suivie d'une hydrolyse ainsi qu'une acétylation fournissent **28**, **29** et l'acétate du tétradécèn-10 ol-1 *cis* (**47**) l'attirant sexuel de *l'Archips semiferanus* (Walker). On a pu réussir une synthèse de Wittig renversée de **47** par la réaction du polymère **10** avec la triphénylphosphine fondue, suivie d'une réaction avec une base et d'un traitement avec le butyraldéhyde. Une coupure subséquente, suivie d'une acétylation, conduit à **47** avec un bon rendement et une bonne stéréosélectivité et contenant plus que 91% de l'isomère *cis*.

[Traduit par le journal]

Introduction

Insoluble polymer supports are widely used in the synthesis of polypeptides (1) and have been applied to polynucleotide (2) and polysaccharide (3) syntheses as well. All of these syntheses involve the preparation of biopolymers by the repetition of a very few well characterized

[1]For part VII see ref. 8.

[2]Presented in part at the 59th Canadian Chemical Conference of the Chemical Institute of Canada, London, Ont., June 1976.

[3]Author to whom correspondence should be addressed.

[4]Holder of NRCC studentships 1974–1977.

chemical transformations. Although the *number* of reactions required for the synthesis of a typical natural product is relatively small, compared to the synthesis of a polypeptide, such as ribonuclease A (4), the *variety* of chemical reactions is large. Thus one would expect the synthesis of a natural product in eight different steps to be considerably more difficult than that of a pentapeptide involving eight steps but only two different steps. Syntheses of natural products, in general, have not been attempted on solid phases despite the inherent advantages of this method (1, 2, 5), possibly due to the fact that each reaction in the synthetic scheme must be carefully examined with respect to its compatibility with the heterogeneous reaction medium, even though the given reaction under investigation was highly successful in homogeneous phase.

Insect sex attractants (6) of Lepidoptera, having the general formula shown below, are particularly suitable molecules to prepare on solid phases. Not only can one exploit the 'general' advantages of solid phase synthesis described by Merrifield (1) and Letsinger *et al.* (5) (simplicity of reactions, ease of work-up conditions, adaptability to automation), but we and others had previously shown how insoluble polymer supports can be used as monoprotecting groups of symmetrical dials (7, 8) and diols (refs. 9 and 10 and for recent reviews see ref. 11), the simple starting materials used in the synthesis of insect sex attractants.

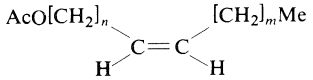

In a preliminary report of this work (12), we described the synthesis of insect sex attractants on solid phases by an alkyne coupling route. In this report we present the details of the solid phase alkyne route (12) along with several modifications and alternative solid phase syntheses of insect sex attractants based on Wittig condensations.

Results and Discussion

The Alkyne Route

A 2% crosslinked divinylbenzene–styrene copolymer, incorporating trityl chloride functional groups, (**1**) (13), was prepared by our direct lithiation method (9). Polymer **1** was treated with 1,6-hexanediol (**2**), 1,8-octanediol (**3**), and 1,10-decanediol (**4**) for 48 h in pyridine at room temperature to give monoprotected polymer-bound diols **5–7** respectively. It was not possible at this stage to wash out liberated HCl and still maintain unreacted residual polymer-bound trityl chloride (**1**) for the determination of unreacted **1**. The amounts of diols **2–4** attached to polymers **5–7** were determined by cleavage of **5–7** with dry HCl in dioxane, having a titration value of 0.35 *M* HCl (Table 1).

Lithioalkynes can be readily coupled to alkyl halides in tetrahydrofuran – hexamethylphosphoric triamide (THF–HMPT) (14) and hence it was desirable to convert **5–7** to polymer-bound halides. Treatment of **7** with $SOCl_2$ in pyridine or dioxane–pyridine, PBr_3 in pyridine or dioxane–pyridine, PPh_3Br_2 in dimethylformamide (DMF), or even PPh_3 in CCl_4 (15) resulted in complete or partial cleavage of the diol from the polymer and hence these standard procedures for conversion of primary alcohols to halides had to be abandoned. Mesylation of **5–7** with methanesulfonyl chloride in pyridine for 48 h at room temperature gave the polymer-bound symmetrical diol monomesylates **8–10** respectively. The polymer turns brown at this stage and cannot be washed free of all impurities and hence sulfur analysis of **8–10**, for example, would give meaningless results. Acid cleavage of **8–10** as before gave 1,6-hexanediol monomesylate (**11**), 1,8-octanediol monomesylate (**12**), and 1,10-decanediol monomesylate (**13**) in yields of ~30%, ω-chloro-1-alkanols (from displacement of mesylate by Cl^- during cleavage) in yields of ~30%, and some recovered diol (Table 1). Since one can never be certain of the purity of a polymer-bound product we base our yields on cleaved products and intermediates only.[5] It should be mentioned that certain losses occur in the work-up of the products so that the summation of yields of products and recovered starting material usually remains less than 100% of the diol initially bound to the polymer. We feel that small losses occur due to

[5]It may also be true, as a referee suggested, that cleavage is incomplete, but we feel that this viewpoint is unlikely as repetitive cleavages liberate no additional products. In addition, if some diol is uncleavable, then some diol would be irretrievably lost only in the first cycle. If additional diol became uncleavable in subsequent cycles the capacity of the polymer would diminish with each cycle, which is not the case.

TABLE 1. Yields of insect attractants and intermediates prepared on solid phases via the alkyne route

Insect attractant	Diol initially bound to polymers **5–7**[a] (mmol/g)	Diol monomesylates and ω-chloro-1-alkanols[b] (mmol/g)	Quantity of alkyn-1-ol[c] (mmol/g)	Recovered diol monomesylate[c] (mmol/g)	Recovered diol[c] (mmol/g)	Attractant[d] (mmol/g)	Overall yield of attractant (%)	Overall conversion to attractant[e] (%)	Overall yield by solution methods (%)
28	0.44	0.15	0.14	0.02	0.20	0.12	27	55	30[f], 4[g]
29	0.42	0.21	0.17	0.02	0.15	0.15	36	60	16[h]
30	0.52	0.28	0.21	0.03	0.13	0.19	36	53	—[i]

[a]Determined by cleavage of samples of **5–7** with 0.35 *M* HCl in dioxane.
[b]Determined by cleavage of samples of **8–10** with 0.35 *M* HCl in dioxane.
[c]Recovered from acid cleavage of **18–20**.
[d]Obtained by the reduction and acetylation of the alkyn-1-ols.
[e]Yield if recovered diol and mesylate are recycled.
[f]From ref. 18 based on 6-chlorohexan-1-ol.
[g]From ref. 35 based on $TsO(CH_2)_5CH(OMe)_2$.
[h]From ref. 19 based on 8-chlorooctan-1-ol.
[i]No yields are given in ref. 20.

cleavage of diol and products from the polymer in intermediate steps in the synthesis. The combined yields of monomesylate and ω-chloro-1-alkanol represent high conversion of **5–7** to **8–10** (and hence **11–13**) as the recovered diols were likely doubly bound to the polymer (9). As previously shown (9) it is possible to prepare a polymer-bound trityl chloride to which symmetrical diols can be bound exclusively at one end only. Acetylation of the free alcohol end gives an almost quantitative yield of the symmetrical diol monoacetate upon cleavage from the polymer. Thus we concluded (9) that the acetylation reaction goes to completion. The acetylation reaction on polymer **1** used in this paper gives us approximately 60% yields of symmetrical diol monoacetates as previously reported (9). We had suggested (9) that the remaining diol was likely doubly-bound since we know that the acetylation reaction is nearly quantitative. In this paper our combined yields of ω-chloro-1-alkanols and symmetrical diol monomesylates via polymer **1** are close to 60% and we feel that these results parallel the acetylation results previously reported (9) and lead us again to the conclusion that the recovered diol was due to double binding to the polymer. Polymer-bound monomesylate (**10**) could be directly converted to a polymer-bound aliphatic bromide (**14**) or iodide (**15**) by treatment of **10** with NaBr or NaI, respectively, in HMPT at 70°C for 48 h in the dark. Halide analysis of polymer-bound aliphatic halides **14** and **15** was achieved using potassium *tert*-butyl alcohol under reflux overnight to ensure complete liberation of halide. These analyses of polymer-bound aliphatic halides are useful in that they distinguish aliphatic halides from ionic, benzylic, or trityl halides. These conditions are much more vigorous than those used in the modified Volhard analysis of polymeric benzylic halides (16), characteristic of Merrifield's polymer (1) or polymer **1**. Since some model preliminary experiments indicated that all attempted reactions on polymer-bound monomesylate **10** worked as well or better than polymer-bound bromide **14** or iodide **15**, all subsequent reactions were done exclusively on mesylates, thus eliminating one step in the reaction sequence.

Polymer-bound monomesylates **8** and **9** were added to 1-lithio-1-hexyne (**16**) and **10** to 1-lithio-1-butyne (**17**) in THF–HMPT (1:1) at −10°C and allowed to stir overnight at room temperature to give polymer-bound alkynes **18–20**, respectively (Scheme 1). Liberation of the alkynes from polymers **18–20** as before gave recovered polymer-bound trityl alcohol (**21**) and the acetylenic alcohols, 7-dodecyn-1-ol (**22**), 9-tetradecyn-1-ol (**23**), and 11-tetradecyn-1-ol (**24**), respectively. Crude **22–24** contaminated with some unreacted **2–4** and **11–13**, were purified at this stage by preparative tlc.[6] Hydrogenation of **22–24** with Pd–$CaCO_3$ treated with quinoline (17) gave 7-dodecen-1-ol (**25**), 9-tetradecen-1-ol (**26**), and 11-tetradecen-1-ol (**27**). Acetylation of **25–27** afforded (Table 1)

[6]Since the only major products recovered at this stage were the single desired product and recovered diol, these compounds could presumably be separated by distillation if the reactions were done on a larger scale.

7-dodecen-1-ol acetate (18) (**28**), 9-tetradecen-1-ol acetate (19) (**29**), and 11-tetradecen-1-ol acetate (20) (**30**), the *cis* isomers of which are the sex attractants of the cabbage looper, *Trichoplusia ni* (Hübner), the fall army worm moth, *Spodoptera frugiperda* (J. E. Smith), and the red-banded leaf roller, *Argyrotaenia velutinana* (Walker), respectively. Attractant **30** was also prepared from **24** by acetylation, followed by hydrogenation, but **30**, prepared by this reverse sequence of chemical reactions, was contaminated by considerable amounts of alkyne, alkane, and the *trans* isomer.

Vapour phase chromatography (vpc) on a 10% Silar C column of **29–30** showed significant amounts of their *trans* isomers (Table 2) as well as small amounts of unreacted alkyne and over-reduced alkane-1-ol acetates. High pressure liquid chromatography (hplc), using a μ Bondapak C-18 reverse phase column, has recently been used in the separation of *cis* and *trans* isomers of insect sex attractants (21). Analysis by hplc, confirmed the vpc results entirely for attractants **28–30**, showing that these compounds contained significant amounts of the *trans* isomer. It was recognized that catalytic hydrogenation of **23** to give **26** was not completely stereoselective for the *cis* isomer (18).

It is known that reduction of alkynes with boranes (22) yields *cis*-alkenes exclusively and this procedure has been applied to the stereoselective synthesis of insect sex attractants (23). Hence, treatment[7] of **23** and **24** with 9-BBN in THF gave **26** and **27**, which on acetylation gave exclusively the *cis* isomers of **29** and **30**, as analyzed by hplc and infrared spectroscopy. The mass spectra, taken at an ionization potential of 16 eV, of **28–30** exhibited weak, but detectable parent ions and base peaks corresponding to the loss of acetic acid.

The Wittig Route

The synthesis of insect sex attractants by Wittig reactions in homogeneous phase has been described (25, 26) and we wished to apply this mode of synthesis to solid phases. Polymer **1** reacted with 1,7-heptanediol (**31**), 1,9-nonanediol (**32**), and 1,10-decanediol (**4**) as described above to give the monoprotected polymer-bound diols **33**, **34**, and **7**, respectively. The amounts of diol contained in polymers **33**, **34**, and **7** were determined by acid cleavage with HCl in dioxane (Table 3). Due to the acid

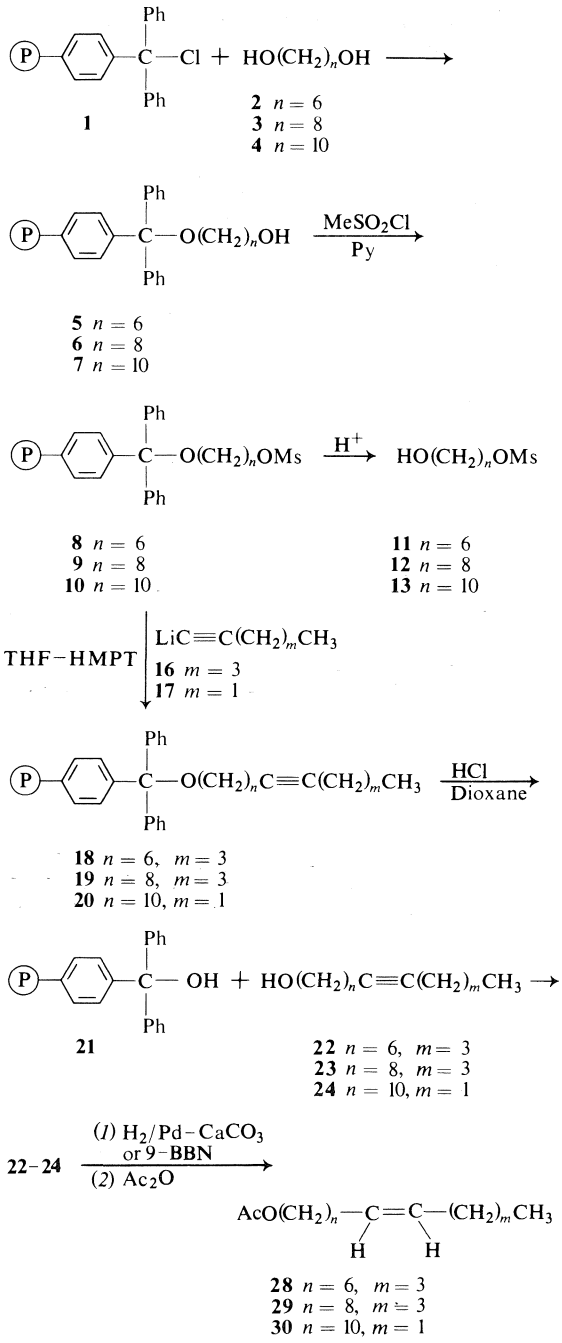

SCHEME 1

[7]Preliminary experiments designed to effect the direct reduction of polymer-bound alkyne **20** to a polymer-bound *cis*-alkene using the homogeneous reducing agents 9-BBN in THF or diisobutylaluminum hydride (24) (DIBAH) in benzene have so far given inconsistent results.

TABLE 2. Purity of insect attractants prepared on solid phases via the alkyne route as determined by vpc and hplc

Attractant	Alkene (%)	*cis* Isomer[a] (%)	Alkyne impurity[b] (%)	Alkane impurity[c] (%)
28[d]	93.5	75.5	—	3.5
29[d]	84.0	84.8	6.5	7.4
29[e]	89.4	100	10.6	—
30[d]	88.0	83.0[f]	12.0	—
30[e]	>99.0	>98.0[f]	<1.0	—
30[g]	84.0	48.0[f]	7.0	9.0

[a]As a percentage of total alkene.
[b]Alkyne unreduced by catalytic or 9-BBN reduction.
[c]Alkyne overreduced to alkane.
[d]Prepared by catalytic reduction of the alkyn-1-ol and acetylation.
[e]Prepared by 9-BBN reduction of the alkyn-1-ol.
[f]Determined by hplc only.
[g]Prepared by catalytic reduction of an alkyn-1-ol acetate.

sensitive trityl blocking group of the polymer, oxidation of **33**, **34**, and **7** to the corresponding aldehydes had to be accomplished under basic or neutral conditions. Furthermore, many oxidizing agents are used in mixtures that are heterogeneous at the beginning of the reaction or precipitate chromium salts during the course of the oxidation. The heterogeneous nature of the oxidizing agent coupled with the insoluble polymer substrate would make the oxidations unfavourable, if not impossible, and precipitated chromium salts would be difficult to separate from the polymer under non-acidic conditions. In addition, since the products of any reaction on the insoluble polymer cannot be purified at intermediate stages in the synthesis it is desirable that each reaction proceed in high yield and be free of side products. We found that these requirements were met using the Sharpless reagent (27) (CrO_2Cl_2, *tert*-butyl alcohol, pyridine in CH_2Cl_2). Thus oxidation of **33**, **34**, and **7** with the Sharpless reagent in CH_2Cl_2 at room temperature overnight gave the polymer-bound aldehydes **35**–**37** respectively. These polymers exhibited strong infrared absorption at 1730 cm^{-1} indicative of an aliphatic aldehyde. Acid hydrolysis of **35**–**37** gave some 7-hydroxyheptanal (28) (**38**), 9-hydroxynonanal (28) (**39**), and 10-hydroxydecanal (28) (**40**), respectively, on purification by preparative tlc but considerable polymerization of **38**–**40** had occurred during the hydrolysis. Due to considerable by-product formation upon cleavage it is difficult to determine yields of **38**–**40** but we can be fairly certain that it cannot be more than approximately 60% of loaded diol since we had previously shown that these polymers contain

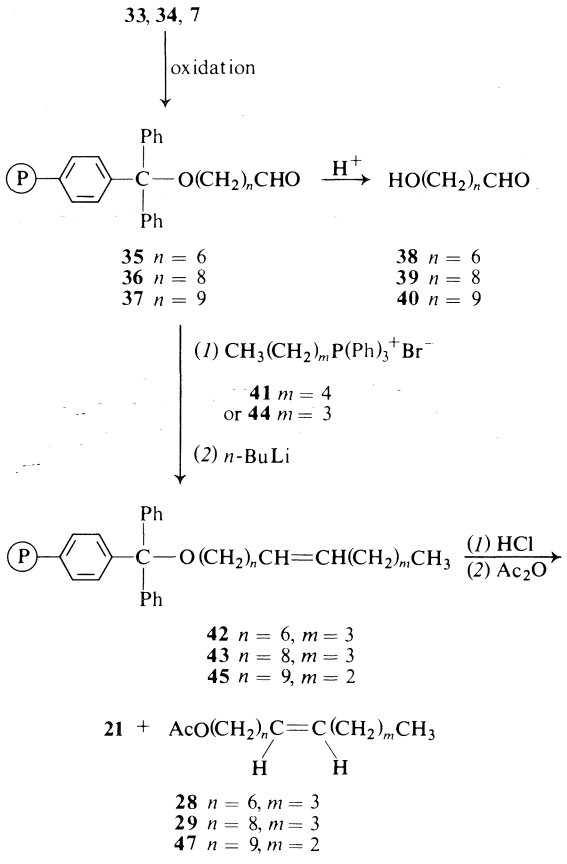

SCHEME 2

about 40% doubly bound diol (9). The Wittig reactions of **35** and **36** using *n*-pentyltriphenylphosphonium bromide (**41**) with *n*-BuLi in THF at room temperature overnight have polymer-bound alkenes **42** and **43**. Acid hydrol-

TABLE 3. Yields of insect attractants prepared on solid phases by the Wittig and 'reverse' Wittig routes

Insect attractant	Diol initially bound to polymers **33**, **34**, and **7**[a] (mmol/g)	Alken-1-ol[b] (mmol/g)	Recovered diol[b] (mmol/g)	Attractant[c] (mmol/g)	Overall yield of attractant[d] (%)	Overall conversion to attractant (%)	Overall yield by solution methods (%)
28	0.75	0.18	0.42	0.17	23	52	66[e]
29	0.85	0.32	0.27	0.30	36	52	57[f], 30[g]
47	0.52	0.18	0.16	0.17	33	48	—[h]
47[i]	0.65	0.25	0.24	0.25	35	56	—[h]
47[i]	0.52	0.18	0.16	0.18	33	47	—[h]
47[i]	0.52	0.19	0.16	0.19	35	50	—[h]

[a]Determined by cleavage of **33**, **34**, **7**, and **48–50** respectively with 0.35 *M* HCl in dioxane.
[b]Recovered on acid cleavage of **42**, **43**, and **45**.
[c]Obtained by the acetylation of the alken-1-ols.
[d]Yield if recovered diol is recycled.
[e]From ref. 38 based on $Cl(CH_2)_6CO_2H$.
[f]From ref. 38 based on $Cl(CH_2)_8CO_2H$.
[g]From ref. 26 based on oleyl alcohol.
[h]No yields are given in ref. 29.
[i]From 'reverse' Wittig reactions.

ysis of **42** and **43** with HCl in dioxane[8] gave 7-dodecen-1-ol (**25**) and 9-tetradecen-1-ol (**26**), which on acetylation yielded on 7-dodecen-1-ol acetate (18) (**28**), and 9-tetradecen-1-ol acetate (19) (**29**) (Scheme 2). Similarly, **37** reacted with *n*-butyltriphenylphosphonium bromide (**44**) to give a polymer-bound alkene (**45**), which after cleavage from the polymer gave 10-tetradecen-1-ol (**46**). Acetylation yielded 10-tetradecen-1-ol acetate (29) (**47**), the *cis* isomer of which is the sex attractant of the oak leaf roller, *Archips semiferanus* Walker. It is known that the Wittig reaction can afford a predominance of the *cis* isomer and reaction conditions have been worked out giving *cis* products of high stereoselectivity (30). Although we had not concerned ourselves with details of achieving high stereoselectivity in these sequences the ratio of *cis* to *trans* isomers was quite high as determined by vpc and hplc (Table 4).

The 'Reverse' Wittig Route

Since we were successful in synthesizing insect sex attractants by condensation of Wittig reagents with polymer-bound aldehydes, we were interested to see if the Wittig reaction would work in the reverse sense, *i.e.* reaction of a polymer-bound Wittig reagent with aliphatic aldehydes. Treatment of polymer-bound bromide **14** or iodide **15**, derived from polymer-bound 1,10-decanediol (**10**), with triphenylphosphine in refluxing xylene did *not* yield a polymer containing ionic halide. It is possible that the polymer-bound halides **14** and **15** are sufficiently sterically constrained that nucleophilic attack by PPh_3 is very slow under normal conditions (31). The concentration of PPh_3 was increased 10-fold to induce salt formation, but no reaction occurred. We felt that replacing the nucleophilic halide counterion by the mesylate anion and increasing the concentration of triphenylphosphine to its limit might favour salt formation. Thus, treatment of **10** with molten triphenylphosphine at 100°C under argon overnight gave the desired polymer-bound phosphonium salt (**48**) as its mesylate. Similarly, treatment of **14** and **15**, containing 0.22 and 0.24 mmol halide/g, gave the polymer-bound phosphonium salts **49** and **50** containing 0.15 and 0.18 mmol ionic halide/g, as their bromide and iodide, respectively. Polymers **48–50** reacted with *n*-BuLi in dry THF at room temperature overnight to give dark purple polymers, which were either washed free of excess reagents under dry argon or used directly. The addition of butyraldehyde to the polymers suspended in THF discharged the colour after 0.5 h and the mixture was stirred for 8 h to give the same polymer **45** prepared by the 'normal' Wittig route (Scheme 3). As before, acid hydrolysis of **45** gave recovered polymer **21** and **46** which on acetylation yielded **47** (Table 3). Analysis by vpc and hplc of **47** prepared by the 'reverse' Wittig route showed 91.2% stereoselectivity for the *cis* isomer (Table 4). It is somewhat surprising that the 'reverse' Wittig route should be so highly stereoselective especially since

[8]Treatment with AcCl in AcOH can give the attractant acetates directly, but the products are difficult to purify by this procedure.

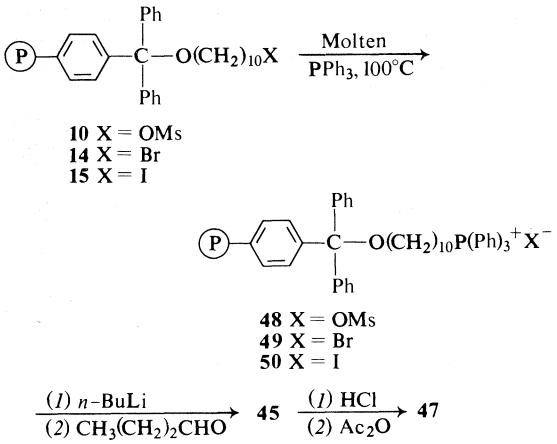

SCHEME 3

special conditions necessary to promote *cis* stereoselectivity (30) were not followed. We thought that at least in the case of **48** the mesylate counterion might be the cause of this stereoselectivity and hence we repeated the preparation of **47** via the normal Wittig route (Scheme 1) but using *n*-butyltriphenylphosphonium *mesylate* (**51**) as the Wittig reagent. The stereoselectivities of the synthesis of **47** via **51** and **44** were very similar (Table 4) and hence the mesylate counterion does not appreciably affect the stereoselectivity of the Wittig reaction. Used polymer **21** recovered from the synthesis of the sex attractants by the alkyne, Wittig, or 'reverse' Wittig routes can be reconverted to polymer **1** and recycled with no loss of activity (9).[9] It appears that the acid cleavage step strips the polymers of most impurities acquired during the synthetic route and liberates **21** with no reduction in capacity.

Bioassay of 28

A behavioural bioassay (32) performed on **28**, the sex attractant of the cabbage looper, prepared by both the alkyne and Wittig routes showed intense response in over 80% of the males in the 8–10 day age group.

Conclusions

The synthesis of natural products in general and insect sex attractants in particular on solid phases has been demonstrated by three independent routes in yields at least comparable with solution phase methods, despite the fact that most solution phase methods use comparatively expensive or poorly accessible starting materials such as ω-chloro-1-alkanols or ω-chloroalkanoic acids and our solid phase method uses inexpensive 1,ω-alkanediols (Tables 1 and 3). Although problems are sometimes encountered in the restriction that chemical reagents must be soluble and that certain reactions are sluggish under mild conditions, reagents and reaction conditions can usually be found that are compatible with the heterogeneity of reactions on solid phases. On the other hand, unexpected benefits (now becoming more common) sometimes accrue to the researcher attempting synthesis on solid phases. These benefits often include increased stability of chemical intermediates attached to solid phases and, as shown in this paper, enhanced stereoselectivity in a Wittig reaction.

TABLE 4. The amount of *cis* and *trans* isomers of insect attractants prepared on solid phases by the Wittig and 'reverse' Wittig routes as determined by vpc and hplc

Attractant (%)	Alkene (%)	*cis* Isomer (%)
28	98.7	68.6
29	98.6	82.7
47	99.6	67.4
47[a]	92.6	91.2
47[b]	—	90[c]
47[d]	—	78[c]

[a]Prepared via **48**.
[b]Prepared via **49**.
[c]Determined by hplc only.
[d]Prepared via **50**.

Experimental

A Bausch and Lomb Abbé 3L refractometer was used to record the refractive indices. Infrared spectra were recorded on a Unicam SP1000 ir spectrophotometer as neat films between NaCl discs unless otherwise specified. Nuclear magnetic resonance spectra were recorded on a Varian EM360 spectrometer using deuterochloroform as solvent and tetramethylsilane as internal standard. Mass spectra were recorded on a Perkin-Elmer–Hitachi RMU6E mass spectrometer. Silica gel was used for all thin and preparative layer chromatography. Fractions were extracted with ether in a Soxhlet extractor. Filtration was done under vacuum through sintered glass Buchner funnels. Filtration under an inert atmosphere was done as previously described (9). Microanalyses were performed by G. Gygli of Toronto.

[9]Once used polymer often gives higher yields than fresh polymer and we attribute this phenomenon to the cleaning of the polymer, from monomer and other impurities, during the reaction sequence.

Vapour phase chromatograms were run with a Perkin Elmer 990 instrument using a 15 ft × $\frac{1}{8}$ in. column of 10% Silar C on Gaschrom Q(60/80) at a temperature of 170°C and a nitrogen flow rate of 15 ml/min. High pressure liquid chromatograms were run with a Waters Associates model 440 instrument, with an R-400 refractive index detector. A 30 × 0.4 cm reverse phase μ Bondapak C-18 column using 30% water in acetonitrile for C-14 acetates or 40% water in acetonitrile for **28** at a flow rate of 0.8–1.0 ml/min. Spectral and analytical data are given for all new compounds and for known compounds where data are unreported.

Preparation of Polymer-bound Diols ***5–7***, ***33***, *and* ***34***

The above monoprotected polymer-bound diols were prepared by a previously described procedure (9). The amounts of diol/g of polymer were determined by acid cleavage (9) and are listed in Tables 1 and 3.

Preparation of Polymer-bound Diol Monomesylates ***8–10***

In a typical procedure 5 g of **7**, containing 2.6 mmol of **4**, was suspended in 80 ml of dry pyridine and 2.5 ml (32 mmol) of methanesulfonyl chloride and stirred for 48 h at room temperature under anhydrous conditions ($CaCl_2$ drying tube). The polymer was filtered, washed with three 40 ml portions of dry pyridine, three 40 ml portions of ethanol, five 40 ml portions of water, two 20 ml portions of ethanol, two 30 ml portions of dioxane, four 30 ml portions of ether, and dried under vacuum overnight or by heating in benzene under reflux for 3–4 h in a Soxhlet extractor, containing 3A molecular sieves in the thimble, giving polymer-bound monomesylate **10**: ir (KBr) 1180 (broad, w) (O—SO_2) and 1360 cm^{-1} (broad, w) (O—SO_2).

Polymers **8** and **9**, prepared in an identical manner, exhibited similar infrared spectra.

Preparation of Diol Monomesylates ***11–13***

Acid cleavage of 1.0 g of **10** with 0.35 *M* HCl in dioxane as previously described (9) and purification of the filtrate on preparative tlc (eluant ether–benzene, 2:3) afforded, from the slowest moving band, 23 mg of recovered 1,10-decanediol (**4**), from the fastest moving band, 27 mg of 10-chloro-1-decanol, n_D^{25} 1.4575 (lit. (33), n_D^{25} 1.4578), and from the middle band, 35 mg of 1,10-decanediol monomesylate (**13**); mp 45–46°C; ir (KBr) 1170 (O—SO_2), 1360 (O—SO_2) and 3400 cm^{-1} (OH); nmr δ 4.1 (t, 2, J = 8 Hz, CH_2OSO_2), 3.6 (m, 3, CH_2OH), 3.0 (s, 3, CH_3SO_2), and 1.8–1.2 (m, 16). *Anal.* calcd. for $C_{11}H_{24}O_4S$: C 52.35, H 9.59, S 12.71; found: C 52.80, H 9.43, S 12.97.

Similarly, **8** yielded 28 mg of recovered **2**, 10 mg of 6-chloro-1-hexanol, n_D^{25} 1.4548 (lit. (33) n_D^{25} 1.4550), and 15 mg of 1,6-hexanediol monomesylate (**11**) as an oil; ir 1170 (O—SO_2), 1360 (O—SO_2), and 3400 cm^{-1} (OH); nmr δ 4.1 (t, 2, J = 6 Hz, CH_2OSO_2), 3.6 (m, 3, CH_2OH), 3.0 (s, 3, CH_3SO_2), and 1.8–1.2 (m, 8). *Anal.* calcd. for $C_7H_{16}O_4S$: C 42.84, H 8.22, S 16.34; found: C 42.55, H 8.07, S 16.16.

Similarly, **9** gave 27 mg of recovered **3**, 17 mg of 8-chloro-1-octanol, n_D^{25} 1.4558 (lit. (33) n_D^{25} 1.4563), and 24 mg of 1,8-octanediol monomesylate (**12**) as an oil; ir 1170 (O—SO_2), 1360 (O—SO_2), and 3400 cm^{-1} (OH); nmr δ 4.2 (t, 2, J = 8 Hz, CH_2OSO_2), 3.6 (m, 3, CH_2OH), 3.0 (s, 3, CH_3SO_2), and 1.8–1.2 (m, 12). *Anal.* calcd. for $C_9H_{20}O_4S$: C 48.18, H 8.99, S 14.30; found: C 48.46, H 9.14, S 13.92.

Preparation of Polymer-bound Bromide ***14*** *and Iodide* ***15***

In a typical procedure, 1.0 g of polymer-bound monomesylate **10**, containing 0.28 mmol of **13**/g was suspended in 50 ml of HMPT, containing 1.5 g (10 mmol) of sodium iodide, and stirred at 70°C for 48 h in the dark. The polymer was filtered, washed as described for **10**, but omitting the pyridine wash, and dried to give polymer-bound iodide **15**.

Polymer-bound **14** was prepared in a similar manner using sodium bromide. Treatment of 0.2 g of polymers **14** or **15** with 0.5 g of potassium *tert*-butoxide in *tert*-butyl alcohol overnight under reflux and then following the modified Volhard analysis (16) gave values of 0.26 mmol halide/g of **14** and 0.24 mmol/g of **15**.

Preparation of Polymer-bound Alkynes ***18–20***

To a solution of 10 mmol of 1-lithio-1-butyne (**17**), prepared in 40 ml of THF under argon at −10°C from 0.8 ml of 1-butyne in 8 ml THF and 4 ml of 2.5 *M* *n*-butyllithium in 28 ml THF, was added 2.0 g of polymer **10** containing 0.28 mmol of **13**/g of **10**, and 30 ml HMPT. The mixture was stirred overnight at room temperature, filtered, washed with four 25 ml portions of THF–water (1:1), two 25 ml portions of ethanol, two 50 ml portions of water, two 25 ml portions of ethanol, two 25 ml portions of dioxane, and three 25 ml portions of ether, and dried as above to give polymer-bound alkyne **20**.

Polymer-bound alkynes **18** and **19** were prepared in a similar manner using 1-litho-1-hexyne (**16**).

The polymer-bound alkynes **18–20** did not exhibit absorptions at 2200 cm^{-1} typical of a C≡C stretch in infrared spectra.

Preparation of Alkyn-1-ols ***22–24*** *and Their Acetates*

Treatment of 2.0 g of **20**, with acid as described above and purification of the filtrate on preparative tlc (eluant ether–benzene 35:65) afforded 23 mg of recovered diol **4** (R_f 0.15), 8 mg of monomesylate **13** (R_f 0.25), and 44 mg of 11-tetradecyn-1-ol (34) (**24**) (R_f 0.50) as an oil; n_D^{25} 1.4661; ir 1050 (C—O) and 3400 cm^{-1} (OH); nmr δ 3.6 (m, 3, CH_2OH), 20 (m, 4, $CH_2C{\equiv}C$), 18–12 (m, 16), and 0.9 (t, 3, J = 7 Hz, CH_3). Acetylation of 0.1 g of **24**, with 0.5 ml of acetic anhydride in 5 ml of pyridine under reflux for 15 min gave 11-tetradecyn-1-ol acetate as an oil; n_D^{25} 1.4625; ir 1240 (C—O) and 1740 cm^{-1} (ester C=O); nmr δ 4.0 (t, 2, J = 8 Hz, CH_2O), 2.0 (s, 3, $CH_3C{=}O$), 2.0 (m, 4, $CH_2C{\equiv}C$), 1.8–1.2 (m, 16), and 0.9 (t, 3, J = 7.5 Hz, CH_3CH_2); ms (70 eV) *m/e* (rel. intensity) 252(4) (M^+), 192(6.5) (M^+ − AcOH), 43(100). *Anal.* calcd. for $C_{16}H_{28}O_2$: C 76.14, H 11.18; found: C 75.98, H 11.25.

Similarly, **18** yielded 24 mg of **2**, 4 mg of **11**, and 26 mg of 7-dodecyn-1-ol (35) (**22**) as an oil; n_D^{25} 1.4641 (lit. (35) n_D^{25} 1.4638); ir 1060 (C—O) and 3400 cm^{-1} (OH); nmr δ 3.6 (m, 3, CH_2OH), 2.0 (m, 4, $CH_2C{\equiv}C$), 1.8–1.2 (m, 12), and 0.9 (t, 3, J = 5.5 Hz, CH_3). Acetylation of **22** gave 7-dodecyn-1-ol acetate (35) as an oil: n_D^{25} 1.4496 (lit. (35) n_D^{25} 1.4591); ir 1240 (C—O) and 1740 cm^{-1} (ester C—O); nmr δ 4.0 (t, 2, J = 8 Hz, CH_2O), 2.0 (s, 3, $CH_3C{=}O$), 2.0 (m, 4, $CH_2C{\equiv}C$), 1.8–1.1 (m, 12), and 0.9 (t, 3, J = 5 Hz, CH_3CH_2); ms (70 eV) *m/e* (rel. intensity) 224(0.05) (M^+), 164(5.2) (M^+ − AcOH), 43(100).

Similarly, **19** gave 22 mg of **3**, 4 mg of **12** and 36 mg of 9-tetradecyn-1-ol (**23**) as an oil; n_D^{25} 1.4653; ir 1060 (C—O) and 3400 cm^{-1} (OH); nmr δ 3.6 (m, 3, CH_2OH), 2.0 (m, 4, $CH_2C{\equiv}C$), 1.8–1.2 (m, 16), and 0.9 (t, 3,

J = 5.5 Hz, CH_3). *Anal.* calcd. for $C_{14}H_{26}O$: C 79.94, H 12.46; found: C 80.01, H 12.55.

Acetylation of **23** yielded 9-tetradecyn-1-ol acetate as an oil: n_D^{25} 1.4612; ir 1240 (C—O) and 1740 cm^{-1} (ester C=O); nmr δ 4.1 (t, 2, J = 8 Hz, CH_2O), 2.0 (s, 3, CH_3 C=O), 2.0 (m, 4, CH_2 C≡C), 1.8–1.2 (m, 16), and 0.9 (t, 3, J = 5.5 Hz, CH_3); ms (70 eV) *m/e* (rel. intensity) 252(0.025) (M^+), 192(0.23) (M^+ − AcOH), 43(100). *Anal.* calcd. for $C_{16}H_{28}O_2$: C 76.14, H, 11.18; found: C 75.85, H 11.18.

Preparation of Insect Sex Attractants ***28–30***

In a typical procedure (17), 44 mg (0.21 mol) of **24** in 5 ml of ethanol, 15 mg of Pd–$CaCO_3$, and 50 μl quinoline were stirred at room temperature under 1 atm of hydrogen until 1 equiv. (12.7 ml) was taken up. The mixture was filtered, taken up in ether, washed with water, dilute hydrochloric acid, and water, dried ($MgSO_4$), filtered, and evaporated to give *cis*-11-tetradecen-1-ol (**27**) as an unpurified oil. Acetylation of **27** in 0.5 ml of acetic anhydride and 5 ml of pyridine gave an oil, which on purification by preparative tlc (eluant ether–benzene 2:3), yielded 48 mg (0.19 mmol) of pure 11-tetradecen-1-ol acetate (20, 36) (**30**) in high yield (Table 1).

Similarly, hydrogenation and acetylation of **22** gave 7-dodecen-1-ol acetate (18) (**28**); n_D^{25} 1.4476 (lit. (18) n_D^{25} 1.4420); ir 960 (*trans* CH=CH), 1240 (C—O), and 1740 cm^{-1} (ester C=O); nmr δ 5.3 (m, 2, C*H*—C*H*), 4.1 (t, 2, J = 8 Hz, CH_2O), 2.0 (s, 3, CH_3CO), 2.0 (m, 4, $CH_2C{\equiv}C$), 1.8–1.2 (m, 12), and 0.9 (t, 3, J = 5 Hz, CH_3CH_2); ms (16 eV) *m/e* (rel. intensity) 226(0.3) (M^+), 166(100) (M^+ − AcOH), 151(1.1), 137(25), 123(27), 109(48).

Similarly, **23** yielded 9-tetradecen-1-ol acetate (19, 26) (**29**) in high yield (Table 1).

Compounds **28–30** were analyzed by vpc and hplc to determine the amount of *trans* product in the supposedly pure *cis* compounds and the data are recorded in Table 2.

Reduction of Alkyn-1-ols ***22*** *and* ***23*** *with 9-BBN*

In a typical procedure (22, 23), 100 mg (0.48 mmol) of **24** in 2 ml of THF was treated with 5 ml of 9-BBN (0.5 *M*, 2.5 mequiv.) and stirred at room temperature under argon for 4 h. Acetic acid (5 ml) was added, the solution stirred for 2 h, diluted with ether, washed with base, acid, bicarbonate, and saturated sodium chloride, and dried ($MgSO_4$) and evaporated to an oil. To the oil in 5 ml of THF was added 2 ml of 30% sodium hydroxide and 2 ml of 40% hydrogen peroxide and the mixture stirred until cool. The mixture was extracted as above to give an oil which on preparative tlc (eluant ether–benzene 2:3) gave *cis*-11-tetradecen-1-ol (37) (**27**) as an oil; n_D^{25} 1.4598; ir 3400 cm^{-1} (OH); nmr δ 5.3 (m, 2, C*H*≡C*H*), 3.6 (m, 3, CH_2OH), 2.3–2.1 (m, 4, CH_2CH=CHO), 1.8–1.2 (m, 16), and 0.9 (t, 3, J = 7.5 Hz, CH_3-CH_2). *Anal.* calcd. for $C_{14}H_{28}O$: C 79.18, H 13.29; found: C 79.11, H 13.14.

Similarly, reduction of **23** gave pure *cis*-**26**. Alken-1-ols **26** and **27** were acetylated to pure *cis*-**29** and *cis*-**30**, respectively, and analyzed by hplc, showing that **29** and **30** contained not less than 98% of the pure *cis* isomers.

Preparation of Monoprotected Polymer-bound Aldehydes ***35–37***

In a typical procedure, 5 mequiv. of di-*tert*-butyl chromate, prepared according to Sharpless and Akashi (27) in 25 ml of methylene chloride was transferred by a syringe to 2.5 g of polymer **33** in 40 ml of methylene chloride. The very dark mixture was stirred overnight at room temperature, filtered, washed with four 25 ml portions of methylene chloride and twice with 25 ml of ether, and air dried to give the polymer-bound aldehyde **35**; ir (KBr) 1730 cm^{-1} (aldehyde C=O). Polymers **36** and **37**, prepared in a similar manner, exhibited similar infrared spectra.

Preparation of ω*-Hydroxyaldehydes* ***38–40***

Cleavage of **35–37** with HCl in dioxane as before gave crude products. Preparative tlc (eluant ether–benzene 2:3) of the crude mixtures derived from **35–37** gave small amounts, at an R_f value of 0.35, of 6-hydroxyhexanal (**38**), 8-hydroxyoctanal (**39**), and 10-hydroxydecanal (**40**), identical in properties to those previously described (28). Since cleavage of **35–37** resulted in considerably by-product formation the absolute loading of aldehyde on the polymer could not be determined, but could obviously not be more than the polymer-bound diol, and is likely about 60% of the loaded diol value.

Polymer-bound Trityl Ether Alkenes ***42***, ***43***, *and* ***45***

To a mixture of 2.5 g (6 mmol) of *n*-pentyltriphenylphosphonium bromide (**41**) and 2.4 ml of 2.5 *M n*-butyllithium (in hexane) in 60 ml of THF under argon was added 2.0 g, containing not more than 0.9 mmol of aldehyde, (60% of loaded diol) of polymer **35** in 10 ml of THF. The mixture was stirred overnight, quenched with THF–water 1:1, filtered, and washed with two 20 ml portions of THF, one 20 ml portion of ethanol, four 20 ml portions of water, two 20 ml portions of ethanol, two 20 ml portions of dioxane, and three 20 ml portions of ether, and air dried to give polymer-bound alkene **42**, which did not exhibit a carbonyl absorption in its infrared spectrum.

Similarly, the Wittig reaction of **41** with 2.0 g of **36**, containing not more than 1.0 mmol of aldehyde, yielded polymer-bound alkene **43**.

Similarly, the Wittig reaction of *n*-butyltriphenylphosphonium bromide (**44**) with 2.0 g of **37**, containing not more than 0.6 mmol of aldehyde, (60% of loaded diol) yielded polymer-bound alkene **45**.

Preparation of Alken-1-ols ***25***, ***26***, *and* ***46***

Acid hydrolysis of 2.0 g of **42** as before yielded a mixture, which on preparative tlc (eluant ether–benzene 35:65) gave 110 mg (0.84 mmol) of recovered **31** (R_f, 0.15), and 66 mg (0.36 mmol) of 7-dodecen-1-ol (38) (**25**) as an oil; n_D^{25} 1.4538 (lit. (38) n_D^{25} 1.4554); ir 960 (w, *trans*-CH=CH) and 3400 cm^{-1} (OH); nmr δ 5.3 (m, 2, C*H*=C*H*), 3.6 (m, 3, CH_2OH), 2.0 (m, 4, CH_2CH=CH), 1.7–1.2 (m, 12), and 0.9 (t, 3, J = 5 Hz, CH_3CH_2).

Similarly, acid hydrolysis of 2.0 g of **43** gave 86 mg (0.54 mmol) of recovered diol **32** and 134 mg (0.64 mol) of 9-tetradecen-1-ol (38) (**26**) as an oil: n_D^{25} 1.4577 (lit. (38) n_D^{25} 1.4584); ir 960 (w, *trans*-CH=CH) and 3400 cm^{-1} (OH); nmr δ 5.25 (m, 2, C*H*=C*H*), 3.6 (m, 3, CH_2OH), 2.0 (m, 4, CH_2CH=CH), 1.8–1.2 (m, 16), and 0.9 (t, 3, J = 6 Hz, CH_3CH_2).

Similarly, acid hydrolysis of 2.0 g of **45** gave 56 mg (0.32 mmol) of recovered **4** and 76 mg (0.36 mmol) of 10-tetradecen-1-ol (29) (**46**) as an oil; n_D^{25} 1.4589; ir 960 (w, *trans*-CH=CH) and 3400 cm^{-1} (OH); nmr δ 5.25 (m, 2, C*H*=C*H*), 3.6 (m, 3, CH_2OH), 2.0 (m, 4,

$CH_2CH{=}CH$), 1.8–1.2 (m, 16), and 0.9 (t, 3, J = 6.5 Hz, CH_3CH_2). *Anal.* calcd. for $C_{14}H_{28}O$: C 79.18, H 13.29; found: C 79.41, H 13.16.

Preparation of Attractants ***28***, ***29***, *and* ***47*** *by the Wittig Route*

Acetylation of **25**, **26**, and **46** as above yielded attractants **28** and **29**, previously prepared via the alkyne route and a different attractant, 10-tetradecen-1-ol acetate (29) (**47**) as an oil: n_D^{25} 1.4492; ir 960 (w, *trans*-CH=CH), 1240 (C—O), and 1740 cm^{-1} (ester C=O); nmr δ 5.4 (m, 2, $CH{=}CH$), 4.1 (t, 2, J = 8 Hz, CH_2O), 2.0 (m, 4, $CH_2CH{=}CH$), 1.8–1.2 (m, 16), and 0.9 (t, 3, J = 6 Hz, CH_3CH_2); ms (16 eV) *m/e* (rel. intensity) 254(4) (M^+), 194(100) (M^+ − AcOH). *Anal.* calcd. for $C_{16}H_{30}O_2$: C 75.54, H 11.80; found: C 75.34, H 11.70.

Analysis of **28**, **29**, and **47** by vpc and hplc determined the purity and isomeric distribution of the products (Table 4).

Preparation of Polymer-bound Phosphonium Salts ***48–50***

A mixture of 2.5 g of **10**, containing 0.65 mmol of mesylate, and 25 g of triphenylphosphine was heated to 100°C under argon and stirred overnight. The mixture was cooled to 80°C and poured into a Soxhlet thimble. A Soxhlet extraction for 4 h with ether removed the excess triphenylphosphine and gave the polymer-bound phosphonium mesylate (**48**).

Similarly, treatment of polymer-bound bromide (**14**) and iodide (**15**) with molten triphenylphosphine yielded the polymer-bound phosphonium bromide (**49**) and iodide (**50**), respectively. The infrared spectra of **48–50** were uninformative. Analysis of **49** and **50** for ionic halide ion was readily accomplished by treatment of **49** and **50** with 0.1 *M* sodium hydroxide in dioxane–water (1:1), followed by standard analysis (16), to give 0.26 mmol of halide/g of **49** or **50**. These analysis conditions are specific for ionic halide as liberation of halide from **14** or **15** required more drastic treatment (see above).

Preparation of Polymer-bound Alkene ***45*** *by the 'Reverse' Wittig Route*

A suspension of 2 g of polymer-bound phosphonium mesylate (**48**) in 50 ml of dry THF was treated with 2.5 ml (4 mequiv.) of 1.6 *M n*-butyllithium in hexane and stirred overnight at room temperature. The polymer was filtered and washed with three 10 ml portions of dry THF under inert atmosphere conditions (9), to give a dark purple polymer. To the polymer, resuspended in 50 ml of THF was added 2 ml (22 mmol) of butyraldehyde. The dark colour of the polymer was discharged after 0.5 h but the mixture was stirred for an additional 7.5 h. The mixture was filtered, washed as before for polymer **45**, and air dried to give polymer-bound alkene **45**.

Similarly, polymer-bound bromide (**49**) or iodide (**50**), gave polymer **45**. In some experiments, the polymer-bound ylides prepared from **48–50** were not filtered and washed but used directly in reactions with butyraldehyde, giving similar results as before.

Acid cleavage of **45**, prepared from **48–50** gave different samples of alkene-1-ols **46**. Acetylation of the different samples of **46** as before gave samples of the sex attractant **47**, which were analyzed by vpc and hplc (Table 4).

Acknowledgements

This research was supported by a grant from the National Research Council of Canada and the Canadian Forestry Service of Environment Canada. One of us (T.M.F.) wishes to thank the National Research Council of Canada for a postgraduate scholarship.

1. R. B. Merrifield. Science, **150**, 178 (1965); G. R. Marshall and R. B. Merrifield. *In* Biochemical aspects of reactions of solid supports. *Edited by* G. R. Stark. Academic Press, New York, NY. 1971. pp. 111–169.
2. R. L. Letsinger and V. Mahadevan. J. Am. Chem. Soc. **88**, 5319 (1966).
3. J. M. Fréchet and C. Schuerch. J. Am. Chem. Soc. **93**, 492 (1971).
4. B. Gutte and R. B. Merrifield. J. Am. Chem. Soc. **91**, 501 (1969).
5. R. L. Letsinger, M. J. Kornet, V. Mahadevan, and D. M. Jerina. J. Am. Chem. Soc. **86**, 5163 (1964).
6. D. A. Evans and C. L. Green. Chem. Soc. Rev. **2**, 75 (1973).
7. C. C. Leznoff and J. Y. Wong. Can. J. Chem. **51**, 2756 (1973).
8. C. C. Leznoff and S. Greenberg. Can. J. Chem. **54**, 3824 (1976).
9. T. M. Fyles and C. C. Leznoff. Can. J. Chem. **54**, 935 (1976).
10. C. C. Leznoff and J. Y. Wong. Can. J. Chem. **50**, 2892 (1972); J. Y. Wong and C. C. Leznoff. Can. J. Chem. **51**, 2452 (1973); J. M. J. Fréchet and L. J. Nuyens. Can. J. Chem. **54**, 926 (1976).
11. C. U. Pittman, Jr. and G. O. Evans. Chem. Technol. 560 (1973); C. C. Leznoff. Chem. Soc. Rev. **3**, 65 (1974); C. G. Overberger and K. N. Sannes. Angew. Chem. Int. Ed. Engl. **13**, 159 (1974); A. Patchornik and M. A. Kraus. Pure Appl. Chem. **43**, 503 (1975); D. C. Neckers. J. Chem. Educ. **52**, 695 (1975); J. I. Crowley and H. Rapoport. Acc. Chem. Res. **9**, 135 (1976).
12. C. C. Leznoff and T. M. Fyles. J. Chem. Soc. Chem. Commun. 251 (1976).
13. L. R. Melby and D. R. Strobach. J. Am. Chem. Soc. **89**, 450 (1967); F. Cramer and H. Köster. Angew. Chem. Int. Ed. Engl. **7**, 473 (1968); J. M. J. Fréchet and K. E. Haque. Tetrahedron Lett. 3055 (1975).
14. H. Normant. Angew. Chem. Int. Ed. Engl. **6**, 1046 (1967); M. Schwarz and R. M. Waters. Synthesis, 567 (1972).
15. J. B. Lee and T. J. Nolan. Can. J. Chem. **44**, 1331 (1966); R. Appel. Angew. Chem. Int. Ed. Engl. **14**, 801 (1975).
16. J. M. Stewart and J. D. Young. Solid phase peptide syntheses. W. H. Freeman Ltd., San Francisco, CA. 1969. p. 58.
17. R. L. Augustine. Catalytic hydrogenation. Marcel Dekker, Inc., New York, NY. 1965. p. 71.
18. R. S. Berger. Ann. Entomol. Soc. Am. **59**, 767 (1966); N. Green, M. Jacobson, T. J. Henneberry, and A. N. Kishaba. J. Med. Chem. **10**, 533 (1967).
19. D. Warthen. J. Med. Chem. **11**, 371 (1968).

20. W. L. ROELOFS and H. ARN. Nature, **219**, 513 (1968).
21. J. D. WARTHEN, JR. J. Am. Oil Chem. Soc. **52**, 151 (1975).
22. H. C. BROWN and G. ZWEIFEL. J. Am. Chem. Soc. **83**, 3834 (1961); H. C. BROWN and S. K. GUPTA. J. Am. Chem. Soc. **97**, 5249 (1975); G. G. SCOUTEN. Ph.D. Thesis, Purdue University, Lafayette, IN. 1976.
23. G. HOLAN and D. F. O'KEEFE. Tetrahedron Lett. 673 (1973).
24. E. WINTERFELDT. Synthesis, 617 (1975).
25. J. O. RODIN, R. M. SILVERSTEIN, W. E. BURKHOLDER, and J. E. GORMAN. Science, **165**, 904 (1969).
26. H. J. BESTMANN, P. RANGE, and R. KUNSTMANN. Chem. Ber. **104**, 65 (1971).
27. K. B. SHARPLESS and K. AKASHI. J. Am. Chem. Soc. **97**, 5927 (1975).
28. J. COLONGE, L. COTTIER, and G. DESCOTES. C.R. Acad. Sci. Paris Ser. C, **268**, 1155 (1969) and references cited.
29. L. B. HENDRY, J. JUGOVICH, L. ROMAN, M. E. ANDERSON, and R. O. MUMMA. Experientia, **36**, 886 (1974).
30. A. W. JOHNSON. Ylid chemistry. Academic Press, New York and London. 1966. p. 171; L. D. BERGELSON, L. I. BARSUKOV, and M. M. SHEMYAKIN. Tetrahedron, 2709 (1967); P. SONNET. Org. Prep. Proced. Int. **6**, 269 (1974).
31. P. BECK. *In* Organic phosphorous compounds. *Edited by* G. M. Kosolapoff and L. Maier. Wiley-Interscience, New York, NY. 1972. pp. 189–194.
32. M. JACOBSON. Insect sex phenomones. Academic Press, New York and London. 1972. pp. 141–144.
33. G. M. BENNET and A. N. MOSSES. J. Chem. Soc. 170 (1931).
34. W. L. ROELOFS and A. COMEAU. J. Insect. Physiol. **17**, 435 (1971); J. A. KLUN and J. R. ROBINSON. Ann. Entomol. Soc. Am. **65**, 1337 (1972).
35. B. G. KOVALEV and R. I. ISHCHENKO. J. Org. Chem. USSR, **10**, 468 (1974).
36. G. M. MEIJER, F. J. RITTER, C. J. PERSOONS, A. K. MINKS, and S. VOERMAN. Science, **175**, 1469 (1972).
37. W. L. ROELOFS and A. COMEAU. J. Insect Physiol.. **17**, 1969 (1971).
38. A. S. KOVALEVA, V. M. BULINA, L. L. IVANOV, YU. B. PYATNOVA, and R. P. EVSTIGNEEVA. J. Org. Chem. USSR, **10**, 700 (1974).

Some thermodynamic properties of the solutions of $ZrCl_4$ and $HfCl_4$ in CsCl melts

D. A. ASVESTAS, P. PINT,[1] AND S. N. FLENGAS

Department of Metallurgy and Materials Science, University of Toronto, Toronto, Ont., Canada M5S 1A4

Received June 21, 1976

D. A. ASVESTAS, P. PINT, and S. N. FLENGAS. Can. J. Chem. **55**, 1154 (1977).

The binary equilibrium phase diagrams of the systems CsCl–Cs_2ZrCl_6, CsCl–Cs_2HfCl_6, and CsCl–KF were established by cryoscopy. A portion of the ternary CsCl–KF–$ZrCl_4$ has also been determined.

Equilibrium vapour pressures of the two pure compounds Cs_2ZrCl_6 and Cs_2HfCl_6, as well as of mixtures of Cs_2HfCl_6 with CsCl, have been measured. The equilibrium reaction is given as

$$Cs_2MCl_6 \rightleftarrows 2CsCl + MCl_4$$

where M represents Zr or Hf.

From the results, activities of CsCl, Cs_2HfCl_6, and $HfCl_4$ were calculated at 825 °C.

The low escaping tendency of the MCl_4 vapour from the CsCl–Cs_2MCl_6 type melts makes these solutions suitable as electrolytes for the recovery of Zr and Hf metal by fused salt electrolysis.

D. A. ASVESTAS, P. PINT et S. N. FLENGAS. Can. J. Chem. **55**, 1154 (1977).

On a établi par cryoscopie les diagrammes de phase d'équilibre binaire des systèmes CsCl–Cs_2ZrCl_6, CsCl–Cs_2HfCl_6 et CsCl–KF. On a aussi déterminé une portion du diagramme ternaire CsCl–KF–$ZrCl_4$.

On a mesuré les pressions de vapeur à l'équilibre des deux composés purs Cs_2ZrCl_6 et Cs_2HfCl_6 de même que celles de mélanges de Cs_2HfCl_6 avec CsCl. On peut représenter la réaction d'équilibre par l'équation

$$Cs_2MCl_6 \rightleftarrows 2CsCl + MCl_4$$

où M est égal à Zr ou Hf.

A partir des résultats, on a calculé, à 825 °C, les activités de CsCl, Cs_2HfCl_6 et $HfCl_4$.

La faible tendance que présente la vapeur de MCl_4 à s'échapper de CsCl–Cs_2MCl_6 fondu rend ces solutions appropriées comme électrolytes pour la récupération des métaux Zr et Hf par l'électrolyse des sels fondus.

[Traduit par le journal]

Introduction

In previous publications from this laboratory (1, 2) the vapour pressures of $ZrCl_4$ in equilibrium with solutions of $ZrCl_4$ and alkali chlorides, such as LiCl, NaCl, and KCl, and of $HfCl_4$ in equilibrium with solutions containing $HfCl_4$ and LiCl, have been determined by a direct experimental technique involving the use of a molten tin isoteniscope.

In the present investigation the technique has been applied to the determination of the vapour pressures of $ZrCl_4$ and of $HfCl_4$ in equilibrium with solutions of $ZrCl_4$ and of $HfCl_4$ in CsCl.

In addition, part of the phase diagrams of the systems CsCl–$ZrCl_4$, CsCl–$HfCl_4$, CsCl–$ZrCl_4$–KF and of the system CsCl–KF have been determined by cryoscopy. The CsCl–$ZrCl_4$–KF system was investigated for the purpose of finding the effect of KF on the solubility of Cs_2ZrCl_6 in CsCl bearing melts.

These systems are of interest as they may be considered as potential electrolytes for the recovery of Zr and Hf metals by fused salt electrolysis (3), as well as for the separation of Zr from Hf through the vapour transport process established previously in this laboratory (4).

From the results of this study, various thermodynamic properties of the systems have been calculated.

Experimental

At specific partial pressures and temperatures, the vapours of $ZrCl_4$ and $HfCl_4$ react with solid CsCl and produce the stoichiometric solid complex compounds of the general formula Cs_2MCl_6, where M is Zr or Hf, respectively.

[1]Present address: International Nickel Company, Research Laboratories, Sheridan Park, Ontario.

The corresponding reactions may be written as:

[1] $2CsCl\ (solid) + MCl_4\ (vapour) \rightarrow Cs_2MCl_6\ (solid)$
at P, T at P, T at P, T

It should be noted that these complex compounds also exist as congruently melting and appear in the phase diagrams of the corresponding MCl_4–CsCl binary systems.

The method applied for the preparation of the pure stoichiometric compounds was developed in this laboratory earlier (1, 2) and the preparation was conducted in the simple apparatus shown in Fig. 1.

In this process a known amount of CsCl is ground to particle size of less then 325 mesh and is reacted with either $ZrCl_4$ or $HfCl_4$ vapours at a pressure of 1 atm in the previously sealed two compartment reaction cell shown in Fig. 1.

The temperature T_1 in compartment I is adjusted to be the sublimation temperature of $ZrCl_4$ or $HfCl_4$, respectively, and in this manner the pressure of the corresponding MCl_4 vapour in the entire system is kept always at 1 atm. The amounts of MCl_4 and CsCl placed in compartments I and II should be such that the mole ratio MCl_4/CsCl should be greater than the 1/2 predicted by reaction 1, and the reation then should always be able to proceed to completion.

The temperature T_2 in compartment II is the reaction temperature characteristic of a given system and should always be greater than T_1.

For the reaction to be possible thermodynamically the equilibrium pressure of MCl_4 vapour created by the thermal decomposition of the compound Cs_2MCl_6 in compartment II should always be less than the applied pressure of the vapour MCl_4 which is 1 atm.

It is also important to satisfy kinetic requirements and for a given system it is necessary to conduct the reaction at temperatures as high as possible provided that the thermodynamic requirements are not violated.

However, when T_2 is very high in compartment II particle sintering is taking place and the reaction becomes slow. Once sintering has taken place it is necessary to open the cell in a dry box, grind the partially reacted sample, and repeat the reaction until the stoichiometry of the product remains unchanged. The optimum conditions for the preparation of the pure stoichiometric compounds Cs_2ZrCl_6 and Cs_2HfCl_6 were established after several tests. Thus, for Cs_2ZrCl_6 the temperatures T_1 and T_2 were 331 and 475 °C, respectively, while for Cs_2HfCl_6 these were 318 and 475 °C.

At the end of a reaction, the unreacted MCl_4 vapour which remains in the free volume of the apparatus in both compartments I and II is totally condensed in compartment I by a stepwise decrease of the temperatures in the two compartments.

Thus, first the reaction temperature T_2 in compartment II is decreased until it becomes slightly higher than T_1, and then both T_1 and T_2 are decreased stepwise by 20 °C, until room temperature is attained. In this manner all the unreacted MCl_4 vapour is transferred into compartment I without ever decomposing the complex compound Cs_2MCl_6 present in compartment II. The stoichiometry of each compound and its composition is determined simply by weighing the amount of material in compartment II, Fig. 1, before and after reaction.

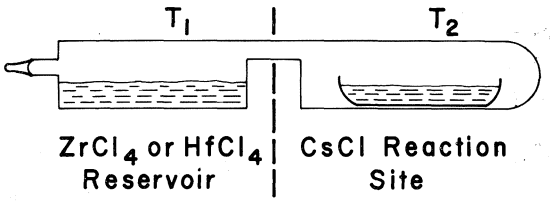

FIG. 1. Reaction cell for the preparation of the compounds Cs_2ZrCl_6 and Cs_2HfCl_6. The reagents are first transferred into their respective compartments and the cell is evacuated and sealed under vacuum prior to heating.

When a reaction has reached completion, the excess weight indicates the amount of MCl_4 vapour reacted with CsCl, and the corresponding mole ratio of CsCl/MCl_4 should be 2/1.

The CsCl used in this work was reaction grade which analyzed 99.9% CsCl after fusion and was pretreated with anhydrous gaseous HCl at 800 °C, followed by evacuation and sublimation to remove all volatile impurities. The KF was of 99% purity reagent grade and was dried under vacuum at 750 °C.

The $ZrCl_4$ and $HfCl_4$ salts were reactor grade and were obtained from the Wah Chung Corporation of America, Albany, NY. Those were further purified by repeated sublimations in vacuum through a molten tin plug, as reported earlier (2).

Solutions of various compositions were prepared by mixing CsCl with the compound Cs_2MCl_6. All handling of materials, preparation of samples, and transfers to the reaction cells were conducted in a dry box filled with argon gas.

The apparatus for the measurement of the vapour pressures of $ZrCl_4$ and $HfCl_4$ in equilibrium with their corresponding solutions in alkali chlorides has been described elsewhere (2). In brief, all vapour pressures were measured by a static method employing a simple isoteniscope with molten tin.

The apparatus is shown in Fig. 2. It consists essentially of a quartz glass cell, A, containing the sample the temperature of which is measured by means of a calibrated chromel–alumel thermocouple, C, placed in the well at the centre. The cell is connected through a graded seal to a Pyrex U-tube, E, filled with molten tin.

The temperature of the hot box containing the molten tin isoteniscope was monitored by two thermocouples to insure that the entire isoteniscope was above the condensation point of the tetrachlorides.

Equilibrium pressure measurements were made during heating and cooling cycles and the values for each individual cycle were in very good agreement at high pressures and temperatures. At temperatures below 600 °C the reproducibility was less satisfactory, as the equilibrium pressures obtained during cooling were always slightly less than those obtained during heating.

The apparatus for determining the phase diagrams for those systems has also been described elsewhere (1, 2). The containers for the mixtures to be measured were heart-shaped quartz cells having the thermocouple well at the centre of the charge and were sealed under vacuum. Cooling rates were 3/4 °C to 1 °C per min.

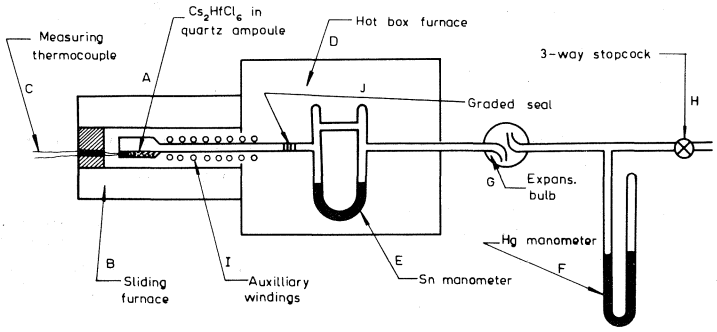

FIG. 2. Apparatus for the measurement of the equilibrium vapour pressures of $ZrCl_4$ and $HfCl_4$ in the CsCl solutions.

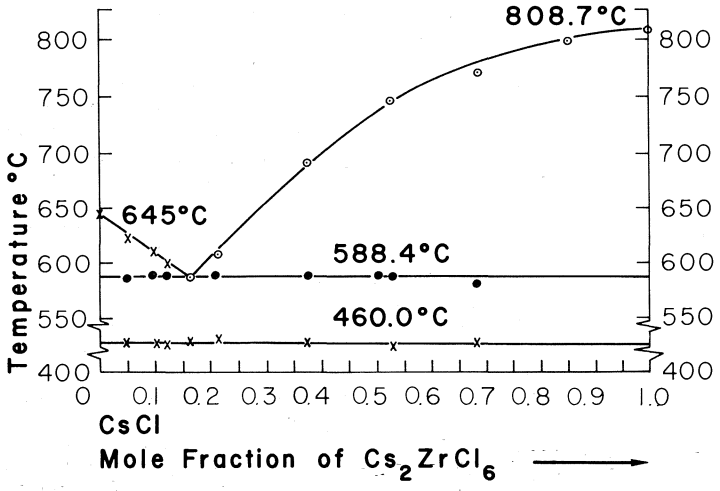

FIG. 3. Phase diagram of the binary system CsCl–Cs_2ZrCl_6.

Experimental Results

Determination of Phase Diagrams

The part of the phase diagrams representing the CsCl–Cs_2ZrCl_6 and the CsCl–Cs_2HfCl_6 subsystems are shown respectively in Figs. 3 and 4.

The characteristic data for these diagrams are given in Table 1. The phase diagram for the subsystem CsCl–Cs_2ZrCl_6 is relatively simple, having one eutectic composition at $X_{Cs_2ZrCl_6} = 0.162$.

The liquidus temperature arrests observed for melts rich in Cs_2ZrCl_6 were poorly defined and in most cases the liquidus at any one composition was repeated four times. The same degree of difficulty was not encountered with melts rich in CsCl. In most cases the eutectic temperature was very well defined except when the melt compositions were far removed from the eutectic composition. The CsCl solid–solid transformation was readily seen on the CsCl-rich side of the diagram and is occurring at 460 °C. No indication of complex compounds other than Cs_2ZrCl_6 was evident.

The phase diagram determined in this work disagrees with the only other available measurements by Morozov and Sun-In-Chzhu (5). In the latter the eutectic was found to be at 21.8 mol% of Cs_2ZrCl_6 instead of 16.2 mol% reported in this work. Similarly the melting point for pure Cs_2ZrCl_6 was given as 805 °C and the eutectic temperature as 572 °C, instead of the values of 808.7 and 588.4 °C, respectively, reported in the present work.

The disagreement may be attributed to the presence of impurities in the Cs_2ZrCl_6, probably in the form of hydrated zirconium oxychlorides, used by those workers. Their method of preparing Cs_2ZrCl_6 consisted of intimately mixing the stoichiometric amounts of $ZrCl_4$ and CsCl

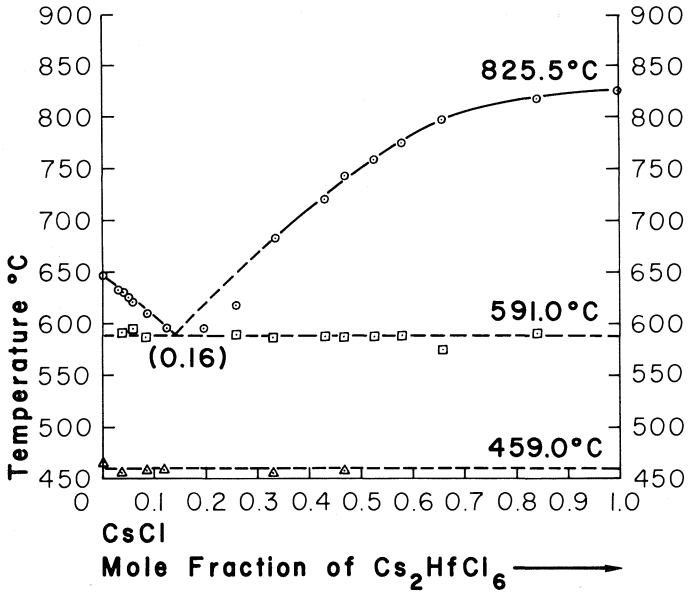

FIG. 4. Phase diagram of the binary system CsCl–Cs_2HfCl_6.

TABLE 1. Characteristics of the phase diagram of the binary systems CsCl–Cs_2ZrCl_6, CsCl–Cs_2HfCl_6, and CsCl–KF

Binary system	Eutectic composition X_{CsCl}	T, eutectic (°C)	T, melting point of Cs_2MCl_6 (°C)
CsCl–Cs_2ZrCl_6	83.8	588.4	808.7
CsCl–Cs_2HfCl_6	84.0	591.0	825.5
CsCl–KF	64.0	500.0	

and the hydrated oxychlorides which are always present in 'pure' zirconium tetrachloride would be expected to remain in the mixture.

The phase diagram of the subsystem CsCl–Cs_2HfCl_6 is shown in Fig. 4.

The melting point of pure Cs_2HfCl_6 given in Fig. 4 is higher than that reported by Morozov and Sun-In-Chzhu (5) by about 5 °C. The Cs_2HfCl_6 used by those authors was again obtained by mixing the stoichiometric amounts of $HfCl_4$ and CsCl and, hence, could contain the aforementioned impurities.

As in the case of the Cs_2ZrCl_6–CsCl subsystem the Cs_2HfCl_6-rich side of the phase diagram was obtained with more difficulty than the CsCl-rich side. The CsCl solid–solid transformation is seen here at 459 °C.

The Cs_2HfCl_6–CsCl subsystem is characterized by a single eutectic at 591 ± 2 °C and at 16.0 mol% Cs_2HfCl_6. The congruently melting compound Cs_2HfCl_6 has a melting point at 825 °C.

Neither phase diagram shows evidence of solid solubility on either side of the eutectic and they resemble the phase diagrams of the other alkali–chlorozirconate or alkali–chlorohafnate systems investigated previously (1, 2).

As indicated earlier, the quartz heart-shaped cells used for containing these melts were sealed under vacuum prior to their use for the cryoscopic measurement. Therefore the phase diagrams reported herein were obtained under the equilibrium pressures of the $ZrCl_4$ or $HfCl_4$ vapours present and not at constant atmospheric pressure.

The phase diagrams of the CsCl–Cs_2ZrCl_6 and CsCl–Cs_2HfCl_6 subsystems are part of the overall binary systems CsCl–$ZrCl_4$ and CsCl–$HfCl_4$, in which the Cs_2ZrCl_6 and Cs_2HfCl_6, respectively, are appearing as con-

TABLE 2. Part of the phase diagram for the system KF–CsCl–$ZrCl_4$

Composition	First temperature arrest (°C)	Second temperature arrest (°C)	Third temperature arrest (°C)
$X_{CsCl} = 0.74$ $X_{KF} = 0.23$ $X_{ZrCl_4} = 0.03$	601		
$X_{CsCl} = 0.86$ $X_{KF} = 0.09$ $X_{ZrCl_4} = 0.05$	626	516	
$X_{CsCl} = 0.75$ $X_{KF} = 0.20$ $X_{ZrCl_4} = 0.05$	607		
$X_{CsCl} = 0.66$ $X_{KF} = 0.30$ $X_{ZrCl_4} = 0.04$	595	537	
$X_{CsCl} = 0.76$ $X_{KF} = 0.10$ $X_{ZrCl_4} = 0.14$	554		485
$X_{CsCl} = 0.68$ $X_{KF} = 0.20$ $X_{ZrCl_4} = 0.12$	535	519	502
$X_{CsCl} = 0.68$ $X_{KF} = 0.20$ $X_{ZrCl_4} = 0.12$	537	522	495
$X_{CsCl} = 0.87$ $X_{KF} = 0.10$ $X_{ZrCl_4} = 0.03$	621	532	

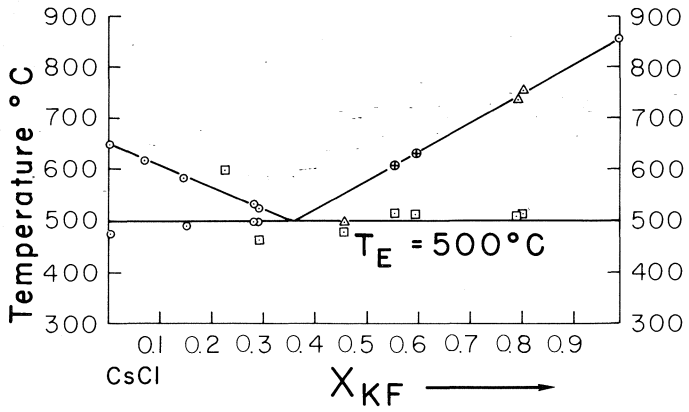

FIG. 5. Phase diagram of the binary system CsCl–KF.

gruently melting compounds. Compositions rich in $ZrCl_4$ or $HfCl_4$ at $X_{MCl_4} > 0.33$ could not be investigated as the solutions exhibit very high decomposition pressures at temperatures higher than about 350 °C.

The binary CsCl–KF system and part of the ternary phase diagram for the system CsCl–$ZrCl_4$–KF were also investigated and the results are given in Figs. 5 and 6, respectively. It is seen that the binary system CsCl–KF is of the simple eutectic type. Its characteristic temperatures are included in Table 1. Details of the characteristic temperatures in the ternary system are given in Table 2. The first temperature arrest represents the ternary liquidus. It may be seen that $ZrCl_4$ has a substantial solubility of about 12–14 mol% in melts containing CsCl and KF at temperatures higher than 550 °C.

Vapour Pressure Measurements

The vapour pressures of $ZrCl_4$ and $HfCl_4$ in equilibrium with the pure compounds

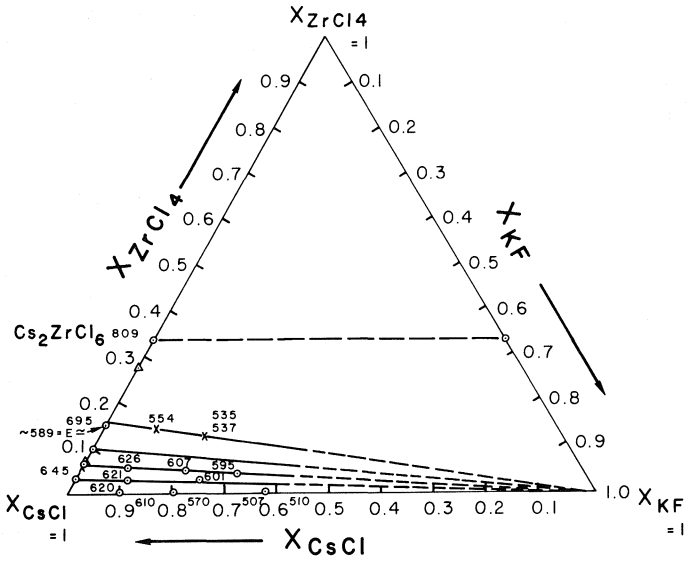

FIG. 6. Part of the phase diagram of the ternary system CsCl–KF–$ZrCl_4$.

Cs_2ZrCl_6 and Cs_2HfCl_6, respectively, have been determined and are shown in Fig. 7. The results are plotted as log P_{MCl_4} *vs.* $1/T$ and the lines shown on the graphs are calculated by the least-squares method while the points are experimental. The corresponding equations for the various equilibria were calculated and are given in Table 3. Reaction 1 in Table 3 defines the equilibrium pressure of $ZrCl_4$ over pure solid Cs_2ZrCl_6 at temperatures higher than the eutectic temperature shown in the phase diagram given in Fig. 3.

During an actual pressure measurement, the $ZrCl_4$ vapour present in the pressure measuring apparatus is created by the thermal decomposition of Cs_2ZrCl_6, and it is inevitable that some small amount of CsCl shall be present. The CsCl thus produced reacts with Cs_2ZrCl_6 to form the liquid phase predicted by the phase diagram. In this sense, the pressures of $ZrCl_4$ reported represent the saturated solutions of Cs_2ZrCl_6 in CsCl. Reaction 2 in Table 3 represents the equilibrium over pure molten Cs_2ZrCl_6 at temperatures higher than its melting point.

Similar considerations apply to Reactions 3 and 4 for Cs_2HfCl_6, given in Table 3. It should be noted that the two linear portions of the pressure curves for Cs_2ZrCl_6 and Cs_2HfCl_6 in Fig. 7 intercept at temperatures which are in agreement with the melting points of the compounds Cs_2ZrCl_6 and Cs_2HfCl_6, respectively.

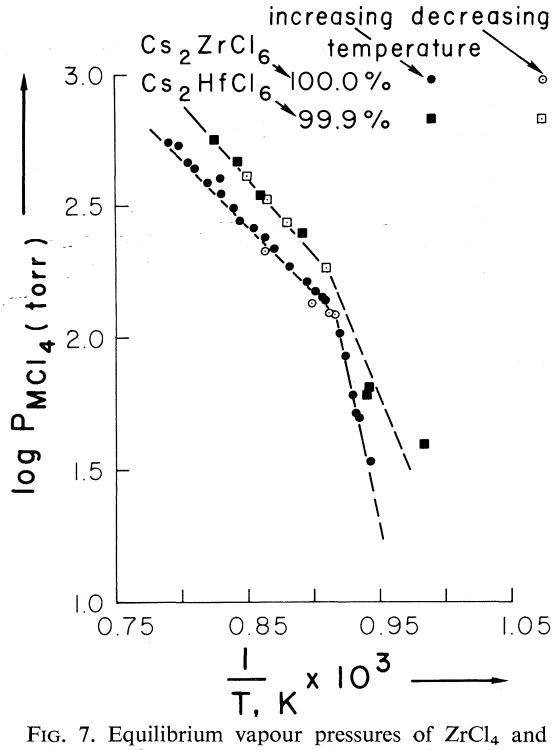

FIG. 7. Equilibrium vapour pressures of $ZrCl_4$ and $HfCl_4$ over the pure compounds Cs_2ZrCl_6 and Cs_2HfCl_6, respectively, given as log P (torr) *vs.* $1/T$ (K).

The vapour pressures in equilibrium with solutions containing Cs_2HfCl_6 and CsCl were also investigated and the plots of P_{HfCl_4} in torr *vs.* T in °C for three compositions on the

TABLE 3. Equilibrium vapour pressures of $ZrCl_4$ and $HfCl_4$ over the systems $CsCl$–Cs_2ZrCl_6 and $CsCl$–Cs_2HfCl_6, respectively

Equilibrium reactions	Cs_2MCl_6 (mol%)	Temperature range (K)	$\log P_{MCl_4} = A + \frac{B}{T}$ (torr)		
			A	$B \times 10^{-3}$	St. error of estimate
1. Cs_2ZrCl_6 (solid) $\rightleftarrows$ 2CsCl (in solution) + $ZrCl_4$ (vap.)	100	1060–1082	21.51	−2.119	±0.0216
2. Cs_2ZrCl_6 (liquid) $\rightleftarrows$ 2CsCl (in solution) + $ZrCl_4$ (vap.)	100	1082–1243	6.909	−0.5263	±0.0163
3. Cs_2HfCl_6 (solid) $\rightleftarrows$ 2CsCl (in solution) + $HfCl_4$ (vap.)	99.9*	—	—	—	—
4. Cs_2HfCl_6 (liquid) $\rightleftarrows$ 2CsCl (in solution) + $HfCl_4$ (vap.)	99.9	1121–1211	6.751	−0.4882	±0.0301
5. Cs_2HfCl_6 (in solution) $\rightleftarrows$ 2CsCl (in solution) + $HfCl_4$ (vap.)	95.0	1109–1187	7.865	−0.6203	±0.0085
6. Cs_2HfCl_6 (in solution) $\rightleftarrows$ 2CsCl (in solution) + $HfCl_4$ (vap.)	70.0	1104–1232	8.934	−0.8081	±0.0316
7. Cs_2HfCl_6 (in solution) $\rightleftarrows$ 2CsCl (in solution) + $HfCl_4$ (vap.)	62.5	1119–1271	6.152	−0.5149	±0.1258

*Pressure data for this range are shown in Fig. 7. Their accuracy did not warrant a least-squares calculation.

Cs_2HfCl_6-rich side of the eutectic as well as for the pure compound, are given in Fig. 8.

At temperatures $T < T_E$ all four compositions should yield a common vapour pressure curve. The equilibrium then is represented by the reaction

[2] Cs_2HfCl_6 (pure solid) $\rightleftarrows$ CsCl (pure solid) + $HfCl_4$ (vapour)

However, at these low temperatures the equilibrium pressures of $HfCl_4$ are very low and the accuracy of the measurement is affected by the presence of foreign gases which are absorbed by the solid powders used for those experiments, hence the observed scatter of points.

At temperatures above the eutectic and up to the corresponding melting point of a given solution, all compositions are expected to have a common vapour pressure curve since the equilibria which determine such pressures are given by reaction 3 in Table 3.

As the temperature is increased for a given composition the pressure curves are expected to branch off at the corresponding liquidus temperatures. This behaviour was found to be common with all the hexachlorozirconate and hexachlorohafnate systems investigated so far (1, 2).

It should be noted that the accuracy of the measurements of the vapour pressures over the three phase equilibria representing the saturated solutions of Cs_2HfCl_6 was rather poor, as seen from the scatter of points in Fig. 8.

This is probably due to the difficulty of reaching exact equilibrium in a system which changes composition with temperature. However, the expected trends were evident. In the all liquid range the equilibria are given by reactions 4, 5, 6, and 7 in Table 3.

For temperatures corresponding to the homogeneous liquid range, the measured equilibria represent only a liquid and a gas phase, both of which have fixed compositions, and the pressure measurements are extremely reproducible. An exception is the composition containing 62.5 mol% Cs_2HfCl_6, in which some CsCl vaporizes in the pressure measuring cell at the high temperatures of these measurements.

The corresponding equations expressing log P_{HfCl_4} *vs.* $1/T$ for the compositions investigated are also given in Table 3.

Discussion

A. Cryoscopic Calculations

For the dilute solutions of the complex

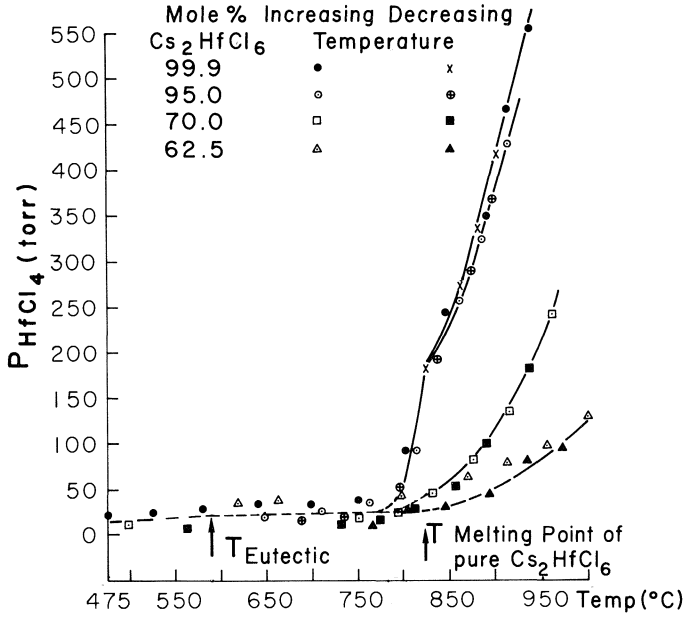

FIG. 8. Equilibrium vapour pressures of $HfCl_4$ over solutions of Cs_2HfCl_6 with CsCl.

compounds of the type Cs_2MCl_6 in CsCl, the depression of the melting point of CsCl is given by the expression

$$[3] \qquad \Delta T = V \frac{RT_F}{\Delta H_F} X_{solute}$$

where V represents the number of foreign ions other than those present in the solvent melt. The derivation of this equation is based on the applicability of Temkin's (6) ideal solution concept to ionic fused salt systems. T_F is the melting point of CsCl; ΔH_F is the heat of fusion of CsCl which is given (7) as 4.9 ± 0.1 kcal/mol, and X_{solute} is the mole fraction of the solute Cs_2MCl_6. This equation was found applicable to the CsCl-rich side of the corresponding phase diagrams for the systems, $CsCl–Cs_2ZrCl_6$ and $CsCl–Cs_2HfCl_6$, for $V = 1$.

This is seen in Fig. 9, where the theoretical liquidus curve calculated from [3] is compared with experimental values for concentrations up to 12 mol% Cs_2MCl_6. For $V = 1$, a number of dissociation schemes may be considered, such as:

$$[4a] \qquad Cs_2MCl_6 \rightleftarrows 2Cs^+ + MCl_6^{2-}$$

or

$$[4b] \qquad Cs_2MCl_6 \rightleftarrows 2Cs^+ + Cl^- + MCl_5^-$$

$$[4c] \qquad Cs_2MCl_6 \rightleftarrows 2Cl^- + (MCl_4) + 2Cs^+$$

Although [3] cannot distinguish between these dissociation schemes, it is clearly indicated that ion-association does not occur in these melts as the latter would require a value for V less than unity.

B. Calculation of Activities

Activities of Cs_2HfCl_6, CsCl, and $HfCl_4$ can be calculated by combining the vapour pressure and phase diagram data. Activities of the complex compound Cs_2HfCl_6 in the $CsCl–Cs_2HfCl_6$ melts may be calculated from the present results following a previously established mathematical treatment (9). Considering the equilibrium

$$Cs_2HfCl_6 \text{ (in solution)} \rightleftarrows 2CsCl \text{ (in solution)} + HfCl_4 \text{ (vapour)}$$

the equilibrium constant is

$$[5] \qquad K = \frac{a_{CsCl}^2 \cdot P_{HfCl_4}}{a_{Cs_2HfCl_6}}$$

Along any isotherm in the homogeneous liquid region of the phase diagram for the system $CsCl–Cs_2HfCl_6$, T = constant, d ln k = 0, and,

$$[6] \qquad 2 \, d \ln a_{CsCl} + d \ln P_{HfCl_4} = d \ln a_{Cs_2HfCl_6}$$

For the overall binary system $CsCl–HfCl_4$, the Gibbs–Duhem expression is written as

$$[7] \qquad X'_{HfCl_4} \, d \ln a_{HfCl_4} + X'_{CsCl} \, d \ln a_{CsCl} = 0$$

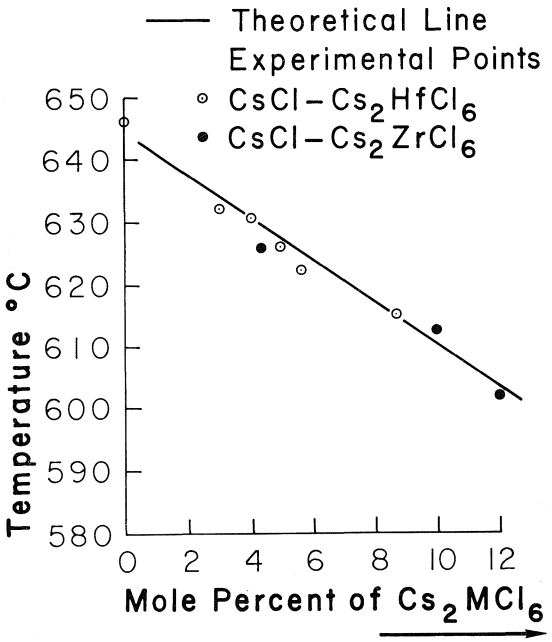

FIG. 9. Comparison of the theoretical liquidus line for $V = 1$ with the experimental data for the systems $CsCl–Cs_2ZrCl_6$ and $CsCl–Cs_2HfCl_6$.

where primed X's represent the mole fractions in the overall system.

It has been shown in a previous publication (8) that at compositions at which X_{MCl_4} is less than 0.33, the Gibbs–Duhem relationship is also applicable to the subsystem $CsCl–Cs_2HfCl_6$ provided that the equation is written as

$$[8] \quad X_{CsCl}\, d \ln a_{CsCl} + X_{Cs_2HfCl_6}\, d \ln a_{Cs_2HfCl_6} = 0$$

where unprimed X's are the new mole fractions which define the composition in the subsystem $CsCl–Cs_2HfCl_6$. Since the subsystem $CsCl–Cs_2HfCl_6$ is created by reacting all the $HfCl_4$ present with excess CsCl according to

$$[9] \quad 2CsCl + HfCl_4 \rightarrow Cs_2HfCl_6$$

the relationship between primed and unprimed X's is found by a mass balance calculation based on the stoichiometry of reaction 9.

These are:

$$[10] \quad X'_{CsCl} = \frac{2 - X_{CsCl}}{3 - 2X_{CsCl}} \qquad X'_{HfCl_4} = \frac{1 - X_{CsCl}}{3 - 2X_{CsCl}}$$

The final expression for the activity of Cs_2HfCl_6 is obtained from eqs. 6 and 8, and is given as,

$$[11] \quad d \ln a_{Cs_2HfCl_6} = \frac{X_{CsCl}}{1 + X_{Cs_2HfCl_6}}\, d \ln P_{HfCl_4}$$

which is applicable at T = constant. This expression may be integrated graphically for solutions at temperatures in the homogeneous liquid range.

Thus for $X_{Cs_2HfCl_6} = 1$ and $a_{Cs_2HfCl_6} = 1$

$$Q = \frac{X_{CsCl}}{1 + X_{Cs_2HfCl_6}} = 0$$

where Q is a concentration parameter. Then P_{HfCl_4} is the vapour pressure of $HfCl_4$ measured over pure molten Cs_2HfCl_6 at the chosen temperature. At $X_{Cs_2HfCl_6} = 0$, $a_{Cs_2HfCl_6} = 0$, and

$$Q = \frac{X_{CsCl}}{1 + X_{Cs_2HfCl_6}} = 1$$

Hence the integral is well defined at one end.

The standard states of the components CsCl and Cs_2HfCl_6 for activities calculated by this method are the real states of the components at the temperature at which the integration is conducted. For the gaseous $HfCl_4$, the standard state is the vapour at 1 atm pressure at all temperatures.

Values of P_{HfCl_4} at 825, 875, 900, and 925 °C were calculated from the log P_{HfCl_4} expressions shown in Table 3 and are given in Fig. 10 for compositions from 99.9 mol% to 62.5 mol% of Cs_2HfCl_6. The plot of Q *vs.* log P_{HfCl_4} obtained from the pressure data at 825 °C is shown in Fig. 11. The area under the curve yields the activities of Cs_2HfCl_6 at the corresponding compositions.

At 825.5 °C, which is the melting point of Cs_2HfCl_6, pure CsCl is molten, and solid Cs_2HfCl_6 is in equilibrium with liquid. Hence the standard states calculated at this isotherm should be the pure solid or liquid Cs_2HfCl_6 at the melting point and the pure liquid CsCl.

Activities calculated at 825 °C and at compositions between 99.9 and 62.5 mol% Cs_2HfCl_6 are given in Fig. 12.

Activities for Cs_2HfCl_6 may also be calculated from the phase diagram using the van't Hoff relationship in the form;

$$[12] \quad \ln a_{Cs_2HfCl_6} = -\frac{\Delta H_F}{R}\left(\frac{1}{T_L} - \frac{1}{T_F}\right)$$

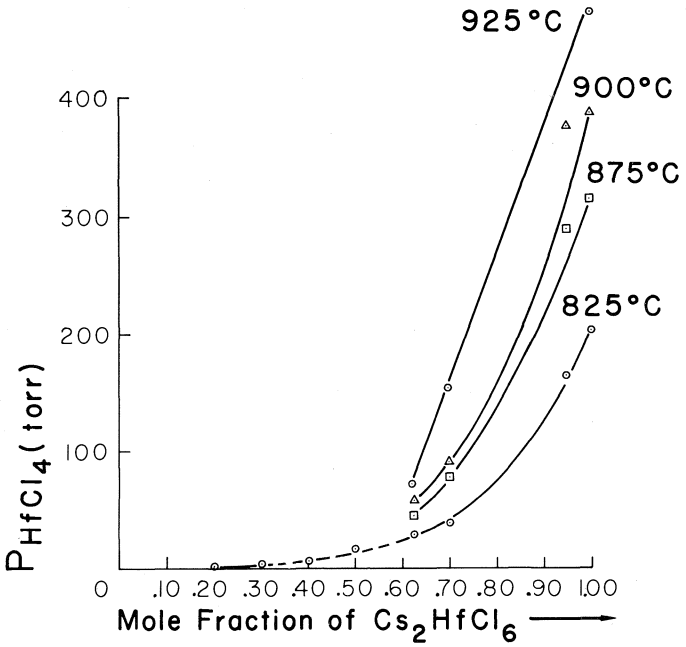

FIG. 10. Equilibrium vapour pressures of $HfCl_4$ plotted *vs.* the mole fraction of Cs_2HfCl_6 at the temperatures of 825, 875, 900, and 925 °C. The dotted line for 825 °C represents pressures calculated from the equilibrium constant K.

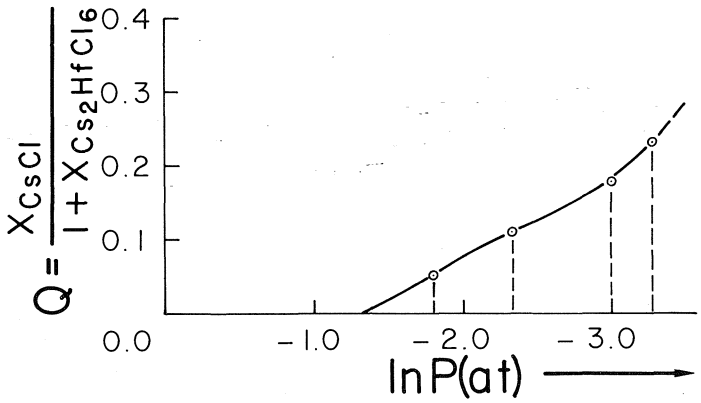

FIG. 11. Plot of the concentration parameter $Q = X_{CsCl}/(1 + X_{Cs_2HfCl_6})$ *vs.* ln P_{HfCl_4} (atm). The area under the curve allows the calculation of activities for Cs_2HfCl_6.

where ΔH_F is the heat of fusion of Cs_2HfCl_6. Although this value is not available in the literature, it has been assumed (9) that it should be similar to the heat of fusion of Cs_2ZrCl_6 which has been measured calorimetrically previously and is given as 17.53 ± 0.58 kcal/mol (10).

The activities for Cs_2HfCl_6 calculated from the phase diagram for compositions between 30 to 100 mol% Cs_2ZrCl_6 are also included in Fig. 12. Although these activities are non-isothermal, they represent a temperature range of about 150 °C, and compare well with those determined from pressure at 825 °C.

The activity data for Cs_2HfCl_6 in Fig. 12 indicate positive deviations from ideality at the Cs_2HfCl_6-rich end, while solutions containing less than 50 mol% Cs_2HfCl_6 behave ideally.

TABLE 4. Calculated activities of Cs_2HfCl_6, CsCl, and of $HfCl_4$ at 825 °C

$X_{Cs_2HfCl_6}$	$a_{Cs_2HfCl_6}$	a_{CsCl}	P_{HfCl_4} (torr)	$a_{HfCl_4} \times 10^6$	$K \times 10^3$
0.9	0.9880	0.137	126	13.3	3.2
0.8	0.9470	0.180	75	7.9	3.4
0.7	0.859	0.245	39	4.1	3.6
0.6	0.750	0.318	24	2.5	4.2
0.5	0.580*	0.438	8	0.9	
0.4	0.400*	0.598	3	0.3	
0.3	0.300*	0.700	2	0.2	
0.2	0.20*	0.803	1		
0.1	0.10*	0.910			

*From cryoscopic data.

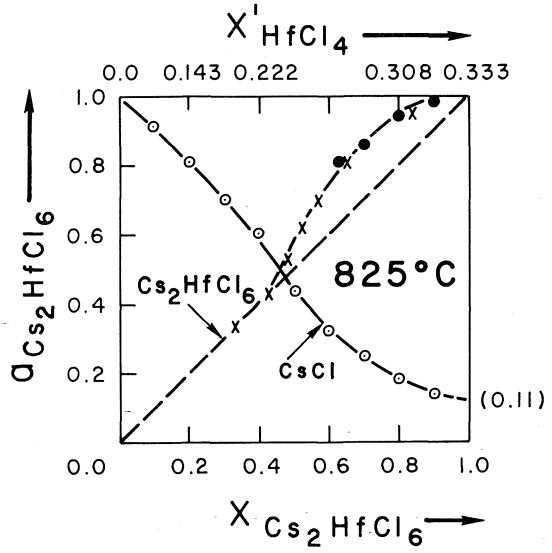

FIG. 12. The activities of Cs_2HfCl_6 and of CsCl at 825 °C. Lower concentration scale refers to the CsCl–Cs_2HfCl_6 subsystem while the upper concentration scale corresponds to the overall system CsCl–$HfCl_4$. The extrapolated activity for CsCl at $X_{Cs_2HfCl_6} = 1$ given as 0.11 represents the activity of CsCl in pure liquid Cs_2HfCl_6.

This ideal behaviour indicates an increased stabilization of $HfCl_4$ in CsCl-rich solutions, and also indicates that Cs_2HfCl_6 dissociates in melts containing more than 50 mol% CsCl into the species Cs^+ and the $HfCl_6^{2-}$.

Approximate activities of CsCl in the CsCl–Cs_2HfCl_6 subsystem have also been calculated at 825 °C using the Gibbs–Duhem eq. 8, and the results of these calculations are given in Fig. 12 and Table 4.

Activities of $HfCl_4$ in the CsCl–Cs_2HfCl_6 binary system have been calculated at 825 °C from the well known expression

$$[13] \qquad a_{HfCl_4} = \frac{P_{HfCl_4}}{P^0_{HfCl_4}}$$

where P_{HfCl_4} is the vapour pressure in equilibrium with a solution of given composition and temperature, and $P^0_{HfCl_4}$ is the pressure in equilibrium with pure solid $HfCl_4$ at the same temperature. This is given (7) by

$$[14] \qquad \log P^0_{HfCl_4}(\text{torr}) = -\frac{5197}{T} + 11.71$$

This equation is strictly valid only in the temperature range 476 to 681 K, and extrapolations were made when necessary.

To calculate the activities, the values for P_{HfCl_4} were selected at the mole fractions 1.0, 0.9, 0.8, 0.7, and 0.6. The results of these calculations for compositions in the investigated range are given in Table 4 and represent approximate values for the a_{HfCl_4} because of the long extrapolations involved in the calculation of $P^0_{HfCl_4}$ at the selected temperatures.

For these calculations, pressures were used instead of fugacities since the $HfCl_4$ vapour has been found to be monomeric and to obey the ideal gas laws at high temperatures (7).

The activities for $HfCl_4$ shown in Table 4 are very low and indicate the pronounced chemical stability of $HfCl_4$ in the CsCl–$HfCl_4$ solutions. Thus, at 700 °C, a solution containing 29 mol% of $HfCl_4$ has a decomposition pressure of 17 torr while pure $HfCl_4$ at the same temperature is calculated to have an equilibrium pressure of 2.33×10^6 torr.

This pronounced chemical stabilization of $HfCl_4$ in CsCl melts should be attributed to the presence of the complex compound Cs_2HfCl_6. Activities of $ZrCl_4$ and of Cs_2ZrCl_6 in the CsCl–Cs_2ZrCl_6 system have not been calculated, as the pressures of $ZrCl_4$ vapour in

equilibrium with solution containing various amounts of CsCl have not been measured.

From the activity values in Fig. 12 and the available equilibrium pressure data, the equilibrium constant K for the reaction

$$Cs_2HfCl_6 \text{ (solid)} \rightarrow 2CsCl \text{ (liquid)} + HfCl_4 \text{ (vapour)}$$

has been calculated at 825 °C from the data for the four compositions investigated, and the values are given in Table 4. It is seen that K is almost constant in the concentration range studied, and had the average value of $3.6 \pm 0.6 \times 10^{-3}$.

K may be used to calculate the equilibrium pressures of $HfCl_4$ at 825 °C over solutions containing less than 60 mol% of Cs_2HfCl_6. Those pressure values have also been included in Fig. 12.

It is of interest to compare the thermodynamic stability for all the alkali and alkaline earth chlorozirconate and chlorohafnate systems investigated so far in this laboratory.

Table 5 contains a list of the compounds of $ZrCl_4$ and $HfCl_4$ with various alkali, and alkaline earth chlorides. T_{dec} describes the temperature at which the pressure of $ZrCl_4$ or $HfCl_4$ in equilibrium with a given compound reaches 1 atm.

If T_{dec} is taken as a measure of thermal stability, then it is apparent that the zirconium and hafnium compounds with CsCl are the most stable of the series. Comparing the zirconium with the corresponding hafnium compounds, it is also seen that while Li_2ZrCl_6 is less stable than Li_2HfCl_6, Cs_2ZrCl_6 is more stable than Cs_2HfCl_6.

TABLE 5. Thermal stability of hexachlorozirconates and hexachlorohafnates, expressed as T_{dec} °C, as a function of the ionic radius of the complexing alkali or alkaline earth metal

Compound	T_{dec} (°C)	Ionic radius* for alkali and alkaline earth metal cation in Å
$SrZrCl_6$	410	1.13
$BaZrCl_6$	455	1.35
Li_2ZrCl_6	501	0.60
Li_2HfCl_6	513	
Na_2ZrCl_6	634	0.95
K_2ZrCl_6	831	1.33
Rb_2ZrCl_6	904	1.48
Cs_2ZrCl_6	1040	1.69
Cs_2HfCl_6	953	

*These are the crystal radii of Pauling (11).

Considering the effect of the size of the alkali metal cation on the thermodynamic stability of a given A_2MCl_6 type compound, the available data for the zirconium compounds indicate that their stability increases with increasing size of the alkali metal cation. This reflects a strengthening in the Zr—Cl bonds, and is the result of decreasing attraction between the alkali cations and the chloride species in the complex compound. It is also evident from the data in Table 5 that the compounds with the divalent alkaline earth chlorides are the least stable of the series, as expected.

Conclusions

From the results it has been established that $ZrCl_4$ and $HfCl_4$ have extended solubility in melts containing CsCl or CsCl and KF, and the solutions are thermodynamically stable. This becomes evident from the low values of the equilibrium vapour pressures of $ZrCl_4$ and $HfCl_4$ over such melts. The pure compounds Cs_2ZrCl_6 and Cs_2HfCl_6 have been synthesized.

From the measured vapour pressures of $HfCl_4$ in equilibrium with CsCl–Cs_2HfCl_6 melts at different compositions and temperatures, and from the cryoscopic data, the activities of Cs_2HfCl_4, CsCl, and $HfCl_4$ were calculated at 825 °C.

It has been found for solutions rich in Cs_2HfCl_6 the activity of Cs_2HfCl_6 exhibits positive deviations from ideality, while for solutions containing less than 50 mol% Cs_2HfCl_6 the solutions behave ideally.

The activities for $HfCl_4$ are extremely low, indicating the high stability of the melts due to the formation of the complex compound Cs_2HfCl_6. The equilibrium constant K for the decomposition of this compound has been calculated to be $(3.6 \pm 0.6) \times 10^{-3}$ at 825 °C.

A comparison between available data indicates that the Cs_2ZrCl_6 and Cs_2HfCl_6 compounds are the most stable of the alkali and alkaline earth series.

The CsCl–Cs_2ZrCl_6, or CsCl–Cs_2HfCl_6 mixtures with or without KF appear to be suitable as electrolytes for the recovery of Zr or Hf metals by fused salt electrolysis as they represent thermodynamically stable solutions of the volatile vapours of $ZrCl_4$ or $HfCl_4$. In addition, the cryoscopic results indicate the ionic character of those systems.

Acknowledgements

The authors are grateful to the National Research Council of Canada for its financial support in the form of a PRAI Grant obtained for the purpose of investigating the recovery of Zr and Hf metals by fused salt electrolysis.

1. R. L. LISTER and S. N. FLENGAS. Can. J. Chem. **43**, 2947 (1965).
2. J. E. DUTRIZAC and S. N. FLENGAS. Advance in Extractive Metallurgy Symposium, Paper 24, April 17–20. The Institution of Mining and Metallurgy, London, England. 1967.
3. S. N. FLENGAS and P. PINT. Can. Metall. Q. **8**, No. 2, 1969. p. 151.
4. J. E. DUTRIZAC and S. N. FLENGAS. Canadian Patent, 863258 (1971).
5. I. S. MOROZOV and SUN-IN-CHZHU. Zh. Neorg. Khim. **4**, 678 (1959) (Transl.: Russ. J. Inorg. Chem. **4**, 307 (1959)).
6. M. TEMKIN. Trans. from Zh. Fiz. Khim. **20**, No. 1, 165 (1946).
7. O. KUBASCHEWSKI, E. L. EVANS, and C. B. ALCOCK. Metallurgical thermochemistry. Fourth Edition. Pergamon Press, England. 1967.
8. S. N. FLENGAS, J. E. DUTRIZAC, and R. L. LISTER. Can. J. Chem. **46**, 495 (1968).
9. J. E. DUTRIZAC and S. N. FLENGAS. Can. J. Chem. **45**, 2312 (1967).
10. A. S. KUCHARSKI and S. N. FLENGAS. Can. J. Chem. **52**, 946 (1974).
11. A. F. WELLS. Structural inorganic chemistry. 3rd ed. Oxford University Press. 1962. p. 7.

Nuclear magnetic resonance study of catalyzed intermolecular fluorine exchange in the methyltetrafluorosilicate anion[1]

RONALD KIRK MARAT AND ALEXANDER F. JANZEN
Department of Chemistry, University of Manitoba, Winnipeg, Man., Canada R3T 2N2

Received September 27, 1976

RONALD KIRK MARAT and ALEXANDER F. JANZEN. Can. J. Chem. **55**, 1167 (1977).

The effect of HF, MeOH, H_2O, F^-, pyridine, $Pr_4N^+MeSiF_4^-$, and temperature on the rate of intermolecular fluorine exchange in the methyltetrafluorosilicate anion has been studied by the dynamic nuclear magnetic resonance technique. The exchange was found to be catalyzed by HF and, to a lesser extent, MeOH and H_2O, but inhibited by F^-, pyridine, and $Pr_4N^+MeSiF_4^-$. The results are analyzed in terms of the coordination model of reaction mechanisms.

RONALD KIRK MARAT et ALEXANDER F. JANZEN. Can. J. Chem. **55**, 1167 (1977).

On a étudié, par la technique de la résonance magnétique nucléaire dynamique, l'effet de HF, MeOH, H_2O, F^-, pyridine, $Pr_4N^+MeSiF_4^-$ et de la température sur les vitesses d'échange de fluor intermoléculaire dans l'anion méthyltétrafluorosilicate. On a trouvé que l'échange est catalysé par HF et à un degré moindre par MeOH et H_2O mais est inhibé par F^-, la pyridine et $Pr_4N^+MeSiF_4^-$. On analyse les résultats en termes d'un modèle de coordination des mécanismes de réaction.

[Traduit par le journal]

Introduction

Ligand exchange processes in phosphorus, sulfur, and silicon compounds are rapid in the presence of H_2O, HF, and base catalysts (1–3) and we have described the results in terms of the coordination model of reaction mechanisms[2] which emphasizes the coordination changes of the elements during a chemical reaction and classifies such changes into intermolecular or intramolecular (*n*-center) reactions.

As a further test of these mechanistic proposals we have studied catalyzed intermolecular fluorine exchange in $(n\text{-}C_3H_7)_4N^+CH_3SiF_4^-$, particularly the effect of HF, CH_3OH, H_2O, F^-, and pyridine on the rate of silicon–fluorine bond cleavage in $CH_3SiF_4^-$. This compound was first prepared by Klanberg and Muetterties who found that $CH_3SiF_4^-$ underwent both axial–equatorial and intermolecular fluorine exchange (4). The axial–equatorial exchange is typical of trigonal bipyramidal molecules and the structure of $CH_3SiF_4^-$, while not yet determined, is probably trigonal bipyramidal in view of the structure of analogous compounds such as $(C_6H_5)_2SiF_3^-$ (4), SiF_5^- (5), and isoelectronic CH_3PF_4 (6). Rapid axial–equatorial exchange equilibrates the four fluorine substituents in $CH_3SiF_4^-$ and simplifies the calculation of the methyl resonance line shape for the intermolecular exchange process.

Results

Calculation of the Exchange Broadened Spectra

It was necessary to generate proton magnetic resonance line shapes for a group of three equivalent protons coupled to a group of four equivalent fluorines undergoing intermolecular exchange. Line shapes were calculated by a matrix formulation of the McConnell–Bloch equations, similar to that of Reeves and Shaw (7). The Bloch equations, although not strictly valid for cases of spin–spin coupling, may be used since all nuclear spin isochromats are independent except for the effects of chemical exchange.

The F–Si–C–H coupling constant, in the absence of intermolecular exchange, is 4.73 ± 0.05 Hz and is independent, within experimental error, of temperature and concentration. The ^{29}Si–C–H coupling constant is 9.3 ± 0.2 Hz in the slow and fast exchange limits. Chemical shifts were found to be constant to within 2 Hz over the temperature and concentration range studied. Satellite peaks resulting from the ^{29}Si compound (relative abundance 4.67%) were included in all line shape calculations. Examples

[1]Presented at the 59th Canadian Chemical Conference of the Chemical Institute of Canada, London, Ont., June 6–9, 1976.

[2]A. F. Janzen. The coordination model of reaction mechanisms; manuscript submitted for publication.

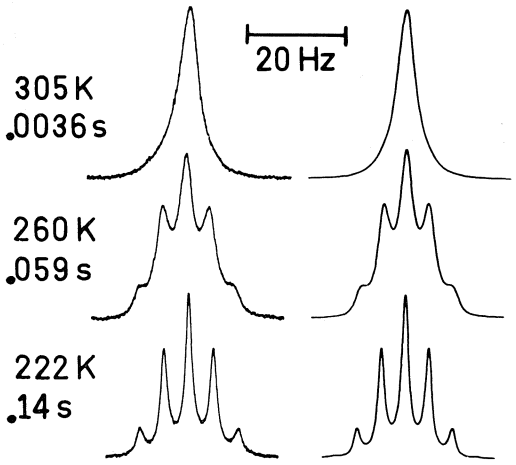

FIG. 1. A comparison of the calculated (right) and experimental (left) methyl proton resonance of $CH_3SiF_4^-$ undergoing intermolecular fluorine exchange. Sample contained $(n\text{-}C_3H_7)_4N^+CH_3SiF_4^-$ (1.0 *M*) and CH_3OH (1.0 *M*) in CH_2Cl_2 solvent.

of calculated[3] and experimental spectra are shown in Fig. 1.

Effect of HF, MeOH, H_2O, $Pr_4N^+MeSiF_4^-$, F^-, Pyridine, and Temperature on the Exchange Rate

The pre-exchange lifetime (τ) may be related to the kinetics of the exchange reaction by [1],

$$[1] \qquad (f\tau)^{-1} = k[A]^{a-1}[B]^b[C]^c \ldots$$

where A is the species being observed (Pr_4N^+-$MeSiF_4^-$) and B, C, ... are other species involved in the exchange reaction but not observed in the exchange broadened nmr spectrum; *a*, *b*, *c*, ... are the kinetic orders, *k* is the specific rate constant, and *f* is a statistical factor which relates the magnetic pre-exchange lifetime (τ) of A to the chemical preexchange lifetime (9). *f* includes a factor of $\frac{1}{4}$ because four fluorines can undergo exchange, and a factor of $\frac{1}{2}$ because there is a 50% probability that after exchange the fluorine may have the same spin state. Our calculations include the factor of $\frac{1}{2}$ in the exchange probability matrix.

The effect of any reagent on the fluorine exchange process in $MeSiF_4^-$ may thus be determined by varying the concentration of the reagent and observing its influence on τ; a plot of ln $1/\tau$ *vs.* ln [concentration] then gives the order in that reagent. This technique was used in the following experiments.

(i) Effect of HF

Figure 2 shows a plot of ln [HF] *vs.* ln $1/\tau$ at three temperatures. The slopes (least square) and orders in HF are 2.5 ± 0.2 at +33°C, 2.9 ± 0.2 at +3°C and, 3.4 ± 0.3 at −7°C, thus the orders increase at lower temperature. HF produced a very rapid rate of exchange and therefore studies were carried out at low HF concentration, generally from 10^{-1} to 10^{-3} *M*. The difficulty of working with such small quantities of HF is assumed to be the main reason for the large experimental errors in Fig. 2. Reaction of HF with the glass wall of the nmr tube is a minor cause for error because samples could be left at room temperature for several hours without appreciable change in the exchange rate.

(ii) Effect of Methanol

Figure 3 shows a plot of ln [MeOH] *vs.* ln $1/\tau$ at two temperatures. The orders in MeOH are 1.95 ± 0.05 at +31.5°C and 2.5 ± 0.1 at 0°C, thus the order increases at lower temperature. A comparison of HF (Fig. 2) and MeOH (Fig. 3) catalyzed reactions shows that about 10^2 to 10^3 times as much MeOH as HF must be used to produce comparable rates of exchange.

(iii) Effect of Water

The effect of water on the exchange rate was

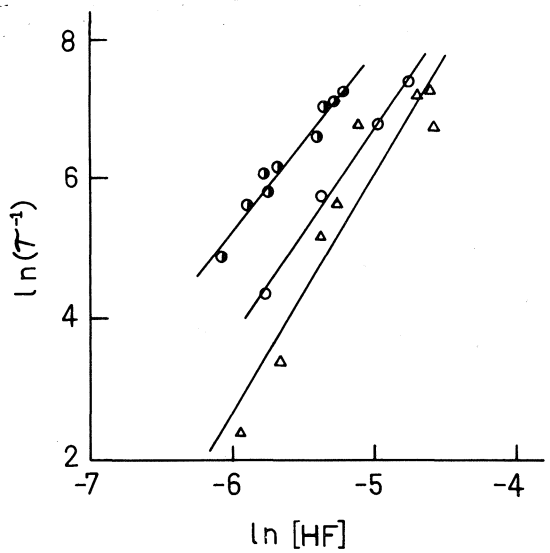

FIG. 2. Plot of ln $1/\tau$ *vs.* ln [HF] at three temperatures and at 0.66 *M* $(n\text{-}C_3H_7)_4N^+CH_3SiF_4^-$: ◑ +33°C; ○ +3°C; △ −7°C.

[3]A detailed description of the line shape calculations is found in ref. 8.

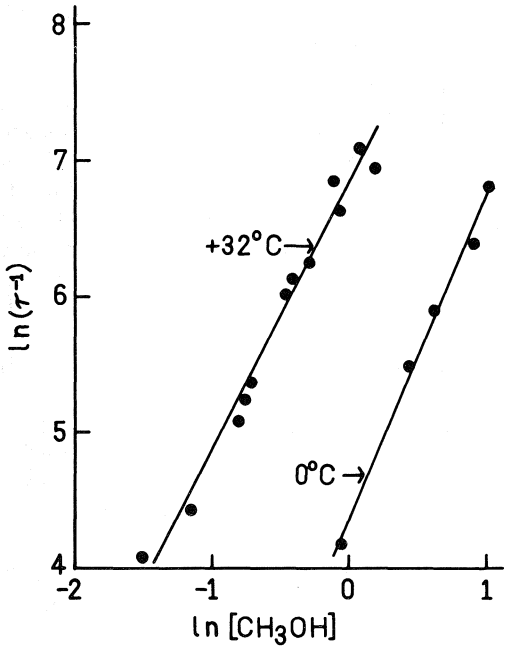

FIG. 3. Plot of ln $1/\tau$ *vs.* ln [CH_3OH] at two temperatures and 0.66 *M* $(n\text{-}C_3H_7)_4N^+CH_3SiF_4^-$.

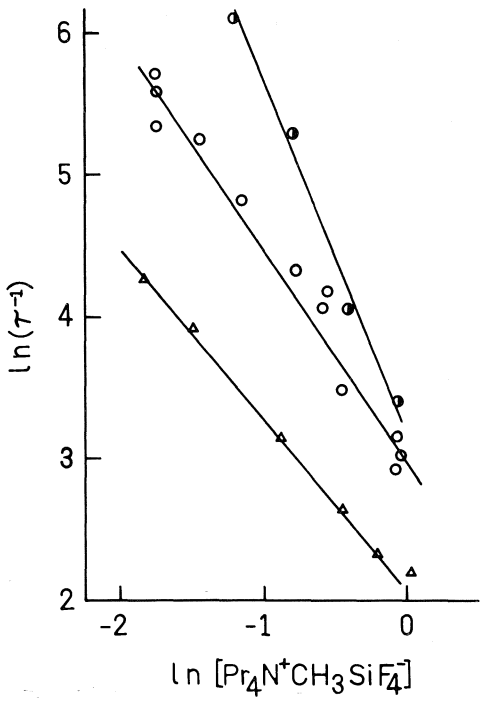

FIG. 4. Plot of ln $1/\tau$ *vs.* ln $[(n\text{-}C_3H_7)_4N^+CH_3SiF_4^-]$ for HF and CH_3OH catalyzed exchange reactions: ◑ [HF] = 2.2×10^{-3} *M*, +31.5°C; ○ [CH_3OH] = 1.0 *M*, −17°C; △ [CH_3OH] = 1.0 *M*, −25°C.

briefly studied and found to be similar to that of MeOH. A comparison of the rates of HF, MeOH, and H_2O catalyzed reactions at constant temperature and $Pr_4N^+MeSiF_4^-$ concentration is shown in Table 1. It may be seen that HF, at only 5.0×10^{-3} *M*, produces a $1/\tau$ value of 2300 s^{-1}, whereas 1.0 *M* MeOH and H_2O produce $1/\tau$ values of 800 and 900 s^{-1}, respectively.

(iv) Effect of $Pr_4N^+MeSiF_4^-$

Figure 4 shows a plot of ln $1/\tau$ *vs.* ln [$Pr_4N^+MeSiF_4^-$] for HF and MeOH catalyzed reactions, the latter at two temperatures. It may be seen that addition of $Pr_4N^+MeSiF_4^-$ inhibits exchange and the orders ($a - 1$ in eq. 1) in this reagent are -1.5 ± 0.2 at +31.5°C for HF catalyzed exchange, and -0.5 ± 0.2 at −17°C and -0.2 ± 0.1 at −25°C for MeOH catalyzed exchange. Inhibition is more pronounced for the HF than for the MeOH catalyzed reaction.

TABLE 1. Relative rates of exchange at +31.5°C and 0.66 *M* $(n\text{-}C_3H_7)_4N^+CH_3SiF_4^-$

Reagent	Concentration	$1/\tau(\pm 10\%)$
HF	5.0×10^{-3} *M*	2300
H_2O	1.0 *M*	900
CH_3OH	1.0 *M*	800

(v) Effect of Fluoride Ion and Pyridine

Figure 5 shows a plot of $1/\tau$ *vs.* fluoride ion (as $Pr_4N^+F^-$) or pyridine for the HF and MeOH catalyzed reactions. Both F^- and pyridine inhibit exchange in the HF and MeOH catalyzed reactions, but the concentrations of $Pr_4N^+F^-$ and HF are approximately 10^2 to 10^3 times lower than concentrations of pyridine and MeOH. The most effective inhibition is produced by addition of F^- to HF catalyzed reactions, *e.g.*, it may be estimated from Fig. 5 that $1/\tau$ is reduced by 50% after addition of about 1.3×10^{-3} *M* F^- to a sample containing 3.95×10^{-3} *M* HF.

(vi) Effect of Temperature

Figure 6 shows a plot of ln $1/\tau$ *vs.* $1/T$ for HF and MeOH catalyzed exchange reactions. The temperature dependency of the two systems is very similar, but the concentration of HF is only 3.3×10^{-3} *M* whereas that of MeOH is 1.0 *M*. The high temperature straight line portion of the plot (above ~ -25°C) gives an apparent activation energy $E_a = 12.3 \pm 0.4$ kcal/mol for the HF catalyzed reaction and $E_a = 10.2 \pm 0.3$

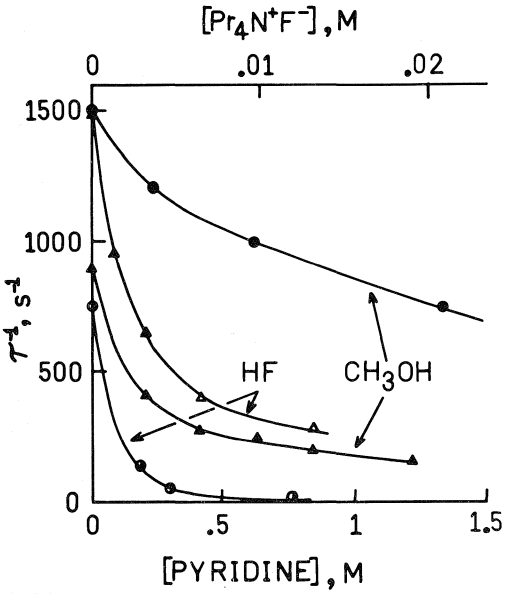

FIG. 5. Inhibition of HF and CH_3OH catalyzed exchange reactions by $(n\text{-}C_3H_7)_4N^+F^-$ and pyridine at +33°C and 0.66 *M* $(n\text{-}C_3H_7)_4N^+CH_3SiF_4^-$: ● $[CH_3OH] = 1.65$ *M*, F^- inhibition; ◑ $[HF] = 3.95 \times 10^{-3}$ *M*, F^- inhibition; △ $[HF] = 5.25 \times 10^{-3}$ *M*, pyridine inhibition; ▲ $[CH_3OH] = 1.0$ *M*, pyridine inhibition.

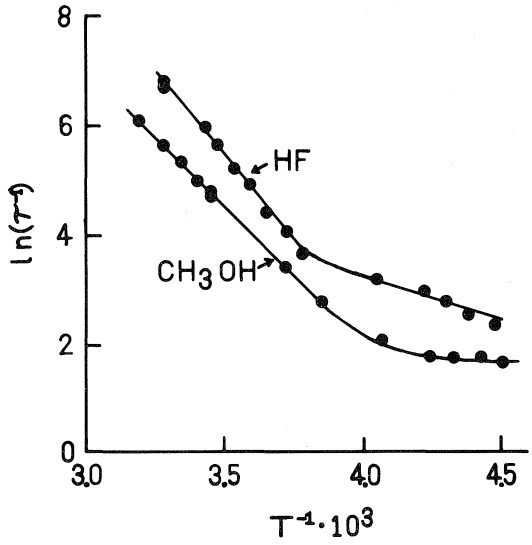

FIG. 6. The effect of temperature on the HF and CH_3OH catalyzed exchange reactions at 1.0 *M* $(n\text{-}C_3H_7)_4N^+CH_3SiF_4^-$: $[HF] = 3.3 \times 10^{-3}$ *M* and $[CH_3OH] = 1.0$ *M*.

kcal/mol for the MeOH catalyzed reaction. At lower temperatures (below ~ −25°C), the apparent activation energy is about 2 kcal/mol for the HF catalyzed reaction and about 0.4 kcal/mol for the MeOH catalyzed reaction.

(vii) Effect of 2,6-Di-tert-butylpyridine

A sample containing 0.66 *M* $Pr_4N^+MeSiF_4^-$ and 1.0 *M* MeOH showed no discernible change in the exchange rate upon addition of 2,6-di-*tert*-butylpyridine over a concentration range 0 to 0.52 *M*.

(viii) Effect of Hexamethyldisilazane

Fluorine exchange in an HF catalyzed reaction was immediately stopped on addition of $[Me_3Si]_2NH$; some Me_3SiF was produced and identified by nmr. In a separate experiment it was shown that $[Me_3Si]_2NH$ reacts very rapidly with a dilute solution of HF to produce Me_3SiF. Fluorine exchange in a MeOH catalyzed reaction was also slowed down, but at a reduced rate; some Me_3SiF was formed and it was separated on the vacuum line and identified by nmr and mass spectrometry. In a separate experiment it was shown that $[Me_3Si]_2NH$ reacts very slowly, over a period of several days, with MeOH.

Discussion

Possible Mechanism of Catalyzed Intermolecular Fluorine Exchange

The experimental results discussed above, particularly the high orders in HF and MeOH, the negative fractional order in $Pr_4N^+MeSiF_4^-$, and the change in order with temperature, suggest that intermolecular fluorine exchange in $MeSiF_4^-$ is a complex process and a quantitative kinetic analysis will not be attempted. Nevertheless, it is possible to offer a qualitative but consistent explanation of the experimental results.

In the first place, the results definitely show that unimolecular ionization of $MeSiF_4^-$, [2],

$$[2] \qquad MeSiF_4^- \rightleftharpoons MeSiF_3 + F^-$$

or bimolecular fluorine exchange of $MeSiF_4^-$, [3], cannot be mechanisms of exchange which

$$[3] \quad MeSiF_4^- + MeSiF^*{}_4^- \rightleftharpoons MeSiF_3F^{*-} + MeSiF^*{}_3F^-$$

are rapid on the nmr time scale because negligible exchange occurs unless HF, MeOH, or H_2O are added. Since $MeSiF_4^-$ is actually prepared from $MeSiF_3$ and F^-, it must be concluded that [2] lies essentially to the left and that loss of F^- is hindered by a high activation barrier.

Secondly, it can be stated quite confidently that HF is responsible for very rapid fluorine

exchange in $MeSiF_4^-$; Table 1 and Figs. 2 and 3 demonstrate that much lower concentrations of HF than MeOH or H_2O are required to bring about comparable rates of exchange, therefore, it is reasonable to conclude that MeOH or H_2O reacts with $MeSiF_4^-$ to generate HF, [4] and [5], and HF then becomes the dominant fluorine

[4] $MeSiF_4^- + MeOH \rightleftharpoons MeSiF_3OMe^- + HF$

[5] $MeSiF_4^- + H_2O \rightleftharpoons MeSiF_3OH^- + HF$

transfer reagent in the exchange reaction. The equilibrium of [4] and [5] must lie predominantly to the left to explain the decrease of 10^2 to 10^3 in the rate of MeOH or H_2O catalyzed exchange, furthermore, the synthesis of $MeSiF_4^-$ may be carried out in methanol solution without any apparent formation of $MeSiF_3OMe^-$, and there is only a small change in the chemical shift (less than 2 Hz) of $MeSiF_4^-$ as MeOH is added.

If HF is responsible for rapid fluorine exchange then any reduction in its equilibrium concentration must result in a reduced rate of exchange. Thus adding $[Me_3Si]_2NH$ to a MeOH or HF catalyzed reaction removes HF as Me_3SiF, [6], while addition of small amounts of

[6] $[Me_3Si]_2NH + 2HF \rightleftharpoons 2Me_3SiF + NH_3$

fluoride, as $Pr_4N^+F^-$, inhibits exchange (Fig. 5) because HF is converted to bifluoride, [7]. There

[7] $F^- + HF \rightleftharpoons F—H—F^-$

are many reports in the literature that HF may be complexed as bifluoride and that fluorine exchange is slowed down by this procedure.

Pyridine may also tie up HF as $C_5H_5NH^+F^-$ or, in view of the large amount of pyridine that must be added to observe inhibition (Fig. 5), it is also possible that inhibition is due to the formation of $MeSiF_4(base)^-$, [8]. Previous nmr and

[8] $MeSiF_4^- + base \rightleftharpoons MeSiF_4(base)^-$

thermochemical studies have shown that bases such as NH_3 and amines may interact strongly with SiF_5^- to give six-coordinate silicon adducts (1, 10). That inhibition is not observed with bases such as 2,6-di-*tert*-butylpyridine suggests that this base is probably too bulky to coordinate to $MeSiF_4^-$ and too weakly basic to complex out HF (11).

In order to account for some of the more complex features of the exchange process, such as the high orders in HF and MeOH (Figs. 2 and 3), negative order in $Pr_4N^+MeSiF_4^-$ (Fig. 4), and temperature effects (Fig. 6), it is useful to consider the most likely coordination changes[2] of all elements taking part in the reactions; these are probably[4] Si $4 \rightleftharpoons 5 \rightleftharpoons 6$, H $1 \rightleftharpoons 2$, F $1 \rightleftharpoons 2$, and O $2 \rightleftharpoons 3$. The coordination changes may occur via the fluorine exchange mechanism of [9] which postulates initial attack of HF, MeOH, or H_2O on $MeSiF_4^-$ to give a six-coordinate intermediate (i) i-**2**, followed by a four-center reaction to give i-**3**. X—H bond cleavage and loss of HF then gives i-**5**.

[9]

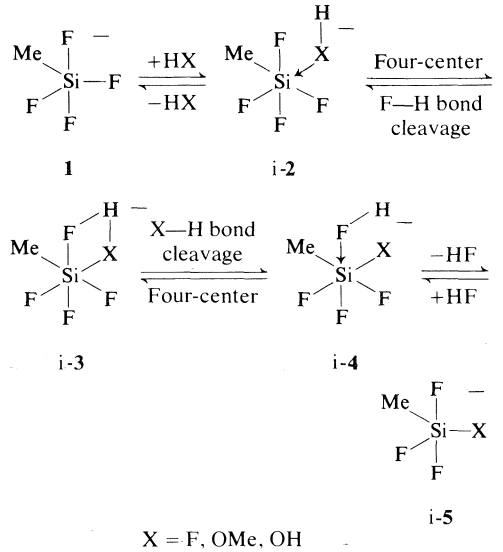

1 i-**2** i-**3** i-**4** i-**5**

X = F, OMe, OH

The high order in HF could be ascribed to $(HF)_n$ aggregates, or, it may reflect the reaction of HF with $Pr_4N^+MeSiF_4^-$ which may shift the equilibrium, [10], to the right. The molecular

[10] $Pr_4N^+MeSiF_4^- + nHF \rightleftharpoons Pr_4N^+ + MeSiF_4(HF)_n^-$

weight of $Pr_4N^+MeSiF_4^-$ in CH_2Cl_2 solution was found to be 330 ± 20, as determined by vapour pressure measurement, *i.e.* about 8% greater than the molecular weight of the ion-pair. Previously, Brownstein and Bornais found that $Bu_4N^+PF_6^-$ and $Bu_4N^+AsF_6^-$ had apparent

[4]That hydrogen and fluorine may form two-coordinate intermediates is reasonable in view of the many stable compounds of similar coordination number, *e.g.*, FHF^-, B_2H_6, $(CO)_5CrHCr(CO)_5^-$ (12), $Et_3AlFAlEt_3^-$(13), polymeric SbF_5, etc. Three-coordinate oxygen is found in H_3O^+, R_3O^+, and dimeric $(RO)_3Al$ and six-coordinate silicon in SiF_6^{2-}, $Si(acac)_3^+$ and $SiX_4 \cdot 2base$. Corriu and Leard's study of racemization of chlorosilanes (14) provides a good example of coordination changes Si $4 \rightleftharpoons 5 \rightleftharpoons 6$.

molecular weights about 5% greater than the formula weight (15).

If HF is produced in the MeOH catalyzed reaction, [4], then the order in MeOH should be one-half[5] that of the order in HF. This is in reasonable agreement with experiment since the orders in MeOH are 1.95 ± 0.05 to 2.5 ± 0.1 (Fig. 3) while the orders in HF are 2.5 ± 0.2 to 3.4 ± 0.3 (Fig. 2).

At lower temperature the order in HF (Fig. 2) and MeOH (Fig. 3) increases, perhaps because the average number of associated HF molecules in $MeSiF_4(HF)_n^-$ increases. Increasing the concentration of $Pr_4N^+MeSiF_4^-$ at constant HF concentration may result in a decreased rate of fluorine exchange (Fig. 4) because more HF is tied up as $MeSiF_4(HF)_n^-$. That inhibition by $Pr_4N^+MeSiF_4^-$ is less pronounced for the MeOH than for the HF catalyzed reaction (Fig. 4) suggests that the large concentration of MeOH might favour the production of $MeSiF_4(HOMe)_n^-$, rather than $MeSiF_4(HF)_n^-$, therefore, the equilibrium concentration of HF would not be reduced as effectively in a MeOH catalyzed reaction. Complexes such as $SiF_4 \cdot 4MeOH$ have been described previously by Guertin and Onyszchuk (16).

The mechanism of [9], modified to include intermediates such as $MeSiF_4(HF)_n^-$, is assumed to be responsible for rapid HF catalyzed exchange and all the results discussed above appear to be consistent with this view. The activation energy plot (Fig. 6), however, suggests that there are two parallel pathways of fluorine exchange, one dominant above $\sim -25°C$, with apparent activation energy 10.2–12.3 kcal/mol, which is assumed to be the HF catalyzed process discussed so far, the other, dominant below $\sim -25°C$, has an apparent activation energy of about 0.4 to 2 kcal/mol. Other reactions which might also produce fluorine exchange are [11] and [12]. Recent studies in our laboratory have

$$[11] \qquad MeSiF_4^- + HF \rightleftharpoons MeSiF_3 + FHF^-$$

$$[12] \qquad MeSiF_4^- + MeSiF^*{}_3 \rightleftharpoons MeSiF_3 + MeSiF^*{}_3F^-$$

shown that fluorine exchange, in the absence of catalysts, is very rapid in the system $MeSiF_4^-$–$MeSiF_3$ (17), therefore, any reaction which liberates $MeSiF_3$, even in small amounts, may be an important pathway of fluorine exchange.

Comparison with Other Catalyzed Exchange Processes

Fluorine exchange occurs in an acidified aqueous solution of $(NH_4)_2SiF_6$ (18) and SiF_5^- salts can be precipitated from fluorosilicic acid solutions (19). Presumably, H_3O^+ and SiF_6^{2-} give intermediate-**6**, which may undergo cleavage at three-coordinate oxygen and two-coordinate hydrogen (O 2 ⇌ 3, H 1 ⇌ 2). Loss of H_2O from i-**6** gives an intermediate which is entirely analogous to intermediate-**2** in [9]. In the absence of an acid catalyst, H_2O and SiF_6^{2-} probably give intermediate-**7**, but cleavage of the F—H bond in i-**7** (F 1 ⇌ 2, H 1 ⇌ 2) does not result in fluorine transfer.

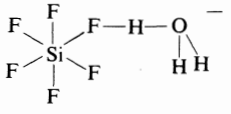

i-**6**

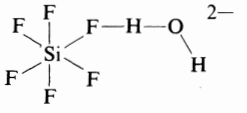

i-**7**

It may appear contradictory that exchange in $MeSiF_4^-$ is inhibited by fluoride or pyridine, whereas other reactions of silicon or phosphorus compounds are generally catalyzed by bases, *e.g.*, hydrolysis and fluorine exchange of Me_3SiF is catalyzed by diethylamine (3), reaction of alcohols with R_3SiH is catalyzed by fluoride or alkoxide (20), and decomposition of phosphonium salts is catalyzed by hydroxide (21). However, this apparent conflict may be resolved by assuming that four-center reactions are accelerated if the central silicon or phosphorus atom achieves six coordination.[2] In that case, Me_3SiF, R_3SiH, or $R_3(C_6H_5CH_2)P^+$ require base catalysts in order to increase the coordination around silicon or phosphorus. The formation of intermediates such as i-**8**, i-**9**, and i-**10** may then be

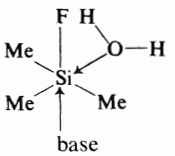

i-**8**

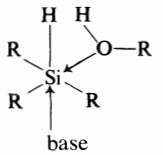

i-**9**

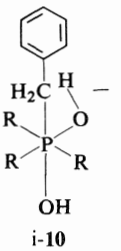

i-**10**

followed by rapid four-center reactions and loss of HF from i-**8** (Si 4 ⇌ 5 ⇌ 6, H 1 ⇌ 2, F 1 ⇌ 2, O 2 ⇌ 3), loss of H_2 from i-**9** (Si 4 ⇌

[5]If [HF] = [$MeSiF_3OMe^-$] and [$MeSiF_4^-$] is constant in the equilibrium constant expression for [4], then [HF] $\propto K_{eq}^{1/2}$[MeOH]$^{1/2}$. If rate $\propto$ [HF]^n, then rate $\propto K_{eq}^{1/2\,n}$[MeOH]$^{1/2\,n}$.

$5 \rightleftharpoons 6$, H $1 \rightleftharpoons 2$, O $2 \rightleftharpoons 3$), and loss of toluene from i-**10** (P $4 \rightleftharpoons 5 \rightleftharpoons 6$, H $1 \rightleftharpoons 2$, O $1 \rightleftharpoons 2$, C $4 \rightleftharpoons 5$). Since $MeSiF_4^-$ is already five-coordinate, any attack on silicon by a base such as pyridine will merely compete with reagents such as water, alcohol, or hydrogen fluoride and inhibit further reaction.

Experimental

Materials

Methyltrifluorosilane (PCR), 10% aqueous $(n\text{-}C_3H_7)_4NOH$ (Eastman), 49% aqueous HF (Fisher), anhydrous HF (Matheson), and hexamethyldisilazane (Aldrich) were used without further purification. Methanol was distilled from sodium, methylene chloride from P_2O_5, and 1,2-dimethoxyethane was poured through a column of 3A molecular sieves and distilled from lithium aluminum hydride; all were stored over 3A molecular sieves prior to use, including acetonitrile.

Dilute solutions of HF were prepared by bubbling gaseous anhydrous HF into a 1:1 (v/v) mixture of acetonitrile and methylene chloride, in which HF was readily soluble. These solutions were standardized acidimetrically and, when stored at 0°C, showed no decomposition after several weeks. In a separate experiment it was shown that addition of acetonitrile had no effect on the exchange rate. Dilute solutions of water were made up in a 10% (v/v) mixture of acetonitrile and methylene chloride.

Tetra-*n*-propylammonium methyltetrafluorosilicate was prepared by the method of Klanberg and Muetterties (4). Neutralization of $(n\text{-}C_3H_7)_4NOH$ (75 ml of a 3% solution) with 1% aqueous HF was monitored with a glass electrode p*H* meter to ensure that no excess HF was introduced. The white, hygroscopic powder, $(n\text{-}C_3H_7)_4N^+F^-$ (2.7 g) was handled in a dry box at all times. $(n\text{-}C_3H_7)_4N^+CH_3SiF_4^-$ (40–50% yield) was recrystallized from 1,2-dimethoxyethane, washed with diethyl ether, and identified by its ^1H and ^{19}F nmr spectrum (4) and mp 157–159°C (lit. (4) mp 161–164°C).

Samples of $(n\text{-}C_3H_7)_4N^+CH_3SiF_4^-$ with $1/\tau$ values less than 2 or 3 s^{-1} at +33°C were sufficiently pure for kinetic studies. On a number of occasions, however, only impure samples were obtained, most likely because of the introduction of HF or H_2O or perhaps because of the presence of CH_3SiF_3 or methylchlorofluorosilanes (from reaction of SbF_3 with CH_3SiCl_3). Chloride contamination of $(CH_3)_4N^+F^-$ has been mentioned previously (4).

Preparation of Nuclear Magnetic Resonance Samples

The 5 mm nmr tubes, calibrated to contain exactly 0.3 or 0.4 ml, were cleaned with CH_2Cl_2, treated with hexamethyldisilazane (1), and dried at 220°C for at least 24 h. $(n\text{-}C_3H_7)_4N^+CH_3SiF_4^-$ was weighed into the nmr tube, catalysts or other reagents were added by means of a microlitre syringe, and the total volume adjusted by adding CH_2Cl_2 up to the calibration mark. The tube was capped, inverted several times to ensure thorough mixing, and equilibrated for 20 min at probe temperature.

During concentration runs the volume of reagent added (2–10 μl) was always small compared to the total sample volume (300 or 400 μl) and the error of ~3% was ignored. Volume changes with temperature were also ignored. Samples for the determination of activation parameters were sealed under vacuum and stored at −196°C until required. This was necessary to avoid the effects of sample aging.

Instrumental

All proton magnetic resonance spectra were recorded on a Varian HA-100-D spectrometer at 100 MHz using CH_2Cl_2 as the internal lock. Frequencies were measured with a Hewlett-Packard 5323-A frequency counter and are considered accurate to ±0.02 Hz. Spectra were recorded at a sweep rate of 0.1 Hz/s and a sweep width of 2 Hz/cm with a minimum amount of filtering. The R.F. field strength was 0.025 mG as determined by the method of Harris and Worvill (22). Spectra run with a threefold increase in field strength showed negligible distortion due to saturation effects. Every point in the figures represents the average of at least three, sometimes up to seven, scans of the nmr spectrum.

Wilmad 503-ps nmr tubes were chosen for their reproducible spinning characteristics and were employed for all nmr studies. Temperatures were determined with an iron–constantan thermocouple placed at sample depth in a 'dummy' sample of CH_2Cl_2.

Mass spectra were obtained on a Finnigan 1015 quadrupole mass spectrometer.

Calculation of Line Shapes

All calculated spectra were produced with a modified version of Dr. G. M. Whitesides' computer program EXCHYS (23). The computations were performed with an IBM 370-158 computer and the Fortran-H compiler. The digital output was plotted on a Calcomp 750-563 or Versatec D1200-A plotter.

Due to the large number of spectra that had to be compared and the high symmetry of the spectra, a numerical procedure was employed for comparison of the spectra. For spectra past the point of coalescence, the half-height width of the experimental spectrum was compared with a graph of calculated half-height widths as a function of $1/\tau$. Graphs of this type were made for a number of different T_2 values. T_2 values were estimated from natural abundance $^{13}CH_2Cl_2$ and varied from 0.5 to 1.3 s. For slower exchange rates, graphs were prepared of 'valley-to-peak' ratios as a function of $1/\tau$ for a range of T_2 values. Spectra at intermediate exchange rates were analyzed by visual comparison of experimental and calculated spectra.[3] The lifetime values determined by this method are considered accurate to ±10%.

Acknowledgements

The financial assistance of the National Research Council of Canada and the Research Board of the University of Manitoba is gratefully acknowledged.

1. J. A. Gibson, D. G. Ibbott, and A. F. Janzen. Can. J. Chem. **51**, 3203 (1973).
2. D. G. Ibbott and A. F. Janzen. Can. J. Chem. **50**, 2428 (1972); A. F. Janzen, J. A. Gibson, and D. G. Ibbott. Inorg. Chem. **11**, 2853 (1972); R. E. Wasylishen, G. S. Birdi, and A. F. Janzen. Inorg. Chem. **15**, 3054 (1976).
3. J. A. Gibson and A. F. Janzen. Can. J. Chem. **50**, 3087 (1972).

4. F. KLANBERG and E. L. MUETTERTIES. Inorg. Chem. **7**, 155 (1968).
5. P. BIRD, J. F. HARROD, and K. A. THAN. J. Am. Chem. Soc. **96**, 1222 (1974).
6. L. S. BARTELL and K. W. HANSEN. Inorg. Chem. **4**, 1777 (1965).
7. L. W. REEVES and K. N. SHAW. Can. J. Chem. **48**, 3641 (1970).
8. R. K. MARAT. M.Sc. Thesis, University of Manitoba, Man. 1976.
9. G. BINSCH. Dynamic nuclear magnetic resonance spectroscopy. *Edited* by L. M. Jackman and F. A. Cotton. Academic Press, New York, NY. 1975; N. S. Ham and T. Mole. Progress in NMR spectroscopy. Vol. 4. *Edited* by J. W. Emsley, J. Feeney, and L. H. Sutcliffe. Pergamon Press, New York, NY. 1969. p. 91; A. A. FROST and R. G. PEARSON. Kinetics and mechanism. 2nd ed. Wiley, New York, NY. 1961; L. W. REEVES. Adv. Phys. Org. Chem. **3**, 187 (1965).
10. I. WHARF and M. ONYSZCHUK. Can. J. Chem. **50**, 3450 (1972); I. WHARF and M. ONYSZCHUK. Can. J. Chem. **48**, 2250 (1970).
11. H. C. BROWN and B. KANNER. J. Am. Chem. Soc. **88**, 986 (1966).
12. L. B. HANDY, P. M. TREICHEL, and L. F. DAHL. J. Am. Chem. Soc. **88**, 366 (1966).
13. G. ALLEGRA and G. PEREGO. Acta Crystallogr. **16**, 185 (1963).
14. R. J. P. CORRIU and M. LEARD. Chem. Commun. 1086 (1971).
15. S. BROWNSTEIN and J. BORNAIS. Can. J. Chem. **46**, 225 (1968).
16. J. P. GUERTIN and M. ONYSZCHUK. Can. J. Chem. **41**, 1477 (1963).
17. R. K. MARAT and A. F. JANZEN. In press.
18. E. L. MUETTERTIES and W. D. PHILLIPS. J. Am. Chem. Soc. **81**, 1084 (1959).
19. K. BEHRENDS and G. KIEL. Naturwissenschaften, **54**, 537 (1967).
20. I. S. AKHREM, M. DENE, and M. E. VOL'PIN. IZV. Akad. Nauk SSSR, Ser. Khim. 932 (1973).
21. M. ZANGER, C. A. VANDER WERF, and W. E. MCEWEN. J. Am. Chem. Soc. **81**, 3806 (1959).
22. R. K. HARRIS and K. M. WORVILL. J. Magn. Reson. **9**, 383 (1973).
23. J. K. KRIEGER. Ph.D. Thesis, Massachusetts Institute of Technology, Cambridge, MA. 1971.

An electron spin resonance and CIDNP study of the structure and reactivity of some excited triplet biphenyl ketones

HARISH M. VYAS AND JEFFREY K. S. WAN

Department of Chemistry, Queen's University, Kingston, Ont., Canada K7L 3N6

Received September 20, 1976

HARISH M. VYAS and JEFFREY K. S. WAN. Can. J. Chem. **55**, 1175 (1977).

The correlation of structure and reactivity of some excited triplet biphenyl ketones was approached by a combined esr and CIDNP study. The low temperature esr study confirmed the assignment of the triplet π,π^* as the lowest triplet state in these biphenyl ketones. An analysis of the zero-field energies suggests that these π,π^* triplets have a structure with both the biphenyl and the carbonyl groups being coplanar. Consequently a substantial unpaired spin density may result at the carbonyl oxygen atom which could lead to abstraction reactions. The CIDNP results are consistent with the triplet photoreduction mechanism. The polarization is mainly due to the cage products and the polarization magnitude is therefore dependent upon the light intensity.

HARISH M. VYAS et JEFFREY K. S. WAN. Can. J. Chem. **55**, 1175 (1977).

On a examiné une corrélation de structure et de réactivité de quelques triplets excités de biphényl cétones à l'aide d'une étude combinée de rpe et de CIDNP. Des études de rpe à basse température ont confirmé l'attribution de l'état triplet π,π^* comme étant l'état triplet le plus bas de ces biphényl cétones. Une analyse des énergies à champ zéro suggère que ces états triplets π,π^* ont une structure dans laquelle les groupes biphényles et carbonyles sont coplanaires. En conséquence, une densité importante de spin non-pairé peut se retrouver au niveau de l'atome d'oxygène du carbonyle ce qui pourrait conduire alors aux réactions d'enlèvement. Les résultats CINDP sont en accord avec le mécanisme de la photoréduction triplet. La polarisation est principalement due aux produits formés dans la cage et l'amplitude de la polarisation dépend donc de l'intensité lumineuse.

[Traduit par le journal]

Introduction

The structure and reactivity of excited organic triplet states in photochemical reactions have received much theoretical and experimental attention in the past 15 years. In liquid photochemical systems the triplet state is normally populated via rapid intersystem crossing from the lowest excited singlet to the sublevels of the triplet state. When more than one triplet state are available below the first excited singlet, it is not easy to establish which of the triplet states is mainly responsible for the observed chemical reaction. A classical example is the photochemistry of 4-benzoylbiphenyl. This system has been extensively studied (1). Some of the interesting features known are that 4-benzoylbiphenyl has two excited triplet states below the first excited singlet and the lowest triplet is characteristic of a π,π^* state. Turro and Lee (2) have demonstrated that this triplet state can abstract hydrogen atoms from alcohol solvent, although its reactivity is much less than that of the corresponding n,π^* triplet reaction of benzophenone. Arguments have been put forward (1*b*, 3) that the low lying π,π^* triplet states have some intrinsic chemical property. Direct evidence, however, is still lacking.

Recently we have been concerned with the establishment of the role of the triplet state in CIDEP (4) and CIDNP (5) systems involving carbonyl compounds. We wish to extend the application of esr and magnetic polarization studies to the correlation of structure and reactivity of the 4-benzoylbiphenyl triplet. The triplet esr study reveals a systematic and subtle correlation between biphenyl and a series of 4-phenyl substituted aromatic and alkyl aromatic ketones. The meager intrinsic chemical property of these ketones may be related to the structures of their characteristic π,π^* triplets. The high sensitivity of CIDNP technique in the present study afforded the direct investigation of the minor chemical reactions of these π,π^* triplets. No experimental evidence of CIDEP was observed in the 4-benzoylbiphenyl system and this is consistent with our theory (4) since the chemical rate involving the π,π^* triplet is too slow compared to its depolarization rate via spin–lattice relaxation.

TABLE 1. Experimental zero-field parameters (in 10^{-4} cm^{-1}) for triplet biphenyl ketones in ethanol glass at 77 K

Parameter	Biphenyl	4-Benzoyl biphenyl	4-Phenyl acetophenone	*p*-Phenyl γ-methyl valerophenone	Benzophenone[a] (n,π* triplet)
D	1096[b]	946±7	954±7	978[c]	−1596
E	−36[b]	−87±5	−82±6	−74[c]	+174
x	400	402	400	400	
y	329	228	236	252	
z	−730	−630	−636	−652	
$z + y$	−401	−402	−400	−400	
τ(s)	4.2	0.24±0.03	0.23±0.03	0.37[c]	~0.001

[a]The D and E values for benzophenone n,π* triplet are taken from ref. 19 and are given here for comparison.
[b]The values are taken from ref. 11.
[c]The values are taken from ref. 12.

Experimental

Samples of the carbonyl compounds were repeatedly recrystallized before use. For the triplet esr studies, ethanol solutions containing approximately 0.01 M of the carbonyl compound in 3 mm suprasil tubes were degassed under vacuum. The samples were irradiated at 77 K within the cavity of a Varian E-3 spectrometer. The light source was a 1 kW super pressure mercury lamp. The triplet spectra were recorded at 9.30 GHz and were calibrated against the known triplet biphenyl spectrum. Kinetic measurements of the triplets were made at a constant field ($\Delta M = 2$) using a rotating sector and an instrument computer described previously (6).

CIDNP studies were carried out using a Bruker HX60 nmr spectrometer and a modified probe to allow light irradiation via a reflecting mirror and lens assembly. The light source was the 1 kW mercury lamp. Sample solutions were degassed before use. Isopropanol used in the CIDNP experiments was purified by passing through an alumina column. Variation of light intensity in the CIDNP experiments was accomplished by using a set of calibrated screen filters.

Results and Discussion

1. Triplet Electron Spin Resonance Studies at 77 K

Photolysis at 77 K of both 4-phenylacetophenone and 4-benzoylbiphenyl, respectively, gave readily detectable $\Delta M = 2$ esr signals. Of the six possible high field ($\Delta M = 1$) signals only four (corresponding to the x and y features) were observed. The z features were too weak for detection as they are usually the weakest of the high field transitions. The approximate values of the zero field parameters $|D|$ and $|E|$ can, however, be calculated from the observed x and y transitions, which have a doublet splitting approximately equal to $(D - 3E)$ and $(D + 3E)$, respectively. These values are given in Table 1.

The decay kinetics of the triplet 4-phenylacetophenone and 4-benzoylbiphenyl were found to be first-order with a half-life τ of 0.23 s for the triplet phenylacetophenone and 0.24 s for the triplet benzoylbiphenyl. The long half-life values together with the observed zero-field parameters strongly suggest that the lowest triplet state of these two ketones is the π,π* configuration. This assignment is consistent with those reported in literature (1, 7). However, in the case of 4-benzoylbiphenyl the π,π* triplet state was assigned to the biphenyl moiety exclusively (1*a*), as concluded from the evidence that the phosphorescence spectrum of 4-benzoylbiphenyl is very similar to that of hydroxybiphenyl. An alternative assignment to the conjugated system involving both the biphenyl and the carbonyl groups was rejected by the authors (1*a*) based on the infrared spectroscopic evidence that the carbonyl and the biphenyl groups are non-coplanar in the ground state molecule (8). Since the geometry of the triplet molecule need not be the same as that of the ground state, we must argue that the conjugation between the carbonyl and the biphenyl moieties in the triplet 4-benzoylbiphenyl cannot be excluded by the phosphorescence study alone. For example, while the ground state of the molecule biphenyl is known to be nonplanar (9), Wagner (10) has shown that the triplet biphenyl is planar.

Similar triplet esr observations were made in the photolysis of *p*-phenyl-γ-methylvalerophenone. Table 1 presents a correlation of the zero-field parameters between biphenyl and the three biphenyl ketones. The coordinates for the biphenyl ketones are the same as those in biphenyl (11). Hence $D = -\frac{3}{2}z$ and $E = (y - x)/2$. The high field lines will then appear in the order $H_z^- < H_x^- < H_y^- < H_y^+ < H_x^+ < H_z^+$, here

the superscripts + and − refer to the higher and lower magnetic field.

The correlation presented in Table 1 reveals a few very important points. The zero-field energies x and $(z + y)$ have almost identical values for biphenyl and the ketones. Furthermore, the experimental observation showed that the positions of the high field signals H_x^- and H_x^+ appeared at nearly the same magnetic field for all these compounds and that the corresponding separations $H_x^+ - H_x^-$ are always equal to $-\frac{3}{2}$ (z − x + y). On the other hand, the zero-field energies y and z for the ketones are significantly different from the values of biphenyl. However, the relative changes in y and z values for the ketones are comparable to the corresponding change in biphenyl. This implies that the free spin delocalization in the xz and the xy molecular planes of the biphenyl ketones occurs to the same extent, as in biphenyl. Among the series of the biphenyl ketones studied, the results indicated that the zero-field energies are not affected by the group R bonded to the carbonyl.

In order to understand the significance of the correlation between the biphenyl and the biphenyl ketones listed in Table 1, it is worthwhile to consider a similar relationship between the zero-field parameters of biphenyl and *p*-terphenyl. Here we take the D and E values of the biphenyl and *p*-terphenyl from a theoretical calculation by Orloff and Brinen (13) and we work out the corresponding energies for x, y, z, and $(z + x)$. It should be noted that the theoretical values of E were given a positive sign by the authors (13) but their coordinate systems were the same as used throughout this paper. Despite the difference in the sign of the E values, we will show that the trend of the zero-field energies will give some insight to the structure of the biphenyl ketone triplets. The calculated energies for biphenyl and *p*-terphenyl are given in Table 2. It can be seen that the presumed order in which the $\Delta M = 1$ signals appear should be the same as that observed in the biphenyl ketone triplets. The calculated values for y and for $(z + x)$ are almost identical for both biphenyl and *p*-terphenyl. Thus the high field signals H_y^- and H_y^+ for both biphenyl and *p*-terphenyl would appear at approximately the same field and their doublet splittings $H_y^+ - H_y^-$ would be approximately equal to $-\frac{3}{2}(z + x - y)$. The relative changes in the parameters between the biphenyl and *p*-terphenyl are similar in trend and in magnitude as those between biphenyl and the biphenyl ketones. The similarity is indeed striking. In Table 1 the near stationary values of the signals H_x^- and H_x^+ are observed. In Table 2 the predicted stationary lines are the H_y^- and H_y^+. This is merely due to the different signs for the E values used in the two tables.

TABLE 2. Calculated zero-field parameters (in 10^{-4} cm^{-1}) for the triplet biphenyl and the triplet *p*-terphenyl

Parameter	Biphenyl	*p*-Terphenyl
D	1160[a]	1030[a]
E	60[a]	10[a]
x	440	350
y	320	330
z	−760	−680
$z + x$	−320	−330

[a]These values are taken from the theoretical calculations in ref. 13.

The correlation presented in Table 2 takes into account the planarity of the biphenyl and the terphenyl triplets and the consequent assumption of a double bond character for the carbon–carbon bond between the phenyl rings. It is expected that the zero-field energies are sensitive to a torsion of the central bond and to the nature of the carbon–carbon bond between the rings (13). The lower D and E values in *p*-terphenyl relative to the biphenyl clearly reflect the free spin delocalization onto the third coplanar phenyl ring. By analogy, the observed lower values in the biphenyl ketones as compared to biphenyl suggest some delocalization of the free spin onto the carbonyl group, probably achieved in a similar manner as in *p*-terphenyl:

$^3\pi\pi^*$ **B**

Here the triplet biphenyl ketone represented by the valence bond resonance structure **B** requires that the biphenyl and the carbonyl groups be coplanar with substantial spin density at the carbonyl oxygen atom. It is thought that it is the contribution of this resonance structure in the triplet that leads to the hydrogen abstraction reaction. It should be noted that the resonance structure **B** may also be derived from the n,π* triplet state, but the extent of the contribution

may be entirely different in different triplet states.

CIDNP Studies

Despite the low overall chemical reactivity of the triplet biphenyl ketones, the extremely high sensitivity of the CIDNP technique afforded a direct probe of the mechanism of these chemical reactions. During the photolysis of a 0.01 *M* solution of 4-benzoylbiphenyl in isopropanol, the aromatic protons of the parent ketone exhibited CIDNP in the enhanced absorption mode (Fig. 1). When a similar isopropanol solution of 4-phenylacetophenone was photolyzed, only the methyl protons of the ketone exhibited polarization in the emissive mode. However, when pentachlorophenol was added to the solution as a more efficient hydrogen donor, both the methyl protons and the aromatic protons of the ketone showed polarization with the methyl protons in emission and the *ortho* protons enhanced absorption (Fig. 2). The polarization of the methyl protons observed in the presence of pentachlorophenol as the hydrogen donor was very much larger than that in isopropanol alone. Similarly,

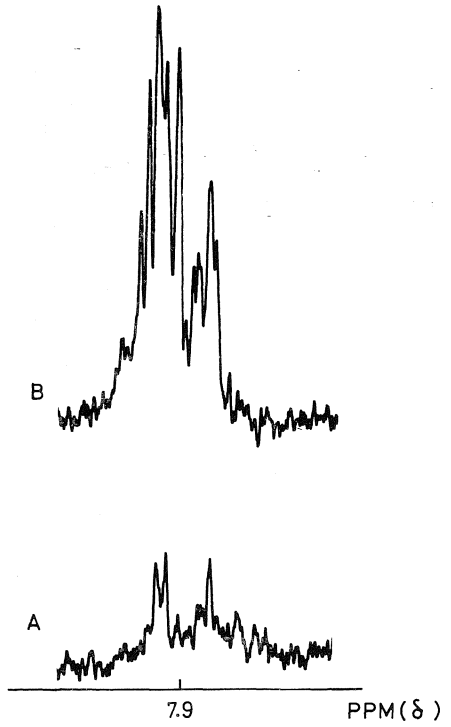

FIG. 1. Nuclear magnetic resonance spectra recorded before (A) and during (B) the photolysis of 4-benzoylbiphenyl in isopropanol.

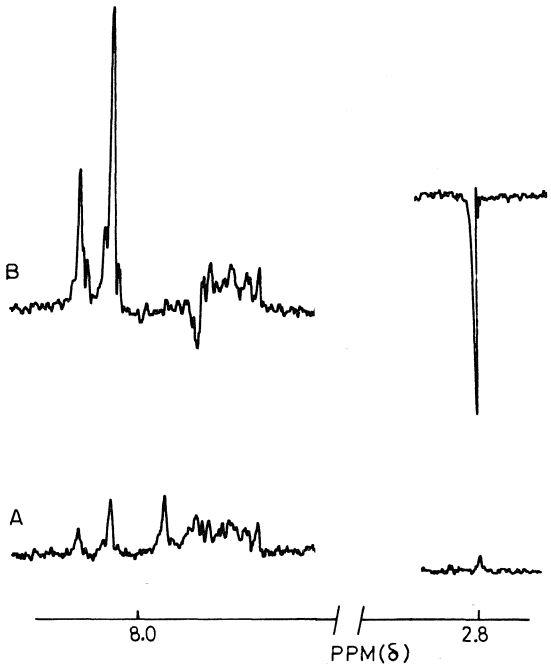

FIG. 2. Nuclear magnetic resonance spectra recorded before (A) and during (B) the photolysis of 4-phenylacetophenone and pentachlorophenol in isopropanol. The methyl proton spectrum at δ 2.8 was recorded at a much lower sensitivity than that of the aromatic protons at δ 8.0.

the addition of pentachlorophenol to the isopropanol solution of 4-benzoylbiphenyl increased the polarization magnitude.

These CIDNP observations in the biphenyl ketone – chlorophenyl systems can be readily explained by the Kaptein's rules at high field (14) according to the following reaction scheme:

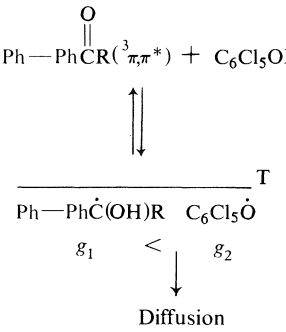

For the 4-benzoylbiphenyl, R is a phenyl group. For the 4-phenylacetophenone, R is a methyl group. From esr measurements it was found that the *g*-value for the pentachlorophenoxy radical is greater than that of the ketyl radical. By

analogy to the benzophenone (15) and isopropyl ketyl radicals (16), the hyperfine coupling constants are assumed to be positive for the methyl protons ($a_{CH_3} = +17$ G) and the *meta* protons ($a_H^{meta} = +1.2$ G), and negative for the *ortho* and *para* protons ($a_H^{ortho} = -3.24$ G, $a_H^{para} = -3.7$ G). With these parameters and the triplet ketone as the precursor, the cage product (which is the parent ketone) would exhibit CIDNP with the methyl protons strongly emissive and the *ortho* protons enhanced absorptive.

Further evidence that the observed CIDNP originates from the cage reaction is provided by the steady-state CIDNP intensity dependence on the irradiating light intensity. This is shown in Fig. 3 for the methyl proton CIDNP intensity as a linear function of light intensity.

It should be mentioned here that during the photolysis of 4-phenylacetophenone and pentachlorophenol in acetone-d_6 or in CD_3CN, no CIDNP from the enol of the parent ketone was ever observed.

While the presence of the ketyl and phenoxy radical intermediates can be inferred from the CIDNP experiments, the primary photochemical abstraction reactions of the triplet biphenyl ketones can be studied directly by esr. For example, during the photolysis of 4-benzoylbiphenyl in the presence of 2,6-di-*tert*-butylphenol, the esr spectrum of the corresponding phenoxy radical was readily observed. However, unlike the benzophenone and phenol system (17), the counter phenoxy radical did not exhibit any polarization. CIDEP was not expected to be observed in the present systems, since the chemical reaction rate would be too slow compared to the triplet depolarization rate.

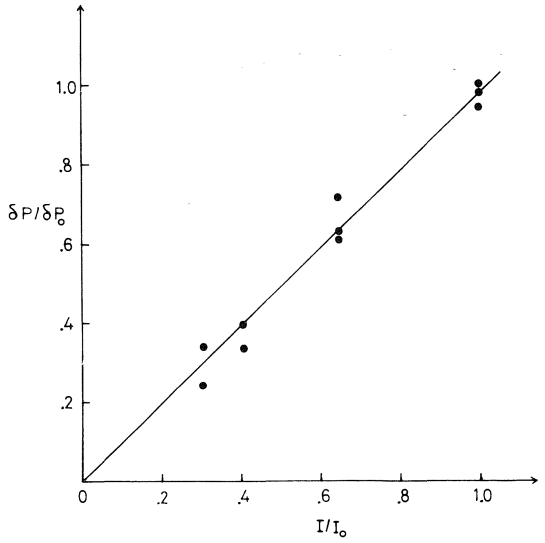

FIG. 3. The CIDNP intensity ($\delta P/\delta P_0$) of the methyl protons in the photolysis of 4-phenylacetophenone as a function of light intensity (I/I_0). δP is the steady-state emission intensity at light intensity I; δP_0 is the corresponding CIDNP intensity at the unattenuated light intensity I_0.

The CIDNP experiments together with the triplet esr study clearly demonstrated that the biphenyl ketones with their lowest π,π^* triplet states can undergo photoreduction, similar to those ketones with lowest n,π^* triplet states. An immediate question arose. Does the chemical reactivity of the biphenyl ketones truly involve the lowest π,π^* triplet? Wagner and co-workers (12) have discussed the various probable pathways by which triplet reactivity can manifest in phenyl ketones with lowest triplet π,π^* state. Analysis of the reactivity of various *p*-methoxy phenyl ketones (7) strongly suggests that the hydrogen abstraction reaction involves the upper n,π^* triplet state, populated via a thermal equilibration with the lower π,π^* triplet state. The thermal relaxation mechanism in these methoxy phenyl ketone systems is not unreasonable, since the separation between the upper n,π^* and the lower π,π^* triplet states is of the order of 3 kcal/mol (7). However, in the present biphenyl ketone systems the separation between the two triplet states can be as high as 9 to 14 kcal/mol, as estimated from the phosphorescence data (1*a*, 4). It would then appear unlikely that the photoreduction of these biphenyl ketones involves the upper n,π^* triplets via thermal relaxation from the lower π,π^* triplets.

Another mechanism which can impart triplet reactivity for ketones with lowest π,π^* triplet state is the vibronic coupling between the lower π,π^* and the upper n,π^* triplet states (18). This mechanism is again not likely to be significant in the biphenyl ketone systems due to the large separation between the two triplet states. Furthermore, the relative insensitivity of the phosphorescence life-times of the biphenyl ketones (1*b*, 7, 12) to the nature of the medium supports this conclusion.

Finally, we are inclined to believe that in these biphenyl ketones the photoreduction originates from the lower π,π^* triplet without the involvement of the upper n,π^* triplet state. The chemical reactivity of these π,π^* triplets may well be

due to their coplanar structure which leads to a substantial unpaired spin density at the carbonyl oxygen atom.

Acknowledgment

This research is supported by the National Research Council of Canada.

1. (*a*) V. L. ERMOLAEV and A. N. TERENIN. Sov. Phys. Usp. Engl. Transl. **3**, 423 (1960); (*b*) G. PORTER and P. SUPPAN. Trans. Faraday Soc. **61**, 1664 (1965); (*c*) L. H. PIETTE, J. H. SHARP, T. KUWANA, and J. N. PITTS, JR. J. Chem. Phys. **36**, 3094 (1962); (*d*) J. N. PITTS, JR., H. W. JOHNSON, JR., and T. KUWANA. J. Phys. Chem. **66**, 2465 (1962).
2. N. J. TURRO and C. G. LEE. Mol. Photochem. **4**, 427 (1972).
3. J. A. BARLTROP and J. D. COYLE. J. Chem. Soc. B, 251 (1971).
4. J. K. S. WAN, S. K. WONG, and D. A. HUTCHINSON. Acc. Chem. Res. **7**, 58 (1974); J. Chem. Phys. **58**, 985 (1973).
5. H. M. VYAS and J. K. S. WAN. Chem. Phys. Lett. **34**, 470 (1975); F. J. ADRIAN, H. M. VYAS, and J. K. S. WAN. J. Chem. Phys. **65**, 1454 (1976).
6. H. M. VYAS and J. K. S. WAN. Int. J. Chem. Kinet. **6**, 125 (1974).
7. R. N. GRIFFIN. Photochem. Photobiol. **7**, 159 (1968).
8. I. YA. POSTOVSKII, L. F. TREFILOVA, YU. N. SHEINKER, and S. G. BOGOMOLOV. Dokl. Akad. Nauk. SSSR, **113**, 347 (1957).
9. S. KWUN, T. REE, and H. EYRING. J. Chem. Phys. **40**, 3320 (1964).
10. P. J. WAGNER. J. Am. Chem. Soc. **89**, 2820 (1967).
11. J. MISPELTER. Chem. Phys. Lett. **10**, 539 (1971).
12. P. J. WAGNER, A. E. KEMPPAINEN, and H. N. SCOTT. J. Am. Chem. Soc. **95**, 5604 (1973).
13. M. K. ORLOFF and J. S. BRINEN. J. Chem. Phys. **47**, 3999 (1967).
14. R. KAPTEIN. J. Am. Chem. Soc. **94**, 6251 (1972).
15. R. WILSON. J. Chem. Soc. B, 84 (1968); 1581 (1968).
16. H. PAUL and H. FISCHER. Chem. Commun. 1038 (1971).
17. S. K. WONG and J. K. S. WAN. J. Chem. Phys. **59**, 3859 (1973).
18. N. C. YANG and R. DUSENBERY. J. Am. Chem. Soc. **90**, 5899 (1968).
19. R. M. HOCHSTRASSER, G. W. SCOTT, and A. H. ZEWAIL. J. Chem. Phys. **58**, 393 (1973).

Uniform quality constrained gaussian basis sets

PAUL G. MEZEY AND IMRE G. CSIZMADIA
Department of Chemistry, University of Toronto, Toronto, Ont., Canada M5S 1A1

Received October 8, 1976

PAUL G. MEZEY and IMRE G. CSIZMADIA. Can. J. Chem. **55**, 1181 (1977).

Uniformly balanced (6^s3^p), (7^s3^p), and (8^s4^p) gaussian basis sets with identical exponent sets for functions describing the $2s$ and $2p$ subshells have been obtained for the first row atoms. The basis sets have been determined using a direct optimization technique; they are thoroughly balanced and satisfy a rigorous quality criterion. These uniform quality constrained basis sets were designed for applications in *ab initio* programs of the type of the GAUSSIAN 70 program system, that may utilize the integration-time saving constraint $\alpha_{2s} = \alpha_{2p}$.

PAUL G. MEZEY et IMRE G. CSIZMADIA. Can. J. Chem. **55**, 1181 (1977).

On a obtenu des ensembles (6^s3^p), (7^s3^p) et (8^s4^p) à base gaussienne balancés d'une façon uniforme comportant des ensembles d'exposants identiques pour les fonctions décrivant les sous-couches $2s$ et $2p$ des atomes de la première rangée. On a déterminé les ensembles de base en utilisant une technique d'optimisation directe; ils sont bien balancés et satisfont un critère de qualité rigoureux. On a développé ces ensembles de base de qualité uniforme contrainte afin de les utiliser dans des programmes *ab initio* du type du système de programme "Gaussian 70" qui peuvent être utilisés pour la contrainte $\alpha_{2s} = \alpha_{2p}$ qui permet de sauver du temps lors de l'intégration.

[Traduit par le journal]

Introduction

Since the introduction of gaussian basis sets with identical radial parts for $2s$ and $2p$ type functions (1), the simplification thus resulted in the evaluation of integrals in *ab initio* calculations has brought about a dramatic increase in the number of *ab initio* MO studies undertaken. The fact that this constraint introduced in the basis sets has only a relatively minor effect on the accuracy of the calculated results and also the ready applicability of the Gaussian 70 program system, developed by Pople and co-workers (2) for the utilization of such basis sets, encouraged many theoretical investigations, mostly in the field of organic chemistry. Consequently, the application of constrained basis sets has proven to be a major breakthrough in computational theoretical chemistry.

In a recent study on gaussian basis sets (3, 4) several uniform quality bases have been proposed for a series of atoms. The quality of these basis sets has been defined in terms of the "balance" of the exponents, as expressed by the logarithmic energy gradients (with components $G_i = \partial E/\partial \log \alpha_i$) in the space of the orbital exponents, α_i. For a fully optimized basis set these "forces" in the exponent space are at "balance", *i.e.* the gradient vector $\boldsymbol{G}$ is zero. The degree of optimization, the quality or "balance" of any basis set may be characterized by these "forces", *i.e.* by the length of the corresponding gradient vector. Previous studies (5) indicated that a "5×10^{-5} quality" (*i.e.* $|\boldsymbol{g}| \equiv |\boldsymbol{G}|/\sqrt{n} \leqslant 5 \times 10^{-5}$) is sufficient to ensure the convergence of total energy as well as various one-electron properties to the limits inherent in the size (n) of the basis set.

Results and Discussion

Due to the particular importance of constrained basis sets this study has been undertaken to apply the above quality characterization and the uniform quality principle to constrained gaussian bases. For the gaussian type functions describing the $2s$ and $2p$ subshells the integration-time saving $\alpha_{2s} = \alpha_{2p}$ constraint has been applied. In the present work three series of uniform quality *constrained* basis sets are reported for the first row atoms from B to F. These constrained basis sets are compatible with previously published uniform quality basis sets for Li and Be (and H) where the constraint does not apply (3, 4). The previously unpublished (7^s) Li and Be bases are reported here.

In the direct optimization procedure for the open shell energy functional $E(\alpha)$ described elsewhere (5) appropriate modifications have been carried out to accomodate this constraint.

Since the conjugate gradient optimization technique (6) in the basis set optimization method is applicable to unconstrained variables only, exponents $\alpha_{i(2s)}$, $\alpha_{i(2p_x)}$, $\alpha_{i(2p_y)}$, and $\alpha_{i(2p_z)}$ were regarded as one single variable α_i. The corresponding element of the gradient was taken as

$$[1] \quad G_i = \frac{\partial E}{\partial \log \alpha_i} = \frac{\partial E}{\partial \log \alpha_{i(2s)}} + \frac{\partial E}{\partial \log \alpha_{i(2p_x)}} + \frac{\partial E}{\partial \log \alpha_{i(2p_y)}} + \frac{\partial E}{\partial \log \alpha_{i(2p_z)}}$$

This definition of component G_i results in appropriate weighting as compared to components belonging to the 1*s* subset.

In general, the optimum of a fully relaxed basis set ($\alpha_{i(2s)} \neq \alpha_{i(2p)}$ allowed) is different from the optimum of a constrained basis ($\alpha_{i(2s)} = \alpha_{i(2p)}$). At the optimum of a fully relaxed basis set the individual terms on the right side of eq. 1 are all zero. For a constrained set, however, only the sum of these terms is required to be zero. The individual energy-gradient components have been calculated using the same technique as described earlier (5). For the joint optimization of the linear parameters (MO coefficients) and nonlinear parameters (orbital exponents) a combination of Roothaan's open shell technique (7) and the method of conjugate gradients has been used (5).

A computer program has been developed for the outlined quasi-constrained optimization problem of the open shell energy functional. All calculations reported in the present study have been carried out on the IBM 370/165 computer at the University of Toronto.

Throughout the optimizations the condition

$$|g| \leqslant 5 \times 10^{-5}$$

has been regarded as the final quality criterion. The optimized (6^s3^p), (7^s3^p), and (8^s4^p) uniform quality (U.Q.) constrained gaussian basis sets are listed in Tables 1, 2, and 3, respectively. Along the orbital exponents the calculated total energy, orbital energies and virial coefficient are also included in the tables.[1]

It is noteworthy that at the actual optimum points of the various basis spaces, the additive terms on the right side of expression [1], *i.e.* most of the gradient components formally belonging to the valence shell, are rather large. A magnitude of the order of 2×10^{-2} is characteristic. As gradient lengths of this order are characteristic of rather crude basis sets, this finding indicates that optima of the constrained sets are, indeed, far from being balanced if the constraints are removed.

A close inspection of the linear coefficients of the calculated optimum wavefunctions revealed several "natural" contraction schemes for the U.Q. constrained bases. These natural contractions follow the most closely the grouping and general pattern of uncontracted linear coefficients as shown by their sign changes and ratios. The various contraction schemes and contraction coefficients for basis series (6^s3^p), (7^s3^p), and (8^s4^p) are presented in Tables 4, 5, and 6, respectively. While "split valence shell" contractions (B), (C), and (D) are recommended for MO calculations, "minimum" contraction (A) appears to represent the valence region poorly. Any different "non-natural" minimum contraction scheme, however, may introduce a significant strain on the carefully balanced exponent set itself and the uniform quality principle would no longer apply. This type of interrelation between optimum contractions and optimum exponent sets is the subject of a study, now under way (8).

In Table 7 total energies calculated with previously published, *unconstrained* uniform quality basis sets (3, 4) are compared with the present values. In general, the constraint results in a larger increase in energy if more electrons are in the valence shell. For the (6^s3^p) basis series the energy difference appears to be roughly proportional to the calculated total energy, the (8^s4^p) series shows larger deviations from such a proportionality. Also, for the latter series the deviations are significantly larger, indicating that for larger basis sets the constraint represents a more serious restriction. Though for $n \rightarrow \infty$ the energies calculated with constrained and unconstrained basis sets both converge to the *sp* limit, the above observation casts some doubt on the overall effectiveness of applying the constraint on significantly larger basis sets, as the improvement of the $n \rightarrow n + 1$ extension of a constrained basis relative to that of the unconstrained basis may become much too inferior for larger *n*.

[1]The FORTRAN subroutines that incorporate the new basis sets and are compatible with the corresponding GAUSSIAN 70 routines will be submitted to QCPE (Indiana University, Bloomington, IN) shortly.

TABLE 1. Orbital exponents of uniform quality constrained (6^s3^p) gaussian basis sets for the first row atoms

Gaussian function	Atom H[a]	Li[b]	Be[a]	B	C	N	O	F
s_1	4.5003393E+0	2.6201879E+2	5.0379423E+2	3.3827048E+2	4.9923412E+2	6.9389159E+2	9.1010591E+2	1.1622727E+3
s_2	6.8128531E-1	3.9428547E+1	7.5823293E+1	5.0982791E+1	7.5253389E+1	1.0459998E+2	1.3719746E+2	1.7521557E+2
s_3	1.5137521E-1	8.9077969E+0	1.7187786E+1	1.1390648E+1	1.6865227E+1	2.3489776E+1	3.0852873E+1	3.9443650E+1
sp_4		2.4068059E+0	4.7133062E+0	3.0317733E+0	4.5265710E+0	6.3344778E+0	8.3506785E+0	1.0699126E+1
sp_5		7.0577803E-1	1.4188045E+0	5.6711546E-1	8.9738894E-1	1.2906681E+0	1.7288645E+0	2.2356404E+0
sp_6		4.7792113E-2	1.0454887E-1	1.4236177E-1	2.1746646E-1	3.0741878E-1	3.9954862E-1	5.0747169E-1
Total Energy (a.u.)	-0.49697925	-7.42785720	-14.55637909	-24.48776606	-37.61828057	-54.28819008	-74.63088688	-99.14416701
Orbital Energies (a.u.)								
1s		-2.47633921	-4.73031919	-7.67525175	-11.29917248	-15.59627229	-20.62235010	-26.32337143
2s		-0.19498886	-0.30077995	-0.48569933	-0.69111536	-0.92456599	-1.20969580	-1.52356394
2p				-0.30458971	-0.42033215	-0.54580402	-0.59516407	-0.67626459
Virial	-2.00000130	-1.99999559	-2.00000002	-2.00000035	-2.00000009	-2.00000031	-2.00000002	-1.99999983

[a]Values taken from Ref. 3.

[b]Values taken from Ref. 4.

TABLE 2. Orbital exponents of uniform quality constrained (7^s3^p) gaussian basis sets for the first row atoms

Gaussian function	Atom H[a]	Li	Be	B	C	N	O	F
s_1	1.3007804E+1	2.7087721E+2	5.2352286E+2	8.1445043E+2	1.2611106E+3	1.8379944E+3	2.4852908E+3	3.2613686E+3
s_2	1.9620797E+0	4.0763784E+1	7.8762698E+1	1.2253684E+2	1.8970866E+2	2.7644414E+2	3.7377706E+2	4.9044689E+2
s_3	4.4452610E-1	9.2075190E+0	1.7837960E+1	2.7779296E+1	4.3042165E+1	6.2749943E+1	8.4861693E+1	1.1136376E+2
s_4	1.2194923E-1	2.4906831E+0	4.8814088E+0	7.6601343E+0	1.1913771E+1	1.7400276E+1	2.3553994E+1	3.0920903E+1
sp_5		7.3372838E-1	1.4672334E+0	2.3572123E+0	3.6715984E+0	5.3499987E+0	7.2311925E+0	9.4687627E+0
sp_6		7.5163939E-2	1.8003843E-1	4.6935753E-1	7.7353222E-1	1.1465393E+0	1.5607872E+0	2.0489457E+0
sp_7		3.0295450E-2	5.9925230E-2	1.2603362E-1	1.9775148E-1	2.8496897E-1	3.7366028E-1	4.7895342E-1
Total Energy (a.u.)	-0.49927841	-7.42935771	-14.56724496	-24.51171607	-37.65167787	-54.33197499	-74.68755294	-99.21456424
Orbital Energies (a.u.)								
1s	-0.49927841	-2.47524361	-4.72918883	-7.69127710	-11.32302239	-15.62826436	-20.66468595	-26.37578183
2s		-0.19620255	-0.30892007	-0.49099042	-0.69892887	-0.93448087	-1.22282215	-1.53924793
2p				-0.30455090	-0.42221199	-0.54916730	-0.60070169	-0.68357392
Virial	-1.99999874	-1.99996978	-2.00000019	-2.00000002	-2.00000008	-2.00000000	-1.99999995	-1.99999972

[a]Values taken from Ref. 3.

TABLE 3. Orbital exponents of uniform quality constrained (8^s4^p) gaussian basis sets for the first row atoms

Gaussian function	Atom H[a]	Li[b]	Be[a]	B	C	N	O	F
s_1	1.3007804E+1	6.4708254E+2	1.2801984E+3	1.5564523E+3	2.3244303E+3	3.3862833E+3	4.5310574E+3	5.9494099E+3
s_2	1.9620797E+0	9.7153248E+1	1.9231394E+2	2.3385280E+2	3.4919703E+2	5.0858182E+2	6.8047642E+2	8.9435691E+2
s_3	4.4452610E-1	2.2082029E+1	4.3744413E+1	5.3137147E+1	7.9295146E+1	1.1540574E+2	1.5430800E+2	2.0284776E+2
s_4	1.2194923E-1	6.1770176E+0	1.2272144E+1	1.4798473E+1	2.2004892E+1	3.1912016E+1	4.2518257E+1	5.5739272E+1
sp_5		1.9207573E+0	3.8585893E+0	4.5727831E+0	6.7038232E+0	9.6070026E+0	1.2663803E+1	1.6456766E+1
sp_6		6.3101307E-1	1.2881969E+0	1.4650699E+0	2.0353844E+0	2.8366515E+0	3.6105889E+0	4.6013855E+0
sp_7		7.2449052E-2	1.8027863E-1	3.9516884E-1	5.9444227E-1	8.4088294E-1	1.0751200E+0	1.3638590E+0
sp_8		2.8098019E-2	5.9068041E-2	1.1158048E-1	1.6608713E-1	2.3256222E-1	2.9134154E-1	3.6372193E-1
Total Energy (a.u.)	-0.49927841	-7.43174938	-14.57123581	-24.52182163	-37.67393752	-54.37474502	-74.76487832	-99.34038417
Orbital Energies (a.u.)								
1s	-0.49927841	-2.47702396	-4.73166422	-7.69204895	-11.32172309	-15.62437589	-20.66090272	-26.37161040
2s		-0.19628989	-0.30901592	-0.49236977	-0.70243566	-0.94081737	-1.23618494	-1.56054678
2p				-0.30796225	-0.42899835	-0.56066208	-0.62086715	-0.71411819
Virial	-1.99999874	-2.00000814	-2.00000182	-2.00000031	-2.00000017	-2.00000007	-1.99999949	-2.00000054

[a]Values taken from Ref. 3.

[b]Values taken from Ref. 4.

TABLE 4. Coefficients for minimum (A), split valence shell (B), (C), and (D) contractions of uniform quality constrained (6^s3^p) bases

Contraction	Function	Primitive	Atom H	Li	Be	B	C	N	O	F
A	S_1	s_1	0.07047600	0.00652506	0.00610520	0.01794770	0.01765640	0.01737913	0.01738840	0.01728362
		s_2	0.40788710	0.04793004	0.04502018	0.12428016	0.12282758	0.12134671	0.12159014	0.12107092
		s_3	0.64767370	0.20271358	0.19454359	0.43460941	0.43373349	0.43213014	0.43391525	0.43376920
	----	s_4		0.48126490	0.47339130	0.55967468	0.56063372	0.56274856	0.56035813	0.56061627
		s_5		0.41720605	0.43070170	0.21628857	0.22859251	0.23623083	0.26143481	0.27479939
	S_2	s_6		1.00000000	1.00000000	0.83351517	0.82551782	0.82031965	0.80150569	0.79165703
	P_1	p_1				0.09315910	0.10495470	0.11305510	0.12036979	0.12547200
		p_2				0.42980620	0.44824499	0.45963851	0.46209457	0.46640200
		p_3				0.65746960	0.63870899	0.62584731	0.62396375	0.61965900
B	S_1	s_1	0.15631155	0.00973907	0.00932934	0.01794990	0.01765640	0.01737913	0.01738840	0.01728362
		s_2	0.90466920	0.07153866	0.06879515	0.12428016	0.12282758	0.12134671	0.12159014	0.12107092
		s_3	1.00000000	0.30256301	0.29728126	0.43460941	0.43373349	0.43213014	0.43391525	0.43376920
	----	s_4		0.71831870	0.72338730	0.55967468	0.56063372	0.56274856	0.56035813	0.56061627
	S_2	s_5		1.00000000	1.00000000	1.00000000	1.00000000	1.00000000	1.00000000	1.00000000
	S_3	s_6		1.00000000	1.00000000	1.00000000	1.00000000	1.00000000	1.00000000	1.00000000
	P_1	p_1				0.19437240	0.20713654	0.21571630	0.22629884	0.23240412
		p_2				0.89677190	0.88464756	0.87701939	0.86875175	0.86388793
	P_2	p_3				1.00000000	1.00000000	1.00000000	1.00000000	1.00000000

TABLE 4 (*Concluded*)

C	S_1	s_1	0.15631155	0.02718502	0.02659390	0.03368999	0.03326936	0.03291998	0.03281322	0.03265004
		s_2	0.90466920	0.19968847	0.19610517	0.23328879	0.23143979	0.22985789	0.22944976	0.22871195
	S_2	s_3	1.00000000	0.84455521	0.84742005	0.81581406	0.81726912	0.81855143	0.81883077	0.81942217
	S_3	s_4		1.00000000	1.00000000	1.0000000	1.00000000	1.00000000	1.00000000	1.00000000
	S_4	s_5		1.00000000	1.00000000	1.0000000	1.00000000	1.00000000	1.00000000	1.00000000
		s_6		1.00000000	1.00000000	1.0000000	1.00000000	1.00000000	1.00000000	1.00000000
	P_1	p_1				0.19437240	0.20713654	0.21571630	0.22629884	0.23240412
	P_2	p_2				0.89677190	0.88464756	0.87701939	0.86875175	0.86388793
		p_3				1.00000000	1.00000000	1.00000000	1.00000000	1.00000000
D	S_1	s_1	0.15631155	0.02718502	0.02659390	0.03368999	0.03326936	0.03291998	0.03281332	0.03265004
		s_2	0.90466920	0.19968847	0.19610517	0.23328879	0.23143979	0.22985789	0.22944976	0.22871195
	S_2	s_3	1.00000000	0.84455521	0.84742005	0.81581406	0.81726912	0.81855143	0.81883077	0.81942217
	S_3	s_4		1.00000000	1.00000000	1.00000000	1.00000000	1.00000000	1.00000000	1.00000000
	S_4	s_5		1.00000000	1.00000000	1.00000000	1.00000000	1.00000000	1.00000000	1.00000000
		s_6		1.00000000	1.00000000	1.0000000	1.00000000	1.00000000	1.00000000	1.00000000
	P_1	p_1				1.0000000	1.00000000	1.00000000	1.00000000	1.00000000
	P_2	p_2				1.0000000	1.00000000	1.00000000	1.00000000	1.00000000
	P_3	p_3				1.0000000	1.00000000	1.00000000	1.00000000	1.00000000

TABLE 5. Coefficients for minimum (A), and split valence shell (B), (C), and (D) contractions of uniform quality constrained (7^s3^p) bases

Contraction	Function	Primitive	Atom H	Li	Be	B	C	N	O	F
A	S_1	s_1	0.01968640	0.00628301	0.00584543	0.00599488	0.00556281	0.00517214	0.00499193	0.00480445
		s_2	0.13797140	0.04626570	0.04328726	0.04446663	0.04144372	0.03867461	0.03740121	0.03606299
		s_3	0.47831519	0.19703426	0.18831040	0.19368875	0.18329154	0.17331627	0.16876058	0.16381139
		s_4	0.50110059	0.47487239	0.46967697	0.47880848	0.46893064	0.45832839	0.45401528	0.44869310
	----	s_5		0.42942174	0.4411181	0.42322519	0.44378872	0.46479224	0.47373674	0.48415892
	S_2	s_6		0.48410382	0.48973978	0.33336506	0.32010759	0.30880232	0.32462680	0.32882403
		s_7		0.55242626	0.56247929	0.72822812	0.74386957	0.75594299	0.74512548	0.74340262
	P_1	p_1				0.12166760	0.13074760	0.13497660	0.13989770	0.14252399
		p_2				0.46662469	0.47295150	0.47768259	0.47584829	0.47735377
		p_3				0.59817058	0.59255451	0.58916909	0.59378258	0.59438007
B	S_1	s_1	0.03349240	0.00628301	0.00584543	0.00599488	0.00556281	0.00517214	0.00499193	0.00480445
		s_2	0.23473023	0.04626570	0.04328726	0.04446663	0.04144372	0.03867461	0.03740121	0.03606299
		s_3	0.81375586	0.19703426	0.18831040	0.19368875	0.18329154	0.17331627	0.16876058	0.16381139
		s_4	1.00000000	0.47487239	0.46967697	0.47880848	0.46893064	0.45832839	0.45401528	0.44869310
	----	s_5		0.42942174	0.4411181	0.42322519	0.44378872	0.46479224	0.47373674	0.48415892
	S_2	s_6		1.00000000	1.00000000	1.00000000	1.00000000	1.00000000	1.000000000	1.00000000
	S_3	s_7		1.00000000	1.00000000	1.0000000	1.00000000	1.00000000	1.000000000	1.00000000
	P_1	p_1				0.22718751	0.23764624	0.24170135	0.24966627	0.25282220
		p_2				0.87131912	0.85963449	0.85538182	0.84921534	0.84677414
	P_2	p_3				1.00000000	1.00000000	1.00000000	1.00000000	1.00000000

TABLE 5 (*Concluded*)

C	S_1	s_1	0.13142994	0.00954933	0.00907310	0.00909850	0.00870934	0.00836556	0.00819091	0.00801750
		s_2	0.92112181	0.07031758	0.06718925	0.06748753	0.06488580	0.06255332	0.06136905	0.06018072
		s_3	1.00000000	0.29946532	0.29229004	0.29396371	0.28696793	0.28032620	0.27690749	0.27336300
	----	s_4	1.00000000	0.72174153	0.72901923	0.72669329	0.73417494	0.74131218	0.74496209	0.74876412
	S_2	s_5		1.00000000	1.00000000	1.00000000	1.00000000	1.00000000	1.00000000	1.00000000
	S_3	s_6		1.00000000	1.00000000	1.00000000	1.00000000	1.00000000	1.00000000	1.00000000
	S_4	s_7		1.00000000	1.00000000	1.00000000	1.00000000	1.00000000	1.00000000	1.00000000
		p_1				0.22718751	0.23764624	0.24170135	0.24966627	0.25282220
	P_1	p_2				0.87131912	0.85963449	0.85538182	0.84921534	0.84677414
	P_2	p_3				1.00000000	1.00000000	1.00000000	1.00000000	1.00000000
D	S_1	s_1	0.13142994	0.00954933	0.00907310	0.00909850	0.00870934	0.00836556	0.00819091	0.00801750
		s_2	0.92112181	0.07031758	0.06718925	0.06748753	0.06488580	0.06255332	0.06136905	0.06018072
		s_3	1.00000000	0.29946532	0.29229004	0.29396371	0.28696793	0.28032620	0.27690749	0.27336300
	----	s_4	1.00000000	0.72174153	0.72901923	0.72669329	0.73417494	0.74131218	0.74496209	0.74876412
	S_2	s_5		1.00000000	1.00000000	1.00000000	1.00000000	1.00000000	1.00000000	1.00000000
	S_3	s_6		1.00000000	1.00000000	1.00000000	1.00000000	1.00000000	1.00000000	1.00000000
	S_4	s_7		1.00000000	1.00000000	1.00000000	1.00000000	1.00000000	1.00000000	1.00000000
	P_1	p_1				1.00000000	1.00000000	1.00000000	1.00000000	1.00000000
	P_2	p_2				1.00000000	1.00000000	1.00000000	1.00000000	1.00000000
	P_3	p_3				1.00000000	1.00000000	1.00000000	1.00000000	1.00000000

TABLE 6. Coefficients for minimum (A), and split valence shell (B), (C), and (D) contractions of uniform quality constrained (8^s4^p) bases

Contraction	Function	Primitive	Atom H	Li	Be	B	C	N	O	F
A	S_1	s_1	0.01968640	0.00213181	0.00192366	0.00264993	0.00255265	0.00236047	0.00230007	0.00220400
		s_2	0.13797140	0.01622407	0.01467118	0.02011091	0.01940426	0.01798372	0.01754052	0.01680280
		s_3	0.47831519	0.07775647	0.07118272	0.09581925	0.09313516	0.08715987	0.08542794	0.08223380
		s_4	0.50110059	0.24783167	0.23477326	0.30146113	0.30020987	0.28973076	0.28880720	0.28333067
		s_5		0.47336413	0.46892564	0.51660829	0.52911693	0.53662163	0.54466920	0.54982563
	----	s_6		0.34006862	0.35989946	0.22101959	0.21452025	0.22528391	0.22138666	0.22605455
	S_2	s_7		0.54828027	0.50110045	0.45216500	0.48213074	0.49273304	0.53906026	0.56004286
		s_8		0.49128695	0.55264409	0.61380791	0.58585875	0.57648735	0.53262318	0.51306210
	P_1	p_1				0.03733610	0.04867740	0.05303790	0.05842010	0.06087630
		p_2				0.14734099	0.17542941	0.19124551	0.21162850	0.22305850
		p_3				0.47824138	0.48705812	0.49226954	0.48788239	0.48843289
		p_4				0.54063648	0.50482262	0.48631044	0.47633680	0.46854909
B	S_1	s_1	0.03349240	0.00213181	0.00192366	0.00264993	0.00255265	0.00236047	0.00230007	0.00220400
		s_2	0.23473023	0.01622407	0.01467118	0.02011091	0.01940426	0.01798372	0.01754052	0.01680280
		s_3	0.81375586	0.07775647	0.07118272	0.09581925	0.09313516	0.08715987	0.08542794	0.08223380
		s_4	1.00000000	0.24783167	0.23477326	0.30146113	0.30020987	0.28973076	0.28880720	0.28333067
		s_5		0.47336413	0.46892564	0.51660829	0.52911693	0.53662163	0.54466920	0.54982563
	----	s_6		0.34006862	0.35989946	0.22101959	0.21452025	0.22528391	0.22138666	0.22605455
	S_2	s_7		1.00000000	1.00000000	1.00000000	1.00000000	1.00000000	1.00000000	1.00000000
	S_3	s_8		1.00000000	1.00000000	1.00000000	1.00000000	1.00000000	1.00000000	1.00000000
	P_1	p_1				0.06290302	0.07682543	0.08107641	0.08730420	0.08956035
		p_2				0.24823680	0.27687260	0.29234753	0.31626200	0.32816051
	----	p_3				0.80573034	0.76870265	0.75250802	0.72910153	0.71857557
	P_2	p_4				1.00000000	1.00000000	1.00000000	1.00000000	1.00000000

TABLE 6 (*Concluded*)

C	S_1	s_1	0.13142994	0.00669964	0.00643350	0.00682633	0.00664413	0.00641473	0.00629681	0.00617821
		s_2	0.92112181	0.05098736	0.04906642	0.05180649	0.05050615	0.04887184	0.04802001	0.04710125
		s_3	1.00000000	0.24436514	0.23806410	0.24683415	0.24241582	0.23686214	0.23387278	0.23051609
		s_4	1.00000000	0.77886018	0.78517769	0.77657568	0.78139793	0.78736063	0.79065633	0.79422669
	S_2	s_5		0.61224800	0.59476739	0.73277902	0.74647232	0.74093465	0.74931804	0.74809385
		s_6		0.43984392	0.45648274	0.31350352	0.30264280	0.31105838	0.30456838	0.30757027
	S_3	s_7		1.00000000	1.00000000	1.00000000	1.00000000	1.00000000	1.00000000	1.00000000
	S_4	s_8		1.00000000	1.00000000	1.00000000	1.00000000	1.00000000	1.00000000	1.00000000
	P	p_1				0.06290302	0.07682543	0.08107641	0.08730420	0.08956035
		p_2				0.24823680	0.27687260	0.29234753	0.31626200	0.32816051
	P_2	p_3				0.80573034	0.76870265	0.75250802	0.72910153	0.71857557
		p_4				1.00000000	1.00000000	1.00000000	1.00000000	1.00000000
D	S_1	s_1	0.13142994	0.00669964	0.00643350	0.00682633	0.00664413	0.00641473	0.00629681	0.00617821
		s_2	0.92112181	0.05098736	0.04906642	0.05180649	0.05050615	0.04887184	0.04802001	0.04710125
		s_3	1.00000000	0.24436514	0.23806410	0.24683415	0.24241582	0.23686214	0.23387278	0.23051609
		s_4	1.00000000	0.77886018	0.78517769	0.77657568	0.78139793	0.78736063	0.79065633	0.79422669
	S_2	s_5		0.61224800	0.59476739	0.73277902	0.74647232	0.74093465	0.74931804	0.74809385
		s_6		0.43984392	0.45648274	0.31350352	0.30264280	0.31105838	0.30456838	0.30757027
	S_3	s_7		1.00000000	1.00000000	1.00000000	1.00000000	1.00000000	1.00000000	1.00000000
	S_4	s_8		1.00000000	1.00000000	1.00000000	1.00000000	1.00000000	1.00000000	1.00000000
	P_1	p_1				0.21346439	0.23109901	0.23154411	0.23135118	0.22955833
		p_2				0.84240336	0.83286207	0.83490805	0.83807634	0.84113090
	P_2	p_3				1.00000000	1.00000000	1.00000000	1.00000000	1.00000000
	P_3	p_4				1.00000000	1.00000000	1.00000000	1.00000000	1.00000000

TABLE 7. Comparison of total energy values (in au) obtained with constrained and unconstrained uniform quality (6^s3^p) and (8^s4^p) bases

	Basis	H[a]	Li[a]	Be[a]	B	C	N	O	F
(6^s3^p)	Constrained				-24.48776606	-37.61828657	-54.28819008	-74.63088688	-99.14416701
	Unconstrained	-0.49697925[b]	-7.42785720[c]	-14.55637909[b]	-24.49197372[b]	-37.62296576[c]	-54.29461100[c]	-74.64241258[c]	-99.16103032[c]
	Difference				0.00420766	0.00467919	0.00642092	0.01152570	0.01686331
(8^s4^p)	Constrained				-24.52182163	-37.67393752	-54.37474502	-74.76487832	-99.34038417
	Unconstrained	-0.49927841[b]	-7.43174938[c]	-14.57123581[b]	-24.52486442	-37.67993863	-54.38504476	-74.78174746	-99.36540660
	Difference				0.00304279	0.00600111	0.01029974	0.01686914	0.02502243

[a]The $\alpha_{2s} = \alpha_{2p}$ constraint does not apply to the ground states of these atoms

[b]Values taken from Ref. 3

[c]Values taken from Ref. 4

Acknowledgement

The authors are deeply indebted to the National Research Council of Canada for continuing financial support.

1. (*a*) W. J. HEHRE, R. F. STEWART, and J. A. POPLE. J. Chem. Phys. **51**, 2657 (1969). (*b*) R. DITCHFIELD, W. J. HEHRE, and J. A. POPLE. J. Chem. Phys. **54**, 724 (1971).
2. W. J. HEHRE, W. A. LATHAN, R. DITCHFIELD, M. D. NEWTON, and J. A. POPLE. GAUSSIAN 70, QCPE, Indiana University, Bloomington, Indiana.
3. P. G. MEZEY, R. E. KARI, and I. G. CSIZMADIA. J. Chem. Phys. **66**, 964 (1977).
4. P. G. MEZEY, I. G. CSIZMADIA, and R. E. KARI. J. Chem. Phys. In press.
5. (*a*) R. E. KARI, P. G. MEZEY, and I. G. CSIZMADIA. J. Chem. Phys. **63**, 581 (1975). (*b*) R. E. KARI, P. G. MEZEY, and I. G. CSIZMADIA. J. Chem. Phys. **64**, 632 (1976).
6. (*a*) R. FLETCHER and M. J. D. POWELL. Comput. J. **6**, 163 (1963). (*b*) W. C. DAVIDON. Variable metric method for minimization. A.E.C. Research and Development Report, ANL 5990 (Rev.). 1959.
7. C. C. J. ROOTHAAN. Rev. Mod. Phys. **32**, 179 (1960).
8. P. G. MEZEY, R. E. KARI, and I. G. CSIZMADIA. To be published.

Cathodic luminescence of oxide covered aluminium and tantalum electrodes

JOUKO J. KANKARE,[1] DOUGLAS E. RYAN,[2] AND BERNHARD J. FÜRST
Trace Analysis Research Centre, Chemistry Department, Dalhousie University, Halifax, N.S., Canada B3H 4J1

Received September 13, 1976

JOUKO J. KANKARE, DOUGLAS E. RYAN, and BERNHARD J. FÜRST. Can. J. Chem. **55**, 1193 (1977).

Cathodic luminescence of oxide covered aluminium and tantalum electrodes in various electrolyte solutions was measured at low amplitude (0 to 10 V) ac excitation. Oxygen or hydrogen peroxide are necessary constituents of the solution for high levels of light emission. For the aluminium electrode in tartrate solutions, copper enhanced light emission at concentrations down to 10 ppb.

The tantalum electrode gave fairly high luminescence in solutions containing sodium perchlorate, perchloric acid, and hydrogen peroxide, but copper had no influence on the luminescence output. A mechanism based on the electrogeneration of singlet oxygen and its subsequent radiative transition to the triplet state is suggested.

JOUKO J. KANKARE, DOUGLAS E. RYAN et BERNHARD J. FÜRST. Can. J. Chem. **55**, 1193 (1977).

On a mesuré à des amplitudes basses (0 à 10 V) d'excitation ac, la luminescence cathodique dans diverses solutions d'électrolytes, d'électrodes d'aluminium et de tantale couvertes par de l'oxyde. La présence d'oxygène ou de peroxyde d'hydrogène est nécessaire dans les solutions pour obtenir des hauts niveaux d'émission de lumière. Dans le cas d'électrodes d'aluminium dans des solutions de tartrate, le cuivre augmente l'émission de lumière à des concentrations allant jusqu'à 10 ppb.

L'électrode de tantale fournit des luminescences assez élevées dans des solutions contenant du perchlorate de sodium, d'acide perchlorique et du peroxyde d'hydrogène mais le cuivre n'a aucune influence sur le rendement de luminescence. On suggère un mécanisme basé sur une électrogénération de l'oxygène à l'état singulet et sa transition radiative subséquente vers l'état triplet.

[Traduit par le journal]

The electroluminescence or galvanoluminescence of valve metals, of which Al and Ta are the most familiar, has been known for a long time (1). By placing two electrodes into an electrolyte solution, one of which is aluminium (and the other any conductive material), and applying direct current so that the aluminium electrode is positive, light is emitted from the aluminium surface at sufficiently high voltages. It was later noted that light was emitted momentarily also when the polarity was changed. Aluminium could be substituted by other metals capable of forming insulating oxide coatings, although light was brightest with aluminium.

Electroluminescence of valve metals has not been a subject of intensive research work and the number of articles dealing with this phenomenon is relatively low. However, various theories have been put forth about the origin of light. The first hypothesis (2) was that the light was due to electric discharges inside the minute gas bubbles formed on the surface of the electrode. This hypothesis was later rejected by Anderson (3) because the spectrum of light was found to be independent of the composition of the solution. Anderson's theory was based on the combination of ionic and electronic currents with the radiation being due to the electron–hole recombination within the supposedly semiconducting oxide layer. Though published in the early forties, the theory was surprisingly modern and it was subject to only minor modifications as a result of the extensive studies of van Geel and co-workers (4) in 1957. Further support for the solid state electroluminescence character of the anodic luminescence was provided by two rather recent articles by Ganley and co-workers (5, 6). Ganley showed that the spectrum of the light emitted by an aluminium anode depends on the impurities in the metal. The striking discovery was that the spectrum of the cathodic luminescence was essentially independent of the impurities. Ganley suggested that the cathodic luminescence may

[1]On sabbatical leave from the University of Turku, Finland.

[2]To whom correspondence should be addressed.

not be electroluminescence at all but did not give any hypothesis on an alternative mechanism. A comprehensive and up-to-date review article on the subject is available (7).

This study was initially undertaken in order to find possible analytical applications of electroluminescence. Later on, when certain interesting results emerged from the study, the character of the work became of a more fundamental nature.

Methods of Measurement

Both direct and alternating currents have been used in studies of electroluminescence. The use of dc has been mostly confined to anodic luminescence, partly because the 'continuous cathodic glow' is extremely weak. The oxide layer is gradually damaged during the continuous cathodic high current conditions. With ac, a kind of steady state (where the oxide layer is restored during the positive half-periods) is hopefully achieved. In order to render the capacitive effects harmless and also to be able to sample the dark current of the photomultiplier tube, it is useful to include a region with zero volts between the pulses. The pulse train of the shape shown in Fig. 1 has also been used by van Geel and co-workers (4); this allows the use of a lock-in amplifier, a powerful tool in picking up a weak signal from the background noise. The total period of the pulse train is four times the original period.

There are two different approaches for measuring the light emission from the electrode. One is to apply a pulse train of a constant amplitude and record the decay of the light emission as a function of time. Another method is to scan the amplitude of the pulses and record the light intensity.

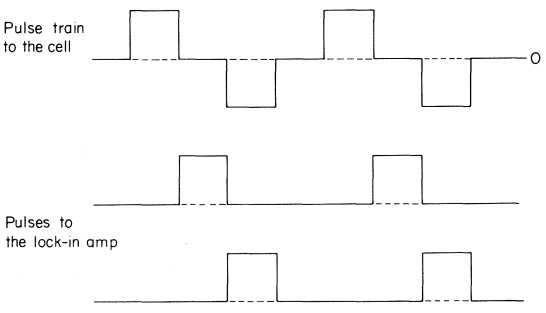

FIG. 1. Pulse trains applied to the cell and the lock-in amplifier.

Experimental

Cell

Figure 2 shows the structure of the cell and electrodes. The valve metal electrode was a 20 mm diameter circle cut from metal foil of 0.25 mm thickness. The foil was cemented to a brass shaft using silver-epoxy. The brass shaft was embedded and cemented into a Teflon® piece to insulate it from the solution. The materials used for the electrodes were aluminium of 99.999% purity (Alfa-Ventron) and tantalum of 99.98% purity (Alfa-Ventron).

The electrodes were polished mechanically using γ-alumina (Gamal®, Fisher, particle size <0.1 μm). The aluminium electrode was polished chemically in a mixture of 14 parts of 85% *o*-phosphoric acid, 5 parts of 18 F sulfuric acid and 1 part of 12 F nitric acid at 85°C. The composition of the solution used for chemical polishing of tantalum was 5 parts of sulfuric acid, 2 parts of nitric acid, and 2 parts of 50% hydrofluoric acid.

The anodization of the aluminium electrode was performed in the same supporting electrolyte as in the accompanying experiments. The anodization was done at a constant current (*ca.* 1 mA/cm^2) until a cell voltage of 11.5 V was attained and continued at this voltage until the current was below 50 μA. In the case of the tantalum electrode, the anodization was done in 0.1 *M* sulfuric acid until a 3 to 4 μA current was attained.

Apparatus

Figure 3 shows a block diagram of the apparatus used. The normal square wave from a function generator (Wavetek, Model 180) was divided by four in order to obtain the gate pulses for the lock-in amplifier and waveform generator. The wavelength generator consists of an adjustable ramp generator and a power amplifier. The photomultiplier (PM) tube was EMI 9592 B with an S 10 spectral response. The power supply for the PM tube was Kepco ABC 1500. The output of the PM tube was amplified by using a simple FET switched lock-in amplifier and recorded on a Fisher X–Y recorder (Model 100 XY).

A Jarrell-Ash monochromator (Model 82-410), with both the input and output slits removed, was used to record the spectrum. The spectral resolution of *ca.* 40 nm was determined using a mercury calibration

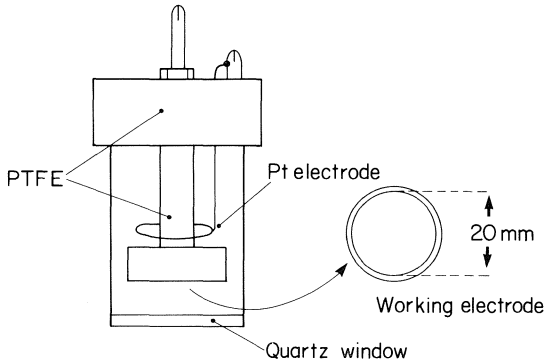

FIG. 2. The cell and electrodes.

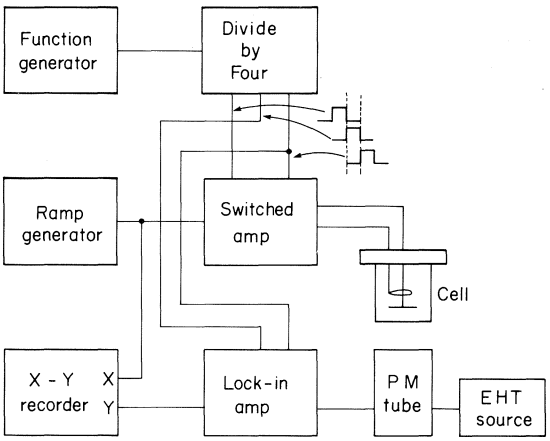

FIG. 3. The block diagram of the electroluminescence apparatus.

source. In this case the output from the lock-in amplifier was integrated using a simple op amp integrator.

Results and Discussion

Aluminium Electrode

Measurements in tartrate solutions were made at *ca.* p*H* 6, because the influence of copper on the light intensity had a broad maximum at this p*H*. The length of the pulses applied to the cell was maintained at 10 ms; no radical change in the light intensity or curve shape was found on varying the pulse length from 50 to 2 ms.

In order to swamp the possible influence of the supporting electrolyte, its concentration was maintained at 0.1 *M* in all of the experiments. Figure 4 shows the influence of 0.1 ppm copper on the luminescence. The shape of the curve bears some resemblance to the voltammetric curves on a stationary electrode and suggests a diffusion controlled process. The removal of oxygen by bubbling nitrogen through the solution had a profound effect on the light intensity (Fig. 5).

These experimental results suggest that the cathodic luminescence, at voltage levels of less than −10 V, is due to electrogenerated chemiluminescence. Luminescence is, however, observed in such different kinds of solutions that it restricts the possible chemiluminescent reactions to the electrogeneration of singlet oxygen, $^1O_2$, and its subsequent radiative transition to the triplet ground state. Search of previous publications shows that none of the authors has paid particular attention to removing oxygen from their solutions.

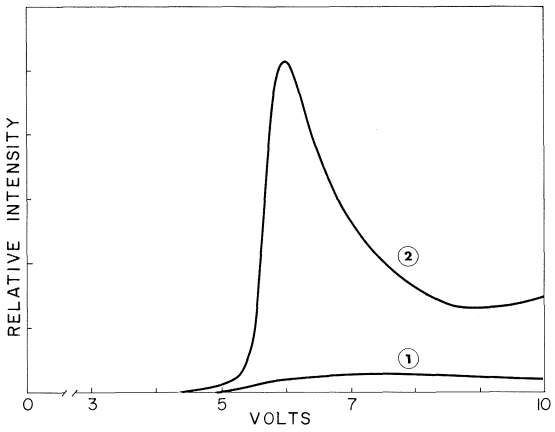

FIG. 4. Influence of copper on the electroluminescence. Curve *1*: 0.1 *M* solution of sodium tartrate at p*H* 6.2. Curve *2*: 0.1 ppm Cu(II) added to the solution.

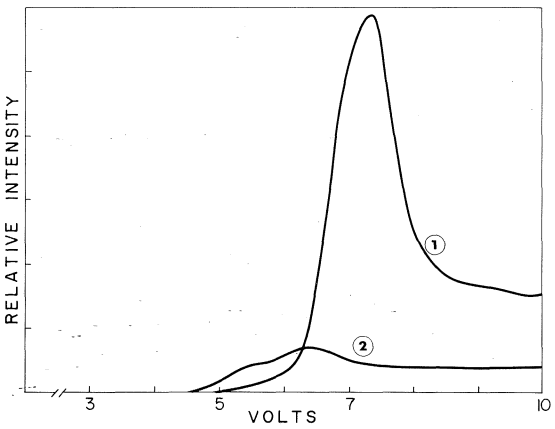

FIG. 5. Influence of the removal of oxygen on the electroluminescence. Curve *1*: 0.1 ppm Cu(II) in 0.1 *M* sodium tartrate at p*H* 6.2. Curve *2*: the same solution but nitrogen bubbled through for 30 min.

Some examples of copper catalyzed chemiluminescent reactions are reported in the literature. Stauff and co-worker showed that copper catalyzes the auto-oxidation of sulfite (8) and cystein (9) reactions which produce light. They proposed a mechanism which is based on the generation and radiative transition of singlet oxygen dimer. The role of the copper complex is to form mixed ligand complexes with oxygen radicals HO· and HO_2· thus prolonging their lifetime. In the present study, the possible copper complex may be either homogeneous copper tartrate in solution or a copper species adsorbed on the surface of the electrode. In the latter case the surface would become com-

pletely covered at a low concentration level and the light intensity would level off with increasing copper concentration.

That this is indeed the case can be seen in Fig. 6. The plot of light intensity *vs.* copper concentration is quite linear up to *ca.* 10^{-5} *M*, has a maximum at *ca.* 3×10^{-5} *M*, and then the intensity continuously decreases with increasing copper concentration. This decrease can be explained on the basis of competition of the surface-bound and soluble copper for HO· and HO_2· radicals. If the phenomenon is due to a sorbed copper species, there are several alternatives as to the structure of the species. The simplest possibility is copper chemisorbed on alumina. Aluminium oxide is known to form fairly stable complexes with copper(II) ions (10). The presence of this species could be checked by studying the influence of supporting electrolyte. If the catalyzing species is copper chemisorbed on alumina, then the better the complexing agent used as electrolyte the weaker should be the influence of copper on the light emission. This was tested by using a series of three dicarboxylic acids (tartaric, malic, and succinic acids); these acids were selected because of their similar carbon skeletons, but different complexing abilities. In the presence of malic and succinic acids (measured at p*H* 6.1 to 6.3 in 0.1 *M* solutions) copper does not enhance the luminescence, although the stability constants of the copper malate and succinate are considerably lower than that of copper tartrate.

An additional experiment with acetate showed that also in this medium, copper did not enhance the luminescence. Thus the catalyzing species presumably is not copper chemisorbed on alumina.

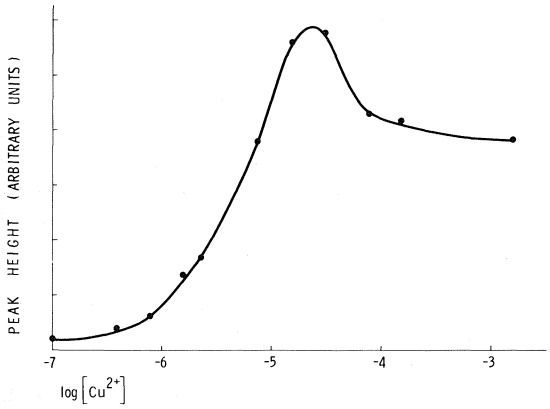

FIG. 6. Influence of copper on the peak height of the electroluminescence curve. Supporting electrolyte is 0.1 *M* sodium tartrate at p*H* 6.2.

The second possible structure for the copper species is chemisorbed copper tartrate. This complexation may occur in two different ways:

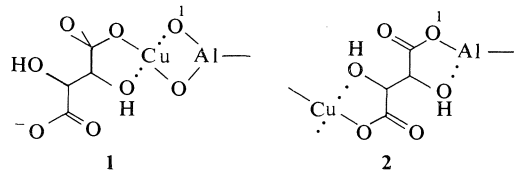

1 2

There are facts in support of structure **2**. Structure **1** does not explain the special status of tartrate; there are no obvious reasons why the other ligands are ineffective in promoting luminescence together with copper ions. On the other hand, copper ions and tartrate are known to form polymeric complexes, and it is assumed that in these complexes there is an analogous tartrate bridge as in structure **2** (11).

Malate forms also a dimeric complex with copper but in this complex the two copper atoms are linked together by an oxygen bridge. Thus structure **2** seems to have a capability of explaining the unique behaviour of tartrate.

Tantalum Electrode

The surface of aluminium is easily corroded and during the experiments the surface must be frequently polished and reanodized. Tantalum is chemically more resistant; it forms a tough oxide layer and it is known to be electroluminescent. In the hope that more reproducible results could be obtained, further experiments were directed to the study of the feasibility of the tantalum electrode. Surprisingly, the first experiments with several electrolytes using a freshly anodized electrode gave nearly no luminescence. After several repeated scans from 0 to 10 V, during which the light emission continuously increased, the output curve of the emission attained a constant form. As with aluminium, it was also found that the intensity of the light emission was highly dependent on the concentration of oxygen in the solution; oxygen could be replaced by hydrogen peroxide and its concentration could be more easily varied.

Tartrate was found to provide a favourable medium for electroluminescence studies with the tantalum electrode. Copper, however, had no significant influence on the intensity of the

light emission (this might be attributed to the poor chemisorption of copper tartrate on the tantalum pentoxide surface).

Studies were now directed to electroluminescence in perchlorate solutions. This medium was chosen because it was felt that more information could be gained about the basic phenomenon in a simple inorganic non-complexing solution. In the first experiments the acidity was varied and the ionic strength was maintained at one with sodium perchlorate; the concentration of hydrogen peroxide was 10^{-3} *M*. Figure 7 shows the electroluminescence curves obtained by scanning the pulse amplitude. The curve at the lowest acid concentration, 0.002 *M*, is seen to be composed of one peak or two overlapping peaks. At higher acid concentrations, the peaks are separated so that the position of the peak at lower voltage is maintained nearly constant whereas the peak at higher voltage is shifted, flattened, and eventually disappears. The reduction of the light intensity to nearly zero at higher voltages cannot be easily explained by solid state electroluminescence. If the origin of light is solid state electroluminescence then it is probable that the light intensity is a monotonously increasing function of current. However, the Faradaic current (as estimated from an oscilloscopic trace) is *ca.* five times higher at 9 V than at 4 V, although the light intensity itself is nearly zero (Fig. 7). If we adopt the *ad hoc* hypothesis that the light arises from a chemiluminescent reaction involving oxygen radicals, there are several alternative explanations.

One possibility is that the two maxima are due to two different reduction mechanisms

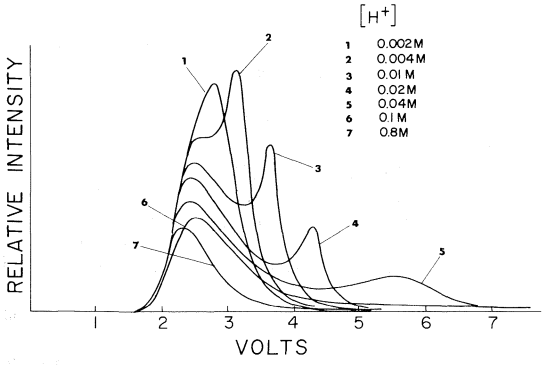

FIG. 7. Electroluminescence curves of the tantalum electrode at different acid concentrations. $[ClO^-_4] = 1\ M$ $[H_2O_2] = 10^{-3}\ M$.

which become prevalent at different voltages. The last stage before the very fast light emitting step should be the electron transfer to the substrate, because no light is emitted during the positive pulses. The reduction step should be a one-electron transfer in order to lead to light emitting species (9). However, it is not easily conceivable that from the same reagent (hydrogen peroxide) we get the same product (singlet oxygen) via two different mechanisms. It is more likely that one of the peaks is due to the reduction of hydrogen peroxide, the other due to oxygen. Schematically, without taking into account the possible complex formation with tantalum pentoxide, we can write the mechanisms:

$$H_2O_2 + e \rightarrow HO\cdot + HO^-$$

$$H_2O_2 + HO\cdot \rightarrow HO_2\cdot + H_2O$$

$$O_2 + e \rightarrow O_2^-$$

$$O_2^- + H^+ \rightleftarrows HO_2\cdot$$

$$2HO_2\cdot \rightarrow H_2O_2 + {}^1O_2$$

$$2{}^1O_2 \rightarrow ({}^1O_2)_2 \rightarrow 2{}^3O_2 + h\nu$$

At higher potential the rate of the electrochemical reduction of the oxygen radicals competes with the formation of singlet oxygen thus reducing the chemiluminescence.

The other alternative is that the first peak is due to the reduction of chemisorbed hydrogen peroxide (or oxygen) and the second peak due to the diffusion controlled reaction. In order to study this possibility, an experimental arrangement analogous to chronocoulometric measurement was assembled. The cell was subjected to a constant amplitude pulse train and the output from the lock-in amplifier was integrated before recording on the X–Y recorder. At low potential (3 V) the integral is a strictly linear function of time showing that diffusion is not the rate determining step in the reaction chain leading to light emission; at higher potentials, the linear relationship does not hold. If the reaction is diffusion controlled, the integral of the light emission should be a linear function of the square root of time. This is not the case, however, and the curves seem to be composed of two straight lines (Fig. 8); this may be due to the slow rate of chemisorption.

If the light emission is due to singlet oxygen, it should have a characteristic spectrum (12). There are two principal difficulties, however,

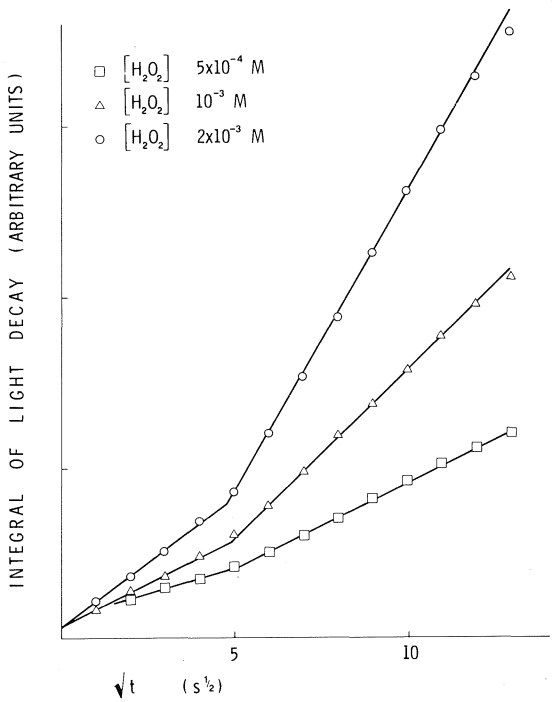

FIG. 8. Integrals of the light decay curves measured with the tantalum electrode in solutions which contain 0.96 mol of $NaClO_4$ and 0.04 mol of $HClO_4$ per ℓ and varying amounts of H_2O_2. The amplitude of the pulses is 6 V.

in determining this spectrum. Firstly, the intensity is very low so that a long integration time should be used for each spectrum point.

Secondly, the light emission is time-dependent unless very low voltages are used. At 3 V, the light intensity given by a tantalum electrode is relatively constant although small. Figure 9 shows the spectrum recorded for the electroluminescence of the tantalum electrode in a solution containing 0.02 *M* H_2O_2 and 0.04 *M* $HClO_4$ in 1 *M* $NaClO_4$. The known maxima of the emission spectrum of singlet oxygen are shown in Fig. 9 as a column diagram. The relative intensities of the maxima are known to vary depending upon the source and medium of singlet oxygen. Due to the poor resolution the spectrum does not provide the unambiguous answer, but it does not preclude the leading role of singlet oxygen.

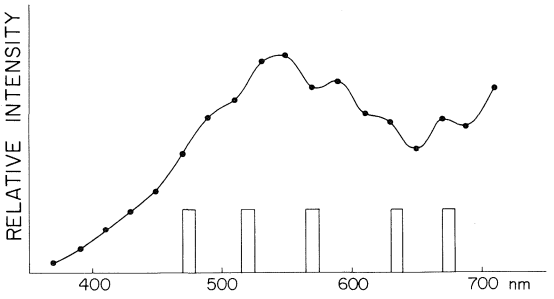

FIG. 9. The spectrum of the cathodic luminescence of the tantalum electrode in a solution which contains 0.04 mol of $HClO_4$, 0.96 mol of $NaClO_4$, and 0.02 mol of H_2O_2 per ℓ.

Conclusions

Cathodic luminescence at low voltages can be explained by the generation and radiative transition of singlet oxygen. The phenomena described are observed only at voltages of less than 10 V; this may be why they have escaped the attention of previous workers who used voltages greater than 30 V (for higher light intensity). It may be that electrogenerated chemiluminescence is predominant at low voltages and solid state luminescence at high.

The influence of trace concentrations of copper on the luminescence with an aluminium cathode in tartrate solutions is of analytical interest. However, the rather poor reproducibility (of electrode surface) and the sensitivity limit of 0.1 μg ml^{-1} makes its practical use questionable.

The high sensitivity of luminescence, with the tantalum electrode, to oxygen and hydrogen peroxide may be of analytical value.

Acknowledgements

This work was supported by a National Research Council of Canada grant to D. E. Ryan. It is a pleasure to acknowledge also the indebtedness to Dalhousie University for the award of a Senior Killam Fellowship to J. J. Kankare.

1. F. BRAUN. Ann. Phys. Chem. **65**, 361 (1898).
2. A. GUNTHERSCHULTZE. Ann. Phys. **21**, 929 (1906).
3. S. ANDERSON. J. Appl. Phys. **14**, 601 (1943).
4. W. VAN GEEL, C. A. PISTORIUS, and B. C. BOUMA. Philips Res. Rep. **12**, 465 (1957).
5. W. P. GANLEY, P. M. MOONEY, and D. HUMINIK. Thin Solid Films, **3**, 377 (1969).
6. W. P. GANLEY. Thin Solid Films, **11**, 91 (1972).
7. S. IKONOPISOV. Electrochim. Acta, **20**, 783 (1975).
8. J. STAUFF. Photochem. Photobiol. **4**, 1199 (1965).
9. J. STAUFF and F. NIMMERFALL. Z. Naturforsch. Teil B, **24**, 852 (1969).
10. H. HOHL and W. STUMM. J. Colloid Interface Sci. **55**, 281 (1976).
11. K. RAJAN and A. MARTELL, J. Inorg. Nucl. Chem. **29**, 463 (1967).
12. M. NAKANO, K. TAKAYAMA, Y. SHIMIZU, Y. TSUJI, H. INABA, and T. MIGITA. J. Am. Chem. Soc. **98**, 1974 (1976).

Nuclear magnetic resonance investigation of the conformational dynamic properties of benzocycloheptenones and related compounds

G. BODENNEC[1] AND M. ST-JACQUES[2]

Département de Chimie, Université de Montréal, Montréal (Qué.), Canada H3C 3V1

Received October 19, 1976

G. BODENNEC and M. ST-JACQUES. Can. J. Chem. **55**, 1199 (1977).

Free energy barriers for ring inversion were determined from dnmr studies of 3,4-benzocycloheptenone (**4**) and for deuterated derivatives **6** and **7** of 4,5-benzocycloheptenone (**5**). The investigation of 2,3-benzocycloheptenone (**3**) revealed negative results. The magnitude of $\Delta G^{\ddagger}$ for **4** and the trend observed for **5**, **6**, and **7** strongly suggest that the chair conformation of these molecules interconverts through a wagging motion of the C(5) end of the benzocycloheptene seven-membered ring.

G. BODENNEC et M. ST-JACQUES. Can. J. Chem. **55**, 1199 (1977).

On a déterminé les barrières d'énergie libre pour l'inversion de cycles à partir d'études rmn dynamique de la benzo-3,4 cyclohepténone (**4**) et des dérivés deutérés **6** et **7** de la benzo-4,5 cyclohepténone (**5**). L'étude de la benzo-2,3 cyclohepténone (**3**) n'a apportée que des résultats négatifs. L'amplitude de $\Delta G^{\ddagger}$ pour **4** et la tendance observée pour **5**, **6** et **7** suggèrent fortement que la conformation chaise de ces molécules s'interconvertit par un mouvement de battement de la portion C(5) du cycle à sept chaînons du benzocycloheptène.

[Traduit par le journal]

We have witnessed, in the last decade, a constant progression of our knowledge of the stereochemical, conformational, and dynamic properties of several classes of seven-membered cyclic molecules (1–18). The dnmr method (1), in particular, has been extremely useful to study those molecules possessing conformational averaging processes characterized by free energies of activation barriers greater than 5 kcal/mol. Among the various classes of compounds studied, cycloheptene (**1**) and benzocycloheptene (**2**) have received much attention because of their limited number of possible conformations characterized by readily defined geometries and symmetry properties together with reasonably high interconversion activation energies. It is now well known that both **1** and **2** exist preferentially in the chair conformation (11, 14) characterized by different inversion $\Delta G^{\ddagger}$, namely 5.0 kcal/mol (13) for **1** and 10.9 kcal/mol (18) for **2**.

Attempts to rationalize this large $\Delta G^{\ddagger}$ difference diverge in their description of the dynamic behaviour of benzocycloheptene. Different conformational energy calculations (7–10) agree in their suggestion that the cycloheptene chair interconverts through a wagging motion of the double bond. As for benzocycloheptene, Allinger and Sprague (7) have suggested that it also inverts through a wagging motion of the benzo double bond and that the smaller relief of torsional strain about the C(sp^2)—C(sp^3) bonds compared to cycloheptene accounts for the higher barrier of **2**. In contrast, Favini and Nava (10), have calculated, using the MINDO/2 approximation, that the C(5) wagging motion is easier than the benzo wag and conclude that the change in inversion mechanism is responsible for the large $\Delta G^{\ddagger}$ difference.

Experimental data bearing on this question appear to be scarce. A dnmr study (15) of the substituent effect of *gem*-dimethyl groups revealed parallel $\Delta G^{\ddagger}$ trends for analogous derivatives in each series and this observation was interpreted in terms of similar inversion pathways for both groups of compounds. However, owing to the small $\Delta G^{\ddagger}$ variations observed within each series, it seemed desirable, in light of recent calculations (10), to obtain additional data bearing on the divergent point.

We now wish to report the results of our dnmr study of the simple derivatives **3**, **4**, **5**, **6**, and **7** of benzocycloheptene.

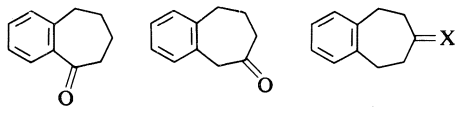

3 **4** **5** X = O; **6** X = CH_2; **7** X = CCl_2

[1]Scientist on leave (1974–1975) from the Université de Lyon, France.

[2]Author to whom correspondence should be addressed.

Results

Selectively deuterated derivatives of **5**, **6**, and **7** were prepared for easier analysis of the ^{1}Hmr spectral modifications occurring at low temperatures. The key reaction involved a catalytic reduction of double bonds with deuterium gas; it is expected to place vicinal deuterium atoms in a predominantly *cis* arrangement (14, 16). As these compounds were prepared at different times, the isotopic purity varied according to the experimental conditions. Attempts to maximize isotopic purity were not always made when the dynamic parameters could be obtained reliably from samples containing several identified isotopic species.

Scheme 1 illustrates the preparation of compounds identified as **5**-d_6, **6**-d_6, and **7**-d_6 but for which mass spectral analysis indicated the presence of appreciable quantities of d_4 and d_5 species and for which the ^{1}Hmr spectral region of the benzylic protons showed two peaks separated by 2.2 Hz, thus suggesting that the species CH_2CD_2 give rise to the taller lowfield line while the species $CHDCD_2$ give rise to the smaller upfield line as seen clearly in the spectrum at 25°C for **6**-d_6 (Fig. 1). The separation between these peaks is the normal isotopic shift of the α-deuterium atom (19).

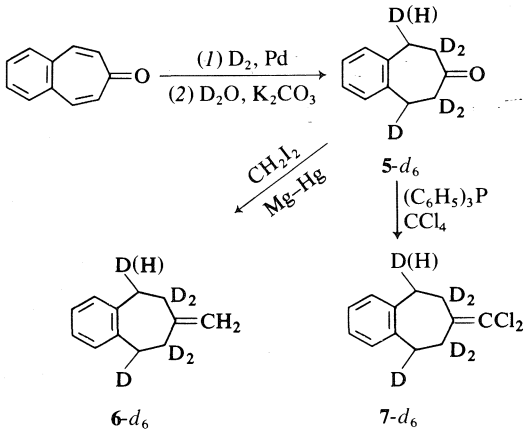

SCHEME 1

Changing the solvent from ethanol to anhydrous tetrahydrofuran improved the isotopic composition of **5**-d_4 which, however, still contained appreciable quantities of d_3 and d_5 species (see Experimental section). The deuterium content was nevertheless sufficient for our proposed ^{1}Hmr investigation of **5**-d_4, **6**-d_4, and **7**-d_4 (Scheme 2) as will be described later.

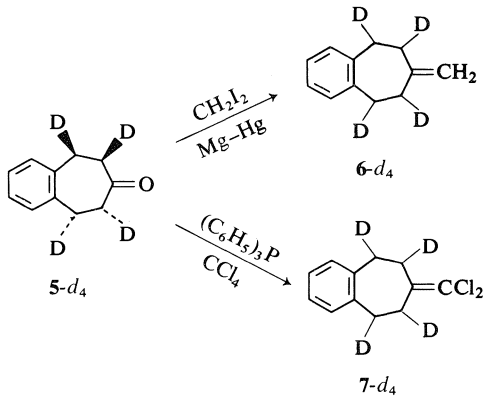

SCHEME 2

It is important to point out that each of the compounds prepared actually contains essentially equal amounts of *syn* and *anti* isomers, but because the ^{1}Hmr signals of each side of the ring are essentially independent (14, 16), only the *anti* isomers have been shown in the schemes.

Spectral Analysis

Spectral changes were observed for compounds **4**, **6**-d_4, **6**-d_6, and **7**-d_4, whereas the ^{1}Hmr spectra of **3**, **5**, **5**-d_4, **5**-d_6, and **7**-d_6 showed no discernable spectral modification (down to −170°C) resulting from the slowing down of conformational averaging processes.

The ^{1}Hmr spectral behaviour of the non-aromatic signals of 3,4-benzocycloheptenone (**4**) (2-benzosuberone) in CHF_2Cl at low temperatures has revealed that both the lowfield singlet (δ 3.67) and the high field multiplet (centered at δ 1.98) show clearcut splitting below −162°C. The lowfield singlet, attributed to protons on C-2, has split into two broad bands separated by about 90 Hz at −168°C. The low temperature spectrum actually consists of a broadened AB pattern whose lines could not all be resolved at such low temperatures. Nevertheless, the use of approximate equations (20) for two exchanging sites and a transmission coefficient of one give an estimate of 5.1 kcal/mol for $\Delta G^{\ddagger}$ at −162°C (T_c).

Figure 1 shows the spectra of benzylic signal of **6**-d_6 in CHF_2Cl at several temperatures. The spectrum at 25°C indicates the presence of two singlets separated by 2.2 Hz; the taller line is due to CH_2CD_2 species while the shorter starred line arises from $CHDCD_2$ species. Both lines split at low temperatures, the taller giving an AB quartet (J = −14.3 Hz and $\Delta\nu$ = 11.7 Hz)

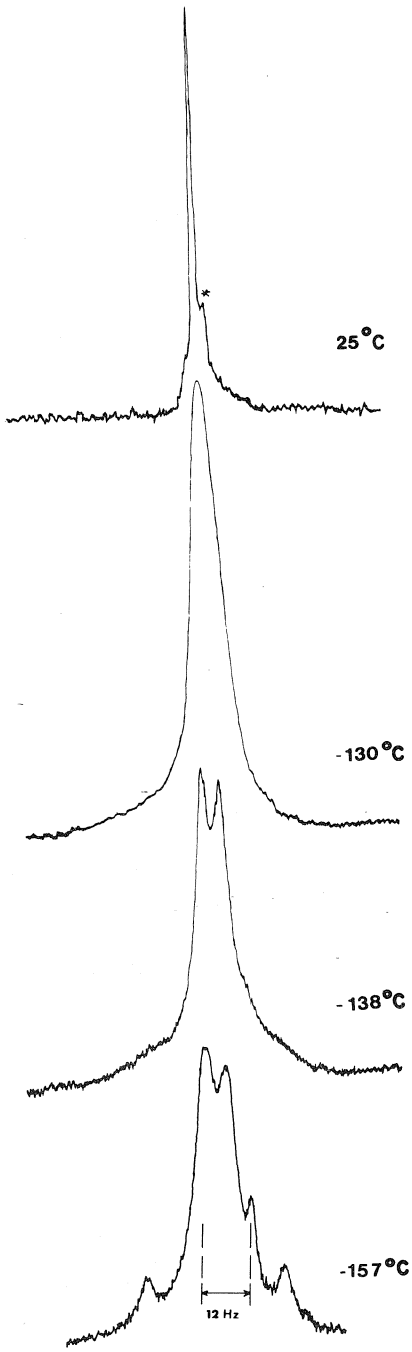

FIG. 1. 100 MHz deuterium decoupled ^{1}Hmr spectra of **6**-d_6 (10% in CHF_2Cl) at several temperatures. The stick diagram under the spectra at -157°C identifies the doublet arising from the splitting of the starred line in the spectrum at 25°C.

at -157°C and the shorter giving a doublet identified by the stick diagram. Standard equations (20) afforded a $\Delta G^{\ddagger}$ value of 6.9 kcal/mol at -130°C (T_c). A series of spectra for **7**-d_6 down to -170°C showed broadening greater than for the TMS line but no clearcut splitting was observed.

The low temperature spectrum of non-deuterated **6** gave indications that the chemical shift separation is larger for the two non-equivalent methylene protons next to the *exo* double bond than at the benzylic positions. Consequently a comparative study of **6**-d_4 and **7**-d_4 was undertaken.

Figure 2 shows several ^{1}Hmr spectra for **6**-d_4 (right side) and **7**-d_4 (left side). It is readily apparent that the isotopic purity of these compounds is not sufficient (see Experimental section) to give the AX pattern at $+25$°C for CHDCHD (*cis*) arrangements expected for each compound (14, 16). Nevertheless the extent of deuteration is sufficient to remove much of the strong coupling and thus enable relatively easy detection and overall analysis of the splitting observed for the high field band. It is seen that the upfield signal of **6**-d_4 splits into two broad bands separated by about 65 Hz below -122°C (T_c). The use of standard equations (20) provided the estimate $\Delta G^{\ddagger} = 7.1$ kcal/mol. The observation that this value is very close to the $\Delta G^{\ddagger}$ value calculated earlier for **6**-d_6 (Fig. 1) suggests that the approach using **6**-d_4 and **7**-d_4 should lead to acceptable $\Delta G^{\ddagger}$ estimates.

Solubility problems made the study of **7**-d_4 slightly more difficult but a spectral change (Fig. 2 left side) was nevertheless observed for a solution in a mixture of CHF_2Cl–$CHFCl_2$ (1:1) and a direct comparison with that of **6**-d_4 shows that $T_c \approx -155$°C and $\Delta\nu \approx 60$ Hz so that $\Delta G^{\ddagger} = 5.5$ kcal/mol can be calculated.

A careful examination of the ^{1}Hmr spectrum of **5**-d_4 in CCl_4 at room temperature showed several lines attributable to isotopic impurities of the type CHD—CHD (*cis*) CHD—CHD (*trans*), $CHDCH_2$, and $CHDCD_2$ as anticipated (14) and confirmed by the mass spectral analysis which revealed the presence of significant amounts of d_3, d_4, and d_5 species (namely 25, 42, and 24% respectively). Having identified the peaks belonging to $CHDCH_2$ species from the spectrum of a sample of 3,6-dideutero-4,5-benzocycloheptenone it was possible to identify the more intense doublets of the AX pattern of the

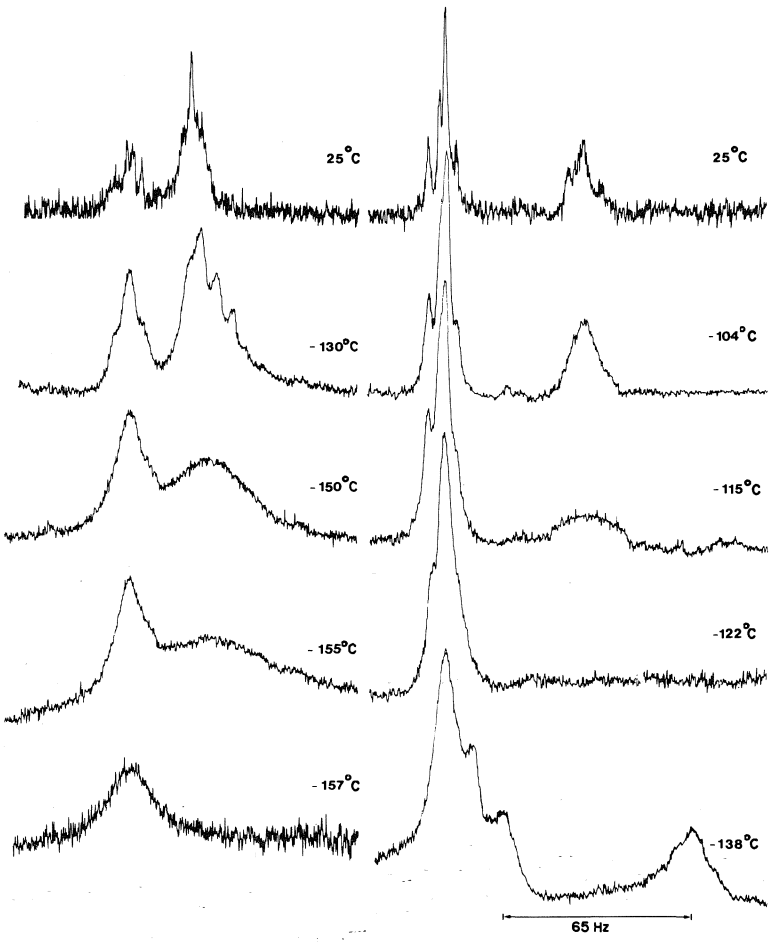

FIG. 2. 100 MHz deuterium decoupled ^{1}Hmr spectra of **6**-d_4 (10% in CHF_2Cl) (right side) and **7**-d_4 (3% in a 1:1 mixture of CHF_2Cl and $CHFCl_2$) (left side) at several temperatures. Both series of spectra were recorded on the same scale.

CHDCHD (*cis*) species (14) whose splitting is equal to the averaged coupling constant J_{cis} = 2.2 Hz, as well as the less intense doublets of the AX pattern of the CHDCHD (*trans*) species characterized by the averaged coupling constant J_{trans} = 9.9 Hz. The R-value (21) $R = J_{trans}/J_{cis} = 4.5$ was calculated with a reasonable degree of confidence based on the verification of this approach for a similarly deuterated benzocycloheptene derivative (14, 16).

The spectra of **6**-d_4 and **7**-d_4 were much less well defined than that of **5**-d_4 owing to a greater isotopic distribution so that R cannot be calculated reliably. As seen in Fig. 2 only the lowfield signal of **6**-d_4 at +25°C reveals clearly the doublet components of the two AX patterns in question.

Discussion

It is well known that benzocycloheptene exists in the chair conformation (14) and it has been deduced from dipole moment studies (6) that **5** exists as a mixture of chair (92%) and boat (8%) conformations in benzene solution. Owing to the inherent uncertainties associated with that method, the exact amount of boat conformation is open to question and in fact may be quite small. There is, however, no reason to believe that the chair is not the predominant conformation. Consequently the R-value of 4.5 calculated

from the ^{1}Hmr spectrum of **5**-d_4 suggests that the carbonyl group has flattened the chair relative to that of benzocycloheptene (14) for which $R = 8.7$. In fact, this change in R-value corresponds to a reduction of the internal torsional angle (21) (ψ) from 74° in benzocycloheptene to 68° in the conformation of **5**. This angular change is very similar to the flattening effect of the carbonyl group in cyclohexanone ($\psi = 50°$) relative to cyclohexane ($\psi = 56$–$58°$) (21).

Although R-values could not be obtained confidently for **6**-d_4 and **7**-d_4, an estimated value from the lowfield signal in the spectrum of **6**-d_4 at +25° (Fig. 2) suggests that it is very similar to that of **5**-d_4. Furthermore, the benzylic coupling of 14.3 Hz determined for **6**-d_6 (Fig. 1) is very similar to the value of 14.1 Hz determined for the chair conformation of benzocycloheptene (14). It therefore appears certain that **4**, **5**, **6**, and **7** exist predominantly as chair conformations.

The nature of the most stable conformation of **3** is more uncertain. Nuclear Overhauser enhancement experiments (22) on two isomeric tetrabromo-2,3-benzocycloheptenones were interpreted in terms of a skew and a twist-boat conformation. The significance of these results with respect to the conformation of **3** is not obvious. The dnmr results having been negative for **3**, we are unable to specify unambiguously the geometry of its most stable conformation.

The inversion scheme for benzocycloheptene has already been described (23). It involves a rate-determining chair-to-boat step and a less energetic pseudorotation motion between boat and twist-boat forms. Two different pathways have been suggested for the rate determining chair-to-boat step (7, 10). Scheme 3 illustrates the difference clearly. It is shown that one possibility involves the wagging motion of the benzo group through conformation A which possesses six coplanar ring carbon atoms. The other possibility involves the wagging of C(5) through conformation B having five coplanar ring carbon atoms. (The numbering convention used in this section refers to the parent compound even when used for its derivatives. It should not be associated with the nomenclature numbering convention of the derivatives investigated.)

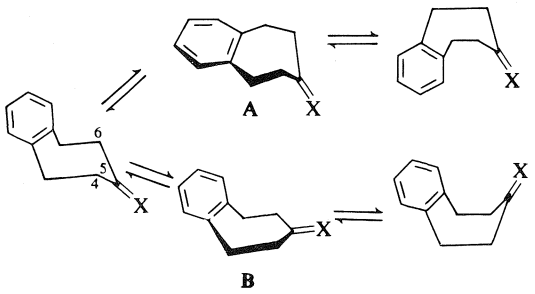

SCHEME 3

It is seen that only pathway B involves appreciable rotation of the C(4)—C(5) and C(5)—C(6) bonds in the rate determining step. Provided rotational energy is an important contributor to the activation energy, any structural modification resulting in easier rotation about these bonds is expected to decrease the overall $\Delta G^{\ddagger}$ for ring inversion of molecules favoring this path. In fact it has been shown (4*a*) that torsional energy accounts for a large part of the energy difference between the chair and the inversion transition state of cyclohexane. The variation in $\Delta G^{\ddagger}$ values of the six-membered cyclic compounds listed in Table 1 was consequently rationalized convincingly in terms of the ease of rotation of the bonds adjacent to the sp^2 carbon (24, 25).

Table 1 reveals a very similar trend for both the six- and seven-membered cyclic compounds listed, such that it is very tempting to suggest that inversion in the second series of compounds also proceeds through a pathway involving appreciable rotation of the bonds adjacent to the sp^2 carbon atom and consequently that the chair conformation of these compounds inter-

TABLE 1. Summary of $\Delta G^{\ddagger}$ values for the ring inversion of some six, seven, and eight-membered compounds

Compound	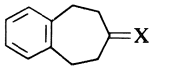	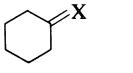	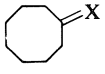
X = H_2	10.9[a]	10.3[b]	8.1[d]
X = O	<5	4.0[c]	7.5[d]
X = CH_2	7.0	8.4[b]	8.1[d]
X = CCl_2	5.5	5.4[b]	~7.5[e]

[a]Reference 18.
[b]Reference 24 and references cited therein.
[c]Reference 30.
[d]Reference 2, pp. 568 and 599. The values reported characterize the ring inversion process of the boat–chair conformation. The pseudorotation barrier for these compounds is significantly lower.
[e]Estimate from unpublished dnmr results by G. Bodennec.

convert via pathway B. Supporting evidence is provided by the observation that the same chemical modifications in the eight-membered compounds listed in Table 1 do not lead to a significant variation in $\Delta G^{\ddagger}$ for ring inversion, most probably because the rate determining step involves little rotation about the bonds adjacent to the sp^2 carbon (ref. 2, p. 568).

Furthermore, the higher $\Delta G^{\ddagger}$ value determined for **4** compared to **5** is consistent with a C(5) wag. Reaching B involves appreciable rotation about only one bond adjacent to the carbonyl group of **4**, whereas two such bonds rotate in **5**.

While it appears certain that the chair conformations of **4**, **5**, **6**, and **7** invert through a C(5) wag, it is not as clear that the extrapolation to **2** suggested by the data in Table 1 is a valid one. In fact calculations (7–10) have shown that both the benzo and the C(5) wags should be more energetic than the double bond wag of cycloheptene and it is possible that both A and B would require very similar energy for benzocycloheptene. Unfortunately Allinger's calculations (7) were not sufficiently complete to prove otherwise while Favini's calculations (10) suggest that the C(5) wag is the easier process but, because agreement with the experimental barrier is very poor (6.0 kcal/mol compared to the 10.9 kcal/mol observed for **3**), it is difficult to be convinced. Recent calculations (26) for 1,5-cyclooctadiene and its dibenzo analog afford a better estimate of the energy difference between a double bond wag and benzo wag as involved for the boat-to-chair interconversion. The enthalpy values calculated are 5.2 and 11.4 kcal/mol for the diene and dibenzo compound respectively. These results together with the data in Table 1 suggest that both pathways A and B for benzocycloheptene might indeed be of comparable energy.

The lack of knowledge on the geometry of the most stable conformation of **3**, the negative dnmr results, and the better stabilization expected for some conformations through resonance between the carbonyl group and the aromatic ring suggest that the conformational dynamic properties of **3** may be different from those of **4** and **5**.

We therefore conclude that **1** inverts through pathway A while **4**, **5**, **6**, and **7** invert through pathway B. As for **2**, it is clear that both pathways are expected to involve relatively higher and comparable activation energies and it appears that the qualitative interpretation of the substituent effects determined in this work cannot tell with certainty which of the two ring motions is rate determining.

Experimental

The vpc analyses and separations were carried out on a Varian-aerograph A90-P3 instrument using ¼ in. silicone DC 550 (15%) columns and helium as carrier gas. Mass spectral analyses were performed on an Hitachi–Perkin-Elmer model RMU-6D instrument operating at 70 and 12 eV.

Routine analytical ^{1}Hmr spectra were recorded on a JEOL C-60H spectrometer operating at 60 MHz in the external lock mode. The low temperature ^{1}Hmr spectra were obtained at 100 MHz using a JEOL JNM-4H-100 spectrometer. Solutions containing a small quantity of TMS were degassed and sealed. Deuterium decoupling, when required, was effected by means of the JEOL Hetero Spin Decoupler model JNM-SD-HC.

Temperatures were monitored by means of a JEOL temperature control unit model JES-VT-3 and determined accurately with a calibrated thermocouple placed inside a solvent-containing dummy nmr tube.

2,3-Benzocycloheptenone (3)

This compound was obtained from Aldrich Chemical Co. as 1-benzosuberone and used without further purification.

3,4-Benzocycloheptenone (4)

This compound was prepared from **3** by the method of Huisgen *et al.* (27). Its ^{1}Hmr spectrum in $CDCl_3$ at 60 MHz is entirely consistent with that expected for **4**: δ 7.1 (4H, aromatic), 3.65 (2H, s), 2.90 (2H, m), 2.47 (2H, t), and 1.95 (2H, m).

4,5-Benzotropone

This compound was prepared as previously described (6, 14) and found to be identical to other samples previously prepared in this laboratory.

Preparation of 6-d_6 and 7-d_6 (Scheme 1)

A solution of 4,5-benzotropone (2.1 g) in 120 ml of ethanol containing 0.60 g of paladium-on-charcoal (5%) catalyst was placed in a compact deuteration apparatus (14) for about 16 h. Deuterium gas absorption had then ceased and the mixture was filtered on diatomaceous earth. Evaporation of the solvent gave a product which was shown by vpc analysis to have a retention time equal to that of authentic 4,5-benzocycloheptenone (14).

The above ketone was then added to a solution of 4.0 g of potassium carbonate in 40 ml of D_2O. After 5 h of reflux, the product was isolated in the usual manner (14). This procedure was repeated once and the product expected to be **5**-d_6 was isolated. The deuterium decoupled 100 MHz ^{1}Hmr spectrum in CHF_2Cl showed two benzylic singlets (near δ 2.8) separated by 2.2 Hz and in the ratio 70:30 (peak heights). Thus the sample contained a large quantity of CH_2CD_2 species (more

intense lowfield line) and $CHDCD_2$ species (less intense upfield line).

Compound **6**-d_6 was prepared from the above sample of **5**-d_6 by the reaction of methylene iodide and magnesium amalgam as previously described by Bertini *et al.* (28). An ether solution (20 ml) of 0.50 g (3.0 mmol) of ketone **5**-d_6 and 0.88 g (3.3 mmol) of methylene iodide was added with stirring, at room temperature under a nitrogen atmosphere, to previously prepared magnesium amalgam (0.160 g of Mg and 5 ml of Hg). After reaction work-up (28) and evaporation of the ether solvent, a vpc analysis of the crude product revealed a mixture of **6**-d_6 (70%) and the starting ketone (30%). Chemically pure **6**-d_6 was obtained by preparative vpc and its deuterium decoupled ^{1}Hmr spectrum (10% in CHF_2Cl) showed a characteristic singlet at δ 4.7 ($C{=}CH_2$) and another signal at δ 2.8 (benzylic CH_2CD_2 and $CHDCD_2$) in the ratio 2:2.2. The upfield signal (Fig. 1) consists of two singlets separated by 2.2 Hz, the more intense line belonging to CH_2CD_2 species and the other one to the $CHDCD_2$ species. A mass spectral analysis at 12 eV revealed the following isotopic distribution: d_3 = 5%, d_4 = 42%, d_5 = 23%, d_6 = 21%, d_7 = 7%, d_8 = 2%.

Compound **7**-d_6 was prepared from **5**-d_6 by a reaction with carbon tetrachloride and triphenylphosphine according to the method of Rabinowitz and Marcus (29). Thus, a solution of 0.48 g of **5**-d_6 (3 mmol) and 1.6 g of triphenylphosphine in 30 ml of carbon tetrachloride was heated to 80°C for 10 h. After work-up (29), 0.35 g of crude product was obtained. Analysis by vpc showed that it possessed a retention time equal to that of authentic 5-exodichloromethylenebenzocycloheptene (**7**) mp 103–104°C. The mass spectrum showed a cluster of peaks near *m/e* 232 thus confirming the identity of the compound, but we were not able to get a very meaningful isotopic distribution.

Preparation of **5**-d_4, **6**-d_4, *and* **7**-d_4 *(Scheme 3)*

A solution of 4,5-benzotropone (1.6 g) in 90 ml of tetrahydrofuran (freshly distilled over $LiAlH_4$) containing 100 mg of palladium-on-charcoal (5%) catalyst was reacted with deuterium gas as described earlier. After filtration of the catalyst and evaporation of the solvent, 1.5 g of ketone expected to be **5**-d_4 was obtained. Analysis by vpc showed a retention time identical to authentic 4,5-benzocycloheptenone (14). The deuterium decoupled ^{1}Hmr spectrum at 100 MHz (5% in CHF_2Cl) showed two characteristic signals for the non-aromatic protons: δ 2.5 (H next to carbonyl) and δ 2.8 (benzylic H) of essentially equal surface. A mass spectral analysis revealed the following isotopic distribution: d_1 = 4%, d_2 = 5%, d_3 = 25%, d_4 = 42%, d_5 = 24%.

Compound **6**-d_4 was prepared from a sample of 0.6 g of **5**-d_4 by a reaction with methylene iodide and magnesium amalgam as described earlier. After work-up 0.45 g of crude product was obtained. Chemically pure **6**-d_4 was obtained by vpc purification. A 100 MHz deuterium decoupled ^{1}Hmr spectrum of **6**-d_4 (Fig. 2) as a 10% solution in CHF_2Cl showed the following characteristic signals: δ 2.3 (H next to $C{=}CH_2$) 2.8 (benzylic H), and 4.7 ($=CH_2$). The mass spectral analysis revealed the following isotopic composition: d_1 = 1%, d_2 = 9%, d_3 = 27%, d_4 = 35%, d_5 = 19%, d_6 = 7%, d_7 = 2%.

Compound **7**-d_4 was prepared from a sample of 0.41 g of **5**-d_4 by a reaction with 1.3 g of triphenylphosphine in 30 ml of carbon tetrachloride as previously described. The product was identified by comparison of its vpc retention time with a sample of authentic 5-dichloromethylenebenzocycloheptene and then purified by preparative vpc. The 100 MHz deuterium decoupled ^{1}Hmr spectrum of this compound (Fig. 2) in a mixture of CHF_2Cl and $CHFCl_2$ (1:1) showed two non-aromatic signals at δ 2.6 (protons next to $C{=}CCl_2$) and 2.8 (benzylic protons). The mass spectrum showed a cluster of peaks near *m/e* 230 thus confirming the identity of the compound, but we were not able to get a very meaningful isotopic distribution.

Acknowledgment

We wish to acknowledge the collaboration of D. Montecalvo and C. Vaziri in the preliminary stages of this work, and R. Mayer for assistance in recording the low temperature spectra. We are very grateful for the financial assistance of the National Research Council of Canada and of the Quebec government for a Quebec–France exchange fellowship to G.B.

1. W. Tochermann. Fortschr. Chem. Forsch. **15**, 378 (1970).
2. F. A. L. Anet. *In* Dynamic nuclear magnetic resonance spectroscopy. *Edited by* L. M. Jackman and F. A. Cotton. Academic Press, New York, NY. 1975.
3. P. Groth. Acta Chem. Scand. **21**, 2031 (1967).
4. J. B. Hendrickson. (*a*) J. Am. Chem. Soc. **89**, 7036 (1967); (*b*) **89**, 7043 (1967); (*c*) **89**, 7047 (1967).
5. E. S. Glazer, R. Knorr, C. Ganter, and J. D. Roberts. J. Am. Chem. Soc. **94**, 6026 (1972).
6. N. L. Allinger and W. Szkrybalo. J. Org. Chem. **27**, 722 (1962).
7. N. L. Allinger and J. T. Sprague. J. Am. Chem. Soc. **94**, 5734 (1972).
8. G. Favini, G. Buemi, and M. Ramondi. J. Mol. Struct. **2**, 137 (1968).
9. G. Favini and A. Nava. Theor. Chim. Acta, **31**, 261 (1973).
10. G. Favini and A. Nava. Gazz. Chim. Ital. **104**, 621 (1974).
11. N. Neto, C. DiLauro, and S. Califano. Spectrochim, Acta Ser. A, **26**, 1489 (1970).
12. R. J. Abraham, L. J. Kricka, and A. Ledwith. J. Chem. Soc. Perkin Trans. II, 1648 (1974).
13. M. St-Jacques and C. Vaziri. Can. J. Chem. **49**, 1256 (1971).
14. M. St-Jacques and C. Vaziri. Org. Magn. Reson. **4**, 77 (1972).
15. M. St-Jacques and C. Vaziri. Can. J. Chem. **51**, 1192 (1973).
16. L. Canuel and M. St-Jacques. Can. J. Chem. **52**, 3581 (1974).
17. M. St-Jacques, C. Vaziri, D. A. Frenette, A. Goursot, and S. Fliszar. J. Am. Chem. Soc. **98**, 5759 (1976).

18. S. KABUSS, H. FRIEBOLIN, and H. SCHMID. Tetrahedron Lett. 469 (1965).
19. H. BATIZ-HERNANDEZ and R. A. BERNHEIM. *In* Progress in N.M.R. spectroscopy. Vol. 3. *Edited by* J. W. Emsley, J. Feeney, and L. H. Sutcliffe. Pergamon Press, New York, NY. 1967. Chapt. 2.
20. D. KOST, E. H. CARLSON, and M. RABAN. Chem. Commun. 656 (1971).
21. J. B. LAMBERT. Acc. Chem. Res. **4**, 87 (1971).
22. M. C. WOODS, S. EBINE, M. HOSHINA, K. TAKAHASHI, and I. MIURA. Tetrahedron Lett. 2879 (1969).
23. S. KABUSS, H. G. SCHMID, H. FRIEBOLIN, and W. FAISST. Org. Magn. Reson. **2**, 19 (1970).
24. M. BERNARD and M. ST-JACQUES. Can. J. Chem. **48**, 3039 (1970).
25. J. T. GERIG and R. A. RIMERMAN. J. Am. Chem. Soc. **92**, 1219 (1970).
26. N. L. ALLINGER and J. T. SPRAGUE. Tetrahedron, **31**, 21 (1975).
27. R. HUISGEN, E. RAUENBUSH, G. SEIDL, and I. WIMMER. Justus Liebigs Ann. Chem. **671**, 41 (1964).
28. F. BERTINI, P. GRASSELI, G. ZUBIANI, and G. CAINELLI. Tetrahedron, **26**, 1281 (1970).
29. R. RABINOWITZ and R. MARCUS. J. Am. Chem. Soc. **84**, 1312 (1962).
30. F. A. L. ANET, G. N. CHMURNY, and J. KRANE. J. Am. Chem. Soc. **95**, 4423 (1973).

The photoreduction of hexaaquoiron(III) perchlorate in the presence of tertiary aliphatic alcohols. The effect of added copper

JOHN H. CAREY AND BARRY G. OLIVER[1]

Water Chemistry Section, Canada Centre for Inland Waters, P.O. Box 5050, Burlington, Ont., Canada L7R 4A6

AND

COOPER H. LANGFORD

Department of Chemistry, Carleton University, Ottawa, Ont., Canada K1S 5B6

Received October 25, 1976

JOHN H. CAREY, BARRY G. OLIVER, and COOPER H. LANGFORD. Can. J. Chem. **55**, 1207 (1977).

The irradiation of ferric perchlorate in the presence of *tert*-amyl alcohol produces Fe(II) with a quantum yield of 0.110 ± 0.002, 12% lower than the yield obtained when *tert*-butyl alcohol was used as scavenger. Other tertiary alcohols studied, 3-methyl-2-pentanol and 3-ethyl-3-pentanol, exhibited similar lower yields. It is shown that this reduction is due to the formation of γ-hydroxyalkyl radicals which do not reduce ferric ion to ferrous. The addition of copper causes these radicals to be oxidized. The Fe(II) quantum yield for the irradiation with tertiary amyl alcohol as scavenger in the presence of copper is in good agreement with the tertiary butyl alcohol results in the absence of copper (0.124 ± 0.003).

Quantum yields are observed which are independent of scavenger concentration indicating outer sphere photooxidations are not taking place. This result supports the suggestion that an H on the carbon bearing oxygen is necessary for direct reaction between scavenger and the ferric charge transfer excited state.

JOHN H. CAREY, BARRY G. OLIVER et COOPER H. LANGFORD. Can. J. Chem. **55**, 1207 (1977).

L'irradiation du perchlorate ferrique en présence d'alcool amylique tertiaire conduit à la formation de Fe(II) avec un rendement quantique de 0.110 ± 0.002 soit 12% de moins que le rendement obtenu quand on utilise l'alcool butylique tertiaire comme piège. Les autres alcools tertiaires étudiés, soit le méthyl-3 pentanol-2 et l'éthyl-3 pentanol-3, présentent aussi des rendements plus bas. On montre que cette réduction est due à la formation de radicaux γ-hydroxyalkyles qui ne réduisent pas l'ion ferrique en ion ferreux. L'addition de cuivre cause l'oxydation de ces radicaux. Le rendement quantique de Fe(II) pour l'irradiation avec l'alcool amylique tertiaire comme piège en présence de cuivre est en bon accord avec les résultats obtenus pour l'alcool butylique tertiaire en absence de cuivre (0.124 ± 0.003).

On a observé des rendements quantiques qui sont indépendants de la concentration de piège; ces résultats indiquent qu'il n'y a pas de photooxydation qui se produit dans les couches extérieures. Ces résultats supportent l'hypothèse qu'un hydrogène sur le carbone portant l'oxygène est nécessaire pour la réaction directe entre le piège et l'état excité de transfert de charge de l'ion ferrique.

[Traduit par le journal]

Introduction

The ultraviolet irradiation of strongly acidic solutions of ferric perchlorate leads to the production of hydroxyl radicals by a process represented by reaction 1

$$[1] \qquad Fe^{3+}_{aq} \underset{k_{-1}}{\overset{h\nu}{\rightleftharpoons}} Fe^{3+*}_{aq} \xrightarrow[H_2O]{k_1} Fe^{2+}_{aq} + H^+ + \cdot OH$$

In the absence of scavengers, a back reaction represented by reaction 2 predominates and the net iron(II) yield is very low.

$$[2] \qquad \cdot OH + Fe^{2+}_{aq} + H^+ \xrightarrow{k_2} Fe^{3+}_{aq} + H_2O$$

In order to determine the quantum yield of the primary photochemical processes, organic molecules may be added as hydroxyl radical scavengers. Adamson *et al.* (1) have discussed the requirements for successful use of such scavengers. Since the scavanger molecule invariably forms a new radical in the scavenging reaction, it is essential that the chemistry of the new radical be known so that its fate can be accurately predicted. Other requirements are that no new light absorbing species be introduced in the system

[1] To whom correspondence should be addressed.

and that the scavenger itself be photochemically inert in the wavelength region of interest.

A further complication in the use of scavengers is that at the high concentrations necessary for complete scavenging, reactions may occur between the scavenger and excited state (2). Such a reaction has now been observed in the ferric perchlorate/perchloric acid system when methanol, isopropanol, and formic acid were used as scavengers (3, 4). Of the scavengers studied, *tert*-butyl alcohol was the only one that was efficient enough to react with all hydroxyl radicals and yet not undergo reaction directly with the excited state. It seemed likely that an H on the hydroxyl-bearing C was a requirement for the reaction between scavenger and excited state (4). The reaction path for *tert*-butyl alcohol can be represented by:

$$[3]\quad \cdot OH + HOC(CH_3)_3 \xrightarrow{k_3} H_2O + HOC(CH_3)_2CH_2\cdot$$

$$[4]\quad HOC(CH_3)_2CH_2\cdot + Fe^{3+}_{aq} \xrightarrow{k_4} Fe^{2+}_{aq} + \text{products}$$

The establishment of structure-reactivity relationships such as this can aid in evaluating the importance of the photochemical process in complex systems such as natural waters. To explore this relationship further, we have studied the irradiation of ferric perchlorate in the presence of other alcohols lacking an α-hydrogen.

Experimental

Irradiation Procedures

Solutions to be irradiated were 0.02 *M* ferric perchlorate, 2.00 *M* $HClO_4$, and various copper and alcohol concentrations. Commercial ferric perchlorate (K and K, non-yellow) and cupric perchlorate (Alfa) were used to prepared stock solutions, the concentrations of which were determined by atomic absorption techniques. Spectrophotometric grade *tert*-butyl alcohol was used without further purification whereas *tert*-amyl alcohol (Fisher, reagent), 3-methyl-3-pentanol (Eastman), and 3-ethyl-3-pentanol (Eastman) were fractionally distilled prior to use. Irradiations were performed in a cylindrical quartz cell with an outer jacket through which distilled water from a heating bath could be circulated to maintain the photolyte temperature at 30.0 ± 0.1°C. High purity nitrogen was passed through the solutions for 20 min prior to irradiation. The photoreactor (Ultraviolet Products Inc., San Gabriel, CA) contained four low pressure mercury lamps. Light intensities were determined by ferrioxalate actinometry (6) with potassium ferrioxalate (K and K) recrystallized twice from water.

Analytical Procedures

The iron(II) yields were determined using *o*-phenanthroline and the neutralization dilution technique previously described (3). When copper was present, a blue crystalline precipitate usually formed during the analysis. A check of the analytical system, using samples containing ferrous ammonium sulfate revealed that the precipitate did not contain iron(II). A calibration plot obtained by measuring the absorbance of the supernatant after allowing the blue precipitate to settle gave a molar absorptivity of 1.09×10^4 at 510 nm based on iron(II) concentration. This is in excellent agreement with the value of 1.10×10^4 reported by Hatchard and Parker (5). Thus, the blue precipitate and the presence of copper did not interfere with the iron(II) determination at 510 nm. It was necessary at high copper concentrations to increase the quantity of phenanthroline used in order to achieve complete complexation of the ferrous ion. This behaviour leads us to conclude that the blue precipitate was a copper-phenanthroline complex, probably precipitated as the perchlorate salt.

Photolyte samples were analyzed for products by gas chromatography. After neutralization, the aqueous samples were injected directly into a gas chromatograph equipped with either a Tenax-GC (Enka N.V., Holland) or Chromosorb 101 (Johns-Manville) column and flame ionization detectors.

For example, a sample of the photolysis solution containing 0.10 *M* *tert*-butyl alcohol was irradiated to 10% conversion based on iron. The photolyte was neutralized with KOH and the precipitate (iron oxide and potassium perchlorate) was removed by decantation. The clear, colourless supernatant was injected directly onto a 1.83 m Tenax column operated at 170°C. Adequate separation of the resulting products from the much larger parent alcohol peak could be achieved at this temperature for both the *tert*-butyl and *tert*-amyl alcohol systems. Alternatively, the neutralized supernatant could be evaporated under vacuum at 35°C and the residue extracted several times with ether.

To obtain the mass spectra of the products, concentrated samples were injected into a Finnigan GC-MS system with TENAX column. Mass spectra and gas chromatographic behaviour of the observed products were compared with those of the following diols.

Isobutylene Glycol: Synthesized from methallyl alcohol (Pfaltz and Bauer) following literature procedures (6).

2-Methyl-1,2-butanediol and 2-methyl-2,3-butanediol: Synthesized from 2-methyl-1-butene and 2-methyl-2-butene, respectively, by akaline permanganate oxidation at low temperature.

2,7-Dimethyl-2,7-octanediol (ICN Pharmaceuticals) and 3-methyl-1,3-butanediol (BASF) were used as received.

The identity of the three synthesized glycols was confirmed by periodate cleavage (7) and analysis of the resulting carbonyl products by thin layer chromatography of their 2,4-dinitrophenylhydrazine derivatives on alumina with solvent cyclohexane–nitrobenzene (2:1). Cleavage of isobutylene glycol led to formaldehyde and acetone, while 2-methyl-1,2-butanediol gave formaldehyde and methyl ethyl ketone and cleavage of 2-methyl-2,3-butanediol yielded acetaldehyde and acetone.

Results and Discussion

Previous studies on the 2537 Å irradiation of ferric perchlorate in the presence of *tert*-butyl alcohol, performed on undegassed solutions

over a temperature range of 35–40°C, established a limiting quantum yield for iron(III) reduction to be 0.130 ± 0.003 (3). From this value, a primary quantum yield for free ·OH was calculated to be 0.065. We have studied the scavenging behaviour of three other tertiary alcohols in this system by irradiating a deaerated photolyte at a temperature of 30.0 ± 0.1°C. For the purpose of comparison, *tert*-butyl alcohol was also studied under these conditions. For all tertiary alcohols studied, the concentration of iron(II) increases linearly with irradiation time for conversions less than 10%. Although concentrations were limited by solubility, in all cases a yield could be reached which was independent of scavenger concentration. These yields are summarized in Table 1. It can be seen that the limiting yield for iron(II) production drops as substitution on the alcohol increases. Such an effect is unexpected based on reaction scheme 1–4.

It may be possible for tertiary alcohol structure to exert some influence on the primary reaction by affecting k_1 and k_{-1}. Since it was previously demonstrated (4) that methanol, isopropyl alcohol, and *tert*-butyl alcohol did not enter the primary coordination sphere of the iron, such an effect is unlikely. Instead, it seems probable that the reaction of hydroxyl radicals with higher tertiary alcohols produces some radicals, which do not react with Fe(III) to produce Fe(II) via reaction 4.

Walling and co-workers (8–10) have discussed the types of radicals formed in the Fenton's reagent (ferrous ion – hydrogen peroxide) oxidation of alcohols and characterized them according to their reaction with Fe(III). He has concluded that radicals formed by abstraction of an α-hydrogen from alcohols are oxidized by Fe(III) at diffusion controlled rates, while radicals which arise by abstraction of β-hydrogens are oxidized with more difficulty. Radicals formed by abstraction of hydrogens further removed from the hydroxyl group resemble alkyl radicals in that neither is oxidized by Fe(III). These radicals can, however, be oxidized by Cu(II) which will produce Fe(II) via reactions 5 and 6.

$$[5] \qquad R\cdot + Cu^{2+}_{aq} \xrightarrow[H_2O]{} ROH + Cu^{+}_{aq} + H^{+}$$

$$[6] \qquad Cu^{+}_{aq} + Fe^{3+}_{aq} \rightarrow Cu^{2+}_{aq} + Fe^{2+}_{aq}$$

The addition of copper can, however, cause other changes in the reaction mechanism. Bhatia and Schuler (11) found that the hydroxycyclohexadienyl radical could be quantitatively oxidized by ferricyanide, while lower yields and other complications were present when copper was used as oxidant. Some of these complications were due to the buildup of cuprous ion in the system. Such a buildup will not occur in the present system since the cuprous ion will react with Fe(III).

Walling *et al.* (10) have reported that the addition of high copper concentrations can affect results in the Fenton's reagent system in a manner suggestive of the reaction of hydroxyl radicals with Cu(II).

$$[7] \qquad Cu^{2+}_{aq} + \cdot OH \rightleftarrows Cu(III) + OH^{-}$$

In acid solution, Cu(III) rapidly reverts to hydroxyl radicals and Cu(II) (12). Since the present studies were performed in 2 *M* $HClO_4$, if any Cu(III) formed, it should decompose too rapidly to oxidize Fe(II) and thus affect the Fe(II) yield.

In order to check the effect of adding copper on the *tert*-butyl alcohol scavenging system, studies were performed at 30.0°C over a range of copper concentrations from 0.01 to 0.05 *M*. The concentrations of *tert*-butyl alcohol used were previously shown to be sufficient to scavenge all hydroxyl radicals (3). The quantum yield for iron(II) production is 0.124 ± 0.003 and is independent of copper concentration.

The addition of copper to the tertiary amyl system caused an increase in the rate at which Fe(II) was formed on irradiation. Identical results were obtained for a copper concentration of 0.002 and 0.005 *M*. The quantum yield is calculated to be 0.124 ± 0.002, in good agreement with the value obtained for *tert*-butyl alcohol scavenging at this temperature. The quantum yields for the other tertiary alcohols also exhibited a similar increase. These results are summarized in Table 1.

Attempts were made to identify the organic products resulting from both *tert*-butyl and *tert*-amyl alcohol scavenging in this system. In a previous paper (3), it was reasoned that isobutylene glycol and Fe(II) were the likely products from the reaction of a 2-methyl-2-hydroxypropyl radical with Fe(III). Similarly, reaction between Fe(III) and radicals produced by β-hydrogen abstraction from *tert*-amyl alcohol may also lead to diols as expected products.

TABLE 1

(*a*) Quantum yields for photoreduction at various scavenger concentrations

Scavenger	Scavenger concentration (mol/ℓ)	Copper concentration (mol/ℓ)	$\Phi_{Fe(II)}$
tert-Butyl alcohol	0.106	0	0.126±0.003
	0.536	0	0.125±0.003
	0.536	0.005	0.122±0.003
	0.536	0.010	0.124±0.002
	0.536	0.040	0.123±0.002
	0.536	0.050	0.125±0.002
tert-Amyl alcohol	0.184	0	0.107±0.002
	0.275	0	0.108±0.002
	0.367	0	0.113±0.002
	0.643	0	0.110±0.002
	0.275	0.002	0.121±0.002
	0.367	0.002	0.125±0.003
	0.459	0.002	0.123±0.002
	0.184	0.005	0.124±0.002
	0.275	0.005	0.124±0.002
	0.367	0.005	0.123±0.002
	0.459	0.005	0.125±0.002
	0.643	0.005	0.126±0.002
3-Methyl-3-pentanol	0.081	0	0.109±0.001
	0.162	0	0.107±0.002
	0.081	0.005	0.122±0.002
	0.162	0.005	0.121±0.002
3-Ethyl-3-pentanol	0.0072	0	0.103±0.002
	0.0144	0	0.104±0.002
	0.0144	0.005	0.122±0.002

(*b*) Prominent peaks in mass spectra of products for tertiary amyl alcohol scavenging

	Intensty (%)					
AMU	Product A[a]	2-Methyl-2,3-butanediol[b]	Product B[a]	2-Methyl-1,2-butanediol[b]	Product C[a]	3-Methyl-1,3-butanediol[b]
39	17.4	13.7	28.1	13.1	20.8	13.2
41	37.7	34.7	31.2	26.3	33.8	—
42	18.6	7.9	10.4	3.2	14.5	6.3
43	92.3	76.8	70.8	42.0	100.0	100.0
45	20.9	21.1	29.2	22.1	—	—
55	—	—	100.0[c]	48.4[c]	5.3	7.4
56	—	—	9.4	3.7	5.5	5.8
57	—	—	59.1	42.0	—	—
58	13.8	—	—	9.5	12.5	6.8
59	100.0	100.0	—	—	49.1	79.0
71	11.1	24.2	5.2	10.5	13.3	14.2
73	—	—	88.5[c]	100.0[c]	—	—
75	—	—	35.4	36.8	—	—
89	6.1	9.5	5.2	5.3	8.0	7.4

[a] $[HClO_4] = 2.00\ M$, $[Fe^{3+}] = 0.02\ M$, $[Cu^{2+}] = 0.005\ M$. Spectra determined on Finnigan GC/MS System by subtraction of baseline from that of peak.

[b] Spectra of synthetic samples run by direct injection on a Hitachi-Perkin Elmer RMU6L Mass Spectrometer.

[c] Peaks at *m/e* 55 and 73 are related by loss of H_2O from the ion. The base peak has shifted because the two instruments operate under different conditions, *e.g.*, temperature, which affects rate of loss of H_2O.

TABLE 1 (*Concluded*)

(*c*) Mass spectrum of product for *tert*-butyl alcohol scavenging[d]

	Intensity (%)	
AMU	Photo-product	Isobutylene glycol
42	6.1	6.2
43	19.3	20.9
44	21.9	21.0
45	100.0	100.0
75	16.7	15.6
76	6.6	7.2

[d]Obtained by subtraction of mass spectrum baseline from that of peak.

[8] $$\cdot CH_2-\underset{\displaystyle CH_3}{\overset{\displaystyle OH}{\overset{|}{\underset{|}{C}}}}-CH_2CH_3 + Fe^{3+}_{aq} \rightarrow \underset{\displaystyle HO}{\overset{|}{CH_2}}-\underset{\displaystyle CH_3}{\overset{\displaystyle OH}{\overset{|}{\underset{|}{C}}}}-CH_2CH_3 + Fe^{2+}_{aq} + H^+$$

1

[9] $$CH_3-\underset{\displaystyle CH_3}{\overset{\displaystyle OH}{\overset{|}{\underset{|}{C}}}}-\dot{C}HCH_3 + Fe^{3+}_{aq} \rightarrow CH_3-\underset{\displaystyle CH_3}{\overset{\displaystyle HO}{\overset{|}{\underset{|}{C}}}}-\overset{\displaystyle OH}{\overset{|}{CH}}CH_3 + Fe^{2+}_{aq} + H^+$$

2

The reaction of the 3-methyl-3-hydroxybutyl radical with Cu(II) will likewise result in diol formation.

[10] $$CH_3-\underset{\displaystyle CH_3}{\overset{\displaystyle OH}{\overset{|}{\underset{|}{C}}}}-CH_2\dot{C}H_2 + Cu^{2+}_{aq} \rightarrow CH_3-\underset{\displaystyle CH_3}{\overset{\displaystyle HO}{\overset{|}{\underset{|}{C}}}}-\overset{\displaystyle OH}{\overset{|}{CH_2}}CH_2 + Cu^{+}_{aq} + H^+$$

3

For *tert*-butyl alcohol, comparison of retention times and mass spectra of the scavenging product and a synthetic sample of isobutylene glycol confirm that the latter is the major organic product of the photolysis. There was no noticeable difference between aerated and deaerated samples, with or without copper.

In the *tert*-amyl alcohol case, two products are easily detected by gas chromatography of a photolyte containing no copper. A third product can be observed at higher temperature and long retention times. The first two observed products have retention times and mass spectra identical to synthetic samples of the expected glycols 2-methyl-1,2-butanediol (**1**) and 2-methyl-2,3-butanediol (**2**). The third product has identical retention times on two different GC columns to a commercial sample of 2,7-dimethyl-2,7-octanediol and indicates that in the absence of copper, the 3-methyl-3-hydroxybutyl radical undergoes a radical–radical reaction 11.

[11] $$2\ CH_3-\underset{\displaystyle CH_3}{\overset{\displaystyle OH}{\overset{|}{\underset{|}{C}}}}-CH_2\dot{C}H_2 \longrightarrow CH_3-\underset{\displaystyle CH_3}{\overset{\displaystyle OH}{\overset{|}{\underset{|}{C}}}}-CH_2CH_2CH_2CH_2-\underset{\displaystyle CH_3}{\overset{\displaystyle OH}{\overset{|}{\underset{|}{C}}}}-CH_3$$

4

Products **1** and **2** are also found in the photolysis of a solution containing copper. No change in the ratio or position of the peaks was apparent. Product **4** from the radical–radical reaction is not present in the photolyte containing copper but has been replaced by a new product of only slightly longer GC retention time than **2**. Comparison of GC retention times and mass spectra of this product with a commercial sample reveals that this product is 3-methyl-1,3-butanediol **3**. Since the glycol products could be susceptible to pinacol type rearrangements in the acid medium, no attempt was made to determine quantum yields of the organic products. The mass spectra obtained for the reaction products and synthesized diols are shown in Table 1 (*b*) and (*c*).

In the irradiation of 0.01 *M* ferric perchlorate in the presence of benzoic acid, it was found that *o*-, *m*-, and *p*-hydroxybenzoic acids were formed corresponding to the statistical 2:2:1 ratio (13). To evaluate the possibility that the hydroxyl radical abstracts hydrogen from these tertiary alcohols on a statistical basis, we have calculated the fraction of γ-hydrogens relative to the total number of β- and γ-hydrogens in the molecule and from these values predicted quantum yields for Fe(II) based on statistical abstraction. These yields were 0.105 for *tert*-amyl alcohol, 0.094 for 3-methyl-3-pentanol, and 0.085 for 3-ethyl-3-pentanol. For the latter two alcohols, the observed yields in Table 1 are higher than those predicted, indicating some preference towards the abstraction of β-hydrogen rather than γ.

A recent esr study of the photolysis of ferric perchlorate in neat alcohol glasses revealed that methyl radicals were formed from *tert*-butyl alcohol (14). Methyl radicals are inert towards iron(III) and would dimerize without producing iron(II). However, in the presence of copper, the reaction of methyl radicals with copper(II) would result in iron(II) production via reaction 6. It can be seen in Table 1 that there is no effect of copper on the iron yield for *tert*-butyl alcohol scavenging and thus methyl radicals are not produced in the photolysis in aqueous solution. The methyl radicals observed in neat alcohol glasses may result from excitation of an alcohol-to-iron charge transfer transition. Such a transition is unlikely in dilute aqueous solution where it has previously been demonstrated that *tert*-butyl alcohol does not enter the primary coordination sphere of iron(III) (4).

There is no evidence for outer-sphere reaction between any of the tertiary alcohols studied and the ferric CT excited state. This result supports the suggestion that an H on the carbon bearing oxygen is necessary for the excited state reaction (4).

It is evident that differences in reactivity of radicals towards various metal oxidants may allow individual radicals to be observed. This may prove to be an important tool for mechanistic interpretation. We intend to explore this possibility further.

Acknowledgements

We thank William M. J. Strachan, Michael E. Comba, and Michael E. Fox, Canada Centre for Inland Waters, for obtaining the mass spectra and BASF Corporation for the gift of 3-methyl-1,3-butanediol.

C.H.L. thanks the National Research Council of Canada for grants and acknowledges a research agreement with the Inland Waters Directorate, Environment Canada.

1. M. G. Adamson, D. L. Baulch, and F. S. Dainton. Trans. Faraday Soc. **58**, 1388 (1962).
2. H. P. Waits and G. S. Hammond. J. Am. Chem. Soc. **86**, 1911 (1964).
3. C. H. Langford and J. H. Carey. Can. J. Chem. **53**, 2430 (1975).
4. J. H. Carey and C. H. Langford. Can. J. Chem. **53**, 2436 (1975).
5. C. G. Hatchard and A. C. Parker. Proc. R. Soc. A, **235**, 518 (1956).
6. G. Hearne, M. Tamell, and W. Converso. Ind. Eng. Chem. **33**, 805 (1941).
7. W. H. Evans and A. Dennis. Analyst, **98**, 782 (1973).
8. C. Walling and S. Kato. J. Am. Chem. Soc. **93**, 4275 (1971).
9. C. Walling and G. El-Taliawi. J. Am. Chem. Soc. **95**, 844 (1973).
10. C. Walling, G. El-Taliawi, and R. Johnson. J. Am. Chem. Soc. **96**, 133 (1974).
11. K. Bhatia and R. Schuler. J. Phys. Chem. **78**, 2335 (1974).
12. D. Meyerstein. Inorg. Chem. **10**, 638 (1971).
13. H. G. C. Bates and N. Uri. J. Am. Chem. Soc. **75**, 2754 (1953).
14. A. Cox and T. J. Kemp. J. Chem. Soc. Faraday Trans. I, **71**, 2490 (1975).

Crystal structure of a dimeric 1-methylcytosine mercuric chloride complex

MONIQUE AUTHIER-MARTIN AND ANDRÉ L. BEAUCHAMP

Département de Chimie, Université de Montréal, Montréal (Qué.), Canada H3C 3V1

Received August 12, 1976

MONIQUE AUTHIER-MARTIN and ANDRÉ L. BEAUCHAMP. Can. J. Chem. **55**, 1213 (1977).

Di-μ-chloro-bis[chloro(1-methylcytosine-O,N^3)mercury(II)] belongs to space group $P2_1/c$ with cell dimensions $a = 9.932(2)$, $b = 14.051(3)$, $c = 9.198(2)$ Å, and $\beta = 135.41(2)°$. The structure was solved by the heavy-atom method and refined to an R factor of 0.027 for 1271 independent reflections. The crystal is composed of centrosymmetric dimeric molecules in which two mercury atoms are attached by a pair of symmetrical chlorine bridges. The 1-methylcytosine ligand is bidentate *via* N(3) and O(2). The metal atom has a (2 + 3) coordination with a very distorted trigonal bipyramid geometry. A chlorine atom at 2.322(3) Å and ring nitrogen N(3) at 2.17(1) Å form strong axial bonds with mercury. Two bridging chlorine atoms at 2.719(2) and 2.745(3) Å, and carbonyl oxygen O(2) at 2.84(1) Å form weaker equatorial bonds. The amino group is hydrogen-bonded to a bridging chlorine of the same molecule (N···Cl = 3.23(1) Å) and a carbonyl oxygen of a neighboring molecule (N···O = 2.86(2) Å).

MONIQUE AUTHIER-MARTIN et ANDRÉ L. BEAUCHAMP. Can. J. Chem. **55**, 1213 (1977).

Les cristaux de di-μ-chloro-bis[chloro(méthyl-1-cytosine-O,N^3)mercure(II)] appartiennent au groupe spatial $P2_1/c$ et les dimensions de la maille élémentaire sont $a = 9.932(2)$, $b = 14.051(3)$, $c = 9.198(2)$ Å et $\beta = 135.41(2)°$. La structure a été résolue par la méthode de l'atome lourd. L'affinement effectué au moyen de 1271 réflexions indépendantes a convergé à un facteur R de 0.027. Le cristal est constitué de molécules dimères centrosymétriques dans lesquelles les deux atomes de mercure sont réunis par deux ponts chlore symétriques. La méthyl-1-cytosine forme un chélate par l'intermédiaire de N(3) et O(2). Le métal possède une coordination (2 + 3) correspondant à une bipyramide triangulaire très déformée. Un atome de chlore à 2.322(3) Å et l'atome N(3) du coordinat à 2.17(1) Å forment des liaisons axiales fortes avec le mercure. Les deux atomes de chlore des ponts à 2.719(2) et 2.745(3) Å, ainsi que l'atome O(2) du groupement carbonyle à 2.84(1) Å, établissent les liaisons équatoriales plus faibles. Les deux atomes d'hydrogène du groupement amino participent à des liaisons hydrogène, l'une intramoléculaire avec le chlore d'un pont (N···Cl = 3.23(1) Å), l'autre intermoléculaire avec l'oxygène du groupement carbonyle (N···O = 2.86(2) Å).

Introduction

As part of our research on metal complexes with purine and pyrimidine bases of DNA, mercuric chloride was found to form a 1:1 addition compound with 1-methylcytosine. Other workers (1) have identified ring nitrogen N(3) as the primary target for Hg^{2+} and CH_3Hg^+ ions in solutions of N(1)-substituted cytosines. X-Ray work on complexes with other metals (2–4) has also shown binding at N(3), but in some cases chelate formation through the adjacent carbonyl group takes place. The present crystal structure was studied in order to ascertain N(3)-coordination and to determine whether the carbonyl group is bonded to mercury.

Experimental

Crystal Data

$C_5H_7N_3OCl_2Hg$ f.w. = 396.63

Monoclinic, space group $P2_1/c$, $a = 9.932(2)$, $b = 14.051(3)$, $c = 9.198(2)$ Å, $\beta = 135.41(2)°$, $V = 901.1$ Å^3, $Z = 4$ monomers (or 2 dimers), $D_c = 2.924$ g cm^{-3}, $D_o = 2.91(1)$ g cm^{-3} (flotation in $CHBr_3$–$Br_2CHCHBr_2$ mixture), $\mu(MoK\alpha) = 171$ cm^{-1}, $\lambda(MoK\bar{\alpha}) = 0.71068$ (graphite monochromator), $t = 23°C$.

Preparation

Mercuric chloride and 1-methylcytosine (0.4 mmol each) were dissolved in 40 ml of water at 80°C. Upon cooling at room temperature, colorless crystals of composition $(MC)HgCl_2$ (where MC = 1-methylcytosine) precipitated. *Anal.* calcd.: Hg 50.57, Cl 17.88, C 15.14, N 10.60, H 1.78; found (Schwarzkopf Lab.): Hg 50.14, Cl 17.50, C 14.96, N 10.81, H 2.04.

The crystal chosen for data collection was a small plate of dimensions 0.37 mm × 0.04 mm × 0.15 mm measured perpendicular to {001}, {010}, and {31$\bar{2}$}. The last set of very small faces was not identified unambiguously, but the absorption correction is not sensitive to its exact positioning.

Crystallographic Measurements

Space group $P2_1/c$ and preliminary cell constants were determined from precession photographs. Refined cell parameters and intensity measurements were obtained

TABLE 1. Refined fractional coordinates ($\times 10^3$, Cl $\times 10^4$, Hg $\times 10^5$) and anisotropic temperature factors ($\times 10^3$, Hg $\times 10^4$), t.f. = exp $\{-(U_{11}a^{*2}h^2 + U_{22}b^{*2}k^2 + U_{33}c^{*2}l^2 + 2U_{12}a^*b^*hk + 2U_{13}a^*c^*hl + 2U_{23}b^*c^*kl)$. Extinction coefficient = $4.7(3)\times 10^3$

Atom	x	y	z	U_{11}	U_{22}	U_{33}	U_{12}	U_{13}	U_{23}
Hg	21691(6)	9437(2)	18546(4)	342(2)	280(2)	481(2)	38(2)	321(2)	−2(2)
Cl(1)	1155(4)	2238(1)	2443(4)	55(2)	33(1)	65(2)	6(1)	50(2)	1(1)
Cl(2)	624(4)	−523(1)	2252(3)	35(1)	37(1)	36(1)	4(1)	28(1)	1(1)
N(1)	683(1)	65(1)	255(1)	31(5)	36(3)	55(5)	0(3)	35(4)	0(3)
C(1)	789(2)	136(1)	253(2)	47(7)	58(6)	61(7)	−11(5)	44(7)	−6(5)
C(2)	549(1)	94(1)	250(1)	34(5)	27(4)	48(5)	−2(4)	31(5)	−3(4)
O(2)	511(1)	178(1)	240(1)	50(5)	21(3)	77(5)	7(3)	50(4)	8(3)
N(3)	448(1)	24(1)	248(1)	27(4)	24(3)	43(4)	4(3)	27(4)	5(3)
C(4)	489(1)	−66(1)	262(1)	32(6)	29(4)	44(5)	2(4)	27(5)	4(4)
N(4)	393(1)	−130(1)	265(1)	55(6)	28(3)	79(6)	6(4)	57(6)	0(4)
C(5)	632(1)	−95(1)	274(1)	37(6)	27(4)	48(5)	5(4)	31(5)	−4(4)
C(6)	728(1)	−28(1)	271(1)	30(6)	44(5)	42(5)	7(4)	30(5)	7(4)

with a Syntex P$\bar{1}$ automatic diffractometer. A set of 15 reflections ($11 < 2\theta < 24°$) were automatically centered and indexed according to the standard procedure. Least-squares refinement on the setting angles of those reflections led to the cell parameters given above and to the orientation matrix for data collection. Oscillation photographs taken along each of the three axes showed the expected symmetry and spacing, and confirmed our choice of axes.

All hkl and $hk\bar{l}$ reflections within a sphere of $2\theta < 50°$ were measured. The $\theta/2\theta$ scan technique was used and the scan speed (from 1° to 24° (2θ)/mn) was automatically selected according to peak height. The 2θ scan was from $[2\theta(K\alpha_1) - 1.2°]$ to $[2\theta(K\alpha_2) + 1.2°]$ (Syntex autocollection program). Background counts were taken at each limit and the background time-to-scan time ratio was 0.4. Three standard reflections (002, $\bar{1}\bar{1}1$, $\bar{1}02$) measured every 45 reflections showed variations $< \pm 5\%$ from their respective means. The reduced set of data consisted of 1589 unique reflections. A total of 1271 reflections with net intensities $I \geq 2.5\sigma(I)$ (5) were used to solve the structure. The data were corrected for Lorentz and polarization effects. Absorption corrections based on the equations of the crystal faces were applied at a later stage. A grid of $5 \times 5 \times 10$ was used and the transmission factor ranged from 0.10 to 0.49 (Program NRC-3, Ahmed and Singh).

Resolution of the Structure

The structure was solved by the heavy-atom method. Successive Fourier maps and structure factor calculations revealed the positions of all nonhydrogen atoms. The function minimized in least-squares calculations was $\sum w(|F_o| - |F_c|)^2$. Full-matrix refinement with isotropic temperature factors and weights $w = 1.0$ converged to

$$R = \sum||F_o| - |F_c||/\sum|F_o| = 0.166$$

An absorption correction was introduced and R decreased to 0.086. Anisotropic refinement of all nonhydrogen atoms was carried out using block-diagonal least squares. At this stage, all hydrogen atoms were visible on a ΔF map. They were placed at their calculated positions (C—H and N—H = 0.95 Å) with temperature factors $B = 6.0$ Å^2 ($U = 0.076$ Å^2). Their parameters were not refined, but the shifts on the coordinates of the corresponding carbon or nitrogen atoms were applied to those of hydrogen as well.[1] In the last cycles of refinement, individual weights $w = 1/\sigma_F^2$ (5) were applied to each reflection. Refinement of the scale factor, the secondary extinction coefficient (6), the coordinates, and anisotropic temperature factors of all nonhydrogen atoms converged to $R = 0.027$ and

$$R_w = [\sum w(|F_o| - |F_c|)^2/\sum w|F_o|^2]^{1/2} = 0.031$$

The validity of the weighting scheme was confirmed by the absence of systematic variations of $w(|F_o| - |F_c|)^2$ as a function of $\sin\theta/\lambda$ and $|F_o|$. The final ΔF map showed a few peaks of 1.0 e/Å^3 near mercury and one peak of 0.9 e/Å^3 in the neighborhood of O(2). Elsewhere, the background was lower than ± 0.6 e/Å^3.

The refined parameters are given in Table 1 and a list of structure factors is available upon request.[1] The scattering curves used were those of Cromer and Waber (7) for nonhydrogen atoms and of Stewart *et al.* (8) for hydrogen. The anomalous dispersion coefficients $\Delta f'$ and $\Delta f''$ of Hg and Cl (9) were included in the calculations.

Local versions of the following computer programs were used in this work: F. R. Ahmed and C. P. Huber, NRC-2 (Data Reduction); F. R. Ahmed and P. Singh, NRC-3 (Absorption Correction); R. J. Doedens and J. A. Ibers, NUCLS (Least-squares refinement), with block-diagonal option introduced by J. Sygusch; A. Zalkin, FORDAP (Fourier maps); C. K. Johnson, ORTEP (Stereo drawings).

Description of the Structure and Discussion

The structure consists of centrosymmetric chlorine-bridged dimers where 1-methylcytosine acts as a bidentate ligand (Fig. 1). The five

[1]The structure factor table and the list of hydrogen coordinates are available, at a nominal charge, from the Depository of Unpublished Data, CISTI, National Research Council of Canada, Ottawa, Canada K1A 0S2.

TABLE 2. Distances and angles around mercury

Atoms	Distance (Å)	Bonds	Angle (deg)
Hg—Cl(1)	2.322(3)	Cl(1)—Hg—N(3)	148.0(3)
Hg—Cl(2)	2.745(3)	Cl(1)—Hg—Cl(2)	100.4(1)
Hg—Cl(2)[a]	2.719(2)	Cl(1)—Hg—Cl(2)[a]	108.2(1)
Hg—N(3)	2.17(1)	Cl(1)—Hg—O(2)	101.3(2)
Hg—O(2)	2.84(1)	Cl(2)—Hg—Cl(2)[a]	84.6(1)
		Cl(2)—Hg—N(3)	102.1(3)
		Cl(2)—Hg—O(2)	152.8(2)
		Cl(2)[a]—Hg—N(3)	96.3(3)
		Cl(2)[a]—Hg—O(2)	103.9(2)
		N(3)—Hg—O(2)	51.8(4)

[a] $a = x,y,z$.

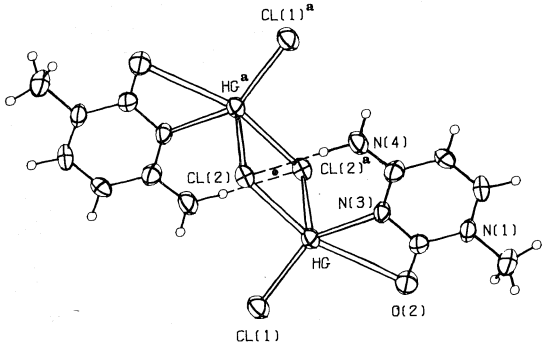

FIG. 1. Structure of the dimer. The left part of the molecule is related to the right part by a crystallographic inversion center shown as a black spot. Dashed lines represent hydrogen bonds. $a = (\bar{x}, \bar{y}, \bar{z})$.

donor atoms within bonding distances do not define a regular polyhedron around mercury (Table 2). On the basis of bond strength, the compound is best described in terms of a (2 + 3) coordination with a highly distorted trigonal bipyramid geometry. Mercury is strongly bonded to Cl(1) and N(3) occupying 'axial positions', whereas O(2) and two crystallographically equivalent Cl(2) atoms form three weaker bonds in the 'equatorial plane'.

It is common to recognize two sets of bonds in the coordination sphere of mercury. For instance, a number of addition compounds contain Cl—Hg—Cl units with strong bonds at ~180° and as many as four weak bonds or contacts in the equatorial plane completing a (2 + 4) octahedral coordination (11–15). The Hg—Cl(1) distance observed here (2.322(3) Å) is typical of such strong bonds. The most unexpected feature of the present structure is that the second strong bond is formed with N(3) instead of Cl(2). The Hg—N(3) distance (2.17(1) Å) is normal for pyridine-type nitrogen (16). Shorter distances, as observed in bis(1-methylthyminato)mercury(II) (2.04 Å) (17), are normally found only when mercury reacts by substitution of an acidic hydrogen atom.

The two Hg—Cl(2) bonds in the equatorial plane are much stronger than Hg—O(2). This produces a displacement of the axial bonds in the direction that increases the Cl(2)—Hg–axial angles above 90° and, as a consequence, the axial–Hg–axial angle is reduced to 148.0(3)°.

The Hg—O(2) distance (2.84(1) Å) is less, although not much, than the sum of the van der Waals radii (3.0 Å) (11). Similar or slightly shorter distances have been reported for complexes with uracil (2.71 Å) (18), dihydrouracil (2.88 Å) (18), and cyclohexanedione (2.79 Å) (14). Consequently, there is a significant oxygen–metal interaction as found in copper–cytosine complexes (3). A comparison of these chelates with the monodentate platinum complex (4) reveals a striking difference between the exocyclic angles at N(3). Pt—N(3)—C(2) and Pt—N(3)—C(4) are 115.3 and 125.1° respectively. The difference of 10° is probably due to steric effect of hydrogen atoms which make the amino group bulkier than a carbonyl group. In the copper complexes, the angles differ by 17.5° and 22.2° (3) and a still greater difference (24°) is found here. This is probably due to chelate formation because such large differences in exocyclic angles are needed to take the carbonyl oxygen close enough to the metal atom. The C(2)—O(2)—Hg angle of 80.6(8)° would also be acceptable, the direction of maximum basicity theoretically predicted by Bonaccorsi *et al.* (19) being at 55° from the C—O bond. In the present case, unequal exocyclic angles also promote intramolecular hydrogen bonding of the amino group with a bridging chlorine

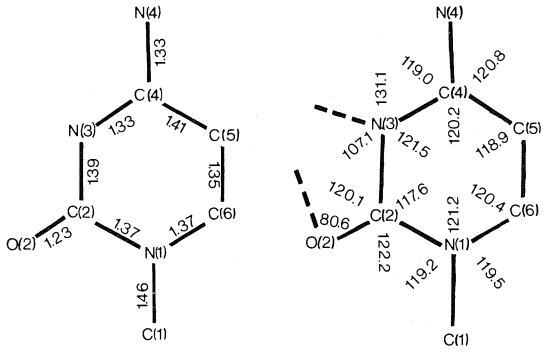

FIG. 2. Interatomic distances and bond angles of the coordinated ligand. The e.s.d.'s are 0.01–0.02 Å on bond lengths and 1.0° on bond angles.

atom: Cl(2)—N(4) = 3.23(1) Å, C(4)—N(4)—Cl(2) = 117.0(9)°.

Most of the Hg—Cl—Hg bridges reported in the literature are either symmetrical, as observed here, with two equivalent Hg—Cl distances of ~2.8 Å, or highly unsymmetrical with one short bond of ~2.3 Å and one weak contact >3.0 Å. The latter type, which is more common, is observed in $HgCl_2$ (11), many of its addition compounds (11–15) and the complex of Cl_3CHgCl with 1,10-phenanthroline (20). Both types of bridges are present in $MHgCl_3$ salts (with M = univalent cation), where octahedral $HgCl_6$ units sharing edges form infinite chains or ribbons (11, 21). To our knowledge, this is the first example of mercury being symmetrically bridged by a pair of chlorine atoms in a discrete molecule.

The geometry of the coordinated ligand is shown in Fig. 2. Bond lengths and bond angles in neutral and protonated cytosine rings have been discussed by Sundaralingam and coworkers (10). The two forms exhibit differences in bond lengths not much greater than the e.s.d.'s of the present work. Our values do not differ significantly from those of either type of ring, except for C(2)—N(3) (1.39(1) Å), which is probably greater than the distance of the neutral form (1.356 Å) and close to that of the protonated form (1.389 Å). In the case of angles, our e.s.d.'s are smaller compared with the differences for the most sensitive angles. Our results (N(1)—C(2)—N(3) = 117.6(1.0)°, C(2)—N(3)—C(4) = 121.5(9)°, N(3)—C(4)—C(5) = 120.2(1.0)°) are more like those of the neutral form (119.1, 120.2, 121.7°) than those of the protonated form (114.8, 124.8, 117.7°).

The amino and methyl groups are in the plane of the six-membered ring within 1σ and their exocyclic angles are normal. The carbonyl group is significantly out of that plane with distances of 0.026 Å (3σ) and 0.042 Å (6σ) for C(2) and O(2) respectively. The exocyclic angles around C(2) are affected by protonation, complexation at N(3), and hydrogen bonding (3, 22). In this case, additional effects are expected from chelation and our results cannot be related in a simple manner to those various phenomena.

A packing diagram (Fig. 3) shows dimers linked by strong intermolecular N—H···O hydrogen bonds: N—O = 2.86(2) Å, C(4)—N(4)—O(2) = 112.5(9)°. All other contacts are normal. It is noteworthy that the organic ligands are approximately parallel within the dimer and in the rest of the structure. Neverthe-

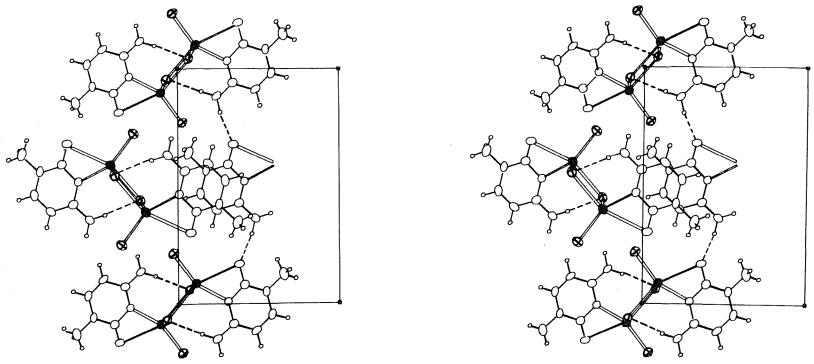

FIG. 3. Projection of the unit cell down the *c* axis. The origin is at the lower left corner, *a* is horizontal, *b* is vertical, and *c* points toward the reader. The atoms can be identified by comparison with Fig. 1.

less, the rings are not above each other and there is apparently little direct effect of base stacking as frequently observed with this type of ligands.

Acknowledgments

We wish to thank Dr. Fernande Rochon for permission to use the diffractometer and her valuable assistance in collecting data. This work was supported by the National Research Council of Canada and the Ministère de l'Education du Québec.

1. G. L. EICHHORN. Inorganic biochemistry. Vol. 2. Elsevier, New York. 1973. p. 1205; S. MANSY, T. E. WOOD, J. C. SPROWLES, and R. S. TOBIAS. J. Am. Chem. Soc. **96**, 1762 (1974); K. W. JENNETTE, S. J. LIPPARD, and D. A. UCKO. Biochim. Biophys. Acta, **402**, 403 (1975).
2. M. SUNDARALINGAM and J. A. CARRABINE. J. Mol. Biol. **61**, 287 (1971); G. R. CLARK and J. D. ORBELL. J. Chem. Soc. Chem. Commun. 697 (1975); D. M. L. GOODGAME, J. JEEVES, and C. D. REYNOLDS. Biochem. J. **151**, 467 (1975); K. SAITO, R. TERASHIMA, T. SAKAKI, and K. TOMITA. Biochem. Biophys. Res. Commun. **61**, 83 (1974).
3. T. J. KISTENMACHER, D. J. SZALDA, and L. G. MARZILLI. Acta Cryst. B, **31**, 2416 (1975); D. J. SZALDA, L. G. MARZILLI, and T. J. KISTENMACHER. Inorg. Chem. **14**, 2076 (1975).
4. C. J. L. LOCK, R. A. SPERANZINI, and J. POWELL. Can. J. Chem. **54**, 53 (1976).
5. G. H. STOUT and L. H. JENSEN. X-Ray structure determination. Macmillan, New York. 1968. p. 454.
6. P. COPPENS and W. C. HAMILTON. Acta Crystallogr. A, **26**, 71 (1970).
7. D. T. CROMER and J. T. WABER. Acta Crystallogr. **18**, 104 (1965).
8. R. F. STEWART, E. DAVIDSON, and W. T. SIMPSON. J. Chem. Phys. **42**, 3175 (1965).
9. D. T. CROMER. Acta Crystallogr. **18**, 17 (1965).
10. M. A. VISWAMITRA, B. S. REDDY, G. H. Y. LIN, and M. SUNDARALINGAM. J. Am. Chem. Soc. **93**, 4565 (1971).
11. D. GRDENIC. Q. Rev. **19**, 303 (1965).
12. R. S. MCEWEN and G. A. SIM. J. Chem. Soc. A, 1897 (1969).
13. R. S. MCEWEN, G. A. SIM, and C. R. JOHNSON. J. Chem. Soc. Chem. Commun. 885 (1967) and references therein.
14. P. GROTH and O. HASSEL. Acta Chem. Scand. **18**, 1327 (1964).
15. R. J. MAJESTE and L. M. TREFONAS. Inorg. Chem. **11**, 1834 (1972).
16. S. KULPE. Z. Anorg. Allg. Chem. **349**, 314 (1967).
17. L. D. KOSTURKO, C. FOLZER, and R. F. STEWART. Biochemistry, **13**, 3949 (1974).
18. J. A. CARRABINE and M. SUNDARALINGAM. Biochemistry, **10**, 292 (1971).
19. R. BONACCORSI, A. PULLMAN, E. SCROCCO, and J. TOMASI. Theor. Chim. Acta (Berlin), **24**, 51 (1972).
20. A. D. REDHOUSE. J. Chem. Soc. Chem. Commun. 1119 (1972).
21. M. AUTHIER-MARTIN and A. L. BEAUCHAMP. Can. J. Chem. **53**, 2345 (1975).

The stereochemistry of the Wittig reactions of allylic phosphoranes and phosphonate esters with aldehydes

RICHARD NEVILLE GEDYE, KENNETH CHARLES WESTAWAY, PARKASH ARORA, ROBERT BISSON, AND ALY HAMDY KHALIL

Department of Chemistry, Laurentian University, Sudbury, Ont., Canada P3E 2C6

Received July 23, 1976

RICHARD NEVILLE GEDYE, KENNETH CHARLES WESTAWAY, PARKASH ARORA, ROBERT BISSON, and ALY HAMDY KHALIL. Can. J. Chem. **55**, 1218 (1977).

Methyl *Z*- and *E*-4-bromo-3-methylbut-2-enoate **13** and **14** react with triethyl phosphite stereospecifically with retention of configuration to give the corresponding *Z*- and *E*-phosphonate esters **8** and **9**. The *Z*- and *E*-phosphonates react with aldehydes with extensive stereomutation of the double bond. Rapid equilibration to a mixture of one part *E*-phosphonate to two parts *Z*-phosphonate occurs when either geometric isomer is treated with base. Despite this, the *E*-2,*E*-4 ester **16** is the chief product of the reaction. Methyl *E*-β-ionylideneacetate **16***b* is the major product of the reaction of either isomer with β-cyclocitral and with cyclohexene carboxaldehyde only the *E*-2,*E*-4 isomer **16***c* is formed. Benzaldehyde reacts with the phosphonates to give a mixture of the *E*-2,*E*-4 and *Z*-2,*E*-4 isomers **16***a* and **15***a* in a 4:1 ratio. Although the corresponding *Z*- and *E*-phosphonium salts **6** and **7**, obtained stereospecifically from the bromo esters, react by the same general mechanism as the phosphonates the main product with benzaldehyde is the *Z*-2,*Z*-4 isomer **17***a*.

RICHARD NEVILLE GEDYE, KENNETH CHARLES WESTAWAY, PARKASH ARORA, ROBERT BISSON et ALY HAMDY KHALIL. Can. J. Chem. **55**, 1218 (1977).

Les *Z* et *E* bromo-4 méthyl-3 buténoate-2 de méthyle (**13** et **14**) réagissent stéréospécifiquement avec le triéthyle phosphite avec rétention de configuration pour conduire aux phosphonates esters *Z* et *E* correspondants (**8** et **9**). Les phosphonates *Z* et *E* réagissent avec les aldéhydes avec une grande stéréomutation de la double liaison. L'équilibration rapide vers un mélange d'une partie de phosphonate *E* par rapport à deux parties de phosphonate *Z* se produit chaque fois qu'un des isomères géométriques est traité avec une base. Malgré ces résultats, l'ester *E*-2,*E*-4 est le produit principal de la réaction. Le *E*-β-ionylidèneacétate de méthyle **16***b* est le produit majeur de la réaction de chacun des isomères avec le β-cyclocitral; avec le cyclohexène carboxaldéhyde, il n'y a que l'isomère *E*-2,*E*-4 (**16***c*) qui est formé. Le benzaldéhyde réagit avec les phosphonates pour conduire à un mélange des isomères *E*-2,*E*-4 et *Z*-2,*E*-4 (**16***a* et **15***a*) dans un rapport de 4:1. Quoique les sels de phosphonium *Z* et *E* correspondants (**6** et **7**), obtenus stéréospécifiquement à partir des bromo esters, réagissent par le même mécanisme général que les phosphonates, le produit principal avec le benzaldéhyde est l'isomère de *Z*-2,*Z*-4 (**17***a*).

[Traduit par le journal]

The Wittig reaction of β-ionylideneacetaldehyde with the phosphorane derived from (3-methoxycarbonylprop-2-enyl)triphenylphosphonium bromide (1), and the Horner modification of the Wittig reaction using β-ionylideneacetaldehyde and triesters of 4-phosphono-3-methylbut-2-enoic acid (2, 3) have been used in the synthesis of vitamin A and related compounds. Until recently however, little attention has been given to the stereochemical aspects of these reactions.

Of the methods available for the synthesis of the vitamin A precursor, β-ionylideneacetic acid, the Reformatsky reaction (4–9) and modified Wittig reactions (10, 11) have received particular attention. These reactions are not generally stereospecific and tend to give a mixture of the *Z*- and *E*-isomers of β-ionylideneacetic acid **1** and **2**. The *Z*- and *E*-β-ionylideneacetic acids have recently been prepared stereospecifically in good yield by the reaction of the Wittig reagent **3**, from triphenyl-β-cyclogeranylphosphonium bromide, with 4-hydroxy-3-methylbut-2-enolide **4** and methyl *E*-formylcrotonate **5**, respectively (9). Since the starting materials for these syntheses are not readily available and are tedious to prepare, an alternate stereospecific route is desirable.

The Wittig reactions of the pure *Z*- and *E*-phosphonium bromides **6** and **7** and of the pure *Z*- and *E*-phosphonate esters **8** and **9** in the Horner modification of the Wittig reaction with β-cyclocitral appeared to provide attractive

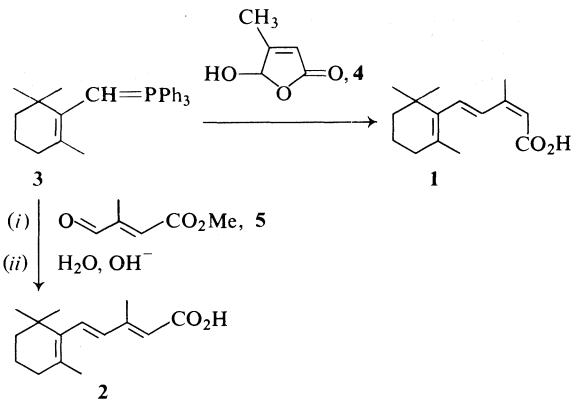

routes to a stereospecific synthesis of the *Z*- and *E*-β-ionylideneacetic acids, and hence to the geometrical isomers of vitamin A. In the present study, the stereochemistry of the Wittig reactions of **6**–**9** with β-cyclocitral **10** and other aldehydes has been investigated.

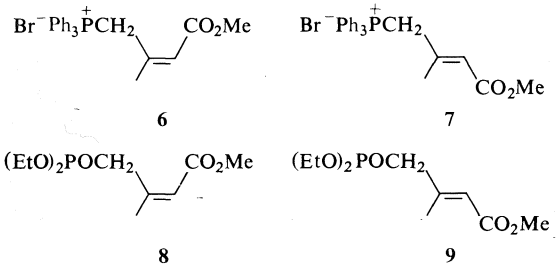

The stereospecificity of the formation of allylic Wittig reagents by the reaction of triphenylphosphine with allylic halides and of the subsequent condensations with carbonyl compounds appears to be in doubt. In an attempted preparation of *Z*-allylic Wittig reagents from the allylic bromide formed by treating methyl *Z*-2-methylbut-2-enoate **11** with *N*-bromosuccinimide, and from methyl *Z*-4-chlorobut-2-enoate, Pattenden and Weedon (12) observed complete inversion of configuration resulting in the formation of the corresponding *E*-phosphonium salts.

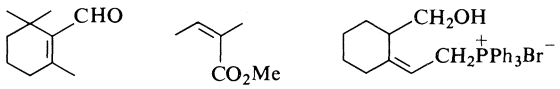

Howe (13) observed retention of configuration during the conversion of mixtures of *Z*- and *E*-isomers of ethyl 4-bromo-3-methylbut-2-enoate to the corresponding phosphonium salts, but found that the *Z*- and *E*-phosphonium salts gave the same mixture of products when condensed with benzaldehyde in the presence of base. Harrison and Lythgoe (14), observed almost complete retention of configuration during the reaction of the *Z*-phosphonium salt **12** with a ketone. It should be noted, however, that the ylide from **12** does not have a resonance stabilizing carbomethoxy group.

In the present study, the *Z*- and the *E*-isomers of methyl 4-bromo-3-methylbut-2-enoate (9), **13** and **14**, were converted with complete retention of configuration into the corresponding phosphonium bromides **6** and **7** at room temperature.

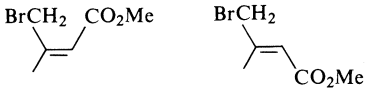

This conclusion was based on the evidence obtained from the nmr spectra of the bromoesters and the phosphonium salts (13, 15).

Attention was then focused on the stereochemistry of the Wittig reactions of the phosphonium salts **6** and **7**, in the presence of sodium methoxide, with benzaldehyde and β-cyclocitral. The reactions of the *Z*- and *E*-phosphonium salts with benzaldehyde in the presence of sodium methoxide, although carried out under milder conditions than those conducted by Howe (at 20°C rather than at reflux temperatures), proved to be completely non-stereospecific. The same mixture of isomeric products **15***a*–**18***a* were formed from both **6** and **7** with the *Z*-2,*Z*-4 isomer **17***a* being the principal product.

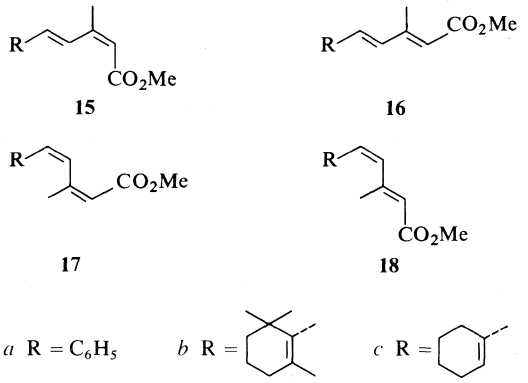

In order to further investigate the observed stereomutations in these Wittig reactions, the ylide **19** was prepared by treating a suspension of the *Z*- and *E*-phosphonium salts **6** and **7** in benzene with an equimolar amount of dilute aque-

ous alkali. The solid isolated from both reactions had identical ir, uv, and nmr spectra. Moreover the nmr spectrum showed only one type of β-methyl group, a situation which would be different if it was a mixture of *Z*- and *E*-isomers (13, 15). Thus it was concluded that **6** and **7** gave the same phosphorane. The isolated phosphorane is a yellow solid which is stable enough to be kept for long periods without decomposition. Participation of the ester group in charge delocalization is evident from the shift of the carbonyl absorption in the infrared from 1700 cm^{-1} in the salt, to 1669 cm^{-1} in the phosphorane.

Corey and Erickson (15) isolated a phosphorane of considerably lower melting point (near 135°C) than that obtained in this investigation (176–180°C). Their product which was formed in basic aqueous acetonitrile was shown by nmr analysis to be a 2:1 mixture of the *Z*- and *E*-phosphoranes, for which the structures **19***b* and **19***a*, respectively, were assigned.

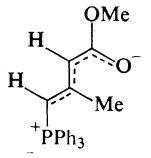

19*a*

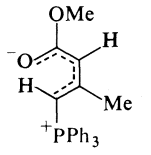

19*b*

The nmr spectrum of the crystalline ylide formed in the present study was similar to that of the *Z*-isomer **19***b* (13, 15) and no signals corresponding to those quoted for the *E*-isomer were observed.

The formation of predominantly *Z*-2 isomers in the above Wittig reaction is consistent with the formation, *in situ*, of mainly the *Z*-ylide **19***b* from both the *Z*- and *E*-phosphonium salts **6** and **7**. It should be noted that the isolated ylide reacted with benzaldehyde in benzene solution to give essentially the same isomeric mixture as that obtained in the condensation of **6** and **7** with benzaldehyde.

β-cyclocitral, on the other hand, failed to react with the phosphonium salts **6** and **7** under normal conditions, and on prolonged refluxing with the isolated ylide gave a complex mixture of products. Because of this lack of reactivity, attention was turned to the reactions of the allylic phosphonate esters **8** and **9** with aldehydes since it has been reported (16) that phosphonate carbanions are generally more reactive than the conventional Wittig reagents towards carbonyl compounds.

In their studies of the synthesis of compounds related to vitamin A using triesters of 4-phosphono-3-methylbut-2-enoic acid, Machleidt and Wessendorf (3) have suggested that the reaction may be stereospecific and that the stereochemistry of the product depends on the *Z*- to *E*-ratio of the phosphonate used. Pattenden and Weedon (17), however, found that in the reaction of the *E*-phosphonate **9** with certain aldehydes the expected *E*-2-esters were formed whereas similar reactions with the *Z*-phosphonate **8** were accompanied by extensive stereomutation and only *ca.* 25% of the resulting esters possessed the *Z*-2 configuration. Corey and Erickson (15), on the other hand, found that even the *E*-phosphonate **9** did not give a stereochemically pure product since they observed that the reaction of *n*-hexanal with the *E*-phosphonate gave a mixture of the *E*-2,*E*-4 and *Z*-2,*E*-4 isomers in a 6:1 ratio.

The *Z*- and *E*-phosphonates were prepared by the Michaelis–Arbuzov reaction (18) of the corresponding *Z*- and *E*-isomers of methyl 4-bromo-3-methylbut-2-enoate (9) **13** and **14** with triethyl phosphite. In agreement with the work of Corey and Erickson (15), it was shown by glc and nmr spectroscopy that these reactions occurred with complete retention of configuration. It should be noted that retention of configuration has also been reported in the reaction of nerol bromide with triethyl phosphite (19).

The reactions of the *Z*- and *E*-phosphonates **8** and **9** with benzaldehyde gave results which differed from those of Pattenden and Weedon in that each isomer gave an identical mixture of products. The reactions were carried out in the presence of sodium methoxide in a mixture of methanol and dimethyl formamide and gave, in each case, a mixture of approximately 80% of the *E*-2,*E*-4 isomer **16***a* and 20% of the *Z*-2,*E*-4 isomer **15***a*. Similar results were obtained using sodium amide in tetrahydrofuran.

The reactions of the *Z*- and *E*-phosphonates with β-cyclocitral in the presence of sodium methoxide in methanol and dimethylformamide failed to give any of the expected isomers of methyl-β-ionylideneacetate. When the reactions were carried out using the stronger base sodium amide in tetrahydrofuran a rather complex mixture of products was obtained, of which methyl *E*-β-ionylideneacetate **16***b* was the main com-

ponent. A small amount of the *Z*-isomer **15***b* was also detected. While the product ratio varied slightly in different runs, it was apparent that the *Z*- and *E*-phosphonates again gave essentially the same products.

Both the *Z*- and *E*-phosphonates reacted with cyclohexene carboxaldehyde in the presence of sodium amide in tetrahydrofuran to give a high yield of methyl 5-(cyclohexen-1-yl)-3-methylpenta-*E*-2,*E*-4-dienoate **16***c*. No other isomers were detected by glc or nmr.

It was observed, using a glc analysis, that a rapid isomerization of the *Z*- and *E*-phosphonates giving a mixture of about two parts of the *Z*- to one part of the *E*-isomer occurred in the early stages of the reaction between the phosphonates and these aldehydes. Further investigations showed that the phosphonates equilibrated rapidly with several different bases including aqueous sodium hydroxide, sodium methoxide in methanol, and sodium amide in tetrahydrofuran. In every case a ratio of *Z*- to *E*-phosphonate of approximately 2:1 was obtained. It was noted also that no appreciable equilibration occurred in these solvents in the absence of base. Contrary to previous reports (3, 17), this isomerization would suggest that any particular aldehyde should react with the equilibrium mixture of the *Z*- and *E*-phosphonates to give the same mixture of isomeric products. This is in fact, what was observed.

It is generally accepted (20) that the Horner modification of the Wittig reaction involves the formation of a phosphonate carbanion which then undergoes nucleophilic attack on the carbonyl compound. The presence of the phosphonate anions in this reaction was demonstrated by deuterium exchange studies (see below) and by the fact that treatment of the *Z*- and *E*-phosphonate esters with excess *n*-butyllithium in diethyl ether led to new absorptions at longer wavelength in the uv. The *Z*-phosphonate (λ_{max} 226 nm, ε 6500) gave a new absorption initially at 280 nm while the *E*-phosphonate (λ_{max} 219 nm, ε 14 000) gave a new absorption initially at 340 nm. The increase in the λ_{max} is larger for the *E*-isomer which forms a more linear carbanion than the *Z*-isomer (21). On standing, both of the longer wavelength absorptions were observed, thus confirming that the phosphonate esters were isomerizing under the conditions of the experiment. The stronger absorption at 280 nm is consistent with the *Z*-phosphonate ester anion being in higher yield at equilibrium (the *E*-anion should have the larger extinction coefficient (21)). The greater stability of the carbanion from the *Z*-phosphonate, which is U-shaped, than that of the carbanion from the *E*-phosphonate, which is W-shaped, follows observed stabilities of simple allylic carbanions (22).

Since the *Z*- and *E*-phosphonate esters **8** and **9** isomerized rapidly with sodium methoxide in methanol, and since the methylene protons were expected to be quite acidic it was thought that the *Z*- and *E*-carbanions would be present in fairly high concentrations. Three experiments illustrated that this was not the case. First, it was impossible to titrate either the *Z*- or the *E*-phosphonate with sodium methoxide, *i.e.* no measurable amount of the anions was formed. Secondly, it was not possible to detect the uv absorptions of either the *Z*- or the *E*-carbanion when the phosphonate esters were treated with an excess of sodium methoxide in methanol. Thirdly, when an excess of a much stronger base, *n*-butyllithium, was added to a solution of the phosphonate esters in ether, the uv absorbance of the phosphonate ester was not appreciably reduced even though the new absorptions resulting from the carbanions were observed. Thus the isomerization and condensation reaction must occur via the carbanion intermediate which is present in very low concentration. It should also be noted that in selected cases of the Wittig–Horner reaction, carbanion formation does not occur unless the carbonyl reactant is present in solution (20).

Although the isomerization of the phosphonate esters could occur in two ways, it is certain that it must involve the delocalized carbanion **20**. The α,β bond in the anion **20** will only have partial double bond character and thus one possibility is that isomerization could occur by rotation about this bond.

A second possibility is that the isomerization reaction occurs by way of the β,γ-unsaturated ester **21**, which would form if the carbanion **20** was protonated at the α-carbon.

This mechanism is possible because a deuterium exchange study of both the *Z*- and *E*-phosphonate esters using sodium methoxide in CH_3OD demonstrated that the reactions shown in the above equation were occurring. These exchange tests also illustrated that the rates of

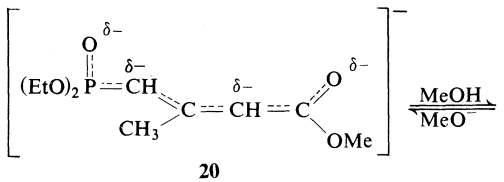

20

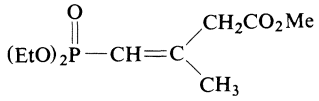

21

exchange were different; the methylene protons adjacent to the phosphonate group were exchanged almost instantaneously whereas the vinyl hydrogen was exchanged at a much lower rate.

The relative rates of exchange and isomerization were determined in an attempt to distinguish between the two possible mechanisms. If isomerization occurred by way of the β,γ-unsaturated ester **21**, exchange at the vinyl hydrogen would have to occur at least as rapidly as the isomerization. It was found that exchange of the vinyl hydrogen was complete before the equilibrium of the *Z*- and *E*-phosphonates was fully established (Table 1). Since these results indicate that **21** is an intermediate in this reaction and since exchange occurs faster than isomerization, it is probable that isomerization occurs via rotation about the α,β bond in **21**.

The fact that the *Z*-phosphonate predominates in the base-catalyzed equilibration is thought to be due to the increased steric crowding that exists in the *E*-phosphonate. Space-filling models indicate that the steric hindrance between the CH_3 group (at C-3) and the $-CO_2CH_3$ group in the *E*-isomer is larger than between the $-CH_2PO(OEt)_2$ group and the $-CO_2CH_3$ group in the *Z*-isomer. In order to check this hypothesis stereomutation studies were also carried out on the *Z*- and *E*-phosphonates **8***a* and **9***a* derived from the reaction of the *Z*- and *E*-isomers of methyl 4-bromocrotonate with triethylphosphite. The previously unreported methyl *Z*-4-bromo-3-methylcrotonate was obtained in small amounts when the product of the reaction of methyl crotonate and *N*-bromosuccinimide was distilled on an annular spinning band column. The stereochemistry of both the *Z*-bromo ester and the *Z*-phosphonate **8***a* was confirmed by nmr studies which showed a considerable downfield shift in the absorption of the $-CH_2Br$ and the $-CH_2PO$ protons in the *Z*-isomers compared with the corresponding *E*-isomers. This is due to a greater degree of deshielding of the methylene protons by the carboxymethyl group in the *Z*-isomers (21). It was shown, using a glc analysis, that both **8***a* and **9***a* isomerized rapidly in the presence of a catalytic amount of sodium methoxide in methanol[1] giving a mixture of ten parts of the *E*-isomer **9***a* to one part of the *Z*-isomer **8***a*.

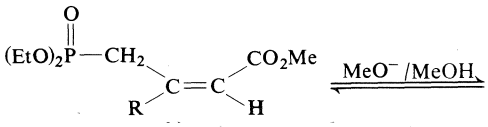

8 (R = CH_3) 65%
8*a* (R = H) 10%

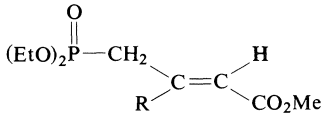

9 (R = CH_3) 36%
9*a* (R = H) 90%

These results substantiate the above hypothesis[2] because replacement of the CH_3 (in **9**) by H (in **9***a*) would remove the steric hindrance between the substituent at C-3 and the carbometh-

TABLE 1. Exchange and isomerization studies[a] in the reactions of methyl *Z*-and *E*-4-phosphono-3-methylbut-2-enoate, **8** and **9**, with CH_3ONa in CH_3OD (analysis by nmr)

Starting ester	*Z*-Isomer (%)	*E*-Isomer (%)	Exchange at vinyl CH (%)
Z	81	19	44
Z	78	22	60
Z	71	29	100
Z	64	36	100
E	50	50	60
E	62	38	100
E	63	37	100

[a]The equilibrium mixture contained 64% of the *Z*-isomer and 36% of the *E*-isomer.

[1]These isomers did not appear to be stable in the presence of sodium methoxide, since neither isomer could be detected in the reaction mixture after standing for 1 h.

[2]A second possibility to explain the relative stabilities of the *Z*- and *E*-isomers *i.e.* that a six-membered ring in which the carbonyl oxygen is coordinated with the phosphorus as in the ylide **19***b*, was ruled out because the frequencies of the infrared absorptions of both the C=O and the P=O groups were identical in both the *Z*- and *E*-phosphonates **8** and **9** and also because of the results of these stereomutation studies.

oxy group and would result in increased stability of the *E*-isomer. In the case of the 4-phosphonocrotonates steric hindrance would only be expected to be significant in the *Z*-isomer, where the $—CH_2PO(OEt)_2$ and the $—CO_2Me$ group are on the same side of the double bond. Thus the *Z*-isomer should be much less stable than the *E*-isomer. This is illustrated by the high concentration of the *E*-isomer **9***a* in the base-catalyzed equilibrium mixture, and by the fact that the *Z*-isomer isomerized to give an appreciable amount of the *E*-isomer on standing at room temperature for a few days.

Attention was then turned to the stereochemistry of the condensation of the *Z*- and *E*-phosphonate esters **8** and **9** with benzaldehyde, β-cyclocitral, and cyclohexene carboxaldehyde. The product ratio in the base-catalyzed isomerization of the methyl 4-phosphono-3-methylbut-2-enoates might lead to the prediction that predominantly *Z*-2,*E*-4 products would be formed in these modified Wittig reactions regardless of the stereochemistry of the initial phosphonate ester. However, in all the reactions investigated, the *E*-2,*E*-4 products predominated, suggesting either that a second stereomutation of the products occurred or that the *E*-phosphonate anion reacts more rapidly than the *Z*-phosphonate anion with aldehydes.

Control experiments (Table 2) showed that methyl *Z*-2,*E*-4-5-phenyl-2,4-pentadienoate **15***a* underwent a slow isomerization in the presence of sodium methoxide in methanol and dimethylformamide to give an equilibrium mixture of 35% of the *Z*-2,*E*-4 isomer and 65% of the *E*-2,*E*-4 isomer **16***a* (by glc).

On the other hand, the reaction of benzaldehyde with either the *Z*-phosphonate **8** or the *E*-phosphonate **9** (Table 3) gave, after a few minutes, a small amount of a mixture of approximately 85% of the *E*-2,*E*-4 isomer **16***a* and 15% of the *Z*-2,*E*-4 isomer **15***a*. These proportions cannot be explained by a second stereomutation of **15***a* or **16***a* since the control experiment above showed that such a stereomutation would be comparatively slow. The gradual decrease of the proportion of the *E*-2,*E*-4 isomer with time (Table 3) is consistent with the results of the control experiment. It must be concluded, therefore, that the *E*-phosphonate anion reacts more rapidly with aldehydes than the *Z*-phosphonate anion. The fact that the newly formed double bond (at C-4) had entirely the *E*-configuration is consistent with the stereochemical course proposed by Boutagy and Thomas (20) for the Wittig–Horner reaction (Scheme 1).

TABLE 2. Isomerization of methyl *Z*-2,*E*-4-5-phenyl-2,4-pentadienoate with sodium methoxide in methanol and DMF at 25°C (analysis by glc)

Time (h)	*Z*-2,*E*-4 Isomer (%)	*E*-2,*E*-4 Isomer (%)
0	100	0
1	46	54
4	39	61
8	38	62
12.5	37	63
24	35	65

TABLE 3. Product ratios observed from the reaction of methyl *Z*- and *E*-4-phosphono-3-methylbut-2-enoate with benzaldehyde in the presence of sodium methoxide in methanol and DMF at 25°C (by glc)

Time (min)	Ratio *Z*-2,*E*-4/*E*-2,*E*-4 from *Z* (%)	Ratio *Z*-2,*E*-4/*E*-2,*E*-4 from *E* (%)
2	16/84	14/86
30	20/80	21/79
60	25/75	25/75

The formation of the *Z*-and *E-threo* betaines **20** and **21** by the addition of the *Z*- and *E*-phosphonate carbanions to benzaldehyde would be expected to be faster than the formation of the *Z*- and *E-erythro* betaines, which are more sterically hindered. Since the rate of decomposition of the *threo* betaines would also be expected to be greater than that of the *erythro* betaines (20), the *Z*-2,*E*-4 and *E*-2,*E*-4 **15***a* and **16***a* isomers would be expected to be the chief products of the reaction.

The fact that the *E*-2,*E*-4 isomer **16***a* is formed more rapidly than the *Z*-2,*E*-4 isomer **15***a*, despite the lower equilibrium concentration of the *E*-phosphonate can be explained by the greater steric crowding in the *Z-threo* betaine **20** than in the *E-threo* betaine **21**. Also, since the *E*-2,*E*-4 isomer is thermodynamically more stable than the *Z*-2,*E*-4 isomer, it would be expected to be the chief product of the reaction under equilibrium conditions.

In conclusion, these studies have illustrated the following points.

(*a*) The reactions of the *Z*- and *E*-phosphonium salts **6** and **7** with aldehydes proceed with

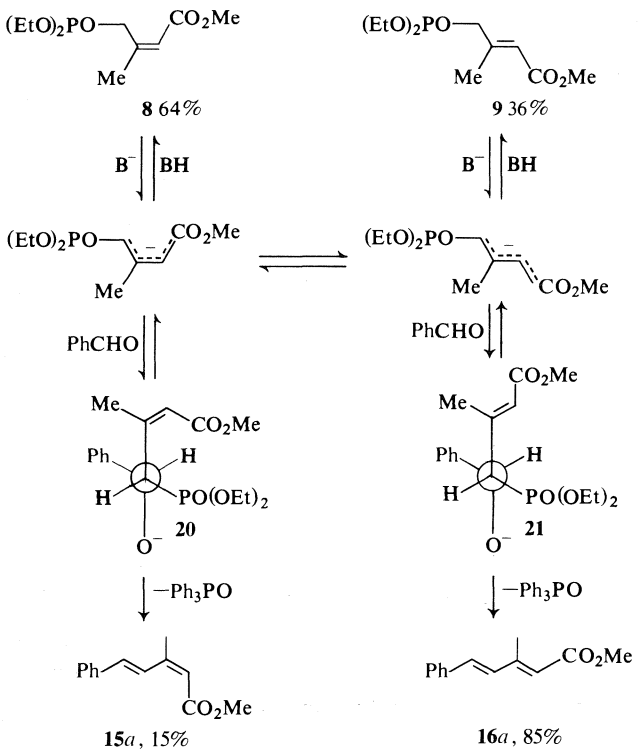

SCHEME 1

extensive stereomutation giving the same mixture of products from either isomer. The reaction involves the intermediate formation of the *Z*-ylide and in the case of the reaction with benzaldehyde results in products with predominantly the *Z*-2 configuration.

(*b*) The Horner phosphonate ester modification of the Wittig reaction gives the same mixture of isomeric products when either the *Z*- or the *E*-phosphonate esters **8** and **9** are reacted with a particular aldehyde. This result is observed because the carbanion, which is present in a low concentration, isomerizes rapidly to give an equilibrium mixture of the phosphonate esters in the initial stages of the reaction.

(*c*) The above reactions thus do not offer an improved route for the synthesis of vitamin A or its precursors because of their lack of stereospecificity. Although the *E*,*E*-isomer is the principle product from Horner modification of the Wittig reaction with β-cyclocitral, the yield is only fair under the conditions used in this investigation.

Experimental

All boiling points and melting points are uncorrected. Infrared spectra were recorded with a Beckman IR-10 double beam spectrophotometer. The nmr spectra were obtained with a Varian A-60 in deuterochloroform unless otherwise stated, with tetramethylsilane as an internal reference. Ultraviolet spectra were recorded with a Hitachi–Perkin-Elmer model 124 double beam spectrophotometer. Gas chromatography was carried out on a Varian Aerograph model 90-P using a 160 × 6 mm column of 3% SE-30 silicone gum rubber on Chromosorb W. Elemental analyses were carried out in the School of Chemistry, University of Bristol, England.

(Z-3-Methoxycarbonyl-2-methylprop-2-enyl)triphenylphosphonium Bromide **6**

To a well stirred suspension of triphenylphosphine (26.6 g, 0.1 mol) in dry ether or dry benzene (150 ml) was added dropwise methyl *Z*-4-bromo-3-methylbut-2-enoate (9) **13** (19.3 g, 0.1 mol) in dry ether (30 ml). The mixture was stirred for 24 h at room temperature. The crude phosphonium salt was filtered, washed with dry ether, and finally dried for 6 h at 40°C/10 torr, giving the *Z*-phosphonium salt **6** (38.0 g, 83%), mp 140–143°C. The analytical sample, obtained by recrystallization from methanol – ethyl acetate and dried at 40°C/10 torr for 6 h, had mp 134–136°C, λ_{max} (EtOH) 203, 222.5, 262, 267.5, and 275 nm; ν_{max} (KBr) 1705vs, 1645s, 1585w, 1480m, 1438vs,

1385m, 1360m, 1245s, 1225vs, 1195w, 1168m, 1150vs, 1105vs, 1030s, 990m, 895s, 850m, 745vs, 715s, 703m-s, 682s, and 650s cm^{-1}; nmr ($F_3C—CO_2H$) δ 7.65–7.80 (m, aryl H), 6.07 (br d, J = 5 Hz, C:CH), 4.87 (d, J = 16 Hz, $\overset{+}{P}CH_2$), 3.45 (s, OMe), and 1.97 (m, MeC:C). *Anal.* calcd. for $C_{24}H_{24}BrO_2P$: C 63.29, H 5.31, Br 17.55; found: C 62.96, H 5.56, Br 17.23.

(E-3-Methoxycarbonyl-2-methylprop-2-enyl)triphenylphosphonium Bromide 7

Repetition of the above procedure using *E*-bromoester **14** gave the *E*-phosphonium salt **7** (40.0 g, 99%), mp 178–181°C. The analytical sample which was obtained by recrystallization from methanol – ethyl acetate and dried at 40°C/10 torr for 6 h, had mp 177–179°C, (lit. (15) bp 183–184°C); λ_{max} (EtOH) 204, 224, 268, and 275 nm; ν_{max} (KBr) 1700vs, 1645s, 1545w, 1440s, 1430s, 1280vs, 1155w, 1105vs, 1032w, 885w, 815w, 768s, 750s, 740m, 712s, and 680 cm^{-1}; nmr ($F_3C—CO_2H$) δ 7.77–7.92 (m, aryl H), 5.92 (br d, J = 5 Hz, C:CH), 4.27 (d, J = 16 Hz, $\overset{+}{P}CH_2$), 3.90 (s, OMe), and 2.08 (MeC:C). *Anal.* found: C 63.27, H 5.40, Br 17.89.

When an unseparated mixture of *Z*- and *E*-bromoesters, **13** and **14** was treated in the same manner as above a phosphonium salt of mp 162°C was obtained (lit. (24) mp 160°C). Nuclear magnetic resonance spectroscopy showed that this salt is a mixture of the phosphonium salts **6** and **7**.

Z-Diethyl 3-Methoxycarbonyl-2-methylprop-2-enylphosphonate 8

The *Z*-bromoester **13** (38.6 g, 0.2 mol) was added slowly to triethyl phosphite (33.2 g, 0.2 mol). The mixture was heated gradually to 150°C and maintained at this temperature for 1 h. Distillation of the residue gave only the *Z*-phosphonate ester **8** (43.5 g, 87%) bp 99–100°C/1 torr; glc showed only one peak; n_D^{24} 1.4590 (lit. (12) bp 82°C (bath/10^{-2} torr, n_D^{21} 1.4591); λ_{max} (MeOH) 227 nm (ε 6.5 × 10^3); ν_{max} (neat) 1714vs, 1650s, 1436s 1249vs, 1161vs, 1051vs, 1030vs, 960s, and 780mw cm^{-1}; nmr δ 5.83 (br d, J = 5 Hz, C=CH), 4.11 (2, J = 7 Hz, O—CH_2Me), 3.70 (s, OMe), 3.47 (d, J = 23 Hz, CH_2, —PO<), 2.07 (dd, J = 1.5 and *ca.* 4 Hz, MeC=C), 1.29 (t, J = 7 Hz, CH_3CH_2O—). *Anal.* calcd. for $C_{10}H_{19}O_5$: C 48.0, H 7.61; found: C 47.9, H 7.7.

E-Diethyl 3-Methoxycarbonyl-2-methylprop-2-enylphosphonate 9

Repetition of the preceding experiment using *E*-bromoester **14** gave the *E*-phosphonate **9**, bp 107–108°C/1 torr (lit. (15) bp 112°C/0.12 torr); glc showed only one peak of longer retention time than the *Z*-phosphonate **8**; n_D^{24} 1.4617; λ_{max} (MeOH) 219 nm (ε 13.8 × 10^3); ν_{max} (neat) 1719vs, 1650s, 1438s, 1243vs, 1216vs, 1150vs, 1050vs, 1030vs, 960s, 870m, 850w, 833w, 780m cm^{-1}; nmr δ 5.83 (br d, J = 5 Hz, C=CH—), 4.14 (q, J = 7 Hz, O—CH_2Me), 3.71 (s, OMe), 2.69 (d, J = 23 Hz, CH_2—PO<), 2.30 (dd, J = 1.5 and *ca.* 4 Hz, Me—C=C), and 1.31 (t, J = 7 Hz, CH_3CH_2O—). *Anal.* calcd. for $C_{10}H_{19}O_5$: C 48.0, H 7.61; found: C 47.8, H 7.65.

(3-Methoxycarbonyl-2-methylprop-2-enyllidene)triphenylphosphorane 19

(*E*-3-Methoxycarbonyl-2-methylprop-2-enyl)triphenyl phosphonium bromide **7** (45.5 g, 0.1 mol) was suspended in water (200 ml) and benzene (250 ml) was added. The well stirred mixture was brought to the phenolphthalein equivalence point by the addition of aqueous sodium hydroxide solution (3%). The two layers were separated. The deep yellow coloured benzene layer was dried over anhydrous sodium sulphate, and concentrated to a small volume. Careful addition of dry petroleum ether (bp 30–60°C) caused crystallization of the ylide **19** as shiny yellow needles. The ylide was filtered and dried at 25°C/10 torr for 1 h giving 26.3 g (70%), mp 174–180°C with sintering at 166°C (lit. (15) mp near 135°C); λ_{max} (CH_3CN) 227 nm; ν_{max} (KBr) 1669vs, 1645vs, 1503vs, 1448vs, 1390m, 1210w, 1181s, 1119vs, 1095m, 1015m, 999w, 932m, 899m, 805w, 775w, 715s, and 690 cm^{-1}; nmr δ 7.33–7.93 (m, aryl H), 4.70 (br, C=CH—), 3.62 (s, OMe), 3.41 (only half of the —CH=P— doublet can be seen), and 1.63 (MeC=C). *Anal.* calcd. for $C_{24}H_{23}O_2P$: C 76.99, H 6.19; found: C 76.75, H 6.23.

When the above experiment was repeated using (*Z*-methoxycarbonyl-2-methylprop-2-enyl)triphenylphosphonium bromide **6** the same ylide **19** was obtained as shown by uv, ir, and nmr spectroscopy.

The Wittig Reaction of the Z-and E-Phosphonium Salts 6 and 7 with Benzaldehyde

(*i*) A stirred solution of (*Z*-3-methoxycarbonyl-2-methylprop-2-enyl)triphenylphosphonium bromide **6** (0.2 g, 0.4 mmol) in 1 ml of absolute methanol was treated with a solution of sodium methoxide (0.4 mmol) (from 10 mg sodium in 1 ml absolute methanol) whereupon the yellow colour of the ylide developed immediately. The yellow solution was stirred for 15–20 min at 20°C, and then benzaldehyde (44 mg, 0.4 mmol) in methanol (1 ml) was added rapidly. The reaction mixture was stirred for 3 h, concentrated under reduced pressure, and the residue was taken up in ether. The ethereal solution was washed with water, dried over anhydrous sodium sulphate, evaporated, and then extracted with hexane. Evaporation of the hexane gave a semi solid product of which the solid portion was shown to be mainly triphenylphosphine oxide. Gas–liquid chromatography of the liquid portion showed three peaks in an approximately 6:1:1 ratio. The first peak was shown to be due to a mixture of the *Z*-2,*Z*-4 ester **17***a* and the *E*-2,*Z*-4 isomer **18***a*, the second peak the *Z*-2,*E*-4 isomer **15***a*, and the third peak the *E*-2,*E*-4 isomer **16***a* by comparison with reference compounds (see below). The nmr spectrum (in CCl_4) was taken and compared with the spectra of the reference compounds which agreed with the literature values (25). The analysis was performed by integration of the signals due to the 3-methyl groups which appeared at δ 1.76 (*Z*-2,*Z*-4 isomer), δ 2.10 (*Z*-2,*E*-4 and *E*-2,*Z*-4 isomers), and δ 2.36 (*E*-2,*E*-4 isomer). A combination of the glc and nmr analyses showed that the product contained 48% *Z*-2,*Z*-4 **17***a*, 23% *E*-2,*Z*-4 **18***a* 15% *Z*-2,*E*-4 **15***a*, and 14% *E*-2,*E*-4 **16***a* isomers of methyl 3-methyl-5-phenylpenta-2,4-dienoate.

(*ii*) Repetition of the above procedure using the *E*-phosphonium salt gave a product of the same composition (glc assay) as that obtained in the above experiment.

The Wittig Reaction of the Ylide 19 with Benzaldehyde

To the ylide **19** (14.0 g, 0.037 mol) in dry benzene (100 ml) was added benzaldehyde (7.84 g, 0.074 mol) in ben-

zene (25 ml). The mixture was stirred for 1 h under nitrogen at room temperature and then refluxed for 72 h. The excess solvent was evaporated under reduced pressure, the residue diluted with 100 ml of petroleum ether (bp 30–60°C), and the precipitated triphenylphosphine oxide (mp 157–158°C) collected by filtration. The filtrate was dried over anhydrous sodium sulphate. Evaporation of the solvent and distillation of the residue gave a pale yellow oil (3.97 g), bp 110–114°C/1 torr. The product was shown by glc to be a mixture of 45% *Z*-2,*Z*-4 **17***a*, 25% *E*-2,*Z*-4 **18***a*, 14% *Z*-2,*E*-4 **15***a*, and 14% *E*-2,*E*-4 **16***a* isomers of methyl 3-methyl-5-phenylpenta-2,4-dienoate (yield 53%).

The yield was slightly improved (61%) when the reaction was carried out in a sealed tube at 170°C in the presence of benzoic acid and excess benzaldehyde (2 equiv.) (26).

*Reaction of the Z- and E-Phosphonate Esters **8** and **9** with Benzaldehyde*

(*i*) To a well stirred suspension of sodium amide (1.0 g, 0.025 mol) in tetrahydrofuran (20 ml) was added a mixture of benzaldehyde (2.65 g, 0.025 mol) and the *Z*-phosphonate **8** (5.48 g, 0.022 mol) in tetrahydrofuran (20 ml) during 15 min. The reaction mixture was stirred at 0°C for 30 min, and then at 30–40°C for an additional 30 min. The mixture was cooled to 0°C, and then saturated sodium chloride solution (50 ml) added. The product was taken up in petroleum ether (bp 30–60°C), washed with water, dried, and evaporated. Distillation of the residue gave a pale yellow oil (4.5 g) bp 85–90°C/0.03 torr. The product was shown by glc to be a mixture of 20% *Z*-2,*E*-4 **15***a* and 80% *E*-2,*E*-4 **16***a*, isomers of methyl 3-methyl-5-phenylpenta-2,4-dienoate (yield 82%).

(*ii*) Repetition of the preceding reaction with the *E*-phosphonate gave a colourless oil (4.2 g) bp 86–90°C/0.03 torr. The product was shown by glc to be a mixture of 20% *Z*-2,*E*-4 **15***a* and 80% of the *E*-2,*E*-4 **16***a*, isomers of methyl 3-methyl-5-phenyl-2,4-dienoate (yield 76%).

(*iii*) To a solution of benzaldehyde (40 mg, 0.38 mmol) and the *Z*-phosphonate **8** (130 mg, 0.52 mmol) in dimethylformamide (5 ml) was added dropwise over a period of 5 min a solution of sodium (0.015 g) in methanol (1 ml) (0.65 mmol of sodium methoxide). The mixture was stirred at room temperature for 1 h, aliquots being taken at various time intervals and analyzed by glc (Table 3). The product was diluted with water and extracted with petroleum ether (bp 60–80°C). The extracts were evaporated, washed with sodium chloride solution, dried over anhydrous magnesium sulfate, and evaporated giving a yellow oil. Gas–liquid chromatographic analysis of the oil showed the presence of methyl *E*-2,*E*-4-3-methyl-5-phenylpenta-2,4-dienoate **16***a* (80%) and the *Z*-2,*E*-4 isomer **17***a* (20%). Nuclear magnetic resonance spectroscopy (by integration of the CH_3—C= signal) showed the presence of 84% of the *E*-2,*E*-4-isomer and 16% of the *Z*-2,*E*-4 isomer.

(*iv*) Repetition of the above reaction using the *E*-phosphonate **9** gave a yellow oil, shown by glc and nmr analysis to contain the *E*-2,*E*-4 isomer (79%) and the *Z*-2,*E*-4 isomer (21%).

Isomerization of Methyl Z-2,E-4-3-Methyl-5-phenylpenta-2,4-dienoate with Sodium Methoxide

To the diene ester (50 mg, 0.25 mmol) in dimethylformamide (5 ml) was added a solution of sodium (7 mg) in methanol (1 ml) (0.3 mmol of CH_3ONa) over a period of 4 min. The mixture was stirred at room temperature for 24 h and aliquots taken at various time intervals. The percentage of the *Z*-2,*E*-4 and *E*-2,*E*-4 isomers **15***a* and **16***a* in the aliquots were determined by glc analysis (Table 2).

*The Reaction of the Z- and E-phosphonates **8** and **9** with β-cyclocitral*

(*i*) A mixture of β-cyclocitral (3.8 g; 0.025 mol) and *Z*-diethyl 3-methoxycarbonyl-2-methylprop-2-enylphosphonate **8** (6.5 g, 0.027 mol) in tetrahydrofuran (20 ml) was added during 15 min to a well stirred suspension of sodium amide (1.0 g, 0.025 mol) in tetrahydrofuran (20 ml) at 0°C. The reaction mixture was stirred at 0°C for 30 min, and then at 30–40°C for an additional 30 min. The mixture was cooled to 0°C, and saturated sodium chloride solution (50 ml) was added. The product was taken up in petroleum ether (bp 30–60°C), washed thoroughly with water, dried, and then evaporated. Distillation of the residue gave a pale yellow oil (4.9 g), bp 156–162°C/5 torr. The product was shown by glc to contain about 50% methyl *E*-β-ionylideneacetate, 10% methyl *Z*-β-ionylideneacetate and several other unidentified products.

(*ii*) Repetition of the preceding experiment with the *E*-phosphonate **9** gave a pale yellow oil (4.5 g), bp 158–164°C/5 torr. The product was shown by glc to have the same composition as that obtained above from the *Z*-phosphonate.

(*iii*) To a solution of β-cyclocitral (68 mg, 0.45 mmol) and the *Z*-phosphonate **8** (130 mg, 0.52 mmol) in dimethylformamide (5 ml), was added dropwise over a period of 5 min a solution of sodium (15 mg) in methanol (1 ml) (0.65 mmol of sodium methoxide). The mixture, which became orange after a few minutes, was stirred for 1 h at room temperature, diluted with sodium chloride solution, and extracted with petroleum ether. The extracts were washed with water, dried over anhydrous magnesium sulfate, and evaporated giving a viscous pale green oil. The product was shown to contain no methyl *Z*- or *E*-β-ionylideneacetate, although two products with much longer retention times were detected by glc analysis.

(*iv*) The above experiment was repeated using the *E*-phosphonate **9**. Similar results were obtained.

*The Reaction of Cyclohexenecarboxaldehyde with the Z- and E-Phosphonates **8** and **9***

(*i*) A mixture of cyclohexenecarboxyldehyde (2.75 g, 0.025 mol) and *Z*-diethyl 3-methoxycarbonyl-2-methylprop-2-enylphosphonate (6.5 g, 0.027 mol) in tetrahydrofuran (20 ml) was added during 15 min to a well stirred suspension of sodium amide (1.0 g, 0.025 mol) in tetrahydrofuran (20 ml) at 0°C. The reaction mixture was stirred at 0°C for 30 min, and then at 30–40°C for an additional 30 min. The mixture was cooled to 0°C, and saturated sodium chloride solution (50 ml) was added. The product was taken up in petroleum ether (bp 30–60°C), washed thoroughly with water, dried, and then evaporated. Distillation of the residue gave an oil (4.8 g, 92%), bp 116–119°C/3 torr. The product was shown by glc and nmr spectroscopy to be methyl 5-(cyclohexen-2-yl)-3-methylpenta-*E*-2,*E*-4-dienoate **16***c* when compared with a sample prepared from methyl *E*-formylcrotonate (9).

(*ii*) On repetition of the preceding experiment using the *Z*-phosphonate, only the *E*-2,*E*-4 isomer was obtained. No other isomer could be detected by glc or nmr.

*Isomerization and Exchange Studies on the Z- and E-Phosphonates **8** and **9***

(i) With Sodium Methoxide in Methanol

The *E*-phosphonate (71 mg, 0.28 mmol) in methanol (0.1 ml) was treated with 0.4 ml of a solution of sodium (15 mg) in methanol (1 ml) (0.26 mmol of CH_3ONa). Aliquots of the reaction were analyzed on glc after 1 min, 2 min, and 10 min. In each case the mixture contained 65% of the *Z*-phosphonate and 35% of the *E*-phosphonate (higher retention time).

Repetition of the reaction using the *Z*-phosphonate gave the same proportion of isomers. The use of a catalytic amount of sodium methoxide also gave the same product ratio.

(ii) With Other Bases

A similar isomerization was observed using sodium amide, sodium hydride, or sodium hydroxide as the base, and in each case an approximately 2:1 ratio of the *Z*- to *E*-isomer was detected using glc analysis.

(iii) With Sodium Methoxide in CH_3OD

In a typical procedure the *Z*-phosphonate (26 mg, 0.1 mmol) was treated with sodium methoxide (3 mg, 0.05 mmol) in CH_3OD (7 ml). The reaction was quenched by adding DCl in D_2O after 3 min. The mixture was extracted with ether and the ether extracts washed with D_2O, dried over anhydrous magnesium sulfate, and evaporated giving a pale yellow oil, which was analyzed by nmr spectroscopy. Integration of the peaks at δ 2.07 ppm ($CH_3C{=}C$, *Z*-isomer) and δ 2.30 ppm ($CH_3C{=}C$, *E*-isomer) showed the presence of the *Z*-isomer (81%) and the *E*-isomer (19%). Integration of the peak at δ 5.83 ppm (C=CH, *Z*- and *E*-isomer) showed that the vinyl hydrogen was 44% exchanged. The absence of the peaks at δ 3.47 ppm (CH_3PO, *Z*-isomer) and 2.69 ppm (CH_2PO, *E*-isomer) showed that the methylene protons were completely exchanged. For a summary of results of different runs, see Table 1.

Methyl Z- and E-4-Bromocrotonate

Methyl crotonate (28.5 g, 0.285 mol) in anhydrous carbon tetrachloride (100 ml) was refluxed with *N*-bromosuccinimide (46 g, 0.26 mol) in the presence of benzoyl peroxide (0.1 g) for 12 h. The succinimide was collected by filtration and the filtrate evaporated. Distillation gave a methyl 4-bromocrotonate (33.3 g, 72%) bp 82–91°C/12 torr. A glc analysis of the distillate indicated that the product was a mixture of approximately 1 part of the *Z*-isomer (lower retention time) to 20 parts of the *E*-isomer.

The product was fractionated using an annular spinning band column with approximately 100 theoretical plates giving two main fractions: (*1*) 0.30 g, bp 56–57°C/8.5 torr (>90% *Z*-isomer, glc and nmr); (*2*) 12.5 g, bp 66–67°C/8.5 torr (pure *E*-isomer, glc and nmr) (lit. (27) bp 83.5–85.5°C/15 torr). Fraction *1*: ir ν_{max} 1726vs, 1648s, 1441s, 1400s, 1296m, 1200vs, 1075m, 940m, 920s, 735m cm^{-1}; nmr δ 6.20 (br, HC= at C-3), 5.63 (d, J = 12 Hz, $=CHCO_2Me$), 4.40 (d, J = 7 Hz, CH_2Br), 3.59 (s, CO_2CH_3). Fraction *2*: ir ν_{max} 1729s, 1660s, 1439s, 1320s, 1280s, 1200s, 1135s, 1034s, 1007m, 975s, 722s cm^{-1}; nmr δ 6.81 (q, J = 7.6 Hz, HC= at C-3), 5.92 (d, J = 15 Hz, =CH—CO_2Me), 3.97 (e, J = 7.2 Hz, $BrCH_2$—), 3.60 (s, CO_2CH_3).

Methyl Z- and E-4-Phosphonocrotonate

(*i*) A mixture of methyl 4-bromocrotonate (14.6 g, 0.08 mol) (containing approximately 20 parts of the *E*- to 1 part of the *Z*-isomer) and triethylphosphite (13.7 g, 0.08 mol) was heated gradually to 150°C during 2 h. The product was distilled giving methyl 4-phosphonocrotonate (17.7 g, 95%) bp 127–134°C/3 torr (lit. (28) 115–130°C/0.3 torr). Gas–liquid chromatographic analysis indicated an approximate ratio of 1 part of the *Z*- to 20 parts of the *E*-isomer. Fractionation of the product using the annular spinning band column gave the following main fractions: (*1*) 0.25 g, bp 121–122°C/3 torr (glc 90% *Z*-isomer); (*2*) 0.95 g, bp 127–132°C/3 torr (glc mixture of *Z*-, *E*-, and a third component; (*3*) 8.5 g, bp 134–135°C/3 torr (glc 95% *E*-isomer); nmr 6.78 (m, 1H, CH vinyl), 5.90 (br d, 1H, J = 14 Hz, CH vinyl), 4.10 (q, 4H, J = 8 Hz, OCH_2Me), 3.72 (s, 3H, CO_2CH_3), 2.75 (dd, 2H, J = 8 Hz, CH_2PO) and 1.33 (t, 6H, J = 6 Hz, OCH_2CH_3). Fraction *1*, assumed to be chiefly the *Z*-isomer proved unstable and after 24 h isomerized to give about 50% *E*-isomer.

(*ii*) A mixture of methyl *Z*-4-bromocrotonate (0.76 g, 4.2 mmol) and triethylphosphite (0.75 g, 4.5 mmol) was heated gradually to 120°C during 1 h. Gas–liquid chromatographic analysis showed the presence of the *Z*-isomer **8***a* with a trace of the *E*-isomer **8***b* (higher retention time); nmr (neat) 5.75–6.63 (m, 2H, vinyl CH), 4.06 (q, 4H, J = 8 Hz, OCH_2Me) 3.74 (s, 3H, CO_2CH_3), 3.32 (dd, 2H, J = 5 and 7 Hz, CH_2PO) and 1.33 (t, 6H, J = 6 Hz, OCH_2CH_3).

*Isomerization of Methyl Z- and E-4-Phosphonocrotonate **8a** and **9a** with Sodium Methoxide*

The *Z*-phosphonate (10 mg, 0.042 mmol) in methanol (0.03 ml) was treated with 0.01 ml (0.0065 mmol) of a solution of sodium (15 mg) in methanol (1 ml). After 1 min the solution was analyzed by glc, and shown to be a mixture of the *Z*-isomer (10%) and the *E*-isomer (90%). No further change in the product composition was observed after 10 min. (On standing longer the peaks due to both isomers gradually decreased in size, with the appearance of new peaks in the glc. When equimolar amounts of phosphonate and sodium methoxide were mixed, only a small amount of the isomers could be detected after a few minutes.)

Repetition of the experiment using the *E*-isomer gave the same product composition.

Preparation of the Reference Compounds

*The Geometrical Isomers of Methyl 3-Methyl-5-phenylpenta-2,4-dienoate (**15a**, **16a**, **17a**, and **18a**)*

The four isomeric acids (*Z*-2,*E*-4, *E*-2,*E*-4, *Z*-2,*Z*-4, and *E*-2,*Z*-4 isomers) were prepared according to the method of Pattenden and Weedon (17) and converted into the corresponding methyl esters with diazomethane (9).

*Methyl Z- and E-β-Ionylideneacetate (**15b** and **16b**)*

(*i*) The *Z*- and *E*-isomers **15***b* and **16***b* were prepared by the reaction of triphenylcyclogeranyl bromide with 4-hydroxy-3-methylbut-2-enolide and methyl *E*-3-formylcrotonate respectively (9). The *Z*-acid formed in the first of these reactions was converted into the methyl ester with diazomethane.

(*ii*) *Z*-β-Ionylideneacetic acid was prepared by the hy-

drolysis of the δ-lactone of 5-hydroxy-3-methyl-5-(2,6,6-trimethyl-1-cyclohexen-1-yl)-2-pentonoic acid (9), and converted to the methyl **15***b* using diazomethane.

(*iii*) *E*-β-Ionylideneacetic acid was prepared by the method of Ishikawa (10) and converted into the methyl ester **16***b* with diazomethane.

*The Z-2,E-4 and E-2,E-4 Isomers of Methyl 3-Methyl-5-(cyclohexen-1-yl)pentadienoic Acid (**15***a and **16***a)*

These compounds were prepared according to the procedures in (*i*) for methyl *Z*- and *E*-β-ionylideneacetate (above (9)).

1. G. WITTIG. Experientia, **12**, 48 (1956).
2. H. POMMER. Angew. Chem. **72**, 811 (1960).
3. H. MACHLEIDT and R. WESSENDORF. Ann. **679**, 20 (1964).
4. P. KARRER, H. SALOMON, R. MORF, and O. WALKER. Helv. Chim. Acta, **15**, 878 (1932).
5. C. D. ROBESON, J. D. COWLEY, L. WEISLER, M. H. STERN, C. C. EDDINGER, and A. J. CHECHAK. J. Am. Chem. Soc. **77**, 4111 (1955).
6. S. H. HARPER and J. F. OUGHTON. Chem. Ind. 574 (1952).
7. S. YOSHIDA and K. TANABE. Japan Patent No. 8420 (1957); Chem. Abstr. **52**, 14673d (1958).
8. K. EITER, E. TRUSCHEIT, and H. OEDINGER. Angew. Chem. **72**, 948 (1960).
9. R. N. GEDYE, P. ARORA, and A. H. KHALIL. Can. J. Chem. **53**, 1943 (1975).
10. Y. ISHIKAWA. Bull. Chem. Soc. Jpn. **36**, 1527 (1963).
11. F. R. ATHERTON. Brit. Patent No. 1,206,440 (1969); Chem. Abstr. **73**, 120189 (1970).
12. G. PATTENDON and B. C. L. WEEDON. J. Chem. Soc. C, 1984 (1968).
13. R. K. HOWE. J. Am. Chem. Soc. **93**, 3457 (1971).
14. I. T. HARRISON and B. LYTHGOE. J. Chem. Soc. 843 (1958).
15. E. J. COREY and B. W. ERICKSON. J. Org. Chem. **39**, 821 (1974).
16. W. S. WADSWORTH and W. D. EMMONDS. J. Am. Chem. Soc. **83**, 1733 (1961).
17. G. PATTENDEN and B. C. L. WEEDON. J. Chem. Soc. C, 1997 (1968).
18. G. M. KOSOLAPOFF. Organo phosphorus compounds. 1st ed. Wiley and Sons Inc., New York, NY. 1950. p. 121.
19. N. F. BLAU, T. T. WANG, and C. M. BUESS. J. Chem. Eng. Data, **15**, 206 (1970).
20. J. BOUTAGY and R. THOMAS. Chem. Rev. **74**, 87 (1974).
21. V. M. PARIKH. Absorption spectroscopy of organic molecules. Addison Wesley, Don Mills, Ont. 1974. p. 28.
22. G. J. HEISWOLF, J. A. A. VAN DRUNEN, and H. KLOOSTERZIEL. Recl. Trav. Chim. **88**, 1377 (1969).
23. L. M. JACKMAN and R. H. WILEY. J. Chem. Soc. 2881 (1960).
24. G. WITTIG and H. POMMER. Ger. Patent No. 250,552 (1958); Chem. Abstr. **53**, 436 (1959).
25. R. H. WILEY, T. H. CRAWFORD, and C. E. STABLES. J. Org. Chem. **27**, 1535 (1962).
26. G. FODOR and I. TOMOSKOZI. Tetrahedron Lett. 579 (1961).
27. R. N. GEDYE and A. NECHVATAL. J. Chem. Soc. 5925 (1964).
28. R. S. BURDEN and L. CROMBIE. J. Chem. Soc. C, 2477 (1969).

Effect of aza-substitution on the geometry and electrocyclization of pentadienyl anions: an apparent exception to the Woodward–Hoffmann rules?

D. H. HUNTER, S. K. SIM,[1] AND R. P. STEINER[2]

Department of Chemistry, University of Western Ontario, London, Ont., Canada N6A 5B7

Received August 13, 1976

D. H. HUNTER, S. K. SIM, and R. P. STEINER. Can. J. Chem. **55**, 1229 (1977).

Two geometrical isomers of 1,3,5-triphenyl-1,3-pentadiene **1** have been prepared and characterized; *trans,cis*-**1** and *trans,trans*-**1**. These have been used to prepare and characterize the 1,3,5-triphenylpentadienyl anion by quenching the lithium salt in THF and by following hydrogen–deuterium exchange in methanol-*O-d* with potassium methoxide. Attempts to induce electrocyclization (130°C in THF or 200°C in KO*t*Bu–HO*t*Bu) have proven unsuccessful. A comparison of the behaviour of this anion with the 2-aza and 2,4-diaza analogues has helped in elucidating the mechanisms for their electrocyclization and the apparent exception to the Woodward–Hoffmann rules.

D. H. HUNTER, S. K. SIM et R. P. STEINER. Can. J. Chem. **55**, 1229 (1977).

On a préparé et caractérisé deux isomères géométriques du triphényl-1,3,5 pentadiène-1,3 (**1**); il s'agit des isomères *trans,cis* **1** et *trans,trans* **1**. On les a utilisé pour préparer et caractériser l'anion triphényl-1,3,5 pentadiényle en piégeant le sel de lithium dans le THF et en faisant suivre cette réaction par un échange hydrogène–deutérium dans le méthanol *O-d* avec le méthylate de potassium. Tous les essais effectués dans le but d'induire de l'électrocyclisation (130°C, dans du THF ou 200°C, dans le KO*t*Bu–*t*BuOH) se sont soldés par des insuccès. Une comparaison du comportement de cet anion avec ses analogues aza-2 et diaza-2,4 a permis d'élucider les mécanismes de leurs électrocyclisations et l'exception apparente aux règles de Woodward–Hoffmann.

[Traduit par le journal]

Introduction

Many examples of electrocyclization reactions of delocalized carbanions have appeared in recent years (1) and these have provided evidence on the thermodynamics, the dynamics, and the stereochemistry of these reactions. In contrast to the three center system (*e.g.*, allyl ⇌ cyclopropyl) and the seven center system (*e.g.*, heptatrienyl ⇌ cycloheptadienyl), there have been significantly fewer examples from the five center system (*e.g.*, pentadienyl ⇌ cyclopentenyl). Although many open-chain pentadienyl anions have been prepared and characterized, with but one exception (2), cyclization has not been observed. The cycloreversion reactions of cyclopentenyl anions have not been reported to date.

Electrocyclization reactions involving pentadienyl anions in cyclic systems have been observed in two cases; the cyclooctadienyl anion (3) and the cyclohexadienyl (4) anion. These show opposite thermodynamics, the anion in the eight-membered ring prefers the closed form

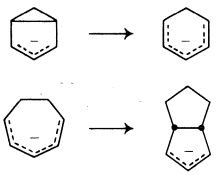

but the six-membered ring prefers the open form. These contrasting results are presumably a consequence of the strain peculiar to these ring sizes. Both reactions occur in the anticipated disrotatory manner (5) but this stereochemistry is also imposed by ring strain. In fact, there are a number (6) of electrocyclic reactions that occur in the direction required by ring strain in spite of contrary orbital symmetry demands.

In contrast to the all-carbon systems, aza-substitution at the 2 and 4 position in pentadienyl anions suffices to induce electrocyclization (7, 8). It has also been possible to observe the stereochemistry of these reactions and marked changes have been observed in both the rate and stereoselectivity of the electrocyclization process. In an attempt to sort out the factors responsible for these changes, the all-carbon system has now been prepared and studied. We wish to report on the behaviour of the 1,3,5-triphenylpenta-

[1]Present address: Department of Chemistry, University of Alberta, Edmonton, Alberta.

[2]Present address: Department of Chemistry, Fort Lewis College, Durango, CO, U.S.A. 81301.

dienyl anion **5** to compare and contrast its behaviour with the 1,3,5-triphenyl-2-azapentadienyl anion **6** and the 1,3,5-triphenyl-2,4-diazapentadienyl anion **7**.

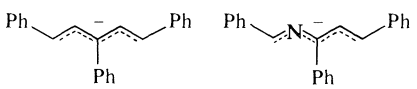

5 **6**

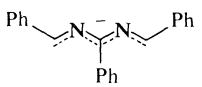

7

Results

Preparation and Characterization of the 1,3,5-Triphenyl-1,3-pentadienes

As illustrated in Scheme 1 both 1,3,5-triphenyl-*trans,trans*-1,3-pentadiene (*trans,trans*-**1**) and 1,3,5-triphenyl-*trans,cis*-1,3-pentadiene (*trans,cis*-**1**) were prepared from chalcone using variants of the Wittig reaction. Reaction of the Wittig reagent from (2-phenylethyl)triphenylphosphonium bromide with an equimolar amount of chalcone provided an initial mixture of *trans,trans*-**1** and *trans,cis*-**1** in a ratio of 6:1. A 30% yield of *trans,trans*-**1** was obtained after purification. In contrast, the reagent from diethyl 2-phenylethylphosphonate with chalcone produced a 1:7 mixture of *trans,trans*-**1** to *trans,cis*-**1** which provided a 16% yield of purified *trans,cis*-**1**. The ^{1}H nmr spectra of both dienes were consistent with a *trans* configuration at the terminal double bond ($J_{12} \sim 17$ Hz). The configuration at the internal double bond was assigned from the relative reactivity of the two dienes with dienophiles with the assumption that *trans,cis*-**1** would be more reluctant than *trans,trans*-**1** to adopt the conformation needed for a Diels–Alder reaction.

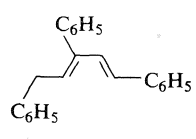

trans,trans-**1**

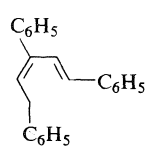

trans,cis-**1**

The relative reactivity of *trans,trans*-**1** and *trans,cis*-**1** with dienophiles was measured by nmr monitoring of changes in the ratio of *trans,trans*-**1** to *trans,cis*-**1** upon addition of less than an equimolar amount of a dienophile. As indicated in Table 1 three dienophiles were used to test the generality of the reactivity preference. With 2-butyne, benzoquinone, and *N*-phenylmaleimide one of the dienes was consistently more reactive than the other. The more reactive diene was assigned the *trans,trans* configuration in accord with the expected conformational preferences. The apparent differences in relative reactivity of *trans,trans*-**1** and *trans,cis*-**1** upon changing the dienophile are probably not significant. These rate ratios are minimum values since the observed ratio of unreacted dienes will be sensitive to the extent of reaction.

To clarify further the relative reactivities, the two dienes were reacted separately with *N*-phenylmaleimide. Treatment of *trans,trans*-**1** in benzene with *N*-phenylmaleimide at 80°C for 42 h provided the Diels–Alder adduct in 74% isolated yield. In contrast, heating to 155°C for 74 h was required to result in reaction of *trans,cis*-**1**. This reaction yielded a mixture which seemed, by mass spectrometry, to contain a 1:1 adduct but no pure component could be isolated. Thus *trans,trans*-**1** reacts cleanly to give a Diels–Alder adduct while *trans,cis*-**1** is much less reactive and less selective when it finally reacts.

Geometry of the Pentadienes and Azapentadienes

The relative stability of *trans,trans*-**1** and *trans,cis*-**1** was determined by equilibration at 60°C in potassium methoxide – methanol. Starting with either diene the same mixture was obtained (73% *trans,trans*-**1** and 27% *trans,cis*-**1**) as indicated by the results of runs 1–6 of Table 2. Figure 1 summarizes the results obtained for the analogous azapentadienes and diazapentadiene. In the case of **4** only one geometry has been observed (7) although it has been treated under the same conditions which equilibrated the geometries of **1**, **2**, and **3** and which resulted in hydrogen–deuterium exchange of **4**. Attempts to induce geometrical isomerization in **4** by irradiation, both sensitized (triphenylene) and unsensitized, also failed. Thus it is probable that

TABLE 1. Changes in the ratio of *trans,trans*-**1** to *trans,cis*-**1** on reaction[a] with a dieneophile

Dieneophile	*trans,trans*-**1**/*trans,cis*-**1**		
	Initial	Final[b]	Rate ratio
N-Phenylmaleimide	7	0.25	28
Benzoquinone	2	0.3	7
2-Butyne	2	0.1	20

[a]Reaction run in CCl_4 at 60°C.
[b]The unreacted dienes were isolated as the lead band from tlc.

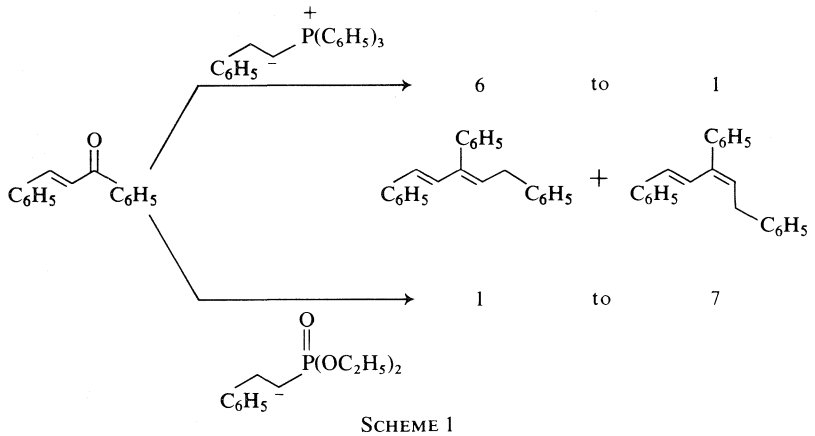

SCHEME 1

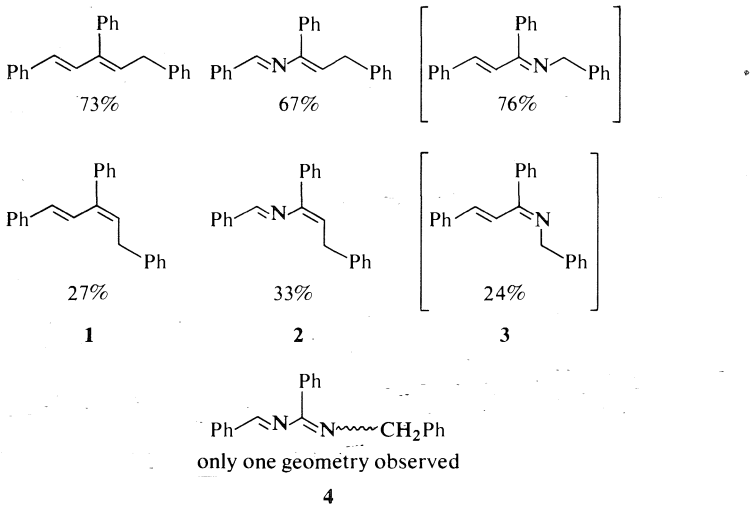

FIG. 1. Equilibrium percentages of azapentadienes and pentadienes at 60°C in $KOCH_3$–$HOCH_3$.

the one geometry observed for **4** is the thermodynamically preferred geometry but its actual configuration remains undetermined.

As described previously (8), the geometries of **1** and also **2** were assigned using Diels–Alder relative reactivity. The geometries of **3** could not be assigned in a similar manner and thus remain uncertain except for the *trans* arrangement across the carbon–carbon double bond. Analogy with **1** and **2** led to the assumption shown in brackets in Fig. 1.

Geometry of the Pentadienyl and Azapentadienyl Anions

Treatment of either *trans,trans*-**1** or *trans,cis*-**1** with lithium 2,2,6,6-tetramethylpiperidide (LiTMP) in THF led to a deep blue solution which was characterized by quenching experiments (acetic acid) and variable temperature nmr (9). As indicated in runs 7–11 of Table 2 quenching of the anion from either geometry of **1** at varying times led to the same mixture of *trans,trans*-**1** (45%) and *trans,cis*-**1** (55%). A material balance of run 8 resulted in a 93% recovery of **1** and quenching with acetic acid-*O*-*d* resulted in **1** containing 94%-d_1 and 6%-d_0 by mass spectrometry.

A variable temperature ^1H and ^{13}C nmr study (9) of 1,3,5-triphenylpentadienyllithium **5** in THF-d_8 indicated the presence of both the S and W shapes with the S predominating by a factor of about 2.3. The nmr and quenching results are summarized in Scheme 2. If the rate of quenching exceeds the rate of interconversion of S and W

TABLE 2. Base-catalyzed interconversion of *trans,trans*-**1** and *trans,cis*-**1**

Run	Substrate[a]	Base[b]–solvent	T (°C)	Time (h)	Product (%)	
					trans,trans-**1**	*trans,cis*-**1**
1	*trans,trans*-**1**	$KOCH_3$–$HOCH_3$	60	24	80	20
2	*trans,trans*-**1**	$KOCH_3$–$HOCH_3$	60	72	78	22
3	*trans,trans*-**1**	$KOCH_3$–$HOCH_3$	60	216	73	27
4	*trans,cis*-**1**	$KOCH_3$–$HOCH_3$	60	23	58	42
5	*trans,cis*-**1**	$KOCH_3$–$HOCH_3$	60	68	72	28
6	*trans,cis*-**1**	$KOCH_3$–$HOCH_3$	60	216	74	26
7	*trans,trans*-**1**	LiTMP–THF	25	24	45	55
8	*trans,cis*-**1**	LiTMP–THF	25	3	45[c]	55
9	*trans,cis*-**1**	LiTMP–THF	25	24	44	56
10	*trans,cis*-**1**	LiTMP–THF	120°	24	45[d]	56
11	*trans,trans*-**1**	LiTMP–THF	120°	24	43[d]	57

[a]0.15 M in runs 1–6; ~0.1 M in runs 7–11.
[b]0.22 M in runs 1–6.
[c]Both *trans,trans*-**1** and *trans,cis*-**1** obtained in 93% total yield.
[d]Both *trans,trans*-**1** and *trans,cis*-**1** obtained in 50% total yield.

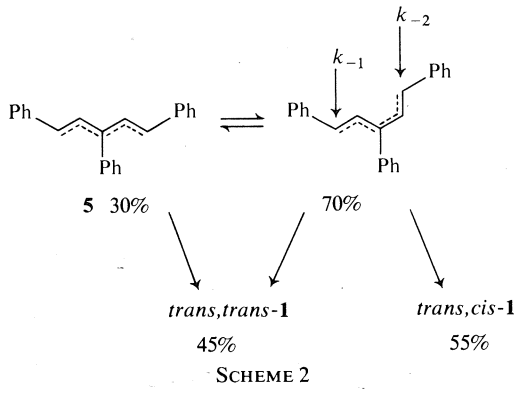

SCHEME 2

shapes (k_1(S ⇌ W) ~ 10^3 s^{-1} at 25°C), then the quenching preference of the S shape can be calculated. From the anion composition and the proportions of **1** upon quenching, it is found that k_{-1}/k_{-2} ~ 0.3. As with the 2-azapentadienyl anions (from **2** and **3**) and the 2,4-diazapentadienyl anion (from **4** and hydrobenzamide **8**), no products are observed due to protonation at the central carbon. This contrasts with the behaviour of cyclohexadienyl anions (10) (*e.g.*, in Birch reductions).

Analogous quenching results are observed for 2-azapentadienyllithium **6** in THF (8). Since **6** electrocyclizes near 0°C, it was not studied by nmr and quenching with acetic acid was used to determine the geometries of **6**. The products of quench (Scheme 3) clearly indicate the presence of more than one geometry for **6**. Although there are insufficient data to calculate the actual proportions of the geometries of **6** that are present, the S forms are present and may predominate as in the case of **5**.

Attempts to characterize the geometries of 2,4-diazapentadienyllithium **7** have proven much less successful because of its propensity to electrocyclize (7). Attempts were made to generate **7** from hydrobenzamide **8** and to quench before electrocyclization. Using organolithium bases in THF down to the freezing point of THF (~ −110°C), intense color was observed but quenching showed that anion formation was the slow step and, at most, only traces (<1%) of quench product **4** could be obtained. In a further effort to characterize **7**, potassium piperidide in α-methyltetrahydrofuran down to −130°C has now been used. This is clearly a kinetically much more active base since no unreacted starting material **8** was recovered even upon quenching at 5 min with trifluoroacetic acid. Again, however, in spite of intense color no **4** could be observed (<5%) accompanying the product of electrocyclization, amarine.

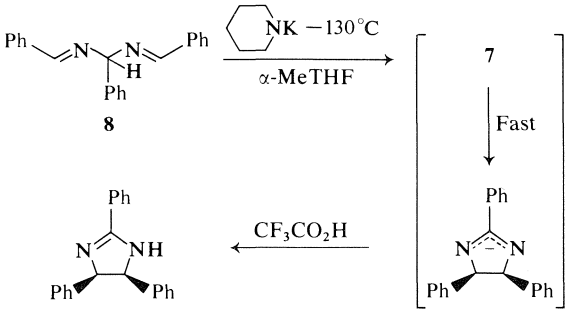

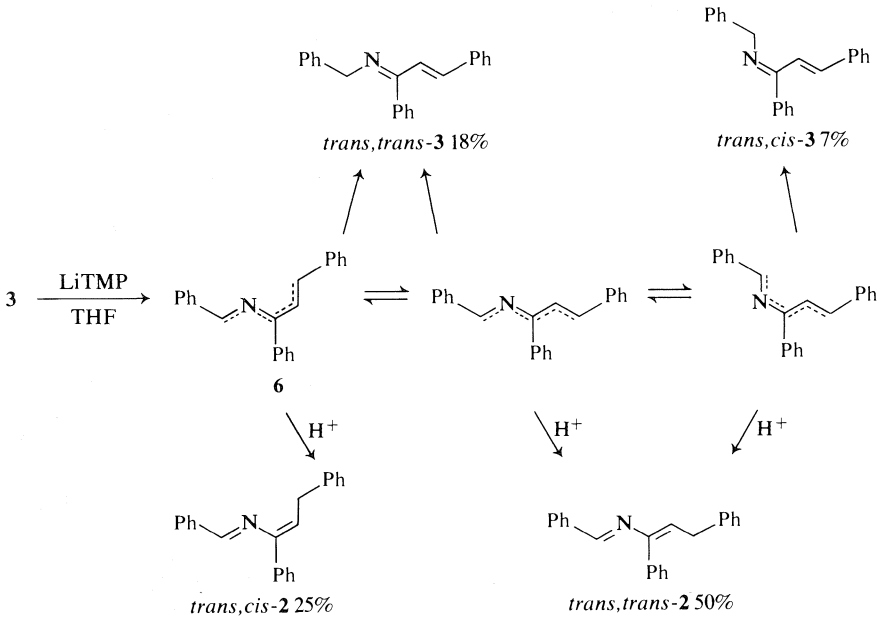

SCHEME 3

The results of the nmr and quenching studies of the three anions **5**, **6**, and **7** show that both **5** and **6** exist in more than one geometry and these geometries are of comparable stability. One of these geometries is unsymmetrical, the S-shape,

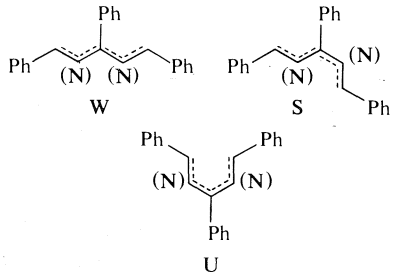

and the other symmetrical, the W- or U-shapes. Of the two possibilities for the symmetrical species, the W seems more probable than the U, first, from inspection of space-filling models and second, since a variety of pentadienyl anions have been shown to adopt the W-shape some with a small amount of the S-shape present (1*b*). The geometrical preferences of **7** could not be observed because of its reactivity but can only be inferred by analogy with **5** and **6**.

Kinetic Acidity of the Pentadienes

The base-catalyzed H–D exchange and isomerization reactions of the structurally related pentadiene (*trans,cis*-**1**), azapentadiene (**3**), and diazapentadiene (**4**) have been followed in CH_3OK–CH_3OD at 60°C. A comparison of the ease of deprotonation in the three systems should yield a rough estimate of the relative stabilities of the anions **5**, **6**, and **7**. As detailed in Table 3, the rate of total exchange and isomerization of the thermodynamically less stable *trans,cis*-**1** to *trans,trans*-**1** was followed by a combination of nmr and mass spectrometry. Qualitatively, exchange was somewhat faster than isomerization in agreement with the quenching experiments for the S-shape ($k_{-1}/k_{-2} \sim 0.3$). A maximum of 3 atoms D/molecule was observed under these conditions and exchange occurred exclusively at the 1 and 5 positions consistent with reaction via **5**. On the basis of the data in Table 3, a rough estimate of the rate constant for H–D exchange could be made (Fig. 2).

The azapentadienes have also been studied and Fig. 2 contains the rate constant for H–D exchange for the 4-aza isomer (**3**) which is by far the minor component at equilibrium with the 2-aza isomer (**2**). Exchange of **2** occurs more slowly than **3** and although not determined directly seems to be more comparable in rate to **4**. It should be noted that a direct comparison of *trans,cis*-**3** with *trans,cis*-**1** cannot be made since the first reaction of **3** under these conditions

TABLE 3. Base-catalyzed exchange and isomerization of *trans,cis*-**1** in $KOCH_3$–$DOCH_3$[a] at 60°C

Run	Time (min)	Isomerization[b] (%)	Isotopic analysis (%) d_0	d_1	d_2	d_3
12	60	6	41	44	12	3
13	120	15	23	46	24	7
14	1140	37	0	6	37	51

[a]0.28 *M* in base, 0.02 *M* in *trans,cis*-**1**.
[b]As determined by nmr.
[c]Mass spectrum on mixture of *trans-trans*-**1** and *trans,cis*-**1**.

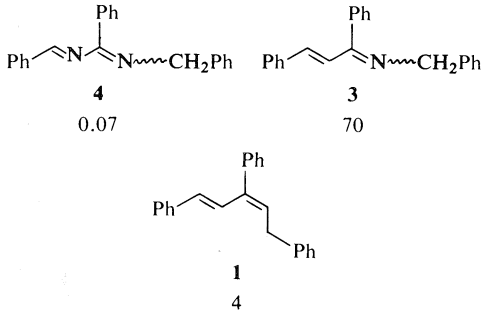

FIG. 2. Second-order rate constants ($\times 10^4$) M^{-1} s^{-1} for hydrogen–deuterium exchange in $KOCH_3$–$DOCH_3$ at 60°C.

is *syn–anti* equilibration and so the reported rate constant is for the mixture of geometries.

The rate constant for exchange of the diazapentadiene (**4**) is also shown in Fig. 2 but in the case of **4**, both electrocyclization and exchange occur competitively through anion **7**. Thus, exchange only measures about one-third of the acts of carbanion formation, which implies that the actual kinetic acidity is about three times greater ($k_2 \sim 0.2 \times 10^{-4}$ M^{-1} s^{-1}) than indicated in Fig. 2. Again in the case of **4** it is not clear which geometry is adopted although in this case only one geometrical isomer is observed.

However, in spite of the uncertainty as to the geometry of **3** and **4**, it seems clear that **1**, **3**, and **4** all deprotonate within a reactivity range of about 300. In as far as anion stabilities can be deduced from kinetic acidities, these exchange rates imply that the anions **5**, **6**, and **7** are of comparable stability relative to the dienes **1**, **3**, and **4**. Thus aza-substitution at the 2 and 4 positions in a pentadienyl anion has modest effects on the stability of the anion. This is in accord with simple valence bond or molecular orbital concepts which place the negative charge at the 1, 3, and 5 positions in a pentadienyl chain.

Electrocyclization of **5**

Attempts to induce **5** to cyclize both thermally and photochemically resulted in failure. As indicated in runs 10 and 11 of Table 2, heating of THF solutions of **5** to 120°C resulted in reduced yields of recovered **1**, but no other 'monomeric' products could be observed. Upon heating to 150°C for 16 h followed by quenching, no dienes **1** could be observed and at the same time no monomeric hydrocarbons could be isolated. Similarly heating of *trans,trans*-**1** in a degassed solution of 0.7 *M* potassium *tert*-butoxide in *tert*-butyl alcohol for 18 h at 200°C resulted in nearly complete loss of **1** and no product attributable to cyclization could be isolated. Reaction at lower temperature resulted in varying loss of **1** but no product of cyclization.

Solutions of **5** in both THF and *N,N,N',N'*-tetramethylethylenediamine in quartz cells were irradiated using a Hanovia 1000 W high pressure mercury lamp. Experiments were attempted both isolating the long wavelength absorption band of **5** at 585 nm and using the total wavelength range available. In these experiments only **1** was obtained on quenching. Thus all attempts to persuade **5** to electrocyclize were unsuccessful although **6** and **7** react with ease.

Discussion

The preparation of the *trans,trans* and *trans,cis* isomers of **1** and of the derived anion **5** has provided the final comparison in evaluating the significance of 2- and 4-aza substitution of the reactivity of pentadienyl anions. Effects upon the geometry and stability of the open-chain anion and the dienes are not large, but dramatic effects have been noted for the electrocyclization reaction. There are marked changes in both the propensity to undergo cyclization and in the stereochemistry of the product of cyclization. In dis-

cussing the results of the study of **5**, their impact upon the electrocyclization reactions will be emphasized, first by comparing and contrasting the diaza, monoaza, and all-carbon systems. Then, possible mechanistic interpretations of the observed reactivity pattern will be presented in light of these new results.

Rates of Electrocyclization

The lithium salts of the open-chain 1,3,5-triphenylpentadienyl anions and their aza analogues (**5**, **6**, and **7**) have been prepared in THF from the corresponding carbon acids using amide bases at low temperatures. The all-carbon anion **5** undergoes no conversion to a cyclic form in the temperature range of −80 to +130°C. The 2-aza anion **6**, on the other hand, remains in the open-chain form at temperatures below 0°C but in the temperature range 0 to 25°C converts completely to cyclic isomers. Remarkably the 2,4-diaza anion **7** has only been observed as a fleeting intermediate on the way to cyclized product at temperatures as low as −130°C. The evidences for the existence of **7** are: the intense color (λ_{max} = 592 nm) observed; the isolation in one case (the tris *p*-Cl compound) of small amounts (~1%) of the quench product, tri-*p*-Cl-**4**, and its hydrolysis product; and, of course, chemical intuition as to the most likely proton abstraction reaction.

Reactions in protic media provide a further comparison of the relative rates of cyclization of **6** and **7**. As mentioned earlier KOMe–HOMe at 60°C suffices to produce **6** or **7** from the corresponding carbon acids at similar rates, but the rate of production of cyclized product is quite different. As judged from the fact that hydrogen–deuterium exchange and cyclization are competitive for **4**, the diaza anion **7** would seem to cyclize and protonate at about the same rate. Thus cyclization of **7** must be occurring with a rate constant (k_1) of at least 10^5 s^{-1} (11). In contrast while KOMe–DOMe at 60°C suffices to effect exchange and isomerization of **3**, KO*t*Bu–HO*t*Bu at 120°C must be used to generate cyclized product. Since KO*t*Bu–HO*t*Bu is judged to be a kinetically much stronger base than KOMe–HOMe (12), it is possible to estimate that cyclization is occurring some 10^6 slower than protonation.

It seems likely that the large changes in rate upon aza substitution reflect changes in the

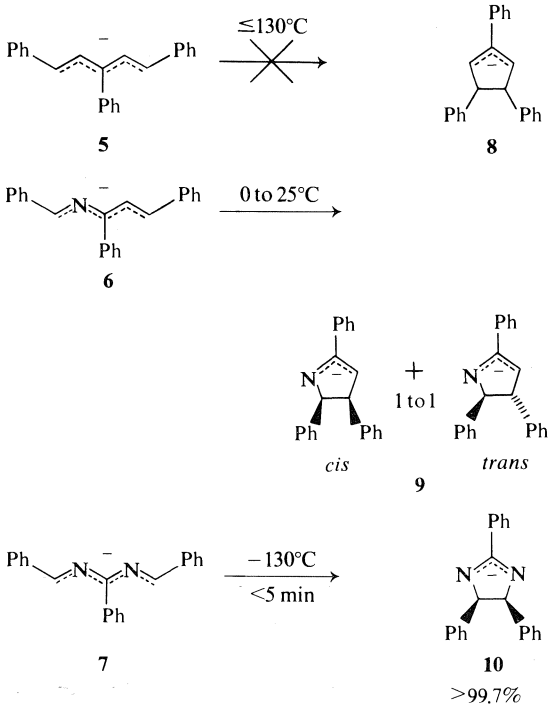

5 **8** **6** **9** **7** **10**

thermodynamic stability of the cyclic anions relative to the open-chain anions. As presented earlier, the rate of formation of the open-chain anions (**5**, **6**, and **7**) by base-catalyzed deprotonation with CH_3OK–CH_3OH covers a range of about 300. In contrast, the cyclization reaction rates for **6** and **7** differ by about 10^6 and **5** does not cyclize. On this basis it seems more reasonable to attribute the changes in the cyclization rates to changes in the stability of the cyclized form with the open-chain anions having comparable relative stabilities.

It is possible to construct a qualitative free energy diagram (Fig. 3) consistent with the observed results. Although none of the spacings are known directly, several approximate free energy values can be assigned by analogy. It is likely that the cyclopentene forms are more stable than the pentadiene forms since cyclopentene (ΔG_f^{298}(g) = 26.48 kcal/mol) is 8.36 kcal/mol more stable than *trans*-1,3-pentadiene (ΔG_f^{298}(g) = 34.84) (13). The phenyl substituents should presumably serve to narrow this gap. The introduction of one nitrogen should have similar effects upon both the open and closed forms while in the diaza case delocalization should serve to selectively stabilize the cy-

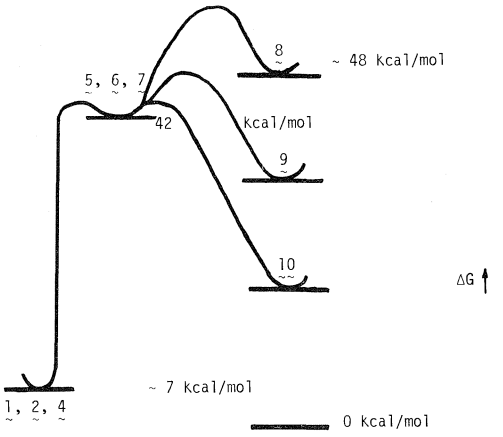

FIG. 3. Free energy profile showing effect of aza-substitution on the cyclization reactions.

clized form. The extent of this stabilization is not certain.

The free energy of the open-chain anions relative to the dienes is available through an estimate of the pK_a. All three pentadienes have kinetic acidities similar to methyl acetates (14) which places their pK_a near 26. The free energy of the all-carbon closed anion relative to the cyclopentene is also available through a pK_a estimate of propene ($\sim$35) (15). We were unable to find estimates for the pK_a of imines or amidines[3] but the fact that the cyclization reactions occur, places their energy below that of the open form. Undoubtedly the amidines will be more acidic than imines. From this kind of analysis, admittedly approximate in nature, it is certainly tempting to suggest that it is the product stability that determines the cyclization reaction rate.

The reluctance of the all-carbon anion to cyclize is consistent with the observations for other pentadienyl anions. Recent gas phase measurements of proton affinities of 1,3-pentadiene (18) and propene (19) suggest that the open form of the anion would be favoured at equilibrium. The only example (2) of a possible cyclization involves the 1,5-diphenylpentadienyl anion which can be postulated as an intermediate in the high temperature Wolf–Kishner reduction of dibenzylidene acetone yielding diphenylcyclopentenes. The results with dibenzylidene acetone could well reflect kinetic rather than thermodynamic control, if the reaction does proceed through anionic intermediates.

[3]Alkyl and arylamidines are reported to form salts with $NaNH_2$ and KNH_2 (16) while *N,N'*-diarylformamidines are converted to their salts by OH^- (17).

Stereochemistry of Electrocyclization

Concurrent with the marked change in cyclization rates, there is a marked change in cyclization stereochemistry. The diaza anion **7** cyclizes to produce (7) the *cis* isomer **10** exclusively (>99.7%) whereas the monoaza anion **6** produces (8) both the *cis* and *trans* isomers (*cis*-**9** and *trans*-**9**) in approximately equal amounts. In both cases, **9** and **10**, the *cis* form is thermodynamically less favoured than the *trans* form ($K_{eq} \approx 25$). So while cyclization *rates* reflect product stability, cyclization *stereochemistry* does not.

The cyclization stereochemistry of **7** does not show any observable temperature sensitivity since reaction at −130°C (THF) or at 60°C (KOMe–HOMe) produces only the *cis* product. The 1:1 mixture of *cis*- and *trans*-**9** does not change significantly with extent of reaction, consistent with kinetic control without subsequent conversion of *cis* to *trans* isomers. These controls point to a real difference in the mode of cyclization of the diaza anion **7** and the monoaza anion **6**, with the relative rates of production of the *cis* and *trans* closed forms changing by at least 300.

The cyclization reactions of **6** and **7** seem best categorized as electrocyclization reactions and consequently the stereoselectivity of the reactions can be analyzed in terms of orbital symmetry control. The typical approach to the analysis of electrocyclization reactions involves considering interconversion of the all-*cis* open form with the cyclic form. With this premise both the Woodward–Hoffmann rules and orbital correlation using simple Huckel molecular orbitals predict a disrotatory mode of ring closure for the pentadienyl anion **5** as well as the diaza and monoaza anions, **6** and **7**. Clearly the dramatic change in

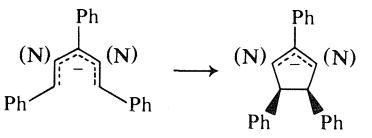

reaction stereochemistry with aza-substitution requires a modification from this simple approach. Two possible explanations seem appropriate: more than one geometry of the open-

chain anions is involved or a more sophisticated orbital correlation analysis is needed.

Role of Anion Geometries

The formation of both the *cis* and *trans* forms of the closed anion **9** can be rationalized by assuming that reaction occurs from more than one geometry of **6** but always in a disrotatory manner while in contrast, the diaza anion **7** should be reacting from just one geometry. Thus it seemed desirable to explore the effect of aza-substitution on the geometries adopted by the open-chain anions. Unfortunately, as mentioned earlier, **7** reacts so fast that neither nmr nor quenching experiments could be used successfully to determine the geometry of **7**.

The intermediate reactivity of **6** allowed quenching experiments to be carried out and these were consistent with the presence of more than one geometry of **6**. In fact, it appeared that the W (or U) form and both the S forms were present and these were present in similar amounts. The lack of reactivity of **5** ruled out a study of the cyclization stereochemistry, but allowed a determination of the geometry of **5** both by nmr and quenching. A comparison of **5** and **6** should then show whether aza-substitution greatly effects the geometry adopted by pentadienyl anions. Nuclear magnetic resonance and quenching results on **5** were consistent with the presence of both the S and W (or U) forms with the S predominating by about a factor of 2. The similarity between the geometries adopted by both **5** and **6**, thus, provides no support for the proposal of a unique geometry of **7**. Nonetheless, it is worth considering specific mechanistic possibilities involving different geometries.

One geometrical modification of the all-*cis* U-form involves isomerism around the terminal bonds which results in three possible isomers, of which the *E-E* form should be the most stable. A mechanism consistent with the observations would have anion **7** react exclusively through the *E-E* form but **6** react roughly equally through the *E-E* and *E-Z* forms. It is this kind of proposal that seems inconsistent with the geometrical observation on **5** and **6**. Aza-substitution does not greatly effect geometrical preferences.

A second modification involves rotation around the inner bonds of the *E-E* form to produce the W and S forms. The nmr study (9) of the lithium salt of **5** in THF-d_8 shows that the W

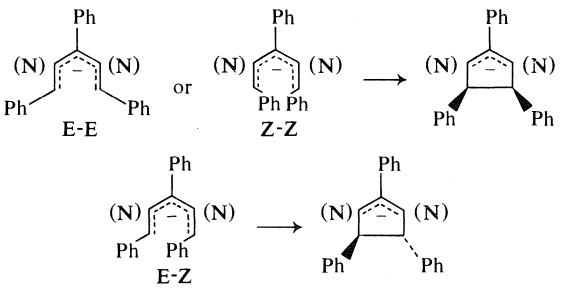

and S forms are of roughly equal energy and the rate constants for isomerization are about 10^2 to 10^3 at -20 to -5°C. While, in principle, the W and U forms could lead directly to the *cis*-closed isomer and the S could lead to the *trans*-closed isomer, again it becomes necessary to postulate an unsubstantiated unique geometry for the diaza anion **7**. Direct cyclization from either the W or S forms also seems unlikely in terms of the large distance between one and five carbon atoms and the number of atoms that would have to move in such a concerted process.

If the anion geometries are interconverting rapidly before cyclization occurs, an analysis involving the Hammond–Leffler postulate may be valid (the validity of this postulate has been seriously questioned recently, see ref. 20). For the most exothermic reaction (**7** → **10**) the transition state leading to the less stable isomer is observed to be lower in energy than the transition state leading to the more stable (*trans*-**10**) isomer. As the reaction becomes less exothermic (**6** → **9**) the stability of the products could become more important in determining the relative reaction rates. Consequently the transition state leading to the more stable isomer (*trans*-**9**) could approach that leading to the less stable isomer (*cis*-**9**) and result in lower stereoselectivity as observed. While the trend in the stereoselectivity is consistent with this analysis, the results seem unusual in two respects: first, the change in stereoselectivity (≥ 300) is rather large for two exothermic processes and, second, the more exothermic process is the one that shows the higher stereoselectivity.

Concurrent Disrotatory and Conrotatory Reactions

If indeed both **6** and **7** adopt the same geometries for cyclization, then it becomes necessary to postulate a violation of the Woodward–Hoffmann rules. Such a suggestion is not without

precedent although direct analogies are not yet available. The simplest approach is to assume that all reaction occurs through the *E-E* configuration of the U-form but while **7** reacts in just a disrotatory manner, **6** proceeds in both a conrotatory and disrotatory mode. The basis for this proposal resides in the fact that **7** is a symmetrical species (C_{2v}) while **6** has no analogous symmetry. Both Schilling and Snyder (21) using extended Huckel or CNDO/INDO and Epiotis (22) using configuration interaction have concluded that asymmetric substitution of electron-withdrawing or -donating groups can lead, in the extreme, to a reversal of the stereochemistry of an electrocyclic reaction. However, *we* are not in a position to estimate whether the aza-substitution discussed here represents a sufficient perturbation.

As must be clear by now, the stereochemistry of electrocyclization of the symmetrical all-carbon anion **5** would have provided more conclusive evidence as to the correct explanation for the observed changes. However, **5** refused to electrocyclize. Interestingly cyclization during the high temperature Wolf–Kishner reduction of *trans, trans*-dibenzylidene acetone has been observed (2). The 1,5-diphenylpentadienyl anion has been postulated as an intermediate in this reaction which is run at 225°C using powdered potassium *tert*-butoxide, sodium methoxide, or potassium hydroxide. In all cases both the *cis*- and *trans*-

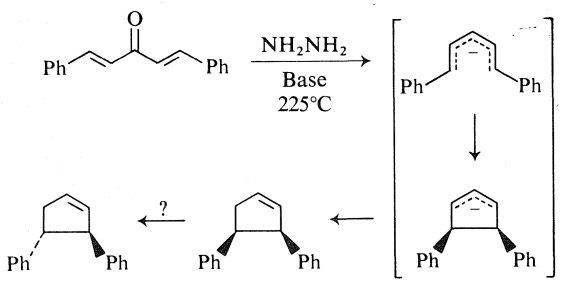

3,4-diphenyl cyclopentenes were among the reaction products. However, controls established that the products isomerize under the reaction conditions, leaving ambiguous the kinetic stereoselectivity in this cyclization reaction. Indeed, as the author suggests, the reaction may be proceeding initially through the *cis* anion, but at the present this is merely conjectural.

In summary, the study of the 1,3,5-triphenylpentadienyl anion has helped confirm the geometrical preferences for such open-chain delocalized anions and, indirectly, provided support for the hypothesis that molecular asymmetry can lead to a change in the stereochemical demands imposed by orbital symmetry.

Experimental

Solvents and Bases

The methanol was distilled from magnesium and the methanol-*O-d* was prepared from dimethylcarbonate (23). Base solutions were prepared by reaction of the alcohol under argon with freshly cut potassium. Tetrahydrofuran was freshly distilled from lithium aluminum hydride before use. THF and α-methyltetrahydrofuran used for bulb-to-bulb distillation were stored over sodium/potassium alloy with added benzophenone as indicator.

Solutions of potassium piperidide in THF or α-methyl THF were prepared by dissolving the residue obtained after evaporating the solvent from an aliquot of a solution of potassium piperidide in piperidine (~1 *M*). The potassium piperidide in piperidine was prepared by heating potassium hydride (washed free of oil) with piperidine (freshly distilled from potassium) at reflux for about 1 h under argon. Although colored, these solutions of potassium piperidide in piperidine remained active for up to 3 weeks without significantly changing their titre.

Preparation of trans,cis-1,3,5-Triphenyl-1,3-pentadiene

(a) Diethyl 2-Phenylethylphosphonate

A mixture of triethylphosphite (freshly distilled, 5.5 g, 33 mmol) and 2-phenylethylbromide (6 g, 33 mmol) was heated under an argon atmosphere first at 130°C for 1 h, then at 170°C for 1 h, and then at 220°C for 3 h. After cooling the reaction mixture was distilled and the fraction of bp 130–134°C/0.03 torr was collected yielding 4.1 g (17 mmol, 51% yield) of product.

The mass spectrum gave *m/e* 242 for the molecular ion. The nmr spectrum (CCl_4) showed the following: δ 1.01 (6H, t), 1.5–3.1 (4H, m), 4.0 (4H, m) 7.03 (5H, s). The infrared spectrum (neat) gave major bands at 3004, 1248, 1030, and 962 cm^{-1}.

(b) trans,cis-1,3,5-Triphenyl-1,3-pentadiene

To the diethyl 2-phenylethylphosphonate (2.7 g, 11 mmol) in 25 ml of THF (freshly distilled) at −20°C was added 11 mmol of *n*-butyllithium. After stirring at −20°C for 4 h the solution was warmed to ambient temperature and chalcone (2.4 g, 11 mmol) in 25 ml THF was added. Stirring was continued for 15 h followed by work-up using an ether–water extraction. The crude oil obtained after solvent removal was chromatographed (silica gel, 10% ether–pentane) and the *trans,cis*-**1** was recrystallized from pentane to yield white needles of mp 72–75°C (16% yield).

The mass spectrum gave *m/e* 296 for the molecular ion. The nmr spectrum (CCl_4) showed an AX_2 with ν_A = 5.68 ppm, ν_X = 3.75 ppm, and J_{AX} = 7.0 Hz; an AB with one half visible with ν_A = 6.38 ppm and J_{AB} = 17 Hz; and a 16 H multiplet in the region 7.0–7.4 ppm. The infrared spectrum ($CHCl_3$, cm^{-1}) showed major bands at 3021, 2970, 1600, 1500, 1449, and 972.

An analysis of the nmr spectrum of the crude reaction product indicated a ratio of *trans,cis*-**1** to *trans,trans*-**1** of 7.

Preparation of trans, trans-1,3,5-Triphenyl-1,3-pentadiene

(a) Triphenyl-(2-phenylethyl)phosphonium Bromide

After refluxing for 6 days a solution of 2-phenylethyl bromide (5 g, 27 mmol) and triphenylphosphine (6.9 g, 27 mmol) in 125 ml of benzene under argon, the reaction mixture was allowed to crystallize by cooling for several hours. After filtration the filtrate yielded 0.7 g of unreacted 2-phenylethyl bromide. The crystals, after washing with cold benzene, yielded 4.5 g (42% yield) of product of mp 78–83°C. This hygroscopic material was used without further purification.

The nmr spectrum ($CDCl_3$, δ) showed the following: 2.8–3.2 (2H, m), 3.8–4.2 (2H, m), and 6.8–8.0 ppm (20H, m). The infrared spectrum ($CHCl_3$, cm^{-1}) showed major bands at 2910, 1440, and 1100.

(b) trans,trans-1,3,5-Triphenyl-1,3-pentadiene

To the previously prepared phosphonium salt (4.5 g, 10 mmol) suspended in 120 ml of THF (freshly distilled from $LiAlH_4$) under an argon atmosphere at −20°C was added 11 mmol of *n*-butyllithium in hexane. At this point all the material had gone into solution. After stirring for an additional 90 min at −20°C, the solution was warmed to ambient temperature and chalcone (2.1 g, 10 mmol) in 20 ml of THF was added. After stirring for 15 min, water was added to quench the reaction mixture and the reaction was worked up using an ether–water extraction. The residual oil obtained after solvent removal was chromatographed (silica gel eluted with 10% ether in pentane) and the appropriate material was recrystallized from pentane to yield 0.84 g (30% yield) of white plates mp 75–77°C.

The mass spectrum gave *m/e* 296 for the molecular ion. The nmr spectrum (CCl_4) showed an AX_2 with ν_A = 5.91 ppm, ν_X = 3.26 ppm, and J_{AX} = 7.5 Hz; an AB with ν_A = 5.97 ppm, ν_B = 6.90 ppm, and J_{ab} = 16.3 Hz; and a 15 H multiplet δ 7.0–7.4 ppm. The infrared spectrum ($CHCl_3$, cm^{-1}) showed major bands at 3090, 3070, 3040, 3010, 1595, 1492, 1444, 972, and 695.

An analysis of the nmr spectrum of the crude reaction product indicated a ratio of *trans,trans*-**1** to *trans,cis*-**1** of about 6.

Diels–Alder Reactions of 1

(a) With N-Phenylmaleimide

(i) trans,trans-1—A solution of 58 mg (0.34 mmol) of purified *N*-phenylmaleimide and 100 mg (0.34 mmol) *trans,trans*-**1** in 4 ml of benzene was sealed in an evacuated thick-walled tube after degassing. After heating at 80°C for 42 h, the benzene was evaporated and the residue recrystallized from ether to yield 93 mg. A second crop was obtained after tlc (silica gel, chloroform) and recrystallization to provide a total yield of 117 mg (74%) of mp 190–192°C.

The mass spectrum showed a molecular ion at *m/e* 469 consistent with a 1:1 adduct. The nmr spectrum (CCl_4) was complex with δ 7.1–7.9 (20 H, m), 6.2–6.3 (1H, m), and 2.7–3.9 ppm (6H, m). The composition of the 6H multiplet was clarified through the use of europium shift reagent ($Eu(fod)_3$) which separated it into six distinct signals. These signals were assigned on the basis of decoupling experiments and their multiplicity and a typical spectrum showed H_e (6.23 ppm, t), H_f (5.44 ppm, q), H_a (4.74 ppm, t), H_d (4.57 ppm, d of d), H_c (3.95 ppm, m);

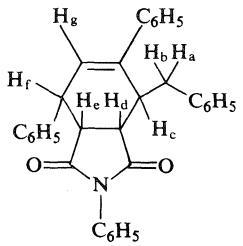

and H_b (3.64 ppm, d of d). No attempt was made to obtain coupling constants since the multiplets were not first order. The infrared spectrum ($CHCl_3$, cm^{-1}) showed major bands at 2924, 1670, 1590, 1455, 1432, 1360, 1150, and 700 cm^{-1}.

(ii) trans,cis-1—In sealed evacuated tubes, degassed solutions of *trans,cis*-**1** and *N*-phenylmaleimide in equimolar amounts in benzene were heated for 22 h at 80°C and 69 h at 125°C. Nuclear magnetic resonance analysis of the reaction mixture indicated little to no reaction had occurred. Heating for 74 h at 155°C resulted in loss of starting materials and production of a white crystalline solid which proved to be a mixture. Purification by tlc (silica gel, methylene chloride) and repeated recrystallization from hexane resulted in isolation of material with a broad melting range (82–86°C).

The mass spectrum of this material was consistent with a 1:1 adduct (molecular ion *m/e* 469) and showed a fragmentation pattern very similar to the 1:1 adduct obtained from *trans,trans*-**1** and *N*-phenylmaleimide. However, we were unable to isolate any single pure material, perhaps because of a mixture of diastereomers or because of rearrangement during purification.

(iii) trans,trans-1 and trans,cis-1—A mixture of the dienes (120 mg, 0.4 mmol, 7:1 ratio of *trans,trans*-**1** to *trans,cis*-**1**) and *N*-phenylmaleimide (60 mg, 0.35 mmol) in 0.5 ml of carbon tetrachloride was refluxed for 4 h. After separation by tlc (silica gel, 10% ether in hexane), the lead band containing both dienes showed a ratio of 1:4.25 of *trans,trans*-**1** *to trans,cis*-**1** by nmr integration. The baseline band yielded material identical to the 1:1 adduct of *trans,trans*-**1** and *N*-phenylmaleimide as shown by mixture mp and mp.

(b) With Benzoquinone

To a mixture of *trans,trans*-**1** and *trans,cis*-**1** in a ratio of 2:1 (50 mg, 0.17 mmol) in 0.5 ml of carbon tetrachloride in an nmr tube was added 6 mg (0.06 mmol) of benzoquinone. After heating to 60°C for 4–5 h, the progress of the reaction was monitored by nmr. Over a 37 h period 30 mg of benzoquinone was added and the reaction mixture was then separated by tlc (silica gel, 10% ether in hexane). The lead fraction containing the dienes was analyzed to be a 1:3 mixture of *trans,trans*-**1** to *trans,cis*-**1**. No attempt was made to isolate or characterize the adduct.

(c) With 2-Butyne

As above 50 mg of a 2:1 mixture of *trans,trans*-**1** and *trans,cis*-**1** was heated in an nmr tube with a twofold excess of 2-butyne in 0.5 ml of carbon tetrachloride. After 6 days at 60°C, the diene mixture was separated by tlc and showed a ratio of 1:10 favouring *trans,cis*-**1**. No attempt was made to isolate and characterize the adduct.

*Isomerization and Exchange of **1** in Methanol (Tables 2 and 3)*

To either *trans,trans*-**1** or *trans,cis*-**1** dissolved in ~25 μl of THF, was added 0.22 *M* potassium methoxide–methanol (or methanol-*O-d*). This solution was cooled to −80°C, twice degassed, and an argon atmosphere introduced. The solution was then warmed to 60°C for the reported time period. The reaction was quenched by pouring into ether–H_2O. After the ether layer was washed twice with H_2O, once with saturated sodium chloride, and dried with magnesium sulfate, the solvent was evaporated. The proportions of the isomers of **1** was determined by nmr with careful and repeated integration.

Material for mass spectrometric analyses was further treated by tlc and a mass spectrum was obtained on the mixture of isomers of **1**. A combination of nmr and mass spectrometry allowed an estimate of the percentage of isomerization and of isotopic exchange.

*Isomerization and Exchange of **1** using Lithium 2,2,6,6-Tetramethylpiperidide (Table 2)*

A one-necked reaction vessel to which was attached either an nmr tube, a quartz cell, or a reaction tube was used for the reactions not run near room temperature. For those reactions to be run in sealed tubes or cells the selected isomer of **1** was placed in the tube and the solution of lithium tetramethylpiperidide (TMP) in THF was prepared in the reaction vessel. Solutions of lithium TMP in THF (1–2 *M*) were prepared by adding a 1.1-fold amount of *n*-butyllithium (Ventron) to a cooled solution (~ −20°C) of TMP in THF followed by stirring for 1 h from −20°C up to ambient temperature. This base solution was then tipped into the tube or cell which was then sealed. For those reactions run at 25°C, the selected isomers of **1** in a small amount of THF was added to the base solution.

The reactions were quenched by adding a slight excess of acetic acid or acetic acid-*O-d*. Work-up involved pouring the now colorless reaction mixture into ether–water. The ether layer was washed twice with water, once with saturated sodium chloride, dried with magnesium sulfate, and the solvent evaporated. This material was analyzed by nmr before and after tlc.

Reaction of Hydrobenzamide with Potassium Piperidide

The reaction vessel consisted of two bulbs connected by a neck with a sintered glass frit. The reaction bulb was equipped with a side arm through which the hydrobenzamide **8** (~100 mg) in 1.5 ml of α-methyltetrahydrofuran (MTHF) could be added. This side arm had a break seal and the solution of **8** had been prepared by bulb-to-bulb distillation of MTHF. The reaction bulb also had a side arm with a Teflon Rotaflo stopcock for the introduction of MTHF by bulb-to-bulb distillation, the evaporation of solvent, the introduction of argon, and the introduction of deuterochloroform by bulb-to-bulb distillation. The second bulb was equipped with an nmr tube and a side arm with a Rotaflo stopcock for evacuation purposes.

The reaction was run by cooling a solution of LiTMP in MTHF to −130°C and introducing the solution of **8** by breaking the break seal. Color formation (purple) was immediate. After stirring the reaction for about 5 min an argon atmosphere was introduced followed by a 1.1 excess of dried trifluoroacetic acid. Complete loss of color usually took about 2–3 min. The solvent was then evaporated and dried deuterochloroform was introduced. This solution was then filtered into the second bulb and sealed in the nmr tube.

The contents of the nmr tube were analyzed and revealed no starting material or products expected to arise from quenching of the open-chain anion. Instead, the sole product appeared to be amarine, the closed form with *cis*-phenyl rings.

Acknowledgment

The authors wish to thank the National Research Council of Canada for their financial support.

1. (*a*) E. Buncel. Carbanions: mechanistic and isotopic aspects. Elsevier, Amsterdam. 1975; (*b*) D. H. Hunter. Isotopes in carbanion rearrangements. *In* Isotopes in molecular rearrangements. *Edited by* E. Buncel and C. C. Lee. Elsevier, New York, NY. 1974.
2. (*a*) C. W. Shoppee and G. N. Hendersen. J. Chem. Soc. Perkin Trans. I, 765 (1975); (*b*) C. W. Shoppee and G. N. Hendersen. J. Chem. Soc. Chem. Commun. 561 (1974).
3. (*a*) P. R. Stapp and R. F. Kleinschmidt. J. Org. Chem. **30**, 3006 (1965); (*b*) L. H. Slaugh. J. Org. Chem. **32**, 108 (1968); (*c*) R. B. Bates and D. A. McCombs. Tetrahedron Lett. 199 (1969); (*d*) H. Kloosterziel and J. A. A. VanDrunen. Recl. Trav. Chim. Pays-Bas, **89**, 368 (1970).
4. (*a*) D. J. Atkinson, M. J. Perkins, and P. Ward. Chem. Commun. 1390 (1969); (*b*) S. W. Staley and J. P. Erdman. J. Am. Chem. Soc. **92**, 3832 (1970).
5. R. B. Woodward and R. Hoffmann. The conservation of orbital symmetry. Academic Press, Weinheim. 1971.
6. (*a*) G. Wittig, V. Rautenstrauch, and F. Winger. Tetrahedron Suppl. **7**, 189 (1966); (*b*) M. E. Londrigan and J. E. Mulvaney. J. Org. Chem. **37**, 2823 (1972); (*c*) W. T. Ford and M. Newcomb. J. Am. Chem. Soc. **95**, 6277 (1973); (*d*) M. Newcomb and W. T. Ford. J. Am. Chem. Soc. **95**, 7186 (1973).
7. (*a*) D. H. Hunter and S. K. Sim. Can. J. Chem. **50**, 669 (1971); (*b*) D. H. Hunter and S. K. Sim. Can. J. Chem. **50**, 678 (1971).
8. D. H. Hunter and R. P. Steiner. Can. J. Chem. **53**, 355 (1975).
9. D. H. Hunter, R. E. Klinck, R. P. Steiner, and J. B. Stothers. Can. J. Chem. **54**, 1464 (1976).
10. (*a*) R. B. Bates, R. H. Carnighan, and C. E. Staples. J. Am. Chem. Soc. **85**, 3032 (1963); (*b*) R. B. Bates, D. W. Gosselink, and J. A. Kaczynski. Tetrahedron Lett. 199 (1967); (*c*) A. J. Birch and G. S. Rao. Advances in organic chemistry. Vol. 8. Wiley-Interscience, New York, NY. 1972. p. 1.
11. C. D. Ritchie and R. E. Uschold. J. Am. Chem. Soc. **90**, 3415 (1968).
12. (*a*) D. J. Cram, B. Rickborn, C. A. Kingsbury, and P. Haberfield. J. Am. Chem. Soc. **83**, 3678 (1961); (*b*) K. Bowden. Chem. Rev. **66**, 119 (1966).
13. American Petroleum Institute, Project 44. Selected values of properties of hydrocarbons and related com-

pounds. College Station, TX. Thermodynamics Research Center, Texas A & M University. 1973.
14. (*a*) J. HINE and P. D. HALSIN. J. Am. Chem. Soc. **94**, 6998 (1972); (*b*) R. G. PEARSON and R. L. DILLON. J. Am. Chem. Soc. **75**, 2439 (1953).
15. D. J. CRAM. Fundamentals of carbanion chemistry. Academic Press, New York, NY. 1965.
16. P. A. S. SMITH. Open-chain nitrogen compounds. Vol. 1. Benjamin, New York, NY. 1965. p. 178.
17. R. H. DE WOLFE. J. Am. Chem. Soc. **86**, 864 (1964).
18. T. B. MCMAHON and P. KEBARLE. J. Am. Chem. Soc. **98**, 3399 (1976).
19. D. K. BOHME, E. LEE-RUFF, and L. B. YOUNG. J. Am. Chem. Soc. **94**, 5153 (1972).
20. C. J. JOHNSON. Chem. Rev. **75**, 755 (1975).
21. B. SCHILLING and J. P. SNYDER. J. Am. Chem. Soc. **97**, 4422 (1975).
22. (*a*) N. D. EPIOTIS. Angew. Chem. Int. Ed. Engl. **13**, 751 (1974); (*b*) N. C. EPIOTIS. J. Am. Chem. Soc. **95**, 1200 (1973).
23. A. E. STREITWIESER, JR., L. VERBIT, and P. STANG. J. Org. Chem. **29**, 3706 (1969).

Raman study of the structural properties of KNO_3(II)

M. H. BROOKER

Chemistry Department, Memorial University of Newfoundland, St. John's, Nfld., Canada A1C 5S7

Received August 13, 1976

M. H. BROOKER. Can. J. Chem. **55**, 1242 (1977).

Raman spectra of oriented single crystals of KNO_3(II) have been recorded at 298 and 77 K. At both temperatures the data are in excellent agreement with the factor group analysis based on the generally accepted *Pmcn* space group. Additional spectral features observed near room temperature suggest the presence of a significant number of disordered nitrate groups on alternate lattice sites, although the majority of nitrate groups occupy the ordered sites. As the temperature is lowered, the disordered groups freeze out until near the temperature of reported electrical anomalies (213 K) only the ordered sites are occupied. Improved resolution has resulted in detection of a number of new spectral features while improved depolarization data have resulted in reassignment of several peaks.

M. H. BROOKER. Can. J. Chem. **55**, 1242 (1977).

On a enregistré, à 298 et à 77 K, les spectres Raman de cristaux uniques orientés de KNO_3(II). Aux deux températures les données sont en excellent accord avec l'analyse de facteur de groupe basée sur le groupe d'espace *Pmcn* généralement accepté. Des données spectrales additionnelles observées près de la température de la pièce suggèrent la présence d'un nombre important de groupes nitrates désordonnés à des sites alternés du réseau; toutefois la majorité des groupes nitrates occupent des sites ordonnés. A mesure que la température est abaissée, les groupes désordonnés sont gelés jusqu'à une température proche de celle rapportée pour des anomalies électriques (213 K) alors que les sites ordonnés sont les seuls qui soient occupés. Une résolution accrue a permis de détecter un certain nombre de caractéristiques spectrales nouvelles alors que des donnés de dépolarisation améliorées ont permis une réattribution de divers pics.

[Traduit par le journal]

Elucidation of the mechanisms of solid–solid and solid–liquid phase transformations requires the knowledge of all possible structural properties of the various phases. Although considerable effort has been expended on the structure of KNO_3 in the room temperature phase (KNO_3(II)) several anomalies remain. Accurate X-ray analysis of KNO_3 by Nimmo and Lucas (1) confirmed the *Pmcn* space group proposed by Edwards (2) but these authors reported that the nitrate group was non-planar and did not have its horizontal mirror plane coincident with the *ab* crystallographic plane. Fermor and Kjekshus (3) reported anomalous values for electrical resistivity and dielectric measurements as a function of temperature and suggested the existence of a phase transition in the vicinity of 213 K and tentatively designated the low temperature phase as KNO_3(VIII). Limited X-ray data were insufficient to determine whether the low temperature phase belonged to a different space group from that of phase II. The same authors (4) reported similar results for the other anhydrous univalent nitrates but subsequent calorimetric and neutron diffraction studies on $RbNO_3$ and $CsNO_3$ by Owen and Kennard (5) failed to reveal any transitions and the electrical anomalies of Fermor and Kjekshus were ascribed to thermal hysteresis. Recently, however, Badr *et al.* (6) detected subtle changes in the Raman spectra for the region of the external lattice modes of $RbNO_3$ and $CsNO_3$ which occurred close to the temperature of the low-temperature anomaly of the electrical measurements. The same authors (7) have proposed that the room temperature forms of $NaNO_3$ and $CsNO_3$ contain a significant number of NO_3^- groups on disordered alternate sites which freeze out at lower temperatures.

Previous vibrational studies of KNO_3(II) have been primarily restricted to room temperature and above (8–15) although Karpov and Shultin (11, 12) have measured the infrared spectrum at 77 K. Raman studies of oriented single crystals have been performed (8–10, 15) but poor depolarization measurements have resulted in several uncertain assignments and were of little use for assessment of the reported anomalies. Accurate oriented single crystal

Raman studies at 298 and 77 K were undertaken to investigate the nature of the reported phase transition at 213 K and to ascertain whether the poor depolarization ratios measured in previous studies were due to crystal imperfections and misalignment, or to real structural features of the type described by Nimmo and Lucas.

Experimental

Single crystals of KNO_3(II) were grown from saturated aqueous solution by slow evaporation at room temperature. Experiments were performed on a number of large crystals of varied dimensions. Orientations were determined from crystal morphology (16). Crystals grew with well developed 010 planes; 110, 100, and 001 planes were easily identified; however, 100 and 001 faces of suitable size could only be obtained by polishing. The structure of KNO_3(II) is normally reported in the non-standard setting *Pmcn*; $a = 5.414$, $b = 9.164$, and $c = 6.431$; $z = 4$. In this setting '*a*' has been chosen as the axis of highest symmetry and the crystallographic mirror plane is in *bc*. The horizontal plane of the NO_3^- group is in *ab*. Normally one would classify as B_{1g}, normal modes which are symmetric with respect to the mirror plane of the D_{2h} factor group which in this case is *bc* (17). However, it has been accepted practice to identify as B_{1g} those modes which are symmetric to the NO_3^- plane, the *ab* plane. The full factor group analysis for KNO_3 has been given by a number of workers (9–11, 13, 15) and will not be reproduced here.

Polarized Raman spectra were measured with a Coderg PHO Raman spectrometer after sample excitation with the 488.0 nm line of a Control Laser, model 553A argon ion laser. Plasma lines from the laser were removed with a narrow-band-pass interference filter. Peak positions were calibrated against laser plasma lines and are probably accurate to ± 0.5 cm^{-1}. Power levels at the sample were approximately 600 mW. Polarization of the incident beam was controlled by a half-wave plate, and the scattered light was analyzed with a Polaroid film placed before the monochromator slit. Crystals were carefully mounted on the metal tip of a vacuum cryostat (18) and spectra were obtained for samples at room temperature, ice temperature, dry ice temperature, and liquid nitrogen temperature. Quoted temperature values are for the coolant. The actual sample temperatures were difficult to determine accurately but calibration with compounds with known melting points and phase transition temperatures suggested that the sample temperatures were within 5° of the coolant temperature. For high temperature studies crystals were sealed in glass tubing and heated with a coil of nichrome wire. Temperatures were monitored with a chromel–alumel thermocouple outside the tube. Spectra were recorded for light scattered at 90°, *i.e.* $x(zz)y$, and for light scattered at 180° (back scattering, *i.e.* $x(zz)x$) to the incident beam. The back scattering technique had the advantage of permitting measurement of pairs of symmetric tensors without realignment of the crystal. The crystals were aligned roughly by inspection and then adjusted by carefully minimizing the depolarization ratios for peaks at 1050 cm^{-1}, α_{ab}/α_{aa}; 52 cm^{-1}, α_{bc}/α_{ac}; and 1359, α_{ab}/α_{aa}. Depolarization data were extremely sensitive to crystal quality and orientation but excellent depolarization ratios were obtained from a number of large ($1 \times 2 \times 3$ mm) clear crystals. In this regard it would appear that the poor depolarization ratios obtained by previous authors were due to crystal imperfections. Potassium nitrate tends to occlude water to give a striated crystal with grains along the *c* axis and crystals of this type gave much poorer depolarization ratios. Relative intensities (peak height times half-width) for each setting were first normalized to the off-diagonal α_{ac} component at 83 cm^{-1} (298 K), 91.4 cm^{-1} (77 K). Within experimental error the α_{aa} and α_{bb} components of ν_1 (A_g) were identical and both were set equal to 1000. For the 77 K intensity data, 1.0 cm^{-1} slits were employed and 2.0 cm^{-1} slits for the 298 K data. Half-widths were not corrected but if necessary relative intensities were corrected for the difference in grating response for the $\parallel$ and $\perp$ scattered light since a polarization scrambler was not employed. Resolution of components of peaks ~ 90 cm^{-1} and 715 cm^{-1} was achieved with 0.25 cm^{-1} slits.

Raman spectra were also obtained for samples of ^{15}N-enriched ($\sim 98\%$, ^{15}N) KNO_3 at 77 K to aid the assignment of the lattice modes. Spectra of oriented single crystals of $K^{14}NO_3$ and $K^{15}NO_3$ were recorded for the $c(bc)b$ orientation (spill-over from α_{ba} and α_{ac} was evident). Each sample was recorded twice in alternate fashion and peak positions calibrated to the 221.7 argon – ion plasma line. Lower laser power was employed as a precaution to guard against localized heating since the $K^{15}NO_3$ crystal was not of highest optical quality. A precision of ± 0.1 cm was realized.

Results and Discussion

Raman spectra for KNO_3(II) are shown in Figs. 1 to 4, while peak position, intensity, and half-width data for 298 and 77 K are collected in Tables 1 and 2. Although minor but significant differences exist between the spectra obtained at 298 and 77 K both sets of data are in excellent agreement with the predictions of a factor group analysis based on the *Pmcn* space group. It would appear that the differences between the 298 and 77 K results are due to minor structural changes. Relative intensity data represent the best extinction of unwanted lines obtained and is an average of at least two independent measurements, but even at this the actual values are probably uncertain by 10%. Spill-over of α_{ab} into the α_{bb} spectra and of α_{bc} into α_{ac} was most severe but was eliminated for several exceptionally clear crystals. Spill-over was somewhat worse for samples recorded at 77 K since most crystals fractured on cooling. Nevertheless, it was possible to show that the mode at 52 cm^{-1} is active only in α_{ac} but not in α_{bc} and that the 1344 cm^{-1} mode is active only

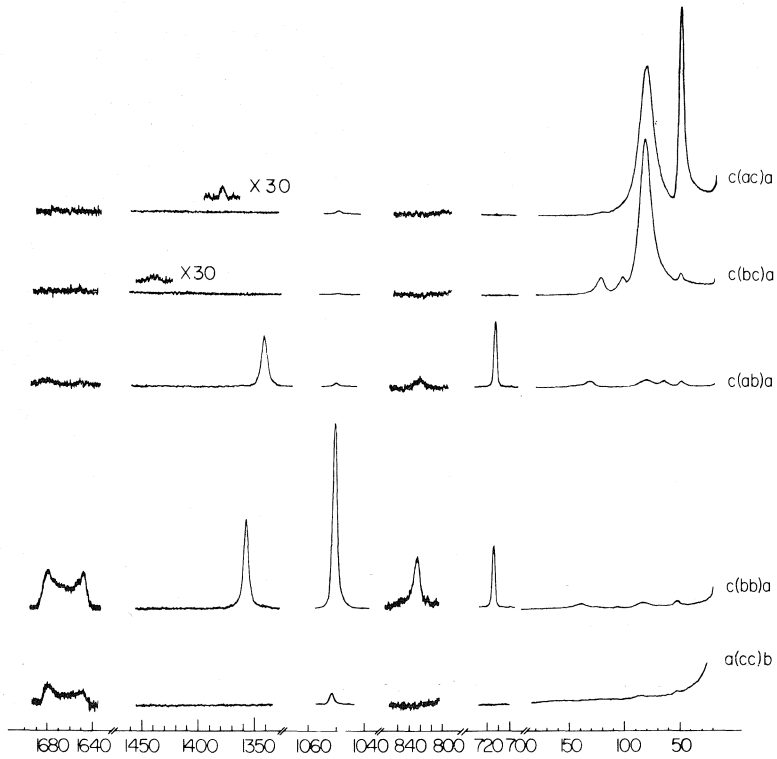

FIG. 1. Raman spectra obtained from oriented single crystals of KNO_3(II) at 298 K. Relative intensities within spectral regions are comparable. Slit-widths were 1.0 cm^{-1} for the 1050 cm^{-1} region, 4.0 cm^{-1} for the 800 cm^{-1} region, and 2.0 cm^{-1} for other regions.

in α_{ab} while the 1359 cm^{-1} mode is active in α_{aa} and α_{bb} (Figs. 1, 2; Tables 1, 2). The present room temperature data are in reasonable agreement with previous work although weak peaks at 108 cm^{-1} (A_g) and 150 cm^{-1} (B_{1g}) have not previously been reported. Raman data for KNO_3 at 77 K have not previously been reported and our spectra show peaks at 122.6 cm^{-1} (B_{1g}), 137.0 cm^{-1} (B_{3g}), 158.2 (B_{1g}), and 162.5 (B_{3g}) which have no counterpart in the room temperature spectrum. A weak peak of B_{2g} or B_{3g} symmetry was occasionally detected at 81 cm^{-1}. The peak at ~90 cm^{-1} has been resolved into two components 91.8 (B_{2g}) and 93.4 (B_{3g}) and two components have clearly been resolved in the ν_4 region 713.2 (B_{1g}) and 714.5 (A_{1g}), Fig. 3. With the exception of the $2\nu_2$ region the A_g modes were essentially absent for α_{cc}. Two other significant observations of the room temperature study were the presence of a weak shoulder of A_g symmetry on the ν_1 (A_g) peak and a broad asymmetry on the low frequency side of the lattice mode at 52 cm^{-1}. Both features were absent from the spectra obtained at liquid nitrogen temperature (Fig. 4).

Raman peaks for $K^{15}NO_3$ were observed at 55.3, 72.4, 91.8, 93.4, 111.2, 132.3, 713, 1051, 1312 (B_{1g}), 1326 (A_g), 1354 (vw, B_{2g}), 1415 (vw, B_{3g}), 1428 ($2\nu_4$), 1608, and 1637 cm^{-1} ($2\nu_2$). No special effort was made to detect the weaker lattice modes since the uncertainty of measurement of these weak peaks would have resulted in little additional information.

Internal Modes

ν_1 *Region*

In the ν_1 symmetric stretching mode of the NO_3^- ion, two infrared and two Raman modes are predicted by the unit cell group analysis. Karpov and Shultin (11) have identified infrared components B_{1u}, 1051.0 cm^{-1} and B_{2u}, 1049.9 cm^{-1}. The A_g mode occurs at 1050.6 in the Raman with $\alpha_{aa} \simeq \alpha_{bb} \gg \alpha_{cc}$ but the B_{3g} mode has not been detected. The values of α_{aa}, α_{bb}, and α_{cc} suggest that the σ_h plane of NO_3^- does not depart significantly from the *ab*

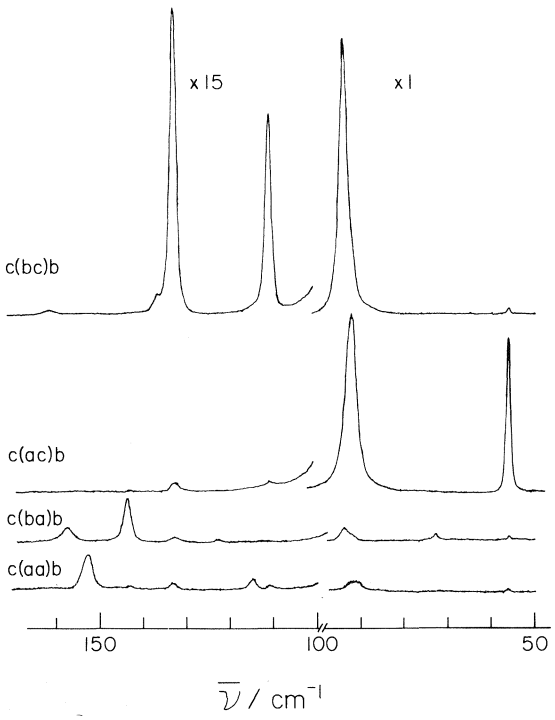

FIG. 2. Raman spectra of lattice region of KNO_3(II) at 77 K. Silt-width was 1.0 cm^{-1} from 0 to 100 cm^{-1}, 2 cm^{-1} from 100 to 170 cm^{-1}.

crystallographic plane. Previously (14) we have assigned the weak shoulder on the ν_1 mode of a number of metal nitrates at room temperature to a correlation field component and in particular for KNO_3 a shoulder at $\sim$1047 cm^{-1} was assigned to the B_{3g} component. Although the assignment for the cubic nitrates, $Ca(NO_3)_2$, $Sr(NO_3)_2$, and $Pb(NO_3)_2$, appears valid and F_{2g} symmetry has been confirmed by depolarization measurements (19),[1] for the alkali metal, silver and thallium nitrates the shoulders have A_g symmetry and *cannot* be due to correlation field components and these features must be reassigned. Badr *et al.* (7) have observed similar features in $NaNO_3$ and $CsNO_3$ crystals. These authors observed that the ratio of the intensity of the low frequency component, I', to the high frequency component, I, increased with increased temperature but could be frozen out at 213 K. "Energetically distinguishable alternate structures" were proposed with different types of coordination which were responsible for differences between the local fields and altered the frequency of the vibration. Clusters with aragonite and calcite coordination were proposed. James *et al.* (20) have assigned similar features to hot bands. Our studies support the alternate structures explanation. Limited temperature variation studies for KNO_3(II) indicate that I'/I increases with increased temperature with values 0, 0.05_4, 0.070, 0.08_5, and 0.13 at 195, 275, 300, 335, and 383 K, respectively.[2] A hot band of the type $\nu_1 = 1 \rightarrow \nu_1 = 2$ is unlikely since the observed intensity is over ten times that expected by Boltzman distribution although a 3 cm^{-1} anharmonicity would not be too large. A hot band involving a combination of ν_1 with a lattice mode 'hot band' is more difficult to discount. However, one would not expect these modes to freeze out at temperatures as high as 213 K since upper states of lattice modes are still appreciably populated at this temperature. The marked temperature dependence near phase transitions (7) is not consistent with a hot band origin for these peaks. It should be noted that although the peak separation is almost identical for $NaNO_3$, KNO_3, and $CsNO_3$, 4, 3, and 3 cm^{-1}, the intensity ratio I'/I at room temperature is not constant but increases with cation size, 0.05_8, 0.07_0, and 0.09_5.

It is interesting to note that the temperature at which the low frequency shoulder freezes out for KNO_3 is approximately equal to the temperature of the phase transition (213 K) reported by Fermor and Kjekshus (3) from dielectric and conductivity studies. Phase transitions of a similar type for all of the alkali metal nitrates have been reported by Fermor and Kjekshus (4) but these have previously received little credence since no evidence for a structural change was detected from neutron diffraction studies (5). Badr *et al.* (6) have since shown that subtle change in Raman peak intensities of two peaks near 38 cm^{-1} of $RbNO_3$ occurs between 203 and 205 K which is near the transition temperature of 228 K reported by Fermor and Kjekshus. The possibility must be considered that these transitions are associated with the final 'freezing out' of a small fraction of 'disordered' sites. The presence of such sites would be difficult to detect by con-

[1]It is possible that weak shoulders also exist for the cubic nitrates but they would be obscured by the F_g mode.

[2]Integrated intensities were measured from band areas.

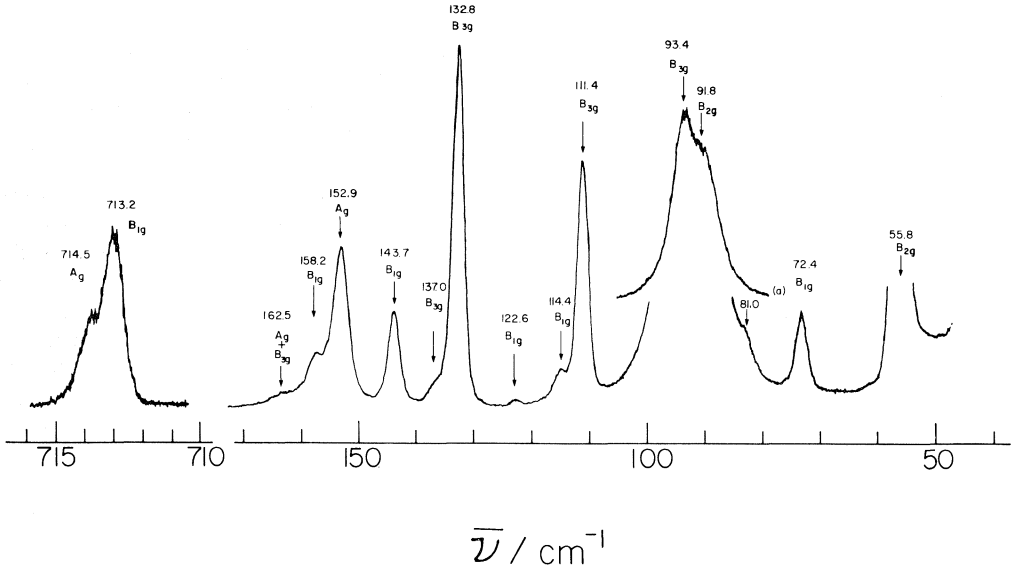

FIG. 3. Raman spectra for a poorly oriented KNO_3(II) crystal at 77 K. The orientation is primarily *c*(*ba*)*b*. The insert at about 90 cm^{-1} has abcissa expansion of 2×. Slits were 0.5 cm^{-1} for the 90 and 715 cm^{-1} regions, 1.0 cm^{-1} from 30 to 90 cm^{-1}, and 2 cm^{-1} from 100 to 170 cm^{-1}.

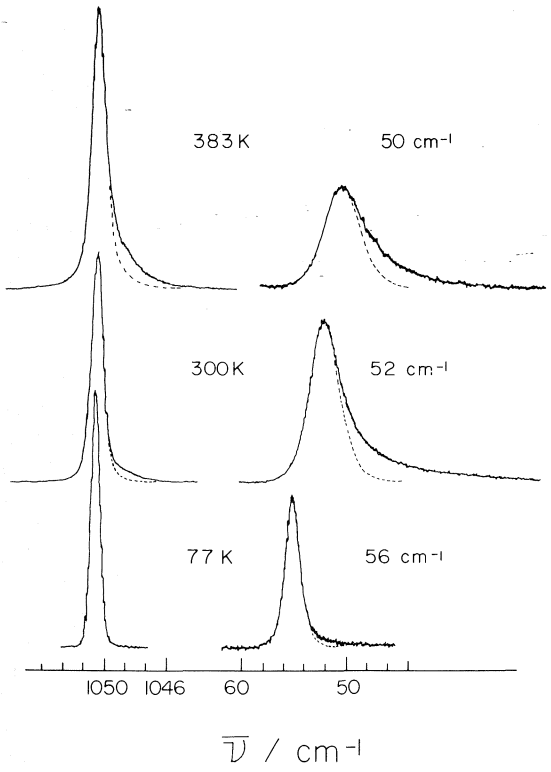

FIG. 4. Raman spectra of the 1050 and 50 cm^{-1} regions at selected temperatures.

ventional diffraction or spectroscopic methods since both phases would have identical crystal structures. For instance, in the present study there is no indication that the space group of KNO_3(II) is other than *Pmcn* at both room temperature and liquid nitrogen temperature but the shoulder on the ν_1 mode and the asymmetry of the 52 cm^{-1} lattice mode suggest the presence of a small fraction of alternate sites in KNO_3 at room temperature. Multiple site occupancy by anions in simple crystals is not unusual; in fact, for $RbNO_3$ and $CsNO_3$ the space group requires the NO_3^- groups to be on three sets of non-equivalent C_1 sites (21, 22) and peak multiplicity due to this multiple site effect has been detected by infrared (21) and Raman (23) spectroscopy. A two-site model has been proposed (24) for the disordered high temperature phase, KNO_3(I), and Strømme (25) has suggested that even the ordered phase, KNO_3(III), contains NO_3^- groups statistically distributed between two twofold disordered non-equivalent positions. Our Raman results[3] for KNO_3(I) and KNO_3(III) support Strømme's model and further suggest that KNO_3(II) has a small fraction of NO_3^- groups on disordered positions.

[3]M. H. Brooker. Unpublished work.

TABLE 1. Raman peak position (cm^{-1}), half-width, and relative intensity data for KNO_3 at 298 K

Peak position (cm^{-1})	Relative intensity[a]						Half-width[b] $w_{1/2}$ (cm^{-1})	Assignment	
	aa	*bb*	*cc*	*ab*	*ac*	*bc*			
52	(40)	(35)	(11)	(16)	1100	(15)	4.8	B_{2g}	Trans.
67	0	0	0	30	0	0	10.0	B_{1g}	Rot. about *c*?
83	(98)	(92)	(40)	(40)	1850	—	15.0	B_{2g}	Rot. about *b*
84					—	1800	12.0	B_{3g}	Rot. about *a*
104	0	0	0	0	0	75	7.0	B_{3g}	Trans.
108	4	4	0	(1)	0	0	~5	A_g	
125	0	0	0	0	0	109	8.0	B_{3g}	Trans.
134	0	0	0	38	0	0	10.0	B_{1g}	
141	40	39	0	0	0	0	13.0	A_g	
150	0	0	(1)	11	0	0	10.0	B_{1g}	
715	55	53	0	56	0	0	3.2	$A_g + B_{1g}$	ν_4
826	0.3	0.3	0	(0.05)	0	0	4.0	A_g	ν_2
1030	5	5	1	1	1	1	3.0	A_g	$N^{18}O^{16}O_2^-$
1047	70	70	6	(2)	—	—	4.0	A_g	Disordered site
1050	1000	1000	80	(35)	(3)	(4)	3.0	A_g	ν_1
1344	0	0	0	76	0	0	6.2	B_{1g}	ν_3
1359	75	75	0	0	0	0	4.8	A_g	
1385	0	0	0	0	0.6	0	4.5	B_{2g}	
1446	0	0	0	0	0	0.2	6.0	B_{3g}	
1431	0.5	0.5	0	0	0	0	~5	A_g	$2\nu_4$
1652	2.5	2.5	1.6	0	0	0	~6	A_g	$2\nu_2$
1686	4.5	4.5	3.0	0	0	0	~10	A_g	

[a]Normalized to 1000 for ν_1 (A_g) α_{aa}, α_{bb}; parentheses indicate non-zero value due to spill-over.
[b]Full-width at half-height (2.0 cm^{-1} slit-width).

ν_2 *Region*

Two infrared and two Raman modes are predicted for the ν_2 region of KNO_3(II). Karpov and Shultin (11) have assigned the infrared modes at 829 cm^{-1} (B_{1u}) and 844 cm^{-1} (B_{2u}) and from dipole sum calculations (12) estimated the Raman modes to be at 844.6 cm^{-1} (B_{3g}) and 825 cm^{-1} (A_g). We have observed the A_g mode at 825.2 cm^{-1} for both α_{aa} and α_{bb} ($\alpha_{cc} \simeq 0$) but the B_{3g} mode could not be detected in α_{bc}. Occasionally, in poorly aligned samples we observed a weak feature ~843 cm^{-1} in α_{ab} which may be B_{3g}; however, the depolarization characteristics were never correct. We have been unable to confirm the presence of a peak at 829 cm^{-1} which Frech and Devlin (15) have assigned to B_{3g}. Often in a poorly aligned crystal the 825 cm^{-1} peak was observed in α_{ab} where it appeared somewhat broader than in α_{aa} but we did not detect any frequency shift for this mode for different tensor components.

The overtone region, $2\nu_2$, also suggests the essential correctness of the Shultin and Karpov assignments since a broad envelope is observed with peak maxima at 1652 and 1691 cm^{-1} at 77 K which correspond to 2×826 and 2×845 cm^{-1}. Considerable intensity occurs between the maxima but no attempt has been made to further resolve this envelope in the present study. This intensity may be due to combinations involving non-zone-centre modes. The static field value of ν_2 appears to be approximately 835 cm^{-1} which is close to the value of ν_2 for $LiNO_3$ and $NaNO_3$. It is interesting that the high frequency component of $2\nu_2$ shifts from 1686 to 1691 cm^{-1} when the crystal is cooled from 298 to 77 K, whereas, the 1652 cm^{-1} component remains constant. Shultin and Karpov report an analogous result for the ν_2 fundamental region with the peak at 843 shifting to 846 cm^{-1} when the crystal was cooled to 77 K.

ν_3 *Region*

Assignment of the five observed Raman peaks in the ν_3 region are identical to those reported by Frech and Devlin (15). The B_{2g} and B_{3g} modes are associated with non-planar motions of the nitrate group. The extremely small relative intensity values of these peaks suggest that nitrate retains its planar character

TABLE 2. Raman peak position (cm^{-1}), half-width, and relative intensity data for KNO_3 at 77 K

Peak position (cm^{-1})[a]	Relative intensity[b]						Half-width[c] $w_{1/2}$ (cm^{-1})	Assignment	
	aa	*bb*	*cc*	*ab*	*ac*	*bc*			
55.8	(12)	(10)	(6)	(4)	420	(17)	2.0	B_{2g}	Trans.
72.4	(1)	0	0	15	0	0	2.5	B_{1g}	Rot. about *c*?
91.8	(37)	(35)	(12)	(12)	1250	—	3.8	B_{2g}	Rot. about *b*
93.4	(38)	(35)	(12)	(12)	—	1368	3.0	B_{3g}	Rot. about *a*
111.4	(5)	(5)	0	0	0	114	2.1	B_{3g}	Trans.
114.4	6	6	0	0	0	0	2.5	A_g	
122.6	0	0	0	2	0	0	~4	B_{1g}	
132.8	(11)	0	0	0	0	170	2.1	B_{3g}	Trans.
137.0	0	0	0	0	0	7	3.0	B_{3g}	
143.7	(2)	0	0	25	0	0	2.5	B_{1g}	
152.9	20	18	0	(1)	0	0	3.0	A_g	
158.2	(1)	0	0	12	0	0	4.0	B_{1g}	
162.5	2	2	0	0	0	3	~5	$B_{3g} + A_g$	
713.2	0	0	0	57	0	(1)	1.6	B_{1g}	ν_4
714.5	65	60	0	0	(1)	0	1.6	A_g	
825.2	0.4	0.4	0	(0.1)	0	0	3.0	A_{1g}	ν_2
1030.5	5	5						A_g	$N^{18}O^{16}O_2^-$
1050.6	1000	1000	60	(40)	(4)	(10)	1.3	A_g	ν_1
1342.5	(2)	(2)	0	58	0	0	2.0	B_{1g}	
1356.8	60	60	0	(2)	0	0	2.0	A_g	ν_3
1388.0	0	0	0	0	0.5	0	4.0	B_{2g}	
1451.5	0	0	0	0	0	0.2	5.0	B_{3g}	
1431	0.4	0.4	0	0	0	0	~4	A_g	$2\nu_4$
1652	3	3	2	0	0	0	6	A_g	$2\nu_4$
1691	5	5	3	0	0	0	10	A_g	

[a]Accuracy quoted is primarily for comparison within regions.
[b]Normalized to 1000 for ν_1 (A_g) α_{aa}, α_{bb}; parentheses indicate non-zero value due to spill-over.
[c]Full-width at half-height (1.0 cm^{-1} slit-width).

in KNO_3. Two infrared peaks at 1340 and 1375 cm^{-1} have been identified but no assignments were possible (13). The most intense longitudinal optional (LO) mode of ν_3 has been detected at 1445 cm^{-1} in the infrared spectrum (26). Since KNO_3(II) is centrosymmetric LO peaks are not Raman allowed. A weak peak at 1431 cm^{-1} with A_g symmetry was assigned to $2\nu_4$.

ν_4 Region

Only two of the four predicted Raman peaks have been detected in this region. At 77 K the assignments are 713.2 (B_{1g}) and 714.5 (A_g) which implies a site splitting of 1.3 cm^{-1} which is larger than the 0.5 cm^{-1} value estimated by Frech and Devlin (15). The intensities of the out-of-plane modes B_{2g} and B_{3g} appear to be identically zero. Karpov and Shultin (11) have reported infrared peaks at 715.2 (B_{2u}) and 714.5 (B_{3u}). The B_{1u} mode although theoretically allowed was not detected.

External Region

Even at 77 K only 13 of the 18 predicted Raman modes were observed. Improved depolarization studies indicate that the 55.8 cm^{-1} mode has B_{2g} symmetry only while the band ~90 cm^{-1} contains two components 91.8 (B_{2g}) and 93.4 (B_{3g}). The 93.4 cm^{-1} mode has been assigned to a rotatory mode of nitrate about the *a* axis while the 91.8 cm^{-1} mode has been assigned to the rotatory mode of nitrate about *b*. It is interesting to note that the relative intensities of the two components are about equal but the higher frequency mode of the pair has a 20% smaller halfwidth than the lower frequency component. The similarity of the two components is in accord with the crystal packing since KNO_3(II) has a pseudo-hexagonal unit cell. The optical anisotropy in the *ab* plane is very small with refractive indices of 1.513, 1.512, and 1.336. The rotatory motion of the nitrate group about the *c* axis should be active in α_{ab} and it is possible that the weak peak at 72.4 cm^{-1} corresponds to this mode. A rotatory motion about the C_3 axis will have a small polarizability change associated with it and one would expect a weak, broad peak at lower energy than rotatory motions about *a* or *b*. The 55.8 cm^{-1} (B_{2g}) mode has been assigned to a trans-

latory motion of the K^+ sublattice against the NO_3^- sublattice. Most of the peaks above 100 cm^{-1} must belong to other translatory modes. When ^{15}N was substituted for ^{14}N the peaks at 55.8, 111.4, and 132.8 were shifted by 0.5, 0.2, and 0.5 cm^{-1} but the peaks 72.4, 91.8, and 93.4 cm^{-1} remained unshifted ($\sim$0.1 cm^{-1}). These results are consistent with the above assignments. Simple harmonic oscillator calculations suggest that translatory modes should shift by $\sim$0.8% and rotatory modes should remain unshifted. Rousseau *et al.* (27) have obtained similar results for lattice modes of $NaNO_3$ and confirmed that the rotatory mode of NO_3^- was at 185 cm^{-1}, whereas the translatory mode was at a lower position, 98 cm^{-1}.

The most significant changes that occur in the Raman spectrum between 298 and 77 K occur in the lattice region. The halfwidths and relative intensities of all of the peaks decreased considerably with decreased temperature and several new components were detected. Peak positions increased by about 10% when the temperature was lowered from 298 to 77 K and this effect can probably be attributed to lattice contraction. It would appear that at room temperature the thermal motion is quite considerable. In the room temperature phase of $AgNO_3$, X-ray studies suggest that the NO_3^- ion has a root mean square oscillation of $\sim$8° (28). Undoubtedly the thermal disorder contributes significantly to the marked asymmetry of the 52 cm^{-1} mode at room temperature. It is doubtful that the asymmetry can be assigned to simple hot bands since calculations based on Boltzmann statistics do not reproduce the asymmetry even for large values of the anharmonicity constant. If one assumes a symmetric peak about the peak maximum, the excess area, I', may be used as an indication of asymmetry. The value of I'/I_{total} has a minimum, almost zero, value at 77 K and increases to a maximum value of 0.33 at 390 K; at 401 K the phase transition to KNO_3(I) occurs and the peak abruptly disappears. Values of I'/I_{total} obtained were: 0.075 at 77 K; 0.19 at 195 K; 0.26 at 275 K; 0.30 at 300 K; 0.33 at 370 K; and 0.35 at 390 K.[4] A possible explanation for the observed asymmetry is that it is associated with disordered sites of the lattice. Since the 52 cm^{-1} peak appears to be due to a lattice translatory mode, disordering of the K^+ and NO_3^- positions could give rise to a range of modes in this region. Wegdam *et al.* (29)[5] have shown that low energy phonons in warm crystals have amplitudes which are an appreciable fraction of the magnitude of the lattice distances. As a result of the large amplitudes local symmetries will change continuously within the time interval of the phonon lifetime. Thus a large amplitude and anharmonicity of the 52 cm^{-1} mode could explain the asymmetry in this mode and also result in a range of symmetries available to the NO_3^- groups which would contribute to the ν_1 band asymmetry. Although the anomalous features of the 1050 cm^{-1} and 52 cm^{-1} peaks are similar there is not a direct correspondence since the intensity ratio changes of the two features do not match.

The considerable decrease in halfwidth which occurs for all lattice modes when the temperature is lowered to 77 K and the corresponding intensity decrease of the 52 and 83 cm^{-1} modes (Tables 1 and 2) suggest that in the room temperature form of KNO_3(II) thermal motion is quite significant. There is no evidence to suggest that the NO_3^- group loses its planarity nor was there any evidence to suggest that the plane of the NO_3^- is not on the *ab* crystallographic plane although it must be admitted that Raman spectroscopy does not measure positional properties with accuracy. Possibly the anomalous features of the X-ray determination are due to the positional and thermal disordering noted above. Anharmonicities in the thermally induced motions of the NO_3^- groups could easily account for the small departure from planarity of the NO_3^- as determined from the X-ray analysis. The observed temperature dependence of the out-of-plane character of the nitrogen atom (0.019 Å at 298 K, 0.036 Å at 398 K) as determined in the X-ray analysis (1) is consistent with the concept of thermally induced anharmonic motions and a moderate degree of disorder in the room temperature phase. The fact that the Raman spectra for KNO_3 at both 77 and 298 K are best interpreted in terms of the *Pmcn* space-group suggests that the phase transition at 213 K proposed by Fermor and Kjekshus involves only a minor structural

[4]Values of I'/I may be used to estimate activation energies of the alternate orientations. See ref. 7. If this is done the present data lead to a value of approximately 1.6 kcal mol^{-1} at 298 K.

[5]The applicability of this reference was suggested by one of the referees.

change, quite possibly the "freezing out" of the disordered nitrate groups. Since X-ray measurements are time-averaged over a long time it is not surprising that the disorder was not detected by X-ray diffraction.

Acknowledgement

This work was supported by the National Research Council of Canada.

1. J. K. NIMMO and B. W. LUCAS. Nature Phys. Sci. **237**, 61 (1972); J. Phys. C, **6**, 201 (1973).
2. D. A. EDWARDS. Z. Kristallogr. A, **80**, 154 (1931).
3. J. H. FERMOR and A. KJEKSHUS. Acta Chem. Scand. **22**, 836 (1968).
4. J. H. FERMOR and A. KJEKSHUS. Acta Chem. Scand. **22**, 2054 (1968).
5. W. R. OWEN and C. H. L. KENNARD. Aust. J. Chem. **24**, 1295 (1971).
6. YA. A.-KH. BADR, S. V. KARPOV, and A. A. SHULTIN. Sov. Phys. Solid State, **16**, 1515 (1975); Fiz. Tverd. Tela, **16**, 2327 (1974).
7. YA. A.-KH. BADR, S. V. KARPOV, and A. A. SHULTIN. Sov. Phys. Solid State, **15**, 1692 (1974); Fiz. Tverd. Tela, **15**, 2541 (1973).
8. T. M. K. NEDUNGADI. Proc. Indian Acad. Sci. **14**A, 242 (1941).
9. L. COUTURE. Ann. Phys. XII, 5 (1947).
10. M. BALKANSKI, M. K. TENG, and M. NUSIMOVICI. Phys. Rev. **176**, 1098 (1968).
11. S. V. KARPOV and A. A. SHULTIN. J. Phys. Chem. Solids, **29**, 475 (1968).
12. A. A. SHULTIN and S. V. KARPOV. J. Phys. Chem. Solids, **30**, 1981 (1969).
13. M. H. BROOKER and D. E. IRISH. Can. J. Chem. **48**, 1183 (1970).
14. M. H. BROOKER. J. Chem. Phys. **53**, 2670 (1970).
15. R. FRECH and J. P. DEVLIN. Chem. Phys. Lett. **38**, 79 (1976).
16. P. GROTH. Chemische krystallographic. Vol. 2. The Groth Institute, University Park, PA. 1959.
17. M. H. BROOKER. Appl. Spectrosc. **29**, 528 (1975).
18. J. B. BATES. Appl. Spectrosc. **25**, 380 (1971).
19. M. H. BROOKER and J. B. BATES. Spectrochim. Acta, **29**A, 439 (1973).
20. D. W. JAMES, M. T. CARRICK, and H. F. SHURVELL. Aust. J. Chem. **28**, 1129 (1975).
21. S. V. KARPOV and A. A. SHULTIN. Phys. Status Solidi, **39**, 33 (1970).
22. T. P. DELACY and C. H. L. KENNARD. Aust. J. Chem. **24**, 165 (1971).
23. M. H. BROOKER. J. Chem. Phys. **59**, 5828 (1973).
24. Y. SHINNAKA. J. Phys. Soc. Jpn. **17**, 820 (1962).
25. K. O. STRØMME. Acta Chem. Scand. **23**, 1625 (1969).
26. J. B. BATES and M. H. BROOKER. Chem. Phys. Lett. **21**, 349 (1973).
27. D. L. ROUSSEAU, R. E. MILLER, and G. E. LEROI. J. Chem. Phys. **48**, 3409 (1968).
28. C. S. GIBBONS and J. TROTTER. J. Chem. Soc. A, 2058 (1971).
29. G. H. WEGDAM, J. B. TE BEEK, H. VAN DER LINDEN, and J. VAN DER ELSKEN. J. Chem. Phys. **55**, 5207 (1971).

Nucleic acid related compounds. 24. Transformation of tubercidin 2′,3′-*O*-orthoacetate into halo, deoxy, epoxide, and unsaturated sugar nucleosides[1,2]

MORRIS J. ROBINS, ROGER A. JONES, AND RUDOLF MENGEL[3]

Department of Chemistry, The University of Alberta, Edmonton, Alta., Canada T6G 2G2

Received November 4, 1976

MORRIS J. ROBINS, ROGER A. JONES, and RUDOLF MENGEL. Can. J. Chem. **55**, 1251 (1977).

Treatment of tubercidin (4-amino-7-β-D-ribofuranosylpyrrolo[2,3-*d*]pyrimidine) (**1**) with methyl orthoacetate gave the 2′,3′-*O*-orthoester, **2**. Pivalic acid chloride in refluxing pyridine converted **2** into a mixture containing 4-*N*-pivalamido-7-(3-chloro-3-deoxy-2-*O*-acetyl-5-*O*-pivalyl-β-D-xylofuranosyl)pyrrolo[2,3-*d*)pyrimidine (**3***a*) and the corresponding 2′-*O*-(4,4-dimethyl-3-pivaloxypent-2-enoyl) (DMPP) compound (**3***b*) via acetoxonium ion intermediates. Treatment of **2** with sodium iodide/pivalyl chloride/pyridine gave the iodo analog (**3***c*) of DMPP derivative **3***b* plus the 3′,4′-unsaturated nucleoside (**5***a*). Treatment of **3***a–c* with methanolic sodium methoxide gave the *ribo*-epoxide **4**, which underwent $N^1 \rightarrow 3'$ intramolecular cyclization readily. Dehalogenation of **3** and deprotection gave 3′-deoxytubercidin (**8**). Deblocking of **5***a* gave **5***b* which was hydrogenated to give **8** plus its 4′-epimer **9**. Heating of **3***c* or **5***a* produced 4-*N*-pivalamido-7-(5-pivaloxymethylfuran-2-yl)pyrrolo[2,3-*d*]pyrimidine (**10***a*). Deblocking of **10***a* gave **10***d* which was hydrogenated to give racemic 4-amino-7-(2,3-dideoxy-β-D,L-*glycero*-pentofuranosyl)pyrrolo[2,3-*d*]pyrimidine (**7**,**11**). The 2′,3′-unsaturated nucleoside (**6**) was obtained and hydrogenated to produce 2′,3′-dideoxytubercidin (**7**). Spectroscopic identification of products, epoxide instability, and comparison with other procedures are discussed.

MORRIS J. ROBINS, ROGER A. JONES et RUDOLF MENGEL. Can. J. Chem. **55**, 1251 (1977).

La réaction de la tubercidine (amino-4 β-D-ribofuranosyl-7 pyrrolo[2,3-*d*]pyrimidine (**1**)) avec l'orthoacétate de méthyle donne l'*O*-orthoester-2′,3′. Celui-ci est transformé en un mélange contenant la *N*-pivalamido-4 (chloro-3 déoxy-3 *O*-acétyl-2 *O*-pivalyl-5 β-D-xylofuranosyl)-7 pyrrolo[2,3-*d*]pyrimidine (**3***a*) et le composé correspondant *O*-(diméthyl-4,4 pivaloxy-3 pentènoyl-2)-2′ (DMPP) (**3***b*), via l'intermédiaire d'ions acétoxonium, par action du chlorure de pivalyle dans la pyridine à reflux. L'action sur **2** du mélange iodure de sodium/chlorure de pivalyle/pyridine donne l'analogue iodé (**3***c*) du dérivé DMPP **3***b* plus le nucléoside insaturé-3′,4′ (**5***a*). Par traitement de **3***a–c* avec le méthylate de sodium méthanolique, l'époxyde *ribo* **4** est obtenu, ce dernier subissant une cyclisation $N^1 \rightarrow 3'$ intramoléculaire rapide. Déhalogénation de **3** et déprotection donne la déoxy-3′ tubercidine (**8**). Déblocage de **5***a* donne **5***b* qui est hydrogéné et donne **8** avec son épimère-4′ (**9**). La *N*-pivalamido-4 (pivaloxyméthyl-5 furanyl-2)-7 pyrrolo[2,3-*d*]pyrimidine (**10***a*) est produire lors du chauffage de **3***c* ou **5***a*. Déblocage de **10***a* donne **10***d* qui est hydrogéné et donne le racémique amino-4 (didéoxy-2,3 β-D,L-*glycero*-pentofuranosyl)-7 pyrrolo[2,3-*d*]pyrimidine (**7**,**11**). Le nucléoside insaturé-2′,3′ (**6**) est obtenu et, hydrogéné, donne la didéoxy-2′,3′ tubercidine (**7**). L'identification spectroscopique des produits, l'instabilité de l'époxyde et la comparaison avec d'autres procédés sont discutées.

The nucleoside antibiotic tubercidin (7-deazaadenosine; 4-amino-7-β-D-ribofuranosylpyrrolo-[2,3-*d*]pyrimidine) (**1**) has been studied extensively both chemically and from a biochemical-medical viewpoint. An excellent comprehensive review covers both aspects (1). Tubercidin is closely related to adenosine structurally and chemically, and is a substrate for many enzymes concerned with biosynthetic processes involving adenosine and phosphorylated metabolites. Two notable exceptions are its complete resistance to adenosine deaminase and the absence of enzymic phosphorolysis of the glycosyl bond (1). The latter two pathways represent major catabolic degradation (inactivation) modes for adenosine and biologically active analogs. Modification of the heterocyclic base of tubercidin has been studied systematically (2), and coupling syntheses of the pyrrolo[2,3-*d*]pyrimidine anti-

[1]Abstracted in part from the Ph.D. dissertation of R. A. Jones, The University of Alberta, Edmonton, Alta., Spring, 1974.

[2]For the previous paper in this series see ref. 12.

[3]Postdoctoral Fellow, 1969–1971. Present address: Fachbereich Chemie, Universität Konstanz, 7750 Konstanz, West Germany.

biotics have been achieved (2*c*). However, little work has been reported concerning the sugar moiety of tubercidin (3–6). Although the well established sugar–base coupling methods have been used extensively in the synthesis of modified sugar analogs of adenosine (7), no such parallel studies have appeared with related tubercidin compounds. The lack of coupling stereoselectivity with certain sugars, the instability of unsaturated carbohydrate derivatives, and the extensive heterocyclic transformations involved before and after coupling in the total synthesis routes make this approach rather uninviting for the study of a variety of modified-sugar nucleoside antibiotics.

We have been interested in developing procedures and reactions for the transformation of the sugar moiety of intact nucleosides into stereochemically inverted, unsaturated, and deoxy derivatives. This allows the retention of pre-existing stereochemistry at non-functionalized sites and the use of starting materials which are accessible on a practical scale via fermentation. We now wish to describe details of the successful application of the ortho ester – acyl halide (acyloxonium ion) approach to the sugar modification of tubercidin (for a preliminary account see ref. 8).

Treatment of tubercidin (**1**) with trimethyl orthoacetate under acid catalysis gave 2′,3′-*O*-methoxyethylidenetubercidin (**2**) quantitatively as a mixture of orthoester diastereomers. (See Scheme 1.) This product mixture was treated with pivalic acid chloride in refluxing pyridine (9) to give 4-*N*-pivalamido-7-(3-chloro-3-deoxy-2-*O*-acetyl-5-*O*-pivalyl-β-D-xylofuranosyl)-pyrrolo[2,3-*d*]pyrimidine (**3***a*) and the corresponding 2′-*O*-(4,4-dimethyl-3-pivaloxypent-2-enoyl) (DMPP) derivative **3***b* in 89% combined yield and in a ratio of ~16:1, respectively. In contrast to the corresponding reaction of the adenosine orthoester (9), no 2′-chloro isomers were detected. The absence of nucleophilic attack at the 2′-position of tubercidin has been noted previously in acetoxonium ion mediated reactions (5, 6). The use of free radical dechlorination conditions (10) (tri-*n*-butyltin hydride plus α,α′-azobisisobutyronitrile as initiator) with **3***a* followed by deblocking gave 3′-deoxytubercidin (**8**) (5, 6) in 51% yield. This allows use of the blocked chloro nucleosides for syntheses of specific deoxy derivatives whereas catalytic hydrogenolysis of chloro compounds has been generally unsuccessful (6, 11). Treatment of the unpurified mixture of **3***a*,**3***b* with methanolic sodium methoxide gave the *ribo*-epoxide (2′,3′-anhydrotubercidin) (**4**) (6, 8) in 72% overall yield from **1**. This verified the *trans* orientation of the 3′-chloro and 2′-acyloxy groups and provided alternative access to the useful intermediate **4**.

Reaction of **2** with excess sodium iodide and pivalyl chloride in refluxing pyridine gave 4-*N*-pivalamido-7-(3-iodo-3-deoxy-2-*O*-[4,4-dimethyl-3-pivaloxypent-2-enoyl]-5-*O*-pivalyl-β-D-xylofuranosyl)pyrrolo[2,3-*d*]pyrimidine (**3***c*) plus a small quantity of the 3′,4′-unsaturated product **5***a* formed by loss of hydrogen iodide from **3***c*. As in the corresponding adenosine series (9), no 2′-*O*-acetyl product was formed using pivalyl iodide (generated *in situ*). In contrast, detectable 2′-iodo substitution did not occur. Treatment of **3***c* with methanolic sodium methoxide gave a product which was identical to **4** by thin layer chromatography (tlc) and mass spectroscopy. Hydrogenolysis of **3***c* followed by deblocking gave **8** in 79% yield. Treatment of **3***c* in refluxing pyridine or with 1,5-diazabicyclo-[4.3.0]non-5-ene (DBN) in pyridine at ambient temperature gave a mixture of **5***a* and the furan derivative **10***a*. Selective elimination of hydrogen iodide from **3***c* was effected smoothly using silver acetate (12) to give **5***a* quantitatively. Deblocking of **5***a* gave crystalline 4-amino-7-(3-deoxy-β-D-*glycero*-pent-3-enofuranosyl)pyrrolo[2,3,-*d*]-pyrimidine (**5***b*). Hydrogenation of **5***b* gave **8** plus its 4′-epimer (**9**) in a ratio of 1:1.4 and in 91% combined yield. These epimers were separated cleanly and conveniently on the Dekker anion exchange column (13).

Extended heating of **3***c* in pyridine or neat fusion of **5***a* at 180°C gave **10***a*. Hydrogenolysis of the pivaloxy–methyl bond of **10***a* occurred very readily to give **10***b* which was deblocked to give 4-amino-7-(5-methylfuran-2-yl)pyrrolo[2,3-*d*]pyrimidine (**10***c*). Prior deblocking of **10***a* gave the hydroxymethylfuran derivative (**10***d*) which underwent hydrogenation of the furan ring to give racemic 4-amino-7-(2,3-dideoxy-β-D,L-*glycero*-pentofuranosyl)pyrrolo[2,3-*d*]pyrimidine (**7**,**11**). The *cis* orientation of the base (1′) and hydroxymethyl (4′) substituents of **7**,**11** was verified by 5′-*O*-tosylation followed by quantitative cyclization (tlc, uv) to the $N^1 \rightarrow 5'$-cyclonucleosides (3, 9, 14). Selective deblocking of the 2′-hydroxyl of **3***c* was effected by oxidative

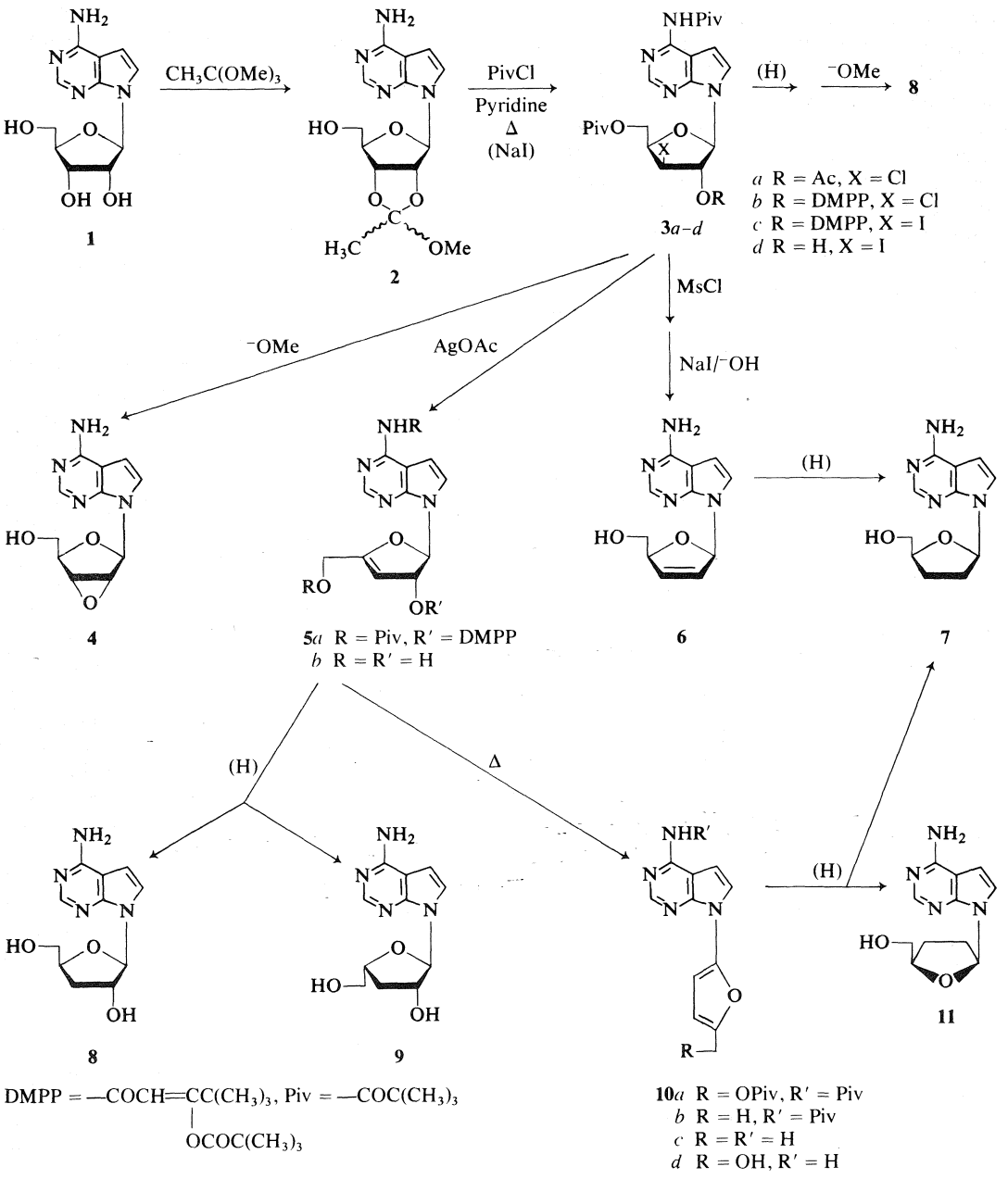

SCHEME 1

removal of the DMPP group using potassium permanganate in cold aqueous pyridine (12). The resulting *trans* iodohydrin (**3***d*) was mesylated and then treated with sodium iodide in cold aqueous base. Elimination of iodo and mesylate with concomitant deblocking occurred (12) to give 4-amino-7-(2,3-dideoxy-β-D-*glycero*-pent-2-enofuranosyl)pyrrolo[2,3-*d*]pyrimidine (**6**) in 55% yield. Hydrogenation of **6** gave amorphous 2′,3′-dideoxytubercidin (**7**), which was previously reported (also in a non-crystalline state) as a by-product of the hydrogenolysis of a blocked 3′-bromo-2′-*O*-acetyl xylo derivative (6).

Although not mentioned by Moffatt and co-workers (6), 2′,3′-anhydrotubercidin (**4**) is an extremely sensitive compound which readily

undergoes intramolecular degradation especially in hydroxylic solvents. By analogy with the adenosine *ribo*-epoxide (15), it is assumed that nucleophilic attack by N-1 at C-3′ of the epoxide gives transitory $N^1 \rightarrow 3'$-cyclonucleoside formation. Attack of water at C-2 of the positively charged pyrimidine ring followed by ring opening would be expected to lead to an amino carboxamidine substituted pyrrole. However, the expected product of this degradation apparently undergoes further reactions and a red-purple coloration slowly develops in crystalline samples of **4**, and rapidly in amorphous products or solutions. As seen in Fig. 1, the kinetic degradation of **4** (uv λ_{max} ~270 nm) to product(s) (uv λ_{max} > 300 nm) in aqueous solution qualitatively parallels that of the analogous adenosine *ribo*-epoxide (15). However, the reaction proceeds much more readily and attempts to isolate and purify the product were unsuccessful. The absence of a sharp isosbestic point at ~290 nm suggests the possible formation of more than one ring-opened species. Evaporation of a warmed solution of **4** in methanol followed by drying the residue *in vacuo* gave a solid whose mass spectrum contained peaks at *m/e* 238.1069 (calcd. for $C_{10}H_{14}N_4O_3$: 238.1066) and *m/e* 221.0813 (calcd. for $C_{10}H_{11}N_3O_3$: 221.0800). By analogy

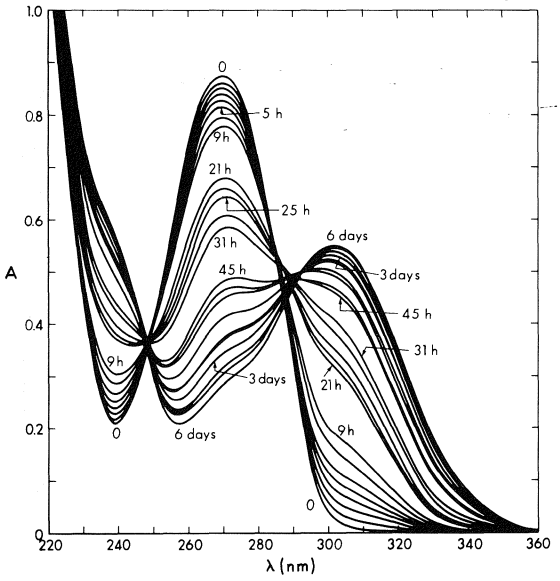

FIG. 1. Ultraviolet absorption *vs.* wavelength of an aqueous solution (1.9 mg/100 ml) of **4** at room temperature measured at various times. At 80°C the change in spectra (from 0 – corresponding to 6 days) was complete in 1 h.

with the adenosine series, these formulas could correspond to structures **i** and **ii**, respectively. It

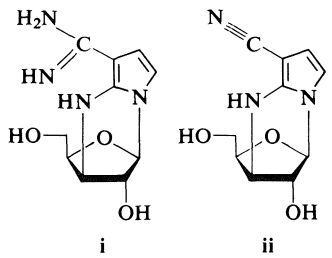

is noteworthy that the peaks at *m/e* 221 and 238 do not appear in the mass spectrum of a carefully purified sample of **4**. However, the presence of the *m/e* 221 ion was noted in the previously reported mass spectrum of **4** and attributed to the loss of HCN from the parent ion (6). It appears unlikely that this postulated fragmentation would occur with **4** since in an extensive mass spectral investigation of adenosine derivatives and analogs the loss of HCN was shown to arise later from the B+H ion (16). An alternative explanation for the presence of the *m/e* 221 peak in the reported (6) spectrum of **4** is partial prior decomposition of **4** to **i** which in turn could give rise to **ii** (*m/e* 221). Nucleophilic substitution reactions of **4** at C-3′ could not be effected directly in practical yields owing to the rapid rate of decomposition, whereas several such reactions were successful with the corresponding adenosine epoxide (15).

Mass and ^1H nmr spectra of all tubercidin compounds described in this study are closely analogous to their adenosine counterparts (9, 12). The mass spectra can generally be inferred from those of the adenosine analogs with all heterocyclic base-containing fragments occurring at one atomic mass unit lower in this series (^{14}N *vs.* $^{12}C^1H$ at the 7-position, adenosine numbering). The mechanisms of the ortho-ester – pivalyl halide reactions involving acyloxonium ion and ketene acetal intermediates and proofs of structures of the products are discussed in detail in ref. 9. The pertinent literature and new procedures for deoxy and unsaturated compounds are described in ref. 12.

The present study demonstrates that carbohydrate transformations of naturally occurring nucleoside antibiotics into halo, deoxy, epoxy, and unsaturated sugar products can be effected directly on a practically convenient scale using chloro and iodo intermediates generated from

the methyl-2′,3′-*O*-orthoacetate and pivalyl halides. Thus, a viable semisynthetic alternative to sugar–base coupling has been realized with this fermentation derived biomolecule.

Experimental

Melting points were determined on a Reichert microstage apparatus and are uncorrected. ^{1}H nmr spectra were recorded on Varian A-60 and HA-100 instruments with TMS as internal reference. Furan protons are given primed numbers corresponding to nucleoside sugar numbering in nmr data. Ultraviolet (uv) spectra were recorded on Cary 14 or 15 spectrophotometers. Accurately weighed uv spectral samples were dissolved in a minimum volume of MeOH and then diluted with at least 9 volumes of the designated solvent or solution. Optical rotations were measured on a Perkin-Elmer model 141 polarimeter using a 10 cm, 1 ml microcell. Mass spectra were obtained by the mass spectroscopy laboratory of this department on AEI MS-2, MS-9, or MS-12 instruments via direct probe sample introduction at 70 eV and 150 to 230°C. Elemental analyses were determined by the microanalytical laboratory of this department or by Schwarzkopf Microanalytical Laboratory, Woodside, NY. Thin layer chromatography (tlc) was performed on Eastman Chromatogram sheets (silica gel No. 13181, indicator No. 6060). Developed chromatograms were evaluated under uv (2537 Å) light. Evaporations were carried out using a Büchler rotating evaporator with a dry ice cooled Dewar condenser under aspirator or oil pump vacuum, at 40°C or less. Hydrogenations were effected using a Parr shaking apparatus at room temperature, under the specified hydrogen pressure with Matheson, Coleman and Bell 5 or 10% palladium-on-carbon as catalyst. Silica column chromatography was performed on Mallinckrodt SilicAR CC-7 or Woelm (0.063–0.1 mm) silica gel. Unless specified, 'silica' refers to the Mallinckrodt CC-7 adsorbent. Carbon chromatography was effected on Barnebey-Cheney AU-4 carbon which was refluxed with 1 *N* HCl for several hours, washed with water, and refluxed with 1 *N* NaOH. The carbon was then washed with water until the filtrate was neutral, followed by methanol, chloroform, and methylene chloride, and allowed to air dry. 'Ether' refers to Mallinckrodt diethyl ether in all cases. Pyridine was refluxed over and then distilled from calcium hydride and stored over linde 4A molecular sieves (dried at 200°C). Sodium iodide was dried in the presence of phosphorous pentoxide at room temperature under high vacuum for at least 24 h. Pivalyl chloride was distilled before use. Tubercidin was purchased from the Upjohn Company, Kalamazoo, Michigan.

'Diffusion crystallization' (9, 17) was effected using methanol–ether. A concentrated solution of the nucleoside (warming was sometimes necessary) in methanol contained in a beaker or small wide mouth Erlenmeyer flask was allowed to stand in a closed desiccator containing a large volume of ether. Crystallization was allowed to proceed at room temperature for 2–5 days and the crystals were then collected, without cooling. In no case was it necessary to collect more than two crops, with the first crop generally giving ~90% of the material obtained.

2′,3′-O-Methoxyethylidenetubercidin (2)

To a suspension of 2.6 g (0.0098 mol) of **1** in 50 ml of dry dioxane was added 4.75 g (0.040 mol) of trimethyl orthoacetate and 4.5 g (0.028 mol) of trichloracetic acid. The mixture was heated at 50°C for 15 min and the resulting clear solution was cooled and neutralized with 30 ml of 10% aqueous $NaHCO_3$ plus 5 drops of 25% aqueous NH_3. Most of the dioxane was evaporated and the aqueous solution was extracted with 5 × 40 ml of $CHCl_3$. The combined organic phase was dried over Na_2SO_4, filtered, and evaporated to give a colorless solid foam (quantitative). This crude material could be used without further purification in subsequent reactions. Purification of this product was effected by chromatography on a column (2.3 × 15 cm, 24 g) of Woelm silica gel packed in $CHCl_3$ containing 1.5% of saturated MeOH–NH_3 and developed with the same solvent mixture. Fractions (50 ml) 6–14 gave (after evaporation and drying at 0.1 torr) 2.09 g (66%) of **2** as a colorless solid foam. A sample of this material was dissolved in H_2O (adjusted to and maintained at p*H* 8 with NH_4OH) and the solution was frozen. On melting, colorless crystals of **2** were obtained, mp 97–98°C; uv (MeOH)-λ_{max} 268 nm (ε 12 100); nmr (DMSO-d_6) δ 1.51, 1.63 (*exo*, *endo*, s, s, 3, C-CH_3), 3.34, 3.16 (*exo*, *endo*, s, s, 3, OCH_3), 3.56 (m, 2, H-5′, H-5″), 4.10 (m, 1, H-4′), 4.84–5.38 (m, 3, H-2′, H-3′, 5′-OH), 6.34, 6.16 (*exo*, *endo*, d, d, $J_{1'-2'}$ = 4 Hz, 1, H-1′), 6.60 (d, J_{5-6} = 4 Hz, 1, H-5), 7.35 (d, J_{6-5} = 4 Hz, 1, H-6), 7.04 (s, 2, 4-NH_2), 8.04 (s, 1, H-2); ratio of *exo*:*endo* diastereomers 1:2. *Anal.* calcd. for $C_{14}H_{18}N_4O_5$: C 52.17, H 5.63, N 17.38; found: C 51.88, H 5.38, N 17.07.

4-N-Pivalamido-7-(3-chloro-3-deoxy-2-O-acetyl-5-O-pivalyl-β-D-xylofuranosyl)pyrrolo[2,3-d]pyrimidine (3a) and 4-N-Pivalamido-7-(3-chloro-3-deoxy-5-O-pivalyl-2-O-[4,4-dimethyl-3-pivaloxypent-2-enoyl]-β-D-xylofuranosyl)pyrrolo[2,3-d]pyrimidine (3b)

To a solution of 1 g (0.003 mol) of crude **2** in 100 ml of pyridine was added 5.5 ml (0.045 mol) of pivalyl chloride with stirring and cooling. The mixture was heated at 80°C for 5 min and the solution was then refluxed for 1 h. After cooling in an ice bath, 10 ml of MeOH was added slowly and the mixture was stirred at room temperature for 10 min. The solution was evaporated until precipitation of solid began and then 150 ml of Et_2O was added. The mixture was filtered and the filtrate was washed with 100 ml of 10% aqueous $NaHCO_3$ solution. The aqueous phase was separated and extracted with Et_2O. The combined organic phase was dried over Na_2SO_4, filtered, and evaporated to give a pale yellow solid foam composed primarily of **3***a* and **3***b*. This foam was applied to a silica gel column (2.4 × 42 cm, 60 g) packed in Et_2O – petroleum ether 1:1. The column was developed successively with 300 ml portions of this solvent mixture, Et_2O – petroleum ether 3:1, and then Et_2O. Fractions (25 ml) 13–16 contained **3***b*, 17–27 a mixture of several components (tlc) which were not identified, and 28–40 contained **3***a*.

Evaporation of the first combined fractions and drying the residue at 0.1 torr gave 103 mg (5.2%) of **3***b*. This material melted at ~82°C (dec.); uv (MeOH)λ_{max} 285; 219 (ε 8820; 45 400), shoulder 229 nm (ε 28 200); nmr ($CDCl_3$) δ 1.12 (s, 9, C=C-*tert*-Bu) 1.20 and 1.23 (s and s, 9 and 9, 5′-OPiv and C=COPiv), 1.36 (s, 9, 4-NPiv),

4.32–4.66 (m, 4, H-3′–H-5′′), 5.46 (m, 1, H-2′), 5.75 (s, 1, CH=C), 6.59 (d, $J_{1'-2'} \sim 3$ Hz, 1, H-1′), 7.08 (d, $J_{5-6} = 4$ Hz, 1, H-5), 7.52 (d, $J_{6-5} = 4$ Hz, 1, H-6), 8.16 (s, 1, H-2), 8.46 (s, 1, 4-NH); ms calcd. for M^+: 662.3083; found (*m/e*): 662.3062 (^{35}Cl). *Anal.* calcd. for $C_{33}H_{47}ClN_4O_8$: C 59.76, H 7.15, N 8.45; found: C 60.00, H 7.15, N 8.39.

Analogous treatment of the third combined fractions gave 1.25 g (84%) of **3***a* which melted at ~75°C; uv (MeOH) λ_{max} 285; 218 (ε 8400; 32 700) shoulder 229 nm (ε 17 500); nmr ($CDCl_3$) δ 1.23 (s, 9, 5′-OPiv), 1.39 (s, 9, 4-NPiv), 2.16 (s, 3, 2′-OAc), 4.38–4.62 (m, 4, H-3′–H-5′′), 5.54 (m, 1, H-2′), 6.58 (d, $J_{1'-2'} \sim 4$ Hz, 1, H-1′), 7.13 (d, $J_{5-6} = 4$ Hz, 1, H-5), 7.53 (d, $J_{6-5} = 4$ Hz, 1, H-6), 8.18 (br s, 1, 4-NH), 8.50 (s, 1, H-2); ms calcd. for M^+: 494.1933; found (*m/e*): 494.1925. *Anal.* calcd. for $C_{23}H_{31}ClN_4O_6$: C 55.81, H 6.31, N 11.32; found: C 55.78, H 6.37, N 11.32.

4-Amino-7-(2,3-anhydro-β-D-ribofuranosyl)pyrrolo-[2,3-d]pyrimidine (4)

A 1.2 g (0.0045 mol) sample of **1** was converted to **2** and then to **3***a* + **3***b* as described above without purification of intermediates. The solid glass (**3***a*,*b*) was dissolved in 100 ml of MeOH and a solution of 3 g of NaOMe in 50 ml of MeOH was added. The solution was allowed to stand for 20 h at room temperature and then was neutralized with HOAc and evaporated to dryness. The residue was partitioned between H_2O and Et_2O. The aqueous layer was evaporated to dryness and the residue was stirred with 2 × 125 ml of boiling EtOAc (dry). Insoluble salts were filtered and the filtrate was cooled to 0°C. A brown precipitate which separated upon standing was filtered and discarded. The filtrate was dried over $MgSO_4$ and Na_2SO_4, filtered, and evaporated to give 0.80 g (72% overall from **1**) of crude **4** as an off-white solid. This chromatographically homogeneous (tlc) material was dissolved in dry EtOAc, filtered through Na_2SO_4, and the filtrate was partially evaporated. Crystallization of **4** occurred to give product, mp 167–170°C (dec.); $[\alpha]_D^{24}$ −71.8° (*c* 1, H_2O) during first ~20 min, rising to +1.3° after 3 days; tlc and spectroscopic properties identical to those of a sample prepared by a different procedure (18). *Anal.* calcd. for $C_{11}H_{12}N_4O_3$: C 53.22, H 4.86, N 22.57; found: C 53.50, H 4.82, N 22.87.

4-N-Pivalamido-7-(3-iodo-3-deoxy-5-O-pivalyl-2-O-[4,4-dimethyl-3-pivaloxypent-2-enoyl]-β-D-xylo-furanosyl)pyrrolo[2,3-d]pyrimidine (3c)

To a solution of 644 mg (0.002 mol) of **2** in 40 ml of pyridine was added 6 g (0.04 mol) of NaI and the vigorously stirred solution was heated to reflux. Pivalyl chloride (2.4 ml, 0.02 mol) was added and the mixture was heated at reflux for 4 min, allowed to cool for 20 min, and 10 ml of MeOH was added. The red solution was stirred for ~3 h and poured into 100 ml of H_2O containing 5 g of $NaHCO_3$ and 0.5 g of $Na_2S_2O_3$. The resulting yellow solution was extracted with 100 ml of Et_2O. The ether phase was washed with H_2O and back extracted as indicated by tlc. The combined organic phase was evaporated and the resulting gum was co-evaporated using toluene and then 98% EtOH to give 1.38 g of a yellow solid foam. This material was dissolved in EtOAc and applied to a column (2.2 × 28 cm, 40 g) of activated carbon packed in EtOAc and eluted with $CHCl_3$–EtOAc (1:1). Fractions comprising 100 to 500 ml contained 987 mg (65%) of **3***c* as a white solid foam containing only a trace amount of **5***a* (tlc, silica, 20% pentane – Et_2O). An analytically pure sample of **3***c* was obtained by chromatography of 500 mg of this material on a silica column (2.2 × 31 cm, 52 g) packed in Et_2O–pentane (1:1) and eluted with 275 ml of this mixture followed by 225 ml of 25% pentane – Et_2O. Evaporation of fractions from 350 to 500 ml gave 380 mg of pure **3***c* as a white solid foam, uv (MeOH)λ_{max} 287; 219 (ε 8700; 45 600) shoulder 229 (ε 29 800)λ_{min} 256 (ε 5600), (0.1 *N* HCl)λ_{max} 291; 222 (ε 11 700; 40 300)λ_{min} 263 (ε 9900), (0.1 *N* NaOH)λ_{max} 285–305; 243 (ε 10 600; 29 900) shoulder 232 (ε 27 300)λ_{min} 268 nm (ε 10 000); nmr ($CDCl_3$) δ 1.11 (s, 9, C=C-*tert*-Bu), 1.21 and 1.23 (s and s, 9 and 9, 5′-OPiv and C=COPiv), 1.35 (s, 9, 4-NPiv), 3.88 (m, 1, H-4′), 4.32 (m, 3, H-3′–H-5′′), 5.69 (d of d, $J_{2'-1'} = 3.5$ Hz, $J_{2'-3'} = 2$ Hz, 1, H-2′), 5.74 (s, 1, CH=C), 6.53 (d, $J_{1'-2'} = 3.5$ Hz, 1, H-1′), 7.10 (d, $J_{5-6} = 4$ Hz, 1, H-5), 7.64 (d, $J_{6-5} = 4$ Hz, 1, *H*-6), 8.23 (s, 1, 4-NH), 8.50 (s, 1, H-2); ms calcd. for M^+: 754.2339; found (*m/e*): 754.2376. *Anal.* calcd. for $C_{33}H_{47}IN_4O_8$: C 52.52, H 6.28, I 16.82, N 7.43; found: C 52.45, H 6.40, I 16.98, N 7.37.

A 6 g (0.023 mol) sample of **1** was subjected to the above conditions (**1** → **2** → **3***c*) without purification of **2**. A 62.5% overall yield of pure **3***c* (after chromatography on silica gel) was obtained.

4-N-Pivalamido-7-(3-deoxy-5-O-pivalyl-2-O-[4,4-dimethyl-3-pivaloxypent-2-enoyl]-β-D-glycero-pent-3-enofuranosyl)pyrrolo[2,3-d]pyrimidine (5a)

A 1.51 g (0.002 mol) portion of **3***c* and 1.67 g (0.01 mol) of silver acetate were dissolved in 60 ml of pyridine and stirred in a water bath at 16°C for ~19 h. The resulting dark solution was poured into 120 ml of 5% aqueous $NaHCO_3$. The mixture, containing precipitated silver salts, was extracted with Et_2O and the organic layer was washed with H_2O. The combined organic phase was evaporated and coevaporated using toluene and then 98% EtOH. The residue was dissolved in $CHCl_3$, filtered through Celite, and evaporated to give 1.3 g of a brown solid foam. This material was dissolved in 25% pentane – Et_2O and applied to a silica gel column (2.2 × 46 cm, 75 g) packed in and eluted with the same solvent mixture. Fractions comprising 150 to 270 ml were evaporated to give 1.26 g (quantitative) of **5***a* as a white solid foam, uv (MeOH)λ_{max} 287; 218 (ε 9000; 50 500) shoulder 230 (ε 32 000)λ_{min}254 nm (ε 5200); nmr ($CDCl_3$) δ 1.15 (s, 9, C=C-*tert*-Bu), 1.22 and 1.28 (s and s, 9 and 9, 5′-OPiv and C=COPiv), 1.39 (s, 9, 4-NPiv), 4.70 (s, 2, H-5′, H-5′′), 5.38 (m, 1, H-3′), 5.74 (s, 1, CH=C), 5.94 (m, 1, H-2′), 6.94 (d, $J_{1'-2'} = 2.0$ Hz, 1, H-1′), 7.02 (d, $J_{5-6} = 4.0$ Hz, 1, H-5), 7.12 (d, $J_{6-5} = 4.0$ Hz, 1, H-6), 8.57 (s, 1, 4-NH), 8.89 (s, 1, H-2). *Anal.* calcd. for $C_{33}H_{46}N_4O_8$: C 63.24, H 7.40, N 8.94; found: C 63.26, H 7.60, N 8.84.

4-Amino-7-(3-deoxy-β-D-glycero-pent-3-enofuranosyl)-pyrrolo[2,3-d]pyrimidine (5b)

To 1.26 g (0.002 mol) of **5***a* dissolved in 20 ml of MeOH was added 0.5 g of NaOMe. The reaction was stirred overnight at room temperature and evaporated to dryness. The residue was dissolved in H_2O, applied to a column (1.3 × 16 cm) of Dowex 1-X2(OH^-) resin, and

eluted with 650 ml of H_2O followed by 300 ml of 30% MeOH–H_2O. Evaporation of fractions comprising 300 to 950 ml gave 376 mg (75%) of **5***b*. Crystallization of this material from MeOH (with diffusion of Et_2O) gave 257 mg, mp 196–198°C; $[\alpha]_D^{26}$ −413° (*c* 0.12, H_2O), −457° (*c* 0.98, DMF); uv (MeOH or H_2O)λ_{max} 268 (ε 13 900)-λ_{min} 238 (ε 3100), (0.1 *N* HCl)λ_{max} 270; 226 (ε 12 700; 27 900)λ_{min} 246 (ε 5400), (0.1 *N* NaOH)λ_{max} 268 (ε 13 400) λ_{min} 240 nm (ε 3700); nmr (DMSO-d_6)δ 3.99 (d, $J_{5',5''-OH}$ = 5.5 Hz, 2, H-5′, H-5″), 5.03 (m, 1, H-2′), 5.20 (m, 2, H-3′, 5′-OH), 5.64 (d, $J_{OH-2'}$ = 6 Hz, 1, 2′-OH), 6.45 (d, $J_{1'-2'}$ = 2.5 Hz, 1, H-1′), 6.64 (d, J_{5-6} = 3.5 Hz, H-5), 7.04 (m, 3, 4-NH_2, H-6), 8.07 (s, 1, H-2). *Anal.* calcd. for $C_{11}H_{12}N_4O_3$: C 53.22, H 4.87, N 22.57; found: C 53.43, H 5.05, N 22.46.

*3′-Deoxytubercidin (**8**) and 4-amino-7-(3-deoxy-α-L-threo-pentofuranosyl)pyrrolo[2,3-d]pyrimidine (**9**)*

A 248 mg (0.001 mol) sample of **5***b*, 250 mg of 10% Pd/C, and 50 ml of H_2O–EtOH (1:1) were hydrogenated at 10 psi for 2 h. The mixture was filtered through Celite, the catalyst was washed with 50 ml of H_2O–EtOH (1:1), and the filtrate was evaporated. The residue was dissolved in 30% MeOH–H_2O and applied to a column (2.4 × 95 cm) of Dowex 1-X2(OH^-) resin packed in and eluted with the same solvent mixture. Evaporation of fractions from 2100 to 2900 ml gave 94 mg (38%) of solid. Crystallization of this product from MeOH (with diffusion of Et_2O) gave 80 mg of **8**, mp 182–183°C; $[\alpha]_D^{26}$ −73.4° (*c* 0.93, 95% EtOH); uv (MeOH or 0.1 *N* NaOH)λ_{max} 269 (ε 11 400) λ_{min} 239 (ε 2700), (0.1 *N* HCl)λ_{max} 272; 227 (ε 10 700; 24 000) λ_{min} 246 nm (ε 4300); nmr (DMSO-d_6) δ 1.89 (d of q, $J_{3''-3'}$ = 13 Hz, $J_{3''-2'}$ = 6.5 Hz, $J_{3''-4'}$ = 4 Hz, 1, H-3″) 2.19 ('septet', $J_{3'-3''}$ = 13 Hz, $J_{3'-2'}$ = 8 Hz, $J_{3'-4'}$ = 6 Hz, 1, H-3′), 3.56 (m, 2, H-5′, H-5″), 4.33 (m, 2, H-2′, H-4′), 5.05 (t, $J_{OH-5',5''}$ = 5.5 Hz, 1, 5′-OH), 5.50 (d, $J_{OH-2'}$ = 5.5 Hz, 1, 2′-OH), 6.01 (d, $J_{1'-2'}$ = 3 Hz, 1, H-1′), 6.57 (d, J_{5-6} = 4 Hz, 1, H-5), 6.98 (s, 2, 4-NH_2), 7.32 (d, J_{6-5} = 4 Hz, 1, H-6), 8.09 (s, 1, H-2), (lit. (5) mp 180–181°C; $[\alpha]_D^{27}$ −75.1° (*c* 1, EtOH)). *Anal.* calcd. for $C_{11}H_{14}N_4O_3$: C 52.79, H 5.64, N 22.39; found: C 52.78, H 5.66 N 22.12.

Evaporation of fractions from 4800 to 6300 ml gave 133 mg (58%) of solid. Crystallization of this material from MeOH (with diffusion of Et_2O) gave 102 mg of **9**, mp 191–193°C; $[\alpha]_D^{26}$ −80.0° (*c* 0.73, 95% EtOH); uv (MeOH or 0.1 *N* NaOH) λ_{max} 269 (ε 11 200) λ_{min} 239 (ε 2600), (0.1 *N* HCl) λ_{max} 271; 227 (ε 10 300; 23 500) λ_{min} 246 nm (ε 4200); nmr (DMSO-d_6) δ 1.82 ('quintet', $J_{3''-3'}$ = 13 Hz, $J_{3''-4'}$ = 7 Hz, $J_{3''-2'}$ = 5 Hz, 1, H-3″), 2.34 (m, $J_{3'-4'} = J_{3'-2'}$ = 6 Hz, 1, H-3′), 3.51 ('t', $J_{apparent}$ = 5 Hz, 2, H-5′, H-5″), 4.39 (m, 1, H-4′), 4.66 (m, 1, H-2′), 4.92 (t, $J_{OH-5',5''}$ = 5.5 Hz, 1, 5′-OH), 5.52 (d, $J_{OH-2'}$ = 5.5 Hz, 1, 2′-OH), 6.05 (d, $J_{1'-2'}$ = 4 Hz, 1, H-1′), 6.60 (d, J_{5-6} = 4 Hz, 1, H-5), 6.97 (s, 2, 4-NH_2), 7.14 (d, J_{6-5} = 4 Hz, 1, H-6), 8.90 (s, 1, H-2). *Anal.* calcd. for $C_{11}H_{14}N_4O_3$: C 52.79, H 5.64, N 22.39; found: C 52.78, H 5.37, N 22.09.

*3′-Deoxytubercidin (**8**)*

Method A

To 0.47 g (0.00095 mol) of **3***a* dissolved in 25 ml of benzene was added 30 mg of α-α′-azobisisobutyronitrile and 1.5 ml of tri-*n*-butyltin hydride. The mixture was heated for 1.5 h at reflux, evaporated, and the residue was triturated with 2 × 15 ml of pentane. The pentane washes were discarded and 40 ml of 2.5% NaOMe–MeOH solution was added to the residue. The mixture was stirred for 20 h at room temperature, evaporated, and the residue was dissolved in H_2O and applied to a column (2.3 × 43 cm) of Dowex 1-X2(OH^-) resin packed in H_2O. The column was developed with 400 ml of H_2O followed by 15% MeOH–H_2O. The appropriate fractions (15% MeOH–H_2O) were evaporated and the residue was crystallized from EtOAc to give 0.12 g (51%) of **8**, mp 176–179°C. This product was identical to that prepared above (**5***b* → **8** + **9**) by tlc, uv, nmr, and ms. *Anal.* calcd. for $C_{11}H_{14}N_4O_3$: C 52.79, H 5.64, N 22.39; found: C 52.64, H 5.58, N 22.40.

Method B

A mixture of 2.8 g (0.0037 mol) of **3***c*, 3 g (0.036 mol) of $NaHCO_3$, 3 g of 5% Pd/C, and 130 ml of EtOH–H_2O (10:3) was hydrogenated at 50 psi until hydrogen uptake ceased. The mixture was filtered and the catalyst was washed with EtOH. The combined filtrate was evaporated, H_2O and Et_2O were added, and the mixture was stirred until all solids dissolved. The ether layer was separated, dried over Na_2SO_4, filtered, and the filtrate was evaporated to give 2.03 g (87%) of 4-*N*-pivalamido-7-(3-deoxy-5-*O*-pivalyl-2-*O*-[4,4-dimethyl-3-pivaloxypent-2-enoyl]-β-D-*erythro*-pentofuranosyl)pyrrolo[2,3-*d*]pyrimidine as a colorless solid foam, uv (MeOH) λ_{max} 289 (ε 7100) shoulder 230 nm (ε 24 000); nmr ($CDCl_3$) δ 1.12 (s, 9, C═C-*tert*-Bu), 1.21 and 1.26 (s and s, 9 and 9, 5′-OPiv and C═COPiv), 1.36 (s, 9, 4-NPiv), 2.28 (br m, 2, H-3′, H-3″), 4.28 (m, 2, H-5′, H-5″), 4.54 (m, 1, H-4′), 5.50 (sextet, 1, H-2′), 5.73 (s, 1, CH═C), 6.37 (d, $J_{1'-2'}$ = 2.2 Hz, 1, H-1′), 7.16 (d of d, J_{5-6} ~ 4 Hz, 2, H-5, H-6), 8.26 (s, 1, 4-NH), 8.51 (s, 1, H-2); ms (M^+ = 628) analogous to that of the adenosine analog (**9**) (with B-containing (*m/e* 133) peaks at 1-amu lower than with B = adeninyl (*m/e* 134)).

The above solid glass and 2 g of NaOMe were dissolved in 200 ml of MeOH, stirred for 12 h at room temperature, and evaporated to dryness. The residue was treated with 120 ml of H_2O, neutralized with IRC-50(H^+) resin, and extracted with Et_2O. The aqueous layer was evaporated and the residue was refluxed with 2 × 200 ml of dry EtOAc. The insoluble residue was filtered and the combined filtrate was evaporated to yield **8** as a tan solid. This material was recrystallized from EtOAc to give 0.73 g (79% overall from **3***c*) of **8**; mp 178–180°C; $[\alpha]_D^{24}$ −77.5° (*c* 1, H_2O); spectral and tlc properties were identical to those of the sample prepared by method A. *Anal.* found: C 52.73, H 5.50, N 22.09.

*4-N-Pivalamido-7-(3-iodo-3-deoxy-5-O-pivalyl-β-D-xylofuranosyl)pyrrolo[2,3-d]pyrimidine (**3***d*)*

To a cooled (−5°C), stirred solution of 4.03 g (0.0053 mol) of **3***c* in 140 ml of pyridine–H_2O (5:2) was added 4 g (0.025 mol) of $KMnO_4$. After 90 min the reaction mixture was allowed to warm to 0°C, and 40 ml of 95% EtOH was added. After stirring overnight, the MnO_2 was filtered using a Celite pad and the filter cake was washed with EtOH. The combined filtrate was evaporated to give a brown residue which was stirred with Et_2O and H_2O. The organic layer was separated and washed with H_2O. The combined aqueous layers were extracted with Et_2O. The combined organic phase was evaporated and the

residue was dissolved in Et_2O and applied to a silica column (2.2 × 44 cm, 50 g) packed in and eluted with Et_2O. Fractions (50 ml) 3–8 were evaporated and the resulting colorless solid foam was dried at 0.1 torr to give 2.08 g (72%) of **3***d*. A 100 mg sample of this material was dissolved in 1 ml of Et_2O and 0.8 ml of pentane was added. The supernatant was decanted from the oily product which was washed with 2 ml of pentane and then dried over Paraffin to give a colorless solid foam; uv (MeOH) λ_{max} 285; 218 (ε 8500; 33 600) shoulder 230 (ε 19 600) λ_{min} 253 nm (ε 4400); nmr ($CDCl_3$) δ 1.08 (s, 9, 5′-OPiv), 1.36 (s, 9, 4-NPiv), 4.42 (m, 4, H-3′–H-5′′), 4.88 (m, 1, H-2′), 6.00 (d, $J_{1'-2'} \sim 5$ Hz, 1, H-1′), 7.04 (d, $J_{5-6} \sim 4$ Hz, 1, H-5), 7.42 (d, $J_{6-5} \sim 4$ Hz, 1, H-6), 8.18 (br, 1, 4-NH), 8.24 (s, 1, H-2); ms calcd. for M^+: 544.1283; found (*m*/*e*): 544.1255. *Anal.* calcd. for $C_{21}H_{29}IN_4O_5$: C 46.37, H 5.37, N 10.30; found: C 46.56, H 5.28, N 10.20.

*4-Amino-7-(2,3-dideoxy-β-D-glycero-pent-2-enofuranosyl)pyrrolo[2,3-d]pyrimidine (**6**)*

To an ice-cold solution of 1.09 g (0.002 mol) of **3***d* in 5 ml of pyridine was added 1 ml (0.013 mol) of mesyl chloride and the solution was stirred for 1 h at 0°C. A solution of 1.8 g (0.0045 mol) of NaOH and 1.5 g (0.01 mol) of NaI in 25 ml of ice-cold water was added and stirring was continued for 1 h at 0°C and then at room temperature for 16 h. The red-brown mixture was evaporated and the residue (in ~30 ml of H_2O) was applied to a column (3 × 83 cm) of Dowex 1-X8(OH^-) packed in H_2O. The column was developed with 1400 ml of H_2O, 100 ml of 5%, 1250 ml of 10%, 320 ml of 20%, 3 ℓ of 30%, and 700 ml of 40% MeOH–H_2O. Evaporation of the appropriate fractions (30% MeOH) gave 257 mg (55%) of a colorless product, mp 202–203°C. Recrystallization of a sample of this solid from MeOH–Et_2O followed by drying at 60°C/0.1 torr gave colorless needles of **6**, mp 206–208°C; $[\alpha]_D^{23}$ −27.3° (*c* 0.8, MeOH); uv (p*H* 1) λ_{max} 271; 226 (ε 11 400; 24 600) λ_{min} 243 (ε 3400), (p*H* 7) λ_{max} 269 (ε 11 400) λ_{min} 238 nm (ε 3000); nmr (DMSO-d_6) δ 3.54 (m, 2, H-5′, H-5′′), 4.79 (m, 1, H-4′), 4.95 ('t', $J_{OH-5',5''} = 5.5$ Hz, 1, 5′-OH), 6.01 (d of d of d, $J_{3'-2'} \sim 6$ Hz, $J_{3'-4'} \sim 2$ Hz, $J_{3'-1'} \sim 1.5$ Hz, 1, H-3′), 6.44 (d of d of d, $J_{2'-3'} \sim 6$ Hz, $J_{2'-1'} \sim 2$ Hz, $J_{2'-4'} \sim 1.5$ Hz, 1, H-2′), 6.56 (d, $J_{5-6} = 4$ Hz, 1, H-5), 6.96 (s, 2, 4-NH_2), 7.10 (m, overlapped with H-6, decoupling shows $J_{1'-2'} \sim 2$ Hz, $J_{1'-3'} \sim 1.5$ Hz, 1, H-1′), 7.17 (d, $J_{6-5} = 4$ Hz, 1, H-6), 8.06 (s, 1, H-2); ms calcd. for M^+: 232.0960; found (*m*/*e*): 232.0967. *Anal.* calcd. for $C_{11}H_{12}N_4O_2$: C 56.89, H 5.21, N 24.13; found: C 56.76, H 5.21, N 23.87.

*4-N-Pivalamido-7-(5-pivaloxymethylfuran-2-yl)pyrrolo-[2,3-d]pyrimidine (**10***a*)*

A 626 mg (0.001 mol) sample of **5***a* was heated in an oil bath at 180°C for 2 min. The residue was cooled, dissolved in $CHCl_3$, and evaporated to a yellow powder. Ether (15 ml) was added and the mixture was filtered to give a first crop of 130 mg of **10***a*. Concentration of the mother liquors gave an additional 150 mg (in three crops) for a total yield of 280 mg (71%) of small white crystals of **10***a*, mp 159–160°C; uv (MeOH λ_{max} 262; 218 (ε 28 600; 24 300) shoulder 290 (ε 8400) λ_{min} 233 (ε 12 700), (0.1 *N* NaOH) shoulders 280; 248 (ε 15 400; 20 000), (0.1 *N* HCl) λ_{max} 286; 235 (ε 24 900; 17 500) shoulder 265 (ε 21 300), λ_{min} 245; 220 nm (ε 15 400; 15 400); nmr ($CDCl_3$) δ 1.16 (s, 9, 5′-OPiv), 1.33 (s, 9, 4-NPiv), 5.03 (s, 2, H-5′, H-5′′), 6.49 (d, $J_{3'-2'} = 3$ Hz, 1, H-3′), 6.68 (d, $J_{2'-3'} = 3$ Hz, 1, H-2′), 7.14 (d, $J_{5-6} = 4$ Hz, 1, H-5), 7.50 (d, $J_{6-5} = 4$ Hz, 1, H-6), 8.20 (br, 1, 4-NH), 8.56 (s, 1, H-2). *Anal.* calcd. for $C_{12}H_{26}N_4O_4$: C 63.30, H 6.58, N 14.06; found: C 63.37, H 6.87, N 13.92.

*4-N-Pivalamido-7-(5-methylfuran-2-yl)pyrrolo[2,3-d]-pyrimidine (**10***b*)*

A 100 mg (0.00025 mol) sample of **10***a*, 84 mg (0.001 mol) of $NaHCO_3$, 100 mg of 5% Pd/C, and 50 ml of H_2O–EtOH (1:4) were hydrogenated at 3 psi for 3 min. The mixture was filtered through Celite and the catalyst was washed with MeOH and then $CHCl_3$. After evaporation of the combined filtrate, the residue was partitioned between H_2O and $CHCl_3$. The water layer was extracted with $CHCl_3$ and the combined organic phase was evaporated to give 81 mg of a yellow gum. This gum was dissolved in Et_2O and applied to a silica column (1.3 × 20 cm, 10 g), packed in, and eluted with Et_2O. Upon evaporation of the fractions comprising 20 to 50 ml, 61 mg (82%) of **10***b* crystallized, mp 127–128°C; uv (MeOH) λ_{max} 262; 217 (ε 22 800; 28 100) shoulder 295 (ε 7400) λ_{min} 238 nm (ε 13 200); nmr ($CDCl_3$) δ 1.38 (s, 9, 4-NPiv), 2.33 (d, $J_{CH_3-3'} = 1$ Hz, 3, 5′-CH_3), 6.07 (d of q, $J_{3'-CH_3} = 1$ Hz, $J_{3'-2'} = 3$ Hz, 1, H-3′), 6.49 (d, $J_{2'-3'} = 3$ Hz, 1, H-2′), 7.11 (d, $J_{5-6} = 4$ Hz, 1, H-5), 7.41 (d, $J_{6-5} = 4$ Hz, 1, H-6), 8.30 (br, 1, 4-NH), 8.56 (s, 1, H-2). *Anal.* calcd. for $C_{16}H_{18}N_4O_2$: C 64.41, H 6.08, N 18.78; found: C 64.66, H 6.21, N 18.82.

*4-Amino-7-(5-methylfuran-2-yl)pyrrolo[2,3-d]pyrimidine (**10***c*)*

A 150 mg (0.0005 mol) sample of **10***b* was dissolved in 100 ml of MeOH–Et_3N–H_2O (45:10:45) and stirred at room temperature for 2 days. The solution was evaporated to dryness and the residue crystallized from 5 ml of MeOH (with diffusion of Et_2O) to give a first crop of 66 mg of **10***c*. The mother liquors were evaporated to dryness and the residue dissolved in 3% MeOH–$CHCl_3$ and applied to a column of silica gel (0.8 × 16 cm, 3 g) packed in and eluted with the same solvent mixture. Upon evaporation of the fractions comprising 10 to 30 ml, 36 mg of **10***c* crystallized, for a total yield of 102 mg (94%), mp 127–130°C; uv (MeOH) λ_{max} 248 (ε 25 000) shoulder 285 (ε 9400) λ_{min} 223 (ε 16 200), (0.1 *N* HCl) λ_{max} 253; 221 (ε 23 000; 15 100) λ_{min} 232 (ε 13 300), (0.1 *N* NaOH) λ_{max} 246 (ε 20 900) shoulders 232; 280 nm (ε 16 800; 10 300); nmr (DMSO-d_6) δ 2.26 (d, $J_{CH_3-3'} = 1$ Hz, 3, 5′-CH_3), 6.18 (d of q, $J_{3'-CH_3} = 1$ Hz, $J_{3'-2'} = 3$ Hz, 1, H-3′), 6.43 (d, $J_{2'-3'} = 3$ Hz, 1, H-2′), 6.73 (d, $J_{5-6} = 4$ Hz, 1, H-5), 7.17 (br, 2, 4-NH_2), 7.54 (d, $J_{6-5} = 4$ Hz, 1, H-6), 8.11 (s, 1, H-2), 1.07 (t, $J = 7$ Hz, 0.75, OCH_2CH_3), 2.94 (q, $J = 7$ Hz, 0.5, OCH_2CH_3). *Anal.* calcd. for $C_{11}H_{10}N_4O \cdot \frac{1}{4}Et_2O$: C 61.92, H 5.41, N 24.07; found: C 61.80, H 5.44, N 24.12.

*4-Amino-7-(5-hydroxymethylfuran-2-yl)pyrrolo[2,3-d]-pyrimidine (**10***d*)*

To 796 mg (0.002 mol) of **10***a* dissolved in 20 ml of MeOH was added 250 mg of NaOMe. The mixture was stirred at room temperature for 18 h and evaporated to dryness. The residue was stirred with 15 ml of H_2O and filtered. The filter cake was washed with H_2O until the

filtrate was neutral (~15 ml) and then was crystallized from MeOH and Et_2O to give 426 mg (93%) of **10***d* in two crops, mp 178–180°C; uv (MeOH) λ_{max} 249 (ε 28 500) shoulder 285 (ε 10 300) λ_{min} 223 nm (ε 15 700); nmr (DMSO-d_6) δ 4.40 (s, 2, H-5′, H-5″), 5.25 (br, 1, 5′-OH), 6.42 (d, $J_{3'-2'}$ = 3.5 Hz, 1, H-3′), 6.54 (d, $J_{2'-3'}$ = 3.5 Hz, 1, H-2′), 6.77 (d, J_{5-6} = 4 Hz, 1, H-5), 7.17 (s, 2, 4-NH_2), 7.40 (d, J_{6-5} = 4 Hz, 1, H-6), 8.16 (s, 1, H-2). *Anal.* calcd. for $C_{11}H_{10}N_4O_2$: C 57.38, H 4.38, N 24.34; found: C 57.11, H 4.26, N 24.28.

4-Amino-7-(2,3-dideoxy-β-D,L-glycero-pentofuranosyl)-pyrrolo[2,3-d]pyrimidine (7,11)

A mixture of 230 mg (0.001 mol) of **10***d*, 250 mg (0.003 mol) of $NaHCO_3$, 460 mg of 10% Pd/C, and 50 ml of H_2O–MeOH (1:4) was hydrogenated at 60 psi for 16 h. The mixture was filtered through Celite and the catalyst was washed with MeOH. The filtrate was evaporated to dryness, dissolved in H_2O, and applied to a column (1.3 × 43 cm) of Dowex 1-X2(OH^-) resin packed in H_2O and eluted with 60 ml of H_2O followed by 90 ml of 30% MeOH–H_2O. Evaporation of fractions from 40 to 140 ml gave 181 mg (77%) of **7,11**. Crystallization of this racemate from MeOH (with diffusion of Et_2O) gave 90 mg of fine crystals, mp 70–73°C; uv (MeOH or 0.1 *N* NaOH) λ_{max} 270 (ε 11 400) λ_{min} 240 (ε 2700), (0.1 *N* HCl) λ_{max} 272; 227 (ε 10 600; 24 000) λ_{min} 246 nm (ε 4100); nmr (DMSO-d_6) δ 2.03 (m, 2, H-3′, H-3″), 2.26 (m, 2, H-2′, H-2″), 3.52 (m, 2, H-5′, H-5″), 4.04 (m, 1, H-4′), 4.96 (m, 1, 5′-OH), 6.33 ('t', $J_{apparent}$ = 6 Hz, 1, H-1′), 6.56 (d, J_{5-6} = 3.5 Hz, 1, H-5), 6.95 (s, 2, 4-NH_2), 7.32 (d, J_{6-5} = 3.5 Hz, 1, H-6), 8.05 (s, 1, H-2). *Anal.* calcd. for $C_{11}H_{14}N_4O_2$: C 56.40, H 6.02, N 23.92; found: C 56.22, H 6.10, N 23.71.

The nmr spectrum reported (6) for **7** is in agreement with that of this racemate. Treatment of a small sample of this racemate with tosyl chloride in pyridine followed by heating the isolated tosylate in acetone to effect cyclonucleoside formation (14) proceeded quantitatively (tlc) and gave a product having uv (H_2O) λ_{max} 293, shoulder 273 nm (3).

2′,3′-Dideoxytubercidin (7)

To a solution of 165 mg (0.71 mmol) of **6** and 180 mg of $NaHCO_3$ in 30 ml of EtOH–H_2O (1:1) was added 400 mg of 5% Pd/C and the mixture was hydrogenated at 40 psi for 24 h. The mixture was filtered using a Celite pad and the filter cake was washed with EtOH. The filtrate was evaporated and the residue was dissolved in H_2O and applied to a column (2.3 × 15 cm) of Dowex 1-X2(OH^-) resin packed in H_2O. The column was eluted with 300 ml of H_2O followed by 15% MeOH–H_2O. The appropriate fractions (15% MeOH) were pooled and evaporated. The residue resisted crystallization and was dissolved in H_2O and freeze-dried. The amorphous solid was dried over P_2O_5 at room temperature/0.1 torr for 2 days to give 115 mg (69%) of **7**, $[\alpha]_D^{23}$ −35.6° (*c* 0.28, MeOH); uv and ^1H nmr spectral properties were the same as for the above **7,11** racemate. *Anal.* calcd. for $C_{11}H_{14}N_4O_2$: C 56.40, H 6.02, N 23.92; found: C 56.11, H 6.01, N 23.94.

Acknowledgments

Generous financial support from the National Cancer Institute of Canada, the National Research Council of Canada (A5890), and The University of Alberta is gratefully acknowledged.

1. R. J. SUHADOLNIK. Nucleoside antibiotics. Wiley-Interscience, New York, NY. 1970. Chapt. 8.
2. (*a*) J. F. GERSTER, B. CARPENTER, R. K. ROBINS, and L. B. TOWNSEND. J. Med. Chem. **10**, 326 (1967); (*b*) R. L. TOLMAN, R. K. ROBINS, and L. B. TOWNSEND. J. Heterocycl. Chem. **4**, 230 (1967); (*c*) R. L. TOLMAN, R. K. ROBINS, and L. B. TOWNSEND. J. Am. Chem. Soc. **90**, 524 (1968); **91**, 2102 (1969); (*d*) B. C. HINSHAW, J. F. GERSTER, R. K. ROBINS, and L. B. TOWNSEND. J. Heterocycl. Chem. **6**, 215 (1969); (*e*) B. C. HINSHAW, J. F. GERSTER, R. K. ROBINS, and L. B. TOWNSEND. J. Org. Chem. **35**, 236 (1970); (*f*) K. H. SCHRAM and L. B. TOWNSEND. J. Chem. Soc. Perkin Trans. 1, 1253 (1975); and references therein.
3. K. ANZAI and M. MATSUI. Bull. Chem. Soc. Jpn., **46**, 618 (1973).
4. K. ANZAI and M. MATSUI. Agr. Biol. Chem. **37**, 345 (1973).
5. M. J. ROBINS, J. R. MCCARTHY, JR., R. A. JONES, and R. MENGEL. Can. J. Chem. **51**, 1313 (1973).
6. T. C. JAIN, A. F. RUSSELL, and J. G. MOFFATT. J. Org. Chem. **38**, 3179 (1973).
7. L. GOODMAN. *In* Basic principles in nucleic acid chemistry. Vol. I. *Edited by* P. O. P. Ts'o. Academic Press, New York, NY. 1974. pp. 93–208.
8. M. J. ROBINS, R. MENGEL, and R. A. JONES. J. Am. Chem. Soc. **95**, 4074 (1973).
9. M. J. ROBINS, R. MENGEL, R. A. JONES, and Y. FOURON. J. Am. Chem. Soc. **98**, 8204 (1976).
10. H. G. KUIVILA. Synthesis, 499 (1970); J. FARKAŠ and F. ŠORM. Coll. Czech. Chem. Commun. **32**, 2663 (1967).
11. A. F. RUSSELL, S. GREENBERG, and J. G. MOFFATT. J. Am. Chem. Soc. **95**, 4025 (1973).
12. M. J. ROBINS, R. A. JONES, and R. MENGEL. J. Am. Chem. Soc. **98**, 8213 (1976).
13. C. A. DEKKER. J. Am. Chem. Soc. **87**, 4027 (1965).
14. V. M. CLARK, A. R. TODD, and J. ZUSSMAN. J. Chem. Soc. 2952 (1951).
15. M. J. ROBINS, Y. FOURON, and R. MENGEL. J. Org. Chem. **39**, 1564 (1974).
16. S. J. SHAW, D. M. DESIDERIO, K. TSUBOYAMA, and J. A. MCCLOSKEY. J. Am. Chem. Soc. **92**, 2510 (1970).
17. J. N. BROWN and L. M. TREFONAS. Org. Prep. Proced. **2**, 317 (1970).
18. M. J. ROBINS, Y. FOURON, and W. H. MUHS. Can. J. Chem. This issue.

Nucleic acid related compounds. 25. Syntheses of arabino, xylo, and lyxo-anhydro sugar nucleosides from tubercidin ribo-epoxide[1,2]

MORRIS J. ROBINS, YVES FOURON, AND WOLFGANG H. MUHS[3]

Department of Chemistry, The University of Alberta, Edmonton, Alta., Canada T6G 2G2

Received December 3, 1976

MORRIS J. ROBINS, YVES FOURON, and WOLFGANG H. MUHS. Can J. Chem. **55**, 1260 (1977).

Treatment of the *trans* iodohydrin acetate, 4-amino-7-(3-iodo-3-deoxy-2-*O*-acetyl-5-*O*-[2,5,5-trimethyl-1,3-dioxolan-4-on-2-yl]-β-D-xylofuranosyl)pyrrolo[2,3-*d*]pyrimidine (**2**) with methanolic ammonia gave 2′,3′-anhydrotubercidin (**3**) in 96% yield. N^4,N^4,$O^{5'}$-Tribenzoylation of **3** gave **4**, which is stabilized against intramolecular cyclization. Treatment of **4** with boron trifluoride etherate (3′,5′-benzoxonium ion formation) followed by deblocking gave 4-amino-7-β-D-xylofuranosylpyrrolo[2,3-*d*]pyrimidine (**5**) in 91% overall yield from tubercidin (**1**). The 3′,5′-*O*-isopropylidene derivative (**6***a*) of **5** was mesylated to give **6***b* which was deprotected in acid and the resulting *trans* hydroxy mesylate was treated with base to give 4-amino-7-(2,3-anhydro-β-D-lyxofuranosyl)pyrrolo[2,3-*d*]pyrimidine (**7**). This *lyxo* epoxide was treated with sodium benzoate in DMF to give 4-amino-7-β-D-arabinofuranosylpyrrolo[2,3-*d*]pyrimidine (**8**). Biochemical, spectroscopic, and chemical properties of these semisynthetic antibiotic analogues of biologically active adenine nucleosides are discussed.

MORRIS J. ROBINS, YVES FOURON et WOLFGANG H. MUHS. Can. J. Chem. **55**, 1260 (1977).

Par traitement de l'acétate de *trans* iodohydrine, amino-4 (iodo-3 deoxy-3 *O*-acétyl-2-*O* [triméthyl-2,5,5 dioxolan-1,3 on-4 yl-2]-5 β-D-xylofuranosyl)-7 pyrrolo[2,3-*d*]pyrimidine (**2**) avec de l'ammoniac méthanolique on obtient, avec un rendement de 96%, l'anhydro-2′,3′ tubercidine (**3**). Par tribenzoylation en N^4,N^4,$O^{5'}$, **3** conduit à **4** qui est ainsi stabilisé contre une cyclisation intramoléculaire. Par traitement de **4** avec l'éthérate de trifluorure de bore (formation de l'ion benzoxonium-3′,5′), suivit du déblocage, on obtient l'amino-4 β-D-xylofuranosyl-7 pyrrolo[2,3-*d*]pyrimidine (**5**) avec un rendement global, à partir de la tubercidine (**1**), de 91%. Le dérivé *O*-isopropylidène-3′,5′ (**6***a*) de **5** est mésylé et donne **6***b* qui est déprotégé en milieu acide. Le *trans* hydroxy mésylate résultant, par traitement basique, donne l'amino-4 (anhydro-2,3 β-D-lyxofuranosyl)-7 pyrrolo[2,3-*d*]pyrimidine (**7**). Cet époxyde *lyxo* fournit l'amino-4 β-D-arabinofuranosyl-7 pyrrolo[2,3-*d*]pyrimidine (**8**) sous l'action du benzoate de sodium dans la DMF. Les propriétés biochimiques, spectroscopiques, et chimiques de ces analogues semi-synthétiques de nucléosides à activité biologique de l'adénine sont discutées.

Tubercidin (4-amino-7-β-D-ribofuranosylpyrrolo[2,3-*d*]pyrimidine) (**1**), the 7-deaza analog of adenosine, is closely related to adenosine chemically as well as structurally. This antibiotic is also found to act as a substrate for many enzymes involved with biosynthetic reactions of adenosine and phosphorylated adenosine biomolecules. Two significant exceptions are the complete resistance of **1** to deamination by adenosine deaminase, and to phosphorolytic cleavage of the glycosyl bond. An excellent review covers both chemical and biological aspects (1). Since deamination and phosphorolysis of the sugar–base bond represent major catabolic degradation (inactivation) modes for adenosine and most biologically active derivatives, the corresponding tubercidin products represent significant 'rational drug design' targets. The well established sugar–base coupling methods have been used extensively in syntheses of modified sugar analogs of adenosine (2), and this approach was successfully employed using ribose in syntheses of the naturally occurring pyrrolo[2,3-*d*]pyrimidine antibiotics (3). However, the lack of 'correct' stereospecificity in coupling reactions with certain diastereomeric sugar derivatives (see, for example, ref. 4) and the extensive heterocyclic transformations involved before and after coupling in the total synthesis routes (3) make this approach rather uninviting for preparation of arabinosyl and xylosyl sugar analogs; which probably accounts for the previous absence of their synthesis and biological evaluation. We now wish to describe their syntheses using acyloxonium ion mediated transformations of preformed nucleosides (5, 6).

[1]Abstracted in part from the Ph.D. dissertation of Y. Fouron, The University of Alberta, spring, 1975.

[2]For the previous paper in this series see ref. 5*g*.

[3]Postdoctoral Fellow, 1975–present.

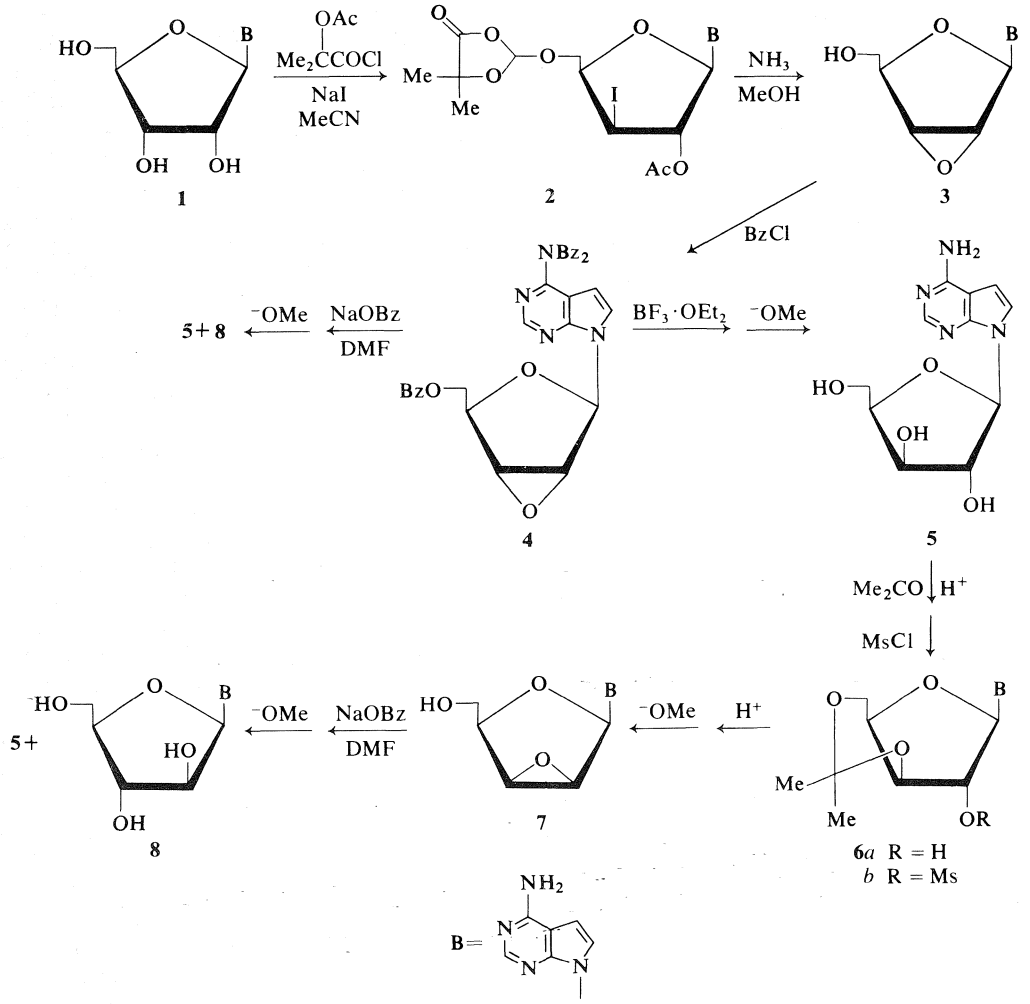

SCHEME 1

Although treatment of the crude mixture of 4-*N*-pivalamido-7-(3-chloro-3-deoxy-2-*O*-acetyl-5-*O*-pivalyl-β-D-xylofuranosyl)pyrrolo[2,3-*d*]-pyrimidine and its 2′-*O*-(4,4-dimethyl-3-pivaloxypent-2-enoyl) derivative (5*g*) with methanolic sodium methoxide gave 2′,3′-anhydrotubercidin (**3**); yields (maximum 72%) were variable and significant degradation via N-1→C-3′ intramolecular cyclization (5*d*,*g*) frequently occurred. It was found to be more experimentally convenient and economical to use the iodo product **2**, obtained by treatment of tubercidin (**1**) with α-acetoxyisobutyryl chloride and excess sodium iodide (5*b*). This is in contrast with reactions involving *adenosine* in which the orthoester/pivalyl chloride route proceeds smoothly (5*d*) and avoids problems of incomplete reaction, multiple acylation, and significant glycosyl bond cleavage noted with the Mattocks–Moffatt procedure (6, 7).

In situ generation of α-acetoxyisobutyryl iodide in acetonitrile provided smooth reaction with **1** at room temperature to give 4-amino-7-(3-iodo-3-deoxy-2-*O*-acetyl-5-*O*-[2,5,5-trimethyldioxolan-4-on-2-yl]-β-D-xylofuranosyl)-pyrrolo[2,3-*d*]pyrimidine (**2**) in quantitative yield (5*b*) (see Scheme 1). Treatment of the amorphous product (**2**) with methanolic ammonia at room temperature gave the *ribo*-epoxide (**3**) in 96% yield after column chromatographic purification. Deblocking of **2** occurred in methanolic ammonia at −20°C to give crystalline 4-amino-7-

(3-iodo-3-deoxy-β-D-xylofuranosyl)pyrrolo-[2,3-*d*]pyrimidine (66%).

Benzoylation of **3** produced the stable (5*d*) and readily crystallized tribenzoyl derivative (presumably (8) dibenzimide **4**) quantitatively (89% crystalline). Treatment of **4** with sodium benzoate in hot moist *N*,*N*-dimethylformamide (DMF) (9) followed by deblocking gave 4-amino-7-β-D-xylofuranosylpyrrolo[2,3-*d*]pyrimidine (xyloTb) (**5**) in 68% crystalline yield after purification on the Dekker anion exchange column (10). Unexpectedly, elution of the column with 70% methanol–water gave 6.8% of the arabino isomer, **8**. Although a minor amount of 9-β-D-arabinofuranosyladenine is produced in the parallel reaction with 2′,3′-anhydroadenosine (11), no nucleophilic reactions at C-2′ of tubercidin have been observed previously (5*a*,*b*,*g*, 12), and only very recently has an intramolecular participation route provided access to the elusive 2′-deoxytubercidin (13). Treatment of **4** with boron trifluoride etherate in acetonitrile gave a benzoate ester, presumably via the 3′,5′-benzoxonium ion species (**i**) (14), which was deblocked with methanolic sodium methoxide to give **5**, exclusively, in 95% yield (91% overall from **1**).

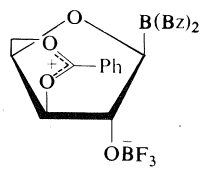

i

It had been reported (15) that the *arabino* and *xylo* diastereomers of adenosine were incompletely resolved on the Dekker column. Two mixtures of araA and xyloA with ratios of 1:11 and 11:1 were prepared and subjected to the ion exchange conditions used to separate **5** and **8**. In both cases, the isomers were resolved cleanly and completely as indicated by the uv absorption profiles and quantitative recovery of electrophoretically homogeneous (*vide infra*) products upon evaporation of appropriately pooled fractions (11). Acid-catalyzed hydrolysis of these separated nucleosides and paper chromatographic analysis (16) of the aldopentose sugars released, corroborated the complete separation efficiency (11).

Blocking of **5** with acetone and 2,2-dimethoxypropane gave **6***a* quantitatively and this crystalline 3′,5′-*O*-isopropylidene derivative was mesylated to give amorphous **6***b*. Deketalization of **6***b* proceeded smoothly in 90% trifluoroacetic acid – water (17) and the resulting *trans* hydroxy mesylate was cyclized in methanolic sodium methoxide to give 4-amino-7-(2,3-anhydro-β-D-lyxofuranosyl)pyrrolo[2,3-*d*]pyrimidine (**7**) in 82% yield. Treatment of the *lyxo*-epoxide (**7**) with sodium benzoate – DMF followed by deblocking gave crystalline 4-amino-7-β-D-arabinofuranosylpyrrolo[2,3-*d*]pyrimidine (araTb) (**8**) in 73% yield plus 4.5% of xyloTb (**5**). It is interesting to note that comparable yields of the minor products are formed presumably by nucleophilic attack of benzoate at C-2′ of the *ribo* (**4**→**8**) and *lyxo* (**7**→**5**) epoxides. The base at C-1′ of **4** is *cis* to the incoming benzoate nucleophile whereas *trans* (base to benzoate) attack occurs with **7**. In contrast, presumed nucleophilic attack on a *lyxo* 2′,3′-thiiranium ion species (episulfonium ion) gave a ratio of ~3:2 for C-3′ to C-2′ substitution by benzoate (13). A complex balance of steric (short C-1′—N-7 glycosyl bond) (see ref. 18*a* and, for a comparison of glycosyl bond lengths, ref. 18*b*), electronic (including extent of bond formation *vs.* breaking) (19) and hydrophobic factors apparently control the normally prohibited nucleophilic attack at C-2′ of tubercidin derivatives (5*a*,*b*,*g*, 12).

The structures indicated in these transformations are compatible with uv, nmr, and mass spectral data as well as elemental analyses. As noted previously (5*d*, 6, 12), there is no observed coupling of H-1′ and H-2′ in the *ribo*-epoxides of adenosine or tubercidin. However, it is noteworthy to point out that there is also no observed coupling of H-1′ and H-2′ in the *lyxo*-epoxides of adenosine (5*d*) or tubercidin (see Experimental section). It has been generally assumed that a coupling constant of less than 1 Hz was diagnostic for a *trans* orientation of H-1′ and H-2′ in a furanosyl nucleoside (20). Compound **7** and the analogous adenosine series product (5*d*) clearly violate this empirical expectation. An X-ray crystallographic study of these diastereomeric epoxide products would be of interest.

The nmr and mass spectroscopic patterns of **5** and **8** (see Experimental section) are closely analogous to those of the corresponding 9-β-D-xylofuranosyl- and arabinofuranosyladenine nucleosides (21–23) and are individually unique from those of the ribofuranosyl products. As well, **5** and **8** do not react detectably in 5 h with

sodium periodate solution (24) (whereas the *cis* diol **1** cleaves completely within 20 min under identical conditions). Paper electrophoresis of **5** in a borate buffer at p*H* 9 shows migration toward the anode comparable to that of **1**, whereas borate addition has a much smaller effect on the migration of **8** (*i.e.* formation of a 3′,5′-*O*-borate complex with **5** is comparable to that of the 2′,3′-*O*-borate complex of **1**). Paper chromatographic (25) mobilities of the adenosine and tubercidin compounds are also parallel (see Table 1).

The synthesis (9, 26) and biological inhibitory activity (27, 28) of 9-β-D-arabinofuranosyladenine (araA) were reported several years before its isolation from microbiological culture fermentation (29) and evaluation as a promising antiviral drug (30). Synthetic 9-β-D-xylofuranosyladenine (xyloA) (4*b*, 31) was also shown to exhibit inhibitory activity against neoplastic cells (32). However, both araA and xyloA are rapidly converted to the corresponding 6-oxo (hypoxanthine) analogs by adenosine deaminase (33–35), an enzyme with high activity in both mammalian blood and intestinal loci. The incorporation of radioactivity into inosine monophosphate (IMP) and ribonucleic acid (RNA) after treatment with purine-labeled araA has subsequently been shown to result from enzymatic deamination, glycosyl bond cleavage (presumably phosphorolysis), and effective reutilization of the purine moiety as 'salvaged' ribonucleotides (34, 35). The absence of substrate activity of tubercidin with adenosine deaminase and glycosyl phosphorolysis enzymes (1) renders the presumably degradation resistant araTb (**8**) and xyloTb (**5**) compounds of heightened biochemical and biological interest. As anticipated, even high levels of adenosine deaminase had no effect on **5** or **8** as indicated by uv spectroscopy.

TABLE 1. Paper chromatography and electrophoresis of isomeric nucleosides

Compound	Paper chromatography[a] (R_{araA} or R^{*}_{araTb})[b]	Electrophoretic mobility[c] Distance (mm) migrated toward anode
riboA	0.86	80
araA	1.0	0
xyloA	0.86	75
riboTb (**1**)	0.67	97
araTb (**8**)	1.0	32
xyloTb (**5**)	0.90	85

[a]Descending on the same sheet of Whatman No. 1 paper using 60 ml of (1 *M* NH_4OAc containing 0.01 *M* EDTA disodium salt adjusted to p*H* 9 with NH_4OH and saturated with sodium tetraborate) mixed with 140 ml of 90% EtOH. The mixture was allowed to stand for 1 h and was then filtered before use (25).

[b]$R_{arabino} = R_{F(compound)}/R_{F(arabino)}$

[c]Performed on a Savant flatplate apparatus (HV-3000A) using Whatman No. 1 paper and 0.1 *M* sodium borate at p*H* 9 at 1.5 KV (27 V/cm) 30–35 mA, 90 min.

The present study demonstrates that transformations of naturally occurring nucleoside antibiotics into epoxide sugar products can be effected in high yields on a practically convenient scale. Application of benzoate nucleophilic displacement or boron trifluoride induced acyloxonium participation on 2′,3′-anhydro (epoxide) nucleosides provides configurationally inverted antibiotic structures. Such *arabino* and *xylo* diastereomers, even in the purine series, were available prior to our work (5*d*) only through base–sugar coupling sequences (4*b*,*c*, 9, 23, 26, 31, 36). Successful application of these acyloxonium ion–nucleophilic displacement procedures to other commonly occurring nucleosides[4] (14*b*, 37) and results of biological and biochemical investigations will be reported separately.

Experimental

General methods are described in detail in ref. 5*g*. J. T. Baker 3405 silica gel was used for column chromatography. All nmr spectra were determined in Me_2SO-d_6 with Me_4Si internal standard. See refs. 5*e*,*g*, and 38 for descriptions of 'diffusion crystallization'. Tubercidin was purchased from the Upjohn Company, Kalamazoo, Michigan. Adenosine deaminase (Grade II) was purchased from Sigma Chemical Company, St. Louis, MO.

*4-Amino-7-(3-iodo-3-deoxy-*β*-D-xylofuranosyl)pyrrolo[2,3-d]pyrimidine*

A 0.54 g (0.001 mol) sample of **2** (5*b*) was dissolved in 100 ml of MeOH presaturated with NH_3 at −20°C and allowed to stand at that temperature for 3 h. Ammonia was evaporated *in vacuo* at −20°C and 2 g of silica gel was added to the solution. The mixture was evaporated to dryness and the impregnated powder was added to a column (2 × 26 cm, 40 g) of silica. The column was washed with $CHCl_3$ and the wash discarded. The product was eluted using $CHCl_3$–MeOH (98:2). Evaporation of appropriate fractions gave 0.25 g (66%) of the title compound as a white powder. A sample for analysis was recrystallized from 95% EtOH (with diffusion of Et_2O) and had mp 175–176°C; $[\alpha]_D^{24}$ −5° (*c* 0.6, DMF); uv (0.1 *N* HCl) λ_{max} 265; 225 (ε 11 300; 22 200) λ_{min} 245 (ε 5250), (H_2O) λ_{max} 268 (ε 12 300) λ_{min} 238 (ε 3200), (0.1 *N* NaOH) λ_{max} 268 (ε 11 700) λ_{min} 242 nm (ε 6000); nmr δ 3.70 (br, s, 2, H-5′, H-5″), 3.90 (m, 1, H-4′), 4.46 ('t', $J_{3'-2'} = J_{3'-4'} = 5.5$ Hz, 1, H-3′), 4.83 (m, 1, H-2′), 5.40 ('t', $J_{OH-5',5''} = 5.5$ Hz, 1, 5′-OH), 5.91 (d, $J_{1'-2'} = 5$ Hz,

[4]R. Mengel *et al.*, work to be published.

1, H-1′), 6.14 (d, $J_{OH-2'} \sim 3$ Hz, 1, 2′-OH), 6.65 (d, $J_{5-6} = 4$ Hz, 1, H-5), 7.10 (br s, 2, 4-NH_2), 7.40 (d, $J_{6-5} = 4$ Hz, 1, H-6), 8.10 (s, 1, H-2); ms (180°C) *m/e* (relative intensity, ion) 376(8, M), 248(8, $M-128$), 230(4, $M-(128+18)$), 219(12, $M-(127+30)$), 189(2), 164(44, BHCHO(1′)), 147(4, BCH_2), 135(28, B+2H), 134(100, B+H). *Anal.* calcd. for $C_{11}H_{13}IN_4O_3$: C 35.12, H 3.48, I 33.74, N 14.89; found: C 35.12, H 3.84, I 33.87, N 14.61.

4-Amino-7-(2,3-anhydro-β-D-ribofuranosyl)pyrrolo[2,3-d]pyrimidine (3)

To 100 ml of absolute MeOH saturated with NH_3 (at −5°C) was added 1.64 g (0.003 mol) of **2** (*5b*). The flask was securely stoppered and allowed to stand at room temperature for 6 h. Completion of the reaction was verified by tlc (silica gel, 5% MeOH–$CHCl_3$). The solution was evaporated (water aspirator) to ~20 ml and 4 g of silica gel was added. The mixture was evaporated to dryness at room temperature and the impregnated powder was added to a column (4 × 20 cm, 60 g) of silica gel. The column was washed with 2000 ml of CH_2Cl_2[5] and the wash was discarded. The product was eluted using CH_2Cl_2–MeOH (20:1) and 100 ml fractions were collected. Evaporation (at room temperature) of fractions 9–14 gave a white powder which was dried *in vacuo* for 12 h at room temperature to give 0.765 g (96%) of **3**·monohydrate (^{1}H nmr). A sample for analysis was *rapidly* (*5d,g*) recrystallized from 95% EtOH (with diffusion of Et_2O) to give **3** as white needles, mp 170–173°C; $[\alpha]_D^{24}$ −46° (*c* 0.22, MeOH); uv (MeOH) λ_{max} 271 (ε 11 500) λ_{min} 227 nm (ε 2410); nmr δ 3.50 (m, 2, H-5′, H-5″), 4.12 (t, $J_{4'-5',5''} \sim 6$ Hz, 1, H-4′), 4.20 (d, $J_{3'-2'} = 2.5$ Hz, 1, H-3′), 4.28 (d, $J_{2'-3'} \sim 2.5$ Hz, 1, H-2′), 5.04 (br s, 1, 5′-OH), 6.28 (s, 1, H-1′), 6.60 (d, 1, H-5), 7.05 (s, 2, 4-NH_2), 7.35 (d, 1, H-6), 8.08 (s, 1, H-2); ms (190°C) *m/e* (% relative intensity, ion) 248(11.5, M), 218(2, $M-CHO(5')$), 217(3, $M-31$), 201(0.5, $M-CHO-17$), 189(3), 163(50, BHCHO(1′)), 147(6.5, BCH_2), 135(21, B+2H), 134(100, B+H); (lit. (12) mp 145–176°C; $[\alpha]_D^{23}$ −42.6° (*c* 0.2, MeOH)). *Anal.* calcd. for $C_{11}H_{12}N_4O_3$; C 53.22, H 4.86, N 22.57; found: C 53.17, H 4.62, N 22.34.

4-N,N-Dibenzimido-7-(5-O-benzoyl-2,3-anhydro-β-D-ribofuranosyl)pyrrolo[2,3-d]pyrimidine (4)

To a suspension of 1 g (0.004 mol) of crude **3** in 30 ml of dry pyridine was added 3 ml (0.026 mol) of freshly distilled benzoyl chloride and the resulting clear solution was stirred for 8 h at room temperature. Ice chips were added and the solution was poured slowly into 2000 ml of ice and H_2O with vigorous stirring. The resulting white precipitate was filtered, washed with 1000 ml of cold H_2O, and dried (finally *in vacuo* at 50°C) to give 2 g (89%) of **4**. Recrystallization of 65 mg of this product from 5 ml of EtOH–$CHCl_3$ gave 60 mg of pure **4**, mp 201–202°C; uv (MeOH) shoulder 270 (ε 17 500), λ_{max} 215 nm (ε 59 500); nmr δ 4.2–4.6 (m, 5, H-2′–H-5″), 6.38 (d, $J_{5-6} = 4$ Hz, 1, H-5), 6.48 (s, 1, H-1′), 7.3–7.95 (m, 16, benzoate, H-6), 8.56 (s, 1, H-2); ms (200°C) *m/e* (relative intensity, ion) 560(68, M), 455(100, $M-COC_6H_5$), 439(23, $M-OCOC_6H_5$), 218(40, sugar fragment). *Anal.* calcd. for $C_{32}H_{24}N_4O_6$: C 68.56, H 4.31, N 9.99; found: C 68.43, H 4.54, N 10.27.

4-Amino-7-β-D-xylofuranosylpyrrolo[2,3-d]pyrimidine (5) (xyloTb)

Method A

To a solution of 0.56 g (0.001 mol) of **4** in 50 ml of DMF containing 1 ml of H_2O was added 0.35 g (0.002 mol) of sodium benzoate. This mixture was heated with stirring at 100°C for 34 h and was then evaporated *in vacuo*. The resulting gum was dissolved in 240 ml of MeOH and 0.6 g (0.025 g at.) of sodium was added. The solution was stirred for 21 h at room temperature, neutralized with HOAc, and evaporated. The residue was partitioned between H_2O and Et_2O and the aqueous phase was applied to a column (2.5 × 22 cm) of Dowex 1-X2(OH^-) resin packed in H_2O. The column was washed with H_2O (2 ℓ) and then with 10% MeOH–H_2O. The amount of MeOH in H_2O was gradually increased to 60% which eluted the product. Evaporation of the appropriate fractions gave 0.19 g (71%) of **5** which was crystallized from MeOH (with diffusion of Et_2O) to give 0.18 g (68%) of **5**, mp 223–224°C; $[\alpha]_D^{24}$ −135°C (*c* 0.5, DMF); uv (0.1 *N* HCl) λ_{max} 270; 227 (ε 10 600; 22 400) λ_{min} 245 (ε 3950), (H_2O) λ_{max} 270 (ε 11 500) λ_{min} 237 (ε 1950), (0.1 *N* NaOH) λ_{max} 270 (ε 11 400) λ_{min} 240 nm (ε 3550); nmr δ 3.6–3.7 (m, 2, H-5′, H-5″), 3.95–4.10 (m, 2, H-3′, H-4′), 4.22 (br s, 1, H-2′), 5.15 ('t', $J_{OH-5',5''} \sim 5$ Hz, 1, 5′-OH), 5.7 (d, 1, 2′-OH), 5.88 (s, 1, 3′-OH), 5.94 (d, $J_{1'-2'} = 2$ Hz, 1, H-1′), 6.55 (d, $J_{5-6} = 4$ Hz, 1, H-5), 7.0 (br s, 2, 4-NH_2), 7.38 (d, 1, $J_{6-5} = 4$ Hz, H-6), 8.08 (s, 1, H-2); ms (170°C) *m/e* (relative intensity, ion) 266(3, M), 177(45, $BHCH_2CHO$), 163(66, BHCHO(1′)), 147(19.5, BCH_2), 135(2, B+2H), 134(100, B+H). *Anal.* calcd. for $C_{11}H_{14}N_4O_4$: C 49.62, H 5.30, N 21.04; found: C 49.42, H 5.32, N 20.75.

Further elution with 70% MeOH–H_2O gave 0.018 g (6.8%) of the arabino isomer **8**. This product had identical mobility to a sample of **8** (prepared below) by tlc, paper chromatography, and electrophoresis. The mass spectrum was identical to that of **8** and the nmr spectrum of the product obtained from similar experimental runs was identical to that of **8** (H-1′ at δ 6.42, $J_{1'-2'} = 4$ Hz).

Method B

To a solution of 280 mg (0.5 mmol) of **4** in 10 ml of dry MeCN (distilled from P_2O_5 and stored over 3A molecular sieves) was added 1 ml of freshly distilled $BF_3 \cdot OEt_2$ and the mixture was stirred for 10 min at room temperature. Absolute MeOH (5 ml) was added and stirring was continued for 1 h. The mixture was poured into 100 ml of saturated aqueous $NaHCO_3$ solution and the milky suspension was extracted with 3 × 50 ml of CH_2Cl_2. The combined organic phase was washed with 50 ml of H_2O, dried over Na_2SO_4, and evaporated to dryness. The resulting yellow glass (homogeneous on tlc, cyclohexane–Me_2CO 1:1) (300 mg) was stirred for 15 h at room temperature with 0.2 *N* NaOMe – MeOH. This solution was neutralized with 600 mg of HOAc and evaporated to a heavy oil. This residue was partitioned between H_2O and Et_2O, and the organic phase was extracted with an additional 30 ml of H_2O. The combined aqueous phase was evaporated to ~10 ml and applied to a column (2 × 25 cm) of Dowex 1-X2(OH^-). Elution was effected using 1 ℓ of H_2O, 300 ml each of 10%, 20%, and

[5]The use of methylene chloride appears to be essential. Substitution of chloroform resulted in lower yields of less pure epoxide.

30%, 1.5 ℓ of 40%, 1 ℓ of 50%, and 2 ℓ of 70% MeOH–H_2O. Fractions (20 ml) 113–160 were pooled and evaporated to give 126 mg (95%) of **5** after drying *in vacuo*. This solid product had identical spectral, chromatographic, and electrophoretic properties to that of method A and could be used without further purification.

No araTb (**8**) was detected in the 70% MeOH–H_2O or earlier eluates.

*4-Amino-7-(3,5-O-isopropylidene-β-D-xylofuranosyl)pyrrolo[2,3-d]pyrimidine (**6a**)*

To a stirred solution of 6 ml of freshly distilled acetone containing 0.84 g of *p*-toluenesulfonic acid and 1.5 ml (0.014 mol) of 2,2-dimethoxypropane was added 0.3 g (0.0011 mol) of **5**. The flask was stoppered and stirred for 20 h. The red solution was poured into a stirred solution (30 ml) of saturated aqueous $NaHCO_3$. This solution was extracted with 7 × 30 ml of $CHCl_3$. White crystals separated upon concentration of the combined organic phase. These were filtered to yield 0.34 g (100%) of **6a**, mp 251–252°C; $[\alpha]_D^{24}$ −81.5° (*c* 0.5, DMF); uv (0.1 *N* HCl) λ_{max} 266; 225 (ε 10 300; 21 400) λ_{min} 242 (ε 4000); (H_2O) λ_{max} 270 (ε 11 100) λ_{min} 237 (ε 280), (0.1 *N* NaOH) λ_{max} 267 (ε 10 800) λ_{min} 240 nm (ε 4000); nmr δ 1.34, 1.44 (s, s; 3, 3; CMe_2), 3.8–4.3 (m, 5, H-2′–H5′′), 5.90 (br s, 1, 2′-OH), 6.16 (s, 1, H-1′), 6.52 (d, J_{5-6} = 4 Hz, 1, H-5), 6.96 (br s, 2, 4-NH_2), 7.42 (d, J_{6-5} = 4 Hz, 1, H-6), 8.08 (s, 1, H-2); ms (185°C) *m/e* (% relative intensity, ion) 306(8.5, M), 291(4, *M*−15), 219(1), 193(2), 177(5.5, $BHCH_2CHO$), 163(70, BHCHO(1′)), 147(3, BCH_2), 135(32, B+2H), 134(100, B+H). *Anal.* calcd. for $C_{14}H_{18}N_4O_4$: C 54.89, H 5.92, N 18.29; found: C 55.09, H 6.13, N 18.02.

*4-Amino-7-(3,5-O-isopropylidene-2-O-methanesulfonyl-β-D-xylofuranosyl)pyrrolo[2,3-d]pyrimidine (**6b**)*

To a stirred solution of 0.6 g (0.0019 mol) of **6a** in 10 ml of dry freshly distilled pyridine was added 0.6 ml (0.007 mol) of mesyl chloride. The flask was stoppered and stirred for 3 h. The solution was poured into 150 ml of ice and H_2O and this mixture was extracted with 4 × 50 ml of $CHCl_3$. The combined organic phase was washed with saturated aqueous $NaHCO_3$, H_2O, dried over Na_2SO_4, filtered, and evaporated *in vacuo* to give a white powder. This powder was dissolved in 5 ml of $CHCl_3$ and applied to a column of silica (2.3 × 50 cm, 100 g). The column was washed with 200 ml of $CHCl_3$ and the compound was then eluted with MeOH–$CHCl_3$ (3:97). The appropriate fractions were evaporated to give 0.58 g (79%) of **6b** as a white powder, mp 80–83°C; uv (MeOH) λ_{max} 270 (ε 11 200) λ_{min} 230 nm (ε 3670); nmr δ 1.32, 1.50 (s, s; 3, 3; CMe_2), 3.48 (s, 3, OMs), 3.9–4.3 (m, 3, H-4′–H-5′′), 4.65 (d, $J_{3'-4'}$ = 2 Hz, 1, H-3′), 5.05 (s, 1, H-2′), 6.40 (s, 1, H-1′), 6.60 (d, J_{5-6} ~ 3.8 Hz, 1, H-5), 7.1 (br s, 2, 4-NH_2), 7.40 (d, J_{6-5} ~ 3.8 Hz, 1, H-6), 8.08 (s, 1, H-2); ms (180°C) calcd. for M^+ ($C_{15}H_{20}N_4O_6S$): 384.1103; found (*m/e*): 384.1111; *m/e* (% relative intensity, ion) 384(5.5, M), 369(3.5, *M*−15), 247(5.5), 231(7), 217(2), 201(11), 163(95, BHCHO(1′)), 147(9, BCH_2), 135(32, B+2H), 134(100, B+H).

4-Amino-7-(2-O-methanesulfonyl-β-D-xylofuranosyl)pyrrolo[2,3-d]pyrimidine

A 0.55 g (0.0014 mol) sample of **6b** was dissolved in 50 ml of 90% trifluoroacetic acid – H_2O. The solution was stirred at room temperature for 20 min and was then evaporated. After removal of traces of H_2O and acid by coevaporation of the residue with benzene, 0.42 g (87%) of the title compound was obtained as a white solid foam, mp 179–180°C; uv (MeOH) λ_{max} 270 (ε 11 200) λ_{min} 230 nm (ε 3670); nmr δ 3.22 (s, 3, OMs), 3.71 (m, 2, H-5′, H-5′′), 4.09 (m, 1, H-4′), 4.42 (m, 1, H-3′), 4.91 ('t', $J_{OH-5',5''}$ = 5 Hz, 1, 5′-OH), 5.21 ('t', $J_{2'-3'} = J_{2'-1'}$ = 2.5 Hz, 1, H-2′), 6.25 (d, $J_{1'-2'}$ = 2.5 Hz, 1, H-1′), 6.35 (d, $J_{OH-2'}$ = 5.5 Hz, 1, 2′-OH), 6.60 (d, J_{5-6} = 4 Hz, 1, H-5), 7.12 (br s, 2, 4-NH_2), 7.36 (d, J_{6-5} = 4 Hz, 1, H-6), 8.08 (s, 1, H-2); ms (200°C) calcd. for M^+: 344.0791; found (*m/e*): 344.0798; *m/e* (% relative intensity, ion) 344(2.5, M), 248(27, M−(OMs and OH)), 217(7, 248–31), 201(6), 189(9), 163(93, BHCHO(1′)), 147(18, BCH_2), 135(50, B + 2H), 134(100, B + H). *Anal.* calcd. for $C_{12}H_{16}N_4O_6S$: C 41.85, H 4.68, N 16.27, S 9.31; found: C 41.67, H 4.47, N 16.00, S 9.28.

*4-Amino-7-(2,3-anhydro-β-D-lyxofuranosyl)pyrrolo[2,3-d]pyrimidine (**7**)*

To a solution of 0.237 g (0.0007 mol) of the above mesylate product in 80 ml of MeOH was added 0.2 g (0.009 g at.) of sodium. The solution was stirred at room temperature for 12 h, neutralized with HOAc, and evaporated to dryness. The residue was dissolved in 25 ml of H_2O and the solution was applied to a column (2 × 60 cm) of Dowex 1-X2(OH^-) resin. Elution with H_2O and evaporation of appropriately pooled fractions gave 0.14 g (82%) of **7**. Recrystallization of this material from 95% EtOH gave crystals of **7**, mp 110–112°C (dec.); $[\alpha]_D^{24}$ −50.5° (*c* 0.4, DMF); uv (0.1 *N* HCl) λ_{max} 270; 225 (ε 11 100; 23 000) λ_{min} 245 (ε 4250), (H_2O) λ_{max} 270 (ε 12 500) λ_{min} 247 (ε 7500), (0.1 *N* NaOH) λ_{max} 270 (ε 12 000) λ_{min} 238 nm (ε 4100); nmr δ 3.58 (d, 2, H-5′, H-5′′), 3.95–4.2 (m, 3, H-2′–H-4′), 5.00 (br s, 1, 5′-OH), 6.40 (s, 1, H-1′), 6.65 (d, J_{5-6} = 4 Hz, 1, H-5), 7.08 (br s, 2, 4-NH_2), 7.30 (d, J_{6-5} = 4 Hz, 1, H-6), 8.12 (s, 1, H-2); ms (140°C) calcd. for M^+: 248.0909; found (*m/e*): 248.0905; *m/e* (% relative intensity, ion) 248 (12, M), 231(1.5, *M* − 17), 218(5.5, *MH* − CHO(5′)), 217(8.5, *M* − 31), 201(5.5, *MH* − CHO − 17), 189(8.5), 163(97, BHCHO(1′)), 147(23, BCH_2), 135(49, B + 2H), 134(100, B + H). *Anal.* calcd. for $C_{11}H_{12}N_4O_3$: C 53.22, H 4.86, N 22.57; found: C 53.04, H 5.09, N 22.81.

*4-Amino-7-β-D-arabinofuranosylpyrrolo[2,3-d]pyrimidine (**8**) (araTb)*

To a solution of 0.13 g (0.0005 mol) of **7** in 25 ml of DMF containing 1 ml of H_2O was added 0.15 g (0.001 mol) of sodium benzoate. This mixture was heated at 100°C for 12 h with stirring and was then evaporated *in vacuo*. The residue was dissolved in 40 ml of MeOH and 0.07 g (0.003 g at.) of sodium was added. The solution was stirred for 1 h at room temperature, neutralized with HOAc, and evaporated. The residue was dissolved in 25 ml of H_2O and the solution was applied to a column (2 × 32 cm) of Dowex 1-X2(OH^-) resin. The column was washed with H_2O (2 ℓ) and then with 10% MeOH–H_2O. The concentration of MeOH in H_2O was gradually increased. A small quantity, 0.006 g (4.5%) of material identical to **5** by tlc, paper chromatography, electrophoresis, mass spectrometry, and nmr was eluted with 60% MeOH–H_2O. Further elution gave 0.102 g (77%) of **8**. Recrystallization of 0.1 g of this material from MeOH

(with diffusion of Et_2O) gave 0.095 g of crystalline **8**, mp 125–126°C; $[\alpha]_D^{24}$ 6.9° (*c* 0.5, DMF); uv (0.1 *N* HCl) λ_{max} 268; 225 (ε 11 100; 23 800) λ_{min} 245 (ε 4150), (H_2O) λ_{max} 268 (ε 11 900) λ_{min} 240 (ε 4500), (0.1 *N* NaOH) λ_{max} 270 (ε 11 200) λ_{min} 240 nm (ε 4150); nmr δ 3.55–3.80 (m, 3, H-3′, H-5′, H-5″), 3.95–4.20 (m, 2, H-2′, H-4′), 5.01 (t, 1, 5′-OH), 5.41 (d, 2, 2′-OH, 3′-OH), 6.42 (d, $J_{1'-2'}$ = 4 Hz, 1, H-1′), 6.52 (d, J_{5-6} = 4 Hz, 1, H-5), 6.90 (br s, 2, 4-NH_2), 7.29 (d, J_{6-5} = 4 Hz, 1, H-6), 8.05 (s, 1, H-2), ms (200°C) *m/e* (% relative intensity, ion) 266(7, M), 236(1, *MH* − CHO(5′)), 193(1), 190(0.5), 177(11, $BHCH_2$-CHO), 163(60, BHCHO(1′)), 147(8, BCH_2), 135(32, B + 2H), 134(100, B + H). *Anal.* calcd. for $C_{11}H_{14}N_4O_4$: C 49.62, H 5.30, N 21.04; found: C 49.92, H 5.40, N 20.86.

*Treatment of **1**, **5**, and **8** with periodate*

Solutions of **1**, **5**, and **8** in H_2O were placed (sequentially) in a cuvette and an aqueous solution of $NaIO_4$ was added. The solutions were mixed rapidly and the cuvette was placed in a uv spectrometer. The change in optical density at 227 nm was observed as a function of time as described (24).

Tubercidin (**1**) was oxidized completely in ~20 min, whereas **5** and **8** caused no change in the uv absorption of the periodate ion over an extended period of time.

*Treatment of **1**, **5**, and **8** with Adenosine Deaminase*

Solutions of **1**, **5**, and **8** in 0.05 *M* KH_2PO_4 buffer (p*H* 7.0) were treated with a solution of adenosine deaminase[6] in 0.05 *M* Tris-HCl buffer (p*H* 8). After standing at room temperature for 30 h, aliquots were diluted, and uv spectra were determined. These spectra were superimposable with those of control solutions of **1**, **5**, and **8**. Under these conditions, adenosine was *rapidly* and completely converted to inosine ($\Delta\varepsilon_{265\ nm} \sim -8600$).

Acknowledgments

Generous financial support from the National Cancer Institute of Canada, the National Research Council of Canada (A5890), and The University of Alberta is gratefully acknowledged.

1. R. J. SUHADOLNIK. Nucleoside antibiotics. Wiley–Interscience, New York, NY. 1970. Chapt. 8.
2. L. GOODMAN. *In* Basic principles in nucleic acid chemistry. Vol. I. *Edited by* P. O. P. Ts'o. Academic Press, New York, NY. 1974. pp. 93–208.
3. R. L. TOLMAN, R. K. ROBINS, and L. B. TOWNSEND. J. Am. Chem. Soc. **90**, 524 (1968); **91**, 2102 (1969).
4. (*a*) B. R. BAKER. *In* Chemistry and biology of purines. A Ciba foundation symposium. *Edited by* G. E. W. Wolstenholme and D. M. O'Connor. J. & A. Churchill Ltd., London. 1957. pp. 120–133; (*b*) W. W. LEE, A. P. MARTINEZ, G. L. TONG, and L. GOODMAN. Chem. Ind. (London), 2007 (1963); (*c*) C. P. J. GLAUDEMANS and H. G. FLETCHER, JR. J. Org. Chem. **28**, 3004 (1963).
5. (*a*) M. J. ROBINS, R. MENGEL, and R. A. JONES. J. Am. Chem. Soc. **95**, 4074 (1973); (*b*) M. J. ROBINS, J. R. MCCARTHY, JR., R. A. JONES, and R. MENGEL. Can. J. Chem. **51**, 1313 (1973); (*c*) M. J. ROBINS and R. A. JONES. J. Org. Chem. **39**, 113 (1974); (*d*) M. J. ROBINS, Y. FOURON, and R. MENGEL. J. Org. Chem. **39**, 1564 (1974); (*e*) M. J. ROBINS, R. MENGEL, R. A. JONES, and Y. FOURON. J. Am. Chem. Soc. **98**, 8204 (1976); (*f*) M. J. ROBINS, R. A. JONES, and R. MENGEL, J. Am. Chem. Soc. **98**, 8213 (1976); (*g*) M. J. ROBINS, R. A. JONES, and R. MENGEL. Can. J. Chem. This issue.
6. A. F. RUSSELL, S. GREENBERG, and J. G. MOFFATT. J. Am. Chem. Soc. **95**, 4025 (1973).
7. F. W. LICHTENTHALER, K. KITAHARA, and K. STROBEL. Synthesis, 860 (1974).
8. (*a*) K. ANZAI and M. MATSUI. Agr. Biol. Chem. **37**, 301 (1973); K. ANZAI and M. MATSUI. Bull. Chem. Soc. Jpn. **46**, 3228 (1973); (*b*) P. A. LYON and C. B. REESE. J. Chem. Soc. Perkin Trans. 1, 2645 (1974).
9. W. W. LEE, A. BENITEZ, L. GOODMAN, and B. R. BAKER. J. Am. Chem. Soc. **82**, 2648 (1960).
10. C. A. DEKKER. J. Am. Chem. Soc. **87**, 4027 (1965).
11. Y. FOURON. Ph.D. Dissertation, The University of Alberta, Edmonton, Alta. 1975.
12. T. C. JAIN, A. F. RUSSELL, and J. G. MOFFATT. J. Org. Chem. **38**, 3179 (1973).
13. M. J. ROBINS and W. H. MUHS. J. Chem. Soc. Chem. Commun. 269 (1976).
14. (*a*) J. G. BUCHANAN and A. R. EDGAR. Chem. Commun. 29 (1967); (*b*) R. MENGEL and W. MUHS. Nucleic Acids Res. (Spec. Publ. No. 1), s41 (1975).
15. E. J. REIST, D. F. CALKINS, and L. GOODMAN. J. Org. Chem. **32**, 169 (1967).
16. R. H. HALL. Anal. Biochem. **4**, 395 (1962).
17. J. E. CHRISTENSEN and L. GOODMAN. Carbohydr. Res. **7**, 510 (1968).
18. (*a*) J. ABOLA and M. SUNDARALINGAM. Acta Crystallogr. Sect. B, **29**, 697 (1973); (*b*) P. SINGH and D. J. HODGSON. J. Am. Chem. Soc. **96**, 5276 (1974).
19. R. E. PARKER and N. S. ISAACS. Chem. Rev. **59**, 737 (1959).
20. (*a*) K. L. RINEHART, JR., W. S. CHILTON, M. HICHENS, and W. VON PHILLIPSBORN. J. Am. Chem. Soc. **84**, 3216 (1962); (*b*) R. U. LEMIEUX and D. R. LINEBACK. Ann. Rev. Biochem. **32**, 155 (1963); (*c*) L. B. TOWNSEND. *In* Synthetic procedures in nucleic acid chemistry. Vol. 2. *Edited by* W. W. Zorbach and R. S. Tipson. Wiley–Interscience, New York, N.Y. 1973. pp. 330–331.
21. S. J. SHAW, D. M. DESIDERIO, K. TSUBOYAMA, and J. A. MCCLOSKEY. J. Am. Chem. Soc. **92**, 2510 (1970).
22. L. B. TOWNSEND. *In* Synthetic procedures in nucleic acid chemistry. Vol. 2. *Edited by* W. W. Zorbach and R. S. Tipson. Wiley–Interscience, New York, NY. 1973. pp. 322, 334, 356.
23. M. IKEHARA, Y. NAKAHARA, and S. YAMADA. Chem. Pharm. Bull. **19**, 538 (1971).
24. J. S. DIXON and D. LIPKIN. Anal. Chem. **26**, 1092 (1954).
25. I. SMITH (*Editor*). Chromatographic and electrophoretic techniques. Vol. 1. 3rd ed. Interscience Publishers, New York, NY. 1969. p. 298.
26. E. J. REIST, A. BENITEZ, L. GOODMAN, B. R. BAKER, and W. W. LEE. J. Org. Chem. **27**, 3274 (1962).
27. J. J. BRINK and G. A. LEPAGE. Cancer Res. **24**, 312 (1964); **24**, 1042 (1964).

[6]A concentration of enzyme 300 fold that of the highest range employed in ref. 39 was used.

28. S. S. COHEN. Progr. Nucleic Acid Res. Mol. Biol. **5**, 1 (1966).
29. Parke, Davis and Company, British Patent No. 1,159,290 (1969); Chem. Abstr. **71**, 79757z (1969).
30. (*a*) F. M. SCHABEL, JR. Chemotherapy, **13**, 321 (1968); (*b*) D. PAVAN-LANGSTON, R. A. BUCHANAN, and C. A. ALFORD, JR. (*Editors*). Adenine arabinoside: an antiviral agent. Raven Press, New York, NY. 1975.
31. B. R. BAKER and K. HEWSON. J. Org. Chem. **22**, 966 (1957).
32. D. B. ELLIS and G. A. LEPAGE. Can. J. Biochem. **43**, 617 (1965); D. B. ELLIS and G. A. LEPAGE. Mol. Pharmacol. **1**, 231 (1965).
33. A. BLOCH, M. J. ROBINS, and J. R. MCCARTHY, JR. J. Med. Chem. **10**, 908 (1967).
34. G. A. LEPAGE. Can. J. Biochem. **48**, 75 (1970).
35. J. C. DRACH, J. S. BUS, S. K. SCHULTZ, and J. N. SANDBERG. Biochem. Pharmacol. **23**, 2761 (1974).
36. (*a*) R. BARKER and H. G. FLETCHER, JR. J. Org. Chem. **26**, 4605 (1961); C. P. J. GLAUDEMANS and H. G. FLETCHER, JR. J. Org. Chem. **29**, 3286 (1964); (*b*) E. J. REIST, V. J. BARTUSKA, and L. GOODMAN. J. Org. Chem. **29**, 3725 (1964); (*c*) P. CHANG and B. LYTHGOE. J. Chem. Soc. 1992 (1950).
37. R. MENGEL and H. WIEDNER. Chem. Ber. **109**, 433 (1976); **109**, 1395 (1976).
38. J. N. BROWN and L. M. TREFONAS. Organic Prep. Proced. **2**, 317 (1970).
39. M. J. ROBINS and G. L. BASOM. Can. J. Chem. **51**, 3161 (1973).

Formation of ketenes from carboxylic acids in strong acids. Intermediacy of ketenes in the acid-catalyzed α-chlorination of carboxylic acids[1]

YOSHIRO OGATA, TAIRA HARADA, AND TOSHIYUKI SUGIMOTO

Department of Applied Chemistry, Faculty of Engineering, Nagoya University, Chikusa-ku, Nagoya, Japan

Received August 31, 1976

YOSHIRO OGATA, TAIRA HARADA, and TOSHIYUKI SUGIMOTO. Can. J. Chem. **55**, 1268 (1977).

Evidence (chemical trapping by aniline, and nmr and laser–Raman spectroscopy) is presented for the presence of ketenes in heated solutions of carboxylic acids in fuming H_2SO_4. The intermediacy of ketenes in α-chlorination catalyzed by strong acids is suggested.

YOSHIRO OGATA, TAIRA HARADA et TOSHIYUKI SUGIMOTO. Can. J. Chem. **55**, 1268 (1977).

On présente quelques résultats (piégeage chimique par l'aniline et spectres Raman–laser et rmn) indiquant la présence de cétènes dans des solutions d'acides carboxyliques chauffés en présence d'acide sulfurique fumant. On suggère que des cétènes sont présents sous forme d'intermédiaire lors de la chloration-α catalysée par des acides forts.

[Traduit par le journal]

The α-halogenation of ketones and aldehydes, and probably acid halides, is said to proceed through the corresponding enols. The present authors recently reported a novel method for α-chlorination of aliphatic acids in the presence of molecular oxygen, chlorosulfonic acid, and chloranil which may also proceed via enolized acids (1, 2). The enols of acids $RCH{=}C(OH)_2$ when dehydrated, may produce ketenes which may then participate in this halogenation (3, 4). Little *et al.* (3) suggested two mechanisms for the PCl_3-catalyzed α-chlorination of cyclohexanecarboxylic acid, one involving enolization of the acid chloride followed by rate-determining addition of chlorine and the other involving ketenes, but no evidence for either suggestion has been presented.

The present authors have studied the behavior of fatty acids in fuming H_2SO_4 and wish to report evidence that ketenes may be involved in the acid-catalyzed chlorination. The behavior of carboxylic acids in these strong acids has been studied earlier (5–9); in particular, Deno *et al.* used nmr spectroscopy to observe protonated carboxylic acids and acyl cations, the latter being predominant in solutions containing more than 20% SO_3 in H_2SO_4 (8*a*). They also predicted an equilibrium formation of ketenes from acyl

[1] $$RCH_2CO_2H + H^+ \rightleftharpoons RCH_2\overset{+}{C}(OH)_2 \rightleftharpoons RCH_2\overset{+}{C}O + H_2O$$

[2] $$RCH_2\overset{+}{C}O \rightleftharpoons RCH{=}C{=}O + \overset{+}{H}$$

cations. Recently, Deno and Friedman[2] found evidence in favor of the presence of ketenes: (*a*) a decrease of the nmr band (3.29 δ), characteristic of CH_3CO^+, on the addition of D_2SO_4, which suggests the conversion:

$$CH_3CO^+ \overset{-H^+}{\rightleftharpoons} CH_2{=}C{=}O \overset{D^+}{\rightleftharpoons} CH_2D\overset{+}{C}O$$

(*b*) similar nmr observation of H–D exchange at the α-CH_2 of $CH_3CH_2CO^+$ but no exchange at the β-CH_3, (*c*) H–D exchange at the C-4 methyl, but no exchange at C-2 and C-3 of the crotonyl cation, suggesting 4-proton elimination:

$$CH_3CH{=}CH{-}\overset{+}{C}O \overset{-H^+}{\rightleftharpoons} CH_2{=}CH{-}CH{=}C{=}O$$

(*d*) the same nmr spectrum was obtained for both *cis*- and *trans*-crotonic acid dissolved in fuming H_2SO_4, suggesting the presence of $CH_2{=}CH{-}CH{=}C{=}O$.

Discussion of Results

The present authors wished to confirm the presence of ketenes from carboxylic acids in strong acid media by way of (*i*) the trap of a ketene by aniline, (*ii*) nmr spectroscopy, and (*iii*) laser–Raman spectroscopy.

(*i*) A mixture of fuming H_2SO_4 and acetic acid was heated at 80°C and the vapor was introduced into aniline with N_2 under reduced pressure as a

[1]Contribution No. 226 from the Department of Applied Chemistry, Faculty of Engineering, Nagoya University.

[2]N. C. Deno and N. Friedman, personal communication.

carrier. Product analysis by glc indicated the presence of acetanilide, whereas a mixture of acetic acid and aniline gave no acetanilide in these conditions even in the presence of a catalytic amount of fuming H_2SO_4. This confirms the formation of ketene which acetylates aniline (10). The possibility of participation of acetic anhydride in this acetylation (11) was also ruled out by the following results. (*a*) The nmr spectrum of a mixture of acetic acid and fuming H_2SO_4 after heating at 80°C showed no peaks due to the acetic anhydride or protonated acetic anhydride, but only a singlet at 3.93 δ due to the acyl cation, $CH_3—\overset{+}{C}=O$ (8), in agreement with the reported chemical shift. (*b*) Vapors from a heated mixture of acetic anhydride and fuming H_2SO_4 were passed, using N_2, into aniline, but no acetanilide was detected. The observed low yield of acetanilide could be ascribed to the unfavorable equilibrium for formation of ketene (reaction 2) in this system and presumably to side reactions of the ketene produced in hot fuming H_2SO_4. Ketene has been reported to react with sulfuric acid to give acetylsulfoacetic acid as a red viscous oil (12).

$$H_2SO_4 + 2CH_2=C=O \rightarrow CH_3CO_2SO_2CH_2CO_2H$$

Indeed, the nmr spectrum of the red viscous oil which was obtained as a residue after heating acetic acid in fuming H_2SO_4 showed only two singlets at 4.41 (2H) and 2.63 δ (3H); this implies the formation of acetylsulfoacetic acid as a side product. Attempts to collect ketene vapor in a cold trap were unsuccessful, probably because ketene itself has a very low boiling point (−56°C), so that most would be expelled by carrier N_2, even with cooling. The authors also attempted to trap dimethylketene, assuming its formation from isobutyric acid in fuming H_2SO_4 by an analogous method, but the isolation of acetylated product, $PhNH—CO—CH(CH_3)_2$, was unsuccessful, probably because of the higher boiling point (34°C) and the higher solubility of dimethylketene in fuming H_2SO_4 compared with that of ketene itself.

(*ii*) The details of the nmr spectrum of a mixture of isobutyric acid and fuming H_2SO_4 (50% SO_3) are as follows: δ 1.92 (d, J = 7.1 Hz, 6H), 4.20 (septet, J = 7.1 Hz, 1H), 1.67 (s, ~1H), 1.80 (s, ~1H), and 3.90 (s, ~1H). The septet centered at 4.20 δ and the doublet centered at 1.92 δ were assigned to α-H and β-H of the acyl cation **1**, respectively. Deno reported that isobutyric acid was completely converted to the corresponding acyl cation **1** in 50% SO_3 in H_2SO_4 and that chemical shifts of α-H and β-H for the acyl cation are 4.23 (septet, J = 7.0 Hz) and 1.90 δ (d, J = 7.1 Hz), respectively (8), which agrees with our results.

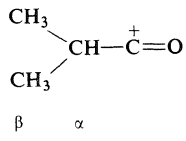

1

It is known that ketoketenes $R_2C=C=O$ dimerize to cyclobutane-type dimers (13). The observed two weak singlets at 1.67 and 1.80 δ suggest the presence of a dimer of the type 2,2,4,4-tetramethyl-1,3-butanedione (**2**). The nmr shift of **2** in $CDCl_3$ was reported to be 1.29 δ because of the oscillation of the flexible four-membered ring between **2***a* and **2***b* (15). The dimer,

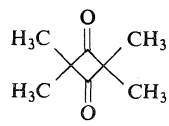

2

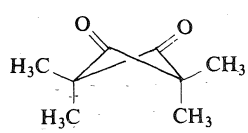

2*a*

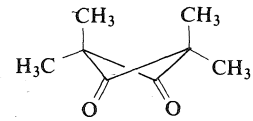

2*b*

prepared in our hands (14), gave the same peaks at 1.83 and 1.68 δ in fuming H_2SO_4, but gave only one peak at 1.80 δ in 95% H_2SO_4 as shown in Table 1. This value (1.83 δ), which is larger than 1.30, implies *O*-protonation in strong acid, because a similar phenomenon was observed in simple ketones; *e.g.*, the peak due to the methyl protons of acetone in SbF_5/HSO_3F appears at 3.25 δ which is considerably deshielded (*ca.* 1.2 δ) compared with that in ordinary organic solvents (16). The peak at 1.68 δ may be caused by an unknown product derived from the dimer **2**.

The nmr peak at 3.90 δ is ascribed to the dimethylketene monomer or its derivative on the basis of the following. On introduction of dimethylketene, prepared by an alternative method (17), to fuming H_2SO_4 at room temperature the nmr spectrum of the resulting solution exhibited the 3.90 δ peak: δ 3.90 (sharp s), 4.00 (br s), and

TABLE 1. The nmr spectrum of a solution of 2,2,4,4-tetramethyl-1,3-butanedione (**2**) in 95% H_2SO_4 or fuming H_2SO_4

Solvent system		
SO_3 (%)	H_2SO_4 (%)	Spectral data
30	70	1.83(s), 1.68(s)*
15	85	1.83(s), 1.67(s)
10	90	1.82(s), 1.65(s)
7	93	1.78(s), 3.26(septet, J=7 Hz, 1H), 1.30(d, J=7 Hz, 6H)
—	95†	1.80(s), 3.36(septet, J=7 Hz, 1H), 1.31(d, J=7 Hz, 6H)

*The peak at 1.68 δ increased in size when the solution was heated at 110°C for 10 min, and other weak peaks appeared at 5.47, 4.81, and 4.00 δ.
†5% H_2O.

5.10 (br s). The dimer **2** can decompose on heating to its monomer, $(CH_3)_2C{=}C{=}O$ (18). The solution of isobutyric acid in fuming H_2SO_4 was heated to 50°C for 30 min as in the chlorination system (2), and the observed nmr shifts are as follows: δ 1.62 (weak s), 1.74 (weak s), 3.90 (sharp s, 1.5H), 4.00 (br s, 2H), 4.85 (br s, 3H), 5.45 (br s, 2H). This shows that the peaks due to the acyl cation **1** have disappeared, while the two weak singlets at 1.62 and 1.74 δ still remained, suggesting the presence of dimer **2**. The peaks at

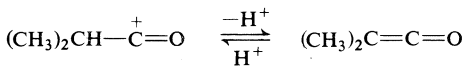

1

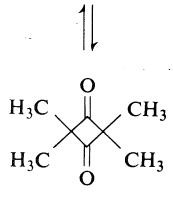

2

5.45, 4.85, and 4.00 δ for isobutyric acid in heated fuming H_2SO_4 cannot be assigned, but they suggest the presence of unknown products from dimer **2** in fuming H_2SO_4, since similar peaks of 5.47, 4.81, and 4.00 δ were also observed in a heated solution of dimer **2** in fuming H_2SO_4.

(*iii*) The laser–Raman spectrum of isobutyric acid in fuming H_2SO_4 (molar ratio 1:5.7) which had been heated at 50°C for 10 min had a sharp and strong band at 2160 cm^{-1} and this band was assigned to the asymmetric C=C=O stretch, since liquid samples of ketenes have generally a band at 2116 cm^{-1} (19). It was confirmed that other major bands (Fig. 1) were due to fuming H_2SO_4 by direct comparison with an authentic sample. The sample which gave the Raman band at 2160 cm^{-1} gave no nmr peaks corresponding to acyl cation **1**, but only the peaks corresponding to ketene monomer and its dimer and the above-mentioned peaks at 5.45, 4.85, and 4.00 δ. Hence this band cannot be assigned to the acyl cation.

It is concluded from these results that ketene may be formed according to reactions 1 and 2 in our reaction conditions. The authors have previously reported that fuming H_2SO_4-catalyzed chlorination of isovaleric acid by molecular chlorine gave the corresponding α-chlorination (20). Therefore, the authors suggest that α-chlorination of a carboxylic acid may proceed via the corresponding ketenes, since the enol, *i.e.* ketene hydrated at C=O, seems to be more unstable in fuming H_2SO_4 and hence is present, if at all, at a lower concentration. Indeed, reaction of ketene with molecular chlorine has been reported to give α-chlorinated acetyl chloride (21).

Experimental

General

Glacial acetic acid (bp 47°C/48 torr), isobutyric acid (bp 70–72°C/29 torr), acetic anhydride (bp 138–139°C), and aniline (bp 86–87°C/20 torr) were commercial reagents and were distilled before use. 2,2,4,4-Tetramethyl-1,3-butanedione (**2**) was prepared according to the literature (15), mp 114–116°C (lit. (15) mp 115–116°C). Commercially available (1st grade) fuming sulfuric acid (50% SO_3) was used without further purification.

Nuclear magnetic resonance spectra were measured on a 60 MHz JEOL C 60 HL nmr spectrometer at 25°C using capillary benzene as an external standard and a 60 MHz Hitachi R-24B nmr spectrometer at 35°C using TMS in $CHCl_3$ as an external standard. Chemical shifts (δ) are expressed in ppm.

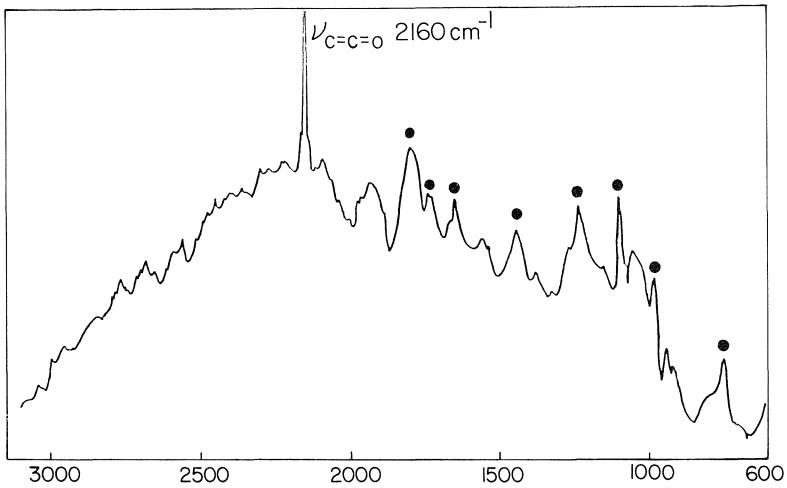

FIG. 1. The Raman spectrum, at room temperature, of the 3200–600 cm^{-1} region of dimethylketene produced from the isobutyric acid – fuming H_2SO_4 system. It was confirmed that marked (●) bands were due to fuming H_2SO_4 by direct comparison with an authentic sample.

The laser–Raman spectra were measured at room temperature by a JASCO R-300 laser–Raman spectrophotometer with an argon ion model 251 CW laser source. The 5145 Å exciting line was used for the 4000–600 cm^{-1} spectral region.

Analysis of reaction products was done on a Yanagimoto model GCG 550 gas chromatograph employing a flame ionization detector. The columns were a 1.3 m × 3 mm copper column packed with PEG 20 M 10% on Chromosorb W, 60–80 mesh, and a 1.5 m × 3 mm copper column packed with Apiezon grease L 15% on Celite 545, 80–100 mesh. The glc analysis conditions were as follows: N_2 flow rate was 30 ml/min and the temperature programmed at 8°C/min from 50–240°C.

Trapping of Ketene with Aniline

To stirred and cooled (0°C) glacial acetic acid (14.8 g, 0.25 mol) was added 2.0 g of fuming H_2SO_4 (50% SO_3) dropwise over a 0.5 h period. Stirring at 0°C was continued for additional 1 h. Immediately after warming to room temperature over a 0.5 h period, the system was evacuated (*ca.* 250 torr) and the temperature of the mixture rose slowly to 80°C. Dry nitrogen was bubbled gradually into this flask and then into aniline (23.0 g, 0.25 mol); after 5 h, the procedure was stopped. The resulting aniline solution was then analyzed by glc on the above mentioned two columns; the peak due to the acetanilide produced was identified by comparison with an authentic sample and the yield (*ca.* 2.3% based on acetic acid) was determined by the internal standard method. The reaction of aniline (8.0 g, 0.086 mol) with glacial acetic acid (0.32 g, 0.005 mol) was attempted for 6 h with magnetic stirring at room temperature and the solution obtained was analyzed by glc on a column packed with PEG 20M; no peak due to acetanilide was found. A similar result was obtained even on addition of a few drops of fuming sulfuric acid to the aniline – acetic acid mixture. Attempts to acetylate aniline with acetic anhydride were carried out as follows. Acetic anhydride (3.8 g, 0.037 mol) was added dropwise to cooled (0°C) fuming H_2SO_4 (14.0 g). The system was evacuated (*ca.* 250 torr) and allowed to warm to 80°C. The N_2 was bubbled gradually to this system and thence into aniline (20.0 g, 0.125 mol) for 5 h. No acetanilide was detected by glc analysis of the resulting aniline solution.

Acknowledgment

The authors wish to thank Mitsubishi Kasei Co. and Toagosei Co. for their gifts of materials and to M. Inaishi for his aid in experiments.

1. Y. OGATA and K. MATSUYAMA. Tetrahedron, **26**, 5929 (1970).
2. Y. OGATA, T. HARADA, K. MATSUYAMA, and T. IKEJIRI. J. Org. Chem. **40**, 2960 (1975).
3. J. C. LITTLE, A. R. SEXTON, Y. L. CHANG TONG, and T. E. ZURAWIC. J. Am. Chem. Soc. **91**, 7098 (1969).
4. (*a*) C. C. PRICE, C. D. BEARD, and K. AKUNE. J. Am. Chem. Soc. **92**, 5916 (1970); (*b*) C. C. PRICE and C. D. BEARD. J. Am. Chem. Soc. **92**, 5921 (1970).
5. J. T. EDWARD and I. C. WANG. Can. J. Chem. **40**, 966 (1962).
6. R. STEWART and K. YATES. J. Am. Chem. Soc. **82**, 4059 (1960).
7. H. HOSOYA and S. NAGAKURA. Spectrochim. Acta, **17**, 324 (1961).
8. (*a*) N. C. DENO, C. U. PITTMAN, JR., and M. J. WISOTSKY. J. Am. Chem. Soc. **86**, 4370 (1964); (*b*) N. FRIEDMAN. Ph.D. Thesis, Pennsylvania State University, University Park, PA. 1965.
9. G. A. OLAH and A. M. WHITE. J. Am. Chem. Soc. **89**, 3591 (1967).
10. R. N. LACEY. Adv. Org. Chem. **2**, 213 (1960).
11. J. MARCH. Advanced organic chemistry: reactions,

mechanisms, and structure. McGraw-Hill, New York, NY. 1968. p. 336.
12. T. F. DOUMANI and J. E. CUNEO. U.S. Patent No. 2,411,823 (1946); Chem. Abstr. **41**, 1234d (1947).
13. R. ADAMS, W. E. BACHMANN, J. R. JOHNSON, L. F. FIESER, and H. R. SNYDER. Organic reactions. Vol. 3. Wiley, New York, NY. 1946. p. 127.
14. L. L. MILLER and J. R. JOHNSON. J. Org. Chem. **1**, 135 (1936).
15. C. Y. CHEN and R. J. W. LEFÈVRE. Aust. J. Chem. **18**, 1293 (1965).
16. T. BIRCHALL and R. J. GILLESPIE. Can. J. Chem. **43**, 1045 (1965).
17. C. W. SMITH and D. G. NORTON. Organic syntheses. Coll. Vol. IV. Wiley, New York, NY. 1963. p. 348.
18. H. STAUDINGER, F. FELIX, P. MEYER, H. HARDER, and E. STIRNEMANN. Helv. Chim. Acta, **8**, 322 (1925).
19. F. R. DOLLISH, W. G. FATELEY, and F. F. BENTLEY. Characteristic Raman frequencies of organic compounds. Wiley, New York, NY. 1974. p. 144.
20. Y. OGATA and T. IKEJIRI. Nippon Kagaku Kaishi, 1517 (1975).
21. F. B. ERICKSON and E. J. PRILL. J. Org. Chem. **23**, 141 (1958).

Studies on thermodynamics of solution by gas chromatography: solubility measurements of hydrocarbons in cycloalkanols

RAKESH K. KUCHHAL, KANAI L. MALLIK,[1] AND PYARE L. GUPTA[2]

Indian Institute of Petroleum, Dehradun-248005, India

Received July 6, 1976

RAKESH K. KUCHHAL, KANAI L. MALLIK, and PYARE L. GUPTA. Can. J. Chem. **55**, 1273 (1977).

Activity coefficients at infinite dilution have been determined by gas–liquid chromatography for nine hydrocarbons solutes in cyclopentanol, cyclohexanol, cycloheptanol, benzyl alcohol, and *n*-heptanol at 25 °C. Experimental results for cyclopentane and cyclohexane in cycloalkanols compare favourably with the values obtained by extrapolation to infinite dilution of activity coefficient data calculated from Benson *et al.*'s static (vapour–liquid equilibrium) measurements. Some characteristics of the solute–solvent interaction in the systems are discussed in light of statistical approaches (thermal and athermal contributions).

RAKESH K. KUCHHAL, KANAI L. MALLIK et PYARE L. GUPTA. Can. J. Chem. **55**, 1273 (1977).

On a déterminé les coefficients d'activité à dilution infinie en faisant appel à la chromatographie gaz–liquide; ces mesures ont été faites pour neuf hydrocarbures en solution dans le cyclopentanol, le cyclohexanol, le cycloheptanol, l'alcool benzylique et le *n*-heptanol à 25 °C. Les résultats expérimentaux obtenus pour le cyclopentane et le cyclohexane dans les cycloalkanols se comparent avantageusement avec les valeurs obtenues par extrapolation à dilution infinie de coefficients d'activité calculés à partir des mesures statiques (équilibre liquide–vapeur) effectuées par Benson et ses collaborateurs. On discute, à la lumière d'approches statistiques (contributions thermiques et athermiques), de quelques caractéristiques de l'interaction soluté–solvant dans les systèmes.

[Traduit par le journal]

Introduction

Studies on thermodynamics of solution comprising alcohol–hydrocarbon systems have been undertaken by several investigators during the last twenty-five years (1–7). Most of the studies in this field were devoted to aliphatic/aromatic alcohol–hydrocarbon mixtures, and little information is available for cycloalkanol–hydrocarbon systems (8) and there remains a paucity of thermodynamic data in this area. Such thermodynamic data are of considerable importance as they can indicate the potential use of the certain solvents as extraction agents. It is worth mentioning that use of cyclohexanol has already been reported as an extraction solvent for the recovery of cyclohexane from benzene-rich petroleum fractions (9).

The gas chromatographic (GC) technique has been well established as an advantageous method for determination of the thermodynamic properties at infinite dilution for binary non-electrolyte solutions (10–13). Such thermodynamic data may be conveniently determined by using a conventional GC equipment, employing cycloalkanols or other alcohols as the stationary phase. In the present paper, attempts have been made to study activity coefficients at infinite dilution for nine hydrocarbons in three cycloalkanols (cyclopentanol, cyclohexanol, and cycloheptanol) and two other aliphatic and aromatic alcohols, namely, *n*-heptyl and benzyl alcohols at 25 °C.

Experimental Section

The gas chromatographic apparatus and experimental procedure used for determining solute specific retention volumes have been reported in an earlier communication (11). Stationary phases (solvent components) (five solvents) obtained either from Fluka (Germany) or BDH (England): cyclopentanol, cyclohexanol, cycloheptanol, *n*-heptyl alcohol, and benzyl alcohol were used without any further treatment. The physical properties of the solvents (mostly literature values) are shown in Table 1. Approximately 25–30% coating on Chromosorb P (60–80 mesh size) were used for the present studies. To eliminate the problem of solvent depletion, caution was taken to connect a precolumn (about 20 cm in length and 3 mm in diameter) packed with about 35% of the desired solvent-coated support material with the

[1]Present Address: Research and Development Centre, Indian Oil Corporation, Sector-13, Faridabad-121002, Haryana.

[2]To whom correspondence should be addressed.

TABLE 1. Selected physical properties of solvents studied

Compound	Molecular weight	Boiling point at 760 mm (°C)	Refractive index n_D^{20}	Density d_4^{25} (ml/g)	Vapour pressure at 25 °C in mm
Cyclopentanol	86.14	140.83	1.4530	0.9430	2.20
Cyclohexanol	100.16	161.1	1.4641	0.9454	<1
Cycloheptanol	114.19	185.0	1.4705	0.9589	<1
n-Heptanol	116.20	176.0	1.4225	0.8186	<1
Benzyl alcohol	108.13	205.10	1.5404	1.0416	<1

main column. The carrier gas (H_2) was thus saturated with solvent prior to the point of injection. As in earlier cases (11, 12), satisfactory functioning of the presaturator column was observed in the present studies. The temperature of the column oven was maintained at 25 °C with variation of 0.1 °C as checked with an ASTM thermometer periodically.

Results

Solute activity coefficients at infinite dilution in the liquid phase ($\gamma_{2,p}^{\infty}$) were determined from the expression (14),

$$[1] \qquad \gamma_{2,p}^{\infty} = \frac{1.704 \times 10^7}{M p_0 V_g^0}$$

where $\gamma_{2,p}$ = activity coefficient for solute, M = solvent molecular weight, p_0 = vapour pressure of the pure saturated solute vapour in torr, and V_g^0 = specific retention volume of solute in ml, of carrier gas per gram of liquid in ml. This equation was discussed in detail elsewhere (11). The vapour pressures were calculated from the Antoine equation using the constants as reported in Dreisbach compilation (15).

Activity coefficients corrected for vapour phase nonideality ($\gamma_{2,f}^{\infty}$), is given by (16)

$$[2] \quad \ln \gamma_{2,f}^{\infty} = \ln \gamma_{2,p}^{\infty} + \frac{(V_2 - \beta_{22})(p_0 - p_1)}{RT} + \frac{\beta_{22}^2(p_0^2 - p_1^2)}{(RT)^2}$$

where $\gamma_{2,f}$ = activity coefficient corrected for vapour phase imperfection, superscript ∞ denotes infinite dilution, V_2 = molar volume of solute in ml, β_{22} = second virial coefficient for pure solute, 2, at temperature T in cm^3 mol^{-1}, p_0 = vapour pressure of pure solute in torr, p_1 = vapour pressure of pure solvent, in torr (negligible at operating temperature (Table 1)). Furthermore the last term of eq. 2 can be ignored as β_{22}^2 makes an insignificant contribution. The virial coefficients were computed from the modified corresponding states equation of McGlashan and co-workers (17, 18).

$$[3] \quad \frac{\beta_{22}}{V_c} = 0.430 - 0.886\left(\frac{T_c}{T}\right) - 0.694\left(\frac{T_c}{T}\right)^2 - 0.0375(n-1)\left(\frac{T_c}{T}\right)^{4.5}$$

where V_c and T_c are the critical volume and critical temperature of solute, n the effective carbon number of the solute. V_c and T_c data are obtained from Dreishbach's compilation (15).

Discussion

When used as stationary phases, all the five solvents could resolve the lower hydrocarbon mixture in a relatively short time. The chromatogram of all these compounds showed symmetrical peaks useful for analytical purposes.

The validity of any data under the equilibrium conditions can be substantiated by comparison with existing results in the literature but no direct data for comparison from GC or from conventional classical techniques, are available for these solvents. However, it was considered worthwhile to compare our results with the extrapolated values of activity coefficients obtained from the vapour liquid equilibrium data reported by Benson *et al.* (8, 19). Activity coefficients at finite concentrations were calculated from vapour–liquid equilibrium data, using the well known expression

$$[4] \qquad \gamma_{2,p} = \frac{y_2 P}{x_2 p_0}$$

where y_2 = mole fraction of solute in vapour phase, x_2 = mole fraction of solute in liquid phase, P = total vapour pressure in torr. The $\gamma_{2,p}^{\infty}$ values thus obtained were found to be in fair agreement as is evident from Table 2. Chevalley (20) also reported activity coeffi-

TABLE 2. Comparison of activity coefficients data at 25 °C

Solute	Solvent	GC value: Present work	GC value: Calculated from data of Benson *et al.* data (8, 19)
Cyclohexane	Cyclopentanol	4.15	4.11
Cyclohexane	Cyclohexanol	3.51	3.63
Cyclopentane	Cyclopentanol	4.00	3.73
Cyclopentane	Cyclohexanol	3.30	3.16

TABLE 3. Activity coefficients at infinite dilution for hydrocarbons at 25 °C

Solute	Cyclopentanol		Cyclohexanol		Cycloheptanol		*n*-Heptanol		Benzyl alcohol	
	$\gamma_{2,p}^{\infty}$	$\gamma_{2,f}^{\infty}$	$\gamma_{2,p}^{\infty}$	$\gamma_{2,f}^{\infty}$	$\gamma_{2,p}^{\infty}$	$\gamma_{2,f}^{\infty}$	$\gamma_{2,p}^{\infty}$	$\gamma_{2,f}^{\infty}$	$\gamma_{2,p}^{\infty}$	$\gamma_{2,f}^{\infty}$
Propane	4.20	4.66	4.10	4.56	3.70	4.12	2.25	2.50	7.21	8.02
Isobutane	5.05	5.44	4.81	5.20	4.53	4.89	2.71	2.93	10.24	11.07
n-Butane	5.00	5.30	4.55	4.83	4.31	4.57	2.51	2.67	9.00	9.55
n-Pentane	5.78	5.95	5.29	5.45	4.77	4.91	2.82	2.90	11.20	11.53
n-Hexane	6.50	6.58	6.14	6.22	5.13	5.20	3.06	3.10	13.30	13.46
Cyclopentane	4.00	4.08	3.30	3.37	2.87	2.93	2.18	2.22	5.76	5.88
Methyl cyclopentane	4.40	4.45	3.80	3.85	3.33	3.37	2.54	2.57	7.96	8.05
Cyclohexane	4.15	4.19	3.51	3.55	3.12	3.15	2.47	2.50	7.64	7.72
Benzene	2.96	2.99	2.78	2.80	2.56	2.58	2.10	2.12	2.35	2.37

cients at finite concentration for the cyclohexane–cyclohexanol system in the temperature range of 35–55 °C. By extrapolating their values to 25 °C, the $\gamma_{2,p}^{\infty}$ value comes out to be 3.7, which compares favourably to our experimental data of 3.51. Similarly, our GC data on benzene–*n*-heptyl alcohol system also show the same consistent trend in $\gamma_{2,p}^{\infty}$ values when compared with the extrapolated data of Wehe and Coates (21) for the benzene–*n*-alcohol systems at their boiling points. Thus, the activity coefficient of benzene in methanol system was found to be 13.26, benzene–ethanol 10.48, and benzene–*n*-butanol 3.84 as compared to our datum, 2.12 in benzene–*n*-heptanol.

Table 3 lists the activity coefficients at infinite dilution for nine hydrocarbons at 25 °C. Data reported here are the mean of at least three experimental runs. The reproducibility of $\gamma_{2,p}^{\infty}$ was found to be within 2–3%. The data indicate that all the compounds studied exhibit a marked positive deviation from Raoult's law. Interestingly, $\gamma_{2,f}^{\infty}$ values of saturated hydrocarbons in cycloalkanols lie in between those of benzyl alcohol and *n*-heptanol. The activity coefficient is related to the excess partial molar free energy $\Delta\bar{g}_e^{\infty}$ by the well known relation

$$[5] \qquad \Delta\bar{g}_e^{\infty} = RT \ln \gamma_{2,f}^{\infty}$$

As $\Delta\bar{g}_e^{\infty}$ is exponentially related to the activity coefficient, the trends observed in Table 3 are somewhat normalized in Fig. 1 showing an incremental relationship between free energy and molecular structure for hydrocarbon solutes at 25 °C. It is evident from Table 3 that $\gamma_{2,f}^{\infty}$ values in all the cycloalkanols are larger for the *n*-alkanes than for the aromatic hydrocarbon solute which can be best explained on the basis of their respective cohesive energy densities (22, 23). Another interesting aspect of the data is that the activity coefficients at infinite dilution of all the solutes are decreasing numerically from cyclopentanol to cycloheptanol (and as a matter of fact in *n*-heptanol also), indicating the decrease in polarity of the solvent. Comparing the $\gamma_{2,f}^{\infty}$ data for cyclohexane and benzene in any one of the alcohols, it is evident that nonideality is less in the case of benzene solution. Depending upon environments, hydroxyl group can act both as proton donor or acceptor. It is usually observed that the proton accepting ability of hydroxyl group is very strong (24), but in the vicinity of benzene

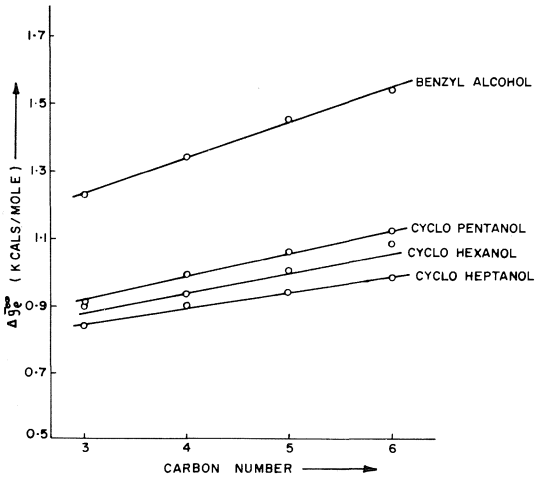

FIG. 1. Incremental relation between excess free energy and molecular structure for *n*-paraffins in monohydroxy solvents.

molecule it acts as a proton donor as benzene may act here as proton acceptor (25), causing C—OH- - -π interaction. Interestingly, $\gamma_{2,f}^{\infty}$ for benzene in benzyl alcohol is found to be lower than that in cycloalkanols, whereas for other hydrocarbon solutes it is always higher in benzyl alcohol. This observation is in accordance with the theoretical consideration for π-bond interactions.

Experimental determination of thermodynamic parameters serves as an important check on the various theories. The GC technique, which provides a rapid and convenient means to determine thermodynamic parameter, has also now been widely used (26) in testing the solution theories, particularly in very low concentration region where other methods like vapour pressure measurements (27, 28) or sensitive microbalance techniques (16) are least accurate. A number of theories have been put forward to predict the solution behaviour. Some of them are quite elaborate and require detailed information about the physical properties of solute and solvent molecules. Based on quasi-lattice theory, Everett and co-workers (29, 30) have explained the deviation from Raoult's law as due to combination of two completely independent factors, namely disparity in molecular size of solute and solvent (combinatorial or configurational term or the athermal part) and secondly, due to difference in intermolecular forces (the thermal part).

$$[6] \quad \ln \gamma_{2,f}^{\infty} = \ln \gamma_2^{\infty,\text{config}} + \ln \gamma_2^{\infty,\text{therm}}$$

The configurational term can be calculated from the Flory–Huggins equation (derived from a lattice model)

$$[7] \quad \ln \gamma_2^{\infty,\text{config}} = \ln \frac{1}{r} + \left(1 - \frac{1}{r}\right)$$

where r is taken as the ratio of the molar volume of the solvent to that of the solute V_1/V_2. Values for $\ln \gamma_2^{\infty,\text{config}}$ calculated to 25 °C are tabulated in Table 4.

According to the Flory–Huggins theory, the thermal term, $\ln \gamma_2^{\infty,\text{therm}}$ is directly related to the interaction parameter which is strictly a free energy term (30, 31)

$$[8] \quad \ln \gamma_2^{\infty,\text{therm}} = \chi \phi_1^2$$

where χ = interaction parameter; at infinite dilution, $\phi_1 = 1$, where ϕ_1 represents volume fraction of solvent.

By subtracting the thermal contribution, $\ln \gamma_2^{\infty,\text{config}}$, given in Table 4 from the logarithm of the experimental activity coefficient, the interaction parameters at 25 °C can be determined and are also presented in Table 4. The combinatorial part, as expected, indicates negative contribution to solution non-ideality. The data further show that the interaction parameter is positive for all the systems studied indicating that overall interchange free energies are positive. Two features of the interaction parameter data are worth mentioning. χ is increasing uniformly for *n*-paraffins in a particular solvent which means that as the number of contact sites or segments increase in a system the interaction parameter also increases thus providing that either the contact point lattice model (32) or the Barkers' model (33) can explain the phenomenon. The other interesting point to note is that for a particular solute the interaction parameter decreases with increase in molecular weight of the cycloalkanol solvent, which is a little difficult to explain with the experimental data available at the moment. It is likely that with increase in the molecular weight, some of the contact points may not be fully accessible for interaction.

Based on an earlier statistical approach of Longuet-Higgins (34), Martire *et al.* (35) have proposed that the interaction parameter χ can be obtained from the perturbation treatment, where the difference in intermolecular attrac-

tions between two solutes, a reference and a perturbed one in a solvent at infinite dilution, is given by the expression

$$[9] \quad \chi = \chi' = \frac{V_2'}{RT}\left[\frac{E_1}{V_1} - \frac{E_2'}{V_2'}\right]\left[\frac{T_{c,2}}{T_{c,2}'} - 1\right]$$

where V = molar volume in ml, E = molar intermolecular cohesive energy, R = gas constant, subscripts 1 and 2 refer to solvent and solute, respectively, and primed and unprimed terms represent the reference and perturbed state, respectively. This model was suggested on the assumption that the two solute states, the reference and the perturbed ones, differ only in intermolecular attractions between primed solute–solvent and unprimed solute–solvent molecules. It is evident that the interaction parameter for a series of solutes in a given solvent at a particular temperature should show a linear relationship with the solute critical temperature, $T_{c,2}$ or with potential well depth for the bigger molecules. Figure 2 demonstrates the linearity between χ values for our systems *vs.* the critical temperature of the solutes studied indicating that this model can also work for such systems.

Another simpler approach, Regular solution model, based on the cohesive energy density

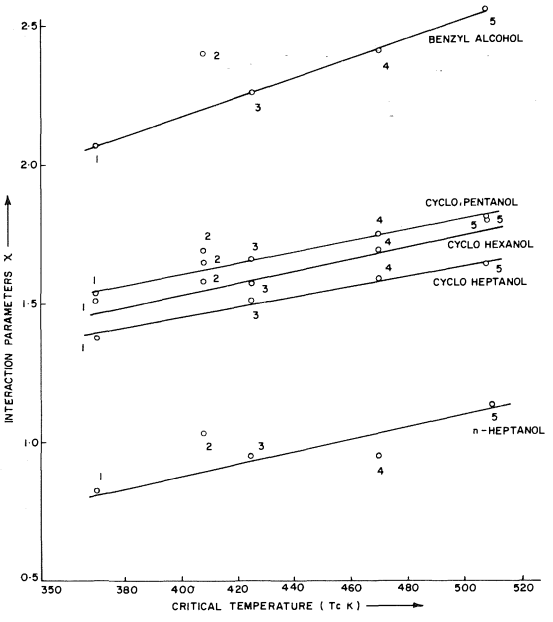

FIG. 2. Interaction parameters *vs.* critical temperature of solutes: *1*, propane; *2*, isobutane; *3*, *n*-butane; *4*, *n*-pentane; *5*, *n*-hexane.

TABLE 4. Combinatorial and thermal contributions to activity coefficients at 25 °C

Solute	Cyclopentanol		Cyclohexanol		Cycloheptanol		*n*-Heptanol		Benzyl alcohol	
	$-\ln \gamma_2^{\infty,\text{config}}$	$\ln \gamma_2^{\infty,\text{therm}}$	$-\ln \gamma_2^{\infty,\text{config}}$	$\ln \gamma_2^{\infty,\text{therm}}$	$-\ln \gamma_2^{\infty,\text{config}}$	$\ln \gamma_2^{\infty,\text{therm}}$	$-\ln \gamma_2^{\infty,\text{config}}$	$\ln \gamma_2^{\infty,\text{therm}}$	$-\ln \gamma_2^{\infty,\text{config}}$	$\ln \gamma_2^{\infty,\text{therm}}$
Propane	0.000	1.54	0.014	1.51	0.035	1.38	0.092	0.82	0.011	2.07
Isobutane	0.002	1.69	0.000	1.65	0.007	1.58	0.040	1.03	0.000	2.40
n-Butane	0.006	1.66	0.001	1.57	0.012	1.51	0.051	0.95	0.000	2.26
n-Pentane	0.031	1.75	0.005	1.69	0.000	1.59	0.019	0.95	0.006	2.41
n-Hexane	0.076	1.81	0.026	1.80	0.005	1.64	0.003	1.13	0.030	2.56
Cyclopentane	0.001	1.41	0.006	1.21	0.024	1.05	0.072	0.73	0.004	1.77
Methyl cyclopentane	0.025	1.47	0.002	1.35	0.001	1.21	0.024	0.92	0.004	2.08
Cyclohexane	0.016	1.42	0.000	1.27	0.004	1.14	0.033	0.88	0.000	2.05
Benzene	0.000	1.10	0.014	1.03	0.035	0.91	0.092	0.66	0.011	0.86

concept initially proposed by Hildebrand and Scott (36), which was later extended by Weimer and Prausnitz (37), was also tested on the cyclohexanol and benzyl alcohol systems (for other alcohols, accurate solubility parameter data were not available in the literature). In the case of the nonpolar–polar mixture, the interaction parameter χ can be expressed as

$$[10] \quad \chi = \frac{V_2}{RT}[(\lambda_1 - \lambda_2)^2 + \Gamma_1^2 - 2\psi_{12}]$$

where λ and Γ represent the nonpolar and polar solubility parameters, and ψ_{12} is an adjustable parameter. Except the ψ_{12} term, other terms on the right hand side of the equation are known. The data for ψ_{12} were taken from the published literature (37–39). Appreciable differences between the experimental and calculated χ values were observed. However, with a limited objective, this model provides a good approach for the qualitative picture of a solute–solvent system. The limited usefulness of the solubility parameter theory has also been observed by Scott (40).

1. G. SCATCHARD. Chem. Rev. **44**, 7 (1949).
2. J. H. HILDEBRAND and R. L. SCOTT. Solubility of non-electrolytes. Reinhold, New York. 1950.
3. C. G. SAVINI, D. R. WINTERHALTER, and H. C. VAN NESS. J. Chem. Eng. Data, **10**, 168 (1965); **10**, 171 (1965).
4. H. RENON and J. M. PRAUSNITZ. Chem. Eng. Sci. **22**, 299 (1967).
5. I. A. WIEHE and E. B. BAGLEY. Ind. Eng. Chem. (Fundamentals), **6**, 209 (1967).
6. T. W. LEE, R. A. GREENKORN, and K. C. CHAO. Chem. Eng. Sci. **28**, 1005 (1973).
7. F. DOLEZALEK. Z. Phys. Chem. **64**, 727 (1908).
8. G. C. BENSON, S. C. ANAND, and O. KIYOHARA. J. Chem. Eng. Data, **19**, 258 (1974).
9. H. SOLANGE and Y. L. GLADEL. Fr. Patent, 1,540,277 (Sept. 27, 1968), Chem. Abstr. **71**, 80795*s* (1969).
10. (*a*) J. C. GIDDINGS and K. L. MALLIK. Ind. Eng. Chem. **59**(4), 18 (1967). (*b*) K. L. MALLIK. An introduction to nonanalytical application of gas chromatography. Peacock Press, New Delhi. 1976.
11. R. K. KUCHHAL and K. L. MALLIK. J. Chem. Eng. Data, **17**, 49 (1972).
12. (*a*) R. K. KUCHHAL and K. L. MALLIK. J. Appl. Chem. Biotechnol. **26**, 67 (1976). (*b*) B. S. RAWAT, K. L. MALLIK, and I. B. GULATI. J. Appl. Chem. Biotechnol. **22**, 1001 (1972).
13. R. K. KUCHHAL. Ph.D. Thesis, Meerut University. 1973.
14. D. E. MARTIRE. Gas chromatography. *Edited by* L. Fowler. Academic Press, New York, N.Y. 1963. p. 33.
15. R. R. DREISBACH. Physical properties of chemical compounds. Advances in Chemistry Series, No. 15, American Chemical Society, Washington D.C., 1955; No. 22., 1959.
16. A. J. ASHWORTH. J. Chem. Soc. Faraday Trans. I, **69**, 459 (1973).
17. M. L. MCGLASHAN and D. J. B. POTTER. Proc. R. Soc. Ser. A, **267**, 478 (1962).
18. M. L. MCGLASHAN and C. J. WORMALD. Trans. Faraday Soc. **60**, 646 (1964).
19. D. E. G. JONES, I. A. WEEKS, S. C. ANAND, R. W. WETMORE, and G. C. BENSON. J. Chem. Eng. Data, **17**, 501 (1972).
20. M. J. CHEVALLEY. Bull. Soc. Chim. Fr. 510 (1961).
21. A. H. WEHE and J. COATES. Am. Inst. Chem. Eng. J. **1**, 241 (1955).
22. J. M. PRAUSNITZ. Molecular thermodynamics of fluid-phase equilibria. Prentice-Hall, N.J. 1969. p. 273.
23. J. W. KING and P. R. QUINNEY. J. Phys. Chem. **78**, 2635 (1974).
24. K. NAKANISHI, S. ICHINOSE, and H. SHIRAI. Ind. Eng. Chem. (Fundamental), **7**, 382 (1968).
25. J. S. ROWLINSON. Molecular interactions in liquids and solutions. Gas chromatography. *Edited by* A. Goldup. The Institute of Petroleum. 1964. p. 217.
26. Y. B. TEWARI, J. P. SHERIDAN, and D. E. MARTIRE. J. Phys. Chem. **74**, 3263 (1970).
27. D. H. EVERETT and M. F. PENNY. Proc. R. Soc. Ser. A, **212**, 164 (1952).
28. M. L. MCGLASHAN and A. G. WILLIAMSON. Trans. Faraday Soc. **57**, 588 (1961).
29. A. J. ASHWORTH and D. H. EVERETT. Trans. Faraday Soc. **56**, 1609 (1960).
30. D. H. EVERETT and R. J. MUNN. Trans. Faraday Soc. **60**, 1951 (1964).
31. E. A. GUGGENHEIM. Trans. Faraday Soc. **44**, 1007 (1948).
32. E. A. GUGGENHEIM. Mixtures. Oxford University Press, London. 1952. Chapts. X and XI; H. Tompa. Polymer solutions. Butterworths, England. 1956. Chapt. IV.
33. J. A. BARKER. J. Chem. Phys. **20**, 1526 (1952); **21**, 1391 (1953).
34. H. C. LONGUET-HIGGINS. Discuss. Faraday Soc. **15**, 73 (1953).
35. (*a*) G. R. LUCKHURST and D. E. MARTIRE. Trans. Faraday Soc. **65**, 1248 (1969); (*b*) Y. B. TEWARI, D. E. MARTIRE, and J. P. SHERIDAN. J. Phys. Chem. **74**, 2345 (1970).
36. J. H. HILDEBRAND and R. L. SCOTT. Regular solution. Prentice Hall, Englewood Cliffs, N.J. 1962; The solubility of nonelectrolytes. Dover Publications Inc., N.Y. 1964.
37. R. F. WEIMER and J. M. PRAUSNITZ. Hydrocarbon Process. Pet. Refiner, **44**, 237 (1965).
38. J. C. HELPINSTILL and M. VAN WINKLE. Ind. Eng. Chem. Proc. Des. Develop. **7**, 213 (1968).
39. P. R. KIEZYK and D. MCKAY. Can. J. Chem. Eng. **51**, 741 (1973).
40. R. L. SCOTT. J. Phys. Chem. **52**, 136 (1958).

Canadian Journal of Chemistry

Published by
THE NATIONAL RESEARCH COUNCIL OF CANADA

Volume 55 Number 8 April 15, 1977

Journal canadien de chimie

Publié par
LE CONSEIL NATIONAL DE RECHERCHES DU CANADA

Volume 55 numéro 8 15 avril 1977

X-Ray photoelectron spectroscopy of monosubstituted perfluorobenzenes

BARRY C. TRUDELL AND S. JAMES W. PRICE[1]

Department of Chemistry, University of Windsor, Windsor, Ont., Canada N9B 3P4

Received September 1, 1976

BARRY C. TRUDELL and S. JAMES W. PRICE. Can. J. Chem. **55**, 1279 (1977).

The gas phase X-ray photoelectron spectra, XPS, were observed for the series C_6F_5X (X = F, Cl, I, Br, H). Binding energies were determined from the spectra using the ESCAPLOT Program. Charge calculations were carried out using Equalization of Electronegativity, CNDO/2, and ACHARGE approaches on each molecule. The more sophisticated analysis leads to the following equation correlating the (C 1*s*) binding energies and the atomic charges q_i

$$E_i(\text{C } 1s) = 290.23 + 22.32q_i + \sum_{i \neq j} q_j/R_{ij}$$

BARRY C. TRUDELL et S. JAMES W. PRICE. Can. J. Chem. **55**, 1279 (1977).

On a observé les spectres photoélectroniques de rayons-X en phase gazeuse (XPS) pour une série de C_6F_5X (X = F, Cl, I, Br, H). On a déterminé les énergies de liaison à partir des spectres et faisant appel au programme ESCAPLOT. On a effectué des calculs de charge, pour chaque molécule, à l'aide des approaches d'égalisation d'électronégativé, CNDO/2 et ACHARGE. Les analyses les plus sophistiquées conduisent à l'équation suivante qui permet de relier les énergies de liaison (C 1*s*) et les charges atomiques q_i

$$E_i(\text{C } 1s) = 290.23 + 22.32q_i + \sum_{i \neq j} q_j/R_{ij}$$

[Traduit par le journal]

Introduction

One of the most sought after characteristics of a molecule is its charge distribution and the changes of this distribution with substitution of different groups. Until the development of XPS, the charge distributions were usually derived theoretically, but now since it has been well established that 'chemical shifts' in XPS are definitely and precisely related to the charge distributions in molecules, we can calculate the charges on atoms in a molecule using experimental data.

Several investigations of this nature have been carried out on benzene derivatives. Clark *et al.* (1, 2) have studied both the fluoro and chlorobenzenes in the frozen solid state and correlated the CNDO/2 charge distribution with observed binding energies. However such solid studies are affected by 'solid state effects', so that there is always some doubt in the analyses of the data. Thomas (3) and Davis *et al.* (4) have all studied the fluorobenzenes and Ohta and co-workers (5) have studied the monosubstituted benzenes in the gaseous state. All have studied the charge distribution in the molecules by means of XPS.

In this paper we report the XPS data for a series of monosubstituted perfluorobenzenes and will discuss the result in terms of the electrostatic potential model, equalization of electronegativity calculation, and CNDO/2 results.

[1]To whom correspondence should be addressed.

Experimental

All of the perfluorobenzenes were obtained from the Imperial Smelting Corporation. The chemicals were distilled twice, with only middle fractions taken to ensure purity. Boiling points agreed with literature values (6).

Spectra were measured using a McPherson Esca 36 spectrometer[2] employing MgK_α radiation (1253.6 eV). The sample was out-gassed by freezing and pumping, and introduced into the spectrometer by means of a needle valve. The sample pressure in the vacuum chamber was always 5×10^{-5} torr. An additional 2×10^{-5} torr of argon was added as a standard (7) (argon $2p_{3/2}$ = 248.62 eV). The actual pressure in the collision region near the inlet nozzle was probably around two orders of magnitude greater; however we were not able to measure the pressure at that point and we assume that the pressure in the vacuum chamber reflects that of the nozzle region, *i.e.* they are proportional. The spectra for each level were reproducible to within ± 0.1 eV.

Raw data from the spectrometer were converted from "odd bit" to "even bit" using a PDP11 computer and then were fed into an IBM 360/65 computer along with the ESCAPLOT program.[3] This program deconvolutes and returns data on each individual peak as well as plotting out the spectra on a Calcomp 65 plotter. All of the spectra were also plotted out by the spectrometer. The data returned by the program includes XMAX (peak position in eV), YMAX (height of peak in number of counts), FWHM (line width at half height), GFAC (gaussian fraction; the program assumes the peak to be a Gauss–Lorentz combination band), and AREA (area of the peak).

Results and Discussion

The result of taking benzene spectra at various pressures is presented in Table 1. No significant pressure effects as reported by Siegbahn *et al.* (8) could be detected in the range presented in agreement with the results of Davis *et al.* (4).The binding energies of the C_6F_5X series are reported in Table 2. A calibration of the spectrometer with C_6H_6, Ar, and CF_4 ensured the linearity of the energy scale. The linearity of the spectrometer showed a deviation not greater than ± 0.1 eV over the range 248–700 eV. Although we have reported some energy levels lower than 248.0 eV we see no reason to doubt the validity of these numbers.

Figure 1 shows (*a*) spectra plotted by the spectrometer and (*b*) the deconvoluted spectra

[2]Located at the University of Western Ontario, London, Ontario.

[3]The ESCAPLOT program accepts the modified spectrometer data (*i.e.* binding energy *vs.* number of counts) and given initial estimates of XMAX, YMAX, GFAC, and FWHM for each peak then iterates until values for XMAX, YMAX, GFAC, FWHM, and AREA are returned with a convergence criteria of 0.00001. A number of baseline types may also be chosen.

TABLE 1. C 1*s* binding energies for benzene vapor relative to Ar $2p_{3/2}$ = 284.62 eV at various pressures

Binding energies[a] (eV)	Pressure[b] (torr)
290.4	1×10^{-4}
290.4	5×10^{-5}
290.3	3×10^{-5}
290.3	1×10^{-5}
290.3	8.5×10^{-6}
290.3	5×10^{-6}

[a]Corrected to Ar $2P_{3/2}$ = 248.62 eV.
[b]Plus 2×10^{-5} torr argon. Pressures given are vacuum chamber pressures. Pressure in the region of the inlet nozzle is probably about two orders of magnitude greater.

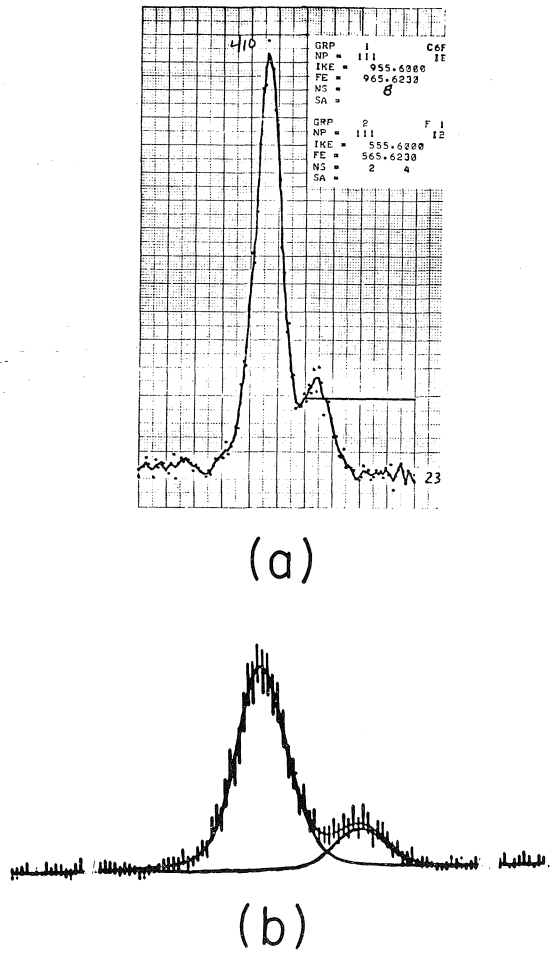

FIG. 1. (*a*) Machine spectra of the C 1*s* peaks in C_6F_5I. (*b*) Spectra of the C 1*s* peaks in C_6F_5I calculated by the ESCAPLOT program.

TABLE 2. Binding energies in compounds of the type C_6F_5X at 5×10^{-5} torr

Compound	Level	B.E.[a,b]	YMAX	GFAC	FWHM	AREA[a]
C_6F_6	C 1*s*	294.22(0.02)	255.9	0.631	1.03	342(12)
	F 1*s*	694.13(0.02)	128.5	0.695	1.27	198(10)
C_6F_5Cl	C 1*s*	292.95(0.09)	40.5	0.801	1.10	53(18)
		294.05(0.02)	204.4	0.311	0.91	263(18)
	F 1*s*	694.06(0.03)	69.3	0.849	1.48	117(9)
	Cl $2p_{1/2}$	208.96(0.07)	20.3	0.765	1.24	30(9)
	Cl $2p_{3/2}$	207.36(0.05)	42.0	0.479	1.20	69(9)
	Cl 2*s*	278.14(0.07)	41.2	0.756	1.61	128(46)
C_6F_5Br	C 1*s*	292.57(0.08)	21.8	0.207	1.05	34(10)
		293.92(0.03)	88.0	0.600	1.04	113(11)
	F 1*s*	693.93(0.01)	301.4	0.508	1.39	550(17)
	Br 3*s*	264.27(0.01)	34.2	0.989	3.38	123(12)
	Br $3p_{1/2}$	197.37(0.06)	68.8	0.356	2.50	239(38)
	Br $3p_{3/2}$	190.76(0.03)	147.0	0.203	2.23	429(21)
	Br $3d_{3/2}$	78.33(0.05)	79.1	0.247	1.02	117(15)
	Br $3d_{5/2}$	77.30(0.04)	103.2	0.548	1.17	157(15)
C_6F_5I	C 1*s*	292.01(0.04)	72.5	0.999	1.11	86(8)
		293.80(0.01)	370.3	0.689	1.11	498(17)
	F 1*s*	693.84(0.01)	349.0	0.456	1.34	625(19)
	I $3d_{3/2}$	638.76(0.01)	870.3	0.233	1.12	1411(44)
	I $3d_{5/2}$	627.27(0.01)	1298.1	0.279	1.09	2020(35)
	I $4d_{3/2}$	59.30(0.02)	200.0	0.152	1.20	358(25)
	I $4d_{5/2}$	57.58(0.02)	256.8	0.643	1.27	407(22)
C_6F_5H	C 1*s*	291.71(0.03)	90.6	0.210	1.08	143(18)
		293.92(0.01)	457.5	0.558	1.04	615(19)
	F 1*s*	693.88(0.01)	413.7	0.426	1.27	714(18)

[a]Values in parentheses are the uncertainties calculated by the ESCAPLOT program.
[b]All binding energies relative to argon $2p_{3/2} = 248.62$ eV.

produced by the ESCAPLOT program for the C 1*s* levels of C_6F_5I. The straight lines in the computer spectra are error bars. In addition to error calculations the program refines the binding energy values and permits comparison of peak area ratios with the theoretical values.

The values of C 1*s* (C_6H_6) and F 1*s* (C_6F_6) binding energies agree with those of Davis *et al.* (4). The C 1*s* peaks in C_6F_5X (X = H, I, Br, Cl) were assigned on the basis of peak areas which were in reasonable agreement with the theoretical value of 5:1 within the error limits.

Differences in the F 1*s* binding energies in the ortho, meta, and para positions of the molecules were too small to be detected as separate peaks. The resulting single peaks are however somewhat broader in the case of C_6F_5Cl, C_6F_5Br, and C_6F_5I.

The pattern of the chemical shifts relative to benzene for the C 1*s* levels of the carbon to which X is attached (C_1) is what one would expect, *i.e.* the shifts are in the order F > Cl > Br > I > H.

In all cases the C_1 1*s* binding energies are higher than in the equivalent C_6H_5X compound. This is presumably a result of the general environment created by the fluorine atoms and of their electron withdrawing power moderated by back donation of electron density by a +M (mesomeric) effect. When charge distributions calculated by CNDO/2 for C_6F_5H, C_6F_5Cl, and C_6F_6 are compared with those for C_6H_6, C_6H_5Cl, and C_6H_5F respectively an almost constant difference (0.08–0.09) is obtained for the C_1 carbons. This would seem to imply a fairly constant +M effect in the C_6F_5X compounds.

Equalization of Electronegativity Calculations

The method of Huheey (9) can be used to calculate partial atomic charges in molecules. In order to calculate the charge on the carbon atom bonded to X in the series C_6F_5X (X = F, Cl, Br, I, H) it is convenient to assume that the C_5F_5 part of the molecule is identical in each case. Looking at the C 1*s* and F 1*s* binding energy levels one can see little variation of the values from molecule to molecule which perhaps supports this concept.

In Huheey's method, the orbital electronegativity is defined as:

$$\chi = a + b\delta$$

where a and b are known parameters and δ is the partial charge of the atom in question. For example, for the C—Cl bond in C_6F_5Cl we have:

$$\chi_C = 8.79 + 13.67\delta_C$$

$$\chi_{Cl} = 9.38 + 11.30\delta_{Cl}$$

and

$$\delta_C + \delta_{Cl} = 0 \quad \text{(neutral molecule)}$$

$$8.79 + 13.67\delta_C = 9.38 - 11.30\delta_C$$

$$\delta_C = +0.024$$

The results for such a calculation for each molecule are shown in Table 3. These partial charges are not absolute values as those calculated by CNDO/2 or the electrostatic potential model given later, but do provide a simple good correlation with the binding energy data as shown in Fig. 2. The line of best fit for the data given, gives the following equation

[1] Partial charge = 0.0588 (Binding energy) − 17.146

CNDO/2 Calculations and Chemical Shifts

According to the electrostatic potential model, the binding energy of a core electron E_i, is given by the following equation

$$[2] \qquad E_i = E_0 + k_A q_i + \sum_{i \neq j} q_j/R_{ij}$$

when E_0 and k_A are constants dependent on the kind of atom and R_{ij} is the internuclear distance and q_i the charge. The values of these two constants have been established by Ohta (5) for monosubstituted benzenes to be 22.67 for k_A and 290.2 eV for E_0 for the carbon atoms.

TABLE 3. Relative partial charges in the carbon atom attached to X in C_6F_5X (X = H, I, Br, Cl, F)

X	δ_C	δ_C' [a]
H	−0.060	0.0
I	−0.035	0.025
Br	−0.017	0.043
Cl	0.024	0.084
F	0.109	0.169

[a]Value of δ_C C_6F_5H set equal to 0.0.

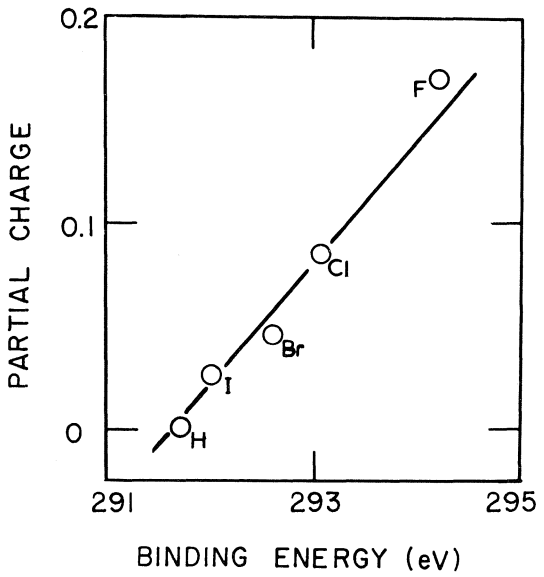

FIG. 2. Partial atomic charge on the carbon attached to X in C_6F_5X as a function of the C 1*s* binding energy of this carbon atom. Partial charge was calculated assuming a constant contribution from C_5F_5 and is expressed relative to the corresponding C 1*s* value in C_6F_5H.

Equation 2 may be rewritten in the form

$$[3] \qquad E_i - \sum_{i \neq j} q_j/R_{ij} = E_0 + k_A q_i$$

Thus a plot of the term on the left *vs.* q_i should yield a straight line with slope k_A and intercept E_0. To do this one needs q and R_{ij} values.

We have obtained the charge densities of the atoms in the series C_6F_5X (X = H, I, Br, Cl, F) using the CNDO/2 calculation. The calculation was carried out using QCPE No. 290[4] which varies the geometry of the molecule to obtain a minimum of energy. The basis set for the calculation involves 1*s* for H; 2*s*, 2*p* for C, F; 3*s*, 2*p*, 3*d* for Cl; 4*s*, 4*p*, and 3*d* for Br; and 5*s*, 5*p*, and 4*d* for I. We believe this to be the first calculation of this type on Br and I used in conjunction with XPS. The CNDO/2 charges are reported in Table 4.

Substituting the values for q_i calculated by CNDO/2 and the necessary R_{ij} one obtains the plot in Fig. 3. As can be seen the values for C_6F_5Br are far off the line. Deviations similar to this have been noted by Ohta (5) for C 1*s* cal-

[4]Developed by Dr. D. Rinaldi, Université de Nancy. Available through Quantum Chemistry Program Exchange, University of Indiana.

TABLE 4. Charge densities of 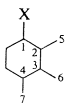 as determined by CNDO/2

Compound	Atom	Charge density	Atom	Charge density
C_6F_5I	C_1	−0.045	F_5	−0.176
	C_2	0.186	F_6	−0.166
	C_3	0.146	F_7	−0.163
	C_4	0.160	X	0.066
C_6F_5Br	C_1	−0.435	F_5	−0.245
	C_2	0.201	F_6	−0.191
	C_3	0.122	F_7	−0.190
	C_4	0.141	X	0.712
C_6F_5Cl	C_1	−0.004	F_5	−0.164
	C_2	0.216	F_6	−0.159
	C_3	0.137	F_7	−0.156
	C_4	0.171	X	−0.079
C_6F_6	C	0.157	F	−0.157
C_6F_5H	C_1	−0.082	F_5	−0.178
	C_2	0.208	F_6	−0.162
	C_3	0.136	F_7	−0.162
	C_4	0.174	X	0.062

culations when the group attached to the carbon atom is Cl, NO_2, or CN. Inadequate parameters for these groups in the CNDO/2 programmes were held responsible. Omitting the points for C_6F_5Br, least squares analysis of the data gives

$$[4] \quad E_i(\text{C } 1s) = 290.19 + 22.24q_i + \sum_{j \neq i} q_j/R_{ij}$$

which is in excellent agreement with Ohta's results of

$$[5] \quad E_i(\text{C } 1s) = 290.2 + 22.67q_i + \sum_{j \neq i} q_j/R_{ij}$$

for C 1*s* binding energies in benzene type systems.

Because of the discrepancies with the charge distribution in C_6F_5Br we decided to calculate the charge distribution using the electrostatic potential model.

Atomic Charge Analysis

Using chemical shift data and a knowledge of molecular geometry atomic charges may also be calculated by ACHARGE analysis (1–5). In the present cases ΔE is required for C 1*s* and F 1*s* levels.

In the preceding section we calculated the E_0 and k_A values for C 1*s* only. A variety of values

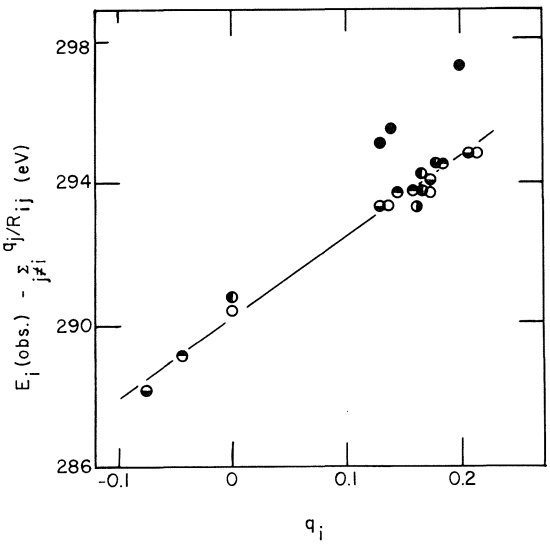

FIG. 3. Binding energies of C 1*s* electrons in C_6F_5X (X = F, Cl, Br, I, H) corrected for interatomic potentials *vs.* the charge on the respective carbon atom. ◑ C_6F_6, ○ C_6F_5Cl, ● C_6F_5Br, ○ C_6F_5I, ○ C_5F_6H. All preceding points are based on q_i values from CNDO/2 calculations. ◐ C_6F_5Br from ACHARGE.

for E_0 and k_A for F 1*s* levels has been used. We have decided to use Siegbahn's value (8) of $k_F = 35.1$ eV/e and have calculated E_0 for F 1*s* to be 697.4 eV in a method similar to that in the paper of Davis *et al.* (4). There is no need to know the E_0 and k_A values for the 'X' substituent, if we assume that

$$[6] \quad \sum_j q_j = 0$$

i.e. neutrality of the molecule. We may also reduce the problem from a 12 × 12 matrix to a 8 × 8 matrix by symmetry.

The charge densities calculated by the analyses of the C 1*s* and F 1*s* levels of the C_6F_5X series are shown in Table 5. In all of the compounds, except C_6F_5Br, there is satisfactory agreement between the ACHARGE and CNDO/2 results.

In both the ACHARGE and CNDO/2 charge calculations, the carbon atom joined to X in C_6F_5X (X = H, I, Br, Cl) is the least positive carbons in the structures in agreement with the +M effects of the fluorines. Also in the CNDO/2 charges the *o*, *p* carbons are more positive than the meta carbon consistent with this idea. The

TABLE 5. Charge densities of 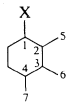 as determined by ACHARGE

Molecule	Atom	Charge density	Atom	Charge density
C_6F_6	C	0.157	F	−0.157
C_6F_5Br	C_1	−0.010	F_5	−0.137
	C_2	0.176	F_6	−0.182
	C_3	0.153	F_7	−0.141
	C_4	0.152	X	−0.022
C_6F_5Cl	C_1	0.014	F_5	−0.144
	C_2	0.176	F_6	−0.190
	C_3	0.160	F_7	−0.147
	C_4	0.158	X	−0.028
C_6F_5I	C_1	−0.047	F_5	−0.131
	C_2	0.181	F_6	−0.176
	C_3	0.148	F_7	−0.136
	C_4	0.148	X	−0.007
C_6F_5H	C_1	−0.136	F_5	−0.155
	C_2	0.205	F_6	−0.200
	C_3	0.160	F_7	−0.154
	C_4	0.162	X	0.108

ACHARGE analysis does not show these trends as clearly.

In order to clarify the results of the charge calculation of C_6F_5Br, it was decided to put the ACHARGE charge densities for this molecule to an analysis identical to the CNDO/2 charges. It was found that the points calculated with the ACHARGE values fit very well on the graph on Fig. 3.

Because of the agreement between the CNDO/2 and ACHARGE calculations for every molecule except C_6F_5Br, we offer this as evidence that the CNDO/2 calculation for this molecule may be in error. It is recognized that if there are any excited state contributions to the experimental C 1*s* bonding energies this will be reflected in the ACHARGE calculation and would lead to disagreement with CNDO/2 results. However, it seems unlikely that in the series of C_6F_5X compounds studied excited state contributions in C_6F_5Br should be of such a unique character. The equation for the line derived by a least squares calculation including the points for C_6F_5Br derived from ACHARGE calculations yields the following equation

$$[7] \quad E_i(\mathrm{C}\,1s) = 290.23 + 22.32q_i + \sum_{i \neq j} q_j/R_{ij}$$

which is still in excellent agreement with previous published work on aromatic systems and quite similar to eq. 4. We regard eq. 7 as the general equation for perfluorobenzene systems.

In conclusion, it would seem that the Equalization of Electronegativity calculations, although easily carried out with good correlations with the present XPS data, provide little realistic information about the molecule. On the other hand, XPS data are used to calculate charge distributions on molecules in the ACHARGE approach and these are usually comparable to CNDO/2 calculations.

1. D. T. CLARK, D. KILCAST, D. B. ADAMS, and W. K. R. MUSGRAVE. J. Electron Spectrosc. **1**, 227 (1972/73).
2. D. T. CLARK, D. KILCAST, D. B. ADAMS, and W. K. R. MUSGRAVE. J. Electron Spectrosc. **6**, 117 (1975).
3. T. D. THOMAS. J. Chem. Phys. **52**, 1373 (1970).
4. D. W. DAVIS, D. A. SHIRLEY, and T. D. THOMAS. J. Am. Chem. Soc. **94**, 6565 (1972).
5. T. OHTA, T. FUJIKAWA, and H. KURODA. Bull. Chem. Soc. Jpn. **48**, 2017 (1975).
6. Highly Fluorinated Aromatic and Alicyclic Compounds. Imperial Smelting Co., St. Andrews Rd., Avonmouth, Bristol BS11 9HP, England.
7. K. SIEGBAHN *et al.* J. Electron Spectrosc. Relat. Phenom. **2**, 295 (1973).
8. K. SIEGBAHN *et al.* ESCA applied to free molecules. North Holland Publishing Co., Amsterdam. 1969. pp. 18–21.
9. J. HUHEEY. J. Phys. Chem. **69**, 3284 (1965).

Toward an understanding of rates of crystal nucleation from solution with a variable driving force

RONALD E. MASSEY AND O. E. HILEMAN, JR.

Department of Chemistry, McMaster University, Hamilton, Ont., Canada L8S 4M1

Received July 7, 1975[1]

RONALD E. MASSEY and O. E. HILEMAN, JR. Can. J. Chem. **55**, 1285 (1977).

'Number-time' data obtained during studies on the nucleation from aqueous solution of $CaSO_4 \cdot 2H_2O$ (gypsum) using the droplet technique and a variable driving force are reported. Sulfate ion was generated, *in situ*, by the reaction between $S_2O_8^{2-}$ and $S_2O_3^{2-}$ in the presence of Ca^{2+}. The rate of the reaction was determined from polarographic data. The stoichiometry and solubility of the precipitate in the aqueous matrix were determined.

Problems which arise during analysis of 'number-time' data obtained from droplet experiments with a large spread in individual droplet volumes and a variable driving force using techniques suggested in the literature are commented upon. A new technique was developed and applied to the analysis of our data. The effects of a non-steady state rate of nucleation, variable lag times and a decreasing cation:anion ratio on the derived results are discussed.

RONALD E. MASSEY et O. E. HILEMAN, JR. Can. J. Chem. **55**, 1285 (1977).

On rapporte des données de "nombre-temps" obtenues durant des études sur la nucléation à partir de solution aqueuse de $CaSO_4 \cdot 2H_2O$ (gypsum) utilisant la technique des gouttelettes et une force motrice variable. On a généré l'ion sulfate *in situ* par la réaction entre $S_2O_8^{2-}$ et $S_2O_3^{2-}$ en présence de Ca^{2+}. On a déterminé la vitesse de la réaction à partir de données polarographiques. On a déterminé la stoechiométrie et la solubilité du précipité dans la matrice aqueuse.

On fait des commentaires sur les problèmes qui se développent au cours de l'analyse des données de "nombre-temps" obtenues à partir d'expériences avec des gouttelettes impliquant un large éventail dans le volume des gouttelettes individuelles et une force matrice variable et utilisant les techniques suggérées dans la littérature. On a développé une nouvelle technique et on l'a appliquée à l'analyse de nos données. On discute des effets d'un état de non-équilibre de vitesse de nucléation, de temps de retard variables et d'un décroissement du rapport cation/anion sur les résultats qui en découlent.

[Traduit par le journal]

Introduction

Data obtained during nucleation studies employing miniaturization techniques are usually collected as increasing number of detected events occurring in the droplet population as a function of increasing experimental time. Interpretation of such "number-time" data has been the subject of several publications (1–5). Generally, the problem is considered from a probabilistic point of view and the results are summarized by expressions similar to [1].

$$[1] \qquad J(t_e) = \frac{1}{v}\frac{1}{N - n_{t,v}}\frac{dn_{t,v}}{dt_e}$$

where J is a theoretical rate of nucleation dependent on supersaturation and temperature but independent of matrix effects, t_e is time lapse from the initiation of the nucleation experiment, v is droplet volume, N is the total number of droplets of the same volume in a population, and $n_{t,v}$ is the total number of droplets in a population with a certain volume which contain crystals at a given time.

Variations with time of one or both of the driving force and the nucleation rate as well as a supersaturation dependent 'time-lag' limit the applicability of this type of approach. Time-dependent supersaturation levels and the "time-lag" have been considered by several authors (3, 6–8). Carte (3), for example, suggested that eq. 1 be modified into the form shown as eq. 2 for data analysis in systems with a time-dependent supersaturation.

$$[2] \qquad J(S,t_e) = \frac{1}{v}\frac{1}{N - n_{t,v}}\frac{\partial n_{t,v}}{\partial S}\frac{\partial S}{\partial t_e}$$

where S is supersaturation level = $[(\text{I.P.}) \times (K_{sp}^{-1})]^{1/2}$ (I.P. = ion product = $[Ca^{2+}][SO_4^{2-}]$).

[1]Revision received September 17, 1976.

Kashchiev (6) extended the applicability of the Zeldovich equation (9), using Szilard's scheme for embryo build-up (10), to nucleation rates and total numbers of nuclei formed in systems undergoing homogeneous nucleation at a linear time-dependent supersaturation. Frisch and Carlier (8) have presented a theoretical derivation showing the relationship between the time lag and the time-independent supersaturation being experienced by a system.

Recently, results from work in our laboratory focused on crystal nucleation from solution using modifications of Vonegut's droplet technique have revealed difficulties which arise when using interpretive schemes based on eqs. 1 and 2 and 'pooled data'. In this paper, we report a general interpretive approach applicable to "number-time" data. The new scheme is applied to the interpretation of data obtained during studies on $CaSO_4 \cdot 2H_2O$ nucleation from solution under conditions of a variable driving force and an initial non-steady state nucleation rate. The influences of a non-steady state nucleation rate and a variable time lag on the magnitude of derived macroscopic parameters are discussed.

Experimental

A droplet experiment can be divided into a series of steps: preparation of an aqueous solution containing the precursors for generation of the supersaturation; dispersion of a small, known amount of this solution in an immiscible oil; selection and subsequent preparation of a population of droplets for microscopic observation; generation of the supersaturation; notation of "number-time" data and subsequent data analysis and interpretation. Additionally, the rate of formation of the supersaturation and the equilibrium solubility of the crystalline product in the aqueous medium must be measured.

The reaction between $S_2O_3^{2-}$ and an excess of $S_2O_8^{2-}$ was used to generate SO_4^{2-}, *in situ*, in the presence of Ca^{2+}. Results obtained from polarographic analysis of 'beaker' experiments performed in parallel were used to infer supersaturation data for a droplet population. The appearance of crystals within the droplet population was recorded photomicrographically. For analysis, the 'number-time' data were separated on the basis of narrow droplet volume ranges.

Reagents and Apparatus

Reagents

All salts ($Ca(NO_3)_2 \cdot 4H_2O$ (Baker), $K_2S_2O_8$ (Allied), $Na_2S_2O_3 \cdot 5H_2O$ (BDH), and EDTA (Fisher)) were of 'Reagent grade' quality. Solutions prepared from them were pressure filtered (N_2) through a 0.3 μ PVC filter (Sartorius). Solution 'A' was prepared by mixing, immediately before use, equal volumes of the $Ca(NO_3)_2 \cdot 4H_2O$ and the $K_2S_2O_8$ solutions. Solution 'B' contained $Na_2S_2O_3$. Light and heavy mineral oils (BDH) were used as supplied.

Apparatus

Dispersions of the aqueous solutions were made with the aid of a Virtis micro-homogenizer (Fisher) in a 6 ml homogenizing flask.

Isolation of certain droplet size ranges was accomplished by using a centrifuge (International Clinical Centrifuge) and a 15 ml centrifuge tube.

The observation vessel was a Nessler cup of 31 mm OD, 26 mm height with an optically flat bottom. The inside bottom surface was made hydrophobic with a coating of Drifilm SC-87 (Pierce Chemical Co.).

One of the two microscopes used was a Vickers M15 polarizing microscope (Vickers Instruments) with a magnification of 75× (5× objective, 10× eyepiece, 1½× analyser). The light source was a 500 W super-high pressure mercury vapour lamp (Philips Electronics). Cooling water was pumped through a water jacket housing the lamp and primary condenser; the polarizer was protected by two heat absorbing filters. The other microscope used was a Vickers M41 (Vickers Instruments) with a magnification of 200× (250×) (20× objective, 10× eyepiece, 1.00× (1.25×) analyser). The light source was a 12 V, 100 W tungsten–halogen lamp (Philips Electronics). The lamp unit had its own heat and light filters. A dark field illumination technique was used.

Nessler cups were fitted into cell holders, then placed onto a micrometer stage (Vickers Instruments) equipped with a micrometer dial of range 0.01 to 20 mm.

A thermostatted cell holder, which would hold a Nessler cup, was manufactured from an aluminum rod (Fig. 1). A tight fitting O-ring was attached to the Nessler cup before it was placed in the cell holder. An outside collar, with an opening greater than the diameter of the Nessler cup, was screwed down thereby forcing the O-ring onto a lip and sealing the inner compartment formed by the walls of the Nessler cup and the cell holder.

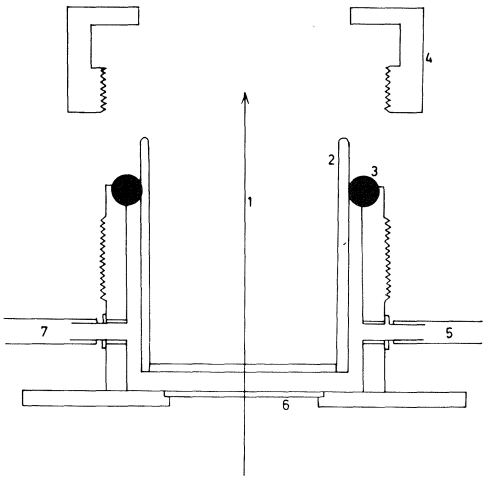

FIG. 1. The thermostatted cell holder for droplet observation under the microscope. *1*, optical axis; *2*, Nessler cup; *3*, O ring; *4*, collar; *5*, inlet; *6*, window; *7*, outlet.

TABLE 1. Summary of experimental conditions for nucleation experiments

Experiment[a]	Concentration (mol/ℓ)						
	Ca^{2+}	$S_2O_8^{2-}$	$S_2O_3^{2-}$	K^+	Na^+	NO_3^-	μ^b
E_1	0.250	0.100	0.250	0.200	0.500	0.500	1.80
E_2	0.475	0.157	0.433	0.314	0.866	0.950	3.20

[a]Experiments performed at 295 ± 1 K.
[b]μ = ionic strength of the solution from which the crystals formed.

Thermostatted water was passed through this compartment via nozzles placed directly opposite each other. The base of the cell holder was formed from an aluminum plate, with a 25 mm diameter window into which a thin quartz circular cover glass was affixed.

The camera, an Autowind 35 mm (Vickers Instruments), was controlled by an autoexposure unit J-35 (Vickers Instruments). Ansochrome D-500 and D-200 colour reversal film (G.A.F.) was used.

The photomicrographs were projected onto a pinboard (60 × 90 cm) using a Pradovit projector (Lietz), equipped with either a 150 mm or a 50 mm lens, and a Ansochrome 940 projector (G.A.F.), equipped with a 150 mm lens.

Solubility of $CaSO_4 \cdot 2H_2O$

A synthetic matrix was prepared which contained 0.2 *M* $Na_2S_4O_6$ and 0.05 *M* $Na_2S_2O_3$. An excess of freshly prepared $CaSO_4 \cdot 2H_2O$ was added, the solution was stirred for 24 h, then pressure filtered. Aliquots of the resulting filtrate were titrated with 0.0100 *M* EDTA to an EBT end point.

Determination of Supersaturation Data

The rate of change in the thiosulfate concentration in solution was determined polarographically using the free dissolution wave of Hg ($E_{1/2} = -0.2$ V *vs.* SCE) as the indicator. The sulfate ion concentration was calculated from the resulting data.

Calibration

A thiosulfate solution was prepared and standardized against $K_2Cr_2O_7$. Exactly 0, 5, 10, 20 and 25 ml portions of this solution were pipetted into separate 250 ml volumetric flasks containing approximately 200 ml of KNO_3 solution, enough $S_2O_8^{2-}$ to duplicate the initial conditions of each experiment, and Triton-X100. After dilution to volume the polarograms were determined over a range of +0.1 to −0.5 V *vs.* SCE.

Procedure

Solutions A and B, previously described, were mixed and at certain time intervals 3.0 ml of the solution were transferred into separate 250 ml volumetric flasks containing 200 ml of water to quench the reaction. After addition of KNO_3 and Triton-X100 and upon dilution to volume, the polarograms of these solutions were recorded. The diffusion current of each solution was measured at the same potential as the calibration standards. The diffusion current of the first aliquot was observed initially and was subsequently recorded over a period of 2 h.

Droplet Experiments

The following procedure was used to prepare a large population of non-communicating droplets. The population must exhibit a narrow volume range and, to aid in microscopic observation of events taking place within it, the population should be situated on an optically flat surface. The experimental conditions used are summarized in Table 1.

Procedure

Both solution A, containing calcium and peroxydisulfate, and solution B, containing thiosulfate, were pressure filtered through a 0.3 μ PVC filter. Equal aliquots of each were withdrawn, combined together and thoroughly mixed. This solution was drawn into a dropping pipette and 2 drops of it were placed in a 6 ml homogenizing flask containing 5 ml of light mineral oil. The solution was dispersed by means of a microhomogenizer rotating at approximately 40 000 rpm for 10 s. The contents of the homogenizing flask were then poured into a 15 ml centrifuge tube containing 11 ml of heavy mineral oil. This mixture was rotated at 4000 rpm in a centrifuge for 2–5 min. An eye dropper was used to transfer 3–4 ml of the mixture to the bottom of a Nessler cup which contained 1 ml of the heavier oil. The cup and contents were rotated at 4000 rpm for 3–4 min and then the oil was decanted off until a depth of 3 mm remained.

The observation cup was placed in a cell holder on the microscope stage and fields of view were selected for observation. Micrometer dial settings for each field of view were noted so that accurate readjustment for observation of multiple fields of view was possible.

Each field of view was photographed and the time, relative to experimental time zero, was recorded. Data recording was terminated when most of the droplets contained crystals or at the lapse of a predetermined time interval. Finally, a photograph was taken of a millimeter slide using the same magnification factor.

Data Collection

The 35 mm slides were sorted into fields of view, arranged into correct time sequence, labelled, and mounted in trays. The absolute droplet sizes were measured by comparing observed diameters with the distance measured between rulings on the projected millimeter slide.

A slide showing all the droplets from one field of view was projected on the screen and the droplet population was divided into volume ranges. The droplets in each range were identified with pins of a specific colour. All the slides taken of the one field of view were then projected in correct time sequence. As each slide was displayed, a search was made for those droplets which contained a crystal not visible in the previous slide. If such a droplet were found, the pin associated with it was removed and placed in a container holding all those

removed for that particular slide. This procedure was repeated for all slides in all fields of view.

The data observed from corresponding volumes and times from all fields of view were combined. These data were then summed over time to give $n_{t,v}$, the total number of droplets of volume 'v' containing crystals at time 't_e'.

Results

Preliminary experiments established $CaSO_4 \cdot 2H_2O$ to be the sparingly soluble product of reaction between $S_2O_3^{2-}$ and $S_2O_8^{2-}$ in the presence of Ca^{2+}. The measured K_{sp} value for $CaSO_4 \cdot 2H_2O$ at 295 ± 1 K was found to be invariant, within experimental error, as the ionic strength of the aqueous matrix changed from 1.80 to 3.20. Thus, an average value of 8.47×10^{-4} was used in the calculation of the supersaturation levels reported in this study.

Supersaturation *vs.* time data calculated from results of the polarographic determination of $S_2O_3^{2-}$ concentration levels in bulk reaction mixtures are shown in Fig. 2. The maximum supersaturation attained for experiments E_1 and E_2 was found to be 7.7 and 13, respectively. These supersaturation values were obtained at an ionic strength of 1.80 (E_1) and 3.20 (E_2).

Typical results selected from droplet experiments performed under each set of experimental conditions listed in Table 1 are shown as $n_{t,v}/N$ *vs.* time curves in Figs. 3 and 4. The data for each curve are taken from one experimental run with the total population divided into several volume ranges. For statistical reasons, the minimum population for each volume range required for subsequent data analysis was 100 droplets; data arising from volume ranges with fewer than 100 droplets were disregarded.

Discussion

Bigg (2) suggests that $n_{t,v}$ *vs.* time data collected by observation of nucleation events in a droplet population comprised of a multiplicity of individual droplet volumes may be combined if the mean crystallization time in each volume range is reduced to that of a droplet of standard size. From the following argument, in contrast, we conclude that rate calculations must be performed within each individual volume range.

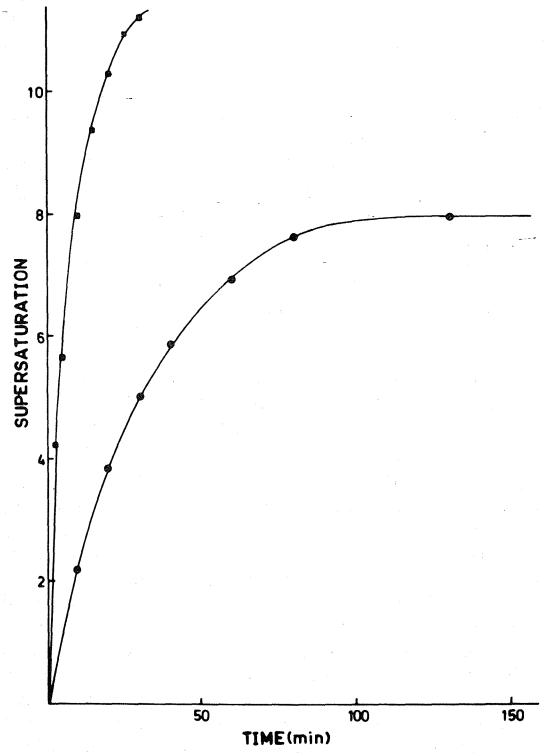

FIG. 2. Plots of the supersaturation *vs.* time for experiments E_1 and E_2: ● = E_1, ■ = E_2.

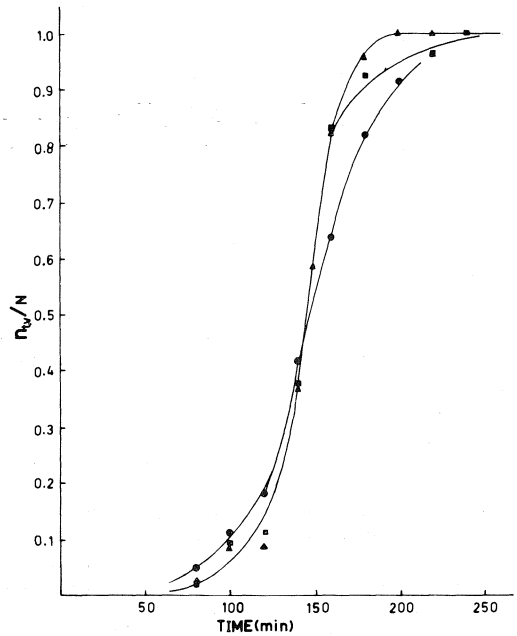

FIG. 3. Plots of $n_{t,v}/N$ *vs.* time measured for three volume ranges in experiment E_1. Legend: ●, $v = 2.57 \times 10^{-9}$ cm^3; ■, $v = 4.85 \times 10^{-9}$ cm^3; ▲, $v = 8.18 \times 10^{-9}$ cm^3.

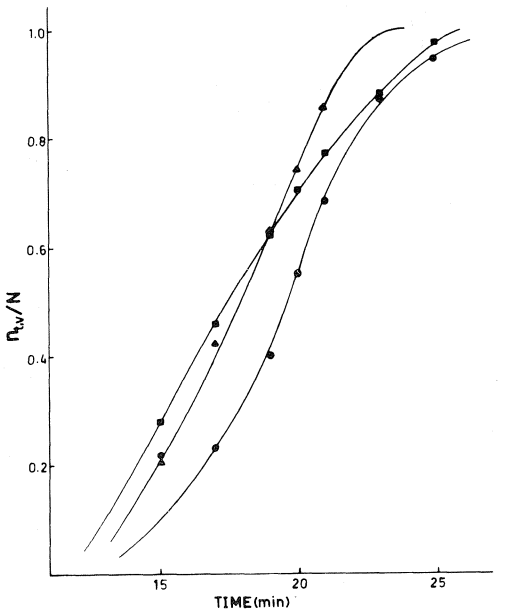

FIG. 4. Plots of $n_{t,v}/N$ *vs.* time measured for three volume ranges in experiment E_2. Legend: ●, $v = 5.24 \times 10^{-10}$ cm^3; ■, $v = 4.19 \times 10^{-9}$ cm^3; ▲, $v = 1.41 \times 10^{-8}$ cm^3.

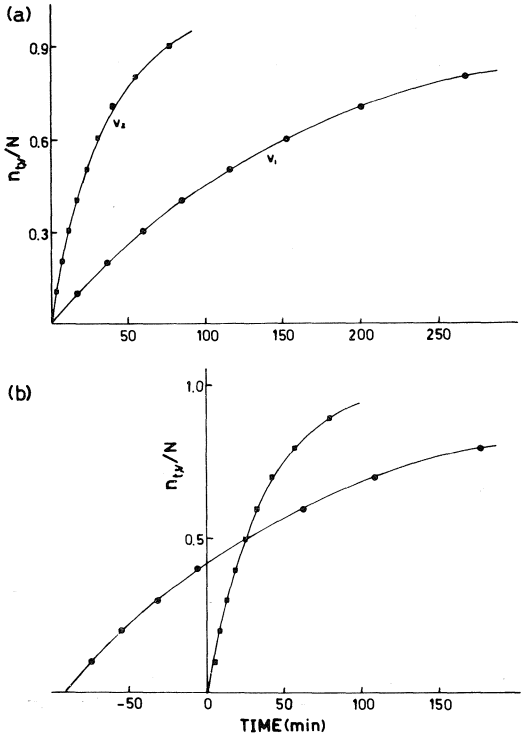

FIG. 5. (*a*) The $n_{t,v}/N$ *vs.* time plots of two droplet populations v_1 and v_2. (*b*) The mean crystallization time of v_1 reduced to that of v_2. Legend: ●, $v_1 = 1.0 \times 10^{-10}$ cm^3; ■, $v_2 = 5.0 \times 10^{-10}$ cm^3.

If the supersaturation is constant during the nucleation experiment, eq. 1 may be integrated over time to give eq. 3.

$$[3] \qquad n_{t,v} = N[1 - \exp(-Jvt_e)]$$

By setting $J = 10^6$ cm^{-3} s^{-1}, selecting various values of v and using [3], hypothetical 'number-time' data for each droplet volume range can be generated. Sample data for $v_1 = 1 \times 10^{-10}$ cm^3 and $v_2 = 5 \times 10^{-10}$ cm^3 are shown in Fig. 5*a*. The mean crystallization time, defined as that point in experimental time when $n_{t,v}/N = 0.5$, for these data is 6930 s for v_1 and 1380 s for v_2. The curve labelled v_1 in Fig. 5 was shifted along the time axis using the procedure suggested by Bigg (2): 5550 s were subtracted from all t_e values. The result is shown as Fig. 5*b*. Summation of the two curves in this figure produces a distorted, S-shaped curve with an apparent initial non-steady state rate of nucleation even though the data were generated assuming a steady-state rate. Such manipulations, therefore, do not seem to be useful as the basis of a scheme for the analysis and interpretation of number-time data obtained from experiments with droplet populations made up of diverse individual volumes. In this study, the data observed for the individual volume ranges were not combined together for subsequent data analysis and parameter estimation.

More serious problems arise in the interpretation of number-time data if the supersaturation level being experienced by the system significantly changes with time during the nucleation experiment. A suggested scheme for the analysis of data gathered under this condition follows.

Figure 6 depicts, in three dimensions, the inter-relationships between the laboratory observables $n_{t,v}$, S, and t_e during a hypothetical nucleation experiment that has such a variable driving force. A dummy variable, z, is introduced for ease of algebraic manipulation. The vector components of dn_z, the tangential vector, are $dn_{t,v}$, dS, and dt_e. The orthogonal projection of dn_z onto the S,t_e plane is dz. If the angle between dz and dt_e is θ, the following trigonometric relations will then hold:

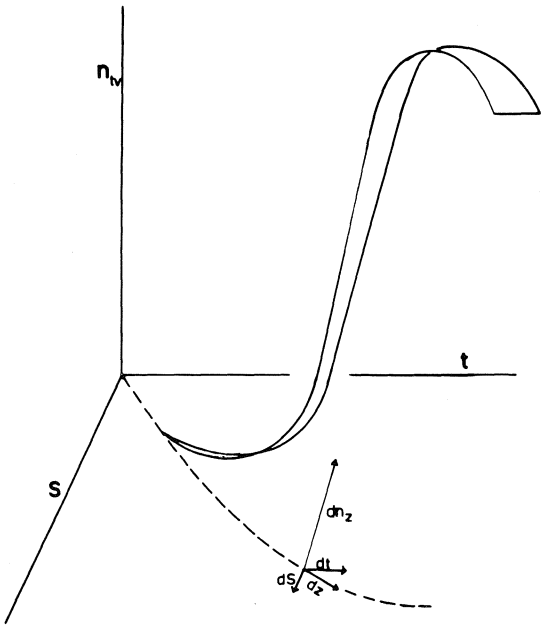

FIG. 6. The inter-relationships between $n_{t,v}$, t, and S in an experiment that has a variable driving force.

$$\frac{dt_e}{dz} = \cos\theta$$

$$\frac{dS}{dz} = \sin\theta$$

$$\frac{dS}{dt_e} = \tan\theta$$

A dimensional analysis of the above relations suggests that dt_e, dS, and dz must be dimensionless. Thus a dimensionless quantity 't' is introduced such that

$$t = \frac{t_e}{t_{0.5} - t_0}$$

where t_0 is the time (t_e) at which the curve given by eq. 3 fitted to the steady state portion of the $n_{t,v}/N$ *vs.* t_e curve intersects the t_e axis, and $t_{0.5}$ is the time (t_e) at which $n_{t,v}/N$ attained a value of 0.5. Then,

[4] $$\frac{dn_{t,v}}{dz} = \frac{\partial n_{t,v}}{\partial t}\cos\theta = \frac{\partial n_{t,v}}{\partial t}\left[\left(\frac{dS}{dt}\right)^2 + 1\right]^{-1/2}$$

and

[5] $$\frac{dn_{t,v}}{dz} = \frac{\partial n_{t,v}}{\partial S}\sin\theta = \frac{\partial n_{t,v}}{\partial S}\left[\left(\frac{dS}{dt}\right)^{-2} + 1\right]^{-1/2}$$

To an observer in the S,t plane the rate of nucleation would appear to obey eq. 6.

[6] $$J'(z) = \frac{1}{v}\frac{1}{N - n_{t,v}}\frac{dn_{t,v}}{dz}$$

where J' = an experimental rate of nucleation calculated from each datum point on the $n_{t,v}/N$ *vs.* time curve which reflects the effects of variable non-steady state rates, cation:anion ratios, lag times, and other matrix effects.

Substitution, in turn, of eqs. 4 and 5 into eq. 6 yields, respectively,

[7] $$J'(S,t) = \frac{1}{v}\frac{1}{N - n_{t,v}}\frac{\partial n_{t,v}}{\partial t} \times \left[\left(\frac{dS}{dt}\right)^2 + 1\right]^{-1/2}$$

and

[8] $$J'(S,t) = \frac{1}{v}\frac{1}{N - n_{t,v}}\frac{\partial n_{t,v}}{\partial S} \times \left[\left(\frac{dS}{dt}\right)^{-2} + 1\right]^{-1/2}$$

At very low dS/dt, that is, as $[(dS/dt)^2 + 1]^{-1/2}$ approaches one, and as $[(dS/dt)^{-2} + 1]^{-1/2}$ approaches dS/dt, eqs. 7 and 8 reduce to eqs. 9 and 10 respectively.

[9] $$J'(t) = \frac{1}{v}\frac{1}{N - n_{t,v}}\frac{\partial n_{t,v}}{\partial t}$$

[10] $$J'(S,t) = \frac{1}{v}\frac{1}{N - n_{t,v}}\frac{\partial n_{t,v}}{\partial S}\frac{dS}{dt}$$

At very high dS/dt, that is as $[(dS/dt)^2 + 1]^{-1/2}$ approaches (dt/dS), and as $[(dS/dt)^{-2} + 1]^{-1/2}$ approaches one, eqs. 7 and 8 reduce to eqs. 11 and 12 respectively.

[11] $$J'(S,t) = \frac{1}{v}\frac{1}{N - n_{t,v}}\frac{\partial n_{t,v}}{\partial t}\frac{dt}{dS}$$

[12] $$J'(S) = \frac{1}{v}\frac{1}{N - n_{t,v}}\frac{\partial n_{t,v}}{\partial S}$$

Equation 2, therefore, is a special case of a more general expression for the rate of nucleation with a variable driving force. And, compared with

TABLE 2. Selected data for experiments E_1 and E_2

Parameter	Value					
	E_1			E_2		
	v_1	v_2	v_3	v_1	v_2	v_3
V (cm^3)	2.57×10^{-9}	4.85×10^{-9}	8.18×10^{-9}	5.24×10^{-10}	4.19×10^{-9}	1.41×10^{-8}
t_0 (s)	6540	7380	7380	987	732	834
$t_{0.5}$ (s)	8820	8700	8700	1176	1047	1080
$\frac{dS}{dt}$[a]	0.25	0.090	0.090	0.83	2.1	1.3
$\left[\left(\frac{dS}{dt}\right)^2+1\right]^{-1/2}$	0.97	1.0	1.0	0.77	0.44	0.60
$\left[\left(\frac{dS}{dt}\right)^{-2}+1\right]^{-1/2}$	0.24	0.090	0.090	0.64	0.90	0.80
$J_f'v$ (s^{-1})[b]	6.6×10^{-4}	5.1×10^{-4}	1.3×10^{-3}	6.8×10^{-3}	6.2×10^{-3}	5.1×10^{-3}

[a]These values taken at the t_0 time for each volume range.
[b]J_f' is an experimental rate of nucleation calculated by fitting eq. 3 to the 'number-time' data which reflects the effect of variable non-steady state rates, cation:anion ratios, lag times, and other matrix effects.

eq. 9, it is less appropriate for use in data analysis because of the errors introduced by multiplying together a large number $\partial n_{t,v}/\partial S$ and a small number dS/dt.

Shown in Table 2 are the data required for the calculation of a dimensionless time scale and the selection of an appropriate model to be used in the calculation of J' for three typical volume ranges in each of experiments E_1 and E_2. Best values of $J_f'v$ estimated by fitting [3] to the data are also included in Table 2.

Experiment E_1 was performed under conditions of low dS/dt (Table 2); hence eq. 9 was used to calculate values of J'. These values coupled with S *vs.* time data were used to prepare the E_1 plots in Figs. 7 and 8. Experiment E_2 was performed under conditions of moderate dS/dt (Table 2); hence neither set of approximate relations, eqs. 9 and 10 nor eqs. 11 and 12, would appear appropriate for the calculation of J' values. But, owing to the scatter in the 'number-time' data, the slope and intercept values of the ln J' *vs.* $(\ln S)^{-2}$ and ln J' *vs.* ln S plots prepared using J' values calculated with eq. 7 did not exhibit statistically significant differences from these parameters of the same plots prepared using J' values calculated with eq. 9. Consequently the E_2 plots in Figs. 7 and 8 were prepared from J' values calculated using eq. 9.

The apparent discrepancy within the parameters listed in Table 3, derived from the $n_{t,v}/N$ *vs.* time data collected under conditions of low dS/dt (E_1) and moderate dS/dt (E_2) must arise from additional factors not included in the

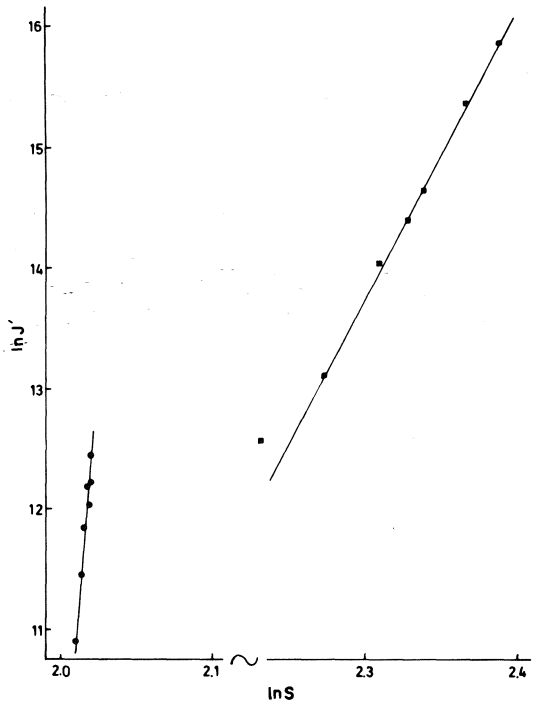

FIG. 7. Plots of ln J' *vs.* ln S for experiments E_1 and E_2: ● = E_1, ■ = E_2.

TABLE 3. Values of various macroscopic parameters calculated from the data shown in Figs. 7 and 8[a]

Experiment[b]	S^*	(S_b^*)	σ (ergs cm^{-2}) $\times 10^9$	n^*	r^* (nm)	ΔG^* (ergs) $\times 10^{12}$	ln A
E_1	7.02±0.35	(7.20±0.20)	56.8±1.7	186±37	1.76±0.14	7.39±0.8	78.9±4.8
E_2	5.57±0.33	(6.13±0.11)	34.4±1.0	45±9	1.10±0.09	1.74±0.2	42.7±2.6

[a]S^*, S_b^*: a critical supersaturation, n^* is critical number of monomers in an embryo, r^* is critical radius of an embryo, ± values are the 95% confidence level.
[b]Figure 6 shows the nature of the variation with time and the extent of the supersaturation for each experiment.

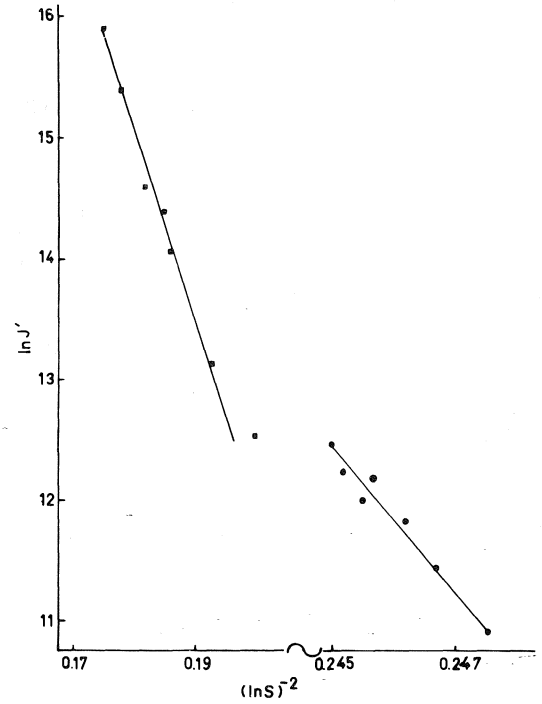

FIG. 8. Plots of ln J' *vs.* (ln S)$^{-2}$ for experiments E_1 and E_2: ● = E_1, ■ = E_2.

model. Some of these factors may be: changing Ca^{2+}:SO_4^{2-} ratios during an experiment, non-steady state rates of nucleation, and changing lag times.

Calcium ion was in excess from the beginning of each experiment but the Ca^{2+}:SO_4^{2-} ratio approached one as the experiments proceeded. In a subsequent report, it will be shown that the nucleation rate at any one ion product varies with the Ca^{2+}:SO_4^{2-} ratio. Measurement of the rate of nucleation as the cation:anion ratio was decreasing had the effect of increasing the slope of the ln J' *vs.* (ln S)$^{-2}$ plot. The curve would also be shifted upwards if the critical supersaturation were reached simultaneously with that Ca^{2+}:SO_4^{2-} ratio which gives a maximum rate.

Non-steady state rates of nucleation of $CaSO_4 \cdot 2H_2O$ generally occurred at very low supersaturations and high values of the Ca^{2+}:SO_4^{2-} ratio. This effectively lengthened the lag time.

Large, but rapidly decreasing, lag times resulting from low, but increasing, supersaturations that exist early in variable driving force experiments are a major source of uncertainty in the analysis of 'number-time' data. Frisch and Carlier (8) have shown that the lag time is a complex function of (ln S)$^{-2}$; thus, our calculated nucleation rates correspond to S measurements of a prior time and this gap increases at lower supersaturation levels. The gap narrows as S increases and eventually becomes negligible.

'Number-time' data will exhibit the influence of a changing lag time during their collection through deviations in both the shape of the $n_{t,v}/N$ *vs.* time curve and the apparent lag time from those expected when S is not changing. These deviations lead to an ever decreasing underestimation of J at increasing values of S; this results in non-linear ln J' *vs.* (ln S)$^{-2}$ curves and overestimation of σ, ΔG^*, S^*, and A (σ = a surface energy, ΔG^* = critical free energy of an embryo, S^* = a critical supersaturation, and A = pre-exponential factor). The data of Table 3 tend to confirm this.

The design of successful nucleation from solution experiments employing a variable driving force depends upon a comparison between the effects of supersaturation and the rate of change of supersaturation on the laboratory observables. The former effects become significant as supersaturation increases whereas the latter are major at lower supersaturations. In most cases, then, it is necessary to achieve some optimum balance between the two. Con-

sequently for our studies on calcium sulfate nucleation from solution using a variable driving force, it seems necessary to generate high final supersaturation levels rapidly thereby causing negligible lag times and non-steady state rate effects.

Acknowledgements

The authors acknowledge the financial assistance provided by the National Advisory Committee on Water Resources Research of the Department of Energy, Mines, and Resources and the National Research Council of Canada. We also acknowledge the helpful discussions with Dr. S. S. QueHee and Mr. D. M. Keller during the revision of the paper.

1. D. TURNBULL. J. Chem. Phys. **18**, 768 (1950).
2. E. K. BIGG. Phys. Soc. Proc. **66**B, 688 (1953).
3. A. E. CARTE. Proc. Phys. Soc. London, **73**, 324 (1959).
4. I. E. KUHNS and B. J. MASON. Proc. R. Soc. A, **302**, 437 (1968).
5. G. R. WOOD and A. G. WALTON. J. Appl. Phys. **41**, 3027 (1970).
6. D. KASHCHIEV. (*a*) Surf. Sci. **18**, 293 (1969); (*b*) **22**, 319 (1970).
7. S. TOSCHEV and I. MARKOV. Ber. Bunsenges. **73**, 184 (1969).
8. H. L. FRISCH and C. C. CARLIER. J. Chem. Phys. **54**, 4326 (1971).
9. J. B. ZELDOVICH. Acta Physicochim. USSR, **18**, 1 (1943).
10. L. SZILARD. (see ref. 11).
11. L. FARKAS. Z. Phys. Chem. (Leipzig) A, **125**, 326 (1927).

Polymorphism in phenol under pressure: dielectric properties and molar polarizations of polycrystalline phenol I and II

JOHN E. BERTIE AND PETER R. TREMAINE[1]

Department of Chemistry, University of Alberta, Edmonton, Alta., Canada T6G 2G2

Received November 12, 1976

JOHN E. BERTIE and PETER R. TREMAINE. Can. J. Chem. **55**, 1294 (1977).

The dielectric properties of phenol I have been measured as isothermal functions of pressure between 140 and 1520 bar and between +35 and −10°C. No dielectric relaxation was observed. The static (50 kHz) permittivity at 10°C is given with a precision of 0.3% by

$$\varepsilon_0' = 2.882 + 4.4 \times 10^{-5}P - 3 \times 10^{-9}P^2$$

where P is in bar. The extrapolated value at 1 bar is 2.882 ± 0.009 which compares with literature values between 2.74 and 2.84. The 50 kHz molar polarization, $\bar{P}$, at 10°C is given by

$$\bar{P}/\text{cm}^3 = 20.30 + 11.75\ V/V_0$$

where V and V_0 are the molar volumes at pressures P and 1 bar, respectively. At 10°C and 1 bar, the electronic and atomic polarizations are estimated to be 26.9 ± 0.3 cm³ and 5.1 ± 0.4 cm³, respectively. Expressions for the isobaric temperature dependence of ε_0' are reported for several pressures. Below 1500 bar, $(\partial\varepsilon_0'/\partial T)_P$ is negative, as expected from the density change but in contrast with previous results and with results obtained while varying the temperature under a constant applied pressure of 1 kbar. The accuracy of the temperature dependence at 1 bar is not high, judging from the thermal expansivity calculated from it.

ε_0' of phenol II at 10°C and an estimated pressure of 2000 bar is 3.10 ± 0.06, with the corresponding molar polarization 30.75 ± 0.5 cm³. No intrinsic dielectric relaxation was observed in phenol II and the molar polarization shows no marked discontinuity at the transition. Phenol II is, therefore, like phenol I, a hydrogen-bonded solid in which the hydroxyl hydrogen atoms are ordered, either fully or in chains. The dielectric parameters and Arrhenius activation energies of two transient dispersions which appeared whenever phenol II formed are discussed.

JOHN E. BERTIE et PETER R. TREMAINE. Can. J. Chem, **55**, 1294 (1977).

On a mesuré les propriétés diélectriques du phénol I comme une fonction isotherme de la pression entre 140 et 1520 bar et entre +35 et −10°C. On n'a observé aucune relaxation diélectrique. On rapporte la permitivité statique (50 kHz) à 10°C avec une précision de 0.3% par l'équation

$$\varepsilon_0' = 2.882 + 4.4 \times 10^{-5}P - 3 \times 10^{-9}P^2$$

où P est exprimé en bar. La valeur extrapolée à 1 bar est de 2.882 ± 0.009 qui se compare avec les valeurs de 2.74 à 2.84 trouvées dans la littérature. La polarisation molaire 50 kHz, $\bar{P}$, à 10°C est représentée par l'équation

$$\bar{P}/\text{cm}^3 = 20.30 + 11.75\ V/V_0$$

où V et V_0 représentent les volumes molaires respectivement aux pressions P et 1 bar. A 10°C et une bar, on estime que les polarisations électroniques et atomiques sont respectivement de 26.9 ± 0.3 cm³ et 5.1 ± 0.4 cm³. On rapporte pour plusieurs pressions des expressions pour la relation isobarique entre la température et ε_0'. Tel que prévu à partir des changements de densité mais en opposition avec les résultats antérieurs et les résultats obtenus lorsque l'on fait varier la température à pression appliquée constante de 1 kbar, la valeur de $(\partial\varepsilon_0'/\partial T)_P$ est négative en dessous de 1500 bar. La précision de la dépendance sur la température à 1 bar n'est pas élevée si l'on en juge à partir de l'expansivité thermique que l'on peut calculer à partir de cette valeur.

ε_0' du phénol II à 10°C et une pression estimée de 2000 bar est de 3.10 ± 0.06 avec une polarisation molaire correspondante de 30.75 ± 0.5 cm³. On n'a observé aucune relaxation diélectrique intrinsèque dans le phénol II et la polarisation molaire ne montre aucune discontinuité importante au niveau de la transition. Le phénol II est donc, comme le phénol I, un

---

[1]Present address: Research Chemistry Branch, Atomic Energy of Canada Limited, Whiteshell Nuclear Research Establishment, Pinawa, Man., Canada R0E 1L0.

solide lié par des ponts hydrogène dans lesquels les atomes de l'hydrogène de l'hydroxyle sont ordonnés soit complètement soit en chaînes. On discute des paramètres diélectriques et des énergies d'activation d'Arrhénius des deux dispersions transitoires qui apparaissent chaque fois que la phénol II est formé.

[Traduit par le journal]

Introduction

The literature concerning the physico-chemical properties and polymorphs of phenol under pressure has been summarized in previous papers (1, 2) which presented results from this study (3).[2] This paper reports the dielectric properties at frequencies below 100 kHz of polycrystalline phenol I and its high pressure polymorph phenol II. Specifically, the static (50 kHz) dielectric permittivity is reported for phenol I at temperatures between -10 and ± 35°C and pressures up to 1.5 kbar, and for phenol II at 10°C and 2 kbar. The corresponding molar polarizations, or Clausius–Mossotti functions, are reported for each phase at 10°C. Also reported are the parameters of two transient dispersions which appeared after the phenol I to II transition had occurred.

The dielectric properties of phenol under pressure have not been studied previously. The dielectric constant of phenol I at atmospheric pressure has been reported to increase slightly with decreasing frequency between 60 and 0.2 kHz (4–6), undoubtedly due to space charge polarization effects (7–9), and to decrease (4, 5), or to remain essentially constant (6), with decreasing temperature from a value of 2.79 $\pm$ 0.05 at $+10$°C and 50 to 60 kHz (4, 5). Although exceptions are known (10–12) the dielectric constant of a solid is expected to increase as the density increases with decreasing temperature (13), but the temperature dependence reported (4–6) for phenol is commonly observed when the solid is at atmospheric pressure because of the formation of cracks in the sample (13–15). The correct temperature dependence can be obtained if the solid is above atmospheric pressure (14, 15).

Experimental

Analar analytical reagent grade phenol was purified in evacuated glass tubes, by directional freezing followed by zone refining in the dark (3). Like Timmermans and Hennaut-Roland (16) we found the melting point to be an unreliable criterion of purity. The purified samples contained less than 0.02 weight percent of water (Karl Fischer titration). The sodium-D line refractive index of the purified samples was 1.5401 at 45.6°C compared with 1.5404 for the commercial product, both measured in a dry atmosphere to an estimated accuracy of ± 0.0001. Timmermans' (16) value is 1.5400. The specific conductivity at 10 kHz decreased from 3.5×10^{-5} μmho cm^{-1} for the commercial product to less than 1.5×10^{-5} μmho cm^{-1} after purification. Mallinckrodt analytical reagent grade phenol was found to be distinctly less pure than the Analar phenol by the above criteria but the samples purified from the two commercial products were identical.

Two piston and cylinder, three terminal, high-pressure dielectric cells were used in conjunction with the 20 ton press which, with the pressure calibration, has been described (1). The coaxial dielectric cell was similar to that described by Whalley *et al.* (17), and is shown in Fig. 1. The cylinder and all steel parts were of Vascomax 350, 18% Ni maraging steel, heat treated to 54 Rockwell C. The taper on electrode a reduced the considerable nonuniformity of the pressure in the cell. Electrode a was joined to its support b by epoxy resin about a mica insulator, which formed an 'unsupported area' pressure seal (18). The two brass backing rings between parts g and h were 0.030 in. apart in the middle of the annulus. The nonconducting coolant which filled the thermostat jacket j was kerosene, either pure or mixed with Skelly C petroleum ether for temperatures below -20°C. The temperature was measured by a calibrated (1) (to ± 0.1°C) thermocouple set in a copper block clamped around the cylinder The parallel-plate cell was that described previously (1), slightly modified to reduce the 'dead space', *i.e.* the cell volume when the electrodes touch, and to reduce intrusion of the sample between the electrodes and the pistons. This cell was thermostatted and its temperature was measured in the way described for the coaxial cell. Temperature gradients were found to occur across both cells and, consequently, the temperatures are only accurate to ± 0.5°C at -40°C and ± 0.1°C at $+10$°C.

Capacitance and conductance were measured by a General Radio 1615A capacitance bridge in conjunction with a General Radio 1310B oscillator, a Rhode and Schwartz UBM tunable indicating amplifier, and a Hewlett-Packard 5321B frequency counter. All connections were coaxial cable whose shields were joined to the common ground of the capacitance bridge through General Radio 847 connectors. The bridge was calibrated against a General Radio 1404B, 100 pF reference standard capacitor, and reproduced the capacitances of a factory-calibrated General Radio 1422CD precision variable capacitor to within 0.003 pF in the 1 to 20 pF capacitance range used in this work. The factory calibration of the dissipation factor, D, and conductance, G, controls was used; values of the dielectric loss calculated from D agreed with those calculated from G to within 1%.

[2]Available from CISTI, the National Research Council of Canada, Ottawa, Canada K1A 0S2. Accession number 21126.

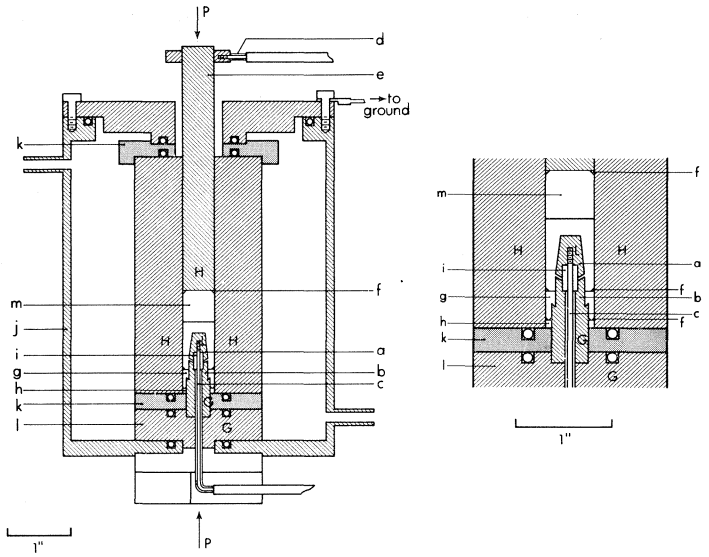

FIG. 1. The coaxial, three terminal, high-pressure dielectric cell. The letters indicate: H, L, G, high, low, and ground potentials; a, steel electrode; b, steel support and guard electrode; c, teflon-insulated low potential lead; d, high potential lead; e, steel piston; f, brass backing ring; g, teflon support; h, bakelite support; i, teflon cylinder; j, stainless steel thermostat jacket; k, bakelite discs; l, steel support disc; m, teflon plug; p, applied pressure. The open circles are Buna-N O-rings.

Cell Constants

Calibration of the coaxial cell with Baker, and Eastman, spectrograde carbon tetrachloride and cyclohexane as dielectric constant standards (19) showed the lead capacitance to be negligible. Therefore the cell constant at atmospheric pressure, about 1 pF, was measured with the cell containing air. This was done at each frequency, because the bridge calibration changed by about 0.8% from 20 to 100 kHz. The cell constant was independent of temperature to within 0.05% between 10 and 35°C and was assumed to remain so to −10°C. The cell constant was also constant provided the top piston was at least 0.5 in. away from the top of the central electrode, a in Fig. 1. The piston was therefore kept 0.75 in. away from the central electrode and the 0.5 in. long teflon plug, m, was used to minimize friction.

The pressure dependence of the coaxial cell constant was calculated from the values 29.1×10^6 p.s.i., 0.26, and 7.17×10^{-7} bar^{-1} for Youngs modulus (20), Poisson's ratio (20), and the compressibility (21), respectively, of the maraging steel. The formula (22)

$$\frac{C}{C_0} = \frac{L}{L_0}\frac{\log (a_0/r_0)}{\log (a/r)}$$

was used, where C, L, r, and a denote the cell constant, length and radius of the inner electrode (a in Fig. 1), and the radius of the bore of the pressure vessel, respectively, at pressure P, and the subscripted entries denote the corresponding atmospheric pressure values. The pressure expansion of the bore of the pressure vessel, $a - a_0$, was taken as 0.75 of the ideal elastic expansion which was calculated as described previously (2). The factor 0.75 was selected because the sample's length-to-radius ratio was 2.8 in the coaxial cell compared with 0.5 in the compression cell for which the factor was, experimentally (2), 0.38. An error of ±0.25 in this factor causes errors of 0.03% and 0.08% in the cell constants at 1000 and 3000 bar, respectively. The length and radius of the inner electrode at pressure P were calculated by multiplying the atmospheric pressure values by $(1 - \beta P/3)$, where β is the compressibility. The radius of the inner electrode varied uniformly from 0.146 in. to 0.115 in. over its length; this electrode was regarded as n cylindrical electrodes in parallel, and $n = 10$ gave sufficient precision. C_0/C varied essentially linearly with pressure and was 1.00288 at 2000 bar.

The cell constant of the parallel-plate cell was only required for +10°C. The capacitance of this cell containing a sample of dielectric constant ε is (23)

$$C = 8.854 \times 10^{-2}\, \varepsilon A/S \text{ pF}$$

The area of the guarded electrode, A (cm^2), was determined from the cell dimensions and was assumed to be independent of pressure. The distance between the electrodes, S (cm), was determined at 750 bar from the measured capacitance and the dielectric constant of phenol at 750 bar and 10°C which was determined using the coaxial cell. The volume of phenol present at 750 bar was calculated from the equation

$$V_{750} = \pi a_{750}^2 S + k$$

where a_{750} is the radius of the bore of the pressure vessel at 750 bar and k is the dead space. k was calculated from the cell dimensions to be 0.11068 ± 0.00010 cm^3 and was assumed to be independent of pressure. The radius, a_{750}, was calculated from the atmospheric pressure value as described previously (2), using 0.38 of ideal elastic expansion because the length-to-radius ratio of the dielec-

TABLE 1. The dielectric constant of phenol I at 50 kHz as a function of pressure for various temperatures

Sample	T(°C)	Dielectric constant (ε')[a]	Highest and lowest pressures (bar)	No. of points
Sample 1	6.5	$2.8758+4.5862\times10^{-5}P-1.7431\times10^{-9}P^2$	344, 1248	8
	24.5	$2.8685+4.9873\times10^{-5}P-3.4037\times10^{-9}P^2$	485, 1519	9
	35.0	$2.8809+4.1352\times10^{-5}P-6.8752\times10^{-10}P^2$	518, 1498	8
	10.0[b]	$2.8773+4.2181\times10^{-5}P-1.2020\times10^{-9}P^2$	346, 1322	8
Sample 2	34.9	$2.8909+3.5462\times10^{-5}P+1.7092\times10^{-10}P^2$	290, 1400	8
	25.0	$2.8823+4.2153\times10^{-5}P-1.4414\times10^{-9}P^2$	337, 1324	8
	10.0	$2.8803+4.2720\times10^{-5}P-3.5512\times10^{-9}P^2$	260, 1324	8
	−0.3	$2.8848+3.6878\times10^{-5}P-2.3062\times10^{-9}P^2$	318, 1362	7
Sample 3	20.2	$2.8889+4.7756\times10^{-5}P-2.4621\times10^{-9}P^2$	140, 1399	11
	10.1	$2.8896+4.7935\times10^{-5}P-4.0375\times10^{-9}P^2$	242, 1312	9
	−0.7	$2.8976+3.6906\times10^{-5}P-3.6226\times10^{-10}P^2$	228, 1156	7
	−10.2	$2.9002+3.6662\times10^{-5}P-1.1885\times10^{-9}P^2$	306, 1288	7

[a] P is the pressure in bar.
[b] The data were taken after phenol II had been formed and transformed back to phenol I, and ε was smaller than at 6.5 and 24.5°C indicating that the cell constant had changed in the transitions. The data were corrected by multiplying by 1.00183, on the assumption that ε at 750 bar varies linearly with temperature between 6.5 and 24.5°C.

tric sample was close to that of the compression sample (2). At other pressures, P, the volume of the sample was calculated from the compression results (2) so the dielectric constant was calculated from the equation

$$\varepsilon_P = \varepsilon_{750}(C_P/C_{750})[(V_P - k)/(V_{750} - k)](a_{750}^2/a_P^2)$$

where C_P and C_{750} are the capacitances of the cell at P and 750 bar, respectively.

Results and Discussion

Phenol I: General

The coaxial cell was assembled under dry nitrogen, using about 2 g of polycrystalline phenol. Each sample was annealed overnight at +35°C and an apparent pressure of 1500 bar. The dielectric constant and loss of phenol I between 100 Hz and 100 kHz were then determined isothermally as functions of increasing pressure and decreasing pressure, neglecting the pressure dependence of the cell constant. The apparent pressure was changed by 125 bar every half hour, and the measurements were made 25 min after the pressure change. When phenol I had been studied at each required temperature, phenol II was formed at +35°C and 2000 bar and was studied as described later.

No dielectric relaxation between 10^2 and 10^5 Hz was found in phenol I between −70 and +40°C. The dielectric constants at 50 kHz were not affected by space charge polarization, except at the lowest pressures when the temperature was above 30°C, so they are used as the static dielectric constants, ε_0'. For each sample at each temperature, ε_0' was plotted against apparent pressure on large graphs, smooth curves were drawn through the points, and the approximately 500 bar hysteresis in the apparent pressure for a given value of ε_0' was removed by averaging the two apparent pressures. The dielectric constants and the averaged pressures were corrected for the deformation of the cell under pressure, and ε_0' was fitted to quadratic equations in pressure by the least-squares method. In all cases the standard and maximum deviations of the observed and calculated dielectric constants were less than 0.00012 and 0.00018 respectively, and the individual deviations were random. The resulting equations are given in Table 1, with the highest and lowest average pressures of the data, and the number of points used to derive each equation. The original dielectric constants and further details are given elsewhere (3).

Phenol I at 10°C

The three equations for 10.0 ± 0.1°C (Table 1) were averaged to give

$$[1]\quad \varepsilon_0' = 2.8824 + 4.4278\times10^{-5}P - 2.9302\times10^{-9}P^2$$

where P is in bar, for the static (50 kHz) dielectric constant of phenol I. Averaged values of ε_0' and $(\partial\varepsilon_0'/\partial P)_{10°C}$ are given in Table 2, with the maximum deviations from the average; the average data have precisions of about 0.3% and 8% which are satisfyingly close, although inferior, to those obtained for alkali halides (11,

TABLE 2. Dielectric constants and molar polarizations of phenol I at 10°C and 50 kHz

		Dielectric constant		$(\partial\varepsilon_0'/\partial P)_{10°C} \times 10^5$/bar^{-1}		Molar polarization/cm^3	
P/bar	V/V_0[a]	Mean	Maximum deviation	Mean	Maximum deviation	Mean	Maximum deviation
0	1.000	2.882	0.008	4.4	0.4	32.05	0.08
250	0.9942	2.893	0.008	4.3	0.3	31.98	0.09
500	0.9888	2.904	0.009	4.1	0.3	31.92	0.10
750	0.9838	2.914	0.009	4.0	0.2	31.86	0.10
1000	0.9791	2.924	0.010	3.8	0.3	31.80	0.10
1250	0.9747	2.933	0.010	3.7	0.3	31.75	0.10
1500	0.9707	2.942	0.010	3.5	0.3	31.71	0.10

[a]From ref. 2.

12, 24) by the superior (25) techniques that can be used for those solids.

Estimates of $(\partial\varepsilon_0'/\partial P)_{10°C}$ were also obtained using the parallel-plate cell. The 50 kHz capacitance of about 5 g of phenol at 10°C was determined as a function of average pressure (the hysteresis was ~350 bar), and was converted to dielectric constant as described earlier, assuming that $\varepsilon' = 2.914$ (eq. 1 and Table 2) at 750 bar. The results are compared in Fig. 2 with the line given by eq. 1. The values of $(\partial\varepsilon_0'/\partial P)_{10°C}$ measured using the two cells disagree by more than the estimated errors, particularly below 750 bar, suggesting that the accuracy of the values listed in Table 2 may be considerably poorer than the precision. This disagreement presumably arises from the defects of both types of cell (25) for such measurements.

The molar polarization, $\bar{P}$, of phenol I at 10°C was calculated from ε_0' (Table 2) through the Clausius–Mossotti equation. The molar volumes at pressures P and atmospheric, V and V_0, were calculated from the volume compressions (2) and the value, 1.132 g cm^{-3} (26), of the density at atmospheric pressure and 25°C, assuming this to be unchanged at 10°C. The molar polarizations in cm^3 are described by the equation

$$[2] \qquad \bar{P} = 20.30 + 11.75\, V/V_0$$

are tabulated in Table 2 and shown in Fig. 3. No dielectric relaxation was detected between +40 and −70°C below 100 kHz in either cell, so the polarization is undoubtedly the sum of electronic and atomic polarizations only. The reduction in the polarization with increasing pressure is the dependence usually observed (11, 12, 24, 25, 27), and it may indicate a reduction in the electronic and atomic polarizations or reflect the inadequacy of the Lorentz local field

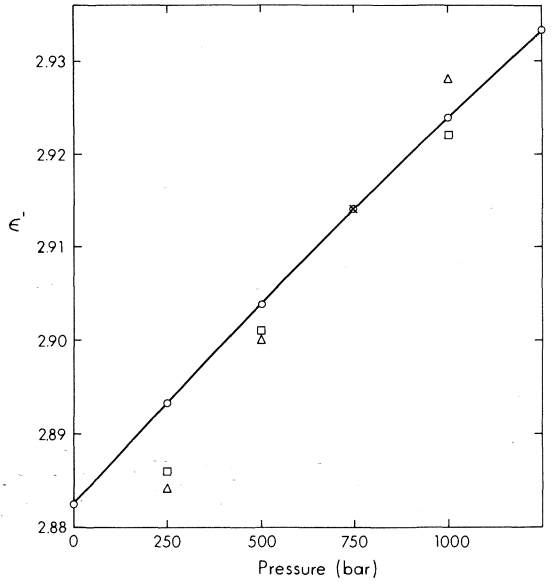

FIG. 2. The 50 kHz dielectric constant of phenol I at 10°C measured using the coaxial cell (line and circles) and the parallel-plate cell (squares and triangles). The values from the two cells were forced to agree at 750 bar.

for the monoclinic (pseudo-orthorhombic) (2 and references cited therein) phenol I. At atmospheric pressure, $\bar{P}$ is 32.05 ± 0.1 cm^3, the electronic polarization was estimated to be 26.9 ± 0.3 cm^3 as described in the next paragraph, so the atomic polarization is 5.1 ± 0.4 cm^3.

The refractive indices are known as a function of wavelength for liquid phenol at 45°C and atmospheric pressure (16, 28) and were fitted to within 0.0002 by the Sellmeier equation (29)

$$n^2 = n_\infty{}^2 + \frac{B}{\lambda^2 - \lambda_0{}^2}$$

where n and n_∞ are the refractive indices at

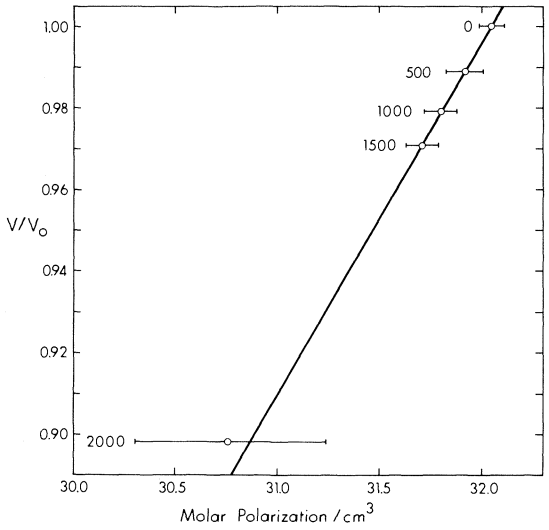

FIG. 3. The 50 kHz molar polarization of phenol I at 10°C plotted against the fractional molar volumes at the pressures (bar) shown to the left of the points. The error bars show the standard deviations. The line represents eq. 2. The 2000 bar point is for phenol II.

wavelengths λ and infinity, $B = 2.4132 \times 10^4$ nm^2, $\lambda_0 = 184.43$ nm, and $n_\infty = 1.5151$. This value of n_∞ and the density of liquid phenol at 45°C, 1.05446 g cm^{-3} (16, 28), yield 26.91 $\pm$ 0.02 cm^3 for the electronic polarization of liquid phenol at 45°C, through the Lorentz–Lorentz equation (30). The only refractive index of phenol I that is known is 1.5930 at the melting point, where that of the liquid is 1.5400; these values were reported (31) for 41°C and unspecified, but probably sodium-D, radiation and, from a comparison with Timmermans' values (16, 28), are probably accurate to $\pm$0.0025. If the density of phenol I at 41°C is assumed to be the same as at 25°C, 1.132 g cm^{-3} (26), the molar polarization of phenol I at 41°C for sodium-D radiation is 28.2 $\pm$ 0.1 cm^3, within 1% of that of liquid phenol at 41°C which is, from Timmermans' data (16, 28), 28.0 $\pm$ 0.2 cm^3. We therefore assume that the electronic polarization of phenol I at 10°C is within 1% of that of liquid phenol at 45°C, and is 26.9 $\pm$ 0.3 cm^3.

Phenol I: Temperature Dependence

The isobaric temperature dependence of ε_0' was calculated from the expressions in Table 1. The expressions for each temperature were multiplied by 1.00196, 1.00127, and 0.99682 for samples 1, 2, and 3, respectively, the factors being those required to yield 2.914 for the dielectric constant at 10°C and 750 bar for each sample. The justification for this is that about half of the difference between different samples appeared to be due to errors in the cell constant. The resulting expressions gave the data shown in Fig. 4. The 50 kHz dielectric constants above 30°C were influenced by electrode polarization, and the same was probably true of the values for sample 2 at 25.0°C. These points were omitted from least-squares fits of the data which gave the expressions shown in Table 3 and the lines drawn in Fig. 4.

The positive value of $(\partial\varepsilon_0'/\partial T)_{1500\text{ bar}}$ (Table 3, Fig. 4, line *A*) is clearly unreliable, because the standard deviation of the fit is of the order of the total change in the dielectric constant. At the lower pressures $(\partial\varepsilon_0'/\partial T)_P$ is negative as expected, confirming that the opposite temperature dependences previously reported (Introduction) are incorrect. Further, the dielectric constant at 10°C and atmospheric pressure found in this work,

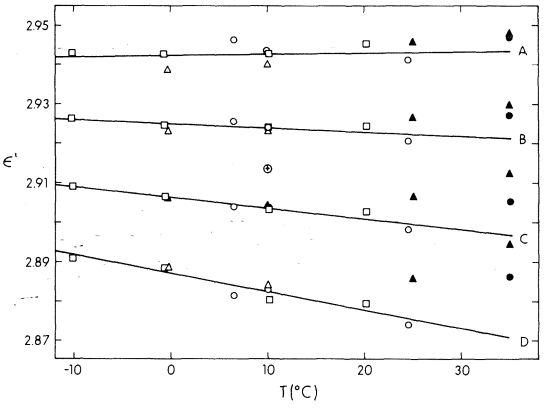

FIG. 4. The 50 kHz dielectric constants of phenol I at *A*, 1500 bar; *B*, 1000 bar; *C*, 500 bar; and *D*, 1 bar, corrected for errors in the cell constants. Symbols ○, △, □, and ⊕ indicate data from samples 1, 2, and 3, respectively, and the value common to all samples. The solid lines represent the expressions given in Table 3.

TABLE 3. Expressions for the isobaric temperature dependence of the 50 kHz dielectric constant of phenol I

Pressure (bar)	Dielectric constant (ε')[a]	Standard deviation
1	$2.8870-4.66\times10^{-4}\,T$	0.0018
500	$2.9063-2.63\times10^{-4}\,T$	0.0010
1000	$2.9248-9.69\times10^{-5}\,T$	0.0014
1500	$2.9424+3.81\times10^{-5}\,T$	0.0026

[a]Calculated from all of the data below 24.9°C. *T* is the temperature (°C).

2.882, is higher than that reported previously, 2.79 ± 0.5 (4, 5), which suggests (13–15) that the previous errors were due to cracks in the samples.

Following Chan and Chew (14, 15) ε_0' of phenol I was also measured as a function of temperature under a constant apparent pressure of 1000 bar in the coaxial cell. The results obtained are shown in Fig. 5 as the curves *XY* (cooling curve) and *YZX* (warming curve) together with Smyth and Hitchcock's data (4) as curve *A*, and the 1000 bar and 1 bar isobars from Fig. 4 and Table 3 as lines *B* and *D*. It is clear that cracks formed in the sample even under a constant apparent pressure of 1 kbar. Thus, although the correct temperature dependence of the dielectric constant of plastic crystals can be determined by applying a small (~10 bar) constant pressure to the sample (14), far more care is required for the more common, harder molecular crystals like phenol and the low-temperature phases of compounds that form plastic crystals (15).

The accuracies of the isobaric temperature dependences of ε_0' below 1500 bar (Table 3, Fig. 4) cannot be high and are difficult to assess. A rough evaluation was made for $(\partial\varepsilon/\partial T)_0$ by using it, through the Clausius–Mossotti equation, to calculate the isobaric thermal expansivity at atmospheric pressure, $\alpha = 1/V_0(\partial V/\partial T)_0$, where V_0 is the molar volume at atmospheric pressure. The molar polarization, $\bar{P}$, was first assumed to be independent of temperature, and this yielded (14) $\alpha = 1.5 \times 10^{-4}$ $(K)^{-1}$ at +10°C. Second, $\bar{P}$ was assumed to depend only on density, so that $(\partial\bar{P}/\partial V)_P = (\partial\bar{P}/\partial V)_T = (1/V_0)(\partial\bar{P}/\partial(V/V_0))_T$ and the following equation was obtained.

$$\alpha = \frac{\dfrac{V}{V_0}\dfrac{-3}{(\varepsilon - 1)(\varepsilon + 2)}\left(\dfrac{\partial\varepsilon}{\partial T}\right)_P}{1 - \dfrac{V}{V_0}\dfrac{1}{\bar{P}}\left(\dfrac{\partial\bar{P}}{\partial(V/V_0)}\right)_T}$$

where V, ε, and $\bar{P}$ are the molar volume, dielectric constant, and molar polarization at pressure P. For atmospheric pressure V/V_0 is unity, $(\partial\bar{P}/\partial(V/V_0))_{10°C}$ is 11.75 ± 0.01 cm^3 for all pressures (eq. 2), and the remaining data given in Tables 2 and 3 yield $\alpha = 2.4 \times 10^{-4}$ $(K)^{-1}$ at 10°C. The only known value of the thermal expansivity of phenol is the mean expansivity between −190°C and +20°C at atmospheric pressure, which is $(2.6 \pm 0.8) \times 10^{-4}$ $(K)^{-1}$ from X-ray data (2). The thermal expansivity increases with increasing temperature, so its value at +10°C must be considerably greater than 2.6×10^{-4} $(K)^{-1}$. We must conclude that either the magnitude of $(\partial\varepsilon_0'/\partial T)_0$ given in Table 3 is too small, or the assumptions used to relate it to the thermal expansivity are poor.

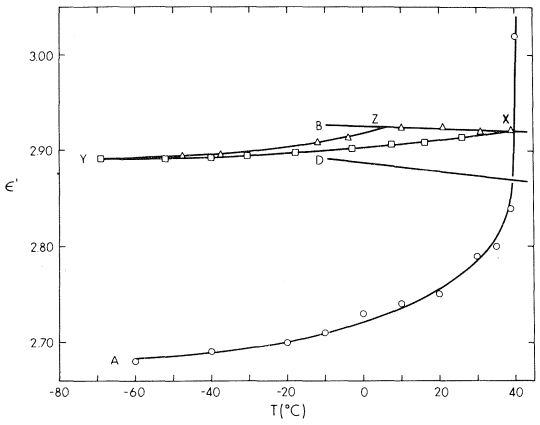

FIG. 5. The dielectric constant of phenol I as a function of temperature. Curve *A* is from ref. 4. Lines *B* and *D* are the 1000 and 1 bar isobars from Fig. 4 and Table 3. *XY* is the cooling and *YZX* the warming curve for phenol under a constant applied pressure of 1 kbar in the coaxial cell.

Phenol II at 10°C

Phenol I was converted to phenol II at +38°C over several hours. These conditions minimized the amplitude of a transient dispersion which always accompanied the formation of phenol II and which is discussed later. Phenol II was then left at +38°C and 2000 bar for the several days required for the dispersion to decrease sufficiently not to influence the measured dielectric constants. The capacitance and conductance were measured at +10°C as functions of frequency, for increasing and decreasing apparent pressures between 1250 and 6000 bar in the coaxial cell and between 1250 and 2500 bar in the parallel-plate cell. The apparent pressure was changed by 300 bar for the coaxial cell, and 125 bar for the parallel-plate cell, every 30 min and the measurements were made 25 min later.

No intrinsic (permanent) dielectric relaxation was detected in phenol II at 10°C between 0.1 and 100 kHz. The apparent pressure ranges used were the maximum available but the 50 kHz capacitance showed little pressure dependence and no pressure-hysteresis in either cell. The pressure dependence of the dielectric constant

of phenol II could not, therefore, be determined. It was argued that the essentially constant measured capacitance was appropriate to a pressure close to the transition pressure, since the pressure uniformity in the cell should be greatest during the transition, and the measured capacitance at an apparent pressure of 2000 bar was assumed to correspond to a true pressure of 2000 bar. The average of three measurements in the coaxial cell and two in the parallel-plate cell gave the 50 kHz dielectric constant of phenol II at +10°C and approximately 2000 bar as 3.10 with a standard deviation of 0.06. From this value, the molar polarization is 30.75 ± 0.5 cm^3 since, from the data used earlier, the density of phenol II at +10°C and 2000 bar is 1.260 g cm^{-3}. This value is included in Fig. 3, and the polarization clearly does not change its volume dependence greatly at the phase transition. This, plus the absence of intrinsic dielectric relaxation in either phase, suggests that phenol II is like phenol I, a hydrogen-bonded solid in which the hydroxyl hydrogen atoms are ordered, either fully or in chains (2 and references cited therein), and are not free to change positions readily. Our failure to observe any pressure dependence of the capacitance of the cells containing phenol II indicates that phenol II is much harder than phenol I.

Phenol II: Transient Dielectric Dispersion

The transient dielectric loss which accompanied the formation of phenol II showed two maxima, at 9 kHz and above 100 kHz at 10°C, and yielded two incompletely resolved Cole–Cole arcs. Its decay with time varied from sample to sample, and in some samples it did not disappear completely. The lower frequency of maximum loss, at a given temperature and pressure, did not change as the loss decayed. The magnitude of the loss was smallest when phenol II was made at high temperature, and the rate of decay was fastest when it occurred at high temperature and low pressure. To determine the Arrhenius activation energies, the real, C', and imaginary, C'', capacitances were measured as functions of temperature for two samples in the parallel-plate cell at a constant apparent pressure of 2000 bar. The data were inadequate to permit an analytical resolution (32) of the two dispersions, so the high- or low-frequency points on the Cole–Cole plots were fitted to a circular arc by bisecting chords drawn between data points. The data from one sample and the fitted arcs are shown in Fig. 6. The relaxation times were calculated from the parameters which defined the circular arcs by the method of Cole and Cole (33, 34), and their logarithms are plotted against reciprocal temperature in Fig. 7. The lines drawn were fitted by the method of least-squares and correspond to the equations

$$[3] \quad \log \tau_1 = 2.730 \times 10^3/T - 14.278$$

and

$$[4] \quad \log \tau_2 = 1.094 \times 10^3/T - 10.213$$

for the low and high frequency dispersions, with standard deviations 0.086 and 0.076 and corresponding Arrhenius activation energies 12.5 ± 0.6 and 5.0 ± 0.5 kcal/mol, respectively.

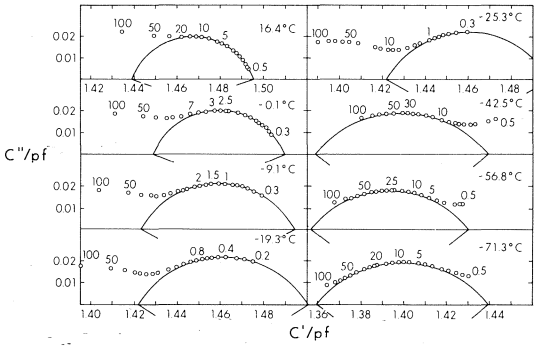

FIG. 6. Cole–Cole plots of the transient dielectric dispersion in phenol II at a constant apparent pressure of 2000 bar in the parallel-plate cell. The numbers beside the points give the frequencies in kHz. The circular arcs fitted to the data are shown.

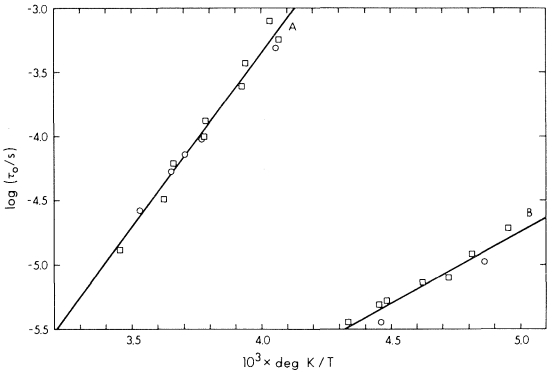

FIG. 7. The temperature dependence of the relaxation times of the two transient dispersions in phenol II at an apparent pressure of 2000 bar. The squares and circles indicate data from different samples. Lines *A* and *B* correspond to eqs. 3 and 4.

These transient dispersions may be due to Maxwell–Wagner effects caused by the precipitation of impurities during the transition (1), and/or to dipolar reorientation at either the phenol II – impurity interface or the phenol II – phenol II interface. Since there were two distinct dispersions, neither of which appeared alone, both mechanisms were likely present. The decay of the Maxwell–Wagner dispersion would result from the slow (1) redissolution of the impurities or from their coalescence from parallel sheets along the particle boundaries into spheres (35). The decay of the interfacial relaxation would result from the decrease in the impurity – phenol II contact area accompanying the above processes, or from an increase in the phenol II particle size by self-annealing which is undoubtedly slow since phenol II is very hard (see above). The well-resolved non-spotty X-ray diffraction lines which we obtained from unground samples of quenched phenol II (2, 3) indicate that phenol II formed with a particle size of 10 to 0.1 μm (36). The room temperature value for τ_1 is typical of Maxwell–Wagner dispersions (35). The 5.0 kcal mol^{-1} activation energy of the high frequency dispersion is consistent with an activation step involving breaking one hydrogen bond to permit hydroxyl rotation at the phenol II interface.

Acknowledgements

We thank the National Research Council of Canada for financial support and for the award of a 1967 Science Scholarship to P.R.T.

1. J. E. Bertie and P. R. Tremaine. J. Chem. Phys. **58**, 854 (1973).
2. J. E. Bertie and P. R. Tremaine. J. Chem. Phys. **63**, 3334 (1975).
3. P. R. Tremaine. Ph.D. Thesis, University of Alberta, Edmonton, Alta. 1974.
4. C. P. Smyth and C. S. Hitchcock. J. Am. Chem. Soc. **54**, 4631 (1932).
5. S. E. Kamerling and C. P. Smyth. J. Am. Chem. Soc. **55**, 462 (1933).
6. V. A. Tolkachev and V. I. Kovalevskii. Zh. Fiz. Khim. **44**, 1365 (1970); Russ. J. Phys. Chem. **44**, 768 (1970).
7. J. F. Johnson and R. H. Cole. J. Am. Chem. Soc. **73**, 4536 (1951).
8. W. Dannhauser and R. H. Cole. J. Am. Chem. Soc. **74**, 6105 (1952).
9. M. Davies. *In* Dielectric properties and molecular behaviour. *Edited by* N. E. Hill, W. E. Vaughan, A. H. Price, and M. Davies. Van Nostrand Reinhold Company, London. 1969. Chapt. 5, p. 280.
10. S. R. Gough. Can. J. Chem. **50**, 3046 (1972).
11. K. F. Young and H. P. R. Frederikse. J. Appl. Phys. **40**, 3115 (1969).
12. P. A. Smith and D. H. Riehl. J. Phys. Chem. Solids, **35**, 1327 (1974).
13. C. P. Smyth. *In* Physics and chemistry of the organic solid state. Vol. 1. *Edited by* D. Fox, M. M. Labes, and A. Weissberger. Interscience. 1963. Chapt. 12, Sections IIIB and C.
14. R. K. Chan and H. A. Chew. Can. J. Chem. **47**, 2249 (1969).
15. H. A. Chew and R. K. Chan. Can. J. Chem. **51**, 2141 (1973).
16. J. Timmermans and Mme. Hennaut-Roland. J. Chim. Phys. **34**, 693 (1937).
17. E. Whalley, J. B. R. Heath, and D. W. Davidson. J. Chem. Phys. **48**, 2362 (1968).
18. P. W. Bridgman. Proc. Am. Acad. Arts Sci. **49**, 627 (1914).
19. A. A. Maryott and E. R. Smith. Tables of dielectric constants of pure liquids. N.B.S. Circular 514. 1951.
20. Preliminary Data, 18% Nickel 350 Maraging Steel. International Nickel Company of Canada, Toronto. 1968.
21. R. J. Roark. Formulas for stress and strain. Fourth ed. McGraw-Hill Book Company, New York. 1964. p. 91.
22. C. P. Smyth. Dielectric behaviour and structure. McGraw-Hill Book Company, New York. 1955. p. 204.
23. F. W. Sears. Electricity and magnetism. Addison-Wesley, Reading, MA. 1951. p. 205.
24. B. W. Jones. Philos. Mag. **16**, 1085 (1967).
25. E. Whalley. *In* Advances in high pressure research. Vol. 1. *Edited by* R. S. Bradley. Academic Press, NY. 1966. Chapt. 3. p. 143.
26. R. J. L. Andon, D. P. Biddiscombe, J. D. Cox, R. Handley, D. Harrop, E. F. G. Herington, and J. F. Martin. J. Chem. Soc. (London), **1960**, 5246 (1960).
27. M. S. Costantino and W. B. Daniels. J. Chem. Phys. **62**, 764 (1975) and references cited therein.
28. J. Timmermans. Physico-chemical constants of pure organic compounds. Vol. 1. Elsevier, New York. 1950. p. 459.
29. A. H. Price. *In* Dielectric properties and molecular behaviour. *Edited by* N. E. Hill, W. E. Vaughan, A. H. Price, and M. Davies. Van Nostrand Reinhold Company, London. 1969. Chapt. 4. p. 236.
30. A. H. Price. *In* Dielectric properties and molecular behaviour. *Edited by* N. E. Hill, W. E. Vaughan, A. H. Price, and M. Davies. Van Nostrand Reinhold Company, London. 1969. Chapt. 3. p. 191.
31. F. Nechai. Soviet Phys.-Tech. Phys. **1**, 423 (1956); Zhurnal Teknicheskoi Fiz. **26**, 436 (1956).
32. W. Dannhauser. J. Chem. Phys. **55**, 629 (1971).
33. K. S. Cole and R. H. Cole. J. Chem. Phys. **9**, 341 (1941).
34. M. Davies. *In* Dielectric properties and molecular behaviour. *Edited by* N. E. Hill, W. E. Vaughan, A. H. Price, and M. Davies. Van Nostrand Reinhold Company, London. 1969. p. 290.
35. L. K. H. van Beck. Progress in Dielectrics, **7**, 69 (1969).
36. L. V. Azaroff and M. J. Buerger. The powder method in X-ray crystallography. McGraw-Hill, New York, Toronto, London. 1958.

Nuclear magnetic resonance relaxation and anisotropic reorientation in liquid dimethylmercury

CLAUDE R. LASSIGNE AND E. J. WELLS

Chemistry Department, Simon Fraser University, Burnaby 2, B.C., Canada V5A 1S6

Received October 29, 1976

CLAUDE R. LASSIGNE and E. J. WELLS. Can. J. Chem. **55**, 1303 (1977).

Spin–lattice relaxation times of ^{1}H, D, and ^{199}Hg have been measured between 234 and 333 K in liquid dimethylmercury and its isotopic modifications. These measurements have allowed the relaxation mechanisms to be separated. It was found that the spin–rotation interaction is the dominating mechanism for the ^{199}Hg relaxation at 14.1 kG even at low temperatures. We have estimated the spin–rotation constants, $C_{\parallel} = -120 \pm 60$ kHz and $C_{\perp} = -23 \pm 3$ kHz along with the chemical shift anisotropy $\Delta\sigma = \sigma_{\parallel} - \sigma_{\perp} = +4600 \pm 1000$ ppm. It is concluded that reorientation about the symmetry axis is not well described by molecular diffusion. Reorientation of the methyl group about its symmetry axis is found to be approximately forty times faster than the reorientation about the perpendicular axis.

CLAUDE R. LASSIGNE et E. J. WELLS. Can. J. Chem. **55**, 1303 (1977).

On a mesuré, entre 234 et 333 K, les temps de relaxation spin–réseau de ^{1}H, D et ^{199}Hg dans le diméthylmercure liquide et dans ses modifications isotopiques. Ces mesures ont permis de séparer les mécanismes de relaxation. On a trouvé que l'interaction spin–rotation est le mécanisme dominant pour la relaxation du ^{199}Hg à 14.1 kG même à basse température. On a estimé les valeurs des constantes spin–rotation $C_{\parallel} = -120 \pm 60$ kHz et $C_{\perp} = -23 \pm 3$ kHz ainsi que l'anisotropie du déplacement chimique $\Delta\sigma = \sigma_{\parallel} - \sigma_{\perp} = +4600 \pm 1000$ ppm. On en conclut que la réorientation autour de l'axe de symétrie n'est pas bien décrite par la diffusion moléculaire. La réorientation du groupe méthyle autour de l'axe de symétrie est approximativement 40 fois plus rapide que la réorientation autour de l'axe perpendiculaire.

[Traduit par le journal]

Introduction

Nuclear magnetic resonance is a convenient probe for the study of the rotation of molecules in liquids (1) because the nuclear spin-relaxation time depends on the molecular motion although there is still some question as to the validity of the various proposed models. In a molecule in the liquid phase, the more nuclei whose relaxation time can be measured, the more information one can obtain about the motions of that particular molecule (2, 3). For nuclei of spin $I \geq 1$ the quadrupolar relaxation is generally the dominant mechanism in the spin–lattice relaxation time. However, for nuclei of spin 1/2 the problem is more complicated because of the various possible mechanisms which may contribute to the total relaxation rate.

In a number of studies involving nuclei of spin 1/2, ^{13}C (4–7), ^{19}F (8), ^{31}P (9), ^{15}N (10), ^{119}Sn (11, 12), and ^{207}Pb (13), it has been shown that the spin–rotation contribution to the spin–lattice relaxation rate is the dominant mechanism. There appears to be a trend showing that the spin–rotation interaction ($I \cdot C_0 \cdot J$) becomes more important for the higher Z nuclei of spin 1/2, however, studies involving these higher Z nuclei have rarely been reported in the literature. If indeed this interaction is large it should be reflected in the value for the spin–rotation constant C_0 for the ^{199}Hg nucleus in $Hg(CH_3)_2$.

Along with the study of the relaxation of the ^{199}Hg nucleus we have also studied the ^{1}H and D temperature dependence of the spin–lattice relaxation times and thus derived the anisotropic reorientational motion of the dimethylmercury molecule.

Experimental

Measurement of Relaxation Times

The proton spin–lattice relaxation times T_1 were measured by the saturation recovery method (14) and rapid adiabatic passage with sampling (15) on a Varian A56/60 high resolution nmr spectrometer operating at 60 MHz. The D spin–lattice relaxation times were measured at 15.4 MHz by rapid adiabatic passage with sampling on a Varian XL-100 nmr spectrometer.

The ^{199}Hg (16.84%, $I = 1/2$) relaxation times were measured indirectly by the modified rotary echo method of Wells and Abramson (16*a*) and Chan (16*b*) on the *proton* multiplet components. $R_{2r}(\equiv T_{2r}^{-1})$ for protons

was obtained at 60 MHz (14.1 kG). The relaxation rate is given in the rotating frame by

$$[1] \qquad R_{2r} = \tfrac{1}{2}(R_{1H} + R_{2H})$$

Therefore by performing a selective rotary echo experiment on the central proton signal due to the dimethylmercury molecules containing non-magnetic Hg ($I = 0$) we obtain,

$$[2] \qquad R_{2r}^{I} = \tfrac{1}{2}(R_{1H}^{I} + R_{2H}^{I})$$

For this case the value of $R_{2r}(H)$ was found to be the same as $R_1(H)$ which means that $R_{1H}^{I} = R_{2H}^{I}$.

Also performing a selective rotary echo experiment on either member of the proton doublet due to $^{199}Hg(CH_3)_2$ molecules (see Fig. 1) we obtain

$$[3] \qquad R_{2r}^{II} = \tfrac{1}{2}(R_{1H}^{II} + R_{2H}^{II})$$

Here $R_{1H}^{II} = R_{1H}^{I}$ since both dipole and scalar T_1 contributions from ^{199}Hg to ^1H are negligible, and $R_{2H}^{II} = R_{1H}^{II} + R_1(^{199}Hg)$; where $R_1(^{199}Hg)$ is the mercury-199 scalar contribution to the proton R_{2H} in the slow relaxation limit ($R_1(^{199}Hg) \ll 2\pi J_{^1H-^{199}Hg}$) which is well satisfied here.

The ^{201}Hg isotope (13.22%, $I = 3/2$) is scalar coupled to ^1H but collapsed in the spectrum, and affords a scalar R_2 mechanism to the ^1H which is included with the rotary echo measurement on Hg ($I = 0$) resonance. Assuming the reasonable value of 500 MHz for the quadrupole coupling constant of ^{201}Hg in $Hg(CH_3)_2$, we estimate $T_1(^{201}Hg) \approx 10^{-7}$ s and since $J_{^{201}Hg-H}$ is ≈ 38 Hz, it can be shown that the effect of the collapsed ^{201}Hg multiplet on the central ^1H component is to modify the observed R_2 by only a negligible 2%.

Therefore using these two selective rotary echo experiments we can indirectly obtain values of $R_1(^{199}Hg)$.

$$[4] \quad R_1(^{119}Hg) = 2(\Delta R_{2r}) = 2(R_{2r}^{II} - R_{2r}^{I})$$

For the mixtures of $Hg(CH_3)_2$ and $Hg(CD_3)_2$ there was no evidence of any of the mixed species such as CH_3—Hg—CH_2D etc. or CH_3—Hg—CD_3 so that in the separation of the various mechanisms possible H–D or CH_3–CD_3 exchange could be neglected.

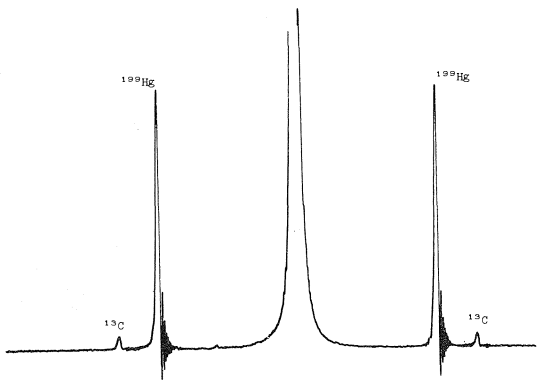

FIG. 1. ^1H spectrum of neat liquid $Hg(CH_3)_2$ at 60 MHz.

Temperature control was accomplished using the Varian V-6040 temperature nmr probe accessory. Temperatures were measured using a copper constantan thermocouple and temperature readings were stable to $\pm 1°C$.

Synthesis of $Hg(CD_3)_2$

The dimethylmercury-d_6 was prepared according to Gilman and Brown's Grignard method (17) with minor modifications. In a dry 100 cc flask fitted with "Drierite" was added 2.0 g of Mg turnings. To this was added 10 cc of dry (absolute) ether and 2.0 g of dry methyl iodide-d_3 (Merck, Sharp and Dohme of Canada). As soon as the reaction had started, a solution of 8.0 g of CD_3I in 40 cc of dry (absolute) ether was slowly added. An ice bath was used to cool the reaction flask when the reaction proceeded too vigorously. When spontaneous refluxing had ceased, the mixture was further refluxed for 30 min to drive the reaction to completion.

The Grignard reagent was carefully decanted from the excess Mg into a 500 cc flask fitted with a condenser and heated until refluxing had begun. To this was attached a Soxhlet extractor containing 7.15 g of $HgCl_2$; 75 cc of dry (absolute) ether was added to the flask. This was allowed to reflux for 3 days to improve the yield of the dimethylmercury-d_6.

After 3 days of refluxing the solution was cooled in ice and the excess Grignard reagent was destroyed by the addition of about 25 cc of water through the condenser. The water had to be carefully added to keep the reaction from becoming too vigorous. Next the ether layer was separated and the aqueous layer extracted with 20 cc of dry (absolute) ether. The combined ether extract was washed with 25 cc of water, separated, and dried over $CaCl_2$. The ether was carefully distilled off using a 'spiral' column. The remaining traces of ether were separated out using preparative vapor phase chromatography. The yield was 3.92 g of $Hg(CD_3)_2$ (57% yield); bp 88–89°C (uncorrected).

The $Hg(CH_3)_2$ was obtained from Alfa Inorganics. The samples were degassed in 5 mm tubes by the usual freeze–pump–thaw cycles under vacuum. The viscosity and density were measured by standard methods.

Spin–Spin Coupling Constants and Chemical Shifts in $Hg(CH_3)_2$ and $Hg(CD_3)_2$

We have measured the various nuclear spin–spin coupling constants for $Hg(CH_3)_2$ and $Hg(CD_3)_2$ using ^1H and ^{13}C nmr. These values are tabulated in Table 1.

The first four coupling constants are in excellent agreement with the results of Dean and McFarlane (18). The last two coupling constants have not been previously reported. The value of $H_{^1H-^2D} = 1.9 \pm 0.1$ Hz indicates that the $\angle$H—C—D is very close to 109.5° since the geminal coupling constant is very sensitive to small changes in the $\angle$H—C—H angle (19).

The ratio J_{C-H}/J_{C-D} is always close to the value predicted by the gyromagnetic ratios $\gamma_H/\gamma_D =$

TABLE 1. Nuclear spin–spin coupling constants in $Hg(CH_3)_2$ and $Hg(CD_3)_2$*

Parameter	Value (Hz)	Source
$^1J_{^1H-^{13}C}$	129.5 ±0.2	^1H spectrum
$^2J_{^1H-^{199}Hg}$	101.5 ±0.2	^1H spectrum
$^1J_{^{13}C-^{199}Hg}$	684.6 ±0.3	^{13}C–{^1H} decoupled
$^4J_{^1H-^1H}$	0.43±0.03	^1H spectrum
$^1J_{^1H-^2D}$	1.9 ±0.1	^1H spectrum
$^1J_{^{13}C-^2D}$	19.8 ±0.6	^{13}C undecoupled spectrum

*^1H spectrum obtained on Varian A56/60 at 60 MHz and ^{13}C spectrum obtained on XL-100 operating at 25.1 MHz in FT mode.

6.5144 (20). We find the value of $J_{C-H} - 6.5144 \times J_{C-D}$ as $+0.6 \pm 4.0$ Hz. Thus it appears that there is no significant isotope effect on the coupling constants. These results are in agreement with those observed for a variety of deuterated organic compounds (21).

We have also measured the deuterium isotope shift on both ^{13}C and ^1H resonances of $Hg(CH_3)_2$ and modified species. The values obtained are $\delta_{isot}(^{13}C) = 0.95 \pm 0.07$ ppm (upfield on deuteration) and $\delta_{isot}(^1H)$ $(CH_3 \rightarrow CHD_2) = 0.040 \pm 0.003$ ppm (also upfield). The isotope shifts in the ^1H and ^{13}C spectra are representative of the differences of ranges in chemical shifts ($^{13}C \approx 600$ ppm and $^1H \approx 20$ ppm).

Results and Analysis

For most nuclei of spin 1/2 the relaxation is caused by a combination of mechanisms: intermolecular and intramolecular dipolar coupling, spin–rotation interaction, and possibly chemical shift anisotropy. The proton relaxation data in Table 2 and Fig. 2 indicate the presence of at least two mechanisms in the relaxation rate.

The form of the chemical shift anisotropy contribution is

$$R_1^{CSA} = \frac{2}{15}\gamma^2 H_0^2(\sigma_{\parallel} - \sigma_{\perp})^2\tau_c$$

since $\tau_c \approx 10^{-12}$ s and $(\sigma_{\parallel} - \sigma_{\perp}) \approx 1$–5 ppm for protons usually, $R_1^{CSA} \approx 10^{-9}$ s^{-1} for protons is negligible. For ^{199}Hg the chemical shift anisotropy $(\sigma_{\parallel} - \sigma_{\perp})$ may be as large as 5000 ppm. This value gives $R_1^{CSA} \approx 0.1$ s^{-1} which is small but may not be negligible.

Extrapolation from data by standard type of dilution studies (22) of $Hg(CH_3)_2$ in $Hg(CD_3)_2$ allows the separation of intermolecular dipole–dipole effects from intramolecular mechanisms for protons. In the ^{199}Hg relaxation in dimethylmercury it is safe to assume that the intermolecular ^1H–^{199}Hg dipole–dipole relaxation is insignificant as in the ^{13}C relaxation (23) because of the much increased intermolecular nuclear separation. Thus we are left with the separation of the intramolecular contributions to both the ^1H and ^{199}Hg relaxation rates.

TABLE 2. R_1 relaxation data for liquid $Hg(CH_3)_2$–$Hg(CD_3)_2$ mixtures*

	R_1 (s^{-1}), ^1H of		
T (K)	100% $Hg(CH_3)_2$	60% of $Hg(CH_3)_2$	27% of $Hg(CH_3)_2$
333	0.109	0.099	0.085
315	0.118	0.108	0.093
296	0.139	0.128	0.114
282	0.156	0.135	0.117
270	0.183	0.157	0.120
258	0.203	0.160	0.143
250	0.220	0.170	0.148
234	0.271	0.211	0.182

*In $Hg(CD_3)_2$. Error in measured relaxation rates is ±5%.

D in $Hg(CD_3)_2$		^{199}Hg in $Hg(CH_3)_2$	
T (K)	R_1 (s^{-1})	T (K)	R_1 (s^{-1})
333	0.410	333	1.150
311	0.422	315	0.970
298	0.459	296	0.850
267	0.557	282	0.780
263	0.570	270	0.774
245	0.641	258	0.670
240	0.684	250	0.600
234	0.743	234	0.571
219	0.828		

Proton Relaxation

The temperature-dependent proton relaxation times are shown in Fig. 2 for pure $Hg(CH_3)_2$ and mixtures containing 27 and 60% mole fraction $Hg(CH_3)_2$ in $Hg(CD_3)_2$ respectively. The intermolecular relaxation rate for the mixtures is given as,

$$[5] \quad R_{1inter}^{H} = R_{1inter}^{H-H} + R_{1inter}^{H-D} + R_{1inter}^{^1H-^{199}Hg}$$

Since $\gamma_H^2 = 42.5\gamma_D^2$ and the spin values are different, the deuterium in dimethylmercury-d_6 will contribute 1/24 as much to the intermolecular relaxation as the hydrogens in dimethylmercury-h_6. The total proton relaxation is then

$$[6] \quad R_{1total}^{H} = \frac{23C + 1}{24} R_{1inter}^{H-H} + R_{1inter}^{^1H-^{199}Hg} + R_{1intra}^{dd} + R_1^{SR}$$

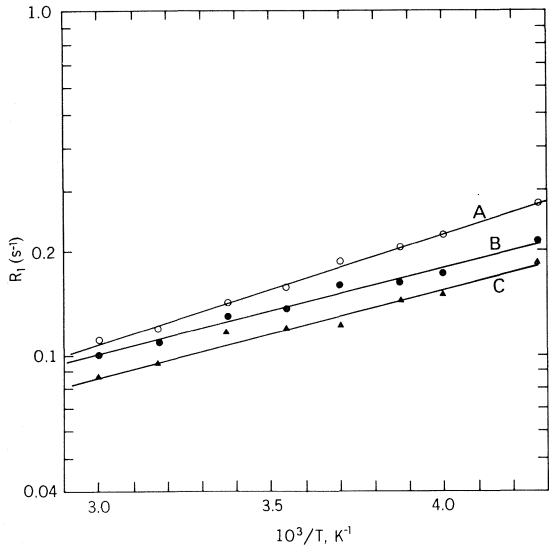

FIG. 2. Experimental relaxation rates for ^1H in dimethylmercury; (*A*) neat $Hg(CH_3)_2$; (*B*) 60% $Hg(CH_3)_2$ in $Hg(CD_3)_2$; (*C*) 27% $Hg(CH_3)_2$ in $Hg(CD_3)_2$.

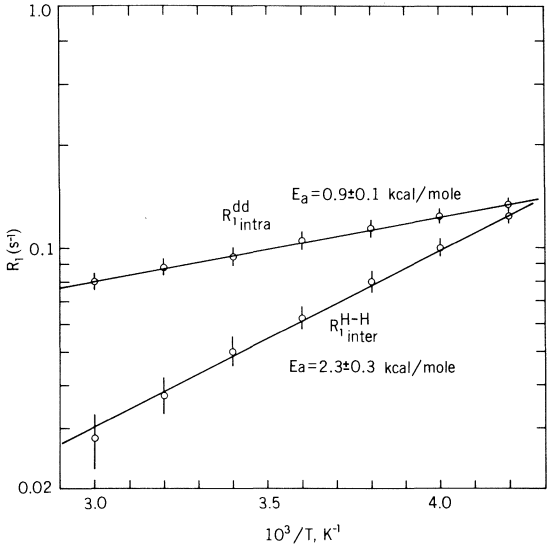

FIG. 3. Separation of $R_{1\,inter}^{H-H}$ from R_{intra}^{dd} for the ^1H relaxation rate in $Hg(CH_3)_2$.

where C is the mole fraction of dimethylmercury-h_6. A plot of $R_1{}^H$ *vs.* $23C/24$ yields

$$[7] \qquad \text{Slope} = R_{1\,inter}^{H-H}$$

$$[8] \qquad \text{Intercept} = \tfrac{1}{24} R_{1\,inter}^{H-H} + R_{1\,inter}^{H-^{199}Hg} + R_{1\,intra}^{dd} + R_1{}^{SR}$$

We may eliminate $R_{1\,inter}^{H-^{199}Hg}$ if we assume that d^0_{H-Hg} equals d^0_{H-H} (in fact d^0_{H-Hg} will actually be greater than d^0_{H-H}), we must also keep in mind that ^{199}Hg is only 16.86% natural abundance, whence

$$[9] \qquad R_{1\,inter}^{H-^{199}Hg} \approx 0.024 R_{1\,inter}^{H-H}$$

We are then left with separating $R_{1\,intra}^{dd}$ from $R_1{}^{SR}$. The plots of Fig. 2 show no curvature, which would normally be present if we had a mixture of intramolecular dipole–dipole and spin–rotation interactions since these two mechanisms have opposite temperature dependence. It appears safe to assume that at least over the temperature range studied the spin–rotation contribution is negligible for protons and that the only relaxation mechanisms present are those due to inter- and intramolecular dipole–dipole interactions. The separation of these two mechanisms is shown in Fig. 3. For the intermolecular interaction the energy of activation is 2.3 ± 0.3 kcal/mol and for the intramolecular dipole–dipole it is 0.9 ± 0.1 kcal/mol. The data indicate the intermolecular dipole–dipole mechanism to be predominant at the higher temperatures.

Anisotropic Rotational Diffusion Tensor for $Hg(CD_3)_2$

The usual method of obtaining the anisotropic rotational diffusion tensor of a symmetric top molecule involves the measurement of the relaxation time of two quadrupolar nuclei which have different bond angles with respect to the symmetry axis of the molecule (24–27). Thus in our molecule we could determine the anisotropic rotational diffusion tensor for dimethylmercury-d_6 from quadrupolar relaxation of both D and ^{201}Hg. The equations that relate the measured relaxation rate of a nucleus to the diffusion tensor components and the relative orientation to the electric field gradient are, in the rotational diffusion limit (28):

$$[10] \qquad R_{1Q} = \frac{3\pi^2(2I+3)}{10I^2(2I-1)} (e^2qQ/h)^2 \tau_c$$

$$[11] \qquad \tau_c = \frac{\frac{1}{4}(3\cos^2\theta - 1)^2}{6D_\perp} + \frac{3\sin^2\theta\cos^2\theta}{5D_\perp + D_\parallel} + \frac{\frac{3}{4}\sin^4\theta}{2D_\perp + 4D_\parallel}$$

The problem is that the ^{201}Hg resonance is not observable either directly or indirectly because of its very short relaxation time due to its pre-

sumably large quadrupole coupling constant. We must therefore find a different method of obtaining $D_\perp$ and $D_\parallel$. First we use the D relaxation times of Fig. 4, the approximate D quadrupole coupling constant for molecules containing methyl groups (165 kHz) and eq. 10 to obtain τ_c(D).

It has been shown experimentally (29) that $D_\parallel$ is invariant to deuteration in acetonitrile and we assume the same to be true here. However, this does not matter much since τ_c(H–H) and τ_c(D) are quite insensitive to changes in $D_\parallel$ because in the calculation of τ_c(H–H) and τ_c(D) using eq. 11 $\sim$90% and $\sim$70% respectively come from the first term which is solely dependent on $D_\perp$. The term $D_\perp$ has been found to be about 7% different in going from CH_3CN to CD_3CN (29) and for our $Hg(CH_3)_2$ case we calculate the difference in $D_\perp$'s to be $\sim$12% which we will assume is negligible. With these points in mind we will proceed with our analysis for $D_\parallel$ and $D_\perp$.

We use Powles' expression (30),

$$[12] \qquad R_{1\,\mathrm{intra}}^{\mathrm{H-H}} = \frac{3\gamma_H{}^4\hbar^2}{r_{\mathrm{H-H}}^6}\,\tau_c(\mathrm{H\text{–}H})$$

(which assumes independent pairwise interactions and neglects symmetry effects) to obtain τ_c(H–H). This is the effective correlation time for reorientation of the proton internuclear vector. For this correlation time $\theta = 90°$ in eq. 11 because the pertinent proton relaxation interaction occurs in the plane of the methyl hydrogens. This plane is normal to the major axis. Using the appropriate values for the constants and $r_{\mathrm{H-H}}$ (from Table 3) in eq. 12 we obtain

$$[13] \qquad R_{1\,\mathrm{intra}}^{\mathrm{H-H}} = 4.86 \times 10^{10}\tau_c(\mathrm{H\text{–}H})$$

Using eq. 11, the experimental values for τ_c(H–H), τ_c(D), $\theta = 90°$ for τ_c(H–H) and $\theta = 109° 28'$ for τ_c(D) we can solve for the temperature dependence of both $D_\perp$ and $D_\parallel$. These are given in Fig. 5. We find E_a for $D_\perp$ is 0.85 $\pm$ 0.15 kcal/mol and for $D_\parallel$, E_a = 1.30 $\pm$ 0.60 kcal/mol. Also the reorientation *about* the figure axis is about forty times faster than reorientation *of* the figure axis. The values for $D_\parallel$ have a great uncertainty because τ_c(D) and τ_c(H–H) are largely dependent on the value of $D_\perp$; hence large changes in $D_\parallel$ have very little effect on either τ_c(D) or τ_c(H–H). The value of $E_a(D_\parallel)$ = 1.30 $\pm$ 0.60 kcal/mol would appear a bit high since in most cases involving methyl group reorientation $E_a(D_\parallel) = \sim$0.8 kcal/mol (2, 4, 7, 24, 25), however a value of 0.8 kcal/mol is *within* the uncertainty of our analysis.

The error limits given for the $D_\parallel$ and $D_\perp$ activation energies are derived from the assumptions that the correlation times τ_c(H–H) and τ_c(D) have a $\pm$5% error and thus in the solution of the two simultaneous equations one obtains a range of $D_\perp$'s and $D_\parallel$'s and thus error limits in the E_a's.

Although our E_a's for $D_\parallel$ and $D_\perp$ appear quite different from that found for CH_3CN and CH_3I (2, 4) there are reasonable explanations. In CH_3CN and CH_3I (2, 4) the energy of activation for $D_\perp$ was found to be $\sim$1.7 kcal/mol while in

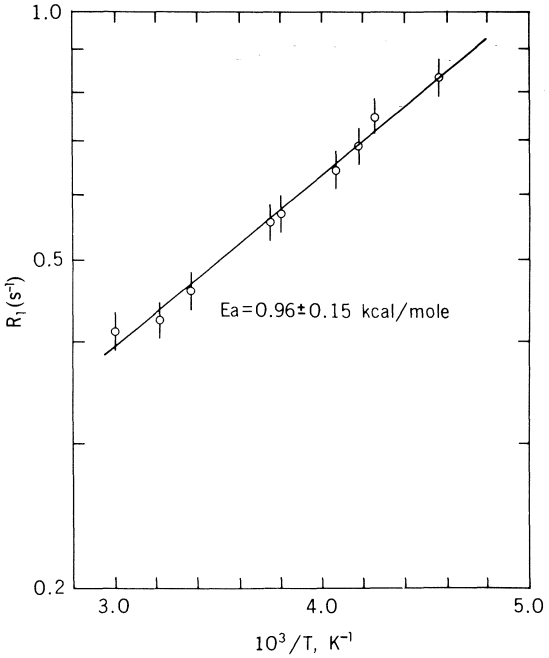

FIG. 4. D spin–lattice relaxation rate in $Hg(CD_3)_2$.

TABLE 3. Geometric parameters and moments of inertia for $Hg(CH_3)_2$

Parameter	Value
r_{C-H}*	1.096 Å
r_{H-H}*	1.81 Å
r_{Hg-C}†	2.094 Å
r_{Hg-H}	2.62 Å (calculated)
∠H—C—H*	109.5°
∠C—Hg—C†	180°
$I_\parallel$	11.0×10^{-40} g cm²
$I_\perp$†	240.8×10^{-40} g cm²

*Typical values of average $-CH_3$ group.
†Reference 48.

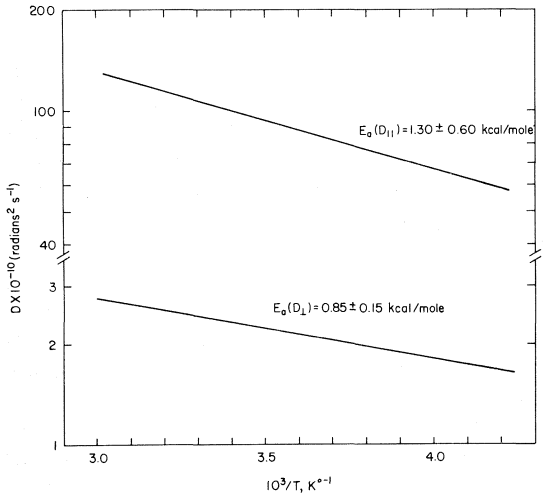

FIG. 5. Rotational rate constants ($D_{\|}$, $D_{\perp}$) for Hg-$(CD_3)_2$.

dimethylmercury we found $E_a(D_{\perp})$ to be only 0.9 kcal/mol. A possible reason for this low value may have been that at the higher temperatures a small amount of spin–rotation may have been present in the proton relaxation rate. Subtraction of this R_1^{SR} contribution from $R_{1\,intra}^{H}$ would give us a smaller $R_{1\,intra}^{dd}$ and thus a smaller value for the correlation time τ_c(H–H) which would mean $E_a(D_{\perp})$ would then be greater than the measured 0.9 kcal/mol.

In the past the nmr rotational correlation time, τ_θ, for the isotropic rotation of a spherical molecule was given in terms of the viscosity η,

$$[14] \qquad \tau_\theta = \frac{4\pi a^3 \eta}{3kT}$$

However, it has been found that the activation energies (31, 32) of τ_θ and η/T do not always agree, as is the case here, $E_a(\eta/T) \cong 2$ kcal/mol while $E_a(\tau_\theta) \approx 0.9$ kcal/mol. This is not surprising since τ_θ is a measure of the rotational motion and η is a measure of the translational motion. The inadequacy of eq. 14 has recently been observed in the pressure dependence of τ_θ and η (33–36). The conclusions were that agreement between the temperature and pressure dependences of η/T and τ_θ will only occur if the rotational and translational motions are highly coupled. Their results on monosubstituted benzenes (35) and toluene-d_8 (36) indicate that molecular shape is the decisive factor in determining the degree of coupling between the rotational and translational motions in liquids.

χ-*Test*

Since eqs. 10 and 11 are derived from the assumption of rotational diffusion, we can test the results by the so-called χ-test (27) to check that this method is a good approximation of the reorientations. The χ-test consists of calculating the ratio of the reorientational correlation time about a particular axis to the theoretical free gas reorientational time about the same axis assuming rotational equipartition. If χ is large compared to 1, the rotational diffusion limit applies. For dimethylmercury application of the χ-test to the perpendicular motion gives values ranging from 15–22 indicating rotational diffusion for this motion. However for the parallel motion the range of $\chi_{\|}$ is only 1.4–3.0 indicating possible inertial effects due to the much smaller moment of inertia about this axis.

^{199}*Hg Spin–Lattice Relaxation*

For the ^{199}Hg relaxation it is safe to assume that the intermolecular dipole–dipole relaxation is insignificant as previously mentioned. Therefore the T_1's of ^{199}Hg in dimethylmercury (Fig. 6) come only from intramolecular interactions. The dipolar contribution can be written as,

$$[15] \qquad R_{1\,intra}^{dd} = \frac{6\gamma_H{}^2\gamma_{^{199}Hg}{}^2\hbar^2}{r_{H-Hg}^6}\tau_c(\text{Hg–H})$$

Using the appropriate values for the constants and intermolecular distances (Table 3) we obtain

$$[16] \qquad R_{1\,intra}^{dd} = 3.36 \times 10^8 \tau_c(\text{Hg–H})$$

where τ_c(Hg–H) can be calculated using eq. 11

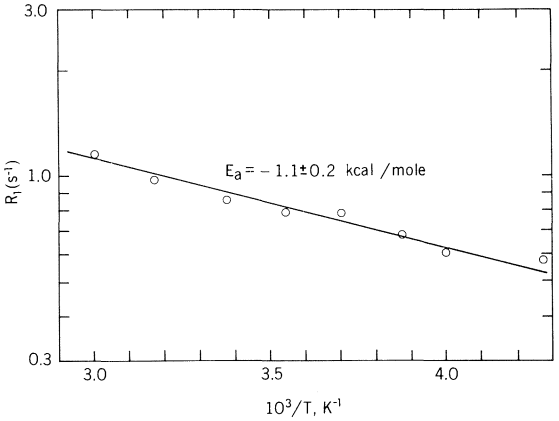

FIG. 6. ^{199}Hg spin–lattice relaxation rate in ^{199}Hg-$(CH_3)_2$.

along with $D_\perp$, $D_\parallel$, and $\theta = 23.5°$. The calculated contribution at 313 K is $R_{1\,\text{intra}}^{\text{dd}} = 0.0014$ s^{-1} which is negligible, due to the large Hg–H separation. The temperature dependence in Fig. 6 indicates that the major operative spin–lattice relaxation mechanism is that due to the spin–rotation interaction. It shows an Arrhenius behaviour with an energy of activation of -1.1 ± 0.2 kcal/mol. There is a slight contribution due to the chemical shift anisotropy mechanism which will be discussed in a later section.

Discussion

Proton–Proton Intermolecular Dipole Relaxation

An approximate isotropic theory of translational diffusion of a spherical molecule through a viscous medium leads (37) to the following expression for the intermolecular dipole relaxation,

$$[17] \qquad R_{1\,\text{inter}}^{\text{H–H}} = \frac{9\pi^2\hbar^2\gamma_H{}^4\eta N}{2kT}$$

Here η is the viscosity and N is the number density of molecules. Our measured values of the temperature dependence of the density and viscosity are given in Table 4. These values in eq. 17 yield the calculated values of intermolecular dipole relaxation times that are compared in Table 5 with the measured values from the dilution extrapolation. The agreement is surprisingly good, and perhaps fortuitous in view of the simplified model. The calculated activation energy for the interaction is 2.2 kcal/mol and the experimental value is 2.3 ± 0.3 kcal/mol.

^{199}Hg Spin–Rotation Constants

Since we have established that the relaxation of the ^{199}Hg nucleus in dimethylmercury is governed mainly by the spin–rotation interaction we should be able to obtain the spin–rotation tensor.

Bender and Zeidler (38) have derived an equation relating the spin–rotation relaxation of a nucleus in symmetric top molecules to the rotational diffusion constants of the molecule. Their result is

$$[18] \quad R_1^{\text{SR}} = \frac{8\pi^2}{3\hbar^2}(I_\parallel{}^2 C_\parallel{}^2 D_\parallel + 2I_\perp{}^2 C_\perp{}^2 D_\perp)$$

where all symbols have their usual meaning. The derivation of this equation is based on the assumption that both diffusion constants are in the rotational diffusion limit, which is reasonable for $D_\perp$ but possibly not for $D_\parallel$ because of possible inertial effects for this motion. However, with this in mind we will proceed with this treatment.

Table 4. Density and viscosity for liquid $Hg(CH_3)_2$

T (K)	ρ (g/ml)	η (cP)
273	3.1403	1.308
288	3.0903	1.115
298	3.0787	1.040
308	3.0620	0.956

Table 5. Theoretical and experimental values for $T_{1\,\text{inter}}^{\text{H–H}}$

	Value (s)	
T (K)	Theory	Experimental
273	13.9	15.1
288	17.5	18.9
298	19.6	21.7
308	22.2	24.6

If the temperature dependent data for $D_\parallel$, $D_\perp$, and R_1^{SR} are known, one can obtain the values for $C_\parallel$ and $C_\perp$ using eq. 18. From eq. 18 and the necessary values for R_1^{SR}, $D_\parallel$, and $D_\perp$ we obtain,

At 313 K

$$[19a] \quad C_\parallel{}^2 + 19.3C_\perp{}^2 = 2.70 \times 10^{10}$$

At 238 K

$$[19b] \quad C_\parallel{}^2 + 26.3C_\perp{}^2 = 3.15 \times 10^{10}$$

The values for $C_\parallel$ and $C_\perp$ are obtained from the intersection of the temperature dependent ellipses plotted in Fig. 7. The values obtained are:

$$|C_\parallel| = 120 \pm 60 \text{ kHz}$$

and

$$|C_\perp| = 26 \pm 3 \text{ kHz}$$

We emphasize that although $D_\perp$ is in the rotational diffusion limit, $D_\parallel$ probably *is not* and one must be cautious with the value obtained for $C_\parallel$ in view of the large error associated with the solution for $D_\parallel$ through τ_c(H–H) and τ_c(D) in eq. 11.

Absolute Shielding Scale of ^{199}Hg

The magnetic shielding constant has been related to the spin–rotation constant through the second order paramagnetic term of Ram-

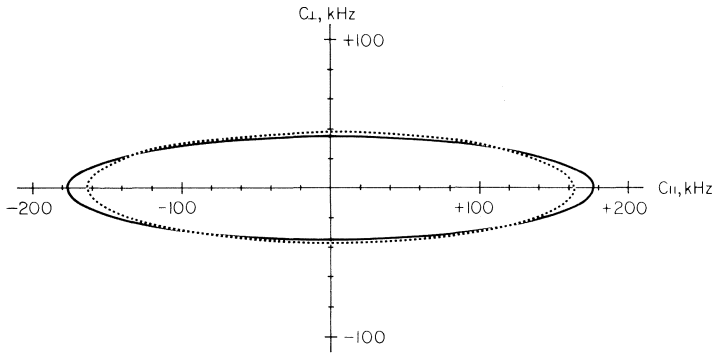

FIG. 7. Temperature dependent ellipses (----313 K and —238 K) of $C_{\parallel}$ and $C_{\perp}$ for ^{199}Hg in $Hg(CH_3)_2$.

sey's shielding expression (39–41). Deverell (42) has rewritten this expression for symmetric top molecules,

$$[20]\quad \sigma_{ave} = \sigma_d' + \sigma_p' = \frac{e^2}{3mc^2} \times \left\{\left\langle 0 \left| \sum_k \frac{1}{r_k} \right| 0 \right\rangle - \sum_j (Z_j/r_{ij})\right\} + \frac{e^2}{6mc^2}\left\{\frac{\pi}{m\mu_N\gamma_I}(2C_{\perp}I_{\perp} + C_{\parallel}I_{\parallel})\right\}$$

using Deverell's notation. This relation has been used to obtain the absolute chemical shift scale for ^{31}P (42, 43); ^{19}F (42); ^{119}Sn (11); and ^{207}Pb (44). The above expression suggests that the σ_p' is the only portion of the shielding constant that is sensitive to the chemical environment changes and thus changes in the spin–rotation constant (C).

Using the second term of eq. 20 along with the appropriate values for the constants, $C_{\parallel}$ and $C_{\perp}$, we obtain σ_p' for ^{199}Hg in $Hg(CH_3)_2$. We assume σ_p' to be negative in order to have a net deshielding effect and thus there are two solutions for σ_p':

If

$$C_{\parallel} = -120 \text{ kHz}$$

$$C_{\perp} = -26 \text{ kHz}$$

Then

$$\sigma_p' = -5050 \text{ ppm}$$

If

$$C_{\parallel} = +120 \text{ kHz}$$

$$C_{\perp} = -26 \text{ kHz}$$

Then

$$\sigma_p' = -4100 \text{ ppm}$$

The average total shielding constant can be calculated from Deverell's formula along with the value of σ_d' for the free atom tabulated by Ramsey (40). Ramsey gives $\sigma_d' = 9650$ ppm for Hg and therefore $\sigma_{ave} = 4600$ or 5550 ppm. The shielding scale obtained is shown in Fig. 8 and shows that the resonances of the non-metallic mercury compounds are found between the resonances of the bare nucleus and the free mercury atom.

Chemical Shift Anisotropy

If we use the paramagnetic term of eq. 20 along with the relationship,

$$\sigma_p' = \tfrac{1}{3}(2\sigma_{\perp} + \sigma_{\parallel})$$

we obtain for the ^{199}Hg nucleus,

$$[21]\quad 2\sigma_{\perp} + \sigma_{\parallel} = 1.10 \times 10^{31}(2I_{\perp}C_{\perp} + I_{\parallel}C_{\parallel})$$

and therefore

$$[22a]\qquad \sigma_{\perp} = 1.10 \times 10^{31} I_{\perp}C_{\perp}$$

$$[22b]\qquad \sigma_{\parallel} = 1.10 \times 10^{31} I_{\parallel}C_{\parallel}$$

Making use of eqs. [22*a*, *b*] along with the moments of inertia and spin–rotation constants we can calculate the chemical shift anisotropy ($\Delta\sigma = \sigma_{\parallel} - \sigma_{\perp}$). If we use $C_{\parallel} = -120$ kHz and $C_{\perp} = -26$ kHz we obtain $\Delta\sigma = +5415 \pm 1515$ ppm, while the second set of solutions $C_{\parallel} = +120$ kHz and $C_{\perp} = -26$ kHz yields $\Delta\sigma = +8300 \pm 1515$ ppm. From these estimates of $\Delta\sigma$ for the ^{199}Hg nucleus we can estimate the chemical shift anisotropy contribution to the ^{199}Hg spin–lattice relaxation rate. These various contributions are shown in Table 6.

As is shown in Fig. 6 there is no sign of any curvature in the temperature dependence of $R_1(^{199}\text{Hg})$ which indicates that almost all relaxation is due to the spin–rotation interaction and there appears to be very little chemical shift

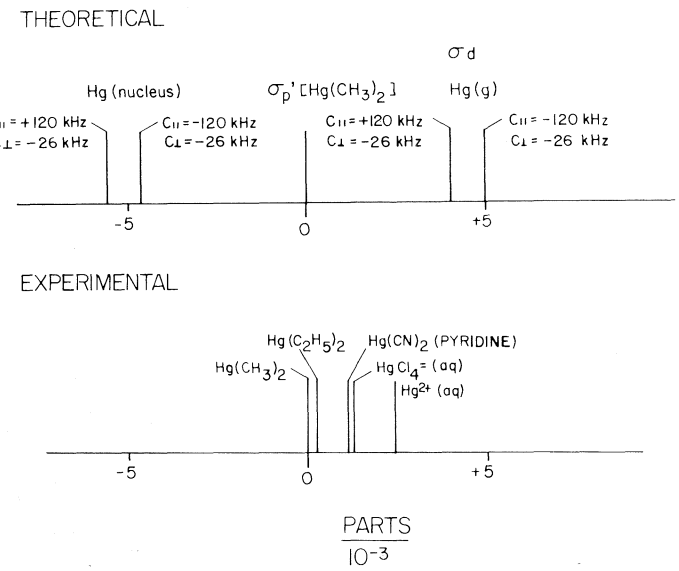

FIG. 8. ^{199}Hg shielding scales. Experimental scale values obtained from ref. 42. Theoretical scale derived from experimental values for $C_{\|}$ and $C_{\perp}$ along with eq. 19.

TABLE 6. Chemical shift anisotropy contributions to the relaxation rate of the ^{199}Hg nucleus at 14.1 kG*

τ_c ($\times 10^{12}$ s)	T (K)	$\Delta\sigma$ (ppm)	R_1^{CSA} (s^{-1})
6.7	300	+3900	0.061
6.7	300	+5400	0.117
6.7	300	+6900	0.192
6.7	300	+8300	0.275
10.2	234	+3900	0.093
10.2	234	+5400	0.178
10.2	234	+6900	0.292
10.2	234	+8300	0.419

*$\tau_c = (6D_{\perp})^{-1}$ for Hg atom since it lies on the main symmetry axis and $\theta = 0°$.

anisotropy contribution. This would then certainly eliminate $\Delta\sigma = +8300$ ppm since this would contribute significantly to the ^{199}Hg relaxation at low temperatures.

In Table 7 are shown the chemical shift anisotropy (CSA) and spin–rotation (SR) contributions to the ^{199}Hg relaxation rate for the most reasonable values of $C_{\|}$, $C_{\perp}$, and $\Delta\sigma$. Comparison of these calculated values of $R_1^{total}(^{199}Hg)$ with the experimental $R_1(^{199}Hg)$ values at both temperatures indicates that the most reasonable choice is that of $\Delta\sigma = +4640$ ppm and $C_{\|} = -120$ kHz and $C_{\perp} = -23$ kHz. For this value of $\Delta\sigma$ at 300 K the CSA mechanism would contribute only 10% to the total relaxation rate and at 234 K it would be 20%. Our final value of $\Delta\sigma = +4600$ ppm appears quite reasonable by comparison with the only other measurement of $\Delta\sigma(^{199}Hg) = +5345 \pm 25$ ppm by Kennedy and McFarlane (45) in CH_3HgBr. Thus our best estimates for the spin–rotation tensor are: $C_{\|} = -120 \pm 60$ kHz and $C_{\perp} = -23 \pm 3$ kHz. Use of these values along with $D_{\|}$ and $D_{\perp}$ in eq. 18 shows that about 50% of the ^{199}Hg spin–rotation interaction comes from the methyl group reorientation and 50% from the overall tumbling motion of the dimethylmercury molecule.

It has been pointed out (46) that the (**IC**) tensor for ^{13}C spins in many non-linear molecules is near isotropic *i.e.* $(\mathbf{IC})_t \cong I_{\|}C_{\|} \cong I_{\perp}C_{\perp}$. This is true only for the cases where $\Delta\sigma$ is small compared to σ_p'. We emphasize that such is not the case for ^{199}Hg in dimethylmercury since $\Delta\sigma = +4600$ ppm and $\sigma_p' = -4500$ ppm. In fact for our case $(\mathbf{IC})_{\perp}$ is about four times $(\mathbf{IC})_{\|}$.

Using our values of $\Delta\sigma$, $C_{\|}$, and $C_{\perp}$ we can estimate the point at which $R_1^{SR} = R_1^{CSA}$ at 23.5 kG (*i.e.* the point at which $R_1(^{199}Hg)$ reaches a maximum). This should occur at about −45°C calculated from our values of $\Delta\sigma$ and spin–rotation constants. Thus $R_1(^{199}Hg)$ behaviour at higher fields should display observable effects due to the large chemical shift anisotropy in $Hg(CH_3)_2$.

TABLE 7. Chemical shift anisotropy and spin–rotation contributions to the relaxation rate of the ^{199}Hg nucleus (at 14.1 kG) for various values of $C_{\parallel}$ and $C_{\perp}$*

(*a*) At 300 K

$C_{\parallel}$ (kHz)	$C_{\perp}$ (kHz)	$\Delta\sigma$ (ppm)	R_1^{SR} (s^{-1})	R_1^{CSA} (s^{-1})	R_1^{total} (s^{-1})
−60	−23	+5366	0.466	0.117	0.583
−120	−23	+4640	0.775	0.087	0.862
−180	−23	+3914	1.290	0.061	1.351
−180	−26	+4712	1.390	0.091	1.481
−120	−26	+5438	0.875	0.117	0.992

(*b*) At 234 K

$C_{\parallel}$ (kHz)	$C_{\perp}$ (kHz)	$\Delta\sigma$ (ppm)	R_1^{SR} (s^{-1})	R_1^{CSA} (s^{-1})	R_1^{total} (s^{-1})
−60	−23	+5366	0.313	0.175	0.488
−120	−23	+4640	0.505	0.132	0.637
−180	−23	+3914	0.825	0.093	0.918
−180	−26	+4712	0.892	0.138	1.030
−120	−26	+5438	0.572	0.178	0.760

*R_1^{SR} calculated using eq. 17.

A recent nmr study of ^{199}Hg (47) has yielded an atomic reference scale for all measured nmr line shifts of mercury. The resulting shielding constant is $\sigma_p' = -4686$ ppm for $^{199}Hg(CH_3)_2$ *vs.* ^{199}Hg atom. Using our best fit values for $C_{\perp}$ and $C_{\parallel}$ ($C_{\parallel} = -120$ kHz and $C_{\perp} = -23$ kHz) along with eq. 21 and the relationship $\sigma_p' = \frac{1}{3}(2\sigma_{\perp} + \sigma_{\parallel})$ we obtain $\sigma_p' = -4550$ ppm, in excellent agreement with the reported value of −4686 ppm.

Acknowledgments

We thank the Canadian Donner Foundation for an equipment grant toward the pulse spectrometer, and the National Research Council of Canada for continued operating support.

1. A. ABRAGAM. The principles of nuclear magnetism. Clarendon Press, London. 1961.
2. T. T. BOPP. J. Chem. Phys. **47**, 3621 (1964).
3. M. D. ZEIDLER. Ber. Buns. Ges. **69**, 659 (1965).
4. K. T. GILLEN, M. SCHWARTZ, and J. H. NOGGLE. Mol. Phys. **20**, 899 (1971).
5. T. C. FARRAR, S. J. DRUCK, R. R. SHOUP, and E. D. BECKER. J. Am. Chem. Soc. **94**, 699 (1972).
6. J. R. LYERLA, JR., D. M. GRANT, and C. H. WANG. J. Chem. Phys. **55**, 4676 (1971).
7. E. J. WELLS and C. R. LASSIGNE. Can. J. Chem. In press.
8. R. L. ARMSTRONG and J. A. COURTNEY. Can. J. Phys. **50**, 1262 (1972).
9. D. W. SAWYER and J. G. POWLES. Mol. Phys. **21**, 83 (1971).
10. W. M. LITCHMAN and M. ALEI, JR. J. Chem. Phys. **56**, 5818 (1972).
11. R. R. SHARP. J. Chem. Phys. **57**, 5321 (1972).
12. R. R. SHARP. Private communication.
13. R. HAWK. Ph.D. Thesis, University of Michigan, Michigan. 1973.
14. A. L. VAN GEET and D. N. HUME. Anal. Chem. **37**, 983 (1965).
15. R. G. PARKER and J. JONAS. Rev. Sci. Instrum. **41**, 319 (1970).
16. (*a*) E. J. WELLS and K. H. ABRAMSON. J. Mag. Resn. **1**, 378 (1969); (*b*) S. O. CHAN. Ph.D. Thesis, Simon Fraser University, Burnaby, B.C. 1969.
17. H. GILMAN and R. E. BROWN. J. Am. Chem. Soc. **51**, 928 (1929).
18. R. R. DEAN and W. MCFARLAND. Mol. Phys. **13**, 343 (1967).
19. H. S. GUTOWSKY, M. KARPLUS, and D. M. GRANT. J. Chem. Phys. **31**, 1278 (1959).
20. T. F. WIMMETT. Phys. Rev. **91**, 476 (1953).
21. V. GOLD, H. N. COLLI, and J. E. PEARSON. J. Chem. Soc. Chem. Commun. 408 (1973).
22. G. BONERA and A. RIGAMONTI. J. Chem. Phys. **42**, 171 (1965).
23. K. F. KUHLAMNN, D. M. GRANT, and R. K. HARRIS. J. Chem. Phys. **52**, 3439 (1970).
24. D. E. WOESSNER, B. S. SNOWDEN, and E. T. STROM. Mol. Phys. **14**, 265 (1968).
25. J. JONAS and J. M. DIGENNARO. J. Chem. Phys. **50**, 2392 (1969).
26. A. ALLERHAND. J. Chem. Phys. **52**, 3596 (1970).
27. K. T. GILLEN and J. H. NOGGLE. J. Chem. Phys. **53**, 801 (1970).
28. W. T. HUNTRESS, JR. J. Chem. Phys. **48**, 3524 (1968).
29. T. K. LEIPERT, J. H. NOGGLE, and K. T. GILLEN. J. Mat. Resn. **13**, 158 (1974).
30. J. G. POWLES. Ber. Buns. Ges. **67**, 328 (1963).
31. D. E. O'REILLY and G. E. SCHACHER. J. Chem. Phys. **39**, 1768 (1963).
32. J. G. POWLES and R. FIGGINS. Mol. Phys. **10**, 155 (1966).
33. T. E. BULL and J. JONAS. J. Chem. Phys. **52**, 2779 (1970).

34. T. E. BULL and J. JONAS. J. Chem. Phys. **52**, 4553 (1970).
35. R. A. ASSINK, J. DEZWAAN, and J. JONAS. J. Chem. Phys. **56**, 4975 (1972).
36. D. J. WILBUR and J. JONAS. J. Chem. Phys. **62**, 2800 (1975).
37. R. W. MITCHELL and M. EISNER. J. Chem. Phys. **33**, 86 (1960).
38. H. J. BENDER and M. ZEIDLER. Ber. Buns. Ges. **75**, 236 (1971).
39. N. F. RAMSEY. Phys. Rev. **78**, 699 (1950).
40. N. F. RAMSEY. Molecular beams. Oxford Press, London. 1956.
41. W. H. FLYGARE. J. Chem. Phys. **41**, 793 (1964).
42. C. DEVERELL. Mol. Phys. **18**, 319 (1970).
43. K. T. GILLEN. J. Chem. Phys. **56**, 1573 (1972).
44. R. R. SHARP and R. HAWK. J. Chem. Phys. **60**, 1009 (1974).
45. J. D. KENNEDY and W. MCFARLANE. J. Chem. Soc. Chem. Commun. 595 (1974).
46. J. R. LYERLA, JR., D. M. GRANT, and C. H. WANG. J. Chem. Phys. **55**, 4674 (1971).
47. H. KRUGER, O. LUTZ, A. NOLLE, and A. SCWENK. Z. Phys. A, **273**, 325 (1975).
48. K. SURYANARAYANA RAO, B. P. STOICHEFF, and R. TURNER. Can. J. Phys. **38**, 1516 (1960).

The hydrolysis of 1- and 2-adamantyl nitrate in water: limiting values of $\Delta C_p^{\neq}$ for displacement of the nitrate ion in water

KALAVELIL MATTHEW KOSHY,[1] RAJANI KANTA MOHANTY,[2] AND ROSS ELMORE ROBERTSON[3]

Department of Chemistry, University of Calgary, Calgary, Alta., Canada T2N 1N4

Received July 13, 1976

KALAVELIL MATTHEW KOSHY, RAJANI KANTA MOHANTY, and ROSS ELMORE ROBERTSON. Can. J. Chem. **55**, 1314 (1977).

Values of $\Delta C_p^{\neq}$ have been obtained for the hydrolysis of 1- and 2-adamantyl nitrate in water and of 1-adamantyl nitrate in 0.2 mol fraction ethanol–water and acetonitrile–water. The limiting value of $\Delta C_p^{\neq}$ for displacement of the NO_3^- ions in water is more negative than -130 cal mol^{-1} deg^{-1}. Much less negative values in mixed solvents show that the large negative values obtained for hydrolysis in water derive in some manner from the structural properties of water. The mechanistic implications of these facts are discussed.

KALAVELIL MATTHEW KOSHY, RAJANI KANTA MOHANTY et ROSS ELMORE ROBERTSON. Can. J. Chem. **55,** 1314 (1977).

On a obtenu des valeurs de $\Delta C_p^{\neq}$ pour l'hydrolyse des nitrates d'adamantyle-1 et -2 dans l'eau et du nitrate d'adamantyle-1 dans des mélanges éthanol–eau et acétonitrile–eau de 0.2 fraction molaire. La valeur limite de $\Delta C_p^{\neq}$ pour le déplacement des ions NO_3^- dans l'eau est plus négative que -130 cal mol^{-1} deg^{-1}. Des valeurs beaucoup plus négatives dans les solvants mixtes montrent que les valeurs très négatives obtenues pour l'hydrolyse dans l'eau proviennent d'une manière quelconque des propriétés structurales de l'eau. On discute des implications mécanistiques de ces faits.

[Traduit par le journal]

In this paper we examine the mechanistic implications of the values of $\Delta C_p^{\neq}$ derived from the hydrolysis of the 1- and 2-adamantyl nitrates in water and in mixed solvents. In solvolytic displacement reactions, the adamantyl structure ensures the absence of rear-side nucleophilic interaction (1) and since participation by H or Me is unlikely (2), displacement from the adamantyl structure makes certain that the mechanism is S_N1 (3–5), Lim (6), or k_c (7), as one chooses. Because the 2-adamantyl structure thus eliminates the possibility of 'border-line mechanism' and mixed kinetics (ref. 5, pp. 320–321) which had been recognized in earlier discussions of displacement from secondary carbons, the 2-adamantyl structure was proposed by Schleyer *et al.* as a limiting standard for evaluating the mechanism for displacement from secondary carbons (2).

The mechanism of such solvolytic S_N displacements is recognized to depend on the structure of the reactant, the group being displaced, and the nucleophilic and ionizing properties of the solvent. The latter consideration, though long recognized (9), is not always observed. Water is a unique solvent in this respect. Because of the tendency to form transient structures about weakly polar solutes (10) and the further characteristic that these structures are sensitive to temperature and to the development of charge on the anion, we are provided, through $\Delta C_p^{\neq}$ values, with a 'handle' for evaluating the degree of charge development at the transition state (11).

Very early in studying their proposed S_N1/S_N2 mechanistic classification of nucleophilic displacement reactions, Hughes and Ingold recognized the need for a range of charge development at the transition state and for the possibility of 'shielding' and mixed kinetics (5). This logical extension of the simplistic S_N1/S_N2 mechanistic classification was provided with a formalism and a firmer experimental justification by Winstein and co-workers in the course of an extensive investigation, largely in the solvent acetic acid (12, 13). The possible existence of parallel pathways (k_Δ, k_s, k_c, in Winstein's nomenclature (7)) for hydrolytic displacement from secon-

[1]Present address: Scarborough College, University of Toronto, West Hill, Toronto, Ont.

[2]Research Assistant, University of Calgary, Calgary, Alta. 1974–1976. On leave of absence from Ravenshaw College, Cuttack, Orissa, India.

[3]Author to whom correspondence should be addressed.

TABLE 1. Empirical constants for the equation $\log k = A_1 + A_2/T + A_3 \log T$*

Substrate	Solvent	A_1	$-A_2$	$-A_3$
1-Adamantyl nitrate	Pure water	241.6144	15645.39	77.17005
	0.2 mol fraction EtOH 0.8 mol fraction water	80.47522	8156.765	22.9635
	0.2 mol fraction MeCN 0.8 mol fraction water	49.9976	7112.224	12.0758
2-Adamantyl nitrate	Pure water	212.6713	17049.474	66.0285
4-Methylbenzyl nitrate†	0.1 mol fraction acetonitrile in water	61.7977	7459.339	16.5609

*T in Kelvins.
†$\Delta C_p^{\ddagger}$ in water = 101 cal mol^{-1} deg^{-1}.

dary substrates in water would be expected to alter values of $\Delta C_p^{\ddagger}$ to less negative values (14). Hence the proposal that 2-adamantyl-X provided a 'standard' for evaluating the displacement of other secondaries was intriguing and encouraged us to determine the $\Delta C_p^{\ddagger}$ for the hydrolysis of 2-adamantyl nitrate in water. While in one sense the results obtained were not too surprising since we already knew the value of $\Delta C_p^{\ddagger}$ for the hydrolysis of 1-adamantyl nitrate, we believe these results raise important questions with regard to the interpretation of $\Delta C_p^{\ddagger}$ not only with reference to those reported here but with respect to the significance of this coefficient as a mechanistic probe in general (11).

The rate data were determined as previously (15) and the rate–temperature relationships were obtained by fitting these data to the empirical equation

$$[1] \qquad \log k_1 = A_1 + A_2/T + A_3 \log T$$

The values of the constants are given in Table 1. Derived values (11) of $\Delta H^{\ddagger}$, $\Delta S^{\ddagger}$, and $\Delta C_p^{\ddagger}$ are given in Table 2. The value of $\Delta C_p^{\ddagger}$ for 1-adamantyl nitrate is at once seen to be the most negative value of this coefficient reported to date. The value of $\Delta C_p^{\ddagger}$ found for the 2-adamantyl nitrate is about the same as was found for the 2,6-dimethylbenzyl nitrate (16) and possibly a little less negative than that of the 1-adamantyl nitrate. Such a small difference would be consistent with the smaller 'm' value and k_{EtOH}/k_{AcOH} ratio reported in Schleyer's paper (2).

In accord with our earlier assumption that large negative values of $\Delta C_p^{\ddagger}$ reflected a correspondingly large reorganization of the water structure adjacent to the developing nitrate ion in the activation process (11), and following earlier experience with *tert*-BuCl (17) $\Delta C_p^{\ddagger}$ values were determined for the hydrolysis of the 1-adamantyl nitrate and 4-Me-benzyl nitrate in 0.2 mol fraction acetonitrile in water and in 0.2 mol fraction ethanol in water. The values of $\Delta C_p^{\ddagger}$ obtained in these mixed solvents may be compared with those found for *tert*-butyl chloride hydrolyzing in the same media (Table 3). For reasons which will be apparent, it was not considered necessary to repeat this work with the 2-adamantyl nitrate, since there is no cause to believe that the results would be significantly different.

The values of $\Delta C_p^{\ddagger}$ found for the solvolysis of 1- and 2-adamantyl nitrate hydrolyzing in water are far more negative than what was previously regarded as limiting (18). That such large negative values could be attributed to the breakdown of the total hydrophobic solvent shell is unacceptable, even though Ahlywalia and co-workers have shown (19, 20) that $\Delta C^0_{p,s}$ for the solvation of tetra-*n*-butyl ammonium chloride changes on the addition of co-solvent in the same manner as $\Delta C_p^{\ddagger}$ reported here (Table 2). The large values of $\Delta C^0_{p,s}$ for the solvation of the ammonium salts in water relate to the temperature sensitivity of the hydrophobic shell about the cation while in the kinetic study, the larger the cation the more likely the initial state solvation will be shielded from the effects of charge development in the activation process and hence remain unchanged.

In Table (4) the values of $\Delta C^0_{p,s}$ are given for a number of alkali nitrates. If +30 cal mol^{-1}

TABLE 2. Derived pseudo-thermodynamic parameters for solvolysis in water and mixed solvents

Substrate	Solvent	Temp. (°C)	$k \times 10^5$ (s^{-1})	$\Delta H^{\ddagger}$ (cal mol^{-1})	$\Delta S^{\ddagger}$ (cal mol^{-1} deg^{-1})	$-\Delta C_p^{\ddagger}$ (cal mol^{-1} deg^{-1})
1-Adamantyl nitrate	Water	10	141.3	28 380 ± 52	26.0 ± 0.1	
		25	1 585.0	25 274 ± 135	17.9 ± 0.5	155 ± 9
		50	63 100.0	21 390 ± 360	5.4 ± 1.2	
	0.2 mol fraction EtOH	10	2.239	23 839 ± 112	4.5 ± 0.4	
	0.8 mol fraction water					
		25	19.95	23 124 ± 33	2.1 ± 0.1	48 ± 7
		50	446.7	21 934 ± 170	−1.8 ± 0.5	
	0.2 mol fraction MeCN	10	1.862	25 186 ± 77	8.9 ± 0.3	
	0.8 mol fraction water	25	18.20	24 796 ± 46	7.5 ± 0.1	26 ± 8
		50	512.9	24 146 ± 232	5.4 ± 0.7	
2-Adamantyl nitrate	Water	50	0.1778	34 969 ± 650	23.0 ± 1.9	
		75	6.683	31 640 ± 150	13.1 ± 0.4	133 ± 21
		90	47.32	29 642 ± 203	7.5 ± 0.5	
4-Methylbenzyl nitrate	0.1 mol fraction acetonitrile in water	10		24 250 ± 141	3.6 ± 0.5	
		25		23 730 ± 28	1.8 ± 0.1	35 ± 8
		50				

deg^{-1} is taken as a reasonable estimate for the values $\Delta C_{p,s}^{0}$ associated with hydrophobic solvation of the neutral NO_3 group,[4] the values of $\Delta C_p^{\ddagger}$ reported in Table 2 for the hydrolysis of adamantyl nitrates are seen to be far more negative that can be accounted for by the separation of a fully charged nitrate ion.[5] It seems reasonable that experimental values of $\Delta C_p^{\ddagger}$ in the range $-130 \rightarrow -150$ must contain factors derived from kinetic complexities and the nature of the limiting mechanism in water.

Several authors have recognized that if solvolytic reactions partition between two pathways having different critical energies, there will be a positive contribution to $\Delta C_p^{\ddagger}$ (14, 22, 23) but only for the case of ion-pair return is a negative 'spurious' contribution anticipated (24).[6]

While Albery and Robinson (24) neglected the possibility of a contribution to $\Delta C_p^{\ddagger}$ from solvent reorganization, they noted that where there was an equilibrium involving ion-pair return, such as proposed by Winstein and coworkers, a negative temperature coefficient would be found. This suggestion provides a ready explanation for that part of $\Delta C_p^{\ddagger}$ to be attributed to kinetic complexity. But there are difficulties with this hypothesis, the most obvious being to account for the large reduction in $\Delta C_p^{\ddagger}$ on the addition of a co-solvent (Table 2, and refs. 17 and 18). Winstein and his coworkers showed that ion-pair return depends markedly on the solvent employed (13, 25) and that this phenomenon was favoured by solvents of low solvating power and weak nucleophilicity. Water fits neither category. Our results show that on changing to a more favorable environment for ion-pair return, the effect in question largely disappears. Nor is it clear that water in a solvent-separated ion-pair will not be a stronger nucleophile rather than otherwise. Such enhanced nucleophilicity predicates no ion-pair return after initial front-side displacement. Here our evidence involves product forma-

[4]It is assumed that this +30 cal mol^{-1} deg^{-1} would contribute −30 cal mol^{-1} deg^{-1} to $\Delta C_p^{\ddagger}$ in the activation process (11).

[5]A probable value might be 80 cal mol^{-1} deg^{-1} based on −30 as a base value unrelated to water structure, −30 from hydrophobic bonding about neutral NO_3, and −20 from Table 4.

[6]A discussion of various possible contributions to $\Delta C_p^{\ddagger}$ from such kinetic complexities is given in a previous paper (23).

TABLE 3. $\Delta C_p^{\ddagger}$ values for solvolysis of *tert*-butyl chloride

Substrate	Solvent	Temp. (°C)	$\Delta H^{\ddagger}$ (cal mol^{-1})	$\Delta S^{\ddagger}$ (cal mol^{-1} deg^{-1})	$-\Delta C_p^{\ddagger}$ (cal mol^{-1} deg^{-1})
tert-BuCl	Water*	10	23 830	14.4	83 ± 4.5
	0.2 mol fraction EtOH* 0.8 mol fraction water*	10	19 430	−3.1	40 ± 3
	0.2 mol fraction acetonitrile 0.8 mol fraction water	10	21 366	−1.2 ± 0.1	39 ± 2

*Reference 18.
†Reference 17.

TABLE 4. Estimated values of heat capacity for solution of alkali nitrates (21)

Nitrate	$\phi C = 0$ (cal mol^{-1} deg^{-1})
$NaNO_3$	−9.6
KNO_3	−15.5
$RbNO_3$	−17.4
$CsNO_3$	−18.8

tion with the activated methyl rather than the adamantyl group. In the reaction of methyl iodide catalyzed by Ag^+ ion, the rate of reaction was found to be accelerated by excess nitrate ion. Hammond and co-workers (26) and Colcleugh and Moelwyn-Hughes (27) postulated the formation of an intermediate of the form $(NO_3^-)MeI(Ag^+)$. Since methanol was the only organic product, an alternative hypothesis would postulate $NO_3^- \cdots H_2O \cdots Me \cdots I \cdots Ag^+$, the Ag^+ being partially desolvated but the nucleophilic water molecule forming part of the NO_3^- solvation shell. This water molecule is then rendered more active by the presence of the NO_3^- group. Such a possibility is not inconsistent with the specific salt effects reported by Bunton and co-workers (28, 29) and provides a guide to the probable reason that evidence for ion-pair return from the solvent-separated ion-pair is not observed in solvents of fair nucleophilicity. Both of the foregoing arguments weigh against the ion-pair return hypothesis as a logical possibility to account for the large negative values of $\Delta C_p^{\ddagger}$ reported here but provide no clear alternative.

These arguments do not exclude the existence of contributions to $\Delta C_p^{\ddagger}$ from kinetic complexities associated with front-side displacement and water structure. Hence, in the absence of a better understanding, the significance of this empirical term ($\Delta C_p^{\ddagger}$) can still serve as a useful mechanistic probe giving an indication of the degree of charge development where the mechanism involves some degree of nucleophilic interaction and signalling front-side displacement where structural features permit or require this alternative.

Experimental

1-Adamantyl Nitrate

This compound was prepared from 1-adamantyl bromide (Aldrich Chemical Co. Inc.). 1-Adamantyl bromide (8 g, 0.041 mol) dissolved in 50 ml of dry ether was stirred with 10 g (0.059 mol) of powdered silver nitrate for 12 h at room temperature. After removal of the precipitated silver bromide the product was recovered by evaporation of the ether. Recrystallization from cyclohexane gave 5 g of 1-adamantyl nitrate. It was further purified by vacuum sublimation (65°C/0.1 torr), mp 103–104°C, nmr_{TMS} (CCl_4) δ 2.4–2.95 (m, 9, CH_2, CH), 2.05 (m, 6, CH_2). *Anal.* calcd. for $C_{10}H_{15}NO_3$: C 60.91, H 7.61, N 7.11; found: C 60.93, H 7.82, N 7.12.

2-Adamantyl Nitrate

A 2-adamantanol (Aldrich Chem. Co. Inc.) solution was refluxed with 48% HBr in the presence of concentrated H_2SO_4, for 24 h. The bromide thus obtained (95% yield) was extracted with ether. The nitrate was prepared from the bromide following the same procedure as in the case of 1-adamantyl nitrate, except for the fact that the stirring with silver nitrate was done for 24 h. The conversion was found to be 100% (no C—Br peak in the ir). The nitrate was crystallized from ether by removing part of the ether under vacuum. Further purification was done by vacuum sublimation; mp 30°C. *Anal.* calcd.: C 60.91, H 7.61, N 7.11; found: C 60.86, H 7.63, N 7.12.

para-Methylbenzyl nitrate was prepared and purified as before (8).

Solvent Mixtures

All solvent mixtures were prepared by mixing the two components, the volumes of which were calculated on the basis of their densities at the temperature of mixing (20°C). Ethanol was obtained from Standard Chemicals (absolute alcohol, 99.9%) and was used as such. Acetoni-

trile was of spectro quality obtained from Matheson, Coleman and Bell.

The water used was distilled water passed through an ion exchange column (Rexyn R208-1-300-H-OH).

Acknowledgments

The authors wish to acknowledge useful discussions with Professor J. M. W. Scott of Memorial University. In addition we wish to acknowledge the financial assistance of the National Research Council of Canada for part of this work.

1. P. v. R. Schleyer and R. Nicholas. J. Am. Chem. Soc. **83**, 2700 (1961).
2. J. L. Fry, C. J. Lancelot, L. K. M. Lam, J. M. Harris, R. C. Bingham, D. J. Raber, R. E. Hall, and P. v. R. Schleyer. J. Am. Chem. Soc. **92**, 2538 (1970).
3. E. D. Hughes, C. K. Ingold, and C. S. Patel. J. Chem. Soc. 526 (1933).
4. E. D. Hughes. J. Am. Chem. Soc. **57**, 708 (1935).
5. C. K. Ingold. Structure and mechanism in organic chemistry. Cornell University Press, Ithaca, NY. 1953. Chapt. 7.
6. S. Winstein, E. Grunwald, and H. W. Jones. J. Am. Chem. Soc. **73**, 2700 (1951).
7. P. v. R. Schleyer, J. L. Fry, L. K. M. Lam, and C. J. Lancelot. J. Am. Chem. Soc. **92**, 2542 (1970).
8. K. Koshy and R. E. Robertson. Can. J. Chem. **52**, 2485 (1974).
9. E. D. Hughes. Discuss. Faraday Soc. **37**, 603 (1941).
10. H. S. Frank and W. Y. Wen. Discuss. Faraday Soc. **24**, 133 (1957).
11. R. E. Robertson. Progress in physical organic chemistry. Vol. 4. *Edited by* A. Streitwieser, Jr. and R. Taft. Interscience, John Wiley, New York, NY. 1967. p. 213.
12. S. Winstein, E. Clippinger, A. H. Fainberg, and G. C. Robinson. J. Am. Chem. Soc. **76**, 2597 (1954).
13. S. Winstein, B. Appel, R. Baker, and A. Diaz. Chem. Soc. (London) Spec. Publ. **19**, 109 (1965).
14. G. Kohnstam. Adv. Phys. Org. Chem. **5**, 121 (1967).
15. R. E. Robertson and S. E. Sugamori. J. Am. Chem. Soc. **91**, 7254 (1969).
16. K. M. Koshy, R. E. Robertson, G. S. Dyson, and S. Singh. Can. J. Chem. **54**, 3614 (1976).
17. R. E. Robertson and S. E. Sugamori. Can. J. Chem. **50**, 1353 (1972).
18. E. A. Moelwyn-Hughes, S. E. Sugamori, and R. E. Robertson. J. Chem. Soc. 1965 (1965).
19. R. K. Mohanty, T. S. Sarma, S. Subramanian, and J. C. Ahlywalia. Trans. Faraday Soc. **67**, 305 (1971).
20. R. K. Mohanty, S. Sunder, and J. C. Ahlywalia. J. Phys. Chem. **76**, 2577 (1972).
21. V. B. Parker. Natl. Bur. Stand. No. 2 (1965).
22. J. R. Hulett. Q. Rev. Chem. Soc. London, **18**, 227 (1964).
23. J. M. W. Scott and R. E. Robertson. Can. J. Chem. **50**, 167 (1972).
24. W. J. Albery and B. H. Robinson. Trans. Faraday Soc. **65**, 980 (1969).
25. S. Winstein and G. C. Robinson. J. Am. Chem. Soc. **80**, 169 (1958).
26. G. S. Hammond, M. F. Hawthorne, J. H. Waters, and B. M. Graybill. J. Am. Chem. Soc. **82**, 704 (1960).
27. D. W. Colcleugh and E. A. Moelwyn-Hughes. J. Chem. Soc. 2542 (1964).
28. C. A. Bunton, J. H. Crabtree, and L. Robinson. J. Chem. Soc. **90**, 1258 (1968).
29. C. A. Bunton and L. Robinson. J. Am. Chem. Soc. **90**, 5965 (1968).

An examination of two solvation parameters: $\Delta C_p^{\ddagger}$ and '*m*'

RAJANI KANTA MOHANTY[1] AND ROSS ELMORE ROBERTSON[2]

Department of Chemistry, University of Calgary, Calgary, Alta., Canada T2N 1N4

Received August 31, 1976

RAJANI KANTA MOHANTY and ROSS ELMORE ROBERTSON. Can. J. Chem. **55**, 1319 (1977).

The empirical '*m*' values from the Grunwald–Winstein solvent correlation equation for S_N displacement reactons show a fair correlation with corresponding $\Delta C_p^{\ddagger}$ values obtained from hydrolysis in water. The correlation plots separate according to the nature of the displaced groups, a consequence of different relative effects of anions on water structure. The mechanistic significance of the correlation is examined.

RAJANI KANTA MOHANTY et ROSS ELMORE ROBERTSON. Can. J. Chem. **55**, 1319 (1977).

Les valeurs '*m*' empiriques obtenues à partir de l'équation de corrélation de solvant de Grunwald–Winstein pour des réactions de déplacements S_N montrent une bonne relation avec les valeurs correspondants de $\Delta C_p^{\ddagger}$ obtenues à partir de l'hydrolyse dans l'eau. Les courbes de corrélation se séparent, suivant la nature des groupes déplacés; ce résultat est une conséquence des différents effets relatifs des anions sur la structure de l'eau. On examine la signification mécanistique de cette corrélation.

[Traduit par le journal]

A qualitative relationship between the ionizing properties of solvolyzing media and the rate of S_N displacement reactions was published over 40 years ago by Hughes and Ingold (1). During the intervening years various attempts have been made to formulate a more quantitative correlation (2–7). Among these, the linear free energy solvent correlation

$$[1] \qquad (\log k = \log k_0 + mY)$$

of Grunwald and Winstein has attracted the most lasting attention, possibly because of its apparent simplicity. The authors, themselves, recognized that this correlation was not entirely satisfactory (4, 8), a fact they illustrated by showing that various solvent mixtures produced a dispersion of plots (see also refs. 9–11). Equation 1 illustrates the inherent difficulty in attempting to reduce a number of interacting complexities to a simple expression. In such a simplification fine structure tends to be neglected.

While these more general attempts were being made to compass solvent effects on S_N reactions, we have examined the solvent effects on ionogenic S_N reactions hydrolyzing, mainly in water, using the semi-empirical parameter, $\Delta C_p^{\ddagger}$, as a measure of charge development at the transition state (12). Originally we thought that this coefficient ($d\Delta H^{\ddagger}/dT = \Delta C_p^{\ddagger}$) was determined wholly by the difference in heat capacity between the initial and transition states of the surrounding aqueous solvent shell ($\Delta C_p^{\ddagger} = (\bar{C}_{p\ \text{T.S.}} - \bar{C}_{p\ \text{I.S.}})$ induced by the external effects of charge development on the activated quasi-ion pair. This is an over-simplification. The temperature coefficient of $\Delta H^{\ddagger}$ is necessarily complex and empirical in spite of the apparent certitude engendered by transition state terminology. The latter fact may limit but does not cancel the value of $\Delta C_p^{\ddagger}$ as a useful indicator of the detailed mechanism of hydrolysis in water. Among the modifications to the initial hypothesis (13) was the recognition that a base value of about -30 cal mol^{-1} deg^{-1} was present apparently unrelated to solvent structure in water and that $\Delta C_p^{\ddagger}{}_{\text{str}} = (\Delta C_p^{\ddagger} - 30)$ was determined largely (if not entirely) by charge development on the quasi anion (14). The latter modification was based in part on the observation that those reactants, RX, in which R possessed the greatest capacity to distribute positive charge and hinder nucleophilic attack (*e.g.*, 1-adamantyl nitrate (15, 16)) were just those which yielded the most negative values of $\Delta C_p^{\ddagger}$ yet were also just those cases where the positive charge was least likely to break down water structure. One of the more illuminating studies correlating $\Delta C_p^{\ddagger}$ with the probable charge on the quasi anion at the transition state and with corresponding changes on the central carbon atom at the transition state was published in two papers by Koshy and Robert-

[1]Research Associate on leave from Ravenshaw College, Cuttack, India.

[2]Author to whom correspondence should be addressed.

son (13, 17). From these, and related data it was concluded that for such displacements the transition state corresponded to some critical level of positive charge becoming available[3] on the central carbon. This simple operative condition provides an external mechanism (S_N2) for a reduction of internal electrostatic interaction and a transfer of electrons permitting the eventual front-side displacement of X. The kinetic solvent isotope effect (19) and the above noted correlation (17) both support the conclusion that the transition state coincides with the initial establishment of nucleophilic interaction *and* if nucleophilic interaction is possible it will be established.[4] The alternative to that seeming tautology will be the limiting mechanism where front-side displacement precedes nucleophilic interaction. We shall return to this point in connection with the hydrolysis of *tert*-butyl chloride. It follows that the more efficient the charge dispersal in $R^{\delta+}$ of the activated RX, the greater the reduction in internal electrostatic interaction between $R^{\delta+}$ and $X^{\delta-}$. Such dispersal will have two important mechanistic consequences. (*i*) There will be a corresponding enhancement of external effects of $X^{\delta-}$ on the adjacent solvent shell (the ionizing properties of the solvent will become increasingly important) and (*ii*) there will be a delay in establishing nucleophilic interaction relative to the reaction coordinate. This simple analysis was sufficient to account for the $\Delta C_p^{\ddagger}$ *vs.* k_H/k_D correlation (17) noted above for the hydrolysis of a series of benzyl nitrates in water and we would assume will apply also to solvolysis in organo–aqueous mixtures. Solvolysis in acetic acid and similar media tends to enhance the possibility of ion-pair complications (20, 21) which are not important in water and hence are neglected here. The above hypothesis at once provides a basis for understanding why the transition state is reached at a later stage for displacement through the series *prim* < *sec* < *tert* and why there is a corresponding shift to more negative values of $\Delta C_p^{\ddagger}$ and leads to the structural condition predicating a limiting mechanism. These general conclusions reached from a consideration of $\Delta C_p^{\ddagger}$ values provide a basis for examining the '*m*' values of the Grunwald–Winstein correlation [1].

Granted the above analysis for hydrolytic S_N displacements in water approximates solvolytic displacements in general, then '*m*' is necessarily complex. This term reflects the ability of the R groups to disperse electron deficiency, steric factors which influence the initiation of nucleophilic interaction, and some portion of inherent nucleophilic activity of the solvent not included in *Y*.

Originally (2, 3) the *Y*-values were expected to characterize the ionizing properties of the solvent. However, since it is doubtful if *tert*-butyl chloride hydrolyzes by a limiting mechanism in water (see below) it is less likely to do so in 80/20 v/v ethanol–water, the original standard solvent. Hence *Y* will contain some varying specific nucleophilic contribution and the dispersion noted by Grunwald and co-workers is not surprising. What was much less obvious at first sight was that '*m*' values determined using the displacement of a halide or a tosylate were about the same (16) when we knew that the interaction of these displaced groups on hydrolysis in water was quite different (1, 5). It was this seeming contradiction which led to the present comparison between $\Delta C_p^{\ddagger}$ and '*m*' values for hydrolysis.

Results and Discussion

The $\Delta C_p^{\ddagger}$ values were known for a series of substituted benzyl nitrates in water (13) and since these provided a basis for the mechanistic conclusions outlined above, corresponding '*m*' values were determined from solvolytic rate data obtained in various (two or three) ethanol–water mixtures by a conductance method (22). This limited series together with the water data was judged sufficient for an approximate value of '*m*' in view of the inherent uncertainties in the latter term (8). With the exception of the 2,6-dimethyl substituent the benzyl series had the advantage of low, and similar steric requirements. Rate data and corresponding '*m*' values are given in Table 1. A plot of the latter *vs.* $\Delta C_p^{\ddagger}$ for hydrolysis in water is given in Fig. 1. On the same figure are included plots for corresponding data for a number of halides and sulfonates. It is at once evident that a fair correlation exists, divided according to the nature of the displaced groups. This division is the natural consequence of the fact that $\Delta C_p^{\ddagger}$ reflects the specific exter-

[3]In the general case, 'available' will include allowance for steric factors which in the noted benzyl series were low with exception of the 2,6-dimethyl substituent (15, 18).

[4]NOTE ADDED IN PROOF: J. L. Kurn reaches a similar conclusion from a different premise (Acc. Chem. Res. **5**, 1 (1972)).

TABLE 1. Rate data and corresponding '*m*' values

Substrate (nitrate)	Temp. (°C)	'*m*'*	$\Delta C_p^{\neq}$ (cal mol^{-1} deg^{-1})	k_H/k_D (per two D atoms)	$k \times 10^5$ (s^{-1})†	Reference for $\Delta C_p^{\neq}$
1-Adamantyl	48.10	1.22	155±9		53 090 (water) 354.8 (44.7% E) 3.548 (80% E)	26
2-Adamantyl	69.97	1.09	133±21		3.162 (water) 1.589 (5% E) 1.381 (10% E)	26
2,6-Dimethyl benzyl	48.10	1.00	134±4	1.394	5888 (water) 244.4 (40% E) 39.81 (60% E)	15
4-Methyl benzyl	48.10	0.86	101±5	1.384	1096 (water) 53.47 (40% E) 1.496 (80% E)	13
2-Methyl benzyl	48.10	0.92	86±8	1.324	234.4 (water) 76.04 (20% E) 14.76 (40% E)	15
Benzyl	48.10	0.70	62±1	1.240	12.59 (water) 1.622 (40% E) 0.2818 (60% E)	13
3-Trifluoro methylbenzyl	73.45	0.65	57±10	0.976	7.079 (water) 5.623 (10% E) 3.791 (20% E)	13
3-Methyl benzyl	48.10	0.84	54±5		29.85 (water) 12.75 (20% E) 2.666 (40% E)	13
4-Nitrobenzyl	73.44	0.35	35±12		1.905 (water) 1.413 (20% E) 0.6411 (40% E)	13
2,4-Dimethyl benzyl	43.63	0.79			522.4 (40% E) 199.5 (50% E) 71.66 (60% E)	—
2-Butyl	69.97	0.70			2.831 (20% E) 0.7044 (40% E)	—

*Reference, this work.
†E is ethanol.

nal effects of a given charge on the particular group being displaced while '*m*' reflects the *relative* effect of particular displacement to that corresponding to an assumed limiting case for the same anion.

The correlation of $\Delta C_p^{\neq}$ and '*m*' for the benzyl nitrate series is seen to be quite satisfactory while that for the sulfonates shows a lack of sensitivity presumably because the internal charge dispersal in the sulfonate group reduces internal interaction and at the same time minimizes external effects (12, 19, 23). The '*m*' values reflect the degree of overall charge on the R group when the critical charge on the central carbon corresponds to that necessary to initiate nucleophilic interaction.[5] The examples on the halide plot show a greater degree of scatter. This was expected since there is considerable variation in the steric contribution to '*m*' through this series. A notable example is *tert*-butyl chloride which is more widely displaced than might be expected. We attribute this to the fact that *tert*-butyl chloride in water does not give a limiting value of $\Delta C_p^{\neq}$ for displacement of a halide (24), a fact which suggests that the mechanism of hydrolysis for this compound in water is not limiting; *i.e.* in the absence of obtrusive steric factors nucleo-

[5]The kinetic solvent isotope effects (k_{H_2O}/k_{D_2O}) for displacement of the sulfonic group are about 1.1 in all cases examined (19).

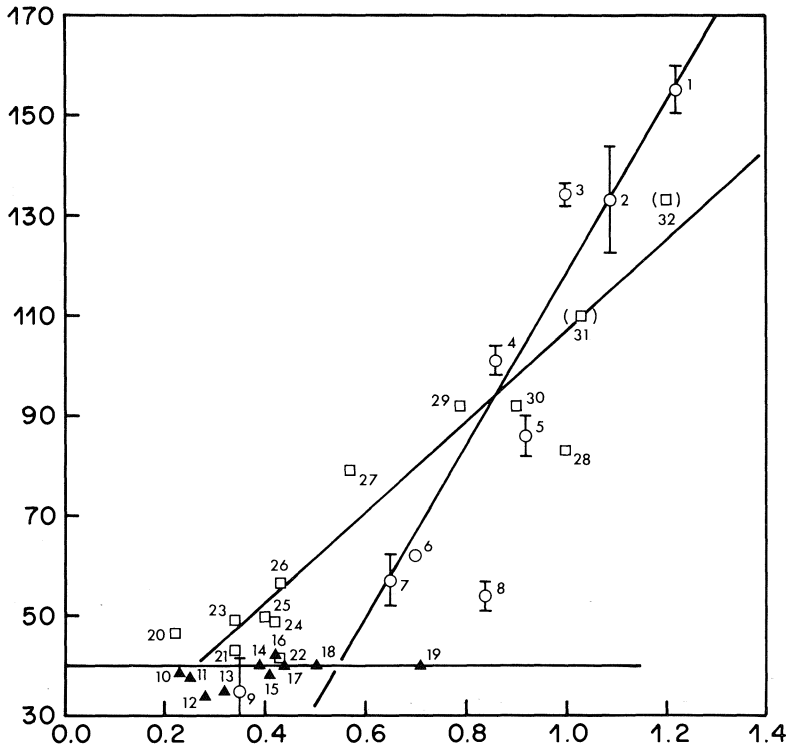

FIG. 1. A correlation of $\Delta C_p^{\ddagger}$ and 'm' for the solvolytic displacement of a series of nitrates, halides, and sulfonates: (*1*) 1-adamantyl nitrate (this work, Table 1); (*2*) 2-adamantyl nitrate (this work, Table 1); (*3*) 2,6-dimethylbenzyl nitrate (this work, Table 1); (*4*) 4-methylbenzyl nitrate (this work, Table 1); (*5*) 2-methylbenzyl nitrate (this work, Table 1); (*6*) benzyl nitrate (this work, Table 1); (*7*) trifluoromethylbenzyl nitrate (this work, Table 1); (*8*) 3-methylbenzyl nitrate (this work, Table 1); (*9*) 4-nitrobenzyl nitrate (this work, Table 1); (*10*) methyl tosylate (12, 27); (*11*) ethyl tosylate (12, 27); (*12*) ethyl benzenesulfonate (12, 28); (*13*) *n*-butyl brosylate (12, 28); (*14*) benzyl tosylate ($\Delta C_p^{\ddagger}$ assumed) (12, 28); (*15*) 2-propyl brosylate (12, 28); (*16*) 2-propyl tosylate (12, 27); (*17*) cyclohexyl tosylate ($\Delta C_p^{\ddagger}$ assumed) (27); (*18*) cyclopropyl tosylate ($\Delta C_p^{\ddagger}$ assumed) (29); (*19*) 3,3-dimethyl-2-butyl brosylate ($\Delta C_p^{\ddagger}$ assumed) (30); (*20*) methyl bromide (12, 16); (*21*) *n*-propyl bromide (12, 28); (*22*) benzyl chloride (28, 32); (*23*) ethyl bromide (12, 16); (*24*) β-methylallyl chloride (28, 31); (*25*) allyl chloride (28, 31); (*26*) 2-propyl bromide (12, 16); (*27*) 4-methylbenzyl chloride (28, 32); (*28*) *tert*-butyl chloride (2, 12); (*29*) α-methylallyl chloride (28, 31); (*30*) *tert*-amyl bromide ($\Delta C_p^{\ddagger}$ assumed) (12, 28); (*31*) 2-adamantyl bromide ($\Delta C_p^{\ddagger}$ estimated) (16); (*32*) 1-adamantyl bromide ($\Delta C_p^{\ddagger}$ estimated) (16).

The values of $\Delta C_p^{\ddagger}$ for all sulfonates examined are in the range 35 ± 6 cal mol^{-1} deg^{-1}. $\Delta C_p^{\ddagger}$ for 4-methylbenzyl chloride was 20 cal mol^{-1} deg^{-1} less negative than the value for the corresponding nitrate. This fact provided the basis for the estimated values of the adamantyl bromides, which regrettably were too insoluble in water to study.

philic interaction is established (and transition state reached) prior to full charge development on the Cl^- ion. We do not have a $\Delta C_p^{\ddagger}$ value for 1-adamantyl bromide (which would certainly react by a limiting mechanism) but judging from the difference in $\Delta C_p^{\ddagger}$ for *p*-methylbenzyl nitrate and chloride (13) the point for this limiting compound would lie very close to the curve shown for the halides. Where the same difference in $\Delta C_p^{\ddagger}$ is allowed between 2-adamantyl nitrate and bromide as between 4-methyl benzyl nitrate and chloride, the point for 2-adamantyl bromide falls on the halide plot. A direct determination of $\Delta C_p^{\ddagger}$ for 2-adamantyl bromide failed because of solubility problems.

That 'm' and $\Delta C_p^{\ddagger}$ are found to show a fair correlation dependent on the displaced group provides a method for estimating the probable value of $\Delta C_p^{\ddagger}$ for hydrolysis in water without the necessity of a rather demanding kinetic study, or for cases where such a study is impractical. In our view, the much greater value of this

study comes from the insight which the comparison provides with regard to the critical condition necessary for S_N displacement reactions and for the significance of '*m*'.

Experimental

Water

Ordinary distilled water was passed through an ion exchange resin (Fisher Research Grade Rexyn I-300) and subsequently redistilled.

Ethanol

Absolute ethanol supplied by Standard Chemicals, 99.9% pure, was used as such.

Nitrate Esters

All nitrate esters were prepared by either the heterogeneous or homogeneous method (17) starting from the chloride or the bromide, except for *ortho*, *meta*, and *para* and 2,4-dimethyl benzyl nitrates which were available. They were purified before use either by distillation under reduced pressure (25) or by crystallization from a suitable solvent depending on whether the nitrate was a liquid or solid. Details have been reported (26). The different solvent mixtures were prepared by mixing the two components (v/v) at room temperature. The first-order rate constants were determined by using Queen type cells either at one common temperature (48°C) or through extrapolation from other temperatures. Extrapolation was not attempted in cases where the rate was either too slow or too fast because of the high error involved. The rate data were obtained by a conductance method. The error involved in the rates was much less than $\pm 0.5\%$ except in case of *p*-NO_2-benzyl nitrate and 2-butyl nitrate where an error of ± 0.7 to $\pm 0.8\%$ was encountered in some of the rates.

The *Y* values for different solvent mixtures were obtained from the literature (4). The '*m*' values were obtained from the plots of log *k* in water and at least two aqueous ethanol solvents *vs.* *Y* (slope = '*m*'). A good straight line was obtained in most cases except for *p*-methylbenzyl nitrate where the best possible straight line was used.

1. E. D. Hughes and C. K. Ingold. J. Chem. Soc. 244 (1935).
2. E. Grunwald and S. Winstein. J. Am. Chem. Soc. **70**, 846 (1948).
3. S. Winstein, E. Grunwald, and H. W. Jones. J. Am. Chem. Soc. **73**, 2700 (1951).
4. A. H. Fainberg and S. Winstein. J. Am. Chem. Soc. **78**, 2770 (1956).
5. C. G. Swain and D. C. Dittmer. J. Am. Chem. Soc. **75**, 4627 (1953).
6. C. G. Swain, R. B. Mosely, and D. E. Bown. J. Am. Chem. Soc. **77**, 3731 (1955).
7. C. G. Swain and R. B. Mosely. J. Am. Chem. Soc. **77**, 3727 (1955).
8. T. W. Bentley, F. L. Schadt, and P. v. R. Schleyer. J. Am. Chem. Soc. **94**, 992 (1972).
9. S. Winstein, A. H. Fainberg, and E. Grunwald. J. Am. Chem. Soc. **79**, 4146 (1957).
10. F. Spieth, W. C. Ruebsamen, and A. R. Olson. J. Am. Chem. Soc. **76**, 6253 (1954).
11. L. Wilputte-Steinert and P. J. C. Fierens. Bull. Soc. Chim. Belg. **64**, 308 (1955).
12. R. E. Robertson. Prog. Phys. Org. Chem. **4**, 213 (1967).
13. K. M. Koshy and R. E. Robertson. Can. J. Chem. **52**, 2485 (1974).
14. S. Singh and R. E. Robertson. Can. J. Chem. **54**, 1246 (1976).
15. K. M. Koshy, R. E. Robertson, G. S. Dyson, and S. Singh. Can. J. Chem. **54**, 3614 (1976).
16. D. J. Raber, R. C. Bingham, J. M. Harris, J. L. Fry, and P. v. R. Schleyer. J. Am. Chem. Soc. **92**, 5977 (1970).
17. K. M. Koshy and R. E. Robertson. J. Am. Chem. Soc. **96**, 914 (1974).
18. J. C. Charlton and E. D. Hughes. J. Chem. Soc. 850 (1956).
19. P. M. Laughton and R. E. Robertson. *In* Solute–solvent interactions. *Edited by* J. F. Coetzee and C. D. Ritchie. Marcel Dekker, New York, NY. 1969. Chapt. 7.
20. S. Winstein, E. Clippinger, A. H. Fainberg, and G. C. Robinson. J. Am. Chem. Soc. **76**, 2597 (1954).
21. D. J. Raber, J. M. Harris, and P. v. R. Schleyer. *In* Ions and ion pairs in organic reactions. Vol. 2. *Edited by* M. Szwarc. Wiley, New York, NY. 1974.
22. R. E. Robertson and S. E. Sugamori. J. Am. Chem. Soc. **91**, 7254 (1969).
23. H. M. R. Hoffmann. J. Chem. Soc. 6753 (1965).
24. R. E. Robertson, S. Singh, and A. Annessa. In preparation.
25. K. M. Koshy. Ph.D. Thesis, The University of Calgary, Calgary, Alta. 1973.
26. K. M. Koshy, R. K. Mohanty, and R. E. Robertson. Can. J. Chem. This issue.
27. J. L. Fry, C. J. Lancelot, L. K. M. Lam, J. H. Harris, R. C. Bingham, D. J. Raber, R. E. Hall, and P. v. R. Schleyer. J. Am. Chem. Soc. **92**, 2538 (1970).
28. A. Streitwieser, Jr. Solvolytic displacement reactions. McGraw-Hill, New York, NY. 1962. pp. 46, 64, and 78.
29. P. v. R. Schleyer, W. F. Sliwinski, G. W. Van Dine, U. Schöllkopf, J. Paust, and K. Fellenberger. J. Am. Chem. Soc. **94**, 125 (1972).
30. S. Winstein and H. Marshall. J. Am. Chem. Soc. **74**, 1120 (1952).
31. L. J. Brubacher, L. Treindl, and R. E. Robertson. J. Am. Chem. Soc. **90**, 4611 (1968).
32. K. M. Koshy, R. E. Robertson, and W. M. J. Strachan. Can. J. Chem. **51**, 2958 (1973).

C-Alkylation of 1,3-dihydroxyanthraquinones. Total syntheses of (±)-averufin and (±)-bipolarin

ANDRÉ CASTONGUAY AND PAUL BRASSARD

Département de Chimie, Université Laval, Québec (Qué.), Canada G1K 7P4

Received July 19, 1976

ANDRÉ CASTONGUAY and PAUL BRASSARD. Can. J. Chem. **55**, 1324 (1977).

Various methods of substituting 1,3-dihydroxyanthraquinones in the 2-position were investigated. It was eventually found that direct hydroxyalkylation in the presence of definite amounts of sodium bicarbonate could be carried out. The reaction of 1,3,6,8-tetrahydroxyanthraquinone with 5-oxohexanal or 4-hydroxybutanal gave, respectively, among other products, (±)-averufin and (±)-bipolarin.

ANDRÉ CASTONGUAY et PAUL BRASSARD. Can. J. Chem. **55**, 1324 (1977).

Diverses façons de substituer les dihydroxy-1,3 anthraquinones en position 2 ont été étudiées. Eventuellement, l'hydroxyalkylation directe s'est avérée réalisable en présence de quantités définies de bicarbonate de sodium dans l'eau. Ainsi les réactions de la tétrahydroxy-1,3,6,8 anthraquinone avec l'oxo-5 hexanal ou l'hydroxy-4 butanal donnent respectivement, entre autres produits, l'(±)-avérufine et la (±)-bipolarine.

A number of naturally occurring anthraquinones such as averantin (1), bipolarin (2), avermutin (1), versicorufin (3), and averufin (1) and its derivatives (2, 3) can be considered formally as hydroxyalkylation products of 1,3,6,8-tetrahydroxyanthraquinone (**25**). Averantin has previously been prepared by the reduction of solorinic acid (4), however none of the other proposed structures have been obtained or confirmed by synthesis. Hydroxymethylation of xanthopurpurin or its derivatives has been successful (5) but no reaction using higher homologs of formaldehyde appears to have been described.

Even though 1,3,6,8-tetrahydroxyanthraquinone has recently become quite readily available (6), most work of an exploratory nature was carried out with the more common xanthopurpurin (**1**). Several methods of preparing this compound exist, but in our hands only one, very succinct, was found to be satisfactory (7). This procedure involving the hydrosulfite reduction of the commercial dye purpurin was found to be simple and to give a high yield (85%) of the desired product.

The first attempts to do substitution on the system centered on the alkylation, with 1-chloro-1-methoxybutane, or the acylation of 1,3,9,10-tetraacetoxyanthracene (**2**). Various modifications of Friedel–Crafts conditions produced no useful result; however, a Fries rearrangement of the substrate did give the 2-acetyl derivative (**3**) in low yield (15%) which could not be improved.

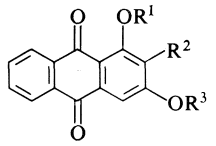

1 $R^1 = R^2 = R^3 = H$
3 $R^1 = R^3 = H, R^2 = COCH_3$
4 $R^1 = R^2 = H, R^3 = CH_2OCH_3$
5 $R^1 = R^3 = CH_2OCH_3, R^2 = H$
10 $R^1 = R^3 = H, R^2 = CH_2OH$
11 $R^1 = R^3 = CH_3, R^2 = CH_2OH$
12 $R^1 = R^3 = CH_3, R^2 = CHO$
13 $R^1 = CH_3, R^2 = CH{=}CH(CH_2)_3CH_3, R^3 = C_4H_9$
14 $R^1 = R^3 = CH_3, R^2 = CH{=}CH(CH_2)_3CH_3$
15 $R^1 = R^3 = H, R^2 = CHO$
16 $R^1 = CH_2CH{=}CH_2, R^2 = H, R^3 = CH_3$
17 $R^1 = CH_2CH{=}CH_2, R^2 = H, R^3 =$ 
18 $R^1 = R^2 = H, R^3 = CH_2CH{=}CH_2$
19 $R^1 = H, R^2 = CH_2CH{=}CH_2, R^3 = CH_3$
20 $R^1 = R^3 = H, R^2 = CH_2CH{=}CH_2$
21 $R^1 = R^3 = H, R^2 = CH{=}CH{-}CH_3$
22 $R^1 = R^3 = H, R^2 = CHOHCHOHCH_3$
27 $R^1 = R^3 = H, R^2 =$ 
28 $R^1 = R^3 = H, R^2 = CH{=}CH(CH_2)_2CH_2OH$
31 $R^1 = R^3 = H, R^2 = CH{=}CH(CH_2)_3CH_3$

Attempts to carry out the process photochemically did not give the expected product.

Alkylation of the anthracene nucleus at the required position was next envisaged by first lithiating the 1,3,9,10-tetramethoxy derivative (**7**). It is well known that di-*O*-methylresorcinol

is metallated in position 2 (8) and although anthracene itself gives rise to a 9,10-addition of ethyllithium (9), it was expected that the methoxyl groups would decrease the affinity of these positions sufficiently to permit the desired metallation. The reactions of 1,3,9,10-tetramethoxyanthracene with either butyl- or phenyllithium gave products unsubstituted in position 2 and which obviously were produced by 9,10-addition of the reagents followed by elimination of lithium methoxide. Electronic effects allowed the prediction that the alkyl or aryl group would occupy the 9-position. This was confirmed at least in the case of the phenyl derivative since the nmr spectrum shows a strong upfield shift for the 1-methoxyl group (δ 3.37).

In was then sought to modify the anthraquinoid structure by converting it to the diketal. This could conveniently be carried out by electrochemical oxidation of the corresponding hydroquinone diether. Modification of earlier work (10) improved the yield of anthraquinone tetramethyl diketal (78%), however, some of the monoketal was also isolated (15%). An attempt to extend the reaction to 1,3,9,10-tetramethoxyanthracene proved to be impractical since a large number of products were detected.

Use of the Wittig reaction in the course of the alkylation of xanthopurpurin was also investigated since lucidin (**10**) and its analogs can readily be prepared (5). Methylation of the hydroxymethylated compound **10** and oxidation gave the aldehyde **12** which reacted with *n*-pentylenetriphenylphosphorane. Under the conditions used, a 70% yield of the expected di-*O*-methyl-bis-deoxyaverythrin (**14**) was obtained along with 12% of 3-butoxy 2-(*trans*-hex-1-enyl)-1-methoxyanthraquinone (**13**), the product of an unusual type of transetherification (the identity of the latter is derived mainly from its mass and the nmr spectrum which shows in particular the disappearance of the 3-methoxyl group and the presence of a triplet at δ 3.92 attributed to the oxymethylene part of the butoxy substituent). An extended use of this method depended on the possibility of protecting the phenolic groups reversibly during the condensation and all attempts at methoxymethylation of both lucidin (**10**) and nordamnacanthal (**15**) succeeded only in O-alkylating the 3-hydroxyl functions.

The Claisen rearrangement provides another versatile method for alkylating anthraquinones and its use has been illustrated in a recent synthesis of islandicin (11). More hindered systems such as 1-allyloxy-3-methoxyanthraquinone (**16**) and 1-allyloxy-3-(tetrahydropyran-2-yloxy)anthraquinone (**17**) have now been found to rearrange smoothly to the expected products **19** and **20** in boiling 1,2-dichlorobenzene (in the latter case with loss of the protecting group). Moreover xanthopurpurin can be selectively O-allylated in position 3 and then converted although slowly upon heating to the 2-allyl derivative (**20**). Isomerization of the double bond in this compound into conjugation with the aromatic ring proved to be surprisingly difficult but was eventually carried out with the use of rhodium trichloride (12). The resulting 2-(*trans*-prop-1-enyl) derivative (**21**) when treated with osmium tetroxide gave a *threo*-diol (**22**) having one of the partial arrangements analogous to those required in an eventual synthesis of nidurufin. One attempt to introduce a longer side-chain by O-alkylating xanthopurpurin with 3-chlorohex-1-ene was unsuccessful and only the rearranged hex-2-enyl diether could be isolated.

Attention was then turned to the hydroxyalkylation of 1,3-dihydroxyanthraquinones by

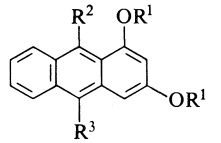

2 $R^1 = COCH_3$, $R^2 = R^3 = OCOCH_3$
6 $R^1 = CH_2OCH_3$, $R^2 = R^3 = OCH_3$
7 $R^1 = CH_3$, $R^2 = R^3 = OCH_3$
8 $R^1 = CH_3$, $R^2 = C_6H_5$, $R^3 = OCH_3$
9 $R^1 = CH_3$, $R^2 = C_4H_9$, $R^3 = OCH_3$

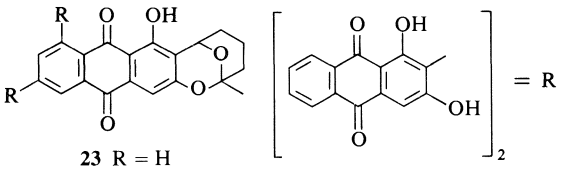

23 R = H
26 R = OH

24 $R = CH(CH_2)_3COCH_3$
29 $R = CH(CH_2)_3CH_2OH$
32 $R = CH(CH_2)_4CH_3$

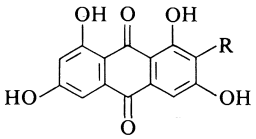

25 R = H

30 R =

aldehydes in basic media. The method had previously been successful in the case of formaldehyde, but attempts to apply it to other aldehydes under a variety of conditions did not provide a trace of the expected product. A number of hypotheses were then made which eventually led to successful hydroxyalkylations: (*a*) the products of C-hydroxyalkylation were assumed to be highly hindered and particularly prone to fragmentation, (*b*) strong or excess base was expected to promote the reverse reaction, (*c*) the presence of another function capable of trapping the secondary alcohol or the corresponding carbonium ion was thought to favor the reaction, and finally (*d*) it was anticipated that the use of a polar protic solvent would facilitate C-alkylation by strongly solvating the aryl oxide oxygen.

These prerequisites were taken into account in an experiment involving xanthopurpurin, 1 equiv. of sodium bicarbonate, and an excess of 5-oxohexanal in water at about 95°C. It was expected that if hydroxyalkylation occurred the secondary alcohol would combine with the ketone and form a fairly stable cyclic hemiketal (Scheme 1). Chromatography of the crude reaction product provided three compounds, one of which revealed that the reaction had indeed gone one step further than anticipated and had given an 11% yield of the analog of averufin, bis-deoxyaverufin (**23**). The nmr spectrum of this substance is in good agreement in part with that of averufin while its mass spectrum is almost superimposable on that of the latter when shifted by 32 mass units. From the top of the column a very polar and highly insoluble compound (31%) was isolated and converted to the tetramethyl ether. This derivative was identified as the 6,6-di(1,3-dimethoxyanthraquinon-2-yl)hexan-2-one (**24**) by its molecular mass (632) and its nmr spectrum which shows an acetyl group (δ 2.11), a single benzylic proton as a triplet (δ 5.13), and the absence of the characteristic signal for 2-H in xanthopurpurin. Forty percent of the starting material was also recovered from a median fraction.

The synthesis of (±)-averufin (**26**) required 1,3,6,8-tetrahydroxyanthraquinone (**25**) which was obtained in a 92% yield from the tetramethyl ether (6) by a brief treatment with a molten mixture of sodium and aluminum chlorides. The hydroxyalkylation of this quinone with 5-oxohexanal was found to require 2 equiv. of bicarbonate, a much longer reaction time (11 h) and a lower temperature (~85°C). Under these conditions a 6.5% yield of the desired product was isolated along with a large amount of unreacted starting material (48%). Some of the corresponding dianthraquinonylhexanone was also undoubtedly formed but was not isolated. Racemic averufin was indistinguishable from the natural product (tlc in four solvent systems and comparison of the ir and mass spectra).

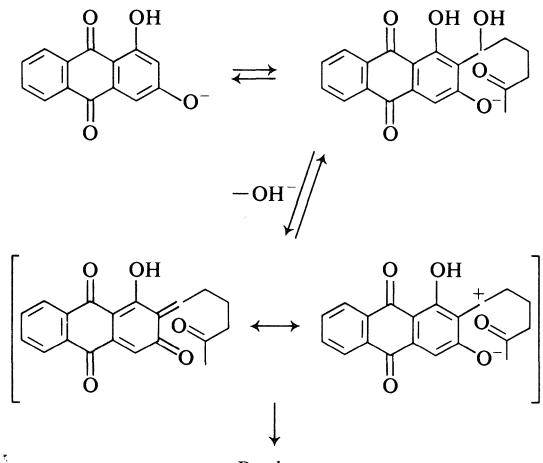

SCHEME 1

The ketoaldehyde used in the preceding syntheses was then replaced by the readily accessible 5-hydroxypentanal in order to determine whether 2-(tetrahydropyran-2-yl) derivatives of 1,3-dihydroxyanthraquinone of the type of avermutin could be obtained by this modification of the method. Dry column chromatography of the crude products gave a fast moving zone which, when rechromatographed, gave a substance (20%) identified as bis-deoxynoravermutin (**27**). The nature of the substance was confirmed by its mass spectrum which shows a fragmentation pattern almost identical to that of avermutin but shifted by 46 mass units. In the nmr spectrum, the absence of a signal corresponding to the proton in position 2 and the presence of a broad doublet at δ 5.05 (J_{aa} = 8 Hz), a multiplet at δ 3.64 collapsing to a broad doublet (J_{gem} = 11 Hz) by irradiation of the other axial hydrogens, and a broad doublet at δ 4.24 corresponding respectively to the 2′ axial, 6′ axial, and 6′ equatorial protons corroborate the assigned structure. The data also suggest that the tetrahydropyranyl ring is essentially rigid and attached to the anthraquinone in the equatorial position.

From the second column, 26% of the starting material was also recovered along with a small

amount (5%) of a dehydration product, 2-(5-hydroxy-*trans*-pent-1-enyl)-1,3-dihydroxyanthraquinone (**28**) which was identified straightforwardly from the spectra of the corresponding dimethyl ether. Finally a fourth product, the dianthraquinonylpentanol (**29**) was isolated from the top of the first column.

The foregoing results suggested that the racemic modification of another natural product, bipolarin (**30**), could now be prepared very easily by this method. The required 4-hydroxybutanal was obtained in a crude form by reducing γ-butyrolactone with diisobutylaluminum hydride (13) and reacted with 1,3,6,8-tetrahydroxyanthraquinone under conditions similar to those used for the synthesis of (±)-averufin. Preparative thin layer chromatography of the crude products gave a fast moving zone which consisted of (±)-bipolarin (**30**) (22%). Some starting material (8%) was recovered from a second band but other fractions were not examined. An authentic sample of bipolarin was unavailable but the physical and spectral properties of the synthetic substance are in excellent agreement with those of the natural product (with the exception of one ir band obtained by a different method).

Under the described conditions, aldehydes incapable of forming cyclic derivatives were nonetheless found to react with xanthopurpurin. With *n*-hexanal the process was very slow but afforded a 23% yield of bis-deoxyaverythrin (2-(*trans*-hex-1-enyl)-1,3-dihydroxyanthraquinone (**31**)) which after methylation was found to be identical to a product prepared earlier by a Wittig reaction. Other experiments carried out in media containing substances capable of intercepting the intermediate benzylic alcohol were unsuccessful. In aqueous acetone the reaction proceeded more rapidly than in water. The same product (26%) was obtained as before but uncontaminated with starting material. A 4% yield of a second unidentified product was also obtained which according to the mass spectrum is dimeric. In a 1:1 mixture of methanol and water a very little (4.5%) of the usual product was encountered along with the dianthraquinonylhexane (**32**) and much starting material. All attempts to substitute 1,3,6,8-tetrahydroxyanthraquinone by analogous means failed.

Experimental

Melting points were taken for samples in capillary tubes with a Thomas–Hoover apparatus (calibrated thermometer). The ir and uv spectra were determined with Beckman IR-12 and DK-1A spectrophotometers respectively. The nmr spectra were recorded with Varian A-60 and Bruker HX-90 spectrometers (tetramethylsilane as internal standard). The mass spectra were obtained with a Varian M-66 spectrometer. Davison silica gel No. 923 was used for column chromatography, Baker-7G silica gel for preparative tlc, and Woelm silica gel, activity III, for dry column chromatography.

*Xanthopurpurin (**1**)*

To a solution of purpurin (50.0 g, 0.195 mol) in water (2 ℓ) and concentrated ammonia (100 ml) at 0–5°C was added sodium hydrosulfite (100 g) over a period of 1 h. The mixture was stirred at this temperature for 4.5 h, allowed to stand overnight, aerated for 12 h, acidified with hydrochloric acid, and filtered. The washed and dried residue can be recrystallized in portions from a large volume of 1,2-dichloroethane and consists of xanthopurpurin (40 g, 85%), mp 270–271°C (lit. (14) mp 262–263°C; lit. (15) mp 268–270°C); δ (90 MHz, C_5D_5N) 6.93 (1H, d, J = 2.5 Hz, 2-H), 7.39–7.78 (2H, m, 6,7-H), 7.62 (1H, d, J = 2.5 Hz, 4-H), and 8.00–8.42 (2H, m, 5,8-H); *m/e* 240 (M^+), 212, 184.

*1,3,9,10-Tetraacetoxyanthracene (**2**)*

A mixture of 1,3-diacetoxyanthraquinone (3.72 g, 11.5 mmol), anhydrous sodium acetate (220 mg, 2.68 mmol), activated zinc (11 g), and acetic anhydride (100 ml) was refluxed for 35 min, filtered, poured into water, and neutralized with sodium bicarbonate. Extraction of the aqueous suspension with benzene gave the tetraacetate **2** (4.0 g, 85%), mp 191–193°C (toluene); λ_{max} ($CHCl_3$) 252, 258, 360, 375, 395 nm (log ε 4.97, 5.25, 3.73, 3.83, 3.82); ν_{max} (KBr) 1760 (acetate) and 1635 (aromatic C=C) cm^{-1}; δ (60 MHz, $CDCl_3$) 2.32, 2.42, 2.50, and 2.57 (4 × 3H, 4s, 1,3,9,10-OAc), 7.02 (1H, d, J = 2.5 Hz, 2-H), 7.40 (1H, d, J = 2.5 Hz, 4-H), 7.48–7.66 (2H, m, 6,7-H), and 7.72–7.95 (2H, m, 5,8-H); *m/e* 410 (M^+), 368, 326, 284. *Anal.* calcd. for $C_{22}H_{18}O_8$: C 64.39, H 4.42; found: C 64.58, H 4.32.

*2-Acetyl-1,3-dihydroxyanthraquinone (**3**)*

1,3,9,10-Tetraacetoxyanthracene (**2**) (410 mg, 1.00 mmol) was added to anhydrous aluminum chloride (665 mg, 5.00 mmol) in nitrobenzene (2 g) at 0–5°C. The mixture was stirred at room temperature for 15 h and poured into water (100 ml). After elimination of the nitrobenzene by washing with petroleum ether (bp 30–60°C), the aqueous phase was extracted with ethyl acetate (3 × 100 ml). The residue obtained after evaporation of the solvent was chromatographed on silica gel (dry column, chloroform – ethyl acetate 4:1) and gave the rearranged quinone (**3**) (41 mg, 15%), mp 188–189°C (1,2-dichloroethane); λ_{max} (chloroform) 258, 298, 430 nm (log ε 4.50, 4.27, 3.77); ν_{max} (KBr) 1670 (quinone C=O) and 1620 (chelated C=O) cm^{-1}; δ (90 MHz, $CDCl_3$) 2.82 (3H, s, $COCH_3$), 7.31 (1H, s, 4-H), 7.72–7.91 (2H, m, 6,7-H), and 8.19–8.38 (2H, m, 5,8-H); *m/e* 282 (M^+), 267. Diacetate (Ac_2O:H_2SO_4), mp 185–186°C (ethanol–water). *Anal.* calcd. for $C_{20}H_{14}O_7$: C 65.57, H 3.85; found: C 65.35, H 3.73.

*1-Hydroxy-3-(methoxymethoxy)anthraquinone (**4**)*

The silver salt of xanthopurpurin was first prepared from a solution of the quinone (240 mg, 1.00 mmol) in

aqueous 0.2 *N* sodium hydroxide by addition of silver nitrate (170 mg, 1.00 mmol) in water (3 ml). A suspension of the well dried silver salt in a mixture of chloromethoxymethane (240 mg, 3 mmol) and anhydrous benzene (10 ml) was stirred at room temperature for 2 days and then poured into water. The residue of the ether extract was chromatographed on silica gel (dry column, benzene) and gave the 3-methoxymethyl ether (**4**) (228 mg, 80%), mp 135–136°C (toluene); ν_{max} (KBr) 1670 (quinone C=O) and 1630 (chelated C=O) cm^{-1}; δ (60 MHz, $CDCl_3$) 3.48 (3H, s, OCH_3), 5.23 (2H, s, $—OCH_2O—$), 6.80 (1H, d, J = 2.5 Hz, 2-H), 7.38 (1H, d, J = 2.5 Hz, 4-H), 7.50–7.80 (2H, m, 6,7-H), and 8.05–8.33 (2H, m, 5,8-H); *m/e* 284 (M^+). *Anal.* calcd. for $C_{16}H_{12}O_5$: C 67.50, H 4.26; found: C 67.46, H 4.22.

*1,3-Di(methoxymethoxy)anthraquinone (**5**)*

The disodium salt of xanthopurpurin was obtained by evaporating to dryness a solution of the quinone (240 mg, 1.00 mmol) and sodium hydroxide (80 mg, 2.00 mmol) in aqueous methanol. To a stirred suspension of the dried salt in chloromethoxymethane (160 mg, 2.00 mmol) and anhydrous 1,2-dimethoxyethane (10 ml) were added alternately small portions of sodium and chloromethoxymethane until the yellow colour of the mixture was no longer altered by addition of the metal (24 h). Dilution of the reaction mixture with chloroform, extraction with 1% aqueous sodium hydroxide, and evaporation of the organic solvents gave the mixed diacetal **5** (297 mg, 90%), mp 158–159°C (ether – petroleum ether, bp 30–60°C); ν_{max} (KBr) 1655 (quinone C=O) cm^{-1}; δ (60 MHz, $CDCl_3$) 3.48 and 3.55 (2 × 3H, 2s, OCH_3), 5.27 and 5.33 (2 × 2H, 2s, $—OCH_2O—$), 7.13 (1H, d, J = 3.0 Hz, 2-H), 7.60 (1H, d, J = 3.0 Hz, 4-H), 7.55–7.87 (2H, m, 6,7-H), and 8.05–8.38 (2H, m, 5,8-H); *m/e* 328 (M^+), 313. *Anal.* calcd. for $C_{18}H_{16}O_6$: C 65.85, H 4.91; found: C 65.63, H 4.97.

*9,10-Dimethoxy-1,3-di(methoxymethoxy)anthracene (**6**)*

To a mixture of 1,3-di(methoxymethoxy)anthraquinone (264 mg, 0.80 mmol), absolute ethanol (0.5 ml), 20% aqueous sodium hydroxide (2 ml), and activated zinc (80 mg), stirred under nitrogen and kept at 86°C, was added methyl *p*-toluenesulfonate (1.45 g) in portions over a period of 3 h. After one more hour the reaction mixture was extracted several times with benzene and the latter evaporated. The residue was chromatographed on basic alumina (Brockman, activity I) and gave the anthracene **6** as an unstable oil (125 mg, 43%); δ (60 MHz, $CDCl_3$) 3.47 and 3.55 (2 × 3H, 2s, $—CH_2OCH_3$), 3.95 and 3.97 (2 × 3H, 2 s, 9,10-OCH_3), 5.25 and 5.32 (2 × 2H, 2s, $—OCH_2O—$), 6.82 (1H, d, J = 2.5 Hz, 2-H), 7.18–7.47 (2H, m, 6,7-H), 7.40 (1H, d, J = 2.5 Hz, 4-H), and 7.90–8.38 (2H, m, 5,8-H).

*1,3,9,10-Tetramethoxyanthracene (**7**)*

To a mixture of 1,3-dimethoxyanthraquinone (1.13 g, 4.22 mmol), ethanol (2.5 ml), 20% aqueous sodium hydroxide (10 ml), and activated zinc (415 mg), heated to refluxing under nitrogen for 4 h was added methyl *p*-toluenesulfonate (8.05 g) in portions over a period of 3 h. The residue obtained by evaporation of a chloroform extract of the reaction mixture was chromatographed on neutral alumina (50 g) (Woelm, activity I) (benzene–ether 1:1) and gave the tetramethyl ether **7** (683 mg, 54%), mp 120–121°C (ether); δ (60 MHz, $CDCl_3$–C_6D_6 4:1) 3.82, 3.85, 3.90, and 3.93 (4 × 3H, 4s, 1,3,9,10-OCH_3), 6.42 (1H, d, J = 2.5 Hz, 2-H), 7.07 (1H, d, J = 2.5 Hz, 4-H), 7.02–7.47 (2H, m, 6,7-H), and 8.03–8.43 (2H, m, 5,8-H); *m/e* 298 (M^+), 283. *Anal.* calcd. for $C_{18}H_{18}O_4$: C 72.46, H 6.08; found: C 72.53, H 5.93.

*1,3,10-Trimethoxy-9-phenylanthracene (**8**)*

To a well stirred solution of 1,3,9,10-tetramethoxyanthracene (149 mg, 0.50 mmol) in anhydrous ether (2 ml) was added under nitrogen an ether solution of phenyllithium (0.5 mmol). The reaction mixture was allowed to stand for several hours and poured into water (50 ml). The crude solid was chromatographed on neutral alumina (20 g, Woelm, activity I) (benzene–chloroform) and gave the phenylanthracene **8** (130 mg, 76%), mp 190–192°C (ether); δ (60 MHz, $CDCl_3$) 3.37 (3H, s, 1-OCH_3), 3.97 and 4.12 (2 × 3H, 2s, 3,10-OCH_3), 6.37 (1H, d, J = 2.5 Hz, 2-H), 7.20 (1H, d, J = 2.5 Hz, 4-H), 7.33 (5H, s, 9-C_6H_5), 7.27–7.50 (2H, m, 6,7-H), and 8.17–8.40 (2H, m, 5,8-H); *m/e* 344 (M^+), 329, 314. *Anal.* calcd. for $C_{23}H_{20}O_3$: C 80.21, H 5.85; found: C 80.47, H 5.86.

*9-Butyl-1,3,10-trimethoxyanthracene (**9**)*

An analogous preparation (1.00 mmol of 1,3,9,10-tetramethoxyanthracene and 1.00 mmol of butyllithium) gave the butylanthracene **9** (322 mg, 99%); δ (60 MHz, $CDCl_3$) 1.03 (3H, t, J = 7.0 Hz, 4′-H_3), 1.30 and 1.66 (6H, 2m, 1′,2′,3′-H_2), 3.80, 3.87, and 3.97 (3 × 3H, 3s, 1,3,10-OCH_3), 6.40 (1H, d, J = 3.0 Hz, 2-H), 7.10 (1H, d, J = 3.0 Hz, 4-H), 7.25–7.48 (2H, m, 6,7-H), and 8.07–8.33 (2H, m, 5,8-H); *m/e* 324 (M^+). *Anal.* calcd. for $C_{21}H_{24}O_3$: C 77.75, H 7.46; found: C 77.83, H 7.60.

*2-Hydroxymethyl-1,3-dimethoxyanthraquinone (**11**)*

Methylation of lucidin (5) (**10**) (270 mg, 1.00 mmol) by a standard procedure (anhydrous potassium carbonate (6.0 g), dimethyl sulfate (0.5 ml), and boiling acetone (200 ml) (24 h)) gave the dimethyl ether **11** (212 mg, 71%), after chromatography of the crude product on silica gel (benzene – ethyl acetate 1:1), mp 173.5–174.0°C (lit. (16) mp 175°C) (ether – petroleum ether, bp 30–60°C); λ_{max} ($CHCl_3$) 247, 274, 390 nm (log ε 4.24, 4.42, 3.56); ν_{max} (KBr) 3440 (hydroxyl) and 1670 (quinone C=O) cm^{-1}; δ (60 MHz, $CDCl_3$) 3.98 and 4.02 (2 × 3H, 2s, 1,3-OCH_3), 4.84 (2H, s, 2-CH_2), 7.65 (1H, s, 4-H), 7.60–7.85 (2H, m 6,7-H) and 8.07–8.42 (2H, m, 5,8-H); *m/e* 298 (M^+).

*2-Formyl-1,3-dimethoxyanthraquinone (**12**)*

A mixture of lucidin 1,3-dimethyl ether (**11**) (298 mg, 1.00 mmol), activated manganese dioxide (17) (1.2 g), and anhydrous benzene (50 ml) when refluxed for 16 h, filtered, and evaporated, gave the aldehyde **12** (264 mg, 89%), mp 184.5–185.5°C (ethanol); λ_{max} ($CHCl_3$) 280, 335, 370, 490 nm (log ε 4.45, 3.65, 3.53, 3.20); ν_{max} (KBr) 1695 (aldehyde) and 1670 (quinone C=O) cm^{-1}; δ (90 MHz, $CDCl_3$) 4.05 and 4.09 (2 × 3H, 2s, 1,3-OCH_3), 7.71 (1H, s, 4-H), 7.63–7.85 (2H, m, 6,7-H), 8.17–8.37 (2H, m, 5,8-H), and 10.52 (1H, s, CHO); *m/e* 296 (M^+). *Anal.* calcd. for $C_{17}H_{12}O_5$: C 68.91, H 4.08; found: C 68.78, H 4.06.

*2-(trans-Hex-1-enyl)-1,3-dimethoxyanthraquinone (**14**)*

To a stirred suspension of *n*-pentyltriphenylphosphonium bromide (413 mg, 1.00 mmol) in anhydrous tetrahydrofuran (20 ml) under nitrogen was added an ether

solution of butyllithium (1.25 mmol) followed at 0°C by 2-formyl-1,3-dimethoxyanthraquinone (**12**) (296 mg, 1.00 mmol). The reaction mixture was stirred for 20 min, poured into water, and extracted with ether. The crude products were separated by preparative thin-layer chromatography (silica gel – benzene). A fast-moving band consisted of 3-butoxy-2-(hex-1-enyl)-1-methoxyanthraquinone (**13**) (47 mg, 12%), mp 121–122°C (ethanol–water); λ_{max} ($CHCl_3$) 290, 299 sh, 380 nm (log ε 4.46, 4.27, 3.77); ν_{max} (KBr) 1665 (quinone C=O) cm^{-1}; δ (90 MHz, $CDCl_3$) 1.01 (6H, t, J = ~6.5 Hz, 4′,6′′-H_3), 1.33–2.04 (8H, m, 2′,3′,4′′,5′′-H_2), 2.14–2.38 (2H, m, 3′′-H_2), 3.92 (2H, t, J = 7.0 Hz, 1′-H_2), 4.02 (3H, s, 3-OCH_3), 6.69 [2H, AB part of an ABX_2 system, J_{AB} = 16.0 Hz (Δν = 17.9 Hz), J_{BX} = 6.0 Hz, 1′′-H (6.49) and 2′′-H (6.89)], 7.62 (1H, s, 4-H), 7.58–7.78 (2H, m, 6,7-H), and 8.12–8.32 (2H, m, 5,8-H); *m/e* 392 (M^+), 335, 279. *Anal.* calcd. for $C_{25}H_{28}O_4$: C 76.50, H 7.19; found: C 76.38, H 7.21.

A second zone contained the expected hexenylanthraquinone **14** (244 mg, 70%), mp 112–113°C (ethanol–water); λ_{max} ($CHCl_3$) 291, 300, 390 nm (log ε 4.59, 4.58, 3.68); ν_{max} (KBr) 1665 (quinone C=O) cm^{-1}; δ (90 MHz, $CDCl_3$) 0.93 (3H, t, J = ~7.0 Hz, 6′-H_3), 1.20–1.70 (4H, m, 4′,5′-H_2), 2.14–2.42 (2H, m, 3′-H_2), 3.85 (3H, s, 3-OCH_3), 4.02 (3H, s, 1-OCH_3), 6.72 [2H, AB part of an ABX_2 system, J_{AX} = 16.5 Hz (Δν = 20.7 Hz), J_{BX} = 6.0 Hz, 1′-H (6.49) and 2′-H (6.95)], 7.63 (1H, s, 4-H), 7.63–7.85 (2H, m, 6,7-H), and 8.12–8.33 (2H, m, 5,8-H); *m/e* 350 (M^+), 335. *Anal.* calcd. for $C_{22}H_{22}O_4$: C 75.41, H 6.33; found: C 75.53, H 6.45.

*1-Allyloxy-3-methoxyanthraquinone (**16**)*

The crude 3-methyl ether obtained from xanthopurpurin (960 mg, 4.00 mmol), dimethyl sulfate (1 g, 8 mmol), anhydrous potassium carbonate (1.38 mg, 1.00 mmol), and 1,2-dimethoxyethane (40 ml) at 50°C (8 h) was heated to reflux for 10 h with allyl bromide (1.74 g, 14.4 mmol), potassium iodide (2.0 g, 12.0 mmol), and anhydrous potassium carbonate (1.6 g, 11.6 mmol) in 1,2-dimethoxyethane (25 ml). The crude product was chromatographed on silica gel (dry column, benzene – ethyl acetate 4:1) and gave the allyl ether **16** (782 mg, 66%), mp 146–147°C (methanol); λ_{max} (ethanol) 230 sh, 238, 247 sh, 277, 330, 390 nm (log ε 4.25, 4.27, 4.22, 4.80, 3.50, 3.67); ν_{max} (KBr) 1665 (quinone C=O) cm^{-1}; δ (90 MHz, $CDCl_3$) 3.92 (3H, s, 3-OCH_3), 4.62–4.78 (2H, m, 1′-H_2), 5.27–5.80 (2H, m, 3′-H_2), 6.22 (1H, m, 2′-H), 6.76 (1H, d, J = 3.0 Hz, 2-H), 7.43 (1H, d, J = 3.0 Hz, 4-H), 7.61–7.78 (2H, m, 6,7-H) and 8.11–8.31 (2H, m, 5,8-H); *m/e* 294 (M^+). *Anal.* calcd. for $C_{18}H_{14}O_4$: C 73.46, H 4.80; found: C 73.29, H 5.01.

1-Hydroxy-3-(tetrahydropyran-2-yloxy)anthraquinone

A mixture of xanthopurpurin (240 mg, 1.00 mmol), dihydropyran (2 ml), a trace of *p*-toluenesulfonic acid, and chloroform (1 ml), was stirred at room temperature for 2 h, washed with water, evaporated, and gave the 3-(tetrahydropyran-2-yl) ether (293 mg, 90%), mp 151–152°C (ethanol–water), λ_{max} (ethanol) 230, 240, 245, 264, 277, 331, 400 nm (log ε 4.24, 4.37, 4.36, 4.30, 4.29, 3.28, 3.75); ν_{max} (KBr) 1670 (quinone C=O) and 1630 (chelated C=O) cm^{-1}; δ (60 MHz, $CDCl_3$) 1.47–2.03 (6H, m, 3′,4′,5′-H_2), 3.57–3.90 (2H, m, 6′-H_2), 5.43–5.66 (1H, m, 2′-H), 6.85 (1H, d, J = 2.5 Hz, 2-H), 7.40 (1H, d, J = 2.5 Hz, 4-H), 7.57–7.87 (2H, m, 6,7-H), 8.03–8.40 (2H, m, 5,8-H), and 12.75 (1H, s, 1-OH); *m/e* 324 (M^+). *Anal.* calcd. for $C_{19}H_{16}O_5$: C 70.36, H 4.98; found: C 70.46, H 5.02.

*1-Allyloxy-3-(tetrahydropyran-2-yloxy)anthraquinone (**17**)*

In a preparation analogous to that of the allyl ether **16**, the foregoing quinone (1.0 g, 3.1 mmol), allyl bromide (1.45 g, 12.0 mmol), potassium iodide (1.98 g, 11.9 mmol), anhydrous potassium carbonate (4.14 g, 30.0 mmol), and 1,2-dimethoxyethane (25 ml) at reflux temperature (8 h) gave the allyl ether **17** (933 mg, 83%), mp 121.5–122.5°C (methanol); λ_{max} (ethanol) 230, 238, 245 sh, 276, 327, 395 nm (log ε 4.34, 4.36, 4.32, 4.41, 3.57, 3.73); ν_{max} (KBr) 1660 (quinone C=O) cm^{-1}; δ (90 MHz, $CDCl_3$) 1.48–2.00 (6H, m, 3′′,4′′,5′′-H_2), 3.47–3.91 (2H, m, 6′′-H_2), 4.73 (2H, dt, J = 4.5, 1.5 Hz, 1′-H_2), 5.28–5.82 (2H, m, 3′-H_2), 5.61 (1H, m, 2′′-H), 6.12 (1H, m, 2′-H), 6.95 (1H, d, J = 2.5 Hz, 2-H), 7.59 (1H, d, J = 2.5 Hz, 4-H), 7.57–7.78 (2H, m, 6,7-H), and 8.13–8.33 (2H, m, 5,8-H); *m/e* 364 (M^+), 280. *Anal.* calcd. for $C_{22}H_{20}O_5$: C 72.51, H 5.53; found: C 72.48, H 5.58.

*3-Allyloxy-1-hydroxyanthraquinone (**18**)*

The direct O-allylation of xanthopurpurin by the foregoing method gave the 3-allyl ether, mp 155–156°C (ether – petroleum ether, bp 30–60°C); λ_{max} (ethanol) 231, 241, 245, 266, 280, 324, 405 nm (log ε 4.32, 4.38, 4.42, 4.31, 4.36, 3.46, 3.84); ν_{max} (KBr) 1670 (quinone C=O) and 1635 (chelated C=O) cm^{-1}; δ (90 MHz, $CDCl_3$) 4.65 (2H, dt, J = 5.5, 1.0 Hz, 1′-H_2), 5.25–5.59 (2H, m, 3′-H_2), 6.28 (1H, m, 2′-H), 6.69 (1H, d, J = 2.5 Hz, 2-H), 7.35 (1H, d, J = 2.5 Hz, 4-H), 7.68–7.89 (2H, m, 6,7-H), and 8.17–8.39 (2H, m, 5,8-H); *m/e* 280 (M^+). *Anal.* calcd. for $C_{17}H_{12}O_4$: C 72.85, H 4.32; found: C 72.56, H 4.41.

*2-Allyl-1-hydroxy-3-methoxyanthraquinone (**19**)*

A solution of 1-allyloxy-3-methoxyanthraquinone (**16**) (100 mg, 0.340 mmol) in *o*-dichlorobenzene (25 ml) was refluxed for 16 h and evaporated under vacuum (0.5 torr). Chromatography of the residue on silica gel (dry column, benzene) gave the rearranged product **19** (76 mg, 76%), mp 140–141°C (ether – petroleum ether, bp 30–60°C); λ_{max} (ethanol) 241 sh, 246, 274, 335, 410 (log ε 4.32, 4.34, 4.49, 3.45, 3.82); ν_{max} (KBr) 1660 (quinone C=O), and 1630 (chelated C=O) cm^{-1}; δ (90 MHz, $CDCl_3$) 3.47 (2H, dt, J = 6.0, 1.5 Hz, 1′-H_2), 3.97 (3H, s, 3-OCH_3), 4.90–5.21 (2H, m, 3′-H_2), 5.93 (1H, m, 2′-H), 7.36 (1H, s, 4-H), 7.66–7.83 (2H, m, 6,7-H), 8.11–8.33 (2H, m, 5,8-H), and 12.87 (1H, s, 1-OH); *m/e* 294 (M^+). *Anal.* calcd. for $C_{18}H_{14}O_4$: C 73.46, H 4.80; found: C 73.45, H 4.87.

*2-Allyl-1,3-dihydroxyanthraquinone (**20**)*

An analogous reaction with the allyl ether **17** (20.3 g, 55.8 mmol) and *o*-dichlorobenzene (900 ml) (15 h) gave the crude 2-allylanthraquinone **20** which was recrystallized from a mixture of 1,2-dichloroethane and ethyl acetate (12.6 g, 81%), mp 256–257°C (1,2-dichloroethane); λ_{max} (chloroform) 249, 281, 420 nm (log ε 4.38, 4.44, 3.80); ν_{max} (KBr) 3395 (hydroxyl), 1660 (quinone C=O), and 1635 (chelated C=O) cm^{-1}; δ (90 MHz, C_5D_5N) 3.85 (2H, dt, J = 6.0, 1.0 Hz, 1′-H_2), 5.04–5.80 (2H, m,

3′-H_2), 6.23 (1H, m, 2′-H), 7.63 (1H, s, 4-H), 7.50–7.77 (2H, m, 6,7-H), and 8.12–8.37 (2H, m, 5,8-H); *m/e* 280 (M^+). *Anal.* calcd. for $C_{17}H_{12}O_4$: C 72.85, H 4.32; found: C 72.61, H 4.55.

The same product and yield were obtained from xanthopurpurin 3-allyl ether **18** (900 mg) after refluxing for 46 h in the same solvent (50 ml) and purifying the crude product by chromatography on silica gel (dry column, benzene – chloroform – ethyl acetate 5:3:2).

2-Allyl-1,3-dimethoxyanthraquinone

The dimethyl ether was obtained in the usual way from the 2-allyl compound **20** (679 mg, 2.43 mmol) dimethyl sulfate (1.2 ml), anhydrous sodium carbonate (3.0 g), and refluxing acetone (100 ml, 7.5 h) after chromatography on silica gel (dry column, benzene – ethyl acetate 4:1) (668 mg, 89%), mp 132.5–133.5°C (methanol); λ_{max} (ethanol 239, 245, 275, 350 nm (log ε 4.13, 4.09, 4.58, 3.63); ν_{max} (KBr) 1670 (quinone C=O) and 1640 (vinyl) cm^{-1}; δ (60 MHz, $CDCl_3$) 3.53 (2H, dt, J = 6.0, 1.0 Hz, 1′-H_2), 3.92 and 3.98 (2 × 3H, 2s, 1,3-OCH_3), 4.83–5.27 (2H, m, 3′-H_2), 5.99 (1H, m, 2′-H), 7.60 (1H, s, 4-H), 7.60–7.83 (2H, m, 6,7-H), and 8.03–8.38 (2H, m, 5,8-H); *m/e* 308 (M^+). *Anal.* calcd. for $C_{19}H_{16}O_4$: C 74.01, H 5.23; found: C 73.87, H 5.31.

*1,3-Dihydroxy-2-(trans-prop-1-enyl)anthraquinone (**21**)*

A mixture of 2-allyl-1,3-dihydroxyanthraquinone (**20**) (500 mg, 1.79 mmol), rhodium trichloride trihydrate (25 mg), and absolute ethanol (25 ml) stirred at 75°C for 2 h, diluted with boiling water, cooled, and filtered gave the isomerized quinone **21** (363 mg, 73%), mp 237–238°C (1,2-dichloroethane); λ_{max} (chloroform) 253, 299, 430 nm (log ε 4.64, 4.74, 4.20); ν_{max} (KBr) 3340 (hydroxyl), 1665 (quinone C=O), and 1645 (chelated C=O) cm^{-1}; δ (90 MHz, C_5D_5N) 0.95 (3H, d, J = 6.0 Hz, 3′-H_3), 6.94–7.38 (2H, m, 1′,2′-H), 7.51–7.77 (2H, m, 6,7-H), 7.70 (1H, s, 4-H), and 8.17–8.41 (2H, m, 5,8-H). *Anal.* calcd. for $C_{17}H_{12}O_4$: C 72.85, H 4.32; found: C 72.75, H 4.53.

*1,3-Dihydroxy-2-(threo-1,2-dihydroxypropyl)anthraquinone (**22**)*

A mixture of 1,3-dihydroxy-2-(*trans*-prop-1-enyl)anthraquinone (**21**) (281 mg, 1.00 mmol) and osmium tetroxide (256 mg, 1.01 mmol) in pyridine (4 ml) was stirred at room temperature for 30 min. The reaction mixture, after addition of pyridine (4.8 ml) and an aqueous solution (8 ml) of sodium bisulfite (460 mg, 4.42 mmol), was allowed to stand for 5 min then diluted with water (100 ml) and extracted with ethyl acetate. The residue obtained by evaporation of the organic solvent was chromatographed on silica gel (50 g) (ethyl acetate) and gave the diol **22** (252 mg, 80%), mp 260–261°C (1,2-dichloroethane); λ_{max} (ethanol) 246, 281, 405 nm (lo ε 4.85, 4.47, 3.89); ν_{max} (KBr) 3500, 3200 (hydroxyls), 1680 (quinone C=O), and 1625 (chelated C=O) cm^{-1}; δ (90 MHz, $(CD_3)_2SO$) 1.11 (3H, d, J = 6.5 Hz, 3′-H_3). 4.05 (1H, dq, J = 5.5, 6.5 Hz, 2′-H; collapses to a doublet (J = 5.5 Hz) by irradiation at δ 1.11 and to a quartet (J = 6.5 Hz) by irradiation at δ 4.95), 4.95 (1H, d, J = 5.5 Hz, 1′-H), 7.78–7.95 (2H, m, 6,7-H), and 8.00–8.31 (2H, m, 5,8-H); *m/e* 314 (M^+). *Anal.* calcd. for $C_{17}H_{12}O_6$: C 64.96, H 4.49; found: C 64.80, H 4.49.

Hydroxyalkylation of Xanthopurpurin with 5-Oxohexanal

A mixture of xanthopurpurin (480 mg, 2.00 mmol), sodium bicarbonate (178 mg, 2.12 mmol), 5-oxohexanal (18) (456 mg, 4.00 mmol), and water (4 ml) was stirred under nitrogen and kept at an external temperature of 100°C for 2.5 h. Two more portion (480 mg each) of the aldehyde were added after 1 h and 1.5 h. The reaction mixture was then poured into water and acidified with dilute hydrochloric acid. Cyclohexenone (528 mg) can be isolated from the filtrate after saturating with salt and extracting repeatedly with ether. The crude products were chromatographed on silica gel (dry column, benzene) and gave a fast moving band consisting of 5-hydroxy-2-methyl-2,4-propano-6,11-dihydro-4*H*-anthra[2,3-*d*]*m*-dioxine-6,11-dione (bis-deoxyaverufin) (**23**) (73 mg, 11%), mp 179.0–179.5°C (ether – petroleum ether, bp 30–60°C); λ_{max} ($CHCl_3$) 247, 281, 400 nm (log ε 4.59, 4.57, 3.94); ν_{max} (KBr) 1665 (quinone C=O) and 1625 (chelated C=O) cm^{-1}; δ (90 MHz, $CDCl_3$) 1.58 (3H, s, 2-CH_3), 1.55–2.17 (6H, m, 2,4-propano), 5.36 (1H, m, 4-H), 7.23 (1H, s, 12-H), 7.68–7.82 (2H, m, 8,9-H), 8.17–8.31 (2H, m, 7,10-H), and 13.00 (1H, s, 5-OH); *m/e* 336 (M^+), 318, 293, 279, 278, 265, 254, 253. *Anal.* calcd. for $C_{20}H_{16}O_5$: C 71.42, H 4 80; found: C 71.45, H 4.73. Xanthopurpurin (187 mg, 39%) can be recovered from a median zone.

From the top of the column was extracted 6,6-bis-(1,3-dihydroxyanthraquinone-2-yl)hexan-2-one (**24**) (178 mg, 31%) which was converted in the usual way (dimethyl sulfate, anhydrous potassium carbonate, and acetone) to the tetramethyl ether, mp 210–212°C (aqueous ethanol); λ_{max} (ethanol) 281, 360 nm (log ε 5.04, 4.21); ν_{max} (KBr) 1710 (aliphatic C=O) and 1670 (quinone C=O) cm^{-1}; δ (90 MHz, $CDCl_3$) 1 50–1.83 (4H, m, 4,5-H_2), 2.11 (3H, s, 1-H_3), 2.51 (2H, t, J = 7.5 Hz, 3-H_2), 3.63 (6H, s, 3′,3″-OCH_3), 4.03 (6H, s, 1′,1″-OCH_3), 5.13 (1H, t, J = 7.5 Hz, 6-H), 7.61–7.75 (4H, m, 6′,6″, 7′,7″-H), 7.66 (2H, s, 4′,4″-H), and 8.28 (4H, m, 5′,5″,8′,8″-H); *m/e* 632 (M^+), 546, 281. *Anal.* calcd. for $C_{38}H_{32}O_9$: C 72.14, H 5.10; found: C 71.84, H 5.24.

*1,3,6,8-Tetrahydroxyanthraquinone (**25**)*

1,3,6,8-Tetramethoxyanthraquinone (2.82 g, 8.60 mmol) was added to a melt of anhydrous aluminum chloride (282 g) and sodium chloride (56 g) at 140°C. The temperature was then raised to 180°C for 30 s. The residue obtained from an ethyl acetate extract of the crude product was chromatographed on silica gel (100 g, benzene – ethyl acetate 4:1) and gave the tetrahydroxy compound **25** (2.13 g, 91%), mp >340°C (lit. (19, 20) mp >360°C; lit. (21) dec. 353°C); λ_{max} (ethanol) 220, 251, 262, 294, 318, 450 nm (log ε 4.48, 3.89, 3.85, 4.34, 3.85, 3.81); ν_{max} (KBr) 3350 (hydroxyl), 1670 (quinone C=O), and 1620 (chelated C=O) cm^{-1}; δ (90 MHz, C_5D_5N) 6.93 (2H, d, J = 2.5 Hz, 2,7-H) and 7.60 (2H, d, J = 2.5 Hz, 4,5-H).

*(±)-Averufin (**26**)*

A solution of 1,3,6,8-tetrahydroxyanthraquinone (**25**) (400 mg, 1.47 mmol), sodium bicarbonate (248 mg, 2.95 mmol), and 5-oxohexanal (18) (336 mg, 2.95 mmol) was stirred under nitrogen at an external temperature of 90°C for 14 h. Seven similar portions of aldehyde were added at regular intervals. The reaction mixture was then poured into water and extracted with ethyl acetate. The crude

products were chromatographed on silica gel (dry column, benzene – ethyl acetate 1:1). A fast moving zone contained a small amount of an unidentified yellow product. The median zone was purified by preparative tlc on silica gel (benzene – ethyl acetate 50:1, 4 migrations) and gave (±)-averufin (35 mg, 6.5%) (acetone–benzene) which decomposes >280°C (lit. (22) mp dec. 280–282°C; lit. (2) mp 280°C, lit. (23) dec. 283–289°C); λ_{max} (ethanol) 223, 255, 265, 294, 320, 451 nm (log ε 4.46, 4.15, 4.20, 4.43, 4.14, 3.94); ν_{max} (KBr) 3360 (hydroxyl), 1670 (quinone C=O) and 1625 (chelated C=O) cm^{-1}; δ (90 MHz, $(CD_3)_2SO$) 1.52 (3H, s, 2-CH_3), 1.44–2.17 (6H, m, 2,4-propano-), 5.11–5.28 (1H, m, 4-H), 6.50 (1H, d, J = 2.5 Hz, 8-H), 6.89 (1H, s, 12-H), and 7.00 (1H, d, J = 2.5 Hz, 10-H); *m/e* 368 (M^+), 350, 325, 311, 310, 297, 286, 285. *Anal.* calcd. for $C_{20}H_{16}O_7$: C 65.21, H 4.38; found: C 65.13, H 4.60. From the top of the original column a large part of tetrahydroxyanthraquinone (191 mg, 48%) could be recovered by extraction (benzene – ethyl acetate 5:1).

Hydroxyalkylation of Xanthopurpurin with 5-Hydroxypentanal

A mixture of xanthopurpurin (480 mg, 2.00 mmol), sodium bicarbonate (178 mg, 2.12 mmol), and 5-hydroxypentanal (24) (408 mg, 4.00 mmol) in water (4 ml) was stirred under nitrogen at an external temperature of 100°C for 7 h. Two more portions of aldehyde (400 mg each) were added after the first and second hours. The reaction mixture was then poured into water, acidified, and extracted with ethyl acetate. The crude products were chromatographed on silica gel (dry column, benzene – ethyl acetate 9:1). A fast moving band was rechromatographed by the same procedure and allowed the separation of three products. The substance with the highest R_f was identified as 1,3-dihydroxy-2-(tetrahydropyran-2-yl)anthraquinone (bis-deoxynoravermutin) (**27**) (130 mg, 20%), mp 190.5–191.5°C (ether); λ_{max} ($CHCl_3$) 280, 410 nm (log ε 4.47, 3.89); ν_{max} (KBr) 3210 (hydroxyl), 1680 (quinone C=O) and 1620 (chelated C=O) cm^{-1}; δ (90 MHz, $CDCl_3$) 1.51–2.17 (6H, 2m, 3′,4′,5′-H_2), 3.46–3.82 (1H, m, 6′-H axial; collapses to a broad doublet by irradiation at δ 1.69, J_{gem} = 11.0 Hz), 4.24 (1H, br d, 6′-H equatorial; gives a doublet by irradiation at δ 1.69, J_{gem} = 11.0Hz), 5.05 (1H, br d, J = 8.0 Hz, 2′-H axial), 7.21 (1H, s, 4-H), 7.61–7.81 (2H, m, 6,7-H), 8.11–8.31 (2H, m, 5,8-H), 9.72 (1H, s, 3-OH), and 13.23 (1H, s, 1-OH); *m/e* 324 (M+), 306, 279, 278, 267, 265, 254, 253, 241, 240. *Anal.* calcd. for $C_{19}H_{16}O_5$: C 70.36, H 4.98; found: C 70.39, H 4.89. A second band consisted of xanthopurpurin (124 mg, 26%). Extraction of the top of this second column with ethyl acetate gave 1,3-dihydroxy-2-(5-hydroxy-*trans*-pent-1-enyl)anthraquinone (**28**) (31 mg, 4.8%), mp 212–213°C (ethyl acetate – benzene); λ_{max} ($CHCl_3$) 250, 291, 420 nm (log ε 4.30, 4.34, 3.75); ν_{max} (KBr) 3500 (hydroxyl), 1650 (quinone C=O) and 1620 (chelated C=O) cm^{-1}. Methylation of this product (dimethyl sulfate, anhydrous sodium carbonate and acetone) gave the corresponding 1,3-dimethyl ether, mp 140.0–141.5°C (ether – petroleum ether, bp 30–60°C), λ_{max} (chloroform) 291, 300, 390 nm (log ε 4.59, 4.58, 3.68); δ (90 MHz, $CDCl_3$) 1.63–1.98 (2H, m, 4′-H_2), 2.29–2.55 (2H, m, 3′-H_2), 3.74 (2H, t, J = 6.5 Hz, 5′-H_2), 3.81 (3H, s, 3-OCH_3), 4.03 (3H, s, 1-OCH_3), 6.77 [2H, AB part of an ABX_2 system, J_{AB} = 17.0 Hz ($\Delta\nu$ = 16.9 Hz), J_{BX} = 5.5 Hz, 1′-H (6.63) and 2′-H (6.90)], 7.63–7.89 (2H, m, 6,7-H), 7.66 (1H, s, 4-H), and 8.16–8.33 (2H, m, 5,8-H). *Anal.* calcd. for $C_{21}H_{22}O_6 \cdot H_2O$: C 68.09, H 5.99; found: C 68.36, H 5.54.

From the top of the first column a red oil was obtained by extraction with absolute ethanol, which was methylated in the usual way and gave, after chromatography on silica gel (dry column, benzene – ethyl acetate 2:1), a trimethyl ether of 5,5-bis-(1,3-dihydroxyanthraquinon-2-yl) pentanol-1 (**29**), mp 144–145°C (ethanol); λ_{max} (chloroform) 285, 395 nm (log ε 4.96, 4.08); ν_{max} (KBr) 1670 (quinone C=O) and 1630 (chelated C=O) cm^{-1}; δ (90 MHz, $CDCl_3$) 1.41–1.91 (6H, m, 2,3,4-H_2), 3.66 (2H, t, J = 6.0 Hz, 1-H), 3.80 and 3.92 (2 × 3H, 2s, 3′,3″-OCH_3), 3.97 (3H, s, 1″-OCH_3), 5.10 (1H, t, J = 7.5 Hz, 5-H), 7.37 (1H, s, 4′-H), 7.61 (1H, s, 4″-H), 7.60–7.83 (4H, m, 6′,6″,7′,7″-H), 8.11–8.33 (4H, m, 5′,5″,8′,8″-H), and 13.32 (1H, s, 1′-OH). *Anal.* calcd. for $C_{36}H_{30}O_9$: C 71.28, H 4.99; found: C 71.26, H 4.95.

4-Hydroxybutanal

To a well stirred solution of γ-butyrolactone (8.6 g, 0.1 mol) in pentane at −63°C and under dry nitrogen was added over a period of 1 h a 20% solution of diisobutylaluminum hydride in hexane (21.3 g, 0.15 mol). After 2 h, the reaction mixture was allowed to come to room temperature, diluted with 2-propanol (5 ml) and water (5 ml), filtered, and evaporated. The residue was constituted essentially of 4-hydroxybutanal (2.85 g, 32%); ν_{max} (film) 3390 (hydroxyl) cm^{-1}; δ (60 MHz, $CDCl_3$) 1.55–1.97 (4H, m, 2,3-H_2), 3.47–4.12 (2H, m, 4-H_2), and 5.18–5.60 (2H, 2m, 1-H and 1-OH). The substance is known to be unstable and could not be further purified (25).

*(±)-Bipolarin (**30**)*

A solution of 1,3,6,8-tetrahydroxyanthraquinone (**25**) (300 mg, 1.10 mmol), 4-hydroxybutanal (540 mg, 6.14 mmol), and sodium bicarbonate (186 mg, 2.21 mmol) in water (3 ml) was stirred under nitrogen for 16 h at an external temperature of 90°C. Supplemental portions of hydroxybutanal (540 mg each) were added after 0.5, 1, 2, 4, and 8 h. The crude products obtained after dilution of the reaction mixture with water (100 ml) and acidification were separated by preparative tlc (silica gel, benzene – ethyl acetate 20:1, 3 migrations). The band with the highest R_f consisted of (±)-bipolarin (**30**), (95 mg, 25%), mp 261–262°C (acetone) (lit. (2) mp 261°C); λ_{max} (ethanol) 223, 254, 265, 293, 320, 450 nm (log ε 4.45, 4.12, 4.18, 4.42, 4.02, 3.90); ν_{max} (KBr) 3400 (hydroxyl), 1665 (quinone C=O) and 1625 (chelated C=O) cm^{-1}; δ (90 MHz, $(CD_3)_2SO$) 1.81–2.26 (4H, m, 3′,4′-H_2), 3.62–4.20 (2H, 2m, 5′-H_2), 5.17–5.41 (1H, m, 2′-H), 6.52 (1H, d, J = 2.0 Hz, 7-H), 7.05 (1H, d, J = 2.0 Hz, 5-H), and 7.13 (1H, s, 4-H); *m/e* 342 (M^+), 314, 311, 299, 297, 286, 285, 272. *Anal.* calcd. for $C_{18}H_{14}O_7$: C 63.16, H 4.12; found: C 63.27, H 4.43. A small amount of 1,3,6,8-tetrahydroxyanthraquinone (25 mg, 8%) can also be recovered.

Alkylation of Xanthopurpurin with n-Hexanal

Method A

A solution of xanthopurpurin (120 mg, 0.50 mmol), *n*-hexanal (100 mg, 1.00 mmol), and sodium bicarbonate

(42 mg, 0.50 mmol) in water (1 ml) was stirred at 100°C (external) for 95 h. Further portions of aldehyde (2 × 100 mg and 2 × 200 mg) were added after 2, 5, 26, and 48 h. The crude product was chromatographed on silica gel (dry column, benzene – ethyl acetate 25:1). Separation of a fast moving zone by preparative tlc (silica gel, benzene – ethyl acetate 50:1, 2 migrations) gave 2-(*trans*-hex-1-enyl)-1,3-dihydroxyanthraquinone (**31**) (38 mg, 24%), mp 210.0–211.5°C (ether – petroleum ether bp 30–60°C); λ_{max} (chloroform) 252, 295, 430 nm (log ε 4.35, 4.40, 3.74); ν_{max} (KBr) 3380 (hydroxyl), 1660 (quinone C=O) and 1640 (chelated C=O) cm^{-1}; δ (90 MHz, $(CD_3)_2SO$) 1.90 (3H, t, J = 6.0 Hz, 6′-H_3), 1.16–1.50 (4H, m, 4′,5′-H_2), 2.04–2.37 (2H, m, 3′-H_2), 6.77 [2H, AB part of an ABX_2 system, J_{AB} = 17.0 Hz ($\Delta\nu$ = 25.9 Hz) J_{BX} = 6.5 Hz, 1′-H (6.63) and 2′-H (6.81)], 7.29 (1H, s, 4-H), 7.81–8.00 (2H, m, 6,7-H), and 8.00–8.24 (2H, m, 5,8-H); *m/e* 322 (M^+), 293, 279, 265, 253. *Anal.* calcd. for $C_{20}H_{18}O_4$: C 74.52, H 5.63; found: C 74.27, H 5.52. Methylation of this product gave a substance identical to that prepared earlier.

Method B

When the foregoing reaction between xanthopurpurin (2.00 mmol), *n*-hexanal (12 mmol), and sodium bicarbonate (2.00 mmol) was conducted in water (3 ml) and acetone (1 ml) under pressure (sealed tube) for 112 h at 100°C, the principal product, obtained by chromatography (silica gel, benzene – ethyl acetate 50:1), was the same hexenyl compound **31** (170 mg, 26%). Elution with benzene – ethyl acetate 25:1 gave an unidentified red solid purified by preparative tlc (silica gel, benzene – ethyl acetate 100:1), mp 178–179°C (26 mg); λ_{max} (chloroform) 274, 278, 420 nm (log ε 4.74, 4.86, 4.22); ν_{max} (KBr) 3380, 1665, 1625, 1590, 1475 cm^{-1}; *m/e* 644, 573, 391, 323, 293, 279, 265, 253.

Method C

The preceding experiment was conducted (24 h) in a mixture of methanol (2 ml) and water (2 ml) and the crude products were chromatographed on silica gel (dry column, benzene – ethyl acetate 9:1). Separation of a fast moving zone by preparative tlc gave xanthopurpurin (259 mg, 54%) and 2-(*trans*-hex-1-enyl)-1,3-dihydroxyanthraquinone (**31**), (29 mg, 4.5%). The top of the original column contained 1,1-bis(1,3-dihydroxyanthraquinon-2-yl)hexane (**32**). Methylation of this material by the usual means (dimethyl sulfate, anhydrous sodium carbonate, and acetone) gave the corresponding tetramethyl ether, mp 214.5–215.0°C (ether – petroleum ether, bp 30–60°C); λ_{max} (chloroform) 274, 281, 360 nm (log ε 4.96, 4.97, 4.15); ν_{max} (KBr) 1670 (quinone C=O) cm^{-1}; δ (90 MHz, $CDCl_3$) 0.88 (3H, t, J = 6.0 Hz, 6-H_3), 1.22–1.48 (8H, m, 2,3,4,5-H_2), 3.66 (6H, s, 3′,3″-OCH_3), 4.05 (6H, s, 1′,1″-OCH_3), 5.17 (1H, t, J = 7.5 Hz, 1-H), 7.58–7.73 (4H, m, 6′,6″,7′,7″-H), 7.66 (2H, s, 4′,4″-H), and 8.09–8.26 (4H, m, 5′,5″,8′,8″-H). *Anal.* calcd. for $C_{38}H_{34}O_8$: C 73.77, H 5.54; found: C 73.72, H 5.58.

Acknowledgments

The authors wish to thank Dr. P. S. Steyn for a sample of averufin. Financial support from the Ministère de l'Education du Québec and the award of National Research Council of Canada scholarships to one of us (A.C.) are acknowledged.

1. R. H. THOMSON. Naturally occurring quinones. 2nd ed. Academic Press, London and New York. 1971. pp. 482–487.
2. P. J. AUCAMP and C. W. HOLZAPFEL. J. S. Afr. Chem. Inst. **23**, 40 (1970).
3. J. GRANDJEAN, J. JADOT, and J. RAMAUT. Bull. Soc. Chim. Belg. **81**, 521 (1972); Y. BERGER, J. JADOT, and J. RAMAUT. Bull. Soc. Chim. Belg. **85**, 161 (1976).
4. M. V. SARGENT, D. O'N. SMITH, J. A. ELIX, and P. ROFFEY. J. Chem. Soc. C, 2763 (1969).
5. German Patent No. 184,786; Frdl., 1X, 694; N. R. AYYANGAR and K. VENKATARAMAN. J. Sci. Ind. Res. India, **15B**, 359 (1956); N. R. AYYANGAR, B. S. JOSHI, and K. VENKATARAMAN. Tetrahedron, **6**, 331 (1959).
6. A. CASTONGUAY and P. BRASSARD. Synth. Commun. **5**, 377 (1975).
7. E. DEB. BARNETT and J. W. COOK. J. Chem. Soc. 1376 (1922).
8. G. WITTIG, U. POCKELS, and H. DROEGE. Chem. Ber. **71**, 1903 (1938); H. GILMAN, H. B. WILLIS, T. H. COOK, F. J. WEBB, and R. N. MEALS. J. Am. Chem. Soc. **62**, 667 (1940).
9. R. G. HARVEY and C. C. DAVIS. J. Org. Chem. **34**, 3607 (1969).
10. N. L. WEINBERG and B. BELLEAU. Tetrahedron, **29**, 279 (1973).
11. A. S. KENDE, J. L. BELLETIRE, and E. L. HUME. Tetrahedron Lett. **31**, 2935 (1973).
12. E. BERTELE and P. SCHUDEL. Helv. Chim. Acta, **50**, 2445 (1967).
13. G. SAUCY and R. BORER. Helv. Chim. Acta, **54**, 2121 (1971).
14. H. PLATH. Chem. Ber. **9**, 1204 (1876).
15. A. G. PERKIN and C. W. H. STORY. J. Chem. Soc. 1399 (1929).
16. B. S. JOSHI, N. PARKASH, and K. VENKATARAMAN. J. Sci. Ind. Res. India, **14B**, 87 (1955).
17. S. BALL, T. W. GOODWIN, and R. A. MORTON. Biochem. J. **42**, 516 (1948).
18. R. I. LONGLEY, JR. and W. S. EMERSON. J. Am. Chem. Soc. **72**, 3079 (1950); B. G. KOVALEV, N. P. DORMIDONTOVA, E. M. AL'TMARK, and A. A. SHAMSHURIN. Probl. Poluch. Poluprod. Prom. Org. Sin. Akad. Nauk SSSR, Otd. Obshch. Tekh. Khim. 53 (1967); Chem. Abstr. **68**, 113993y (1968).
19. E. BULLOCK, D. KIRKALDY, J. C. ROBERTS, and J. G. UNDERWOOD. J. Chem. Soc. 829 (1963).
20. M. D. SUTHERLAND and J. W. WELLS. Chem. Ind. 291 (1959).
21. S. SHIBATA. J. Pharm. Soc. Jpn. **61**, 320 (1941); Chem. Abstr. **44**, 9396g (1950).
22. D. F. G. PUSEY and J. C. ROBERTS. J. Chem. Soc. 3542 (1963).
23. J. A. DONKERSLOOT, R. I. MATELES, and S. S. YANG. Biochem. Biophys. Res. Commun. **47**, 1051 (1972).
24. G. F. WOODS, JR. Org. Synth. **27**, 43 (1947).
25. R. PAUL and S. TCHELITCHEFF. Bull. Soc. Chim. Fr. 197 (1948); R. PAUL, M. FLUCHAIRE, and C. COLLARDEAU. Bull. Soc. Chim. Fr. 668 (1950).

The reflection method in predissociation

ANDRÉ D. BANDRAUK AND JEAN-PIERRE LAPLANTE[1]

Département de chimie, Université de Sherbrooke, Sherbrooke (Qué.), Canada J1K 2R1

Received November 29, 1976

ANDRÉ D. BANDRAUK and JEAN-PIERRE LAPLANTE. Can. J. Chem. **55**, 1333 (1977).

The reflection method is used to calculate energy shifts and linewidths in predissociation by a linear continuum. The analytic results of this method are compared to the exact analytic calculations. It is found that, as in semiclassical calculations, energy shifts and linewidths usually vanish at the same energies. The spectroscopic implications of this finding are pointed out.

ANDRÉ D. BANDRAUK et JEAN-PIERRE LAPLANTE. Can. J. Chem. **55**, 1333 (1977).

La méthode de réflexion est appliquée aux calculs de déplacement d'énergie et de largeur des raies pour des systèmes prédissociés par un continuum linéaire. Les résultats analytiques de cette méthode sont comparés aux résultats exacts. En général, les déplacements d'énergie et les largeurs sont nul aux mêmes énergies. Les implications de ce résultat sont soulignés pour la spectroscopie de prédissociation.

Introduction

Predissociation is now a well established phenomenon in the electronic spectroscopy of molecules (1, 2). It is an example of a bound state embedded in a continuum. The influence of the continuum on such a discrete level is observed in the absorption spectra by the broadening and the shift of the level. Recent analytical expressions have been obtained for the linewidth Γ, responsible for the broadening, and the energy shift ΔE of such levels (3). It was found that these results compare well to a previous semiclassical treatment of this phenomenon (4).

In as much as one is dealing with transitions from a bound state to a continuum in a process such as predissociation, such transitions involve calculations of overlap integrals between bound state wave functions and rapidly oscillating continuum functions. One popular approximation, called the reflection method, corresponds to replacing the continuum function by a delta function. This method was analyzed by numerical calculations originally by Coolidge *et al.* (5) in a study of the Franck–Condon principle. These authors pointed out that this method appears to be very satisfactory, despite the difficulty of setting up a formal justification for it. Since then this method has been used many times in Franck–Condon factor calculations (6–8), in resonant Raman scattering by a continuum (9, 10), as well as in photodissociation (11). In a recent communication (12) we have shown the approximations inherent in such an approach by using a model depicted in Fig. 1. Thus in this model one has a bound state function $\phi_r(X)$ interacting with a continuum function $\phi_c(X)$. As the continuum is assumed to be linear around the interaction or crossing point X_c, the functions $\phi_c(X)$ are the well-known Airy functions (13, 14). In this way we were able to show that the reflection method corresponds to neglecting the kinetic energy of the nuclei in the continuum state. This is therefore a *rigorous* justification for the classical ideas of Condon (5). This model also enabled us to derive the appropriate corrections to the reflection method in the linear potential approximation.

In this work we wish to apply this method to predissociation in a diatomic molecule as shown in Fig. 1. Previous studies of this phenomenon were done assuming that both the bound state potential $V_r(X)$ and the continuum potential $V_c(X)$ were linear around the crossing point X_c, (3, 4, 15). This is therefore inaccurate for low lying vibrational levels, in particular for the ground vibrational state $v = 0$. We shall therefore first apply the reflection method to the linear model of the bound state and compare it to the rigorous analytic results obtained in ref. 3. Finally we shall calculate by the reflection method the predissociation linewidth Γ and the energy shift ΔE for a harmonic oscillator as a function of vibrational quantum number.

[1]Present address: Service de Chimie Physique II, Université Libre, Bruxelles, Belgium.

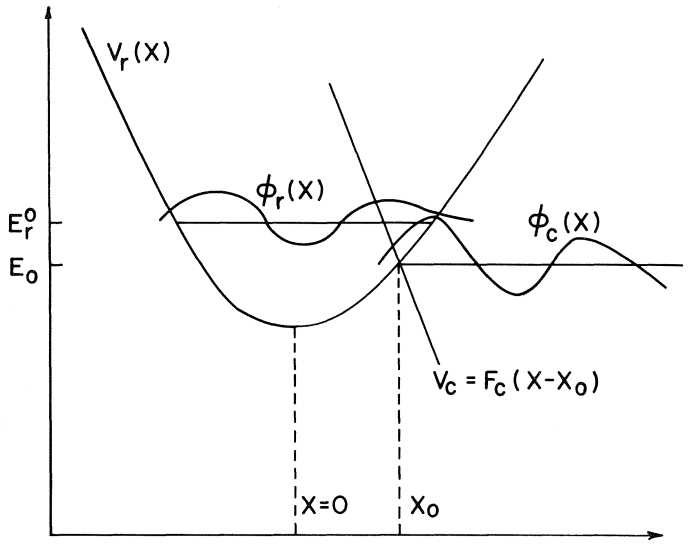

FIG. 1. Potentials and functions in X-space.

Linear Potentials and the Reflection Method

We consider the potential system illustrated in Fig. 1, where we have a potential $V_r(X)$, supporting bound states with functions $\phi_r(X)$, intersected by a linear continuum potential $V_c(X)$ with functions $\phi_c(X)$. X is the internuclear coordinate for a particular vibration in a molecule.

The continuum eigenfunctions $\phi_c(X)$ are the eigensolutions for the linear potential defined by

$$V_c(X) = E_0 - F_c(X - X_0) \quad [1]$$

where E_0 is the crossing point energy with respect to the minimum of the bound state potential, X_0 is the crossing point, and F_c is the absolute value of the slope of $V_c(X)$. The Schröedinger equation in momentum space becomes for this potential (we set $\hbar = 1$)

$$\left[\frac{p^2}{2\mu} + \left(E_0 + F_cX_0 - iF_c\frac{d}{dp}\right)\right]\phi_c(E_c,p) = E_c\phi_c(E_c,p) \quad [2]$$

where $\phi_c(E_c,p)$ is the Fourier momentum transform of $\phi_c(E_c,X)$ and μ is the reduced mass. We thus obtain,

$$\phi_c(E_c,X) = 2\pi^{1/2}N_cA_i(-q_c) \quad [3]$$

where

$$q_c = a_c\left(X + \frac{E_c - (E_0 + F_cX_0)}{F_c}\right)$$

$$N_c = a_c/(2\pi F_c)^{1/2} \quad [4]$$

$$a_c = (2\mu F_c)^{1/3}$$

$A_i(-q)$ is the Airy function defined in ref. 14 by,

$$2\pi^{1/2}A_i(-q) = \int_{-\infty}^{\infty} \exp\left[i(p^3/3 - pq)\right] dp \quad [5]$$

The continuum functions are normalized to the energy delta function, *i.e.*

$$\langle\phi_c(E_c',X)|\phi_c(E_c,X)\rangle = \delta(E_c - E_c') \quad [6]$$

It is to be noted that the factor $p^3/3$ in the exponential of [5] comes from integrating the kinetic energy term $p^2/2\mu$, in [2]. Hence, setting this kinetic term equal to zero, or correspondingly $p^3 \equiv 0$, one obtains

$$\phi_c(E_c,X) = (F_c)^{-1/2}\delta(X - X_c) \quad [7]$$

X_c is the classical turning point, *i.e.* where $q_c \equiv 0$, so that from [4] we have,

$$X_c = \frac{E_0 + F_cX_0 - E_c}{F_c} \quad [8]$$

This simple model shows us that the reflection method comes from neglecting the nuclear kinetic energy of the continuum state.

Having defined the linear potential eigenfunctions, we will now use these to calculate the relevant parameters in predissociation, *i.e.* the linewidth Γ and the energy shift ΔE. These are obtainable in second order perturbation theory from the integral (2)

$$G(E) = (\alpha_n)^2 \lim_{\varepsilon \to 0} \int_{-\infty}^{\infty} \frac{|\langle \phi_r(E_r^0,X)|\phi_c(E_c,X)\rangle|^2}{E - E_c + i\varepsilon} dE_c \quad [9]$$

where α_n is the nonadiabatic electronic matrix element assumed to be independent of nuclear distance, and the limit is taken after the integration is performed in order to avoid the singularity in the denominator. The expressions for the energy shift ΔE and linewidth Γ follow directly from the integral $G(E)$ in eq. 9,

$$\Delta E = \text{Re } G(E) = \alpha_n^2 \text{ PP} \int_{-\infty}^{\infty} \frac{|\langle \phi_r(E_r^0,X)|\phi_c(E_c,X)\rangle|^2}{E - E_c} dE_c$$

$$\tfrac{1}{2}\Gamma(E) = -\text{Im } G(E) = \alpha_n^2\pi \int \delta(E - E_c)|\langle \phi_r(E_r^0,X)|\phi_c(E_c,X)\rangle|^2 dE_c \quad [10]$$

where Re and Im stand for real and imaginary parts, and finally PP is the principal part integral.

We will now assume that the potential $V_r(X)$ is linear around the bound state energy E_r^0. This should be acceptable for high vibrational quantum levels. In particular, this model leads to Landau–Zener predissociation when treated by semiclassical scattering theory (4). Thus, from Fig. 1, we define

$$V_r(X) = E_0 + F_r(X - X_0) \quad [11]$$

The slope F_r is now positive as compared to the potential $V_c(X)$ in [1]. The eigenfunctions of $V_r(X)$ now become also Airy functions,

$$\phi_r(E_r^0,X) = 2\pi^{1/2}N_rA_i(-q_r) \quad [12]$$

where

$$q_r = a_r\left(X - \frac{E_r^0 - (E_0 - F_rX_0)}{F_r}\right)$$

$$N_r = \frac{(\pi\omega_r)^{1/2}a_r}{2\pi(F_r)^{1/2}} \quad [13]$$

$$a_r = (2\mu F_r)^{1/3}$$

and ω_r is the frequency of the bound state at E_r^0.

The normalization of these functions is such that (13)

$$\langle \phi_r(E_r^0,X)|\phi_r(E_r^0,X)\rangle = 1 \quad [14]$$

Introducing the functions [3] and [12] into the integral [9], one obtains (Appendix I),

[15] $$G(E) = -(1 + i)\frac{\omega_r\alpha_n^2}{2F_r}\left(\frac{\pi}{2aF_c}\right)^{1/2}\int_0^\infty t^{-1/2}\exp(-ibt^3 + i\kappa t)\,dt$$

where

$$a = \frac{1}{2\mu}\left(\frac{1}{F_c} + \frac{1}{F_r}\right)$$

[16] $$b = aF_c^3/12$$

$$\kappa = \frac{(E_r^0 - E^0)F_c}{F_r} + E - E_0$$

The singular integral in [15] can be recognized as the linear potential Green's function studied by Aspnes (16). Using his results one obtains (3)

[17] $$G(E_r^0) = \frac{\pi\omega_r\alpha_n^2}{(F_rF_c)^{1/3}}\left(\frac{2\mu}{F_r + F_c}\right)^{2/3}[-iA_i^2(-k) - A_i(-k)B_i(-k)]$$

where

[18] $$k = (2\mu)^{1/3}\left(\frac{F_rF_c}{F_rF_c}\right)^{2/3}(E_r^0 - E_0)$$

The functions A_i and B_i are the regular and irregular Airy functions defined in ref. 14. This gives for ΔE and Γ, following the definitions in [10],

[19] $$\Delta E(E_r^0) = -\alpha A_i(-k)B_i(-k)$$
$$\tfrac{1}{2}\Gamma(E_r^0) = \alpha A_i^2(-k)$$

where

$$\alpha = \frac{\pi\omega_r\alpha_n^2}{(F_rF_c)^{1/3}}\left(\frac{2\mu}{F_r + F_c}\right)^{2/3}$$

Let us now do this calculation in the reflection method, *i.e.* we set in the integral [9] for the continuum functions $\phi_o(E_c,X)$,

[20] $$\exp(ip^3/6\mu F_c) = 1$$

As shown in Appendix I, this has the effect of converting the factor a as defined in [16] to

[21] $$a = a_r' = (\tfrac{1}{2}\mu F_r)$$

It is to be observed that one could have obtained this result by setting $F_c \to \infty$ in the definition of a, *i.e.* the reflection method becomes *exact* for steep potentials. This result had been anticipated by Coolidge *et al.* (5) in their numerical calculations. Our derivation gives therefore a formal justification for this conclusion.

The final result for G_R obtained by the reflection method is therefore (Appendix I),

[22] $$G_R(E_r^0) = \alpha_R[-iA_i^2(-k_R) - A_i(-k_R)B_i(-k_R)]$$

where

$$k_R = (2\mu)^{1/3}\frac{(F_r + F_c)}{F_cF_r^{2/3}}(E_r^0 - E^0)$$

[23] $$\alpha_R = \frac{\pi\omega_r\alpha_n^2(2\mu)^{2/3}}{F_c(F_r)^{1/3}}$$

From our definitions of the linewidth and energy shifts in [10] we obtain,

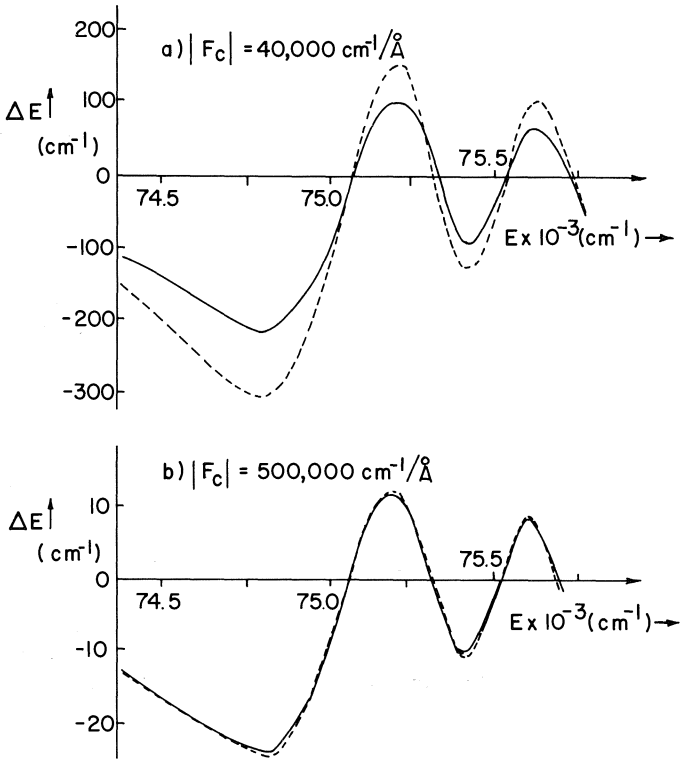

FIG. 2. $\Delta E_r(E)$ for $E_r^0 = 75\,000\ \text{cm}^{-1}$, $E_0 = 74\,800\ \text{cm}^{-1}$, $\omega_r = 1000\ \text{cm}^{-1}$, $\mu = 7.5$, $\alpha_n = 300\ \text{cm}^{-1}$, $F_r = 28\,000\ \text{cm}^{-1}/\text{Å}$; exact calculations (—), reflection method (-----).

[24]
$$\tfrac{1}{2}\Gamma(E_r^0) = +\alpha_R A_i^2(-k_R)$$
$$\Delta E_R(E_r^0) = -\alpha_R A_i(-k_R) B_i(-k_R)$$

A comparison of the two expressions shows that in the limit $F_c \gg F_r$, the exact result in [19] goes over into the reflection results in [24].

In Fig. 2, a numerical comparison of the two methods is illustrated for ΔE. The curves for the steep continuum, Fig. 2*b*, corroborate the conclusion that in this case the reflection method is excellent. In the intermediate slope case, Fig. 2*a*, the reflection method tends to overestimate the integrals. In other words, this method neglects the oscillatory tail of the continuum formations which diminish the integrals. The numerical calculations of Coolidge *et al.* (5) on reflection absorption intensities indicate that this method always overestimates absorption intensities. Our calculations show therefore that this is a general feature of this method. Nevertheless, what is *remarkable*, is that the reflection method follows faithfully the oscillatory pattern of ΔE and Γ obtained exactly. This can be seen readily in the mathematical expressions [19] and [24] for these parameters. The argument of the Airy functions changes only in magnitude but not in phase. The immediate conclusion from this is that ΔE and Γ will have identical zeroes occurring at the zeroes of $A_i(-k)$.

Another possibility is to apply a total reflection method, *i.e.* to both functions ϕ_r and ϕ_c. This could happen for instance in the case of heavy molecules. Since the singular integrand in the integral [15] is very large at small t, then an expansion of $\exp(-ibt^3)$ in powers of b should converge for large μ since $b \propto \mu^{-1}$ (eq. 16). We therefore write

[25]
$$\exp(-ibt^3) = \sum_{n=0}^{\infty} \frac{(-ib)^n}{n!} t^{3n}$$

and using the definition of the gamma function (14)

$$[26] \qquad \Gamma(Z) = k^Z \int_0^\infty t^{Z-1} e^{-kt} dt$$

one arrives at the following result for $G(E)$, eq. 15,

$$[27] \qquad G(E) = \frac{-i\omega_r(\pi\mu)^{1/2}}{[2F_r(F_r + F_c)]^{1/2}} \sum_{n=0}^{\infty} (-1)^n \left(\frac{F_r + F_c}{4\mu F_r F_c}\right)^n \frac{\Gamma(3n + \frac{1}{2})}{n!\kappa^{3n+\frac{1}{2}}}$$

κ has been defined in eq. 16.

Taking the first term, $n = 0$, of this series corresponds to using the total reflection method. The other terms are therefore the corrections arising from the nuclear kinetic energy. Thus, in the total reflection method, one obtains from the $n = 0$ term in [27],

$$[28] \qquad \Delta E = \frac{-i\omega_r\alpha_n{}^2\pi\mu^{1/2}}{[2F_r(F_r + F_c)]^{1/2}} \kappa^{-1/2}$$

This result is only valid provided $E_r{}^0 < E_0$, *i.e.* for energies below the crossing point. In fact the expression [27] is discontinuous, going from real values for $\kappa < 0$ to purely imaginary values for $\kappa > 0$. Therefore it cannot be used for $E_r{}^0 > E_0$ as the series then becomes incorrect.

The result (eq. 28) is interesting in that it was first derived by Ben-Aryeh (15) for the predissociation in the NO molecule by using asymptotic expressions for the Airy functions at large negative parameters in [10]. One therefore sees that this expression is only valid for large mass systems as it is an expansion in powers of μ^{-1}. In particular this approximation at the resonance energy $E_r{}^0$ gives

$$[29] \qquad \Delta E(E_r{}^0) = \frac{-\omega_r\alpha_n{}^2\pi\mu^{1/2}}{\sqrt{2}(F_r + F_c)|E_r{}^0 - E_0|^{1/2}}$$

In as much as $\omega_r \propto \mu^{-1/2}$, one sees that this approximation gives very little isotope dependence in the energy shifts.

The Harmonic Oscillator

We will now discuss predissociation of the harmonic oscillator in the reflection method. Our starting point will be the definition in [7] of the continuum function $\phi_c(E_c,X)$ in the delta function approximation. Hence any overlap integral with the vth eigenfunction of the oscillator will be

$$[30] \qquad \langle\phi_v(E_v{}^0,X)|\phi_c(E_c,X)\rangle = N_v F_c{}^{-1/2} H_v(\sqrt{\beta}X_c) \exp\left[-\tfrac{1}{2}(\sqrt{\beta}X_c)^2\right]$$

where

$$\beta = \sqrt{\mu k}$$

$$N_v = [\sqrt{\beta/\pi}/2^v v!]^{1/2}$$

are the usual parameters for a harmonic oscillator of force constant k, and H_v is the Hermite polynomial for the level v. X_c corresponds to the classical turning point of the linear potential at energy E_c and has been defined in [8].

In this model, the integral $G(E)$ of [9] can be shown to reduce to (Appendix II),

$$[31] \qquad G(E) = \frac{N_v{}^2}{F_c} \lim_{\varepsilon \to 0} \int_{-\infty}^{\infty} \frac{(H_v(X))^2 e^{-X^2}}{E' - X + i\varepsilon} dX$$

where

$$[32] \qquad E' = \frac{\sqrt{\beta}}{F_c}(E - E_0 - F_c X_0)$$

It should be mentioned in passing that this integral can also be used to calculate resonant Raman scattering cross sections by a continuum since the integrals are formally the same (9, 17). Using the

integral representation for the denominator,

$$[33] \qquad \frac{1}{E' - X + i\varepsilon} = -i \int_0^\infty e^{it(E' - X + i\varepsilon)}\, dt$$

one obtains the following results from Appendix II.

$v = 0$:

$$[34] \qquad G_0(E) = \frac{\alpha_n^2 N_0^2}{F_c}\left[-i\pi\, e^{-E'^2} + 2\pi^{1/2}\, e^{-E'^2} \sum_{n=0}^{\infty} \frac{(E')^{2n+1}}{(2n+1)n!} \right]$$

$v \neq 0$:

$$[35] \quad G_v(E) = \frac{\alpha_n^2 N_v^2}{F_c}\left[-i\pi\, e^{-E'^2}[H_v(E')]^2 + \frac{\pi}{\sqrt{2}} e^{-E'^2} H_v(E')[H_{v+1}(E') - 2vH_{v-1}(E')] \right]$$

Defining $E' = -X_E\sqrt{\beta}$ where E' is given in [32], one has finally, from the definitions in [35],

$$\Delta E_v(E) = \frac{\alpha_n^2 N_v^2 \pi}{F_c\sqrt{2}} e^{-\beta X_E^2}\{H_v(-\sqrt{\beta}X_E)[H_{v+1}(-\sqrt{\beta}X_E) - 2vH_{v-1}(-\sqrt{\beta}X_E)]\}$$

$$[36] \qquad \tfrac{1}{2}\Gamma_0(E) = \frac{\alpha_n^2 N_v^2 \pi}{F_c} e^{-\beta X_E^2}[H_v(-\sqrt{\beta}X_E)]^2$$

Comparing these results to the exact results for the linear potential models, eq. 19, one notices the formal similarity between the two. In other words, both ΔE and Γ have a common energy dependence in the functions A_i or H_v. The implications of this result is that these parameters will have similar oscillatory behavior with common zeroes. Subsidiary zeroes may appear for ΔE, *i.e.* the energy shift is a more rapidly varying parameter than the linewidth Γ as reflected in [36]. Our results for the predissociation of the harmonic oscillator therefore corroborate the numerical findings of Julienne and Krauss (18) for O_2 that Γ and ΔE are oscillatory functions even for low vibrational levels.

Conclusions

We have derived analytic expressions in the reflection method for linewidths Γ and energy shifts ΔE for two different models: a linear potential model valid for high vibrational quanta and the harmonic oscillator potential valid for low vibrational quanta. The mathematical structure illustrated in [19] and [30] shows that in all cases Γ and ΔE have common zeroes. In addition ΔE has additional zeroes which imply that this parameter is a more sensitive function of energy than the linewidth Γ. As shown previously for the linear potential model, this can introduce important asymmetries in lineshapes (3).

We have furthermore shown that the reflection method should be an excellent approximation for steep repulsive potentials. The method tends to overestimate the Franck–Condon factors and therefore the parameters ΔE and Γ for intermediate slopes. On the other hand, the reflection method seems to preserve the phase oscillations of these parameters when compared to the exact results. Furthermore a total reflection method, *i.e.* applied to both bound states and continuum states, results in discontinuous and therefore erroneous results for ΔE.

As a final conclusion we wish to reiterate an important finding. We have seen that Γ and ΔE have common zeroes, *i.e.* they vanish at identical energies. From an experimental viewpoint, this means that sharp levels in a predissociated spectrum undergo no energy shifts. Hence one should be able to reconstruct the 'unperturbed' potential curve by just analysing the positions of sharp levels. From thereon, one should be able to calculate from the spectrum the energy shifts of the broadened levels with respect to the unperturbed potential levels and thus calculate the perturbation parameters via our formulae.

Acknowledgements

The authors wish to thank the National Research Council of Canada and the Ministère de l'Education du Québec for grants supporting this research.

1. G. HERZBERG. Spectra of diatomic molecules. Van Nostrand, New York, NY. 1950; Electronic spectra of polyatomic molecules. Van Nostrand, New York, NY. 1967.
2. R. S. MULLIKEN. J. Chem. Phys. **33**, 247 (1960).
3. A. D. BANDRAUK and J. P. LAPLANTE. J. Chem. Phys. **65**, 2592 (1976); **65**, 2602 (1976).
4. A. D. BANDRAUK and M. S. CHILD. Mol. Phys. **19**, 95 (1970).
5. A. S. COOLIDGE, H. M. JAMES, and R. D. PRESENT. J. Chem. Phys. **4**, 193 (1936).
6. I. RIESS. J. Chem. Phys. **56**, 1613 (1972).
7. E. A. GISLASON. J. Chem. Phys. **58**, 3702 (1973).
8. F. H. MIES and A. L. SMITH. J. Chem. Phys. **45**, 994 (1966).
9. M. MINGARDI and W. SIEBRAND. Chem. Phys. Lett. **23**, 1 (1973); **24**, 492 (1974).
10. M. JACON and D. VAN LABEKE. Mol. Phys. **29**, 4 (1975).
11. G. H. DUNN. Phys. Rev. **172**, 1 (1968).
12. J. P. LAPLANTE and A. D. BANDRAUK. Chem. Phys. Lett. **42**, 184 (1976).
13. L. D. LANDAU and E. M. LIFSCHITZ. Non-relativistic quantum mechanics. Addison-Wesley, Reading, MA. 1958. Sect. 87.
14. M. ABRAMOWITZ and I. A. STEGUN. Handbook of mathematical functions. Dover, New York, NY. 1965.
15. Y. BEN-ARYEH. J. Quant. Spectrosc. Radiat. Transfer, **13**, 1441 (1973).
16. D. E. ASPNES. Phys. Rev. **147**, 554 (1966).
17. J. P. LAPLANTE and A. D. BANDRAUK. J. Raman Spectrosc. 1976.
18. P. S. JULIENNE and M. KRAUSS. J. Mol. Spectrosc. **56**, 270 (1975).
19. A. ERDELYI. Tables of integral transforms. McGraw-Hill, New York, NY. 1965.

Appendix I

We wish to evaluate the integral $G(E)$, eq. 9, which becomes, after introducing the appropriate functions and the integral representation, eq. 33,

$$[I.1]\quad G(E) = \frac{-i\omega_r}{2\pi F_r F_c} \lim_{\varepsilon\to 0} \int_0^\infty \int_{-\infty}^\infty \int_{-\infty}^\infty dt\, dp\, dp' \exp\left[it(E + i\varepsilon)\right] \times \exp\left[ia\left(\frac{-p^3}{3} + \frac{p'^3}{3}\right) + i(p - p')\left(\frac{E_r^0 - E_0}{F_r} - \frac{E_0}{F_c}\right)\right] \int_{-\infty}^\infty \exp iE_c\left(\frac{p}{F_c} - t - \frac{p'}{F_r}\right) dE_c$$

where

$$a = \frac{1}{2\mu}(1/F_c + 1/F_r) = a_r' + a_c'$$

Since the coefficient a multiplies the p^3 terms in the exponential, then setting $F_c = \infty$, *i.e.* $a = a_r'$, corresponds to neglecting the p^3 terms and hence the kinetic energy in the continuum functions $\phi_c(E_c, p)$. This is therefore the *reflection* method for the continuum.

The last integral in $G(E)$ reduces to a delta function. The ensuing calculation gives

$$[I.2]\quad G(E) = \frac{-i\omega_r}{2F_r} \lim_{\varepsilon\to 0} \int_0^\infty dt \exp\left[it(E + i\varepsilon)\right] \exp\left[-ia\frac{F_c^3 t^3}{3} + iF_c t\left(\frac{E_r^0 - E_0}{F_r} - \frac{E_0}{F_c}\right)\right] \times \int_{-\infty}^\infty dp \exp\left[-iaF_c tp^2 + iaF_c^2 t^2 p\right]$$

Furthermore, setting $r = F_c t$, the last integral gives

$$[I.3]\quad \int_{-\infty}^\infty \exp\left[-irap^2 + ira^2 p\right] dp = \left(\frac{\pi}{ra}\right)^{1/2} (1 - i) \exp\left(\frac{ira^3}{4}\right)$$

With this result, $G(E)$ finally becomes

$$[I.4]\quad G(E) = -(1 + i)\frac{\omega_r}{2F_r}\left(\frac{\pi}{2aF_c}\right)^{1/2} \int_0^\infty t^{-1/2} \exp\left[-ibt^3 + it(\kappa + i\varepsilon)\right] dt$$

where

$$b = aF_c^3/12$$

$$\kappa = (E_r^0 - E_0)(F_c/F_r) + (E - E_0)$$

Appendix II

We wish to evaluate the integral

$$[II.1] \qquad I(E) = \lim_{\varepsilon \to 0} \int_{-\infty}^{\infty} \frac{[H_v(X)]^2}{(E - X + i\varepsilon)} e^{-X^2} dX$$

By introducing the integral representation [33] for the denominator, $I(E)$ now becomes the double integral,

$$[II.2] \qquad I(E) = -i \lim_{\varepsilon \to 0} \int_0^{\infty} e^{-\varepsilon t} dt \int_{-\infty}^{\infty} [H_v(X)]^2 \exp(-X^2 - iXt) dX$$

From tables of integral transforms (19), we rapidly evaluate the Fourier transform in the integral to give,

$$[II.3] \qquad I(E) = -i2^v \pi^{1/2} v! \int_0^{\infty} dt\, L_v(t^2/2) \exp(iEt - \varepsilon t - t^2/4)$$

where L_v is the generalized Laguerre polynomial (14)

$$[II.4] \qquad L_v(t) = (v!)^{-1} e^t \frac{d^v}{dt^v}(t^v e^{-t})$$

The integral [II.3] is tabulated in Erdelyi (19) in terms of sine and cosine Fourier transforms. Using these results one obtains finally

$$[II.5] \qquad I(E) = -i\pi e^{-E^2}[H_v(E)]^2 + \frac{\pi}{\sqrt{2}} e^{-E^2} H_v(E)[H_{v+1}(E) - 2vH_{v-1}(E)]$$

The case $v = 0$ requires a more careful calculation since one cannot use recurrence formulae for $L_0(t)$. We start with eq. II.3,

$$[II.6] \qquad I_1(E) = \lim_{\varepsilon \to 0} \int_0^{\infty} t^v \exp(-t^2/4 - \varepsilon t) \cos Et\, dt = \pi^{1/2} e^{-E^2} H_v(E)$$

$$[II.7] \qquad I_2(E) = i \lim_{\varepsilon \to 0} \int_0^{\infty} t^v \exp(-t^2/4 - \varepsilon t) \sin Et\, dt$$

$$= 2^{v+1}\Gamma\left(\frac{v+2}{2}\right) E e^{-E^2} {}_1F_1\left[\frac{1}{2} - \frac{v}{2}; \frac{3}{2}; E^2\right]$$

where ${}_1F_1(a;b;z)$ is the confluent hypergeometric function defined in (14). Evaluating this function, one obtains for $v = 0$,

$$[II.8] \qquad {}_1F_1\left(\frac{1}{2}; \frac{3}{2}; E^2\right) = \sum_{n=0}^{\infty} \frac{E^{2n}}{(2n+1)n!}$$

Collecting the results [II.6] and [II.7] one obtains for $v = 0$,

$$[II.9] \qquad I(E) = i\pi e^{-E^2} + 2\pi^{1/2} e^{-E^2} \sum_{n=0}^{\infty} \frac{E^{2n+1}}{(2n+1)n!}$$

Kinetics and mechanism of decarboxylation of some pyridinecarboxylic acids in aqueous solution. II

GERALD E. DUNN AND HARALD F. THIMM

Department of Chemistry, University of Manitoba, Winnipeg, Manitoba, Canada R3T 2N2

Received July 12, 1976

GERALD E. DUNN and HARALD F. THIMM. Can. J. Chem. **55**, 1342 (1977).

Six 3-substituted picolinic acids were synthesized and decarboxylated in buffered aqueous solutions of ionic strength 1.0 at 150 and/or 95°C. 3-Amino- and 3-hydroxypicolinic acids appear to decarboxylate by initial protonation, but the others fit the requirements of the Hammick mechanism for picolinic acid decarboxylation. Both electron-withdrawing and electron-releasing 3-substituents accelerate decarboxylation in picolinic acids but inhibit decarboxylation in their anions. Acceleration in the acids is considered to be the result of interference by 3-substituents with coplanarity of the carboxyl group and the aromatic nucleus. This reduces the order of the bond between the carboxyl group and the ring, thus facilitating bond breaking. In decarboxylation of the anions water appears to play a critical role, since picolinate ions have not been observed to decarboxylate in any other solvent, including ethylene glycol. It is proposed that water forms a hydrogen-bonded bridge between carboxylate oxygen and aromatic nitrogen, so that as the carbon–carbon bond breaks a nitrogen–hydrogen bond is formed. This may provide a lower energy path through an ylide intermediate than would be required if the picolinate ion were to decarboxylate to a 2-pyridyl carbanion.

GERALD E. DUNN et HARALD F. THIMM. Can. J. Chem. **55**, 1342 (1977).

On a synthétisé six acides picoliniques substitués en position 3 et on les a décarboxylés dans des solutions aqueuses tamponnés de force ionique 1.0, à 150 et/ou 95°C. Il semble que les acides amino-3 et hydroxy-3 picoliniques se décarboxylent par une protonation initiale; toutefois les autres présentent les caractéristiques nécessaires pour le mécanisme proposé par Hammick pour la décarboxylation de l'acide picolinique. Les substituants en position 3 qui attirent les électrons ainsi que ceux qui repoussent les électrons accélèrent la décarboxylation des acides picoliniques mais inhibent la décarboxylation de leurs anions. On considère que l'accélération dans les acides provient d'une interférence, par les substituants en position 3, sur la coplanarité du groupe carboxyle et du noyau aromatique. Cet effet réduit l'ordre de la liaison entre le groupement carboxyle et le cycle et facilite ainsi le bris du lien. Dans le cas de la décarboxylation des anions, il semble que l'eau joue un rôle critique puisque l'on n'a jamais observé la décarboxylation des ions picolinates dans d'autres solvants, même l'éthylène glycol. On suggère que l'eau forme des ponts hydrogène entre l'oxygène du carboxylate et l'azote du cycle aromatique provoquant la formation d'un lien azote–hydrogène au moment où le lien carbone–carbone se brise. Ce processus pourrait fournir une voie requérant une énergie plus basse, via un ylide intermédiaire, que celle qui serait requise si l'ion picolinate se décarboxylait par l'intermédiaire d'un carbanion pyridyle-2.

[Traduit par le journal]

Introduction

The mechanism first proposed by Hammick for the decarboxylation of picolinic and quinaldinic acids in organic solvents, is that shown in reaction 1, with Hammick's preference being for path *2* (1). Others have favored path *1* (2, 3).

A previous paper from this laboratory reported a study of the reaction in aqueous solution (4). The rate *vs.* p*H* curve goes through a maximum at the isoelectric p*H*, and there is a ^{13}C kinetic isotope effect at p*H*'s both above and below the isoelectric point. These observations are predicted by the Hammick mechanism, but others are not so readily interpreted. For example, since the Hammick mechanism depends on

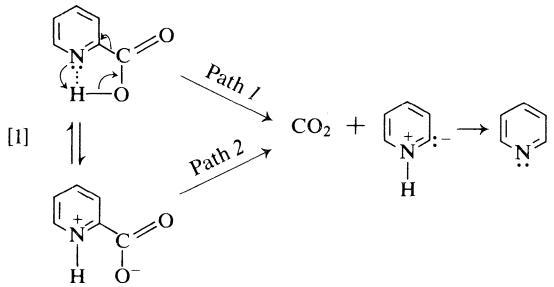

positively charged nitrogen for stabilization of the transition state leading to the ylide, it was surprising to find that the picolinate anion, for which no such stabilization is apparent, decarboxylates almost half as fast as the acid itself.

On the other hand, homarine, the methylbetaine of picolinic acid, where positive charge on nitrogen is assured, was found to decarboxylate about a hundred times faster than picolinic acid. Thus, in its decarboxylation picolinic acid appears to resemble its anion more than its betaine. This was at first thought to mean that at the reaction temperature (150°C) picolinic acid is mainly in the non-zwitterionic form, but ultraviolet spectra at that temperature did not support this hypothesis.

Even the 100-fold increase in rate produced by N-methylation appeared surprisingly small when it was found that quinolinic acid under the same conditions decarboxylates at least a thousand times faster than picolinic acid. (4) Thus a 3-carboxyl group has a tenfold larger effect on the rate of decarboxylation than does quaternization of the 1-nitrogen atom. On the other hand, 4-, 5-, and 6-carboxyl, 5-nitro, and 6-methyl groups have very small effects (factor of two) on the rate of decarboxylation of picolinic acid. The present work was undertaken in an attempt to sort out the factors involved in substituent effects on the decarboxylation of picolinic acids.

Results

In previous work a 3-carboxyl substituent had produced what appeared to be an anomalously large rate increase (4), so attention was concentrated on 3-substituents. Six 3-substituted picolinic acids were synthesized: amino, benzoyl, bromo, hydroxy, methyl, and nitro. These were decarboxylated in buffered aqueous solutions of ionic strength 1.0 at 150 and/or 95°C. The 3-amino- and 3-hydroxypicolinic acids gave p*H*–rate profiles very different from those of picolinic and the other substituted picolinic acids. It is thought that they decarboxylate by a different mechanism from the rest, probably a ring-protonation mechanism like those of the amino- and hydroxybenzoic acids, and they will not be discussed further here.

3-Methylpicolinic Acid

The p*H*–rate profile for 3-methylpicolinic acid at 150°C is given in Fig. 1. It shows the same rate maximum at intermediate p*H* as that shown by picolinic acid (4) but, unlike the curve for picolinic acid, this one does not level off at high p*H*. Apparently the 3-methylpicolinate anion does not decarboxylate. To confirm this difference between picolinic and 3-methylpicolinic acids, both were run at p*H* 9.2. For picolinic acid the rate constant was 5×10^{-7} s^{-1}; for 3-methylpicolinic no reaction was detected after 330 h ($k < 1 \times 10^{-8}$ s^{-1}).

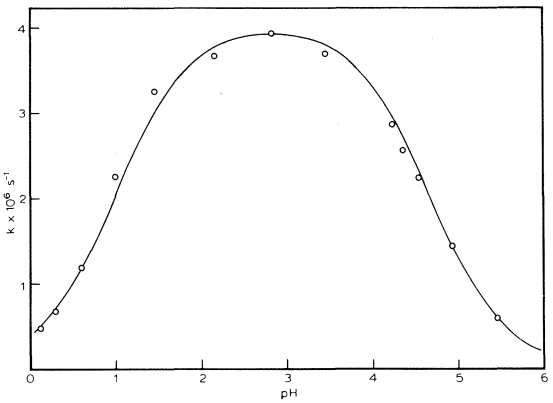

FIG. 1. First-order rate constants for the decarboxylation of 3-methylpicolinic acid at 150°C, $\mu = 1.0$. Circles represent experimental points and the solid line is calculated from [6].

To derive the p*H* dependence of rate constant for the Hammick mechanism, let H_2A^+ represent protonated amino acid, HA represent isoelectric species (neutral acid plus zwitterion), and A^- represent amino acid anion. k_{HA} is the rate constant for decarboxylation of the isoelectric species and k_A that for the anion. Then [2] and [3] define the amino acid ionization constants and [4] gives the stoichiometric concentration of amino acid [C].

$$[2] \qquad H_2A^+ \overset{K_1}{\rightleftharpoons} H^+ + HA$$

$$[3] \qquad HA \overset{K_2}{\rightleftharpoons} H^+ + A^-$$

$$[4] \qquad [H_2A^+] + [HA] + [A^-] = [C]$$

If only the isoelectric species decarboxylates, the rate may be expressed in terms of either [C] or [HA], as in [5].

$$[5] \qquad d[CO_2]/dt = k[C] = k_{HA}[HA]$$

Combination of [2]–[5] gives [6], the dependence of the stoichiometric rate constant, k, on hydrogen-ion concentration:

$$[6] \qquad k = \frac{k_{HA}}{\frac{[H^+]}{K_1} + 1 + \frac{K_2}{[H^+]}}$$

At low p*H*, where $[H^+] \gg K_2$, [6] reduces to [7]

$$[7] \qquad \frac{1}{k} = \frac{[H^+]}{k_{HA}K_1} + \frac{1}{k_{HA}}$$

and at high pH, where $[H^+] \ll K_1$, [6] reduces to [8]

$$[8] \qquad \frac{1}{k} = \frac{K_2}{k_{HA}[H^+]} + \frac{1}{k_{HA}}$$

The data for 3-methylpicolinic acid give straight-line plots for [7] and [8] in the pH regions 0–2.1 and 2.8–5.5, respectively. The values found for k_{HA} are 4.08×10^{-6} s^{-1} from [7] and 4.00×10^{-6} s^{-1} from [8]. The same plots give $pK_1 = 0.99$ and $pK_2 = 4.68$. Use of these three numbers in [6] generates the solid line in Fig. 1.

Other 3-Substituted Picolinic Acids

Decarboxylation of 3-bromopicolinic acid was studied by the method used for the 3-methyl derivative, but the reaction is much faster, so the reaction temperature was lowered to 95°C to get convenient rates. 3-Bromopicolinic acid is light sensitive, so the uncertainty in rate constants is estimated to be about ±7% instead of the usual ±2%.

A complete rate profile was not done for 3-benzoylpicolinic acid. Rate constants at 150°C and $\mu = 1.0$ were 2.0×10^4, 4.5×10^{-4}, and 3.0×10^{-4} s^{-1} at pH's of 0.37, 1.22, and 2.19, respectively, from which it is evident that $k_{HA} \geq 4.5 \times 10^{-4}$ s^{-1}.

3-Nitropicolinic acid decarboxylated so rapidly, even at 95°C, that accurate measurements were not possible. At pH 0.3 decarboxylation was complete in 2 h, so that $k > 1 \times 10^{-3}$ s^{-1} and, of course, $k_{HA} \geq k$. Both the 3-nitro and 5-nitro anions underwent some reaction other than decarboxylation at pH 9.2.

None of the 3-substituted picolinate anions examined in this work decarboxylated detectably at 150°C and pH 9.2 during a period equal to ten or more half-lives of the isoelectric species. These results, together with some previously reported (4), are collected in Table 1.

TABLE 1. First-order rate constants for decarboxylation of substituted picolinic acids at ionic strength 1.0

Substituent	Temperature (°C)	Acid k_{HA} (s^{-1})	Anion k_A (s^{-1})
None	150	1.1×10^{-6}	5.0×10^{-7}
1-Methyl	150	1.3×10^{-4}	
3-Methyl	150	4.0×10^{-6}	Very small*
5-Methyl	150	4.4×10^{-7}	3×10^{-8}
6-Methyl	150	7.7×10^{-7}	3.7×10^{-7}
3-Benzoyl	150	$\geq 4.5 \times 10^{-4}$	Very small*
4-Carboxyl	150	1.5×10^{-6}	
5-Carboxyl	150	1.8×10^{-6}	
5-Nitro	150	2.2×10^{-6}	$< 3.8 \times 10^{-7}$
6-Carboxyl	150	1.3×10^{-6}	
3-Carboxyl	150	$\geq 1.2 \times 10^{-3}$	
	95	3.3×10^{-6}	1.0×10^{-6}
3-Bromo	95	1.5×10^{-5}	Very small*
3-Nitro	95	$\geq 1 \times 10^{-3}$	Very small*

*Very small means $k_A \leq k_{HA} \times 10^{-3}$.

Discussion

It had been noted in previous work (4) that a carboxyl substituent anywhere on the ring increases the rate of decarboxylation of picolinic acid, but the effect is a thousand times greater in the 3-position than elsewhere. This could be an electronic, steric, or neighboring-group effect. The data on Table 1 show that other electron-withdrawing 3-substituents cause similar or larger rate increases although their structures are very different. This makes it very unlikely that the acceleration is a neighboring-group effect.

The data for 6-methyl, 5-nitro, and 4-, 5-, and 6-carboxyl substituents show that the usual electronic effects found in aromatic systems (Hammett's σ) are present, but small. Electron-withdrawing substituents accelerate, and electron-releasing substituents retard, as might be expected from the Hammick mechanism in which there is an increase of negative charge at the 2-position of the transition state.

The effect of substituents at the 3-position is quite different, however. Electron-attracting substituents (3-benzoyl, 3-carboxyl, 3-bromo, 3-nitro) produce rate increases of several orders of magnitude. This effect is at least partly steric, since a methyl substituent switches from retarding in the 5- and 6-positions to accelerating in the 3-position. However, it is also largely electronic, as is shown by the much larger rate increase produced by 3-bromo than by 3-methyl, although they are comparable in size. Furthermore, the electronic effect must be composed more of electrostatic (inductive and/or field) effects than delocalization (resonance) effects, since nitro and carboxyl substituents have such enormously larger effects in the 3- than in the 5-position. These observations are consistent with the Hammick mechanism, in which negative charge at the 2-position of an ylide-like transition state can be stabilized electrostatically by positive charge at the 1- or 3-positions, but cannot be delocalized by the usual resonance structures on to

substituents at the 3- or 5-positions except by making the 2-position a carbene.

The steric accelerating effect of a 3-methyl group shows that the more pronounced accelerating effect of a 1-methyl group is not entirely due to the positive charge introduced on nitrogen by quaternization. In previous work (4) it was thought surprising that the 1-methylpicolinate betaine (homarine) decarboxylates more than a hundred times faster than the picolinic acid zwitterion, although both have a unit positive charge on nitrogen. It is now evident that a fairer comparison would be between the betaine and 3-methylpicolinic acid, where the ratio is only 33. It has been estimated (4) that the fraction of picolinic acid present as zwitterion at 150°C and $\mu = 1.0$ may be as low as 40%. A similar percentage for the 3-methyl acid would leave a ratio of only 10–15 to be explained by solvation or other effects.

The most significant feature of the data in Table 1 is found in the column for picolinate anion decarboxylation. The anions of picolinic acid and its 6-methyl, 3-carboxy, 5-methyl, and 5-nitro derivatives decarboxylate slower than the corresponding acids by factors of about two to ten, but none of the other 3-substituted acids decarboxylate detectably at all. Since the 3-carboxy mono-anion is probably a zwitterion as indicated in reaction 9, it is safe to say that no

[9] 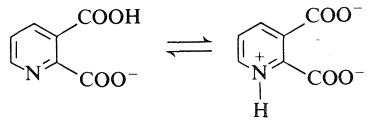

3-substituted picolinic acid decarboxylates as anion (neither nitrogen or carboxyl protonated). The contrast between the behavior of the acids, where all 3-substituents accelerate, and their anions, where all 3-substituents inhibit, is very striking.

Since both the acceleration for acids and inhibition for anions occur with either electron-releasing or electron-attracting substituents, both effects would appear to be at least partly steric. The obvious steric effect of a 3-substituent is to prevent coplanarity between the 2-carboxyl group and the aromatic nucleus, thus reducing the order of the bond between carboxyl group and ring. It could also interfere with hydrogen bonding between carboxyl group and aromatic nitrogen. The reduced bond order would contribute to the accelerating effect of a 3-substituent on the acid by any mechanism but, according to the Hammick mechanism, [1], a decrease of hydrogen bonding should have a retarding effect on path *1* by interfering with the cyclic intramolecular electron shift. Evidently intramolecular hydrogen bonding is not an important feature of picolinic acid decarboxylation in water.

Clearly, neither decreased bond order nor decreased intramolecular hydrogen bonding can account for the inhibitory effect of a 3-substituent on decarboxylation of picolinate anions. There remains the possibility that a 3-substituent interferes with the approach of solvent molecules to the carboxylate group. It is noteworthy, in this respect, that in the many studies of picolinic acid decarboxylation in organic solvents no mention has been made of decarboxylation of picolinate anion. In fact, Brown and Hammick have reported that quinaldinate ion does not decarboxylate at 184.4°C in ethylene glycol, although the acid readily does so. (5) Attempts to determine whether or not quinaldinic acid decarboxylates in aqueous base at 150°C failed because both the acid and quinoline undergo some other reaction under these conditions. As an alternative, the behavior of picolinate ion in ethylene glycol was investigated. A 2×10^{-4} *M* solution of sodium picolinate in glycol showed no decarboxylation after 48 h, a period in which the acid would be 75% decarboxylated (6). In other words, if k_A is the rate constant for decarboxylation of the anion, $k_A < 0.015\, k_{HA}$. Apparently aqueous solvent is essential to the decarboxylation of picolinate anion, and a 3-substituent interferes with the action of the solvent.

The role of water in the decarboxylation is difficult to determine. Several possibilities come to mind. Water or hydroxide ion could add to the carboxylate group, leading to loss of bicarbonate as in reaction 10. A 3-substituent could interfere with formation of the tetrahedral intermediate. Clark has long maintained that decar-

[10] 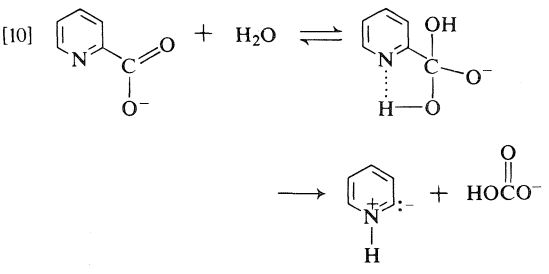

boxylation of picolinic and other acids in the isoelectric form involves nucleophilic attack by solvent on the carboxyl carbon (2), but the nucleophilic solvent is not limited to water and it is difficult to see why glycol could not play this role.

Another possibility is that water forms a hydrogen-bonded bridge between the carboxylate oxygen and ring nitrogen as in reaction 11. A

[11] 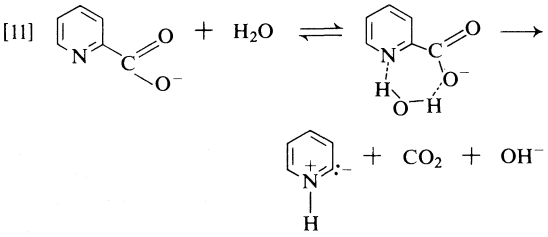

3-substituent, by pushing the carboxylate group out of coplanarity with the ring, could interfere with the formation of the hydrogen-bonded complex. Both mechanisms have the advantage that the intermediate formed on loss of carbon dioxide is an ylide rather than an aryl carbanion. The mechanism of [11] has the additional advantage that the geometry of the complex could be such as to make water a unique solvent for the decarboxylation of picolinate anions.

In the preceding paper on picolinic acid decarboxylation (4) concern was expressed over an apparent discrepancy between the relative ease of formation of 2- and 6-pyridyl carbanions by decarboxylation ($2 \gg 4$) and by deprotonation ($4 > 2$) as evidenced by base-catalyzed deuterium exchange. (7) It is now noteworthy that, if either of the above mechanisms for picolinate anion decarboxylation is correct, the discrepancy disappears. This is because these mechanisms make ylide rather than carbanion the immediate product of decarboxylation of the picolinate anion as well as of picolinic acid, and the relative ease of formation of the ylides is $2 \gg 4$ by either decarboxylation or deprotonation (7).

In conclusion, then, the opposite effects of 3-substitution on the rates of decarboxylation of picolinic acid and its anion may be accounted for by mechanisms such as those represented by [10] and [11], with [11] having some advantages over [10]. On the other hand, the unique ability of water to facilitate decarboxylation of the picolinate anion may reside in its polarity and geometry which in some way make it especially suitable for solvation of a transition state with developing negative charge at position 2, or for providing proton at position 2. The mechanism represented by [11] is attractive, but by no means compelling.

Experimental

Materials

The acids listed below were synthesized as described; others were commercial products.

3-Methylpicolinic Acid

2-Amino-3-picoline was diazotized and converted to 2-bromo-3-picoline by the method of Craig (8) in 57% yield. This, in turn, was converted to 2-cyano-3-picoline by the procedure of Friedman and Shechter, method *C*, (9) in 95% yield. The 2-cyano-3-picoline was hydrolyzed by refluxing in 13 *M* HCl for 4 h. Removal of the solvent under reduced pressure left light tan crystals (86%). These were purified by sublimation at 20 torr, followed by two recrystallizations from 95% ethanol, to give fine white crystals, mp 117–118°C (lit. (10) mp 111°C). *Anal.* calcd. for $C_7H_7NO_2 \cdot H_2O$: C 54.2, H 5.81, N 9.04, neut. equiv. 155.1; found: C 54.2, H 5.85, N 9.18, neut. equiv. 155.4.

3-Aminopicolinic Acid

3-Aminopicolinic acid, mp 211–212°C (lit. (11) mp 210°C) was prepared from quinolinic anhydride by the method of Sucharda (11).

3-Bromopicolinic Acid

3-Aminopicolinic acid (10 g) was diazotized in 48% HBr (30 ml) containing ice by dropwise addition of sodium nitrite (6 g in 40 ml H_2O) at 0–1°C. The resulting solution was poured into a solution of cuprous bromide (8.8 g) in 48% HBr (20 ml) containing ice (100 g). When reaction was complete a silvery blue precipitate was filtered off and washed with cold water. An aqueous suspension of this solid was decomposed with H_2S, the cupric sulfide filtered off, and the filtrate reduced to low volume on a rotary evaporator. Its p*H* was adjusted to 2–3 and, on standing, brown crystals were collected, recrystallized from water, and sublimed at 0.2 torr to yield a white powder (0.7 g, 10%), mp 130–131°C (dec.). *Anal.* calcd. for $C_6H_4NO_2Br$: C 35.6, H 1.98, N 6.94, Br 39.6; found: C 35.9, H 2.01, N 6.77, Br 39.6.

3-Benzoylpicolinic Acid

This acid was synthesized from quinolinic anhydride by the method of Jeiteles (12), mp 148.5–149.5°C (lit. (12) mp 147°C).

3-Nitropicolinic Acid

This compound was obtained by oxidation of 3-nitropicoline prepared from 2-chloro-3-nitropyridine by treatment with sodium diethylmalonate.

Sodium metal (3.5 g) was added to diethylmalonate (75 g) at 60°C. 2-Chloro-3-nitropyridine (25 g) was added with cooling to keep the temperature below 95°C. The mixture was kept at 60°C for 2 h, then allowed to stand at room temperature for 24 h. Excess starting materials were removed by fractionation at 1 torr (38–52°C), leaving a red-brown oil and sodium chloride. The oil gave the right mass and nmr spectra for 2-(3-nitropyridyl)diethylmalonate, and was hydrolyzed without further purification by heating 5 h on a steam bath with water (32 ml) and sulfuric acid (18 ml). After standing overnight, the

mixture was made alkaline with solid sodium carbonate and steam distilled. The steam distillate was extracted with ether and the extract dried and evaporated to leave a yellow oil with the right mass and nmr spectra for 3-nitro-2-picoline (70%). The crude 3-nitro-2-picoline was oxidized to 3-nitropicolinic acid with potassium permanganate as described by Brown (13). Yield 8%, mp 120–121°C (lit. (14) mp 105°C). Because of the discrepancy with the literature melting point, the product was analyzed. *Anal.* calcd. for $C_6H_4N_2O_4$: C 42.9, H 2.40, N 16.7; found: C 43.0, H 2.51, N 16.5. Mass spectrum, *m/e* (relative intensity): 168(1), 151(1.5), 124(50), 94(17), 78(100).

5-Methylpicolinic Acid

2,5-Lutidine (7.7 g) was refluxed with selenium dioxide (14.3 g) and pyridine (40 ml) for 2 h, then filtered and steam distilled. The residue was acidified with glacial acetic acid (10 ml) and concentrated to 15 ml under reduced pressure. This was filtered into a suspension of cupric acetate (20 g) in water (100 ml). After standing a day, the precipitate was filtered off, washed with water, and treated in aqueous suspension with H_2S. CuS was filtered off and washed with water. Combined filtrate and washings were taken to low volume under reduced pressure, filtered, and evaporated to dryness. The residue was recrystallized from benzene to give white crystals (9%), mp 166–168°C (lit. (14) mp 163–164°C), ms, *m/e* (relative intensity): 137(5), 93(100), 92(30), 66(52), 65(55).

Rate Measurements

Rates were followed spectrophotometrically as previously described (4) in solutions buffered with HCl, NaH_2PO_4, Na_2HPO_4, and adjusted to constant ionic strength with KCl. Good first-order plots were obtained up to at least 3 half-lives, and the ultraviolet spectrum of the product coincided with that of the appropriate substituted pyridine in each case.

Acknowledgment

The authors are grateful to the National Research Council of Canada for financial support.

1. P. Dyson and D. L. Hammick. J. Chem. Soc. 1724 (1937); M. F. R. Ashworth, R. P. Daffern, and D. L. Hammick. J. Chem. Soc. 809 (1939).
2. L. W. Clark. J. Phys. Chem. **66**, 125 (1962); **67**, 138 (1963); **68**, 3048 (1964); **69**, 2277 (1965).
3. E. V. Brown and R. J. Moser. J. Org. Chem. **36**, 454 (1971).
4. G. E. Dunn, G. K. J. Lee, and H. Thimm. Can. J. Chem. **50**, 3017 (1972).
5. B. R. Brown and D. L. Hammick. J. Chem. Soc. 659 (1949).
6. P. Haake and J. Mantecon. J. Am. Chem. Soc. **86**, 5230 (1964).
7. J. A. Zoltewicz and C. L. Smith. J. Am. Chem. Soc. **89**, 3358 (1967).
8. L. C. Craig. J. Am. Chem. Soc. **56**, 231 (1934).
9. L. Friedman and H. Shechter. J. Org. Chem. **26**, 2522 (1961).
10. T. Zinke and E. Winzheimer. Ann. **290**, 321 (1896).
11. E. Sucharda. Ber. **58**, 1727 (1925).
12. B. Jeiteles. Monatsh. Chem. **17**, 515 (1896).
13. E. V. Brown. J. Am. Chem. Soc. **76**, 3167 (1954).
14. D. Jerchel, J. Heider, and H. Wagner. Ann. **613**, 153 (1958).

The preparation of some potential intermediates for syntheses of aminopolydeoxy sugars related to antibiotics[1]

HANS H. BAER AND FAWZY F. Z. GEORGES
Department of Chemistry, University of Ottawa, Ont., Canada K1N 6N5

Received December 20, 1976

HANS H. BAER and FAWZY F. Z. GEORGES. Can. J. Chem. **55**, 1348 (1977).

Starting from methyl 3,6-dideoxy-3-nitro-α-D-glucopyranoside (**1**) and proceeding through its 4-mesylate (**2**) and 2,4-dimesylate (**3**), respectively, methyl 3,4,6-trideoxy-3-nitro-α-D-*xylo*-hexopyranoside (**4**) and methyl 2-*O*-acetyl-3,4,6-trideoxy-3-nitro-α-D-*threo*-hex-3-enopyranoside (**5**) were prepared. The 4,6-*O*-benzylidene derivatives (**6**, **8**, and **10**) of methyl 2-*O*-acetyl-3-deoxy-3-nitro-β-D-glucopyranoside, methyl 3-deoxy-3-nitro-α-D-glucopyranoside, and methyl 2,3-dideoxy-3-nitro-α-D-*arabino*-hexopyranoside were found to undergo without difficulty the Hanessian–Hullar reaction with *N*-bromosuccinimide, to give good yields of the corresponding 6-bromo-4-benzoates (**7**, **9**, and **11**). Partial anomerization giving the β-anomer **12** of **11** was observed under certain circumstances.

HANS H. BAER et FAWZY F. Z. GEORGES. Can. J. Chem. **55**, 1348 (1977).

En partant du méthyle 3,6-didésoxy-3-nitro-α-D-glucopyranoside (**1**) et en passant par le 4-mésylate (**2**) et le 2,4-dimésylate (**3**), respectivement, on a preparé le méthyle 3,4,6-tridésoxy-3-nitro-α-D-*xylo*-hexopyranoside (**4**) et le méthyle 2-*O*-acétyl-3,4,6-tridésoxy-3-nitro-α-D-*thréo*-hex-3-énopyranoside (**5**). On a trouvé que les dérivés 4,6-*O*-benzylidénés (**6**, **8**, et **10**) du méthyle 2-*O*-acétyl-3-désoxy-3-nitro-β-D-glucopyranoside, du méthyle 3-désoxy-3-nitro-α-D-glucopyranoside, et du méthyle 2,3-didésoxy-3-nitro-α-D-*arabino*-hexopyranoside réagissaient sans difficultés avec la *N*-bromosuccinimide par la réaction de Hanessian–Hullar et donnaient en bons rendements les 6-bromo-4-benzoates correspondants. Dans certains cas on a observé anomérisation partielle donnant l'anomère **12** du composé **11**.

Previous work in this laboratory has dealt with the utilization of nitro sugars as readily accessible points of departure for syntheses of aminopolydeoxy sugars that represent building stones of antibiotics or are structurally related to such natural products. We obtained by this approach the following sugars, as free amines, hydrochlorides, or *N*-acetyl derivatives: 3-amino-2,3,6-trideoxy-D-*lyxo*-hexose (D-daunosamine) (1) and its D-*arabino* isomer (D-acosamine) (1, 2), 2,3,6-trideoxy-3-dimethylamino-D-*arabino*-hexose (D-angolosamine) (2), 3,4,6-trideoxy-3-dimethylamino-L-*xylo*-hexose (L-desosamine) (3), and methyl 3-amino-3,4,6-trideoxy-2-*O*-methyl-α-L-*xylo*-hexopyranoside (4) which is a positional isomer of methyl actinosaminide, the corresponding 2,3,6-trideoxy-4-*O*-methyl-L-*arabino* derivative (5). Facile synthetic access to carbohydrate moieties of this kind should aid in research directed toward the modification of biological properties in antibiotics by partial syntheses using modified components, as has been done successfully for instance in studies on daunorubicin and adriamycin (6).

We now report the preparation of some further nitro sugar derivatives which should be convertible without difficulty into amino sugars by procedures already well established. For a synthesis of the natural D-enantiomer of desosamine analogous to the recently described (3) synthesis of the L-enantiomer, methyl 3,4,6-trideoxy-3-nitro-α-D-*xylo*-hexopyranoside (**4**) would be the required precursor. The L-enantiomer of **4** had been prepared (3) by a nearly quantitative reduction, with sodium borohydride, of the corresponding 3,4-unsaturated glycoside but, unfortunately, the latter was obtained (7) in only about 10% over-all yield from a primary starting compound, methyl 3,6-dideoxy-3-nitro-α-L-glucopyranoside.[2] Performance in the D-series called for a more economical utilization of the costlier methyl 3,6-dideoxy-3-nitro-α-D-glucopyranoside (**1**) whose practical preparation (2) is somewhat

[1]Part 38 in a series on reactions of nitro sugars. For part 37 see ref. 8.

[2]The ultimate source of this readily prepared starting compound is reasonably priced, commercial L-rhamnose. This factor, and the nearly complete recovery, for possible recycling, of unreacted nitro glycoside in the olefination step mitigated the disadvantage of the low yield.

more involved. A superior way of generating the desired 4-deoxy function has now emanated from our studies on nitro sugar methanesulfonates (8) in the course of which the 2,4-di-*O*-methylsulfonyl derivative **3** of **1** had been obtained. The rate of mesylation in **1** has now been found to be considerably greater at position 4 than at position 2, so that upon interruption of the reaction after an appropriate period of time the 4-mono-*O*-mesyl derivative **2** could be isolated in 36% yield, with 60% of unchanged **1** being recoverable for re-use. The site of preferential mesylation followed from non-identity of the product (mp 93–94.5°C, $[\alpha]_D$ + 96.6°) with the known (8) 2-*O*-mesyl isomer (mp 106–107°C, $[\alpha]_D$ +148°). Reductive dehydromethylsulfonyloxylation (2) of **2** with sodium borohydride then afforded a 60% yield of crystalline **4**, identified by comparison with the known L-enantiomer. Compound **4** should be convertible into the dimethylamino sugar, D-desosamine, as elaborated (3) in the L-series.

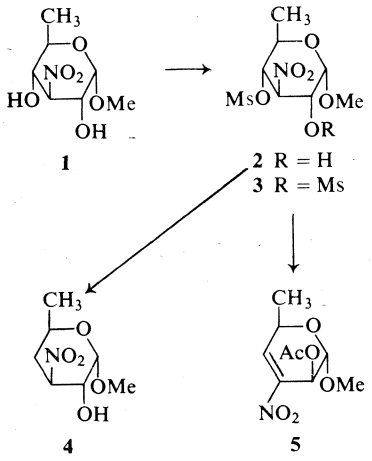

The preparative usefulness of nitro sugar mesylates (2, 8, 9) was underscored by another interesting, and surprisingly facile, transformation. When the dimesylate **3** was heated for 10 min in acetone containing acetic acid and sodium acetate, methyl 2-*O*-acetyl-3,4,6-trideoxy-3-nitro-α-D-*threo*-hex-3-enopyranoside (**5**) was produced in 75% yield. Evidently, configurational inversion at C-2 accompanied the constitutional change. This was not unexpected in view of earlier observations. Thus, the L-enantiomer of **5** had been produced (7) in modest yield (21%) from the corresponding 2,4-diacetate having the α-D-*gluco* configuration, by prolonged treatment with sodium bicarbonate in refluxing benzene (40 h), and the remarkable inversion at C-2 was considered to be a manifestation of the $A^{(1,2)}$ effect (10) that renders a pseudoaxial substituent vicinal to an endocyclic nitroalkene grouping more favorable than a pseudoequatorial one. A mechanism for the formation of the α-L-*threo* product in that reaction has been proposed (11), and it may be applied *mutatis mutandis* to the present case (Scheme 1). The product **5** doubtless arises by a first elimination of a molecule of methanesulfonic acid to give unsaturated monomesylate, either A or B, or both, and subsequent addition of acetate ion with concomitant elimination of the second mesylate function, to give **5** and (or) its isomer C. The latter, if formed, would isomerize to **5** by acetate elimination–addition. It is an open question whether the reaction takes both of the pathways shown or favors one. (In the aforementioned dehydroacetoxylation, which gave mainly L-**5**, the 2-acetate corresponding to B was isolated as a minor product in 4% yield.) Both of the primary structures A and B are encumbered by $A^{(1,2)}$ strain which should provide part of the driving force for their transformation into **5** and C, respectively. Isomerization of C to **5** is thought to be favored electronically; the inductive effect of the anomeric center will enhance electron deficiency at C-2, promoting nucleophilic attack at that site and rendering **5** more stable than C. The rearrangement could be induced by an intermolecular attack of acetate ion as depicted or, alternatively, could involve intramolecular acetoxy group migration through a six-membered, cyclic transition state. Compound **5** should be a potential preparative precursor for the D-*lyxo* isomer of D-desosamine.

In order to explore possibilities of entry into the series of nitrogenous 6-deoxy-D-hexose derivatives through key intermediates other than **1** it was envisaged to depart from readily available 4,6-*O*-benzylidenated 3-deoxy-3-nitro-D-hexopyranosides (12) and examine whether the elegant method (13) of converting such acetals by *N*-bromosuccinimide into 6-bromo-6-deoxy-4-benzoates is applicable in this particular case. Methyl 2-*O*-acetyl-4,6-*O*-benzylidene-3-deoxy-3-nitro-β-D-glucopyranoside (**6**), methyl 4,6-*O*-benzylidene-3-deoxy-3-nitro-α-D-glucopyranoside (**8**), and methyl 4,6-*O*-benzylidene-2,3-dideoxy-3-nitro-α-D-*arabino*-hexopyranoside (**10**) were selected as objects of study. The question as to whether nitro sugars such as these would without

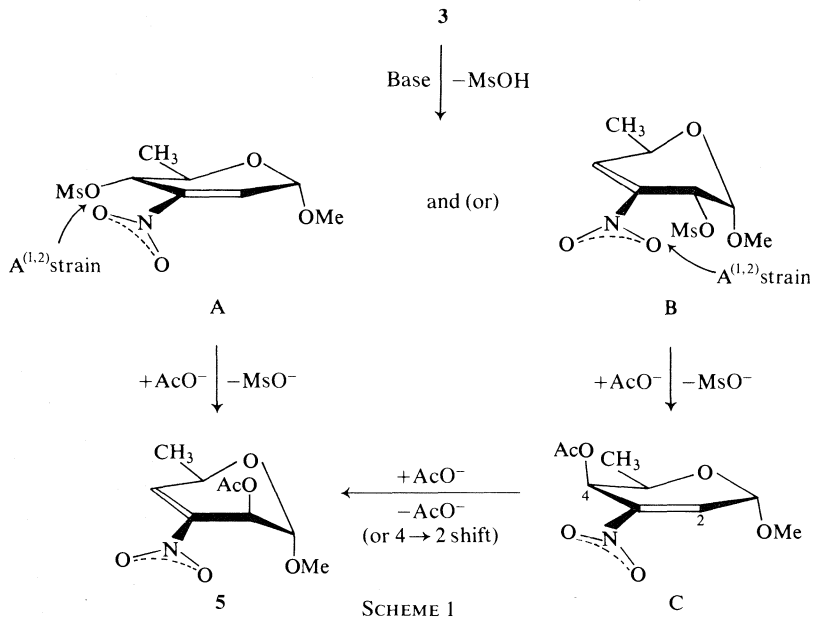

SCHEME 1

complications be compatible with the planned operation was not a trivial one in view of possible competing bromination at the nitromethine carbon atom (14). Compound **6** and numerous similar compounds had proved to undergo bromination at C-3 by the action of *N*-bromoacetamide (and in the one case examined also by *N*-bromosuccinimide) to give *gem*-bromonitro derivatives while the benzylidene acetal structure remained unaffected.[3] However, the conditions under which the geminal halogenations were performed differed from those of the Hanessian reaction in that they promoted an ionic process (protic solvent and catalysis by sodium acetate). It has now been found that **6**, **8**, and **10** do react with NBS in refluxing carbon tetrachloride in the presence of barium carbonate, affording the desired 6-bromo-6-deoxy-4-*O*-benzoyl derivatives in yields of 56–80%. Whereas single products (**7** and **9**) were obtained from **6** and **8**, respectively, the 2-deoxy sugar **10** in first experiments gave the expected α-glycoside **11** (64%) but also a second product which was revealed to be the β-glycoside **12** (16%). Evidently, traces of acid engendered in the medium and not efficaciously neutralized by solid barium carbonate were responsible for partial anomerization. 2-Deoxyglycosides are generally more prone to acid-catalyzed anomerization than ordinary glycosides; a similar observation had been made (1) in a reductive debromination of a 6-bromo-2,6-dideoxy glycoside. The formation of **12** was suppressed by an increased amount of acid scavenger. Configurational correlation of **11** and **12** was made on the basis of specific ro-

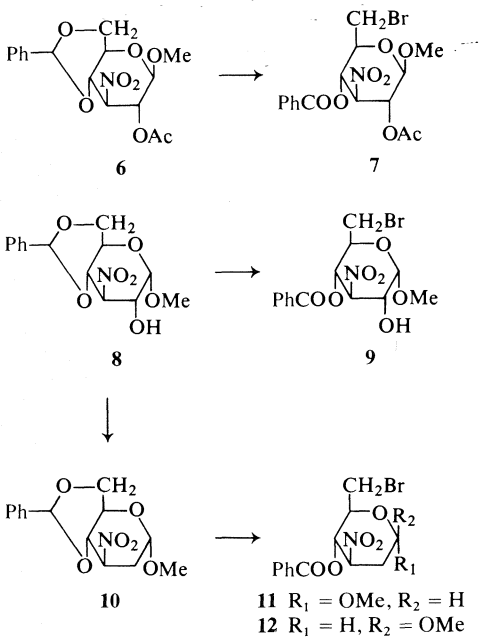

[3]The α-D-glucoside **8** resisted this type of bromination. The 2-deoxy derivative **10** was not examined but its β-anomer as well as α- and β-D-*lyxo* isomers reacted readily.

tations (+71.5° and +26.5°, respectively), and by nmr spectra which showed for the anomeric proton in **11** a narrow multiplet ($J_{1,2a}$ and $J_{1,2e}$ both small) and in **12**, a quartet ($J_{1,2a}$ = 10, $J_{1,2e}$ = 2 Hz) indicating equatorial and axial orientations, respectively, for H-1. In accord with this, the signals of the anomeric methoxyl protons (τ 6.56 in **11**, 6.41 in **12**; in chloroform-*d*) were in the relative positions normally found in α- and β-glycosides of this type (14).

Incidentally the glycoside **10**, which had previously been synthesized from **8** by the sequence of *O*-acetylation followed by dehydroacetoxylation and reduction, can now be prepared more conveniently thanks to the new, smooth olefination (8, 9) with methanesulfonyl chloride followed by borohydride reduction. We record here its preparation from **8**, achieved in 91% yield without isolation of intermediates.

Experimental

All reactions were monitored by tlc on 7.5-cm plates coated with silica gel G and irrigated, unless otherwise specified, with (v/v) 1:4 ethyl acetate – carbon tetrachloride (solvent *A*), 1:20 methanol–chloroform (solvent *B*), or 1:2 ethyl acetate – petroleum ether (solvent *C*). The spots were made visible by use of a spray of 1% ceric sulfate in 10% sulfuric acid, and heating the plates. Infrared data refer to spectra of Nujol mulls. Optical rotations were recorded at room temperature from chloroform solutions, *c* 0.4–1.3. The nmr data refer to 100 MHz spectra of $CDCl_3$ solutions containing tetramethylsilane as internal standard.

Methyl 3,6-Dideoxy-4-O-methylsulfonyl-3-nitro-α-D-glucopyranoside (2)

The glycoside **1** (2) (2.0 g) and methylsulfonyl chloride (0.75 ml, 1 mol equiv.) were stirred together in dichloromethane (60 ml), with external cooling to 10–15°C, and triethylamine (1.3 ml) was added after 5 min. As no sign of reaction was detected by tlc (solvent *B*) after another 5 min, cooling was discontinued and three additional 0.7-ml portions of mesyl chloride along with equivalent amounts of triethylamine were introduced in 15-min intervals. Gradually during this operation a faster spot representing **2** appeared in tlc, and the intensity of the spot due to **1** diminished. Eventually a faint spot (still faster) corresponding to known (8) dimesylate **3** began to show. At this stage the reaction was quenched by the addition of methanol (5 ml), and after 1 h the mixture was evaporated. Several portions of 1-propanol were successively added to and evaporated from the syrupy residue which was finally dissolved in chloroform (3 ml) and chromatographed on silica gel (85 g) by means of chloroform as eluent. Fractions containing the fast-moving, minor product **3** were discarded. The subsequent fractions that contained only **2** were combined and evaporated to give a syrup which crystallized overnight upon trituration with hexane (10 ml). The material (1.00 g, 36%) was recrystallized from ethyl acetate – petroleum ether giving sharp needles, mp 93–93.5°C; $[\alpha]_D$ +96.6°; ν_{max} 3300 (OH), 1550 (NO_2), and 1170 cm^{-1} (OMs). The nmr data: δ 4.75–5.00 (m, 3H, ill resolved, H-1, H-3, H-4), 4.2 (br m, H-2), 3.85 (br m, H-5), 3.49 (s, 3H, OMe), 2.96 (s, 3H, OMs), 2.48 (d, *J* = 11 Hz, removable with D_2O, OH), 1.43 (d, 3H, *J* = 6 Hz, C-Me). *Anal.* calcd. for $C_8H_{15}NO_8S$ (285.2): C 33.68, H 5.30, S 11.24; found: C 33.74, H 5.30, 11.15. Continued elution of the column with ether furnished 1.20 g (60%) of unchanged **1**.

Methyl 3,4,6-Trideoxy-3-nitro-α-D-xylo-hexopyranoside (4)

To a magnetically stirred, ice cooled solution of the mesylate **2** (800 mg) in ethanol (20 ml) was added sodium borohydride (0.14 g) in small portions. The reaction was then allowed to continue for 30 min at 25°C. Examination by tlc (solvent *C*) revealed total consumption of **2** and formation of a fast-moving product (**4**) accompanied by traces of faster and slower impurities. The solution was deionized with 5 ml of Amberlite IR-120(H^+) whereby it became acidic. It was neutralized carefully with triethylamine and evaporated. Numerous portions of methanol were then evaporated from the residue for removal of boric acid, after which the material was chromatographed on a column of silica gel (17 g) by use of chloroform as eluent. Early fractions containing the high-mobility contaminants were discarded, and the fractions containing the main product were evaporated to give 320 mg (60%) of a colorless syrup of **4**. It crystallized from ether – petroleum ether as long needles, mp 55–56°C, $[\alpha]_D$ +197°. Reported (3) for L-**4**, mp 56–57°C and $[\alpha]_D$ −198°. Spectral data of **4** accorded with those of the enantiomer.

Methyl 2-O-Acetyl-3,4,6-trideoxy-3-nitro-α-D-threo-hex-3-enopyranoside (5)

A mixture of the 2,4-di-*O*-mesyl glycoside **3** (8) (200 mg), sodium acetate (50 mg), and glacial acetic acid (10 small drops) in acetone (5 ml) was heated at reflux for 10 min. Complete conversion of **3** into a new product was revealed by tlc (chloroform). The reaction mixture was evaporated and the residue extracted with ether. The filtered extract was coevaporated with several portions of ethanol to give a syrup which was taken up in ethanol (0.5 ml) and kept overnight at 0°C. Compound **5** (95 mg, 75%) was deposited in crystalline form and recrystallized from ethyl acetate – petroleum ether; mp 81–82°C, $[\alpha]_D$ +163°. Reported (7) for L-**5**: mp 81–81.5°C, $[\alpha]_D$ −165°.

Methyl 2-O-Acetyl-4-O-benzoyl-6-bromo-3,6-dideoxy-3-nitro-β-D-glucopyranoside (7)

A suspension of benzylidene acetal **6** (12) (1.00 g) and barium carbonate (0.50 g) in carbon tetrachloride (25 ml) containing *N*-bromosuccinimide (0.70 g) was refluxed with magnetic stirring for 2 h. The hot reaction mixture was filtered and the solid residue washed with hot carbon tetrachloride (2 × 15 ml). The combined filtrate was evaporated to dryness and a solution of the resultant syrup in ether (25 ml) was washed with water (15 ml) and dried ($CaCl_2$). Partial evaporation of solvent then furnished several crops of crystalline **7**. The concentrated mother liquor was treated with some pentane which produced a yellowish oil that was decanted and triturated with fresh pentane; this gave an additional crop of crystals, the total yield being 0.67 g (56%). Recrystallized from chloroform – petroleum ether the product showed

mp 181–182°C, $[\alpha]_D$ −45.7°, ν_{max} 1715 (CO) and 1565 cm^{-1} (NO_2). The nmr data: δ 7.95 and 7.47 (m, 2 + 3H, PhCO), 5.65 (t, $J_{3,4} = J_{4,5} = 10$ Hz, H-4), 5.48 (q, $J_{1,2} = 8$, $J_{2,3} = 10$ Hz, H-2), 4.98 (t, $J = 10$ Hz, H-3), 4.56 (d, $J_{1,2} = 8$ Hz, H-1), 3.90 (m, H-5), 3.59 (s, 3H, OMe), 3.54–3.46 (m, 2H, H-6, H-6′), 2.10 (s, 3H, OAc). *Anal.* calcd. for $C_{16}H_{18}BrNO_8$ (432.2): C 44.46, H 4.19, Br 18.49; found: C 44.28, H 4.07, Br 18.38.

*Methyl 4-O-Benzoyl-6-bromo-3,6-dideoxy-3-nitro-α-D-glucopyranoside (**9**)*

The benzylidene acetal **8** (15) (2.00 g), *N*-bromosuccinimide (1.50 g), and barium carbonate (1.0 g) were refluxed with magnetic stirring in carbon tetrachloride (100 ml) for 3 h. The hot solution was filtered, the inorganic residue washed with hot carbon tetrachloride (2 × 20 ml), and the filtrate evaporated. The syrupy product was purified by passage through a column of silica gel (50 g) with solvent *A* and was thereafter crystallized from carbon tetrachloride at 0°C. The prisms (1.50 g, 60%) had mp 126°C, $[\alpha]_D$ +84°; ν_{max} 3470 (OH), 1720 (CO), and 1560 cm^{-1} (NO_2). The nmr data: δ 7.95 and 7.45 (m, 2 + 3H, PhCO), 5.56 (t, $J_{3,4} = J_{4,5} = 10$ Hz, H-4), 4.97 (t, $J_{2,3} = J_{3,4} = 10$ Hz, H-3), 4.95 (d, $J_{1,2} = 4$ Hz, H-1), 4.30 (octet, $J_{1,2} = 4$, $J_{2,3} = 10$, $J_{2,OH} = 11$ Hz, collapsing to q on D_2O exchange–H-2), 4.10 (septet, H-5), 3.60 (s, 3H, OMe), 3.51–3.44 (m, 2H, H-6, H-6′), 2.46 (d, $J = 11$ Hz, removed on D_2O exchange, O-H). *Anal.* calcd. for $C_{14}H_{16}BrNO_7$ (390.2): C 43.09, H 4.13, Br 20.48; found: C 43.05, H 4.04, Br 20.72.

*Methyl 4,6-O-Benzylidene-2,3-dideoxy-3-nitro-α-D-arabino-hexopyranoside (**10**)*

A solution of **8** (15) (1.80 g) in anhydrous ether (50 ml) containing triethylamine (2.7 ml) was cooled to 10–15°C, and methylsulfonyl chloride (1.3 ml) was added dropwise with stirring during 30 min. Thin layer chromatography (solvent *C*) then indicated complete conversion of **8** into the faster-moving product of dehydration (see ref. 8). The reaction mixture was filtered and the filtrate evaporated to give a yellowish oil which was dissolved in dichloromethane (10 ml). Careful addition of triethylamine (2 ml) at 10–15°C, followed by anhydrous ether (25 ml) gave a precipitate of salts. This was filtered off and the filtrate set aside. The precipitate was washed with water in which it largely dissolved (to be discarded), and the water-insoluble part was dissolved in ether (3 ml) and, after drying over $CaCl_2$, combined with the main solution containing the product. Solvent evaporation gave a solid which was immediately dissolved in absolute ethanol (50 ml) and treated with sodium borohydride (1.0 g) in small portions at 15°C. After stirring for 2 h the reaction mixture was filtered, the filter residue washed with ethanol (2 × 10 ml), and the combined filtrate evaporated. The syrupy material containing some solid was extracted twice with 15 ml of ethyl acetate. Evaporation of the extract furnished crystalline **10** (1.55 g, 91%), mp 107–109°C, $[\alpha]_D$ +68.5° (lit. (16) mp 108–111°C, $[\alpha]_D$ +67.0°).

*Methyl 4-O-Benzoyl-6-bromo-2,3,6-trideoxy-3-nitro-α-D-arabino-hexopyranoside (**11**)*

The acetal **10** (1.55 g), *N*-bromosuccinimide (1.60 g), and barium carbonate (2.0 g) were magnetically stirred in boiling carbon tetrachloride (100 ml) for 3 h. Filtration, washing of the residue with hot chloroform (10 ml), and evaporation of the combined filtrate gave a yellow syrup. This was dissolved in ether (20 ml) which was then washed with water (2 × 5 ml), dried (Na_2SO_4), and evaporated again. The pale yellow residue was taken up in methanol (5 ml) from which **11** crystallized as needles after several hours at 0°C. The air-dried product (1.57 g, 80%) had mp 93–93.5°C, $[\alpha]_D$ +70.5°.

In an earlier experiment, 2.00 g of **10** and 1.50 g of *N*-bromosuccinimide but only 1.0 g of barium carbonate were used under conditions otherwise identical with those just described. Thin layer chromatography (solvent *A*) indicated the presence of a more slowly moving by-product (**12**) besides **11**. The syrup obtained upon solvent evaporation was therefore chromatographed on a column of silica gel (50 g) using solvent *A* as irrigant. The fractions containing the (faster moving) main product furnished **11**, which crystallized from methanol as above, in a yield of 1.63 g (64%); mp 93°C, $[\alpha]_D$ +71.5; ν_{max} 1732 (CO) and 1550 cm^{-1} (NO_2). The nmr data: δ 8.0 and 7.5 (m, 2 + 3H, PhCO), 5.58 (t, $J_{3,4} = J_{4,5} = 10$ Hz, H-4), 5.2 (m, $J_{3,4} = 10$, $J_{2a,3} = 6$, $J_{2e,3} = 4$ Hz, H-3), 5.00 (narrow m, H-1), 4.1 (m, $J_{4,5} = 10$ Hz, H-5), 3.5 region (overlapping signals, 5H, H-6, H-6′ and, at δ 3.44, OMe), 2.6–2.2 (m, ill resolved, 2H, H-2, H-2′). *Anal.* calcd. for $C_{14}H_{16}BrNO_6$ (374.2): C 44.93, H 4.31, Br 21.36; found: C 45.06, H 4.19, Br 21.61.

*Methyl 4-O-Benzoyl-6-bromo-2,3,6-trideoxy-3-nitro-β-D-arabino-hexopyranoside (**12**)*

Continued elution of the column mentioned in the second experiment of the preceding section yielded the β-anomer **12** which crystallized upon solvent evaporation and was recrystallized from ethyl acetate – petroleum ether. The yield was 400 mg (16%), mp 182–183°C, $[\alpha]_D$ +26.5°, ν_{max} 1715 (CO) and 1560 cm^{-1} (NO_2). The nmr data: δ 8.00 and 7.55 (m, 2 + 3H, PhCO), 5.57 (t, $J_{3,4} = J_{4,5} = 10$ Hz, H-4), 4.87 (octet, $J_{3,4} = 10$, $J_{2a,3} = 8$, $J_{2e,3} = 5$ Hz, H-3), 4.60 (q, $J_{1,2a} = 10$, $J_{1,2e} = 2$ Hz, H-1), 3.79 (m, $J_{4,5} = 10$ Hz, H-5), 3.59 (s, 3H, OMe), 3.53 (m, 2H, overlapping the OMe signal, H-6, H-6′), 2.5 region (br m, 2H, H-2, H-2′). *Anal.* calcd. for $C_{14}H_{16}BrNO_6$ (374.2): C 44.93, H 4.31, N 3.74; found: C 44.59, H 4.43, N 3.82.

Acknowledgment

Support of this research by the National Research Council of Canada is gratefully acknowledged.

1. H. H. Baer, K. Čapek, and M. C. Cook. Can. J. Chem. **47**, 89 (1969).
2. H. H. Baer and F. F. Z. Georges. Can. J. Chem. **55**, 1100 (1977).
3. H. H. Baer and C. W. Chiu. Can. J. Chem. **52**, 122 (1974).
4. H. H. Baer and C. W. Chiu. Carbohydr. Res. **31**, 347 (1973).
5. N. N. Lomakina, I. A. Spiridonova, I. Yu. Sheinker, and T. F. Vlasova. Khim. Prir. Soedin. **9**, 101 (1973); Chem. Abstr. **78**, 148170m (1973).
6. F. Arcamone, S. Penco, A. Vigevani, S. Redaelli, G. Franchi, A. DiMarco, A. M. Casazza, T.

DASDIA, F. FORMELLI, A. NECCO, and C. SORANZO. J. Med. Chem. **18**, 703 (1975). F. ARCAMONE, A. BARGIOTTI, G. CASSINELLI, S. PENCO, and S. HANESSIAN. Carbohydr. Res. **46**, C3 (1976).
7. H. H. BAER and C. W. CHIU. Can. J. Chem. **52**, 111 (1974).
8. H. H. BAER and F. F. Z. GEORGES. J. Org. Chem. **41**, 3474 (1976).
9. Y. TACHIMORI, T. TAKAMOTO, and R. SUDOH. Chem. Lett. 483 (1976).
10. F. JOHNSON. Chem. Rev. **68**, 378 (1968).
11. H. H. BAER. Proceedings of American Chemical Society, Carbohydrate Division, Centennial Symposium, New York, NY., April 1976, Marcel Dekker, Inc. In press.
12. H. H. BAER. Methods Carbohydr. Chem. **6**, 302 (1972); H. H. BAER and T. NEILSON. Can. J. Chem. **43**, 840 (1965).
13. S. HANESSIAN. Carbohydr. Res. **2**, 86 (1966); D. L. FAILLA, T. L. HULLAR, and S. B. SISKIN. Chem. Commun. 716 (1966); S. HANESSIAN and N. R. PLESSAS. J. Org. Chem. **34**, 1035 (1969); **34**, 1045 (1969); T. L. HULLAR and S. B. SISKIN. J. Org. Chem. **35**, 225 (1970).
14. H. H. BAER and W. RANK. Can. J. Chem. **51**, 2001 (1973); **52**, 2257 (1974).
15. H. H. BAER and W. RANK. Can. J. Chem. **50**, 1216 (1972).
16. H. H. BAER and W. RANK. Can. J. Chem. **50**, 1292 (1972).

Excess enthalpies and volumes of water + tetrahydrofuran mixtures at 298.15 K[1]

OSAMU KIYOHARA[2] AND GEORGE C. BENSON

Division of Chemistry, National Research Council of Canada, Ottawa, Ont., Canada K1A 0R6

Received October 22, 1976

OSAMU KIYOHARA and GEORGE C. BENSON. Can. J. Chem. **55**, 1354 (1977).

Excess enthalpies and volumes of water + tetrahydrofuran mixtures were measured at 298.15 K, using an LKB flow microcalorimeter and a successive dilution dilatometer. The effect of flow rate on the enthalpy results was investigated. Partial molar excess enthalpies and volumes were derived from the results, and their significance is discussed with reference to the molecular interactions in the mixture.

OSAMU KIYOHARA et GEORGE C. BENSON. Can. J. Chem. **55**, 1354 (1977).

On a mesuré, à 298.15 K, les enthalpies et les volumes d'excès de mélange eau + tétrahydrofuranne en utilisant un microcalorimètre continue LKB et un dilatomètre à dilutions successives. On a étudié l'effet de la vitesse d'écoulement sur les résultats d'enthalpie. On a dérivé des enthalpies et des volumes d'excès molaires partiels à partir des résultats et on discute de leur signification par rapport aux interactions moléculaires dans le mélange.

[Traduit par le journal]

A number of investigations of the interactions between nonelectrolytes and water have examined the thermodynamic properties of aqueous tetrahydrofuran (THF) mixtures (1–6). At 298.15 K the excess enthalpy curve is S-shaped with a zero value near 0.4 mole fraction of H_2O (1–3). The excess Gibbs free energy is positive (5) and the excess entropy and volume are negative (4–6) over the whole mole fraction range.

The thermal behavior of the system H_2O + THF is of special interest because its determination has been suggested as a test of mixing calorimeters (7). There are, however, fairly large discrepancies between the published excess enthalpy results (1–3), and it is evident that further independent studies are needed before this system can be established as a calorimetric standard.

Our laboratory is currently investigating the thermodynamic properties of H_2O + THF mixtures. The present paper reports the results of careful determinations of excess enthalpy and excess volume, both at 298.15 K.

Experimental

Materials

Tetrahydrofuran (Fisher Scientific Co., certified reagent) was further purified by glc using a column containing 20% silicone oil DC200 on Chromosorb P. It was stored over a molecular sieve (BDH Type 4A, 8–12 mesh beads) and under dry nitrogen gas. The final product had a very slight yellow tinge, but at 298.15 K its density, $d = 881.95\ \mathrm{kg\ m^{-3}}$, and refractive index, $n_D = 1.40474$, were in reasonable agreement with literature data (d/kg m^{-3}: 882.2 (4), 882.1 (5), 882.3 (8), 881.94 (9); n_D: 1.4051 (4), 1.4048 (5), 1.4041 (8), 1.4045 (9)).

Mixtures were made with deionized distilled water. Both components were partially degassed by agitation under reduced pressure prior to their use.

Calorimetric Measurements

Excess enthalpies, H^E, were determined in an LKB flow microcalorimeter (Model 10700-1). Details of the equipment and operating procedure have been described previously (10). The error of the determination of H^E/J mol^{-1} is estimated to be less than $0.1 + 0.005|H^E/\mathrm{J\ mol^{-1}}|$.

For the present system it was not appropriate to assume that the calibration constant for a mixture was a volume fraction average of the constants determined for the pure components at the same flow rate. Instead, it was necessary to determine calibration constants with several mixtures of known composition flowing through the calorimeter at various flow rates. These results were smoothed so that appropriate calibration constants for other mixtures could be interpolated. Despite this precaution, we found that the values of H^E depended on the total flow rate used in their determination, particularly in the water-rich region. This variation appeared to be due to incomplete mixing. Although a total flow rate $f = 5.0\ \mathrm{mm^3\ s^{-1}}$ (stated in terms of the unmixed components) had been satisfactory in most of our previous work, it was necessary to operate at lower rates for H_2O + THF and measurements were made with $f = 2.0$, 1.5, and $1.0\ \mathrm{mm^3\ s^{-1}}$. For x_1 (the mole fraction of H_2O) ≤ 0.6, the values of H^E measured at the

[1]NRCC No. 15597. This work was presented in part at the 31st Annual Calorimetry Conference, Argonne National Laboratory, Argonne, Illinois, U.S.A., September 29 – October 2, 1976.

[2]NRCC Research Associate from 1975.

three flow rates agreed within their estimated experimental error; but for $x_1 > 0.6$, significant systematic differences appeared, with the absolute values of H^E increasing with decreasing flow rate. Empirically it was found that the results for H^E at these low flow rates varied approximately linearly with the square of the flow rate, and this fact was used to extrapolate the results to zero flow. The differences of the extrapolated values from the results at the lowest flow rate are in most cases less than their estimated experimental error, but we believe that the observed systematic variation justifies the extrapolation.

Dilatometric Measurements

Excess volumes, V^E, were determined at constant pressure by a successive dilution method using a micrometer syringe dilatometer. The apparatus and operating technique have been described by Tanaka *et al.* (11). For the present system, the error of the determination of $V^E/cm^3\ mol^{-1}$ is estimated to be less than $0.0003 + 0.001|V^E/cm^3\ mol^{-1}|$.

Results

Excess Enthalpies

Values of H^E for H_2O (1) + THF (2) mixtures at 298.15 K are listed in Table 1, where x_1 indicates the mole fraction of H_2O. All the results given for mixtures with $x_1 \leq 0.6$ were determined at the same total flow rate $f = 2.0\ mm^3\ s^{-1}$, since as pointed out above, the results of exploratory measurements at lower flow rates were not significantly different in this mole fraction range. For $x_1 > 0.6$, measurements were made with flow rates of 2.0, 1.5, and 1.0 $mm^3\ s^{-1}$, but only the results at the lowest flow rate are reported in detail.

The empirical equation

$$[1]\quad H^E/J\ mol^{-1} = x_1(1 - x_1)\sum_{j=1}^{n} a_j(1 - 2x_1)^{j-1}$$

was fitted to the results for $x_1 \leq 0.6$ combined with each set for $x_1 > 0.6$. Values of the coefficients were determined by the method of least-squares with all points weighted equally. The three sets of coefficients a_j, each labelled with the relevant flow rate, are given in Table 2, along with the standard error

$$[2]\quad \sigma = \{\sum[H^E - H^E(\text{eq. } 1)]^2/(m - n)\}^{1/2}$$

where m is the number of results and n is the number of coefficients in the representation by [1].

The results for $f = 1.0\ mm^3\ s^{-1}$ were extrapolated to zero flow rate as described in the preceding section. The corrections applied in this extrapolation are given in parentheses in Table 1.

TABLE 1. Molar excess enthalpies of H_2O (1) + THF (2) mixtures at 298.15 K*

x_1	$H^E/J\ mol^{-1}$	x_1	$H^E/J\ mol^{-1}$
0.0400	151.83	0.5000	−210.37
0.0600	208.51	0.5400	−289.77
0.0800	253.14	0.5800	−367.94
0.1000	283.04	0.6200	−443.05 (−0.15)
0.1200	302.92	0.6600	−513.51 (−0.44)
0.1400	310.08	0.7000	−578.39 (−0.88)
0.1600	310.42	0.7400	−635.64 (−1.41)
0.1800	302.11	0.7600	−662.01 (−1.68)
0.2000	289.35	0.7800	−686.40 (−1.94)
0.2200	270.62	0.8000	−706.59 (−2.14)
0.2400	246.78	0.8200	−723.71 (−2.29)
0.2600	221.00	0.8400	−736.20 (−2.35)
0.3000	160.86	0.8600	−740.18 (−2.30)
0.3400	94.26	0.8800	−733.51 (−2.14)
0.3800	23.22	0.9000	−708.48 (−1.86)
0.4000	−14.21	0.9200	−662.39 (−1.47)
0.4200	−52.31	0.9400	−581.55 (−1.01)
0.4600	−131.11	0.9600	−455.06 (−0.54)
0.5000	−210.49	0.9800	−266.58 (−0.15)

*Results for $x_1 \leq 0.6$ determined at $f = 2.0\ mm^3\ s^{-1}$. Results for $x_1 > 0.6$ determined at $f = 1.0\ mm^3\ s^{-1}$; add values in parentheses to correct to zero flow.

Table 1. Coefficients for the representation of the extrapolated values by [1] are included in Table 2. The extrema of the H^E curve (for $f = 0$) are 311.8 J mol^{-1} at $x_1 = 0.150$ and −743.1 J mol^{-1} at $x_1 = 0.858$; H^E vanishes near $x_1 = 0.392$.

Deviations of the results given in Table 1 from the smoothing function for zero flow rate are plotted in Fig. 1. The solid curves in this figure show deviations of the smoothed results at $f = 2.0$, 1.5, and 1.0 $mm^3\ s^{-1}$. For the highest flow rate, discrepancies of more than 1% occur.

There have been several previous investigations of the excess enthalpy of H_2O + THF mixtures at 298.15 K (1–3). These results, apart from those of Erva (1) which are only reported graphically, are included in Fig. 1 for comparison. The results of Glew and Watts (3) are within 1% of ours over most of the mole fraction range. Deviations of the results reported by Nakayama and Shinoda (2) are mainly negative and relatively large.

Excess Volumes

The experimental values of V^E are summarized in Table 3. Some difficulty was experienced in finding a suitable smoothing equation for these results. Representation by a form analogous to [1] required the use of a large number of coefficients. Replacing mole fractions by volume or mass fractions led to better representations

TABLE 2. Coefficients and standard errors for least-squares representations of H^E and V^E

	H^E/J mol^{-1} (eq. 1)				V^E/cm^3 mol^{-1}
	$f = 2.0$	$f = 1.5$	$f = 1.0$	$f = 0$	(eq 3)
a_1	−840.32	−840.37	−840.04	−839.92	−1.57734
a_2	4018.21	4014.13	4015.96	4013.97	−55.7535
a_3	−925.79	−927.12	−952.63	−958.35	220.952
a_4	1516.16	1614.06	1663.26	1717.84	−350.758
a_5	865.59	723.88	725.44	664.05	253.377
a_6	4558.61	4471.32	4419.39	4369.86	−67.6829
a_7	−4812.70	−4660.44	−4638.35	−4568.70	
σ	0.66	0.61	0.66	0.66	0.0022

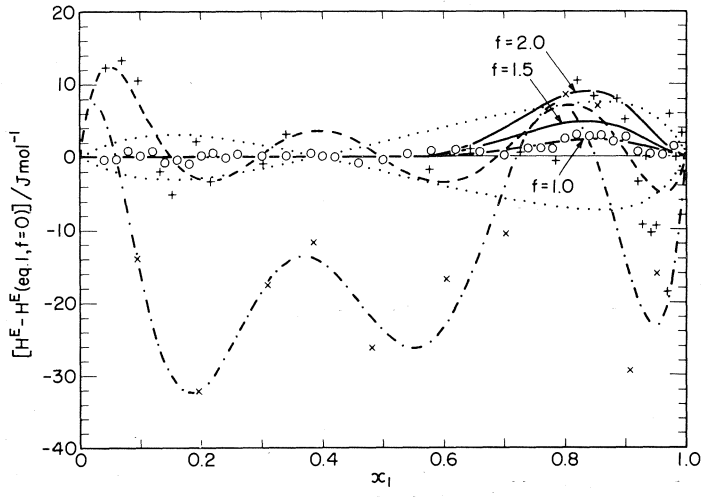

FIG. 1. Comparison of experimental results for the molar excess enthalpy of H_2O (1) + THF (2) mixtures at 298.15 K. Points and curves represent deviations from eq. 1 with coefficients for $f = 0$. Points: ○, present work; +, Glew and Watts (3); ×, Nakayama and Shinoda (2). Curves are smoothed results: —, present work (at flow rates 2.0, 1.5, and 1.0 mm^3 s^{-1}); ---, ref. 3; -·-, ref. 2. The dotted curves correspond to deviations of ±1%.

with fewer coefficients. However, the best representation was obtained with the form

$$[3] \quad V^E/\text{cm}^3\ \text{mol}^{-1} = x_1(1 - x_1) \sum_{j=1}^{n} a_j(1 - x_1)^{(j-1)/2}$$

Values of the coefficients and standard error for this representetation are given in the last column of Table 2.

Figure 2 shows that the deviations of our results from their representation by [3] are, for the most part, less than 1%; however, they appear to vary systematically with mole fraction and are larger on a percentage basis at both ends of the range. Deviations of V^E results from the literature (4–6) are also plotted in Fig. 2. Most of the results of Singer *et al.* (5) give large negative deviations which fall below the lower limit of the plot, but the other sets of data (4, 6) are in fair agreement with our results.

Discussion

In discussing the present results it is convenient to refer to the partial molar excess enthalpies $H_i^E(x_1)$ and volumes $V_i^E(x_1)$. Plots of these derived quantities are given in Figs. 3 and 4. Although the representations of H^E and V^E by [1] and [3] are adequate for most purposes, they are not very suitable for evaluating the slopes of these functions (particularly of V^E) near the ends of the mole fraction range. The curves for the partial molar excess enthalpies and volumes were therefore obtained from least-

TABLE 3. Molar excess volumes of H_2O (1) + THF (2) mixtures at 298.15 K

x_1	V^E/cm^3 mol^{-1}	x_1	V^E/cm^3 mol^{-1}	x_1	V^E/cm^3 mol^{-1}
0.0119	−0.0150	0.7063	−0.8373	0.9477	−0.3131
0.0383	−0.0552	0.7317	−0.8236	0.9541	−0.2768
0.0752	−0.1193	0.7576	−0.8062	0.9560	−0.2655
0.1129	−0.1912	0.7779	−0.7874	0.9573	−0.2570
0.1656	−0.2959	0.7956	−0.7676	0.9634	−0.2202
0.1766	−0.3171	0.8090	−0.7488	0.9688	−0.1858
0.1808	−0.3252	0.8237	−0.7255	0.9712	−0.1705
0.2380	−0.4341	0.8261	−0.7208	0.9742	−0.1524
0.3230	−0.5781	0.8373	−0.7007	0.9794	−0.1182
0.3238	−0.5796	0.8446	−0.6860	0.9830	−0.0956
0.3937	−0.6779	0.8501	−0.6741	0.9851	−0.0833
0.4486	−0.7409	0.8602	−0.6508	0.9855	−0.0806
0.4614	−0.7538	0.8728	−0.6182	0.9897	−0.0555
0.5025	−0.7899	0.8733	−0.6168	0.9928	−0.0373
0.5399	−0.8157	0.8937	−0.5554	0.9956	−0.0222
0.5545	−0.8241	0.9117	−0.4880	0.9974	−0.0130
0.5984	−0.8429	0.9225	−0.4407	0.9990	−0.0050
0.6261	−0.8497	0.9281	−0.4152	0.9997	−0.0017
0.6396	−0.8510	0.9418	−0.3463		
0.6741	−0.8471	0.9441	−0.3335		

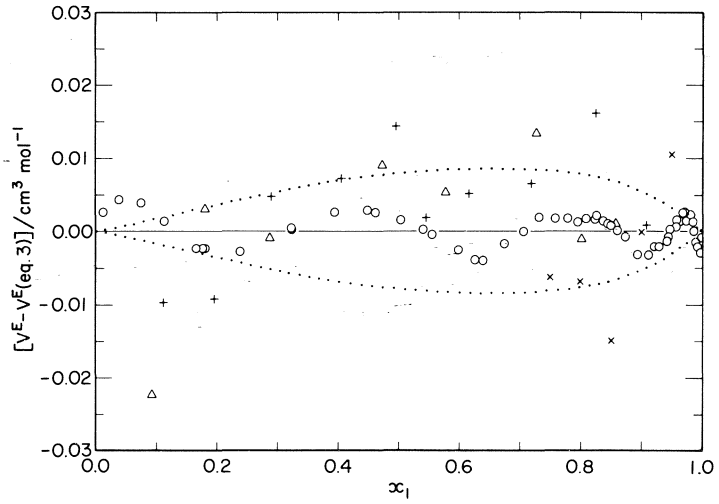

FIG. 2. Comparison of experimental results for the molar excess volume of H_2O (1) + THF (2) mixtures at 298.15 K. Points represent deviations from eq. 3: ○, present work; +, Morcom and Smith (6); ×, Singer *et al.* (5); △, Matouš *et al.* (4). The dotted curves correspond to deviations of ±1%.

squares analyses in which the experimental results were fitted with a set of cubic splines (12).

At infinite dilution, our value of $H_2^E(1) = -15.3$ kJ mol^{-1} is about 0.4 kJ mol^{-1} lower than the value (-14.93 ± 0.17) kJ mol^{-1} determined by Franks *et al.* (13). The insert to Fig. 4 shows the behavior of $V_2^E(x_1)$ for dilute THF mixtures. The intercept $V_2^E(1) = -4.8$ cm^3 mol^{-1} is in good agreement with the results of magnetic float densitometer studies (−4.68 cm^3 mol^{-1} (13) and −4.9 cm^3 mol^{-1} (14)). A sharp minimum of $V_2^E(x_1)$ occurs near $x_1 = 0.975$ and a broad minimum of $V_1^E(x_1)$ at low mole fractions of water. The latter behavior is similar to that observed for several other water + nonelectrolyte mixtures (15, 16).

A qualitative interpretation of our results can be given in terms of the so-called "flickering

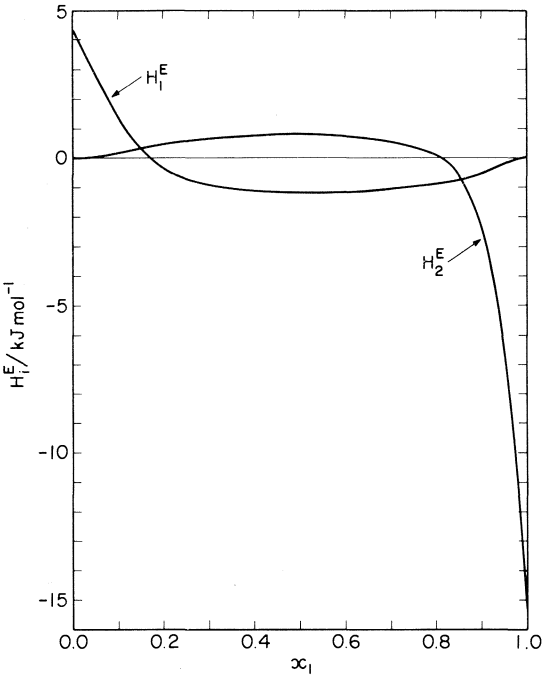

FIG. 3. Partial molar excess enthalpies of water and THF in H_2O (1) + THF (2) mixtures at 298.15 K. Curves calculated from least-squares splines.

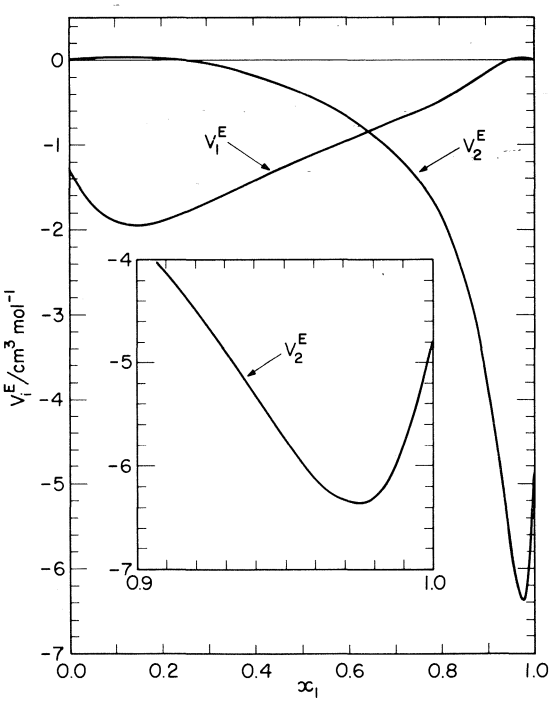

FIG. 4. Partial molar excess volumes of water and THF in H_2O (1) + THF (2) mixtures at 298.15 K. Curves calculated from least-squares splines.

cluster" model of liquid water (17). According to this model, water is composed of microscopic clusters of hydrogen-bonded molecules in dynamic equilibrium with more weakly bonded water molecules occupying cavities within the clusters and interstitial positions between them. Although the structural details of the model are still controversial, its general features are in accord with a variety of experimental results.

When water is the solvent for a nonelectrolyte, deviations of the properties of the solution from ideality in the water-rich region reflect the influence of the added species on the cluster equilibrium. The addition of an apolar or mixed type of nonelectrolyte (18) may initially promote or stabilize cluster formation in a cooperative manner since the solute tends to occupy the cavities and to displace the weakly bonded water molecules which can form more hydrogen-bonded clusters. In the present system the large negative values of $H_2^E(x_1)$ for water-rich mixtures are a consequence of enhanced hydrogen bonding. It has been suggested that the minimum in the $V_2^E(x_1)$ curve occurs when there are no more cavities to support the full structuring ability of the solute molecules (18). Further solute addition then has a disruptive influence on the water structure.

Figure 3 shows that over a broad central mole fraction range, $H_1^E(x_1)$ and $H_2^E(x_1)$ become nearly constant. A similar region has been observed for H_2O + ethanol mixtures, and Larkin has described it as a pseudo two-phase system (19). In the present case, the pseudo phases consist of the stabilized water clusters in equilibrium with a random mixture of H_2O + THF. The molecular environment experienced by added quantities of H_2O or THF remains essentially constant since only the relative amounts of the phases are changed. When water is added to pure THF, water–water hydrogen bonds are broken and water–THF hydrogen bonds are formed. The positive values of $H_1^E(x_1)$ observed at low x_1 suggest that the mixed bonding is weaker (or less extensive) than the bonding in pure water.

Finally, we wish to express some reservations about the suitability of using H_2O + THF to test mixing calorimeters. Apart from the problem of obtaining and storing THF in a suitably pure state, our work indicates that it is inherently difficult to form homogeneous H_2O + THF mixtures with $x_1 > 0.6$. It is known that this system has regions of limited

solubility above 345 K (4) and below 286 K (20), and it seems likely that an incipient phase separation (demixing) occurs even at 298.15 K. It appears that the time needed to establish equilibrium on a microscopic level can lead to erroneous H^E results, particularly in flow type mixing calorimeters. It is very desirable to have a variety of test mixtures, but it is important to make clear the nature of the test which each provides. The thermal behavior of the mixture selected to test a calorimeter should be reasonably similar to that of the mixture which it is proposed to measure. From this point of view we believe that, in many cases, H_2O + THF may present an unnecessary challenge.

Acknowledgements

We are indebted to Dr. R. Tanaka for helpful discussions, and also to Mr. P. J. D'Arcy and Mr. C. J. Halpin for technical assistance during this investigation.

1. J. Erva. Suom. Kemistil. B**28**, 131 (1955).
2. H. Nakayama and K. Shinoda. J. Chem. Thermodyn. **3**, 401 (1971).
3. D. N. Glew and H. Watts. Can. J. Chem. **51**, 1933 (1973).
4. J. Matouš, J. P. Novák, J. Šobr, and J. Pick. Collect. Czech. Chem. Commun. **37**, 2653 (1972).
5. R. Singer, H. Arm, and H. Daeniker. Helv. Chim. Acta, **52**, 2347 (1969).
6. K. W. Morcom and R. W. Smith. Trans. Faraday Soc. **66**, 1073 (1970).
7. Standards Committee of the Calorimetry Conference (U.S.A.) Report dated July 25, 1974. Bull. Thermodyn. Thermochem. **18**, 681 (1975).
8. S. Murakami, M. Koyama, and R. Fujishiro. Bull. Chem. Soc. Jpn. **41**, 1540 (1968).
9. W. Hayduk, H. Laudie, and O. H. Smith. J. Chem. Eng. Data, **18**, 373 (1973).
10. R. Tanaka, P. J. D'Arcy, and G. C. Benson. Thermochim. Acta, **11**, 163 (1975).
11. R. Tanaka, O. Kiyohara, P. J. D'Arcy, and G. C. Benson. Can. J. Chem. **53**, 2262 (1975).
12. J. H. Ahlberg, E. N. Nilson, and J. L. Walsh. The theory of splines and their applications. Academic Press, New York, NY. 1967.
13. F. Franks, M. A. J. Quickenden, D. S. Reid, and B. Watson. Trans. Faraday Soc. **66**, 582 (1970).
14. S. Cabani, G. Conti, and L. Lepori. J. Phys. Chem. **76**, 1338 (1972).
15. D. A. Armitage, M. J. Blandamer, M. J. Foster, N. J. Hidden, K. W. Morcom, M. C. R. Symons, and M. J. Wootten. Trans. Faraday Soc. **64**, 1193 (1968).
16. M. J. Blandamer, N. J. Hidden, K. W. Morcom, R. W. Smith, N. C. Treloar, and M. J. Wootten. Trans. Faraday Soc. **65**, 2633 (1969).
17. H. S. Frank and W.-Y. Wen. Discuss. Faraday Soc. **24**, 133 (1957).
18. F. Franks and D. S. Reid. *In* Water, a comprehensive treatise. Vol. 2. *Edited by* F. Franks. Plenum Press, New York, NY. 1973. Chapt. 5.
19. J. A. Larkin. J. Chem. Thermodyn. **7**, 137 (1975).
20. L. Carbonnel and J.-C. Rosso. J. Solid State Chem. **8**, 304 (1973).

Viscosities of mixtures of SnR_4 compounds and of some other large globular molecules. Effect of size difference

CLAUDE JAMBON[1] AND GENEVIÈVE DELMAS

Université du Québec à Montréal, Département de chimie, C.P. 8888, Montréal (Qué), Canada H3C 3P8

Received July 5, 1976

CLAUDE JAMBON and GENEVIÈVE DELMAS. Can. J. Chem. **55**, 1360 (1977).

Solution viscosities have been measured at 25 °C on seven I systems of SnR_4 compounds: $SnBut_4$ with $SnMe_4$, $SnEt_4$, $SnPr_4$, $SnOct_4$, $SnLaur_4$ and $SnLaur_4$ with $SnEt_4$ and $SnPr_4$. The effect of shape difference on excess solution viscosities was investigated. The experimental value $\Delta \ln \eta_{exp} = \ln \eta_s - x_1 \ln \eta_1 - x_2 \ln \eta_2$ was compared to $\Delta \ln \eta_{th}$. $\Delta \ln \eta_{th}$ was obtained using ΔG_M(mixing) in place of $G_M^{\neq}$(activation) and free volume theories. Experimental heats of mixing have been measured and are used in $\Delta \ln \eta_{th}$. It was found that with the Van der Waals model for the energy, the difference $\Delta \ln \eta_{exp} - \Delta \ln \eta_{th}$, indicative of the agreement between the predicted and experimental value, is relatively small for mixtures of molecules not having a large size difference. However, for systems different in size, $\Delta \ln \eta_{exp} - \Delta \ln \eta_{th}$ is positive and large and is shown to be an increasing function of the size difference. $\Delta \ln \eta_{th}$ could be adjusted to $\Delta \ln \eta_{exp}$ by adding a term $\ln \eta_{\Delta V^*} = c(V_1^{*1/2} - V_2^{*1/2})^2$ where V^* is the core volume. To confirm the validity of $\ln \eta_{\Delta V^*}$, the seven II systems chosen in order to present a large range $(V_1^{*1/2} - V_2^{*1/2})$ were measured: $SnBut_4$ + squalane, $Si(OEt)_4$ + $Si(OOct)_4$, n-C_{10} + $Si(OOct)_4$, $Si(OEt)_4$ + squalane, n-C_{12} + $SnOct_4$, $Si(OMe)_4$ + $Si(OOct)_4$, n-C_{16} + benzene. A c value of 5.3×10^{-3} cm^3 appears to be adequate for all the systems studied in this work. The 'condensation effect' of $SnEt_4$ and $SnPr_4$ observed by calorimetry is possibly seen here in the series $SnLaur_4$ with $SnEt_4$, $SnPr_4$, $SnBut_4$.

CLAUDE JAMBON et GENEVIÈVE DELMAS. Can. J. Chem. **55**, 1360 (1977).

Des mesures de viscosités ont été faites sur les composés SnR_4 et leurs mélanges. Sept systèmes I $SnBut_4$ avec $SnMe_4$, $SnEt_4$, $SnPr_4$, $SnOct_4$, $SnLaur_4$ ainsi que $SnLaur_4$ avec $SnEt_4$ et $SnPr_4$ ont été étudiés. Nous nous interessions à l'effet de la forme des molécules sur la viscosité d'excès. La valeur expérimentale $\Delta \ln \eta_{exp} = \ln \eta_s - x_1 \ln \eta_1 - x_2 \ln \eta_2$ est comparée à $\Delta \ln \eta_{th}$. Pour obtenir $\Delta \ln \eta_{th}$, on se sert de théories de volume libre et de ΔG_M(énergie libre de mélange) au lieu de $G_M^{\neq}$ d'activation. Les chaleurs de mélanges utilisées dans $\Delta \ln \eta_{th}$ ont été mesurées. On trouve qu'avec le modèle de Van der Waals pour l'energie, la différence $\Delta \ln \eta_{exp} - \Delta \ln \eta_{th}$, caractéristique du bon accord entre les valeurs expérimentales et théoriques, est petite pour les mélanges de molécules qui ont des tailles assez voisines. Au contraire pour des mélanges de molécules de tailles différentes, la valeur de $\Delta \ln \eta_{exp} - \Delta \ln \eta_{th}$ est grande et positive; elle est aussi une fonction croissante de la différence de taille. $\Delta \ln \eta_{th}$ peut être ajusté à $\Delta \ln \eta_{exp}$ en ajoutant un terme $\ln \eta_{\Delta V^*} = c(V_1^{*1/2} - V_2^{*1/2})$ où V^* est le volume à 0 K. Pour confirmer l'expression pour $\ln \eta_{\Delta V^*}$, sept autres systèmes II ont été étudiés. Les systèmes (II) ont été choisis de façon à avoir une grande différence de V^*. Ce sont: $SnBut_4$ + squalane, $Si(OEt)_4$ + $Si(OOct)_4$, n-C_{10} + $Si(OOct)_4$, $Si(OEt)_4$ + squalane, n-C_{12} + $SnOct_4$, $Si(OMe)_4$ + $Si(OOct)_4$, n-C_{16} + benzène. Une valeur de c de 5.3×10^{-3} cm^3 semble convenir approximativement pour les systems présentés ici. L'effet de condensation de $SnEt_4$ et $SnPr_4$, observé par calorimétrie, peut sans doute se voir sur la série, $SnLaur_4$ avec $SnEt_4$, $SnPr_4$, $SnBut_4$.

Introduction

Recent theories of solutions (1–4) have emphasized the importance of the free volume difference between the two components of the mixture. The diverse contributions arising from the free volume difference can be understood qualitatively in the following way. The more volatile compound is 'condensed' in the presence of the denser one or its free volume is diminished. As a result, there is a negative contribution to the excess volumes and a negative or exothermic contribution to the heats of mixing and to the entropies of mixing. The contribution to the heats or to the volumes of mixing derived from the difference in cohesive energy of the two components cannot yet be calculated adequately. However, a test of the free volume theories can be made by using the experimental heats of mixing. In this case, the predicted excess volumes, for instance, are in good agreement with the experimental ones.

[1]Present address: Laboratoire de Chimie Analytique I, Département de chimie et biochimie de L'Université Claude-Bernard de Lyon I, 43, boulevard du 11-novembre 1918, 69621 Villeurbanne.

It would be interesting to investigate if measurements of viscosities of binary mixtures combined with free volume theories could give some information on the importance of free volume terms in viscosities of mixtures. Bloomfield and Dewan (5) have used the calculated free energy of mixing as an approximation to the free energy of activation. They have shown, on systems with relatively small differences in free volume, that there is a good agreement between the calculated and experimental excess viscosities. Recently (6), it has been shown that the free volume theory using a Van der Waals model gives quite good excess viscosity predictions even for systems with large free volume differences. This later work seemed to show that excess viscosities were sensitive to the shape of the molecules.

It has seemed worthwhile to us to study the viscosities of mixtures of non-polar globular molecules such as the SnR_4 compounds. Heats of mixing (7) of SnR_4 (with R = CH_3, C_2H_5, C_4H_9) with the alkanes have shown that these compounds have properties similar to those of the alkanes. Furthermore, the shape of the molecules of the SnR_4 compounds is changed gradually from globular to elongated when the chain-length of the R group is increased. This work presents the results of excess viscosity measurements of seven SnR_4 mixtures (I). Since the difference between experimental and calculated excess viscosities shows a correlation with the difference of size of the two components, six other systems have been studied to confirm this correlation. These systems (II) were chosen mainly because of size differences. The seven I systems are $SnBut_4$ with $SnMe_4$, $SnEt_4$, $SnPr_4$, $SnOct_4$, $SnLaur_4$ and $SnLaur_4$ with $SnEt_4$ and $SnPr_4$, the six II systems are $SnBut_4$ + squalane ($C_{30}H_{62}$), $Si(OMe)_4$ + $Si(OOct)_4$, $Si(OEt)_4$ + $Si(OOct)_4$, $Si(OEt)_4$ + squalane, $Si(OOct)_4$ + n-C_{10}, $SnOct_4$ + n-C_{12}. The seventh II system n-C_{16} + benzene was in the literature.

Experimental

Apparatus

The viscosimeters were of the Ubbelholde type from the Cannon Instrument Co. (State College, PA). The flow times were not lower than 80 s. Calibration of the viscosimeters was made as in previous work (6). For highly viscous liquids, the calibration constants were checked by measurements of viscosities of viscous liquids reported in the literature, such as oleic acid. Special care was taken with liquids of high viscosities to assure a good mixing of the solutions. The calorimeter used for heats of mixing measurements and the densitometer used for density and expansion coefficient measurements have been described previously (7).

Solvents

The methyl, ethyl, propyl derivatives were obtained from the K and K Co. (99%). Tetrabutyl tin was either from the Aldrich or K and K Companies. The octyl and lauryl derivatives were obtained at the Chemical Procurement Laboratories (College Point, N.Y.). The alkanes were purchased from the Aldrich Co.; the squalane and the $Si(OR)_4$ from the K and K Co. Densities of the compounds were measured as a test of their purity.

Table 1 gives some physicochemical data and parameters about the pure components: density, expansion coefficient, viscosity, pressure reduction parameter P^*, volume reduction parameter V^*. The calculations to obtain V^* and P^* are described later. The density of $SnOct_4$ has been omitted because it was outside the range of literature values. However, the two systems with $SnOct_4$ have been kept since they seemed to follow the general trend on Fig. 1.

Theory

Theories relate the viscosities of liquids either to the activation energy required for the molecule to overcome the attractive forces of its neighbours and flow to a new position (absolute reaction rate theory) or the probability that an empty site exists near a molecule (free volume theory). In a recent theory, Macedo and Litovitz (8) have made the hypothesis that the two effects are combined so that the probability for viscous flow is taken as the product of probabilities for acquiring sufficient activation energy and of the occurrence of an empty site. Similar assumptions are made for the solutions. Furthermore, a bridge can be made to the thermodynamic functions of mixing by assuming a simple relation between the solution activation energy $\Delta G,^{\neq}$ the pure liquid activation energies $\Delta G_1^{\neq}$, $\Delta G_2^{\neq}$, and the excess free energy of mixing ΔG_M^R.

$$[1] \quad \Delta G^{\neq} = x_1 \Delta G_1^{\neq} + x_2 \Delta G_2^{\neq} - \Delta G_M^R$$

For the pure components and the solution the viscosities η_i are defined as:

$$[2] \quad \eta_i = A \exp [\Delta G_i^{\neq}/RT + (\tilde{v}_i - 1)^{-1}]$$

where $\tilde{v}_i$ is the reduced volume.

$$[3] \quad \ln \eta_i = \ln A + \Delta G_i^{\neq}/RT + (\tilde{v}_i - 1)^{-1}$$

Equation 3 can be applied to the solution and the pure components to obtain:

$$[4] \quad \Delta \ln \eta = \ln \eta_{sol} - (x_1 \ln \eta_1 + x_2 \ln \eta_2)$$

If eqs. 1 and 2 are used in eq. 4, the activation energies are eliminated and $\Delta \ln \eta$ is related to the free energy of mixing by:

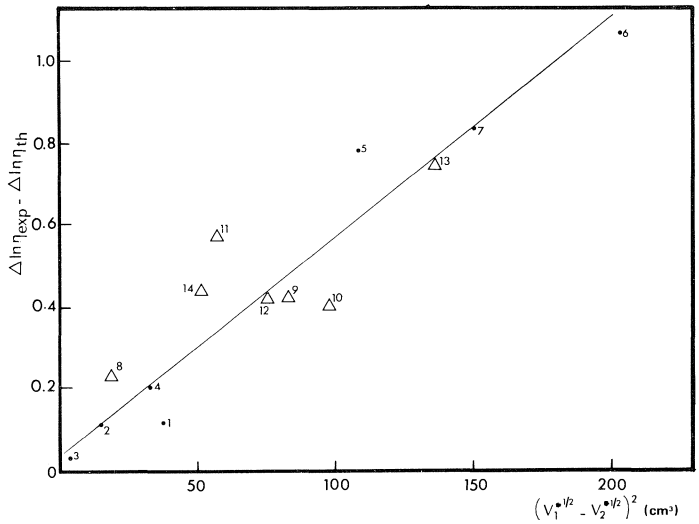

FIG. 1. $\Delta \ln \eta_{exp} - \Delta \ln \eta_{th}$ from eqs. 4 and 5 *vs.* the difference in core volume of the two components $(V_1^{*1/2} - V_2^{*1/2})^2$, ● SnR_4 systems (points 1 to 7), △, other systems (points 8 to 14). The systems corresponding to the numbers can be found in Table 2.

$$[5] \quad \Delta \ln \eta_{th} = -\Delta G_M^R/RT + \frac{1}{\tilde{v} - 1} - \frac{x_1}{\tilde{v}_1 - 1} - \frac{x_2}{\tilde{v}_2 - 1}$$

$\tilde{v}$ is the reduced volume of the solution. One can say here that if the reduced volumes of the two components are not the same, the solution is not ideal from the viscosity point of view ($\Delta \ln \eta \neq 0$) even if $\Delta G_M^R = 0$. Comparison between experiment and theory will be made between eq. 5 and the experimental quantity $\Delta \ln \eta_{exp} = \ln \eta_{sol} - x_1 \ln \eta_1 - x_2 \ln \eta_2$ where η_{sol}, η_1, and η_2 are the measured values.

For ΔG_M^R in eq. 5, the experimental ΔH_M will be used and ΔS_M calculated. Different models (4) have been proposed for the energy–volume relationship but the Van der Waals relation $U = -1/V$, widely used by Flory (3), gives good results with relatively simple calculations. The $\tilde{v}$ of the solution depends not only on the difference in the reduced volume of the pure components $\tilde{v}_1$ and $\tilde{v}_2$ but also on the heats of mixing of the solution through the X_{12} parameter (eq. 38 of ref. 3*b*). In this work, $\tilde{v}$ is obtained by a simpler approximation detailed in refs. 4 and 9. The expression for ΔS_M^R, the excess entropy of mixing is (3):

$$[6] \quad \Delta S_M^R = 3x_1 \frac{P_1^* V_1^*}{RT_1^*} \ln \frac{\tilde{v}_1^{1/3} - 1}{\tilde{v}^{1/3} - 1} + 3x_2 \frac{P_2^* V_2^*}{RT_2^*} \ln \frac{\tilde{v}_2^{1/3} - 1}{\tilde{v}^{1/3} - 1}$$

P^*, V^*, and T^* are respectively the pressure, volume, temperature reduction parameters. They are obtained for the pure component as described below. To simplify, the following nomenclature is used:

$$[7] \quad \Delta \ln \eta_{th} = -\frac{\Delta H_M}{RT} + \frac{\Delta S_M^R}{R} + f(\tilde{v}) = \ln \eta_H + \ln \eta_S + \ln \eta_V$$

where

$$\ln \eta_H = -\Delta H_M/RT$$

$$\ln \eta_S = \Delta S_M^R/R$$

and

$$\ln \eta_V = f(\tilde{v}) = \frac{1}{\tilde{v} - 1} - \frac{x_1}{\tilde{v}_1 - 1} - \frac{x_2}{\tilde{v}_2 - 1}$$

Parameters for the Pure Components

The expansion coefficient and the density are necessary to obtain (3) $\tilde{v}$ and V^* through the equations

$$\tilde{v}^{1/3} = (\tfrac{4}{3}\alpha T + 1)/(\alpha T + 1)$$

and

$$V^* = V/\tilde{v}$$

$\tilde{T}$ is obtained by $\tilde{T} = \tilde{v}^{-1}(1 - \tilde{v}^{-1/3})$ and $T^* = T/\tilde{T}$. P^* is derived by the thermal pressure coefficient γ and $P^* = \gamma \tilde{v}^2 T$. For systems with little free volume differences, $\tilde{v}$ is near $\tilde{v}_1$ and $\tilde{v}_2$ which makes small the contribution of the term containing P^*, $\ln \eta_s$, in eq 7. Table 1 gives the parameters used in the calculations. The T^* have not been tabulated because they can be obtained easily from the above equations.

TABLE 1. Physico-chemical parameters for the pure components at 25 °C

Compound	This laboratory d (g cm^{-3})	α (10^3 K^{-1})	η (cP)	P^* (J cm^{-3})	V^* (cm^3)
$SnMe_4$	1.2865	1.28	0.36	415[a]	107.7
$SnEt_4$	1.1877	1.00	0.68	455[a]	159.0
$SnPr_4$	1.1013	0.890	1.25	481[a]	213.6
$SnBut_4$	1.0492	0.818	2.30	439[a]	271.6
$SnOct_4$	—	0.790	15.2	486[a]	494.7
$SnLaur_4$	0.9170	0.775	36.8	475[a]	723.6
Squalane	0.8051	0.815	28.9	457[b]	432.7
$Si(OMe)_4$	1.0234	1.283	0.59	523[a]	114.2
$Si(OEt)_4$	0.9301	1.168	0.66	459[a]	174.8
$Si(OOct)_4$	0.8806	0.829	9.51	453[a]	544.9
n-C_{10}	0.7259	1.05	0.84	439[c]	155.6
n-C_{12}	0.7449	0.98	1.34	455[c]	183.7

[a]From γ measured in this laboratory by R. Philippe.
[b]From ref. 15.
[c]From ref. 3.

Results and Discussion

Pure Viscosities

Viscosities of the pure components are given in Table 1. Viscosities of the *n*-alkanes agree with published literature values (10). It is interesting to note that the viscosities depend so much on molecular shape and flexibility of the atomic bonds. The comparison of the viscosities (in cP) of four molecules having not too different molecular weights such as squalane (η = 28.9), $SnOct_4$ (η = 15.2), $Si(OOct)_4$ (η = 9.51), and 9*n*-octylheptadecane (η = 10.0) (11) illustrates this point. Low viscosities seem to be a characteristic of molecules with a central atom tetrasubstituted with identical groups.

Solution Viscosities

Table 2 shows the overall results for the systems. The different columns of Table 2 give respectively the maximum of $\Delta \ln \eta_{exp}$, the concentration at which the maximum occurs, the coefficients A_0, A_1, A_2, of the experimental concentration dependance of $\Delta \ln \eta_{exp}$:

$$[8] \quad \Delta \ln \eta_{exp} = x_1 x_2 (A_0 + A_1 x_1 + A_2 x_2^2)$$

$\Delta \ln \eta_{th}$ and the different contributions in eq. 7, $\ln \eta_H$, $\ln \eta_S$, $\ln \eta_V$, are tabulated in the other columns. The contact energy parameter X_{12} has been calculated (12) and is given in the next column divided by s_1, the surface-to-volume ratio of component 1. The last three columns give $\Delta \ln \eta_{exp} - \Delta \ln \eta_{th}$, $(V_1^{*1/2} - V_2^{*1/2})^2$ a function of the difference in core volume of 1 and 2 and the number corresponding to each system on the graph. The experimental heats of mixing, used to obtain values of $\ln \eta_H$, are published separately (12) or will be published later (for the II systems).

The maximum of the heats has been used and no correction has been made for the fact that the maximum of $\Delta \ln \eta$ is not exactly at the same concentration as the maximum of the heats.

Characteristics of the SnR_4 Mixtures (Seven Systems)

(*1*) For the first system, $SnBut_4 + SnMe_4$, where there is a relatively large free volume difference, $\Delta \ln \eta$ is positive and large, due to the free volume contribution. This result had been found in the previous work (6). (*2*) For the next three systems for which the heats of mixing and free volume differences are small, $\Delta \ln \eta$ is predicted to be very small while the experimental values are larger and positive (for two systems). (*3*) For the last three systems of class I, the negative contribution coming from the large heats of mixing is almost balanced by the positive one due to the difference in free volume, so that $\Delta \ln \eta_{th}$ is predicted to be quite small. It is then surprising to obtain experimentally very large positive values of $\Delta \ln \eta$. This result had not been seen or was not so apparent in mixtures of $SnBut_4$ and long alkanes (6) for which a large heat of mixing was accompanied by a negative value of $\Delta \ln \eta$. Inspection of Table 2 indicates that the value of the difference $\Delta \ln \eta_{exp} - \Delta \ln \eta_{th}$ is an increasing function of the difference of volumes between the two components.

It has been shown that long chain alkanes (7), long chain alcohols (14), and long chain tin com-

TABLE 2. Experimental and calculated $\Delta \ln \eta$ at 25 °C for the series I (SnR_4 compounds) and the series II (mixtures with large size differences between the components)

	Experimental					Calculated						
System	$\Delta \ln \eta_{exp}$	x_{1max}	A_0	A_1	A_2	$\Delta \ln \eta_{th}$	$\ln \eta_H$[b]	$\ln \eta_S$	$\ln \eta_V$	$X_{12}{s_1}^{-1}$[c] (J cm^{-3} Å^{-1})	$\Delta \ln \eta_{exp} - \Delta \ln \eta_{th}$	$(V_1^{*1/2} - V_2^{*1/2})^2$ (cm^3)	Numbers on Fig. 1
Series I													
$SnBut_4$ + $SnMe_4$	0.29	0.45	1.5185	−0.5886	−0.4065	0.170	−0.026	−0.069	0.260	3.82	0.12	87.2	1
+ $SnEt_4$	0.15	0.40	0.5618	0.1965	−0.2965	0.038	−0.018	−0.014	0.070	1.52	0.11	14.9	2
+ $SnPr_4$	0.03	0.37	0.0912	0.4674	0.9232	0.003	−0.007	−0.002	0.013	0.46	0.03	3.5	3
+ $SnOct_4$	0.16	0.62	0.5414	−0.0251	0.3425	−0.042	−0.097	0.010	0.044	2.60	0.20	33.2	4
+ $SnLaur_4$	0.63	0.60	1.6989	1.0928	0.7496	0.154	−0.228	0.041	0.033	5.72	0.78	108.6	5
$SnEt_4$ + $SnLaur_4$	1.19	0.50	8.6008	−12.089	7.0478	0.121	−0.161	−0.010	0.292	5.83	1.07	204.2	6
$SnPr_4$ + $SnLaur_4$	0.82	0.60	5.4593	−6.5059	3.4565	0.009	−0.159	0.016	0.133	4.87	0.83	151.0	7
Series II													
$SnBut_4$ + squalane	0.19	0.65	0.7348	−0.5608	1.1057	−0.032	−0.037	0.007	−0.019	1.80	0.23	18.7	8
$Si(OEt)_4$ + $Si(OOct)_4$	0.41	0.60	2.2253	−1.5408	0.5705	−0.001	−0.201	−0.011	0.211	8.06	0.42	83.1	9
n-C_{10} + $Si(OOct)_4$	0.47	0.50	2.7371	−2.3078	0.8583	0.034	−0.081	0.000	0.115	3.55	0.40	98.1	10
$Si(OEt)_4$ + squalane	0.32	0.55	1.6844	−1.0522	0.3757	−0.144	−0.428	0.009	0.274	19.4	0.57	56.8	11
n-C_{12} + $SnOct_4$	0.30	0.45	1.4524	−0.6889	0.2084	−0.121	−0.280	−0.027	0.132	10.7	0.42	75.4	12
$Si(OMe)_4$ + $Si(OOct)_4$	0.56	0.60	3.5433	−4.0732	2.4100	−0.249	−0.610	0.079	0.282	29.0	0.74	136.5	13
n-C_{16} + benzene[a]	0.15	0.45	—	—	—	−0.291	−0.445	0.021	0.176	40.0	0.44	51.4	14

[a] $\Delta \ln \eta$ measured in ref. 10(*b*).
[b] $\ln \eta_H = -\Delta H_M/RT$, ΔH_M being reported in ref. 12.
[c] Calculated as in ref. 12.

pounds (13) exhibit an order between the chains. A branched alkane, on the other hand, and presumably a tin derivative with a branched alkyl substituent, does not show this order due to its more isotropic character. It does not seem possible, as in ref. 6, to explain from these results the specific effect of the shape difference between the globular shorter tin derivatives and the ordered $SnLaur_4$ on $\Delta \ln \eta_{exp} - \Delta \ln \eta_{th}$. The reason for this must be that, in the I systems, the molecules with shape differences have, in addition, very large size differences. The size effect must mask the shape effect. Comparison of $\Delta \ln \eta_{exp} - \Delta \ln \eta_{th}$ for two compounds having the same size but different shapes such as $SnLaur_4$ and one of its branched isomers would be informative but is not possible due to the non-availability of one of these isomers.

Effect of the Size Difference on Excess Viscosities

To obtain a more quantitative correlation between the size difference and the 'error' in the theory, $\Delta \ln \eta_{exp} - \Delta \ln \eta_{th}$ was plotted in Fig. 1 against the values $(V_1^{*1/2} - V_2^{*1/2})^2$. For the seven I systems, there is a reasonably linear relationship. The extrapolation to 0 of $\Delta \ln \eta_{exp} - \Delta \ln \eta_{th}$ when $V_1^* = V_2^*$ shows that the value of $\ln \eta_{th}$, as calculated by eq. 7, describes the experimental results well, except for large size differences. To correct for this, one should add the term $\ln \eta_{\Delta V^*}$ to the calculated value so that

$$[9] \quad \Delta \ln \eta_{th} = \ln \eta_H + \ln \eta_S + \ln \eta_V + \ln \eta_{\Delta V^*}$$

$$\ln \eta_{\Delta V^*} = c(V_1^{*1/2} - V_2^{*1/2})^2$$

This expression was tried by analogy with the cohesive energy difference in solution.

Confirmation with Other Systems of the Validity of the Empirical Term $\ln \eta_{\Delta V^*}$ Added in Eq. 9

The next six systems have been chosen so that their $(V_1^{*1/2} - V_2^{*1/2})^2$ values would be spread between 50 and 200 cm^3. Heats of mixing, excess viscosities, and excess volumes have been measured and $\Delta \ln \eta_{th}$ obtained. One can see in Fig. 1 that these points fall reasonably well on the line obtained with the SnR_4 compounds. It is interesting to note that the $\Delta \ln \eta_{exp} - \Delta \ln \eta_{th}$ values agree with the curve of Fig. 1 regardless of the sizes of the other contributions. For two systems, the free volume contributions are large and for three other systems $\Delta \ln \eta_H$ is important. The mixture, n-C_{16} + benzene, was added in Table 2, the agreement with eq. 9 being quite good even for this moderately polar system.

The scatter of the points on Fig. 1 around the straight line reflects undoubtedly the too great a simplicity of the expression for $\ln \eta_{\Delta V^*}$. One would have liked to have several slopes in Fig. 1 related to the shape of the mixed molecules but more experiments seem necessary to test this possibility. On the theoretical side, it would be interesting to understand the origin of $\ln \eta_{\Delta V^*}$. It is possible that the solution viscosity is increased when the molecules have large size differences because the probability of a suitable empty site near a molecule diminishes. On the other hand, excess volume measurements[2] show that a negative contribution occurs for the same systems for which $\ln \eta_{\Delta V^*}$ is important. In this case, it is likely that a good fitting of the small molecules in between the spaces left by the large ones is the source of the increased viscosity and decreased volume.

Condensation Effect with $SnEt_4$ and $SnPr_4$

Heats of mixing of the first four homologs of the SnR_4 series with the ordered chain compound $SnLaur_4$ have shown that there is a minimum of the heats per mole with $SnEt_4$ and $SnPr_4$. The same result is found if another ordered liquid like hexadecane is mixed with the same series. This is interpreted as the presence of an exothermic contribution to the heats which is larger for $SnEt_4$ and $SnPr_4$ than for the other members. Due to the presence of four alkyl groups on the Sn atom, $SnEt_4$ and $SnPr_4$ are sterically hindered and have low mobilities and large cohesive energies. The higher values of P^* for $SnEt_4$ (455) and $SnPr_4$ (481) J cm^{-3} compared to the values for the two nearest members of the same series $SnMe_4$ (415) and $SnBut_4$ (439) are macroscopic evidences of this distinctive character of $SnEt_4$ and $SnPr_4$. When they are mixed with a chain molecule as n-C_{16} or even a shorter alkane, they have the ability to diminish the mobility or 'condense' the other molecule. This characteristic has been found recently (16) on other sterically hindered molecules such as the alkanes substituted on the same carbon atom or neighbouring carbon atoms. The condensation effect gives a definite contribution to the excess volume: the diminution of the mobility is accompanied by a contraction which decreases the total volume.[2] It would be interesting to see if the excess viscosities would show a special contribution due to

[2]Cl. Jambon, G. Delmas, and Nguyen Hong Phuong. To be published.

the condensation effect. One would have liked to see a special contribution for the systems involving the $SnEt_4$ and $SnPr_4$ compared to the $SnBut_4$ and $SnMe_4$ ones. The system $SnLaur_4$ + $SnMe_4$ has not been investigated because the different contributions $\Delta \ln \eta_{th}$, $\ln \eta_H$, $\ln \eta_V$, $\ln \eta_{\Delta V^*}$ are so large that $\Delta \ln \eta_{exp} - \Delta \ln \eta_{th}$ would perhaps not have been very significant. However, inspection of the three other systems (points 5, 6, 7) on Fig. 1 shows that there is indeed an irregularity in the series; the points corresponding to $SnEt_4$ and $SnPr_4$ are lower than that for $SnBut_4$ as it would be expected from a contribution coming from the condensation effect. On the other end, the low values of $\ln \eta_{exp} - \ln \eta_{th}$ for the points 6 and 7 may be related to an inadequacy of $\ln \eta_{\Delta V^*}$ for large values of $(V_1^{*1/2} - V_2^{*1/2})^2$ and not to the condensation effect. Another test of the presence of this effect was made using n-C_{16} as the condensable molecule instead of $SnLaur_4$. In the mixtures of n-C_{16} with $SnEt_4$, $SnPr_4$, and $SnBut_4$, the molar volumes of the two components are similar so that $\ln \eta_{\Delta V^*}$ is negligible. The same calculations as for the other systems give, respectively for $\Delta \ln \eta_{exp} - \Delta \ln \eta_{th}$, 0.169, 0.112, 0.124. This time, it appears, that the system involving $SnPr_4$ is not in between those with $SnEt_4$ and $SnBut_4$ as would have been expected. However, the difference with the expected value is rather small and does not permit a definite conclusion. The condensation effect is related to some kind of couplage between the motions of the condensing molecule (SnR_4) and the condensated ($SnLaur_4$, n-C_{16}). Since the short SnR_4 molecules have the same shape it is possible that the maximum of the effect does not happen with the same SnR_4 when the condensated molecule is changed. The condensation effect may have some importance in other terms of the excess viscosities not included in the change of the reduced volume ($\ln \eta_v$) and of the free energy ($\ln \eta_H + \Delta \ln \eta_S$) with the mixing.

Acknowledgments

This work was supported by the France-Québec scientific program which gave financial assistance to the stay of Dr Claude Jambon at UQUAM and by the National Research Council of Canada, to whom we are grateful. We thank Nguyen Hong Phuong for her collaboration.

1. I. Prigogine, A. Bellemans, and V. Mathot. The molecular theory of solutions. North Holland, Amsterdam, and Interscience, New York. 1957.
2. D. Patterson, G. Delmas, and T. Somcynsky. J. Polymer Sci. **57**, 79 (1962).
3. (*a*) P. J. Flory, R. A. Orwoll, and A. Vrij. J. Am. Chem. Soc. **86**, 3515 (1964). (*b*) P. J. Flory. J. Am. Chem. Soc. **87**, 1833 (1965).
4. G. Delmas and D. Patterson. Discuss. Faraday Soc. **49**, 98 (1970).
5. V. A. Bloomfield and R. K. Dewan. J. Phys. Chem. **75**, 3113 (1971).
6. G. Delmas, P. Purves, and P. de Saint-Romain. J. Phys. Chem. **79**, 1970 (1975).
7. G. Delmas and S. Turrell. J. Chem. Soc. Faraday I, **70**, 572 (1974).
8. P. B. Macedo and T. A. Litovitz. J. Chem. Phys. **31**, 1164 (1965).
9. G. Delmas, P. de Saint-Romain, and P. Purves. J. Chem. Soc. Faraday I, **79**, 1181 (1975).
10. (*a*) E. Meeussen, C. Debeuf, and P. Huyskens. Bull. Soc. Chim. Belg. **76**, 145 (1967). (*b*) E. L. Heric and J. G. Brewer. J. Chem. Eng. Data, **12**, 574 (1967).
11. E. M. Griest, W. Webb, and R. Schiessler. J. Chem. Phys. **29**, 711 (1958).
12. N. T. Thanh and G. Delmas. J. Phys. Chem. To be published.
13. G. Delmas and N. T. Thanh. J. Chem. Soc. Faraday I, **71**, 172 (1975).
14. G. Delmas and N. T. Thanh. J. Chim. Phys. **72**, 1285 (1975).
15. G. Gee, D. Mangaraj, D. Sims, and G. J. Wilson. Polymer, **1**, 467 (1960).
16. P. Tancrède, P. Bothorel, P. de Saint-Romain, and D. Patterson. J. Chem. Soc. Faraday II, **73**, 15 (1976).

Anatoxin-*a*, a toxic alkaloid from *Anabaena flos-aquae* NRC-44h[1]

J. P. DEVLIN,[2] O. E. EDWARDS,[3] P. R. GORHAM,[4]
N. R. HUNTER,[2] R. K. PIKE,[2] AND B. STAVRIC[2]

Division of Biological Sciences, National Research Council of Canada, Ottawa, Ont., Canada K1A 0R6

Received September 9, 1976

J. P. DEVLIN, O. E. EDWARDS, P. R. GORHAM, N. R. HUNTER, R. K. PIKE, and B. STAVRIC. Can. J. Chem. **55**, 1367 (1977).

A toxic alkaloid, anatoxin-*a*, has been isolated from mass cultures of a unialgal clone, NRC-44h, of the freshwater blue-green algae *Anabaena flos-aquae* (Lyngb.) de Bréb., and its structure determined.

J. P. DEVLIN, O. E. EDWARDS, P. R. GORHAM, N. R. HUNTER, R. K. PIKE et B. STAVRIC. Can. J. Chem. **55**, 1367 (1977).

On a isolé et déterminé la structure d'un alcaloïde toxique, l'anatoxine *a*, extrait de cultures massives d'un clone à une algue, NRC-44h, de l'algue bleue-verte d'eau potable *Anabaena flos-aquae* (Lyngb.) de Bréb.

[Traduit par le journal]

Ingestion of blooms of toxic freshwater algae are periodically responsible for the death of livestock, waterfowl, fish, and other wildlife (1–4). The chemical nature of the toxins from at least six species of freshwater algae have been studied to date (4–11).

Toxic strains of the filamentous blue-green alga, *Anabaena flos-aquae* (Lyngb.) de Bréb., have been obtained from a bloom that had poisoned cattle (12). They produced a toxin that killed mice in 2 to 5 min, preceded by gasps and tremors. It was called, therefore, Very Fast Death Factor (VFDF), and was shown by comparative tests to be indistinguishable in its effects from other toxic blooms that had killed livestock, waterfowl, and other species of wildlife (13). Using the medium and techniques worked out for the mass culture and bio-assay of the toxicity of these toxic strains, the following study was carried out to determine the structure of anatoxin-*a* (VFDF) produced by a unialgal clone NRC-44h that was obtained by a single-filament isolation from toxic strain NRC-44. Assay by intraperitoneal (ip) injection of mice was used to monitor toxin production and to follow the early stages of isolation.

In a preliminary study (14) Stavric and Gorham showed that the toxin was a low molecular weight amine probably containing an enone system (λ_{max} 227 nm). In subsequent work this absorption and a characteristic infrared band at 1670 cm^{-1} were used to monitor the final stages of purification of the toxin. The highest toxicity observed was LD_{min} (ip, mouse) of 0.25 mg/kg.

A variety of techniques were explored for the isolation and enrichment of the toxin. Because significant amounts of toxin were produced only as cultures matured (14 days) and 20 to 90% might be found in the medium at that time (14) it was decided to lyse the alga and isolate the toxin from the resulting aqueous suspension by ion-exchange chromatography. The simplest lysing technique proved to be the addition of Triton-X to the aqueous suspension. The toxin was absorbed from the lysed suspension onto the acid form of the carboxylic acid ion-exchange resin, Duolite. It was then eluted from the resin using alcoholic hydrogen chloride. Gentle concentration of the eluate *in vacuo* gave a syrup. A cold, aqueous solution of this syrup was adjusted to p*H* 8.5–9, the base rapidly extracted into methylene chloride, then at once reextracted into dilute hydrochloric acid. Evaporation of the acid solution left a glass rich in toxin hydrochloride (30% recovery of toxic material).

[1]Issued as NRCC No. 15801.

[2]NRCC postdoctoral fellows.

[3]To whom enquiries about chemistry should be addressed.

[4]Present address, Department of Botany, the University of Alberta, Edmonton, Alta. T6G 2E9. To whom enquiries about phycology and toxinology should be addressed.

Alternatively, the first syrup was triturated with benzene to remove neutral components, then triturated repeatedly with ¾% ethanol in chloroform. The latter removed much of the toxin hydrochloride.

However, the most efficient and reliable isolation procedure was to adjust the p*H* of the suspension of the mature algae to 5, concentrate this, then finally freeze-dry. The resulting green powder was extracted with dilute hydrogen chloride in methanol. Gentle evaporation of the extract left a syrup which was treated by the benzene–chloroform trituration described above. By this procedure a 73% recovery of toxin as hydrochloride was realized, as estimated by the LD_{min} for mice. Final purification was achieved by preparative thin-layer chromatography on silica gel using 20% methanol in chloroform for development.

Properties and Structure

The toxin hydrochloride was a nearly colorless glass with strong $R_2NH_2^+$ absorption below 3000 cm^{-1} and peaks at 1665 (str), 1638 (wk), and 1580 (med) cm^{-1} for a chloroform solution. This and its uv absorption (λ_{max} 227 nm, ε approximately 10 000) suggested the presence of a disubstituted α,β-unsaturated ketone. Since the toxin gave *N*-benzoyl and *N*-acetyl derivatives which had no NH group (ir) it was a secondary base. It absorbed only 1 mol of hydrogen over platinum, and its ^{13}C nmr spectrum showed the presence of only one C–C double bond. Mass spectra[5] and analyses showed its empirical formula to be $C_{10}H_{15}N$, hence it was a bicyclic compound.

Structure **1** was deduced for anatoxin-*a* on the basis of the above evidence and analysis of its ^1H nmr spectrum (see below). This was soon confirmed by X-ray crystallographic analysis of the *N*-acetyl derivative and absolute stereochemistry assigned (15). Because of this the arguments leading to structure **1** will be omitted, and only comments on the spectra given.

The vital evidence from chemical shifts and coupling obtained from 100 MHz[6] and 220 MHz ^1H nmr spectra of the *N*-acetyl derivative is illustrated on structure **2**, in which the double-ended arrows indicate demonstrated large coupling constants between the hydrogens. Attempts to demonstrate the vicinal nature of the methylenes resonating near 1.7 and 2.5 Hz failed. The ^{13}C nmr was not definitive for structure proof (see Experimental).

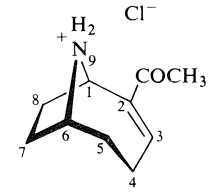

1

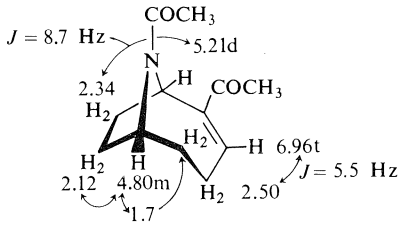

2

TABLE 1. The major fragment ions with high *m/e* of anatoxin-*a*

Formula	Mass	
	Calculated	Found
$C_{10}H_{15}NO$	165.1154	165.1138
$C_9H_{12}NO$	150.0919	150.0971
$C_8H_{10}NO$	136.0762	136.0758
C_7H_8NO	122.0606	122.0601

The major fragment ions with high *m/e* in the electron-impact mass spectrum[5] of anatoxin-*a* are given in Table 1. These were misleading in that they seemed likely to be pyridine derivatives. However, on the basis of **1** we formulate them as **3**, **4**, and **5**. Fragment ions from the *N*-acetyl derivatives are given in Table 2. These probably have structures **6** ($C_{10}H_{12}O^+$), **4** ($C_8H_{10}NO^+$), **7** ($C_8H_{12}N^+$), **8** ($C_8H_9^+$), **9** C_6H_8N), and **10** (C_5H_8N).

A synthesis of anatoxin-*a* from cocaine has now been achieved, confirming both the structure and absolute stereochemistry (16). The activity of the toxin as a post-synaptic depolarizing neuromuscular blocking agent has been reported (17).

A systematic name for anatoxin-*a* is 2-acetyl-9-azabicyclo[4.2.1.]non-2-ene.

[5]We are grateful to Dr. W. D. Jamieson, Atlantic Regional Laboratory, National Research Council of Canada for the high resolution mass spectra.

[6]We thank Dr. R. R. Fraser, Department of Chemistry, University of Ottawa for these decoupling experiments.

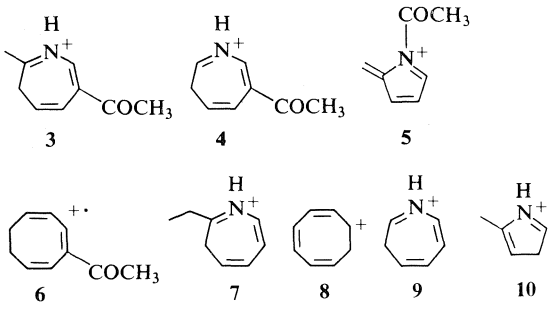

TABLE 2. Fragment ions from the *N*-acetyl derivative

Formula	Mass	
	Calculated	Found
$C_{10}H_{12}O$	148.08882	148.08939
$C_8H_{10}NO$	136.07624	136.0757
$C_8H_{12}N$	122.09697	122.0967
C_8H_9	105.07043	105.0701
C_6H_8N	94.06567	94.06540
C_5H_8N	82.06567	82.06540

Experimental

Bio-assay of Toxin

The regular method was similar to that described previously (7). Duplicate 20-g male mice, Connaught Laboratories or Alberta Laboratory Animal Services strains, were given graded dosages of algal suspensions or extracts by intraperitoneal injection. They were observed for toxinological signs and survival times for periods of 30 min or longer. Since the toxin has virtually an all-or-none effect, minimum lethal dose LD_{min} or LD_{100}, rather than 50% lethal dose, LD_{50}, was used to express toxicity. Mouse units (MU) used to determine recoveries were calculated on the basis of minimal dosage to kill a 25-g mouse. A few extracts were assayed using five replicates per dose to establish the LD_{min}'s a bit more precisely.

Anabaena flos-aquae NRC-44h

The toxic unialgal (bacterized) clone, *Anabaena flos-aquae* NRC-44h, was obtained by single-filament isolation in ASM-1 medium from the toxic colony isolate NRC-44 (14). *Anabaena flos-aquae* NRC-44 was one of eight toxic strains out of 12 that grew in shake flasks in ASM medium, 22°C, 1750 lux continuous, cool white fluorescent lamps, from a sample of a poisonous bloom collected from Burton Lake, Saskatchewan, June 20, 1961 (14). The bloom had an LD_{min} (ip) mouse = 80 mg/kg and an LD_{min} (oral) mouse = 800 mg/kg. Survival times were 5 to 6 min (ip or oral) preceded by a few gasps or tremors without violent convulsions. There were no detectable changes upon autopsy. Strain NRC-44 had an LD_{min} (ip) mouse = 640 mg/kg (12). It produced the same signs and survival times as the parent bloom. NRC-44h was the one clone out of 18, all toxic to varying degrees, which produced the greatest amount of anatoxin-*a* (90 to 120 MU/ℓ) when mass-cultured for 14 days in ASM-1 medium. Therefore, it was selected for further study.

Mass culture of Anabaena flos-aquae NRC-44h

Mass cultures were grown in 9-ℓ Pyrex bottles fitted with glass aerators inserted through a hole in the large rubber stopper that plugged the mouth. Eight litres of ASM-1 medium (12), p*H* 7.8, was autoclaved for 1 h in the bottle, cooled, and 100 ml of mature inoculum, that had been grown in shake flasks under similar conditions, was added aseptically. Batch cultures consisting of many bottles were grown in a temperature-controlled room at 21 ± 1°C with continuous illumination from three rows of 40-W cool white fluorescent lamps that were situated behind or between the bottles (Fig. 2 of ref. 18). The cultures were continuously aerated and stirred by sparging with filtered compressed air at 5 psi (0.35 kg/cm²) supplied from distribution manifolds at 1.0 to 1.5 ℓ/min.

Cultures were inoculated and harvested singly or in groups, as required, at about the peak of algal growth and toxin production, which was 14 days. If not lysed and treated with ion-exchange resin, mass cultures were acidified with HCl to p*H* 5 or 6, concentrated by vacuum distillation at 35°C with a Majonnier evaporator or a small cyclic still, and then freeze-dried from a starting temperature of −40°C or lower in a large commercial or a small laboratory apparatus. Frozen concentrates were sometimes stored at −40°C for several days or weeks prior to freeze-drying without loss of potency. Freeze-dried cultures were ground in a mortar to remove lumps, and stored in dark bottles at 5°C until used. There was a measurable loss of potency if stored for many months under these conditions, however. Different batches of freeze-dried NRC-44h had initial LD_{min}'s that varied from 80 to 160 mg/kg or even higher. The cause of this variability was subsequently shown to be the bacterial contaminants (19).

Isolation of the Toxin

(*A1*) To each 8 ℓ bottle of culture was added 1 ml of Triton-X followed by 25–30 g of the carboxylic acid ion-exchange resin Duolite C-100 (40–100 mesh, previously washed successively with sodium hydroxide solution, water, 3 *N* hydrochloric acid, ethanol, then water). The suspension was stirred for 17 h, then the solids separated by filtration through a sand bed in a glass chromatographic column. The bed of solids was washed with one column volume of water, then the toxin was eluted with 200 ml of 1.5 *N* hydrochloric acid in 50% ethanol–water. The eluate was evaporated in a Craig rotating evaporator in a 35°C bath. The residual syrup now contained an average of 52% of the original toxic compound (mouse assay). The cold aqueous solution of the syrup was quickly adjusted to p*H* 9, the toxin extracted rapidly into methylene chloride, then immediately back into 1 *N* hydrochloric acid. The acid solution was evaporated on a rotating evaporator (35°C bath), leaving a thick brown syrup, which now contained an average of 29% of the original toxicity. The final enrichment was by preparative thin layer chromatography on methanol-washed, reactivated fluorescent Chromar sheets using 1:8 methanol in methylene chloride (R_f 0.45) or on fluorescent (G_{254}) silica gel plates using 1:4 methanol–chloroform

for elution (R_f 0.3). The toxin rich zone was replated once for further enrichment.

An alternate procedure was devised to avoid the handling of the free base.

(*A2*) The syrup recovered from the ion-exchange resin (see *A1*) was triturated with benzene, which removed less polar non-toxic components. The insoluble part was dissolved in a minimum amount of ethanol, then chloroform added until precipitation stopped. The bulk of the toxin remained in the chloroform. After filtration, the filtrate was evaporated. The residue was resuspended in chloroform (¾% ethanol) and the solution filtered through sodium sulfate, then evaporated. The resulting gum was suspended in water containing a trace of hydrochloric acid, then filtered. The markedly enriched extract (LD_{min} = 25 mg/kg) recovered by evaporation of the filtrate on a rotating evaporator, was further enriched by preparative thin layer chromatography as described in *A1*.

(*B*) An 8 ℓ culture of algae was freeze-dried and ground (see above) leaving a free-flowing green powder (13.8 g, LD_{min} = 160 mg/kg, 3450 MU). This was shaken for 0.5 h with 200 ml of ¾% ethanol in chloroform. The suspension was filtered, then the extraction repeated twice. Evaporation of the reddish green chloroform solution in a bath at room temperature left a gum. This was taken up in 100 ml of methanol and the p*H* adjusted to 2 using 3 *N* hydrochloric acid in methanol. The suspension was filtered and the filtrate evaporated under reduced pressure. The residue was distributed between 150 ml of water and 50 ml of chloroform, then the chloroform washed with 150 ml of water. The combined aqueous layers were washed with 25 ml of chloroform. The aqueous solution was evaporated to dryness, then the bulk of the toxin extracted from the residue by two triturations with ¾% ethanol in chloroform giving 28 mg of chloroform-soluble material. This was again extracted with chloroform followed by filtration through sodium sulfate to give 22 mg (LD_{min} = 0.3 mg/kg) with λ_{max} at 225 nm (ε 6000) (2900 MU). Preparative tlc purification of this gave 13 mg containing 2600 MU (near 100% purity, recovery 70% of original toxic component). If the p*H* of the culture was not reduced to below 7 before the removal of the water, much loss of toxin resulted.

Properties of Anatoxin-a Hydrochloride

The purest material from preparative tlc had LD_{min} (intraperitoneal mouse assay) of 0.25 mg/kg; λ_{max} ($CHCl_3$) 2300–2800 (NH_2^+), 1670 (str), 1645 (wk), and 1588 (med) cm^{-1}; λ_{max} (95% ethanol) 227 nm, ε near 10 000. Its 60 MHz proton nmr spectrum in deuterium oxide had 1H signals at δ 7.1 (t, J = 6 Hz), 4.7 (d, J = 6 Hz) and 3.9 (br) relative to a 3H singlet arbitrarily set at δ 2.0 ($COCH_3$). The mass spectrum of the hydrochloride (direct inlet, 98°C) had peaks at *m/e* (relative intensity): 166(22), 165(100), 164(9), 151(6), 150(28), 137(22), 136(38), 123(10), 122(54), 108(12), 94(26), 93(7), 83(8), 82(31), 81(8), 69(31), 68(28), 67(10). Its ^{13}C nmr spectrum in D_2O had signals at 24.5, 25.9, 28.0, 28.5, 31.0, 53.9, 60.7, 143.9, 152.0, 207.5 ppm from TMS.

Anatoxin-a

The base was recovered by addition of ice-cold sodium hydroxide solution to a cold aqueous solution of the hydrochloride, followed by rapid extraction into pure ether. The resulting oil had ν_{max} (CH_2Cl_2) 1664 cm^{-1}. Its high resolution mass spectrum (direct inlet, −5°C) gave peaks at 165.1138 ($C_{10}H_{15}NO$), 150.0917 ($C_9H_{12}NO$), 136.0758 ($C_8H_{10}NO$), and 122.0601 (C_7H_8NO).

Dihydroanatoxin-a Hydrochloride

Anatoxin-*a* hydrochloride (10 mg) was added to 3 ml of acetic acid containing platinum from 10 mg of Adam's platinum oxide under a hydrogen atmosphere. After 1.5 h stirring at room temperature 1.0 mol equiv. of hydrogen had been absorbed. The catalyst was removed by filtration then the solvent removed *in vacuo*. The amorphous product had ν_{max} (CH_2Cl_2) 1717 cm^{-1}.

N-Benzoyl Anatoxin-a

Benzoyl chloride (300 mg) was added to a solution of 33 mg of anatoxin-*a* hydrochloride in 2 ml of pyridine at 0°C. The temperature was raised gradually to 50°C and maintained there for 4 h. After cooling, then the addition of 3 ml of water, the solution was stirred for 5 h. The product was extracted into methylene chloride, and the organic layers washed with 1 *N* sulfuric acid (3 × 4 ml), water (4 ml), and 5% sodium carbonate (2 × 4 ml). The dried methylene chloride solution yielded 25 mg of viscous oil, which was distilled over a short path at 120°C/1 × 10^{-5} torr. It had ν_{max} (methylene chloride) 1667 and 1625 cm^{-1}. Its high resolution mass spectrum[5] had peaks at 269.1411 ($C_{17}H_{19}NO_2$), 166.1237 ($C_{10}H_{16}NO$), and 164.1086 ($C_{10}H_{14}NO$).

N-Acetyl Anatoxin-a

To 0.5 ml of acetic anhydride containing 100 mg of anhydrous sodium acetate was added 18 mg of anatoxin-*a* hydrochloride. The mixture was maintained at 60°C for 3 h, then left overnight at room temperature. The bulk of the acetic anhydride was removed under reduced pressure. One millilitre of methanol was added. After 0.5 h the methanol was removed under reduced pressure then the residue taken up in 0.5 ml of water. The solution was made basic using solid sodium carbonate, then the product extracted into methylene chloride. The 22 mg of pale brown gum crystallized spontaneously. This was distilled over a short path at 85°C/5 × 10^{-4} torr giving a mixture of crystals and oil. A small amount of dry ether removed 3 mg of oil leaving 12 mg of colorless crystals. After two recrystallizations from acetone–hexane the *N*-acetyl derivative melted at 117–118°C and had $[\alpha]_D$ −127° (*c*, 4.8 in ethanol). It had ν_{max} ($CHCl_3$) 1664 (med) and 1624 (str) cm^{-1}, and λ_{max} 226 nm, ε 10 500. Its 60 MHz ^1H nmr spectrum had signals at δ 7.05 (1H, *t*, J = 6 Hz), 5.28 (1H, d, J = 8 Hz), 4.83 (1H, $W_{1/2}$ = 12 Hz), 2.35 (3H, s), and 1.98 (3H, s). Chemical shift assignments and coupling constants derived from its 220 MHz ^1H nmr spectrum with spin decoupling studies are displayed on formula **2**. Its mass spectrum (direct inlet) had peaks at *m/e* (relative intensity): 207(100), 165(89), 164(62), 150(56), 149(64). The accurate mass[5] of other important ions in the electron impact mass spectrum of *N*-acetyl anatoxin-*a* are given in Table 2.

Acknowledgements

The authors wish to express their gratitude for the expert technical assistance of Mr. D'Arcy Wright who carried out most of the mass culturing and toxicity assays. Dr. W. E. Sneader

worked on the development of the methods for large-scale lysis and ion-exchange chromatography. Messrs. A. Holland and P. Hurdle, and Dr. W. W. Carmichael deserve thanks for their help in the final stages of the investigation. We thank Mr. H. Seguin for microanalyses, Dr. W. G. Jamieson for the high resolution mass spectra, and Dr. I. C. P. Smith and associates for the ^{13}C nmr spectra.

1. P. R. GORHAM. *In* Algae and man. *Edited by* D. F. Jackson. Plenum Press, New York, NY. 1964. p. 307.
2. M. SCHWIMMER and D. SCHWIMMER. *In* Algae, man and the environment. *Edited by* D. F. Jackson. Plenum Press, New York, NY. 1968. p. 279.
3. J. G. GENTILE. *In* Microbiol toxins. Vol. 7. *Edited by* S. Kadis, A. Ciegler, and A. J. Ajl. Academic Press, New York, NY. 1971. p. 27.
4. M. SHILO. *In* Microbiol toxins. Vol. 7. *Edited by* S. Kadis, A. Ciegler, and S. J. Ajl. Academic Press, New York, NY. 1971. p. 67.
5. P. G. J. LOUW. S. Afr. Ind. Chem. **4**, 62 (1950).
6. H. KONST, P. D. MCKERCHER, P. R. GORHAM, A. ROBERTSON, and J. HOWELL. Can. J. Comp. Med. Vet. Sci. **29**, 221 (1965).
7. C. T. BISHOP, E. F. L. J. ANET, and P. R. GORHAM. Can. J. Biochem. Physiol. **37**, 453 (1959).
8. J. RAMA MURTHY and J. B. CAPINDALE. Can. J. Biochem. **48**, 508 (1970).
9. G. W. PRESCOTT. Hydrobiology, **1**, 1 (1948).
10. M. ALAM, M. IKAWA, J. J. SASNER, JR., and P. J. SAWYER. Toxicon, **11**, 65 (1973).
11. Y. HASHIMOTO, T. OKAISHI, L. D. DANG, and T. NOGUCHI. Bull. Jpn. Soc. Sci. Fish. **34**, 528 (1968).
12. P. R. GORHAM, J. MCLACHLAN, U. T. HAMMER, and W. K. KIM. Verh. Int. Verein. Limnol. **15**, 796 (1964).
13. W. W. CARMICHAEL and P. R. GORHAM. J. Phycol. **10**, 238 (1974).
14. B. STAVRIC and P. R. GORHAM. Proceedings, Can. Soc. Plant Physiol. Annual Meeting, University of British Columbia, Abstracts. 1966. p. 20.
15. C. S. HUBER. Acta Crystallogr. Ser. B, **78**, 2577 (1972).
16. H. F. CAMPBELL, O. E. EDWARDS, and R. KOLT. Can. J. Chem. This issue.
17. W. W. CARMICHAEL, D. F. BIGGS, and P. R. GORHAM. Science, **187**, 542 (1975).
18. P. R. GORHAM. Can. Vet. J. **1**, 235 (1960).
19. W. W. CARMICHAEL. *Anabaena flos-aquae* toxin: its toxicology and mechanism of action. Ph.D. dissertation, University of Alberta, Edmonton, Alta. 1974.

Synthesis of nor-anatoxin-*a* and anatoxin-*a*[1]

HENRY F. CAMPBELL,[2] OLIVER E. EDWARDS, AND RALPH KOLT

Division of Biological Sciences, National Research Council of Canada, Ottawa, Ont., Canada K1A 0R6

Received September 9, 1976

HENRY F. CAMPBELL, OLIVER E. EDWARDS, and RALPH KOLT. Can. J. Chem. **55**, 1372 (1977).

The neuro-muscular post-synaptic depolarizing agent anatoxin-*a* from *Anabaena flos-aquae* (Lyngb.) de Bréb. has been synthesized from cocaine.

HENRY F. CAMPBELL, OLIVER E. EDWARDS et RALPH KOLT. Can. J. Chem. **55**, 1372 (1977).

On a synthétisé, à partir de la cocaine, l'agent dépolarisant post-synaptique neuro-musculaire, anatoxine-*a*, obtenu à partir de l'*Anabaena flos-aquae* (Lyngb.) de Bréb.

[Traduit par le journal]

Some strains of the fresh-water blue-green algae *Anabaena flos-aquae* (Lyngb.) de Bréb. produce a toxin which has been named anatoxin-*a*. This proved to be a homotropane derivative **1** (1, 2). Anatoxin is of considerable pharmacological interest because of its activity as a post-synaptic depolarizing agent (3). We now report a synthesis of optically active anatoxin-*a* from cocaine (**2**). Since the absolute configuration of the toxin had been determined by X-ray analysis (2), the synthesis confirms the absolute stereochemistry which had been assigned to cocaine (4).

Cocaine was converted by known procedures (5) into the α,β-unsaturated acid **3**. Reaction of the lithium salt of **3** with methyllithium (6) produced the methyl ketone **4** in 76% yield. When this ketone was treated with sodium dimethyloxosulfonium methylide in dimethyl sulfoxide (7) it gave a 65% yield of the *endo* cyclopropane derivative **5** and 35% of the *exo* isomer **6**. Occasionally small amounts of a product with properties corresponding to those expected for the epoxide **7** were produced.

The structures of the two cyclopropanes were assigned on the basis of the ^{1}H nmr shifts shown on the figures. The greater proximity of the acetyl group to the *N*-methyl group and one bridgehead hydrogen, resulting in downfield shifts, identifies the *endo* isomer. The course of the photolysis of the two isomers (see below) made the assignments certain.

Attempts to remove the *N*-methyl group of **5** using 2,2,2-trichloroethyl chloroformate or phosgene led to complications apparently due to attack on the cyclopropane ring. The *exo* isomer **6** proved inert to 2,2,2-trichloroethyl chloroformate at room temperature. Hence the demethylation was deferred to a later stage.

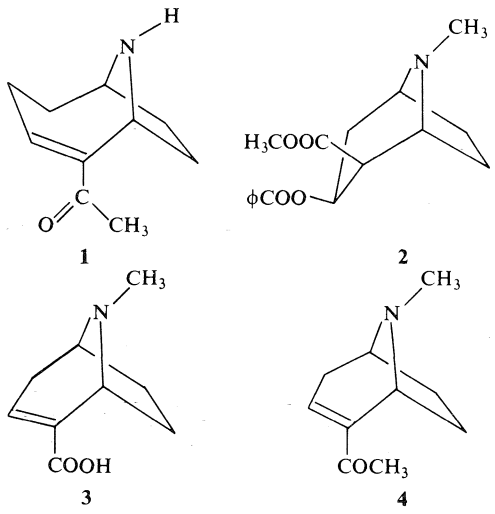

Two methods were successful in opening of the cyclopropane ring of **5**, reductive fission using lithium in liquid ammonia or photolytic cleavage. There was reason to expect that the reductive opening of **5** would result in the ring expanded product (see Discussion). Indeed, the action of lithium in ammonia did convert **5** into the enolate anions of the saturated ketone **8**. These were directly converted by acetic anhydride into mixtures of the two enol acetates **9** and **10**. Alternatively, the ketone **8** was isolated, then converted into the enol acetates by acetic anhydride in the presence of hydrogen bromide. Addition of bromine to the enol acetates, followed by aqueous work-up gave the bromo ketone **11**. Elimination of hydrogen bromide

[1]Issued as NRCC No. 15802.

[2]NRCC Postdoctoral Fellow. Present address: William H. Rorer Inc., 500 Virginia Drive, Fort Washington, PA, U.S.A.

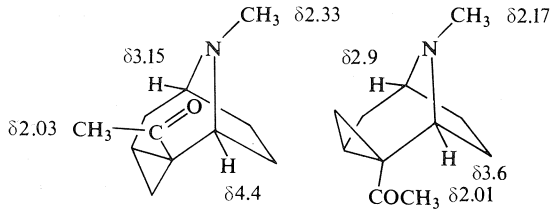

5 6

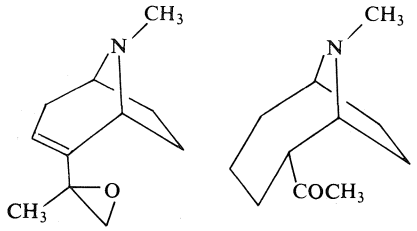

7 8

from **11** was achieved by the action of lithium bromide and lithium carbonate in dimethyl formamide, giving *N*-methyl anatoxin-*a* (**12**).

In contrast to the behavior of the *endo* isomer, the action of lithium in ammonia on the *exo* isomer **6** only resulted in reduction of the carbonyl group.

There was literature precedent for the photolytic opening of cyclopropyl ketones to the α,β-unsaturated ketone[3] (8–10). When an aqueous solution of the hydrochloride of the *endo* isomer **5** was irradiated using light with maximum intensity at 300 nm, a 75% yield of the ring expanded *N*-methyl anatoxin-*a* (**12**) resulted.

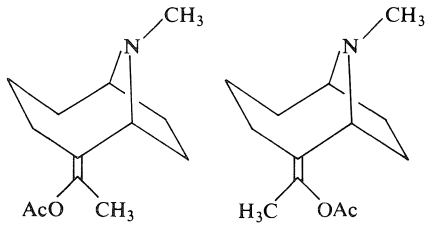

9 10

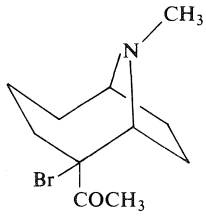

11

[3]We are grateful to Dr. P. W. Jeffs for drawing our attention to this possibility.

The *exo* isomer **6** photolyzed much more slowly than **5** under comparable conditions, and the reaction took a different course (see below).

De-*N*-methylation of *N*-methyl anatoxin using 2,2,2-trichloroethoxycarbonyl chloride (11) proved to be erratic, and the zinc deblocking of the nitrogen was not clean, so this method was not pursued further.

De-*N*-methylation using phosgene has been reported (13). Preliminary experiments with the methyl ketone **4** (*N*-methyl nor-anatoxin-*a*) showed that phosgene in benzene at room temperature gave extensive demethylation in 0.5 h. The major product, nor-anatoxin-*a* (14) was characterized as its hydrochloride after work-up. However, comparable treatment of *N*-methyl anatoxin-*a* gave messy mixtures of products which have not been characterized.

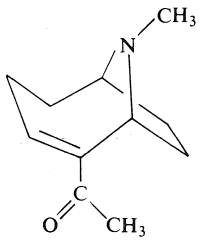

12

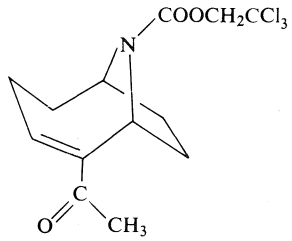

13

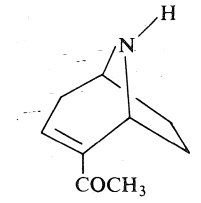

14

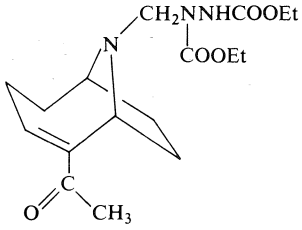

15

The successful preparation of anatoxin-*a* resulted from the action of diethyl azodicarboxylate (diethyl azodiformate) on the *N*-methyl derivative (14). A benzene solution of **12** and the azo compound was refluxed for 2.5 h, the intermediate (presumably **15**) was hydrolyzed by hydrogen chloride in aqueous ethanol and the products separated by preparative tlc. A 30% yield of anatoxin-*a* hydrochloride was obtained. Its infrared, ultraviolet, and nmr spectra and its toxicity[4] coincided with those of natural anatoxin-*a* hydrochloride. The base was converted to its crystalline *N*-acetyl derivative, which had a melting

[4]Personal communication from Professor P. R. Gorham.

point, spectra, and rotation identical to those of the *N*-acetyl derivative of natural anatoxin-*a* (1).

The photolysis of the *exo*-cyclopropylketone **6** gave no significant amount of enone. Instead two alcohols isomeric with the parent ketone were produced. The ^{1}H and ^{13}C nmr spectra gave convincing evidence that the structures of these were the epimeric alcohols **16** and **17**.

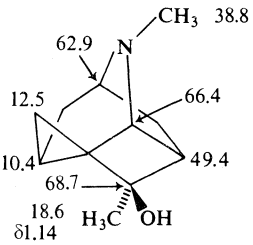

16

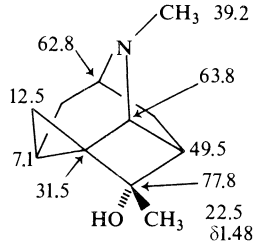

17

Discussion

In reaction **1** we outline the possible routes for lithium–ammonia reduction of a cyclopropyl ketone. An equilibrium has been written for path (*c*) since this would only approach delocalization (resonance) if the geometry was ideal for overlap. Path *a* is written as irreversible since the charge repulsion would make the charge-separated ring-opened structure of considerably lower energy.

The accumulated evidence (15, 16) seems only consistent with rapid reduction to the dianion (path *a*). If the geometry is ideal for overlap of the unshared pair on carbon with one bond of the cyclopropane ring, the ring opening may be synchronous with the addition of the second electron.

We are surprised that the reversible process *c* is not more important. Indeed for a number of cases, including that of the *endo* isomer **5**, one could argue that it is the more stable ring-open radical anion which is being preferentially formed. However the observation of Dauben and Wolff (16) that *trans* 1-acetyl-2-methylcyclopropane gave 94% of *tert*-butyl acetone is incompatible with this possibility.

The simple reduction of the carbonyl in the case of the *exo* isomer **6** appears to result from poor overlap of the carbanion with the bonds of the cyclopropane ring. It is hence protonated on the carbonyl carbon as in path *b*.

The generally accepted picture of the photoreaction of conjugated cyclopropyl ketones involves excitation to an n–π* singlet followed by transformation into a triplet diradical [2] (17). The question of which of the two possible cyclopropane bonds is cleaved depends on their ability to overlap with the π orbitals of the carbonyl, and the sensing in the transition state of the relative stability of the two possible diradicals (18, 19). Our observations can be explained using these factors and a third, the proximity to the oxygen of an abstractable hydrogen.

The overlap in the favored rotamer **18** and the higher stability of the secondary rather than primary radical combine to cause predominant formation of the ring-expanded product **12** from the *endo* isomer **5**. The formation of an α,β

[1]

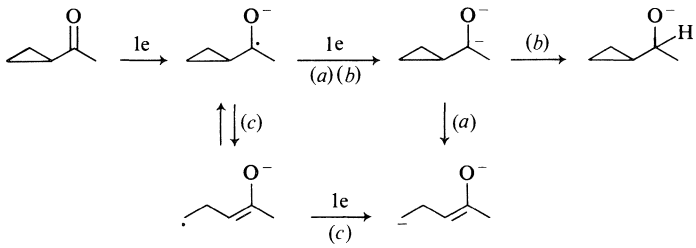

[2]

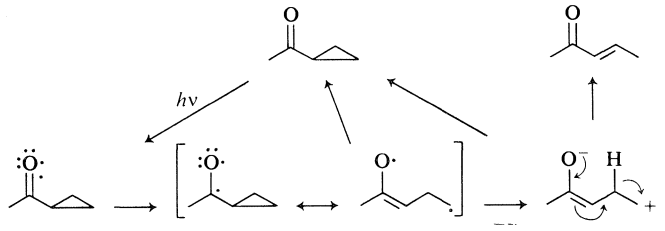

unsaturated ketone from a diradical is most attractively explained [2] by a 1,3-electron jump to give the zwitterion **19**. The zwitterion **19** derived from **18** then undergoes a 1,2-hydride shift to give the observed product. The postulated 1,3-electron jump corresponds to the 'electron

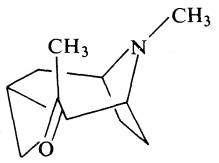

18

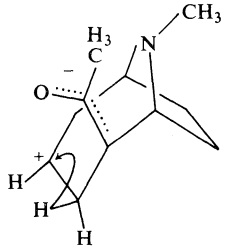

19

demotion' concept of Zimmerman and co-workers (12). Winter and Lindauer have produced evidence that the conjugated enones are formed by 1,2 hydrogen shifts (9).

The fate of the *exo* isomer **6** seems to be the resultant of the fact that the most favorable rotamers **20** and **21** would lead to a higher-energy primary radical on ring fission, and that the *endo* hydrogen on C-8 can be brought into

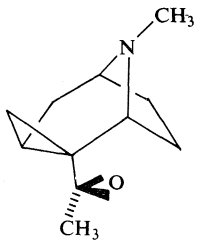

20

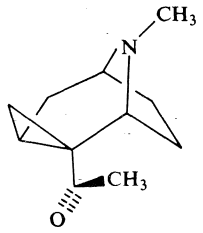

21

close proximity to the carbonyl oxygen. Consequently hydrogen abstraction followed by cyclization was the dominant reaction [3]. This striking difference in photochemical behavior is so clearly associated with the different geometry of the two isomers, that no ambiguity is left as to which is which.

[3] 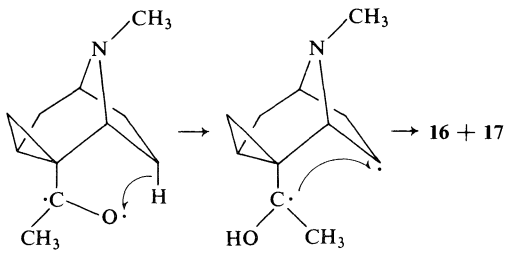 → **16** + **17**

Experimental

Infrared spectra were of chloroform solutions, ultraviolet spectra of solutions in 95% ethanol, and unless otherwise stated ^{1}H nmr and ^{13}C nmr spectra were of deuterochloroform solutions with TMS as internal reference. Thin layer and preparative layer chromatography were done using silica gel containing a fluorescent indicator (G_{254}). Gas–liquid chromatography (glc) was on 6 ft × $\frac{1}{4}$ in. column of 10% silicone rubber on silanized Chromosorb W (SE30).

*Anhydroecgonine (**3**)*

This was prepared by hydrolysis of cocaine (**2**) in refluxing concentrated hydrochloric acid (5). It was converted to its methyl ester using dry methanol saturated with anhydrous hydrogen chloride at 0°C. This distilled at 55°C/0.5 torr, and had ν_{max} 1710 and 1640 cm^{-1}, λ_{max} 218 nm (ε 10 850), $[\alpha]_D$ −43° (*c* 1.5, methanol), and gave ^{1}H nmr signals at δ 2.38 (s, 3H), 3.75 (s, 3H), and 6.85 (1H).

Lithium Salt of Anhydroecgonine

To a solution of 3.62 g (20 mmol) of redistilled methyl ester of anhydroecgonine in 10 ml of 5% water in methanol was added 880 mg of lithium hydroxide monohydrate (20.1 mmol). After 2 h refluxing the solvent was removed and the solid dried *in vacuo*. After two triturations with ether it was redried at 80°C/0.1 torr for 4 h giving 3.46 g (100%).

Alternatively, an aqueous solution of the hydrochloride of anhydroecgonine was treated with 2 mol equiv. of lithium hydroxide, the water removed under reduced pressure, and the mixture of salts dried at 100°C under 0.1 torr pressure.

*Methyl Ketone **4***

To a stirred suspension of 2.9 g (16.8 mmol) of the lithium salt of anhydroecgonine in 50 ml of pure dry 1,2-dimethoxyethane under nitrogen at 5°C was added 13.5 ml of methyllithium solution (1.8 *M* in ether). The mixture was stirred for 5 h at room temperature then taken to near dryness under reduced pressure. The products were distributed between ice-cold 2 *N* hydrochloric acid and ether. The aqueous layers were made basic and the product extracted into methylene chloride, giving 2.1 g of nearly pure methyl ketone (79%).

This was converted to its hydrochloride, which after recrystallization from ethanol – ethyl acetate mixture had mp 161–163°C and $[\alpha]_D$ −70°C (*c* 1, methanol). It had λ_{max} 224 nm (ε 12 000). *Anal.* calcd. for $C_{10}H_{16}ClNO$: C 59.54, H 8.00, N 6.95, Cl 17.58; found: C 59.36, H 8.08, N 7.01, Cl 17.34. The free base recovered from the hydrochloride had ν_{max} ($CHCl_3$) 1665 and 1630 cm^{-1} and ^{1}H nmr signals at δ 2.32 (3H), 2.38 (3H), 3.35 (m, 1H), 4.0 (br d, 1H), 6.93 (t, 1H).

Cyclopropyl Ketone Formation

A mineral oil dispersion of sodium hydride (1.01 g, 50%, 21 mmol) was washed three times with pentane. To this was added 4.62 g of trimethyloxosulfonium iodide (21 mmol) then the flask flushed thoroughly with nitrogen. Dry dimethyl sulfoxide (25 ml) was added slowly through a septum using a syringe, while the mixture was stirred magnetically. After 20 min stirring at room temperature,

vigorous hydrogen evolution had ceased. A solution of 3.30 g (20 mmol) of the α,β-unsaturated ketone **4** in 5 ml of dioxane was added through the septum. The reaction mixture was stirred under nitrogen for 2 h at room temperature then 1 h at 50°C. It was poured into 80 ml of cold water then extracted five times with ether. The oil remaining after removal of the ether was distilled. The main fraction, collected between 55 and 80°C under 0.05 torr weighed 2.82 g. Gas–liquid chromatography on SE-30 at 170°C showed this to consist of starting material (9% recovery) and a mixture of the *endo* cyclopropyl ketone **5** (43% yield) and the *exo* isomer **6** (27% yield).

The mixture of products could be partially separated by chromatography on a 65-fold ratio of tlc silica gel using a 10:1 mixture of chloroform and methanol. The order of elution was *exo* isomer, starting material, then *endo* isomer. A slightly better resolution was achieved using a 35-fold ratio of neutral alumina (activity II) and pentane–ether mixtures for elution. The same elution order was observed. In one run a sizeable by-product was observed. It was isolated by chromatography of the base hydrochlorides on silica gel using 3:1 methanol – acetic acid for elution. It was tentatively assigned the epoxide structure **7**.

Epoxide 7

The free base had no carbonyl absorption in its infrared spectrum. Its ^{1}H nmr spectrum had peaks at δ 1.31 (3H), 2.35 (3H), and 5.55 (1H, t, J = 4 Hz).

Endo Cyclopropyl Ketone 5

This was distilled over a short path at 80°C/0.1 torr. It had ν_{max} 1680 cm^{-1} and gave ^{1}H nmr signals at δ 2.03 (s, 3H) and 2.33 (s, 3H) and broad 1H signals at δ 3.15 and 4.4. Its hydrochloride after recrystallization from methanol – ethyl acetate had mp 188–193°C, $[\alpha]_D$ +99° (*c* 1, methanol) and λ_{max} 271 nm (ε 20 with ε_{210} 710). It gave ^{1}H nmr signals (in D_2O, HOD set at δ 4.70) at 2.0 and 2.7 (3H, s's) and 3.8 and 5.0 (1H, m's).

Exo Cyclopropyl Ketone 6

The early eluates from the chromatograms were nearly pure *exo* isomer. This was distilled over a short path at 80°C/1 torr pressure. It had ν_{max} 1680 cm^{-1} and gave ^{1}H nmr signals at δ 2.01 (s, 3H), 2.17 (s, 3H) and broad 1H signals at 2.9 and 3.6.

It gave a hydrochloride which after recrystallization from methanol – ethyl acetate had mp 192–194°C, $[\alpha]_D^{20}$ −76° (*c* 1, methanol) and λ_{max} 275 nm (ε 25, with ε_{210} 1220). It gave ^{1}H nmr signals (in D_2O, HOD set at δ 4.70) at 2.01 and 2.75 (3H, s's) and 3.8 and 4.4 (1H, m's). *Anal.* calcd. for $C_{11}H_{18}ClNO$: C 61.25, H 8.41, N 6.50; found: C 61.38, H 8.38, N 6.30.

Reactions of the Endo Isomer 5

Lithium–Ammonia Reduction

Approximately 500 ml of liquid ammonia, distilled from sodium, was collected in a double-walled 2 ℓ flask under a dry ice condensor. The flask was flushed with dry nitrogen, then 4.16 g (60 mmol) of clean lithium metal was added. The mixture was stirred briefly, then a solution of 6.0 g of the *endo* isomer in 150 ml of ether was added slowly with stirring. The mixture was stirred for 3 h, then 67 g of ammonium chloride added. The ammonia was evaporated overnight in a slow stream of nitrogen. The residue was taken up in 900 ml of ether and 900 ml of saturated aqueous sodium chloride solution. The aqueous phase was extracted four times with ether. The dried ether layers gave 5.6 g of crude product (93%). This was placed on top of a column of 500 g of tlc silica gel, then eluted with a 10:1 benzene–diethylamine mixture. The composition of the fractions was monitored using glc (SE-30 at 170°C). After somewhat impure fractions (439 mg) the main product (3.5 g, 58%) was eluted, followed by fractions contaminated with alcohols.

De-N-methylation of Endo Cyclopropyl Ketone 5

A solution of 99 mg of *endo* cyclopropyl ketone **5** and 125 mg of diethylazodicarboxylate (DAD) in 7.5 ml of dry benzene was refluxed for 11 h. At this point only a small amount of starting material remained (tlc in 4:1 benzene–methanol). An extra 30 mg of DAD was added, the solution refluxed for 15 min, then left at room temperature for 10 h. The benzene was removed *in vacuo*, then a solution of the residue in a mixture of 2.5 ml of 2 *N* hydrochloric acid and 2.5 ml of 95% ethanol refluxed for 2.5 h. The resulting solution was taken to a syrup on a rotating evaporator *in vacuo*. The residue was chromatographed on two 20 × 20 cm 500 μm plates using methanol for development. A zone with R_f 0.2–0.5 was extracted with hot 3:2 methanol – acetic acid mixture. Removal of the solvent gave 62 mg of the hydrochloride of the desired de-*N*-methylated base. It had a sharp ^{1}H nmr signal at δ 1.90 relative to the HOD signal (set at δ 4.7).

The corresponding base had ν_{max} 1675 cm^{-1} and gave ^{1}H nmr signals at 2.10 (3H, s) and 0.85, 3.5, and 4.7 (1H, m's).

Ring Expanded Ketone 8

The major product from the lithium–ammonia reduction had ν_{max} 1705 cm^{-1} and gave ^{1}H nmr signals at δ 2.09 and 2.12 (s's, ratio 1:2), 2.38 and 2.48 (s's, ratio 1:2) corresponding to two epimeric ketones. The bases were converted to hydrochlorides using hydrogen chloride in methanol. The major component gave a salt with mp 152–155°C, $[\alpha]_D$ −11° (*c* 1, methanol). The salt gave ^{1}H nmr signals in heavy water with δ 2.22 (s, 3H) and 2.91 (s, 3H) relative to DSS.

Enol Acetates 9 and 10

(*a*) The lithium in ammonia reduction of the *endo* cyclopropyl ketone **5** (895 mg, 5.0 mmol) was conducted as described above, but the ammonium chloride addition was done carefully until the blue color was just destroyed. The ammonia was then evaporated over 4.5 h in a stream of dry nitrogen. The residue was suspended in 50 ml of pure 1,2-dimethoxyethane, the solution cooled in an ice bath, then added to 5 ml of acetic anhydride. The mixture was stirred for 3 h at room temperature, then poured into a cold mixture of saturated sodium bicarbonate solution and ether. This mixture was stirred for 0.5 h. The ether layer was separated and the aqueous layer extracted twice with fresh ether. The dried ether layers yielded 1.0 g of yellow liquid.

Gas–liquid chromatography (SE-30, 175°C) showed the absence of cyclopropyl ketone and the presence of only a few percent of ring-expanded ketone. Two enol acetates were present in the ratio of 1:3 (identities unknown). A sample distilled over a short path at 100–125°C/0.02 torr had ν_{max} 1740, 1670 cm^{-1}. The bulk of residual acetic anhydride was removed under 0.05 torr during 6 h. The resulting oil gave ^{1}H nmr singlets at δ 2.51 (N—CH_3),

2.13 (CH_3COO), and 2.00 (CH_3—C═C). Signals at δ 2.18 and 1.90 appear to arise from the minor isomer.

(*b*) Ketone **8** hydrochloride (365 mg) was dissolved in 10 ml of acetic anhydride. Hydrogen bromide was bubbled through the solution for 1 min (*ca.* 1 bubble/s). The solution was then heated at 80°C for 24 h. It was evaporated under reduced pressure giving 487 mg of the desired enol acetates as hydrobromides. The mixture had ν_{max} 1755 and 1670 cm^{-1} and gave ^1H nmr signals at δ 1.91 (vinyl methyl), 2.22 (acetate), and a pair of doublets (J = 5 Hz) centered at δ 2.25 and δ 3.0 attributable to the N-CH_3 in the isomers.

*Bromo Ketone **11***

A 0.174 *M* solution of bromine in chloroform was prepared. Ten millilitres of this at 0°C was added to 461 mg of the enol acetate hydrobromides (**9** + **10**) during the course of 15 min. After 2 h at room temperature the ^1H nmr spectrum showed complete bromination. Water was added and the mixture stirred for 1 h, then the solvents evaporated under reduced pressure. The 569 mg of crude bromo ketone hydrobromide was a mixture of two isomers as shown by ^1H nmr signals at δ 1.68 and 1.74 and at δ 2.15 and 2.22 (relative to HOD set at 4.70). One component (the isomer giving the lower-field N-CH_3 and CH_3CO signals) crystallized from acetone giving 224 mg (49%), mp 138–141°C. It gave ^1H nmr signals at δ 2.57 (3H), 2.97 (3H), 5.0 (br s, 1H) and 5.5 (br s, 1H). *Anal.* calcd. for $C_{11}H_{19}Br_3NO$: C 38.74, H 5.61, N 4.11, Br 46.85; found: C 38.59, H 5.72, N 4.19, Br 46.69.

*Dehydrobromination of **11** (N-Methyl Anatoxin-a)*

Bromo ketone hydrobromide (569 mg, 1.67 mmol) and 610 mg (7 mmol) of dry lithium bromide was dried briefly at 100°C/1 × 10^{-2} torr, then 16 ml of dry dimethyl formamide added. The mixture was heated at 60°C for 17 h, and at 130°C for 1 h. The bulk of the dimethyl formamide was removed at 70°C/0.5 torr pressure. The residue was dissolved in 5 ml of water, made basic with solid sodium carbonate, then strongly alkaline with ice-cold 40% sodium hydroxide solution. The product was quickly extracted into ether (4–10 ml portions). After drying and distillation of the ether, the product was converted to its hydrobromide in methanol. This was purified on four 1000 μm plates using 2:1 chloroform–methanol. The most visible band under uv light was collected. This gave 173 mg rich in α,β unsaturated ketone (**12**). This had ν_{max} 1670 cm^{-1} and gave ^1H nmr signals (D_2O) at δ 2.35 (s, 3H), 2.75 (s, 3H), and 7.50 (t, J = 7 Hz, 1H). Repeated purification attempts using silica gel plates failed to remove saturated ketone (ν_{max} 1705 cm^{-1}) and other impurities completely.

*Photolysis of Endo Hydrochloride **5** (N-Methyl Anatoxin-a)*

The *endo* cyclopropyl ketone **5** (105 mg) was converted to its hydrochloride. This was dissolved in 10 ml of water and irradiated in a Vycor flask at 20°C using a Rayonet apparatus with lamps giving peak emission at 300 nm. Reaction was complete in 24 h. The water was removed *in vacuo*, then the product purified using two 20 cm^2, 1 mm thick plates using 4:1 chloroform–methanol as eluate under argon. The broad uv active zone with R_f 0.2 yielded 48 mg (46%) rich in *N*-methyl anatoxin-*a*. This was dissolved in 10:1 chloroform–methanol, filtered, then evaporated and dried *in vacuo*. The glassy solid had $[\alpha]_D$ +42° (*c* 1, methanol); ν_{max} 1670 cm^{-1}; λ_{max} 228 nm (ε 6200); ^1H nmr signals at 2.38 (s, 3H), 2.60 (s, 3H), 3.9 (m, 1H), 4.9 (br d, 1H), and 7.3 (t, J = 6 Hz, 1H).

*De-N-methylation of **12** (Anatoxin-a)*

N-Methyl anatoxin-*a* (**12**) hydrochloride (155 mg) was dissolved in 5 ml of water, the solution made strongly alkaline with cold sodium hydroxide solution, then the base extracted rapidly into methylene chloride. After drying and removal of the solvent, the base was dissolved in 10 ml of dry benzene. After addition of 190 mg of diethylazodicarboxylate the solution was refluxed for 2.5 h. The benzene was removed under reduced pressure and the residue taken up in a mixture of 4 ml of 95% ethanol and 4 ml of 2 *N* hydrochloric acid. This was refluxed for 3 h, then evaporated to dryness on a rotating evaporator. The products were separated on three 20 cm × 20 cm plates (thickness 1 mm) using 4:1 chloroform–methanol under argon. The desired product had R_f approximately 0.2. This zone (65 mg) was replated on one 20 cm × 20 cm × 1 mm plate under the same conditions giving 42 mg (29%) of quite pure anatoxin-*a* hydrochloride (**1**). This had $[\alpha]_D$ +36° (*c* 0.85, ethanol); λ_{max} 226 nm (ε 8500); ν_{max} 1670, 1642, and 1588 cm^{-1}. Its ^1H nmr spectrum had signals at δ 2.40 (s, 3H), 4.4 (m, 1H), 5.3 (m, 1H), 7.3 (t, J = 5 Hz, 1H), and a broad 2H signal between δ 8.3 and 9.0 (2H). These spectra corresponded well to those of natural anatoxin-*a* (**1**).

*N-Acetyl Derivative of **1** (N-Acetyl Anatoxin-a)*

The above hydrochloride (42 mg) was dissolved in 1 ml of acetic anhydride containing 200 mg of sodium acetate. This was heated 1 h at 60°C then left for 60 h at room temperature. The excess anhydride was removed under reduced pressure, the residue warmed with methanol, and the evaporation repeated. The residue was distributed between 5% sodium carbonate and methylene chloride. The organic phase gave 35 mg of product. This crystallized in part from acetone–hexane. The crystals were sublimed over a short path at 95°C/1 × 10^{-4} torr. The crystalline sublimate was washed once with ether, leaving 10 mg of crystals. These were recrystallized once from acetone–hexane. The *N*-acetyl derivative had mp 113–114°C, $[\alpha]_D$ −125 (*c* 0.6, ethanol), ν_{max} 1622 and 1663 cm^{-1} and λ_{max} 226 nm (ε 10 800). Its ^1H nmr spectrum had signals at δ 2.0 (s, 3H), 2.37 (s, 3H), 4.81 (br m, 1H), 5.29 (d, J = 8 Hz, 1H), and 7.02 (t, J = 6 Hz, 1H). Its spectra were identical to those of *N*-acetyl anatoxin-*a* (**1**) and a mixture mp showed no depression. *Anal.* calcd. for $C_{12}H_{17}O_2N$: C 69.54, H 8.27, N 6.75; found: C 69.71, H 8.39, N 6.58.

*Nor-anatoxin-a (**14**)*

(*a*) The *N*-methyl ketone **4** (98 mg, 9.59 mmol) in 1 ml of dry benzene and 0.2 ml of a benzene solution of phosgene (1 mmol) were mixed in an nmr tube in an ice bath, a small precipitate formed. After 30 min at 20°C the *N*-methyl signal had disappeared and a new methyl signal at lower field had appeared (CH_3Cl). After a further 30 min at 20°C the solvent was removed under reduced pressure. The residue was dissolved in water, and the solution left overnight at room temperature. After removal of the water, the product was sublimed at 100°C/1 × 10^{-4} torr. The partially crystalline sublimate was recrystallized from methanol – ethyl acetate mixture giving 15 mg, mp 232–235°C and 40 mg of less pure product.

The crystals had $[\alpha]_D$ −80° (*c* 1.62, methanol) and λ_{max} 225 nm (ε 10 600). Their ^1H nmr spectrum in D_2O had a 3H singlet 2.3 ppm upfield from the HOD signal (approximately δ 4.70) and a 1H triplet 2.45 ppm downfield from this reference signal. *Anal.* calcd. for $C_9H_{14}ClNO$: C 57.60, H 7.52, N 7.46; found: C 57.42, H 7.50, N 7.92.

The ^1H nmr spectrum of the free base **14** had signals at δ 2.27 (3H, s), 3.70 (1H, m), 4.27 (1H, m), and 6.68 (1H, t, J = 4 Hz).

(*b*) A solution of 207 mg of the *N*-methyl ketone **4** and 366 mg of diethylazodicarboxylate in 10 ml of dry benzene was refluxed for 18 h. After removal of the benzene *in vacuo* the residue was dissolved in a mixture of 6 ml of 2 *N* hydrochloric acid and 6 ml of 95% ethanol. The solution was refluxed for 4.5 h, then concentrated *in vacuo*, dilute sodium hydroxide added, and the base extracted into benzene. It was quickly reconverted to the hydrochloride. Only part was soluble in water, hence the solution was filtered. The filtrate was taken to dryness *in vacuo* then the residue crystallized from methanol – ethyl acetate giving 81 mg of nor-anatoxin-*a* hydrochloride mp 229–231°C. It proved identical to the product from (*a*).

Reactions of Exo Cyclopropyl Ketone ***6***

Photolysis of Exo Cyclopropyl Ketone ***6***

A solution of 373 mg of the hydrochloride of **6** in 12 ml of methanol was irradiated in a Vycor flask with lamps peaked at 300 nm in a Rayonet apparatus for 28 h. At the end of this time tlc showed absence of starting material and the presence of two more polar compounds as major products. The solvent was removed under reduced pressure, aqueous sodium hydroxide added, and the base extracted into methylene chloride. It was purified using six 0.5 mm × 20 cm × 20 cm plates with chloroform, acetone, methanol, and diethylamine (15:10:5:1) as developing solvent. The two major products had R_f 0.7 (84 mg) and 0.5 (114 mg). On some silica gel plates (more acidic?) the fast moving product appeared to be destroyed giving a more polar unsaturated alcohol which has not been fully characterized. Photolysis in water gave essentially the same products as above.

Tetracyclic Alcohol ***17***

The compound with high R_f was sublimed at 100°C 0.1 torr; mp 131°C $[\alpha]_D$ −54° (*c* 1.71, methanol), ν_{max} 3595 cm^{-1}. Its ^1H nmr spectrum had signals at δ 3.27 (d, J = 4 Hz, H_A), 3.17 (br m, $W_{1/2}$ 12 Hz, H_B), 2.87 (br m, $W_{1/2}$ 16 Hz, H_C), 2.28 (1H, s, OH), 2.10 (s, NCH_3), 1.50 (s, 3H), and signals for 2.7 hydrogens between δ 0.5 and 1.1. Tentative ^{13}C nmr chemical shift assignments based in part on multiplicities determined using off-resonance decoupling are indicated on the structure **17**. *Anal.* calcd. for $C_{11}H_{19}NO$: C 73.70, H 9.56, N 7.81; found: C 73.58, H 9.70, N 7.69. Yield 22%.

Tetracyclic Alcohol ***16***

The compound with lower R_f from the photolysis of **6** was distilled over a short path at 100°C/0.1 torr. The distillate crystallized in part. It had $[\alpha]_D$ −43° (*c* 0.97 methanol) and ν_{max} 3595 cm^{-1}. Its ^1H nmr spectrum had signals at 3.94 (d, J = 4 Hz, H_A), 3.1 (br m, $W_{1/2}$ = 14 Hz, H_B), 2.8 (br m, $W_{1/2}$ = 17 Hz, H_C), 2.46 (s, OH), 2.10 (s, N—CH_3), 1.13 (s, CH_3) and signals for 3.3H between δ 0.3 and 1.05. Tentative assignments of its ^{13}C nmr spectrum based on multiplicities from an off-resonance decoupled spectrum are indicated on the structure **16**. *Anal.* calcd. for $C_{11}H_{19}NO$: C 73.70, H 9.56, N 7.81; found: C 73.56, H 9.76, N 7.66. Yield 31%.

Lithium in Ammonia on Exo-cyclopropyl Ketone ***6***

A solution of 1.2 g of lithium in 250 ml of liquid ammonia (distilled over sodium) was prepared in a double-walled flask. To this was slowly added 1.57 g of the *exo* isomer **6** (>90% purity) in 50 ml of ether. The mixture was stirred for 3.5 h after completion of the addition, then 20 g of ammonium chloride added cautiously. After disappearance of the blue color the ammonia was evaporated in a stream of nitrogen. Water (100 ml) was cautiously added to the residue. This was saturated with sodium chloride, then extracted with five 100 ml portions of ether. The ether layers yielded 1.2 g (76%) of product consisting mainly of alcohols (ν_{max} 3600 cm^{-1}) but containing some unchanged cyclopropyl ketones (ν_{max} 1680 cm^{-1}). Its ^1H nmr spectrum had signals at δ 1.02 (d, J = 6 Hz) and 1.2 (d, J = 6 Hz) of almost equal intensity, total 3H; 2.14 (s, 3H) and a 6-line multiplet (probably a pair of partially superimposed quartets) at δ 3.9. There were signals for approximately two hydrogens between δ 0.25 and 1.0 (cyclopropane hydrogens).

The structure of these alcohols as simple products of reduction of the carbonyl was confirmed by oxidation. A solution of 113 mg of the alcohol mixture and 53 mg of chromium trioxide in 2 ml of acetic acid and 0.2 ml of water was heated at 45°C for 15 min, then stirred for 1 h at room temperature. The excess reagent was destroyed with methanol then the bulk of the solvents removed under reduced pressure. The residue was made strongly basic with 15% sodium hydroxide solution, then extracted with ether. The 78 mg of product had M^+ 179, and ^1H nmr and ir spectra nearly identical to those of *exo*-cyclopropyl ketone **6**.

Sodium in ethanol reduction of the *exo*-cyclopropyl ketone also gave a 1:1 mixture of the two alcohols.

Acknowledgements

We thank Mr. H. Séguin for microanalyses and mass spectra, and Dr. I. C. P. Smith and associates for ^{13}C nmr spectra. We are grateful to Dr. N. R. Hunter for preliminary work on the degradation of cocaine.

1. J. P. Devlin, O. E. Edwards, P. R. Gorham, N. R. Hunter, and B. Stavric. Can. J. Chem. This issue.
2. C. S. Huber. Acta Crystallogr. Sect. B, **28**, 2577 (1972).
3. W. W. Carmichael, D. F. Biggs, and P. R. Gorham. Science, **187**, 542 (1975).
4. E. Hardegger and H. Ott. Helv. Chim. Acta, **38**, 312 (1955).
5. C. L. Zirkle, T. A. Geissman, M. Bloom, P. N. Craig, F. R. Gerns, Z. K. Indik, and A. M. Pavloff. J. Org. Chem. **27**, 1269 (1962).
6. C. H. DePuy, G. M. Dappen, K. L. Eilers, and R. A. Klein. J. Org. Chem. **29**, 2813 (1964).
7. E. J. Corey and M. Chaykovsky. J. Am. Chem. Soc. **84**, 867 (1962).
8. J. N. Pitts, Jr. and I. Norman. J. Am. Chem. Soc. **76**, 4815 (1954).

9. R. E. K. WINTER and R. J. LINDAUER. Tetrahedron Lett. 2345 (1967).
10. W. G. DAUBEN, L. SCHUTTE, and R. E. WOLF. J. Org. Chem. **34**, 1849 (1969).
11. R. B. WOODWARD, K. HEUSLER, J. GOSTELI, P. NAEGELI, W. OPPOLZER, R. RAMAGE, S. RANGANATHAN, and H. VORBRUGGEN. J. Am. Chem. Soc. **88**, 852 (1966); T. A. MONTZKA, J. D. MATISKELLAR, and R. A. PARTYKA. Tetrahedron Lett. 1325 (1974).
12. H. E. ZIMMERMAN, R. D. RIEKE, and J. R. SCHEFFER. J. Am. Chem. Soc. **89**, 2033 (1967).
13. Boehringer and Son, Ingelheim, Germany. British patent Nos. 1,166,798 (October, 1969) and 1,167,688 (October, 1969); Chem. Abstr. **72**, P32102n (1970); **72**, P43965x (1970).
14. E. E. SMISSMAN and A. MAKRIYANNIS. J. Org. Chem. **38**, 1652 (1973).
15. S. W. STALEY. *In* Selective organic transformations. Vol. 2. *Edited by* B. S. Thyagarajan. Wiley-Interscience, New York. 1972. pp. 309–348.
16. W. G. DAUBEN and R. E. WOLF. J. Org. Chem. **35**, 374 (1970).
17. H. E. ZIMMERMAN, K. G. HANCOCK, and G. C. LICKE. J. Am. Chem. Soc. **90**, 4892 (1968).
18. H. E. ZIMMERMAN and R. L. MORSE. J. Am. Chem. Soc. **90**, 954 (1968).
19. W. G. DAUBEN, L. SCHUTTE, R. E. WOLF, and E. J. DEVINY. J. Org. Chem. **34**, 2512 (1969).

The photodissociation of ammonia in the $\tilde{A} \leftarrow \tilde{X}$ absorption system. Part I. Deuterium isotope effects in the photodissociation[1]

S. KODA[2] AND R. A. BACK

Division of Chemistry, National Research Council of Canada, Ottawa, Ont., Canada K1A 0R6

Received August 9, 1976

S. KODA and R. A. BACK. Can. J. Chem. **55**, 1380 (1977).

The photolyses of mixtures of NH_3, NH_2D, NHD_2, and ND_3 have been studied at wavelengths of 2144, 2139, 2062, and 1850 Å in the presence of C_3H_8 as a hydrogen atom scavenger. Quantum yields of dissociation have the same values for all four species, presumably unity. Analysis of the H_2 and HD produced permitted evaluation of intramolecular deuterium isotope effects in the photodissociation of NH_2D and ND_2H. At the two shortest wavelengths dissociation of H was favored by a factor of 2 or 3, while at 2144 and 2139 Å the isotope effect was much larger. Implications for the mechanism of the predissociation of the $\tilde{A}$-state of ammonia are discussed briefly. The system does not appear to be useful for the photochemical separation of deuterium.

S. KODA et R. A. BACK. Can. J. Chem. **55**, 1380 (1977).

On a étudié la photolyse de mélanges de NH_3, NH_2D, NHD_2 et ND_3 à des longueurs d'onde de 2144, 2139, 2062 et 1850 Å en présence de C_3H_8 servant de piège pour les atomes d'hydrogène. Les rendements quantiques de dissociation ont les mêmes valeurs pour les quatre espèces et sont probablement égales à l'unité. L'analyse de H_2 et de HD permet d'évaluer les effets isotopiques intramoléculaires du deutérium dans la photodissociation de NH_2D et ND_2H. Aux deux longueurs d'onde les plus courtes, la dissociation de H est favorisée par un facteur de 2 ou 3 alors qu'à 2144 et 2139 Å l'effet isotopique est beaucoup plus grand. On discute brièvement des implications pour le mécanisme de la prédissociation de l'état $\tilde{A}$ de l'ammoniac. Ce système ne semble pas utile pour la séparation photochimique du deutérium.

[Traduit par le journal]

Introduction

The photolysis of ammonia in its first absorption region ($\tilde{A} \leftarrow \tilde{X}$, ~2200–1700 Å) has been extensively studied, and the general features of the primary photodissociation are well established (1–3). The dissociation products are almost exclusively (>99%) H + NH_2, and the quantum yield is close to unity and independent of pressure. The absorption spectrum shows well-resolved vibrational bands in a long progression arising from excitation of the symmetric out-of-plane bending mode (ν_2') of the planar $\tilde{A}$ state (4, 5). In the case of NH_3 these bands are almost completely diffuse, showing no rotational fine structure; with ND_3, however, rotational lines are well resolved in the bands corresponding to $v_2' = 0$ or 1 (all higher members of the progression are diffuse) (5). It is apparent that the upper state is strongly predissociated, even in ND_3, as the rotational lines are considerably broadened, and the quantum yield of dissociation of unity, independent of pressure, confirms that the excited state must be very short-lived.

While it is agreed that the photolysis of ammonia proceeds through a predissociation, there is some uncertainty about the repulsive state involved, and the precise details of the predissociation are not clear (4–6). The striking difference in the spectra of NH_3 and ND_3 suggests that there could be a large deuterium isotope effect in the photodissociation, and the present work was undertaken to explore this possibility, and to gain a better understanding of the predissociation process. A further purpose was to explore the potential of the ammonia photolysis for photochemical isotope separation.

Experimental and Results

Apparatus

Ammonia was photolyzed in several cylindrical quartz reaction vessels, 5 cm in diameter, with plane Suprasil windows, and varying from 1 to 20 cm in length. These were sometimes used

[1]NRCC No. 15813.

[2]NRCC Postdoctoral Fellow, 1972–1974; present address: Division of Reaction Chemistry, Faculty of Engineering, University of Tokyo, Tokyo, Japan.

in simple static systems, and in other experiments were incorporated into a closed circulation loop with a ballast volume. Conditions were chosen, contingent upon the wavelength of the exciting light, the extinction coefficients, the light intensity, and the ammonia pressure, to ensure low conversion and moderately homogeneous absorption of light.

Light Sources

Four light sources were employed:

(*i*) A flat-spiral cadmium resonance lamp operated at 280°C. A 1 cm filter cell containing cadmium vapor at 500°C removed the 2288 Å resonance line, so that the effective light was almost entirely at 2144 Å.

(*ii*) A Philips Spectral zinc lamp, used with a 1 cm filter cell filled with about 75 torr each of NH_3 and ND_3. The filter removed the 2026 Å line completely and reduced the 2062 Å line to less than 0.4% of the 2139 Å radiation; the effective light was essentially pure 2139 Å radiation.

(*iii*) An iodine–argon microwave discharge lamp with a liquid water filter, which gave virtually monochromatic 2062 Å radiation (7).

(*iv*) A low-pressure flat-spiral mercury-resonance lamp, used as a source of 1850 Å radiation. The light path was flushed with N_2 to prevent absorption by O_2, O_3, and water vapor, and the system was mercury-free to avoid photosensitization by 1850 or 2537 Å light. Ammonia is transparent to the latter, so that the effective light was almost pure 1850 Å radiation.

The spectral purity of the light sources was determined with a 0.5 m grating monochromator and a photomultiplier, which were also used to monitor light intensity and absorption during the photolyses. A platinum-cathode phototube was sometimes used for the latter purpose with the iodine lamp (8).

Analysis

After irradiation, N_2 and H_2 were removed through a trap at −196°C and measured in a gas burette. The composition of the gas was determined by separating H_2 through a hot palladium thimble. When necessary, the isotopic composition of the hydrogen was measured by gas chromatography, using an alumina column, treated with $MnCl_3$, at −196°C (9). Isotopic composition of deuteriated ammonia was determined by decomposing the gas by a Tesla discharge, at the same time removing hydrogen through a hot palladium thimble, until the decomposition was complete, and finally measuring the isotopic composition of the hydrogen by gas chromatography as before.

Materials

Ammonia was obtained from Matheson, and ammonia-d_3 (99 atom% D) from Merck, Sharp and Dohme of Canada Ltd. Both were used after rigorous degassing and trap-to-trap distillation. The partially deuteriated ammonias, NH_2D and NHD_2, cannot be isolated, as H–D equilibration occurs within seconds of mixing the gases. To study these species, NH_3 and ND_3 were mixed in a known ratio, and equilibrium concentrations were calculated from equations based on the data of Pyper *et al.* (10). All the spectroscopic and photochemical experiments with NH_2D and NHD_2 were done with the four ammonias present at equilibrium; by suitable variation of the initial proportions of NH_3 and ND_3 and thence of the two mixed species, the properties of each of the latter could be determined, essentially in each case by solving two equations in two unknowns.

Propane was Research-grade, obtained from Matheson, and used without further purification. Gas chromatography confirmed that olefin content was negligible.

Ultraviolet Absorption Spectra

While the photographic spectra of both NH_3 and ND_3 are well known, quantitative extinction coefficients have apparently been reported only for NH_3 (11). The only information about the spectra of NH_2D and ND_2H comes from the work of Walsh and Warsop (4), who measured the wavelength of a few band heads from a plate in which the spectra of the four isotopic ammonias were badly overlapped. Since the present study required quantitative absorption spectra for the four species, low resolution spectra were measured on a Cary spectrophotometer, and are shown in Figs. 1 and 2. Each of the two isotopically mixed ammonias required a special technique to separate its spectrum from those of the other three components always present. Thus to measure the spectrum of NH_2D, NH_3 and ND_3 were mixed in a ratio of ~4/1, giving an $NH_3/NH_2D/NHD_2/ND_3$ ratio of about 50/39/10/1 in the sample cell. The reference cell of the double-beam instrument was then filled with NH_3 at a pressure calculated to balance exactly the partial pressure of NH_3 in the

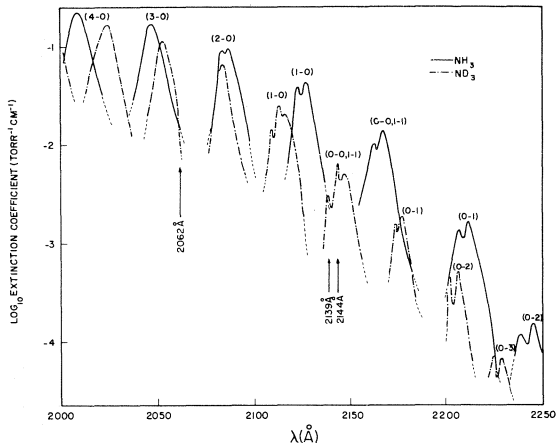

FIG. 1. Low resolution absorption spectra of NH_3 and ND_3. Values of v_2' and v_2'' are shown in parentheses for each band.

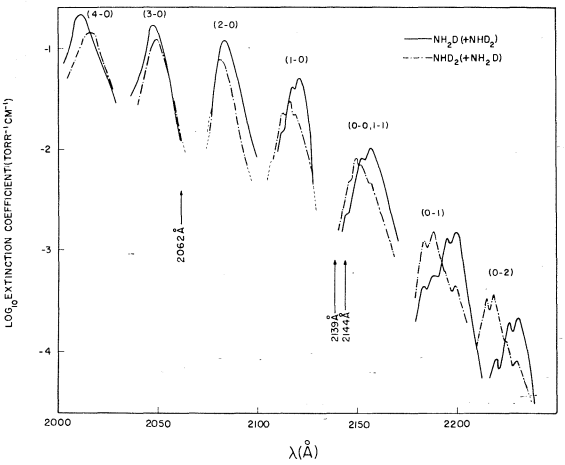

FIG. 2. Low resolution absorption spectra of NH_2D and NHD_2. Values of v_2' and v_2'' are shown in parentheses for each band.

sample, so that the measured difference spectrum was that of NH_2D with a small (20%) NHD_2 component and an almost negligible (2%) amount of ND_3. The spectrum of NHD_2 was obtained in a similar way with ND_3 in the reference cell. The spectra of the mixed ammonias in Fig. 2 have not been corrected for the minor component, and the ND_3 spectrum in Fig. 1 has not been corrected for the presence of a 12% ND_2H impurity.

The photolysis experiments required accurate values of the extinction coefficients for each of the isotopic ammonias at each of the four wavelengths employed. These were measured in the photolysis cells, using the photolytic light sources and a 0.5 m monochromator and photomultiplier to measure transmitted light intensity. Accurately linear Beer's Law behaviour was observed over a wide range of pressure and for each of a number of isotopic compositions. Values of ε for NH_3 were obtained directly, and those for ND_3 almost directly with only a small correction for the 3% of NDH_2 impurity. For the mixed ammonias, NH_3 and ND_3 were mixed in known proportions, and equilibrium compositions calculated. From Beer's Law plots at several compositions, making corrections for absorption by NH_3 and ND_3, extinction coefficients for NH_2D and NHD_2 were obtained by solving pairs of equations in two unknowns. Values of the molar decadic extinction coefficients for the four ammonias at the four photolysis wavelengths are shown in Table 1.

TABLE 1. Molar decadic extinction coefficients of isotopic ammonias

Wavelength (Å)	ε			
	NH_3	NH_2D	NHD_2	ND_3
2144	16.2	9.51	39.1	46.3
2139	43.2	13.8	9.25	31.7
2062	292	279	221	250
1850	1330	2500	3085	1750

While it is known that in the spectrum of ND_3, bands arising from $v_2' = 0$ or 1 show well-resolved rotational fine structure, and that with NH_3 all bands are almost completely diffuse,[3] the behaviour of NH_2D and NHD_2 had not been established, although it seemed probable that their spectra would be diffuse. Spectra of NH_3–ND_3 mixtures were therefore photographed at high dispersion, using the first order of a 10 m grating spectrograph.[4] From Fig. 2 it was possible to identify the bands due to the mixed ammonias, and it was clear that neither NH_2D nor NHD_2 shows any rotational fine structure. This was seen most clearly for the 0,1 band of ND_2H, which is almost free of overlap by the same band of ND_3. Other bands are more badly overlapped, but in no instance were sharp rotational features observed which

[3]Dixon (12) observed extremely faint rotational structure in the spectrum of NH_3. All four isotopic ammonias show broad rotational features at low resolution (Figs. 1 and 2) the double-headed band contours for all bands with $v_2' \leq 2$ arising from the P and R branch structure.

[4]We are grateful to Mr. F. Alberti of the Herzberg Institute for photographing these spectra.

could not be assigned to ND_3. Thus it appears that substitution of a single atom of D by H in ND_3 increases the rate of predissociation enough to completely obscure the rotational fine structure through the line broadening associated with the reduced lifetime of the excited state.

Photochemical Measurements

In order to measure the rate of the primary dissociation,

[1] $$NH_3 + h\nu \rightarrow NH_2 + H$$

the reaction with propane

[2] $$H + C_3H_8 \rightarrow H_2 + C_3H_7$$

was used, and the hydrogen produced was easily separated and measured. This system has been thoroughly studied by Schindler and coworkers (2, 3) and our results are in good accord with theirs. In order to make reaction 2 quantitative and therefore the H_2 a true measure of reaction 1, conditions must be carefully controlled. Propane pressure must be high enough, and the light intensity low enough, that loss of H by reaction with C_3H_7 or NH_2 is negligible. Conversion must also be kept low enough to avoid build-up of propylene from the disproportionation of C_3H_7 to concentrations at which loss of H by addition to the olefin becomes significant, and also to avoid secondary photolysis of hydrazine or propylamine. Figure 3 shows typical plots of $H_2 + HD$ and N_2 *vs.* propane pressure from the photolysis of an equimolar NH_3–ND_3 mixture, and it is seen that the yield of $H_2 + HD$ becomes constant above about 200 torr. It was also observed that under these conditions production of $H_2 + HD$ was a linear function of time and of light intensity, showing that the secondary reactions of products (which would be time-dependent) and reactions of H with C_3H_7 or NH_2 (which would be intensity dependent) were not important. It appears from these observations that essentially all of the H atoms formed in reaction 1 were reacting to form H_2.

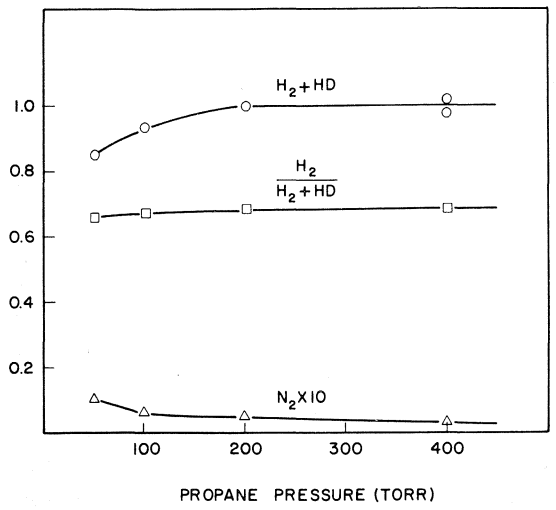

FIG. 3. Dependence of product yields on propane pressure, for photolysis of equimolar NH_3–ND_3 at 20 torr pressure, irradiated at 2139 Å.

Before the yield of H_2 can be equated to the rate of reaction 1, the possibility of direct formation of H_2 as a primary photolysis product must be considered. It is well established that reaction 1 is the main process, and the present study confirms this. However, very careful measurements of the yield of D_2 from the photolysis of ND_3 in the presence of excess propane or ethylene (13) indicate the occurrence of a molecular process with a quantum yield ranging from ≤ 0.003 at 2139 Å to ≤ 0.009 at 1849 Å. Very small corrections for this process have been applied to the present results, assuming that these quantum yields are the same in the four isotopic ammonias.

Finally, in the experiments with the isotopically mixed ammonias, it is essential that H or D atoms produced in the primary photodissociation do not undergo exchange with either propane or ammonia before reacting with propane, so that the yields of HD and H_2 accurately reflect the primary yields of D and H respectively. Absence of exchange with propane is shown by the low yields of H_2 in the photolysis of ND_3 in the presence of propane which corresponded closely to that expected from the isotopic H impurity in the ND_3. Absence of exchange with ammonia is less easily demonstrated, but the self-consistent behaviour of the isotopically mixed systems over a wide range of conditions and the agreement with calculations that presume no such exchange are probably the best proof. Another possible source of error in the isotopic experiments is the reaction of H or D with hydrazine; the very low yields of D_2 from the photolysis of ND_3 in the presence of propane, in which hydrazine would be largely N_2D_4, show that this did not occur. Hydrazine concentration was low in the present system because of the low light intensity and high

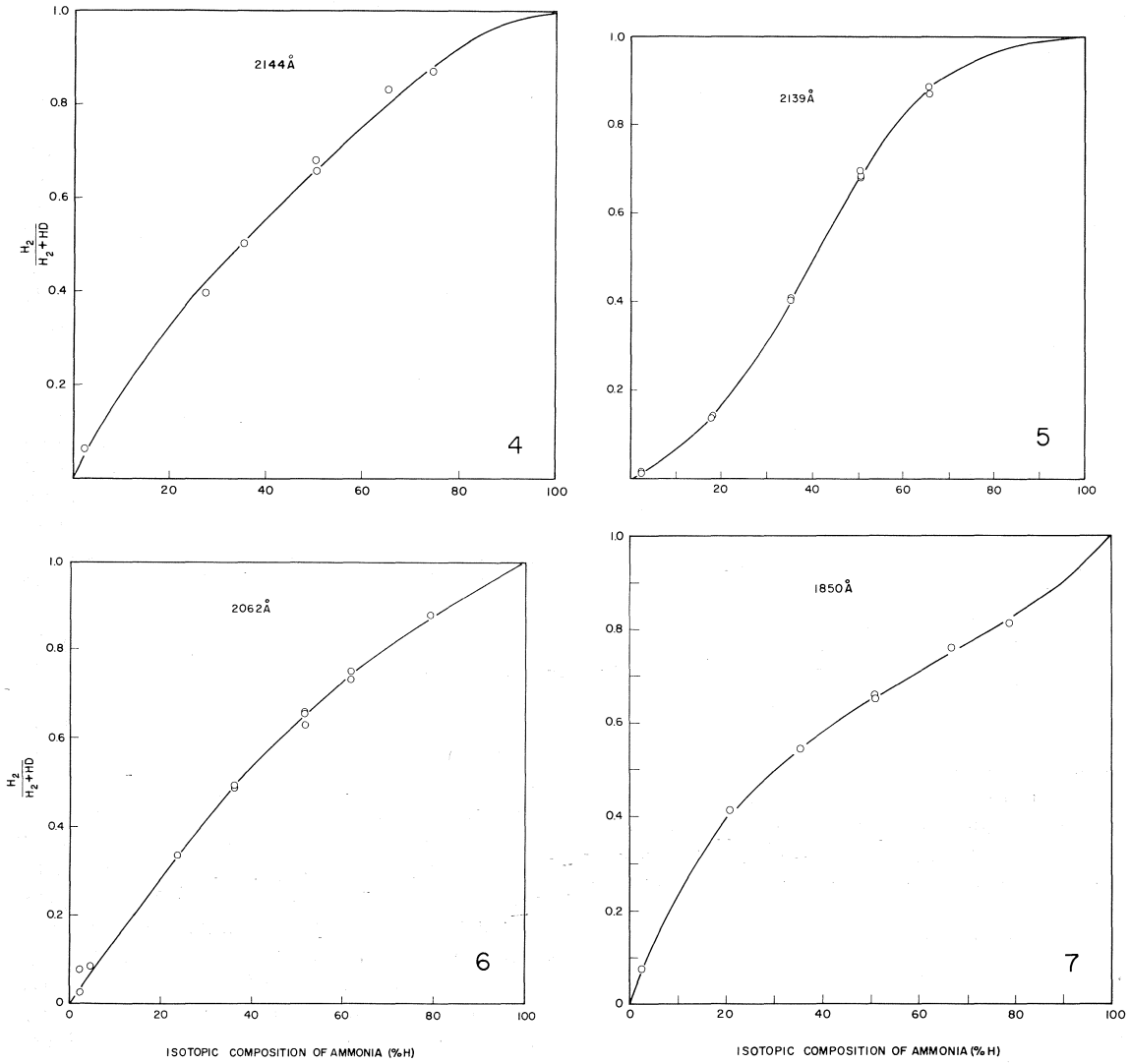

FIGS. 4, 5, 6, and 7. Isotopic composition of hydrogen from the photolysis of NH_3, NH_2D, NHD_2, and ND_3 in the presence of C_3H_8. Points are experimental, curves are calculated (see text).

propane pressure, which favor reaction of NH_2 radicals with propane rather than combination to form hydrazine (2); destruction of hydrazine by reaction with propyl radicals, leading eventually to N_2, is also a factor. The low yield of N_2 observed (Fig. 3) reflects the low concentration of hydrazine in the system.

Primary photodissociation yields of H and D atoms, based on the production of H_2 and HD by reaction with propane, were measured for mixtures of the isotopic ammonias ranging from pure NH_3 to 97% ND_3. The results are shown in Figs. 4, 5, 6, and 7 for photolysis at 2144, 2139, 2062, and 1850 Å respectively. In each figure are shown plots of the ratio $H_2/(H_2 + HD)$ against the atom% H in the ammonia mixture. The quantum yields of H_2 and HD were measured relative to that of H_2 from NH_3, taking this to be unity; no absolute quantum yields were measured. The quantum yield of total hydrogen (H_2 + HD) was independent of isotopic composition, showing that the quantum yield of dissociation has the same value in each of the four isotopic species (presumably unity) and therefore no intermolecular isotope effect can be observed.

Discussion

The photodissociation processes occurring in the mixtures of isotopic ammonias are the following:

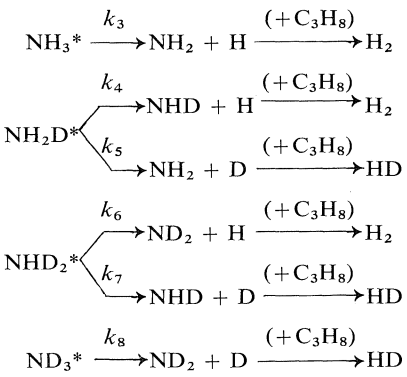

[3] $NH_3^* \xrightarrow{k_3} NH_2 + H \xrightarrow{(+C_3H_8)} H_2$

[4] $NH_2D^* \xrightarrow{k_4} NHD + H \xrightarrow{(+C_3H_8)} H_2$

[5] $NH_2D^* \xrightarrow{k_5} NH_2 + D \xrightarrow{(+C_3H_8)} HD$

[6] $NHD_2^* \xrightarrow{k_6} ND_2 + H \xrightarrow{(+C_3H_8)} H_2$

[7] $NHD_2^* \xrightarrow{k_7} NHD + D \xrightarrow{(+C_3H_8)} HD$

[8] $ND_3^* \xrightarrow{k_8} ND_2 + D \xrightarrow{(+C_3H_8)} HD$

The variation of $H_2/(H_2 + HD)$ with isotopic composition at each wavelength depends on the extinction coefficients for each of the four ammonias, and on the intramolecular isotope effect in the photodissociation of NH_2D and NHD_2. The data points in Figs. 4 to 7 are experimental values; the smooth curves through them are calculated, in the following way. For a given atom% D in the ammonia mixture, relative concentrations of NH_3, NH_2D, NHD_2, and ND_3 were calculated from the equilibrium constants. Relative absorption of light by each species at each wavelength was then calculated, using the measured extinction coefficients (Table 1); then, assuming a quantum yield of unity, the relative amount of each species dissociated was obtained. Dissociation of NH_3 and ND_3 lead unambiguously to H_2 and HD respectively in amounts that are thus simply calculated. The remainder of the H_2 and HD must then arise from dissociation of the two mixed ammonias, reactions 4 to 7. The primary intramolecular isotope effect, I, in the photodissociation may be defined as $I_{NH_2D} = k_4/2k_5$ for NH_2D, and $I_{NHD_2} = 2k_6/k_7$ for NHD_2. For any two data points shown in Figs. 4 to 7, values of I_{NH_2D} and I_{NHD_2} can be obtained by solving two equations in two unknowns. In practice, the values of I for the two species were varied until the best least-squares fit to all the experimental points was achieved at each wavelength. The calculated curves shown in Figs. 4 to 7 correspond to these values, which are summarized in Table 2; also listed in parentheses are estimated limits of uncertainty.

TABLE 2. Intramolecular isotope effect, I, in the photolysis of NH_2D and NHD_2

λ (Å)	v_2'	I_{NH_2D}	I_{NHD_2}
2144	0, 1	Large	8.05 (6.3–10.7)
2139	0, 1	10.9 (2.1–large)	2.64 (1.5–19.3)
2062	3	1.90 (1.55–2.16)	2.32 (2.06–2.68)
1850	9, 10	1.95 (1.62–2.41)	3.15 (2.63–3.81)

Values of I_{NH_2D} are listed as 'large' when the yield of HD was entirely accounted for by the estimated production of D atoms from the other isotopic ammonias, leaving a yield of zero, within experimental accuracy, from the photolysis of NH_2D. The values of I in Table 2 show a significant dependence on the exciting wavelength. For the two shortest wavelengths the best estimates are within the range 1.9–3.2, which can be regarded as a fairly normal primary kinetic deuterium isotope effect. There is also probably a significant difference between NH_2D and NHD_2 at these wavelengths, which can be interpreted as a preference for the dissociation of the lone hydrogen isotope from each species, *i.e.*, D from NH_2D and H from NHD_2, superimposed on the primary isotope effect. Values of I at 2139 Å are rather uncertain because of the small fraction of light absorbed by the mixed species (Table 1) and consequent large correction for H and D produced by dissociation of NH_3 and ND_3. The data are not incompatible, however, with fairly large values of I. At 2144 Å, I is unmistakably much larger than at the two shorter wavelengths.

The present experiments thus show a sizeable intramolecular deuterium isotope effect in the photodecomposition of NH_2D and NHD_2, complementing the earlier spectroscopic observation of a large intermolecular isotope effect between NH_3 and ND_3. It is interesting that the abnormally large effects at 2139 and 2144 Å correspond to dissociation from the $v_2' = 0$ and $v_2' = 1$ levels of the $\tilde{A}$ state, the same levels which in ND_3 show resolved rotational structure indicative of a long lifetime. The large isotope effect suggests a tunnelling process, either through a barrier or between potential energy surfaces, while the lower, more normal values of I at 2062 and 1850 Å are more characteristic

of passage over a potential barrier. The detailed mechanism of the predissociation will be discussed in a subsequent paper (13).

Finally, the possibility of using the photolysis of ammonia for hydrogen–deuterium separation may be assessed. It is clear that separation of deuterium by selective photolysis of the ~0.03% of NH_2D present in natural ammonia is not promising. Overlap of the spectra of NH_3 and NH_2D (Figs. 1 and 2) would probably limit selectivity in the absorption of light in an equimolar mixture to no better than a factor of 10; it has been seen that dissociation of H rather than D from NH_2D is strongly favored, and it is not apparent how to trap the NHD fragment in a form which will not readily exchange its hydrogen with ammonia, the starting material. On the other hand, photochemical removal of quite small fractions of NHD_2 from ND_3 appears much more favorable; the discrete nature of the ND_3 spectrum would permit highly selective photolysis of NHD_2 at appropriate wavelengths, and the H atoms preferentially dissociated in the photolysis could be easily trapped by a hydrocarbon scavenger, or, with some loss of efficiency, simply by reaction with the hydrazine formed in the photolysis. There would seem to be little practical value in such a separation, however, unless for some reason ND_3 of very high isotopic purity were required.

1. J. G. Calvert and J. N. Pitts, Jr. Photochemistry. John Wiley and Sons Inc., New York, NY. 1966.
2. W. E. Groth, U. Schurath, and R. N. Schindler. J. Phys. Chem. **72**, 3914 (1968).
3. U. Schurath and R. N. Schindler. Ber. Bunsen Geselschaft Phys. Chem. **72**, 1027 (1968).
4. A. D. Walsh and P. A. Warsop. Trans. Faraday Soc. **57**, 345 (1961).
5. A. E. Douglas. Discuss. Faraday Soc. **35**, 158 (1963).
6. G. Herzberg. Electronic spectra of polyatomic molecules. D. van Nostrand Co., Princeton, NJ. 1966.
7. R. A. Back and T. Yokota. Intern. J. Chem. Kinet. **5**, 1039 (1973).
8. W. D. Woolley and R. A. Back. Can. J. Chem. **46**, 295 (1968).
9. T. Terao and R. A. Back. J. Phys. Chem. **73**, 3884 (1969).
10. J. W. Pyper, R. S. Newbury, and G. W. Barton, Jr. J. Chem. Phys. **47**, 1179 (1967).
11. B. A. Thompson, P. Harteck, and R. R. Reeves, Jr. J. Geophys. Res. **68**, 6431 (1963).
12. J. K. Dixon. Phys. Rev. **43**, 711 (1933).
13. R. A. Back and S. Koda. Can. J. Chem. This issue.

The photodissociation of ammonia in the $\tilde{A} \leftarrow \tilde{X}$ absorption system. Part II. Translational excitation of the hydrogen atoms produced, and the mechanism of the predissociation[1]

R. A. BACK AND S. KODA[2]

Division of Chemistry, National Research Council of Canada, Ottawa, Ont., Canada K1A 0R6

Received August 9, 1976

R. A. BACK and S. KODA. Can. J. Chem. **55**, 1387 (1977).

The photolyses of NH_3 and ND_3 have been studied at 2139, 2062, and 1850 Å in the presence of propane and ethylene. Upper limits (none was actually observed) were established for the quantum yields of molecular dissociation of D_2 from ND_3 of 0.003 and 0.004 at 2139 and 2062 Å, while at 1850 Å a definite yield of 0.009 was obtained. Similar results were observed with NH_3. From the dependence of hydrogen yields on the ratio of ethylene to propane, it was concluded that H and D atoms were produced in the photolysis with excess translational energy. Values of the integrated reaction probability (IRP) of hot H atoms with propane were estimated to be 0.078, 0.070, and 0.045 at 2139, 2062, and 1850 Å respectively, while corresponding values for hot D atoms from ND_3 were 0.083, 0.062, and 0.029. Implications of the decrease in IRP with increasing photon energy are discussed, and it is concluded that at the shorter wavelengths a second dissociation channel leading to $NH_2(^2A_1)$ becomes important. A mechanism for the predissociation of the $\tilde{A}$-state of ammonia is presented which accounts for this behaviour and for the deuterium isotope effects observed previously. It is suggested that the dissociation does not follow the state correlation rules for dissociation in the plane of the molecule, at least when the ν_2 out-of-plane bending vibration in the $\tilde{A}$-state is excited to levels of $v_2 = 2$ or higher.

R. A. BACK et S. KODA. Can. J. Chem. **55**, 1387 (1977).

On a étudié la photolyse de NH_3 et ND_3 à 2139, 2062 et 1850 Å en présence du propane et d'éthylène. On a établi que les limites supérieures (en fait aucun n'a été observé) pour les rendements quantiques de la dissociation moléculaire de D_2 à partir de ND_3 sont égales à 0.003 et 0.004 à 2139 et 2062 Å alors qu'à 1850 Å un rendement bien défini de 0.009 peut être obtenu. On a pu observé des résultats semblables avec NH_3. A partir de la dépendance des rendements d'hydrogène sur les rapports d'éthylène sur propane, on peut conclure que les atomes de H et de D peuvent être produits lors de la photolyse avec une énergie de translation en excès. On a estimé que les valeurs des probabilités de réaction intégrée (PRI) des atomes d'hydrogène chauds avec le propane sont respectivement de 0.078, 0.070 et 0.045 à 2139, 2062 et 1850 Å alors que les valeurs correspondantes pour les atomes de deutérium chauds à partir de ND_3 sont 0.083, 0.062 et 0.029. On discute des implications de la diminution des PRI avec une augmentation de l'énergie photonique et on en conclut qu'aux longueurs d'ondes les plus courtes, un second chemin de dissociation conduisant à $NH_2(^2A_1)$ devient important. On présente un mécanisme pour la prédissociation de l'état $\tilde{A}$ de l'ammoniac qui tient compte de ce comportement ainsi que des effets isotopiques du deutérium observés antérieurement. On suggère que la dissociation ne suit pas les règles de corrélation d'état pour la dissociation dans le plan de la molécule, au moins lorsque la vibration de déformation angulaire hors-plan, ν_2, de l'état $\tilde{A}$ est excité à des niveaux de $v_2 = 2$ ou plus élevé.

[Traduit par le journal]

Introduction

The present papers are concerned with the mechanism of the photodissociation of ammonia in its first absorption band, the $\tilde{A} \leftarrow \tilde{X}$ transition. Part I described the measurement of deuterium isotope effects in the photodissociation (1). It is well established that much of the excess energy released in the photolysis of simple hydrides such as HBr, HI, or H_2S appears as translational energy of the hydrogen atoms produced (2–13). With increasing molecular complexity, more of the excess energy may be distributed among the vibrational and rotational modes of the fragments, and knowledge of the translational energy of the hydrogen atoms should yield valuable information about this distribution and about the way in which the molecule dissociates. The present paper describes an experimental estimation of the

[1]NRCC No. 15814.

[2]NRCC Postdoctoral Fellow, 1972–1974. Present address: Division of Reaction Chemistry, Faculty of Engineering, University of Tokyo, Tokyo, Japan.

translational energy of the hydrogen atoms formed in the photodissociation of ammonia.

Experimental

Light sources, reaction vessels, and experimental procedures were essentially as previously described (1). Wavelengths employed were 2139, 2062, and 1850 Å, and all experiments were at 295 K. Ammonia pressures were low (5 to 20 torr) and in most experiments a high pressure, usually 300 torr, of propane was present; light intensities and conversions were such that in the absence of ethylene, essentially all the hydrogen atoms produced reacted with propane to form H_2 (1). The translational energy of the hydrogen atoms was estimated by adding ethylene to the system and studying the competition between their reactions with ethylene and propane. Other experiments were done with ammonia–ethylene mixtures, without propane, to assess the yield of molecular H_2 in the photodissociation, and appropriate blank experiments were done to permit corrections to be made for H or H_2 arising from the photolysis of propane or ethylene. Quantum yields were measured relative to the yield of H_2 from photolysis of NH_3 in the presence of 300 torr of propane, which was assumed to be unity (1).

Results and Discussion

Molecular Hydrogen Formation

Because formation of molecular hydrogen in the photodissociation can lead to experimental observations in the ammonia–propane–ethylene system very similar to those expected for translationally hot hydrogen atoms, this will be dealt with first. Ethylene is known to react rapidly with thermal hydrogen atoms to form ethyl radicals which disappear in secondary reactions yielding no H_2. In the photolysis of ammonia–ethylene mixtures, limiting yields of H_2 at high pressures of ethylene can arise from (*a*) photodissociation of ammonia to yield H_2, (*b*) photodissociation of ethylene to yield H_2, (*c*) abstraction of H from ethylene by hot H atoms, and (*d*) abstraction of H from ammonia by hot H atoms. Process (*b*) can be corrected for by blank photolyses of ethylene alone, and the best estimates of (*a*) come from experiments with ND_3–C_2H_4 mixtures, in which the yield of D_2 should be an unambiguous measure of the molecular dissociation if (*d*) can be neglected. Results are shown in Table 1. At the two longest wavelengths, total noncondensible gas was barely measurable and could not be analyzed for D_2 content; only upper limits for the yield of D_2 are shown, and there is no positive evidence that molecular elimination of D_2 occurs at all. At 1850 Å, however, there is definite evidence for molecular elimination with a quantum yield of about 0.009. The low yields of D_2 at 2139 and 2062 Å put upper limits on (*d*), the abstraction of D from ND_3 by translationally hot D atoms. It will be seen that this is probably even less likely at 1850 Å, as the D atoms have less translational energy, and there is no evidence that it occurs at all.

Values of the quantum yield of D_2 in Table 1 should at least be firm upper limits for the molecular dissociation of D_2 from ND_3. Experiments with NH_3 were in substantial agreement, although less accurate, and there seems to be no large isotope effect in this process. The upper limit of 0.003 at 2062 Å is in good agreement with similar limits of 0.003 and 0.005 for ND_3 and NH_3 respectively reported by Schindler and co-workers (14) and confirm that molecular elimination is virtually negligible at this wavelength. Our value of 0.009 at 1850 Å is significantly lower than the value $<4\%$ reported by McNesby *et al.* (15) for NH_3. The latter value, however, was based on a yield of H_2 from a NH_3–C_2D_4 mixture, which was about 3.5% of that from pure NH_3; the quantum yield of H_2 from pure NH_3 is certainly less than unity (14), and could be as low as 0.3 at the relatively high light intensities employed, which would lead to an absolute quantum yield for molecular H_2 production of about 1%, in good agreement with our value.

Estimation of Translational Energy of Hydrogen Atoms

Figure 1 shows Φ_{H_2}/Φ_H in the NH_3–C_3H_8–C_2H_4 system, plotted against the C_2H_4/C_3H_8 ratio, for photolysis at 2139, 2062, and 1850 Å. Values of Φ_H are based on the hydrogen yield from the system in the absence of ethylene, under conditions where H atoms are quantitatively converted to H_2 (1). Both Φ_H and Φ_{H_2} at 2062 and 1850 Å are corrected for maximum molecular hydrogen formed directly from the photolysis of NH_3, C_2H_4, and C_3H_8, evaluated in suitable blank experiments as discussed above. The vertical bars indicate the uncertainty associated with this correction, which becomes appreciable at 1850 as the photolysis of ethylene becomes more important. Corrections at 2139 were well within the accuracy of the measurement and none were made.

If the reduction in Φ_{H_2}/Φ_H shown in Fig. 1 arose from a simple competition between ethylene and propane for thermally equilibrated H

TABLE 1. Hydrogen yields from photolysis of ND_3–C_2H_4 mixtures

λ (Å)	P_{ND_3} (torr)	$P_{C_2H_4}$ (torr)	Yield (%) H_2	HD	D_2	D_2 (quantum yield)
2139	11.2	53.2	(Not measurable)			<0.0030
	10.9	126.6	(Not measurable)			<0.0026
2062	10.9	142.4	(Not measurable)			<0.0036
	11.1	50.6	(Not measurable)			<0.0044
1850	10.2	53.3	93.8	—	6.2	<0.0085
	10.1	142.4	97.1	—	2.9	<0.0099

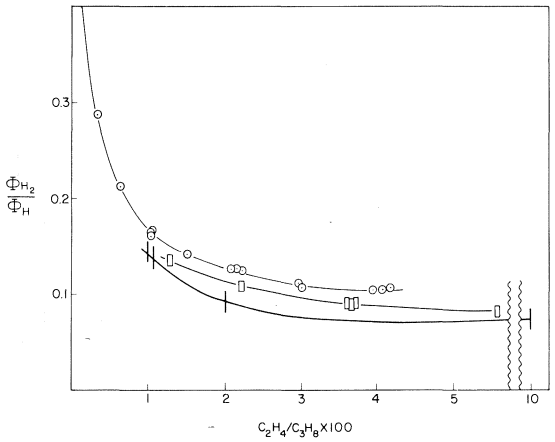

FIG. 1. Dependence of H_2 yield from the photolysis of NH_3 on the ethylene/propane ratio. Propane pressure = 200–500 torr, NH_3 pressure = 5–20 torr. ○ = 2139 Å, □ = 2062 Å, ■ = 1850 Å.

atoms, a steady reduction with increasing C_2H_4/C_3H_8 ratio would be expected, tending in the limit towards zero. It can easily be shown also that a reciprocal plot of the same data should be linear with an intercept of unity; Fig. 2 shows such a plot. It is clear from Figs. 1 and 2 that the behaviour observed is not characteristic of thermal H atoms; in simple terms, the H atoms become progressively more difficult to scavenge with ethylene as more and more ethylene is added. It has been seen that formation of molecular hydrogen, which might account for these observations, is small and has been corrected for, and it appears that the presence of translationally excited H atoms offers the only reasonable explanation. The following reactions must then be considered in the NH_3–C_2H_4–C_3H_8 system:

[1] $NH_3 + h\nu \rightarrow NH_2 + H^*$

[2] $H^* + C_3H_8 \rightarrow H_2 + C_3H_7$

[3] $\rightarrow H + C_3H_8$

[4] $H^* + C_2H_4 \rightarrow C_2H_5$

[5] $\rightarrow H + C_2H_4$

[6] $H + C_3H_8 \rightarrow H_2 + C_3H_7$

[7] $H + C_2H_4 \rightarrow C_2H_5$

where H^* represents a translationally hot hydrogen atom. It can be seen that

[8] $$\Phi_{H_2} = \frac{k_2P + [k_6P(k_3P + k_5E)/(k_6P + k_7E)]}{(k_2 + k_3)P + (k_4 + k_5)E}$$

where P and E are pressures of propane and

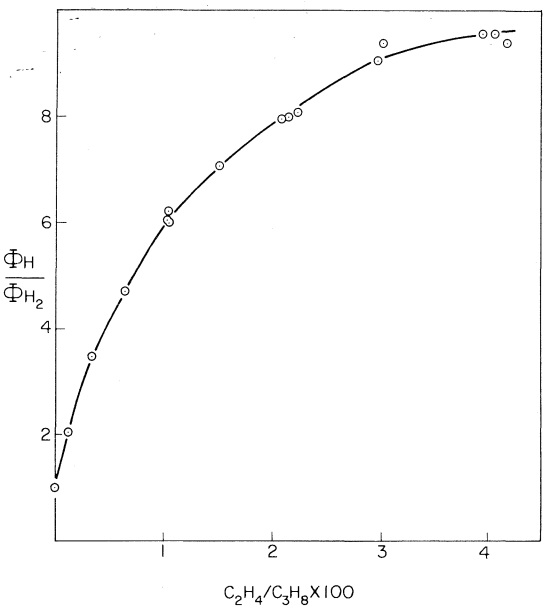

FIG. 2. Reciprocal plot of the data from Fig. 1; this should be linear for H-atoms with thermal energies.

ethylene, from which one obtains

$$[9]\quad \frac{\Phi_{H_2}}{1-\Phi_{H_2}} = \frac{(k_2+k_3)k_6P^2 + (k_2k_7+k_5k_6)PE}{(k_4k_6+k_3k_7)PE + (k_4+k_5)k_7E^2}$$

If k_3, k_4, and k_5 are all about the same order of magnitude, as seems probable, and $P \gg E$ as in the present experiments, the second term in the denominator can to a good approximation be neglected. Then

$$[10]\quad \phi/(1-\phi) = \alpha + \beta(P/E)$$

where

$$\alpha = (k_2k_7 + k_5k_6)/(k_4k_6 + k_3k_7) \approx k_2/k_3$$

(as it will be seen that $k_2k_7 \gg k_5k_6$ and $k_3k_7 \gg k_4k_6$) and

$$\beta = (k_2+k_3)k_6/(k_4k_6+k_3k_7) \approx (k_6/k_7) \times (1 + (k_2/k_3))$$

(since $k_7 \gg k_6$). Figure 3 shows plots of $\phi/(1-\phi)$ *vs.* P/E for both NH_3 and ND_3 for the photolysis at 2139 Å; these are linear within the accuracy of the data. Figure 4 shows similar plots for the less accurate and less extensive data at the two shorter wavelengths together with the straight lines taken from Fig. 3 for comparison. Table 2 shows values of α and β, and approximate values of k_2/k_3 and k_6/k_7 derived from the plots in Figs. 3 and 4 via eq. 10. Values of the integrated reaction probability (IRP) for reaction with propane, given in our system by $k_2/(k_2+k_3)$ are also shown, and in Table 3 values of IRP are shown which were obtained with some diatomic photolytic sources of hot H or D atoms in which the translational energy was well defined.

The foregoing treatment of the experimental data is an approximate one, but sufficiently accurate for present purposes. It should be noted that k_2, k_3, k_4, and k_5 are not simple rate constants but are effective mean values appropriate to the actual distribution of translational energies of atoms in the system. The latter is a complex function of the original distribution formed in the photolysis, the energy-loss processes (reactions 3 and 5) which reduce the translational energy towards its thermal equilibrium value, and the reactions, 2 and 4, which remove atoms from the system. The IRP is the average probability that an atom will react with propane to form H_2 between the time of its formation in the photolysis and the time at which its energy has been reduced to the thermal equilibrium value (6). The values of k_6/k_7 obtained (Table 2) are in fair agreement, con-

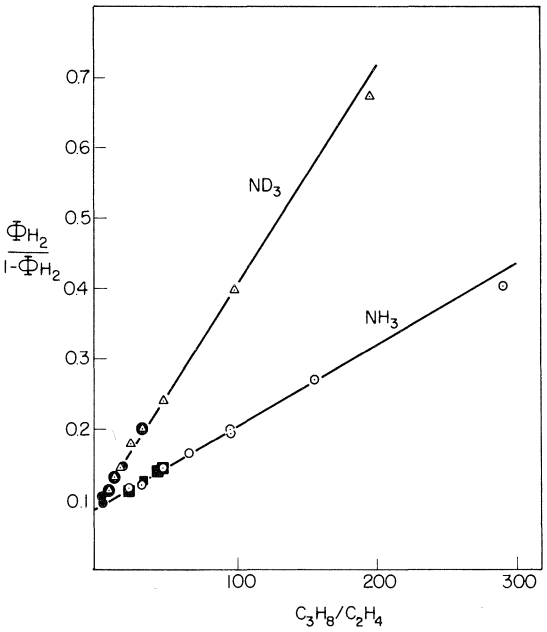

FIG. 3. Plot of eq. 9 for the photolysis of NH_3 and ND_3 at 2139 Å: ○ = 5 torr NH_3 + 200–500 torr C_3H_8, ■ = 10 torr NH_3 + 300 torr C_3H_8, △ = 5 torr ND_3 + 300 torr C_3H_8, ● = 10 torr ND_3 + 300 torr C_3H_8.

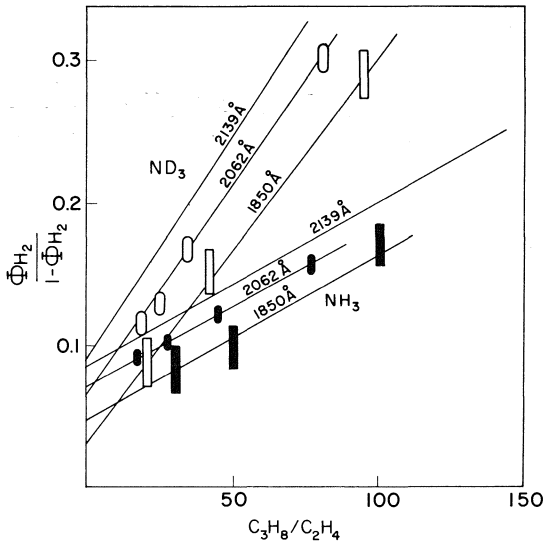

FIG. 4. Plot of eq. 9 for the photolysis of NH_3 and ND_3 at 2139, 2062, and 1850 Å.

TABLE 2. Slopes and intercepts from Fig. 4 and derived rate parameters

System	λ (Å)	α (= k_2/k_3)	β × 10^3	k_6/k_7 × 10^3	IRP
NH_3	2139	0.085	1.15	1.06	0.078
NH_3	2062	0.075	1.12	1.04	0.070
NH_3	1850	0.047	1.16	1.11	0.045
ND_3	2139	0.090	3.13	2.87	0.083
ND_3	2062	0.066	2.93	2.75	0.062
ND_3	1850	0.030	2.70	2.62	0.029

TABLE 3. Some comparable values of IRP from the literature

System	Excess translational energy of atoms (kcal/mol)	IRP	Reference
DI + C_2H_6	41.5 and 20.8	0.188*	2
DI + C_5H_{12}	41.5 and 20.8	0.172*	2
DBr + C_4H_{10}	24.4	0.296	8
DBr + C_4H_{10}	36.4	0.364	8
DBr + C_4H_{10}	65.3	0.441	8
HBr + C_4D_{10}	19.6	~0.09†	13
HBr + C_4D_{10}	46	~0.165†	13

*Estimated from values of intercept.
†Estimated from published figure.

sidering the errors and approximations involved, with a value of about 0.6×10^{-3} for H atoms which may be extrapolated from Yang's measurements (16). It is interesting to note the inverse isotope effect of about 2.7 in the k_6/k_7 ratio. Since one expects a normal isotope effect in both reactions, the inverse effect in the ratio must arise from a difference between the two, which probably implies a quite large normal isotope effect in the addition reaction.

The present results provide strong evidence for the formation of translationally hot hydrogen atoms in the photolysis of ammonia. The values of the IRP obtained are lower than those reported for other hot-atom systems (Table 3), so that the latter cannot provide an accurate calibration for the present system. A comparison of the data, however, suggest that the highest values of the IRP observed (at 2139 Å) must correspond to translational energies of no more than 20 kcal/mol and probably rather less; this may be compared with a theoretical maximum value of about 26 kcal/mol. The most striking feature of the data in Table 2 is the decrease in IRP, and thence presumably in the translational energy of H or D, with decreasing wavelength. This result was unexpected and difficult to explain, and will be seen to lead to important conclusions about the mechanism of the predissociation. It is not an artifact of our treatment of the data; it is evident from the simple experimental results in Fig. 1 that hydrogen atoms are more easily scavenged by ethylene at the shorter wavelengths. While the uncertainty in the data at 2062 and 1850 Å is considerable, the downward trend in the IRP seems well beyond the limits of experimental error.

The values of the IRP are closely similar in the NH_3 and ND_3 systems, with those in the latter perhaps falling off significantly faster with decreasing wavelength. The maximum energy theoretically available for translational excitation of H and D is almost the same, so that the similar IRP values imply small isotope effects in the k_2/k_3 ratio. Since both reactions 2 and 3 might be expected to show sizeable isotope effects, these must approximately cancel in the ratio.

The Mechanism of the Predissociation

There has been some uncertainty about the electronic structure of the first excited singlet state, $\tilde{A}$, of ammonia and the mechanism of its predissociation (17–20). It has been shown that the $\tilde{A}$-state is planar (D_{3h}) with electronic symmetry A_2''. It is agreed that it is formed by excitation of a lone-pair electron to an orbital of a_1' symmetry and thus has an electron configuration $\ldots (2a_1')^2\sigma_{N-H}.(1e')^4\sigma_{N-H}.(1a_2'')n.(3a_1')$. The uncertainty has concerned the identity and nature of the $3a_1'$ orbital. As Walsh and Warsop pointed out (17), there will be two valence-shell orbitals (*i.e.*, derived from the 2*p* orbitals of N), essentially antibonding (σ^*), complimentary to the bonding $2a_1'$ and $1e'$ orbitals, and the lowest of these will be of a a_1' symmetry. There will also be a Rydberg orbital, again of a_1' symmetry, derived from and closely resembling the 3*s* orbital of the N atom. Walsh suggested that the $\tilde{A}$-state was the Rydberg state formed by excitation of a lone-pair electron to this orbital and that it was predissociated by interaction with the σ^* state formed by excitation to the σ^* orbital. Others (18, 19) have argued that there is only one orbital of a_1' symmetry expected at this energy level, and therefore only a single excited state. Robin (20), however, has discussed such "conjugate pairs" of Rydberg and valence-shell orbitals in some detail, and it seems clear that there should indeed

be two distinct orbitals, both with a_1' symmetry and having very similar nodal structure; the bonding properties however will be quite different, with the Rydberg orbital almost non-bonding and the σ^* orbital strongly anti-bonding.

While the existence of two distinct orbitals, Rydberg and σ^*, seems clear, they are probably very strongly mixed in the $\tilde{A}$-state (20). Calculations by Horsley and Flouquet (21) for example indicated a state largely Rydberg in character at small H—NH_2 displacements and mostly σ^* as the H—NH_2 bond is stretched. Thus the two states interact so strongly that the crossing will be totally avoided, and the predissociation cannot be described as that of one state by another, but rather as the homogeneous vibrational predissociation of a single state (Herzberg's Case II predissociation (19)). This description of the $\tilde{A}$-state is in accord with the fact that it is strongly bound with respect to symmetric bending; vibrational structure arising from excitation of ν_2' remains well defined throughout the absorption band, showing in fact slight negative anharmonicity (17) and a value of ν_2' not greatly reduced from that in the ground state. The symmetric stretching vibration is also probably excited in the transition (22, 23). Yet the molecule is strongly predissociated even from the (0000) level. The description is also in accord with the observation that the $\tilde{A}$-state is much less subject to pressure broadening than would be expected for a pure Rydberg state although showing typical Rydberg behaviour in some other respects (20).

Any model for the predissociation of the $\tilde{A}$-state must take into account the following observations:

(*1*) Decomposition into $NH_2 + H$ occurs with a quantum yield of one from all levels of the $\tilde{A}$-state. Lifetimes of 2 and 7 ps can be estimated from linewidths (18, 23) for the (0000) and (0100) vibrational levels of ND_3, *i.e.*, the (0000) level decomposes *faster* than the vibrationally excited (0100) level. Higher levels of ND_3 are all much shorter lived, while the longest lifetime of any excited level of NH_3 must be less than about 0.5 ps. The lifetimes of ND_3 in its two lowest levels are short but nevertheless correspond to many vibrations of the molecule; there must therefore be a potential well of appreciable depth in the D—ND_2 co-ordinate.

(*2*) There is a very large intramolecular isotope effect in the decomposition of NH_2D and NHD_2 from $v_2' = 0$ and 1, favouring the dissociation of H; from higher vibrational levels a more normal value of 2 or 3 is found (1). There is also a very large intermolecular isotope effect between NH_3 and ND_3, again evident only in the lowest vibrational levels.

(*3*) The present study has shown that the translational energy of the H or D atom produced in the photolysis *decreases* with increasing photon energy, from 2139 to 2062 to 1850 Å.

The simplest model that might be considered for the predissociation is shown in Fig. 5 for ND_3; this is very similar to that suggested by Douglas (18). If the potential barrier in the $\tilde{A}$-state lies between $v_2 = 1$ and $v_2 = 2$, then dissociation from $v_2 \geq 2$ would involve simple passage over the barrier, accounting for the short lifetime and the small isotope effect. Dissociation from $v_2 = 0$ or 1 would have to occur by "tunnelling" through the barrier, a slower process typically associated with a large deuterium isotope effect, as observed. The observation that decomposition from the $v_2 = 0$ level is about 3 times faster than from $v_2 = 1$ is

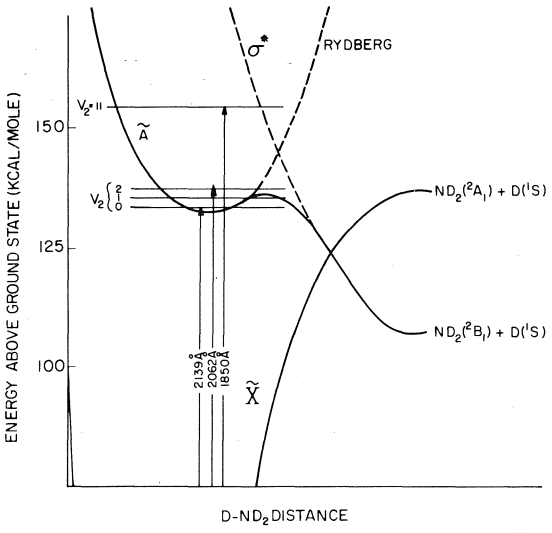

FIG. 5. Model for the predissociation of the $\tilde{A}$-state of ND_3. Correlation with products is for dissociation in the plane of the molecule. Energy levels are accurate, based on $\Delta H_f^0(ND_2) = 46.2$ kcal/mol at 0 K, and spectroscopic data for the $\tilde{A}$-state (18) and ND_2 (27). Potential curves are qualitative. Dotted lines represent hypothetical unperturbed Rydberg and σ^* states.

most plausibly explained by the fact, first pointed out by Longuet-Higgins (as quoted by Herzberg (ref. 19, p. 466)), that dissociation into ND_2 and D in their ground states is vibronically forbidden for odd values of v_2.

While the model shown in Fig. 5 can thus account for most of the features of the predissociation, it appears incapable of explaining the decrease in translational energy of the D or H atoms with increasing photon energy. It can be argued that the excess energy is initially in the v_2 out-of-plane bending vibration, and on dissociation will tend to go into rotational and vibrational excitation of the ND_2 or NH_2 radical rather than appearing as translational energy of the dissociating fragments. While this could lead to a hydrogen atom energy almost independent of photon energy, it is difficult to see how it could yield the observed inverse dependence. The most probable explanation of the latter would appear to be decomposition of the $\tilde{A}$-state by two channels, forming not only the ground-state products as shown in Fig. 5, but also $ND_2(^2A_1) + D$. At 2139 Å only the ground-state channel is energetically possible, but at 2062 and 1850 Å, ND_2 or NH_2 could be excited to the $^2A_1$ state. In the latter process much less translational energy could be imparted to the fragments, and if this channel became progressively more important at 2062 and 1850 Å, the observed dependence of translational energy on wavelength could be accounted for. Formation of excited ND_2 radicals by dissociation of the $\tilde{A}$-state is of course not allowed by the symmetry correlations shown in Fig. 5. These correlations however are based on dissociation in the plane of the molecule (18), and it may be questioned how strictly they apply if dissociation occurs out of the molecular plane, as appears not unlikely at 2062 and 1850 Å when the out-of-plane vibration is highly excited ($v_2 = 3$ and 9 respectively). There is some quite independent evidence that the planar state-correlations are not in fact obeyed in the ammonia system. From Fig. 5 it is clear that in-plane interaction of H with NH_2 in their ground states would not correlate with the ground state of NH_3, and one would expect the combination reaction to be slow, involving an intersystem crossing and probably a potential barrier. There is good experimental evidence that this and other combination reactions of NH_2 which would encounter the same difficulty are in fact very fast, occurring almost at the collision rate. Evleth has very recently considered this problem (25) and has shown by potential surface calculations that if the interaction is not constrained to planar geometry, NH_2 and H in their ground states interact on a smooth attractive surface to form the ground state of NH_3; *i.e.*, the $\tilde{A}$-state and the ground state interact strongly near their dissociation limits and the crossing shown in Fig. 5 is totally avoided. A corollary of course is that the $\tilde{A}$-state when not restricted to dissociation in the molecular plane can correlate with $NH_2(^2A_1) + H$. This leads to a model for the predissociation of the $\tilde{A}$-state, shown in Fig. 6 for ND_3, which appears to offer a much more satisfactory explanation of the experimental facts. The potential curve for the $\tilde{A}$-state is now determined by the interaction of 3 electronic states; the Rydberg and the valence-shell states strongly mixed as before, and what is formally the ground state in planar geometry interacting strongly as the dissociation limit is approached, leading to dissociation into $ND_2(^2A_1) + D$. The rapid predissociation of all levels of the $\tilde{A}$-state with $v_2 > 1$ now has a simple explanation; if $\Delta H_f^0(ND_2)$ at 0 K = 46.2 kcal/mol, a value which can be roughly estimated from $\Delta H_f^0(NH_2)$ at 298 K = 45.0 (26), then the dissociation limit of the $\tilde{A}$-state lies between $v_2 = 1$

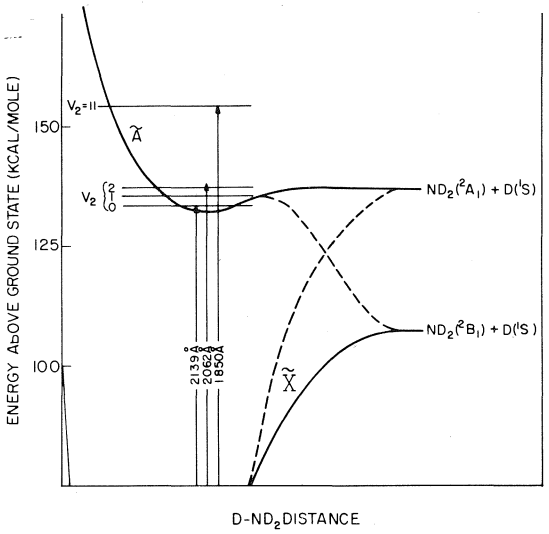

FIG. 6. Model for the predissociation of the $\tilde{A}$-state of ND_3, as in Fig. 5 but with product correlations for non-planar dissociation.

and $v_2 = 2$, so that above $v_2 = 1$ the molecule can dissociate rapidly by a vibrational predissociation, *i.e.* a simple unimolecular decomposition. For the $v_2 = 0$ and 1 levels this is energetically impossible and the predissociation must proceed by crossing to the ground state; this will be slower and should show a strong deuterium isotope effect, as observed, as the H or D atom tunnels between the potential surfaces. Dissociation to ground-state products from these levels may also be favoured because the out-of-plane vibration is not highly excited and the dissociation will therefore tend to occur not far out of the molecular plane and to follow the channel predicted by the planar symmetry correlations. The slower dissociation from the $v_2 = 1$ level can probably be explained as before by the influence of vibronic selection rules.

The predissociation mechanism shown in Fig. 6 provides a reasonable explanation of the translational excitation of the D or H atoms produced. At 2139 Å the $\tilde{A}$-state is excited to the $v_2 = 0$ level in ND_3 and the $v_2 = 0$ or 1 levels in NH_3, in which absorption in the $(0100) \leftarrow (01^+00)$ hot band is appreciable. Energy of about 28 to 30 kcal/mol is released on dissociation to ground-state $NH_2 + H$ or $ND_2 + D$, and from conservation of momentum a maximum of between 25 and 28 kcal/mol could be converted to translational energy of the H or D atom. As noted earlier the present experiments did not permit a precise measurement of translational energies, but it was probably something less than 20 kcal/mol at 2139 Å. The remainder of the energy released may be assumed to go into vibrational and rotational excitation of the amino radical in what appears a reasonable partition of energy. Dissociation at 2062 Å ($v_2 = 3$) to give amino radicals in the $^2A_1$ state can release very little translational energy, no more than 3 kcal/mol, and the observed reduction in the translational energy of the H and D atoms can be attributed to the onset of this process. The fact that there is still evidently considerable hot-atom reaction at 2062 Å indicates that some of the dissociation is still proceeding by the lower channel. The further decrease in translational energy at 1850 Å suggests that predissociation by the lower channel competes less and less effectively with the unimolecular decomposition as the latter becomes faster with increasing vibrational excitation of the $\tilde{A}$-state. Little of the energy of excitation of ν_2 will be converted to translational energy of the fragments in the latter process because in a unimolecular decomposition of this sort the molecule will tend to dissociate with minimal energy in the reaction co-ordinate, only slightly in excess of the dissociation energy. The suggested competition between the two dissociation channels can also account for the sharper fall-off in translation energy of D from ND_3 evident in Table 2; the predissociation of ND_3 is slower than that of NH_3, so that predissociation to ground-state products will compete less effectively with the higher-energy channel as the latter should show a smaller isotope effect.

The mechanism that thus emerges for the predissociation of the $\tilde{A}$-state may be summarized. Excitation to levels of $v_2 = 0$ or 1 leads to relatively slow predissociation essentially by an intersystem crossing to the ground state, yielding $H + NH_2(^2B_1)$. At levels above $v_2 = 1$, the higher-energy channel leading to $H + NH_2(^2A_1)$ becomes accessible, and the $\tilde{A}$-state begins to dissociate by a simple unimolecular decomposition in competition with the lower-energy channel. With increasing photon energy, ν_2 and probably ν_1 are excited to higher levels, the unimolecular decomposition becomes faster, and the low-energy channel competes less and less effectively. This mechanism appears to offer the most plausible explanation of the experimental facts. It is of course an oversimplification of a complex system; in particular, no single potential energy curve such as those of Figs. 5 and 6 can predict the dynamics of the predissociation as the out-of-plane angle of the dissociation co-ordinate is varied widely. The latter angle may be closely coupled to the level of excitation of ν_2, and it is possible that the predissociation from low levels of ν_2 may approximate more closely to the model in Fig. 5, while with increasing excitation of ν_2 the system will tend to follow the model in Fig. 6. A dynamic calculation based on potential energy surfaces for each level of excitation of ν_2 and for a range of out-of-plane dissociation angles would be required to settle this question. The proposed mechanism predicts that emission from the $(^2A_1)$ state of the amino radical should be observed at all excitation wavelengths below about 2100 Å. Okabe and Lenzi (24) failed to observe such emission, but their detection system was only sensitive to about 6000 Å. For excitation at 2062 and 1850 Å, the minimum *possible* wavelengths for NH_2 emission are about 9400 and 6000 Å

respectively, and the Franck–Condon factors in the transition will shift the emission *maximum* far to the red. Observation of emission at these wavelengths could be difficult experimentally but would lend strong support to the proposed mechanism. Quantitative measurements of the emission could yield detailed information about the predissociation, and it is hoped to attempt such measurements in the near future.

1. S. KODA and R. A. BACK. Can. J. Chem. This issue.
2. R. J. CARTER, W. H. HAMILL, and R. R. WILLIAMS, JR. J. Am. Chem. Soc. **77**, 6457 (1955).
3. R. M. MARTIN and J. E. WILLARD. J. Chem. Phys. **40**, 3007 (1964).
4. A. KUPPERMANN and J. M. WHITE. J. Chem. Phys. **44**, 4352 (1966).
5. C. C. CHOU and F. S. ROWLAND. J. Am. Chem. Soc. **88**, 2616 (1966).
6. R. G. GANN and J. DUBRIN. J. Chem. Phys. **47**, 1867 (1967); **50**, 535 (1969).
7. G. P. STURM and J. M. WHITE. J. Chem. Phys. **50**, 5035 (1969).
8. L. E. COMPTON and R. M. MARTIN. J. Chem. Phys. **52**, 1613 (1970).
9. L. E. COMPTON, J. L. GOLE, and R. M. MARTIN. J. Phys. Chem. **73**, 1158 (1969).
10. B. G. DZANTIEV, A. K. LYUBIMOVA, and A. V. SHISHKOV. Khim. Vys. Energ. **3**, 478 (1969).
11. R. D. PENZHORN, E. LISSI, I. RIVAS, and H. SOTO. Z. Phys. Chem. Frankfurt am Main, **83**, 200 (1973).
12. G. A. OLDERSHAW and D. A. PORTER. J. Chem. Soc. Faraday Trans. 1, **70**, 1240 (1974).
13. L. E. COMPTON and R. M. MARTIN. J. Phys. Chem. **73**, 3474 (1969).
14. U. SCHURATH, P. TIEDEMANN, and R. N. SCHINDLER. J. Phys. Chem. **73**, 456 (1969).
15. J. R. MCNESBY, I. TANAKA, and H. OKABE. J. Chem. Phys. **36**, 605 (1962).
16. K. YANG. J. Phys. Chem. **67**, 562 (1963).
17. A. O. WALSH and P. A. WARSOP. Trans. Faraday Soc. **57**, 345 (1961).
18. A. E. DOUGLAS. Discuss. Faraday Soc. **35**, 158 (1963).
19. G. HERZBERG. Electronic spectra of polyatomic molecules. Van Nostrand, Princeton, NJ. 1966.
20. M. B. ROBIN. Higher excited states of polyatomic molecules. Vol. I. Academic Press, New York, NY. 1974.
21. J. A. HORSLEY and F. FLOUQUET. Chem. Phys. Lett. **5**, 165 (1970).
22. W. R. HARSHBARGER. J. Chem. Phys. **53**, 903 (1970).
23. P. A. HACKETT, R. A. BACK, and S. KODA. J. Chem. Phys. **65**, 5103 (1976).
24. H. OKABE and M. LENZI. J. Chem. Phys. **47**, 5241 (1967).
25. E. M. EVLETH. Chem. Phys. Lett. **38**, 516 (1976).
26. S. W. BENSON and H. E. O'NEAL. Kinetic data on gas phase unimolecular reactions. NSRDS-NBS 21, U.S. Government Printing Office, Washington, DC. 1970.
27. K. DRESSLER and D. A. RAMSAY. Phil. Trans. R. Soc. London, A**251**, 553 (1959).

The ultraviolet absorption spectrum of methyl diimide vapor[1]

S.K. VIDYARTHI,[2] C. WILLIS, AND R.A. BACK

Division of Chemistry, National Research Council of Canada, Ottawa, Ont., Canada K1A 0R6

Received October 22, 1976

S. K. VIDYARTHI, C. WILLIS, and R. A. BACK. Can. J. Chem. **55**, 1396 (1977).

The vapor phase absorption spectra of $CH_3N{=}NH$ and $CH_3N{=}ND$ have been measured from 160–450 nm. There are three prominent features centered at 360 nm ($\varepsilon = 6\ M^{-1}\ cm^{-1}$), 208 nm ($\varepsilon = 710\ M^{-1}\ cm^{-1}$), and 170 nm ($\varepsilon = 2080\ M^{-1}\ cm^{-1}$). The weak near-uv band is assigned to the valence shell transition $\pi^* \leftarrow n_+$ while the two far-uv bands are attributed to the $3s \leftarrow n_+$ and $3p \leftarrow n_+$ Rydberg transitions. The band at 208 nm has resolved vibrational structure on the long wavelength tail and a vibrational analysis shows the main progression excited is the ν_{10}' CNN deformation mode.

S. K. VIDYARTHI, C. WILLIS et R. A. BACK. Can. J. Chem. **55**, 1396 (1977).

On a mesuré, de 160–450 nm, le spectre d'absorption en phase vapeur de $CH_3N{=}NH$ et $CH_3N{=}ND$. Il y a trois caractéristiques principales qui sont centrées à 360 nm ($\varepsilon = 6\ M^{-1}\ cm^{-1}$), 208 nm ($\varepsilon = 710\ M^{-1}\ cm^{-1}$) et 170 nm ($\varepsilon = 2080\ M^{-1}\ cm^{-1}$). On a attribué la bande faible dans le proche ultra-violet à une transition de couche de valence $\pi^* \leftarrow n_+$ alors que les deux bandes d'ultra-violet lointain sont attribuées à des transitions $3s \leftarrow n_+$ et $3p \leftarrow n_+$ de Rydberg. La bande à 208 nm a une structure vibrationnelle résolue sur la queue à grande longueur d'onde et une analyse vibrationnelle montre que la progression principale qui est excitée est le mode de déformation CNN ν_{10}'.

[Traduit par le journal]

Introduction

There has been sustained interest in the ultraviolet spectroscopy of azo compounds including the prototype molecule diimide, N_2H_2. Methyldiimide, $CH_3N{=}NH$, is the first member of a series of unstable monoalkyl diimides which have been prepared by Ackermann and coworkers (1), Kosower (2), and others. These compounds show typical weak azo absorption in the near ultraviolet but their far-uv absorption spectra have not been reported. Methyldiimide is of particular interest as a compound intermediate between diimide and azomethane whose far-uv spectra have both been studied in some detail (3–5) and the photoelectron spectrum of all three have recently been reported (6).

Experimental

Samples of $CH_3N{=}NH$ and $CH_3N{=}ND$ were prepared as described elsewhere (7). Traces of ammonia were removed by treatment with P_2O_5. Methyldiimide decays both thermally and photochemically to form N_2 and CH_4, both transparent above 160 nm so that a useful criterion of purity was the absence of residual absorption after complete decomposition of the sample. Absolute extinction coefficients were based on measurement of final pressures of N_2 and CH_4; because of the thermal instability of methyldiimide and its great sensitivity to light, there is an uncertainty of $\pm 10\%$ in these absolute values.

Absorption spectra above 200 nm were measured in a Cary-15 spectrophotometer, and below 200 nm with a helium-flushed McPherson 0.5 m grating monochromator system using absorption cells with sapphire windows. Spectra above 200 nm were also photographed with a medium Hilger quartz-prism spectrograph.

Results

The near-uv spectrum of $CH_3N{=}NH$, measured at room temperature and about 50 torr pressure is shown in Fig. 1. The molar decadic extinction coefficient at the maximum at 360 nm was $6 \pm 2\ M^{-1}\ cm^{-1}$. Essentially the same spectrum was observed with $CH_3N{=}ND$. No fine structure was discernible in the spectrum of either compound, either in the spectrophotometer traces or in the photographic spectra of the same region. The spectrum is apparently completely diffuse,[3] like that of azomethane, showing none of the sharp vibrational structure evident with N_2H_2.

[1]NRCC No. 15799.

[2]NRCC Postdoctoral Fellow 1973–1975. Present address: Domtar Research, Senneville, P.Q.

[3]Ackermann and co-workers reported faint structure in the near-uv band of $CH_3N{=}NH$; it seems possible that this was due to the presence of a small N_2H_2 impurity, as there is some evidence that this can be formed in the synthesis of $CH_3N{=}NH$ by the method employed (8).

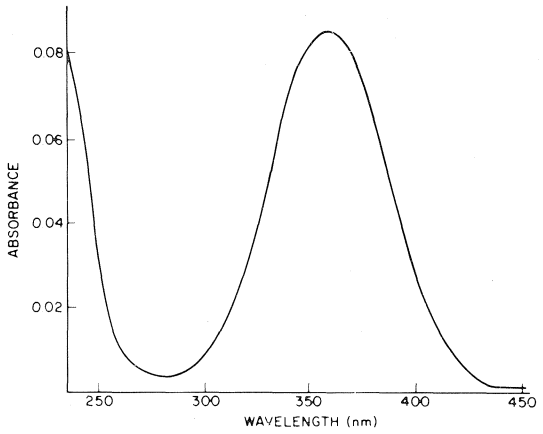

FIG. 1. Near-uv absorption spectrum of methyldiimide.

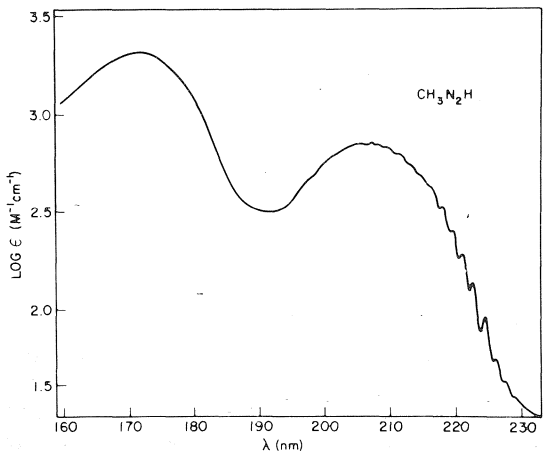

FIG. 2. Far-uv absorption spectrum of methyldiimide.

Two much stronger broad absorption bands were observed in the far-uv spectrum (Fig. 2) with maxima at 208 and 172 nm, and values of ε_{max} of about 710 and 2080 M^{-1} cm^{-1} respectively. The band at 208 nm shows vibrational structure on the long-wavelength side, while the band at 172 nm is completely diffuse. The 208 nm band is shown at higher resolution in Fig. 3 for both $CH_3N{=}NH$ and $CH_3N{=}ND$, exhibiting a blue shift of about 2 nm on deuteriation. The frequencies of the vibrational band maxima were measured from photographic plates, calibrated with a standard iron arc, and are listed in Tables 1 and 2 for $CH_3N{=}NH$ and $CH_3N{=}ND$.

Discussion

Vibrational Analysis of the 208 nm Band

The vibrational structure in the 208 nm band

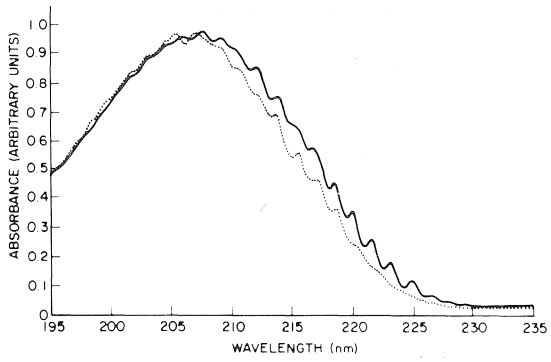

FIG. 3. The 208 nm band of methyldiimide and methyldiimide-d_1; solid line, $CH_3N{=}NH$; dotted line, $CH_3N{=}ND$.

of $CH_3N{=}NH$ consists largely of a single long strong progression which is evident in Fig. 3. Upon closer inspection of the photographic spectrum, however, it could be seen that this was overlapped by two other weaker progressions having the same band interval. Band frequencies and intervals for the three progressions are listed in Table 1. The first, strong progression is in column 1; the second, in column 2, was much weaker; while the third (column 3) was weaker still with fewer members detectable. The average band interval from all three progressions is 324 cm^{-1}. The spectrum of $CH_3N{=}ND$ follows an entirely analogous pattern (Table 2) with a band interval of 326 cm^{-1}. The considerable scatter in the values for the intervals between bands for both molecules reflects the inaccuracy in estimating the positions of the band maxima for bands which were largely overlapped, often weak, and distorted by the sharp increase in the absorption with decreasing wavelength.

The only reasonable interpretation of the long progressions in Tables 1 and 2 is that they arise from excitation of the ν_{10}' CNN deformation (bending) vibration of the upper state. In the ground state this has a frequency of 557 cm^{-1} (1), and the observed value of 325 cm^{-1} represents a very considerable reduction. Excitation of the equivalent CNN bending vibration has been suggested recently in the analogous transition in azomethane (4), with frequencies of 470 and 590 cm^{-1} in the upper and ground states respectively, while in both the near- (9) and far- (3) uv transitions of N_2H_2, the symmetric HNN bending vibration is strongly excited.

The two weaker progressions (columns 2 and

TABLE 1. Frequencies of vibrational band maxima for the 208 nm band of $CH_3N{=}NH$, with intervals between bands in parentheses*

	Frequency for $v_{15}'' =$				
V_{10}'	0		1		2
0	43675	(210)	43465		
	(354)		(346)		
1	44029	(218)	43811		
	(333)		(320)		
2	44362	(231)	44131	(234)	43897
	(301)		(330)		(314)
3	44663	(202)	44461	(250)	44211
	(329)		(351)		(328)
4	44992	(180)	44812	(273)	44539
	(314)		(292)		(367)
5	45306	(202)	45104	(198)	44906
	(318)		(363)		(309)
6	45624	(157)	45467	(252)	45215
	(312)		(301)		
7	45936	(168)	45768		
	(300)		(290)		
8	46236	(178)	46058		
	(338)		(333)		
9	46574	(183)	46391		
	(308)				
10	46882				
Average	(321)		(325)		(330)
intervals		(193)		(241)	

*Average $\nu_{10}' = 324\ cm^{-1}$; average $\nu_{15}'' = 209\ cm^{-1}$.

3) are most probably hot bands arising from thermal excitation of ν_{15}'', the methyl torsional vibration, in the ground state, which has been tentatively identified by Ackermann and coworkers (1) from combination bands in the ir spectrum. Its frequency of about $170\ cm^{-1}$ is reasonably close, within the accuracy of the two measurements, to the average separation of $204\ cm^{-1}$ between the progressions in Tables 1 and 2, and the Boltzmann factors of ~0.4 and ~0.2 at 25°C for $v_{15}'' = 1$ and 2 are in approximate accord with the relative intensities of the three progressions. Spectra measured at 85°C showed no marked change from room temperature, which is not incompatible with the presence of ν_{15}'' hot bands, since the expected increases of about 10 and 30% in these weak, overlapped bands in the second and third progressions would have been difficult to detect. This probably does rule out the alternative possibility that the weak progressions arise from thermal excitation of ν_{10}'' in the ground state; the average interval between the progressions could be $204 + 325 = 529\ cm^{-1}$, not far from the infrared value of 557 for ν_{10}'', but raising the temperature to 85°C should have increased the intensity of the $v_{10}'' = 1$ hot bands by 50% and increased that for $v_{10}'' = 2$ by a factor of 2.5, which should have been detected. It also does not appear reasonable to assign the weak progressions to excitation of a second vibration, the N—N stretch for example, in the excited state, as this would require displacement of the progressions relative to one another in an impossible manner.

Values of v_{10}' in Tables 1 and 2 have been assigned on the assumption that the first bands in the first two progressions in each case correspond to $v_{10}' = 0$ corresponding to band origins of 43 675 and 43 668 cm^{-1} for $CH_3N{=}NH$ and $CH_3N{=}ND$ respectively. This is probably correct, as no other bands could be detected at longer wavelengths, but must be regarded as still somewhat tentative.

Assignment of the Electronic Transitions

By analogy with the equivalent absorptions in *trans*-N_2H_2 (λ_{max} = 365 nm (9)) and in *trans*-azomethane (λ_{max} = 340 nm (10)), the weak

TABLE 2. Frequencies of vibrational band maxima for the 206 nm band of $CH_3N{=}ND$, with intervals between bands in parentheses*

	Frequency for $v_{15}'' =$				
V_{10}'	0		1		2
0	43668	(203)	43465		
	(343)		(319)		
1	44011	(227)	43784		
	(330)		(344)		
2	44341	(213)	44128		
	(310)		(339)		
3	44651	(184)	44467	(236)	44231
	(338)		(317)		(271)
4	44989	(205)	44784	(282)	44502
	(310)		(321)		(367)
5	45299	(194)	45105	(236)	44869
	(319)		(348)		(331)
6	45618	(165)	45453	(253)	45200
	(316)		(304)		(337)
7	45934	(177)	45757	(220)	45537
	(305)		(335)		
8	46238	(146)	46092		
	(361)		(308)		
9	46599	(199)	46400		
	(332)		(334)		
10	46931	(197)	46734		
	(301)				
11	47232				
Average intervals	(324)	(192)	(327)	(245)	(327)

*Average $\nu_{10}' = 326\ cm^{-1}$; average $\nu_{15}'' = 209\ cm^{-1}$.

TABLE 3. Rydberg term values and quantum deficiencies (δ) in $CH_3N{=}NH$ and $CH_3N{=}NCH_3$

Compound	Absorption maximum (nm)	Assignment	Term value[a] (cm^{-1})	Quantum deficiency (δ)	Extinction coefficient ($M^{-1}\ cm^{-1}$)
$CH_3N{=}NH$	208	$3s \leftarrow n_+$	28500 ± 500	1.0_6	710
	170	$3p \leftarrow n_+$	19000 ± 500	0.6_0	2080
$CH_3N{=}NCH_3$	227	$3s \leftarrow n_+$[b]	28400	1.0_3	≤ 0.5[c]
	185	$3p \leftarrow n_+$[b]	18400	0.5_6	≈ 7000

[a]Derived from $E_{vert}^{p.e.} - E_{vert}^{uv} = R/(n - \delta)^2$ where $E_{vert}^{p.e.}$ is the vertical IP taken from photoelectron spectrum (6) and E_{vert}^{uv} is maximum of uv absorption.
[b]These assignments are taken from Robin (5).
[c]See ref. 12.

structureless band in methyldiimide with $\lambda_{max} = 360$ nm can comfortably be assigned to the $\pi^* \leftarrow n_+$ transition.

The two far-uv absorption bands can probably be assigned respectively to $3s \leftarrow n_+$ and $3p \leftarrow n_+$ Rydberg transitions. The term values and quantum defects, given in Table 3, are what would be expected and agree closely with those derived from the absorption spectra of azomethane for which Robin (5) convincingly argues that the first two short wavelength absorptions (weak shoulder with $E_{max} = 44\,100\ cm^{-1}$ and strong band with $E_{max} = 54\,000\ cm^{-1}$) are Rydberg in nature. The very different relative intensities for the absorption due to the $3s \leftarrow n_+$ transition in azomethane and methyldiimide is as expected. The transition is $g \leftarrow g$ parity forbidden for C_{2h} symmetry (azomethane) but fully allowed for C_s symmetry (methyldiimide). Although the second short wavelength band in methyldiimide

centered around 170 nm fits very well with the assignment to the $3p \leftarrow n_+$ transition, involvement of the valence shell transition $\pi^* \leftarrow n_-$ cannot be ruled out. The observed band maximum is $E_{max} = 58\,000\ cm^{-1}$ which is very close to that predicted for the $^1(\pi^* \leftarrow n_-)$ transition in diimide (11). It has been recently suggested (6) that the 170 nm band in N_2H_2 can be assigned to the $3p \leftarrow n_+$ Rydberg transition.

1. M.N. ACKERMANN, J.J. BURDGE, and N.C. CRAIG. J. Chem. Phys. **58**, 203 (1973).
2. E.M. KOSOWER. Acc. Chem. Res. **4**, 193 (1971).
3. A. TROMBETTI. Can. J. Phys. **46**, 1005 (1968).
4. A.M. BASS and A.H. LAUFER. J. Photochem. **2**, 465 (1973).
5. M.B. ROBIN. Higher excited states of polyatomic molecules. Vol. II. Academic Press, New York, NY. 1975. pp. 68–73.
6. D.C. FROST, S.T. LEE, C.A. MCDOWELL, and N.P.C WESTWOOD. J. Chem. Phys. **64**, 4719 (1976).
7. S.K. VIDYARTHI, C. WILLIS, and R.A. BACK. J. Phys. Chem. **80**, 559 (1976).
8. W.E. STEINMETZ, D.H. ROBINSON, and M.N. ACKERMANN. Inorg. Chem. **14**, 421 (1975).
9. R.A. BACK, C. WILLIS, and D.A. RAMSAY. Can. J. Chem. **52**, 1006 (1974).
10. J.G. CALVERT and J.N. PITTS. Photochemistry. J. Wiley and Sons, New York. 1966. p. 453.
11. (*a*) N. C. BAIRD and J. R. SWENSON. Can. J. Chem. **51**, 3097 (1973). (*b*) M. B. ROBIN, R. R. HART, and N. A. KUEBLER. J. Am. Chem. Soc. **89**, 1564 (1967).
12. O. A. MOSHER, M. S. FOSTER, W. M. FLICKER, J. L. BEAUCHAMP, and A. KUPPERMAN. J. Chem. Phys. **62**, 3424 (1975).

Solvent effect correlations and the mechanism of solvolysis of alkyl chlorosulfates[1]

ERWIN BUNCEL, J. PETER MILLINGTON, AND JAMES F. WILTSHIRE
Department of Chemistry, Queen's University, Kingston, Ont., Canada K7L 3N6

Received September 15, 1976

ERWIN BUNCEL, J. PETER MILLINGTON, and JAMES F. WILTSHIRE. Can. J. Chem. **55**, 1401 (1977).

The rate of hydrolysis of the series of alkyl chlorosulfates $ROSO_2Cl$ (R = ethyl, *n*-propyl, isobutyl, neopentyl) has been measured as a function of solvent composition in dioxane–water media. The solvent effect is examined from the viewpoint of dielectric constant, solvation number, and solvent ionizing power. The results point to a continuous variation of solvolytic mechanisms (from S_N2, through borderline, to S_N1) along the series. The correlations are also considered with respect to the 'entropy criterion' for multiple bond scission previously advanced for solvolysis of the alkyl chlorosulfates. Solute–solvent interactions are identified as a possible alternative origin of the abnormally large $\Delta S^{\neq}$ values observed in chlorosulfate solvolysis.

ERWIN BUNCEL, J. PETER MILLINGTON et JAMES F. WILTSHIRE. Can. J. Chem. **55**, 1401 (1977).

On a mesuré les vitesses d'hydrolyse d'une série de chlorosulfates d'alkyles $ROSCO_2Cl$ (R = éthyle, *n*-propyle, isobutyle, néopentyle) en fonction de la composition du solvant dans un milieu dioxanne–eau. On a examiné l'effet du solvant à partir du point de vue de la constante diélectrique, du nombre de solvatation et du pouvoir ionisant du solvant. Les résultats indiquent qu'il y a une variation continue des mécanismes de solvolyse (à partir de S_N2 et passant par des cas intermédiaires jusqu'à S_N1) tout le long de la série. On considère aussi des corrélations par rapport avec le 'critère d'entropie' pour les scissions de liens multiples qui ont été proposé antérieurement pour la solvolyse des chlorosulfates d'alkyles. On a identifié les interactions soluté–solvant comme une origine alternative possible pour les valeurs de $\Delta S^{\neq}$ qui sont anormalement grandes et qui ont été observées pour la solvolyse des chlorosulfates.
[Traduit par le journal]

Although many discussions of solvent effects on reaction rates of nucleophilic substitution processes have been reported, systematic investigations of reaction series are relatively few in number (1–5). Previously we reported on the mechanism of solvolysis of a series of primary alkyl chlorosulfates, $ROSO_2Cl$, in aqueous dioxane (6–8). A normal mode of solvolysis, that is bimolecular or unimolecular displacement on carbon with $^-OSO_2Cl$ as the leaving group, was indicated by (*i*) the effect of nucleophiles on the rate of hydrolysis of *n*-propyl chlorosulfate; (*ii*) the observation of a large lyate ion effect ($k_{OH^-}/k_{H_2O} = 380$) for *n*-propyl chlorosulfate but an absence of a lyate ion effect ($k_{OH^-}/k_{H_2O} = 1$) for neopentyl chlorosulfate; (*iii*) the occurrence of rearrangement in the hydrolysis of neopentyl chlorosulfate; (*iv*) the relative reactivities of the series of primary alkyl chlorosulfates (methyl > ethyl > *n*-propyl > isobutyl > neopentyl). These observations were in accord with the solvolytic transition states **1** and **2** (uni- and bimolecular mechanisms, respectively, with Nu as the nucleophilic species). However, the observation of 'abnormally' large entropies of activation suggested that ternary fission (fragmentation (9)) was occurring, *i.e.* transition states **3** and **4** with both carbon–oxygen and sulfur–chlorine bond weakenings.

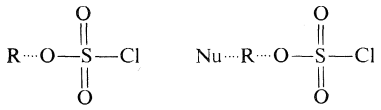

1

2

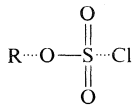

3

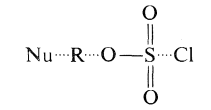

4

Further work has been undertaken in order to obtain additional information on the nature of the solvolytic mechanism of alkyl chlorosulfates, and to shed light on the validity of the entropy criterion of fragmentation. The present paper describes the results of the application of solvent

[1]Bond scission in sulfur compounds. Part XI. For part X see ref. 42.

TABLE 1. Rates of hydrolysis of alkyl chlorosulfates at 25°C as function of water molarity, dielectric constant, and solvent ionizing power

$ROSO_2Cl$	$[H_2O]$ (M/l)	ε[a]	Y[b]	$k \times 10^4$ s^{-1}	$\Delta H^{\ddagger}$ (kcal)	$\Delta S^{\ddagger}$ (25°C) (eu)	$\Delta F^{\ddagger}$ (25°C) (kcal)
Ethyl	10.00[c]	8.7	−1.04	71.7	12.6	−26.0	20.4
	14.97	15.0	−0.23	104.0			
	19.95	22.3	0.40	154.0			
	29.93	38.0	1.55	213.0			
	34.91	46.0	1.91	242.0			
n-Propyl	10.00[c]	8.7	−1.04	39.8	13.6	−24.0	20.7
	13.45	12.8	−0.36	55.0			
	19.95	22.2	0.40	88.1			
	28.85	37.3	1.44	130.0			
	39.65	53.7	2.15	186.0			
Isobutyl	10.00[c]	8.7	−1.04	3.09	17.6	−15.5	22.2
	19.90	22.2	0.40	10.4			
	29.83	38.0	1.54	20.5			
	42.00	55.5	2.27	43.9			
Neopentyl	9.93[c]	8.6	−1.04	0.168	24.0	0.1	24.0
	19.85	22.2	0.40	1.15			
	29.99	38.0	1.55	4.18			
	43.00	57.7	2.31	9.96			

[a]Data from ref. 43.
[b]From ref. 33*a*.
[c]From ref. 7.

effect correlations to the problem. Related mechanistic studies of chlorosulfates have been reported from this as well as other laboratories (10–12). Solvolytic studies of sulfonyl chlorides (13–16) also have a bearing on this work.

Results and Discussion

In Table 1 are presented the data for the conductimetrically determined rates of hydrolysis of ethyl, *n*-propyl, isobutyl, and neopentyl chlorosulfate in various dioxane–water media at 25°C. In the ensuing discussion, the influence of solvent composition on velocity of reaction will be considered from the following viewpoints: (*1*) electrostatic theory; (*2*) solvation numbers; (*3*) solvent ionizing power. The information derived from these treatments will then be considered with respect to the abnormal $\Delta S^{\ddagger}$ values which have been observed for this reaction series. Finally, we will consider the application of the $\Delta S^{\ddagger}$ criterion in other systems. The availability of comparable data in the literature on the response of reaction rates to medium changes serves as a useful reference point in interpretation of the present results.

Correlations with Dielectric Constant

According to electrostatic theory of reaction kinetics, the velocity of a solvolytic reaction should increase with increasing dielectric constant of the medium (17–20). For an S_N1 reaction occurring in a medium of dielectric constant ε the electrostatic component of the free energy of activation, $\Delta G_{es}^{\ddagger}$, is given by (20) [1][2] in which σ is the separation of charges z_Ae and z_Be in the quasi-ionic activated complex, which is assumed to be in the form of a double sphere with radii r_A and r_B:

$$[1] \qquad \Delta G_{es}^{\ddagger} = \frac{z_A^2e^2}{2\varepsilon r_A} + \frac{z_B^2e^2}{2\varepsilon r_B} + \frac{z_Az_Be^2}{\sigma\varepsilon}$$

For the simplified case that $r_A = r_B = r$, $\sigma = 2r$ and $z_A = 1$, $z_B = -1$, this expression reduces to

$$[2] \qquad \Delta G_{es}^{\ddagger} = \frac{e^2}{2\varepsilon r}$$

Equation 2 predicts that a linear plot will result between the logarithm of the rate constant and the reciprocal of the dielectric constant, with slope $e^2/2r$. In practice such plots are somewhat

[2]Equation 1 corresponds to the 'double sphere' model of ref. 20, which is deemed to be more applicable to the present problem than the 'single sphere' model (20). The final expressions for the two models, however, only differ by a small numerical factor. The derivations are based on the assumption of a continuous dielectric medium (*cf.* ref. 21).

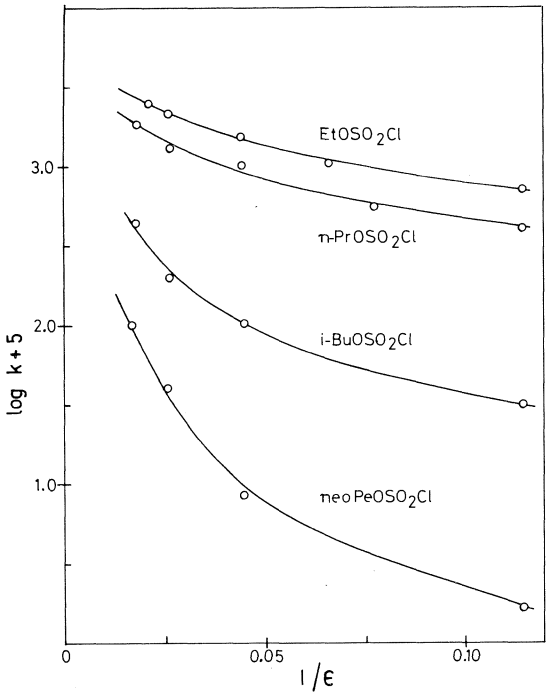

FIG. 1. Correlation between the logarithm of the rate constant and the inverse of the dielectric constant for the hydrolysis of alkyl chlorosulfates in dioxane–water mixtures.

curved, the slope decreasing in the region of low ε values, and it may be suggested that this is caused by the intrusion of S_N2 character in media of low polarity.

The log *k vs.* 1/ε plots for solvolysis of the alkyl chlorosulfates are presented in Fig. 1. The plots reveal a family of curves with increasing dependence of rate on dielectric constant, the dependence being least for ethyl chlorosulfate and greatest for neopentyl chlorosulfate. This behaviour can be rationalized by the designation of a bimolecular (S_N2) and a unimolecular (S_N1) mechanism to the two extreme types of behaviour, with a borderline or intermediate ($S_N1/2$) mechanism in between. Specifically, the increments in the magnitudes of the initial slope values along the series (Table 2) are indicative of the following operative mechanisms: bimolecular for ethyl and *n*-propyl chlorosulfate, unimolecular for neopentyl, and intermediate for the isobutyl compound.

Table 2 presents, in addition to data for the chlorosulfate series, the slopes of log *k vs.* 1/ε plots and the derived $r_\pm$ values (20) for solvolysis of some alkyl halides, based on measurements

TABLE 2. Dielectric constant correlations: comparison of slopes and $r_\pm$ values[a]

	d(log *k*)/d (1/ε)	$r_\pm$ (Å)
$EtOSO_2Cl$	−11.8	9.74
n-$PrOSO_2Cl$	−14.0	8.21
i-$BuOSO_2Cl$	−29.5	3.90
neoPeOSO_2Cl	−40.5	2.84
EtBr	−122.1	1.00
tert-BuCl	−423.5	0.29
tert-BuBr	−238.4	0.51

[a]Calculations according to ref. 20; the data for EtBr, *tert*-BuCl and *tert*-BuBr are taken from refs. 20 and 22*c*.

in the high dielectric constant region of acetone–water mixtures (22*c*). The larger $r_\pm$ value for ethyl bromide compared with the *tert*-butyl halides is in accord with the bimolecular mechanism of solvolysis. Comparison of the data for the chlorosulfates with those for the alkyl halides shows that for the former the slopes are much smaller and the $r_\pm$ values are much greater.

The large $r_\pm$ values for the chlorosulfate series are consistent with the proposal of multiple bond scission in the transition state. The ion pair formed by ternary scission, $[R^+SO_3\ Cl^-]$, would have the ionic species separated by a greater distance than in the case of a simple ion pair such as $[R^+Cl^-]$; this would lead to a greater effective radius of the activated complex and hence a larger apparent $r_\pm$ value for chlorosulfate solvolysis. Hence, according to this treatment the reason for the smaller slope in the log *k vs.* 1/ε plot for neopentyl chlorosulfate as compared to the *tert*-butyl chloride or bromide case is a greater effective $r_\pm$ value due to multiple bond scission. For ethyl and *n*-propyl chlorosulfate the $r_\pm$ values appear to be unreasonably large, but this is probably an artifact of the model used, as it is noted that [1] is not strictly applicable to the bimolecular mechanism of solvolysis.

A weakness of the electrostatic model is that it treats the medium as a continuous dielectric and thus ignores the operation of specific solute–solvent interactions. Alternative approaches employ empirical solvent parameters, and since these are based on selected model processes (*e.g.*, the solvolysis of *tert*-butyl chloride), they can serve as probes of solute–solvent interactions. An investigation, using these alternative approaches, of the solute–solvent interactions in the hydrolysis of alkyl chlorosulfates is given below.

TABLE 3. Comparison of solvation numbers and $\Delta S^{\neq}$ values for chlorosulfates and other alkyl derivatives in aqueous dioxane or aqueous acetone[a]

	n	$\Delta S^{\neq}$ (eu)	Medium	Temperature (°C)	Reference
Ethyl chlorosulfate	1.01	−26.0	aq. dioxane	25	This work
n-Propyl chlorosulfate	1.10	−24.0	aq. dioxane	25	This work
Ethyl bromide	2.3	−37	aq. acetone	25	22*b*
Methanesulfonyl chloride	2.4	−30	aq. dioxane	25	14*b*
Ethanesulfonyl chloride	2.6	−37	aq. dioxane	25	14*b*
Ethyl benzenesulfonate	3.3	−20	aq. dioxane	25	22*b*
i-Butyl chlorosulfate	1.81	−15.5	aq. dioxane	25	This work
i-Propyl benzenesulfonate	4.3	−14	aq. dioxane	25	22*b*
Neopentyl chlorosulfate	2.86	0.1	aq. dioxane	25	This work
α-Phenylethyl chloride	4.7	−16	aq. dioxane	50	33*b*
tert-Butyl bromide	5.7	−14	aq. acetone	25	22*c*
Benzhydryl chloride	6.3	−15	aq. acetone	50	33*d*
tert-Butyl chloride	6.7	−12	aq. dioxane	50	33*a*

[a]Solvation numbers (n) are derived from kinetic data (via [3]) over a range of solvent compositions, while $\Delta S^{\neq}$ values refer to media with a 10 M water content.

Solvation Numbers

Solvation numbers, n, derived from [3] in which k_1 is the measured pseudo first-order rate constant, have been obtained for many hydrolytic reactions in dioxane–water or acetone–water mixtures.[3] Although for a number of reasons n cannot be directly equated with molecularity with respect to water (*e.g.*, use of activities rather

$$[3] \qquad \log k_1 = \log k' + n \log [H_2O]$$

than concentrations leads to much steeper curves), nevertheless values of n provide a useful empirical criterion of mechanism (22–26). Thus unimolecular solvolysis is associated with larger solvation numbers than bimolecular solvolysis. The data in Table 3 show that for common alkyl derivatives n is typically 5–7 in unimolecular solvolysis and 2–3 in bimolecular solvolysis.[4] These results may be attributed to a specific solvation of the transition state by the water molecules, bearing in mind that in the unimolecular mechanism the carbonium ion is formed within a solvation shell of water. The critical number of water molecules required in the unimolecular mechanism will be greater than in the bimolecular mechanism, since in the latter case the role of water molecules is limited to solvation of the incipient anion and to nucleophilic participation.

The log k *vs.* log $[H_2O]$ plots for the alkyl chlorosulfates (Fig. 2) are linear; the derived n values are given in Table 3. The striking aspect about the data of Table 3 are the low n values for the alkyl chlorosulfates. It appears that in the chlorosulfate series the bimolecular mechanism is associated with $n = 1$ and the unimolecular mechanism with $n = 3$. It has been noted previously (24, 27) that substrates which are highly solvated due to hydrogen bonding require fewer additional water molecules in solvation of the transition state, so that a lesser degree of solvent reorganization is entailed. This could provide a possible explanation for the low solvation numbers with the alkyl chlorosulfates since the polar OSO_2Cl group is expected to be extensively solvated.[5] For ethyl or *n*-propyl chlorosulfate the molecules of water which would solvate the departing anion are already present in the initial state and only one additional water molecule is needed to act as the nucleophile in the displacement process. Similarly, the unimolecularly reacting neopentyl chlorosulfate would require the reorganization of fewer water molecules in comparison with *tert*-butyl chloride, for example, which should be reflected in a smaller n value, as is observed.

m–Y Correlations

A plot of log k *vs.* Y, the solvent ionizing

[3]Alternative derivations of solvation numbers are given by Moelwyn-Hughes (23) and by Kohnstam (24).

[4]In Table 3 reactions which can be supposed to proceed by the S_N2, an intermediate ($S_N1/2$), and the S_N1 mechanism have been grouped together.

[5]A dissection of the initial state and the transition state solvation terms is possible through measurement of thermodynamic transfer functions (29–32).

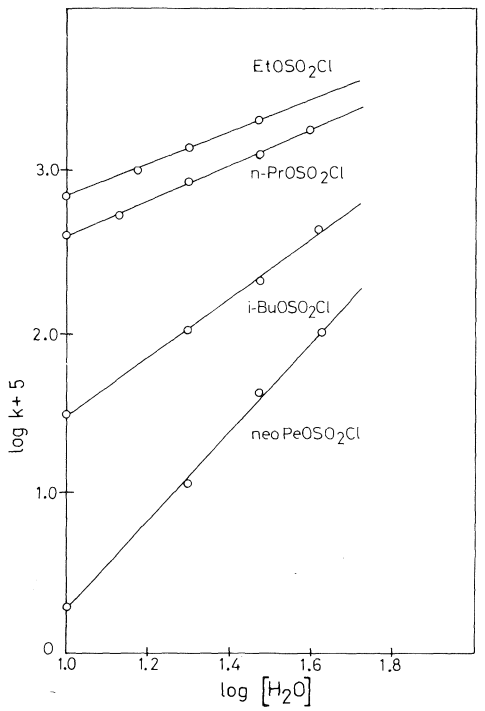

FIG. 2. Correlation between the logarithm of the rate constant and the logarithm of the water molarity for the hydrolysis of alkyl chlorosulfates in aqueous dioxane.

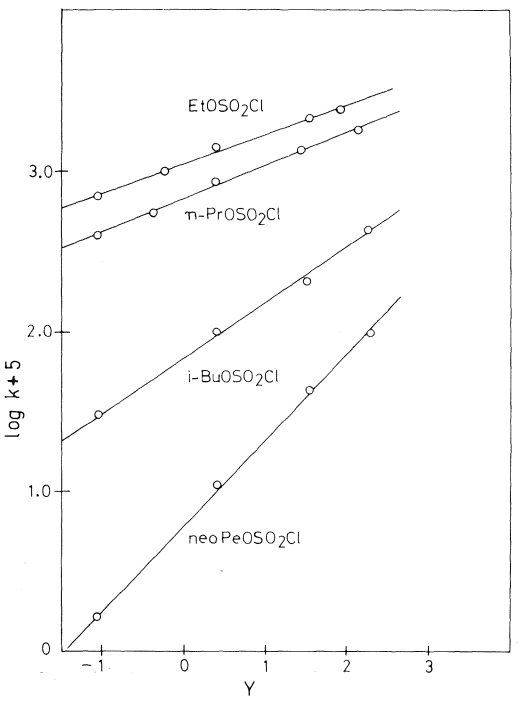

FIG. 3. Correlation between the logarithm of the rate constant and the medium ionizing power Y for hydrolysis of alkyl chlorosulfates in aqueous dioxane.

power (33*a*), for the series of alkyl chlorosulfates is shown in Fig. 3. The similarity with the log k *vs.* log [H_2O] plot (Fig. 2) is striking. However, the similarity is a consequence of the fact that, for the solvent range under consideration, Y is linearly related to log [H_2O]. The derived values of m, the substrate constant, are shown in Table 4 together with corresponding values for other alkyl derivatives, which were taken directly from the sources quoted or calculated from data therein.

The m values for the chlorosulfates are seen to be generally lower than for other alkyl derivatives solvolyzing by a particular mechanism. For S_N2 solvolysis in the chlorosulfate series $m \simeq 0.2$, compared with 0.3–0.4 for the arenesulfonates and halides. For S_N1 solvolysis $m \simeq 0.5$ for the chlorosulfates, 0.5–0.7 for the arenesulfonates, and 0.9–1.1 for the halides. The obvious deduction is that the chlorosulfates are less dependent on the inonizing power of the medium than are other alkyl derivatives. This could be interpreted to mean that the chlorosulfates fit into the part of the mechanistic spectrum between S_N2 and the borderline region. However, such an interpretation is contrary to previous conclusions (6–8). A more plausible explanation is connected with the low solvation number values. Since Y and log [H_2O] vary correspondingly over the range of solvent composition studied, the relative insensitivity of solvolysis rates of the alkyl chlorosulfates to the ionizing power of the medium appears to be due to the more extensive solvation of the initial state.[6] The relevance of this solvation factor to $\Delta S^{\neq}$ in chlorosulfate solvolysis is considered in the next section.

$\Delta S^{\neq}$ *in Chlorosulfate Solvolysis: Multiple Bond Scission vs. Initial State Solvation*

In our first investigation of the solvolysis of the alkyl chlorosulfates, the discovery of abnormally large $\Delta S^{\neq}$ values led to the proposal of multiple bond scission (7, 8). It appeared plausible that $\Delta S^{\neq}$ could provide a criterion of the concerted fragmentation pathway, due to the

[6]Similarly, the lower m values observed for alkyl arenesulfonates in comparison with alkyl halides are in accord with a greater solvation of the initial state in the former series (27); see, however, ref. 28 for the possible effect of neighbouring group participation on m values.

TABLE 4. Comparison of m values for solvolysis of chlorosulfates and other alkyl derivatives in aqueous dioxane and aqueous acetone

	m	T (°C)	Medium	Reference
Ethyl chlorosulfate	0.178	25	aq. dioxane	This work
n-Propyl chlorosulfate	0.209	25		This work
i-Butyl chlorosulfate	0.345	25		This work
Neopentyl chlorosulfate	0.523	25		This work
Methanesulfonyl chloride	0.332	25		14*b*
Ethanesulfonyl chloride	0.372	25		14*b*
Ethyl bromide	0.339	25	aq. acetone	22*c*
Ethyl benzenesulfonate	0.440	25	aq. dioxane	22*b*
i-Propyl benzenesulfonate	0.707	50		22*b*
p-Methoxyneophyl tosylate	0.560	25		33*e*
tert-Butyl chloride	1.007	50		33*a*
α-Phenylethyl chloride	1.136	25		33*b*
Neophyl chloride	0.961	50		33*c*
Neophyl bromide	0.925	50	aq. acetone	33*c*

increase in the degrees of freedom expected in the transition state of a process involving the formation of several particles. In the present study support has been obtained for the above proposal by application of an electrostatic treatment to the effect of solvent composition on the rate of reaction. The treatment shows in effect that chlorosulfate solvolysis is characterized by the large $r_{\pm}$ values which would be expected if multiple bond scission were operative.

It now becomes pertinent to consider the alternate possibility that the large initial state solvation of the alkyl chlorosulfates, which is reflected in low substrate values (m) and in small solvation numbers (n), might be responsible for the abnormally large entropies of activation characteristic of chlorosulfate solvolysis. Solvation numbers reflect the degree of reorganization of solvent molecules necessary in the formation of the transition state; the greater the solvent reorganization, the more negative might $\Delta S^{\ddagger}$ be expected to be (27, 34). Hence the abnormally positive $\Delta S^{\ddagger}$ values for chlorosulfate solvolysis might be considered to be due to the relatively small solvation numbers. The literature data for a number of alkyl derivatives given in Table 3 can be interpreted on that basis. It is seen that within each of the S_N2 and S_N1 groupings the abnormally positive (or less negative) $\Delta S^{\ddagger}$ values for the chlorosulfate derivatives are indeed paralleled by relatively small n values. This parallelism between $\Delta S^{\ddagger}$ and n values supports the contention that the abnormal values exhibited by the chlorosulfate derivatives may arise from the same factor, *i.e.* extensive initial state solvation. It is noted that this correlation is not obscured by the different ranges of $\Delta S^{\ddagger}$ values which are characteristic of the S_N1/S_N2 pathways. Thus it is found that initial state solvation is in fact a reasonable alternative origin of the abnormal $\Delta S^{\ddagger}$ values in chlorosulfate solvolysis.

At present a choice between the alternatives of multiple bond scission or initial state solvation (or the further possibility that both are operative factors) cannot readily be made. The major drawback is that there is no independent criterion for fragmentation in the solvolysis of chlorosulfates, such as could be provided by the measurement of kinetic isotope effects or $\Delta V^{\ddagger}$ values (*vide infra*). Furthermore, the differing viewpoints held by different workers (1–5) on solvation effects in solvolytic processes attest to the intrinsic difficulty in correlating more quantitatively $\Delta S^{\ddagger}$ and n values in solvolytic processes.

The Application of the $\Delta S^{\ddagger}$ Fragmentation Criterion in Other Systems

Since the entropy of activation criterion was first proposed as a result of our investigation of chlorosulfate solvolysis (7, 8) several studies have appeared in the literature (35–39) relating to application of this mechanistic criterion to other systems. Of closest analogy are the studies with the structurally related chloroformates (36) and chlorosulfites (37). The entropy of activation for the solvolysis–decomposition of 1-adamantyl chloroformate in 80% aqueous ethanol has been found to be 16–20 eu more positive than cor-

responding values for solvolysis of 1-adamantyl halides in this solvent (36), in accord with an ionization–fragmentation process:

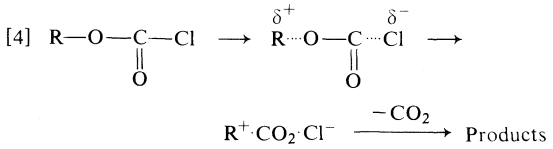

The cleavage reaction of cyclic ethers by alkyl chlorosulfites in benzene proceeds with a more positive $\Delta S^{\neq}$ (10–20 eu) compared with analogous S_N2 displacements and this has been interpreted on the basis of the fragmentation mechanism in [5] which entails simultaneous

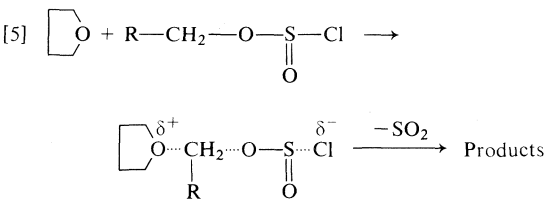

fission of C—O and S—Cl bonds (37). Formation of incipient SO_2 in the transition state is considered to provide substantial driving force for the reaction. In view of the results obtained in the present study, an investigation of the importance of solvent effects in the systems [4] and [5] would be in order to ascertain whether solute–solvent interactions could provide a valid alternative explanation of the abnormally large $\Delta S^{\neq}$ values.

The point was made previously by us that in certain structural situations the parallelism between fragmentation and abnormal $\Delta S^{\neq}$ values is not expected to hold.[7] It has also been noted that the nature of the leaving group can have a marked effect on entropies of activation and hence on the interpretation of abnormally large $\Delta S^{\neq}$ values (40).[8] Especially important in this regard is the study of le Noble *et al.* (41), which relates to the *volume of activation* ($\Delta V^{\neq}$) as a criterion of fragmentation. In this study it was stressed that beyond the intuitive nature of the $\Delta V^{\neq}$ criterion, a number of relevant factors must be explicitly considered in the evaluation of any given reaction system. It is clear that such an approach should also be taken when using the $\Delta S^{\neq}$ criterion.

Conclusions

Examination of the solvolysis of alkyl chlorosulfates from different viewpoints has provided alternative interpretations of the solvolytic mechanism. Application of electrostatic theory to the rate variation as a function of solvent composition in aqueous dioxane mixtures leads to the designation of bimolecular, unimolecular, and intermediate mechanistic types along the reaction series. Furthermore, comparison of the data for the chlorosulfates with those for alkyl halides via [1] and [2] points to the operation of a fragmentation mechanism for the chlorosulfate series, previously advanced on the basis of the abnormally large entropies of activation (6–8). However, the solvation numbers (n) derived via [3] are smaller than for other alkyl derivatives, and application of Winstein's m–Y correlation also yields lower m values for the alkyl chlorosulfates. It is proposed that the relatively small n and m values arise as a result of extensive initial state solvation and that the abnormally large $\Delta S^{\neq}$ values in chlorosulfate solvolysis may also have this factor as origin. Since independent criteria of multiple bond fission in these and in related solvolytic processes are lacking, it is suggested that caution be exercised in application of $\Delta S^{\neq}$ values as an indication of the fragmentation mechanism, *e.g.*, in reactions of chloroformates (36) or chlorosulfites (37). Similar caution has recently been advocated in application of volumes of activation as indications of fragmentation in solvolytic processes (41).

Experimental

The alkyl chlorosulfates were prepared from the respective alcohols and sulfuryl chloride as described previously (6) and were stored at 0–5°C. Dioxane was purified by refluxing over sodium and fractional distillation. The water used was distilled and deionized using a mixed bed ion exchange resin.

The kinetic data were determined conductimetrically.

[7]It was noted (39) that it is conceivable that multiple bond fission may create steric *restrictions* in the transition state, as in the case of a departing phenyl group which stabilizes the transition state by charge delocalization and is consequently restricted to a given spatial orientation (38). In such cases unusually high entropies of activation would, of course, not be expected; in fact $\Delta S^{\neq}$ values smaller than the normal size may result from the reduction in internal degrees of freedom in the transition state.

[8]D. N. Kevill, K. C. Kolwych, D. M. Shold, and C.-B. Kim, unpublished results quoted in ref. 40, footnote 218.

A Phillips P.R. 9501 direct reading conductivity bridge was used and was coupled to a chart recorder for measurement of relatively fast reaction rates. A dip-type conductivity cell was employed. The concentration of chlorosulfate used was *ca.* 0.01 *M*. Reaction solutions were thermostatted to ± 0.01°C. The rate data were calculated as previously described (6, 7).

Acknowledgment

The authors thank the National Research Council of Canada for the award of a scholarship (J.P.M.) and an operating grant. Helpful discussions with Professor C. A. Grob and R. E. Robertson are also acknowledged.

1. C. K. INGOLD. Structure and mechanism in organic chemistry. 2nd ed. Cornell University Press, Ithaca, NY. 1969.
2. S. R. HARTSHORN. Aliphatic-nucleophilic substitution. Cambridge University Press. 1973.
3. R. E. ROBERTSON. Prog. Phys. Org. Chem. **4**, 213 (1967).
4. M. H. ABRAHAM. Prog. Phys. Org. Chem. **11**, 1 (1974).
5. J. M. HARRIS. Prog. Phys. Org. Chem. **11**, 89 (1974).
6. E. BUNCEL and J. P. MILLINGTON. Can. J. Chem. **43**, 547 (1965).
7. E. BUNCEL and J. P. MILLINGTON. Can. J. Chem. **43**, 556 (1965).
8. E. BUNCEL and J. P. MILLINGTON. Proc. Chem. Soc. 406 (1964).
9. C. A. GROB. Angew. Chem. Int. Ed. Engl. **8**, 535 (1969).
10. (*a*) E. BUNCEL and J. P. MILLINGTON. Can. J. Chem. **47**, 2145 (1969); (*b*) E. BUNCEL, L. I. CHOONG, and A. RAOULT. J. Chem. Soc. Perkin Trans. II, 691 (1972); (*c*) E. BUNCEL and A. RAOULT. Can. J. Chem. **50**, 1907 (1972); (*d*) E. BUNCEL, A. RAOULT, and L. I. LANCASTER. J. Am. Chem. Soc. **95**, 5964 (1973).
11. E. C. F. KO and R. E. ROBERTSON. Can. J. Chem. **50**, 434 (1972).
12. S. KOBAYASHI, T. ASHIDA, and T. SAEGUSA. Bull. Chem. Soc. Jpn. **47**, 1233 (1974).
13. (*a*) R. E. ROBERTSON and B. ROSSALL. Can. J. Chem. **49**, 1441 (1971); (*b*) B. ROSSALL and R. E. ROBERTSON. Can. J. Chem. **49**, 1451 (1971).
14. (*a*) F. E. JENKINS and A. N. HAMBLY. Aust. J. Chem. **14**, 190, 205 (1961); (*b*) R. FOON and A. N. HAMBLY. Aust. J. Chem. **15**, 668 (1962); (*c*) M. L. TONNET and A. N. HAMBLY. Aust. J. Chem. **24**, 703 (1971); (*d*) R. FOON and A. N. HAMBLY. Aust. J. Chem. **24**, 713 (1971).
15. A. R. HAUGHTON, R. M. LAIRD, and M. J. SPENCE. J. Chem. Soc. Perkin Trans. II, 637 (1975).
16. (*a*) O. ROGNE. J. Chem. Soc. B, 1294 (1968); (*b*) O. ROGNE. J. Chem. Soc. Perkin Trans. II, 1486 (1975).
17. K. J. LAIDLER and H. EYRING. Ann. N.Y. Acad. Sci. **39**, 303 (1940).
18. K. B. WIBERG. Physical organic chemistry. Wiley, New York, NY. 1964. p. 379.
19. E. S. AMIS. Solvent effects on reaction rates and mechanisms. Academic Press, New York, NY. 1966.
20. K. J. LAIDLER. Suomen Kem. A, **33**, 44 (1960).
21. J. B. HYNE, R. WILLS, and R. E. WONKKA. J. Am. Chem. Soc. **84**, 2914 (1962).
22. (*a*) E. TOMMILA and E. MERIKALLIO. Suomen Kem. B, **26**, 79 (1953); (*b*) E. TOMMILA. Acta Chem. Scand. **9**, 975 (1955); (*c*) E. TOMMILA, M. TIILIKAINEN, and A. VOIPIO. Ann. Acad. Sci. Fenn. A II, **65** (1955); (*d*) E. TOMMILA, E. PAAKKALA, U. K. VIRTANEN, A. ERVA, and S. VARILA. Ann. Acad. Sci. Fenn. A II, **91** (1959).
23. E. A. MOELWYN-HUGHES. J. Chem. Soc. 4301 (1962).
24. G. KOHNSTAM. *In* The transition state. Special Publication No. 16. The Chemical Society. London. 1962.
25. D. A. BROWN and R. F. HUDSON. J. Chem. Soc. 3352 (1953).
26. R. V. VIZGERT. Russ. Chem. Rev. **32**, 1 (1963).
27. R. E. ROBERTSON, R. L. HEPPOLETTE, and J. M. W. SCOTT. Can. J. Chem. **37**, 803 (1959).
28. R. C. BINGHAM and P. v. R. SCHLEYER. J. Am. Chem. Soc. **93**, 3189 (1971).
29. E. M. ARNETT, W. G. BENTRUDE, J. J. BURKE, and P. MCC. DUGGLEBY. J. Am. Chem. Soc. **87**, 1541 (1965).
30. P. HABERFIELD, J. FRIEDMAN, and M. F. PINKSTON. J. Am. Chem. Soc. **94**, 71 (1972).
31. R. FUCHS, C. P. HAGAN, and R. F. RODEWALD. J. Phys. Chem. **78**, 1509 (1974).
32. E. BUNCEL and E. A. SYMONS. J. Am. Chem. Soc. **98**, 656 (1976); E. BUNCEL and H. WILSON. Adv. Phys. Org. Chem. In press.
33. (*a*) A. H. FAINBERG and S. WINSTEIN. J. Am. Chem. Soc. **78**, 2770 (1956); (*b*) A. H. FAINBERG and S. WINSTEIN. J. Am. Chem. Soc. **79**, 1597 (1957); (*c*) A. H. FAINBERG and S. WINSTEIN. J. Am. Chem. Soc. **79**, 1608 (1957). (*d*) S. WINSTEIN, A. H. FAINBERG, and E. GRUNWALD. J. Am. Chem. Soc. **79**, 4146 (1957); (*e*) S. G. SMITH, A. H. FAINBERG, and S. WINSTEIN. J. Am. Chem. Soc. **83**, 618 (1961).
34. R. E. ROBERTSON. Suomen Kem. A, **33**, 63 (1960).
35. J. F. KING and D. J. H. SMITH. J. Am. Chem. Soc. **89**, 4803 (1967).
36. D. N. KEVILL and F. L. WEITL. J. Am. Chem. Soc. **90**, 6416 (1968); D. N. KEVILL and F. L. WEITL. Tetrahedron Lett. 707 (1971).
37. Y. HARA and M. MATSUDA. J. Org. Chem. **40**, 2786 (1975).
38. S. SELTZER and F. T. DUNNE. J. Am. Chem. Soc. **87**, 2628 (1965).
39. E. BUNCEL. Chem. Rev. **70**, 323 (1970).
40. D. J. RABER, J. M. HARRIS, and P. v. R. SCHLEYER. *In* Ions and ion pairs in organic reactions. Vol. 2, *Edited by* M. Szwarc. Wiley, New York, NY. 1974. Chapt. 3.
41. W. J. LE NOBLE, H. GUGGISBERG, T. ASANO, L. CHO, and C. A. GROB. J. Am. Chem. Soc. **98**, 920 (1976).
42. E. BUNCEL and C. CHUAQUI. Can. J. Chem. **53**, 1275 (1975).
43. F. E. CRITCHFIELD, J. A. GIBSON, JR., and J. L. HALL. J. Am. Chem. Soc. **75**, 1991 (1953).

Transition metal complexes of deprotonated 2-mercaptobenzoxazole. Study of the thiol–thioketo form equilibrium

CARLO PRETI AND GIUSEPPE TOSI

Istituto di Chimica Generale ed Inorganica, University of Modena, 41100 Modena, Italy

Received October 6, 1976

CARLO PRETI and GIUSEPPE TOSI. Can. J. Chem. **55**, 1409 (1977).

Complexes of 2-mercaptobenzoxazole (mbo) with Zn(II), Cd(II), Hg(II), Cu(I), Ag(I), Au(I), Ni(II), Pd(II), Pt(II), Co(II), Rh(III), and Ir(III) were prepared and characterized. Their structures have been assigned on the basis of chemical analysis, ir and far ir spectroscopy, electronic spectra, and magnetic susceptibility measurements. The ligand always bonds through both the sulphur and the nitrogen heteroatoms. The ligand field parameters have been evaluated and are in keeping with the proposed structures confirming the presence of MS_2N_2 and MS_3N_3 chromophores.

CARLO PRETI et GIUSEPPE TOSI. Can. J. Chem. **55**, 1409 (1977).

On a préparé et caractérisé les complexes du mercapto-2 benzoxazole (mbo) avec Zn(II), Cd(II), Hg(II), Cu(I), Ag(I), Au(I), Ni(II), Pd(II), Pt(II), Co(II), Rh(III) et Ir(III). On leur a attribué des structures en se basant sur l'analyse chimique, la spectroscopie ir et ir lointain, les spectres électroniques et des mesures de susceptibilité magnétique. Le ligand est toujours attaché par l'intermédiaire des hétéroatomes du soufre et d'azote. On a évalué les paramètres de champ de ligands et ils sont en accord avec les structures proposées confirmant aisni la présence de chromophores MS_2N_2 et MS_3N_3.

[Traduit par le journal]

Introduction

In view of the importance of the oxazole group in biological systems, in industry, and in medicine and as an analytical reagent (1–5) we are interested in the study of the coordination behaviour of 2-mercaptobenzoxazole (mbo).

The complexing properties of the HNCS group with metal ions have been studied in our laboratory and we have obtained a variety of interesting complexes with the ligand acting as N-bonding (6, 7). The ligand exists as two tautomeric conformations exhibiting thiol–thione isomerism involving —N=C—SH and —NH—C=S groups in a thione–thiol equilibrium:

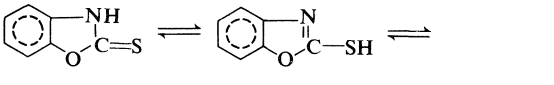

a *b*

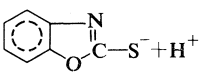

c

The examination of the complexing properties of the mbo ligand with metal ions is the aim of the present paper in order to further our present knowledge in the field of ligands which exhibit the thiol–thione equilibrium reported above (8, 9).

It is possible that in this molecule only two atoms could act as bonding sites, *i.e.* the sulphur exocyclic atom and the cyclic nitrogen atom. Since the lone pairs on the oxygen atom present in the skeleton of the ring are involved in the resonating structures of the molecule, it is expected that it should have very weak coordinating ability (10).

We present in this work the investigation of the structural aspects of the complexes of deprotonated 2-mercaptobenzoxazole with the metal ions Zn(II), Cd(II), Hg(II), Cu(I), Ag(I), Au(I), Ni(II), Pd(II), Pt(II), Co(II), Rh(III), and Ir(III). Their structures have been tentatively assigned on the basis of chemical analysis, ir and far ir spectroscopy, electronic spectra, and magnetic susceptibility data.

Results and Discussion

The complexes, their analytical data, room temperature magnetic moments, and other physical properties are reported in Table 1. The solid state electronic spectra are listed in Table 2, while the most important ir bands in the range 4000–50 cm^{-1} are listed in Table 3. The complexes are powdery and insoluble in the most common organic solvents. This insolubility suggests that these derivatives could be polymeric with more than one ligand molecule coordinated to the metal ion. Because of the general in-

TABLE 1. Analytical data and other physical properties

Compound	Colour	Calculated (%)			Found (%)			Dec. point (°C)	μ_B
		C	H	X[a]	C	H	X[a]		
$Zn(mbo)_2$	pink–white	46.0	2.2	17.9	45.2	2.3	17.6	217–220	dia.
$Cd(mbo)_2 \cdot H_2O$	pink–white	39.0	2.3	26.1	38.7	2.3	26.0	233–235	dia.
$Hg(mbo)_2 \cdot 2H_2O$	white	31.3	2.2	37.4	31.1	2.2	37.8	180–183	dia.
Cumbo	ivory	39.3	1.9	6.6	39.2	1.8	6.8	288–290	dia.
Agmbo	white	32.6	1.6	5.4	31.7	1.6	5.6	>350	dia.
$Aumbo \cdot H_2O$	white	23.0	1.6	3.8	23.2	1.6	3.7	268–270	dia.
$Ni(mbo)_2 \cdot H_2O$	dark green	44.6	2.7	7.4	44.8	2.6	7.3	>350	dia.
$Pd(mbo)_2 \cdot H_2O$	hazel–brown	39.6	2.4	6.6	39.3	1.9	6.7	>350	dia.
$Pt(mbo)_2$	yellow	33.9	1.6	5.6	33.8	1.8	5.7	>350	dia.
$Co(mbo)_2 \cdot 2H_2O$	turquoise	42.5	3.1	7.1	42.5	2.7	6.9	207–210	4.4
$Rh(mbo)_3 \cdot 2H_2O$	orange–brown	42.8	2.7	7.1	42.9	2.7	6.9	>350	dia.
$Ir(mbo)_3 \cdot 5H_2O$	yellow	34.4	3.0	5.7	34.2	3.1	5.8	>350	dia.

[a]X = metal for zinc, cadmium, and mercury derivatives; X = nitrogen for all the remaining derivatives.

solubility of the complexes, studies by such means as nmr, molecular weight, and molar conductivity measurements have not been carried out.

Electronic Spectra and Magnetic Susceptibility Studies

The spectral and magnetic properties of the complexes were studied in order to understand the spatial arrangement of the ligands around the metal ions. The derivatives of zinc(II), cadmium(II), mercury(II), copper(I), silver(I), and gold(I) were found to be diamagnetic which is expected as these metal ions belong to a d^{10} system. These metals do not show *d–d* transitions and therefore the stereochemistry of their complexes cannot be derived from diffuse reflectance spectra.

The nickel complex $Ni(mbo)_2 \cdot H_2O$ is diamagnetic; this fact could be indicative of a spatial arrangement of the mbo around the nickel ion in a square planar or five-coordinated geometry. The five-coordination should be possible only with water coordinated to the metal, but this fact can be excluded, because, from a detailed analysis of the infrared spectra, see below, the water observed is clearly uncoordinated lattice water. Furthermore, this water is lost at 100°C while, if coordinated, should be lost near 150°C (11).

The absence of electronic transitions below 10 000 cm^{-1} indicates very strongly that the spatial arrangement of the mbo around the nickel ion is square planar. The assignment of the bands in the electronic spectrum, Table 2, is made by assuming the convention that the metal *x*- and *y*-axes lie between the metal–ligand bonds (12). The band at 25 000 cm^{-1} is charge transfer in character and not a *d–d* transition because of its high intensity.

The calculated orbital parameter Δ_1 (13) from the $x^2 - y^2 \rightarrow xy$ in-plane transition is in the 19 000–20 000 cm^{-1} range, assuming reasonable values for the correction factor, thus placing the ligand in the expected sulphur and nitrogen donor range (14, 15).

The magnetic moment of the inner cobalt derivative, 4.4 μ_B, lies well within the range of tetrahedral complexes (16); the turquoise colour of the complex also indicates the tetrahedral geometry of this derivative. The reflectance spectrum shows two bands at 7635 (ν_2) and 16 890 cm^{-1} (ν_3) typical of a tetrahedral configuration. It is reasonable to suppose its structure to be that of an infinite polymer with the ligand forming bridges between cobalt ions. A similar structure has been suggested for inner complexes of cobalt(II) with imidazole and benzimidazole (17, 18). Using the values of ν_2 and ν_3, the ligand field parameters *Dq* and *B'* have been evaluated (Table 2).

By comparison of *Dq* values reported for CoL_4 groups, we can see that for CoS_4 chromophores *Dq* lies in the range 316–425 cm^{-1}, while the corresponding range for CoN_4 chromophores is 467–538 cm^{-1}; the complex $Co(mbo)_2 \cdot H_2O$ shows a *Dq* value that is, using the 'law of the average environment', typical of a CoS_2N_2 chromophore (14, 19).

The Pd(II) and Pt(II) ions, with d^8 configuration, have square planar arrangements of ligand molecules around them in a large number of their

TABLE 2. Ultraviolet–visible spectra and ligand field parameters (cm^{-1})

Compound	*d–d* Transitions	Wavenumbers	Ligand field[b] Parameter	Value
$Co(mbo)_2 \cdot H_2O$	$^4A_2(F) \rightarrow {}^4T_1(P)$	16 890	*Dq*	440
	$^4A_2(F) \rightarrow {}^4T_1(F)$	7 635	*B'*	747
	$^4A_2(F) \rightarrow {}^4T_2(F)$	4 440[a]	β	0.77
$Ni(mbo)_2 \cdot H_2O$	Charge transfer	25 000		
	$^1A_g \rightarrow {}^1B_{1g}$	17 035	Δ_1	19 835
$Pd(mbo)_2 \cdot H_2O$	$^1A_g \rightarrow {}^1B_{1g}$	23 255	Δ_1	25 355
$Rh(mbo)_3 \cdot 2H_2O$	$^1A_{1g} \rightarrow {}^1T_{2g}$	30 960	Δ	28 270
	$^1A_{1g} \rightarrow {}^1T_{1g}$	26 670	*B'*	283
			β	0.39
			*Z**	0.20
$Ir(mbo)_3 \cdot 5H_2O$	$^1A_{1g} \rightarrow {}^1T_{2g}$	31 865	Δ	28 670
	$^1A_{1g} \rightarrow {}^1T_{1g}$	27 400	*B'*	295
	$^1A_{1g} \rightarrow {}^3T_{1g}$	23 255	β	0.45

[a]Calculated value.
[b]*B* is taken to be 967, 720, and 660 cm^{-1} for the Co^{2+}, Rh^{3+}, and Ir^{3+} free ions respectively.

complexes. In the electronic spectrum of the palladium(II) derivative, recorded in the solid state as a Nujol mull, only the band at 23 255 cm^{-1} can be considered a *d–d* transition of the type $^1A_g \rightarrow {}^1B_{1g}$ ($x^2 - y^2 \rightarrow xy$). The value of Δ_1, by the standard treatment, is 26 355 cm^{-1} (20). Assignments have not been possible in the case of the platinum(II) derivative.

The derivatives $Rh(mbo)_3 \cdot 2H_2O$ and $Ir(mbo)_3 \cdot 5H_2O$ are low-spin type (t_{2g}^6). Solid state electronic spectra confirm an octahedral symmetry of the central atom. The two observed absorption bands are in the ranges expected for the two spin-allowed transitions from the ground state $^1A_{1g}$; the ratio ν_2/ν_1 is 1.16 both for rhodium and iridium complexes. By means of the equations (21):

$$\nu_1 = \Delta - 4B' + 86(B')^2/\Delta$$

and

$$\nu_2 = \Delta + 12B' + 2(B')^2/\Delta$$

the ligand field parameters Δ, *B'*, and β have been evaluated and have been reported in Table 2. The value of Δ is higher than those found for the rhodium and iridium complexes with sulphur containing ligands (22) and could be indicative of an octahedral symmetry with metal–nitrogen and metal–sulphur bonds in polymeric materials. The *B'* values of the order of 39 and 45% of the free ion value in rhodium and iridium derivatives, respectively, suggest a strong covalency in the metal–ligand σ bond.

It is known that decreasing values of β are associated with a reduction in the effective positive charge of the metal ion and with an increasing tendency to be reduced to the next lower oxidation state. For the second-row transition metals the variation of the Racah interelectronic repulsion parameter with cation charge *Z** and the number *q* of electrons in the partly filled *d* shell, is expressed by the relation (21):

$$B'(cm^{-1}) = 472 + 28q + 50(Z^* + 1) - 500/(Z^* + 1)$$

This gave the effective ionic charge in the rhodium derivative as 0.20, considerably below the formal +3 oxidation state of the metal.

Infrared Spectra

The infrared spectra of the complexes do not display the bands due to ν(NH) and δ(NH), clearly indicating the absence of imino-hydrogen in these derivatives. Furthermore it is worthwhile examining the fact that the mode of coordination of the ligand could be distinguished by the analysis of the positions and intensities of the thioamide bands (23–26) and of the bands at 1095 cm^{-1} and 820 cm^{-1} attributed to the prevailing contribution of ν(COC) asymmetric and symmetric, Table 3. The directions of the shifts of all the bands in the spectra of the complexes are the same and this fact clearly indicates that the bonding pattern must be the same in all the complexes.

TABLE 3. Infrared absorption bands (cm^{-1})

Compound	Thioamide I	Thioamide II	ν(COC) asym.	Thioamide III	ν(COC) sym.	Thioamide IV	ν(M—N)	ν(M—S)	Other bands
mbo solid	1505vs	1245ms	1095vs	1010s	820ms	745vs	—	—	425ms, 264m, 237m
$Zn(mbo)_2$	1482s	1250vs	1100vs	1012ms	820ms	638ms	216m	340m	422ms, 275m, 240m
$Cd(mbo)_2 \cdot H_2O$	1480vs	1250vs	1100vs	1010s	818ms	635ms	200s	310m	420ms, 260m, 236m
$Hg(mbo)_2 \cdot 2H_2O$	1485ms	1255vs	1095s	1010m	812ms	630m	190m, 164m	290m, 226m	420ms, 275m, 239m
Cumbo	1481ms	1250s	1100ms	1010m	820m	640m	218m	330m	425ms, 266m, 233m
Agmbo	1480s	1250vs	1100s	1010s	820s	639ms	410s	250m	436m, 272mw, 236mw
$Aumbo \cdot H_2O$	1480s	1270vs	1105ms	1010ms	825ms	642m	290ms	267vs[a]	424ms, 235m
$Ni(mbo)_2 \cdot H_2O$	1485s	1255vs	1100vs	1010ms	822ms	640m	292ms, 281s	378s, 313s	420ms, 260sh, 233m
$Pd(mbo)_2 \cdot H_2O$	1482vs	1255vs	1100vs	1010s	820s	641m	297m, 273m	343m	421m, 267m, 239m
$Pt(mbo)_2$	1480s	1265vs	1100vs	1010s	822ms	643m	263s	317m	423m, 253m, 231m
$Co(mbo)_2 \cdot 2H_2O$	1481s	1250vs	1100vs	1010ms	820ms	640m	286ms, 255ms	382m, 302ms	419ms, 269m, 236m
$Rh(mbo)_3 \cdot 2H_2O$	1480ms	1260s	1100s	1010ms	811ms	630m	283m	324m	427ms, 260m, 240m
$Ir(mbo)_3 \cdot 5H_2O$	1480ms	1250s	1100s	1010ms	810ms	631m	295m, 270m	330m, 305m	428m, 260m, 236m

[a]Overlapping a ligand band which is markedly reinforced.

Thioamide I band has a predominant contribution from ν(C═N) + δ(CH), band II has a predominant contribution from ν(C⋯N) + δ(CH) + ν(C⋯S), band III has a contribution from ν(C⋯N) + ν(C⋯S), while thioamide IV has a major contribution from ν(C⋯S). The major changes in the spectra of the complexes as compared to that of the ligand are a red shift of the thioamide I band of about 20 cm^{-1} and a blue shift of band II. The thioamide III band appears unchanged at the same wavenumbers, while the thioamide IV band undergoes a red shift.

The bands at 1095 and 820 cm^{-1} attributed to the prevailing contribution of ν(COC) asymmetric and symmetric are at the same wavenumbers or show small positive shifts, thus excluding the possibility of coordination through the oxygen atom of the oxazole ring.

According to literature data (8, 27–30) the shifts reported above clearly allow us to suggest both N- and S-coordination. A chelate form is difficult to envisage because of the high strain that appears from the molecular model of a four-membered ring of the type , taking into account that the carbon and nitrogen atoms already belong to a five-membered ring. We propose, for all the complexes, a bridged configuration with the ligands linked to two different metal atoms.

The low frequency spectral data give further confirmation of N- and S-bonding to the metals. In the spectra of N-bonded and S-bonded complexes, absorptions due to ν(M—N) and ν(M—S) are usually present in the range 350–150 cm^{-1}. In our spectra new bands are present in the low frequency region, Table 3, that are assigned to ν(M—N) and ν(M—S) according to literature data for similar complexes (8, 31–41).

In all the water containing complexes, bands due to ν(OH) and δ(HOH) are present at 3500 cm^{-1} (broad) and at 1600 cm^{-1} (broad) clearly indicating the presence of lattice water. Twisting, wagging, and rocking, vibrational modes of the coordinated water are not present in the expected ranges (11).

Conclusions

It appears that in acid medium this ligand

coordinates in the form **a** through the nitrogen heteroatom only (6, 7); when operating in basic medium the anionic ligand **c** obtained from the form **b** bonds via both sulphur and nitrogen. This behaviour could be explained by an attack of the sulphur anion, followed by the coordination of the cyclic nitrogen.

We can propose for the diamagnetic derivatives $Zn(mbo)_2$, $Cd(mbo)_2 \cdot H_2O$, and $Hg(mbo)_2 \cdot 2H_2O$ a tetrahedral arrangement of the ligand molecules in polymeric structures. On the basis of ir studies the structure of the copper(I) complex may be represented in the form of a polymeric structure through ligand bridging, sulphur and nitrogen bonded, in which Cu(I) tends to achieve its maximum coordination number. The formation of the chelate with a four-membered ring structure is not very probable because of its high strain. Silver(I) and gold(I) complexes have a linear structure of the type:

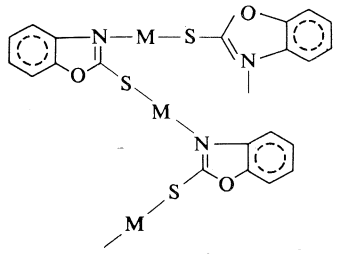

The derivatives of nickel(II), palladium(II), and platinum(II) are square planar, while the cobalt(II) complex is tetrahedral; rhodium(III) and iridium(III) complexes are of low-spin type in an octahedral symmetry. Rhodium(III) salts afford with mbo only substitution reactions, although the presence of thiol, a classical reducing agent, can also lead to reduction of the metal. This fact could be explained by admitting that the octahedral environment of the complex $Rh(mbo)_3 \cdot 2H_2O$ stabilizes the d^6 electronic configuration.

The insolubility of these derivatives in water and even in organic solvents provides further confirmation of a polymeric intermolecular linkage of the ligand.

In general the structures suggested seem the most reasonable ones; however, these suggestions are only tentative as the evidence supporting, for example, bridging ligands is at the moment not sufficient to be definitive.

Experimental

Purification of the Ligand

2-Mercaptobenzoxazole (mbo), supplied by Fluka, was purified by recrystallization from ethanol; mp 192–194°C (lit. (42) mp 193°C).

Preparation of the Complexes

Method A

An aqueous solution of the metal chloride or nitrate or acetate, maintained at a p*H* value lower than that of precipitation of the corresponding hydroxide, was treated with an aqueous ethanol solution of the ligand with the metal:ligand stoichiometric ratio of 1:1, 1:2, and 1:3 depending on the oxidation number of the starting metal. The p*H* value was checked by a p*H*meter Polymetron 42B during the preparation. The chloride, nitrate, or acetate ions were never present in the resulting complexes.

Method B

The metal salts were dissolved in ethanol and added dropwise to a stirred solution of mbo in a mixture of ethanol and dimethyl sulfoxide in the ratio 20:3.

The complexes obtained were purified by means of repeated washing with ethanol and dried over P_4O_{10}.

Infrared Measurements

The ir spectra were recorded in the range 4000–50 cm^{-1} with Perkin-Elmer 457 and 225 and Hitachi–Perkin-Elmer FIS3 spectrophotometers. The spectra in the range 4000–400 cm^{-1} were measured as KBr discs or a $CHCl_3$ solution. Far ir spectra were measured as Nujol mulls supported between polyethylene sheets. Atmospheric water was removed from the spectrophotometer housing by flushing with dry nitrogen.

Ultraviolet–Visible Spectra

The electronic spectra were recorded with a Shimadzu MPS-50L spectrophotometer in the solid state in the range 4000–35000 cm^{-1}.

Magnetic Susceptibility Measurements

These were carried out by Gouy's method at room temperature. Molecular susceptibilities were corrected for diamagnetism of the component atoms by use of Pascal's constants (43). This correction was not used for the temperature independent paramagnetism because it does not influence the assignment of the configurations, and, in any event, is not very accurate.

Acknowledgements

We thank Dr. S. Camellini for his experimental work, Mr. G. Pistoni for elemental analyses, and the National Research Council (C.N.R.) of Italy for financial support.

1. M. Tamura, H. Hada, J. Noguchi, and S. Hayashi. J. Phys. Chem. **66**, 559 (1962) and references therein.
2. P. Bassignana, C. Cogrossi, and M. Gandino. Spectrochim. Acta, **19**, 1885 (1963).
3. C. Runti. Fondamenti di chimica farmaceutica. Vol. I, II, and III. Lint inc., Trieste. 1971.
4. L. S. Goodman and A. Gilman. The pharmacological basis of therapeutics. MacMillan Company, Toronto, Ont. 1971.

5. D. E. RYAN. Anal. Chem. **22**, 599 (1950).
6. C. PRETI and G. TOSI. Can. J. Chem. **54**, 85 (1976).
7. C. PRETI and G. TOSI. J. Inorg. Nucl. Chem. **38**, 1125 (1976).
8. C. PRETI and G. TOSI. Can. J. Chem. **54**, 1558 (1976).
9. M. ST. C. FLETT. J. Chem. Soc. 347 (1953).
10. R. T. MORRISON and R. N. BOYD. Organic chemistry. Allyn and Bacon Inc., Boston, MA. 1963.
11. C. PRETI and G. TOSI. Spectrochim. Acta Ser. A, **31**, 1139 (1975).
12. O. SIIMANN and J. FRESCO. J. Am. Chem. Soc. **92**, 2652 (1970).
13. H. B. GRAY and C. J. BALLHAUSEN. J. Am. Chem. Soc. **85**, 260 (1963).
14. A. B. P. LEVER. Inorganic electronic spectroscopy. *Edited by* M. F. Lappert. Elsevier, Amsterdam. 1968.
15. C. K. JORGENSEN. Absorption spectra and chemical bonding in complexes. Pergamon Press, Oxford. 1964.
16. B. N. FIGGIS and J. LEWIS. Prog. Inorg. Chem. **6**, 192 (1964).
17. W. J. EILBECK, F. HOLMES, and A. E. UNDERHILL. J. Chem. Soc. A, 757 (1967).
18. M. GOODGAME and F. A. COTTON. J. Am. Chem. Soc. **84**, 1543 (1962).
19. B. P. KENNEDY and A. B. P. LEVER. Can. J. Chem. **50**, 3488 (1972).
20. A. R. LATHAM, V. HASCALL, and H. B. GRAY. Inorg. Chem. **4**, 788 (1965).
21. C. K. JORGENSEN. Prog. Inorg. Chem. **4**, 73 (1972).
22. G. MARCOTRIGIANO, G. C. PELLACANI, C. PRETI, and G. TOSI. Bull. Chem. Soc. Jpn. **48**, 1018 (1975).
23. E. LIEBER, C. N. R. RAO, C. N. PILLAI, and R. D. HITES. Can. J. Chem. **36**, 801 (1958).
24. L. J. BELLAMY. The infrared spectra of complex molecules. J. Wiley, New York, NY. 1966.
25. C. N. R. RAO and R. VENKATARAGHAVAN. Spectrochim. Acta, **18**, 541 (1962).
26. C. N. R. RAO, R. VENKATARAGHAVAN, and T. R. KASTURI. Can. J. Chem. **42**, 36 (1964).
27. K. JENSEN and P. H. NIELSEN. Acta Chem. Scand. **20**, 597 (1966).
28. B. SINGH and R. SINGH. J. Inorg. Nucl. Chem. **34**, 3449 (1972).
29. B. SINGH and K. P. THAKUR. J. Inorg. Nucl. Chem. **36**, 1735 (1974).
30. J. DEHAND and J. JORDANOV. Inorg. Chim. Acta, **17**, 37 (1976).
31. D. DE FILIPPO and C. PRETI. J. Chem. Soc. A, 1904 (1970).
32. J. R. FERRARO. Low frequency vibrations of inorganic and coordination compounds. Plenum Press, New York, NY. 1971.
33. D. M. ADAMS. Metal–ligand and related vibrations. E. Arnold, London. 1967.
34. I. S. AHUJA. J. Inorg. Nucl. Chem. **29**, 2091 (1967).
35. J. A. WEAVER, P. HAMBRIGHT, P. T. TALBERT, E. KANG, and A. T. THORPE. Inorg. Chem. **9**, 268 (1970).
36. C. D. FLINT and M. GOODGAME. J. Chem. Soc. A, 1718 (1967).
37. C. PRETI and D. DE FILIPPO. J. Chem. Soc. A, 1901 (1970).
38. C. POSTMUS, J. R. FERRARO, and W. WOZNIAK. Inorg. Chem. **6**, 2030 (1967).
39. D. M. L. GOODGAME, M. GOODGAME, P. J. HAYWARD, and G. W. RAYNER-CANHAM. Inorg. Chem. **7**, 2447 (1968).
40. R. J. H. CLARK and C. S. WILLIAMS. Inorg. Chem. **4**, 350 (1965).
41. I. P. KHULLAR and U. AGARWALA. Can. J. Chem. **53**, 1165 (1975).
42. R. C. WEAST (*Editor*). Handbook of chemistry and physics. 49th ed. The Chemical Rubber Co., Cleveland, OH. 1968–1969. p. C204.
43. B. N. FIGGIS and J. LEWIS. Modern co-ordination chemistry. Interscience, New York, NY. 1959. p. 403.

A laser interferometric study of the diffusion of O_2, N_2, H_2, and Ar into water

ROBERT NEVILLE O'BRIEN AND WILLIAM FRANK HYSLOP

Chemistry Department, University of Victoria, P.O. Box 1700, Victoria, B.C., Canada V8W 2Y2

Received November 11, 1976

ROBERT NEVILLE O'BRIEN and WILLIAM FRANK HYSLOP. Can. J. Chem. **55**, 1415 (1977).

The diffusion constants of O_2, N_2, H_2, and Ar at 24°C in H_2O are calculated from interferometric data. The question of surface resistance to diffusion of O_2 into water is discussed. There appears to be no such resistance.

ROBERT NEVILLE O'BRIEN et WILLIAM FRANK HYSLOP. Can. J. Chem. **55**, 1415 (1977).

Utilisant des données interférométriques, on a calculé, à 24°C, les constantes de diffusion de O_2, N_2, H_2 et Ar dans H_2O. On discute de la question de la résistance de surface à la diffusion de l'oxygène dans l'eau. Il semble qu'une telle résistance n'existe pas.

[Traduit par le journal]

The diffusion of gases into liquids has been studied for a very long time, but until recently gas analysis has been laborious and often inaccurate. This has resulted in a wide scatter in published results. The diffusion coefficients of gases in liquids and the scatter of the data has been recorded by Himmeblau (1) in 1964 and more recently by Tham, Walker, and Gubbins (2) in 1970. Further indications of the uncertainties are given by Danckwerts (3) and by the recent (1972) publication (4) of data for the O_2–H_2O system differing by seventy percent from the "generally accepted value".

The interest in good diffusion data arises from many sources of which the following are topical. The fuel cell which is currently most used is the hydrogen–oxygen cell and diffusion rates of dissolved gases are necessary data for design calculations. The rate of ingress of O_2 in natural waters limits the safe man-induced biological or chemical oxygen demand that can be tolerated. The rate of diffusional relaxation of supersaturation downstream from dams on natural waterways influences the incidence of fish bubble disease in the fish in these waters, and the rate of aerobic oxidation of sewage in sewage oxidation systems is dependent finally on oxygen diffusion rates in water.

All of the methods of measuring gas diffusion in water to date have depended on measuring the bulk concentration after a predetermined and rather long time. The extended times produce problems such as securing homogeneity in the solution, maintaining constant pressure and temperature, and general isolation of the system from the surroundings.

Multiple beam interferometry runs are of the order of minutes rather than hours and transient systems can be followed for very long relative times because the method requires no destructive sampling and determinations are made at motion picture camera speed, *i.e.* 16 frames per second. Zero time is easily found and, since a concentration gradient results, various regions of the liquid layer can be investigated including positions very near the surface. The literature has several references to an apparent surface resistance (3, 5, 6) which interferometry is uniquely capable of investigating.

Theory

The diffusion constant D ($cm^2\ s^{-1}$) of a species is determined by the nature of the medium as embodied in the viscosity, η ($g\ cm^{-1}\ s^{-1}$), the size of the diffusing species, r (cm), and the temperature, T (K). Usually the first two are fixed, but viscosity of course varies with temperature. Fick's Second Law expression which arises from closer consideration of the rate of change of concentration by diffusion

$$\frac{\partial C}{\partial t} = D\frac{\partial^2 C}{\partial x^2} \qquad [1]$$

where C is the concentration ($mol\ cm^{-3}$), t is the time (s), and x is the distance perpendicular to the gas–liquid interface (cm) must be solved for the initial conditions

$$C = C_0 \quad x > 0, t = 0$$

It is assumed as a boundary condition that the surface layer of liquid is immediately saturated

with gas or $C = C_s$ at a sudden pressure increase. It is also assumed that before a sudden increase in pressure the concentration of gas is uniform throughout the mass of solution ($C = C_0$) and that at a great distance ($x = \infty$) from the interface the concentration is still C_0 for the time the experiment lasts or the boundary conditions for semi-infinite or unrestricted diffusion are

$$t > 0, x \to \infty; \quad C \to C_0$$
$$t > 0, x = 0; \quad C = C_s$$

The solution of eq. 1 by Laplace transforms for these boundary conditions is

$$[2] \qquad C - C_0 = (C_s - C_0) \operatorname{erfc} \frac{x}{2\sqrt{Dt}}$$

Here erfc is the complement of the error function whose values are tabulated in a number of publications (3, 6). If Henry's Law is assumed (a good approximation for sparingly soluble gases) then

$$[3] \qquad m = kp$$

where m is the mass of gas dissolved by a unit volume of solution (mol ℓ^{-1}), k is the Henry's Law constant (mol ℓ^{-1} atm^{-1}), and p is the pressure (atm). There are plenty of data in the literature (3) and handbooks to provide C_0 and C_s. Concentration *vs.* refractive index plots are available (8). The mathematical manipulations leading to the solution of eq. 1 are also available (8).

A further assumption is made that no natural convection occurs. Since the liquid is heavier than the gas as in the case of O_2 dissolving in water, it is assumed that the oxygen solution is lighter than the pure water resulting in stable, density-layering down from the interface. This has been proven to be true. The refractive index of unreactive gas–water solutions is less than water (8) and from the Lorentz–Lorenz Law

$$[4] \qquad R = \frac{M}{\rho}\left(\frac{n^2 - 1}{n^2 + 2}\right)$$

where R is the molar refraction (cm^3), M the molecular weight (g), ρ the density (g cm^{-3}), and n is the refractive index of the pure water or solution; it is clear that it should be so. Indeed densities have been calculated from refractive index data (9).

Experimental

The apparatus used, a specially designed Fabry-Perot interferometer enclosed in a pressure jacket and partially filled with water, has been described previously (7). Briefly the coated glass flats were 5 cm apart and each had a 90% reflecting dichroic coating on the inner surfaces and anti-reflection coatings on the outer surfaces. The interferometer body was of stainless steel, the pressure compensating jacket was of mild steel. A special gas diffusing inlet allowed pressure to be applied rapidly by the quick opening valve with only moderate agitation of the water. The pressure system was arranged so that a high quality gas from a cylinder could be held in a large enough separate reservoir at the desired pressure so that on opening the fast opening valve, the pressure drop was undetectable.

Fringes were obtained vertically oriented to the meniscus and conveniently spaced at about 3 fringes per mm. The interferograms were recorded with a Bolex Paillard 16 mm camera at 16 frames per s for an initial

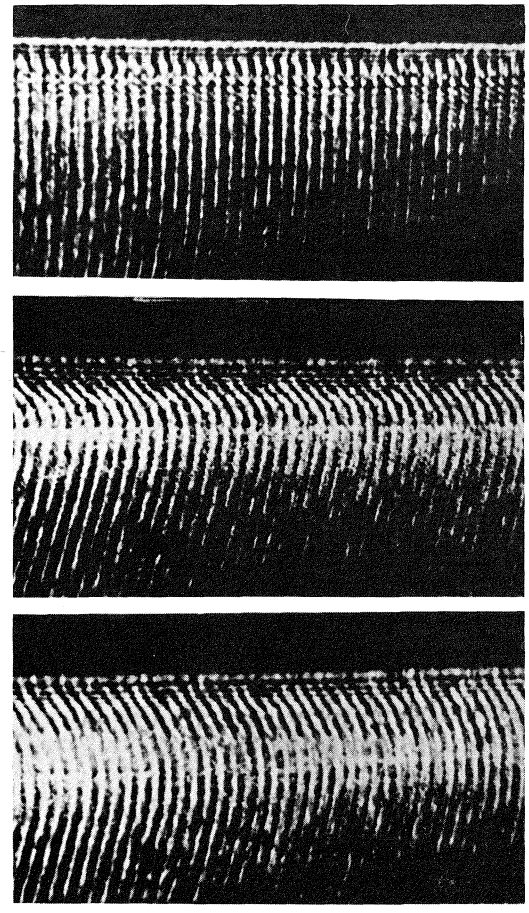

FIG. 1. Interferograms recorded at 0.0 s, 120 s, and 300 s after application of 8.27×10^5 N m^{-2}, O_2 pressure to a 0.5 M solution of Me_4NBr.

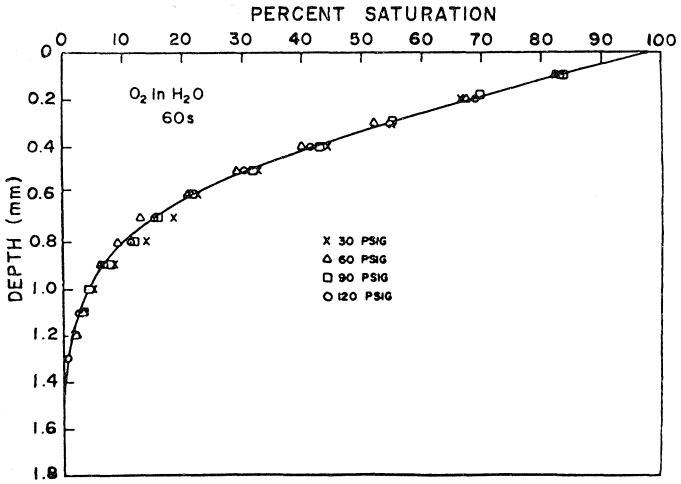

FIG. 2. Percent saturation of a solution of O_2 in H_2O *vs.* depth of H_2O at 60 s. The pressures used were 2.07×10^5 N m^{-2} (×), 4.14×10^5 N m^{-2} (△), 6.21×10^5 N m^{-2} (□), 8.27×10^5 N m^{-2} (○). The solid line was computer generated using $D = 2.0 \times 10^{-5}$ cm^2 s^{-1}.

15 s burst, then in 10 s bursts around the time at which it was desired to analyse a frame.

On application of the pressure jump, the gas temperature as measured by a miniature thermistor rose as much as 5°C. In the liquid the temperature rose 0.03°C, calculated from the refractive index change, and relaxed in about 1 to 1.5 s. The agreement of the known thermal conductivity (10) of water with the relaxation times permitted a rough calculation of the work of compression on the gas above the liquid. With allowance made for thermal capacity and conductivity of the metal walls reasonable agreement was found.

In a typical run, no thermal isolation was attempted. The room was thermostatted at 22 ± 0.5°C but no variation in the temperature of the solution was detected either by thermistor or optically over the 10–30 min of a run.

After a 100 ft roll of film had been developed, frames at selected times were analysed by projecting the frames onto a plotting table. The fringes were hand drawn at magnifications of ×50 or ×100 on large size mm graph paper and fringe shifts converted to concentration using refractive index *vs.* concentration data (7) and a modified Bragg expression

$$[5] \qquad 2nd \cos\theta = N\lambda$$

where n is the refractive index, d the thickness (cm), cos θ is almost exactly one since the angle of incidence must not deviate appreciably from 90° for good fringes, and N is the order of interference or twice the number of wavelengths λ (cm) in the thickness t.

At the pressure jump, the solution was compressed as well as heated. The compressibility of water at these low pressures (0–10 atm applied pressure) was obtained and has been published (9). The compressibility of solutions of O_2 was also obtained and is shown in Table 1. It is to be compared to $K_t \times 10^{10} = 3.97$ Pa for pure water (7) or for higher pressures Bridgman's value (11) of $K_t \times 10^{10} = 4.42$ or Kell's 4.39 (12). The average values for O_2 saturated solutions at 22°C were: at 1.03×10^5 Pa, 4.01; at 2.07×10^5 Pa, 3.91; and at 4.14×10^5 Pa, 3.99. It seems likely that the effect of O_2 in the solution is small.

TABLE 1. Isothermal compressibility of water saturated with oxygen at 4.14×10^5 Pa^{-1}

Applied pressure in psig	Pa^{-1}	F	$\Delta\rho$/N m^{-2} (× 10^7)	$10^{10} K_t$ (Pa^{-1})
14	0.965	2.25	4.035	4.046
15	1.034	2.35	2.390	3.941
29	1.909	4.55	3.937	3.948
30	2.069	4.80	4.016	4.027
44	3.033	7.00	3.992	4.003
46	3.171	7.20	3.928	3.939
60	4.137	9.50	3.974	3.985
78	5.377	12.50	4.022	4.033
81	5.583	13.0	4.027	4.038

Results and Discussion

Figure 1 is a series of interferograms at 8.3×10^5 Pa O_2 pressure in 0.5 M tetramethyl ammonium bromide solution at 22°C. They were photographed at 0 s, 120 s, and 300 s. They are presented as typical of the interferograms obtained during this study. The field of view was approximately 8 × 5 mm; the major change in fringe direction in the second frame is at about 1 mm depth.

Figures 2 and 3 give a measure of the precision of measurement. Figure 2 is percent saturation of water with O_2 *vs.* depth at 22°C and 2.07, 4.13,

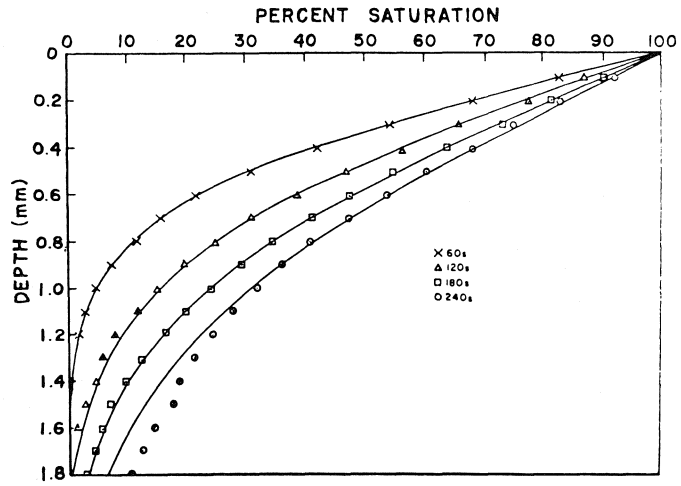

FIG. 3. Complete averaging at various times (60 s (×), 120 s (△), 180 s (□), 240 s (○)) *vs.* depth of all runs at all four pressures used, 2.07, 4.14, 6.21, and 8.27 × 10^5 N m^{-2}. The solid line was computer generated using $D = 2.0 \times 10^{-5}$ cm^2 s^{-1}.

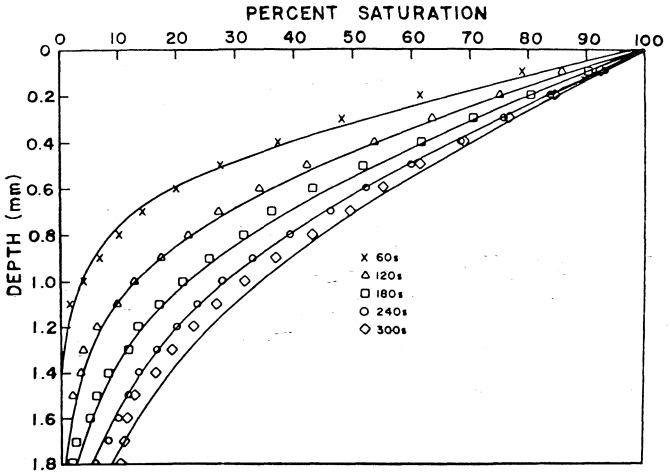

FIG. 4. Average percent saturation of N_2 in H_2O *vs.* depth for several runs at four pressures (2.07, 4.14, 6.21, 8.27 × 10^5 N m^{-2}) at 60 s (×), 120 s (△), 180 s (□), 240 s (○), and 300 s (◇). The solid line was computer generated using $D = 2.0 \times 10^{-5}$ cm^2 s^{-1}.

6.20 and 8.27 × 10^5 Pa pressure and 60 s. Figure 3 shows the same systems (except for 6.20 × 10^5 Pa) at 120 s, but completely averaged for all times and all pressures. The solid line in both cases is computer-generated from eq. 2. If averages are now taken and longer times considered, serious deviation begins at 240 s. This is believed to be due to having so short an extent of straight fringe in the frame that it is difficult to decide what represents zero change in refractive index or this is a systematic mechanical measurement error. A test of reproducibility of data was arranged by re-evaluating several runs after six months had elapsed. The reproducibility for short times was about ±0.6%.

The plot for N_2 average percent saturations in H_2O at 22°C at various depths for 8.27 × 10^5 Pa (120 psig) shows (Fig. 4) the same inaccuracies at longer times. Argon (Fig. 5) shows deviation from the theoretical at shorter times and hydrogen (Fig. 6) has only one time, 60 s, when good agreement is obtained.

This is the expected trend for more rapid diffusion rates which result in shorter straight

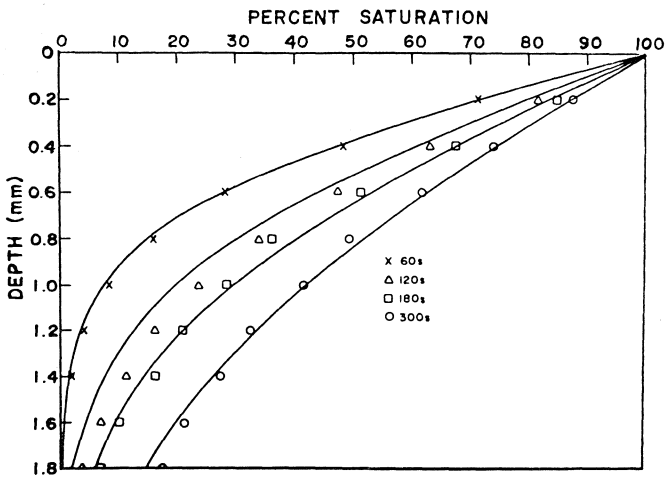

FIG. 5. Average percent saturation of Ar in H_2O *vs.* depth for several runs at various pressures (2.07, 4.14, and 6.21 × 10^5 N m^{-2}) at 60 s (×), 120 s (△), 180 s (□), 300 s (○). The solid line was computer generated using 2.5 × 10^{-5} cm^2 s^{-1}.

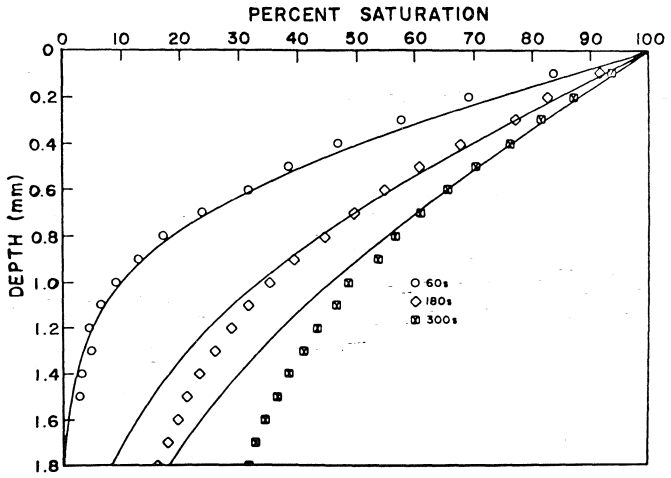

FIG. 6. Average percent saturation of H_2 in H_2O *vs.* depth for several runs at various pressures (2.07, 4.14, and 6.21 × 10^5 N m^{-2}) at 60 s (○), 180 s (□), and 300 s (⊠). The solid line was computer generated using D = 3.0 × 10^{-5} cm^2 s^{-1}.

portions of fringe in the field of view. It is also the natural result of a careful hand-measuring by a conscientious person attempting to fail safe. New machine measuring techniques presently being tested reduce the reproducibility range markedly and also are expected to effectively eliminate this problem. Figure 7 shows percent saturation of O_2 in H_2O at 1 mm and 1.5 mm depths at long times, up to 5400 s. The experiment was an attempt to link the present transient experiments with equilibrium type experiments. The fringes at 1.5 mm passed behind a fiduciary point placed in the optical system soon after 600 s. Only about 1.5% deviation from the theoretical line was found at 90 h (nearly 4 days), and 80% saturation, or there is reason to believe that values obtained by this transient method would be acceptably near equilibrium values found by other, bulk value methods.

Table 2 presents the values of diffusion constants found. The method of arriving at these values was to pick reasonable values of D the diffusion constant for the various systems, calculate the concentration expected at a given

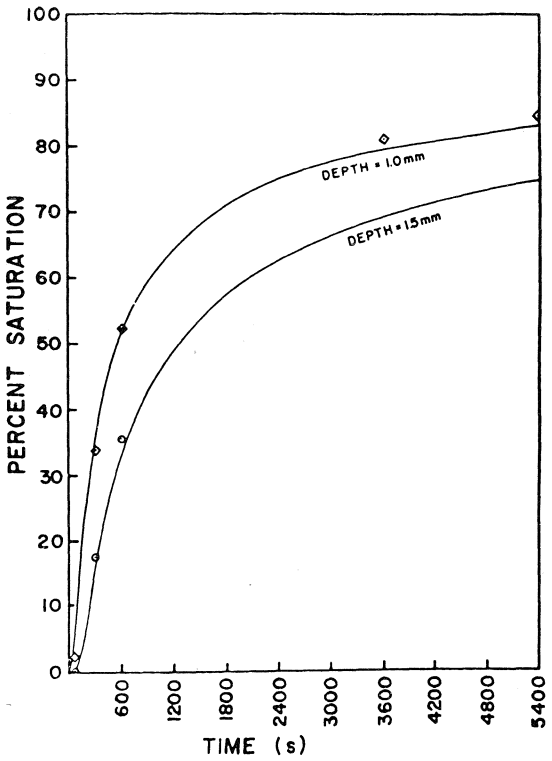

FIG. 7. Percent saturation of O_2 in H_2O at long times at two depths, 1.0 mm (◇) and 1.5 mm (○). The solid lines were computer generated using $D = 2.0 \times 10^{-5}$ cm^2 s^{-1}.

depth and time using eq. 2, and subtract these from the experimentally determined value. Figure 8 shows such a plot for O_2 in H_2O at 22°C, 60 psig for various depths and various values of D. $D = 2.0 \times 10^{-5}$ cm^2 s^{-1} obviously

TABLE 2. Diffusion coefficients of gases in liquids

Gas	Solvent	Temperature (°C)	D (cm^2 s^{-1})
Oxygen	Water	22	2.0×10^{-5}
Nitrogen	Water	22	1.8×10^{-5}
Argon	Water	22	2.5×10^{-5}
Hydrogen	Water	22	3.0×10^{-5}

fits the data best and the scatter suggests the data do not merit refinement to 2.05 or 1.95. A least-squares approximation of data showed minimum deviation at 2.0 with the deviations close to symmetrical about that value. All other systems were evaluated in the same way. The values in Table 2 agree well with the best literature values except our hydrogen–water value is slightly low. The optical anomalies investigated by McLarnon, Muller, and Tobias (13) which suggest that in cells of thickness of several centimetres significant errors could occur for refractive index gradients of 1×10^{-2} cm^{-1} do not apply since our gradient $\simeq 2.3 \times 10^{-3}$ cm^{-1}.

Conclusions

No significant deviation from theoretically calculated values at short distances below the surface were found. Nor were there short time anomalies. It is therefore concluded that no surface resistance exists at clean surfaces, though it has been shown that a monolayer of surfactant does create an appreciable barrier (14). Because of the good agreement with literature values found by other methods it is concluded that transient experiments by interferometry are as accurate as and more convenient than equili-

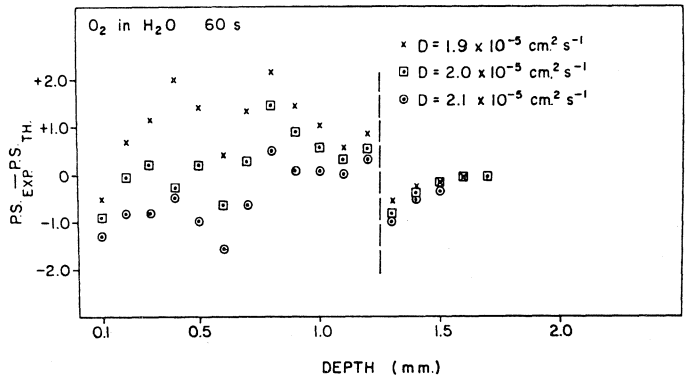

FIG. 8. The difference between experimental ($P.S._{exp}$) and calculated ($P.S._{th}$) percent saturation for O_2 in H_2O *vs.* depth at 60 s for various calculated values using $D = 1.9 \times 10^{-5}$ cm s^{-1} (×), $D = 2.0 \times 10^{-5}$ cm^2 s^{-1}, and $D = 2.1 \times 10^{-5}$ cm^2 s^{-1}.

brium values. Recently experiments have been recorded on video tape and an automatic system of evaluation of interferograms seems possible which should make the system more accurate and also much faster. Future experiments will explore other systems at other temperatures including solutions such as those in Fig. 1 and gas clathrates.

Acknowledgements

We thank the National Research Council of Canada for supporting this work with a Fellowship to one of us (W.F.H.) and Environment Canada for contract support. We also thank C. W. Tobias for the original suggestion and early encouragement of the work.

1. D. M. HIMMELBLAU. Chem. Rev. **64**, 527 (1964).
2. M. K. THAM, R. D. WALKER, and K. E. GUBBINS. J. Phys. Chem. **74**, 1747 (1970).
3. P. V. DANCKWERTS. Gas–liquid reactions. McGraw-Hill Book Co., New York. 1970. p. 66.
4. G. W. HUNG and R. H. DINIUS. J. Chem. Eng. Data, **17**, 449 (1972).
5. S. H. CHIANG and H. L. TOOR. A. I. Ch. E. J. **5**, 165 (1959).
6. E. A. HARVEY and W. SMITH. Chem. Eng. Sci. **10**, 274 (1959).
7. R. N. O'BRIEN and W. F. HYSLOP. A Fabry-Perot interferometer for monitoring gas–liquid exchange. *In* Chemistry and physics of aqueous gas solutions. *Edited by* W. A. Adams. The Electrochemical Soc., Inc., Princeton, NJ. 1975.
8. W. F. HYSLOP. Doctoral Dissertation, University of Victoria, Victoria, B.C. 1975; J. Crank. The mathematics of diffusion. 2nd ed. Clarendon, Oxford. 1975. p. 20.
9. R. N. O'BRIEN and W. F. HYSLOP. J. Chem. Eng. Data. To be published.
10. H. J. V. TYRRELL. Diffusion and heat flow in liquids. Butterworths, London. 1961. p. 126.
11. P. W. BRIDGMAN. Proc. Am. Acad. Arts Sci. **48**, 309 (1912).
12. G. S. KELL. J. Chem. Eng. Data, **15**, 119 (1970).
13. F. R. MCLARNON, R. H. MULLER, and C. W. TOBIAS. J. Electrochem. Soc. **122**, 59 (1975).
14. R. N. O'BRIEN, A. I. FEHER, K. L. LI, and W. C. TAN. Can. J. Chem. To be published.

Photochemistry of 1,4-diphenyl-1,4-epoxy-1,4-dihydronaphthalene 2-carboxylate and 2,3-dicarboxylate esters[1,2]

R. A. F. MATHESON, A. W. MCCULLOCH, A. G. MCINNES, AND D. G. SMITH

Atlantic Regional Laboratory, National Research Council of Canada, Halifax, N.S., Canada B3H 3Z1

Received November 19, 1976

R. A. F. MATHESON, A. W. MCCULLOCH, A. G. MCINNES, and D. G. SMITH. Can. J. Chem. **55**, 1422 (1977).

Direct irradiation (2537 Å) of methyl 1,4-diphenyl-1,4-epoxy-1,4-dihydronaphthalene-2-carboxylate (**13***b*) affords methyl 2,4-diphenyl-3-benzoxepine-1-carboxylate (**17***b*) and methyl 1-benzoyl-3-phenylindene-2-carboxylate (**19***b*), while acetone-sensitized irradiation yields chiefly **19***b*. The latter can be converted to methyl 3-phenylindene-2-carboxylate (**21***b*).

Direct irradiation of dimethyl 1,4-diphenyl-1,4-epoxy-1,4-dihydronaphthalene-2,3-dicarboxylate (**13***a*) affords a mixture of dimethyl 2,4-diphenyl-3-benzoxepine-1,5-dicarboxylate (**17***a*), dimethyl 1-benzoyl-3-phenylindene-1,2-dicarboxylate (**19***a*), and dimethyl 1-benzoyl-2-phenylindene-1,3-dicarboxylate (**18**). The latter two products cleave readily to give dimethyl 3-phenylindene-1,2-dicarboxylate (**21***a*) and dimethyl 2-phenylindene-1,3-dicarboxylate (**20**) respectively. Sensitized irradiation yields mainly **19***a*. The formation of **19***a* and **19***b* as major products of photorearrangement of **13***a* and **13***b* is consistent with a di-π-methane pathway producing methyl 4,6-diphenyl-5-oxatetracyclo[5.4.0.0.^{2,4}0^{3,6}]undeca-1(7),8,10-triene 2-carboxylate and 2,3-dicarboxylate (**25***a*,*b*), intermediates similar to those previously observed by other workers for benzonorbornadienes and 7-azabenzonorbornadienes. Compound **18** is derived by photo-induced rearrangement of the benzoxepine **17***a*.

The $AlCl_3$-catalyzed rearrangement of **13***a* yields a mixture of dimethyl 2,4-diphenyl-1(2*H*)-naphthalenone-2,3-dicarboxylate (**15**) and methyl 1,3-diphenyl-4-hydroxynaphthalene-2-carboxylate (**16**), while that of **13***b* affords only **16**.

R. A. F. MATHESON, A. W. MCCULLOCH, A. G. MCINNES et D. G. SMITH. Can. J. Chem. **55**, 1422 (1977).

L'irradiation directe (2537 Å) du diphényl-1,4 époxy-1,4 dihydro-1,4 naphtalènecarboxylate-2 de méthyle (**13***b*) conduit au diphényl-2,4 benzoxépine-3 carboxylate-1 de méthyle (**17***b*) et au benzoyl-1 phényl-3 indènecarboxylate-2 de méthyle (**19***b*) alors que l'irradiation sensibilisée par l'acétone fournit principalement **19***b*. On peut convertir ce dernier en phényl-3 indènecarboxylate-2 de méthyle (**21***b*).

L'irradiation directe du diphényl-1,4 époxy-1,4 dihydro-1,4 naphtalènedicarboxylate-2,3 de méthyle (**13***a*) conduit à un mélange de diphényl-2,4 benzoxépine-3 dicarboxylate-1,5 de méthyle (**17***a*), du benzoyl-1 phényl-3 indènedicarboxylate-1,2 de méthyle (**19***a*) et du benzoyl-1 phényl-2 indènedicarboxylate-1,3 de méthyle (**18**). Ces deux derniers produits se coupent rapidement pour conduire respectivement au phényl-3 indènedicarboxylate-1,2 de méthyle (**21***a*) et au phényl-2 indènedicarboxylate-1,3 de méthyle (**20**). L'irradiation sensibilisée conduit principalement à **19***a*. La formation de **19***a* et de **19***b* comme produits majeurs des photoréarrangements de **13***a* et de **13***b* est en accord avec un chemin di-π-méthane produisant les diphényl-4,6 oxa-5 tétracyclo[5.4.0.0.^{2,4}0^{3,6}]undécatriène-1(7),8,10 carboxylate-2 et dicarboxylate-2,3 de méthyle (**25***a*,*b*), des intermédiaires semblables à ceux observés antérieurement par d'autres chercheurs pour des benzonorbornadiènes et des aza-7 benzonorbornadiènes. Le composé **18** dérive d'un réarrangement photoinduit de la benzoxépine **17***a*.

Le réarrangement catalysé par $AlCl_3$ de **13***a* conduit à un mélange de diphényl-2,4 1(2*H*) napthtalènonedicarboxylate-2,3 de méthyle (**15**) et de diphényl-1,3 hydroxy-4 naphtalènecarboxylate-2 de méthyle (**16**) alors que celle de **13***b* conduit uniquement à **16**.

[Traduit par le journal]

Introduction

There has been considerable interest in recent years in the photochemistry of the benzonorbornadiene system (1–8). Sensitized irradiation of benzonorbornadiene **1***a* (1) and some substituted derivatives **1***b–e* (2) has been shown to afford good yields of the corresponding tetracyclic compounds **2***a–e*.

Prinzbach and his co-workers have studied the photochemical behavior of the three 7-azabenzonorbornadiene derivatives **3***a–c*. Direct irradia-

[1]NRCC No. 15811.

[2]Taken in part from the Ph.D. thesis of R.A.F.M. (supervisor A.G.M.), Dalhousie University, Halifax, N.S., 1973.

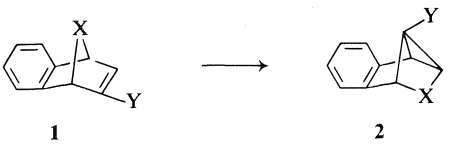

1 2

a, X = CH_2 Y = H

b, X = C(cyclopropyl) Y = H

c, X = C(Me)(Me) Y = H

d, X = C(ϕ)(ϕ) Y = H

e, X = CH_2 Y = CH(Me)(Me)

tion of **3***a*,*b* gave chiefly the anticipated benzazepine **4***a*,*b*, while irradiation of **3***c* afforded a mixture of **4***c* (9%) and the benzofulvene **5***c* (40%). Acetone-sensitized irradiation of **3***a* gave a mixture of the isomeric fulvenes **5***a* and **6***a* (3). Recent work by Swenton and his co-workers on the direct and sensitized photochemistry of the 7-aza derivative **3***d* has clarified the behavior of the above compounds (5, 6). While direct irradiation of **3***d* gave the benzazepine **4***d*, the acetone-sensitized reaction under carefully controlled conditions led to isolation of the tetracyclic azetidine **7***d* (94%), which underwent facile (acid-catalyzed) isomerization to the benzofulvene **5***d*. All attempts to isolate compounds of type **7** from the reactions of **3***a* or the 1,4-dimethyl derivative of **3***d* were unsuccessful, and it was suggested that this was probably due to their instability (6).

The photochemical behavior of simple 7-oxabenzonorbornadienes has received relatively little attention.[3] Ziegler and Hammond found that direct irradiation of 7-oxabenzonorbornadiene **9** afforded the corresponding benzoxepine **10** (4–6%), while the sensitized reaction gave a dimer (8%) resulting from intermolecular 2 + 2 cycloaddition of **9**, together with a large amount of intractable material (7, 8). Edman has suggested that formation of polymer in the latter reaction may be due to formation of the reactive tetracyclic ether **11** (1).

In the course of an investigation of the influence of $AlCl_3$ on the Diels–Alder reactions of a number of heterocyclic dienes, we have studied the reactions of 1,3-diphenylisobenzofuran **12** with dimethyl acetylenedicarboxylate (DMAD) and methyl propiolate (MP). We have also carried out a study of the photochemical behavior of the 1,4-diphenyl-1,4-epoxy-1,4-dihydronaphthalene adducts **13***a* and **13***b*. These 7-oxabenzonorbornadienes are of particular interest since it was anticipated that the presence of the bridgehead aryl substituents might enhance the stability of certain radical intermediates, and would certainly preclude formation of a benzofulvene. Our results are given below, together with some discussion of the $AlCl_3$-catalyzed rearrangements of these compounds.

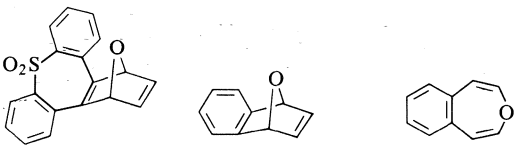

8 9 10

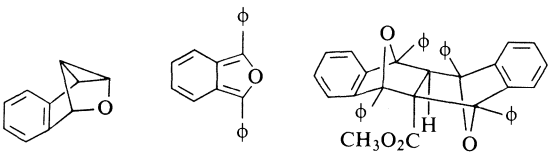

11 12 14

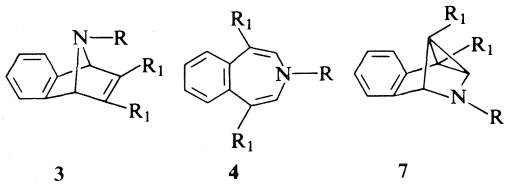

3 4 7

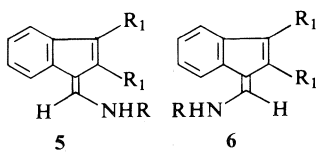

5 6

a, R = CO_2CH_3 R_1 = H
b, R = Tos R_1 = H
c, R = CO_2CH_3 R_1 = CO_2CH_3
d, R = $CO_2{}^tBu$ R_1 = H

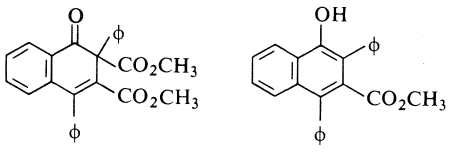

15 16

[3]Prinzbach *et al.* have studied the photochemistry of the annellated oxanorbornadiene **8** (9).

Results and Discussion

Preparation of the 7-Oxabenzonorbornadienes 13a,b

Diene **12** reacted readily with DMAD or MP to give the expected Diels–Alder adducts **13***a* and **13***b*. It was difficult to stop the reaction at this stage in the case of **13***b* due to the enhanced dienophilicity of the oxanorbornadiene-2-carboxylate system (*cf.* ref. 10). Formation of **13***b* was favored at low temperatures and high dienophile concentration: at higher reaction temperatures and lower concentrations of MP the diadduct **14** was favored. A diacid analogous to **14**, resulting from the reaction of **12** with acetylenedicarboxylic acid, has been previously reported by Berson (11).

As expected $AlCl_3$ caused a significant enhancement in the rate of Diels–Alder addition of **12** to both dienophiles. Reactions of **12** with DMAD in the presence of $AlCl_3$ gave, depending on the reaction parameters (see Table 1), the adduct **13***a*, the naphthalenone **15**, and the naphthol **16**. Similar reactions of **12** with MP gave **13***b*, **14**, and **16**. Additional experiments established that **15** and **16** could be obtained in good yield on treatment of **13***a* and **13***b*, respectively, with Lewis acids. Mechanisms for this type of rearrangement have been discussed previously (12–15).

The isolation of **16** from reaction of **12** with DMAD is, however, unexpected. This product must arise via decarboxylation of the β-keto ester **15**, and indeed we have shown that treatment of **15** with $AlCl_3$ gives **16**.

Photochemistry of the 7-Oxabenzonorbornadienes 13a,b

Observations

Direct irradiation (2537 Å; Et_2O) of **13***b* gave as major product (40%) the indene **19***b* together with the benzoxepine **17***b* (20%); the yield of **19***b* increased (55%) in the acetone-sensitized reaction.

Direct irradiation (Et_2O or CH_2Cl_2) of **13***a* gave the benzoxepine **17***a* as a minor product (15–20% yield, based on the amount of starting material consumed).[4] The major component of the crude reaction product, the indene **19***a*, was readily converted to **21***a* during work-up. A third product, indene **18**, was similarly converted to **20** (see Experimental). Because of their reactivity we were unable to obtain **18** and **19***a* in pure state. The conversions of **18** and **19***a* to **20** and **21***a* took place slowly on standing and were catalyzed by acid or base.[5] Benzoic acid was identified as a by-product in each case. The facility of the rearrangements of **18** and **19***a* is consistent with their β-keto ester structures. In contrast, compound **19***b*, which does not possess a β-keto ester moiety, proved to be relatively stable to acid, base, and moisture; it was, however, converted in part to **21***b* during thin-layer chromatography on alumina plates.

Acetone-sensitized irradiation of **13***a* gave as predominant product the indene **19***a* and only a small amount of **17***a*. The percentage of light capture by the sensitizer during both this irradiation and the acetone-sensitized irradiation of **13***b* above was calculated to be 90–95%.

For comparison purposes we investigated the acetone-sensitized irradiation of the diaryl-substituted oxanorbornadiene **22**. We had previously shown that this compound was converted on direct irradiation chiefly to the oxepine **23***a*, with a small amount of the 6-hydroxyfulvene **24** as by-product (16). Use of acetone as a sensitizer caused reversal of the product ratio, the product now being almost exclusively **24**, with only a very low yield of **23***a*.

The light-catalyzed reaction of **22** in the presence of iodine is known to proceed readily to give a high yield of **24** (16). The benzo derivative **13***a* was, however, surprisingly inert under similar experimental conditions.

Mechanisms

Triplet-sensitized irradiations of benzonor-

TABLE 1. Reaction of 1,3-diphenylisobenzofuran (**12**) with DMAD in the presence of $AlCl_3$ (molar ratio of reactants 1:1:2)[a]

Time (min)	T (°C)	Product yields (%)[b] **13***a*	**15**	**16**
10	−20	81	9	—
30	0	18	75	—
30	25	7	69	15
300	25	—	48	34
240	40	—	5	75

[a]Concentration of **12** 0.061 *M* in CH_2Cl_2.
[b]Yields based on **12**.

[4]Prinzbach *et al.* have reported that direct irradiation of **13***a* produces a 40–50% conversion to **17***a*, although no details were given (footnote in ref. 3).

[5]Although the base-catalyzed reactions proceeded rapidly the products were base-sensitive. In the case of **21***a*, the 1-hydroxyindene **29** was identified as an oxidative breakdown product (see Experimental).

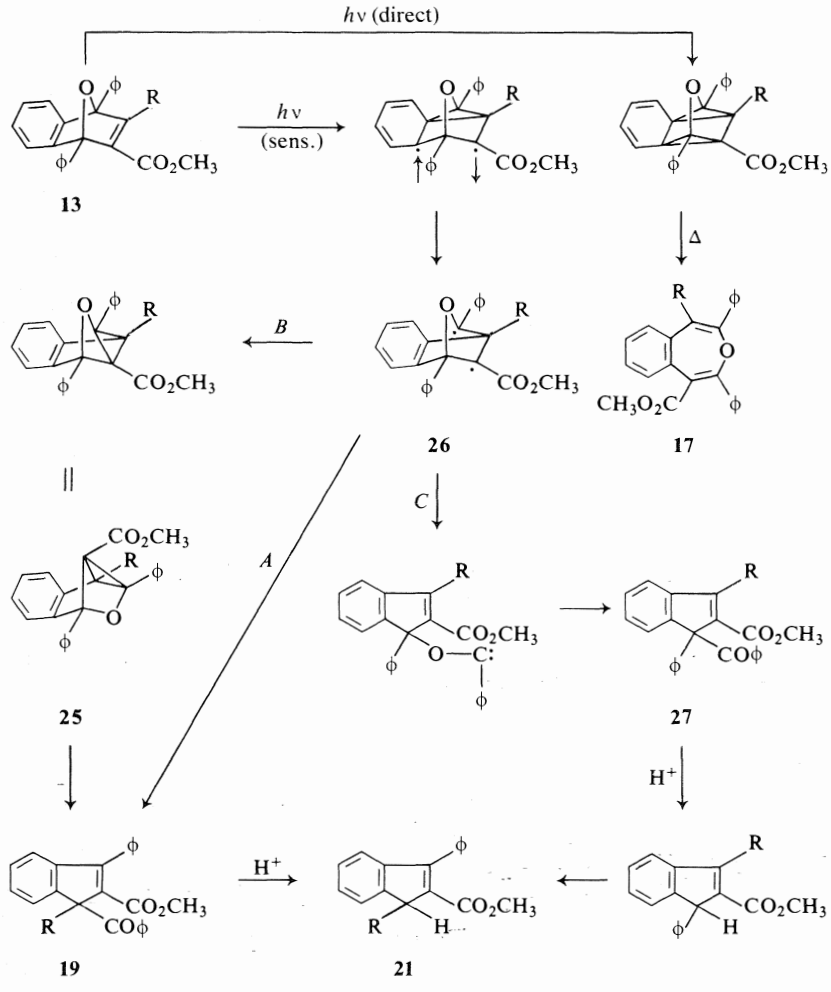

a, R = CO_2CH_3 *b*, R = H

SCHEME 1

bornadienes **1** (1, 2) and of the 7-aza analog **3***d* (6) afford the tetracyclic products **2** and **7***d*, respectively. The observed subsequent rearrangement of **7***d* to the benzofulvene **5***d* must proceed by way of a tautomeric indene intermediate (6). If the sensitized photorearrangements of **13***a* and **13***b* are to parallel those above we would expect (*i*) formation of the tetracyclic oxetanes **25***a* and **25***b* via the di-π-methane intermediates **26***a* and **26***b* (Scheme 1, pathway *B*), and (*ii*) their subsequent rearrangement to the keto indenes **19***a* and **19***b*.

Alternative less likely mechanisms of indene formation from **13** via intermediate **26** (*cf.* refs. 6, 16–18) are 1,4-radical cleavage leading directly to **19** (Scheme 1, pathway *A*) and 1,2-cleavage to a carbene intermediate and migration to give **27** (Scheme 1, pathway *C*). Hydrolytic cleavage of **27** could afford **21***a* via its tautomer.

None of the pathways shown in Scheme 1 account for the formation of indene **18**. We have found that this compound arises through photorearrangement of the benzoxepine **17***a*. A ring-contraction mechanism, involving transannular 1,4-bond formation similar to that observed during photo-induced rearrangement of simple oxepines and azepines (19) and of 1-benzothiepine (20), is shown in Scheme 2.

Structures of Products

The structures of all products were based mainly on spectroscopic evidence (see Experi-

TABLE 2. ^{1}H nmr (60 MHz) data ($CDCl_3$)

Compound	Chemical shifts δ (integrated intensity, multiplicity)[a]			
	$-CO_2CH_3$	Aromatic *H*	Ring *H*	O*H*
13*a*	3.66(6H,s)	7.00–7.90(14H,m)		
13*b*	3.64(3H,s)	6.95–7.15(3H,m), 7.30–7.95(11H,m)	8.03(1H,s)	
14	3.20(3H,s)	6.65–8.10(28H,m)	4.70(1H,s)	
15	3.35(3H,s), 3.78(3H,s)	6.75–8.05(14H,m)		
16	3.19(3H,s)	7.30–7.70(13H,m), 8.33(1H,m)		5.68(1H,s)
17*a*	3.63(6H,s)	7.05–7.55(14H,m)		
17*b*	3.60(3H,s)	7.00–7.75(14H,m)	6.83(1H,s)	
18	3.69(3H,s), 3.73(3H,s)	7.00–8.00(14H,m)		
19*a*	3.57(3H,s), 3.85(3H,s)	7.10–7.95(14H,m)		
19*b*	3.53(3H,s)	7.20–8.10(14H,m)	5.73(1H,s)	
20	3.52(3H,s), 3.78(3H,s)	7.05–7.90(9H,m)	4.94(1H,bs)	
21*a*	3.67(3H,s), 3.75(3H,s)	7.20–7.70(9H,m)	4.87(1H,bs)	
21*b*	3.70(3H,s)	7.20–7.70(9H,m)	3.88(2H,s)	
29	3.65(3H,s), 3.70(3H,s)	7.10–7.50(9H,m)		4.30(1H,s)

[a]b = broad, s = singlet, m = multiplet.

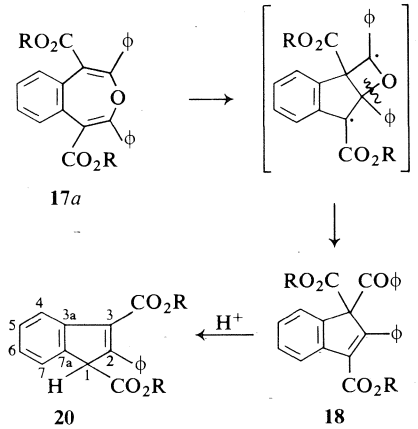

SCHEME 2

mental). ^{1}H nmr data are detailed in Table 2 and relevant ^{13}C nmr data have been included in the experimental section. Detailed tabulated ^{13}C data (in $CDCl_3$) for compounds **15**, **16**, **17***a*, **17***b*, **19***b*, **20**, **21***a*, **21***b*, and **29**, as well as for indene itself, have been deposited in the Depository of Unpublished Data.[6]

(a) Adducts 13a, 13b, and 14

These compounds are all formed via well-recognized pathways. Their mass spectra show weak molecular ions and as expected are also characterized by strong ions at *m/e* 270 derived by Diels–Alder retrogression to **12**. In addition these compounds show the anticipated ^{1}H nmr signals for aromatic, carbomethoxyl, olefinic (**13***b*), and ring-junction (**14**) hydrogens. No attempt was made to unequivocally establish the stereochemistry of the central ring-junction in **14**, although by analogy with our previous work on the Diels–Alder additions of furans to oxonorbornadienes (10, 21), we have tentatively assigned the *endo–exo* stereochemistry shown.

(b) Naphthalenone 15 and Naphthol 16

The acid-catalyzed rearrangement of fully substituted oxanorbornadienes to cyclohexadienones is known (12), as is the corresponding rearrangement of lesser substituted oxanorbornadienes to substituted phenols (12–15). Analogous rearrangements of **13***a* and **13***b* would be expected to yield **15** and **16**, respectively. The spectroscopic evidence given below established that these products were in fact obtained.

In the case of **16** the presence of a phenolic hydroxyl group is indicated by its ir (3540 cm^{-1}) and ^{1}H nmr (δ 5.68, exchangeable by D_2O) spectra. This hydroxyl is not hydrogen bonded to the conjugated ester group (1724 cm^{-1}), establishing that these two substituents are not in an *ortho* relationship. Strong evidence that the hydroxyl group is located at C-1 is derived from the low-field shift (δ 8.33) of one aromatic proton (H-5), a characteristic of 1-naphthol (22). Finally, the exceptionally high-field shift (δ 3.19) of the protons of the carbomethoxyl group is consistent with shielding by two vicinal aryl substituents (*cf.* ref. 14).

In the case of the naphthalenone **15** the ir

[6]The tabular data are available, at a nominal charge, from the Depository of Unpublished Data, CISTI, National Research Council of Canada, Ottawa, Canada K1A 0S2.

spectrum shows absorptions for conjugated ester (1698 cm^{-1}), non-conjugated ester (1734 cm^{-1}), and ketone (1668 cm^{-1}) carbonyl groups. The ^1H nmr spectrum shows two methoxyl resonances, at δ 3.78 and 3.35. The high-field shift of the latter is again due to its shielding by the *ortho* phenyl substituent. The conversion of **15** to **16** on treatment with Lewis acids suggests that the ketone carbonyl must be at C-1 of the naphthalene ring, and the ease of this decarboxylative conversion strongly indicates the presence of a β-keto ester system in **15**.

Although it is impossible to assign most of the individual carbon resonances of **15** and **16**, due to extensive signal overlap in their high-resolution ^{13}C nmr spectra, some significant observations can be made which serve to confirm these structures. In the case of **16** the signal for the hydroxyl-substituted C-1 appears as expected at low field (147.9 ppm). This chemical shift is similar to that of C-1 in 1-naphthol (23). The signal for C-2 of **16** is at 118.3 ppm, due to a combination of shielding by the hydroxyl group at C-1 (*cf.* C-2 of 1-naphthol (23)) and deshielding by the attached aryl substituent. The main features of the spectrum of **15** are the three carbonyl resonances at 167.0 and 169.5 (both ester), and 193.9 (ring ketone) ppm, and the saturated carbon resonance (C-2) at 68.0 ppm.

(c) Benzoxepines 17a and 17b

The spectral properties of these compounds are similar to those of the related oxepines **23***a*,*b* (16). The mass spectra show the expected molecular ions, with base peaks at *m*/*e* 105, due to the tendency of these molecules to readily lose a benzoyl fragment. The ir spectra show absorptions for conjugated ester carbonyl groups and the ^1H nmr spectra are characterized in each case by an aromatic envelope (14H) and by the appropriate signals for methoxyl (6H singlet for **17***a*) and oxepine ring (**17***b*) hydrogens. The ^{13}C nmr spectra especially that of **17***b*, are complicated by overlapping signals for the many aromatic resonances. The carbons directly attached to the ring oxygen and also substituted by aryl groups (C-2 and C-4) appear as expected well downfield at 157–159 ppm. In the case of **17***b* the unsubstituted ring carbon (C-5) resonates at 114.1 ppm (^1J = 156.8 Hz) consistent with its position β to the ring oxygen.

Indenes 18, 19a, 19b, 20, 21a, 21b, and 29

The structure of **21***a* was unequivocally established by X-ray analysis, full details of which will be published elsewhere (28). Prior spectroscopic evidence strongly indicative of this structure included: (*a*) a molecular ion in the mass spectrum corresponding to the molecular formula $C_{19}H_{16}O_4$; (*b*) ir absorptions for α,β-unsaturated (1721 cm^{-1}) and non-conjugated (1735 cm^{-1}) ester carbonyl groups; (*c*) strong ultraviolet absorption maxima at *ca.* 235 and 290 nm, consistent with its substituted indene chromophore; (*d*) ^1H nmr signals for nine aromatic hydrogens (envelope), two methoxyl groups, and a single methine proton (δ 4.87); and (*e*) its ^{13}C nmr spectrum which is consistent with the types of carbons present (indene, phenyl, and carbomethoxyl) and is similar in many respects to the spectrum of indene itself.

Although it is not possible to make unambiguous assignments of all the carbons of the indene skeleton of **21***a*, due to signal overlap in the high-resolution spectrum, such assignments can be readily made in the case of C-1, C-2, and C-3. The methine carbon (C-1) appears at 55.7 ppm, reflecting the deshielding effect of the carbomethoxyl substituent. The resonance for C-2 can be assigned on the basis of its chemical shift (129.6 ppm; deshielded by the attached ester group, but shielded by the β-phenyl substituent). This carbon is geminally coupled (^2J = 6.1 Hz) to H-1.[7] As expected the phenyl-substituted carbon, C-3, appears well downfield (155.2 ppm; deshielded by both the phenyl group and the ester substituent at C-2) as a multiplet (possible coupling with the *ortho* hydrogens of the aryl substituent as well as to H-1 and H-4).

The ester carbonyl carbon bonded to C-1 can also be differentiated on the basis of its geminal coupling (^2J = 11.0 Hz) with H-1.

Compound **21***a* has been suggested previously as a product of photolysis of **28** (27). The similarity between the recorded properties and those of our product confirms this assignment.

The structures of the four indene derivatives **19***b*, **20**, **21***b*, and **29**, have been deduced mainly through comparison of their ^{13}C nmr spectra with that of **21***a* (see below). Supporting evidence for each structure is also obtained (see Experimental) from: (*a*) their mass spectra, each of which exhibits a molecular ion corresponding to the expected molecular formula; (*b*) their ir

[7]The observation of similar spacing (5.8 Hz) in the resonance at 133.9 ppm in the spectrum of indene confirms its assignment to C-2. This resonance has previously been assigned to C-2 (24, 25) or C-3 (26).

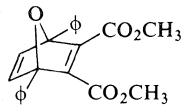

22

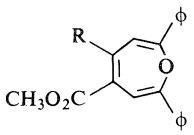

23
a, R = CO_2CH_3
b, R = H

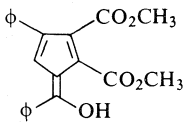

24

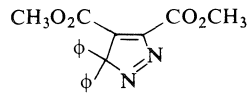

28

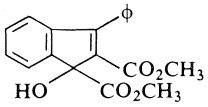

29

spectra which show absorptions for α,β-unsaturated ester (all four compounds), non-conjugated ester (**20**), and ketonic (**19***b*) carbonyl groups; (*c*) their uv absorption spectra all of which have comparable maxima at *ca.* 235 and 290 nm; and (*d*) their ^{1}H nmr spectra (Table 2) which are characterized by the expected signals for aromatic, methoxyl, and methine (or methylene) hydrogens.

As stated above the structures of **19***b*, **20**, **21***b*, and **29** were elucidated largely on the basis of their ^{13}C nmr spectra and comparison with the data obtained for the established structure **21***a*. In the case of the structurally-related **21***b* most of the carbon resonances can be readily compared to those of the corresponding carbons of **21***a*. The most significant features of **21***b* are: (*i*) the chemical shift and multiplicity of C-1, confirming the methylene nature of this carbon, and (*ii*) the characteristic geminal coupling between C-2 (130.6 ppm, triplet, ^2J = 6.9 Hz) and the two hydrogens at C-1. The chemical shift and the absence of any other observable long-range coupling involving C-2 proves that the ester grouping must be at this carbon.

The structure of the 1-benzoyl indene **19***b*, which is a direct precursor of **21***b* and must therefore have the same relative orientation of the ester and phenyl substituents as the latter, follows again from comparison of its ^{13}C nmr spectrum with that of **21***a*. In this case it was not possible to determine the coupling between C-2 and H-1 (due to signal overlap), but the geminal coupling between H-1 and the ketone carbonyl carbon at C-1 (^2J = 8.1 Hz) could be readily observed.

In the case of the 1-hydroxy derivative **29** the only major ^{13}C nmr spectral differences are (*i*) the chemical shift of C-1, now moved downfield (to 83.9 ppm) in accord with deshielding by the hydroxyl substituent, and (*ii*) the absence of geminal coupling in the ester carbonyl carbon which is bonded to C-1, which shows that the hydroxyl is located at C-1. The presence of the hydroxyl group is confirmed by ir absorption at 3480 cm^{-1}, and a ^{1}H nmr signal at δ 4.30, replaceable by D_2O.

The isomeric nature of **20** and **21***a* is clearly evidenced by their ir, uv, ^{1}H nmr, and ^{13}C nmr spectra. Since the geminal coupling in the ester carbonyl carbon and the chemical shift of C-1 are essentially the same in both compounds the difference can only be in the position of the ester and phenyl substituents. Thus **20** must have the ester grouping at C-3, and in accord with this both C-2 and C-3 now appear as multiplets since both of these carbons will now be long-range coupled to at least two hydrogens.

As mentioned previously compounds **18** and **19***a* could not be isolated in a pure state due to their ease of rearrangement to **20** and **21***a*. However, by analogy with the closely related conversion of **19***b* to **21***b*, we can assign precursors **18** and **19***a* the structures shown. Supporting evidence was obtained from studies of samples rich in these compounds. The ^{1}H nmr spectra both show aromatic envelopes and singlets for the hydrogens of two methoxyl groups; the mass spectra show strong ions at *m/e* 105 (base peak), reflecting the very facile cleavage of the benzoyl grouping.

Experimental

The ^{1}H nmr spectra were obtained on a Varian A-60A spectrometer, using $CDCl_3$ as solvent and tetramethylsilane as internal standard. ^{13}C nmr spectra at 25.16 MHz were recorded in $CDCl_3$ on a Varian XL-100-15 spectrometer equipped with a VFT-100 data system. The deuterium resonance from the solvent was used for field-frequency lock. Spectral width was 5120 Hz with an acquisition time of 0.8 s, and an 8K transform was used. In addition to proton noise decoupled spectra, high-resolution spectra enhanced by gated noise decoupling were used to obtain coupling constants ($J_{^{13}C-^1H}$).

Infrared absorptions (in $CHCl_3$ solution, unless otherwise stated) were measured on a Perkin–Elmer 521 spectrometer. Ultraviolet spectra were recorded in 95% EtOH on a Unicam SP 8000 spectrophotometer. The high-resolution mass spectral measurements were made

using a Dupont-C.E.C. 21-110B double focussing mass spectrometer.

All column chromatography was carried out using Mallinckrodt silicic acid (100 mesh) with $CHCl_3$ as eluant unless stated otherwise. Preparative thin-layer chromatography (plc) was performed on Merck silica gel F-254 precoated plates using 2 mm layers.

Irradiation experiments were conducted in a Rayonet photochemical reactor, using quartz reaction vessels, a 2537 Å light source, and an operating temperature of 30°C. Fisher spectral grade acetone (ε at 254 nm = 11) was employed in the sensitized irradiations.

Reaction of 1,3-Diphenylisobenzofuran with Dimethyl Acetylenedicarboxylate (DMAD)

(a) Thermal Reaction

A mixture of **12** (3.25 g, 0.012 mol) and DMAD (1.88 g, 0.013 mol) was refluxed in benzene (125 ml) for 4 h. Removal of the solvent and recrystallization of the crude product from ethyl acetate – pentane gave the 7-oxabenzonorbornadiene **13***a* as cream-colored prisms (4.30 g, 87%), mp 158–160°C. Molecular ion (< 1%) at *m/e* 412.1310 ($C_{26}H_{20}O_5$ requires 412.13108); base peak at *m/e* 105 ($C_6H_5CO^+$); significant ions at *m/e* (%) 380(5), 336(5), 270(36), 241(6), 239(4), 189(7), 165(5), 135(4), and 77(19). ν_{max} 1718, 1626 cm^{-1}. λ_{max} (ε) 207 (36 900), 218 (30 400) nm; ε at 254 nm, 2900.

(b) $AlCl_3$-Promoted Reaction

The Lewis acid promoted reaction was conducted using a variety of reaction parameters: a summary of the experimental conditions and product compositions is given in Table 1. A typical procedure follows.

A solution of **12** (2.07 g, 0.0077 mol) in CH_2Cl_2 (25 ml) was added to a stirred mixture of DMAD (1.16 g, 0.0082 mol) and $AlCl_3$ (2.22 g, 0.0167 mol) in CH_2Cl_2 (100 ml) at 25°C. Reaction was allowed to continue for 30 min, and was terminated by pouring into ice-water. The organic layer was separated, dried (Na_2SO_4), and the solvent removed under reduced pressure. The oily residue (3.08 g) was chromatographed. From the column, in order of elution, were obtained: (*i*) unreacted DMAD (0.12 g); (*ii*) adduct **13***a* (0.22 g, 7%); (*iii*) the naphthalenone **15**, isolated as a colorless solid (2.18 g, 69%), mp 206–207°C. Molecular ion (29%) at *m/e* 412.1302 ($C_{26}H_{20}O_5$ requires 412.13108); base peak at *m/e* 293; significant ions at *m/e* (%) 380(31), 352(68), 321(73), 265(57), 263(30), and 105(22). ν_{max} 1734, 1698, 1668 cm^{-1}. δ_c (ppm) 68.0 (br t, 3.0, C-2), 167.0 (q, 4.0, ester C=O), 169.5 (q, 4.1, ester C=O), 193.9 (dd, 3.6, 1.6, C-1); (*iv*) a fraction which was further purified by plc (25% acetone – petroleum ether) to give the naphthol **16** as a colorless solid (0.41 g, 15%), mp 92–94°C. Molecular ion (100%) at *m/e* 354.1254 ($C_{24}H_{18}O_3$ requires 354.12560); significant ions at *m/e* (%) 323(14), 321(12), 265(13), 209(12), 161(9), 147(20), 85(8), 83(11), and 59(8). ν_{max} 3540, 1724, 1589, 1570 cm^{-1}. δ_c (ppm) 118.3 (s, C-2), 147.9 (br s, C-1).

Reaction of 1,3-Diphenylisobenzofuran with Methyl Propiolate (MP)

(a) Thermal Reaction

To a stirred solution of MP (2.61 g, 0.0311 mol) in CH_2Cl_2 (10 ml) at 0°C was added dropwise over a period of 30 min a solution of **12** (1.06 g, 0.0039 mol) in CH_2Cl_2 (25 ml). The mixture was stirred for a further 1 h at 0°C and the solvent then removed at low temperature under reduced pressure. Column chromatography of the yellow oily residue afforded the following, in order of elution.

(*i*) A colorless solid (823 mg), crystallization of which from ethyl acetate – petroleum ether gave the 2:1 adduct **14** as colorless prisms (732 mg, 59%), mp 220–222°C (dependent on rate of heating). Molecular ion (≪1%) at *m/e* 624 ($C_{44}H_{32}O_4$ requires 624); base peak at *m/e* 270 (1,3-diphenylisobenzofuran$^+$); significant ions at *m/e* (%) 241(21), 239(17), 218(5), 189(10), 165(13), 135(11), 105(69), and 77(14). ν_{max} 1721, 1600 cm^{-1}.

(*ii*) A colorless oil (448 mg), crystallization of which from ethyl acetate – petroleum ether gave the mono-adduct **13***b* as cream-colored prisms (357 mg, 26%), double mp, with partial liquefaction at 121–125°C and melting at 142–146°C. Molecular ion (3%) at *m/e* 354.1247 ($C_{24}H_{18}O_3$ requires 354.12560); base peak at *m/e* 105 ($C_6H_5CO^+$); significant ions at *m/e* (%) 322(4), 294(4), 270(29), 241(4), 239(4), 218(5), 189(10), 165(5), 135(3), and 77(15). ν_{max} 1720, 1604, 1584 cm^{-1}. λ_{max} (ε) 208 (35 400), 218 (33 300) nm; ε at 254 nm, 2300.

Reaction of equimolar amounts of **12** and MP at 40°C for 90 min gave a 77% yield of **14** and negligible **13***b*.

(b) $AlCl_3$-Promoted Reaction

Compound **12** (1.05 g, 0.0039 mol) in CH_2Cl_2 (30 ml) was cooled to −30°C and added dropwise over 2 min to a similarly cooled, vigorously stirred mixture of MP (0.33 g, 0.0039 mol) and $AlCl_3$ (1.04 g, 0.0078 mol) in CH_2Cl_2 (50 ml). The reaction mixture was stirred at −30°C for a further 8 min, and then treated with ice water (20 ml). The organic layer was separated, dried (Na_2SO_4), and the solvent evaporated under reduced pressure. The dark oily residue was chromatographed and fractions recovered as follows: (*i*) unreacted MP (0.13 g); (*ii*) a mixture of **13***b* and **14**. Preparative thin-layer chromatography (25% acetone – petroleum ether) gave **13***b* (0.12 g, 9%) and **14** (0.63 g, 52%); (*iii*) the naphthol **16** (0.11 g, 8%).

*Reaction of **13***b* with 1,3-Diphenylisobenzofuran*

Adduct **13***b* (0.36 g, 0.001 mol) and **12** (0.27 g, 0.001 mol) were heated at 40°C in CH_2Cl_2 (15 ml) for 2 h. Evaporation of the solvent and crystallization of the residue from petroleum ether gave **14** (0.48 g, 77%).

*Rearrangement of **13***a* to **15***

(*a*) The benzonorbornadiene **13***a* (0.73 g, 0.0018 mol) and $AlCl_3$ (0.49 g, 0.0037 mol) in CH_2Cl_2 (30 ml) were stirred at 25°C for 90 min. Ice water (15 ml) was added to destroy the $AlCl_3$ and the organic layer then separated, dried (Na_2SO_4), and evaporated. The crude product was chromatographed. Collected from the column, in order of elution, were unreacted **13***a* (0.08 g), **15** (0.48 g, 66%), and **16** (0.11 g, 17%).

(*b*) Gaseous BF_3 was bubbled through a solution of **13***a* (0.73 g) in CH_2Cl_2 (30 ml) for 10 min. Work-up and chromatography as above afforded starting material (0.15 g) and **15** (0.51 g, 70%).

*Rearrangement of **13***b* to **16***

$AlCl_3$ (0.49 g, 0.0037 mol) was added to a solution of **13***b* (0.41 g, 0.0012 mol) in CH_2Cl_2 (30 ml), and the stirred mixture heated at 40°C for 30 min. After hydrolysis with ice water, the organic layer was separated, dried

(Na_2SO_4), and the solvent removed under reduced pressure. Chromatography afforded **16** (0.23 g, 56%).

*Rearrangement of **15** to **16***

Naphthalenone **15** (0.54 g, 0.0013 mol) and $AlCl_3$ (0.57 g, 0.0043 mol) in CH_2Cl_2 (25 ml) were stirred at 40°C for 3 h. After removal of the Lewis acid by ice water, the organic layer was separated, dried (Na_2SO_4), and evaporated. Column chromatography afforded unreacted **15** (0.19 g) and the naphthol **16** (0.22 g, 48%).

*Direct Irradiation of Oxabenzonorbornadiene **13b***

A solution of **13***b* (150 mg, 0.00042 mol) in ether (150 ml) was irradiated for 6 h. The residue obtained on removal of the solvent was chromatographed. Fractions eluted as follows.

(*i*) Benzoxepine **17***b* (30 mg, 20%), obtained as a colorless solid, mp 117–119°C. Molecular ion (7%) at *m/e* 354 ($C_{24}H_{18}O_3$ requires 354); base peak at *m/e* 105 ($C_6H_5CO^+$); *m/e* 77(27%); all other ions <4%. ν_{max} 1719 cm^{-1}. λ_{max} (ε) 205 (32 500), 273 (34 300), 315 sh (7500) nm. δ_c (ppm) 114.1 (br d, 156.8, C-5), 157.5 (q, 4.4, C-4), 158.2 (m, C-2).

(*ii*) A 1:1 mixture (26 mg) of **17***b* and **13***b*.

(*iii*) Slightly impure **19***b* (61 mg) (see below).

*Sensitized Irradiation of **13b***

Compound **13***b* (500 mg, 0.00141 mol) in acetone (300 ml) was irradiated for 3 h. The yellow oil obtained on evaporation was submitted to plc ($CHCl_3$). This afforded the following.

(*i*) A mixture (41 mg) of **13***b* and **17***b*.

(*ii*) Slightly impure **19***b* (316 mg). Repeated plc as above gave **19***b* as a yellow oil (276 mg, 55%) which could not be induced to crystallize, but was obtained as a glassy solid, liquefying <55°C. Molecular ion (2%) at *m/e* 354.1251 ($C_{24}H_{18}O_3$ requires 354.12560); base peak at *m/e* 105 ($C_6H_5CO^+$); significant ions at *m/e* (%) 322(7), 286(2), 265(3), 233(8), 218(8), 189(10), and 77(23). ν_{max} 1717, 1686 cm^{-1}. λ_{max} (ε) 205 (34 600), 241 (19 300), 287 (9800) nm. δ_c (ppm) 59.5 (br d, 133.7, C-1), 132.0 (m not observable, C-2), 155.5 (m, C-3), 164.2 (q, 3.7, ester C=O at C-2), 195.9 (dt, 8.1, 3.9, ketone C=O at C-1).

*Direct Irradiation of 7-Oxabenzonorbornadiene **13a***

(*a*) A solution of **13***a* (3.00 g, 0.0073 mol) in ether (425 ml) was irradiated for 3½ h. Removal of the solvent gave a yellow oil. Compounds **18** and **19***a* were indicated as major products (ratio *ca.* 1:5) by ^1H nmr signals for their methoxyl protons, while the absence of **20** and **21***a* was confirmed by the lack of signals between 4.0 and 6.0 δ. Treatment of the crude product with cyclohexane gave a colorless solid (212 mg); recrystallization from ethyl acetate – pentane gave the benzoxepine **17***a* as colorless prisms (166 mg, 6%), mp 174–176°C. Molecular ion (1%) at *m/e* 412.1298 ($C_{26}H_{20}O_5$ requires 412.13108); base peak at *m/e* 105 ($C_6H_5CO^+$); *m/e* 77 (16%), all other ions <3%. ν_{max} 1724 cm^{-1}. λ_{max} (ε) 205 (35 900), 271 (42 400), 312 sh (9200) nm. δ_c (ppm) 123.1 (d, 4.4, C-1/C-5), 159.0 (t, 4.0, C-2/C-4).

The remainder of the product was chromatographed (successive elutions with 2%, 10%, and 20% $CHCl_3$–benzene). Significant fractions obtained from the column were as follows.

Fraction *i*. Crystallization from petroleum ether gave unreacted. **13***a* (696 mg).

Fraction *ii*. Initial treatment with cyclohexane, followed by recrystallization (ethyl acetate – pentane) gave further **17***a* (103 mg, 3.4%); treatment of the residue from the mother liquors with petroleum ether afforded **13***a* (100 mg).

Fraction *iii*. Initial treatment and crystallization as in *ii* above gave **17***a* (82 mg, 2.7%). The pentane-insoluble portion (45 mg) of the remainder of this fraction was characterized by strong methoxyl signals at 3.67 and 3.71 δ; during purification these signals decreased in intensity and were replaced by signals for **20**. Repeated plc (30% acetone – petroleum ether) gave **20**, slightly contaminated by **18**, as a colorless solid (22 mg), and a fraction (12 mg) of lower R_f, consisting mainly of **18**. (Molecular ion at *m/e* 412 (<1%), base peak at *m/e* 105 ($C_6H_5CO^+$), *m/e* 77 (21%), all other ions <5%.) Final purification by plc (30% acetone – petroleum ether; 0.25 mm layer) afforded pure **20** as colorless prisms (9 mg), mp 135–137°C. Molecular ion (100%) at *m/e* 308.1039 ($C_{19}H_{16}O_4$ requires 308.10486); significant ions at *m/e* (%) 276(81), 249(87), 218(43), 205(30), and 189(71). ν_{max} ($CHCl_3$) 1735 cm^{-1} (broad); (KBr) 1732, 1714 cm^{-1}. λ_{max} (ε) 205 (24 600), 235 (14 400), 303 (10 500) nm. δ_c (ppm) 59.1 (dd, 133.5, 2.4, C-1), 132.5 (m, C-3), 151.0 (m, C-2), 165.3 (q, 3.9, ester C=O at C-3), 169.7 (dq, 10.8, 4.1, ester C=O at C-1).

Fraction *iv*. 168 mg, consisting mainly of the indene **18**.

Fraction *v*. 511 mg, consisting mainly of the indene **21***a*.

Fraction *vi*. 490 mg, being predominantly a mixture of **21***a* and benzoic acid. Removal of the acid by washing with $NaHCO_3$ gave **21***a* (307 mg). Crystallization from ethyl acetate – petroleum ether gave colorless prisms, mp 88–90°C (lit. (27) mp 93–94°C). Molecular ion (77%) at *m/e* 308.1048 ($C_{19}H_{16}O_4$ requires 308.10485); base peak at *m/e* 249.0919 ($C_{17}H_{13}O_2$ requires 249.09156); significant ions at *m/e* (%) 276(27), 250(23), 232(16), 221(25), 219(36), 218(28), 205(45), 189(70), and 94.5(20). ν_{max} ($CHCl_3$) 1735, 1721 cm^{-1}; (KBr) 1740, 1710 cm^{-1}. λ_{max} (ε) 206 (24 400), 234 (15 900), 293 (12 900) nm. δ_c (ppm) 55.7 (br d, 135.6, C-1), 129.6 (d, 6.1, C-2), 155.2 (m, C-3), 164.4 (q, 3.8, ester C=O at C-2), 170.2 (dq, 11.0, 4.0, ester C=O at C-1).

The benzoic acid was recovered after reacidification of the bicarbonate washings and ether extraction, as a colorless solid, identified by mp, mixture mp (121–123°C), and ^1H nmr.

In a separate experiment plc (30% acetone – petroleum ether) afforded a fraction (24 mg) rich in compound **19***a*. (Molecular ion at *m/e* 412, very intense base peak at *m/e* 105, with strong peak at *m/e* 77. Ease of conversion to **21***a* results in appearance of *m/e* 308 and other peaks due to **21***a*.)

(*b*) Adduct **13***a* (310 mg, 0.00075 mol) in CH_2Cl_2 (200 ml) was irradiated for 5 h. Evaporation gave a viscous yellow oil. This was dissolved in methanol (20 ml) and water (1 ml) and concentrated HCl (6 drops) added. The mixture was allowed to stand at room temperature for 72 h. Concentration and extraction with CH_2Cl_2 afforded a yellow oil. Trituration with ethyl acetate – petroleum ether gave **17***a* as a colorless solid (57 mg, 18%). The soluble fraction on repeated plc ($CHCl_3$; 2% MeOH–$CHCl_3$) gave the indenes **21***a* (115 mg, 50%) and **20** (28 mg, 12%).

*Sensitized Irradiation of **13a***

Compound **13***a* (500 mg, 0.0012 mol) in acetone (400 ml) was irradiated for 5 h. The crude product, a

yellow oil, appeared from ^{1}H nmr to consist of **13***a*, **17***a*, and **19***a* in a ratio of 19:14:67. This was taken up in methanol (20 ml) and water (1 ml) and concentrated HCl (10 drops) added. The mixture was then allowed to stand for 72 h. The benzoxepine **17***a* (27 mg, 5%) crystallized from solution. Evaporation gave a yellow gum, repeated plc ($CHCl_3$) of which afforded **21***a* (332 mg, 66%).

*Attempted Rearrangement of **13***a* in the Presence of Iodine*

Compound **13***a* (200 mg, 0.00049 mol) and iodine (43 mg, 0.00017 mol) in ether (40 ml) were allowed to stand in daylight for 30 min. The mixture was washed with sodium bisulfite, then water, and dried (Na_2SO_4). Evaporation of solvent gave a colorless solid (194 mg), shown by ^{1}H nmr to be unreacted **13***a*.

Reactions for 4 days at room temperature, or for 10 h in refluxing cyclohexane, were also unsuccessful.

*Sensitized Irradiation of Dimethyl 1,4-Diphenyl-7-Oxanorbornadiene-2,3-dicarboxylate **22***

The oxanorbornadiene **22** (100 mg, 0.00028 mol) in acetone (100 ml) was irradiated for 3 h. Removal of the solvent and successive plc (1% MeOH–$CHCl_3$; 30% acetone–benzene) gave dimethyl 3,6-diphenyl-6-hydroxyfulvene 1,2-dicarboxylate **24** as a bright orange solid (70 mg, 70%) mp 141–142°C, and only a very small quantity of dimethyl 2,7-diphenyloxepine-4,5-dicarboxylate **23***a* (*cf.* ref. 16).

*Irradiation of the Benzoxepine **17***a*

A solution of **17***a* (100 mg, 0.00024 mol) in CH_2Cl_2 (300 ml) was irradiated for 3¼ h. Evaporation gave a yellow oil, shown by ^{1}H nmr to be mainly **18**. This product was dissolved in methanol (10 ml) and water (1 ml) and concentrated HCl (6 drops) added. The mixture was allowed to stand for 72 h. After evaporation and extraction with CH_2Cl_2 the product was submitted to repeated plc (2% MeOH–$CHCl_3$); this afforded **20** (30 mg, 40%).

*Conversion of **21***a* to **29***

A solution of **21***a* (115 mg, 0.00037 mol) in methanol (10 ml) was treated with 2 *N* NaOH (10 drops). The now deep yellow solution was allowed to stand at room temperature for 2 h. The solution was concentrated and the residue taken up in ether. Drying (Na_2SO_4) and evaporation gave a yellow oily residue, plc (2% MeOH–$CHCl_3$) of which gave (*i*) unreacted **21***a* (43 mg), and (*ii*) **29** as an almost colorless oil (46 mg, 38%) which slowly crystallized. Recrystallization from ethyl acetate – petroleum ether gave colorless cubes, mp 157–158°C. Molecular ion (1%) at *m/e* 324.0998 ($C_{19}H_{16}O_5$ requires 324.09978); base peak at *m/e* 233; significant ions at *m/e* (%) 308(1), 276(1), 265(15), 249(2), 176(15), and 151(6). ν_{max} (KBr): 3480, 1723, 1693 cm^{-1}. δ_c (ppm) 83.9 (br s, C-1), 132.6 or 133.2 (m not observable, C-2), 155.8 (m, C-3), 164.0 (q, 3.9, ester C=O at C-2), 173.3 (quint., 3.9, ester C=O at C-1).

The above reaction was repeated under a N_2 atmosphere for 4 h. In this case **21***a* was recovered quantitatively.

*Rearrangements of **18** to **20** and of **19***a* to **21***a*

These conversions occurred slowly on standing at room temperature. They were most efficiently carried out by treatment with aqueous methanolic HCl (see above). Both rearrangements occurred rapidly on treatment of a methanolic solution with a few drops of NaOH, but the products, especially **21***a*, were base-sensitive (see above).

*Attempted Rearrangement of **19***b* to **21***b*

(*a*) A solution of **19***b* (150 mg) in MeOH (5 ml) was treated with 2 *N* NaOH (8 drops). The now bright orange solution was allowed to stand at room temperature for 4 h. Acidification, evaporation, and extraction with CH_2Cl_2 gave an almost quantitative recovery of **19***b*.

(*b*) A solution of **19***b* (150 mg) in MeOH (8 ml) and H_2O (1 ml) was treated with concentrated HCl (6 drops). The yellow solution was allowed to stand at room temperature for 96 h. Evaporation and extraction with CH_2Cl_2 afforded only unreacted **19***b* in near quantitative yield.

*Rearrangement of **19***b* to **21***b*

Attempted purification of **19***b* (300 mg, 0.00085 mol) on alumina plates (Merck aluminum oxide GF 254 Type E, 1.25 mm; 30% acetone – petroleum ether) gave a main band (169 mg). Further plc (SiO_2; $CHCl_3$) afforded **21***b* (30 mg, 14%) which was crystallized from ethyl acetate – petroleum ether as cream-colored needles, mp 113.5–115°C. Molecular ion (64%) at *m/e* 250.0987 ($C_{17}H_{14}O_2$ requires 250.09938); base peak at *m/e* 191 $(M - CO_2CH_3)^+$; significant ions at *m/e* (%) 235(4), 219(12), 218(11), 189(32), and 165(11). ν_{max} 1704 cm^{-1}. λ_{max} (ε) 206 (23 700), 233 (12 700), 293 (14 200) nm. δ_c (ppm) 39.5 (td, 130.9, 2.5, C-1), 130.6 (t, 6.9, C-2), 153.6 (m, C-3), 165.3 (q, 3.9, ester C=O).

Acknowledgments

We wish to acknowledge the excellent technical assistance of Mr. J. Van Ingen. We also thank Miss J. Riley (NRCC summer student, 1973) for her contribution to this work. Our thanks go also to Mr. D. J. Embree (for high-resolution mass spectra), Dr. I. Oxton (for assistance with infrared measurements), and Mrs. M. G. Flack (for experimental assistance).

We are grateful to Dr. A. W. Hanson of the Division of Biological Sciences, National Research Council of Canada, Ottawa, for the X-ray structural information on the indene **21***a*.

1. J. R. Edman. J. Am. Chem. Soc. **91**, 7103 (1969).
2. W. Eberbach, P. Würsch, and H. Prinzbach. Helv. Chim. Acta, **53**, 1235 (1970).
3. G. Kaupp, J. Perreten, R. Leute, and H. Prinzbach. Chem. Ber. **103**, 2288 (1970).
4. L. A. Paquette, D. M. Cottrell, R. A. Snow, K. B. Gifkins, and J. Clardy. J. Am. Chem. Soc. **97**, 3275 (1975).
5. P. D. Rosso, J. Oberdier, and J. S. Swenton. Tetrahedron Lett. 3947 (1971); P. D. Rosso. Ph.D. Thesis, Ohio State University, Columbus, OH. 1973.
6. J. S. Swenton, J. Oberdier, and P. D. Rosso. J. Org. Chem. **39**, 1038 (1974).
7. G. R. Ziegler and G. S. Hammond. J. Am. Chem. Soc. **90**, 513 (1968).
8. G. R. Ziegler. J. Am. Chem. Soc. **91**, 446 (1969).
9. H. Prinzbach, P. Würsch, P. Vogel, W. Tochtermann, and C. Franke. Helv. Chim. Acta, **51**, 911 (1968).

10. A. W. McCULLOCH and A. G. McINNES. Can. J. Chem. **53**, 1496 (1975).
11. J. A. BERSON. J. Am. Chem. Soc. **75**, 1240 (1953).
12. P. VOGEL, B. WILLHALM, and H. PRINZBACH. Helv. Chim. Acta, **52**, 584 (1969).
13. A. W. McCULLOCH, B. STANOVNIK, D. G. SMITH, and A. G. McINNES. Can. J. Chem. **47**, 4319 (1969).
14. A. W. McCULLOCH and A. G. McINNES. Can. J. Chem. **52**, 143 (1974).
15. E. WOLTHIUS, B. BOSSENBROEK, G. DEWALL, E. GEELS, and A. LEEGWATER. J. Org. Chem. **28**, 148 (1962).
16. R. K. BANSAL, A. W. McCULLOCH, P. W. RASMUSSEN, and A. G. McINNES. Can. J. Chem. **53**, 138 (1975).
17. G. KAUPP. Justus Liebig's Ann. Chem. 844 (1973).
18. D. STUSCHE and H. PRINZBACH. Chem. Ber. **106**, 3817 (1973).
19. L. A. PAQUETTE and J. H. BARRETT. J. Am. Chem. Soc. **88**, 1718 (1966).
20. H. HOFMANN and B. MEYER. Tetrahedron Lett. 4597 (1972).
21. A. W. McCULLOCH, D. G. SMITH, and A. G. McINNES. Can. J. Chem. **51**, 4125 (1973); **52**, 1013 (1974).
22. J. W. EMSLEY, S. R. SALMAN, and R. A. STOREY. J. Chem. Soc. B, 1513 (1970).
23. L. ERNST. Chem. Ber. **108**, 2030 (1975).
24. U. EDLUND. Chem. Scripta, **7**, 85 (1975).
25. Y. N. LUZIKOV, N. M. SERGEYEV, and Y. A. USTYNYUK. J. Organomet. Chem. **65**, 303 (1974).
26. F. H. KÖHLER. Chem. Ber. **107**, 570 (1974).
27. G. EGE. Tetrahedron Lett. 1667 (1963).
28. A. W. HANSON. Acta Crystallogr. In press.

N-Ethylamino acid synthesis and *N*-acylamino acid cleavage using Meerwein's reagent[1]

FRANCIS M.F. CHEN AND N. LEO BENOITON

Department of Biochemistry, University of Ottawa, Ottawa, Ont., Canada K1N 9A9

Received July 8, 1976[2]

FRANCIS M. F. CHEN and N. LEO BENOITON. Can. J. Chem. **55**, 1433 (1977).

N-Ethylamino acids have been prepared by reaction of *N*-acetylamino acids with trimethyloxonium tetrafluoroborate (Meerwein's reagent) giving imino ether fluoroborates, followed by reduction with sodium borohydride. The use of Meerwein's reagent for the deacylation of *N*-acylamino and *N*-acyl,*N*-methylamino acid derivatives has been investigated.

FRANCIS M. F. CHEN et N. LEO BENOITON. Can. J. Chem. **55**, 1433 (1977).

On a préparé des acides *N*-éthylaminés par réaction des acides *N*-acétylaminés avec le tétrafluoroborate de triméthyloxonium (réactif de Meerwein) conduisant aux fluoroborates iminoéthers qui sont ensuite réduits par le borohydrure de sodium. On a étudié l'utilisation du réactif de Meerwein pour la déacylation des dérivés acides *N*-acylaminés et *N*-acyl,*N*-méthylaminés.

[Traduit par le journal]

The alkylating power of trialkyloxonium tetrafluoroborate (Meerwein's reagent) is well known (1, 2). Amongst other things, it reacts with an amide to give an imino ether fluoroborate, thus converting the rather intractable amide into a highly reactive and versatile intermediate for further synthetic manoeuvers. In this paper, we describe studies on two applications of this in the amino acid field, namely, the conversion of *N*-acetylamino acids into *N*-ethylamino acids, and the use of Meerwein's reagent for the deacylation of amino and *N*-methylamino acid derivatives.

Direct ethylation of a free amino acid is likely to give mixed products of mono- and diethylation (3),[3,4] while ethylation of an *N*-protected amino acid is complicated by the side reaction of β-elimination of the ethylating agent.[5]

N-Ethylamino acids have been obtained here in moderate yields by reaction of *N*-acetylamino acids with trimethyloxonium tetrafluoroborate followed by reduction of the resulting imino ether fluoroborate with sodium borohydride. The results are given in Table 1. Each product

$$CH_3—CO—NH—CHR—COOH \xrightarrow{Me_3OBF_4}$$

$$CH_3—C(OMe)=\overset{+}{N}H—CHR—COOH\cdot BF_4^- \xrightarrow{NaBH_4}$$

$$CH_3—CH_2—NH—CHR—COOH$$

contained 0.6–0.8% of unalkylated amino acid as contaminant. The small amount (10–15%) of ester formed during the alkylation (1) was removed during the work-up. The chirality of the starting material was preserved during the reaction for *N*-ethylleucine but not for *N*-ethylphenylalanine. A sample of L-valine obtained by hydrolysis of the corresponding imino ether intermediate was shown (9) to have an optical purity of ≃96% (2% D-isomer). Borch has converted amides to amines in good yield in this manner (10). Monteiro applied this to a synthesis of L-proline from L-pyroglutamic acid (11). We have confirmed the latter work, with similar results. We have also observed in a control experiment that *N*-acetylleucine was converted into *N*-ethylleucine in 6% yield by sodium borohydride even in the absence of Meerwein's reagent.

The free amino acid side product from each reaction is probably the result of hydrolysis of

[1]Supported by a grant from the Medical Research Council of Canada. N.L.B. is an Associate of the MRCC.

[2]Revision received January 20, 1977.

[3]Reductive methylation of amines leads to dimethylation (3, 4).

[4]Kanao (5) synthesized several *N*-ethyl- and *N*,*N*-diethylamino acids by reductive alkylation using hydrogen and a platinum oxide catalyst giving very few details. Bowman (6) obtained monoethylation for valine and diethylation for alanine by the same reaction under nonforcing condition.

[5]Complete *N*-methylation of an *N*-benzyloxycarbonylamino acid is easily achieved using methyl iodide and sodium hydride (7), but *N*-ethylation is far from complete.

TABLE 1. Properties of *N*-ethylamino acids

Compound	Yield (%) A[a]	Yield (%) B[b]	Analysis (%) Calculated C	Calculated H	Calculated N	Found C	Found H	Found N	Chromatographic data[c] Color constant	Chromatographic data[c] Elution time (min)
DL-EtAla	56	41	51.3	9.5	11.6	51.7	9.8	11.8	0.7	65
DL-EtVal	71	50	57.9	10.4	9.6	57.7	10.7	9.6	0.2	69
DL-EtLeu	75	55	60.3	10.8	8.8	60.2	11.0	8.6	1.0	74
L-EtLeu		46[d]								
DL-EtPhe[e]		53	68.4	7.8	7.3	68.5	7.9	7.1	0.7	96
MeLeu									13.4	75

[a]Based on analysis with the amino acid analyzer.
[b]Isolated material.
[c]Long column of a Beckman amino acid analyzer eluted with p*H* 4.25 buffer at half-normal flow rate (8).
[d]$[\alpha]_D$ +22° (*c* 0.5, H_2O) (lit. (4) $[\alpha]_D$ +25°).
[e]Obtained from the enantiomer. $[\alpha]_D$ +2.8° (H_2O).

the imino ether fluoroborate by moisture. It is known that imino ether fluoroborates are readily hydrolyzed to free amino groups in aqueous acid or base (12, 13). This in fact led to our interest in the second application of these intermediates. We were interested in finding some means for removing acetyl and/or benzoyl groups from amino and *N*-methylamino acids, with the hope of achieving selectivity if possible. Muxfeldt *et al.* have cleaved a benzamide (12) and Hanessian, *N*-acetamino sugars (13) in good yield by this method. The high sensitivity to hydrolysis of imino ether fluoroborates of tertiary amides has been pointed out (10).

$$R'—CO—NR''—CHR—COOMe \xrightarrow{Me_3OBF_4} R'—C(OMe)=\overset{+}{N}R''—CHR—COOMe\cdot BF_4^- \xrightarrow[H^+ \text{ or } OH^-]{H_2O} R'—COOMe + R''NH—CHR—COOMe$$

R′ = Me or Ph R″ = H or Me

Experiments were monitored by nmr[6] spectroscopy, and carried out on the acylamino acid methyl esters to simplify quantitation. The results appear in Table 2. The conversion to imino ether intermediate was never complete, under the conditions employed, even in the presence of excess reagent. On hydrolysis, most of the intermediate gave rise to deacylated product, but a small portion (5–15%) was converted back into starting material. The amount of starting material recovered was 25–35% for the acetyl derivatives, whether methylated or unmethylated (R′ = Me; R″ = H or Me), less for the *N*-benzoyl,*N*-methyl derivatives (R′ = Ph; R″ = Me), and twice as much for the unmethylated benzoyl derivatives (R′ = Ph; R″ = H). No clear selectivity between amino and *N*-methylamino acid derivatives was obtained; only a large difference in reactivity between the benzoyl derivatives. The relative susceptibility to cleavage is therefore Bz-MeX-OR > Ac-MeX-OR = Ac-X-OR > Bz-X-OR where X = an amino acid residue. It is seen in Table 2 that, except for undergoing partial esterification, an unesterified derivative gave the same result. Because of the incomplete reaction, this approach for cleavage of acylamino acid derivatives leaves much to be desired, but it might find use when other methods are inapplicable.

The results are in general agreement with those of Pilotti *et al.* (14) who succeeded with the deacetylation but failed with the debenzoylation of acylamines, and Hanessian (13) who cleaved acetamino sugars by this method. They are also in agreement with the synthetic work of Borch (10). But one difference or discrepancy exists in that both Borch (10) and Muxfeldt *et al.* (12) reported a high reactivity for a secondary benzoylamide.

Experimental

The *N*-acylamino acid esters were obtained from the acids using methanolic HCl; the *N*-methylamino acid derivatives, from the same acids using methyl iodide and sodium hydride (15).

Acylamino Acid Ester Cleavage

A suspension of substrate (1 mmol) and trimethyloxonium tetrafluoroborate (1.1 mmol) (2) in 20 ml of dichloromethane (dried over $CaCl_2$, and distilled) was stirred at room temperature under nitrogen for 24 h. The solvent was removed under reduced pressure, and

[6]Proton nuclear magnetic resonance (60 MHz).

TABLE 2. Cleavage of acylamines via imino ether fluoroborates

Compound	After alkylation[a]		After hydrolysis[a]	
	A Imino ether intermediate	*B* Starting material	*C* Deacylated product	*D* Starting material
Ac-Val-OMe	77, 80[b]	23, 20[b]	73	26
Ac-Leu-OMe	75, 85[b]	25, 15[b]	66	34
Ac-MeLeu-OMe	71	29	66	34
Bz-Leu-OMe	26, 33[b]	74, 67[b]	24	76
Bz-Val-OMe	30	70	33	67
Bz-MeLeu-OMe	> 90		90	10
Bz-MeVal-OMe	> 90		80	20
Ac-Val-OH			61[c]	26[c]

[a]Percent, determined by nmr, assuming $A + B = 100$; $C + D = 100$. D corresponds to $B + (A - C)$. Hydrolysis with 3% aqueous acetic acid.
[b]100% excess reagent.
[c]13% of ester formed.

an nmr spectrum was recorded to determine the ratio between the amount of imino ether product and the amount of starting material. The mixture was then stirred in 20 ml of 3% aqueous acetic acid for 3 h. A second nmr spectrum recorded after removal of the solvents gave the ratio between the amount of deacylated product and the amount of starting material. There was no evidence for side-reactions other than those discussed.

Synthesis of N-Ethylamino Acids

A solution of *N*-acetylamino acid (0.01 mol) and trimethyloxonium tetrafluoroborate (0.011 mol) in 20 ml of dichloromethane was stirred under nitrogen at 23°C for 16 h. The solvent was removed under reduced pressure, the residue was dissolved in 25 ml of ethanol, the solution was cooled in an ice-bath, and 1 g of powdered sodium borohydride was added in small portions to the stirred solution. After stirring an additional 30 min in the cold and 30 min at 23°C, the mixture was acidified to Congo red with ethanolic HCl. The precipitate was filtered off and the filtrate was evaporated to dryness. The residue was analyzed for amino acid at this stage (8) or the product was isolated from an aqueous solution by absorption on to a resin (Dowex 50, 20–50 mesh; 50 ml) followed by elution with 50 ml of 5 *N* NH_4OH. The *N*-ethylamino acid was obtained by crystallization from ethanol after evaporation of the eluate. All products had nmr spectra (D_2O) consistent with their assigned structures.

1. H. MEERWEIN, G. HINZ, P. HOFMANN, E. KRONING, and E. PFEIL. J. Prakt. Chem. **147**, 17 (1937).
2. T.J. CURPHEY. Org. Synth. **51**, 142 (1971).
3. W.S. EMERSON. Org. React. **4**, 174 (1948); G.E. MEANS and R.E. FEENEY. Biochemistry, **7**, 2192 (1968).
4. M.L. MOORE. Org. React. **5**, 301 (1949); R.E. BOWMAN and H.H. STROUD. J. Chem. Soc. 1342 (1950).
5. S. KANAO. J. Pharm. Soc. Jpn. **66**, 4 (1946).
6. R. E. BOWMAN. J. Chem. Soc. 1346 (1950).
7. J.R. MCDERMOTT and N.L. BENOITON. Can. J. Chem. **51**, 1915 (1973).
8. J.R. COGGINS and N.L. BENOITON. J. Chromatogr. **52**, 251 (1970).
9. S. T. CHEUNG and N. L. BENOITON. Can. J. Chem. **55**, 911 (1977).
10. R. F. BORCH. Tetrahedron Lett. 61 (1968).
11. H.J. MONTEIRO. Synthesis, 137 (1974).
12. H. MUXFELDT and W. ROGALSKI. J. Am. Chem. Soc. **87**, 933 (1965); H. MUXFELDT, J. BEHLING, G. GRETHE, and W. ROGALSKI. J. Am. Chem. Soc. **89**, 4991 (1967).
13. S. HANESSIAN. Tetrahedron Lett. 1549 (1967).
14. A. PILOTTI, A. REUTERHALL, K. TORSSELL, and C-G. LINDBLAD. Acta Chem. Scand. **23**, 818 (1969).
15. J.R. COGGINS and N.L. BENOITON. Can. J. Chem. **49**, 1968 (1971).

Erratum: Thermodynamics of basic ionization of some aminoethers in water

SHEILA TERESA LOBO AND ROSS ELMORE ROBERTSON
Department of Chemistry, University of Calgary, Calgary, Alta., Canada T2N 1N4
Received February 7, 1977
(Ref.: Can. J. Chem. **54**, 3600 (1976))

Aside from the units, the heading for the last column of Table 1 should be $\Lambda_0(BH^+OH^-)$.

Erratum: Thermodynamic parameters for the basic ionization of some cyclic amines in water

SHEILA TERESA LOBO, TANIKELLA S. S. R. MURTY, AND ROSS ELMORE ROBERTSON
Department of Chemistry, University of Calgary, Calgary, Alta., Canada T2N 1N4
Received February 7, 1977
(Ref.: Can. J. Chem. **54**, 3607 (1976))

The sentence beginning on line 7 following eq. 3, p. 3609, erroneously refers to "amine hydrochlorides"; it should refer to "amine hydroxides".

Aside from the units, the heading for the last column of Table 1 should be $\Lambda_0(BH^+OH^-)$.

Canadian Journal of Chemistry

Published by
THE NATIONAL RESEARCH COUNCIL OF CANADA

Journal canadien de chimie

Publié par
LE CONSEIL NATIONAL DE RECHERCHES DU CANADA

Volume 55 Number 9 May 1, 1977

Volume 55 numéro 9 1 mai 1977

Sign reversal of geminal $^{13}CH_3$–C–^{15}N coupling in configurationally isomeric fragments[1]

GERALD W. BUCHANAN AND BRIAN A. DAWSON

Department of Chemistry, Carleton University, Ottawa, Ont., Canada K1S 5B6

Received November 25, 1976

GERALD W. BUCHANAN and BRIAN A. DAWSON. Can. J. Chem. **55**, 1437 (1977).

The signs of geminal ^{15}N–C–$^{13}CH_3$ couplings in configurationally isomeric acetophenone oximes have been determined relative to those of the vicinal ^{15}N–C–C–H interactions using an off resonance proton decoupling technique. In the *Z*-isomer where the nitrogen lone pair is *cis* to the coupled carbon, the coupling is large and negative, whereas in the *E*-isomer, the geminal ^{15}N–C–$^{13}CH_3$ coupling is small and positive in sign.

GERALD W. BUCHANAN et BRIAN A. DAWSON. Can. J. Chem. **55**, 1437 (1977).

On a déterminé les signes des couplages ^{15}N–C–$^{13}CH_3$ géminés dans des oximes de l'acétophénone qui sont isomères au point de vue configurationnel; ces déterminations ont été effectuées par rapport à celles des interactions ^{15}N–C–C–H vicinales en faisant appel à la technique "off resonance" de découplage du proton. Dans l'isomère *Z*, où la paire libre de l'azote est *cis* par rapport au carbone qui est couplé, le couplage est grand et négatif alors que dans l'isomère *E* le couplage géminé ^{15}N–C–$^{13}CH_3$ est petit et de signe positif.

[Traduit par le journal]

Introduction

There has been a good deal of recent interest in the magnitudes and signs of geminal coupling constants involving ^{15}N and other magnetic nuclei. The influence of the nitrogen lone pair is clearly pronounced (1). For both saturated and unsaturated compounds, $^2J_{^{15}N-H}$ is calculated to be large and negative when the nitrogen lone pair is *cis* to the coupled proton, whereas this coupling is small and can be of either sign when the lone pair is *trans* to the coupled proton (2). In the case of formaldoxime, $^2J_{^{15}N-H}$ is -13.8 Hz for the former coupling and $+2.7$ Hz for the latter (3). A similar trend has been observed for isomeric acetaldoximes (4, 5).

With regard to geminal ^{13}C–^{15}N interactions,

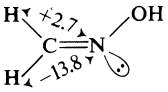

Lichter *et al.* (6) have demonstrated the sensitivity of this parameter to N lone pair geometry in the *Z*- and *E*-2-cyclohexenone oximes shown below.

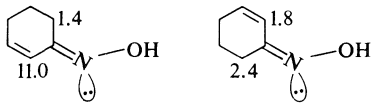

In an earlier study Bundgaard and Jakobsen (7) determined the sign of $^2J_{^{13}C^{15}N}$ relative to $^3J_{^{15}NH}$ in ^{15}N-enriched pyridine and some derivatives. These authors predicted, that in cases where a geometrically rigid CCN fragment was present, a sign change in the geminal ^{13}C–^{15}N coupling would be observed between members of an isomeric pair. We wish to report the first

[1]Presented in part at the 59th Canadian Chemical Conference of the Chemical Institute of Canada, London, Ontario, June 1976.

experimental verification of this prediction using *Z*- and *E*-acetophenone oximes as model compounds. This work represents an extension of our earlier study (8) which involved exclusively *E*-isomers.

Results and Discussion

(a) Chemical Shifts

Below are compared the ^{13}C chemical shifts (δ_c from TMS ± 0.1) for the *Z*- and *E*-isomers. Most notable is the increased shielding of the CH_3 resonance of 9 ppm in the *E*-isomer relative to the *Z* case, which reflects its *syn* relationship to the OH function in the former compound. Similar findings have been reported by Roberts and co-workers (9) for other configurationally isomeric oximes. In the *Z*-isomer the quaternary aromatic carbon is shielded by 2.5 ppm relative to the *E* case, again a consequence of the *syn*-OH moiety.

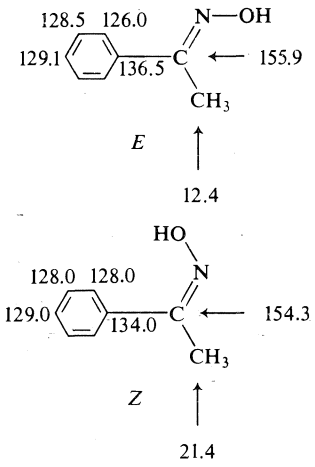

(b) Coupling Constants

The absolute values of the ^{13}C–^{15}N *J*'s are presented below. For the *Z*-isomer it was not possible to measure the vicinal coupling to the *ortho* carbons due to peak overlap with the *meta* resonance. Clearly there is a dramatic effect of N lone pair geometry on the magnitude of the geminal interactions. When the lone pair is *cis* to the coupled carbon, as in the quaternary carbon of the *E*-isomer and the CH_3 of the *Z*, the absolute values of ^2J are much greater than in the cases where the lone pair is *trans*.

In this work we have used the off resonance proton decoupling procedure described by Jakobsen *et al.* (7, 10, 11) to determine the signs of the geminal ^{15}N–C–$^{13}CH_3$ couplings relative

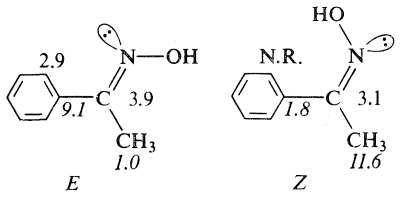

to those for the vicinal ^{15}N–C–C–H interactions. The latter are known to be negative (3) in isomeric acetaldoximes and are assumed negative for the present acetophenone oximes due to the close agreement in experimental findings for the isomeric pairs illustrated. Additional support for

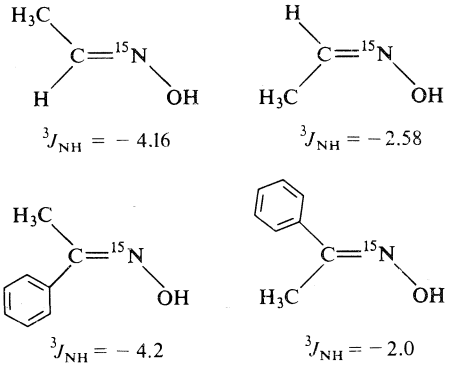

this assumption comes from the results of INDO MO calculations (2) which indicate negative vicinal ^{15}N–H *J*'s in fragments such as these.

The Jakobsen technique (10) is applicable for determining the relative sign of $^nJ_{CX}$ and the corresponding $^{n+1}J_{HX}$ spin couplings, where X is a spin $\frac{1}{2}$ nucleus (*i.e.* ^{15}N). Use is made of the *difference* observed for the reduced splittings, $J_{\text{residual (CH)}} = 2\pi\Delta\nu J_{CH}/\gamma H_2$ in the ^{13}C spectrum of the $J_{^{13}C-X}$ doublet. In the case of the *Z*-isomer, off resonance ^1H decoupling on the high field side ($\Delta\nu = 65$ Hz, $\gamma H_2 \approx 1600$), caused a reduction in the residual coupling for the high field lines indicating the same sign for $^3J_{NH}$ and $^2J_{CN}$ (*i.e.* negative). As a check, off resonance decoupling on the low field side did indeed cause a reduction of the residual J_{CH} for the low field lines.

Conversely for the *E*-isomer, off resonance decoupling on the high field side ($\Delta\nu \approx 50$, $\gamma H_2 \approx 2000$) reduced J_{CH} preferentially on the low field side, whereas low field irradiation reduced J_{CH} on the high field side. Therefore in the *E*-isomer, $^2J_{CN}$ must be positive. A typical spectrum is shown in Fig. 1, illustrating the result of high field ^1H irradiation. Since $^2J_{CN}$ will

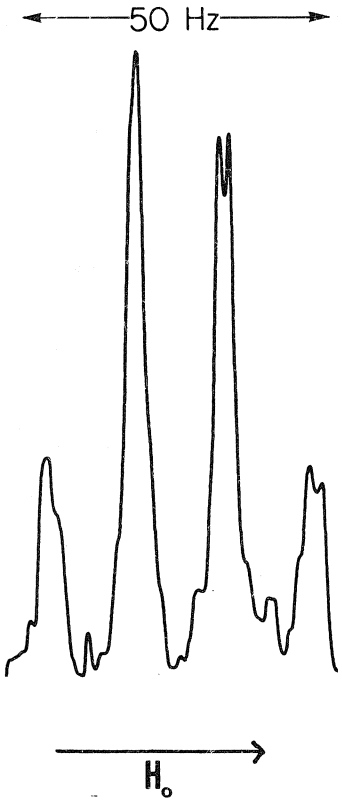

FIG. 1. Methyl region of the ^{13}C spectrum for ^{15}N enriched *E*-acetophenone oxime. Spectrum recorded with off resonance ^1H decoupling, $\gamma H_2 \approx 2000$ and $\Delta\nu \approx 50$ Hz to the high field side of the ^1H resonance of the CH_3 group.

not be affected by ^1H decoupling, the reduced splitting on the low field side must be due to a preferential reduction of $^1J_{CH}$.

The present results for $^2J_{CN}$ in oximes parallel those for $^2J_{NH}$. Specifically, geminal J's are large and negative when the N lone pair is *cis* to the coupled carbon, and small and positive when the lone pair is *trans* to the $^{13}CH_3$.

Recently Schulman and Venanzi (13), have demonstrated that $^2J_{CN}$ and $^3J_{CN}$ are dominated by the Fermi contact term in contrast to $^1J_{CN}$ for a variety of compounds, although the only oxime considered has been that derived from formaldehyde. At present, we are carrying out INDO MO calculations to evaluate the Fermi contact contributions to the observed couplings in aromatic oximes and related materials. Results will be communicated in the near future.

Experimental

Materials

Preparation of the *E*-isomer was reported in our previous study (8). The *Z*-isomer was prepared according to the procedure of Smith and Kaiser (14), using 95% ^{15}N enriched hydroxylamine hydrochloride obtained from Merck, Sharpe, and Dohme (Canada).

Spectra

Spectra were recorded using a Varian XL-100-12 nmr spectrometer equipped with the Nicolet TT-100 Fourier transform data system. Samples were examined as 0.1 *M* solutions in $CDCl_3$ solution in 5 mm sample tubes. Spectral widths were commonly 2000 Hz and a minimum of 8K data points were used. For the off resonance experiments the noise modulation was removed and the decoupler high power level reduced to 50% which gave a γH_2 value of *ca.* 1600.

1. R. WASYLISHEN. *In* Nuclear magnetic resonance spectroscopy of nuclei other than protons. *Edited by* T. Axenrod and G. A. Webb. Wiley–Interscience, New York, NY. 1974. Chapt. 8. p. 105.
2. R. WASYLISHEN and T. SCHAEFER. Can. J. Chem. **50**, 2989 (1972).
3. D. CREPAUX, J. M. LEHN, and R. R. DEAN. Mol. Phys. **16**, 225 (1969).
4. J. P. KINTZINGER and J. M. LEHN. Chem. Commun. 660 (1967).
5. D. CREPAUX and J. M. LEHN. Mol. Phys. **14**, 547 (1968).
6. R. L. LICHTER, D. E. DORMAN, and R. WASYLISHEN. J. Am. Chem. Soc. **96**, 930 (1974).
7. T. BUNDGAARD and H. J. JAKOBSEN. Tetrahedron Lett. 1621 (1976).
8. G. W. BUCHANAN and B. A. DAWSON. Can. J. Chem. **54**, 790 (1976).
9. G. E. HAWKES, K. HERWIG, and J. D. ROBERTS. J. Org. Chem. **39**, 1017 (1974).
10. H. J. JAKOBSEN, T. BUNDGAARD, and R. S. HANSEN. Mol. Phys. **23**, 197 (1972).
11. S. SORENSEN, R. S. HANSEN, and H. J. JAKOBSEN. J. Am. Chem. Soc. **95**, 5080 (1973).
12. R. L. LICHTER and J. D. ROBERTS. J. Am. Chem. Soc. **93**, 5218 (1971).
13. J. M. SCHULMAN and T. VENANZI. J. Am. Chem. Soc. **98**, 4701 (1976).
14. J. H. SMITH and E. T. KAISER. J. Org. Chem. **39**, 728 (1974).

On the molecular conformation of the bis-1,3-dioxolyl molecule in decahydronaphthalene and benzene solutions

ERNST BOCK, GARNETTE SUTHERLAND, AND DAVID MCKINNON
Parker Chemistry Laboratory, University of Manitoba, Winnipeg, Man., Canada R3T 2N2
AND
EDWARD TOMCHUK
Department of Physics, University of Winnipeg, Winnipeg, Man., Canada R3B 2E9
Received May 21, 1976[1]

ERNST BOCK, GARNETTE SUTHERLAND, DAVID MCKINNON, and EDWARD TOMCHUK. Can. J. Chem. **55**, 1440 (1977).

The electric dipole moments of the bis-1,3-dioxolyl molecule were determined in dilute decahydronaphthalene solution at 25 and 100°C and in dilute benzene solution at 25°C. From the temperature dependence of the dipole moment it is concluded that the *trans* rotamer of the molecule is more stable in both solvents than the *gauche* rotamer by ~4.5 kJ mol^{-1}. The conformational behavior of the molecule is discussed in terms of a recently proposed solvation theory.

ERNST BOCK, GARNETTE SUTHERLAND, DAVID MCKINNON et EDWARD TOMCHUK. Can. J. Chem. **55**, 1440 (1977).

On a déterminé, en solution diluée de décahydronaphtalène, à 25 et à 100°C, et dans des solutions diluées de benzène, à 25°C, les moments électriques dipolaires de la molécule bis-dioxolyl-1,3. En se basant sur la dépendance du moment dipolaire sur la température, on en conclut que le rotamère *trans* de la molécule est plus stable, dans les deux solvants, que le rotamère *gauche*; la différence est ~4.5 kJ mol^{-1}. On discute du comportement conformationnel de la molécule en termes d'une théorie de solvatation qui a été proposée récemment.
[Traduit par le journal]

Introduction

In a recent paper published in this journal (1) it was suggested that in acetone solution the *trans* rotamer of bis-1,3-dioxolyl is more stable than the *gauche* rotamer and that the difference in enthalpy between the two rotamers in acetone was approximately 700–1300 J mol^{-1}. The above authors based their conclusions on the temperature dependence of certain proton nmr coupling constants. But because it proved impossible to measure independently the coupling constants for the two rotamers the authors could obtain an approximate value only for the conformational energy difference. However, the marked increase in the value of ^3J(H,H) with decrease in temperature suggested strongly that the *trans* conformer was the energetically more favoured one, at least in acetone solution.

Another technique which may be used to determine relative stabilities of rotamers makes use of molecular electric dipole moments. Although this technique suffers from a number of disadvantages compared to the nmr technique, *viz.*, solution dipole moments can rarely be determined with an accuracy of better than 3.33×10^{-32} C m (0.01 D), both conformers may have dipole moments of comparable magnitude, etc., it is nevertheless particularly suitable in this case because the *trans* rotamer has no dipole moment whereas the *gauche* rotamer can be expected to have a dipole moment of $5.0 \times 10^{-30} - 6.7 \times 10^{-30}$ C m (1.5 – 2.0 D) as calculated by the INDO–MO theory (1) and estimated from bond-moment vector-model calculations. (See Fig. 1.) Details of the INDO–MO calculations are given in ref. 1 and need not be repeated here. The vector-model dipole moment was estimated using the following bond moments: C—O 0.7 D, C^-—H^+ 0.4 D, C=C^-—H^+ 0.7 D (2), and the molecular coordinates for the *gauche* rotamer of Schaefer *et al.* (1). Thus if the energy barrier separating the two rotamers is not too large, *i.e.*, if a significant change in the population of the two forms can be realised in a reasonable temperature interval, then it is possible to obtain the energy difference between the two forms from the observed temperature dependence of the

[1]Revision received January 24, 1977.

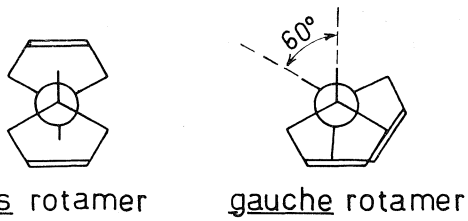

FIG. 1. The *trans* and *gauche* rotamers of bis-1,3-dioxolyl.

molecular dipole moment. The relationship between the dipole moments and the energy difference, $\Delta E = E_g - E_t$, of the *gauche* and *trans* rotamers respectively, the measured dipole moment, m, at a temperature, T, is given by (3):

$$[1] \qquad m^2 = \frac{\mu_t^2 + \mu_g^2 \omega\, e^{-\Delta E/RT}}{1 + \omega\, e^{-\Delta E/RT}}$$

Here ω is the ratio of the partition functions of the *gauche* to *trans* rotamers. In the absence of microwave and infrared data ω may be approximated to the product of the ratio of the statistical weights of the two rotamers and the square root of the ratio of the products of the principal moments of inertia of the two rotamers; *i.e.*, we assume here that the vibrational contributions to the partition functions are the same for both rotamers. The statistical weight of the *gauche* rotamer is 2 since there are two non-superimposable forms of this rotamer. And the statistical weight of the *trans* rotamer is 1. Using the coordinates of Schaefer *et al.* (1) for the two rotamers the product of the principal moments of inertia, $I_A I_B I_C$, of the *gauche* and *trans* rotamer results as 2.94×10^{-38} kg m^2 and 1.82×10^{-38} kg m^2, respectively. Combination of these values then yield a value for $\omega = 2.54$. With this approximation and setting μ_t equal to zero [1] becomes:

$$[2] \qquad m^2 = \frac{2.54\mu_g^2\, e^{-\Delta E/RT}}{1 + 2.54\, e^{-\Delta E/RT}}$$

Equation 2 contains two unknown quantities: ΔE and μ_g. Both can be determined by measuring the dipole moment, m, at two different and preferably widely separated temperatures. It is this method which we chose for the determination of ΔE.

Experimental

The experimental technique used in the determination of the solution dipole moment has been described elsewhere (4). The bis-1,3-dioxolyl was prepared after the method of Fuchs and Hauptmann (5). To ensure as wide a temperature interval as possible decahydronaphthalene was chosen as solvent. The choice of solvent was dictated by its low volatility, nonpolarity, and ready availability in highly purified state. It was obtained from Fisher Scientific Co., under their label 'Spectroquality', and was used without further purification. The uncertainty in the experimental dipole moment is estimated to be 3.3×10^{-32} C m (0.01 D). The estimate of the uncertainty is based on the sum of the measured standard deviations in the Smith (6) polarization parameters α and ν. The error in the temperature was less than 0.01°C and the error in the weight fraction was negligibly small.

Results and Discussion

The experimental results are shown in Table 1 and the derived quantities based on these results are summarized in Table 2. INDO–MO calculations predict the *gauche* form to be more stable in the vapor phase but experimental measurements in solution show that the *trans* form is more stable. The experimental observations are in qualitative agreement with the nmr studies referred to above (1).

It is interesting to speculate on the reasons for

TABLE 1. Weight fraction, W, dielectric constant, ε, refractive index, n, and Smith's polarization parameters α and ν for solutions of bis-1,3-bioxolyl in decahydronaphthalene at 25 and 100°C and benzene at 25°C

$W \times 10^3$	ε	n	α	ν
In decahydronaphthalene solution at 25°C				
0.839	2.1586	1.4710	0.739	−0.111
1.993	2.1595	1.4710		
3.838	2.1609	1.4709		
5.86	2.1624	1.4709		
7.788	2.1637	1.4708		
11.972	—	1.4705		
25.212	—	1.4701		
In decahydronaphthalene at 100°C				
0.976	2.0748	1.4390	0.671	−0.100
1.775	2.0752	1.4388		
3.742	2.0766	1.4387		
6.441	2.0785	1.4386		
7.826	2.0792	1.4385		
29.976	—	1.4379		
48.795	—	1.4372		
In benzene solution at 25°C				
1.175	2.2747	1.4980	0.638	−0.083
2.541	2.2756	1.4980		
4.068	2.2766	1.4980		
5.579	2.2776	1.4980		
7.535	2.2788	1.4978		
10.226	—	1.4975		
21.262	—	1.4972		
44.392	—	1.4968		

TABLE 2. Summary of observed and calculated data

Solvent	μ_{exp} (C m × 10^{30}) 25°C	100°C	μ_{gauche} (C m × 10^{30})	ΔE (kJ mol^{-1})
$C_{10}H_{18}$	3.61	4.07	6.68	4.5
C_6H_6	3.24	—		5.2
INDO			5.31	−4.2

the observed conformational preference in solution.

According to a recently proposed solvation theory (7), which regards the solvent as a dielectric continuum and the solvent molecule as a collection of electric charges, the solute–solvent interaction energy may be written as a sum of three interaction terms, *viz.*, a polar term, a dipolar term, and a quadrupolar term. The polar term is usually small and for nonpolar solvents may be set equal to zero. The dipolar term is proportional to the square of the dipole moment of the solute molecule; this term therefore, in the present case, will favour the *gauche* form because the *trans* form has a zero dipole moment. Finally, the quadrupolar term is proportional to the square of the molecular quadrupole moment and will stabilize the rotamer with the largest molecular quadrupole moment. It is relatively easy to compute the dipolar term. The computation of the quadrupolar term is much more complicated. However, from an examination of molecular models and from a comparison of calculated molecular quadrupole moments of *sym* tetrasubstituted ethanes (7), molecules the structures of which are similar to the structure of bis-1,3-dioxolyl, it is clear that in the present case the quadrupolar term must be considerably larger for the *trans* conformer compared to the *gauche* conformer. Thus the stabilization of the *trans* conformer in solution must be due entirely to the quadrupolar interaction. The energy of this interaction may be estimated as follows. Using the dipole moment of the *gauche* form as calculated by [2], and a molecular radius of 3.2×10^{-10} m, as estimated from molecular models and standard bond lengths, and published bond polarizability data (8) one obtains the following values for the k and l parameters of Abraham (7): $k = 8.0$ kJ mol^{-1}, $l = 0.75$. Using these values and setting $x = 0.218$ the dipolar interaction results as 2.1 kJ mol^{-1}. If this value is subtracted from the difference of the conformational energy difference in the vapour and solution phase, respectively, one obtains an estimate for the quadrupolar interaction term, *i.e.*,

$$\Delta E^v - \Delta E^s - \text{dipolar term} = \text{quadrupolar term}$$

Here ΔE^v and ΔE^s are the energy differences between the *gauche* and *trans* conformations in the vapor and solution phase, respectively. In the absence of experimental data for ΔE^v we set this term equal to the INDO calculated value, *i.e.* $\Delta E^v = -4.2$ kJ mol^{-1}. From Table 2 ΔE^s in decahydronaphthalene is 4.5 kJ mol^{-1}. Thus the quadrupolar term in this solvent results as -10.8 kJ mol^{-1}. This seems a rather large value for this interaction; it implies an unreasonably large quadrupole parameter, h, of some 75 kJ mol^{-1}. However, it should be kept in mind that this estimate is critically dependent on the correct estimate of ΔE^v. Now it is well known that INDO–MO predicted conformational energy differences are not always reliable since they are derived from the difference of two very large numbers (the total molecular energies of each conformer) of almost equal magnitude (9). For instance, in the present case, the total energy, *i.e.*, the energy of the molecule relative to the free nuclei and electrons, is -3.0479735×10^5 kJ mol^{-1} and -3.0479317×10^5 kJ mol^{-1} for the *gauche* and *trans* conformer, respectively, which gives

$$\Delta E = E_g - E_t = -4.2 \text{ kJ mol}^{-1}$$

Thus a small error in one or both total energy estimates may result in quite a large error in ΔE.

Acknowledgements

The financial assistance of the National Research Council of Canada and the Faculty of Graduate Studies and Research of the University of Manitoba is very much appreciated.

1. T. SCHAEFER, K. CHUM, D. MCKINNON, and M. S. CHAUHAN. Can. J. Chem. **53**, 2734 (1975).
2. V. I. MINKIN, O. A. OSIPOV, and YU. A. SHDANOV. Dipole moments in organic chemistry. Plenum Press, New York, London. 1970. p. 88.
3. S. MIZUSHIMA. Structure of molecules and internal rotation. Academic Press Inc., New York, NY. 1954. p. 34.
4. E. BOCK and E. F. DOJAK. Can. J. Chem. **45**, 1097 (1967).
5. B. FUCHS and S. HAUPTMANN. Chem. Commun. 705 (1971).
6. J. W. SMITH. Trans. Faraday Soc. **46**, 394 (1950).
7. R. J. ABRAHAM and E. BRETSCHNEIDER. *In* Internal rotation in molecules. *Edited by* W. J. Orville-Thomas. J. Wiley and Sons, New York, NY. 1974. Chapt. 13.
8. R. J. W. LE FEVRE and K. D. STEEL. Chem. Ind. London, 670 (1961).
9. W. DANCHURA, T. SCHAEFER, J. B. ROWBOTHAM, and D. J. WOOD. Can. J. Chem. **52**, 3986 (1974).

The resonance Raman spectra and excitation profiles of some 4-sulfamylazobenzenes[1]

KAMAL KUMAR AND P. R. CAREY[2]

Division of Biological Sciences, National Research Council of Canada, Ottawa, Ont., Canada K1A 0R6

Received November 17, 1976

KAMAL KUMAR and P. R. CAREY. Can. J. Chem. **55**, 1444 (1977).

The resonance Raman spectra of three pharmacologically important sulfonamides, 4-sulfamyl-4′-dimethylaminoazobenzene (**1**), 4-sulfamyl-4′-hydroxyazobenzene (**2**), and 4-sulfamyl-4′-aminoazobenzene (**3**), are compared with those of analogues lacking the sulfonamide group. The $—SO_2NH_2$ moiety does not directly contribute intense or moderately intense bands to the resonance Raman spectra of **1**, **2**, and **3**. However, $—SO_2NH_2$ ionization is reflected by frequency changes in a band near 1140 cm^{-1} and intensity changes in the 1420 cm^{-1} region. The normal Raman spectrum of **2** confirms that the intensity changes reflect $—SO_2NH_2$ ionization rather than unrelated changes in vibronic coupling. The effect of —OH ionization on the resonance Raman spectrum of **2** emphasizes that caution must be exercised when relating spectral perturbations to changes in contributions from valence bond type structures. Resonance Raman excitation profiles for the 1138, 1387, and 1416 cm^{-1} bands of **2** show that these bands gain intensity by coupling with the electronic transitions in the 240 to 450 nm region and that, more than 1000 cm^{-1} to the red of λ_{max}, the wavelength dependence can be closely reproduced by the F_B type terms of Albrecht and Hutley. The excitation profile for each band shows evidence for structure in the 470 nm region, although lack of sufficient excitation wavelengths prevents accurate estimation of the spacing. Under conditions of rigorous resonance the intense Raman lines all occur in the 1400 cm^{-1} region, *i.e.* they are 'bunched' in the region known to contain the —N=N— stretching vibration.

KAMAL KUMAR et P. R. CAREY. Can. J. Chem. **55**, 1444 (1977).

On compare les spectres de résonance Raman de trois sulfonamides pharmacologiquement importantes, sulfamyl-4 diméthylamino-4′ azobenzène (**1**), sulfamyl-4 hydroxy-4′ azobenzène (**2**) et sulfamyl-4 amino-4′ azobenzène (**3**) avec ceux d'analogues ne contenant pas le groupe sulfonamide. La portion $—SO_2NH_2$ ne contribue pas directement de bandes intenses ou modérément intenses au spectre de résonance Raman de **1**, **2** et **3**. Toutefois l'ionization de $—SO_2NH_2$ se réflète par des changements de fréquence dans la bande près de 1140 cm^{-1} et par des changements d'intensité dans la région de 1420 cm^{-1}. Le spectre Raman normal de **2** confirme que les changements d'intensité sont un reflet de l'ionization du $—SO_2NH_2$ plutôt que des changements du couplage vibronique qui ne sont pas reliés à l'ionisation. L'effet de l'ionization du —OH sur le spectre de résonance Raman de **2** met en relief les précautions qui doivent être prises lorsqu'on essaie de relier des perturbations de spectre avec des changements dans la contribution provenant de structures de type de lien de valence. Les profils d'excitation de la résonance Raman pour les bandes à 1138, 1387 et 1416 cm^{-1} de **2** montrent que ces bandes gagnent de l'intensité par couplage avec les transitions électroniques dans la région de 240 à 450 nm et que plus de 1000 cm^{-1} vers le rouge du λ_{max}, la relation avec la longueur d'onde peut être très bien reproduite par des termes du type F_B de Albrecht et Hutley. Le profil d'excitation de chaque bande montre des indications pour la structure dans la région de 470 nm quoique un manque de suffisantes longueurs d'onde pour l'excitation empêche un estimé précis de l'espacement. Dans des conditions de résonance rigoureuse, les lignes Raman intenses se produisent toutes dans la région de 1400 cm^{-1} c'est-à-dire qu'elles sont toutes concentrées dans la région qui est connue pour contenir les vibrations de fréquence —N=N—.

[Traduit par le journal]

Introduction

Certain aromatic sulfonamides are very powerful and selective inhibitors of the enzyme carbonic anhydrase (1). Because of their highly specific interaction with the active site they have proved extremely useful in work on the physicochemistry and mechanism of action of carbonic anhydrase (2). Comparison of the resonance Raman spectra of free aqueous aromatic sulfonamides with those of the drugs bound to the enzyme reveals several differences in band posi-

[1]NRCC No. 15825.

[2]To whom correspondence should be addressed.

tions and intensities (3, 4). These spectral differences may be used to delineate the chemical changes occurring in the sulfonamide molecule upon binding. The aim of the present paper is to establish several points relating the chemistry of **1**, **2**, and **3** (Fig. 1) to their resonance Raman spectra which were omitted or only touched upon in the earlier biochemically oriented work (3, 4). Furthermore, the variation of Raman intensities with excitation wavelength, the excitation profiles, have been measured for **2** to provide a quantitative estimate of Raman intensity enhancement for comparison with existing theories.

Materials and Methods

The azobenzene sulfonamides studied in this work are shown in Fig. 1. Compounds **1**, **2**, and **3** were synthesized and generously donated by Dr. R. W. King; **4** and **5** were purchased from Eastman Kodak Co., Rochester, NY; **6** was purchased from K and K, Plainview, NY, and **7** and **8** were purchased from Pfaltz and Bauer, Flushing, NY; *p*-carboxybenzenesulfonamide was purchased from Aldrich, Milwaukee, WI.

Raman spectra were obtained with a Jarrell-Ash 25-400 spectrophotometer using a RCA 310304A-02 photomultiplier tube and photon counting detection. The excitation sources were Spectra-Physics Model 185 He–Cd ion and Model 164 Ar^+ and Kr^+ lasers. Peak frequencies were calibrated using emission lines from Ar, Xe, and Ne lamps and are believed to be accurate to ± 2 cm^{-1} for well resolved bands. In the 1100 cm^{-1} region the accuracy is ± 1 cm^{-1}. Band intensities were measured by band heights and intensities reported for the excitation profiles are the average of at least three runs. Solutions for the excitation profile measurements contained *N*/10 KOH and 25% MeOH. The MeOH band at 1017 cm^{-1} was taken as an internal reference. Since the internal standard was close to the lines measured and solutions were of low optical density (~ 0.6 at 457.9 nm) neither a λ^4 correction nor a self-absorption correction was necessary.

The Raman spectra showed excellent reproducibility and neither photodecomposition nor photoisomerisation were detected. Absorption spectra were recorded on Cary 14 and 15 spectrophotometers and infrared spectra were recorded on a Perkin Elmer 521 grating spectrophotometer. The IR band positions are accurate to ± 2 cm^{-1}.

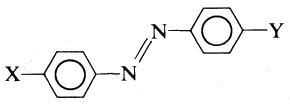

1 X = —$N(CH_3)_2$; Y = —SO_2NH_2
2 X = —O^-; Y = —SO_2NH_2
3 X = —NH_2; Y = —SO_2NH_2
4 X = —NH_2; Y = —H
5 X = —$N(CH_3)_2$; Y = —H
6 X = —NH_2; Y = —CO_2^-
7 X = —NH_2; Y = —SO_3^-
8 X = —NH_2; Y = —AsO_3^{2-}

FIG. 1. The structures of the compounds studied.

Results and Discussion

The Absorption Spectra

Above 300 nm the compounds **1** → **8** have similar absorption spectra with two features between 300 and 500 nm (Fig. 2, refs. 3 and 4). For **3** → **8** the spectra are characterized by a λ_{max} near 380 nm with a shoulder near 430 nm. **1** has a λ_{max} near 470 nm and a shoulder close to 440 nm while for **2** λ_{max} is near 450 nm with a shoulder near 425 nm. It is probable that mixing of the electronic transitions occurs and each of the above bands contains contributions from more than one transition, thus definitive assignments are not possible at present. However, the following comments may be made. The high energy band near 400 nm is probably related to the transition found in azobenzene near 320 nm (5) while the band near 450 nm may be identified with the 440 nm $n \rightarrow \pi^*$ transition of azobenzene (5) which in the present compounds gains intensity by mixing with the available $\pi \rightarrow \pi^*$ transitions. The appearance in the resonance Raman spectra (*vide infra*) of intense features from the benzene and azo moieties suggests that both chromophores make important contributions to the absorption spectra in the 450 nm region.

*Evidence that Intense Features from —SO_2NH_2 do not Appear in the Resonance Raman Spectra of **1**, **2**, and **3***

This evidence is obtained from analogues in which the —SO_2NH_2 is absent, from the comparison of ir and Raman data and from the Raman spectrum of **2** when —OH → —O^-. The resonance Raman spectra of **6**, **7**, and **8** (Fig. 3), where the —SO_2NH_2 of **3** is replaced by —CO_2^-, —SO_3^-, and AsO_3^{2-} respectively are very similar and exhibit all the features seen in the spectrum of the —SO_2NH_2 compound; thus there are no extra features in the latter spectrum to assign to contributions from the sulfonamide group. The band at 1130 (**6**), 1122 (**7**), and 1096 cm^{-1} (**8**) is probably a variable CH in plane bending mode (*vide infra*) and is present, as a weak feature, in **1**, **2**, and **3** (Fig. 4 and refs. 3 and 4). Comparison of the resonance Raman spectrum of **3** with that of **4** where H replaces —SO_2NH_2 (Fig. 4) shows that the only additional feature in the sulfonamide spectrum is at

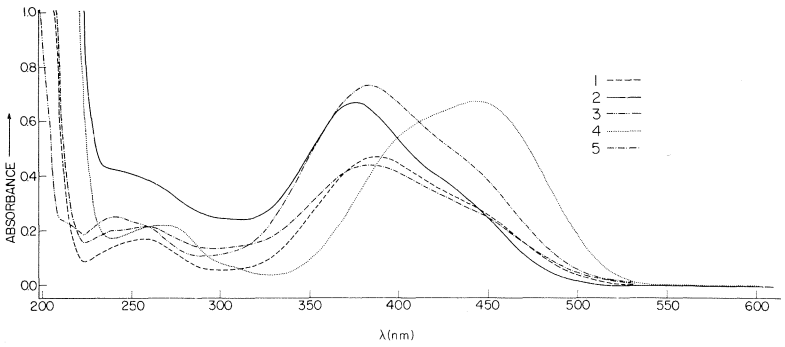

FIG. 2. Absorption spectra of (*1*) **7**, 3.7×10^{-5} *M*, tris-HCl buffer, p*H* 8.3; (*2*) **4**, 1.5×10^{-4} *M*, H_2O; (*3*) **8**, 3.4×10^{-5} *M*, *N*/10 KOH; (*4*) **2**, 1.9×10^{-5} *M* in 75% *N*/10 KOH, 25% methanol; (*5*) **6**, 3.5×10^{-5} *M*, tris-HCl, p*H* 8.2.

1398 cm^{-1}, this is almost certainly a ring mode characteristic of a *p*—*p'* substituted azobenzene (Fig. 3, ref. 6) and does not contain a significant contribution from $—SO_2NH_2$. Comparison of **1** and **5** (not shown) yields an identical result; there are no additional features in the spectrum of **1** attributable to $—SO_2NH_2$.

In the infrared the $—SO_2—$ symmetric stretch of $—SO_2NH_2$ has been assigned by a number of workers (7) to the range 1152–1169 cm^{-1}. The infrared spectra of **1**, **2**, and **3** (Fig. 5) all show an intense peak in this region and on the basis of the literature values (see, *e.g.*, ref. 7) these are assigned to the $—SO_2—$ symmetric stretch with the added possibility that a CH in plane bend (8) may make a minor contribution to the main $—SO_2—$ peak. The intense ir peak near 1140 cm^{-1} for **1**, **2**, and **3** (Fig. 5) coincides, within experimental error, with the Raman band assigned to Ph—N stretch (3, 4). Because **1** and **3** had high luminescent backgrounds only **2** gave a satisfactory Raman spectrum in the solid phase for comparison with the infrared data. For solid **2**, neither the normal (4) nor the resonance (Fig. 6 and ref. 4) Raman spectra have an intense peak near 1165 cm^{-1}. The very weak peak near 1165 cm^{-1} (Fig. 6) could possibly be $—SO_2—$ stretch but, on the basis of comparison of the three forms of **2** —OH,$—SO_2NH_2$; $—O^-$,$—SO_2NH_2$; and O^-,$—SO_2NH^-$, it is more likely to be a CH in plane bending mode (see next section). Additional evidence for the absence of the $—SO_2—$ mode comes from the normal Raman spectrum of $^-O_2C—Ph—SO_2NH_2$ (Fig. 7); no band is detected near 1160 cm^{-1} where the $—SO_2—$ stretch, insensitive to substituent effects (7), is expected.

In summary it appears certain that the $—SO_2NH_2$ does not contribute an intense or even a moderately intense mode to the resonance Raman spectra of **1**, **2**, or **3**. However, if distortion takes place in the $—SO_2NH_2$ group, increased conjugation between the sulfonamide and the ring could produce an intensity enhanced sulfonamide or Ph—S mode and this has been proposed as the mechanism for the appearance of a new resonance Raman band near 1125 cm^{-1} when **1**, **2**, and **3** separately bind to the enzyme carbonic anhydrase (4).

Effect of —OH and $—SO_2NH_2$ Ionization on the Resonance Raman Spectrum of 2

The high quality resonance Raman spectra of **2** in its HO—Ph—N=N—Ph—SO_2NH_2, O^-—Ph—N=N—Ph—SO_2NH_2, and O^-—Ph—N=N—Ph—SO_2NH^- forms (Fig. 6) permit an assessment of the effect of group ionization on the spectra. In particular the validity of correlating spectral changes with the relative importance of valence bond structures such as quinonoid (9) may be tested.

Ionization of —OH

There is a substantial body of evidence indicating that the Raman and resonance Raman spectra of *p*–*p'* disubstituted azobenzenes contain a feature with a high degree of —N=N— stretch near 1430 cm^{-1} and a mode with a high degree of Ph—N stretch occurs near 1140 cm^{-1} (3, 4, 10, 11, and references therein). For HO—Ph—N=N—Ph—SO_2NH_2 these modes are ascribed to the 1438 and 1139 cm^{-1} features respectively (Fig. 6). The marked change in the absorption spectrum of **2** when —OH → $—O^-$ (λ_{max} goes from ~360 to ~450 nm) is accom-

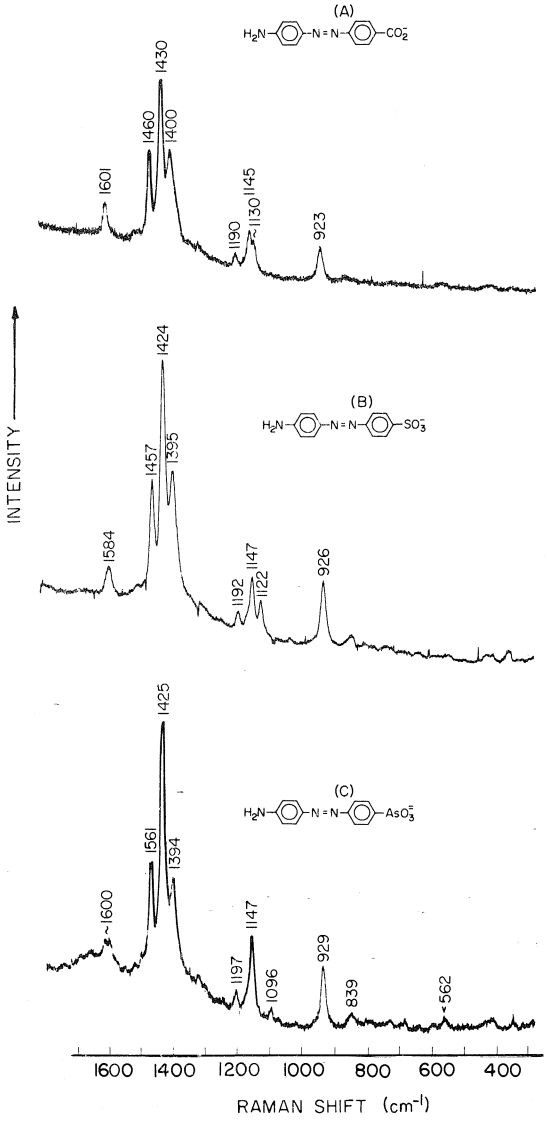

FIG. 3. Resonance Raman spectra (441.6 nm excitation) of (*A*) **6**, 3.3×10^{-4} *M* in *N*/10 KOH; (*B*) **7**, 6.9×10^{-4} *M* in tris buffer p*H* 7.4; (*C*) **8**, 2×10^{-5} *M* in *N*/10 KOH. Laser power ~60 mW, spectral slit width ~9 cm^{-1}, scan speed 0.5 cm^{-1}/s.

panied by striking changes in the relative intensities of the resonance Raman bands (Fig. 6). Two classes of frequency changes are detected in the resonance Raman spectrum upon ionization. The three bands in the —N=N— stretching region, 1400–1465 cm^{-1}, move approximately 20 cm^{-1} to low frequency while shifts to low frequency of 0–8 cm^{-1} are observed for the main Ph—N mode at 1139 cm^{-1} and its satellites at

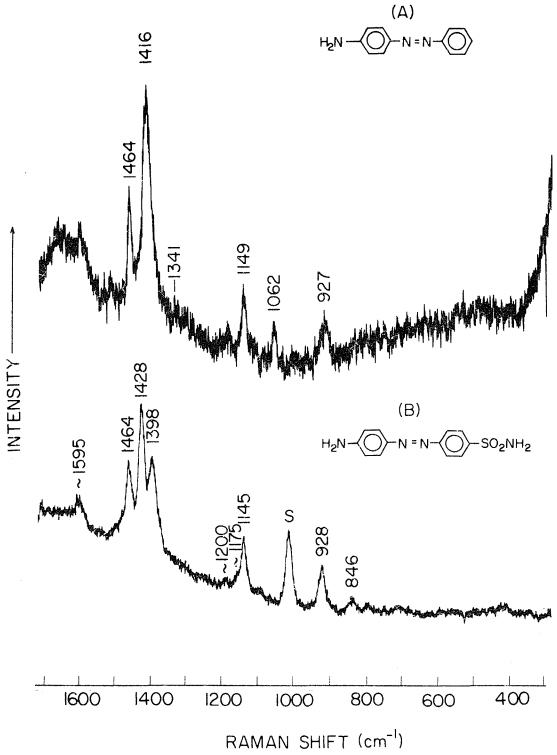

FIG. 4. Resonance Raman spectra (441.6 nm excitation) of (*A*) saturated solution of **4**, p*H* 13.0; (*B*) **3**, 4×10^{-5} *M*, p*H* 7.0, tris buffer 75%, methanol 25% (v/v). 40 mW laser power, spectral slit width 9 cm^{-1}, scan speed 0.5 cm^{-1}/s.

~1165 and 1098 cm^{-1}. The observed shifts for the N=N is compatible with the simple idea of a decrease in —N=N— bond order caused by increased importance of quinonoid forms of the type

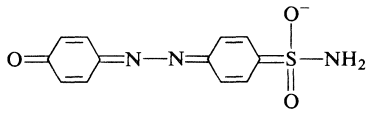

However, for Ph—N the observed shift is clearly incompatible with the increased bond order expected on the basis of the quinonoid arguments. This emphasises that considerable care needs to be exercised when interpreting spectral changes in terms of contributions from valence bond structures. The bands flanking the N=N mode, at 1465, 1400 cm^{-1} in —OH and 1446, 1384 cm^{-1} in —O^-, are assigned to benzene ring modes, each ring contributing one band. Upon —OH → O^- the marked intensity gain of

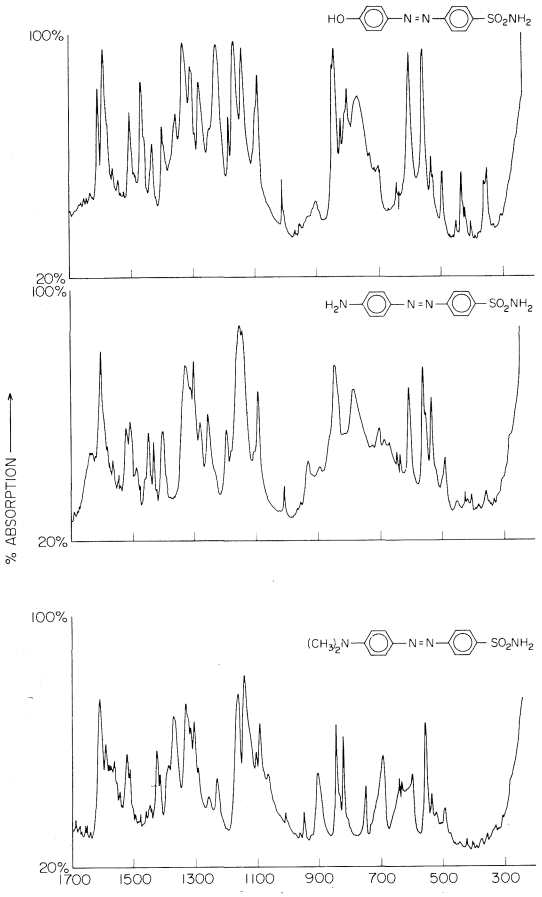

FIG. 5. Infrared spectra of compounds **1**, **2**, and **3** in KBr matrices.

these bands is evidence that they are coupled to the chromophore or chromophores responsible for intensity enhancement in the $—O^-$ form, while their frequency shifts similar to N=N indicate that they are vibrationally coupled to the N=N. This vibrational coupling may provide a mechanism for intensity enhancement of the ring modes. The 1165 and 1098 cm^{-1} bands flanking the intense 1139 cm^{-1} Ph—N feature in the —OH (Fig. 6) are ascribed to CH in plane bending modes 9*a* and 18*b* (or 15 see ref. 8) for *p–p′* disubstituted benzenes. The intensity increase for the 1190 cm^{-1}, in addition to the 1165 and 1098 cm^{-1} bands, upon OH → O^-, suggests that all three features share a common origin and may be CH in plane bends which are intensity-enhanced by coupling to the Ph—N stretching vibration. Further evidence for a coupling of this nature is found in the Raman spectral changes seen upon $—SO_2NH_2$ ionization.

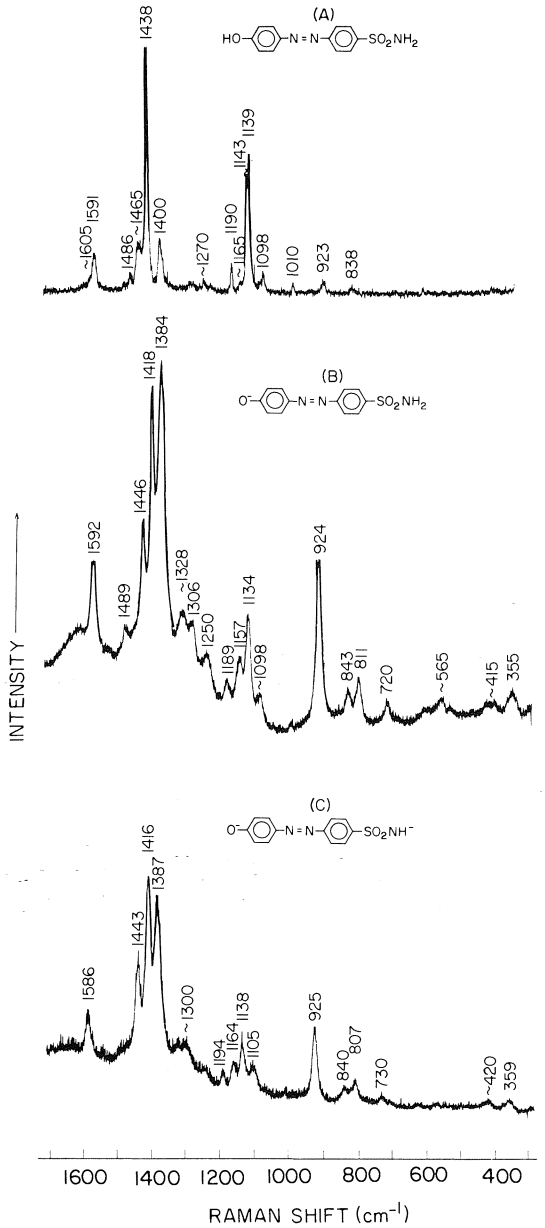

FIG. 6. Resonance Raman (441.6 nm excitation) spectra of compound **2** (*A*) solid (—OH, SO_2NH_2 form), (*B*) 1.1×10^{-4} *M* in tris-sulfate buffer p*H* 8.2 ($—O^-$, $—SO_2NH_2$ form), (*C*) 7.7×10^{-5} *M*, *N*/10 KOH ($—O^-$, $—SO_2NH^-$ form). Laser power ~40 mW. Spectral slit width (*A*) ~4 cm^{-1}, (*B*) ~5 cm^{-1}, (*C*) ~9 cm^{-1}, scan speed 0.5 cm^{-1}/s.

Ionization of $—SO_2NH_2$

The changes in the resonance Raman spectrum of **2** upon sulfonamide ionization have been dealt with at some length (3, 4) and only the 1150 cm^{-1} region will be mentioned here. The

TABLE 1. Tentative assignments (800–1600 cm^{-1} region) for compounds **1**, **2**, and **3**. Band positions are in cm^{-1} and are for aqueous solution at p$H \approx 9.0$. Wilson's mode numbering is followed

Assignment		Frequency		
		Sulfonamide **1**	Sulfonamide **2**	Sulfonamide **3**
	8*b*	1593 w	1592 m	~1595 w
	19*a*		1488 w	
Coupled	19*b**	1446 m	1445 s	1464 s
Coupled	N=N	1419 vs	1417 vs	1428 vs
Coupled	19*b**	1392 s	1384 vs	1398 s
Coupled	Ph—NMe_2	1370 m		
	14		1328 w	
	3	~1318 vw	1306 w	
	Ph—O ?		1250 w	
Coupled	X sens 7*a*	1202 vw	1183 w	~1200 vw
Coupled	9*a*	~1160 sh	1157 w	~1175 sh
Coupled	Ph—N	1139 m	1134 m	1145 m
Coupled	18*b*	1097 w	1098 w	
	5	921 m	924 m	928 m
	10*a*	826 w	843 w	846 w
	11		811 w	

*Possibly both benzene rings contribute a 19*b* feature.

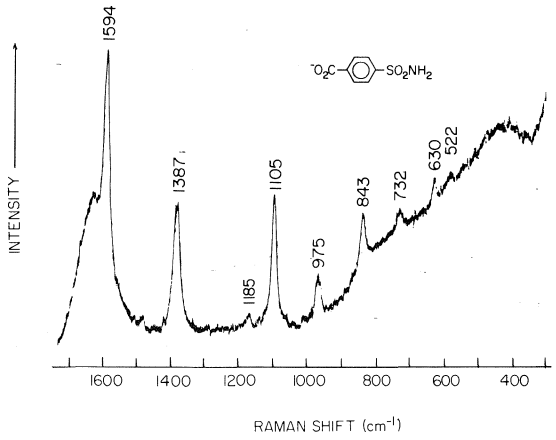

FIG. 7. Normal Raman spectra (441.6 nm excitation) of O_2^-C—Ph—SO_2NH^-, aqueous solution pH 12.6. Laser power 60 mW, spectral slit width ~9 cm^{-1}, scan speed 0.5 cm^{-1}/s.

main Ph—N band at 1134 cm^{-1} (Fig. 6) moves to 1138 cm^{-1} in —SO_2NH^-; this small shift is real and is reproduced in the 20 spectra obtained at various times with differing laser excitation wavelengths. Additionally the weak bands at 1157, 1098, and 1195 cm^{-1} assigned to CH in plane bending modes move to a higher frequency by approximately 7 cm^{-1} in the —SO_2NH^- providing further evidence for coupling to the Ph—N stretch.

It is interesting that for both —OH and —SO_2NH_2 ionization the lines grouped around the main —N=N— and Ph—N modes appear to act in concert.

Possible assignments for **1**, **2**, and **3**, based on Raman, ir, and literature data are summarized in Table 1, using Wilson's mode numbering (given in ref. 12, p. 341). It must be stressed that the assignments are tentative and that the bands in the 1400 and 1150 cm^{-1} regions are probably highly mixed. It is suggested that the great majority of the ring modes seen come from the ring containing the —O^-, —NH_2, or —$N(CH_3)_2$ chromophore. The other benzene ring is thought to make a major contribution only in the 1400 cm^{-1} region of the resonance Raman spectrum. The band at 1370 cm^{-1} in **1** is ascribed to the Ph—$N(CH_3)_2$ group and may arise as a result of the very strong conjugation between the dimethylamino and phenyl systems. The assignments suggested here are in substantive agreement with those tentatively proposed by Dupaix *et al.* (13).

*Evidence that Intensity Changes in the Resonance Raman Spectra of **1**, **2**, and **3** may be used to Follow Sulfonamide Ionization Independently of Vibronic Effects*

For compounds **1**, **2**, and **3** upon —SO_2NH_2 becoming —SO_2NH^- the ratio of the resonance Raman band intensities for the features near 1420 and 1390 cm^{-1} increases (4). This resonance Raman intensity change may be used to follow ionization of the sulfonamide group upon

binding to the enzyme carbonic anhydrase. It is thus important to find out if it is a reliable monitor of the change in chemistry or whether it simply reflects an unrelated change in vibronic coupling ensuing from the different absorption spectrum of the $-SO_2NH^-$ form (3, 4). The normal Raman spectra of **2** with 647.1 nm excitation (Fig. 8), which are not expected to be subject to subtle changes in vibronic interactions, indicate the increase of Int$\sim$1420/Int$\sim$1390 can be taken as a reliable monitor of sulfonamide ionization. Figure 8 shows that Int$\sim$1420/$\sim$1390 goes from 0.72 to 0.94, upon ionization, compared to 0.97 and 1.16 in the respective resonance (441.6 nm excitation) cases (4). Band positions in the normal and resonance Raman spectra are the same to within the limits of experimental error.

Excitation Profiles

The variation of Raman intensities with excitation wavelength, the excitation profile, is capable of providing information on vibronic structure which lies unresolved in an absorption spectrum. Excitation profiles can indicate the identity of an absorption band responsible for the intensity enhancement of Raman bands, the position of the vibronic component (*e.g.*, 0–0) responsible for maximum enhancement (14) and, in favorable cases, the 0–0 to 0–1 to 0–2 etc. spacing (15). It is also of considerable current interest to compare experimental Raman intensity enhancements with those predicted by theory.

The frequency dependence of the Raman lines in the preresonance region can be computed from the form of the scattering tensor derived by Albrecht and co-worker (16). Albrecht and Hutley derived two frequency dependent factors F_A and F_B which involve one and two excited electronic states respectively:

$$F_A = \nu^2 \frac{(\nu_e^2 + \nu_0^2)}{(\nu_e^2 - \nu_0^2)^2}$$

$$F_B = 2\nu^2 \frac{(\nu_e\nu_s + \nu_0^2)}{(\nu_e^2 - \nu_0^2)(\nu_s^2 - \nu_0^2)}$$

where ν_0 is the excitation frequency, ν_e is the frequency of the major active virtual electronic state (made equal to the frequency of the coupled lowest energy electronic transition), and ν_s is the frequency of another virtual state

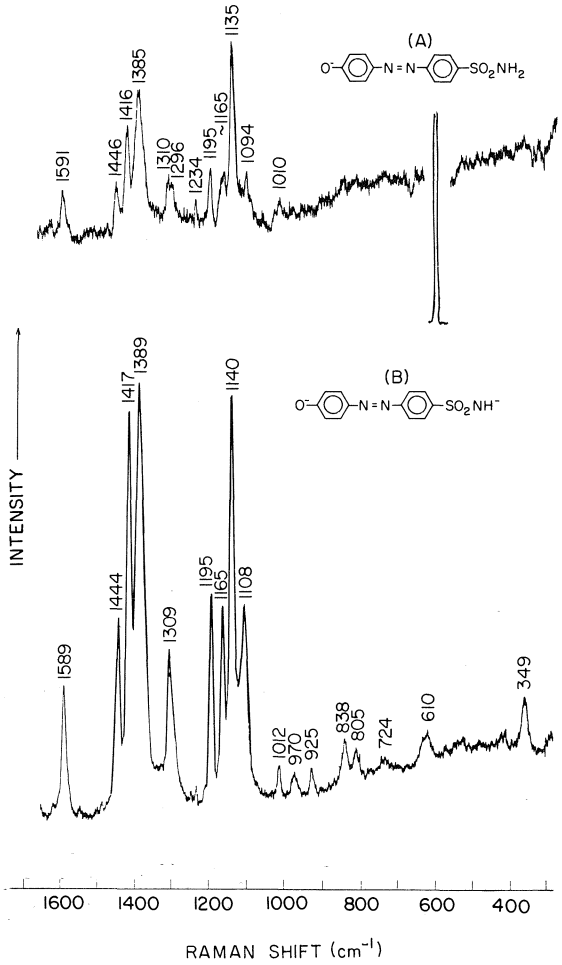

FIG. 8. Normal Raman spectra (647.1 nm excitation) of (*A*) $\sim 2.5 \times 10^{-2}$ *M* O^-—Ph—N=N—$PhSO_2NH_2$ in tris-sulfate buffer p*H* 9.1, (*B*) $\sim 7 \times 10^{-2}$ *M* $^-$O—Ph—N=N—$PhSO_2NH^-$ in *N*/10 KOH. Laser power $\sim$80 mW, spectral slit 5 cm^{-1}.

(derived from the higher energy absorption spectrum).

The frequency dependence of the intensity of a transition, I_{mn} is given by

$$I_{mn} \propto F_A^2 \quad \text{or} \quad I_{mn} \propto F_B^2$$

Albrecht and Hutley's formulism requires that only one diagonal component of the polarizability tensor be active. This criterion may be tested by measuring depolarization ratios. Under resonance conditions if only one component of the tensor is responsible for scattering the depolarization ratio is 0.33 (17). The average of two sets of measurements for **2** (at p*H* 8.0, with

TABLE 2. Comparison of experimental and theoretical (16) Raman intensities as a function of exciting wavelength (λ_0), for the 1416, 1387, and 1138 cm^{-1} lines of compound **2**. Intensities for 514.5 nm excitation are arbitrarily taken as 1.0. pH = 13.0

	Raman intensity			Raman intensity			Raman intensity		
		Theoretical*			Theoretical*			Theoretical*	
ν_0 (kK) (λ_0 (nm))	Experimental $[I\nu_0/I_{19.43}]_{1416}$	$(F_A^2)_{1416}$	$(F_B^2)_{1416}$	Experimental $[I\nu_0/I_{19.43}]_{1387}$	$(F_A^2)_{1387}$	$(F_B^2)_{1387}$	Experimental $[I\nu_0/I_{19.43}]_{1138}$	$(F_A^2)_{1138}$	$(F_B^2)_{1138}$
17.60 (568.2)	0.21	0.10	0.21	0.18	0.10	0.21	0.33	0.10	0.22
18.84 (530.8)	0.52	0.43	0.58	0.53	0.43	0.58	0.75	0.43	0.58
19.43 (514.5)	1	1	1	1	1	1	1	1	1
19.93 (501.7)	1.68	1.84	1.67	1.58	1.85	1.67	1.35	1.85	1.66
20.14 (496.5)	2.07	3.34	1.74	1.88	3.34	1.74	1.55	3.34	2.09
20.49 (488.0)	2.47	6.94	3.28	2.22	6.93	3.28	1.74	6.93	3.27
20.98 (476.5)	2.97	23.96	6.62	2.41	23.84	6.62	1.98	23.80	6.59
21.15 (472.7)	2.71	40.17	9.01	2.08	40.08	9.01	1.82	40.08	8.96
21.47 (465.8)	3.20	129.84	17.23	2.38	129.73	17.23	1.93	129.35	17.14
21.83 (457.9)	3.43	831.38	46.70	2.37	830.90	47.82	1.77	826.12	46.39

*For the calculation of frequency factors ν_e = 22.47 kK and ν_s = 37.31 kK.

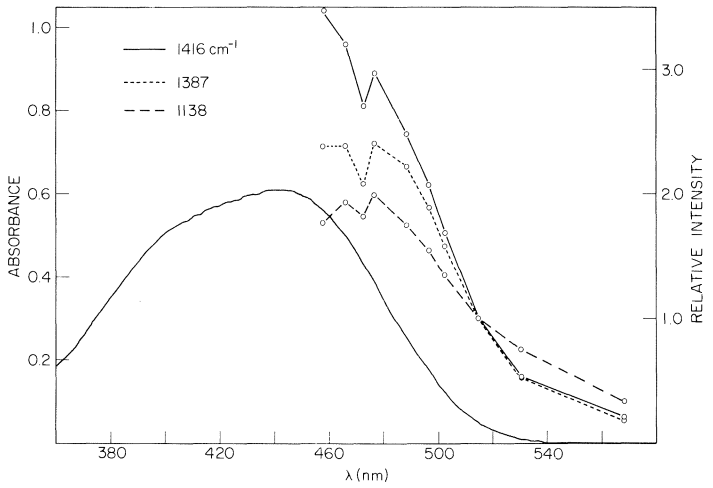

FIG. 9. Absorption spectrum and excitation profiles (for 1416, 1387, and 1138 cm^{-1} lines) of compound **2** p*H* 13.0, $\sim 2 \times 10^{-5}$ *M*.

441.6 nm excitation) gave $\rho_{1134} = 0.32 \pm 0.03$, $\rho_{1384} = 0.34 \pm 0.03$, $\rho_{1417} = 0.33 \pm 0.03$. Thus it is very likely that only one component of the polarizability tensor is dominant under resonance conditions.

Table 2 shows the calculated and measured intensities of the 1138, 1387, and 1416 cm^{-1} bands of **2**. Each band gains intensity with decrease in excitation wavelength with the 1387 and 1416 cm^{-1} features showing the greater increase. The results show that the intensity variations are better determined by F_B rather than F_A term. The point at which the pre-resonance Raman region moves into the rigorous resonance Raman case has not been well defined. For the rigorous resonance Raman case damping constants, obtainable from structured absorption spectra or overtones in the Raman spectra, must be used to calculate relative intensity enhancement. The unavailability of this experimental data prevented the use of damping constants in the present work and without this it is apparent that the agreement between theoretical F_B^2 terms and experimental intensities breaks down at about 1000 cm^{-1} from λ_{max}, or when $\lambda_{exciting}$ is lower than 488.0 nm. This point may, of course, be taken as the simple empirical definition of the boundary between pre- and rigorous-resonance.

The development of structure in the excitation profile is evident in Table 2 and Fig. 9; all three of the lines measured show a minimum at 472.6 nm excitation. Measurements at additional wavelengths, unobtainable with our existing equipment, are needed to quantify the spacing in the structure. However small spacing evident from the present data does indicate that vibrational spacing, rather than two electronic transitions, is being resolved.

Finally it is noted, as an experimental observation, that under rigorous resonance Raman conditions, most of the Raman intensity is seen in the 1400 cm^{-1} region, where the stretching vibration of the N=N group occurs.

Acknowledgements

The authors are grateful to Dr. R. W. King for providing some of the compounds, to Mr. R. G. Carriere for recording the excitation profiles, and to Dr. R. N. Jones for the use of a Perkin Elmer 521 infrared spectrophotometer.

1. T. MANN and D. KEILIN. Nature (London), **146**, 164 (1940).
2. J. E. COLEMAN. *In* Inorganic biochemistry. Vol. 1. *Edited by* G. L. Eichhorn. Elsevier, Amsterdam. 1973. Chapt. 16.
3. K. KUMAR, R. W. KING, and P. R. CAREY. FEBS Lett. **48**, 283 (1974).
4. K. KUMAR, R. W. KING, and P. R. CAREY. Biochemistry, **15**, 2195 (1976).
5. H. H. JAFFÉ, S.-J. YEH, and R. W. GARDNER. J. Mol. Spectrosc. **2**, 120 (1958).
6. H. H. HACKER. Inaugural Dissertation, University of Munich, Munich, West Germany. 1968.
7. L. J. BELLAMY. Advances in infrared group frequen-

cies. Methuen, London. 1968. p. 233 and references therein.
8. G. VARSÁNYI. Vibrational spectra of benzene derivatives. Academic Press, New York, NY. 1969. p. 204.
9. Y. SAITO, B.-K. KIM, K. MACHIDA, and T. UNO. Bull. Chem. Soc. Jpn. **47**, 2111 (1974).
10. P. R. CAREY, H. SCHNEIDER, and H. J. BERNSTEIN. Biochem. Biophys. Res. Commun. **47**, 588 (1972).
11. P. R. CAREY, A. FROESE, and H. SCHNEIDER. Biochemistry, **12**, 2198 (1973).
12. L. M. SVERDLOV, M. A. KOVNER, and E. P. KRAINOV. Vibrational spectra of polyatomic molecules. Wiley, New York, NY. 1974.
13. A. DUPAIX, J.-J. BECHET, J. YON, J.-C. MERLIN, M. DELHAYE, and M. HILL. Proc. Nat. Acad. Sci. USA, **72**, 4223 (1975).
14. V. R. SALARES, R. MENDELSOHN, P. R. CAREY, and H. J. BERNSTEIN. J. Phys. Chem. **80**, 1137 (1976).
15. B. P. GABER, V. MISKOWSKI, and T. G. SPIRO. J. Am. Chem. Soc. **96**, 6868 (1974).
16. A. C. ALBRECHT and M. C. HUTLEY. J. Chem. Phys. **55**, 4438 (1971).
17. K. KUMAR and P. R. CAREY. J. Chem. Phys. **63**, 3697 (1975).

Crystal and molecular structures of spiro-3,4′-*R*-(3,3-dideoxy-1,2:5,6-di-*O*-isopropylidene-α-D-*ribo*-hexafuranose)-3′-*S*(and 3′-*R*)-acetamido-2′-pyrrolidone

STEVEN J. RETTIG AND JAMES TROTTER

Department of Chemistry, University of British Columbia, 2075 Wesbrook Mall, Vancouver, B.C., Canada V6T 1W5

Received September 8, 1976

STEVEN J. RETTIG and JAMES TROTTER. Can. J. Chem. **55**, 1454 (1977).

Crystals of the 3′-*S* isomer of the title compound are orthorhombic, $a = 23.004(5)$, $b = 11.103(1)$, $c = 7.616(3)$ Å, $Z = 4$, space group $P2_12_12_1$. Crystals of the 3′-*R* isomer are orthorhombic, $a = 24.898(1)$, $b = 10.4122(4)$, $c = 7.6467(6)$ Å, $Z = 4$, space group $P2_12_12_1$. The structures were solved by direct methods and were refined by full-matrix least squares procedures to final *R* values of 0.038 for 1466 and 1996 reflections with $I \geq 3\sigma(I)$ for the 3′-*S* and 3′-*R* isomers respectively. Both crystal structures consist of discrete molecules linked by systems of intermolecular N—H...O hydrogen bonds and possible weak C—H...O interactions.

STEVEN J. RETTIG et JAMES TROTTER. Can. J. Chem. **55**, 1454 (1977).

Les cristaux de l'isomère 3′-*S* du composé mentionné dans le titre sont orthorhombiques, $a = 23.004(5)$, $b = 11.103(1)$, $c = 7.616(3)$ Å, $Z = 4$, groupe d'espace $P2_12_12_1$. Les cristaux de l'isomère 3′-*R* sont orthorhombiques, $a = 24.898(1)$, $b = 10.4122(4)$, $c = 7.6467(6)$ Å, $Z = 4$, groupe d'espace $P2_12_12_1$. On a résolu les structures par des méthodes directes et on les a affinées par la méthode des moindres carrés (matrice complète) jusqu'à des valeurs finales de *R* respectives de 0.038 pour 1466 et 1996 réflexions avec $I \geq 3\sigma(I)$ pour les isomères 3′-*S* et 3′-*R*. Les deux structures cristallines comprennent des molécules distinctes liées par des systèmes de ponts hydrogène N—H...O intermoléculaires et possiblement des interactions C—H...O qui sont faibles.

[Traduit par le journal]

Introduction

The reaction of (*Z*)-3-deoxy-3-*C*-methoxycarbonylmethylene-1,2:5,6-di-*O*-isopropylidene-α-D-*ribo*-hexafuranose, **1**, with diazomethane followed by hydrogenation was found to yield four diastereomeric pyrrolidones **2**, **4**, **6**, and **8** (1). Conversion of these four compounds to the *N*-acetyl derivatives afforded the crystalline products **3**, **5**, **7**, and **9**. Because of uncertainties in structural assignments by conventional methods the X-ray crystallographic analysis of two of these products, namely **7** and **9**, has been undertaken.

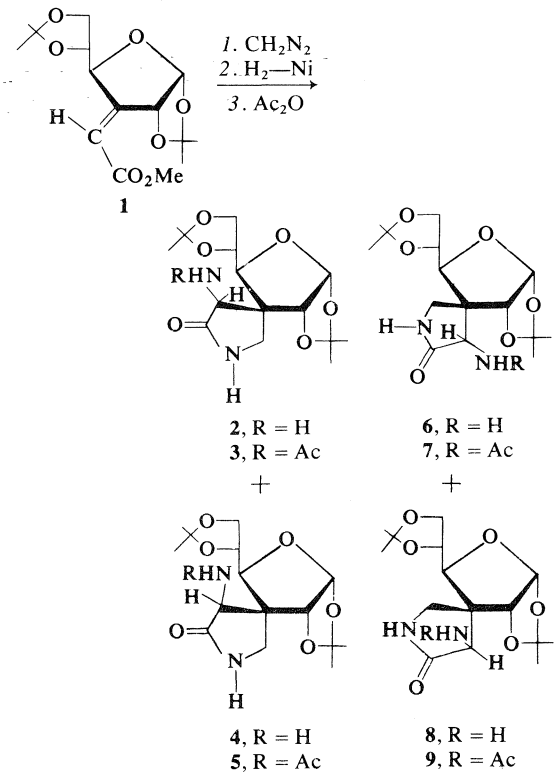

Experimental

3′-S Isomer (9)

The crystal chosen for study was mounted with *c* parallel to the goniostat axis and had dimensions of *ca.* 0.4 × 0.4 × 0.6 mm. Unit-cell and space group data were obtained from film and diffractometer measurements. The unit-cell parameters were refined by a least squares treatment of $\sin^2\theta$ values for 12 reflections measured on a diffractometer with Cu K_α radiation. Crystal data are:

$C_{17}H_{26}N_2O_7$ fw = 370.4

Orthorhombic, $a = 23.004(5)$, $b = 11.103(1)$, $c = 7.616(3)$ Å, $V = 1945.2(9)$ Å^3, $Z = 4$, $\rho_c = 1.265(1)$ g cm^{-3}, $F(000) = 792$ (22°C, Cu K_α, $\lambda = 1.5418$ Å, $\mu = 8.4$ cm^{-1}), mp 284–286°C, $[\alpha]_D^{25}$ +98.3°. Absent reflections:

$h00$, $h \neq 2n$, $0k0$, $k \neq 2n$, and $00l$, $l \neq 2n$ define uniquely the space group $P2_12_12_1$ (D_2^4, No. 19).

Intensities were measured with nickel-filtered Cu K_α radiation on a Datex-automated General Electric XRD-6 diffractometer. A θ–2θ scan at 2° min^{-1} over a range of $(1.80 + 0.86 \tan \theta)$ degrees in 2θ was employed. Background counts of 20 s were measured at each end of the scan. Data were measured to $2\theta = 145°$ (minimum interplanar spacing 0.81 Å). The intensity of the check reflection, measured every 40 reflections throughout the data collection, remained constant to within ±2%. Lorentz and polarization corrections and check reflection scaling

TABLE 1. Final positional parameters (fractional × 10^4, $H \times 10^3$) with estimated standard deviations in parentheses

Atom	x	y	z
	3′-*S* isomer		
O(1)	1879(1)	3024(3)	7861(4)
O(2)	2141(1)	−502(3)	7721(6)
O(3)	1201(1)	85(2)	7496(5)
O(4)	2049(1)	4364(3)	10178(4)
O(5)	1192(1)	3607(2)	11200(3)
O(6)	−392(1)	1021(3)	7577(5)
O(7)	−76(1)	1912(2)	12549(4)
N(2)	459(1)	1154(3)	10332(4)
N(1′)	199(2)	2353(3)	6139(5)
C(1)	1706(2)	4109(4)	8698(6)
C(2)	1095(2)	3908(3)	9391(5)
C(3)	885(2)	2801(3)	8375(5)
C(4)	1467(2)	2097(3)	8283(6)
C(5)	1543(2)	1101(4)	6945(7)
C(6)	2164(2)	613(5)	6844(10)
C(7)	1573(2)	−965(4)	7511(7)
C(8)	1712(2)	4214(3)	11750(6)
C(3′)	354(2)	2142(3)	9155(5)
C(2′)	−1(2)	1750(3)	7554(6)
C(5′)	668(2)	3178(4)	6530(6)
C(12)	213(2)	1090(3)	11944(5)
C(13)	316(3)	−69(5)	12929(8)
C(14)	1516(3)	−1635(6)	5793(11)
C(15)	1425(3)	−1708(6)	9103(11)
C(16)	2039(2)	3404(5)	12999(8)
C(17)	1573(2)	5424(4)	12541(11)
H(N2)	68(2)	53(3)	992(5)
H(N1′)	2(2)	216(5)	507(9)
H(1)	179(2)	479(4)	781(7)
H(2)	84(2)	461(3)	939(6)
H(4)	157(2)	175(3)	937(6)
H(5)	140(2)	133(4)	592(7)
H(6a)	229(3)	47(5)	547(10)
H(6b)	242(2)	110(4)	747(7)
H(3′)	9(1)	266(3)	977(5)
H(5′a)	52(2)	400(4)	648(5)
H(5′b)	100(2)	315(4)	562(7)
H(13a)	34(3)	5(6)	1422(11)
H(13b)	64(2)	−54(5)	1249(7)
H(13c)	−3(3)	−46(6)	1296(11)
H(14a)	184(2)	−227(5)	592(8)
H(14b)	162(3)	−109(7)	487(8)
H(14c)	112(2)	−180(4)	558(6)
H(15a)	103(3)	−206(5)	896(8)
H(15b)	165(3)	−237(6)	923(9)
H(15c)	149(3)	−113(7)	1025(9)
H(16a)	212(2)	272(5)	1224(8)
H(16b)	183(3)	328(5)	1420(10)
H(16c)	240(2)	377(4)	1333(7)
H(17a)	136(2)	586(4)	1168(7)
H(17b)	194(2)	582(4)	1286(6)
H(17c)	131(3)	536(6)	1357(9)
	3′-*R* isomer		
O(1)	1912(1)	1969(2)	7820(3)
O(2)	2042(1)	5651(2)	7524(4)
O(3)	1209(1)	5004(2)	8341(3)
O(4)	2074(1)	532(2)	5504(3)
O(5)	1271(1)	1294(2)	4540(2)
O(6)	−94(1)	4358(2)	7941(2)
O(7)	146(1)	3096(2)	3038(2)
N(2)	149(1)	1988(2)	5559(2)
N(1′)	373(1)	2819(2)	9442(2)
C(1)	1768(1)	807(3)	6991(4)
C(2)	1194(1)	962(2)	6336(3)
C(3)	989(1)	2143(2)	7310(3)
C(4)	1514(1)	2929(2)	7413(3)
C(5)	1568(1)	3986(3)	8768(4)
C(6)	2119(2)	4621(4)	8705(6)
C(7)	1509(1)	6091(3)	7779(6)
C(8)	1766(1)	752(3)	3957(4)
C(3′)	517(1)	2859(2)	6460(2)
C(2′)	228(1)	3460(2)	8029(3)
C(5′)	761(1)	1799(2)	9132(3)
C(12)	18(1)	2141(2)	3876(3)
C(13)	−294(2)	1055(3)	3073(4)
C(14)	1465(3)	7127(5)	9108(15)
C(15)	1273(5)	6472(10)	5992(14)
C(16)	2046(1)	1706(4)	2788(6)
C(17)	1669(2)	−506(3)	3026(7)
H(N2)	9(1)	120(3)	609(4)
H(N1′)	20(1)	298(3)	1051(5)
H(1)	181(2)	12(4)	781(5)
H(2)	94(1)	27(3)	643(4)
H(4)	161(1)	322(3)	622(4)
H(5)	149(1)	364(3)	999(4)
H(6a)	217(2)	511(5)	983(7)
H(6b)	238(1)	410(4)	827(5)
H(3′)	62(1)	352(3)	567(3)
H(5′a)	57(1)	96(2)	911(3)
H(5′b)	103(1)	181(2)	1001(3)
H(13a)	2(2)	43(5)	273(8)
H(13b)	−49(2)	52(4)	393(6)
H(13c)	−53(2)	137(6)	228(8)
H(14a)	176(3)	766(7)	877(9)
H(14b)	172(2)	659(5)	1006(6)
H(14c)	116(2)	738(5)	958(7)
H(15a)	87(4)	701(9)	699(13)
H(15b)	151(3)	700(6)	566(9)
H(15c)	142(3)	572(8)	492(12)
H(16a)	212(2)	233(5)	358(6)
H(16b)	177(2)	194(4)	181(6)
H(16c)	243(1)	136(4)	234(5)
H(17a)	144(1)	−100(4)	368(5)
H(17b)	200(2)	−87(4)	277(6)
H(17c)	137(2)	−35(6)	186(9)

TABLE 2. Final thermal parameters and their estimated standard deviations

(*a*) Anisotropic thermal parameters ($U_{ij} \times 10^3$ Å^2)

Atom	U_{11}	U_{22}	U_{33}	U_{12}	U_{13}	U_{23}
			3′-*S* isomer			
O(1)	61(1)	73(2)	80(2)	−15(1)	13(1)	4(2)
O(2)	58(2)	82(2)	109(3)	9(1)	0(2)	−10(2)
O(3)	58(1)	54(1)	93(2)	6(1)	8(2)	−12(2)
O(4)	72(2)	108(2)	69(2)	−45(2)	0(2)	6(2)
O(5)	53(1)	52(1)	53(1)	−10(1)	−5(1)	2(1)
O(6)	90(2)	75(2)	82(2)	−36(2)	−20(2)	4(2)
O(7)	87(2)	66(2)	52(1)	12(1)	8(2)	0(2)
N(2)	52(2)	44(1)	58(2)	0(1)	5(2)	2(1)
N(1′)	69(2)	55(2)	55(2)	−5(2)	−8(2)	−2(2)
C(1)	72(3)	60(2)	68(3)	−18(2)	0(2)	11(2)
C(2)	57(2)	43(2)	60(2)	−9(2)	−1(2)	3(2)
C(3)	54(2)	42(2)	52(2)	−4(2)	−3(2)	5(2)
C(4)	50(2)	52(2)	62(3)	−4(2)	1(2)	5(2)
C(5)	64(2)	67(2)	67(3)	−2(2)	13(2)	−4(2)
C(6)	71(3)	77(3)	112(5)	2(3)	25(3)	−14(3)
C(7)	55(2)	65(2)	86(3)	9(2)	−4(2)	−9(3)
C(8)	50(2)	52(2)	69(2)	−15(2)	0(2)	0(2)
C(3′)	52(2)	37(2)	47(2)	1(2)	−2(2)	−2(2)
C(2′)	61(2)	46(2)	60(2)	−5(2)	−3(2)	−1(2)
C(5′)	72(3)	50(2)	55(2)	−5(2)	−2(2)	7(2)
C(12)	58(2)	48(2)	52(2)	−8(2)	2(2)	5(2)
C(13)	118(5)	66(3)	67(4)	7(3)	14(3)	15(3)
C(14)	88(4)	98(4)	118(6)	23(4)	−3(4)	−41(4)
C(15)	82(4)	90(4)	125(6)	−2(3)	1(4)	19(4)
C(16)	58(2)	82(3)	89(4)	−5(2)	−14(3)	5(3)
C(17)	77(3)	64(3)	121(5)	−10(3)	−17(4)	−15(3)
			3′-*R* isomer			
O(1)	46(1)	51(1)	87(1)	7(1)	−18(1)	4(1)
O(2)	76(1)	65(1)	127(2)	−23(1)	22(1)	−6(2)
O(3)	62(1)	33(1)	73(1)	−10(1)	−5(1)	−2(1)
O(4)	53(1)	103(2)	67(1)	41(1)	1(1)	8(1)
O(5)	39(1)	47(1)	50(1)	11(1)	2(1)	−4(1)
O(6)	61(1)	45(1)	52(1)	19(1)	0(1)	−13(1)
O(7)	118(2)	43(1)	30(1)	−13(1)	−4(1)	6(1)
N(2)	42(1)	27(1)	31(1)	−1(1)	0(1)	1(1)
N(1′)	59(1)	41(1)	33(1)	3(1)	5(1)	−2(1)
C(1)	52(1)	41(1)	64(2)	12(1)	−1(1)	9(1)
C(2)	45(1)	27(1)	54(1)	6(1)	5(1)	1(1)
C(3)	41(1)	25(1)	40(1)	1(1)	−2(1)	1(1)
C(4)	40(1)	36(1)	53(1)	0(1)	−7(1)	4(1)
C(5)	62(1)	44(1)	54(1)	−9(1)	−15(1)	3(1)
C(6)	68(2)	72(2)	102(3)	−17(2)	−28(2)	−11(2)
C(7)	84(2)	42(1)	117(3)	−12(1)	23(2)	13(2)
C(8)	37(1)	47(1)	61(1)	10(1)	6(1)	1(1)
C(3′)	38(1)	26(1)	31(1)	0(1)	1(1)	1(1)
C(2′)	43(1)	33(1)	39(1)	2(1)	0(1)	−7(1)
C(5′)	53(1)	36(1)	40(1)	0(1)	−3(1)	9(1)
C(12)	62(1)	32(1)	31(1)	0(1)	0(1)	−2(1)
C(13)	109(3)	56(2)	49(1)	−25(2)	−16(2)	−7(1)
C(14)	117(4)	63(3)	288(11)	−38(3)	65(6)	−75(5)
C(15)	211(9)	163(8)	175(8)	17(7)	13(7)	120(7)
C(16)	50(1)	69(2)	86(2)	1(1)	6(2)	13(2)
C(17)	72(2)	53(2)	113(3)	9(2)	24(2)	−23(2)

TABLE 2 (*Concluded*)

(*b*) Isotropic thermal parameters

Atom	U (Å^2)	Atom	U (Å^2)
	3′-*S* isomer ($U \times 10^2$)		
H(N2)	6(1)	H(13c)	14(3)
H(N1′)	11(2)	H(14a)	10(2)
H(1)	9(1)	H(14b)	13(3)
H(2)	6(1)	H(14c)	7(1)
H(4)	5(1)	H(15a)	12(2)
H(5)	7(1)	H(15b)	11(2)
H(6a)	14(2)	H(15c)	13(3)
H(6b)	8(1)	H(16a)	11(2)
H(3′)	3(1)	H(16b)	13(2)
H(5′a)	6(1)	H(16c)	11(2)
H(5′b)	9(2)	H(17a)	8(2)
H(13a)	14(2)	H(17b)	7(1)
H(13b)	11(2)	H(17c)	13(3)
	3′-*R* isomer ($U \times 10^3$)		
H(N2)	62(8)	H(13c)	150(22)
H(N1′)	72(9)	H(14a)	173(24)
H(1)	75(10)	H(14b)	99(17)
H(2)	49(7)	H(14c)	123(18)
H(4)	51(8)	H(15a)	250(43)
H(5)	54(8)	H(15b)	137(24)
H(6a)	125(17)	H(15c)	182(34)
H(6b)	71(10)	H(16a)	111(17)
H(3′)	45(6)	H(16b)	100(13)
H(5′a)	44(6)	H(16c)	82(10)
H(5′b)	31(5)	H(17a)	76(11)
H(13a)	116(16)	H(17b)	90(12)
H(13b)	100(12)	H(17c)	170(23)

were applied, and the structure amplitudes were derived. No absorption correction was made in view of the low value of μ. Of the 2229 independent reflections measured, 1478 had intensities greater than $3\sigma(I)$ above background where $\sigma^2(I) = S + B + (0.06S)^2$ with S = scan count and B = time averaged background count. These reflections were used in the solution and refinement of the structure.

The structure was solved by direct methods using tangent formula refinement (2–4).[1] Thirty-two sets of phases for 322 reflections with $|E| \geq 1.425$ were determined. One set of phases was outstanding in that it had the lowest value of R_k (0.25) and the greatest number of phases determined (296). An *E*-map calculated from this set of phases clearly gave the positions of the 26 non-hydrogen atoms among the 29 highest peaks. Two cycles of full-matrix least-squares refinement of the positional and isotropic thermal parameters of the non-hydrogen atoms gave $R = 0.130$. Three cycles of anisotropic refinement reduced R to 0.080. The coordinates of the 26 hydrogen atoms were revealed on a difference map calculated at this point. The entire structure (H atoms with isotropic temperature factors) was refined for 6 cycles giving a final R of 0.038 and R_w of 0.048 for 1466 reflections with $I \geq 3\sigma(I)$ (1 unobserved and 12 observed reflections which had $|F_o| - |F_c| > 3\sigma(F)$ were removed from the data set in the final stages of refinement; for all 2229 reflections $R = 0.070$ and $R_w = 0.060$).

The least squares refinement was based on the minimization of $\Sigma w[|F_o| - |F_c|/(1 + gI)|]^2$ where g is the extinction parameter and I the uncorrected intensity. The final value of g was $2.4(1) \times 10^{-7}$. The scattering factors of ref. 5 were used for the non-hydrogen atoms and those of ref. 6 for the hydrogen atoms. Anomalous scattering factors from ref. 7 were used for the non-hydrogen atoms. The anisotropic thermal parameters employed in the refinement are U_{ij} in the expression:

$$f = f^0 \exp[-2\pi^2(U_{11}h^2a^{*2} + U_{22}k^2b^{*2} + U_{33}l^2c^{*2} + 2U_{12}hka^*b^* + 2U_{13}hla^*c^* + 2U_{23}klb^*c^*)]$$

where f^0 is the tabulated scattering factor and f is that corrected for thermal motion (for H atoms $f = f^0 \exp[-8\pi^2 U \sin^2\theta/\lambda^2]$). The weighting scheme: $w = 1/\sigma^2(F)$ where $\sigma^2(F)$ is derived from the previously defined $\sigma^2(I)$ gave uniform average values of $w(|F_o| - |F_c|)^2$ over ranges of $|F_c|$ and was employed in the final stages of refinement. The absolute configuration of the molecule was determined from that known for the D-*ribo*-hexafuranose moiety.

On the final cycle of refinement the mean parameter shift was 0.10σ with no shifts greater than 0.43σ. The mean error in an observation of unit weight was 1.095. A

[1]Also from M. G. B. Drew, private communication.

final difference map showed maximum fluctuations of ± 0.2 e Å^{-3}.

3′-R Isomer (7)

Experimental details are the same as for the 3′-*S* isomer except where noted. The crystal used for data collection was mounted with *c* parallel to the goniostat axis and had dimensions of *ca.* 0.4 × 0.5 × 0.8 mm. Twenty-one reflections were used in the refinement of the unit-cell parameters. Crystal data are:

Orthorhombic, $a = 24.898(1)$, $b = 10.4122(4)$, $c = 7.6467(6)$ Å, $V = 1982.3(2)$ Å^3, $Z = 4$, $\rho_c = 1.2411(3)$ g cm^{-3}, $\mu = 8.2$ cm^{-1}, space group $P2_12_12_1$, mp 261–263°C, $[\alpha]_D^{25} +108.5°$.

The intensity of the check reflection remained constant to within ±2.5% during the data collection. Of 2268 independent reflections measured, 2011 had intensities greater than $3\sigma(I)$ above background.

The structure was solved by direct methods. Four sets of phases for 328 reflections with $|E| \geq 1.40$ were determined. One set was outstanding in that it had the lowest value of R_k (0.20) and the greatest number of phases determined (316). An *E*-map calculated from this set of phases gave the positions of the 26 non-hydrogen atoms among the 36 highest peaks. Three cycles of isotropic refinement of the C, N, and O atoms gave $R = 0.149$. Two cycles of anisotropic refinement reduced *R* to 0.070 and a difference map revealed the positions of 23 of the 26 hydrogen atoms. The remaining hydrogen coordinates (all associated with C(15)) were placed in staggered positions. The entire structure was refined for 8 cycles giving a final *R* of 0.038 and R_w of 0.048 for 1996 reflections with $I \geq 3\sigma(I)$ (15 observed and 3 unobserved reflections which had $(|F_o| - |F_c|) > 3\sigma(F)$ were removed from the data set in the final stages of refinement; for all 2268 reflections $R = 0.050$ and $R_w = 0.053$). The final value of the extinction parameter *g* was $4.07(15) \times 10^{-7}$ and the mean error in an observation of unit weight was 1.270. The final positional parameters for both compounds are given in Table 1 and the thermal parameters in Table 2. Measured and calculated structure factors have been placed in the Depository of Unpublished Data.[2]

The thermal motions of both compounds have been analysed in terms of rigid-body modes of translation, libration, and screw motion (8) using the computer program MGTLS. Rigid-body analyses were successful for the 15 atom group O(1), O(4), O(5), N(1′), N(2), C(1)–C(5), C(8), C(2′), C(3′), C(5′), and C(12) (rms $\sigma U_{ij} = 0.0024$ and 0.0023 Å^2, rms $\Delta U_{ij} = 0.0046$ and 0.0062 Å^2 respectively for the 3′-*S* and 3′-*R* isomers). There is considerable thermal motion in the 'free' isopropylidene group of the 3′-*R* isomer. The C(7) coordination group (C(7), O(2), O(3), C(14), and C(15)) behaves as a rigid-body in the 3′-*R* isomer (rms $\Delta U_{ij} = 0.0042$ Å^2), but not in the 3′-*S* isomer where the libration tensor is not positive-definite. Bond distances have been corrected for libration (9, 10) and independent motion based on the ΔU_{ij} (11, 12) and appear along with uncorrected values in Table 3.

[2]The structure factor table is available, at a nominal charge, from the Depository of Unpublished Data, CISTI, National Research Council of Canada, Ottawa, Canada K1A 0S2.

TABLE 3. Bond lengths (Å) with estimated standard deviations in parentheses*

(*a*) Non-hydrogen atoms

Bond	3′-*S* isomer Uncorr.†	3′-*R* isomer Uncorr.†	3′-*R* isomer Corr.
O(1)—C(1)	1.419(5)	1.412(4)	
O(1)—C(4)	1.435(4)	1.442(3)	
O(2)—C(6)	1.408(7)	1.415(5)	[1.442]
O(2)—C(7)	1.412(5)	1.416(4)	[1.436]
O(3)—C(5)	1.437(5)	1.424(3)	[1.441]
O(3)—C(7)	1.446(5)	1.422(3)	[1.451]
O(4)—C(1)	1.405(5)	1.399(4)	
O(4)—C(8)	1.436(5)	1.428(3)	
O(5)—C(2)	1.436(5)	1.429(3)	
O(5)—C(8)	1.435(4)	1.428(3)	
O(6)—C(2′)	1.211(4)	1.233(3)	
O(7)—C(12)	1.220(4)	1.225(3)	
N(2)—C(3′)	1.438(5)	1.460(3)	
N(2)—C(12)	1.354(5)	1.338(3)	
N(1′)—C(2′)	1.350(6)	1.321(3)	
N(1′)—C(5′)	1.446(5)	1.455(3)	
C(1)—C(2)	1.518(6)	1.522(4)	
C(2)—C(3)	1.531(5)	1.526(3)	
C(3)—C(4)	1.553(5)	1.545(3)	
C(3)—C(3′)	1.542(5)	1.536(3)	
C(3)—C(5′)	1.549(6)	1.547(3)	
C(4)—C(5)	1.514(6)	1.517(4)	
C(5)—C(6)	1.530(7)	1.526(4)	
C(7)—C(14)	1.510(8)	1.487(8)	[1.514]
C(7)—C(15)	1.505(8)	1.539(10)	[1.573]
C(8)—C(16)	1.509(6)	1.507(4)	
C(8)—C(17)	1.506(6)	1.510(4)	
C(3′)—C(2′)	1.530(6)	1.532(3)	
C(12)—C(13)	1.508(6)	1.503(4)	

*Table 3(*b*) (Bonds involving hydrogen atoms) is lodged with the Depository of Unpublished Data. See footnote 2 in text for getting a copy.

†Thermal libration correction increases the distances by a maximum of 0.004 Å, except for the values shown in square brackets.

(*c*) Summary of bond lengths involving hydrogen

Bond	Distance (Å)	Mean (Å)
N—H	0.92–0.94(3–7)	0.93
C—H	0.84–1.38(2–10)	0.98

Results and Discussion

Figures 1 and 2 show general views of the 3′-*S* and 3′-*R* isomers respectively and the packing arrangements viewed in the *b* direction are shown in Figs. 3 and 4. Bond angles are given in Table 4 and intraannular torsion angles in Table 5. Table 6 gives details of the hydrogen-bonding schemes and selected nonbonded distances. Individual bond lengths (Table 3*b*) and angles

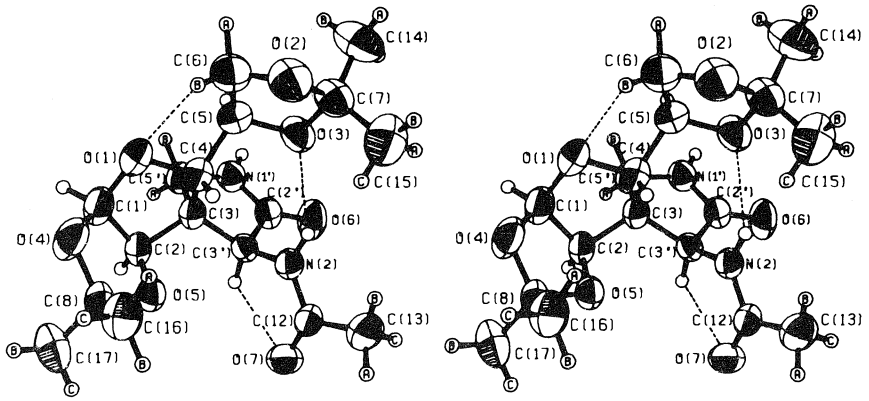

FIG. 1. A stereo view of the 3′-*S* isomer. 50% ellipsoids are shown for the non-hydrogen atoms.

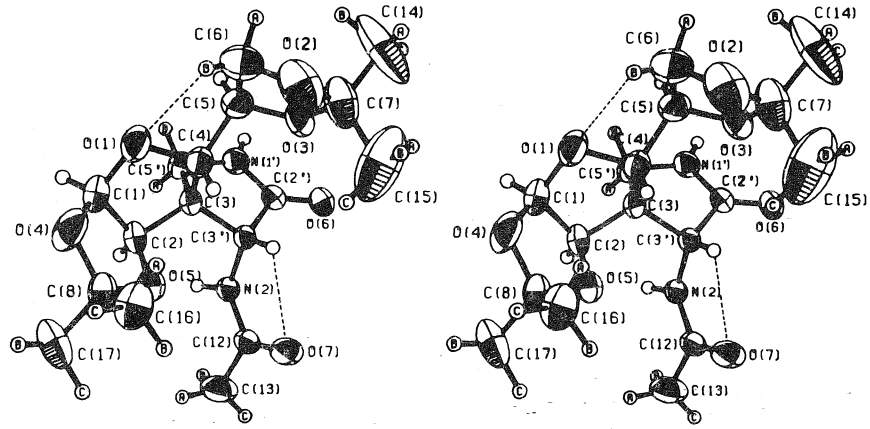

FIG. 2. A stereo view of the 3′-*R* isomer. 50% ellipsoids are shown for the non-hydrogen atoms.

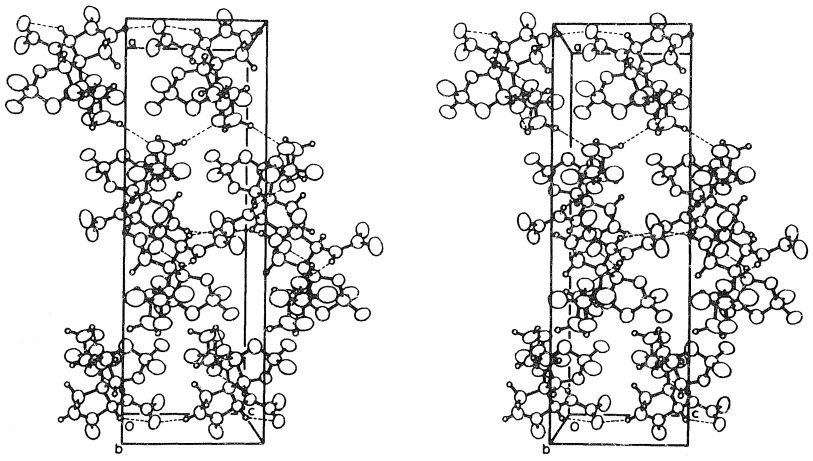

FIG. 3. The crystal structure of the 3′-*S* isomer viewed in the *b* direction. Broken lines represent hydrogen bonds.

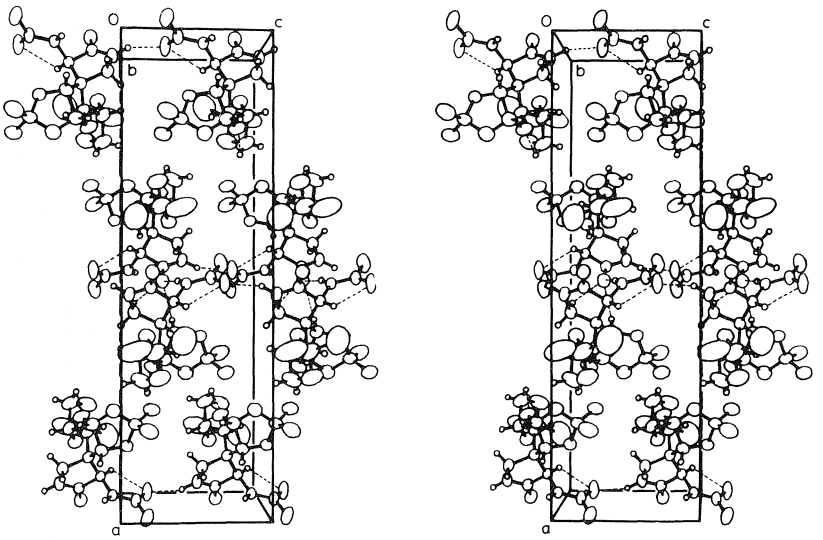

FIG. 4. The crystal structure of the 3′-*R* isomer viewed in the *b* direction. Broken lines represent hydrogen bonds.

(Table 4*b*) involving hydrogen atoms and equations of weighted least-squares mean planes (Table 7) have been deposited along with the structure factors (see footnote 2).

The structural identification of compounds **7** and **9** has enabled the structural assignments to be made by chemical tests for the two remaining pyrrolidones **3** and **5** which have *S* rather than *R* chirality at the spiro junction (C(3)) (1).

Both crystal structures consist of discrete molecules linked by a network of N—H...O hydrogen bonds, with some possible weak C—H...O interactions. There is remarkable similarity between the packing arrangements for the two isomers (see Figs. 3 and 4). Both isomers feature intermolecular N(1′)—H(N1′)...O(7) hydrogen bonds (N...O = 2.849(5) Å for the 3′-*S* isomer and 2.822(3) Å for the 3′-*R* isomer) and possible weak intermolecular C—H...O interactions, C(2)—H(2)...O(6) and C(5′)—H(5′)...O(6) (C...O = 3.219(5) and 3.292(5) Å for the 3′-*S* isomer and 3.256(3) and 3.425(3) Å for the 3′-*R* isomer), as well as two intramolecular C—H...O interactions, C(6)—H(6)...O(1) and C(3′)—H(3′)...O(7). The major difference is that H(N2) is involved in an intramolecular N—H...O hydrogen bond with O(3) in the 3′-*S* isomer (N...O = 2.998(4) Å) and an intermolecular hydrogen bond with O(6) in the 3′-*R* isomer (N...O = 2.972(2) Å). The 3′-*S* isomer has a third possible C—H...O interaction C(6)—H(6a)...O(2) (C...O = 3.520(6) Å) which is not present in the 3′-*R* isomer. The large thermal motion of the C(7) coordination group, apparent in the 3′-*R* isomer, is considerably subdued by the intramolecular N—H...O hydrogen bond (and possibly by the intermolecular C(6)—H(6a)...O(2) interaction) in the 3′-*S* isomer.

The furanose rings in the two isomeric molecules have similar, but significantly different, conformations (see Table 5). The bond lengths and angles in the furanose rings of the two molecules are equal within experimental error, while some of the exocyclic angles at ring junction atoms C(1), C(2), and C(3) differ significantly. In both rings the C(1)—O(1) bond is significantly shorter than the C(4)—O(1) bond. The C(3)—C(4) bonds (1.557(5) and 1.549(3) Å for the 3′-*S* and 3′-*R* isomers respectively) are longer, and the C(4)—C(5) bonds (1.516(6) and 1.519(4) Å) are shorter than usual. These differences probably arise from a combination of steric and σ-hybridization effects (13).

Bond lengths and angles in both fused and free isopropylidene rings of the two structures are in good agreement with the mean values tabulated for isopropylidene groups fused to sugar molecules (14). The weighted mean C—C, C—O, and C—CH_3 distances (standard deviation of the mean in parentheses) are: 1.526(2), 1.432(3), and 1.513(7) Å in the present structures compared to

TABLE 4. Bond angles (deg) with estimated standard deviations in parentheses*

(*a*) Non-hydrogen atoms

Bonds	Angle (deg) 3′-*S* isomer	3′-*R* isomer
C(1)—O(1)—C(4)	108.9(3)	108.8(2)
C(6)—O(2)—C(7)	107.6(4)	106.6(3)
C(5)—O(3)—C(7)	108.2(3)	109.4(2)
C(1)—O(4)—C(8)	110.0(3)	110.3(2)
C(2)—O(5)—C(8)	107.5(3)	108.7(2)
C(3′)—N(2)—C(12)	122.3(3)	122.2(2)
C(2′)—N(1′)—C(5′)	113.8(4)	114.6(2)
O(1)—C(1)—O(4)	112.0(4)	113.7(2)
O(1)—C(1)—C(2)	106.9(3)	107.2(2)
O(4)—C(1)—C(2)	105.7(3)	105.4(2)
O(5)—C(2)—C(1)	102.9(3)	102.5(2)
O(5)—C(2)—C(3)	110.3(3)	108.6(2)
C(1)—C(2)—C(3)	103.6(3)	103.9(2)
C(2)—C(3)—C(4)	98.9(3)	99.7(2)
C(2)—C(3)—C(3′)	115.9(3)	116.2(2)
C(2)—C(3)—C(5′)	110.0(3)	112.1(2)
C(4)—C(3)—C(3′)	117.6(3)	114.3(2)
C(4)—C(3)—C(5′)	111.8(3)	112.8(2)
C(3′)—C(3)—C(5′)	102.9(3)	102.3(2)
O(1)—C(4)—C(3)	102.7(3)	103.1(2)
O(1)—C(4)—C(5)	107.3(3)	107.1(2)
C(3)—C(4)—C(5)	119.8(3)	119.6(2)
O(3)—C(5)—C(4)	108.3(3)	109.2(2)
O(3)—C(5)—C(6)	104.3(4)	103.5(2)
C(4)—C(5)—C(6)	113.6(4)	111.8(3)
O(2)—C(6)—C(5)	104.6(4)	103.0(3)
O(2)—C(7)—O(3)	104.7(3)	106.0(2)
O(2)—C(7)—C(14)	110.9(5)	113.5(4)
O(2)—C(7)—C(15)	108.5(4)	108.6(5)
O(3)—C(7)—C(14)	109.8(4)	109.4(4)
O(3)—C(7)—C(15)	108.3(4)	105.9(5)
C(14)—C(7)—C(15)	114.1(5)	113.0(7)
O(4)—C(8)—O(5)	105.1(3)	105.5(2)
O(4)—C(8)—C(16)	109.0(4)	110.4(2)
O(4)—C(8)—C(17)	110.1(4)	109.7(3)
O(5)—C(8)—C(16)	108.6(3)	108.9(2)
O(5)—C(8)—C(17)	111.0(3)	110.6(2)
C(16)—C(8)—C(17)	112.7(5)	111.5(3)
N(2)—C(3′)—C(3)	117.9(3)	112.1(2)
N(2)—C(3′)—C(2′)	111.7(3)	109.2(2)
C(3)—C(3′)—C(2′)	104.5(3)	103.1(2)
O(6)—C(2′)—N(1′)	126.6(4)	127.2(2)
O(6)—C(2′)—C(3′)	125.1(4)	124.9(2)
N(1′)—C(2′)—C(3′)	108.3(3)	107.8(2)
N(1′)—C(5′)—C(3)	104.8(3)	102.8(2)
O(7)—C(12)—N(2)	122.1(3)	122.5(2)
O(7)—C(12)—C(13)	122.4(4)	122.1(2)
N(2)—C(12)—C(13)	115.5(4)	115.5(2)

*Table 4(*b*) (Angles involving hydrogen atoms) is lodged with the Depository of Unpublished Data. See footnote 2 in text for getting a copy.

mean values of 1.533(8), 1.425(12), and 1.509(13) Å from ref. 14. The corresponding isopropylidene ring conformations differ significantly in the two isomers as shown by the torsion angles in Table 5.

TABLE 5. Intra-annular torsion angles (deg). Five-membered rings

Bond	Angle (deg) 3′-*S* isomer	3′-*R* isomer
C(1)—C(2)	−21.8(3)	−23.7(2)
C(2)—O(5)	29.9(3)	27.7(2)
O(5)—C(8)	−26.8(3)	−21.6(2)
C(8)—O(4)	12.3(3)	5.4(2)
O(4)—C(1)	6.0(4)	11.5(2)
C(1)—C(2)	−17.3(4)	−15.3(2)
C(2)—C(3)	35.9(3)	33.8(2)
C(3)—C(4)	−43.0(3)	−41.3(2)
C(4)—O(1)	34.6(3)	33.9(2)
O(1)—C(1)	−11.2(4)	−11.9(2)
C(3)—C(3′)	22.3(3)	29.2(2)
C(3′)—C(2′)	−14.3(3)	−20.3(2)
C(2′)—N(1′)	−0.8(4)	1.9(2)
N(1′)—C(5′)	15.4(4)	17.2(2)
C(5′)—C(3)	−22.8(3)	−28.1(2)
C(5)—C(6)	−13.5(4)	−26.3(3)
C(6)—O(2)	29.3(4)	34.3(3)
O(2)—C(7)	−33.8(4)	−29.4(3)
C(7)—O(3)	24.4(4)	11.6(3)
O(3)—C(5)	−6.6(4)	9.1(3)

The pyrrolidone rings in the two molecules both have envelope conformation with C(3) out of the plane of the other four atoms. The four atom group C(5′), N(1′), C(2′), and C(3′) is planar within experimental error in the 3′-*S* isomer and is slightly, but significantly, non-planar in the 3′-*R* isomer. The difference in chirality at C(3′) and the resultant changes in the hydrogen bonding schemes appear to be responsible for significant differences between corresponding bond lengths in the pyrrolidone rings and *N*-acetyl side chains. The strong N(2)—H(N2)...O(6) intermolecular hydrogen bond which exists in the 3′-*R* isomer is believed to be responsible for a significant lengthening of the C(3′)—N(2) and C(2′)—O(6) bonds (1.462(3) and 1.233(3) Å) and a shortening of the C(2′)—N(1′) and N(2)—C(12) bonds (1.322(3) and 1.339(3) Å) relative to the distances of 1.441(5), 1.213(4), 1.352(6), and 1.355(5) Å respectively in the 3′-*S* isomer. The geometry of the amide groups is normal. The coordination groups of the four sp^2 atoms (N(1′), N(2), C(2′), and C(12)) are planar within experimental error in the 3′-*S* isomer while only the C(12) group is rigorously planar in the 3′-*R* isomer.

TABLE 6

(*a*) Selected intra- and intermolecular contacts

Atoms	3′-*S* isomer distance	3′-*R* isomer distance
	Intramolecular	
O(5)...C(4)	2.854(5)	2.844(3)
O(5)...C(3′)	2.965(4)	2.888(3)
N(2)...C(4)	2.985(5)	
C(6)...C(14)	3.013(10)	3.092(8)
H(5)...H(5′b)	2.22(7)	2.21(4)
H(6a)...H(14b)	2.39(9)	1.90(7)
	Intermolecular*	
O(4)...H(16c)[1]	2.80(6)	2.71(4)
C(12)...H(N1′)[2]	2.70(6)	2.76(4)
H(5)...H(16b)[3]		2.36(5)
H(5′b)...H(16b)[3]	2.21(9)	2.30(5)

(*b*) Hydrogen-bond data and possible C—H...O interactions* (distances in Å and angles in deg)

D—H...A	Distance H...A	Distance D...A	∠DHA	∠XAH
		3′-*S* isomer		
N(1′)—H(N1′)...O(7)[3]	1.95(7)	2.849(5)	160(5)	115(2)
N(2)—H(N2)...O(3)	2.25(4)	2.998(4)	138(3)	111(1), 119(1)
C(6)—H(6b)...O(1)	2.49(4)	2.863(6)	104(3)	157(1), 75(1)
C(6)—H(6a)...O(2)[1]	2.46(8)	3.520(6)	162(5)	112(1), 126(1)
C(2)—H(2)...O(6)[4]	2.40(4)	3.219(5)	141(3)	136(1)
C(5′)—H(5′a)...O(6)[4]	2.38(4)	3.292(5)	156(3)	138(1)
C(3′)—H(3′)...O(7)	2.31(3)	2.779(5)	109(2)	81(1)
		3′-*R* isomer		
N(1′)—H(N1′)...O(7)[3]	1.95(4)	2.822(3)	156(3)	119(1)
N(2)—H(N2)...O(6)[4]	2.05(3)	2.972(2)	169(3)	133.4(9)
C(2)—H(2)...O(6)[4]	2.35(3)	3.256(3)	155(2)	150.9(7)
C(5′)—H(5′a)...O(6)[4]	2.58(3)	3.425(3)	143(2)	145.4(6)
C(6)—H(6b)...O(1)	2.53(4)	2.890(4)	104(3)	158(1), 75(1)
C(3′)—H(3′)...O(7)	2.37(3)	2.786(3)	106(2)	80.6(7)

*Superscripts refer to atoms at positions: [1]1/2 $-x$, $-y$, 1/2$+z$; [2]x, y, $z-1$; [3]x, y, 1$+z$; [4]$-x$, $y-1/2$, 3/2 $-z$.

Acknowledgements

We thank Professor A. Rosenthal and Mr. K. Dooley for suggesting the problem and providing the samples. We are indebted to the National Research Council of Canada for financial support and to the University of British Columbia Computing Centre for assistance.

1. A. ROSENTHAL and K. DOOLEY. Carbohyd. Res. **52**, 79 (1976).
2. J. KARLE and H. HAUPTMAN. Acta Crystallogr. **9**, 635 (1965).
3. J. KARLE and I. L. KARLE. Acta Crystallogr. **21**, 849 (1966).
4. M. G. B. DREW, D. H. TEMPLETON, and A. ZALKIN. Acta Crystallogr. Sect. B, **25**, 261 (1969).
5. D. T. CROMER and J. B. MANN. Acta Crystallogr. Sect. A, **24**, 321 (1968).
6. R. F. STEWART, E. R. DAVIDSON, and W. T. SIMPSON. J. Chem. Phys. **42**, 3175 (1965).
7. D. T. CROMER and D. LIBERMAN. J. Chem. Phys. **53**, 1891 (1970).
8. V. SCHOMAKER and K. N. TRUEBLOOD. Acta Crystallogr. Sect. B, **24**, 63 (1969).
9. D. W. J. CRUICKSHANK. Acta Crystallogr. **9**, 747 (1956); **9**, 754 (1956).
10. D. W. J. CRUICKSHANK. Acta Crystallogr. **14**, 896 (1961).
11. W. R. BUSING and H. A. LEVY. Acta Crystallogr. **17**, 142 (1964).
12. C. K. JOHNSON. *In* Crystallographic computing. Munksgaard, Copenhagen. 1970. pp. 207–226.
13. S. J. RETTIG. Ph.D. Thesis. University of British Columbia, Vancouver, B.C. 1974.
14. C. RICHE and C. PASCARD-BILLY. Acta Crystallogr. Sect. B, **31**, 2565 (1975).

The autoxidation of optically active 1-bromo-2-methylbutane[1]

J. A. HOWARD, J. H. B. CHENIER, AND D. A. HOLDEN
Division of Chemistry, National Research Council of Canada, Ottawa, Ont., Canada K1A 0R9

Received November 22, 1976

J. A. HOWARD, J. H. B. CHENIER, and D. A. HOLDEN. Can. J. Chem. **55**, 1463 (1977).

(+)-1-Bromo-2-methylbutane undergoes autoxidation at 1 atm of oxygen and 30°C to give, after reduction with triphenylphosphine, 1-bromo-2-methyl-2-butanol with a (+) to (−) enantiomer ratio of 1.9 ± 0.2. The optically active 1-bromo-2-methyl-2-butyl radical is, therefore, partially trapped by oxygen at this pressure before it has time to completely racemize. The half-life for racemization of the preferred conformation is approximately 2×10^{-8} s^{-1} at 30°C. At 100 atm of oxygen the yield of (+)-$CH_3CH_2COH(CH_3)CH_2Br$ is >90% and the reaction appears to proceed with retention of configuration. A small percentage of (−)-1-bromo-2-methyl-2-butanol is, however, still produced, presumably by inversion of configuration.

J. A. HOWARD, J. H. B. CHENIER et D. A. HOLDEN. Can. J. Chem. **55**, 1463 (1977).

Le (+) bromo-1 méthyl-2 butane subit une autoxydation à 1 atm d'oxygène et à 30°C pour conduire après réduction avec la triphénylphosphine au bromo-1 méthyl-2 butanol-2 avec un rapport d'énantiomères (+) à (−) de 1.9 ± 0.2. On peut donc en conclure que le radical optiquement actif bromo-1 méthyl-2 butyle-2 est partiellement piégé par l'oxygène à cette pression avant d'avoir le temps de se racémiser complètement. La demi-vie pour la racémisation de la conformation privilégiée est approximativement 2×10^{-8} s^{-1} à 30°C. A 100 atm d'oxygène, le rendement de (+)-$CH_3CH_2COH(CH_3)CH_2Br$ est >90% et il semble que la réaction se produit avec rétention de configuration. Toutefois un petit pourcentage de (−)-bromo-1 méthyl-2 butanol-2 se produit, probablement par une inversion de configuration.
[Traduit par le journal]

Introduction

Free-radical metathesis reactions are generally nonstereospecific because the intermediate radical either has a planar arrangement of atoms attached to the radical centre or because it has a very low energy barrier to inversion (1–3). Autoxidations are consistent with this generalization since optically active organic (4) and organometallic (5, 6) compounds produce optically inactive products although Bartlett and co-workers (7) have shown that the *cis*-decalyl radical can be trapped by high pressures of oxygen during thermolysis of *cis*-9-carbo-*tert*-butylperoxydecalin.

The majority of exceptions to this rule have been observed in free-radical brominations (8, 9). Thus Skell and Shea found that bromination of (+)-$CH_3CH_2CH(CH_3)CH_2Br$ and (+)-$CH_3CH_2CH(CH_3)CH_2Cl$ occurs with a high degree of stereochemical control. Retention of optical activity in these reactions has been attributed to the intermediacy of unsymmetrically 'bridged' β-haloalkyl radicals (8, 9).

If 'bridged' β-haloalkyl radicals are a general phenomenon in free-radical chemistry, autoxidation of optically active alkyl halides such as (+)-$CH_3CH_2CH(CH_3)CH_2Br$ at the asymmetric centre should give an optically active hydroperoxide, provided reaction of the radical with oxygen is faster than racemization.

We report here a product study of the autoxidation of (+)-1-bromo-2-methylbutane which confirms this prediction and which also confirms the half-life for racemization of optically active 1-bromo-2-methyl-2-butyl that was estimated from the bromination studies (9).

Results

(+)-1-Bromo-2-methylbutane (8.08 *M*) containing α,α′-azobisisobutyronitrile (0.18 *M*) absorbed oxygen at atmospheric pressure and 30°C with an initial rate of 6.12×10^{-8} *M* s^{-1}, implying a kinetic chain length of about three. After 59 days 0.31 *M* of oxygen had been absorbed. The final reaction mixture gave an iodometric titration for active oxygen of 0.24 *M*, indicating that hydroperoxide was formed in ~80% yield based on the oxygen absorbed. Reduction of the hydroperoxide with a slight excess of triphenylphosphine gave 1-bromo-2-

[1]Issued as NRCC No. 15835.

methyl-2-butanol (0.25 *M*). We can, therefore, conclude that (+)-$CH_3CH_2CH(CH_3)CH_2Br$ undergoes autoxidation almost exclusively at the carbon β to the bromine substituent.

$$CH_3CH_2CH(CH_3)CH_2Br \xrightarrow{O_2} CH_3CH_2\underset{\displaystyle OOH}{\underset{|}{C}}(CH_3)CH_2Br \xrightarrow{Ph_3P} CH_3CH_2\underset{\displaystyle OH}{\underset{|}{C}}(CH_3)CH_2Br$$

1-Bromo-2-methyl-2-butanol was isolated 99% pure by preparative gas-liquid chromatography. Specific rotations of carbon tetrachloride solutions of the starting and recovered alkyl bromide and the bromohydrin were determined and are given in Table 1. The bromohydrin was quite clearly dextrorotatory and some optical activity was, therefore, retained upon autoxidation at the asymmetric centre.

The nmr spectrum of the recovered bromohydrin was recorded in the absence and presence of the optically active lanthanide shift reagent tris[3 - heptafluoropropylhydroxymethylene - *d* - camphorato]europium, $Eu(HFC)_3$. The spectrum of the bromohydrin in the presence of $Eu(HFC)_3$ was shifted downfield relative to the uncoordinated compound. Moreover, some of the transitions, especially the triplet from the primary protons of the ethyl group, were split into contributions from (+) and (−) forms of $CH_3CH_2COH(CH_3)CH_2Br$. The nmr transitions from these protons for the racemic alcohol and the alcohol prepared at 1 atm of O_2 are shown in Figs. 1*A* and 1*B*. It is obvious from a comparison of these two spectra that the bromohydrin prepared by autoxidation of the alkyl bromide is richer in one of the enantiomers. Since the recovered bromohydrin was dextrorotatory this must be (+)-$CH_3CH_2COH(CH_3)CH_2Br$. The ratio of (+) to (−) enantiomers prepared by autoxidation was estimated from an expanded form of the nmr spectrum and found to be 1.9 ± 0.2.

TABLE 1. Specific rotations of the 1-bromo-2-methyl-2-butanol produced by autoxidation of (+)-1-bromo-2-methylbutane at different oxygen pressures[a]

		[α] (deg.)		
O_2 pressure (atm)	λ (nm)	Starting material	Recovered bromide	1-Bromo-2-methyl-2-butanol
1	589	+3.86	+3.87	+1.39
	365	+9.82	+9.91	+4.12
10	589	+3.7	+3.77	+2.44
	365	—	+9.24	+7.77
100	589	+3.91	+3.72	+2.87
	365	—	+9.07	+9.33

[a]Specific rotation at 30°C in carbon tetrachloride.

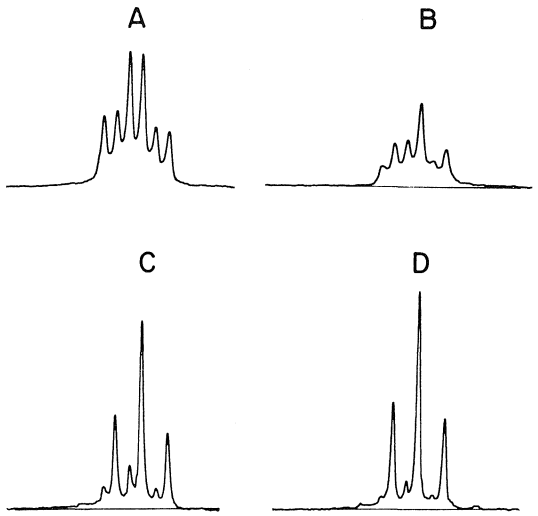

FIG. 1. Part of the ^1H nmr spectrum of 1-bromo-2-methyl-2-butanol (~0.5 *M*, CCl_4) in the presence of $Eu(HFC)_3$ (~0.07 *M*): racemic alcohol (*A*); prepared by autoxidation of (+)-$CH_3CH_2CH(CH_3)CH_2Br$ at 1 atm of O_2 (*B*); at 10 atm of O_2 (*C*); and at 100 atm of O_2 (*D*).

This result proves conclusively that the optically active 1-bromo-2-methyl-2-butyl radical formed during autoxidation of (+)-$CH_3CH_2CH(CH_3)CH_2Br$ can be trapped stereospecifically by oxygen before it undergoes complete racemization. Since there will be a competition between these two processes, increasing the oxygen concentration should favour the bimolecular reaction. Autoxidations were performed at 10 and 100 atm of oxygen and the optical activity of the recovered bromohydrin and ratio of (+)- to (−)-$CH_3CH_2COH(CH_3)CH_2Br$ were measured and they were both found to increase as expected (Tables 1 and 2).

Discussion

We believe that autoxidation of (+)-$CH_3CH_2CH(CH_3)CH_2Br$ to an optically active hydroperoxide is the first example of stereochemical control for this reaction. This result is, however, not unexpected in view of Skell's work on the photobromination of this compound. Thus if optically active 1-bromo-2-methyl-2-butyl

TABLE 2. Products[a] of autoxidation of (+)-$CH_3CH_2CH(CH_3)CH_2Br$ at different oxygen pressures at 30°C

O_2 pressure (atm)	$CH_3CH_2COH(CH_3)CH_2Br$ (M)		
	(+)	(−)	[+]/[−]
1	0.162	0.087	1.9±0.2[b]
10	0.176	0.034	5.2±0.5
100	0.186	0.014	13.3±1.0

[a]After triphenylphosphine reduction.
[b]The error is based on the accuracy of the curve fitting procedure used to estimate relative yields.

radicals live long enough to abstract a bromine atom from bromine they should live long enough to react stereospecifically with oxygen. The present work is, however, of intrinsic importance because it does confirm Skell's postulation that this β-bromoalkyl radical is formed in a preferred conformation for a reaction that is mechanistically less ambiguous than photobromination.

Skell (9) found that photobromination of (+)-$CH_3CH_2CH(CH_3)CH_2Br$ gave (−)-$CH_3CH_2CBr(CH_3)CH_2Br$ and invoked Brewster's rules (10) to conclude that the reaction proceeded with retention of configuration. By analogy autoxidation of (+)-$CH_3CH_2CH(CH_3)CH_2Br$ should also occur with retention of configuration. This would appear to be the case since (+)-$CH_3CH_2COH(CH_3)CH_2Br$ is the major reaction product and according to Brewster's rules, replacement of H by OH in (+)-$CH_3CH_2CH(CH_3)CH_2Br$ without changing the configuration should give a bromohydrin with retention of sign and a slightly smaller specific rotation.

The optically active 1-bromo-2-methylbutane used in our study was prepared from (−)-2-methyl-1-butanol which has been shown to have an *S* configuration (11).[2] The configuration of (+)-$CH_3CH_2CH(CH_3)CH_2Br$ should also be *S* and may be represented by conformations **i, ii,** and **iii**.

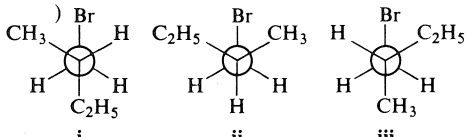

Although conformer stability increases in the order **ii** < **iii** < **i** the chain propagating radical must react preferentially with **ii** because of the influence of the β-bromine substituent on the rate of reaction with peroxy radicals. Thus the relative rate constants for abstraction of the tertiary hydrogen from $CH_3CH_2CH(CH_3)CH_2Br$ and $CH_3CH_2CH(CH_3)CH_2CH_3$ by the *tert*-butylperoxy radical are 2.8:1.[3] There must, therefore, be a specific interaction between the bromine substituent and the semioccupied orbital which stabilizes the incipient radical. Furthermore, reaction with **i** and **iii** would lead to a product with inversion of configuration while the principal product appears to have retained the configuration of the reactant (*vide supra*).

The 1-bromo-2-methyl-2-butyl radical produced from **ii** in the rate controlling propagation reaction can be represented by **iv** and it will

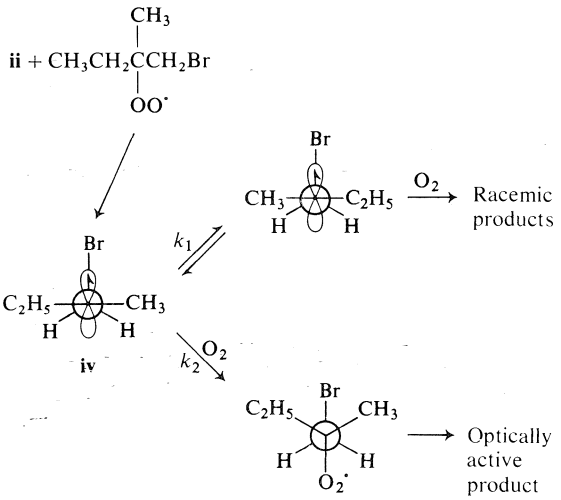

either react stereospecifically with oxygen by backside attack to give an optically active product with retention of configuration or racemize to give a racemic mixture of products. The ratio of (+)- to (−)-enantiomeric products should, therefore, be given by

$$[1]\quad \frac{[(+)\text{-}CH_3CH_2COH(CH_3)CH_2Br]}{[(-)\text{-}CH_3CH_2COH(CH_3)CH_2Br]} = \frac{2k_2[O_2]}{k_1} + 1$$

[2]We thank Professor A. G. Davies for bringing this to our attention. Some of the stereochemical arguments presented in this paper are based on suggestions by Professor Davies.

[3]The absolute rate constants for abstraction of the tertiary hydrogen from $CH_3CH_2CH(CH_3)CH_2Br$ and $CH_3CH_2CH(CH_3)CH_2CH_3$ by $(CH_3)_3COO\cdot$ at 30°C are 0.018 M^{-1} s^{-1} and 0.0064 M^{-1} s^{-1}, respectively (J. A. Howard, J. H. B. Chenier, and D. A. Holden, unpublished results).

This equation must, however, give an oversimplified description of the relative product ratio because if $[(+)]/[(-)] = 1.9$ at 1 atm of O_2 it should be ~ 190 at 100 atm whereas it is ~ 13 (Table 2). We originally believed this discrepancy was due to levorotatory impurity in the starting material. However, the alcohol from which the bromide was prepared had a specific rotation, $(\alpha)_D^{23} = -5.8°$ (lit. (12) $[\alpha]_D^{20} = -5.9°$) and was, therefore, optically pure. Since there is no reason to believe that any optical activity was lost in the preparation of (+)-$CH_3CH_2CH(CH_3)CH_2Br$ we can assume that this compound was optically pure.

There are two plausible explanations for the $\sim 7\%$ yield of (−)-$CH_3CH_2COH(CH_3)CH_2Br$ at 100 atm of O_2. First, there could be some reaction with conformers **i** and **iii** to give this product. Secondly, although oxygen probably reacts with **iv** by backside attack a small amount of (−)-$CH_3CH_2COH(CH_3)CH_2Br$ could be produced by frontside attack, since reaction of most alkyl radicals with oxygen occurs on every encounter (13). At the present time we cannot distinguish between these two possibilities but the least favoured process appears to account for *ca.* 7% of the product.

If the ratio of (+)-$CH_3CH_2COH(CH_3)CH_2Br$ to (−)-$CH_3CH_2COH(CH_3)CH_2Br$ produced at ~ 1 atm of O_2 is corrected for (−) enantiomer formed in a stereospecific reaction, [1] can be used to calculate a value of k_1 (the rate constant for racemization) $= 3.7 \times 10^7\ s^{-1}$, taking $k_2 = 10^{9.5}\ M^{-1}\ s^{-1}$ (13) and $[O_2] = 10^{-5} \times$ the pressure of oxygen in torr (14). The half-life for racemization of optically active 1-bromo-2-methyl-2-butyl is, therefore, approximately 2×10^{-8} s at 30°C which is in excellent agreement with the value of 10^{-8} s calculated by Skell from his bromination studies (9). If we make the same correction to the ratio of enantiomers produced at 10 atm of O_2 a value of $k_2 = 5.8 \times 10^7\ M^{-1}\ s^{-1}$ can be calculated which is in reasonable agreement with the lower pressure value.

Experimental

Materials

(−)-*2-Methyl-1-butanol* (Aldrich) $[\alpha]_D^{23}$ (obsvd.) $= -5.8°$ (undiluted) (lit. (12) $[\alpha]_D^{20} = -5.90°$) was used after drying over barium oxide. (+)-*1-Bromo-2-methylbutane* was prepared from (−)-2-methylbutanol and PBr_3 by the method of Crombie and Harper (15) and was purified by glpc. The specific rotations of this compound are given in Table 1. It is difficult to ascertain the optical purity of this compound because of the discrepancy in published specific rotations (2, 12, 16, 17). It does, however, seem reasonable to assume that it has the same optical purity as the starting alcohol, *viz.*, 100%. *1-Bromo-2-methyl-2-butanol* was synthesized from isopentene by the method of Suter and Zook (18).

Products

(+)-1-Bromo-2-methylbutane (5.0 ml) and α,α′-azobisisobutyronitrile (0.15 g) were allowed to react at 30°C with 1, 10, and 100 atm of oxygen above the liquid. Reactions at 1 atm were conducted in our automatic recording oxygen absorption apparatus (19), while high pressure experiments were performed in glass-lined stainless steel vessels. The reactions were allowed to proceed for 40–60 days after which time the hydroperoxide concentration was determined by iodometric titration. The hydroperoxide was reduced with a slight excess of freshly sublimed triphenylphosphine (20). The reaction mixture was then pumped into a trap maintained at the temperature of liquid nitrogen. The yield of alcohol was determined by gas-liquid chromatography (Varian 2800) relative to standard solutions of authentic 1-bromo-2-methyl-2-butanol. The alcohol was separated from the reaction mixture by preparative glc and was >99% by analytical glc. The optical activity was measured on a Perkin Elmer digital polarimeter at 30°C and λ 589 nm and 365 nm. The nmr signals of the (+) and (−) enantiomers resolved with the aid of the optically active lanthanide shift reagent tris[3-heptafluoropropylhydroxymethylene)-*d*-camphorato]europium (Stohler Isotope Chemicals) (21, 22). Relative concentrations were estimated from expanded spectra using a line shape simulation programme (23).

Acknowledgement

We are indebted to Dr. S. K. Brownstein and Mr. J. Bornais for the nuclear magnetic resonance spectra and to the referees for their extremely lucid criticisms.

1. H. C. Brown, M. S. Kharasch, and T. H. Chao. J. Am. Chem. Soc. **62**, 3435 (1940).
2. D. D. Tanner, H. Yabuuchi, and E. V. Blackburn. J. Am. Chem. Soc. **93**, 4802 (1971).
3. D. D. Tanner, T. C. S. Ruo, and E. V. Blackburn. Can. J. Chem. **52**, 2242 (1974).
4. A. G. Davies and J. E. Packer. J. Chem. Soc. 4390 (1961).
5. A. G. Davies and B. P. Roberts. Chem. Commun. 298 (1966).
6. A. G. Davies and B. P. Roberts. J. Chem. Soc. B, 17 (1967).
7. P. D. Bartlett, R. E. Pincock, J. H. Rolston, W. G. Shindel, and L. A. Singer. J. Am. Chem. Soc. **87**, 2590 (1965).
8. P. S. Skell and K. J. Shea. Isr. J. Chem. **10**, 493 (1972).
9. P. S. Skell and K. J. Shea. Free radicals. Vol. II. *Edited by* J. K. Kochi. Wiley, New York, NY. 1973. Chapt. 26.
10. J. H. Brewster. J. Am. Chem. Soc. **81**, 5475 (1959).

11. W. KLYNE and J. BUCKINGHAM. Atlas of stereochemistry. Chapman and Hall. 1974. p. 31.
12. Handbook of Chemistry and Physics. 56th ed. Chemical Rubber Co., Cleveland, OH. 1975–1976.
13. J. A. HOWARD. Free radicals. Vol. II. *Edited by* J. K. Kochi. Wiley, New York, NY. 1973. Chapt. 1.
14. F. R. MAYO and A. A. MILLER. J. Am. Chem. Soc. **80**, 2480 (1958).
15. L. CROMBIE and S. H. HARPER. J. Chem. Soc. 2685 (1950).
16. P. S. SKELL, D. L. TULEEN, and P. D. READIO. J. Am. Chem. Soc. **85**, 2849 (1963).
17. Handbook of Chemistry and Physics. 44th ed. Chemical Rubber Co., Cleveland, OH. 1963.
18. C. M. SUTER and H. D. ZOOK. J. Am. Chem. Soc. **66**, 738 (1944).
19. J. A. HOWARD and K. U. INGOLD. Can. J. Chem. **47**, 3809 (1969).
20. L. HORNER and W. JURGELEIT. Justus Liebigs Ann. Chem. **591**, 138 (1955).
21. A. F. COCKERILL, G. L. O. DAVIES, R. C. HARDEN, and D. M. RACKHAM. Chem. Rev. **73**, 553 (1973).
22. R. E. SIEVERS. Nuclear magnetic resonance shift reagents. Academic Press, New York, NY. 1973.
23. R. LEFEBVRE and J. MARUANI. J. Chem. Phys. **42**, 1480 (1965).

Flow nuclear magnetic resonance detection and characterization of an intermediate on the reaction pathway in a nucleophilic aromatic substitution reaction

C. A. FYFE, A. KOLL, S. W. H. DAMJI, C. D. MALKIEWICH, AND P. A. FORTE

Guelph–Waterloo Centre for Graduate Work in Chemistry, Guelph Campus, Department of Chemistry, University of Guelph, Guelph, Ont., Canada N1G 2W1

Received October 26, 1976

C. A. FYFE, A. KOLL, S. W. H. DAMJI, C. D. MALKIEWICH, and P. A. FORTE. Can. J. Chem. **55**, 1468 (1977).

The use of high resolution flow nmr has made possible the detection and characterization by nmr of the transient intermediate σ-complex on the actual substitution pathway in the nucleophilic aromatic substitution reaction of 1-ethoxy-2,4-dinitronaphthalene (**3**) with *n*-butylamine, and the assignment of its uv–visible spectrum. The intermediate is unambiguously identified as the σ-complex (**4**) and the reaction is one where the two-step mechanism is clearly applicable.

C. A. FYFE, A. KOLL, S. W. H. DAMJI, C. D. MALKIEWICH et P. A. FORTE. Can. J. Chem. **55**, 1468 (1977).

L'utilisation de la rmn continue à haute résolution a rendu possible la détection et la caractérisation par rmn de complexes σ intermédiaires de transition sur le chemin de substitution réel lors de la réaction de substitution aromatique nucléophile de l'éthoxy-1 dinitro-2,4 naphtalène (**3**) par la *n*-butylamine et l'attribution de son spectre uv–visible. On a identifié d'une façon non-ambigue l'intermédiaire comme étant un complexe σ (**4**) et la réaction en est une où le mécanisme en deux étapes peut très bien être appliqué.

[Traduit par le journal]

Introduction

There has been interest for several years in the mechanism of nucleophilic aromatic substitution reactions (1), particularly in the correctness of the 'two-step' mechanism for the reaction proposed by Bunnett and Zahler (2). Considerable effort has been made in the investigation and characterization of Meisenheimer complexes (3) which are formally analogous to the σ-complex postulated in the two-step mechanism, but where further reaction is unfavourable. It has been found generally that uv–visible spectroscopy and nuclear magnetic resonance spectroscopy are the best techniques for the detection and characterization of these species.

More recently, there have been claims of the successful detection of these species during actual substitution reactions. Thus, in an investigation using optical spectroscopy it has been claimed (5) that the complex **1** had been detected during the reaction of picrylchloride with methoxide ion because a two-banded spectrum characteristic of a trinitro-substituted Meisenheimer complex was observed. However, it was subsequently shown by Crampton *et al.* (4) using nmr spectroscopy that the σ-complex formed was in fact probably the 1,3-complex **2**, although the conditions of the two experiments were somewhat different. This example illustrates the difficulties involved with structural assignments based on uv–visible spectroscopy.

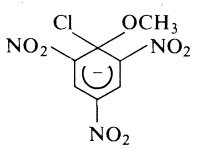

1

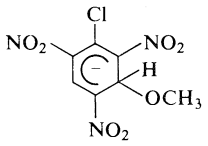

2

More recently, Orvik and Bunnett (6) have reported the detection, using uv–visible spectroscopy, of an intermediate species in the reaction of 1-ethoxy-2,4-dinitronaphthalene (**3**) with *n*-butylamine in dimethyl sulphoxide (DMSO) solution and examined the kinetics of its decomposition. On the basis of its uv–visible spectrum, they proposed structure **4** for this species.

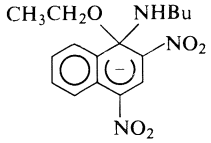

4

Sekiguchi and co-workers have examined the interaction of the same substrate with secondary amines (7, 8) and have concluded that complexes analogous to **4** are formed and that they are quite stable when secondary amines are used.

We have developed and used the technique of flow nmr spectroscopy which allows good high resolution nmr spectra of reliable intensities to be measured in rapidly flowing, chemically reacting mixtures (9, 10). We have used this technique in the past to detect and to characterize transient species (11–15) in several different organic reactions. Nuclear magnetic resonance is in general a much superior technique to uv–visible spectroscopy for the characterization of chemical compounds and the development of flow nmr techniques transfers this advantage to the characterization of very short-lived species.

The purpose of the present work was to use these techniques to try and detect the transient species reported by Bunnett and to determine unambiguously its structure by high resolution nmr.

Experimental

Nuclear magnetic resonance spectra were recorded on a Varian HA100 spectrometer and uv–visible spectra on a Unicam SP800 spectrometer. With the exception of 1-ethoxy-2,4-dinitronaphthalene, all materials were from commercial sources or were prepared by literature techniques and had mp's and nmr spectra consistent with their proposed structures.

Flow nmr and uv spectra were obtained using the techniques and equipment previously described (9, 10). In the flow nmr technique, the flow nmr tube is not spun, giving somewhat broader lines than usual. There is additional line-broadening from the flow, but the spectra are quite adequate for structural assignments. In particular, since the reactants are preequilibrated in the magnetic field, the relative intensities of the lines are reasonably reliable and will be proportional to the concentrations of the appropriate species.

Preparation of 1-Ethoxy-2,4-dinitronaphthalene (3)

Difficulties were encountered in the preparation of this compound by literature procedures from 1-chloro-2,4-dinitronaphthalene and the following alternative procedure was developed.

2,4-Dinitronaphthol (100 g, 0.427 mol) was added to 300 ml *N*,*N*-diethylaniline in a 1 ℓ round bottomed flask fitted with a reflux condenser. The temperature of the solution was raised to 80°C with constant stirring and 95 g toluenesulphonyl chloride (0.5 mol) added. The solution was then continuously stirred at 80°C for 8 h. The reaction mixture was poured onto 500 ml of ice – aqueous acid yielding a brownish precipitate. This was collected by filtration, washed with ice-cold aqueous acid, twice with cold water, and then dried overnight in a vacuum desiccator. This crude material consists of mainly 2,4-dinitronaphthyl tosylate with some 1-chloro-2,4-dinitronaphthalene.

This material was dissolved in the minimum quantity of DMSO and an equivalent amount of freshly prepared 2 *M* sodium ethoxide in ethanol was added. After stirring for 1 h, the mixture was poured into aqueous acid. A solid and some oily material precipitated and the oil later solidified. After filtration and washing with ice-cold water, the crude product was dissolved in benzene and shaken with 10% aqueous $NaHCO_3$ in a separatory funnel. An orange precipitate resulted which was the sodium salt of 2,4-dinitronaphthol from unreacted starting material. After removal of this precipitate the benzene solution was washed twice with water in the separating funnel and dried over anhydrous Na_2SO_4. The volume of the solution was reduced by evaporation and light petroleum ether added until an oily solid precipitated. The solid was filtered and then recrystallized from 95% ethanol yielding 70.6 g of 1-ethoxy-2,4-dinitronaphthalene (60% overall yield) mp 90°C.

Results and Discussion

(A) Flow Nuclear Magnetic Resonance Measurements

These were made at 20°C using DMSO as solvent and at 0°C in a solvent mixture of 75% DMSO and 25% methanol. The latter system was chosen to obtain lower temperatures and also to see if the reaction mechanism would be altered by the presence of a substantial proportion of alcoholic solvent. Essentially the same results were obtained in both cases. Figure 1 shows representative spectra obtained in the mixed solvent system at 0°C, using a 4:1 ratio of amine–substrate.

The top spectrum in Fig. 1 shows the ring proton absorptions of 1-ethoxy-2,4-dinitronaphthalene obtained under static conditions. The proton H_3 between the two nitro groups is at δ 8.8 and is easily identified by its lowfield shift and lack of large couplings to any other nuclei. The middle spectra were obtained under flowing conditions at the indicated time intervals after mixing and all three show signals due to three species, one of which is the reactant. This may be deduced from the presence at low field of three single absorptions at δ 8.8, 8.9, and 9.1 which must be due to the hydrogen H_3 between the two nitro groups in three different species as only H_3 shows no large couplings to other nuclei.

On stopping the flow, there is the immediate appearance of the bottom spectrum, which is that of the product mixture from the reaction and the species responsible for the absorption

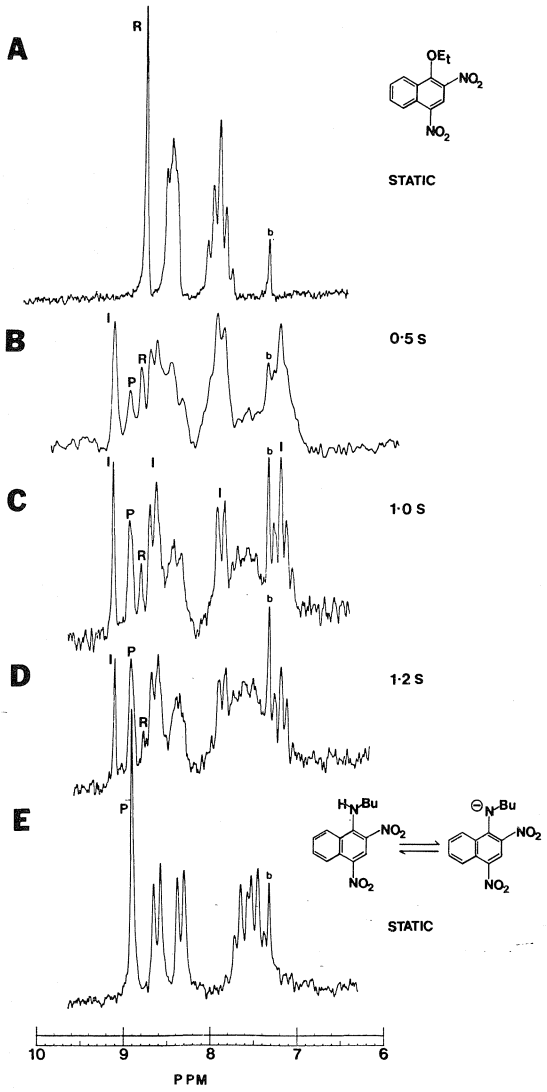

FIG. 1. 100 MHz proton nmr spectra of the aromatic region during the reaction of 0.20 *M* 1-ethoxy-2,4-dinitronaphthalene (in 75% DMSO – 25% MeOH) with *n*-butylamine (0.8 *M* in 75% DMSO – 25% MeOH) at 0°C: (A) 1-ethoxy-2,4-dinitronaphthalene. Static spectrum before mixing; (B) flow nmr spectrum, 0.5 s after mixing; (C) flow nmr spectrum, 1.0 s after mixing; (D) flow nmr spectrum, 1.2 s after mixing; (E) static spectrum immediately on stopping the flow. The small peak at δ 7.3(b) is due to a benzene reference.

at δ 8.9 in the flowing spectrum. By comparison of the three spectra, the signals due to the transient intermediate in the flowing spectrum may be identified. This species shows signals at δ 9.09 (s, H_3), 8.62 (d, H_8), 7.83 (d, H_5), and 7.14 (m, H_6,H_7). Compared to the reactant molecule, there has been a downfield shift of H_3 which is characteristic of the formation of a Meisenheimer complex based on the spectra of known Meisenheimer complexes in these systems (3). The other signals are shifted to higher fields, again characteristic of such complexes. The results are in agreement with the intermediate species having structure **4**. In particular, the presence of the H_3 resonance at low fields rules out the possibility that a σ-complex might have been formed from attack at C_3 as in the case of picryl chloride, as this species would have given a spectrum with a single sharp resonance due to H_3 at high field.

In some chemical systems the intermediates are long enough lived that their decay can be measured by stopping the flow and quickly and repeatedly scanning a small spectral region containing one signal due to the intermediate and one due to the product. In the present case, however, the intermediate is very short-lived and its decay must be measured in a continuously flowing system. The time between mixing and observation can be altered both by changing the flow-rate and also by increasing the distance (and thus the volume of solution) between the mixing chamber and detection coils by the use of spacers (12). The permutation of these two variables should yield a self consistent set of data, and the complete time-evolution of the system may be determined (Fig. 2). Figure 2 shows the complete time dependence of the relative concentrations of the reactant, intermediate, and product species, and thus illustrates an additional advantage of using nmr for investigations of reaction mechanisms, which is that the concentrations of several species may be monitored independently and simultaneously. The general profiles for the reactant, intermediate, and product concentrations are in agreement with the proposed reaction scheme [1] although it must be emphasized that this detection of an intermediate species in a reaction mixture does not prove that it is involved in the reaction pathway yielding the products, as a scheme with a side equilibrium involving this species would give exactly the same kinetic behaviour. The concentration of the intermediate reaches a maximum after only 1 s and then very quickly decays. Thus, characterization of this species by nmr spectroscopy can only be made using the present techniques.

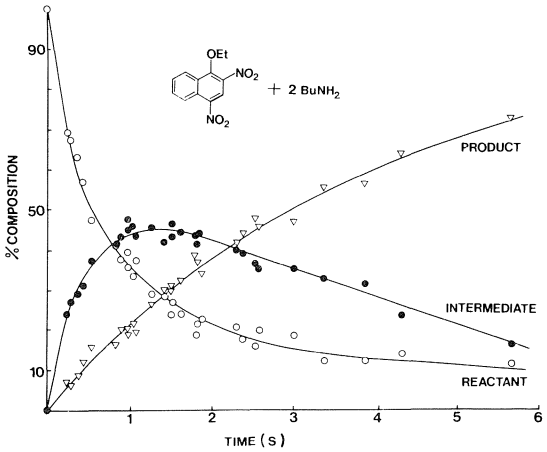

FIG. 2. Percentage composition of the reaction mixture during the reaction of 0.20 *M* 1-ethoxy-2,4-dinitronaphthalene (75% DMSO – 25% MeOH) with *n*-butylamine (0.4 *M* in 75% DMSO – 25% MeOH) at 0°C, from measurement of the relative intensities of the singlet low field absorptions assigned to the H_3 protons of the reactant, intermediate, and product species.

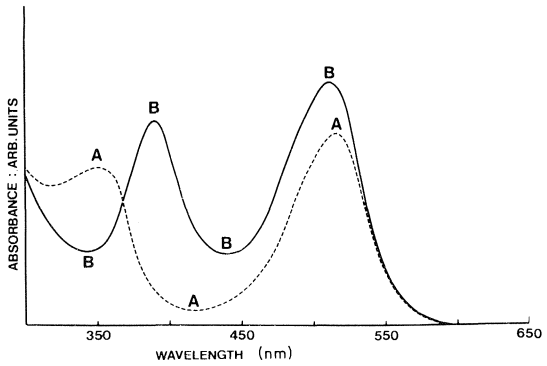

FIG. 3. Ultraviolet–visible spectral changes during the reaction of 1-ethoxy-2,4-dinitronaphthalene (0.01 *M* in 75% DMSO – 25% MeOH) with *n*-butylamine (0.1 *M* in 75% DMSO – 25% MeOH) at 0°C: (A) flow uv–visible spectrum recorded approximately 0.3 s after mixing; (B) static spectrum of the equilibrium product mixture recorded 3 min after reaction.

(B) Flow Ultraviolet–Visible Measurements

The extinction coefficient of the intermediate species is so large that it was not possible to use solutions of exactly the same concentration as used in the nmr experiments even using the very short pathlength flow uv cell previously described. The maximum possible concentration that could be used was 0.01 *M* in substrate. It was checked that there were no substantial changes in the general sequence of spectral changes observed during the reaction over a hundred fold change in concentration up to 0.01 *M* and it was assumed that there would be no change up to the nmr concentration. The results of the flow uv–visible investigation are shown in Fig. 3. Curve A shows the spectrum recorded during the reaction of 0.01 *M* 1-ethoxy-2,4-dinitronaphthalene with a tenfold excess of *n*-butylamine at 0°C in 75% DMSO – 25% MeOH. The spectrum was recorded under flowing conditions at a flow rate of 60 ml/min (approximately 0.3 s after mixing). Curve B shows the spectrum of this solution static after reaction and represents the limiting spectrum for the system at equilibrium. The general spectral profiles and changes observed are very similar to those reported by Orvik and Bunnett. There is the immediate appearance of a large single absorption (λ_{max} 520 nm) and a smaller broad absorption (λ_{max} 350 nm) (Curve A). The equilibrium spectrum shows a large single absorption (λ_{max} 514 nm) and a smaller single absorption (λ_{max} 390 nm). Curve A is thought to be due mainly to the intermediate σ-complex although there may be a small amount of reactant present as it shows a weak absorption at 350 nm. It is unlikely that there is any product species present as there is no absorption evident at 390 nm. Curve B is due to the equilibrium product mixture in which it is known both **5** and **6** are present. The use of 4:1 and 2:1 excesses of amine gives the same two absorptions in the spectra of the equilibrium mixtures, but the peak at 390 nm increases in intensity relative to that at 514 nm and shows evidence of a shoulder developing on the high wavelength side. Thus, the neutral product must contribute to the 390 nm absorption in curve B. It was not possible to increase the amine concentration to a large enough excess to convert all of the product to the anion species as in the previous uv–visible investigation. Taking into account the changes which will be caused by the difference in concentration from that used in previous work, it is thought that the uv–visible spectral changes observed here are similar to those reported previously for dilute solutions and that this, together with the flow nmr data, indicates that the colour producing species are mainly **4** and **6**.

(C) Quenching Experiments: Product Identification

Quenching the product mixture by addition

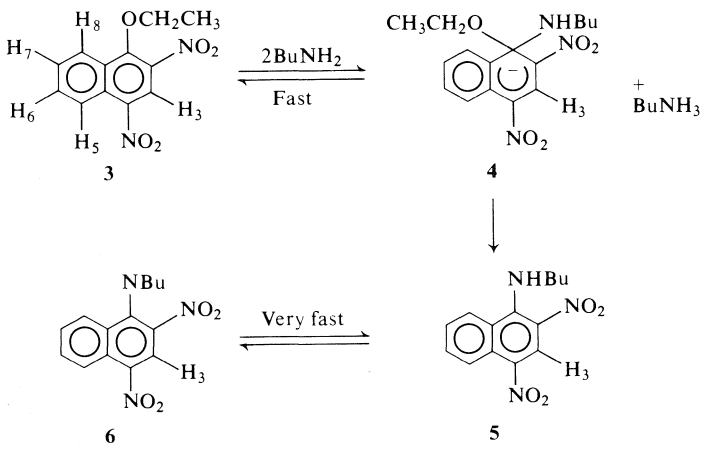

[1]

of water or aqueous acid yielded 1-(*N*-butylamino)-2,4-dinitronaphthalene (**5**) identified by its mp and nmr spectrum. The nmr spectrum of **5** is, however, different from that of the final product mixture shown in Fig. 1. In the reaction excess amine is present, and **5** will be in equilibrium with its conjugate base **6** as discussed by Bunnett (6). The spectrum of isolated **5** redissolved in the solvent mixture (0.2 *M* in 75% DMS; 25% MeOH) with 1 equiv. of *n*-butylamine added is identical to that from the product mixture shown in Fig. 1, confirming this assignment.

(D) Conclusions

The results obtained are all compatible with reaction [1] originally proposed by Orvik and Bunnett (6). In particular, the flow nmr data are quite diagnostic of the structure of the intermediate **4** and it is felt that this system is one where the 'two-step' mechanism is clearly applicable for the substitution which occurs. The nmr spectra of the intermediate could only be obtained by the flow nmr technique.

The complexity of the nmr spectra in this type of system makes it relatively difficult to use nmr techniques and we have investigated the reaction of 2,4,6-trinitroanisole by the flow nmr technique under similar conditions to try to obtain data of this type on other systems where the nmr spectra obtained will be much simpler.[1]

[1]C. A. Fyfe, A. Koll, and S. W. H. Damji, work to be published.

1. C. F. Bernasconi. *In* M.T.P. International review of science. Organic chemistry, series one. Vol. 3. *Edited by* H. Zollinger. Butterworths, London and University Park Press, Baltimore. 1973. p. 33.
2. J. F. Bunnett and R. E. Zahler. Chem. Rev. **49**, 275 (1951).
3. (*a*) R. Foster and C. A. Fyfe. Rev. Pure. Appl. Chem. **16**, 61 (1966); (*b*) E. Buncel, A. R. Norris, and K. E. Russell. Q. Rev. Chem. Soc. **22**, 123 (1968); (*c*) M. R. Crampton. Adv. Phys. Org. Chem. **7**, 211 (1969); (*d*) M. J. Strauss. Chem. Rev. **70**, 667 (1970); (*e*) C. A. Fyfe. *In* The chemistry of the hydroxyl group. *Edited by* S. Patai. Interscience, London. 1971.
4. M. R. Crampton, M. A. El Ghariani, and H. A. Khan. J. Chem. Soc. D, 834 (1971).
5. R. Gaboriaud and R. Schaal. Bull. Soc. Chim. Fr. 2683 (1969).
6. J. A. Orvik and J. F. Bunnett. J. Am. Chem. Soc. **92**, 2417 (1970).
7. S. Sekiguchi, K. Shinozaki, T. Hirose, K. Matsui, and K. Sekine. Bull. Chem. Soc. Jpn. **49**, 2264 (1974).
8. S. Sekiguchi, T. Itagaki, T. Hirose, K. Matsui, and K. Sekine. Tetrahedron, **29**, 3527 (1973).
9. S. W. H. Damji. Ph.D. Thesis, University of Guelph, Guelph, Ont. (1975).
10. C. A. Fyfe, M. Cocivera, and S. W. H. Damji. J. Magn. Reson. **23**, 377 (1976).
11. C. A. Fyfe, M. Cocivera, and S. W. H. Damji. J. Chem. Soc. Chem. Commun. 743 (1973).
12. C. A. Fyfe, M. Cocivera, and S. W. H. Damji. J. Am. Chem. Soc. **97**, 5707 (1975).
13. M. Cocivera, C. A. Fyfe, H. E. Chen, and S. P. Vaish. J. Am. Chem. Soc. **96**, 1611 (1974).
14. M. Cocivera, C. A. Fyfe, H. E. Chen, S. P. Vaish, and A. Effio. J. Am. Chem. Soc. **97**, 5707 (1975).
15. C. A. Fyfe, C. D. Malkiewich, S. W. H. Damji, and A. R. Norris. J. Am. Chem. Soc. **98**, 6983 (1976).

Cryoscopic and nuclear magnetic resonance studies of interaction between acetylacetone and water in benzene

MASANAO KATO, HITOSHI WATARAI, AND NOBUO SUZUKI[1]

Department of Chemistry, Faculty of Science, Tohoku University, Sendai, 980 Japan

Received January 5, 1976[2]

MASANAO KATO, HITOSHI WATARAI, and NOBUO SUZUKI. Can. J. Chem. **55**, 1473 (1977).

The interaction between acetylacetone and water in benzene solution has been examined by freezing point depression and nuclear magnetic resonance spectroscopy. The experimental results suggest that a 1:1 associated complex between acetylacetone and water is formed in benzene solution saturated with water, and the association constant is estimated to be 2.4 ± 0.1 (kg solvent/mol). By comparison with the results of methylacetylacetone and dimethylacetylacetone, it is suggested that the enol tautomer of acetylacetone preferentially associates with water.

MASANAO KATO, HITOSHI WATARAI et NOBUO SUZUKI. Can. J. Chem. **55**, 1473 (1977).

On a étudié l'interaction entre l'acétylacétone et l'eau dans des solutions benzéniques par la méthode cryoscopique et par spectrométrie rmn. Les résultats expérimentaux suggèrent qu'il y a formation d'un complexe d'association 1:1 entre l'acétylacétone et l'eau dans des solutions benzéniques saturées par de l'eau et que l'on peut estimer la constante d'association à 2.4 ± 0.1 (kg solvent/mol). Par comparaison de ces résultats avec ceux obtenus avec la méthylacétylacétone et la diméthylacétylacétone, on croit que le tautomère énolique de l'acétylacétone s'associe d'une façon préférentielle avec l'eau.

[Traduit par le journal]

Introduction

Many research works on the liquid–liquid extraction systems involving β-diketones has been made. In most studies, however, the liquid–liquid distribution of acetylacetone between aqueous and organic phases has been represented by the following simple scheme

[1]
$$\begin{array}{ll} HAA & \text{org.} \\ \uparrow\downarrow & \\ HAA \rightleftharpoons AA^- + H^+ & \text{aq.} \end{array}$$

where HAA denotes acetylacetone and org. and aq. indicate organic and aqueous phases, respectively. The partition coefficient of acetylacetone is ordinarily defined as concentration ratio of undissociated form in two phases. But it is necessary to consider that acetylacetone exists as a mixture of keto and enol tautomers. Furthermore, in order to clarify the mechanism of distribution of acetylacetone, an interaction between acetylacetone and water must be considered.

Lin *et al.* (1) have suggested the existence of the associated complexes between acetylacetone and water in carbon tetrachloride solution by liquid–liquid partition method. However, they did not pay any attention to the keto–enol tautomerism of acetylacetone. It has been suggested from nmr spectroscopic measurements that acetylacetone associates with some protic solvents (2–4), but an interaction between acetylacetone and water has not yet been studied in detail.

In this study we estimated the association constant between acetylacetone and water by freezing point depression method in benzene solution, and examined the structure of the associated complex by nmr spectroscopy. The freezing point depression method has been adopted because an activity of solvent can be precisely measured by a simple apparatus. Benzene is employed as non-aqueous solvent because it is widely used in liquid–liquid partition experiments and dissolves a proper amount of water in present investigation. In order to examine the preferential interaction of one of two tautomers of acetylacetone with water, methylacetylacetone (MAA; 3-methyl-2,4-pentanedione) and dimethylacetylacetone (DMAA; 3,3-dimethyl-2,4-pentanedione) were synthesized and employed for measurement of nmr spectra and freezing point depression of benzene solution.

[1]To whom correspondence should be addressed.

[2]Revision received January 3, 1977.

Experimental

Materials

Acetylacetone (Wako Junyaku GR) was washed by diluted aqueous ammonia and water, dried with anhydrous Na_2SO_4 or $CaSO_4$ (Drierite), and then fractionally distilled under dried nitrogen atmosphere prior to use ($d_4^{25} = 0.9678$).

Redistilled water was used.

Benzene (Wako Junyaku GR) was fractionally crystallized and dried with metal sodium, and then fractionally distilled prior to use.

Impurity did not appear on gas chromatography in all substances.

MAA and DMAA were synthesized by Bloomfield's stepwise reaction (5). MAA was purified twice by fractional distillation under reduced pressure. DMAA was purified by recrystallization and fractional distillation under reduced pressure. The products were identified by nmr spectra and no impurity was observed by gas chromatography.

Instruments

Freezing point depressions have been measured by a Beckman thermometer attached to Teflon capped freezing tube in a thermostated room at 25 ± 1°C. The contents in the inner tube were agitated by an externally driven Teflon coated magnetic stirrer. Although the freezing point depression was not measured under dry atmosphere, the water content change in test solutions through the measurement did not exceed 0.0008 mol/kg solvent. The observed values are the average of two independent measurements. The reproducibility of experimental values were ±0.004°C for binary systems and ±0.006°C for ternary systems.

All solutions were prepared by weight.

The concentration of water was determined by Karl Fischer titration. Since the keto tautomer of acetylacetone does not exert an appreciable interference to the end point in this titration, an ordinary Karl Fischer reagent was used for samples containing acetylacetone (Mitsubishi Chem. Ind., Karl Fischer reagent SS and unhydrated methanol). For samples containing MAA or DMAA a modified Karl Fischer reagent (Mitsubishi Chem. Ind., unhydrated solvent PE) was used to avoid the fading of the end point.

Nuclear magnetic resonance spectra were obtained on Varian A-60 spectrometer. The measurement of benzene solution was performed at 5.5°C and the main peak of benzene protons was employed as internal standard. The chemical shifts are reported in cps units within ±1 cps. Equilibrium constants of tautomerism have been obtained from intensity ratio of resonance peaks of methyl protons of both tautomers. For the system composed of acetylacetone and water, the chemical shifts and equilibrium constants of keto–enol tautomerism have been measured at 39 ± 1°C. Methyl groups of enol tautomer were used as the internal standard without employing an auxiliary standard like tetramethylsilane, after having verified that the methyl signal was not affected by water concentration.

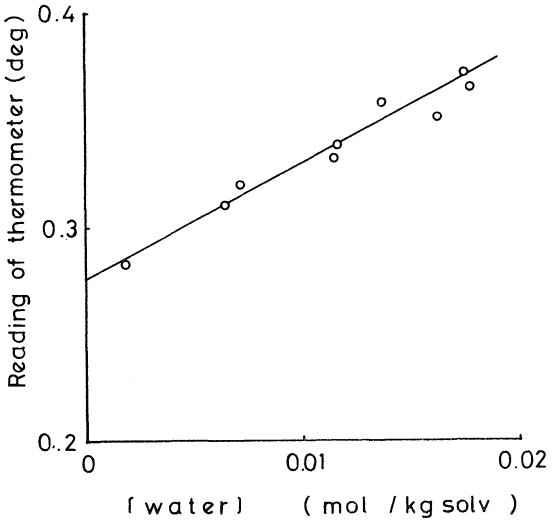

FIG. 1. Freezing point depressions of benzene by water.

Results and Discussion[3]

Freezing Point Depression Measurements

The observed freezing point depressions of benzene solutions of water are shown in Fig. 1. The slope of 5.130 (deg/mol/kg solvent) agrees with the molar freezing point depression constant of benzene ($K_f = 5.128$) (6). This proves that the dissolved water in benzene behaves as monomer in the concentration range up to 0.02 mol/kg solvent (7).

In Table 1 and Fig. 2, the observed freezing point depressions of benzene solutions of acetylacetone are demonstrated in the concentration range up to nearly 1 mol/kg solvent. The plots show a curved line departing from the straight line of slope 5.128.

Generally, the freezing point depression of solution is represented in terms of solvent activity coefficient, γ_s.

$$[2] \qquad \frac{\theta}{T} = -\frac{T_s^m R}{\Delta H_s^m} \ln X_s \gamma_s$$

where T_s^m, H_s^m, and X_s indicate the freezing point of solvent, the latent heat of fusion of solvent, and the mole fraction of solvent, respectively; and θ and T denote the freezing point depression and the freezing point of solu-

[3]The original freezing point data of the binary and ternary systems, a detailed calculation of the estimation of the formation constants for the parallel reactions between acetylacetone and water, chemical shifts of β-diketones and water concentration of the binary and ternary systems are available, at a nominal charge, from the Depository of Unpublished Data, CISTI, National Research Council of Canada, Ottawa, Canada K1A 0S2.

TABLE 1. Freezing point depressions of acetylacetone–benzene systems

Acetylaceton concentration (mol/kg solvent)	θ (°C)
0.128	0.638
0.196	0.965
0.294	1.429
0.471	2.209
0.746	3.393
0.899	4.031

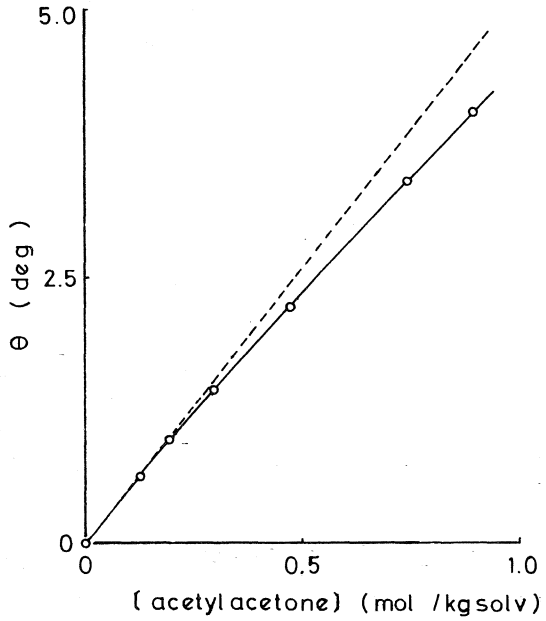

FIG. 2. Freezing point depressions of benzene by acetylacetone.

tion. Since the logarithmic term of eq. 2 can be expanded in powers of solute mole fraction, $X_i = 1 - X_s$, as follows

$$[3] \quad \ln X_s\gamma_s = -X_i - \tfrac{1}{2}X_i^2 - \tfrac{1}{3}X_i^3 - \ldots \ldots + \frac{1}{RT}(\alpha X_i^2 + \alpha' X_i^3 + \ldots)$$

the next approximated equation is obtained by neglecting the higher terms,

$$[4] \quad \frac{\theta}{X_i} = \frac{T^2R}{\Delta H_s^m}\left\{1 + \left(\frac{1}{2} - \frac{\alpha}{RT}\right)X_i\right\}$$

in which T_s^m is assumed to be identical to T. The parameter α represents the extent of the interaction including solute–solute and solute–solvent interaction. The observed freezing point data for the benzene–acetylacetone system are plotted in Fig. 3 on the basis of eq. 4. A linear relation obtained in dilute region shows that eq. 4 is a good approximation up to $X_i \simeq 0.03$. From the slope, α is obtained as 920 cal/mol. In this study we are concerned with the activity coefficient of benzene in relatively concentrated solution and disregard to a polymerization of acetylacetone which was suggested by Lin *et al.* (1) based on the postulation of solution ideality.

The observed freezing point depressions of the acetylacetone–water–benzene ternary system are shown in Fig. 4 and Table 2. The acetylacetone concentration varied up to 0.14 mol/kg solvent but the water concentration in benzene was held constant at 0.0188 ± 0.0002 mol/kg solvent which is below the saturation concentration of water. The line 0 in Fig. 4 indicates the ideal case in which no association between the components occurs and the activity coefficient of benzene is equal to unity. The line *1* indicates a hypothetical case that acetylacetone molecules completely associate with water. The observed freezing point depressions are less than the predicted values from the next equation derived by assuming no interaction between water (X_w) and acetylacetone (X_A).

$$[5] \quad \theta = \frac{T^2R}{\Delta H_s^m}\left\{X_w + X_A + \tfrac{1}{2}(X_w + X_A)^2 - \frac{920}{RT}X_A^2\right\}$$

So it is suggested that acetylacetone associates with water in benzene. Figure 4 seems to suggest that an associated complex predominantly consists of one molecule of acetylacetone and one molecule of water in accordance with the analysis of Kaufman and Singleterry (8).

Estimation of the Association Constant

The freezing point depressions of non-associ-

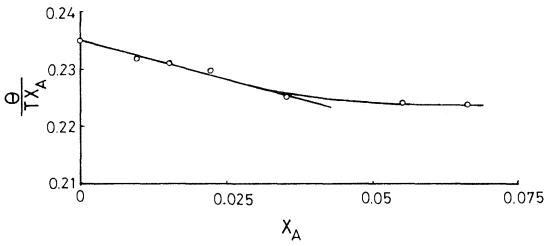

FIG. 3. Relation between acetylacetone mole fraction, X_A, and the term of θ/TX_A.

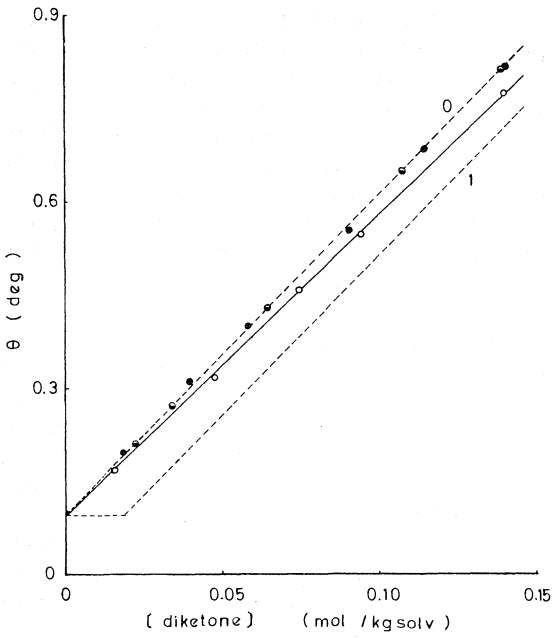

FIG. 4. Freezing point depressions of acetylacetone–water–benzene (○), MAA–water–benzene (◒), and DMAA–water–benzene (●) systems. Water concentration is 0.0188 mol/kg solvent.

TABLE 2. Freezing point depressions of water–acetylacetone–benzene systems

Acetylacetone concentration (mol/kg solvent)	Water concentration (mol/kg solvent)	θ (°C)
0.0156	0.0188	0.168
0.0477	0.0188	0.322
0.0746	0.0188	0.460
0.0945	0.0188	0.548
0.1401	0.0188	0.776

ated solutions are given by eq. 5. Similarly, the observed freezing point depressions, θ_{obs}, of the associated solutions are represented by

$$[6] \qquad \theta_{obs} = -\frac{RT^2}{\Delta H_s^{m}} \ln X_s' \gamma_s$$

where X_s' is the mole fraction of benzene in the associated solution. In eq. 6, the activity coefficient of benzene in associated solution is assumed to be equal to that in non-associated solution. The difference between θ and θ_{obs} is related to the ratio of X_s/X_s',

$$[7] \qquad \theta - \theta_{obs} = -\frac{RT^2}{\Delta H_s^{m}} \ln \frac{X_s}{X_s'}$$

The mole fraction X_s is given by

$$[8] \qquad X_s = \frac{n_s}{n_s + n_a^{0} + n_w^{0}}$$

where n_s, n_a^{0}, and n_w^{0} are the number of moles of benzene, acetylacetone, and water, respectively. On the other hand, X_s' is represented by eq. 9 considering the following equilibria,

$$\mathrm{HAA} + \mathrm{H_2O} \rightleftharpoons (\mathrm{HAA})(\mathrm{H_2O})$$
$$2\mathrm{HAA} + \mathrm{H_2O} \rightleftharpoons (\mathrm{HAA})_2(\mathrm{H_2O})$$
$$\vdots \qquad\qquad \vdots$$
$$j\mathrm{HAA} + k\mathrm{H_2O} \rightleftharpoons (\mathrm{HAA})_j(\mathrm{H_2O})_k$$

$$[9] \qquad X_s' = \frac{n_s}{n_s + n_a + n_w + \sum_{j,k} n_{jk}}$$

where n_a, n_w are the number of moles of free acetylacetone and free water respectively and n_{jk} is that of the associated complex $(\mathrm{HAA})_j(\mathrm{H_2O})_k$. From above relations the next equation is derived,

$$[10] \qquad -\ln \frac{X_s}{X_s'} = \ln \left\{ 1 + \sum_{j,k} (j + k - 1) X_{jk} \right\}$$

where X_{jk} is the mole fraction of the associated complex. By substituting the eq. 10 into eq. 7 and expanding the logarithmic term, we get the next equation,

$$[11] \qquad \theta - \theta_{obs} = \frac{RT^2}{\Delta H_s^{m}} \sum_{j,k} (j + k - 1) X_{jk}$$

or on a molality scale, m,

$$[12] \qquad \theta - \theta_{obs} = K_f \sum_{j,k} (j + k - 1) m_{jk}$$

where K_f is the molar freezing point depression constant. Here we can represent the association constant, $K_{jk} = m_{jk}/m_a^{j} m_w^{k}$, by

$$[13] \qquad K_{jk} = \frac{m_{jk}}{\left(m_a^{0} - \sum_{j,k} j m_{jk} \right)^{j} \left(m_w^{0} - \sum_{j,k} k m_{jk} \right)^{k}}$$

TABLE 3. Estimation of association constants from the observed freezing point depressions[a]

Acetylacetone concentration (mol/kg solvent)	$\frac{\theta - \theta_{obs}}{K_f}$[b] (mol/kg solvent)	K_{11}[c] (kg solvent/mol)^2	K_{21}[c] (kg solvent/mol)^2	K_{12}[c] (kg solvent/mol)^2	m_{11}[c,d] (K_{11} = 2.4)
0.0156	0.00144	5.8_7	199	321	0.00065
0.0477	0.00302	4.2_9	43	131	0.00186
0.0746	0.00234	1.9_7	25.0_4	588	0.00276
0.0945	0.00442	3.4_2	1.4_8	110	0.00337
0.1401	0.00360	1.7_4	5.6_8	56	0.00461

[a]Water concentration is 0.0188 mol/kg solvent.
[b]Total concentration of associated complexes obtained from eq. 12.
[c]Estimated association constant from assumption of only one associated complex.
[d]The best values of calculated complex concentration at $K_{11} = 2.4 \pm 0.1$ and $\sigma = 0.006$.

The calculated association constant for each process of K_{11}, K_{21}, K_{12} are summarized in Table 3. We tried also to estimate the association constant for a higher associated complex which might also be present, but the calculation gives negative association constants. From Table 3, the association between two molecules of acetylacetone and one molecule of water is unlikely because the calculated association constants, K_{21}, do not give a constant value at different concentrations, and also the association of one molecule of acetylacetone and two molecules of water is impossible since the data for K_{12} are too large and show fairly large scatter. So it is most reasonable to assume that the association of one molecule of acetylacetone and one molecule of water occurs in this system.

The best fit calculation of the K_{11} was carried out as follows. In this case, the concentrations of associated complex, $m_{11}{}^c$, are represented from eq. 13 as follows.

$$[14] \qquad m_{11}{}^c = \frac{K_{11}(m_a{}^0 + m_w{}^0) + 1 - \sqrt{\{K_{11}(m_a{}^0 + m_w{}^0) + 1\}^2 - 4K_{11}m_a{}^0m_w{}^0}}{2K_{11}}$$

Hence, the difference between calculated and observed freezing point depression, $d\theta$, is defined as a function of K_{11}. So, the fittest value of K_{11} is determined by minimizing the deviation of the calculated freezing point depression, $\theta - K_f m_{11}{}^c$, from the observed one. The deviation, σ, is defined as

$$[15] \qquad \sigma = \sqrt{\frac{d\theta^2}{N - 2}}$$

where N is the number of observed points. The obtained best value is 2.4 ± 0.1 (kg solvent/mol), as shown in Table 3. The smooth line in Fig. 4 is a calculated one for $K_{11} = 2.4$.

Comparison with MAA and DMAA

The observed freezing point depressions of benzene by MAA and DMAA are plotted in Fig. 5 together with that for naphthalene. The straight line with slope of 5.130 means that these β-diketones cause no change of benzene activity up to nearly 0.15 mol/kg solvent.

In Fig. 4, the observed freezing point depressions of MAA–water–benzene and DMAA–water–benzene ternary systems are shown. Since all the observed values are on line *0*, it is found that MAA and DMAA do not associate with water. Taking into account that these β-diketones are nearly composed of keto tautomer, we can expect that the keto tautomer of acetylacetone does not participate in the association of

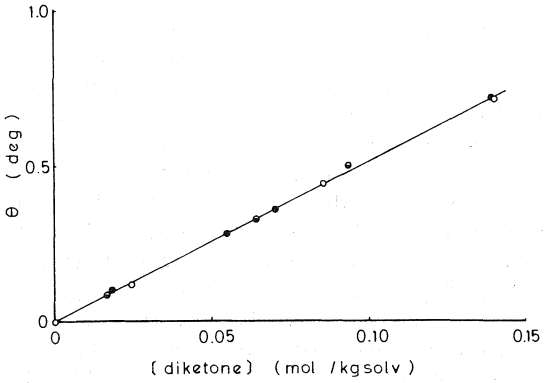

FIG. 5. Freezing point depressions of benzene by MAA (●), DMAA (○), and naphthalene (◒).

TABLE 4. Water concentration dependence of chemical shift and band width of hydroxyl proton of enol tautomer of acetylacetone and methylacetylacetone in benzene solution at 5.5°C

Acetylacetone (X_{AA} = 0.0154 ± 0.0002)			Methylacetylacetone (X_{MAA} = 0.00837 ± 0.00005)		
X_w	ν (Hz)[a]	Δν (Hz)	X_w	ν (Hz)	Δν (Hz)
0.00054	550 ± 1	8 ± 0.3	0.00074	611 ± 1	3 ± 0.3
0.00082	550	18	0.00093	612	3
0.00101	550	42	0.00118	611	3
0.00115	550	—[b]	0.00139	612	3
0.00143	550	—[b]			

[a]The main peak of benzene, which is observed at 409 Hz lower than TMS signal, is chosen as an internal standard.
[b]The signal can not be analyzed because of its ambiguous S/N ratio.

TABLE 5. Water concentration dependence of chemical shift and band width of hydroxyl proton of enol tautomer in acetylacetone–water system[a]

Mole fraction of water (X_w)	Chemical shift (ν)[b] (Hz)	Band width at half intensity (Δν) (Hz)	Ratio of peak area $\frac{A(\text{—OH})}{A(\text{—CH=})}$
0.0	813 ± 1	2.0 ± 0.5	1.000
0.0314	777	12.5	1.008
0.0457	747	15.0	1.024
0.0669	709	20.0	1.111
0.0889	676	26.0	1.133
0.1191	633	28.0	1.235
0.1339	613	30.0	1.276

[a]At 39 ± 1°C.
[b]Chemical shifts are relative to the methyl protons of enol form.

acetylacetone with water. Accordingly, it is presumed that the 1:1 associated complex between acetylacetone and water may consist of enol tautomer and water.

This argument is supported by the nmr study of the water concentration dependence of the chemical shifts of enol tautomer.

Nuclear Magnetic Resonance Measurements

In order to investigate the structure of the associated complex, the water concentration dependence of the chemical shifts of acetylacetone and MAA in benzene at 5.5°C were examined. The results are shown in Table 4. It is found that the chemical shifts of acetylacetone and MAA are independent of water concentration. In preliminary experiment, a distinct high-field shift of the hydroxyl proton of enol tautomer of acetylacetone in carbontetrachloride was observed with increasing water concentration. Thus it seems that the chemical shift of the hydroxyl proton in benzene solution is affected by the paramagnetic effect of benzene ring as proposed by Rogers and Burdett (9). The enol content of acetylacetone is 93.1% and that of MAA is 20.1% under the condition described in Table 4. But the signal width at half intensity of hydroxyl proton of acetylacetone is broadening with increasing water concentration. Signals of the other protons of acetylacetone and MAA, however, remain constant and the signal of water proton is not observed. These results suggest a hydrogen bonding interaction between water and the enol tautomer of acetylacetone.

Since the nmr spectra of acetylacetone–benzene–water ternary system did not give clear information about the interaction between acetylacetone and water because of a poor S/N ratio, we investigated the acetylacetone–water binary system. The water concentration dependence of the nmr spectra of acetylacetone was examined and the results are shown in Table 5 and Fig. 6. The signal of the hydroxyl proton of enol tautomer shifts to high magnetic field and broadens with an increase of water concentration. The peak area of its signal also increases with an increase of water concentration. Chemi-

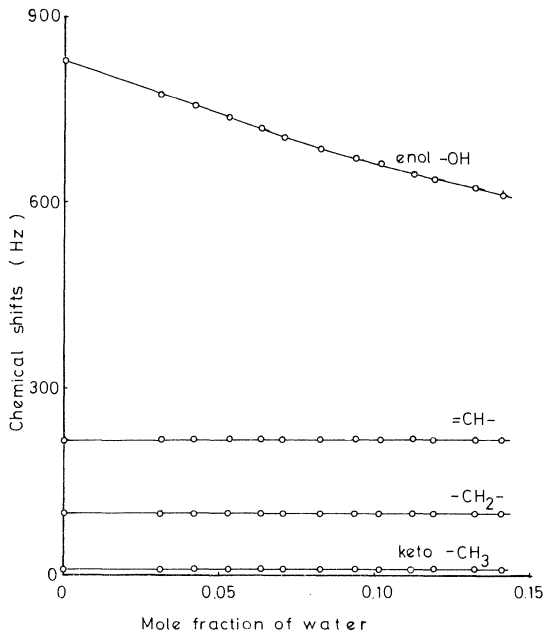

FIG. 6. The water concentration dependence of the chemical shifts of acetylacetone at 39°C. Chemical shifts are relative to the methyl protons of enol form.

cal shifts of other protons, however, remain constant and the signal of water protons is not observed individually because of the probable exchange with the hydroxyl proton of enol tautomer as shown in Table 5. Enol content in acetylacetone–water system also remains constant at 78.8% in the concentration range of water up to $X_w = 0.1339$. These results emphasize the interaction between water and enol tautomer as described above. The evidence on the interaction between water and keto tautomer was not obtained since the chemical shifts of keto tautomer remained constant as concentration of water was varied.

Interpretation from the nmr spectra agrees with the results of the other systems (2, 4). In the acetylacetone–dimethylamine system (2), it has been reported that the signal of the enol hydroxyl proton shifts to high magnetic field with increasing concentration of dimethylamine. This result and the fact that acetylacetone forms no associated complex with triethylamine (4), which is a strong aprotic base, support the present conclusion that protons of water molecule play an essential role in interaction between enol tautomer and water.

Partition of Acetylacetone

Now the apparent partition coefficient, P, of undissociated forms of acetylacetone is expressed as follows

$$[16] \qquad P = \frac{[HAA]_{org}}{[HAA]_{aq}}$$

$$[17] \qquad = \frac{[keto]_{org} + [enol]_{org} + [enol - H_2O]_{org}}{[keto]_{aq} + [enol - H_2O]_{aq}}$$

The fraction of unhydrated enol tautomer in aqueous phase may be negligible in a diluted solution of acetylacetone. When a benzene solution of acetylacetone, for example 0.001 mol/kg solvent, was equilibrated with water, about 10% of acetylacetone in benzene phase may occur as the 1:1 associated complex with water. As a conclusion, the formation of the associated complex in benzene phase should not be overlooked in exact understanding of the partition equilibrium involving acetylacetone.

1. T. F. LIN, S. D. CHRISTIAN, and H. E. AFFSPRUNG. J. Phys. Chem. **71**, 968 (1967).
2. L. W. REEVES and W. G. SCHNEIDER. Can. J. Chem. **36**, 793 (1958).
3. H. JOHANSSON and J. RYDBERG. Acta Chem. Scand. **23**, 2797 (1969).
4. L. W. REEVES. Can. J. Chem. **35**, 1351 (1957); K. KONDO, Y. KONDO, T. TAKEMOTO, and T. IKENOUE. Kogyo Kagaku Zasshi, **68**, 1404 (1965).
5. J. J. BLOOMFIELD. J. Org. Chem. **26**, 4112 (1961).
6. A. R. GLASGOW, A. J. STREIFF, and F. D. ROSSINI. J. Res. Natl. Bur. Stand. **35**, 355 (1945).
7. W. L. MASTERTON and M. C. GENDRANO. J. Phys. Chem. **70**, 2895 (1966); S. D. CHRISTIAN, H. E. AFFSPRUNG, and J. R. JOHNSON. J. Chem. Soc. 1896 (1963).
8. S. KAUFMAN and C. R. SINGLETERRY. J. Phys. Chem. **56**, 604 (1952).
9. M. T. ROGERS and J. L. BURDETT. Can. J. Chem. **43**, 1516 (1965).

Straining strained molecules. II.[1] The syntheses and spectral properties of some ace-bridged naphthalenes[2]

REGINALD H. MITCHELL,[3] THOMAS FYLES, AND LEONARD M. RALPH

Department of Chemistry, University of Victoria, Victoria, B.C., Canada V8W 2Y2

Received October 27, 1976

REGINALD H. MITCHELL, THOMAS FYLES, and LEONARD M. RALPH. Can. J. Chem. **55**, 1480 (1977).

Reaction of both *peri*-dilithionaphthalene and *peri*-dilithioacenaphthalene with acenaphthenequinone and pyracenequinone yielded the dihydroxy derivatives of acenaphth[1,2-*a*]-acenaphthylene **11***a*, **11***b*, **11***c* with no, one, and two ace-bridges respectively. These could be converted either by the Corey thionocarbonate method or with anhydrous liquid hydrogen fluoride to the three alkenes **12***a,b,c* and with $Pb(OAc)_4$ to the three diketones **13***a,b,c*. The latter on Wolff-Kishner reduction yielded alkenes **12***a,b* and mono ketones **15***b,c*. The uv, ir, ^{1}Hmr spectra and electrode reduction potentials for the four series of compounds in which the ace-bridges add increments of strain were examined and possible effects which might be due to strain were noted. Several areas in which theoretical calculations are lacking were noted.

REGINALD H. MITCHELL, THOMAS FYLES et LEONARD M. RALPH. Can. J. Chem. **55**, 1480 (1977).

La réaction des *péri*-dilithionaphtalènes et *péri*-dilithioacénaphtalènes avec l'acénaphtènequinone et pyracènequinone conduit aux dérivés dihydroxylés **11***a*, **11***b* et **11***c* de l'acénaphtène[1,2-*a*]acénaphthylène qui comportent respectivement aucun, un et deux ponts acé. Ces composés peuvent conduire, soit par la méthode des thionocarbonates de Corey soit avec l'aide de l'acide fluorhydrique liquide anhydre, aux trois alcènes **12***a,b,c*, et, avec $Pb(OAc)_4$, trois dicétones **13***a,b,c*. La réduction de Wolff–Kishner de ces dernières conduit aux alcènes **12***a,b* et aux mono-cétones **15***b,c*. On a examiné les spectres uv, ir, et rm^{1}H et les potentiels de réduction d'électrode des quatre séries de composés dans lesquelles les ponts acé ajoutent des éléments de contraintes et on a noté les effets qui peuvent ressortir de ces contraintes. On note plusieurs champs dans lesquels il manque des calculs théoriques.

[Traduit par le journal]

Introduction

One of the more interesting aspects of naphthalene chemistry is the so-called *peri*-interaction which occurs between 1,8-disubstituted naphthalenes due to the restricted geometry imposed by the naphthalene nucleus (for an extensive review see ref. 1). The effects are summarized as shown in Table 1.

In naphthalene itself the distance between the 1,8(*peri*) hydrogens is 244 pm. Substitution of these hydrogens by methyls increases this distance to 293 pm, and distorts the naphthalene framework, the angles α and β opening some 4–5° while the opposite angles δ and γ close by several degrees. Correspondingly when the X—X distance is shortened to 154 pm as in acenaphthene, angles α and β close considerably while δ opens. It can be seen that the strain introduced in the molecule is accommodated by this scissor movement of the central naphthalene carbons. Addition of the second bridge in pyracene clearly prevents this relief of strain and while the X—X distance now lengthens a little beyond the normal C—C bond length to 159 pm, the angles α and β remain severely distorted from the normal 120° values. Pyracene **1** is thus strained, and indeed up until 1952 when Anderson and Wade (2) synthesized it, it was thought that this geometrical scissoring would be sufficiently exacting to prevent closure of the second five-membered ring. Whilst no strain energy calculations appear to have been made on **1**, Dauben (3) has calculated the strain energy of pyracylene **3** to be *ca.* 50 kcal/mol. Using Dauben's potential function (3, 4) we calculate the strain in pyracene due to the bond angle deformations to be about 36 kcal/mol. This seems reasonable in that introduction of unsaturation into the *peri*-bridges would be expected to shorten the X—X distance to *ca.* 135 pm (5) and hence introduce more angle strain. Indeed, although Anderson

[1]For part I see ref. 84.

[2]Presented in preliminary form at the 30th Northwest Regional Meeting of the American Chemical Society, University of Hawaii, June 13, 1975.

[3]Author to whom correspondence should be addressed.

(6) was able to synthesize 1,2-dihydropyracylene **2** in 1957, it was a further 10 years before Trost and co-workers (7, 8) reported the synthesis of pyracylene **3** itself. Whereas pyracene **1** is quite stable, **2** decomposes slowly at room temperature in the solid state, and pyracylene **3** could only be isolated in solution, nicely reflecting the increasing strain in the series **1–3**.

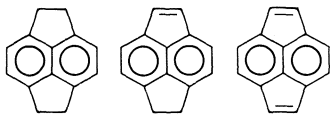

1 **2** **3**

A further potentially interesting series in which to study the effects of strain is derived from the interesting hydrocarbon acenaphth[1,2-*a*]acenaphthylene **4** first reported by Letsinger and Gilpin (9) in 1964. Addition of bridges across the *peri*-positions of **4** leads to the series of compounds **5–8** which should have progressively increased strains. Compound **8** is of further special interest since it consists of two pyracylene molecules ('4*n*' compounds) fused along one edge and thus should (10) be an aromatic '4*n* + 2' compound. Examples of fused ('4*n* + 4*n*') compounds are rare in the literature (see, for example, ref. 11) and on the whole have proved disappointingly olefinic as Wilcox *et al.* (12) point out. However such examples do not contain benzenoid rings which, at least as far as 4*n* and 4*n* + 2 systems are concerned, seem to exert a stabilizing effect (for example see refs. 4 and 8). Compounds containing a pentalene nucleus are non-alternate hydrocarbons and ones with a potential (4*n* + 2) π periphery such as **8** are indeed rare, Vogel's (13) dicyclohepta-[*cd*,*gh*]pentalene being the only example known to us. In fact, despite the myriad (see, for example, ref. 14) of calculations on similar systems both known and hypothetical, **8** seems to have been neglected.

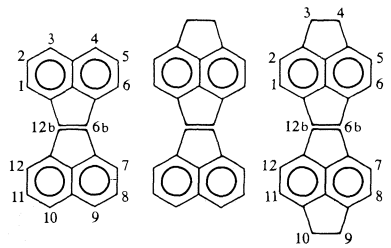

4 **5** **6**

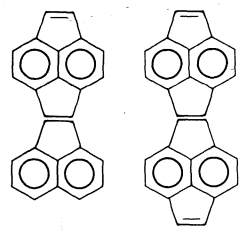

7 **8**

This paper reports the synthesis of **5** and **6** and another synthesis of **4** and our interpretation of their spectral properties in terms of strain, as well as our (as yet unsuccessful) attempts to convert **6** to the fully unsaturated hydrocarbon **8**.

Nomenclature

Since all of the following derivatives of **4** have unwieldy names and as comparisons will be made between the three series of compounds corresponding to **4**, **5**, and **6** we will refer to **4** as an unbridged-alkene and its derivatives will all have *a* numbers, **5** as a monobridged-alkene, the *b* series and **6** as a bisbridged-alkene, the *c* series. In this way for example the diols all have the number **11**, and **11***a* is unbridged-diol, **11***b* is monobridged-diol, and so on. For each compound a probable Chemical Abstract name is given in the experimental section.

Results

I. Syntheses

Unbridged-alkene **4** has been synthesized (9, 15) by two routes from the unbridged-diol **11***a*, derived from condensation of 1,8-dilithionaphthalene **9***a* (16) with acenaphthenequinone **10***a*. Since the second route (15) involves a transannular intramolecular ring closure across the *peri*-positions of **13***a*, we expected that it might be sensitive to the distance between the carbonyl groups of **13** and bring about a synthetic verification of our predictions derived from Table 1.

We found that 1,8-dilithionaphthalene **9***a* was more conveniently prepared from 1,8-diiodonaphthalene (17) and then, using essentially Letsinger's conditions, we obtained unbridged-diol **11***a* from **9***a* and **10***a* in 12–14% yield, monobridged-diol **11***b* from 5,6-dilithioacenaphthene **9***c*[4] and **10***a* in 10–20% yield, and bisbridged-diol **11***c* from **9***c* and pyracene-

[4]Letsinger (16) also attempted to prepare 5,6-dilithioacenaphthene, but was using 3,5-dibromoacenaphthene (mp 138–140°C) (18) and not authentic 5,6-dibromoacenaphthene (19, 20) best prepared from 5-bromoacenaphthene (21).

TABLE 1. Bond lengths and angles in *peri*-substituted naphthalenes

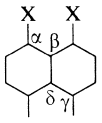

	X—X (pm)	α (deg.)	β (deg.)	δ (deg.)	γ (deg.)	Ref.
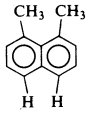	293	124.8	125.2	119.5	112	63
	244	*	121.5	121.5	*	85
	154	108.6	112.4	128.4	115.5	49
	159	107.5	115	115	107.5	86

*Not explicitly stated, but probably close to 120°.

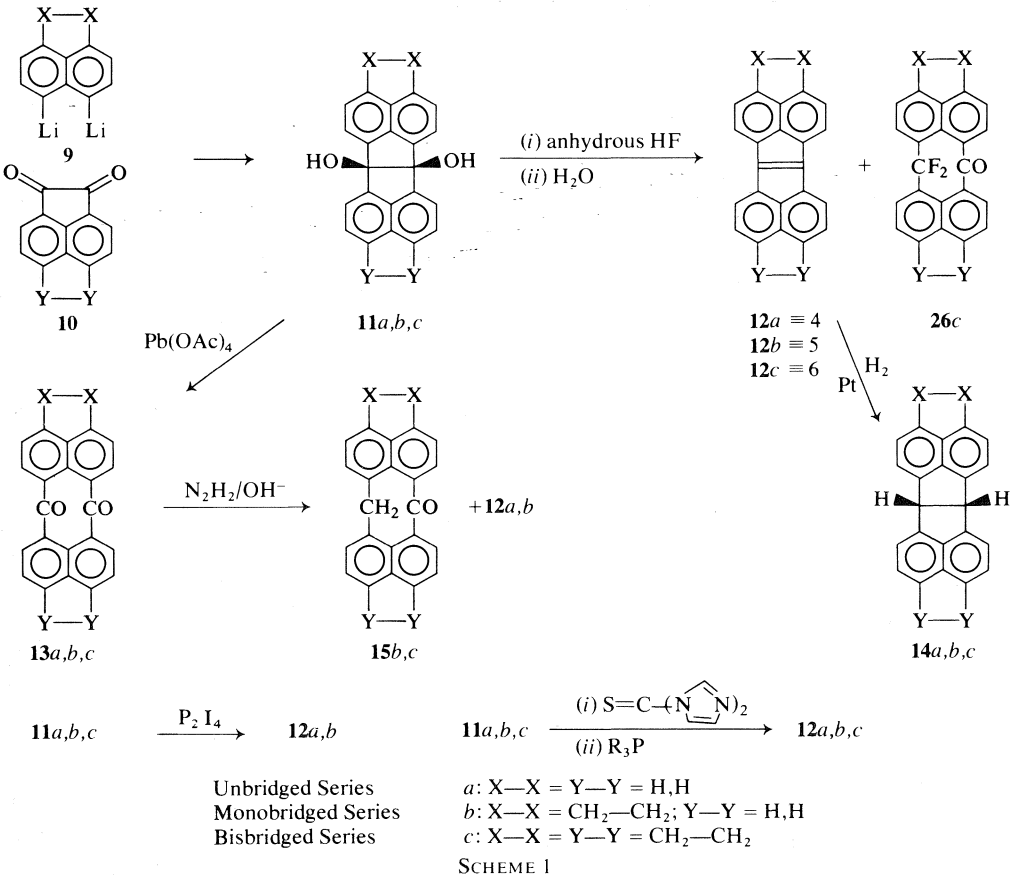

Unbridged Series — *a*: X—X = Y—Y = H,H
Monobridged Series — *b*: X—X = CH_2—CH_2; Y—Y = H,H
Bisbridged Series — *c*: X—X = Y—Y = CH_2—CH_2

SCHEME 1

quinone **10***c* (22) in 13–26% yield. All three diols show an absence of carbonyl absorption, strong —OH stretch bands at *ca.* 3350 cm^{-1} in their infrared spectra and strong M^+ molecular ions in their mass spectra. Their uv spectra, which are similar, will be discussed below.[5]

Preparation of the Alkenes Through the Wolff–Kishner Route

Unlike (9) unbridged-diol **11***a*, lead tetraacetate cleavage of monobridged-diol **11***b* to monobridged-diketone **13***b* was both sluggish and low yielding and moreover almost no **13***c* was formed from the bisbridged-diol **11***c*. Addition of trichloroacetic acid (23), however, completed all three reactions in *ca.* 30 min in 71–76% yields. The structures of the diketones **13** were readily confirmed by the absence of —OH bands and presence of strong C=O absorption *ca.* 1690 cm^{-1} in their ir spectra, base peak molecular ions in their mass spectra, and similarities in their uv spectra.

Reaction of unbridged-diketone **13***a* with hydrazine as described by Agosta (15), but using a longer reaction time, improved the yield of **12***a* to 83%. The uv spectrum of purple **12***a* agrees with the maxima that are reported (9, 15), except that both papers omitted to report a number of maxima (log ε 2–3) in the 500–620 nm region.

Agreeing with Agosta's (15) observation we usually obtained a small amount (~4%) of unbridged-alkane **14***a* as a by-product. We could not isolate any unbridged-monoketone **15***a* in this reaction (*cf.* below).

When monobridged-diketone **13***b* was subjected to these reaction conditions the purple monobridged-alkene **12***b* (≡5), mp 274–276°C was obtained in 22% yield. Its structure was proved by its uv (very similar to that of **12***a*, see below), by its ^{1}Hmr spectrum (essentially first order), and its correct molecular ion at *m/e* 302 in its mass spectrum. There was also obtained the yellow monobridged-monoketone **15***b*, mp 233–234°C in 33% yield. Its structure was assigned on the basis of the molecular ion at *m/e* 320 in the mass spectrum, with peaks corresponding to loss of CO and CHO, the strong ir band 1665 cm^{-1}, and the ^{1}Hmr spectrum in which two non-equivalent methylene protons can be seen as doublets, J = 14 Hz at δ 4.96 and 4.38. Consideration of the geometry of **15***b* clearly indicates that the two hydrogens at C-14 should be different, H_{endo} being in the shielding

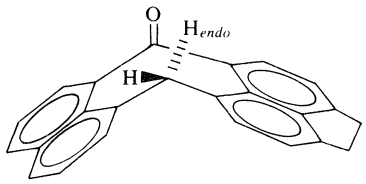

15*b*

cone (24) of the C-7 carbonyl group. These results are in excellent agreement with the spectra obtained for the known (25*a*) 6-methyl derivative of **15***a* and are consistent with the spectra obtained for the corresponding thiocin derivative (C=O replaced by S=O) reported by Johnson and Vegh (25*b*) and the 7,12-dihydropleidenes (25*c*) where similar geometries exist. Extending the initial heating period of **13***b* with hydrazine increased the yield of **12***b* to 27%, when only little ketone **15***b* was detected. Finally, reaction of the bisbridged-diketone **13***c* gave no purple products, even after long reflux times, the only product isolated being the yellow bisbridged-monoketone **15***c*, mp 284–287°C (dec.) in 29% yield. The structure was again assigned on the basis of the molecular ion at *m/e* 346 in the mass spectrum, with peaks corresponding to loss of CO and CHO, the strong ir band at 1660 cm^{-1} (C=O), and the ^{1}Hmr spectrum which showed the 14-protons as an AB double doublet at δ 4.85 and 4.35, with H_{endo} being shielded.

These results are interesting in view of Agosta's (15) mechanism for the transformation of **13***a* into **12***a* in which he proposes the monohydrazone **16***a* to be an intermediate, which undergoes transannular attack on the carbonyl group to give **17***a* which after loss of N_2 gives alcohol **18***a* (isolable) and hence the alkene **12***a*. He could not (and neither could we) isolate any unbridged-monoketone **15***a*. Addition of the extra *peri*-bridges must, as we suggest, widen the distance across the bridge, making the transannular attack more difficult for **16***b*, consistent with the longer reflux time necessary for the reaction. In the case of **16***c*, transannular reaction seems not to occur at all. There could, however, be a more interesting alternative explanation: alcohol **18** could be regarded as the 'homoenol' of ketone **15**, and as

[5]Only spectral information relative to the structure will be given here. More detailed comparisons between series will be made in the sections to follow. Unless otherwise stated all new compounds gave satisfactory analyses (see Experimental), and correct molecular ions in their mass spectra.

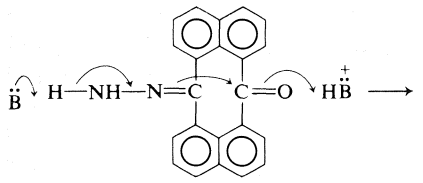

16*a*

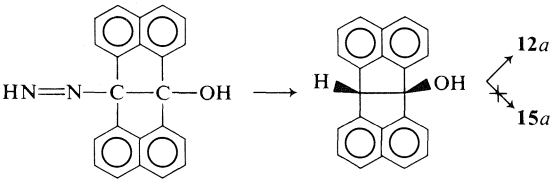

17*a* 18

such could ketonize to **15** breaking the transannular bond, thus relieving strain rather than dehydrating to alkene **12**. In the *c* series the strain should be greatest and hence we are more likely to observe ketone **15***c* as the product rather than alkene **12***c*; the intermediate monobridged *b* series giving both **15***b* and **12***b*. Though we could not isolate any alcohol **18***b* or **18***c* to support this argument (Agosta did isolate **18***a* and showed it gave **12***a* under the reaction conditions and not **15***a*), it does not prevent this mechanism from being the operative one. We were unable to conclusively isolate any fully reduced products *i.e.* **19***b* or *c*, which might be expected to form by further reaction of the monohydrazone **16***b*,*c* to bishydrazones and hence on to product **19**. We could in fact see a short lived

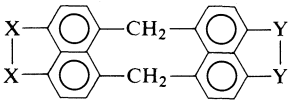

19

product in the ^{1}Hmr spectrum of the crude reaction mixture leading to **15***c*, which showed AB doublets at δ 5.87 and 4.12 (J = 15 Hz) as well as the aromatic and *peri*-bridged protons. Unfortunately we could not isolate this product after chromatography. The ^{1}Hmr spectrum is consistent with the structure of **19***c* and agrees very well with that reported (25*a*) for the 6-methyl derivative of **19***a*.

Preparation of the Alkenes Through Halide and Other Intermediates

With the failure of the Wolff–Kishner conditions to yield bisbridged-alkene **12***c*, we decided that a more likely route would probably stem directly from the diols **11** themselves, since the **6***b*–**12***b* bridge is already in place, and hence a part of the strain present in **12** is already overcome. A likely approach seemed conversion of diols **11** into dihalides and subsequent dehalogenation to alkenes **12**. In fact Kuhn and Winterstein (26) had introduced P_2I_4 as a reagent to effect this very transformation in one step in 1928. Indeed for unbridged and monobridged-diols **11***a*,*b* the reaction succeeded and gave the previously obtained alkenes **12***a*,*b* in yields that ranged from 16–96% for no apparent reason. An average yield over ten experiments was *ca.* 50%. Consistently, however, we could not generate any bisbridged-alkene **12***c*.

Surprisingly, neither thionyl chloride nor anhydrous HCl in chloroform gave isolable dichloride from **11***a*,*b* and no alkene **12***a*,*b* could be detected when the product was treated with NaI in acetone (27, 28), a procedure that was successful for the preparation of 1,2-diphenylacenaphthylene from 1,2-diphenylacenaphthene-1,2-diol (28). Similarly, no dihalide was obtained when **11***a* was treated with dimethylsulphide and *N*-chlorosuccinimide (Corey *et al.* (29)) or triphenylphosphine dibromide in dimethylformamide (Wiley *et al.* (30)) or phosphorous tribromide. Further, the products of these reactions did not give alkene **12***a* on treatment with Cr(II) (31). It appears that neither an S_N2 displacement in which attack from the back would have to be between the V of the aromatic rings, nor an S_N1 process, which by consideration of molecular models indicates that the monocation derived from **11***a* is more strained than **11***a* itself, are favoured.

Application of Corey's (32) thionocarbonate procedure (in which a *cis*-1,2-diol **20** is refluxed in xylene with *N*,*N*′-thiocarbonyldiimidazole to yield the cyclic thionocarbonate **21** and then subsequently refluxed with trimethylphosphite to yield the alkene), on the three *cis*-diols **11***a*,*b*,*c*

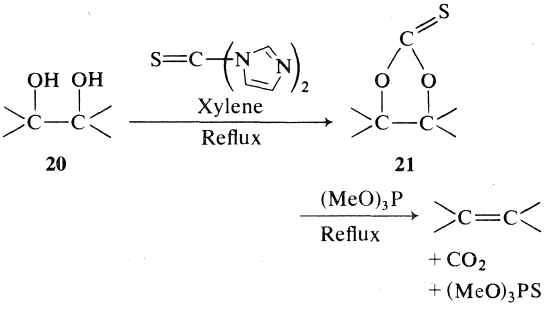

20 21

successfully gave the three alkenes **12***a,b,c* in yields from 12–20%. We found that use of the more reactive (33) tris(diethylamino)phosphine in place of trimethyl phosphite in the second step increased the yields of **12** to about 30% for each alkene. We did not find prior isolation of the *N,N'*-thiocarbonyldiimidazole **22** very easy nor necessary, since the compound seems to decompose even on standing in the freezer. However, we confirmed Pullukat and Urry's report (34) that it is easier to isolate **22** from the reaction of trimethylsilylimidazole and thiophosgene than from imidazole and thiophosgene itself (35).

In our procedure we prepared **22** *in situ* from imidazole and thiophosgene and used it in xylene without prior isolation with diols **11** with no decrease in yield. Alternative methods of decomposing the intermediate thionocarbonates (21) have been described more recently, however, we found that use of iron pentacarbonyl in place of phosphine as described by Daub *et al.* (36) gave reduced yield of alkenes **12** (12–20%) whereas use of isopropyl iodide – zinc as described by Vedejs and Wu (37) gave no alkenes.

The structure of the now obtained bisbridged-alkene **12***c*, obtained as purple crystals, mp > 350°C, followed from its ^{1}Hmr spectrum which showed an aromatic AB quartet at δ 8.00 and 7.45 with the methylene protons at δ 3.52, the mass spectrum with parent molecular ion at *m/e* 328 as base peak, and the uv spectrum very similar to that of alkenes **12***a,b*.

Attempted use of the low valent titanium species described by McMurrey and Fleming (38) to reduce ketones and *vic*-diols to alkenes gave 15% yield of the monobridged-alkane **14***b*, identical to that obtained on hydrogenating alkene **12***b*. However, we were later (39) to learn that this reagent has proved highly variable depending on the bottle of $TiCl_3$ used, and a better reagent, probably Ti(0) from the action of potassium on $TiCl_3$ gives more reliable results. We also tried a number of other methods of converting 1,2-diols into olefins (40) but in our hands these were not successful.

Reaction of Diols 11 with Anhydrous Hydrogen Fluoride: Simplest Preparation of Alkenes 12

Le singer (9) reported that diol **11***a* gave a 29% yield of alkene **12***a* on treatment with liquid hydrogen fluoride in a copper vessel at 0°C for 45 min followed by ice water quench. We have found that this yield can be increased to 68% by allowing the diol **11***a* to stand in liquid hydrogen fluoride in a polyethylene flask overnight such that all of the HF has evaporated before water is added. A dark precipitate is obtained which slowly dissolves in CH_2Cl_2–aq-Na_2CO_3 solution on shaking to give a deep red organic layer containing the alkene **12**. Very few (41) reactions have been described in which a 1,2-diol is converted to an alkene under such conditions, more commonly halide intermediates (see above) are utilized, and it is thus interesting to speculate on the nature of the intermediate. One possibility is a dication **23**. It has been

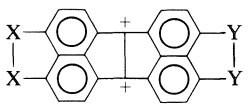

23

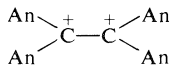

24

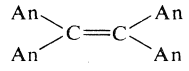

25

An = *p*-MeO—C_6H_5—

claimed (42) that dication **24** forms alkene **25** under similar conditions, though we have not yet been able to repeat this to our satisfaction (43).[6] Forsyth and Olah (44) have shown that aromatic dications can readily form in strongly acidic media, and in the case of **23** such a dication could be planar and hence stabilized. In a future paper we hope to describe the generation of the dications of **12** (*i.e.* **23**) as well as the radical cations and anions to compare with this reaction intermediate in the hope that we can elucidate the mechanism of thi s reaction.

Also obtained from the reaction of bisbridged-diol **11***c* with liquid HF as described above was 2% of a yellow compound mp > 350°C, which showed a molecular ion in its mass spectrum at *m/e* 382 with peaks corresponding to loss of H, O, F, and CO from M^+. Its uv spectrum was very similar to the bisbridged-monoketone **15***c*, and together with the presence of a strong carbonyl absorption at 1680 cm^{-1} in its ir spectrum led us to assign the structure of the difluoro ketone **26***c* to this compound. This was supported by its ^{1}Hmr spectrum in which the lowfield absorption at δ 7.83 corresponds to H-1 and 13 with coupling to the *ortho* H-2 (7.5 Hz) as well as the F-14 (1.5 Hz), a doublet at δ 7.64 corre-

[6]Manuscript in preparation.

sponds to H-6 and 8, deshielded by the adjacent carbonyl and coupled to the *ortho* H-5 or -9 (7.2 Hz), coincidental doublets at δ 7.27 (J = 7–7.5 Hz) corresponding to H-2, 5, 9, and 12, and

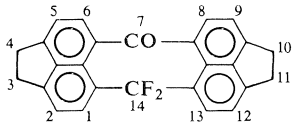

26*c*

a singlet at δ 3.30 for H-3, 4, 10, 12. The main difference between the ir spectra of **15***c* and **26***c* is a strong band at 1043 cm^{-1}; this is consistent with a C—F stretch (45).

'Magic-acid', FSO_3H, gave only a 15% yield of **12***a* from **11***a*.

Hydrogenation of the Alkenes ***12***

Hydrogenation in benzene using PtO_2 (not pre-reduced) was most convenient and essentially gave quantitative reduction in less than 2 h. The three alkenes **14** were readily identified by the appearance of the 6b,12b-methine protons close to δ 6 in their ^{1}Hmr spectra, and the correct molecular ions in their mass spectra. They gave similar uv spectra, and that of **14***a* agreed with that reported (15).

Attempted Dehydrogenation of Bisbridged-alkene ***6*** *(****12****c) to Pyrace[1,2-a]pyracylene(****8****)*

Harvey and Cho (46) have shown that a variety of dihydroaromatic compounds (*e.g.*, acenaphthene, 9,10-dihydrophenanthrene, 4,5,-9,10-tetrahydropyrene) readily form dianions in the presence of alkyllithium–TMEDA complex, and that on addition of oxidant (*e.g.*, Cu(II)), the corresponding aromatic compounds (*i.e.* acenaphthylene, phenanthrene, and pyrene, respectively) are formed in good yields. Trost *et al.* (47) have also shown that with *n*-butyllithium (with or without TMEDA) 1,2-dihydropyracylene **2** forms pyracylene dianion (green in solution) which on protonation reforms **2**. However, the report does not indicate whether **3** could be obtained by addition of oxidant to the green solution of $\mathbf{3}^{2-}$.

In the event, when we added *n*-BuLi/TMEDA to a cyclohexane solution of **6** a deep blue colour formed immediately and this, after standing at room temperature for *ca.* 12 h or after reflux for 1 h, turned deep red in colour. Quenching experiments with water did not return any of **6**; mainly a tar was formed. On such addition of Cu(II) the colour turns dark green and subsequently black. After protonation yellowish-red products which rapidly tarred were obtained, none of which could be identified.

Trost *et al.* (8) were able to convert pyracene **1** into pyracylene **3** by a bromination–debromination sequence.

Reaction of bisbridged-alkene **6** with **5** mol equiv. of bromine in CCl_4 under irradiation with a tungsten lamp gave a yellow solid which in its ^{1}Hmr spectrum showed an AB double doublet at δ 7.88 and 7.57 (8H, J = 7 Hz, aromatic protons) and two singlets at δ 5.85 and 5.81 (~2H each, -CHBr) which is consistent with the structure of the hexabromide **27** as a *cis/trans* mixture. For comparison, the methine protons of 1,2-dibromoacenaphthene **28** occur at δ 5.98. However, we were not able to

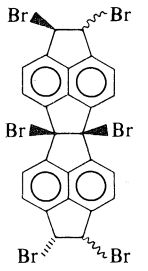

27

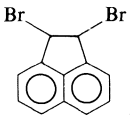

28

obtain a satisfactory mass spectrum for **27**. Reaction of **27** with NaI and $Na_2S_2O_3$ in acetone as described by Trost (8) or in DMF or by the use of Zn dust or Cr(II) in DMF has not yet yielded product that can be assigned structure **8**. However, we intend to pursue our efforts to obtain this compound, as well as **7** from **5**, which were likewise unsuccessful.

II. Discussion of Spectra in Terms of Strain

Unfortunately X-ray crystallographic structures of 1,2-dihydropyracylene **2** and unbridged-alkene **4** have not yet been reported, and further acenaphthylene forms a disordered crystal (48), so calculations of the strain energy of **4**–**6** would at best be guesses. Indeed even with such data they are hazardous, for example using the X-ray crystal data (49) for acenaphthene and Dauben's potential function mentioned earlier we calculate the strain energy of acenaphthene to be about 15 kcal/mol, whereas heat of formation measurements (50) suggest that it is in the order of 9 kcal/mol. However, such calculations rely on the accuracy of the X-ray data and that for acenaphthene has

TABLE 2. *p*-Band shifts in the uv spectra

Compound	*p*-Band (nm)				Shift $\Delta\nu$ (cm^{-1})		Ref.
Naphthalene	275	}			1762		87*
Acenaphthene	289						
Pyracene	295	}			704		87†
Naphthalene	275	}			1276		87*
1,8-Dimethylnaphthalene	285						1
1,4,5,8-Tetramethylnaphthalene	296	}			1304		1
Acenaphthylene	340	} 1479	334	} 1531	323	} 1805	87‡
1,2-Dihydropyracylene	358		352		343		2
12*a*	388	} 1383	380	} 1378	367	} 1247	
12*b*	410		401		384.5		
12*c*	434	} 1349	425	} 1409	404.5	} 1279	

*Spectrum E1/1.
†Spectrum E1/16.
‡Spectrum E6/12.

changed markedly over the years (49). Using the data for 1,8-dimethylnaphthalene (Table 1) which were obtained in 1973, much better agreement between calculated (6 kcal/mol) and actual (7 kcal/mol (50)) strain energy is obtained. Since the X-ray structure of pyracene was performed back in 1960, the calculated strain energy may also be over-estimated as in the case for acenaphthene. However, there can be no doubt that addition of the second *peri*-bridge to acenaphthene substantially increases the strain energy, and hence can be expected to do the same for compound **4**.

The remainder of this paper will be spent discussing the changes in properties that occur on *peri*-bridging **4** and assessing any likelihood that they are related to strain.

Ultraviolet and Visible Spectra

It has been well documented (51) that introduction of a methyl group into an alternate hydrocarbon results in a bathochromic shift of the *para*-band[7] (52) in the ultraviolet spectrum, and this can be quite well accounted for theoretically (53). In a non-alternate hydrocarbon, however, the shift can be either bathochromic or hypsochromic depending on the position of substitution (54). If introduction of the substituent strains the molecule, further complications arise; both hypsochromic (55) and bathochromic (53) shifts have been observed and either a loss (56) or gain (57) in fine structure can occur. The latter are more clearly defined than the former. When substituents are present which prevent the molecule from becoming planar, *i.e.* reduce the π-orbital overlap, a loss of fine structure is usually observed together with a bathochromic shift *e.g.*, in certain methyl phenanthrenes, benzophenanthrenes, and chrysenes (53, 56) as well as in many of the cyclophanes (58).

However, when substituents are present such as methylene or dimethylene (ace) bridges which do not deform the molecule from planarity, but introduce strain, then usually an increase in fine structure results (57). Lewis and Calvin (59) explain this effect in terms of 'loose bolts', *i.e.* when a system has saturated substituents the dissipation of the energy of the electronically activated system is facilitated by the many possible vibrationally active states. Introduction of a strained bridge hinders this dissipation of energy resulting in the appearance of the fine structure, and usually a bathochromic shift somewhat greater than the effect of the corresponding dimethyl derivative (51).

For acenaphthene, addition of a second bridge to form pyracene causes a considerably smaller bathochromic shift (*ca.* 700 cm^{-1}) (see Table 2) in the *p*-band than the *ca.* 1800 cm^{-1} shift of adding the first bridge to naphthalene, whereas addition of two and then a further two methyl groups to naphthalene gives nearly equal shifts of *ca.* 1300 cm^{-1} each; the total shift for two ace-bridges or 4-methyl groups being about the same. It would be interesting to know whether this is caused by the change in bond angles of the naphthalene ring or whether it is due to the relative abilities of the methyl group and the

[7]Clar's (52) *p*-bands are the intense (log ε 3–4) long wavelength bands associated with the HOMO–LUMO transition.

ace-bridge to hyperconjugate with the ring. The behaviour of the three alkenes, **12**, is quite different, producing nearly equal shifts for each bridge addition; the shifts comparing quite well with those for ace-bridging acenaphthylene to give 1,2-dihydropyracylene. This may be a result of the lower flexibility of the alkene bridge present in these systems, indicating an increase in strain.

The spectra (see Fig. 1) also reveal a considerable increase in fine structure on adding ace-bridges to **12***a* consistent with the molecule remaining nearly planar but being held more rigidly as discussed above. Although calculations (60, 62) have been carried out on **12***a*, the 'purple band' (probably a combination difference band (61) and not the HOMO–LUMO transition as suggested (60)) is not well accounted for and no attention has been paid to the actual geometry of the system. Since there now exist a number of papers (63) which can compute the best geometries with minimum strain, it would be interesting to recalculate the spectra using such data, though at present this is beyond our capabilities here.

All of the other compounds to be discussed are bent and belong to the two classes of compounds of type A and B. The diols **11** (X = OH) and alkanes **14** (X = H) are of type A. Agosta (15) has reproduced the spectra of both **11***a* and **14***a* and compared them to acenaphthene. In fact the spectra are quite different from the latter, the position of the main maxima being both bathochromically shifted some 15–30 nm and

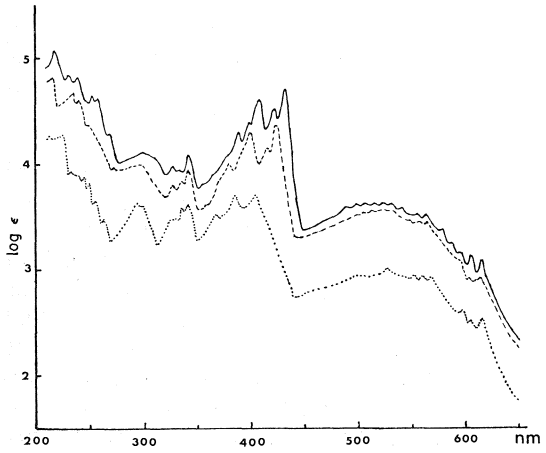

FIG. 1. Ultraviolet absorption spectra in cyclohexane solution for **12***c*—(log ε displaced +0.5); **12***b* --- ; **12***a* · · · (log ε displaced −0.5).

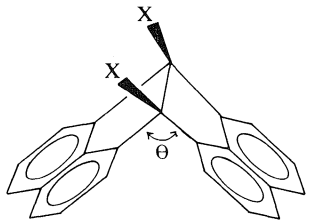

A

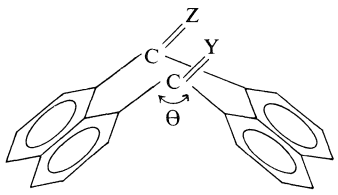

B

twice as intense. This is consistent with extensive interactions between the π systems of the two naphthalene rings as is seen in the naphthalene derivative **29** (64) and resembles that seen in the cyclophanes (58, 65) except that since the aromatic rings are not expected to be bent in A no loss of intensity is seen.

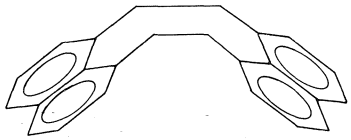

29

For both the diol **11***a* and alkane **14***a* addition of the first acebridge to give **11***b* and **14***b*, respectively, produces only a small 4–7 nm (535–780 cm^{-1}) bathochromic shift in each *p*-band absorption, similar to that discussed above for pyracene. Addition of the second ace-bridge to give **11***c* and **14***c* respectively produces an even smaller shift of 1–5 nm (108–601 cm^{-1}), in contrast to the case for the alkenes. This would appear to suggest that the saturated central bridge does accommodate the strain better than an unsaturated bridge, especially in light of the fact that the overall shape (*i.e.* number of maxima and relative intensities) of the spectra of **11** and **14** hardly change on bridging. This would seem to indicate that both the interactions between the rings are not affected, *i.e.* presumably the inter-ring angle θ does not change by much, and the molecule is not 'tightened up' much. This is interesting considering the bond angle changes that have to occur in the naphthalene nucleus.

TABLE 3. Selected infrared bands

Compound	C=C band (cm^{-1})	Compound	C=O band (cm^{-1})	Ref.
Tetraphenylethylene	1600	**13***a*	1689	
1,2-Diphenylacenaphthylene	1602	**13***b*	1688	
12*a*	1604	**13***c*	1690	
12*b*	1610	6-Me-**15***a*	1655	25*b*
12*c*	1615	**15***b*	1660	
		15*c*	1660	
		26*c*	1675	
		1,8-Dibenzoylnaphthalene	1664	9
		Di-1-naphthylketone	1653	66
		Benzophenone	1645	66

The diketones (B, Y=Z=O) also show this same effect where in the absence of a central bridge, the molecule should be able to twist. This twisting seems more severe in the monoketones **15***b,c* in which H_{endo} projects towards the carbonyl group, when an additional intense ($\varepsilon \sim 10^4$) maximum at *ca.* 360 nm appears (also in difluoroketone **26***c*) (probably an electron transfer band). This twisting is further supported by the ir data.

Infrared Spectra

For the planar alkenes **12** the 1600 cm^{-1} 'aromatic' (ref. 45, p. 69) band is intense and well defined. Qualitatively, all other things being equal, one would expect this to move to higher frequency as the stiffness in each C=C bond increased. Indeed for the alkenes **12** this is exactly what happens (Table 3). Addition of each bridge to **12***a* produces a small (5–6 cm^{-1}) shift to higher frequency, consistent with the idea that each bond tightens up to absorb the strain on introducing the bridge indicated in the uv spectra above. Whilst in general the 1600 cm^{-1} band can appear between 1625–1575 cm^{-1} for most aromatics (ref. 45, p. 71), it would seem that on comparison to the two model compounds tetraphenylethylene and 1,2-diphenylacenaphthylene there is a definite shift. Whilst it is doubtful that much can be drawn from the ir spectra of the bent alkanes **14***a,b,c*, it is interesting that they show bands at 1596, 1584, and 1585 cm^{-1}, respectively, consistent with Cram's idea (66) that an out of plane distortion of the aromatic ring as in [2.2]paracyclophane, shifts the band to lower frequencies.

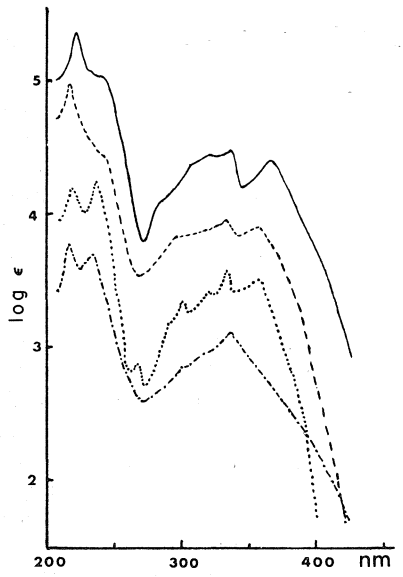

FIG. 2. Ultraviolet absorption spectra in cyclohexane solution for **15***c* — (log ε displaced +1); **15***b* --- (log ε displaced +0.5); **26***c* ··· ; **13***c* ·-·-·- (log ε displaced −0.5).

The absorptions due to the carbonyl bands in compounds **13**, **15**, and **26***c* are interesting (Table 3). Aryl conjugation to the carbonyl group reduces the frequency provided the groups can become co-planar (ref. 45, p. 137). Letsinger (9) pointed out that diketone **13***a* absorbed at 25 cm^{-1} higher than in 1,8-dibenzoylnaphthalene, which in fact itself absorbs considerably higher than benzophenone (67). Addition of the bridges to **13***a* to give **13***b,c* does not affect the carbonyl absorption, supporting the uv data that θ of B does not change very much. Of considerable significance, however, is the fact that the $\diagdown$C=O$\diagup$ band for the monoketones **15** is close to 1660 cm^{-1}, comparable to that in 1,8-dibenzoylnaphthalene. This supports the uv data and clearly indicates that the carbonyl

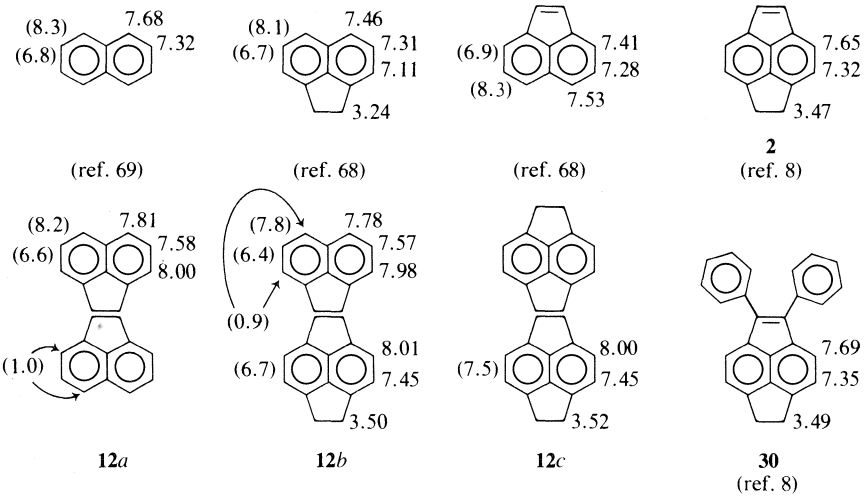

CHART 1. Proton chemical shifts, δ, and coupling constants (Hz).

group is conjugating with the ring. The change of one carbonyl group of **13** to the methylene group of **15** must twist the rings more than simple (Dreiding) molecular models would suggest. The higher frequency $\rangle C{=}O$ of **26***c* (1675 cm^{-1}) is consistent with the shorter wavelength λ_{max} in the uv spectrum, indicating a partial twist in this compound.

Nuclear Magnetic Resonance Spectra

The assignment of ^{1}Hmr spectra was made on the basis of known coupling constants and chemical shifts for the parent systems and for compound **2** and are shown in Chart 1.

Whilst evidence has been found (69, 70) for a steric effect on proton ^3J coupling constants, the values obtained in the series studied do not seem to be exceptional, however, some of the observed chemical shifts are of note. In 1,2-dihydropyracylene **2** and 5,6-dihydro-1,2-diphenylpyracylene **30** the chemical shifts of the naphthalene protons correspond within *ca.* 0.04 ppm, and are deshielded somewhat from those of acenaphthylene. The protons of **12**, however, are all considerably deshielded beyond those of **30**. In particular the protons next to the pentalene rings (H-1, 6, 7, 12) appear at δ 8.02–7.98, deshielded by 0.6–0.8 ppm from typical β-naphthene protons. Whilst the other ring protons are also deshielded, the effect is not so marked. Such large deshielding effects are most commonly seen (71) where protons suffer steric compression as in the 4,5-protons of phenanthrene **31**, δ 8.42, (69) and the 3,4-protons of perylene **32**, δ 8.03, (69). An alternative explanation is of course that the deshielding observed is due to the

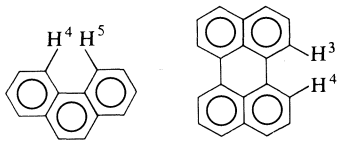

31 **32**

sum of all the ring currents involved and is larger for **12** than **2** because of the increase in rings. Some comment is then required for **30**: if steric effects prevent coplanarity of the benzene rings with the acenaphthylene system then clearly the protons would not feel the deshielding effects of the substituent rings, whereas in compounds **12** they are planar and thus the full effect could be felt. Whilst calculations to substantiate this idea are well advanced for benzenoid systems (see, for example, ref. 72) application to other systems is more recent and not easy (see, for example, ref. 73). Analyses of the ^{13}Cmr spectra of aromatic compounds have appeared (74) and both chemical shifts and coupling constants appear useful in elucidating steric effects. The ^{13}Cmr spectra for the alkenes **12** are shown in Chart 2 together with the calculated spectra (in parentheses) using Trost and Herdle's (75) additivity relationships. Clearly, excellent agreement is obtained. The values for the quaternary carbon atoms which might be expected to show the greatest strain effect have not yet been determined because of low solubility and long relaxation times,

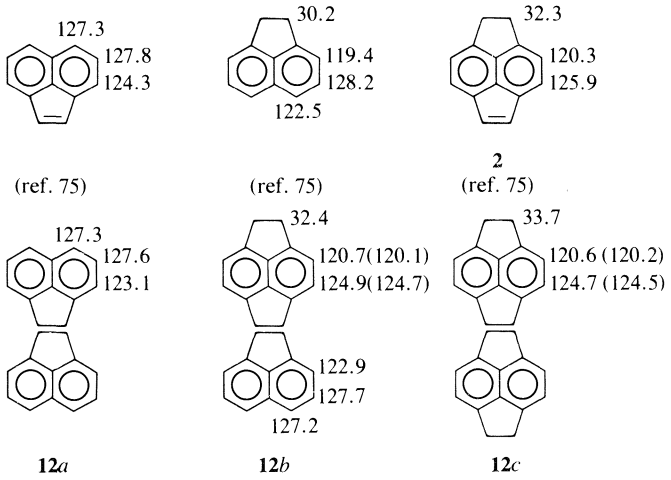

CHART 2. ^{13}C chemical shifts of proton decoupled spectra. All chemical shifts are given in ppm downfield from TMS, recorded in $CDCl_3$ on a Nicolet TT-14 60 MHz ft-spectrometer. Values in parentheses are calculated using additivity relationships (75).

although we have not given up hope of obtaining this data.

Apart from compounds **12**, the other fused naphthalenes are all bent as in structures A and B. A normal consequence of bringing aromatic rings face to face is to see a shielding of the aromatic protons (58, 64, 76, 77). By contrast the chemical shifts of the aromatic protons of compounds **11**, **13**, **14**, and **15** seem unexceptional. It is possible that the deshielding observed in compounds **12** is present also in these compounds and counteracts the above shielding. An alternative is that overlap of benzenoid rings must be extensive before any effect is observed.

Electrode Reduction Potentials

The three alkenes **12***a*,*b*,*c* can be reduced at the dropping mercury electrode and give reproducible (± 0.003 V) half-wave potentials. Each alkene gives two reduction waves corresponding to addition of one and two electrons to the compound. The measurements were made in 100% dimethylformamide to overcome solubility problems, but Given (78) has shown that such values only differ by a few hundredths of a volt from other solvents such as aqueous dioxane. The results are shown in Table 4 and are consistent with values for related systems (ref. 61, p. 178).

Macoll (79) was one of the earliest to point out that polarographic half wave reduction potentials ($\varepsilon_{1/2}$) are linearly correlated with the HMO energy of the lowest unoccupied MO (LUMO). Arising from this, it has been shown (80; also ref. 61, p. 176) that for a large number of aromatic hydrocarbons, even including some nonalternate ones that the $\varepsilon_{1/2}$ values so obtained (in aqueous dioxane) are related to the energy of the LUMO, $\varepsilon_{m+1} = \alpha + m_{m+1}\beta$, by the equation

$$[1] \qquad \varepsilon_{1/2} = 2.368 m_{m+1} - 0.924$$

where the effective value of β is about -55 kcal/mol. Since Watson and Matsen (81) have also shown that there is an excellent linear correlation between the frequency of the *p*-band in the uv spectrum and the $\varepsilon_{1/2}$ values for aromatic hydrocarbons, and that a plot of the frequency of the *p*-band against the HMO energy difference between the highest occupied orbital (HOMO) and the LUMO shows an excellent linear correlation given by equation 2 (ref. 61, p. 217)

$$[2] \quad \nu(p\text{-band, cm}^{-1}) = 19020\Delta m + 10520$$

where

$$\varepsilon_m = \alpha + m_m\beta$$

and

$$[3] \qquad \Delta m = m_m - m_{m+1}$$

(again β has value *ca.* -55 kcal/mol), we can use a combination of these equations to determine experimentally the energy of the HOMO, $\varepsilon_m = \alpha + m_m\beta$.

It can be seen from Table 4 that the results give

TABLE 4. Half-wave electrode reduction potentials and molecular orbital energies

Compound	$-\varepsilon_{1/2}$ *vs.* SCE (V)	$-m_{m+1}$*	ν *p*-band (cm^{-1})	Δm*	m_m*
12*a*	1.33 (2.14)†	0.171	23,041	0.747	0.576
12*b*	1.40 (2.18)†	0.201	23,529	0.684	0.483
12*c*	1.45 (2.21)†	0.222	24,722	0.658	0.436

*See text, calculated from [1] ($-m_{m+1}$), [2] (Δm), and [3] (m_m).
†Second wave.

for **12***a* a value of $m_m = 0.58$ which compares reasonably well with the calculated value (60) of 0.50 when the approximations involved[8] are considered.

It can be seen that the values obtained for m_m and m_{m+1} are not just opposite in sign but of greatly different magnitude. This is correct for non-alternate hydrocarbons (ref. 61, p. 46).

We can see from Table 4 that addition of the ace-bridges makes reduction more difficult. This is consistent with previous data (ref. 61, p. 178) where the difference between naphthalene and acenaphthene, $-\Delta\varepsilon_{1/2} = 0.17$ V. Addition of a methyl group to acenaphthene gives $-\Delta\varepsilon_{1/2} = 0.11$ V. The $-\Delta\varepsilon_{1/2}$ values for ace-bridging **12***a* are 0.05 to 0.07 V, somewhat smaller than expected from above. This might be indicative of strain in the system changing the σ-bonding which in turn will affect the π-bonding and hence the orbital energies or alternatively it suggests that the incoming electron goes into an orbital in this system in which the coefficients of the atoms to which the bridges are attached are small.

That however is not consistent with the published (82) LUMO and HOMO shown schematically. Consider the lowest antibonding orbital (ψ_a). Electron density in the radical anion of **12***a* will be high at the *peri*-positions despite the destabilizing effects of the alkyl groups. The small increase in $\varepsilon_{1/2}$ values observed relative to other systems may be because there is a node between the 6b–12b carbons. Bridging the *peri*-positions tends to stretch the 6b–12b bond and thus perhaps lowers the energy of ψ_a relative to ψ_b where it is strongly bonded. This effect may counteract the normal destabilizing effect of the alkyl groups on ψ_a relative to ψ_b and hence reduce $\varepsilon_{1/2}$. The proposed 'strain effect' of the ace-bridges is thus opposite in effect to the more normally observed 'inductive/hyperconjugative effect' of alkyl groups, and thus may support the unusual uv data in which addition of bridges to alkenes **12** produces approximately equal bathochromic shifts, whereas in all the other systems discussed which have no central π-bridge, the bathochromic shift for the second bridge is much smaller than that for the first.

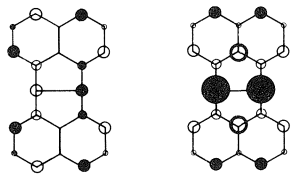

LUMO ψ_a HOMO ψ_b

[8]The equations 1 and 2 apply strictly to alternate hydrocarbons, though they work well for some non-alternates such as fluoranthenes (ref. 61, pp. 181, 217). Comparison of orbital energies when in one case an electron is promoted from a lower to a higher orbital and in a second an extra electron is added is perhaps dangerous, anyway.

Conclusions

We have prepared four series of strained compounds in which the differences amount to adding first one and then a second ace-bridge in the *peri*-positions such that further increments of strain are added and have documented changes in uv, ir, and ^{1}Hmr spectra and $\varepsilon_{1/2}$ values that we observe. We have then attempted to explain these changes in properties by relation to structurally similar molecules and hence suggest effects which might be strain related. The results so obtained have pointed out several areas in which good calculations are lacking and should receive attention by competent theoreticians.

Experimental

All melting points were determined on a Kofler hot stage and are uncorrected. The ^{1}Hmr spectra were determined in $CDCl_3$ (unless otherwise stated) on a Perkin-Elmer R12A (60 MHz) or R32 (90 MHz) spectrometer

and reported in ppm downfield from tetramethylsilane as internal standard. Mass spectra[9] were determined on a Hitachi–Perkin-Elmer RMU-7 or Finnigan 3300 mass spectrometer at 70 eV. The ir[9] spectra were recorded on a Pye-Unicam SP1000 spectrophotometer and the uv spectra on a Cary 17 spectrophotometer. The ir bands quoted in Table 2 were measured on a Beckman IR-4 as an average of ten values calibrated with polystyrene. Microanalyses were performed by this department. All evaporations were carried out under reduced pressure on a rotary evaporator at *ca.* 40°C. Extracts were dried with anhydrous sodium sulfate.

5-Bromoacenaphthene

This was prepared in 84% yield by the method of Ross *et al.* (21) from acenaphthene and *N*-bromosuccinimide in dimethylformamide, as white crystals from ethanol, mp 53.5–55°C (lit. (21) mp 51–52°C); ^{1}Hmr δ (60 MHz), 7.8–6.9 (5H, m, Ar*H*), and 3.25 (4H, s, -CH_2-).

5,6-Dibromoacenaphthene

This was obtained in 30–60% crude yield by the method of Constantine *et al.* (20) using 5-bromoacenaphthene, bromine, and Ag_2SO_4 in dioxane – perchloric acid solvent. Extensive chromatography on silica gel was required to remove all traces of the major impurity, orange acenaphthylenes. The pure product so obtained (25–40% yield) as very pale yellow crystals from benzene had mp 173–175°C (lit. (20) mp 165–168°C; (19) mp 173–174°C); ^{1}Hmr δ (60 MHz) 7.78 (2H, d, J = 8 Hz, *o*-Br-Ar*H*), 7.04 (2H, d, J = 8Hz, *o*-CH_2-Ar*H*), and 3.24 (4H, s, -CH_2-).

Unbridged-diol ***11a****, cis-6b,12b-Dihydroxy-6b,12b-dihydroacenaphth[1,2-a]acenaphthylene*

This was prepared essentially by the method of Letsinger and Gilpin (9) with modifications to make it more convenient. *n*-BuLi (46 mmol in 25 ml hexane) was injected into a solution of 1,8-diiodonaphthalene (17) (8.62 g, 22.7 mmol) in anhydrous ether (400 ml) and stirred under N_2 for 15–30 min to generate 1,8-dilithionaphthalene **9***a*. Acenaphthenequinone **10***a* (Aldrich, 4.14 g, 22.7 mmol) was then added and the reaction mixture stirred at room temperature for 14 h and/or refluxed for 6 h. After addition of saturated NH_4Cl solution the organic layer was separated, dried and evaporated. Any residue remaining in the aqueous layer was extracted with CH_2Cl_2. The combined residues from the organic layers were extracted with hot $CHCl_3$ and cooled, when nearly colourless product deposited in 12–14% yield, mp 300–305°C, almost free of carbonyl absorption in its ir spectrum. A further recrystallization from $CHCl_3$ gave pure product, mp > 310°C (lit. (9) mp 319–321°C); ^{1}Hmr δ (90 MHz) 8.0–7.5 (aromatic protons; -OH protons could not be clearly seen, sample only slightly soluble); uv (cyclohexane) λ_{max} (log ε_{max}) 323 nm (4.10), 320 sh (4.08), 308 (4.09), 281 (3.87), 270 (3.76), 260 (3.52), 250 sh (3.39), and 226 sh (4.67).

[9]Infrared bands and mass spectral data are available, at a nominal charge, from the Depository of Unpublished Data, CISTI, National Research Council of Canada, Ottawa, Canada K1A 0S2.

Monobridged-diol ***11b****, cis-6b,12b-Dihydroxy-3,4,6b,12b-tetrahydrocyclopent[f,g]acenaphth[1,2-a]acenaphthylene*

From *n*-BuLi (65 mmol in 35 ml hexane), 5,6-dibromoacenaphthene (10.0 g, 32.1 mmol), anhydrous ether (900 ml) and acenaphthenequinone (Aldrich, 5.85 g, 32.1 mmol) product **11***b* could be isolated in 10–20% yield as described above for **11***a*, as off-white crystals mp 290–295°C. Recrystallization from acetone or chloroform gave **11***b* as a white powder mp 304–308°C (dec.); ^{1}Hmr δ (60 MHz) 7.9–7.2(m, aromatic protons) and 3.38 (s, -CH_2-) the -OH protons could not be clearly discerned, the sample being only slightly soluble; uv (cyclohexane) λ_{max} (log ε_{max}) 329 nm (4.12), 315 (4.08), 286 (3.84), 274 (3.72), 264 (3.51), 254 sh (3.32), and 227 sh (4.19); *Anal.* calcd. for $C_{24}H_{16}O_2$: C 85.69, H 4.79; found: C 85.46, H 5.01.

Bisbridged-diol ***11c****, cis-6b,12b-Dihydroxy-3,4,6b,9,10,12b-hexahydrodicyclopent[f,g:f′,g′]acenaphth[1,2-a]-acenaphthylene*

This was carried out exactly as described above for **11***b* except that pyracenequinone **10***c* (22) (6.68 g, 32.1 mmol) replaced the acenaphthenequinone. The product **11***c* was obtained in 13–26% yield as a cream powder mp 295–305°C. Recrystallization from $CHCl_3$ gave white powdery crystals, mp 316–320°C (dec.); ^{1}Hmr δ (90 MHz, DMSO-d_6) 7.96 (4H, d, J = 7 Hz, 1-Ar*H*), 7.58 (4H, d, J = 7 Hz, 2-ArH), 6.34 (2H, s, -OH), and 3.60 (8H, s, -CH_2-); uv (cyclohexane) λ_{max} (log ε_{max}) 333 nm (3.83), 319 (3.78), 291 (3.55). 279 (3.36), 268 (3.10), 259 sh (2.86), and 228 (4.36). *Anal.* calcd. for $C_{26}H_{18}O_2$: C 86.17, H 5.01; found: C 85.98, C 4.97.

Unbridged-diketone ***13a****, 1,8-(1′,8′)-Naphthalylnaphthalene*

This was prepared essentially as described by Letsinger (9) except that the reaction was carried out at room temperature for 4 h. Crystallization of the product from benzene yielded 75% of **13***a*, mp 334–334.5°C (lit. (9) mp 333–334°C); ^{1}Hmr δ (90 MHz) 8.00–7.75 (4H, m, α-Ar-*H*) and 7.65–7.30 (8H, m, β-Ar*H*); uv (cyclohexane) λ_{max} (log ε_{max}) 318 nm sh (4.10), 311 (4.11), 282 sh (3.84), 268 sh (3.78) 224 (4.80), and 210 (4.98).

Monobridged-diketone ***13b****, 5,6-(1′,8′)-Naphthalylacenaphthene*

This could be prepared as described for **13***a* above in 30–60% yield. The following procedure was found to be more efficient. Lead tetraacetate (5 g, 11 mmol) was added to a stirred suspension of diol **11***b* (1.75 g, 5.22 mmol) and trichloracetic acid (20 mg) in dry (Na) benzene (250 ml) at room temperature. After 30 min CH_2Cl_2 and dilute HCl were added. The organic layer was washed (aqueous HCl, aqueous NaOH, H_2O), dried, and evaporated. The residue was recrystallized from benzene to yield 1.32 g (76%) of product **13***b* as pale yellow crystals, mp 330–334°C (dec.); ^{1}Hmr δ (60 MHz) 8.0–7.6 (2H, m, α-ArH), 7.6–7.2 (8H, m, β-ArH), and 3.39 (4H, s, -CH_2-); uv (cyclohexane) λ_{max} (log ε_{max}) 331 nm (4.07), 324 sh (4.05) 282 sh (3.81) 276 sh (3.72) 226 sh (4.66), and 213 (4.82); *Anal.* calcd. for $C_{24}H_{14}O_2$: C 86.21, H 4.22; found: C 85.88, H 4.27.

Bisbridged-diketone ***13c****, 5,6-(5′,6′)-Acenaphthalyl-acenaphthene*

This was carried out using CCl_3COOH as catalyst exactly as described above for **13***a*, and gave a 71% yield of product **13***c* as yellow crystals from benzene–chloroform, mp > 330°C (dec.); ^{1}Hmr δ (90 MHz, CD_2Cl_2) 7.45 (4H, d, J = 7 Hz, *o*-CO-Ar*H*), 7.30 (4H, d, J = 7 Hz, *o*-CH_2-Ar*H*), and 3.34 (8H, s, -CH_2-); uv (cyclohexane) λ_{max} (log ε_{max}) 336 nm (4.12), 301 sh (3.86), 232 (4.70), and 215 (4.78); *Anal.* calcd. for $C_{26}H_{26}O_2$: C 86.65, H 4.47; found: C 86.80, H 4.76.

Wolff–Kishner Reduction of ***13a****: Preparation of Unbridged-alkene* ***12a****, Acenaphth[1,2-a]acenaphthylene*

This was carried out essentially as described by Agosta (15). After chromatography on silica gel, recrystallization of the product from xylene yielded 83% of **13***a*, mp 287–288°C (lit. (15) mp 284–286°C; (9) mp 285–286.5°C); ^{1}Hmr (90 MHz, CD_2Cl_2), see Chart 1; uv (cyclohexane) λ_{max} (log ε_{max}) 616 nm (2.62), 605 (2.59), 597 (2.61), 568 (2.92), 560 (2.92), 551 (2.92), 528 (3.00), 500 sh (2.93), 404.5 (4.21), 384.5 (4.21), 367 (4.02), 342 (4.12), 336.5 (4.09), 330 (3.97), 325 sh (3.96), 322 sh (3.92), 300 sh (4.10), 294 (4.14), 263 (3.97), 255 (4.15), 250 (4.30), 245 (4.37), 240 sh (4.38), 232.5 (4.43), 225 (4.78), 220 sh (4.75), and 212.5 (4.76); *Anal.* calcd. for $C_{22}H_{12}$: C 95.62, H 4.38; found: C 95.75, H 4.28.

The mother liquors from the above recrystallization usually contained a little of the dihydrocompound **14***a* as noted by Agosta (15).

Wolff–Kishner Reduction of ***13b****: Preparation of Monobridged-alkene* ***12b****, Pyraceno[1,2-a]acenaphthylene, (3,4-Dihydrocyclopent[f,g]acenaphth[1,2-a]acenaphthylene) and Monobridged-monoketone* ***15b****, 3,4-Dihydrocyclopent[d,e]naphtho[2,3,4-i,j]naphtho[6,7,8-d′,e′]cyclooctan-7-one*

(a) Short Reflux: Less Alkene ***12b****, More Ketone* ***15b***

Monobridged-diketone **13***b* (109 mg, 0.33 mmol), KOH (0.25 g), 97% hydrazine hydrate (1 ml, 20 mmol), ethylene glycol (5 ml), and water (2.5 ml) were heated to *ca.* 110°C for 1 h under N_2. The water was then distilled out in a N_2 stream, the temperature rising to about 180°C when it was purple. After 2 h at 180°C, the reaction was cooled and diluted with water. The products were extracted into CH_2Cl_2 and the organic layer was washed, dried, and evaporated. The residue was chromatographed on silica gel using benzene as eluant.

Eluted first was the mono-bridged alkene **12***b*, which, after removal of solvent, yielded 22 mg (22%) of purple crystals. Recrystallization from xylene yielded 10 mg (10%) of dark purple crystals, mp 274–276°C; ^{1}Hmr (90 MHz, CD_2Cl_2), see Chart 1; uv (cyclohexane) λ_{max} (log ε_{max}) 615 nm (2.54), 605 (2.54), 595 (2.58), 566 (2.94), 558 (2.94), 550 (2.95), 540 sh (2.99), 533 sh (3.04), 526 (3.05), 520 sh (3.04), 512 (3.03), 505 (3.02), 499 sh (3.01), 425 (4.35), 416 (4.13), 401 (4.28), 393 sh (4.10), 380 (3.99), 380 (3.82), 373 sh (3.82), 361 sh (3.63), 343 (3.94), 336 (3.83), 327 (3.80), 320 sh (3.69), 297 (39.8), 271 (3.90), 250 sh (4.36), 246 (4.36), 236 (4.60), 229 (4.67), and 213 (4.82); *Anal.* calcd. for $C_{24}H_{14}$: C 95.33, H 4.67; found: C 95.21, H 4.41.

Eluted next was a yellow band which on concentration and crystallization from $CHCl_3$–acetone gave bright yellow crystals of monobridged-monoketone **15***b* (34 mg, 33%), mp 233–234°C; ^{1}Hmr δ (90 MHz) 7.8–7.1 (10H, m, Ar*H*), 4.96 (1H, d, J = 14 Hz, *exo*-14-H), 4.38 (1H, d, J = 14 Hz, *endo*-14-H), and 3.24 (4H, s, -CH_2-); uv (cyclohexane) λ_{max} (log ε_{max}) 356 nm (3.91), 332 (3.96), 325 sh (3.91), 317 sh (3.89), 295 (3.83), 241 sh (4.49), and 216 (4.97); *Anal.* calcd. for $C_{24}H_{16}O$: C 89.97, H 5.03; found: C 90.28, H 5.09.

(b) Long Reflux: More Alkene ***12b****, Less Ketone* ***15b***

Monobridged-diketone **13***b* (1.25 g, 3.74 mmol), KOH (18 g), 97% hydrazine hydrate (35 ml, 0.7 mol), ethylene glycol (190 ml), and water (45 ml) were heated at 110–120°C for 8 h under N_2. The reaction was continued as described in (*a*) above, heating at 180–210°C for 3 h. After work-up and chromatography the red band yielded on crystallization from benzene 325 mg (27%) of dark purple crystals of **12***b*. Rechromatography over silica gel of the mother liquors from this crystallization using pentane as eluant gave first a yellow band, which on crystallization yielded 47 mg (4%) of pale yellow needles, mp 223–226°C, found to be identical to the monobridged-alkane **14***b*, obtained by hydrogenation of **12***b* described below. Next, more (5–10%) of the purple alkene **12***b* was eluted.

Wolff–Kishner Reduction of ***13c****: Preparation of Bisbridged-monoketone* ***15c****, (3,4,10,11-Tetrahydrodicyclopent[d,e:d′,e′]dinaphthocyclooctan-7-one)*

Bisbridged-diketone **13***c* (250 mg, 0.69 mmol), KOH (8 g), 97% hydrazine hydrate (15 ml, 0.3 mol), ethylene glycol (50 ml), and water (20 ml) were heated at *ca.* 120°C for 6 h under N_2. The water was then distilled out in a N_2 stream, the temperature rising to 180°C over 90 min. The reaction was heated at *ca.* 180°C for 12 h, during which time a bright yellow precipitate formed but no purple colour. After cooling H_2O and CH_2Cl_2 were added. The organic layer was washed, dried, and evaporated. Crystallization of the yellow residue from acetone–tetrahydrofuran (1:3) gave product **15***c* as bright yellow crystals 70 mg (29%) mp 284–287°C (dec.); ^{1}Hmr δ (90 MHz) 7.6–7.1 (8H, m, ArH), 4.85 (1H, d, J = 14 Hz, *exo*-7-H), 4.35 (1H, d, J = 14 Hz, *endo*-7-H), and 3.27 (8H, s, -CH_2-); uv (cyclohexane) λ_{max} (log ε_{max}) 364 nm (3.92), 334 (3.98), 320 (3.95), 305 sh (3.87), 282 sh (3.61), 239 sh (4.54), 230 sh (4.63), and 219 (4.86); *Anal.* calcd. for $C_{26}H_{18}O$: C 90.14, H 5.24; found: C 90.28, H 5.08.

Reaction of Diols ***11a****,* ***11b****,* ***11c*** *with HF*
General Procedure

Liquid anhydrous H_2F_2 (Matheson, 50 ml) was added directly from a cylinder to the diol in a polyethylene flask under N_2 cooled to −70°C. The reaction mixture, which went dark instantly, was allowed to warm to room temperature overnight in a N_2 stream such that all the H_2F_2 evaporated. The dark residue was then taken up in CH_2Cl_2 and aqueous Na_2CO_3 solution added. The organic layer became redder over a period of hours (0.5–6 h), after which it was washed, dried, and evaporated. Each residue was treated as described below.

(a) Diol ***11a****: Preparation of Unbridged-alkene* ***12a***—From diol **11***a* (50 mg, 0.16 mmol) after filtration through a silica gel column in benzene there was obtained 31 mg (68%) of alkene **12***a*, identical to the sample previously obtained.

(b) Diol ***11b****: Preparation of Monobridged-alkene* ***12b***—From diol **11***b* (600 mg, 1.8 mmol) after chromatography

on silica gel using benzene as eluant there was obtained 228 mg (42%) of alkene **12***b*, identical to the sample previously obtained.

*(c) Diol **11**c: Preparation of Bisbridged-alkene **12**c, Pyraceno[1,2-a]-5,6-dihydropyracylene (3,4,9,10-Tetrahydrodicyclopent[f,g:f′,g′]acenaphth[1,2-a]acenaphthylene)*— From diol **11***c*, (1.4 g, 3.9 mmol) after chromatography on silica gel using CH_2Cl_2 as eluant the red band yielded 400 mg (32%) of alkene **12***c*, as dark purple crystals mp > 350°C from benzene (or xylene); ^{1}Hmr (90 MHz, CD_2Cl_2) see Chart 1; uv (cyclohexane) λ_{max} (log ε_{max}) 615 nm (2.56), 606 (2.62), 596 (2.65), 587 (2.74), 578 sh (2.86), 565 (3.00), 556 (3.01), 542 (3.07), 533 (3.11), 524 (3.12), 516 (3.12), 506 (3.12), 498 sh (3.11), 490 sh (3.09), 434 (4.20), 424 (4.01), 410 (4.10), 401 (3.88), 388 (3.79), 380 sh (3.56), 368 sh (3.39), 360 sh (3.20), 343 (3.59), 334 (3.44), 328 (3.47), 311 sh (3.55), 305 sh (3.55), 305 sh (3.59), 300 (3.60), 269 (3.79), 258.5 (4.12), 252 (4.14), 246 (4.10), 239 (4.32), 231 (4.34), and 217 (4.56); *Anal.* calcd. for $C_{26}H_{16}$: C 95.09, H 4.91; found: C 95.16, H 4.84.

Eluted next from the column was a yellow band which after concentration and crystallization from benzene and then chloroform yielded 28 mg (2%) of pale yellow crystals, mp > 350°C assigned the structure of the bisbridged-difluoro monoketone **26***c*, 3,4,10,11-tetrahydrodicyclopent[*d*,*e*:*d*′,*e*′]dinaphtho-14,14-difluorocyclooctan-7-one; ^{1}Hmr (90 MHz) see text; uv (cyclohexane) λ_{max} (log ε_{max}) 356 nm (4.02), 332 (4.08), 318 (3.93), 300 (3.85), 289 sh (3.74), 267 sh (3.37), 257 (3.39), 250 sh (3.94), 231 (4.75), and 217 (4.70); *Anal.* calcd. for $C_{26}H_{16}F_2O$: C 81.67, H 4.22; found: C 81.88, H 4.23.

*Reaction of Unbridged-diol **11**a with 'Magic Acid'*

The diol **11***a* (50 mg, 0.16 mmol) was added at 0°C under N_2 to FSO_3H (Magic acid, 5 ml). The reaction turned black at once, and was stirred at 0°C for 2 h before pouring onto ice. The products were extracted with CH_2Cl_2, washed, dried, and evaporated. A quantitative uv indicated 6.6 mg of product **12***a* was present, a yield of 15%.

*Preparation of the Alkenes **12**a, **12**b, and **12**c Through the Corey Thionocarbonate Procedure (32)*

An In Situ General Procedure

Thiophosgene (0.1 ml, 1.3 mmol) was injected into a solution of imidazole (340 mg, 5 mmol) in 20 ml of *o*-xylene (dry) under N_2 at room temperature. After stirring for 2 h the suspension was removed by filtration and the diol (50 mg) was added to the filtrate and heated to 100°C for 12 h. Tris(diethylamino)phosphine (1 ml) was then added and the reaction heated to reflux for 2 h. After cooling and addition of H_2O and CH_2Cl_2 the organic layer was washed, dried, and evaporated. The residue was chromatographed on a small column of silica gel in benzene, the red-purple band yielding on concentration crystalline product in *ca.* 30% yield for each alkene **12***a*, **12***b*, and **12***c* identical to the samples previously obtained.

*Reaction of the Diols **11**a, **11**b, and **11**c wtih P_2I_4: Preparation of Alkenes **12**a and **12**b*

General Procedure

The diol (500 mg) and P_2I_4 (83) (500 mg) were stirred for 12 h in dry ether (100 ml) or THF (80 ml) and then the red-orange solution was heated under reflux for 4 h. After cooling the iodine was removed by washing with $Na_2S_2O_3$ solution; CH_2Cl_2 was added if necessary. The organic layer was washed, dried, and evaporated and the residue chromatographed on silica gel in benzene. Concentration of the red-purple band yielded crystalline product. The yields were very variable and ranged from 16–96% for alkenes **12***a* and **12***b*; none of alkene **12***c* could be detected. The average yield over ten experiments was 49% for **12***b*.

*Reaction of Monobridged-diol **11**b, with Low-valent Titanium Species (38): Preparation of the Monobridged Alkane **14**b*

$LiAlH_4$ (65 mg, 1.7 mmol) was added to a suspension of $TiCl_3$ (400 mg, 2.6 mmol) in dry THF (15 ml) and stirred under N_2 for 30 min. The diol **11***b* (95 mg, 0.28 mmol) was then added and the mixture heated under reflux for 6 h. After cooling, CH_2Cl_2 and H_2O were added and the orange organic layer was washed, dried, and evaporated. The residue was chromatographed on silica gel. From the first yellow band there was obtained 13 mg (15%) of monobridged-alkane **14***b*.

*Hydrogenation of the Alkenes **12**a, **12**b, and **12**c: Preparation of the Alkanes **14**a, **14**b, and **14**c*

The alkene (80 mg) in benzene (25–50 ml) was stirred under a hydrogen atmosphere (770 torr) in presence of PtO_2 (~25 mg). The purple colour faded to yellow within 2 h. Removal of catalyst and then solvent left crystals of product alkanes in near quantitative yield. The products were recrystallized from cyclohexane to yield the following.

(*a*) From alkene **12***a* unbridged-alkane **14***a*, *cis*-6b,12b-dihydroacenaphth[1,2-*a*]acenaphthylene as long white needles, mp 213–215°C (lit. (15) mp 216–219°C); ^{1}Hmr δ (90 MHz) 7.8–7.4 (12H, m, ArH) and 5.71 (2H, s, —CH—); uv (cyclohexane) λ_{max} (log ε_{max}), 308 nm (4.05), 303 (4.08), 296 (4.11), 282 (3.96), 271 (3.76), 260 (3.60), 222 sh (5.06), and 217 (5.09).

(*b*) From alkene **12***b*, monobridged-alkane **14***b*, pyraceno[1,2-*a*]acenaphthene (3,4,6b,12b-tetrahydrocyclopent[f,g]acenaphth[1,2-*a*]acenaphthylene) as fluffy white needles mp 233–235°C; ^{1}Hmr δ (90 MHz) 7.6–7.0 (10H, m, ArH), 5.73 (2H, s, —CH—), and 3.36 (4H, s, -CH_2-); uv (cyclohexane) λ_{max} (log ε_{max}) 360 nm (2.94), 343 (3.07), 316 sh (4.04), 314 (4.04), 308 (4,08), 303 (4.11), 291 sh (3.97), 286 sh (3.96), 275 sh (3.71), 264 sh (3.61), and 223 (5.05); *Anal.* calcd. for $C_{24}H_{16}$: C 94.70, H 5.30; found: C 94.51, H 5.40.

(*c*) From alkene **12***c*, bisbridged-alkane **14***c*, pyraceno-[1,2-*a*]pyracene, (3,4,6b,9,10,12b-hexahydrodicyclopent-[f,g:f′,g′]acenaphth[1,2-*a*]acenaphthylene) as white crystals mp 282–283°C; ^{1}Hmr δ (90 MHz) 7.48 (4H, d, J = 7 Hz, H-1,6,7,12), 7.18 (4H, d, J = 7 Hz, H-2,5,8,11), 5.93 (2H, s, —CH—), and 3.31 (8H, s, -CH_2-); uv (cyclohexane) λ_{max} (log ε_{max}) 327 nm (3.91), 317 (4.11), 310 (4.14), 304 (4.16), 290 (4.02), 280 sh (3.80), 268 sh (3.61), 255 (3.51), and 228 (5.00); *Anal.* calcd. for $C_{26}H_{18}$: C 94.51, H 5.49; found: C 93.99, H 5.41. (This sample burnt with extreme difficulty.)

Measurement of Electrode Reduction Potentials

The values quoted in Table 4 were measured on a Metrohm-Polarecord E261 as 0.002 *M* solutions of hydrocarbon in anhydrous dimethylformamide which was 0.175 *M* in tetra *n*-butylammonium iodide using a dropping mercury electrode relative to the standard calomel electrode.

Acknowledgments

We thank the National Research Council of Canada and the University of Victoria for their support of this work.

1. V. Balasubramaniyan. Chem. Rev. **66**, 567 (1966).
2. A. G. Anderson, Jr. and R. H. Wade. J. Am. Chem. Soc. **74**, 2274 (1952).
3. H. J. Dauben and A. G. Osborne. Abstracts of the 130th National Meeting of the American Chemical Society, Atlantic City, NJ. 1956. p. 370.
4. B. M. Trost, P. L. Kinson, C. A. Maier, and I. C. Paul. J. Am. Chem. Soc. **93**, 7275 (1971).
5. H. Yamaguchi and T. Nakajima. Bull. Chem. Soc. Jpn. **44**, 682 (1971).
6. A. G. Anderson, Jr. and R. G. Anderson. J. Org. Chem. **23**, 517 (1958).
7. B. M. Trost and G. M. Bright. J. Am. Chem. Soc. **89**, 4244 (1967).
8. B. M. Trost, G. M. Bright, C. Frihart, and D. Brittelli. J. Am. Chem. Soc. **93**, 737 (1971).
9. R. L. Letsinger and J. A. Gilpin. J. Org. Chem. **29**, 243 (1964).
10. J. D. Roberts, A. Streitwieser, Jr., and C. M. Regan. J. Am. Chem. Soc. **74**, 4579 (1952); A. Rosowsky, H. Fleischer, S. T. Young, R. Partch, W. H. Saunders, Jr., and V. Boekelheide. Tetrahedron, **11**, 121 (1960); R. Breslow. Chem. Eng. News, **43**, 90 (1965).
11. R. Breslow, W. Horspool, H. Sugiyama, and W. Vitale. J. Am. Chem. Soc. **88**, 3677 (1966); R. Breslow, W. Vitale, and K. Wendel. Tetrahedron Lett. 365 (1965); G. Schröder and H. Röttele. Angew. Chem. Int. Ed. Engl. **7**, 635 (1968); R. R. Jones and R. G. Bergman. J. Am. Chem. Soc. **94**, 660 (1972); R. Breslow, M. Oda, and T. Sugimoto. J. Am. Chem. Soc. **96**, 1640 (1974); J. A. Elix, M. V. Sargent, and F. Sondheimer. J. Am. Chem. Soc. **89**, 5080 (1967); G. Schröder, S. R. Ramadas, and P. Nikoloff. Chem. Ber. **105**, 1072 (1972); P. J. Garratt and R. H. Mitchell. Chem. Commun. 719 (1968); P. J. Garratt, K. P. C. Volhardt, and R. H. Mitchell. J. Chem. Soc. C, 2137 (1970); R. Breslow, J. Napierski, and T. C. Clarke. J. Am. Chem. Soc. **97**, 6275 (1975).
12. C. F. Wilcox, Jr., J. P. Uetrecht, G. D. Grantham, and K. G. Grohmann. J. Am. Chem. Soc. **97**, 1914 (1975).
13. H. Reel and E. Vogel. Angew. Chem. Int. Ed. Engl. **11**, 1013 (1972).
14. M. J. S. Dewar and N. Trinajstic. Collec. Czech. Chem. Commun. **35**, 3484 (1970); R. D. Brown. J. Chem. Soc. 2391 (1951); B. A. Hess, Jr. and L. J. Schaad. J. Org. Chem. **36**, 3418 (1971); J. Am. Chem. Soc. **93**, 2413 (1971); R. S. Sheldrake and W. C. Herndon. Tetrahedron Lett. 775 (1975) and references therein; A. Graovic, I. Gutman, M. Randić, and N. Trinajstic. J. Am. Chem. Soc. **95**, 6267 (1973).
15. W. C. Agosta. J. Am. Chem. Soc. **89**, 3505 (1967); Tetrahedron Lett. 3635 (1966).
16. R. L. Letsinger, J. A. Gilpin, and W. J. Vullo. J. Org. Chem. **27**, 672 (1962).
17. H. H. Hodgson and J. S. Whitehurst. J. Chem. Soc. 80 (1947).
18. R. Avoyan and Yu. Struckov. Zh. Strukt. Khim. **3**, 605 (1962).
19. G. P. Petrenko, V. G. Usachenko, and A. P. Karushin. Zh. Org. Khim. **4**, 2190 (1968); J. Org. Chem. (USSR), 2113 (1968).
20. P. R. Constantine, L. W. Deady, and R. D. Topsom. J. Org. Chem. **34**, 1113 (1969).
21. S. D. Ross, M. Finkelstein, and R. C. Petersen. J. Am. Chem. Soc. **80**, 4327 (1958).
22. B. M. Trost. J. Am. Chem. Soc. **91**, 918 (1969).
23. R. P. Bell, V. G. Rivlin, and W. A. Waters. J. Chem. Soc. 1696 (1958); C. A. Grob and P. W. Schiess. Helv. Chim. Acta, **43**, 1546 (1960).
24. L. M. Jackman and S. Sternhell. Applications of nuclear magnetic resonance spectroscopy in organic chemistry. Pergamon Press, Oxford. 1969. p. 92.
25. (*a*) P. T. Lansbury and M. Klein. Tetrahedron Lett. 1981 (1968); (*b*) C. R. Johnson and D. C. Vegh. Chem. Commun. 557 (1969); (*c*) P. T. Lansbury, J. F. Bieron, and M. Klein. J. Am. Chem. Soc. **88**, 1477 (1966); P. T. Lansbury, A. J. Lacher, and F. D. Saeva. J. Am. Chem. Soc. **89**, 4360 (1969).
26. R. Kuhn and A. Winterstein. Helv. Chim. Acta, **11**, 106 (1928); R. Kuhn and K. Wallenfels. Chem. Ber. **71**, 1899 (1938); R. Kuhn and K. L. Scholler. Chem. Ber. **87**, 598 (1954).
27. L. F. Fieser and M. Fieser. Reagents for organic synthesis. Vol. 1. J. Wiley, New York, NY. 1967. p. 1160; R. Schoenheimer. J. Biol. Chem. **110**, 461 (1935); D. H. R. Barton and E. Miller. J. Am. Chem. Soc. **72**, 1066 (1950); C. L. Stevens and J. C. French. J. Am. Chem. Soc. **75**, 657 (1953).
28. W. E. Bachmann and E. J. H. Chu. J. Am. Chem. Soc. **58**, 1118 (1936).
29. E. J. Corey, C. U. Kim, and M. Taheda. Tetrahedron Lett. 4339 (1972).
30. G. A. Wiley, R. L. Hershkowitz, B. M. Rhein, and B. C. Chung. J. Am. Chem. Soc. **86**, 964 (1964).
31. C. E. Castro. J. Am. Chem. Soc. **83**, 3262 (1961); C. E. Castro and W. C. Kray, Jr. J. Am. Chem. Soc. **86**, 4603 (1964); I. M. Mathai, K. Schug, and S. I. Miller. J. Org. Chem. **35**, 1733 (1970).
32. E. J. Corey and R. A. Winter. J. Am. Chem. Soc. **85**, 2677 (1963).
33. R. H. Mitchell. Can. J. Chem. **54**, 238 (1976).
34. T. J. Pullukat and G. Urry. Tetrahedron Lett. 1953 (1967).
35. H. A. Staab and G. Walther. Ann. **657**, 98 (1962).
36. J. Daub, V. Trautz, and U. Erhardt. Tetrahedron Lett. 4435 (1972).
37. E. Vedejs and E. S. C. Wu. J. Org. Chem. **39**, 3641 (1974).
38. J. E. McMurrey and M. P. Fleming. J. Am. Chem. Soc. **96**, 4708 (1974).
39. J. E. McMurrey and M. P. Fleming. J. Org. Chem. **41**, 896 (1976); J. E. McMurrey. Paper S28, The 31st

Meeting of the Northwest Region of the American Chemical Society, Reno, Nevada, June 14, 1976.
40. F. W. EASTWOOD, K. J. HARRINGTON, J. S. JOSAN, and J. L. PURA. Tetrahedron Lett. 5223 (1970); J. S. JOSAN and F. W. EASTWOOD. Aust. J. Chem. **21**, 2013 (1968); J. N. HINES, M. J. PEAGRAM, G. H. WHITHAM, and M. WRIGHT. Chem. Commun. 1593 (1968).
41. M. GOMBERG and W. E. BACKMANN. J. Am. Chem. Soc. **49**, 236 (1927).
42. R. E. BUCKLES and W. D. WOMER. J. Am. Chem. Soc. **80**, 5055 (1958); R. E. BUCKLES, R. E. ERIKSON, J. D. SNYDER, and W. B. PERSON. J. Am. Chem. Soc. **82**, 2444 (1960); N. C. BAENZIGER, R. E. BUCKLES, and T. D. SIMPSON. J. Am. Chem. Soc. **89**, 3405 (1967); L. EBERSON and L. G. GONZALEZ. Acta Chem. Scand. **27**, 1255 (1973).
43. L. MAZUCH, R. H. MITCHELL, and P. R. WEST. Chem. Ind. 399 (1975).
44. D. A. FORSYTH and G. A. OLAH. J. Am. Chem. Soc. **98**, 4086 (1976).
45. L. J. BELLAMY. The infrared spectra of complex molecules. 2nd ed. Methuen and Co. Ltd, London. 1958. p. 330.
46. R. G. HARVEY and H. CHO. J. Am. Chem. Soc. **96**, 2434 (1974).
47. B. M. TROST, D. BUHNER, and G. M. BRIGHT. Tetrahedron Lett. 2787 (1973).
48. T. R. WELBERRY. Proc. R. Soc. Ser. A, **334**, 19 (1973).
49. H. W. W. EHRLICH. Acta Crystallogr. **10**, 699 (1957).
50. W. D. GOOD. J. Chem. Thermodyn. **5**, 715 (1973).
51. R. N. JONES. Chem. Rev. **32**, 1 (1943).
52. E. CLAR. J. Chem. Phys. **17**, 741 (1949); Chem. Ber. **82**, 495 (1949); Spectrochim. Acta, **4**, 116 (1950).
53. D. PETERS. J. Chem. Soc. 646 (1957) and references therein.
54. H. C. LONGUET HIGGINS and R. G. SOWDEN. J. Chem. Soc. 1404 (1952); VON PL. A. PLATTNER and E. HEILBRONNER. Helv. Chim. Acta, **30**, 910 (1947).
55. W. L. MOSBY. J. Am. Chem. Soc. **75**, 3348 (1953) and references quoted therein.
56. R. N. JONES. J. Am. Chem. Soc. **63**, 313 (1941); G. M. BADGER, J. E. CAMPBELL, J. W. COOK, R. A. RAPHAEL, and A. J. SCOTT. J. Chem. Soc. 2326 (1950); E. M. ARNETT, M. E. STREM, and R. A. FRIEDEL. Tetrahedron Lett. 658 (1961).
57. R. N. JONES. J. Am. Chem. Soc. **67**, 2127 (1945); G. H. BEAVEN, D. M. HALL, M. S. LESSLIE, and E. E. TURNER. J. Chem. Soc. 854 (1952).
58. B. H. SMITH. Bridged aromatic compounds. Academic Press, New York, NY. 1964. Chapt. 6, p. 359.
59. G. N. LEWIS and M. CALVIN. Chem. Rev. **25**, 273 (1939).
60. S. K. BOSE. Theor. Chim. Acta (Berlin), **5**, 84 (1966).
61. A. STREITWIESER, JR. Molecular orbital theory for organic chemists. John Wiley, New York, NY. 1961. p. 220.
62. A. DASGUPTA and N. K. DASGUPTA. J. Mol. Struct. **27**, 113 (1975).
63. D. BRIGHT, I. E. MAXWELL, and J. DE BOER. J. Chem. Soc. Perkin Trans. II, 2103 (1973); R. H. BOYD. J. Chem. Phys. **49**, 2574 (1968); N. L. ALLINGER and J. T. SPRAGUE. J. Am. Chem. Soc. **95**, 3893 (1973).
64. R. H. MITCHELL and F. SONDHEIMER. J. Am. Chem. Soc. **90**, 530 (1968).
65. D. J. CRAM, N. L. ALLINGER, and H. STEINBERG. J. Am. Chem. Soc. **76**, 6132 (1954); D. J. CRAM, C. K. DALTON, and G. R. KNOX. J. Am. Chem. Soc. **85**, 1088 (1962).
66. D. J. CRAM and H. STEINBERG. J. Am. Chem. Soc. **73**, 5691 (1951).
67. L. HORNER and F. MAURER. Ann. **736**, 145 (1970).
68. A. J. JONES, T. D. ALGER, D. M. GRANT, and W. M. LITCHMAN. J. Am. Chem. Soc. **92**, 2386 (1970); M. J. S. DEWAR and R. C. FAHEY. J. Am. Chem. Soc. **85**, 2704 (1963).
69. M. A. COOPER and S. L. MANATT. J. Am. Chem. Soc. **91**, 6325 (1969).
70. S. CASTELLANO and R. KOSTELNIK. Tetrahedron Lett. 5211 (1967).
71. B. V. CHENEY. J. Am. Chem. Soc. **90**, 5386 (1968) and references quoted therein.
72. C. W. HAIGH, R. B. MALLION, and E. A. G. ARMOUR. Mol. Phys. **18**, 751 (1970) and references therein.
73. C. A. COULSON and R. B. MALLION. J. Am. Chem. Soc. **98**, 592 (1976).
74. T. D. ALGER, D. M. GRANT, and E. G. PAUL. J. Am. Chem. Soc. **88**, 5397 (1966); A. J. JONES, T. D. ALGER, D. M. GRANT, and W. M. LITCHMAN. J. Am. Chem. Soc. **92**, 2386 (1970); H. GUNTHER and W. HERRIG. J. Am. Chem. Soc. **97**, 5594 (1975) and references therein.
75. B. M. TROST and W. B. HERDLE. J. Am. Chem. Soc. **98**, 4080 (1976).
76. D. J. CRAM, C. K. DALTON, and G. R. KNOX. J. Am. Chem. Soc. **85**, 1088 (1963); D. J. CRAM and R. C. HELGESON. J. Am. Chem. Soc. **88**, 3515 (1966).
77. R. H. MITCHELL and V. BOEKELHEIDE. J. Am. Chem. Soc. **96**, 1547 (1974).
78. P. H. GIVEN. J. Chem. Soc. 2684 (1952).
79. A. MACCOLL. Nature, **163**, 178 (1949).
80. G. J. HOIJTINK. Rec. Trav. Chim. **74**, 1525 (1955).
81. A. T. WATSON and F. A. MATSEN. J. Chem. Phys. **18**, 1305 (1950).
82. F. GERSON and J. H. HAMMONS. *In* Nonbenzenoid aromatics. Vol. 2. *Edited by* J. P. Snyder. Academic Press, New York, NY. 1971. Chapt. 2, p. 117.
83. F. E. E. GERMANN and R. N. TRAXLER. J. Am. Chem. Soc. **49**, 310 (1927).
84. R. H. MITCHELL, R. J. CARRUTHERS, and J. C. M. ZWINKELS. Tetrahedron Lett. 2585 (1976).
85. D. W. J. CRUICKSHANK and R. A. SPARKS. Proc. R. Soc. Ser. A, **258**, 270 (1960).
86. G. L. SIMMONS and E. C. LINGAFELTER. Acta Crystallogr. **14**, 872 (1961).
87. DMS UV Atlas. Butterworths, London. 1967.

A theoretical study of the Curtius rearrangement. The electronic structures and interconversions of the CHNO species

ARVI RAUK AND PAUL F. ALEWOOD

Department of Chemistry, The University of Calgary, Calgary, Alta., Canada T2N 1N4

Received June 10, 1976[1]

ARVI RAUK and PAUL F. ALEWOOD. Can. J. Chem. **55**, 1498 (1977).

The thermal and photochemical decomposition of formyl azide in the Curtius rearrangement has been studied by means of RHF–LCAO–MO–SCF calculations augmented by CI. The lower electronic states of carbonyl azides, carbonyl nitrenes, isocyanates, cyanates, oxazirenes, nitrile oxides (fulminates), and isofulminates are discussed on the basis of the results for formyl azide and the corresponding isomers of formula CHNO. The discovery of two nearly degenerate states of A'' symmetry for formyl azide which may channel decomposition products directly to both isocyanates and carbonyl nitrenes explains some puzzling features of the photolytic Curtius rearrangement. The interconvertibility of the CHNO isomers (and the RCNO isomers) is discussed in terms of the energetics and intended correlations of the accessible electronic states of these species.

ARVI RAUK et PAUL F. ALEWOOD. Can. J. Chem. **55**, 1498 (1977).

Faisant appel à des calculs RHF–LCAO–MO–SCF complétés par CI, on a étudié les décompositions thermiques et photochimiques de l'azoture de formyle au cours du réarrangement de Curtius. On discute des états électroniques les plus bas des azotures de carbonyle, des nitrènes de carbonyle, des isocyanates, des cyanates, des oxazirènes des oxydes de nitrile (fulminates) et des isofulminates sur la base des résultats obtenus avec l'azoture de formyle et des isomères correspondants de formule CHNO. La découverte de deux états presque dégénérés de symétrie A'' pour l'azoture de formyle, qui peuvent servir directement de canaux pour les produits de décompositions tant pour les isocyanates que les nitrènes de carbonyle, explique quelques caractéristiques embarrassantes du réarrangement de Curtius photochimique. On discute de l'interconvertibilité des isomères CHNO (et des isomères RCNO) en termes des corrélations énergétiques et perspectives des états électroniques accessibles de ces espèces.

[Traduit par le journal]

Introduction

Electron deficient substances are rarely stable and rarely amenable to direct study. Their intermediacy is often postulated in reactions which frequently involve intricate rearrangements of the molecular skeleton. The proof of their intermediacy is far more than just an academic exercise but lends valuable and difficult-to-obtain evidence regarding their chemical and physical properties.

In Scheme 1 are summarized the synthetically important Curtius, Hofmann, and Lossen rearrangements (1). For each of these reactions, a mechanism can be written which involves an intermediate carbonyl nitrene that subsequently rearranges to an isocyanate. Evidence, in the form of insertion and abstraction products, for the intermediacy of carbonyl nitrenes in the photolytic Curtius rearrangement is well documented. Likewise, thermal decomposition of 'rigid' azides such as azidoformates leads to the formation of nitrene trapping products. However, thermolysis of other acyl azides leads initially only to isocyanates (2, 3). The scope of the Curtius reaction is summarized in Scheme 2.

Failure to observe nitrene trapping products has led to the current thinking that migration of the alkyl or acyl group is concurrent with loss of halide in the Hofmann rearrangement and with loss of hydroxide (or carboxylate) in the case of the Lossen rearrangement. Because of the similarity of the three reactions (Scheme 1) the question arises as to whether, in the case of the Curtius reaction, the nitrenes are being generated by an alternative and competing decomposition of the acyl azide, with rearrangement to isocyanate being simultaneous with loss of nitrogen, in a manner completely analogous to the mechanism proposed for the Hofmann and Lossen reactions. Certainly, the migrating group is never kinetically free (4–6). An elegant study of isotope effects in the decomposition

[1]Revision received January 3, 1977.

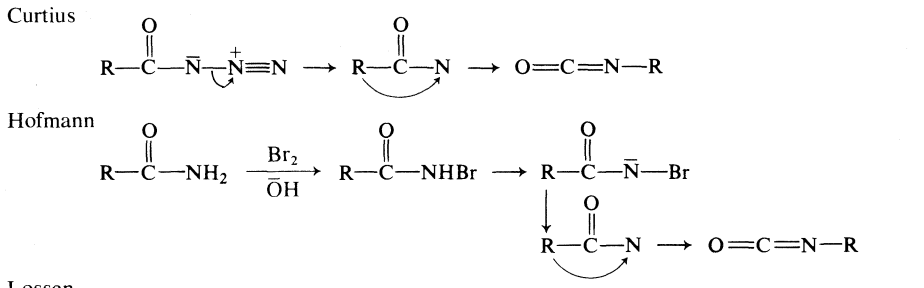

SCHEME 1

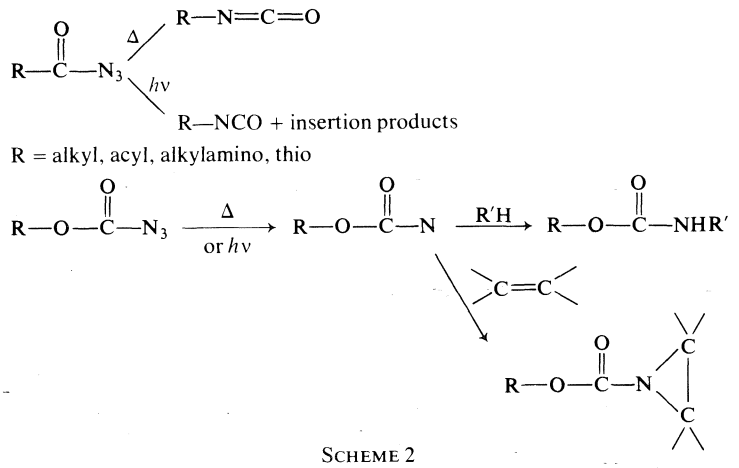

SCHEME 2

and rearrangement of benzoyl azide provides compelling evidence for the view that rearrangement and expulsion of nitrogen occur concurrently (7). That nitrenes may be generated by a different route is also supported by a study of the photolysis of pivaloyl azide in a variety of solvents (3). In this case the yields of isocyanate were essentially constant under all conditions while the yield of nitrene trapping products varied appreciably. Similar results have been obtained during the photolysis of benzoyl azide (8).

However, earlier evidence which suggested a non-concerted mechanism for the rearrangement-decomposition cannot easily be reinterpreted. Kinetic measurements of the thermally induced decomposition-rearrangement of *m*- and *p*-substituted benzoyl azides revealed no Hammett correlation (9). The substituents influenced the rate of nitrogen evolution in an unpredictable fashion (9). The results are contrary to the results obtained for the Hofmann and Lossen rearrangements (10, 11), and can be interpreted as evidence for a lack of aryl migration in the transition state. In the same vein, a small positive value in the volume change of activation in the thermal Curtius rearrangement of benzoyl azide has been cited as evidence that the reaction has a non-polar transition state in which extensive bond breaking (*i.e.* leading to nitrene) has taken place (12). Theoretical (13, 14) and experimental (15) investigations into the mechanism of the entirely analogous Wolff rearrangement (Scheme 3) has led to the general conclusion that the rearrangement is not concerted. From computed MO and state energies together with symmetry correlation it was concluded that the Wolff rearrangement does involve a ketocarbene, but when performed photolytically an oxirene intermediate is also involved. An oxirene intermediate is not formed in the thermal decomposition as the initially formed ketocarbene lacks sufficient vibrational energy to achieve cyclization.

Just and Zehetner (16, 17) have demonstrated the formation of acyl nitrenes as well as isocyanates upon irradiation of *O*-methylpodo-carponitrile oxide and mesitonitrile oxides. They suggested the mechanistic pathway shown in Scheme 4 and showed that isocyanate was

Wolff rearrangement

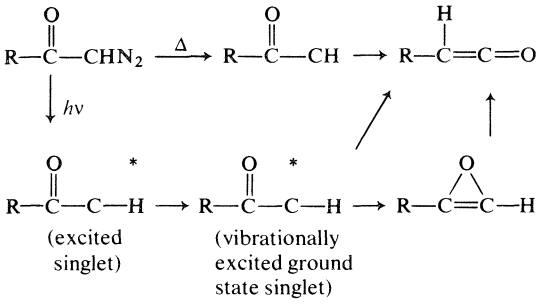

SCHEME 3

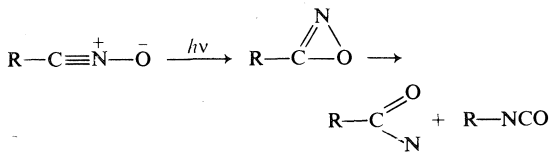

SCHEME 4

not appreciably converted to acylnitrene under the reaction conditions. The *thermal* isomerization of nitrile oxides (17) to isocyanates has been known for more than sixty years and has been recently reinvestigated by Grundmann and Dean (18) who achieved the clean rearrangement of substituted aryl nitrile oxides by refluxing them in a high boiling solvent. It was demonstrated that the mechanism involves an intramolecular rearrangement in which bond breaking and bond making are apparently synchronous (19). Grundmann suggested the following mechanism for the rearrangement:

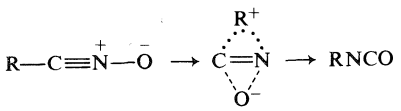

Alkyl isocyanates R—NCO are also readily produced from alkyl cyanates (20), ROCN, by an exothermic rearrangement (21). The tendency toward isomerization can be minimized if the alkyl carbonium ion R^+ is primary or bridgehead (21). Aryl cyanates do not rearrange thermally to aryl isocyanates. By analogy to the well studied thiocyanate to isothiocyanate rearrangement, the mechanism probably involves heterolytic bond cleavage, as below:

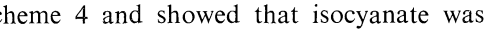

The electronic structures of carbonyl nitrenes have been studied by means of non-empirical MO computations (22, 23) and the mechanism of insertion and abstraction reactions discussed (22). We here present a study of the thermal and photolytic decomposition of formyl azide and the electronic structures and energetics of compounds isomeric to isocyanic acid, and discuss the possible pathways of interconversion.

Method

Restricted Hartree–Fock–Roothaan LCAO–MO–SCF (24) calculations were performed on the following compounds whose structures are shown in Fig. 1: formyl azide **1**, formyl nitrene **2**, isocyanic acid **3**, cyanic acid **4**, oxazirene **5**, fulminic acid **6**, and isofulminic acid **7**. Calculations on formyl nitrene **2** have previously

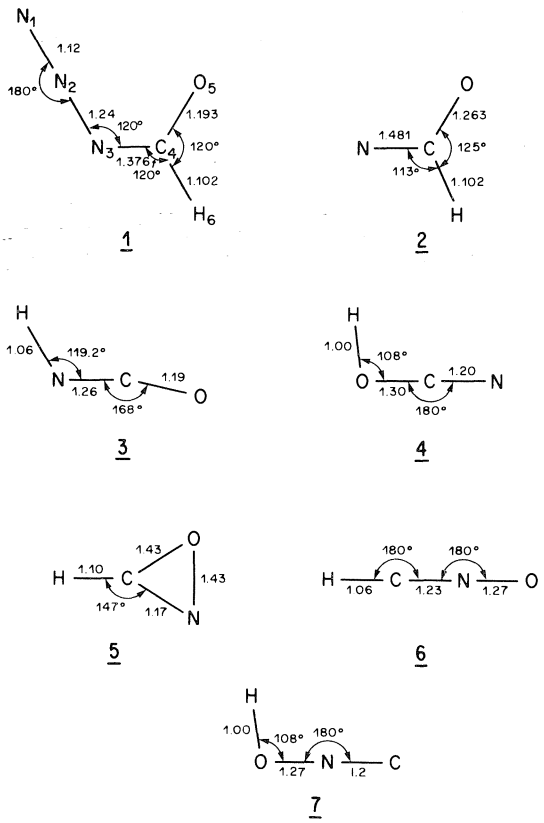

FIG. 1. Structures of the compounds **1**–**7** used in the study: bond lengths in Angstroms; angles in degrees.

been reported (22, 23). The geometry of **2** has been optimized by Harrison and Shalhoub (23). Further geometry variations were performed on **2** in order to establish which deformations of this molecule are relatively unhindered. Although the geometry of **3** has been reported (25), some geometry variation was performed on this system as a consequence of recent experimental (on ClNCO) (26) and theoretical (27, 28) indications that the NCO fragment may be appreciably non-linear. Limited geometry searches were performed on compounds **4** and **5** for which specific experimental data on geometries are lacking. The experimental geometry for **6** (29) and an 'idealized' geometry for **7** were adopted. For **1**, bond lengths were taken from formamide (30) and methyl azide (30) and idealized angles of 120° were used. Some geometry variation, to be discussed later, was performed. The geometries of the compounds for which results are reported in the text and in other figures are shown in Fig. 1.

In the present *ab initio* method, all one- and two-centre integrals are computed over a minimal basis set of exponential-type functions (STO). All three- and four-centre integrals are computed using Pople's (31) STO-3G Gaussian expansion of the STO's[2]. Slater exponents were employed for all atoms except hydrogen where an exponent of 1.2 was chosen. For reasons which are discussed below, calculations were also performed on compounds **2** and **3** using an extended basis set ($9s5p/4s$ contracted to $4s2p/2s$ (32)).

Since recent reports on electron deficient cationic systems (33, 34) have suggested that correlation energy may not adequately cancel when comparing calculated RHF energies of constitutional isomers, we decided to include correlation energies for the ground states of various species by perturbation theory. The correlation energy is taken as the second order correction to the RHF energy, which implies inclusion of all double excited configurations. The relative advantages and disadvantages of Rayleigh–Schrödinger (RS) and Brillouin–Wigner (BW) expansions and of Moller–Plesset (MP) and Epstein–Nesbet (EN) partitions of the Hamiltonian have recently been discussed by Ostlund and Bowen (34) and will not be repeated here. Suffice it to say that the BW–EN combination gives better convergence and includes higher order terms in a many-body sense than other combinations and is equivalent to the exact diagonalization of the double excited CI matrix if one neglects non-zero elements between double excited configurations. Use of the BW–EN procedure allows one to incorporate most of the correlation energy, for a given basis. This is the procedure we have adopted. All single determinantal double excited configurations except those involving core orbitals are included.

In the calculation of the energies of the excited states, all single excitations, excluding those involving core orbitals, are included. In many cases, heavy mixing between different single excited configurations occurs. It was necessary to include those configurations in the zero order description of the excited state and perform the exact diagonalization of the zero-order block of the CI matrix. The contributions of those configurations which mix only weakly were incorporated through Rayleigh–Schrödinger perturbation theory as second order corrections to the energy.

Excitation energies were calculated as the difference between the all-single-excitations CI energy for the excited state and the ground state RHF–SCF energy, rather than the energy which includes the correlation correction. This procedure is justified theoretically because terms coming from triply-excited configuration contributions to the excited state largely cancel those from doubly-excited configuration contributions to the ground state (35). As seen below, where comparisons can be made, good agreement with experimentally obtained excitation energies is obtained.

Results and Discussion

The results of Mulliken population analyses on the SCF configurations of compounds **1–7** are shown in Fig. 2. The valence molecular orbitals of compounds **3–6**, displayed as linear combinations of hybridized atomic orbitals, are shown in Figs. 3–6, respectively, as are the energies of the individual molecular orbitals. The orbitals have been classified as belonging to one or the other of the irreducible representations (a' or σ, a'' or π) of the point group C_s. Special features of the seven structures are dis-

[2]It was earlier determined (22) by using the STO-4G expansion that approximation of the smaller three- and four-centre integrals in this way does not lead to anomalous results in the electronic structure or relative energies.

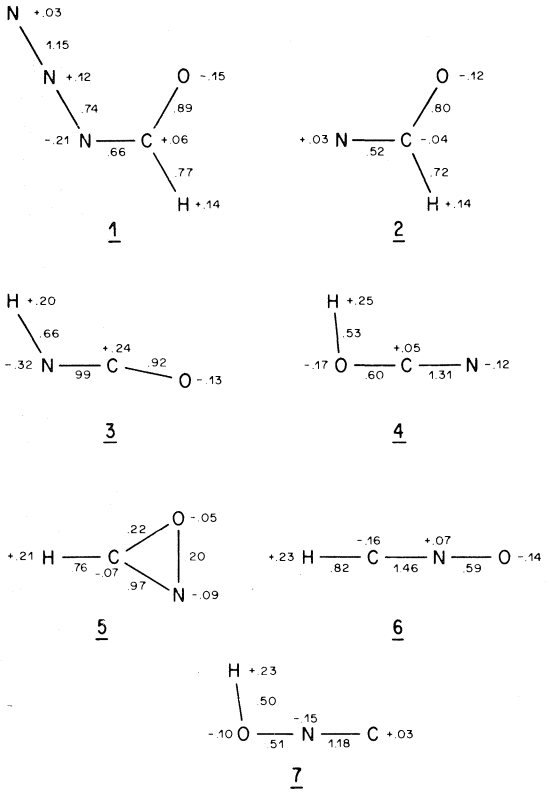

FIG. 2. Mulliken population analyses for compounds **1–7**. Net charges are indicated at the atomic positions and bond overlap populations on the bonds.

cussed separately in the sections immediately following. This is followed by a general discussion of the possible roles of these substances in the thermal and photolytic Curtius reactions.

Formyl Azide 1

The results of a Mulliken population analysis (Fig. 2) indicate that, of the various resonance forms for **1**, the

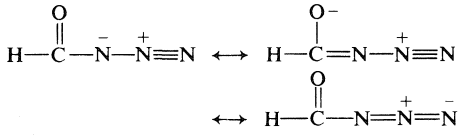

last shown is the least important. The ground state configuration of the molecule is $...(14\sigma)^2(15\sigma)^2(3\pi)^2$. The highest occupied molecular orbital in the ground state configuration (3π) is a π MO localized largely to the $N_1—N_2—N_3$ fragment with a node close to N_2. The second highest occupied MO (15σ, Fig. 7) is also π-like in the $N_1—N_2—N_3$ fragment, with a node near N_2, but has a contribution from an in-plane p orbital on oxygen.

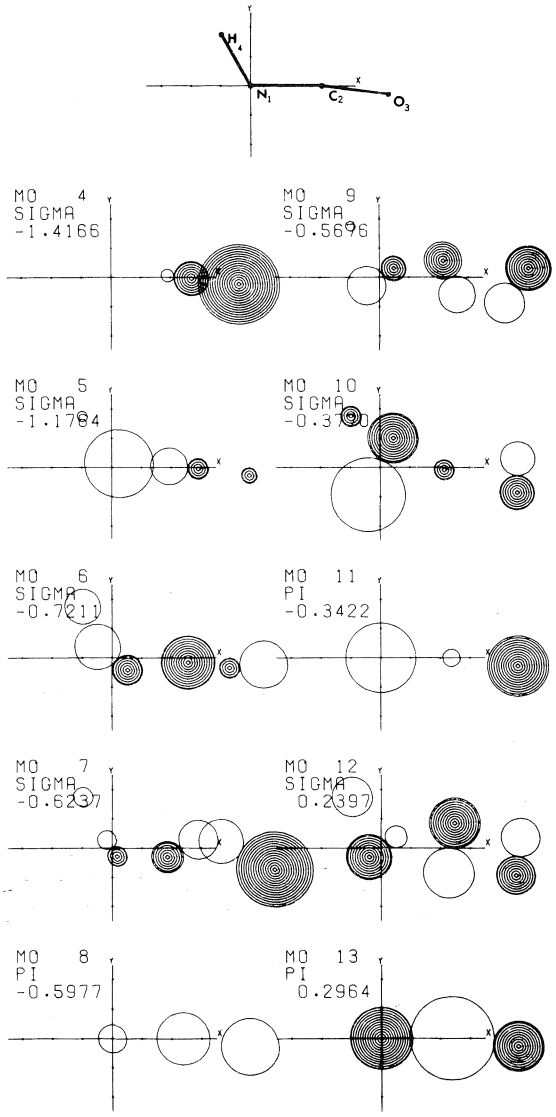

FIG. 3. The valence molecular orbitals of isocyanic acid **3** are displayed as linear combinations of hybridized atomic orbitals. The magnitude of each atomic orbital is directly proportional to the magnitude of its coefficient in the LCAO expansion of the MO. Only the top lobes of each PI (a'') orbital are shown. The MO energy is in hartree units (1 hartree = 627.71 kcal/mol = 27.21 eV).

Calculations allowing interaction among all singly excited configurations (except those involving excitations from the five core orbitals) yield four excited singlet states that lie less than 7 eV above the ground state. These are: $^1A_1''$

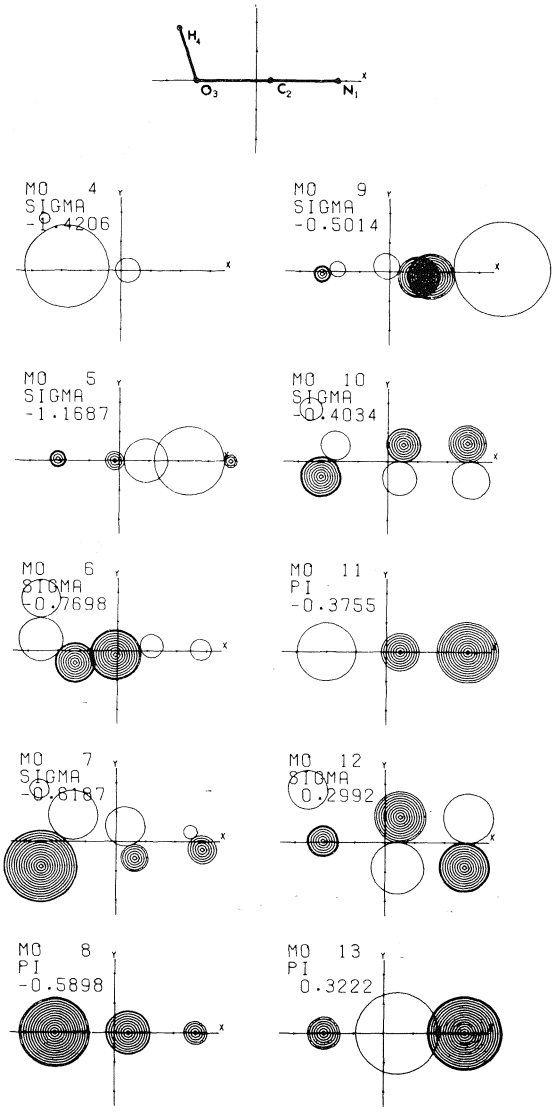

FIG. 4. The valence molecular orbitals of cyanic acid **4** are displayed as linear combinations of hybridized atomic orbitals. The magnitude of each atomic orbital is directly proportional to the magnitude of its coefficient in the LCAO expansion of the MO. Only the top lobes of each PI (a'') orbital are shown. The MO energy is in hartree units (1 hartree = 627.71 kcal/mol = 27.21 eV).

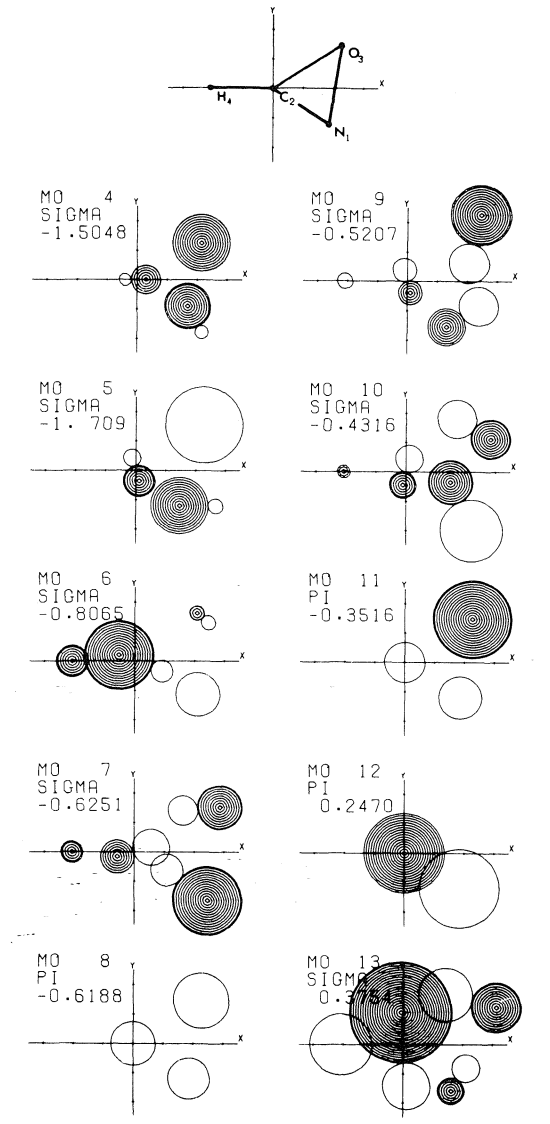

FIG. 5. The valence molecular orbitals of oxazirene **5** are displayed as linear combinations of hybridized atomic orbitals. The magnitude of each atomic orbital is directly proportional to the magnitude of its coefficient in the LCAO expansion of the MO. Only the top lobes of each PI (a'') orbital are shown. The MO energy is in hartree units (1 hartree = 627.71 kcal/mol = 27.21 eV).

4.44 eV; $^1A_2''$ 4.60 eV; $^1A_2'$ 5.96 eV; $^1A_3''$ 6.69 eV. In spite of the extensive photochemical studies of acyl azides that have been reported, we can find no reports of the uv spectra of these compounds. Methyl azidoformate, $CH_3OC(O)N_3$, has a weak band ($\varepsilon \sim 40$) at 4.8 eV (36). Alkyl azides exhibit two absorption bands in the near-uv region, a weak band ($\varepsilon \sim 25$) at 4.3 eV and a stronger band ($\varepsilon \sim 500$) at 5.7 eV (37). Both transitions are assigned to $\pi_x \rightarrow \pi_y^*$-type transitions ($A''$ symmetry) of the azide group, which correlate with orbital symmetry forbidden transitions of the azide anion. Our calculations indicate that the origin of the two

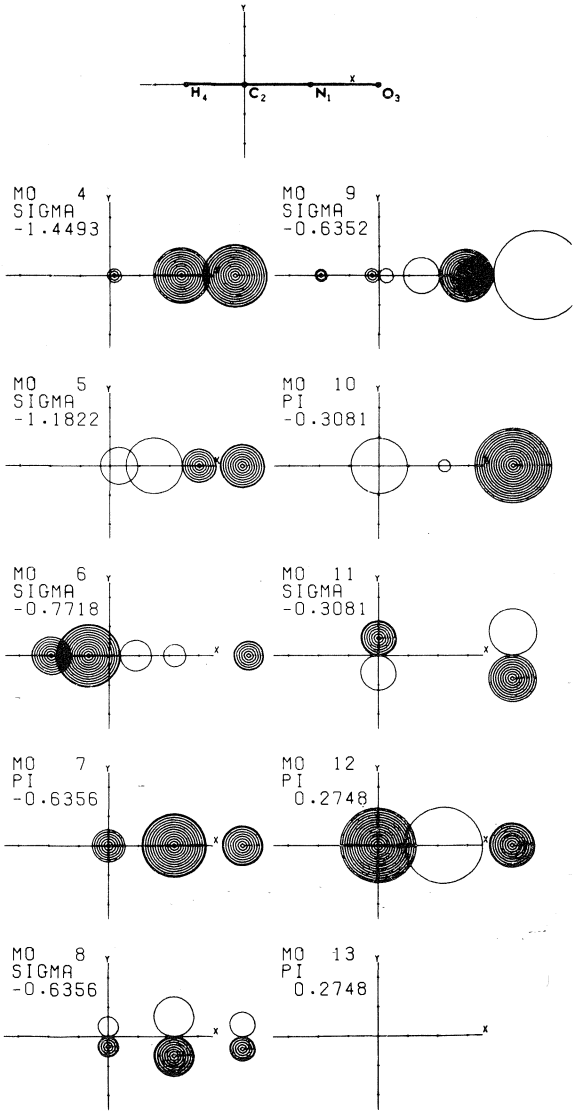

FIG. 6. The valence molecular orbitals of fulminic acid **6** are displayed as linear combinations of hybridized atomic orbitals. The magnitude of each atomic orbital is directly proportional to the magnitude of its coefficient in the LCAO expansion of the MO. Only the top lobes of each PI (a'') orbital are shown. The MO energy is in hartree units (1 hartree = 627.71 kcal/mol = 27.21 eV).

lowest nearly degenerate A'' transitions of formyl azide **1** is the same except that considerable mixing of other configurations of the same symmetry occurs. The transitions which give rise to the principal configurations for the two states $^1A_1''$ and $^1A_2''$, as well as the $^1A_2'$ state, are shown schematically in Fig. 7. The $^1A_2'$ state has almost equal contributions from

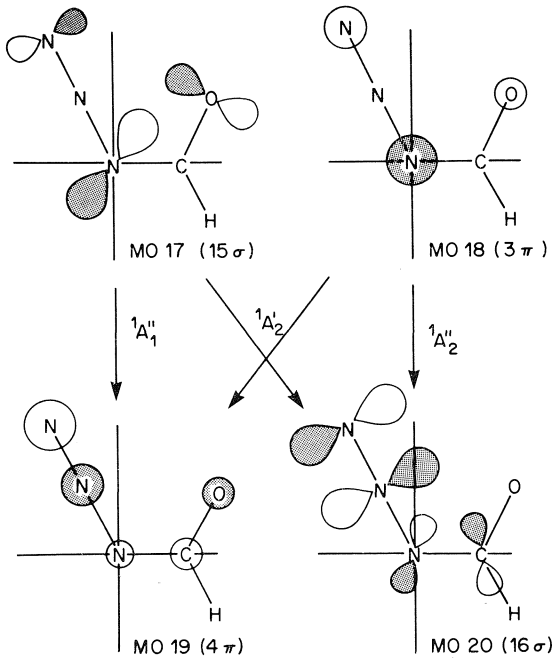

FIG. 7. The two highest occupied and two lowest unoccupied MO's of formyl azide **1**. The excitations which make major contributions to the first three excited states of **1** are indicated by the arrows.

the two configurations arising from the two $\pi \rightarrow \pi^*$-like transitions shown in Fig. 7.

The thermal and photolytic decomposition of the azide is discussed in the second to last section.

Formyl Nitrene 2

Although formyl nitrene has been discussed in detail previously (22, 23) some of the salient features bear repeating in the present context. The results of a Mulliken population analysis (Fig. 2) indicate that the nitrogen atom, though electron-deficient, does not compete effectively with oxygen for electrons. The contribution of the resonance structure

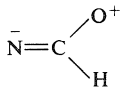

to the electronic structure of **2** is unimportant.

Examination of Fig. 2 of ref. 22 reveals that the electrons are missing from a non-bonded σ orbital (MO 12) highly localized to the nitrogen.[3]

[3]Electron spin resonance evidence (38) confirms that the extra electron in acetyl nitrene radical anion is in a nitrogen p orbital in the carbonyl plane.

There are four electrons in the π system of **2** (MO's 8 and 11). A resonance structure such as that above would only be important if either of MO 10 (oxygen non-bonded electron pair) or MO 11 (nitrogen non-bonded electron pair) were unoccupied.

One expects that the doubly-excited electronic configuration $...(1\pi)^2(8\sigma)^2(9\sigma)^2(2\pi)^0(10\sigma)^2$ would contribute strongly to the electronic structure of the $^1A_1'$ state of **2**, thereby reducing the anisotropy in the electron distribution about nitrogen. Recent natural orbital calculations by Harrison and Shalhoub (23) suggest an occupancy of 0.74 electrons for the natural orbital corresponding to MO 12 of the SCF calculation. Indeed, Harrison and Shalhoub find that the electronic state whose dominant configuration is that shown above is only 1.52 eV above the lowest singlet state of **2**. Since straightforward interaction of the SCF configuration with the $...(9\sigma)^2(10\sigma)^2$ configuration, when the latter is constructed from the orbitals of the former, yields the result that the states so generated are separated by 6.91 eV (6.83 eV with the larger basis set), it was necessary to perform an MCSCF (39) calculation involving the two configurations. Using the larger basis set, the energy of the lower closed shell singlet state is reduced relative to the SCF value by a small amount, 0.0166 hartree, yielding the MSCF energy −167.5613 hartree. However, the energy of the upper closed shell singlet is lowered to −167.4901 hartree. Thus the energy separation calculated by the MCSCF procedure is 1.83 eV, in satisfactory agreement with that found by Harrison and Shalhoub (23). Likewise, the composition of the lower state, $^1A_1'$, corresponds to 73% of the $...(9\sigma)^2(2\pi)^2$ configuration and 27% of the $...(9\sigma)^2(10\sigma)^2$ configuration. The upper closed shell state, $^1A_2'$, has the composition, 29% $...(9\sigma)^2(2\pi)^2$, 71% $...(9\sigma)^2(10\sigma)^2$. The $^1A_1''$ state of **2** is calculated to be 0.09 eV above the $^1A_1'$ state if one includes the lowering of the latter due to the MCSCF calculation. The dominant configuration of the $^1A_1''$ state is $...(9\sigma)^2(2\pi)^1(10\sigma)^1$. The fourth singlet state, $^1A_3'$, is 3.16 eV above the $^1A_1'$ state and corresponds mainly to the configuration $...(9\sigma)^1(2\pi)^2(10\sigma)^1$. The fifth state, $^1A_2''$, is 5.74 eV above the first singlet state and arises from the configuration $...(9\sigma)^1(2\pi)^2(3\pi)^1$. Except for the position of the $^1A_2'$ state, as explained above, similar results are obtained using the smaller STO basis, without MCSCF. The energies (in eV) obtained with the STO basis, relative to the $^1A_1'$ state are: $^1A_1''$ −0.82; $^1A_3'$ 3.32; $^1A_2''$ 4.21.

The possible intermediacy of carbonyl nitrenes, such as **2** in the thermal and photolytic Curtius reaction, is discussed later.

Isocyanic Acid **3**

Isocyanic acid is calculated to be the most stable isomer of formula HNCO, 91 kcal/mol more stable than formyl nitrene **2**. Separate calculations using various values for the CNO angle verified previous reports (26–28) that this angle in isocyanates is appreciably non-linear. Although one would not expect linearity of the heavy atom skeleton in any of the systems **1**, **3**–**7**, except **6**, since the NCO units (N_3 for **1**) do not reside in an axially symmetric potential, it was of interest to determine the extent of non-linearity and look for the cause of the unusually large deviation. The equilibrium value of the NCO angle of **3** (Fig. 1) is found to be 168°. The ground state electron distribution (Fig. 2) shows that the central carbon atom is much more electron deficient than in any of the other species considered. This is due to the fact that the two highest occupied molecular orbitals (MO's 10 and 11) are π-like orbitals with a node very near the carbon atom, and has the consequence that the NCO fragment has a very low bending force constant (40).

The calculated dipole moment is 1.70 D, in reasonable agreement with the experimental value of 2.1 D (41).

The near ultraviolet absorption spectrum of isocyanic acid **3** (as well as alkyl and inorganic isocyanates) has been previously analyzed (42, 43). Although only the first transition in isocyanic acid is observable (at 5.90 eV), many more states of the closely related alkyl isocyanates are seen. Excitation energies (in eV), computed with the large basis, are as follows (experimental values (42) for ethyl isocyanate are in parentheses): $^1A_1''$ 5.89 (5.95); $^1A_2'$ 7.38 (6.82); $^1A_2''$ 8.53 (7.13). The values obtained using the STO basis are: $^1A_1''$ 5.06; $^1A_2'$ 6.88; $^1A_2''$ 7.95.

The states $^1A_1''$ and $^1A_2''$ originate almost entirely from the transitions $2\pi \rightarrow 10\sigma$ (MO 11 to MO 12, Fig. 3) and $9\sigma \rightarrow 3\pi$ (MO 10 to MO 13, Fig. 3), respectively. The same four orbitals are involved in the description of the

state, $^1A_2'$, whose major configuration is that from $9\sigma \rightarrow 10\sigma$ but which has 42% contribution from the $2\pi \rightarrow 3\pi$ configuration.

Cyanic Acid **4**

Cyanic acid is computed to be 1 kcal/mol less stable than isocyanic acid. The results of population analysis of cyanic acid, shown in Fig. 2, and the molecular orbitals, shown in Fig. 4, support the usual valence bond description, C—O single bond, C—N triple bond.

The energies in eV, relative to the ground state, of the three lowest singlet states of cyanic acid are: A'' 6.78; A' 7.84; A'' 8.14. There are no published experimental uv spectroscopic data on **4** or alkyl cyanates.

The dipole moment of **4** is computed to be 2.96 D.

Oxazirene **5**

The anti-aromatic character expected for a conjugated three membered ring with 4π electrons is evident upon inspection of the results of population analysis of oxazirene (Fig. 2). The second occupied π orbital has a node which bisects the C—O and N—O bonds and leads to very small bond overlap populations for these two bonds. The total electronic energy of oxazirene is computed to be within 1 kcal/mol of the closed shell $^1A_1'$ state of formyl nitrene. The computations reveal that there are no singlet electronic states of oxazirene that are less than 7 eV above its ground state. There are no experimental data on this compound.

The dipole moment of **5** is computed to be 2.16 D.

Fulminic Acid **6**

Fulminic acid, a model for alkyl nitrile oxides is calculated to be 60 kcal/mol less stable than isocyanic acid.[4] The population analysis shown in Fig. 2 supports the usual valence bond description: C—N triple bond, N—O single bond. However, the charge separation in the N—O bond is not nearly as great as might have been expected of a formal dative bond. Molecular orbitals of **6** are shown in Fig. 6.

The computed dipole moment is 3.65 D (experimental 3.06 D (*29a*)).

[4]Not much significance should be attached to the absolute and relative energies of **3**, **6**, and **7** since no geometry optimization was performed on either **6** or **7**.

The gas phase uv spectrum of **6** shows a band progression between 4.4 and 5.1 eV (44). The two lowest excited singlet states, A_2 and E_1, are 4.95 and 5.52 eV, respectively, above the ground state. Both states are primarily linear combinations of configurations derived from the $\pi \rightarrow \pi^*$ transitions from the two highest occupied MO's of **6** to the two lowest unoccupied MO's (Fig. 6).

Isofulminic Acid **7**

Isofulminic acid is included for the sake of completeness. It is computed to be 13 kcal/mol more stable than fulminic acid and 47 kcal/mol less stable than isocyanic acid.[4] The population analysis (Fig. 2) indicates the electronic structure of the ground state as best described by the first resonance structure below with little contribution from the second.

$$\text{H—O—N=C} \leftrightarrow \text{H—O—}\overset{+}{\text{N}}\equiv\overset{-}{\text{C}}$$

The lowest unoccupied molecular orbital is a π^*-like orbital of the N—C fragment in the plane of the molecule. The largest single contribution to the LUMO is a p orbital of the carbon suggesting that the compound should be highly susceptible to nucleophilic attack at that site. Although alkyl isofulminates are not known, typical reactions of alkyl isonitriles, RNC do involve addition of nucleophiles to the carbon atom.

The computed dipole moment is 3.09 D.

The energies in eV, of the three lowest lying singlet excited states, relative to the ground state are: $^1A_1''$ 6.29; $^1A_2'$ 7.24; $^1A_2''$ 7.46.

The Curtius Reaction

In Fig. 8 is shown the molecular orbital energy level diagram for formyl azide **1**, N_2, formylnitrene **2**, and isocyanic acid **3**. The correlations are based on inspection of the phase properties of the molecular orbitals. There is no indication from the diagram in Fig. 8 that **1** should not decompose thermally to yield formyl nitrene or isocyanic acid directly in their ground states. The state correlation diagram for the decomposition of **1** to formyl nitrene + N_2 and isocyanic acid is shown in Fig. 9. The decomposition of **1** is simulated by stretching the N_2—N_3 bond (Fig. 1) by 0.26 Å, 0.53 Å, and 1.94 Å (points *b*, *c*, and *d*, respectively, in Fig. 9) beyond the equilibrium value

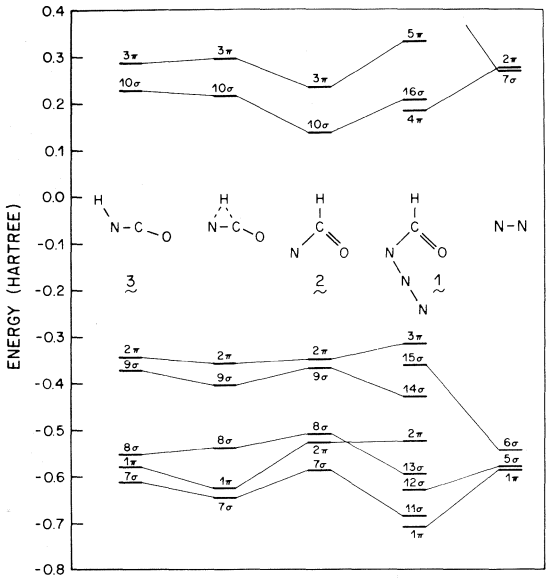

FIG. 8. The molecular orbital correlation diagram for the decomposition of formyl azide **1**.

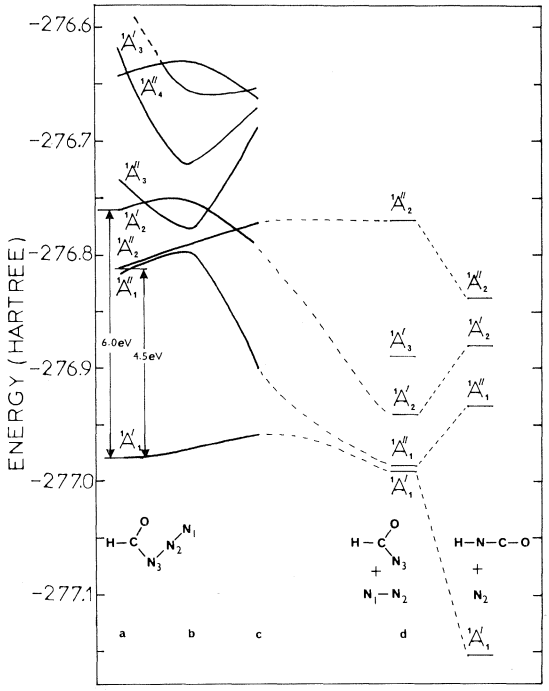

FIG. 9. The state correlation diagram for the decomposition of formyl azide **1**: point *a*, structure shown in Fig. 1; point *b*, same structure as at point *a* except that N_2—N_3 is stretched by 0.26 Å; point *c*, same structure as at point *a* except that N_2—N_3 is stretched by 0.53 Å; point *d*, N_2 and N_3 are 3.18 Å apart, the structure of **2** is as given in Fig. 1, and N_1—N_2 is the experimental value for elemental nitrogen.

(point *a* in Fig. 9).[5] Besides the N_2—N_3 bond, the geometry of the rest of the system is that of **1** for points *b* and *c*. It was not feasible to optimize the geometry at points *b* and *c*. As a result, the energies of the ground and excited states at the initial stages of decomposition are probably higher than they should be, relative to the energy of **1**. At the last point, *d*, decomposition is essentially complete. The geometry of the nitrene fragment is the same as **2** (Fig. 1) and the experimental bond length (30) of N_2 (1.098 Å) is used. The total SCF energy at point *d* is 2.5 kcal/mol higher than the sum of the SCF energies from separate calculations on **2** and N_2. The energy of the $^1A_1'$ state of isocyanic acid **3** was positioned in Fig. 9 by comparing the relative BW–EN corrected $^1A_1'$ state energies of **2** and **3** in the same (STO) basis. The positions of the other electronic states of **2** and **3** plotted in Fig. 9 were obtained from the larger basis set results, although the conclusions are not altered if one uses the smaller basis set data.

The first excited state of N_2 is calculated to be at 9.0 eV (experimental value 9.3 eV (45)) and is not shown. Pyrolysis of the azide to nitrene is calculated to be essentially isoenergetic with a low activation energy. Since the usual light sources for photolysis (*e.g.*, Rayonet reactor or Hanover lamps) provide energy in the vicinity of 4.5 eV and virtually nothing above 6.5 eV, the decomposition, whether thermal or photolytic, must eject the N_2 in its ground state.

The ground state of the azide $^1A_1'$ correlates directly with the $^1A_1'$ state of formyl nitrene. The nitrene in this state is calculated to have an anisotropic charge distribution about the nitrogen atom. The [1,2]-sigmatropic shift of hydride (or alkyl) group in this state is an orbital symmetry allowed process and computations on an intermediate structure (Fig. 8) suggest that, as in carbo cationic systems, there is little or no activation energy for the process. As the nitrene would probably be reached in a vibrationally excited state in the thermal Curtius reaction, it is likely that the highly exothermic rearrange-

[5]Calculations were also performed on the *trans* geometry of **1**. The ordering and positions of the excited states of the *trans* isomer were essentially the same as for the *cis* isomer at all stages of the simulated decomposition. Accordingly, only the data for the slightly more stable *cis* form are illustrated in Fig. 9 and discussed in the text.

ment to isocyanate takes place spontaneously or perhaps more likely still, is concerted with expulsion of N_2. This would explain the universal lack of evidence for nitrene intermediates in the thermolysis of acyl azides.

The two lowest excited states of the acyl azide **1** are nearly degenerate, at about 4.5 eV above the ground state. As stated earlier, both can be identified with transitions of the azide group which are electric dipole forbidden in the azide anion. Although the basis set is too crude to yield reliable values for electric dipole oscillator strengths, the calculations do indicate that the oscillator strengths for those two states, as well as the $^1A_2'$ state at 6.0 eV, are about $f \simeq 0.001$, corresponding to weakly allowed transitions. Since the radiation typically used in photolysis has energy of 4.9 eV (Hg 253.7 nm line), it is probable that the photolytic Curtius reaction proceeds entirely by excitation to the $^1A_1''$ and $^1A_2''$ states.

The behavior of the $^1A_1''$ and $^1A_2''$ states during the decomposition is of special significance. The near degeneracy suggests that the two states should both be populated upon photolysis, or by equilibration after photolysis. The two states remain nearly degenerate in the early part of the decomposition (in fact there is a weakly avoided crossing) and then diverge rapidly. One correlates with the $^1A_1''$ state of **2** whose dominant configuration is $...(9\sigma)^2(2\pi)^1(10\sigma)^1$ in a highly exothermic process. The other correlates with the $^1A_2''$ state whose dominant configuration is $...(9\sigma)^1(2\pi)^2(3\pi)^1$ which corresponds to the $n \rightarrow \pi^*$ transition of the carbonyl moiety.

The descending $^1A_1''$ state of the decomposing azide yields the $^1A_1''$ state of the nitrene. Rearrangement to the $^1A_1''$ state of isocyanic acid is an endothermic process and should be hindered if collisional deactivation is rapid. The fate of the reactive nitrene intermediate will depend on the nature of the solvent and the presence of nitrene traps.

On the other hand, the $^1A_2''$ state of the acyl azide correlates with the $^1A_2''$ state of the carbonyl nitrene. The nitrene can rearrange to the isocyanate in a substantially exothermic process. It was not possible to do geometry optimization (energy minimization) along the reaction coordinate so it is probable that the calculated activation energies for the decomposition of the acyl azide states $^1A_1''$ and $^1A_2''$ are not as high as calculated. It is intriguing that if decomposition along the two pathways were competitive, the $^1A_2''$ path would lead directly to isocyanate and the yield of isocyanate would depend only on the internal partitioning of the photolyzed azide between the two states, rather than on external effects. It was found in photolyses of pivaloyl azide (3) and benzoyl azide (8) that yields of isocyanate were essentially constant under a variety of conditions but that yields of nitrene trapping products were sensitive to reaction conditions.

Interconversions Between the HCNO Isomers

Compounds **2**–**7** represent the only isomers of HCNO for which reasonable valence bond structures can be written. At least some alkyl or aryl derivatives of all except **5** and **7** are known. As discussed in the Introduction, clean rearrangements can be effected between all known isomeric forms. However, without quantitative calculations of the complete HCNO hypersurface for each of the electronic states of the generalized HCNO structure, it is not possible to make more than some general remarks about the interconversions of the isomeric species.

The calculated energies of ground and excited states of **2**–**7**, rearranged for the sake of the discussion which follows, are shown plotted on the same energy scale in Fig. 10. Intended correlations between states of species which are close together on the potential hypersurface can in some cases be deduced by connecting states of like symmetry and by taking into account the nodal and symmetry properties of the molecular orbitals from which the principal contributing configurations are derived. The latter distinction is difficult to make if, as happens often in the present system, the CI calculations indicate that two or more configurations contribute strongly to the description of the state wave function.

We enumerate here, without detailed rationalization, those interconversions which can be expected with reasonable confidence on the basis of the calculations performed in the present study. These remarks should also apply to the alkyl derivatives of the parent HCNO structures.

(*1*) **2** $\rightleftarrows$ **3**. Carbonyl nitrenes **2** will rearrange to isocyanates **3** via their $^1A_1'$ states with little or no activation energy. Isocyanates should be convertible to nitrenes via their $^1A_1''$ states.

(*2*) **3** $\rightleftarrows$ **4**. The ground states, $^1A_1'$, of cyanates

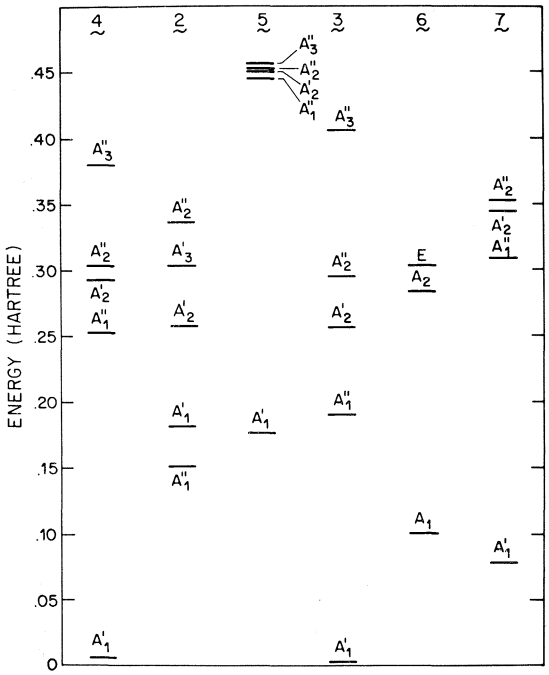

FIG. 10. The calculated state energies of compounds **2**–**7** shown on the same scale.

and isocyanates do not correlate with each other. Our results support the conclusion, stated previously, that the observed rearrangement of alkyl cyanates to isocyanates (20) probably occurs by a dissociative mechanism involving carbonium ions. The equilibrium favours the isocyanate, apparently by more than the calculated amount of 1 kcal/mol. There appears to be no direct photochemical route for interconversion either, since the $^1A_1''$ states do not correlate with each other (46).

(*3*) **3** ⇄ **6**. Fulminic acid and isocyanic acid are not close to each other on the potential hypersurface but, as reviewed in the Introduction, nitrile oxides have been reported to rearrange to isocyanates both thermally (17–19) and photochemically (16, 17). In the thermal rearrangement, a transition state in which both oxygen and alkyl group migration occur simultaneously has been implicated by studies of isotope effects (19). To explore the possibility of such a low energy pathway would require an extensive search of the nuclear configuration space and is beyond the scope of the present study. The stepwise rearrangement **6** → **5** → **2** → **3** does not appear to be feasible on energetic and electronic grounds.

Any rearrangement which involves **5** must proceed by way of the ground state of this species. Since the $^1A_2$ state of **6** does correlate directly with the $^1A_1'$ state of **5** we expect nitrile oxides to be converted to oxazirenes upon photolysis. The oxazirenes should be metastable since the $^1A_1'$ state of **5** would tend to correlate with a higher $^1A'$ state of **2**. An avoided crossing ultimately connects the $^1A_1'$ states of **5** and **2** and allows rearrangement to the more stable isocyanate **3**. The observation of nitrene trapping products in the photochemical conversion of nitrile oxides to isocyanates supports this route (16).

Acknowledgments

We are indebted to the National Research Council of Canada for financial support of this work, and to the University of Calgary for the receipt of a generous computing grant. We give special thanks to José M. Barriel who wrote the computer programs for the configuration interaction part of the study, and to M. A. Robb, Queen Elizabeth College, University of London, who did the MCSCF calculations for us.

1. J. MARCH. Advanced organic chemistry. McGraw-Hill, New York, NY. 1968. p. 816.
2. R. K. SMALLEY and T. E. BINGHAM. J. Chem. Soc. C, 2481 (1969).
3. S. LINKE, G. T. TISUE, and W. LWOWSKI. J. Am. Chem. Soc. **89**, 6308 (1967); G. R. FELT and W. LWOWSKI. J. Org. Chem. **41**, 96 (1976).
4. J. KENYON, H. PHILLIPS, and V. P. PITTMAN. J. Chem. Soc. 1972 (1935).
5. F. BELL. J. Chem. Soc. 835 (1934).
6. M. B. HOCKING. Can. J. Chem. **46**, 2275 (1968).
7. J. C. WRIGHT and A. FRY. Diss. Abstr. Int. B, 770 (1969).
8. Y. HAYASHI and D. SWERN. J. Am. Chem. Soc. **95**, 5205 (1973).
9. Y. YUKAWA and Y. TSUNO. J. Am. Chem. Soc. **79**, 5530 (1957).
10. (*a*) R. D. BRIGHT and C. R. HAUSER. J. Am. Chem. Soc. **61**, 618 (1939); (*b*) W. B. RENFROW, JR., and C. R. HAUSER. J. Am. Chem. Soc. **59**, 2308 (1937).
11. C. R. HAUSER and W. B. RENFROW, Jr. J. Am. Chem. Soc. **59**, 121 (1937).
12. K. R. BROWER. J. Am. Chem. Soc. **83**, 4370 (1961); **85**, 1401 (1963).
13. I. G. CSIZMADIA, H. E. GUNNING, R. K. GOSAVI, and O. P. STRAUSZ. J. Am. Chem. Soc. **95**, 133 (1973).
14. A. C. HOPKINSON. J. Chem. Soc. Perkin II, 794 (1973).
15. J. FENWICK, G. FRATER, K. OGI, and O. P. STRAUSZ. J. Am. Chem. Soc. **95**, 124 (1973) and references therein.
16. G. JUST and W. ZEHETNER. Tetrahedron Lett. **35**, 3389 (1967).

17. C. GRUNDMANN. Fortschr. Chem. Forsch. **7**, 62 (1966).
18. C. GRUNDMANN and J. M. DEAN. J. Org. Chem. **30**, 2809 (1965).
19. C. GRUNDMANN and P. KOCHS. Angew. Chem. Int. Ed. Engl. **9**, 635 (1970).
20. E. GRIGAT and R. PÜTTER. Newer methods of preparative organic chemistry. *Edited by* W. Foerst. 1971. p. 166.
21. J. C. KAUER and W. W. HENDERSON. J. Am. Chem. Soc. **86**, 4732 (1964).
22. P. F. ALEWOOD, P. M. KAZMAIER, and A. RAUK. J. Am. Chem. Soc. **95**, 5466 (1973).
23. J. F. HARRISON and G. SHALHOUB. J. Am. Chem. Soc. **97**, 4172 (1975).
24. C. C. J. ROOTHAAN. Rev. Mod. Phys. **23**, 69 (1951).
25. L. H. JONES, J. N. SHOOLERY, R. G. SHULMAN, and D. M. YOST. J. Chem. Phys. **18**, 990 (1950).
26. H. OBERHAMMER. Z. Naturforsch. A, **26**, 280 (1971).
27. B. M. RODE, W. KOSMUS, and E. NACHBAUR. Chem. Phys. Lett. **17**, 186 (1972).
28. B. M. RODE, W. KOSMUS, and E. NACHBAUR. Z. Naturforsch. A, **29**, 650 (1974).
29. (*a*) M. WINNEWISSER and H. K. BODENSEH. Z. Naturforsch. A, **22**, 1724 (1967); (*b*) H. K. BODENSEH and M. WINNEWISSER. Z. Naturforsch. A, **24**, 1973 (1969).
30. L. E. SUTTON (*Editor*). Chem. Soc. Spec. Publ. No 11. 1958; No 18. 1965.
31. W. J. HEHRE, R. F. STEWART, and J. A. POPLE. J. Chem. Phys. **51**, 2657 (1969).
32. T. H. DUNNING, JR. J. Chem. Phys. **53**, 2823 (1970).
33. B. ZURAWSKI, R. AHLRICHS, and W. KUTZELNIGG. Chem. Phys. Lett. **21**, 309 (1973).
34. N. S. OSTLUND and M. F. BOWEN. Theor. Chim. Acta, **40**, 175 (1975).
35. J. P. MALRIEU, P. CLAVERIE, and S. DINER. Theor. Chim. Acta, **8**, 404 (1967).
36. Y. N. SHEINKER. Dokl. Akad. Nauk, SSSR, **77**, 1043 (1951).
37. A. REISER and H. M. WAGNER. *In* The chemistry of azido group. *Edited by* S. Patai. Interscience Publisher, Toronto, Ont. 1971. Chapt. 8.
38. R. W. FESSENDEN. Chem. Phys. Lett. **29**, 364 (1974).
39. G. DAS and A. C. WAHL. J. Chem. Phys. **56**, 1769 (1972) and references therein.
40. J. M. R. STONE. J. Mol. Spectrosc. **54**, 1 (1975).
41. W. H. HOCKING, M. C. L. GERRY, and G. WINNEWISSER. Astrophys. J. **187**, L89 (1974).
42. J. W. RABELAIS, J. R. MCDONALD, and S. P. MCGLYNN. J. Chem. Phys. **51**, 5103 (1969).
43. R. N. DIXON and G. H. KIRBY. Trans. Faraday Soc. **64**, 2002 (1968).
44. W. D. SHEASLEY and C. W. MATHEWS. J. Mol. Spectrosc. **43**, 467 (1972).
45. J. T. VANDERSLICE, S. G. TILFORD, and P. G. WILKINSON. Astrophys. J. **142**, 1227 (1965).
46. M. HARA, T. FUJIMOTO, Y. ODAIRA, and S. TSUTSUMI. Chem. Abstr. **69**, 35607e; Nippon Kagaku Zasshi, **86**, 1091 (1967).

The crystal structure and polarised Raman spectrum of Rb_2AgI_3

IAN DAVID BROWN, HELEN ELAINE HOWARD-LOCK, AND MAHADEVAN NATARAJAN

Institute for Materials Research, McMaster University, Hamilton, Ont., Canada L8S 4M1

Received October 19, 1976

IAN DAVID BROWN, HELEN ELAINE HOWARD-LOCK, and MAHADEVAN NATARAJAN. Can. J. Chem. **55**, 1511 (1977).

The crystal structure of Rb_2AgI_3, space group *Pnma*, $a = 10.258(2)$, $b = 4.886(4)$, $c = 20.063(10)$ Å, has been refined. It is isostructural with K_2AgI_3 with chains of corner linked AgI_4 tetrahedra (Ag—I(bridge) = 2.881 Å, Ag—I(terminal) = 2.834 Å) running along *b*. The average bonding distance around the two seven coordinate Rb atoms is 3.722 Å. The polarised Raman spectrum shows the expected 36 modes which are assigned to four different symmetry species. All modes occur with frequencies less than 112 cm^{-1}.

IAN DAVID BROWN, HELEN ELAINE HOWARD-LOCK et MAHADEVAN NATARAJAN. Can. J. Chem. **55**, 1511 (1977).

On a affiné la structure cristalline de Rb_2AgI_3, groupe d'espace *Pnma*, $a = 10.258(2)$, $b = 4.886(4)$, $c = 20.063(10)$ Å. Elle est isostructurale avec celle du K_2AgI_3 et comporte des chaînes de AgI_4 tétraédriques reliées par les coins (Ag—I(pont) = 2.881 Å, Ag—I(bout de chaine) = 2.834 Å) le long de l'axe *b*. La distance de liaison moyenne autour des deux atomes de Rb heptacoordonnés est de 3.722 Å. Le spectre Raman polarisé présente les 36 modes attendus qui sont attribués aux quatre espèces de symétrie différente. Tous les modes se produisent avec des fréquences de moins de 112 cm^{-1}.

[Traduit par le journal]

Introduction

In 1952 Brink and Stenfert Kroese (1) reported that Rb_2AgI_3 was isostructural with K_2AgI_3. We have undertaken the refinement of this structure because of the paucity of accurate measurements of Rb—I distances. The spectral work reported in this paper is part of a study on the lattice vibrations of moderately complex inorganic solids.

Procedures and Discussion

X-Ray Procedure

Following the method of Brink and Stenfert Kroese (1), crystals of Rb_2AgI_3 were grown from a warm saturated aqueous solution of RbI with AgI. The resulting colourless needles of Rb_2AgI_3 elongated along *b* were used for the structure refinement. Precession photographs showed orthorhombic symmetry and systematic absences $hk0$, $h = 2n + 1$; $0kl$, $k + l = 2n + 1$, indicating space groups *Pnma* or $Pn2_1a$. The former space group was assumed following Brink and Stenfert Kroese (1) and was found to give a satisfactory refinement. Accurate lattice parameters (Table 1) were obtained by a least-squares fit to the angular settings of 15 reflections ($20° < 2\theta < 30°$) measured on a syntex $P\bar{1}$ diffractometer with graphite crystal monochromated MoKα radiation ($\lambda = 0.71069$ Å). X-ray intensities of 2499 reflections in a single quadrant (hkl and $hk\bar{l}$) were measured on the same instrument from a crystal ground to a sphere of radius 0.05 mm. The intensities were corrected for absorption ($\mu R = 1.06$), Lorentz and polarization effects, and symmetry related reflections were averaged to give 1321 non-equivalent intensities.

TABLE 1. Crystal data for Rb_2AgI_3 (CAS Registry Number 17218-08-5)*

Parameter	Value
a	10.258(2) Å
b	4.886(4) Å
c	20.063(10) Å
Z	4
D_x	4.35
D_m	4.23 ± 0.05†

*Orthorhombic, space group *Pnma* (D_{2h}^{16} No. 62).
†Measured by displacement in methylene iodide.

The atomic parameters taken from K_2AgI_3 (1) were then refined by the locally written full-matrix least-squares program CUDLS (CDC 6400) to yield final agreement indices $R_1 (= \sum ||F_o| - |F_c|| / \sum |F_o|) = 0.089$ and $R_2 (= \sum \omega (F_o - F_c)^2 / \sum \omega F_o^2)^{1/2} = 0.069$. In the final round $\omega = (\sigma_c^2 + (0.2F_o)^2)^{-1}$ where σ_c is the standard

TABLE 2. Atomic positional and thermal coordinates* for Rb_2AgI_3

Atom	x	y	z	$U(1,1)$	$U(2,2)$	$U(3,3)$	$U(1,3)$
Rb(1)	0.4217(3)	0.75	0.7113(1)	0.029(2)	0.028(2)	0.041(2)	0.000(1)
Rb(2)	0.2522(3)	0.25	0.4570(1)	0.034(2)	0.035(2)	0.028(2)	0.009(1)
Ag	0.1362(3)	0.25	0.1360(1)	0.032(1)	0.044(2)	0.039(1)	0.000(1)
I(1)	0.1879(2)	0.25	0.2753(1)	0.028(1)	0.035(1)	0.023(1)	0.000(1)
I(2)	0.3803(2)	0.25	0.0710(1)	0.026(1)	0.038(1)	0.026(1)	0.002(1)
I(3)	0.0033(2)	0.75	0.1018(1)	0.030(1)	0.024(1)	0.035(1)	−0.001(1)

*The temperature factor is given by $T = \exp(-2\pi^2 \Sigma_i \Sigma_j U_{ij} H_i H_j a_i^* a_j^*)$, where U_{ij} are the thermal coordinates.

deviation arising from the counting statistics. The final atom parameters are given in Table 2, those not fixed by symmetry were refined together with a scale factor and the parameter used in the extinction correction $F^* = F(1 + 1.3 \times 10^{-7} \times \beta(2\sigma)F^2)^{1/2}$ (2). The scattering curves for Rb^+, Ag^+, and I^- ions corrected for anomalous dispersion were taken from International Tables for X-ray Crystallography (3). The observed and final calculated structure factors have been placed in the Depository of Unpublished Data.[1]

Discussion of the Structure

Bond lengths and angles are presented in Table 3. Rb_2AgI_3 is isostructural with K_2AgI_3 which has been well described by Shoemaker (4). The temperature factors indicate no large anisotropic motion, the rms deviation of all atoms from their mean position lying between 0.15 and 0.21 Å. The temperature factor for Ag is slightly, but significantly larger than that of the other atoms, a result also found in K_2AgI_3 (5). A bond valence analysis (Table 4) gives valence sums around each atom that show a standard deviation of 0.07 valence units from the atomic valence. As in K_2AgI_3, the angles at the silver atom deviate significantly from tetrahedral but in a sense opposite to that usually found (6). The large I(bridging)—Ag—I(bridging) angle (116°) is determined by the b axis length while the smaller I(terminal)—Ag—I(terminal) angle (107°) is opposite the only edge of the tetrahedron that is shared with two other coordination polyhedra. Figure 1 shows a projection of the unit cell of Rb_2AgI_3 in the ac plane.

Polarised Raman Spectrum of Rb_2AgI_3

The factor group of crystalline Rb_2AgI_3 is

[1]Photocopies may be obtained upon request, at a nominal charge, from the Depository of Unpublished Data, CISTI, National Research Council of Canada, Ottawa, Canada K1A 0S2.

TABLE 3. Bond lengths (Å) and angles (deg)

Bond	Length (Å)	
Ag—I(1)	2.845(3)	
Ag—I(2)	2.823(3)	
Ag—I(3)	2.881(2)	(×2)
Rb(1)—I(1)	3.656(3)	(×2)
Rb(1)—I(1)′	3.674(3)	(×2)
Rb(1)—I(2)	3.751(3)	(×2)
Rb(1)—I(3)	3.842(3)	
Rb(2)—I(1)	3.705(3)	
Rb(2)—I(2)	3.612(2)	(×2)
Rb(2)—I(2)′	3.856(4)	
Rb(2)—I(3)	3.741(3)	(×2)
Rb(2)—I(3)′	3.838(3)	

Bonds	Angle (deg)
I(1)—Ag—I(2)	106.8(1)
I(1)—Ag—I(3)	108.8(1)
I(2)—Ag—I(3)	108.1(1)
Ag—I(3)—Ag′	116.0(1)

D_{2h} for which the Raman active modes all have g symmetry and the infrared modes u symmetry. Since the AgI_3 moiety of the structure exists in the form of chains of corner shared AgI_4 tetrahedra it is inappropriate to divide the modes into internal and lattice modes. The number of Raman active modes and their symmetries are shown by factor group analysis to be

$$12A_g + 6B_{1g} + 12B_{2g} + 6B_{3g}$$

Following the procedure outlined by Adams and Newton (9) the translatory lattice modes are found to be

$$2A_g + B_{1g} + 2B_{2g} + B_{3g} + A_u + 2B_{1u} + B_{2u} + 2B_{3u}$$

of which $B_{1u} + B_{2u} + B_{3u}$ are the three acoustic modes. All 36 g modes are active and symmetry-allowed in the Raman spectrum.

TABLE 4. Bond valence*

	Rb(1)	Rb(2)	Ag	Σ
I(1)	0.17 (×2) 0.17 (×2)	0.16	0.25	1.09
I(2)	0.14 (×2)	0.19 (×2) 0.12	0.26	1.04
I(3)	0.12	0.16 (×2) 0.12	0.23 (×2)	1.02
Σ	1.08	1.10	0.97	

*The valences (S) were calculated from the distances (R) by means of the expression $S = (R/R_0)^{-N}$ (7) where $R_0 = 2.843$, $N = 7$ for Rb—I(8) and $R_0 = 2.362$, $N = 7.5$ for Ag—I.

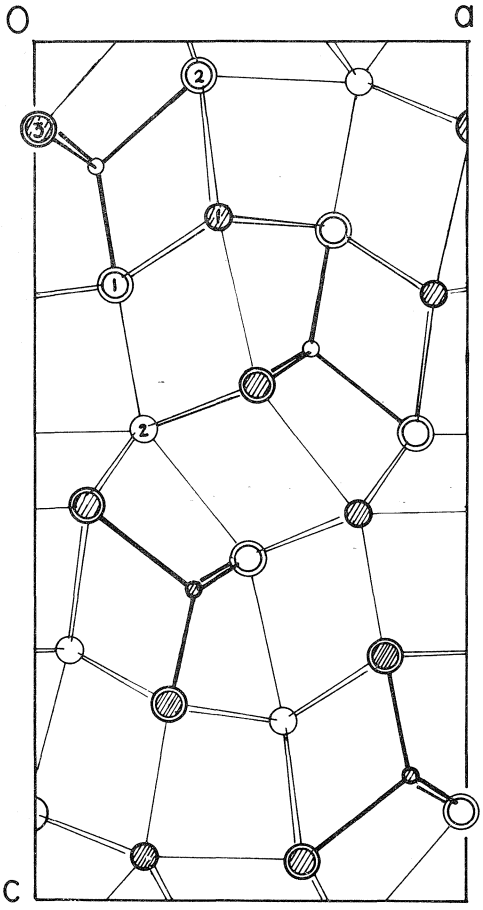

FIG. 1. Rb_2AgI_3 projected down the b axis. The double circles are I, large circles Rb, small circles Ag. Atoms at $y = 3/4$ are shaded; those at $y = 1/4$ are unshaded.

Raman Procedure

Single crystals of Rb_2AgI_3 approximately 3 mm on an edge were polished on the faces perpendicular to the crystallographic axes and mounted on an X-ray goniometer. All spectra were measured at room temperature. An argon ion laser provided plane polarised radiation of 100 mW at 5145 Å. The laser beam was focused onto the crystal which had been mounted with one of the crystallographic axes parallel to the incoming beam. A Babinet compensator before the sample and a polariser in the scattered beam permitted the selection of various components of the Raman tensor. The spectrum of the scattered light was analysed with a SPEX 1400 double monochromator, the total instrumental width (laser and spectrometer) being 1.5 cm^{-1} for a slit width of 200 μm.

Discussion of Raman Spectrum

The scattering geometry can be described by the symbol $x(uv)y$ where x is the crystal axis parallel to the direction of the incident beam, y that parallel to the scattered beam, and u and v are the crystallographic axes parallel to the direction of polarisation of the incident and scattered beam respectively.

The spectra are shown in Fig. 2. The scattering geometry $a(bb)c$ (Fig. 2a) should give the $12A_g$ modes. The spectrum shows 12 or 13 lines some of which may be overtone modes. The geometry $a(ba)b$ (Fig. 2b) should show the $6B_{1g}$ modes and six lines can be seen. Similarly $a(ca)c$ (Fig. 2c) shows the expected 12 lines of the B_{2g} spectrum and $a(cb)c$ (Fig. 2d) shows the expected 6 lines of the B_{3g} spectrum.

Two features of the spectra are noteworthy; namely, the absence of any lines at frequencies above 112 cm^{-1} (none of the spectra show any features between 112 cm^{-1} and 1800 cm^{-1}), and the broadening of the higher frequency peaks.

The absence of high frequency modes is expected for a crystal with weak bonds. Table 5 lists a series of stretching force constants determined spectroscopically for a number of bonds

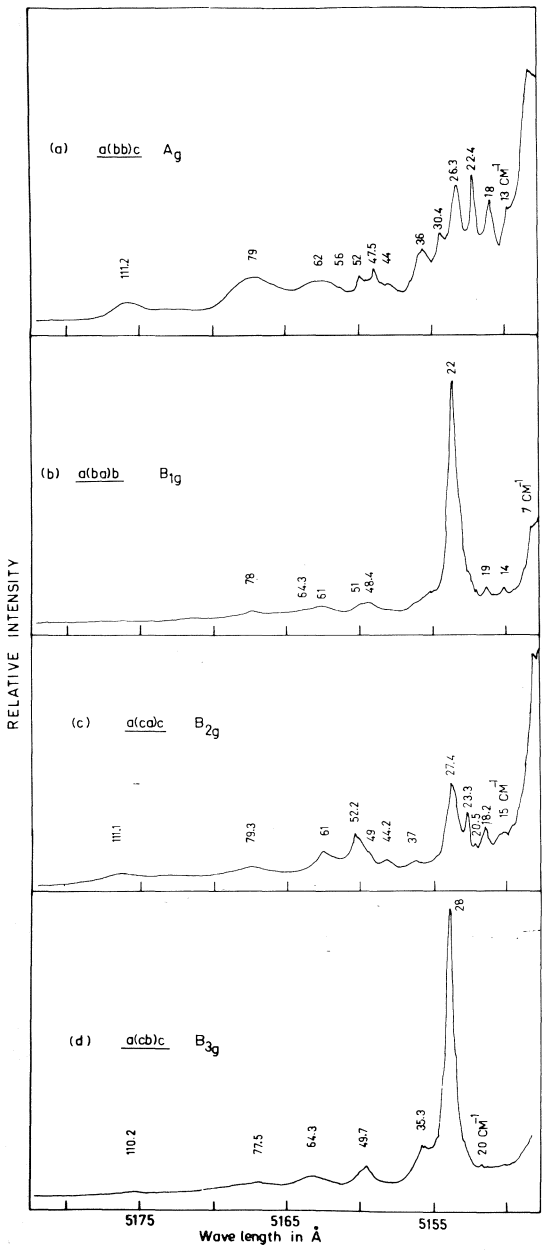

FIG. 2. Polarized Raman spectrum of Rb_2AgI_3. The scattering geometry and the corresponding symmetry species are indicated in the figure. The observed line positions are also marked in wave numbers, cm^{-1}.

with relatively small bond valence. There is a correlation between bond valence and force constant which allows one to estimate stretching force constants of around 0.30 mdyn $Å^{-1}$ (30 N m^{-1}) for Ag—I and 0.12 mdyn $Å^{-1}$ (12 N m^{-1}) for Rb—I. For such force constants the Ag—I stretching vibration would be around 93 cm^{-1} and the Rb—I stretching vibration around 63 cm^{-1}. Since the stretching vibrations generally have the highest frequency we do not expect to find lines much above 100 cm^{-1}. The Ag—I(terminal) stretching vibration will lie entirely in the mirror plane and, therefore, will appear in A_g or B_{2g}. The band at 111 cm^{-1} appears in both and probably represents factor group splitting of the Ag—I symmetric stretching vibration. Because there are many possibilities for two phonon and overtone bands, it is not possible to definitely assign such bands with any certainty.

TABLE 5. Stretching force constants and valences observed for weak bonds

Bond	Valence	k (mdyn/Å)	
Sn—I	1.0	1.36	*
B—Br	0.75	1.10	*
Cd—S	0.5	1.00–1.03	†
In—S	0.5	0.55–0.67	†
Cd—S	0.5	1.30–1.50	†
Cr—S	0.5	0.83–0.91	†
Lu—O	0.32–0.47	0.48–0.68	‡
Lu—O	0.36–0.45	0.47–0.62	‡
Y—O	0.32–0.49	0.35	‡

*Reference 10.
†Reference 11.
‡Reference 12.

Acknowledgements

We wish to thank Mr. R. Faggiani for his assistance in the structure determination, Dr. M. Pezolet for assistance in measuring the Raman spectrum, and the National Research Council of Canada for operating grants.

1. C. BRINK and H. A. STENFERT KROESE. Acta Crystallogr. **5**, 433 (1952).
2. A. C. LARSON. Acta Crystallogr. **23**, 664 (1967).
3. International Tables for X-ray Crystallography. Vol. 4. Kynoch Press, Birmingham. 1974. p. 71.
4. CLARA BRINK SHOEMAKER. Z. Kristallogr. **137**, 15 (1973); Acta Crystallogr. B**32**, 1619 (1976).
5. M. M. THACKERAY and J. COETZER. Acta Crystallogr. B**31**, 2339 (1975).
6. I. D. BROWN. Acta. Crystallogr. In press.
7. I. D. BROWN and R. D. SHANNON. Acta Crystallogr. A**29**, 266 (1973).
8. M. NATARAJAN, R. FAGGIANI, and I. D. BROWN. Acta Crystallogr. B**33**, 129 (1977).
9. D. M. ADAMS and D. C. NEWTON. Tables for factor group and point group analysis. Beckman, RIIC Ltd., England. 1970.
10. A. MÜLLER and B. KREBS. J. Mol. Spectrosc. **24**, 180 (1976).
11. H. SHIMIZU, Y. OHBABYASHI, K. YAMAMOTO, and K. ABE. J. Phys. Soc. Jpn. **38**, 750 (1975).
12. A. ARMBUSTER. J. Phys. Chem. Solids, **37**, 321 (1976).

Résonance quadripolaire nucléaire du brome dans des composés organomagnésiens

JACKY KRESS[1]

Laboratoire de Spectrochimie Infrarouge et Raman du C.N.R.S., 2, rue Henri Dunant, F-94320 Thiais, France

ET

LUCIEN GUIBÉ[2]

Laboratoire d'Electronique Fondamentale (associé au C.N.R.S.), Bâtiment 220, Université Paris XI, F-91405 Orsay Cédex, France

Reçu le 17 novembre 1976

JACKY KRESS et LUCIEN GUIBÉ. Can. J. Chem. **55**, 1515 (1977).

Des signaux de résonance quadripolaire nucléaire du brome (isotopes 79 et 81) ont été observés, à 77 K, dans quelques composés organomagnésiens cristallisés du type $RMgBr{\cdot}nR'_2O$, et dans $MgBr_2{\cdot}nEt_2O$. Les fréquences correspondantes, relativement basses (de l'ordre de 33 MHz pour le ^{81}Br, à comparer avec 220 MHz pour une liaison $\diagdown C—Br$) montrent le caractère fortement ionique de la liaison —Mg—Br, tandis que leur regroupement dans un intervalle restreint (30–42 MHz) suggère que la liaison Mg—Br est peu affectée par les changements des radicaux R ou R′ dans la série étudiée. Cependant l'évolution de la fréquence de résonance dans cet intervalle peut s'interpréter en fonction de la nature des groupes R et R′.

JACKY KRESS and LUCIEN GUIBÉ. Can. J. Chem. **55**, 1515 (1977).

Bromine nuclear quadrupole resonance signals corresponding to both isotopes ^{79}Br and ^{81}Br have been observed, at 77 K, in some crystallized organomagnesium bromides of formula $RMgBr{\cdot}nR'_2O$, and in $MgBr_2{\cdot}nEt_2O$. The low value of the resonance frequencies, of about 33 MHz to be compared to 220 MHz for a typical $\diagdown C—Br$ bond, shows the ionic character of the Mg—Br bond. The fact that the resonance frequencies are found within a restricted frequency range, between 30 and 42 MHz, shows that the Mg—Br bond is only slightly affected by the nature of the radicals R and R′ through the series studied. However the variation of the bromine resonance frequency in this series may be interpreted in terms of the nature of R and R′.

Introduction

Le grand nombre d'études physicochimiques déjà consacrées aux composés organomagnésiens s'explique par l'importance de ces composés en synthèse organique et par la complexité des problèmes que soulève leur constitution; la connaissance de cette dernière est évidemment d'un intérêt fondamental pour l'étude des réactions chimiques. Ces études physicochimiques ont porté non seulement sur les solutions organomagnésiennes, mais aussi sur les cristaux isolables à partir de ces solutions et elles ont fait appel à des techniques les plus diverses. La diffraction des rayons X, en particulier, a permis d'établir la structure des composés définis solides, obtenus à partir des solutions dans les éthers, et de montrer que ce sont des complexes moléculaires contenant une ou plusieurs molécules de solvant coordonnées au magnésium; c'est notamment le cas du diéthérate de bromure d'éthylmagnésium, $EtMgBr{\cdot}2Et_2O$ (1). Les spectrométries infra-rouge et Raman ont récemment permis de montrer que ces mêmes complexes constituent généralement l'espèce dominante dans les solutions et que les résultats obtenus sur les organomagnésiens cristallisés (1) peuvent souvent être étendus aux composés en solution (2).

Il nous a semblé souhaitable de compléter l'étude de ces complexes en faisant appel à une autre technique d'étude de l'état cristallisé, la résonance quadripolaire nucléaire (rqn), qui constitue une méthode de recherche particulièrement adaptée à l'étude des liaisons chimiques et des distributions de charges électriques autour des noyaux résonnants. Elle ne semble pas encore

[1]Adresse actuelle: Laboratoire de Chimie Moléculaire Inorganique et de Catalyse, Institut de Chimie, Université Louis Pasteur, 4, rue Blaise Pascal, Boîte Postale 296/R8, F-67008 Strasbourg Cédex, France.

[2]Auteur auquel doit être adressée la correspondance concernant cet article.

avoir été utilisée pour l'étude de dérivés magnésiens, bien que les noyaux d'halogènes présents dans les halogénures de magnésium et les organomagnésiens mixtes possèdent un moment quadripolaire favorable et aient été largement étudiés dans des nombreux composés organiques et minéraux.

Nous présentons ici les premiers résultats obtenus sur des complexes bromés afin de tenter (*i*) de les caractériser et d'analyser leur structure, (*ii*) de préciser l'ionicité de la liaison magnésium–halogène et d'apporter ainsi un support expérimental aux conclusions des calculs de chimie quantique (3), (*iii*) d'examiner l'influence de la nature du ligand organique et du solvant sur la répartition des électrons dans ces complexes.

Aspects expérimentaux

A. Préparation des composés

Les composés étudiés étant très sensibles à l'oxygène et à l'humidité de l'air, toutes les manipulations ont été effectuées sous atmosphère inerte. Les solvants et les halogénures organiques de départ ont été distillés sous azote juste avant leur utilisation.

Les solutions des organomagnésiens mixtes MeMgBr, EtMgBr, *tert*-BuMgBr, PhMgBr, MeMgI et EtMgI dans l'éther éthylique, PhMgBr dans le tétrahydrofuranne et EtMgBr dans l'éther isopropylique ont été obtenues par la méthode classique (4) d'addition des halogénures MeBr, EtBr, *tert*-BuBr, PhBr, MeI et EtI sur le magnésium dans le solvant approprié; les solutions de $MgBr_2$ et de MgI_2 dans l'éther éthylique l'ont été par addition de dibromoéthane et d'iode, respectivement (5).

Les composés définis $MeMgBr{\cdot}2Et_2O$ (6), $EtMgBr{\cdot}2Et_2O$ (1), $MeMgI{\cdot}2Et_2O$ (6), $EtMgI{\cdot}2Et_2O$ (2), $PhMgBr{\cdot}2Et_2O$ (7), PhMgBr·2THF (8), $[EtMgBr{\cdot}(iso\text{-}Pr)_2O]_2$ (9), $MgBr_2$ (10) et $MgI_2{\cdot}2Et_2O$ (5) ont été isolés à l'état cristallisé à partir de ces solutions selon les procédés décrits dans les références citées. Les cinq premiers sont liquides à la température ambiante (2, 6, 7). Les complexes $MgBr_2{\cdot}Me_2O$ et $MgBr_2{\cdot}2Me_2O$ ont été obtenus par piégeage d'éther méthylique sur le bromure de magnésium non solvaté (10).

A partir des solutions de bromure de magnésium dans l'éther éthylique on peut obtenir, selon les conditions expérimentales, trois complexes de stoechiométrie 1–1, 1–2 et 1–3 (11). Notre étude a porté sur trois échantillons différents: les cristaux obtenus par refroidissement d'une solution concentrée et maintenus au contact du solvant (I), ceux obtenus par une évaporation limitée de l'éther à la rampe à vide et conservés en atmosphère d'éther (II) et ceux obtenus par un pompage plus poussé de l'éther à température ambiante (III) pour lesquels la microanalyse a montré qu'il s'agit du monoéthérate $MgBr_2{\cdot}Et_2O$.

Dans le cas du bromure de tertiobutylmagnésium, le magnésien n'a jamais été isolé de sa solution dans l'éther éthylique. Nous avons d'une part étudié les cristaux obtenus par refroidissement d'une solution concentrée et maintenus au contact du solvant (I) et, d'autre part, le solide obtenu par évaporation poussée de l'éther à la rampe à vide à 25°C (II).

B. Obtention des spectres de rqn

Les signaux de résonance ont été recherchés à l'aide d'un spectromètre à superréaction de type classique avec stabilisation du niveau de bruit, modulation Zeeman antisymétrique, amplification sélective, détection de phase et enregistrement. Tous les composés préparés, contenus dans des ampoules de verre Pyrex scellées, ont été étudiés à 77 K.

Les échantillons liquides à la température ambiante ont été refroidis avec précaution pour éviter la formation d'un verre; en particulier, pour les échantillons $MgBr_2{\cdot}nEt_2O$(I) et *tert*-$BuMgBr{\cdot}nEt_2O$(I), les raies non trouvées au cours d'une première recherche, n'ont pu être observées qu'à la suite d'une recristallisation par réchauffage modéré (début de fusion) et refroidissement lent de ces échantillons.

Les premiers essais, effectués sur $MgBr_2$ et $MgBr_2{\cdot}nEt_2O$(II), ont couvert une gamme de fréquence étendue, car l'ordre de grandeur des fréquences de résonance du brome dans ce type de composé était difficile à évaluer à priori. Les autres échantillons ont été étudiés entre 30 et 50 MHz environ.

Les fréquences des signaux ont été mesurées à l'aide d'un générateur haute fréquence relié à un fréquencemètre compteur à quartz. Malgré la grande précision de cet instrument, la précision des déterminations de fréquences de résonance n'excède pas ± 30 kHz, en raison de la largeur des raies, de leur faible rapport signal/bruit compris le plus souvent entre 4 et 10 et de la difficulté de repérer la position exacte de la composante centrale dans le spectre de superréaction. L'exactitude des pointés a pu être contrôlée par l'observation independante des signaux des deux isotopes ^{79}Br et ^{81}Br du brome dont les fréquences de résonance sont dans le rapport, 1.197, des moments quadripolaires.

Résultats et discussion

Des signaux ont été observés dans 9 échantillons parmi les 16 préparés et étudiés; les raies dues aux deux isotopes ^{79}Br et ^{81}Br ont été observées dans la majorité des cas. Les tableaux 1 et 2 donnent les fréquences de tous les signaux observés; cependant, seules celles de l'isotope ^{81}Br seront considérées au cours de la discussion. Les composés dans lesquels aucune résonance n'a été détectée sont les suivants: $MgBr_2$ (4.7–55), $MgBr_2{\cdot}2Me_2O$ (20–50), $MgBr_2{\cdot}Me_2O$ (25.8–59.6), $MeMgBr{\cdot}2Et_2O$ (24.3–59.4), $MgI_2{\cdot}2Et_2O$ (13.6–47.8), $MeMgI{\cdot}2Et_2O$ (30.6–50.1), $EtMgI{\cdot}2Et_2O$ (31.9–42); les nombres entre parenthèses indiquent les limites, en MHz, de la gamme de fréquence explorée pour chaque composé.

A. Remarques générales

(*1*) L'observation d'un signal unique, pour chacun des isotopes du brome, dans les quatre premiers composés du tableau 1 qui ont fait par ailleurs l'objet d'études radiocristallographiques est compatible avec les structures cristallines déterminées (1, 7–9) et montre que tous les

TABLEAU 1. Fréquences (MHz) des rqn de ^{79}Br et ^{81}Br dans des composés organomagnésiens à 77 K

Composés*	^{81}Br	^{79}Br
$EtMgBr{\cdot}2Et_2O$	30.55	36.56
$PhMgBr{\cdot}2Et_2O$	33.53	40.08
PhMgBr·2THF	31.14	37.27
$EtMgBr{\cdot}[(iso\text{-}Pr)_2O]_2$	30.23	36.43
$MgBr_2{\cdot}nEt_2O$†	35.57	42.59
tert-$BuMgBr{\cdot}nEt_2O$ (I)	33.72	40.38
(II)	31.75‡	—
	32.66	39.04

*Et = ethyl-; Ph = phényl-; THF = tétrahydrofuranne; iso-Pr = isopropyl-; *tert*-Bu = tertiobutyl-.
†Pour $MgBr \cdot nEt_2O$ seule une valeur moyenne de la fréquence de résonance de chaque isotope est donnée ici. Les valeurs de chacune des résonances observées sont données dans le tableau 2.
‡Signal très faible, la raie de ^{79}Br n'a pas été recherchée.

atomes de brome sont équivalents dans chacun de ces complexes.

Par contre, l'observation de deux résonances distantes d'environ 8 MHz dans le complexe $MgBr_2{\cdot}2Et_2O$ (*cf. B-3*, plus loin) indique l'existence de deux liaisons Mg—Br différentes et semble en contradiction avec l'étude radiocristallographique (12) qui montre quatre distances Mg–Br nettement différentes dans la maille cristalline.

(*2*) La fréquence moyenne de résonance dans les différents composés est d'environ 33 MHz et peut être comparée aux fréquences du brome dans des composés organiques à liaison essentiellement covalente, de l'ordre de 200 à 300 MHz (13), dans des complexes d'un autre métal tel que l'aluminium, 83.5 MHz pour $AlBr_3{\cdot}Et_2O$ (14), et dans des sels ioniques comme $BaBr_2{\cdot}nH_2O$ ($n = 0, 1, 2$): $3.8 < f < 22$ MHz (15).

Cette comparaison permet d'apprécier le caractère ionique de la liaison Mg—Br dans les composés organomagnésiens étudiés. Les fréquences de rqn du brome y sont particulièrement basses, apportant la preuve expérimentale directe d'une ionicité importante. Cette observation est en accord avec la faible électronégativité du magnésium et avec les résultats des études théoriques effectuées sur des molécules modèles linéaires (3).

Il est possible d'obtenir une valeur de l'ionicité par application de la théorie de Townes et Dailey (16, 17) prise sous sa forme simplifiée

$$e^2Qq = (1 - s^2)(1 - I)e^2Qq_{at}$$

s^2 mesurant le taux d'hybridation "*s*" de la liaison Mg—Br sur le brome, est pris égal à 0.25 par analogie avec le cas du chlore (17); e^2Qq_{at} est le couplage atomique du $^{81}Br \simeq -643$ MHz (16) et e^2Qq est le couplage du composé étudié valant deux fois la fréquence de résonance mesurée quand on néglige l'asymétrie η du couplage quadripolaire, soit $\simeq 66$ MHz. Il vient alors $I = 0.86$. Cette valeur doit être considérée avec précaution étant donné les nombreuses approximations faites dans le calcul. Elle est toutefois très voisine de celle obtenue à partir de la différence d'électronégativité suivant la relation (16) $I = (x_A - x_B)/2 = 0.80$ avec $x_{Br} = 2.8$ et $x_{Mg} = 1.2$, bien que cette dernière néglige en particulier l'effet des molécules d'éther coordonnées au magnésium.

(*3*) Les fréquences des différentes raies se situent toutes entre 30 et 42 MHz (*cf.* tableau 1) et restent ainsi bien groupées, suggérant que, malgré la faible valeur du gradient de champ électrique à l'emplacement des noyaux de brome, ce sont les électrons de la liaison Mg—Br qui y apportent la principale contribution bien plus que le champ cristallin. La liaison Mg—Br présente ainsi, dans la série étudiée, une structure bien définie, caractérisée par la fréquence de résonance quadripolaire du ^{81}Br voisine de 35 MHz et peu modifiée quand les radicaux R et R′ sont changés.

B. Etude particulière des différents composés

(*1*) Les trois composés $EtMgBr{\cdot}2Et_2O$, $PhMgBr{\cdot}2Et_2O$ et PhMgBr·2THF possèdent une structure moléculaire analogue comportant des motifs monomères dans lesquels les quatre ligands forment un arrangement tétraédrique autour du magnésium (1, 7, 8). Les fréquences de résonance du brome doivent donc refléter essentiellement les effets inductifs dus aux trois autres ligands portés par le magnésium et doivent permettre d'analyser directement l'influence de la nature du groupe organique et du solvant sur la distribution des électrons dans les complexes.

Effectivement, les variations de fréquence observées à la suite de la substitution de l'un des ligands s'interprètent bien en termes d'effets inductifs. D'une part le remplacement d'un groupe éthyle par un groupe phényle, plus électronégatif, entraîne une élévation de fréquence de 3 MHz (tableau 1) résultant d'un déplacement des électrons du brome vers le magnésium et le groupe phényle. Un effet analogue est observé pour la fréquence de résonance du chlore lors du passage de $EtCH_2Cl$ (32.968 MHz) à $PhCH_2Cl$ (33.627 MHz) ou de EtCl (32.704 MHz) à PhCl (34.622 MHz) (13).

D'autre part, le remplacement des molécules d'éther éthylique par celles de tétrahydrofuranne, meilleur donneur d'électrons, entraîne un abaissement de fréquence de 2.3 MHz (tableau 1) indiquant que les électrons se déplacent, cette fois, vers le brome. Une telle variation est compatible avec la différence observée entre les fréquences moyennes des bromes terminaux du dimère Al_2Br_6 (95.740 MHz) (13) et celles du complexe $AlBr_3 \cdot Et_2O$ (83.5 MHz) (14); l'abaissement de la fréquence est dans ce cas dû au déplacement d'électrons vers le brome à la suite de la fixation d'une molécule d'éther éthylique sur l'aluminium.

Ces observations sont en bon accord avec les conclusions du paragraphe *A-3* ci-dessus. Elles montrent en effet que ce sont bien les électrons de liaison qui sont principalement responsables du gradient de champ électrique vu par le noyau de brome; elles indiquent en outre que le magnésium transmet jusqu'au brome les effets des déplacements de charge induits par le remplacement du groupement organique R ou des molécules de solvant liées au magnésium et ceci malgré le caractère peu covalent des liaisons dans ces composés organomagnésiens.

(*2*) Le composé $[EtMgBr \cdot (iso\text{-}Pr)_2O]_2$ est constitué de dimères formés par l'intermédiaire de deux ponts brome entre deux atomes de magnésium. Chaque magnésium est tétracoordonné et lié à un groupe éthyle, une molécule d'éther isopropylique, et deux atomes de brome (9). La fréquence de résonance des atomes de brome en pont entre deux autres atomes étant, en principe, inférieure à celle des bromes terminaux (17), comme cela a été observé pour le dimère Al_2Br_6 dont les bromes en pont résonnent à 81.815 MHz et les bromes terminaux à 96.426 et 95.055 MHz (13, 17), la fréquence du brome de l'organomagnésien est de ce point de vue attendue à une valeur inférieure à celle du complexe $EtMgBr \cdot 2Et_2O$. Par contre, le remplacement dans la sphère de coordination du magnésium des deux molécules d'éther éthylique par un atome de brome et une molécule d'éther isopropylique, tous les deux plus faibles donneurs d'électrons que l'éther éthylique, laisse prévoir par effet inductif une fréquence de résonance supérieure à celle de $EtMgBr \cdot 2Et_2O$. La fréquence obtenue, 30.23 MHz, est en fait voisine de celle du composé $EtMgBr \cdot 2Et_2O$, ce qui est compatible avec l'existence des deux effets précédents qui semblent se compenser.

(*3*) Les trois échantillons I, II et III de complexes $MgBr_2 \cdot nEt_2O$ donnent lieu à des spectres différents, bien que les fréquences de certains signaux semblent très voisines. Ainsi, les signaux à 33.71 et 41.94 MHz dans I sont très voisins des signaux à 33.72 et 42.13 MHz dans II; de même les signaux à 31.79 et 32.66 MHz dans II sont voisins des signaux à 31.84 et 32.67 MHz dans III ($MgBr_2 \cdot Et_2O$). Ces ressemblances entre les spectres apparaissent de manière plus nette sur le diagramme de la fig. 1, où les différents groupes de raies ont été repérés par les lettres minuscules *a*, *b*, *c* et *d*; elles sont vraisemblablement dues à la présence de mélanges des trois complexes (11) déjà signalés à propos de la préparation des composés et les petits écarts de fréquence constatés sont dans les limites de précision de la détermination des fréquences, rendue difficile par la largeur ($\simeq 20$ kHz) des raies enregistrées. Compte tenu des conditions de préparation des trois échantillons, l'échantillon I contiendrait les composés les plus solvatés $MgBr_2 \cdot 2Et_2O$ et $MgBr_2 \cdot 3Et_2O$, ce dernier donnant lieu à la raie à 38.12 MHz, et l'échantillon II les composés $MgBr_2 \cdot Et_2O$ et $MgBr_2 \cdot 2Et_2O$, tandis que l'échantillon III est du monoéthérate. Les raies *a* étant dues au monoéthérate, les raies *b* correspondent donc au diéthérate et les raies *c* au triéthérate; les raies *d*, apparues dans l'échantillon I après que celui-ci ait été recristallisé (I′), sont de fréquences proches de celles des raies *a* du monoéthérate, mais néanmoins suffisamment éloignées, par rapport à la marge d'erreur dans la détermination des fré-

TABLEAU 2. Fréquences (MHz) des rqn de ^{79}Br et ^{81}Br dans les composés $MgBr_2 \cdot nEt_2O$ à 77 K

Composés	^{81}Br	^{79}Br	Fréquence*
$MgBr_2 \cdot nEt_2O$ (I)	33.71	40.35	*b*
	38.12	45.67	*c*
	41.94	50.35	*b*
(I′)	32.37	38.75	*d*
	32.87	39.35	*d*
	33.72	40.40	*b*
	38.23	45.73	*c*
	42.13	50.43	*b*
(II)	31.79	38.06	*a*
	32.66	39.01	*a*
	33.74	40.37	*b*
	42.13	50.52	*b*
(III)	31.84	38.08	*a*
	32.67	39.14	*a*

*Les fréquences *a*, *b* et *c* correspondent respectivement au mono-, di- et triéthérate de $MgBr_2$. Les fréquences *d* seraient dues à une variété cristalline du monoéthérate.

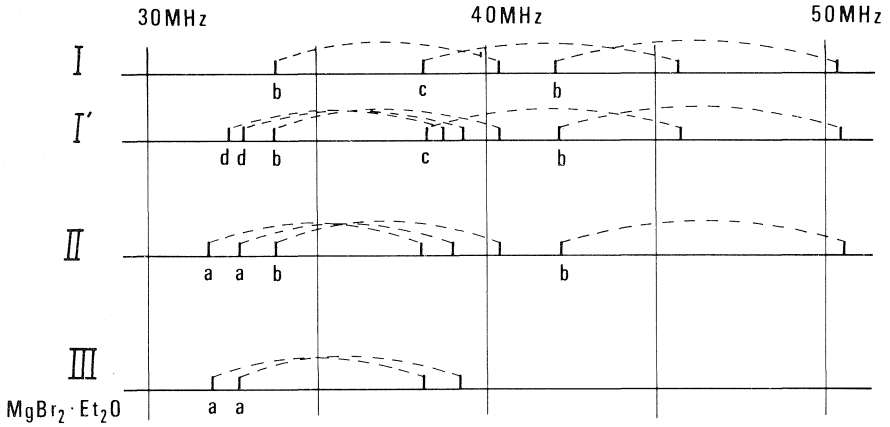

FIG. 1. Comparaison des spectres des différents échantillons I, I′, II et III de $MgBr_2 \cdot n Et_2O$ étudiés. Les raies correspondant aux deux isotopes ^{79}Br et ^{81}Br sont reliées par une ligne pointillée. La raie en pointillé dans le spectre I′ n'a pas été observée par suite de la présence, à cet endroit, d'une raie parasite intense.

quences, pour que les deux groupes de raies ne puissent être confondus. Elles correspondent, très vraisemblablement à une autre variété cristalline du monoéthérate.

La fréquence moyenne des résonances dans ces complexes de $MgBr_2$, environ 35 MHz, est supérieure à celle des composés précédents comme le laisse prévoir l'électronégativité du brome supérieure à celle des groupes éthyle et phényle. Des différences analogues ont été observées par ailleurs pour la fréquence de ^{79}Br dans Me_2InBr (68.75 MHz) et dans $MeInBr_2$ (102.92 MHz) (18), ainsi que pour la fréquence de ^{35}Cl dans $EtCH_2Cl$ (32.968 MHz) et $BrCH_2Cl$ (36.14 MHz) (13).

(*4*) Les deux échantillons de *tert*-BuMgBr·$n Et_2O$ donnent aussi lieu à des signaux de fréquences différentes, indiquant une composition ou une structure différente. Remarquons que leurs fréquences sont supérieures à celles des complexes EtMgBr·$2Et_2O$ et $[EtMgBr \cdot (iso\text{-}Pr)_2O]_2$. Or, un groupe tertiobutyle étant considéré comme moins électronégatif qu'un groupe éthyle, le remplacement du second par le premier devrait entraîner un abaissement de fréquence comme celui observé pour le chlore dans *tert*-BuCl (31.065 MHz) comparé à EtCl (32.704 MHz) (13). Les fréquences des deux échantillons de *tert*-BuMgBr·$n Et_2O$ ne semblent donc pas compatibles avec l'existence ni d'un diéthérate monomère *tert*-BuMgBr·$2Et_2O$ semblable à EtMgBr·$2Et_2O$, ni d'un monoéthérate dimère $[tert\text{-}BuMgBr \cdot Et_2O]_2$ semblable à $[EtMgBr \cdot (iso\text{-}Pr)_2O]_2$; d'autant plus que dans ce dernier cas, le remplacement des molécules $(iso\text{-}Pr)_2O$ par des molécules Et_2O, meilleurs donneurs d'électrons, serait un facteur supplémentaire d'abaissement de la fréquence de résonance du brome.

Par contre les fréquences de 33.72 MHz pour l'échantillon I, de 31.75 et 32.66 MHz pour l'échantillon II, sont très voisines des fréquences des signaux correspondants à $MgBr_2 \cdot 2Et_2O$ et $MgBr_2 \cdot Et_2O$ respectivement. Cette double coïncidence n'est certainement pas fortuite mais suggère que le magnésien mixte s'est dismuté en bromure de magnésium et ditertiobutylmagnésium selon un processus analogue à celui observé pour les halogénures de méthylmagnésium (6). Le bromure de magnésium ainsi obtenu serait disolvaté dans l'échantillon I et monosolvaté dans l'échantillon II pour lequel l'éther éthylique en excès a été évacué par pompage sur la rampe à vide. Cette description nous paraît très vraisemblable quoique tous les signaux de rqn des deux complexes de $MgBr_2$ (à une et deux molécules d'éther) n'aient pas été observés (le rapport signal sur bruit des signaux cités dans le tableau est faible), et elle semble confirmée par une étude parallèle (non publiée) des spectres Raman.

Conclusion

Cette première étude d'organomagnésien par rqn met en évidence les possibilités de cette technique pour l'étude de leur structure électronique et moléculaire, ainsi que pour l'identification des complexes présents dans un échantillon solide comme dans le cas des complexes de

$MgBr_2$ avec l'éther éthylique. A la suite de cette première étude, la poursuite de recherches sur ces composés apparaît souhaitable pour que la discussion des résultats obtenus repose sur une base expérimentale élargie.

1. L. J. GUGGENBERGER et R. E. RUNDLE. J. Am. Chem. Soc. **90**, 5375 (1968).
2. J. KRESS et A. NOVAK. J. Organometal. Chem. **86**, 281 (1975).
3. M. ASTIER et P. MILLIE. J. Organometal. Chem. **31**, 139 (1971).
4. M. S. KHARASCH et O. REINMUTH. Grignard reactions of nonmetallic substances. Prentice Hall, Inc. New-York, NY. 1954.
5. E. C. ASHBY et R. C. ARNOTT. J. Organometal. Chem. **14**, 1 (1968).
6. J. KRESS et A. NOVAK. J. Organometal. Chem. **99**, 199 (1975).
7. G. STUCKY et R. E. RUNDLE. J. Am. Chem. Soc. **86**, 4825 (1964).
8. F. A. SCHRODER. Chem. Ber. **102**, 2035 (1969).
9. A. L. SPEK, P. VOORBERGEN, G. SCHATT, C. BLOMBERG et F. BICKELHAUPT. J. Organometal. Chem. **77**, 147 (1974).
10. J. KRESS et J. GUILLERMET. Spectrochim. Acta Ser. A, **29**, 1717 (1973).
11. G. B. RAVICH et I. MANYSHAROVA. Zh. Struk. Khim. **2**, 449 (1961).
12. H. SCHIBILLA et M. T. LE BIHAN. Acta Crystallogr. **23**, 332 (1967).
13. I. P. BIRYUKOV, M. G. VORONKOV et I. A. SAFIN. Tables of nuclear quadrupole resonance frequencies. Translated from Russian. Israel Program for Scientific Translation, Jerusalem. 1969.
14. YU. K. MAKSYUTIN, E. V. BRYUKHOVA, G. K. SEMIN et E. N. GUR'YANOVA. Izv. Akad. Nauk SSSR Ser. Khim. **11**, 2658 (1968).
15. A. F. VOLKOV et N. I. SMIRNOV. Dokl. Akad. Nauk SSSR, **211**, 1377 (1973).
16. T. P. DAS et E. L. HAHN. NQR spectroscopy. Supplement I to Solid State Physics. Academic Press, New York, NY. 1958.
17. E. A. C. LUCKEN. Nuclear quadrupole coupling constants. Academic Press, Londres et New York. 1969.
18. D. P. PATTERSON et A. CARNEVALE. Inorg. Chem. **13**, 1479 (1974).

Coefficients *B* de viscosité dans les systèmes ternaires aqueux. I. NaCl – alcool *tert*-butylique – eau et Bu_4NBr – alcool *tert*-butylique – eau à 25°C

MARC PALMA ET JEAN-PIERRE MOREL

Laboratoire d'Etude des Interactions Solutés–Solvants, Groupe de Chimie Physique, Université de Clermont, Les Cézeaux, B.P. 45, 63170 Aubière, France

Reçu le 27 septembre 1976

MARC PALMA et JEAN-PIERRE MOREL. Can. J. Chem. **55**, 1521 (1977).

Nous avons mesuré le coefficient *B* de viscosité des électrolytes NaCl et Bu_4NBr dans les mélanges hydroorganiques contenant jusqu'à 40% en poids d'alcool *tert*-butylique (TBA), ainsi que celui du non-électrolyte TBA dans les solutions aqueuses salines de NaCl et de Bu_4NBr. Les variations de *B* sont comparées à celles des grandeurs thermodynamiques de transfert ΔH_t^0 et ΔS_t^0 des solutés étudiés dans ces différents milieux. La contribution du soluté à l'enthalpie libre d'activation de viscosité est également calculée.

MARC PALMA and JEAN-PIERRE MOREL. Can. J. Chem. **55**, 1521 (1977).

We have measured the viscosity coefficient *B* of the electrolytes NaCl and Bu_4NBr in aqueous-organic mixtures containing up to 40% by weight of *tert*-butyl alcohol (TBA), as well as that of the non-electrolyte TBA in aqueous solutions of the salts NaCl and Bu_4NBr. The variations of *B* were compared with those of the thermodynamic quantities ΔH_t^0 and ΔS_t^0 of the solutes studied in these different media. The contribution of the solute to the free enthalpy of activation of viscosity has also been calculated.

[Journal translation]

Introduction

Le coefficient *B* de viscosité des électrolytes en mélange hydroorganique n'a pas fait l'objet de nombreuses études systématiques. La plupart des auteurs qui ont abordé ce sujet sont cités dans la revue de Padova (1) qui traite de la solvatation en milieux non aqueux et mixtes. Le travail le plus complet dans le domaine a été publié récemment par Feakins *et al.* (2) qui ont étudié les chlorures alcalins en milieu eau–méthanol.

La grandeur *B* peut se définir comme la limite lorsque la concentration molaire *c* tend vers 0 de:

$$\frac{\eta/\eta_0 - 1 - A\sqrt{c}}{c}$$

où η et η_0 sont les viscosités de la solution et du solvant, *A* le coefficient de la loi limite de Falkenhagen (3) qui rend compte des interactions ioniques pour ce phénomène. (Pour les non électrolytes: $A = 0$.)

Ainsi, en solution diluée, la viscosité relative obéit-elle en général à la loi de Jones–Dole (4):

$$[1] \qquad \eta_r = \eta/\eta_0 = 1 + A\sqrt{c} + Bc$$

B, caractéristique des interactions soluté–solvant comme le montre son additivité, peut donner des informations précieuses sur la solvatation. En solution aqueuse, les déterminations de *B* concernant tant les électrolytes que les non-électrolytes sont d'ailleurs fort nombreuses (5–10).

Nous avons mis au point un dispositif automatique de mesure de la viscosité des solutions qui devrait nous permettre d'acquérir un assez grand nombre de données suffisamment précises dans le domaine des mélanges hydroorganiques. Nous abordons ce projet avec l'étude des électrolytes types NaCl et Bu_4NBr dans les mélanges aqueux contenant jusqu'à 40% en poids d'alcool *tert*-butylique (TBA). Les propriétés thermodynamiques de nombreux solutés, et en particulier des halogénures alcalins, dans ces solvants, ont fait l'objet de travaux au laboratoire (11, 12); il nous sera ainsi possible de confronter ces grandeurs à la propriété de transport *B*. Afin de pouvoir examiner ces systèmes sous l'angle des interactions soluté–cosolvant où les deux espèces jouent un rôle symétrique, nous avons également mesuré le coefficient *B* du TBA dans les solutions salines de NaCl et de Bu_4NBr; cette approche a également fait l'objet de récents travaux dans le domaine des propriétés thermodynamiques (13).

Partie expérimentale

Dispositif

Notre dispositif permet de mesurer simultanément la viscosité et la masse volumique d'un liquide à une température donnée. Sa description détaillée a déjà été faite

dans une précédente publication (14). Il est constitué essentiellement (*i*) d'un viscosimètre à capillaire type Ubbelohde (diamètre intérieur du capillaire: 0.5 mm), (*ii*) d'un densimètre digital Anton Paar, (*iii*) d'une burette à dilution.

Il suffit d'introduire une masse déterminée de solvant dans le réservoir du viscosimètre et de remplir la burette d'une solution de concentration connue. La suite de la manipulation (mesure des temps d'écoulement, de la période du densimètre, neuf répétitions, six dilutions et impressions) se fait de façon entièrement automatique selon un programme prédéterminé. Afin que la composition du mélange reste constante pendant la durée des mesures, des saturateurs contenant un solvant identique à celui étudié isolent l'intérieur du dispositif de l'air atmosphérique. Le circuit de régulation thermique du densimètre et du viscosimètre donne sur une longue période une stabilité de $\pm 2 \times 10^{-3}$ K.

Réactifs

L'alcool *tert*-butylique a été purifié au laboratoire selon la méthode habituelle (15). Le chlorure de sodium est un produit pur pour analyses 'Prolabo' et le bromure de tétrabutyl-ammonium a été recristallisé dans l'acétate d'éthyle. L'eau est tridistillée dans un appareil en quartz. Toutes les solutions ont été filtrées sur un verre fritté de porosité n° 4.

Viscosités

La viscosité relative η_r se détermine par

$$[2] \qquad \eta_r = \eta/\eta_0 = \rho t/\rho_0 t_0$$

masses volumiques et temps d'écoulement relatifs respectivement à la solution et au solvant. Le volume de la boule de mesure du viscosimètre étant faible, la correction d'énergie cinétique d'Hagenbach (16) est négligeable. Nous avons déjà exposé ailleurs (14) de façon détaillée notre méthode d'exploitation des données numériques et en particulier la façon de déterminer le coefficient B. Nous traçons systématiquement les graphes $(\eta_r - 1)/\sqrt{c} = f(\sqrt{c})$ et $(\eta_r - 1 - A\sqrt{c})/c = f(c)$. Les coefficients A de la loi de Jones–Dole pour les différents mélanges ont été calculés à l'aide de la formule de Falkenhagen (3) et des données de la littérature (17). Le tracé des graphes $(\eta_r - 1)/\sqrt{c} = f(\sqrt{c})$ nous a permis de constater un accord satisfaisant entre les valeurs expérimentales et calculées du coefficient A. Les coefficients B de TBA dans eau–NaCl et eau–Bu_4NBr ont été obtenus à l'aide d'une mesure effectuée sur le solvant pur et six mesures à des concentrations variant de 0.01 à 0.1 M environ. Les graphes $(\eta_r - 1 - A\sqrt{c})/c = B + Dc$ montrent un coefficient D (14) nul à la précision des mesures. Quant à Bu_4NBr dans eau–TBA, la détermination a été effectuée dans un domaine de concentration un peu plus élevé: 0.025 à 0.25 M environ. En effet, dans un intervalle de concentration compris en moyenne entre 0 et 0.06 M, la loi de Jones–Dole n'est pas vérifiée.

Ce phénomène a déjà été signalé par Kay (18) et Desnoyers (7). Enfin, NaCl dans eau–TBA montre un coefficient D non négligeable pour certains mélanges.

Les incertitudes relatives moyennes sur les mesures sont inférieures aux valeurs suivantes: (*i*) molarité c (de 0.01 à 0.25 M): $\pm 5 \times 10^{-3}$, (*ii*) temps d'écoulement (de 100 à 500 s): $\pm 5 \times 10^{-5}$, (*iii*) masses volumiques ρ (de l'ordre de 1 g cm^{-3}): $\pm 2 \times 10^{-5}$.

Volumes molaires

A partir des masses volumiques utilisées pour le calcul des viscosités, nous pouvons déterminer les volumes molaires apparents par la méthode classique (19). En ce qui concerne NaCl et Bu_4NBr dans eau–TBA, l'accord avec la littérature est satisfaisant (20); de même pour TBA dans les solutions salines (13).

Résultats et discussion

Pour les résultats voir les tableaux 1 et 2. Les variations du coefficient B des divers solutés avec la concentration en cosolvant, exprimée par sa molalité dans l'eau, sont représentées sur les figs 1 et 2. Pour les deux électrolytes, dans les mélanges eau–TBA, on observe des courbes décroissantes à point d'inflexion plus ou moins marqué vers $m_{TBA} = 2.5$ soit environ 16% en poids d'alcool dans le solvant; pour NaCl, B passe par un minimum vers $m_{TBA} = 4$ soit 23%. Pour TBA, le coefficient B décroît de façon sensiblement linéaire avec m_{NaCl}; avec m_{Bu_4NBr} les variations sont qualitativement et quantitativement comparables à celles de B (Bu_4NBr) dans eau–TBA.

Deux constatations s'imposent: (*i*) Bu_4NBr et TBA jouent des rôles symétriques et les variations de B, qui sont importantes, sont sans doute gouvernées par les interactions hydrophobes des chaînes hydrocarbonées des deux espèces; (*ii*) Pour NaCl et TBA, on observe que les variations de B ($^s\delta B$) sont analogues dans leurs formes à celles des enthalpies de transfert: $\Delta H^\theta_{t(w\rightarrow w+TBA)}$ de NaCl et $\Delta H^\theta_{t(w\rightarrow w+NaCl)}$ de TBA (13), ceci au signe près.

Si aucune théorie satisfaisante du coefficient B n'a été proposée, on peut dire, en résumé, que sa valeur est déterminée par deux contributions: celle due aux interactions soluté–solvant qui

TABLEAU 1. Coefficients A et B des électrolytes NaCl et Bu_4NBr dans eau – alcool *tert*-butylique

		NaCl		Bu_4NBr	
x*	m†	A calculé	B ℓ mol^{-1}	A calculé	B ℓ mol^{-1}
0	0	0.0060	0.079	0.0091	1.20
5	0.71	0.0059	0.075	0.0090	1.11
10	1.50	0.0056	0.060	0.0089	1.01
15	2.38	0.00545	0.036	0.0088	0.870
20	3.37	0.00535	0.009	0.00885	0.720
25	4.50	0.00535	0.002	0.0089	
30	5.78	0.0055	0.0245	0.00905	0.545
35	7.26	0.0056	0.040	0.0093	
40	8.99	0.0062	0.051	0.0097	0.450

*x: pourcentage en poids de TBA.
†m: molalité en TBA.

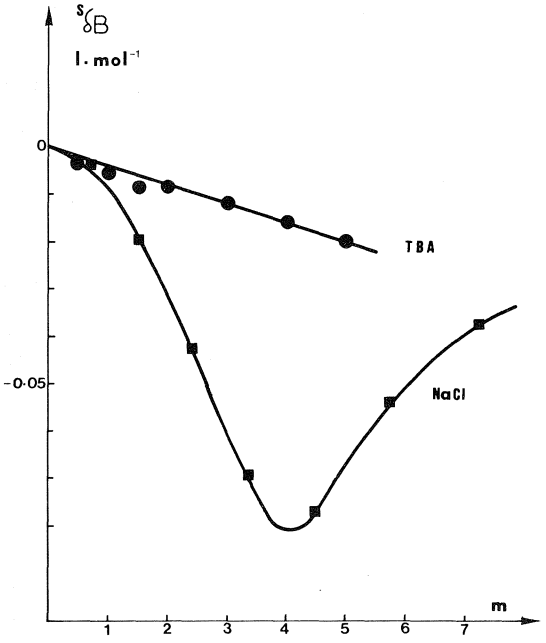

FIG. 1. Variations du coefficient B de NaCl et TBA respectivement avec les molalités en TBA et NaCl dans l'eau.

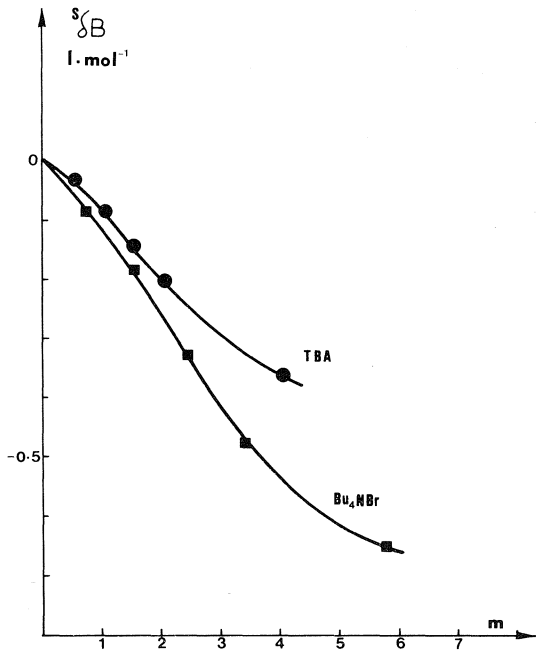

FIG. 2. Variations du coefficient B de Bu_4NBr et de TBA respectivement avec les molalités en TBA et Bu_4NBr dans l'eau.

modifient la structure du milieu et par suite sa viscosité; celle due au volume propre de l'espèce soluté dont le modèle macroscopique d'Einstein peut rendre compte. La première est prépondérante pour les petits ions minéraux; la deuxième, positive, prend de l'importance lorsque la molécule de soluté devient plus grosse que la molécule de solvant. Dans le premier cas, qui s'applique à NaCl, une corrélation intéressante a été proposée par Nightingale (21): dans l'eau, B varie linéairement avec l'entropie d'hydratation des ions. Quel que soit l'ion, ou l'électrolyte, on peut écrire:

$$[3] \qquad B = a + k\Delta S_h^{\theta}$$

On a observé que pour NaCl dans eau–TBA, $^{s}\delta B$ varie comme ΔH_t^{θ}, c'est-à-dire également comme ΔS_t^{θ} (12); aussi, comme nous le constatons sur la fig. 3, on observe une bonne corrélation linéaire en portant $^{s}\delta B$ en fonction de ΔS_t^{θ}. La relation de Nightingale peut fournir une explication, si elle reste valable dans les solvants concernés avec les mêmes valeurs de a et k; on aurait alors immédiatement:

$$[4] \qquad {}^{s}\delta B = k\Delta S_t^{\theta}$$

Malheureusement, la pente de la droite obtenue fig. 3 (5.3×10^{-3} ℓ J^{-1} K) n'est pas identique à celle de la corrélation de Nightingale (1.8×10^{-3} ℓ J^{-1} K). L'explication n'est donc pas aussi simple.

Avec pour modèle du processus de transport celui développé par Eyring (22), le coefficient B permet de calculer une grandeur d'activation: l'enthalpie libre d'activation de l'écoulement visqueux d'une solution de concentration donnée. Cette théorie a été appliquée par Nightingale et Benck (23) aux électrolytes dans l'eau et, récemment, par Feakins (2) aux solutions dans les mélanges eau–méthanol. Sans reprendre en détail un développement analogue à celui conduit par cet auteur, nous allons établir une expression qui conserve la forme logarithmique de $(1 + B)$ et reste satisfaisante lorsque B n'est pas petit devant 1.

La différence d'enthalpie libre d'activation entre 1 mol de solution de molarité c_i et 1 mol de solvant est:

$$[5] \qquad RT \ln (1 + Bc_i)\,\overline{V}/\overline{V}^0$$

où le volume molaire de la solution s'écrit en fonction de celui $\overline{V}^0$ du solvant:

$$[6] \qquad \overline{V} = \overline{V}^0 + x_i(\overline{V}_i - \overline{V}^0)$$

TABLEAU 2. Coefficients B de l'alcool *tert*-butylique dans les solutions salines

m*	Eau–NaCl	Eau–Bu_4NBr
0	0.387	0.387
0.5	0.3825	0.355
1	0.381	0.300
1.5	0.378	0.240
2	0.378	0.180
3	0.375	
4	0.371	0.024
5	0.367	

*m: molalité des sels respectifs dans l'eau.

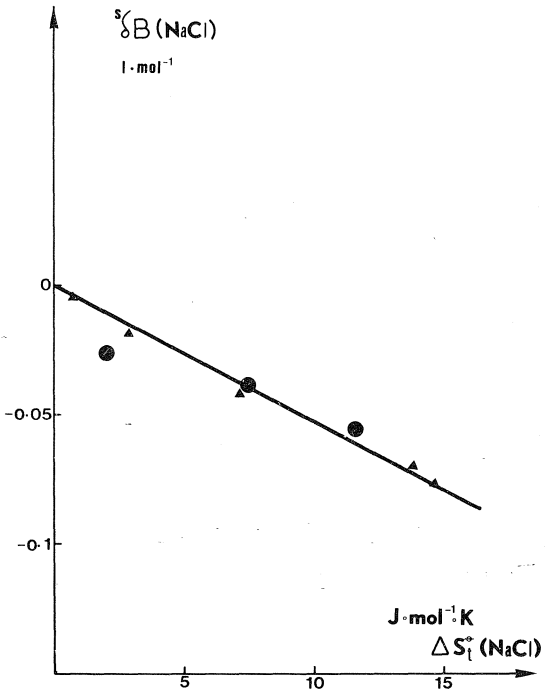

FIG. 3. Variations du coefficient B en fonction de l'entropie molaire de transfert pour NaCl dans les milieux eau–TBA: % en poids de TBA: ▲ 5, 10, 15, 20, 25; ● 30, 35, 40.

x_i est la fraction molaire en soluté de volume molaire partiel $\overline{V}_i$.

La différence ci-dessus est due au remplacement de x_i mole de solvant par x_i de soluté; elle est donc égale à $x_i(\Delta\mu_i^{\neq} - \Delta\mu_0^{\neq})$ où les $\Delta\mu^{\neq}$ représentent respectivement les contributions molaires du soluté et du solvant à l'enthalpie libre d'activation d'une solution. Dans la formule [5] n'intervient pas le terme $A\sqrt{c}$ puisque l'on s'intéresse uniquement aux interactions soluté–solvant, c'est-à-dire qu'on choisit comme état de référence la solution infiniment diluée; en complétant la définition de cet état de référence par la convention $c = 1$ on a alors:

$\overline{V}_i = \overline{V}_i^{\theta}$ volume molaire à dilution infinie

$x_i = c_i\overline{V}^0$ en solution diluée (avec $\overline{V}^0$ en ℓ mol^{-1})

$$[7]\quad \overline{V}/\overline{V}^0 = 1 + c_i(\overline{V}_i^{\theta} - \overline{V}^0) = 1 + c_i\Delta\overline{V}$$

et par suite:

$$[8]\quad \Delta\mu_i^{\neq} - \Delta\mu_0^{\neq} = \frac{RT}{\overline{V}^0}\ln(1 + B)(1 + \Delta\overline{V})$$

Cette expression donne donc la variation d'enthalpie libre d'activation quand on remplace 1 mol de solvant par 1 mol de soluté pour obtenir une solution idéale de molarité unité. En faisant les approximations $\ln(1 + \varepsilon) = \varepsilon$, on obtient l'expression proposée par Feakins:

$$[9]\quad \Delta\mu_i^{\neq} - \Delta\mu_0^{\neq} = \frac{RT}{\overline{V}^0}(B + \Delta\overline{V})$$

Dans cette expression, on peut considérer que le premier membre constitue la contribution à B d'interactions soluté–solvant; $\Delta\overline{V}$ est une contribution de volume telle que si $\Delta\overline{V} > 0$ (volume molaire partiel du soluté supérieur à celui du solvant) la valeur de B est diminuée d'autant. On voit donc que cette dernière contribution ne s'apparente en rien à l'effet de volume tel que le prévoit la relation d'Einstein dans laquelle B croît avec le volume du soluté.

Dans l'eau, (*i*) pour NaCl: $B = 79 \times 10^{-3}$ et $\Delta\overline{V} = -1.45 \times 10^{-3}$, (*ii*) pour Bu_4NBr: $B = 1200 \times 10^{-3}$ et $\Delta\overline{V} = 282 \times 10^{-3}$. Pour ce dernier sel, la contribution de volume n'est donc pas négligeable; de même pour le non-électrolyte TBA: $B = 387 \times 10^{-3}$ et $\Delta\overline{V} = 69 \times 10^{-3}$. L'importance relative des deux contributions a été analysée par Feakins (2).

Intéressons-nous maintenant à l'effet d'un changement de solvant. Comme l'a souligné l'auteur précédent, dans la mesure où l'on s'intéresse à l'interaction soluté–solvant, ce sont les variations de $\Delta\mu_i^{\neq}$ qui sont intéressantes. B varie d'un solvant à l'autre du fait des variations de $\Delta\mu_i^{\neq}$ mais aussi des caractéristiques propres du solvant: $\overline{V}^0$ et $\Delta\mu_0^{\neq}$; il dépend aussi des variations de $\Delta\overline{V}$. Par exemple, dans le mélange contenant 20% en poids de TBA on a:

$$\Delta\overline{V}(\text{NaCl}) = -1.86 \times 10^{-3}$$

$$B(\text{NaCl}) = 9 \times 10^{-3}$$

$$\Delta\overline{V}(Bu_4NBr) = 278 \times 10^{-3}$$

$$B(Bu_4NBr) = 720 \times 10^{-3}$$

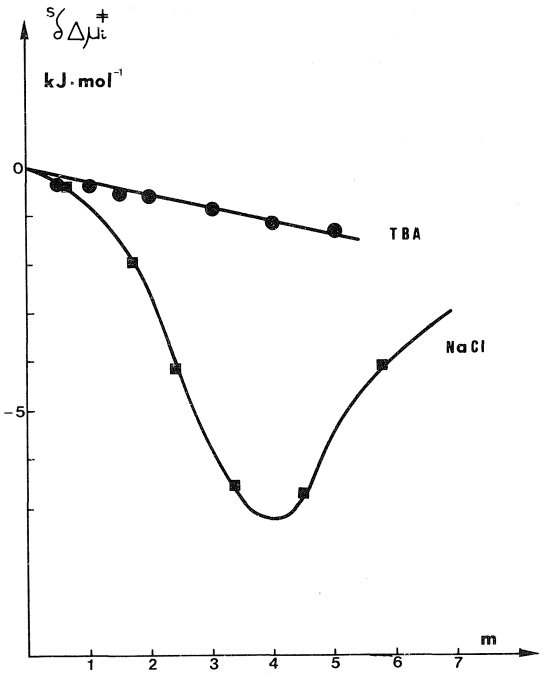

FIG. 4. Variations de la contribution molaire des solutés à l'enthalpie libre d'activation des solutions molaires de NaCl et TBA dans les mélanges de molalité m respectivement en TBA et NaCl.

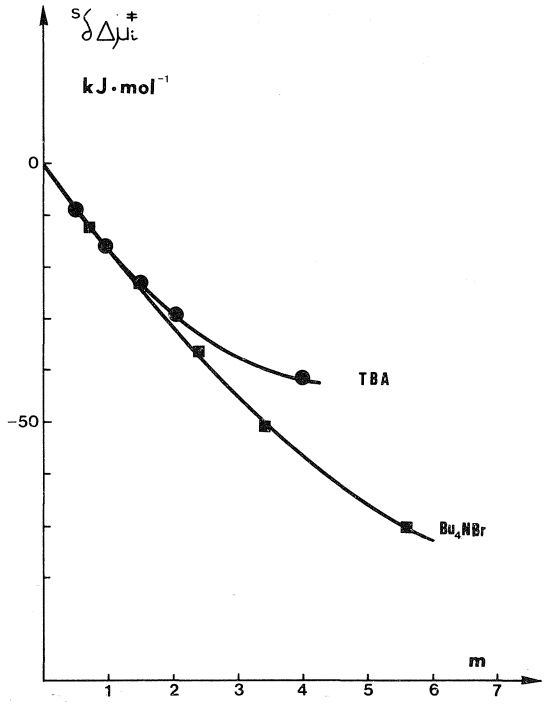

FIG. 5. Variations de la contribution molaire des solutés à l'enthalpie libre d'activation des solutions molaires de Bu_4NBr et TBA dans les mélanges de molalité m respectivement en TBA et Bu_4NBr.

En comparant avec les valeurs dans l'eau données ci-dessus, on voit que dans les deux cas les variations de $\Delta\overline{V}$ avec le solvant sont négligeables devant celles de B.

Sur les figs 4 et 5 nous avons tracé les variations des $\Delta\mu_i^{\neq}$($^{s}\delta\Delta\mu_i^{\neq}$) avec la composition du solvant; on voit que ces variations, quant à leurs formes et amplitudes relatives, sont très semblables à celles des coefficients B correspondants.

Dans le cas du système Bu_4NBr–TBA, on constate que, jusqu'à $m = 1.5$ les variations relatives à l'électrolyte en présence de non-électrolyte et, réciproquement, celle du nonélectrolyte en présence de l'électrolyte, coïncident; ceci contrairement aux variations $^{s}\delta B$ correspondantes. On peut rapprocher ce comportement de la grandeur d'activation $\Delta\mu_i^{\neq}$ de celui constaté pour les grandeurs thermodynamiques (13). Ainsi, sur la base du modèle d'Eyring, dans les solvants étudiés, les variations de B rendent essentiellement compte des variations de l'enthalpie libre molaire partielle d'activation du soluté. Donc, dans ces milieux, cette quantité varie proportionnellement à l'entropie du soluté dans l'état fondamental comme le montre la relation [4].

En conclusion, on voit que des relations intéressantes existent entre les propriétés thermodynamiques du soluté dans l'état fondamental et la propriété de transport B, ou la grandeur d'activation qui en découle à travers le modèle d'Eyring. Ces relations ne sont pas immédiatement prévisibles à partir des propriétés connues.

Des données expérimentales supplémentaires sont au moins nécessaires pour espérer une meilleure compréhension.

1. J. I. PADOVA. *Dans* Modern aspects of electrochemistry. Vol. 7. *Edité par* B. E. Conway et J. O'M. Bockris. Butterworths, Londres. 1972.
2. D. FEAKINS, D. J. FREEMANTLE et K. G. LAWRENCE. J. Chem. Soc. Faraday Trans. 1, **70**, 795 (1974).
3. H. FALKENHAGEN et E. L. VERNON. Phys. Z. 33 (1932).
4. G. JONES et M. DOLE. J. Am. Chem. Soc. **51**, 2950 (1929).
5. W. M. COX et J. H. WOLFENDEN. Proc. R. Soc. Ser. A, **145**, 475 (1934).
6. M. KAMINSKY. Z. Phys. Chem. **5**, 154 (1955); **8**, 173 (1956); **12**, 206 (1957).
7. J. E. DESNOYERS et G. PERRON. J. Solution Chem. **1**, 199 (1972).
8. J. E. DESNOYERS, M. AREL et P. A. LEDUC. Can. J. Chem. **47**, 547 (1969).
9. R. I. PATEL, K. J. PATIL et M. V. KAULGUD. Z. Phys. Chem. **86**, 67 (1973).

10. T. T. HERSKOVITS et T. M. KELLY. J. Phys. Chem. **77**, 381 (1973).
11. Y. POINTUD, J. JUILLARD, J. P. MOREL et L. AVEDIKIAN. Electrochim. Acta, **19**, 229 (1974).
12. Y. POINTUD, J. JUILLARD, L. AVEDIKIAN, J. P. MOREL et M. DUCROS. Thermochim. Acta, **8**, 423 (1974).
13. J. E. DESNOYERS, G. PERRON, J. P. MOREL et L. AVEDIKIAN. Chemistry and physics of aqueous gas solutions. *Edité par* W. A. Adams. Electrochemical Society, Princeton, NJ. 1975. p. 172.
14. M. PALMA et J. P. MOREL. J. Chim. Phys. **73**, 645 (1976).
15. J. P. MOREL et J. MORIN. J. Chim. Phys. **67**, 2018 (1970).
16. E. HAGENBACH. Pogg. Ann. **109**, 385 (1860).
17. T. L. BROADWATER et R. L. KAY. J. Phys. Chem. **74**, 21 (1970); **74**, 3802 (1970).
18. R. L. KAY, T. VITUCCIO, C. ZAWOYSKI et D. F. EVANS. J. Phys. Chem. **70**, 2336 (1966).
19. O. REDLICH et D. MEYER. Chem. Rev. **64**, 221 (1964).
20. L. AVEDIKIAN, G. PERRON et J. E. DESNOYERS. J. Solution Chem. **4**, 331 (1975).
21. E. R. NIGHTINGALE, JR. J. Phys. Chem. **63**, 1381 (1959).
22. S. GLASSTONE, K. J. LAIDLER et H. EYRING. The theory of rate processes. McGraw-Hill. 1941. p. 477.
23. E. R. NIGHTINGALE, JR. et R. F. BENCK. J. Phys. Chem. **63**, 1777 (1959).

Coordination compounds of indium. Part XXXIII. X-Ray photoelectron spectroscopy of neutral and anionic indium halide species

BRIAN H. FREELAND,[1] JACOB J. HABEEB, AND DENNIS G. TUCK

Department of Chemistry, University of Windsor, Windsor, Ont., Canada N9B 3P4

Received October 14, 1976

BRIAN H. FREELAND, JACOB J. HABEEB, and DENNIS G. TUCK. Can. J. Chem. **55**, 1527 (1977).

The X-ray photoelectron spectra (metal and halogen energy levels) have been recorded for binary halides of indium in the +I, +II, and +III states, and for anionic halide complexes of indium(I) and (III). The results are internally consistent in terms of the relation between metal and ligand levels, but lattice effects prevent any detailed interpretation of indium levels in terms of oxidation state, ligand electronegativity, and/or coordination number.

BRIAN H. FREELAND, JACOB J. HABEEB et DENNIS G. TUCK. Can. J. Chem. **55**, 1527 (1977).

On a enregistré les spectres photoélectroniques de rayons-X (les niveaux d'énergie du métal et des halogènes) d'halogénures binaires d'indium dans les états +I, +II et +III et pour les halogénures complexes anioniques de l'indium(I) et (III). Les résultats sont en accord interne en termes de la relation entre les niveaux du métal et du ligand, mais des effets de réseaux empêchent toutes interprétations plus détaillées des niveaux de l'indium en termes d'états d'oxydation, d'électronégativité du ligand et/ou du nombre de coordination.

[Traduit par le journal]

Introduction

The literature now contains a number of papers on the use of X-ray photoelectron spectroscopy (ESCA) in studies of the structure and bonding in inorganic molecules. As part of a programme of studies of main group metallic elements, we have recently carried out a series of measurements of electron binding energies in compounds of indium with chlorine, bromine, and iodine. The species studied included the neutral halides of indium in the +III, +II, and +I states, and the anionic complexes of indium(I) and (III).

There has been little previous work on the electron spectroscopy of indium complexes. McGuire, Schweitzer, and Carlson (1) have measured the $3d_{5/2}$ and $3p_{3/2}$ levels in indium metal and a number of binary compounds, and have compared the results with those for the analogous compounds of other Group III metals. In general our results are in agreement with those reported by these authors.

Experimental

Preparative

The neutral indium(III) and indium(I) halides were prepared by methods reported previously (2, 3). Indium(II) halides were obtained from the reduction of InX_3 by indium metal in xylene (4). The preparation of the anionic halide complexes followed previously described procedures (5–7). The identity of the compounds was confirmed where necessary by elemental analysis.

Spectroscopy

Electron binding energies were measured on a McPherson ESCA-36 photoelectron spectrometer operated jointly by the Universities of Toronto, Western Ontario, and Windsor. Magnesium K_α X-radiation (1253.6 eV) was the exciting radiation.

Samples were inserted into a vacuum-locked target chamber as thin smears on platinum discs, and were in some cases covered with vacuum-deposited thin films of gold for calibration purposes. The preparation of these discs, and all other handling of samples, was carried out in a dry nitrogen atmosphere in order to prevent hydrolysis or oxidation of the indium compounds.

Electron energy measurements were recorded on tape, and were also obtained in graphical form after appropriate accumulation of results. In view of the accuracy of the binding energies (see below), it was not considered worthwhile to analyse the data by any computing procedure, and the results quoted below were obtained by measuring the peak height energy manually from the printed spectra. As a measure of the reliability of this procedure, five results for the $3d_{5/2}$ level in $InCl_3$ gave 446.1, 445.6, 446.1, 446.2, and 445.9 eV; the mean of these five values is $446.0 \pm 0.1_1$ (σ). For each spectrum we routinely measured the $3d_{5/2}$ and $3d_{3/2}$ levels of indium, the half-widths of each of these lines, the energies of Pt $4f_{7/2}$ or Au $4f_{7/2}$ as appropriate, and the most easily characterized line of the halide present (Cl $2p_{3/2}$; Br $3p_{3/2}$; I $3d_{5/2}$). The separation between $3d_{3/2}$ and $3d_{5/2}$ of indium was essentially constant in all the compounds studied, at 7.5 ± 0.2 eV. All experimental values quoted

[1]Present address: Department of Chemistry, University of Western Ontario, London, Ont., Canada.

are taken to be subject to a probable error of ± 0.1 eV unless otherwise noted. In view of the other uncertainties associated with the interpretation of these results, this is not an unduly large problem.

Results and Discussion

The original aim of the present work was to establish the effects of parameters such as oxidation state, coordination number, and ligand electronegativity upon the electron energy levels of indium in its complexes. As the results described show, this aim has not been realized, and some of the reasons for this are not hard to identify. One major problem of ESCA studies on solids is the appreciable line widths involved, with the resultant decrease in the accuracy of measurements of the binding energy, and this is certainly a significant factor in the present work (see below). Equally important is the nature of the energy relationships involved. The general treatment (8) shows that the incident energy $h\nu$ is distributed amongst electron binding (E_b), kinetic (E_k), and lattice or (Madelung) energy terms, *i.e.*

$$h\nu = E_k + (E_b + E_{lattice})$$

Clearly then in discussing atomic energy levels (E_b) derived from ESCA studies of solids, the effect of the Madelung terms cannot safely be ignored. A comparison of the results for (say) indium in different solids may therefore not be meaningful unless the lattices concerned are sufficiently similar for the assumption of a constant value for $E_{lattice}$ to be valid.

The results obtained are listed in Tables 1–4. The values for In $3d_{5/2}$ are in general similar to those reported by McGuire *et al.* (1), although there are some detailed differences which we note below. In order to examine the implications of these results in terms of indium–halogen bonding, we have plotted the indium $3d_{5/2}$ level *vs.* the appropriate halogen level for the neutral halides, and for those indium(I) and (III) complexes for which results are available. Figure 1 shows that within experimental error there is a monotonic increase in the levels of both metal and halogen, for each halogen, irrespective of oxidation state and/or coordination number of the indium. Comparison of the halogen levels with published results indicates that the bonding is strongly ionic. Thus for chlorine the range of 198.5–199.5 eV is substantially lower than in the neutral covalent silicon or germanium chlorides and organochlorides (9) (205–207 eV), but higher than in the alkali metal halides (8) (193–195 eV). The conclusion that the bonding in indium(I) and (III) halides is of the order of 50% ionic is in keeping with earlier discussions of the bonding based on force constant calculations (10) (and with nqr studies of tin(IV) species (11), in which the metal is formally isoelectronic with indium(III)).

TABLE 1. Indium and halogen energy levels (in eV) in neutral indium halides (relative to Pt $4f_{7/2} = 71.2$ eV)

Compound		In $3d_{5/2}$	In $3d_{3/2}$	Halogen[a]
1	InCl	445.2	452.8	198.5
2	InBr	445.2	452.9	182.5
3	InI	444.0	451.9	619.1
4	$InCl_2$	445.5	453.2	198.9
5	$InBr_2$	445.9	453.4	182.8
6	InI_2	445.1	452.7	619.4
7	$InCl_3$	446.0	453.5	199.1
8	$InBr_3$	445.8	453.4	183.0
9	InI_3[b]	445.1	452.8	619.2

[a]Chlorine $2p_{3/2}$; bromine $3p_{3/2}$; iodine $3d_{5/2}$.
[b]'Yellow' allotrope.

TABLE 2. Indium and halogen energy levels (in eV) in anionic indium(III) complexes (relative to Au $4f_{7/2} = 84.0$ eV)

Complex		In $d_{5/2}$	In $d_{3/2}$	Halogen[a]
10	$(MeNH_3)_4InCl_7$	446.2	454.2	
11	$(Me_2NH_2)_4InCl_7$	445.5	453.2	
12	$(Me_3NH)_3InCl_6$	445.7	453.2	199.2
13	$(Me_4N)_2InCl_5$	445.3	452.8	
14	Et_4NInCl_4	445.7	453.1	199.1
15	$(MeNH_3)_4InBr_7$	445.4	453.0	
16	$(Me_4N)_2InBr_5$	446.0	453.6	182.7
17	Me_4NInBr_4	445.7	453.3	182.6

[a]Chlorine $2p_{3/2}$; bromine $3p_{3/2}$.

TABLE 3. Indium, carbon, and halogen energy levels (in eV) in n-$Pr_4N[InX_4]$ complexes (X = Cl, Br, I) (relative to Pt $4f_{7/2} = 71.2$ eV)

Anion		In $d_{5/2}$	In $d_{3/2}$	C(1*s*)	Halogen[a]
18	$InCl_4^-$	446.2	453.8	285.2	199.4
19	$InBr_4^-$	446.2	453.8	285.1	183.1
20	InI_4^-	445.9	453.6	285.3	620.1

[a]Chlorine $2p_{3/2}$; bromine $3p_{3/2}$; iodine $3d_{5/2}$.

TABLE 4. Indium, carbon, and halogen energy levels (in eV) in indium(I) anionic complexes (relative to Pt $4f_{7/2}$ = 71.2 eV)

Compound		In $3d_{5/2}$	In $3d_{3/2}$	C(1*s*)	Halogen[b]
21	$Et_4N[InCl_2]$	445.7	453.4	285.3	199.2
22	$Et_4N[InBr_2]$	446.6	454.8	285.7	183.1
23	$Et_4N[InI_2]$	446.5	453.8	[c]	620.9
24	$(Me_2diphos)[InI_3]$[a]	445.3	452.9	284.9	619.9

[a] Me_2diphos = bis(diphenylmethyl)-1,2-phosphonio-ethane cation.
[b] Chlorine $2p_{3/2}$; bromine $3p_{3/2}$; iodine $3d_{5/2}$.
[c] Not recorded.

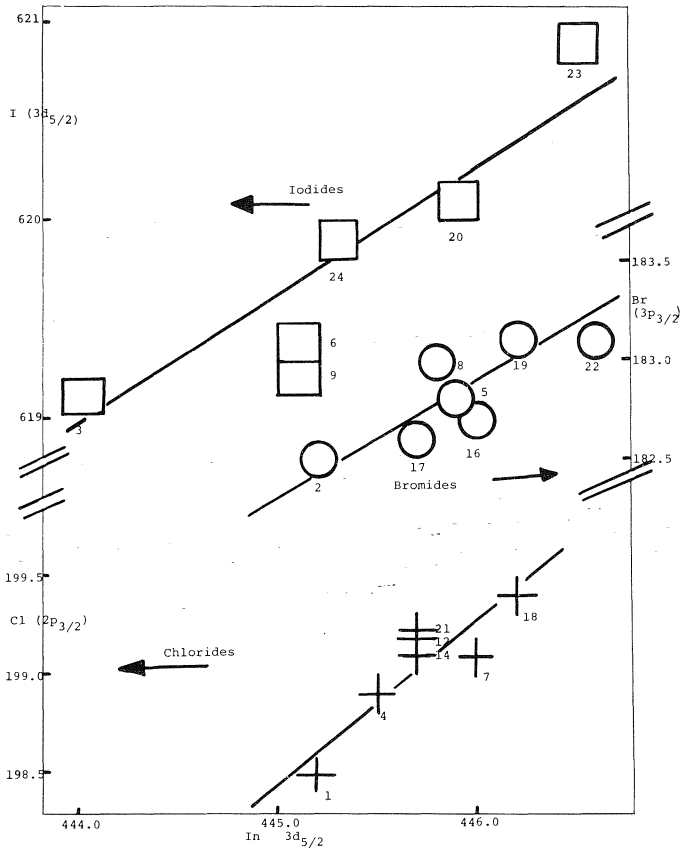

FIG. 1. Relationship between indium $3d_{5/2}$ and halogen energy levels (in eV) in indium halide compounds. Numbers identify compounds in Tables 1–4.

Given this model of bonding, it is not surprising that in each series of halogen compounds the monohalide involves the weakest interaction. There is no general ordering of the levels by oxidation state beyond the monohalides, no doubt because of perturbations imposed on any such order by lattice effects. As an example of such effects, we note that there are two sets of results for the $InCl_4^-$ anion, in salts with Et_4N^+ and n-Pr_4N^+ cations. These two sets of values are not identical (see Tables 2 and 3), but both lie reasonably on the plotted line in Fig. 1, establishing that both indium and chlorine levels are affected by the different $E_{lattice}$ terms for the two salts, but that the In–Cl interaction is the same in both cases. The emphasis which

this approach places on relationships between two atoms within a single molecule, rather than the levels for a given atom in a series of molecules, seems entirely appropriate in studying ionic solids. Some of the correlations of atomic levels claimed in the earlier literature may well flounder on the incorrect assumption that the lattice terms can be safely ignored.

Effect of Oxidation State, etc., on Indium Levels

One of the disappointing conclusions to be drawn from the above discussion is that one cannot use the energy levels measured in solid state ESCA experiments in order to determine the oxidation state of indium in a given compound. However, it is interesting to examine the overall effect of the oxidation state on these levels in a series of simple compounds, namely the binary halides. The results for these compounds are given in Table 1. Our value for InCl is close to that reported by McGuire *et al.* (1) (445.1 ± 0.3 eV), but their results for the trihalides are consistently higher than ours by approximately 1.1 eV. The reasons for this are not immediately apparent.

A number of authors have presented refined treatments of ESCA data (and more particularly of photoelectron spectra) whereby the levels are related to calculated atomic charges in molecules (8, 9, 12, 13). In view of the small range of experimental values and the relatively low accuracy achieved with crystalline samples, it does not seem worthwhile to pursue such arguments in the present case. Rather we have followed the simpler procedure of plotting E_b for indium against the sum of the atomic electronegatives of the ligand(s) concerned; the electronegativities are those quoted by Allred (14), namely Cl 3.16, Br 2.96, I 2.66. Figure 2 shows that five of the nine points lie on a straight line, which also extends to indium metal (E_b $3d_{5/2}$ 448.1 eV, from ref. 1).

Of those compounds studied, indium trichloride and tribromide involve six-coordination of indium by halide ions in a chromium trichloride structure (ref. 15, p. 235). Indium monochloride has a distorted sodium chloride structure while the monobromide and monoiodide have the thallium iodide structure, in which five halide nearest neighbours are at the vertices of an octahedron centred on the metal (ref. 15, p. 349). Indium triiodide exists as the iodide-bridged dimer In_2I_6 in the solid state (16),

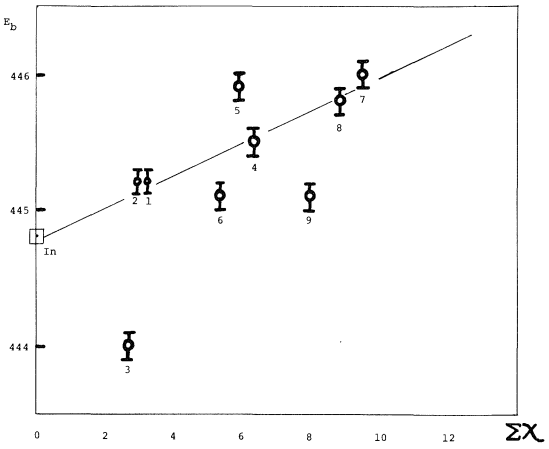

FIG. 2. Dependence of indium $3d_{5/2}$ energy levels (E_b, in eV) in indium halide compounds on ligand electronegativity ($\Sigma\chi$). Numbers identify compounds in Table 1.

with four-coordinate indium(III). Indium(II) bromide and iodide have been formulated as $In[InX_4]$ (X = Br, I) on the basis of the Raman spectra of the solids (3); indium dichloride has been assigned various structures, involving $[InCl_4]^-$, $[InCl_6]^{3-}$, or $[In_2Cl_9]^{3-}$ units with the appropriate number of indium(I) cations. Such ionic formulations are inevitably over-simplifications but for the present the more important point is that $InCl_2$ is structurally different from the related pair $InBr_2$ and InI_2.

The overall conclusion from an examination of Fig. 2 must be that indium $3d_{5/2}$ binding energies do indeed increase with the increasing (integrated) electronegativity of the environment, and hence with the presumed positive charge on the metal, within the limits discussed. There is no basis for predicting that a linear relationship would apply, but a monotonic dependence of energy level on ligand properties seems entirely reasonable. The compounds which lie on, or close to, the line drawn are those in which indium is in an ionic octahedral environment. The compounds $InBr_2$, InI_2, and InI_3 do not fit into this category, and here again lattice effects are presumably the source of the difficulties. The most serious remaining problem is then with InI, for which no explanation is forthcoming.

The results in Tables 3 and 4 show that with the two series n-$Pr_4N[InX_4]$ and $Et_4N[InX_2]$ the overall effect of increasing ligand electronegativity is to raise the indium energy level

TABLE 5. Widths at half-height (in eV) for indium levels in binary indium halides

Compound		$3d_{5/2}$	$3d_{3/2}$
1	InCl	1.7	1.6
2	InBr	1.5	1.5
3	InI	2.0	2.0
4	$InCl_2$	1.5	1.4
5	$InBr_2$	1.4	1.3
6	InI_2	1.4	1.3
7	$InCl_3$	1.4	1.3
8	$InBr_3$	1.2	1.2
9	InI_3	1.5	1.4

slightly. The salt $Et_4N[InCl_2]$ is a notable exception to this rule, even though the results for this compound apparently show a good correlation with other indium chloride species in Fig. 1. In view of the difficulties noted above for the neutral halides, we do not feel justified in extending the argument to a discussion of the results for the anionic halide complexes of indium(I) and (III). It is *a fortiori* impossible to discuss the effect of coordination number in such complexes, since changes in coordination number are necessarily accompanied by, and indeed are in part the result of, changes in cation and hence of lattice.

Such qualifications as expressed above clearly reduce, or remove completely, the value of ESCA studies of indium halides as a tool for structural investigation, due in the main to uncertainties as to the significance of lattice energy terms in any given situation.

Indium(II) Compounds

As noted earlier, the compounds InX_2 present an interesting structural problem, since they do not contain In^{2+} ions, being generally formulated as ionic dimers involving two indium species in the oxidation states I and III in the lattice. (See refs. 3 and 17 for a review of the evidence on this point.) We therefore examined the spectra of these compounds with particular interest in the hope of identifying two distinct binding energies. In fact, in none of the compounds $InCl_2$, $InBr_2$, or InI_2 did we detect more than a single indium level. The line shapes did not differ significantly from those for the other binary halides, and the half-widths were no larger than in other halides (Table 5). Given that the indium $3d_{5/2}$ levels in InCl and $InCl_3$ are 445.2 and 446.0 eV (Table 1), one could reasonably expect some indication of the presence of two oxidation states in $InCl_2$, and similar arguments can be advanced for $InBr_2$ and InI_2. The results clearly underline the statement made elsewhere (3, 17), that the ionic formulations noted earlier represent gross over-simplification of the structures involved, despite spectral evidence as to the nature of the indium(III) anionic complexes present.

We may note in the context of line-width measurements that the iodine results for indium(III) iodide, $I_2InI_2InI_2$, show no evidence for the existence of terminal and bridging iodide as required by the crystal structure (17). The line widths for $3d_{3/2}$ and $3d_{5/2}$ are 1.4 and 1.5 eV, with a separation of 11.5 eV; for the compound n-$Pr_4N.InI_4$ the comparable values are 1.5, 1.5, and 11.4 eV. Other iodine species show similar values. These results serve to emphasize the very considerable limits which must be conceded in X-ray photoelectron spectroscopy studies of crystalline solids.

Acknowledgements

It is a pleasure to acknowledge helpful discussions with Dr. J. E. Drake, and the help of the laboratory personnel at the University of Western Ontario. This research was supported in part by Operating and Capital Equipment Grants from the National Research Council of Canada.

1. G. E. McGUIRE, G. K. SCHWEITZER, and T. A. CARLSON. Inorg. Chem. **12**, 2450 (1973).
2. A. J. CARTY and D. G. TUCK. J. Chem. Soc. A, 1081 (1966).
3. J. G. CONTRERAS, J. S. POLAND, and D. G. TUCK. J. Chem. Soc. Dalton, 922 (1973).
4. B. H. FREELAND and D. G. TUCK. Inorg. Chem. **15**, 475 (1976).
5. J. GISLASON, M. H. LLOYD, and D. G. TUCK. Inorg. Chem. **10**, 1907 (1971).
6. J. J. HABEEB and D. G. TUCK. Chem. Commun. 600 (1975).
7. J. J. HABEEB and D. G. TUCK. J. Chem. Soc. Dalton, 866 (1976).
8. P. H. CITRIN, R. L. SHAW, A. PACKER, and T. D. THOMAS. *In* Electron spectroscopy. *Edited by* D. A. Shirley. American Elsevier, New York. 1972. p. 691.
9. J. E. DRAKE, C. RIDDLE, and L. COATSWORTH. Can. J. Chem. **53**, 3602 (1975).
10. J. G. CONTRERAS and D. G. TUCK. Inorg. Chem. **11**, 2967 (1972).

11. M. KUBO and D. NAKAMURA. Adv. Inorg. Chem. Radiochem. **8**, 257 (1966).
12. L. B. PERRY and W. L. JOLLY. Inorg. Chem. **13**, 1215 (1974).
13. L. B. PERRY and W. L. JOLLY. J. Am. Chem. Soc. **95**, 5442 (1973).
14. A. L. ALLRED. J. Inorg. Nucl. Chem. **17**, 215 (1961).
15. A. F. WELLS. Structural inorganic chemistry. 4th ed. Oxford University Press, Oxford. 1975.
16. J. D. FORRESTER, A. ZALKIN, and D. H. TEMPLETON. Inorg. Chem. **3**, 63 (1964).
17. A. J. CARTY and D. G. TUCK. Prog. Inorg. Chem. **19**, 245 (1975).

Theoretical study of the vibrational structure of the $^1(n, \pi^*)$ transition in diimide: potential curves and Franck–Condon analysis

M. PERIĆ, R. J. BUENKER, AND S. D. PEYERIMHOFF

Lehrstuhl für Theoretische Chemie der Universität Bonn and Institut für Physikalische Chemie der Universität Bonn, Wegelerstr. 12, 5300 Bonn, Germany

Received November 11, 1976

M. PERIĆ, R. J. BUENKER, and S. D. PEYERIMHOFF. Can. J. Chem. **55**, 1533 (1977).

Ab initio CI potential curves are reported for the ground and $^1(n,\pi^*)$ excited states of diimide for each of the six possible internal coordinates. These results are then used to obtain vibrational wavefunctions and frequencies for both states, which in turn are combined with electronic transition moment data to allow a Franck–Condon analysis of the band structure of the (dipole-forbidden) n–π^* absorption system. This procedure allows one to reproduce the main features of the observed spectra of N_2H_2 and N_2D_2 and indicates that the majority of the vibrational transitions seen are vibronically induced via the antisymmetric NH stretching mode ν_5. The calculations are in essential agreement with the earlier experimental interpretation of the vibrational structure of this transition in terms of progressions in the symmetric bending (ν_2) and NN stretching (ν_3) frequencies, except that they indicate that the previous v_2' numbering should be altered by three units. According to this interpretation the isotope shift for the vibronic origin is 672 cm^{-1} compared with the corresponding calculated value of 666 cm^{-1}. It is argued that several other weaker transitions seen experimentally arise via a different inducement mechanism, namely the torsion (ν_4) mode, and as such are only observed in energy regions where ν_5-induced transitions cannot occur.

M. PERIĆ, R. J. BUENKER et S. D. PEYERIMHOFF. Can. J. Chem. **55**, 1533 (1977).

On rapporte des courbes de potentiel IC *ab initio* pour les états fondamentaux et excités $^1(n,\pi^*)$ de la diimide pour chacune des six coordonnées internes possibles. On utilise alors ces résultats pour obtenir des fonctions d'ondes vibrationnelles et des fréquences pour les deux états qui à leur tour sont combinées avec des données de moment de transition électronique pour permettre une analyse de Franck–Condon de la structure de bande du système d'absorption n–π^* (dipole-interdite). Ce procédé permet de reproduire les caractéristiques principales des spectres observés pour N_2H_2 et N_2D_2 et indique que la majorité des transitions vibrationnelles qui sont détectées sont induites par un processus vibronique par l'intermédiaire d'un mode de vibration antisymétrique de valence du NH (ν_5). Ces calculs sont en accord général avec l'interprétation expérimentale antérieure de la structure vibrationnelle de cette transition en termes de progression dans les fréquences de déformation angulaire symétrique (ν_2) et de vibration de valence (ν_3); toutefois ils indiquent que la numérotation antérieure v_2' devrait être modifieé par trois unités. D'après cette interprétation, le déplacement isotopique pour l'origine vibronique est 672 cm^{-1} comparé avec la valeur calculée correspondante de 666 cm^{-1}. On présente plusieurs arguments indiquant que plusieurs autres transitions faibles qui sont détectées expérimentalement dérivent d'un mécanisme d'induction différent soit le mode de torsion (ν_4) et que comme telles elles sont observées uniquement dans des régions d'énergie où des transitions induites ν_5 ne peuvent pas se produire.

[Traduit par le journal]

Introduction

The absorption spectra of N_2H_2 and N_2D_2 (diimide) in the 3000–4300 Å region generally believed to correspond to the $^1(n,\pi^*)$ $^1B_g \leftarrow {}^1A_g$ transition have recently been reported by Back, Willis, and Ramsay (1). At roughly the same time *ab initio* SCF and CI calculations at the approximate (*trans*) ground state equilibrium geometry of this system were carried out by Vasudevan *et al.* (2) for a large number of electronic states for this molecule. In comparing these experimental and theoretical results for the $^1(n,\pi^*)$ transition it was noted, however, that the calculated vertical electronic energy difference for this species was some 0.6 eV *smaller* than the observed location of the absolute intensity maxima in the corresponding absorption systems (2). Because of the Franck–Condon Principle one normally expects the vertical electronic energy difference to very

nearly coincide with the energy of maximum transition probability and hence this result might be taken to indicate that the calculations were simply in error in this respect by roughly the entire 0.6 eV margin. On the other hand experience with this type of CI treatment for other systems such as formaldehyde (3), ethylene (4), and water (5), for example, indicates that the error limits for such calculated transition energy results should not exceed the 0.2–0.3 eV range. It was thereupon argued by Vasudevan *et al.* (2) that there is a strong likelihood that the *true* vertical electronic transition actually occurs well *below* the observed location of the absorption maximum in this case, especially since the $^1(n,\pi^*)$ system is electronically dipole-forbidden for the ground state equilibrium nuclear conformation (C_{2h} point group).

In order to investigate this hypothesis in more detail from the theoretical side it is necessary to calculate potential surfaces for both ground and $^1(n,\pi^*)$ excited states of N_2H_2 so as to allow for a vibrational analysis of this electronic transition. Clearly one of the key objectives in such a study is to determine the mechanism by which this formally dipole-forbidden transition gains sufficient intensity to be observed at all. In addition it is hoped that through this type of analysis a good correlation between calculated and experimental results for the band structure of the $^1(n,\pi^*)$ system will be obtained which allows for a definite assignment of the vibrational progressions observed in this spectral region (1). The present paper reports the results of such an *ab initio* CI treatment of the $^1(n,\pi^*)$ transition of diimide, in which all six possible vibrational modes are given explicit consideration.

Description of the Theoretical Treatment

Details of the AO basis (double-zeta plus Rydberg) and CI treatment employed in the present calculations have already been given in earlier work (2). One change has been made, however, namely in that approximate natural orbitals (NO's) are used (6, 7) for each of the CI states rather than simply the corresponding SCF MO's employed previously. This improvement in the CI treatment leads to an increase in the vertical transition energy of about 0.1 eV, but still not by a great enough amount to change any of the qualitative conclusions referred to in the Introduction. The sizes of the configuration spaces treated, for which secular equation eigenvalues have been obtained to an estimated accuracy of 0.01 eV (8), range from 15 000 to 25 000 in the present study.

The method employed for the vibrational analysis is similar to that used for ethylene and O_2 in previous work (9, 10) and is summarized below. In accordance with the Born–Oppenheimer (and Franck–Condon) Approximation the total wavefunction Ψ is first assumed to be separable into an electronic (ψ_e) and a vibrational (ψ_v) part. A further simplification is introduced by assuming that the six vibrational modes of diimide are independent of one another, that is

$$[1] \qquad \psi_v = \prod_{j=1}^{6} \psi_v^{(j)}(R_j)$$

where R_j is a (symmetrized) internal coordinate.[1] Under these conditions the transition moment for a given vibrational species can be written as:

$$[2] \quad \langle r \rangle = \int \cdots \int \prod_j \psi_{v'}^{(j)} \boldsymbol{R}_{e'e''} \psi_{v''}^{(j)} \, d\tau_v$$

where $\boldsymbol{R}_{e'e''} = \int \psi_{e'} \boldsymbol{r} \psi_{e''} \, d\tau_e$ is the electronic transition moment (with the usual primed notation being employed to distinguish between ground and excited species in each instance).

In principle the electronic transition moment should be a function of all six vibrational coordinates but in this work it is assumed that this quantity is independent of all such species except the inducing mode in each case, *i.e.* that vibrational excitation which makes the overall transition vibronically allowed under the dipole selection rules.[2] Whereupon one obtains the result:

$$[3] \quad \langle \boldsymbol{r} \rangle_{e'v'e''v''} = \prod_{j \neq I} S_{v'v''}^{(j)} \times \int \psi_{v'}^{(I)} \boldsymbol{R}_{e'e''}(R_I) \psi_{v''}^{(I)} \, dR_I$$

in which the subscript I denotes the inducing

[1]Note that the species used correspond to pure NN or NH stretch or analogous bending motions and therefore do not strictly satisfy the Eckart conditions, *i.e.* they are not completely orthogonal to the various translational and rotational modes.

[2]Note that the usual subsidiary assumption employed in deriving the Franck–Condon Principle for *allowed* transitions states that $\boldsymbol{R}_{e'e''}$ is independent of *all* vibrational species.

mode, and the quantities $S_{v'v''}^{(j)}$ are the vibrational overlaps for the various noninducing modes in a given vibrational transition. The corresponding f value or transition probability is then given in the usual way as

$$[4] \quad f_{e'v'e''v''} = \tfrac{2}{3}|\langle r\rangle_{e'v'e''v''}|^2 \cdot \Delta E_{e'v'e''v''}$$

where ΔE is the transition energy.

The necessary vibrational wavefunctions and energies are obtained (in the framework of the Born–Oppenheimer approximation) by solving the Schrödinger equation in which a given electronic energy curve serves as the potential for the nuclear motion. Since the present approach assumes that the various vibrational modes are independent of one another it is consistent to simply calculate appropriate sets of one-dimensional potential curves (with all other coordinates held fixed in a given case), and substitute these data in the corresponding Schrödinger equations for each type of nuclear motion. The requirement of choosing a set of fixed values for the (five) complementary coordinates in each case introduces a certain amount of ambiguity into the procedure since in practice there is some coupling observed between the various vibrational modes, but since the geometry changes encountered in going from ground to the $^1(n,\pi^*)$ excited states in diimide are relatively small this problem is not expected to be very critical in the present study.[3] Finally, to complete the vibrational analysis it is necessary to calculate the electronic transition moment $\boldsymbol{R}_{e'e''}$ as a function of each of the three antisymmetrical internal coordinates in *trans*-diimide.

Vibrational Frequencies and $R_{e'e''}$ Values

The CI potential curves calculated for the six vibrational coordinates in the ground and $^1(n,\pi^*)$ states of diimide are shown in Fig. 1 *a*, *b*; corresponding vibrational energy levels are also indicated in each case. The first three modes ν_1 to ν_3 are of a_g symmetry, corresponding respectively to (symmetric) NH stretch, HNN bending, and NN stretch. The torsional vibration ν_4 belongs to a_u while ν_5 (antisymmetric NH stretch) and ν_6 (antisymmetric HNN bending) are of b_u symmetry.

The calculated equilibrium values for each of the internal coordinates of ground and excited state are collected in Table 1. Significant distinctions are noted in the NN bond lengths and HNN angles of the two states as well as in the shapes of their respective torsional potential curves. The calculated increase in R_{NN} of 0.09 bohr ($\sim$0.05 Å) upon excitation[4] is in very good agreement with the experimental estimate for this quantity (0.05 Å) given by Back *et al.* (1), but the change in bond angle predicted by the calculations (13° toward a less bent geometry) is only about half that cited by the latter authors based on their assignment of the observed $^1(n,\pi^*)$ vibrational structure. The present result, however, is in very good agreement with the value of $\Delta\varphi = 12°$ obtained by Baird and Swenson (11) in an earlier theoretical treatment. Each state is calculated to possess equal NH bond lengths and HNN bond angles, with R_{NH} for the upper species being only 0.024 bohr smaller than the corresponding ground state value. Finally the CI energy of the ground state for its global potential minimum is found to be -110.166 hartree, which is 2.554 eV below the excited state minimum energy (all results based on curve fitting procedures).

The calculated vibrational frequencies for the various ground and excited state species are given in Table 2 and are compared with the corresponding observed values wherever possible (12,1); data for N_2D_2 have also been calculated and are likewise contained in the table. Two theoretical values are given in each case, one equal to the 0–1 frequency and the other obtained by doubling the calculated zero-point energy; the discrepancies between these results are a measure of the degree of anharmonicity present in the associated potential curves.

In general it appears that the calculations can reproduce the experimental frequencies to within

[3]In general (but not always) the values of the ground state equilibrium conformation are employed for these fixed parameters because of the emphasis which the Franck–Condon Principle places on the nuclear arrangement of the lower state.

[4]The absolute value calculated for R_{NN} in the N_2H_2 ground state is somewhat too large (2.366 bohr experimentally) because NN bond functions (or equivalent polarization functions) are not included in the AO basis set. Nevertheless this omission should have essentially the same effect on ground and excited state, and hence the calculations are expected to give a good estimate of the *change* in this geometrical coordinate which occurs during the $^1(n,\pi^*)$ transition.

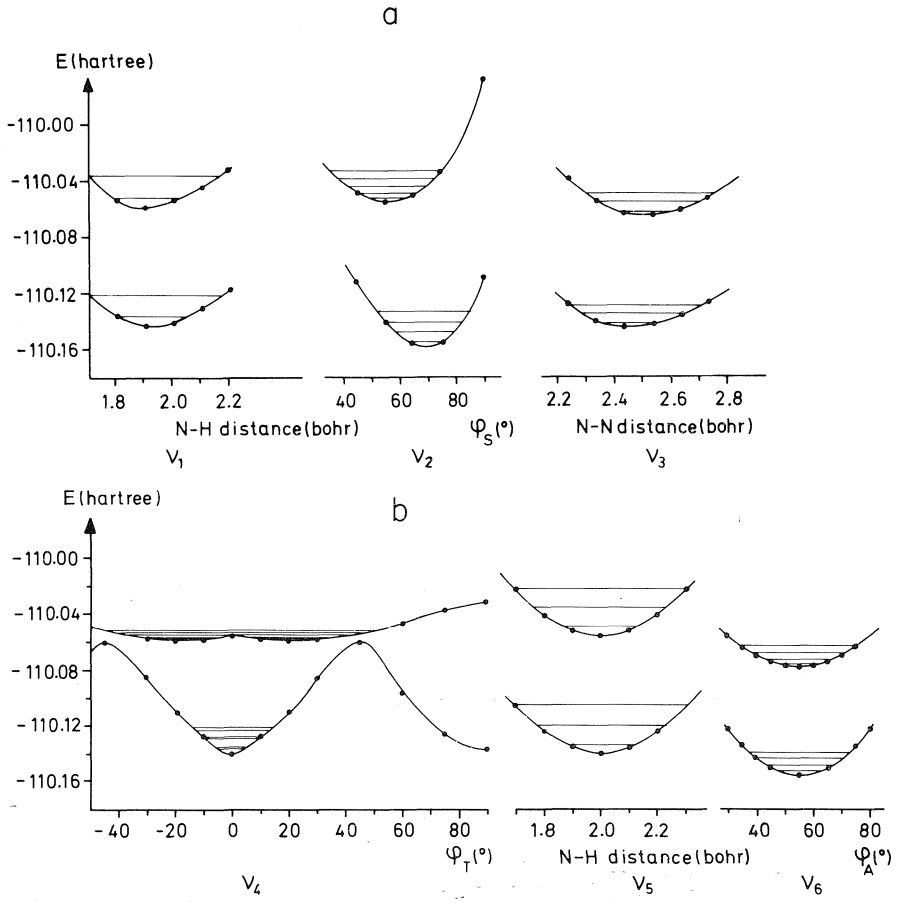

FIG. 1. CI potential curves calculated for the six vibrational coordinates in ground and $^1(n,\pi^*)$ excited state of diimide; vibrational energy levels are also indicated.

TABLE 1. Calculated equilibrium values for each of the internal coordinates of N_2H_2 obtained from a polynomial fit to the CI data displayed in Fig. 1

Parameter	Ground state	$^1(n,\pi^*)$ state
NH (bohr)[a]	1.932	1.908
Bending angle NNH	110°	123°
NN (bohr)	2.443	2.533
Torsional angle	0°	28°
Relationship between NH bond lengths	Equal	Equal
Relationship between HNN bond angles	Equal	Equal

[a]1 bohr = 0.52917 Å.

an error of 50–250 cm^{-1} in all cases; the largest discrepancies occur for ν_1 and ν_6. Considering the underlying assumptions in the theoretical procedure used, especially the failure to consider coupling between the various modes, such agreement between calculation and experiment for both ground and excited state frequencies appears to be quite reasonable; in particular, the results would seem to be of sufficient accuracy to allow for an unambiguous assignment of the band structure observed for this electronic transition (1).

Finally, the calculated $^1(n,\pi^*)$ transition moment results are given in Table 3 as a function of each of the three antisymmetric vibrational coordinates of diimide. For small excursions away from the symmetric (C_{2h}) nuclear conformation it is found that this quantity is largest in absolute value for the NH stretch species ν_5 and smallest for the corresponding antisymmetric bending mode ν_6. The transition moment ultimately becomes much larger upon torsion as the system approaches the *cis* limit ($\varphi_t = 90°$, C_{2v} symmetry), in which case the transition in question becomes dipole allowed ($^1B_1 \leftarrow {}^1A_1$).

TABLE 2. Calculated vibrational frequencies (in cm^{-1}) for the various modes in N_2H_2 and N_2D_2 and comparison with experiment

Vibrational modes	N_2H_2			N_2D_2		
	Calcd.[a]		Exptl.[b]	Calcd.[a]		Exptl.[b]
Ground state						
ν_1 (NH sym)	3467	3371	3128	2452	2391	(2320)[c]
ν_2 (φ sym)	1465	1456	1583	1035	1031	1215
ν_3 (NN)	1566	1522	1529	1516	1475	(1539)[d]
ν_4 (torsion)	1714	1476	—[e]	1218	1149	—
ν_5 (NH antisym)	3086	3092	3120	2182	2184	2315
ν_6 (φ antisym)	1039	1042	1286	734	735	946
$^1(n,\pi^*)$ state						
ν_1	3662	3525	—	2589	2491	—
ν_2	1066	1050	1215 (1135–1170)	754	746	910 (880–909)
ν_3	1407	1341	1550 (1546–1548)	1360	1301	1440 (1437–1443)
ν_4	388	40	—	306	9	—
ν_5	3132	3120	—	2217	2212	—
ν_6	902	885	—	642	632	—

[a]The first column gives twice the calculated zero-point energy, while the second contains the calculated 0–1 transition energy.
[b]Experimental ground state data are from ref. 12; corresponding $^1(n,\pi^*)$ values are from ref. 1. The ranges given in parentheses for the upper state ν_2' and ν_3' frequencies are average differences observed within several progressions (1).
[c]Estimated value, ref. 12.
[d]Somewhat uncertain, ref. 1.
[e]Two indirect references given in refs. 12 and 13 to unpublished work by Trombetti indicate that ν_4 lies in the region 1250–1350 cm^{-1}; the assignment seems far from certain, however (14).

TABLE 3. Calculated electronic transition moment $\boldsymbol{R}_{e'e''}$ as a function of the antisymmetric vibrational modes in N_2H_2

(*a*) NH stretch, ν_5

Δ(NH)	$R^y_{e'e''}$
0.0	0.0
±0.1	0.0511
±0.2	0.0619
±0.3	0.0783

(*b*) NH bending, ν_6

$\Delta\varphi_a$ (deg)	$R^y_{e'e''}$
0	0.0
±5	0.0076
±10	0.0110
±25	0.0012

(*c*) Torsion, ν_4

$\Delta\varphi_t$ (deg)	$R^x_{e'e''}$	$R^z_{e'e''}$
0	0.0	0.0
±10	0.0357	0.0260
±20	0.0511	0.0446
±30	0.0459	0.0565
±45	0.0655	−0.0167
±60	0.1999	−0.0600
±75	0.3066	−0.0369
±90	0.3534	0.0

No experimental results for $\boldsymbol{R}_{e'e''}$ in diimide have yet been reported.

Vibrational Overlap and Transition Probability Integrals

In order to calculate an intensity distribution for the $^1(n,\pi^*)$ transition it is necessary to combine the vibrational wavefunctions obtained in the last section with the electronic transition moment data so as to evaluate the various integrals required on the right-hand side of eq. 3. The results of these computations are given in Table 4 for N_2H_2 and N_2D_2 respectively. The magnitudes of the dipole moment matrix elements in Table 4 are of special interest in the present study since these quantities ultimately determine the overall strength of transitions induced via a vibronic mechanism. The data for the NH stretching and bending antisymmetric modes ν_5 and ν_6 indicate quite strongly in each instance that only the $1 \leftarrow 0$ ($v' \leftarrow v''$) vibrational transitions are of sufficient magnitude to be of experimental significance. The fact that all other vibrational species ($n \leftarrow 0$) are much less probable is of course tied up with the result that for both modes the ground and excited state potential curves show minima at the same value of the internal coordinate (namely zero, *i.e.* for a symmetric equilibrium geometry). The finding that only the $1 \leftarrow 0$ ν_6 transition should be

TABLE 4. Vibrational overlaps and $\langle \psi_{v'} \boldsymbol{R}_{e'e''} \psi_{v''} \rangle$ values for the various vibrational modes of N_2H_2 and N_2D_2 (notation $0.n-a$ signifies $0.n \times 10^{-a}$)

Mode	Integral	Isomer	Overlap for upper vibrational quantum number = 0	1	2	3	4	5	6	7
ν_1	$\langle \psi_{0''} \vert \psi_{v'} \rangle$	N_2H_2	0.998	0.057	0.006	0.003	0.005	0.001		
		N_2D_2	0.997	0.073	0.003	0.004	0.004	0.001		
ν_2	$\langle \psi_{0''} \vert \psi_{v'} \rangle$	N_2H_2	0.324	0.480	0.509	0.446	0.341	0.236	0.151	0.091
		N_2D_2	0.205	0.361	0.453	0.466	0.419	0.339	0.252	0.175
ν_3	$\langle \psi_{0''} \vert \psi_{v'} \rangle$	N_2H_2	0.822	0.493	0.249	0.120	0.061	0.035	0.017	0.007
		N_2D_2	0.817	0.497	0.254	0.123	0.062	0.035	0.018	0.007
ν_4	$\langle \psi_{0''} \vert \psi_{v'} \rangle$	N_2H_2	0.435	0	0.697	0	0.451			
		N_2D_2	0.247	0	0.677	0	0.536			
	$\langle \psi_{0''} \vert R^x_{e'e''} \vert \psi_{v'} \rangle$	N_2H_2	0	0.0154	0	0.007	0			
		N_2D_2	0	0.0118	0	0.007	0			
	$\langle \psi_{0''} \vert R^z_{e'e''} \vert \psi_{v'} \rangle$	N_2H_2	0	0.0155	0	0.002	0			
		N_2D_2	0	0.0123	0	0.002	0			
ν_5	$\langle \psi_{0''} \vert \psi_{v'} \rangle$	N_2H_2	1.0	0	0.003	0	0.001	0	0.000	
		N_2D_2	1.0	0	0.004	0	0.001	0	0.000	
	$\langle \psi_{0''} \vert R^y_{e'e''} \vert \psi_{v'} \rangle$	N_2H_2	0	0.0367	0	0.0045	0	0.4–4	0	
		N_2D_2	0	0.0322	0	0.0025	0	0.5–4	0	
ν_6	$\langle \psi_{0''} \vert \psi_{v'} \rangle$	N_2H_2	0.998	0	0.057	0	0.002	0	0.5–3	0
		N_2D_2	0.998	0	0.053	0	0.002	0	0.3–3	0
	$\langle \psi_{0''} \vert R^y_{e'e''} \vert \psi_{v'} \rangle$	N_2H_2	0.0	0.0058	0.0	0.0012	0	0.0003	0	0.000
		N_2D_2	0.0	0.0051	0.0	0.0008	0	0.0001	0	0.000

observable in the entire $^1(n,\pi^*)$ manifold clearly puts to rest the speculation by Vasudevan *et al.* (2) to the effect that this species is actually responsible for the three long 1100 cm^{-1} progressions found by Back *et al.* (1) for this spectrum.

The situation for the third antisymmetric variable (ν_4, torsion) is less clear, however; primarily because of the extremely flat potential curve which characterizes the $^1(n,\pi^*)$ upper state upon vibrating in this mode (see Fig. 1*a* and also the work of Baird and Swenson (11)). The main difficulty therein is that the vibrational overlap integrals for higher upper state quantum numbers are quite sensitive to the shape of the torsional potential curve at relatively large angles, particularly in the region of the energy maximum for the *cis* conformation.[5] Since the electronic transition moment increases by an order of magnitude as the angle of torsion varies from 10° to 90° (*cis*) the magnitude of the dipole matrix elements for large ν_4' is critically dependent on the manner in which these overlap integrals decrease over the same region. The present calculations do not rule out the possibility that the dipole integrals increase for the higher torsional levels (beyond $\nu_4' = 4$). On the other hand, if such behavior were observed experimentally progressions in $2\omega_4'$ (200–500 cm^{-1}, see Table 2) would be detected; since such activity does not appear in the experimental diimide absorption spectrum it therefore seems unlikely that such considerations play a decisive role in arriving at a satisfactory assignment of the band systems contained therein.

In any event it seems clear from the calculations that the most probable inducing mode for the $^1(n,\pi^*)$ transition in *trans*-diimide is the $(1 \leftarrow 0)$ NH antisymmetric stretching mode ν_5. The *f* value for this species (see eq. 4) is 1.0×10^{-4}, some three times larger than the corresponding result for the most probable $(1 \leftarrow 0)$ torsion-induced system and 40 times greater than the analogous ν_6 quantity (Table 5). Moreover, the calculated intensity for the ν_5-induced complex seems to be at least qualitatively consistent with the overall strength of the observed transition. The corresponding *f* value for the (dipole-allowed) $^1(n,\pi^*)$ transition in *cis*-diimide is 9×10^{-3} for example, only 90 times greater than the ν_5 vibronically-induced oscillator strength for the *trans* isomer. Given the well-known weakness of both quadrupole and mag-

[5]Note that the structural parameters of the *trans* conformer are employed exclusively in calculating this potential curve.

TABLE 5. Calculated oscillator strengths for key vibronic transitions in the N_2H_2 $^1(n,\pi^*)$ system (see eq. 4)[a]

Inducing mode ($v' \leftarrow v''$)	$f_{e'v'e''v''}$	Ratio
$1 \leftarrow 0$, ν_5	1.0×10^{-4}	1/1
$1 \leftarrow 0$, ν_4	0.3×10^{-5}	1/3
$3 \leftarrow 0$, ν_4	0.4×10^{-6}	1/23
$1 \leftarrow 0$, ν_6	0.2×10^{-6}	1/40

[a]The corresponding f value for the (allowed) $^1(n,\pi^*)$ transition in the *cis* conformer (torsion 90°) is 0.9×10^{-2}, *i.e.* 90 times stronger than the $1 \leftarrow 0$, ν_5 (reference) value for *trans*-diimide.

netic dipole-allowed transitions, and also the fact that diimide apparently exists almost exclusively in the *trans* form (13), it is thus the clear indication of the present calculations that at least the major features of the observed diimide spectrum in the 3000–4300 Å region are vibronically induced through the $(1 \leftarrow 0)$ NH antisymmetric stretching species.

The vibrational overlap integrals of Table 4 for the six possible N_2H_2 modes indicate further that the intensity distribution for the symmetric NH stretching species ν_1 should be localized in a single transition while the data for the ν_2 and ν_3 vibrational modes (of relatively high frequency, see Table 2) predict that in these instances the intensity of the corresponding transitions should be distributed over a fairly large wavelength region. Significantly large NN stretching (ν_3) overlap integrals are calculated from $v' = 0$ up to at least $v' = 2$ (Table 4), with similarly large values for the symmetric bending ν_2 mode occurring from $v' = 0$ up to as high as $v' = 7$ and 8 for N_2H_2 and N_2D_2 respectively.

Intensity Distribution for the $^1(n,\pi^*)$ ν_5-induced Portion of the Spectrum

The band structure observed for the 3000–4300 Å region of the diimide spectrum has been assigned (1) in terms of progressions in the upper state ν_2 (symmetric bending) and ν_3 (NN stretching) frequencies. The present calculations are seen to be in general agreement with this interpretation, complete with the finding that the short progression in the spectrum should be assigned to ν_3 and the long to ν_2 (see Table 4). They indicate further that the transitions are most likely vibronically induced via the NH stretching mode ν_5 $(1 \leftarrow 0)$. To obtain a more detailed correlation between calculation and experiment in this regard the results of Table 4 can be substituted into eqs. 3 and 4 in order to calculate an intensity distribution for this electronic transition in both N_2H_2 and N_2D_2. The most important feature of this analysis can then be given rather concisely in terms of a table

TABLE 6. Products of Franck–Condon overlap integrals $\langle\psi_{0''}|\psi_{v_2'}\rangle$ $\langle\psi_{0''}|\psi_{v_3'}\rangle$ for the $v' \leftarrow v'' = 0$ transitions for the symmetric bending (ν_2) and the NN stretching (ν_3) vibrational modes for the $^1(n,\pi^*)$ system in N_2H_2 (part *a*) and N_2D_2 (part *b*)

		Overlap integral for $v_3' =$			
System	v_2'	0	1	2	3
(*a*) N_2H_2	0	0.266	0.160	0.081	0.039
	1	0.395	0.237	0.120	0.058
	2	0.418	0.251	0.127	0.061
	3	0.367	0.220	0.111	0.054
	4	0.280	0.168	0.085	0.041
	5	0.194	0.116	0.059	0.028
	6	0.124	0.074	0.038	0.018
	7	0.075	0.045	0.023	0.011
(*b*) N_2D_2	0	0.167	0.102	0.052	0.025
	1	0.295	0.179	0.092	0.044
	2	0.370	0.225	0.115	0.056
	3	0.381	0.232	0.118	0.057
	4	0.342	0.208	0.106	0.052
	5	0.277	0.168	0.086	0.042
	6	0.206	0.125	0.064	0.031
	7	0.143	0.087	0.044	0.022

TABLE 7. Calculated vibrational transition energies (cm^{-1}) for various (v_2',v_3') combinations for the $1 \leftarrow 0$ ν_5-induced $^1(n,\pi^*)$ system in N_2H_2 (part *a*) and N_2D_2 (part *b*). The energy differences between successive transitions are always given in parentheses[a]

		Vibrational transition energy for $v_3' =$				
System	v_2'	0		1		2
(*a*) N_2H_2	0	22 833	(1 341)	24 174	(1 260)	25 434
		(1 050)				
	1	23 883		25 224		26 484
		(1 034)				
	2	24 917		26 258		27 518[b]
		(1 016)				
	3	25 933[b]		27 274[b]		28 534
		(996)				
	4	26 929		28 270		29 530
		(974)				
	5	27 903		29 244		30 504
		(951)				
	6	28 854		30 195		31 455
		(941)				
	7	29 795		31 136		32 396
(*b*) N_2D_2	0	22 167	(1 301)	23 468	(1 226)	24 694
		(746)				
	1	22 913		24 214		25 440
		(738)				
	2	23 651		24 952		26 178
		(729)				
	3	24 380		25 681		26 907
		(721)				
	4	25 101		26 402[b]		27 628
		(711)				
	5	25 812[b]		27 113		28 339
		(701)				
	6	26 513		27 814		29 040
		(692)				
	7	27 205		28 506		29 732

[a]Note that while the discrepancies between calculated and experimental (1) energy values in the present assignment are only roughly 1000 cm^{-1} for the (0,0) species in N_2H_2 and N_2D_2, they become progressively larger toward higher quantum numbers because the calculated vibrational frequencies are underestimated by 100–200 cm^{-1} (Table 2).

[b]This level corresponds to the strongest band observed experimentally (1) in a given progression.

of products of Franck–Condon overlaps for the two vibrational modes ν_2 and ν_3 which appear to be involved in the observed progressions (Table 6). The corresponding energies for the $(1 \leftarrow 0)$ ν_5-induced vibronic transitions (assuming that only the lowest transitions in the other three modes are observed[6]) are then listed in Table 7. For all practical purposes the oscillator strength for each $(v_2',v_3') \leftarrow (0,0)$ transition in this $(1 \leftarrow 0)$ ν_5-induced series (complex) can be obtained by multiplying the square of the corresponding product of Franck–Condon overlaps of Table 6 by the total calculated f value of 1×10^{-4} listed in Table 5.

The (0,0) transitions[7] in this complex are thus calculated to occur at 22 833 cm^{-1} and 22 167 cm^{-1} for N_2H_2 and N_2D_2 respectively. According to the interpretation of Back *et al.* (1) the corresponding (0,0) experimental lines are not

[6]The $2 \leftarrow 0$ ν_4 transition would have perhaps been a more logical choice (Table 4) but since the corresponding $0 \leftarrow 0$ species lies only 320 cm^{-1} lower in N_2H_2 and 225 cm^{-1} lower in N_2D_2 very little of quantitative significance would be changed in Table 7 as a result of this alteration.

[7]Hereafter the notation (v_2',v_3') is used to indicate the vibronically-induced transition from $v_2'' = 0$ to v_2' and from $v_3'' = 0$ to v_3'; for the ν_5-induced series a transition from $v_5'' = 0$ to $v_5' = 1$ is always assumed.

observed but can be expected at roughly 20 330 cm^{-1} and 20 530 cm^{-1} respectively based on extrapolations in the ν_2' frequencies of N_2H_2 (1170 cm^{-1}) and N_2D_2 (880 cm^{-1}).

In the experimental assignment (1) transitions from $v_3'' = 0$ to $v_3' = 0$ and 1 are found to be about equally strong while a third progression involving the upper $v_3' = 2$ state is said to be rather weak. The calculated results of Tables 4 and 6 are in reasonably good agreement with this assignment, except that the $v_3' = 1$ Franck–Condon factor is found to be smaller than that for $v_3' = 0$. The calculated ν_3' frequency fits in well with the experimental values in both N_2H_2 and N_2D_2 (Table 2).

The situation for the symmetric bending (long) progression is less obvious, however. In this case the interpretation of Back *et al.* (1) associates the most probable transition with the upper quantum number $v_2' = 6$ in N_2H_2 and $v_2' = 8$ in N_2D_2, thereby putting the energy difference between absorption maximum and 0–0 transition in this progression at roughly 7100 cm^{-1} in both systems. According to the Franck–Condon Principle this energy difference should correspond roughly to the relaxation energy of the $^1(n,\pi^*)$ state reached exclusively through the bending vibration following vertical excitation from the ground state equilibrium conformation. Since *ab initio* calculations at both the SCF and CI levels predict that the actual symmetric bending relaxation energy is less than half this amount, Vasudevan *et al.* (2) called into question this aspect of the experimental interpretation. In at least qualitative support of this argument the present vibrational treatment indicates that the most probable transition occurs for $v_2' = 2$ for N_2H_2 and $v_2' = 3$ for N_2D_2 (Table 4) rather than for quantum numbers 6 and 8.

Considering both the theoretical and experimental evidence available (including some doubts expressed about the exact numbering for the ν_2' species in ref. 1) it seems advisable to reassign the members of each observed long progression in the following manner. In the $(v_2',0)$ species the longest-wavelength transition reported to be *certain* for N_2H_2 (occurring at 23 840 cm^{-1}) is assigned in the notation of Back *et al.* as $v_2' = 3$; the situation is equivalent in N_2D_2. Since the calculations indicate that these progressions should be shorter by at least three v_2' levels it seems reasonable to assign these species instead as $v_2' = 0$ (in both isotopes). This procedure would result in an assignment of the most intense line observed in the $v_3' = 0$ progressions as $v_2' = 3$ and 5 for N_2H_2 and N_2D_2,[8] respectively, compared with the corresponding calculated results of $v_2' = 2$ and 3. Given the error limits in both the *ab initio* calculations and in the experimental intensity measurements such discrepancies seem well within reason. According to this assignment the measured isotope shift for the (0,0) transition in this system is thus indicated to be 672 cm^{-1} (Fig. 2), with the N_2H_2 species occurring at the higher frequency, which result in turn compares rather well with the corresponding calculated quantity of 666 cm^{-1} (Table 7) in both magnitude and sign.

According to this interpretation the absolute error in the calculated ν_5-induced (0,0) transition energies is 1007 cm^{-1} for N_2H_2 and 1001 cm^{-1} for N_2D_2, an underestimation of some 0.12 eV in both cases. This finding is consistent with the position taken earlier (2) in which error limits in the calculations are claimed to be considerably smaller than the roughly 0.6 eV value indicated by a direct comparison of the calculated vertical electronic energy difference with the location of the measured absorption maximum. A small portion of the decrease in this quantity (roughly 0.1 eV) comes about because of the use of natural orbitals in the present CI study in contrast to the earlier theoretical treatment, but the rest of the improvement is traced to more fundamental considerations. Although the energy of the *strictly vertical* ν_5 excitation agrees quite closely with that of the corresponding $0 \leftarrow 0$ transition, the *most probable observed* vibrational ν_5 species is $1 \leftarrow 0$, occurring at one ν_5' quantum (3120 cm^{-1} or 0.4 eV; Table 2, N_2H_2) *higher* in energy; thus it is clear that use of the vertical energy difference between the two states to predict the location of the absorption maximum for this formally forbidden band is not a good approximation in this instance. In summary then, although the present calculations quite definitely rule out the occurrence of a progression in the antisymmetric bending frequency ν_6, as speculated earlier (2), they do support the two basic conclusions of the earlier theoretical work

[8]Note also that in the $v_3' = 1$ progression of N_2D_2 the reported maximum occurs for one v_2' quantum lower than in the $v_3' = 0$ series, thus coming into even better agreement with the present calculations.

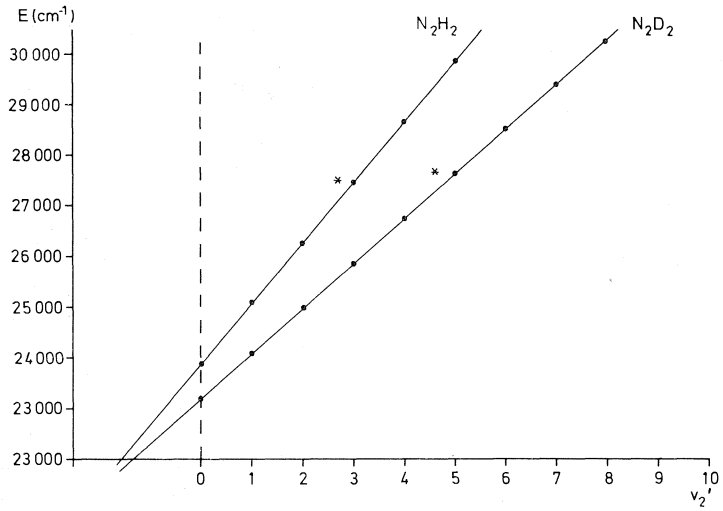

FIG. 2. Extrapolation of the first observed v_2' progression in N_2H_2 and N_2D_2 using the numbering of the present assignment. (The strongest bands are denoted by an asterisk.) The isotope shift for the respective 0–0 bands is 672 cm^{-1}.

TABLE 8. Experimental lines (1) which do not fit into the three ν_5-induced progressions given in Table 7

System	Observed[a] band center E_a (cm^{-1})	Assignment[b] according to ref. 1	Present assignment[b] as ν_4-induced	Observed band center E_b (cm^{-1}) of associated ν_5-induced[c] transition	$E_b - E_a$ (cm^{-1})
N_2H_2	23 296	(1,1)	(2,0)	26 262	2 966
	24 433	(2,1)	(3,0)	27 455	3 022
	—				
	[23 622]	(0,2)	(1,1)	26 631	3 009
	24 912	(1,2)	(2,1)	27 801	2 889
	25 973	(2,2)	(3,1)	28 992	3 019
	—				
	[22 794]	(2,0)	?	?	
N_2D_2	23 601	(2,1)	(3,0)	25 857	2 256

[a]Values in square brackets are reported to be less certain (1).
[b]Given are the (v_2',v_3') assignments.
[c]According to the present assignment this transition differs from the corresponding species in the first column only in the mode of inducement (the lower-energy (E_a) transition is induced through ν_4, the higher (E_b) through ν_5).

(2) to the effect that: (*a*) error limits for the CI transition energy results seem to fall uniformally in the 0.2 eV range; and (*b*) the width of the v_2' symmetric bending progressions does not exceed 0.4 eV from the position of the absorption maximum to the corresponding 0–0 member.

Possible ν_4-induced Vibronic Transitions

The analysis of the preceding section alone is not capable of accounting for all the known vibrational transitions observed in the region of the diimide spectrum, in particular those which have been assigned by Back *et al.* (1) with $v_2' <$ 3; the wavenumbers of the band centers falling in this category are given in Table 8. If one accepts the premise that the ν_2' progressions are not as long as claimed earlier (1) it is necessary to find another explanation for the occurrence of these vibrational transitions. Since the band systems in question appear to fit in reasonably well with the same type of two-dimensional frequency analysis as has been discussed previously it seems fairly unlikely that the lower electronic state is different than in the other cases, that is, that the *cis* isomer could somehow be involved. Instead it seems considerably more

plausible that the levels in question simply arise through a different vibronic mechanism, whereupon the calculations suggest that the most likely candidate for such a secondary inducing mode is the $1 \leftarrow 0$ torsion (ν_4) species (see Table 5).

If this hypothesis is correct the intensity distribution for such torsional-induced transitions should resemble quite closely that of their counterparts with $v_5' = 1$ treated in the preceding section. Ideally one would expect that the corresponding transitions of the two types possessing the same (v_2',v_3') set of quantum numbers would differ in energy by an amount roughly equal to the difference in their inducing mode frequencies $(\nu_5' - \nu_4')$. In addition the intensity *ratio* for each such pair of transitions should always have essentially the same value, with the calculations indicating that the ν_4-induced species should generally be about three times weaker than the corresponding ν_5 species (see Table 5).

According to Table 2 the difference between ν_5' and ν_4' is $(3120 - 40) = 3080\ cm^{-1}$ for N_2H_2 and $(2212 - 9) = 2203\ cm^{-1}$ for N_2D_2.[9] If one adds the appropriate value of $(\nu_5' - \nu_4')$ to the frequencies of the transitions listed in Table 8 the new energy result does in fact in all but a single case (the very weak 22 794 cm^{-1} species) agree quite well with that of another observed transition within the ν_5-induced complex discussed earlier. Furthermore, the fact that *all* the observed transitions can be arranged in a single two-dimensional (v_2,v_3) frequency table points out the near equality between the quantity $(\nu_5' - \nu_4')$ and an integral combination of the key progression frequencies ν_2' and ν_3' in both N_2H_2 and N_2D_2, namely $\nu_5' - \nu_4' \cong 4\nu_2' - \nu_3'$ in each case.[10] In other words, each ν_5-induced transition with $v_3' > 0$ has a (weaker) ν_4-induced counterpart at nearly the same frequency with a v_2' value four units higher and v_3' one unit smaller.

There is in fact some doubling observed in the $v_3' = 2$ progression of N_2D_2 (1) but if this phenomenon were caused by such multiply-induced transitions, the 30 368 and 30 478 cm^{-1} pair, for example, would have to be assigned as the (5,2) ν_5-induced and (9,1) ν_4-induced species on this basis; the observation of the latter transition would be unexpected, however, since the corresponding (9,1) ν_5-induced line has not been seen experimentally ((12,1) in the notation of Back *et al.*). On the other hand the earlier suggestion (1) that such doubling arises in N_2D_2 because there $\nu_1' \approx \nu_2' + \nu_3'$ seems very unlikely on the basis of the present calculations since this hypothesis seemingly requires that transitions with $\nu_1' \neq 0$ be observed even though one estimates from Table 4*b* that the largest Franck–Condon factor of this type is roughly 300 times smaller than that for $\nu_1' = 0$. A third possibility which is probably more realistic than either of the foregoing is that a progression in the very small torsional frequency is involved (according to this view the respective transitions would be ν_5-induced). In any event it seems very difficult to explain such phenomena with any high degree of certainty based on the evidence presently available.

The hypothesis of nearly coincident transitions induced by two different asymmetric modes does appear to receive some additional support from the experiments in another context, however. In the earlier view (1) the lines reported at 25 973 and 26 985 cm^{-1} in the N_2H_2 spectrum (for $v_2' = 2$ and 3) should differ by a single v_2' quantum; the actual energy difference of 1012 cm^{-1} on the other hand does not agree very well with the other values in the same progression, particularly with the succeeding case in which $\nu_2' = 1208\ cm^{-1}$. By contrast in the present hypothesis there is a more complicated relationship between the above two transitions, since it is at this point that the ν_5-induced series (responsible for the 26 985 cm^{-1} line, with $v_3' = 2$) should end and the ν_4-induced progression of different v_3' quantum numbers should begin. Clearly such observations neither prove nor disprove either of the interpretations discussed, but it seems somewhat more than coincidence that the long progressions found by Back *et al.* should show their greatest deviation from

[9]In this computation the $1 \leftarrow 0$ frequencies of Table 2 are used since the energy difference sought actually involves ν_5 and ν_4 transitions between these levels; other values for this difference would emerge if one uses the so-called zero-point frequencies for this computation, a practice which does not fully conform to the physical situation under discussion.

[10]In N_2H_2 the actual measured energy differences for such pairs of transitions vary from 2900 cm^{-1} to 3200 cm^{-1} and similar consistency is noted in N_2D_2 (Table 8). Furthermore in each case the higher-energy transition in the correspondence turns out to be one of the most intense species found in the spectrum.

the harmonic condition precisely at the point where the calculations predict a break in the normal pattern to be most probable.[11]

The last point which still would seem to require discussion is the assignment of the feature observed at 22 794 cm^{-1} in the N_2H_2 spectrum; it is the shortest-wavelength line reported (1) and is said to be very weak. As such it might be best explained as a totally extraneous feature, but if one proceeds under the assumption that it is a *bona fide* diimide transition it is clear that it does not fit in well with either of the ν_5- and ν_4-induced series previously discussed; in the first case its assignment would require $v_2' = -1$, whereas in the torsion-induced series it would correspond to $v_3' = -1$. This result would seem to narrow the possibilities for a vibrationally-induced transition down to a single choice, namely via the $1 \leftarrow 0$ ν_6 mode. Using the same type of arguments as before such an assignment would require that the frequency of the band center in question to differ from that of an observed ν_5-induced species by an amount equal to roughly $\nu_6' - \nu_5'$ or 2235 cm^{-1} according to the present calculations (Table 2). Adding this amount to the value of 22 794 cm^{-1} yields a frequency which in fact differs by only 44 cm^{-1} from that of the band center of Back *et al.*'s (4,0) transition (the (1,0) ν_5-induced species according to the present interpretation). Again the occurrence of such a possible coincidence is seen to be tied up with the fact that the difference in the pertinent inducing frequencies is close to being an integral combination of the experimental progression frequencies, in this case approximately $2\nu_2'$. Since the calculations indicate that such ν_6-induced transitions should be much weaker (by a factor of about 40) than the corresponding ν_5-induced lines it is certainly plausible that they could be observed only under extremely favorable conditions, in particular in an area of the spectrum where no other strong transition is found. As with the discussion of the doubling phenomena in N_2D_2, however, it seems extremely difficult to devise an experimental test which could provide a definitive basis on which to determine whether such an assignment for the 22 794 cm^{-1} feature is actually justified.

[11]In the $v_3' = 1$ progression of N_2H_2 no such obvious break is observed, but in the $v_3' = 0$ series v_2' is reported to change from 1233 cm^{-1} to only 1046 cm^{-1} across the analogous border (1). In N_2D_2 a change from 976 cm^{-1} to 891 cm^{-1} is reported at an equivalent point in the $v_3' = 1$ progression.

Conclusion

In summary the present calculations indicate that the major portion of the 3000–4300 Å spectrum of diimide arises through vibronic inducement via the $1 \leftarrow 0$ transition in the NH antisymmetric stretching mode. Within this framework the individual vibrational transitions can be assigned in a very straightforward manner on the basis of progressions in v_2' and v_3', much as Back, Willis, and Ramsay have argued in their original paper; the only difference in the present interpretation is that its v_2' assignments are always three units lower than those given earlier (1). The calculations indicate further that $1 \leftarrow 0$ torsion (ν_4)-induced transitions overlap quite closely with ν_5-induced species in the $v_3' = 1$ and 2 progressions, and in fact occur as separate transitions in spectral regions lying outside the range in which such $v_5' = 1$ species can occur. According to this interpretation the calculated 0–0 vibrational transition energies obtained in the present CI treatment are found to lie about 1000 cm^{-1} below their measured values.

Acknowledgements

The authors wish to thank Professor D. A. Ramsay for some lively correspondence and discussions on the subject treated in this paper. One of us (M.P.) is grateful for the hospitality shown him at the University of Bonn and for the financial support given to him by the DAAD. The services and computer time made available by the University of Bonn Computer Center have been essential to this study and are gratefully acknowledged.

1. R. A. Back, C. Willis, and D. A. Ramsay. Can. J. Chem. **52**, 1006 (1974).
2. K. Vasudevan, S. D. Peyerimhoff, R. J. Buenker, W. E. Kammer, and H. Hsu. Chem. Phys. **7**, 187 (1975).
3. S. D. Peyerimhoff, R. J. Buenker, W. E. Kammer, and H. Hsu. Chem. Phys. Lett. **8**, 129 (1971).
4. U. Fischbach, R. J. Buenker, and S. D. Peyerimhoff. Chem. Phys. **5**, 265 (1974).
5. R. J. Buenker and S. D. Peyerimhoff. Chem. Phys. Lett. **29**, 253 (1974).
6. R. J. Buenker and S. D. Peyerimhoff. Theor. Chim. Acta, Berlin, **35**, 33 (1974).
7. K. H. Thunemann, J. Römelt, S. D. Peyerimhoff, and R. J. Buenker. Int. J. Quant. Chem. In press.

8. R. J. BUENKER and S. D. PEYERIMHOFF. Theoret. Chim. Acta, Berlin, **39**, 217 (1975).
9. S. D. PEYERIMHOFF and R. J. BUENKER. Theoret. Chim. Acta, Berlin, **27**, 243 (1972).
10. R. J. BUENKER, S. D. PEYERIMHOFF, and M. PERIĆ. Chem. Phys. Lett. **42**, 383 (1976).
11. N. C. BAIRD and J. R. SWENSON. Can. J. Chem. **51**, 3097 (1973).
12. V. E. BONDYBEY and J. W. NIBLER. J. Chem. Phys. **58**, 2125 (1973).
13. M. CARLOTTI, J. W. C. JOHNS, and A. TROMBETTI. Can. J. Phys. **52**, 340 (1974).
14. J. W. NIBLER and V. E. BONDYBEY. J. Chem. Phys. **60**, 1307 (1974).

Intermediates in the photolysis of alkyl sulfides and disulfides in dilute glass matrices

FRANK C. ADAM AND ALLEN JOHN ELLIOT[1]

Department of Chemistry, University of Calgary, Calgary, Alta., Canada T2N 1N4

Received June 15, 1976[2]

FRANK C. ADAM and ALLEN JOHN ELLIOT. Can. J. Chem. **55**, 1546 (1977).

Simple alkyl sulfides and disulfides have been photolysed at 253.7 nm in dilute rigid glasses of 3-methylpentane, and the reactions which occur both at 77 K and in the glass at higher temperatures have been studied using epr and optical spectroscopy. The end products of photolysis have been determined using glc at room temperature. In sulfides, C—S bond cleavage leads to 'hot' radical pairs that react with each other giving rise to the main diamagnetic products observed, or react with nearby solvent molecules in the matrix by hydrogen abstraction yielding RSH and the solvent derived radicals (M·) which dominate the initial epr spectrum at 77 K. Thiyl radicals (RS·) are produced in significant amounts only after the sulfide glasses have been warmed slightly to allow the cage reaction,

$$RSH + M\cdot \rightarrow RS\cdot + MH$$

to occur. Pethiyl radicals ($RS_2\cdot$) are not ordinarily observed in sulfide photolyses. Photolysis of disulfide-containing glasses gives rise to S—S bond rupture and mainly diamagnetic products, or to C—S bond cleavage resulting in the formation of solvent radicals and $RS_2\cdot$. Very little RS· is generated on warming the matrices. As with ethyl mercaptan photolysis, radicals corresponding to α-hydrogen abstraction of the substrate are obtained for both ethyl sulfide and disulfide. The spectral characteristics and photolytic behaviour of the sulfur containing radical species have been investigated where possible.

FRANK C. ADAM et ALLEN JOHN ELLIOT. Can. J. Chem. **55**, 1546 (1977).

On a effectué la photolyse, à 253.7 nm, de sulfures et de disulfures simples d'alkyles; ces études ont été réalisées dans des verres rigides et dilués de méthyl-3 pentane et on a évalué les réactions qui se produisent à 77 K et dans le verre à des températures plus élevées par rpe et par spectroscopie optique. Les produits finaux des photolyses ont été déterminés en utilisant la chromatographie en phase gazeuse à température de la pièce. Dans le cas des sulfures, la coupure du lien C—S conduit à des paires de radicaux "chauds" qui réagissent les uns avec les autres pour conduire aux principaux produits diamagnétiques qui ont pu être observés ou qui réagissent avec des molécules environnantes de solvant dans la matrice par enlèvement de l'hydrogène avec formation de RSH et des radicaux dérivés du solvant (M·) qui dominent le spectre rpe initial à 77 K. Il n'y a formation de radicaux thiyles (RS·) en quantité appréciable qu'uniquement après que les verres de sulfure ont été légèrement réchauffés de façon à permettre la réaction en cage:

$$RSH + M\cdot \rightarrow RS\cdot + MH$$

On n'observe généralement pas la formation de radicaux perthiyles ($RS_2\cdot$) lors de la photolyse des sulfures. La photolyse de verres contenant des disulfures donne lieu à la rupture du lien S—S et conduit principalement à la formation de produits diamagnétiques ou à la rupture du lien C—S avec formation de radicaux de solvants et de $RS_2\cdot$. Lorsque l'on réchauffe les matrices, les radicaux RS· ne sont formés qu'en faible quantité. Comme dans le cas de la photolyse de l'éthylmercaptan, les radicaux correspondants à l'enlèvement d'un hydrogène en α du substrat peuvent être obtenus à partir des sulfures ainsi que des disulfures d'éthyle. Lorsque de telles possibilités existent, on a étudié les caractéristiques spectrales et les comportements photolytiques des espèces radicalaires contenant du soufre.

[Traduit par le journal]

Introduction

The radical scavenging ability of thiols may play an important role in the protection and repair of living biological materials subjected to the effects of ionizing radiation (1). The thiyl radical produced during this scavenging process may also be involved in the degradation of the charged species resulting from such radiation. For instance the process

$$(RSSR)^- \rightarrow RS\cdot + RS^-$$

has been reported (2) to occur with amino acids

[1]Present address: Department of Chemistry, Queens University, Kingston, Ont., Canada.

[2]Revision received November 23, 1976.

such as cystine in the aqueous phase. In order to further the understanding of the formation and the reactions of the thiyl radical in a variety of surroundings, we have undertaken to study the photolysis of simple alkyl sulfides and disulfides in dilute rigid glasses. The solid state is chosen so that the transient species may be readily trapped and studied by conventional techniques. The matrices are dilute so as to minimize solute–solute interactions.

In an earlier publication (3), it was found that alkyl mercaptans undergo a number of interesting cage reactions when photolysed as solutes in dilute (0.01 mol dm^{-3}) glass solutions of 3-methylpentane (3MP) at 77 K. The thiyl radical produced by 253.7 nm radiation results from S—H cleavage; it is 'hot' in the sense that it is very reactive and immediately abstracts a hydrogen atom from a nearby solvent molecule, regenerating the thiol molecule.

The hydrogen atoms may also be kinetically hot, and abstract from the nearby solvent to produce a second solvent radical, or may be thermalized, diffusing away to eventually yield molecular hydrogen or to interact with a distant photodamaged centre in the matrix. Each photolysed mercaptan (RSH) is therefore associated with a solvent cage containing either one or two solvent radicals. As a result, the epr spectrum at 77 K is mainly due to solvent radicals (M·); thiyl radicals (RS·) result only when the matrix is relaxed by warming so as to allow the 'repair' reaction 1 to occur

$$\text{RSH} + \text{M}\cdot \rightarrow \text{RS}\cdot + \text{MH} \qquad [1]$$

within the still rigid solvent cage. When a second M· radical is present in the same cage, one gets recombination to the thioether RSM

$$\text{RS}\cdot + \text{M}\cdot \rightarrow \text{RSM} \qquad [2]$$

The thiyl radical itself is characterized by a yellow color (3, 4) with $\lambda_{max} \simeq 400$ nm; single crystal studies (5) have established that this radical has an axial g-tensor ($g_{\parallel} \simeq 2.2, g_{\perp} \simeq 2.0$) and an isotropic β-hydrogen coupling constant with $a_{max} \simeq 48$ G. The epr of rigid randomly oriented RS· is accordingly very broad and at low concentrations would be expected to give only a weak asymmetric resonance near $g \simeq 2.00$ due to those molecules situated with C—S bonds perpendicular to the magnetic field (*i.e.* $g_{obs} \simeq g_{\perp}$).

In more concentrated mercaptan glasses (0.1 mol dm^{-3}) a second species is also observed. It is thought to be the non-linear perthiyl radical $RS_2\cdot$ and is characterized by an anisotropic g-tensor with principal values near 2.06, 2.025, and 2.00, and for those radicals with an α-methylene group, a 6–10 G doublet proton hyperfine coupling. These parameters match those observed for photolysed (6) or γ-radiolysed cystine single crystals (7, 8) and were unambiguously assigned by Gordy and co-worker (9) to $CyS_2\cdot$ by virtue of their ^{33}S and proton hyperfine structures. A second resonance (α) was also assigned by Gordy to CyS·, but this may be in error since the characteristic g-values ($g_{\parallel} \simeq 2.06$, $g_{\perp} \simeq 2.00$) do not correspond to those given above and a comparison of the photolytic behaviour of this species in ref. 8 shows it to be different from that exhibited by CyS· in ref. 5 or from the thiyl radicals studied in the present research.

From liquid (10) or gas phase (11) studies it is known that sulfides undergo the primary photolytic process

$$\text{RSR} \xrightarrow{h\nu} \text{R}\cdot + \text{RS}\cdot \qquad [3]$$

while for disulfides

$$\text{RSSR} \xrightarrow{h\nu} 2\text{RS}\cdot \qquad [4]$$

with a minor contribution from C—S cleavage

$$\text{RSSR} \xrightarrow{h\nu} \text{R}\cdot + \text{RS}_2\cdot \qquad [5]$$

If such processes can be made to occur in dilute glassy matrices of RSR or RSSR in 3MP, then large concentrations of either thiyl and/or perthiyl radicals may be built up for further characterization and study. The object of the present investigation is to produce by photolytic action damage centres containing either a one-sulphur species (from a sulfide) or a two-sulfur atom intermediate (from a disulfide) isolated in a rigid solvent cage. In this way it was hoped to avoid the association effects observed for mercaptans in either the low temperature hydrocarbon–thiol glasses, or in the undiluted crystalline state where both monomer (one-sulfur) and dimer (two-sulfur) cages may be formed at the same time. Since neither sulfides nor disulfides are expected to dimerize in dilute solution, a satisfactory correlation with the concentration effects observed in the thiol studies of ref. 3 would reinforce the conclusions reached there.

Experimental

The procedures and apparatus used were essentially the same as those described in ref. 3. The symmetrical methyl,

ethyl, *i*-propyl, *n*-butyl, *i*-butyl, and *t*-butyl disulfides were distilled before use, as were the ethyl, *n*-propyl, *i*-propyl, and *i*-butyl sulfides studied. Both low temperature epr and optical spectra were obtained using samples prepared and sealed off from a high vacuum line. Ethyl and *i*-propyl sulfide and disulfide glasses (0.1 mol dm^{-3} in 3MP) were photolysed for 90 min at 77 K using the 253.7 nm mercury resonance line, and were subsequently melted, warmed to room temperature, unsealed, and analysed by glc, using 3% squalane or 3% SE30 on Chromosorb W for the heavy fractions (longer retention times than the solvent) and Poropak Q for the lighter hydrocarbon ends. Hydrogen gas analyses were carried out as in ref. 3.

An attempt has been made to keep photolytic conversion to a minimum. Even so, the quantum efficiency for the formation of trapped paramagnetic species is lower for both sulfides and disulfides than it was for thiols. This means that somewhat long photolysis times and higher concentrations (0.1 mol dm^{-3}) must be used to obtain satisfactory epr, optical, and product analyses.

Results

On the basis of eqs. 3–5 one would expect the initial epr spectrum of photolysed sulfides to contain the alkyl fragment R· and the thiyl radical RS·. In the case of disulfides RS_2· would be produced as well. In no case were the spectra of the combination of radicals predicted by these equations obtained simultaneously. Upon completion of the 253.7 nm photolysis, there were no intense optical absorptions near 400 nm, and the epr spectra of the isomeric propyl and butyl derivatives give hyperfine structure characteristic of the solvent radical M· rather than that of the alkyl radical R· expected. While most of the alkyl radicals have even-line spectra, and may be difficult to detect in the presence of the six line hyperfine pattern of M· (12), the isobutyl radical is known to have an odd line hyperfine spectrum in a rigid medium (13) and should therefore be readily detectable in this system. In fact the initial epr spectra of the propyl and butyl sulfides and the high field portion of the disulfide spectra are to all intents and purposes identical. The ethyl and methyl derivatives behave slightly differently and will be considered separately.

In no case were epr signals due to trapped hydrogen atoms obtained, nor half-field resonances due to trapped radical pairs ($\Delta M = \pm 2$) observed in normal operation of the spectrometer (14). None of the processes to be described is thermally reversible.

The experiments are divided up according to the following scheme:

Phase I: Photolysis of glass at 77 K with 253.7 nm light.

Phase II: Warming the glass to allow cage reactions ($\simeq$80 K) and diffusion of smaller species such as Et· etc.

Phase III: Warming toward softening point of glass (85–90 K). This allows the diffusion of larger species, and eventual annihilation of all paramagnetic compounds.

Phase IV: A (fresh) Phase II glass is recooled to 77 K and subjected to photobleaching experiments on the species produced in the first warming.

Phase V: A Phase IV glass is warmed slightly to allow the cage reactions of photobleached species ($\simeq$80 K). Further warming leads to annihilation as in Phase III.

A. Alkyl Sulfides

As noted above each of the higher alkyl sulfides in 3MP give (Phase I) epr spectra which are very similar; that of *n*-Pr_2S–3MP is given in Fig. 1, curve *a*. It is virtually identical to the six line proton hyperfine spectrum obtained by photolysis of any of the dilute (0.01 mol dm^{-3}) alkyl thiol–3MP or H_2S–3MP glasses studied in ref. 3, and is accordingly assigned to the solvent radical M·. In this particular instance *n*-Pr· would have been expected (13) to give rise to a 1:3:4:4:3:1 sextet, compared to the 1:9:19.5:19.7:11.5:1.75 sextet obtained here. The *g* values (2.002) and splittings ($\simeq$23 G) are similar for each. Apart from the fact that the main constituent of the epr spectrum appears to be M· and not R·, it is important to note there is the epr absorption at $g = 2.06$ and there is no gross asymmetry in the spectrum near $g = 2.00$. The same applies to the Et_2S–3MP glass which gives an absorption as in curve *a* of Fig. 2. Although Fig. 2*a* is still basically a six line hyperfine pattern, it has considerably more detail, most of which can be ascribed to the ethyl radical. The splittings (a(3H) = 28.8 G, a(2H) = 22.3 G) are similar to those obtained by γ-radiolysis of ethyl halides at 77 K (13). Generally speaking the Phase I epr spectra contain only hydrocarbon radicals such as M· or Et·. The optical spectra of Phase I sulfide glasses typically contain two weak absorptions, one at 400 nm, the other at 520 nm, and a representative spectrum is shown in Fig. 3, curve *a*. The 520 nm peak is ascribed to the n–π* transition of a thiocarbonyl, expected to absorb in this region (15, 16), while the 400 nm peak will be considered below.

Warming the photolysed glasses slightly (79–

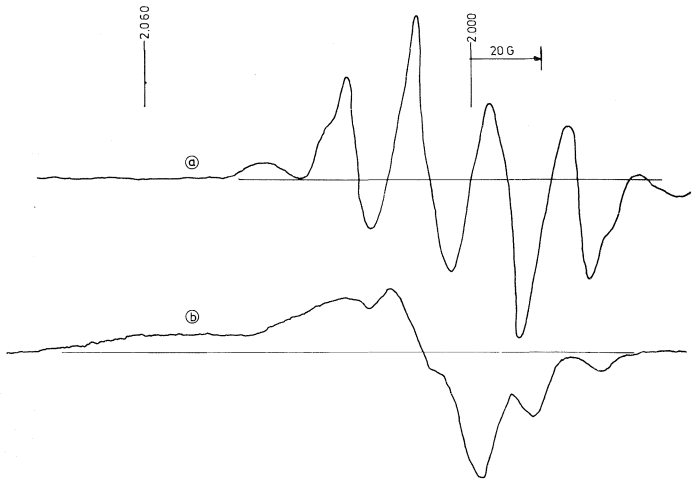

FIG. 1. (*a*) Initial (Phase I) epr spectrum of 0.1 mol dm^{-3} *n*-Pr_2S in 3MP photolysed at 253.7 nm for 180 min, showing solvent radical M·. (*b*) Phase II spectrum obtained by warming sample (*a*) slightly, showing spectrum of RS· and some residual M·.

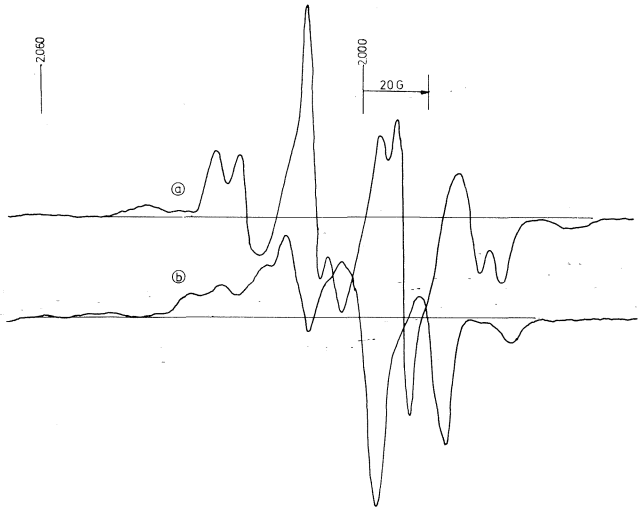

FIG. 2. (*a*) Initial (Phase I) epr spectrum of 0.1 mol dm^{-3} Et_2S in 3MP photolysed for 180 min at 77 K showing hyperfine structure of Et·. (*b*) Phase II spectrum of sample in (*a*) after slight warming, demonstrating five line hyperfine pattern of $CH_3\dot{C}HSX$ and asymmetry due to EtS·.

80 K) gives Phase II; the glasses become intensely yellow as typified in curve *b* of Fig. 3, and the hydrocarbon radicals M· or Et· initially present, decay, to be replaced by a broad asymmetric resonance depicted in Fig. 1*b*. This resonance is assigned to the RS· radicals formed by the reaction 1. In the case of Et_2S a similar spectrum to Fig. 1*b* results upon decay of the Et· radicals, presumably by an analogous process. When Et_2S has undergone a longer Phase I photolysis ($\simeq$1.5 h) an additional five line hyperfine spectrum as in Fig. 2*b* is observed. It is similar to radical C of ref. 3 ($g_{iso} \simeq 2.004$, $a(4H) = 19.7$ G, $\Delta H_{pp} = 6$ G) which was assigned to a species of the sort $CH_3\dot{C}HSX$, with X being H, R, or M. The basis of this assignment is that it is not observed with other alkyl sulfides and the hyperfine splittings are close to the weighted means of those observed for such components in the liquid phase ($a(1H) = 16.8$ G, $a(3H) = 19.8$ G) (17) or in γ-irradiated urea clathrates of Et_2S (18) with $a(1H)_{\parallel} = 24.6$ G, $a(1H)_{\perp} = 12.8$ G; $a(3H)_{\parallel} =$

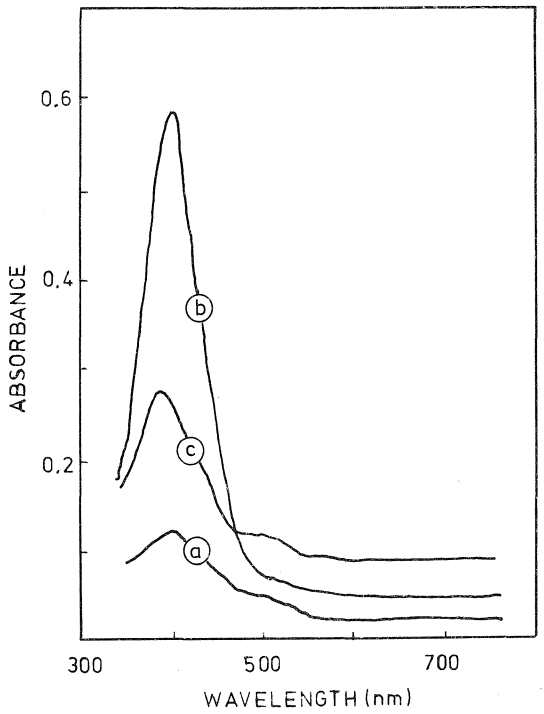

FIG. 3. (*a*) Initial (Phase I) optical spectrum of 0.1 mol dm^{-3} *i*-Pr_2S in 3MP photolysed for 60 min at 253.6 nm. Absorptions due to $(CH_3)_2C{=}S$ (520 nm) and *i*-$PrS_2\cdot$ (405 nm). (*b*) Phase II spectrum of sample in (*a*) warmed slightly. Absorption at 410 nm due to *i*-$PrS\cdot$. (*c*) Phase IV spectrum of sample in (*b*) obtained by recooling to 77 K and 30 min 253.7 nm photolysis. Absorption due to *i*-$PrS_2\cdot$ at 405 nm and $(CH_3)_2C{=}S$ at 520 nm.

21.8 G, $a(3H)_\perp$ = 19.4 G. The asymmetry of the five line spectrum in Fig. 2*b*, and the intense yellow of the glass can be ascribed to EtS· which is also present. As with all other sulfide–3MP glasses, there is little epr absorption near g = 2.06 for the Phase II glass of Fig. 2*b*.

Phase III is obtained by warming the glass toward the softening point of the matrix. It is characterized by the gradual loss in intensity of all of the absorptions represented by Figs. 1*b*, 2*b*, or 3*b* with little change in the line shapes. No new epr absorptions appear in the region near g = 2.06.

The photolytic behaviour of RS· can be studied by resort to Phase IV conditions. Such photolysis is distinct from either Phase I or II. The intensity of the yellow color is diminished and shifts to the blue to give a new absorption maximum, as seen in Fig. 3, curve *c*. This new maximum corresponds in wavelength to the weak absorption originally observed in curve *a* of Phase I. Meanwhile in epr samples, the resonance of Fig. 1*b* is replaced by a complex hyperfine pattern apparently characteristic of the solute (since it is quite different from that obtained in Phase I) and, in addition, signals appear to the low field end of the spectrum near g = 2.06. Apart from this last feature, the spectrum obtained from EtS· is similar to that in Fig. 2*a* and can again be assigned to the ethyl radical. This Phase IV photolysis is also quite different from that in Phase I, however. Besides generating the low field $EtS_2\cdot$ hyperfine doublet at g = 2.0596, a 5–10 min Phase IV photolysis will produce about the same amount of ethyl radical as was obtained in a 30 min Phase I photolysis. It is apparent from the visual bleaching that the EtS· species is being photolysed by 253.7 nm radiation during this step to yield Et· and ^3P sulfur atoms, as was suggested in ref. 3. It is thought that these sulfur atoms are able to diffuse in 3MP glasses at 77 K and react according to the scheme,

$$\mathrm{RS}\cdot \underset{\Delta}{\overset{h\nu}{\rightleftarrows}} \mathrm{R}\cdot + \mathrm{S}:$$

$$\mathrm{RS}\cdot + \mathrm{S}: \rightarrow \mathrm{RS_2}\cdot$$

$$n\mathrm{S}: \rightarrow \cdot\mathrm{S}_n\cdot$$

That the first of these reactions is thermally reversible is easily demonstrated by warming a Phase IV glass. This is Phase V and is typified by loss of all alkyl radical signal, slight intensification of the $RS_2\cdot$ absorption, and a partial recovery of the spectral characteristics attributed to RS·. The various systems can be recycled between Phases IV and V several times, the only apparent differences between successive spectra being that $RS_2\cdot$ signals continue to grow, while the overall intensities of the remaining absorptions diminish and the glasses assume a more distinct and permanent yellow colouration. The photolysis of RS· has been observed in analogous single crystal studies; CyS· was photolysed to give a carbon centred radical with an isotopic g value near g = 2.004 (5, 19) and CyS· was reformed on warming.

It is apparent from the optical spectra that both RS· and $RS_2\cdot$ absorb near 400 nm, although the actual maxima are slightly different for each alkyl function. For the various sulfides in 3MP, the RS· and $RS_2\cdot$ maxima are given, respectively, by Et_2S (405, 398 nm), *i*-Pr_2S (410, 405), *n*-Pr_2S (405, 395), and *i*-Bu_2S (415, 410 nm). The weak peak occurring near 400 nm in Fig. 3*a* must also

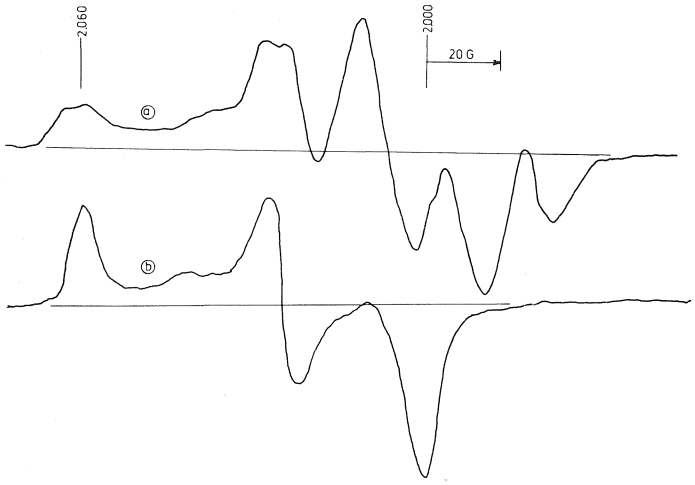

FIG. 4. (*a*) Initial (Phase I) epr spectrum of 0.1 mol dm^{-3} *n*-Bu_2S_2 in 3MP, 180 min 253.7 nm photolysis at 77 K showing absorptions due to *n*-$BuS_2\cdot$ and M· superimposed. (*b*) Phase II epr spectrum obtained from 0.1 mol dm^{-3} *t*-Bu_2S_2 in 3MP, 180 min 253.7 nm photolysis at 77 K and warmed slightly. The absorption is due to *t*-$BuS_2\cdot$.

be attributed to *n*-$PrS_2\cdot$ being formed during Phase I. This possibly results from photolysis of *n*-PrS· obtained from localized Phase II type warming in the large optical samples, a condition which is not replicated in the smaller epr samples which are in better thermal contact with the refrigerant.

The photobleaching of the $CH_3\dot{C}HSEt$ spectra found in Et_2S–3MP glasses has also been studied. Following a longer 3 h Phase I photolysis (to enhance the yield relative to the other photoproducts discussed above), it was found that photobleaching with 253.7 nm light in Phase IV reduced the intensity of the five line absorption. Ethyl radicals were still the major product of this photobleach. The five line spectrum is regenerated upon warming the matrix in Phase V, suggesting the following equilibrium

$$CH_3\dot{C}HSEt \underset{\Delta}{\overset{h\nu}{\rightleftarrows}} CH_3CH{=}S + Et\cdot$$

B. Alkyl Disulfides

When the higher dialkyl disulfides are photolysed in 3MP glasses at 77 K, the initial Phase I epr spectrum indicates that both $RS_2\cdot$ and M· are produced. These disulfides, including *i*-Bu_2S_2, all give similar spectra of which that for *n*-Bu_2S_2 is a representative example and is shown in Fig. 4*a*. It should be compared to the spectrum of a corresponding sulfide in Fig. 1*a*, especially near $g = 2.06$. The M· hyperfine spectrum is of much lower intensity compared to the photolysed sulfides. With Et_2S_2–3MP glasses, a strong hyperfine quintet is obtained, which has, within the experimental limits of these measurements, the same splitting and *g* value as observed in Fig. 2*b*. Because it arises from a substrate with two sulfur atoms, it is assigned to the species $CH_3\dot{C}HSSX$, the justification being that an analogous species observed in liquid solution has virtually the same splitting as does its $CH_3\dot{C}HSX$ counterpart (17). Me_2S_2 gives a hyperfine triplet with a similar splitting, and both demonstrate epr absorptions in the $g = 2.06$ region.

The optical spectra of all disulfides are similar to curve *a* of Fig. 3 in that two absorptions are obtained at 400 and 520 nm. In the case of *t*-Bu_2S_2, the latter is very weak; the former peak is probably stronger than in the case of the sulfides, but analysis is made difficult due to the onset of absorption by the substrate in this spectral region.

In contrast to the sulfide and thiol glasses, warming of disulfide glasses in Phase II produces neither the spectacular growth of yellow colouration, nor does the asymmetry in the epr spectrum at $g = 2.00$ increase. In the epr spectrum of *t*-Bu_2S_2 the solvent radicals decay to reveal the complete perthiyl spectrum of Fig. 4*b*. In this case the absorption at 380 nm is essentially unchanged during warmup as is the intensity of the $RS_2\cdot$ resonance in the epr spectrum. The $g = 2.06$ peak shows a 5–10 G doublet splitting for only those perthiyl radicals with an α-methylene

group. The epr signals fade as the matrix is warmed to its melting point in Phase III.

If a freshly photolysed Et_2S_2 glass is warmed slightly, recooled, and then subjected to a second Phase IV 253.7 nm photolysis, one can detect growth of weak hyperfine lines corresponding to Et· with little other change in the epr spectrum. This implies that EtS· is also formed in the disulfide photolysis, but that there is very little of it, correlating with the above observation in that there is no intensification of the yellow colour on warming, and that any asymmetry in the epr spectra that may be observed at $g = 2.00$ is due to RS_2· and not RS·. The five line hyperfine spectrum is unaffected by this second photolysis, a feature which is in contrast to that observed with the sulfides, and which supports the assignment made above.

C. Product Analysis

A somewhat greater variety of products were obtained by the glc than might have been expected from the simple photolytic process indicated in the Introduction, and the situation is clearly much more complex than had been hoped. The amounts of these products vary according to the substrate, concentration, photolysis time, and sample size, but the values in Table 1 are representative. The results for the 30 min photolysis of a 0.01 mol dm^{-3} *i*-PrSH glass have been included for comparison. The sulfide and disulfide results are for 0.1 mol dm^{-3} glasses and 90 min photolysis. All concentrations in Table 1 are in mmol dm^{-3}, referred to room temperature. Many other peaks are obtained in the glc chromatogram which had very much lower peak height than those reported. In some instances these peaks can be assigned to species such as CH_3SR, MSH, etc., but they individually form only a small part of the total. A mass balance is not possible since products (such as RSH) with similar retention times to the solvent could not be assayed. The fate of the thiocarbonyls formed is not known but is presumed to be high molecular weight polymers (16) or disulfides resulting from reaction with the alkyl mercaptans also produced in the photolysis. Authentic samples of RSM were not available so the total area of the three peaks was related to concentration using the corresponding RSSR conversion factors multiplied by the inverse ratio of the number of carbon atoms.

TABLE 1. Product yields for 90 min photolysis of 0.1 *M* sulfide and disulfide glasses, and for 30 min photolysis of a 0.01 *M* mercaptan glass at 77 K using 253.7 nm light

	Yield (mmol ℓ^{-1}) for substrate =			
Product	Et_2S	*i*-Pr_2S	*i*-Pr_2S_2	*i*-PrSH
H_2	0.3	0.5	0.5	1.1
CH_4	0.2	0.46	0.3	1.7
C_2H_4	0.9	0.09	0.03	0.15
C_2H_6	0.4	0.10	0.04	0.7
C_3H_6	<0.01	1.6	0.12	0.06
C_3H_8	<0.01	0.6	0.07	0.09
RSSR	0.22	0.08	—	0.3
RSM	(0.13)	(0.16)	(0.12)	(0.73)
C=S	0.7	0.7	1.5	<0.5

Thiocarbonyl concentrations were estimated using the known extinction coefficients of stable thioketones (15).

The amount of C—S bond rupture in *i*-Pr_2S can be estimated from the alkene (R′) and alkane (RH) yields. For the conditions given in Table 1 it is about 1–3% of the total sulfide. The amount of C—S bond rupture in disulfides is significantly less, being 0.1 to 0.2% of the total disulfide. From the hydrogen yield, the conversion of thiol to damage centres is 10–15%.

In the glc there is no material change in the substrate heights caused by photolysis of either *i*-Pr_2S or *i*-Pr_2S_2 glasses so that the overall conversion of these substances is within the experimental accuracy of the method (~10%).

Discussion

There are a number of points of difficulty which must be considered before proceeding to an analysis of the experimental results. These are as follows: (*a*) the radical pairs predicted from the liquid and gas phase work in eqs. 3–5 are not those radicals immobilized in the glassy matrix at 77 K following photolysis. (*b*) While the primary radicals are produced in pairs, not all decay by cage recombinations although in many instances the two radicals would be much too large to be able to diffuse out of their original cage and into the 3MP matrix at temperatures below 84 K. (*c*) There are products obtained in Table 1 which are unexpected on the basis of eqs. 3–5.

The observation that very little thiyl radical is present following photolysis is consistent with the suggestion made in ref. 3 which supposes that RS· can carry off a larger-than-normal share of the photon energy because of the availability of an energetically low lying electronic state. Since the photons have energies of 469 kJ mol^{-1} and

TABLE 2. Cage reactions of divalent sulfur compounds in a rigid hydrocarbon (MH) medium; *A*, thiols; *B*, sulfides; *C*, disulfide S—S cleavage; *D*, disulfide C—S cleavage. Asterisks denote kinetically hot species R″ is an alkene and R′CH = a subsidiary radical formed from the (normal) alkyl group R

	Cage reaction				
Medium	[6] X* + Y*	[7] Y* + X*	[8] Y* + MH + X	[9] X* + MH + Y	[10] X* + Y* + 2MH
A, Thiols Y = H· X = RS·	H_2 + S=CHR′		H_2 + RSM	RSH + M· + H_{th}·	RSH + H_2 + 2M·
B, Sulfides Y = R· X = RS·	RSH + R″	RH + S=CHR′	RH + RSM	RSH + RM*	RSH + RH + 2M·
C, Disulfides Y = RS· X = RS·	RSH + S=CHR′		RSH + RSM		2RSH + 2M·
D, Disulfides Y = R· X = RS_2·	RS_2H + R″	RSSR*	M· + RS_2· + RH	RS_2H + RM*	RS_2H + RH + 2M·

the C—S and S—S bonds have energies of only about 293 kJ mol^{-1} (1) then the excess energy available to the separated fragments far exceeds 4 kJ mol^{-1} required to effect H-atom abstraction from the geminal radical or from a neighbouring solvent molecule (20). Photolytic scission of the C—S bond may also produce a kinetically 'hot' alkyl radical in a fashion analogous to the photolysis of alkyl halides in 3MP (21) which give at 77 K solvent radicals M· as the trapped metastable species rather than the appropriate alkyl radical R·. In keeping with the idea that either one or both of the photolytic fragments may be born with energies in excess of thermal, Table 2 has been drawn up to give in general terms the cage reactions most likely to occur in a rigid medium following the photolytic rupture in Phase I,

$$XY \xrightarrow{h\nu} X\cdot^* + Y\cdot^*$$

Included are bond dissociations for S—H (*i.e.* mercaptans in row *A*), C—S (for sulfides, *B*, and disulfides, *D*) and for S—S rupture (disulfides in row *C*). Reactions 6 and 7 (columns 2 and 3) represent α-hydrogen abstractions for primary alkyl groups, and would not be expected to be important for the tertiary alkyl function. Reaction 8*B* is taken to mean that hot R· (Y*) attacks the solvent MH in the presence of thermalized RS· (X) and so on. The entries are chosen to correspond to the usual situation where relatively little R· or RS· is observed at the cessation of photolysis, while M· and RS_2· are detected experimentally. The occurrence of the appropriate thiocarbonyl, alkane RH, alkene R″, and thioether RSM are seen to result in an obvious way from cage processes.

This brings up the second difficulty. With the exception of cage type [9*A*], warming the matrix should result in loss of all paramagnetic species because the residual radicals are all large molecules, occur as proximal pairs in cages such as given by [10], and should decay by "composite first order" kinetics (22). The fact that epr signals and radical conversions are observed right up to the melting point of the matrix clearly contradicts this supposition, and some mechanism must be found which will allow for the formation of stable populations of isolated radicals at 77 K. The most plausible explanations involve secondary photolysis of the caged products. While we have not been able to produce paramagnetic species by the photolysis of a stable thioketone in 3MP at 77 K, products which are known to be photochemically active to 253.7 nm radiation are butyl radicals (23), M· (24), RS· (3), RSH (3), and probably RSSH. The solvent radicals have been reported to rupture giving CH_3· (24*a*) or C_2H_5· (24*b*) leaving an alkene trapped in the matrix.

$$CH_3CHCHC_2H_5 \xrightarrow{h\nu} CH_3CH{=}CH + C_2H_5\cdot$$

This rearrangement would effectively remove one radical from a cage such as reaction 10*B* with the result that annealing the residual cage would give

RS· rather than the RSM which would result from the unmodified cage. The liberated Et· could then produce a second thiyl radical by a diffusion encounter with RSH in an inactive cage during the annealing. Secondary photolysis of RSH is another possibility. It would create a type [9*A*] cage from one such as [9*B*], liberating a thermal hydrogen atom, which is mobile in 3MP at 77 K (25), and which could perform a function similar to the mobile ethyl radical mentioned above, but at a lower temperature. The mobile species could also react with other radicals, thiocarbonyls, or with distant solvent molecules (20).

With regard to the unexpectedly diverse variety of the products formed, there appear to be hydrocarbon fragments resulting from both the solute and solvent molecules. A great number of modes exist for their formation, for instance by decomposition of excited molecules produced as a result of radical recombinations (*e.g.* M*, RM*, or M_2* resulting from cage reactions in Table 2), or from photolysis of M·. The situation is clearly too complex to be sorted out on the basis of the present evidence. As will be seen below, we have tried to relate all these secondary products in isopropyl sulfide and disulfide photolyses back to those occurring in the primary photolysis of *i*-PrSH, not because this is felt to be the only operative mechanism but because many of the accompanying processes, such as photolysis of M·, would be expected to give very similar product distributions in these very diverse systems.

A. Sulfide Photolysis

The primary reactions cited in Table 2 can be justified by the results which appear in Table 1, except that it is necessary to sort out which of the products are due to the primary process and which are due to secondary photolytic processes. Columns 1 and 4 of Table 1 show relatively small amounts of propane and propene result from Et_2S and *i*-PrSH photolysis, or from solvent fragmentation. These are, however, the main products in the photolysis of *i*-Pr_2S (column 2) and justify the primary products of [6*B*] and [7*B*]. For reasons given in the previous section the remaining products are considered to be equivalent to mercaptan photolysis. A rough estimate of the magnitude of this effect can be obtained by scaling down the results in column 4 of Table 1 to correspond to the situation actually met in the sulfide photolysis. The total sulfide decomposition must exceed the amount of propane and propene recovered (2.2 mmol dm^{-3}) whereas the analysed sulfur amounts to 1.02 mmol dm^{-3}. If the remaining sulfur appears as *i*-PrSH as Table 2 would suggest, then the total *i*-PrSH yield must exceed 1.18 mmol dm^{-3}, or a mean mercaptan concentration of 0.6 mmol dm^{-3}. Thus a 90 min *i*-Pr_2S photolysis should produce sufficient mercaptan to be equivalent to a 30 min photolysis of 10 mmol dm^{-3} *i*-PrSH, scaled down by a factor somewhat greater than 0.18. Since in both systems, disulfide can result only from thiyl recombination, and this has been assumed to result only from mercaptan photolysis, a comparison of disulfide yields should give a more reliable scaling factor. One obtains 0.27 as the proportion of secondary process in sulfides to primary process in mercaptan. By multiplying column 4 of Table 1 by this factor and subtracting it from column 2, one obtains a relatively good agreement for all products except H_2 which is too low (by 0.2 mmol dm^{-3}) and RH which is also too low to explain the thione yield by process [7*B*]. If in addition a molecular reaction is included,

$$\text{RSR} \xrightarrow{h\nu} \text{R}'' + \text{R}'\text{CH}{=}\text{S} + \text{H}_2 \qquad [11]$$

then all yields are brought into correspondence. The analysis suggests that *i*-Pr_2S photolysis proceeds 60% by [6*B*], 22% by [7*B*], 8.5% by [11], 6% by [9*B*], and 3.5% by [10*B*] and represents reaction of 2.3% of the sulfide initially present. Of the total mercaptan produced by these processes, about 20% is subject to secondary photolysis. From the M· signal in the epr spectrum, an estimate of ~0.5 mmol dm^{-3} can be made for this paramagnetic transient (23*b*), in reasonable agreement with the amount required to produce the observed RSSR and RSM (0.38 mmol dm^{-3}). Viewed from another point, over 90% of the sulfide decomposition gives diamagnetic products directly, the remainder involving detectable paramagnetic intermediates. Of these, roughly a third undergo a repair reaction such as [1].

The five line hyperfine spectrum observed following decay of the Et· and M· radicals in the Et_2S photolysis can be attributed to radicals resulting from attack of the thioaldehyde present as a result of reactions 7*B* or 11. During the primary photolysis at 77 K,

$$\text{H}_{\text{th}}\cdot + \text{S}{=}\text{CHCH}_3 \rightarrow \text{HS}\dot{\text{C}}\text{HCH}_3$$

while during warmup,

$$Et\cdot + S{=}CHCH_3 \rightarrow EtS\dot{C}HCH_3$$

or

$$M\cdot + S{=}CHCH_3 \rightarrow MS\dot{C}HCH_3$$

The formation of the first will be obscured by the presence of M· or Et· but might be expected to give rise to a similar five line hyperfine spectrum as the other $CH_3\dot{C}HSX$ species, and since their appearance depends upon the buildup of a secondary species, their observation will be favoured by longer photolysis times. Radicals of this size remain immobilized in the matrix until it softens, and can subsequently be repaired by photolytically produced thiol at higher temperatures. As a result, the ethyl disulfide yield eventually obtained at room temperature is probably undiminished by the formation of this type of radical.

B. Alkyl Disulfides

The disulfide–3MP photolysis is somewhat more complicated since there is a greater number of primary processes possible, as can be seen from Table 2. While the diversity of products is at least as great with the sulfides and thiols, their yields are only slightly lower, and the production of RS· is substantially reduced in the case of the disulfides. Since there is a strong possibility that each of the primary products RSH and RSSH will undergo secondary photolysis, and hence act as a source of thermal hydrogen atoms, then an analysis similar to that of the last section can be carried out, at least as far as the fragmentation products are concerned. By using a scaling factor of 0.2 to relate column 4 to column 3 of Table 1, and assuming a molecular process similar to [11] namely:

$$[12] \qquad RSSR \xrightarrow{h\nu} RSSR^* \rightarrow 2R'CH{=}S + H_2$$

one finds a reasonable fit for the isopropyl disulfide data. Of the assayed products, about 25% of the primary S—S cleavage occurs by [12] and about 75% by [6*C*], [7*C*]. Of the decomposed disulfide assayed, 12% gives $RS_2\cdot$ and RSSH by C—S bond rupture. No estimates of the processes [10*C*] or [9*D*] can be made. This particular analysis suggests that the contribution from reaction [8*C*], [9*C*] is very small so that most of the thiol produced by S—S cleavage is present in a cage as a geminal thiol pair [10*C*] or is combined with a thiocarbonyl compound as in [6*C*], [7*C*]. On absorption of a second photon, these cages would appear to regenerate the parent disulfide or to give rise to a diffusible hydrogen atom and intermediates similar to those found in the photolysed thiol systems (3). For [10*C*]

$$2RSH \xrightarrow{h\nu} R\dot{S}S(H)R + H_{th}\cdot$$

$$R\dot{S}S(H)R \xrightarrow{h\nu?} RS_2\cdot + RH$$

$$\rightarrow RSSR + H_{th}\cdot$$

These reactions have already been considered in [3] and occur in concentrated thiol glasses which contain dimers of the mercaptan. For cages typefied by [6*C*] one obtains

$$RSH + S{=}CHR' \xrightarrow{h\nu} RSS\dot{C}HR' + H_{th}\cdot$$

This last reaction would give rise in the case of ethyl and methyl disulfide, a hyperfine quintet and triplet, respectively, as observed in the Phase I epr spectra of these compounds photolysed at 77 K.

Although $CH_3CH_2SS\dot{C}HCH_3$ gives an epr spectrum essentially identical to that of the molecules $CH_3\dot{C}HSH$ and $CH_3\dot{C}HSC_2H_5$ produced in the sulfide or mercaptan photolysis, it is generated under circumstances which would photolyse the latter compounds. Such radicals are neither expected nor found in *t*-Bu_2S_2 photolysis.

Conclusions and Summary

One of the reasons for which the present research was undertaken was to provide a positive identification and determine the reaction characteristics of the neutral intermediate species which may be involved in the γ-radiolysis of divalent compounds in the solid state. Both the thiyl and perthiyl radicals are implicated in the radiolysis of cysteine, for instance, which forms cystine even in the crystalline state (26) and which also gives stable perthiyl radicals at room temperature (5).

Although the divalent sulfur compounds undergo a very complex set of reactions when photolysed in dilute matrices, the following facts now appear verified:

(*a*) Thiyl radicals are preferentially formed from photolysed sulfides and monomeric thiols (3) which contain a single S atom in the reactive cage. As produced photolytically RS· is kinetic-

ally hot and may damage surrounding molecules by H-atom abstraction.

(*b*) In the glassy state thiyl radicals have a single broad unsymmetrical epr absorption near $g = 2.00$.

(*c*) Thiyl radicals may be photolysed by 253.7 nm radiation to give alkyl radicals and ^3P sulfur atoms. Wavelengths much longer than 350 nm are ineffectual, although these radicals also have strong absorption near 400 nm.

(*d*) ^3P sulfur atoms diffuse in 3MP matrices at 77 K.

(*e*) Perthiyl radicals will not be produced in dilute mercaptan (3) or sulfide systems unless ^3P sulfur atoms are liberated by photolysis of thiyl radicals.

(*f*) RS· has a tautomeric form R′ĊHSH which does not appear to be the preferred isomer in 3MP at 77 K. The reverse is true for the oxygen analogues, methoxyl (27), and ethoxyl (28) radicals.

(*g*) The α-abstraction product of Et_2S, $CH_3\dot{C}HSC_2H_5$ has been observed. It is photodecomposed by 253.7 nm radiation to give Et· and thiocarbonyl at 77 K, and reforms by a cage reaction on warming.

(*h*) The perthiyl radical is preferentially formed from photolysed disulfides or from mercaptan dimers where the sulfur atoms appear as 'pairs' in an otherwise dilute matrix.

(*i*) RS_2· is characterized in esr by an anisotropic *g*-tensor with principal values near 2.00, 2.025, and 2.06, and doublet hyperfine splitting of 5–10 G when the R-group contains an α-methylene group. In the optical spectrum, there appears to be reasonably strong absorption in the 375–400 nm region. RS_2· is not photolabile above 240 nm.

(*j*) The α-abstraction product of disulfides is photochemically stable to 253.7 nm, and has epr hyperfine spectra similar to the compound in (*g*). Neither has strong visible absorption.

(*k*) The above paramagnetic species constitute only a small fraction of the total sulfide or disulfide photo-decomposition, being $\simeq 10\%$ and less than 12% respectively. The remainder are diamagnetic products such as mercaptans, thiocarbonyl, mixed thioethers, and alkanes or alkenes corresponding to the R group of the original substrate.

(*l*) Mercaptan produced in Et_2S and Et_2S_2 may be subject to secondary photolysis, leading to EtS· in sulfides, and to $EtSS\dot{C}HCH_3$ or EtS_2· in the case of disulfides.

There are many points of agreement between the present work and other research where sulfides and disulfides have been photolysed under widely different experimental conditions. Included in these studies are the room temperature liquid phase photolysis carried out with or without dilution of the substrates by a hydrocarbon solvent. It must be recognized that under such conditions cage processes such as [8*B*] forming RSM will have reduced significance and that all reactions which occur in Phase I through Phase V in the glassy state will be proceeding simultaneously in fluid media. Thus while mercaptans are the major products obtained from room temperature photolytic cleavage of the S—S bonds in disulfides (1), this mercaptan will scavenge other mobile radical products such as M·, R′ĊHSSR, etc. giving rise to thermal RS·. RS· will itself be photolysed during the experiment and, by virtue of the atomic sulfur released, will eventually lead to the formation of the mono-, tri-, and tetrasulfide products observed (10). It is perhaps significant that the RSH concentration reaches a steady state maximum during disulfide photolysis (29). This was assumed due to secondary RSH photolysis much as has been suggested by the present results. Evidence of H_2 formation and unexpected hydrocarbon residues is also found in the room temperature photolysis of both sulfide and disulfides (30).

With regard to research carried out in the rigid matrices, it is now apparent that Rosengren, who used only optical and glc methods to study the photolysis of alkyl disulfides in hydrocarbon glasses at 77 K (16) did not have RS· but rather RS_2· as the species which absorbed near 400 nm. We are in agreement that the major photoreaction is that given by [6*C*], [7*C*].

There is also agreement between our work and that of Bolman *et al.* (31) and of Windle and coworker (32) who photolysed at 77 K a variety of mercaptans, sulfides, and disulfides as polycrystalline solids or adsorbed on Vicor plates. Their spectra of mercaptans and disulfides agree with earlier (3) and present work, respectively, in that RS_2· is produced in both concentrated RSH and in R_2S_2 matrices along with other species which exhibit proton hyperfine coupling. However, photolysis of *n*-decyl sulfide (32) produces

$RS_2\cdot$ along with an eight line hyperfine pattern due to an alkyl radical. This result would be anticipated if the stronger binding of the sulfide in the crystalline lattice led to formation of a higher proportion of thermalized alkyl thiyl radicals which are then subsequently photolysed to liberate free sulfur atoms much as in our Phase IV experiments.

Reference has already been made to the correspondence between our results and those for photolysed or γ-irradiated cysteine and cysteine single crystals.

Acknowledgement

The authors would like to credit, with many thanks, the financial aid of the National Research Council of Canada.

1. P. C. JOCELYN. Biochemistry of the SH group. Academic Press, London. 1972.
2. M. Z. HOFFMAN and E. HAYON. J. Am. Chem. Soc. **94**, 7950 (1972).
3. A. J. ELLIOT and F. C. ADAM. Can. J. Chem. **52**, 102 (1974).
4. W. KARMANN, A. GRANZOW, G. MEISSNER, and A. HENGLEIN. Int. J. Radiat. Phys. Chem. **1**, 395 (1969).
5. R. F. WHEATON and M. G. ORMEROD. Trans. Faraday Soc. **65**, 1638 (1968).
6. E. L. THOMSEN and S. O. NIELSEN. J. Chem. Phys. **57**, 1095 (1972).
7. K. AKASAKA, S. OHNISHI, T. SUITA, and I. NITTA. J. Chem. Phys. **40**, 3110 (1964).
8. V. G. KRIVENKO, L. P. KAYUSHIN, and M. K. PULATOVA. Biofizika, **14**, 615 (1969).
9. J. H. HADLEY and W. GORDY. Proc. Nat. Acad. Sci. USA, **71**, 3106 (1974).
10. B. MILLIGAN, D. E. RIVETT, and W. E. SAVAGE. Aust. J. Chem. **16**, 1020 (1963).
11. (*a*) P. M. RAO and A. R. KNIGHT. Can. J. Chem. **50**, 844 (1972). (*b*) P. M. RAO, J. A. COPECK, and A. R. KNIGHT. Can. J. Chem. **45**, 1369 (1967).
12. (*a*) S. ADITYA and J. E. WILLARD. J. Am. Chem. Soc. **88**, 229 (1966). (*b*) K. FUEKI and Z. KURI. J. Am. Chem. Soc. **87**, 923 (1965).
13. (*a*) R. F. C. CLARIDGE and J. E. WILLARD. J. Am. Chem. Soc. **87**, 4992 (1965). (*b*) P. B. AYSCOUGH and C. THOMSEN. Trans. Faraday Soc. **58**, 1471 (1962).
14. D. P. LIN and J. E. WILLARD. J. Phys. Chem. **78**, 2233 (1974).
15. J. W. GREIDANUS. Can. J. Chem. **48**, 3530 (1970).
16. K. ROSINGREN. Acta Chem. Scand. **16**, 1401 (1962).
17. J. Q. ADAMS. J. Am. Chem. Soc. **92**, 4535 (1970).
18. O. H. GRIFFITH and M. H. MALLON. J. Chem. Phys. **47**, 837 (1967).
19. H. C. BOX, H. G. FREUND, and E. E. BUDZINSKI. J. Chem. Phys. **45**, 809 (1965).
20. M. A. NEISS, E. D. SPRAGUE, and J. E. WILLARD. J. Chem. Phys. **63**, 1118 (1965).
21. D. J. HENDERSON and J. E. WILLARD. J. Phys. Chem. **91**, 3014 (1969).
22. M. SHIROM and J. E. WILLARD. J. Phys. Chem. **72**, 1702 (1968).
23. (*a*) M. IWASAKI and K. TORIYANA. J. Chem. Phys. **46**, 2852 (1967). (*b*) F. C. ADAM and I. R. H. MARSHALL. Can. J. Chem. **54**, 3833 (1976).
24. (*a*) F. W. FROBEN and J. E. WILLARD. J. Phys. Chem. **75**, 35 (1971). (*b*) M. YA. MEL'NIKOV, V. I. SKLYARENKO, and N. V. FOK. Dokl. Akad. Nauk. SSR, **218**, 875 (1974).
25. D. TIMM and J. E. WILLARD. J. Phys. Chem. **73**, 2403 (1969).
26. D. B. PETERSON, J. HOLIAN, and W. M. GARRISON. J. Chem. Phys. **73**, 1568 (1969).
27. B. SMALLER and M. S. MATHESON. J. Chem. Phys. **28**, 1169 (1958).
28. R. S. ALGER, T. H. ANDERSON, and L. A. WEBB. J. Chem. Phys. **30**, 695 (1959).
29. C. WALLING and R. RABINOWITZ. J. Am. Chem. Soc. **81**, 1137 (1959).
30. W. E. HAINES, G. L. COOK, and J. S. BALL. J. Am. Chem. Soc. **78**, 5213 (1956).
31. P. S. H. BOLMAN, I. SAFARIK, D. A. STILES, W. J. R. TYERMAN, and O. P. STRAUSZ. Can. J. Chem. **48**, 3872 (1970).
32. J. J. WINDLE and A. K. WIERSEMA. J. Chem. Phys. **41**, 1996 (1964).

Determination of motional asymmetry of methyl rotators from ^{13}C spin dynamics

LAWRENCE G. WERBELOW AND DAVID M. GRANT
Department of Chemistry, University of Utah, Salt Lake City, UT, U.S.A. 84112

Received December 11, 1976

LAWRENCE G. WERBELOW and DAVID M. GRANT. Can. J. Chem. **55**, 1558 (1977).

Recent advances in the theory of dipolar relaxation in multispin systems are applied to studies of methyl rotators in isotropic fluids. A simple methodology is outlined which is very attractive for the investigation of anisotropic methyl group reorientation. It is demonstrated that this approach does not suffer from many of the inherent limitations of conventional applications of dipolar relaxation to such studies. Analogous extensions of the propounded method become temptingly obvious.

LAWRENCE G. WERBELOW et DAVID M. GRANT. Can. J. Chem. **55**, 1558 (1977).

On a appliqué des connaissances acquises récemment dans le domaine de la théorie de la relaxation dipolaire de systèmes multispin pour étudier des rotors méthyles dans des fluides isotropes. On décrit une méthodologie simple qui est très attrayante pour l'étude de la réorientation anisotrope du groupe méthyle. On démontre que plusieurs des limitations inhérentes des applications conventionnelles de la relaxation dipolaire à de telles études ne se retrouvent pas dans cette approche. Des extensions analogues de la méthode proposée deviennent rapidement évidentes.

[Traduit par le journal]

Introduction

The investigation of the dynamical features of methyl rotators in liquid media has provided the central theme for numerous recent experimental applications of transient effects in magnetic resonance studies (1). However, recent advances in the theory of dipolar relaxation in multispin systems (2, 3) have yet to be routinely applied in such seemingly inviting experimental investigations of related topics. It is the intent of this work to emphasize how differential recovery rates of individual components in a fully coupled $^{13}CH_3$ subspectrum can yield detailed information on the motional asymmetry of methyl rotators.

In proton decoupled $^{13}CH_3$ spin systems, the apparently exponential (4)[1] recovery rate of the inverted collapsed quartet is related to molecular parameters by the following expression

$$[1]\quad \ln\left(\frac{\langle I_z^{C}(t)\rangle}{\langle I_z^{C}(0)\rangle}\right) \simeq \ln(5\gamma_H/\gamma_C) - \ln(10+\zeta_C) - J_{CH}(10+\zeta_C)t$$

The dipolar spectral density, J_{CH}, can be written in the specialized form,

$$[2a]\quad \frac{J_{CH}}{\alpha\chi} = \frac{1}{16} + \left(\frac{1}{5+\xi}\right) + 2\left(\frac{1}{2+4\xi}\right)$$

Nondipolar contributions to the carbon relaxation rate are approximated as random field interactions. The contribution of such interactions to the longitudinal relaxation rate of spin 'i' is conveniently represented by the term $R_1^{0}(i)$. The unitless interaction ratio appearing in [1] can be related to this quantity by the expression

$$[2b]\quad \zeta_C = \frac{R_1^{0}(C)}{J_{CH}}$$

The parameters α, χ, and ξ appearing in [2a] are defined by the following relationships

$$[3]\quad \alpha = 32/27$$

$$\chi = \frac{3}{40D_0}\left(\frac{\gamma_H\gamma_C\hbar}{r_{CH}^{3}}\right)^2$$

$$\xi = \frac{D_{int}}{D_0} + 1$$

Internuclear distances and magnetogyric ratios are conventionally defined.

For simplicity, it is assumed that the methyl rotator is affixed to a framework completely described by the isotropic rotational diffusion constant D_0. Superimposed upon this three dimensional isotropic motion is a one dimensional internal diffusional rotation of the proton triad about the threefold symmetry axis. This secondary motion, quantified by the rotational diffusion constant D_{int}, is assumed not to couple

[1]The cautionary remarks expressed in ref. 4 relating to the general validity of [1] should be carefully noted.

with the overall motion.[2] It is also important to note that expressions 1 and 2 imply the assumption of a featureless power density in which all frequency dependence of the power density has been suppressed.

The measurable kinetic equation [1] contains three unknown parameters, ζ_C, χ, and ξ. The conventional transcription (1) of this problem normally deduces χ from the dipolar recovery rate of an independent C—H dipolar interaction which is reflective of only the motions of the molecular framework. Once χ has been determined, ζ_C and ξ in principle can be determined from the simple linear form expressed in [1].

Although this conventional approach is very convenient and straightforward, it does suffer from the limitation that there may be instances when such an approach will yield misleading information (4).[1] Furthermore, unless D_0 and D_{int} are of comparable order of magnitude, it is not feasible to quantitatively determine the motional asymmetry of the methyl rotator. Equation 2*a* clearly indicates that if $\xi \gg 1$, then J_{CH} is independent of this parameter. In such instances, dynamic information may be limited to motions perpendicular to the rotator's principal axis. These motions are characterized by the parameter χ. One possible alternative approach which does not suffer from this latter limitation is the analysis of the spin rotation contribution to the relaxation rate of the carbon nucleus (5). Unfortunately, the dynamical information associated with spin rotation interactions are not as well understood at the present time as those arising from the intramolecular dipolar interaction.

Theory

There is a wealth of motional and structural information encoded in the time evolution equations of methyl groups which is generally ignored in the transient magnetic resonance experiment. When the kinetic analysis is done correctly, it can be shown that the time evolution of the fully coupled carbon quartet is of the general form (6)

$$[4]\quad \ln\langle I_z^C\rangle = f(J_{CH}, J_{HH}, J_{HCH}, J_{HHH}, J_{CHH}, J_{CHHH}, R_1^0(C), R_1^0(H); t)$$

The various auto and cross correlated dipolar spectral densities are defined in the notation of refs. 2 and 6. Assuming, for convenience, a tetrahedral geometry ($r_{HH} = (\sqrt{8}/\sqrt{3})r_{CH}$) and $\gamma_H/\gamma_C = 4$, these spectral terms can be written in the following abbreviated forms

$$\frac{J_{HCH}}{\alpha\chi} = \frac{1}{16} - \frac{1}{2}\left(\frac{1}{5+\xi}\right) - \left(\frac{1}{2+4\xi}\right)$$

$$\frac{\alpha J_{HH}}{\chi} = \frac{1}{6} + 3\left(\frac{1}{2+4\xi}\right)$$

$$[5]\quad \frac{\alpha J_{HHH}}{\chi} = \frac{1}{6} - \frac{3}{2}\left(\frac{1}{2+4\xi}\right)$$

$$\frac{\sqrt{\alpha} J_{CHH}}{\chi} = \frac{1}{9} + \frac{4}{3}\left(\frac{1}{2+4\xi}\right)$$

$$\frac{\sqrt{\alpha} J_{CHHH}}{\chi} = \frac{1}{9} - \frac{8}{3}\left(\frac{1}{2+4\xi}\right)$$

Figure 1 plots the amplitude of the six unique spectral densities defined by the previous equations *vs.* the motional asymmetry parameter, ξ. It is interesting to comment that conventional applications of magnetic relaxation phenomena to the problem of methyl rotator dynamics employ either the HH or CH autocorrelation power densities (the uppermost two curves in Fig. 1). A comparison of these two approaches indicates that it is advantageous to exploit CH interactions rather than HH interactions because of a twofold enhancement in motional sensitivity of the locked *vs.* freely rotating methyl spectral densities. Furthermore, the J_{HH} curve becomes experimentally insensitive to differences in ξ for values of this parameter larger than a factor of five or ten. A realistic upper limit for the usefulness of CH interactions is two or three times this value, and thus, relative values of D_{int} to D_0 may be studied up to a ratio of 10 to 20.

Also note that cross correlation spectral densities need not be intrinsically positive. Theories of rotational diffusion yield spectral representations of lattice correlations which are described as a superposition of *positive* amplitude Lorentzians. For autocorrelation densities, all weighting factors are non-negative geometrical constants. However, for the interference or cross

[2]When comparing the dynamical features of rigid, symmetric top rotators and internal rotators affixed to an otherwise isotropically rotating framework, it proves convenient to make the conventional identifications, $D_0 \sim D_\perp$ and $D_{int} \sim D_\parallel - D_\perp$ (for example, see ref. 9). However, the notations (D_{int}, D_0) and ($D_\parallel$, $D_\perp$) *imply* different physical models and hence the redundancy in variables is justifiable. It should be noted that $D_\parallel/D_\perp = 1 + D_{int}/D_0$. The notation introduced by [3] is chosen to render the definition of ξ compatible with previous and relatively standardized notation (*e.g.*, see ref. 4).

correlation spectral densities, no such restriction is imposed on the various weighting coefficients. Although puzzling to the uninitiated, this fact presents no anomalies of definition or in associated physical meaning (2). The interlevel transition rates are positive constraining the systems response to an arbitrary perturbation as a superposition of damping rather than oscillatory factors.

Comparison of [1] and [4] clearly indicates that considerably more information may be harvested from the fully coupled experiment (eq. 4) in contrast to the conventional approach (eq. 1). Under the geometrical and motional constraints imposed by the various assumptions, one may not presume that all of the spectral densities are independent, *e.g.*,

$$\frac{2}{27\sqrt{\alpha}}(7J_{HH} + 2J_{HHH}) = J_{CHH}$$

and

$$\frac{28}{27\sqrt{\alpha}}\left(J_{HHH} - \frac{5}{14}J_{HH}\right) = J_{CHHH}$$

If the model assumed for the internal motion is one of time modulated 120° random jumps, there would be only two independent power densities. Regardless of this linear dependence, there is no corresponding reduction in the complexity of [4].

It has been shown (6) that these additional power densities cause differential recovery rates of symmetrically positioned components in the carbon manifold.[3] Such effects are easily incorporated into the evolution equations by introducing a 'multiplet asymmetry magnetization' defined by the expression,

$$[6a]\quad \langle I_z^{\Delta}\rangle \equiv 4\langle I_z^{C}I_z^{H}I_z^{H'} + I_z^{C}I_z^{H}I_z^{H''} + I_z^{C}I_z^{H'}I_z^{H''}\rangle$$

$$[6b]\quad \langle I_z^{\Delta}\rangle \equiv 2(3(P_{\frac{3}{2},\frac{3}{2},\frac{1}{2}} - P_{\frac{3}{2},\frac{3}{2},-\frac{1}{2}}) - (P_{\frac{3}{2},\frac{1}{2},\frac{1}{2}} - P_{\frac{3}{2},\frac{1}{2},-\frac{1}{2}}) - 2(P_{\frac{1}{2},\frac{1}{2},\frac{1}{2}} - P_{\frac{1}{2},\frac{1}{2},-\frac{1}{2}}))$$

where P_{I^H,I_z^H,I_z^C} is the population of the symmetrized eigenstate characterized by a coupled proton spin I^H, a projection of I_z^H, and a carbon projection, I_z^C. No kinetic distinction between the symmetric and antisymmetric proton doublet states is necessary. Equality 6*b* identifies I_z^{Δ} as three times the sum of the outer components minus the intensity of the central components in the carbon quartet. Note for $\langle I_z^{\Delta}\rangle$, the thermal equilibrium value vanishes identically.

As demonstrated in the following section, the experimental determination of the time evolution of the multiplet asymmetry provides an enticing means to probe the dynamical features of mobile spin groupings.

[3]These differential effects are in no way related to the effects discussed by Schaublin *et al.* (10).

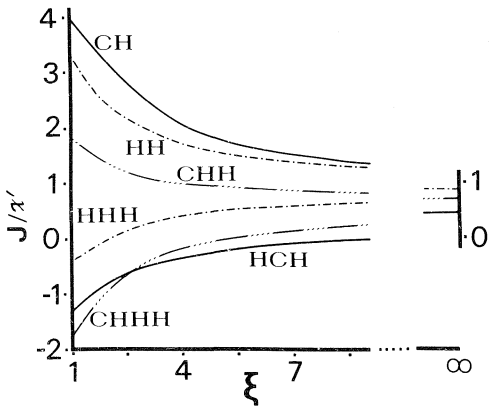

FIG. 1. Plot of the six unique dipolar spectral densities which characterize the spin kinetics of the $^{13}CH_3$ spin grouping *vs.* the motional asymmetry parameter, $\xi(\equiv 1 + D_{int}/D_0)$. The power densities are measured in units of $(\gamma_C\gamma_H\hbar/r_{CH}^3)^2(1/80D_0) \equiv \chi'$. In the limit as $\xi \to \infty$, it is explicitly noted that $J_{CH} = J_{HCH}$, $J_{HH} = J_{HHH}$, and $J_{CHH} = J_{CHHH}$. The various J's are defined in [2*a*] and [5] in the text.

Results and Discussion

Since the response of the multiplet asymmetry magnetization to an arbitrary homogenous perturbation is correctly described as a weighted sum of six exponential terms whose time constants may be determined by the solution of a sextic equation, it might be surmised that any approach utilizing this parameter does not warrant the increased numerical complications even though an expanded description is obtained. Figures 2, 3, and 4 illustrate that such pessimism is not justified. These figures are expanded versions of similar plots given in ref. 6 and depict the transient behaviour of the multiplet asymmetry magnetization subsequent to complete inversion of the proton spectral doublet for various anisotropy factors, ξ. Figure 2 assumes both the proton and carbon spins are relaxed solely by the intramolecular dipolar interaction. Conversely, Figs. 3 and 4 assume a fully correlated random field-type interaction (*e.g.* spin rotation, dilute paramagnetics, etc.) competes favourably with dipolar interactions in providing effective relaxation pathways for the carbon or hydrogen nuclei respectively. For clarity, the dynamics of I_z^{Δ} have been reproduced only from the point in time of maximum deviation onwards. The initial spin evolution can be deduced by noting that the

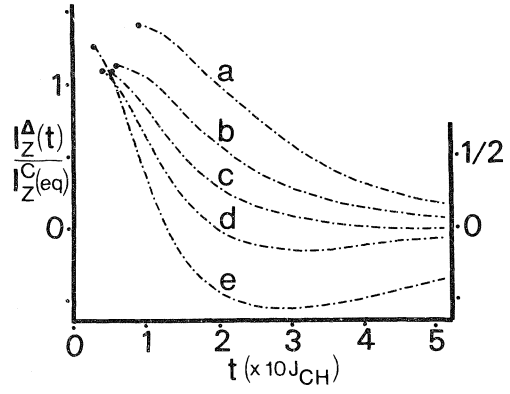

FIG. 2. Plot of the multiplet asymmetry magnetization as a function of time subsequent to complete inversion of the proton spectral doublet. Both the dependent and independent variables are measured in the natural units of the system which are $\langle I_z^{C}(eq)\rangle$ and $10J_{CH}^{-1}$, respectively. Curves *a*, *b*, *c*, *d*, and *e* correspond to a motional asymmetry (ξ) equal to 1, 4, 8, 16, and 100, respectively. Motional and geometrical assumptions are noted in the text. For clarity, the initial growth of I_z^{Δ} is not reproduced in the individual curves. Time dependent spin interactions other than the intramolecular dipolar coupling are assumed negligible.

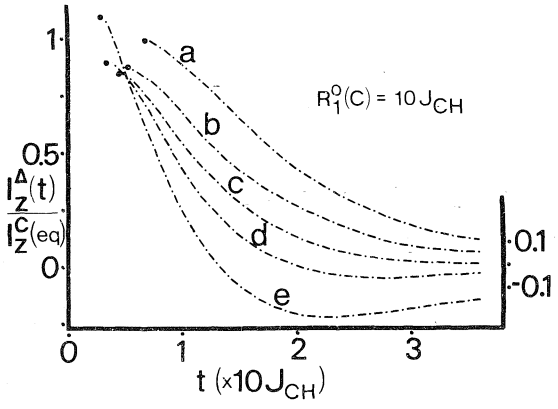

FIG. 3. Notation is identical to that described for Fig. 2. It is assumed that the carbon spin is relaxed by dipolar and random field interactions of equal magnitude. The protons are relaxed solely by intramolecular dipolar couplings.

initial values for the asymmetry magnetization must be zero whenever the perturbing influence is homogenous across each multiplet.

There are numerous reasons for preferring a spin preparation generated by a hard π-pulse on the proton spectral doublet. It can be shown (6) that I_z^{Δ} is coupled to I_z^{H} by the three spin power density, J_{CHH}. For the methyl rotator geometry, this spectral parameter is always characterized by an appreciable magnitude over the effective range of ξ. In contrast, Fig. 1 reveals that the

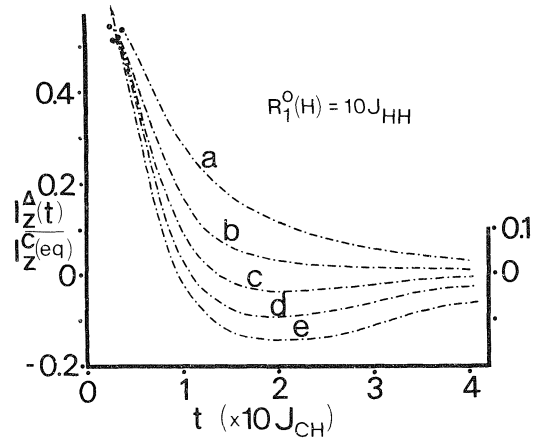

FIG. 4. Notation is identical to that described for Fig. 2. It is assumed that the protons are relaxed by dipolar and random field interactions of magnitudes $10(J_{HH} + \frac{1}{3}J_{CH})$ and $10J_{HH}$, respectively. The ^{13}C spin is relaxed exclusively by the dipolar mechanism.

other multispin power densities such as J_{CHH}, J_{HHH}, and J_{CHHH} become vanishingly small over certain motional ranges. For instance, I_z^{Δ} is directly coupled to I_z^{C} by the three spin power density, J_{HCH}. Hence, inversion of the carbon quartet results in a very weak transfer of magnetization into I_z^{Δ} over a considerable range of ξ. Indeed, for $\xi \cong 9$, this coupling vanishes, and stimulation of I_z^{C} only perturbs I_z^{Δ} inefficiently by second-order indirect couplings to other normal modes of magnetization.

Another benefit of inverting the proton magnetization is sensitivity. By stimulating the total proton magnetization a transient Overhauser enhancement is generated in the carbon and multiplet asymmetry magnetization reservoirs. For times much less that the intrinsic relaxation rates[4] (2) of the proton or carbon spins, the growth of I_z^{Δ} following a proton π-pulse is approximated as[5]

$$[7a] \quad (d/dt)\langle I_z^{\Delta}(t \to 0)\rangle \simeq -24J_{CHH}\langle I_z^{H}\rangle \simeq 24\left(\frac{\gamma_H}{\gamma_C}\right) J_{CHH}\langle I_z^{C}(eq)\rangle$$

[4]The intrinsic relaxation rate for the protons and carbon spins are $10J_{HH} + \frac{10}{3}J_{HCH} + R_1^{0}(H)$ and $10J_{HCH} + R_1^{0}(C)$ respectively. Continued usage of the implicative notation of T_{1H}^{-1} and T_{1C}^{-1} for these respective parameters is undoubtedly misleading and probably should be discouraged.

[5]Note the obvious but inconsequential omission of signs in eqs. 40–45 in ref. 6.

whereas following a homogenous carbon π-pulse

$$[7b] \quad (\mathrm{d}/\mathrm{d}t)\langle I_z^{\Delta}(t \to 0)\rangle \simeq \frac{10}{3} J_{\mathrm{HCH}} \langle I_z^{\mathrm{C}}(\mathrm{eq})\rangle$$

Noting that the absolute magnitude of J_{CHH} is always larger than J_{HCH}, it is rationalized that proton inversions are often orders of magnitude more stimulating than carbon inversions.

Figures 2, 3, and 4 demonstrate some very interesting and useful evolution characteristics of I_z^{Δ} subsequent to a hard π-pulse on the protons. It should be noted that if the parameter J_{HCH} is negative ($\xi \gtrsim 9$), then the normalized intensity of the outermost lines is invariably greater than the normalized intensity of the innermost lines. From the assumed spin preparation and previous discussion, it is apparent that the outer lines are always characterized by an initial transient rate which is greater in magnitude than the central components. However, if J_{HCH} is positive, then the normalized intensity of the central lines will invariably overcompensate for this initial inequity, and in fact, excede the normalized intensity of the outer lines. The existence of possible random field interactions does not significantly alter this generalization.

The effects of random field interactions are reflected in Figs. 3 and 4. Although not explicitly demonstrated by the various plots due to the suppression of the short time behaviour, the initial growth of $I_z^{\Delta}(t)$ is invariant with respect to random field interactions (*cf.* eq. 7*a*). Since the coupling coefficient between I_z^{H} and I_z^{Δ} is independent of both proton and random field interactions, it can be inferred to a good approximation that the amount of magnetization funneled into the multiplet asymmetry mode is limited by the intrinsic rate of the deviation decay of I_z^{H} and hence is reflective of various factors which determine this rate. This is clearly indicated by contrasting Figs. 2 and 4. Note that in the latter figure, the magnitude of magnetization transferred is about one-half of that transferred for the assumed intrinsic proton relaxation rate depicted in the former figure which is roughly one-half as efficient.

As a first approximation, a moderate random field contribution to the carbon spin dynamics does not influence significantly the amplitude of I_z^{Δ}. The primary effect of such interactions causes a contraction in the time domain since $R_1^0(\mathrm{C})$ contributes directly to the intrinsic relaxation rate of I_z^{Δ}. This behaviour is noted by contrasting Figs. 2 and 3.

If $R_1^0(\mathrm{H})$ dominates the spin kinetics, then I_z^{H} is relaxed so efficiently that very little magnetization is allowed to escape from this reservoir into I_z^{Δ} before the reestablishment of thermal equilibrium. On the other hand, if $R_1^0(\mathrm{C})$ dominates the spin kinetics, then I_z^{Δ} is relaxed so efficiently that very little magnetization is allowed to accumulate in this reservoir before being dissipated. In either of these instances utilization of the multiplet asymmetry magnetization will prove to be ineffective. Of course these generalizations presume a spin system prepared by a proton inversion. If one can tolerate the aforementioned limitations of carbon inversion, then it is also possible to observe useful cross correlation effects under different restrictions (4).

For large motional anisotropies, the thermal deviation of I_z^{H} decays at a rate which is roughly four times slower than for small anisotropies. Likewise, the coupling coefficient, $4J_{\mathrm{CHH}}$, is reduced by a factor of three. These counterbalancing effects result in a startling consistency in the observed maximum intensity of I_z^{Δ} for a given random field contribution.

Also note that there is much more variability in the relaxation kinetics for large ξ. This is a consequence of large magnetizations being generated in all six coupled normal mode reservoirs including the modes composed of degenerate proton transitions which are connected to I_z^{H} via J_{HHH} cross terms. Whereas autocorrelation spectral densities must decrease in amplitude with increasing internal degrees of freedom thus spreading a given area over a broader range of frequencies, cross correlation spectral densities are not bound to such limitations and may increase or decrease in magnitude depending upon the relative orientation of the internuclear vectors with respect to the principal axes of diffusion.

The true time behavior is somewhat misrepresented by these plots because the normalization factor, $10J_{\mathrm{CH}}$. In the limit where ξ becomes quite large, the abscissa is in reality contracted by a factor of 9 relative to the limit characterized by ξ equal to unity. This is simply a quantitative restatement of the fact that the longitudinal relaxation is sensitive to those molecular frequencies closest to the natural Larmor frequency of the system.

As mentioned earlier, the spectral density,

J_{CHH}, is always positive for any assumed ξ. Hence, it is rationalized that at times small compared to $(10J_{CH} + R_1^0(H))^{-1}$, the outer lines always grow relative to the central components due to a transient Overhauser effect. Likewise, the total carbon magnetization initially increases by the same reasoning. Comparison of the initial growth rates of the multiplet asymmetry magnetization and the total carbon magnetization would provide a useful experimental feature which can provide an initial estimate of the importance of cross correlation effects. The ratio of rates is given by the following equation

$$[8] \qquad \frac{-(d/dt)\langle I_z^A(t \to 0)\rangle}{-(d/dt)\langle I_z^C(t \to 0)\rangle} \cong \frac{12J_{CHH}}{5J_{CH}}$$

This valuable ratio is independent of χ and R_1^0(C, H) and yields ξ directly. Figure 5 plots this ratio as a function of ξ. It is noted that this experiment provides an excellent means to determine the magnitude of large motional anisotropies.

Using the simultaneous coupled differential equations presented in ref. 6, $(-d/dt)\nu(t) = \Gamma\nu(t)$, a solution may be obtained of the form $\nu(t) = \mathbf{B} \exp(-\mathbf{B}^{-1}\Gamma\mathbf{B})\mathbf{B}^{-1}\nu(0)$ where $\mathbf{B}$ is a unitary matrix composed of the eigenvectors of Γ and the matrix $\mathbf{B}^{-1}\Gamma\mathbf{B}$ is the diagonalized eigenvalue matrix of Γ. It becomes a straightforward task to generate comparative evolution plots of I_z^A from these solutions. With a suitable manifold of simulated evolution rates for I_z^A and some experience with the solutions, the experimentalist may deduce a fairly detailed view of the spin dynamics in the methyl rotator. Such simple comparative methods may provide sufficient information to the investigator and thereby obviate resorting to more exact but complex nonlinear least squares techniques (7). Applications of analogous graphical methods for more general dynamical investigations of three and four spin one-half systems are apparent even though the complexity of such treatments may be a serious deterrent.

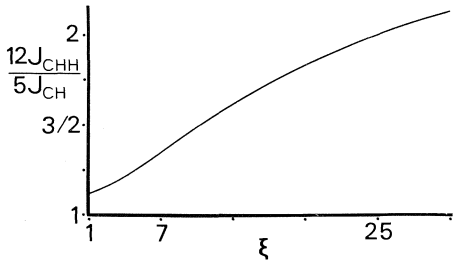

FIG. 5. The initial rate ratio

$$\frac{(-d/dt)I_z^A(t \to 0)}{(-d/dt)I_z^C(t \to 0)} = \frac{12J_{CHH}}{5J_{CH}}$$

following complete inversion of the proton spectral doublet is plotted as a function of the motional asymmetry parameter, ξ.

Conclusions

It is hoped that the suggested graphical approach and related discussion provide a meaningful approach to a study of rotationally anisotropic methyl groups and in general, by extrapolation, to the nature and practical consequences of multispin correlations in polyspin systems. An exhaustive discussion or exposition of the various ideas developed in the previous sections was neither attempted nor achieved; the primary motivation of this presentation was to merely introduce some basic lines of reasoning. The rather restrictive conditions hypothetically assumed for the methyl spin dynamics need not limit the approach as extensions to methyl groups attached to symmetric or asymmetric top rotators is straightforward (8) though less convenient in their application.

Acknowledgements

This work was supported by the National Institutes of Health under Grant GM08521. Helpful discussions with Dr. Charlie Mayne on experimental studies in progress are also gratefully acknowledged. Thanks are extended to a pair of conscientious referees.

1. (*a*) K. H. LADNER, D. K. DALLING, and D. M. GRANT. J. Phys. Chem. **80**, 1783 (1976); (*b*) D. E. AXELSON and C. E. HOLLOWAY. Can. J. Chem. **54**, 2820 (1976); (*c*) S. W. COLLINS, T. D. ALGER, D. M. GRANT, K. F. KUHLMANN, and J. C. SMITH. J. Phys. Chem. **79**, 2031 (1975).
2. L. G. WERBELOW and D. M. GRANT. Adv. Magn. Reson. Vol. IX, 189 (1977).
3. R. R. VOLD and R. L. VOLD. Prog. NMR Spect. To be published.
4. L. G. WERBELOW and D. M. GRANT. J. Chem. Phys. **63**, 4742 (1975).
5. A. P. ZENS and P. D. ELLIS. J. Am. Chem. Soc. **97**, 5685 (1975).
6. L. G. WERBELOW and D. M. GRANT. J. Chem. Phys. **63**, 544 (1975).
7. C. L. MAYNE and D. M. GRANT. J. Chem. Phys. To be published.
8. L. G. WERBELOW and A. G. MARSHALL. J. Magn. Reson. **11**, 299 (1973); L. G. WERBELOW and D. M. GRANT. J. Magn. Reson. **21**, 369 (1976).
9. L. G. WERBELOW. J. Am. Chem. Soc. **96**, 4747 (1974).
10. S. SCHAUBLIN, A. HOHENER, and R. R. ERNST. J. Magn. Reson. **13**, 196 (1974).

Comparison of ^{13}C and ^{1}H *N*-alkyl shifts of isomeric alkyl tetrazoles: some ambident benzylations

R. N. BUTLER[1] AND T. M. MCEVOY
Department of Chemistry, University College, Galway, Ireland
AND
F. L. SCOTT AND J. C. TOBIN
Department of Chemistry, University College, Cork, Ireland

Received July 6, 1976[2]

R. N. BUTLER, T. M. MCEVOY, F. L. SCOTT, and J. C. TOBIN. Can. J. Chem. **55**, 1564 (1977).

^{13}C nmr alkyl shifts of *N*-alkyl tetrazoles and azoles follow the pattern of proton shifts. The shielding of the *N*-alkyl group increases for the structural units

$$=N-N(R)-N= \; < \; =N-N(R)-\underset{|}{C}= \; < \; =\underset{|}{C}-N(R)-\underset{|}{C}=$$

The carbon spectra are more reliable for structural assignment. Synthesis of a number of mono- and dibenzyl derivatives of benzaldehyde tetrazol-5-ylhydrazone are reported.

R. N. BUTLER, T. M. MCEVOY, F. L. SCOTT et J. C. TOBIN. Can. J. Chem. **55**, 1564 (1977).

Les déplacements alkyles, en rmn du ^{13}C, des groupes des *N*-alkyltétrazoles et -azoles correspondent à ceux observés pour les déplacements du proton. Le blindage des groupes *N*-alkyles augmente pour les unités de structure

$$=N-N(R)-N= \; < \; =N-N(R)-\underset{|}{C}= \; < \; =\underset{|}{C}-N(R)-\underset{|}{C}=$$

Les spectres du carbone sont plus fiables pour l'attribution des structures. On rapporte la synthèse d'un certain nombre de dérivés mono- et dibenzylés de la tétrazolylhydrazone-5 de la benzaldéhyde.

[Traduit par le journal]

Proton nmr alkyl shifts have proved useful for distinguishing between *N*-alkyl isomers in the azole series due to increased shielding of the alkyl group in the structural units (1)

$$\underset{C}{=N-N(R)-N=} \; < \; \underset{B}{\overset{|}{=}C-N(R)-N=} \; < \; \overset{|}{=}C-N(R)-\underset{|}{C}=$$
$$A$$

However, these trends may break down when substituents containing special anisotropic effects are present. For example, in the tetrazole series, for 5-substituents such as —NH—N=CHAr and —NHCOMe, a 1-*N*-alkyl group (I) may be deshielded to the same region as the corresponding 2-*N*-alkyl isomer (II) and a distinction by proton nmr is not always possible (2, 3).

With a number of benzyl derivatives of benzaldehyde tetrazol-5-ylhydrazone (Table 1, compounds **9**–**12**) we have now found that the correlation previously noted (1) is reversed due to the anisotropic effects of the 5-hydrazono substituent at the 1-*N*-alkyl site. As far as we are

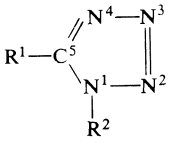

I

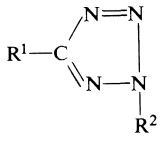

II

aware, these are the only reported examples where a 2-*N*-alkyl tetrazole isomer is more shielded than the corresponding 1-*N*-alkyl compound. ^{13}C nmr alkyl shifts have, however, proved more useful for structural assignments with these isomeric systems. The data in Table 1 clearly suggest that the same structural – chemical shift trends, which we noted (1) in proton spectra of *N*-alkyl azoles, also apply in the carbon spectra. There is consistently higher shielding of the C-1 atom of *N*-alkyl groups for the structural moieties A > B > C in diazoles,

[1]Author to whom correspondence should be addressed.
[2]Revision received January 25, 1977.

TABLE 1. ^{13}C and ^{1}H shifts of *N*-alkyl tetrazoles

Compound	Tetrazole R¹	Tetrazole R²	Type	*N*-alkyl shift (structural unit) ^{13}C (ppm from TMS)	^{1}H (τ)
1[a]	NH_2	Me	I	31.4 (B)	6.18 (B)
2[a]	NH_2	Me	II	39–41 (C)[f]	5.84 (C)
3[a]	NH_2	Bz	I	48.0 (B)	4.66 (B)
4[a]	NH_2	Bz	II	55.5 (C)	4.46 (C)
5[b]	H	Me	I	33.7 (B)	5.73 (B)
6[b]	H	Me	II	38.8 (C)	5.54 (C)
7[c,d]	Ph	Me	I	35.0 (B)	5.84 (B)
8[c,d]	Ph	Me	II	39.4 (C)	5.75 (C)
9[d]	NH·N:CHPh	Bz	I	51.7 (B)	4.08 (B)
10[d]	NH·N:CHPh	Bz	II	56.9 (C)	4.36 (C)
11[d]	N(Bz)·N=CHPh	Bz	I	52.6 (B)[h]	4.08 (B)[h]
12[d]	N(Bz)·N=CHPh	Bz	II	56.9 (C)[i]	4.34 (C)[i]
13[a]	N(Bz)·N=CHPh	H	—	—	4.64 (*exo*)
	Triazoles and Diazoles				
14[b]	4-Methyl-1,2,4 triazole			30.7 (A)	—[g]
15[b]	1-Methyl-1,2,4-triazole			36.0 (B)	—
16[b]	2-Methyl-1,2,3-triazole			41.5 (C)	—
17[b]	1-Methyl-1,2,3-triazole			35.7 (B)	—
18[b]	1-Methylimidazole			32.6 (A)	—
19[b,e]	1-Methylpyrazole			38.1 (B)	—

[a]Solvent DMSO.
[b]From ref. 10, solvent dioxane.
[c]From ref. 11.
[d]Solvent $CDCl_3$.
[e]See ref. 12.
[f]Solvent overlap.
[g]See ref. 1.
[h]*exo* CH_2, 51.5 ppm and 4.62τ.
[i]*exo* CH_2, 51.1 ppm and 4.62τ.

triazoles, and tetrazoles. Furthermore, for tetrazoles with 5-substituents, which caused reversal of the shielding order for 1-*N*-alkyl protons (compounds **9–12**, Table 1), the deshielding anisotropic influence of the 5-substituent did not reach the 1-alkyl carbon atom and the normal shift pattern was retained. These results suggest that proton *N*-alkyl shifts need to be viewed with some caution for assigning isomeric *N*-alkyl tetrazoles, particularly when the 5-substituent contains >C=N or >C=O groups, and that ^{13}C nmr shifts are more reliable.

Benzylations

The new tetrazole benzyl isomers were obtained by direct benzylation reactions. Benzylation of the ambident anion of benzaldehyde tetrazol-5-ylhydrazone with benzyl chloride was endocyclic and occurred at the 1- and 2-tetrazole positions in the ratio of *ca.* 3:1, respectively, giving compounds **9** and **10** (Table 1). Benzylations of the anions of these 1- and 2-monobenzyl derivatives of the hydrazone were exclusively exocyclic, occurring at the 6-*N*-position giving compounds **11** and **12**, respectively. Benzylation of the anion of 6-monobenzyl derivative **13** was also endocyclic and occurred at both the 1- and 2-tetrazole positions in the ratio of *ca.* 2.5:1, respectively. The structures of the monobenzylated isomers, **9, 10,** and **13** were established by unequivocal preparations. The structures of the dibenzyl isomers **11** and **12** were proved from independent preparations by further benzylation of each of the possible monobenzyl precursors. The benzylation patterns observed were, in general, similar to those previously reported (3–6) for alkylations of other 5-aminotetrazole systems.

Experimental

Infrared spectra were measured for KBr discs or mulls with Perkin-Elmer 377 and 457 spectrophotometers. Nuclear magnetic resonance spectra were measured with JEOL JNM-MH-100 and FX 60 FT spectrometers. Benzaldehyde tetrazol-5-ylhydrazone (7) and the other tetrazoles **1–4** (8) were prepared by the literature procedure. The compound **13** (mp 239°C) was obtained by stirring 5-benzylnitrosoaminotetrazole (9) with zinc dust in glacial acetic acid followed by addition of benzaldehyde in ethanol. *Anal.* calcd. for $C_{15}H_{14}N_6$: C 64.75, H 5.05, N 30.2; found: C 64.85, H 5.1, N 30.1.

Benzylation Reactions

Benzylation of Benzaldehyde Tetrazol-5-ylhydrazone

A solution of the hydrazone (18.8 g) in a mixture of 10% sodium hydroxide (40 ml), absolute alcohol (80 ml), and water (40 ml) was treated with benzyl chloride (12 ml) and heated under reflux for 6 h after which the alcohol was distilled off. The remaining aqueous solution containing a white solid mass was cooled overnight and the solid was removed, washed with water, and stirred for 1 h in 10% sodium hydroxide (40 ml). The alkali insoluble material (solid A) was removed and after acidification of the alkaline filtrate, starting hydrazone (7.8 g, 42%, mp 238°C) separated. The solid A was washed with water and stirred in cold chloroform (100 ml) when compound **9** (6.65 g, mp 204–206°C) remained undissolved. The chloroform filtrate was evaporated under reduced pressure and the semi-solid residue treated with acetone and chilled to −40°C to initiate precipitation. After equilibrating for 1 h at ambient temperatures, a further crop (0.25 g) of compound **9** separated (total yield, 6.9 g, 25%) mp 208°C (from glacial acetic acid). *Anal.* calcd. for $C_{15}H_{14}N_6$: C 64.75, H 5.05, N 30.2; found: C 64.65, H 5.05, N 30.2.

Evaporation of the acetone filtrate gave a gum which, when treated with absolute alcohol (100 ml) followed by cooling to −40°C, yielded the dibenzyl derivative **11** (6.4 g, 17.5%, mp 127°C after repeated recrystallizations from absolute alcohol). *Anal.* calcd. for $C_{22}H_{20}N_6$: C 71.7, H 5.45, N 22.8; found: C 71.75, H 5.5, N 23.15. The alcoholic filtrate after evaporation yielded the 2-benzylhydrazone **10** (2.08 g, 7.5%) which was washed with ether and after recrystallization from alcohol had mp 145°C. *Anal.* calcd. for $C_{15}H_{14}N_6$: C 64.75, H 5.05, N 30.2; found: C 65.05, H 5.15, N 30.6.

Benzylation of Benzaldehyde 1- and 2-Benzyltetrazol-5-ylhydrazones

A suspension of the hydrazone **9** (1.4 g) in a mixture of 10% sodium hydroxide (2 ml), absolute alcohol (4 ml), and water (2 ml) was treated with benzyl chloride (0.6 ml), heated under reflux for 4 h, and poured into ice cold water (100 ml). Compound **11** (1.56 g, 85%) separated. The mp was raised to 130°C by repeated recrystallizations from absolute alcohol and the compound was identical (mixture mp and ir spectra) with that obtained from the benzylation of benzaldehyde tetrazol-5-ylhydrazone above. *Anal.* calcd. as above; found: C 71.75, H 5.45, N 22.85.

A similar treatment of the 2-benzylhydrazone **10** gave compound **12** (88%), mp 150–151°C (from absolute alcohol). *Anal.* calcd. for $C_{22}H_{20}N_6$: C 71.7, H 5.45, N 22.8; found: C 71.5, H 5.5, N 23.05.

Benzylation of the benzaldehyde 6-benzyltetrazol-5-ylhydrazone, **13**, in the manner described gave compound **12** (16%) and compound **11**, (41%) along with a 30% recovery of compound **13**.

All of the compounds **9–13** showed two >C=N ir stretch bands at 1600 and 1640 cm^{-1}. The compounds **9** and **10** showed N—H stretch bands at 3260–3280 cm^{-1} which were absent in compounds **11** and **12**. The following ^1H and ^{13}C nmr signals (in $CDCl_2$) were also observed: **9**, 1.93τ, 145.4 ppm (CH=N); **10**, 2.04τ, 143.5 ppm (CH=N) and 165.8 ppm (tetrazole 5-C); **11**, 2.53τ, 140.0 ppm (CH=N) and 156.1 ppm (tetrazole 5-C); **12**, 2.30τ, 138.3 ppm (CH=N) and 168.6 ppm (tetrazole 5-C). Compounds **9**, **10**, and **13** were also prepared by unequivocal routes which we have developed previously (3, 9) for methyl isomers.

Acknowledgment

T.M.McE. and J.C.T. acknowledge State Grants for Research.

1. R. N. Butler. Can. J. Chem. **51**, 2315 (1973).
2. F. L. Scott, R. N. Butler, and J. Feeney. J. Chem. Soc. B, 919 (1967).
3. R. N. Butler and F. L. Scott. J. Org. Chem. **31**, 3182 (1966).
4. R. N. Butler. Leicester Chem. Rev. **10**, 12 (1969); Chem. Abstr. **73**, 55991m (1970).
5. F. L. Scott and J. C. Tobin. J. Chem. Soc. C, 703 (1971).
6. R. A. Henry and W. G. Finnegan. J. Am. Chem. Soc. **76**, 923 (1954).
7. F. L. Scott, W. N. Morrish, and J. Reilly. J. Org. Chem. **27**, 692 (1957).
8. R. N. Butler. Adv. Heterocycl. Chem. **21**, 323 (1977).
9. R. N. Butler, T. M. Lambe, J. C. Tobin, and F. L. Scott. J. Chem. Soc. Perkin Trans. I, 1357 (1973).
10. J. Elguero, C. Marzin, and J. D. Roberts. J. Org. Chem. **39**, 357 (1974).
11. M. Begtrup. Acta Chem. Scand. **27**, 3101 (1973).
12. R. G. Rees and M. J. Green. J. Chem. Soc. B, 387 (1968).

Ab initio calculations on 4-substituted benzoic acids; a further theoretical investigation into the nature of substituent effects in aromatic derivatives

PAUL G. MEZEY AND WILLIAM F. REYNOLDS

Department of Chemistry, University of Toronto, Toronto, Ont., Canada M5S 1A1

Received October 19, 1976

PAUL G. MEZEY and WILLIAM F. REYNOLDS. Can. J. Chem. **55**, 1567 (1977).

Ab initio (STO-3G) molecular orbital calculations for 4-substituted benzoic acids and XCH_3–HCO_2H pairs are used to derive a theoretical field, T_F, and resonance, $T_{R(BA)}$, substituent scale. Comparison with previous calculations for 4-substituted styrenes shows that a common field scale can be used for different systems but that different resonance scales are necessary, depending upon the electronic nature of the probe group. The field effect primarily reflects the direct electrostatic interaction between the substituent and the carboxylic acid. However, there are also significant contributions due to field-induced polarization of the intervening phenyl π electron system. By contrast, the π polarization effect seems to be the dominant field effect in the case of non-interacting probes (such as carbon atomic charges or chemical shifts). A very close parallel is noted between substituent effects upon atomic charges and acid dissociation energies.

PAUL G. MEZEY et WILLIAM F. REYNOLDS. Can. J. Chem. **55**, 1567 (1977).

Des calculs *ab initio* d'orbitales moléculaires (STO-3G) sur des acides benzoïques substitués en position 4 et sur des paires XCH_3–HCO_2H sont utilisés pour établir une échelle théorique pour les substituants impliquants deux paramètres soit T_F et $T_{R(BA)}$. Une comparaison avec des calculs antérieurs, sur des styrènes substitués en position 4, montre qu'une échelle de champ commune peut être utilisée pour différents systèmes mais que différentes échelles de résonance sont nécessaires suivant la nature électronique du groupe examiné. L'effet de champ est premièrement un reflet de l'interaction électrostatique directe entre le substituant et l'acide carboxylique. Toutefois il y a aussi des contributions importantes qui sont dues à la polarisation induite par le champ du système d'électrons π du groupement phényle impliqué. Par opposition, l'effet de polarisation π semble être l'effet de champ le plus important dans le cas de groupements qui n'interagissent pas (telles que les charges atomiques du carbone ou les déplacements chimiques). On note un parallélisme très important entre les effets des substituants sur les charges atomiques et les énergies de dissociation des acides.

[Traduit par le journal]

Introduction

In a previous paper (1), we have shown that *ab initio* (STO-3G minimal basis set) calculations of atomic charges in 4-substituted styrenes can be used to derive a theoretical dual (field and resonance) substituent parameter scale, T_F and T_R^0, which closely parallels the σ_I,σ_R^0 scale of Taft and co-workers (2) and the *F*,*R* scale of Swain and Lupton (3). While both *F* and σ_I are claimed to be applicable to all aromatic derivatives, there is a significant difference between the two resonance scales. While the *R* parameter scale is claimed to also be applicable to all aromatic systems (3), Taft has concluded that different resonance scales are necessary, depending upon the electronic nature of the probe group (2). In addition, the relationship between substituent effects upon atomic charges and upon energy effects is not entirely clear. Both the original Hammett σ scale (4) and the *F*,*R* scale (3) were based upon energy changes. While the σ_I,σ_R^0 scale is based partially on ^{19}F chemical shifts (2) and while numerous correlations of ^1H, ^{13}C, and ^{19}F chemical shifts (5–7) and atomic charges (7) with substituent parameters have been reported, there is not always a direct parallel between energy changes and changes in atomic charges (8). Consequently, it was decided to carry out a theoretical investigation of substituent effects on energy changes in aromatic compounds, both to check the universality of field and resonance substituent scales and to check the relationship between substituent effects upon energies and upon atomic charges. In addition, it was hoped that the calculations would provide further insight into the mechanisms of transmission of polar substituent effects. The system chosen was a series of 4-substituted benzoic acids. Energy changes were calculated for the isodesmic (9) reaction [1]. Defined in this

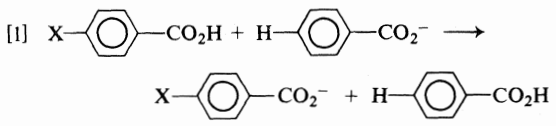

manner, the energy change, $\Delta E_{BA}{}^0$, for [1] measures the effect of the substituent upon the acid dissociation energy. This system was chosen because it is the original system chosen to define the Hammett equation (4) and because experimental energies are available for [1] in the gas phase (10), allowing a check of the accuracy of the calculations.

Results and Discussion

Energy changes associated with [1] are tabulated in Table 1. Calculations were performed for planar and pyramidal NH_2 groups, OH, CHO, CH_3, F, CF_3, CN, and NO_2. These correspond to the minimal substituent set of Taft (2) with planar NH_2, OH, and CHO substituting for $N(CH_3)_2$, OCH_3, and $COCH_3$ for reasons of computational economy. Calculated energies for several substituents are compared with experimental energies for [1] in the gas phase (1) in Table 1. There is a close parallel between experimental (10) and calculated energies for [1]. Although the two sets of energies are not strictly comparable (since the calculations correspond to the hypothetical vibrationless state at 0 K), the close parallel lends confidence to the accuracy of the calculations.

By contrast with styrene (1), there is no obvious way to separate and isolate field and resonance effects upon the ionization energies of benzoic acid derivatives. Experimentally, field effects on acid dissociation constants have been estimated for 4-substituted bicyclo[2.2.2]octane-1-carboxylic acids (3, 11, 12). While these compounds could also be investigated theoretically, basically the same information can be obtained at much lower computational cost by carrying out calculations for ionization energies of CH_3X–HCO_2H pairs with the C—X bond and the CO_2H group in the same relative orientation as in benzoic acid (Fig. 1). These calculations should estimate the through-space field effect of the substituent while eliminating resonance effects and other through-bond effects.

TABLE 1. Comparison of experimental and calculated energies, ΔE_{BA} for [1] (in kcal/mol)

Substituent	Calculated energy	Experimental energy[a]
NH_2(pl)[d]	+5.14[b]	—
NH_2(py)[e]	+3.10	+2.3
OH	+0.60	+0.75[c]
CH_3	+1.10	+1.05
F	−1.51	−2.9
CHO	−4.53	—
CF_3	−5.26	—
CN	−9.87	−10.3
NO_2	−13.55	−11.1

[a]From ref. 10.
[b]Positive sign indicates weaker acidity.
[c]Experimental value for OCH_3 derivative (10). In OH derivatives the proton transfer [1] involves phenolic hydrogen.
[d]Planar NH_2 group.
[e]Pyramidal NH_2 group.

The calculated energies, $\Delta E_{IM}{}^0$ (where IM refers to isolated molecules, *i.e.* CH_3X–HCO_2H pairs) are summarized in Table 2. These calculated energies are directly proportional to the theoretical field substituent parameter scale, $T_F(q)$ derived from the differences in β hydrogen atomic charges in 4-substituted styrenes (1):

$$[2] \quad T_F(q) = -0.139\Delta E_{IM}{}^0 \quad (r = 0.9979)$$

The slope from [2] can be used to convert $\Delta E_{IM}{}^0$ to a field substituent parameter scale based upon energies, $T_F(E)$ (see Table 2).

It is seen that there is nearly perfect agreement between the theoretical field effect parameters, T_F, estimated from the ionization energies for CH_3X–HCO_2H pairs and from atomic charges from 4-substituted styrenes. There is also good agreement with σ_I although field effects are overestimated for CN and NO_2 (possible reasons for these deviations have been discussed previously (1)).[1] Two important conclusions follow from these observations. Firstly, the data for these two systems indicate that field substituent parameters are essentially identical for different systems, in agreement with the assumptions of both Taft and co-workers (2) and Swain and Lupton (3). Secondly, the results indicate that, at least in these systems, the same field substituent parameter can be used to investigate substituent effects upon charge densities and upon dissociation energies.

Unfortunately, the field contributions to ionization energies of CH_3X–HCO_2H pairs cannot be directly subtracted from the ionization energies for the corresponding benzoic acids to obtain resonance contributions to the latter

[1]Taft and co-workers have calculated proton affinities for β-substituted ethylamines (13). The proton affinities correlate reasonably well with σ_I but the effect of CN and particularly NO_2 also appear overestimated in this system.

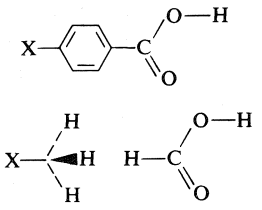

FIG. 1. Geometries for 4-substituted benzoic acids and XCH_3–HCO_2H pairs.

TABLE 2. Substituent effect upon acid dissociation energy for XCH_3–HCO_2H pairs, ΔE_{IM}, and theoretical parameters based upon ΔE_{IM}, and atomic charges for 4-substituted styrenes

Substituent	$\Delta E_{IM}{}^0$ (kcal/mol)	$T_F(E)^a$	$T_F(q)^b$	$\sigma_I{}^c$
NH_2(pl)	+0.16	−0.02	−0.01	+0.06
NH_2(py)	−0.40	+0.06	+0.07	+0.12
OH	−1.72	+0.24	+0.27	+0.27
CH_3	+0.08	−0.01	−0.04	−0.04
F	−2.52	+0.35	+0.38	+0.50
CHO	−2.04	+0.28	+0.25	+0.30
CF_3	−2.82	+0.39	+0.39	+0.45
CN	−5.36	+0.75	+0.72	+0.56
NO_2	−7.53	+1.05	+1.06	+0.65

[a] T_F values derived by multiplying $\Delta E_{IM}{}^0$ by −0.139, the slope from the correlation of $T_F(q)$ with $\Delta E_{IM}{}^0$ (see [2]).
[b] T_F values based on atomic charges (1). Values derived by scaling β hydrogen atomic charge difference for 4-hydroxystyrene to 0.27, the experimental σ_I value for OH (2). Values differ slightly from those in ref. 1 due to C—O bond length optimization for the OH derivative (see Experimental).
[c] From ref. 2.

ionization energies. The reason that this cannot be done is the dependence of the magnitude of the field effect upon the effective dielectric constant of the intervening medium (14, 15). Previous theoretical investigations for similar molecules in the gas phase suggest that the field effect should be enhanced due to transmission through the phenyl group (1, 15, 16).

Since it is difficult to predict the magnitude of the field enhancement factor, an alternative approach to separating field and resonance contributions was attempted. Since there is a direct relationship between T_F values based upon atomic charges and acid dissociation energies, it was felt that a similar relationship might exist for resonance effects. It has previously been shown that there is a good linear relationship between $\sigma_R{}^0$ and $\sum q_c\pi$ (the substituent induced change in carbon π electron density) for substituted benzenes (7, 17) and styrenes (1, 18). In the case of benzoic acid derivatives, there is a different substituent-induced change in π electron density for the neutral compound, $\sum q_\pi n$, and the benzoate anion, $\sum q_\pi{}^-$ (see Table 3). Previous experimental data for benzoic acid dissociation constants in solution indicate that the resonance effect of a substituent upon acidity is mainly determined by resonance interactions in the neutral molecule (19). Consequently, it was anticipated that $\sum q_\pi n$ would provide the appropriate measure of the resonance effect on the ionization energy. However, to check this point, dual substituent parameter correlations were performed for $\Delta E_{BA}{}^0$ *vs.* $\Delta E_{IM}{}^0$ plus $\sum q_\pi n$ and $\Delta E_{BA}{}^0$ *vs.* $\Delta E_{IM}{}^0 + \sum q_\pi{}^-$, to see which parameter gave the better fit (this is the technique recommended by Taft and co-workers to determine which σ_R scale is best suited to a particular experimental system (2)).

The correlations were:

$$[3]\quad \Delta E_{BA} = 1.714\Delta E_{IM} - 37.36\sum q_\pi n \qquad (r = 0.9998)\quad \text{s.d.} = 0.12 \text{ kcal/mol}$$

$$[4]\quad \Delta E_{BA} = 1.68\Delta E_{IM} - 39.4\sum q_\pi{}^- \qquad (r = 0.9974)\quad \text{s.d.} = 0.66 \text{ kcal/mol}$$

While both correlations are very good, there is a clear discrimination in favour of the correlation with $\sum q_\pi n$, as anticipated (the discrimination is particularly apparent in the standard deviations).

Several conclusions can be drawn from these correlations. First, the existence of a precise correlation such as [3] provides strong support for the basic concept of separating substituent effects into field and resonance components. Second, [3] indicates that there is a very substantial enhancement of the polar effect of the substituent (71%) in benzoic acid, relative to the CH_3X–HCO_2H pairs. The significance of this large enhancement factor is discussed below. Equation 3 also indicates a very close relationship between resonance effects upon acid dissociation energies and upon atomic charges (since a resonance parameter based upon π electron density changes quantitatively predicts acid dissociation energies). Assuming that the very minor deviations in the correlation arise because this relationship is not perfect, this equation can be recast to estimate resonance contributions to acid dissociation energies, $\Delta E_{res}{}^0$:

$$[5]\quad \Delta E_{res}{}^0 = \Delta E_{BA}{}^0 - \Delta E_{field}{}^0 = \Delta E_{BA}{}^0 - 1.714\Delta E_{IM}{}^0$$

These values are also given in Table 3.

In the case of 4-substituted styrenes, $\sum q_\pi$ was used to derive a theoretical resonance parameter,

TABLE 3. Substituent-induced changes in total π electron density for neutral and anionic benzoic acid and comparison of theoretical resonance (π charge transfer) substituent constants for styrene and benzoic acid

Substituent	$\Sigma q_\pi n^a$	$\Sigma q_\pi{}^{-b}$	$\Delta E_{res}{}^{0c}$	$T_{R(BA)}q^d$	$T_{R(BA)}E^e$	$\sigma_{R(BA)}{}^f$	$\Sigma q_\pi c^g$	$T_R{}^{0h}$	$\sigma_R{}^{0f}$
NH_2(pl)	−1269	−962	+4.87	−0.80	−0.84	−0.83	−1202	−0.58	−0.52
NH_2(py)	−982	−734	+3.79	−0.62	−0.65	−0.82	−930	−0.46	−0.48
OH	−966	−764	+3.55	−0.61	−0.61	−0.61	−922	−0.45	−0.45
F	−823	−682	+2.81	−0.52	−0.48	−0.45	−787	−0.38	−0.34
CH_3	−97	−30	+0.96	−0.06	−0.16	−0.11	−82	−0.04	−0.11
CHO	+268	+556	−1.04	+0.17	+0.18	+0.16	+331	+0.16	+0.16
CF_3	+102	+178	−0.42	+0.06	+0.07	+0.08	+120	+0.06	+0.08
CN	+201	+446	−0.67	+0.13	+0.12	+0.13	+257	+0.13	+0.13
NO_2	+190	+387	−0.64	+0.12	+0.11	+0.15	+234	+0.12	+0.15

[a]Substituent induced change in total π electron density for entire π electron system of neutral benzoic acid (×10⁴). Negative sign indicates increased electron density.
[b]Change in total π electron density for benzoate anion (×10⁴).
[c]Resonance contribution to substituent-induced change in acid dissociation energy as given by [5] (in kcal/mol).
[d]$T_{R(BA)}q$ scale based upon $\Sigma q_\pi n$ with $T_{R(BA)}$ for OH taken as −0.61 (see text).
[e]$T_{R(BA)}E$ scale based upon $\Delta E_{res}{}^0$ with $T_{R(BA)}$ for OH taken as −0.61 (see text).
[f]From ref. 2.
[g]Substituent-induced change in total π electron density for styrene (×10⁴) (1). First three entries are different than those in ref. 1 due to C—X bond length optimization (see Experimental).
[h]$T_R{}^0$ scale based upon $\Sigma q_\pi c$ with $\Sigma q_\pi c$ for the OH derivative scaled to −0.45, the $\sigma_R{}^0$ value for OCH_3 (2). Values differ slightly from ref. 1 due to change in $\Sigma q_\pi c$ for OH derivative (see footnote *g*).

$T_R{}^0$, which is analogous to the experimental $\sigma_R{}^0$ scale for aromatic molecules containing neutral probe groups (2). This was done by scaling Σq_π for OH (-922×10^4)[2] to $\sigma_R{}^0$ for OCH_3 (−0.45). A similar theoretical resonance scale, $T_{R(BA)}$, for benzoic acid can be derived by scaling either $\Sigma q_\pi n$ or $\Delta E_{res}{}^0$ for the OH group to −0.61, the experimental $\sigma_{R(BA)}$ value for OCH_3 (2). These $T_{R(BA)}$ scales can then be compared with $\sigma_{R(BA)}$ (2).

These comparisons are presented in Table 3, along with $\sigma_R{}^0$ and $T_R{}^0$ scales. A comparison of $T_{R(BA)}$ and $T_R{}^0$ scales indicates that the former scale predicts enhanced effects of π donor groups (*e.g.* NH_2), relative to π acceptor groups, in agreement with $\sigma_{R(BA)}$ relative to $\sigma_R{}^0$ (2). Thus our results indicate that resonance parameters depend upon the nature of the probe groups while field parameters do not. This supports the fundamental model of dual substituent parameters proposed by Taft and co-workers (2) but is contradictory to the assumption of Swain and Lupton that there is a universal resonance parameter (3). In general there is a close parallel between $\sigma_R{}^0$ and $T_R{}^0$ and between $\sigma_{R(BA)}$ and $T_{R(BA)}$. The major deviation is for pyramidal NH_2 in the $T_{R(BA)}$ scale. This deviation may be in part due to the use of fixed substituent geometries. Other calculations indicate that the amino group becomes more nearly planar when electron-withdrawing groups are substituted in the *para* position of aniline (20); this would increase the magnitude of $T_{R(BA)}$ for this group to a value closer to that for planar NH_2.

The most striking feature of the results in both Tables 2 and 3 is the very close parallel between substituent parameters based upon energies and upon atomic charges. This provides further justification for the use of chemical shifts in substituent parameter correlations (in cases where substituent-induced chemical shift changes parallel changes in ground state atomic charges),[3] even though σ constants were originally defined from energy changes (4). However, one cautionary note is necessary. Although [3] indicates a quite precise relationship between energy changes and π electron density changes, preliminary results of calculations to estimate the relative ability of substituents to stabilize benzoic acid and benzoate anions suggest that the origins of this apparently simple relationship may be quite complex.[4]

The calculations also provide further insights into the nature of transmission of polar substituent effects. The $\sigma_{R(BA)}$ scale is defined so that

[2]The value of Σq_π for OH is different than that previously reported (1), due to optimization of the C—O bond length in the styrene derivative (see Experimental). This results in a change in the $T_R{}^0$ scale from that previously reported (1).

[3]For a detailed discussion of the origins and limitations of chemical shift – charge density correlations in aromatic derivatives, see ref. 21. We have previously suggested that substituent-induced ^{13}C and ^1H chemical shifts can be used to monitor changes in ground state atomic charges in aromatic derivatives provided that a large number of substituents are included and provided that the substituent is at least three bonds removed from the probe nucleus (22–24).

[4]W. F. Reynolds and P. G. Mezey, work in progress.

polar and resonance contributions to acid dissociation energies are equal for benzoic acid derivatives in H_2O (2):

$$[6]\quad \Delta G_{BA}{}^0 = -1.36\sigma_I - 1.36\sigma_{R(BA)} \qquad (\rho_R/\rho_I = 1.00)$$

When [2] is redefined in terms of T_F and $T_{R(BA)}$ it is seen that while both field and resonance effects are enhanced in the gas phase relative to aqueous solutions, the enhancement is greater for field effects:

$$[7]\quad \Delta E_{BA}{}^0 = -12.3T_F - 5.9T_{R(BA)} \qquad (\rho_R/\rho_I = 0.48)$$

A similar result is obtained when gas phase ionization energies (10) are correlated with σ_I and $\sigma_{R(BA)}$.[5]

$$[8]\quad \Delta G_{BA}{}^0 = -14.1\sigma_I - 7.2\sigma_{R(BA)} \qquad (\rho_R/\rho_I = 0.51)$$

There are several previous reports of solvation decreasing substituent effects by up to a factor of ten (10, 25, 26). The relatively greater decrease for polar effects on going from the gas phase to solution may partly reflect specific solvation of the polar substituents. Solvation of the CO_2^- group should also decrease the field effect since this effect is mainly due to electrostatic interactions of the substituent with CO_2^- (see below). However, another factor may be involved. The calculations of Hermann show that the field effect of a substituent is enhanced when transmitted through a dielectric sphere surrounded by a vacuum (15) (as confirmed by [2]). However, according to the Kirkwood–Westheimer model (14), the field effect is decreased when the surrounding medium is of higher dielectric constant than the sphere. The gas phase measurements and measurements in H_2O should respectively correspond to the former and latter cases. Thus there should be a less effective transmission of field effects in solution than in the gas phase. Finally, the smaller decrease in resonance effects may partly

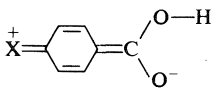

1

be due to solvent enhancement of donor–acceptor interactions as in **1**. This type of interaction should be favoured in polar solvents since it involves an increase in dipole moment. It has previously been suggested that this is an important interaction in solution (19, 27) but probably not in the gas phase (10).

It is also instructive to consider the relative importance of field effects on benzoic acid derivatives and upon charge densities in aromatic derivatives. There are structural similarities between benzoic acid and styrene derivatives:

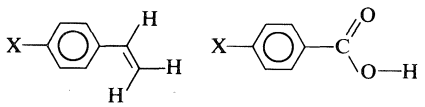

The correlation of $q_{C(\beta)}\pi$, the β carbon charge density of styrene (1) with T_F and $T_R{}^0$ reveals

$$[9]\quad q_{C(\beta)}\pi = +0.023T_F + 0.035T_R{}^0 \qquad (\rho_R/\rho_I = 1.53)$$

A similar result is obtained if the ^{13}C chemical shifts for C(β) of styrene derivatives (measured in an inert solvent (18)) are correlated with σ_I and $\sigma_R{}^0$:

$$[10]\quad \delta_C(\beta) = 5.09\sigma_I + 8.33\sigma_R{}^0 \quad (\rho_R/\rho_I = 1.64)$$

It is seen that, in relative terms, there is a much greater field dependence on the dissociation energy for benzoic acid in the gas phase than on the C(β) π electron density (and chemical shift) for styrene (comparing [7] and [8] with [9] and [10]). This reflects a fundamental difference in the transmission of field effects in the two systems. In benzoic acid, the energy change is primarily a result of a direct electrostatic interaction between the polar substituent and a changing probe group (28). In styrene (and other aromatic systems) one is dealing with a non-interacting probe (carbon atomic charges or chemical shift). In these systems, the main mechanism of transmission of polar substituent effects is believed to be a charge redistribution of the π electron system (without π charge transfer to or from the substituent), *i.e.* a π inductive effect (29, 30).[6] A

[5]The experimental measurements are based upon equilibrium constants and therefore represent free energy changes while the calculations reflect internal energy changes. However, the gas phase results should be comparable since entropy changes are generally very small for gas phase proton transfer reactions (10). The solution values are also comparable if one makes the usual assumption of a linear free energy relationship (4). The negative signs in [6]–[8] result because the equations are expressed in energy changes rather than in terms of log *K*.

[6]Similar observations concerning the different mechanisms of transmission of polar effects in these two cases have been made by Fukunaga and Taft (31).

particularly important mechanism is polarization of the π electron system due to the electric field of the substituent (22, 24, 32–34). Until recently, this was regarded as a relatively unimportant mechanism of transmission of polar substituent effects in aromatic derivatives (29). The main reason was that most earlier investigations involved acid dissociation constants (where direct electrostatic interactions dominate (14, 15, 28)) or infrared measurements (where resonance effects dominate (35)). It was only with the advent of ^{13}C nmr spectroscopy, where (in appropriate cases) the chemical shifts can be used to monitor charge density changes at each carbon, that evidence for significant π polarization effects in aromatic derivatives was obtained (15).

Although direct electrostatic effects undoubtedly dominate, π inductive effects should also contribute to the field dependence of benzoic acid dissociation energies. The latter effect should contribute in the same way as resonance effects. In particular, π polarization of the intervening phenyl groups may account for part of the calculated enhanced field dependence for benzoic acid relative to XCH_3–HCO_2H. Since the direct field effect depends upon the distance of the ionizable proton from the substituent (28), the difference in dissociation energies ($\Delta\Delta E_{IM}^0$) for *syn* and *anti* conformations of formic acid (see Fig. 2) should also be directly proportional to the field effect. Similarly $\Delta\Delta E_{BA}^0$ for benzoic acid should also be directly proportional to the direct field effect in this system since through-bond effects should affect both conformations equally. (This is precisely analogous to the estimation of direct field effects in styrenes from the β vinyl proton charge density difference (1)). Values for $\Delta\Delta E_{IM}^0$ are given in Table 4. Correlation of $\Delta\Delta E_{IM}^0$ *vs.* ΔE_{IM}^0 for the *anti* conformation of the proton shows the expected parallel:

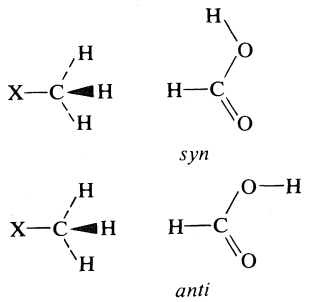

FIG. 2. The *syn* and *anti* conformations for formic acid.

[11] $\Delta E_{IM}^0(anti) = 17.9\Delta\Delta E_{IM}^0 \quad (r = 0.998)$

In the case of benzoic acid, calculations were only performed for the highly polar CN and NO_2 derivatives due to cost limitations. Comparing $\Delta\Delta E_{BA}^0$ and $\Delta\Delta E_{IM}^0$ for these two derivatives indicates an average 47% enhancement of the direct field effect in the former system (a very similar direct field enhancement factor was estimated in the case of styrene (1)). Since the total enhancement is 71%, (see [3]), approximately one third of this enhancement must be due to polarization of the phenyl group, suggesting a small but significant π polarization effect on benzoic acid dissociation energies.

One surprising feature is the very small magnitude of $\Delta\Delta E_{IM}^0$. As first pointed out by Bjerrum (28)), the substituent effect upon an acid dissociation energy can be estimated from the energy required to remove the proton from the vicinity of a dipolar substituent:

[12] $$\Delta E^0 = \frac{e\mu \cos\theta}{r^2}$$

where the parameters are as shown below:

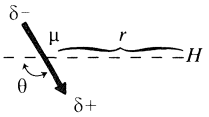

2

(The Kirkwood–Westheimer modification of [11] includes a term on the bottom for the effective dielectric constant, D_E, of the cavity (14). However, this term should be unnecessary for CH_3X–HCO_2H pairs.

This equation predicts larger ΔE_{IM}^0 values for the *syn* conformation than for the *anti* conformation of the OH bond, due to the closer proximity of the *syn* hydrogen. However, the values for $\Delta\Delta E_{IM}$ from [11] are much larger than those from the STO-3G calculations while the individual values are smaller. (Table 5 shows typical values for the cyano derivative.) It appears that these discrepancies occur because the Bjerrum model is a gross oversimplification. The protonation of the acid function induces considerable charge redistribution within this group. In fact, far better agreement is obtained with the results of the STO-3G calculations if one calculates the energy of interaction of the CN dipole with the entire atomic charge distribution for neutral formic acid and for the formate anion (Table 5).

TABLE 4. Comparison of substituent-induced changes in acid dissociation energies for *syn* and *anti* OH conformations in XCH_3–HCO_2H pairs and for two derivatives of benzoic acid

Substituent	$\Delta E_{IM}^0(syn)$	$\Delta E_{IM}^0(anti)$	$\Delta\Delta E_{IM}^{0\,b}$	$\Delta\Delta E_{BA}^{0\,b}$	$\Delta\Delta E_{BA}^0/\Delta\Delta E_{IM}^0$
NH_2(pl)	+0.17[a]	+0.16	+0.01	—	—
NH_2(py)	−0.42	−0.40	−0.02	—	—
OH	−1.80	−1.72	−0.08	—	—
CH_3	+0.09	+0.08	+0.01	—	—
F	−2.65	−2.52	−0.13	—	—
CHO	−2.14	−2.03	−0.11	—	—
CF_3	−2.99	−2.82	−0.17	—	—
CN	−5.66	−5.36	−0.30	−0.43	1.42
NO_2	−7.94	−7.53	−0.41	−0.63	1.52

[a]In kcal/mol. Positive sign indicates weaker acid.
[b]$\Delta\Delta E^0 = \Delta E^0(syn) - \Delta E^0(anti)$.

TABLE 5. Comparison of substituent-induced changes in acid dissociation energies for *syn* and *anti* OH conformations of CH_3CN–HCO_2H pairs as estimated by STO-3G calculations and from the Bjerrum equation (26)

Calculation	$\Delta E_{IM}(syn)$	$\Delta E_{IM}(anti)$	$\Delta\Delta E_{IM}^b$
STO-3G	−5.66[a]	−5.36	−0.30
[12][c]	−4.42	−3.29	−1.15
[12] using complete formic acid charge distribution[d]	−5.06	−4.88	−0.18

[a]In kcal/mol (negative sign indicates stronger acid).
[b]$\Delta\Delta E_{IM}^0 = \Delta E_{IM}^0(syn) - \Delta E_{IM}^0(anti)$.
[c]Energy required to remove a unit positive charge from the vicinity of the C≡N dipole (μ = 3.09 D (1)). The dipole was considered to be located at the mid-point of the C≡N bond while the unit positive charge was located respectively at the position of the syn and anti protons.
[d]Energy of interaction of C≡N dipole with atomic charge distribution for formate anion minus energy of interaction with atomic charge distribution of formic acid. Atomic charge distributions taken from STO-3G calculations for CH_3CN–HCO_2H pairs.

The calculations also suggest that the major interaction of the substituent dipole is with the anion; the CN group stabilizes the anion (−4.50 kcal/mol) while slightly destabilizing neutral formic acid (respectively, +0.38 kcal/mol and +0.56 kcal/mol for *anti* and *syn* conformations).

The dipolar field effect of the substituent also alters the electron distribution within the probe group (1). However, it appears that this makes a negligible contribution to the acid dissociation energy of CH_3X–HCO_2H pairs. For example, if one performs the same calculation as in line 3 of Table 5 but uses the atomic charges calculated for isolated HCO_2H and HCO_2^- rather than those obtained from CH_3CN–HCO_2H and CH_3CN–HCO_2^-, the calculated acid dissociation energies are changed by only 0.03 kcal/mol. Thus, although there is a very close parallel between field effects upon atomic charges and upon acid dissociation energies (Table 2), this does not appear to be a cause–effect relationship. Rather the parallel changes in the two parameters occur because field effects upon both atomic charges (36, 37) and acid dissociation energies (28) both depend directly upon the substituent dipole moment. Davis and Shirley have recently concluded that substituent-induced changes in atomic charges play an important role in determining the proton affinities of methanol derivatives (38). However, the latter involve close range interactions where inductive effects may dominate over field effects (1). Thus their conclusions and ours are probably not contradictory.

In summary, calculated acid dissociation energies for 4-substituted benzoic acids and for XCH_3–HCO_2H pairs have been used to derive a theoretical dual substituent parameter scale which is in good agreement with the σ_I,$\sigma_{R(BA)}$ scale of Taft. The results of this and a previous investigation show that the same field substituent parameter scale can be used for different systems, but different resonance parameters are necessary for different systems, in agreement with the proposals of Taft (2). The results also confirm that identical substituent parameter scales can be used for acid dissociation energies and atomic charges (or chemical shifts where these parallel atomic charges). The field effect of a substituent upon the acid dissociation energy of an aromatic acid primarily reflects electrostatic interactions between the substituent and the CO_2^- group, but field induced polarization of the intervening π electron system also contributes. Finally, the results support the basic concept of the separability of field and resonance substituent effects in aromatic derivatives.

Details of Calculations

Throughout this study an STO-3G basis set as contracted to a minimal basis (39) was used in

calculations. All *ab initio* SCF MO calculations were carried out on an IBM370/165 computer using a version of the Gaussian 70 program (40).

Standard bond lengths were assumed for benzoic acid and the benzoate anion (41) with all bond angles of 120°. Fixed substituent geometries were assumed for most substituents (42). In the case of strongly conjugating groups (planar and pyramidal NH_2 and OH), energy minimization calculations were performed for 4-substituted styrene derivatives, optimizing the C—X bond length only. Optimum bond lengths were 1.406 Å for planar NH_2, 1.428 Å for pyramidal NH_2, and 1.389 Å for OH, compared to values of 1.40 Å, 1.43 Å, and 1.36 Å used previously (1). Energy optimization calculations for the OH derivative of benzoic acid gave a C—O bond length change of less than 0.003 Å from the corresponding styrene derivatives. Consequently the optimized styrene substituent bond lengths were used for the benzoic acid calculations.

Acknowledgments

Financial support from the National Research Council of Canada is gratefully acknowledged (W.F.R.). We thank Professor R. W. Taft and R. D. Topsom for supplying copies of manuscripts prior to publication.

1. W. F. Reynolds, P. G. Mezey, and G. K. Hamer. Can. J. Chem. **55**, 522 (1977).
2. R. T. C. Brownlee, S. Ehrenson, and R. W. Taft. Prog. Phys. Org. Chem. **10**, 1 (1973).
3. C. G. Swain and E. P. Lupton. J. Am. Chem. Soc. **90**, 4328 (1968).
4. L. P. Hammett. Chem. Rev. **17**, 125 (1935).
5. W. T. Raynes. *In* The Chemical Society Specialist Reports on Nuclear Magnetic Resonance. Vols. 1–3. London. 1972–1974.
6. M. T. Tribble and J. G. Traynham. *In* Advances in linear free energy relationships. *Edited by* N. B. Chapman and J. Shorter. Plenum Press, New York, NY. 1972.
7. W. J. Hehre, R. W. Taft, and R. D. Topsom. Prog. Phys. Org. Chem. In press.
8. J. F. Wolf, P. G. Haren, R. W. Taft, and W. J. Hehre. J. Am. Chem. Soc. **97**, 2902 (1975).
9. W. J. Hehre, R. Ditchfield, L. Radom, and J. A. Pople. J. Am. Chem. Soc. **92**, 4796 (1970).
10. R. Yamdagni, T. B. McMahon, and P. Kebarle. J. Am. Chem. Soc. **96**, 4035 (1974).
11. J. D. Roberts and W. T. Moreland. J. Am. Chem. Soc. **75**, 2167 (1953).
12. H. D. Holtz and L. M. Stock. J. Am. Chem. Soc. **86**, 5188 (1964).
13. M. Taagepera, W. J. Hehre, R. D. Topsom, and R. W. Taft. J. Am. Chem. Soc. **98**, 7438 (1976).
14. (*a*) J. G. Kirkwood and F. H. Westheimer. J. Chem. Phys. **6**, 506 (1938); (*b*) F. H. Westheimer and J. G. Kirkwood. J. Chem. Phys. **6**, 513 (1938).
15. R. B. Hermann. J. Am. Chem. Soc. **91**, 3152 (1969).
16. G. K. Hamer, I. R. Peat, and W. F. Reynolds. Can. J. Chem. **51**, 915 (1973).
17. R. T. C. Brownlee and R. W. Taft. J. Am. Chem. Soc. **92**, 7007 (1970).
18. G. K. Hamer, I. R. Peat, and W. F. Reynolds. Can. J. Chem. **51**, 897 (1973).
19. R. W. Taft. J. Phys. Chem. **64**, 1805 (1960).
20. W. J. Hehre, L. Radom, and J. A. Pople. J. Chem. Soc. Chem. Commun. 669 (1972).
21. D. G. Farnum. Adv. Phys. Org. Chem. **11**, 123 (1975).
22. W. F. Reynolds, I. R. Peat, M. H. Freedman, and J. R. Lyerla. Can. J. Chem. **51**, 1857 (1973).
23. D. A. Dawson and W. F. Reynolds. Can. J. Chem. **52**, 39 (1974).
24. D. A. Dawson and W. F. Reynolds. Can. J. Chem. **53**, 373 (1975).
25. R. W. Taft. *In* Proton transfer reactions. *Edited by* E. F. Caldin and V. Gold. Chapman and Hall, London. 1975.
26. J. M. McKelvey, S. Alexandratos, A. Streitwieser, J-L. M. Abboud, and W. J. Hehre. J. Am. Chem. Soc. **98**, 244 (1976).
27. H. Van Bekkum, P. E. Verkade, and B. M. Wepster. Recl. Trav. Chim. Pays-Bas, **78**, 815 (1959).
28. N. Bjerrum. Z. Phys. Chem. **106**, 219 (1923).
29. A. R. Katritzky and R. D. Topsom. J. Chem. Educ. **49**, 400 (1972).
30. R. D. Topsom. Prog. Phys. Org. Chem. **12**, 1 (1976).
31. J. Fukunaga and R. W. Taft. J. Am. Chem. Soc. **97**, 1612 (1975).
32. W. F. Reynolds and G. K. Hamer. J. Am. Chem. Soc. **98**, 7296 (1976).
33. W. Adcock, B. D. Gupta, and W. Kitching. J. Org. Chem. **41**, 1498 (1976).
34. R. T. C. Brownlee, G. Butt, M. P. Chan, and R. D. Topsom. J. Chem. Soc. Perkin Trans. II, 1486 (1976).
35. A. R. Katritzky and R. D. Topsom. *In* Linear free energy relationships. *Edited by* N. B. Chapman and J. Shorter. Plenum Press, New York, NY. 1972.
36. A. D. Buckingham. Can. J. Chem. **38**, 300 (1960).
37. G. K. Hamer and W. F. Reynolds. J. Chem. Soc. Chem. Commun. 1218 (1971).
38. D. W. Davis and D. A. Shirley. J. Am. Chem. Soc. **98**, 7898 (1976).
39. W. J. Hehre, R. F. Stewart, and J. A. Pople. J. Chem. Phys. **51**, 2657 (1969).
40. W. J. Hehre, W. A. Lathan, R. Ditchfield, M. A. Newton, and J. A. Pople. Gaussian 70, Quantum Chemistry Program Exchange, Indiana University, Bloomington, IN.
41. J. A. Pople and M. Gordon. J. Am. Chem. Soc. **89**, 4253 (1967).
42. G. K. Hamer. Ph.D. Thesis, University of Toronto, Toronto, Ont. 1973.

Chemical constituents of the physodes of brown algae. Characterization by ^{1}H and ^{13}C nuclear magnetic resonance spectroscopy of oligomers of phloroglucinol from *Fucus vesiculosus* (L.)[1]

JAMES S. CRAIGIE, A. GAVIN MCINNES, MARK A. RAGAN,[2] AND JOHN A. WALTER

Atlantic Regional Laboratory, National Research Council of Canada, Halifax, N.S., Canada B3H 3Z1

Received December 22, 1976

JAMES S. CRAIGIE, A. GAVIN MCINNES, MARK A. RAGAN, and JOHN A. WALTER. Can. J. Chem. **55**, 1575 (1977).

Alcoholic extracts of *Fucus vesiculosus* contain small quantities of low molecular weight polyphenols derived from phloroglucinol and 2,2′,4,4′,6,6′-hexahydroxybiphenyl. ^{1}H and ^{13}C nmr were used to identify two of these as 4-(2″,4″,6″-trihydroxyphenoxy)-2,2′,4′,6,6′-pentahydroxybiphenyl and 4-(2″-(2‴,4‴,6‴-trihydroxyphenoxy)-4″,6″-dihydroxyphenoxy)-2,2′,4′,6,6′-pentahydroxybiphenyl.

JAMES S. CRAIGIE, A. GAVIN MCINNES, MARK A. RAGAN et JOHN A. WALTER. Can. J. Chem. **55**, 1575 (1977).

Les produits obtenus par extractions alcooliques du *Fucus vesiculosus* contiennent des petites quantités de polyphénols de bas poids moléculaires dérivés du phloroglucinol et de l'hexahydroxy-2,2′,4,4′,6,6′ biphényle. On a utilisé la rmn ^{1}H et ^{13}C pour en identifier deux qui sont le (trihydroxy-2″,4″,6″ phénoxy)-4 pentahydroxy-2,2′,4′,6,6′ biphényle et le [(trihydroxy-2‴,4‴,6‴ phénoxy)-2″ dihydroxy-4″,6″ phénoxy]-4 pentahydroxy-2,2′,4′,6,6′ biphényle.

[Traduit par le journal]

Introduction

In 1892 it was demonstrated (1) that brown algal subcellular bodies, called physodes, gave a fiery red colour with the Lindt reagent (vanillin–HCl). This distinctive reaction led to the generally accepted belief that brown algae contained phloroglucinol **1***a* or related compounds (2).[3] Chemical evidence that brown algal cells produce **1***a*, however, was lacking until quite recently when it was demonstrated in hydrolysates of the tannins of *Sargassum ringgoldianum* (3), exudates of *Fucus vesiculosus* (4), and in the direct extracts of seventeen algal species (5). In a previous communication (6) we showed that extracts of Nova Scotian *F. vesiculosus* contained **1***a* and 2,2′,4,4′,6,6′-hexahydroxybiphenyl **2***a* ('dimer'), other oligomers, and high molecular weight polymers composed of **1***a* and **2***a*. Glombitza *et al.* (7) have independently identified the peracetylated derivatives of **1***a* and **2***a* in acetylated

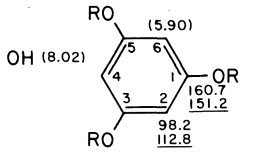

1a R = H[a]
1b R = $COCH_3$ [a,b]

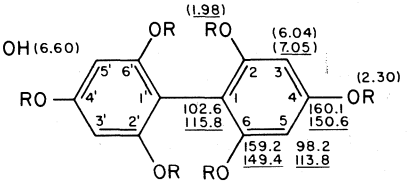

2a R = H[a]
2b R = $COCH_3$ [a,b]

extracts of *F. vesiculosus*, and also claimed the presence of a terphenyl and two quaterphenyls presumably derived from residues of **1***a*. However, on the basis of their published data it is

[1]NRCC No. 15848.

[2]Institute of Marine Biochemistry, University of Trondheim, N-7034, Trondheim, Norway.

[3]In the structures illustrated the superscripts *a–f* refer to the following: *a*, numbers in parentheses are δ (TMS) (ppm); numbers not in parentheses are δ_c (TMS or TSP) (ppm); underlined numbers refer to R = CH_3CO; numbers not underlined to R = H; *b*, resonances for ^{13}C nuclei in CH_3CO— groups have not been individually assigned; *c*, data from ref. 13; *d*, data from ref. 8; *e*, data from ref. 19; ^{13}C resonances were reassigned by comparison with **5***b*, using the substituent effect of a CH_3CO_2 group at C-4′ (from **9** and **10**, see text); *f*, data from ref. 17.

difficult to assess the validity of the latter structures. Structure **3***b* has also been proposed (8) and ether linked derivatives of **1***a* have been identified in the extracts of the brown seaweeds *Bifurcaria bifurcata* (9, 10) and *Halidrys siliquosa* (11). We now report ^1H and ^{13}C nuclear magnetic resonance (nmr) evidence for the structures of two compounds, isolated from the extracts of *F. vesiculosus*, containing **1***a* and **2***a* linked through oxygen in the ratio of 1:1 (**3***a*) and 2:1 (**4***a*).

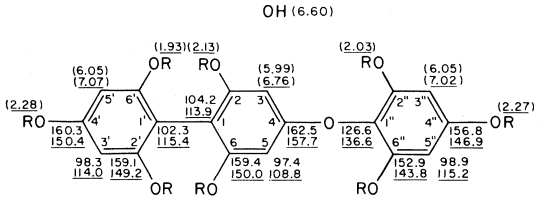

3a R = H[a]

3b R = $COCH_3$[a,b]

3c R = $Si(CH_3)_3$

Experimental

^1H nmr spectra were recorded at 100 MHz with a Varian HA-100 continuous-wave spectrometer, and ^{13}C nmr spectra with a Varian XL-100/15 pulse Fourier-transform instrument (25.16 MHz, spectral width 5120 Hz, acquisition time 0.8 to 1.6 s, flip angle 40°, ^1H-decoupling field strength $\gamma H_2/2\pi = 3800$ Hz, internal ^2H pulse lock). Broadband ^1H-decoupling from ^{13}C was accomplished by phase modulation of the decoupling field from 0 to 180° at 150 Hz (12). High-resolution (h.r.) ^{13}C spectra were recorded with retained nuclear Overhauser enhancement by applying the decoupling field for 1.6 s between data acquisition periods (13).

Mass spectra were obtained from a Consolidated Electrodynamics Corporation 21-110B spectrometer, and precise masses were measured by the peak matching method using an ion in the spectrum of perfluorokerosene as a standard.

Fucus vesiculosus (L.) was collected near Morris Point, Halifax Co., Nova Scotia and its alcoholic extracts were fractionated on Avicel columns as described in our earlier report (6). Compounds in the acetone eluate were purified by repeated preparative chromatography on layers of SilicAR TLC-7GF (Mallinckrodt) until chromatographically homogenous on silica gel or polyamide tlc plates (6). Bands were detected by ultraviolet absorption (254 nm) or by spraying guide strips with vanillin–HCl. Final purification was accomplished on columns (1.5 × 15 cm) of Woelm polyamide developed with methanol–water (3:1 v/v). Typically 70 mg of **3***a* and 40 mg of **4***a* could be recovered in this manner from 8 kg of fresh alga. Acetates were prepared routinely (6), and the trimethylsilyl ethers used for mass spectrometry were formed using Tri-Sil (Pierce Chemical Co.). Compounds **2***a*, **2***b* (6), and **5***b* (14) were synthesized.

Proton chemical shifts, δ (ppm) referenced to tetramethylsilane (TMS) contained in a concentric tube in the case of the hydroxy compounds (solvent H_2O), or to internal TMS (acetylated derivatives in acetone-d_6), are enclosed in parentheses. ^{13}C chemical shifts (δ_c) of the hydroxy compounds were referenced to internal sodium 3-trimethylsilylpropionate 2,2,3,3-d_4 (TSP) (solvent H_2O containing a small amount of HOD); the shifts of the acetylated compounds (solvent acetone-d_6) to internal TMS.

Results and Discussion[3]

Precise mass measurements of the molecular ions observed as intense peaks in the mass spectra of the trimethylsilyl derivatives (**3***c*, **4***c*) of the unknowns **3***a* and **4***a* established the molecular formula $C_{42}H_{78}O_9Si_8$ (*m/e* 950.3788 ± 0.0029; calcd.: 950.37996) for **3***c* and $C_{54}H_{98}O_{12}Si_{10}$ (*m/e* 1218.471 ± 0.004; calcd.: 1218.475) for **4***c*. Thus **3***a* possesses eight hydroxy groups and the molecular formula $C_{18}H_{14}O_9$, while **4***a* contains ten hydroxy groups and has a molecular formula of $C_{24}H_{18}O_{12}$ (15). The molecular ions in the mass spectra of **3***a*, **3***b*, **4***a*, and **4***b* were of low intensity.

^1H and ^{13}C chemical shift data from our experiments and other sources as indicated are shown on the structural diagrams, with the data for acetylated derivatives being underlined. Spin–spin coupling constants $J_{^{13}C^1H}$ measured from high-resolution ^{13}C spectra are listed in Table 1.

A comparison of the ^1H nmr spectra data for **3***b* with those for the model compounds **2***b*, **5***b*, and **7***b* showed that three resonances (δ 2.03–2.06, 6H, CH_3CO_2; δ 2.25–2.27, 3H, CH_3CO_2; δ 7.02–7.04, 2H, aromatic H), were common to the spectra of **3***b*, **5***b*, and **7***b*. The signals originated from hydrogens associated with a 2,4,6-triacetoxyphenoxy residue in the case of both **5***b* and **7***b*, thus the presence of this structural unit may be inferred for **3***b*. The five resonances remaining for **3***b* were consistent with the presence of a biphenyl ring system substituted as in **2***b*, but possessing a 2,4,6-triacetoxyphenoxy substituent at C-4. Three of the signals (δ 1.93, 6H, CH_3CO_2 at C-2′,C-6′; δ 2.28, 3H, CH_3CO_2 at C-4′; δ 7.07, 2H, H-3′,H-5′) were essentially identical to those obtained for **2***b* (δ 1.98, δ 2.30, and δ 7.05), thus confirming the presence, and substitution pattern, of one of the biphenyl rings. The shift of the signal for the remaining two chemically equivalent aromatic hydrogens of **3***b* (δ 6.76) closely resembled that for H-2′,H-6′ of **7***b* (δ 6.72), which would be almost unaffected if the acetoxy group attached to C-4′ was replaced

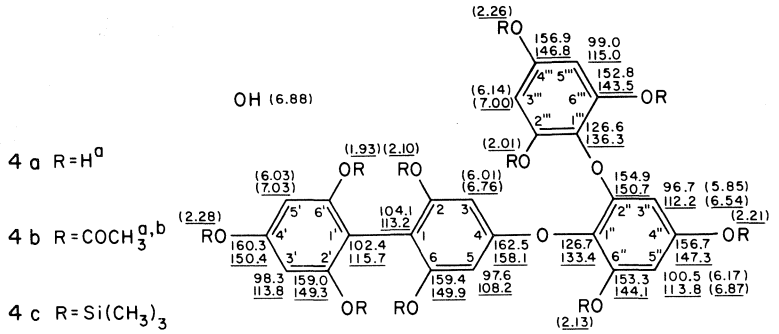

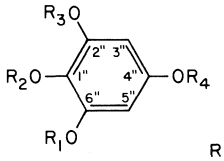

	R_1	R_2	R_3	R_4
4 d		R	R	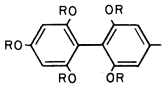
4 e	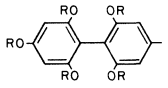	R		R
4 f	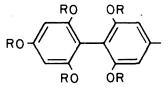		R	R
4 g	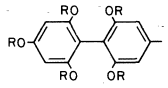	R	R	
4 h	R	R	R	R

by a phenyl substituent (16). Each of the **3***b* hydrogens (H-3, H-5) would, therefore, lie between a phenoxy and an acetoxy (δ 2.13, 3H) substituent, like H-2′ and H-6′ of **7***b*. The presence of only two signals with chemical shifts $\delta \geqq 2.20$ from acetoxy methyl groups in **3***b* excluded the possibility of a 3,4,5-triacetoxyphenoxy substituent as in **7***b*, the spectrum of which contains three such signals. In both **5***b* and **7***b*, a phenoxy substituent shields the protons of adjacent acetoxy groups. This eliminates **6***a* and **6***b* as possible structures. The combined ^{1}H nmr results favour structure **3***a* for the unknown and **3***b* for its acetate derivative.

The structures of **3***a* and **3***b* were finally established by comparing their ^{13}C spectra with those for the model compounds **1***a*, **1***b*, **2***a*, **2***b*, **5***a*, and **5***b*. All of the model compounds possessed symmetry elements which resulted in a reduction in the number of signals observed for the aromatic carbons. Thus the ^{13}C spectra of **1***a* and **1***b* contained only two resonances for such carbons, the one arising from those bearing hydrogen being easily recognized because it was split by one-bond ^{13}C–H spin–spin coupling

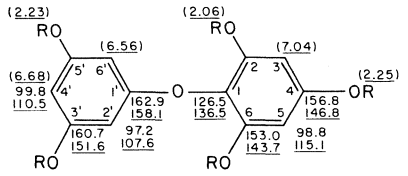

5 a R = H[a]

5 b R = COCH3[a,b,c]

TABLE 1. ^{13}C–^{1}H spin–spin couplings (±0.4 Hz) for **3***a*, **3***b*, **4***a*, **4***b* and model compounds **1***a*, **1***b*, **2***a*, **2***b*, **5***a*, **5***b**

	C-1,1′	*C-2,2′,6,6′*	*C-3,3′,5,5′*	*C-4,4′*			*C-2,4,6*	*C-1,3,5*						
2*a*	^{3}J5.3t	ma	^{1}J160.0d ^{3}J4.7d	^{2}J3.5t		**1***a*	^{1}J160.5d ^{3}J4.6t	m,$w_{1/2}\simeq 9$						
2*b*	^{3}J5.5t	mb	^{1}J168.3d ^{3}J5.0d	^{2}J5.0t		**1***b*	^{1}J167.6d ^{3}J4.9t	$^{2}J\simeq 4.0$t $^{4}J\simeq 3.0$d						
					C-4′	*C-3′,5′*	*C-2′,6′*	*C-1′*	*C-1*	*C-2,6*	*C-3,5*	*C-4*		
				5*a*	†	†	^{1}J161.9d $^{3}J4\pm 1$t	†	†	†	^{1}J161.6d ^{3}J5.3d	†		
				5*b*	^{1}J167.9d ^{3}J5.3t	mb	^{1}J165.9d ^{3}J4.7t	^{2}J4.4t	^{3}J7.4t	mb	^{1}J168.1d ^{3}J5.6d	^{2}J5.3t		
	C-1′	*C-2′,6′*	*C-3′,5′*	*C-4′*	*C-1*	*C-2,6*	*C-3,5*	*C-4*	*C-1″*	*C-2″,6″*	*C-3″,5″*	*C-4″*		
3*a*	^{3}J5.0t	ma	^{1}J160.1d ^{3}J5.0d	^{2}J3.7t	^{3}J5.0t	ma	^{1}J161.4d ^{3}J4.0d	^{2}J3.8t	^{3}J7.3t	ma	^{1}J161.1d ^{3}J5.1d	^{2}J3.8t		
3*b*	^{3}J5.0t	mb	^{1}J168.7d ^{3}J5.0d	^{2}J5.0t	^{3}J5.0t	mb	^{1}J166.2d ^{3}J5.0d	^{2}J4.7t	^{3}J7.3t	mb	^{1}J168.1d ^{3}J5.6d	^{2}J5.3t		
	C-1′	*C-2′,6′*	*C-3′,5′*	*C-4′*	*C-1*	*C-2,6*	*C-3,5*	*C-4*	*C-1‴*	*C-2‴,6‴*	*C-3‴,5‴*	*C-4‴*		
4*a*	^{3}J4.9t	ma	^{1}J160.3d ^{3}J4.7d	^{2}J3.5t	^{3}J5.1t	ma	^{1}J161.9d ^{3}J4.6d	^{2}J4.1t	^{3}J7.1t	ma	^{1}J160.7d ^{3}J5.0d	^{2}J4.3t		
4*b*	^{3}J5.5t	mb	^{1}J168.3d ^{3}J5.0d	^{2}J4.8t	$^{3}J5\pm 1$t	mb	^{1}J166.2d $^{3}J5\pm 1$d	$^{2}J5\pm 1$d	^{3}J7.5t	mb	^{1}J168.4d ^{3}J5.0d	^{2}J5.5t		
									C-1″	*C-2″*	*C-3″*	*C-4″*	*C-5″*	*C-6″*
								4*a*	^{3}J7.2t	^{2}J or ^{4}J3.8d	^{1}J161.6d ^{3}J5.3d	^{2}J4.3t	^{1}J161.2d ^{3}J5.6d	^{2}J or ^{4}J3.7d
								4*b*	^{3}J7.2t	m	$^{1}J170\pm 2$d ^{3}J5.5d	^{2}J5.2t	^{1}J168.3d ^{3}J5.0d	m

*For the carbons of acetate groups, spin–spin coupling constants (Hz) were: $^{13}CH_3$, $^{1}J_{CH}$ 130.4q; $^{13}C{=}O$, ^{2}J 6.9q. ma: characteristic multiplet (doublet of doublets) due to coupling to one *ortho* and one *para* proton in h.r. spectra of hydroxy compounds; mb: similar multiplet for acetylated compounds; m: multiplet; d: doublet; t: triplet; q:quartet; $w_{1/2}$ line width at half height.
†Poor S/N due to insufficient material for h.r. spectrum.

($^1J_{CH}$) in the h.r. spectra, and occurred at higher field than the signal due to the ring carbons bonded to oxygen, in accord with known ^{13}C substituent effects (17). Similarly, four resonances were observed for the biphenyl ring carbons of **2***a* and **2***b*, the two at highest field arising from quaternary carbons (C-1, C-1′) and carbons carrying hydrogens (C-3, C-3′, C-5, C-5′; $^1J_{CH}$). The remaining resonances due to the two types of carbon bonded to oxygen occurred at low field as expected, and could be assigned because the signal for C-2, C-2′, C-6, and C-6′ was about twice the intensity of the one arising from C-4 and C-4′, the relative intensities of the two sets of resonances being independent of the conditions used to record the spectra.

Compound **5***b* was synthesized in 5% yield following Glombitza *et al.* (14). Its ^{13}C spectrum contained three signals arising from aromatic carbons bearing hydrogen. Two which appeared as doublets ($^1J_{CH}$) of triplets ($^3J_{CH}$ to two hydrogens) could be assigned to C-4′ (δ_c 110.5) and C-2′,C-6′ (δ_c 107.6), the relative intensity of the former resonance being approximately half that of the latter, a result independent of experimental conditions. The signal for C-3,C-5 was a doublet ($^1J_{CH}$) of doublets ($^3J_{CH}$ to one hydrogen) as expected. Resonances at δ_c 167.9 to δ_c 168.5 were readily ascribed to the acetoxyl carbonyl carbons, and one at δ_c 158.1 clearly belonged to C-1′ (the corresponding carbon in diphenyl ether resonates at δ_c 157.9 (17)). A low-intensity signal at δ_c 136.5 could be ascribed to the poorly-relaxed carbon C-1, which is shielded by a *para* and two *ortho* acetoxy substituents. The resonance at δ_c 151.6 could be assigned to C-3′, C-5′ as their chemical shift should not differ significantly from that of C-1,C-3,C-5 (δ_c 151.2) in **1***b*, the *meta* substituent effects of acetoxy and phenoxy groups being small (17). The remaining

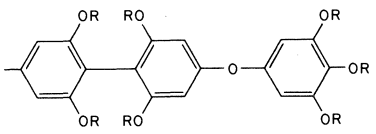

6a R = H
6b R = $COCH_3$

two resonances at δ_c 146.8 and δ_c 143.7 were assigned to C-4 and C-2,C-6, respectively. the relative intensity of the former signal being approximately half that of the latter under a variety of experimental conditions. Additional support for this assignment is provided by the spectrum of diphenyl ether (17), where C-2,C-6 (δ_c 119.3) is shielded to a greater extent than C-4 (δ_c 123.6). It is reasonable to assume that the corresponding carbons in **5***b* would show comparable differences in chemical shift. A similar analysis assigned the resonances in the ^{13}C spectrum of **5***a*, although there was insufficient sample for a h.r. spectrum of the carbons not bonded to hydrogen.

The 18 carbons of **3***a* gave rise to 12 resonances in the aromatic region of the ^1H broadband-decoupled ^{13}C spectrum. This is consistent with the ^1H nmr results discussed above which showed that **3***a* was symmetrical, and indirectly but unequivocally established the presence of at least six pairs of chemically equivalent aromatic carbons. Twelve resonances for the aromatic carbons were also observed in the high resolution ^{13}C spectrum of **3***b*, but the ^1H broadband-decoupled ^{13}C spectrum contained only ten resonances due to superposition of signals (C-1 hidden by C-3′,C-5′ and C-1′ by C-3″,C-5″).

It was apparent from the ^{13}C chemical shift and spin–spin coupling data (Table 1) that **3***a* (**3***b*) possessed three sets of aromatic carbons. Each set contained two chemically non-equivalent, plus two pairs of chemically equivalent, carbons and gave rise to four resonances. The ^{13}C data for one set of carbons (**3***a*, **3***b*; C-1′ through C-6′) was virtually identical to that for **2***a* (**2***b*), and that of another set (**3***a*, **3***b*; C-1 through C-6) differed only slightly, and predictably (see comments on chemical shift calculations below). Similarly the ^{13}C data for the carbons in the remaining set (**3***a*, **3***b*; C-1″ through C-6″) were almost indistinguishable from those obtained for C-1 through C-6 of **5***a* (**5***b*).

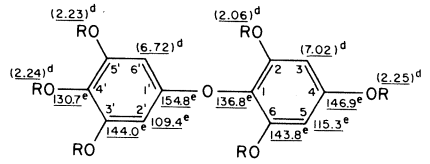

7a R = H[a]
7b R = $COCH_3$[a,b,d,e]

The ^{13}C chemical shifts expected for C-1 through C-6 of **3***a* and **3***b* were calculated from the known chemical shifts for **1***a*, **1***b*, **2***a*, **2***b*, **5***a*, and **5***b* as follows. Comparison of **1***a*,**1***b* and **5***a*,**5***b* yields the changes in chemical shift at all

the carbons of **1***a*,**1***b* due to replacement of one hydroxy (or acetoxy) substituent by a 2,4,6-trihydroxy (or triacetoxy) phenoxy group: at the directly bonded carbon +2.2(+6.9) ppm; *ortho* −1.0(−5.2) ppm; *meta* 0.0(+0.4) ppm; *para* +1.6(−2.3) ppm. These chemical shift changes applied to **2***a*,**2***b* for the same change of substitution at C-4 predict the following chemical shifts for C-1 through C-6 of **3***a*,**3***b*. The close correspondence of measured and predicted (in parentheses) shifts provides further support for the ^{13}C resonance assignments and the structures: **3***a* C-1 104.2 (104.2), C-2,C-6 159.4 (159.2), C-3,C-5 97.4 (97.2), C-4 162.5 (162.3); **3***b* C-1 113.9 (113.5), C-2,C-6 150.0 (149.8), C-3,C-5 108.8 (108.6), C-4 157.7 (157.5).

In addition, hydrogen to deuterium exchange in D_2O eliminated ^{13}C–^{1}H spin–spin coupling from all resonances except those assigned to C-1 through C-6 of **3***a*, which partially retained coupling. This confirms that the latter carbons belonged to the same ring. The centre ring of **3***a* would be expected to exchange hydrogen less rapidly, as it provides less opportunity for keto–enol tautomerism. The combined evidence therefore establishes that **3***a* is 4-(2″,4″,6″-trihydroxyphenoxy)-2,2′,4′,6,6′,-pentahydroxybiphenyl.

The ^{1}H nmr spectrum for **4***a* (solvent acetone-d_6) contained three singlet resonances at δ 6.01, 6.03, and 6.14 due to three pairs of chemically equivalent aromatic hydrogens. Two of these (δ 6.01, 6.03) corresponded closely to the signals for hydrogens at C-3, C-3′, C-5, C-5′ of **2***a* and C-3, C-3′, C-5, C-5′, C-3″, C-5″ of **3***a*, while the third (δ 6.14) was similar apart from a small downfield shift. The spectrum also contained an AB multiplet for two *meta*-coupled aromatic hydrogens (centroid δ 6.01, Δν 32.7 Hz, $^{3}J_{HH}$ 2.8 Hz) and a broad OH signal (δ 6.88) integrating for 10 protons.

The ^{13}C spectrum of **4***a* contained 18 resonances, 12 of which corresponded almost exactly in chemical shift, relative intensity (recorded under widely varying conditions), and ^{13}C–H coupling (Table 1) with the resonances for **3***a*. This information combined with the known molecular formula established that **4***a* contained 2,2′,4′,6,6′-pentahydroxybiphenoxy and 2,4,6-trihydroxyphenoxy residues, which were asymmetrically substituted on another aromatic ring containing $C_6H_4O_3$. Similarly the ^{13}C spectrum of **4***b* supported these conclusions.

The presence of two *meta*-coupled hydrogens limits the choice of structure of the acetylated material to five possibilities, **4***b*, and **4***d* to **4***g*. The choice of **4***b* as the correct structure was based on a comparison of the measured ^{13}C chemical shifts for the carbons of the asymmetrically substituted aromatic ring (C-1″ to C-6″) with predicted shifts derived from measurements of acetylated model compounds, as follows. Firstly, three independent predictions were made of the ^{13}C shifts for **4***h*.

(*a*) The average effect of replacement of an acetoxy substituent on a ring by a 2,4,6-triacetoxyphenoxy group was estimated by comparing the measured δ_c values for **1***b*, **5***b*; **2***b*, **3***b*; **1***b*, **8** (18); **5***b*, **8** (18): at substituent +6.9 ± 0.2 ppm; *ortho* −5.4 ± 0.4 ppm; *meta* +0.4 ± 0.2 ppm; *para* −2.6 ± 0.7 ppm. This information was then used to predict the ^{13}C chemical shifts for **4***h* by applying the substituent effects above, in reverse, to allow for substitution of an acetoxy group at C-1′ of **7***b*.

(*b*) The measured shifts of **5***b* and **7***b* were compared to estimate the substituent effects of acetoxy-substitution at C-4′ of **5***b* and these were applied to predict the result of substitution of an acetoxy group at C-2 of **1***b*.

(*c*) **1***b* and **9** were compared to obtain the effects of acetoxy substitution at C-5 of **9**, and these were used to predict the effect of acetoxy substitution at C-5 of **10**. The averages of these predictions (*a*,*b*,*c*) of the δ_c values for **4***h* were: C-1″ 132.2 ± 0.9; C-2″,6″ 143.3 ± 0.6; C-3″,5″ 114.4 ± 0.5; C-4″ 147.5 ± 0.6 ppm. When these values were compared with the measured δ_c values for C-1″ to C-6″ of **3***b*, the effect of replacing an acetoxy substituent by a (2,2′,4′,6,6′)-pentaacetoxy biphenoxy group was obtainable: at substituent +4.4(±0.9); *ortho* +0.5(±0.6); *meta* +0.8(±0.5); *para* −0.6(±0.6) ppm. The predicted δ_c for **4***h* and the substituent effects above were used to predict the chemical shifts for the five alternative structures **4***b*, **4***d* to **4***g*. For example, δ_c for C-1″ of **4***b* is given by δ_c for C-1″ of **4***h* (132.2 ppm), plus the effect of replacing the acetoxy substituent at C-1″ with a 2,2′,4′,6,6′-pentaacetoxy biphenoxy group (+4.4 ppm) and the effect of replacing the *ortho*-acetoxy at C-2″ by a 2,4,6-triacetoxyphenoxy substituent (−5.4 ppm). The total, 131.2 ppm, is the predicted δ_c. The nearest experimental δ_c values for this ring are compared with predictions in Table 2, which also shows the sum of

TABLE 2. Comparison of experimental δ_c (ppm) for C-1″ through C-6″ of **4***b*, **4***d–g* with nearest predicted values

Experimental δ_c (ppm)	Nearest predicted δ_c for alternative structures (ppm)				
	4*b*	**4***d*	**4***e*	**4***f*	**4***g*
112.2	109.8 C-3″	109.5 C-5″	108.4 C-3″	114.2 C-3″	108.4 C-3″
113.8	112.6 C-5″	112.3 C-3″	112.3 C-5″	115.3 C-5″	109.5 C-5″
133.4	131.2 C-1″	126.2 C-1″	127.3 C-1″	138.7 C-2″	130.1 C-1″
144.1	144.2 C-6″	144.5 C-2″	148.1 C-6″	139.6 C-1″	144.5 C-2″
147.3	147.3 C-4″	151.0 C-6″	148.7 C-4″	142.3 C-6″	148.1 C-6″
150.7	150.7 C-2″	152.3 C-4″	151.0 C-2″	145.7 C-4″	155.2 C-4″
Σ |(Exptl. − predicted)|	5.9	17.1	17.1	23.3	17.3

TABLE 3. Predicted δ_c for C-1″ to C-6″ of **4***a* and **4***b* (ppm)

		C-1″	C-2″	C-3″	C-4″	C-5″	C-6″
4*a*	Predicted	125.7	155.2	98.0	156.9	100.5	153.0
	Measured	126.7	154.9	96.7	156.7	100.5	153.3
4*b*	Predicted	131.2	150.7	109.8	147.3	112.6	144.2
	Measured	133.4	150.7	112.2	147.3	113.8	144.1

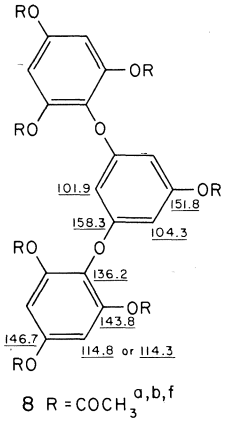

8 R = $COCH_3$ a,b,f

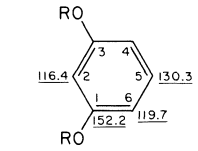

9 R = $COCH_3$ a,b

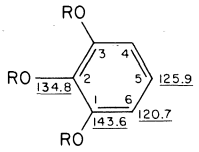

10 R = $COCH_3$ a,b

the absolute magnitudes of the differences between predicted and experimental values. Thus, structure **4***b* is clearly favoured. The predicted shifts for **4***b* (or **4***a*) may also be calculated from the experimental shifts for **3***b* (**3***a*) and the substituent effects under (*a*) above (or the corresponding substituent effect for replacement of OH by a 2,4,6-trihydroxyphenoxy substituent, estimated from experimental data for **1***a*,**5***a*; **2***a*,**3***a*), again giving close agreement (Table 3) with the other predicted shifts (Table 2, structure **4***b*) and with the experimentally measured values.

F. vesiculosus from Nova Scotia has been shown to contain 4-(2″,4″,6″-trihydroxyphenoxy)-2,2′,4′,6,6′-pentahydroxybiphenyl **3***a* and 4-(2″-(2‴,4‴,6‴-trihydroxyphenoxy)-4″,6″-dihydroxyphenoxy)-2,2′,4′,6,6′-pentahydroxybiphenyl **4***a* in addition to compounds **1***a* and **2***a* (6). If a terphenyl or quaterphenyls (7) were present in our extracts, their trimethylsilyl ethers should appear at *m/e* 1022 and 1362, respectively. In fact, only a trace of an otherwise unidentified compound appeared at *m/e* 1022, and no *m/e* 1362 ion was observed following gc/ms (Ragan and Craigie, unpublished) and high resolution ms with photoplate ion beam integration. Similarly, the ether linked C_{12} and C_{18} polyphloroglucinols reported from *Bifurcaria bifurcata* (9, 10), *Cystoseira tamariscifolia* (14), *Halidrys siliquosa* (11), and *Laminaria ochroleuca* (18) must occur only in minute quantities, if at all, in our *F. vesiculosus*.

Acknowledgments

We thank Dr. W. D. Jamieson and Mr. D. Embree for the high resolution mass measurements and for helpful discussions. M.A.R. acknowledges financial support for his graduate studies from Dalhousie University and the National Research Council of Canada.

1. E. CRATO. Ber. Dtsch. Bot. Ges. **10**, 295 (1892).
2. M. A. RAGAN. Bot. Mar. **19**, 145 (1976).
3. C. OGINO and Y. TAKI. J. Tokyo Univ. Fish. **43**, 1 (1957).
4. J. S. CRAIGIE and J. MCLACHLAN. Can. J. Bot. **42**, 23 (1964).

5. K.-W. GLOMBITZA, H.-U. RÖSENER, H. VILTER, and W. RAUWALD. Planta Med. **24**, 301 (1973).
6. M. A. RAGAN and J. S. CRAIGIE. Can. J. Biochem. **54**, 66 (1976).
7. K.-W. GLOMBITZA, H.-W. RAUWALD, and G. ECKHARDT. Phytochemistry, **14**, 1403 (1975).
8. K.-W. GLOMBITZA. VIIIth International Seaweed Symposium, Bangor, Wales. 1974.
9. K.-W. GLOMBITZA and H.-U. RÖSENER. Phytochemistry, **13**, 1245 (1974).
10. K.-W. GLOMBITZA, H.-U. RÖSENER, and M. KOCH. Phytochemistry, **15**, 1279 (1976).
11. K.-W. GLOMBITZA and E. SATTLER. Tetrahedron Lett. **43**, 4277 (1973).
12. J. B. GRUTZNER and R. E. SANTINI. J. Magn. Reson. **19**, 173 (1975).
13. G. C. LEVY and G. L. NELSON. Carbon-13 nuclear magnetic resonance for organic chemists. Wiley-Interscience, New York, NY. 1972.
14. K.-W. GLOMBITZA, H.-U. RÖSENER, and D. MÜLLER. Phytochemistry, **14**, 1115 (1975).
15. M. A. RAGAN. Physodes and the phenolic compounds of brown algae. Ph.D. thesis, Dalhousie University, Halifax, N.S. 1976.
16. L. M. JACKMAN and S. STERNHELL. Applications of nuclear magnetic resonance spectroscopy in organic chemistry. 2nd ed. Pergamon, New York, NY. 1969.
17. J. B. STOTHERS. Carbon-13 NMR spectroscopy. Academic Press, New York, NY. 1972.
18. K.-W. GLOMBITZA, M. KOCH, and G. ECKHARDT. Phytochemistry, **15**, 1082 (1976).
19. E. SATTLER. Thesis, Reinischen Friedrich-Wilhelms-Universität zu Bonn. 1974.

Synthesis and structure of dichlorobis(thiosemicarbazide)mercury(II)

CHUNG CHIEH

Guelph–Waterloo Centre for Graduate Work in Chemistry, University of Waterloo, Waterloo, Ont., Canada N2L 3G1

Received December 29, 1976

CHUNG CHIEH. Can. J. Chem. **55**, 1583 (1977).

The reaction between mercury(II) chloride and thiosemicarbazide (1:2 molar ratio) in ethanol–water (1:1 by volume) gave, almost quantitatively, dichlorobis(thiosemicarbazide)-mercury(II), $HgCl_2(tsc)_2$. There was a trace of unidentified black material as a side product. The crystals of $HgCl_2(tsc)_2$ are orthorhombic with $a = 8.675(7)$, $b = 8.123(6)$, $c = 15.786(11)$ Å, $Z = 4$, and space group *Pbcn*. The $HgCl_2(tsc)_2$ molecule in the crystal has a twofold axis and the mercury atom is bonded to two chlorine atoms at 2.841(3) Å, and two sulfur atoms at 2.417(3) Å, in a highly distorted tetrahedron. The bond angles are: S—Hg—S = 160.7(1)°; Cl—Hg—Cl = 96.6(1)°; S—Hg—Cl = 89.5(1)° (twice) and 103.4(1)° (twice). However, if the close contacts, Hg···Cl = 3.250(3) Å, were counted, the coordination around the Hg atom would be an approximate octahedron.

CHUNG CHIEH. Can. J. Chem. **55**, 1583 (1977).

La réaction du chlorure mercurique(II) avec la thiosemicarbazide (rapport molaire 1:2) dans un mélange éthanol–eau (1:1 par volume) donne, presque quantitativement, le dichloro bis(thiosemicarbazide) mercurique(II), $HgCl_2(tsc)_2$. On a retrouvé comme sous-produit une trace d'un composé noir non-identifié. Les cristaux de $HgCl_2(tsc)_2$ sont orthorhombiques avec $a = 8.675(7)$, $b = 8.123(6)$, $c = 15.786(11)$ Å, $Z = 4$ et groupe d'espace *Pbcn*. La molécule de $HgCl_2(tsc)_2$ dans le cristal possède un axe binaire et l'atome de mercure est lié aux deux atomes de chlore distant de 2.841(3) Å, et à deux atomes de soufre qui se trouvent à 2.417(3) Å à l'intérieur d'un tétraèdre fortement déformé. Les angles de liaison sont: S—Hg—S = 160.7(1)°; Cl—Hg—Cl = 96.6(1)°; S—Hg—Cl = 89.5(1)° (deux fois) et 103.4(1)° (deux fois). Toutefois si les contacts immédiats Hg···Cl = 3.250(3) Å sont comptés, la coordination autour de l'atome de Hg serait approximativement octaédrique.

[Traduit par le journal]

Introduction

Like thiourea (tu), thiosemicarbazide (tsc) contains a $\diagdown C{=}S \diagup$ group which can coordinate to mercury. Thiourea forms a series of compounds with formula $HgX_2(tu)_n$ where $n = 1, 2, 3,$ or 4; and X = Cl, Br, or I. The mercury atom is coordinated in an unusual, approximately trigonal planar, arrangement by two equivalent thiourea sulfur atoms and one chlorine atom in $HgCl_2(tu)_2$ (1). However, in $HgI_2(tu)_2$, the mercury atom is coordinated to two sulfur and two iodine atoms in a distorted tetrahedron (2). In $HgCl_2(tu)_3$ (3) and $HgCl_2(tu)_4$ (4), the mercury atom is coordinated to three and four sulfur atoms respectively. These structural studies revealed the complexity of the interaction between the $\diagdown C{=}S \diagup$ group and the mercury(II) ions.

Thiosemicarbazide is different from thiourea in that it can also be a bidentate ligand which forms a five-membered chelating ring in many nickel complexes (5, 6). Although the *cis*- and *trans*-dithiosemicarbazidenickel(II) dinitrate exist in different crystal forms (7), both *cis*- and *trans*-dithiosemicarbazidenickel(II) sulfate are present in one crystal (5). When tsc is a chelating agent, the configuration is different from that of the free molecule (8). However, in the structure of thiosemicarbazidesilver(I) chloride, the ligand is monodentate with only Ag—S bond (9). The configuration of tsc is the same as that of the free molecule. The energy difference between the two configurations has been estimated to be small (9). Our previous study indicated that there is a tendency for organo-mercury to bond to the amino-group of penicillamine (10). It is interesting to see how the NH_2 groups in tsc interact with the mercury(II) ion. Recently, nickel was found to form a 4-coordinated complex with *N*,*N*-diethylphenylazothioformamide, a derivative of thiosemicarbazide. The ligand was bidentate with S and N bonded to the nickel

ion despite the presence of a bulky phenyl group on the nitrogen (11). The configuration of tsc in a complex is therefore very delicately determined by the energy of bonding between the metal and the nitrogen atoms. It is in search of an understanding of the chemical interaction between mercury and tsc that these studies are carried out. Whether compounds of formula $HgX_2(tsc)_n$ with $n = 1$, 2, 3, and 4 can be synthesized is still to be established. This paper reports the synthesis and crystal structure of $HgCl_2(tsc)_2$.

Experimental

Preparation of $HgCl_2(tsc)_2$

Commercial thiosemicarbazide (Fluka) and mercury(II) chloride (Baker) of reagent grade were used and the mixed solvents were made up from equal volumes of absolute ethanol and deionized water. The mixed solvent was chosen because a similiar system was used in the preparation of *N,N'*-diethylthiourea (dietu) complexes of the type $MX_2(dietu)_2$ (M = Zn, Cd, Hg; X = Cl, Br, I) (12). The solubility of tsc in ethanol is small but tsc is very soluble in the mixed solvent. Ethanol is a good carrying solvent for $HgCl_2$ in other types of reactions (13). To 40 ml solution containing 0.3646 g (4 m*M*) of tsc, 0.5431 g (2 m*M*) $HgCl_2$ crystal was added. No stirring was applied to this natural heterogenous mixture. The reaction was left to proceed slowly at room temperature, 25 ± 3°. Some long, fine needles, observed under a 40 × microscope, formed very quickly around the crystals of $HgCl_2$. The reaction vessel was then covered. On the next day, crystals of $HgCl_2$ had disappeared and the long needles were no longer there. In their place were colorless prismatic crystals. There was also a trace of black particles possibly resulted from the formation of HgS or mercury metal. These prisms were separated by filtration, but the bulk sample so obtained was tinged with a brown color because of the presence of the black material. The filtrate was allowed to evaporate in a partially-covered beaker at room temperature and more colorless prismatic crystals were obtained. When the filtrate evaporated totally, there was a trace of tsc crystal left in the beaker, together with some prisms.

Crystallographic Measurement

Rotation, Weissenberg and precession photographs were used to determined the cell constants and space group which was unique, from the systematic absences. Photographic data also confirmed that crystals obtained in the first batch are the same as those obtained from the filtrate. Crystals are usually prisms with (±100) and (00 ±1) planes developed. The {111} type planes are developed on the ends of slightly elongated crystals. The cell constants were refined by least-squares methods from the 2θ values of 17 reflections measured on the diffractometer. Crystal data are as follows:

$C_2H_{10}Cl_2HgN_6S_2$ fw = 453.8

Orthorhombic, $a = 8.675(7)$, $b = 8.123(6)$, $c = 15.786(11)$ Å. $V = 1112.4$ Å^3, $D_o = 2.70$ (by flotation), $Z = 4$, $D_c = 2.709$ g cm^{-3}. Systematic absences: $0kl$: $k = 2n + 1$; $h0l$: $l = 2n + 1$; $hk0$: $h + k = 2n + 1$; space group *Pbcn*. $\mu(MoK\alpha) = 149.3$ cm^{-1}; $\lambda(MoK\alpha) = 0.7107$ Å.

The crystal used for intensity measurements had dimensions of 0.10 × 0.15 × 0.12 mm along *a*, *b*, and *c* directions. It was mounted with *b*-axis along the the φ-axis of the G.E. XRD-6 automatic diffractometer, which was equipped with a pulse height analyser, a scintillation counter, and a Hewlett Packard Scaler Timer (Model 5201L). A total of 975 reflections with $2\theta(MoK\alpha) \leq 50°$ were measured using θ–2θ scan technique at a constant speed of 2° per min. The scan range was ±(0.95 ± 0.43 tan θ) with respect to the calculated 2θ. Backgrounds were counted for 20 s on each side of the scanning range. During data collection, four standard reflections (400, 021, $\bar{1}10$, and $02\bar{7}$) were measured repeatedly between each 100 reflections. The negative indices used for the standard reflections gave four values evenly spread on the φ circle. The variation of intensities for the standard reflections was less than 3%. There were 720 reflections (74%) with integrated intensities (I = count − background) greater than $2\sigma(I)$, and they were considered as observed reflections. The standard deviations $\sigma(I)$ were calculated from counting statistics. No absorption correction was made ($\mu R = 1.05$). Lorentz and polarization factors were applied to derive the structure amplitudes.

From the Patterson synthesis, the mercury atom was found to be located at the special positions, 4*c*, of space group *Pbcn*. It was very difficult to differentiate the corresponding Hg—S from Hg—Cl vector peaks in the Patterson map and two Cl atoms were put in both positions to begin with. The Fourier map revealed all the non-hydrogen atoms. With isotropic temperature factors for all the atoms, the R factor ($= \Sigma||F_o| - |F_c||/\Sigma|F_o|$) was reduced to 0.10. When anisotropic thermal parameters were introduced, the R factor became 0.048. A difference Fourier map calculated at this stage gave two peaks of electron density 2.0 e/Å^3, one at (0.0 0.39 0.25) and another one in the vicinity of the Hg atom. It was not possible to have a water molecule at the point (0.0 0.39 0.25) because this position is only 2.1 Å from two neighboring N(1) and 2.3 Å from two N(2) atoms. In fact, this point would be the position for Hg had the alternative origin been chosen. All other peaks were less than 0.8 e/Å^3 and only two of them were located clearly at possible positions for hydrogen atoms, which were included in the full-matrix least-squares refinements. The revised program written by Doedens and Ibers was used. The atomic scattering factors from Cromer and Waber (14) were used with anomalous dispersion coefficients for Hg from Cromer (15). At the final stage, a weighting function $w^{-1} = (70.0 - |F_o| + 0.01F_o^2)$ was introduced and the final R and R_w ($= [\Sigma w^2(|F_o| - |F_c|)^2/\Sigma w^2F_o^2]^{1/2}$) were 0.046 and 0.057 respectively. The weighting scheme gave uniform errors, $\Sigma w(|F_o| - |F_c|)^2/(m - n)$, in all ranges of F_o and the final atomic coordinates are given in Table 1. The table of structure factors and anisotropic temperature factors is available from the Depository of Unpublished Data.[1]

[1]Photocopies may be obtained, upon request, at a nominal charge from the Depository of Unpublished Data, CISTI, National Research Council of Canada, Ottawa, Canada K1A 0S2.

Results and Discussion

The long fine needles observed at the beginning when mercury(II) chloride was added to the solution of tsc were probably a compound of composition $HgCl_2(tsc)$. Presently, we are using other mole ratios for the synthesis of other compounds $HgCl_2(tsc)_n$, $n = 1$, 3, and 4, in the hope of obtaining a series similiar to that observed in reactions between $HgCl_2$ and thiourea. Spectroscopic evidence has shown that the needles are not the same as the prisms.

The crystals are composed of individual molecules of $HgCl_2(tsc)_2$. The bond lengths and angles are given in Fig. 1, which also shows the thermal anisotropy of the atoms. The molecule is located at a special position, 4*c*, of the space group *Pbcn* (No. 60, International Tables for X-ray Crystallography (16)), and therefore has a twofold rotation axis. The mercury is bonded to two sulfur, Hg—S = 2.417(3), and two chlorine, Hg—Cl = 2.821(3) Å, atoms in a very distorted tetrahedron. The bond angles are: S—Hg—S = 160.7(1)°, Cl—Hg—Cl = 96.6(1)°, S—Hg—Cl = 89.5(1)° (twice) and 103.4(1)° (twice). However, the chlorine is also very close to the mercury atom of a neighboring molecule with Hg· · ·Cl = 3.250(3) Å. This relation can be seen from the stereo-packing diagram, Fig. 2. If these weak interactions are counted, the coordination of the mercury can be described as very distorted octahedral.

The free tsc molecule is planar with a maximum deviation from the least-squares plane of 0.03 Å. The bonded tsc in $HgCl_2(tsc)_2$ is also planar with a displacement of only 0.01 Å. The mercury atom is 1.5 Å from the plane of the tsc. The bond lengths in the ligand are similiar to those of tsc; but C=S is lengthened because of coordination. The bond lengths are 1.74(1) and 1.701(5) Å for the bonded and free tsc respectively. The dihedral angles are 1.1° for NNCN and 2.1° for NNCS.

TABLE 1. Final fractional coordinates ($\times 10^4$) $\pm(xyz, \frac{1}{2}-x\ \frac{1}{2}-y\ \frac{1}{2}+z, \frac{1}{2}+x\ \frac{1}{2}-y\ \bar{z}, \bar{x}\ y\ \frac{1}{2}-z)$

Atom	x	y	z
Hg	1/2	3816.5(9)	1/4
Cl	8320(3)	6126(4)	2893(2)
S	4630(3)	3317(5)	3995(2)
N(1)	0073(11)	3869(13)	3861(7)
N(2)	1620(11)	3441(15)	3702(6)
N(3)	2421(14)	4574(17)	4944(6)
C	2719(13)	3798(15)	4221(7)
H(2)*	174(18)	295(22)	325(11)
H(3)	143(21)	462(21)	509(10)

*For H atomic coordinates, the multiplier is 10^3.

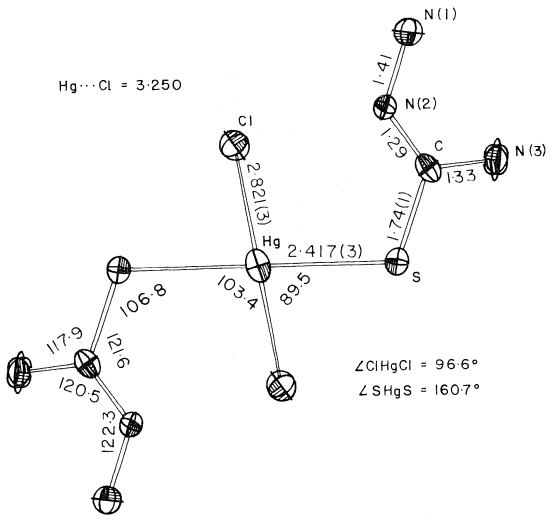

FIG. 1. Bond distances and angles for $HgCl_2(tsc)_2$ with anisotropic thermal ellipsoids. The important standard deviations are given in parentheses and the remainder are: σ(C—N, N—N) = 0.02 Å; σ(angles around Hg) = 0.02°; σ(HgSC) = 0.3°; σ(other angles) = 0.5°.

The comparison of Hg—S and Hg—Cl distances of tsc and thiourea complexes are set out in Table 2. In general, the Hg—S distance increases with coordination number (CN). When there are three or more Hg—S bonds around the Hg atom, the Hg—S distances vary. A similarity was observed in a series of compounds that contain $Hg(SCN)_n^{(n-2)-}$ as part of the molecule (18–20). The four Hg—S distances for $(Ph_4P)_2 \cdot Hg(SCN)_4$ are included in Table 2. A notable similarity in the Hg—S distances between $Hg(SCN)_4^{2-}$ (2.531(40) Å) and $Hg(tu)_4^{2+}$ (2.549(48) Å) exists regardless of the difference in charge for the two species. The values in parentheses are the standard deviations of the mean, $\bar{s}$, calculated by $\bar{s} = ((\sum x^2 - (\sum x)^2/3)/3)^{1/2}$, where the x's represent the bond lengths used to calculate the mean. The angles Hg—S—C for the two series of compounds are different.

The Hg—Cl distance for $HgCl_2(tsc)_2$ is the largest among the compounds listed in Table 2. This may due to the fact that the chlorine atom is unsymmetrically bridged to two mercury(II) ions.

Strong intramolecular hydrogen bonds

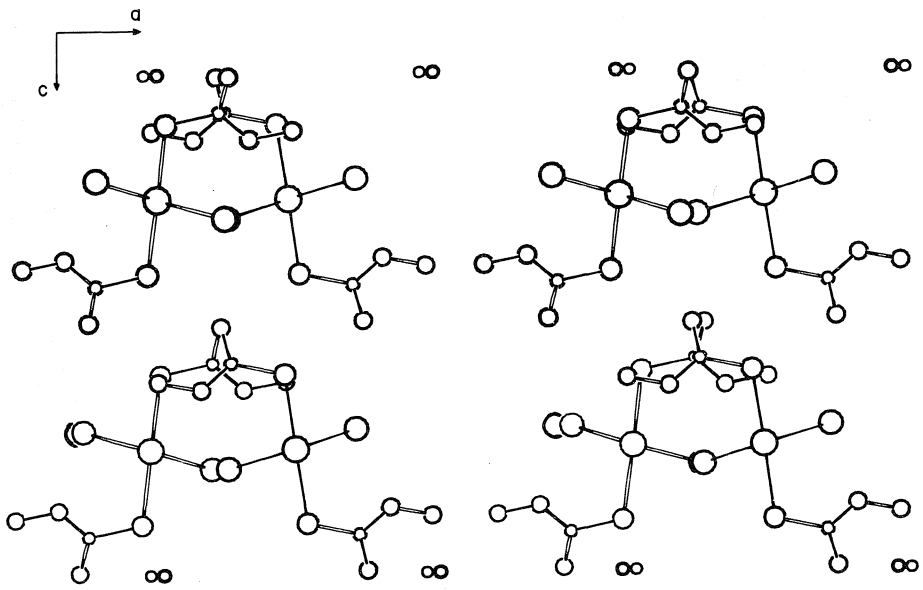

FIG. 2. Stereo-pair of the packing diagram viewed from the twofold axis of the molecules or the *b*-axis of the unit cell.

TABLE 2. Comparison of Hg—S, Hg—Cl distances and ∠Hg—S—C angles

Compound	Hg—S	∠Hg—S—C	Hg—Cl	Coordination geometry	Reference
$HgCl_2(tsc)_2$	2.417(3)	106.8(3)	2.821(3)	Tetrahedral*	
$HgCl_2(tu)_2$	2.417(3)	110.9(8)	2.57(1)	Trigonal planar	1
$HgCl(tu)Cl\cdot\frac{1}{2}HgCl_2$	2.40(2)	116(3)	2.39(2)	Trigonal planar	17
$HgCl_2(tu)_3$	2.37(3)	111(2)†		Trigonal	
	2.61(3)	121(2)†		Bipyramidal	3
	3.10(3)	160(3)†			
$HgCl_2(tu)_4$	2.506(8)	103.3(8)		Tetrahedral	
	2.527(8)	105.5(12)			3
	2.544(8)	108.6(11)			
	2.617(8)	102.3(12)			
$(Ph_4P)_2Hg(SCN)_4$	2.491(3)	98.0(4)		Tetrahedral	20
	2.504(3)	97.9(4)			
	2.552(3)	96.4(4)			
	2.575(3)	103.1(4)			

*Very distorted.
†Values calculated from the coordinates of ref. 3.

may exist between the terminal nitrogens, N(1)···N(3) = 2.72(2) Å, H(3)—N(3) = 0.89 Å, and N(1)···H(3) = 2.3(2) Å. A similar N(1)···N(3) distance of 2.69(12) is found in the free tsc molecule (8). Despite the unfavorable angle, N(2)—N(3)···N(1) = 31° and N(3)—H(3)···N(1) = 105°, the hydrogen bond exists because it forms a six-membered ring. The hydrogen H(2) is bonded to N(2), N(2)—H(2) = 0.83 Å.

The structure consists of layers of $HgCl_2(tsc)_2$ molecules. Each layer, which is perpendicular to the *c*-axis, is composed of three sublayers in the form of a sandwich. The centre layers are two-dimensional Hg—Cl···Hg— linkage networks which hold the tsc layers through strong Hg—S bonds. Intermolecular hydrogen bonds are very weak. The shortest intermolecular distances are: N(1)···N(3) (x, $1-y$, $1-z$) = 3.14(2) Å, and N(1)···Cl ($-0.5+x$, $0.5+y$, $0.5-z$) = 3.37 Å. A packing diagram viewed from the *b*-axis or the twofold axis of the

molecule is given in Fig. 2. Both N(1) and N(3) are oriented toward the S atoms in the structure. This is the same as the packing of the free tsc, in which the hydrogen atoms are pointing toward the S atoms due to electrostatic attraction (8).

Acknowledgements

This work was financed by The National Research Council of Canada. I thank Mr. E. T. McMahon for his help in the synthesis.

1. P. D. Brotherton, P. C. Healy, C. L. Raston, and A. H. White. J. Chem. Soc. Dalton, 334 (1973).
2. A. Korczyanski. Roczn. Chem. **42**, 393 (1968).
3. A. Korczyanski. Roczn. Chem. **42**, 207 (1968).
4. P. D. Brotherton and A. H. White. J. Chem. Soc. Dalton, 2696 (1973).
5. R. G. Hazell. Acta Chem. Scand. **22**, 2171 (1968); **22**, 2809 (1968).
6. R. G. Hazell and S. E. Rasmussen. Acta Chem. Scand. **16**, 2325 (1962).
7. R. G. Hazell. Acta Chem. Scand. **26**, 1365 (1972).
8. F. Hansen and R. G. Hazell. Acta Chem. Scand. **23**, 1359 (1969).
9. G. E. Gasparri, A. Mangia, A. Musatti, and M. Nardelli. Acta Crystallogr. B**24**, 367 (1968).
10. Y. S. Wong, P. C. Chieh, and A. J. Carty. Can. J. Chem. **51**, 2597 (1973).
11. R. G. Hazell. Acta Chem. Scand. A**30**, 322 (1976).
12. G. Marcotrigiano. Z. Anorg. Allg. Chem. **422**, 80 (1976).
13. C. Chieh. Can. J. Chem. **55**, 65 (1977).
14. D. T. Cromer and J. T. Waber. Acta Crystallogr. **18**, 104 (1965).
15. D. T. Cromer. Acta Crystallogr. **18**, 17 (1965).
16. International Tables for X-ray Crystallography. Vol. I, 3rd ed. Kynoch Press, Birmingham. 1969.
17. P. D. Brotherton and A. H. White. J. Chem. Soc. Dalton, 2698 (1973).
18. J. Hubert, A. L. Beauchamp, and R. Rivest. Can. J. Chem. **53**, 3383 (1975).
19. A. Sakhri and A. L. Beauchamp. Inorg. Chem. **14**, 740 (1975).
20. A. Sakhri and A. L. Beauchamp. Acta Crystallogr. B**31**, 409 (1975).

Entropy production in bulk isothermal relaxation

ANDREW W. YAU AND HUW O. PRITCHARD

Centre for Research in Experimental Space Science, York University, Downsview, Ont., Canada M3J 1P3

Received November 4, 1976

ANDREW W. YAU and HUW O. PRITCHARD. Can. J. Chem. **55**, 1588 (1977).

Four theorems relating to complete monotonicity of entropy production in isothermal bulk relaxation have been proved, and in another two cases, it is shown by numerical experiment that the entropy production is probably monotonic also. The total entropy and the total energy do not in general relax with the same rate constant, and under many conditions the time constant for entropy relaxation approaches twice the time constant for energy relaxation. We speculate that the maximum entropy principle used in the information-theoretic approach to bulk relaxation may be synonymous with the principle of complete monotonicity of entropy production.

ANDREW W. YAU et HUW O. PRITCHARD. Can. J. Chem. **55**, 1588 (1977).

On a prouvé quatre théorèmes reliant la monotonicité complète de la production d'entropie lors de la relaxation globale isotherme et, dans deux autres cas, on montre par des expériences numériques que la production d'entropie est aussi probablement monotone. L'entropie totale et l'énergie totale ne se détentent pas d'une façon générale avec la même constante de vitesse et dans plusieurs conditions la constante de temps pour la détente de l'entropie approche une valeur à peu près deux fois plus grande que la constante de temps pour la relaxation de l'énergie. On croit que le principe d'entropie maximum utilisé dans une approche information-théorique à la détente globale peut être synonyme du principe de monotonicité complète de la production d'entropie.

[Traduit par le journal]

Introduction

Following from a conjecture by McKean in 1966 (1) we have investigated the time-dependence of the total entropy in a number of model relaxations (2, 3) and found that often they seem to be in conformity with McKean's supposition, *i.e.*

$$[1] \quad (-1)^n \mathrm{d}^n S/\mathrm{d}t^n \leq 0 \qquad n = 1, 2, 3, \ldots$$

where S is the total entropy and t is the time; an extensive list of references to other work of a similar nature, particularly by Harris and by Simons, can be found in ref. 2. However, eq. 1 is by no means a universal rule, and there are frequent exceptions. For example, the exception of (isothermal) autocatalytic processes (and consequently also of oscillatory processes) is readily demonstrated; also, Lissi (4) has recently noted another class of exceptions, that of highly exothermic processes taking place adiabatically, a point we also confirmed by numerical integration for the explosive thermal decomposition of methyl isocyanide (5).

A process conforming to [1] is said to be "completely monotonic". In this paper, we present a summary of cases of complete monotonicity proved for an assembly of molecules undergoing bulk rotational and/or vibrational relaxation under isothermal conditions: the cases are presented under two headings, those which can be proved algebraically in the normal fashion, and those which we have only been able to demonstrate as plausibly correct (3) by numerical experiment; the details of these proofs will be made available in thesis form subsequently (6).

Following our existing notation[1] (7), the evolution of population distribution in an isothermal relaxation is given by

$$[2] \quad n_i(t) = \tilde{n}_i^{1/2} \sum_j S_{ij} \, \mathrm{e}^{\lambda_j t} \sum_k S_{kj} \tilde{n}_k^{-1/2} n_k(0)$$

We then write, following Bernstein and Levine (8), an expression for the total entropy as

$$[3] \qquad S(t) = -\boldsymbol{k} \sum_i n_i(t) \ln [n_i(t)/\tilde{n}_i]$$

whence

$$[4] \quad S^{(l+1)} = \frac{\mathrm{d}^{l+1} S}{\mathrm{d}t^{l+1}} = -\boldsymbol{k} \sum_i \sum_{m=0}^{l} \binom{l}{m} \frac{\mathrm{d}^m}{\mathrm{d}t^m} \ln \left(\frac{n_i(t)}{\tilde{n}_i} \right) \times \frac{\mathrm{d}^{l-m+1}}{\mathrm{d}t^{l-m+1}} n_i(t)$$

[1] Briefly, $n_i(t)$ is the population at time t, $\tilde{n}_i$ is the equilibrium population, and λ_j and S_{ij} are respectively the eigenvalues and eigenvectors of the relaxation matrix.

A. Cases Proved Analytically

A1. Canonically Invariant Relaxation

The properties of a canonically invariant relaxing system have been established by Andersen, Oppenheim, Shuler, and Weiss (9). For such a system, the mean energy $\langle E(t)\rangle$ relaxes as $\exp(-\mu t)$ where

$$[5] \qquad \mu = Z[M]\,P_{0\leftarrow 1}[1 - a\mathrm{e}^{-\tilde{\beta}\varepsilon_1}]$$

(a being related to state degeneracy factors) and the population evolution is characterised by the time-dependent inverse temperature $\beta(t) = [\boldsymbol{k}T(t)]^{-1}$, *viz.*,

$$[6] \qquad n_i(t) = [Q(t)]^{-1} g_i \exp[-\beta(t)\varepsilon_i]$$

where $Q(t)$ is the partition function. Hence

$$[7] \quad S^{(1)} = \boldsymbol{k}\beta^{(1)}(t)[\tilde{\beta} - \beta(t)] \times [\langle E^2(t)\rangle - \langle E(t)\rangle^2]$$

where $\langle E^2(t)\rangle$ is the mean square energy at time t. Since

$$[8] \qquad \frac{\mathrm{d}\langle E(t)\rangle}{\mathrm{d}t} = \frac{\mathrm{d}\langle E(t)\rangle}{\mathrm{d}\beta}\frac{\mathrm{d}\beta}{\mathrm{d}t}$$

and

$$[8a] \quad \frac{\mathrm{d}\langle E(t)\rangle}{\mathrm{d}\beta} = [\langle E(t)\rangle^2 - \langle E^2(t)\rangle] < 0$$

eq. 7 becomes

$$[7a] \quad S^{(1)} = -\boldsymbol{k}[\tilde{\beta} - \beta(t)]\frac{\mathrm{d}\langle E(t)\rangle}{\mathrm{d}t} \geq 0$$

Differentiating further

$$[9] \quad S^{(l)} = -\boldsymbol{k}\sum_{m=0}^{l-1}\binom{l-1}{m}\frac{\mathrm{d}^{l-m}}{\mathrm{d}t^{l-m}}\langle E(t)\rangle \cdot \frac{\mathrm{d}^m}{\mathrm{d}t^m}[\tilde{\beta} - \beta(t)]$$

and since the inverse temperature $\beta(t)$ has already been derived by Andersen *et al.* (9) and is monotonic, then [9] itself can be shown (6) to be *completely monotonic*.

A2. Canonically Invariant Relaxation

In our previous numerical examination of bulk relaxation (10), it was found (11) that there often did not appear to be any simple connection between the relaxation rates for entropy and energy. Consequently, we examined this relationship and can show (6), using eq. 7*a*, that whereas in a canonically invariant process the total energy decays as $\exp(-\mu t)$, *the total entropy decays as* $\exp(-2\mu t)$ *in the limit as* $t \to \infty$. This suggests that it may be possible to introduce the concept of a relaxation time for the total entropy: certainly, almost pure exponential behaviour of the total entropy at long time has been observed previously (2), but any simple relationship of the rate with the rate of energy relaxation escaped notice.

A3. $(N-1)$-fold Degenerate System

In our previous paper (7), we showed that if the relaxation matrix had $(N-1)$ degenerate eigenvalues of magnitude μ, eq. 2 becomes

$$[10] \qquad n_i(t) = \tilde{n}_i + (n_i(0) - \tilde{n}_i)\mathrm{e}^{-\mu t}$$

Writing

$$\gamma_i = n_i(t)/\tilde{n}_i$$

and

$$\Delta_i = (n_i(0) - \tilde{n}_i)/\tilde{n}_i$$

we can put

$$[11] \qquad S^{(1)} = \boldsymbol{k}\sum_i \tilde{n}_i S_i^{(1)}$$

where[2]

$$[12] \quad S_i^{(1)} = -\ln\gamma_i\frac{\mathrm{d}\gamma_i}{\mathrm{d}t} = \mu\Delta_i\,\mathrm{e}^{-\mu t}\ln(1 + \Delta_i\mathrm{e}^{-\mu t})$$

It is a simple matter to show that successive derivatives of [12] alternate in sign and therefore that S itself is *completely monotonic*; the monotonicity of the individual S_i-terms probably stems from the absence of overshoot or fluctuation in the degenerate system. Notice, as in *A2*, the long-time behaviour of the entropy is $\exp(-2\mu t)$.

A4. General Relaxing System at Long Time

As $t \to \infty$, the population vector [2] can be written as

$$[13] \qquad n_i(t) = \tilde{n}_i(1 + \phi_i(t))$$

If $\phi_i(t)$ is sufficiently small that we can assume

$$[14] \qquad \ln n_i(t) = \ln\tilde{n}_i + \phi_i(t)$$

then

$$[15] \quad \lim_{t\to\infty} S = -\tfrac{1}{2}\boldsymbol{k}\sum_{j=0}^{N-2}\mathrm{e}^{2\lambda_j t} \times \left[\sum_\alpha S_{\alpha j}\tilde{n}_\alpha^{-1/2}n_\alpha(0)\right]^2$$

Since [15] is in normal-mode form, *viz.*

$$[16] \qquad S = -\boldsymbol{k}\sum_i a_i\mathrm{e}^{-b_i t}$$

[2]Note that the subscript i here denotes an index for each level in the system (not the internal entropy).

and all the a_i are positive, then by Descartes' rule of sign for a sequence of exponentials [15] is *completely monotonic*. Notice again, as in *A2*, the appearance of $2\lambda_j$ in the expression for the relaxation time for the total entropy.

B. Cases Established Numerically

The four cases noted above represent the limit of the new theorems of entropy production which we have been able to establish by conventional means: unfortunately, three of them (*A1*, *A2*, and *A3*) refer to rather idealised systems, but the correspondence between *A2* and *A4* is suggestive enough that we should examine numerically some more realistic cases. Following our previous approach (3), we constructed analytical formulae for the first *six* derivatives of the total entropy and examined their behaviour for a series of practical relaxations: in this way, the following 'rules' were established.

B1. Transition Probabilities Obeying the Sum Rule

We examined both vibrational and rotational relaxations, using a wide variety of starting distributions including delta-distributions and bimodal delta-distributions. In many cases, populations of levels overshot, often in succession, but of course the energy does not overshoot since the sum rule guarantees exponential decay of the energy. *In all cases eq. 1 held up to* $n = 6$.

B2. Transition Probabilities of Linear Surprisal Form with Minimum Eigenvalue Spread

As discussed previously (7), this form of the transition-probability matrix often yields energy relaxation which is close to exponential: only rotational relaxation was examined.

(*a*) In simple heating or cooling processes *eq. 1 holds up to* $n = 6$; inspection of the population vectors during the relaxation shows that the systems are *not canonically invariant*, although there are no overshoots in either population or energy.

(*b*) In relaxations from delta- or bimodal delta-distributions, *eq. 1 fails randomly at some value of* $3 \leq n \leq 6$: the greater the number of levels overshooting or the greater the magnitude of the energy overshoot, the lower the value of n at which [1] appears to fail; nevertheless, the failure is only temporary, and the system soon gets back on a monotonic path.

B3. Mixed Rotation–Vibration Relaxation with our Standard Set (10) of Transition Probabilities

The results are essentially as in *B2*(*a*) and *B2*(*b*) although, because of the much greater range of eigenvalues (7), the decay departs more seriously from a pure exponential and the overshoots are more frequent and/or severe.

B4. The Time Scale for Entropy Relaxation

Theorems *A2*, *A3*, and *A4* above suggest that the total entropy relaxes exponentially in the limit, and with a characteristic time which is *half* of that for the energy relaxation. Numerical examination shows that this factor of two relating the relaxation times for the total energy and the total entropy is a persistent feature. Figure 1 compares the energy relaxation and the entropy relaxation for two sum-rule cases: (*a*) a simple temperature change in which the total-entropy relaxation (open circles) is almost indistinguishable from a pure exponential having twice the time constant of that associated with the energy relaxation; (*b*) one in which the initial distribution is a delta function, where it is seen that

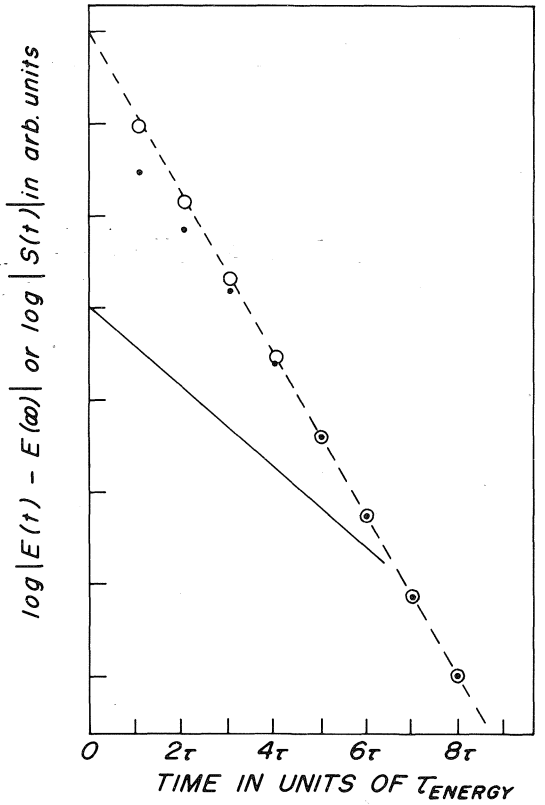

FIG. 1. Comparison of energy and entropy production rates in rotational relaxation, with transition probabilities obeying the sum rule. —, total energy; ---, line having exactly twice the slope of the solid line; ○, total entropy for a simple temperature change; ●, total entropy for a delta-function as the initial population distribution.

beyond $t \approx 3\tau_{energy}$ the total entropy (dots) approaches very closely to that in case (*a*). Other cases of simple temperature relaxation, either assuming canonical invariance, assuming $(N-1)$-fold degeneracy, or assuming probabilities with a small eigenvalue range, would be indistinguishable from curve (*a*) and are not reproduced here. However, using our standard set of transition probabilities (10) having a very wide range of eigenvalues (7), the limiting behaviour shown in Fig. 1 is not reached before all numerical accuracy is lost, and all we can see in these cases is that the *internal* entropy, in the limit, relaxes with the same time constant as does the total energy (which can also be shown analytically as a step in establishing *A4*, *cf.* also *A2*).

Speculation

Clearly the monotonicity principle does not hold for all isothermal relaxing systems, but it does appear to hold for many systems for most of the time. In the cases we examined, it seems that such departures as exist are only 'weak' in the sense that they are temporary, and they appear to be self-correcting. One is reminded here of other examples of relaxations which seem to get on to the same track in their approach to equilibrium, regardless of the starting distribution (12).

Furthermore, the results depicted in Fig. 1 suggest that there does appear to be such a concept of a maximum rate of entropy production, having a limiting value of the time constant exactly twice that of the time constant for the decay of the energy. In no case that we examined did the time constant for the relaxation of the entropy exceed twice that for the relaxation of the energy. Noting that under the conditions when the entropy relaxation rate most nearly approaches the limit of twice the energy relaxation rate the monotonicity principle appears to be most strongly obeyed, we suppose that maximum entropy production and monotonicity are intimately related. Moreover, because of the non-negativeness of the a_i in [15] and [16], there would be no 'negative' contributions to the entropy production rate, and we would fulfill, at least intuitively, the requirement for a maximum rate of production. Again, one is reminded of the information-theoretic description of bulk relaxation in which the entropy is maximised against some assumed dynamical constraints, such as the pure-exponential relaxation of the energy (13). Since in fact these dynamical constraints are all embodied in the master equation and in the way in which it operates on the initial distribution, perhaps the monotonicity of entropy production is synonymous with that maximum entropy principle, but without any explicit reference to the constraints. Moreover, it is relevant to note in further consideration of the results of Fig. 1 that, as conjectured by Andersen *et al.* (9) and proved by Cukier and Deutch (14), a canonical distribution minimises $S^{(1)}$ at a fixed value of $S(t)$ against all other distributions $n_i(t)$.

Acknowledgement

This work was supported by the National Research Council of Canada.

1. H. McKean. Arch. Ratl. Mech. Anal. **21**, 343 (1966).
2. H. O. Pritchard, N. I. Labib, and D. L. S. McElwain. Can. J. Chem. **52**, 2618 (1974).
3. H. O. Pritchard. Can. J. Chem. **53**, 1756 (1975).
4. E. Lissi. Can. J. Chem. **54**, 1995 (1976).
5. K. L. Holtze and H. O. Pritchard. Unpublished results.
6. A. W. Yau. Thesis, York University, Downsview, Ontario. To be submitted.
7. A. W. Yau and H. O. Pritchard. Can. J. Chem. **55**, 737 (1977).
8. R. B. Bernstein and R. D. Levine. Advances in atomic and molecular physics. Vol. 11. Academic Press, New York. 1975. p. 215.
9. H. C. Andersen, I. Oppenheim, K. E. Shuler, and G. H. Weiss. J. Math. Phys. **5**, 522 (1964); J. Chem. Phys. **41**, 3012 (1964).
10. H. O. Pritchard. Can. J. Chem. **54**, 2372 (1976).
11. H. O. Pritchard. Unpublished results.
12. H. O. Pritchard. Specialist periodical reports, reaction kinetics. Vol. 1. The Chemical Society, London. 1975. p. 243.
13. I. Procaccia and R. D. Levine. J. Chem. Phys. **62**, 2496 (1975); **63**, 4261 (1975); Chem. Phys. Lett. **33**, 5 (1975).
14. R. Cukier and J. Deutch. J. Chem. Phys. **46**, 3686 (1967).

Erratum: The trifluoroacetic acid solvent system. Part V. Cryoscopic measurements

MICHAEL G. HARRISS AND JOHN B. MILNE
Department of Chemistry, University of Ottawa, Ottawa, Canada K1N 6N5

Received February 8, 1977
(Ref.: Can. J. Chem. **54**, 3031 (1976))

Equation 4 (p. 3034) should read

$$\nu = \frac{[MX] + 2[M^+]}{C_{MX}}$$

Equation 7 (p. 3034) should read

$$\nu = \frac{[MX] + 2[M^+] + 2[M_2X^+]}{C_{MX}}$$

Equation 10 on p. 3035 should read

$$y_{\pm} = \frac{10^{-14.534\sqrt{I}/(1+1.0044a_0\sqrt{I})}}{1 + \frac{0.001C_{MX}\nu(114 - W_s)}{1.5732}}$$

In eq. 6, p. 3034, W_s is the molecular weight of the solute.

COMMUNICATIONS

The perturbation by anesthetics of hydrogen bonds involving water

A. NAGYRÉVI AND C. SANDORFY

Département de Chimie, Université de Montréal, Montréal (Qué.), Canada H3C 3V1

Received February 17, 1977

A. NAGYRÉVI and C. SANDORFY. Can. J. Chem. **55**, 1593 (1977).

It is shown through the measurement of infrared spectra at low temperatures, on the examples of two fluorocarbon anesthetics and a protein denaturing agent, that such compounds shift the association equilibrium in hydrogen bonds involving water in favor of free or less hydrogen bonded species.

A. NAGYRÉVI et C. SANDORFY. Can. J. Chem. **55**, 1593 (1977).

On montre par des spectres infrarouges mesurés en solution à basse température que des anesthésiques comme le chloroforme ou l'halothane aussi bien que la tétraméthylurée déplacent vers les espèces libre ou plus faiblement associées l'équilibre d'association dans des liaisons hydrogène que forment les molécules d'eau.

In previous publications from this laboratory attention has been drawn to the fact that halofluorocarbon anesthetics "break" hydrogen bonds (HB) of the N—H---N, O—H---O or N—H---O=C type in solution (1, 2). In other words these halofluorocarbons shift the equilibrium of association in favor of the "free" or less associated species. It has been suggested that this observation could be relevant for the elucidation of the mechanism of inhalation anesthesia. It is then natural to inquire whether similar observations can be made on hydrogen bonds involving water.

The means of doing this has been, as before, measuring infrared spectra and using low temperature measurements in order to magnify the effects. For this we needed a solvent in which polar molecules dissolve more easily than in the solvents which we used previously. Thus we were led to use 2-methyltetrahydrofuran (MTF) which can be cooled down to liquid nitrogen temperature where it is a glass. Even after thorough dehydration MTF contains a small amount of water, estimated to be 0.004 *M*. In our experiments some more water has been added to have a H_2O concentration about ten times higher. The HB breakers were chloroform, halothane (CF_3—CHClBr), and tetramethylurea. The two former are well known anesthetics. Urea is known as a protein denaturing agent; we had to use its tetramethylderivative which is soluble in MTF.

Figure 1 shows the infrared spectrum of 0.04 *M* water in MTF at 22°C and at −190°C. At 22°C the main peaks are at about 3575 and 3490 cm^{-1}. The band at higher frequency is probably due to the weak HB in which the oxygen in the MTF molecule is the proton acceptor while the band at lower frequency is likely to involve water–water bonding as well. Upon lowering the temperature more highly associated species become preponderant as shown by the spectacular changes in the spectrum.

The changes that occur upon addition of 0.5–1 *M* chloroform or halothane, or tetramethylurea at room temperature are slight. Upon lowering the temperature, however, con-

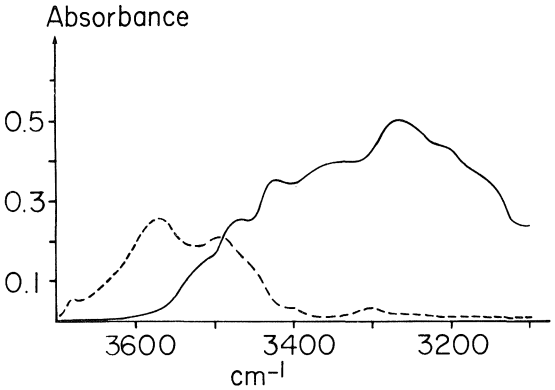

FIG. 1. The infrared spectrum of a 0.04 *M* solution of water in 2-methyltetrahydrofuran: --- at 22°C; — at −190°C.

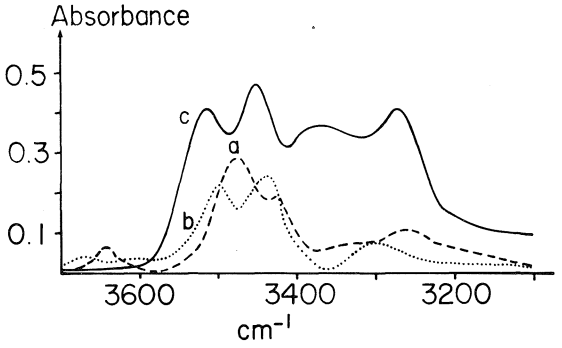

FIG. 2. The infrared spectrum of (*a*) 0.03 *M* water + 1.02 *M* chloroform in 2-methyltetrahydrofuran at −190°C. (*b*) 0.04 *M* water + 0.87 *M* halothane in 2-methyltetrahydrofuran at −190°C. (*c*) 0.04 *M* water + 0.60 *M* tetramethylurea in 2-methyltetrahydrofuran at −190°C.

spicuous changes occur (Fig. 2). They are different with the three hydrogen bond breakers but the change invariably favors the less associated species. (Compare the spectra in Fig. 2 with the low temperature spectrum in Fig. 1.)

We are making no attempt to assign the numerous bands present in these spectra. The only point we wish to make is that HB's involving water are just as sensitive to perturbation by halogenated anesthetics and other "HB breakers" as the other types of hydrogen bonds mentioned above. The changes occur gradually with decreasing temperature. They only become spectacular at very low temperatures; it is our belief, however, that the lesser changes occurring at normal temperature might be sufficient for biological action. The reason why HB's are broken might be the formation of other HB's or other types of aggregates but discussion on this will also be reserved for a later publication.

Experimental

2-Methyltetrahydrofuran was purchased from the Eastman-Kodak Company and was purified according to a prescription given by Fieser and Fieser (3). Its purity was checked by taking the boiling point (78°C) and by its known infrared spectrum (4). The samples were prepared and stored under dry nitrogen atmosphere and were kept on P_2O_5. Chloroform was washed with water, dried and distilled. Halothane and tetramethylurea were high purity commercial products and were not purified further. The spectra were measured on a Perkin-Elmer model 621 infrared spectrometer. The low temperature techniques have been described before (5).

Acknowledgements

Our thanks are due to Dr. R. Massuda for introducing A.N. into the techniques of low temperature infrared measurements.

We are indebted to the Procter and Gamble Company in Worms, Germany for a grant enabling A.N. to carry out research work in our laboratory. We acknowledge financial help by the National Research Council of Canada.

1. T. DI PAOLO and C. SANDORFY. Can. J. Chem. **52**, 3612 (1974).
2. T. DI PAOLO and C. SANDORFY. J. Med. Chem. **17**, 809 (1974).
3. L. F. FIESER and M. FIESER. Reagents for organic syntheses. Vol. 1. 1968. p. 1140.
4. G. M. BARROW and S. SEARLES. J. Am. Chem. Soc. **75**, 1175 (1953).
5. M. ASSELIN and C. SANDORFY. J. Chem. Phys. **52**, 6130 (1970).

Canadian Journal of Chemistry

Published by
THE NATIONAL RESEARCH COUNCIL OF CANADA

Journal canadien de chimie

Publié par
LE CONSEIL NATIONAL DE RECHERCHES DU CANADA

Volume 55 Number 10 May 15, 1977

Volume 55 numéro 10 15 mai 1977

The unimolecular isomerisation of monofluorocyclopropane: a reaction with multiple fall-off characteristics?

MOHAMMAD H. BAGHAL-VAYJOOEE, ANDREW W. YAU, AND HUW O. PRITCHARD

Centre for Research in Experimental Space Science, York University, Downsview, Ont., Canada M3J 1P3

Received November 15, 1976

MOHAMMAD H. BAGHAL-VAYJOOEE, ANDREW W. YAU, and HUW O. PRITCHARD. Can. J. Chem. **55**, 1595 (1977).

Monofluorocyclopropane isomerises at 475°C to give four products, *cis*-1-fluoropropene, *trans*-1-fluoropropene, 2-fluoropropene, and 3-fluoropropene; the ratios of product formation are not independent of pressure and it is shown that, using the Kassel representation, the individual fall-off curves correspond to values of the parameter $s = 9$, 6, 4, and 4 respectively. It is shown that although conventional RRKM theory can account satisfactorily for the difference in fall-off behaviour between the *cis*- and *trans*-1-propene yields, it cannot account for the pressure dependence of the formation of 2- and 3-fluoropropene; the latter behaviour is, however, easily understood in terms of the master-equation approach.

MOHAMMAD H. BAGHAL-VAYJOOEE, ANDREW W. YAU et HUW O. PRITCHARD. Can. J. Chem. **55**, 1595 (1977).

Le fluorocyclopropane s'isomérise à 475°C pour conduire à quatre produits: le fluoro-1 propène *cis*, le fluoro-1 propène *trans*, le fluoro-2 propène et le fluoro-3 propène; les rapports des produits formés ne sont pas indépendants de la pression et on montre qu'à l'aide d'une représentation de Kassel les courbes individuelles de décroissance correspondent respectivement aux valeurs des paramètres $s = 9$, 6, 4 et 4. Quoique la théorie RRKM conventionnelle peut tenir compte d'une façon satisfaisante des différences dans les comportements de décroissance entre les rendements des propènes-1 *cis* et *trans*, on peut montrer qu'elle ne peut tenir compte de la dépendance qui existe entre la pression et la formation des fluoro-2 (et -3) propènes. Toutefois ce dernier comportement peut être facilement compris en termes d'une approche d'une équation maîtresse.

[Traduit par le journal]

Many unimolecular reactions yield more than one product (1, 2), but despite the intrinsic interest in studying comparative fall-off behaviour for the decomposition of a single molecule to several products (3), there exists very little information of this kind. A question of interest is whether the same molecule could exhibit *markedly* different fall-off behaviour in respect of its alternative reaction paths?

The thermal isomerisation of monofluorocyclopropane to four distinct isomeric products was studied at 475°C by Casas, Kerr, and Trotman-Dickenson (4) over a pressure range from 464 to 0.167 Torr, and the individual rates of production of the four products are shown in Fig. 1. The solid lines drawn through these points are the best Kassel curves (5) which will fit the data, having values of $s = 9$, 6, 4, and 4 for *cis*-1-, *trans*-1-, 2-, and 3-fluoropropene respectively. In presenting their experimental results, Casas, Kerr, and Trotman-Dickenson *presumed* that the much sharper fall-off behaviour of the 2- and 3-fluoropropene production rates was due to some loss (by polymerisation) of these two products at low pressures, although apparently there was no firm evidence to indicate

TABLE 1. Unimolecular behaviour in the thermal isomerisation of monofluorocyclopropane

Reaction designation	Product	Kassel s	$P_{1/2}$ (Torr)	Reaction order at 0.2 Torr
[1c]	*cis*-1-Fluoropropene	9	0.4	1.3
[1t]	*trans*-1-Fluoropropene	6	1.2	1.6
[2]	2-Fluoropropene	4	~16	~1.8
[3]	3-Fluoropropene	4	~16	~1.8

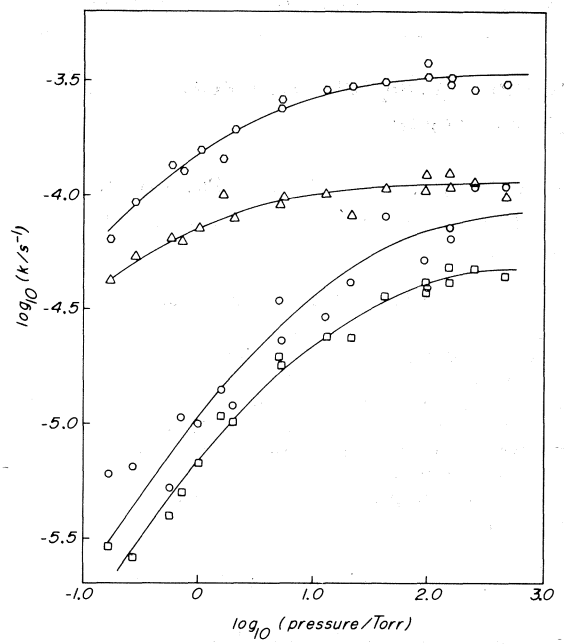

FIG. 1. Experimental rates, taken from the work of Casas, Kerr, and Trotman-Dickenson, for the formation of *cis*-1-fluoropropene (△), *trans*-1-fluoropropene (○), 2-fluoropropene (□), and 3-fluoropropene (○) from monofluorocyclopropane as a function of total pressure, at 475°C. The solid lines are Kassel curves having s = 9, 6, 4, and 4 respectively (a slight shift in the pressure axis being apparent between the latter two cases).

that these two molecules were lost preferentially by polymerisation. We will argue that an equally plausible assumption is that Fig. 1 represents a case of a molecule showing distinctly different fall-off behaviour for different reaction channels, and in support of this hypothesis, we present a set of consistency tests, summarised in Table 1. The four products certainly exhibit the normal expected patterns in respect of the number of effective oscillators and the half-pressure ($P_{1/2}$), or the reaction order at some fixed pressure in the fall-off region and, despite the difficulties inherent in this particular experiment, Table 1 presents at least a *prima facie* case for considering that each channel exhibits genuinely different fall-off behaviour.

A further consistency test can be applied to reactions [1c] and [1t]. If we assume that the rate constant for the ith unimolecular reaction channel obeys strict Arrhenius form

$$[4] \qquad k_{\infty,i} = A_i \exp(-E_{a,i}/RT)$$

then the specific rate constant is given by (6, 7)

$$[5] \qquad k_i(E) = \frac{A_i N(E - E_{a,i})}{N(E)}$$

where $N(E - E_{a,i})$ is the density of states of the molecule at $(E - E_{a,i})$. We will show later (8) using the master-equation formulation (9) that it is possible to relate the half-pressure $P_{1/2}$ to the function $k_i(E)$, whence if we assume that reactions [1c] and [1t] have the same critical energy E_a

$$[6] \qquad \frac{P_{1/2}[1t]}{P_{1/2}[1c]} \sim \frac{k_{1t}(E)}{k_{1c}(E)} \equiv \frac{A[1t]}{A[1c]} = \frac{k_\infty[1t]}{k_\infty[1c]} \simeq \frac{k_{464\,\mathrm{Torr}}[1t]}{k_{464\,\mathrm{Torr}}[1c]} = \frac{54.8}{17.6} = 3.1$$

The ratio of the half-pressures shown in Table 1 and Fig. 1 is 3: thus, the discrimination in the fall-off behaviour between the products *cis*- and *trans*-1-fluoropropene (which Casas, Kerr, and Trotman-Dickenson (4) state is a kinetic effect, and not due to any subsequent *cis–trans* isomerisation after the initial formation) is clearly consistent with current ideas of unimolecular reaction behaviour.

The question then is: can RRKM theory account for the much more severe fall-off in the formation of 2- and 3-fluoropropene? The simple answer, using *conventional* RRKM theory (1) is no, as is shown by the following set of calculations. The forms of the normal modes of vibration for a cyclopropyl halide molecule are

known (10) and normal-mode vibrational analyses have been made for cyclopropyl chloride, bromide, and iodide (11) and of course for cyclopropane itself (12). From this information, we have estimated by conventional comparative techniques (13) the frequencies of the 21 normal vibrational modes for monofluorocyclopropane, and carried out a series of RRKM calculations. Modern efficient methods for calculating the sum of states (14, 15) are about two orders of magnitude faster than the conventional method, as programmed by Robinson and Holbrook (1) for 21 oscillators, and it is not necessary to perform any grouping of the frequencies as is normally the case with such complicated molecules.

Figure 2 shows the theoretical fall-off curves for the four products, compared with the experimental curves (now plotted in conventional k/k_∞ form), calculated using the "ring breathing" frequency (16) of 1200 cm^{-1} as the one removed to define the activated complex. It can be seen that this calculation represents the fall-off behaviour for the *cis*- and *trans*-1-fluoropropene channels excellently, as would of course be expected because of the earlier agreement in eq. 6. However, the fall-off curves for the other two channels are much too shallow, shallower in fact that the 1-fluoropropene curves when in fact they should be much steeper. Isolation of either of two other frequencies, the "C—F deformation" near 300 cm^{-1} or the "asymmetric C—F stretch" near 3000 cm^{-1} leads to calculated fall-off curves for the formation of 2- and 3-fluoropropene very similar to those shown in Fig. 2. Such gross insensitivity of the calculated fall-off has already been noted in less extreme form by others (16–18) and in this particular reaction, in order to reproduce the fall-off behaviour for the production rates of 2- and 3-fluoropropene given the values of k_∞, one would have to choose critical energies in the region of 75 kcal/mol for both channels; this is clearly at variance with the experimental observations (4) which place the critical energies at *about* 4 kcal and 1 kcal respectively above the 1-fluoropropene threshold.

The difficulty here, as is well recognised in chemical activation studies (19), is that one cannot apply conventional RRKM theory to a second reaction channel placed above the first because the decay via the first channel distorts the population distribution below the second threshold, and the normal RRKM assumptions become invalid for this second channel. King,

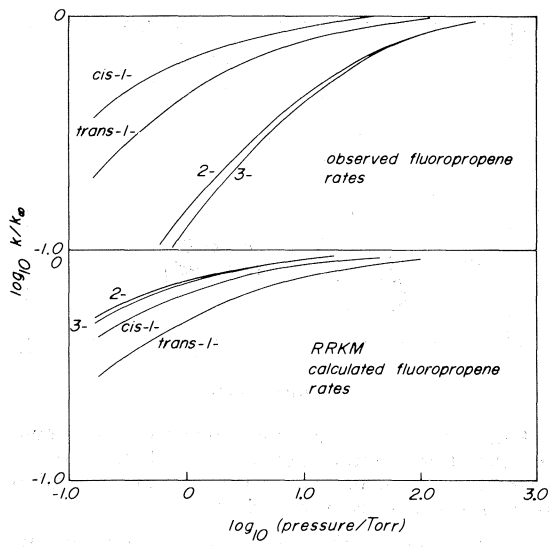

FIG. 2. Comparison of experimental data from Fig. 1 with the results of RRKM calculations. In these calculations the following parameters were used: collision efficiency $\lambda = 0.2$; critical energy (all reactions) = 61 kcal/mol; log (A_∞/s^{-1}) = 13.85, 14.37, 13.54, and 13.64 for *cis*-1-, *trans*-1-, 2-, and 3-fluoropropene respectively; vibration frequencies (cm^{-1}); $\nu_1 = 3100$; $\nu_2 = 3020$; $\nu_3 = 2980$; $\nu_4 = 1450$; $\nu_5 = 1305$; $\nu_6 = 1200$; $\nu_7 = 1090$; $\nu_8 = 1025$; $\nu_9 = 885$; $\nu_{10} = 770$; $\nu_{11} = 865$; $\nu_{12} = 325$; $\nu_{13} = 3095$; $\nu_{14} = 3065$; $\nu_{15} = 1415$; $\nu_{16} = 1275$; $\nu_{17} = 1165$; $\nu_{18} = 1045$; $\nu_{19} = 935$; $\nu_{20} = 810$; $\nu_{21} = 355$; (the numbering of the modes is as in ref. 10). Frequency isolated in this calculation, ν_6; frequencies isolated in other calculations were ν_3 and ν_{12}.

Golden, Spokes, and Benson (20) have discussed a generalisation of the Kassel formulation in the competitive pyrolysis of the two propyl iodides, and an analogous generalisation of the RRKM formulation would be straightforward. However, neither generalisation could take into account properly the mutual perturbation of one channel by the other, whereas it is automatically included in our master-equation formulation (9). Using a very simple extension (8) of the pentadiagonal master-equation model (*i.e.* non-nearest-neighbour transitions included) depicted in Fig. 1*b* of ref. 9, the results of a numerical simulation are as shown in Fig. 3. The curve labelled "channel I" shows the fall-off behaviour for a single decay channel placed at $E = 60$ kcal/mol (with channel II closed): the curve marked "channel II" shows the fall-off behaviour for a single channel placed at $E = 62$ kcal/mol *with channel I closed*; the properties of the probability matrices were chosen so that these fall-off curves would be disposed with respect

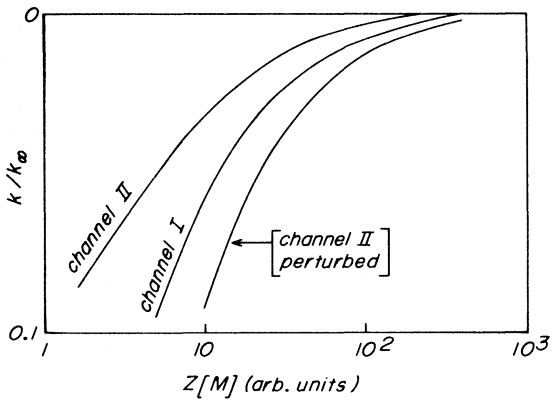

FIG. 3. Results of a master-equation calculation showing the strong perturbation of the fall-off curve for channel II depending upon whether channel I, slightly below it in energy, is open or closed.

to each other rather like those calculated by RRKM theory in Fig. 2, say for 1- and 2-fluoropropene respectively. When the calculation is repeated with both channels open, the fall-off behaviour of channel I remains virtually unchanged, but that of channel II moves markedly to the position denoted by "channel II perturbed", which is in fact in a position very like that observed for 2- and 3-fluoropropene in its relationship to the 1-fluoropropene channel(s). We conclude, therefore, that a plausible interpretation of the thermal isomerisation data for monofluorocyclopropane is that of the four channels available two, leading to *cis*- and *trans*-1-fluoropropene, have the same critical energy and their fall-off behaviour is well represented by RRKM methods; the two other channels, leading to 2- and 3-fluoropropene, have slightly higher critical energies, and their fall-off curves are severely perturbed by the existence of the lower channel(s), giving them a much sharper curvature than would be normal in a molecule of this complexity, for the given values of the critical energy.

Acknowledgements

This work was supported by the National Research Council of Canada; we would also thank Drs. J. A. Kerr and A. F. Trotman-Dickenson for helpful correspondence.

1. P. J. ROBINSON and K. A. HOLBROOK. Unimolecular reactions. John Wiley, London. 1972.
2. P. J. ROBINSON. Spec. Per. Repts. Chem. Soc. London. Reaction kinetics. Vol. 1. 1975. p. 93.
3. H. O. PRITCHARD. *In* Transfer and storage of energy. Vol. 2. John Wiley, London. 1969. p. 368.
4. F. CASAS, J. A. KERR, and A. F. TROTMAN-DICKENSON. J. Chem. Soc. 3655 (1964).
5. G. EMANUEL. Int. J. Chem. Kinet. **4**, 591 (1972).
6. N. B. SLATER. Proc. Leeds Phil. Soc. (Scientific Section), **6**, 259 (1955).
7. W. FORST. *In* Reaction transition states. *Edited by* J. E. Dubois. Gordon and Breach, London. 1972. p. 75.
8. A. W. YAU. Thesis, York University, Downsview, Ont. To be submitted.
9. H. O. PRITCHARD. Can. J. Chem. **55**, 284 (1977).
10. W. G. ROTHSCHILD. J. Chem. Phys. **44**, 3875 (1966).
11. T. HIROKAWA, M. HAYASHI, and H. MURATA. J. Sci. Hiroshima Univ. A **37**, 301 (1973).
12. P. M. MATHAI, G. G. SHEPHERD, and H. L. WELSH. Can. J. Phys. **34**, 1448 (1956).
13. G. HERZBERG. Infrared and Raman spectra. D. Van Nostrand, New York. 1945. p. 315.
14. S. E. STEIN and B. S. RABINOVITCH. J. Chem. Phys. **58**, 2438 (1973).
15. A. W. YAU and H. O. PRITCHARD. Can. J. Chem. **55**, 992 (1977).
16. K. A. HOLBROOK, J. S. PALMER, K. A. W. PARRY, and P. J. ROBINSON. Trans. Faraday Soc. **66**, 869 (1970).
17. B. NOBLE, H. CARMICHAEL, and C. L. BUMGARDNER. J. Phys. Chem. **76**, 1680 (1972).
18. B. D. NEELY and H. CARMICHAEL. J. Phys. Chem. **77**, 307 (1973).
19. D. C. TARDY, B. S. RABINOVITCH, and C. W. LARSON. J. Chem. Phys. **45**, 1163 (1966).
20. K. D. KING, D. M. GOLDEN, G. N. SPOKES, and S. W. BENSON. Int. J. Chem. Kinet. **3**, 411 (1971).

Analysis of a proposal for nitric-oxide abatement in jet-aircraft engines

ROGER A. CRAIG

National Aeronautics and Space Administration, Ames Research Center, Moffett Field, CA, U.S.A. 94035

AND

HUW O. PRITCHARD

Centre for Research in Experimental Space Science, York University, Downsview, Ont., Canada M3J 1P3

Received December 10, 1976

ROGER A. CRAIG and HUW O. PRITCHARD. Can. J. Chem. **55**, 1599 (1977).

Modifications are reported to a conventional gas-kinetics computer program which allow for the continuous addition of chemical species to the flowing gas. This is necessary in modelling the gas flows in a jet engine where air is continuously entrained with the burnt or burning gases, and it also facilitates the investigation of introducing chemical additives into a flowing reaction mixture.

The program is used to compare, under the same *one-dimensional* modelling approximations, the nitric-oxide emissions from a conventional jet engine and from a proposed lean-burning modification, and it is concluded that the lean-burning model has potential for reducing nitric-oxide emission by more than two orders of magnitude.

ROGER A. CRAIG et HUW O. PRITCHARD. Can. J. Chem. **55**, 1599 (1977).

On rapporte des modifications à un programme conventionnel d'ordinateur pour la cinétique en phase gazeus qui permettent de tenir compte de l'addition continue d'espèces chimiques à un gaz en mouvement; ces modifications sont nécessaires si l'on veut développer un modèle pour des gaz qui se déplacent dans un réacteur où l'air est entraîné d'une façon continue aux côtés des gaz qui ont déjà brûlé et de ceux qui sont en train de brûlés; cette modification facilite aussi l'étude de l'effet produit par l'introduction d'additifs chimiques dans un mélange réactionnel en déplacement.

On utilise ce programme pour comparer, dans les mêmes approximations d'un modèle unidimentionnel, les émissions d'oxyde nitrique provenant d'un réacteur conventionnel avec celles d'un système de combustion à mélange pauvre qui est proposé; on en conclut que le système de combustion à mélange pauvre pourrait permettre de réduire les émissions d'oxyde nitrique par au moins deux ordres de grandeur.

[Traduit par le journal]

Introduction

The importance of minimising nitric-oxide emissions from both aircraft and automobile engines needs no amplification (1, 2). The basic problem is that whilst most engine pollutants are the result of incomplete combustion, and can (in principle) be suppressed by improving combustion efficiency, nitric oxide is synthesised from air itself when it is exposed to the high temperatures normally accompanying the combustion. It is well known (3, 4), again in principle, that the formation of nitric oxide can be lessened by carrying out the combustion at much lower temperatures, which would mean using much leaner combustion mixtures than are normally feasible (5). If we now confine our attention to the (axially symmetric) turbine aircraft engine, which is a considerably less difficult modelling problem than is the reciprocating automobile engine, there are two difficulties associated with using much leaner combustion mixtures. First, and most important, the flame becomes unstable, and may blow out; second, the combustion becomes slower, and it may be difficult to achieve complete combustion either within the length of a normal combustion chamber, or even at all (6, 7).

There have been at least three different proposals for achieving complete and stable combustion at low equivalence ratios (ϕ = molar ratio of fuel to air, with the stoichiometric ratio being $\phi = 1$). Roffe and Ferri (6) have experimented with a preheat system in which the air used in the combustion is heated to a higher temperature than is typical in a normal jet engine (1100–1200 K as opposed to, say, 700 K). Oppenheim and co-workers (8) have examined the feasibility of stabilising the combustion by heat recirculation from the later stages of the combustion. A third suggestion is that stabilisa-

tion can be achieved by using a small pilot flame burning under conditions that produce large numbers of free radicals which will support a lean combustion when it would otherwise die (9). This paper presents a brief summary of this proposal, together with the modification of the usual gas-dynamic equations which are necessary for such a study. We emphasise that this analysis uses a highly simplified description of the flow processes in a turbine engine (as discussed more fully below) but the calculated reduction in the nitric-oxide formation is so dramatic that we believe it could persist even when proper account is taken of the neglected complexities.

It should be noted that combustion at low equivalence ratio is not the only possible attack on the problem of reducing nitric-oxide emissions. Staged combustion, in which a slightly fuel-rich mixture is burnt first and the remaining air required to complete the reaction added later, is known to reduce nitric-oxide formation by a factor of 2 or so and has been used in steam-generating plants (10): similar proposals have been made for aircraft-borne power plants (11). Water injection, which has the general effect of lowering the gas temperatures, has been shown to reduce nitric-oxide emissions from turbine combustors (12–14). However, large amounts of water are required and so this approach is unattractive for continuous use with power plants in aircraft. On the other hand, water injection has been used on take-off in some aircraft, causing unacceptable smoke problems. Another idea is the swirl-can combustor (1) which attempts to achieve a very rapid combustion followed by a very rapid quenching, and there have also been proposals which try to blend together the concepts of staged and swirling combustions (15, 16). Entrainment of suitable additives intended to catalyse the reformation of oxygen and nitrogen from nitric oxide is also a common idea. Metallic or ammonium formates or oxalates have been claimed to be effective (17), but one can see many operational difficulties to be overcome before such additives could be used in aircraft engines. We ourselves have examined several plausible additives (*e.g.* O_3), but so far have found none which would appear to be effective (9). Finally one need not, in principle, have to modify the combustion process since (18) the flow patterns of the exhaust gases around the turbine blades are such that a suitable catalytic coating on the blades could destroy all the nitric oxide present, but again there are many technical details to be solved.

The Computer Program

The combustor is modelled conventionally as consisting of two major zones, illustrated in Fig. 1: a primary zone in which combustion is achieved, and a secondary zone in which air is entrained to cool the combustion products. Fuel and air are pre-mixed at the inlet conditions and then flow through the combustor, with the combustion defined by kinetic chemical reactions. The conservation equations used to describe this process are:

Mass

$$[1] \qquad \frac{1}{\rho VA}\frac{\mathrm{D}}{\mathrm{D}t}(\rho VA) = \frac{\mu}{\rho}$$

Species

$$[2] \qquad \frac{\mathrm{D}}{\mathrm{D}t}\frac{C_i}{\rho} = \frac{1}{\rho}\left(r_i + \frac{\mu_i}{M_i} - \frac{C_i\mu}{\rho}\right) \qquad i = 1, \ldots N$$

Momentum

$$[3] \qquad \rho\frac{\mathrm{D}V}{\mathrm{D}t} + \frac{1}{V}\frac{\mathrm{D}p}{\mathrm{D}t} = \mu(V_\mathrm{p} - V)$$

Energy

$$[4] \qquad \rho\frac{\mathrm{D}}{\mathrm{D}t}\left(h + \frac{V^2}{2}\right) = \mu[h_\mathrm{p} - h + \tfrac{1}{2}(V_\mathrm{p}^2 - V^2)]$$

and gas ideality is assumed

$$[5] \qquad P = \rho\frac{RT}{M_\mathrm{w}}$$

In eqs. 1–5, P is the pressure, ρ is the density, R is the gas constant, V is the axial velocity, A is the local area, M_i are the species molecular weights, and M_w is the mean molecular weight, all in g, cm, and s units; h is the enthalpy per g, and quantities labelled with a subscript p refer to combustor inlet conditions. The C_i are the individual species concentrations in mol cm^{-3}, the r_i are the rates of production in mol $cm^{-3}\,s^{-1}$, the μ_i represent the local rates of introduction of mass of each individual species due to entrainment in g cm^{-3} s^{-1}, and μ is the sum over all species of the μ_i. Equations 1–5 describe a chemically reacting one-dimensional flow which is assumed to be inviscid and adiabatic, and transport is by convection only. In the secondary zone, the entraining air is injected uniformly around the wall of the combustor and instantaneous radial mixing with the bulk of the flow is

assumed; the composition of the entraining gas is specified by the μ_i terms in eq. 2, enabling chemical additives introduced along with the cooling air to be treated very simply. A fuller account of the derivation and solution of these equations is available in thesis form (9).

The computer program used in this work was the NASA-Lewis General Chemical Kinetics Program (19), modified as outlined in eqs. 2 and 3 above to allow for the entrainment of air or the inclusion of additives in the flow, and extensively tested for consistency (9). Since the main aim of this work was to compare overall nitric-oxide formation rates in two very different model combustions, rather than to examine the combustion processes themselves, a number of fairly drastic approximations were made. Probably the most drastic assumption (from an engineering point of view) was the complete neglect of turbulence, which has been included in some other modelling studies (20, 21), and which is known to correlate to some extent with nitric-oxide formation rates (3). This sensitivity to turbulence can be rationalised qualitatively by regarding the macroscopic turbulent process as a series of microscopic staged combustions. The neglect of turbulence, which is a very important part of any practical combustion process, was justified *a posteriori* by the fact that the calculated difference between the two models was much greater than any expected variation in nitric-oxide formation rates arising from turbulent effects (22). For similar reasons, we chose to model the much simpler combustion of hydrogen in air, rather than jet fuel in air, simulating the practical process by adding a portion of argon as a diluent so as to match simultaneously both the equivalence ratio and the flame temperature of the real combustion; in fact, it is known not only that jet engines which ordinarily operate on kerosene will perform reasonably well on gaseous hydrogen (23) but that similar amounts of nitric oxide are emitted using either hydrogen or jet fuel (24).

For the modelling calculations, we chose to use the specific flow rates of fuel and air characteristic of a typical commercial gas turbine at a fairly high power setting (20), as shown in Table 1,[1] and the first task was to establish the conditions under which the model would mimic the practical combustion. The rate constants chosen for the hydrogen–oxygen combustion processes (25) are shown in Table 2. Some of these rate constants may be somewhat imprecise, but as is now well established, the overall rates of complex chemical reaction schemes are often rather insensitive to the rates of many of the detailed processes, and as long as the dominant processes are reasonably correct, an acceptable computed rate will emerge (26). Finally, the calculation includes one adjustable parameter, the amount of recirculation in the primary zone, depicted by the two vortex arrows in Fig. 1. A mixture of air and hydrogen will not sustain combustion unless some of the heat of combustion is transferred back (as it is in a real flame by a variety of complex processes) so as to raise the initial temperature of the reaction mixture. Thus, a fraction (15–18% depending on ϕ) of the combusted gas was assumed to be recirculated so as to bring the inlet temperature of the gases up to

TABLE 1. The JT8D combustion chamber

(*a*) Approximate dimensions

Parameter	Value
Diameter	19 cm
Cross-sectional area	297 cm²
Overall length	38 cm
Primary zone length	8 cm
Secondary zone length	30 cm

(*b*) Inlet conditions

Parameter	Value
Overall air flow	7700 g/s
	267 mol/s
Temperature	700 K
Pressure	15 atm

(*c*) Computed flow parameters (typical)

Parameter		Value
Induction times	$\phi = 1$	0.7 ms
	$\phi = 0.8, 1.2$	1.1 ms
Primary zone residence time		4–5 ms
Secondary zone		
Residence time		10–12 ms
Initial temperature	$\phi = 0.8$	2390 K
	$\phi = 1.0$	2600 K
	$\phi = 1.2$	2590 K
Initial velocity	$\phi = 0.8$	2800 cm/s
	$\phi = 1.0$	3200 cm/s
	$\phi = 1.2$	3300 cm/s

[1]The JT8D engine is used in such aircraft as the Boeing 727, Douglas DC9, and Sud Caravelle 10, and a complete engine consists of nine combustor cans (such as depicted in Table 1), arranged symmetrically about the engine axis.

TABLE 2. Combustion reactions*

	Reaction	Rate parameters		
		A	n	E (kcal/mol)
[*i*]	$H_2 + OH \rightleftarrows H_2O + H$	2.2×10^{13}	0	5.1
[*ii*]	$H + O_2 \rightleftarrows OH + O$	1.26×10^{14}	0	16.3
[*iii*]	$O + H_2 \rightleftarrows OH + H$	1.74×10^{13}	0	9.4
[*iv*]	$M + H + O_2 \rightleftarrows HO_2 + M$	1.0×10^{15}	0	−1
[*v*]	$M + H_2 \rightleftarrows H + H + M$	2.23×10^{12}	$\frac{1}{2}$	92.6
[*vi*]	$H_2 + HO_2 \rightleftarrows H_2O_2 + H$	9.6×10^{12}	0	24
[*vii*]	$M + H_2O_2 \rightleftarrows OH + OH + M$	1.17×10^{17}	0	45.5
[*viii*]	$H + HO_2 \rightleftarrows OH + OH$	7×10^{13}	0	0
[*ix*]	$M + H + OH \rightleftarrows H_2O + M$	1×10^{19}	−1	0
[*x*]	$M + O + O \rightleftarrows O_2 + M$	1.38×10^{18}	−1	0.34
[*xi*]	$O + H_2O \rightleftarrows OH + OH$	8.4×10^{13}	0	18
[*xii*]	$OH + HO_2 \rightleftarrows H_2O + O_2$	6×10^{12}	0	0
[*xiii*]	$O + HO_2 \rightleftarrows OH + O_2$	6×10^{12}	0	0
[*xiv*]	$HO_2 + HO_2 \rightleftarrows H_2O_2 + O_2$	1.8×10^{12}	0	0
[*xv*]	$H_2 + O_2 \rightleftarrows OH + OH$	1.0×10^{14}	0	47.6
[*xvi*]	$H_2 + O_2 \rightleftarrows H + HO_2$	2×10^{14}	0	67
[*xvii*]	$OH + H_2O_2 \rightleftarrows H_2O + HO_2$	1×10^{13}	0	1.8
[*xviii*]	$O + H_2O_2 \rightleftarrows OH + HO_2$	8×10^{13}	0	1
[*xix*]	$H + H_2O_2 \rightleftarrows H_2O + OH$	3×10^{14}	0	9

*Rate constants (in units of mol, cm^3, and s) are for the forward direction and are given by $k = AT^n \exp(-E/RT)$. All third body efficiencies are 1.0 except for reaction *iv* in which the efficiency of H_2 is taken as 3.3 and of H_2O as 21.

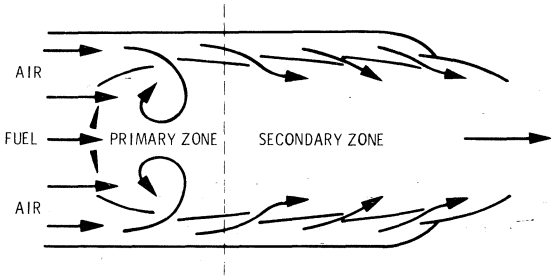

FIG. 1. Schematic representation of a jet-engine combustor can.

the design inlet temperature of 1000 K (14). This gives a self-sustaining stable combustion with an acceptable induction time and flame-front thickness; more extensive discussion of this recirculation procedure can be found in ref. 7 where our program has been used to model the methanol–air combustion in an engine, and in ref. 9. Moreover, not only are the induction times acceptable, but so are their relationships with equivalence ratio and inlet pressure when compared with observed data (9). Hence, it would seem that extension of this model to include nitric-oxide forming reactions is warranted, particularly so since the temperature history of the nitrogen–oxygen mixture is the principal determinant of the final nitric-oxide mass flow.

The reaction rates involved in the formation of nitric oxide (25, 27, 28) are shown in Table 3. Again, some of these rates are still rather uncertain at the present time, but with the exception of reaction *xxii* (which is discussed further below), are thought to be accurate within a factor of two (29). Only 9 chemical reactions are included in Table 3, other reactions (such as $NO_2 + O \rightleftarrows NO + O_2$, $M + NO_2 \rightleftarrows M + NO + O$) were discarded as making no significant contribution to the nitric-oxide mass flow (9). This gives a total of 28 chemical reaction-rate equations to be integrated, coupled with the eqs. 1–5 describing the flow and the air entrainment, using our modification of the NASA–Lewis General Chemical Kinetics Program (9, 19). With appropriate integration step lengths, determined by the error criteria in the usual way, a typical computer run would take about 200 s on a CDC 7600 machine.

Results

First we present very briefly the results obtained for a conventional combustor design: many details of the combustion itself will not be discussed here, only those pertaining to the formation of nitric oxide. Smooth combustion is achieved (as noted above) by recirculating 15–

TABLE 3. Nitric-oxide formation reactions*

	Reaction	Rate parameters		
		A	n	E (kcal/mol)
[xx]	$N + NO \rightleftarrows N_2 + O$	3.1×10^{13}	0	0.33
[xxi]	$N + O_2 \rightleftarrows NO + O$	6.43×10^{9}	1	6.2
[xxii]	$N + OH \rightleftarrows NO + H$	4×10^{13}	0	0
[xxiii]	$H + N_2O \rightleftarrows N_2 + OH$	3×10^{13}	0	10.8
[xxiv]	$O + N_2O \rightleftarrows N_2 + O_2$	3.6×10^{13}	0	24
[xxv]	$O + N_2O \rightleftarrows NO + NO$	5×10^{13}	0	24
[xxvi]	$M + N + O \rightleftarrows NO + M$	6.4×10^{16}	$-\frac{1}{2}$	0
[xxvii]	$M + N_2O \rightleftarrows N_2 + O + M$	2×10^{15}	0	57.6
[xxviii]	$M + N + N \rightleftarrows N_2 + M$	7×10^{14}	0	0

*Rate constants (in units of mol, cm³, and s) are for the forward directions and are given by $k = AT^n \exp(-E/RT)$.

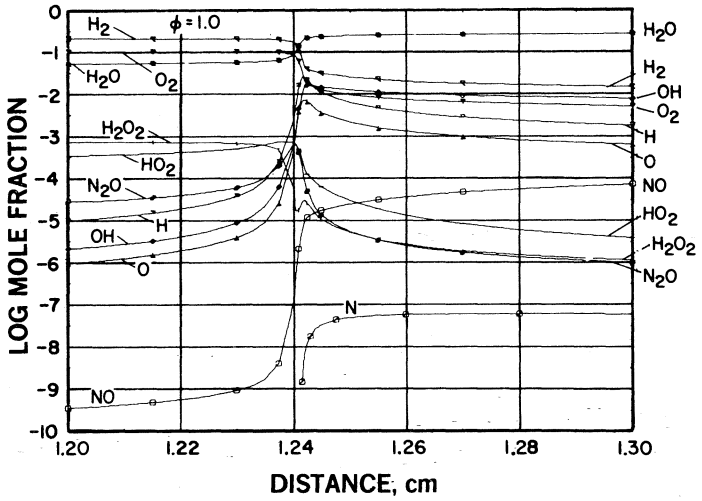

FIG. 2. Calculated species mole fractions in the combustion region of the primary zone for the case $\phi = 1.0$; note that the primary zone is approximately 8 cm long.

18% of the gas in the primary zone (7, 9) giving an effective inlet temperature in the steady state of 1000 K. Under these conditions, there is a short induction period, clearly shown in Figs. 2, 3, and 5: *cf.* also Table 1. During this time, the concentrations of various free radicals (O, OH, H, HO_2) increase, and when their concentrations become high enough, combustion occurs quite abruptly, after which most species relax to their equilibrium levels: a typical plot of the individual species concentrations through the flame front for an equivalence ratio $\phi = 1.0$ is shown in Fig. 2. Nitric oxide, however, does not equilibrate as quickly as the other species, and its concentration climbs slowly from a low value at the flame zone towards its equilibrium level. The net rates of the various nitric-oxide producing reactions are shown in Fig. 3 for the primary zone and in Fig. 4 for the secondary zone, using in each case three trial values of overall equivalence ratio (lean, $\phi = 0.8$; stoichiometric, $\phi = 1.0$; rich, $\phi = 1.2$). There is negligible production before the combustion zone, and thereafter, three reactions are responsible for the formation of nitric oxide, which are, in decreasing order of importance

[6] $O + N_2 \rightarrow NO + N$ (*xx*, reverse)

[7] $N + OH \rightarrow NO + H$ (*xxii*)

[8] $N + O_2 \rightarrow NO + O$ (*xxi*)

with the latter one only being significant under fuel-lean conditions (Fig. 3). The importance of reaction 7 has not been recognised until recently,

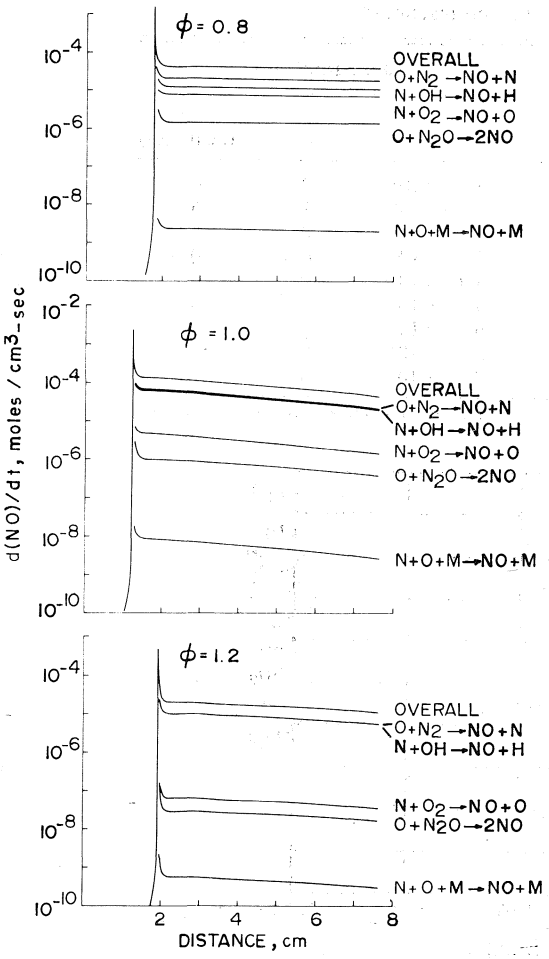

FIG. 3. Calculated overall and individual nitric-oxide production rates in the primary zone.

although its inclusion in model reaction schemes is now commonplace (7, 8, 30, 31), and the reaction scheme [6]–[8] is now often termed the extended Zeldovich mechanism (32). Moreover, we have assumed for reaction 7 the room-temperature rate constant with no activation energy, so its importance could well be underestimated in these calculations.[2] We may rationalise the results shown in Fig. 4 in the following way. In the fuel-lean case ($\phi = 0.8$), combustion is already complete at the 8 cm mark and the nitric-oxide formation rates continue to decline. On the other hand, the addition of more air to the fuel-rich case ($\phi = 1.2$) causes the combustion to proceed further, and along with it, all rates of nitric-oxide forming processes increase to maxima before falling off; the behaviour of the stoichiometric case ($\phi = 1.0$) is intermediate between the other two. Figure 5 shows an enlarged segment of Fig. 3 for the $\phi = 1.0$ case; similar plots for the other cases are available in thesis form (9).

Figure 6 presents a summary of the results in the form of nitric-oxide mass flows and temperature profiles for the conventional combustor. As we have seen in Figs. 2–5, the production of nitric oxide commences in the primary combustion zone, and the production rate is greatest in the stoichiometric case; in both this and the fuel-lean case, most of the production of nitric oxide occurs in the primary zone. However, in the fuel-rich case, there is a rather low rate of nitric-oxide production in the primary zone, since the concentrations of O_2 and O are low in this region, but a large amount is generated when the excess fuel is burned in the initial entraining air; in this burning zone, there is an excess of free radicals and a large amount of new O_2 to enhance the nitric-oxide production rate. Figure 6 also shows that in all three cases, nitric-oxide production ceases when the gas is cooled below about 2200 K in the secondary zone, and no significant amounts of nitric oxide are formed or destroyed after the 2200 K freezing mark is passed (9, 35). This effect becomes rather obvious when the results are presented as mass flow of nitric oxide rather than, as is usually done, the relative concentration of nitric oxide where the dilution effect of the entraining air obscures the real freezing points.

Before proceeding to examine the alternative model combustion, it is necessary to know that this, albeit, very simple model of the conventional combustor does not predict nitric-oxide flow rates which are wildly in error. In fact, they agree quite well with those found in practice, being very similar (9) to measurements made on an experimental combustor using hydrogen as a fuel (36), and about a factor of 2–4 greater than the observed values[3] for the JT8D combustor

[2]Nonetheless, since this work was completed, measurements of the reverse reaction have been made at high temperatures (2400–4200 K) by Flower (33) and the rate for reaction 7 used in our calculations is consistent with these measurements: Flower's results correspond to a value of k_7 of 3.5, 4.4, and 5.0×10^{13} mol^{-1} cm^3 s^{-1} at 1500, 2000, and 2500 K respectively, compared with the constant value of 4.0×10^{13} mol^{-1} cm^3 s^{-1} shown in [*xxii*] of Table 2.

[3]Recently, it has been suggested (38) that these measured nitric-oxide flow rates could be too low by a factor of between 2 and 5.

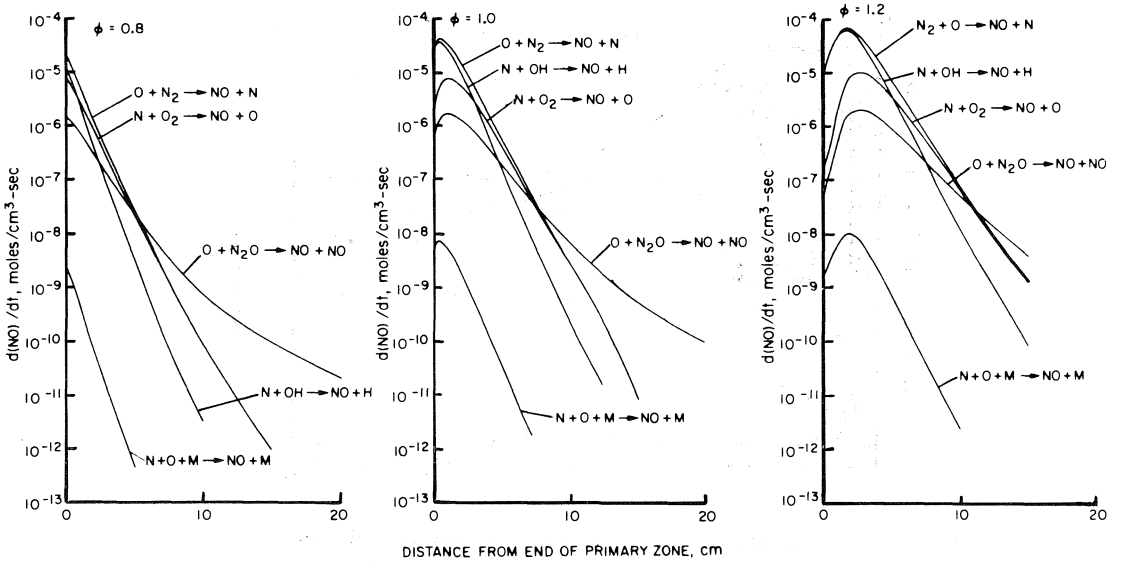

FIG. 4. Calculated nitric-oxide production rates in the secondary zone.

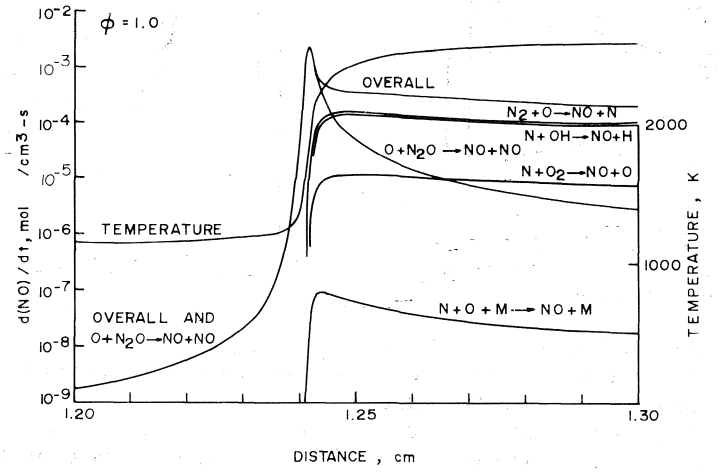

FIG. 5. Calculated temperature and nitric-oxide production rates in the combustion region of the primary zone for the case $\phi = 1.0$. Note that the oxidation of nitrous oxide appears to be an important early source of nitric oxide in all three calculations ($\phi = 0.8$, 1.0, and 1.2), but it is not clear whether this is a significant conclusion. It is marginally consistent with the observation that nitrous oxide is an important source of nitric oxide in fuel-lean systems at low temperatures (31), but at variance with the observation that "prompt NO" does not occur in hydrogen nor carbon-monoxide flames (34); the rate constant used for reaction *xxv* agrees with that most recently recommended (29), but no "sensitivity tests" were carried out on this reaction.

itself using jet fuel at the same inlet temperature (37). It would appear, therefore, that on these criteria, as well as other tests of the model (7, 9), the present reaction scheme and flow model should be adequate to test the likely success of the proposal for reducing nitric-oxide emissions using a pilot flame, rich in free radicals, to support a lean combustion (9).

There are many possible practical configurations for the support of a lean combustion by a pilot flame, but we are restricted in our computer program to those having axial symmetry. Hence, we examined the idealised model depicted in Fig. 7, having the length, exit diameter, and the fuel and air flows exactly the same as for the conventional combustor just described. Com-

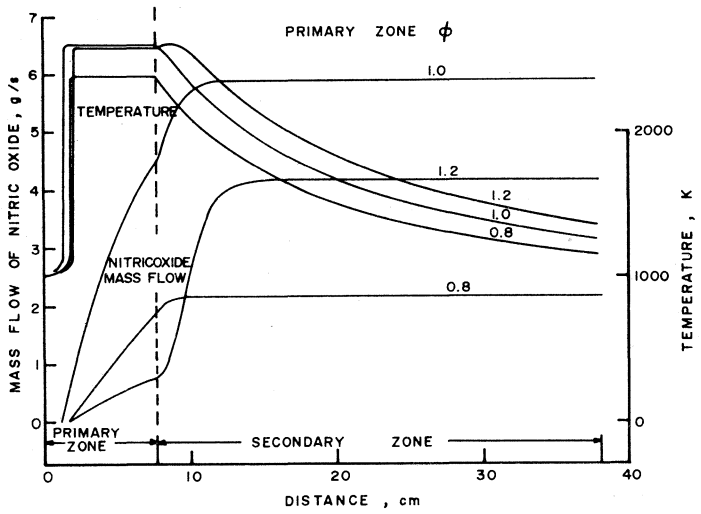

FIG. 6. Calculated temperature and nitric-oxide mass flow along the entire combustor.

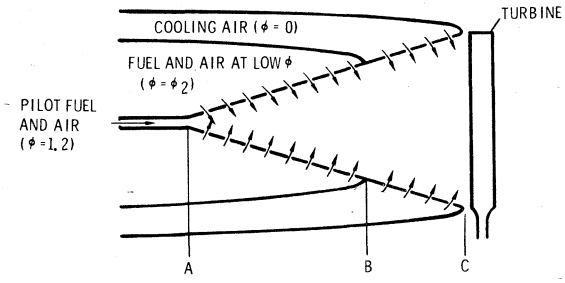

FIG. 7. Schematic representation of the novel combustor for low nitric-oxide emissions.

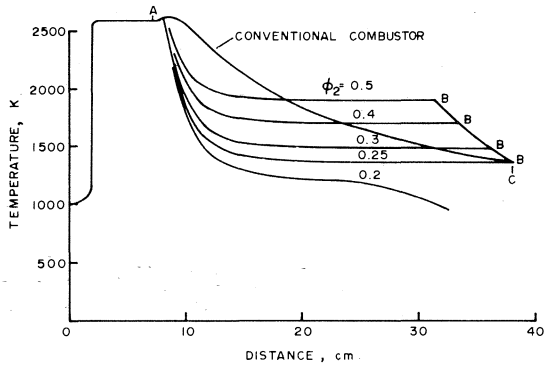

FIG. 8. Calculated temperature profiles along the conventional and the novel combustors.

bustion is established by burning a small portion of the fuel and air in a primary, or pilot stage. This pilot stage is assumed to have the same axial properties as the primary stage of the conventional combustor, but the diameter is reduced from 19 cm to 1 cm. The equivalence ratio in the pilot stage is 1.2, and the specific fuel and air flows are the same as in the conventional combustor. The remainder of the fuel is then burned in the conical section extending from A to B. The fuel is premixed with air at low equivalence ratios ϕ_2 and at normal air-entrainment conditions, and is introduced into the flow uniformly along the section A to B; the smaller ϕ_2, the greater is the distance between A and B. After all the fuel has been entrained, the remaining air is introduced between B and C in the normal manner. Figure 8 shows the calculated axial variation of temperature for this novel combustor, compared with the conventional combustor. The pilot stage temperature is just the temperature for the conventional combustor primary zone. The parameter ϕ_2 is varied from 0.5 to 0.2, but in each case the same total amount of fuel and air flows through the combustor. Thus, if all the fuel is burnt, the exit conditions (pressure, temperature, mass flow, thrust, etc.) will be the same as in the conventional combustor. The pilot gas is hot and rich in the free radicals required for combustion, so the fuel and air mixture introduced between A and B burns very rapidly although at a lower temperature. As ϕ_2 is reduced more and more below 0.5, combustion proceeds at successively lower temperatures, but nevertheless it proceeds! However, at $\phi_2 = 0.2$, the cooling effect of the entraining air overwhelms the heat liberated in the combustion

reactions and the combustion freezes near the 20 cm mark, leading to a very low exit temperature, large concentrations of unburnt gas, and of course low efficiency. The combustion does not extinguish itself in this way at $\phi_2 = 0.25$ or above.

Figure 9 shows the calculated nitric-oxide mass flow along this novel combustor, confirming that there is a much lower production of nitric oxide by as much as perhaps a factor of 100. However, the production of nitric oxide does not freeze at 2200 K as it does in the conventional combustor. This is because of the protracted combustion which, although the temperature is somewhat lower, still contains high concentrations of radicals; examination of the radical profiles shows that OH and HO_2 radicals have much higher concentrations in these lean flames than they do in the conventional ones. Thus, in the early stages of this novel combustor nitric oxide continues to be formed by reactions 6, 7, and 8 giving rise to the steep increase in the mass-flow curves just after point A. However, these reactions then become quenched and the curves bend over fairly sharply, leaving only reaction *xxv*, the oxidation of nitrous oxide as the important formation reaction. This reaction, it will be recalled, was the one apparently responsible for the peak nitric-oxide production in the flame zone of the conventional combustor, *cf.* Fig. 5.

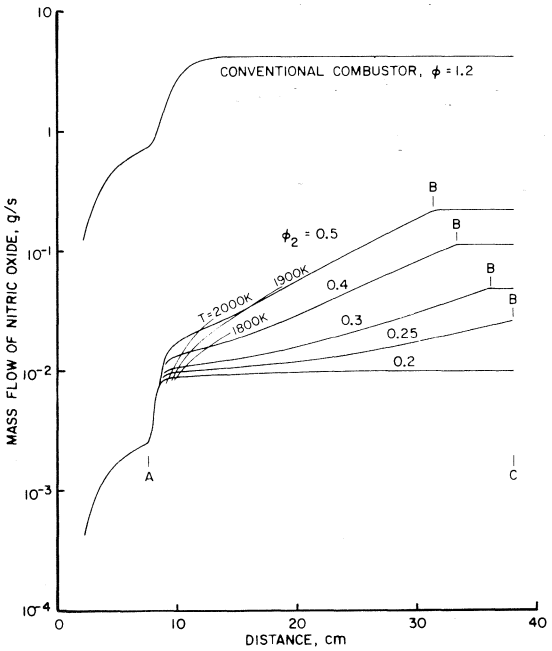

FIG. 9. Calculated nitric-oxide mass flow rates along the conventional and the novel combustors; (conventional combustor data taken from Fig. 6).

As was noted above, there appears to be a limit of about $\phi_2 = 0.25$ below which the flame dies and combustion is incomplete, but all the same, the system should be very resistant to a complete flame-out, since any downstream disturbance of this kind should encounter more and more difficulty propagating backwards and extinguishing the pilot flame. Also, one might expect that, although our calculations show that combustion is virtually complete at the exit for the $\phi_2 = 0.25$ case, a somewhat higher ϕ_2 might be needed to achieve a satisfactorily complete combustion in a real engine.

Conclusion

All the numerical tests we have undertaken show that our modifications of the NASA-Lewis General Chemical Kinetics Program to allow for the entrainment of air or the inclusion of additives into the flow are correct. The program was used to examine in a comparative way, making the same approximations in each case, a conventional and a proposed lean-burning combustion, and it would appear that using the lean-burning process, reductions of nitric-oxide emission of over a factor of 100 might be possible. In this design the combustion is protracted to low temperatures, and the (often neglected) details of the combustion may not be ignored. The super-equilibrium concentrations of free radicals during this combustion are important, and the nitric oxide produced from such a combustor cannot be estimated from equilibrium or from steady-state assumptions, but requires an analysis including the kinetics of the combustion reactions (*cf.* also ref. 39). Thus, in practical application, the extent of the improvement in nitric-oxide emissions using piloted flame techniques will be somewhat dependent on the nature of the fuel, but a significant improvement appears guaranteed by the fact that the overall temperature profile of the combustion is lower.

Acknowledgement

Part of this research was supported by the National Research Council of Canada.

1. Proceedings of the third conference on the climatic impact assessment program (CIAP). DOT-TSC-OST-74-15. U.S. Department of Transportation, Washington, DC. 1974.

2. J. B. HEYWOOD and J. C. KECK. Environ. Sci. Technol. **7**, 216 (1973).
3. I. L. DRELL and F. E. BELLES. Survey of Hydrogen Combustion Properties. National Advisory Committee for Aeronautics, Report 1383, 1958.
4. ANON. Basic considerations in the combustion of hydrocarbon fuels with air, National Advisory Committee for Aeronautics, Report 1300, 1957.
5. A. FERRI. Astronaut. Aeronaut. July 1972. p. 37.
6. G. ROFFE and A. FERRI. Prevaporization and premixing to obtain low oxides of nitrogen in gas turbine combustors. NASA CR-2495, 1975; Effect of premixing quality on oxides of nitrogen in gas turbine combustors. NASA CR-2657, 1976.
7. H. G. ADELAMN, L. H. BROWNING, and R. K. PEFLEY. AIAA J. **14**, 793 (1976).
8. A. J. GANJI, J. SHORT, M. C. BRANCH, and A. K. OPPENHEIM. AIAA J. **14**, 809 (1976).
9. R. A. CRAIG. Ph.D. Thesis, York University, Downsview, Ont. 1974; R. A. CRAIG and H. O. PRITCHARD. U.S. Patent pending.
10. ANON. Power, September 1972. p. 83.
11. G. H. SCHWEDERSKY. U.S. Patent 3,729,285. April 1973.
12. N. R. DEBELIUS, M. B. HILT, and R. H. JOHNSON. Am. Soc. Mech. Eng. Pap. 71-GT-58, 1971.
13. N. R. MARCHIONNA, L. A. DIEHL, and A. M. TROUT. The effect of water injection on nitric oxide emissions of a gas turbine combustor burning ASTM Jet-A fuel. NASA TMX-2958. 1973.
14. R. KOLLRACK and L. D. ACETO. J. Air Pollution Control Assoc. **23**, 116 (1973).
15. S. J. MARKOWSKI. U.S. Patent 3,788,065. January 1974.
16. R. P. LOHMANN and S. J. MARKOWSKI. U.S. Patent 3,872,664. March 1975.
17. M. P. STENGEL. U.S. Patent 3,746,498. July 1973.
18. R. A. CRAIG. Unpublished.
19. D. A. BITTKER and V. J. SCULLIN. General chemical kinetics computer program for static and flow reactions, with application to combustion and shock-tube kinetics. NASA, TN D - 6586 (1972).
20. R. S. FLETCHER and J. B. HEYWOOD. AIAA Paper No. 71-123, AIAA 9th Aerospace Sciences Meeting, 1971.
21. J. B. HEYWOOD. AIAA Paper No. 71-712, AIAA 9th Aerospace Sciences Meeting, 1971.
22. F. C. GOULDIN. Comb. Sci. Tech. **9**, 17 (1974).
23. ANON. Hydrogen for turbojet and ramjet powered flight. National Advisory Committee for Aeronautics, RM E 57 D 23. 1957.
24. J. GROBMAN, C. NORGREN, and D. ANDERSON. Turbojet emissions, hydrogen *vs*. JP. NASA TMX-68258 (1973).
25. D. L. BAULCH, D. D. DRYSDALE, D. G. HORNE, and A. C. LLOYD. Evaluated kinetic data for high temperature reactions. Vols. 1 and 2. The Chemical Rubber Co., Cleveland, Ohio. 1972, 1973.
26. H. O. PRITCHARD. Spec. Period. Rep., React. Kinet. **1**, 243 (1975).
27. G. A. LAVOIE, J. B. HEYWOOD, and J. C. KECK. Combust. Sci. Technol. **1**, 313 (1970).
28. I. M. CAMPBELL and B. A. THRUSH. Trans. Faraday Soc. **64**, 1265 (1968).
29. Chemical kinetic and photochemical data for modelling atmospheric chemistry. National Bureau of Standards, Technical Note 866, 1975.
30. N. P. CERNANSKY and R. F. SAWYER. Fifteenth Symposium (International) on Combustion. The Combustion Institute, Pittsburgh, PA. 1975. p. 1039.
31. P. C. MALTE and D. T. PRATT. Combust. Sci. Technol. **9**, 221 (1974); Fifteenth Symposium (International) on Combustion. The Combustion Institute, Pittsburgh, PA. 1975. p. 1061.
32. T. TAKAGI, M. OGASAWARA, K. FUJII, and M. DAIZO. Fifteenth Symposium (International) on Combustion. The Combustion Institute, Pittsburgh, PA. 1975. p. 1051.
33. W. L. FLOWER. Experimental study of nitric oxide – hydrogen reaction kinetics. HTGL Report No. 103. Stanford University. March 1976.
34. C. P. FENIMORE. Thirteenth Symposium (International) on Combustion. The Combustion Institute, Pittsburgh, PA. 1971. p. 373.
35. R. ROBERTS, L. D. ACETO, R. KOLLRACK, D. P. TEIXEIRA, and J. M. BONNELL. AIAA J. **10**, 820 (1972).
36. C. T. NORGREN and R. D. INGEBO. Emissions of nitrogen oxides from an experimental hydrogen-fuelled gas turbine combustor. NASA TMX-X-2997 (1975).
37. F. W. LIPPERT. Am. Soc. Mech. Eng. Pap. 72-GT-60 (1972).
38. National Aeronautics and Space Administration. Atmospheric programs, Bulletin 76-1, January 1976.
39. H. F. NELSON. AIAA J. **14**, 1177 (1976).

Solvent effects on thermodynamics and mechanism of dissociation of the monocomplex of nickel(II) with thiocyanate

PRAPHULLA KUMAR CHATTOPADHYAY AND BYRON KRATOCHVIL

Department of Chemistry, University of Alberta, Edmonton, Alta., Canada T6G 2G2

Received November 24, 1976

PRAPHULLA KUMAR CHATTOPADHYAY and BYRON KRATOCHVIL. Can. J. Chem. **55**, 1609 (1977).

Rate constants and associated activation parameters for dissociation of $(NiSCN)^+$ were measured kinetically in methanol and dimethylsulfoxide by stopped-flow spectrophotometry using copper(II) as the decomposing ion. The data along with previous results by others on dissociation of $(NiSCN)^+$ in water, acetonitrile, and *N*,*N*-dimethylformamide are discussed mechanistically by considering the effect of solvent donor properties on the activation enthalpy for the dissociation process. Rate constants for dissociation at a single temperature are not systematically related to the Gutmann donor number of the solvent, but the enthalpy of activation for the dissociation process shows a linear inverse relation to the donor number. Pathways for dissociation of $(NiSCN)^+$ in these solvents are accommodated within an I_d-type mechanism.

PRAPHULLA KUMAR CHATTOPADHYAY et BYRON KRATOCHVIL. Can. J. Chem. **55**, 1609 (1977).

Opérant dans le méthanol et le diméthylsulfoxyde, faisant appel à la spectrométrie de flux stoppé et au cuivre(II) comme ion de décomposition, on a mesuré la cinétique, les constantes de vitesse et les paramètres d'activation qui sont associés avec la dissociation de $(NiSCN)^+$. Les données obtenues, de concert avec des résultats obtenus antérieurement par d'autres sur la dissociation de $(NiSCN)^+$ dans l'eau, dans l'acétonitrile et dans le *N*,*N*-diméthylformamide, peuvent être discutées du point de vue mécanistique en considérant l'effet des propriétés donneurs du solvant sur l'enthalpie d'activation pour le processus de dissociation. Les constantes de vitesse pour la dissociation à une température donnée ne sont pas reliées d'une facon systématique avec le nombre donneur de Gutmann du solvant mais l'enthalpie d'activation pour le processus de dissociation présente une relation linéaire inverse avec le nombre donneur. On peut accommoder les chemins de dissociation de $(NiSCN)^+$ dans ces solvants à l'intérieur d'un mécanisme du type I_d.

[Traduit par le journal]

Introduction

It was shown (1) recently that the pathways for dissociation of the $(S_5NiIsoquinoline)^{2+}$ ion in water, methanol, acetonitrile, propylene carbonate, dimethylsulfoxide, and *N*,*N*-dimethylformamide can be accommodated within an I_d-type mechanism represented by

$$[1] \quad L{-}NiS_5 + S \rightleftarrows \underset{\substack{\text{Outer}\\\text{sphere}\\\text{complex}}}{S,S_5Ni{-}L} \rightleftarrows S{-}NiS_5,L$$

where S is a solvent molecule, L is isoquinoline, and charges have been omitted. It was also pointed out that for this system dissociation rate constants at any single temperature do not show a systematic trend with the donicities of the solvents, as has been observed for the $(S_5NiSCN)^+$ ion (2), but enthalpies of activation ($\Delta H_d^{\ddagger}$) for dissociation of $(S_5NiIsoquinoline)^{2+}$ do bear a linear relation with Gutmann donor numbers (3) of the solvents. From this relation the best values for the donor numbers of methanol and water were suggested to be 9 and 18. To test whether results for the $(S_5NiIsoquinoline)^{2+}$ ion can be applied to other simple monocomplexes of nickel(II), similar investigations with different ligands are needed.

Although considerable data have been collected on rate constants and activation parameters for the formation of various labile complexes of nickel(II), only a few isolated studies of dissociation of these species have been reported, and systematic data on solvent effects are limited. Particularly needed are data on dissociation in systems where the ligand is an inorganic anion.

Recently Coetzee and Hsu (4) reported a stopped-flow spectrophotometric investigation of rates of formation and dissociation of $NiSCN^+$ in dimethylsulfoxide. They repeated some earlier studies (2, 5), and proposed that the reaction of nickel(II) with thiocyanate ion proceeds by an I_d-type mechanism. Although the formation rate

constant (k_f) of the reaction at 20°C reported by them agrees with the results of Dickert, Hoffmann, and Janjic (2) within 11%, the enthalpies of activation ($\Delta H_f^{\ddagger}$) for the reaction do not (7.8 ± 0.6 *vs.* 13.1 kcal). Coetzee and Hsu (4) also reported dissociation rate constants (k_b) and associated activation parameters ($\Delta H_b^{\ddagger}$ and $\Delta S_b^{\ddagger}$) for dissociation of S_5NiSCN^+ ion in dimethylsulfoxide as solvent. These values were obtained indirectly by calculation from stopped-flow spectrophotometrically measured formation rate constants (k_f) and spectrophotometrically measured overall equilibrium constants (K_{eq}) for the reaction. The uncertainty in $\Delta H_b^{\ddagger}$, 16.6 ± 2 kcal, is relatively high, owing to uncertainties in the measurement of k_f and K_{eq} as well as in the value used for a, the distance of closest approach between ions in the Fuoss-Eigen equation (6). Dickert, Hoffmann, and Janjic also reported values of $\Delta H_b^{\ddagger}$ and $\Delta S_b^{\ddagger}$ for dissociation of $NiSCN^+$ in water, acetonitrile, methanol, and *N*,*N*-dimethylformamide, and k_b at 20°C for this reaction in dimethylsulfoxide (2). These data were obtained by pressure-jump measurements, and estimates of uncertainties in the values were not given.

As shown before (1), a plot of $\Delta H_b^{\ddagger}$ for $(S_5NiIsoquinoline)^{2+}$ in various solvents against the Gutmann donor numbers of the solvents is linear, with methanol and dimethylsulfoxide lying near the ends of the donicity scale of the solvents considered. Because an improved understanding of the fine structure of the mechanism of dissociation of labile nickel(II) complexes may accrue from consideration of the donor properties of the solvents coordinated to the nickel(II) ion, accurate values of the dissociation rate constants and associated enthalpies of activation are needed, especially for solvents located at the ends of the donicity scale. An uncertainty in $\Delta H_b^{\ddagger}$ values of no more than ±1 kcal seems desirable. For these reasons, and because of the discrepancy of 5.3 kcal in $\Delta H_f^{\ddagger}$ values pointed out earlier, we decided to determine directly rate constants and associated activation parameters for dissociation of the $(S_5NiSCN)^+$ ion in methanol and dimethylsulfoxide. This was done by stopped-flow spectrophotometry, a high concentration of copper(II) ion being used as the decomposing species. Our results, in conjunction with earlier results in water, acetonitrile, and *N*,*N*-dimethylformamide (2), are discussed from a mechanistic point of view by considering the effect of solvent donor properties on the enthalpy of activation for the dissociation process.

Experimental Section

Solvents

Methanol (Fisher, ACS grade) was distilled fractionally over N_2. The middle fraction boiling at 64.3°C was decanted onto dry CaO after being dried over 3 Å molecular sieves (Linde) for 1 day, and was distilled fractionally from CaO over N_2. The middle fraction from this distillation, boiling point 64.5°C, was finally distilled from Mg metal over N_2 and the middle fraction was collected for the kinetic studies. Dimethylsulfoxide was purified as before (1).

Reagents

In methanol as solvent nickel(II) was introduced as nickel(II) perchlorate monohydrate, which was obtained from recrystallized hexahydrate (G. F. Smith) by heating at 90 ± 5°C under vacuum. In dimethylsulfoxide as solvent $Ni(ClO_4)_2 \cdot 6DMSO$ was prepared (7) and used. The concentration of each nickel(II) solution was determined by EDTA titration as before (1). Hexakis(acetonitrile)copper(II) perchlorate (8) was used in both methanol and dimethylsulfoxide as solvents. Potassium thiocyanate (J. T. Baker, Baker Analyzed Reagent, assay 100%) was dried at 60°C under vacuum for 2 days. Sodium perchlorate (Fisher) was recrystallized from distilled demineralized water and dried under vacuum at 65°C for 3 days.

Instrumentation and Experimental Procedure

All solvents were used within 3 days of purification. All nonaqueous solutions were prepared and dispensed in a dry box (Kewaunee Scientific) under dry N_2, using glassware that had been oven-dried at 110°C for several days. All other standard procedures for handling nonaqueous solutions were followed. Pseudo-first-order rate constants for formation of $CuSCN^+$ ion were obtained by measuring the rate of change of transmittance of the solution with time upon mixing of a copper(II) solution with a solution of the monocomplex of nickel(II) with thiocyanate ion at 394 nm in methanol and 375 nm in dimethylsulfoxide (where the absorbance is primarily due to $CuSCN^+$). Kinetic measurements were made with a stopped-flow spectrophotometer (Durrum Instrument Co., Model D-110). A description of the instrument and methods of recording the change in transmittance with time has been reported (9*a*), along with modifications for improved temperature control (9*b*). In methanol as solvent, concentrations of nickel(II) and thiocyanate ion were held constant at 2.5×10^{-3} *M* and 2.0×10^{-4} *M* respectively; copper(II) concentrations were varied from 2.5×10^{-2} *M* to 1.28×10^{-1} *M*. Ionic strengths of the solutions were varied from 0.082 *M* to 0.384 *M*; sodium perchlorate was added to adjust ionic strength levels. In dimethylsulfoxide as solvent, concentrations of nickel(II) and thiocyanate ion were held constant at 2.0×10^{-3} *M* and 1×10^{-3} *M* respectively, and the copper(II) concentrations were varied in five steps from 5×10^{-3} *M* to 20×10^{-3} *M*. All concentrations refer to final values after mixing in the stopped-flow cell. Each experiment was repeated with different batches of solvent and

TABLE 1. Pseudo-first-order rate constants for dissociation of $NiSCN^+$ in methanol[a]

Set No.	$[Cu(ClO_4)_2]$ (M)	$[NaClO_4]$ (M)	Ionic strength	k_{obs}, s^{-1} 15°C	25°C	35°C	45°C
A	0.03027	—	0.091	—	0.495[b]	—	—
	0.06054	—	0.182	—	0.541[b]	—	—
	0.09038	—	0.271	—	0.608[b]	—	—
	0.1280	—	0.384	—	0.673[b]	—	—
B	0.02507	0.225	0.300	—	0.654	—	—
	0.0507	0.150	0.302	—	0.660	—	—
	0.0758	0.075	0.302	—	0.660	—	—
	0.1010	—	0.303	—	0.658	—	—
C	0.0274	—	0.082	0.159_3	0.488	—	—
	0.0274	0.033	0.115	0.175_4	0.517	—	—
	0.0274	0.082	0.164	0.192_5	0.573	—	—
	0.0274	0.164	0.246	0.210	0.654	—	—
D	0.0280	—	0.084	—	—	1.47_8	3.85_0
	0.0280	0.018	0.102	—	—	1.54_0	3.93_4
	0.0280	0.045	0.129	—	—	1.61_2	4.07_6
	0.0280	0.090	0.174	—	—	1.69_0	4.20_0
Values of k_b extrapolated to $I = 0$				0.123	0.404[c]	1.30_5	3.54_5

[a]Concentration of nickel(II) and thiocyanate ion held constant at 2.5×10^{-3} and 2.0×10^{-4} M respectively.
[b]Results at 25.2°C.
[c]Additional value: 0.430 at 25.2°C.

reagents; results of duplicate sets of experiments agreed within ±2% in all cases.

Results and Discussion

Under the experimental conditions selected only monocomplexes of nickel(II) and copper(II) are expected to form (2, 4). Table 1 lists the observed pseudo-first-order rate constants (k_{obs}) for dissociation of $NiSCN^+$ ion in methanol by use of copper(II) as the decomposing ion at various temperatures, ionic strengths, and concentrations of copper(II). In all experiments, the concentrations of nickel(II) and thiocyanate ion were held constant. Figure 1 shows the variation in k_{obs} with ionic strength of the medium at a fixed concentration of copper(II) at 25°C and 15°C in methanol. Table 2 contains the values of observed pseudo-first-order rate constants at different temperatures in dimethylsulfoxide. The major features of the results in Table 1 and Table 2 are:

(*1*). Observed pseudo-first-order rate constants in methanol vary linearly with the first power of the ionic strength of the medium but are independent of the concentration of copper(II) ion as long as it is sufficiently high compared to the concentration of nickel(II); this is shown in the results of the experiments in Sets A, B, and C in Table 1. Contrary to observations in methanol, in dimethylsulfoxide observed pseudo-first-order rate constants are independent of the ionic strength of the medium and the concentrations of both copper(II) and nickel(II) (Table 2), as long as the copper(II) concentrations are much higher than the concentration of nickel(II).

(*2*). In methanol, observed pseudo-first-order rate constants at zero ionic strength and 25°C are the same whether the ionic strength is varied by addition of $Cu(ClO_4)_2$, (Set A, Table 1) or by addition of $NaClO_4$ (Set C, Table 1), assuming $NaClO_4$ and $Cu(ClO_4)_2$ are completely dissociated. The results of Sets A and C in Table 1 indicate that 0.128 M $Cu(ClO_4)_2$ and 0.164 M $NaClO_4$ are completely dissociated in methanol at 25°C.

(*3*). From the results of Sets C and D in Table 1, a plot of k_{obs} against the first power of the ionic strength of the medium (I) at 15°C shows curvature at higher concentrations (Fig. 1), while k_{obs} varies linearly with ionic strength at 25, 35, and 45°C.

The dependence of k_{obs} on ionic strength in methanol as solvent can be explained by assuming ion-pair association between $(S_5NiSCN)^+$ and ClO_4^- in methanol, the extent of association increasing with increasing ClO_4^- concentration. It is not possible on the basis of this work to state whether the association is 'contact' or

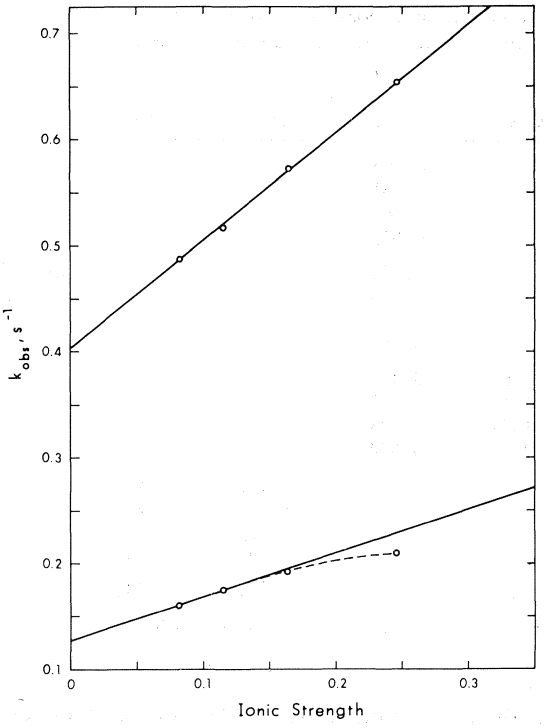

FIG. 1. Variation in observed pseudo-first-order rate constants (k_{obs}) for dissociation of $(S_5NiSCN)^+$ in methanol as function of ionic strength at 15°C (lower line) and 25°C (upper line). Concentrations of copper(II), nickel(II), and SCN^- held constant at 0.0274 *M*, 2.5×10^{-3} *M*, and 2.0×10^{-4} *M*.

TABLE 2. Pseudo-first-order rate constants for dissociation of $NiSCN^+$ in dimethylsulfoxide[a]

$[Cu^{2+}]$ (*M*)	Total ionic strength, *I*	k_{obs}, s^{-1} 19°C	25°C	30°C
0.005	0.015	67.9_8	$109._3$	167
0.010	0.030	67.2_8	$111._8$	165
0.015	0.045	67.2_8	$110._9$	165
0.020	0.060	67.2_8	$111._8$	167
0.020	0.060	—	$110._9$	—
Median values of k_b at $I = 0$		67.3[b]	$110._9$	166

[a]Concentrations of nickel(II) and thiocyanate ion held constant at 2×10^{-3} *M* and 1×10^{-3} *M* respectively.
[b]Value of k_b at $I = 0$ and 20°C is 73.4 s^{-1} (from plot of log k_b *vs.* $1/T$, *T* in K).

'solvent-separated' in nature, but it can be assumed that the effect of increasing concentrations of ClO_4^- on the extent of either type of association will be of the same type. Interaction between nickel(II) and SCN^- in the $(S_5NiSCN)^+$ ion in solution may be partly covalent and partly electrostatic in nature. The electrostatic interaction would be expected to be greater in methanol than in dimethylsulfoxide because of the lower dielectric constant of methanol. Because electrostatic interaction depends in part on the charge density of the interacting ions in a medium, association of ClO_4^- with nickel(II) in $(S_5NiSCN)^+$ may decrease the extent of electrostatic interaction between nickel(II) and SCN^-. The intensity of chemical interaction depends mainly on the intrinsic Lewis-acid character of the central coordinating atom relative to the intrinsic Lewis-base character of the donor atom in the ligand rather than on the overall magnitude of the charges on the reacting ions. In addition, the 'electrostatic' interaction would be expected to be weaker than the 'chemical' interaction, and so it can be predicted that the 'softer' electrostatic interaction will be most affected by association of ClO_4^- with nickel(II) in $(S_5NiSCN)^+$. The conclusion that electrostatic considerations are the important factor in ionic strength effects on observed rates is supported by the absence of ionic strength effects on k_{obs} for the dissociation of the monocomplexes of isoquinoline and 4-phenylpyridine with nickel(II) in methanol (1, 10).

It has been established that substitution reactions in acetonitrile (11) and methanol (11*a*, 12) for formation of labile complexes of nickel(II) with many ligands, including 2,2′,2″-terpyridine and thiocyanate ion, proceed by a dissociative (I_d) type of interchange mechanism (13), as was initially proposed and verified for similar reactions in aqueous solution by Eigen and Wilkins (14). From the observed effect of anions like Cl^-, Br^-, I^-, SCN^-, NO_3^-, CH_3COO^-, and $C_6H_5COO^-$ in the inner sphere of nickel(II) on ternary complex formation of nickel(II) in acetonitrile and methanol, it can be concluded that the effect of the presence of these anions in the inner sphere of nickel(II) on solvent-exchange rates in acetonitrile (15) is some 10 to 50 times higher than the corresponding effect in methanol (16). The effect observed with ClO_4^- in the inner sphere of nickel(II) is very small in acetonitrile (17). From this we conclude that in methanol the effect of ClO_4^- in the inner sphere of nickel(II), either as a contact or solvent-separated ion pair, has a negligibly small effect on the solvent exchange rate of methanol on nickel(II). This explains the absence of an ionic strength effect on the rate of formation of

nickel(II) with terpyridine in methanol (11). The absence of an ionic strength effect on the solvent exchange rate of nickel(II) in methanol was also observed in an investigation of the formation of labile complexes of nickel(II) with various ligands, including SCN^-, in methanol by Pearson and Ellegen (12*a*). From these pieces of evidence we conclude that in anhydrous methanol an ion pair exists between ClO_4^- and nickel(II) in $(S_5NiSCN)^+$ which, by decreasing the intensity of the electrostatic interaction between nickel(II) and SCN^- (without noticeably affecting the 'chemical' interaction involved in $(S_5NiSCN)^+$), increases the observed pseudo-first-order rate constant for dissociation of $(S_5NiSCN)^+$. Since the extent of ion-pair formation increases proportionally with increasing concentration of ClO_4^- in the medium, values of k_{obs} for dissociation of $(S_5NiSCN)^+$ in methanol vary directly with the ionic strength of the medium as adjusted by addition of $NaClO_4$.

In dimethylsulfoxide the electrostatic interaction involved in $(S_5NiSCN)^+$ will be smaller than in methanol because of the higher dielectric constant. Dimethylsulfoxide is also a better donor toward nickel(II) than is methanol. It is therefore expected that in dimethylsulfoxide ion-pair formation between nickel(II) in $(S_5NiSCN)^+$ and ClO_4^- will be less, and those ion pairs that do form likely will be mainly solvent separated. The combination of high dielectric constant and bulky size of DMSO would be expected to result in little or no ion-pair interaction between ClO_4^- and nickel(II) in that solvent, and consequently, ion-pairing effects on the weak electrostatic interaction involved in $(S_5NiSCN)^+$ should be negligibly small. This could explain why, contrary to what is observed in methanol, high concentrations of ClO_4^- in dimethylsulfoxide have no effect on the dissociation of $(S_5NiSCN)^+$ in that solvent. In methanol plots of ionic strength against observed pseudo-first-order rate constants for dissociation of $(S_5NiSCN)^+$ were linear at ionic concentrations up to 0.38 *M* at 25, 35, and 45°C, and up to 0.164 *M* at 15°C. Above 0.16 *M* at 15°C a deviation from linearity was observed that can be explained by assuming incomplete dissociation of $NaClO_4$. From the extent of deviation the association constant of $NaClO_4$ in methanol was calculated to be 3 at 15°C and 0 at 25°C. These values are reasonable relative to related systems (18).

The copper(II)-induced dissociation of $(S_5NiSCN)^+$ in methanol and dimethylsulfoxide can be represented by

$$[2] \qquad NiSCN^+ \underset{k_f}{\overset{k_b}{\rightleftharpoons}} Ni^{2+} + SCN^-$$

$$[3] \qquad Cu^{2+} + SCN^- \overset{k_1}{\rightleftharpoons} CuSCN^+$$

Solvent molecules associated with Ni^{2+} and Cu^{2+} are omitted for convenience. This scheme is the same as observed for copper(II)-induced dissociation of the monocomplex of nickel(II) with isoquinoline in propylene carbonate and acetonitrile (1), and for dissociation of the monocomplex of manganese(II) with bipyridine, terpyridine, and phenanthroline using H^+ and Hg^{2+} as electrophiles in anhydrous methanol (19).

From reactions 2 and 3 it can be shown that when $[Cu^{2+}] \gg [SCN^-]$, as used in this work, k_{obs} is given by

$$[4] \quad k_{obs} = k_b k_1 [Cu^{2+}]/(k_f[Ni^{2+}] + k_1[Cu^{2+}])$$

where k_{obs} is an experimentally determined pseudo-first-order rate constant. If, at high concentrations of copper(II), $k_f[Ni^{2+}] \ll k_1[Cu^{2+}]$, then k_{obs} is equal to k_b and is independent of $[Cu^{2+}]$, $[Ni^{2+}]$, and $[SCN^-]$. If the ionic strength of the medium does not influence the dissociation process by changing k_b in the rate-determining step, then k_{obs} is directly equal to the true k_b. This is the case in dimethylsulfoxide. On the other hand, if the rate-determining step is influenced by the ionic strength of the medium, as in methanol, k_{obs} will be affected. In such a case true values of k_b should be obtained by extrapolating values of k_{obs} to zero ionic strength of the medium. Under our experimental conditions k_{obs} was independent of $[Cu^{2+}]$, $[SCN^-]$, and $[Ni^{2+}]$. Also, if the influence of ionic strength on the magnitude of k_{obs} in methanol is assumed to stem from the effect of ion pairing between ClO_4^- and nickel(II) on the electrostatic interaction involved in $(S_5NiSCN)^+$, a plot of k_{obs} against ionic strength is expected to be a straight line. This is indeed observed (Fig. 1).

Rate constants for dissociation of $(S_5NiSCN)^+$ in dimethylsulfoxide and methanol at different temperatures and zero ionic strength are summarized at the bottom of Tables 1 and 2. Table 3 lists dissociation rate constants at

TABLE 3. Comparison of activation parameters for dissociation of $(S_5NiSCN)^+$ and $(S_5NiIsoquinoline)^{2+}$ in different solvents[a]

Solvent	k_b[b] (s^{-1})	$(S_5NiSCN)^+$ ΔH_b^* (kcal)	$(S_5NiSCN)^+$ ΔS_b^* (cal deg^{-1} mol^{-1})	$(S_5NiIsoquinoline)^{2+}$ ΔH_b^* (kcal)	$(S_5NiIsoquinoline)^{2+}$ ΔS_b^* (cal deg^{-1} mol^{-1})	Donicity
Water	450	17.5[c]	+13.1[c]	16.1±0.6[e]	+2±2[e]	18
Methanol	0.227_5	19.9±0.2[d]	+6.4±0.7[d]	19.3±0.2[e]	+7.5±0.7[e]	9
Acetonitrile	0.3	18[c]	+0.25[c]	17.2±0.5[e]	−5±2[e]	14.1
Dimethylsulfoxide	73.4_5	13.9±0.1[d,f]	−2.6±0.4[d,f]	13.5±0.4[e]	−4±1[e]	29.6
N,N-Dimethyl-formamide	15	15.2[c]	−1.5[c]	13.9±0.4[e]	−5±1[e]	26.8

[a]All data at 25°C.
[b]Results at 20°C. Where necessary, values calculated from plots of log k_b *vs.* $1/T$, T in K.
[c]Reference 2.
[d]This work.
[e]Reference 1.
[f]$\Delta H^{\ddagger} = 16.6 \pm 2$ kcal and $\Delta S^{\ddagger} = 6 \pm 6$ reported by Coetzee and Hsu (4).

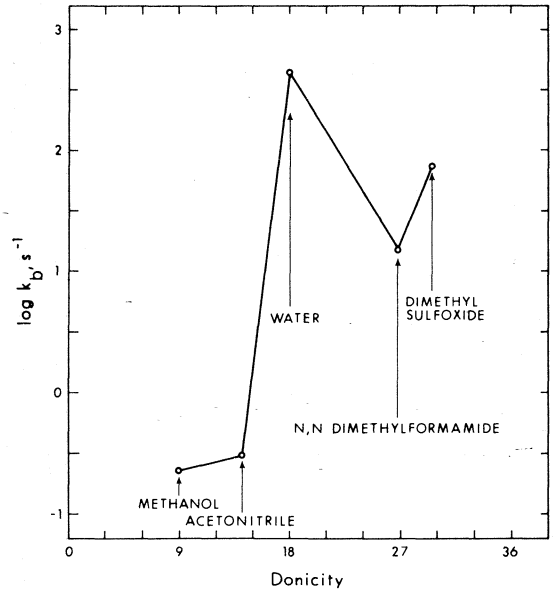

FIG. 2. Relation between log rate constants for dissociation of $(S_5NiSCN)^+$ in various donor solvents and the donicity of the solvent.

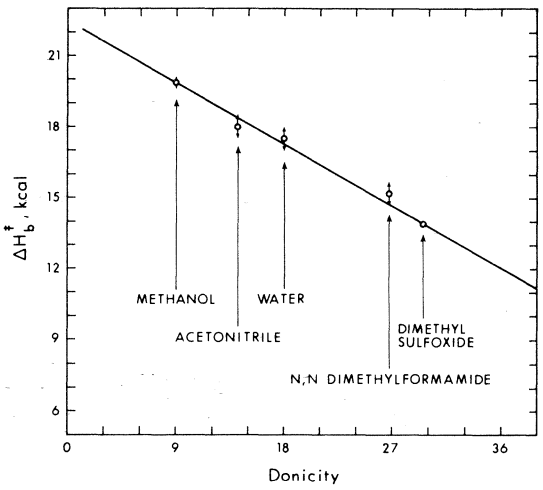

FIG. 3. Relation between enthalpy of activation ($\Delta H_b^{\ddagger}$) for dissociation of $(S_5NiSCN)^+$ in various donor solvents and the donicity of the solvent. (For acetonitrile, water, and dimethylformamide, arrows indicate ±0.5 kcal.)

20°C and associated activation parameters in different donor solvents. The value for k_b in dimethylsulfoxide at 25°C agrees with earlier work (4) within experimental error. The dissociation rate constants do not show a systematic relation with donicity of solvent (Fig. 2), but the enthalpy of activation for dissociation does show a linear correlation (Fig. 3). From Fig. 3 the donor numbers of methanol and water are best represented by values of 9 and 18. These results agree with those found earlier in the study of solvent effects on dissociation of the monocomplex of nickel(II) with isoquinoline (1). Recently Tanaka (20) predicted a value in the neighbourhood of 10 for the donor number of methanol from plots of (*a*) ΔH_{SbCl_5} against ΔH_{PhOH}, (*b*) ΔH_{SbCl_5} against ΔH_{I_2}, and (*c*) ΔH_{SbCl_5} against $C_B E_B$ for a variety of organic solvents. Values for ΔH_{PhOH}, ΔH_{I_2}, C_B, and C_E were those of Drago and co-workers (21). Values close to 9 and 18 for the donor numbers of methanol and water can also be predicted from recent measurements of downfield nmr chemical shifts of $CsClO_4$ in different solvents (22), though these results do not agree with values of 26 for methanol and 33 for water predicted from sodium-23 nmr chemical shifts for $NaClO_4$

in several donor solvents (23). The reasons for the differences in these nmr data are unclear, but the lower charge density of the cesium ion might give more meaningful results in comparisons of the donor properties of structured hydroxylic solvents such as water and methanol. Hinton also has predicted a value near 20 for the donor number of water on the basis of measurements of the infinite dilution resonance frequency of thallium-205 ion in several solvents (25).

Table 3 also summarizes the activation parameters for dissociation of monocomplexes of nickel(II) with thiocyanate ion and isoquinoline. Comparison of the enthalpies of activation suggests that the pathways for dissociation of $(S_5NiSCN)^+$ in the solvents considered can be accommodated within the I_d-type mechanism represented by eq. 1, as was observed for $(S_5NiIsoquinoline)^{2+}$. It was pointed out earlier (1) that for an I_d mechanism represented by eq. 1 the activation enthalpy for dissociation will depend upon both the Lewis-acid character of $(S_5Ni)^{2+}$ (24) and the Lewis-base character of the ligand relative to the free solvent molecule. If S is a solvent molecule coordinated to nickel(II) in the inner sphere, and it has little or no interaction with bulk solvent structure, the Lewis-acid character of $(NiS_5)^{2+}$ will be inversely related to the donicity of S, and $\Delta H_b^{\neq}$ for dissociation of $(S_5NiSCN)^+$ will increase with decreasing donicity of the solvent. The value of $\Delta H_b^{\neq}$ for dissociation of a nickel(II) monocomplex in a solvent S would be expected to increase with an increase in donicity of the donor atom in the ligand. Nitrogen is a better donor towards nickel(II) than sulfur. Thus $\Delta H_b^{\neq}$ for dissociation of $(S_5NiIsoquinoline)^{2+}$, in which N is the donor atom, is expected to be higher than the corresponding quantity for dissociation of $(S_5NiSCN)^+$, in which sulfur is the donor atom, in any solvent if only the Lewis-base property or donicity of the ligand coordinating site is considered. From Table 3 $\Delta H_b^{\neq}$ for $(S_5NiSCN)^+$ is greater than for $(S_5NiIsoquinoline)^{2+}$ in all the solvents considered. This trend in $\Delta H_b^{\neq}$ values is the opposite of that expected from consideration of the donicity of the ligands only, and suggests that in $(S_5NiSCN)^+$ an electrostatic effect is indeed involved. The electrostatic force between nickel(II) and thiocyanate ion causes $\Delta H_b^{\neq}$ for dissociation of $(S_5NiSCN)^+$ to be larger than for dissociation of $(S_5NiIsoquinoline)^{2+}$ in all solvents (Table 3). The same conclusion is supported by the results for dissociation of $(S_5Ni4\text{-phenylpyridine})^{2+}$ in different solvents (10).

Information on the position of other solvents on this scale would be useful. In tetrahydrofuran the copper salts used in this work were not adequately soluble, however, and in propylene carbonate a fine yellow-orange suspension, barely visible to the eye, appeared in solutions of $(S_5NiSCN)^+$ after 2 to 3 h. Benzonitrile absorbs strongly in the wavelength region where the isoquinoline and thiocyanate complexes absorb, and so spectral data on these systems in this solvent also could not be obtained.

In summary, we conclude that the pathway for dissociation of $(S_5NiSCN)^+$ in the solvents studied is best represented by an I_d-type mechanism, as observed previously for dissociation of $(S_5NiIsoquinoline)^{2+}$. Rate constants for dissociation at any particular temperature are not systematically related to the donicity of the solvent, but the enthalpy of activation for dissociation of $(S_5NiSCN)^+$ is inversely related to the Gutmann donor number of the solvent. Additional evidence is given in support of a value of 9 for the donor number of methanol, and of 18 for water. The meaning of such low donor numbers for these solvents is not clear at this time. Additional data on other systems in these solvents, as well as measurements in related hydroxylic solvents, are needed to provide further insight into the question.

1. P. K. CHATTOPADHYAY and B. KRATOCHVIL. Inorg. Chem. **15**, 3104 (1976).
2. F. DICKERT, H. HOFFMANN, and T. JANJIC. Ber. Bunsenges. Phys. Chem. **78**, 712 (1974).
3. V. GUTMANN. Topics Curr. Chem. **27**, 59 (1972).
4. J. F. COETZEE and E. HSU. J. Solution Chem. **4**, 45 (1975).
5. C. H. LANGFORD and H. G. TSIANG. Inorg. Chem. **9**, 2345 (1970).
6. (*a*) M. EIGEN. Z. Phys. Chem. (Frankfurt am Main), **1**, 176 (1954); (*b*) R. M. FUOSS. J. Am. Chem. Soc. **80**, 5059 (1958).
7. J. SELBIN, W. E. BULL, and L. H. HOLMES, JR. J. Inorg. Nucl. Chem. **16**, 219 (1961).
8. B. KRATOCHVIL, D. A. ZATKO, and R. MARKUSEWSKI. Anal. Chem. **38**, 770 (1966).
9. (*a*) P. K. CHATTOPADHYAY and B. KRATOCHVIL. Can. J. Chem. **54**, 2540 (1976); (*b*) P. K. CHATTOPADHYAY and J. F. COETZEE. Anal. Chem. **44**, 2117 (1972).
10. P. K. CHATTOPADHYAY and B. KRATOCHVIL. Unpublished results.
11. (*a*) P. K. CHATTOPADHYAY and J. F. COETZEE. Inorg. Chem. **12**, 113 (1973); (*b*) P. K. CHATTOPADHYAY and J. F. COETZEE. Anal. Chem. **46**, 2014 (1974).

12. (*a*) R. G. PEARSON and P. ELLEGEN. Inorg. Chem. **6**, 1379 (1967); (*b*) F. DICKERT, H. HOFFMANN, and W. JAENICKE. Ber. Bunsenges. Phys. Chem. **74**, 500 (1970).
13. C. H. LANGFORD and H. B. GRAY. Ligand substitution processes. W. A. Benjamin, New York, NY. 1965.
14. (*a*) M. EIGEN and R. G. WILKINS. Adv. Chem. Ser. No. 49, 55 (1965); (*b*) R. G. WILKINS. Acc. Chem. Res. **3**, 408 (1970).
15. P. K. CHATTOPADHYAY and J. F. COETZEE. Inorg. Chem. **15**, 400 (1976).
16. J. F. COETZEE and D. M. GILLES. Inorg. Chem. **15**, 405 (1976).
17. P. K. CHATTOPADHYAY and J. F. COETZEE. Unpublished results.
18. B. KRATOCHVIL and H. YEAGER. Topics Curr. Chem. **27**, 1 (1972).
19. D. J. BENTON and P. MOORE. J. Chem. Soc. Dalton Trans. 399 (1973).
20. M. TANAKA. Private communication.
21. (*a*) R. S. DRAGO and B. B. WAYLAND. J. Am. Chem. Soc. **87**, 3571 (1965); (*b*) R. S. DRAGO, G. C. VOGEL, and T. E. NEEDHAM. J. Am. Chem. Soc. **93**, 6014 (1971).
22. A. I. POPOV. Paper presented at 172nd National Meeting, American Chemical Society, San Francisco, Sept., 1976.
23. (*a*) R. H. ERLICH, E. ROCH, and A. I. POPOV. J. Am. Chem. Soc. **92**, 4989 (1970); (*b*) R. H. ERLICH and A. I. POPOV. J. Am. Chem. Soc. **93**, 5620 (1971); (*c*) M. S. GREENBERG, R. L. BONDER, and A. I. POPOV. J. Phys. Chem. **77**, 2449 (1973).
24. C. H. LANGFORD and J. P. K. TONG. Can. J. Chem. **53**, 702 (1975).
25. J. F. HINTON. Private communication.

Matrix effect on the structure of $\dot{G}e(CH_3)_3$

LYDIA BONAZZOLA, NICOLE LERAY, AND JACQUES RONCIN

Laboratoire de Résonance Electronique et Ionique, Associé au CNRS, Université de Paris-Sud, Bâtiment 350, Orsay, France 91405

Received November 2, 1976

LYDIA BONAZZOLA, NICOLE LERAY, and JACQUES RONCIN. Can. J. Chem. **55**, 1617 (1977).

An important matrix effect which can be correlated with the polarisability of radicals is observed for the ^{73}Ge coupling constant of $\dot{G}e(CH_3)_3$ radical.

LYDIA BONAZZOLA, NICOLE LERAY et JACQUES RONCIN. Can. J. Chem. **55**, 1617 (1977).

Un important effet de matrice est observé pour le couplage RPE du ^{73}Ge dans le radical $(CH_3)_3\dot{G}e$. Il peut être relié à la polarisabilité du radical.

It has been shown some years ago (1) that the unpaired spin density at the Si nucleus of $Cl_n\dot{S}i(CH_3)_{3-n}$ radicals and probably the geometry of the radical site were strongly dependent on the trapping matrix: the esr hyperfine coupling of ^{29}Si nucleus in $^{29}\dot{S}i(CH_3)_3$ varies from 172.5 G in a nonpolar $Si(CH_3)_4$ matrix to 129 G in a $ClSi(CH_3)_3$ matrix ($\mu = 2$ Debye).

Another example of the trapping matrix influence on the hyperfine coupling of an atom of group IV of the Periodic Table, bearing the unpaired electron is the $^{119}\dot{S}n(CH_3)_3$ radical: Lloyd and Rogers (2) find 1983 G for the ^{119}Sn coupling when the radical is trapped in an adamantane matrix. For the same radical in a $ClSn(CH_3)_3$ matrix ($\mu = 3.5$ Debye) ^{119}Sn coupling is found to be 1611 G (3).

We have looked for a possible extension of these results to other atoms of group IV and we have investigated the influence of the trapping matrix on the couplings of ^{73}Ge when $^{73}\dot{G}e(CH_3)_3$ radicals are trapped in a $Ge(CH_3)_4$ nonpolar matrix and a $ClGe(CH_3)_3$ polar matrix. The experimental conditions[1] are the same as those used for silicon compounds (1). The esr spectra are shown on Fig. 1 and the couplings tabulated in Table 1. These data show that ^{73}Ge coupling decreases when the dipole moment of the matrix increases.

The matrix effect observed in $\dot{S}i(CH_3)_3$ (1), $\dot{S}n(CH_3)_3$ (2), and $\dot{G}e(CH_3)_3$ (this work) is quite important: around 20% variation of the coupling from one matrix to the other. In contrast, such matrix effects have never been ob-

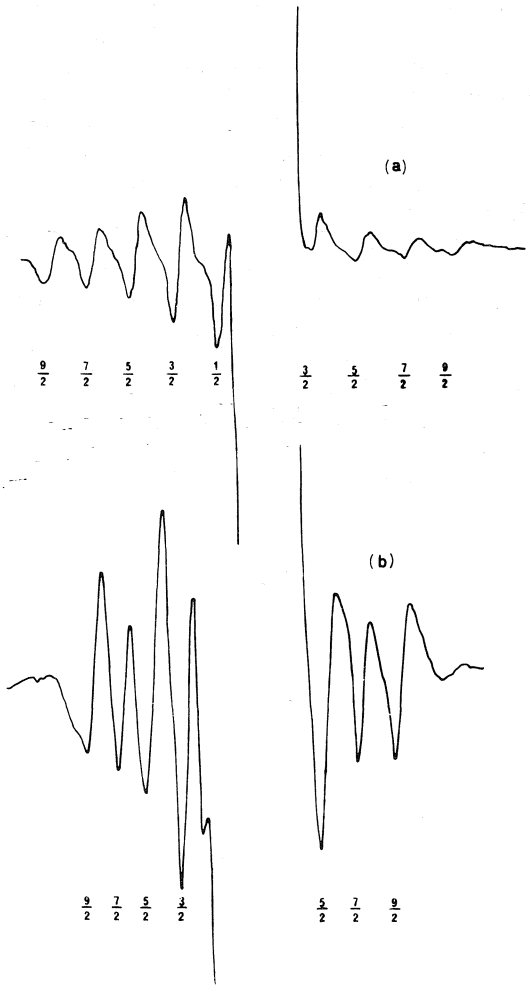

FIG. 1. Electron spin resonance spectra of $^{73}\dot{G}e(CH_3)_3$ radicals in $Ge(CH_3)_4$ (*a*) and $ClGe(CH_3)_3$ (*b*).

[1] $\dot{G}eCl(CH_3)_3$ was kindly provided by Professor Satge of Université Paul Sabatier, Toulouse, France.

TABLE 1. a_X couplings for $\dot{X}(CH_3)_3$ radicals (X = Si, Ge, Sn) in different matrices

Radical	Matrix	Coupling (Gauss)	μ (Debye)	Reference
$Si(CH_3)_3$	$Si(CH_3)_4$	172.5	0	1
	$ClSi(CH_3)_3$	129	2.09	1
$Ge(CH_3)_3$	$Ge(CH_3)_4$	83	0	This work
	Adamantane	84.7	0	2
	$ClGe(CH_3)_3$	63	—	This work
$Sn(CH_3)_3$	Adamantane	1983	0	2
	$ClSn(CH_3)_3$	1611	3.5	3

served on uncharged hydrocarbon radicals except in the case of radicals adsorbed on solid surfaces, such as porous glass (4, 5).

In a previous paper, we have suggested that these couplings and structure variations might be related to the field due to the dipoles of the molecules of the matrix. If so, the different behaviour of hydrocarbon radicals may arise from the low polarisability of carbon compared to other elements in group IV of the Periodic Table.

Similar effects are to be expected whenever the polarisability of the atom bearing the unpaired electron is of the same order of magnitude or larger than that of group IV elements. Unfortunately esr data relative to the coupling of a radical in different matrices are scarce. The only data we have found concern $\dot{P}\varphi_2$ and $\dot{P}\varphi_3^+$ radicals and they confirm the above statement: ^{31}P coupling of $\dot{P}\varphi_2$ radical is 93 G when the trapping matrix is $PO\varphi_3$ (6) and 103 G when the matrix is $\varphi_2P(S)H$ (6). Similarly ^{31}P coupling of the radical ion $\dot{P}\varphi_3^+$ changes from 396 G (7) in a φ_3PBCl_3 matrix to 342 G (8) in φ_3PBF_3 matrix.

1. C. HESSE, N. LERAY, and J. RONCIN. J. Chem. Phys. **57**, 749 (1972).
2. R. V. LLOYD and M. T. ROGERS. J. Am. Chem. Soc. **95**, 2459 (1973).
3. J. E. BENNET and J. A. HOWARD. Chem. Phys. Lett. **15**, 322 (1972).
4. G. B. GARBUTT, H. D. GESSER, and M. FUJIMOTO. J. Chem. Phys. **48**, 4605 (1968).
5. N. SHIMAMOTO, Y. FUJITA, and T. KWAN. Bull. Chem. Soc. Jpn. **43**, 580 (1970).
6. M. GEOFFROY, E. A. C. LUCKEN, and C. MAZELINE. Mol. Phys. **28**, 839 (1974).
7. T. BERCLAZ, M. GEOFFROY, and E. A. C. LUCKEN. Chem. Phys. Lett. **36**, 677 (1975).
8. T. BERCLAZ and M. GEOFFROY. Mol. Phys. **30**, 549 (1975).

Structure and conformation of hydroxylubimin, a sesquiterpenoid phytoalexin[1]

GEORGE I. BIRNBAUM

Division of Biological Sciences, National Research Council of Canada, Ottawa, Ont., Canada K1A 0R6

Received December 2, 1976

GEORGE I. BIRNBAUM. Can. J. Chem. **55**, 1619 (1977).

In order to determine the orientation of the isopropenyl group and confirm the stereochemistry at other chiral centers in lubimin (**1**) and hydroxylubimin (**2**), two antifungal sesquiterpenes, an X-ray structure analysis of **2** was carried out. Crystals of **2** are orthorhombic, space group $P2_12_12_1$, $a = 6.190$, $b = 7.210$, $c = 63.082$ Å, $Z = 8$. The structure was solved by direct methods and refined to $R = 0.045$. In both independent molecules the six-membered ring is chair-shaped with all four substituents equatorially oriented. The five-membered ring, attached by a spiro junction, is a half-chair with the isopropenyl substituent in an equatorial position. This side-chain is *trans* to the methyl-bearing carbon in the six-membered ring.

GEORGE I. BIRNBAUM. Can. J. Chem. **55**, 1619 (1977).

Afin de déterminer l'orientation du groupe isopropényle et pour confirmer la stéréochimie au niveau d'autres centres chiraux de la lubimine (**1**) et de l'hydroxylubimine (**2**), deux sesquiterpènes fungicides, on a effectué une analyse de structure de rayon-X de **2**. Les cristaux de **2** sont orthorhombiques, groupe spatial $P2_12_12_1$, $a = 6.190$, $b = 7.210$, $c = 63.082$ Å, $Z = 8$. On a résolu la structure par des méthodes directes et on l'a affinée jusqu'à une valeur de $R = 0.045$. Dans les deux molécules indépendantes, le cycle à six chaînons est dans une forme chaise avec les quatre substituants orientés en position équatoriale. Le cycle à cinq chaînons, attaché par une junction spiro, est en forme de demi-chaise avec le groupe isopropényle en position équatoriale. Cette chaîne latérale est *trans* par rapport au carbone portant le méthyle dans le cycle à six chaînons.

[Traduit par le journal]

Phytoalexins are stress compounds produced by a plant as a result of fungal infection. They inhibit fungal growth, thereby preventing the full development of the disease (1). Lubimin (**1**) and hydroxylubimin (**2**) are two sesquiterpenoid phytoalexins which have been isolated from several species of the *Solanaceae* family, such as potatoes (*Solanum tuberosum*), egg plants (*Solanum melongena*), and thorn apples (*Datura stramonium*) (2–4). Stoessl *et al.* (3), and subsequently Masamune and his collaborators (4), proposed the correct skeleton structure of **1**. The latter authors also concluded that **2** was the 3-hydroxy derivative of **1**. The stereochemistry at most chiral centers of **1** and **2** was published later (5), but the orientation of the isopropenyl group could not be determined from spectroscopic data. In order to establish this feature, and to confirm the earlier stereochemical assignment, we undertook an X-ray analysis of **2**. A preliminary report of our investigation was recently published (6); it showed the relative and absolute configurations of **1** and **2**. The absolute configuration was assumed by analogy with related sesquiterpenoids.[2] It was recently verified by an application of the benzoate rule in the interpretation of a CD spectrum (7).

Experimental

3-Hydroxylubimin, $C_{15}H_{24}O_3$, was crystallized from ether/petroleum ether to give colorless prisms, mp 96.5–99.5°C. Precession photographs showed the following systematic absences: $h00$ for odd h, $0k0$ for odd k, and $00l$ for odd l. The space group was thus uniquely determined to be $P2_12_12_1$. A crystal fragment measuring 0.15 × 0.25 × 0.45 mm was mounted along the c axis on a card-controlled Picker four-circle diffractometer and the following crystal data were obtained.

$C_{15}H_{24}O_3$ fw = 252.3
Orthorhombic, $a = 6.190(1)$, $b = 7.210(1)$, $c = 63.082(2)$ Å, $V = 2815.3$ Å^3, $D_m = 1.18$ g cm^{-3}, $Z = 8$, $D_x = 1.19$ g cm^{-3} (22°C; CuKα_1, $\lambda = 1.54051$ Å, CuKα_2, $\lambda = 1.54433$ Å), $F(000) = 1104$, μ(CuKα) = 6.6 cm^{-1}.

The moving-crystal – moving-counter method (θ–2θ scan) was used to measure the intensity data. Monochromatization was achieved by the use of a nickel filter and a pulse-height analyzer. The 130 reflection was monitored at regular intervals; its intensity decreased by 5% during the data collection. A net count of 60 or 10% of the background, whichever was higher, was determined as threshold intensity below which reflections were considered unobserved. There were 2868 unique reflections accessible to the diffractometer ($2\theta \leq 130°$) of which 2301 had intensities above threshold values. The intensities were corrected for Lorentz and polarization factors; absorption corrections were considered unnecessary in view of the low value of μ.

[1]NRCC No. 15815.
[2]A. Stoessl, private communication.

TABLE 1. Final fractional coordinates and thermal parameters (Å²)

(*a*) Nonhydrogen atoms[a]

Atom	10^4x	10^4y	10^5z	10^4U_{11}	10^4U_{22}	10^4U_{33}	10^4U_{23}	10^4U_{13}	10^4U_{12}
C(A,1)	6732(6)	6429(4)	8449(5)	596(19)	360(15)	571(20)	−35(13)	−94(16)	33(16)
C(A,2)	8416(5)	6296(4)	10189(5)	474(17)	429(16)	456(20)	−95(13)	−24(14)	2(15)
C(A,3)	8958(5)	4281(4)	10590(4)	399(15)	472(15)	373(20)	33(12)	−16(12)	−55(15)
C(A,4)	9804(5)	3330(4)	8603(4)	381(15)	397(14)	423(20)	21(12)	37(12)	−36(14)
C(A,5)	8129(5)	3411(4)	6752(4)	433(15)	346(13)	408(20)	0(12)	29(12)	−17(14)
C(A,6)	9138(6)	2591(5)	4700(5)	530(17)	494(17)	402(20)	−3(13)	61(14)	−23(16)
C(A,7)	8006(6)	728(5)	4311(5)	523(17)	450(15)	422(20)	−16(13)	6(14)	−6(16)
C(A,8)	5705(6)	1121(4)	5102(5)	511(18)	439(16)	520(20)	−12(14)	−12(15)	−61(16)
C(A,9)	6095(5)	2201(4)	7162(5)	405(15)	452(16)	499(20)	−62(13)	52(13)	−29(15)
C(A,10)	7494(6)	5494(4)	6421(5)	622(20)	398(15)	412(20)	74(12)	−34(15)	−13(16)
C(A,11)	8248(7)	21(5)	2051(5)	711(22)	435(16)	469(20)	−49(14)	22(17)	−13(18)
C(A,12)	9718(10)	−1253(7)	1604(7)	1202(40)	799(29)	629(20)	−78(21)	213(26)	249(32)
C(A,13)	6857(9)	811(8)	389(6)	980(33)	944(31)	549(20)	−129(21)	−105(22)	57(32)
C(A,14)	10597(6)	1381(5)	9086(5)	554(19)	485(17)	538(20)	11(15)	2(16)	74(17)
C(A,15)	5807(7)	5687(5)	4709(6)	865(27)	464(17)	562(20)	10(15)	−151(19)	106(21)
O(A,1)	7754(4)	7185(4)	12091(4)	523(13)	668(15)	595(20)	−267(12)	−59(11)	54(13)
O(A,2)	10577(4)	4148(4)	12207(3)	528(13)	700(14)	435(20)	−34(10)	−131(10)	49(13)
O(A,3)	3989(6)	6165(5)	4983(5)	889(20)	904(21)	846(20)	−86(16)	−367(17)	252(19)
C(B,1)	5700(6)	5159(6)	35682(5)	492(17)	747(22)	408(20)	24(15)	37(14)	56(19)
C(B,2)	7441(6)	3721(6)	35892(5)	457(17)	787(23)	406(20)	122(15)	−15(14)	64(19)
C(B,3)	8108(5)	2989(5)	33742(5)	441(16)	570(18)	468(20)	68(14)	−61(14)	20(17)
C(B,4)	8781(5)	4535(5)	32238(4)	371(14)	632(19)	388(20)	−28(14)	−31(12)	−75(16)
C(B,5)	6995(5)	6031(5)	31950(4)	418(15)	512(17)	367(20)	1(13)	−24(12)	−66(15)
C(B,6)	7845(5)	7666(5)	30570(5)	454(16)	595(19)	497(20)	52(15)	−83(14)	−113(17)
C(B,7)	6577(6)	7588(5)	28468(5)	515(17)	603(19)	448(20)	0(14)	−26(14)	−39(18)
C(B,8)	4400(6)	6854(6)	29160(5)	529(19)	761(22)	469(20)	61(16)	−134(15)	−129(20)
C(B,9)	4980(5)	5331(5)	30738(5)	452(16)	609(19)	428(20)	−12(14)	−35(13)	−126(17)
C(B,10)	6332(6)	6726(5)	34208(5)	499(18)	579(18)	426(20)	−68(14)	−72(13)	−63(17)
C(B,11)	6622(7)	9402(6)	27253(5)	742(24)	661(21)	406(20)	56(15)	−51(17)	−68(22)
C(B,12)	4991(9)	10581(7)	27191(8)	891(31)	805(28)	907(20)	200(24)	−72(26)	59(30)
C(B,13)	8680(10)	9801(7)	26169(7)	1077(36)	779(28)	735(20)	242(22)	213(26)	−108(30)
C(B,14)	9585(6)	3725(5)	30168(5)	532(18)	675(21)	492(20)	−30(16)	76(15)	3(19)
C(B,15)	4559(8)	8146(6)	34142(6)	874(28)	558(20)	593(20)	−37(16)	70(20)	44(22)
O(B,1)	6609(4)	2262(5)	37211(4)	570(14)	977(20)	667(20)	396(15)	101(13)	220(16)
O(B,2)	9756(5)	1610(4)	33953(4)	712(16)	774(17)	627(20)	98(13)	−16(13)	203(16)
O(B,3)	2768(5)	7905(5)	34779(5)	818(19)	868(19)	723(20)	13(15)	151(15)	292(19)

[a]The thermal vibration parameters are expressed as $\exp[-2\pi^2(U_{11}h^2a^{*2} + U_{22}k^2b^{*2} + U_{33}l^2c^{*2} + 2U_{23}klb^*c^* + 2U_{13}hla^*c^* + 2U_{12}hka^*b^*)]$.

The structure was determined by direct methods with a multisolution procedure similar to that described by Kennard *et al.* (8). With $\alpha_{min} = 2.21$ and $t_{min} = 0.3$ one of the 64 permutations yielded $R_E = 0.18$ for 323 reflections with $E \geq 1.50$ after a tangent refinement was carried out in three stages. The E map revealed the positions of all 36 nonhydrogen atoms in the two crystallographically independent molecules. Atomic parameters were refined by block-diagonal least squares. All scattering factors were taken from the International Tables for X-Ray Crystallography (9) and the oxygen curve was corrected for anomalous dispersion. All hydrogen atoms were located on difference Fourier maps and their parameters were refined isotropically. Throughout the refinement the function $\Sigma w(|F_o| - |F_c|)^2$ was minimized and the following weighting scheme was used during the final stages: $w = w_1w_2$, where $w_1 = 1$ for $|F_o| \leq 11.5$, $w_1 = 11.5/|F_o|$ for $|F_o| > 11.5$; $w_2 = \sin^2\theta/0.35$ for $\sin^2\theta < 0.35$, $w_2 = 1$ for $\sin^2\theta \geq 0.35$. Six strong reflections suffered severely from extinction effects and they were given zero weights. After the final cycle the average parameter shift equalled 0.08σ and the largest one 0.65σ. The conventional residual index R ($\Sigma|\Delta F|/\Sigma|F_o|$) is 0.045 and the weighted index R' ($\Sigma w\Delta F^2/\Sigma wF_o^2$) is 0.057 for 2330 reflections, including 35 unobserved ones for which $|F_o| < |F_c|$. A final difference Fourier map was featureless.

The final coordinates and temperature parameters, as well as their estimated standard deviations, are listed in Table 1. Table 2 lists the observed and calculated structure factors.[3] Bond lengths and endocyclic torsional angles are shown in Fig. 1 while bond angles are given in Fig. 2.

Discussion

A stereoscopic view of one of the molecules (A) is shown in Fig. 3. In each of the two inde-

[3]Table 2 may be obtained, at a nominal charge, from the Depository of Unpublished Data, CISTI, National Research Council of Canada, Ottawa, Canada K1A 0S2.

TABLE 1 (*Concluded*)

(*b*) Hydrogen atoms

Atom	10^3x	10^3y	10^4z	B
H(A1,1)	543(5)	596(4)	891(5)	3.0(0.6)
H(A1,2)	650(6)	771(5)	817(5)	4.2(0.7)
H(A2,1)	968(5)	691(4)	970(4)	2.3(0.5)
H(A01,1)	657(10)	707(8)	1228(8)	7.8(1.3)
H(A3,1)	774(5)	377(4)	1110(4)	2.2(0.5)
H(A02,1)	1001(9)	446(7)	1312(8)	7.3(1.2)
H(A4,1)	1094(6)	399(5)	816(5)	3.8(0.7)
H(A6,1)	1070(6)	247(5)	482(6)	4.7(0.8)
H(A6,2)	885(6)	352(5)	353(5)	3.6(0.7)
H(A7,1)	872(6)	−17(5)	528(5)	3.8(0.7)
H(A8,1)	485(7)	−5(6)	530(6)	5.7(0.9)
H(A8,2)	503(6)	194(5)	406(5)	4.4(0.8)
H(A9,1)	632(5)	131(4)	842(4)	2.9(0.6)
H(A9,2)	489(6)	296(5)	768(5)	3.5(0.6)
H(A10,1)	875(7)	608(6)	586(6)	4.9(0.8)
H(A12,1)	1063(8)	−190(7)	279(7)	6.8(1.1)
H(A12,2)	985(7)	−183(5)	15(6)	4.9(0.8)
H(A13,1)	684(8)	234(8)	47(7)	7.0(1.1)
H(A13,2)	539(8)	55(7)	69(7)	6.7(1.1)
H(A13,3)	713(10)	31(8)	−103(8)	8.3(1.3)
H(A14,1)	949(5)	65(5)	979(5)	3.3(0.6)
H(A14,2)	1112(6)	73(5)	788(5)	3.6(0.7)
H(A14,3)	1182(7)	133(5)	994(6)	4.9(0.8)
H(A15,1)	638(8)	557(7)	328(8)	7.2(1.1)
H(B1,1)	443(6)	462(5)	3514(5)	4.3(0.7)
H(B1,2)	529(8)	561(6)	3712(7)	6.0(1.0)
H(B2,1)	874(6)	426(5)	3665(5)	3.9(0.7)
H(B01,1)	739(9)	135(7)	3731(7)	7.3(1.2)
H(B3,1)	692(6)	235(5)	3310(5)	4.3(0.7)
H(B02,1)	1062(8)	196(7)	3497(7)	6.5(1.0)
H(B4,1)	995(5)	516(4)	3302(5)	3.3(0.6)
H(B6,1)	931(6)	754(5)	3053(5)	4.3(0.7)
H(B6,2)	758(6)	888(5)	3128(5)	4.0(0.7)
H(B7,1)	703(5)	660(4)	2757(4)	2.9(0.6)
H(B8,1)	362(6)	636(5)	2797(6)	4.6(0.8)
H(B8,2)	364(8)	793(7)	3012(7)	6.7(1.0)
H(B9,1)	522(7)	426(6)	2987(6)	5.0(0.8)
H(B9,2)	378(6)	502(5)	3173(5)	4.0(0.7)
H(B10,1)	747(6)	743(5)	3474(5)	3.8(0.7)
H(B12,1)	357(10)	1035(9)	2819(9)	8.8(1.4)
H(B12,2)	505(8)	1183(7)	2628(7)	6.5(1.0)
H(B13,1)	870(8)	1102(7)	2560(7)	6.5(1.0)
H(B13,2)	899(9)	895(8)	2497(8)	8.4(1.4)
H(B13,3)	980(11)	974(9)	2741(9)	9.2(1.5)
H(B14,1)	1074(7)	283(6)	3045(6)	5.7(0.9)
H(B14,2)	845(8)	304(7)	2937(7)	6.7(1.0)
H(B14,3)	993(6)	469(5)	2914(5)	4.1(0.7)
H(B15,1)	482(8)	932(6)	3360(7)	6.1(1.0)

pendent molecules the six-membered ring is chair-shaped and all four substituents are equatorially oriented. All torsion angles are within a few degrees of 55.9°, the value observed in cyclohexane, indicating that there is very little strain. The conformation of the five-membered rings can be expressed by their phase angles of pseudorotation (10). In molecule A $\Delta = 74.0°$ which is almost identical with the value (72°) corresponding to a perfect half-chair. C(7) and C(8) are displaced by 0.324 and 0.359 Å, respectively, to the opposite sides of the plane defined by C(5), C(6), and C(9). In molecule B the displacements of C(7) and C(8) amount to 0.269 and 0.392 Å, respectively, while $\Delta = 79.5°$ indicates a slightly distorted half-chair. The Newman

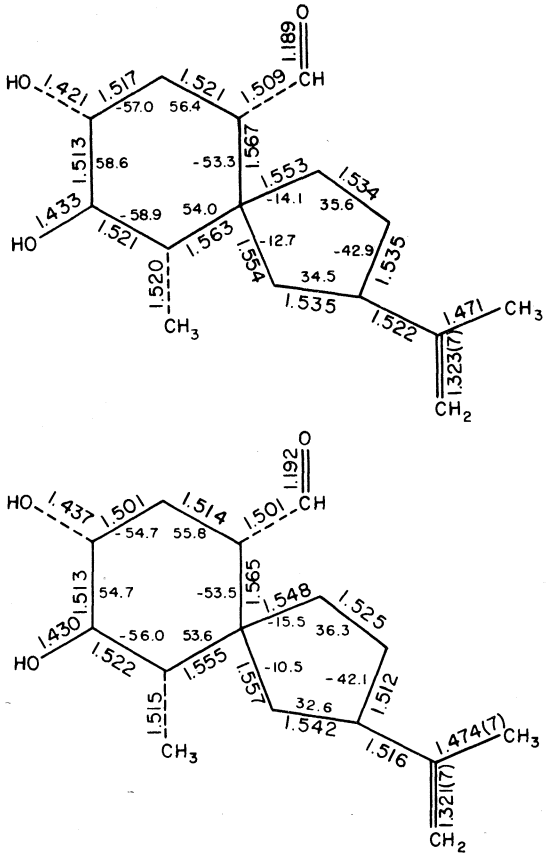

FIG. 1. Bond lengths and torsional angles in molecules A (top) and B (bottom). Unless otherwise indicated, the e.s.d.'s are 0.004–0.006 Å and 0.2–0.3°, respectively.

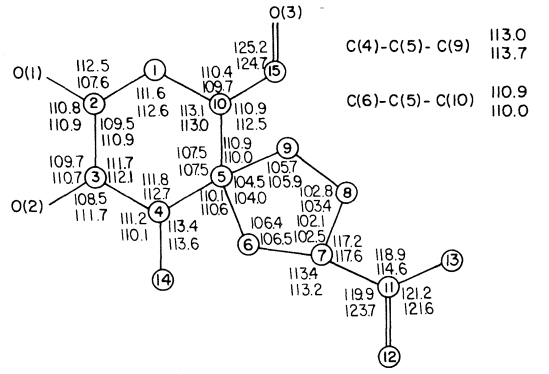

FIG. 2. Bond angles in molecules A (top) and B (bottom). The e.s.d.'s are 0.2–0.4°.

projections in Fig. 4 show the conformations of the aldehyde and isopropenyl groups attached to the two rings in each molecule. In the case of the aldehyde group the two projections look very similar, indicating a preferred conformation. This preference can be explained in terms of non-bonded intramolecular contacts. A clockwise rotation of the C=O group about the C(15)—C(10) bond would decrease the distances between O(3) and H(9,2) and between H(10,1) and H(15,1), 2.9 and 2.2 Å, respectively. On the other hand, a counterclockwise rotation would result in decreasing the distances between O(3) and H(1,1) (2.6 Å) and between H(15,1) and H(6,2) (2.2 Å). Of these four distances, the latter three are very close to van der Waals contacts. Consequently, the range of allowable conformation is very narrow. The conformation of the isopropenyl group is substantially different in the two molecules: there are no short contacts in molecule A, while in molecule B the H(8,2)···H(12,1) distance is 2.13 Å.

Equivalent bonds have the same lengths, within experimental error, in both molecules, except for the C(7)—C(8) bond which is significantly longer in molecule A than in molecule B. The reason is not quite clear, but it may be related to the difference in the conformation of the isopropenyl groups. None of the bond lengths are unusual. As expected, the longest ones are at the spiro junction, reflecting the high degree of substitution. The short C(11)—C(13) bond can be ascribed to the strong thermal vibration of the latter atom; in capsidiol, a closely related sesquiterpenoid phytoalexin isolated from sweet peppers, this bond was even shorter, 1.438 Å (11).

Two bond angles involving oxygen atoms, C(1)—C(2)—O(1) and C(4)—C(3)—O(2), are significantly different in the two molecules. This may be attributable to the different hydrogen bonds in which each molecule participates (see below). The large C(7)—C(11)—C(12) angle and the small C(7)—C(11)—C(13) angle in molecule B are presumably due to the fact that C(8) and C(12) are almost eclipsed. It is somewhat surprising that this interaction is not relieved by a rotation about the C(7)—C(11) bond.

The geometry of the hydrogen bonds in the crystal structure is given in Table 3. Both hydroxyl groups in each molecule act as proton donors and acceptors. However, only in molecule B does the aldehyde oxygen accept a proton from a hydroxyl group. This proton is shared by two acceptors and consequently the H···O distances are somewhat long. A bifurcated hydrogen bond with a similar geometry was encountered in the *trans–syn* photodimer of methyl orotate (12). Each molecule has a polar 'head' and a nonpolar 'tail' and the molecules are

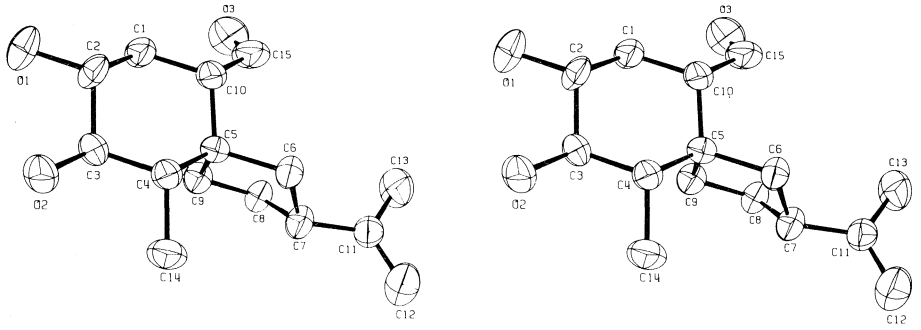

FIG. 3. Stereoscopic view of molecule A; the ellipsoids include 50% probability.

TABLE 3. Geometry of hydrogen bonds

Bonds	Length (Å)		Angle (deg)	
	$D\cdots A$	$H\cdots A$	D—$H\cdots A$	H—$D\cdots A$
O(A,1)—H···O(B,1)$(1-x,\frac{1}{2}+y,\frac{1}{2}-z)$	2.734	1.99	171	7
O(A,2)—H···O(B,2)$(2-x,\frac{1}{2}+y,\frac{1}{2}-z)$	3.008	2.36	144	28
O(A,2)—H···O(B,3)$(1-x,-\frac{1}{2}+y,\frac{1}{2}-z)$	2.950	2.44	126	42
O(B,1)—H···O(A,2)$(2-x,-\frac{1}{2}+y,\frac{1}{2}-z)$	2.862	2.03	175	4
O(B,2)—H···O(A,1)$(2-x,-\frac{1}{2}+y,\frac{1}{2}-z)$	2.962	2.09	165	10

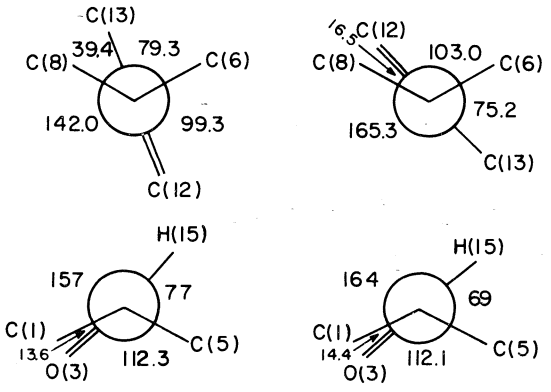

FIG. 4. Newman projections along C(7)—C(11) (top) and C(10)—C(15) (bottom) in molecules A (left) and B (right).

packed 'head' to 'head' and 'tail' to 'tail' along z in the sequence —A—B—B—A—. The isopropenyl groups, representing the non-polar 'tails', are close to the screw axes parallel to y. The hydrogen bonds join the polar 'heads' of molecules A and B to each other, thus forming chains of hydrogen-bonded molecules —A—B—A—B— parallel to x. Apart from these hydrogen bonds there are no intermolecular contacts which are shorter than normal van der Waals distances.

Acknowledgments

I am grateful to Dr. A. Stoessl, Agriculture Canada, for suggesting this investigation and for supplying me with crystals of hydroxylubimin. Figure 3 was drawn with the help of the ORTEP program by C. K. Johnson. All other crystallographic computations were performed with programs written by F. R. Ahmed, S. R. Hall, M. E. Pippy, and C. P. Huber.

1. A. STOESSL, J. B. STOTHERS, and E. W. B. WARD. Phytochemistry, **15**, 855 (1976).
2. L. V. METLITSKII, O. L. OZERETSKOVSKAYA, N. S. VUL'FSON, and L. I. CHALOVA. Dokl. Akad. Nauk SSSR, **200**, 1970 (1971).
3. A. STOESSL, J. B. STOTHERS, and E. W. B. WARD. J. Chem. Soc. Chem. Commun. 709 (1974).
4. N. KATSUI, A. MATSUNAGA, and T. MASAMUNE. Tetrahedron Lett. 4483 (1974).
5. A. STOESSL, J. B. STOTHERS, and E. W. B. WARD. J. Chem. Soc. Chem. Commun. 431 (1976).
6. G. I. BIRNBAUM, C. P. HUBER, M. L. POST, J. B. STOTHERS, J. R. ROBINSON, A. STOESSL, and E. W. B. WARD. J. Chem. Soc. Chem. Commun. 330 (1976).
7. N. KATSUI, H. KITAHARA, F. YAGIHASHI, A. MATSUNAGA, and T. MASAMUNE. Chem. Lett. Jpn. 861 (1976).
8. O. KENNARD, N. W. ISAACS, W. D. S. MOTHERWELL, J. C. COPPOLA, D. L. WAMPLER, A. C. LARSON, and D. G. WATSON. Proc. R. Soc. A, **325**, 401 (1971).
9. International Tables for X-Ray Crystallography. Vol. 4. *Edited by* J. A. Ibers and W. C. Hamilton. Kynoch Press, Birmingham. 1974.
10. C. ALTONA, H. J. GEISE, and C. ROMERS. Tetrahedron, **24**, 13 (1968).
11. G. I. BIRNBAUM, A. STOESSL, S. H. GROVER, and J. B. STOTHERS. Can. J. Chem. **52**, 993 (1974).
12. G. I. BIRNBAUM. Acta Crystallogr. Sect. B, **28**, 1248 (1972).

The thermal decomposition of methane. III. Methyl radical exchange in CH_4–CD_4 mixtures[1]

C.-J. CHEN AND M. H. BACK

Chemistry Department, University of Ottawa, Ottawa, Ont., Canada K1N 6N5

AND

R. A. BACK

Chemistry Division, National Research Council of Canada, Ottawa, Ont., Canada K1A 0R9

Received November 4, 1976

C.-J. CHEN, M. H. BACK, and R. A. BACK. Can. J. Chem. **55**, 1624 (1977).

The thermal methyl-radical exchange reaction, $CH_4 + CD_4 \rightarrow CH_3D + CD_3H$, has been studied in a static system at temperatures from 880 to 1103 K, with equimolar mixtures at a pressure of 440 Torr. The exchange occurs by a methyl-radical chain mechanism, propagated by the reactions $CH_3 + CD_4 \rightarrow CH_3D + CD_3$ and $CD_3 + CH_4 \rightarrow CD_3H + CH_3$. Values of an average rate constant for these reactions have been estimated; $k_X = 1.42 \times 10^6$ ℓ mol^{-1} s^{-1} at 995 K. Comparison with shock tube data and photochemical measurements, at higher and lower temperatures respectively, indicates pronounced non-Arrhenius behaviour.

C.-J. CHEN, M. H. BACK et R. A. BACK. Can. J. Chem. **55**, 1624 (1977).

Utilisant des mélanges équimoléculaires à une pression de 440 Torr, on a étudié, dans un système statique et à des températures allant de 880 à 1103 K, la réaction d'échange thermique du radical méthyle $CH_4 + CD_4 \rightarrow CH_3D + CD_3H$. La réaction se produit par un mécanisme en chaîne du radical méthyle propagé par les réactions $CH_3 + CD_4 \rightarrow CH_3D + CD_3$ et $CD_3 + CH_4 \rightarrow CD_3H + CH_3$. On a évalué que les valeurs moyennes des constantes de vitesse de ces réactions sont $k_X = 1.42 \times 10^6$ ℓ mol^{-1} s^{-1} à 995 K. Une comparaison avec des données de tube de choc et des mesures photochimiques respectivement à des températures plus élevées et plus basses, indique que le comportement diffère considérablement de celui prédit par la théorie d'Arrhénius.

[Traduit par le journal]

Introduction

Non-Arrhenius behaviour in the rate constants for hydrogen abstraction has been observed in several recent studies where the measurements have been made at high temperatures (>1000 K) (1–7). Clark and Dove (8) have offered the most quantitative explanation of this effect, using the BEBO method to show that tunnelling corrections and quantum effects can account reasonably well for the observed curvature. The effect is of great interest in the understanding of the activated complex in chemical reactions, and more data for this type of reaction in the high-temperature region are needed.

The methyl radical exchange reaction in mixtures of CH_4 and CD_4 was studied some years ago by Burcat and Lifshitz (9) using a shock tube in the temperature range 1340–1745 K. They concluded that the exchange proceeded through a methyl-radical chain mechanism propagated by the reactions

[A] $CH_3 + CD_4 \rightarrow CH_3D + CD_3$

[B] $CD_3 + CH_4 \rightarrow CD_3H + CH_3$

and their measurement of an average rate constant for these reactions was considerably higher than an extrapolated value from measurements in a lower temperature region (500–800 K) (10). In a recent study in these laboratories of the thermal decomposition of methane (11), mixtures of CH_4 and CD_4 were used in some experiments to determine whether molecular hydrogen was formed in the primary dissociation. In the course of these experiments it was noted that an efficient H–D exchange was occurring, much faster than the decomposition itself, which closely followed the simple stoichiometry

$$CH_4 + CD_4 \rightarrow CH_3D + CD_3H$$

The present paper describes kinetic measurements of this exchange reaction in the static pyrolysis system at temperatures from 880 to 1103 K. The results are in substantial agreement

[1]NRCC No. 15865.

with the earlier results of Burcat and Lifshitz (9) and confirm their observation of non-Arrhenius behaviour in this reaction.

Experimental

Apparatus, techniques, and product analysis have already been described (11). Experiments were performed over the temperature range 880–1103 K with equimolar mixtures of CH_4 and CD_4 at a pressure of 440 Torr. Samples of methane were analyzed for isotopic composition by mass spectrometry.[2] Hydrogen was analyzed for H_2, HD, and D_2 by gas chromatography (11).

Results

Analysis of methane after the reaction showed that CH_3D and CD_3H were the only isotopic methanes produced in significant yields; CH_2D_2 was negligible when the extent of the exchange was $<20\%$. Figures 1 and 2 show typical first-order plots for the disappearance of CH_4 and CD_4 and the formation of the mixed methanes. Within experimental error, $-d[CH_4]/dt = -d[CD_4]/dt = d[CH_3D]/dt = d[CD_3H]/dt$ as required for the simple exchange mechanism suggested. There seems little doubt that the radical chain mechanism is operative in the present system.

In the thermal decomposition of CH_4, we have shown (7, 11) that the methyl radical concentration in the early stages is determined by the following reactions:

[1] $$CH_4 \rightarrow CH_3 + H$$

[2] $$H + CH_4 \rightarrow H_2 + CH_3$$

[3] $$2CH_3 \rightleftharpoons C_2H_6$$

[4] $$CH_3 + C_2H_6 \rightarrow CH_4 + C_2H_5$$

[5] $$C_2H_5 \rightarrow C_2H_4 + H$$

Reaction 1 is slow and rate controlling, and is always followed by reactions 2 and 3, so that the steady-state methyl radical concentration is given by

[6] $$[CH_3] = \{(k_1[CH_4] + k_{-3}[C_2H_6])/k_3\}^{1/2}$$

Initially, $[CH_3]$ is determined by reactions 1 and 3 alone, but as ethane accumulates reaction -3 becomes important. Ethane is formed by reaction 3 at a rate equal to that of reaction 1, and begins to disappear by reaction 4 as its concentration rises. The ethane concentration will be given by the differential equation

[7] $$d[C_2H_6]/dt = k_1[CH_4] - k_4[CH_3][C_2H_6]$$

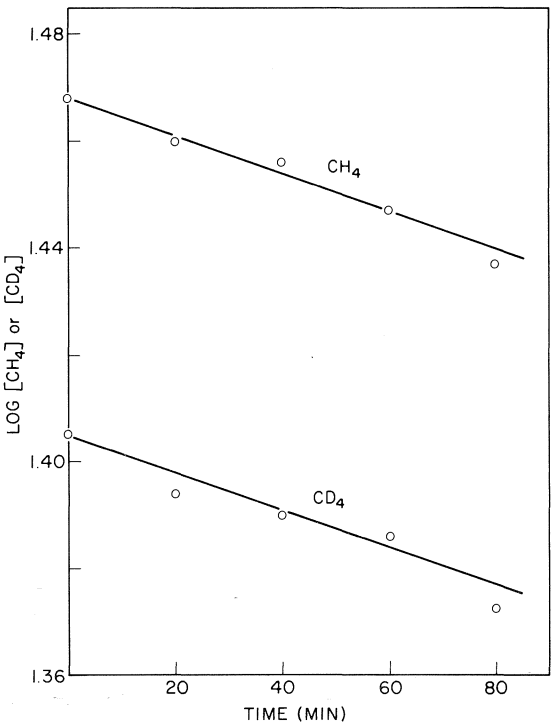

FIG. 1. First order plots for disappearance of CH_4 and CD_4 at 957 K. Initial pressure 440 Torr.

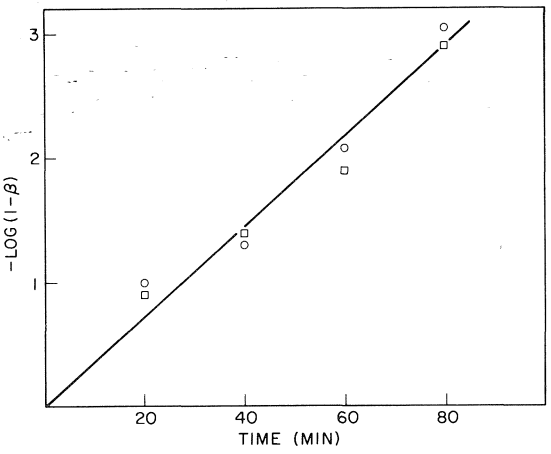

FIG. 2. First order plots for formation of CD_3H (○) and CH_3D (□), at 957 K where $\beta = 1 - [CD_3H]/[CD_4]$ or $1 - [CH_3D]/[CH_4]$ respectively. Initial pressure 440 Torr.

Calculation of the Rate Constant for Exchange

Equation 6 can be applied to the CH_4–CD_4

[2]We are grateful to Mr. Roger Pilon for assistance in the mass spectrometry.

system, after appropriate modifications to take into account kinetic isotopic effects in reactions 1 and 3, to calculate the total radical concentration, $[CH_3] + [CD_3]$. It is more difficult to determine the concentration of each radical. Because reactions A and B are much faster than reaction 1, the chain length of the exchange reaction is large, and the relative concentrations of CH_3 and CD_3 will adjust themselves to maintain the relation $k_A[CH_3][CD_4] = k_B[CD_3][CH_4]$. Values of k_A and k_B could in principle be obtained from the system in two ways. Measurements of the yields of C_2H_6 and C_2D_6 could be used to evaluate $[CH_3]$ and $[CD_3]$, making suitable assumptions about the relative combination rates. Alternatively, experiments could be done with $[CH_4] \gg [CD_4]$ so that $[CH_3] \gg [CD_3]$, and $[CH_3]$ could then be obtained simply from eq. 6, and k_A evaluated from the exchange rate; analogous experiments with $[CD_4] \gg [CH_4]$ could be used to determine k_B. Both these methods are thwarted by experimental difficulties inherent in the methane pyrolysis. In the first case, accurate isotopic analysis of the very small yields of ethane was impossible in the presence of the large excess of methane, while in the second method the exchange reaction became too slow compared to the thermal decomposition. The separate evaluation of k_A and k_B was therefore abandoned and the data treated instead in terms of an average rate constant for exchange, k_X, defined by the usual relation

$$[8] \quad \frac{d[CD_3H]}{dt} + \frac{d[CH_3D]}{dt} = \frac{2k_X[CD_4][CH_4]}{[CD_4] + [CH_4]}([CH_3] + [CD_3])$$

To evaluate k_X from eq. 8, the total methyl radical concentration must be estimated from eq. 6, taking account of all the isotopic species involved. While values of k_1, k_3, and k_{-3} are known with some confidence for the CH_4 system (7, 11) the corresponding values of k_1 for CD_4, k_3 for $CH_3 + CD_3$ and $CD_3 + CD_3$, and k_{-3} for CH_3CD_3, are not. The deuterium isotope effect in k_1 is undoubtedly in the normal direction, as will be seen from the isotopic composition of the hydrogen formed (below). A small inverse secondary deuterium isotope effect has recently been reported in k_{-3} for C_2H_6 and C_2D_6 (12); the isotope effect in k_3 is probably very small. The kinetic isotope effects in reactions 1 and -3 are thus in opposite directions, and the terms in eq. 6 involving k_1 and k_{-3} are of comparable importance at the ethane concentrations attained in the present experiments. It was therefore concluded that no large error would be introduced by simply ignoring all kinetic isotope effects in k_1, k_3, and k_{-3}, and calculating the total radical concentrations using equation 6 and the known rate constants used previously (7) for the CH_4 pyrolysis system. Details of the calculation of radical concentration and values of k_X obtained from eq. 8 are shown in Table 1. Radical concentrations used were simple averages of the initial value and the value corresponding to the steady-state in ethane, as the rate of the exchange reaction was measured between $t = 0$ and the attainment of the steady state. The first-order rate plots were linear, within experimental scatter (Figs. 1 and 2), although some upward curvature, as expected from the increasing radical concentration (Table 1) was perhaps evident in some of the experiments. Average rates and average radical concentrations were used to obtain k_X, and the absolute errors arising from the approximations involved, including the neglect of isotope effects, are probably less than $\pm 20\%$.

Isotope Effects in Reactions 1 and 2

The initial yields of H_2, HD, and D_2 from the pyrolysis of equimolar CH_4–CD_4 mixtures are shown in Table 2. Kinetic isotope effects in both reactions 1 and 2 combine to determine the isotopic composition of the hydrogen. The pertinent reactions are

$$[1A] \quad CH_4 \rightarrow CH_3 + H$$

$$[1B] \quad CD_4 \rightarrow CD_3 + D$$

$$[2A] \quad H + CH_4 \rightarrow H_2 + CH_3$$

$$[2B] \quad H + CD_4 \rightarrow HD + CD_3$$

$$[2C] \quad D + CH_4 \rightarrow HD + CH_3$$

$$[2D] \quad D + CD_4 \rightarrow D_2 + CD_3$$

To separate the isotope effects of the two reactions, some simplification must be made. If it is assumed that $k_{2A}/k_{2B} = k_{2C}/k_{2D} = Y$, and putting $k_{1A}/k_{1B} = X$, it can be shown that for equimolar CH_4–CD_4 mixtures,

$$[9] \quad XY = [H_2]/[D_2]$$

$$[10] \quad [D_2]X^2 - [HD]X + [H_2] = 0$$

$$[11] \quad [D_2]Y^2 - [HD]Y + [H_2] = 0$$

Equations 10 and 11 are identical in X and Y and can be solved when $[HD]^2 > 4[H_2][D_2]$, as was

TABLE 1. Values of the average rate constant, k_X, for methyl-radical exchange, measured in equimolar CH_4–CD_4 mixtures at 400 Torr

T (K)	$([CH_3]+[CD_3])\times 10^{11}$ (mol ℓ^{-1}) Initial	Steady state	Average	$[C_2H_6]_{55}\times 10^7$ (mol ℓ^{-1})	$k_1\times 10^8$ (s^{-1})	$k_{-3}\times 10^3$ [a] (s^{-1})	$k_3\times 10^{-10}$ [b] (ℓ mol^{-1} s^{-1})	$k_X\times 10^{-5}$ (ℓ mol^{-1} s^{-1})
880[c]	—	—	4.03	190	0.00207[d]	0.0039	3.51	2.90
957	1.99	2.38	2.18	0.337	0.247[d]	0.210	3.36	11.8
995	5.61	10.2	7.89	2.30	2.40	1.32	3.22	14.2
1038	16.1	37.0	24.1	3.77	18.6	8.50	3.17	15.5
1068	38.2	73.0	55.6	4.40	70.8	27.6	3.10	21.8
1103	85.9	188	137	8.38	30.2	101.8	2.58	30.6

[a]Calculated as described in refs. 7 and 13.
[b]k_3 was taken as 4.0×10^{10} ℓ mol^{-1} s^{-1} in the high-pressure limit. The extent of fall-off was taken equal to that for k_{-3}. For a discussion of these values see ref. 14.
[c]0.24% ethane added.
[d]Calculated from RRKM equation of ref. 11.

TABLE 2. Yields of H_2, HD, and D_2

T (K)	Time (min)	Yield $\times 10^8$ (mol ℓ^{-1}) H_2	HD	D_2	$\frac{[HD]^2}{[H_2][D_2]}$
1068	0.50	9.44	10.9	2.49	5.0
	1.01	17.4	20.7	4.60	5.4
	2.00	29.8	51.3	23.0	3.8
	3.51	73.7	93.4	26.2	4.5
	5.01	107	151	46.4	4.6
1103	0.26	18.0	22.1	5.14	5.3
	0.40	29.2	36.6	8.91	5.1
	0.51	36.2	48.5	14.5	4.5
	0.77	67.1	78.1	25.0	3.6
	1.01	91.3	123	36.5	4.6
	1.51	154	204	65.2	4.2

found experimentally, to yield 2 roots. The initial rates, estimated from the data in Table 2, gave average values of $[H_2]/[D_2]$ of 3.6 ± 0.4 and of $[HD]^2/[H_2][D_2]$ of 5.2 ± 0.5, and from eqs. 9 and 11 values of X and Y of 1.2 and 3.0 were obtained. This implies that the overall isotope effect of 3.6 is unequally shared between reactions 1 and 2, but there is nothing to indicate which value belongs to which reaction. It should also be noted that the conclusion that X and Y are unequal depends on the value of $[HD]^2/[H_2][D_2]$ being significantly greater than 4, which considering the scatter in the data may be seriously questioned. A perhaps more accurate estimate of the kinetic isotope effect in reaction 1 can be obtained from the yields of ethane; it has been shown that the initial yield of ethane is an accurate measure of reaction 1 in the pyrolysis of methane (11), and the measurements of total initial ethane from equimolar CH_4–CD_4 mixtures showed this to be about 20% less than that expected from pure CH_4 at both 1068 and 1103 K. This corresponds to an isotope effect in reaction 1 of about 1.7 which combined with eq. 9 would suggest an isotope effect in reaction 2 of 2.2. There are considerable uncertainties in both these estimates of isotope effects, particularly in the measurement of the small quantities of deuterium in the initial stages of the reaction. It may be concluded only that the kinetic isotope effects in both reactions are normal in direction and magnitude, and that for reaction 2 is probably greater than that for reaction 1.

Discussion

In Fig. 3 our values of k_X are compared with data obtained at both lower and higher temperatures. The low-temperature data (425–800 K) were obtained by photolysis methods and have been recently reviewed by Kerr and Parsonage

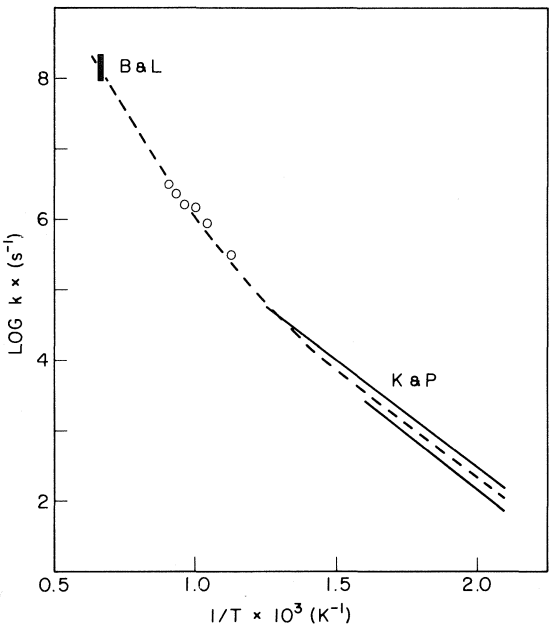

FIG. 3. Comparison of present experiments (○) with shock-tube data of Burcat and Lifshitz (B & L) (9) and the photochemical data compiled by Kerr and Parsonage (K & P) (10).

(10). The two lines shown in Fig. 3 are their recommended values for the rate constants for the reactions, CH_3 (or CD_3) + CH_4, and CH_3 (or CD_3) + CD_4 (secondary isotope effects were considered negligible in their assessment). The average rate constant, k_X, as defined in the present experiments, should fall about midway between the two lines.

The high-temperature value shown is based on an average of two experiments (No. 2 and 3) at 1500 K with equimolar CH_4–CD_4 mixtures reported by Burcat and Lifshitz (9) which appear to be representative of their measurements. These authors did not report values of k_X directly, but values are implicit in their comparison with low-temperature data. In this comparison they assumed reaction -3 to be unimportant, and their steady-state equation (VIII) is in error by a factor of 2; the neglect of reaction -3, and the error in their equation VII tend to cancel one another, and their estimate of methyl radical concentration is not greatly in error. Reaction -3 is far from negligible in their experiments, and in fact the second term in the numerator of the r.h.s. of eq. 6 becomes dominant at an early stage of the reaction, so that $[CH_3]$ approaches a value corresponding to the equilibrium $C_2H_6 \rightleftharpoons 2CH_3$. To estimate $[CH_3]$ accurately via eq. 6, it would be necessary to calculate an average value of $[C_2H_6]$ by integration of eq. 7. Because k_4 is not accurately known at this temperature, we have instead calculated lower and upper limits for $[CH_3]$, assuming in the first case that reaction -3 is negligible (which underestimates $[CH_3]$), and in the second that reaction 4 is negligible (which overestimates $[CH_3]$). The vertical bar in Fig. 3 corresponds to the range of k_X obtained between these two limiting values of $[CH_3]$. In the calculation, a value of $k_1 = 3.16 \times 10^9\ s^{-1}$ at 1500 K was taken, based on measurements in this laboratory (11), extrapolated by RRKM calculations, assuming argon to be 1/3 as efficient as CH_4 as a collision partner, which gives values in good agreement with experiment. Values of $k_3 = 4 \times 10^{10}\ M^{-1}\ s^{-1}$ and $k_3/k_{-3} = 7.7 \times 10^9\ M^{-1}$ (7) were also employed. The true value of k_X measured by Burcat and Lifshitz should lie well between the calculated limits, probably rather closer to the lower one.

The data in Fig. 3 appear to constitute strong evidence for non-Arrhenius behaviour in the reaction of methyl radicals with methane. While there is considerable uncertainty in all the rate constants shown, the curvature seems well beyond any reasonable estimate of the experimental error. There now appears to be good evidence for such behaviour in a number of simple hydrogen abstraction reactions (1–7).

1. P. D. PACEY and J. H. PURNELL. J. Chem. Soc. Faraday Trans. I, **68**, 1462 (1972).
2. T. C. CLARK and J. E. DOVE. Can. J. Chem. **51**, 2155 (1973).
3. P. D. PACEY. Can. J. Chem. **51**, 2415 (1973); **53**, 2742 (1975).
4. R. ZELLNER and W. STEINERT. Int. J. Chem. Kinet. **8**, 397 (1976).
5. M. B. COLKET, D. W. NAEGELI, and I. GLASSMAN. Int. J. Chem. Kinet. **7**, 223 (1975).
6. T. BERCES and F. MARTA. Int. J. Chem. Kinet. **8**, 295 (1976).
7. C.-J. CHEN, M. H. BACK, and R. A. BACK. Can. J. Chem. **54**, 3175 (1976).
8. T. C. CLARK and J. E. DOVE. Can. J. Chem. **51**, 2147 (1973).
9. A. BURCAT and A. LIFSHITZ. J. Chem. Phys. **52**, 3613 (1970).
10. J. A. KERR and M. J. PARSONAGE. Evaluated kinetic data on gas phase hydrogen transfer reactions of methyl radicals. Butterworths, London. 1976.
11. C.-J. CHEN, M. H. BACK, and R. A. BACK. Can. J. Chem. **53**, 3580 (1975).
12. J. A. CLARK and C. P. QUINN. J. Chem. Soc. Faraday Trans. I, **72**, 706 (1976).
13. M. C. LIN and K. J. LAIDLER. Trans. Faraday Soc. **64**, 79 (1968).
14. E. V. WAAGE and B. S. RABINOVITCH. Int. J. Chem. Kinet. **3**, 105 (1971).

Intramolecular alkylation of a ketone by 1,2-epoxide groups of differing stereochemistry

E. W. WARNHOFF AND V. SRINIVASAN

Department of Chemistry, University of Western Ontario, London, Ont., Canada N6A 5B7

Received December 13, 1976

E. W. WARNHOFF and V. SRINIVASAN. Can. J. Chem. **55**, 1629 (1977).

The intramolecular alkylation of a ketone by three epoxide stereoisomers of **1** has been studied. Although a variety of products are possible *a priori*, in *tert*-BuOH–H_2O–KOH each reaction yields a preponderant product. The course of these reactions can be rationalized by considering the accessibility of both faces of the three possible enolates to the backside of each carbon of the epoxide group for the S_N2 reaction.

E. W. WARNHOFF et V. SRINIVASAN. Can. J. Chem. **55**, 1629 (1977).

On a étudié l'alkylation intramoléculaire d'une cétone par trois époxydes stéréoisomères de **1**. Quoiqu'un grand nombre de produits soit possibles *à priori*, dans le milieu réactionnel *tert*-BuOH–H_2O–KOH, chaque réaction conduit à un produit principal. On peut rationaliser le cours de ces réactions en considérant l'accessibilité de chaque face des trois énolates possibles vis-à-vis une attaque par l'arrière de chaque atome de carbone du groupe époxyde pour la réaction du type S_N2.

[Traduit par le journal]

During the recently reported study (1) of base-catalyzed intramolecular opening of the epoxide ring of some derivatives of the sesquiterpene caryophyllene, the opportunity was provided to examine the base-catalyzed intramolecular alkylation of a ketone by the epoxide group. This reaction has been useful on occasion (2–7), and it seemed worthwhile to explore its stereodependence with the available stereoisomers of the keto oxide **1**.

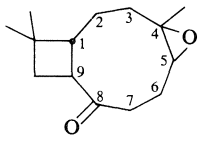

1

For each of the three isomers **2**, **6**, and **9** there was the possibility of reaction at either α-carbon of the ketone and at either carbon of the epoxide to yield a 3-, 4-, 5-, or 6-membered ring. Although either enolate could in principle be alkylated from either side, in fact there was one preponderant product formed in each reaction, as already noted for epoxide **2** by Barton and Lindsey (2). Structural assignments to products (Scheme 1) were readily made with ir (OH, C=O, and cyclopropyl CH), uv (C=O conjugated with cyclopropyl), and ^{1}Hmr spectra (C*H*OH, cyclopropyl H, see Table 1) in conjunction with acetylation and oxidation experiments. For two of the stereoisomers, the product distribution depended on the base–solvent system used. Thus with epoxide **2** in methanolic KOH the major product was **3** as found by Barton and Lindsey in the course of the structure determination of caryophyllene (2). However, there was also ~5% each of two other isomers formed, mp 119°C and 146°C, and in the *tert*-butyl alcohol–water–KOH system, the amount of one of the minor products (mp 119°C) was increased to 27%. The product of mp 146°C was a tertiary hydroxy cyclopropyl ketone and is assigned the stereostructure **5** on the assumptions of inversion during oxide ring opening and formation of the most stable configurations at the two enolizable α-positions of the ketone.

The third ketol isomer of mp 119°C was found to be the artifact **4** derived from the major product **3** by base-catalyzed intramolecular hydride transfer (9, 10).[1] Its structure follows from oxidation to the same dione **12** obtained by oxidation of **3**, and from photochemical cleavage (Scheme 2) which produced lactone **13** via intramolecular hydrogen abstraction in the diradical and cyclization of the resulting ketene. The ^{1}Hmr spectrum of this lactone contained a methyl

[1]Some of the facts (and consequently their interpretation) regarding the ketols of mp 119 and 130°C given in this paper and in refs. 9 and 10 differ from those given in ref. 8; the facts presented here and in ref. 10 are correct.

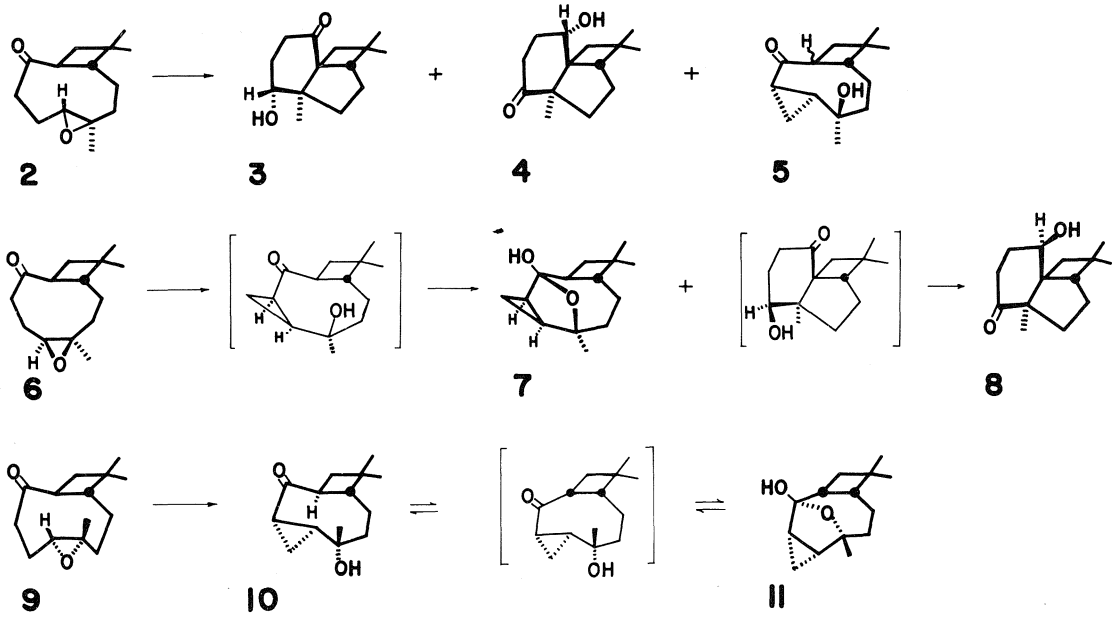

SCHEME 1

doublet at δ 0.91 (J = 6 Hz) in addition to the *gem*-dimethyl group. Irradiation of ketol **3** (Scheme 2) also produced a lactone **14** which, however, exhibited three methyl singlets in its ^{1}Hmr spectrum.

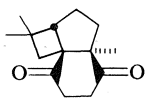

12

In the methanolic potassium hydroxide system, *cis*-keto oxide-a **6** gave a complex mixture of at least nine products, but in *tert*-butyl alcohol – water – potassium hydroxide only two products were formed. The major one (~60%), which had no carbonyl infrared absorption, was assigned the cyclopropyl hemiketal structure **7**. A monoacetate was formed at reflux in acetic anhydride – pyridine. Although the configuration at the cyclobutane ring fusion is epimerizable, it should be *trans* as shown because the *cis*-configuration would have more unfavorable non-bonded interactions on the α-face of the molecule.

The second product of the reaction formed in only 4% yield was **8**, mp 130°C, whose origin is discussed in the following paper (10).

The *cis*-keto oxide-b **9** gave a single alkylation product in both the methanolic potassium hydroxide and the *tert*-butyl alcohol – water – potassium hydroxide media. This product was a cyclopropyl ketone which was partially isomerized by base to a hemiketal. The isomerization was shown to be a true equilibration by obtaining the same 2:1 mixture of **10** and **11** starting with each pure compound. The geometry (Dreiding models) is much better for hemiketalization if the cyclobutane ring is *cis*-fused. The slow rate of hemiketalization is best explained if the cyclopropyl ketone **10** has a *trans*-fused cyclobutane ring and the hemiketal has a *cis*-fused cyclobutane ring so that an epimerization is required before hemiketalization can occur.

These alkylations are true S_N2 displacements of an enolate on the oxide group, and not solvolytic openings of the oxide with concomitant reaction of the enol(ate), because the oxide groups of caryophyllene monoxide (**2**, with $=CH_2$ in place of $=O$) and isocaryophyllene monoxides (**6** and **9** with $=CH_2$ in place of $=O$) are stable to these reaction conditions. The products found accord with expectations from examination of Dreiding models. The simplest case is that of *cis*-keto oxide-b **9** for which the C-9-enolate can not get within bonding distance of the back of either C-4 or C-5 of the oxide group, and hence only alkylation by the C-7-enolate can occur. Although in principle alkylation could occur with the enolate in the *cis*- or

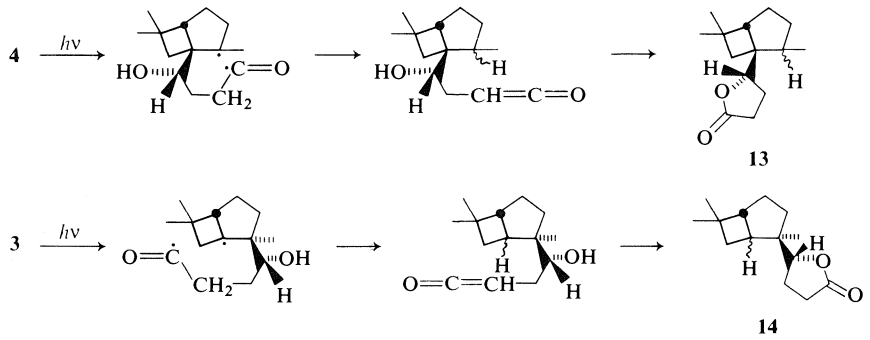

SCHEME 2

TABLE 1. ^{1}Hmr data[a,b]

Compound	Methyl groups[c]	Other	
Cyclopropyl ketol **5**	0.97, 0.97, 1.03	3.13 (1H, m, ketone α-H)	0.7–0.95 (m, cyclopropyl H)
Cyclopropyl ketol **7**	0.92, 1.17, 1.21	—	0.4–0.8 (m, cyclopropyl H)
Cyclopropyl ketol **7** acetate	0.91, 1.13, 1.26	1.99 (CH_3C=O)	0.4–0.8 (m, cyclopropyl H)
Cyclopropyl ketol **10**	0.96, 1.05, 1.26	3.16 (1H, m, ketone α-H)	0.6–0.95 (m, cyclopropyl H)
Cyclopropyl hemiketal **11**	1.07, 1.15, 1.25	—	0.3–0.7 (m, cyclopropyl H)
Cyclopropyl hemiketal **11** acetate	1.06, 1.13, 1.31	2.00 (CH_3=O)	0.35–0.75 (m, cyclopropyl H)
Diketone **12**	0.91, 1.03, 1.08	—	—
γ-Lactone **13**	0.91, 1.18, 0.91 (d, J = 6)	4.64 (1H, q, CHOC=O)	
γ-Lactone **14**	0.86, 0.86, 1.16	4.25 (1H, t, CHOC=O)	

[a]Chemical shifts are given in ppm from tetramethylsilane (δ), and coupling constants are given in Hz for $CDCl_3$ solutions; d = doublet t = triplet, q = quartet, m = multiplet.
[b]For data on ketols **3**, **4**, and **8** see the following paper; for data on keto oxides **2**, **6**, and **9** see ref. 13.
[c]All peaks were singlets except as noted.

trans-configuration and with the cyclobutane fusion either *cis* or *trans*, only the transition state involving the *cis*-enolate and the *trans*-cyclobutane fusion (→**10**) has the proper orientation of the enolate α-carbon at the backside of C-5 without unfavorable transannular hydrogen interactions. The cyclopropyl ketol **10** with the *trans*-cyclobutane fusion might have been expected to form a hemiketal, but Dreiding models clearly show this hemiketal to be more strained than **11** with the *cis*-fused cyclobutane.

For the *cis*-keto oxide-a **6**, it is apparently not possible to get the α-face of the C-9-enolate properly positioned behind C-5 for S_N2 displacement, nor is it possible to get the β-face properly oriented behind either C-4 or C-5. However, the α-face of the C-9-enolate can approach the back of the tertiary C-4 correctly, and this path eventually produces the minor product **8** (10). With the C-7-enolate of **6**, when the cyclobutane fusion is *trans*, the *cis*-enolate is well situated for displacement at the backside of C-5 leading to **7** as the major product. Cyclopropane formation may predominate in this case because the transition state for the formation of the other product **8** has an unfavorable interaction of α-C-4-methyl with the α-hydrogen of the cyclobutane methylene group.

In contrast, the α-face of the C-9-enolate of the *trans*-keto oxide **2** has no unfavorable interactions for alkylation at tertiary C-4, and this path leads to the major product **3** observed. Attack of the C-9-enolate at secondary C-5 is apparently prohibited because strain prevents C-9 from getting properly oriented at the back of C-5. The alkylation of the β-face of the *cis*-C-7-enolate by C-5 to give cyclopropane **5** competes only to a minor extent with the formation of **3**.[2]

[2]Of the three products with the same structure, **5**, **10**, and the ketol precursor of **7**, only **5** gives no evidence of hemiketal formation. The probable reason for this situation is that, if the cyclobutane fusion in **5** is *trans*, hemiketal ring closure would increase the unfavorable nonbonded interactions (6αH ↔ 2αH ↔ 9αH) already present on the α-face of the molecule. On the other hand if the cyclobutane fusion is *cis*, hemiketal formation would jam the 6αH into the 2αH, while the uncyclized ketol structure can assume a conformation which minimizes these α-repulsions.

Experimental

General

Procedures and apparatus are the same as for ref. 1. Woelm neutral alumina was used for column chromatography and its activity is specified in parentheses. The colors specified for tlc spots are for incompletely charred plates. The following abbreviations were used: Py for pyridine, PE for petroleum ether, THF for tetrahydrofuran, EtOAc for ethyl acetate, Ac_2O for acetic anhydride, MeOH for methanol, and *tert*-BuOH for *tert*-butyl alcohol.

Isomerization of Caryophyllene Keto Epoxide **2**

Keto oxide **2** was prepared by the procedure of Treibs (2, 11).

(a) tert-BuOH–Water–KOH

A solution of 8.62 g (38 mmol) of **2**, mp 62.5–63°C, in 100 ml of *tert*-BuOH containing 7 ml of water and 18 g of KOH was refluxed for 64 h. Dilution with water and extraction with ether yielded 8.30 g (96%) of a light yellow solid whose tlc examination (EtOAc:PE, 65:35) revealed three intense spots: R_f 0.75 (brown), 0.55 (dark green), and 0.35 (light brown).

Recrystallization of the crude product from PE gave a first crop of 4.15 g (50%) of **3**, mp 144–146°C, R_f 0.55 (single spot). A second recrystallization raised the mp to 147–148.5°C, $[\alpha]_D$ −32.8° (*c* 3.12, $CHCl_3$) (lit. (2) mp 148–149°C, $[\alpha]_D^{22}$ −32° (*c* 4.68, $CHCl_3$)); $\nu_{max}(CHCl_3)$ 3600 and 3460 (OH), and 1700 cm^{-1} (6-ring C=O).

The mother liquor left from the first crop was concentrated and chromatographed on 100 g of alumina (IV). Elution with PE–benzene (50:50) afforded 2.30 g (27%) of **4**, R_f 0.75 (single spot). Two recrystallizations from PE furnished 1.60 g of small plates of **4**, mp 118–119°C, $[\alpha]_D^{17}$ +17.8° (*c* 3.11, $CHCl_3$); λ_{max}(EtOH) 292 nm (ε 34); $\nu_{max}(CS_2)$ 3600 and 3500 (OH), and 1705 cm^{-1} (6-ring C=O). *Anal.* calcd. for $C_{14}H_{22}O_2$ (222.3): C 75.63, H 9.97; found: C 75.53, H 9.90.

Further elution of the column with benzene gave 1.15 g of a mixture of **3** and **4** (ratio of 95:5). Elution with MeOH washed off 400 mg (4.8%) of a yellow oil, R_f 0.35, trituration of which with ether followed by three recrystallizations from PE gave small colorless crystals of **5**, mp 145–146°C (crystal change at 123–125°C), $[\alpha]_D^{18}$ +73° (*c* 3.04, $CHCl_3$); λ_{max}(EtOH) 280 nm (ε 158); $\nu_{max}(CHCl_3)$ 3580 and 3420 (OH), 3000 (cyclopropane CH_2), and 1695 cm^{-1} (8-ring C=O conjugated with Δ). *Anal.* calcd. for $C_{14}H_{22}O_2$ (222.3): C 75.63, H 9.97; found: C 75.21, H 10.13.

The cyclopropyl ketone **5** was recovered unchanged in 88% yield when a solution of 47 mg of **5** in 5 ml of MeOH containing 1 g of KOH was refluxed for 12 h. Examination of the recovered material by ir, tlc, and ^{1}Hmr gave no indication of any other compound.

(b) MeOH–KOH (Procedure of Barton and Lindsey (2))

A solution of 225 mg of **2** in 5 ml of MeOH containing 1 g of KOH was refluxed for 6 h, after which time the reaction mixture was worked-up (2) to give 200 mg (90%) of white solid. Thin layer chromatographic examination of the crude product revealed the presence of three spots with the same R_f and charring behaviour as the spots from the reaction in *tert*-BuOH, but since signals from **4** and **5** could not be clearly distinguished in the ^{1}Hmr spectrum of the total product, the amounts of **4** and **5** are estimated to be less than ~5% each.

Diketone **12**

A solution of 201 mg of **4** in 2 ml of Py was added to the orange mixture of 180 mg of CrO_3 in 2 ml of Py at room temperature. After 27 h the reaction mixture was diluted with CH_2Cl_2 and passed through alumina (IV). Evaporation of the solvent left 190 mg of an oil which was chromatographed on 15 g of neutral alumina (IV). PE eluted 190 mg (95%) of an oil (single tlc spot). Two recrystallizations from PE gave long colorless needles of *diketone* **12**, mp 51.5–52°C, $[\alpha]_D^{17}$ −161° (*c* 3.65, $CHCl_3$); $\nu_{max}(CS_2)$ 1700 cm^{-1} (6-ring C=O), identical (mmp, ir, tlc, ^{1}Hmr) with a specimen prepared by oxidation of **3**. *Anal.* calcd. for $C_{14}H_{20}O_2$ (220.3): C 76.33, H 9.15; found: C 76.80, H 9.25.

Photochemical Cleavage of Ketol **3**

A solution of 530 mg of pure **3** in 18 ml of thiophene-free benzene under a N_2 atmosphere in a quartz cell was irradiated with an 85 W Hanovia C-H-3 ultraviolet lamp for 17 h (30 cm from lamp to cell). Evaporation of the yellow solution left 530 mg of colorless solid which tlc examination (EtOAc:PE, 65:35) revealed to consist of one product, R_f 0.55, and starting material **3**, R_f 0.35. Partition between ether and H_2O–MeOH–KOH gave 300 mg of pure recovered **3**. Acidification (aqueous HCl) of the basic solution and extraction with ether yielded 170 mg of colorless solid (single tlc spot R_f 0.55). Two recrystallizations from PE gave 100 mg of lactone **14**, mp 93–94.5°C, $[\alpha]_D^{21}$ −62° (*c* 3.08, $CHCl_3$); $\nu_{max}(CS_2)$ 1770 cm^{-1} (γ-lactone C=O); ord (*c* 0.80, MeOH) $[\phi]_{450}$ −86°, $[\phi]_{350}$ −162°, and $[\phi]_{250}$ −287°. *Anal.* calcd. for $C_{14}H_{22}O_2$ (222.3): C 75.63, H 9.97; found: C 75.22, H 10.18.

Photochemical Cleavage of Ketol **4**

A solution of 300 mg of pure **4** in 12 ml of thiophene-free benzene under a N_2 atmosphere was irradiated in the same cell and with the same lamp (same distance from lamp to cell) as in the previous experiment with **4** except that the irradiation time was 23 h. Evaporation of the solution left 300 mg of a liquid whose tlc examination gave a single spot different from that of starting material. Partition of 150 mg of the liquid between ether and base (as above) gave 100 mg of lactone recovered by acidification of the basic layer and 20 mg of neutral material (two spots, neither was **4**) from the ether layer. The lactone **13** was evaporatively distilled at 90–95°C/0.4 torr and gave a single tlc spot, R_f 0.65, $[\alpha]_D^{18}$ +5.8° (*c* 3.11, $CHCl_3$); $\nu_{max}(CS_2)$ 1775 cm^{-1} (γ-lactone); ord (*c* 1.99, MeOH) $[\phi]_{450}$ +10°, $[\phi]_{350}$ +12°, and $[\phi]_{250}$ −110°. *Anal.* calcd. for $C_{14}H_{22}O_2$ (222.3): C 75.63, H 9.97; found: C 75.76, H 10.01.

Isomerization of Isocaryophyllene Keto Epoxide-a **6**

Liquid keto epoxide **6** was prepared by the $KMnO_4$ oxidation of pure crystalline isocaryophyllene oxide-a (12).

(a) tert-BuOH–Water–KOH

A solution of 1.21 g of **6** in 18 ml of *tert*-BuOH containing 1 ml of water and 3.5 g of KOH was refluxed for 70 h. Dilution with water and extraction with ether yielded 1.17 g (98%) of oily product whose tlc examination ($CHCl_3$:MeOH, 90:10) revealed four spots, R_f 0.90 (mauve, **6**), 0.80 (**8**), 0.70 (**7**) and a faint more polar spot. Chromatography on 30 g of alumina (IV) gave 135 mg (12%) of recovered **6** in the PE eluate. Further elution with PE:benzene (25:75) gave 790 mg (68%) of an oil.

Crystallization from PE gave 45 mg (4%) of colorless **8**, mp 129–130°C, unchanged on further recrystallization, $[\alpha]_D^{17}$ −44° (*c* 2.29, $CHCl_3$); $\nu_{max}(CS_2)$ 3600 and 3480 (OH), and 1708 cm^{-1} (6-ring C=O). *Anal.* calcd. for $C_{14}H_{22}O_2$ (222.3): C 75.63, H 9.97; found: C 76.08, H 10.19.

The mother liquors from the crystallization were concentrated to obtain 350 mg (32%) of colorless prisms of hemi-ketal **7**, mp 115–116°C. Two recrystallizations from PE raised the mp to 116–117°C, $[\alpha]_D^{17}$ −8.7° (*c* 2.87, $CHCl_3$); $\nu_{max}(CS_2)$ 3580 and 3400 (OH), 3060 and 3030 cm^{-1} (cyclopropane CH_2), no C=O absorption. *Anal.* calcd. for $C_{14}H_{22}O_2$ (222.3): C 75.63, H 9.97; found: C 76.09, H 10.36.

The mother liquor left from crystallizing **7** was found (tlc and infrared) to be mostly **7** with a minor amount of **8**.

(b) MeOH–KOH

A solution of 200 mg of **6** in 5 ml of MeOH containing 1 g of KOH was refluxed for 5.5 h. Dilution with water and ether extraction gave 180 mg of an oil. Thin layer chromatographic examination (EtOAc:PE 65:35) revealed at least nine spots, and the ^{1}Hmr spectrum of the oil contained methoxyl signals. The reaction was not investigated further.

*Hemiketal Acetate **7** (OAc for OH)*

Compound **7** was not acetylated when 80 mg in 1 ml of Py and 1 ml of Ac_2O was allowed to stand at room temperature for 24 h. However, when 175 mg of **7** in 5 ml of Py and 1 ml of Ac_2O was refluxed for 48 h, reaction occurred to give 208 mg (100%) of crude liquid after work-up. Thin layer chromatographic examination (EtOAc:PE, 65:35) revealed two spots, R_f 0.70 (major) and R_f 0.55 (trace of starting material **7**). Chromatography on 5 g of alumina (II) gave 125 mg of crystals in the PE eluate. Recrystallization from PE gave colorless needles of the monoacetate, mp 100–100.5°C, $[\alpha]_D^{17}$ −93° (*c* 2.00, $CHCl_3$); $\nu_{max}(CS_2)$ 3015 and 3000 (cyclopropane CH_2), and 1735 cm^{-1} (ester C=O). *Anal.* calcd. for $C_{16}H_{24}O_3$ (264.4): C 72.69, H 9.15; found: C 73.14, H 9.53.

*Oxidation of Hydroxy Ketone **8***

A solution of 11 mg of **8** in 0.5 ml of Py was added to the complex prepared from 25 mg of CrO_3 and 1 ml of Py. After 24 h at room temperature the reaction mixture was diluted with CH_2Cl_2 and passed through alumina (IV). Evaporation of the eluate left 7 mg of solid. One recrystallization from PE gave colorless crystals of **12**, mp 50–52°C, undepressed on admixture with the authentic specimen prepared from **3**.

*Isomerization of Isocaryophyllene Keto Epoxide-b **9***

Keto epoxide **9** was prepared by the $KMnO_4$ oxidation of isocaryophyllene oxide-b (12). The crude product was chromatographed on alumina (IV), and the PE eluate was recrystallized thrice from PE to give pure keto epoxide **9**, mp 77–78°C (lit. (12) mp 78–79°C).

(a) MeOH–KOH

A solution of 715 mg of pure **9** in 30 ml of MeOH containing 6 g of KOH was refluxed for 24 h. Dilution with water and extraction with ether yielded 720 mg of a colorless oil whose tlc examination (EtOAc:PE, 35:65) revealed only two spots, R_f 0.45 and 0.35, both different from starting material **9**, R_f 0.40. Chromatography on 20 g of alumina (III) gave 500 mg (69%) of colorless liquid hemiketal **11** (single tlc spot) in the PE eluate. A sample was evaporatively distilled at 60–65°C/0.1 torr for analysis, $[\alpha]_D^{18}$ −35° (*c* 3.72, $CHCl_3$); $\nu_{max}(CS_2)$ 3580 and 3440 (OH), and 3040 and 3070 cm^{-1} (cyclopropane CH_2). *Anal.* calcd. for $C_{14}H_{22}O_2$ (222.3): C 75.63, H 9.97; found: C 75.22, H 10.14.

Further elution of the chromatogram with benzene gave 185 mg (25%) of the hydroxy cyclopropyl ketone **10** (single tlc spot). Two recrystallizations from PE gave colorless clusters of small needles of **10**, mp 131–132°C, $[\alpha]_D^{20}$ +71° (*c* 2.13, $CHCl_3$), λ_{max}(EtOH) 280 nm (ε 147), ε_{200} 4100, ε_{210} 2300; $\nu_{max}(CHCl_3)$ 3580 and 3440 (OH), and 1685 cm^{-1} (cyclopropyl conjugated C=O). *Anal.* calcd. for $C_{14}H_{22}O_2$ (222.3): C 75.63, H 9.97; found: C 75.40, H 9.88.

The hydroxy cyclopropyl ketone **10** was not acetylated when 112 mg in 1 ml of Py and 1 ml of Ac_2O was allowed to stand at room temperature for 24 h.

(b) tert-BuOH–KOH

A solution of 111 mg of **9** in 5 ml of *tert*-BuOH containing 0.5 ml of water and 1 g of KOH was refluxed for 14 h. Dilution with water and extraction with ether yielded 110 mg of oily product whose tlc examination revealed only two spots identical in R_f with the two products from the reaction in MeOH–KOH. Chromatography on alumina (III) gave 65 mg of **11** and 28 mg of **10**, mp 130–132°C, undepressed by the sample from the reaction in MeOH–KOH.

*Hemiketal Acetate **11** (OAc for OH)*

The hemiketal **11** was not acetylated when 57 mg in 1 ml of Py and 1 ml of Ac_2O was allowed to stand at room temperature for 24 h. However, when 200 mg of **11** in 5 ml of Py and 1 ml of Ac_2O was refluxed for 48 h, reaction occurred to give 200 mg (84%) of liquid product which solidified on cooling. Thin layer chromatographic examination (EtOAc:PE, 35:65) revealed an intense spot, R_f 0.75, and a faint spot, R_f 0.55, corresponding to **11**. Two recrystallizations from PE (bp 30–60°C) gave colorless needles of the monoacetate, mp 66–66.5°C, $[\alpha]_D^{18}$ −23° (*c* 1.27 $CHCl_3$); $\nu_{max}(CS_2)$ 3000 and 3030 (CH_2 of cyclopropane, and 1730 cm^{-1} (ester C=O). *Mol. Ion* calcd. for $C_{16}H_{24}O_3$: 264.1726; found: 264.1725.

*Equilibration of **10** and **11***

(a) A solution of 111 mg of hydroxy ketone **10** in 7 ml of MeOH containing 1.3 g of KOH was refluxed for 43 h. Dilution with water and extraction with ether yielded 105 mg of a mixture of **10** and **11** only (tlc). Chromatography on 7 g of alumina (III) gave 70 mg (66%) of liquid hemiketal **11** in the PE eluate and 28 mg (27%) of recovered hydroxy ketone **10**, mp 129–131°C, in the benzene–ether eluate.

(b) A solution of 78 mg of pure liquid **11** in 5 ml of MeOH containing 1 g of KOH was refluxed for 45 h. Dilution with water and extraction with ether gave 73 mg of a mixture of **10** and **11** only (tlc). Chromatography on 5 g of alumina (III) gave 48 mg (66%) of recovered hemiketal **11** in the PE eluate, and 21 mg (29%) of hydroxy ketone **10**, mp 128–130°C, in the benzene–ether eluate.

1. V. Srinivasan and E. W. Warnhoff. Can. J. Chem. **54**, 1372 (1976).
2. D. H. R. Barton and A. S. Lindsey. J. Chem. Soc. 2988 (1951).

3. J. K. CRANDALL, R. D. HUNTINGTON, and G. L. BRUNNER. J. Org. Chem. **37**, 2911 (1972).
4. (*a*) J. E. MCMURRY. Tetrahedron Lett. 3731 (1970); (*b*) J. E. MCMURRY and S. J. ISSER. J. Am. Chem. Soc. **94**, 7132 (1972).
5. J. E. MEINWALD and O. L. CHAPMAN. J. Am. Chem. Soc. **81**, 5800 (1959).
6. G. L. HODGSON, D. F. MACSWEENEY, and T. MONEY. Tetrahedron Lett. 3683 (1972).
7. R. B. WOODWARD, T. FUKUNAGA, and R. C. KELLY. J. Am. Chem. Soc. **86**, 3162 (1964).
8. V. SRINIVASAN. Ph.D. Thesis, University of Western Ontario, London, Ont., Canada. 1968.
9. E. W. WARNHOFF. J. Chem. Soc. Chem. Commun. 517 (1976).
10. E. W. WARNHOFF. Can. J. Chem. This issue.
11. W. TREIBS. Ber. **80**, 56 (1947).
12. G. R. RAMAGE and R. WHITEHEAD. J. Chem. Soc. 4336 (1954).
13. E. W. WARNHOFF and V. SRINIVASAN. Can. J. Chem. **51**, 3955 (1973).

Intramolecular hydride shifts in 4-hydroxycyclohexanones

E. W. WARNHOFF

Department of Chemistry, University of Western Ontario, London, Ont., Canada N6A 5B7

Received December 13, 1976

E. W. WARNHOFF. Can. J. Chem. **55**, 1635 (1977).

The two reversible base-catalyzed ketol rearrangements **1** ⇌ **2** and **3** ⇌ **4** have been proved to occur by intramolecular hydrogen (probably hydride) transfer. A combination of evidence including reduction studies, ^{1}Hmr data, and determination of absolute configuration has shown that both ketol pairs have the stereochemistry required for suprafacial hydride migration. In the course of this work, the anomalous sodium–1-propanol reduction of dione **9** has been reinvestigated.

E. W. WARNHOFF. Can. J. Chem. **55**, 1635 (1977).

On a prouvé que les deux réarrangements de cétols catalysés par les bases, **1** ⇌ **2** et **3** ⇌ **4**, se produisent par transfert intramoléculaire d'hydrogène (probablement un hydrure). Une combinaison de données incluant des études de réduction, les données de rm^{1}H et de détermination de configuration absolue a permis de montrer que les deux paires de cétols ont la stéréochimie requise pour une migration d'hydrure suprafaciale. Dans le cadre de ce travail, on a réexaminé la réduction anormale par le sodium et le propanol-1, de la dione **9**.

[Traduit par le journal]

There are a number of examples of base-catalyzed intramolecular hydride transfers of the Meerwein-Ponndorf–Oppenauer type which occur readily when C*H*OH and ketone groups are proximately disposed as pictured below in Fig. 1. These include geometrically favorable 1,4- and 1,5-hydride shifts across single and fused rings.[1] Recently, we reported an unambiguous case (**1** ⇌ **2**, Scheme 1) of such an intramolecular 1,4-hydride shift within a cyclohexanone ring (8) in several basic media. In this paper is presented detailed evidence that the transfer **1** ⇌ **2** is indeed intramolecular with the required suprafacial stereochemistry and, moreover, that **3** and **4**, the hydroxyl epimers of **1** and **2**, constitute another pair of ketols undergoing this type of hydride transfer.

The functional group positions in the interconvertible ketols **1** and **2** were verified by photochemical cleavage to the two lactones **5** and **6** (8, 9), but independent proof of hydroxyl stereochemistry in each was necessary to demonstrate the suprafaciality of the hydride shift required by an intramolecular process. The hydroxyl configuration of Barton's ketol **1** was already firmly established by Horeau's method (10) and by its mode of genesis which does not disturb the known configuration at this carbon atom in the keto oxide precursor (11). This α-configuration has the more stable equatorial conformation since we find that ketol **1** is the major product (~90%) from reduction of the 8,8-ethylene ketal **11** by sodium–1-propanol followed by hydrolysis. The application of Horeau's method to the 121° ketol from isomerization of **1** gave an excess of (−) enantiomer in the recovered α-phenylbutyric acid as expected for the *S* configuration at C-8 depicted in **2**. However, additional confirmatory evidence for the hydroxyl configuration in **2** was less directly obtained because the 5-carbonyl group in this compound is hindered. Initially we had hoped to carry out reductive experiments on the 5,5-ethylene ketal **12** to be prepared in turn from **2**, but it was found that the hydroxy ketal obtained from **2** was a product

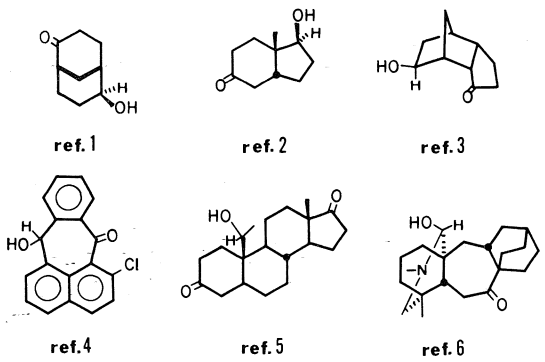

FIG. 1. Compounds in which base-catalyzed intramolecular hydride transfer occurs.

[1]There is even a postulated case of 1,3-hydride transfer during the saponification of a limonoid pointed out to us by Professor D. A. H. Taylor (7). However, the evidence is not conclusive.

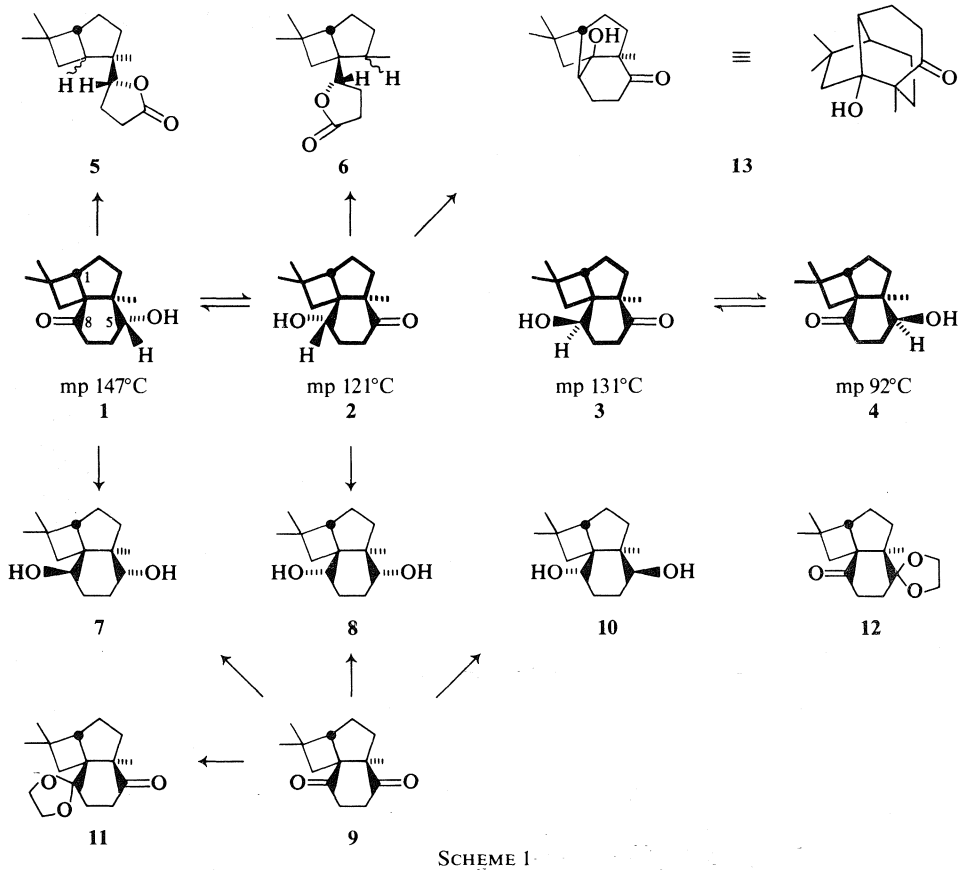

SCHEME 1

of rearrangement since hydrolysis furnished a ketol in which the hydroxyl group was now tertiary (no C*H*OH in ^{1}Hmr, no oxidation by Cr(VI)).[2] The structure **13** is assigned to this product in analogy with the rearrangement of **14**

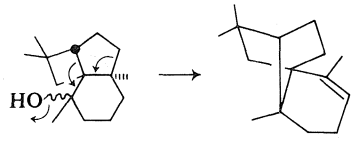

to **15** (12). For rearrangement to be initiated by the loss of a *secondary* hydroxyl group under such mild conditions is evidence for the α-hydroxyl stereochemistry (*anti* to the migrating alkyl carbon atom) as in **2**. Still milder conditions sufficient to ketalize **1** gave only recovered starting material with **2**. Direct evidence that the 5-keto group is more hindered than the 8-keto group was provided by ketalization of the dione **9** which produced only the 8,8-monoketal **11**.

Reductive experiments with the two ketols and their acetates further strengthened the hydroxyl assignment in **2**. On the premise that borohydride reduction of **1** and **2** should add hydride mainly from the less hindered carbonyl side, inspection of Dreiding models revealed that reduction of **2** should give **8** with the same C-5-stereochemistry as in **1**, but reduction of **1** should give **7** with the opposite configuration at C-8 from that in **2**. In agreement, two different diols were obtained. The hydroxyl groups already present in **1** and **2** were not involved in any orienting effect during reduction because hydride reduction of the ketol acetates **1** (*OAc for OH*) and **2** (*OAc for OH*) followed by saponification produced, in each case, the same diol as obtained from the corresponding ketol. Proof that it was the hydroxyl configuration at C-8 alone that was responsible for the difference between the two diols came from two experi-

[2]At the time of our earlier submission (8) it was not known that rearrangement had occurred.

ments. Borohydride reduction of the 8,8-monoketal **11** afforded 82% of ketol **1** after hydrolysis and recrystallization, and oxidation of the diol from ketol **1** with 1 equiv. of Cr(VI) gave a mixture of four compounds: dione, recovered diol, ketol **1**, and a second ketol which was not **2**.

A further check on the configuration at C-8 was provided by reduction of the acetate of ketol **1** with sodium amalgam in acetic acid, a reaction that should produce the more stable equatorial hydroxyl configuration.[3] The product was the 5-monoacetate of the 162° diol **7** obtained from the borohydride reduction of **1**. This result is in agreement with that of Barton *et al.*, who obtained the same diol by reduction of **1** with sodium and 1-propanol (13).[3]

All of this interlocking evidence allows the confident assignment of the β-equatorial hydroxyl configuration in the flattened chair cyclohexane conformation shown in **16** to the

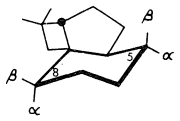

16

reduced C-8 carbonyl group, and therefore the 8α-axial hydroxyl configuration in ketol **2**. The half height band widths of the α-oxygenated carbinyl protons in the ^{1}Hmr spectra of these various derivatives (Fig. 2 and Table 1) are all in agreement with the chair conformation **16** deduced from the chemical data.

The fact that reduction of the 8-carbonyl group gave the opposite stereochemistry from that in **2** allowed preparation of a third ketol in this series by the sequence of reactions in Scheme 2. Surprisingly, this third ketol **3**, mp 131°C, proved to be identical with a minor product of base treatment of the keto oxide from *cis*-caryophyllene oxide-a (9). Therefore, during that alkylation reaction, the initial product **4** must have undergone hydride shift to **3** contrary to what was thought earlier (8). The reason for the mistaken conclusion became clear when **3** was isomerized in KOH – isopropyl alcohol. The equilibrium ratio of products **3**:**4** was 54:46 from ^{1}Hmr spectra, but both ketols had almost identical tlc R_f values. Pure 131° ketol **3** could be

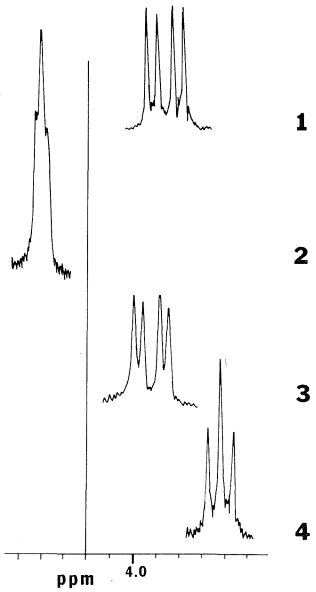

FIG. 2. The patterns of the C*H*OH signal in the four ketols **1**–**4** at 100 MHz.

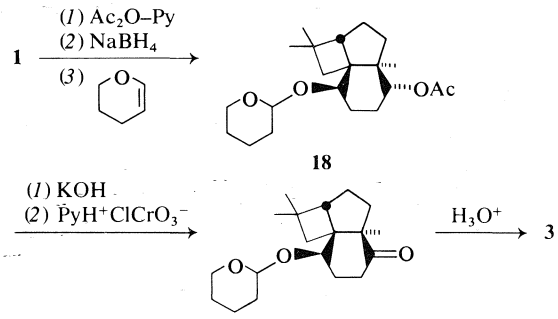

SCHEME 2

crystallized from the product mixture,[4] but the lower-melting ketol **4** could not be isolated in pure form from the mother liquors by crystallization or chromatography. However, pure ketol **4**, mp 92°C, was separated from the 90:10 mixture of **1**:**4** formed by borohydride reduction of ketal **11** followed by hydrolysis. The structure and stereochemistry of **4** follow from the fact that it is oxidized to the dione **9**, and with this carbon–oxygen skeleton there is no longer any alternative left.

The formal possibility of accounting for these isomerizations by homoenolization via **17** has

[3]The acetate was used instead of the ketol to avoid any ambiguity due to possible intramolecular protonation by the C-5 hydroxyl group during reduction.

[4]It was this behaviour together with the single, only slightly ellipsoidal tlc spot for the ketol mixture which caused us to think earlier (8) that the ketol pair **3** and **4** did not undergo hydride shift.

TABLE 1. 100 MHz ^{1}Hmr data[a]

Compound	Methyl groups[b]	C_5-H	C_8-H	$CH_3C{=}O$
Ketol **1**	0.85, 0.91, 1.02	3.87 ($J_{AX} + J_{BX} = 16$, $w_{1/2} = 18$, axH)	—	—
Ketol **2**	0.90, 1.17, 1.19	—	4.40 (nm, $w_{1/2} = 6$, eqH)	—
Ketol **3**	0.92, 1.02, 1.21	—	3.92 ($J_{AX} + J_{BX} = 16$, $w_{1/2} = 18$, axH)	—
Ketol **4**	0.90, 0.91, 1.02	3.63 ($J_{AX} + J_{BX} = 11$, $w_{1/2} = 12$, eqH)	—	—
Ketol **13**	1.02, 1.04, 1.20	—	—	—
1 (OAc for OH)	0.89, 0.89, 1.00	5.09 ($J_{AX} + J_{BX} = 16$, $w_{1/2} = 18$, axH)	—	2.07
2 (OAc for OH)	0.88, 1.14, 1.21	—	5.58 (nm, $w_{1/2} = 7$, eqH)	2.10
Diol **7**	0.82, 0.92, 1.20	3.32 (m, $w_{1/2} = 18$, axH)	3.45 (m, $w_{1/2} = 18$, axH)	—
Diol **8**	0.88, 0.94, 1.16	3.40 (m, $w_{1/2} = 17$, axH)	4.19 (nm, $w_{1/2} = 6$, eqH)	—
Diol **10**	0.90, 0.91, 1.20	3.60 (nm, $w_{1/2} = 12$ (or 9), eqH)	3.60 (nm, $w_{1/2} = 9$ (or 12), eqH)	—
7 (5-OAc for 5-OH)	0.89, 0.90, 1.20	4.60 (m, $w_{1/2} = 17$, axH)	3.44 (m, $w_{1/2} = 17$, axH)	2.03
8 (8-OAc for 8-OH)	0.87, 0.93, 1.19	3.42 (m, $w_{1/2} = 17$, axH)	5.40 (nm, $w_{1/2} = 5$, eqH)	2.03

[a]Chemical shifts are given in ppm from tetramethylsilane (δ), and coupling constants and half widths ($w_{1/2}$) are given in Hz for $CDCl_3$ solutions; m = multiplet, nm = narrow multiplet.
[b]All methyl peaks were singlets.

17

been excluded by failure to exchange the C*H*OH proton of **1** in KOD–*tert*-BuOD–D_2O (8), and therefore, by exclusion, these isomerizations must be hydride transfers. Both intra- and intermolecular transfers have been found to occur, but the much greater rate of the intramolecular process is evident from several observations. First, over periods of several hours in the hot basic isomerization media, the only products detectable by tlc and ^{1}Hmr are the respective ketol pair having the required suprafacial relationship. For **1** ⇌ **2** (or **3** ⇌ **4**) there are no traces of other (known) products expected from intermolecular hydride transfer reactions: dione **9**, diols such as **7** and **8**, or the ketols **3** and **4** (or **1** and **2**). Second, during this 'clean' period, **1** and **2** do not accept hydride from isopropyl alcohol solvent, nor do they donate hydride to added carbonyl compounds (2,2-dimethylcyclohexanone and fluorenone (14)). Third, if the isomerization **1** ⇌ **2** is continued for longer periods with higher KOH concentrations, either under nitrogen or not, then other intermolecular reaction products do build up. The first extra product is the 162° diol **7** which has the proper stereochemistry to have been formed by hydride donation from 2-propanol to the carbonyl group of **1** which was shown above to be less hindered than the carbonyl group of **2**. Then, more slowly the 155° diol **8**, probably from 2-propanol reduction of ketol **2**, begins to appear together with several other less polar products apparently resulting from aldol condensation of the newly formed acetone with **1** and/or **2** (see Experimental).

Although the *cis* fusion of the ketol ring to the cyclopentane ring would facilitate attainment of a boat-like transition state necessary for easy intramolecular hydride transfer in either pair of ketols, how important this factor is remains to be seen. Perhaps such 1,4-hydride shifts in 4-hydroxycyclohexanones are general.

Finally, some evidence is offered that our concern over complications during the reductive experiments was not excessive. In Barton's earlier work (13) it was found that sodium–1-propanol reduction of ketol **1** and dione **9** gave

different diols, and this result was apparently responsible for the incorrect assignment of stereochemistry to the ketol at that time (13, 15). In the expectation that this reduction method should have given the more stable equatorial hydroxyl configuration and therefore the same diol from **1** and **9**, the actual experimental result is puzzling. Our sodium amalgam reduction of the acetate of **1** was consistent with the earlier sodium reduction of **1**, and therefore we have re-examined the sodium–1-propanol reduction of dione **9**. The product was found to be a mixture of comparable amounts of four compounds, two of which corresponded in tlc behavior to diols **7** and **8**. When the crude product was recrystallized from chloroform as done previously (13), a third, higher-melting diol (probably **10**) corresponding to that reported (13) crystallized cleanly from the mixture even though it constituted a minor amount of the total product. Why such a mélange of products is formed in this reduction is not immediately obvious, but certainly no stereochemical conclusions can be drawn from the reaction.

Experimental

Melting points were taken on a Reichert Kofler microscope hot-stage and are corrected. Infrared spectra were obtained on a Beckman Acculab 4 spectrometer; ^{1}Hmr spectra were obtained by Mrs. Heather Schroder on a Varian HA-100 instrument; mass spectra were obtained by Mr. Doug Hairsine on a MAT 311A instrument; optical rotations taken with a 1-dm tube on a Rudolph Model 80 polarimeter by P.R.W. All thin and thick layer chromatograms were run on Merck GF_{254} silica gel developed in EtOAc:PE (67:33). Woelm neutral alumina was used and the grade is specified in parentheses. Pyridinium chlorochromate was obtained from the Aldrich Chemical Company. Organic solutions were washed to neutrality and dried by shaking with saturated NaCl solution and standing over anhydrous $MgSO_4$. For most of the new compounds, precise mass determinations for the molecular ion of a pure sample were obtained instead of combustion analyses. Purity was determined from constancy of mp together with ^{1}Hmr, ir, and tlc data. The following abbreviations were used: PE = petroleum ether of bp 60–80°C, p.e. = petroleum ether of bp 36–45°C, Py = pyridine, MeOH = methanol, *tert*-BuOH = *tert*-butyl alcohol, *i*-PrOH = 2-propanol, Ac_2O = acetic anhydride, EtOAc = ethyl acetate, and *p*-TsOH = *p*-toluene sulfonic acid.

Isomerization of Ketol ***1***

(a) tert-BuOH–H_2O–KOH

A solution of 140 mg of pure **1** in 7 ml of *tert*-BuOH containing 0.2 ml of water and 6 KOH pellets was refluxed for 47 h. Dilution with water and extraction with ether yielded 140 mg of solid whose tlc showed only two spots corresponding to **1** and **2**. Separation on a thick plate yielded 95 mg (68%) of recovered **1** and 46 mg (32%) of isomer **2**, mp 119–121°C after recrystallization from ether–PE. The 100 MHz ^{1}Hmr spectrum of the latter was identical with that of the product from the reaction of caryophyllene keto oxide with hydroxide (9), and the mixture mp was not depressed.

(b) tert-BuOD–D_2O–KOD

To a solution of 217 mg of K metal dissolved in 8 ml of *tert*-BuOD was added 1 ml of D_2O and 200 mg of pure **1**. The mixture was refluxed for 40 h with one evaporation and replacement of *tert*-BuOD–D_2O. The cooled reaction mixture was poured into a H_2O–HOAc–NaOAc buffer and extracted with ether to give 105 mg of deuterated product. Separation on a thick plate as in (*a*) followed by recrystallization from ether–PE gave 28 mg of pure **2** (42% d_4, 40% d_3, 15% d_2, 3% d_1) and 23 mg of pure **1** (40% d_4, 35% d_3, 19% d_2, 4.6% d_1). The 100 MHz ^{1}Hmr spectrum of the **2**-d_4 sample contained ~18H by integration. The C*H*OH proton of **2**-d_4 at δ 4.39 was a slightly broadened singlet of 1H intensity by integration (comparison with CH_3 signal). The 100 MHz ^{1}Hmr spectrum of the **1**-d_4 sample contained ~19H by integration. The C*H*OH proton of **1**-d_4 at δ 3.85 was a slightly broadened singlet (broadened base) of 1H intensity by integration (comparison with CH_3 signal).

(c) Fluorenone–tert-BuOH–H_2O–KOH (14)

A solution of 50 mg of **1**, 168 mg of fluorenone, and 6 KOH pellets in 7 ml of *tert*-BuOH and 0.2 ml of water was refluxed for 30 h. Dilution of the reaction mixture with water and extraction with ether yielded 176 mg of golden solid whose tlc showed spots corresponding to **1** and **2** but not to dione **9** or to any of its diol reduction products which are more polar than **3**. Thick layer chromatography in the same solvent system gave 47 mg of recovered **1** + **2**.

(d) 2,2-Dimethylcyclohexanone–tert-BuOH–H_2O–KOH

A solution of 50 mg of **1**, 0.5 ml of 2,2-dimethylcyclohexanone, and 6 KOH pellets in 7 ml of *tert*-BuOH and 0.2 ml of water was refluxed for 50 h. Dilution of the reaction mixture with water and extraction with ether yielded, after evaporation of most of the 2,2-dimethylcyclohexanone, 62 mg of oily solid whose tlc showed spots corresponding to **1** and **2**, but not to dione **9** or to any of its diol reduction products, or to 2,2-dimethylcyclohexanol.

Isomerization of Ketol ***2***

(a) tert-BuOH–H_2O–KOH

When 40 mg of **2** was refluxed with a mixture of 6 KOH pellets, 0.2 ml of H_2O and 7 ml of *tert*-BuOH for 50 h and worked-up as for the isomerization of **1**, 38 mg of a 63:37 ratio (^{1}Hmr integration of CHOH signals) of **1**:**2** was obtained.

(b) i-PrOH–KOH

When 35 mg of **2** was refluxed with a solution of 8 KOH pellets in 7 ml of *i*-PrOH for 14 h, it was transformed into 34 mg of the equilibrated mixture of **1**:**2** (69:31 from integration of the 100 MHz ^{1}Hmr spectrum).

(c) MeOH–KOH

When 18 mg of **2** was refluxed with a solution of 7 KOH pellets in 7 ml of MeOH for 102 h, it was partially isomerized into **1** but not to the extent of reaching equilibrium.

More Vigorous Isomerization of ***1***

A solution of 1.800 g of ketol **1** and 20 KOH pellets in 20 ml of *i*-PrOH was evacuated and put under a nitrogen atmosphere before being refluxed for 16.5 h. After cooling, tlc examination revealed the beginning of formation of diol **7** and the least polar acetone condensation product. Another 20 KOH pellets were added, and the reaction mixture was refluxed under nitrogen for another 23 h. Dilution with water and extraction with ether gave 1.925 g after removal of solvent. Thin layer chromatography R_f values: 0.73, 0.66, 0.59 (**2**), 0.53, 0.46 (**1**), 0.40 (**7** + **8**). Crystallization from ether–PE removed a total of 1.128 g of a mixture of ketols **1** + **7** + **8** which after further recrystallization from $CHCl_3$–PE and from ether gave 307 mg of diol **7** as thin blades, mp 162.5–163°C, 100 MHz ^{1}Hmr spectrum identical with that of **7** prepared by borohydride reduction of **1**.

A 202 mg sample of the material from the mother liquors of the original recrystallization was chromatographed on a thick plate. The most polar band contained 18 mg of **1**, **7**, and **8** (tlc and 100 MHz ^{1}Hmr). The least polar band contained 52 mg of liquid with R_f 0.73, $\nu_{max}(CS_2)$ 3640–3300 (OH) and 1703 cm^{-1} (C=O). *Mol. Ion* calcd. for $C_{17}H_{26}O_2$: 262.1932; found: 262.1933 (**1** or **2** + C_3H_6O − H_2O).

The next two bands of increasing polarity yielded mixtures with components having *m/e* 264.2094 ($C_{17}H_{28}O_2$ = **1** or **2** + C_3H_6O − H_2O + H_2), and 304.2407 ($C_{20}H_{32}O_2$ = **1** or **2** + $2C_3H_6O$ − $2H_2O$ + H_2).

The same order of appearance of the same spots was observed when another reaction of 50 mg of **1** and 3 KOH pellets in 3 ml of *i*-PrOH was refluxed and monitored by tlc over a 4 day period except that no products of condensation of acetone with **1** were observed (air oxidation of acetone enolate?).

Partial Resolution of α-Phenylbutyric Acid by Ketol ***2***

To a solution of 115 mg (0.37 mmol) of (±) α-phenylbutyric anhydride in 1 ml of dry Py was added 40 mg (0.18 mmol) of ketol **2**. After 20 h at room temperature in the dark, 0.1 ml of water was added to the colorless solution, and the excess anhydride was allowed to hydrolyze for 45 min. One millilitre of benzene was added and the reaction mixture was titrated to the phenolphthalein endpoint with 0.0815 *N* NaOH solution (9.10 ml required). The basic solution was extracted with three portions of benzene, acidified with 10% aqueous H_2SO_4, and extracted again with benzene (2 × 10 ml). The latter benzene extracts were washed thrice with water and evaporated to dryness. The residual α-phenylbutyric acid was dissolved in benzene and made up to 2 ml in a volumetric flask, $\alpha_{obs}^{22} = -0.185° \pm 0.022°$ corresponding to 21% levorotatory acid (based on recovered ketol **2**; see below). The blank for the rotation was a hydrolyzed 52 mg sample of the anhydride in benzene.

The benzene washes of the basic solution above were washed with aqueous H_2SO_4, aqueous $NaHCO_3$, and water and dried. Evaporation left 51 mg which tlc and 100 MHz ^{1}Hmr showed to consist of 60% of the α-phenylbutyrate of **2** and 40% of the unesterified ketol **2**.

Ketalization of Ketol ***2***

A solution of 232 mg (1.04 mmol) of ketol **2** and 0.1 g of *p*-TsOH·H_2O in 25 ml of toluene and 5 ml of ethylene glycol was slowly distilled. Fresh toluene was added at intervals to maintain the original volume. After collection of ~100 ml of distillate, the reaction mixture was cooled and partitioned between ether and aqueous $NaHCO_3$ to yield 280 mg (100%) of crude hydroxy ketal which crystallized, $\nu_{max}(CS_2)$ 3560 cm^{-1} (intramolecularly H-bonded OH), no ir C=O absorption. Thin layer chromatography gave a major spot with a trace of a more polar contaminant. Hydrolysis of the crude product in 2 ml of acetone with 0.5 ml of 2% aqueous H_2SO_4 at room temperature afforded 143 mg (98%) of crude product after dilution with water and extraction with ether. Recrystallization from ether–p.e. gave 92 mg of colorless blades of rearranged ketol, presumed to be **13**, mp 127–128°C, $[\alpha]_D^{20}$ −18.7° (*c* 1.05, $CHCl_3$), $\nu_{max}(CS_2)$ 3600–3200 (OH) and 1703 cm^{-1} (C=O). *Mol. Ion* calcd. for $C_{14}H_{22}O_2$: 222.1619; found: 222.1619.

The hydroxy ketal in this experiment was not oxidized by pyridinium chlorochromate in CH_2Cl_2 or by the CrO_3–Py reagent. The 100 MHz ^{1}Hmr spectrum did not contain a C*H*(OH) proton.

Ketol **2** was recovered from attempted ketalization with (*a*) ethylene glycol and γ-collidine·HCl in distilling CH_2Cl_2, and (*b*) ethylene glycol and pyridine·HCl in distilling benzene. This second set of conditions was sufficient to convert **1** into its ketal.

Ketalization of Dione ***9***

A mixture of 209 mg (0.95 mmol) of **9**, 5 ml of ethylene glycol, 100 mg of *p*-TsOH·H_2O, and 60 ml of toluene was slowly distilled. After 50 ml of distillate had been collected, a fresh 50 ml of toluene was added to the reaction mixture, and the distillation was continued until another 50 ml had been collected. The cooled residue was basified with aqueous NaOH and extracted with ether. The ether solution was washed with aqueous $NaHCO_3$, dried, and evaporated to leave 259 mg (98%) of almost pure liquid *monoketal* **11**, single tlc spot, $\nu_{max}(CS_2)$ 1705 cm^{-1} (C=O).

A solution of 250 mg of the monoketal in 10 ml of absolute ethanol was stirred for 1 h with 250 mg of $NaBH_4$. After addition of dilute H_2SO_4 the reaction mixture was allowed to stand for 2 h. Extraction with ether yielded 188 mg (89%) of partly crystalline material consisting mostly of ketol **1** and some (17 mg) recovered dione **9**. A combination of recrystallization (ether–PE) and chromatography gave 123 mg of pure ketol **1**, mp 144–146°C, single tlc spot.

Transformations of Ketol ***1***

Acetylation

A solution of 220 mg of ketol **1** in 2 ml of dry Py and 2 ml of Ac_2O was allowed to stand at room temperature for 47 h. Dilution with ether and extraction with aqueous $NaHCO_3$ and dilute H_2SO_4 gave 257 mg (98%) of pure liquid monoacetate of **1**, single tlc spot. A small sample was finally persuaded to crystallize from p.e., mp 57–59°C, $\nu_{max}(CS_2)$ 1740 (ester C=O) and 1702 cm^{-1} (ketone C=O). *Mol. Ion* calcd. for $C_{16}H_{24}O_3$: 264.1725; found: 264.1730.

Borohydride Reduction

A solution of 50 mg of ketol **1** in 7 ml of 95% ethanol was stirred (magnetic bar) at room temperature with 150 mg of $NaBH_4$ for 45 min. Addition of dilute H_2SO_4 and extraction with ether afforded 49 mg (98%) of white solid whose tlc showed only one spot. The 100 MHz ^{1}Hmr

spectrum also indicated only one diol. After recrystallization from ether,[5] fine white matted needles of *diol* **7** were obtained, mp 162–162.5°C, $[\alpha]_D^{22}$ −78° ± 1° (*c* 0.98, $CHCl_3$) (lit. (13) mp 159.5°C, $[\alpha]_D$ −69°), $\nu_{max}(CHCl_3)$ 3600 cm^{-1} (OH). *Mol. Ion* calcd. for $C_{14}H_{24}O_2$: 224.1776; found: 224.1774.

Borohydride Reduction of Acetate of 1

A solution of 70 mg of the acetate of **1** in 4 ml of absolute ethanol was stirred at room temperature (magnetic bar) with 100 mg of $NaBH_4$ for 40 min. Addition of dilute H_2SO_4 and extraction with ether gave 71 mg (100%)of a colorless solid, $\nu_{max}(CS_2)$ 3640–3400 (OH) and 1735 cm^{-1} (ester C=O), whose tlc showed a single spot. The 100 MHz ^{1}Hmr spectrum also gave evidence of at least 95% of one compound. Recrystallization of a 46 mg aliquot from ether–PE gave 30 mg of colorless blades of the *5-monoacetate of* **7**, mp 100–101°C. *Mol. Ion* calcd. for $C_{16}H_{26}O_3$: 266.1881; found: 266.1876.

A 17 mg portion of this monoacetate dissolved in 1 ml of methanol containing two drops of water and half a KOH pellet was heated at 60°C for 1 h. Extraction with ether gave 16 mg of white solid identical with the *diol* **7** prepared by $NaBH_4$ reduction of **1**. Recrystallization from ether[5] gave fine white matted needles, mp 162–162.5°C.

Sodium Amalgam Reduction of the Acetate of 1

A vigorously stirred (magnetic bar) solution of 133 mg of the acetate of ketol **1** in 15 ml of ether and 5 ml of HOAc was treated with pieces of sodium amalgam. When the mixture became gelatinous from precipitated NaOAc, more ether (10 ml) and HOAc (7 ml) were added, and addition of sodium amalgam was continued. After the equivalent of ~2 g of Na had been added, the mixture was partitioned between ether and water, and the ether layer was washed with aqueous NaOH and water. Evaporation of the dried solution left 135 mg (100%) of a colorless glass whose tlc showed two spots corresponding to starting material (major) and the *5-monoacetate of* **7** (minor). The 100 MHz ^{1}Hmr spectrum showed the latter to be the only detectable reduction product.

Transformations of Ketol 2

Acetylation

A solution of 400 mg of ketol **2** in 2 ml of dry Py and 2 ml of Ac_2O was allowed to stand at room temperature for 27 h. Dilution with ether and extraction with aqueous $NaHCO_3$ gave after evaporation 460 mg of crude acetate. Chromatography on 15 g of grade IV alumina afforded in the PE eluate 370 mg (77%) of pure acetate of **2**, ν_{max}-$(CHCl_3)$ 1736 (ester C=O) and 1708 cm^{-1} (ketone C=O), single tlc spot. Recrystallization from p.e. gave colorless prisms of the acetate **5** (*OAc for OH*), mp 58–58.5°C, $[\alpha]_D^{17}$ +15.8° (*c* 3.46, $CHCl_3$). *Anal.* calcd. for $C_{16}H_{24}O_3$ (264.1): C 72.69, H 9.15; found: C 72.88, H 9.30.

The mixture mp with the acetate of ketol **1** (mp 57–59°C) was depressed to 28–53°C.

Borohydride Reduction

A solution of 45 mg of ketol **2** in 5 ml of absolute ethanol was stirred (magnetic bar) with 105 mg of $NaBH_4$ for 1 h. Addition of dilute H_2SO_4 and extraction with ether afforded 45 mg of white solid whose tlc contained one major spot and two minor less polar spots (one corresponding to **2**). Two recrystallizations from ether–PE gave colorless thin prisms of pure *diol* **8** (major product), mp 154–155°C, $[\alpha]_D^{20}$ −28° (*c* 0.79, $CHCl_3$), $\nu_{max}(CS_2)$ 3640–3560 cm^{-1} (OH). *Mol. Ion* calcd. for $C_{14}H_{24}O_2$: 224.1776; found: 224.1777.

Borohydride Reduction of Acetate of 2

A solution of 100 mg of the acetate of **2** in 4 ml of absolute ethanol was stirred at room temperature for 50 min with 100 mg of $NaBH_4$. Addition of dilute H_2SO_4 and extraction with ether gave 100 mg (100%) of a colorless glass which tlc and ^{1}Hmr showed to be composed of a major product (>90%) R_f 0.53 and a minor product (<10%) R_f 0.66. Thick layer separation of a 75 mg aliquot yielded 58 mg of pure major product which was saponified in 2 ml of methanol containing two KOH pellets at 55–60°C for 3.5 h. Dilution with water and extraction with ether afforded 54 mg of pure *diol* **8**, mp 154.5–155°C after recrystallization from ether–PE, identical with the diol from borohydride reduction of **2**. On the same tlc plate with alternating spots, diol **7** had R_f 0.49 and diol **8** had R_f 0.46.

Partial Oxidation of Diol 7

To a solution of 16 mg (0.16 mmol) of CrO_3 in 3 drops of water and 0.5 ml of HOAc was added a solution of 50 mg (0.22 mmol) of **7** in 1.5 ml of HOAc. After 2 h at room temperature, the bluish green solution was diluted with water and extracted with ether to yield 44 mg (88%) of partially crystalline product. Thin layer chromatography revealed four spots: R_f 0.67 dione **9**, 0.54 ketol **3**, 0.46 ketol **1** (major component ~40%), and 0.40 recovered diol **7**. Three recrystallizations from ether–p.e. isolated pure *ketol* **1**, mp 144–147°C, undepressed on admixture with an authentic specimen.

Synthesis of Ketol 3

A solution of 444 mg (2.00 mmol) of ketol **1** in 3 ml of dry Py and 3 ml of Ac_2O was allowed to stand at room temperature for 48 h. Dilution with ether and extraction with aqueous $NaHCO_3$ and 10% aqueous H_2SO_4 afforded 525 mg (99%) of pure (tlc) colorless acetate of **1**.

The entire sample of acetate was dissolved in 20 ml of 95% ethanol and stirred for 45 min with 530 mg of $NaBH_4$. Addition of dilute H_2SO_4 and extraction with ether yielded 537 mg (100%) of the *5-monoacetate of* **7** as a colorless oil that crystallized, $\nu_{max}(CS_2)$ 3640–3400 (OH) and 1735 cm^{-1} (ester C=O).

A solution of 532 mg of this diol monoacetate in 15 ml of benzene was allowed to react for 8 h at room temperature with 4 ml of freshly distilled dihydropyran and 40 mg of *p*-TsOH·H_2O. Quenching with aqueous NaOH and extraction with ether gave 1.558 g of *tetrahydropyranyl ether* **18** plus impurities from dihydropyran, $\nu_{max}(CS_2)$ 1735 cm^{-1} (ester C=O).

The crude tetrahydropyranyl ether **19** plus impurities (1.488 g) was refluxed for 100 min with 15 KOH pellets in 20 ml of methanol. Dilution with water and extraction with ether furnished 1.347 g of yellow liquid *hydroxy tetrahydropyranyl ether*, $\nu_{max}(CS_2)$ 3640–3400 cm^{-1} (OH), no ir C=O absorption.

The total product was dissolved in 5 ml of CH_2Cl_2 and added to a stirred (magnetic bar) suspension of 1.50 g

[5]It was difficult to persuade this diol to crystallize, apparently because it could not decide whether to reappear as fine matted needles or thin blades.

(6.97 mmol) of pyridinium chlorochromate and 320 mg of anhydrous NaOAc in 10 ml of CH_2Cl_2. After 3 h ether was added and the organic solution was filtered and evaporated to leave 1.339 g of yellow oily *keto tetrahydropyranyl ether* **19** plus impurities. The ether group was removed by dissolving the oil in 15 ml of methanol containing 0.4 ml of concentrated hydrochloric acid. Dilution with water and extraction with ether afforded 744 mg of yellow oily partially crystalline material.

After standing for a week, the impurities in the crude ketol had changed into more polar contaminants which were easily removed by thick layer chromatography followed by recrystallization from ether–PE to yield 254 mg (57% overall from **1**) of ketol **3**, mp 130–131°C with previous sintering, $[\alpha]_D^{21}$ −35° (*c* 0.96, $CHCl_3$), $\nu_{max}(CS_2)$ 3640–3400 (OH) and 1710 cm^{-1} (C=O). *Mol. Ion* calcd. for $C_{14}H_{22}O_2$: 222.1619; found: 222.1621. The crystals require drying at reduced pressure and elevated temperature to remove occluded solvent. The mixture mp with the minor product of base treatment of isocaryophyllene keto oxide-a (mp 129–130°C (9)) was not depressed.

Isomerization of Ketol ***3***

A solution of 115 mg of ketol **3** and 12 KOH pellets in 15 ml of *i*-PrOH was refluxed for 10 h. Dilution with water and extraction with ether gave 121 mg of a glass which crystallized. Its tlc contained one elongated spot. Integration of the 100 MHz ^{1}Hmr spectrum gave the ratio of **3**:**4** as 54:46. Recrystallization of the crude product from ether–PE afforded 61 mg (50%) of thin blades of almost pure **3** (tlc). Thin layer chromatographic examination of the mother liquors now clearly showed two overlapping spots with the more polar predominant. Attempted separation of the components of the mother liquors on a thick layer gave in the most polar band a 26 mg fraction containing about 90% of ketol **4** (^{1}Hmr spectrum), but the 10% of **3** could not be separated by recrystallization.

Keto Ketal ***11***

A solution of 424 mg (1.91 mmol) of pure ketol **1** and 20 mg of *p*-TsOH·H_2O in 50 ml of toluene and 5 ml of ethylene glycol was slowly distilled. Fresh toluene was added at intervals to maintain the original volume. After collection of ~120 ml of distillate, the reaction mixture was cooled, and the residue was basified with aqueous NaOH and extracted with ether. Evaporation of the washed and dried ether layer left 535 mg (105%) of viscous oily *ethylene ketal of* **1** which had only a trace of carbonyl ir absorption. Crystallization of a sample from p.e. gave colorless crystals, mp 85–91°C, $\nu_{max}(CS_2)$ 3620–3200 cm^{-1} (OH).

The crude ketal dissolved in 6 ml of CH_2Cl_2 was added to a stirred (magnetic bar) suspension of 803 mg of Py chlorochromate and 300 mg of anhydrous NaOAc in 3 ml of CH_2Cl_2. After 3 h ether was added and the decanted solution was filtered through a 3-cm column of neutral alumina (IV). Evaporation of solvent left 488 mg (96%) of crystalline ketal. Recrystallization from p.e. gave 298 mg of long needles of *keto ketal* **11**, mp 65–67°C, $\nu_{max}(CHCl_3)$ 1702 cm^{-1} (C=O), no OH ir absorption. *Anal.* calcd. for $C_{16}H_{24}O_3$ (264.4): C 72.69, H 9.15; found: C 72.63, H 8.92.

Sodium–1-Propanol Reduction of Keto Ketal ***11***

A solution of 190 mg of **11** in 6 ml of 1-propanol was heated to boiling, and small pieces of Na metal were added until sodium alkoxide began to crystallize from the hot solution. The cooled reaction mixture was diluted with water and extracted with ether to yield 175 mg (92%) of colorless glass which slowly crystallized, $\nu_{max}(CS_2)$ 3640–3200 cm^{-1} (OH), no ir C=O absorption. A 169 mg portion of the product was hydrolyzed at room temperature for 12 h in a solution of 6 ml of 5% aqueous HCl and 10 ml of 95% ethanol. Dilution with water and extraction with ether gave 135 mg (96%) of solid which tlc showed to be mostly ketol **1**, contaminated by 5–10% of ketol **4**. Thick layer chromatography and recrystallization from $CHCl_3$–PE gave **1** (single tlc spot) whose 100 MHz ^{1}Hmr spectrum was identical with that of authentic **1** except for a trace of contamination by **10** which has the same tlc R_f.[6]

Borohydride Reduction of Keto Ketal ***11***

A solution of 298 mg (1.12 mmol) of pure crystalline **11** in 20 ml of 95% ethanol was stirred (magnetic bar) with 295 mg of $NaBH_4$ for 1 h. Excess $NaBH_4$ was destroyed with acetone, and the reaction mixture was partitioned between water and ether. The crude hydroxy ketal obtained (297 mg) was dissolved in 10 ml of 95% ethanol containing 0.5 ml of 7% aqueous HCl for 12 h at room temperature. Dilution with water and extraction with ether afforded 240 mg (95%) of crude ketol mixture whose tlc showed only two spots corresponding to **1** and **4**. The ratio of **1**:**4** from integration of the 100 MHz ^{1}Hmr spectrum was ~90:10. One recrystallization from $CHCl_3$–PE gave 180 mg of long thin colorless prisms of pure **1**, mp 145.5–146°C.

Isolation of Ketol ***4***

The mother liquors from the recrystallization in the previous experiment (57 mg) were chromatographed on a 10 × 20 cm thick plate bearing 10 g of silica gel. The material from the uppermost band (21 mg of approximately equal amounts of **1** and **4**) was re-chromatographed on a 20 × 20 cm thin plate. The uppermost band from this plate yielded 7 mg of pure **4**. Two recrystallizations from ether–p.e. gave 4 mg of colorless small flat prisms of **4**, mp 91–92°C, $[\alpha]_D^{22}$ −51° (*c* 0.36, $CHCl_3$), $\nu_{max}(CS_2)$ 3640–3300 (OH) and 1700 cm^{-1} (C=O). *Mol. Ion* calcd. for $C_{14}H_{22}O_2$: 222.1619; found: 222.1619.

On a single tlc plate with repeating sequences of spots, the four ketols had the following R_f values: **2** 0.58, **3** 0.53, **4** 0.49, and **1** 0.42.

Oxidation of Ketols

(*a*) To a stirred (magnetic bar) suspension of 91 mg (0.42 mmol) of Py chlorochromate in 1 ml of CH_2Cl_2 was added a solution of 30 mg (0.13 mmol) of ketol **3** in 1 ml of CH_2Cl_2. After 1.5 h the reaction mixture was diluted with ether, and the organic solution was filtered through 2 cm of neutral alumina (IV). Evaporation of solvent left 26 mg (86%) of colorless oily dione **9** which solidified on scratching. Recrystallization from p.e. gave white crystals, mp 51–53°C (lit. (16) mp 51–52°C), undepressed on admixture with authentic dione from oxidation of ketol **1**.

(*b*) A similar oxidation of 14 mg of *ketol* **4** with 50 mg of Py chlorochromate in 1.5 ml of CH_2Cl_2 for 2 h gave

[6]The contaminating diol **10** was presumably formed by reduction of dione **9** present as an impurity in the ketal **11**.

13 mg (93%) of almost colorless oily *dione* **9** (single tlc spot) whose complex 100 MHz ^{1}Hmr spectrum was identical with that of dione from *ketol* **1**.

Sodium–1-Propanol Reduction of Dione **9**

A solution of 108 mg of dione **9** in 6 ml of 1-propanol was heated to boiling, and small pieces of Na metal were added until sodium alkoxide began to crystallize from the hot medium. The cooled solution was diluted with water and extracted with ether to yield 121 mg of partially crystalline product, $\nu_{max}(CS_2)$ 3640–3200 cm^{-1} (OH), no ir C=O absorption. Thin layer chromatography revealed four spots in comparable amounts: R_f 0.52, 0.46, 0.39 (corresponds to **7**), and 0.34 (corresponds to **8**). One recrystallization from $CHCl_3$ gave 30 mg (27%) of almost pure R_f 0.46 material, mp 167–178°C. Three more recrystallizations from the same solvent gave felted needles of *diol* **10**, mp 182–183°C, $[\alpha]_D^{20} - 39° \pm 5°$ (*c* 0.45, $CHCl_3$) (lit. (13) mp 181–182°C, $[\alpha]\alpha - 43°$). *Mol. Ion* calcd. for $C_{14}H_{24}O_2$: 224.1776; found: 224.1783. The assignment of hydroxyl stereochemistry rests on the half widths (9 and 12 Hz) of the ^{1}Hmr absorptions of the protons on the HO-bearing carbon atoms when these signals were shifted apart by the addition of $Eu(FOD)_3$.

1. W. Parker and J. R. Stevenson. J. Chem. Soc. Chem. Commun. 1289 (1969).
2. W. Acklin and V. Prelog. Helv. Chim. Acta, **42**, 1239 (1959).
3. J. M. Shepherd, D. Singh, and P. Wilder. Tetrahedron Lett. 2473 (1974).
4. P. T. Lansbury and F. D. Saeva. J. Am. Chem. Soc. **89**, 1890 (1967).
5. J. Wicha and E. Caspi. J. Org. Chem. **38**, 1280 (1973).
6. D. Dvornik and O. E. Edwards. Proc. Chem. Soc. 280 (1958).
7. D. A. H. Taylor. J. Chem. Soc. C, 336 (1970).
8. E. W. Warnhoff. J. Chem. Soc. Chem. Commun. 517 (1976).
9. E. W. Warnhoff and V. Srinivasan. Can. J. Chem. This issue.
10. A. Horeau and J. K. Sutherland. J. Chem. Soc. C, 247 (1966).
11. D. Rogers and M. Ul-Haque. Proc. Chem. Soc. 371 (1963).
12. T. F. W. McKillop, J. Martin, W. Parker, and J. S. Roberts. Chem. Commun. 162 (1967).
13. D. H. R. Barton, T. Bruun, and A. S. Lindsey. J. Chem. Soc. 2210 (1952).
14. E. W. Warnhoff and P. Reynolds-Warnhoff. J. Org. Chem. **28**, 1431 (1963).
15. D. H. R. Barton and A. Nickon. J. Chem. Soc. 4665 (1954).
16. D. H. R. Barton and A. S. Lindsey. J. Chem. Soc. 2988 (1951).

Metal complexes as antioxidants. IV. Reaction of cupric dialkyldithiophosphates and dialkyldithiocarbamates with alkyl hydroperoxides[1]

JOSEPH HECTOR BERNARD CHENIER, JAMES ANTHONY HOWARD,[2] AND JOHN CHARLES TAIT[3]

Division of Chemistry, National Research Council of Canada, Ottawa, Ont., Canada K1A 0R9

Received November 22, 1976

JOSEPH HECTOR BERNARD CHENIER, JAMES ANTHONY HOWARD, and JOHN CHARLES TAIT. Can. J. Chem. **55**, 1644 (1977).

The initial reaction of cupric dialkyldithiophosphates and dialkyldithiocarbamates with *tert*-butyl hydroperoxide and α-cumyl hydroperoxide is a free radical chain process. Initiation is achieved by a redox reaction between the complex and the hydroperoxide to give alkoxy and alkylperoxy radicals. The alkoxy radicals then abstract a hydrogen from excess hydroperoxide to give alkylperoxy radicals. The cupric complexes are converted to copper sulphate by reaction with peroxy radicals while the hydroperoxide is reduced to alcohol. About 5 mol of hydroperoxide are decomposed by each mole of complex. The decomposition of *tert*-butyl hydroperoxide then stops whereas complete destruction of α-cumene hydroperoxide occurs by a heterogeneous ionic reaction.

The kinetics of the initial reaction are second-order for both complexes. The dithiophosphate reaction is first-order in each reactant while the dithiocarbamate reaction is zero-order in the complex concentration and second-order in the hydroperoxide concentration. Simple kinetics, however, only hold for the initial rates of complex disappearance. Total dithiophosphate decomposition exhibits three stages, an initial fast reaction followed by an induction period and a rapid third stage. The concentration–time profile for dithiocarbamate decomposition is quite different and the overall rate of reaction in some instances increases as the complex concentration decreases.

JOSEPH HECTOR BERNARD CHENIER, JAMES ANTHONY HOWARD et JOHN CHARLES TAIT. Can. J. Chem. **55**, 1644 (1977).

La réaction initiale des dialkyldithiophosphates et dialkyldithiocarbamates cupriques avec l'hydroperoxyde de *tert*-butyl et l'hydroperoxyde d'α-cumène est un processus de radicaux libres en chaîne. L'initiation est obtenue par une réaction rédox entre le complexe et l'hydroperoxyde pour conduire aux radicaux alkoxy et alkylperoxy. Les radicaux alkoxy enlèvent alors un hydrogène de l'hydroperoxyde en excès pour conduire aux radicaux alkylperoxy. Il y a transformation des complexes cupriques en sulphate de cuivre par réaction des radicaux peroxy alors que l'hydroperoxyde est réduit en alcool. Il y a décomposition d'environ 5 mol d'hydroperoxyde par chaque mole de complexe. La décomposition de l'hydroperoxyde de *tert*-butyle s'arrête alors tandis que la destruction complète de l'hydroperoxyde d'α-cumène se produit par une réaction ionique hétérogène.

La cinétique de la réaction initiale est du second ordre pour les deux complexes. La réaction du dithiophosphate est du premier ordre par rapport à chaque réactif alors que la réaction du dithiocarbamate est d'ordre zéro par rapport à la concentration du complexe et du deuxième ordre par rapport à la concentration de l'hydroperoxyde. Des cinétiques simples ne s'appliquent toutefois que pour les vitesses initiales de disparition du complexe. La décomposition totale du dithiophosphate présente trois étapes: une étape initiale rapide suivit par une période d'induction en une troisième étape rapide. La profil de concentration en fonction du temps pour la décomposition du dithiocarbamate est très différente et la vitesse globale de réaction dans quelques cas augmente à mesure que la concentration de complexe diminue.

[Traduit par le journal]

Introduction

The previous paper in this series (1) described a kinetic and product study of the destruction of nickel dialkyldithiocarbamates and dialkyldithiophosphates by alkyl hydroperoxides which revealed that the overall reaction is principally a free radical chain process with at least five elementary reactions. It was suggested that the initial reaction involves electron transfer between the complex (A) and the hydroperoxide (ROOH) to generate alkoxy (RO•) and alkylperoxy (ROO•) radicals ([1] and [2]). In the

[1]NRCC No. 15859.

[2]Author to whom all correspondence should be addressed.

[3]NRCC Research Associate 1976.

presence of excess hydroperoxide the alkoxy radicals abstract the hydroperoxidic hydrogen to give alcohol and peroxy radicals [3]. The peroxy radicals are then scavenged by reactions with the complex, reactions that are the major mode of complex destruction. Two peroxy radical-complex reactions were envisaged; a termination reaction [4] and an oxygen atom transfer reaction, [5], the latter being necessary to explain the fairly long chain lengths for induced hydroperoxide decomposition. The elementary reactions involved in the overall process are presented in Scheme 1.

$$\text{[1]} \quad A + ROOH \xrightarrow{k_1} A^{\cdot+} + RO^{\cdot} + {}^{-}OH$$

$$\text{[2]} \quad A^{\cdot+} + ROOH \rightarrow A + H^{+} + ROO^{\cdot}$$

$$\text{[3]} \quad RO^{\cdot} + ROOH \rightarrow ROH + ROO^{\cdot}$$

$$\text{[4]} \quad ROO^{\cdot} + A \rightarrow \text{Non-radical products}$$

$$\text{[5]} \quad ROO^{\cdot} + A \rightarrow Y^{\cdot}$$

SCHEME 1

where $Y^{\cdot}$ is the alkoxy radical $RO^{\cdot}$ or a radical derived from the ligand capable of abstracting the hydroperoxidic hydrogen from ROOH.

The analogous cupric complexes have received less attention than the nickel complexes. It is, however, known that they react rapidly with alkyl hydroperoxides and that at high ratios of hydroperoxide to complex, products characteristic of heterolytic hydroperoxide decomposition are formed (2, 3). Quantitative kinetic data and reaction products at different reactant ratios are, however, not available.

We have extended our work on metal complex – hydroperoxide reactions to include cupric dithiocarbamates and dithiophosphates and the results of a detailed study of these systems are reported here.

Experimental

Materials

Cupric dialkyldithiocarbamates and dialkyldithiophosphates were prepared by reaction of the sodium salt with copper sulphate. Crude complexes were recrystallized to give products with sharp melting points and satisfactory elemental analyses. The hydroperoxides and solvents were prepared and purified as described previously (1).

Kinetic Procedure

Cupric complex concentrations were monitored continuously using a Varian E-4 epr spectrometer equipped with a variable temperature accessory. In a typical experiment 30 μl of 10^{-2} *M* *tert*-butyl hydroperoxide in chlorobenzene were added to 270 μl of 10^{-4} *M* $Cu(Et_2NCS_2)_2$ in chlorobenzene agitated by a fine stream of argon. The variation in the complex concentration as a function of time was obtained either by scanning the esr spectrum at known intervals of time or by setting the field to coincide with the maximum absorption of the copper $M_I = -\frac{3}{2}$ or $-\frac{1}{2}$ transition with the field sweep switched off. The accumulation of cupric complex products was followed by identical procedures. *tert*-Butyl hydroperoxide concentrations were determined by iodometric titration on aliquots that had been pumped from the copper complex into a trap maintained at the temperature of liquid nitrogen. Control experiments showed that this hydroperoxide could be recovered in 100% yield by this procedure. Rates of hydroperoxide disappearance were also estimated by kinetic infrared spectroscopy $\nu = 3530$ cm^{-1}.

Products

Volatile organic products were identified by gas–liquid chromatography and yields were determined relative to standard authentic samples. Thin layer and liquid chromatography were used to investigate the formation of involatile organic products such as dialkylthiuram disulphides and *O*,*O*′-dialkyldithiophosphoryl disulphides. Copper sulphate was identified by X-ray analysis.

Results and Discussion

I. Cupric Dialkyldithiophosphates

Kinetics

Cupric diisopropyldithiophosphate, $Cu[(i\text{-}PrO)_2PS_2]_2$, is rapidly destroyed by excess *tert*-butyl hydroperoxide in argon saturated chlorobenzene at 30°C. Variations in the concentration of $Cu[(i\text{-}PrO)_2PS_2]_2$ as a function of time in the presence of 0.001 *M* and 0.01 *M* hydroperoxide are shown in Figs. 1*a* and 1*b*. It is apparent from these curves that $-d[Cu[(i\text{-}PrO)_2PS_2]_2]/dt$ is not a simple function of time but proceeds through three stages. There is an initial fast stage which decelerates to a slow second stage which is followed by a third fast stage.

Under these circumstances it is extremely difficult to obtain precise kinetic orders especially as the system has to be thoroughly mixed before measurements can be taken. Plots of ln $[Cu[(i\text{-}PrO)_2PS_2]_2]$ as a function of time during the first stage were, however, linear. Furthermore, initial rates of complex disappearance were approximately first-order with respect to each reactant (Table 1). The following rate law was, therefore, initially obeyed

$$\left(\frac{-d[Cu[(i\text{-}PrO)_2PS_2]_2]}{dt}\right) = k[Cu[(i\text{-}PrO)_2PS_2]_2][(CH_3)_3COOH]$$

with a 'best' value of $k \sim 2.4\ M^{-1}\ s^{-1}$.

Measurements of k over a temperature range

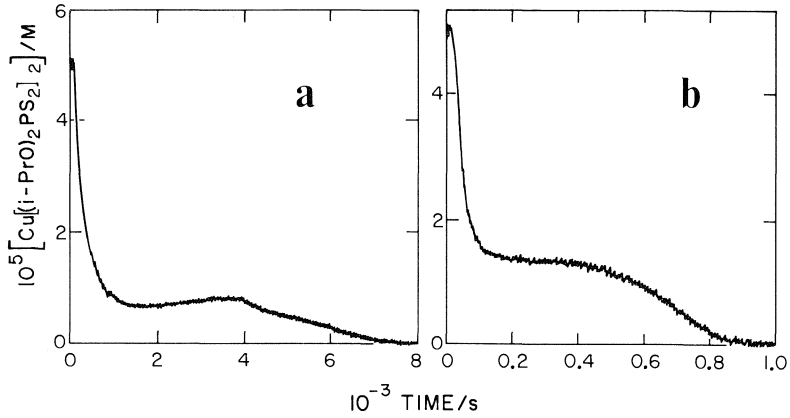

FIG. 1. The change in the concentration of $Cu[(i\text{-}PrO)_2PS_2]_2$ with respect to time after the addition of 0.001 M (*a*) and 0.01 M (*b*) of $(CH_3)_3COOH$ at 30°C.

TABLE 1. Kinetic data for reaction of $Cu[(i\text{-}PrO)_2PS_2]_2$ (A) with $(CH_3)_3COOH$ in argon saturated chlorobenzene at 30°C

$10^5[A]_0$ (M)	$10^3[ROOH]_0$ (M)	10^3k_ψ (s)	$\frac{k_\psi}{[ROOH]}$ (M^{-1} s^{-1})	$10^7(-d[A]/dt)_0$ (M s^{-1})	$\frac{-(d[A]/dt)_0}{[A][ROOH]}$ (M^{-1} s^{-1})
2.5	4	—	—	2.2	2.2
5	1	1.5	1.5	1.16	2.3
5	1	—	—	1.46	2.9
5*	4	—	—	4.4	2.2
5	2	4.1	2.0	—	—
10	2	4	2.0	2	2.1
10†	10	6.5	0.65	—	—

*Saturated with air.
†In the presence of 2,6-di-*tert*-butyl-4-methylphenol (0.011 M).

(253–300 K) gave the Arrhenius equation $\log (k/(M^{-1}\ s^{-1})) = 6.7 - 8.5/\theta$, where $\theta = 2.303RT$ kcal mol^{-1}.

The initial rate of disappearance of $Cu[(i\text{-}PrO)_2PS_2]_2$ was not influenced by oxygen ($\sim 10^{-3}$ M), *tert*-butyl alcohol, or the nature of the hydroperoxide (α-cumyl, α-tetralyl). It was, however, retarded by diisopropyldithiophosphoric acid, $(i\text{-}PrO)_2P(S)SH$, and completely inhibited by *O,O'*-diisopropyldithiophosphoryl disulphide $[(i\text{-}PrO)_2PS_2]_2$. Typical radical scavenging antioxidants such as 2,6-di-*tert*-butyl-4-methylphenol also retarded the initial rate of reaction. There was a very marked influence of solvent on $(-d[Cu[(i\text{-}PrO)_2PS_2]_2]/dt)_0$, the initial rate being a factor of ~25 times slower in benzene and toluene than in chlorobenzene.

The second stage or induction period, τ_{Cu}, began when 70–90% of the complex (depending on the initial ratio of complex to ROOH) had been destroyed. The length of the induction period was very approximately linearly dependent on the complex concentration and inversely proportional to the concentration of ROOH. Addition of *tert*-butyl alcohol to the initial reaction mixture had a marked influence on τ_{Cu} (Table 2).

It is impossible to obtain precise kinetic data for the disappearance of the hydroperoxide in this reaction. It did, however, appear to disappear faster than the complex when stoichiometric reactant concentrations were used.

Destruction of $(CH_3)_3COOH$ ceased when approximately ten times the initial complex concentration had been destroyed. For instance, $Cu[(i\text{-}PrO)_2PS_2]_2$ (10^{-3} M) was destroyed in ~4 h by $(CH_3)_3COOH$ (0.05 M), while the hydroperoxide concentration fell to 0.04 M and remained

TABLE 2. Influence of *tert*-butyl alcohol on the second stage of the destruction of cupric diisopropyldithiophosphate by *tert*-butyl hydroperoxide; $[Cu[i\text{-}PrO)_2PS_2]_2]_0 = 5 \times 10^{-5}$ *M*; $[ROOH]_0 = 10^{-2}$ *M*

$10^4[(CH_3)_3COH]/M$	τ_{Cu}/s
—	360
4.2	207
60	153
530	54

unchanged for 20 days. The stoichiometric factor, $\Delta[ROOH]/\Delta[complex]$, is, therefore, approximately 10.

The *overall* behavior of cumene hydroperoxide was different in that a trace of $Cu[(RO)_2PS_2]_2$ (0.003 *M*) destroyed a large excess of hydroperoxide (0.05 *M*). In this case the disappearance of hydroperoxide followed a three stage reaction pattern analogous to the disappearance of $Cu[(RO)_2PS_2]_2$ but over a considerably longer period of time, *i.e.*, there was an initial fast reaction, a very slow second stage, and a fast third stage. Decomposition of cumene hydroperoxide by $Cu[(i\text{-}PrO)_2PS_2]_2$, therefore, gives a concentration–time profile similar to those observed by Burn *et al.* (4) for $Zn[(RO)_2PS_2]_2$–$C_6H_5C(CH_3)_2OOH$ systems.

Products

tert-Butyl hydroperoxide was quantitatively reduced by $Cu[(i\text{-}PrO)_2PS_2]_2$ to *tert*-butyl alcohol while the cupric ion was precipitated as copper sulphate. Oxygen was not formed in this reaction.

The major reaction products formed from decomposition of cumene hydroperoxide at different initial reactant ratios are summarized in Table 3. The only volatile organic products detected at low ratios of hydroperoxide to complex (runs 1 and 2) were α-cumyl alcohol, acetophenone, and α-methylstyrene with an alcohol to α-methylstyrene ratio of ~5.5 and an acetophenone to alcohol plus α-methylstyrene ratio of 0.1 to 0.2. α-Methylstyrene must arise by dehydration of α-cumyl alcohol and acetophenone by β-scission of cumyloxy radicals. We have shown that cumylperoxy radicals are reduced by $Cu[(RO)_2PS_2]_2$ to these three products.[4] Their formation in the present system is indicative of the intermediacy of cumyloxy and cumylperoxy radicals. It would, however, appear that only about 50% of the hydroperoxide decomposed could be accounted for as volatile organic products implying that the balance of the hydroperoxide derived products were somehow associated with the metal ion.

At higher ratios of hydroperoxide to complex (runs 3, 4, and 5) significant concentrations of phenol and acetone were formed by heterolysis of the hydroperoxide.[5] Heterolysis should give equal concentrations of these two compounds, a situation that was only realized in run 4. α-Methylstyrene, acetophenone, and α-cumyl alcohol were also formed at these reactant ratios. The ratio of α-cumyl alcohol to α-methylstyrene was quite low in these runs presumably because of enhanced dehydration of the alcohol by the Lewis acid responsible for hydroperoxide heterolysis.

The end of the first reaction stage was characterized by the precipitation of an insoluble fraction which was 50% $CuSO_4$ and a so far unidentified brown oil. A cumene hydroperoxide solution from which this precipitate had been removed by filtration was considerably more stable than the original reaction mixture. This precipitate did not decompose *tert*-butyl hydroperoxide whereas it did heterolytically decompose a fresh solution of cumene hydroperoxide.

Conclusions

The initial reaction between $Cu[(RO)_2PS_2]_2$ and ROOH is a free-radical chain process which obeys the rate laws,

$$-\frac{d[A]}{dt} = -\frac{1}{n}\left(\frac{d[ROOH]}{dt}\right) = k[A][ROOH]$$

with *n ca.* 5. The kinetics for this reaction are, therefore, identical with those for the analogous nickel complexes (1) with the value of *k* about an order of magnitude larger.

The reaction mechanism given in Scheme 1 explains most of the salient features of this reac-

[4]J. A. Howard and J. C. Tait, unpublished results.

[5]We have previously stated (1) that traces of nickel dialkyldithiophosphates and dialkyldithiocarbamates do not decompose cumene hydroperoxide to phenol and acetone. This is not strictly true as complete destruction of the hydroperoxide eventually takes place by a heterogeneous ionic process. We were, however, primarily concerned with the *initial* destruction of the complex by excess hydroperoxide which is a homolytic and not a heterolytic process.

TABLE 3. Organic products from the decomposition of cumene hydroperoxide by $Cu[(i\text{-}PrO)_2PS_2]_2$ (A)*

Run No.	$10^2[A]_0$ (M)	$10^2[ROOH]_0$ (M)	$\frac{[ROOH]_0}{[A]_0}$	Product yield × 10^2 (M)				
				Acetone	Phenol	α-Methyl-styrene	Acetophenone	α-Cumyl alcohol
1	0.5	0.5	1.0	—	—	0.02	0.03	0.12
2	1.0	1.16	1.2	—	—	0.08	0.05	0.4
3	0.02	1.0	50	0.2	~1.0	0.07	0.1	0.06
4	0.1	5	50	4.3	4.4	0.36	0.015	0.04
5	2	100	50	80	50	0.85	0.3	0.75
6	0.1†	20	20	1.48	0.74	0.4	0.08	15.4

*Argon saturated benzene or chlorobenzene at 30°C.
†Containing 2,6-di-*tert*-butyl-4-methylphenol (2×10^{-2} M); the reaction was not taken to completion and residual hydroperoxide was reduced to α-cumyl alcohol before analysis.

tion. The reaction of ROO· with A is, however, better described by reactions 6 to 10 since n *ca.* 5

[6] $ROO\cdot + A \rightarrow RO\cdot + A_1$

[7] $ROO\cdot + A_1 \rightarrow RO\cdot + A_2$

[8] $ROO\cdot + A_2 \rightarrow RO\cdot + A_3$

[9] $ROO\cdot + A_3 \rightarrow RO\cdot + A_4$

[10] $ROO\cdot + A_4 \rightarrow$ Non-radical products

where A_1, A_2, A_3, and A_4 are oxidized forms of A. Under steady state conditions reactions 1 to 10 give the rate expressions presented above with $n = 5.5$ and $k = 2k_1$.

The nickel complexes did, however, appear to disappear completely by a pseudo first-order process in the presence of excess hydroperoxide (1) whereas $Cu[(RO)_2PS_2]_2$ did not disappear *completely* under these conditions. Instead, reaction ceased after a fraction of the complex had disappeared and commenced again after an induction period, τ_{Cu}. The dependence of τ_{Cu} on the reactant concentrations suggests the accumulation of radical scavengers in the system which prevents homolytic destruction of the chelate or to the regeneration of the complex at a rate equal to its rate of destruction.

The decomposition of $(CH_3)_3COOH$ by $Cu[(RO)_2PS_2]_2$ stops completely when the chelate has been destroyed and there is no evidence for heterolytic decomposition. The cumene hydroperoxide reaction initially follows a similar concentration–time profile; excess hydroperoxide is, however, eventually destroyed by a heterolytic process. The end of the homolytic reaction is marked by precipitation of an insoluble copper salt. In the case of *tert*-butyl hydroperoxide all the copper ions could be accounted for as copper sulphate while the precipitate produced by cumene hydroperoxide was more complex and contained organic ligands in addition to sulphate ions. This latter precipitate is the active catalyst for heterolytic decomposition of cumene hydroperoxide although it is not active enough to decompose *tert*-butyl hydroperoxide. This may be because cumene hydroperoxide undergoes O—O heterolysis while *tert*-butyl hydroperoxide undergoes C—O heterolysis (5).

Copper sulphate suspended in chlorobenzene does not decompose cumene hydroperoxide. It does, however, react with a mixture of diisopropyldithiophosphoric acid and *O,O'*-diisopropyldithiophosphoryl disulphide to give cupric diisopropyldithiophosphate although $CuSO_4$ does not react with these compounds individually. Yordanov and co-workers (6) have recently reported that production of $Cu[(RO)_2PS_2]_2$ from cupric salts and $[(RO)_2PS_2]_2$ requires the presence of a reductant. A reaction of this nature could be the reason for τ_{Cu}.

II. Cupric Dialkyldithiocarbamates

Kinetics

Cupric diethyldithiocarbamate was rapidly destroyed by excess *tert*-butyl hydroperoxide (see, *e.g.*, Fig. 2). Plots of ln $[Cu(Et_2NCS_2)_2]_t$ and $[Cu(Et_2NCS_2)_2]_t^{0.5}$ against time exhibited very pronounced downward curvatures indicative of a reaction that is neither first nor half-order in the complex concentration; in fact rates were close to zero-order. However, in many runs the rate increased as the complex was consumed. Changes in the hydroperoxide concentration had a pronounced effect on $(-d[Cu(Et_2NCS_2)_2]/dt)_0$ and the reaction was second-order in this reactant. Typical kinetic data for this system are presented in Table 4 and appear to support a rate expression of the form

$$-\frac{d[Cu(Et_2NCS_2)_2]}{dt} = k[ROOH]^2$$

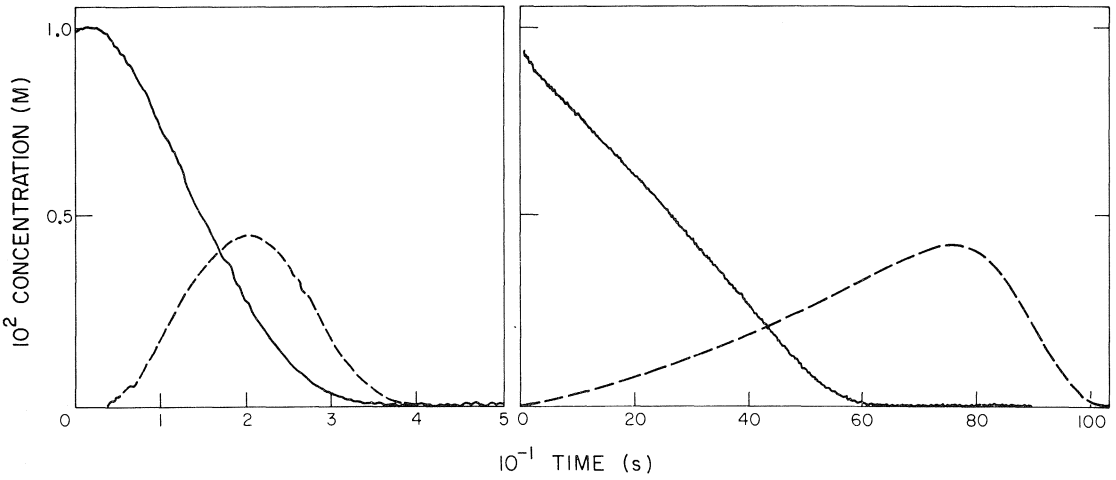

FIG. 2. The change in the concentration of $Cu[Et_2NCS_2]_2$ with respect to time after the addition of 0.11 *M* (*a*) and 0.011 *M* (*b*) $(CH_3)_3COOH$ at 30°C. The broken line illustrates the accumulation of the major transient Cu(II)product.

TABLE 4. Kinetic data for reaction of cupric diethyldithiocarbamate with *tert*-butyl hydroperoxide*

$10^4[Cu(Et_2NCS_2)_2]_0$ (*M*)	$10^3[(CH_3)_3COOH]_0$ (*M*)	$10^7(-d[Cu(Et_2NCS_2)_2]/dt)_0$ ($M\ s^{-1}$)
0.92	2	0.26
1.0	10	1.24
1.0	110	47
9.0	110	90
9.0	10	1.0
500	50	25
1.0†	110	30
1.0‡	110	1

*Argon saturated chlorobenzene at 30°C.
†Air saturated chlorobenzene.
‡Containing 2,6-di-*tert*-butyl-4-methylphenol (0.2 *M*).

Oxygen, the nature of the non-coordinating solvent (toluene, chlorobenzene, and CCl_4), the nature of the alkyl groups in the dialkyldithiocarbamate ligands (Me, Et, *i*-Pr, and *n*-Bu), and the nature of the hydroperoxide (*tert*-butyl, α-cumyl, and α-tetralyl) had very little influence on $(-d[Cu(R_2NCS_2)_2]/dt)_0$.

The rate of disappearance of $Cu(i\text{-}Pr_2NCS_2)_2$ in the presence of excess *tert*-butyl hydroperoxide was inhibited by 2,6-di-*tert*-butyl-4-methylphenol. The initial inhibited rate was zero-order with respect to $Cu(i\text{-}Pr_2NCS_2)_2$ and second-order with respect to ROOH (Table 5). Inhibition by a radical scavenger is consistent with a reaction mechanism in which the principal mode of complex destruction is by alkylperoxy radical attack.

The initial rate of hydroperoxide disappearance was about 10 times faster than the initial rate of complex disappearance implying an induced decomposition with a stoichiometric factor of ~10.

The kinetics for the initial reaction of $Cu(R_2NCS_2)_2$ with alkyl hydroperoxides, zero-order in dithiocarbamate and second-order in ROOH, are anomalous when compared with the kinetics for destruction of $Ni(R_2NCS_2)_2$, $Ni[(RO)_2PS_2]_2$, and $Cu[(RO)_2PS_2]_2$. They imply that free-radical initiation is independent of the complex and occurs by decomposition of a hydroperoxide dimer. The copper complex then functions solely as a radical scavenger. Such an explanation is, however, unacceptable and we prefer to conclude at the present time that the apparent kinetics for this system are influenced by factors that are not immediately obvious. We should note that copper complex – hydroperoxide adducts have been invoked in these and related systems (7). We could, however, find no

TABLE 5. Kinetic data for reaction of $Cu(i\text{-}Pr_2NCS_2)_2$ with $(CH_3)_3COOH$ in the presence of 2,6-di-*tert*-butyl-4-methylphenol* at 30°C

$10^5[Cu(i\text{-}Pr_2NCS_2)_2]_0$ (M)	$10^3[(CH_3)_3COOH]_0$ (M)	$10^8(-d[Cu(i\text{-}Pr_2NCS_2)_2]/dt)$ ($M\ s^{-1}$)
5.0	5.0	4.0
5.0	20	50
100	20	65

*$[BMP]_0 = 1.1 \times 10^{-2}$ M.

esr evidence for the formation of such adducts since the isotropic and anisotropic spectra of $Cu(R_2NCS_2)_2$ were identical in the presence and absence of a large excess of ROOH.[6]

Products

tert-Butyl hydroperoxide was reduced quantitatively to *tert*-butyl alcohol by $Cu(Et_2NCS_2)_2$ while the dithiocarbamate was converted to $CuSO_4$ by excess hydroperoxide; no oxygen was evolved. The disappearance of the dithiocarbamate was accompanied by the appearance of a transient cupric complex, I (see Fig. 2). This complex had the isotropic esr parameters $g = 2.0651$ and $a_{Cu} = 77.1$ G, both parameters being different from those for $Cu(Et_2NCS_2)_2$ ($g = 2.0445$ and $a_{Cu} = 78.64$ G). The rate of appearance of this transient was equal to $(-d[Cu(Et_2NCS_2)_2]/dt)_0$ implying that it is the initial oxidation product. Its concentration reached a maximum when the dithiocarbamate had almost disappeared and it was then destroyed by excess ROOH. Vinogradova and Maizus (8, 9) have also observed the production of a transient cupric complex ($g = 2.066$, $a_{Cu} = 80.2$ G) during reaction of α-phenylethyl hydroperoxide with cupric hexamethyleniminedithiocarbamate and during the $Cu(Et_2NCS_2)_2$ inhibited autoxidation of ethylbenzene and have attributed it to the alkylperoxo dialkyldithiocarbamato copper, $PhCH(Me)OOCuS_2CNEt_2$, formed by displacement of $Et_2NCS_2^{\bullet}$ from the complex by $PhCH(Me)OO^{\bullet}$.

The concentration–time profiles for $Cu(Et_2NCS_2)_2$ and I for reaction of $Cu(Et_2NCS_2)_2$ (0.01 M) with less than a stoichiometric amount of *tert*-butyl hydroperoxide (0.056 M) are shown in Fig. 3. The carbamate was destroyed in approximately 700 s and at this time I had reached a maximum concentration and was then rapidly destroyed. There was then a period when two additional cupric complexes, with g-factors higher than I appeared in the esr spectrum of the reaction mixture, the total concentration of soluble Cu(II) species was, however, quite low during this period. The transient species I was then regenerated, reached a maximum concentration, and finally disappeared completely from the system. $Cu(Et_2NCS_2)_2$ was also regenerated and reached a steady-state concentration when about 75% of the initial concentration had been formed. A possible mechanism for regeneration of $Cu(Et_2NCS_2)_2$ in this system is reaction of diethyldithiuram disulphide, $(Et_2NCS_2)_2$, with cupric ions. Vinogradova and Maizus (9) have reported that this disulphide is formed during inhibition of ethylbenzene autoxidation by $Cu(Et_2NCS_2)_2$. However, their work suggests that it is not stable in the reaction mixture and follows a concentration–time profile that coin-

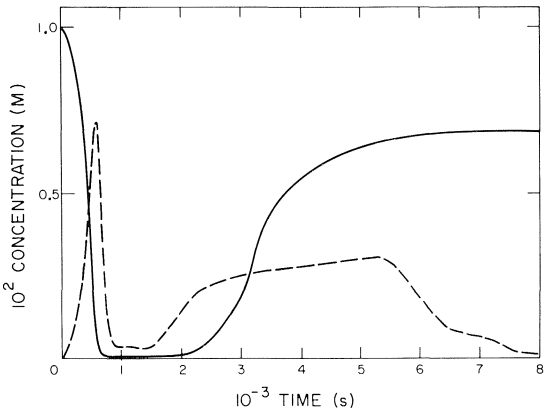

FIG. 3. The changes in the concentrations of $Cu(Et_2NCS_2)_2$ and the major transient Cu(II) product (broken line) during reaction of $Cu(Et_2NCS_2)_2$ (0.01 M) with $(CH_3)_3COOH$ (0.056 M) in argon saturated chlorobenzene at 30°C.

[6]NOTE ADDED IN PROOF—The ^{65}Cu hyperfine was studied on a 10^{-4} M $Cu[Et_2NCS_2]_2$ solution in toluene and 10 and 30% *tert*-butyl hydroperoxide – toluene from 263–233 K. The variation of the hyperfine with temperature was linear and identical for both solutions, the slope of $d|a_0|/dt > 0$ being characteristic for a non-coordinating solvent (F. G. Herring and R. L. Tapping, Can. J. Chem., **52**, 4016 (1974)). Line widths in both solutions were virtually identical.

TABLE 6. Volatile organic products from the decomposition of cumene hydroperoxide by $Cu(Et_2NCS_2)_2$*

Run No.	$10^2[A]_0$ (M)	$10^2[ROOH]_0$ (M)	$\frac{[ROOH]_0}{[A]_0}$	Product yield × 10^2 (M)				
				Acetone	Phenol	α-Methyl-styrene	Acetophenone	α-Cumyl alcohol
1	1	1.2	1.2	—	—	0.22	0.08	0.79
2	0.7	2	2.8_6	—	—	0.5	0.04	1.5
3	0.1	1.2	12	—	—	0.15	0.33	0.35
4	0.02	1.0	50	—	0.008	0.06	—	—
5	2†	100	50	7	5	1.7	0.4	‡
6	0.01	1.2	120	—	—	0.45	0.14	0.25
7	0.1§	20	200	4.8	1.1	0.46	0.04	10

*Solvent: chlorobenzene; temperature: 30°C.
†This reaction was quenched after 5 h.
‡Not measured.
§In the presence of 2,6-di-*tert*-butyl-4-methylphenol. This reaction was quenched after 0.07 M of hydroperoxide had been decomposed.

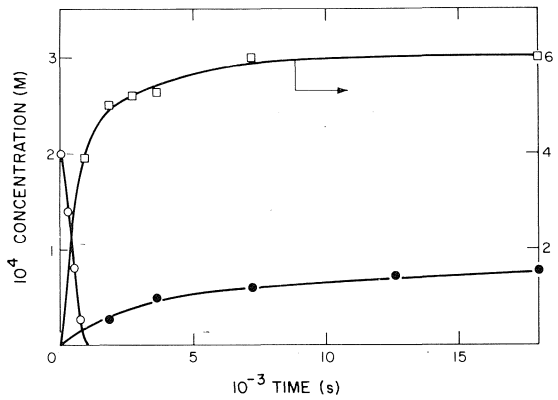

FIG. 4. Concentration–time profiles for production of phenol (●) and α-methylstyrene (□) and disappearance of complex (○) during decomposition of $C_6H_5C(CH_3)_2OOH$ (0.01 M) by $Cu(Et_2NCS_2)_2$ (0.0002 M) at 30°C.

cides with the one for I. We were unable to positively identify $(Et_2NCS_2)_2$ at any stage of the reaction and are, therefore, reluctant to associate regeneration of $Cu(Et_2NCS_2)_2$ with this product.

α-Cumyl alcohol, α-methylstyrene, and acetophenone were the principal volatile organic products from decomposition of α-cumene hydroperoxide at ratios of hydroperoxide to complex less than 10. If, however, this ratio was greater than 10, phenol and acetone were formed and at ratios greater than 50 they were the major final reaction products[5] (Table 6). The accumulation of phenol and α-methylstyrene was followed during the decomposition of $C_6H_5C(CH_3)_2OOH$ (0.01 M) by $Cu(Et_2NCS_2)_2$ (0.0002 M). The concentration–time profiles are shown in Fig. 4 along with the disappearance of the complex. It is quite clear from these curves that α-methylstyrene is formed in the initial reaction whereas phenol is only formed after the complex has disappeared. An insoluble precipitate was deposited after the complex had been destroyed and if this precipitate was filtered from the solution the hydroperoxide was very much more stable. Heterolytic hydroperoxide decomposition is therefore, a heterogeneous process as was suggested by Burn *et al.* (4) for the $Zn[(RO)_2PS_2]_2$–cumene hydroperoxide system. The precipitate does not have the ability to decompose *tert*-butyl hydroperoxide but it does heterolytically decompose a fresh cumene hydroperoxide solution.

Decomposition of cumene hydroperoxide to α-cumyl alcohol, α-methylstyrene, and acetophenone is consistent with reactions 1–10 since reaction 3 gives the alcohol while [6]–[10] give alcohol, α-methylstyrene, and acetophenone[4].

Decomposition of 1,1-diphenylethyl hydroperoxide (0.02 M) by $Cu(i\text{-}Pr_2NCS_2)_2$ (0.01 M) gave 1,1-diphenylethanol (0.0085 M) 1,1-diphenylethylene (0.01 M), acetophenone (0.0026 M), and phenol (0.0023 M). The high yield of alcohol and its dehydration product in this system could be rationalized on the basis of a non-radical deoxygenation of the hydroperoxide analogous to that found with organosulphur compounds such as dialkyl sulphides (5). It is, however, much more likely that this alcohol arises from reaction of 1,1-diphenylethylperoxy radicals with the complex and reaction of 1,1-diphenylethoxy with the hydroperoxide.

The small yields of acetophenone and phenol could be the result of contribution from heterolysis of the hydroperoxide. 1,1-Diphenylethoxy radicals do, however, have a strong tendency to

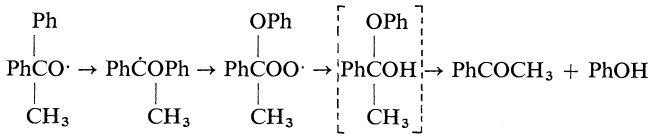

undergo a 1,2-phenyl shift to give 1-phenoxy-1-phenylethyl (10). This radical could combine with oxygen to give the peroxy radical which would be deoxygenated and reduced to the alcohol by the complex. This alcohol would dissociate in solution to acetophenone and phenol.

We favor a homolytic mechanism for the production of acetophenone and phenol in this system because of the absence of a heterolytic process with cumene hydroperoxide at low ratios of hydroperoxide to complex.

Summary

Cupric dialkyldithiophosphates and dialkyldithiocarbamates are converted to copper sulphate by excess *tert*-butyl hydroperoxide while the hydroperoxide is reduced to *tert*-butyl alcohol. The principal reaction mechanism is homolytic with an induced decomposition of the hydroperoxide and destruction of the chelate by alkylperoxy radicals. The most plausible mode of initiation is a redox reaction between the hydroperoxide and complex. The overall behavior of an aralkyl hydroperoxide, such as cumene hydroperoxide, is affected by the formation of a heterogeneous product which is capable of catalyzing the ionic decomposition of cumene hydroperoxide but not *tert*-butyl hydroperoxide.

Simple reaction kinetics only hold for initial rates of complex disappearance. This is because secondary reactions influence the rate of reaction. In the case of the dithiophosphate the rate decelerates, stops completely, and increases rapidly to complete complex destruction. The rate of disappearance of the dithiocarbamate on the other hand appears to increase smoothly as the complex is consumed. The dithiocarbamate is converted to copper sulphate through at least three transient cupric complexes. These complexes are formed by reaction with alkylperoxy radicals and their structure and mechanism for their production will be discussed in a forthcoming publication.

1. J. A. Howard and J. H. B. Chenier. Can. J. Chem. **54**, 390 (1976).
2. J. D. Holdsworth, G. Scott, and D. Williams. J. Chem. Soc. 4692 (1964).
3. G. Scott. Br. Polym. J. **3**, 24 (1971).
4. A. J. Burn, R. Cecil, and V. O. Young. J. Inst. Petrol. **57**, 319 (1971).
5. R. Hiatt. Organic peroxides. Vol. II. *Edited by* D. Swern. John Wiley and Sons, Inc. 1971. Chapt. I.
6. N. Yordanov, N. Nicolov, A. Shishkov, and D. Shopov. Inorg. Nucl. Chem. Lett. **12**, 527 (1976).
7. O. N. Emanuel, D. Kh. Kitaeva, and I. P. Skibida. Izv. Akad. Nauk SSSR, Ser. Khim. 56 (1976).
8. V. G. Vinogradova and Z. K. Maizus. Kinet. Kat. **13**, 298 (1972).
9. A. N. Zverev, V. G. Vinogradova, and Z. K. Maizus. Izv. Akad. Nauk SSSR, Ser. Khim. 2224 (1975).
10. J. A. Howard and K. U. Ingold. Can. J. Chem. **47**, 3797 (1969).

Hydroxymethylbenzimidazole carboxylic acid models of the Asp-His-Ser charge relay system of serine proteases

J. Bryan Jones and Keith E. Taylor

Department of Chemistry, University of Toronto, Toronto, Ont., Canada M5S 1A1

Received November 1, 1976

J. Bryan Jones and Keith E. Taylor. Can. J. Chem. **55**, 1653 (1977).

2-Hydroxymethyl- and 2-acetoxymethylbenzimidazole, and their *C*-4(7)-carboxy derivatives, have been synthesized and characterized for evaluation as chemical models of the Asp-His-Ser triad present at the active sites of several serine proteases. Preliminary studies of the 2-acetoxy compounds, which are analogues of the acyl enzymes, show that the rate of hydrolysis is augmented only 2.5 fold by the carboxylate group of the model charge relay system.

J. Bryan Jones et Keith E. Taylor. Can. J. Chem. **55**, 1653 (1977).

On a synthétisé et caractérisé, pour leur évaluation comme modèle chimique de la triade Asp-His-Ser présente au niveau des sites actifs de plusieurs protéases sérines, les hydroxy-2 méthyl- et acétoxy-2 méthylbenzimidazoles et leurs dérivés *C*-4(7) carboxy. Des études préliminaires sur des composés acétoxy-2, qui sont des analogues des enzymes acyles, montrent que la vitesse d'hydrolyse n'est augmenté que par 2.5 fois par le groupe carboxylate du modèle de système de relais de charge.

[Traduit par le journal]

The serine proteases are hydrolytic enzymes which possess a uniquely reactive serine hydroxyl group at the active site. Although the individual amino acid sequences can be quite dissimilar, the active sites of the enzymes for which X-ray structures are available, *viz.* α-chymotrypsin (1), trypsin (2), elastase (3), and subtilisin (4*a*), each possess an Asp-His-Ser triad in more or less the same geometrical arrangement. This triad has become known as the charge relay system of the serine proteases. Based largely on the chymotrypsin data (1, 5), the operation of the catalytic triad has been interpreted in the manner represented in Scheme 1.[1]

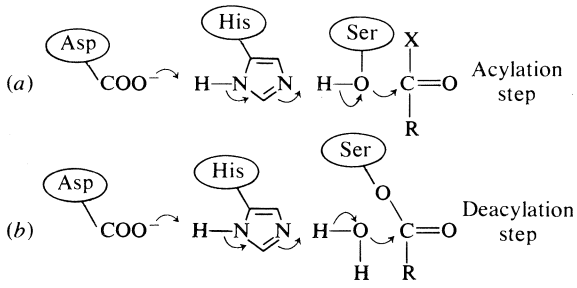

SCHEME 1

The degree to which the carboxylate function is capable of acting as a general base in the Scheme 1 manner is a question which is receiving increasing attention and several model studies have been reported recently (8–11). We felt that benzimidazole derivatives such as **1**–**4**, would serve as good chemical models for the Scheme 1 systems. This paper reports mainly on their synthesis and properties. Some very preliminary data on the rates of deacylation of **2** and **4** have also been obtained.

Results

The benzimidazole derivatives required were prepared in 60–90% yields as outlined in Scheme 2. The dissociation constants of their functional groups were then determined; the pK_a values obtained are summarized in Table 1. The abnormally low pK_{a_1} of **4** was obtained under conditions where $-\log [\mathbf{4}] > pK_a$ and thus may be somewhat insecure (13). However the pK_{a_2} value for **4** is considered reliable.

The rate constants for hydrolysis of the 2-acetoxybenzimidazole derivatives **2** and **4** were determined under pseudo first-order conditions for several half-lives. Data following 15–50% of reaction were used to calculate the rate constants; the same values were obtained when the hydrolyses were allowed to progress up to 80% completion. The results are summarized in Table 2. The fact that hydrolyses of **2** and **4** under the Table 2 conditions were proceeding as expected was confirmed by the isolation of **1** and **3** respectively in >80% yields.

[1]The exact nature of the mechanism of the charge relay system continues to be the topic of considerable debate, particularly with respect to assigning the role played by the asparatate carboxyl(ate) group (1*a*,*b*, 6, 7).

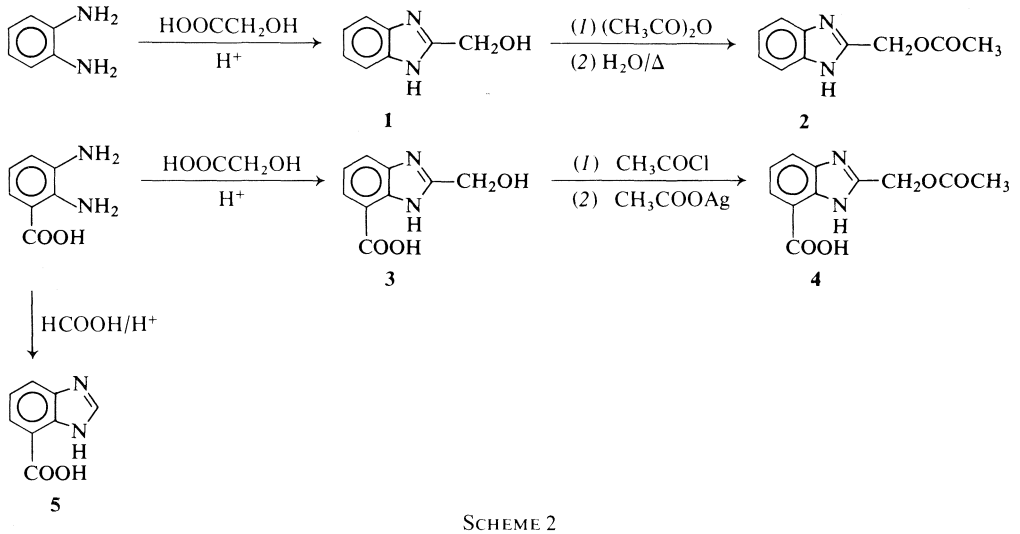

SCHEME 2

TABLE 1. Dissociation constants of benzimidazole derivatives*

Compound	pK_{a_1}	pK_{a_2}
Benzimidazole	5.54±0.02 (5.55 (12))	
1	5.41±0.01 (5.40 (13))	
2	4.54±0.02†	
3·HCl	3.51±0.06†	5.61±0.01†
4	2.23±0.27†	4.85±0.12†
5·HCl	3.21±0.03†	5.52±0.03†

*Dissociation constants were determined at 25°C in aqueous solution.
†Solution 1% v/v in DMSO.

Discussion

Each of the benzimidazoles **1**–**5** was readily prepared. The heterocyclization steps, effected under Phillips-type conditions (14–16), all proceeded in high yield. Selective hydrolysis of the *N*,*O*-diacetyl precursors of **2** and **4** was also achieved without difficulty.

The selection of carboxybenzimidazole structures as suitable models for the Asp-His-Ser triad of serine proteases was influenced by several considerations, including the well-documented evidence for the abilities of imidazoyl and carboxyl groups to participate in hydrolysis reactions (17–20). Furthermore, benzimidazole derivatives have been employed previously in hydrolysis studies (21–24). Analysis of Dreiding models of **4** indicated that the carboxyl-oxygen to N-1 and hydroxymethyl-oxygen to N-3 distances were close to those reported for the His-57-$N^{\delta 1}$ to $O^{\delta 2}$ of Asp-102 (2.8 Å) and His-57-$N^{\varepsilon 2}$ to Ser-195-O^{δ} (3.0 Å) separations in chymotrypsin (1*c*). Charge relays of the Scheme 1 type are thus possible; one possible analogue of the first step of deacylation is depicted in Scheme 3.

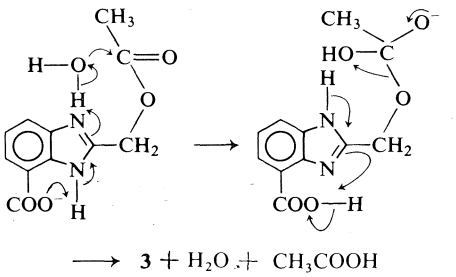

SCHEME 3

Benzimidazole-4(7)-carboxylic acids of this kind have a natural inclination towards intramolecular alignments of the type required for a Scheme 3 orientation as a result of zwitterion formation (25). Analyses of the dissociation constants of Table 1 provide further support for this view. The overall pK_a values are consistent with a Scheme 4 ionization pathway, with the strongly electron-withdrawing protonated imidazolium moiety of **6** perturbing the normal dissociation constant of the carboxyl group. In contrast, the carboxylate group of zwitterions such as **7**[2] has little effect on the imidazolium

[2]The alternative ionization pathway, with the imidazolium group dissociating first merely as a consequence of the presence of a C-4(7) carboxyl group, is extremely improbable. For example, as strong an electron-withdrawing group as nitro is needed at the C-4(7) position in order to induce a lowering of the benzimidazolium pK_a by 2–2.5 units (12).

TABLE 2. Rates of hydrolysis of **2** and **4***

Substrate	p*H*	k ($s^{-1} \times 10^5$)	k_{H_2O} ($s^{-1} \times 10^5$)	k_{-OH} (M^{-1} s^{-1})	k_{H_2O} (**4**:**2**)	k_{-OH} (**4**:**2**)
2	8.0	0.75±0.02	0.62	1.3		
	10.0	13.7 ±0.5†			2.5	0.52
4	8.0	1.62±0.16	1.55	0.68		
	10.0	8.35±0.01†				

*Determined at 25°C under N_2 in aqueous solution 0.1 *M* in KCl and containing 1% v/v DMSO. Each run was performed at least in duplicate and the data were subjected to linear regression analysis. Correlation coefficients were > 0.996 in each case.
†Corrected for uptake of base by glass electrode of p*H* stat.

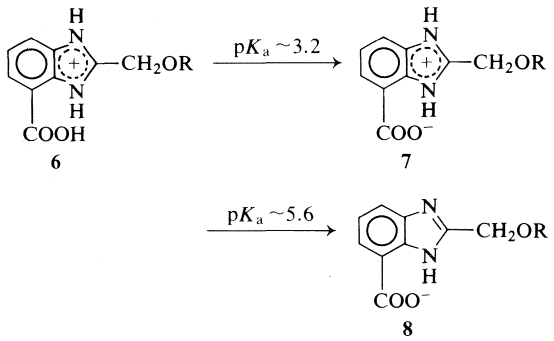

SCHEME 4

ionization. The Table 1 data are consistent with stabilization due to intramolecular hydrogen bonding of zwitterionic forms such as **7** over the corresponding anions **8**.

The Table 1 data also suggest that the CH_2OH and CH_2OCOCH_3 groups of the model compounds maintain themselves in Scheme 3 type orientations. Acetylation of the CH_2OH groups of **1** and **3** results in a lowering of the benzimidazole pK_a by ~0.8 units.[3] This degree of pK_a reduction suggests differential hydrogen bonding as in **9** and **10**. Solvent bridging as in **9** has been invoked previously to account for the low pK_a values of furan- (27) and pyrrole-2-carboxylic acids (24, 28).

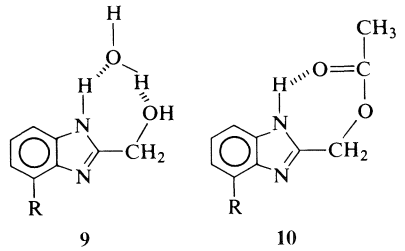

Comparison of the rates of hydrolysis of **2** and **4** shows attack by water of the acyl enzyme model **4** to be only 2.5-fold faster than for **2**, which lacks the *C*-4(7)-carboxyl(ate) function.[4] The true degree of intramolecular acceleration attributable to carboxylate participation may in fact be even smaller than 2.5-fold since no attempt was made to correct for nitrogen basicity differences between **2** and **4** nor to exclude possible effects of elimination pathways (10*b*). Carboxylate participation is evidently not significant under the current assay conditions.[5]

Experimental

All starting chemicals were purchased from Fisher or Aldrich. Nuclear magnetic resonance spectra were obtained on Varian A-60 or T-60 instruments, ir spectra on a Perkin-Elmer 237 spectrophotometer, and mass spectra using an AEI MS-9 spectrometer. Elemental analyses were by A. B. Gygli, Toronto.

2-Hydroxymethylbenzimidazole (1)

O-Phenylenediamine (6 g, 56 mmol) and glycolic acid (6.33 g, 84 mmol) were reacted according to the procedure of Copeland and Day (31) to give a 63% yield of **1**, mp 174–175°C (lit.(31) mp 171–172°C); ir (KBr) 3280, 1062, and 1047 cm^{-1}; nmr (CF_3COOH) δ 5.42 (s, 2H) and 7.70 (m, 4H); (DMSO-$^2H_6$) δ 4.74 (s, 2H) and 7.35 (m, 4H) ppm; ms *m/e* 149.

2-Acetoxymethylbenzimidazole (2)

The procedure used was based on that of Porai-Koshits (32). A solution of 2-hydroxymethylbenzimidazole (**1**; 4.83 g, 32.6 mmol), acetic anhydride (6.5 ml, 69 mmol) and acetic acid (7 ml) was heated for 35 min on a steam bath and then chilled, diluted with water, and filtered. The *N*-1-acetyl-2-acetoxymethylbenzimidazole (5.9 g, 78%) obtained had mp 99–100°C (lit. (32) mp 97–98°C); ir ($CHCl_3$) 1722–1750 cm^{-1} (broad); nmr (C^2HCl_3) δ 2.20 (s, 3H), 2.79 (s, 3H), 5.54 (s, 2H), and 7.52 (m,

[3]A similar acid-strengthening effect has been reported when Ser-195 of chymotrypsin is acetylated (26).

[4]This degree of intramolecular acceleration is of the same magnitude as that observed for the structurally similar (2′-hydroxyphenyl)imidazole models (10*a*). Much larger accelerating effects have been attributed to carboxylate participation in intermolecular model systems (8, 9, 11) but questions have been raised (9*b*, 10*a*) with respect to the relevance of these results to the charge relay hypothesis. Estimates of the maximum rate enhancements to be expected from Asp-COO^- participation in a charge relay triad range from 10 (29) to 5000 (30)

[5]Larger effects should be observed in hydrophobic media.

4H) ppm. This diacetyl compound (5.70 g, 22.6 mmol) and water (20 ml) were refluxed for 10 min and the mixture chilled in ice and scratched to furnish 2-acetoxymethylbenzimidazole (**2**; 3.47 g, 79%), mp 165–166°C (lit. (32) mp 164–165°C); ir ($CHCl_3$) 3442 and 1730 cm^{-1}; nmr (C^2HCl_3) δ 2.05 (s, 3H), 5.40 (s, 2H), and 7.45 (m, 4H) ppm.

2,3-Diaminobenzoic Acid

2-Methyl-6-nitroaniline was acetylated by the procedure of James *et al.* (33) to give a 91% yield of 2-acetamino-3-nitrotoluene, mp 160–161°C (lit. (33) mp 157–158°C); ir ($CHCl_3$) 3445, 1700, 1514, 1480, and 1350 cm^{-1}; nmr (C^2HCl_3) δ 2.18 (s, 3H), 2.30 (s, 3H), and 7.50 (m, 3H) ppm. This was then oxidized with $KMnO_4/MgSO_4$ (31) to give 2-acetamino-3-nitrobenzoic acid (90% yield) which was recrystallized from EtOH and had mp 254–255°C (lit. (33) mp 245°C); ir (Nujol) 3315–2500, 1691, 1513, and 1350 cm^{-1}; nmr (DMSO-$^2H_6$) δ 2.09 (s, 3H), 2.53 (m, 1H), 7.35 (t, J = 7 Hz, 1H), and 8.24 (d, J = 7 Hz, 1H) ppm. The above acetamino compound (32.1 g, 143 mmol) in 5% (v/v) aqueous hydrochloric acid (200 ml) was refluxed for 1 h and then concentrated and cooled. The 2-amino-3-nitrobenzoic acid (94% yield) was recrystallized from water; it had mp 208.5–209°C (lit. (33) mp 205°C); ir ($CHCl_3$) 3470, 3357, 1688, 1559, and 1351 cm^{-1}; uv (MeOH) 234 (ε 13 870), 262 (ε 4940), and 412 nm (ε 6590); nmr (DMSO-$^2H_6$) δ 5.50 (br), 6.76 (t, J = 7 Hz, 1H), and 8.2–8.4 (m, 2H) ppm. 2-Amino-3-nitrobenzoic acid (4.0 g, 22 mmol), $SnCl_2 \cdot 2H_2O$ (15.2 g, 68 mmol), and concentrated hydrochloric acid (25 ml) were heated to 50°C on a steam bath and then placed in an ice bath to maintain the exothermic reaction at 100°C. The solution was then heated for 15 min on the steam bath, cooled, and poured into a solution of NaOH (18.5 g) in water (60 ml). The mixture obtained (pH 7) was filtered and the filtrate brought to pH 1 with concentrated hydrochloric acid. The precipitate of 2,3-diaminobenzoic acid hydrochloride (2.5 g, 75%) was filtered and sublimed (0.5 torr, 100°C) to give material mp 196–198°C (lit. (34, 35) mp 190–191°C (dec.), 201°C (dec.)); ir (Nujol) 3410, 3320, and 1670 cm^{-1}; nmr (DMSO-$^2H_6$) δ 5.73 (broad s, ^2H_2O exchangeable), 6.67 (t, J = 7.7 Hz, 1H), 7.39 (d of d, J = 1.8, 7.7 Hz, 1H), and 7.70 (d of d, J = 1.8, 7.7 Hz, 1H) ppm.

*2-Hydroxymethylbenzimidazole-4(7)-carboxylic Acid (**3**)*

A solution of freshly-sublimed 2,3-diaminobenzoic acid (2.11 g, 13.9 mmol), glycolic acid (3.2 g, 42 mmol), and 4 M aqueous hydrochloric acid (40 ml) was refluxed for 2 h under N_2 and then cooled in ice. The precipitated solid (2.97 g, 94%) was recrystallized twice from 0.5 M aqueous hydrochloric acid, and then thrice from methanol–acetone (1:3) to give **3**·HCl mp > 280°C; ir (KBr) 1695 cm^{-1}; nmr (DMSO-$^2H_6$) δ 5.13 (s, 2H), 7.67 (d of d, J = 2, 6 Hz, 1H), 8.04 (br s, 1H), and 8.15 (d, J = 1.5 Hz, 1H) ppm; ms m/e 193. *Anal.* calcd. for $C_9H_9N_2O_3Cl$: C 47.28, H 3.97, N 12.25, Cl 15.51; found: C 47.29, H 4.04, N 12.14, Cl 15.45.

The methyl ester was prepared by treatment of **3** with diazomethane. After recrystallization from methanol it had mp 166–167°C; ir (KBr) 1690 cm^{-1}; nmr (DMSO-$^2H_6$) δ 3.87 (s), 4.77 (s), and 7.82 (m) ppm; ms m/e 205. *Anal.* calcd. for $C_{10}H_{10}N_2O_3$: C 58.24, H 4.89, N 13.59; found: C 58.46, H 5.06, N 13.41.

*2-Acetoxymethylbenzimidazole-4(7)-carboxylic Acid (**4**)*

2-Hydroxymethylbenzimidazole-4(7)-carboxylic acid hydrochloride (**3**·HCl; 1.21 g, 5.3 mmol) and acetyl chloride (45 ml) were heated for 18 h at 50°C and then concentrated to ~2 ml. The solid which separated was collected (1.49 g); a portion (1 g) was then redissolved in acetic acid and silver acetate was added until no further precipitate formed. The mixture was filtered and the filtrate concentrated to give **4** (515 mg, 61%) mp > 290°C; ir (KBr) 2940–3220, 1729, 1718, and 1686 cm^{-1}; nmr (DMSO-$^2H_6$) δ 2.22 (s, 3H), 5.33 (s, 2H), 7.32 (m, 1H), 7.82 (m, 1H), and 7.95 (m, 1H) ppm; ms m/e 234.0656 (calcd. 234.0641). *Anal.* calcd. for $C_{11}H_{10}N_2O_4$: C 56.41, H 4.30, N 11.96; found: C 56.26, H 4.40, N 11.92.

*Benzimidazole-4(7)-carboxylic Acid (**5**)*

Freshly-sublimed 2,3-diaminobenzoic acid (1.51 g, 9.9 mmol), formic acid (1.20 ml, 29.7 mmol), and 4 M aqueous hydrochloric acid (24 ml) were refluxed for 1 h under N_2 (24, 25). The cooled mixture was then filtered and the precipitate (1.45 g, 73%) was recrystallized from 0.5 M aqueous hydrochloric acid to give **5**·HCl, mp > 300°C (lit. (34) mp > 360°C); ir (KBr) 2865–3570 and 1710 cm^{-1}; nmr (DMSO-$^2H_6$) δ 7.74 (t, J = 8 Hz, 1H), 8.22 (m, 2H), 9.78 (s, 1H), and 12.73 (br, 1H) ppm.

The methyl ester was obtained by reaction of **5**·HCl with diazomethane, mp 214–215°C; ir ($CHCl_3$) 3460, 1730, and 1697 cm^{-1}; nmr (DMSO-$^2H_6$), δ 3.98 (s, 3H), 7.36 and 7.95 (m, 3H), and 8.36 (s, 1H) ppm; ms m/e 176. *Anal.* calcd. for $C_9H_8N_2O_2$: C 61.35, H 4.58, N 15.90; found: C 60.53, H 4.42, N 16.21.

Determination of Dissociation Constants

The dissociation constants of benzimidazole and compounds **1**–**5** were determined by the method of Albert and Serjeant (13). Titration curves for 2–10 mM solutions of substrates, which were also 0.1 M in KCl, against 0.1–0.25 M aqueous NaOH were obtained under N_2 at 25°C using a Radiometer pH-stat. The solutions of **2**–**5** also contained 1% (v/v) DMSO to aid solubility.

*Rates of Hydrolysis of **3** and **4***

The rates of hydrolysis of **3** and **4** were determined, at least in duplicate, at 25°C under N_2 on 0.7–1.5 mM substrate solutions maintained at the selected pH (8 or 10) by automatic addition of 0.05 M aqueous NaOH with a Radiometer pH-stat. The reaction solutions were made up by injecting 100 μl of a DMSO stock solution of **3** or **4** into 10 ml of CO_2-free water. The data were analyzed by linear regression analysis, pseudo first-order plots with correlation coefficients > 0.996 being obtained. The pH 10 results were corrected for base uptake by the glass electrode (36–38). The observed and derived (from $k_{obs} = k_{H_2O} + k_{-OH}[^-OH]$) rate constants are summarized in Table 2. The hydrolysis products, **1** and **2** respectively, of **3** and **4** under the Table 2 conditions were isolated in > 80% yields from representative kinetic runs.

Acknowledgement

We thank Dr. J. W. Bunting for helpful discussions and the National Research Council of Canada for financial support. The award of an NRCC Scholarship (to K.E.T.) is also gratefully acknowledged.

1. (*a*) D. M. BLOW. *In* The enzymes. Vol. 3. 3rd. ed. *Edited by* P. D. Boyer. Academic Press, New York, NY. 1971. pp. 185–212; (*b*) D. M. BLOW. Acc. Chem. Res. **9**, 145 (1976); (*c*) D. M. BLOW, J. J. BIRKTOFT, and B. S. HARTLEY. Nature (London), **221**, 337 (1969).
2. B. KEIL. *In* The enzymes. Vol. 3. 3rd ed. *Edited by* P. D. Boyer. Academic Press, New York, NY. 1971. pp. 250–277.
3. B. S. HARTLEY and D. M. SHOTTON. *In* The enzymes. Vol. 3. 3rd ed. *Edited by* P. D. Boyer. Academic Press, New York, NY. 1971. pp. 323–375.
4. (*a*) J. KRAUT. *In* The enzymes. Vol. 3. 3rd ed. *Edited by* P. D. Boyer. Academic Press, New York, NY. 1971. pp. 547–561; (*b*) J. J. BIRKROFT, J. KRAUT, and S. T. FREER. Biochemistry, **15**, 4481 (1976).
5. G. P. HESS. *In* The enzymes. Vol. 3. 3rd ed. *Edited by* P. D. Boyer. Academic Press, New York, NY. 1971. pp. 213–249.
6. S. SCHEINER, D. A. KLEIER, and W. N. LIPSCOMB. Proc. Natl. Acad. Sci. U.S.A. **72**, 2606 (1975); S. SCHEINER and W. N. LIPSCOMB. Proc. Natl. Acad. Sci. U.S.A. **73**, 432 (1976).
7. R. E. KOEPPE II and R. M. STROUD. Biochemistry, **15**, 3450 (1976); M. KRIEGER, R. E. KOEPPE II, and R. M. STROUD. Biochemistry, **15**, 3458 (1976).
8. G. WALLERBERG, J. BOGER, and P. HAAKE. J. Am. Chem. Soc. **93**, 4938 (1976).
9. (*a*) F. M. MENGER and A. C. VITALE. J. Am. Chem. Soc. **95**, 4931 (1973); (*b*) F. M. MENGER, S. WRENN, and H-S. RHEE. Bioorg. Chem. **4**, 194 (1975).
10. (*a*) G. A. ROGERS and T. C. BRUICE. J. Am. Chem. Soc. **94**, 2473 (1974); (*b*) T. C. BRUICE and T. H. FIFE. J. Am. Chem. Soc. **83**, 1124 (1961).
11. F. D'ANDREA and U. TONELLATO. J. Chem. Soc. Chem. Commun. 659 (1975).
12. D. D. PERRIN. Dissociation constants of organic bases in aqueous solutions. Butterworths, London. 1965.
13. A. ALBERT and E. P. SERJEANT. Determination of ionization constants of acids and bases. Methuen, London. 1962.
14. M. A. PHILLIPS. J. Chem. Soc. 2393 (1928).
15. K. HOFFMAN. Chemistry of heterocyclic compounds. Vol. 6. Part I. Interscience, New York, NY. 1953. Chapt. 8.
16. K. J. MORGAN and A. M. TURNER. Tetrahedron, **25**, 915 (1969).
17. M. L. BENDER. Mechanisms of homogeneous catalysis from protons to proteins. Wiley-Interscience, New York, NY. 1971. Chapt. 16.
18. W. P. JENCKS. Catalysis in chemistry and enzymology. McGraw-Hill, New York, NY. 1969.
19. T. C. BRUICE. *In* The enzymes. Vol. 2. 3rd ed. *Edited by* P. D. Boyer. Academic Press, New York, NY. 1970. Chapt. 4.
20. A. J. KIRBY and A. R. FERSHT. Progress in bioorganic chemistry. Vol. 1. *Edited by* E. T. Kaiser and F. J. Kézdy. Wiley-Interscience, New York, NY. 1971. pp. 1–82.
21. T. C. BRUICE and G. L. SCHMIR. J. Am. Chem. Soc. **80**, 148 (1958).
22. T. KUNITAKE and S. SHINKAI. J. Am. Chem. Soc. **93**, 4247 (1971).
23. R. D. COOK and S. RAZMARA. Tetrahedron Lett. 2905 (1971).
24. A. WILLIAMS and G. SALVADORI. J. Chem. Soc. Perkin Trans. II, 883 (1972).
25. K. J. MORGAN. J. Chem. Soc. 2343 (1961).
26. G. ROBILLARD and R. G. SHULMAN. J. Mol. Biol. **86**, 519 (1974).
27. C. C. PRICE and E. A. DUDLEY. J. Am. Chem. Soc. **78**, 68 (1956).
28. M. K. A. KHAN and K. J. MORGAN. Tetrahedron, **21**, 2197 (1965).
29. A. R. FERSHT and J. SPERLING. J. Mol. Biol. **74**, 137 (1973).
30. R. HENDERSON. Biochem. J. **124**, 13 (1971).
31. R. A. B. COPELAND and A. R. DAY. J. Am. Chem. Soc. **65**, 1072 (1943).
32. B. A. PORAI-KOSHITS. Zh. Obs. Khim. **23**, 1225 (1953); Chem. Abstr. **47**, 12367g (1953).
33. C. W. JAMES, J. KENNER, and W. V. STUBBINGS. J. Chem. Soc. **117**, 775 (1920).
34. B. SCHILLING. Ber. **34**, 902 (1901).
35. J. P. ENGLISH, R. C. CLAPP, Q. P. COLE, I. F. HALVERSTADT, J. O. LAMPEN, and R. O. ROBLIN, JR. J. Am. Chem. Soc. **67**, 295 (1945).
36. H. L. GOERING and H. H. ESPY. J. Am. Chem. Soc. **78**, 1454 (1956).
37. R. G. BATES. Determination of p*H*, theory and practice. J. Wiley and Sons, New York, NY. 1964. pp. 299–302.
38. J. MCMILLAN and R. J. PRYCE. J. Chem. Soc. B, 337 (1970).

The adsorption, desorption, and exchange reactions of oxygen, hydrogen, and water on platinum surfaces. III. Water adsorption and exchange with oxygen and hydrogen

Y. K. PENG AND P. T. DAWSON

Chemistry Department and Institute for Materials Research, McMaster University, Hamilton, Ont., Canada L8S 4M1

Received December 30, 1976

Y. K. PENG and P. T. DAWSON. Can. J. Chem. **55**, 1658 (1977).

Ultra-high vacuum thermal desorption experiments have been carried out on the adsorption of water, and the D_2O/H and $D_2{}^{16}O/{}^{18}O$ exchange reactions on platinum previously characterized by oxygen and hydrogen adsorption studies. Water is weakly adsorbed and only at $T <$ 150 K, an observation confirmed by using H_2 adsorption as a chemical probe for the presence of adsorbed water. The thickness of the adsorbed D_2O layers was determined by a novel method involving monitoring the power output of the temperature programmer. Exchange occurs between adsorbed H and a D_2O overlayer and the extent of exchange increases with the thickness of the overlayer. Isotope distribution studies show that the surface is heterogeneous and the exchange reaction does not occur at uniform rate. Exchange occurs between adsorbed ^{18}O and a $D_2{}^{16}O$ overlayer. The extent of exchange is constant up to $T \sim 300$ K showing that D_2O is more strongly bound on O-covered Pt presumably as a result of H bonding. Heterogeneity also is apparent in the O-exchange reaction. The apparent activation energies for exchange are 1.8 and 2.9 kcal mol^{-1} for the half- and fully-covered surfaces, respectively.

Y. K. PENG et P. T. DAWSON. Can. J. Chem. **55**, 1658 (1977).

On a effectué des expériences de désorption thermique sous de très hauts vides au sujet de l'absorption de l'eau et des réactions d'échange D_2O/H et $D_2{}^{16}O/{}^{18}O$ sur du platine qui avait été caractérisé antérieurement par des études d'adsorption d'oxygène et d'hydrogène. L'eau n'est que faiblement adsorbée et uniquement à des températures < 150 K; cette observation est confirmée en faisant appel à l'adsorption de H_2 comme sonde chimique pour la présence d'eau adsorbée. On a déterminé l'épaisseur des couches de D_2O absorbé par une nouvelle méthode impliquant la mesure de la puissance fournit par le programmeur de température. Il se produit des échanges entre de l'hydrogène adsorbé et une couche superposée de D_2O et la quantité d'échange augmente avec l'épaisseur de la couche superposée. Des études de distribution isotopique montrent que la surface est hétérogène et que la réaction d'échange ne se produit pas à une vitesse uniforme. Les réactions d'échange se produisent entre du ^{18}O adsorbé et une couche superposée de $D_2{}^{16}O$. La quantité d'échange est constante jusqu'à environ 300 K ce qui démontre que le D_2O est adsorbé d'une façon plus forte sur du platine couvert d'oxygène et que ce fait résulte probablement d'un lien hydrogène. L'hétérogénéité est aussi apparente dans la réaction d'échange d'oxygène. Les énergies d'activation apparentes pour les échanges sont respectivement de 1.8 et de 2.9 kcal mol^{-1} pour les surfaces à moitié et complètement couvertes.

[Traduit par le journal]

Introduction

Platinum dispersed on oxide supports is an extremely important practical catalyst. The activity of such catalysts will be determined, in part, by the degree of dispersion of the platinum on the support, *i.e.* the number of exposed platinum atoms per unit area. This important parameter is frequently determined by titration of preadsorbed O_2 with H_2 (1–3). However, many details concerning the correct application of this method remain controversial. In particular, there is considerable disagreement concerning the correct stoichiometry to use for hydrogen chemisorption, oxygen chemisorption, and titration experiments and the relative merits of these methods for determining the dispersion (1–10). Whether or not all the oxygen adsorbed on platinum can be reduced and whether water remains strongly bound to unreacted oxygen or the support or both remain unanswered questions. An enhancement in the uptake of hydrogen by oxygen pretreatment has been inferred from infrared studies on supported catalysts (11–13) and attributed to adsorption of water on the support (11), or re-arrangement of the platinum atoms (12). However, some observations (11) have subsequently been attributed to complications caused by CO impurities (12, 13).

Infrared studies have also been interpreted by the suggestion that the reaction of oxygen with preadsorbed hydrogen produces adsorbed Pt—OH but OH is not formed by either the reverse reaction or the adsorption of water on untreated platinum (14).

In this paper, ultra-high vacuum thermal desorption mass spectrometry experiments on the adsorption of water and the exchange reactions of oxygen and hydrogen with water are described for a pure platinum sample without an oxide support. The sample used has been previously characterized by oxygen and hydrogen adsorption (15, 16). Among the conclusions drawn from this work are that water is very weakly adsorbed on pure platinum but more strongly adsorbed on oxygen-covered platinum.

Experimental Methods

Apparatus

The ultra-high vacuum system used in this work is similar to that described previously (17). The reaction cell, shown schematically in Fig. 1, can be completely immersed in liquid nitrogen. The sample filament, a 12 cm length of 0.01 in. diameter platinum wire (Johnson, Matthey, and Mallory, Grade I), equipped with 0.003 in. diameter platinum sensing leads for temperature measurement and control, was spot welded to heavy tungsten leads. This sample was from the same spool and processed in the same way as that described in papers I and II of this series (15, 16).

Gas Purification

Hydrogen was purified by diffusion through palladium. Oxygen, $^{18}O_2$, with a specified isotopic purity of 99%, was supplied in a Pyrex flask with a break–seal by Stohler Isotope Chemicals and was used without further purification.

Heavy water, D_2O, used exclusively in this work, was supplied by Thompson-Packard Inc. with an isotopic purity of 99.8%. It was pre-purified by vacuum distillation in a bakeable vacuum line and stored in a small Pyrex flask with a break–seal. After this flask had been attached to the system and the system baked out up to the break–seal, further purification was carried out by repeated freezing of the D_2O and pumping. Mass spectrometric analysis showed that D_2O purified in this manner was accompanied by considerable amounts of CO and CO_2 when admitted into the system. The CO and CO_2 may have been present in the purified D_2O or generated within the system when the D_2O came into contact with the stainless steel and glass walls of the system.

In an attempt to further purify the water it was distilled three times over potassium permanganate before carrying out the vacuum distillations described above. However, there was no improvement in the CO and CO_2 contamination level in the system.

The CO and CO_2 contamination is a complication which restricts the type of experiment which can be performed. Thus, on opening valves A and B of Fig. 1 to introduce D_2O into the system, one observes an increase in first the CO and then the CO_2 partial pressures preceding the appearance of D_2O. In such experiments the sample surface would have been contaminated with CO and CO_2 before D_2O adsorption could occur. This problem was minimized in the following way. First a small amount of D_2O was trapped at 77 K in cold finger C and any permanent gases were pumped out. Then the liquid nitrogen coolant was removed for a time period just long enough for the evaporation of CO and CO_2. This was controlled by monitoring the CO and CO_2 partial pressures in the system with the mass spectrometer. Just prior to D_2O evaporation the cold finger was again immersed in liquid nitrogen. This procedure was repeated many times until most of the CO and CO_2 had been removed. It was found that this procedure was more effective the thinner the ice layer. Prior to the introduction of D_2O into the system for dosing, the liquid nitrogen surrounding C was replaced by a Dry Ice/acetone bath. D_2O was dosed onto the platinum sample filament by evaporation from the walls of the reaction cell and thus the total dose was determined by the amount of D_2O introduced into the cell. In this work three different procedures were used to control the size of the dose; in order of increasing magnitude these were as follows:

(*I*) With C immersed in Dry Ice/acetone, valve B was opened for 5 min to allow the D_2O pressure in the cell to come to the equilibrium value corresponding to 195 K, *i.e.* $\sim 10^{-4}$ Torr. Finally, the Dry Ice/acetone bath was replaced by liquid nitrogen and the D_2O trapped for 30 min before closing valve B.

(*II*) This procedure was identical to (*I*) except for the omission of the final trapping step. Consequently the D_2O pressure in the cell was $\sim 10^{-4}$ Torr.

(*III*) The final method used was to remove the Dry Ice/acetone bath from C with valve B open for a desired period of time; this time period determined the size of the subsequent D_2O dose on the sample.

The D_2O was trapped as a thin layer on the reaction

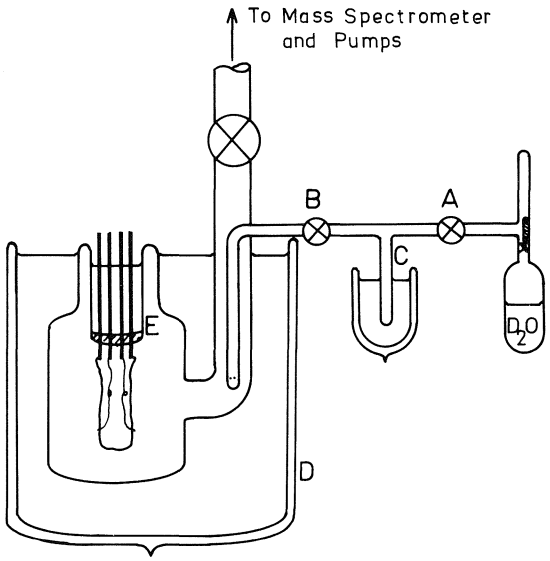

FIG. 1. Schematic diagram of the reaction cell and dosing system.

cell walls by completely surrounding the cell with liquid nitrogen in Dewar D and the procedure described above for removing CO and CO_2 was again repeated several times. Then, with the reaction cell completely immersed in liquid nitrogen, the sample filament was finally flashed clean. The sample surface was dosed with D_2O by removing the liquid nitrogen Dewar D, but leaving Dewar E filled, to keep the filament at low temperature. Consequently, more of the D_2O evaporating from the wall condensed on the larger area of the cold glass surface than on the platinum filament. Monitoring masses 28 and 44 during desorption showed that this dosing procedure successfully reduced the CO and CO_2 contamination to an acceptable level.

Results and Discussion

D_2O Adsorption on Platinum

Mass 20, D_2O, desorption spectra obtained after D_2O adsorption at several platinum filament temperatures in the range 100 to 300 K are shown in Fig. 2. These spectra were all obtained with the reaction cell walls at room temperature, but Dewar E was filled with liquid nitrogen. Consequently, desorbed water was pumped by this cold glass surface. Nevertheless some desorbed D_2O does reach the mass spectrometer as can be seen in spectra (*a*) and (*e*) for adsorption at 100 K. Spectra (*a*)–(*d*) were obtained after a relatively light dose of D_2O using procedure (*II*), *i.e.* the total amount of D_2O in the cell corresponded to a pressure of $\sim 10^{-4}$ Torr, whereas spectrum (*e*) was for a much heavier D_2O dose using procedure (*III*) with the Dry Ice/acetone bath removed for 10 min. It should be noted that a D_2O desorption peak only appears in spectra (*a*) and (*e*) for adsorption at 100 K, and that desorption occurs in the range 150–270 K. The high D_2O partial pressure during desorption caused a reduction in the mass spectrometer emission current which is partly responsible for the rapid decrease in the D_2O peak in spectrum (*e*). Mass 4 has also been monitored during these experiments and no D_2 desorption was observed. These results show that water is adsorbed weakly and nondissociatively on platinum and only at temperatures below 150 K. This is in agreement with recent field emission (18) and photoelectron spectroscopic observations (19). There is no evidence to support a strong adsorption of water at 300 K which has been deduced from contact potential measurements (20), calorimetry (1), and thermal desorption experiments (21) or assumed without verification (7).

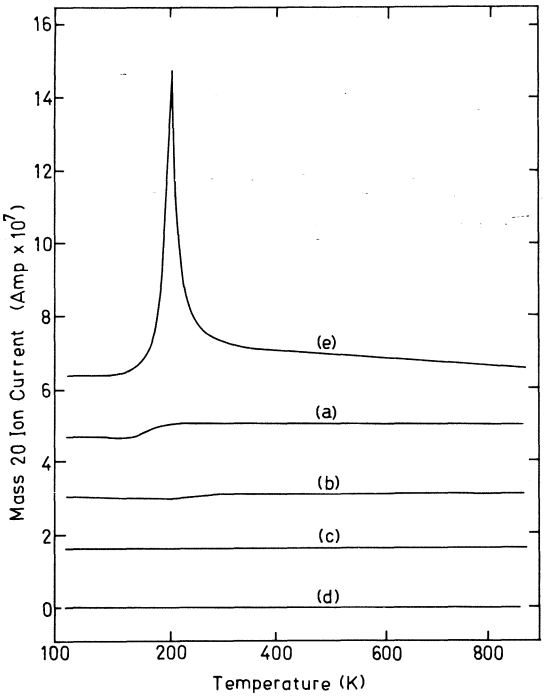

FIG. 2. I_{20}^+ desorption spectra following D_2O adsorption. Spectra (*a*) to (*d*) were for a light dose using procedure (*II*) at 100, 150, 200, and 300 K and spectrum (*e*) followed a heavy dose at 100 K using procedure (*III*) for 10 min. Heating rate 14 deg s^{-1}, curves offset.

H_2 Adsorption on Preadsorbed D_2O

In these experiments, H_2 adsorption was used as a chemical probe for the presence of D_2O on the platinum surface. The D_2O dose was carried out following procedure (*II*) in an identical manner to that used for spectra (*a*) to (*d*) of Fig. 2, but with the sample filament at $\sim$90 K in each case. The reaction cell was next surrounded by liquid nitrogen and then H_2 admitted up to a pressure of 10^{-5} Torr. The sample filament was flashed to 100, 150, 200, or 300 K for 10 s and then allowed to cool to 100 K for 4 min. After pumping out the H_2 from the cell, thermal desorption spectra were obtained with the cell walls at 77 K, monitoring masses 2, 3, and 4 simultaneously. These spectra, shown in Fig. 3, confirm the observation that water is only weakly adsorbed on a platinum surface and only at temperatures below 150 K. It can be seen that H_2 adsorption only occurs to a significant extent at 150 K and higher temperatures and thus does not take place on the D_2O-covered platinum surface. The small de-

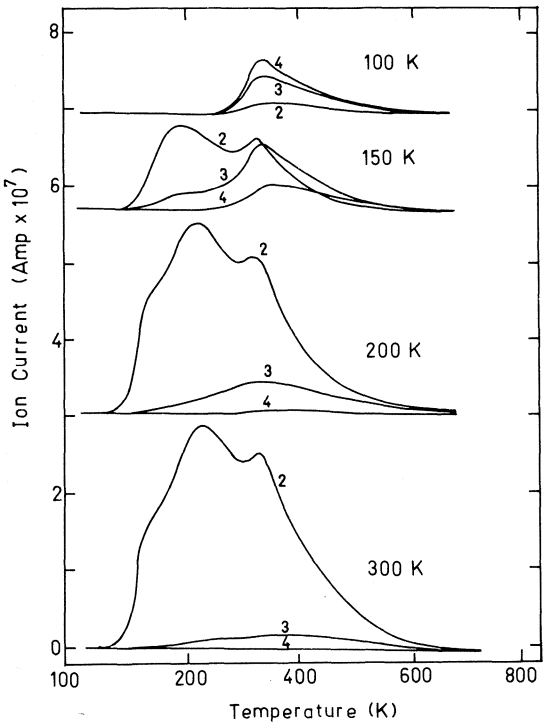

FIG. 3. I_2^+, I_3^+, and I_4^+ desorption spectra following interaction of H_2 with preadsorbed D_2O after heating to the temperatures indicated with the cell wall at 77 K. Heating rate 14 deg s^{-1}, curves offset.

sorption peaks observed after interaction at 100 K are caused by adsorption of background hydrogen gas into the β_3- and β_4-states (16) during the cooling period. This was confirmed by performing a thermal desorption experiment immediately after the filament had cooled to 100 K and without dosing either D_2O or H_2. Also note that the amount of hydrogen observed after adsorption at 150 K is much less than that at 200 K. Desorption of D_2O may be incomplete at 150 K, but the reduced H_2 adsorption is mainly caused by the nonuniform temperature of the filament. When the central portion of the filament is at 150 K the ends will be at temperatures lower than 150 K and therefore partly D_2O-covered. However, at 200 K most of the filament will be at temperatures higher than 150 K. The spectra obtained after heating to 200 K, or higher, are identical to those observed for hydrogen adsorption on clean platinum in paper II of this series (16).

The Thickness of the D_2O Adlayers

The mass 20 desorption spectra of Fig. 2 show qualitatively that D_2O adsorbs on platinum at 100 K and desorbs at temperatures above 150 K, but it would be impossible to analyse these spectra quantitatively to determine the total amount of D_2O desorbing; nor does the dosing method permit the size of the dose to be determined. Fortunately there is an alternative method which can be used to estimate the thickness of the D_2O layers by monitoring the power output of the Kelvin double bridge during desorption. The bridge is programmed to increase the resistance, and hence the temperature, of the central section of the Pt filament linearly with time. The potential drop across the central section, *viz.* IR where R is its resistance and I the current through the filament, is shown as a function of time (temperature) in Fig. 4. Curve

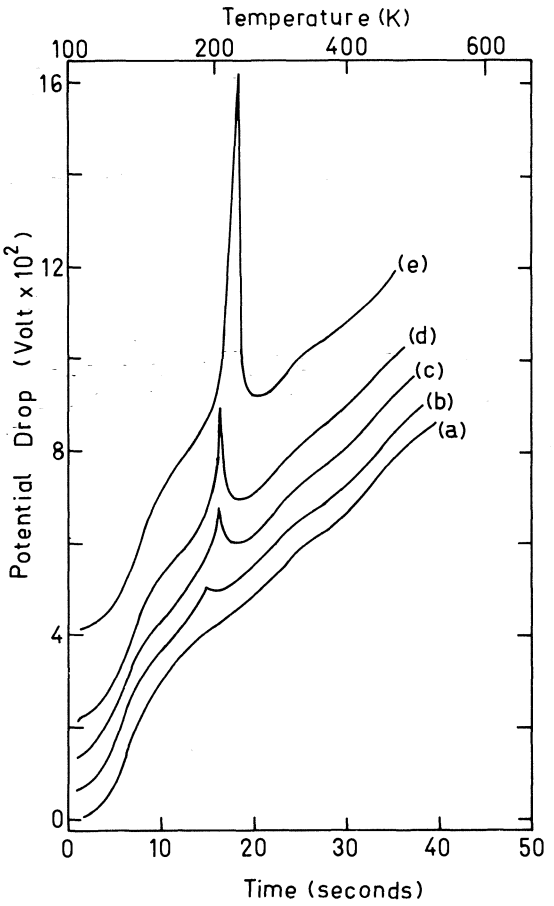

FIG. 4. Potential drop across the central portion of the filament as a function of time (temperature) during the heating of (*a*) a clean surface and also after adsorbing D_2O at 100 K using procedure (*III*) for (*b*) 1, (*c*) 2, (*d*) 3, and (*e*) 10 min. Curves are offset.

(*a*) is for the clean Pt filament. The energy required to desorb an adlayer would place an additional power requirement on the bridge but for monolayer amounts this would be below the detection limit. Curves (*b*)–(*e*) show the corresponding *IR vs.* time curves for steadily increasing D_2O doses, using procedure (*III*) with the Dry Ice/acetone bath removed from cold finger C for 1, 2, 3, and 10 min for spectra (*b*) to (*e*) of Fig. 4 respectively. Clearly there is an increased power requirement over the temperature range where D_2O desorbs, 150–270 K (Fig. 2), and thus the D_2O layer must be quite thick in these experiments. From the measured *IR vs. t* and the known *R vs. t* temperature programme the increased power (I^2R) required to desorb the D_2O layer can be determined. Then from the heat capacity of ice it is an easy matter to calculate the amount of D_2O desorbed and hence estimate the thickness of the ice layer. For the experiments shown in Fig. 4, this thickness varies from $\sim$100 layers for curve (*b*) to $\sim 10^4$ layers for curve (*e*). It is not possible to estimate the magnitude of the lighter doses obtained using procedures (*I*) and (*II*).

The H_2–D_2O Exchange Reaction

A major objective of this study was to obtain information which would improve our understanding of the H_2–D_2O exchange reaction. Conventional approaches in which the rate of production of some species in the gas phase is measured when D_2O interacts with preadsorbed H_2 are complicated by the CO and CO_2 contamination problem. To minimize this problem the sample surface was flash cleaned with the whole reaction vessel immersed in liquid nitrogen and then saturated with H_2 by allowing the filament to cool in an H_2 ambient. Then the D_2O dose was allowed to evaporate from the reaction vessel walls in the manner already described. Blank experiments confirmed that CO does not replace preadsorbed H_2. The extent of the H_2–D_2O exchange was followed by determining the surface isotope composition by thermal desorption.

(a) H_2–D_2O Exchange at 100 K

Following interaction of D_2O with the preadsorbed H adlayer at 100 K, the reaction cell was again cooled in liquid nitrogen. Just prior to commencing the thermal desorption Dewar D was again removed, and during desorption mass 2, 3, or 4 was monitored. It was necessary to obtain the mass 2, 3, and 4 spectra in separate experiments because the spectra contained sharp peaks.

For the spectra shown in Fig. 5, the saturated H adlayer was obtained by adsorbing H_2 at a pressure of 10^{-5} Torr for 4 min with the Pt filament at 100 K. The light D_2O dose was produced using procedure (*II*), *i.e.* the same magnitude as used for spectra (*a*)–(*d*) of Fig. 2. In Fig. 5, the H_2, HD, and D_2 desorption spectra obtained from the H adlayer with a D_2O overlayer can be compared with the H_2 spectrum obtained when H_2 alone was adsorbed on the filament which is shown as a dashed curve. For the D_2O overlayer situation the hydrogen desorption spectra, especially mass 2, have a remarkably sharp peak which coincides with the temperature range over which D_2O evaporates (Figs. 2 and 4) and has a peak maximum temperature at $\sim$188 K. Quite clearly what has happened is that the D_2O overlayer acts as an ice-cap which prevents most of the low temperature H_2 desorption. Once the ice-cap is removed, all the weakly adsorbed hydrogen

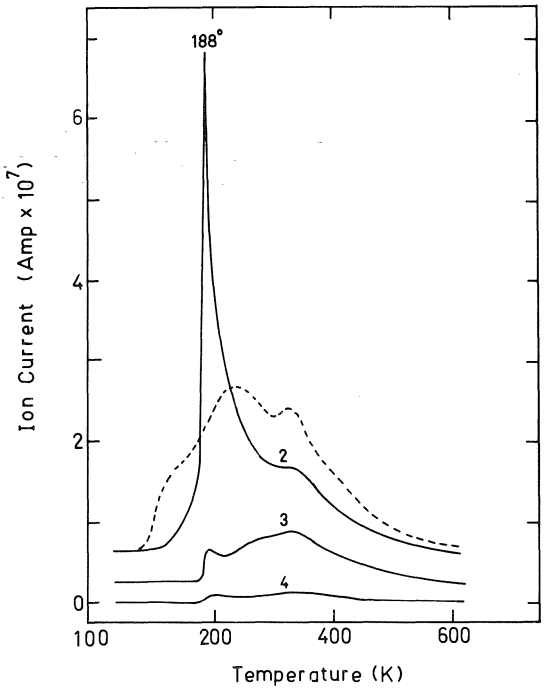

FIG. 5. H/D_2O exchange reaction. Hydrogen was adsorbed at 10^{-5} Torr for 4 min at 100 K followed by a light D_2O dose using procedure (*II*). The H_2, HD, and D_2 desorption spectra were obtained in separate experiments using a heating rate of 14 deg s^{-1}. Curves are offset.

will desorb extremely rapidly and produce the spike observed. It is stressed that since the reaction cell is immersed in liquid nitrogen for these experiments, no D_2O reaches the mass spectrometer and so no drop in electron emission current complicates the interpretation of these results (*cf.* Fig. 2).

The HD and D_2, mass 3 and 4, desorption spectra show that an exchange reaction between the preadsorbed H adlayer and the D_2O overlayer has taken place. In this experiment the extent of the exchange was 27.2%. The D_2O overlayer was relatively thin for the experiments of Fig. 5. As can be seen from the curves of Fig. 4, the thicker the D_2O overlayer the longer is the time required for desorption of the D_2O. Thus it seemed feasible to study the extent of exchange as a function of D_2O overlayer thickness. For thicker overlayers, the contact time between the H adlayer and D_2O overlayer would be increased and extended to higher temperatures and thus might increase the extent of exchange.

In Fig. 6, curve (*a*) is a mass 2 spectrum produced when procedure (*I*) was used to produce the D_2O overlayer. This procedure gives an even lighter dose than procedure (*II*) used for the experiments of Fig. 5 and thus, as expected, the peak maximum is at a lower temperature. For curves (*b*) and (*c*) of Fig. 6, procedure (*III*) was used to produce thicker D_2O overlayers and this produces a steadily increasing peak maximum temperature; peaks (*a*) and (*c*) are 50 K apart. In addition to the peak maximum shift, the thicker D_2O overlayers result in a steadily decreasing amount of preadsorbed H_2 desorbing as H_2, *viz.* the extent of exchange increases. This is confirmed by monitoring the HD and D_2 desorption spectra in addition to that of H_2 as shown in Fig. 7 for the same D_2O overlayer thickness as that for spectrum 6(*c*). For these conditions, the extent of exchange has increased to slightly more than 50%. Thus for thicker D_2O overlayers, the preadsorbed H is forced to stay longer on the surface. This not only increases the time interval during which exchange can take place, but also allows the reaction to proceed at higher temperatures.

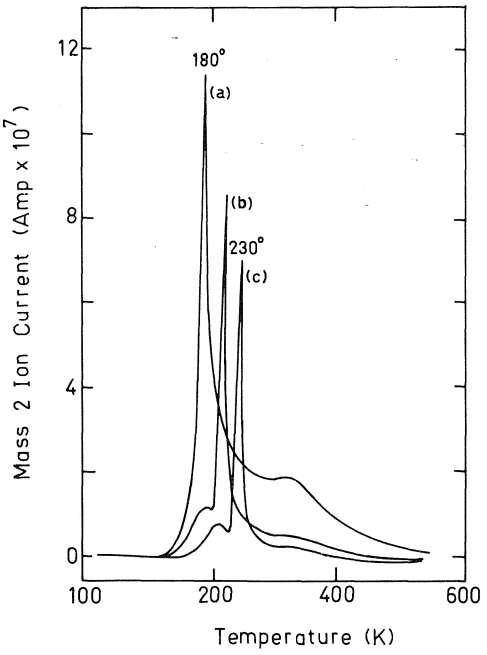

FIG. 6. I_2^+ desorption spectra for H adlayers with D_2O overlayers of varying thickness at 100 K, *cf.* Fig. 5. Curve (*a*) is for a lighter dose using procedure (*I*) whereas curves (*b*) and (*c*) were for procedure (*III*) for 1.5 and 8 min respectively. Heating rate was 14 deg s^{-1}.

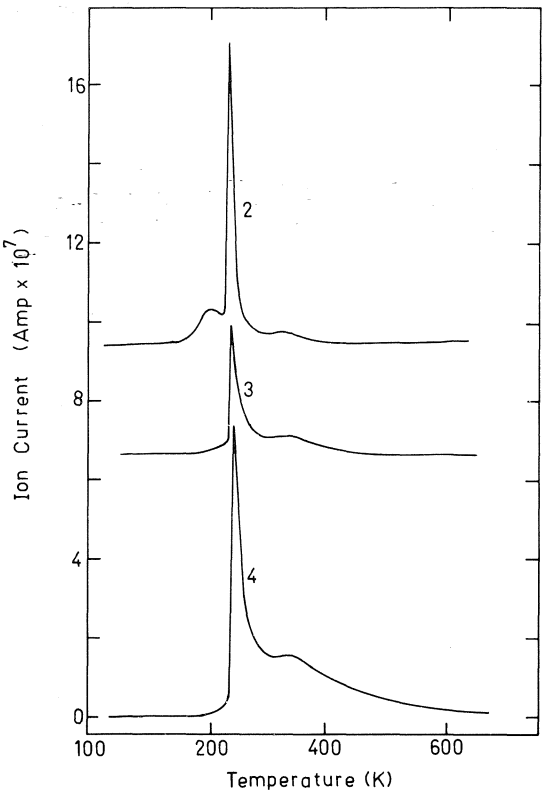

FIG. 7. The mass 2, 3, and 4 desorption spectra for the same experiment as Fig. 6(*c*). Curves are offset.

The mass 2, 3, and 4 spectra of Fig. 7 do not have identical shapes. Furthermore, the amounts of H_2, HD, and D_2 desorbing do not always correspond to the equilibrium statistical distribution of isotopes. For the hydrogens desorbing in the spike, it appears as though the exchange has proceeded beyond statistical in that the HD component is less than one-half of both the H_2 and D_2 components. Undoubtedly this is the result of surface heterogeneity and can be accounted for by a similar explanation to that proposed for the H_2/D_2 exchange reaction reported in paper II of this series (16). On some planes the exchange reaction

$$H_2 + D_2O \rightarrow D_2 + H_2O$$

may be rapid and, in view of the excess D_2O in the system, proceed close to completion. On other planes, exchange may be very slow and the H_2 will desorb substantially unexchanged. The reaction

$$H_2 + D_2O \rightarrow HD + HDO$$

represents an intermediate case. It has already been documented (16) that at the spike temperature the H_2/D_2 exchange reaction is incomplete, and thus the distribution of isotopes observed in Fig. 7 can be understood. Note also that exchange of the hydrogen desorbing at temperatures above that of the spike is more complete and closer to a statistical distribution. This can be also understood in terms of greater H_2–D_2O exchange rates and greater mobility for the adsorbed hydrogen at the higher temperatures (16).

(b) H_2–D_2O Exchange at 150 K

In these experiments the platinum surface was saturated with H_2 at 150 K and then allowed to interact with D_2O desorbing from the reaction vessel walls, in the same manner as for the 100 K exchange experiments. Of course at 150 K the D_2O will not remain on the surface. Figure 8 shows the mass 2, 3, and 4 spectra, monitored simultaneously, for a D_2O dose obtained using procedure (*II*), *i.e.* the same as for Fig. 2 (*a*)–(*d*) and Fig. 5. Also shown in Fig. 8, as a dashed curve, is the desorption spectrum obtained from a pure H adlayer at 150 K.

In this experiment the H + D_2O exchange reaction can take place only during the dosing, and therefore at 150 K. The total amount of exchange is 16.3% and is comparable, apart from the low temperature H_2 desorption which occurs in the mass 2 spike, with that observed in Fig. 5 at 100 K for the same total D_2O dose.

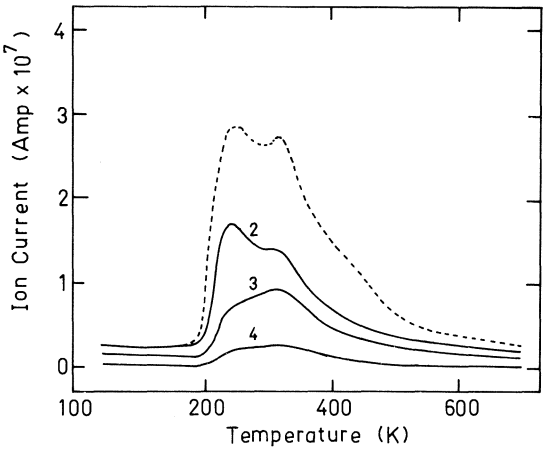

FIG. 8. Mass 2, 3, and 4 desorption spectra following the interaction of D_2O with a saturated H adlayer at 150 K. The D_2O dose was produced using procedure (*II*). The dashed curve shows the desorption spectrum obtained from a pure H adlayer at 150 K. Heating rate 14 deg s^{-1}. Curves are offset.

The ^{18}O–$D_2{}^{16}O$ Exchange Reaction

In these experiments oxygen, $^{18}O_2$, was preadsorbed on the platinum surface and then $D_2{}^{16}O$ was allowed to interact with the preadsorbed ^{18}O by evaporation from the reaction cell walls in the manner already described. This interaction was investigated at different filament temperatures in the range 150–500 K and for two different initial ^{18}O coverages, $N_{18}{}^0 = 3.4 \times 10^{14}$ and $N_{18}{}^0 = 1.6 \times 10^{14}$ atoms cm^{-2} which represent saturated and about half-saturated adlayers respectively (15). An identical $D_2{}^{16}O$ dose was used for each experiment, using procedure (*III*), removing the Dry Ice/acetone bath for 3 min. Oxygen desorption spectra were obtained by monitoring masses 32, 34, and 36 simultaneously. A typical example is shown in Fig. 9 for the interaction of $D_2{}^{16}O$ with a saturated ^{18}O adlayer at 400 K. In this example, the amount of ^{16}O exchanged is 27.3% and the isotopes desorb in a ratio which approximates a statistical distribution. The extent of exchange at different temperatures for the two initial ^{18}O coverages is shown in Fig. 10.

These results have several interesting features.

(*1*) The exchange reaction

$$^{18}O(a) + D_2{}^{16}O(g) \rightarrow {}^{16}O(a) + D_2{}^{18}O$$

does take place.

(*2*) Up to 300 K, the amount of oxygen being exchanged is independent of temperature, but above 300 K the extent of exchange increases considerably with temperature.

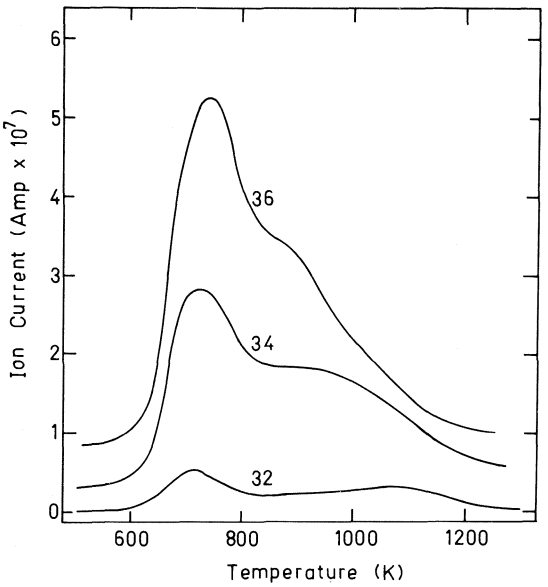

FIG. 9. $^{18}O/D_2{}^{16}O$ exchange reaction. A $D_2{}^{16}O$ dose interacted with a saturated ^{18}O adlayer using procedure (*III*) for 3 min at 400 K. The mass 32, 34, and 36 desorption spectra were obtained simultaneously with a heating rate of 14 deg s^{-1}. Curves are offset.

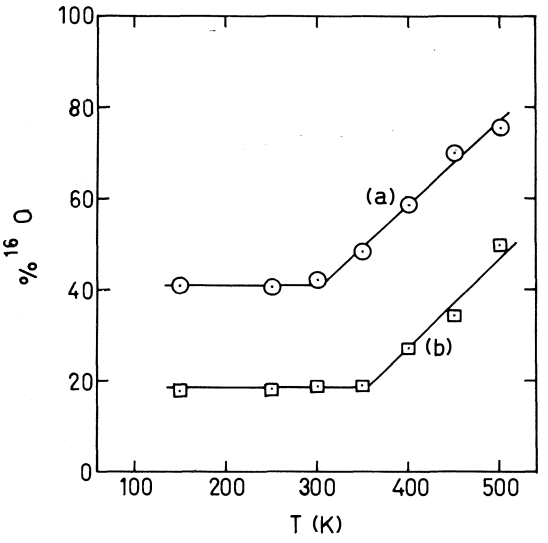

FIG. 10. Percentage ^{16}O in desorption spectra following $^{18}O/D_2{}^{16}O$ exchange experiments typified by Fig. 9 for temperatures in the range 150–500 K and for (*a*) half- and (*b*) fully-saturated ^{18}O adlayers.

(*3*) The % ^{16}O in the desorbing gas for the saturated ^{18}O adlayer is close to one-half that for the half-coverage ^{18}O adlayer. Thus, the actual amount of ^{18}O being exchanged is the same for both ^{18}O coverages. This could imply, most simply, that it is the more tightly bound oxygen which exchanges most rapidly.

The temperature independence of the amount of oxygen being exchanged in the range 150 to 300 K is surprising. If the D_2O does not remain on the surface above 150 K, as already documented for the clean or H-covered surfaces, then it is difficult to understand why the extent of exchange does not increase with temperature in this range. The constant amount of exchange must mean that D_2O is stable on the oxygen-covered surface at least up to 300 K and that the exchange reaction takes place during thermal desorption, prior to desorption of the D_2O at ~300 K. Above 300 K, most of the exchange reaction takes place during dosing, *i.e.* D_2O is not adsorbed, since the extent of exchange does increase with temperature.

In view of the hydrogen bonding possibilities between D_2O and strongly adsorbed oxygen atoms, it is not surprising that preadsorbed oxygen stabilizes the D_2O adlayer.

It is possible to estimate the activation energy for ^{18}O–$D_2{}^{16}O$ exchange from the temperature dependence of the exchange rate for $T > 300$ K. Thus the rate at which ^{16}O is incorporated into the oxygen adlayer can be expressed as

$$\frac{dN_{16}}{dt} = kP_{D_2O}N_{18} = kP_{D_2O}(N_{18}{}^0 - N_{16})$$

where N_{16} and N_{18} are the numbers of ^{16}O and ^{18}O atoms cm^{-2} and $N_{18}{}^0$ is the initial ^{18}O coverage. This rate expression can be integrated to give

$$\ln\left(1 - \frac{N_{16}}{N_{18}{}^0}\right)^{-1} = k\int_0^t P_{D_2O}\,dt = kX$$

where X represents the integrated $D_2{}^{16}O$ dose which is constant for all experiments. If the apparent rate constant, k, is expressed in the usual Arrhenius form, the apparent activation energy for the exchange reaction, $E^{\ddagger}$, can be obtained from the slope of a plot of ln $\{\ln [1 - (N_{16}/N_{18}{}^0)]^{-1}\}$ *vs.* $1/T$. This plot is shown in Fig. 11. The apparent activation energies are 1.8 kcal mol^{-1} for the half-saturated and 2.9 kcal mol^{-1} for the saturated ^{18}O adlayers. A lower activation energy for the half-saturated ^{18}O adlayer suggests that a configuration in which the adsorbed water molecule can interact with both platinum and adsorbed oxygen is more favourable for exchange.

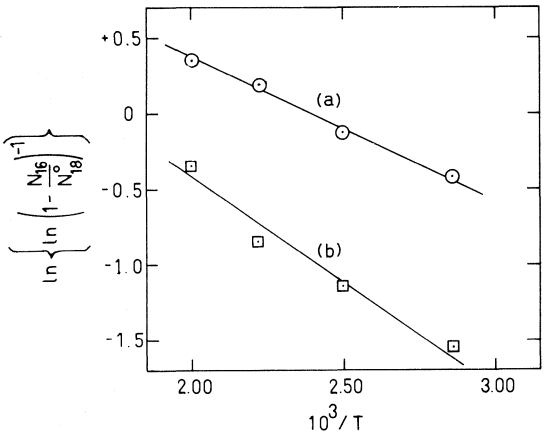

FIG. 11. Arrhenius plot for the data of Fig. 10. The apparent activation energies for $^{18}O/D_2{}^{16}O$ exchange are 1.8 and 2.9 kcal mol^{-1} for the half- and fully-oxygen covered surfaces, (*a*) and (*b*) respectively.

Conclusions

(*1*) Water adsorbs only weakly on clean unsupported platinum and desorbs at temperatures above ~150 K. Hydrogen does not adsorb on the water-covered surface.

(*2*) When D_2O is adsorbed into overlayers of varying thickness onto preadsorbed H, an H/D exchange reaction does take place. The thicker the overlayer, the longer the time and the higher the temperature at which exchange can take place, resulting in an increase in the extent of exchange. The isotope distributions show that the surface is heterogeneous and that exchange takes place at different rates on different areas.

(*3*) $D_2{}^{16}O$ adsorbed into an overlayer on preadsorbed ^{18}O also results in an $^{16}O/^{18}O$ exchange reaction. The constant extent of exchange up to ~300 K shows that water is more strongly adsorbed onto oxygen-covered compared with clean platinum surfaces. The measured activation energies for exchange are 1.8 for half- and 2.9 kcal mol^{-1} for fully-O-covered surfaces. The number of ^{18}O atoms exchanged under given conditions is the same for half and fully saturated ^{18}O adlayers and thus heterogeneity also plays a role in $^{18}O/D_2{}^{16}O$ exchange.

Acknowledgements

The authors wish to thank the National Research Council of Canada and Atomic Energy of Canada Limited, Chalk River Nuclear Laboratories, for their support of this research.

1. H. CHON, R. A. FISHER, E. TOMEZSKO, and J. G. ASTON. Proc. 2nd Congress on Catalysis, Paris, **1**, 217 (1961).
2. H. L. GRUBER. J. Phys. Chem. **66**, 48 (1962).
3. J. E. BENSON and M. BOUDART. J. Catal. **4**, 704 (1965).
4. D. E. MEARS and R. C. HANSFORD. J. Catal. **9**, 125 (1967).
5. G. R. WILSON and W. K. HALL. J. Catal. **17**, 190 (1970); **24**, 306 (1972).
6. Y. BARBAUX, B. ROGER, J-P. BEAUFILS, and J. E. GERMAIN. J. Chim. Phys. **67**, 1035 (1970).
7. M. AKHTAR and F. C. TOMPKINS. Trans. Faraday Soc. **67**, 2454 (1971); **67**, 2461 (1971).
8. J. FREEL. J. Catal. **25**, 149 (1972).
9. R. A. DALLABETTA and M. BOUDART. Proc. 5th Congress on Catalysis, Miami Beach, **2**, 1329 (1973).
10. L. T. DIXON, R. BARTH, R. J. KOKES, and J. W. GRYDER. J. Catal. **37**, 376 (1975).
11. D. D. ELEY, D. M. MORAN, and C. H. ROCHESTER. Trans. Faraday Soc. **64**, 2168 (1968).
12. D. J. DARENSBOURG and R. P. EISHENS, Proc. 5th Congress on Catalysis, Miami Beach, **1**, 371 (1972).
13. L. T. DIXON, R. BARTH, and J. W. GRYDER. J. Catal. **37**, 368 (1975).
14. B. A. MORROW and P. RAMAMURTHY. J. Phys. Chem. **77**, 3052 (1973).
15. Y. K. PENG and P. T. DAWSON. Can. J. Chem. **52**, 3507 (1974).
16. Y. K. PENG and P. T. DAWSON. Can. J. Chem. **53**, 298 (1975).
17. Y. K. PENG and P. T. DAWSON. J. Chem. Phys. **54**, 950 (1971).
18. V. V. GORODETSKI and V. I. SARCHENKO. Proc. 5th Congress on Catalysis, **1**, 527 (1972).
19. P. R. NORTON. J. Catal. **36**, 211 (1975).
20. C. W. JOWETT, P. J. DOBSON, and B. J. HOPKINS. Surf. Sci. **17**, 474 (1969).
21. F. P. NETZER and G. KNERINGER. Surf. Sci. **51**, 526 (1975).

Synthesis, ion-exchange properties, and analytical applications of thermally stable tin(IV) vanadate

MOHSIN QURESHI, SYED ASHFAQ NABI, AND NIGHAT ZEHRA

Department of Chemistry, Aligarh Muslim University, Aligarh-202001, India

Received April 2, 1976[1]

MOHSIN QURESHI, SYED ASHFAQ NABI, and NIGHAT ZEHRA. Can. J. Chem. **55**, 1667 (1977).

Samples of stannic vanadate have been synthesized by varying the mixing ratio of the reagents and p*H* of the mixture. The most stable sample has been synthesized by mixing 0.25 *M* solutions of stannic chloride and sodium metavanadate in the ratio of 2:3 at p*H* 2.5. The material behaves as a weak cation exchanger. This sample has been critically studied for its ion-exchange, chemical, and thermal behaviour. The analytical utility of the material has been demonstrated by achieving some binary separations of metal ions on its column. Arsenate has also been quantitatively removed from a mixture of tungstate, phosphate, and antimonate.

MOHSIN QURESHI, SYED ASHFAQ NABI et NIGHAT ZEHRA. Can. J. Chem. **55**, 1667 (1977).

On a synthétisé des échantillons de vanadate stannique faisant varier le rapport des réactifs mélangés et le p*H* du mélange. L'échantillon le plus stable a été synthétisé en mélangeant des solutions 0.25 *M* de chlorure stannique et métavanadate de sodium dans un rapport de 2:3 à un p*H* 2.5. Le composé se comporte comme un échangeur faible de cations. Cet échantillon a été étudié d'une façon critique pour son comportement comme échangeur d'ions et ses comportements chimique et thermique. On démontre l'utilité analytique de ce composé en effectuant quelques séparations binaires d'ions métalliques sur cette colonne. On a aussi pu enlever d'une façon quantitative l'arsénate à partir d'un mélange de tungstate, de phosphate et d'antimonate.

[Traduit par le journal]

Introduction

Synthetic inorganic ion-exchangers are receiving increasing attention owing to their thermal stability and resistance to radiations. The recent work in this field has been well summarized in the various reviews and monographs (1–3). The selectivity and ion-exchange properties of a material depend considerably on its chemical composition. It is, therefore, always interesting to synthesize new materials and to study their ion-exchange behaviour. Moreover, numerous attempts have been made to study the cation adsorption behaviour of insoluble solids, but very few studies have been made on their anion adsorption properties. In the case of our systematic studies on inorganic ion-exchangers, we found that stannic vanadate selectivity adsorbs the arsenate. Vanadates have not been studied in detail as ion-exchangers. The few studies on the vanadates as ion-exchangers have been summarized recently in the communication on titanium vanadate (4) from this laboratory. As no work on stannic vanadate has been reported so far, hence the present study was taken up.

[1]Revision received January 14, 1977.

Experimental

Reagents

Tin(IV) chloride pentahydrate (Poland) and sodium metavanadate (BDH, England) were used for the synthesis of samples. All other reagents were of AnalaR grade.

Synthesis

Tin(IV) vanadate samples were synthesized by adding 0.25 *M* sodium metavanadate solution in portions to 0.25 *M* solution of tin(IV) chloride with continuous stirring at room temperature (23 ± 3°C). Turbidity appeared in the beginning. The precipitation seemed to increase on subsequent additions of sodium metavanadate solution; when the addition of sodium metavanadate was completed, the p*H* of the mixture was adjusted to the required values by adding either sodium hydroxide or hydrochloric acid solution. The precipitate was allowed to stand for 24 h in the mother liquor. The exact conditions for the synthesis of various samples are given in Table 1. The precipitate was then washed by decantation with demineralized water and finally filtered under suction. The products so obtained were dried at the desired temperatures as indicated in Tables 1 and 2. The dried product on immersing in water gave fine granules which may contain a mixture of Na^+ and H^+ as counter ions. To get the exchanger completely into the H^+ form, the granules were treated with 2 *M* nitric acid in the usual manner (5).

Apparatus

Spectrophotometric, p*H*-metric, and ir studies were performed on the Bausch and Lomb Spectronic-20

TABLE 1. Conditions of synthesis and properties of stannic vanadate samples dried at 40°C*

Sample No.	Mixing ratio (ml) SC:SV	p*H* of mixture	Colour of the dried product	Ion-exchange capacity for K^+ (mequiv/g) p*H* = 6	Chemical composition mol ratio (Sn/V)	Dissolution of the material (mg/50 ml solvent)					
						DMW		2 *M* HNO_3		Formic acid	
						Sn	V	Sn	V	Sn	V
1	1:9	2.5	Greenish-brown	0.80	1.2	0.03	0.51	0.80	3.5	0.00	1.00
2	2:8	2.5	Light brown	0.82	1.2	0.13	0.51	2.5	5.4	0.00	1.50
3	3:7	2.5	Brown	0.78	1.3	0.06	0.47	0.8	1.7	0.00	0.60
4	4:6	2.5	Dark brown	0.85	1.2	0.00	0.04	0.16	0.50	0.05	0.80
5	5:5	2.5	Yellowish-orange	0.66	1.5	0.00	0.04	0.67	0.50	0.00	0.00
6	6:4	2.0	Yellowish-orange	0.60	1.5	0.43	0.00	1.45	9.98	0.00	1.65
7	7:3	2.5	Yellowish-orange	0.60	1.5	0.25	0.50	3.35	8.25	0.22	2.00
8	8:2	2.5	Yellow	0.50	1.6	0.45	4.5	5.00	35.00	0.50	1.65
9†	2:3	2.5	Dark brown	—	—	—	—	—	—	—	—
10	2:3	7.0	Yellowish-orange	0.40	2.8	—	—	—	—	—	—
11	2:3	9.0	Yellowish-orange	0.30	3.0	—	—	—	—	—	—

*SC = stannic chloride, SV = sodium vanadate, DMW = demineralized water.
†Refluxed in excess of sodium vanadate solution (unstable product).

TABLE 2. Effect of drying temperature on ion-exchange capacity of stannic vanadate (sample 4)

Drying temperature (°C)	Colour	Ion-exchange capacity for K^+ (p*H* = 6) (mequiv/g)
40	Brown	0.85
100	Greenish-yellow	0.82
200	Yellowish-green	0.80
400	Green	0.36
700	Dark green	0.10

colorimeter, the Elico p*H* meter model LI-10, and the Perkin Elmer model 137 spectrophotometer respectively. Thermogravimetric analysis was performed on the Stanton thermobalance type H_4. For shaking an electric temperature-controlled Sico Shaker was used.

Analytical Procedure

The Sn(IV) vanadate samples were converted into the H^+ form and then analysed for tin and vanadium. For this purpose 200 mg of the sample was dissolved in concentrated hydrochloric acid. Tin was determined gravimetrically as stannic oxide (ref. 6, p. 1077) and vanadium titrimetrically using potassium permanganate as the titrant (ref. 6, p. 1211). The chemical dissolution was determined by treating a 500 mg sample with 50 ml of the desired solvent. The mixture was then shaken for 6 h in a shaker incubator at room temperature. The amounts of tin and vanadium released in the solution were determined spectrophotometrically using phenyl fluorone (ref. 7, p. 862) and hydrogen peroxide (ref. 7, p. 930) respectively.

Thermal Treatment

Tin(IV) vanadate (sample 4) was dried at different temperatures (Muffle furnace was used for drying at higher temperature) to observe the effect of the drying temperature on the composition and ion-exchange capacity of the sample. Figure 1 shows thermograms of stannic vanadate in the H^+ and K^+ form at the heating rate of 4°C/min.

Infrared Spectra

Infrared absorption spectra were obtained by the KBr disc technique.

pH Titrations

p*H* titrations of the samples in the H^+ form were performed with KCl–KOH and LiCl–LiOH systems by the usual method (8).

Ion-Exchange Capacity

Ion-exchange capacity of various samples of stannic vanadate was determined by the standard column technique (9) at p*H* = 6. The effect of the drying temperature of the product on exchange capacity was also studied. The results are summarized in Tables 1–3.

Sorption Studies

For distribution studies 500 mg of the exchanger in the H^+ form was equilibrated with 50 ml of the required solvent containing the ion under study in an Erlenmeyer flask. The temperature of the shaker was maintained as desired. The amount of metal ions before and after equilibrium was determined by titration with 0.002 *M*

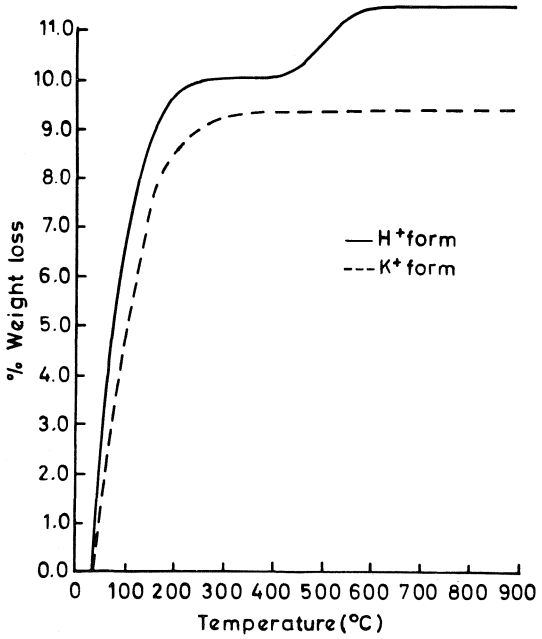

FIG. 1. Thermograms of stannic vanadate (sample 4). (—) H^+ form, (---) K^+ form.

TABLE 3. Ion-exchange capacity of stannic vanadate (sample 4) at pH = 6 for some univalent and bivalent cations

Ion	Hydrated radii (Å)	Ion-exchange capacity (mequiv/g)
Li^+	3.0	0.70
Na^+	2.0	0.78
K^+	1.5	0.85
Mg^{2+}	4.0	0.57
Ca^{2+}	3.0	0.60
Sr^{2+}	2.5	0.75
Ba^{2+}	2.5	0.73

solution of the disodium salt of EDTA. The determinations of arsenate (ref. 7, p. 286), phosphate (ref. 6, p. 819), antimonate (ref. 7, p. 258), and tungstate (ref. 7, p. 886) were done spectrophotometrically. The distribution coefficients were calculated according to the usual formula (4). To study the effect of temperature on the ion-exchange selectivity, the exchange reaction was also carried out in 10^{-3} M HNO_3 at temperatures 25, 40, 60, and 80°C.

Separations

For separation studies, a glass column (id 3.9 mm) filled with 1.5–2.0 g of stannic vanadate in H^+ form on glass wool support was used. The rate of flow of the effluent in all the separations studied was 0.5–0.8 ml/min.

Metal Ion Separations

Binary, separations of Pb^{2+} (400–1360 μg) from Zn^{2+} (1000–2000 μg), Mn^{2+} (800–2000 μg), and Ca^{2+} (500–2000 μg) were achieved quantitatively. The metal ions mixture was poured into the column. It was then allowed to pass through the exchanger with a very slow rate. Then the metal ions absorbed in the exchanger phase were eluted with appropriate eluting reagent Ca^{2+} (500–2000 μg) was also separated from Mg^{2+} (400–1500 μg) in the same manner. The elution curves and the eluting reagents are given in Fig. 3.

Anion Separations

Different amounts of arsenate (100–1000 μg) were quantitatively separated from phosphate, antimonate, and tungstate (200–2000 μg) on a 1 g exchanger column. The procedure was the same as described above. The anions other than arsenate were eluted with demineralized water. Arsenate was also quantitatively removed from a synthetic mixture of phosphate, tungstate, and antimonate.

Results and Discussion

Figure 1 shows the thermograms of stannic vanadate in the H^+ and K^+ forms. It is apparent from the curve for the exchanger in the H^+ form that the exchanger suffers continuous loss in weight, when it is heated to 210°C. The weight becomes constant in the temperature range 210–400°C. The loss in weight is again observed when the temperature is raised further. This continues up to 570°C. No further weight loss is observed beyond this temperature. Therefore the thermogram of stannic vanadate clearly suggests that the loss in weight up to 210°C is due to the removal of external water molecules. The stability of the exchanger is quite significant in the temperature range 210–400°C. When the temperature exceeds 400°C, condensation of OH groups begins resulting in the removal of water molecules. This removal is complete at 570°C. Above this temperature weight remains constant due to the conversion of the material into the oxides. These facts are also well supported by the data on ion-exchange capacity of the exchanger dried at different temperatures (Table 2). It is clear from these observations that there is no change in the capacity when the exchanger is dried at 200°C. The removal of external water molecules has no effect on the exchange capacity. However, when the drying temperature is increased above 400°C, the gradual loss in ion-exchange capacity is observed, as the condensation of OH groups starts. The exchange capacity sharply falls to a negligible value (0.10 mequiv/g) when the drying temperature of the product is 700°C. The thermogram of stannic vanadate in the K^+ form suffers less weight loss than in the H^+ form and shows only one break. After the removal of external

water molecules the weight becomes almost constant. The weight loss due to the removal of internal water molecules is not observed as the condensation is not possible in this case. Therefore the hydroxyl group attached to vanadium is most probably responsible for the cation exchange behaviour of stannic vanadate. This is also supported by the chemical composition data (Table 1). The exchange capacity increased with increase in their vanadium content of the product.

It may be easily inferred from Table 1 that in the preparation of stannic vanadate, variation in the mixing ratio of stannic chloride and sodium vanadate does not have any significant effect on the chemical composition and the ion-exchange capacity of the product, if the p*H* of the mixture is kept constant. However, if the preparation is done in the neutral or basic medium the tin content in the final product is increased. This is probably due to the formation of some stannic hydroxide at higher p*H* values, causing a considerable decrease in the capacity of the sample.

Stannic vanadate is apparently fairly stable in various solvents such as dilute mineral acids, acetic acid, formic acid, dilute alkalies, acetone, alcohols. It is apparent from the chemical dissolution studies of this material with water, dilute nitric acid, and formic acid (Table 1) that stannic vanadate is much more chemically stable than titanium vanadate (4).

A comparison of the effect of drying temperatures on the ion-exchange capacity for some inorganic ion exchangers reveals that stannic vanadate is superior to other ion exchangers as it retains almost 100% exchange capacity up to 200°C. However, the capacity starts decreasing when the drying temperature is further increased. But in fact it shows sufficient ion-exchange capacity even when the drying temperature is raised to 400°C (0.36 mequiv/g). On the other hand, stannic tungstate (10), stannic molybdate (5), titanium selenite (11), titanium arsenate (12), and titanium tungstate (13) lose their capacity sharply as the drying temperature increases and the exchange capacity becomes negligible when the temperature reaches 200°C.

p*H* titration curves apparently show only one inflexion point. Initially when KCl is added in the absence of KOH there is a sharp decrease in p*H* due to the release of hydrogen ions. On the addition of the base, the p*H* increases rapidly, and above p*H* 9 the exchanger begins to hydrolyse. It is also evident from Fig. 2 that in the acidic medium the uptake of the K^+ ion is greater than that of the Li^+ ion. However, the situation is reversed in the p*H* range 7–10.5. The capacity of stannic vanadate increases with increase in p*H* as expected. This is because as the hydrogen ion concentration is increased the exchange reaction tends to proceed in the reverse direction and therefore the adsorption of the metal ions on the exchanger is decreased.

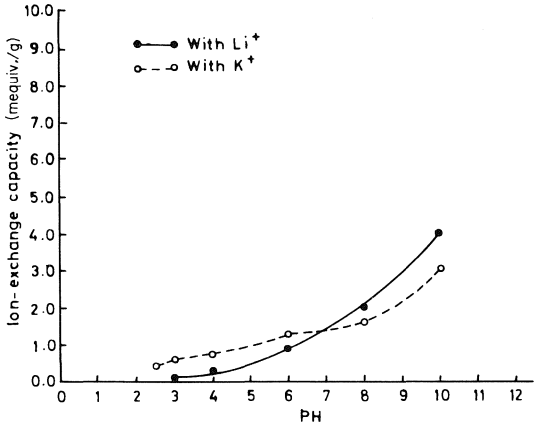

FIG. 2. Ion-exchange capacity as a function of p*H*.

From the ion exchange capacity data (Table 3) it can be concluded that the affinity sequence for monovalent ions is $K^+ > Na^+ > Li^+$ and for bivalent ions is $Ba^{2+} > Sr^{2+} > Ca^{2+} > Mg^{2+}$. This sequence is in accordance with the hydrated radii. Ion-exchange capacity decreases with increase in the hydrated radii. The ions with smaller hydrated radii easily enter the pores of the exchanger, resulting in higher adsorption (14).

The sorption studies on stannic vanadate reveal the possibility of many analytically difficult separations of metal ions and anions. The order of the ion-exchange selectivity in various solvents is as follows:

Demineralized water

$$K^+ > Pb^{2+} > Na^+ > Cd^{2+} \simeq Ca^{2+} > Zn^{2+} > Mn^{2+} > Sr^{2+} > Ba^{2+} > Mg^{2+}$$

0.001 *M* HNO_3

$$K^+ > Pb^{2+} > Na^+ > Zn^{2+} > Ba^{2+} > Cd^{2+} > Ca^{2+} \simeq Mn^{2+} > Sr^{2+} > Mg^{2+}$$

0.005 *M* HNO_3

$$K^+ > Pb^{2+} \simeq Na^+ > Zn^{2+} > Ba^{2+} > Cd^{2+} > Mn^{2+} > Sr^{2+} > Ca^{2+} > Mg^{2+}$$

0.01 *M* HNO_3

$$K^+ > Cd^{2+} > Pb^{2+} > Na^+ > Zn^{2+} > Ba^{2+} > Mn^{2+} > Sr^{2+} > Ca^{2+} > Mg^{2+}$$

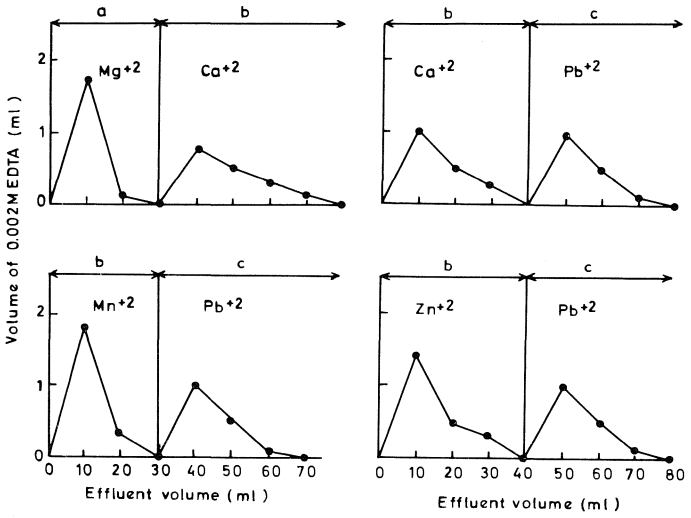

FIG. 3. Separations of metal ions on stannic vanadate columns. a = demineralized water, c = 0.1 M NH_4NO_3 in 0.1 M HNO_3, b = 0.001 M HNO_3.

0.1 M HNO_3

$$Pb^{2+} > K^+ \simeq Na^+ > Mn^{2+} > Cd^{2+} > Zn^{2+} > Sr^{2+} > Ba^{2+} \simeq Ca^{2+} > Mg^{2+}$$

The exchanger has very high affinity for Na^+, K^+, Pb^{2+}, Cd^{2+}, Zn^{2+}, and Ca^{2+} even in the nitric acid medium. Therefore separations of these metal ions are possible from the rest of the ions. The adsorption of Mg^{2+} is very small as compared to other ions and hence it can be easily separated from alkaline earths and other metal ions. Titanium vanadate was found to show the highest affinity for Sr^{2+} ion amongst alkaline earths, but stannic vanadate adsorbs the Ca^{2+} ion more strongly in most solvents. It is also observed that adsorption of ions decreases with increase in nitric acid concentration and can be explained as above. The effect of temperature on the adsorption of metal ions shows that the uptake gradually increases as the equilibrating temperature is increased as usually observed in other ion-exchangers. The following selectivity sequence is observed.

At 25°C

$$Pb^{2+} > Zn^{2+} > Ba^{2+} > Cd^{2+} > Mn^{2+} \simeq Ca^{2+} > Sr^{2+} > Mg^{2+}$$

at 40°C

$$Pb^{2+} > Sr^{2+} > Ba^{2+} > Zn^{2+} > Ca^{2+} > Mn^{2+} > Cd^{2+} > Mg^{2+}$$

at 60°C

$$Pb^{2+} > Sr^{2+} > Zn^{2+} > Ca^{2+} > Cd^{2+} \simeq Mn^{2+} > Ba^{2+} > Mg^{2+}$$

at 80°C

$$Pb^{2+} > Mn^{2+} > Sr^{2+} > Ba^{2+} > Zn^{2+} > Ca^{2+} > Cd^{2+} > Mg^{2+}$$

To demonstrate the practical utility of the exchanger, quantitative separations of Pb^{2+} from Zn^{2+}, Mn^{2+} and Ca^{2+} and of Mg^{2+} from Ca^{2+} have been efficiently achieved on small columns of stannic vanadate.

The anion adsorption studies on stannic vanadate show the specificity for arsenate ion. The reaction is sufficiently fast to be of practical importance. The arsenate which is irreversibly adsorbed has been quantitatively separated from phosphate, antimonate, and tungstate on a 1 g stannic vanadate column. The eluent volumes required to elute phosphate, antimonate, and tungstate are 40, 30, and 30 ml respectively. The arsenate strongly interacts with stannic vanadate and could not be eluted. To understand the mechanism of the reaction the vanadate released was determined and it was found that no excess of vanadate is released and therefore it is probably a case of irreversible adsorption to form either a heteropoly acid salt, *i.e.* stannic vanado-arsenate or to give a mixture of the two insoluble salts, *i.e.* stannic vanadate and stannic arsenate.

Infrared spectrum of stannic vanadate resembles that of titanium vanadate (4). The strong peak between 3000–3600 cm^{-1} with a maximum at 3400 cm^{-1} is due to stretching vibration of interstitial water molecules and OH groups [r_1 (H_2O or OH)] (15). The band between 1600–1700 cm^{-1} with a maximum absorption at 1650 cm^{-1} is due to deformation vibration of M—OH[$\delta_2(H_2O)$]. The peak at 1400 cm^{-1} is due to deformation vibration of

interstitial water [$\delta_1(H_2O)$]. The fourth broad peak with a maximum at 700 cm^{-1} represents the stretching vibration of M—O bond [r_2(Sn—O, V—O)].

1. C. B. AMPHLETT. Inorganic ion exchangers. Elsevier Publishing Co., Amsterdam. 1944.
2. V. VESELY and V. PEKAREK. Talanta Rev. **19**, 219 (1972).
3. J. A. MARINSKY and Y. MARCUS. Ion exchange and solvent extraction. Vol. V. Marcel Dekker, Inc., New York. 1973. p. 1.
4. M. QURESHI, K. G. VARSHNEY, and S. K. KABIRUDDIN. Can. J. Chem. **50**, 2071 (1972).
5. M. QURESHI and J. P. RAWAT. J. Inorg. Nucl. Chem. **30**, 305 (1968).
6. N. H. FURMAN. Standard methods of chemical analyses. 6th ed. D. Van Nostrand and Co., Inc., Princeton, NJ. 1962.
7. E. B. SANDELL. Colorimetric determination of traces of metals. Vol. VIII. 3rd ed. Interscience, New York, NY. 1959.
8. N. E. TOPP and K. W. PEPPER. J. Chem. Soc. 3299 (1949).
9. O. SAMUELSON. Diss. Tekn. Hogskolan. Stockholm. (1944).
10. M. QURESHI and K. G. VARSHNEY. J. Inorg. Nucl. Chem. **30**, 3081 (1968).
11. M. QURESHI, S. A. NABI, N. ZEHRA, and V. KUMAR. Talanta, **20**, 609 (1973).
12. M. QURESHI and S. A. NABI. J. Inorg. Nucl. Chem. **32**, 2059 (1970).
13. M. QURESHI and J. P. GUPTA. J. Chem. Soc. A, **12**, 1755 (1969).
14. C. B. AMPHLETT and L. A. MCDONALD. Proc. Chem. Soc. 276 (1962).
15. S. R. YOGANERASIMHAN. Indian J. Chem. **18**, 360 (1963).

Crystal structure of vanadium(III) tris(metaphosphate)

NORA MIDDLEMISS, FRANK HAWTHORNE, AND CRISPIN CALVO

Institute for Materials Research, McMaster University, Hamilton, Ont., Canada L8S 4M1

Received October 12, 1976

NORA MIDDLEMISS, FRANK HAWTHORNE, and CRISPIN CALVO. Can. J. Chem. **55**, 1673 (1977).

Vanadium(III) tris(metaphosphate), $V(PO_3)_3$, crystallizes in the monoclinic space group *Ic* with lattice parameters $a = 10.615(2)$, $b = 19.095(4)$, $c = 9.432(1)$ Å, $\beta = 97.94(1)°$ with $Z = 12$. The equivalent parameters in the standard space group *Cc* are $a = 13.189(1)$, $b = 19.095(4)$, $c = 9.432(1)$ Å, and $\beta = 127.15(1)°$. The structure was refined by full-matrix least-squares to an $R = 0.091$ ($R_\omega = 0.065$) utilizing 2467 reflections with the atomic positions and their isotropic vibration amplitudes as parameters. The structure consists of infinite chains of PO_4 tetrahedra sharing corners with each other and bridged by VO_6 octahedra. All oxygen atoms are shared between just two cations. The average P—O⟨—P⟩ bond is 1.581 Å while the average of those shared with vanadium is 1.483 Å. The VO_6 group is moderately distorted, with differences of less than 0.06 Å between the longest and shortest V—O bond lengths in any of the three distinct VO_6 groups. The average V—O bond lengths for the three VO_6 groups are 1.995, 1.991, and 1.987 Å. A marked superlattice effect based on a cell with $b/3$ is noted.

NORA MIDDLEMISS, FRANK HAWTHORNE et CRISPIN CALVO. Can. J. Chem. **55**, 1673 (1977).

Le tris(métaphosphate) de vanadium(III), $V(PO_3)_3$, cristallise dans le groupe d'espace monoclinique *Ic* avec des paramètres de maille $a = 10.615(2)$, $b = 19.095(4)$, $c = 9.432(1)$ Å, $\beta = 97.94(1)°$ avec $Z = 12$. Les paramètres équivalents dans le groupe d'espace standard *Cc* sont $a = 13.189(1)$, $b = 19.095(4)$, $c = 9.432(1)$ Å et $\beta = 127.15(1)°$. On a affiné la structure par la méthode des moindres carrés (matrice complète) jusqu'à une valeur de $R = 0.091$ ($R_\omega = 0.065$) utilisant 2467 réflexions et les positions atomiques et leurs amplitudes de vibration isotrope comme paramètres. La structure consiste de chaînes infinies de tétraèdres de PO_4 partageant des coins les uns avec les autres et reliées par un octaèdre de VO_6. Tous les atomes d'oxygène sont partagés uniquement entre deux cations. La longueur moyenne du lien P—O⟨—P⟩ est de 1.581 Å alors que la moyenne des longueurs partagées avec le vanadium est de 1.483 Å. Le groupe VO_6 est modérément déformé; il existe des différences de moins que 0.06 Å entre les longueurs des distances V—O les plus courtes et des plus longues dans chacun des trois groupes VO_6 distincts. Les longueurs moyennes des liens V—O pour les trois groupes VO_6 sont 1.995, 1.991 et 1.987 Å. On note un effet marqué de superstructure basé sur une maille avec $b/3$.

[Traduit par le journal]

Introduction

The systematic study of various solid vanadium oxides has shown that a wide variety can be prepared. In addition to the oxides with vanadium having integral valences, *i.e.* V_2O_3, VO_2, and V_2O_5, series with variable valency for the cation have been prepared. Two well characterized series correspond to V_nO_{2n-1} (1, 2) with $3 \leq n \leq 8$ and V_nO_{2n+1} (3, 4) with $n = 3, 4, 6$. Polymorphic transformations and a variety of changes in physical properties have been noted (2, 4). These structures are characterized by octahedral and/or five-fold coordinate V.

Adding P_2O_5, thus forcing some of the cations into tetrahedral coordination, has to date resulted in a substantially diminished number of phases and variety of solid state properties. This may be due to the instability of stable shear structures based upon tetrahedrally coordinated cations. Among the compositions which do occur are $V(PO_3)_3$, $VO(PO_3)_2$ (5, 6), and VPO_5 (7) with the oxidation state of vanadium progressively increasing in integral steps from 3 to 5. Polymorphs have been reported for only VPO_5 to date and the structures of these have been determined (8, 9). A second tetravalent vanadium compound, $(VO)_2P_2O_7$, whose structure is being studied in this series, has not been reported generally.[1] Surprisingly, only one mixed valency vanadium phosphate system is presently known. This system consists of glasses whose conductivities indicate that polaronic hopping involves an electron hopping from V^{4+} to V^{5+} (11). The structure of these glasses is based upon a

[1]P. Courtine and E. Bordes, private communication.

perturbed α-VPO_5 structure (12). Substitution of phosphorus into metavanadate chains and vanadium into trimetaphosphate rings has been reported (13). However, substitution of V for P in $VO(P_2SiO_8)$ (14, 15), where one might logically expect it, has not been substantiated nor has phosphorus been substituted for tetrahedral V^{5+} in $K_2V_3O_8$ (16). In each case the structure suggests that such substitution, leading to a mixed valency state vanadium in a vanadium phosphate system, should be possible.

The general conclusion available from the details of the preparation of these vanadium phosphorus compounds is that at fixed partial pressure of oxygen the fraction of vanadium reduced increases with temperature (17) as it does with an increased P/V ratio (5, 6, 18) at fixed temperature. The structural studies indicate that as the P/V ratio increases the degree of condensation of the phosphate increases. That is, VPO_5 has non-condensed phosphate groups, and infinite chains of corner sharing PO_4 groups were found (in this laboratory)[2] in $VO(PO_3)_2$ and $V(PO_3)_3$. $VPO_{4.5}$ has both condensed VO_6 groups and P_2O_7 groupings, according to our incomplete studies, while in the vanadium phosphate glasses, prepared from a mixture of $(1 + x)V_2O_5$ and $(1 - x)P_2O_5$, for $x \geq 0$ condensed vanadium polyhedra are proposed to account for the oxygen lost. Although many structures based upon condensed VO_6 groups are possible, in the vanadium phosphate system only a few have been realized. The dearth of mixed valency crystalline vanadium phosphates is worthy of note.

Trivalent metal ion trimetaphosphates have been reported for Al, Ti, Fe, Cr, Mo in addition to V (20–25). The structure of the cubic polymorph, as $Al_4(P_4O_{12})_3$, was reported by Pauling and Sherman (26). Six polymorphs have been reported for $Cr(PO_3)_3$ (25) thus presenting an interesting challenge in both preparing and determining these structures.

Experimental

Crystals of $V(PO_3)_3$ were prepared by reacting a V_2O_5–P_2O_5 mix in an evacuated sealed quartz tube at temperatures near 900°C. The product was found to contain small crystals of $VO(SiP_2O_8)$, $VO(P_2O_7)$, $V(PO_3)_3$ plus at least one additional phase. All the diffraction studies were performed on a crystal from this batch. Crystals with the same lattice parameters and symmetry as reported here were also prepared following the procedure of Lavrov *et al.* (5) and Tofield *et al.* (6).

A small equi-dimensional crystal with a radius of about 0.1 mm was used for the crystallographic study. Unit cell parameters were obtained by measuring both $\pm 2\theta$ values on a Suntex $P2_1$ automatic diffractometer using 2θ values in the range 20 to 30°. Graphite monochromatized MoKα radiation ($\lambda_{\alpha_1} = 0.70926$ Å) was used. The parameters were determined by least-squares refinement methods. Crystal data are as follows:

$V(PO_3)_3$ fw = 287.85
Monoclinic $a = 10.615(2)$, $b = 19.095(4)$, $c = 9.432(1)$ Å, $\beta = 97.94(1)°$, $Z = 12$, $D_m = 3.0 \pm 0.1$ g cm^{-3}, $D_{calcd} = 3.03$ g cm^{-3}. Space group: *Ic* or *I*2/*c*. Absences: $h+k+l$ odd in general and $h0l$ with l odd.

Data were collected with a scintillation counter up to $2\theta = 60°$ using a scan of 2° plus the α_1–α_2 separation. Backgrounds were measured on either side and one degree removed from each peak. The scan rate depended upon the peak intensity. A total of 2847 symmetry independent peaks were scanned and 2467 of these had intensity of positive measure after correcting the peak intensities for background. The latter set was used to determine the structure. All the data were corrected for Lorentz and polarization effects and for absorption based upon a spherical crystal with a radius of 0.1 mm.

At lower 2θ values the diffraction pattern showed reflections indexed with $k \neq 0$ (mod 3) to be substantially weaker than those with $k = 0$ (mod 3). Thus a Patterson function with these latter reflections was used to determine the average atomic positions assuming that the space group of this smaller cell was *I*2/*c*. The structure model at this point showed some P—O bond lengths that were unacceptable and an R value near 0.20. Tofield *et al.* (6) on the basis of a second-harmonic generation signal selected *Cc* as the space group for the standard cell. The final structure was derived in this space group by arbitrarily displacing the atoms sequentially from the average position in conjunction with a decreasing R value.[3] Although the model obtained seemed satisfactory the possibility of a false minimum exists. Therefore, the Patterson function, without the vanadium contribution and a β synthesis (27) based upon the vanadium and phosphorus positions of the model were examined for an alternative structure. None was found. Finally, the structure of $Al(PO_3)_3$ (28), reported recently, is isostructural.

The final atomic parameters, with isotropic thermal parameters, derived by full-matrix least-squares methods, are in Table 1. (The cell has been transformed to one with *Ic* symmetry.) The refinement used scattering curves for neutral atoms (29) and a weighting scheme, ω, so that $\omega(F_o - F_c)^2$ was substantially independent of F_o, *i.e.* $\omega = (46 - 0.53F + 0.0023F^2 + 1000\,(\sigma/F)^2)^{-1}$, where σ is the standard deviation based on counting statistics. (The final R and R_ω were 0.091 and 0.065 respectively considering all reflections and 0.134 and 0.094 considering the $k \neq 0$ (mod 3) reflections only.) Scattering curves were corrected for anomalous dispersion but this

[2]N. Middlemiss and C. Calvo, unpublished results.

[3]A table of calculated and observed structure factors is available, at a nominal charge, from the Depository of Unpublished Data, CISTI, National Research Council of Canada, Ottawa, Canada K1A 0S2.

TABLE 1. Atomic parameters for $V(PO_3)_3$ with estimated standard deviations in parentheses (values are multiplied by 10^4)

Atom	x	y	z	U (Å^2)*
V(*a*)	1/4	0798(2)	1/4	0057(5)
V(*b*)	2529(5)	4115(2)	2479(6)	0049(5)
V(*c*)	2308(3)	7549(2)	2631(4)	0056(6)
P(1)	9756(6)	1442(3)	7657(7)	0059(8)
P(2)	0156(5)	4803(2)	7409(6)	0063(8)
P(3)	0027(5)	8142(2)	7476(6)	0043(7)
P(4)	1026(5)	3018(2)	4494(6)	0051(8)
P(5)	0967(5)	6370(2)	4420(6)	0050(8)
P(6)	1168(6)	9681(3)	4363(7)	0073(9)
P(7)	8791(6)	6965(2)	5748(7)	0056(9)
P(8)	8809(6)	3629(2)	5710(6)	0036(8)
P(9)	8961(5)	0267(3)	5561(6)	0056(8)
O(*a*,2)	9033(10)	5190(6)	7784(13)	0106(21)
O(*a*,3)	0884(10)	1321(5)	2012(12)	0062(19)
O(*a*,6)	1501(12)	9981(6)	2994(14)	0068(22)
O(6,*a*)	2262(13)	0544(7)	0417(16)	0120(26)
O(*a*,7)	8502(11)	6635(6)	7091(13)	0092(20)
O(*a*,8)	7808(10)	6097(6)	9585(13)	0051(20)
O(*b*,2)	1211(11)	4803(7)	1862(13)	0114(22)
O(*b*,3)	8865(12)	8371(7)	8006(15)	0145(24)
O(*b*,4)	1266(12)	3577(6)	3473(15)	0159(24)
O(*b*,5)	2044(11)	3651(6)	0631(13)	0083(20)
O(*b*,9)	8769(11)	9686(6)	6562(13)	0049(19)
O(9,*b*)	8011(11)	9652(6)	9295(13)	0045(20)
O(*c*,1)	0930(13)	8251(7)	2191(15)	0112(24)
O(1,*c*)	8775(11)	1913(6)	8121(13)	0057(21)
O(*c*,4)	2022(12)	7099(7)	0734(15)	0130(24)
O(*c*,5)	1070(10)	6876(5)	3255(12)	0086(19)
O(*c*,7)	7683(11)	2840(6)	9689(14)	0083(21)
O(*c*,8)	8414(10)	3298(6)	6975(13)	0106(21)
O(4,3)	0835(10)	2294(6)	3723(12)	0068(19)
O(4,8)	9695(10)	6892(6)	0056(13)	0091(20)
O(5,2)	0776(10)	5603(5)	3814(11)	0058(18)
O(5,7)	9679(11)	3545(6)	0103(14)	0136(22)
O(6,1)	0125(13)	9079(7)	3906(16)	0091(25)
O(6,9)	0360(11)	9765(6)	0181(13)	0062(21)
O(7,3)	9673(11)	7633(6)	6137(13)	0095(21)
O(8,2)	9770(12)	4235(7)	6178(15)	0138(24)
O(9,1)	9072(12)	0973(7)	6453(15)	0115(25)

*The temperature factor expression is $\exp(-8\pi^2 U \sin^2 0/\lambda^2)$.

effect was not large enough to distinguish the absolute configuration.

Description

The structure is an example of polyhedral packing with three tetrahedra for every octahedron and with each corner shared between two polyhedra. The general bonding motif can be discussed by considering the average structure, shown in projection in Fig. 1, since no new major features arise in the extended structure.

The VO_6 octahedra lie in pseudo-hexagonal arrays with $[10\bar{1}]$ as the normal. Adjacent layers are related by the glide plane. One of the three-fold axes of the octahedra nearly parallels the *b* axis and another nearly parallels the layer direction. Each VO_6 group is bridged to six neighbouring VO_6 groups by phosphate groups. These lie in one of the two adjacent layers and lead to the three dimensional bonding.

The $(PO_3)_n$ chains snake their way between these octahedra while running parallel to *c*. Three distinct PO_4 groups form links in this chain. Although all the PO_4 groups are oriented with a two-fold axis roughly parallel to *b*, the configuration of the central PO_4 group is inverted with respect to the end members of the link. This permits the central PO_4 group to share oxygen atoms with VO_6 groups at the same *y* level and one such bridging occurs between a given VO_6

TABLE 2. Average bond geometry in $V(PO_3)_3$*

Bond	Length (Å)		
	Maximum	Minimum	Average
V—O	2.030(12)	1.949(13)	1.991
P—O—(P)	1.623(13)	1.538(13)	1.581
P—O—(V)	1.501(12)	1.461(14)	1.483
Bonds	**Angle (deg)**		
	Maximum	Minimum	Average
O—V—O (axial)	177.5(5)	170.0(5)	175.2
O—V—O	95.8(5)	84.2(5)	90.0
(P)—O—P—O—(P)	108.1(6)	98.7(7)	102.6
(P)—O—P—O—(V)	114.7(8)	102.6(8)	108.8
(V)—O—P—O—(V)	119.6(7)	115.6(8)	117.7

*A complete table of bond lengths and bond angles is available, at a nominal charge, from the Depository of Unpublished Data, CISTI, National Research Council of Canada, Ottawa, Canada K1A 0S2.

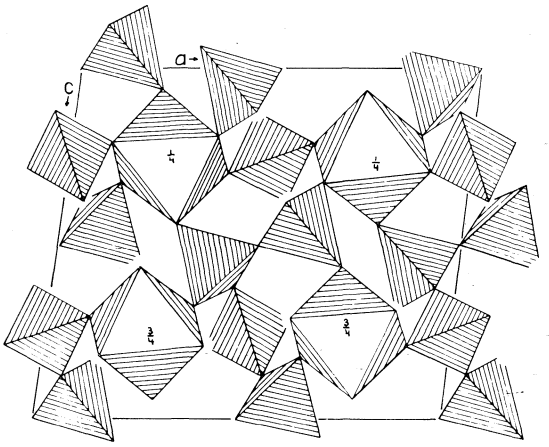

FIG. 1. The average structure of $V(PO_3)_3$ projected down the b axis. The vanadium ion lies within the octahedra and the phosphorus atom within the tetrahedra. The approximate y coordinates of the V^{3+} are shown. Oxygen atoms lie at the corners of the polyhedra.

group and each of its two VO_6 neighbours at the same y level. The remaining phosphate groups are shared between VO_6 groups whose y values differ by $\frac{1}{2}$ of the b axis of the average structure. Each VO_6 has four neighbouring metaphosphate chains. One oxygen is shared with each of the two chains connected to VO_6 at the central phosphate and two oxygens are shared with the other chains. The chains are rectangularly arranged about VO_6, with the rectangle defined by the vectors $\frac{1}{2}a$ and $\frac{1}{2}b$. Adjacent links in the chain have the configurations of the PO_4 groups inverted as required by the glide plane.

In the true structure all the tetrahedra are distorted with the P—O(—V) bond consistently shorter than the P—O(—P). The average values of these are 1.483 and 1.581 Å respectively (Table 2). Although the (V—)O—P—O(—V) bond angles are always the largest within a given tetrahedron, averaging 117.7 ± 0.8°, the deviation from ideality is not solely related to a displacement of the P from the center of the tetrahedron away from the P ions of the nearest neighbouring PO_4 groups. If the deviations, as measured by this angle, are to be considered random, the standard errors would have to increase by a factor of three. Even then, the deviations of the (P—)O—P—O(—P) angle would be significant since they range from 98.7 to 108.1°. Further, this angle is not always the smallest in the congruent PO_4 group. Thus the tetrahedra are not congruent and the deviations, perhaps examined with 3σ in mind, must be related to the angles of the polyhedra at the bridging oxygen. Since the distortions of the PO_4 are thus postulated to be related to the configuration of the four surrounding polyhedra the systematics of the effect is not apparent.

The angle subtended at the oxygen atom by the cations to which it is bonded ranges from 135 to 151° (9 values) when both cations are phosphorus and from 133 to 158° (18 values) otherwise. No strong correlation exists between these angles and the distortions of the polyhedra.

It is conceivable that V^{5+} could substitute for P^{5+} in the PO_4 groups, and this could be the source of some of the polyhedral distortions. The site populations of the tetrahedral cations were

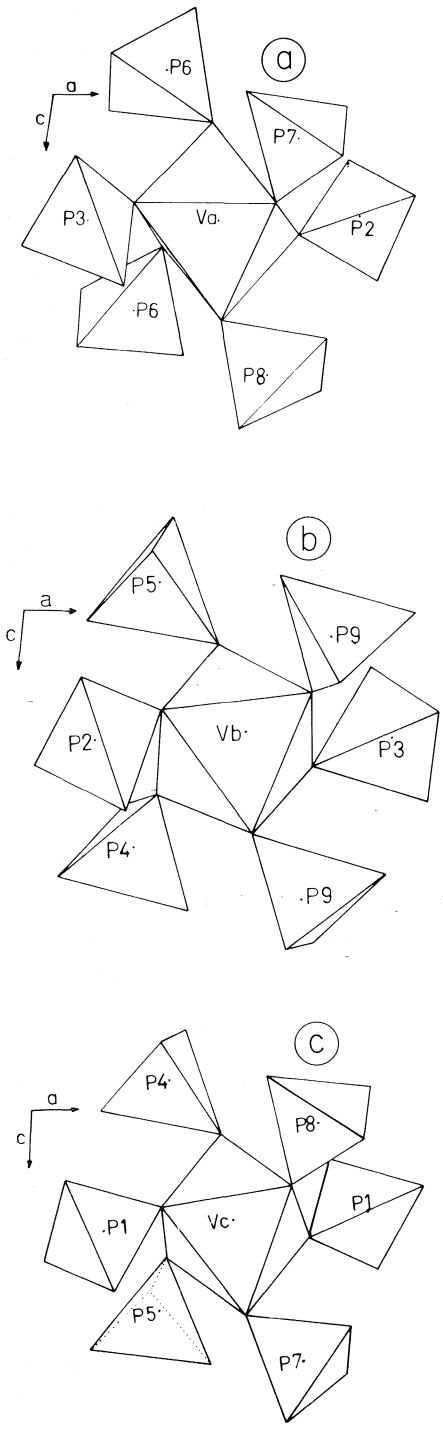

FIG. 2. The environments about the vanadium ions near $x,z = \frac{1}{4}, \frac{1}{4}$ for the three ranges (*a*) $0 \leq y \leq \frac{1}{3}$, (*b*) $\frac{1}{3} \leq y \leq \frac{2}{3}$, (*c*) $\frac{2}{3} \leq y \leq 1$. Oxygen atoms lie at the corners of the polyhedra.

varied. Changes at the 2σ level were found but not considered significant.

The displacement of the atoms from translational equivalence by $b/3$ was calculated. Two of the vanadium ions nearly superimpose, with the third displaced by about $\frac{1}{3}$ Å equatorial to *b*. A similar result applies to the P atoms in the set P(7), P(8), and P(9). The maximum displacement from superposition amongst the set P(4), P(5), and P(6) is $\frac{1}{4}$ Å whereas the set P(1), P(2), and P(3) has the largest set of displacements ranging from 0.16 to 0.51 Å. The major changes occur among the oxygen atoms. This results in a rotation of the polyhedra as shown in Fig. 2 *a*, *b*, *c*. Here the vanadium ions differing by about $\frac{1}{3}b$ and their nearest neighbour PO_4 environments are shown. In every case the phosphate groups sharing oxygen atoms with the upper faces of the VO_6 groups are inverted with respect to those sharing the oxygen atoms of the lower faces. Although the groups in Fig. 2*b* and Fig. 2*c* are substantially nearer to superposing with each other than with those in Fig. 2*a*, the displacements needed for superposition are large. In fact, the largest displacement from superposition of the oxygen atoms is over 1 Å with the average over 0.6 Å. Although it is possible to discuss the mutual angular displacements of each of the polyhedra it is not apparent that this will result in an understanding of the enlarged cell.

The intensities of five strong $k = 0 \pmod 3$ reflections and the 25 strongest $k \neq 0 \pmod 3$ reflections were measured at room temperature, 300°C, and 500°C. The higher temperature intensities were compared to the room temperature ones. The results shown in Fig. 3, indicate that, although the errors are large, the $k \neq 0 \pmod 3$ reflections become substantially weaker with increasing temperature while the $k = 0 \pmod 3$ reflections only weaken slightly. This suggests that the structure tends towards becoming the average structure at high temperatures. This average structure may be modified slightly, possibly through differential axis changes, from the room temperature one since there are some unacceptable bond lengths at room temperature. No evidence of a phase transition at higher temperatures was found by DTA in this laboratory confirming the results of Lavrov *et al.* (5).

Discussion

In light of the many distinct polymorphs of

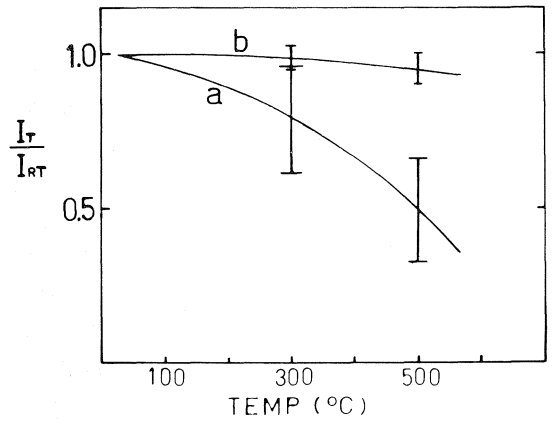

FIG. 3. The ratio of the intensity at various temperatures compared to room temperature for (*a*) 25 strongest reflections with $k \neq 0$ (mod 3) and (*b*) 5 strong reflections with $k = 0$ (mod 3).

$Cr(PO_3)_3$ (25) it is surprising that $V(PO_3)_3$ crystallizes as only one of these. The present structure is one common to one of the polymorphs of Al, Cr, Ti, and Mo trimetaphosphate. The structure of the cubic modification, found for Cr, Al, and Fe as cations, is based upon rings of four tetrahedra and thus bears no direct relationship to the present structure.

Unit cell dimensions of a hexagonal form are known for $Cr(PO_3)_3$ (25) and $Fe(PO_3)_3$. Although the present structure has some features of hexagonal packing, the structure is not easily transformed to a hexagonal or trigonal one. The direction of the chain should lie in a plane perpendicular or parallel to the unique axis of the hexagonal cell. In the present structure these chains are arrayed at the corners of a rectangle normal to the *c* axis and thus a substantial change will be needed to bond the VO_6 with two phosphate groups in each of three chains, as would be required for the hexagonal phase.

Deviations in the bond lengths of the two types of P—O bonds are expected based upon Baur's (30) correlation between bond length and bond strength. Thus the P—O(—P) bond with a bond strength at the oxygen atom of 2.5 will show a longer bond than the P—O(—V) where the bond strength is 1.75. The predicted bond length difference of 0.08 Å is comparable to 0.10 Å as found here.

The V^{3+}—O bond lengths and VO_6 geometry are as found in V_2O_3 (31) and other V_nO_{2n-1} structures (19, 31, 32), as well as for Al^{3+} in $Al(PO_3)_3$ (28). The higher valent vanadium systems are characterized by the short vanadyl bond and as a result, for these systems, the vanadium analogue of structures with the same stoichiometry can often differ. A case in point is MP_2O_7 where for M = Hf, Zr, Sn, Ti, and Si (10) the structures are isostructural and based upon a binary condensation of PO_4 groups. In the vanadium system the structure is written as $VO(PO_3)_2$ to emphasize the vanadyl bond and the infinite chain of corner sharing PO_4 groups.

$V(PO_3)_3$ is one of many structures and structure-types having each oxygen atom shared between only two cations. These structures involve cations with large charges in order to maintain reasonable bond orders on the oxygen atoms. Another structure where the ratio of the numbers of octahedra to tetrahedra is the same as in the present case is $VO(P_2SiO_8)$. This latter structure consists of chains of VO_6 groups containing tetravalent V and bridged by vanadyl groups (14, 15). The PO_4 groups form four membered rings bridged in the chain direction by SiO_4 groups. If P^{5+} were to fully substitute for Si^{4+}, the vanadium would be reduced yielding the same stoichiometry as in the present crystal. This form is unstable presumably because of the instability of the vanadyl bond for trivalent vanadium. Without these bonds the oxygen atom bridging the octahedra would be too underbonded.

Acknowledgment

This research was supported through grants from the National Research Council of Canada.

1. S. KACHI, K. KOSUGE, and H. OKINAKA. J. Solid State Chem. **6**, 258 (1973).
2. H. HORUICHI, M. TOKONAMI, N. MORIMOTO, K. NAGANWAY, Y. BANDO, and T. TAKADA. Mater. Res. Bull. **6**, 833 (1971).
3. (*a*) F. THEOBALT, R. CABALA, and J. BERNARD. C. R. Acad. Sci. (Paris) Ser. C, **266**, 1534 (1968); (*b*) P. D. DERNIER. Mater. Res. Bull. **9**, 955 (1974).
4. (*a*) K.-A. WILHELMI, K. WALTERSSON, and L. KIHLBORG. Acta Chem. Scand. **25**, 2675 (1971); (*b*) K.-A. WILHELMI and K. WALTERSSON. Acta Chem. Scand. **24**, 3409 (1970); (*c*) K. WALTERSSON, B. FORSLUND, and K.-A. WILHELMI. Acta Crystallogr. Sect. B, **30**, 2644 (1974).
5. A. V. LAVROV, L. S. GUZEEVA, and P. M. FEDOROV. Izv. Akad. Nauk SSSR, Neorg. Mater. **10**, 2180 (1974).
6. B. C. TOFIELD, G. R. CRANE, G. A. PASTEUR, and R. C. SHERWOOD. J. Chem. Soc. Dalton Trans. 1806 (1975).
7. J. J. BROWN and F. A. HUMMEL. Trans. Br. Ceram. Soc. **64**, 419 (1965).

8. R. GOPAL and C. CALVO. J. Solid State Chem. **5**, 432 (1972).
9. B. D. JORDAN and C. CALVO. Can. J. Chem. **51**, 2621 (1973).
10. E. TILLMANNS, W. GEBERT, and W. H. BAUR. J. Solid State Chem. **7**, 69 (1973).
11. M. SAYER and A. MANSINGH. Phys. Rev. B, **6**, 4629 (1972).
12. B. D. JORDAN. Ph.D. Thesis, McMaster University, Hamilton, Ontario. 1975.
13. K. L. IDLER. M.Sc. Thesis, McMaster University, Hamilton, Ontario. 1977.
14. C. E. RICE, W. R. ROBINSON, and B. C. TOFIELD. Inorg. Chem. **15**, 345 (1976).
15. N. MIDDLEMISS and C. CALVO. Acta Crystallogr. Sect. B, **32**, 2896 (1976).
16. J. GALY and A. CARPY. Acta Crystallogr. **31**, 1794 (1975).
17. H. HARPER and P. W. MCMILLAN. Phys. Chem. Glasses, **15**, 148 (1974).
18. S. OHASHI and T. MATSUMURA. Bull. Chem. Soc. Jpn. **35**, 501 (1962).
19. M. MAREZIO, P. D. DERNIER, D. B. MCWHAN, and S. KADRI. J. Solid State Chem. **11**, 301 (1974).
20. F. D'YVOIRE. Bull. Soc. Chim. Fr. 1237 (1962).
21. P. REMY and A. BOULLÉ. C. R. Acad. Sci. Paris, **258**, 927 (1964).
22. F. D'YVOIRE. Bull. Soc. Chim. Fr. 1224 (1962).
23. R. M. DOUGLASS and E. STARITZKY. Anal. Chem. **28**, 984 (1957).
24. F. LIEBAU and H. P. WILLIAMS. Angew. Chem. **3**, 315 (1964).
25. P. REMY and A. BOULLÉ. Bull. Soc. Chim. Fr. **6**, 2213 (1972).
26. L. PAULING and J. SHERMAN. Z. Kristallogr. **96**, 481 (1937).
27. G. N. RAMACHANDRAN and R. SRINIVASAN. Fourier methods in crystallography. Wiley–Interscience, New York. 1970.
28. H. VAN DER MEER. Acta Crystallogr. Sect. B, **32**, 2423 (1976).
29. D. T. CROMER and J. B. MANN. Acta Crystallogr. Sect. B, **24**, 321 (1968).
30. W. H. BAUER. Trans. Am. Crystallogr. Assoc. **6**, 129 (1970).
31. W. R. ROBINSON. Acta Crystallogr. **31**, 1153 (1975).
32. H. HORUICHI, M. TOKONAMI, and N. MORIMOTO. Acta Crystallogr. Sect. B, **28**, 1404 (1972).

Studies with inorganic precipitate membranes: Part XIV. Evaluation of effective fixed charge densities

M. Nasim Beg, Fasih A. Siddiqi, and Radhey Shyam

Division of Physical Chemistry, Department of Chemistry, Aligarh Muslim University, Aligarh-202001, India

Received October 25, 1976

M. Nasim Beg, Fasih A. Siddiqi, and Radhey Shyam. Can. J. Chem. **55**, 1680 (1977).

Effective fixed charge densities of cobalt and nickel sulphide (parchment supported) membranes in contact with various 1:1 electrolyte solutions have been evaluated from membrane potential measurements. The methods used for the estimation of charge densities were: (*a*) the Teorell–Meyer–Sievers method (TMS) and (*b*) the methods developed recently by Kobatake and co-workers. The two limiting forms of Kobatake's equation for dilute and concentrated solutions gave identical values of charge densities. The theoretical predictions for membrane potential were borne out quite satisfactorily by experimental results obtained with both the membranes. Apparent transference numbers of coions and permselectivities of the membranes for electrolytes have also been calculated. A method based on permselectivity values for the determination of charge density was also used. It was interesting to note that the charge densities evaluated from different methods of Kobatake and co-workers gave identical values and that the results were comparable to those derived from the TMS method.

M. Nasim Beg, Fasih A. Siddiqi et Radhey Shyam. Can. J. Chem. **55**, 1680 (1977).

On a évalué, à partir de mesures de potentiel de membranes, les densités effectives de charges fixes pour des membranes de sulfures de cobalt et de nickel (supportés sur du parchemin) en contact avec diverses solutions d'électrolytes 1:1. Les méthodes utilisées pour évaluer les densités de charges sont: (*a*) la méthode de Teorell–Meyer–Sievers et (*b*) les méthodes développées récemment par Kobatake et ses collaborateurs. Les deux formes limites de l'équation de Kobatake pour des solutions diluées et concentrées conduisent à des valeurs identiques pour les densités de charge. Les prédictions théoriques pour les potentiels des membranes concordent bien avec les résultats expérimentaux obtenus avec les deux membranes. On a aussi calculé les nombres apparents de transferts des coions et les permsélectivités des membranes pour les électrolytes. On a aussi utilisé une méthode basée sur des valeurs de permsélectivité pour la détermination de la densité de charge. Il est intéressant de noter que les densités de charges évaluées par diverses méthodes de Kobatake et ses collaborateurs conduisent toutes à des valeurs identiques et que les résultats sont comparables à ceux que l'on peut obtenir à partir de la méthode TMS.

[Traduit par le journal]

In a series of communications (1–10) on parchment supported membranes, Siddiqi, Beg, and co-workers (1–6) have, on the basis of the Eisenman–Sherry model of membrane selectivity (11, 12) and by the application of the theory of rate processes to diffusion (13), demonstrated the small density of fixed charge on the membrane matrix. In order to substantiate these findings, membrane potential measurements have been carried out for the evaluation of effective fixed charge density which is an important characteristic of a membrane by various methods (14–16) including those developed recently by Kobatake and co-workers (17–23).

Experimental

Parchment supported cobalt and nickel sulphide membranes were prepared by the method of interaction suggested by Siddiqi, Beg, and co-workers (1–6). To precipitate these substances in the interstices of the parchment paper, a 0.2 *M* solution of sodium sulphide was placed inside a glass tube, to one end of which was tied parchment paper. The tube was suspended for 72 h in a 0.2 *M* solution of either cobalt(II) or nickel(II) chloride. The two solutions were interchanged later and kept for another 72 h. The membranes were washed with deionized water to remove free electrolyte.

Electrochemical cells of the type

Reference electrode Ag–AgCl	Solution C_2	Membrane	Solution C_1	Reference electrode Ag–AgCl

Donnan potential | Donnan potential

←Diffusion→ potential

TABLE 1. Observed membrane potential E_m (mV) across parchment supported cobalt(II) and nickel(II) sulphide membranes in contact with various 1:1 electrolytes at different concentrations (at 25 ± 1°C)

Electrolyte concentration (mol/ℓ)	E_m (mV)							
	Cobalt sulphide				Nickel sulphide			
	KCl	NaCl	LiCl	NH_4Cl	KCl	NaCl	LiCl	NH_4Cl
$1/1 \times 10^{-1}$	5.1	0.6	−12.8	0.8	2.3	−5.3	−11.1	3.8
$5 \times 10^{-1}/5 \times 10^{-2}$	7.6	2.7	−11.5	1.2	3.3	−3.9	−10.8	5.5
$1 \times 10^{-1}/1 \times 10^{-2}$	19.3	15.2	−9.2	8.7	20.8	5.5	0.00	14.1
$5 \times 10^{-2}/5 \times 10^{-3}$	24.8	18.9	0.1	14.0	22.4	10.7	5.4	18.0
$1 \times 10^{-2}/1 \times 10^{-3}$	36.2	24.2	18.9	30.8	31.0	24.9	20.3	30.0
$5 \times 10^{-3}/5 \times 10^{-4}$	36.8	24.7	22.5	33.1	37.0	26.4	25.2	34.0
$1 \times 10^{-3}/1 \times 10^{-4}$	37.0	25.0	23.8	35.1	37.2	26.5	26.0	34.3

were used for measuring membrane potentials. The reference electrodes used were reversible Ag–AgCl standing in chloride solutions. The total potential difference between Ag–AgCl electrodes placed on either side of the membrane is the algebraic sum of the electrode potential, *i.e.* concentration potential and the membrane potential E_m (2, 24). A tenfold difference in concentration of chloride solutions (*i.e.* $C_2/C_1 = 10$) was maintained and measurements were made using a Pye precision potentiometer (No. 7568). The solutions were replaced by fresh solutions and when there was no change in potential with the addition of fresh solutions, with constant vigorous stirring by a pair of magnetic stirrers, it was taken as the true total potential difference across the Ag–AgCl electrodes. In both the membranes it could be reproduced within a few tenths of a mV. The whole cell was immersed in a water thermostat maintained at 25 ± 0.1°C. The various salt solutions (chlorides of Li^+, Na^+, K^+, and NH_4^+) were prepared from B.D.H. A.R. grade chemicals and deionized water. The parchment paper was supplied by M/S Baird and Tatlock (London) Ltd.

Results and Discussion

The values of membrane potential measured across two sulphide membranes in contact with various 1:1 electrolytes are given in Table 1.

When two electrolytic solutions having different concentrations are separated by a membrane, the mobile species penetrate the membrane and various transport phenomena are induced into the system (23). The fixed charge concept of Teorell (14) and Meyer and Sievers (15) (the TMS theory) for charged membranes is a pertinent starting point for the investigation of the actual mechanisms of the ionic or molecular processes which occur in the membrane phase. These authors obtained the following mathematical expression eq. 1 for the emf across a charged membrane by integrating the equation for the emf due to diffusion of ions within a membrane and subsequently adding the two phase-boundary (Donnan) potentials to the intramembrane diffusion potential

$$[1]\quad E_m = 59.2\left[\log \frac{C_2\,(\sqrt{4C_1^2 + \bar{X}^2} + \bar{X})}{C_1\,(\sqrt{4C_2^2 + \bar{X}^2} + \bar{X})} + \bar{U}\log \frac{\sqrt{4C_2^2 + \bar{X}^2} + \bar{X}\bar{U}}{\sqrt{4C_1^2 + \bar{X}^2} + \bar{X}\bar{U}}\right]$$

Here, $\bar{U} = (\bar{u} - \bar{v})/(\bar{u} + \bar{v})$, $\bar{u}$ and $\bar{v}$ are the mobilities of cation and anion, respectively, in the membrane phase, and $\bar{X}$ is the charge on the membrane expressed in equiv./ℓ of imbibed solution. In order to evaluate this parameter for the simple case of a 1:1 electrolyte and a membrane carrying a net negative charge of unity ($\bar{X} = 1$), theoretical concentration potentials E_m existing across the membrane were calculated as a function of C_2, the ratio (C_2/C_1) being kept at a constant value of 10 for different mobility ratios $(\bar{u}/\bar{v})$ and plotted as shown in Fig. 1. The observed membrane potential values for different membranes and KCl electrolyte were plotted in the same graph. The experimental curve for any given membrane was shifted horizontally and ran parallel to one of the theoretical curves. The extent of this shift gave $\log \bar{X}$ and the parallel theoretical curve gave the value for $(\bar{u}/\bar{v})$. The values of $\bar{X}$ and $(\bar{u}/\bar{v})$ derived in this way for the different membranes and electrolytes are given in Table 2.

Recently Kobatake *et al.* (17) derived the following equation for the electrical potential E_m which arises when a negatively-charged membrane separates two solutions of a 1:1 electrolyte of concentrations C_1 and C_2 ($C_1 < C_2$):

$$[2]\quad E_m = -\frac{RT}{F}\left[\frac{1}{\beta}\ln \frac{C_2}{C_1} - \left(1 + \frac{1}{\beta} - 2\alpha\right)\ln\left(\frac{C_2 + \alpha\beta X}{C_1 + \alpha\beta X}\right)\right]\ldots$$

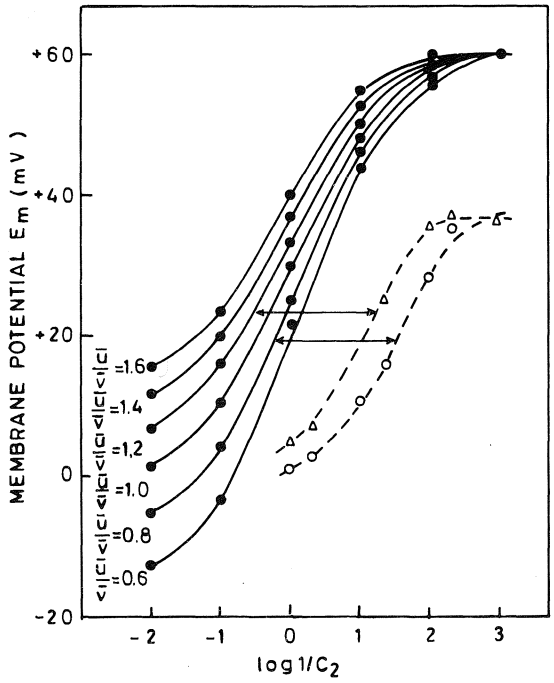

FIG. 1. Evaluation of membrane charge density $\bar{X}$ and the mobility ratio $\bar{u}/\bar{v}$ in the membrane phase. Smooth curves on the left are the theoretical concentration potentials for a cation – selective membrane ($\bar{X} = 1$) using 1:1 electrolytes at different mobility ratios $\bar{u}/\bar{v}$. The experimental values of E_m for (Δ) cobalt and (○) nickel sulphide membranes and KCl electrolyte solution are shown by the broken lines, see text.

TABLE 2. Derived values for membrane parameters ($\bar{X}$) and ($\bar{u}/\bar{v}$) using Teoreil–Meyer–Sievers theory

	Cobalt sulphide		Nickel sulphide	
Electrolyte	$(\bar{X}) \times 10^2$, equiv./ℓ	$\bar{u}/\bar{v}$	$(\bar{X}) \times 10^2$, equiv./ℓ	$\bar{u}/\bar{v}$
KCl	3.8	1.2	2.3	0.8
NaCl	3.0	0.8	1.6	0.6
LiCl	2.5	1.0	2.2	0.8
NH_4Cl	2.2	0.8	1.5	1.0

where

$$\alpha = u/(u + v)$$

$$\beta = 1 + KFX/u$$

F and K represent, respectively, the Faraday constant and a constant dependent upon the viscosity of the solution and structural details of the polymer network of which the membrane is composed. To evaluate the membrane parameters, β and X, two limiting forms of the above equation were derived. When the external salt concentration C is sufficiently small,

$$[3] \quad |E_m^{\sigma}| = \frac{1}{\beta}\ln\gamma - \left(\frac{\gamma - 1}{\alpha\beta\gamma}\right) \times \left(1 + \frac{1}{\beta} - 2\alpha\right)\left(\frac{C_2}{X}\right) + \ldots$$

where

$$|E_m^{\sigma}| = FE_m/RT$$

and

$$\gamma = C_2/C_1$$

When the salt concentration C is high,

$$[4] \quad \frac{1}{t_-} = \frac{1}{1-\alpha} + \frac{(1 + \beta - 2\alpha\beta)(\gamma - 1)}{2(1-\alpha)^2 \ln\gamma}\left(\frac{X}{C_2}\right) + \ldots$$

where t_- is the apparent transference number of coions (anions) in a negatively-charged membrane defined by

$$[5] \quad |E_m^{\sigma}| = (1 - 2t_-)\ln\gamma$$

The values of t_- calculated from observed membrane potentials using [5] are given in Table 3. Equation 3 was used to give the value of β and a relation between α and X by evaluating the intercept and the initial slope of the plot of $|E_m^{\sigma}|$ against C_2 (Fig. 2), while [4] was used to evaluate α from the intercept of a plot of $1/t_-$ against $1/C_2$ (Fig. 3). The value of X (or X_d) was determined by inserting this value of α in the relation between α and X obtained earlier. Once α and β are known in the manner described above, X (or X_c) was also evaluated from the initial slope of $1/t_-$ against $1/C_2$. Kobatake and co-workers (17) have suggested that provided their equation for the membrane potential is correct then the two values of charge densities namely X_c and X_d obtained under opposite limiting conditions (concentrated and dilute) should be the same. In the present case, the two values thus obtained agree well with each other (Table 4), thereby confirming the applicability of the Kobatake and co-workers equation to parchment supported membranes.

Once the values of the parameters α, β, and X for a given membrane electrolyte system have been determined, one can get the theoretical E_m *vs.* C_2 curve using [2] for any given γ (= C_2/C_1) and compare it with the corresponding experimental data. For this comparison eq. 2 can be rewritten in the following form as suggested by Kobatake and co-workers (17)

TABLE 3. Transference number t_- of coions derived from observed membrane potential at various electrolyte concentrations

Electrolyte concentrations (mol/ℓ)	t_- Cobalt sulphide* KCl	NaCl	LiCl	NH_4Cl	Nickel sulphide* KCl	NaCl	LiCl	NH_4Cl
$1/1 \times 10^{-1}$	0.46	0.44	0.65	0.49	0.48	0.55	0.59	0.47
$5 \times 10^{-1}/5 \times 10^{-2}$	0.44	0.48	0.59	0.48	0.47	0.53	0.59	0.45
$1 \times 10^{-1}/1 \times 10^{-2}$	0.34	0.37	0.57	0.42	0.33	0.45	0.50	0.38
$5 \times 10^{-2}/5 \times 10^{-3}$	0.30	0.34	0.50	0.38	0.31	0.41	0.45	0.35
$1 \times 10^{-2}/1 \times 10^{-3}$	0.20	0.30	0.34	0.24	0.24	0.30	0.39	0.25
$5 \times 10^{-3}/5 \times 10^{-4}$	0.19	0.29	0.31	0.22	0.19	0.29	0.29	0.21
$1 \times 10^{-3}/1 \times 10^{-4}$	0.19	0.29	0.30	0.20	0.18	0.28	0.28	0.19

*Membrane.

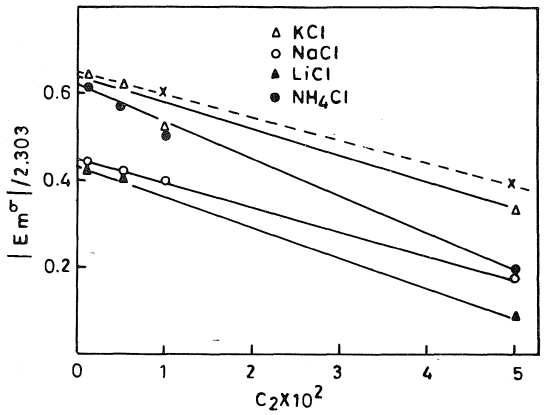

FIG. 2. Plots of $|E_m^\circ|/2.303$ *vs.* $C_2 \times 10^2$ for nickel sulphide membrane (—) in contact with various 1:1 electrolyte solutions and (---) for cobalt sulphide membrane with KCl solutions.

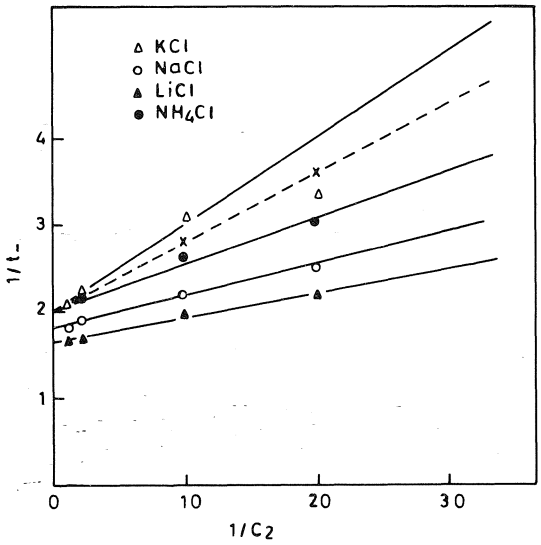

FIG. 3. Plots of $1/t_-$ *vs.* $1/C_2$ for nickel sulphide membrane (—) in contact with various 1:1 electrolyte solutions and cobalt sulphide membrane (---) with KCl solution.

$$[6] \qquad \frac{(\gamma - e^q)}{(e^q - 1)} = Z$$

with q and Z defined by

$$q = \frac{[|E_m^\circ| + (1 - 2\alpha) \ln \gamma]}{1/\beta + (1 - 2\alpha)}$$

and $Z = C_2/\alpha\beta X$. Thus if [6] is valid, the value of $(\gamma - e^q)/(e^q - 1)$ calculated from the measured E_m with predetermined α, β, and X and the given value of γ must fall on a straight line which has a unit slope and passes the co-ordinate origin when plotted against Z. This behaviour should be observed irrespective of the value of γ and the kind of membrane–electrolyte system used. Figure 4 demonstrates that the theoretical prediction of [6] (or eq. 2) is borne out quite satisfactorily by our experimental results on parchment supported membranes.

Kobatake and Kamo (23) derived another equation (eq. 7) for membrane potential using a different set of assumptions, namely: (*a*) the contribution of mass movement is negligible (23), and (*b*) small ions do not behave ideally in a charged membrane (23).

$$[7] \quad E_m = \frac{RT}{F}\left[\ln \frac{C_2}{C_1} + (2\alpha - 1) \times \ln \frac{\sqrt{4C_2^2 + \phi^2 X^2} + (2\alpha - 1)\phi X}{\sqrt{4C_1^2 + \phi^2 X^2} + (2\alpha - 1)\phi X} - \ln \frac{\sqrt{4C_2^2 + \phi^2 X^2} + \phi X}{\sqrt{4C_1^2 + \phi^2 X^2} + \phi X}\right]$$

TABLE 4. Values of the effective fixed charge densities (X_c, X_d, ϕX^* or ϕX) for various membrane electrolyte systems derived from different methods of Kobatake *et al.*

	Value							
	Cobalt sulphide*				Nickel sulphide*			
Parameter‡	KCl†	NaCl†	LiCl†	NH_4Cl†	KCl†	NaCl†	LiCl†	NH_4Cl†
$X_c \times 10^2$ equiv./ℓ (eq. 4)	3.0	2.5	1.7	2.0	2.1	1.5	2.1	1.4
$X_d \times 10^2$ equiv./ℓ (eq. 3)	3.2	2.0	2.2	2.8	2.3	1.8	2.5	3.7
$\phi X^* \times 10^2$ equiv./ℓ (eq. 13)	2.5	1.0	2.9	3.8	2.7	1.9	2.5	3.0
$\phi X \times 10^2$ equiv./ℓ (eq. 10)	2.3	2.7	2.6	4.0	2.8	1.4	1.5	4.0

*Membrane.
†Electrolyte.
‡$X_c = \frac{2(1-\alpha)^2 \ln \gamma}{(1+\beta-2\alpha\beta)(\gamma-1)} \times$ slope; $X_d = \frac{(\gamma-1)(1+1/\beta)}{\alpha\beta\gamma} \times$ slope; ϕX^* is derived from the plot P_s *vs.* log $(C_1 + C_2)/2$; $\phi X = \frac{1-\alpha}{\alpha} \times \left[\frac{\gamma \ln \gamma}{\gamma - 1}\right] \times$ slope.

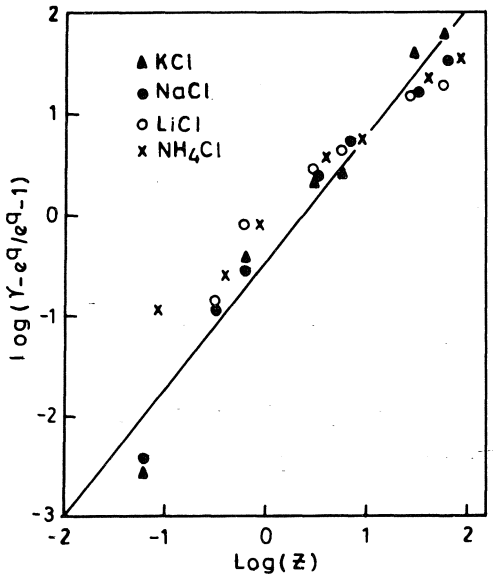

FIG. 4. Plot of log $(\gamma - e^q)/(e^q - 1)$ *vs.* log Z for nickel sulphide membrane in contact with various 1:1 electrolyte solutions.

where ϕ is a characteristic factor of the membrane–electrolyte pair, and represents a fraction of counterions not tightly bound to the membrane skeleton. The product ϕX is termed the thermodynamically effective fixed charge density of a membrane. Other terms have their usual significance. Equation 7 has the same functional form as that given by the TMS theory for the membrane potential E_m (*i.e.* eq. 1) except that the thermodynamically effective fixed charge density ϕX of the membrane is used in place of stoichiometric fixed charge density $\bar{X}$. Equation 7 reduced to the TMS membrane potential for $\phi = 1$. Since it is somewhat troublesome to evaluate ϕX at an arbitrary external electrolyte concentration from the observed membrane potential E_m using [7], Kobatake and Kamo (23) have proposed a simple method using the following approximate equation for the diffusive contribution to the emf of a cell with transport.

$$[8] \qquad E_m = -\frac{RT}{F}(1 - 2\tau_{app}) \ln C_2/C_1$$

where τ_{app} is the transference number of coions in the membrane phase. Comparison of [7] and [8] gives

$$[9] \qquad \tau_{app} = \frac{1-2\alpha}{2} \frac{\ln\left(\frac{\sqrt{4\xi_2^2+1}+2\alpha-1}{\sqrt{4\xi_1^2+1}+2\alpha-1}\right)}{\ln \gamma} + \frac{\ln\left(\frac{\sqrt{4\xi_2^2+1}+1}{\sqrt{4\xi_1^2+1}+1}\right)}{2 \ln \gamma}$$

where $\xi = C/\phi X$, when the concentration of the external salt solution is large as compared to the effective charge density ϕX, *i.e.* when $C_1/\phi X = \xi_1 \gg 1$, [9] is expanded to

$$[10] \qquad 1/\tau_{app} = \frac{1}{1-\alpha} + \frac{\gamma - 1}{\gamma \ln \gamma} \frac{\alpha}{1-\alpha}\left(\frac{\phi X}{C_1}\right) + O\left(\frac{1}{C_1}\right)^2$$

This equation indicates that the plot of $1/\tau_{app}$ *vs.* $1/C_1$ with a fixed γ (or C_2/C_1) should give a straight line, and the values of α and ϕX in the concentrated solution for a given combination of membrane and electrolyte can be determined

from the intercept and the slope of the line. The values of thermodynamically effective fixed charge densities thus derived using Fig. 5 for two sulphide membranes in contact with various 1:1 electrolytes are given in Table 4.

On the other hand (22, 23), the mass-fixed transference number of coions in a negatively-charged membrane immersed in an electrolyte solution of concentration C is defined by

$$[11] \qquad \tau_- = vC_-/(uC_+ + vC_-)$$

where C_+ and C_- are the concentrations of cation and anion respectively in the membrane phase. This equation is transformed to

$$[12] \quad \tau_- = 1 - \alpha\frac{\sqrt{4\xi^2 + 1} + 1}{\sqrt{4\xi^2 + 1} + (2\alpha - 1)}$$

using equations given by Kobatake and co-workers (22, 23) for the activity coefficients, mobilities of small ions in the membrane phase, and the equilibrium condition for electrical neutrality. The difference between τ_{app} calculated from [9] and τ_- from [12] for various reduced concentrations ξ is found to be less than 2%. Therefore τ_{app} and τ_- are considered practically the same. As a result, the apparent transference number τ_{app} evaluated from the membrane potential data permits the determination of the thermodynamically effective fixed charge density ϕX of the membrane at a given average salt concentration C (*i.e.* $(C_1 + C_2)/2$) using [12]. At the same time rearrangement of [12] leads to the definition of permselectivity P_s by the

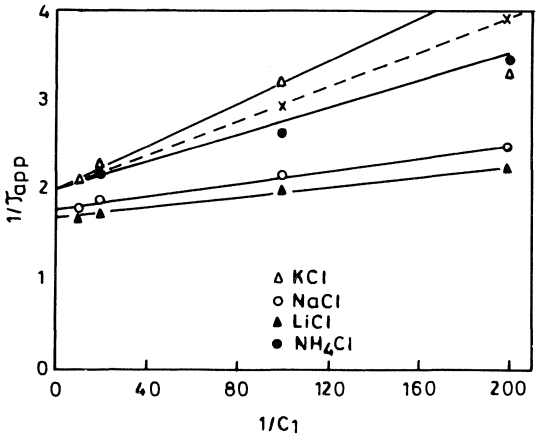

FIG. 5. Plots of $1/\tau_{app}$ *vs.* $1/C_1$ for nickel sulphide membrane (—) in contact with various 1:1 electrolyte solutions and cobalt sulphide membrane (---) with KCl solutions.

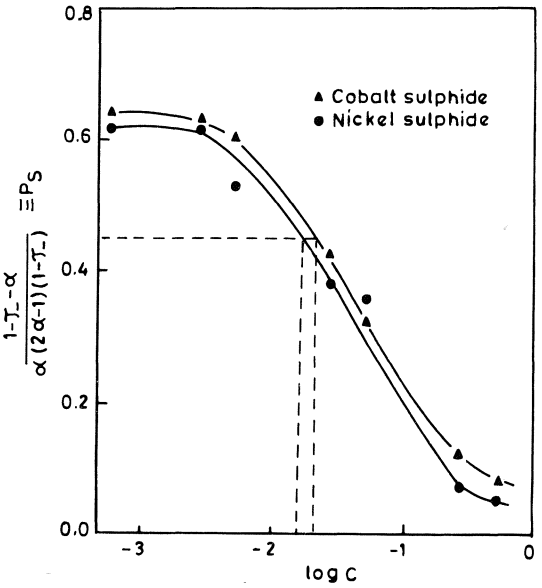

FIG. 6. Plots of P_s *vs.* log $(C_1 + C_2)/2$ for membranes using different concentrations of KCl solutions.

expression

$$[13] \quad \frac{1}{(4\xi^2 + 1)^{1/2}} = \frac{1 - \tau_- - \alpha}{\alpha - (2\alpha - 1)(1 - \tau_-)} \equiv P_s$$

This equation can be used to find the permselectivity P_s from the membrane potential measurements using [8]. If the transport number of coions (τ_- or τ_{app}) is zero, the membrane is perfectly selective and $P_s = 1$, while if the transport number of coions has the value in free solution, $P_s = 0$. The values of P_s obtained using the right-hand side of [13] were plotted against log C. The concentration at which P_s becomes $1/\sqrt{5}$ (*i.e.* $\xi = C/\phi X = 1$) gives the value of the thermodynamically effective fixed charge density ϕX as demanded by the left-hand side of [13]. Figure 6 represents a typical plot of P_s *vs.* log C for two parchment supported sulphide membranes in contact with the KCl electrolyte. The values of ϕX thus derived from both the membranes and 1:1 electrolyte combinations are given in Table 4. Further, it is noted from Tables 2 and 4 that the charge densities found by the three theories are of the same magnitude.

Acknowledgement

Thanks are due to Professor Wasiur Rahman, Head, Department of Chemistry, for providing necessary facilities.

1. F. A. SIDDIQI, N. LAKSHMINARAYANAIAH, and M. N. BEG. J. Polym. Sci. **9**, 2853 (1971).
2. F. A. SIDDIQI, N. LAKSHMINARAYANAIAH, and M. N. BEG. J. Polym. Sci. **9**, 2869 (1971).
3. F. A. SIDDIQI, M. N. BEG, S. P. SINGH, and A. HAQUE. Bull. Chem. Soc. Jpn. **49**(10), 2869 (1976).
4. F. A. SIDDIQI, M. N. BEG, S. P. SINGH, and A. HAQUE. Bull. Chem. Soc. Jpn. **49**(10), 2858 (1976).
5. F. A. SIDDIQI, M. N. BEG, and S. P. SINGH. J. Polym. Sci. In press.
6. F. A. SIDDIQI, M. N. BEG, and P. PRAKASH. J. Electroanal. Chem. In press.
7. F. A. SIDDIQI and S. PRATAP. J. Electroanal. Chem. **23**, 137 (1969).
8. F. A. SIDDIQI and S. PRATAP. J. Electroanal. Chem. **23**, 147 (1969).
9. F. A. SIDDIQI, N. LAKSHMINARAYANAIAH, and S. K. SAKSENA. Z. Phys. Chem. (Frankfurt), **72**, 298 (1970).
10. F. A. SIDDIQI, N. LAKSHMINARAYANAIAH, and S. K. SAKSENA. Z. Phys. Chem. (Frankfurt), **72**, 307 (1970).
11. G. EISENMAN. Membrane transport and metabolism. *Edited by* A. Kleinzer and A. Kotyk. Academic Press, New York, NY. 1961. p. 163; Biophys. J. Suppl. **2**, 259 (1962).
12. H. SHERRY. Ion exchange. Vol. 2. *Edited by* J. A. Marinsky. Dekker, New York, NY. 1968.
13. S. GLASSTONE, K. S. LAIDLER, and H. EYRING. The theory of rate processes. McGraw Hill, New York, NY. 1941. (*a*) p. 525; (*b*) p. 544.
14. T. TEORELL. Proc. Soc. Exp. Biol. **33**, 282 (1935); Proc. Natl. Acad. Sci. (USA), **21**, 152 (1935); Z. Electrochem. **55**, 460 (1951); Prog. Biophys. Chem. **3**, 385 (1953).
15. K. H. MEYER and J. F. SIEVERS. Helv. Chim. Acta, **19**, 649 (1936); **19**, 665 (1936); **19**, 987 (1936).
16. T. TEORELL. Discuss. Faraday Soc. No. 21, 9 (1956).
17. Y. KOBATAKE, T. NORIAKI, Y. TOYOSHIMA, and H. FUJITA. J. Phys. Chem. **69**, 3981 (1965).
18. Y. TOYOSHIMA, M. YUSSA, Y. KOBATAKE, and H. FUJITA. Trans. Faraday Soc. **63**, 2803 (1967); **63**, 2814 (1967).
19. M. YUSSA, Y. KOBATAKE, and H. FUJITA. J. Phys. Chem. **72**, 2871 (1968).
20. N. KAMO, Y. TOYOSHIMA, H. NOZAKI, and Y. KOBATAKE. Kolloid-Z. Z. Polym. **248**, 214 (1971).
21. N. KAMO, Y. TOYOSHIMA, and Y. KOBATAKE. Kolloid-Z. Z. Polym. **249**, 1061 (1971).
22. N. KAMO, M. OCKAWA, and Y. KOBATAKE. J. Phys. Chem. **77**, 92 (1973); **77**, 2995 (1973).
23. Y. KOBATAKE and N. KAMO. Prog. Polym. Sci. Jpn. **5**, 257 (1972).
24. N. LAKSHMINARAYANAIAH. Transport phenomena in membranes. Academic Press, New York, NY. 1969. p. 196.

The pyridinium–dihydropyridine system. I. Synthesis of a series of substituted pyridinium ions and their 1,4-dihydro reduction products and a determination of their stabilities in aqueous buffers

DONALD J. NORRIS AND ROSS STEWART

Department of Chemistry, University of British Columbia, Vancouver, B.C., Canada V6T 1W5

Received October 25, 1976

DONALD J. NORRIS and ROSS STEWART. Can. J. Chem. **55**, 1687 (1977).

Fourteen pyridinium salts, substituted at the 1- and 3-positions, have been prepared and their stabilities determined in aqueous acetate and tris(hydroxymethyl)aminomethane (Tris) buffers. The 1,4-dihydro derivatives of eleven of these have been prepared and characterized and their stabilities likewise determined. The pyridinium ions are stable in acidic solution but undergo either ring attack or amide or ester hydrolysis under basic conditions, whereas the dihydropyridines undergo covalent hydration in acid solution. For only four pairs of compounds and one buffer system (Tris) are there p*H*-ranges in which the pyridinium and dihydropyridine forms are simultaneously stable (less than 10% decomposition in 24 h). These compounds have a carbamoyl or acetyl group at the 3-position and either a methoxymethyl, acetonyl, or carbamoylmethyl group at the 1-position. The acetic acid catalyzed rates of hydration of the 1-alkyl-3-carbamoyl-1,4-dihydropyridines are correlated by σ^* values with a ρ^* of -2.00, consistent with protonation being the rate-controlling step.

DONALD J. NORRIS et ROSS STEWART. Can. J. Chem. **55**, 1687 (1977).

On a préparé 14 sels de pyridinium substitués dans les positions 1 et 3 et on a déterminé leur stabilité dans des tampons d'acétate aqueux et de tris(hydroxyméthyl) aminométhane (Tris). On a préparé les dérivés dihydrogénés en 1,4 d'onze de ces composés et on les a aussi caractérisés et déterminé leur stabilité. Les ions pyridinium sont stables en solution acide mais subissent soit des attaques au niveau du cycle ou des hydrolyses de l'amide ou de l'ester dans des conditions basiques; par ailleurs, les dihydropyridines subissent une hydratation covalente en solution acide. Il n'y a que quatre paires de composés et un système de tampons (Tris) qui fournissent des écarts de p*H* dans lesquels les formes pyridinium et dihydropyridine sont stables d'une façon simultanée (une décomposition de moins de 10% en 24 h). Ces composés possèdent un groupe carbamoyle ou acétyle en position 3 et soit un groupe méthoxyméthyle, acétonyle ou carbamoylméthyle en position 1. Il y a une corrélation entre les vitesses catalysées par l'acide acétique pour l'hydratation des alkyl-1 carbamoyl-3 dihydro-1,4 pyridines et les valeurs σ^*; la valeur de ρ^* de -2.00 est en accord avec une protonation qui agirait comme étape déterminante de la réaction.

[Traduit par le journal]

Introduction

Nicotinamide coenzymes, such as NAD^+, nicotinamide adenine dinucleotide (**1**, $R_1 = CONH_2$, R_2 = adenine dinucleotide), are two-equivalent oxidants which occupy one of the termini of the so-called electron-transport chain in living systems, with oxygen, a one-equivalent oxidant, occupying the other (1). The pyridinium ring in such systems oxidizes alcoholic and other groups by a two-equivalent process which is essentially a hydride transfer, and is converted to a 1,4-dihydropyridine thereby.

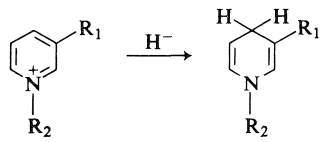

1 **2**

We were interested in determining the effect of substituents in the pyridine ring on the relative free energy levels of the oxidant and reductant, and ultimately, to find NAD^+ model compounds whose equilibrium with flavin nucleotides (the next redox system in the chain) could be directly measured. Accordingly, we have prepared a number of pyridinium and dihydropyridine compounds, **1** and **2** which are models for NAD^+ and its reduction product NADH, and have examined their properties. The present article describes the synthesis of these compounds and a determination of their stabilities in aqueous buffers, the medium in which the redox studies have been made.

Experimental

Synthesis of Quaternary Pyridinium Salts

Quaternary pyridinium salts were prepared from the

corresponding pyridines and alkyl halides. Methyl chloroacetate was prepared from chloroacetic acid and methanol by the method of Clinton and Laskowski (2); isopropyl chloroacetate was similarly prepared by using 2-propanol in place of methanol. All of the other alkyl halides and the pyridines were obtained commercially and used without further purification.

The general method for preparing the pyridinium salts consisted of mixing 30 mmol of each of the pyridine and alkyl halide in 15 ml of solvent (usually acetone or acetone–dimethylformamide) and refluxing for 1–3 days until sufficient crystals had formed. The crystals were filtered, washed with acetone, and dried under aspirator vacuum. Individual variations on this scheme are noted in Table 1. Analytical data appear in Table 2.

Two of the pyridinium compounds, **1***a* and **1***n*, can undergo protonation or deprotonation in the aqueous p*H* range. The p*K* of the carboxylate group of **1***a* was determined to be 1.62 ± 0.12 by monitoring the spectral changes at 250 nm (8). In most aqueous solutions, therefore, **1***a* exists as the dipolar ion. The dissociation constant of the 3-hydroxy group in **1***n* was determined by titration with standard base. A p*K* of 4.69 ± 0.01 was found, close to that for the 3-hydroxypyridinium ion (9). In neutral and basic solutions, therefore, the compound exists predominantly in the dipolar ion form.

Synthesis of 1,4-Dihydropyridines

The 1,4-dihydropyridines were prepared by the classical method of reduction of the corresponding pyridinium salts with sodium dithionite (5, 11–13). The pyridinium salts were used directly as recovered from their preparative reaction mixtures (*vide ante*). Unless stated otherwise crude yields were approximately 50%, and the product crystals could not be stored in contact with air without appreciable decomposition occurring. Compounds **2***m* and **2***n* are expected to be highly unstable in aqueous solution and their attempted preparations were unsuccessful.

In all dihydropyridine syntheses, a solution of 10 mmol of the corresponding pyridinium salt in 15 ml of water was used. These solutions were flushed with nitrogen and then treated by one of the following methods.

Method I

$Na_2S_2O_4$ (2.6 g) was mixed with 20 mmol of sodium or potassium carbonate powder and this mixture was added portionwise to the stirred pyridinium ion solution. Stirring under nitrogen was continued for 15 to 20 min after the first signs of crystallization, after which the crystals were filtered, washed with water, and dried under aspirator vacuum.

*1-Carbamoylmethyl-3-carbamoyl-1,4-dihydropyridine (**2i**)*—The crude crystals were recrystallized from water (30 ml/g) giving an overall 66% yield of yellow, rod-like crystals, which are stable indefinitely in the presence of air at room temperature, mp 179–182°C (dec.). *Anal.* calcd. for $C_8H_{11}N_3O_2$: C 53.04, H 6.07, N 23.20; found: C 52.79, H 6.21, N 23.05.

*1-Carbomethoxymethyl-3-carbamoyl-1,4-dihydropyridine (**2f**)*—The crude product was recrystallized from benzene to give yellow needles, which were stable in air for a few months, mp 128–132°C (dec.). *Anal.* calcd. for $C_9H_{12}N_2O_3$: C 55.12, H 6.12, N 14.29; found: C 55.11, H 6.19, N 14.26.

*1-Cyanomethyl-3-carbamoyl-1,4-dihydropyridine (**2h**)*—The crude crystals were dissolved in refluxing methylene chloride and filtered. Petroleum ether was added until crystallization began. The solution was cooled under nitrogen to yield fluffy, pale yellow crystals, mp 127–130°C (dec.). *Anal.* calcd. for $C_8H_9N_3O$: C 58.89, H 5.52, N 25.77; found: C 58.72, H 5.68, N 25.75.

Method II

Reduction of the pyridinium ions was carried out as in method I, but since the resulting dihydropyridines would not precipitate from the reaction mixture an alternative recovery method was used. After the mixture had turned a bright yellow colour, it was extracted continuously overnight with methylene chloride which had been stored over KOH pellets. The methylene chloride extract was concentrated from about 200 ml to about 20 ml on a rotary evaporator. The remaining solvent was evaporated under aspirator vacuum in a flask fitted with a nitrogen bleed. The nitrogen bleed was necessary in order to recover a crystalline product; without it, evaporation of the remaining methylene chloride left only a yellow oil.

*1-Acetonyl-3-carbamoyl-1,4-dihydropyridine (**2e**)*—The crude product was recrystallized from ethyl acetate, mp 118–121°C (dec.). *Anal.* calcd. for $C_9H_{12}N_2O_2$: C 60.00, H 6.67, N 15.56; found: C 60.38, H 6.68, N 15.20.

*1-Carbamoylmethyl-3-acetyl-1,4-dihydropyridine (**2j**)*—The crude material (64% yield) was recrystallized from ethyl acetate (160 ml/g) under nitrogen to give fine yellow needles, which are stable for several days in air, mp 162–163°C (dec.). *Anal.* calcd. for $C_9H_{12}N_2O_2$: C 60.00, H 6.67, N 15.56; found: C 60.31, H 6.80, N 15.30.

*1-Carbo-i-propoxymethyl-3-carbamoyl-1,4-dihydropyridine (**2g**)*—The crude product was recrystallized from ethyl acetate (20 ml/g) under nitrogen. The crystals appear to require several days of exposure to air for noticeable decomposition, mp 112–114°C (dec.). *Anal.* calcd. for $C_{11}H_{16}N_2O_3$: C 51.06, H 5.80, N 10.83; found: C 50.89, H 5.69, N 10.88.

*1-Methoxymethyl-3-carbamoyl-1,4-dihydropyridine (**2d**)*—The crude crystals (70% yield) were recrystallized twice from ethyl acetate. The recrystallization flask must be scraped with a glass rod before sealing the solution under nitrogen or recrystallization will not occur. The pure crystals are stable for only a few days in the presence of air, mp 106–107°C (dec.). *Anal.* calcd. for $C_8H_{12}N_2O_2$: C 57.14, H 7.14, N 16.67; found: C 57.40, H 7.07, N 16.66.

*1-Carbamoylmethyl-3-cyano-1,4-dihydropyridine (**2k**)*—A small amount of product crystallized from the reaction mixture. These crystals were combined with the extraction product and recrystallized from benzene (100 ml/g). A yield of 70 mg (approximately 10%) of pure product was obtained, mp 139–139.5°C. *Anal.* calcd. for $C_8H_9N_3O$: C 58.89, H 5.52, N 25.77; found: C 59.18, H 5.72, N 25.45.

Method III

The dihydropyridines which are quite acid-labile decompose too rapidly in carbonate solutions for methods I and II to be practical. In these cases, potassium hydroxide was used instead of carbonate. The sodium dithionite and KOH were alternately added to the stirred

TABLE 1. Preparation of pyridinium salts

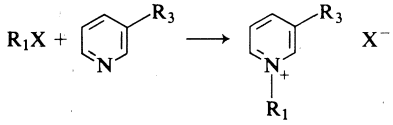

	R_1	R_3	X^-	Reaction solvent	Reaction time (h)	Crude yield (%)	Recrystallization solvent	mp (dec.) found	mp (dec.) lit. (ref.)
1*a*	CH_2COO^-	$CONH_2$	—	MeOH[a]	24	—	H_2O–EtOH	200–203	204–206(3) 206–208(4)
1*b*	CH_3	$CONH_2$	I^-	MeOH	4	81	EtOH	207–210	203(5)
1*c*	CH_2CH_2OH	$CONH_2$	Cl^-	Acetone–DMF(2:1)	48	40	EtOH	195	195.5–196(6) 182(7)
1*d*	CH_2OCH_3	$CONH_2$	Cl^-	Acetone[b]	2	—	—[c]	123–125	
1*e*	CH_2COCH_3	$CONH_2$	Cl^-	Acetone–DMF(1:1)	48	98	MeOH–acetone	202–203	—
1*f*	CH_2COOCH_3	$CONH_2$	Cl^-	Acetone–DMF(2:1)	24	91	MeOH–acetone	165–166	—
1*g*	$CH_2COOCH(CH_3)_2$	$CONH_2$	Cl^-	Acetone–DMF(2:1)	24	92	MeOH–acetone	202–204	—
1*h*	CH_2CN	$CONH_2$	Cl^-[d]	Acetone–DMF(2:1)	48	86	H_2O–EtOH	236–238	—
1*i*	CH_2CONH_2	$CONH_2$	Cl^-	Acetone–DMF(5:1)	24	95	H_2O–EtOH	213–214	—
1*j*	CH_2CONH_2	$COCH_3$	Cl^-	Acetone–DMF(2:1)	24	81	MeOH–acetone	214–214.5	—
1*k*	CH_2CONH_2	CN	Cl^-[d]	Acetone	48	64	EtOH	193–196	
1*l*	CH_2CONH_2	F	Cl^-[d]	Acetone–DMF(3:1)[e]	72	68	EtOH–acetone	160–162	—
1*m*	CH_2CONH_2	H	Cl^-	Acetone	24	87	MeOH–acetone	206–206.5	—
1*n*	CH_2CONH_2	OH	Cl^-	Acetone	24	—	EtOH	197–199	—

[a]Using either sodium chloroacetate or sodium iodoacetate.
[b]The nicotinamide was dissolved in 110 ml of acetone, the chloromethyl methyl ether was added dropwise and the solution was stirred at room temperature while the product slowly crystallized. All recrystallization attempts resulted in decomposition to nicotinamide.
[c]All attempts at recrystallization resulted in decomposition to nicotinamide.
[d]Using a catalytic amount of NaI.
[e]The product separated as a red oil which could be crystallized by seeding or cooling below 0°C, and stirring the oil into acetone.

TABLE 2. Analytical data for pyridinium salts

Compound	Calculated			Found		
	C	H	N	C	H	N
1-Methoxymethyl-3-carbamoylpyridinium chloride (**1***d*)	47.41	5.43	13.83	47.20	5.61	14.00
1-Acetonyl-3-carbamoylpyridinium chloride (**1***e*)	50.35	5.13	13.05	50.42	5.10	13.26
1-Carbomethoxymethyl-3-carbamoylpyridinium chloride (**1***f*)	46.85	4.77	12.15	46.64	5.06	11.80
1-Carbo-*i*-propoxymethyl-3-carbamoylpyridinium chloride (**1***g*)	51.06	5.80	10.83	50.89	5.69	10.88
1-Cyanomethyl-3-carbamoylpyridinium chloride (**1***h*)	48.61	4.05	21.27	48.42	4.14	21.03
1-Carbamoylmethyl-3-carbamoylpyridinium chloride (**1***i*)	44.55	4.64	19.49	44.63	4.85	19.46
1-Carbamoylmethyl-3-acetylpyridinium chloride (**1***j*)	50.35	5.13	13.05	50.33	5.00	12.87
1-Carbamoylmethyl-3-cyanopyridinium chloride (**1***k*)	48.61	4.05	21.27	48.74	4.10	21.23
1-Carbamoylmethyl-3-fluoropyridinium chloride (**1***l*)	44.09	4.20	14.70	43.80	4.17	14.67
1-Carbamoylmethylpyridinium chloride (**1***m*)	48.70	5.22	16.23	48.82	5.08	15.96
1-Carbamoylmethyl-3-hydroxypyridinium chloride (**1***n*)[a]	44.56	4.78	14.85	44.73	4.68	14.80

[a]To confirm that alkylation had not occurred at the hydroxyl group the uv spectrum was compared to that of 1-methyl-3-hydroxypyridinium chloride in acidic and basic solutions. The latter compound has a maximum at 288 nm at p*H* 1 which shifts to 245 and 322 nm at p*H* 13 (10). **1***n* has a maximum at 289 nm at p*H* 1 which shifts to 238 and 313 nm at p*H* 13.

pyridinium ion solution so as to maintain the p*H* close to 10. The products with the exception of **2***l* were recovered as described in method II.

*1-(2′-Hydroxyethyl)-3-carbamoyl-1,4-dihydropyridine (**2***c*)—The product which crystallized from the methylene chloride was filtered, dried, and stored under nitrogen in a dry box. Less than a day's exposure to air is sufficient to cause noticeable discoloration of the crystals, mp 133–133.5°C (dec.); lit. (14) mp 119–121°C. *Anal.* calcd. for $C_8H_{12}N_2O_2$: C 57.14, H 7.14, N 16.67; found: C 56.97, H 6.96, N 16.53.

*1-Methyl-3-carbamoyl-1,4-dihydropyridine (**2***b*)—A yield of 0.4 g (35%) of bright yellow crystals was obtained, mp 73.5–78°C (dec.); lit. (5) mp 84°C, (15) mp 85.3–86.8°C; λ_{max} (ε) = 360 (7820); lit. (15). λ_{max} (ε) = 355 (6680). Attempts to recrystallize the crude product were unsuccessful. The lower extinction coefficient reported in the literature was recorded in water, where this compound decomposes even in the absence of buffer acid. The spectrum of this compound was recorded at p*H* 9.8 in this study to slow down the decomposition reaction, but even at this p*H* a decomposition of a few percent an hour is observable.

*1-Carbamoylmethyl-3-fluoro-1,4-dihydropyridine (**2***l*)—Crystals formed within a few minutes and were filtered immediately. If the crystals were stirred in solution for more than 10 min, they redissolved. Continuous extraction of the filtrate with methylene chloride yielded no product. Presumably the dihydropyridine is so susceptible to acid-catalyzed decomposition that the product must be recovered immediately, even at a p*H* as high as 10. The crude product was recrystallized from benzene (40 ml/g) giving a 10% yield of product, mp 116.5–118°C (dec.). *Anal.* calcd. for $C_7H_9N_2OF$: C 53.85, H 5.77, N 17.95; found: C 53.88, H 5.80, N 17.94.

*1-Carboxymethyl-3-carbamoyl-1,4-dihydropyridine (**2***a*)—This compound could be prepared by method III but it did not prove possible to purify it to analytical standards. When required it was prepared *in situ* by hydrolysis of **2***f* in p*H* 10 buffer for an hour.

Rate Measurements

Kinetic runs were followed by visible or uv absorption spectroscopy. Reactions which had half-lives greater than 5 min were followed on a Cary 16 spectrophotometer. Whenever the absorbance was not being read, the sample cell was removed from the path of the light beam. Reactions which had half-lives less than 5 min were followed on a Bausch and Lomb Spectronic 505 recording spectrophotometer.

Acid-catalyzed Decomposition of 1,4-Dihydropyridines

The rates of decomposition of 1,4-dihydropyridines in acid buffers (acetate or tris(hydroxymethyl)aminomethane, hereafter designated Tris) were measured by following the loss of dihydropyridine absorbance in the region between 300 and 390 nm.

The reaction mixtures were analyzed within a few hours after the decomposition was begun. The p*H* was measured on a Radiometer 26 p*H* meter standardized at p*H* 4 and 7 or 7 and 10. The concentration of acetic acid was determined by titration to a phenolphthalein end point with a standard sodium hydroxide solution. The concentration of protonated Tris was determined by titration to p*H* 10.5 with a standard sodium hydroxide solution.

Absorbance Spectra

Absorbance spectra were recorded on a Cary 16 spectrophotometer between 220 and 520 nm at 10 nm intervals. Spectral determinations were repeated until the extinction coefficients near λ_{max} were reproducible to within 3%. The values of λ_{max} and the corresponding extinction coefficients of most of the compounds used in this study are listed in Table 3. The spectra were recorded in water, except those of **2***a*, **2***b*, **2***c*, and **2***l*, which decompose rapidly in pure water and, therefore, were recorded in p*H* 10 buffer.

Results and Discussion

In view of the ubiquity of NAD^+ and NADH in living systems it is, perhaps, surprising that pyridinium and dihydropyridine rings are subject to ring attack in buffered aqueous systems. A considerable amount of work has been done on these reactions and the pyridinium ring lability been shown to result from nucleophilic

TABLE 3. Ultraviolet absorption data

Compound			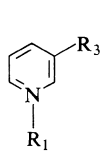		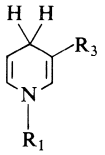	
	R_1	R_3	λ_{max}	ε (M^{-1} cm^{-1})	λ_{max}	ε (M^{-1} cm^{-1})
a	CH_2COO^-	$CONH_2$	—	—	356	7360
b	CH_3	$CONH_2$	—	—	360	7280
c	CH_2CH_2OH	$CONH_2$	265	4340	357	7510
d	CH_2OCH_3	$CONH_2$	264	~4500	338	6490
e	CH_2COCH_3	$CONH_2$	266	4860	353	6300
f	CH_2COOCH_3	$CONH_2$	266	4750	347	6900
g	$CH_2COOCH(CH_3)_2$	$CONH_2$	—	—	349	6360
h	CH_2CN	$CONH_2$	265	4900	340	5820
i	CH_2CONH_2	$CONH_2$	267	4800	351	6800
j	CH_2CONH_2	$COCH_3$	267.5	4450	370	12000
k	CH_2CONH_2	CN	269.5	4670	334	5680
l	CH_2CONH_2	F	—	—	275(sh)	1500

attack at the 2- or 4-positions, reaction 1 (1*b*, 16, 17). The dihydropyridine reaction appears to involve protonation at the 5-position, followed by attack by water or other nucleophile at the 6-position, reaction 2. A second, slower, reaction leads to further decomposition.

[1] 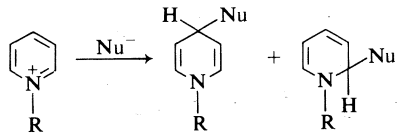

[2] 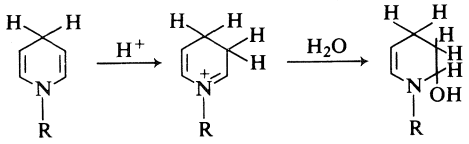

A further cause of instability in aqueous buffers of many of the compounds studied is the lability of the carboxamido and carbalkoxy groups toward hydrolysis (17, 18).

The three principal causes of instability in the model compounds, amide and ester hydrolysis, nucleophilic attack on the pyridinium ring, and acid-catalyzed hydration (or related reaction) of the dihydropyridine ring are discussed below. Since basic conditions favour the first two of these reactions and acidic conditions the third we have sought to define p*H* ranges in which both the oxidized and reduced forms have sufficient stability to enable measurements to be made of redox equilibria involving these compounds.

Amide and Ester Hydrolysis

At p*H* 10.05, 1-carbamoylmethyl-3-fluoropyridinium ion (**1***l*) is slowly converted to a new compound whose polarographic half-wave potential is approximately 200 mV more negative. A similar difference in half-wave potentials is observed between 1-carbamoylmethyl-3-carbamoylpyridinium ion (**1***i*) and 1-carboxymethyl-3-carbamoylpyridinium ion (**1***a*).[1] Thus the

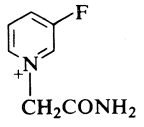

1*l*

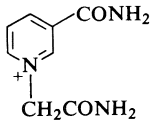

1*i*

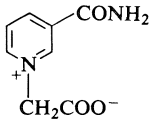

1*a*

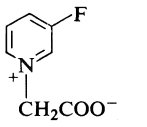

3

half-wave potentials are consistent with hydrolysis of the amide group on the 1-substituent to give 1-carboxymethyl-3-fluoropyridinium ion, **3**. In order to limit the amide hydrolysis rate of **1***l* to 10% or less over a period of 24 h, the cation should not be subjected to a p*H* greater than approximately 9.5.

[1]D. J. Norris and R. Stewart, to be published.

Similar behaviour was observed with solutions of 1-carboxymethyl-3-carbamoylpyridinium ion (**1***a*) and 1-(2′-hydroxyethyl)-3-carbamoylpyridinium ion (**1***c*) left for long periods at p*H*'s near 10. At p*H* 10 the polarographic wave of **1***a* at −1.07 V (*vs.* s.c.e.) disappears with a half-life of 5–6 days and is replaced by a wave at −1.33 V (*vs.* s.c.e.). The polarographic wave of **1***c* decays slightly more rapidly, having a half-life of approximately 3 days at p*H* 9.72 and 10 days at p*H* 10.26. The polarographic half-wave potentials of the products are in the regions one might expect for the dipolar 3-carboxypyridinium ions, **4** and **5**. Thus, the decomposition of **1***a* and **1***c*

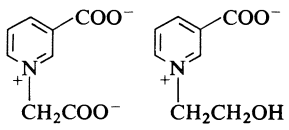

4 **5**

is consistent with hydrolysis of the amide group at the 3-position. In order to limit this decomposition of **1***a* and **1***c* to no more than 10% over a period of 24 h, these ions should not be subjected to p*H*'s greater than 10.1 and 9.9, respectively.

Although no other pyridinium ions were tested for stability in the p*H* region above 10, it is likely that the hydrolysis observed with **1***a*, **1***c*, and **1***l* will occur with any pyridinium ion containing a 1-carbamoylmethyl or 3-carbamoyl group. Consequently, 3-carbamoylpyridinium ions should not be subjected for long periods to p*H*'s greater than 10.0 and 1-carbamoylmethylpyridinium ions to p*H*'s greater than 9.5. Two esters, 1-carbomethoxymethyl- and 1-carbo-*i*-propoxymethyl-3-carbamoylpyridinium ions (**1***f* and **1***g*) underwent rapid decomposition in alkaline solutions. At p*H* 9.2 the methyl ester decomposition had a half-life of approximately 3 min and the *i*-propyl ester reacted about one-sixth as fast. The products from both esters have polarographic half-wave potentials similar to that of 1-carboxymethyl-3-carbamoylpyridinium ion (**1***a*),[1] indicative of hydrolysis of the ester functions. Assuming the hydrolysis rate to be proportional to hydroxide ion concentration over this p*H* range, the decomposition of **1***f* and **1***g* will exceed 10% over a period of 24 h for p*H*'s greater than 5.7 and 6.5, respectively.

Reactions of the Pyridinium Ring

The instability in base of most of the compounds studied was due, in the first instance, to amide or ester hydrolysis. However, in the case of compounds **1***h*, **1***j*, and **1***k*, all of which contain strongly electron-withdrawing groups, the ring is the first site to be attacked as the p*H* is raised.

When **1***h* is mixed with Tris buffer at p*H* 8.2, the solution immediately turns yellow from an increase in absorbance in the region near 340 nm. In more basic solutions, the absorbance at 340 nm is higher still. Upon acidification, the absorbance spectrum reverts to that of **1***h*.

If **1***h* is left at p*H* 8.2 a second, slower reaction occurs with a half-life of approximately 80 min. This reaction is accompanied by further increases in absorbance at 340 nm and decreases in the pyridinium absorbance at 265 nm.

Reaction can also be observed polarographically under the same conditions. Concurrent with the increase in optical density at 340 nm, the polarographic half-wave potential shifts from −800 mV (*vs.* s.c.e.) to −900 mV[1] and the total limiting current of the polarographic wave decreases throughout the reaction to a final value of approximately two thirds of the initial limiting current. The rate of these changes increases with increasing p*H*, but the final value of the limiting current is independent of p*H*. On the other hand, the final value of the absorbance at 340 nm, like the initial value of this quantity, increases with increasing p*H*.

The very rapid, reversible reaction in alkaline solutions probably results from nucleophilic addition of hydroxide to the pyridinium ring (19, 20). (Glycine also appears to react by nucleophilic addition to the ring.) The nature of the subsequent reactions is, however, not clear. In order to avoid these reactions, these cations (**1***h*, **1***j*, **1***k*) should not be subjected to p*H*'s greater than 6.5, 9.5, and 6.5, respectively.

Reactions of the Dihydropyridine Ring

The decomposition of 1,4-dihydropyridines in the presence of acids has been studied by several groups in the past (1*b*, 21–26) and is known to involve several successive reactions (23–25). The primary acid decomposition reaction is a two-step process resulting in hydration of the 5,6-double bond, [2] (21, 26). The first step, which is believed to be rate-determining in aqueous media (21) is protonation at C-5, followed by nucleophilic attack at C-6. In aqueous solutions, the nucleophiles are primarily hydroxide ion and water, although adducts resulting from attack by other nucleophiles are also known (1*b*, 22).

We have measured the rates of the primary acid decomposition reaction for the 1,4-dihydropyridines **2***a–f*, **2***h–l* in acetate and tris(hydroxymethyl)aminomethane (Tris) buffers. The decomposition was followed spectrophotometrically at the λ_{max} of the 1,4-dihydropyridine, near 350 nm. The product generally has an absorbance of approximately 3% of that of the 1,4-dihydropyridine (25) which further decays as the product is consumed in a slower secondary decomposition reaction. Using an absorbance at infinite time, A_∞, of 3% of the initial absorbance, plots of log $(A - A_\infty)$ against time were linear over at least five half-lives as shown in Fig. 1.

The observed rate constants at different p*H*'s and buffer concentrations were analyzed to determine the acetic acid catalytic rate constants using [3] and the results given in Table 4.

$$[3]\quad k_{obs} = k_0 + k_{H^+}[H^+] + k_{AcOH}[AcOH]$$

The uncatalyzed rate, k_0, is a negligible fraction of the rate in acetate buffers, though it does account for a significant fraction of the decomposition in dilute Tris buffers, in which the dihydropyridines are much more stable. The contribution of the term $k_{H^+}[H^+]$ to the overall decomposition rate in 0.1 *M* acetate buffers is less in all cases than that made by the buffer acid term $k_{HOAc}[HOAc]$. 1-Carbamoyl-3-fluoro-1,4-dihydropyridine (**2***l*) decomposed too rapidly in acetate buffer for the reaction to be followed on a recording spectrophotometer. In fact, it underwent the acid decomposition reaction within minutes in unbuffered 1 *M* potassium perchlorate. The decomposition rate in Tris buffer was fast but measurable.

As a result of acid-catalyzed decomposition each 1,4-dihydropyridine will have a minimum allowed p*H* below which it decomposes rapidly enough to interfere with experiments. This value will be to some extent dependent on the choice of buffer. We have calculated a minimum effective p*H* for each dihydropyridine in two buffer systems: acetate ($pK_a = 4.8$), and Tris ($pK_a = 8.1$) (Table 5). (The need to retain buffer capacity places an effective lower limit on such values, one p*H* unit below the p*K* of the buffer acid.)

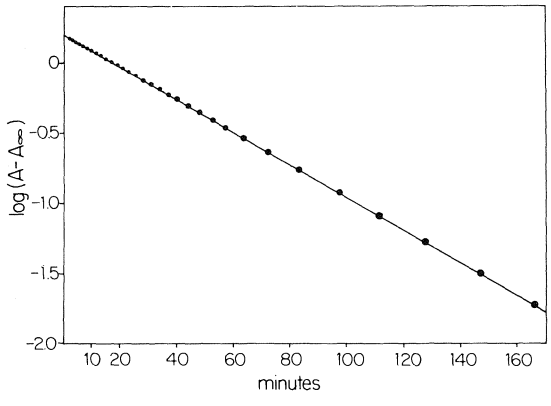

FIG. 1. First-order plots of the rate of hydration of 1-methyl-3-carbamoyl-1,4-dihydropyridine (**2***b*) in 1.0 *M* Tris buffer at p*H* 7.1; *A* is absorbance at 360 nm.

TABLE 4. Acetic acid catalytic coefficients for the hydration of substituted dihydropyridines

Compound	$10^2 k_{HOAc}$ $(M^{-1}\ s^{-1})$	Compound	$10^2 k_{HOAc}$ $(M^{-1}\ s^{-1})$
2*a*	3.3	**2***f*	0.48
2*b*	16	**2***g*	0.03
2*c*	6.2	**2***h*	0.53
2*d*	0.77	**2***i*	0.02
2*e*	0.77	**2***j*	0.02

The minimum allowed p*H* will, of course depend on the decomposition rate which is acceptable. Since some of the equilibration reactions we are concerned with are relatively slow we have arbitrarily chosen a decomposition rate of no more than 10% over 24 h as acceptable for experiments requiring as much as 5 to 6 h. However, for many of the dihydropyridines a decomposition rate this slow cannot be attained in some buffers, the extent of decomposition being as high as 10% in 45 min. Even for these compounds kinetic and other experiments requiring short reaction times can still be conducted with little interference from the decomposition reaction.

The minimum allowed p*H* will depend not only on the choice of buffer system, but also the buffer strength. The values in Table 5 have been calculated assuming a total buffer concentration of 0.1 *M*. Using a lower buffer concentration will generally allow the dihydropyridine to be used at a slightly lower p*H* without increasing the decomposition rate.

The 1,4-dihydropyridines **2***a* through **2***k* can be divided into three groups based on their acid lability. Compounds **2***a*, **2***b*, and **2***c* undergo a relatively rapid decomposition, thus preventing their use in buffers as acidic as acetate or phosphate. Even in Tris buffer, these dihydropyridines are not stable for 24 h (>10% decomposition), although **2***a* does meet the criterion of less than 10% decomposition in 6 h at p*H* 8.5 or higher.

Errata 2 - The captions for Table 4 & 5 should indicate the following: T = 25°C.

TABLE 5. Effective acidity limits for 1,3-substituted pyridinium ions and dihydropyridines[a] in aqueous buffers

				Minimum p*H* for dihydropyridine (**2***a–f, h–l*)	
	R_1	R_3	Maximum p*H* for pyridinium ion (**1***a–l*)	Acetate buffer (p*K* 4.8)	Tris buffer (p*K* 8.1)
a	$CH_2CO_2^-$	$CONH_2$	10	—[b]	—[c]
b	CH_3	$CONH_2$	10	—[b]	—[d]
c	CH_2CH_2OH	$CONH_2$	10	—[b]	—[d]
d	CH_2OCH_3	$CONH_2$	10	—[b]	8.3
e	CH_2COCH_3	$CONH_2$	10	—[b]	8.1
f	$CH_2CO_2CH_3$	$CONH_2$	5.7	—[b]	7.7
g	CH_2CO_2-*i*-Pr	$CONH_2$	6.5		
h	CH_2CN	$CONH_2$	6.5	—[e]	7.1[f]
i	CH_2CONH_2	$CONH_2$	9.5	—[b]	8.1
j	CH_2CONH_2	$COCH_3$	9.5	—[e]	7.1[f]
k	CH_2CONH_2	CN	6.5	—[e]	7.1[f]
l	CH_2CONH_2	F	9.5	—[g]	—[g]

[a]Less than 10% decomposition in 24 h in 0.1 *M* buffer.
[b]Greater than 10% decomposition in 45 min at all p*H* values less than 5.8 (p*K* + 1.0).
[c]10% decomposition in 6 h at p*H* 8.5.
[d]10% decomposition in 3 h at p*H* 8.8 (**2***b*) and p*H* 8.2 (**2***c*).
[e]10% decomposition in 6 h at p*H* 5.6.
[f]Stable over entire buffer range, *i.e.* p*K* ± 1.0.
[g]Extensive decomposition in 24 h at all acidities.

Dihydropyridines **2***h*, **2***j*, and **2***k*, on the other hand, are relatively stable. These compounds show little decomposition for long periods in buffers as basic as Tris, can be expected to show less than 10% decomposition over 24 h in phosphate buffers greater than p*H* 7.8, (based on the relative rates found by Johnston *et al.* for the 1-propyl compound (25)), and can even be used in acetate buffers of p*H* 5.5 for periods of up to 6 h. The remaining dihydropyridines, **2***d*, **2***e*, **2***f*, and **2***i* are too labile to be used in acetate buffers but meet the criterion of less than 10% decomposition over 24 h in Tris buffers.

The acetic acid-catalyzed rate constants for the hydration of the 1-*R*-3-carbamoyl-1,4-dihydropyridines (**2***b*–**2***i*) show a good correlation ($r = 0.991$) with the σ* values (27, 28) for the 1-substituent as shown in Fig. 2. A reaction constant ρ* of −2.00 is observed when the rate constant for 1-carboxymethyl-3-carbamoyl-1,4-dihydropyridine (**2***a*) is excluded. Its exclusion is not unreasonable considering (*a*) the possibility of interaction between the carboxylic acid and carboxylate groups of the mono-basic malonic acid used to define the $\sigma^I_{COO^-}$ value and (*b*) the possibility of non-inductive interactions between the negatively charged carboxylate ion and the dihydropyridine **2***a*.

Johnston *et al.* (25) have made an intensive investigation of the general-acid-catalyzed hydration of 1-propyl-3-carbamoyl-1,4-dihydropyridine in acetate and other buffers. Using −0.06 for the σ* value of the *n*-propyl group (27) and the plot in Fig. 2 a value of −0.84 can be calculated for log k_{AcOH} for this compound, in good agreement with the value of −0.82 measured by Johnston *et al.* (25).

The sign and magnitude of the reaction con-

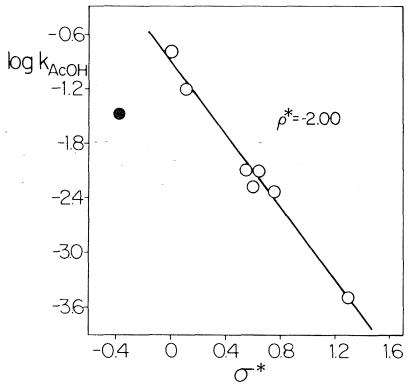

FIG. 2. Hammett plot for the acetic acid catalyzed hydration of 1-substituted 3-carbamoyl-1,4-dihydropyridines; correlation coefficient 0.991. The σ* values were calculated using Charton's σ^I values and the relation $\sigma^*_{(CH_2X)} = \sigma_x^I/0.45$ (27, 28). The point for carboxymethyl (filled circle) was not included in the calculation (see text).

stant ρ* is consistent with protonation at ring carbon being the rate-controlling step in the acid-catalyzed hydration process shown in [2], in agreement with the suggestions of Johnston *et al.* (25) and Kim and Chaykin (21).

Conclusions

The limitations on the p*H* range available for the study of 1,4-dihydropyridines are imposed mainly by the rate of the acid-catalyzed hydration of the 5,6-double bond and therefore represent a lower p*H* limit. The pyridinium ions on the other hand are stable at low p*H*, but undergo a variety of reactions in alkaline solutions. In experiments involving both pyridinium ions and 1,4-dihydropyridines, a narrow p*H*-range will be available for study in some cases. In others there is no p*H* at which the pyridinium ion and the corresponding 1,4-dihydropyridine are stable to the extent of less than 10% decomposition over 24 h. Overlap of the stable p*H*-regions does occur in Tris buffers for four pairs of compounds (*d*, *e*, *i*, and *j*), all of which have similar substituents. The 3-substituent is either carbamoyl or acetyl and the 1-substituent methoxymethyl, acetonyl, or carbamoylmethyl. The σ* values for these three 1-substituents vary only from 0.55 to 0.64 so one might expect rather similar behaviour from them. Dihydropyridines containing more electron-donating groups become very acid-labile while pyridinium ions containing more electron-withdrawing groups become very base-labile with a resulting loss of overlap between the stable p*H*-regions. It is interesting that the coenzyme NAD has the appropriate 1- and 3-substituents that place it among those compounds for which both the pyridinium and 1,4-dihydropyridine forms are relatively stable near neutral p*H*.

Acknowledgment

The financial support of the National Research Council of Canada is gratefully acknowledged.

1. (*a*) U. EISNER and J. KUTHAN. Chem. Rev. **72**, 1 (1972); (*b*) H. SUND. *In* Biological oxidations. *Edited by* T. P. Singer. Interscience Press, New York, NY. 1968; (*c*) R. STEWART. Oxidation mechanisms. W. A. Benjamin Inc., New York, NY. 1964. Chapt. 11.
2. R. O. CLINTON and S. C. LASKOWSKI. J. Am. Chem. Soc. **70**, 3135 (1948).
3. J. H. CRAIG, P. C. HUANG, T. G. SCOTT, and N. J. LEONARD. J. Am. Chem. Soc. **94**, 5872 (1972).
4. K. WALLENFELS, M. GELLICH, and F. KUBOWITZ. Ann. **621**, 137 (1959).
5. P. KARRER, G. SCHWARZENBACH, F. BENZ, and U. SOLMSSEN. Helv. Chim. Acta, **19**, 811 (1936).
6. H. G. WINDMUELLER, C. B. ACKERMAN, H. BAKERMAN, and O. MICKELSON. J. Biol. Chem. **234**, 889 (1959).
7. G. DREHFAHL and K. H. KONIG. Chem. Ber. **87**, 1628 (1954).
8. A. ALBERT and E. P. SERJEANT. The determination of ionisation constants. Chapman and Hall, London. 1971. p. 44.
9. H. H. JAFFE and G. O. DOAK. J. Am. Chem. Soc. **77**, 4441 (1955); A. ALBERT and J. N. PHILLIPS. J. Chem. Soc. 1294 (1956).
10. S. A. HARRIS, T. J. WEBB, and K. FOLKERS. J. Am. Chem. Soc. **62**, 3198 (1940).
11. C. H. SUELTER and D. E. METZLER. Biochem. Biophys. Acta, **44**, 23 (1960).
12. K. SCHENKER and J. DRUEY. Helv. Chim. Acta, **42**, 1960 (1959).
13. B. J-S. WANG and E. R. THORNTON. J. Am. Chem. Soc. **90**, 1216 (1968).
14. O. M. FRIEDMAN, K. POLLACK, and E. KHEDAURI. J. Med. Chem. **6**, 462 (1963).
15. R. F. HUTTON and F. H. WESTHEIMER. Tetrahedron, **3**, 73 (1958).
16. S. P. KOLOWICK, N. D. KAPLAN, and M. M. CIOTTI. J. Biol. Chem. **191**, 447 (1951); F. L. RODKEY. J. Biol. Chem. **213**, 777 (1955); K. WALLENFELS and H. DIECKMANN. Ann. **621**, 166 (1959).
17. T. C. BRUICE and S. J. BENKOVIC. Bioorganic mechanisms. Vol. 2. W. A. Benjamin Inc., New York, NY. 1966. Chapt. 9.
18. R. M. BURTON and N. O. KAPLAN. Arch. Biochem. Biophys. **101**, 139 (1963).
19. S. L. JOHNSON and D. L. MORRISON. J. Biol. Chem. **245**, 4519 (1970).
20. A. G. ANDERSON, JR. and G. BERKELHAMMER. J. Org. Chem. **23**, 1109 (1958).
21. C. S. Y. KIM and S. CHAYKIN. Biochemistry, **7**, 2339 (1968).
22. N. J. OPPENHEIMER and N. O. KAPLAN. Biochemistry, **13**, 4675 (1974).
23. G. W. RAFTER, S. CHAYKIN, and E. G. KREBS. J. Biol. Chem. **208**, 799 (1953).
24. S. G. A. ALIVISATOS, F. UNGER, and G. J. ABRAHAM. Biochemistry, **4**, 2616 (1965).
25. C. C. JOHNSTON, J. L. GARDNER, C. H. SUELTER, and D. E. METZLER. Biochemistry, **2**, 689 (1963).
26. K. S. CHOI and S. G. A. ALIVISATOS. Biochemistry, **7**, 190 (1968).
27. M. CHARTON. J. Org. Chem. **29**, 1222 (1964).
28. R. W. TAFT. J. Am. Chem. Soc. **79**, 1045 (1957); R. W. TAFT. *In* Steric effects in organic chemistry. *Edited by* M. S. Newman. John Wiley and Sons, New York, NY. 1956. Chapt. 13.

Primary isotope effects and mechanism of base initiated β-elimination reactions of di-(*p*-nitrophenyl)fluoroethanes

JAN KURZAWA[1] AND KENNETH T. LEFFEK

Department of Chemistry, Dalhousie University, Halifax, N.S., Canada B3H 4J3

Received September 24, 1976

JAN KURZAWA and KENNETH T. LEFFEK. Can. J. Chem. **55**, 1696 (1977).

The second-order rate constants have been determined for the β-elimination reactions of 2,2-di-(*p*-nitrophenyl)-1,1,1-trifluoroethane, 2,2-di-(*p*-nitrophenyl)-1-fluoroethane, and their β-deuterated analogues with sodium methoxide in methanol. The primary isotope effects and activation parameters for these reactions are reported. It is suggested that the trifluoro-compound reacts via the pre-equilibrium carbanion mechanism $(E1cB)_R$ and that the mono-fluoro compound follows the E2 mechanism via a carbanion-like transition state.

JAN KURZAWA et KENNETH T. LEFFEK. Can. J. Chem. **55**, 1696 (1977).

On a déterminé les constantes de vitesse du deuxième ordre pour les réactions d'élimination β, sous l'influence du méthylate de sodium dans le méthanol, du di-(*p*-nitrophényl)-2,2 tri-fluoro-1,1,1 éthane, du (*p*-nitrophényl)-2,2 fluoro-1 éthane et de leurs analogues deutérés en β. On rapporte les les effets isotopiques primaires et les paramètres d'activation pour ces réactions. On suggère que le composé trifluoré réagit par un mécanisme de carbanion pré-équilibré $(E1cB)_R$ alors que le composé monofluoré suit un mécanisme E2 par l'intermédiaire d'un état de transition ressemblant à un carbanion.

[Traduit par le journal]

Introduction

Considerable attention has been focused recently on the mechanism of β-elimination reactions. The original concerted E2 mechanism, with a transition state **1**, involving simultaneous

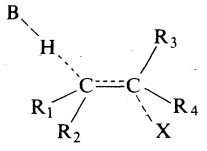

1

breaking of the βC—H bond and the C—X bond where X is the leaving group (1, 2), has been developed into a spectrum of transition states with different extents of C—H and C—X bond rupture, designated carbanion-like or E1cB-like when the βC—H bond breaking is more advanced than the αC—X bond breaking, or carbonium- or E1-like when the opposite situation pertains (3, 4).

Bordwell has proposed (5) that a great many more of these reactions actually proceed via a two step mechanism, [1] and [2], than many current text-books indicate. Bordwell has also suggested that the most common elimination mechanism is the pre-equilibrium anion (reversible anion), $(E1cB)_R$ mechanism which he assumed (5) would occur whenever the leaving group is a poorer leaving group than bromine. Saunders, on the other hand, concludes in a recent review (6) that no major revisions to the current mechanistic assignments are justified. In

$$[1] \qquad B^- + R_1R_2HC{-}CXR_3R_4 \underset{k_{-1}}{\overset{k_1}{\rightleftharpoons}} R_1R_2C^-{-}CXR_3R_4 + BH$$

$$[2] \qquad R_1R_2C^-{-}CXR_3R_4 \xrightarrow{k_2} R_1R_2C{=}CR_3R_4 + X^-$$

the $(E1cB)_R$ mechanism, k_{-1} [BH] is very much greater than k_2. McLennan and Wong (7) have studied the dehydrochlorination of 2,2-di-(*p*-nitrophenyl)-1,1,1-trichloroethane by sodium methoxide in methanol and concluded that the reaction went through an irreversible carbanion mechanism, $(E1cB)_I$, in which $k_2 \gg k_{-1}$ [BH].

In the present work, we have studied the fluoro analogue of the above compound and also the monofluoro derivative in an attempt to observe either a stable carbanion mechanism $(E1)_{anion}$ or a preequilibrium carbanion mechanism, $(E1cB)_R$. The criteria for both these mechanisms (5) are a primary kinetic isotope effect of unity and a substantial leaving group effect on the rate constant. The two mechanisms are distinguished by the kinetics which are first-order for the stable carbanion mechanism $(E1)_{anion}$ and second-order for the $(E1cB)_R$ mechanism.

[1]Postdoctoral Fellow 1975–1976.

TABLE 1. Rate constants and isotopic rate ratios for the reactions of $CF_3CH(p\text{-}C_6H_4NO_2)_2$* ($k_H$) and $CF_3CD(p\text{-}C_6H_4NO_2)_2$* ($k_D$) with sodium methoxide in methanol

Temperature (°C)	$10^3[\bar{O}Me]$ (M)	10^4k_H (s^{-1})	10^4k_D (s^{-1})	k_{2H} ($\ell\ mol^{-1}\ s^{-1}$)	k_{2D} ($\ell\ mol^{-1}\ s^{-1}$)	k_{2H}/k_{2D}
20.4	0.5	0.69	0.73			
	1.0	1.72	1.78			
	1.5	2.75	2.54	0.21	0.21	1.00
	2.5	4.53	4.97			
	5.0	10.33	9.58			
25.0	0.5	1.10	1.45			
	1.0	2.81	3.29			
	1.5	4.85	4.81	0.36	0.355	1.01
	2.5	8.33	8.74			
	5.0	17.28	18.57			
30.0	0.5	1.88	3.13			
	1.0	5.70	5.87			
	1.5	7.83	8.17	0.61	0.62	0.99
	2.5	14.03	15.10			
	5.0	29.16	31.60			
35.8	0.5	5.85	5.08			
	1.0	12.63	9.98			
	1.5	15.20	14.70	1.10	1.10	1.00
	2.5	28.68	27.10			
	5.0	59.16	56.80			
39.8	0.5	5.76	7.71			
	1.0	15.60	17.8			
	1.5	21.83	27.9	1.76	1.75	1.005
	2.5	41.03	44.0			
	5.0	85.00	80.5			

*Initial concentration of substrates = 5×10^{-5} M.

Results and Discussion

Pseudo first-rate constants were determined at five different temperatures by following the appearance of the olefin product at 325 nm for the trifluoro compounds and 380 nm for the monofluoro derivatives in the presence of a large excess of sodium methoxide in methanol. The observed first-order rate constants gave straight lines when plotted against the methoxide concentration, indicating second-order kinetics. The second-order rate constants for both the normal and deuterated compounds are shown in Tables 1 and 2, together with the isotopic rate ratios. The precision of the second-order rate constants is estimated to be $\pm 2\%$.

Since the reactions are second order and no absorption in the visible or uv which could be attributed to the carbanion was observed, neither of the substrates reacts via the stable carbanion mechanism under these conditions. However, the 2,2-di-(*p*-nitrophenyl)-1,1,1-trifluoroethane shows no primary isotope effect, characteristic of the preequilibrium carbanion $(E1cB)_R$ mechanism. An exchange experiment showed that this substrate, recovered after reacting for one half-life, had fallen from an original deuteration level of at least 98% to about 75%. Thus, the trifluoro compound clearly reacts via the $(E1cB)_R$ mechanism which is not inconsistent with McLennan's finding of the irreversible carbanion mechanism $(E1cB)_I$ for the trichloro compound, since chlorine is a better leaving group than fluorine.

The second-order rate constant for the trifluoro compound may be compared to those reported by McLennan and Wong (7) for the substrates 2,2-di-(*p*-R-phenyl)-1,1,1-trichloroethanes reacting with sodium methoxide in methanol at 30°C. These authors demonstrated that these compounds reacted via an irreversible E1cB mechanism by comparison of the Brønsted plot for carbanion formation from hydrocarbons in the same medium, with the dehydrochlorination reaction. McLennan and Wong calculated pK_a values for these substrates using several assumptions (7) which give rise to a large uncertainty in the pK_a. However, a valid comparison can be made between our results and

TABLE 2. Rate constants and isotopic rate ratios for the reaction of $CH_2FCH(p\text{-}C_6H_4NO_2)_2$* ($k_H$) and $CH_2FCD(p\text{-}C_6H_4NO_2)_2$* ($k_D$) with sodium methoxide in methanol

Temperature (°C)	$10^3[\bar{O}Me]$ (M)	10^4k_H (s^{-1})	10^4k_D (s^{-1})	k_{2H} ($\ell\ mol^{-1}\ s^{-1}$)	k_{2D} ($\ell\ mol^{-1}\ s^{-1}$)	k_{2H}/k_{2D}
20.0	1.5	0.85	0.31			
	2.5	1.22	0.41			
	5.0	2.06	0.65	0.030	0.010	3.00
	10.0	3.65	1.14			
	15.0	4.92	1.63			
25.0	1.5	1.39	0.47			
	2.5	1.93	0.67			
	5.0	3.35	1.06	0.046	0.016	2.87
	10.0	5.52	1.92			
	15.0	7.63	2.66			
30.0	1.5	1.85	0.76			
	2.5	2.76	1.02			
	5.0	4.63	1.67	0.073	0.026	2.81
	10.0	8.08	3.02			
	15.0	11.6	4.38			
35.0	1.5	3.65	0.92			
	2.5	5.40	1.35			
	5.0	8.30	2.56	0.112	0.041	2.73
	10.0	14.0	4.50			
	15.0	18.7	6.42			
40.0	1.5	5.23	1.65			
	2.5	7.68	2.25			
	5.0	11.5	3.48	0.167	0.062	2.69
	10.0	21.1	6.83			
	15.0	27.7	8.36			

*Initial concentration of substrates = 2.5×10^{-4} M.

theirs by calculating pK_a values using the same assumptions. On this basis, the trifluoro compound has a pK_a of 11.3 and the monofluoro compound a pK_a of 19.6, and the results are compared in the plot of log k_2 *vs.* pK_a shown in Fig. 1. From this graph it is predicted that if the trifluoro compound were reacting by an irreversible E1cB, the second-order rate constant should be 9.1 $\ell\ mol^{-1}\ s^{-1}$, whereas the point lies well below the line with $k_2 = 0.61\ \ell\ mol^{-1}\ s^{-1}$. Thus, the observed rate of dehydrofluorination is less than the predicted rate of carbanion formation for this compound, consistent with the postulate of an $(E1cB)_R$ mechanism.

The mechanism of the monofluoro compound is clearly different, since it shows a primary isotope effect of $k_H/k_D = 2.8$ at 30°C and also reacts about eight times slower than the trifluoro compound. However, its rate constant of 0.073 $\ell\ mol^{-1}\ s^{-1}$ at 30°C is considerably higher than the value of 0.01 $\ell\ mol^{-1}\ s^{-1}$ predicted by the results of McLennan and Wong (Fig. 1) for the irreversible E1cB mechanism. Thus, the monofluoro compound is observed to react in the

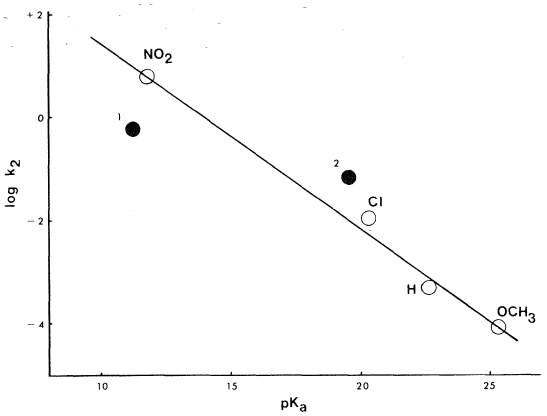

FIG. 1. Plot of log k_2 against pK_a for β-elimination reactions of substrates $(p\text{-}RC_6H_4)_2CHCCl_3$ (○) with sodium methoxide in methanol (●) (1) 2,2-di-(*p*-nitrophenyl)-1,1,1-trifluoroethane, (2) 2,2-di-(*p*-nitrophenyl)-1-fluoroethane.

dehydrofluorination about seven times faster than it is predicted to form carbanions. A mixed mechanism, $(E1cB)_I$ and E2, is excluded by the exact linearity of the activation parameter plots. Therefore, it is concluded that the monofluoro

compound reacts via an E2 mechanism. The small isotope effect of 2.8 shows that the transition state structure is unsymmetrical and there is no doubt, from the observation that di-(*p*-nitrophenyl)methane readily yields a carbanion on treatment with alkoxides in alcohol (8, 9), that the extent of C—H bond rupture must be considerably greater than that of C—F bond rupture. Thus, the mechanism is E2, with a carbanion-like transition state.

The activation parameters calculated from the data in Tables 1 and 2 are given in Table 3, with those for the trichloro compound (10) included for comparison. It can be seen that the dominant factors controlling the rate differences lie in the entropy term. The parameters for the trifluoro compound show a high enthalpy of activation which contains a component arising from the C—F bond rupture whereas the enthalpy of activation for the monofluoro compound is lower and the entropy of activation negative, quite similar to the activation parameters observed in proton transfer reactions from carbon acids (11). This is consistent with a carbanion-like E2 transition state for the monofluoro compound.

The isotope effects on the enthalpy of activation are the same for the monofluoro and trichloro derivatives, while the entropy isotope effects are both small but in the opposite direction. $(\Delta S_D^{\ddagger} - \Delta S_H^{\ddagger})$ for the monofluoro compound is $+1.1$ cal mol^{-1} deg^{-1}, while the corresponding quantity for the trichloro compounds is -1 cal mol^{-1} deg^{-1} (10). Positive values for this quantity are commonly observed and partially cancel the enthalpy difference giving a small isotope effect. Negative values, while unusual, have been reported on several occasions (8, 9, 12, 13) and enhance the rate ratio. However, the activation parameters quoted by McLennan and Wong (10) are based on rate constant measurements at only two different temperatures, so the uncertainties may be large.

TABLE 3. Activation parameters for the β-elimination reactions of 2,2-di-(*p*-nitrophenyl)fluoroethanes with sodium methoxide in methanol

Substrate	$\Delta H^{\ddagger}$ (kcal mol^{-1})	$\Delta S^{\ddagger}$ (cal mol^{-1} deg^{-1})
$CF_3CH(p\text{-}C_6H_4NO_2)_2$	19.1±0.3	+3.6±1.0
$CF_3CD(p\text{-}C_6H_4NO_2)_2$	19.4±0.4	+4.3±1.3
$CH_2FCH(p\text{-}C_6H_4NO_2)_2$	15.2±0.2	−13.7±0.5
$CH_2FCD(p\text{-}C_6H_4NO_2)_2$	16.2±0.2	−12.6±0.5
$CCl_3CH(p\text{-}C_6H_4NO_2)_2$*	17.6	+6
$CCl_3CD(p\text{-}C_6H_4NO_2)_2$*	18.5	+5

*Reference 10.

Experimental

Materials

Anhydrous methanol was prepared by drying commercial absolute methanol with Mg turnings and fractional distillation. The traces of basic material were removed by fractional distillation from anhydrous sulfanilic acid.

Sodium methoxide solutions were prepared by dissolving clean sodium metal in methanol in flasks protected from moisture and carbon dioxide. The concentration of methoxide was determined by titration with standard HCl solution using methyl red as indicator. 2,2-Di-(*p*-nitrophenyl)-1,1,1-trifluoroethane and 2,2-di-(*p*-nitrophenyl)-1-fluoroethane were prepared by methods described by Kaluszyner *et al.* (14) and Bergmann and Kalmus (15). Ethyl esters of trifluoroacetic acid and monofluoroacetic acid were converted to the diphenylcarbinols by treatment with phenylmagnesium bromide on a half mole scale. The reaction with the trifluoroester required refluxing for 1½ h, but the monofluoroester went readily at 0°C in 15 min. The carbinols were reduced with red phosphorous in a mixture of hydriodic and glacial acetic acids by refluxing for 10 days. The diphenylfluoroethanes were finally nitrated with a mixture of nitric and sulfuric acids. The oily products were crystallized several times from methanol. $C_{14}H_9F_3N_2O_4$: mp 120–122°C. *Anal.* calcd.: C 51.5, H 2.8, N 8.6; found: C 51.0, H 2.8, N 8.5; nmr ($CDCl_3$) δ 4.89 (1H, q, J = 8.5 Hz), AA′BB′ pattern 7.4–8.3 (4H). $C_{14}H_{11}FN_2O_4$: mp 82–84°C. *Anal.* calcd.: C 57.9, H 3.8, N 9.6$_5$; found: C 58.1, H 3.7, N 9.7$_5$; nmr ($(CD_3)_2SO$) δ 3.39 (2H, d, J = 8.0 Hz), 4.38 (1H, t, J = 8.0 Hz), AA′BB′ pattern 7.6–8.4 (4H).

The deuterium compounds were prepared from the diphenylcarbinols by reduction with red phosphorous and iodine in deuterated acetic acid. The products were nitrated and crystallized from methanol. The tertiary hydrogen nmr signals at δ 4.89 and 4.38 were completely absent in the deuterated compounds, indicating at least 98% deuteration.

Product Analysis

The reaction of the trifluoro compound was carried out on a 10–20 mg scale and the product was recovered by removal of the methanol, followed by repeated extraction with diethyl ether and then with chloroform. After removal of solvent, the nmr spectrum showed only aromatic hydrogen peaks. The mass spectrum gave a molecular ion at 306 au and the uv absorption a λ_{max} = 325 nm, ε = 15 000. Thus, there is no doubt that the product is the olefin formed by elimination of HF from the substrate molecule.

Kinetic Measurements

The reaction rates were measured using a Unicam SP800 spectrophotometer fitted with a temperature controlled cell block with a capacity of four cells. The absorbance of the olefin products was monitored at a fixed wavelength of 325 nm for the trifluoro and 380 nm

TABLE 4. Run 25.14; temperature 25.0°C; initial concentration $CH_2FCH(p\text{-}C_6H_4NO_2)_2 = 2.5 \times 10^{-4}$ *M*; initial concentration $CH_3\overset{+}{O}\overset{+}{N}a = 0.010$ *M*

Time (min)	x_1 (absorbance)	x_2 (absorbance)
0	0.17	0.84
5	0.33	0.86
10	0.44	0.88
15	0.53	0.90
20	0.60	0.91
25	0.66	0.92
30	0.71	0.93
35	0.75	0.94
40	0.78	0.95
45	0.81	0.96

Guggenheim analysis yields $k_1 = 5.53 \times 10^{-4}$ s^{-1}

for the monofluoro product, which are the maxima of their uv spectra. The absorbance values at definite times were read directly from the chart paper and the first-order rate constants were calculated by the Guggenheim method. Each run was carried out in triplicate with the aid of an automatic cell changer and the rate constants recorded in Tables 1 and 2 are the means of three runs. A sample run is given in Table 4.

Acknowledgment

The authors are grateful for financial support by the National Research Council of Canada.

1. W. HANHART and C. K. INGOLD. J. Chem. Soc. 997 (1927).
2. C. K. INGOLD. Structure and mechanism in organic chemistry. 2nd ed. Cornell University Press, Ithaca, NY. 1969. p. 651.
3. D. J. CRAM, F. B. GREENE, and C. H. DEPUY. J. Am. Chem. Soc. **78**, 790 (1956).
4. J. F. BUNNETT. Angew. Chem. Int. Ed. Engl. **1**, 225 (1962).
5. F. G. BORDWELL. Acc. Chem. Res. **5**, 374 (1972).
6. W. H. SAUNDERS, JR. Acc. Chem. Res. **9**, 19 (1976).
7. D. J. MCLENNAN and R. J. WONG. J. Chem. Soc. Perkin Trans. II, 1373 (1974).
8. J.-H. KIM and K. T. LEFFEK. Can. J. Chem. **51**, 2805 (1973).
9. A. JARCZEWSKI, P. PRUSZYNSKI, and K. T. LEFFEK. Can. J. Chem. **53**, 1176 (1975).
10. D. J. MCLENNAN and R. J. WONG. J. Chem. Soc. Perkin Trans. II, 526 (1974).
11. A. JARCZEWSKI and K. T. LEFFEK. Can. J. Chem. **50**, 24 (1972).
12. P. W. K. FLANAGAN. Diss. Abstr. **18**, 1980 (1958).
13. J. R. KEEFE and N. H. MUNDERLOH. Chem. Commun. 17 (1974).
14. A. KALUSZYNER, S. REUTER, and E. D. BERGMANN. J. Am. Chem. Soc. **77**, 4164 (1955).
15. F. BERGMANN and A. KALMUS. J. Am. Chem. Soc. **76**, 4137 (1954).

Open-chain nitrogen compounds. Part II.[1] Preparation, characterization, and degradation of 1(3)-Aryl-3(1)-methyltriazenes; the effect of substituents on the reaction of diazonium salts with methylamine[2]

T. Patrick Ahern, Handrick Fong, and Keith Vaughan[3]

Department of Chemistry, Saint Mary's University, Halifax, N.S., Canada B3H 3C3

Received December 10, 1976

T. Patrick Ahern, Handrick Fong, and Keith Vaughan. Can. J. Chem. **55**, 1701 (1977).

Treatment of the diazonium salts, $X{\cdot}C_6H_4N_2^+$, with aqueous methylamine affords good yields of the monomethyltriazenes, $X{\cdot}C_6H_4{\cdot}N{=}N{\cdot}NHMe$, when the substituent is a strongly electron-withdrawing group (X = *o*-, *m*-, and *p*-NO_2; *o*-, *m*-, and *p*-CO_2R; *p*-CN and *p*-$COCH_3$). Preparation of the triazene from the *p*-bromobenzene diazonium salt was accompanied by formation of a pentaazadiene. Monomethyltriazenes were not obtained when diazonium salts containing other substituents (X = H, *p*-CH_3, *o*-CF_3, *p*-Cl, *p*-F, *p*-NMe_2, *p*-OH, *p*-OCH_3, *p*-Ph, *p*-$NHCOCH_3$) were treated with methylamine. In these cases the products were either pentaazadiene, or 1,3-diaryltriazenes or unstable materials. The monomethyltriazenes vary considerably in stability and give rise to a number of different degradation products, which were either diaryltriazenes or 3-alkyl-1,3-diaryltriazenes or simply arylamines. 1(3)-(*p*-Nitrophenyl)-3(1)-methyltriazene was found to be a moderately effective methylating agent.

T. Patrick Ahern, Handrick Fong et Keith Vaughan. Can. J. Chem. **55**, 1701 (1977).

Le traitement de sels de diazonium $X{\cdot}C_6H_4N_2^+$ avec de la méthylamine en solution aqueuse conduit avec de bons rendements aux monométhyltriazènes, $X{\cdot}C_6H_4{\cdot}N{=}N{\cdot}NHMe$ quand le substituant est fortement électroaffinitaire (X = *o*-, *m*-, et *p*-NO_2; *o*-, *m*- et *p*-CO_2R; *p*-CN et *p*-$COCH_3$). La préparation du triazène à partir du sel de *p*-bromobenzène diazonium est accompagnée par la formation d'un pentaazadiène. On n'obtient pas de monométhyltriazènes quand on traite les sels de diazonium contenant d'autres substituants (X = H, *p*-CH_3, *o*-CF_3, *p*-Cl, *p*-F, *p*-NMe_2, *p*-OH, *p*-OCH_3, *p*-Ph, *p*-$NHCOCH_3$) par de la méthylamine. Dans ces cas, les produits sont soit un pentaazadiène ou des diaryl-1,3 triazènes ou des composés instables. La stabilité des monométhyltriazènes varie considérablement; leur dégradation conduit à un certain nombre de différents produits qui sont soit des diaryltriazènes ou des alkyl-3 diaryl-1,3 triazènes ou simplement des arylamines. On a trouvé que le *p*-nitrophényl-1(3) méthyl-3(1) triazène est un agent méthylant modérément actif.

[Traduit par le journal]

Introduction

1-Aryl-3-alkyltriazenes can be obtained by the reaction of aryl azides with aliphatic Grignard reagents (3, 4), or, in some instances, by reaction of diazonium salts with alkylamines (1, 5). Monomethyltriazenes have significant carcinogenic activity (6, 7), and have been implicated (8) as metabolites in the carcinogenesis of 1-aryl-3,3-dimethyltriazenes, which have shown considerable potential as antitumour agents (9). The activity of monomethyltriazenes is believed to derive from the facility with which they methylate biological substrates, such as the heterocyclic base units of nucleic acids (10). Chemically, methylation by monomethyltriazenes is also known, as for example in the esterification of carboxylic acids (11). Clearly, an understanding of the formation and properties of monomethyltriazenes is important from both chemical and pharmacological viewpoints.

In part I (1), the reaction of diazotized anthranilate esters with primary aliphatic amines was shown to give excellent yields of semi-stable 1-aryl-3-alkyltriazenes, which were formed without contamination by pentaazadiene. This result was surprising because it has been stated (12, 13) that the reaction of diazonium salts with primary alkylamines is complicated by the formation of pentaazadienes due to further coupling of the diazonium ion with the triazene. In a subsequent communication (2), it was shown that, in general, diazonium salts with strongly electron-withdrawing substituents in the aryl group give rise to pentaazadiene-free triazenes when treated

[1]For part I, see ref. 1.

[2]Preliminary communication, see ref. 2.

[3]Author to whom all correspondence should be sent. (Present address, until August 1977; Department of Pharmacy, University of Aston, Birmingham, England B4 7ET.)

with methylamine. This report gives a full account of the reactions of a number of diazonium salts with methylamine and describes the characterization and degradation of the monomethyltriazenes formed in these reactions.

Experimental

Melting points were recorded on a hot-stage apparatus (Reichert) and are corrected. Infrared spectra were recorded with Nujol suspensions on a Perkin-Elmer model 467 grating spectrophotometer; nmr spectra were measured on a Varian A-60A spectrometer using tetramethylsilane as internal standard. Mass spectra were recorded with a Dupont/C.E.C. Model 21-491 spectrometer using direct insertion.

*1(3)-Aryl-3(1)-methyltriazenes (**2***a–h)*

General Procedure

A solution of the aromatic amine (0.006 mol) in 2 *M* hydrochloric acid (9.0 ml), diluted with water (20 ml), was diazotized at 0°C with sodium nitrite (0.45 g) in water and the resulting solution stirred for 1 h, or until clear. The diazonium salt solution was treated with 40% aqueous methylamine (2.8 ml), whereupon a precipitate of the triazene usually appeared immediately. Sometimes the precipitate was gummy in texture and required careful purification to obtain crystalline material without decomposition. In one case (**2***g*), the triazene was formed initially as a viscous, oily precipitate which was isolated by extraction into chloroform.

This procedure afforded the following triazenes.

*1(3)-(p-Nitrophenyl)-3(1)-methyltriazene (**2***a)*—(0.62–0.95 g, 57–88%), mp 111–113°C (benzene) (lit. (5) mp 114°C); ν_{max} 3180, 3140, 1605, 1600, 1515, 1340 cm^{-1}; δ ($CDCl_3$) 3.5 (br s, 3H, N-Me), 7.4 (br d, 2H, aromatic), 8.13 (d, J = 9 Hz, 2H, aromatic), and 9.2 ppm (br s, 1H, NH); M^+ 180(41%) ($C_7H_8N_4O_2$), *m/e* 165(1%) ($M - CH_3$), 150(77%) ($M - CH_3NH$), 138(97%) ($M - CH_2N_2$), 122(100%) ($C_6H_4NO_2$), 108(20%), 106(12%), and 92(74%).

*1(3)-(p-Cyanophenyl)-3(1)-methyltriazene (**2***b)*—(0.81 g, 83%) mp 135.5–136°C (dec.), (yellow prisms from benzene – petroleum ether); ν_{max} 3185, 3155, 2220, and 1605 cm^{-1}; δ ($CDCl_3$, +55°C) 3.40 (br s, 3H, N-Me), 7.3–7.8 (m, 4H, aromatic), and 8.6 (br s, 1H, NH); δ ($CDCl_3$, −30°C) 3.22 (d, J = 2 Hz, NHMe), 3.62 (s, =N—Me), 7.15–7.85 (m, aromatic), 8.4 (br s, NH), and 9.7 (br s, NH); M^+ 160(31%) ($C_8H_8N_4$), *m/e* 132(16%) ($M - N_2$), 130(34%) ($M - CH_3NH$), 120(1%) (C_7H_6NO), 118(78%) ($M - CH_2N_2$), 102(100%) ($NC{\cdot}C_6H_4$), and 92(17%).

*1(3)-(p-Acetylphenyl)-3-methyltriazene (**2***c)*—(0.77 g, 73%) as a yellow gummy solid which recrystallized from benzene – petroleum ether with mp 90–92°C; ν_{max} 3180, 3160, 1660, and 1600 cm^{-1}; δ ($CDCl_3$) 2.56 (s, 3H, acetyl Me), 3.43 (br s, 3H, N-Me), 7.33 (br d, J = 8 Hz, 2H, aromatic), 7.96 (d, J = 8 Hz, 2H, aromatic), and 8.8 (br s, 1H, NH); M^+ 177(50%) ($C_9H_{11}N_3O$), *m/e* 162 (0.4%) ($M - CH_3$), 149(16%) ($M - N_2$), 147(40%) ($M - CH_3NH$), 135(98%) ($M - CH_2N_2$), 134(53%) ($M - CH_3CO$), 120(100%) (C_7H_6NO), 106(27%), 92 (57%), and 77(37%).

*1(3)-(p-Methoxycarbonylphenyl)-3(1)-methyltriazene (**2***d)*—(0.98 g, 84%), mp 94–96°C (from benzene) (lit. (5) mp 97.5°C); ν_{max} 3180, 3160, 1705, and 1600 cm^{-1}; δ ($CDCl_3$) 3.40 (br s, 3H, N-Me), 3.88 (s, 3H, O-Me), 7.31 (br d, J = 8 Hz, 2H, aromatic), 8.0 (d, J = 8 Hz, 2H, aromatic); M^+ 193(53%) ($C_9H_{11}N_3O_2$), *m/e* 190(0.7%) ($M - H_3$), 165(9%) ($M - N_2$), 151(65%) ($M - CH_2N_2$), 133(13%), 134(17%) ($M - CO_2CH_3$), 120(100%) (C_7H_6NO), 106(3.5%), 103(5%), 92(27%).

*1(3)-(p-Ethoxycarbonylphenyl)-3(1)-methyltriazene (**2***e)*—(yield 64%) mp 83–85°C (benzene – petroleum ether); ν_{max} 3200, 3180, 1710, and 1610 cm^{-1}; δ ($CDCl_3$) 1.35 (t, J = 7 Hz, 3H, C-Me), 3.35 (br s, 3H, N-Me), 4.33 (q, J = 7 Hz, 2H, O-CH_2), 7.30 (br d, J = 8 Hz, 2H, aromatic), and 8.0 (d, J = 8 Hz, 2H, aromatic).

*1(3)-(m-Nitrophenyl)-3(1)-methyltriazene (**2***f)*—(0.65 g, 60%), mp 94–96°C (from ether – petroleum ether); ν_{max} 3380, 1580(W), 1535, and 1345 cm^{-1}; δ ($CDCl_3$) 3.32 (s, 3H, N-Me), 7.3–8.3 (m, 4H, aromatic), and 8.5 (br s, 1H, NH); M^+ 180(41%) ($C_7H_8N_4O_2$); *m/e* 165(0.3%) ($M - CH_3$), 164(0.6%) ($M - O$), 150(77%) ($M - CH_3NH$), 138(36%) ($M - CH_2N_2$), 122(100%) ($C_6H_4NO_2$), 108(4.6%), 106(12%), 92(68%).

*1(3)-(m-Methoxycarbonylphenyl)-3(1)-methyltriazene (**2***g)*—(1.19 g, 90%), mp 107–110°C (from benzene); ν_{max} 3240 and 1720 cm^{-1}; δ ($CDCl_3$) 3.26 (br s, 3H, N-Me), 3.86 (s, 3H, O-Me), 7.3–8.3 (m, 4H, aromatic), and 9.1 (br s, 1H, NH).

*1-Methyl-3-(o-nitrophenyl)triazene (**2***h)*—(0.81 g, 75%), mp 38–40°C; ν_{max} 3330, 1615, 1520, and 1340 cm^{-1}; δ ($CDCl_3$) 3.65 (s, 3H, N-Me), 6.8–8.3 (m, 4H, aromatic), and 11.5 (br s, 1H, NH). The *o*-nitrophenyltriazene decomposed completely within hours of preparation, even when stored in a vacuum desiccator. Some samples were found to contain *o*-nitroaniline after decomposition.

Attempted preparation of 1-(o-Cyanophenyl)-3-methyltriazene

Anthranilonitrile (0.75 g) was dissolved in hot 2.5 *M* hydrochloric acid (10 ml) diluted with water (20 ml), and diazotized at 0°C with sodium nitrite (0.45 g). Aqueous methylamine (2.8 ml of 40%) was added to the clear solution and a yellow colouration developed, followed by the formation of a brown, oily precipitate. The mixture was extracted with chloroform; the residue in the chloroform (yield 0.96 g) displayed triazene characteristics in the ir spectrum, ν_{max} 3400 (NH), 2210 (C≡N), and 1480 (N=N) cm^{-1}, but decomposed immediately.

Reaction of p-Bromobenzene Diazonium Chloride with Methylamine

p-Bromoaniline (1.03 g) was dissolved in 2 *M* hydrochloric acid (9 ml), diluted with water (20 ml), and diazotized at 0°C with sodium nitrite (0.45 g). The clear diazonium salt solution was treated with 40% aqueous methylamine (2.8 ml) in one portion. A yellow precipitate separated immediately, which was filtered to yield a solid mixture of 1(3)-(*p*–bromophenyl)-3(1)-methyltriazene (**2***l*) and 1,5-bis-(*p*–bromophenyl)-3-methylpentaazadiene (**7***b*) (approximate proportion 9:1) (1.02 g), mp 68–70°C; ν_{max} 3190, 3160, 1590, and 1540 cm^{-1}; δ ($CDCl_3$) 3.25 (s, triazene N-Me), 3.76 (s, pentaazadiene N-Me), and 7.1–7.6 (m, aromatic). Recrystallization of the solid mixture from ethanol – dimethyl sulfoxide

resulted in decomposition and formation of a different high melting solid, mp 180–183°C; ν_{max} 1570 (W) cm^{-1}, which could not be identified.

*1,3-Bis-(o-trifluoromethylphenyl)triazene (**4d**)*

o-Aminobenzotrifluoride (0.97 g) in 2 *M* hydrochloric acid (9.0 ml) was diazotized at 0°C with sodium nitrite (0.45 g). The diazonium salt precipitate was dissolved by dilution and 40% aqueous methylamine (2.8 ml) was added in one portion. The yellow solution was stirred for 0.5 h and filtered to afford an off-white solid. Recrystallization from ethanol gave 1,3-bis-(*o*-trifluoromethylphenyl)triazene (51 mg) mp 177–179°C (lit. (19) mp 170–171.5°C); ν_{max} 3355, 1610, and 1590 cm^{-1}; δ ($CDCl_3$) 7.1–7.9 (m, 8H, aromatic), 9.7 (br s, 1H, NH); M^+ 333(1%) ($C_{14}H_9N_3F_6$), *m/e* 314(1%) (*M* − F), 305(16%) (*M* − N_2), 216(1%), 173(48%) ($CF_3C_6H_4N_2$), 160(4%) ($NH{\cdot}C_6H_4CF_3$), 145(100%) ($C_6H_4CF_3$), 131(4%) ($C_7H_5N_3$), 115(4%), 104(4%).

*1,3-Bis-(p-nitrophenyl)-3-methyltriazene (**3a**)*

The *p*-nitrophenyltriazene **2***a* recrystallizes unchanged from benzene when the crystallization is done quickly. Prolonged heating in benzene solution or in alcohol, resulted in decomposition. The product of the decomposition was identified as 1,3-bis-(*p*-nitrophenyl)-3-methyltriazene (yield 31%) mp 228–230°C (from ethanol) (lit. (14) mp 219°C); ν_{max} 1600, 1590, 1500, and 1330 cm^{-1}; δ (DMSO-d_6) 3.35 (s, N-Me), 7.43 (d, *J* = 9 Hz, aromatic), and 7.91 (d, *J* = 9 Hz, aromatic); M^+ 301(2%) ($C_{13}H_{11}N_5O_4$); *m/e* 273(4%) (*M* − N_2), 180(2%) (*M* − $C_6H_3NO_2$), 166(1%) (*M* − $C_6H_3N_2O_2$), 150(76%) ($N_2C_6H_4NO_2$ *or* $CH_2N{\cdot}C_6H_4NO_2$), 122(100%) ($C_6H_4NO_2$), 105(14%), 92(26%).

*1,3-Bis-(o-nitrophenyl)-3-methyltriazene (**3b**)*

1-Methyl-3-(*o*-nitrophenyl)triazene was dissolved in 95% ethanol at room temperature. After standing, a yellow solid separated, which was identified as 1,3-bis-(*o*-nitrophenyl)-3-methyltriazene (yield 3%) mp 107–110°C (from ethanol), ν_{max} 1600, 1520, and 1355 cm^{-1}; M^+ 301(2.4%) ($C_{13}H_{11}N_5O_4$) *m/e* 273(2%) (*M* − N_2), 255(0.4%) (*M* − NO_2), 180(2%) (*M* − $C_6H_3NO_2$), 167(0.6%) (*M* − $C_6H_2N_2O_2$), 150(100%) ($N_2C_6H_4NO_2$ *or* $CH_2NC_6H_4NO_2$), 123(30%) ($C_6H_5NO_2$), 105(4.4%), 92(22%).

*1,3-Bis-(p-methoxycarbonylphenyl)triazene (**4c**)*

The *p*-methoxycarbonylphenyltriazene **2***d* recrystallizes unchanged from benzene when the crystallization is done quickly. However, recrystallization in ethanol, and also on occasion in benzene, when heating is prolonged, results in decomposition. The product of decomposition was identified as the bis-(*p*-methoxycarbonylphenyl)triazene **4***c* (yield 10%) mp 205–210°C (from benzene) (lit. (15) mp 218–219°C); ν_{max} 3230, 1720, 1710, 1690, and 1610 cm^{-1}; δ ($CDCl_3$) 3.93 (s, 6H, O-Me), 7.46 (d, *J* = 8 Hz, 4H, aromatic), and 8.06 (d, *J* = 8 Hz, 4H, aromatic); M^+ 313(0.6%) ($C_{16}H_{15}N_3O_4$), *m/e* 285(7%) (*M* − N_2), 254(8%) (*M* − CH_3CO_2), 194(0.6%) ($C_6H_4N_3C_6H_4$), 163(37%) ($CH_3O_2CC_6H_4N_2$), 135(100%) ($C_6H_4CO_2CH_3$), 120(25%) (C_7H_6NO), 103(25%), 92(7%).

Reaction of o-Nitrobenzenediazonium Salt with Ammonia

o-Nitroaniline (0.83 g) was dissolved in 2 *M* hydrochloric acid (9.0 ml), diluted with water (100 ml), and diazotized at 0°C with sodium nitrite (0.45 g) over a period of 1 h. The clear solution was treated with concentrated ammonia (2.18 ml) in one portion and, after stirring for 5 min, the precipitate was collected to yield an unidentified reddish-brown solid (77 mg), which rapidly decomposed. On standing, further precipitation in the mother liquor produced *o*-nitroaniline (19 mg) identical with a commercial sample.

Reaction of Benzenediazonium Chloride with Methylamine

*(a) 1,5-Diphenyl-3-methylpentaazadiene (**7a**)*

Aniline (0.635 g) was dissolved in 2 *M* hydrochloric acid (9.0 ml), diluted with water (20 ml), and diazotized at 0°C with sodium nitrite (0.45 g). After stirring for 0.75 h, the diazonium salt solution was treated quickly with 40% aqueous methylamine (2.8 ml). The yellow precipitate was filtered to afford the pentaazadiene (0.56 g), mp 109–110°C (lit. (16) mp 112–113°C) (yellow needles from benzene or ethanol); ν_{max} 1580 (W) cm^{-1}; δ ($CDCl_3$) 3.81 (s, 3H, N-Me) and 7.3–7.8 (m, 10H, aromatic).

*(b) 1,3-Diphenyltriazene (**4a**)*

The procedure in (*a*) was repeated with a smaller volume (1.0 ml) of 40% methylamine, added in three successive portions (0.5, 0.3, and 0.2 ml) immediately after the addition of sodium nitrite. A precipitate appeared from the yellow solution after 5 min, and the mixture was filtered to yield 1,3-diphenyltriazene (0.22 g, 27%), identical with a sample prepared below.

Reactions of Benzenediazonium Chloride

(a) With Acetamide

A solution of acetamide (1.5 g) in water was added to a solution of benzene diazonium chloride (0.006 mol) in one portion at 0°C and the solution remained clear. Sodium acetate (6 g) was added, whereupon the solution turned yellow and a precipitate slowly appeared. After stirring for 1 h, the solid was filtered and recrystallized from petroleum ether to give 1,3-diphenyltriazene (0.28 g, 47%), mp 95–97°C (lit. (17) mp 98–99°C), ν_{max} 3150 and 1590 cm^{-1}, identical with a sample prepared by diazotization of aniline alone.

(b) With Urea

Likewise, a solution of benzene diazonium chloride (0.006 mol) was treated with a solution of urea (1.36 g), followed by addition of sodium acetate, whereupon 1,3-diphenyltriazene (78 mg) precipitated.

(c) With Sodium Acetate

Treatment of a solution of benzene diazonium chloride (0.006 mol) with an excess of sodium acetate produced a yellow solution which, after standing for 1 h, afforded a yellow precipitate of 1,3-diphenyltriazene (0.11 g).

*1,3-Bis-(p-tolyl)triazene (**4b**)*

p-Toluidine (0.64 g) was dissolved in 2 *M* hydrochloric acid (9 ml), diluted with water (100 ml), and diazotized at 0°C with sodium nitrite (0.45 g). Aqueous methylamine (2.8 ml of 40%) was added in one portion, whereupon the solution went cloudy. After 5 min, the tan-coloured precipitate was filtered and triturated with methanol. The methanol solution was filtered and the filtrate diluted with water to afford, 1,3-bis-(*p*-tolyl)triazene, mp 116°C (lit. (18) mp 116.5°C), ν_{max} 3170 and 1605 cm^{-1}, identical

with a sample prepared by diazotization of *p*-toluidine alone.

3-Methyl-1,2,3-benzotriazin-4-one

Anthranilic acid (0.86 g), dissolved in 2 *M* hydrochloric acid (9.5 ml) and diluted with water (20 ml), was diazotized at 0°C with sodium nitrite (0.45 g) and treated with 40% aqueous methylamine (2.8 ml). The solution turned yellow, but no immediate precipitate was observed. After standing overnight a white precipitate had formed, which was filtered to yield 3-methyl-1,2,3-benzotriazin-4-one (0.175 g) mp 121–122°C, identical in all respects with an authentic sample (1).

Chloroform extraction of the mother liquor afforded a second batch of the triazinone (0.135 g), mp 116–120°C.

Methylation of 3,5-Dinitrobenzoic Acid

The *p*-nitrophenyltriazene **2***a* (0.63 g, 3.5 mmol) was suspended in ether (10 ml) and stirred at room temperature while a solution of 3,5-dinitrobenzoic acid (0.75 g) in ether (20 ml) was added dropwise. The mixture was left for 17 h at room temperature, filtered, and partially evaporated. The crystalline precipitate was separated to give methyl 3,5-dinitrobenzoate (0.14 g). Evaporation of the ether filtrate gave a red, oily residue which solidified on standing. The solid was scrubbed with 2 *N* hydrochloric acid, filtered, washed with water, scrubbed with 5% aqueous sodium carbonate, filtered, washed with water, and dried to give a second batch of methyl 3,5-dinitrobenzoate (combined yield 0.72 g), which was identical with a sample obtained from reaction of 3,5-dinitrobenzoyl chloride with methanol.

Discussion

Treatment of the *para*-substituted benzene diazonium chlorides **1***a–e* with methylamine in aqueous solution gave good yields of the monomethyltriazenes **2***a–e*. The *meta*-substituted triazenes **2***f* and *g* were also obtained readily from the corresponding diazonium salts **1***f* and *g*. However the *o*-nitrophenyltriazene **2***h* was obtained only with considerable difficulty; treatment of *o*-nitrobenzene diazonium salt with methylamine frequently resulted in decomposition. The *meta*- and *para*-substituted triazenes **2***a–g* are moderately stable yellow solids, but usually decompose on standing, with the exception of the *p*-cyanophenyltriazene **2***b*, which appears to be completely stable. By contrast, the *o*-nitrophenyltriazene **2***h* decomposes very quickly in the solid state and in solution. As previously described (1, 20), the *o*-alkoxycarbonyl- and *o*-acetylphenyltriazenes **2***i* and **2***j* are also unstable and readily cyclize to benzotriazinones and methylenebenzotriazines, respectively. In the present work, the triazene obtained by coupling methylamine with diazotized anthranilic acid cyclized spontaneously to afford 3-methyl-1,2,3-benzotriazin-4-one. The product of the reaction of methylamine with *o*-cyanobenzene diazonium salt displayed ir characteristics of the *o*-cyanophenyltriazene **2** (X = *o*-CN), but decomposed very quickly preventing full characterization.

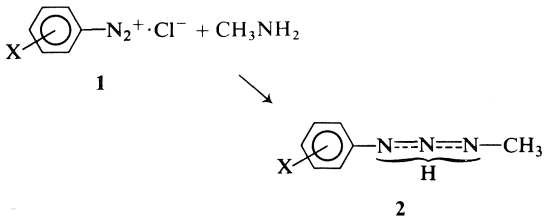

a X = *p*-NO_2	*g* X = *m*-CO_2Me
b X = *p*-CN	*h* X = *o*-NO_2
c X = *p*-$COCH_3$	*i* X = *o*-CO_2R
d X = *p*-CO_2Me	*j* X = *o*-$COCH_3$
e X = *p*-CO_2Et	*k* X = *p*-CH_3
f X = *m*-NO_2	*l* X = *p*-Br

As described more fully elsewhere (21), the spectral properties of the *para*-substituted phenyltriazenes **2***a–e* show that these triazenes exist as a mixture of tautomers in equilibrium (ArN=NNHMe ⇋ ArNHN=NMe). The *N*-methyl proton resonances in the nmr spectra of **2***a–e* are considerably broadened by the tautomeric equilibrium; the presence of both tautomers was confirmed in the case of the *p*-cyano-derivative **2***b* by low temperature nmr measurement. The infrared spectra of these triazenes also give evidence for two tautomers. Two bands appear in the regions 1415–1430 and 1480–1485 cm^{-1}, assigned to the azo-group (N=N) stretching vibration in the 1-aryl- and 3-aryltautomers, respectively. Furthermore, the *para*-substituted triazenes **2***a–e* show two NH absorption bands in the ir at 3140–3160 and 3180–3185 cm^{-1}, whereas the *ortho*-substituted triazenes **2***h* and **2***i* display only one NH band at 3300–3330 cm^{-1}. The low temperature nmr study showed conclusively that the *o*-ethoxycarbonylphenyltriazene **2***i* (R = Et) (and by analogy the *o*-nitrophenyltriazene **2***h*) exists solely as the 3-aryl tautomer.

The structures of the monomethyltriazenes were confirmed, whenever possible, by mass spectral analysis; the observed fragmentation pathways are shown in Scheme 1. The *m*- and *p*-nitrophenyltriazenes have strikingly similar mass spectra showing fragments arising from pathways (*a*) *N*-methyl fragmentation, (*b*) fragmentation at N_2—N_3, (*c*) loss of the fragment diazomethane, CH_2N_2, and (*d*) *N*-aryl

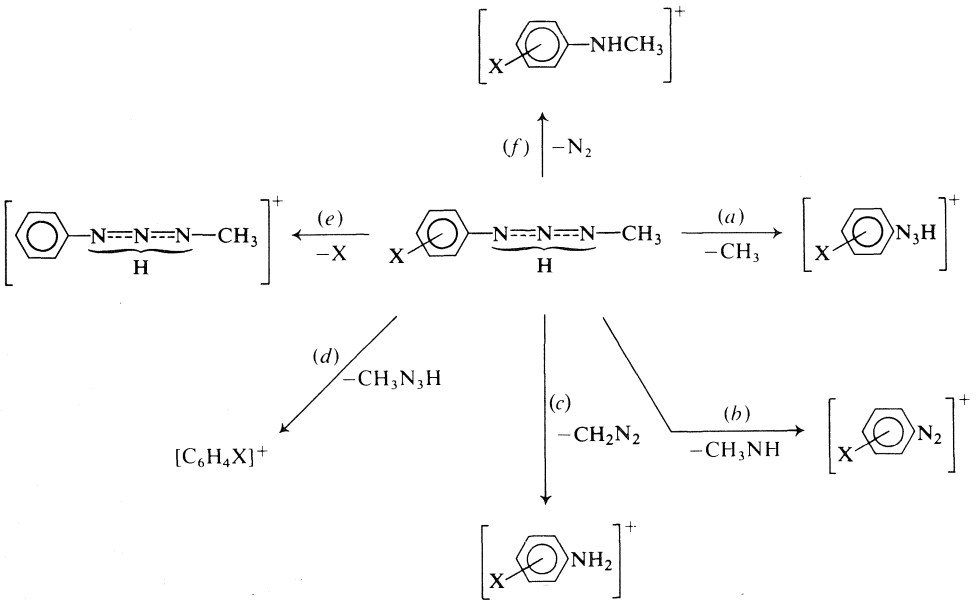

SCHEME 1. Mass spectral fragmentation of 1(3)-Aryl-3(1)-methyltriazenes

fragmentation. Surprisingly, the nitro-derivatives did not show fragmentation by direct loss of N_2 (path *f*), although this pathway was clearly evident in the fragmentation of other *para*-substituted triazenes **2***b*, *c*, and *d*. The *p*-acetyl derivative **2***c* and the ester **2***d* fragmented by loss of the substituent, X, unlike the nitro- and cyanophenyltriazenes. These results are significantly different from the mass spectra reported (22*a*) for the unsubstituted 3-alkyl-1-phenyltriazenes (*e.g.*, **2** X = H), which fragment by the analogous pathways *b*, *c*, and *d*, but did not show fragmentation by loss of N_2 (path *f*) or by breakage of the *N*-alkyl linkage (path *a*).

Several types of decomposition product have been obtained from the unstable triazenes **2**, but the course of the decomposition does not appear to be determined by the reaction medium. The *p*-nitrophenyltriazene **2***a* could be purified by rapid crystallization from benzene, but decomposed when boiled in ethanol to afford the alkyldiaryltriazene **3***a*. The structure of **3***a* was apparent from the ir spectrum, which did not show an NH band, from the nmr spectrum, which displayed *N*-methyl resonance and the expected aromatic pattern, and from the mass spectrum, which showed the molecular ion at M^+ 301. The principal fragments in the mass spectrum of **3***a* showed that fragmentation occurs by path *a* loss of N_2, path *b* fragmentation between N-2 and N-3, and path *c* *N*-aryl fragmentation (Scheme 2).

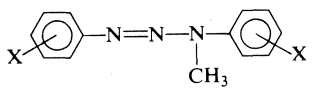

3

a X = *p*-NO_2
b X = *o*-NO_2

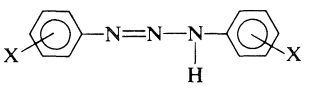

4

a X = H
b X = *p*-CH_3
c X = *p*-CO_2Me
d X = *o*-CF_3

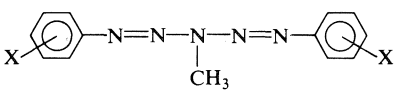

7

a X = H
b X = *p*-Br

The alkyldiaryltriazene **3***b* was similarly obtained when the *o*-nitrophenyltriazene **2***h* was treated with ethanol. **3***b* has a mass spectrum almost identical (in both fragment mass numbers and relative intensities) to that of the *para*-isomer **3***a*. The formation of the alkyldiaryltriazenes **3***a* and *b* in protic media must involve

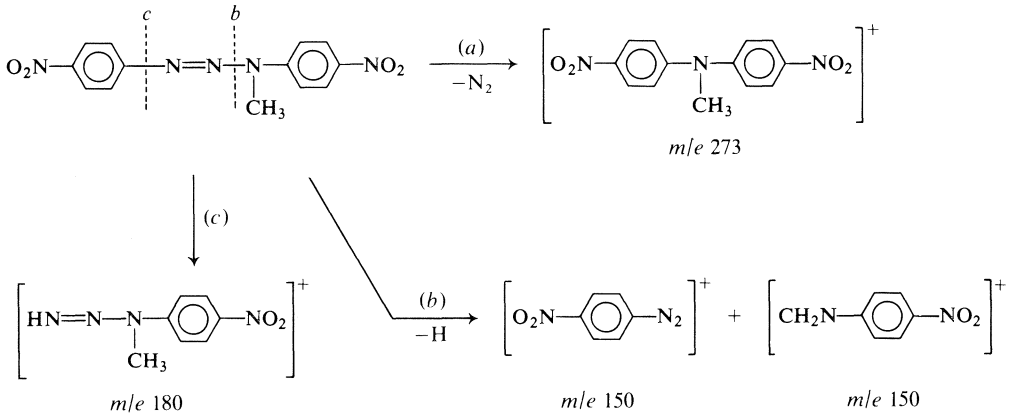

SCHEME 2. Mass spectral fragmentation of 1,3-bis-(*p*-nitrophenyl)-3-methyltriazene

two courses of cleavage (Scheme 3). Thermal loss of nitrogen gives the secondary amine **5** (reaction *ii*), whereas protonation at N-3, followed by retrocoupling (reaction *i*), liberates free aryl diazonium ion, which may then couple with the secondary amine to give the trisubstituted triazene.

Attempted purification of the *o*-nitrophenyltriazene **2***h* in benzene gave only *o*-nitroaniline, which was also the product of solid state decomposition of **2***h*. The facility with which this triazene reverts to the arylamine is possibly a consequence of the preference of **2***h* to exist as the 3-aryl-tautomer, Ar·NH—N=N—R. This preference has been attributed to intramolecular hydrogen bonding (21). *o*-Nitroaniline was also recovered in low yield directly from the reaction of *o*-nitrobenzene diazonium salt with ammonia; in this case the diazonium salt probably couples with NH_3 to give a monoaryltriazene, $Ar{\cdot}N{=}N{\cdot}NH_2$, which would rapidly lose N_2 to give the amine, as has been observed previously when the diazonium salt from *o*-aminoacetophenone was treated with ammonia (20).

A slightly different decomposition course was experienced in the case of the *p*-methoxycarbonylphenyltriazene **2***d*, which reacted in hot ethanol to give the diaryltriazene **4***c*. Analogous decomposition probably occurred when *o*-aminobenzotrifluoride was diazotized and treated with methylamine, in which case the diaryltriazene **4***d* was obtained in low yield, presumably by decomposition of an unstable monomethyltriazene **2** (X = *o*-CF_3). The formation of these diaryltriazenes from monomethyltriazenes must involve protolysis and fragmentation by pathways *i* and *iii* (Scheme 3), giving ArN_2^+ and $ArNH_2$, respectively, followed by coupling of the two fragments. Similar formation of diaryltriazenes and alkyldiaryltriazenes has been

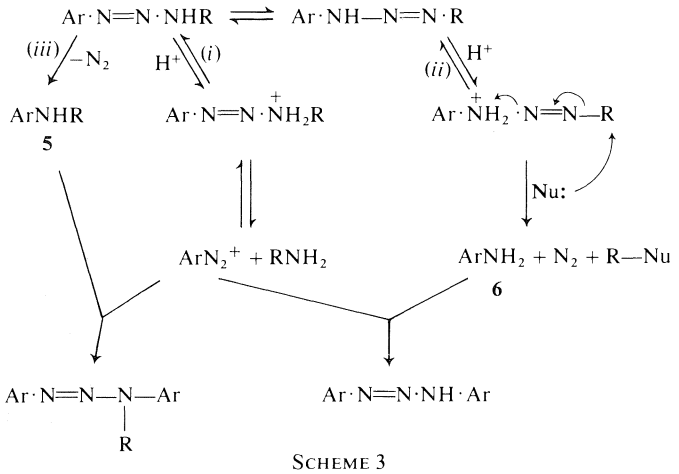

SCHEME 3

observed in the reaction of *p*-nitrobenzene diazonium salt with butylamine (22*b*).

The decomposition mechanism outlined in Scheme 3 has much similarity to the reported reactions of alkyltriazenes with Lewis acids. For example, Kreher and Goth (23) obtained the secondary amine **5** as the major product of reaction of 1-aryl-3-alkyltriazenes with aluminium trihalides, analogous to pathway *ii* (Scheme 3). However when silica gel is used as the catalyst (24), the secondary amine is the minor product, the major product being the primary amine **6**, presumably formed in a manner analogous to pathway *iii*. The carbonium ion-pair mechanism (reaction 1) is favoured to account for the formation of **5**; significantly the tautomer involved here is the 3-aryl-1-methyltriazene.

[1] $Ar\cdot NH—N{=}N—CH_3 \longrightarrow \overset{-}{Ar}NH\cdot\overset{+}{C}H_3 + N_2$

Acidic alumina was found to favour decomposition of the *o*-alkoxycarbonylphenyltriazenes **2***i* by pathway *ii* (1).

The preparation of 1-(*p*-tolyl)-3-methyltriazene (**2***k*) is now described in "Organic Synthesis" (25), but success in this preparation depends upon the addition of the diazonium salt **1***k* solution *to* the methylamine solution at $-10°C$. These reaction conditions are significantly different from those used here to prepare the triazenes **2***a–h*, and when *p*-toluidine was diazotized and treated with methylamine at 0°C, no monomethyltriazene was formed. The only product obtained in this case was the diaryltriazene **4***b*, which could arise by decomposition of the monomethyltriazene **2***k* as in Scheme 3.

The corresponding reaction of benzenediazonium chloride with methylamine proved to be very difficult to reproduce. When a large excess of methylamine was added in one portion to a solution of benzene diazonium chloride, the product was the pentaazadiene **7***a*, no monomethyltriazene being evident; slow addition of methylamine gave no identifiable materials at all. For no obvious reason, the diphenyltriazene **4***a* was obtained when methylamine was added in successive portions to the diazonium salt solution. Diphenyltriazene (**4***a*) was the only product obtained when benzene diazonium chloride solution was treated with (*a*) acetamide followed by sodium acetate, or (*b*) urea followed by sodium acetate, or (*c*) sodium acetate alone.

The unwillingness of benzenediazonium chloride to couple with amides in aqueous solution does not parallel the behaviour in organic solvents. For example, reaction of *p*-chloro- or *p*-bromobenzene diazonium chlorides with formamide in ethereal suspension affords the remarkably stable 1-aryl-3-formyltriazenes **8** (26), reaction 2. The lack of formation of acyl

[2] $Ar\cdot N_2^+ Cl^- + HCO\cdot NH_2 \xrightarrow[NaHCO_3]{\text{Ether}} Ar\cdot N{=}N\cdot NH\cdot CHO + NaCl + H_2O + CO_2$

8

triazenes in the present work is not consistent with a report (27) that acetamide couples with benzenediazonium chloride in the presence of sodium hydroxide to give the *N*-acetyltriazene $CH_3CO\cdot NH\cdot N{=}NC_6H_5$. However, no reaction was observed between acetamide and the diazonium salt from sulfanilic acid (28).

The formation of diphenyltriazene from completely diazotized aniline in the absence of amino compounds can be rationalized in terms of the equilibria involved in the diazotization process (reaction 3) (29). It is generally accepted that the

[3] $Ar\cdot NH_2 \longrightarrow \underset{\mathbf{9}}{ArNH—N{=}O} \rightleftharpoons \underset{\mathbf{10}}{ArN{=}N—OH}$

$\mathbf{9} \downarrow$ $\quad$ $\mathbf{10} \rightleftarrows$

$\underset{\mathbf{4}}{ArNH—N{=}NAr}$ $\quad$ $\underset{\mathbf{11}}{ArN{=}N^+\cdot\overset{-}{O}H}$

equilibrium **9** ⇋ **10** ⇋ **11** is present in diazonium solutions, and addition of base (*e.g.*, sodium acetate) would shift the equilibrium to the left giving a build up of $PhNH\cdot N{=}O$. Condensation of two molecules of this nitrosamine, or a reaction with PhN_2^+, could give the triazene **4**. Although the nature of the conversion **9** → **4** is not fully understood, it clearly does take place in specific cases. Primary nitrosamines have been isolated from diazotization of heterocyclic amines and can be converted into triazenes by simply warming in methanol (30).

The preparation of the *p*-bromophenyltriazene **2***l*, when *p*-bromobenzene diazonium chloride was coupled with methylamine, was accompanied by formation of the pentaazadiene **7***b*. The presence of the pentaazadiene was confirmed by the observation in the nmr spectrum of *N*-methyl resonance at 3.76 ppm, analogous to the *N*-methyl resonance of the pentaazadiene **7***a*.

Attempted purification of the mixture of triazene and pentaazadiene resulted in decomposition. Similarly attempts to prepare the *p*-chloro- and *p*-fluorophenyl-3-methyltriazenes under these conditions gave unstable materials, which could not be characterized.

Attempts to prepare monomethyltriazenes with electron-donating substituents in the aryl group, by this method, were a total failure. Treatment of the diazonium salts **1** (X = Me_2N—, HO—, MeO—, and Ph—) with methylamine at 0°C invariably produced a black oil or tar. Diazotization of *p*-aminoacetanilide and coupling with methylamine afforded a promising solid, which may have been triazene, but it decomposed immediately after filtration.

Monomethyltriazenes are useful chemically as methylating agents, and for example, readily esterify aromatic carboxylic acids (11, 25). The *p*-nitrophenylmethyltriazene **2***a* was found to esterify 3,5-dinitrobenzoic acid, but the reaction was considerably slower than expected. The rapid evolution of nitrogen that is described for the reaction of the *p*-tolyltriazene **2***k* (25) with the dinitrobenzoic acid was certainly not evident in the reaction of the *p*-nitrophenyltriazene, which does not appear to offer any particular advantage as a methylating agent.

Conclusion

These results show that the formation of monomethyltriazenes by addition of methylamine to a diazonium salt solution can be achieved cleanly only when electron-withdrawing substituents are present in the aryl group of the diazonium salt. The non-formation of pentaazadienes in these reactions suggests that the effect of the substituent is to decrease the nucleophilic reactivity of the triazene by a resonance phenomenon [4]. Delocalization of

[4] 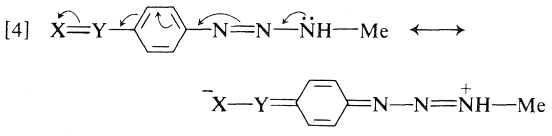

electron density at the alkyl-bearing nitrogen reduces the nucleophilic strength of the triazene moiety, thus rendering it less reactive in the coupling reaction. A similar electron movement, induced by the electron-attracting group, accounts for the shift in the tautomeric equilibrium towards the 3-aryl-tautomer **12** reported previously (21) [5]. A further correlation exists

[5] 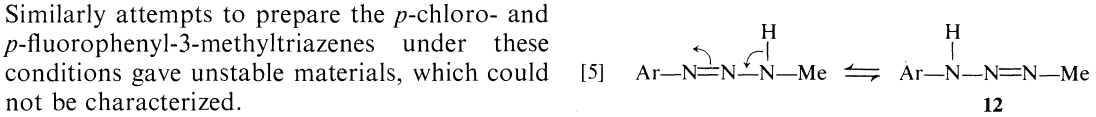

12

between these results and the protolysis experiments of Matrka and co-workers (31); the basicity of the triazene is affected similarly by changes in electron density at N-3 [6].

[6] 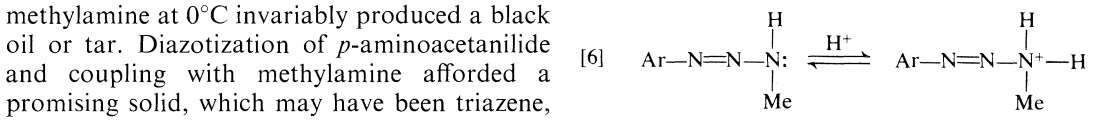

Acknowledgements

The financial assistance of the National Research Council of Canada (in part) is gratefully acknowledged. The authors wish to express their thanks to Dr. Malcolm F. G. Stevens for helpful discussions.

1. R. J. Le Blanc and K. Vaughan. Can. J. Chem. **50**, 2544 (1972).
2. T. P. Ahern and K. Vaughan. Chem. Commun. 701 (1973).
3. O. Dimroth. Ber. **36**, 909 (1903); **38**, 670 (1905); **40**, 2390 (1907).
4. V. Zverina and M. Matrka. Chem. Listy, **63**, 51 (1969).
5. M. Matrka. Cezk. Farm. **21**, 442 (1972).
6. T. M. Ong and F. J. de Serres. Mutat. Res. (Amsterdam), **13**, 276 (1971); **20**, 17 (1973).
7. F. A. Schmid and D. J. Hutchinson. Proc. Am. Assoc. Cancer Res. **14**, 75 (1973).
8. R. Preussman, A. von Hodenburg, and H. Hengy. Biochem. Pharm. **18**, 1 (1969); T. A. Connors, P. M. Goddard, K. Meral, W. C. J. Ross, and D. E. V. Wilman. Biochem. Pharm. **25**, 241 (1976).
9. T. A. Connors. FEBS Lett. **57**, 226 (1975).
10. R. Preussman and A. von Hodenburg. Biochem. Pharm. **19**, 1505 (1970).
11. E. H. White, H. Maskill, D. J. Woodcock, and M. A. Schroeder. Tetrahedron Lett. 1713 (1969).
12. H. Zollinger. Diazo and azo chemistry. Interscience, New York, NY. 1961. p. 179.
13. P. A. S. Smith. Open-chain nitrogen compounds. Vol. II. Benjamin, New York, NY. 1966. p. 285.
14. R. Meldola and F. W. Streatfield. J. Chem. Soc. **53**, 666 (1888).
15. L. Fisera, J. Kovac, E. Komanova, and J. Lesko. Tetrahedron, **30**, 4126 (1974).
16. H. Goldschmidt and V. Badl. Ber. **22**, 934 (1889).
17. C. Suling. Methoden der organisch Chemie (Houben-Weyl). **10/3**, 711, (1965).
18. O. N. Witt. Ber. **10**, 1309 (1877).

19. M. R. PETTITT and J. C. TATLOW. J. Chem. Soc. 1071 (1954).
20. H. FONG and K. VAUGHAN. Can. J. Chem. **53**, 3714 (1975).
21. K. VAUGHAN. J. Chem. Soc. Perkin Trans. II, 17 (1977).
22. (*a*) G. F. KOLAR. Mass spectrometry in biochemistry and medicine. *Edited by* A. Frigerio and N. Castagnoli. Raven Press, New York, NY. 1974. pp. 267–275; (*b*) H. OELSCHLAGER and H. BLUME. Arzneim.-Forsch. **26**, 303 (1976).
23. R. KREHER and K. GOTH. Z. Naturforsch. Teil B, **31**, 217 (1976).
24. M. KAWANISI, I. OTANI, and H. NOZACKI. Tetrahedron Lett. 5575 (1968).
25. E. H. WHITE, A. A. BAUM, and D. E. EITEL. Org. Synth. Coll. Vol. V, 797 (1973).
26. T. IGNASIAK, J. SUSZKO, and B. IGNASIAK. J. Chem. Soc. Perkin Trans. I, 2126 (1975).
27. G. ODDO and A. ALGERINO. Ber, **69**, 279 (1936).
28. H. EAGLE and P. VICKERS. J. Biol. Chem. **114**, 193 (1936).
29. R. N. BUTLER. Chem. Rev. **75**, 241 (1975).
30. J. GOERDELER and M. ROEGLER. Chem. Ber. **103**, 112 (1970).
31. V. ZVERINA, M. REMES, J. DIVIS, J. MARHOLD, and M. MATRKA. Coll. Czech. Chem. Commun. **38**, 251 (1973).

The passivity and overvoltage during hydrogen evolution and indium deposition of metallic indium

ALAN N. CAMPBELL

Department of Chemistry, University of Manitoba, Winnipeg, Man., Canada R3T 2N2

Received October 1, 1976

ALAN N. CAMPBELL. Can. J. Chem. **55,** 1710 (1977).

The passivity and overvoltage during hydrogen evolution and indium deposition of metallic indium have been determined. Although the overvoltage to hydrogen evolution is fairly high and increases with current density in the normal manner, passivity to the solution of indium ions is almost completely absent, in contradistinction to aluminum, whose anodic passivity is complete. A tentative explanation is offered.

ALAN N. CAMPBELL. Can. J. Chem. **55,** 1710 (1977).

On a déterminé la passivité de l'indium métallique et le survoltage durant l'évolution de l'hydrogène et la déposition de l'indium. Quoique le survoltage vis à vis l'évolution de l'hydrogène est assez élevé et augmente d'une façon normale avec la densité du courant, la passivité vis à vis la solution des ions indium est complètement absente; ce comportement est en opposition avec celui de l'aluminium pour lequel la passivité anodique est complète. On offre une explication non définitive.

[Traduit par le journal]

Introduction

Little work seems to have been done on the passivity or overvoltage of metallic indium. Because of the industrial importance of these phenomena, it was thought that the subject merited systematic investigation.

Experimental

Hydrogen Overvoltage

A square sheet of metallic indium was cast in a steel mould at a temperature just above the melting point of indium. The surface was quite bright but it was treated with dilute hydrochloric acid and washed in order to remove any invisible skin of oxide. A platinum wire was embedded in the rear of the indium plate. The plate was then mounted in a frame of plexi-glass, so that the front or conducting surface of the indium was countersunk about 1/4 in. The platinum wire emerged through two sheets of plexi-glass so as to be insulated from the solution. This method ensures that there is no concentration of current on the edges of the indium plate. The area of the conducting plate was 4.94 cm^2.

For measuring the potential of the indium cathode the usual arrangement of a saturated calomel electrode, provided with a Luggin capillary, was used. The anode was a platinum gauze electrode. Various electrolytes were tried but the one finally selected was *N* acetic acid plus *N* KCl. The function of the acetic acid is to act, in conjunction with vigorous stirring, essentially as a buffer. The p*H* remains constant despite the discharge of H^+ ions. The KCl lowers the resistance. Vigorous stirring is necessary to avoid concentration polarisation, as far as possible. A source of constant current was used, an NJE Corporation Rectifier, producing up to 2.5 A at 10 V.

The equilibrium potential of the cell

$$Hg/Hg_2Cl_2 \text{ in sat. } KCl/N \text{ } HAc/H_2/In$$

is 0.3819 V, calculated from the ionisation constant of acetic acid. Current was measured as the drop in potential across a standard resistance, using a sensitive potentiometer.

Experiments were repeated with increasing and with decreasing current and varying time intervals. The results were very consistent, *i.e.* independent of the above factors.

The numerical results are to be found in the Depository of Unpublished Data.[1] The results are expressed graphically in Fig. 1.

Overvoltage of Indium Deposition

The experimental set-up was the same as in the preceding section, but the electrolyte was 0.05 *N* $InBr_3$. Using the value of E^0 for indium previously obtained (1), the emf of the combination.

$$Hg/Hg_2Cl_2, \text{ sat. } KCl/0.05 \text{ } InBr_3/In$$

is calculated to be 0.6478 V. In the present instance, the open circuit potential was found to be 0.6380 V, a difference of 0.0098 V. The hydrogen equilibrium potential is very close to this (0.657 V) but the hydrogen overvoltage at an indium surface (see preceding section) prevents hydrogen evolution.

Results

The current density was raised gradually to 1.890 A/dm^2. The overvoltage was zero up to a current density (c.d.) of 0.567 A/dm^2. It then rose slowly to a value of 0.0552 V at 1.890 A/dm^2.

The experiment was repeated using 0.1 *N* $InCl_3$ (equilibrium potential of combination with

[1]Complete set of the actual experimental data is available, at a nominal charge, from the Depository of Unpublished Data, CISTI, National Research Council of Canada, Ottawa, Canada K1A 0S2.

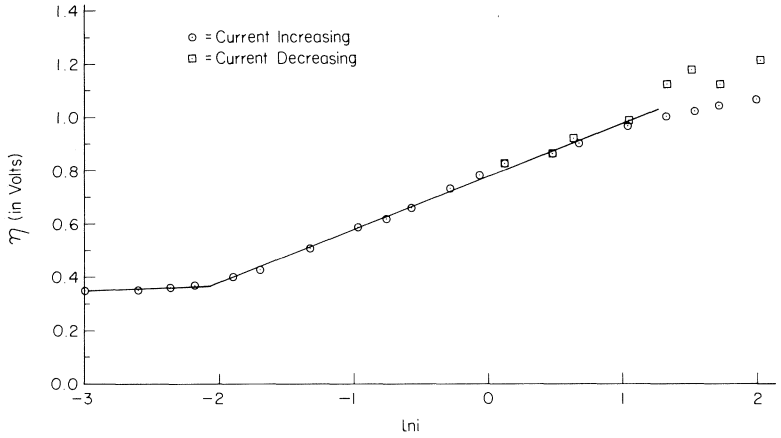

FIG. 1. Plot of η (in V) *vs.* ln *i*.

saturated calomel electrode = 0.6496 V). Again the overvoltage is very slight. A clean crystalline deposit of metallic indium was formed on the cathode (of platinum gauze). The numerical results are to be found elsewhere,[1] the results are expressed graphically in Fig. 2.

Anodic Passivity

The electrolyte first used was 0.1 *N* $InCl_3$, with a platinum gauze cathode and vigorous stirring. No passivity was observed up to a current density of 0.0750 A/dm^2. The passivity ($\eta = E_i - E_{rev}$) then rose slowly to 0.1224 V at a c.d. of 15.12 A/dm^2. The experiment was repeated with *N* $In_2(SO_4)_3$. The passivity attained a maximum value of 0.0270 V at a c.d. of 8.097 A/dm^2. The passivity is very slight.

The numerical results are to be found in the Depository of Unpublished Data.[1] The results are expressed graphically in Fig. 3.

Discussion

Hydrogen Overvoltage

When overvoltage is plotted against the logarithm of the current density (Fig. 1), the curve is seen to consist of two definite straight line portions, (*1*) from 0.0 to 0.1108 A/dm^2 and (*2*) from 0.1108 to 2.718 A/dm^2. After this upper limit, the curve loses slope and ceases to be a straight line. If the equation

$$\eta = a - b \ln i$$

(where η is the overvoltage, *i* the current

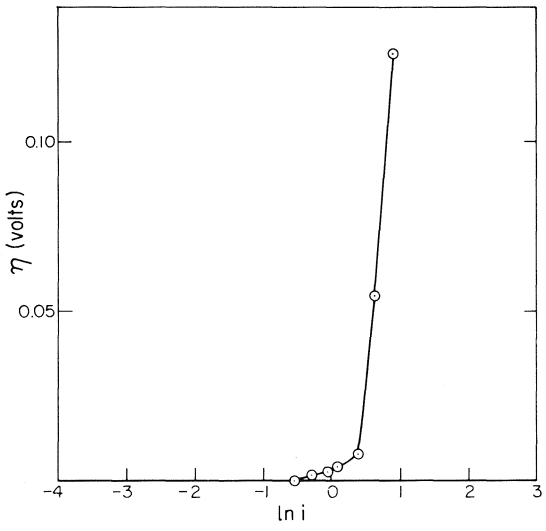

FIG. 2. Overvoltage to indium deposition *vs.* ln *i*.

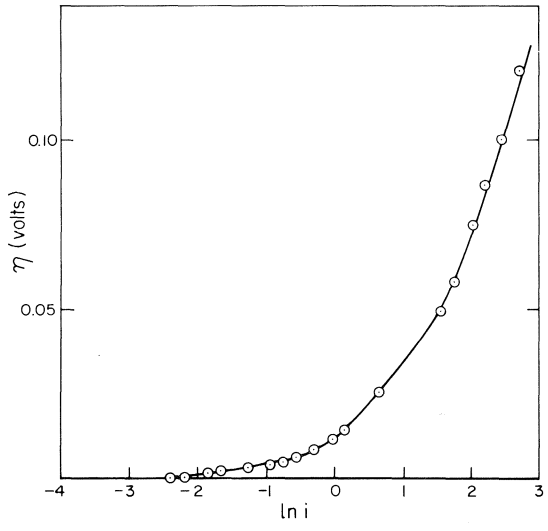

FIG. 3. Passivity of indium anode *vs.* ln *i*.

density, and a and b constants) is applied to the second (higher current density) portion, the constants result as $a = 0.78$ and $b = -0.195$.

The first part of the graph appears to be almost horizontal. If this portion of the graph is neglected, then the lowest overvoltage for hydrogen evolution is 0.37 V. Thiel and Breuning (2) give the overvoltage as 0.533 V, but they do not state the current density. Moreover, their electrolyte was $2N$ H_2SO_4 which must surely have attacked the indium chemically. According to the present results an overvoltage of 0.533 V is attained at a current density of 0.282 A/dm^2, *i.e.* it lies between those of tin and zinc.

Overvoltage to Indium Deposition

This is very slight.

Anodic Passivity

This is very slight and indeed zero up to appreciable current densities. Contrasted with the behaviour of aluminum, this is somewhat surprising. The 'valve' action of aluminum is well known: as anode, aluminum will not pass current up to very high positive potentials. This is no doubt due to the existence on all but recently cut aluminum surfaces of an oxide film (probably not the normal oxide). It has been suggested to me by Professor Sen, that the phenomenon may be due to the relative energy levels of electrons in metallic aluminum and in this aluminum oxide. It is easy to see how electrons could pass in one direction (in this case from oxide to metal) but not in the other. Since passivity is absent from indium, either an oxide layer is not formed (and there is no visual evidence that it is) or the energy levels in metal and in oxide are different from those in aluminum.

An examination of Figs. 1–3, indicates that, though the Tafel relation is obeyed over intermediate ranges of current density, the values increase rather suddenly at high current densities. This is certainly due to the impoverishment of concentration in the immediate neighbourhood of the electrode, despite the vigorous stirring. As to the various mechanisms, competing, simultaneous or successive, described in the texts, the author finds himself unable to make any worthwhile decision.

A lengthy paper by Piercy and Hampson (3), under the title "The Electrochemistry of Indium" contains many valuable references. Among other things, the suggestion is made (4) that the ionization of metallic indium or discharge of indium ion takes place in stages. This is probably true, but the results of this paper show conclusively that both the passivity of anodic solution and the overvoltage to indium deposition are very slight under the experimental conditions described in the paper.

Acknowledgment

The author is indebted to Cominco for a gift of high purity indium metal.

1. A. N. Campbell. Can. J. Chem. **52**, 3769 (1974).
2. A. Thiel and E. Breuning. Z. Anor. Chem. **83**, 337, (1913); **83**, 339 (1913); **83**, 340 (1913).
3. R. Piercy and N. A. Hampson. J. Appl. Electrochem. **5**, 1 (1975).
4. G. M. Budov and V. V. Losev. Dokl. Akad. Nauk. SSSR, **129**, 6 (1959).

Vapour pressures of aqueous solutions of $AgNO_3 + TlNO_3$ by the static method at 98.5°C

MARIE-CHRISTINE TRUDELLE AND MAURICE ABRAHAM

Département de Chimie, Université de Montréal, Montréal (Qué.), Canada H3C 3A7

AND

JAMES SANGSTER[1]

Département de Génie Chimique, Ecole Polytechnique, Campus de l'Université de Montréal, C.P. 6079, Succ. "A" Montréal (Que.), Canada H3C 3A7

Received January 18, 1977

MARIE-CHRISTINE TRUDELLE, MAURICE ABRAHAM, and JAMES SANGSTER. Can. J. Chem. **55**, 1713 (1977).

Vapour pressures of the system $(Ag,Tl)NO_3 + H_2O$ have been measured at 98.5°C by the static method over the complete concentration range for Ag/Tl mole ratio = 1.14. The water activity data can be represented by a modified BET isotherm in the range $0.1 < a_w < 0.7$. The derived BET constants indicate that the salts in this system are very weakly hydrated, probably less so than (for example) $CsNO_3$. The linearity of vapour pressure with water mole ratio R_H, found previously by Tripp and Braunstein for $(Li,K)NO_3 + H_2O$, is absent in the present system. The Henry's law constant for water dissolved in molten $(Ag,Tl)NO_3$ has been deduced. The excess free energy of the system is positive at all concentrations and shows a maximum of 117 cal/mol at water mole fraction 0.66.

MARIE-CHRISTINE TRUDELLE, MAURICE ABRAHAM et JAMES SANGSTER. Can. J. Chem. **55**, 1713 (1977).

On a mesuré les pressions de vapeur du système $(Ag,Tl)NO_3 + H_2O$ à 98.5°C, par une méthode statique, pour tout le domaine de concentration en eau, le rapport molaire Ag/Tl étant fixé à 1.14. On peut représenter les données obtenues pour l'activité de l'eau par une isotherme BET modifiée, dans l'intervalle $0.1 < a_w < 0.7$. Les constantes BET que l'on en dérive indiquent que les sels constituants de ce système sont très faiblement hydratés, probablement moins que, par exemple, $CsNO_3$. Le caractère linéaire de la pression de vapeur fonction du rapport molaire R_H trouvé antérieurement par Tripp et Braunstein pour le système $(Li,K)NO_3 + H_2O$ n'apparaît pas pour le système étudié ici. La constante de la loi de Henry pour l'eau dissoute dans le mélange de sels fondus $(Ag,Tl)NO_3$ a été déduite. L'enthalpie libre d'excès de ce système est positive pour toute concentration en eau avec un maximum de 117 cal/mol pour une fraction molaire en eau de 0.66.

Introduction

Thermodynamic properties of concentrated aqueous electrolyte solutions have in general received less attention than those of dilute solutions, either experimentally or theoretically. Solubility limits have contributed to this difference. Perhaps of greater importance is the fact that there is no theory of aqueous electrolyte solutions as adequate for this concentration region as the Debye–Hückel approach is for dilute solution.

It is significant therefore that more progress in the understanding of concentrated electrolyte solutions has come from the fused salt end of the concentration scale than from the dilute (1, 2). The vapour pressures of very concentrated electrolyte solutions and of aqueous melts have been measured by the isopiestic (3*a*) and differential transpiration (3*b*) methods, mostly for the nitrates and halides of the alkalis and alkaline earths. To complement this small but growing pool of data, we describe here an apparatus for the static measurement of vapour pressures of aqueous solutions above room temperature, and report results for the system $(Ag,Tl)NO_3 + H_2O$ at 98.5°C. This system is convenient for study since, for approximately equimolar Ag and Tl in the mixture, the system is liquid around 100°C over the entire concentration range (4). The choice of this system also marks a departure from all previous work in this area (2, 3) since *both* cations in the salt mixture are probably only weakly hydrated in aqueous solution (previously used mixtures always included Li^+ or Na^+ or Ca^{2+}).

This paper will deal with the apparatus and

[1]To whom correspondence should be addressed.

experimental technique in some detail since, although the principle of the static method is simple and familiar, the components of the apparatus and their manipulation merit special attention.

Experimental

Chemicals and Procedure

The preparation, purification, and storage of the chemicals used, and a detailed description of the experimental procedure are available elsewhere.[2]

Apparatus

The apparatus is represented schematically in Fig. 1. The vacuum system (not shown) comprised a combination diffusion/rotary pump and liquid nitrogen trap. The pressure in the manifold was indicated by a Pirani gauge (Edwards High Vacuum, 10^{-4} to 1 Torr). The sample container was a 100 ml Pyrex flask. The flask was immersed in a bath of water in a Haake Circulating Pump model FS. The sample solution was stirred magnetically. The temperature of the bath was measured with a Hewlett–Packard Quartz Thermometer model 2801A, and read 98.50 ± 0.05°C.

Since the pressure gauge used (quartz spiral type, model 145, 0–50 in. Hg, Texas Instruments) operated at room temperature, an intermediate heated sensing device was necessary to avoid condensation. Thus the sample container was connected, through Pyrex and stainless steel tubing kept at 180°C by heating tape, to one side of a pressure transducer (model DP 15, Validyne Engineering Corp.) kept at 110°C in a thermostated air oven. The other side of the transducer was connected to the pressure gauge and also to a Servo Pressure Controller (model SPC, Volumetrics). Any imbalance signal from the transducer activated the pressure controller to adjust the air pressure presented to the transducer and pressure gauge simultaneously until there was null signal (zero differential pressure). At this point, the vapour pressure of the sample could be read off the pressure gauge as an absolute pressure, the reference side of the gauge being kept evacuated ($\leq 10^{-3}$ Torr) through stopcock 3.

All stopcocks were of the hollow key type; those at room temperature were lubricated with Dow Corning High Vacuum grease, and the heated ones with Apiezon type H.

The dead space above the sample solution was minimized as much as was physically possible; it was estimated to be about 80 cm^3.

The general and degassing techniques and apparatus were tested by measuring the vapour pressure of distilled water. About 25 measurements were taken at temperatures between 50 and 100°C. The values lay within one part per thousand of those in the literature (5).

Calculations

For deriving water activities, the fugacity of the vapour is required. The fugacity f was found from the pressure p by

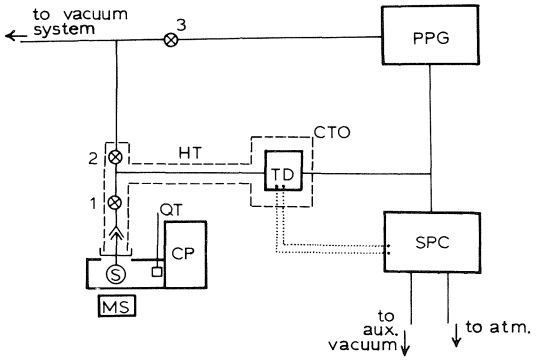

FIG. 1. Block diagram of the apparatus. MS, magnetic stirrer; S, sample flask; CP, circulating pump; QT, quartz thermometer; HT, heating tape; CTO, constant temperature air oven; TD, transducer; PPG, precision pressure gauge; SPC, servo pressure controller; 1, 2, 3, stopcocks.

$$[1] \qquad f = p \exp(Bp/RT)$$

where B is the second virial coefficient of water vapour (6) (-462 cm^3/mol at 98.5°C). Use of the third virial coefficient is not warranted in this work. If f^0 is the fugacity of pure water at 98.5°C, then the water activity $a_w = f/f^0$.

Since the data reported here cover essentially the complete concentration range, free energy parameters have been calculated on both mole fraction and molality scales. If x represents mole fraction, then the activity coefficient of water on the mole fraction scale is $\gamma_w = a_w/x_w$. On the molality scale, the osmotic coefficient ϕ is given by

$$[2] \qquad \phi = -1000 \ln a_w/2mM_w$$

where m is the total molality of salts and M_w is the molar mass of water.

The BET isotherm equation, adapted to aqueous electrolyte solutions, can be written as (7)

$$[3] \quad ma_w/55.51(1 - a_w) = 1/cr + (c - 1)a_w/cr$$

where r is the number of molecules of water adsorbed per complete monolayer on a solute molecule. The constant c is given approximately by $c = \exp[-(E - E_L)/RT]$, where E is the heat of adsorption of water molecules of the monolayer and E_L is the heat of liquefaction of bulk water.

If the mixed solute $(Ag,Tl)NO_3$ be considered as a single solute of molality m, then the measure-

[2]Available upon request, at a nominal charge, from the Depository of Unpublished Data, CISTI, National Research Council of Canada, Ottawa, Canada K1A 0S2.

TABLE 1. Vapour pressures and derived quantities for the system $(Ag,Tl)NO_3 + H_2O$ at 98.5°C*

x_w	m	p	f	a_w	ϕ	γ_w
0.9774	1.284	701.2	691.5	0.9741	0.567	0.997
0.9586	2.397	684.5	675.2	0.9513	0.578	0.992
0.9217	4.716	661.2	652.5	0.9192	0.496	0.997
0.8769	7.792	643.0	634.8	0.8942	0.398	1.020
0.8567	9.285	635.8	627.8	0.8844	0.367	1.032
0.7928	14.51	612.9	605.4	0.8531	0.304	1.076
0.7788	15.77	609.0	601.6	0.8475	0.291	1.088
0.7662	16.94	603.0	595.8	0.8393	0.287	1.095
0.7329	20.23	590.9	584.0	0.8227	0.268	1.122
0.7256	20.99	589.1	582.2	0.8202	0.262	1.130
0.7186	21.74	584.5	577.8	0.8139	0.263	1.133
0.7009	23.69	577.2	570.6	0.8038	0.256	1.147
0.6565	29.04	555.8	549.7	0.7744	0.244	1.180
0.6187	34.21	533.3	527.7	0.7433	0.241	1.201
0.6160	34.60	533.1	527.5	0.7431	0.238	1.206
0.6078	35.82	532.6	527.0	0.7423	0.231	1.221
0.5709	41.72	506.3	501.2	0.7061	0.232	1.237
0.5693	41.99	509.1	504.0	0.7100	0.226	1.247
0.5447	46.40	492.4	487.6	0.6869	0.225	1.260
0.5236	50.50	478.1	473.6	0.6671	0.222	1.274
0.5109	53.14	467.4	463.1	0.6524	0.223	1.277
0.4801	60.11	442.6	438.7	0.6180	0.222	1.287
0.4609	64.93	432.0	428.3	0.6033	0.216	1.309
0.4546	66.60	427.1	423.5	0.5966	0.215	1.312
0.4505	67.71	424.2	420.6	0.5925	0.215	1.315
0.4433	69.71	413.8	410.4	0.5781	0.218	1.304
0.4338	72.45	406.7	403.4	0.5683	0.216	1.310
0.3894	87.04	370.8	368.1	0.5186	0.209	1.332
0.3846	88.82	366.3	363.6	0.5123	0.209	1.332
0.3585	99.33	343.0	340.7	0.4799	0.205	1.339
0.3439	105.9	330.9	328.7	0.4631	0.202	1.347
0.3213	117.3	313.7	311.7	0.4391	0.195	1.367
0.3134	121.6	304.9	303.1	0.4269	0.194	1.362
0.2564	161.0	249.4	248.2	0.3496	0.181	1.364
0.2208	195.9	216.3	215.4	0.3034	0.169	1.374
0.1964	227.1	192.0	191.3	0.2694	0.160	1.372
0.1937	231.1	189.2	188.5	0.2655	0.159	1.370
0.1453	326.5	141.2	140.8	0.1983	0.138	1.365
0.1289	375.1	126.7	126.4	0.1780	0.128	1.381
0.1124	438.3	110.1	109.9	0.1548	0.118	1.377
0.0955	525.7	93.0	92.8	0.1308	0.107	1.369
0.0810	629.8	78.1	78.0	0.1099	0.097	1.356

*Ag/Tl = 1.14 mol/mol; p^0 = 720.15 Torr; f^0 = 709.87 Torr; pressures and fugacities in Torr.

ment of the water activity over the complete concentration range enables the excess free energy G^E to be calculated. Solvent and solute are both liquids in this example, and so G^E is found in the usual way (8) from the equation

$$[4] \quad G^E = x_s RT \int_{x_w=0}^{x_w} (\ln \gamma_w / x_s^2)\, dx_w$$

where $x_s = 1 - x_w$. The integral was evaluated graphically.

Results and Discussion

Vapour Pressures

The vapour pressures and derived thermodynamic parameters are presented in Table 1. Since essentially the complete concentration range is represented, the results may be discussed profitably by using both the osmotic coefficient and activity coefficient of water. Thus Fig. 2 gives the Raoult's law plot of the data; the system shows positive deviations over almost all the

concentration range. This is unusual behaviour for an aqueous electrolyte system, since the vast majority of such systems hitherto studied show strong negative deviations at all compositions (2). The exceptions to this rule are (perhaps not surprisingly) such salts as $AgNO_3$, $RbNO_3$, and $CsNO_3$. For illustration, Fig. 3 shows ϕ and γ_w in the dilute region for $(Ag,Tl)NO_3$ and also for $AgNO_3$ alone at 100°C (9). The substitution of Tl^+ for some of the Ag^+ thus significantly increases γ_w above unity.[3] The behaviour of $RbNO_3$ and $CsNO_3$ solutions is very close to that shown for $AgNO_3$ (10*a*).

Tripp and Braunstein (1, 2, 3*b*) have reported an empirical regularity for $(Li,K)NO_3$ aqueous melts which may or may not be significant for the search for an adequate theoretical model of these systems. They found that the vapour pressure (and a_w) were linear in the 'water mole ratio' R_H = moles H_2O/moles NO_3^- in the region $R_H = 0$ to 1. The same plot is shown in Fig. 4 for the present system $(Ag,Tl)NO_3 + H_2O$. Clearly there is no linearity at all, except[4] perhaps for $R_H < 0.1$. There is as yet no model (statistical or otherwise) to account for this kind of linearity (2), which may depend upon (for example) the presence of a strongly hydrated cation in the mixture.

BET Isotherm

Some time ago Stokes and Robinson (7) pointed out that very concentrated aqueous solutions of strong electrolytes could be described by a suitably adapted BET adsorption isotherm equation. At first thought this may seem quite striking, but the model it implies is a reasonable one and isotherm plots (eq. 3) show good linearity for $a_w < 0.5$ (2, 7). Figure 5 shows the BET isotherm plot for $(Ag,Tl)NO_3 + H_2O$. Also included for comparison are the data for the system $(Li,Cs)NO_3 + H_2O$ at 100°C (3*a*) and $H_2SO_4 + H_2O$ at 25°C (11).

It is noticed immediately that the $(Ag,Tl)NO_3$ isotherm is situated far above all the others (the intercept is 1.33 whereas the others (3*a*) lie below 0.3). The derived BET constants for the present system are given in Table 2, together with those

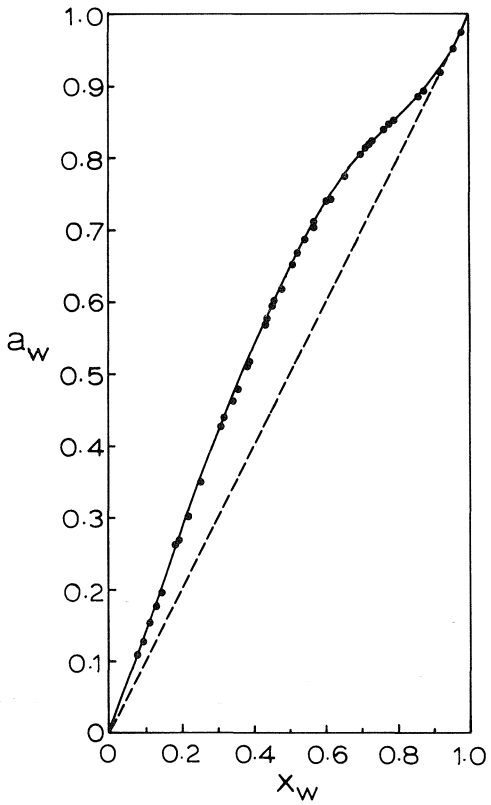

FIG. 2. Raoult's law plot for the system $(Ag,Tl)NO_3 + H_2O$ at 98.5°C. Dashed line represents ideal behaviour.

of a few other representative systems. While the Ag/Tl isotherm is valid in much the same a_w range as the others, the r and c values are very low. If the series $LiNO_3$, $(Li,Cs)NO_3$, $(Ag,Tl)NO_3$ be considered, it may be deduced that the large cations Ag^+, Tl^+, and Cs^+ are all weakly hydrated in comparison with Li^+. Thus if it is assumed that cations are hydrated preferentially over anions then the following approximate values of r at 100°C can be found: Ca^{2+}, 3.6; Li^+, 2.7; Cs^+, 1.3; Ag^+ and Tl^+, 0.3 (using the values of r in refs. 3*a* and 7).

Henry's Law

The BET equation can be written in terms of mole fractions as

$$[5]\quad a_w(1 - x_w)/x_w(1 - a_w) = 1/cr + (c - 1)a_w/cr$$

and thus in the limit as $x_w \to 0$, eq. 5 reduces (2) to

$$[6]\quad (a_w/x_w)_{x_w \to 0} = 1/cr = \gamma_w^{\infty}$$

[3]Figure 3 also suggests that, while γ_w (in contrast to ϕ) is not a sensitive indicator of non-ideality in dilute solution (10*b*), γ_w may become more useful than ϕ in the "water dissolved in molten salt" region.

[4]In the limit as $x_w \to 0$, water exhibits Henry's law behaviour where both vapour pressure and a_w *are* linear in R_H.

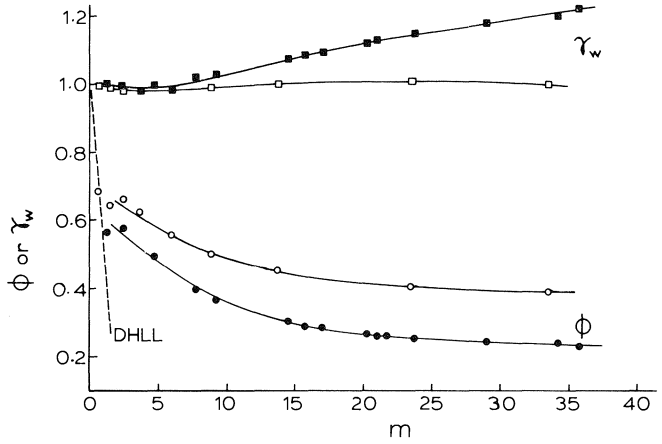

FIG. 3. Solvent free energy parameters for $AgNO_3 + H_2O$ at 100°C (ref. 9), open symbols and $(Ag,Tl)NO_3 + H_2O$ at 98.5°C, closed symbols. □, ■, γ_w; ○, ●, ϕ.

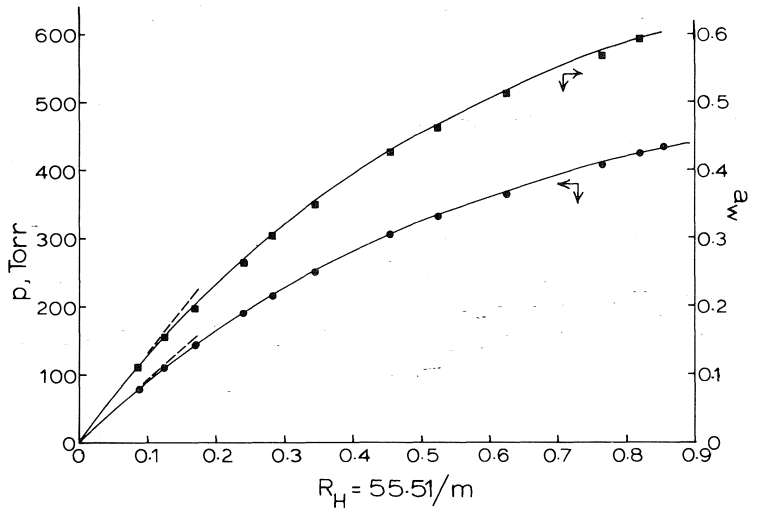

FIG. 4. Vapour pressure and a_w as functions of the water mole ratio R_H. Dashed lines represent linear behaviour extrapolated beyond $R_H = 0.1$. ■, a_w; ●, p.

TABLE 2. Constants of the BET adsorption isotherm (eq. 3) adapted to aqueous solutions of mixed and single electrolytes

Solute	Temperature (°C)	r	c	$-(E - E_L)$ kcal/mol	Reference
$(Ag,Tl)NO_3$[a]	98.5	0.5	1.6	0.3	This work
$(Li,Cs)NO_3$[b]	100	1.7	2.3	0.6	3*a*
$LiNO_3$	100	2.7	5.1	1.2	3*a*
H_2SO_4	25	3.6	28	2.0	11
LiBr	25	3.8	43	2.2	7

[a]Mole ratio Ag/Tl = 1.14.
[b]Mole ratio Li/Cs = 0.98.

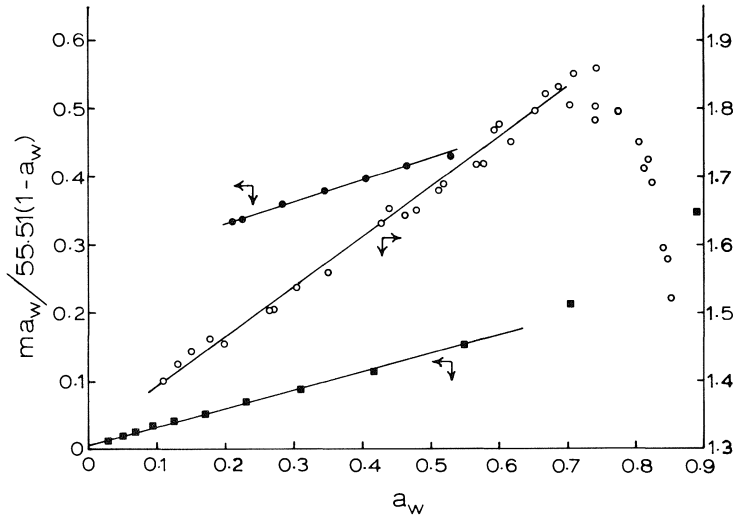

FIG. 5. BET isotherms, adapted for aqueous electrolyte solutions, for three systems: ●, $(Li,Cs)NO_3$ + H_2O at 100°C (ref. 3*a*); ○, $(Ag,Tl)NO_3$ + H_2O at 98.5°C (this work); ■, H_2SO_4 + H_2O at 25°C (ref. 11).

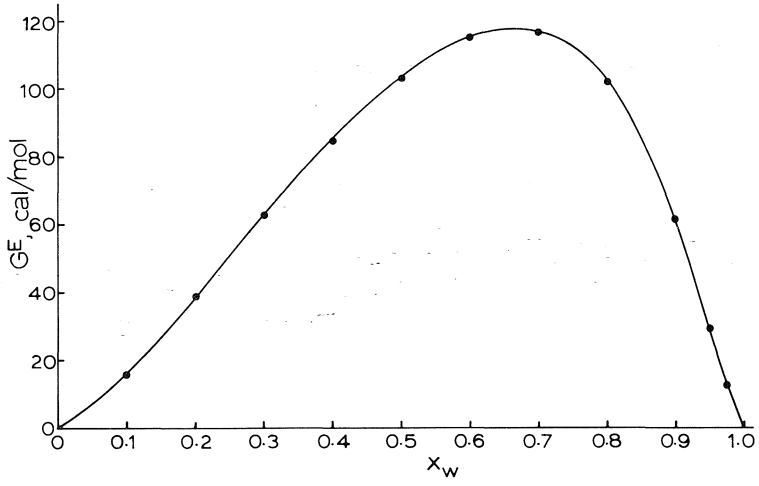

FIG. 6. Excess free energy for the system $(Ag,Tl)NO_3$ + H_2O at 98.5°C as a function of water mole fraction.

where γ_w^∞ is the activity coefficient of water at infinite dilution in molten salt (*i.e.*, the BET intercept). Converting to fugacities, we have

$$[7] \qquad f_w = f_w^0 x_w \gamma_w^\infty = K_H x_w$$

where K_H is Henry's constant for water in molten salt and f_w^0 is the fugacity of pure water. Table 3 gives K_H for water dissolved in a number of molten salts. It is seen that molten salts can differ enormously as 'solvents' for water.

It has not been pointed out previously that the theoretical limit of the BET expression $ma_w/55.51(1 - a_w)$, that is the left side of eq. 3 or eq. 5, as $x_w \to 1$ is 0.5 for 1:1 electrolytes.[5] This is shown quite clearly for dilute solutions of single electrolytes at 25°C (3*a*); it also suggests why the $(Ag,Tl)NO_3$ BET plot deviates *downward* while others (like that for LiBr) deviate *upward* as a_w increases.

[5]In general the limit is $1/\nu$ where ν is the stoichiometric number of ions per electrolyte molecule. This can be deduced easily if a_w is replaced by the 'species mole fraction' $55.51/(55.51 + \nu m)$ and noting that as $m \to 0$, $x_w \to 1 - \nu m/55.51$.

TABLE 3. Henry's law constants K_H (atm) for water dissolved in salts at 100°C calculated according to eq. 7

Salt	K_H	Reference
LiBr	0.010	3*a*
LiCl	0.017	3*a*
$Ca(NO_3)_2$	0.036	3*a*
$LiNO_3$	0.072	3*a*
$(Ca,Cs)NO_3$[a]	0.14	3*a*
$(Li,K)NO_3$[b]	0.21	3*a*
$(Li,Cs)NO_3$[c]	0.25	3*a*
$(Ag,Tl)NO_3$[d]	1.3	This work

[a]Mole ratio Ca/Cs = 0.99.
[b]Mole ratio Li/K = 1.03.
[c]Mole ratio Li/Cs = 0.98.
[d]Mole ratio Ag/Tl = 1.14. For calculating K_H, the γ_w^∞ value at 98.5°C was used.

Excess Free Energy

It is customary, when calculating excess free energies of aqueous electrolyte solutions at ordinary temperatures, to use the ideal solution represented by unity osmotic coefficient ϕ and unity mean ionic activity coefficient $\gamma_\pm$ at all concentrations (12). In this convention solvent obeys Raoult's law and solute obeys Henry's law at infinite dilution, and the pure solute is not chosen as the standard state since it is a solid of limited solubility, possessing properties too different from the solute in solution. This difficulty is absent from the present system since it is liquid at all concentrations. The activity of one component is known over the whole concentration range, and hence the Gibbs–Duhem equation may be integrated from the fused salt end quite easily.

The excess free energy G^E is given by eq. 4 and plotted in Fig. 6. To our knowledge this is the first aqueous electrolyte system to have been treated in this manner. It is seen that G^E is everywhere positive (corresponding to positive Raoult's law deviations) and is a smoothly varying function of composition. The maximum value is 117 cal/mol at $x_w = 0.66$.

Acknowledgments

We thank Le Ministère de l'Education de la Province de Québec and The National Research Council of Canada for financial aid.

1. T. B. TRIPP. *In* Proceedings of the International Symposium on Molten Salts. The Electrochemical Society, Princeton, NJ. 1976. p. 560.
2. J. BRAUNSTEIN. *In* Ionic interactions: from dilute solutions to fused salts. Vol. 1. *Edited by* S. Petrucci. Academic Press, New York. 1971. p. 179.
3. (*a*) H. BRAUNSTEIN and J. BRAUNSTEIN. J. Chem. Thermodyn. **3**, 419 (1971); (*b*) T. B. TRIPP. J. Chem. Thermodyn. **7**, 263 (1975).
4. M. ABRAHAM and J. J. HECHLER. Electrochim. Acta, **17**, 1849 (1972).
5. A. WEXLER and L. GREENSPAN. J. Res. Nat. Bur. Stand. **75**A, 213 (1971).
6. J. P. O'CONNELL and J. M. PRAUSNITZ. Ind. Eng. Chem. Fund. **9**, 579 (1970).
7. R. H. STOKES and R. A. ROBINSON. J. Am. Chem. Soc. **70**, 1870 (1948).
8. H. BLOOM. The chemistry of molten salts. W. A. Benjamin, New York. 1967. p. 49.
9. A. N. CAMPBELL, J. B. FISHMAN, G. RUTHERFORD, T. P. SCHAEFER, and L. ROSS. CAN. J. Chem. **34**, 151 (1956).
10. R. A. ROBINSON and R. C. STOKES. Electrolyte solutions. 2nd ed. (rev.). Butterworths, London. 1965. (*a*) p. 485; (*b*) p. 29.
11. J. A. RARD, A. HABENSCHUSS, and F. H. SPEDDING. J. Chem. Eng. Data, **21**, 374 (1976).
12. H. S. HARNED and R. A. ROBINSON. Multicomponent electrolyte solutions. Pergamon Press, Oxford. 1968. p. 46.

Etude spectroscopique et voltammétrique de l'équilibre existant entre les acides chlorosulfurique et acétosulfurique dans l'acide acétique

BERNARD BRASME, JEAN CLAUDE FISCHER ET MICHEL WARTEL

Université de Lille I, Laboratoire de Chimie Minerale I, Bâtiment C8, B.P. 36, 59650 Villeneuve d'Ascq, France

Reçu le 19 octobre 1976

BERNARD BRASME, JEAN CLAUDE FISCHER et MICHEL WARTEL. Can. J. Chem. **55**, 1720 (1977).

L'étude des spectres Raman d'une solution d'acide chlorosulfurique dans l'acide acétique, soumise à un vide dynamique, révèle l'existence de l'équilibre:

$$HSO_3Cl + HCH_3CO_2 \rightleftarrows HSO_3CH_3CO_2 + HCl$$

dont la constante a été déterminée par l'étude du système:

$$AgCl + HClO_4 + HSO_3CH_3CO_2 + e^- \rightleftarrows Ag + HSO_3Cl + HCH_3CO_2 + ClO_4^-$$

Le traitement mathématique des résultats après affinement par la méthode des moindres carrés conduit à la valeur $K = 10^{0.8\pm0.2}$ mol ℓ^{-1}.

BERNARD BRASME, JEAN CLAUDE FISCHER, and MICHEL WARTEL. Can. J. Chem. **55**, 1720 (1977).

A study of the Raman spectra of a solution of chlorosulfuric acid in acetic acid, under a continuous vacuum, reveals the existence of the equilibrium:

$$ClSO_3H + CH_3COOH \rightleftarrows CH_3COOSO_3H + HCl$$

The equilibrium constant of this reaction was determined from the study of the system:

$$AgCl + HClO_4 + CH_3COOHSO_3 + e^- \rightleftarrows Ag + ClSO_3H + CH_3COOH + ClO_4^-$$

The equilibrium constant derived from a least-squares analysis of the data was found to be $10^{0.8\pm0.2}$ mol ℓ^{-1}.

[Journal translation]

Introduction

Dans un travail précédent (1) nous avons expliqué le caractère diacide de l'acide chlorosulfurique dans le solvant acide acétique (AcOH) en mettant en évidence par spectrométries ir et Raman et par analyse chimique la nature des composés formés lors de la neutralisation d'une solution de HSO_3Cl par une solution d'acétate de pyridinium (PyHAcO). Ce caractère diacide peut être résumé par les trois schémas suivants:

Ionisation

[1] $$HSO_3Cl + AcOH \rightleftarrows AcOH_2^+SO_3Cl^-$$

Réaction acide–base

[2] $$AcOH_2^+SO_3Cl^- + PyH^+AcO^- \rightleftarrows PyH^+SO_3Cl^- + 2AcOH$$

Réaction de complexation

[3] $$PyH^+SO_3Cl^- + PyH^+AcO^- \rightleftarrows PyH^+SO_3AcO^- + PyH^+Cl^-$$

$PyH^+SO_3AcO^-$ symbolise l'acétosulfate de pyridinium. En fait le schéma 3 met en jeu les pouvoirs donneurs de SO_3 des composés SO_3Cl^- et SO_3AcO^-.

En l'absence de la base PyHAcO un échange de SO_3 doit exister entre le chlorosulfate d'acidium acétique formé selon [1] et le solvant soit:

[4] $$AcOH_2^+SO_3Cl^- + 2AcOH \rightleftarrows AcOH_2^+SO_3AcO^- + AcOH_2^+Cl^-$$

que nous pouvons encore écrire:

[5] $$HSO_3Cl + AcOH \rightleftarrows HSO_3AcO + HCl$$

où nous ne présageons pas de l'état de solvatation des différentes espèces.

Résultats et discussion

Existence d'un équilibre entre HSO_3Cl et HSO_3AcO

L'étude par spectroscopie Raman d'une solution 5 *M* de HSO_3Cl (fig. 1, spectre 1) nous permet de mettre en évidence l'existence des espèces $AcOH_2^+$ et SO_3Cl^- et peut être HSO_3Cl par la raie à 415 cm^{-1} (tableau 1).

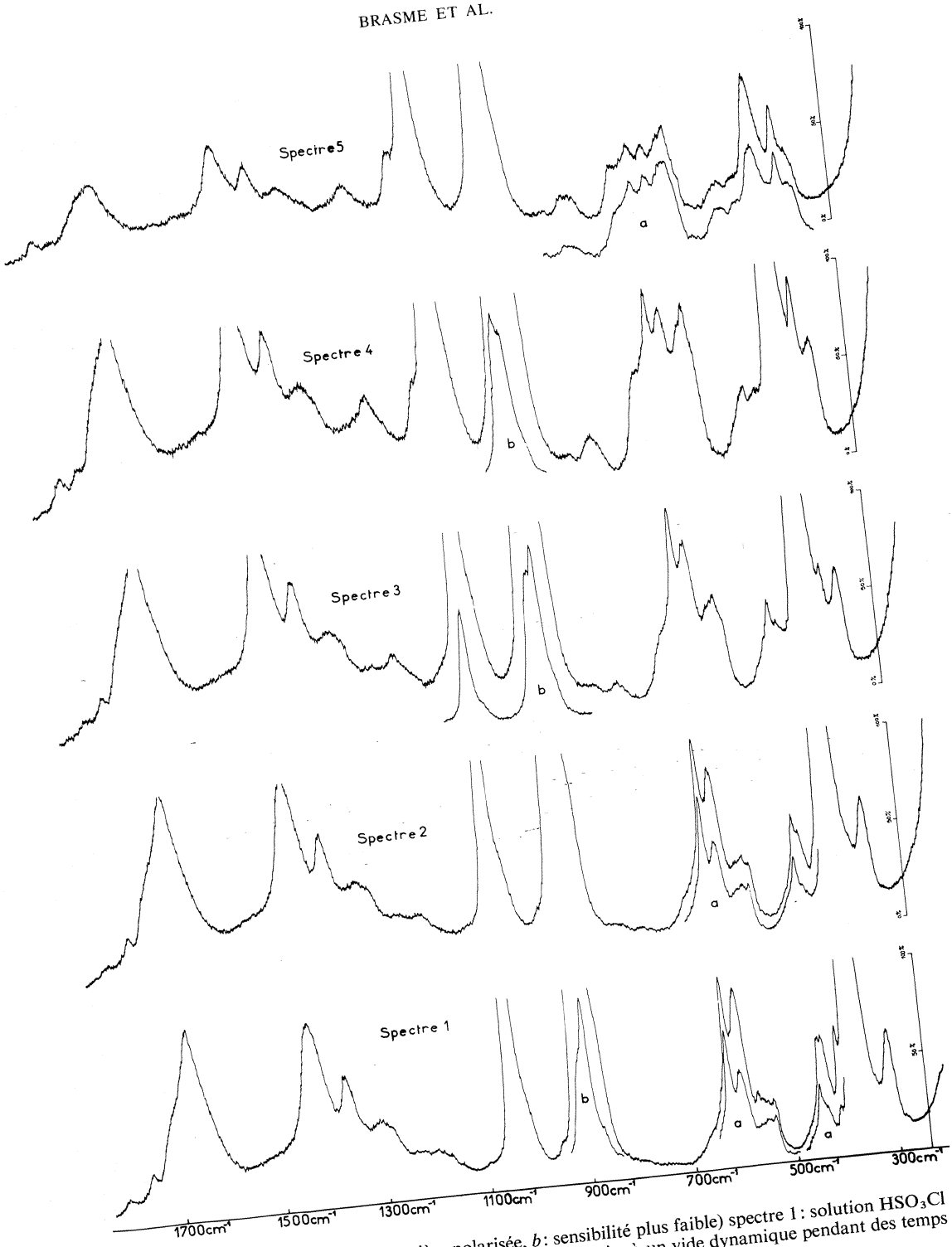

FIG. 1. Spectres Raman (*a*: lumière polarisée, *b*: sensibilité plus faible) spectre 1: solution HSO_3Cl 5 *M* dans AcOH; spectres 2, 3, 4, 5: même solution soumise à un vide dynamique pendant des temps croissants.

TABLEAU 1. Comparaison des fréquences de diffusion Raman du spectre 1 de la fig. 1 à celles du spectre des espèces: HSO_3Cl, AcOH, $AcOH_2^+$, SO_3Cl^- et $AcOSO_3^-$*

Nos résultats			Références			
					$AcOSO_3^-$	
Spectre 1 (fig. 1)	HSO_3Cl	AcOH	$AcOH_2^+$ (5)	SO_3Cl^- (2, 3, 4)	(1)	(6)
					265 m	
310 m	295 à 310 m			312 m		
					340 à 346 F	341 F
					355 à 360 m	
380 F				380 à 430 F		398 f
415 f	415 F					
436 m		436 m				
446 m			450			
	505 f			535		
536 m					545 m	547 F
					554 à 559 F	
				585	568 à 577 m	
598 F		598 m		601 f		
620 F	620 m	619 F	620		612 à 620 f	
630 à 680 (m-f)			645		647 à 655 F	660 m
					737 à 755 m	764 m
					811 f	
						860 f
892 F		892 F				
910 m			908		909 F	906 F
	915 f					
1040 F				1042 F	1043 à 1063 F	1050 F
1150 f	1150 f		1185			
1220					1207 à 1230 f	1220 f
1300 m				1300 f	1280 à 1297 f	1313 f
1365 m		1365 m	1375			
					1400 f	1380 m
1427 F		1427 m			1427 à 1430 f	1440 m
1664 F		1664 m			1680 à 1840 m	1672 à 1800 f

*F: forte, m: moyenne, f: faible.

L'attribution a été réalisée en s'appuyant sur les résultats obtenus par Auger *et al.* (2) et par Gerding et coll. (3, 4) pour SO_3Cl^- et par Casadevall *et al.* (5) pour $AcOH_2^+$.

Toutefois, les fréquences des raies caractéristiques les plus intenses de $AcOSO_3^-$ (regroupées dans le tableau 1) sont trop voisines de celles des raies de SO_3Cl^-, $AcOH_2^+$ et AcOH pour que nous soyons en mesure de prouver la formation d'acide acétosulfurique en quantité décelable selon l'équilibre [5]. Pour montrer que cet équilibre intervenait nous avons tenté de le déplacer vers la droite, par extraction de HCl sous pression réduite.

Nous avons donc réalisé les spectres de diffusion Raman d'une solution 5 *M* d'acide chlorosulfurique dans AcOH soumise à un vide dynamique pendant des temps croissants. Les spectres obtenus sous 10^{-2} Torr après 5 min (spectre 2), 15 min (spectre 3), 1 h (spectre 4) et 6 h (spectre 5) sont comparés à celui de la solution initiale (spectre 1) fig. 1.

Il faut noter qu'en plus du déplacement de l'équilibre, l'abaissement de la pression aura pour effet de faire varier les concentrations par élimination du solvant. Ne disposant pas d'élément de référence privilégié nous avons, au cours de notre étude, augmenté la sensibilité de notre appareillage de manière à maintenir constante dans les quatre premiers spectres l'intensité de la première raie, située vers 310 cm^{-1} (SO_3Cl^-).

Au contraire, dans le cas du spectre 5, nous avons adopté une sensibilité identique à celle utilisée pour réaliser le spectre 1 de manière à disposer d'un élément nous permettant d'ob-

server la modification de l'allure générale du spectre.

Description des spectres

Le spectre 5 comparé au spectre 1 nous permet de constater une nette diminution des intensités des raies caractéristiques de l'espèce SO_3Cl^- (en particulier la raie à 310 cm^{-1} n'apparait plus que sous forme d'un épaulement), ce qui indique un appauvrissement important en chlorosulfate.

L'abaissement de pression a aussi pour effet d'éliminer de la solution une fraction importante du solvant: diminution des intensités des raies situées à 436, 598, 619 et 892 cm^{-1} qui sont attribuables aux mouvements propres de la molécule AcOH.

L'élimination d'une partie du solvant permet d'observer une augmentation de l'intensité des raies caractéristiques de l'espèce $CH_3CO_2H_2^+$ par rapport à celles de l'acide acétique à 446 et 910 cm^{-1}. Nous notons également une augmentation de l'épaulement s'étalant de 625 à 660 cm^{-1}. La concentration de l'espèce $CH_3CO_2H_2^+$ devient suffisante pour rendre visible la raie caractéristique à 1183 cm^{-1} non identifiable sur le spectre 1.

Malgré l'élimination d'une partie du solvant nous enregistrons une augmentation des intensités des raies de diffusion à 1365 et 1427 cm^{-1} (augmentation visible par comparaison de l'intensité de ces raies à celle de la raie à 892 cm^{-1} reportée avec une sensibilité plus faible sur les spectres 1, 3 et 4 de la fig. 1). Ces raies sont attribuables aux mouvements de déformation des liaisons C—H des groupements CH_3. Cette exaltation d'intensité ne peut donc s'expliquer que par l'augmentation des concentrations d'espèces possèdant également des groupements CH_3. (L'espèce $AcOH_2^+$ pouvant être l'une d'elles.)

Même sans tenir compte de cette dernière remarque l'ensemble des résultats nous permet d'affirmer que l'espèce $CH_3CO_2H_2^+$ reste en solution avec une concentration croissante du fait de l'élimination du solvant.

L'espèce cationique $AcOH_2^+$ subsiste alors que l'espèce anionique initiale SO_3Cl^- disparait ce qui implique qu'une autre espèce anionique sera associée au cation acétique.

Cette hypothèse est confirmée par ce qui suit.

(*a*) L'apparition de raies nouvelles à 347, 550, 762 et 1800 cm^{-1}. (*i*) Celle à 347 cm^{-1} n'apparait tout d'abord (spectre 2) que sous forme d'un épaulement de la raie 380 cm^{-1} attribuable à SO_3Cl^- alors que dans le cas du spectre 5 les intensités de ces deux raies sont comparables. (*ii*) La raie à 550 cm^{-1} apparait entre les raies 536 et 570 cm^{-1} caractéristiques de l'espèce SO_3Cl^-. (*iii*) La raie située à 1800 cm^{-1} possède une intensité très faible et sa présence n'est décelable que dans les spectres 3, 4 et 5.

(*b*) Alors que les intensités des autres raies caractéristiques de l'espèce SO_3Cl^- sont artificiellement maintenues constantes (par augmentation de la sensibilité de l'appareillage), celle de la raie à 1040 cm^{-1} augmente et se déplace vers les fréquences plus élevées. Ceci est net quand on compare les intensités relatives des deux raies les plus intenses de SO_3Cl^- à 380 et 1040 cm^{-1} dans les spectres 1 et 5. On peut donc penser qu'apparait en solution une espèce présentant une raie de diffusion à une fréquence légèrement supérieure à 1040 cm^{-1}.

(*c*) Nous enregistrons une modification de l'épaulement situé entre 615 et 650 cm^{-1}. L'intensité relative de celui-ci augmente, ce qui s'explique par l'augmentation de la concentration en $AcOH_2^+$ mais on constate également une modification de sa forme qui se traduit par un élargissement vers des fréquences plus élevées, ce qui peut être expliqué par apparition d'une raie nouvelle vers 660 cm^{-1}.

En résumé: par extraction sous pression réduite: (*a*) la concentration de l'espèce SO_3Cl^- diminue, (*b*) l'espèce $AcOH_2^+$ reste en solution, (*c*) un ensemble de raies nouvelles apparait dans le spectre de la solution à 347, 550, 660, 762, 1050, 1800 cm^{-1} fréquences très voisines des raies caractéristiques les plus intenses observées dans les spectres de l'acétosulfate de sodium, de pyridinium (1) ou d'acidium acétique (6).

En conclusion, même si l'acide chlorosulfurique en solution dans AcOH se trouve sous forme de chlorosulfate d'acidium acétique (spectre 1), cette solution évolue facilement si elle est soumise à un vide dynamique. Les raies nouvelles mises en évidence sur les spectres 2, 3, 4 et 5 peuvent être attribuées à l'ion acétosulfate, malgré les légers déplacements par rapport aux fréquences notées par Commeyras et par rapport à celles des spectres des acétosulfates de sodium et pyridinium réalisés en phase solide.

L'acide chlorosulfurique, en solution dans

l'acide acétique, est donc en équilibre avec l'acide acétosulfurique. Cet équilibre peut être déplacé par une simple extraction de HCl sous pression réduite. Nous avons entrepris dans le paragraphe suivant, l'étude potentiométrique de cet équilibre.

Détermination de la constante de l'équilibre entre les acides HSO_3Cl et HSO_3AcO

L'acide acétique ayant une constante diélectrique égale à 6.2, la dissociation des paires d'ions est faible. Ne pouvant atteindre les constantes d'ionisation, nous ne pouvons déterminer que des constantes de dissociation globale. L'équilibre [5] sera donc toujours écrit sous forme moléculaire.

[5] $HSO_3Cl + AcOH \rightleftarrows HSO_3AcO + HCl$

dont la constante

$$K = \frac{[HSO_3AcO][HCl]}{[HSO_3Cl]} = K^{SO_3}_{HSO_3Cl}/K^{SO_3}_{HSO_3AcO}$$

avec

$$K^{SO_3}_{HSO_3Cl} = \frac{[SO_3][HCl]}{[HSO_3Cl]}$$

et

$$K^{SO_3}_{HSO_3AcO} = \frac{[SO_3]}{[HSO_3AcO]}$$

Ces dernières caractérisant les pouvoirs sulfonants des acides chlorosulfurique et acétosulfurique.

Dans l'acide acétique les constantes de dissociation des électrolytes sont faibles ($<10^{-5}$) (7) et les concentrations des espèces non chargées sont toujours peu élevées ($<5 \times 10^{-2}\ M$) ce qui nous permet d'assimiler activité et concentration. Pour déterminer la constante de [5] nous allons montrer par potentiométrie que l'électrode d'argent est indicatrice de [HCl] dans le solvant AcOH, et utiliser cette propriété vis-à-vis d'un donneur de HCl, l'acide chlorosulfurique.

(1) Etude potentiométrique des solutions de HCl

Les systèmes Ag/Ag^+ et Ag/AgCl sont réversibles, dans AcOH le second système ayant déjà été utilisé comme électrode indicatrice (8) ou comme électrode de référence (9, 10).

Nous avons montré que le système [6] est lui

[6] $AgCl\downarrow + HClO_4 + e^- \rightleftarrows Ag\downarrow + ClO_4^- + HCl$

aussi réversible, par dosage d'une solution ($1.22 \times 10^{-2}\ M$) de HCl par une solution de $AgClO_4$. La courbe de neutralisation, ainsi que le graphe de la transformée logarithmique correspondante sont reproduits sur la fig. 2 (x représentant le rapport $[AgClO_4]$ ajouté/[HCl] initial).

Le potentiel pris par l'électrode, pouvant être traduit par

$$E = E_{HCl}{}^0 + P \log \frac{[HClO_4]}{[HCl][ClO_4^-]}$$

où P représente le coefficient de proportionnalité dans l'équation de Nernst.

Etant données les forces relatives des acides

$HCl(pK^{H^+}_{HCl} = 8.6\,(11))$ $HClO_4(pK^{H^+}_{HClO_4} = 4.85\,(11))$

on peut admettre que $[H^+] \simeq [ClO_4^-]$ ce qui entraine

$$[ClO_4^-] \simeq \sqrt{K^{H^+}_{HClO_4}[H^+ClO_4^-]}$$

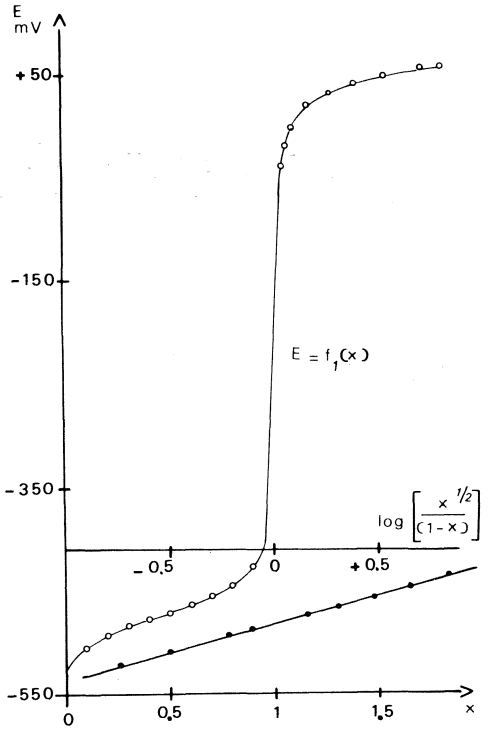

FIG. 2. Dosage d'une solution de HCl par $AgClO_4$ ($E = f_1(x)$). Analyse mathématique de la courbe potentiométrique: courbe (●).

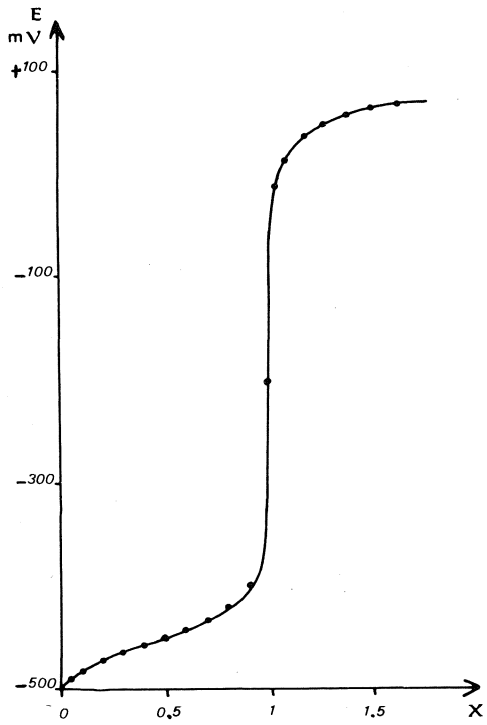

FIG. 3. Dosage d'une solution de HSO_3Cl par $AgClO_4$.

et

$$E = E_{HCl}{}^0 + P \log \left(\frac{x}{1-x}\right) - \frac{P}{2} \log (C_i K^{H^+}_{HClO_4})$$

C_i étant la concentration initiale en HCl.

Par régression linéaire nous obtenons: $P = 56$ mV/unité de log et $E^0 = -669 \pm 2$ mV. La valeur de la pente, proche de la valeur théorique: 59 mV (les manipulations étant effectuées à 25°C) justifie l'hypothèse $[H^+] = [ClO_4{}^-]$. Le système [6] est réversible et peut être utilisé pour

$$(Ag\downarrow + HCl + ClO_4{}^- \rightleftarrows AgCl\downarrow + HClO_4 + e^-)$$

le dosage de complexes donneurs de HCl tels que HSO_3Cl.

(2) Etude voltammétrique du dosage de HSO_3Cl par $AgClO_4$

Nous avons ensuite dosé une solution (2.84×10^{-2} *M*) de HSO_3Cl par une solution de $AgClO_4$ (8.17×10^{-1} *M*). La courbe de neutralisation est présentée sur la fig. 3.

Au cours de ce dosage, nous assistons à la réaction:

[7] $HSO_3Cl + AgClO_4 + AcOH \rightleftarrows AgCl\downarrow + HClO_4 + HAcOSO_3$

à laquelle correspond le système électrochimique:

[8] $AgCl\downarrow + HClO_4 + HAcOSO_3 + e^- \rightleftarrows HSO_3Cl + Ag\downarrow + ClO_4{}^- + AcOH$

L'étude mathématique de la courbe obtenue montre qu'il est nécessaire de tenir compte de l'équilibre [5], HCl libre n'étant pas négligeable devant HSO_3Cl.

En faisant l'hypothèse que SO_3 libre est négligeable devant HSO_3Cl et HSO_3AcO c'est à dire que les constantes $K^{SO_3}_{HSO_3Cl}$ et $K^{SO_3}_{HSO_3AcO}$ sont faibles nous avons: $[HSO_3Cl] + [HSO_3AcO] = C_0'$ avec C_0' concentration initiale en HSO_3Cl. La neutralité électrique donne:

$[Cl^-]$ et $[AcO^-]$ étant négligeable

$$[H^+] = [SO_3Cl^-] + [AcOSO_3{}^-] + [ClO_4{}^-]$$

$$[H^+] = \sqrt{K^{H^+}_{HSO_3Cl}[HSO_3Cl] + K^{H^+}_{HAcOSO_3}[HAcOSO_3] + K^{H^+}_{HClO_4}[HClO_4]}$$

Les résultats d'un travail en cours montrent que les acides chlorosulfurique et acétosulfurique sont tous deux de force très voisine de celle de H_2SO_4, donc non entièrement ionisés et nettement plus faibles que $HClO_4$; résultats analogues à ceux obtenus par Bessière (12) dans l'acide trifluoracétique en ce qui concerne HSO_3Cl et H_2SO_4 ($pK^{H^+}_{HSO_3Cl} - pK^{H^+}_{H_2SO_4} = 0.1$).

En prenant $K^{H^+}_{HSO_3Cl}$ et $K^{H^+}_{HSO_3AcO} = 10^{-7.2}$ constante d'acidité de H_2SO_4 (11) nous obtenons:

$$[H^+] = \sqrt{C_0' \times 10^{-7.2} + x\, C_0' \, 10^{-4.8}} \simeq \sqrt{x\, C_0' \times 10^{-4.8}}$$

si $x > 0.2$ (erreur voisine de 1%); x étant le rapport $[AgClO_4]$ ajouté/$[HSO_3Cl]$ initial.

A partir des équations

$$[HSO_3Cl] + [HSO_3AcO] = C_0'$$

$$K = \frac{[HSO_3AcO][HCl]}{[HSO_3Cl]}$$

$$[HCl] + [HSO_3Cl] = (1 - x)C_0'$$

$$[H^+] = \sqrt{xC_0' \times 10^{-4.8}}$$

la loi de Nernst appliquée au système électrochimique [8] s'écrit:

$$E = E^0 + P \log \frac{2K\sqrt{xC_0'}}{(R - xC_0' - K)\sqrt{10^{-4.8}}}$$

avec

$$R = \sqrt{(xC_0' + K)^2 + 4C_0'K(1 - x)}$$

Afin de déterminer simultanément les valeurs de E^0 et K et vérifier le coefficient de proportionnalité de la loi de Nernst, nous avons utilisé la technique d'affinement par la méthode des moindres carrés. Nous obtenons: $E^0 = -717$ mV, $K = 10^{0.8\pm0.2}$ mol ℓ^{-1}, le coefficient de Nernst = 59 mV.

La comparaison de ce potentiel normal à celui du système

$$AgCl\downarrow + HClO_4 + e^- \rightleftarrows HCl + ClO_4^- + Ag\downarrow$$

conduit à $K = 10^{0.81}$, valeur en très bon accord avec celle déterminée par traitement mathématique, et justifie les hypothèses formulées.

Partie expérimentale

Le solvant utilisé a été préparé selon la méthode déjà décrite (1). Nous n'avons pas utilisé la rectification à l'anhydride acétique (13) afin d'éviter une réaction parasite entre les traces d'anhydride acétique entrainé (14, 15) et HSO_3Cl (16).

L'acide chlorosulfurique Carlo Erba est employé sans purification car sa purification apporte plus d'impuretés (SO_2Cl_2, $S_2O_5Cl_2$, H_2SO_4) qu'elle n'en élimine (17, 18).

Les solutions anhydres d'acide chlorhydrique dans AcOH sont obtenues en faisant passer dans le solvant le chlorure d'hydrogène gazeux obtenu par action de H_3PO_4 anhydre sur NaCl.

$AgClO_4$ (produit Merck) est séché sous pression réduite en présence de P_4O_{10} à 80°C.

$PyHClO_4$ est préparé par addition de pyridine à une solution d'acide perchlorique à 70% dans l'acide acétique. Le solide est séparé par filtration et séché selon la même technique que celle utilisée pour $AgClO_4$.

Le dosage de l'eau des solutions de composés non hydrolysables est effectué par la méthode de Karl Fischer décrite par Bizot (19). La teneur en eau est généralement inférieure à 20 ppm.

L'électrode de référence choisie est l'électrode Tacussel AcHg 10.

Les mesures potentiométriques, sont effectuées sur un millivoltmètre Tacussel ISIS 20 000 couplé à un enregistreur Tacussel EPL2 permettant d'apprécier la stabilité des potentiels.

Conclusion

En conclusion, la valeur élevée de la constante K relative à l'équilibre [5] montre qu'en solution diluée un échange important de SO_3 existe entre l'acide chlorosulfurique et le solvant pour donner l'acide acétosulfurique, si l'on admet comme Casadevall et coll. (21) l'hypothèse que HSO_3AcO est très faiblement donneur de SO_3. HSO_3Cl est donc un donneur de SO_3 légèrement plus fort que l'acide acétosulfurique dans l'acide acétique.

En solution concentrée, la valeur de la constante de l'équilibre [5] déterminée par potentiométrie n'est plus valable, l'activité du solvant ne pouvant plus être considérée comme constante. La seule espèce caractérisée par spectrométrie Raman est le chlorosulfate d'acidium acétique. La formation de cette espèce ionisée est favorisée par l'augmentation du pouvoir dissociant du solvant due à une concentration élevée du soluté (5 M). Cependant, l'équilibre [5] existe encore puisque nous avons montré que par élimination de HCl sous pression réduite le spectre Raman de la solution évolue. On observe une diminution des raies correspondant au chlorosulfate d'acidium acétique et une apparition de nouvelles raies que l'on peut attribuer à l'acétosulfate d'acidium acétique.

La détermination des constantes d'acidité de HSO_3Cl et $HSO_3CH_3CO_2$ ainsi que des constantes de dissociation des sels devrait nous conduire au classement du pouvoir sulfonant de ces différents composés dans l'acide acétique et à la justification du caractère diacide de l'acide chlorosulfurique.

Remerciements

Nous remercions la Délégation Générale à la Recherche Scientifique et Technique pour l'aide financière apportée à ces travaux. Contrat D.G.R.S.T 75–7–02 68.

1. B. Brasme, J. Ogil, J. C. Fischer et M. Wartel. Rev. Chim. Minér. **12**, 175 (1975).
2. Y. Auger, P. Legrand, E. Puskaric, E. Wallart et S. Noel. Spectrochim. Acta, **40**, 350 (1968).
3. D. J. Stufkens et H. Gerding. Recl. Trav. Chim. Pays-Bas, **89**, 417 (1970).
4. R. J. Gillespie et E. A. Robinson. Can. J. Chem. **40**, 644 (1962).

5. S. CASADEVALL, G. CAUQUIL et R. CORRIU. Bull. Soc. Chim. Fr. **2**, 187 (1964).
6. A. COMMEYRAS. Thèse docteur ès sciences. Montpellier, France. 1965.
7. I. M. KOLTHOFF et S. BRUCKEINSTEIN. J. Am. Chem. Soc. **78**, 1 (1956).
8. L. M. MUKHERJEE. J. Am. Chem. Soc. **79**, 4040 (1957).
9. R. A. GLEN. Anal. Chem. **25**, 1916 (1953).
10. A. T. CHENG, R. A. HOWALD et D. L. MILLER. J. Phys. Chem. **67**, 1601 (1963).
11. G. CHARLOT et B. TREMILLON. *Dans* Les réactions chimiques dans les solvants et les sels fondus. *Edité par* Gauthier-Villars, Paris. 1963.
12. J. BESSIERE. Bull. Soc. Chim. Fr. **9**, 3356 (1969).
13. K. J. P. ORTON et A. E. BRADFIELD. J. Chem. Soc. 983 (1927).
14. J. KUCHARSKY et L. SAFARIK. Titrations in non aqueous solvents. Elsevier Publishing Company. 1965.
15. I. GYENES. Titrations in non-aqueous solvents. Iliffe Books, D. Van Nostrand Company, London.
16. E. BAUMSTARK. Lidb. Ann. **140**, 75 (1866).
17. SANGER et RIEGEL. Z. Anorg. Chem. **76**, 75 (1912).
18. E. A. ROBINSON et J. A. CIRUNA. Can. J. Chem. **46**, 1718 (1968).
19. J. BIZOT. Bull. Soc. Chim. Fr. **1**, 151 (1967).
20. I. POPOV. The chemistry of nonaqueous solvents. *Edité par* J. J. Lagowski. Academic Press. 1970.
21. A. CASADEVALL, A. COMMEYRAS, P. PAILLOUS et H. COLLET. Bull. Soc. Chim. Fr. **2**, 719 (1970).

Etude de l'équilibre azido ⇌ tétrazole dans les oxazolo[2,3-*e*], thiazolo[2,3-*e*] et isoxazolo[2,3-*d*]tétrazoles. II.[1] Etude de l'effet de la température par dipolemetrie et résonance magnétique nucléaire

ROBERT FAURE,[2] JEAN-PIERRE GALY ET EMILE-JEAN VINCENT

Laboratoire de Chimie Organique Physique, Université d'Aix-Marseille III, Rue H. Poincaré, 13397 Marseille Cédex 4, France

JEAN-PIERRE FAYET,[2] PIERRE MAURET ET MARIE-CLAIRE VERTUT

Laboratoire de Chimie Organique Structurale, Université Paul Sabatier, 118, route de Narbonne, 31077 Toulouse Cédex, France

ET

JOSÉ ELGUERO

Laboratoire de Chimie Moléculaire, Université d'Aix-Marseille III, Rue H. Poincaré, 13397 Marseille Cédex 4, France

Reçu le 10 décembre 1976

ROBERT FAURE, JEAN-PIERRE GALY, EMILE-JEAN VINCENT, JEAN-PIERRE FAYET, PIERRE MAURET, MARIE-CLAIRE VERTUT et JOSÉ ELGUERO. Can . J. Chem. **55**, 1728 (1977).

La constante d'équilibre azido/tétrazole de cinq azides hétérocycliques (thiazoles, benzothiazole, benzoxazole, isoxazole) dans le dioxanne a été déterminée par rmn du proton et par dipolemétrie. Cette dernière méthode utilise la comparaison des moments dipolaires électriques expérimentaux et des moments théoriques calculés pour l'azide et pour le tétrazole par les méthodes INDO, CNDO/2 et CNDO/S. L'accord est satisfaisant (surtout en utilisant la CNDO/S) aussi bien sur la constante d'équilibre que sur l'effet de la température ($\Delta S \sim 50$ J K^{-1} mol^{-1}). La valeur de l'angle C–N–N ($\alpha = 114°$) des azides est discutée sur la base des énergies, des moments dipolaires et des spectres photoélectroniques expérimentaux et calculés. On démontre la préférence pour la conformation *Z* des azidoimines hétérocycliques.

ROBERT FAURE, JEAN-PIERRE GALY, EMILE-JEAN VINCENT, JEAN-PIERRE FAYET, PIERRE MAURET, MARIE-CLAIRE VERTUT, and JOSÉ ELGUERO. Can. J. Chem. **55**, 1728 (1977).

The equilibrium constant in dioxane between azido and tetrazole isomers has been obtained for five heterocyclic azides (2-azido thiazoles, benzothiazole, benzoxazole, and 3-azido isoxazole) by proton nmr and dipole moment studies. The last method involves a comparison between experimental and calculated (INDO, CNDO/2, CNDO/S) dipole moments. The CNDO/S method gives the best equilibrium constants and entropy factor ($\Delta S \sim 50$ J K^{-1} mol^{-1}). A value of 114° for the C–N–N angle is found to account satisfactorily for certain properties (energy, dipole moment, photoelectron spectra) of aromatic azides. The heterocyclic azidoimines prefer the *Z* conformation.

Introduction

Nous avons montré que la mesure des moments dipolaires pouvait être utilisée pour déterminer la position des équilibres tautomères prototropiques (2–5). Le principe de la méthode est le suivant: pour un équilibre A ⇌ B de constante d'équilibre K_e

$$[1] \qquad K_e = [B]/[A]$$

si P_A est une propriété additive du tautomère A, P_B celle du tautomère B et P_X la propriété expérimentale du mélange en équilibre, on peut écrire:

$$[2] \qquad K_e = \frac{P_A - P_X}{P_X - P_B}$$

La propriété additive, utilisée dans les études précédentes (1–5), est le carré du moment dipolaire (7). Les valeurs des moments dipolaires de chaque forme tautomère, non déterminables expérimentalement, sont évaluées théoriquement à partir de méthodes semi-empiriques de type CNDO.

Dans le cas de la tautomérie prototropique, par suite des échanges rapides du proton entre les différents sites azotés, les constantes d'équilibre évaluées à partir de [2] ne peuvent être controlées par rmn. Afin de tester la validité de cette méthode nous l'avons appliquée au cas de l'isomérie azido ⇌ tétrazole de quelques hétérocycles pentagonaux, **1** à **5**.

[1]Cette publication est la no XXVI de la série "Systèmes aromatiques à 10 électrons π dérivés de l'aza-3a pentalène"; elle a fait l'objet d'une note préliminaire (1).

[2]Auteurs auxquels la correspondance peut être adressée.

TABLEAU 1. Moments dipolaires expérimentaux*

Composé	T(°C)	α	β	RM_D	$P_{2\infty}$	μ_D
1	25	10.97	−0.15	31.74	258.15	3.33
	45	8.61	0	31.74	221.46	3.15
2	25	23.90	−0.24	36.39	582.25	5.17
	45	19.34	−0.30	36.39	492.03	4.88
3	25	12.28	−0.24	47.97	394.22	4.12
	45	9.74	−0.24	47.97	331.53	3.85
4	25	3.26	0	41.83	130.87	2.09
	45	3.11	−0.10	41.83	125.65	2.09
5	25	11.74	−0.14	30.97	270.81	3.42
	45	10.34	−0.15	30.97	249.44	3.38

*Mesurés dans le dioxanne.

Pour ce genre d'équilibre nous avons montré (8, 9) qu'il est possible d'évaluer les proportions relatives de chacune des deux formes tautomères, par une simple étude en résonance magnétique nucléaire du proton.

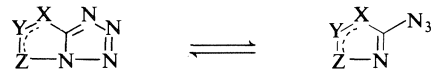

a *b*

1 X = S, Y = CH, Z = CH série du thiazole
2 X = S, Y = CH, Z = C—CH_3 série du thiazole
3 X = S, Y—Z = benzo série du benzothiazole
4 X = O, Y—Z = benzo série du benzoxazole
5 X = CH, Y = C—CH_3, Z = O série de l'isoxazole

Les mesures des moments dipolaires ont été effectuées à deux températures de manière à avoir un ordre de grandeur des paramètres thermodynamiques (ΔH et ΔS) relatifs à cet équilibre. Ces valeurs sont ensuite confontrées avec celles obtenues par une étude de rmn en température variable.

Partie expérimentale

Les moments électriques ont été mesurés dans le dioxanne à la température de 25 et de 45°C. La formule de Debye a été utilisée ainsi que la méthode d'extrapolation d'Halverstadt et Kumler (10) pour le calcul de la polarisation totale du soluté. Les résultats sont donnés dans le tableau 1.

Les spectres de rmn des composés **1**, **2** et **5** ont été enregistrés sur un spectromètre Varian XL-100 à la température de 28°C et ont été analysés au premier ordre; les déplacements chimiques et les constantes de couplage sont donnés avec une précision respective de ±0.01 ppm et de ±0.05 Hz. L'analyse des spectres du tétrazolo[5,1-*b*]benzothiazole **3** et du tétrazolo[5,1-*b*]-benzoxazole **4**, enregistrés respectivement sur des spectromètres Cameca 250 MHz (T = 20°C) et Varian HA-100 (T = 28°C), a été conduite au second ordre à l'aide d'une version modifiée (11) du programme LAOCN3 (12); la déviation moyenne standart est de 0.05 Hz. Les expériences en température variable ont été réalisées sur un spectromètre Perkin-Elmer R32; la précision sur la mesure de la température est estimée à ±1°C. Les constantes d'équilibre ont été déterminées par intégration des raies de résonance relatives à chaque structure et l'erreur sur ces valeurs est inférieure à 10% (9).

Diverses paramétrisations issues du formalisme CNDO ont été appliquées à la détermination théorique des moments dipolaires de ces composés: deux modèles CNDO/2 qui diffèrent entre eux par l'introduction des orbitales *d* dans la base de description de l'atome de soufre, un modèle CNDO/S et, dans le cas des substrats oxygénés (**4** et **5**), un modèle INDO. Les méthodes CNDO/2 (13, 14) et INDO (15) ont été utilisées dans la paramétrisation originale de leurs auteurs. En ce qui concerne la méthode CNDO/S (16), les intégrales bicentriques biélectroniques γ_{AB} ont été évaluées selon le formalisme de Pariser et Parr (17), tandis que les paramètres du soufre (approximation *sp*) sont ceux proposés par Pfister-Gillouzo *et al.* (18).

A l'exception du tétrazolo[5,1-*b*]benzothiazole **3***a* qui a fait l'objet d'une étude cristallographique (19) aucune donnée structurale n'a été publiée sur ces différents composés. Aussi les géométries utilisées dans les calculs théoriques ont été choisies par comparaison avec les données de la littérature concernant des composés similaires (thiazole (20), imidazo[1,2-*b*]thiazole (21), oxadiazole-1,3,4 (22) et −1,2,5 (23)). Nous discuterons ultérieurement du choix de la géométrie du groupement azido, à savoir une structure de type linéaire ou de type angulaire.

Les synthèses des composés **1** à **4** ont été menées selon les méthodes décrites dans la littérature (24–28); l'azido-3 méthyl-5 isoxazole **5** a été obtenu par action de l'azoture de sodium sur le sel de diazonium correspondant. La structure de ce composé a été confirmée par spectrométrie de masse et par résonance magnétique nucléaire du ^{13}C (29).

Résultats et discussion

Equilibre azido/tétrazole: résultats de résonance magnétique nucléaire

Les hétérocycles étudiés dans ce mémoire (composés **1** à **5**) étant peu solubles dans le benzène, nous avons dû utiliser le dioxanne comme solvant pour réaliser les mesures diélectriques. L'étude de rmn a été conduite dans le

TABLEAU 2. Déplacements chimiques, constantes de couplage et constantes d'équilibre:* cas des thiazoles

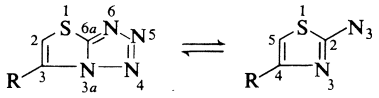

a *b*

	R	Solvant	Forme *a* H_2	Forme *a* R	Forme *a* $J_{H_2R_3}$	Forme *b* H_5	Forme *b* R	Forme *b* $J_{H_5R_4}$	% de forme *a*	$K_e = [b]/[a]$
1	H	dioxanne-d_8	7.50	8.27	$^3J = 4.4$	7.14	7.48	$^3J = 3.5$	31	2.2
2	CH_3	dioxanne-d_8	7.06	2.60	$^4J = 1.4$	6.69	2.31	$^4J = 1.1$	73	0.4

*Les déplacements chimiques sont donnés en ppm et les constantes de couplage en Hz; les spectres ont été enregistrés sur un spectromètre Varian XL-100 à la température de 28°C.

TABLEAU 3. Déplacements chimiques, constantes de couplage et constantes d'équilibre: cas du benzothiazole et du benzoxazole

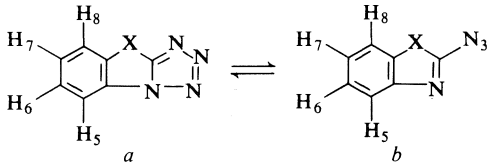

a *b*

	X	Solvant	Forme*	δ (ppm) H_5	H_6	H_7	H_8	*J* (Hz) J_{56}	J_{57}	J_{58}	J_{67}	J_{68}	J_{78}	% de forme *a*	$K_e = [b]/[a]$
3	S	dioxanne-d_8†	*a*	8.27	7.79	7.71	8.22	8.18	1.12	0.64	7.55	1.08	8.33	55.5	0.80
			b	7.81	7.51	7.38	7.96	8.15	1.21	0.67	7.34	1.23	8.06		
		$CDCl_3$‡	*a*	—	—	—	—	—	—	—	—	—	—	<5§	>20
4	O		*b*	7.36	7.08	7.02	7.17	7.99	1.25	0.67	7.67	1.08	8.35		
		DMSO-d_6‡	*a*	—	—	—	—	—	—	—	—	—	—	<5§	>20
			b	7.62	7.37	7.33	7.64	8.09	1.25	0.63	7.68	0.98	8.44		

*Les protons de la forme azide sont numérotés abitrairement pour faciliter la mise en page.
†Ce spectre a été enregistré sur un spectromètre Cameca 250 MHz à la température de 20°C.
‡Ces spectres ont été enregistrés sur un spectromètre Varian HA-100 à la température de 28°C.
§Limite de détection d'une forme tautomère dans les conditions opératoires énoncées ci-dessus.

même solvant pour des raisons de cohérence évidentes.[3]

Dans ce solvant, le comportement des différents produits étudiés est très différent, ainsi que nous le montrent les valeurs expérimentales des constantes d'équilibre déterminées à partir des résultats de résonance magnétique nucléaire du proton (tableaux 2 à 4).

Le thiazolo [2,3-*e*] tétrazole **1** existe principalement sous forme azide, mais l'introduction du groupement méthyle (composé **2**), substituant donneur d'électrons, déplace l'équilibre vers la forme tétrazole (9). En ce qui concerne l'isomérie entre le tétrazolo [5,1-*b*] benzothiazole et l'azido-2 benzothiazole **3** à la température de l'expérience les deux isomères sont en proportion presque équivalente, avec une légère prédominance de la forme tétrazole. Quant aux dérivés oxygénés **4** et **5** ils n'existent que sous la forme azide quel que soit le solvant utilisé.

Par ailleurs tous ces résultats confirment les diverses études qualitatives réalisées par spectroscopie infra-rouge sur l'isomérie azido ⇌ tétrazole dans le cas des hétérocycles à système π excédentaire (24–28, 30).

Angles internucléaires du groupement azide

La détermination théorique des moments

[3]Les spectres de rmn des dérivés oxygénés **4** et **5** ont été enregistrés dans le DMSO-d_6 et le chloroforme deutérié. Dans ces deux solvants seule la forme azide est présente en solution. Nous avons montré (9) que dans le cas des systèmes hétérocycliques pentagonaux le pourcentage de forme tétrazole augmente avec la polarité du solvant. L'absence de cette forme dans le diméthylsulfoxyde est donc une preuve a fortiori de son absence dans le dioxanne.

TABLEAU 4. Déplacements chimiques, constantes de couplage et constantes d'équilibre:* cas de l'isoxazole

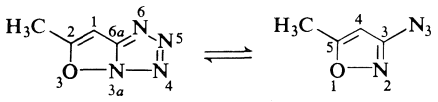

a *b*

	Solvant	Forme *a* H_1	Forme *a* CH_3	Forme *a* J_{12}	Forme *b* H_4	Forme *b* CH_3	Forme *b* J_{45}	% de forme *a*	$K_e = [b]/[a]$
5	$CDCl_3$	—	—	—	5.72	2.34	1.2	<2†	≥50
	DMSO-d_6	—	—	—	6.15	2.36	1.1	<2†	≥50

*Les déplacements chimiques sont donnés en ppm et les constantes de couplage en Hz; les spectres ont été enregistrés sur un spectromètre Varian XL-100 à la température de 28°C.
†Limites de détection d'une forme tautomère dans les conditions opératoires énoncées ci-dessus.

TABLEAU 5. Evolution du module et de la direction du moment dipolaire en fonction de l'angle φ (méthode CNDO)

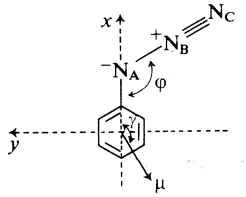

Paramètre	114	140	160	180
μ(D)*	1.34	1.65	1.81	1.90
γ*†	−146	−158	−168	−190
ET_1(eV)‡¶	−2209.57	−2208.94	−2208.11	−2207.81
ET_2(eV)§¶	−2236.47	−2235.60	−2234.75	−2234.44

*Méthode CNDO/S.
†L'angle de la direction du moment dipolaire est compté positivement dans le sens trigonométrique direct par rapport à l'axe de *x*; cette direction du moment dipolaire, donnée par les méthodes de type CNDO, est l'inverse de celle de la définition des chimistes.
‡$ET_1 = E_{elec} + \sum_{A<B}\sum Z_A Z_B/R_{AB}$.
§$ET_2 = E_{elec} + \sum_{A<B}\sum Z_A Z_B\gamma_{AB}$.
¶Méthode CNDO/2.

dipolaires de la forme azide nécessite le choix d'une structure pour le groupement azide, c'est-à-dire le choix de l'angle φ, $\angle RN_AN_B$.

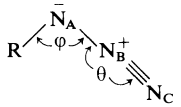

Certains auteurs (31, 32) utilisent dans leurs calculs théoriques une structure linéaire (φ = 180°), en désaccord avec les résultats expérimentaux obtenus par spectroscopie de microonde (33) ou par diffraction X (34, 35) qui indiquent un angle φ voisin de 115°.[4]

Dans l'intention de choisir la géométrie qui conduit au meilleur accord entre moments dipolaires expérimentaux et valeurs théoriques, nous avons étudié l'évolution du module et de la direction du moment dipolaire d'une molécule modèle, le phénylazide, en fonction de la variation de l'angle $\angle RN_AN_B$.

Le moment dipolaire expérimental du phénylazide est de 1.44 D (36) et sa direction est colinéaire à la liaison C—N_A puisque le *p*-bromo phénylazide possède un moment dipolaire nul (37).

Sur le tableau 5 on voit que les résultats obtenus pour un angle φ de 114° (valeur tirée de la réf. 35) sont en bon accord avec l'expérience dans le cadre de la méthode CNDO/S. Il faut cependant noter qu'une variation angulaire de 10 à 20° (par exemple pour φ = 140°) conduit à des résultats encore acceptables pour la valeur et la direction du moment dipolaire, mais la

[4]Pour l'angle θ, $\angle N_AN_BN_C$, nous avons utilisé la valeur de 172° (35).

TABLEAU 6. Spectres photoélectroniques. Comparaison entre valeurs théoriques (méthode CNDO/S) et résultats expérimentaux

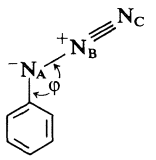

Potentiels d'ionisation théoriques*				Potentiels d'ionisation expérimentaux†
φ = 114°	φ = 140°	φ = 160°	φ = 180°	
8.68(π)	8.60(π)	8.47(π)	8.59(π)	8.72
9.82(π)	9.86(π)	9.53(n)	9.11(n)	9.53
11.16(π)	10.33(n)	9.93(π)	9.98(π)	11.00
11.35(n)	11.12(π)	11.08(π)	11.25(π)	11.35
12.31(σ)	12.38(σ)	12.47(σ)	12.51(σ)	12.30

*Calculés selon le théorème de Koopmans (38); les symboles entre parenthèses indiquent la symétrie des orbitales moléculaires.
†Valeurs de la réf. 32.

structure obtenue est énergétiquement moins stable (méthode CNDO/2).

Cette valeur angulaire de 114° conduit également à un excellent accord avec les résultats de spectroscopie photoélectronique (32) comme on peut le voir dans le tableau 6; les valeurs obtenues en CNDO/2 conduisent à une moins bonne concordance.

Ces résultats montrent que le choix d'une structure angulaire pour le groupement azide est parfaitement justifié; aussi tous les calculs théoriques des formes ouvertes ont été effectués en utilisant pour le groupement azido les données de la réf. 35 φ = 114°, θ = 172°.

Equilibre azido-tétrazole: résultats obtenus à partir des moments dipolaires

Les constantes d'équilibre, évaluées à partir de [2], sont données dans le tableau 7 ainsi que les valeurs théoriques des moments dipolaires de chaque tautomère. Dans ce même tableau nous avons groupé les valeurs expérimentales (rmn) des constantes d'équilibre.

Les conclusions qu'on peut dégager de la comparaison entre valeurs de la constante d'équilibre déterminée par rmn et à l'aide des moments dipolaires (théoriques et expérimentaux) sont les suivantes: (*i*) l'ensemble des méthodes théoriques utilisées permet de rendre compte de l'évolution de l'équilibre azido ⇌ tétrazole, (*ii*) la méthode CNDO/S conduit aux meilleurs résultats (en ce qui concerne les structures **1**, **2** et **5** l'accord est excellent), (*iii*) ces résultats justifient, *a posteriori*, la validité des calculs des constantes d'équilibre (2–5) par cette méthode qui utilise les moments dipolaires théoriques et expérimentaux.

Conformation des azides

Dans l'article déjà cité (35) la structure radiocristallographique de l'azido-3 phényl-4 pyrazole montre que le groupement azido adopte une conformation de type *Z*, **6**. Les calculs précédents ont été réalisés en supposant une même conformation[5] du groupement azide pour les molécules **1***b*, **2***b*, **3***b*, **4***b* et **5***b*. Il est cependant possible que le fait de se trouver en solution ou le changement de noyau hétérocyclique déplace l'équilibre vers la forme *E*.

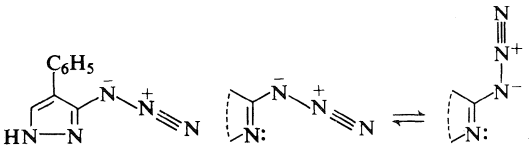

6 *Z* *E*

Nous avons choisi d'étudier le cas de l'azido-3 méthyl-5 isoxazole **5** qui existe en solution exclusivement sous la forme azide **5***b* ($K \geq 50$, tableau 7). Les résultats du tableau 8 montrent d'une part que, quel que soit le modèle énergétique et la méthode utilisée, l'isomère *Z* est toujours favorisé d'environ 0.16 eV (15 kJ mol^{-1}); d'autre part si l'on compare la valeur expérimentale (3.42 D, tableau 1) aux valeurs calculées par la méthode CNDO/S (3.31 et 5.25 D, tableau 8), on voit que l'équilibre est

[5]Nous avons supposé que l'angle dièdre formé par les plans de l'hétérocycle et du groupement azido était nul. En fait pour le produit **6** il est de 13.8° (35).

TABLEAU 7. Moments dipolaires calculés et constantes d'équilibre

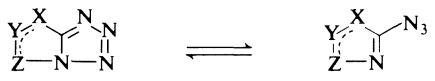

a ⇌ *b*

Composés	Méthodes* théoriques	μ_a	μ_b	Pourcentage de forme *a*†	$K_e = [b]/[a]$‡	$(K_e)_{exp}$§ (T)
	CNDO/2 A	5.36	1.27	35	1.85	2.2 (28°C)
1	CNDO/2 B	5.00	1.05	42	1.40	
	CNDO/S	5.83	1.16	30	2.35	
	CNDO/2 A	5.61	1.50	83	0.20	
2	CNDO/2 B	5.38	1.48	91	0.10	0.4 (28°C)
	CNDO/S	6.11	1.55	69	0.45	
	CNDO/2 A	5.77	1.40	48	1.10	
3	CNDO/2 B	5.91	1.45	45	1.20	0.8 (20°C)
	CNDO/S	6.16	0.78	44	1.30	
	CNDO/2	5.45	0.48	15	6.1	
4	INDO	5.26	0.77	14	6.2	≥20 (28°C)
	CNDO/S	6.14	1.01	9	10.0	
	CNDO/2	6.37	2.96	9	9.8	
5	INDO	6.05	2.96	11	8.5	≥50 (28°C)
	CNDO/S	7.32	3.31	1.5	57	

*A: sans les orbitales *d*; *B*: avec les orbitales *d*.
†Obtenu à partir des moments calculés et expérimentaux.
‡Déterminée à partir de [2]; température: 25°C.
§Déterminée par rmn à partir de [1].

TABLEAU 8. Conformation de l'azido–3 isoxazole

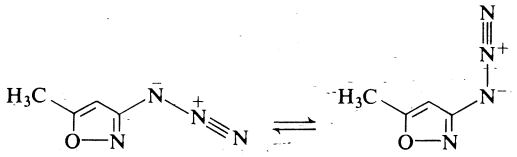

Paramètre		**5***b* (*Z*)	**5***b* (*E*)
Moment dipolaire (D)	CNDO/2	2.96	4.94
	INDO	2.96	4.40
	CNDO/S	3.31	5.25
Energie totale *A** (eV)	CNDO/2	−2623.385	−2623.234
	INDO	−2518.348	−2518.154
Energie totale *B** (eV)	CNDO/2	−2734.527	−2734.397
	INDO	−2629.490	−2629.318

*L'énergie totale est la somme de l'énergie électronique et de l'énergie de répulsion des coeurs; l'énergie de répulsion des coeurs a été évaluée par *A* le modèle des charges ponctuelles, $ER_1 = \sum_{A<B}\sum Z_A Z_B / R_{AB}$ et par *B* le modèle de puits positif, $ER_2 = \sum_{A<B}\sum Z_A Z_B \gamma_{AB}$.

très fortement déplacé vers l'isomère de configuration *Z* (à titre indicatif, l'application de [2] donnerait $K_I = [Z]/[E] \sim 20$, $\Delta G_{25} \sim 8$ kJ mol^{-1}).

Equilibre azido/tétrazole: effets de la température

Les effets de la température sur l'évolution de l'équilibre azido/tétrazole sont bien connus sur le plan qualitatif (déplacement de l'équilibre vers la forme azide par élévation de température (30)), beaucoup moins sur le plan quantitatif. Dans le tableau 9 figurent les différents cas étudiés dans la littérature; à l'exception de l'azido-2 pyridine, décrite par Temple *et al.* (40)

TABLEAU 9. Effet de la température sur l'équilibre azido-tétrazole

Composé	Solvant	No de points	ΔH (kJ mol^{-1})	ΔS (J K^{-1} mol^{-1})	Réf.
Azido-2 diméthyl-4,6 pyrimidine	$CDCl_3$	4	28.2	81.6	39
Azido-2 pyrimidine	DMSO	11	21.6	47.6	40
Azido-2 purine (cyclisation sur N_1)	DMSO	5	19.7	57.3	40
Azido-2 purine (cyclisation sur N_3)	DMSO	5	11.3	46.9	40
Azido-2 chloro-6 pyridine	DMSO	3	14.6	56.9	41
Azido-2 nitro-5 pyridine	DMSO	3	7.1*	22.6	41
Acétyl-1 azido-2 imidazole	DMSO	4	8.3	33.5	42
Azido-2 thiazole **1***b*	DMSO	8	18.8±0.3	48±1	†
Azido-2 thiazole **1***b*	$C_6H_5NO_2$	8	16.0±0.3	57±1	†
Azido-2 méthyl-4 thiazole **2***b*	$C_6H_5NO_2$	8	18.0±0.3	46±1	†
Azido-2 diméthyl-4,5 thiazole **7***b*	$C_6H_5NO_2$	9	20.6±0.7	41±2	†

*La valeur, ΔH = 17.6 kJ mol^{-1}, de la réf. 41 est erronée (T. Sasaki, communication personnelle).
†Ce travail.

les autres composés ont été étudiés avec un nombre insuffisant de mesures.

Nos propres résultats, obtenus comme ceux de la littérature par simple intégration des signaux rmn, figurent également dans le tableau 9 (le domaine de température est compris entre 30 et 120°C.[6] On peut remarquer que l'entropie dépend à la fois du solvant et des substituants. Les spectres des azido-2 thiazoles **1***b*, **2***b* et **7***b*, qui avaient été déjà enregistrés à la température de 30°C dans un grand nombre de solvants (9), ont été enregistrés à la température de 70°C; dans tous les cas, la valeur de l'entropie ΔS est plus grande que zéro, et comprise entre 25 et 75 J K^{-1} mol^{-1}, ce qui interdit définitivement de traiter comme des variables indépendantes le solvant, les substituants et la température.

Nous voyons (tableau 1) que les moments dipolaires des composés **1**, **2** et **3** varient avec la temperature: on a donc un équilibre. La diminution du moment dipolaire de ces dérivés soufrés correspond à un déplacement de l'équilibre vers la forme azide beaucoup moins polaire (tableau 7). Un simple calcul, en utilisant les moments théoriques CNDO/S, conduit aux valeurs suivantes pour l'entropie: **1** ΔS = 30, **2** ΔS = 42, **3** ΔS = 34 J K^{-1} mol^{-1}, valeurs raisonnables, qui montrent une fois de plus la fiabilité de la méthode.

Pour les dérivés oxygénés (**4** et **5**) le moment ne varie pas avec la température, ce qui est en faveur de l'existence d'une seule forme. A partir des calculs théoriques on montre que la forme azide prédomine, ces résultats confirment, en les précisant, les pourcentages évalués en résonance magnétique nucléaire.

[6]A des températures plus élevées les azides se décomposent, parfois d'une façon très violente.

1. J.-P. FAYET, M.-C. VERTUT, P. MAURET, R. FAURE, J.-P. GALY, E.-J. VINCENT et J. ELGUERO. C.R. Acad. Sci. Sér. C, **283**, 157 (1976).
2. P. MAURET, J.-P. FAYET, M. FABRE, J. ELGUERO et M. C. PARDO. J. Chim. Phys. **70**, 1483 (1973); P. MAURET, J.-P. FAYET, M. FABRE, J. ELGUERO et J. DE MENDOZA. J. Chim. Phys. **71**, 115 (1974).
3. J.-P. FAYET, M.-C. VERTUT, P. MAURET, J. DE MENDOZA et J. ELGUERO. J. Heterocycl. Chem. **12**, 197 (1975).
4. R. M. CLARAMUNT, J.-P. FAYET, M.-C. VERTUT, P. MAURET et J. ELGUERO. Tetrahedron, **31**, 545 (1975).
5. J.-P. FAYET, M.-C. VERTUT, R. M. CLARAMUNT, J. M. FABREGA et L. KNUTSSON. Bull. Soc. Chim. Fr. 393 (1975).
6. J. ELGUERO, C. MARZIN, A. R. KATRITZKY et P. LINDA. The tautomerism of heterocycles. *Dans* Advances in heterocyclic chemistry. Suppl. Vol. I. Academic Press, New York, NY. 1976.
7. J. KRAFT et S. WALKER. Physical methods in heterocyclic chemistry. Vol. IV. *Edité par* A. R. Katritzky. Academic Press, London. 1971. p. 237.
8. R. FAURE, J.-P. GALY, G. GIUSTI, E.-J. VINCENT et J. ELGUERO. Org. Magn. Reson. **6**, 485 (1974).
9. J. ELGUERO, R. FAURE, J.-P. GALY et E.-J. VINCENT. Bull. Soc. Chim. Belg. **84**, 1189 (1975).
10. I. F. HALVERSTADT et W. D. KUMLER. J. Am. Chem. Soc. **64**, 2988 (1942).
11. J.-R. LLINAS. D.E.A., Marseille. 1970.
12. S. M. CASTELLANO et A. A. BOTHNER-BY. J. Chem. Phys. **41**, 3863 (1964).
13. J. A. POPLE et G. A. SEGAL. J. Chem. Phys. **44**, 3289 (1966).
14. D. P. SANTRY et G. A. SEGAL. J. Chem. Phys. **47**, 158 (1967).
15. J. A. POPLE, D. L. BEVERIDGE et P. A. DOBOSH. J. Chem. Phys. **47**, 2026 (1967).
16. J. DEL BENE et H. H. JAFFE. J. Chem. Phys. **48**, 1807 (1968).
17. R. G. PARR. Quantum theory of molecular electronic structure. W. A. Benjamin, Inc., New York, NY. 1963.
18. G. PFISTER-GILLOUZO, D. GONBEAU et J. DESCHAMPS. J. Mol. Struct. **14**, 81 (1972).
19. P. DOMIANO et A. MUSATTI. Cryst. Struct. Commun. **3**, 335 (1974).
20. L. NYGAARD, E. ASMUSSEN, J. H. HOG, R. C.

MAHESWARI, C. H. NIELSEN, J. B. PEARSEN, J. RASTRUP-ANDERSEN et G. O. SORENSEN. J. Mol. Struct. **8**, 225 (1971).
21. L. CAVALCA, P. DOMIANO et A. MUSATTI. Cryst. Struct. Commun. **1**, 345 (1972).
22. B. BAK, J. T. NIELSEN, O. F. NIELSEN, L. NYGAARD, J. RASTRUP-ANDERSEN et P. A. STEINER. J. Mol. Spectrosc. **19**, 458 (1966).
23. E. SAEGEBARTH et A. P. COX. J. Chem. Phys. **43**, 166 (1965).
24. G. A. REYNOLDS, J. A. VAN ALLAN et J. F. TINKER. J. Org. Chem. **24**, 1205 (1959).
25. J. H. BOYER et E. J. MILLER. J. Am. Chem. Soc. **81**, 4671 (1959).
26. Y. N. SHEINKER, I. Y. POSTOVSKII, N. P. BEDNYAGINA, L. B. SENYAVINA et L. F. LIPATOVA. Dokl. Akad. Nauk SSSR, **141**, 1388 (1961).
27. L. Y. POCHINOK et L. F. AVRAMENKO. Ukrain. Khim. Zh. **28**, 511 (1962).
28. L. F. AVRAMENKO, T. A. ZAKHAROVA, V. Y. POCHINOK et Y. S. ROZOM. Khim. Geterotskil. Soedin. **4**, 423 (1968).
29. R. FAURE. Résultats non publiés.
30. M. TISLER. Synthesis, 123 (1973); V. Y. POCHINOK, L. F. AVRAMENKO, T. F. GRIGORENKO et V. N. SKOPENKO. Usp. Khim. **44**, 1028 (1975).
31. G. FAVINI. Gazz. Chim. Ital. **91**, 270 (1961).
32. J. BASTIDE, J. P. MAIER et T. KUBOTA. J. Electron Spectrosc. **9**, 307 (1976).
33. M. WINNEWISSER et R. L. COOK. J. Chem. Phys. **41**, 999 (1964).
34. I. E. KNAGGS. Proc. R. Soc. (London), Ser. A, **150**, 576 (1935); D. W. ALLEN, D. J. BUCKLAND et I. W. NOWELL. J. Chem. Soc. Perkin Trans. II, 1610 (1976).
35. P. DOMIANO et A. MUSATTI. Cryst. Struct. Commun. **3**, 713 (1974).
36. YA. K. SYRKIN et E. A. SHOTT-L'VOVA. Dokl. Akad. Nauk SSSR, **87**, 639 (1952).
37. H. O. SPAUSCHUS et J. M. SCOTT. J. Am. Chem. Soc. **73**, 210 (1951).
38. T. KOOPMANS. Physica, **1**, 104 (1933).
39. C. TEMPLE et J. A. MONTGOMERY. J. Org. Chem. **30**, 826 (1965).
40. C. TEMPLE, M. C. THORPE, W. C. COBURN et J. A. MONTGOMERY. J. Org. Chem. **31**, 935 (1966).
41. T. SASAKI, K. KANEMATSU et M. MURATA. Tetrahedron, **27**, 5121 (1971).
42. R. GRANADOS, M. RULL et J. VILARRASA. J. Heterocycl. Chem. **13**, 281 (1976).

Infrared studies of water in crystalline hydrates: $K_2HgCl_4.H_2O$[1]

MICHAEL FALK

Atlantic Regional Laboratory, National Research Council of Canada, Halifax, N.S., Canada B3H 3Z1

AND

OSVALD KNOP

Department of Chemistry, Dalhousie University, Halifax, N.S., Canada B3H 4J3

Received September 22, 1976

MICHAEL FALK and OSVALD KNOP. Can. J. Chem. **55**, 1736 (1977).

Infrared spectra of polycrystalline $K_2HgCl_4.H_2O$ at different degrees of deuteration were recorded, in the 4000–250 cm^{-1} region, at temperatures between liquid-nitrogen and 130°C. The spectra confirm the existence of a single type of water molecule, engaged in two equivalent hydrogen bonds. The value of 2548 cm^{-1} for the isolated O—D stretching frequency leads to an estimate of 3.25(3) Å for the O...Cl hydrogen-bond distance, in excellent agreement with the results of X-ray and neutron diffraction. Dynamic coupling is appreciable for stretch, bend, and librational fundamentals but is weaker than in $CuCl_2.2H_2O$ or $K_2CuCl_4.2H_2O$, in which the water molecules in the crystal are more tightly bonded.

A number of corrected values are reported of isolated O—D stretching frequencies in hydrates studied previously.

MICHAEL FALK et OSVALD KNOP. Can. J. Chem. **55**, 1736 (1977).

On a enregistré les spectres infrarouges du $K_2HgCl_4.H_2O$ polycristallin à différent degré de deutération dans la région de 4000–250 cm^{-1} et à des températures allant de celle de l'azote liquide jusqu'à 130°C. Les spectres confirment l'existence d'un seul type de molécule d'eau qui est impliqué dans deux ponts hydrogène équivalents. La valeur de 2548 cm^{-1} pour la fréquence de valence O—D isolée conduit à un estimé de 3.25(3) Å pour la distance du pont hydrogène entre O...Cl et ceci est en excellent accord avec les résultats de rayons-X et de diffraction neutronique. Le couplage dynamique est assez important pour les vibrations de valence, de déformation angulaire et de libration mais est plus faible que ceux observés dans le $CuCl_2.2H_2O$ ou le $K_2CuCl_4.2H_2O$ dans lesquels les molécules d'eau dans le cristal sont liées d'une façon beaucoup plus intime.

On rapporte un certain nombre de valeurs corrigées pour des fréquences de vibration de valence O—D isolées dans des hydrates qui avaient été étudiés antérieurement.

[Traduit par le journal]

In certain classes of inorganic salt hydrates water molecules link the metal atoms with the anions to form flat infinite chains. Such geometry is particularly favourable for a study of the water molecule in crystals by ir or Raman spectroscopy. Fifer and Schiffer (1) made use of the advantages offered by the isotopic dilution technique in their ir investigation of H_2O in $CuCl_2.2H_2O$, and a similar investigation, in the series $M_2CuCl_4.2H_2O$ (M = K, Rb, NH_4), was carried out in these laboratories (2, 3). In the present paper we describe the ir spectrum of the water molecule in another hydrate containing such chains, $K_2HgCl_4.H_2O$, and compare the results with those obtained for the other compounds.

In the metal–water–anion chains occurring in $MX_2.2H_2O$ and $M_2CuCl_4.2H_2O$ (*cf.* ref. 2) the water molecules are coordinated trigonally, while in $K_2HgCl_4.H_2O$ they are coordinated tetrahedrally (4–7) (Fig. 1). More precisely, in the Hg compound all water molecules are crystallographically equivalent and situated on twofold axes running parallel to the *c*-axis; each molecule is coordinated approximately tetrahedrally by two K and two Cl atoms. There are two types of nearest-neighbour H_2O–H_2O pairs along the chain, (*a*) those separated by the K atoms, with inter-oxygen distances of 4.1 Å, and (*b*) those separated by the Cl atoms, with inter-oxygen distances of 4.8 Å (Fig. 1). The O...O distances for water molecules in different chains are considerably larger, the shortest such distance being 6.9 Å. By contrast, in the other type of chain, one M atom performs the function of two K atoms in $K_2HgCl_4.H_2O$. The O...Cl hydrogen-

[1]NRCC No. 15821.

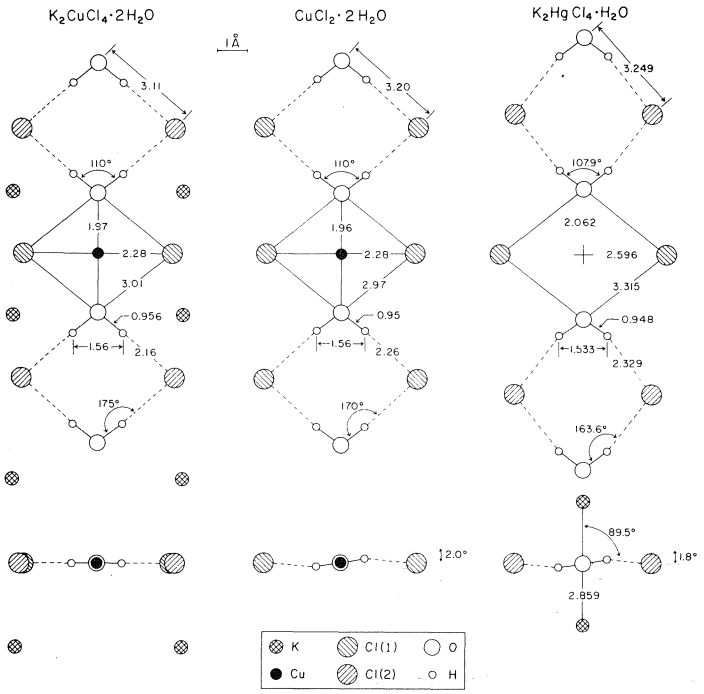

FIG. 1. Plans and elevations of the flat metal–water–chlorine chains in $K_2CuCl_4.2H_2O$ and $CuCl_2.2H_2O$ (after ref. 2) and the analogous chain in $K_2HgCl_4.H_2O$ (after ref. 7). One and a half periods are shown; the interatomic distances are in Å. The water molecule is coordinated trigonally in the Cu compounds but tetrahedrally (∠KOK, 87.7°) in $K_2HgCl_4.H_2O$. The oxygen atoms in H_2O–H_2O pairs of type *a* are separated by a Cu atom in the plane of the chain (in the Cu compounds) or by two K atoms outside that plane (in the Hg compound; the K atoms would project into a position indicated by a cross in the elevation). No metal atoms separate the two oxygens in H_2O–H_2O pairs of type *b*. The plans show the dihedral angles HOH/ClOCl and HOH/KOK.

bond contact in the Hg compound is 3.249(3) Å (7) and thus significantly larger than the corresponding O...Cl distance in $K_2CuCl_4.2H_2O$, 3.11 Å, and somewhat larger than in $CuCl_2.2H_2O$, 3.20 Å, hence hydrogen bonding in $K_2HgCl_4.H_2O$ is expected to be weaker than in either Cu compound. The difference in the hydrogen-bonding strength, in turn, would affect the magnitude of the dynamic coupling of vibrations of water molecules within the chains. Such coupling is appreciable, on evidence from the ir spectra, in the two Cu compounds (2) but not detectable in hydrates in which the water molecules are too far apart to share any nearest-neighbour atoms, *e.g.* $K_2SnCl_4.H_2O$ (8) or $K_2FeCl_5.H_2O$ (9).

Only incomplete descriptions of the vibrational spectrum of $K_2HgCl_4.H_2O$ are found in the literature. Raman lines at 1608, 3411, 3432, and 3475 cm^{-1} have been reported by Weil (10) and fifteen lines, at 415 cm^{-1} and below, by Poulet and Mathieu (11). Infrared bands at 1602 and 3390 cm^{-1} have been reported by by Chihara and Seki (12) and by Glemser and Hartert (13) respectively, and recently Barr and Goldstein (14) presented the Raman and ir spectra below about 350 cm^{-1} of the undeuterated and fully-deuterated compounds, incidental to their study of NH_4HgCl_3. Several studies by nmr also exist (15–19); the angle of inclination of the H–H vector to the crystallographic *b*-axis (*i.e.* of the plane of the water molecule to the 010 plane) obtained from the nmr experiments, 21.4°, is in reasonable agreement with the neutron diffraction result (7), 20.57°, and also with the angle deduced from the Raman spectra (10), 19°.

In addition to describing the results of our ir study of $K_2HgCl_4.H_2O$, we take this opportunity to report the newly re-measured O—D

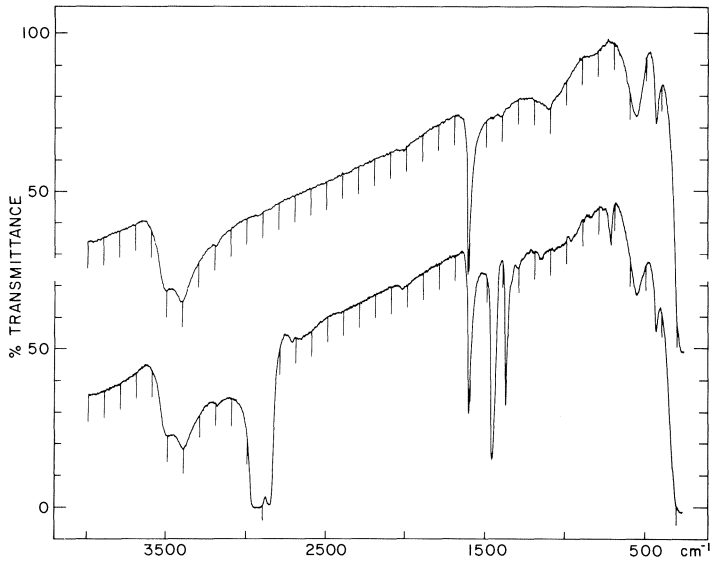

FIG. 2. Survey spectrum of undeuterated $K_2HgCl_4.H_2O$ at room temperature. (*Bottom*) Nujol mull. (*Top*) Pressed pellet of $K_2HgCl_4.H_2O$ in KCl.

stretching frequencies of several hydrates whose spectra were discussed in earlier papers of this series.

Experimental

Crystals of $K_2HgCl_4.H_2O$ were grown by slow evaporation at room temperature of a solution of 10 g KCl and 9 g $HgCl_2$ in 40 ml of a H_2O–D_2O mixture of appropriate composition. The clear colourless crystals, which had formed within a few days, were authenticated by X-ray powder diffraction. The ir spectra of the polycrystalline material dispersed in Nujol and in KCl pellets were similar (Fig. 2), indicating that the structure and composition of the compound were not modified by grinding and pressing with KCl.

In preparing samples of high D content, dry N_2 was bubbled through the solution to exclude atmospheric moisture. As a result of the accelerated evaporation crystals appeared much more rapidly. The low-temperature spectrum of the polycrystalline material obtained in this way showed additional small bands at 3599, 3564, and 3538 cm^{-1} in the O—H and at 2675, 2633, and 2627 cm^{-1} in the O—D stretching region; these small bands were barely detectable in the room-temperature spectra. It seems likely that the additional bands are due to traces of one or both of the two hydrates $KHgCl_3.H_2O$ and $KHg_2Cl_5.2H_2O$ reported by Foot and Levy (20), though we have not been able to show this conclusively. Samples obtained by slow evaporation were usually free of these admixtures.

Pressing pellets of $HgCl_2$ with excess KCl containing a trace of moisture produced H_2O spectra similar to those of $K_2HgCl_4.H_2O$ dispersed in KCl pellets but with additional bands, again presumed to be due to small amounts of the above two compounds. Pressed pellets of $K_2HgCl_4.H_2O$ in KBr gave an entirely different spectrum, similar to that obtained from pellets of $HgBr_2$ in KBr and in agreement with the frequencies reported for $KHgBr_3.H_2O$ (21).

The spectra were recorded on a Perkin-Elmer model 180 spectrophotometer using a model VLT-2 variable-temperature cell holder (Research and Industrial Instruments Company, London).

Results and Discussion

The frequencies of the major bands of H_2O, HDO, and D_2O are listed in Table 1. The spectrum gradually sharpened upon cooling the specimen to liquid-nitrogen temperature. The low-temperature frequencies are more accurate and will be used throughout in the following discussion, except where room-temperature values are required for comparison with the Raman data of refs. 10 and 11.

Bending Vibrations

At low isotopic concentrations the bending fundamentals of H_2O and D_2O are singlets, at 1612 and 1188 cm^{-1} respectively (Fig. 3). This confirms the existence of only one crystallographically distinct type of water molecule. At somewhat higher D contents a feature appears on the low-frequency side of the singlet. For D_2O it occurs at 1185 cm^{-1} and is clearly resolved. For H_2O it occurs at 1610 cm^{-1} and is not resolved from the 1612 cm^{-1} peak, but its frequency is inferred from the overall shift to low frequency with increasing H content. This feature is assigned to the out-of-phase coupled vibrations of certain H_2O–H_2O or D_2O–D_2O

TABLE 1. Vibrational assignments for the water molecule in $K_2HgCl_4 . H_2O$

Mode		Frequency (cm^{-1})[a]						
		H_2O (Raman)[b]	H_2O (ir)		HDO (ir)		D_2O (ir)	
		r.t.	r.t.	l.n.	r.t.	l.n.	r.t.	l.n.
OH stretch	ν_3	— B_{2g}	~3505[c,d]	3473				
		3475 B_{3g}						
	ν_1	3432 A_g			3452	3445		
		3411 B_{1g}	3404 B_{1u}[d]	3412				
OD stretch	ν_3						2612	2602
	ν_1				2548	2544		
							2499	2500
2 × bend			3191	3193			2345	2350
Bend (isolated)			1610	1612		1422		1188
Bend (coupled)		1608 A_g	1608 B_{1u}[d]	1610		1419	1183	1185
		1608 B_{1g}	1616 A_u[e]					
Librations	twist			(630)[f]		602[g]		(440)[f]
	wag		560[c,d]	571	420	431[h]	412	420
	rock	415 B_{2g}	434[c,d]	451	362	378	—	333

[a] r.t., room temperature; l.n., liquid-nitrogen temperature.
[b] From refs. 10 and 11.
[c] B_{2u}, B_{3u}.
[d] Symmetry species assigned from vibrational analysis.
[e] Inactive component; frequency estimated on the assumption that the mean frequency of the factor-group components equals the isotopically isolated frequency (*cf.* refs. 1 and 2). (In an isotopically pure crystal the bending fundamental should be split into one ir-active component B_{1u}, two Raman-active components A_g and B_{1g}, and one inactive component A_u (Fig. 4). For H_2O bending the Raman-active frequencies are known from ref. 10 and the inactive frequency may be estimated after the manner of refs. 1 and 2 by assuming that the average of the frequencies of the four coupled components equals the frequency of the isolated fundamental. However, this calculated frequency, 1616(6) cm^{-1}, is of low accuracy because of combination of experimental errors of the Raman and ir measurements.)
[f] Estimated frequency, see text.
[g] Largely H in-plane motion (*cf.* Fig. 6 of ref. 2).
[h] Largely D in-plane motion.

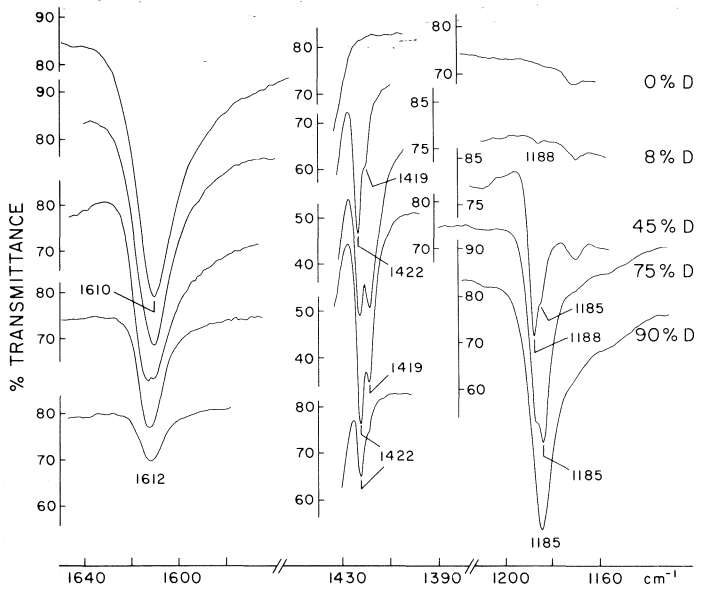

FIG. 3. Spectra of $K_2HgCl_4.H_2O$ (Nujol mulls) at −150°C in the region of the bending vibrations of H_2O, HDO, and D_2O at different D contents.

pairs. Only one feature due to coupling is detected, and the relative intensities of the coupled and uncoupled components are consistent with the coupling being appreciable for only one type of water pair. We identify the pair as one of the nearest-neighbour pairs within the chains, *i.e.* either *a* or *b* (Fig. 1). Pairs *a* and *b* are both centrosymmetric, so in either case the in-phase vibration would be ir inactive (*cf.* discussion in ref. 2).

For the isotopically pure crystals, one of the factor-group components of the bending vibration, B_{1u}, should be ir active (Fig. 4). For both H_2O and D_2O it coincides with the coupled vibration of H_2O or D_2O pairs observed at lower isotopic contents. This confirms that in this hydrate, as in $K_2CuCl_4.2H_2O$ (2) and $CuCl_2.2H_2O$ (1), the coupling of bending vibrations originates almost entirely in *one* type of water pairs within the chain. However, the magnitude of this coupling is considerably smaller in $K_2HgCl_4.H_2O$.

The bending fundamental of HDO at low isotopic concentrations is also a singlet, at 1422 cm^{-1}, which confirms the equivalence of the two hydrogens, consistent with the C_2 site symmetry of the water molecule required by the structure. At higher concentrations of HDO an additional feature, sharp and well-resolved, appears at 1419 cm^{-1}.

Since pairs of type *a* and *b* may exist, in the case of HDO, in either a centrosymmetric or a non-centrosymmetric configuration, the situation is more complex than for H_2O or D_2O pairs. The simplest interpretation of the fact that vibrational coupling results in only one sharp feature at 1419 cm^{-1} at higher HDO contents is

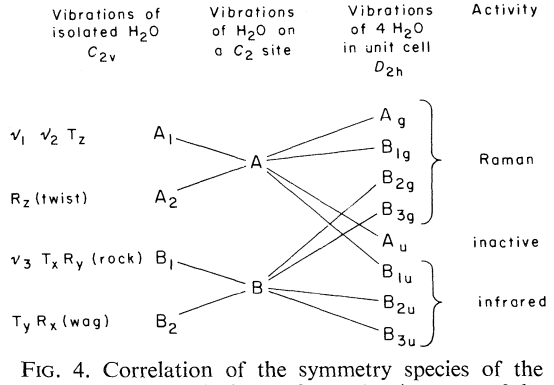

FIG. 4. Correlation of the symmetry species of the molecular (C_{2v}), site (C_2), and factor (D_{2h}) groups of the H_2O fundamentals in $K_2HgCl_4.H_2O$.

to assume that (*i*) the coupling of bending vibrations for HDO, as for H_2O and D_2O, is appreciable for only one type of water pair, *i.e.* either *a* or *b* of Fig. 1; (*ii*) the 1419 cm^{-1} band is due to the out-of-phase coupled vibrations of centrosymmetric and non-centrosymmetric pairs in near coincidence; and (*iii*) the in-phase coupled vibration of the non-centrosymmetric pairs is not observable owing to low intensity. The relative intensities of the 1422 and 1419 cm^{-1} bands at different HDO contents are fully consistent with this interpretation.

It may seem surprising that the strength of dynamic coupling can differ by what appears to be an order of magnitude for pairs of water molecules which do not differ appreciably in their inter-oxygen distances, 4.1 and 4.8 Å. However, the dominant term responsible for the coupling must be of dipole–dipole nature, and so orientation may play a decisive role.

Stretching Vibrations

The vibrationally isolated O—H and O—D fundamentals of isotopically dilute HDO gave rise to sharp singlets at 3445 and 2544 cm^{-1} respectively (Fig. 5). The singlets confirm the equivalence of the two hydrogens, consistent with the C_2 site symmetry of the water molecule.

At intermediate isotopic concentrations the spectrum in the O—D stretching region exhibits several sets of weak bands, of which the most visible are a pair at 2520 and 2565 cm^{-1}. They are assigned to coupled vibrations of HDO–HDO pairs. Unlike for the bending vibrations, the coupling of stretching vibrations appears to be appreciable for more than one type of pair. The corresponding O—H coupled modes of HDO–HDO pairs would be expected to fall near the H_2O stretching frequencies from which they are not resolved.

For undeuterated, or fully deuterated, samples the symmetric and antisymmetric stretching frequencies, ν_1 and ν_3, can be assigned unambiguously by reference to the rules of factor-group splitting (Fig. 4): the Raman bands at 3411 and 3432 cm^{-1} reported in ref. 10 are of symmetry species B_{1g} and A_g and hence must belong to the ν_1 fundamental, while the band at 3475 cm^{-1}, of symmetry species B_{3g}, must belong to the ν_3 fundamental. This establishes that $\nu_3 > \nu_1$, which is the usual order, and leads to the other assignments in the O—H and O—D stretching regions in Table 1. The overtone of

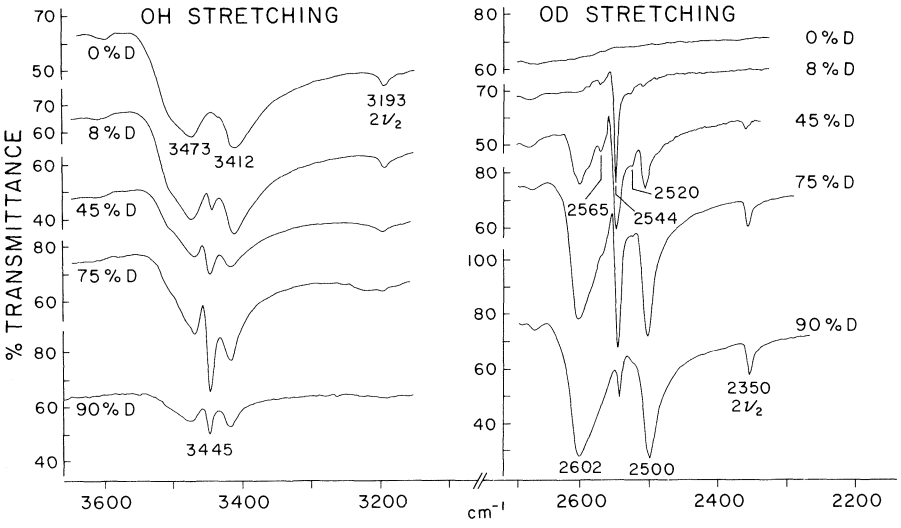

FIG. 5. Spectra of $K_2HgCl_4.H_2O$ (Nujol mulls) at −150°C in the O—H and O—D stretching regions at different D contents.

the bending vibration, $2\nu_2$, at 3193 cm^{-1} for H_2O and 2350 cm^{-1} for D_2O, is clearly enhanced by Fermi resonance with the ν_1 fundamental. The resonance is relatively weak, corresponding to case *a* in Fig. 1 of ref. 22.

We note that dynamic coupling of vibrations is also appreciable for the stretching fundamentals, as witnessed by the frequency differences between the Raman and the ir factor-group components of the ν_1 and ν_3 fundamentals.

Rotational and Translational Vibrations

In the ir spectrum of $K_2HgCl_4.H_2O$ the rocking and wagging librations should yield two, and the twisting libration one, components for a total of five bands (Fig. 6). Only two major features in the H_2O and D_2O spectrum may be assigned to librations. They occur at 571 and 451 cm^{-1} for H_2O and at 420 and 333 cm^{-1} for D_2O, which yields an H_2O/D_2O frequency ratio of about 1.36, characteristic of purely librational motions.[2] The two librations must be the rock and the wag: the twisting fundamental, which is ir inactive under the full C_{2v} symmetry of the undistorted water molecule, is rarely observed in the ir spectra of crystalline hydrates, and the factor-group splitting expected for the librations in $K_2HgCl_4.H_2O$ would be of the order of 1 to 10 cm^{-1}, as for the bending and stretching fundamentals, and certainly not of the order of 100 cm^{-1}.

In crystalline hydrates it is often difficult to decide which of the two is wag and which is rock, but in our case we are helped by the librational frequencies of HDO, 602, 431, and 373 cm^{-1}. Expected qualitative relations between the frequencies of H_2O, D_2O and those of HDO (Fig. 6 of ref. 2) lead us to assign the 571 cm^{-1} band to the wagging libration and the 451 cm^{-1} band, to the rocking libration. The usual sequence of frequencies is rock > wag (23, 24), so the present sequence constitutes another case of reversal (9, 25). The intensity sequence, however, is the usual one, wag > rock ≫ twist (9). The frequency of the twisting libration may be deduced to be approximately 630 cm^{-1} for H_2O and 440 cm^{-1} for D_2O, from a consideration of the scheme presented in Fig. 6 of ref. 2. This scheme places the frequency of the H (or D) out-of-plane libration about midway between those of the wagging and twisting librations of H_2O (or D_2O). Shoulders observed near 630 and 440 cm^{-1} may be due to the twisting mode.

The twisting motion in $K_2HgCl_4.H_2O$ thus appears to correspond to the libration of highest frequency. This is in contrast to $K_2CuCl_4.2H_2O$, in which it is the libration of lowest frequency. The difference may be explained by the forces opposing the twisting motion in a trigonally coordinated water molecule which in the Cu

[2]The intense band at 305 cm^{-1} does not shift upon deuteration, hence it does not belong to the H_2O spectrum of the hydrate.

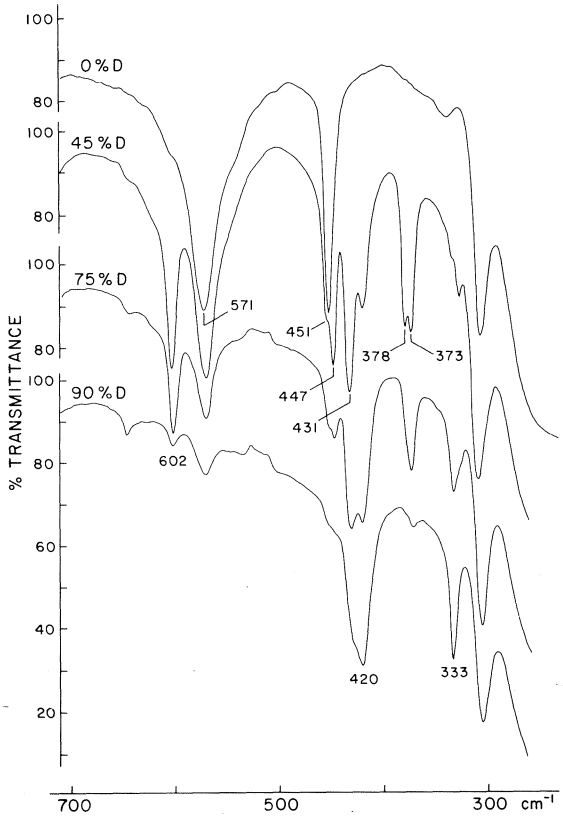

FIG. 6. Spectra of $K_2HgCl_4.H_2O$ (Nujol mulls) at −150°C in the region of the librations of the water molecules, at different D contents.

compound arise only from the hydrogen bonds. In a tetrahedrally coordinated water molecule in the Hg compound this motion is also opposed by the two K–OH_2 contacts. Further work may show whether this is a general rule for other tetrahedrally and trigonally coordinated water molecules in crystals.

Dynamic coupling of vibrations is also appreciable for the librational fundamentals. This is manifested by the difference between the Raman and ir frequencies of the wagging and rocking fundamentals (Table 1), and in the resolution, in the spectra of Fig. 6, of a 'coupled' and an 'isolated' frequency for the H_2O rocking mode at 451/447 cm^{-1}, the HDO mode at 378/373 cm^{-1}, and the D_2O mode at 333/327 cm^{-1}.

In spectra of thicker films broad bands are observed, centred at 1080 and 840 cm^{-1}. They appear to be the first overtones of the wagging and rocking librations respectively. The breadth and the complex shape of these bands show that they are the superpositions of many of the allowed overtones and binary combinations of the four factor-group components of each of these librations (*cf.* ref. 2).

The three translational fundamentals are expected to lie in the 100–300 cm^{-1} region and to give rise to five ir-active and six Raman-active factor-group components (Fig. 4). One of the ir components (at 202 cm^{-1} for H_2O and at 196 cm^{-1} for D_2O) and one of the Raman components (at 157 cm^{-1} for H_2O and at 153 cm^{-1} for D_2O) have been observed in the low-frequency spectra of ref. 14.

The O...Cl Distance

The value of the isolated O—D stretching frequency at room temperature is 2548 cm^{-1}. Using the correlation (26) between the O...X hydrogen-bond distance R and ν(OD) we obtain, for X = Cl, $R = 3.397 + 0.000840[\nu(OD) - 2727] \sim 3.25(3)$ Å, in excellent agreement with the value of 3.249(3) Å resulting from neutron-diffraction work (7). Glemser and Hartert (13) used their 'raw' value of O—H stretching frequency of H_2O, 3390 cm^{-1} (presumably ν_3), to derive, from a similar correlation, R = 3.22 Å. The use of *isolated* O—H or O—D stretching frequency leads to more accurate frequency–distance correlations.

Phase Transition in $K_2HgCl_4.H_2O$

The occurrence of a phase transition at a temperature reported to be as low as 82°C (18) and as high as 114°C (12), presumably depending on the rate of heating, has been described. The transition appears to be accompanied by marked changes in the dielectric properties (18) and by a large enthalpy change (12) but not by dehydration (12) or a volume discontinuity (18). The nature of the transition is not completely understood.

We observed no evidence of a spectral discontinuity in the above temperature region in spectra obtained from $K_2HgCl_4.H_2O$ dispersed in KCl pellets and kept at a predetermined temperature.

Structural Conclusions

1. The existence of a single type of H_2O molecule on a site of symmetry C_2, as determined by X-ray and neutron diffraction, is confirmed.

2. The spectrum of the water molecule in $K_2HgCl_4.H_2O$ grossly contrasts with that in $K_2SnCl_4.H_2O$, which was once incorrectly

TABLE 2. Corrected values of the O—D stretching frequencies (cm^{-1}) of isotopically isolated HDO in hydrates described in refs. 2, 8, 9, and 27

	Frequency[a]				
	Old values			New values	
Compound	r.t.	l.n.	Reference	r.t.	l.n.
$K_2CuCl_4.2H_2O$	2428	2427	2	2425	2425
$K_2FeCl_5.H_2O$	2508	2498	9	2499	2491
$Rb_2FeCl_5.H_2O$	2528	2520	9	2522	2515
$(NH_4)_2FeCl_5.H_2O$	2528	2524	9	2523	2518
$K_2SnCl_4.H_2O$	2604	2608	8	2599	2604
	2554	2546		2550	2541
$KSnCl_3.H_2O$	2653	2666	27	2648	2662
	2621	2638		2617	2634
		2630			2626

[a]r.t., room temperature; l.n., liquid-nitrogen temperature.

thought to be isostructural with the Hg compound (ref. 8 and other references therein).

3. The ν(OD) value of 2548 cm^{-1} for the isolated O—D stretch at room temperature leads to an estimate of 3.25(3) Å for the O...Cl distance involving hydrogen, in excellent agreement with refs. 6 and 7.

4. Dynamic coupling is appreciable for stretch, bend, and librational fundamentals. However, it is smaller in magnitude than in $CuCl_2.2H_2O$ or $K_2CuCl_4.2H_2O$. This might be expected, for the

$$O—\overset{K}{\underset{K}{}}—O$$

interaction is much weaker than the O—Cu—O interaction in the two Cu compounds, and the hydrogen bonding also is weaker.

5. The phase transition reported to occur in the 82–114°C range either does not take place in KCl matrix, and hence is associated with loss of water, or it leads to minimal structural changes in and around the water molecule, such as would not appreciably affect its ir spectrum.

Correction of Earlier Data

We have recently re-checked, using our newly acquired Perkin-Elmer model 180 spectrophotometer, the frequencies of most absorption bands reported in our earlier papers in this series (2, 8, 9, 27). It turned out that for sharp bands the new values generally agree within ± 1 cm^{-1} with the previous values obtained with a Perkin-Elmer model 521 spectrophotometer. However, one important exception was found: the previous values show a systematic error of about $+5$ cm^{-1} in the O—D stretching region, around 2500 cm^{-1}. The error was caused by a local anomaly in the frequency calibration of our model 521 instrument. Because of the importance of having accurate ν(OD) data for frequency–distance correlation purposes, we have gathered in Table 2 the previous and the new, corrected values.

Acknowledgments

We should like to thank Miss Gwen H. Thomas and Mr. P. F. Seto for assistance with the experimental work and Drs. K. Aurivillius and C. Stålhandske for providing us with a preprint of ref. 7. A grant-in-aid of research from the National Research Council of Canada to one of us (O.K.) is acknowledged.

1. R. A. FIFER and J. SCHIFFER. J. Chem. Phys. **54**, 5097 (1971).
2. G. H. THOMAS, M. FALK, and O. KNOP. Can. J. Chem. **52**, 1029 (1974).
3. D. A. OTHEN, O. KNOP, and M. FALK. Unpublished results.
4. C. H. MACGILLAVRY, J. H. DE WILDE, and J. M. BIJVOET. Z. Kristallogr. **100**, 212 (1938).
5. Z. V. ZVONKOVA, V. V. SAMODUROVA, and L. G. VORONTSOVA. Dokl. Akad. Nauk SSSR, **102**, 1155 (1955).
6. K. AURIVILLIUS and C. STÅLHANDSKE. Acta Chem. Scand. **27**, 1086 (1973).
7. K. AURIVILLIUS and C. STÅLHANDSKE. Acta Chem. Scand. A, **30**, 735 (1976).
8. M. FALK, C.-H. HUANG, and O. KNOP. Can. J. Chem. **52**, 2380 (1974).
9. M. FALK, C.-H. HUANG, and O. KNOP. Can. J. Chem. **53**, 51 (1975).
10. A. WEIL. C.R. **236**, 2147 (1953).
11. H. POULET and J.-P. MATHIEU. J. Chim. Phys. **60**, 442 (1963).
12. H. CHIHARA and S. SEKI. Bull. Chem. Soc. Jpn. **32**, 897 (1959).

13. O. GLEMSER and E. HARTERT. Naturwiss. **42**, 534 (1955).
14. R. M. BARR and M. GOLDSTEIN. J. Chem. Soc. Dalton, 1180 (1974).
15. J. ITOH, R. KUSAKA, Y. YAMAGATA, R. KIRIYAMA, and H. IBAMOTO. J. Chem. Phys. **20**, 1503 (1952).
16. J. ITOH, R. KUSAKA, Y. YAMAGATA, R. KIRIYAMA, H. IBAMOTO, T. KANDA, and Y. MASUDA. J. Phys. Soc. Jpn. **8**, 287 (1953).
17. J. ITOH, R. KUSAKA, Y. YAMAGATA, R. KIRIYAMA, and H. IBAMOTO. J. Phys. Soc. Jpn. **8**, 293 (1953).
18. R. KIRIYAMA and H. IBAMOTO. Bull. Chem. Soc. Jpn. **27**, 317 (1954).
19. S. E. SVANSON and P. ALMKVIST. Ark. Kemi, **40**, 165 (1969).
20. H. W. FOOT and L. H. LEVY. Am. Chem. J. **35**, 236 (1906).
21. N. KRAUZMAN and M. KRAUZMAN. Spectrochim. Acta, **29**A, 997 (1973).
22. D. A. OTHEN, O. KNOP, and M. FALK. Can. J. Chem. **53**, 3837 (1975).
23. G. SARTORI, C. FURLANI, and A. DAMIANI. J. Inorg. Nucl. Chem. **8**, 119 (1958).
24. I. NAKAGAWA and T. SHIMANOUCHI. Spectrochim. Acta, **20**, 429 (1964).
25. D. M. ADAMS and P. J. LOCK. J. Chem. Soc. A, 620 (1967).
26. M. FALK and O. KNOP. *In* Water: a comprehensive treatise. Vol. 2. *Edited by* F. Franks. Plenum Press, New York. 1973. Chapt. 2.
27. M. FALK, C.-H. HUANG, and O. KNOP. Can. J. Chem. **52**, 2928 (1974).

Extremal arrangements of points and unit charges on a sphere: equilibrium configurations revisited

THEODOR WILLIAM MELNYK, OSVALD KNOP,[1] AND WILLIAM ROBERT SMITH

Departments of Chemistry and Mathematics, Dalhousie University, Halifax, N.S., Canada B3H 4J3

Received November 15, 1976

THEODOR WILLIAM MELNYK, OSVALD KNOP, and WILLIAM ROBERT SMITH. Can. J. Chem. **55**, 1745 (1977).

We review the formulation and solutions of a number of extremal problems associated with points and unit charges on the surface of a sphere in E^3. For one of these problems, namely

$$U(m,n) = \tfrac{1}{2}k \sum_{p \neq q}^{m} d_{pq}^{-n} = \text{minimum}$$

where d_{pq} is the Euclidean distance between points P and Q and m is the number of points, we discuss the results for $m \leq 16$ and $1 \leq n < \infty$. For the cases $m = 5, 11, 13$–16 we find hitherto undiscovered solutions. Our solutions for $m = 5$ and 11 correct earlier results in the literature. We also sharpen the existing literature results for $m = 7$ and 10.

THEODOR WILLIAM MELNYK, OSVALD KNOP et WILLIAM ROBERT SMITH. Can. J. Chem. **55**, 1745 (1977).

On passe en revue la formulation et les solutions d'un certain nombre de problèmes extrêmes associés avec les charges ponctuelles et unitaires sur la surface d'une sphère en E^3. Pour un de ces problèmes, à savoir

$$U(m,n) = \tfrac{1}{2}k \sum_{p \neq q}^{m} d_{pq}^{-n} = \text{minimum}$$

où d_{pq} est la distance euclidienne entre les points P et Q et m est le nombre de points, on discute des résultats pour $m \leq 16$ et $1 \leq n < \infty$. Pour les cas $m = 5, 11, 13$–16, on trouve des solutions qui n'avaient pas été découvertes jusqu'à maintenant. Nos solutions pour $m = 5$ et 11 corrigent des résultats antérieurs parus dans la littérature. On précise aussi des résultats existants dans la littérature pour $m = 7$ et 10.

[Traduit par le journal]

The problem, and its equivalents and cognates, of how to arrange m points (or equivalent particles or discrete unit charges) on the surface of a three-dimensional sphere to satisfy a prescribed extremal condition, is of importance in stereochemistry (VSEPR theory of directed valency, *cf.* ref. 1) as well as in botany, virology, information theory, and elsewhere (2, 3). However, it is often not appreciated that an 'equilibrium' configuration of the points may in some cases correspond to *several*, quite different, extremal requirements which in general lead to a variety of solutions (*cf.* ref. 4). Furthermore, the extremal requirements are sometimes inadequately specified and their description is confused; it is in fact not entirely clear which particular set of extremal conditions is the most appropriate to use as a basis of stereochemical theory. In view of this and of the fact that the mathematical literature on extremal configurations is quite extensive and at times not easily accessible, we set out, in the following, the various equivalent formulations of the extremal conditions of interest and present as concisely as possible the results, exact or conjectured, that have been reported to date. Against this background we then describe the results of our own investigations of problem *B* below, the extremal problem that has received most attention by chemists.

We have investigated problem *B* for 5 to 16 points by a numerical technique. Rigorous methods (*vide infra*; refs. 2, 3, 6–8) have so far produced solutions for up to 12 points (in an isolated case, for 24 points), and then only for the so-called 'hard-spheres' case, which is of limited importance in stereochemistry. In yielding solutions for 11 and 24 points the geometric method of proof may be approaching its limit of usefulness. On the other hand, the computational time and effort required to deal with 16 points, and the increasing ease with which competing configura-

[1]To whom correspondence should be addressed.

tions can be converted into one another, give us reason to believe that further numerical work may be unprofitable.

We shall not concern ourselves with the importance, relative to other factors, of the stated extremal conditions in determining actual stereochemical configurations.[2]

In this paper, d_{pq} denotes the Euclidean distance between points P and Q on the unit sphere, s_{pq} denotes the corresponding spherical distance (in radians) measured along a great-circle segment connecting P and Q; m is a positive integer and n is a non-negative real number.

Distinct Extremal Problems and Their Formulations

A. Leech (9) posed the following problem: m particles are constrained to the surface of a sphere. Between every pair of them there acts a force which depends only on the distance between them; the law of force is the same for all particles. Which configurations are *balanced* with respect to tangential forces for *any* force law?

B. Which configurations satisfy the condition

$$[1] \quad U(m,n) = \tfrac{1}{2}k \sum_{p \neq q}^{m} {d_{pq}}^{-n} = \text{minimum}$$

If k is dimensionless, the dimension of U is (length)$^{-n}$ and the extremal condition is purely geometrical, involving distances between pairs of points. If the dimension of k is (length)^n, U is dimensionless. If the dimension of k is (energy) × (length)^n, U is the potential energy of a system of m discrete unit charges of equal sign confined to the surface of a sphere. For Coulombic repulsion, $n = 1$.

When $n \to \infty$, U is increasingly dominated by the term(s) corresponding to the smallest d_{pq} and minimizing U becomes equivalent to maximizing the smallest d_{pq}. In this limit the problem is then equivalent to the problem of *densest packing* of equal spheres (or equal circles or spherical caps) on a sphere. This is sometimes referred to as the *hard-spheres* case, while finite values of n pertain to the *soft-spheres* case.

Various equivalent formulations of the *densest-packing* problem are found in the literature (2–4, 6–8): (*1*) Which configuration of m points on a sphere maximizes the minimum distance d_{pq} or s_{pq} between any two of the points? This is the *Tammes problem* of pollen-grain orifices (*cf.* ref. 2, also for results in spaces other than E^3). (*2*) m points are placed on a sphere of radius R_m in such a way that no d_{pq} is less than unity. Find the minimum value of R_m. (*3*) The packing density ρ_m is the ratio of the total area of m equal non-overlapping circles (or spherical caps) on the surface of a sphere to the surface area of the sphere. Find the arrangement(s) of the circles that gives (give) the maximum value of ρ_m. (*4*) Find the largest angular diameter of m equal circles (or spherical caps) which can be packed on the surface of a sphere without overlapping. (*5*) How many cones of given angle can be packed around a point? (*6*) A planet is ruled by m mutually inimical dictators. How are they to distribute their residences so as to maximize the minimum distance between any two of them? (*7*) How can m fuel depots be arranged on a planet so that an accidental explosion of one of them will least endanger the rest?

C. Which configurations satisfy the condition

$$[2] \quad V(m,n) = \tfrac{1}{2}k \sum_{p \neq q}^{m} {d_{pq}}^{n} = \text{maximum}$$

D. Replace in problem *C* the Euclidean distances d_{pq} by the shortest *spherical* distances s_{pq}.

E. The problem of *thinnest covering* of a sphere by m interpenetrating equal spheres (or equal circles or spherical caps):

(*1*) Find the (complete) covering of a sphere by m congruent circles (or spherical caps) having minimum density ρ_m' (analogous to ρ_m in problem *B*(*3*)). (*2*) How should m fuel depots be arranged on a planet so as to minimize the greatest distance between a point of the planet and the nearest depot (*cf.* ref. 6)? (*3*) How should the residences of m allied dictators governing on a planet be placed so as to control the planet as well as possible (*cf.* ref. 6)?

F. How to arrange m interpenetrating equal spheres (or equal circles or spherical caps) of spherical radius s, $0 < s \leq \pi/2$, on a sphere so as to cover the greatest possible area? This case is intermediate between the densest packing and the thinnest covering.

G. How to distribute m points on a sphere so as to maximize the volume of their convex hull? More precisely, (surface of hull)^3/(volume of hull)^2 = minimum.

H. Still other extremal problems have been proposed by Whyte (4), *e.g.*, maximizing the

[2] For a discussion of these other factors see, for example, refs. 1 and 5, and the references quoted therein.

product of distances of all pairs, or finding arrangements which possess extremal properties of any kind, or finding extremal problems which lead to identical solutions.

Known or Conjectured Solutions to Problems *A* to *H* Reported to Date

In the following text and in Tables 2–7, configurations are described either by their proper names (when the configuration corresponds to a familiar convex polyhedron inscribable in a sphere, or when it is obtained by a central projection of the vertices of such a polyhedron onto the sphere)[3] or by symbols indicating the point-group symmetry of the configuration and the way in which the m points are distributed among circles formed by intersections of the sphere with consecutive planes parallel to the equatorial plane. The north–south axis coincides with the principal axis of rotation when the configuration has rotational symmetry. Thus the regular icosahedron, $m = 12$, may be described as $I_h(1:5:5:1)$, with the two single points in the poles and the vertices of the two staggered pentagons in planes parallel to the equatorial plane. Similarly, $C_{4v}(1:4:4:4)$ represents an arrangement of symmetry C_{4v} with one point in a pole and three sets of four coplanar points symmetric about the fourfold axis passing through the pole and the centre of the sphere. This nomenclature is not unique but is in common use and convenient; additional information is provided when ambiguity arises. To save space, the symbols are contracted: $I_h(1:5:5:1)$ becomes $I_h(1^15^21^1)$ and $C_{4v}(1:4:4:4)$ becomes $C_{4v}(1^14^3)$.

The positions of the points in some of the configurations are completely fixed by symmetry. In others, some of the positions vary with n while the point-group symmetry is maintained. The minimum number of n-dependent coordinates (parameters) necessary to describe completely a configuration of a particular point-group symmetry is designated by f. This quantity may be viewed as the *maximum* number of degrees of freedom of the configuration under that symmetry; it is lowered if one or several of the f variable coordinates are *a priori* assigned particular values. Thus removing a vertex of a regular octahedron $O_h(1^14^11^1)(f = 0)$ leaves a square pyramid $C_{4v}(1^14^1)$ ($\equiv$ octahedron $- 1$) in which the relative positions of the five points are completely determined and hence $f = 0$. However, this configuration is only a special case of the square pyramid $C_{4v}(1^14^1)(f = 1)$ inscribed in a sphere and in which the plane of the four points is not fixed relative to the equatorial plane, the geodetic latitude of this plane being the degree of freedom to be specified. Similarly, the removal of a vertex of a regular icosahedron $I_h(1^15^21^1)(f = 0)$ leaves a singly-capped pentagonal antiprism $C_{5v}(1^15^2)(f = 0)$, a special case of the singly-capped pentagonal antiprism $C_{5v}(1^15^2)(f = 2)$ in which the latitudes of the planes containing the two pentagons can assume any admissible values.

A. This problem has been investigated by Leech (9), with the following results. The only solutions are configurations which have rotational symmetry about every diameter through the particles, *i.e.* configurations defined by polyhedra inscribed in the sphere and having all the vertices on axes of rotation. Hence only these possibilities exist: (*a*) Regular polygons with vertices on a great circle. This includes an antipodal pair, $m = 2$. (*b*) Convex Platonic polyhedra $\mathscr{P}\ell(m)$, their duals $\mathscr{D}(m)$, and vertex-figure derivatives $\mathscr{V}(m)$.[4] (*c*) Combinations of configurations of *a* and *b* to give balanced configurations inscribed in the sphere. Construction of such configurations amounts to finding balanced sets of particles having balanced subsets which when removed leave balanced sets. At most three sets from *a* and *b* can be combined. For two sets, the possibilities are two coplanar polygons, or any binary combinations of $\mathscr{P}\ell(m)$, $\mathscr{D}(m)$, and $\mathscr{V}(m)$, or a combination of a polygon and an antipodal pair to a regular bipyramid. For three sets, the possibilities are a combination of $\mathscr{P}\ell(m)$ with its dual $\mathscr{D}(m)$ and vertex-figure polyhedron $\mathscr{V}(m)$, or two coplanar polygons and an antipodal pair combined to a regular bipyramid, or three antipodal pairs in the vertices of an octahedron.

The distinct configurations of class *b* and their combinations are listed in Table 1.

B. The configurations shown in Table 2 for $m = 2$, 3, 4, 6, and 12 are the solutions to the

[3] *Capping* adds vertices above faces perpendicular to the principal axis of symmetry of the polyhedron, *e.g.*, as in a bicapped trigonal prism. *Augmenting* adds vertices above faces perpendicular to the equatorial plane (*e.g.*, trigonal prism + 3) or, occasionally, above other faces.

[4] A dual is defined by the face-centres of a polyhedron. A vertex-figure polyhedron is defined by the midpoints of the edges of a polyhedron.

TABLE 1. Balanced configurations of symmetries O_h, T_d, and I_h (9)

m	Configuration*
4	$\mathscr{P}\ell(4)$ (= tetrahedron T_d)
6	$\mathscr{P}\ell(6)$ (= octahedron O_h)
8	$\mathscr{P}\ell(8)$ (= cube O_h)
10	$\mathscr{P}\ell(4) + \mathscr{V}(4)$
12	$\mathscr{P}\ell(12)$ (= icosahedron I_h), $\mathscr{V}(8)$ (= cuboctahedron O_h)
14	$\mathscr{P}\ell(6) + \mathscr{D}(6)$ (= rhombic dodecahedron or trisoctahedron or tetrahexahedron O_h)
18	$\mathscr{P}\ell(6) + \mathscr{V}(6)$
20	$\mathscr{P}\ell(20)$ (= dodecahedron I_h), $\mathscr{P}\ell(8) + \mathscr{V}(8)$
26	$\mathscr{P}\ell(6) + \mathscr{D}(6) + \mathscr{V}(6)$ (= hexoctahedron O_h)
30	$\mathscr{V}(12)$ (= icosidodecahedron I_h)
32	$\mathscr{P}\ell(12) + \mathscr{D}(12)$ (= rhombic triacontahedron or trisicosahedron I_h)
42	$\mathscr{P}\ell(12) + \mathscr{V}(12)$
50	$\mathscr{P}\ell(20) + \mathscr{V}(20)$
62	$\mathscr{P}\ell(12) + \mathscr{D}(12) + \mathscr{V}(12)$ (= trapezoidal hexecontahedron I_h)

*$\mathscr{P}\ell(6) \equiv \mathscr{D}(8)$, $\mathscr{P}\ell(8) \equiv \mathscr{D}(6)$, $\mathscr{P}\ell(12) \equiv \mathscr{D}(20)$, $\mathscr{P}\ell(20) \equiv \mathscr{D}(12)$.

TABLE 2. Configurations corresponding to the densest packing of congruent hard spheres (solutions to problem B for $n \to \infty$)

m	Configuration	Reference
2	Antipodal pair $D_{\infty h}$	
3	Equilateral triangle D_{3h} inscribed in a great circle	2, 14
4	Tetrahedron T_d	2, 14
5	Trigonal bipyramid D_{3h} or square pyramid[a] $C_{4v}(f = 0)$	2, 14
6	Octahedron O_h	2, 14
7	$C_{3v}(1^1 3^2)$, $s_{\min} = \arccos[\cos\frac{4}{9}\pi/(1 - \cos\frac{4}{9}\pi)]$	7
8[b]	Square antiprism[c] D_{4d}, $s_{\min} = \arccos[(\sqrt{8} - 1)/7]$	7
9	$D_{3h}(3^3)$,[d] $s_{\min} = 2\arccos(\sqrt{6}/3)$	7
10[e]	$C_{2v}(2^1 4^1 2^2)^f$ (proved by L. Danzer)	[i]
11	$C_{5v}(1^1 5^2)^g$ (proved by K. Böröczki)	[i]
12	Icosahedron I_h	2, 14
14	*Not* the trisoctahedron or rhombic dodecahedron or tetrahexahedron O_h[h]	6, 9
20	*Not* the Platonic dodecahedron I_h	6
24	Snub cube O	8
30	*Not* the icosidodecahedron I_h	6, 9
32	*Not* the triacontahedron I_h	6, 9

[a]Octahedron − 1. This is the only instance known for which the solution is not unique: any arrangement between the limiting configurations D_{3h} and C_{4v} ($f = 0$) is admissible (see text).
[b]The *centrosymmetric* solution is the cube (see footnote *i* below).
[c]The triangular faces are *not* equilateral triangles.
[d]Trigonal prism + 3, or a completely truncated trigonal prism.
[e]The *centrosymmetric* solution is a pentagonal antiprism D_{5d}[i].
[f]$s_{\min} = 2\arccos[1 - (1/4R^2)]^{1/2}$, $16R^6 - 44R^4 + 34R^2 - 7 = 0$ (7).
[g]Icosahedron − 1. This is a rigid configuration.
[h]Böröczki (see footnote *i* below) in 1968 proved that this configuration is the *centrosymmetric* solution for $m = 14$.
[i]L. Fejes Tóth. Personal communication to O. Knop.

problem for *any* power law (9) and hence for all values of n. For any other values of m the dependence of the configuration on n must be investigated separately, since the *metric* properties of configurations with $f \neq 0$ change with n or else different ranges of n correspond to different configurations.

The case most extensively studied by rigorous methods is that of the *densest packing*, $n \to \infty$ (2, 10) (Table 2). One might expect, intuitively, that arrangements of the highest symmetry would be the solutions. This is known to be so for $m = 2$ to 6, 9, and 12 but not for $m = 7$, 8, 10, 11, 14, 20, and 24. Furthermore, the conjectured configurations (Table 3) suggest that with increasing m, arrangements of low symmetry are the likely solutions, though in some cases the proposed configurations are not far removed from configurations of the maximum possible symmetry. For $m = 5$, the solution is not unique: any configuration with three of the points on the equatorial circle, with $\pi/2 \leq s_{\min} \leq 2\pi/3$ between pairs, and with the other two points in the poles is equally valid, the limiting

TABLE 3. Conjectured configurations corresponding to the densest packing of congruent hard spheres (conjectured solutions to problem B for $n \to \infty$)

m	Configuration	Reference	m	Configuration	Reference
13	$C_{4v}(1^14^3)$	7	32	$D_5(1^15^61^1)^a$	44
14	$D_{2d}(1^14^12^24^11^1)^a$	7	33	$D_3(3^11)$	45
15	$C_3(3^5)^a$	7	35	$C_{5v}(5^310^15^2)^a$	44
16	$D_{4d}(4^4)^a$	7	36	$C_{5v}(5^310^15^21^1)^a$	44
17	$D_{5h}(1^15^31^1)^a$	40	37	$C_{5v}(1^15^310^15^21^1)^a$	44
18	$D_{4d}(1^14^11^1)^a$	41, 42	40	$D_{5h}(5^310^15^3)^a$	44
19	$C_{3v}(1^13^26^13^2)^f$	43	41	$C_{5v}(1^15^310^15^3)^a$	44
20	$D_{3h}(1^13^26^13^21^1)$	12	42	$D_{5h}(1^15^310^15^31^1)^a$	44
21	$C_3(3^7)$	11, 46	44	$T(1^13^{14}1^1)^b$	g
22	$D_4(1^14^51^1)$	11	48	$O(4^{12})$	17
23	Snub cube − 1, C_1		52	$D_5(1^15^110^45^11^1)^a$	41
25	$D_{5h}(5^5)$	40	60	Snub dodecahedron I	17
26	$C_{5v}(1^15^5)^a$	44	80	$I_h(5^{16})^c$	g
27	$D_{5h}(1^15^51^1)^a$	44	110	$C_3(1^13^{36}1^1)^d$	g
28	$C_4(4^7)$	11	120	$I(5^{24})$	17
30	$D_5(5^6)^a$	44	122	$I_h{}^e$	12
31	$C_5(1^15^6)^a$	44			

[a]Goldberg considered alternative configurations of *axial* symmetry only, of types (w^t), (1^1w^t), and $(1^1w^t1^1)$, $w = 3$, 4, or 5.
[b]This arrangement is obtained by truncating the 4-valent vertices of the rhombic dodecahedron O_h, skewing the resulting hexagonal faces about the stationary 3-valent vertices, and placing a point inside each of the spherical hexagons. Each of these points can occupy one of two equivalent positions inside the hexagon, hence a number of equivalent configurations is possible. The maximum point-group symmetry attainable is T. The minimum spherical distance $s_{min} \sim 0.5565$.
[c]Truncated icosahedron with points above the centers of the hexagonal faces.
[d]This arrangement is derived from the rhombic triacontahedron I_h in a manner analogous to the $m = 44$ case; the truncation takes place at the 5-valent vertices. A number of configurations again are possible. The maximum symmetry attainable is C_3, $s_{min} \sim 0.3508$.
[e]Obtained by central projection of the vertices, edge-midpoints, and face centers of a rhombic triacontahedron I_h onto the sphere. However, this cannot be the best arrangement (ref. 12, erratum; ref. 2, p. 233).
[f]According to ref. 48 (quoted in ref. 47) this result is not correct.
[g]R. M. Robinson. Personal communication to M. Goldberg (unpublished note).

configurations being the trigonal bipyramid D_{3h} and the square pyramid C_{4v} (≡ octahedron − 1).

In general the total number of contacts the spheres (or circles or spherical caps) make with one another, and the average number of contacts per sphere, are rough indications of the efficiency of the densest packing, a large number of contacts at fixed m corresponding to a greater efficiency. However, this is not always so, as shown by Goldberg (11) for two of his conjectured configurations for $m = 21$.

The packing density ρ_m (*cf.* problem $B(3)$) for $m \geq 3$ can be estimated from the inequalities

$$[3] \quad 1 - (1 - g)^{1/2} \leq 2\rho_m/m \leq 1 - \tfrac{1}{2}\,\mathrm{cosec}\,[(m/m - 2)(\pi/6)]$$

where $1/g = (2\sqrt{3})(m/4\pi) + 3(m/4\pi)^{2/3} + 3(m/4\pi)^{1/3}$ (12), with the concomitant condition (13) that ρ_m is always greater than $\frac{5}{4}(2 - \sqrt{2}) \sim 0.732$ except for $m = 5$, where it is equal to this quantity. For $m \to \infty$ the upper bound of ρ_m tends to $\pi/\sqrt{12} \sim 0.907$ (2, 3, 14). The estimate of the upper bound has been sharpened by Robinson (8). Also, the values of $m = 1$ to 4, 6, 8, 9, 12, 24, 48, 60, and 120 are the only ones for which an arrangement of hard congruent spheres on a central sphere can attain its maximum *local* packing density, *i.e.* each sphere will be coordinated by the maximum possible number of like spheres and in contact with them ('maximal' packing) (15). For $m > 3$ these configurations are unique.[5]

For some values of m the known configurations are not remunerative as densest packings. For example, removal of one vertex of a regular octahedron, $m = 6$, yields the C_{4v} solution for $m = 5$: d_{min} is the same in both cases and six equal spheres can therefore be accommodated on the surface of the central sphere just as easily as five. A similar situation exists for $m = 11$. This configuration is obtained by removing one vertex of the regular icosahedron. However, unlike for $m = 5$, the configuration for $m = 11$ is rigid. Robinson (17) tried to prove, unsuccessfully, the conjecture that a similar situation also exists for

[5]The case of 12 spheres congruent with the central sphere was the subject of the celebrated 'thirteen spheres' controversy of 1694 between Newton and Gregory (2, 10). The maximum number of congruent spheres in a *second* 'coordination shell' in which each sphere touches at least one sphere of the twelve, has been bracketted by Fejes Tóth and Heppes (16) between 43 and 50.

$m = 23$, 47, 49, and 119, but that for any other m, $d_{min}(m) > d_{min}(m + 1)$.

At the other end of the n range, for $n = 1$ and $m = 2$ to 8, 10, 12, and 14, the problem was investigated by Föppl (18), at Hilbert's instigation, by methods of the variational calculus. For $m = 2$–6 (D_{3h} for $m = 5$), 8, and 12 the configurations he found were identical with those for the densest packing (Table 2; for $m = 8$, see below). The other configurations he obtained were $D_{5h}(1^1 5^1 1^1)$ for $m = 7$, $D_{4d}(1^1 4^2 1^1)$ for $m = 10$, and $D_{6d}(1^1 6^2 1^1)$ for $m = 14$. He also proposed $D_{4d}(4^1 8^1 4^1)$, $D_{4d}(1^1 4^1 8^1 4^1 1^1)$, and $D_{5d}(5^1 10^1 5^1)$ as the probable best arrangements for $m = 16$, 18, and 20, respectively. From his results he abstracted the following conditions as possible minimum general requirements for a configuration of unit charges to satisfy eq. 1 for the Coulombic case, $n = 1$: (*a*) Existence of an axis of symmetry coincident with the polar axis of the sphere and of order >2 when $m > 2$. (*b*) The charges form an antipodal pair in the polar axis, or regular polygons ('rings') in the equatorial plane or planes parallel to it, or both. (*c*) Neighbouring rings are symmetrically skewed (staggered) relative to one another. (*d*) For large m the problem may not be tractable, but for $m > 14$ that satisfy the condition $m = 2p = 2 + 4q$, where p and q are primes, the probable arrangement corresponds to the partition $1^1 q^1 2 q^1 q^1 1^1$. Such values of m are 22, 46, 94, 118 etc., the difference between successive values being 24 or 48. Five or more rings would be possible for other values of m.

Föppl's configurations must be viewed as corresponding to *local* minima of $U(m,1)$ until proven by rigorous methods to correspond to global minima. The same is true of the other results available for problem *B* so far, including our own.

King (19, 20) summed the absolute values of the Coulombic *forces* acting between pairs of charges and then sought configurations for which this sum was a minimum. His solutions thus correspond to a d^{-2} *potential* and a d^{-3} *force* law, and hence to $n = 2$. Some of the f parameters of the configurations he investigated were arbitrarily fixed and only one or two of them were adjusted to find the minimum of the objective function. Consequently the validity of the resulting configurations as solutions to problem *B* for $n = 2$ cannot be viewed as established. King examined a large number of possible arrangements for $m \leq 16$ and proposed hybrid-orbital schemes with the required point-group symmetry that could be used for bonding in such arrangements.

For $m = 5$ the trigonal bipyramid D_{3h} is believed (21, 22) to yield the lowest $U(5,n)$ for *any* finite n. Specifically, $U(5,n)(D_{3h})$ is lower than the energy corresponding to the octahedron − 1, $C_{4v}(f = 0)$ configuration for any finite n. Moreover, the ratio $U(C_{4v}, f = 0)/U(D_{3h})$ tends to $\frac{4}{3}$ as $n \to \infty$, even though *geometrically* both configurations are equally valid solutions to the *densest packing* problem.

Arrangements for $1 \leq n < \infty$ have been investigated by machine computation for $m = 7$ (21, 23) and 10 (22), with the following results. For $m = 7$, computation using the method of steepest descents (21) confirmed previous results (23) except for the range $2.5 \leq n < 5.6$, where the configuration $C_2(1^1 2^3)$ was found more favourable than $C_{2v}(1^1 4^1 2^1)$, although at $n = 5$ the energy values are equal within the number of digits quoted. The energies of the C_2, C_{2v}, and C_{3v} arrangements at $n = 5.598$ are identical within the accuracy reported in ref. 21. In a similar manner Cohn (24) obtained two arrangements for $n = 1$. For $m = 9$ the result was a trigonal prism + 3, $D_{3h}(3^3)$. His configuration for $m = 11$, $C_{2v}(1^1 2^1 4^1 2^2)$, corresponds to the $B_9C_2H_{11}$ carborane skeleton and possibly also to the $B_{11}H_{11}^{2-}$ skeleton (5).

For $m = 8$ and 9 it has been stated (1, 21, 22), without proof, that the square antiprism $D_{4d}(4^2)$ and the trigonal prism + 3, $D_{3h}(3^3)$, are the respective solutions for all values of n. Indeed, the square antiprism is the solution for $n \to \infty$ and also the arrangement found by Föppl for $n = 1$ (*cf.* also ref. 25). However, the two antiprisms, when inscribed in a unit sphere, are not congruent. A similar situation exists for $m = 9$ (19).

The case of $m = 10$ has been treated by King (20) for $n = 2$ and by Lin and Williams (22) for $1 \leq n \leq 1200$. The configurations proposed by various authors for $m \geq 7$ will be discussed below, together with our own contributions to problem *B*.

C. For $0 < n < 2$ the solution for $m = 4$ is the regular tetrahedron (26, 27). The problem of finding an upper bound of V as a function of m has been investigated by Stolarski (28). For $n = 2$ *any* centrosymmetric polyhedron inscribed in the sphere is a solution (26, 27).

D. When $n = 1$ and $m = 2r$, any centrosym-

metric configuration is a solution and all of them are equally valid (29–31). When $n = 1$ and $m = 2r + 1$, all points which have no antipodal partners must lie on a great circle in such a way that any two semicircles defined by one of the points must contain the same number of points (30; for $m \leq 6$, *cf.* also ref. 31). For $n > 1$ nothing appears to be known.[6]

E. The densest-packing and the thinnest-covering requirements in E^3 (although not necessarily in other spaces, ref. 6) lead to different sets of solutions. Exceptions are the D_{3h} configuration for $m = 5$ and the configurations for $m = 2$, 3, 4, 6, and 12 of Table 2, for which the solutions to the two problems coincide (2, 6, 32);[7] these configurations are also balanced in the sense of problem *A*. The other known solutions to problem *E* are for $m = 7$ (pentagonal bipyramid D_{5h}, ref. 33), 10 (bicapped square antiprism $D_{4d}(1^14^21^1)$, refs. 34 and 35), and 14 (bicapped hexagonal antiprism $D_{6d}(1^16^21^1)$, ref. 34). Conjectured solutions have been proposed for $m = 8$ (square antiprism D_{4d}, not congruent with that of Table 2; refs. 2 and 33), 9 (trigonal prism + 3, $D_{3h}(3^3)$, refs. 34 and 35), 16 (bicapped heptagonal antiprism $D_{7d}(1^17^21^1)$, ref. 34), 20 ($D_{6h}(1^16^31^1)$ with staggered hexagons, ref. 35), and 32 (icosidodecahedron I_h, ref. 34).

It is interesting to note that the configurations for $m = 5$ to 7 are regular bipyramids, while for $m = 10$, 12, and 14 they are bicapped antiprisms.

The *centrosymmetric* solution for $m = 8$ is the hexagonal bipyramid D_{6h}.[6] Favourable centrosymmetric arrangements have been proposed for $m = 10$, 14, and 16 (34): a bicapped tetragonal prism D_{4h} with all faces inscribable in congruent circles, the rhombic dodecahedron O_h, which is also the densest *centrosymmetric* packing arrangement, and a bicapped heptagonal antiprism D_{7d}, which is possibly a solution to problem *E* for $m = 16$.

The covering density ρ_m' for $m \geq 3$ can be estimated from the inequality

$$[4] \quad 2\rho_m'/m \geq 1 - (1/\sqrt{3})\cot[(m/m - 2)(\pi/6)]$$

(3, 32). For $m \to \infty$ the lower bound of ρ_m' from eq. 4 tends to $2\pi/\sqrt{27} \sim 1.209$. This estimate has been slightly sharpened by Fejes Tóth (34). Thus there always is at least about 21% overlap of the congruent circles or caps.

F. Solutions are known for $m = 2$, 3, 4, 6, and 12. They are the same as the solutions to problems *A*, *B*, and *E* (3) and have been referred to as *perfect* distributions of 2, 3, 4, 6, and 12 points on a sphere. It is conjectured (6) that no other values of *m* admit of perfect distributions.

G. The solutions for $m = 4$ to 7 and 12 are, respectively, the regular tetrahedron, trigonal bipyramid D_{3h}, regular octahedron, pentagonal bipyramid D_{5h}, and regular icosahedron. For $m = 8$ the best solution known is a dodecadeltahedron $D_{2d}(2^4)$ with vertex coordinates ($\pm\sin 3\alpha$, 0, $\cos 3\alpha$), (0, $\pm\sin 3\alpha$, $-\cos 3\alpha$), ($\pm\sin\alpha$, 0, $\cos\alpha$), (0, $\pm\sin\alpha$, $-\cos\alpha$), $\cos^2\alpha = (15 + \sqrt{145})/40$, and faces which are not equilateral triangles (36; *cf.* also ref. 25).

H. No investigation seems to have been made of the extremal problems proposed by Whyte (4).

Present Contribution to Problem *B*

Finding the minimum of *U* by numerical computation is complicated by the existence of *local* minima. Since in general the outcome of a minimization by a given numerical technique is predetermined by the choice of starting configuration (≡ starting coordinate values), *all* the local minima must be found and compared to find the global minimum, *i.e. the* solution to problem *B*. For larger values of *m* it is impossible to be certain that all the minima have in fact been found. We feel that, in what follows, we have examined all the local minima of any importance, but we have no proof that we have not missed a local minimum which may in reality be the global minimum of *U* for a given *m* and *n*. The local minimum with the lowest value of *U* obtained will be referred to as the conjectured solution.

Computation Procedure

The problem is to minimize the objective function $U(m,n)$ of eq. 1 taking $k = 1$ (without loss of generality). The distances d_{pq} are given by

$$d_{pq}^2 = 2(1 - \sin\theta_p\cos\phi_p\sin\theta_q\cos\phi_q - \sin\theta_p\sin\phi_p\sin\theta_q\sin\phi_q - \cos\theta_p\cos\theta_q)$$

where θ_p and ϕ_p are the polar and azimuthal angles, respectively, of point *P* in the spherical polar coordinate system with $r = 1$ (without loss of generality). Three degrees of freedom can be eliminated by fixing a rotational origin. One

[6] L. Fejes Tóth. Personal communication to O. Knop.

[7] For $m = 3$ the solution is not unique: the three points are on a great circle but are not necessarily equally spaced.

point and one additional ϕ coordinate can be fixed, leaving $2m - 3$ degrees of freedom for the minimization.

A computer algorithm for minimizing U was written using a modification of a rank one (R1) optimization procedure originally due to Davidon (37[8]–39). This procedure has two distinct advantages over the steepest-descents procedure used by previous authors (21, 22). In general, the convergence of the R1 procedure becomes quadratic near the local minimum, while the convergence of a steepest-descents procedure remains first-order. For our problem the R1 procedure has a special advantage in that it tends to find solutions of low symmetries, which are the most difficult ones to predict. In the steepest-descents procedure a symmetry element, once gained, will be retained from then on, whereas in the R1 procedure symmetry elements can only be gained asymptotically, allowing both the configuration and the positive-definite matrix associated with the procedure, to gain the symmetry element together.

For each value of m an initial configuration containing no symmetry elements was generated by placing the m points on an approximate spiral. Starting from this configuration, $U(m,n)$ was minimized, using all $2m - 3$ degrees of freedom, for two or three values of n. The dependence on n of $U(m,n)$ for the resulting configuration was then examined, within the symmetry constraints of that configuration, using a minimum set of f variable coordinates that describe the configuration. This procedure, also used by Lin and Williams (22), greatly reduces the number of degrees of freedom and the computer time required. For practical reasons the maximum value of n was taken as 400 throughout except for $m = 15$, where it was 1000.

In addition to arrangements found as a result of the minimization using all $2m - 3$ degrees of freedom, $U(m,n)$ of a number of other configurations was minimized within the symmetry constraints of the individual configurations, as above. The values of the coordinates of configurations at the minimum of $U(m,n)$ were then taken as the initial values in a minimization using all $2m - 3$ degrees of freedom at one or more values of n. If the first derivatives of $U(m,n)$ with respect to all $2m - 3$ variables were zero,[9] the configuration was deemed a local minimum and its $U(m,n)$ was then compared with other local minima for the same m and n obtained in the process.

As m becomes large, the number of such symmetry-restricted configurations becomes large. It was then impractical to examine more than a small number of likely-looking arrangements. The configurations investigated (Table 4)[10] contained at least a plane of symmetry and included the configurations conjectured by Föppl (for $n = 1$) and by other authors (for $n \to \infty$, *cf.* Table 3) as solutions of problem *B* for $m \leq 16$.

Results

The arrangements found for $m = 5$ to 16 and the ranges of n in which they are conjectured solutions, are presented in Table 5 and Figs. 1 and 2. In quoting the values (in radians) of the coordinates (θ_p,ϕ_p), the points are numbered as in Fig. 1; $\theta = 0$ corresponds to the north pole and ϕ is measured clockwise from the $+x$ axis of the projection. The θ_p,ϕ_p values at minimum U are listed only for the configurations of Table 5 and then only for one or two representative values of n (Table 6).[10] Variation with n of the minimized energies U of competing configurations is presented, in Figs. 4 to 11, in terms of the ratio $R = U(\text{LMC})/U(\text{reference})$; LMC stands for local-minimum configuration. For U(reference) the symmetry arrangement that is the conjectured solution at $n \to \infty$ is usually employed.

$m = 5$

While the fixed configuration $C_{4v}(f = 0)$ gives a U value which is higher than $U(D_{3h})$ for *any* n (*cf.* above), a C_{4v} configuration with one degree of freedom becomes more favourable than D_{3h} when n exceeds 15.04808, contrary to common belief. The values of the ratios $U(C_{4v}, f = 1)/U(D_{3h})$ and $U(C_{4v},f = 0)/U(C_{4v},f = 1)$ tend to $\frac{2}{3}$ and 2 respectively as $n \to \infty$ (Fig. 4). The minimum of $U(D_{3h})/U(C_{4v},f = 1)$ is at $n \sim 8$. Variation of $\theta_2(C_{4v},f = 1)$ with $1/n$ is shown in Fig. 3.

$m = 6$ and 12

As stated above, the regular octahedron $O_h(1^14^11^1)$ $(f = 0)$ and icosahedron $I_h(1^15^21^1)$ $(f = 0)$ are the respective solutions for all values of n. Figure 5 shows how their $U(m,n)$ vary with n relative to some LMC's.

[8]For discussion of some modifications, see refs. 38 and 39.

[9]Any value less than $10^{-7} \times U$ was considered zero.

[10]This table is available upon request, at a nominal charge, from the Depository of Unpublished Data, CISTI, National Research Council of Canada, Ottawa, Canada K1A 0S2.

TABLE 5. Configurations and validity ranges of n corresponding to the lowest $U(m,n)$ values obtained by computer treatment in this work

m	n	Configuration[a]	d_{min}[b]
5	1		
		Trigonal bipyramid, $D_{3h}(1^1 3^1 1^1)(f = 0)$	d_{12}
	15.04808		
		Square pyramid, $C_{4v}(1^1 4^1)(f = 1)$	$d_{22'}$
	400		
7	1		
		Pentagonal bipyramid, $D_{5h}(1^1 5^1 1^1)(f = 0)$	$d_{22'}$
	~2.00		
		$C_2(1^1 2^3)(f = 5)$	$d_{44'}$
	~5.00		
		$C_{2v}(1^1 4^1 2^1)(f = 3)$	$d_{33'}$
	5.59791		
		$C_{3v}(1^1 3^2)(f = 2)$	d_{12}
	400		
8	1–400	Square antiprism, $D_{4d}(4^2)(f = 1)$	$d_{11'}$
9	1–400	Trigonal prism + 3, $D_{3h}(3^3)(f = 1)$	d_{12}
10	1		
		Bicapped square antiprism, $D_{4d}(1^1 4^2 1^1)(f = 1)$	d_{12}
	8.22402		
		Singly-capped trigonal 'prism', $C_{3v}(1^1 3^3)(f = 3)$	[c]
	24.91438		
		$C_{2v}(2^1 4^1 2^2)(f = 5)$	$d_{22'}$
	400		
11	1		
		$C_{2v}(1^1 2^1 4^1 2^2)(f = 5)$	[d]
	6.16566		
		Singly-capped pentagonal 'antiprism', $C_{5v}(1^1 5^2)(f = 2)$	$d_{33'}$
	400		
13	1		
		$C_{2v}{}^{(1)}(1^1 2^2 4^1 2^2)(f = 6)$	d_{12}
	19.95657		
		$C_{2v}{}^{(2)}(1^1 4^1 2^1 4^1 2^1)(f = 6)$	[e]
	24.70475		
		$C_{4v}(1^1 4^3)(f = 3)$	d_{12}
	400		
14	1		
		$D_{4h}(1^1 4^3 1^1)(f = 1)$	d_{12}
	21.66607		
		$D_{2d}(1^1 4^1 2^2 4^1 1^1)(f = 3)$	d_{23}
	400		
15	1		
		$D_3(3^5)(f = 4)$	d_{24}
	34.02794		
		$C_s(1^1 2^2 1^1 2^3 1^1 2^1)(f = 14)$	[f]
	1000		
16	1–400	$D_{4d}(4^4)(f = 2)$	d_{23}

[a] See Fig. 1.
[b] d_{pq} and its symmetry equivalents in Fig. 1.
[c] d_{12} (~2.824 > n), d_{23} (~2.824 < n).
[d] $d_{33'}$ (~2.872 > n), d_{12} (~2.872 < n).
[e] $d_{44'}$ (~7.768 > n), d_{12} (~7.768 < n).
[f] $d_{77'}$ (~36.86 > n), d_{68} (~36.86 < n).

m = 7

The result obtained by Föppl (18) for $n = 1$ was confirmed but a few minor discrepancies were discovered in the work of Claxton and Benson (21). The cross-over values of n, at which the conjectured solution changes configuration, given by the latter authors have been sharpened. A comparison of values of $U(5,n)$ at the minimum for different configurations is shown in Fig. 6. The C_2 configuration is a local minimum

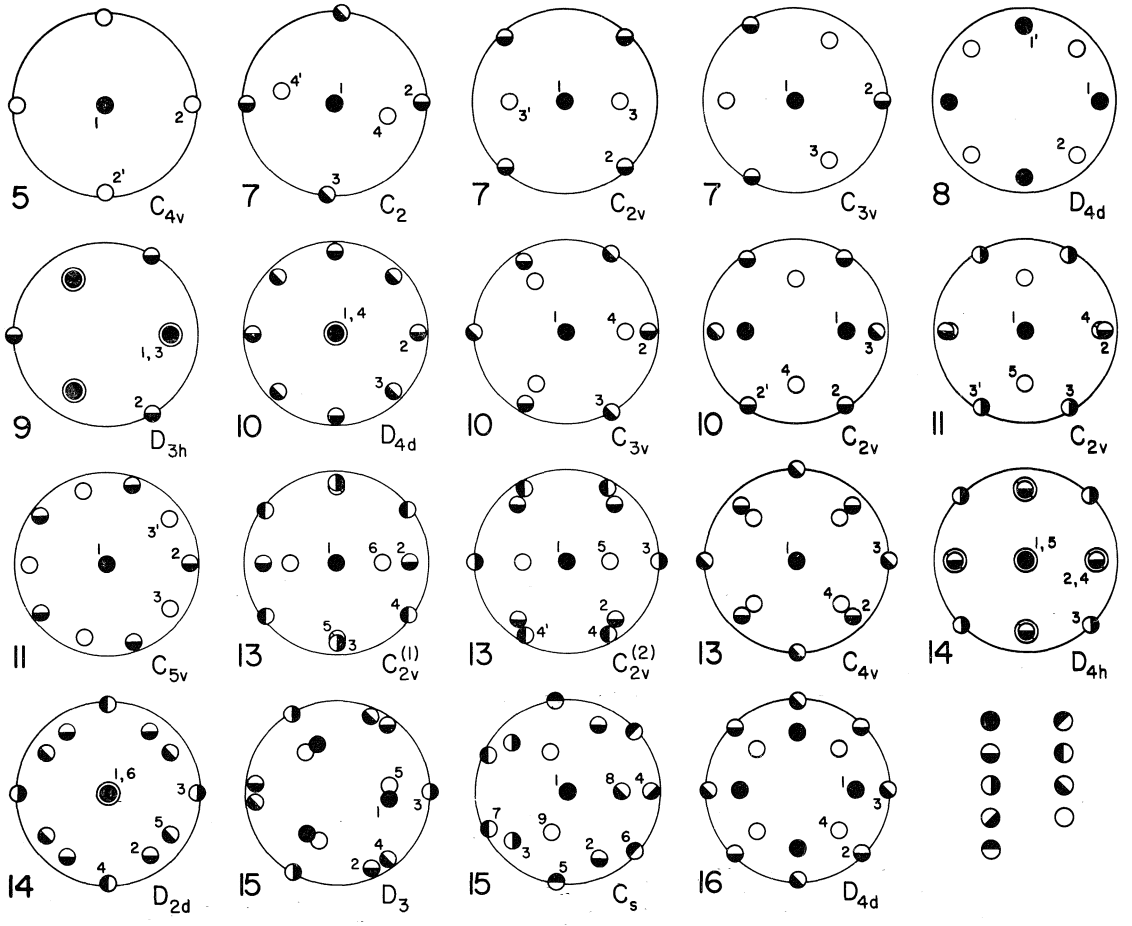

FIG. 1. Parallel projections, along the principal axis of symmetry, of the configurations of Table 5. The coordinates of the highest point on the sphere (the 'north pole') are $\theta = 0$, $\phi = 0$. The points are numbered in the increasing order of θ; the numbering corresponds to that in the text.

in a restricted range of n only. As n decreases, this configuration approaches D_{5h} symmetry and becomes asymptotically indistinguishable from the D_{5h} configuration to one part in 10^{12} in U by $n = 2.00$ and to 1×10^{-8} rad in angular coordinates by $n = 1.84$. With increasing n the C_2 configuration approaches C_{2v} symmetry and becomes asymptotically indistinguishable from the C_{2v} configuration to one part in 10^{12} in U by $n = 4.88$ and to 1×10^{-8} rad in angular coordinates by $n = 5.00$. The C_{2v} configuration remains the lowest minimum ($\equiv$ conjectured solution) until $n \sim 5.59791$, at which point (A of Fig. 6) the C_{3v} configuration becomes the conjectured solution. The angular data given for C_2 by Claxton and Benson (21) were confirmed at $n = 4.0$ but could not be reproduced at $n = 2.0$ and 5.6. Their data for the C_{2v} and C_{3v} configurations were confirmed at these n values.

m = 8

The square antiprism $D_{4d}(4^2)(f = 1)$ is the best arrangement for all values of n (Figs. 3 and 5), confirming previous conjecture.

m = 9

The best arrangement for all values of n is the trigonal prism + 3, $D_{3h}(3^3)(f = 1)$ (Fig. 3), confirming earlier conjectures. At $n = 1$, $\theta_1 \sim 0.790277$, in complete agreement with ref. 24.

m = 10

The three arrangements reported by Lin and Williams (22) have been confirmed and the crossover values of n sharpened (Figs. 3 and 7).[11] The configurations for $n = 1$ and 400 agree with

[11]The angular data given by Lin and Williams for the C_{3v} configuration at $n = 100$ are in fact the correct data for $n = 200$. The value of $U(C_{3v})$ given for $n = 100$ is correct.

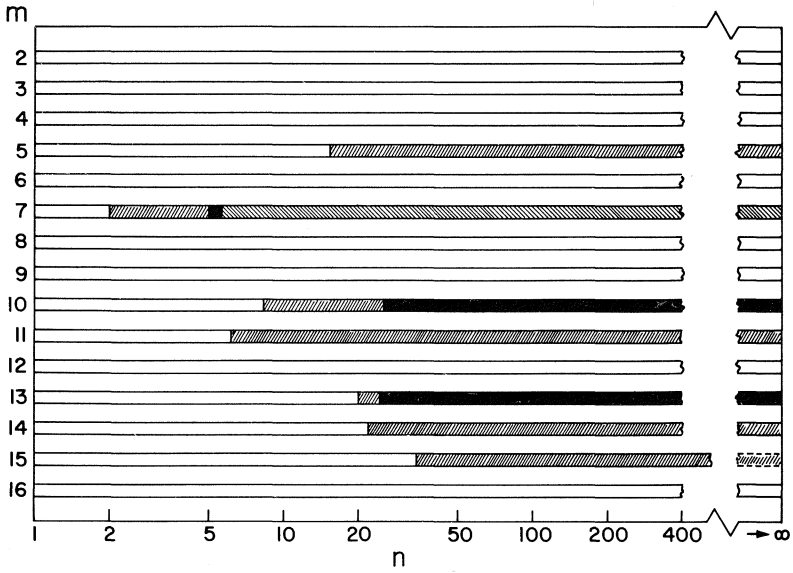

FIG. 2. Synoptic presentation of the ranges of n (on an $n^{-1/2}$ scale) for the solutions, or conjectured solutions, to problem *B*.

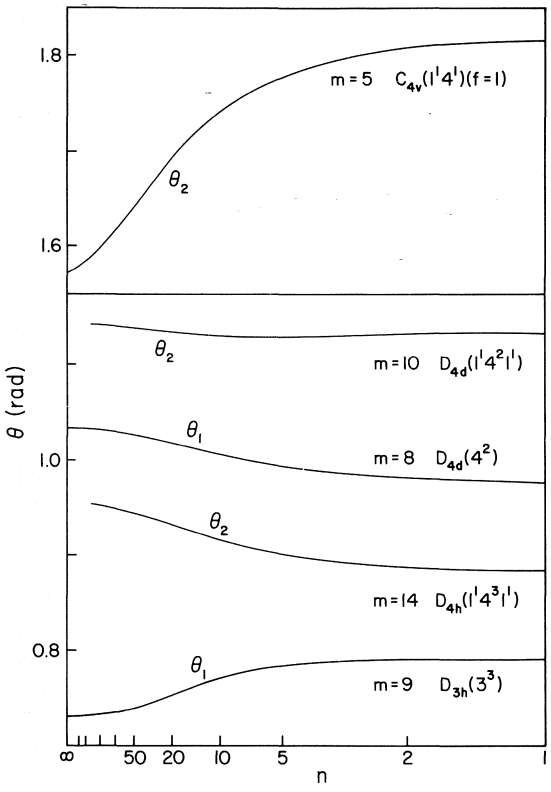

FIG. 3. Variation of θ (rad) with $n^{-1/2}$ for the one-parameter ($f = 1$) configurations of Table 5 at minimized U.

those proposed by Föppl and by Danzer (for $n \to \infty$), respectively.

m = 11

Contrary to the conjecture of Lin and Williams (22) that the densest-packing solution persists for *all* values of n, *two* configurations are solutions at different values of n. At low values, the best arrangement was found to be the $C_{2v}(1^12^14^12^2)$ ($f = 5$) configuration reported for $n = 1$ by Cohn (24), whose numerical results were confirmed. At larger values of n the configuration of minimum $U(11,n)$ is the singly-capped pentagonal 'antiprism' $C_{5v}(1^15^2)(f = 2)$ (Fig. 8); this configuration approaches the icosahedron − 1, $C_{5v}(1^15^2)(f = 0)$ as $n \to \infty$ (*cf.* Table 2). Better than $C_{5v}(1^15^2)(f = 2)$ at low values of n, but not as good as $C_{2v}(1^12^14^12^2)$, is a hitherto unreported configuration of low symmetry, $C_s(1^12^21^12^21^1)$ ($f = 10$). This configuration takes on C_{5v} symmetry at $n \sim 6.144$ and continues with this symmetry for larger values of n (*cf.* inset, Fig. 8).

m = 13

Of the three conjectured solutions found (Figs. 1 and 9), that for large values of n coincides with the $C_{4v}(1^14^3)$ arrangement proposed for $n \to \infty$ by Schütte and van der Waerden (7). The two C_{2v} configurations have not been reported previously.

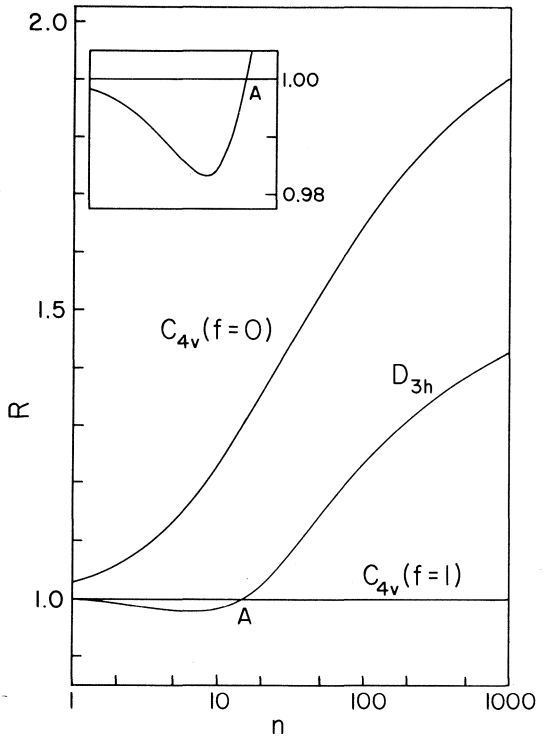

FIG. 4. Variation of $R = U(\text{LMC})/U(C_{4v}, f = 1)$ with $\log n$, $m = 5$. Inset: $U(D_{3h})/U(C_{4v}, f = 1)$ on an expanded scale.

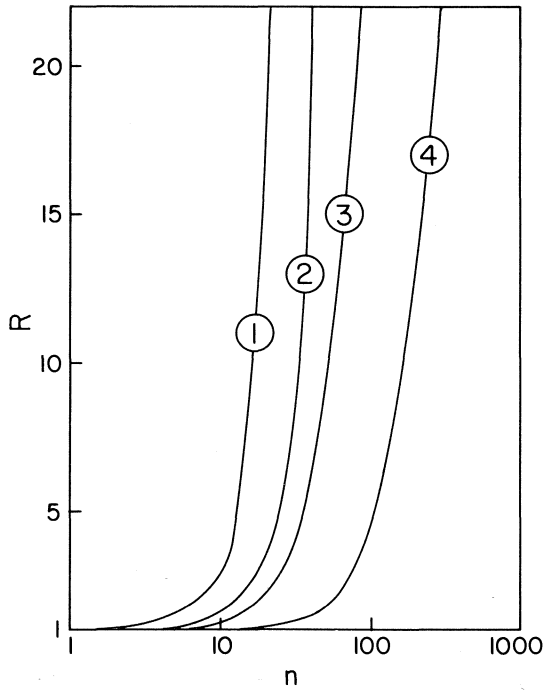

FIG. 5. Variation of $R = U(\text{LMC})/U(\text{MC})$ with $\log n$, $m = 6$, 8, and 12. (*1*) $m = 6$, $U(C_{5v}, f = 1)/U(O_h)$. (*2*) $m = 6$, $U(D_{3h}, f = 1)/U(O_h)$ (trigonal prism *vs.* octahedron). (*3*) $m = 8$, $U(\text{cube } O_h, f = 0)/U(D_{4d}, f = 1)$; $m = 12$, $U(\text{cuboctahedron } O_h, f = 0)/U(I_h, f = 0)$. The two curves are indistinguishable on the scale of this drawing. (*4*) $m = 8$, $U(D_{2d}, f = 2)/U(D_{4d}, f = 1)$.

m = 14

The bicapped hexagonal antiprism $D_{6d}(1^1 6^2 1^1)$ ($f = 1$) found by Föppl for $n = 1$ turned out not to be the best configuration at low n, a bicapped square prism + 4, $D_{4h}(1^1 4^3 1^1)$ ($f = 1$), being better for $n < 21.66607$ (Figs. 1 and 10). At high exponents the D_{2d} configuration proposed by Schütte and van der Waerden (7) for $n \rightarrow \infty$ was confirmed. Interestingly, with decreasing n this configuration became worse than the bicapped hexagonal antiprism at $n \sim 12.60203$ and then disappeared as a local minimum in favour of the latter at $n \sim 11.5110$ (point *C*, Fig. 10). The rhombic dodecahedron $O_h(1^1 4^3 1^1)(f = 0)$ is not the solution at any n.

m = 15

At small values of n the best arrangement is $D_3(3^5)(f = 4)$ (Fig. 11). The $C_3(3^5)$ arrangement proposed by Schütte and van der Waerden (7), in which the central plane of three points is not the equatorial plane, is better than the $D_3(3^5)(f = 4)$ configuration for large n and converges to the D_3 arrangement as n decreases; at $n \sim 54.268$ the U values are indistinguishable to within one part in 10^{12} and the coordinates to within 1.0×10^{-6} rad. However, a new, low-symmetry configuration $C_s(1^1 2^2 1^1 2^3 1^1 2^1)(f = 14)$ was found to be better than both $D_3(3^5)$ and $C_3(3^5)$ for $n > 34.027944$. As n becomes large, the energies of the C_3 and C_s configurations approach each other again and it appears that they might cross over in the range of $n \sim 2000$, which would agree with Schütte and van der Waerden's proposal that C_3 is the solution for $n \rightarrow \infty$.

m = 16

The best arrangement for all values of n is $D_{4d}(4^4)$ ($f = 2$). This is in agreement with the configuration proposed for $n \rightarrow \infty$ by Schütte and van der Waerden but not with Föppl's proposal, $D_{4d}(4^1 8^1 4^1)$, for $n = 1$. The minimized value of U of $D_{4d}(4^1 8^1 4^1)(f = 1)$ exceeds that of $D_{4d}(4^4)(f = 2)$ by about 0.33% at $n = 1$, by 2.6% at $n = 2$, and by 7% at $n = 4$.

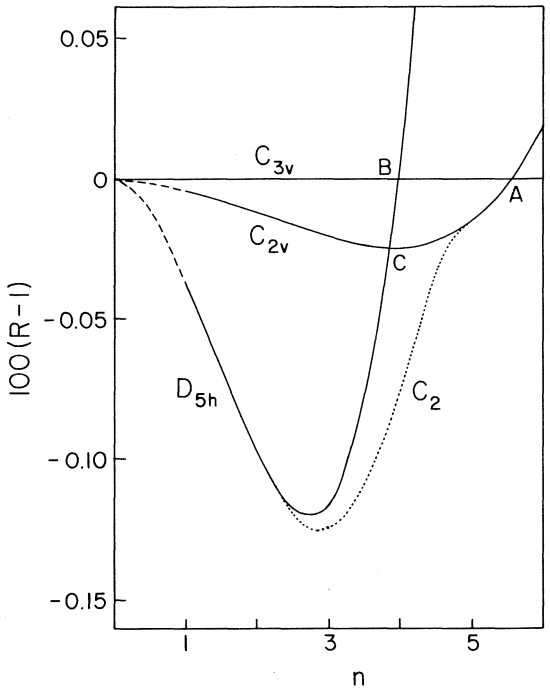

FIG. 6. Variation of $R = U(\text{LMC})/U(C_{3v}, f = 2)$ with n, $m = 7$; $n(A) \sim 5.59791$, $n(B) \sim 3.96$ (this work); $n(C) \sim 3.84165$ (ref. 21).

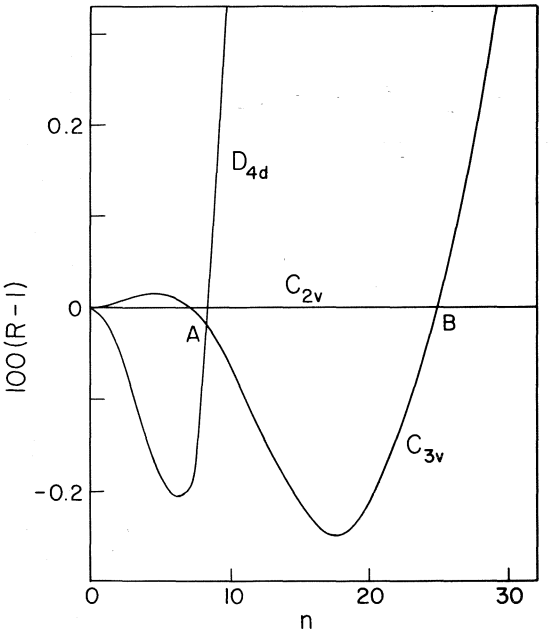

FIG. 7. Variation of $R = U(\text{LMC})/U(C_{2v}, f = 5)$ with n, $m = 10$; $n(A) \sim 8.22402$, $n(B) \sim 24.91438$.

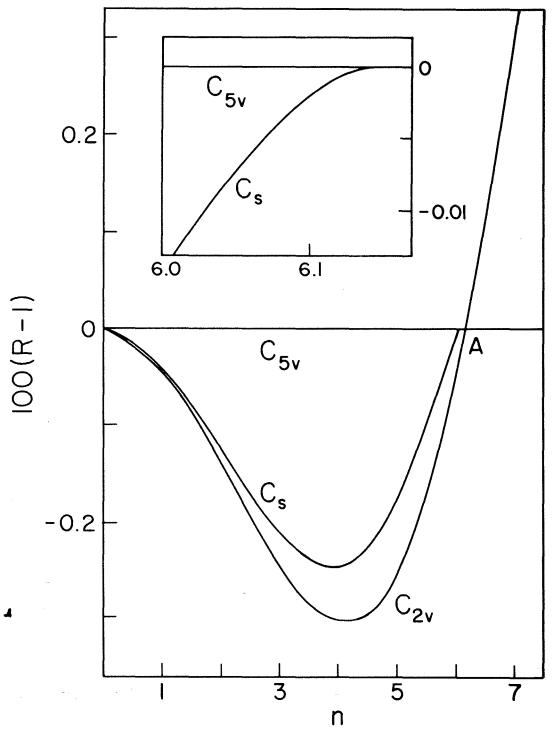

FIG. 8. Variation of $R = U(\text{LMC})/U(C_{5v}, f = 2)$ with n, $m = 11$; $n(A) \sim 6.16566$. Inset: $U(C_s)/U(C_{5v})$ on an expanded scale.

Some Observations on the Results

With one exception the configurations obtained at $n = 400$ always agree with the known or conjectured solutions of problem B for $n \to \infty$, and the $d_{\min}$ and ρ_m values at $n = 400$ and $n \to \infty$ differ, on the average, by only about 0.1–0.2% and by much less for some values of m (Table 7).[10] It is therefore assumed that the configurations listed for $n = 400$ in Table 5 remain valid for $n > 400$. The exception is $m = 15$, where U was minimized up to $n = 1000$, with the result described above.

The configuration found by Föppl for $m = 14$, $n = 1$, does not correspond to the lowest $U(14,1)$, and his prediction of the best configuration for $m = 16$, $n = 1$, has turned out to be wrong. It would seem that his prescription contains too much symmetry, while the solutions to problem B at $n = 1$, and at other values of n, tend to lose elements of high symmetry as m increases.

For $n \to \infty$, where geometrical arguments can be employed, a number of conjectured configurations have been proposed (Table 3). How-

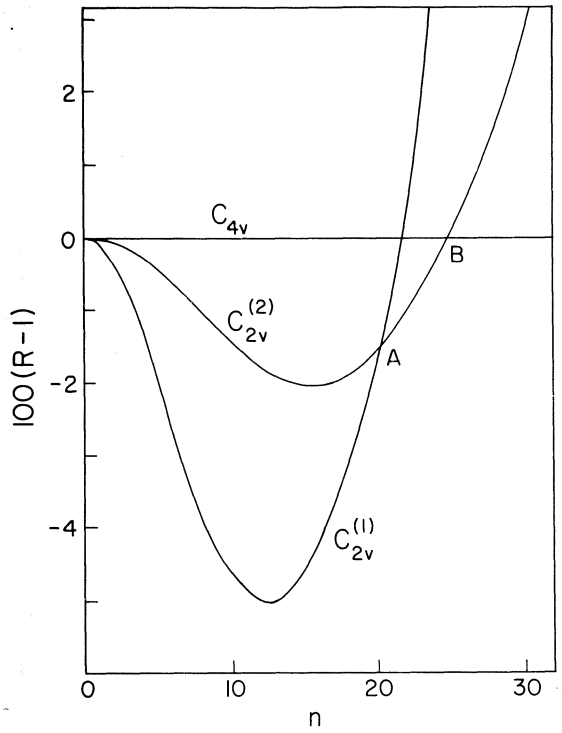

FIG. 9. Variation of $R = U(\text{LMC})/U(C_{4v}, f = 3)$ with n, $m = 13$; $n(A) \sim 19.95657$, $n(B) \sim 24.70475$.

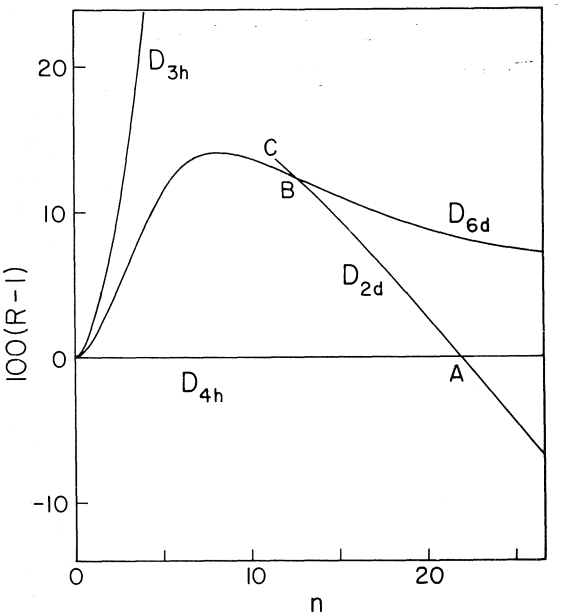

FIG. 10. Variation of $R = U(\text{LMC})/U(D_{4h}, m = 3)$ with n, $m = 14$; $n(A) \sim 21.66607$, $n(B) \sim 12.60203$, $n(C) \sim 11.5110$.

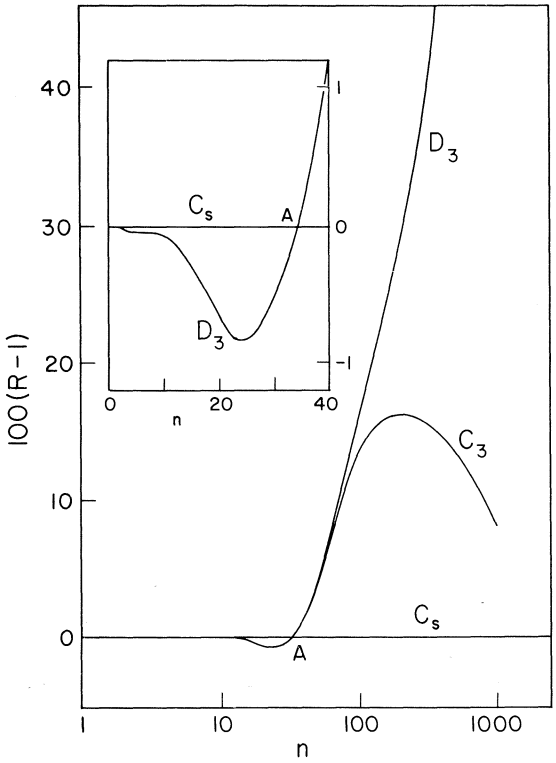

FIG. 11. Variation of $R = U(\text{LMC})/U(C_s, f = 14)$ with $\log n$, $m = 15$; $n(A) \sim 34.02794$.

ever, for *finite* values of n no method of predicting the best configurations for $m > 16$ seems to exist, and the irregular distribution of the cross-over points for $m < 16$ (Fig. 2) makes the possibility of prediction of the validity ranges seem quite remote.

The difference in U between the best and the next-best configurations for a given m,n pair is sometimes very small. Noteworthy are the $D_{5h}|C_2$ and $C_{2v}|C_2$ pairs ($m = 7$) in the $n = 2$ to 5 range (Fig. 6), the triplet $D_{4d}|C_{3v}|C_{2v}$ ($m = 10$) in the region of point A ($n \sim 9$, Fig. 7), the $C_{2v}|C_2$ pair ($m = 11$) between $n = 1$ and 3 and between $n = 5$ and 6, and $D_3|C_s$ ($m = 15$) between $n = 1$ and 10. In the Coulombic case in particular the differences in U between local-minimum and best configurations are seldom pronounced. At the cross-over points the dependence of the arrangement on n is of course critical.

Variation of the *mean* energy of interaction between two charges,

$$[5] \qquad \bar{U}(m,n) = \left[U(m,n) \Big/ \left(\frac{m}{2}\right) \right]^{1/n}$$

in the best configurations is shown in Fig. 12.

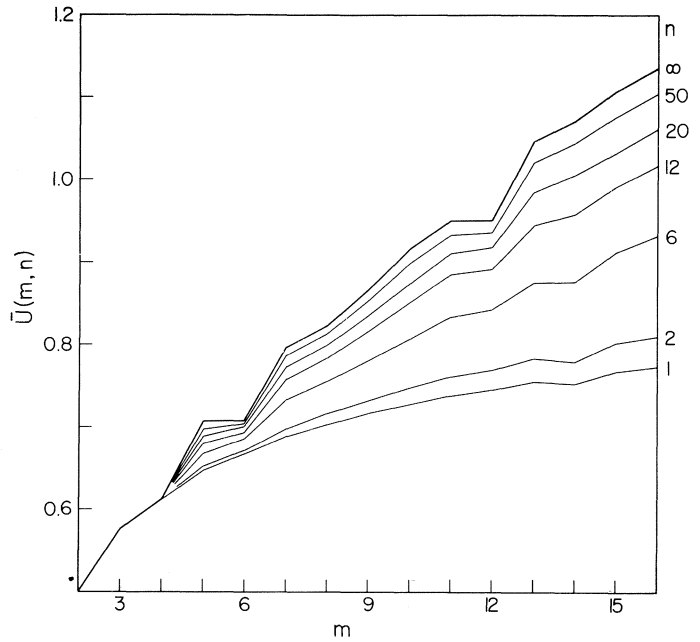

FIG. 12. Variation of the mean energy of interaction $\bar{U}(m,n)$ between two charges in the configuration of minimum $U(m,n)$ (*cf.* eq. 5).

Summary

In this paper we have reviewed the various formulations of a number of extremal problems associated with point charges on the surface of a sphere in E^3 which have appeared in the literature to date. We have summarized existing results for these problems and presented new results for one of these, problem *B*. In that case we have found new solutions for 5, 11, 13, 14, 15, and 16 point charges. We have also sharpened the existing results for $m = 7$ and 10.

Acknowledgments

We thank Professor L. Fejes Tóth and Dr. M. Goldberg for helpful comments on the subject, and the National Research Council of Canada for financial assistance.

NOTE ADDED IN PROOF

The following results reached us too late to be incorporated in the body of the text.

B. In many, though not all, of the previously reported configurations for $n \to \infty$, p of the vertices are arranged on a spiral with the North–South line as axis. Rotating the spiral successively by $2\pi/k$ about this axis produces a set of kp vertices; one or two additional vertices may be located at the poles, giving rise to $m = kp$, $kp + 1$, or $kp + 2$ and configurations of axial (rotational) symmetry C_k or D_k. This observation was used by Karabinta (46, 49)[12] and by Székely (47) to generate, and optimize by computer, a number of conjectured configurations (Table 8), some of them supplanting previous proposals, others for values of m considered for the first time. In a few cases the proposed configurations do not follow the principle of the spiral completely, in that extra points can be accommodated on the sphere in a manner inconsistent with the order of rotation of the generating spiral (*e.g.* for $m = 35$, 40, 59).

It is noteworthy that, when Székely (47) replaced the configuration $C_3(3^{15})$ proposed for $m = 45$ in ref. 46, by an improved configuration $C_4(1^14^{11})$, $s_{\min}$ increased by less than 0.04%, in spite of the complete change of rotational symmetry. This, together with similar though somewhat larger increases for several other m in ref. 47, indicates that with increasing m there will be an increasing number of local extrema and an increasing probability that the global minimum will be of low symmetry, parallelling our findings for small m and intermediate n values. This raises the question of whether a construction principle which presupposes rotational symmetry of order 3 or higher does not from the outset lead to

[12]Reference 49 quoted in refs. 46, 47.

TABLE 8. Supplement to Table 2

m	Configuration	Reference	Supplants reference	m	Configuration	Reference	Supplants reference
17*		49	40	44	C_4 or $D_4(4^{11})$†	46, 49	¶
25	$C_4(1^14^6)$	47	40	45	$C_4(1^14^{11})$	47	46
28	$C_3(1^13^9)$	47	11	50	$D_3(1^16^81^1)$	47	
29	$C_4(1^14^7)$	47		51	$C_5(1^15^{10})$	47	46
34	$C_{3v}(1^16^53^1)$	47		52	$D_5(1^15^{10}1^1)$	47	41
35	$C_{2v}(1^16^54^1)$‡	47	44, 46	53	$C_4(1^14^{13})$	47	
36	C_3 or $D_3(3^{12})$†	46, 49	44	54	C_4 or $D_4(1^14^{13}1^1)$†	47	
37	$C_3(1^13^{12})$	47	44	55	C_5 or $D_5(5^{11})$†	47	
38	$D_{6d}(1^16^61^1)$	47		56	C_6 or $D_6(1^16^91^1)$†	47	
39	C_3 or $D_3(3^{13})$†	46, 49		58	$D_7(1^17^81^1)$	47	
40	$C_3(1^16^63^1)$	47	44, 46	59	$(3^{19}2^1)$§	47	
41	$C_5(1^15^8)$	47	44	60	$C_3(3^{20})$	47	17
42	$D_5(1^15^81^1)$	47	44, 49				

*We have not seen ref. 49; the result is quoted in Table 2 of ref. 47.
†It is not clear from the description in the original paper which point-group symmetry applies.
‡Or $C_{2v}(1^16^52^2)$?
§The configuration is not shown in the original paper.
¶R. M. Robinson. Private communication to M. Goldberg.

configurations containing too much symmetry and not likely to correspond to a global minimum of U.

The Tammes problem has been generalized by Molnár (50 and refs. therein), who introduced the idea of *space-claim*, SC. The SC is a domain associated with each of the m congruent circles C to be packed on the sphere. It consists of one or more circles tangent to C, congruent or incongruent among themselves, though in general the SC can be an arbitrary point set (51). An SC may overlap other SC's but not the C's; it may be viewed as a domain of influence (exclusion) of its C. For one SC per circle the centres of the C's in the extremal arrangements are at the vertices of the five convex Platonic solids, m = 4, 6, 8, 12, 20; the snub cube $O(4^6)$, m = 24; and the snub dodecahedron $I(5^{12})$, m = 60. For two congruent SC's per circle, with all three centres on a great circle, the cuboctahedron $O_h(4^3)$ and the icosidodecahedron $I_h(5^210^15^2)$ are the solutions for m = 12 and 30, respectively. For three SC's per C, two of them congruent and the third smaller, the truncated icosahedron $I_h(5^210^45^2)$ is the solution for m = 60. The icosidodecahedral arrangement for m = 30 and two nonisomorphic arrangements of I_h symmetry constructed by Molnár for m = 180 appear to correspond with the disposition of the features visible on the surface of certain spherical viruses. Molnár remarks that the symmetry of these packings for m = 180 is the direct consequence of the "economy principle", *i.e.* the densest-packing requirement.

The notion that the surface structure of small spherical viruses may be related to the Tammes problem was first explored by Goldberg (44).

C. Computer solutions for n = 1 and m = 5 to 10 have recently been reported by Berman and Hanes (52). The respective configurations coincide with the solutions to B for n = 1 (Table 5) except at m = 7, for which the configuration is a pentagonal bipyramid $C_1(1^7)$ having no symmetry but closely approaching $C_s(1^12^11^12^11^1)$. The $V(7, 1)$ of the $C_1(1^7)$ arrangement differs by only 0.001% from that of the $D_{5h}(1^15^11^1)$ configuration. It is interesting to compare this situation with the configurations of minimum $U(7, n)$ under B (Table 5 and Fig. 6): the configuration corresponding to $U(7, 1)_{\min}$, $D_{5h}(1^15^11^1)$, goes over smoothly into $C_2(1^12^3)$ as n increases, the difference of $U(7, 2.4)$ for the two configurations being less than 0.0007%. The θ_1 value for m = 8, 0.9659 rad, is *below* that of the $D_{4d}(4^2)$ configuration of B for any $n \geq 1$, while θ_1 for m = 9, 0.7911 rad, is *above* that of the $D_{3h}(3^3)$ configuration of B for any $n \geq 1$. For m = 10, the $V(10, 1)$ value quoted in ref. 52 yields a θ_1 comparable with that of the $D_{4d}(1^14^21^1)$ configuration of B at $n \sim 200$.

An estimate of the upper bound of $V(m, 1)$ is given in ref. 53. Additional references relating to C are 53–56.

G. Klee has conjectured that the solution for m = 9 is an augmented trigonal prism $D_{3h}(3^3)$. This configuration has been optimized by Schoen (57):

$$\theta_1 = \arccos [1 - (4/3)c^2]^{1/2} = 0.8213275 \text{ rad}$$

where

$$c = 2(a^2 + b^2)^{1/6} \cos \{[\pi - \arctan(-b/a)]/3\} - (4\sqrt{3})/9$$

$$a = -(121\sqrt{3})/972$$

and

$$b = [(41/54)^3 - 3(121/972)^2]^{1/2}$$

The θ_1 is greater than the corresponding θ_1 for B for any $n \geq 1$.

We thank Professor V. Klee, Dr. M. Goldberg, and Professor L. Fejes Tóth for drawing our attention to the additional references.

1. R. J. Gillespie. Molecular geometry. Van Nostrand Reinhold Co., London. 1972.
2. L. Fejes Tóth. Regular figures. Pergamon-Macmillan, New York. 1964.
3. L. Fejes Tóth. Lagerungen in der Ebene, auf der Kugel und im Raum. 2nd ed. Springer, Berlin. 1972.
4. L. L. Whyte. Am. Math. Monthly, **59**, 606 (1952).
5. E. L. Muetterties and C. M. Wright. Q. Rev. **21**, 109 (1967).
6. L. Fejes Tóth. Period. Math. Hung. **1**, 25 (1971).
7. K. Schütte and B. L. van der Waerden. Math. Ann. **123**, 96 (1951).
8. R. M. Robinson. Math. Ann. **144**, 17 (1961).
9. J. Leech. Math. Gaz. **41**, 81 (1957).
10. H. S. M. Coxeter. Trans. N.Y. Acad. Sci. (II), **24**, 320 (1962).
11. M. Goldberg. Ann. Univ. Sci. Budap. Sect. Math. **12**, 137 (1969).
12. B. L. van der Waerden. Math. Ann. **125**, 213 (1952); **152**, 94 (1963).
13. J. Molnár. Matem. Lapok, **4**, 113 (1953).
14. L. Fejes Tóth. Jahresber. Deutsch. Math.-Ver. **53**, 66 (1943).
15. L. Fejes Tóth. Stud. Sci. Math. Hung. **4**, 441 (1969).
16. L. Fejes Tóth and A. Heppes. Can. J. Math. **19**, 1092 (1967).
17. R. M. Robinson. Math. Ann. **179**, 296 (1969).
18. L. Föppl. J. Reine Angew. Math. **141**, 251 (1912).
19. R. B. King. J. Am. Chem. Soc. **92**, 6455 (1970).
20. R. B. King. J. Am. Chem. Soc. **92**, 6460 (1970).
21. T. A. Claxton and G. C. Benson. Can. J. Chem. **44**, 157 (1966); **44**, 1730 (1966).
22. Y. C. Lin and D. E. Williams. Can. J. Chem. **51**, 312 (1973).
23. D. Britton. Can. J. Chem. **41**, 1632 (1963).
24. H. Cohn. Math. Tables Aids Comput. **10**, 117 (1956).
25. M. Goldberg. Math. Comput. **23**, 785 (1969).
26. L. Fejes Tóth. Acta Math. Acad. Sci. Hung. **7**, 397 (1957).
27. E. Hille. J. Aust. Math. Soc. **6**, 122 (1966).
28. K. B. Stolarsky. Proc. Am. Math. Soc. **35**, 547 (1972); **41**, 575 (1973).
29. G. Sperling. Arch. Math. **11**, 69 (1960).
30. F. Nielsen. Nord. Mat. Tidskr. **13**, 45 (1965).
31. L. Fejes Tóth. Acta Math. Acad. Sci. Hung. **10**, 13 (1959).
32. L. Fejes Tóth. Mat. Fiz. Lapok, **50**, 40 (1943).
33. K. Schütte. Math. Ann. **129**, 181 (1955).
34. G. Fejes Tóth. Stud. Sci. Math. Hung. **4**, 225 (1969).
35. E. Jucovič. Mat.-Fyz. Čas. Slovenske Akad. Vied, **10**, 99 (1960).
36. J. D. Berman and K. Hanes. Math. Ann. **188**, 78 (1970).
37. W. C. Davidon. A.E.C. Res. Dev. Rept. ANL 5990 (1959); Comp. J. **10**, 406 (1968).
38. M. C. Biggs. J. Inst. Math. Appl. **8**, 315 (1971).
39. J. W. Daniel. The approximate minimization of functionals. Prentice-Hall, Inc., Englewood Cliffs, NJ. 1971.
40. E. Jucovič. Mat.-Fyz. Čas. Slovenske Akad. Vied, **9**, 173 (1959).
41. J. Strohmajer. Ann. Univ. Sci. Budap. Sect. Math. **6**, 49 (1963).
42. M. Goldberg. Elem. Math. **20**, 59 (1965).
43. M. Goldberg. Elem. Math. **22**, 108 (1967).
44. M. Goldberg. Ann. Univ. Sci. Budap. Sect. Math. **10**, 37 (1967); J. Mol. Biol. **24**, 337 (1967).
45. M. Goldberg. Elem. Math. **22**, 110 (1967).
46. A. Karabinta and E. Székely. Ann. Univ. Sci. Budap. Sect. Math. **16**, 143 (1973).
47. E. Székely. Ann. Univ. Sci. Budap. Sect. Math. **17**, 157 (1974).
48. K. Bornemissza. Unpublished thesis (in Hungarian). 1968.
49. A. Karabinta. Thèse de doctorat de 3ème cycle. Centre Pédagogique Supérieur, Bamako. 1973.
50. J. Molnár. Publicationes Mathematicae (Debrecen), **22**, 109 (1975).
51. J. Molnár. Magyar Tudom. Akad. III. Oszt. Közl. **14**, 113 (1964); Ann. Univ. Sci. Budap. Sect. Math. **9**, 71 (1966).
52. J. Berman and K. Hanes. Math. Computation. To be published.
53. J. R. Alexander. Acta Math. Acad. Sci. Hungar. **23**, 443 (1972).
54. G. D. Chakerian and M. S. Klamkin. Am. Math. Monthly, **80**, 1009 (1973).
55. J. R. Alexander and K. B. Stolarsky. Trans. Am. Math. Soc. **193**, 1 (1974).
56. K. B. Stolarsky. Pacif. J. Math. **57**, 563 (1975).
57. A. H. Schoen. Personal communication to V. Klee.

Chelating agents in high temperature aqueous chemistry. 1. The kinetics of the thermal decomposition of aqueous nitrilotriacetate (NTA), iminodiacetate (IDA), and *N*-methyliminodiacetate (MIDA)

MEINDERT BOOY[1] AND THOMAS WILSON SWADDLE[2]

Department of Chemistry, The University of Calgary, Calgary, Alta., Canada T2N 1N4

Received November 10, 1976

MEINDERT BOOY and THOMAS WILSON SWADDLE. Can. J. Chem. **55**, 1762 (1977).

Aqueous H_3NTA, H_2MIDA, H_2IDA, and their anions decompose under hydrothermal conditions (400–580 K) according to first order kinetics by successive decarboxylations, oxidation by O_2 being unimportant except at the highest temperatures. In the presence of added H^+, the species H_4NTA^+ and, to a lesser extent, H_3MIDA^+ (but not H_3IDA^+), provide significant decomposition pathways through elimination of a —CH_2COO— group (deacetylation). For $H_nNTA^{(3-n)-}$, first order rate coefficients k_n for decomposition are $k_0 = 4.5 \times 10^{-7}$, $k_1 \sim 1 \times 10^{-6}$, $k_2 \sim 7 \times 10^{-5}$, $k_3 = 2.1 \times 10^{-4}$, and $k_4 = 1.0 \times 10^{-2}$ s^{-1}, at 503 K and ionic strength 2.0 *m*, the spread in rates being due to differences in ΔS^* rather than ΔH^*. H_2MIDA and H_2IDA are comparable in reactivity to H_3NTA, while their anions are much less reactive than the NTA species of the same charge. The good thermal stability of aqueous NTA commends it as a reagent for boiler servicing and for decontamination of water-cooled nuclear reactors. A potentiometric method for the estimation of mono-, di-, and tribasic aminoacids in aqueous mixtures of these is described.

MEINDERT BOOY et THOMAS WILSON SWADDLE. Can. J. Chem. **55**, 1762 (1977).

Des solutions aqueuses de H_3NTA, H_2MIDA, H_2IDA et de leurs anions se décomposent, dans des conditions hydrothermiques (400–580 K), suivant des cinétiques du premier ordre par des décarboxylations successives; l'oxydation par O_2 n'est pas importante exceptée aux plus hautes températures. En présence d'ions H^+ additionnés, les espèces H_4NTA^+ et à un degré moindre H_3MIDA^+ (mais pas H_3IDA^+) fournissent des voies importantes de décompositions par élimination d'un groupe —CH_2COO— (déacétylation). Pour $H_nNTA^{(3-n)-}$, les coefficients de vitesse du premier ordre k_n pour la décomposition sont: $k_0 = 4.5 \times 10^{-7}$, $k_1 \sim 1 \times 10^{-6}$, $k_2 \sim 7 \times 10^{-5}$, $k_3 = 2.1 \times 10^{-4}$ et $k_4 = 1.0 \times 10^{-2}$ s^{-1} à 503 K et une force ionique de 2.0 *m*, les écarts dans les vitesses étant dus à des différences dans les ΔS^* plutôt que dans le ΔH^*. Les H_2MIDA et H_2IDA ont des réactivités comparables à celles du H_3NTA alors que leurs anions sont beaucoup moins réactifs que les espèces NTA ayant la même charge. La bonne stabilité thermique du NTA en solution aqueuse fait qu'on peut le considérer comme un bon réactif pour nettoyer les bouilloires et pour décontaminer des réacteurs nucléaires refroidis à l'eau. On décrit une méthode potentiométrique pour évaluer les aminoacides mono-, di- et tri-basiques dans des mélanges aqueux.

[Traduit par le journal]

Introduction

Our investigations of reagents suitable for high temperature aqueous chemistry (1, 2) have led us to a study of the hydrothermal chemistry of aminopolycarboxylate chelating agents, particularly nitrilotriacetate (NTA). These systems are of potential importance in the nuclear energy field, since chelating agents having high hydrothermal stability could be of use in the on-line removal of cobalt-60 deposits from the heat-transfer circuits of water-cooled nuclear power reactors ("decontamination") (3, 4). It has also been claimed (5, 6) that the addition of chelating agents to boiler water reduces rates of corrosion.

We have therefore examined the products, kinetics, and mechanism of the decomposition of aqueous NTA as functions of temperature and p*H*. The kinetic data also permit the calculation by extrapolation of an upper limit to the thermal lifetime of NTA in natural waters, which may be of interest to environmentalists in the context of the controversy surrounding the use of NTA as a substitute for polyphosphates in detergents (7–10).

Venezky and co-workers studied the rates of decomposition of aqueous ethylenedinitrilotetraacetic acid (H_4EDTA) (11, 12) and H_3NTA (13) and their sodium and lithium salts at 473 K.

[1]Present address: University Chemical Laboratory, the University of Kent, Canterbury, England CT2 7NH.

[2]To whom correspondence should be addressed.

They showed that the salts are more hydrothermally stable than the acids, the rates of decomposition decreasing markedly with increasing pH, and that the EDTA species decompose much more readily than their NTA analogues, this being associated with the presence of internal C–N bonds in EDTA. The hydrothermal decomposition of EDTA, NTA, and nitrilotrimethylenephosphonic acid at pH_{298} 9.5 was studied by Wilson and co-workers (14, 15) using proton magnetic resonance.[3] NTA possessed the highest hydrothermal stability of more than 20 reagents tested, decomposing above 533 K by decarboxylation to *N*-methyliminodiacetate (MIDA) according to first order kinetics. Dioxygen has been reported to cause the oxidation of aqueous EDTA, but not NTA, at 473 K (16), although NTA is oxidized at pH_{298} 8.5 to iminodiacetate (IDA), CO_2, and some oxalate by O_2 at temperatures as low as 358 K in the presence of a palladium–carbon catalyst (17). In the present study, therefore, attention has been given to the influence of the presence of O_2 upon the rate of hydrothermal decomposition of NTA.

Experimental

Materials

Distilled water, further purified by passage through Barnstead deionizer and organic cartridges was used throughout these experiments. All chemicals were reagent grade. Solutions were in general made up by weighing solids and adding water or aqueous acid or alkali with a pipette, and concentrations are therefore expressed on a molal basis (mol kg^{-1}, *m*).

Sodium hydroxide solutions were standardized with potassium hydrogen phthalate solutions using phenolphthalein as indicator. Acids were standardized using red mercuric oxide. Nitrilotriacetic acid (Eastman Kodak) and iminodiacetic acid (Matheson, Coleman, and Bell) were recrystallized from water and dried *in vacuo* for several hours. Hydroxyacetic acid (Fisher) was recrystallized from diethylether. Trifluoromethanesulfonic acid (HTFMS) (3 M Company) was distilled under vacuum. This acid was chosen because it is highly dissociated in water, a poor complexing agent, nonoxidizing (unlike $HClO_4$), and resistant to hydrolysis except at temperatures above about 550 K (2). *N*-Methyliminodiacetic acid (Aldrich), sarcosine hydrochloride (Baker), *N*,*N*-dimethylglycine (K & K), and trisodium nitrilotriacetate hydrate (Aldrich) were used as received. The reactions were carried out in capped Teflon vessels (inner diameter 25 mm, height 36 mm, thickness of walls 1.2 mm) inside stainless steel autoclaves. A Teflon ring provided a seal. These vessels were found suitable for use with aqueous solutions up to 580 K, above which temperature Teflon deformed appreciably. The vessels were filled with 10 ml solution for experiments at 480 K and lower. This left a free volume of 7.7 ml. At higher temperatures, because of the expansion of water, only 5 ml of solution were used, in which case the free volume was 12.7 ml. Unless otherwise stated, the reactions were carried out under air (90 kPa at 294 K, when the vessels were sealed).

Solutions under dinitrogen were prepared by using solvents saturated with N_2, closing the vessels in a glovebox filled with dinitrogen (90 kPa at 294 K). Solutions under dioxygen were made up from solvents saturated with O_2, flushing the vessel with O_2, and capping the vessel quickly, a method which could only give approximate results. The ionic strength was maintained at 2.0 *m* in acid solutions by sodium trifluoromethanesulfonate prepared by neutralizing HTFMS with NaOH and recrystallizing the salt from water, and in alkaline solutions by NaCl.

Thermostating of the pressure vessels was achieved with a Blue M Conwate CW-160HF-1 forced convection oven. The reaction temperature was measured with an iron constantan thermocouple in conjunction with a Leeds-Northrup 7554K4 potentiometer. The cold junction reference was provided by a Thermoelectric 80020 Automated Ice Point Reference. The pressure within the vessels at the reaction temperatures was that of the solvent vapor plus the pressure of the gas present in the free volume on sealing. At selected intervals, vessels were removed from the oven and immediately immersed in cold water.

Gas Liquid Chromatography (glc)

Analyses by glc were performed by the method of Warren and Malec (18). Tabsorb^R (Regis Chemical Company) was used as column material. It was found that this method, employing the *N*-trifluoroacyl derivatives of the butyl esters of the amino acids, did not give quantitatively reproducible analyses for the tertiary amino acids methyliminodiacetate (MIDA) and *N*,*N*-dimethylglycine (DMG). Accordingly, glc was used only for qualitative purposes.

Titration Techniques

All pH measurements and titrations were performed at room temperature (294 K) with a Beckman 39502 combination electrode, standardized against Beckman buffer 22331 (pH = 6.86) and 0.05 *M* potassium diphthalate (Fisher) (pH = 4.01).

The analyses were performed with a Radiometer Model 11 Titrator coupled to a Radiometer Model 28 pH meter. A Radiometer G202 C glass electrode and a K401 saturated calomel electrode were used. The rate of delivery of titrant from a buret was regulated by a magnetic valve and was proportional to the difference of the measured pH and a set endpoint.

Complexometric titrations were performed with copper(II) nitrate and copper(II) chloride solutions standardized against 0.05 *M* Na_2H_2EDTA (Fisher) with murexide (Fisher) as indicator at pH = 8.5 with 0.05 *m* $Na_2B_4O_7 \cdot 10H_2O$ as buffer (19). Solutions in which NTA was dominant gave sharp endpoints. When appreciable

[3]The symbol pH_T refers to the pH of the solution as measured at temperature T kelvins, rather than the reaction temperature.

amounts of di- and monobasic amino acids were present, the colour change was much less distinct.

A potentiometric titration technique was therefore developed for the analysis of mixtures of mono-, di-, and tribasic amino acids, based on the work of Schwarzenbach and Biedermann (20), and Pinzer and Stewart (21). The method utilizes differences in the stability constants of complexes of Ca^{2+}, Zn^{2+}, and Cu^{2+} with the various chelating agents (22). The product solution was washed into a volumetric flask (usually 25 ml) and diluted to the mark. Three aliquots were pipetted, diluted to 40 ml, and neutralized (pH about 6.2) with dilute sodium hydroxide or nitric acid. This left one ionizable proton on the nitrogen atom of each molecule.

To the first aliquot was added an excess of 0.1 *m* copper(II) nitrate solution (pH = 4.15) over the total amount of amino acid expected to be present. The Cu^{2+} ion was able to displace the last proton from all species and neutralization of the liberated protons with 0.1 *m* NaOH gave the total number of moles of amino acid.

To the second aliquot a small excess of 0.1 *m* zinc(II) nitrate (pH = 5.1) was added. This released the protons on nitrogen from di- and tribasic acids only, and these protons were again titrated with 0.1 *m* sodium hydroxide. Pinzer and Stewart (21) used $Pb(NO_3)_2$ instead of $Zn(NO_3)_2$, but Pb^{2+} gave problems with the combination electrode we used, presumably due to precipitation of $PbCl_2$.

To the third aliquot was added an excess of 0.1 *m* $Ca(NO_3)_2$ solution (pH = 5.40). Calcium ion released the last proton only from $HNTA^{2-}$ under these conditions. Neutralization gave the amount of nitrilotriacetate present. The accuracy of the determination of NTA after addition of Ca^{2+} was 99 ± 1%, even when large amounts of dibasic acids were present. The accuracy of the analysis of the dibasic acids MIDA and IDA with Zn^{2+} was 98 ± 2%.

In the cases in which carbon dioxide was expected to be present, the reaction mixture was acidified and heated on a steam bath for 15 min. This was sufficient to remove interfering amounts of carbon dioxide, which caused unsharp endpoints.

Proton Magnetic Resonance Methods

Proton magnetic resonance spectra were obtained on a Varian HA-100 Spectrometer operated in the field sweep mode. The water resonance was used as the lock signal. As the chemical shifts of the methyl and methylene groups are very pH dependent, the solutions of the reaction products were made either alkaline with 3 *m* NaOH or acidic with 2 *m* HCl. Identifications were made by comparing chemical shifts and adding an extra amount of reagent and observing which peaks increased in size.

The use of water as a lock signal had the disadvantage that large amounts of energy were absorbed by the water, which distorted the other signals, so that reliable quantitative measurements could not be made in this way. Analysis of weighed mixtures of aminopolycarboxylates showed deviations from the calculated intensities, measured by integration or by the height of the peaks, by as much as 10%. Martell *et al.* (15) avoided this problem by exchanging hydrogen for deuterium in several steps, and obtaining spectra in D_2O.

Other Analytical Methods

Formaldehyde was detected as its 2,4-dinitrophenylhydrazone and estimated by titration with acid after addition of sulphite (23). Carbon monoxide was detected by mass spectroscopy after correction for the contribution to $m/e = 28$ due to the decomposition of CO_2^+ to CO^+ (2).

Results

1. Products

(*a*) *Gas–Liquid Chromatography*

After heating a solution of 0.10 *m* H_3NTA for 17 h at 473 K IDA, MIDA, GLY, and sarcosine (SARC) were identified as products. Decomposition of H_2IDA under the same conditions produced mainly SARC and some GLY. The spectrum of the decomposition products of methyliminodiacetic acid showed a broad peak at low retention time attributable to *N*,*N*-dimethylglycine (DMG), but small amounts of GLY, SARC, and IDA were also detected. The last compound was probably formed through decomposition of the ammonium salt of MIDA in the chromatograph.

(*b*) *Nuclear Magnetic Resonance*

At low pH IDA, MIDA, formaldehyde, and some formic acid were found as products of the decomposition of NTA. The ratio [IDA]/[MIDA] increased with increasing $[H^+]$, as did the yield of formaldehyde, and the ratio [IDA]/[MIDA] in 2.3 *m* acid was equal to the ratio of the yield of CO to that of CO_2 as determined by mass spectrometry. This indicates that MIDA was formed by decarboxylation, and IDA by a process leading eventually to CO and HCHO. The survival of relatively large concentrations of IDA indicated that its decomposition was markedly slower than that of NTA in acidic solutions. For $pH_{294} > 1.5$ the main mode of decomposition of NTA was decarboxylation, and there was no accumulation of the corresponding product MIDA, which showed that the rates of decarboxylation of MIDA and NTA are similar. Oxidation of NTA by dioxygen resulted in IDA, formaldehyde, and CO_2, but was unimportant except at temperatures above 500 K.

2. Kinetics

It must be recognized that, because of experimental and analytical difficulties, together with complications due to the protonation equilibria and (except at the highest and lowest pH) the

TABLE 1. Pseudo-first order rate coefficients k_{obs} (s^{-1}, $\times 10^5$) for the decomposition of NTA, IDA, and MIDA in acidic solution (HTFMS/NaTFMS) of ionic strength 2.0 *m*

Amino-acid	Temperature (K)	k_{obs} for [HTFMS] (*m*) = 0.0	0.10	0.26	0.52	0.79	1.08	1.80	2.30
NTA	418	0.11±0.05			0.34±0.09		0.36±0.09		0.44±0.10
	433	0.31±0.06		2.6±0.6	2.8±0.7		3.2±0.8		
	453	1.4±0.5		8.4±2.1	12±3	13±3	18±5		19±6
	473	3.1±0.3		29±3	36±2	45±2	49±3		
	487	11±3							
	503	21±6							
IDA	466	3.3±0.8							
	477	4.0±1.4	4.4±1.1		2.1±0.5			1.4±0.4	
	487	9.4±1.3			4.1±1.0				
	503	35±6			16±4			8.4±2.1	
MIDA	466	1.4±0.4							
	473	2.3±0.4	3.5±0.9		3.8±1.0				
	487	3.6±0.3			7.2±1.8				
	503	9.4±1.1			18±4			20±5	

change of p*H* as the decompositions proceeded, the kinetic data reported here are to be regarded as only semiquantitative, except for those referring to NTA^{3-}, $HIDA^-$, and $HMIDA^-$, for which precision was better. They suffice, however, as keys to the mechanism of the reactions, and as empirical guides to the kinetic stability of NTA, IDA, and MIDA over wide ranges of temperature and p*H*.

(*a*) *Isoelectric Species*: *H_3NTA, H_2IDA, and H_2MIDA*

Since ΔH for the acid dissociation of these species is close to zero, and the acids are fairly "weak" at 293 K (22), it was assumed that solutions of the stoichiometric amino acids above contain the isoelectric species to the virtual exclusion of species containing more or fewer protons (*e.g.*, H_4NTA^+, H_2NTA^-), even at ~500 K. Subsequently, it was confirmed that decomposition pathways involving the cationic or anionic species could not contribute significantly to the initial decomposition rate in such solutions, so that the values of the rate coefficients k_{obs} listed in Table 1 under [HTFMS] = 0 can be identified with those governing the decompositions of the isoelectric species themselves.

In these solutions, the fractional extent of decomposition of a given amino acid over a given time interval t was independent of the initial amino acid concentration c_0 for $0.02 < c_0 < 0.3\ m$; thus, the reactions were first order in amino acid concentration. However, the accumulation of basic decomposition products resulted in a rise in p*H* which caused appreciable deviations from the integrated first order rate equation beyond about 40% reaction. This effect was also observed for NTA by Venezky and Moniz (13), who found essentially the same time dependence of [NTA] as reported here except for an "induction time" attributable to solubility problems associated with $c_0 \sim 0.3\ m$. The pseudo-first order rate constants k_{obs} were therefore calculated from the slope of the initially linear parts of plots of $-\ln([NTA]_t/[NTA]_0)$ *vs.* time (Table 1 and Fig. 1). The uncertainties quoted are fairly large because of the pronounced increase in p*H* for the experiments at high temperatures and the large influence of errors in the analyses of experiments at low temperatures in which only the first few percent of reaction could be measured. The presence of dioxygen (up to 90 kPa at 294 K) did not affect the rate of disappearance of the isoelectric or cationic forms of NTA, except at the highest temperature (503 K) with a small volume of solution and an excess of O_2 over NTA.

The temperature dependences of the values of k_{obs} listed in Table 1 under [HTFMS] = 0 for the decompositions of the isoelectric species H_3NTA, H_2IDA, and H_2MIDA (to MIDA, sarcosine, and dimethylglycine, respectively) yield the corresponding values of 106 ± 5,

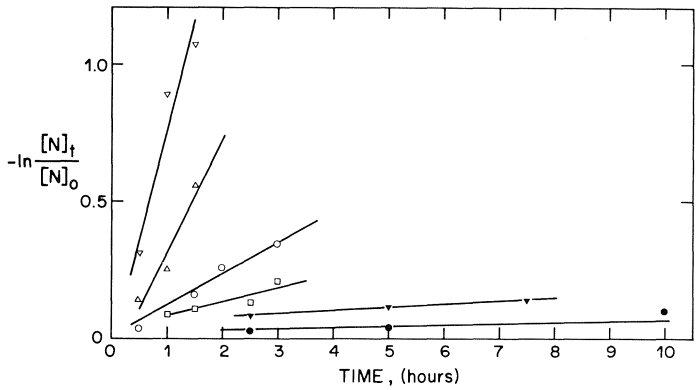

FIG. 1. First order plots of $-\ln [NTA]_t/[NTA]_0$ *vs.* time for the decomposition of H_3NTA; $C_0 = 0.10\ m$; $I = 2.0\ m$ with NaTFMS. ●, 418 K; ▼, 433 K; □, 453 K; ○, 473 K; △, 487 K; ▽, 503 K.

120 ± 14, and 92 ± 9 kJ mol^{-1} for the enthalpies of activation ΔH^* and -109 ± 10, -79 ± 29, and -144 ± 19 J K^{-1} mol^{-1} for the entropies of activation ΔS^*. The kinetic stabilities of these isoelectric acids are thus similar, the slightly lower reactivity of H_2MIDA becoming more evident at the higher temperatures.

(*b*) *Cationic Species*: H_4NTA^+, H_3IDA^+, and H_3MIDA^+

Addition of H^+ to solutions of H_3NTA, H_2IDA, and H_2MIDA produces significant concentrations of the cationic species H_4NTA^+, H_3IDA^+, and H_3MIDA^+ respectively (22), so that both isoelectric and cationic species need to be considered as contributing to the decomposition kinetics of NTA, IDA, and MIDA in solutions containing added acid. Under such conditions, the rate of decomposition of NTA can be described by (Fig. 2)

$$[1] \quad \frac{-d[NTA]}{dt} = \frac{(k_3 + k_4K_4[H^+])[NTA]}{(1 + K_4[H^+])} = k_{obs}[NTA] \text{ at a given } [H^+]$$

adopting a convention whereby k_n is the first-order decomposition rate coefficient of an amino polycarboxylate species having n ionizable protons, and K_n is the nth protonation constant. When $[H^+] > 0.26\ m$, the term involving k_3 may be neglected, and eq. 1 may be linearized to

$$[2] \quad (1/k_{obs}) = (1/k_4) + 1/(k_4K_4[H^+])$$

Plots of k_{obs}^{-1} *vs.* $[HTFMS]^{-1}$ gave good straight lines, and yielded the values of k_4 and K_4 listed in Table 2. On fitting the experimental data for $0.26 \leq [HTFMS] \leq 1.08\ m$ at 473 K and ionic strength 2.0 m to eq. 1 by regression analysis, the values $k_4 = 7.1 \times 10^{-4}$ s^{-1} and $K_4 = 1.7\ m^{-1}$ were obtained, in good agreement with those of Table 2. Values of the decomposition product ratio $[IDA]_t/[MIDA]_t$, calculated on the basis of these kinetic parameters and the assumption that H_4NTA^+ decomposes exclusively to IDA and H_3NTA to MIDA, agreed satisfactorily with those observed experimentally, and served to justify the assumption. The temperature dependence of k_4 (Table 2) gives $\Delta H^* = 150 \pm 14$ kJ mol^{-1} and $\Delta S^* = 11 \pm 32$ J K^{-1} mol^{-1} for the decomposition of H_4NTA^+.

The rates of decomposition of IDA and MIDA in acidified solutions (to sarcosine with traces of glycine, and to a mixture of dimethylglycine and sarcosine, respectively) were also first order in the original amino acids for $c_0 = 0.1$ to $0.3\ m$ at least, and dioxygen did not affect the rates even in 2 m HTFMS. The rate of decomposition of MIDA increased slightly with increasing [HTFMS], and the data of Table 1 suggest $k_3 \sim 2 \times 10^{-4}$ s^{-1} and $K_3 \sim 10\ m^{-1}$ at 503 K. For IDA, however, addition of HTFMS resulted in a *decrease* in the decomposition rate, indicating $k_3 < k_2$, and the values of k_{obs} in Table 1 suggest $K_3 \sim 2\ m^{-1}$ at 470–500 K with $k_2 \geq 10\ k_3$.

TABLE 2. Protonation constants K_4 and first order decomposition rate coefficients k_4 for aqueous H_4NTA^+[a]

Temperature (K)	k_4 (s^{-1}, $\times 10^5$)	K_4 (m^{-1})
293		6[b]
418	0.5±0.1	5.6±2.5
433	3.4±0.2	12.7±3.6
453	23±3	2.1±0.5
473	77±7	1.7±0.3

[a]Calculated from data of Table 1; ionic strength 2.0 m.
[b]Ionic strength 0.1 m (from ref. 22).

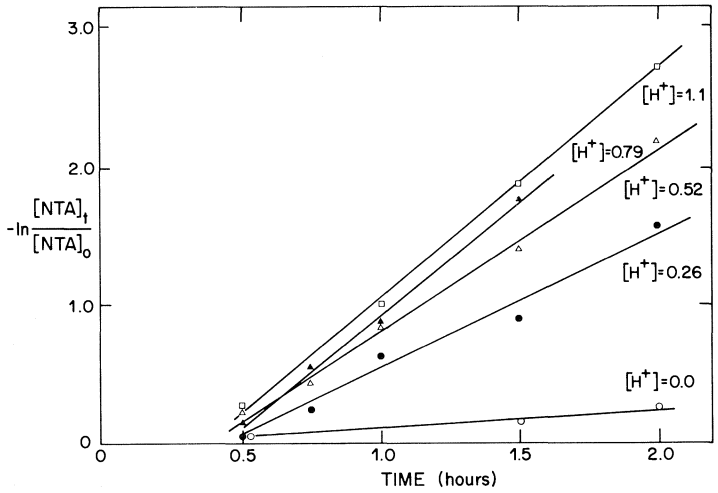

FIG. 2. First order plots for the decomposition of H_3NTA at various $[H^+]$ (m) at 473 K and ionic strength 2.0 m.

(c) Decomposition of the Sodium Salts of NTA, IDA, and MIDA

Solutions of Na_3NTA with initial concentrations from 0.03 to 0.20 m were decomposed at 560 K for 2 h at ionic strength 2.0 m with NaCl under dinitrogen. The slope of a plot of $\ln(-dc_0/dt)$ *vs.* $\ln c_0$ was 0.97 ± 0.07, indicating first order kinetics in Na_3NTA. This correlation was not valid when reactions were carried out under air as the oxidation by dioxygen was fairly rapid relative to these very slow rates of decarboxylation of NTA^{3-}, and all O_2 present was consumed within two hours. Proton magnetic resonance spectra showed much larger amounts of IDA for reactions carried out under pure O_2 than for those under air at the same pressure.

No significant yields of dibasic amino polycarboxylate anions were detected, when aqueous NTA^{3-} was decomposed in the absence of O_2, so that their rates of decomposition were comparable to or faster than that of NTA^{3-}. Semilogarithmic plots of $[NTA^{3-}]$ as time showed a rapid rate over the first few % reaction, presumably due to the presence of traces of oxygen, but subsequently were linear, and first order rate coefficients k_{obs} calculated from the linear portion are listed in Table 3. These coefficients were independent of both ionic strength and $[OH^-]$ for [NaOH] > 0.1 m, so that there was no significant reaction pathway involving nucleophilic attack by OH^- on NTA^{3-}. The data of Table 4 give $\Delta H^* = 103 \pm 5$ kJ mol^{-1} and $\Delta S^* = -166 \pm 8$ J K^{-1} mol^{-1} for the decomposition of NTA^{3-} at ionic strength 2.0 m.

Semi-quantitative experiments showed that the monoprotonated anion $HNTA^{2-}$, prepared in solution by addition of the stoichiometric amount of HCl to Na_3NTA, underwent decarboxylation more rapidly than NTA^{3-} by a factor of about 3 at 541 K and 4 at 575 K (ionic strength 2.0 m). Similar experiments showed that the doubly protonated ion H_2NTA^- was much more reactive, decomposing about one-third as rapidly as H_3NTA at 503 K. Thus,

TABLE 3. First order rate coefficients for the decomposition of NTA^{3-} at ionic strength 2.0 m under dinitrogen[a]

Temperature (K)	$10^5 k_{obs}$[b] (s^{-1})
551	0.44±0.10
561	0.62±0.07
566	0.81±0.02
575	1.14±0.10

[a]Initial $[Na_3NTA] = 0.1$ m.
[b]Uncertainties are standard deviations of semilog plots.

TABLE 4. First order rate coefficients[a] for the decompositions of $HIDA^-$ and $HMIDA^-$ at ionic strength 2.0 m[b]

Temperature (K)	$10^5 k_{obs}$ (s^{-1})	
	NaHIDA	NaHMIDA
541	5.4	3.1
550	11.0	5.7
562	18.5	10.8
573	40.2	21.2

[a]From initial rates.
[b]Initial [chelant] = 0.2 m.

extrapolation of the data of Tables 2 and 3 shows that the relative decomposition rates of NTA^{3-}, $HNTA^{2-}$, H_2NTA^-, H_3NTA, and H_4NTA^+ are $1:3:150:470:2 \times 10^4$ approximately, at 503 K and ionic strength 2.0 *m*.

For IDA^{2-} and $MIDA^{2-}$, the decomposition rates were again very slow but were poorly reproducible. The monoprotonated ions $HIDA^-$ and $HMIDA^-$, however, were respectively some 40 and 20 times more reactive than the dinegative anions at 573 K, and gave the reproducible ($\pm 5\%$) first order rate coefficients k_{obs} of Table 4, from which we calculate $\Delta H^* = 150 \pm 12$ and 148 ± 4 kJ mol^{-1}, and $\Delta S^* = -54 \pm 22$ and -62 ± 7 J K^{-1} mol^{-1}, for the respective decarboxylations.

Rate coefficients for the decomposition of NTA, obtained using both the conditions (566 K, pH_{294} 9.3) and method of computation of Martell *et al.* (15), were somewhat smaller (1.4×10^{-5} s^{-1}) than those reported by these authors (5.3×10^{-5} s^{-1}). It may be that the unlined titanium vessels used by Martell *et al.* (15) caused some catalysis of the reaction, especially since titanium is known to be attacked by alkaline water at high temperatures (4), but the discrepancy is not considered to be serious.

Discussion

This study confirms that the chelating agent NTA possesses good kinetic stability under hydrothermal conditions, especially at high p*H* in the absence of dioxygen. Its decomposition products include MIDA, IDA, DMG, SARC, and GLY. which are also chelating agents but which decompose at rates comparable to that of NTA and do not accumulate in high concentrations as NTA degrades. The ultimate products are CO, CO_2, HCHO, and various methylamines.

The species NTA^{3-}, $HNTA^{2-}$, H_2NTA^-, and H_3NTA all decompose *via* initial elimination of a CO_2 molecule (decarboxylation), but, while the decomposition rate of $HNTA^{2-}$ is only about three times that of NTA^{3-}, and H_3NTA about three times that of H_2NTA^-, H_2NTA^- is fully 70 times more reactive than $HNTA^{2-}$ (at 503 K). Similarly, $HMIDA^-$ is about 40 times less reactive than H_2MIDA, and $HIDA^-$ some 80 times less than H_2IDA at 503 K (from Tables 1 and 4). These observations indicate that decarboxylation is facilitated if at least two ionizable protons are present; since the N atom in an aminopolycarboxylate is always protonated in preference to a $—COO^-$ group, this means that protonation of a $—COO^-$ function is necessary if relatively facile decarboxylation is to occur. This is not surprising, as a proton transfer either within a $—CH_2COOH$ group

[3] 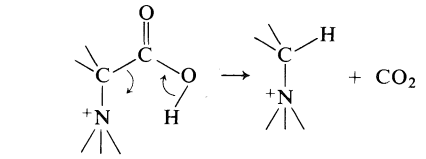

or to $—CH_2COO^-$ from a neighboring $—CH_2COOH$ group

[4] 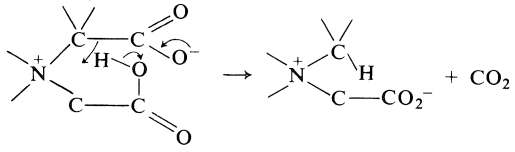

would obviate the development of a carbanion when CO_2 separates. Mechanism 4 seems more likely, especially since protonation of *all* N and $—COO^-$ sites results in a change of mechanism from decarboxylation to deacetylation (from C—C bond fission to C—N bond fission) and, in the case of IDA, a marked *decrease* in reactivity on going from H_2IDA to H_3IDA^+.

The high kinetic stability of NTA^{3-} is due to the strongly negative entropy of activation (-166 J K^{-1} mol^{-1}), as ΔH^* is much the same as for the other decarboxylations (~ 110 kJ mol^{-1}). Conversely, H_4NTA^+ is relatively reactive by virtue of its positive ΔS^* for deacetylation ($\sim +11$ J K^{-1} mol^{-1}), and indeed ΔH^* is rather higher (150 kJ mol^{-1}) than for most comparable decarboxylations, presumably as a result of the difference in mechanism.

The decomposition of aminopolycarboxylic acids by deacetylation might be expected to yield glycollic acid, $HOCH_2COOH$, if direct hydrolysis of the $N—CH_2COOH$ bond were the initial step, but in no case could glycollic acid be detected amongst the decomposition products. Formaldehyde and carbon monoxide were major products, but it was established independently that glycollic acid yields only minor amounts of HCHO under the conditions of these experiments. Formic acid, on the other hand, decomposes extensively to CO and water under these conditions. Thus, the crucial step in these decompositions probably involves the separation of either CO or HCOOH, followed by the release of HCHO.

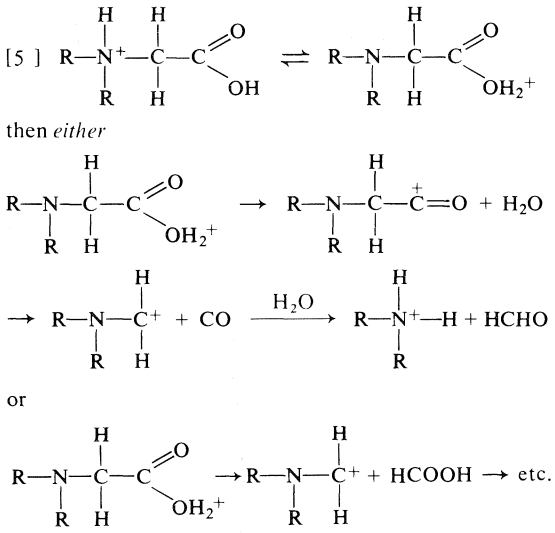

A somewhat similar process has been proposed for the decomposition of glutaric acid (the carbon analogue of IDA) in dilute sulfuric acid (24). Variants of mechanism 5 in which the initiating step is nucleophilic attack of H_2O on the α-carbon atom can be readily devised, but not distinguished operationally.

The formation of the familiar reducing agents, carbon monoxide and formaldehyde, in this pathway serves to emphasize that any organic matter is to be regarded as a potential reductant in aqueous systems at high temperatures, where kinetic barriers are likely to be overcome (2). Similarly, the emergence of dioxygen as an aggressive oxidant in water at high temperatures is illustrated by this work. On the other hand, the high temperature protonation constants K_n estimated here, though approximate, are not very different from those measured at room temperature (22).

Finally, noting that the rate of decomposition of $HNTA^{2-}$, the predominant form of NTA at the pH of natural waters, will be roughly that of NTA^{3-} at low temperatures, we can estimate from the data of Table 3 that the thermal halflife of aqueous NTA in the environment would be on the order of eight million years, since we have shown that oxidation by O_2 is competitive with decarboxylation only at the highest temperatures. Thermal decarboxylation or oxidation of free NTA therefore cannot compete with the photolysis of NTA transition-metal chelates (25, 26) or with biodegradation (18) as mechanisms for the elimination of pollutant NTA from rivers or lakes.

Acknowledgements

We thank the National Research Council of Canada, the University of Calgary, and the Izaak Walton Killam Fund for Advanced Studies for scholarships (to M.B.), and Atomic Energy of Canada, Ltd., for general financial support of this project through Whiteshell Nuclear Research Establishment.

1. M. P. Henderson, V. I. Miasek, and T. W. Swaddle. Can. J. Chem. **49**, 317 (1971).
2. L. Fabes and T. W. Swaddle. Can. J. Chem. **53**, 3053 (1975).
3. M. Tomlinson. Chem. Can. 21 (October, 1974).
4. A. R. Gainsford, M. J. Sisley, T. W. Swaddle, and P. Bayliss. Can. J. Chem. **53**, 12 (1975).
5. J. R. Metcalf. Boiler chelant treatment; an update. Intern. Water Conf., 31st. Annual Meeting, Pittsburgh, PA. 1970.
6. T. C. Margulova, O. I. Martinova, Yu. P. Samoilov, and P. L. Medvedev. Teploenergetika, 65 (1974).
7. A. E. Martell. Pure Appl. Chem. **44**, 81 (1975).
8. P. S. Thayer and C. J. Kensler. C. R. C. Crit. Rev. Environ. Sci. **3**, 375 (1973).
9. A. H. Pickaver. Soil Biol. Biochem. **8**, 13 (1976).
10. H. Mottola. Toxicol. Environ. Chem. Rev. **2**, 99 (1974).
11. D. L. Venezky and W. B. Moniz. U. S. Naval Res. Lab. Rep. No. 6747 (1968); Anal. Chem. **41**, 11 (1969).
12. P. J. Sniegoski and D. L. Venezky. J. Chromatogr. Sci. **12**, 359 (1974).
13. D. L. Venezky and W. B. Moniz. U.S. Naval Res. Lab. Rep. No. 7192 (1970).
14. J. S. Wilson and A. S. Fried. Proc. Am. Power Conf., 35th Ann. Mtg., Chicago, IL. (1973).
15. A. E. Martell, R. J. Motekaitis, A. R. Fried, J. S. Wilson, and D. T. MacMillan. Can. J. Chem. **53**, 3471 (1975).
16. D. L. Venezky. U.S. Naval Res. Lab. Rep. No. 7261 (1971).
17. M. T. Tetenbaum and H. Stone. J. Chem. Soc. Chem. Commun. 1699 (1970).
18. C. B. Warren and E. J. Malec. Science, **176**, 277 (1972); J. Chromatogr. **64**, 219 (1972).
19. A. I. Vogel. Quantitative inorganic analysis. 3rd ed. Longmans, London. 1961.
20. G. Schwarzenbach and W. Biedermann. Helv. Chim. Acta, **31**, 331 (1948).
21. E. A. Pinzer and B. B. Stewart. *In* Encyclopedia of industrial chemical analysis. Vol. 12. *Edited by* F. D. Snell and L. S. Ettre. Interscience, New York, NY. 1967. p. 36.
22. A. E. Martell and R. M. Smith. Critical stability constants. Vol. 1. Plenum Press, New York, NY. 1974.
23. J. F. Walker. Formaldehyde. 3rd ed. Reinhold, New York, NY. 1964. p. 486.
24. R. Kiseleva and M. S. Dudkin. Russ. J. Appl. Chem. **40**, 2405 (1967).
25. T. Trott, R. W. Henwood, and C. H. Langford. Environ. Sci. Technol. **6**, 367 (1972).
26. C. H. Langford, M. Wingham, and V. S. Sastri. Environ. Sci. Technol. **7**, 820 (1973).

Chelating agents in high temperature aqueous chemistry. 2. The thermal decomposition of some transition metal complexes of nitrilotriacetate (NTA)

MEINDERT BOOY[1] AND THOMAS WILSON SWADDLE[2]

Department of Chemistry, The University of Calgary, Calgary, Alta., Canada T2N 1N4

Received November 10, 1976

MEINDERT BOOY and THOMAS WILSON SWADDLE. Can. J. Chem. **55**, 1770 (1977).

The kinetics and mechanism of decomposition of NTA complexes of Fe^{III}, Fe^{II}, Co^{II}, Ni^{II}, and Cu^{II} under hydrothermal conditions (425–573 K) have been examined. The relative rates at 573 K are $Co^{II}NTA^- < NTA^{3-} \lesssim Fe^{II}NTA^- < Ni^{II}NTA^- < Fe^{III}NTA^0 < H_3NTA^0 < Cu^{II}NTA^- < H_4NTA^+$. Aqueous $Co^{II}NTA^-$ and $Fe^{II}NTA^-$, like NTA^{3-}, decomposed at 573 K by decarboxylation, precipitating $Co(OH)_2$ and Fe_3O_4 respectively; $Ni^{II}NTA^-$ precipitated $Ni(OH)_2$ initially but subsequently Ni metal. At 530 K, $Fe^{III}NTA^0$ solutions precipitated $Fe^{II}{}_3(NTA)_2 \cdot H_2O$, but at higher temperatures Fe_3O_4 formed, the NTA ligand being reduced to HCHO and iminodiacetate (IDA) rather than decarboxylated. Similarly, $Cu^{II}NTA^-$ gave IDA and HCHO at temperatures as low as 425 K, forming first Cu^I (which precipitated as CuCl in the presence of Cl^-) and then metallic Cu. The applicability of NTA to corrosion control in boilers and to ^{60}Co removal from water-cooled nuclear reactors is briefly considered. The half-life of $Fe^{III}NTA$ in the hydrosphere is estimated at 80 years (*cf.* 8×10^6 years for free NTA), in the absence of photolysis or biodegradation.

MEINDERT BOOY et THOMAS WILSON SWADDLE. Can. J. Chem. **55**, 1770 (1977).

On a déterminé la cinétique et le mécanisme de décomposition des complexes de NTA avec Fe^{III}, Fe^{II}, Co^{II}, Ni^{II} et du Cu^{II} dans des conditions hydrothermiques (425–573 K). Les vitesses relatives à 573 K sont $Co^{II}NTA^- < NTA^{3-} \lesssim Fe^{II}NTA^- < Ni^{II}NTA^- < Fe^{III}NTA^0 < H_3NTA^0 < Cu^{II}NTA^- < H_4NTA^+$. Comme le fait NTA^{3-}, des solutions aqueuses de $Co^{II}NTA^-$ et de $Fe^{II}NTA^-$ à 573 K se décomposent par décarboxylation et provoquent respectivement la précipitation de $Co(OH)_2$ et de Fe_3O_4; au début de la réaction avec $Ni^{II}NTA^-$, il y a précipitation de $Ni(OH)_2$ mais au fur et à mesure que la réaction progresse, il y a précipitation de nickel métallique. A 530 K, des solutions de $Fe^{III}NTA^-$ provoquent la précipitation de $Fe^{II}{}_3(NTA)_2 \cdot H_2O$ mais à des températures plus élevées, il y a formation de Fe_3O_4 puisque le ligand NTA est réduit en HCHO et iminodiacétate plutôt que d'être décarboxylé. De la même manière, $Cu^{II}NTA^-$ conduit à IDA et HCHO à des températures aussi basses que 425 K conduisant à la formation en premier de Cu^I (qui précipite sous forme de CuCl en présence de Cl^-) et ensuite de Cu sous forme métallique. On a considéré les possibilités d'appliquer le NTA pour contrôler la corrosion dans des bouilloires et pour enlever du ^{60}Co des réacteurs nucléaires refroidis à l'eau. On estime que le temps de demi-vie du $Fe^{III}NTA$ dans l'hydrosphère est d'environ 80 ans (par opposition à 8×10^6 ans pour le NTA à l'état libre) en l'absence de photolyse ou de biodégradation.

[Traduit par le journal]

Introduction

The possibility of using chelating agents, in particular nitrilotriacetate (NTA), in the control of corrosion processes in boilers (1, 2) and of cobalt-60 transport in water-cooled nuclear reactors (3) prompted our study (4) of the kinetics of decomposition of aqueous NTA over a wide range of temperature and p*H*. That study provided incidentally an upper limit to the environmental half-life of free NTA reaching the hydrosphere through its use as a builder in detergents; such NTA may present a biological hazard through mobilization of heavy metals, or through decomposition to secondary amines and thence to carcinogenic *N*-nitrosamines (5–9). The kinetic data provided by the study (4) would not, however, be directly applicable to conditions in boilers, nuclear reactors, or the hydrosphere if the decomposition of NTA were significantly accelerated or retarded by chelation of the metal ions which would inevitably be present.

Accordingly, the present article describes a semi-quantitative study of the effect of chelation of iron(II), iron(III), cobalt(II), nickel(II), and copper(II) upon the kinetics and mechanism of thermal degradation of aqueous NTA. The

[1]Present address: University Chemical Laboratory, The University of Kent, Canterbury, England CT2 7NH.

[2]To whom correspondence should be addressed.

photochemical decomposition of $Fe^{III}NTA$ (10, 11) has been shown to proceed by deacetylation (loss of $—CH_2COO—$) rather than by decarboxylation (loss of CO_2), and the photochemical degradations of $Cu^{II}NTA^-$ (12) and Fe^{III}-$EDTA^-$ (13, 14) have also been examined. The thermal decomposition of aqueous NTA complexes, however, seems to have been little studied, although extensive research in the U.S.S.R. has shown that EDTA complexes of many metal ions have half lives of several hours in water at 473 K, the relative kinetic stabilities being $Na_2CaEDTA \sim Na_2MgEDTA > Na$-$Fe^{III}EDTA > Na_2H_2EDTA > Na_2CuEDTA$ (15, 16), and it has been found (2) that hydrothermal decomposition of iron chelates in boilers can produce corrosion-resistant coatings of magnetite on steel surfaces.

Experimental

Experimental procedures were in general those described previously (4). Unless otherwise stated, analytical grade hydrated transition metal chlorides were used, and shown to be of acceptable purity by complexometric analysis using EDTA. Iron was determined by titration with $K_2Cr_2O_7$ after reduction to iron(II) with $SnCl_2$ (17). Metal chelates were prepared according to Rajabalee (18). Reaction mixtures were made up by weighing the reagents into the PTFE-lined autoclaves, and adding deoxygenated deionized water and closing the vessels under dinitrogen.

For analysis of the chelating agents after reaction, the transition metal ions were removed by addition of sodium hydroxide solution and filtration with a sintered glass funnel. Copper(II) was removed by reduction with a small excess of hydrazine and removal of the yellow product on a sintered glass filter, but the buffer action of the excess hydrazine limited the use of this preliminary procedure to the determinations of di- and tribasic acids using zinc(II) (4), where the endpoints of the titrations are at pH 6.0.

Results

1. Nitrilotriacetatoiron(III)

This complex decomposed readily above 530 K with reduction of iron(III) to iron(II), yielding the solid $Fe^{II}_3(NTA)_2 \cdot H_2O$ (see below) at 530 K, and magnetite at higher temperatures. The rate of reaction was the same whether the starting material was $Fe^{III}NTA \cdot H_2O$ or an equimolar mixture of $FeCl_3$ with Na_3NTA, *i.e.*, it was unaffected by the presence of Na^+ or Cl^-. The proton magnetic resonance spectrum of a solution, initially 0.3 m in each of $FeCl_3$ and Na_3NTA, showed after 2 h at 563 K that iminodiacetate (IDA, formed by deacetylation) and decarboxylation products (notably *N*-methyliminodiacetate, MIDA) were present in small but approximately equal amounts. This indicated that deacetylation was of comparable importance to decarboxylation (in contrast to the decomposition of Na_3NTA, etc. (4)), a conclusion which was verified by the identification of formaldehyde as a major product, and that IDA and MIDA decomposed at rates similar to $Fe^{III}NTA$ and therefore did not accumulate as reaction products.

The rates of disappearance of NTA were first order in $[Fe^{III}NTA]$, and first order rate coefficients k were estimated ($\pm 20\%$) for solutions initially 0.1 m in $Fe^{III}NTA$ and ionic strength 2.0 m (with NaCl) from the expression

$$[1] \qquad kt = \ln([NTA]_0/[NTA]_t)$$

where $[NTA]_t$ represents the total NTA concentration at time t. Values of $10^4 k$ (s^{-1}) of 0.22, 0.60, 0.94, 1.1, and 1.4 were obtained at temperatures of 503, 540, 554, 562, and 573 K respectively, and are represented to within the experimental uncertainty by the enthalpy ΔH^* and entropy ΔS^* of activation given in Table 1.

When $Fe^{III}NTA$ was prepared in solution at 503 K using $Fe(NO_3)_3$ rather than $FeCl_3$, or when $NaNO_3$ was added as such in 1.5:1 molar ratio to $Fe^{III}NTA$, the rate of disappearance of NTA increased about tenfold, the solution of products being bright yellow (due to iron(III)) and a red, non-ferromagnetic precipitate (presumably α-Fe_2O_3) being formed. This occurred even though $NaNO_3$ had no effect on NTA in the absence of iron(III), which indicates that the role of nitrate in promoting the decomposition of $Fe^{III}NTA$ consisted in maintaining the iron in the trivalent state.

In an equimolar mixture of $FeCl_3$ and H_3NTA, decomposition was almost complete in 4.5 h at 503 K, and almost all the iron was reduced to iron(II). Thus, hydrogen ion facilitates the redox (deacetylation) decomposition pathway, the decomposition being only about one-third complete for $Fe^{III}NTA$ alone under these conditions.

2. Nitrilotriacetatoferrate(II) Ion

On heating at 503 K, a solution 0.1 m in $FeCl_2$ and H_3NTA deposited the white solid $Fe_3(NTA)_2 \cdot H_2O$, which was identified by titration and by its infrared spectrum (18), whereas a similar solution of $FeCl_2$ and Na_3NTA precipitated a small amount of a black solid. The

TABLE 1. Pseudo-first order rate coefficients and enthalpies and entropies of activation for the decomposition of aqueous transition metal NTA complexes[a]

Species	Experimental temperature range (K)	ΔH^* (kJ mol^{-1})[b]	ΔS^* (J K^{-1} mol^{-1})[b]	k (s^{-1}) At 473 K	k (s^{-1}) At 573 K
$Fe^{III}NTA$	503–573	60 ± 3	-219 ± 6	8.5×10^{-6}[c]	1.4×10^{-4}
$Fe^{II}NTA^-$					1.6×10^{-5}[d]
$Co^{II}NTA^-$					$\sim 1.6 \times 10^{-6}$[e]
$Ni^{II}NTA^-$					$\sim 5 \times 10^{-5}$[e]
$Cu^{II}NTA^-$[f]	433–473	112 ± 3	-69 ± 7	1.1×10^{-3}	1.8×10^{-1}[c]
NTA^{3-}[g]	540–575	103 ± 5	-166 ± 8	9.0×10^{-8}[c]	1.1×10^{-5}
H_3NTA[g]	418–503	106 ± 5	-109 ± 10	3.1×10^{-5}	5.3×10^{-3}[c]
H_4NTA^+[g]	418–473	150 ± 14	$+11 \pm 32$	7.7×10^{-4}	9.6×10^{-1}[c]

[a]Initial total [NTA] = 0.1 m; ionic strength maintained at 2.0 m with NaCl for $Fe^{III}NTA$, $Fe^{II}NTA^-$, and uncomplexed NTA, but otherwise not controlled.
[b]Uncertainties are standard errors of regression coefficients.
[c]Extrapolated value.
[d]At 566 K; from yields of Fe_3O_4.
[e]Approximate value based on assumption of first order kinetics.
[f]Solutions of NaCuNTA.
[g]Reference 4.

black ferromagnetic solid product obtained at higher temperatures was identified by X-ray diffraction as magnetite, and was seen under the scanning electron microscope to be in the form of good octahedra up to about 50 μm across. The rate of disappearance of NTA was greater when $[Na_3NTA]:[FeCl_2]$ was 2:1 rather than 1:1.

For a variety of initial $[Fe^{II}NTA^-]$, the fractional extent of loss of NTA over a given time interval was the same, at a given temperature, so that the decomposition was first order in $[Fe^{II}NTA^-]$. Unfortunately, a meaningful representation of the time-dependence of the concentration of NTA surviving in solution in terms of the integrated first order rate equation could not be obtained, since the main slow phase of the disappearance of NTA from the solution was preceded by an apparent accelerated initial stage (probably due to the deposition of a small amount of $Fe_3(NTA)_2 \cdot H_2O$, as noted above) and followed by a second accelerated phase. The latter probably originated in heterogeneous catalysis of the decomposition reaction by the precipitated magnetite, as it was established separately that aqueous Na_3NTA decomposed to the extent of 35% in 2 h at 573 K under N_2 in the presence of added magnetite, but only 9% in its absence. This effect was not observed in the decomposition reactions of $Fe^{III}NTA$, which were relatively rapid and qualitatively different from those of $Fe^{II}NTA^-$.

On the other hand, the yield of Fe_3O_4, determined by dissolving the black precipitate in concentrated HCl and analyzing it for total iron (17), indicated that the dissolved iron content declined smoothly in accordance with the integrated first order rate equation, with rate coefficient $k = (1.6 \pm 0.2) \times 10^{-5}$ s^{-1} at 566 K. This rate of decomposition is of the same order of magnitude as that reported by Castle and Thompson (19) for the decomposition of iron(II) hydroxide in aqueous suspensions at 573 K according to the Schikorr reaction

$$[2] \qquad 3Fe(OH)_2 \rightarrow Fe_3O_4 + H_2 + 2H_2O$$

The ^1H nmr spectrum of solutions, initially 0.3 m in each of Na_3NTA and $FeCl_2$, decomposed at 571 K for 2 h, showed the presence of decarboxylation products such as MIDA in small amounts, but no deacetylation products such as IDA could be detected except when the reaction had been carried out under air (when iron(III) was formed). These observations confirmed that deacetylation in non-acidic solutions is associated with oxidation of the ligand by the metal ion.

The addition of HCl or NaOH to solutions of $Fe^{II}NTA^-$ produced modest increases in the rate of disappearance of NTA; thus, at 571 K for solutions initially 0.1 m in $FeCl_2$ and Na_3NTA, 20% NTA was lost after 2 h, as compared with 35% with addition of an equimolar amount of HCl and 42% with NaOH.

3. Nitrilotriacetatocobaltate(II) Ion

The initial decomposition of Co(II)–NTA complexes showed the same behaviour as that of Fe(II)–NTA complexes. At 503 K, $CoCl_2$ + H_3NTA gave $Co_3NTA_2 \cdot H_2O$. Small amounts of

brown solid, most likely oxidized $Co(OH)_2$, were formed upon heating solutions of $CoCl_2$ + Na_3NTA at temperatures above 500 K. After 44 h at 573 K only 10% of the initial amount of cobalt was precipitated. In each case, direct complexometric titration showed that the extent of decomposition of NTA was equal to the extent of formation of $Co(OH)_2$. The ^1H nmr spectrum after reaction for 8 h at 573 K showed the presence of NTA but only very small amounts of decarboxylation products and IDA, the latter most likely due to traces of dioxygen. The precipitation of Co(II) by hydroxide in the analytical procedure (4) was incomplete, and reliable analyses for chelating agents could not be obtained following attempts to remove cobalt(II) by this method. However, all other evidence showed that the $Co(II)NTA^-$ complex was kinetically the most stable of the complexes studied.

4. Nitrilotriacetatonickelate(II) Ion

When solutions containing equimolar amounts of Na_3NTA and $NiCl_2$ were heated at 573 K under N_2, $Ni(OH)_2$ was precipitated initially, but was subsequently reduced to metallic nickel. After 44 h, over 80% of the nickel had been precipitated as the metal, and the solution was almost colorless. Complexometric titrations showed that the NTA content of the solutions was only slightly in excess of the remaining nickel(II) at any time, that is, that the reduction of nickel(II) proceeded at essentially the same rate as the decomposition of NTA, and the two reactions are probably causally connected. The hydrothermal reduction of nickel(II) to the metal by the chelating agents ethylenediamine and diethylenetriamine at about 570 K has been observed in our laboratory by J. C. Arnold.

5. Nitrilotriacetatocuprate(II) Ion

Of the divalent transition metal ions, copper(II) has the highest stability constant for the formation of an NTA complex, and this strong interaction manifests itself (for example) in the dissolution of copper tubing by aqueous NTA at $pH \sim 11$ at room temperature, giving $NaCuNTA \cdot H_2O$ (20). Thus, although copper(II) often acts as an oxidant, *e.g.* of aliphatic amines (21), copper(I) complexes usually disproportionate to copper metal and their copper(II) analogues because of the high thermodynamic stability of the latter (22).

It was therefore not surprising that aqueous $Cu^{II}NTA^-$ decomposed readily at 425 K to deposit essentially pure copper metal; the color of the solution changed from blue to green to yellow as the reaction proceeded. Solutions of $CuCl_2$, similarly treated, showed no change other than the precipitation of a small quantity of a basic copper(II) chloride. When the solutions of $Cu^{II}NTA^-$ were made up from solid $NaCuNTA \cdot H_2O$ (20), the hydrothermally produced copper metal took the form of a fine powder, whereas solutions made from equimolar amounts of Na_3NTA and $CuCl_2$ yielded initially solid CuCl and subsequently large particles of copper metal. The presence of Cl^- also slowed the reduction to copper metal significantly; at 433 K, the amounts of copper produced in 5 h in the presence of 0.0, 0.2, and 1.8 *m* NaCl were 56, 52, and 21% respectively. In a highly acidic solution (initially 0.1 *m* in each of H_3NTA and $CuCl_2$; pH_{293} 1.2), however, the solid product was CuCl (20%) and about 80% of the copper(II) remained in solution after 2 h at 473 K, in which time the decomposition of NTA was about 50% complete; in this case, therefore, the latter reaction proceeded mainly by a pathway *not* involving reduction of copper(II).

An excess of copper(II) over complexing agents in the products was also observed for mixtures of $CuCl_2$ and Na_2H_2EDTA ($pH_{293} = 2$, and also when $pH_{293} = 6$ with NaOH). CuCl was the main product but some Cu metal was also present. Non-oxidative pathways were apparently predominant and the decomposition of $Cu^{II}EDTA^{2-}$ was faster than the decomposition of Cu(II)NTA under the same conditions. Iminodiacetatocopper(II) gave CuCl and Cu metal in a ratio 2:1. The rates of decomposition at 433 K decreased in the order EDTA $\gg$ IDA $>$ NTA.

The decomposition of the organic part of the complexes gave formaldehyde, and the mass spectrum of the gaseous products showed CO_2 and some CO. We also found that at 473 K aqueous $CuCl_2$ was reduced to CuCl by formaldehyde (23). ^1H nmr spectra indicated IDA as the major product and MIDA as a minor product. Only in the case of $H_4Cu(NTA)_2$ at $pH_{293} \sim 2.5$ were significant amounts of aminomonocarboxylic acids (mainly sarcosine) and methylamines (mainly dimethylamine) detected.

The amount of aqueous NTA that was

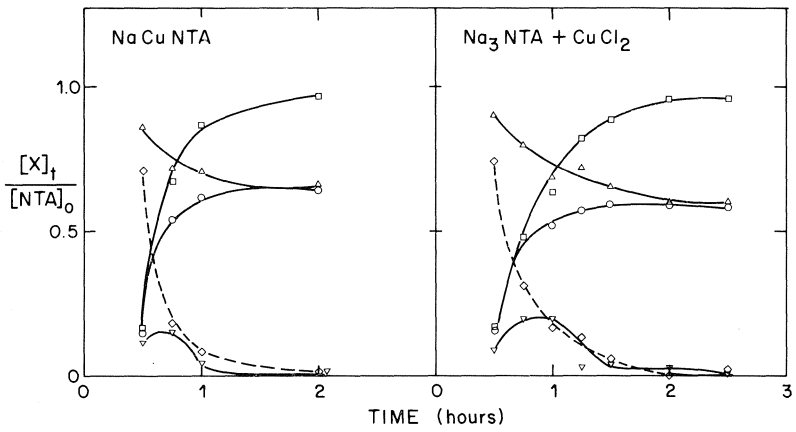

FIG. 1. The decomposition of $Cu^{II}NTA^-$ at 473 K. $[Cu^{2+}]_0 = [NTA^{3-}]_0 = 0.1\ m$. □, $[Cu(0)]_t$, copper metal formed; △, $[L]_t$, total amount of chelating agent; ○, $[L]_t - [Cu(II)L]_t$, uncomplexed chelating agent; ◇, $[Cu(II)]_t = [L]_t - ([L]_t - [Cu(II)L]_t)$; ▽, $[Cu(I)]_t = 1.0 - [Cu(0)]_t - [Cu(II)]_t$.

oxidized by an initially equimolar amount of solid CuCl in 2 h at 473 K was about half that oxidized by the same molar amount of copper(II). The decomposition of 2CuCl + Na_3-NTA progressed somewhat further than for $CuCl_2$ + Na_3NTA after 5 h at 433 K and no CuCl was detected among the products, but for 4CuCl + Na_3NTA considerable amounts of CuCl were still present after the reaction.

In the decomposition of aqueous NaCuNTA, or of $CuCl_2$ + Na_3NTA, complete reduction of copper(II) to the metal resulted in 75% loss of NTA, the remaining 25% of the reduction being accounted for by the further oxidation of the products IDA, HCHO, etc. This is consistent with the stoichiometry

$$[3]\quad Cu^{2+} + \begin{matrix}\diagdown\\ \diagup\end{matrix}\overset{+}{N}H{-}CH_2COO^- + H_2O \rightarrow$$

$$Cu + CO_2 + \begin{matrix}\diagdown\\ \diagup\end{matrix}NH_2^+ + HCHO + H^+$$

which also accounts for the observed initial fall in pH; eventually, however, the pH again rose because of the incursion of non-oxidative degradation of the aminoacids (*e.g.*, decarboxylation). The kinetics of the decompositions were followed at 433, 453, and 473 K (470 K in the last case for $CuCl_2$ + Na_3NTA) with respect to various reactants and products, and are illustrated by Fig. 1. The amount of Cu(II) remaining in solution was calculated from the difference between the total amount of complexing agent (determined after precipitation of copper ions with hydrazine by potentiometric titration after addition of $Zn(NO_3)_2$) and the amount of free ligand (from direct titration of the reaction mixture with $CuCl_2$ and murexide as indicator). The disappearance of Cu(II) followed closely the formation of copper metal. Formally, [Cu(I)] can be expressed as the amount of copper not accounted for by copper metal and Cu(II), and Fig. 1 shows clearly the initial build-up and subsequent decay of copper(I) expected of it as an intermediate in a series of consecutive reactions.

The formation of copper metal followed first order kinetics in $[Cu^{II}NTA^-]$ to 80% conversion with an induction time of about 0.4 h. The rate for this process was faster for NaCuNTA than for $CuCl_2$ + Na_3NTA, presumably because solid CuCl was formed as an intermediate in the latter case and its rate of disappearance was of the same order of magnitude as that of its formation. The rates of formation of copper metal were used to provide approximate first order rate coefficients k (±15%) for the decomposition of $Cu^{II}NTA^-$. For NaCuNTA, $10^4\ k$ (s^{-1}) was 0.7, 2.6, and 10 at 433, 453, and 473 K; for Na_3NTA + $CuCl_2$, $10^4\ k$ was 0.5, 2.5, and 6 at 433, 453, and 470 K.

Discussion

Of the transition metal NTA complexes considered here, only $Co^{II}NTA^-$ decomposed by simple decarboxylation of the ligand and deposition of $Co(OH)_2$, without net reduction or oxidation of the central metal atom. This complex showed remarkable thermal stability, being

less reactive than NTA^{3-} itself by an order of magnitude (Table 1). Thus, in the absence of complicating redox processes, coordination stabilizes the NTA^{3-} ligand.

Nitrilotriacetatoferrate(II) decomposed exclusively by decarboxylation, as did the cobalt(II) complex, but the product $Fe(OH)_2$, being unstable in aqueous systems near 570 K, decomposed to magnetite (19), which appeared to catalyze further decomposition of the NTA to a moderate extent. At low p*H*, $Fe(OH)_2$ formation would be suppressed, and indeed we found the solid product formed under acidic conditions to be $Fe_3(NTA)_2 \cdot H_2O$, which presumably resulted from reaction of $FeNTA^-$ with the $Fe^{2+}(aq)$ released as the ligand decomposed.

Iron(III) oxidized the NTA ligand with the formation of IDA, formaldehyde, and CO_2, whereupon the iron(II) product yielded magnetite as above. The oxidation is rapid relative to the decarboxylation of NTA^{3-}, etc., because the very favorable enthalpy of activation outweighs the strikingly negative entropy of activation in the temperature range of interest.

The decomposition of $Cu^{II}NTA^-$ clearly proceeded via a copper(I) intermediate, which in the presence of chloride yielded solid CuCl but otherwise disproportionated

$$[4] \qquad 2Cu^{II} \rightarrow 2Cu^{I} \begin{cases} \rightarrow Cu^0(s) + Cu^{II} \\ \xrightarrow{Cl^-} 2CuCl(s) \end{cases}$$

Solid CuCl would act as a buffer for Cu(I) in solution. As noted above, the disproportionation of copper(I) is favored by interaction with ligands such as NTA which strongly stabilize copper(II). The stability constant of $Cu^{II}IDA^0$ is much smaller than that of $Cu^{II}NTA^-$ (by a factor of at least 200, at 298 K (24)), so that the IDA formed by oxidation of NTA not only cannot compete effectively with the remaining NTA for coordination to copper(II) but is also less conducive than NTA to reaction 4 even when coordinated. Consequently, IDA accumulated as the chief oxidative degradation product, while the products of lower molecular weight (sarcosine and dimethylamine) were formed by decarboxylation rather than further oxidation of IDA. The oxidation of the NTA ligand in $CuNTA^-$ and in $FeNTA^0$ probably proceeded through successive one-electron transfers, the first being rate determining, and indeed a mechanism of this type has been proposed by Carey and Langford (14) for the photochemical degradation of $Fe^{III}EDTA^-$.

The product distributions in the oxidations of NTA by metal ions were in accordance with the schemes proposed by Langford and co-workers for the photolysis of $Fe^{III}NTA$ (10) and $Cu^{II}NTA^-$ (12), if it is recognized that their experiments were carried out under air and reoxidation of the reduced metal ions could occur (and, in particular, no copper(I) was isolated).

The studies described here and elsewhere (4) demonstrate that the high hydrothermal stabilities of NTA^{3-}, $Fe^{II}NTA^-$, and especially $Co^{II}NTA^-$ augur well for the application of NTA as a decontaminating reagent for the removal of cobalt-60 ferrite deposits in the heat transfer systems of water-cooled nuclear reactors under operating conditions of relatively high temperature and p*H* in conjunction with reducing conditions. Furthermore, the slow deposition of magnetite, copper, and nickel from NTA complexes in solution may lead to the formation of cohesive protective coatings in place of mobile particulate corrosion products. On the other hand, heterolytic catalysis of NTA decomposition on magnetite surfaces was suggested by some of our observations, and radiolysis of aqueous NTA has not been considered. Complete recovery of dissolved $^{60}Co^{II}NTA^-$ from solution may also prove to be technically difficult. It is perhaps more likely that NTA will find application in corrosion control in conventional steam-raising.

Finally, the activation parameters of Table 1 predict that, while NTA itself is expected to have a thermal half-life of some 8 million years in the hydrosphere (assumed 288 K, p*H* 7) (4), complexing with the ubiquitous iron(III) will reduce its environmental half-life to about 80 years as a consequence of the low ΔH^* for decomposition of $Fe^{III}NTA$. The corresponding half-life for $Cu^{II}NTA^-$ is 3000 years. By contrast, photochemical degradation of $Fe^{III}NTA$ or biodegradation of the free ligand should, when available, consume NTA pollutants in a matter of weeks (5–14).

Acknowledgements

We thank the National Research Council of Canada, the University of Calgary, and the

Izaak Walton Killam Fund for Advanced Studies for scholarships (to M.B.), and Atomic Energy of Canada, Ltd., for general financial support of this project through Whiteshell Nuclear Research Establishment.

1. J. R. METCALF. Boiler chelant treatment: an update. 31st Ann. Intern. Water Conf., Pittsburgh, Penn. (1970).
2. T. C. MARGULOVA, O. I. MARTINOVA, YU. P. SAMOILOV, and P. L. MEDVEDEV. Teploenergetika, 65 (1974).
3. M. TOMLINSON. Chem. Can. 21 (October 1974).
4. M. BOOY and T. W. SWADDLE. Can. J. Chem. This issue.
5. P. S. THAYER and C. J. KENSLER. C. R. C. Crit. Rev. Environ. Sci. **3**, 375 (1973).
6. H. MOTTOLA. Toxicol. Environ. Chem. Rev. **2**, 99 (1974).
7. A. E. MARTELL. Pure Appl. Chem. **44**, 81 (1975).
8. S. S. EPSTEIN. Intern. J. Environ. Stud. **2**, 291 (1972); **3**, 13 (1973).
9. A. H. PICKAVER. Soil Biol. Biochem. **8**, 13 (1976).
10. T. TROTT, R. W. HENWOOD, and C. H. LANGFORD. Environ. Sci. Technol. **6**, 367 (1972).
11. R. J. STOLZBERG and D. N. HUME. Environ. Sci. Technol. **9**, 654 (1975).
12. C. H. LANGFORD, M. WINGHAM, and V. S. SASTRI. Environ. Sci. Technol. **7**, 820 (1973).
13. H. B. LOCKHART and R. V. BLAKELEY. Environ. Sci. Technol. **9**, 1035 (1975).
14. J. H. CAREY and C. H. LANGFORD. Can. J. Chem. **51**, 3665 (1973).
15. YU. E. LEBEDEV. Trans. Moscow Energy Inst. **126**, 40 (1972).
16. N. I. KUZ`MENKO and E. M. YAKIMETS. Trudy Ural'sk Politekhn. Inst. **190**, 76 (1970); Energetik, 14 (1974).
17. A. I. VOGEL. Quantitative inorganic analysis. 3rd ed. Longmans, London. 1961.
18. F. J. M. RAJABALEE. Spectrochim. Acta, A**30**, 891 (1974).
19. J. E. CASTLE and R. G. THOMPSON. J. Appl. Chem. **17**, 177 (1967).
20. S. H. WHITLOW. Inorg. Chem. **12**, 2286 (1973).
21. T. A. LANE and J. T. YOKE. Inorg. Chem. **15**, 484 (1976).
22. J. BJERRUM and E. J. NIELSEN. Acta Chem. Scand. **2**, 297 (1948).
23. J. J. BYERLEY and W. K. TEO. Can. J. Chem. **47**, 3355 (1969).
24. A. E. MARTELL and R. M. SMITH. Critical stability constants. Vol. 1. Amino acids. Plenum Press, New York, NY. 1974.

Far infrared absorption and rotational vibrations of the guest molecules in structure I clathrate hydrates between 4.3 and 100 K

JOHN E. BERTIE AND STEPHEN M. JACOBS

Department of Chemistry, University of Alberta, Edmonton, Alta., Canada T6G 2G2

Received December 15, 1976

JOHN E. BERTIE and STEPHEN M. JACOBS. Can. J. Chem. **55**, 1777 (1977).

The infrared spectra between 330 and 15 cm^{-1} of the structure I clathrate hydrates of ethylene oxide, cyclopropane, and trimethylene oxide, at 4.3 K are presented. The spectra have an unusually high signal-to-noise ratio made possible by a Michelson interferometer and a silicon bolometer detector which operates at 1.2 K. Rotational vibrations of the guest molecules were observed at 65.0 and 35.6 cm^{-1} for ethylene oxide and at 69 and 50 cm^{-1} for trimethylene oxide. Inter-guest coupling of rotational vibrations is small and the two frequencies are assigned to vibrations about different inertial axes. The resulting force constants are 487 and 264 ferg rad^{-2} for ethylene oxide and 1190 and 1130 ferg rad^{-2} for trimethylene oxide and are discussed in relation to the barriers to reorientation of the guest molecule. The bands due to these vibrations are fairly sharp at 4.3 K, but are broad and poorly defined at 100 K. The guest and water vibrations interact predominantly through their transition dipoles, although the main contribution to the force constants of the rotational vibrations is from steric forces. The absorption by the water vibrations above 100 cm^{-1} is very similar for ethylene oxide and cyclopropane hydrates but significantly different for trimethylene oxide hydrate. Strong objections exist to the obvious interpretations of this difference which remains unexplained.

JOHN E. BERTIE et STEPHEN M. JACOBS. Can. J. Chem. **55**, 1777 (1977).

On présente les spectres infrarouges, à 4.3 K et entre 330 et 15 cm^{-1}, de la structure I des hydrates de clathrate de l'oxyde d'éthylène, du cyclopropane et de l'oxyde de triméthylène. Les spectres ont un rapport signal à bruit qui est anormalement élevé et qui est rendu possible par un interféromètre de Michelson et un détecteur bolomètre de silice qui opère à 1.2 K. On a observé les vibrations rotationnelles des molécules hôtes à 65.0 et 35.6 cm^{-1} pour l'oxyde d'éthylène et à 69 et 50 cm^{-1} pour l'oxyde de triméthylène. Le couplage des vibrations de rotation entre hôtes est faible et on peut attribuer les deux fréquences à des vibrations autour d'axes d'inertie différents. Les constantes de force qui en résultent sont de 487 et 264 ferg rad^{-2} pour l'oxyde d'éthylène et de 1190 et 1139 ferg rad^{-2} pour de l'oxyde de triméthylène et on les discute par rapport aux barrières de réorientation de la molécule hôte. Les bandes dues à ces vibrations sont assez précises à 4.3 K mais sont plus larges et mal définies à 100 K. Les vibrations de la molécule hôte et de l'eau interagissent d'une façon prédominante par l'intermédiaire de leurs dipoles de transition quoique la contribution principale des constantes de force des vibrations rotationnelles provient de forces stériques. L'absorption par les vibrations de l'eau au-dessus de 100 cm^{-1} est très semblable pour l'oxyde d'éthylène et les hydrates de cyclopropane mais diffère d'une façon importante pour l'hydrate d'oxyde de triméthylène. Des objections très fortes existent au sujet des interprétations qui paraissent évidentes pour ces différences qui demeurent inexpliquées.

[Traduit par le journal]

Introduction

The far-infrared spectra of the structure I clathrate hydrates (1) of ethylene oxide (2) and cyclopropane (3) at 100 K have been reported (4, 5). The rotational vibrations of the ethylene oxide molecules yield diffuse absorption between 100 and about 50 cm^{-1} (4, 5). At 100 K the water molecules have essentially fixed orientations (6) but the ethylene oxide molecular dipoles reorient at about 6 GHz (7). At 4.3 K the ethylene oxide molecules also have essentially fixed orientations (8) so that the clathrate hydrate has an essentially static structure with the water molecules and, probably, the guest molecules (8) orientationally disordered. It was of interest, therefore, to see if the absorption by the rotational vibrations of the guest molecules is sharper at 4.3 K than at 100 K and, if it is sharper, to obtain from the absorption frequencies a measure of the intermolecular forces acting on the guest molecules in the cages of water molecules.

This paper presents the spectra between 120 and about 15 cm^{-1} of the structure I clathrate hydrates and deuterates of ethylene oxide, cyclopropane, and trimethylene oxide (9–11) between

4.3 and 100 K, and spectra between 330 and 120 cm^{-1} of these compounds at 4.3 K.

No previous reports of the far-infrared spectra of structure I hydrates below 100 K exist. While this work was in progress, spectra were reported between 65 and 4 cm^{-1} of the structure II hydrate of tetrahydrofuran between 80 and 17 K (12) and between 100 and 10 cm^{-1} of the mixed structure II hydrates of hydrogen sulfide with carbon tetrachloride, chloroform, and methylene chloride, between 45 and 95 or 290 K (13).

Experimental

The preparation and characterization of the hydrates and deuterates of ethylene oxide (composition used: 6.7 $C_2H_4O{\cdot}46H_2O$ (or D_2O)) and cyclopropane ($6C_3H_6{\cdot}46H_2O$) have been described (4, 5). Structure I trimethylene oxide hydrate and deuterate were prepared by rapidly cooling to 77 K, in vacuum, de-gassed solutions of composition $6C_3H_6O{\cdot}46H_2O$ (or D_2O), then holding them at $-27°C$ for about two weeks before recooling them to 77 K for study (14). X-ray powder diffraction photographs and mid-infrared spectra (5, 14–16) showed the hydrates (deuterates) to be pure. To keep them pure, they were kept under liquid nitrogen and manipulated in a dry, 77–100 K, nitrogen atmosphere.

Spectroscopic pellet samples were made by mixing powdered hydrate and 0.50 g of adamantane in a 0.75 in. diameter piston and cylinder pressure vessel at 77 K, then pressing the powder into a pellet at $-30°C$, $-40°C$, or $-45°C$, all $\pm 5°C$, for ethylene oxide, cyclopropane, or trimethylene oxide hydrates, respectively. A pressure of 1000 bar was applied for at least $1\frac{1}{2}$ h, occasionally releasing it for 5 min. The pellet was cooled to 77 K under pressure to prevent shattering at the adamantane phase transition (17, 18). The pistons were removed and the cylinder, which held the pellet firmly, was placed in the copper sample holder of the infrared cell in a 77 K dry nitrogen atmosphere. The face of one piston of the pressure apparatus was cut at 89.7° to the axis of the piston, to bevel the pellet to reduce interference fringes. Other infrared samples, including all those for study above 120 cm^{-1}, were made by mixing powdered hydrate into 3-methyl pentane at 120 ± 10 K, in a teflon or TPX (Imperial Chemical Industries Ltd. trademark for methyl pentene polymer) cup which was 0.025 in. deep and had a bevelled (4.5°) base. The temperature was then lowered to 77 K and the 3-methyl pentane set to a glass containing powdered hydrate. The cup containing the sample was loaded into the copper sample holder at 77 K. Background spectra (4) were of adamantane pellets or 3-methyl pentane glasses which contained no hydrate, at the same temperature as for the sample spectra.

The infrared cell was a Janis Research Corporation, Inc. model 8DT variable low-temperature research Dewar. In this cell, the copper sample holder is suspended in an atmosphere of helium gas at the bottom of a central tube. At 4.3 K the sample is just above the surface of liquid helium in this tube. At higher temperatures liquid helium is vaporized by a heated diffuser plate and the gas cools the sample. The sample temperatures were measured by factory-calibrated platinum resistance and germanium resistance thermometers mounted in the copper sample holder. The temperatures were controlled to ± 0.1 K at 4.3 K and ± 2 K at higher temperatures, with the aid of two heaters mounted in the copper sample holder and a Cryogenic Research Model TC103 temperature controller which was modified to incorporate a precise decade resistance box. The cell was fitted with windows of crystal quartz for spectra below 120 cm^{-1}, or sapphire for spectra below 330 cm^{-1}, both cut perpendicular to the unique axis and sealed by Indium O-rings against the cold central tube. TPX windows were sealed by buna-N O-rings against the outer jacket of the cell. The cell was kept mounted in the spectrometer and was loaded while cold by carrying the copper sample holder immersed in liquid nitrogen to the cell, then quickly inserting it into the central tube.

Far-infrared spectra were recorded on a modified Beckman-RIIC FS-720 Interferometer described elsewhere (4). The detector was initially a Golay detector but a Molectron Corporation Model D1.5S-720 Silicon Bolometer Cryostat System was used for most of the work. This detector operates at 1.2 K and was found to be reliable, simple to use, and far superior to the Golay.

Results

The Janis cell transmitted far less radiation than the liquid nitrogen cell used previously (4, 5), and the spectra had a very poor signal-to-noise ratio when the Golay detector was used. Curve *a* of Fig. 1 shows a typical absorbance spectrum obtained from a single pair of sample and background interferograms using the Golay detector, and curve *b* shows the average of 14 such spectra. The better performance of the silicon bolometer is illustrated by curve *c*, which was obtained from a single pair of interferograms. Curves *d* and *e* of Fig. 1 show the spectra of 3-methyl pentane glass and an adamantane pellet at 4.3 K.

Figures 2 to 4 show unsmoothed averages of 3 to 5 spectra below 130 cm^{-1} of the structure I hydrates and deuterates of cyclopropane, ethylene oxide, and trimethylene oxide in adamantane pellets between 4.3 and 100 K. The frequencies of the reproducible features at 4.3 K are given in Table 1. In spectra of very strongly absorbing samples the absorbance decreases uniformly from the lowest feature listed to 15 cm^{-1}. The feature (Figs. 2 to 4) at 78, 76.5, or 74 cm^{-1} at 4.3, 50, or 100 K, respectively, is due to imperfect subtraction of the adamantane peak (Fig. 1). The features previously reported (5) at 23, 46, and 68 cm^{-1} for cyclopropane hydrate at 100 K were spurious (Fig. 2). The bands are clearly sharper at 4.3 K than at 100 K, but more detail is observed for ethylene oxide hydrate and deuterate at 100 K (Fig. 3) than was reported previously (4). This is due to the better detector *and*

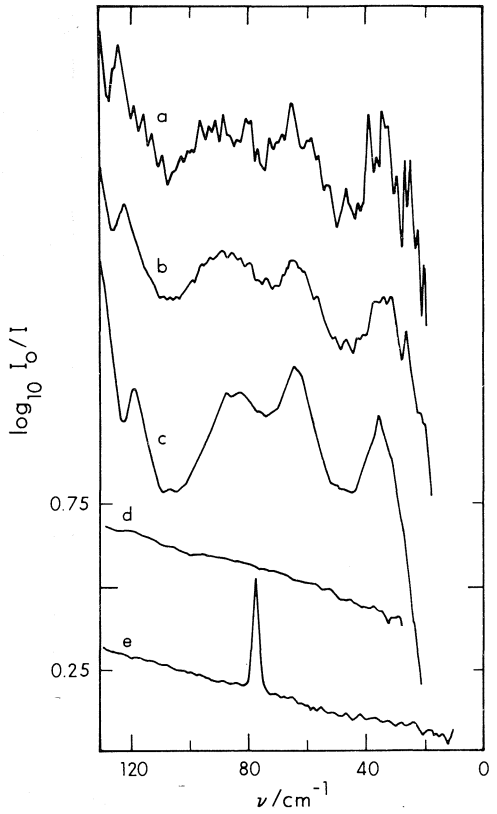

FIG. 1. Curve *a*: spectrum from one pair of sample and background interferograms recorded using the Golay detector. Curve *b*: the average of 14 spectra like curve *a*. Curve *c*: as curve *a* but recorded using the silicon bolometer detector. Curve *d*: spectrum of 3-methyl pentane glass, about $1\frac{1}{4}$ mm thick, at 4.3 K. Curve *e*: spectrum of a 2 mm thick adamantane pellet at 4.3 K. Resolution: 1.5 cm^{-1}. The curves have been offset for clarity.

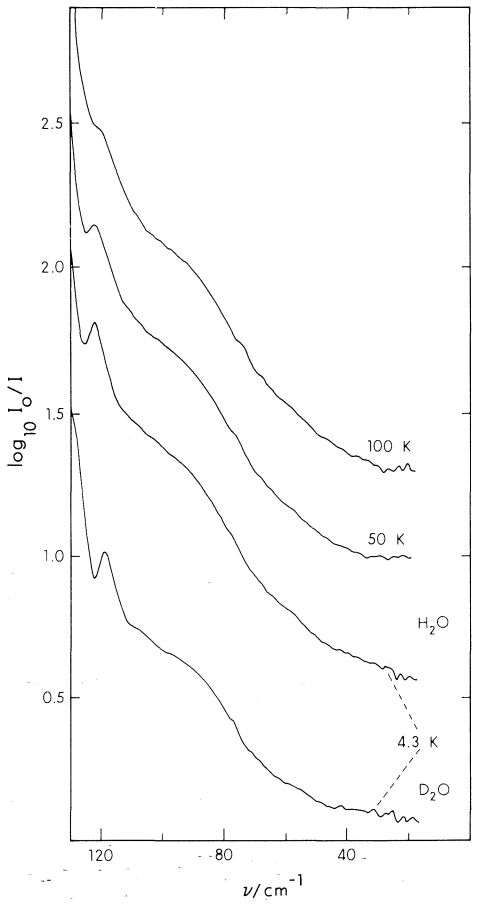

FIG. 2. Spectra of structure I cyclopropane deuterate at 4.3 K (bottom curve) and hydrate at 4.3, 50, and 100 K (top). Resolution: 1.8 cm^{-1}. The hydrate curves have been raised by 0.5 (4.3 K), 0.85 (50 K), and 1.20 (100 K) units for clarity.

to the pellet and glass techniques which allow much more strongly absorbing samples to be used than is possible with mulls (4). The assignment of the peaks and shoulders to water or guest vibrations (Table 1) is based on the isotope shifts, with slight ambiguity in the case of trimethylene oxide hydrate.

The temperature dependences of the spectra of trimethylene oxide hydrate and cyclopropane and ethylene oxide deuterates are similar to those shown (Figs. 2–4). The features above 100 cm^{-1} are all about 2 cm^{-1} lower in frequency at 100 K than at 4.3 K. The temperature shifts of the other features are ± 2 cm^{-1} or less, except for the 65 cm^{-1} band of ethylene oxide hydrate which shifts about 5 cm^{-1} (Fig. 3), and are probably due to increased breadth of the overlapping bands at high temperature.

The following evidence shows that the hydrates did not decompose during the preparation of the adamantane pellets. (*1*) The spectrum of cyclopropane deuterate dispersed in 3-methyl pentane glass at 4.3 K was identical to that of Fig. 2, except that the weak shoulders at 108 and 58 cm^{-1} were about half as prominent. (*2*) A 12.7 mol% aqueous solution of ethylene oxide in a Teflon cup was crystallized completely to yield $6.68C_2H_4O{\cdot}46H_2O$ (19); the Teflon cup was loaded into the cell and yielded spectra of the hydrate identical to those in Fig. 3. (*3*) Cyclopropane and trimethylene oxide hydrates were subjected to the pelleting procedure without adamantane, and were shown to be unchanged by X-ray powder photography (5, 14).

Figure 5 shows unsmoothed averages of three

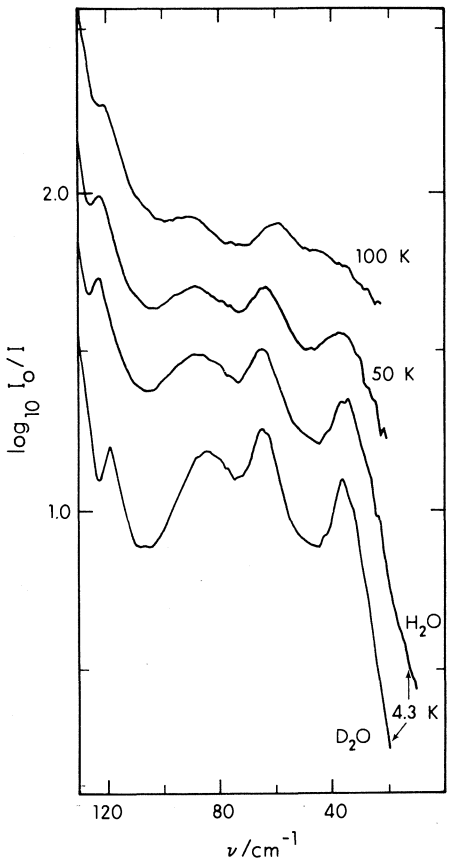

FIG. 3. Spectra of structure I ethylene oxide deuterate at 4.3 K (bottom curve) and hydrate at 4.3, 50, and 100 K (top). Resolution: 1.8 cm^{-1}. The hydrate curves have been raised by 0.4 (4.3 K), 0.65 (50 K), and 0.90 (100 K) units.

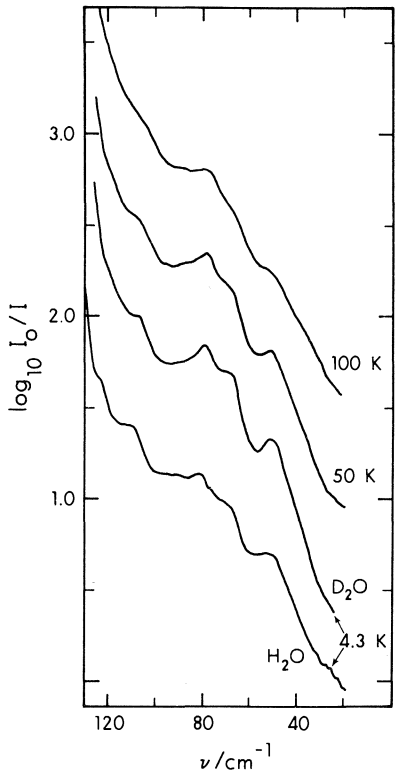

FIG. 4. Spectra of structure I trimethylene oxide hydrate at 4.3 K (bottom curve) and deuterate at 4.3, 50, and 100 K (top). Resolution: 1.8 cm^{-1} for hydrate, 2.8 cm^{-1} for deuterate. The deuterate curves have been raised by 0.25 (4.3 K), 0.75 (50 K), and 1.25 (100 K) units.

spectra of cyclopropane, ethylene oxide, and trimethylene oxide hydrates at 4.3 K between 330 and 100 cm^{-1}. The frequencies of the reproducible features are given in Table 2, with those of the deuterates. Curves *c* and *d* in Fig. 5 are both of cyclopropane hydrate and show that the relative intensity of the main peak is very sensitive to the size of the hydrate particles, increasing with decreasing particle size. The spectrum of very well ground ethylene oxide hydrate at 100 K is the same as reported previously (4, 5) except that the main peak has greater relative intensity. Thus, the frequencies are higher and more structure is resolved when the compounds are at 4.3 K. Curves *c* and *d* also show that the band shapes between 260 and 330 cm^{-1} are uncertain because of different amounts of 3-methyl pentane (curve *e*) in the sample and background glasses. Curve *e* proves that condensation of ice upon the samples was not a problem. Figure 6 shows several spectra of ethylene oxide hydrate at 4.3 K between 220 and 100 cm^{-1}, to prove the existence of the many weak features listed in Table 2.

Discussion

Relaxation data (7, 8, 11, 20, 21) for the hydrates studied (Table 3) indicate that the molecular reorientation rates are below far-infrared frequencies at 100 K. Thus, the perturbed "free" rotation invoked by Hadni and co-workers (13), to explain a band at 40 cm^{-1} in double clathrates, cannot contribute to the present spectra, which must, therefore, be due to absorption by translational (rattling) and rotational vibrations of the guest molecules superimposed on the broad, disorder-allowed absorption by the translational vibrations of the water molecules (4, 5). Whether the absorption by the guest mole-

TABLE 1. Spectral features below 130 cm^{-1} of structure I clathrate hydrates and deuterates at 4.3 K[a]

Compound	Frequency (cm^{-1}) Hydrate		Deuterate	Assignment[b]
Cyclopropane				
			sh 128	w
	125.5	min	122.3	w
	122.5	p	118.7	w
	115	cos	110.8	w
			sh 107.5	w
			cos 101.0	w
	~90	b.sh	~90	w
	58	sh	56.5 (1.5)	w
Ethylene oxide				
	136	sh		
	132	sh	129	w
	126.0	min	122.8	w
	122.6	p	118.9	w
	111.5 cos			w
	105	min	104	w
	87.5 (1.0)	p	84.3 (1.0)	w
	72	min	72	
	65.0	p	64.1	G
	45	min	45	
	35.6	p	35	G
Trimethylene oxide				
			cos 122	w
	124	sh	119	w
	116	cos	110	w
	110	sh	106	w
	100 cos		min 94	w
			sh 90	w
	82	p	80	w
	74.5	cos	73	
	69	sh	68 (2)	G
	60 cos		min 59	
	50 sh		p 51	G
	34	cos?	34	

[a]Frequencies are in cm^{-1} and their accuracy is ±0.5 if quoted to 0.1 or ±1 otherwise, except as noted in parentheses; sh, min, p, cos, and b, indicate shoulder, minimum, peak, change of slope, and broad.
[b]w, water vibration; G, guest vibration.

cules is observed and well-resolved depends on its intensity relative to that of the water molecules.

It is useful to assume that the vibrations of the guest and water molecules do not interact. In this approximation, the water absorption is constant for all structure I hydrates, apart from frequency shifts related to changes in the lattice parameter (5), because it is the density of vibrational states of the empty hydrate lattice weighted by an intensity function (4, 5). It is also useful to assume that the rotational vibrations of each guest molecule occur about the principal axes of inertia of the free molecule. In this case, two of the rotational vibrations of ethylene oxide and trimethylene oxide (22, 23) reorient the dipole moment, and absorb much more radiation than the other four intermolecular vibrations of each guest whose dipole moment derivatives arise solely from intermolecular forces (12). Klug and Whalley (12) analysed the absorption below 70 cm^{-1} by the structure II hydrate of tetrahydrofuran using these assumptions, which appear to hold for that case (24).

It is clear from Figs. 2 to 5 and Tables 1 and 2 that the first assumption holds rather well above 100 cm^{-1} for ethylene oxide and cyclopropane hydrates, but not for trimethylene oxide hydrate. Further, it is not good below 100 cm^{-1}, since the peaks at 87.5 and 82 cm^{-1} in the spectra of ethylene oxide and trimethylene oxide hydrates are sensitive to the water isotope but are replaced

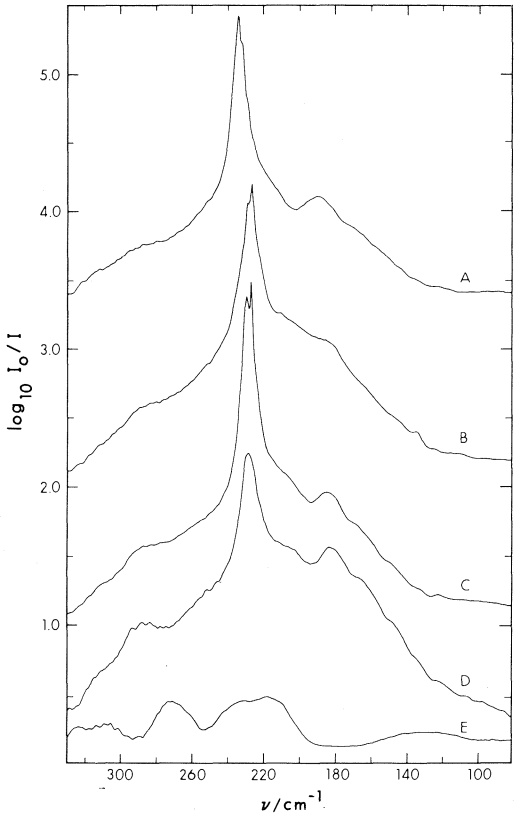

FIG. 5. Spectra of *a*, ethylene oxide hydrate (raised $3\frac{1}{4}$ units), *b*, trimethylene oxide hydrate (raised 2 units), *c*, cyclopropane hydrate (raised 1 unit), *d*, a less-well-ground sample of cyclopropane hydrate (raised $\frac{1}{4}$ unit), and *e*, 3-methyl pentane glass, ($\sim\frac{3}{4}$ mm thick), all at 4.3 K. Resolution: 2 cm^{-1}.

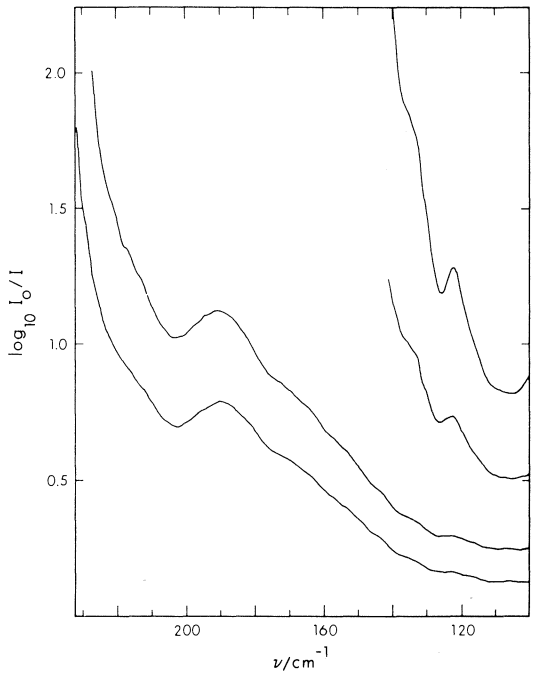

FIG. 6. Spectra of ethylene oxide hydrate at 4.3 K. The curves have been offset for clarity. Resolution: 2 cm^{-1}.

by a broad shoulder in the spectrum of cyclopropane hydrate. They are assigned to translational vibrations of the water which have gained intensity by interacting with the rotational vibrations of the guest. The second assumption is good for these hydrates, since two features in the spectrum of each hydrate with a dipolar guest can be assigned to the vibrations which rotate the dipole, while the other four intermolecular vibrations of each guest molecule are undetectable above 15 cm^{-1}.

The higher and lower frequency guest bands (Table 1) are assigned to the vibrations about the axes of lower and higher inertia, respectively, neglecting intermolecular coupling for the moment. With this assignment and the moments of inertia, *I*, in Table 3, the force constants, *k*, for the two rotational vibrations are calculated from $\nu = (2\pi c)^{-1}[kI^{-1}]^{1/2}$ to be 487 ± 7 and 264 ± 5 ferg rad^{-2} for ethylene oxide hydrate and 1190 ± 20 and 1130 ± 25 ferg rad^{-2} for trimethylene oxide hydrate.

The nearest-neighbor guest–guest intermolecular coupling force constant, *f*, must take a range of values if the orientations of the guest molecules are disordered. The limits of this range are $\pm 2\mu^2/r^3$ in the point-dipole approximation (12), where μ is the dipole moment of the guest molecule (Table 3) and *r* is the distance between the dipoles. For structure I hydrates, each guest molecule in a tetrakaidecahedral cage has two nearest-neighbor guest molecules, in the cages which share a six-sided face with its own cage. Thus, *r* is half of the cubic lattice parameter (Table 3) if the dipoles are central in the cages, and the limits of the interaction constant, *f*, are ±34 and ±35 ferg rad^{-2} for ethylene oxide and trimethylene oxide hydrates, respectively. If the interaction constants were all equal, the nearest-neighbor coupling would yield a range of frequencies from each molecular vibration, the frequencies given in the harmonic approximation by $\nu = (2\pi c)^{-1}[KI^{-1}]^{1/2}$ where *K* varies from $k + 2f$ to $k - 2f$. With the limiting interaction constants given above, these ranges are 60 to 69 cm^{-1} and 31 to 40 cm^{-1} for ethylene oxide hydrate and 66 to 70 and 49 to 52 cm^{-1} for trimethylene oxide hydrate. The ranges for orienta-

TABLE 2. Spectral features between 330 and 115 cm^{-1} of structure I clathrate hydrates and deuterates at 4.3 K[a]

Ethylene oxide			Cyclopropane			Trimethylene oxide		
Hydrate		Deuterate	Hydrate		Deuterate	Hydrate		Deuterate
~300	b.sh	~288	~288	b.sh	~280	~290	b.sh	~280
234.0	p	228	228.5	p	222.5	227.5	p	222.5
230	cos	225	225 cos			225 cos		
229	sh	224	224 sh			223	sh	218
227	cos	221				221	cos	214
225.5 sh						220	sh	213
223.5	cos	215	217 cos			218	cos	210
217 sh			215 sh					
212 sh		sh 208	~212	cos	~210			
208 cos			~205	b.sh	~200	~205	b.sh	~200
203	min	196	193	min	186	194	cos?	184
190	p	183	184	p	178	~180	b.sh	177
186	sh	178 ?	179	sh	174 ?			
182 sh								
176	cos	170	172	cos	166	170	cos	166
171	sh	166	168	sh	163			
164	sh	159	160	sh	~155	162	sh	157
159	cos	155	153	cos	149	155	cos	148
157 sh								
155 cos		sh 147	149	sh	145			
153 sh								
146	cos	142				144	sh	~140
144	sh	139	141	sh	139			
138	cos	134	137.5	cos	133	136.5	min	132.5
136 sh			136	sh	132	134.5	p	131.0
132 sh		sh 129	132	sh	128			
126.0	min	122.8	125.5	min	122.3	128	cos	122
122.6	p	118.9	122.5	p	118.7	124	sh	119

[a]The frequencies are in cm^{-1} and their accuracy is ± 0.5 cm^{-1} if they are quoted to 0.1 or ± 1 otherwise, except where ~ indicates that the feature is hard to define; sh, min, p, cos, and b, indicate shoulder, minimum, peak, change of slope, and broad.

TABLE 3. Parameters of guest molecules and their structure I hydrates

Parameter	Value		
	Cyclopropane	Ethylene oxide	Trimethylene oxide
Van der Waals diameter (Å)[a]	5.5	5.2	5.5, 6.2
Dipole moment (Debye)	0	1.88[b]	1.93[c]
Moments of inertia (amu $Å^2$)[d]		$I_a = 19.83$[b]	$I_b = 43.1$[e]
	—	$I_c = 35.85$	$I_c = 75.1$
Hydrate lattice parameter (Å)[f]	11.97	11.89	11.95
Guest dipole reorientation in hydrate:			
Arrhenius activation energy (kcal/mol)	—	1.4[g]	2.1[h]
Rate at 4.3 K	—	0 Hz[g,i]	0 Hz[h]
Rate at 50 K	—	64 MHz[g]	1 kHz[h]
Rate at 100 K	—	14 GHz[g,j]	20 MHz[h]

[a]Reference 1, which gives only the 5.5 Å diameter for trimethylene oxide. The diameter through the methylenic groups is 6.2 Å.
[b]Reference 28. Beware of incorrect moments of inertia in Table 15, p. 210 of ref. 1.
[c]Reference 22.
[d]About axes perpendicular to the dipolar axis.
[e]Reference 29.
[f]References 5 and 14.
[g]Reference 8 and calculations based thereon.
[h]Reference 11 and calculations based thereon.
[i]This is the calculated frequency of maximum loss But the dispersion is broad, and some dispersion was measurable at audio frequencies at 4.3 K (ref. 8).
[j]Experimentally, 7 GHz at 88 K (ref. 7).

tionally disordered guest molecules must be much smaller than these, probably by a factor of two. Thus, it is clear that inter-guest coupling can only contribute to the breadth of the bands and cannot invalidate the assignments given.

The interaction between the guest and water vibrations precludes a detailed analysis of the shapes of the guest bands such as that of Klug and Whalley (12). However, the bands must also be broadened by static and dynamic forces between the guest and water molecules; that is, by the disorder in the orientations of the water molecules, which causes the force constants, k, of the guest vibrations to vary from cage to cage (12), and by the interaction between the vibrations of the guest and water molecules. This latter interaction also causes the enhanced intensity of the water vibrations near 85 cm^{-1}, and appears to be greater in ethylene oxide hydrate than in trimethylene oxide hydrate. This indicates the predominant dynamic interaction to be between the transition dipoles of the guest (proportional to $\mu/I^{1/2}$) and water vibrations, and not steric interactions. In contrast, Klug and Whalley (12) have argued that the main static forces are non-electrostatic, with repulsive forces between hydrogen atoms on the guest and water molecules being important; the much larger force constants for trimethylene oxide than for ethylene oxide support their conclusion.

The force constants show that for ethylene oxide, trimethylene oxide, and tetrahydrofuran (606 and 465 ferg rad^{-2} (12)) in their hydrates (structures I, I and II, respectively) the rotation of the molecule in its plane meets less resistance than the rotation about the non-dipolar axis in the plane. Further, the force constants for ethylene oxide are both smaller than those for tetrahydrofuran. Thus the curvatures of the potential energy of the molecule with respect to its orientations in the cage are smaller for ethylene oxide, even though the barrier to reorientation of the ethylene oxide dipole (Table 3) is larger than that of the tetrahydrofuran dipole (0.92 kcal/mol (17)). A more quantitative comparison can be made by following Klug and Whalley (12) in assuming that the potential to guest reorientation about each axis is sinusoidal with period $2\pi/n$, and determining n by relating the vibrational quantum to the barrier height by an approximation (12) that is useful if the barrier is large compared to the vibrational quantum. For the in-plane and out-of-plane rotational vibrations, one calculates n to be 3.8 and 4.3 for tetrahydrofuran, using the data in ref. 12, 3.9 and 4.0 for trimethylene oxide, and 2.3 and 3.1 for ethylene oxide; alternatively, the geometric mean frequencies and moments of inertia yield n equal to 4.1 (12), 4.0, and 2.7, respectively. The four-fold potential calculated for tetrahydrofuran in the hexakaidecahedral cages suggested (12) that the guest molecule has minimum energy when its dipole is perpendicular to the four hexagonal faces of the cage, which are tetrahedrally disposed. No such physically appealing conclusions about the equilibrium orientations of ethylene oxide and trimethylene oxide in the tetrakaidecahedral cages are evident from the above values of n and the available approximate calculations (8, 11, 25). The four-fold potentials calculated for the in-plane and out-of-plane motions of trimethylene oxide suggest that the oxygen atom and the methylene groups are indistinguishable to the cage, and that axial and equatorial (8, 11, 25) configurations are equally favoured. Neither of these suggestions is compatible with the calculations (11) or with the existence of an ordering transition (11). For ethylene oxide hydrate, calculations suggest (8) that axial and near-equatorial orientations of the guest molecule are equally likely and it is unclear how two-fold and three-fold barriers arise from this. Thus, the sinusoidal potential is probably too great an approximation for these systems, except to yield the correlation that the relative periodicities calculated for trimethylene oxide and ethylene oxide undoubtedly reflect the large size of trimethylene oxide for the tetrakaidecahedral cage.

The broadening of the guest bands with increasing temperature is of the same magnitude as that observed for tetrahydrofuran hydrate (12), and is greater than is observed (24) for simple molecular crystals under the same conditions. It must arise from the three factors discussed previously (12). Of these, molecular reorientation is too slow (Table 3) to contribute more than about 1 cm^{-1} to the breadth at 100 K. Thus the broadening is due to the anharmonicity of the guest–host interaction potential, which is greater than that of the intermolecular potential of simple molecular crystals. The temperature dependence between 4.3 and 200 K of the spectrum of trimethylene oxide hydrate gave no evidence of the partial ordering transition (11) nor of the ring puckering vibration (23, 26).

Previous discussions of the spectra of ethylene oxide and cyclopropane hydrates between 300 and 100 cm^{-1} (4, 5) apply equally to the present

results. The extra details that are resolved when the samples are at 4.3 K are sufficiently similar in spectra of the two hydrates (Table 2, Figs. 5, 6) to indicate that they arise from features in the density of translational vibrational states of the hypothetical empty hydrate lattice. There are 138 branches of dispersion curves for this lattice so no simple description is possible and the exact origin of the features can only be determined by a calculation of the density of states. Such calculations have been made (27) but further refinement is needed and should be helped by the new data.

The spectra between 330 and 100 cm^{-1} of trimethylene oxide structure I hydrate and deuterate are presented for the first time (Fig. 5). The frequency of the strong central peak is very close to that in the spectrum of cyclopropane hydrate, reflecting (5) the nearly identical lattice parameters of the two hydrates (Table 3). But the spectra of the two hydrates differ between ~200 and 100 cm^{-1}, indicating that trimethylene oxide modifies the absorption by the water molecules. Two possible sources of this modification are evident, but there are strong objections to both. The ring puckering vibration, or an intermolecular vibration, of trimethylene oxide is an unlikely possible source, since its absorption intensity can surely not exceed that of a rotational vibration of trimethylene oxide, which is at least a factor of 10 weaker than the water absorption near 200 cm^{-1} (Figs. 4, 5). The second possible source is that the combination of the large size and the dipole moment of trimethylene oxide perturbs the lattice of water molecules but does not change the lattice parameter significantly from that of cyclopropane hydrate (Table 3). If this were the case, the absorption by the O—D stretching vibrations of HDO molecules isolated in a H_2O lattice, ν_{OD}(HDO), should reflect it. In fact the absorption by ν_{OD}(HDO) at 100 K indicates that both ethylene oxide and trimethylene oxide perturb the water lattice slightly from that of cyclopropane hydrate (14, 16), but gives no indication that trimethylene oxide has a greater effect. Trimethylene oxide structure I hydrate undergoes a partial ordering transition of the guest molecules at ~80 K (11), but neither the ν_{OD}(HDO) absorption nor any other mid-infrared absorption shows any significant change between 100 and 60 K (14). Thus the reason for the modification by trimethylene oxide of the water absorption between 200 and 100 cm^{-1} is unclear.

Acknowledgement

We thank the National Research Council of Canada for support.

1. D. W. Davidson. *In* Water, a comprehensive treatise. Vol. 2. *Edited by* F. Franks. Plenum Press, London. 1973. Chapt. 2.
2. R. K. McMullan and G. A. Jeffrey. J. Chem. Phys. **42**, 2725 (1965).
3. D. R. Hafemann and S. L. Miller. J. Phys. Chem. **73**, 1392 (1969); **73**, 1398 (1969).
4. J. E. Bertie and D. A. Othen. Can. J. Chem. **50**, 3443 (1972).
5. J. E. Bertie, F. E. Bates, and D. K. Hendricksen. Can. J. Chem. **53**, 71 (1975).
6. D. W. Davidson and G. J. Wilson. Can. J. Chem. **41**, 1424 (1963).
7. M. Davies and K. Williams. Trans. Faraday Soc. **64**, 529 (1968).
8. S. K. Garg, B. Morris, and D. W. Davidson. J. Chem. Soc. Faraday Trans. II, **68**, 481 (1972).
9. R. E. Hawkins and D. W. Davidson. J. Phys. Chem. **70**, 1889 (1966).
10. J. C. Rosso and L. Carbonnel. C. R. Acad. Sci. Paris, Ser. C, **274**, 1108 (1972).
11. S. R. Gough, S. K. Garg, and D. W. Davidson. Chem. Phys. **3**, 239 (1974).
12. D. D. Klug and E. Whalley. Can. J. Chem. **51**, 4062 (1973).
13. M. M. X. Gerbaux, C. Barthel, and A. Hadni. Spectrochim. Acta, **31A**, 1901 (1975).
14. P. G. Wright. Ph.D. Thesis, University of Alberta, Edmonton, Alta. 1976. Available from the Canadian Theses Division, Cataloguing Branch, National Library of Canada, 395 Wellington St., Ottawa, Ont. K1A 0N4. Quote Accession Number.
15. J. E. Bertie and D. A. Othen. Can. J. Chem. **51**, 1159 (1973).
16. J. E. Bertie and F. E. Bates. Unpublished results.
17. C. W. F. T. Pistorius and H. C. Snyman. Z. Phys. Chem. Neue Folge, **43**, 278 (1964).
18. E. F. Westrum, Jr. J. Phys. Chem. Solids, **18**, 83 (1961).
19. D. N. Glew and N. S. Rath. J. Chem. Phys. **44**, 1710 (1966).
20. A. W. K. Khanzada and C. A. McDowell. J. Mol. Struct. **16**, 1 (1973).
21. Y. A. Majid, S. K. Garg, and D. W. Davidson. Can. J. Chem. **47**, 4697 (1969).
22. S. I. Chan, J. Zinn, J. Fernandez, and W. D. Gwinn. J. Chem. Phys. **33**, 1643 (1960).
23. R. A. Kydd, H. Weiser, and M. Danyluk. J. Mol. Spectrosc. **44**, 14 (1972).
24. J. E. Bertie and S. M. Jacobs. Unpublished results.
25. D. W. Davidson. Can. J. Chem. **49**, 1224 (1971).
26. S. I. Chan, T. R. Borgers, J. W. Russell, H. L. Strauss, and W. D. Gwinn. J. Chem. Phys. **44**, 1103 (1966).
27. F. W. Birss, R. S. Gay, and J. C. Nash. Private communication.
28. G. L. Cunningham, Jr., A. W. Boyd, R. J. Myers, W. D. Gwinn, and W. I. Levan. J. Chem. Phys. **19**, 676 (1951).
29. S. I. Chan. J. Zinn, and W. D. Gwinn. J. Chem. Phys. **34**, 1919 (1961).

An improved synthesis of ishwarane: conversion of bicyclo[2.2.2]octenes to tricyclo[3.2.1.$0^{2,7}$]octanes via reductive homoallylic cyclization

RONALD B. KELLY AND SANDRA J. ALWARD

Department of Chemistry, University of New Brunswick, P.O. Box 5050, Saint John, N.B., Canada E2L 4L5

Received January 10, 1977

RONALD B. KELLY and SANDRA J. ALWARD. Can. J. Chem. **55**, 1786 (1977).

Conversion of the alcohol **4** into the mesylate **5** and reduction of the latter with $LiAlH_4$ under mild conditions afforded ishwarane **1** in 65% yield, thereby providing a further demonstration of the synthetic utility of such reductive, homoallylic cyclizations and a substantially improved synthesis of ishwarane.

RONALD B. KELLY et SANDRA J. ALWARD. Can. J. Chem. **55**, 1786 (1977).

La transformation de l'alcool **4** en son mésylate **5** et la réduction de ce dernier par $LiAlH_4$ dans des conditions douces fournit l'ishwarane **1** avec un rendement de 65%; cette synthèse fournit une démonstration supplémentaire de l'utilité en synthèse de telles cyclisations homoallyliques réductrices et une synthèse sensiblement améliorée de l'ishwarane.

[Traduit par le journal]

The presence of the tricyclo[3.2.1.$0^{2,7}$]octane system as a structural feature of the terpenoids ishwarane **1** and trachylobane **2** has recently stimulated considerable interest in devising synthetic methods for the construction of this system (1–5). In connection with our total syntheses of ishwarane (1) and trachylobane (2–4) we have described three methods for the conversion of bicyclo[2.2.2]octane systems, readily available by synthesis, into tricyclo[3.2.1.$0^{2,7}$]octanes.[1] All of these methods have been utilized in our total syntheses of trachylobane (2–4) but our reported (1) synthesis of ishwarane involved only the most lengthy of these.

The most convenient synthesis of trachylobane **2** involved reductive, homoallylic cyclization of the mesylate **3** directly to trachylobane (60%) by treatment with $LiAlH_4$ under mild conditions (ref. 4, *cf.* ref. 6). We now wish to bring our synthetic work on the bicyclo[3.2.1.$0^{2,7}$]octane system to a conclusion by reporting the application of this type of cyclization to an improved synthesis of ishwarane **1**. Thus, conversion of the alcohol **4**, the synthesis of which has already been described (1), into the mesylate **5** followed by reduction of the latter with $LiAlH_4$ under mild conditions (refluxing ether, 5 h) afforded ishwarane **1** in 65% yield. The fact that we were successful in converting 47 mg of the alcohol **4** into ishwarane **1** in 65% yield (see Experimental) attests to the amenability of this procedure to small-scale preparations.

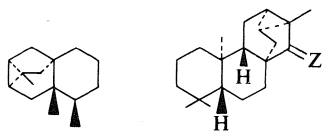

1 **2** Z = H,H; **6** Z = O

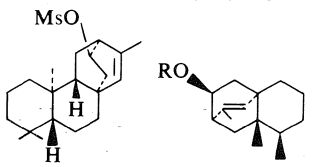

3 **4** R = H; **5** R = Ms

Since the alcohol **4** is a totally synthetic intermediate encountered in our former synthesis of ishwarane **1** (1), its conversion into ishwarane, as just described, represents a new total synthesis of this sesquiterpene. In our former synthesis (1), the conversion of the alcohol **4** into ishwarane **1** required six steps and was accomplished in 23% yield. Hence, the conversion of **4** into ishwarane via the homoallylic cyclization of the mesylate **5** represents a substantially improved total synthesis of this sesquiterpene and further demonstrates the synthetic utility of such cyclizations.[2]

[1]For a discussion of such conversions, with emphasis on mechanism and stereochemistry, see ref. 4.

[2]For another useful type of homoallylic cyclization whereby the mesylate **3** was converted into the ketone **6** see refs. 3 and 4.

Experimental

A solution of 47 mg of the alcohol **4** in 3.5 ml of dry pyridine was cooled to 0°C then treated with 0.13 ml of methanesulfonyl chloride. The solution was left, under nitrogen, at −15°C for 66 h then at 15°C for a further 24 h. Ice was added to the reaction mixture and the resulting cold solution was extracted three times with ether and the ether extracts were washed with cold 1 *N* hydrochloric acid and finally with cold brine. Evaporation of the dried ether extracts afforded 60 mg of the mesylate **5**; ν_{max}(neat) 3020, 1655 and 800 cm^{-1} (olefin), 1345 and 1175 cm^{-1} (mesylate); nmr ($CDCl_3$), δ 0.74 (d, J = 6.5 Hz, 3H, secondary methyl), 0.98 (s, 3H, angular methyl), 1.78 (d, J = 2 Hz, 3H, vinylic methyl), 2.98 (s, 3H, mesylate), 4.75 (m, 1H, SO_2O—C—H), 5.74 (m, 1H, vinylic proton). The mesylate was used directly for the next step.

A solution of 60 mg of the mesylate **5** in 4 ml of ether was added over a period of 30 min to a stirred suspension of 60 mg of lithium aluminum hydride in 4 ml of ether under nitrogen. The mixture was then refluxed for 5 h, cooled, treated with 0.4 ml of brine, stirred for 1 h, then dried by addition of anhydrous sodium sulfate and filtered. Evaporation of the filtrate and purification of the residue by tlc on silica gel with hexane as solvent afforded 28 mg (65%) of (±)-ishwarane. The synthetic sesquiterpene was identical with an authentic sample of ishwarane obtained from natural sources by the following criteria: identity of ir and nmr spectra, single peak on glc when coinjected with an authentic sample.[3]

Acknowledgments

We thank the National Research Council of Canada for a grant in support of this work.

1. R. B. KELLY, J. ZAMECNIK, and B. A. BECKETT. Can. J. Chem. **50**, 3455 (1972).
2. R. B. KELLY, J. EBER, and H. K. HUNG. Can. J. Chem. **51**, 2534 (1973).
3. R. B. KELLY, J. EBER, and H. K. HUNG. J. Chem. Soc. Chem. Commun. 689 (1973).
4. R. B. KELLY, B. A. BECKETT, J. EBER, H. K. HUNG, and J. ZAMECNIK. Can. J. Chem. **53**, 143 (1975).
5. R. M. CORY and D. M. T. CHAN. Tetrahedron Lett. 4441 (1975).
6. R. A. APPLETON, J. C. FAIRLIE, and R. MCCRINDLE. Chem. Commun. 690 (1967).

[3]The properties of ishwarane are given in ref. 1.

The sodium borohydride reduction of *N*-sulfonylpyridinium salts. Synthesis of *N*-sulfonyl-1,4- (1,2-) dihydropyridines

EDWARD E. KNAUS AND KINFE REDDA

Faculty of Pharmacy and Pharmaceutical Sciences, University of Alberta, Edmonton, Alta., Canada T6G 2N8

Received December 23, 1976

EDWARD E. KNAUS and KINFE REDDA. Can. J. Chem. **55**, 1788 (1977).

Reaction of alkyl (aryl) sulfonyl chlorides and sulfonic acid anhydrides with pyridine in the presence of sodium borohydride afford *N*-sulfonyl-1,4-dihydropyridines (**1**) and *N*-sulfonyl-1,2-dihydropyridines (**2**). The ratio of products (**1**:**2**) was dependent upon solvent and temperature. Reaction of **2***d* with 4-phenyl-1,2,4-triazoline-3,5-dione (**4**) afforded the *endo*-adduct **5**.

EDWARD E. KNAUS et KINFE REDDA. Can. J. Chem. **55**, 1788 (1977).

La réaction des chlorures d'alkyle (aryle) sulfonyles et des anhydrides d'acides sulfoniques avec la pyridine en présence de borohydrure de sodium conduit aux *N*-sulfonyldihydro-1,4 pyridines (**1**) et aux *N*-sulfonyldihydro-1,2 pyridines (**2**). Le rapport des produits (**1**:**2**) dépend du solvant et de la température. La réaction de **2***d* avec la phényl-4 triazoline-1,2,4 dione-3,5 (**4**) conduit à l'adduit *endo* **5**.

[Traduit par le journal]

The use of pyridinium salts as precursors for the synthesis of pharmacologically active agents provides an attractive route to reduced pyridine heterocycles. Although the antibacterial activity of some *N*-sulfonylpiperidine derivatives have been studied (1), the preparation of *N*-sulfonyl-1,2-dihydropyridines has not been reported. The synthesis of *N*-benzene (methane) sulfonyl-1,4-dihydropyridine from cyclopentadiene was recently described (2). Many of the benzenesulfonamides already prepared and tested as antibacterial agents possess five- and six-membered heteroaromatic rings as N^1-substituents (1). It would be of interest, therefore, to develop a one-step synthesis of benzenesulfonamides in which the N^1-sulfonamide nitrogen is part of a 1,2- or 1,4-dihydropyridyl ring system. Treatment of a mixture of pyridine and sodium borohydride with alkyl (aryl) sulfonyl chlorides and sulfonic acid anhydrides, using a modification of the procedure reported by Fowler (3) for the preparation of *N*-methoxycarbonyl-1,2-dihydropyridine, now provides a convenient route to *N*-sulfonyl-1,4-dihydropyridines (**1**) and *N*-sulfonyl-1,2-dihydropyridines (**2**).

Reaction of pyridine with methanesulfonyl chloride in methanol at −65°C in the presence of sodium borohydride afforded *N*-methanesulfonyl-1,2-dihydropyridine (**2***a*, 32.1%) as the sole product. A similar reaction employing methane sulfonic anhydride gave **2***a* (37.2%). On the other hand, reaction with benzenesulfonyl chloride using the same conditions, gave rise to an isomeric mixture of **1***b* and **2***b* in a ratio of 1:8 as determined from the integrals of the H-4 and H-2 absorptions at δ 2.68 and 4.16 for the respective compounds.[1] The reaction of benzenesulfonyl chloride with pyridine (both solvent and reactant) in the presence of sodium boro-

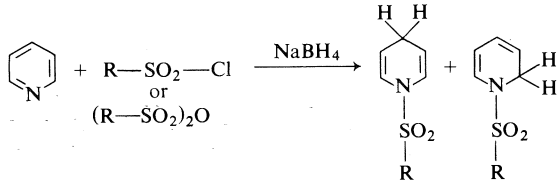

a, R = Me-
b, R = Ph-
c, R = *p*-Me-C_6H_4-
d, R = *p*-MeCONH-C_6H_4-

hydride at 25°C was investigated to determine if the isomeric product ratio **1**:**2** was dependent upon solvent and temperature. Reaction under these conditions gave rise to an isomeric mixture of **1***b* and **2***b* in a ratio of 5:4.[1] The results of similar reactions employing benzenesulfonic anhydride are shown in Table 1.

The reaction of *p*-toluenesulfonyl chloride with pyridine (solvent) at 25°C in the presence of sodium borohydride afforded an isomeric mixture of **1***c* and **2***c* in a ratio of 1:1.[1]

Structure–activity studies of benzenesulfonamides have shown that a N^4-amino group or a group such as a N^4-acetamido group which can

[1]This ratio was determined for the unpurified reaction product since 1,2-dihydropyridines **2** undergo considerable decomposition upon purification.

undergo metabolic biotransformation to a N^4-amino group *in vivo* is required for antibacterial activity. It was therefore of interest to investigate this reaction employing *N*-acetylsulfanilyl chloride. Reaction with pyridine using methanol as solvent at −65°C did not occur probably due to the low solubility of *N*-acetylsulfanilyl chloride. When the reaction was carried out using pyridine as solvent at 25°C an isomeric mixture of **1***d* and **2***d* in a ratio of 2:1 was obtained.[1] The presence of both **1***d* and **2***d* was substantiated further since catalytic reduction with palladium–charcoal and hydrogen gave **3** as a single product which was identical with the product obtained from the reaction of piperidine and *N*-acetylsulfanilyl chloride (4).

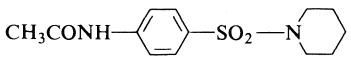

3

A successful separation of **1***d* and **2***d* could not be achieved using column or thin layer chromatography. However pure **1***d* can be obtained by treating a mixture of **1***d* and **2***d* with 4-phenyl-1,2,4-triazoline-3,5-dione (**4**). The 1,2-dihydro isomer **2***d* reacts readily via a ($\pi 2 + \pi 4$) cycloaddition reaction with **4** to give 5-*endo*-*p*-acetylsulfanilyl-2,3,5-triazabicyclo[2.2.2]oct-7-ene-2,3-*endo*-dicarboxylic acid *N*-phenylimide (4) which is consistent with the reported reaction of **2***b* with **4** (5). Compounds **1***d* and **5** are readily separated by preparative thin layer chromatography. Both acidic and alkaline hydrolyses of the N^4-acetamido group of **1***d* to liberate the free amine gave rise to intractable tar even though acidic hydrolysis of the N^4-acetamido group of **3** is known to proceed smoothly (6).

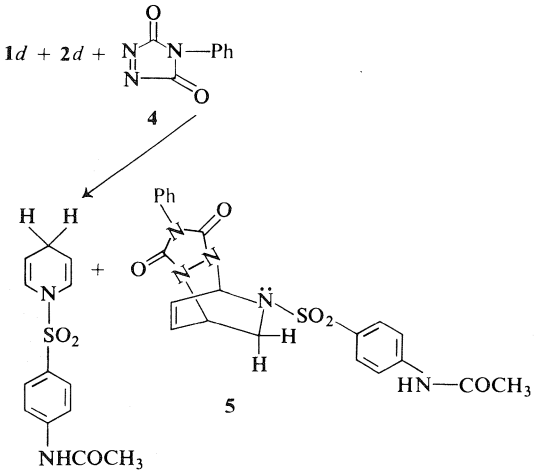

1*d*

TABLE 1. Isomeric product ratio's of 1,4- and 1,2-dihydropyridines

Product mixture	Reactant	Solvent	Reaction temp. (°C)	Reaction time (h)	Ratio **1**:**2**[a]	Ratio **1**:**2**	Yield **1** (%)	Yield **2** (%)
1*b* and **2***b*	$PhSO_2Cl$	MeOH	−65	1.5	1:8	1.8:5.8[b]	1.8[b,d]	5.8[b,d]
1*b* and **2***b*	$PhSO_2Cl$	C_5H_5N	25	15	5:4	12:5[c]	17[c,d]	7.1[c,d]
1*b* and **2***b*	$(PhSO_2)_2O$	MeOH	−65	1.5	4:29	1:5[c]	6.7[c,d]	33.6[c,d]
1*b* and **2***b*	$(PhSO_2)_2O$	C_5H_5N	25	15	7.5:4	3.4:1[c]	23.7[c,d]	7.0[c,d]
1*c* and **2***c*	*p*-Me-C_6H_4-SO_2Cl	C_5H_5N	25	15	1:1	7:5[b]	7.7[b]	6.3[b]
1*d* and **2***d*	*p*-MeCONH-$C_6H_4SO_2Cl$	C_5H_5N	25	15	2:1	4:1[c]	16.7[c]	4.2[c]

[a]Determined from the integrals of the C_2-H and C_2-H of **1** and **2**, respectively, for the unpurified reaction mixture.
[b]Determined from percentage yields of purified isolated products **1** and **2**.
[c]Determined from the integrals of the C_4-H and C_2-H for a purified mixture of **1** and **2**, respectively, eluted from a neutral alumina column.
[d]There is considerable loss of both **1** and **2** during column purification since only 40–60% of **1** and 25–40% of **2** is recovered.

The reduction of *N*-sulfonylpyridinium salts appears to be dependent upon solvent and temperature. Attack by hydride anion occurs predominately or exclusively at the 2-position to give *N*-sulfonyl-1,2-dihydropyridines **2** using methanol as solvent at −65°C whereas attack at the 4-position is usually favoured slightly when pyridine is employed as solvent at 25°C (see Table 1).

The broad spectrum pharmacological screening of **1***d* is presently in progress.

Experimental

Melting points were determined with a Büchi capillary apparatus and are uncorrected. Nuclear magnetic resonance spectra were determined for solutions in deuterochloroform, unless otherwise noted, with TMS as internal standard with a Varian A-60 or HA-100 spectrometer. Infrared spectra (in potassium bromide unless otherwise noted) were taken on a Unicam SP-1000 spectrometer. Mass spectra were measured with an AEI-MS-9 or MS-50 mass spectrometer and these exact mass measurements are sometimes used in lieu of elemental analyses.

*N-Methanesulfonyl-1,2-dihydropyridine (**2***a*)

General Procedure A

Sodium borohydride (0.8 g) was added to a solution of pyridine (1.58 g, 0.02 mol) in methanol (7.5 ml) pre-cooled to −65°C. A solution of methanesulfonyl chloride (2.29 g, 0.02 mol) in dry ether (5 ml) was added dropwise during 15 min. After stirring for 1.5 h at −65°C the reaction mixture was poured onto crushed ice (75 ml) and allowed to come to room temperature. Extraction with chloroform (3 × 30 ml), drying (Na_2SO_4), and removal of the solvent *in vacuo* gave a yellow oil which was chromatographed on a 2.5 × 15 cm neutral alumina column. Elution with 300 ml chloroform gave 1.02 g (32.1%) of **2***a* as a yellow oil: ir (film) 1350, 1160 cm^{-1} (SO_2); nmr δ 6.24–6.62 (1H, m, C_6-H), 5.8–6.18 (1H, m, C_4-H), 5.3–5.73 (2H, m, C_3-H, C_5-H), 4.25 (2H, d ($J_{2,3}$ = 4 Hz) of d ($J_{2,4}$ = 1.5 Hz), C_2-H), 2.92 (3H, s, Me). *Exact Mass* calcd. for $C_6H_9NO_2{}^{32}S$: 159.0354; found: 159.0355.

When the reaction was carried out as described above using 3.48 g (0.02 mol) methanesulfonic anhydride 1.18 g (37.1%) of **1***b* was obtained.

*N-Benzenesulfonyl-1,4-dihydropyridine (**1***b) and N-Benzenesulfonyl-1,2-dihydropyridine (**2***b)*

Sodium borohydride (0.8 g) was added to a solution of pyridine (1.58 g, 0.02 mol) in methanol (20 ml) pre-cooled to −65°C. A solution of benzenesulfonyl chloride (3.52 g, 0.02 mol) in dry ether (10 ml) was added dropwise during 15 min and the reaction was completed as described under procedure A. The reaction product was then chromatographed on a 2.5 × 15 cm neutral alumina column. Elution with benzene (400 ml) gave 0.591 g (13.37%) of an isomeric mixture of **1***b* and **2***b* which was purified further by tlc using five 8 × 8 in. silica gel PF 254 plates, 0.5 mm in thickness, with benzene as development solvent. Extraction of the fraction having an R_f of 0.55–0.6 gave 0.078 g (1.8%) of **1***b*: mp 83–85°C (lit. (2) mp 86–89°C); ir 1352, 1175 cm^{-1} (SO_2); nmr δ 7.58 (5H, m, Ph), 6.47 (2H, d ($J_{2,3}$ = $J_{5,6}$ = 8.5 Hz) of d ($J_{2,4}$ = $J_{4,6}$ = 1.5 Hz), C_2-H, C_6-H), 4.88 (2H, m ($J_{2,3}$ = $J_{5,6}$ = 8.5 Hz), C_3-H, C_5-H), 2.68 (2H, m, C_4-H). *Exact Mass* calcd. for $C_{11}H_{11}NO_2{}^{32}S$: 221.0511; found: 221.0506.

Extraction of the fraction having an R_f of 0.3–0.5 gave 0.257 g (5.8%) of **2***b*: mp 68–69°C; ir 1360, 1340, 1175 cm^{-1} (SO_2); nmr δ 7.62 (5H, m, Ph), 6.63 (1H, d ($J_{5,6}$ = 7.75 Hz) of d ($J_{4,6}$ = 0.8 Hz), C_6-H), 5.8 (1H, m, C_4-H), 5.34 (2H, m, C_3-H, C_5-H), 4.16 (2H, d ($J_{2,3}$ = 4 Hz) of d ($J_{2,4}$ = 1.5 Hz), C_2-H). *Exact Mass* calcd. for $C_{11}H_{11}NO_2{}^{32}S$: 221.0511; found: 221.0506.

General Procedure B

Sodium borohydride (0.8 g) was added to a mixture of pyridine (10 ml) and benzenesulfonyl chloride (3.53 g, 0.02 mol) pre-cooled to 0°C with stirring. The reaction was allowed to proceed for 15 h at 25°C after which it was poured onto crushed ice (100 ml). Extraction with chloroform (4 × 100 ml), drying (Na_2SO_4), and evaporation of the solvent *in vacuo* afforded a brown oil which was subjected to chromatography on a 2.5 × 26 cm neutral alumina column. Elution with benzene (700 ml) afforded 1.06 g of an isomeric mixture composed of 0.75 g (17%) of **1***b* and 0.312 g (7.1%) of **2***b* as determined by the integrals of the C_4-H and C_2-H of **1***b* and **2***b*, respectively.

Reaction of benzenesulfonic anhydride (5.86 g, 0.02 mol) with pyridine (1.58 g, 0.02 mol) in the presence of sodium borohydride (0.8 g) as described under procedure A and purification of the reaction mixture as described above afforded 1.78 g of an isomeric mixture consisting of 0.3 g (6.7%) of **1***b* and 1.49 g (33.6%) of **2***b* as determined by the integrals of the C_4-H and C_2-H of **1***b* and **2***b*, respectively.

Reaction of benzenesulfonic anhydride (5.86 g, 0.02 mol) with pyridine (10 ml) in the presence of sodium borohydride (0.8 g) as described under procedure B and then elution from a neutral alumina column as described above gave 1.36 g of an isomeric mixture composed of 1.05 g (23.7%) of **1***b* and 0.31 g (6.95%) of **2***b* as determined by integrals.

*N-p-Toluenesulfonyl-1,4-dihydropyridine (**1***c) and N-p-Toluenesulfonyl-1,2-dihydropyridine (**2***c)*

Sodium borohydride (0.8 g) was added to a mixture of pyridine (10 ml) and *p*-toluenesulfonyl chloride (3.81 g, 0.02 mol) pre-cooled to 0°C with stirring. The reaction was completed as described under procedure B to give a brown semi-solid which was subjected to chromatography on a 2.5 × 26 cm neutral alumina column. Elution with benzene (250 ml) gave 0.36 g (7.7%) of **1***c*: mp 93–95°C; ir 1370, 1345, 1170 cm^{-1} (SO_2); nmr δ 7.68 (2H, d (J = 8 Hz), *ortho* phenyl hydrogens), 7.38 (2H, d (J = 8 Hz), *meta* phenyl hydrogens), 6.44 (2H, d ($J_{2,3}$ = $J_{5,6}$ = 8.5 Hz), of d ($J_{2,4}$ = $J_{4,6}$ = 1.5 Hz), C_2-H, C_6-H), 4.86 (2H, m ($J_{2,3}$ = $J_{5,6}$ = 8.5 Hz), C_3-H, C_5-H), 2.7 (2H, m, C_4-H), 2.42 (3H, S, CH_3). *Exact Mass* calcd. for $C_{12}H_{13}NO_2{}^{32}S$: 235.0667; found: 235.0659.

Further elution with benzene–ether (1:1 v/v) (250 ml) gave 0.297 g (6.32%) of **2***c*: mp 59–61°C; ir 1350 and 1170 cm^{-1} (SO_2); nmr δ 7.67 (2H, d (J = 8 Hz), *ortho* phenyl hydrogens), 7.38 (2H, d (J = 8 Hz), *meta* phenyl hydrogens), 6.58 (1H, d ($J_{5,6}$ = 7.75) of d ($J_{4,6}$ = 0.8), C_6-H), 5.8 (1H, d ($J_{3,4}$ = 8 Hz) of d ($J_{4,5}$ = 4.5 Hz) of d ($J_{2,4}$ = 1.5 Hz), C_4-H), 5.36 (2H, m, C_3-H, C_5-H), 4.12 (2H, d ($J_{2,3}$ = 4 Hz) of d ($J_{2,4}$ = 1.5 Hz), C_2-H), 2.42 (3H, s,

CH_3). *Exact Mass* calcd. for $C_{12}H_{13}NO_2{}^{32}S$: 235.0667; found: 235.0659.

*N-p-Acetylsulfanilyl-1,4-dihydropyridine (**1d**), N-p-Acetylsulfanilyl-1,2-dihydropyridine (**2d**), and 5-endo-p-Acetylsulfanilyl-2,3,5-triazabicyclo[2.2.2]-oct-7-ene-2,3-endo-dicarboxylic Acid N-phenylimide (**5**)*

Sodium borohydride (0.8 g) was added to a mixture of pyridine (10 ml) and *p*-acetylsulfanilyl chloride (4.67 g, 0.02 mol) pre-cooled to 0°C with stirring. The reaction was completed as described under general procedure B to give a reddish semi-solid which was chromatographed on a 2.5 × 26 cm neutral alumina column. Elution with ether–methanol (6:1 v/v) (300 ml) gave 1.198 g of an isomeric mixture consisting of 0.96 g (16.7%) of **1***d* and 0.24 g (4.2%) of **2***d* as determined from the integrals of the C_4-H and C_2-H of **1***d* and **2***d*, respectively. 4-Phenyl-1,2,4-triazoline-3,5-dione (0.069 g, 0.392 mmol) in methylene chloride (10 ml) was added dropwise with stirring to a solution of 0.543 g of the above mixture of **1***d* and **2***d* (containing 0.109 g, 0.392 mmol of **2***d*) in methylene chloride (20 ml) pre-cooled to 0°C. The reaction was allowed to proceed 1 h, after which the solvent was removed *in vacuo* to give a white solid. Preparative tlc on four 8 × 8 in. silica gel PF 254 plates, 0.5 mm in thickness, with ethyl acetate as development solvent afforded 0.094 g of **1***d* having an R_f of 0.86: mp 138–140°C; ir 1705, 1690 (C=O), 1350, 1168 cm^{-1} (SO_2); nmr δ 9.78 (1H, s, NH, exchanges with deuterium oxide), 7.81 (2H, m, *ortho* phenyl hydrogens), 7.58 (2H, m, *meta* phenyl hydrogens), 6.38 (2H, d ($J_{2,3} = J_{5,6} = 8.5$ Hz) of d ($J_{2,4} = J_{4,6} = 1.5$ Hz), C_2-H, C_6-H), 4.86 (2H, m ($J_{2,3} = J_{5,6} = 8.5$ Hz), C_3-H, C_5-H), 2.67 (2H, m, C_4-H), 2.16 (3H, s, CH_3). *Exact Mass* calcd. for $C_{13}H_{14}N_2O_3{}^{32}S$: 278.0725; found: 278.0721.

Extraction of the fraction having R_f 0.27 gave 0.06 g of **5**: mp 200–204°C; ir 1700 (C=O), 1372, 1160 cm^{-1} (SO_2); nmr (DMSO-d_6) δ 10.5 (1H, s, —NH, exchanges with deuterium oxide), 7.25–8.0 (9H, m, phenyl hydrogens), 5.3–6.68 (3H, m, C_4-H, C_7-H, C_8-H), 4.96 (1H, m, C_1-H), 4.5 (2H, m, C_6-H), 3.15 (3H, s, CH_3). *Anal.* calcd. for $C_{21}H_{19}N_5O_5S$: C 55.63, H 4.19, N 15.45; found: C 55.66, H 4.21, N 15.62.

*N-p-Acetylsulfanilylpiperidine **3***

Catalytic hydrogenation of a 4:1 mixture of **1***d* and **2***d* (95 mg) in methanol (30 ml) was carried out in the presence of palladium-on-charcoal (30 mg) and hydrogen gas at 50 psi for 72 h. Removal of the charcoal by filtration and evaporation of the solvent under reduced pressure afforded 0.055 g (57.1%) of **3** as a white solid, mp 156°C (lit. (5) mp 156°C), identical ir and nmr, with the authentic sample.

Acknowledgments

We are grateful to the Medical Research Council of Canada (Grant MA-4888) for financial support of this work and to the Canadian International Development Agency (CIDA) for a graduate scholarship to K.R.

1. R. G. SHEPHERD. *In* Medicinal chemistry. Part I. *Edited by* A. Burger. Wiley-Interscience, Toronto, Ont. 1970. Chapt. 16. p. 255.
2. D. M. STOUT, T. TAKAYA, and A. I. MEYERS. J. Org. Chem. **40**, 563 (1975).
3. F. W. FOWLER. J. Org. Chem. **37**, 1321 (1972).
4. L. N. GOLDYREV and I. Y. POSTOVIKII. J. Appl. Chem. (USSR), **11**, 316 (1938); Chem. Abstr. **32**, 5801 (1938).
5. E. E. KNAUS, F. M. PASUTTO, C. S. GIAM, and E. A. SWINYARD. J. Heterocycl. Chem. **13**, 481 (1976).
6. H. L. VAUGHN and M. D. ROBBINS. J. Org. Chem. **40**, 1187 (1975).

Multilayer oxidation of polycrystalline platinum

ROBERT J. BERRY

Division of Physics, National Research Council of Canada, Ottawa, Ont., Canada K1A 0R6

Received March 2, 1977

ROBERT J. BERRY. Can. J. Chem. **55**, 1792 (1977).

The formation of a visible oxide film on polycrystalline Pt foil and wire is reported, and positively identified. The conditions for growth and dissociation of the oxide are outlined, and the energy of decomposition is estimated.

ROBERT J. BERRY. Can. J. Chem. **55**, 1792 (1977).

On rapporte et identifie positivement la formation visible d'une couche d'oxyde sur des lames et des fils de platine polycristallins. Les conditions sous lesquelles l'oxyde croît et désassocie sont exposées, et l'energie de décomposition est estimée.

Introduction

Wohler (1), in 1903, reported that Pt black (powder), Pt sponge (finely divided), and smooth Pt foil (all of unstated purity) could be oxidized and indeed visibly darkened in the latter two cases by prolonged heating near 420°C in dry oxygen (pressure unstated, but presumed to be about 1 atm). Since then the oxidation of finely divided Pt has been confirmed by Busch (2) using 1 atm of oxygen at 550°C. However the surface oxidation of Pt foil (or wire) could not be confirmed by Betteridge and Rhys (3) (1961) on high purity Pt, leading them to suggest that Wohler's discolouration of Pt foil might be due to the oxidation of impurities on the Pt surface. Several other authors have concurred with this explanation and the prevailing opinion up to now (*e.g.* ref. 4) has been that heating Pt foil or wire in oxygen or air below 500°C produces only a strongly adherent atomic layer or two of oxygen (or Pt oxide) on its surface.

Under widely different conditions of temperature, pressure, and Pt surface structure than were used by Wohler, there is considerable evidence that Pt will oxidize. For example: Pt foil and wire are known to form a volatile oxide above 800°C in air or oxygen (3); Pt sponge and wire have been oxidized under oxygen pressures of 40–180 atm at 450°C (5); Pt single crystals are reportedly oxidized to the few atomic layer levels under 10^{-8} Torr oxygen at 840°C (6); and evaporated Pt films are reportedly oxidized under about 0.5 Torr oxygen at 400°C (7). Finally we note that, under radically different conditions than Wohler's, Pt has been oxidized when used as electrodes in electrolytic cells (8), and when it has been sputtered onto substrates in oxygen–argon mixtures (9).

In this paper we wish to briefly outline new work that shows conclusively that modern high purity Pt foil and wire will oxidize beyond the few atomic layer levels under something approaching the conditions used by Wohler, and, of interest to thermometrists, under something approaching the conditions often encountered with Pt resistance thermometers.

Results

In our experiments polycrystalline Pt wire (99.99% pure) and Pt foil (99.98% pure), obtained from Sigmund Cohn Corp., U.S.A., have been heated at 450–550°C inside fused silica tubes filled with research grade oxygen at about 1 atm pressure. Within a few days a surface discolouration is visible, and after 1 month or more the surface film is of sufficient thickness (estimated to be about 50–100 atomic layers) that it appears dark blue or black to the naked eye. Microscopic examinations reveal that the surface has a granular colour pattern, indicating that different crystal faces are reacting at different rates.

Evidence that we are dealing with an oxide film is given by the fact that its growth rate depends strongly on oxygen pressure, becoming virtually zero at pressures as low as 10 Torr. In addition, heating a blackened specimen at 600°C or higher in 1 atm of air causes the Pt surface to return to its original bright metallic appearance, undoubtedly due to the dissociation of the oxide film.

To demonstrate conclusively that the film is

not due to the oxides of impurities on the Pt surface, we have stripped the film off a sample of oxidized foil (0.015 mm thick) by immersing it in hot aqua regia. The film was left in the acid for 2 days to ensure that all unoxidized Pt was dissolved, following which it was washed in distilled water many times. A semi-quantitative analysis of the film by the Analytical Chemistry Section of the National Research Council of Canada using optical emission spectroscopy revealed that the only metallic element present beyond the trace impurity level was Pt, which is what one would expect for a Pt oxide film.

This oxidation process was first detected here about two years ago during high precision (0.1 ppm) electrical resistance measurements on Pt resistance thermometers that were specially filled with oxygen to a pressure of 500 Torr (at 22°C). The ice point resistance, $R(0°C)$, was found to increase rapidly when the Pt sensing wire (0.1 mm diameter) was heated in the 450–550°C range and then decreased rapidly in the 600–700°C range. Similar resistance changes have been observed by others during surface oxidation of other metals (4). The usual explanation is that part of the metal is converted into a poorly conducting oxide skin thus reducing the effective cross-sectional area of the metal and increasing its electrical resistance. It was first suspected that we were not dealing with oxidation of trace impurities in the Pt when the measured resistance ratio, $R(100°C)/R(0°C)$, was found to remain constant within ± 15 ppm while $R(0°C)$ changed by up to 0.2%. This resistance ratio is normally very sensitive to changes in the concentration (or oxidation state) of impurities in the Pt (10); however, if the Pt itself is oxidizing one expects the ratio to remain practically unchanged because essentially only the size of the conductor is changing.

It can be readily shown that the change in resistance should be proportional to the thickness of the oxide film to a first approximation (11). Hence by following this very sensitive parameter we have obtained a great deal of information about the surface oxidation of Pt.

Four main points will be mentioned here. Firstly during the initial stages of oxidation the film growth follows the standard logarithmic dependence on time (4). Secondly the heat of decomposition of the oxide has been determined by measuring the temperature for reaction equilibrium (*i.e.* zero oxide growth rate just prior to the onset of dissociation) at a number of oxygen pressures. Using the standard thermodynamical relationships between the dissociation pressure, temperature, and heat of decomposition (12) we estimate the latter to be about 41 ± 2 kcal per mol of oxygen in the region 450–600°C. This value is in reasonable agreement with a value of 32 ± 10 given for solid PtO_2 at 25°C in the "Oxide Handbook" (13). Thirdly, it is also possible to oxidize the Pt in $\frac{1}{2}$ to 1 atm of air at about 450°C at a rate which is easily detected in Pt resistance thermometers. Fourthly the comparatively small oxygen-activated thermal cycling effect found earlier in Pt resistance thermometers in the 0–450°C range by the author (11) is almost certainly due to an initial fractional monolayer of oxide formed on the Pt surface.

A detailed description of the experiments and results outlined here is being prepared for publication. Also further work on the identification of the particular form of oxide involved, and its crystalline structure, is in progress.

Acknowledgments

The author would like to thank Mr. D. G. Kearney for his assistance with the measurements on Pt resistance thermometers, Mr. D. S. Russell and Mr. P. Tymchuk for their spectrographic analysis, and Dr. D. F. Mitchell of the Metallic Corrosion and Oxidation Section for helpful comments on the manuscript.

1. L. Wohler. Ber. Deutsch. Chem. Ges. **36**, 3476 (1903).
2. R. H. Busch. Zeit. Naturforsch. B**5**, 130 (1950).
3. W. Betteridge and D. W. Rhys. First International Congress on Metallic Corrosion. London, April 1961. Butterworth. p. 186.
4. O. Kubaschewski and B. E. Hopkins. Oxidation of metals and alloys. Butterworths, London. 1962. pp. 35, 195, and 248.
5. P. Grandadam. Ann. Chim. Ser. II. **4**, 84 (1935).
6. R. Ducros and R. P. Merril. Surface Sci. **55**, 227 (1976).
7. Ch. Weissmantel, K. Schwabe, and G. Hecht. Werkst. Korros. **12**, 353 (1961).
8. W. Visscher and M. Blijlevens. Electrochim. Acta, **19**, 387 (1974).
9. C. D. Bennewitz, W. D. Westwood, and J. D. Brown. J. Appl. Phys. **46**, 558 (1975).
10. R. J. Berry. Comité International des Poids et Mesures, Comité Consultatif de Thermométrie, Session de 1964. Gauthier-Villars (Paris). Annexe 4, p. T40.
11. R. J. Berry. Temperature measurement 1975. Conference Series No. 26, Institute of Physics, London. 1975. p. 99.
12. O. Kubaschewski, E. L. Evans, and C. B. Alcock. Metallurgical thermochemistry. 4th ed. Pergamon Press, London. 1967. p. 9.
13. G. V. Samsonov. The Oxide Handbook. Plenum, New York. 1973. p. 42.

Canadian Journal of Chemistry

Published by
THE NATIONAL RESEARCH COUNCIL OF CANADA

Journal canadien de chimie

Publié par
LE CONSEIL NATIONAL DE RECHERCHES DU CANADA

Volume 55 Number 11 June 1, 1977

Volume 55 numéro 11 1 juin 1977

Effects of phase density on ionization processes and electron localization in fluids

JOSHUA JORTNER
Department of Chemistry, Tel-Aviv University, Tel-Aviv, Israel
AND
ARIEL GAATHON[1]
Department of Physical Chemistry, The Hebrew University, Jerusalem, Israel

Received November 1, 1976

JOSHUA JORTNER and ARIEL GAATHON. Can. J. Chem. **55**, 1801 (1977).

In this paper we shall be concerned with the energetics of selective ionization processes in simple nonpolar fluids and with the nature of electron localization in polar fluids, studied over a wide density range. The static features of bound Wannier states and of the conduction band in simple solid and fluid insulators were monitored by vacuum-ultraviolet absorption spectroscopy and photoemission studies providing quantitative information concerning the energy of the bottom of the conduction band, impurity ionization potentials, and adiabatic polarization energies. Electron localization in subcritical and supercritical water and ammonia was studied by pulse radiolysis methods. A critical, temperature dependent, density ρ_C for electron localization in ND_3 was observed. The weak density dependence of the maximum of the absorption band of the localized electron in D_2O and ND_3, and the temperature and density dependence of ρ_C in ND_3, provide compelling evidence for the crucial role of density fluctuations on electron localization in polar fluids.

JOSHUA JORTNER et ARIEL GAATHON. Can. J. Chem. **55**, 1801 (1977).

Dans cette publication on est intéressé à l'énergie des processus d'ionisation sélective dans des fluides non-polaires simples et avec la nature de la localisation électronique dans des fluides polaires qui sont étudiés sur un grand écart de densité. On a déterminé les caractéristiques statiques des états Wannier liés et des bandes de conduction dans des solides simples et dans des isolants fluides en faisant appel à la spectroscopie d'absorption dans l'ultra-violet lointain et par des études de photoémission fournissant des informations quantitatives concernant l'énergie au minimum de la bande de conduction, les potentiels d'ionisation des impuretés et les énergies de polarisation adiabatique. On a étudié, par des méthodes de radiolyse pulsées, la localisation d'électrons dans de l'eau et de l'ammoniac à l'état sous-critique et supercritique. On a observé une densité critique, ρ_C, dépendant de la température, pour la localisation d'électrons dans ND_3. La faible dépendance sur la densité du maximum de la bande d'absorption des électrons localisés dans D_2O et ND_3 et les dépendances sur la température et la densité de ρ_C dans ND_3 fournissent des implications importantes sur le rôle crucial des fluctuations de densité sur la localisation des électrons dans des fluides polaires.

[Traduit par le journal]

I. Introduction

The understanding of the nature of excess electron states in fluids (1–3) provides a challenging problem in the general area of the physics and chemistry of disordered materials. In the past decade there has been substantial experimental and theoretical progress in the elucidation of the electronic structure and of electron transport in polar and in nonpolar

[1]Present address: Department of Biological Sciences, Columbia University, New York, NY, U.S.A.

liquids with regard to the molecular composition, the static structure, and the dynamic properties of the medium. An attempt to provide a general classification of excess electron states in fluids is presented in Table 1. The gross features of the quasi-free electron state (3–5) (class 1) as well as localized excess electron states resulting from bubble formation in nonpolar fluids (3–5) (class 5) and via the formation of the solvated electron in polar fluids (1, 2; for a recent review, see ref. 6) (class 6) are well understood. On the other hand, the nature of 'intermediate type' excess electron states with regard to temporal (time-resolved) and structural aspects of electron localization are not yet well established. These include 'quasi-localized' states (class 2) originating from fluctuations in the local electron–medium potential which may result in Anderson localization (3, 7) of the excess electron, self-trapping by small configurational fluctuations (8) (class 3), and electron localization by pre-existing traps (9–11) (class 4). The present paper will be concerned with physical information concerning:

(*1*) The energetics of ionization processes and the features of the quasi-free excess electron states in simple nonpolar solids and fluids. Spectroscopic techniques, utilizing vacuum-ultraviolet optical absorption spectroscopy and electron photoemission to probe energy levels, were applied to these problems.

(*2*) Electron localization in polar fluids, studied by monitoring the yields of localized excess electrons. Conventional time-resolved absorption spectroscopy combined with pulse radiolysis methods for determination of the yields of localized electrons were utilized.

While most of previous studies of excess electron states in fluids focused attention on electrons in liquids, the results of the work reported herein will provide pertinent information regarding the effects of phase density on ionization processes and on electron localization, studied over a broad density range.

II. Selective Ionization Processes in Solids and in Dense Fluids

The optical absorption spectra of pure and of lightly doped simple insulators, such as solid and liquid rare gases, can be analyzed in terms of stable exciton or impurity states converging to the bottom of the conduction band (13, 15; for a recent review see ref. 12). The relative simplicity of these exciton and impurity states makes it possible to gain detailed information regarding ionization processes in a dense medium. The sources of experimental information regarding such selective ionization processes are:

(*A*) Identification of Wannier bound states in pure materials and of Wannier atomic or molecular impurity states in doped insulators by absorption spectroscopy. The Wannier series converges to the bottom of the conduction band.

(*B*) From the convergence limit of the Wannier series studied by absorption spectroscopy one can obtain the band gap, E_G, in the pure substance or the impurity ionization potential, E_G^i, of the impurity in the medium.

(*C*) The energetics of the Wannier states, monitored by absorption spectroscopy, result in basic information regarding the characteristics of the conduction band. In particular, from the effective Rydberg constant of the Wannier series one can deduce the effective mass of the electron near the minimum of the conduction band.

(*D*) The threshold for photoconductivity in the pure solid or liquid results in a direct measurement of E_G, while the photoconductivity threshold E_G^i of the doped insulator yields the ionization potential of the impurity in the medium.

(*E*) The threshold for external photoemission from the pure material, E_{TH}, or from the doped insulator, E_{TH}^i, results in the external ionization potentials. From the combination of optical spectra and photoemission yields in pure or in doped insulators one can determine the energy V_0 of the bottom of the conduction band relative to the vacuum level.

In what follows we shall consider first the energetics of ionization processes in solids where Wannier series are now well documented. Subsequently, we shall consider the application and implication of these results for fluids over a wide density range.

In pure insulators low-lying stable excitons originate from Bloch states near the top of the valence band and in the vicinity of the bottom of the conduction band (16–18). Impurity excited states below interband threshold can be considered in terms of a hole in the energetically flat impurity band correlated with electron states, which are constructed from levels near

TABLE 1. Excess electrons in fluids*

Definition	Physical state of fluid	Nature of electron–fluid interaction	State of excess electron	Time scale	Characteristic systems and physical properties
1. Quasi-free	Structure of fluid unperturbed	Single scattering by fluid structure factor $s(\boldsymbol{Q})$ Multiple scattering off density fluctuations (?)	Extended	Adiabatic injection in *all* fluids Long t scale when $V_0 < E_t^B$	$\mu \geq 10^2\ V^{-1}\ cm^2\ s^{-1}$ All fluids short time Heavy rare gases Ar, Kr, Xe Low density nonpolar (He) and polar (H_2O, NH_3) fluids
2. Quasi-localized	Structure of fluid unperturbed	Strongly changing local potentials	Localized (Anderson model) (?) or extended	Long t scale	$0.1 \leq \mu \leq 10\ V^{-1}\ cm^2\ s^{-1}$ T activated motion Some hydrocarbons (?) Transition range in He gas (?)
3. Self-trapped by small density and/or structural fluctuations	Small configurational fluctuations induced by e	Local attractive potential (homopolaron)	Localized (?)	$t \geq \tau_{MM}$	$0.1 \leq \mu \leq 10\ V^{-1}\ cm^2\ s^{-1}$ T activated Some hydrocarbons (?)
4. Localized by pre-existing 'traps'	Unperturbed pre-existing configurational fluctuations	Local attractive potential of 'trap'	Localized	$t \sim \sigma\langle v\rangle n_{trap}$ $t \leq \tau_{DR}$	$\mu \leq 0.1\ cm^2\ V^{-1}\ s^{-1}$ Polar liquids 'short' times $\tau_{DR} \sim 10^{-10}$–10^{-12} s Polar molecular clusters in hydrocarbons. Polar gases
5. Localized by bubble formation	Formation of microscopic cavity, large configurational changes	Essentially repulsive $V_0 > E_t^B$	Localized	$t \gg \tau_{MM}$	$\mu \sim 10^{-2}$–$10^{-3}\ cm^2\ V^{-1}\ s^{-1}$ Volume expansion Optical spectra Liquid He, Ne
6. Localized by large local configurational changes	Radial and orientational changes induced by e	Bound polaron in polar liquids	Localized	$t \gtrsim \tau_{DR}$	$\mu \sim 10^{-3}\ cm^2\ V^{-1}\ s^{-1}$ Optical spectra, etc. solvated electron in polar liquids

*V_0 = Energy of quasi-free electron (qfe) state; μ = electron mobility; σ = cross section for trapping of qfe by a pre-existing cluster; E_t^B = energy of ground state energy of localized electron (class 5 or 6) in the same fluid; τ_{MM} = time scale for molecular motion; τ_{DR} = dielectric relaxation time.

the bottom of the conduction band. In insulators such as solid rare gases, we are primarily concerned with deep exciton and impurity states, where pseudopotential theory was invoked to rationalize the observation of Wannier states (18). Such highly excited deep exciton and impurity states can be described in terms of the effective mass equation (18, 19). If the edges of both valence and conduction band occur at some point $\boldsymbol{k}_0$ in the Brillouin zone (BZ) and the interband transition is dipole allowed, one is concerned with direct excitons. For impurity excitations $\boldsymbol{k}_0$ corresponding to the minimum of the conduction band and direct impurity excitations are always encountered. In simple insulators $\boldsymbol{k}_0$ correspond to the Γ point in the BZ. The high exciton levels E_n and impurity levels $E_n^{\,i}$ (see Figs. 1 and 2) are described in terms of a hydrogenic series converging to the bottom of the conduction band,

$$E_n = E_G - G/n^2 \quad [1]$$

$$E_n^{\,i} = E_G^{\,i} - G^i/n^2 \quad [2]$$

where E_G corresponds to the interband gap at $\boldsymbol{k}_0$ while $E_G^{\,i}$ is the impurity energy gap (see Figs. 1 and 2). The latter energetic quantity, which in the chemist's language just corresponds to the ionization potential of the impurity in the solid, is given by

$$E_G^{\,i} = I_g + P_+ + V_0 \quad [3]$$

where I_g is the impurity gas phase ionization potential, P_+ is the (adiabatic) medium polarization energy by the impurity positive ion, and V_0 designates the energy of the bottom of the conduction band relative to the vacuum level. G and G^i in [1] and [2] correspond to the effective Rydberg constants for the exciton and for the impurity hydrogenic series, respectively, which are given by

$$G = 13.6(\mu/\varepsilon^2)\ \text{eV} \quad [4]$$

$$G^i = 13.6(m^*/\varepsilon^2)\ \text{eV} \quad [5]$$

$$\mu = m^* m_h/(m^* + m_h) \quad [6]$$

where m^* is the electron effective mass near the bottom of the conduction band, m_h is the hole effective mass, again near $\boldsymbol{k}_0$, while ε is the static dielectric constant of the solid. In view of the large value of m_h we expect that G is close to G^i.

High exciton and impurity states, characterized by the quantum number $n \geq 2$, do not reveal any relation to the atomic or molecular excited states of the constituents in the gas phase, and should be viewed as one-electron excitations of the dense medium below the direct interband threshold. Relevant examples for Wannier exciton states in pure rare-gas solids are presented in Figs. 3 and 4. Focusing attention on Wannier impurity states the following quantitative information concerning the static properties of the conduction band emerges.

(*1*) From the effective Rydberg constant G^i, [5], together with the static dielectric constant, one can deduce m^*. These values are invariant

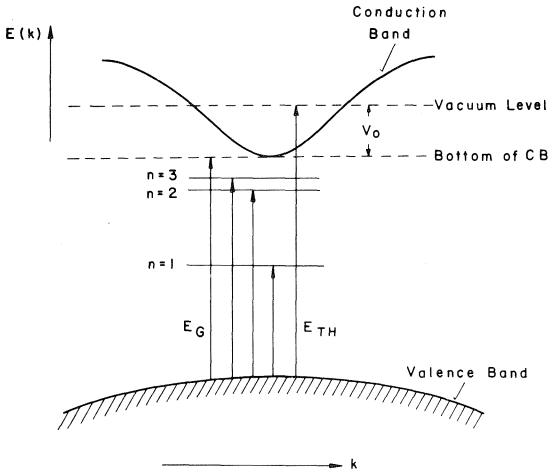

FIG. 1. A schematic representation of the energy levels of a simple pure insulator.

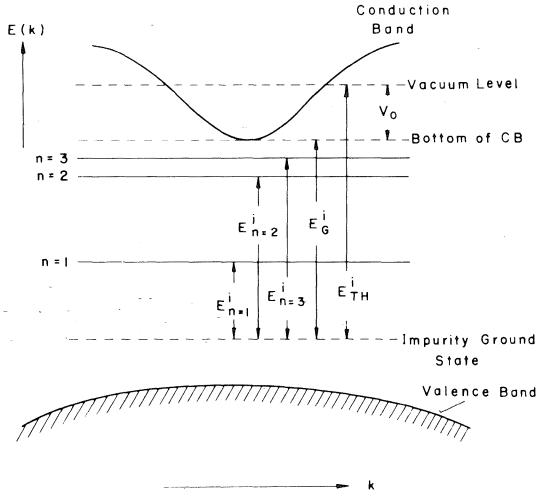

FIG. 2. A schematic representation of the energy levels of Wannier impurity states in an insulator.

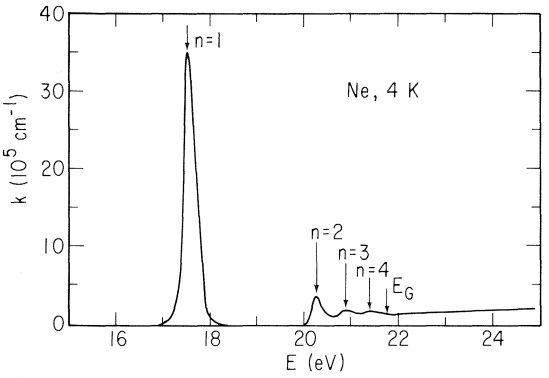

FIG. 3. The absorption spectrum of solid Ne (15, 29).

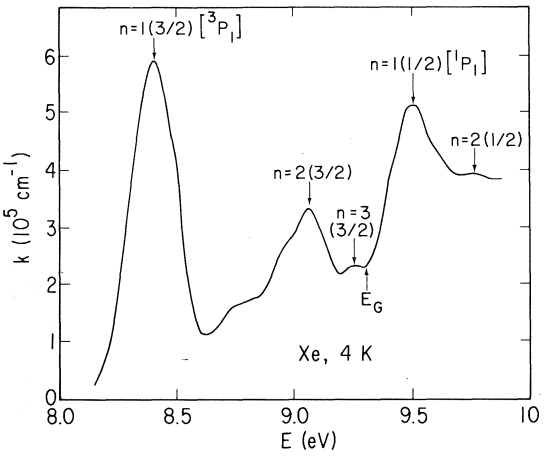

FIG. 4. The absorption spectrum of solid Xe (55).

with respect to the nature of the particular impurity.

(*2*) The convergence limit of the impurity Wannier series results in E_G^i, the impurity ionization potential in the insulator.

(*3*) A direct and reliable approach to derive V_0 rests on the combination of spectroscopic data for E_G^i with photoemission yield data from lightly doped insulators. The photoemission threshold, E_{TH}^i, is

$$E_{TH}^i = I_g^i + P_+ \quad [7]$$

whereupon from [3] and [7] we obtain

$$V_0 = E_G^i - E_{TH}^i \quad [8]$$

An analogous relation of the form

$$V_0 = E_G - E_{TH} \quad [9]$$

holds for the pure solid and liquid insulator.

III. Wannier-type Impurity States in Solid Insulators

We now turn to a brief survey on Wannier impurity states in simple solids. The best known example involves dilute rare-gas alloys (20–22, 14). Typical examples for the absorption spectra of such atomic impurity states (14) are reproduced in Fig. 5. The observation of hydrogenic Wannier impurity states is not limited to rare-gas solids and Xe impurity states were observed in other molecular crystals (23, 24) such as solid H_2, D_2, and CF_4 (Fig. 6). All these spectra pertain to large-radius atomic impurity states. Analogous molecular excitations are also amenable to experimental observation, whereupon extravalence excitations of a molecular impurity in an insulator should exhibit Wannier-type states originating from an electron wavepacket interacting with a molecular positive ion (14). The identification of such molecular excitations is complicated by congestion of vibrational structure, overlap of extravalence

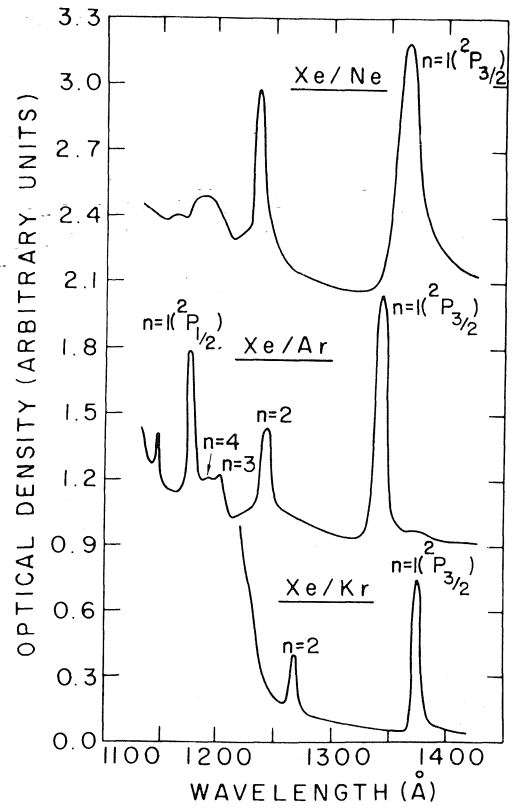

FIG. 5. The absorption spectra of dilute solid rare-gas alloys (14).

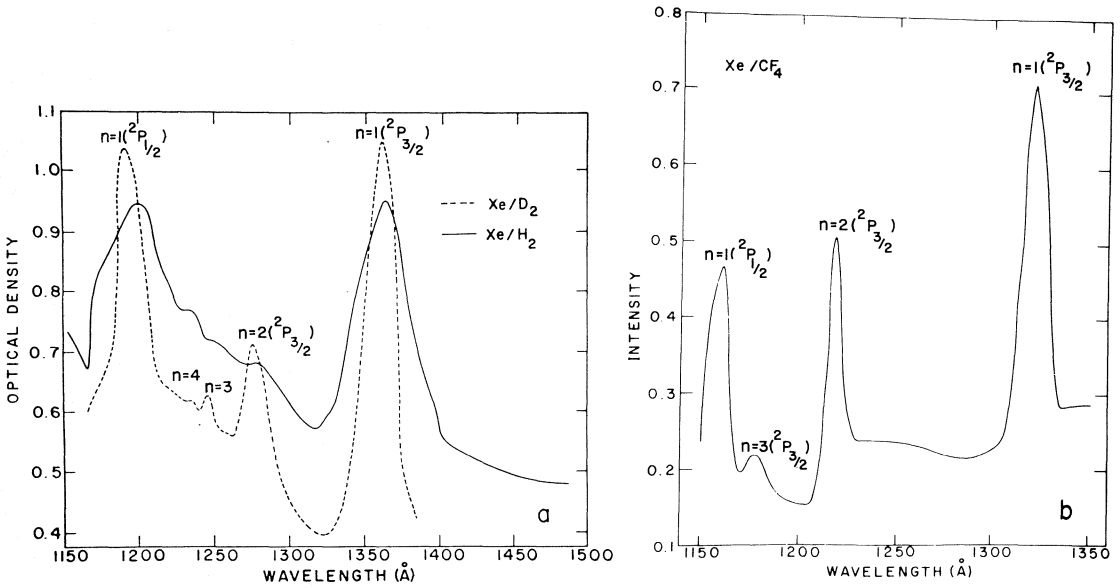

FIG. 6. Absorption spectra of Xe impurity in molecular crystals. (*a*) The absorption spectra of Xe in solid H_2 and D_2 at 6 K. (*b*) The absorption spectrum of Xe in solid CF_4 at 6 K (23).

and intravalence excitations, overlap of extravalence excitations with photodissociative continua, as well as additional line broadening originating from intramolecular electronic relaxation. A typical example for extravalence excitations of the benzene molecule (14) in rare-gas solids is presented in Fig. 7. Analysis of these data according to [2] is demonstrated in Fig. 8.

The physical information derived from solid state absorption spectroscopy is supplemented by the results of photoemission yields from pure solids and from lightly doped insulators (25–30). Figure 9 portrays the energy dependence of the photoemission yield (30) from pure Xe at 20 K. The weak peak at 1380 Å originates from extrinsic effects, while intrinsic photoemission is exhibited below ~1300 Å. Intrinsic photoemission data from atomic and molecular impurity states (26–28) (characterized by $E_{TH}^{i} < E_{TH}$) are presented in Figs. 10–12. Square root extrapolation of the photoemission yield *vs.* energy results in the photoemission thresholds.

In Table 2, we summarize the energetic data characterizing ionization processes in solid rare gases. The following observations are pertinent.

(*a*) E_G^{i} is determined by the nature of the impurity state, according to [3] (see Section II).

(*b*) E_{TH}^{i} is determined by the nature of the impurity state as is evident from [7].

(*c*) The effective Rydberg constants for impurity ionization G^{i} are independent of the nature of the impurity as these are determined by the host dielectric constant and by the features of the conduction band according to [5].

(*d*) The observation that $G^{i} \simeq G$ implies, according to [4]–[6], that $\mu \simeq m^*$, *i.e.* the hole effective mass m_h is large.

(*e*) The V_0 value derived from [8] for doped solids and from [9] for the pure solids corresponds to an intrinsic property of the solid. V_0 is identical, within experimental uncertainty, for the pure and for the doped solids and for the latter it is independent of the nature of the impurity. The self-consistency of the V_0 data provides strong evidence for the validity of the assignment of exciton and Wannier impurity states in insulators.

IV. V_0 Scale for Solid and Liquid Rare Gases

The combination of spectroscopic and photoemission data results in a reliable V_0 scale for solid rare gases. In Table 3, we compare these V_0 values with the experimental data for liquid rare gases recently determined by Tauchert (31). It is apparent that in all cases V_0 in the solid is higher than in the corresponding liquid, indicating that in the former case the contribution of short-range repulsive interactions is

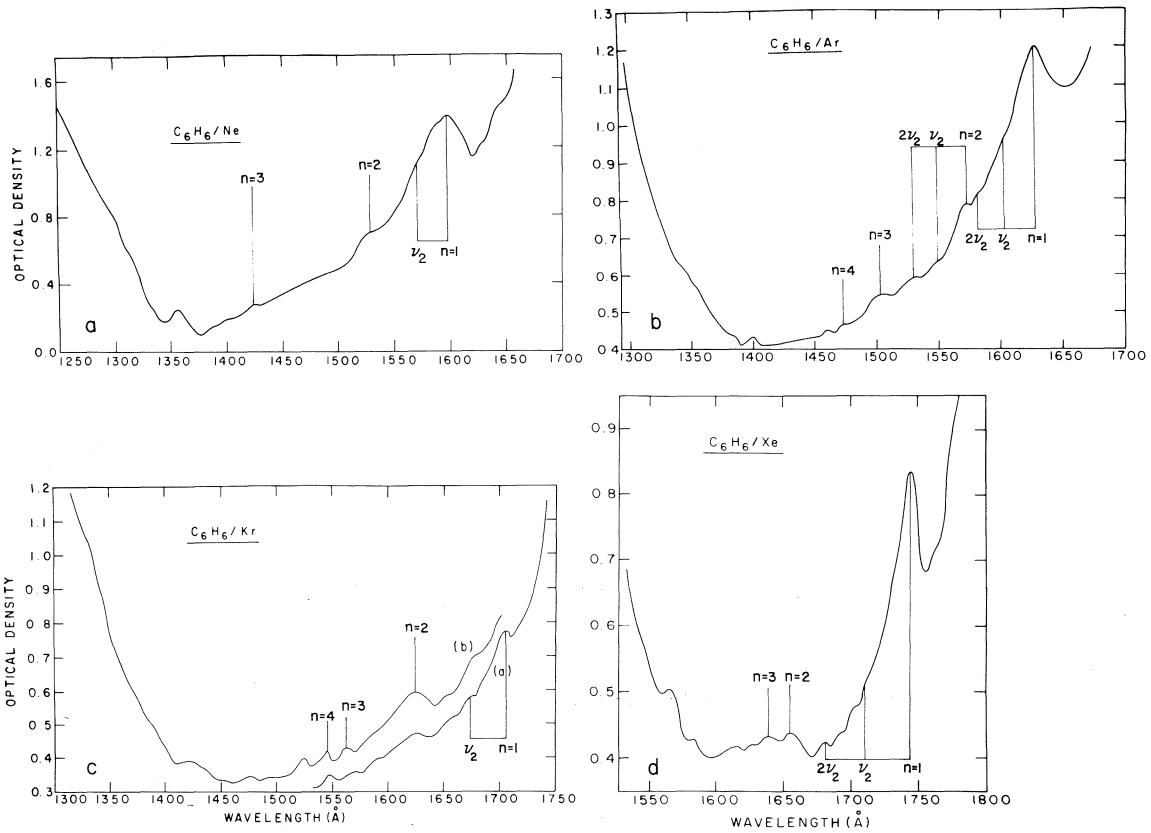

FIG. 7. Extravalence excitations of benzene in solid rare gases (14). (*a*) C_6H_6/Ne; (*b*) C_6H_6/Ar; (*c*) C_6H_6/Kr; (*d*) C_6H_6/Xe.

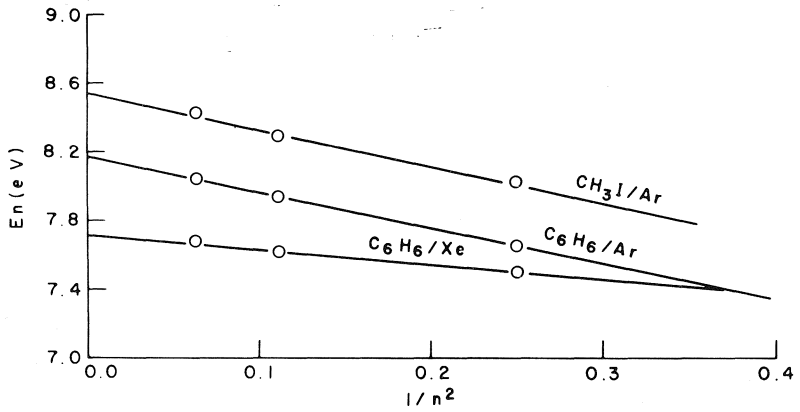

FIG. 8. Plots of E_n *vs.* $1/n^2$ for Wannier molecular impurity states in rare-gas solids.

somewhat higher. It is of interest to confront the experimental V_0 data with the prediction of the simple SJC theory (5). As is well known, the energy of the conduction band minimum for the excess electron consists of two contributions, the background polarization potential U_P and the kinetic energy term T arising from multiple scattering from nearest neighbors, so that $V_0 = T + U_P$. The SJC model provides a simple recipe for the estimate of U_P including

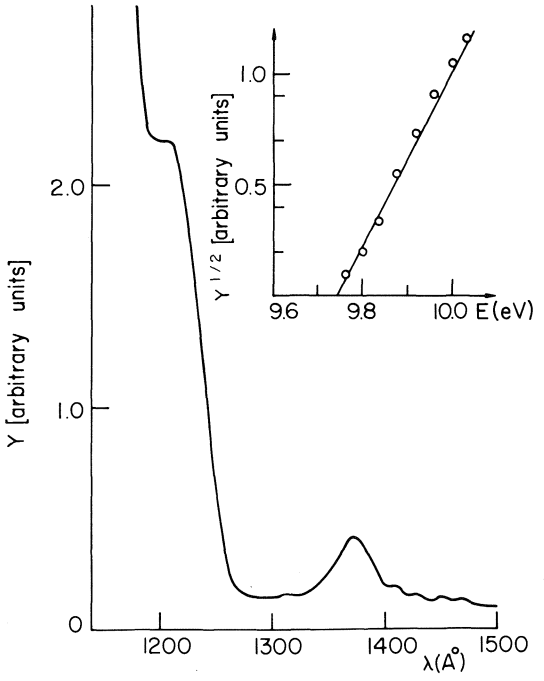

FIG. 9. Photoemission spectrum of pure Xe and 20 K (27, 30).

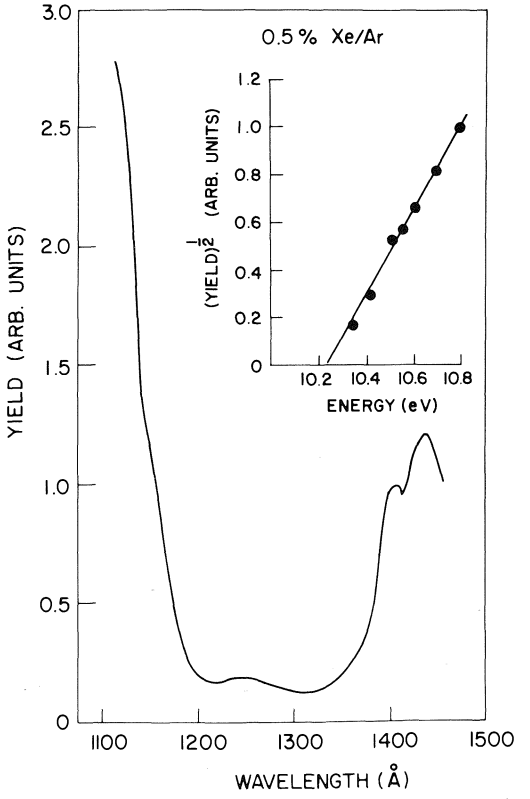

FIG. 10. Photoemission spectrum of Xe in solid Ar (28).

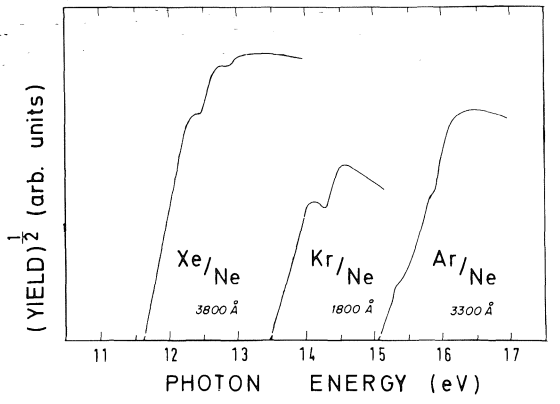

FIG. 11. Photoemission yields of atomic impurities in solid Ne (29).

the screened polarization field of the surrounding atoms and for the evaluation of T by the Wigner–Seitz approximation. Table 4 summarizes the results of such calculations, where the scattering length a of the Hartree–Fock atomic field for He and Ne was taken from theoretical scattering data (5), while for Ar, Kr, and Xe, the value of a was adjusted to fit the liquid V_0 value. These semiquantitative theoretical estimates of V_0 are fraught with difficulties as Table 4 emphasizes how much smaller V_0 is than the T and the U_P terms. These theoretical estimates clearly indicate that the increase of T in the solid is somewhat higher than the corresponding decrease in U_P; however, the SJC model underestimates the relative increase of the short-range repulsive interactions in the solid as is apparent from the result for Ar. Thus this semiquantitative approach (5) should not be considered as an ultimate theory and further theoretical work in this field is required.

V. Impurity Ionization Potentials in Solids

In Table 5 we summarize the available experimental data for the ionization potentials E_G^i of atomic and molecular impurities in solid rare gases obtained from spectroscopic determinations of the convergence limit of Wannier impurity states. Another piece of useful energetic data involves the adiabatic polarization energy of the medium by the positive ion which can be obtained from the relation $P_+ = E_{TH}^i - I_g^i$ provided that the photoemission threshold is known or, alternatively, from [3], $P_+ = E_G^i -$

TABLE 2. Energetic data for pure and doped solid rare gases

System	E_G or E_G^i (eV)	G or G^i (eV)	E_{TH} or E_{TH}^i (eV)	V_0 (eV)
Ne (pure)	21.69	5.24	20.6	1.0 ±0.2
Ar/Ne	16.23	5.27	15.16	1.07±0.1
Kr/Ne	14.76	5.27	13.56	1.2 ±0.1
Xe/Ne	(12.63)		11.67	0.97±0.2
Ar (pure)	14.2	2.4	13.9	0.3 ±0.1
Kr/Ar	12.5		12.2	0.3 ±0.1
Xe/Ar	10.54	2.4	10.23	0.3 ±0.1
Kr (pure)	11.6		11.9	−0.3 ±0.1
Xe/Kr	10.1	1.7	10.3	−0.2 ±0.1
Xe (pure)	9.28	0.88	9.74	−0.46±0.1

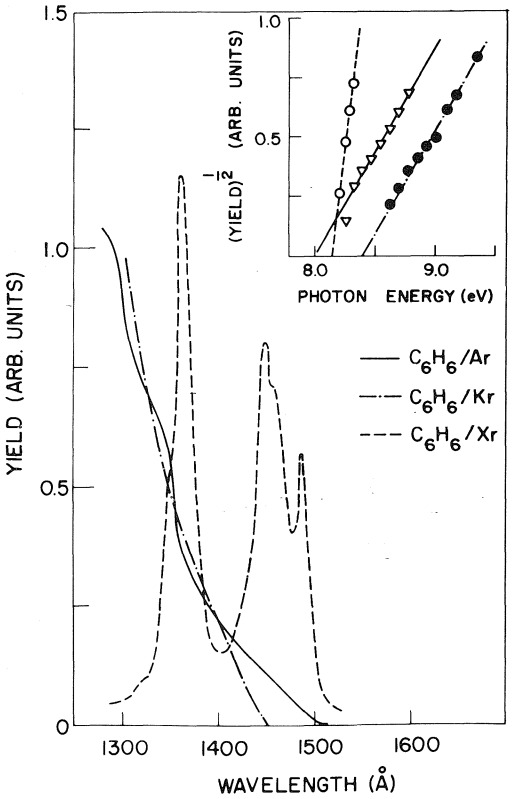

FIG. 12. Photoemission spectra of benzene in solid rare gases (28).

$I_g^i - V_0$ utilizing the experimental V_0 scale (Table 3). The resulting P_+ values are also given in Table 5. From these results we conclude that:

(*A*) The impurity ionization potential in the solid can exceed the gas phase ionization potential provided that V_0 is positive and large. This is the situation for atomic impurity states in solid Ne where $E_g^i > I_g^i$.

(*B*) In a solid characterized by a small positive value of V_0, such as Ar, or where $V_0 < 0$, as is the case for Kr and for Xe, we expect that $P_+ + V_0 < 0$, whereupon $E_g^i < I_g^i$.

(*C*) As $P_+ < 0$ one expects that the external photoemission threshold, [7], is always lower than the gas phase ionization potential, *i.e.* $E_{TH}^i < I_g^i$. This point was discussed by Chia and Delahay (32).

(*D*) For a given impurity in different hosts P_+ roughly increases with increasing optical dielectric constant. A rough approximation for P_+ involves the Born charging energy $P_+ \simeq (e^2/2R)(1 - (\varepsilon_{op})^{-1})$, where R is the effective radius of the impurity. It should be noted that the Born relation does not provide a quantitative account for the experimental P_+ data. Thus, for benzene in Ne, Ar, Kr, and Xe, P_+ exhibits only a weak dependence on the host matrix. Short-range repulsive interactions are of some importance as is evident from the fact that P_+ for Ar^+/Ne is lower than the corresponding values for Kr*/Ne and for

TABLE 3. Experimental V_0 scale for solid and liquid rare gases*

System			V_0 (eV)
Liquid	^{4}He	4.2 K	+1.05
Solid	Ne	4 K	+1.1 ±0.1
Liquid	Ne	25 K	+0.67±0.05
Solid	Ar	6 K	+0.3 ±0.1
Liquid	Ar	87 K	−0.2 ±0.02
Solid	Kr	20 K	−0.25±0.1
Liquid	Kr	123 K	−0.45±0.05
Solid	Xe	40 K	−0.46±0.05
Liquid	Xe	165 K	−0.61±0.05

*Solid state data: absorption and photoemission spectroscopy (Tel-Aviv and DESY work). Liquid data: He, Sommer (53); Ar, Kekner *et al.* (54); Ne, Ar, Kr, Xe, Tauchert (31*a*).

TABLE 4. Application of the SJC theory for the calculation of V_0 in liquid and solid rare gases

System	r_s (Å)	α (Å^3)	a (Å)*	k_0 (Å^{-1})	T (eV)	U_P (eV)	V_0 (eV) Calcd.	V_0 (eV) Exptl.
He(L)	2.22	0.20	0.75	0.66	1.66	−0.38	+1.28	+1.05±0.05
Ne(L)	1.86	0.39	0.56	0.71	1.91	−1.46	+0.45	+0.67±0.05
Ne(S)	1.75	0.39	0.56	0.80	2.44	−1.85	+0.60	+1.1 ±0.1
Ar(L)	2.23	1.63	0.92	0.82	2.53	−2.73	−0.20	−0.2 ±0.02
Ar(S)	2.08	1.63	0.92	0.95	3.46	−3.54	−0.08	+0.3 ±0.1
Kr(L)	2.38	2.46	1.07	0.85	2.73	−3.11	−0.38	−0.40±0.05
Kr(S)	2.21	2.46	1.07	1.00	3.84	−4.05	−0.21	−0.25±0.1
Xe(L)	2.60	4.00	1.26	0.87	2.85	−3.46	−0.61	−0.61±0.1
Xe(S)	2.40	4.00	1.26	1.04	4.12	−4.64	−0.52	−0.46±0.05

*a values for He, Ne from theoretical scattering data, for Ar, Kr, Xe chosen to fit V_0 for liquid.

TABLE 5. Ionization energies and medium polarization energies for atomic and molecular impurities in solid rare gases (all energies in eV)

Guest	Host	E_G^i	I_g^i	P_+
Ar	Ne	16.23	15.68	−0.63
Kr	Ne	14.78	13.92	−0.45
Xe	Ne	12.63	12.08	−0.48
Kr	Ar	12.50	13.92	−1.62
Xe	Ar	10.54	12.08	−1.74
Xe	Kr	10.1	12.08	−1.87
C_6H_6	Ne	(9.20)	9.24	(−1.04)
C_6H_6	Ar	8.51	9.24	−0.93
C_6H_6	Kr	8.18	9.24	−0.96
C_6H_6	Xe	7.75	9.24	−1.03
C_2H_4	Ne	10.43	10.50	−1.07
C_2H_4	Ar	9.13	10.50	−1.57
C_2H_4	Kr	8.88	10.50	−1.42
C_2H_4	Xe	8.14	10.50	−1.90
CH_3I	Ne	9.51	9.49	−0.98
CH_3I	Ar	8.58	9.49	−1.11
CH_3I	Kr	8.13	9.49	−1.16
CH_3I	Xe	—	9.49	—

Xe*/Ne, while P_+ for the latter two systems is practically identical.

VI. Excitons in Fluids

While one-electron excitations in crystalline insulators are quite well understood, the nature of analogous excitations in fluids is not yet elucidated. It was suggested (33) that large-radius Wannier-type exciton states are amenable to experimental observation in a dense fluid where electron–medium interaction is sufficiently weak. Liquid rare gases provide suitable candidates for the search for such electronic excitations which are of considerable interest in relation to general problems of electronic states in disordered materials as well as in the context of deriving quantitative information concerning ionization processes in simple liquids. From the experimental point of view evidence has been reported (34, 35) for the identification of the $n = 2$ exciton in liquid Xe and the $n = 2$ impurity state of Xe in liquid Ar (36). In order to establish the nature of Wannier states in dense simple fluids it will be interesting to obtain a continuous description of the electronic excitations of a guest atom or molecule in a host fluid where the fluid density is varied over a broad density range. One has to distinguish carefully between intravalence excitations, low extravalence impurity excitation, and high extravalence impurity excitations, all of which are exhibited at low and intermediate densities of the host medium, and sort out the large Wannier states which may appear in the high density fluids. The general characteristics of different types of impurity excitations in a host fluid are summarized in Table 6.

Messing (37) has recently studied the absorption spectra of atomic and molecular impurity states in simple dense fluids over a wide density range. The absorption spectra of the Xe/Ar system from the atomic limit up to the solid one is presented in Figs. 13 and 14. At low and at moderate Ar densities (ρ = 0–0.6 g cm^{-3}) five 'atomic' excitations are exhibited (Fig. 13) in the range 1150–1300 Å.

(I) $6s'$ [1/2] $J = 1$ located in the atomic limit at 1296 Å.

(II) $5d$ [1/2] $J = 1$ located in the atomic limit at 1250 Å.

(III) $5d$ [5/2] $J = 3$ which is symmetry forbidden in the isolated atom, being pressure induced around 1210 Å.

(IV) $5d$ [3/2] $J = 1$ located at 1192 Å in the atomic limit.

TABLE 6. Medium effects on absorption spectra of a guest atom in a host fluid and solid*

States of perturbing medium	Guest atomic states		
	(*1*) Intravalence excitations	(*2*) Lowest extravalence $\Delta n_A = 1$ excitations	(*3*) High extravalence $\Delta n_A \geq 2$ excitations
(*A*) Spectral perturbations by a foreign gas at low and at moderate densities	(*a*) Spectral shifts (small red or blue) and line broadening (*b*) Appearance of 'red' or 'blue' satellites (*c*) Symmetry breaking, induction of forbidden transitions	(*a*) Shifts (red at low densities, blue at higher densities) and line broadening (*b*) Appearance of 'red' or of 'blue' satellites (*c*) Symmetry breaking, induction of forbidden transitions	(*a*) Spectral shifts (red or blue) (*b*) States converges into (perturbed) ionization potential
(*B*) Spectral effects of high density fluid or liquid	Same as *1A*	(*a*) Large spectral shifts (blue) (*b*) Satellites disappear, merge with main line into a broad band (*c*) Forbidden transitions exhibited	(*a*) States 'disappear' (*b*) Appearance of high Wannier $n \geq 2$ states (*c*) Wannier states converge into bottom of conduction band
(*C*) Spectral effects in a solid	(*a*), (*b*), (*c*) same as *1A* (*d*) Crystal field splitting of degenerate excited states	Same as *2B*	Same as *3B* Wannier states well resolved due to line narrowing relative to liquid

*n_A, atomic or molecular one-electron quantum number (qn); n, qn for Wannier states.

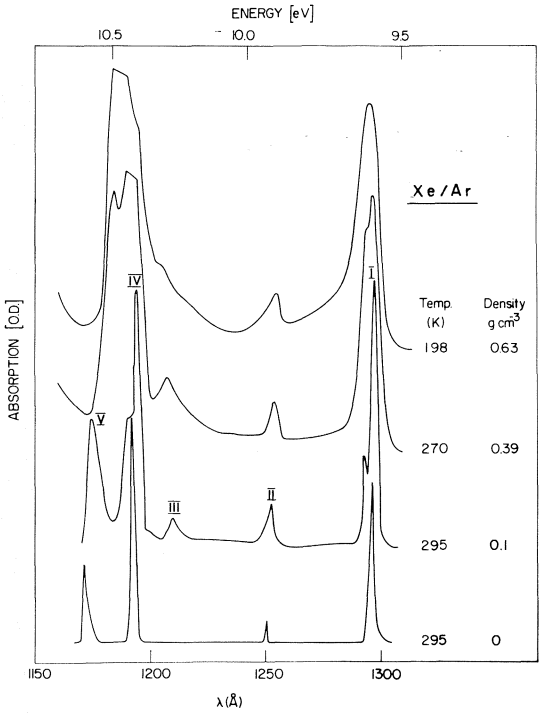

FIG. 13. The absorption spectra of Xe in fluid Ar at low densities (37).

(V) 7*s* [3/2] $J = 1$ located at 1170 Å in the atomic limit.

In the high Ar density region (Fig. 14) the absorption band in the range 1225–1250 Å exhibits an appreciable enhancement for $\rho > 0.8\ \mathrm{g\ cm^{-3}}$. In Fig. 15 we present Messing's results for the intensity ratio of this absorption relative to the intensity of transition I. The intensity enhancement of the 1225–1250 Å band in the Xe/Ar system is entirely different from the behavior of the Xe/Ne system where this intensity ratio reveals only a weak density dependence. Messing (37) assigned the strong absorption band located around 1250 Å in the Xe/Ar system of high Ar densities $\rho > 0.8\ \mathrm{g\ cm^{-3}}$ to the $n = 2$ Wannier impurity states in fluid Ar. Making use of [3] one can then provide an estimate for the Xe impurity ionization potential in liquid Ar assuming that the electron effective mass m^* in the liquid is equal to that in the solid. We then obtain $E_G^{\,i} = 10.9$ eV for Xe in liquid Ar and $P_+ = 1.0 \pm 0.2$ eV for the polarization energy of the liquid.

It is of considerable interest to obtain information regarding the density dependence of the ionization potential of an impurity in a

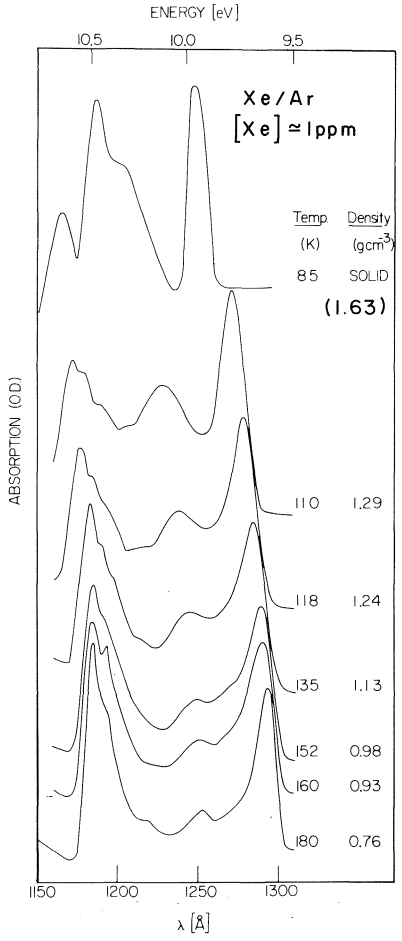

FIG. 14. The absorption spectra of Xe in fluid Ar at high Ar densities (37).

fluid. Messing (37) has studied the vacuum-ultraviolet spectra of CH_3I in Ar over a broad density range. At low densities six Rydberg series are exhibited, three of which converge to the first ionization potential (38). In the Ar density range $\rho = 0$–$0.5\ g\ cm^{-3}$ five members $n = 1$–5 of the Rydberg series could be clearly observed (37). Analysis of these data using the isolated molecule quantum defects (38) results in $G^i = 9.6\ eV$ and $E^i = 9.2\ eV$ for CH_3I at $\rho = 0.34\ g\ cm^{-3}$. In Table 7 we summarize the available experimental information derived from spectroscopic data concerning atomic and ionization potentials in fluids (37). These results demonstrate the gradual decrease of the impurity ionization potential with increasing fluid density. Such a pattern will be exhibited in any fluid where $V_0 < 0$ as is the case for Ar. It is also worthwhile to note that P_+ in the liquid is considerably lower than in the solid, a difference which cannot be reconciled just by the 15% change in the dielectric constant. Obviously, these interesting areas of electronic excitations and ionization processes in fluids deserve further experimental and theoretical effort.

Up to this point we have been concerned with some of the intrinsic features of one-electron excitations in solid and liquid insulators which provide information concerning the energetics of ionization processes in fluids and some static characteristics of the conduction band in such systems. We shall now proceed to discuss some dynamic aspects of electron localization in dense fluids.

VII. Electron Localization in Polar Fluids

Excess electrons in He gas at low temperatures undergo a sharp 'transition' from the quasi-free state to a localized bubble state with increasing density (3, 39–41). Levine and Sanders (39) have demonstrated that the mobility of electrons injected into He gas exhibits a dramatic drop of some four orders of magnitude over a density range of $\sim 10\%$. The nature of the electronic states and electron transport in the transition region were described in terms of the Anderson model (3) by the percolation picture (42) and by a phenomenological model where extended and localized states coexist (43, 44). Electron localization in subcritical and in supercritical polar fluids at sufficiently high densities is expected to be a general phenomenon, while at low densities of a polar fluid the quasi-free excess electron state will be energetically stable. One thus expects that in a polar fluid, as in the case of He, a 'transition' from the localized state to the quasi-free state will be exhibited with decreasing fluid density (45). The problem of electron localization in polar fluids as a function of density (and other thermodynamic variables of state) is of considerable interest (45–49). The following questions are relevant in this context.

(*1*) Can one observe a 'critical' density, ρ_C, for the 'transition' between localized and quasi-free excess electron states in a polar fluid?

(*2*) What are the physical properties of the localized excess electron in a polar fluid over a broad density range where the localized state is thermodynamically stable?

Points *1* and *2* require basic experimental

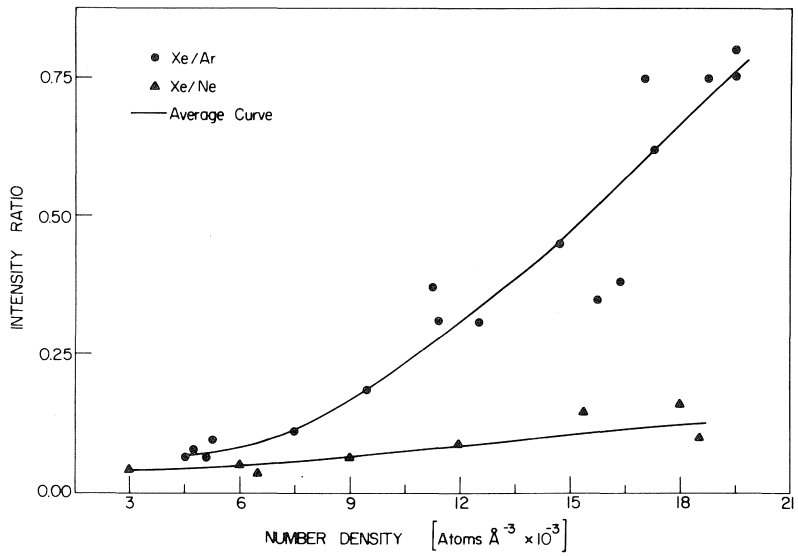

FIG. 15. The density dependence of the intensity ratio of the 1250 Å absorption to the $^1S_0 \rightarrow {}^1P_1$ transition (band I) in Xe/Ar and in Xe/Ne (37).

TABLE 7. Ionization potentials of some atomic and molecular impurities in fluid Ar (from ref. 37*a*) (solid state data are given for comparison)

Guest	Host	E_G^i (eV)	I_g^i (eV)	G (eV)	$P_+ + V_0$ (eV)	P_+ (eV)
Xe	Liquid $\rho = 1.35$ g cm^{-3}	10.9	12.13	(3.0)	−1.23	−1.03
Xe	Solid $\rho = 1.7$ g cm^{-3}	10.54	12.13	2.4	−1.59	−1.79
CH_3I	Supercritical $\rho = 0.34$ g cm^{-3}	9.2	9.55	9.6	−0.35	—
CH_3I	Liquid $\rho = 1.35$ g cm^{-3}	8.7	9.55	(3.0)	−0.85	−0.65
CH_3I	Solid $\rho = 1.7$ g cm^{-3}	8.6	9.55	2.3	−0.95	−1.15
CH_2O	Liquid $\rho = 1.24$ g cm^{-3}	10.2	10.88	3.8	−0.68	—

information. Supplementary theoretical work should be directed towards the elucidation of the following problems.

(*3*) The electron localization process in polar fluids with respect to the role of configurational fluctuations, pre-existing traps, etc.

(*4*) A proper theoretical description of localized excess electron states with regard to the role of short-range and long-range interactions.

A theoretical study of the properties of localized excess electrons and of their thermodynamic stability in a *homogeneous* polar fluid was conducted by Gaathon and co-workers (48, 49). He considered the molecular model for the localized excess electron incorporating short-range attractive and repulsive interactions with the first 'molecular' coordination layer, which consists of N molecules, and long-range polarization interactions with a medium characterized by the mean fluid density beyond the first coordination layer. This homogeneous model results in the following predictions.

(*a*) The critical densities for electron localization in H_2O and NH_3 (Table 8) are obtained

from a modified energetic stability criterion which incorporates entropy changes accompanying the formation of the first coordination layer.

(*b*) The density dependence of the absorption band maximum $h\nu_{max}$ exhibits three distinct regions. (b.1) At high densities (ρ = 1.2–1.0 g cm^{-3} for H_2O) $h\nu_{max}$ drops fast with decreasing ρ. (b.2) Over a broad density range (ρ = 1.0–0.1 g cm^{-3} for H_2O) $h\nu_{max}$ exhibits a weak ρ dependence. (b.3) At lower densities ($\rho < 0.1$ g cm^{-3} in H_2O) $h\nu_{max}$ decreases fast with decreasing ρ.

Experimental studies of the absorption spectra and the yields of localized excess electrons in subcritical and supercritical water and ammonia were conducted by Schindewolf and co-workers (46, 47) and by Gaathon (45, 48, 49). Extensive experimental data for electron localization in D_2O, NH_3, and ND_3 were obtained (49) in the density range $\rho = 1.0\text{–}8 \times 10^{-3}$ g cm^{-3} (p = 1–400 atm, T = 273–670 K) for D_2O and ρ = 0.6–10^{-2} g cm^{-3} (p = 1–200 atm, T = 273–430 K) for NH_3 and ND_3. Pulse radiolysis techniques were employed.

Figures 16 and 17 portray typical absorption spectra (49) of localized electrons in subcritical and supercritical D_2O. The experimental density dependence of $h\nu_{max}$ (corrected for temperature effects) is presented in Fig. 18. In this figure these experimental results are confirmed with the theoretical predictions (Section *b*). We note that the experimental density dependence in region b.1, where a sharp drop of $h\nu_{max}$ is predicted, and in range b.2, where $h\nu_{max}$ exhibits a weak density dependence, is in reasonable agreement with the trend predicted by the homogeneous model. However, in the low density range $\rho < 10^{-1}$ g cm^{-3} the experimental values of $h\nu_{max}$ are practically independent of the fluid density in marked contrast to the expectations based on the homogeneous model which envisions a fast drop of $h\nu_{max}$ with decreasing density in range b.3.

The yields for the formation of localized excess electron states in D_2O and in ND_3 were determined by two independent methods (49). First, time-resolved absorption of the localized electron was found to obey second order decay kinetics and extrapolation of these results to $t = 0$ resulted in the yield. Second, the absorption of the localized electron was monitored during electron pulses of the duration of τ = 0.3 μs and τ = 1.5 μs, the data being analysed

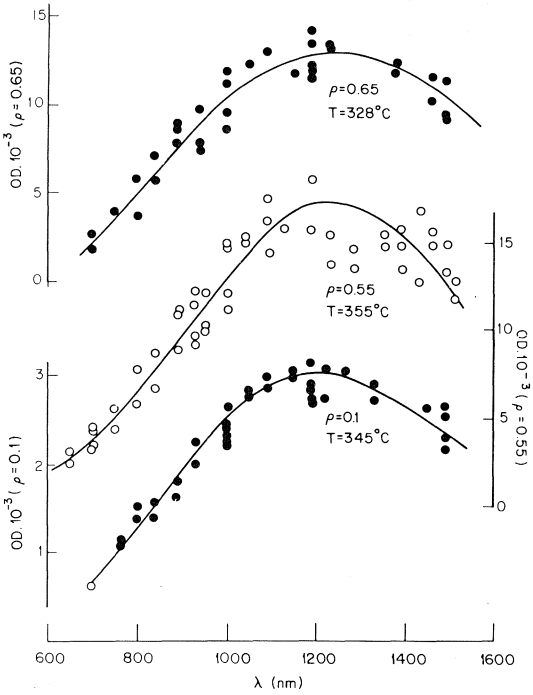

FIG. 16. The absorption spectra of the localized electron in subcritical D_2O (49).

according to the relation $d[e_l]/dt = \alpha\rho I - k[e_l]^2$ where α is the yield of the localized electrons, I is the intensity of the electron beam, ρ is the fluid density, and k is the bimolecular recombination rate constant. The experimental procedures for the determination of the yields of the localized electron provide proper corrections for the 'kinetic instability' of the localized state, originating from efficient recombination, and result in reliable experimental data for the initial yields. The density and temperature dependence of the yields α in D_2O and in ND_3 are displayed in Figs. 19 and 20. From these results we conclude that:

(*1*) In D_2O the localized excess electron state is stable throughout the entire density range 8×10^{-3} g cm$^{-3} < \rho < 1.0$ g cm^{-3} and up to T = 673 K. Thus in supercritical D_2O $\rho_C < 8 \times 10^{-3}$ g cm^{-3}. This experimental result is in conflict with the theoretical prediction of the homogeneous model (Table 8).

(*2*) Electron localization in ND_3 (Fig. 20) exhibits a more complex and more interesting behavior. Near the liquid–vapor coexistence curve (CEC) electron localization is observed up to the lowest density $\rho \simeq 5 \times 10^{-3}$ g cm^{-3}

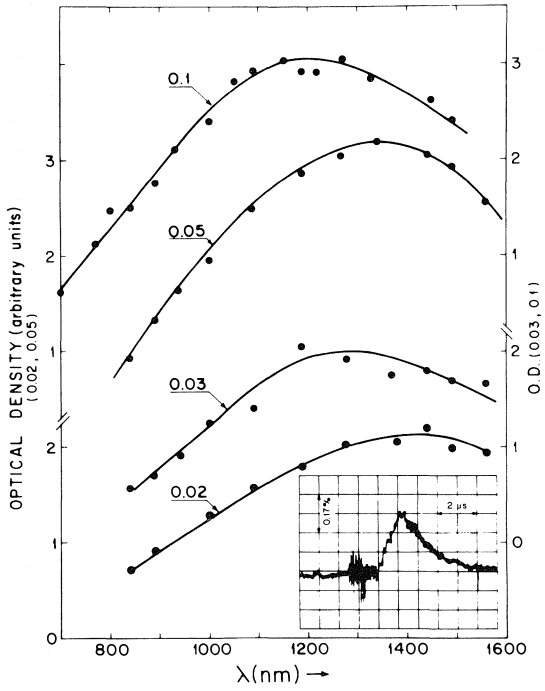

FIG. 17. Absorption spectra of the localized electron in D_2O vapor. The vapor densities (relative to the liquid at 4°C) are indicated by the numbers above the curves (48, 49). (Reprinted with permission from the Journal of Chemical Physics, **58**, 2648 (1973). Copyright by the American Institute of Physics.)

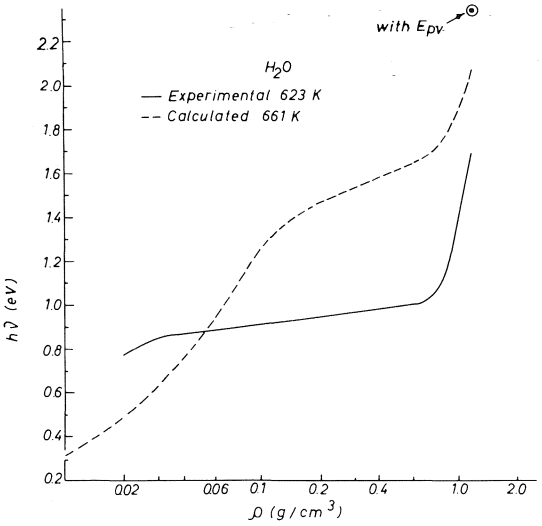

FIG. 18. The density dependence of the band maximum of the localized electron in D_2O (49). Solid curve represents the experimental data at 623 K (corrected for temperature dependence). The dashed curve (49) portrays the prediction of the homogeneous model.

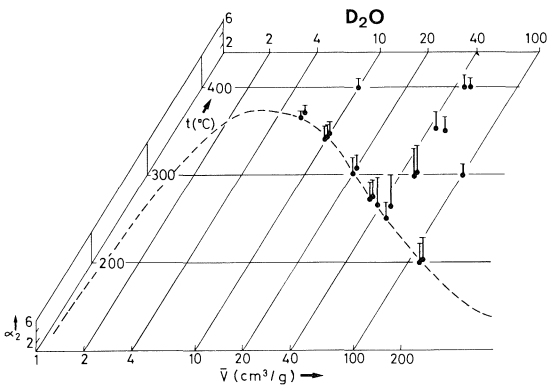

FIG. 19. Density and temperature dependence of the yields and of the localized electrons in D_2O (49). The solid dots represent (ρ, T) points for which experiments were conducted. The vertical lines represent the values of α in arbitrary units. The dashed curve is the liquid–gas CEC. Densities represented in terms of specific volumes $\rho = (\bar{v})^{-1}$.

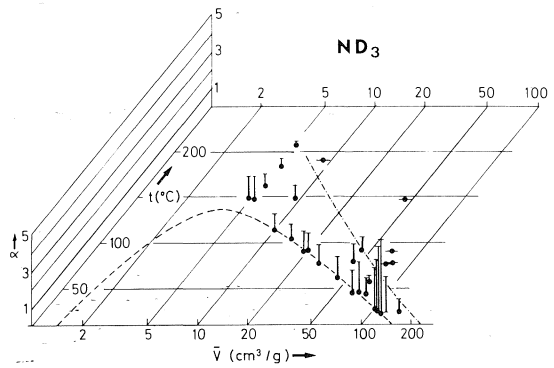

FIG. 20. Density and temperature dependence of the yields of localized electrons in ND_3 (49). Presentation of data identical to those in Fig. 19. Points represented by (—) correspond to ρT values where localized electrons could not be detected. Dashed curve is the liquid–gas CEC. Dotted-dashed curve corresponds to a rough segregation of the ρT plane to two regions where localized states exist and where localized states are thermodynamically unstable.

studied by us, whereupon $\rho_C < 10^{-2}$ g cm^{-3} near the CEC. This observation is again inconsistent with the prediction of the homogeneous model. At high temperatures above the CEC the yield of localized electrons vanishes. In Fig. 20 we have drawn a line in the ρT plane which segregates the range of electron localization from the thermodynamic range where the quasi-free electron state is stable. For these experimental results it is apparent that in supercritical ND_3 ρ_C is determined not only by density but also by the temperature.

TABLE 8. Critical densities for electron localization in polar fluids

	Model calculations		Experimental
	N	ρ_C (g cm^{-3})	ρ_C (g cm^{-3})
H_2O	4	0.044–0.03	$<5\times10^{-3}$
$T = 660$ K	6	0.07–0.05	
NH_3	4	0.08–0.065	$<10^{-2}$ near CEC
$T = 470$ K	6	0.14–0.11	~0.1 40°C above CEC

Although the thermodynamic stability criterion used in the homogeneous model involves a temperature dependence originating from an entropy contribution, the experimental results cannot be accounted for in terms of such a model and in particular the low value of ρ_C near the CEC is striking. On the other hand, at high temperatures above the CEC the predictions of the homogeneous model are not too bad; for example, at 40°C above the CEC $\rho_C \simeq 0.1$ g cm^{-3} in agreement with the observation of Olinger *et al.* (47), in accord with the theoretical prediction (Table 8). However, this minor success does not reconcile the serious discrepancies between the experimental observations and the expectations of the homogeneous model.

These discrepancies between the theoretical homogeneous model and the facts of life can be summarized as follows.

(I) The weak dependence of $h\nu_{max}$ on ρ at low ($\rho < 0.1$ g cm^{-3}) densities is in conflict with the prediction for a sharp drop of $h\nu_{max}$ in that range. This theoretical result originates from the decrease (at $\rho < 0.1$ g cm^{-3}) of the polaron coupling parameter $\beta = \varepsilon_{op}^{-1} - \varepsilon_s^{-1}$ which determines the long-range polarization potential.

(II) The low values of ρ_C observed for D_2O over the entire ρT range and for ND_3 near the CEC. The high value of ρ_C predicted by the homogeneous model originates from the following three causes. First, a cluster of $N = 4$ solvent molecules does not localize the excess electron. Second, the sharp decrease of β with decreasing density at low ρ results in a decrease of the ground state energy. Third, the entropy contribution resulting from formation of the first coordination layer from the homogeneous gas is crucial in determining the thermodynamic stability of the localized state.

(III) The strong temperature dependence of ρ_C for ND_3 is inconsistent with the prediction that the density alone is the primary thermodynamic variable of state which determines the stability of the localized state. We are forced to conclude that the homogeneous model is inadequate and propose that the role of pre-existing density fluctuations is crucial in the electron localization process in polar fluids.

We propose that in polar supercritical fluids of polar molecules the quasi-free electron is trapped by density fluctuations. These density fluctuations can be envisioned as pre-existing clusters which act as electron traps. Similar ideas for dynamics of electron localization in liquids were recently advanced by Kenney-Wallace and Jonah (10) and by Baxendale and Sharpe (11). We address ourselves to a more general problem; as in our one-component system the fluid density can be continuously varied, we inquire when is the amplitude of density fluctuations sufficiently low (*i.e.* the size of the pre-existing clusters is too small) so that electron localization will not occur.

To determine the probability of electron capture by density fluctuations two cardinal points have to be elucidated.

(*A*) What is the minimal size of a pre-existing cluster to insure electron capture?

(*B*) What is the probability for density fluctuations of appropriate amplitude to satisfy condition *A*?

To provide a semiquantitative answer to point *A* we have carried out (49) calculations of the ground state energy of an electron localized in a cluster which consists of $N = 4$ molecules in the first coordination layer and N_D molecules in the second coordination layer. These calculations were conducted (49) using a modified version of Iguchi's method (50). We find that the localized excess electron is stable in a cluster of water molecules consisting of $N = 4$ and $N_D \simeq 2$, while for a cluster of ammonia molecules energetic stability is insured for $N = 4$ and $N_D \simeq 6$. Next we turned to point *B* and utilized (49) the simple thermodynamic fluctuation theory to evaluate the probability distribution for density fluctuations consisting of $N_T = N + N_D$ molecules. This probability distribution is determined by the mean density,

by the isothermal compressibility, by the temperature, and by N_T. Detailed calculations will be presented elsewhere and only some conclusions of this analysis will now be mentioned. As the compressibility is high near the CEC the probability of density fluctuations characterized by a large amplitude is always sufficiently large to insure electron localization both for D_2O and for ND_3 in that region. As $N_T \simeq 10$ for ND_3 and $N_T \simeq 6$ for D_2O we expect that the probability for sufficiently large density fluctuations in the latter case will be large enough over the entire ρT range studied by us. On the other hand, for ND_3 the value of N_T is sufficiently high so that at sufficiently low densities high above the CEC (where the compressibility is low) the probability for the occurrence of large ($N_T \simeq 10$) clusters is low and electron localization will not occur. All these expectations agree with the experimental observations.

We thus conclude that the role of density fluctuations is crucial in determining the energetics and dynamics of electron localization in polar fluids. We have experimentally followed the life story of the electron in the polar fluid on a long (μs) time scale. Thus, the spectroscopic information obtained by us does not pertain, of course, to the initial state of the localized electron trapped in the pre-existing cluster. Following the initial process of electron localization several dynamic processes will be exhibited which will result in further energetic stabilization of the localized state. These will include dielectric relaxation (10, 11) (induced by the field of the localized charge) of the external polar medium. In low density polar fluids ($\rho < 0.1$ g cm^{-3}) this long-range effect may be less important than in normal liquids. More interesting is the possibility of further clustering of polar molecules around the initially formed charged cluster. Such a 'snowball effect' will result in the formation of a trapped electron localized in a large cluster of polar molecules, which is characterized by a high local density. The 'snowball effect' is reminiscent of electrical stabilization of liquid drops in supersaturated vapors.

One of the compelling reasons for the study of excess electron states in fluids is that excess electrons can be used as probes for the study of molecular geometry and molecular dynamics in normal liquids and in subcritical and supercritical fluids. The results reported herein, as well as the recent investigations of the dynamics of electron localization in He gas (39–44) and in normal liquids (9–11, 51, 52), provide the first steps towards that goal.

1. J. JORTNER and N. R. KESTNER (*Editors*). Electrons in fluids. Springer Verlag, Heidelberg. 1973.
2. Proceedings of Colloque Weyl IV. J. Phys. Chem. **75** (1975).
3. H. T. DAVIS and R. G. BROWN. Adv. Chem. Phys. **31**, 392 (1975).
4. J. JORTNER, N. R. KESTNER, S. A. RICE, and M. H. COHEN. J. Chem. Phys. **43**, 2614 (1965).
5. B. E. SPRINGETT, M. H. COHEN, and J. JORTNER. J. Chem. Phys. **48**, 2720 (1968).
6. N. R. KESTNER. J. Phys. Chem. **79**, 2815 (1975).
7. P. W. ANDERSON. Phys. Rev. **102**, 1008 (1958).
8. M. H. COHEN. Can. J. Chem. This issue.
9. J. CHASE and J. HUNT. J. Phys. Chem. **79**, 2835 (1975).
10. G. A. KENNEY-WALLACE and C. D. JONAH. Chem. Phys. Lett. **39**, 596 (1976).
11. J. H. BAXENDALE and P. H. G. SHARPE. Chem. Phys. Lett. **41**, 440 (1976).
12. J. JORTNER. Electronic excitations in molecular crystals. *In* Vacuum ultraviolet radiation physics. *Edited by* E. E. Koch, R. Haensel, and C. Kunz. Pergamon-Vieweg, Braunschweig. 1974. p. 263.
13. G. BALDINI. Phys. Rev. A, **137**, 508 (1965).
14. A. GEDANKEN, B. RAZ, and J. JORTNER. J. Chem. Phys. **58**, 1178 (1973).
15. D. PUDEWILL, F. J. HUMPSEL, V. SAILE, N. SCHWENTNER, M. SKIBOWSKI, and E. E. KOCH. Phys. Status Solidi. In press (1977) and references therein.
16. R. S. KNOX. Theory of excitons. Academic Press, New York. 1963.
17. S. A. RICE and J. JORTNER. *In* Physics and chemistry of the organic solid state. Vol. 3. *Edited by* F. Fox, M. Labes, and A. Weissberger. Interscience Publishers, New York. 1967. Chapt. 4.
18. J. C. PHILLIPS. *In* Solid state physics. Vol. 18. *Edited by* F. Seitz and D. Turnbull. Academic Press, New York. 1966. p. 55.
19. W. KOHN. *In* Solid state physics. Vol. 5. *Edited by* F. Seitz and D. Turnbull. Academic Press, New York. 1957. p. 258.
20. G. BALDINI. Phys. Rev. A, **137**, 508 (1965).
21. G. BALDINI. Jpn. J. Appl. Phys. Suppl. **14**, 613 (1965).
22. A. GOLD and R. S. KNOX. Phys. Rev. **113**, 834 (1959).
23. A. GEDANKEN, B. RAZ, and J. JORTNER. Chem. Phys. Lett. **14**, 172 (1972).
24. A. GEDANKEN, B. RAZ, and J. JORTNER. Chem. Phys. Lett. **14**, 326 (1972).
25. J. F. O'BRIEN and K. J. TEEGARDEN. Phys. Rev. Lett. **17**, 919 (1966).
26. N. SCHWENTNER, M. SKIBOWSKI, and W. STEINMANN. Phys. Rev. B, **8**, 2965 (1973).
27. Z. OPHIR, B. RAZ, and J. JORTNER. Phys. Rev. Lett. **33**, 415 (1974).
28. Z. OPHIR, B. RAZ, J. JORTNER, V. SAILE, N. SCHWENTNER, E. E. KOCH, M. SKIBOWSKI, and W. STEINMANN. J. Chem. Phys. **62**, 650 (1975).

29. D. PUDEWILL, F. J. HUMPSEL, V. SAILE, N. SCHWENTNER, M. SKIBOWSKI, E. E. KOCH, and J. JORTNER. J. Chem. Phys. **65**, 5226 (1976).
30. Z. OPHIR, N. SCHWENTNER, B. RAZ, M. SKIBOWSKI, and J. JORTNER. J. Chem. Phys. **63**, 1072 (1975).
31. (*a*) W. K. TAUCHERT. Ph.D. Thesis, Free University of Berlin, Berlin, W. Germany. 1975. (*b*) W. K. TAUCHERT, H. JUNGBLUT, and W. F. SCHMIDT. Can. J. Chem. This issue.
32. L. CHIA and P. DELAHAY. (*a*) Unpublished. International Conference on Electrons in Fluids, Banff, Canada, Sept. 5–10, 1976. (*b*) J. Electron Spectrosc. In press.
33. S. A. RICE and J. JORTNER. J. Chem. Phys. **44**, 4470 (1966).
34. D. BEAGEHOLE. Phys. Rev. Lett. **15**, 551 (1965).
35. U. ASAF and J. J. STEINBERGER. Phys. Lett. A, **34**, 207 (1971).
36. B. RAZ and J. JORTNER. Proc. R. Soc. London, Ser. A, **317**, 113 (1970).
37. (*a*) I. MESSING. Ph.D. Thesis, Tel-Aviv University, Tel-Aviv, Israel. 1976. (*b*) I. MESSING, B. RAZ, and J. JORTNER. To be published.
38. M. B. ROBIN. Higher excited states of polyatomic molecules. Vol. I. Academic Press, New York. 1974.
39. (*a*) J. L. LEVINE and J. M. SANDERS. Phys. Rev. Lett. **8**, 159 (1962). (*b*) J. L. LEVINE and J. M. SANDERS. Phys. Rev. **154**, 138 (1967).
40. H. R. HARRISON and B. E. SPRINGETT. Chem. Phys. Lett. **10**, 418 (1971); Phys. Lett. **35**, 73 (1971).
41. J. A. JAHNKE and M. SILVER. Chem. Phys. Lett. **19**, 231 (1973).
42. (*a*) T. P. AGGARTER and M. H. COHEN. Phys. Rev. Lett. **25**, 807 (1970); **27**, 129 (1971). (*b*) T. P. AGGARTER. Phys. Rev. A, **5**, 2496 (1972).
43. J. P. HERNANDEZ. Phys. Rev. A, **7**, 1755 (1973).
44. K. W. SCHWARZ. Unpublished. International Conference on Electrons in Fluids, Banff, Canada, Sept. 5–10, 1976.
45. A. GAATHON and J. JORTNER. Electrons in fluids. Springer Verlag, Heidelberg. 1973. p. 429.
46. R. OLINGER, U. SCHINDEWOLF, A. GAATHON, and J. JORTNER. Ber. Bunsenges. Phys. Chem. **75**, 690 (1971).
47. R. OLINGER, S. HAHNE, and U. SCHINDEWOLF. Ber. Bunsenges. Phys. Chem. **76**, 349 (1972).
48. A. GAATHON, G. CZAPSKI, and J. JORTNER. J. Chem. Phys. **58**, 2648 (1973).
49. A. GAATHON. Ph.D. Thesis, The Hebrew University, Jerusalem, Israel. 1974.
50. K. IGUCHI. J. Chem. Phys. **48**, 1735 (1968).
51. P. M. RENTZEPIS, R. JONES, and J. JORTNER. J. Chem. Phys. **59**, 766 (1973).
52. D. HUPPERT, W. S. STURVE, P. M. RENTZEPIS, and J. JORTNER. J. Chem. Phys. **63**, 1205 (1975).
53. W. T. SOMMER. Phys. Rev. Lett. **12**, 271 (1964).
54. J. LEKNER *et al.* Phys. Rev. **156**, 351 (1972).
55. Z. OPHIR. Ph.D. Thesis, Tel-Aviv University, Tel-Aviv, Israel. 1976.

Discussion

L. Kevan: Do you think the "snowball" effect for electron localization should occur in nonpolar liquids doped with polar molecules? In recent experiments on glassy mixtures of alkanes with alcohols we have not yet found evidence for such an effect. And in liquid mixtures I believe Professor Baxendale also does not find such evidence. It may be that the critical experiment has not yet been performed since alcohol forms clusters in alkanes. What is needed is a polar molecule that does not cluster on nonpolar media.

J. Jortner: The proposed "snowball" effect in subcritical and supercritical polar fluids at moderately low densities involves a formation of a localized state by electron attachment to a (sufficiently large) pre-existing cluster, followed by subsequent attachment of polar molecules to that charged cluster. Such effect will not be observed in glasses because of the low diffusion coefficient of the polar molecules. In liquid mixtures of polar and nonpolar molecules at a low concentration of the former such effects can be exhibited. However, the time scale is unknown.

G. A. Kenney-Wallace: Jonah and I have carried out picosecond pulse radiolysis experiments on alcohols diluted in alkanes and, to quote one example, electron solvation in butanol–*n*-hexane (1:5 mol ratio) mixtures definitely appears to be slower than that in pure butanol, by a factor of about 2. The stable spectrum appears within tens of picoseconds, not nanoseconds as might have been expected for a diffusion process; however, even in this concentration range we expect to have large alcohol clusters and so an adequate number of alcohol molecules are already present and available for the solvation sheath. In order to see any "snowball" effects, as Jortner has suggested, we would have to go to much lower concentrations of alcohol.

J. Jortner: Obviously picosecond studies of the systems investigated by you and by Baxendale at low alcohol concentrations are required to settle the point whether 'condensation' of additional polar molecules on a charged cluster occurs.

A. O. Allen: Conductivity studies of dilute (0.01 *M*) methanol in hydrocarbons shows that an equilibrium exists between mobile electrons and methanol-solvated electrons. The evolution of solvation in time is therefore due (at least in part) to passage from smaller to larger clusters through the conductive (unsolvated) state which exists in thermal equilibrium.

J. Jortner: The peaceful coexistence between extended and localized states at thermal equilibrium in methanol–hydrocarbon mixtures bears a close analogy to the recent experiments of Klaus Schwarz on electron drift velocities in He gas where 'slow' and 'fast' electrons were identified.

N. R. Kestner: Whether or not the "snowballing" effect can be observed after the initial cluster is formed (say in Baxendale's experiments) depends on how long range is the effect of the electron on the fluid. If that potential is reasonably short range, the optical spectra may not change significantly after the initial trap is formed especially if the snowballing involves, say, a third or further coordination layer. We now believe that, in fact, the old theoretical models had a potential which was much too long range.

J. Jortner: The "snowball" effect resembles Thompson condensation of charged droplets occurring on a microscopic scale. One has to distinguish carefully between the nature of the potential acting on the localized electron at long times, whose long-range part is affected by density fluctuation, and the interaction of the charged cluster with polar molecules leading to cluster growth. The invariance of the optical spectrum in D_2O in the density range 0.8–0.01 g cm^{-3} reflects the result of a long time experiment where clustering has been already completed.

L. Onsager: Let me argue for the proposition that the "snowball" forms from the outside in. If we regard the trap formation as a process of dielectric relaxation around a delocalized electron, this will proceed at a rate given by the longitudinal relaxation time $\tau_L = \tau_D\varepsilon_\infty/\varepsilon_0$ in the distant part of the fluid (outside the counteracting region of localization), and the equilibrium polarization in the immediate vicinity is established last.

J. Jortner: Your interesting proposal implies that the initial step in electron localization involves the fast response of the polar medium to a large polaron in an extended state and that the long-range polarization field builds up on a time scale which is considerably shorter than the Debye relaxation time. A few years ago Rentzepis, Jones, and myself proposed that the initial step in electron localization in a polar liquid (water) involves the build-up of the long range dipolar polarization field. However, in low density supercritical polar fluids near the liquid–vapor coexistence curve we have to consider the role of pre-existing clusters (originating from density fluctuations), which act as electron traps.

Photoionization energies: liquids and solutions versus gases (Extended Abstract)

LADISLAV NEMEC, LUCILLE CHIA, AND PAUL DELAHAY
Department of Chemistry, New York University, New York, NY, U.S.A. 10003

Received November 22, 1976

We compare the external ionization energies of neutral and ionic species in liquids with the ionization energies of these species in the gas phase. The experimental liquid–gas shifts in ionization energy thus obtained are estimated from simple models.

The external ionization energies for liquids and solutions were obtained by photoelectron spectroscopy by means of a recently developed method (1). The *second* derivative of the quantum yield, with respect to the kinetic energy T of electrons emitted into vacuum, was measured as a function of T. Second derivative curves (sdc) exhibit one or several maxima, each of which corresponds to a photoionization process. The external ionization energy I is related to T_{max} at each sdc maximum by

$$[1] \qquad I = E - T_{max} - 0.52w_{1/2}$$

where E is the photon energy and $w_{1/2}$ is the half-width of the sdc segment on the high-energy side of the maximum. The $w_{1/2}$ correction arises from energy transfer from quasi-free electrons to the liquid medium and is rather small ($w_{1/2} \approx 0.5$ eV).

The energy I for *neutral substances* is lower in the liquid than in the gas phase. The *red shift* (1 to 2 eV) from gas to liquid arises (1) in a major part from the difference between the energies stored in the electrical field of the ion (produced by photoionization) in the liquid and vacuum. This shift depends primarily on the *optical* dielectric constant of the substance being photoionized and does not vary markedly from one substance to another.

Conversely, the energy I for *ions* is higher for solutions than in the gas phase. The *blue shift* from gas to liquid ($\approx$2 to 3 eV) is accounted for, in a major part, by the energy of solvation of the ion. This energy depends on the *static* dielectric constant of the solvent, and consequently the shift for ions can vary appreciably with the nature of the solvent. Detailed experimental results and calculations are presented for a variety of substances.

This work was supported by the National Science Foundation and the Office of Naval Research.

1. L. NEMEC, L. CHIA, and P. DELAHAY. J. Electron Spectrosc. In press.

Discussion

J. Jortner: The general feature of the ionization potential (IP) of a neutral molecule in solution which is red-shifted relative to the gas phase IP pertains to external photoemission to the vacuum. For an internal ionization process the shift can be red or blue depending on the sign and magnitude of V_0.

P. Delahay: Your statement corresponds to my equation for the liquid

$$I_{internal} = I_{external} + V_0$$

where the I's are positive by convention and V_0 is taken with its sign. This relationship does not include the surface potential which was assumed to be zero. V_0 does not matter in the comparison of $I_{external}$ for the liquid with I_{gas} since the final state of the electron is the same in both cases.

A. Henglein: Ionization energies determined by photoelectron spectroscopy are vertical ionization energies which exceed the thermodynamic ones by the reorganization energy of the cation formed (including its solvation shell). The thermodynamic free energies ΔG_i of ionization are important for the understanding of chemical reactions in which an electron is abstracted from a solvent molecule (by a free radical or excited molecule). Free energies of ionization have recently been published (see table) for

Solvent	ΔG_i (eV)	E^0 (V)
Water	7.9	3.4
Ethanol	6.4	1.9
Acetone	6.5	2.0

a few solvents (A. Frank, M. Grätzel, and A. Henglein. Ber. Bunsenges. Phys. Chem. **80**, 593 (1976)). These free energies can be converted into standard redox potentials E^0 using the relation

$$E^0 = -4.5 + \Delta G_i$$

-4.5 V being the potential of an electron in the gas phase on the standard redox potential scale. The standard redox potential of the redox couple H_2O^+/H_2O is 3.4 V.

Effect of temperature and phase on the photoionization energy threshold of TMPD in hydrocarbon solvents

J. BULLOT

Laboratoire de Physico-Chimie des Rayonnements Associé au CNRS, Université Paris-Sud, 91 405 Orsay, France

AND

M. GAUTHIER

E.R. n° 98, Laboratoire de Chimie Physique, Université Paris-Sud, 91 405 Orsay, France

Received September 27, 1976

J. BULLOT and M. GAUTHIER. Can. J. Chem. **55**, 1821 (1977).

The temperature dependence of the TMPD photoionization energy threshold, I, in a set of eight hydrocarbon solvents has been systematically studied, from room temperature down to 77 K. For this purpose ion-pair formation is detected either by measuring the photocurrents in the liquid phase or by measuring the recombination luminescence intensity in the solid phase. It is found that I(liquid) increases linearly when the temperature is decreased down to the liquid–solid transition temperature. At this temperature I undergoes an abrupt increase of 0.2–0.6 eV depending on the hydrocarbon and the nature of the phase transition. Any subsequent solid–solid phase change is accompanied by a new shift towards higher energy. In the low temperature phase of all the studied crystals, I(solid) has a constant value down to 77 K. Glass-forming liquids have a very different behavior: I varies linearly in the liquid and the straight line extrapolates to the I(glass) value at 77 K. The applicability of the two methods is discussed. From the present data it is concluded that the conduction state energy, V_0, is constant in the low-temperature phase of crystals. By calculating the polarization energy due to the $TMPD^+$ cation and from data on the temperature dependence of V_0 in the liquid phase, we have estimated V_0 in crystalline *n*-hexane (0.64 eV) and 2,2,4-trimethylpentane (0.44 eV) and in the plastic phase of cyclohexane (0.47 eV) and 2,2-dimethylbutane (0.01 eV). Finally a correlation of I with the medium density is described.

J. BULLOT et M. GAUTHIER. Can. J. Chem. **55**, 1821 (1977).

Nous avons étudié la variation en fonction de la température du seuil de photoionisation, I, de la TMPD dans huit hydrocarbures, depuis la température ambiante jusqu'à 77 K. La formation des paires d'ions est détectée soit par la mesure des photocourants en phase liquide, soit par la mesure de l'intensité de la luminescence de recombinaison en phase solide. I(liquide) augmente linéairement quand la température décroît, et ceci jusqu'à la température de transition liquide–solide. A ce point I augmente brutalement de 0.2 à 0.6 eV, suivant l'hydrocarbure étudié et la nature de la transition de phase. Toute autre transition de phase solide–solide s'accompagne d'une nouvelle augmentation de I. Dans la phase basse température des cristaux étudiés, I(solide) a une valeur constante jusqu'à 77 K. Les liquides qui donnent des verres ont un comportement très différent: I varie linéairement dans le liquide et les valeurs extrapolées coïncident avec la valeur mesurée à 77 K dans le verre. A partir de ces données on peut conclure que le bas de la bande de conduction, V_0, a une valeur constante dans la phase basse température des cristaux. A partir du calcul de l'énergie de polarisation du cation $TMPD^+$ et des données sur la variation de V_0 en fonction de la température en milieu liquide, nous avons estimé la valeur de V_0 dans les cristaux de *n*-hexane (0.64 eV) et de triméthyl-2,2,4 pentane (0.44 eV) et dans la phase plastique du cyclohexane (0.47 eV) et du diméthyl-2,2 butane (0.01 eV). Enfin nous décrivons une corrélation entre I et la densité du milieu.

1. Introduction

It has long been known that the ionization potential of a solute molecule in a condensed phase is lowered relative to the value measured in the gas phase I_g. Indeed this has been experimentally checked (1–6) by measuring the photoionization threshold of the solute molecule TMPD[1] in some liquid, I(liq.), and in some crystalline or glassy solvents, I(sol.).

[1] *N,N,N′,N′*-Tetramethylparaphenylenediamine.

The early interpretation of Lyons and coworker (7, 8) emphasizes the importance of the polarization of the medium, P_+ around the cation and the ejected electron. More recently, the theoretical model developed by Springett *et al.* (9) for rare gases permits a direct calculation of the energy V_0 of the excess electron in a quasi-free state, which enters the equation giving the photoionization threshold:

$$[1] \qquad I(\text{liq.}) \text{ or } I(\text{sol.}) = I_g + P_+ + V_0$$

This model has been extensively used and extended in the past few years to elucidate some properties of the excess electron in hydrocarbons such as the temperature dependence of V_0 (10, 11), localization criterion (11, 12), and mobility (13–15).

The experimental measurement of I made with TMPD as a solute in various hydrocarbons has shown that I(sol.), measured in the crystal at 77 K, is always higher than I(liq.) measured at room temperature (3). The difference ranges from ~0.6 to 1 eV from one solvent to another. Recently both I(liq.) and V_0 have been found to increase when the temperature is decreased (4*a*, 10), but the V_0 variations are too low to account for the difference, I(sol.) − I(liq.), previously observed.

Therefore it was of interest to study the temperature dependence of the photoionization threshold in the crystal and to look for a specific effect of phase transitions. Some preliminary results (16) have already been published. In the present paper, we report the systematic determination of the TMPD photoionization threshold in various hydrocarbons with special attention (*i*) to the variation of I with temperature either in the crystal or in the liquid and (*ii*) to the effect on I of phase transitions. The solvents have been chosen to cover several types of phase changes, namely liquid–crystal, liquid–glass, and crystal–crystal.

2. Experimental

The experimental techniques used to determine the biphotonic ionization threshold and to detect the ions by the neutralization luminescence have been previously described in detail (1, 16).

In the liquid phase, two photoconduction cells have been used. Each may be fitted into a 10 mm square silica absorption cell C (Fig. 1). In the first cell (Fig. 1*A*), the two stainless steel electrodes E are held 4 mm apart by means of a stumatite[2] spacer ST. The light beam emerging from the monochromator enters through the front silica window S, and is then perpendicular to the applied electric field direction. This set-up was used for most liquid phase measurements. In the second cell (Fig. 1*B*), the electrodes E and G are 1 mm apart. The light enters the cell through the silica window S, fitted into the front stainless steel holder H; the front electrode G is made of a 0.03 mm thick nickel grid welded onto H. This cell was used for some solid-state measurements. Usual care was taken for shielding the measurement cell. The high voltage applied across the sample was taken from a set of batteries, the applied electric field being ~1.5 kV cm^{-1}. The photocurrents were measured by means of a 602 Keithley electrometer. Temperature of the sample was varied by admitting an adjustable flow of cooled nitrogen gas close to cell C. Temperature was known to ±0.2 deg.

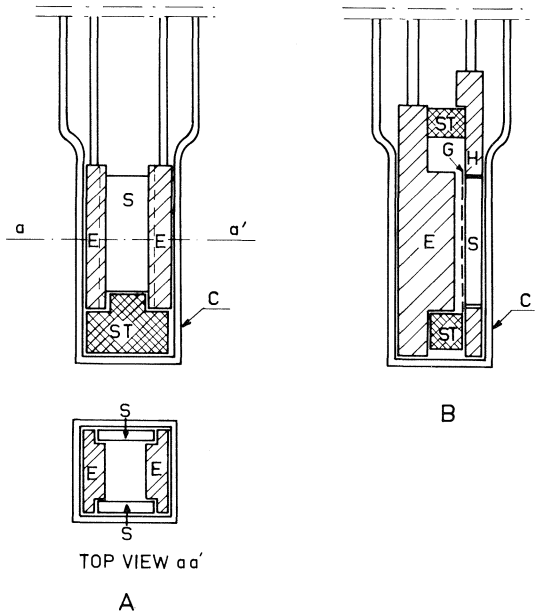

FIG. 1. Details of the photoconduction cell (see text).

The light emerging from a Kern WHS 200 deuterium lamp is passed through a M 25 Huet grating monochromator whose band width is 12 nm This set-up enables accurate measurements up to 195–200 nm. Relative values of the photon flux F *vs.* wavelength were obtained by measuring the fluorescence emitted by a concentrated alcoholic solution of rhodamine B. Absolute values were determined by comparison with the signal obtained at 310 nm with a Kipp thermopile. In the energy range of interest F decreases slowly from 2×10^{12} photons s^{-1} at 270 nm to 0.09×10^{12} photons s^{-1} at 200 nm.

2.1. Chemicals

TMPD (Eastman-Kodak) was liberated from the hydrochloride and sublimated just before use.

The following hydrocarbons (Fluka) were used: 2,2,4-trimethylpentane (TMP); 2,2-dimethylbutane (DMB); *n*-hexane (*n*-Hex); cyclohexane (cy-Hex); neopentane (neo P); tetramethylsilane (TMSi); 3-methylpentane (3-MP); and methylcyclohexane (MCH). They were purified by keeping them at least 24 h on activated molecular sieves (3A + 5A + 13X Linde) in a vacuum system. Afterwards they were slowly distilled into a storage bulb. The efficiency of the treatment was tested by absorption and emission spectroscopy. For photoconductivity measurements, the solution was rapidly prepared in the presence of air, just before use, and poured into the cell C, dehydrated with silica gel. The measurements were done in the presence of air.

[2]Stumatite is a natural lava which, when properly machined, is baked at ~1200°C. The resulting material is hard and has good insulating properties. We had recourse to this material after having experienced great difficulties with Teflon as an insulator which, when immersed in liquid hydrocarbons, yields large dark currents.

3. Results

3.1. The Ionization Efficiency Curves in Liquid and in Solid Hydrocarbons

The shape of the ionization efficiency curves is similar for all the solvents studied. Typical examples are shown in Fig. 2 for liquid MCH and in Fig. 3 for solid cy-Hex. Both refer to the same number of exciting photons at each wavelength.

In the liquid, the concentration has been chosen high enough (5×10^{-4} *M*) to give total absorption whatever the wavelength and it has been verified that for this concentration, the light absorption by the solvent is always negligible, even at short wavelengths. The shape of the curves is consistent with the results reported earlier by Holroyd and Russell (4) but some discrepancies appear in the low and high energy range when comparing the present curves with those of Peterson *et al.* (17).

These authors emphasize the existence of a residual photocurrent in the long wavelength region. Indeed, we observed such currents only in solvents like TMSi or TMP leading to especially high ionization yields. The use of a high pass filter (J280 from MTO which transmits 42% at 280 nm and 67% at 300 nm) reduces the photocurrent measured at 300 nm by a factor of about 20 in TMSi. Since the transmission of the filter becomes negligible only below 230 nm, it appears that the current observed at 300 nm might be totally accounted for by short wavelength stray light which is strongly reduced but not totally cut off by the filter.[3]

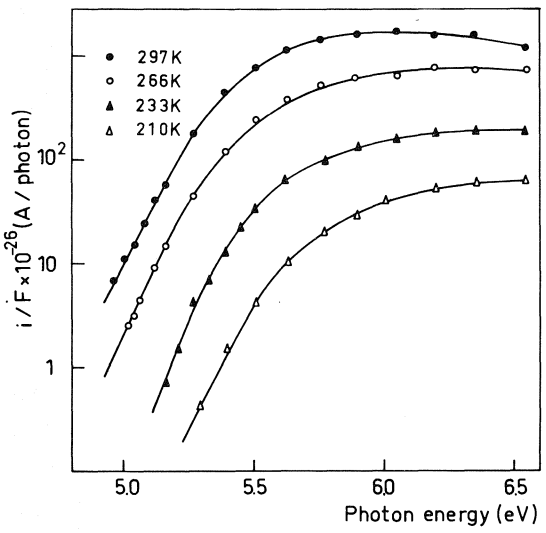

FIG. 2. Photocurrent *vs.* energy curve for liquid MCH at various temperatures.

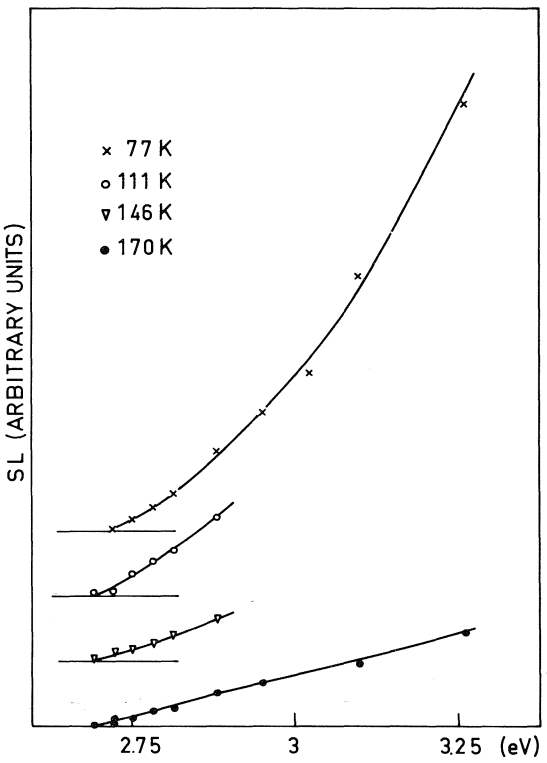

FIG. 3. Neutralization luminescence intensity *vs.* second beam energy curve for crystalline cy-Hex at various temperatures. For sake of clarity the curves have been shifted along the vertical axis. I(sol) is given by $E_T + E_{th}$, where E_T is the energy of the TMPD triplet state (2.8 eV) and E_{th} is the second beam energy threshold.

On the other hand, at high energies, Peterson *et al.* (17) found in every case a drastic decrease of the ionization yield and claimed that it is related to the onset of the third absorption band of TMPD around 6 eV. This fact is not so clear from Holroyd's results (4). In most of our experiments, a maximum has indeed been observed but its wavelength depends on experimental conditions. It has been found that the maximum occurs at a shorter wavelength every time the

[3]It may also be noted that, with a cell fitted with Teflon as an insulator, a monophotonic current was always observed in the 280–350 nm range with a maximum at 305 nm. It was not due to stray light, did not depend on the applied voltage, and its rise time was very long (of the order of minutes). The origin of this signal has not yet been elucidated, but it appears as an experimental artifact since it has never been observed when stumatite was used instead of Teflon.

ionization yield is lowered either by decreasing the temperature or by using solvents in which the ionization yield is low. In a few cases, no more maximum is observable at low temperature and the current rises continuously up to 6.5 eV which corresponds to the maximum of the third absorption band of TMPD. Such an example is shown in Fig. 2 for MCH at 210 K. Thus there is no correlation between the absorption spectrum of TMPD and the photoionization curve. In our opinion, the changes of the shape of the latter may well not be real but may originate from volume recombination effects (4) whose importance increases with ionization yield. Being more interested in the ionization threshold than in the ionization yield, we did not try to overcome this effect.

In the solid, part of the light is scattered by the polycrystalline sample. It is thus quite difficult to determine the number of absorbed photons. It may just be noticed that the incident number of photons is kept constant by adjusting the monochromator slits at each wavelength, and that the *T–T* extinction coefficient being approximately constant in the 400–500 nm range, the curves shown in Fig. 3 truly represent the variation of the ionization efficiency *vs.* energy (6). The increase near the threshold is very rapid; however, due to the small energy range available (it is limited by the onset of the ground state absorption at $\sim$3.3 eV), it is not possible to speculate whether the increase is exponential as in the liquid.

The variations of the ionization yield *vs.* temperature are strikingly different in liquid and solid phases. In the liquid, the yield decreases rapidly with temperature (see Fig. 2 and ref. 4). In the crystal, the variation is more complex. The yield is approximately constant at low temperature and suffers an abrupt decrease in the premelting range. A similar behavior has been observed for all the crystalline solvents studied, the decrease occurring about 10 to 30 deg below any phase transition temperature. It originates in the decrease of the matrix rigidity which shortens the lifetime of the triplet state intermediate and decreases the stability of the trapped electrons which can no longer be detected after excitation.

3.2. *Temperature Dependence of the Photoionization Threshold*

As explained in the experimental section, in the liquid phase the ions were detected by means of the photoconduction technique. In the solid phase, the ions were detected by means of the stimulated luminescence following a biphotonic ionization, except in those cases where the monophotonic ionization of the solute molecule could be detected by means of the photoconduction technique.

The photoionization threshold values given below correspond to the lowest photon energy for which a signal may be detected. In the solid, the detection sensitivity is limited by the intensity and reproducibility of the signal obtained when the first beam is acting alone (1). In the liquid, the detection sensitivity is limited by the value of the dark current ($\sim 3.5 \times 10^{-13}$ A at room temperature) and its stability; typically the lowest detected signals are $\sim 10^{-14}$–10^{-13} A at room temperature, down to 10^{-15}–10^{-14} A at low temperature. Such an approach is justified, in the present work, since we are only concerned with the shift of the photoionization threshold when the temperature is varied and when a new phase is formed. Any other possible definition remains somewhat arbitrary until a better understanding of the meaning of the ionization potential of a solute molecule in a condensed medium is reached.

Plots of I *vs.* temperature for the various solvents are shown in Figs. 4–6. As seen we find that the photoionization threshold in the liquid increases linearly when the temperature is decreased down to the melting point. In the solid phase the I behavior is strikingly different. Within experimental uncertainty ($\sim \pm 0.05$ eV), I(sol.) does not vary with temperature, in a given crystalline phase. This point is clearly seen by examining Figs. 3–5.

In Table 1 are presented the numerical data. In the liquid phase we report the I(liq.) value near room temperature (columns 2 and 3) and in column 4 the slope, $-\mathrm{d}I(\mathrm{liq.})/\mathrm{d}T$; it is seen that the slope changes by ~ 5 when going from a liquid like TMSi, which exhibits quasi-free electron behavior, to glass-forming liquids like 3-MP or MCH in which localized states are anticipated. In the solid phase we report (*i*) the I(sol.) data (columns 5 and 6) obtained by means of the photoconduction method (see Section 3.3) and (*ii*) the average value of I(sol.) measurements (columns 7 and 8) obtained by means of the luminescence method. In columns 9 and 10 the phase transitions are described.

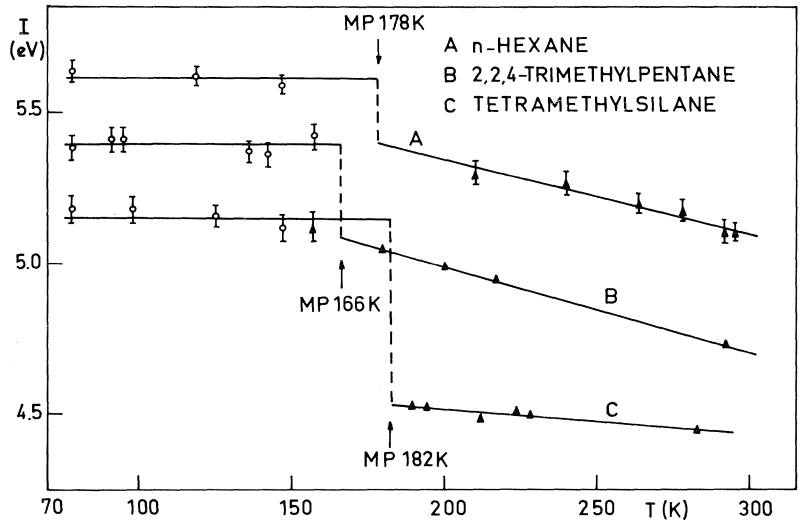

FIG. 4. Temperature dependence of the photoionization threshold energy for TMPD in TMSi, *n*-Hex, and TMP: (▲) data obtained by the photoconduction method; (○) data obtained by the neutralization luminescence method.

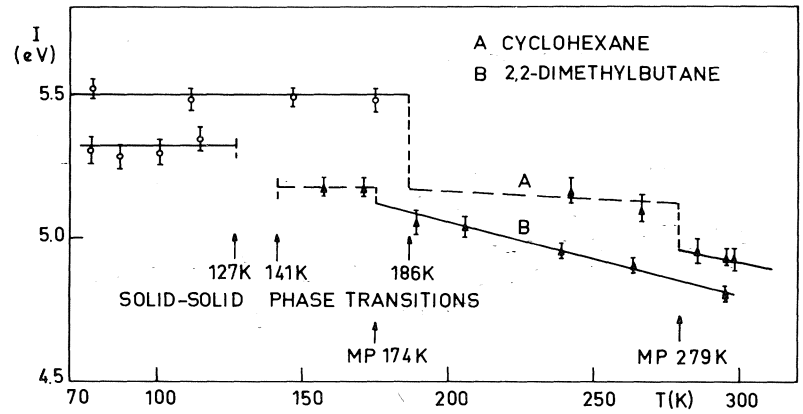

FIG. 5. Temperature dependence of the photoionization threshold energy for TMPD in DMB and cy-Hex. See Fig. 4 for meaning of symbols. For DMB no data could be obtained in the region between the two solid–solid phase transitions.

3.3. Variation of the Photoionization Threshold at a Phase Transition

From Figs. 4 and 5, concerning crystal-forming liquids, it appears that the I *vs.* T curves show discontinuities when the solvent undergoes a phase transition. However, it is necessary to ascertain that the two different methods used for the two phases do not give systematically different values of I at a given temperature and that the observed I shift at a phase transition is not an artifact reflecting some basic difference in the experimental techniques.

Takeda *et al.* (5) stated that, in the liquid phase, mono- and biphotonic ionization yield the same ionization energy values. We have reported before (16) an attempt to measure the TMPD monophotonic threshold in crystalline DMB at 77 K by means of the luminescence technique. However, the accuracy was poor and no conclusion could be drawn.

Evidently, the best method would be to measure the temperature dependence of I from room temperature down to 77 K using the same technique. Unfortunately this is not generally feasible due to the inherent limitations of both experimental methods.

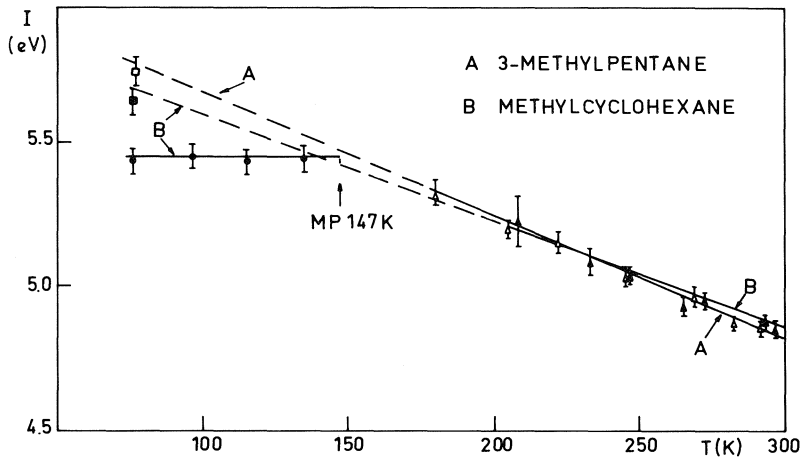

FIG. 6. Temperature dependence of the photoionization threshold energy for TMPD in 3-MP and MCH. Data obtained by the photoconduction method in the liquid: (△) 3-MP; (▲) MCH. Data obtained by the neutralization luminescence method in the glass: (□) 3-MP; (■) MCH; or in the crystal (●) MCH.

As discussed before (Section 3.1), the luminescence technique has a narrow range of applicability and any extension at a higher temperature is precluded. Difficulties are also encountered in extending the photoconduction method to low temperature measurement. As a matter of fact, in most solvents the photocurrent decreases very rapidly with temperature and a further abrupt decrease is expected upon crystallization since most electrons become trapped in the crystal and cannot travel to the electrodes, even in a very thin sample. Finally it is worth noting that since I(sol.) values are significantly higher than I(liq.) ones, the threshold is expected to lie at ~220 nm in solid linear alkanes, *i.e.* within an energy range where the photon flux is dramatically low.

Nevertheless, photocurrents in the solid phase were detected in three favorable cases: TMSi, cy-Hex, and DMB, and the photoionization thresholds could be measured.

In TMSi, for which the photoionization yield is particularly high, a current as high as 8×10^{-13} A at 205 nm could be detected at 156 K, *i.e.* 26 deg below the melting point. A threshold of 5.13 eV was obtained, identical to the average value obtained by means of the biphotonic luminescence technique (Fig. 4). At lower temperatures, the photocurrent intensity decreases rapidly, noise is large, and no accurate measurements could be carried out.

It is well-known that upon crystallization, cy-Hex and DMB give plastic crystals; that is crystals in which molecular reorientation is easy, so that electron trapping is not possible. Moreover, these crystals are almost transparent to light, while at low temperatures opaque polycrystalline samples are obtained. The currents measured at 220 nm were 4×10^{-14} A at 267 K and 5×10^{-13} A at 181 K in cy-Hex and DMB respectively and I(sol.) could be measured (see Table 1). Although a direct comparison with the luminescence technique is not possible in this case, it is important to note that a discontinuity at the melting point is also observed when both liquid and solid I values are obtained by photoconductivity (Fig. 5).

Thus we feel fairly confident in drawing the following conclusions.

(*i*) I(sol.) is always higher than I(liq.). At the liquid–solid phase transition, the I *vs.* T curve presents a discontinuity and the difference $(\Delta I)_{SL} = I(\text{sol.}) - I(\text{liq.})$ is some tenths of an eV. It is larger for rigid crystals (TMSi; *n*-Hex; TMP (16)) than for plastic crystals (cy-Hex; DMB).

(*ii*) From cy-Hex and DMB data it is seen that I(sol.) is higher for the low temperature phase than for the plastic crystal. In cy-Hex there is a discontinuity in the I *vs.* T curve at the solid–solid transition temperature.

(*iii*) For the glass-forming liquids 3-MP and MCH, the I values obtained in the liquid fit a straight line which extrapolates nicely to the I value measured in the glass without any discontinuity at the glass transition temperature.

4. Discussion

4.1. *Ionization Potential and Photoionization Threshold of a Solute Molecule*

The definition of the ionization potential of a molecule in the gas phase—the lowest energy needed for ejecting an electron to infinity with no excess kinetic energy—is no longer valid in a condensed phase. In effect the electron is readily slowed down and gets thermalized in the Coulomb field of the parent cation, and the ionization threshold is related to the ionization potential IP by I(liq. or sol.) = IP(liq. or sol.) + E_c where E_c is the Coulomb energy.

The result is that the energy needed for charge separation is no longer single valued, but reflects the distribution of cation – thermal electron separation distances.

The implication of such a picture may be somewhat different according to the ultimate fate of the electron and according to the detection technique. Let us mention here (*i*) that the only detectable electrons by means of the photoconduction technique are those which have escaped geminate recombination and for which E_c is negligible; and (*ii*) that in a solid matrix the electrons are trapped at such distances that $E_c \simeq 0.1$ eV to 0.2 eV in a glass (1); still lower values are expected in crystals where the density of traps is lower.

Finally we wish to allude to the specific problem of the photoionization threshold and of the shape of the photocurrent *vs.* energy curve. It is indeed a fundamental problem to understand the meaning of the spectral response curve because it contains some basic information concerning the interaction between a solute molecule and the environment. Moreover the proper theoretical description of this curve should provide a clear definition of what the photoionization threshold is, a problem we had to face all along the course of this work.

We are aware of two approaches by Delahay *et al.* (18, 19) and by Peterson *et al.* (17), but no definite conclusion has been reached and no clear definition of the photoionization threshold obtained.

4.2. *The Conduction State Energy V_0 in the Crystal Phase of some Hydrocarbons*

Our experimental results show unambiguously that the photoionization threshold, I(sol.), is constant in the low-temperature crystal phase of all the studied hydrocarbons. In the plastic phase

TABLE 1. Effect of temperature on TMPD photoionization energy threshold

Solvent	Liquid phase			Solid phase					Phase transitions	
				Photoconduction method		Luminescence method				
	T (K)	I(liq.) (eV)	$-dI(liq.)/dT$ (eV K^{-1})	T (K)	I(sol.) (eV)	Temperature range studied (K)	I(sol.) (eV)		T (K)	Nature*
TMSi	283	4.45	8×10^{-4}	156	5.13	146–177	5.15±0.03		182	L–C
TMP	292	4.73	2.8×10^{-3}	—	—	155–177	5.39±0.03		166	L–C
n-Hex	296	5.10	2.4×10^{-3}	—	—	147–177	5.61±0.02		178	L–C
Neo P	—	—	—	—	—	115–177	5.17±0.02		257	L–C
DMB	295	4.80	2.5×10^{-3}	171	5.18	115–177	5.30±0.03		174	L–PC
				157	5.18				141	C–C
									121	C–C
Cy-Hex	298	4.92	2.0×10^{-3}	267	5.10	174–177	5.49±0.02		279	L–PC
				243	5.16				186	C–C
3-MP	292	4.90	3.7×10^{-3}	—	—	77	5.75		77	L–G
MCH	297	4.85	4.0×10^{-3}	—	—	77	5.65		89	L–G
Annealed crystalline MCH	—	—	—	—	—	135–177	5.45±0.02		147	L–C

*L–C: liquid–crystal; L–PC: liquid–plastic crystal; C–C: crystal–crystal; L–G: liquid–glass.

of DMB and cy-Hex, data are too scarce to draw any definite conclusion. Restricting then our discussion to the former well-established result, we wish to comment on the meaning of the constancy of I(sol.).

I(sol.) is related to V_0 and P_+ by [1]. The polarization energy P_+ due to the cation may itself be written as

$$[2] \qquad P_+ = -\frac{e^2}{2r_0}\left(1 - \frac{1}{\varepsilon}\right)$$

where ε is the optical dielectric constant and r_0 the $TMPD^+$ cation radius. In the low temperature phase of crystalline hydrocarbons, the density ρ is not expected to vary much with temperature. Indeed, X-ray crystallographic measurements in the monoclinic phase of cy-Hex at 175 K and 115 K give the same value (20). Then, from the Clausius–Mosotti equation

$$(\varepsilon - 1)/(\varepsilon + 2)M/\rho = P$$

where M is the molecular weight and P the molar polarization, ε may be considered as constant, and consequently P_+ does not vary. Hence from [1] the conclusion is reached that *V_0 is itself constant in the low-temperature phase of hydrocarbons.*

It is of course quite interesting to get an estimate of V_0 in the solid phase. Noda *et al.* (11) and Grand (6*a*) have calculated V_0 in some polar and nonpolar glasses at 77 K, from I(sol.) data published by Bernas *et al.* (1–3) and by Santus *et al.* (21). Bernas and Grand (6*b*) have used the same approach for crystalline hydrocarbons. In refs. 10 and 6 eq. [1] is used: I(sol.) is known and P_+ is calculated from [2]. This indirect way of determining V_0 is straightforward, once the radius r_0 of the $TMPD^+$ cation, which enters [2], is known. Several values have been proposed; Holroyd and Russell (4) deduced an average value $r_0 = 2.49$ Å, while Noda *et al.* (11) used $r_0 = 1.93$ Å. With the latter value these authors calculated $V_0 = 1.20$ and $V_0 = 1.24$ eV in glassy 3-MP and MCH respectively. By using our I(liq.) data for 3-MP (Table 1) and the density data published by Dietrich (22),[4] we obtained a straight line $V_0(T) = 1.60 - 5.44 \times 10^{-3}T$, which extrapolates at 77 K to the $V_0 = 1.20$ eV value given in ref. 11.

A modified version of this indirect method is used below to estimate V_0 in the crystal phase of hydrocarbons. As seen above, an abrupt change $(\Delta I)_{SL}$ of the photoionization threshold energy is observed at the melting point (mp). As a consequence of [1], it may be written that

$$I_{sol} - I_{liq} = P_{+(sol)} - P_{+(liq)} + V_{0(sol)} - V_{0(liq)}$$

or

$$(\Delta I)_{SL} = \Delta P_+ + V_{0(sol)} - V_{0(liq)}$$

where the subscripts sol and liq mean that I, P_+, and V_0 refer respectively to the solid and the liquid at the *melting temperature*. Thus

$$[3] \qquad V_{0(sol)} = V_{0(liq)} + (\Delta I)_{SL} - \Delta P_+$$

From [3], V_0(sol) may be calculated. Here, V_0(liq) is obtained by extrapolating at mp the available liquid V_0 data (10), $(\Delta I)_{SL}$ is measured experimentally, and

$$\Delta P_+ = \frac{e^2}{2r_0}\left(\frac{1}{\varepsilon_{sol}} - \frac{1}{\varepsilon_{liq}}\right)$$

obtained from [2], may be calculated once ε_{sol} and ε_{liq} are known. In the following, ε_{liq} at 293 K is taken as the square of the refractive index. To calculate ε_{liq} and ε_{sol} at mp, first a value of the molar polarization P is obtained from ε_{liq} at 293 K and the known density at 293 K by means of the Clausius–Mosotti equation. Then, using the same equation, the procedure is reversed and ε_{liq} and ε_{sol} at mp are obtained from known values of the fluid density.

One question arises concerning the applicability of [2] giving P_+ in the solid phase. Lyons and Mackie (8) have calculated the energy of the polarization by a positive charge in a crystal by summing over ion-induced dipole interactions and over secondary interactions between induced dipoles. Provided the crystal structure is known, the total polarization energy may be obtained. They found for crystalline *n*-Hex: $P_+ = -1.7$ eV. When we use [2] and calculate ε_{sol} and ε_{liq} for *n*-Hex by the procedure just described, we get $P_+ = -1.65$ eV when choosing $r_0 = 2.49$ Å and $P_+ = -2.13$ eV with $r_0 = 1.93$ Å. Though the situation is different in the case treated in ref. 8—ions are *n*-hexane cations localized at the nodes of the crystal lattice—we simply wish to emphasize that the calculated values of P_+ are of the same order of magnitude.

The above method for calculating V_0(sol) may be used provided the density in the crystal is known. Unfortunately such determinations are

[4]We thank Professor J. E. Willard for kindly supplying these data.

TABLE 2. Calculated values for V_0 in hydrocarbon crystals*

Solvent	T (K)	$(\Delta I)_{SL}$ (eV)	V_0(liq.) at mp (eV) from ref. 5	ΔP_+ (eV)		V_0(sol.) (eV)	
				(*b*)	(*c*)	(*b*)	(*c*)
2,2-DMB	174(*a*)	0.06	−0.14	−0 087	−0 067	0 007	−0 013
2,2,4-TMP	166	0.3	−0 01	−0 168	−0 130	0 46	0 42
Cy-Hex	279(*a*)	0.17	0 27(*d*)	−0 039	−0 030	0.48	0 47
n-Hex	178	0.21	0.26	−0.195	−0.151	0.66	0 62

*(*a*) Plastic phase; (*b*) for $r_0 = 1.93$ Å; (*c*) for $r_0 = 2.49$ Å; (*d*) V_0 has been calculated as explained in the text.

scarce for hydrocarbon crystals. As far as we know, the only data available for the compounds we used are for *n*-Hex (23), cy-Hex (20, 24), and plastic DMB from X-ray studies (23), for TMP and *n*-Hex from pressure–temperature phase diagrams (25), and for plastic cy-Hex from densitometry (26). The results are presented in Table 2. The P_+ calculation has been carried out with two r_0 values 2.49 and 1.93 Å, as discussed above; two sets of V_0(sol.) values result as shown in columns 7 and 8 of Table 2. As no V_0(liq.) data are available for cy-Hex, we have used [1] and [2] to estimate V_0(liq) at mp taking $I_g = 6.6$ eV, $r_0 = 1.93$ Å, and $\varepsilon(293\ \text{K}) = 2.035$.

The method we used to calculate V_0(sol.) from measured $(\Delta I)_{SL}$ escapes the difficulty due to the scattering of data on the gas phase ionization potential of TMPD (27–31). However, due to experimental uncertainties in determining both I and V_0(liq.), the absolute values shown in Table 2 are, in our opinion, a rough estimate. Nonetheless, considering that relative values are meaningful, the following remarks are justified: (*1*) ΔP_+ does not vary much with r_0; (*2*) ΔP_+ is significant but always lower than $\Delta V_0 = V_0(\text{sol}) - V_0(\text{liq})$; (*3*) V_0 suffers an abrupt change when the liquid undergoes crystallization, ΔV_0 being smaller when the liquid yields a plastic phase as in DMB and cy-Hex, than when the liquid directly yields a rigid crystal as in *n*-Hex and TMP.

4.3. *Density Dependence of the Photoionization Threshold*

Previous work on the properties of an excess electron in a fluid or in a solid has demonstrated that they are governed by the density ρ of the medium. This point is clearly evidenced by many experimental results in liquid and solid rare gases (32, 33). The Springett, Jortner, and Cohen model (9) predicts that in rare gases exhibiting quasi-free electron behavior, the energy of the excess electron V_0 is due to two terms: U_p the polarization energy due to the electron and T a kinetic energy term. Both depend upon r_s, the radius of the Wigner–Seitz sphere, defined as $r_s = (3/4\pi\rho)^{1/3}$.

As far as the photoionization threshold is concerned we have seen in the preceding section that P_+, the cation polarization energy in a nonpolar medium, is a function of ρ alone.

All these reasons call for a plot of the photoionization threshold as a function of the density. Such a plot is shown in Fig. 7 for 3-MP, cy-Hex, *n*-Hex, DMB, and TMP. Though our I data do not cover the whole density range (for obvious experimental reasons), it is seen that the I(liq.) data fit a straight line which extrapolates nicely to the point corresponding to the low-temperature crystal phase. In the case of *n*-Hex and cy-Hex the fit is poorer and possibly a different relationship is underlying the density dependence of the photoionization threshold.

The striking difference in the slope between a glass-forming liquid like 3-MP and other crystal-forming hydrocarbons should also be noted.

Undoubtedly such a dependence, though it is not clearly understood at the present time, points out the fundamental role played by the density of the medium upon the properties of the free electron in nonpolar hydrocarbons. Introduction of the molecular quantity $(r_s - a)$, where a is the hard-core radius, used in the SJC model, has been made for correlating V_0 at different temperatures for various hydrocarbons (10) and attempted for I (16). But care should be taken because, as stressed by Jortner (34), in those hydrocarbons where the mobility is low, the electron cannot be considered as quasi-free and the SJC model is inapplicable. The idea underlying Kestner and Jortner's (13) model of a microscopically inhomogeneous fluid, containing 'transparent' and 'opaque' regions regarding electron transport, is very likely a first step to-

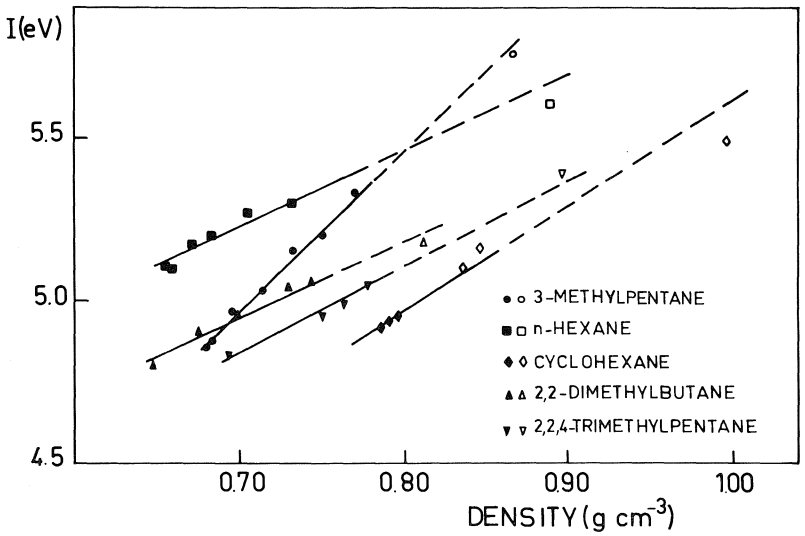

FIG. 7. Plot of the photoionization energy threshold as a function of the medium density.

wards a full understanding of these nonpolar fluids.

Acknowledgments

We are grateful to Mrs. A. Bernas and D. Grand for stimulating discussions.

1. A. BERNAS, M. GAUTHIER, and D. GRAND. J. Phys. Chem. **76**, 2236 (1972).
2. A. BERNAS, M. GAUTHIER, D. GRAND, and G. PARLANT. Chem. Phys. Lett. **17**, 439 (1972).
3. A. BERNAS, J. BLAIS, M. GAUTHIER, and D. GRAND. Chem. Phys. Lett. **30**, 383 (1975).
4. (*a*) R. A. HOLROYD and R. L. RUSSELL. J. Phys. Chem. **78**, 2128 (1974). (*b*) R. A. HOLROYD. J. Chem. Phys. **57**, 3007 (1972).
5. S. S. TAKEDA, N. E. HOUSER, and R. C. JARNAGIN. J. Chem. Phys. **54**, 3195 (1971).
6. (*a*) D. GRAND. Thesis, Université Paris-Sud, Orsay. 1976. (*b*) A. BERNAS and D. GRAND. To be published.
7. L. E. LYONS. J. Chem. Soc. 5001 (1957).
8. L. E. LYONS and J. C. MACKIE. Proc. Chem. Soc. 71 (1962).
9. B. E. SPRINGETT, J. JORTNER, and M. H. COHEN. J. Chem. Phys. **48**, 2720 (1968).
10. R. A. HOLROYD, S. TAMES, and A. KENNEDY. J. Phys. Chem. **79**, 2857 (1975).
11. S. NODA, L. KEVAN, and K. FUEKI. J. Phys. Chem. **79**, 2866 (1975).
12. R. SCHILLER, SZ VASS, and J. MÁNDICS. Int. J. Radiat. Phys. Chem. **5**, 491 (1973).
13. N. R. KESTNER and J. JORTNER. J. Chem. Phys. **59**, 26 (1973).
14. R. SCHILLER and SZ VASS. Int. J. Radiat. Phys. Chem. **7**, 193 (1975).
15. H. T. DAVIS, L.D. SCHMIDT, and R. G. BROWN. Colloque Weyl III. Electrons in fluids. *Edited by* J. Jortner and N. R. Kestner. Springer-Verlag, Berlin. 1973. p. 393.
16. J. BULLOT and M. GAUTHIER. Chem. Phys. Lett. **40**, 402 (1976).
17. S. H. PETERSON, M. YAFFE, J. A. SCHULTZ, and R. C. JARNAGIN. J. Chem. Phys. **63**, 2625 (1975).
18. P. DELAHAY, P. CHARTIER, and L. NEMEC. J. Chem. Phys. **53**, 3126 (1970).
19. P. DELAHAY. J. Chem. Phys. **55**, 4188 (1971).
20. R. KAHN, R. FOURME, D. ANDRE, and M. RENAUD. Acta Crystallogr. Sect. B, **29**, 131 (1973).
21. R. SANTUS, A. HELENE, C. HELENE, and M. PTAK. J. Phys. Chem. **74**, 550 (1970).
22. B. K. DIETRICH. Ph.D. Thesis, University of Wisconsin, Madison. 1971.
23. Landolt–Bornstein Tables. Structure data of organic crystals. Springer-Verlag, Berlin. 1971.
24. M. RENAUD and R. FOURME. J. Chim. Phys. **63**, 27 (1966).
25. A. BONDI. Molecular crystals, liquids and glasses. Wiley, NY. 1968. p. 143.
26. P. F. HIGGINS, R. A. B. IVOR, L. A. K. STAVELEY, and J. J. DES C. VIRDEN. J. Chem. Soc. 5762 (1964).
27. G. BRIEGLEB and J. CZEKALLA. Z. Elektrochem. **63**, 6 (1959).
28. R. FOSTER. Nature, London, **183**, 1253 (1959).
29. M. BATLEY and L. E. LYONS. Mol. Cryst. **3**, 357 (1968).
30. V. K. POTAPOV. Russ. Chem. Rev. **39**, 992 (1970).
31. Y. NAKATO, M. OSAKI, A. EGAWA, and H. TSUBOMURA. Chem. Phys. Lett. **9**, 615 (1971).
32. J. JORTNER. Ber. Bunsenges. **75**, 696 (1971).
33. J. JORTNER. *In* Actions chimiques et biologiques des radiations. Vol. 14. *Edited by* M. Haissinsky. 1970. p. 7.
34. J. JORTNER. Discussion held at Colloque Weyl IV. J. Phys. Chem. **79**, 2860 (1975).

Discussion

J. K. Baird: I noted in your paper that you regarded V_0 to be the energy needed to transfer an electron from a condensed phase to the vacuum. In Professor Delahay's paper, he mentioned a surface energy term which I regarded to be due to a kind of image force. Does his surface term have to be included in your analysis?

M. Gauthier: The results I have presented concern internal photoionization. So a surface energy term has not to be considered. Professor Delahay's results concern photoemission or external photoionization.

J. Jortner: The 'surface polarization' term does not enter into the energetics of either internal or external photoionization process. For an internal ionization V_0 which determines the IP in a dense medium incorporates bulk polarization energy. For external photoemission image charge effects are neglected, of course, for an insulator. The 'surface polarization' energy which was so popular with electrochemists cancels out in the Born–Haber cycle which can be used to describe the energetics of external photoionization.

J.-P. Dodelet: In various hydrocarbon solvents, the IP of TMPD varies with the temperature in the liquid phase. What would be the expected variation of IP of the solvent molecules themselves with the temperature in liquid phase?

M. Gauthier: It has been previously shown that the lowering, with respect to the gas phase, of the ionization potential in a condensed medium is a characteristic of the solvent. So I would say that the same $I_g - I_{liq}$ value is expected for the solvent molecule itself. It amounts to 1 to 2 eV and is expected to vary with temperature in the same way as for TMPD.

G. R. Freeman: The density of the liquid was changed by changing the temperature. Can you distinguish between density and temperature effects?

M. Gauthier: So far we cannot distinguish between temperature and density effects. To that end, it would be necessary to determine the ionization threshold as a function of pressure.

G. Ascarelli: You measured the energy gap of the solid by means of photoionization. If the crystals are not cubic the apparent gap should depend on the direction of incidence of the photon and its polarization with respect to the crystal axis. Did you have single crystals? If so what is the crystal structure of the solidified liquids?

M. Gauthier: All the measurements were done with polycrystalline samples. At any rate, if one attempts to use single crystals, the local perturbation due to the presence of the TMPD impurity molecule would preclude any possibility of studying anisotropy effects. To my knowledge, the crystal structure has been determined only in a few cases. DMB and cyHex are cubic in their high temperature phase. cyHex at low temperature and *n*-Hex are monoclinic.

L. Kevan: In regard to Freeman's question, the changes in ionization energy with temperature depend on the temperature dependence of V_0. Within the framework of the Springett–Jortner–Cohen theory of V_0 this is purely a density effect.

Yield and properties of solvated electrons created by the γ radiolysis of hexamethylphosphorotriamide

M. C. LEBAS, J. SUTTON, AND A. M. KOULKES-PUJO[1]

DRA/SRIRMa and CNRS, Centre d'Etudes Nucléaires de Saclay, 91190 Gif-sur-Yvette, France

Received September 27, 1976

M. C. LEBAS, J. SUTTON, and A. M. KOULKES-PUJO. Can. J. Chem. **55**, 1832 (1977).

According to various authors, the value of the yield of the solvated electron in the pulse radiolysis of hexamethylphosphorotriamide (HMPT) varies from 1.2 to 2.4 and increases to 4.2 or 3.1 in the presence of NaBr. We exposed this compound to γ rays after purification and saturation with N_2O. N_2 was formed with a yield $G(N_2) = 4.4 \pm 0.4$. After elimination of a certain number of processes which might also lead to N_2 formation, it was concluded that this $G(N_2)$ corresponds to the total yield of electrons. This value was confirmed by measuring $G(Br^-)$ obtained by radiolysis of HMPT with *p*-bromophenol as a scavenger. The yield of N_2 remains constant whenever solutes generally known as good electron scavengers are added (H^+, CH_3COCH_3, NO_3^-). An interpretation of the results leads to the suggestion of the formation of a dielectron in this medium.

M. C. LEBAS, J. SUTTON et A. M. KOULKES-PUJO. Can. J. Chem. **55**, 1832 (1977).

Suivant divers auteurs, la valeur du rendement d'électrons solvatés lors de la radiolyse pulsée du HMPT varie de 1.2 à 2.4 et augmente jusqu'à 4.2 ou 3.1 en présence de NaBr. On a soumis ce composé à des rayons γ après purification et saturation avec N_2O. Il y a formation de N_2 avec un rendement de $G(N_2) = 4.4 \pm 0.4$. Après l'élimination d'un certain nombre de processus qui peuvent aussi conduire à la formation de N_2, on a conclu que $G(N_2)$ correspond au rendement total en électrons. On a confirmé cette valeur en mesurant $G(Br^-)$, obtenu par radiolyse de HMPT additionnée de *p*-bromophénol comme capteur d'électrons. Le rendement de N_2 demeure constant quels que soient les solutés ajoutés, connus comme étant de bons capteurs d'électrons (H^+, CH_3COCH_3, NO_3^-). Une interprétation des résultats conduit à la suggestion qu'il y a formation d'un biélectron dans ce milieu.

[Traduit par le journal]

Hexamethylphosphorotriamide (HMPT) is an interesting solvent in that it is polar but also aprotic, *i.e.* it forms no hydrogen bonds. Because of the dipole charge distribution it is also a poor solvating medium for anions but leads to the formation of stable solvated electrons by dissolution of alkali metals. Thus we decided to study the formation and reactions of the solvated electrons formed by γ radiolysis of this compound.

Several previous papers (1–4) on the pulse radiolysis of HMPT give values of the solvated electron yield $G_{e_s^-}$ which vary between 1.2 (1) and 2.3 (2, 4). Moreover addition of NaBr appears to increase this yield to 3.1 (4) and to 4.2 (1).

In view of this disagreement it appeared justifiable to use the classic method of γ radiolysis of the solvent with and without reactive solutes in order to obtain independent information on the solvated electron yield by analysis of final products. We have therefore used N_2O and *p*-bromophenol, taken separately, which lead to the formation of N_2 and Br^- respectively by reaction with solvated electrons. We also radiolyzed solutions containing N_2O plus acid ($HClO_4$, H_2SO_4, HCl), N_2O plus $LiNO_3$, and N_2O plus acetone.

Experimental Method and Results

The experiments were carried out on solutions which were deaerated by saturating with either argon, N_2O, or mixtures of known composition of these two gases at atmospheric pressure. The solvent (Merck) was doubly distilled under vacuum, first over sodium to eliminate H_2O and any chlorinated residues left from the HMPT synthesis. The middle fraction of the second distillation, boiling at 90°C at 4 Torr, was stored in a glove box under dry argon and in the absence of light. The preparation of samples for irradiation was done in the glove box so that the solutions never came in contact with air. The dose rate was $2.7 \pm 0.1 \times 10^{18}$ eV h^{-1} cm^{-3}. The concentration of N_2O in the solution was determined by gas chromatography (column

[1]Author from whom reprints may be obtained.

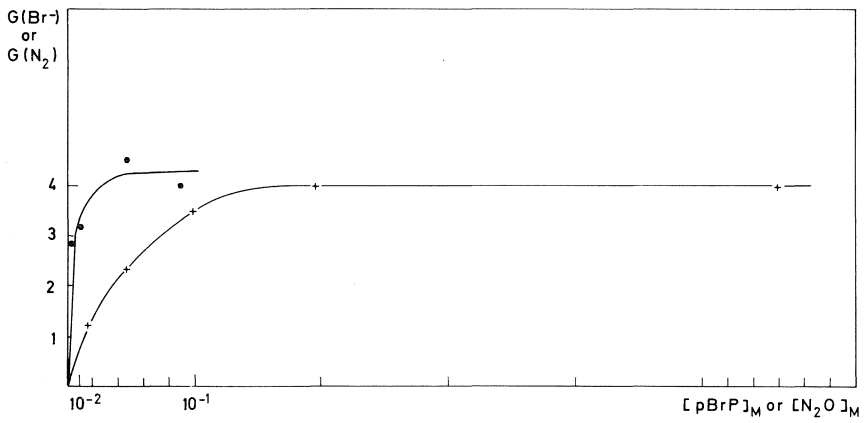

FIG. 1. Yields of N_2 (●) or Br^- (+) *vs.* N_2O or *p*-bromophenol concentrations.

Porapak Q; carrier gas helium). For pure N_2O at atmospheric pressure, it is 9×10^{-2} *M* at 25°C; for mixtures of N_2O/Ar at 1%, 10%, or 50% of N_2O, Henry's law was obeyed and the concentrations in the solutions were respectively 0.9, 9, and 45×10^{-3} *M*. The nitrogen formed by radiolysis of these solutions was determined by gas chromatography.

The radiolysis of solutions of *para*-bromophenol(*p*-BrP) lead to the formation of Br^-, the concentration of which was determined by potentiometric titration using an Orion 801 potentiometer and a specific bromide ion electrode. Although NaBr is fully dissociated in HMPT (5), it was necessary to add water before the titration to obtain a correct response of the electrode with a slope obeying the Nernst's law.

The quantities of N_2 and Br^- formed by irradiation are proportional to the dose over a large range (maximum dose 5.2×10^{19} eV cm^{-3}). The curves representing $G(Br^-)$ and $G(N_2)$ *vs.* the concentration of *p*-BrP or N_2O are presented in Fig. 1. The yields at the plateaux are the same within the limits of experimental error and equal to 4.4 ± 4.0. The addition of 10^{-1} *M* isopropanol or 10^{-1} *M* NaBr to the solutions containing 9×10^{-2} *M* N_2O or *p*-BrP did not change the yields of N_2 or Br^-. We tried to establish a competition between N_2O and H^+ by adding $HClO_4$ or H_2SO_4 which are known to be entirely dissociated in HMPT (6). However, on adding up to 0.35 *M* acid to the solutions containing 9×10^{-4} or 9×10^{-2} *M* N_2O, no variation in the N_2 yield was observed. Thus, if H_s^+ reacts with e_s^-, we can only conclude that the rate constant is very much lower than that of N_2O with e_s^-, contrary to the result obtained in most other solvents. The proton behaviour in this case would be similar to that of the proton in liquid ammonia (7).

Although HCl is not a strong acid in pure HMPT (8), we used this compound in H_2O–HMPT mixtures where it is probably more dissociated. The Cl^- ions so introduced are able to react either with the parent positive ion $HMPT^+$ or with the radical HMPT(-H).

In this case also (0.36 *M* HCl plus 9×10^{-2} *M* N_2O), $G(N_2)$ remained unchanged. These results suggest that Cl^-, contrary to Br^- (which gives Br_2^- on pulse radiolysis (1–4)), does not react with the radicals or ions deriving from $HMPT^+$; however, this seems very unlikely. It is more probable that the electron is scavenged by N_2O and that any other reaction cannot compete with this one. This assumption was supported by the results obtained with solutions containing N_2O and 10^{-1} *M* NaBr, where the N_2 yield again remained constant. We also tried $LiNO_3$ as a second scavenger of electrons in N_2O solutions, but the N_2 yield remained constant.

Acetone (Ac) employed as an electron scavenger represents a special case. Although the addition of 0.47 *M* acetone to solutions containing 9×10^{-2} *M* N_2O did not change $G(N_2)$, addition of the same concentration to a solution containing 9×10^{-4} *M* N_2O increased the value of $G(N_2)$ from 2.3 to 4.4, probably by the intervention of the radical ion Ac^-.

Discussion

Since the plateau value of 4.4 ± 0.4 obtained for $G(N_2)$ or $G(Br^-)$ in the experiments described does not vary on addition of alcohol, it would appear that these products are formed by

reaction of N_2O or *p*-BrP respectively with electrons only and that hydrogen atoms and free radicals make no contribution to these yields. The high G values lead us to assume that N_2O and *p*-BrP at the concentrations employed in the plateau region react with electrons in the spurs before their diffusion. This conclusion is supported (*i*) by the results of Mal'tsev *et al.* (1) who, using pulse radiolysis, directly observed an electron yield of 4.2 in HMPT + 0.3 *M* NaBr and (*ii*) by the fact that addition of 10^{-1} *M* NaBr to 9×10^{-2} *M* N_2O in HMPT leads to no increase in $G(N_2)$. Indeed Shaede *et al.* (4) have given a value $k_{N_2O + e_s^-} = 1.4 \pm 10^{10}$ M^{-1} s^{-1} in HMPT, notably higher than the rate constant for the same process in many other media.

The results obtained by Shaede *et al.* (4) with pyrene as scavenger are more difficult to correlate with ours, the value of $G(Py^-) = 2.4$ remaining constant for pyrene concentrations varying from 3.2×10^{-4} to 1.2×10^{-1} *M*. If N_2O can suppress any recombination of electrons with $HMPT^+$ or HMPT(-H), it seems difficult to admit that Py^- formed by capture of intraspur electrons may undergo a more rapid charge neutralization than the electron itself. In this context the effect of Br^- addition on the yield of Py^- in HMPT may provide valuable information.

Using the theory of Mozumder (9) it is possible to calculate an escape probability for the electron of approximately 0.9 for an effective dielectric constant of 14 (10), *i.e.* approximately 47% of the static dielectric constant. This probability may be compared with that of the hydrated electron (0.5) for an effective dielectric constant in the same proportion. This may be an explanation for the high electron yield found with an appropriate scavenger.

Furthermore, the constancy of the hydrogen yield even in the presence of high concentrations of efficient scavengers of both e_s^- and H lead us to eliminate an overall stoichiometry of the type $2e_s^- \rightarrow H_2 + 2HMPT(-H)^-$. This conclusion is also supported by the stability of the electron in metal–HMPT solutions.

Taking these facts into account, one may suppose that two different forms of electron are produced in HMPT both of which react with N_2O and *p*-BrP but that only one reacts with pyrene. This idea has led us to consider the formation of dielectrons in spite of the uncertain evidence for their existence (except in the case of Eu–NH_3 solutions (11)) and the controversy that arose concerning these species (12). We may admit that they react with N_2O, *p*-BrP, Ac but not rapidly enough with pyrene, anthracene, or biphenyl. In fact, the slow formation of Py^{2-} was recently shown by Engdahl and Rämme (13).

Assuming that the dielectron is formed by successive trapping of two electrons in the same large cavity because of the favourable properties of HMPT, especially its surface energy (33.8 erg cm^{-2} at 20°C) and its molecular volume (207 $Å^3$), we suggest the following mechanism for the radiolysis of this solvent which is consistent with our results and those of other workers.

$$HMPT \xrightarrow{\gamma} HMPT^*$$
$$HMPT \rightarrow HMPT^+, e^-, e_2^{2-}$$
$$HMPT^* \rightarrow H_2 + \text{products}$$
$$HMPT^+ + HMPT \rightarrow HMPT(-H) + HMPT, H^+$$
$$n\text{-}HMPT + e^- \rightarrow e_s^-$$
$$e_2^{2-} + n\text{-}HMPT \rightarrow (e_2^{2-})_s$$
$$e_s^- + HMPT(-H)^\bullet \rightarrow HMPT(-H)^-$$
$$(e_{2_s}^{2-}) + HMPT(-H)^\bullet \rightarrow HMPT(-H)^- + e_s^-$$
$$HMPT(-H)^- + HMPT, H^+ \rightarrow 2HMPT$$
$$HMPT(-H)^\bullet \rightarrow \text{products}$$
$$e_s^- \rightarrow \text{products}$$

1. E. I. Mal'tsev, A. V. Vannikov, and N. A. Bach. Radiat. Eff. **11**, 79 (1971).
2. H. Nauta and C. Van Huis. J. Chem. Soc. Faraday Trans. I, **68**, 647 (1972).
3. A. M. Koulkes-Pujo, L. Gilles, B. Lesigne, J. Sutton, and J. Y. Gal. J. Chem. Soc. Chem. Commun. 71 (1974).
4. E. A. Shaede, L. M. Dorfman, G. Y. Flynn, and D. C. Walker. Can. J. Chem. **51**, 3905 (1973).
5. P. Bruno, M. Della Monica, and E. Righetti. J. Phys. Chem. **77**, 10 (1973).
6. C. Madic and B. Tremillon. Bull. Soc. Chim. 1634 (1968).
7. J. M. Brooks and R. R. Dewald. J. Phys. Chem. **75**, 986 (1971).
8. C. Moliton. Thèse 3e. Cycle, Université de Poitiers, France. 1972.
9. A. Mozumder. J. Chem. Phys. **50**, 3153 (1969).
10. M. C. Lebas. Thèse 3e. Cycle, Université de Paris XI, France. In preparation.
11. R. Catterall and M. C. R. Symons. J. Chem. Soc. Ser. A, 13 (1966).
12. J. L. Dye. Metal Ammonia Solutions, Colloque Weyl II, Ithaca, NY. 1969. *Edited by* J. J. Lagowski and M. J. Sienko. Butterworth, London. 1970. p. 1.
13. K. Å. Engdahl and G. Rämme. Chem. Phys. Lett. **41**, 100 (1976).

Discussion

D. C. Walker: A question about the total electron yield: Do you envisage the proposed reaction between the dielectron and N_2O to give two N_2 molecules?

A. M. Koulkes-Pujo: Yes.

D. C. Walker: With regard to the relative importance of the reactions $e_s^- + e_s^- \rightarrow (e_2^{2-})_s$, $e_s^- + S^+ \rightarrow S$ and $e_s^- + R \rightarrow R^-$ (where R is a radical or molecule product of radiolysis): in the paper by Shaede *et al.* (4) we concluded that the last reaction was most important because when HMPT containing a steady state $[e_s^-]$ from dissolved Na was pulse irradiated, there was an overall net loss of e_s^-. If the first two reactions dominated the decay of e_s^- after radiolysis there would have been no net change in the steady state $[e_s^-]$.

A. M. Koulkes-Pujo: This experiment is perhaps not significant for the presence or absence of e_2^{2-} because your solution contains Na^+ ion and you may have for example other species like e^-, Na^+ pairs.

Effects of very high dose-rates on solvated electron yields (Extended Abstract)

STEFAN KAROLCZAK[1] AND DAVID C. WALKER
Chemistry Department, University of British Columbia, Vancouver, B.C., Canada V6T 1W5
Received October 13, 1976

Upon replacing the electron tube of a 600 kV Febetron 706 accelerator with the dual-tube output attachment of the model 708, a relatively uniform radiation dose can be administered to a sample of thickness-density ~0.45 g cm^{-2}. This enables conventional pulse radiolysis – spectrophotometric studies to be made. Radiation cells were used in which the dose per pulse could readily be changed, as could the optical path length of irradiated solution, so that the same absorbance could be achieved for quite different doses. With the pulse duration fixed at 3 ns, doses from 10^3 to $>10^5$ rad, with dose-rates up to 10^{14} rad s^{-1}, were selected by means of beam attenuators.

For doses less than about 6000 rad the yield of hydrated electrons and their subsequent decay rates in the presence of concentrated electron scavengers were normal and in agreement with published data. At these low doses, too, the formation of CO_3^- in 3 *M* Na_2CO_3/0.3 *M* KNO_3 solutions (due to reaction of OH radicals with CO_3^{2-}) was complete within the 3 ns time resolution of the detector (1P28 photomultiplier) plus oscilloscope (HP 183).

However, at higher doses the yield of e_{eq}^- in water was nonlinear with dose. In fact *G* decreased progressively with increasing dose. Furthermore the absorbance increased after the end of the pulse for 50 to 100 ns, with this post-pulse absorbance often accounting for 30–40% of the maximum observable absorbance. When the product of a hydrated electron reaction, such as Cd^+ in 0.1 *M* Cd^{2+} solutions, was monitored at 300 nm its absorbance showed an analogous effect, namely some immediate and some delayed absorbance. Its yield was also nonlinear with dose. Finally, the CO_3^- radical ion which should be formed in ~10^{-9} s from OH radicals in a 3 *M* Na_2CO_3/0.3 *M* KNO_3 solution also showed delayed absorbance.

In searching for an explanation of these effects we have eliminated the obvious possible electronic or optical artifacts, including (*i*) nonlinear response of the detectors (photodiode and photomultiplier); (*ii*) very rapid shock-wave effects; (*iii*) optical saturation behaviour; or (*iv*) inhomogeneities arising from the beam attenuators. Nor can we find any satisfactory rationalisation for these results in terms of delayed formation of both e_{aq}^- and OH. We could explain all our results, however, if there was significant 'channelling' of the electron beam at high dose-rates. By this we envisage the possibility of electron tracks funnelling together into super-tracks, as a result of the enormous dose-rates and dose from relatively low energy electrons.

If such super-tracks existed they would contain very high concentrations of e_{aq}^- such that these regions would be opaque to visible light, while the surrounding solution was fairly transparent. For 50 or 100 ns after the pulse, these regions would enlarge, due to diffusion of e_{aq}^-, thereby extending the volume of strongly absorbing species and causing a further increase in the measured absorbance. An electron scavenger such as Cd^{2+} at 10^{-2} *M* could capture only a fraction of e_{aq}^- within 5 ns, but over the next decade of time could capture e_{aq}^- as they emerged from the super-track. In this way the absorbance would be essentially constant over about 50 ns before decreasing rapidly, as observed. The very high concentrations of e_{aq}^- and OH in the track will lead to low *G* values as with particles having high LET tracks.

We hesitantly offer this as a possible explanation for the considerable range of data we have on these high dose-rate effects, without knowledge about the plausibility of its physical basis. We know of no information at compara-

[1]On leave from Institute of Radiation Chemistry, Technical University of Łódź, Poland.

ble dose-rates and electron energies which would offer guidance as to whether channelling of electron tracks is expected under these conditions.

Discussion

W. F. Schmidt: From work on breakdown in dielectric liquids it is known that turbulences are created in the liquid due to momentum transfer of charge carriers to the molecules of the liquid. It has also been observed that high energy electron beams create shock waves in the material they are traversing. Isn't it possible that the growing-in of the absorption after the pulse is due to a relaxation of turbulences or other density changes which were created by the high power electron beam and which perturbed the absorption measurement?

S. Karolczak: Shock waves originating at the front of the cell travel across the cell at about the speed of sound, arriving in the observation region after delayed absorbance is complete ($>1\,\mu s$). These temperature/pressure fronts cause a change of refractive index and distort the light beam but such effects occur much later than the phenomena being studied.

Effect of density on the total ionization yields in X-irradiated argon, krypton, and xenon[1]

SAM S.-S. HUANG AND GORDON R. FREEMAN

Chemistry Department, University of Alberta, Edmonton, Alta., Canada T6G 2G2

Received September 27, 1976

SAM S.-S. HUANG and GORDON R. FREEMAN. Can. J. Chem. **55**, 1838 (1977).

The amounts of ionization produced by absorption of X radiation in the liquids xenon, krypton, and argon are respectively 1.5, 1.4, and 1.2 times greater than those produced by the absorption of the same energy in the corresponding low density gases. The yields of free ions in the irradiated liquids were measured at applied electric fields 1–40 kV/cm and extrapolated to infinite field strength. The total number of ionizations per 100 eV absorbed was $G_{tot} = 6.6$ in xenon, 6.0 in krypton, and 4.5 in argon. The reason that the ionization yield is larger in the liquid than in the corresponding low density gas is partly that the energy gap E_g between the top of the valence band and the bottom of the conduction band in the liquid is smaller than the gas phase ionization potential IP. The ratio $IP/E_g = 1.36$ for xenon (Roberts and Wilson), 1.27 for krypton, and 1.17 for argon (from data of Jortner *et al.*). An extra source of ionization in the liquid might be reaction of the higher excited states, $M^* + M \rightarrow [M_2^+ + e^-]$.

SAM S.-S. HUANG et GORDON R. FREEMAN. Can. J. Chem. **55**, 1838 (1977).

Les quantités d'ionisation produites par absorption de radiation X dans le xénon, le krypton et l'argon liquide sont respectivement de 1.5, 1.4 et 1.2 fois plus grandes que celles produites par l'absorption de la même énergie dans les gaz correspondants de faible densité. On a pu mesurer les rendements en ions libres dans les liquides irradiés à des champs électriques appliqués de 1 à 40 kV/cm et les extrapoler à une force de champ infinie. Le nombre total d'ionisations par 100 eV absorbés est $G_{tot} = 6.6$ dans le xénon, 6.0 dans le krypton et 4.5 dans l'argon. Le fait que le rendement d'ionisation est plus grand dans le liquide que dans le gaz correspondant de faible densité provient en partie de la différence d'énergie E_g qui existe entre le sommet de la bande de valence et le bas de la bande de conduction du liquide et qui est plus petite que le potentiel d'ionisation en phase gazeuse IP. Le rapport $IP/E_g = 1.36$ pour le xénon (Roberts et Wilson), 1.27 pour le krypton et 1.17 pour l'argon (à partir de données de Jortner *et al.*). Une source additionnelle d'ionisation dans le liquide peut être la réaction des états excités plus élevés $M^* + M \rightarrow [M_2^+ + e^-]$.

[Traduit par le journal]

Introduction

A problem in radiation chemistry is to know the amount of ionization produced in a liquid or solid exposed to high energy radiation. A useful parameter is W, the average amount of energy expended per ion pair formed. In low density gases the value of W (1–6) is usually about double the first ionization potential (2, 7). Ionization potentials in the condensed phases are often about 2 eV lower than those in the gas phase, due to electronic polarization of the medium around the newly created charges (8–16). One might therefore find an approximately 20% decrease in the value of W on going from the normal gas to the liquid phase, if ionization processes are similar in the two phases.

Product yields from the radiolysis of solutions of an electron scavenger in alcohols (17, 18) and saturated hydrocarbons (19, 20) indicate that the W values in the liquids, ~20 eV, are indeed about 20% lower than those in the corresponding low density gases, ~25 eV (3–6). In aqueous solutions the value of W also appears to be ~20 eV (21–23), whereas the gas phase value is 30 eV (3, 4, 6). This corresponds to an ~33% reduction in W with increasing phase density. The energy gap between the valence and conduction bands in liquid water was recently estimated to be ~9 eV (24), which is ~30% lower than the 12.6 eV gas phase ionization potential (7).

Although the above results indicate that W is smaller in the liquid than in the low density gas there are two major sources of uncertainty in addition to the experimental difficulties. (*a*) The liquid phase values were determined for solutions rather than for pure solvents. If excited neutral

[1]Assisted by the National Research Council of Canada.

molecules react with the solutes the apparent W values would be too small. (*b*) The definition of an ionization in dense phases is ambiguous and not always readily distinguished from that of a highly excited neutral state. For practical purposes we define an ionization as an event during which an electron separates from an ion or molecule, and after which the electron may be considered to have a separate existence for a finite time. This includes geminate ion – electron pairs, in which the electron has not escaped the Coulomb field of the ion but the wave function of the electron is not centered on the ion. If the electrons form localized states they can be detected by optical absorption spectroscopy before they react with geminate ions or other species that happen to be present. However, it has not yet been possible to obtain the value of W for a pure solvent by a spectroscopic method, because it has not been possible to estimate the amount of geminate neutralization that occurs at times shorter than the resolution time of the measurement (including neutralization prior to solvation).

The amount of ionization in a low density gas is measured by applying an electric field across the gas and collecting the charges at electrodes. After an ionization event in a low density gas the electron escapes sufficiently far from its parent ion that geminate neutralization is negligible (25), so essentially all of the charges can be collected at practicable field strengths. This method cannot be used for most liquids because geminate neutralization is not completely eliminated by the application of fields up to 10^5 V/cm. Dielectric breakdown occurs before all the initially formed electrons can be drawn away from their parent ions. Ionization yields measured at high fields may be extrapolated to infinite field strength with the aid of a model (26, 27) based on early work of Onsager (28).

The extrapolation is relatively short when the electrons are able to penetrate relatively long distances from their parent ions. This occurs in liquids made of spherical molecules, such as argon (29–31), krypton, and xenon (31). Unfortunately, the answers obtained by different techniques do not agree with each other (30–33). The problem has therefore been reinvestigated.

Experimental

Materials and Sample Preparation

The stated purities of the gases obtained from Matheson were 99.995% for xenon and krypton, and 99.999% for argon. The same purity of xenon was also obtained from Linde.

The materials were handled in a vacuum rack that was initially evacuated to 0.1 mPa (1×10^{-6} Torr). The gas cylinders were connected to the rack through a vacuum-tight valve that was welded to a piece of flexible stainless steel tubing, which was in turn welded to a Kovar seal. The tubes and rack were flushed twice with gas from the cylinder, then evacuated to 0.1 mPa again with the exception of one portion; the cylinder valve and steel tubing were kept at a pressure in excess of 1 atm (> 100 kPa) by way of a 1 m long manometer tube (2 mm id) that dipped 4 cm beneath the surface of a pool of mercury.

Argon was passed through a 60 cm × 1.5 cm Pyrex U-tube column of activated Molecular Sieves 3A (Fisher Scientific Co) at −78°C, then a 60 cm × 2 cm quartz U-tube of 6–14 mesh activated coconut charcoal (Fisher) at −78°C. The adsorbants had each been activated for 6 days at < 1 mPa, the Molecular Sieves at 290°C, and the charcoal at 600 °C. Upon cooling the adsorbants to −78°C the pressure in the system fell to < 0.1 mPa. The conductance cell was flushed once with purified argon, then filled, using liquid argon refrigerant.

Krypton and xenon were passed through the above type of Molecular Sieves (3A for Kr and 4A for Xe) columns at −78°C. Fresh Sieves were used for each batch, and they were activated for 5 days under 0.1 mPa at 290°C. The purified gas was condensed in one of three potassium-mirrored traps with liquid nitrogen as refrigerant. A slush bath (−150°C isopentane for Kr and −100°C moist ethanol for Xe) was placed around the trap to liquify the material and allow impurities to react with or adsorb on the potassium mirror. After 3 h the krypton or xenon was distilled to a different trap containing a new mirror. Each trap contained a lump of potassium in the bottom; mirrors were regenerated by evacuating the trap to 0.1 mPa and heating the potassium while continuing to evacuate. After 15 three hour treatments some of the material was used to flush the cell, then the rest distilled into it with liquid nitrogen coolant.

The cells were sealed with a flame.

The vacuum line was grease free and was separated from the mercury diffusion pump by two liquid nitrogen traps.

Physical Properties of the Liquids

These are summarized in Table 1. Values were taken or estimated from data in refs. 34–36. The dielectric constant ε was calculated from the polarizability α and the density d, using the Clausius–Mosotti equation (36).

Conductance Cells

The cell used for argon was described in ref. 37. The electrode spacing was $L = 0.49$ cm and the effective area of the collecting electrode was $A = 1.16$ cm^2.

The cell used for krypton and xenon is shown in Fig. 1*b* of ref. 31: $L = 0.30$ cm, $A = 1.77$ cm^2. The exterior of the top half of the cell, which was the collector electrode side, was coated with aquadag and grounded.

The cell constants (L/A, cm^{-1}) were measured conductiometrically, using standard KCl solutions (38).

Cooling Baths

The argon cell was immersed in liquid argon at atmospheric pressure, 87 K.

TABLE 1. Properties of materials

	Ar	Kr	Xe	
T (K)	87	129	164	183
Liquid d (g/cm^3)	1.39	2.34	3.06	2.93
ε	1.50	1.63	1.93	1.87
Vapor pressure (atm)	1.0	2.0	1.0	2.5
Gas α (Å^3)	1.63	2.47	4.01	4.01
IP (eV)	15.7	14.0	12.1	12.1

The krypton and xenon cell was cooled by a regulated stream of cold nitrogen gas in a Styrofoam box. A calibrated thermocouple was glued to the side of the cell. Another thermocouple was placed near the cell and connected to the temperature controller.

Determination of the Free Ion Yields

The free ion yield G_{fi} is the number of pairs of ions and electrons that can be collected at electrodes per 100 eV of energy absorbed by the liquid. The value at a given applied field strength E is designated $G_{fi}{}^{E}$.

The measurement technique was similar to that in ref. 31. Briefly, a 100 ns pulse of 1.7 MeV X rays delivered 1–2 × 10^{10} eV/cm^3 to the sample. The free ions generated by the radiation were swept to electrodes by applying fields of 0.5 to 45 kV/cm. The charge from the sensitive volume ($L \times A$) was integrated and divided by the radiation dose absorbed. The measuring circuit was the same as that in Fig. 2 of ref. 31, except that the 'current integrator and interface circuitry' were replaced by an ultralow bias current integrator (39). The integrator calibration was based on a General Radio type 1422-CD standard capacitor and a Fluke DC Transfer Standard model 731A.

The signal integration time was varied from 50 ms to 5 s, increasing with decreasing applied field and, to a small extent, with decreasing temperature.

Each point in Figs. 1–3 represents the average of 16 signals, from which the average of 16 blanks (no pulse from the accelerator) has been subtracted. Signal and blank measurements alternated each other. This method was developed for other systems in which there was a significant amount of electrical leakage through the sample. The blanks were always zero in argon, krypton, and xenon. Signal averaging was done by a Fabritek model 1062.

The negative power supply used for xenon and krypton was limited to 6 kV.

Dosimetry

The most probable source of error in measuring W or G_{fi} values is in the determination of the amount of energy absorbed by the sample. The energy absorbed per pulse is too small (0.3 ncal) to be measured directly. The dosimetric method must therefore be considered in detail.

X rays were generated by 1.7 MeV electrons striking a gold target. The magnitude of each radiation pulse was monitored by integrating the electron current that flowed from the target to ground. To insulate the target from ions generated in the air, the 3 mm × 50 mm diameter gold disc was glued with epoxy cement into a polystyrene holder that snugly covered one face and the rim. The other face, which received the electron beam, was insulated with Letraset protective coating spray (Letraset Canada Ltd.). The polystyrene holder was mounted into the end of the stainless steel drift tube of the accelerator. A BNC fitting penetrated the holder to make contact with the target. The exterior of the holder was coated with aquadag and thoroughly grounded, as was the accelerator drift tube and the body of the BNC connector. Aquadag was not put on the Letraset coating.

The X rays were roughly collimated by passing through a 10 cm × 10 cm hole in a 10 cm thick lead shield. They then passed through a K filter to remove X radiation emitted from the K shell of the gold target. In the K filter the radiation passed successively through 5.0 mm Pb, 0.4 mm Sn, 0.25 mm Cu, and 1.0 mm Al (41). The ~80 kV radiation from gold or lead would be much more strongly absorbed in xenon than in lithium fluoride and would cause apparent values of G_{fi} in xenon to be too large. An adequate K filter was not used in our earlier experiments (31, 42).

The primary standard for determination of energy absorption was the Fricke dosimeter (40). With it the γ beam from a low intensity ^{60}Co source was calibrated. Doses of 10^{17}–10^{18} eV/g were used for accurate measurement with the Fricke solutions.

The γ beam was then used to calibrate the lithium fluoride crystals of a Harshaw model 2000 thermoluminescent dosimeter. The lowest doses that could be obtained accurately from the γ source, 10^{13}–10^{14} eV/g, were used.

The lithium fluoride crystals served to calibrate the X-ray pulse monitor. The crystals were given 10^{13}–10^{14} eV/g by delivering 10^3–10^4 pulses of X rays, while integrating the total electron current that flowed from the target to ground. The pulse rate was 4/s to assure stability of the system. The ratio (Harshaw reading)/(target monitor reading) sometimes varied for pulse rates > 10/s, so the pulse rate was kept < 10/s.

The dosimeter crystals were used in sets of three or four, contained in thin, flattened glass tubes or wrapped in aluminum foil. The precision of measurement with the crystals was ±2%. Our previous main difficulty had been the estimation of the amount of photoelectric absorption in the high atomic number liquids. We have now used powders of salts that have the same average atomic number as the noble elements to simulate the liquids: KCl for Ar, RbBr for Kr, and CsI for Xe. A hole was drilled in the side of a duplicate cell, the cell was half filled with the appropriate powder, Al foil wrapped LiF crystals were placed midway between the electrodes, and the cell was filled with more powder. The packing densities of the powders were about 25% less than the liquid densities, but an experiment with CsI powder (2.4 g/cm^3) and a large CsI crystal (4.5 g/cm^3) with a small hole drilled into it showed that the density of the salt had little effect on the LiF dosimetry in the geometry used. The rate of generation of primary electrons per unit volume in the salt is proportional to the density, but the electron range is inversely proportional to the density, so the 'equilibrium' flux of high energy electrons is the same.

Results

The measured free ion yields were all in the range $G_{fi}{}^{E}$ = 3 to 7 ion pairs per 100 eV, in-

creasing with applied field strength and increasing from argon to krypton to xenon (Figs. 1–3).

Measurements were made by applying both positive and negative voltages to the high tension electrode. The yields measured with positive applied voltages were larger than those measured with negative voltages; the relative difference increased with increasing voltage (Figs. 1–3). The reason for the difference is not known, but it is not observed for liquids in which electron mobilities are low. It is also smaller when the cell 'dead volume' is smaller. We favor the values obtained with negative voltages because it is easier to think of artifacts that would make the apparent yield too large than too small. For example, positive field penetration into the region between the collector and guard electrodes might draw highly mobile electrons out of that volume, leaving positive ions in the dead volume to drift to the collector and guard. Reversing the field would draw extra electrons into the dead volume, but they would not find extra positive ions to neutralize. The extra electrons would ultimately diffuse to the guard and collector electrodes, relatively unaffected by having entered the dead volume. It is curious that this problem is not discussed in the literature, yet most authors report having used negative applied voltages.

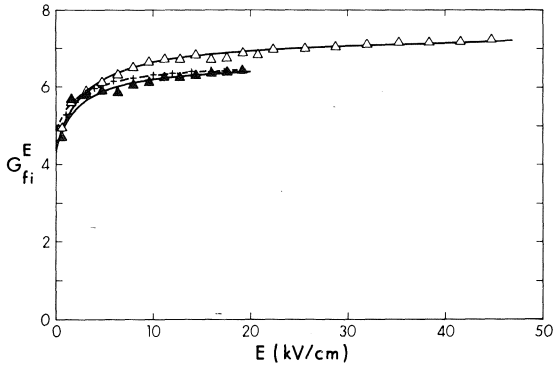

FIG. 1. Free ion yields $G_{fi}{}^{E}$ as a function of applied electric field strength E in liquid xenon at 164 K. △, positive voltage; ▲, negative voltage; +, results for 183 K from ref. 33, negative voltage. The curves were calculated from [9] and [10], using the parameter values in Table 2.

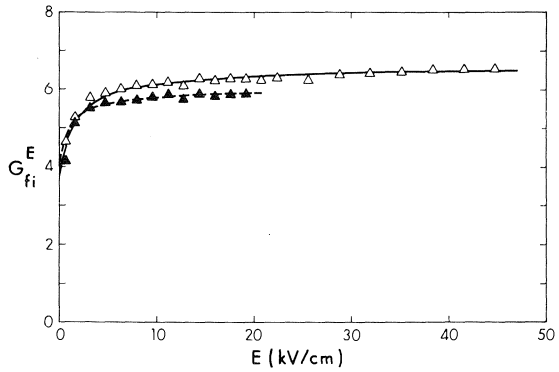

FIG. 2. Free ion yields $G_{fi}{}^{E}$ as a function of applied electric field strength E in liquid krypton at 129 K. △, positive voltage; ▲, negative voltage. The curves were calculated from [9] and [10], using the parameter values in Table 2.

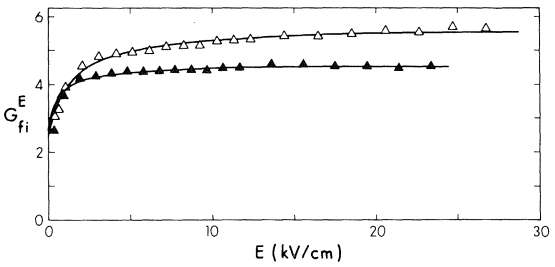

FIG. 3. Free ion yields $G_{fi}{}^{E}$ as a function of applied electric field strength E in liquid argon at 87 K; △, positive voltage; ▲, negative voltage. The curves were calculated from [9] and [10], using the parameter values in Table 2.

Total ionization yields were obtained by extrapolating the measured yields to infinite voltage. The method (26) was based upon early work of Onsager (28) and is discussed below.

Model

In an irradiated system free ions are generated by the following reactions.

[1] $\quad M \rightsquigarrow [M^+ + e^-]$

[2] $\quad [M^+ + e^-] \rightarrow M$, geminate neutralization

[3] $\quad [M^+ + e^-] \rightarrow M^+ + e^-$, free ions

The wiggly arrow in [1] signifies the ionizing radiation. The square brackets indicate that the electron may become thermalized sufficiently close to the ion that the Coulombic attraction between them is not negligible compared to kT. The Coulombic force may draw the ion and electron back together to undergo geminate neutralization (reaction 2). For pairs in which the Coulombic force is not too great, the random thermal motions of the ion and electron may cause them to drift apart (reaction 3). Free ions are those that are sufficiently far apart that the

interaction between them is negligible compared to kT.

The Coulombic energy of attraction E_c between an ion and electron separated by a distance y in a medium of dielectric constant ε is

$$[4] \qquad E_c = \xi^2/\varepsilon y$$

where ξ is the electronic charge.

In the absence of an external field the fraction $\phi(y, 0)$ of ion pairs produced in [1] that become free ions is (28)

$$[5] \qquad \phi(y, 0) = \exp(-E_c/kT)$$

where k is Boltzmann's constant and T is the absolute temperature. Actually, all pairs do not possess the same separation y, so

$$[6] \qquad \phi(0) = \int_0^\infty F(y)\phi(y, 0)\,dy$$

where $F(y)\,dy$ is the fraction of thermalized electron-ion pairs with initial intrapair separation distances between y and $y + dy$.

Application of an external field diminishes the average field between the ion and electron in the randomly oriented pairs. This decreases the extent of geminate neutralization and thereby increases the yield of free ions. The field effect in fluids subjected to densely ionizing radiation, such as alpha particles, was earlier described by Jaffe (43). This model and a later modification of it (44) have sometimes been erroneously applied to systems subjected to sparsely ionizing radiation, such as X rays and high energy electrons. The latter systems were treated by Onsager (28), whose model has been refined through several stages (26, 27, 45). In the presence of an applied field E, the fraction $\phi(y, E)$ of pairs with a given initial separation y that become free ions is

$$[7] \qquad \phi(y, E) = e^{-r/y}\left[1 + e^{-\beta y}\sum_{n=1}^{\infty}\frac{(\beta y)^n}{(n+1)!} \times \sum_{j=0}^{n-1}(n-j)\frac{(r/y)^{j+1}}{(j+1)!}\right]$$

where $r = \xi^2/\varepsilon kT$ and $\beta = \xi E/300kT$.

Averaging over the y distribution one obtains

$$[8] \qquad \phi(E) = \int_0^\infty F(y)\phi(y, E)\,dy$$

The free ion yield is given by

$$[9] \qquad G_{fi}{}^E = \phi(E)G_{tot}$$

where G_{tot} is the yield of reaction 1 and equals $100/W$.

The distribution function $F(y)$ was taken to have the form [10], designated YGP (27).

$$[10] \qquad \begin{cases} F(y) = 0.96\text{YG} & y < 2.4b_{GP} \\ F(y) = 0.96[\text{YG} + 0.5b_{GP}{}^2/y^3] & y > 2.4b_{GP} \end{cases}$$

where 0.96 is a normalization factor, YG is the three dimensional Gaussian function $(4y^2/\pi^{1/2}b_{GP}{}^3)\exp(-y^2/b_{GP}{}^2)$, and b_{GP} is the most probable value of y. The parameter b_{GP} represents an average penetration range of the low energy electrons into the liquid, away from their parent ions, during thermalization.

Equations 9 and 10 were fitted to the experimental data in Figs. 1–3 by using G_{tot} and b_{GP} as adjustable parameters. The value of G_{tot} is somewhat sensitive to the form assumed for $F(y)$. The true form of the distribution is not known, although YGP was devised to fit the experimental field effect on $G_{fi}{}^E$, within this model, in many diverse systems (27). When the range parameter b_{GP} is large, as in the present systems, YGP is practically indistinguishable from the Gaussian YG. A simple exponential form is sometimes used for $F(y)$ (46). It leads to a higher estimate of the value of G_{tot} than does YGP (47).

In the absence of an applied field the free ions neutralize each other and no current is collected on the electrodes.

$$[11] \qquad M^+ + e^- \rightarrow M, \text{ random neutralization}$$

However, at the low radiation doses used, essentially all of the free ions are collected at the electrodes when E is greater than 1 kV/cm. At $E > 1$ kV/cm reaction 11 is negligible, and the increasing yields with field strength are due to the enhancement of reaction 3 at the expense of [2].

Discussion

The values of G_{tot} obtained for xenon, krypton, and argon are listed in Table 2, along with those of the other relevant parameters. Positive applied voltages lead to estimates of G_{tot} that are 10–20% greater than those from negative voltages. The latter are preferred, for reasons given above.

TABLE 2. Parameters of [9] and [10] for curves in Figs. 1–3

Liquid	V	T (K)	ε	G_{tot}	$G_{fi}{}^0$	b_{GP} (Å)
Xe	+	164	1.93	7.3	4.5	1080
	−	164	1.93	6.6	4.4	1300
	−	183	1.87	6.6	4.8	1600
Kr	+	129	1.63	6.5	3.9	1530
	−	129	1.63	6.0	4.0	2030
Ar	+	87	1.50	5.6	2.5	1540
	−	87	1.50	4.5	2.7	2470

The most recent results of Takahashi and coworkers on the ionization of liquid xenon by high energy electrons (33) were converted to $G_{fi}{}^E$ values and included in Fig. 1 for comparison. Negative applied voltages were used and agreement between the two sets of results is satisfactory. Takahashi *et al.* preferred to take the yield $G = 6.4$ measured at 17 kV/cm as the saturation value, although extrapolation to infinite voltage by a yield^{-1} *vs.* V^{-1} plot gave $G = 6.5$ (33). Extrapolation by our method gives $G_{tot} = 6.6$.

In Table 3 ionization energies obtained from the present work are compared with those reported by Takahashi *et al.* (32, 33). The corresponding ratios of gas to liquid energies, W_g/W_l, are listed in Table 4. The value of W_g/W_l decreases slightly on going from xenon to krypton to argon. The ratio for xenon reported in ref. 32 is lower than that in ref. 33, which by the above arguments may itself be too low. By analogy, all of the values in ref. 32 may be low.

The energy gap E_g between the top of the valence band and the bottom of the conduction band in liquid xenon is 8.9 eV (15), which is 0.4 eV smaller than that in solid xenon (11, 16). The values of E_g are 11.6 eV in solid krypton and 14.2 eV in solid argon (16). The electron photoemission threshold energy E_{thresh} drops upon melting the solid, by 0.14 eV in argon and 0.25 eV in krypton (48). The threshold energy corresponds to that required to elevate an electron from the top of the valence band into a vacuum (16),

$$E_{thresh} = E_g - V_0 \quad [12]$$

where V_0 is the energy of the bottom of the conduction band relative to the vacuum level. The value of V_0 in liquid argon, −0.33 eV, is 0.63 eV lower than that in the solid, +0.3 eV (16), so in the liquid phase E_g is (14.2 − 0.14 − 0.63) = 13.4 eV. The value of V_0 in liquid krypton may also be assumed to be lower than that in the solid, due to the decreased repulsive interaction in the less dense phase (16). Hence, $E_g \approx 11$ eV in liquid krypton.

TABLE 3. W_l, the average energy expended per ionization in the noble liquids

		W_l (eV)		
Liquid	V	Present work	Ref. 32	Ref. 33
Xe	+	13.7		
	−	15.2	16.4	15.6(15.2)[a]
Kr	+	15.4		
	−	16.7	20.5	
Ar	+	17.9		
	−	22.0	23.7	

[a]Extrapolated by [9] and [10].

TABLE 4. Ratio of gas and liquid phase W values

			W_g/W_l[b]		
Fluid	W_g (eV)[a]	V	Present work	Ref. 32	Ref. 33
Xe	22.0	+	1.6		
		−	1.5	1.3	1.4(1.5)[c]
Kr	24.2	+	1.6		
		−	1.4	1.2	
Ar	26.4	+	1.5		
		−	1.2	1.1	

[a]Reference 2.
[b]W_l from Table 3.
[c]See Table 3.

TABLE 5. Ratio W_l/E_g for the noble liquids

Liquid	W_l (eV)[a]	E_g (eV)[b]	W_l/E_g	Gas phase W/IP[c]
Xe	15	8.9	1.7	1.82
Kr	17	11	1.5	1.73
Ar	22	13.4	1.6	1.68

[a]Values for negative voltages, from Table 3.
[b]See text.
[c]W from ref. 2, ionization potentials from ref. 7.

The ratio W_l/E_g is analogous to the gas phase ratio W_g/IP, where IP is the ionization potential. The former appears to be slightly lower than the latter (Table 5). In the liquid phase the higher excited states might react by [13], followed by the usual competition between geminate neutralization and free ion formation (*cf.* reactions 2 and 3).

$$M^* + M \rightarrow [M_2^+ + e^-] \quad [13]$$

The energies of the excited states are given by the Wannier equation (8, 11)[2]

$$[14] \quad E_n = E_g - (G/n^2) \qquad n = 1, 2, 3,...$$

where G is a Rydberg-like constant. The value of G in the solids is $\sim$2.1 eV for argon, 1.7 eV for krypton, and 0.9 eV for xenon (11) and should be similar in the liquids. The binding energy of the neutral M_2^* is $\sim$1 eV in the heavier noble solids (49), and that of the ions M_2^+ should be somewhat greater. It is therefore conceivable that states with $n > 1$ contribute to ionization.

The average radii a_n of the excited states are (11)

$$[15] \quad a_n\,(\text{Å}) = 0.53\varepsilon n^2/\mu$$

where $\mu^{-1} = (m_e^*)^{-1} + (m_h^*)^{-1}$, while m_e^* and m_h^* are respectively the effective masses of the electron and positive hole. Assuming that the values of μ in the noble liquids are similar to those in the solids (0.43 in Ar, 0.41 in Kr, and 0.31 in Xe (11)), the value of a_n reaches about 60 Å for $n = 6$ in argon and krypton, and $n = 5$ in xenon. The extent of field induced dissociation of excited states would not be greater than that of geminate pairs with a similar radial distribution. Using an exponential distribution function YE (47) with an inner cut-off at 20 Å, it appears that at $E < 100$ kV/cm there would be $<10\%$ of field induced dissociation of excited states with $a_n < 60$ Å. Field induced dissociation might be a fate alternative to [13] for the highest states at high fields, but the total ionization yield would not be affected.

1. F. W. Spiers. *In* Radiation dosimetry. *Edited by* G. J. Hine and G. L. Brownell. Academic Press, New York. 1956. Chapt. 1.
2. U. Fano. Studies in penetration of charged particles in matter. NAS-NRC Publication 1133, Nat. Acad. Sci., Washington, D.C. 1964. p. 340.
3. G. G. Meisels and D. R. Ethridge. J. Phys. Chem. **76**, 3842 (1972), and references therein.
4. P. Alder and H. K. Bothe. Z. Naturforsch. **20a**, 1700 (1965).
5. R. M. Leblanc and J. A. Herman. J. Chim. Phys. **63**, 1055 (1966).
6. R. Cooper and R. M. Mooring. Aust. J. Chem. **21**, 2417 (1968).
7. R. W. Kiser. Introduction to mass spectrometry and its applications. Prentice-Hall, Englewood Cliffs, N.J. 1965. Appendix IV.
8. G. H. Wannier. Phys. Rev. **52**, 191 (1937).
9. R. J. Elliott. Phys. Rev. **108**, 1384 (1957).
10. D. R. Kearns and M. Calvin. J. Chem. Phys. **34**, 2026 (1961).
11. G. Baldini. Phys. Rev. **128**, 1562 (1962).
12. W. B. Fowler. Phys. Rev. **151**, 657 (1966).
13. N. Geacintov and M. Pope. J. Chem. Phys. **47**, 1194 (1967).
14. (*a*) A. Gedanken, B. Raz, and J. Jortner. J. Chem. Phys. **58**, 1178 (1973); (*b*) A. Gedanken, Z. Karsch, B. Raz, and J. Jortner. Chem. Phys. Lett. **20**, 163 (1973).
15. J. Roberts and E. G. Wilson. J. Phys. C, **6**, 2169 (1973).
16. Z. Ophir, B. Raz, J. Jortner, V. Saile, N. Schwentner, E.-E. Koch, M. Skibowski, and W. Steinmann. J. Chem. Phys. **62**, 650 (1975).
17. K. N. Jha and G. R. Freeman. J. Chem. Phys. **48**, 5480 (1968).
18. T. E. M. Sambrook and G. R. Freeman. Can. J. Chem. **53**, 1521 (1975).
19. M. G. Robinson and G. R. Freeman. J. Chem. Phys. **55**, 5644 (1971).
20. G. R. Freeman and T. E. M. Sambrook. J. Phys. Chem. **78**, 102 (1974).
21. G. V. Buxton. Proc. R. Soc. London, Ser. A, **328**, 9 (1972).
22. Cz. Stradowski and W. H. Hamill. J. Phys. Chem. **80**, 1054 (1976).
23. C. D. Jonah, M. S. Matheson, J. R. Miller, and E. J. Hart. J. Phys. Chem. **80**, 1267 (1976).
24. F. Williams, S. P. Varma, and S. Hillenius. J. Chem. Phys. **64**, 1549 (1976).
25. G. R. Freeman. Radiat. Res. Rev. **1**, 1 (1968).
26. G. R. Freeman. J. Chem. Phys. **39**, 1580 (1963).
27. J.-P. Dodelet, K. Shinsaka, U. Kortsch, and G. R. Freeman. J. Chem. Phys. **59**, 2376 (1973).
28. L. Onsager. Phys. Rev. **54**, 554 (1938).
29. P. H. Tewari and G. R. Freeman. J. Chem. Phys. **51**, 1276 (1969).
30. P. G. Fuochi and G. R. Freeman. J. Chem. Phys. **56**, 2333 (1972).
31. M. G. Robinson and G. R. Freeman. Can. J. Chem. **51**, 641 (1973).
32. T. Takahashi, S. Konno, and T. Doke. J. Phys. C, **7**, 230 (1974).
33. T. Takahashi, S. Konno, T. Hamada, M. Miyajima, S. Kubota, A. Nakamoto, A. Hitachi, E. Shibamura, and T. Doke. Phys. Rev. A, **12**, 1771 (1975).
34. G. A. Cook (*Editor*). Argon, helium and the rare gases. Interscience Publishers, New York. 1961. pp. 151, 360.
35. V. G. Fastovskii, A. E. Rovinskii, and Yu. V. Petrovskii. Inert gases. Israel Program for Scientific Translations, Jerusalem. 1967. pp. 28, 47, 48, 50. Obtainable from U.S. Dept. of Commerce.
36. J. R. Partington. An advanced treatise on physical chemistry. Vol. 5. Longmans, Green and Co., London. 1962. Sect. XI.
37. M. G. Robinson, P. G. Fuochi, and G. R. Freeman. Can. J. Chem. **49**, 3657 (1971).
38. S. Glasstone. Textbook of physical chemistry. 2nd ed. Van Nostrand, Toronto. 1946. Chapt. 12.

[2]Although [14] was derived for crystals (8), it should apply equally well to the present liquids in which the electron scattering cross sections are small. A theoretical problem remains to rationalize the existence of electronic bands in liquids.

39. R. J. GARDNER. Rev. Sci. Inst. To be published.
40. J. W. T. SPINKS and R. J. WOODS. An introduction to radiation chemistry. 2nd ed. Wiley, Toronto. 1976. p. 93.
41. W. J. MEREDITH and J. B. MASSEY. Fundamental physics of radiology. 2nd ed. Wright, Bristol. 1972. Chapt. 13.
42. M. G. ROBINSON and G. R. FREEMAN. Can. J. Chem. **52**, 440 (1974).
43. G. JAFFE. Ann. Phys. **42**, 303 (1913).
44. H. A. KRAMERS. Physica, **18**, 665 (1952).
45. J. TERLECKI and J. FIUTAK. Int. J. Radiat. Phys. Chem. **4**, 469 (1972).
46. G. C. ABELL and K. FUNABASHI. J. Chem. Phys. **58**, 1079 (1973).
47. J.-P. DODELET and G. R. FREEMAN. J. Chem. Phys. **60**, 4657 (1974).
48. B. RAZ and J. JORTNER. Chem. Phys. Lett. **4**, 155 (1969).
49. M. MARTIN. J. Chem. Phys. **54**, 3289 (1971).

Discussion

L. G. Christophorou: A mechanism similar to the one you propose ($M^* + M \rightarrow M_2^+ + e^-$) to account for the extra source of ionization in the liquid noble gases has been suggested by myself (L. G. Christophorou. Atomic and molecular radiation physics. Wiley-Interscience, New York, NY. 1971. Chapt. 2) for the noble gases, to partially account for the increased ionization for the noble gases compared to molecular vapors.

G. R. Freeman: The binding energy of M_2^+ is about 1 eV so the reaction is also possible for the higher Rydberg states in the gas phase. The question is whether a larger fraction of the total number of excited atoms generate ions in the liquid than in the gas.

R. C. Hughes: Could you comment on the fact that in semiconductors like Si and Ge, the energy required for each electron–hole pair is three times the band gap, and for wide band gap materials Rotwarf has predicted that two times the band gap would be required? Your values are even less than two times the band gap.

G. R. Freeman: The gas phase values are also less than two times the ionization potential. Perhaps the semiconductor values were not obtained by extrapolation to infinite field strength, in which case some geminate neutralization might have occurred. This would increase the apparent W values. Furthermore, Si and Ge are already chemically bonded systems, so the equivalent of $M^* + M \rightarrow M_2^+ + e^-$ would not occur in them.

G. Ascarelli: Do you expect field ionization of the excitons?

G. R. Freeman: We have estimated the extent of field induced dissociation of excitons with $n = 6$ in Ar, Kr, and Xe liquids. The fraction that would dissociate at 100 kV/cm would be less than 10%. The highest excitons could be dissociated by high fields, but this process would compete with the bimolecular ionization reaction and would not enhance the total ionization yield.

R. F. Firestone: The proposed contribution of additional free-ion pairs by Hornbeck–Molnar ($Ar^* + Ar \rightarrow Ar_2^+ + e^-$) reactions which you tentatively attribute to the liquid/gaseous phase difference should be observable in the gaseous phase alone. The rate constant for such reactions in the gas is $\sim 10^{-9}$ cm^3 atom^{-1} s^{-1} at room temperature. The radiative decay constant will likely be of the order 10^8 s^{-1} for Ar*. Thus, at 200–300 Torr and 300 K, extra ions from this process will be observed alternative to production of lower excited atomic states. We observe this effect on yields of Ar species in pulse radiolysed Ar gas at 300 K. Thus, it seems unlikely that extra ions will form only at densities characteristic of the liquid phase.

G. R. Freeman: The gas phase W values were probably measured at a few hundred Torr. Although there are the experimental uncertainties that I mentioned in our results, it appears that the reaction is more extensive in the liquid. Ar* refers to a whole manifold of states. The density dependence of the competition between the ionization reaction and other processes may be different for different states.

J. Jortner: Your proposed mechanism for 'Penning type' ionization of bound electron – hole Wannier excitons ($n = 2$) $\rightarrow M_2^+ + e$ (where M is a rare gas atom) is fraught with some difficulties, as the efficiency of this process is determined by the lifetime, τ, of the $n = 2$ state with respect to the $(n = 2) \rightarrow (n = 1)$ nonradiative multiphonon relaxation. Optical emission studies of solid and liquid Ar, Kr, and Xe conducted by us indicate that $\tau \approx 10^{-12}$ s and this expectation is borne out by theoretical calculation.
To the best of my knowledge there is no experimental evidence for extrinsic photoconductivity in liquid Xe below E_g. A search for such effect will provide a conclusive proof for the validity of your suggestion.
Finally, it is possible that cross sections for excitation of metastable exciton states above E_g are higher than the corresponding cross section for excitation of autoionizing states in the gas phase.

G. R. Freeman: Optical emission is a relatively slow reaction on the picosecond time scale and is not a test of the occurrence of the ionization reaction. The geminate neutralization reaction $[M_2^+ + e^-] \rightarrow M_2^*$ could occur in the time range $10^{-12} - 10^{-9}$ s. The longer times correspond to the greater electron penetration ranges; these pairs would be most easily dissociated by the applied fields, so the shorter time neutralizations are the ones that remain at high fields.
The definition of an ionization process in dense phases is ambiguous and not always readily distinguishable from that of a highly excited neutral state. For practical purposes we define an ionization as an event during which an electron separates from an ion or molecule, and after which the electron may be considered to have a separate existence for a finite time. Although the electron has not escaped the Coulomb field of the ion in a geminate pair $[M^+ + e^-]$ we include the pair under the definition of ionization because the wave function of the electron is not centered on the ion. Such electrons are observable in hydrocarbon glasses and in polar liquids and glasses.
Roberts and Wilson did observe photoconductivity in Xe below E_g, but they attributed it, probably correctly, to impurities. However, they made the measurements at rela-

tively low field strengths and would not have dissociated many geminate pairs. Our values were obtained by extrapolation to infinite field strength.

W. F. Schmidt: Klassen and myself have measured saturation currents in liquid argon irradiated with high energy X rays (Can. J. Chem. **47**, 4286 (1969)). Our W value was close to 25 eV and in agreement with data reported by Ullmaier (see above reference) and with those reported by Takahashi *et al.*

G. R. Freeman: We question whether you obtained a saturation current at 13 kV/cm, that is, whether you reduced the amount of geminate neutralization to zero. We had reported G(ionization) ≈ 5, or $W \lesssim 20$ eV (J. Chem. Phys. **51**, 1276 (1969)). Your value agrees with the 1974 value of Takahashi and co-workers. The 1974 value of Takahashi for xenon is higher than that from their more extensive work reported in 1975. If they made the same errors for xenon, krypton, and argon in 1974, all the W values from that study would be too high.

W. F. Schmidt: With respect to the xenon values I should like to ask how dosimetry was performed and whether the Bragg–Gray principle was fulfilled in your experiment.

G. R. Freeman: In the dosimetry we used a powdered salt that has the same average atomic number as the noble liquid in question; CsI for Xe. The samples were thick enough to satisfy the Bragg–Gray principle.

W. F. Schmidt: The difference in currents with positive and negative polarity of the high voltage electrode is, to a large extent, due to irradiation of the dead volume behind the collector electrode – guard ring assembly. Proper shielding reduces this effect to less than 5% difference; sometimes it vanishes completely.

G. R. Freeman: We have a grounded shield behind the collector electrode, at a potential less than 1 mV different from that of the collector. It is difficult to explain the difference in results obtained from positive and negative voltages.

J. W. Warman: I would question the use of the Onsager expression under conditions where the field strengths are high enough (*e.g.* >40 V cm^{-1} in liquid xenon) that the electrons are no longer in thermal equilibrium with the medium. This heating of the electrons should be taken into account as an effective variation of the temperature, *i.e.* the relevant temperature is T_e, the temperature of the electrons not the temperature of the medium.

G. R. Freeman: We have not considered this problem, but will do so. (Using T_e much greater than the liquid temperature increases the value of G_{tot} required to fit the results. See the note added at the end of the article.)

Electron energy loss processes at subelectronic excitation energies in liquids

JOHN L. MAGEE

Chemistry Department and Radiation Laboratory,[1] University of Notre Dame, Notre Dame, IN, U.S.A. 46556

and

Lawrence Berkeley Laboratory, Berkeley, CA, U.S.A. 94720

Received September 27, 1976

JOHN L. MAGEE. Can. J. Chem. **55**, 1847 (1977).

The theory of the processes by which subexcitation electrons lose energy in molecular liquids is considered. It is convenient to classify such losses as resulting from 'indirect' and 'direct' interactions; the former interactions arise from the transient electric field of the electron and the latter from the short range quantum mechanical forces occurring in direct collisions. Indirect processes are considered at some length; Monte Carlo trajectories for electrons are generated and the Fourier spectrum of the electric displacement obtained from which energy loss to dipolar relaxation and infrared-active vibrations are estimated. A tight binding scheme is used to derive an expression for the rate of energy loss to single-phonon excitation in direct collisions; the same theoretical framework is used to discuss electron trapping by the molecules of the liquid. Finally, some attempt is made to relate the loss mechanisms considered to experimentally known facts. It is concluded that the 'direct' processes are probably dominant and that knowledge of elastic scattering is of primary importance for the construction of a satisfactory theory.

JOHN L. MAGEE. Can. J. Chem. **55**, 1847 (1977).

On considère la théorie des processus par lesquels des électrons de subexcitation perdent de l'énergie dans des liquides moléculaires. Il est opportun de classifier de telles pertes comme résultant d'interactions "directes" et "indirectes"; les premières interactions proviennent de champs électriques transitoires de l'électron et les dernières proviennent de forces mécaniques quantiques à courtes distances se produisant lors de collisions directes. On considère longuement les processus indirects à longues distances; on génère des trajectoires de Monte Carlo pour les électrons et on obtient des spectres de Fourier des déplacements d'électron à partir desquels on a pu estimer les pertes d'énergie vers des relaxations dipolaires et les vibrations actives en infrarouge. On utilise un schéma d'association intime pour dériver une expression pour la vitesse de perte d'énergie vers une excitation à phonon simple dans les collisions directes; on utilise le même environnement théorique pour discuter du piégeage des électrons par des molécules du liquide. Enfin on fait quelques essais pour relier les mécanismes considérés pour les pertes avec les faits expérimentaux connus. On en conclut que les processus "directs" sont probablement dominant et que la connaissance de la dispersion élastique est de première importance pour la construction d'une théorie satisfaisante.

[Traduit par le journal]

1. Introduction

Subexcitation electrons can lose energy only in the excitation of the motion of nuclei, *i.e.*, in condensed systems to phonons, and thus in liquids all loss processes must depend upon the electron–phonon coupling. In all molecular media energy can be lost in *direct* or in *distant* or *indirect* collisions. The first mechanism is associated with short-range interactions and is usually the most important loss mechanism. The second mechanism is associated with the transient electric field generated by the motion of the electron. In dipolar media which have large static dielectric constants, under conditions favorable for dielectric relaxation the indirect loss can be very large; in molecular media which have no dielectric relaxation, infrared-active vibrational modes can absorb energy by this mechanism. The indirect loss processes establish a minimum rate of energy loss for electrons in molecular media.

Many investigations of the loss processes of low-energy electrons have been carried out for materials in the solid state, for gases, and for rare gas liquids, but few studies have been made on molecular liquids of interest in radiation chemistry. One of the principal problems of radiation chemistry is the configurations of

[1]Operated under contract with the US Energy Research and Development Authority. This is an ERDA Document NDRL-1706.

charges created by energy deposits immediately after thermalization has been attained. Much effort has been made to infer such configurations from experimental data such as free ion yields, the effect of external fields on free ion yields, the results of scavenger experiments, etc.

The distribution of subelectronic energies in liquids is not known. The function

$$[1] \qquad N(E) = \frac{8I^2}{3(E + I)^3} \qquad 0 \leq E \leq I$$

was proposed for low-energy electrons in molecular media by Magee and Burton (1). Here $N(E)$ is the number of electrons per unit energy interval at E and I is the ionization potential; the spectrum is normalized to unity. This distribution was suggested by a theoretical prediction of the distribution of electrons from photoionization of atoms. A formula for the absorption coefficient of an atom above the ionization limit widely used in opacity calculations of astrophysics was given by Kramers (2) on the basis of quite general considerations. It is

$$[2] \qquad \sigma = C/\nu^3 \qquad h\nu \geq I$$

where C is a constant which depends upon properties of the atom but is of no further relevance to this discussion. The energy of the photoejected electron is given by

$$[3] \qquad h\nu = E + I$$

and so the distribution function of [1] is clearly obtained. Of course, the distribution of electrons arising from particle impact processes is not necessarily expected to be the same and the usefulness of the formula for subexcitation electrons of radiation chemistry had to be established by analyzing experimental data. Platzman (3) investigated the distribution function for gases; it has not been possible to make a meaningful analysis of the data of other phases.

Platzman (3) called attention to the fact that the subexcitation electron spectrum is cut off on the high side at the lowest excited state of the medium, E_x, rather than the ionization potential, I. He analyzed experimental data in rare gases to derive spectra of 'subexcitation' electrons and found functions quite similar to $N(E)$ of [1] except that the high energy limit was E_x instead of I.

According to the distribution function $N(E)$, the average value of E is given by

$$\langle E \rangle = I/3$$

or

$$\langle E \rangle = E_x/3$$

if E_x is substituted for the upper limit. The lowest excitation potentials of molecular liquids are around 6 eV. Radiation chemists think of subexcitation electron energies in the vicinity of 2–3 eV and perhaps this is as reasonable as one knows at the present time.

According to Birkhoff and co-workers (4) and Ritchie *et al.* (5) the absorption of energy from high-energy electrons occurs primarily through a resonant process which forms a plasmon at around 20–24 eV. The case of water has been investigated rather extensively and the plasmon energy has been given as 22 eV; the complex dielectric constant has been obtained throughout this energy region; it is said that the initially created plasmon decays with a mean lifetime of around 10^{-16} s and presumably one of the products is a subexcitation electron. There is no reason to believe that the energy distribution would be given by [1]; in fact, on general grounds it would appear that a Gaussian distribution function would be more reasonable, but no one has considered the matter explicitly.

Interest in the 'initial' geometrical arrangement of the thermalized charged particles in tracks began with Lea (6) and Gray (7, 8). These authors speculated that a subexcitation electron would reach a separation from its parent positive ion of about 150 Å in water before becoming attached to a molecule to form H_2O^- which would subsequently dissociate to the products $H + OH^-$. No calculation of the range or even a consideration of the energy loss mechanisms was made. The value 150 Å was based somehow on interpretation of experimental results for α particles in hexane by Jaffe (9) and no attempt was made to justify the application of this result to water. The first theoretical consideration of the energy loss of a subexcitation electron was made by Fröhlich and Platzman (10). This treatment estimated the loss in *distant* collisions by excitation of polar vibrational modes, *i.e.*, dipolar relaxation. This very sophisticated treatment is not entirely free from objection, however, as we point out in section 2. Samuel and Magee (11) suggested that the energy loss mechanism of subexcitation electrons in water was due to *direct* collisions with the water molecules. These

authors did not present a theoretical treatment in the sense of Fröhlich and Platzman (10), but used gas phase data on fractional energy loss per collision to obtain an estimated loss rate which was large enough to be consistent with parent-ion recapture. The radical diffusion model was beginning to have great success in the explanation of experimental data and it was generally accepted that the reducing entity was the H-atom. Parent-ion recapture seemed to be necessary to explain the initial radical distributions.

After the hydrated electron was discovered a much more elaborate radical diffusion model was constructed by Schwarz (12); all parameters were chosen to be consistent with experimental results and there was no attempt to relate the initial separations of charges to thermalization mechanisms.

In recent years, interest in the behavior of low-energy electrons in organic liquids has been very great. Mozumder and Magee (13) made a study of the free ion yield in hexane which contained an elaborate discussion of the thermalization process for subexcitation electrons. In other studies most authors have been more concerned with the nature of distribution functions which must be assumed in order to obtain agreement with experimental results. Such distribution functions contain indirect information on low-energy electron ranges in the liquids. Mozumder and co-workers (14–16), Abell and Funabashi (17), Hummel (18), Freeman and co-workers (19–22), and Holroyd *et al.* (23), have made many studies of this nature.

Free ion yield studies in molecular liquids involve the difficulty that the amount of energy required to form a primary charge pair is not well known. On general principles it is expected that the energy required is somewhat less for a given compound in the liquid state than in the gas. The situation with respect to the noble gases and their liquids is better understood and has been presented by Huang and Freeman (24).

Most papers treat the high-energy electron track as if it were composed entirely of charge pairs, or that track entities such as short tracks do not exist although on general grounds it is known that they do. All authors are actually aware of the problem, but at the present time there is no real understanding of the role of higher track entities. Mozumder (25) considered the problem explicitly. Mozumder and Magee (13) demonstrated in the case of hexane that the latter had to be taken into account to explain the free ion yield, but many later studies have continued to use the approximation of entities with charge pairs only.

In spite of the various uncertainties regarding energy distribution of subexcitation electrons and track structure, most authors have assumed that it is possible to obtain electron ranges and 'stopping power' information from experimental data. In part this belief is supported by the success of the treatment of electron scavenging and escape using the Smoluchowski and Onsager equations. The question of importance now is this: how do electrons starting at energies from 1 to 5 or 6 eV thermalize in going a distance of 60–100 Å in molecular liquids?

In this paper, we are primarily concerned with the mechanisms of energy loss of subexcitation electrons. The use of the mechanisms to generate range energy relations has not been accomplished.

2. The Theory of Energy Loss: Indirect Processes

The loss of energy by means of the transient electric field generated by the motion of the electron has been considered by Magee and Helman (26). These authors took into account the random motion of the electron as it moves through the molecular medium and made explicit estimates of rates of energy loss to dipolar relaxation and to infrared-active vibrational modes.[2] The earlier treatment of the indirect loss process by Fröhlich and Platzman (10) had been restricted to the dipolar loss mechanism and the electron trajectory had been approximated as linear.

The total energy loss (per unit volume) to a molecule located at a position $\boldsymbol{R}$ in the vicinity of an electron trajectory is given by

$$[4] \qquad L(\boldsymbol{R}) = \frac{1}{4\pi}\int_{-\infty}^{\infty} \boldsymbol{E}(\boldsymbol{R},t)\cdot\frac{\partial \boldsymbol{D}}{\partial t}(\boldsymbol{R},t)\mathrm{d}t$$

where $\boldsymbol{E}$ is the electric field intensity, $\boldsymbol{D}$ the electric displacement, at $\boldsymbol{R}$. It is clear that the energy lost to the molecule depends upon an integral over the entire trajectory of the electron;

[2]This problem has also been considered by H. Sano (unpublished results) using a space–time autocorrelation function. His result is in qualitative agreement with this section.

the interaction pattern of the trajectory cannot be divided into separate 'collisions'.

Fourier transforms of $\boldsymbol{E}$ and $\boldsymbol{D}$ are used and a complex dielectric constant

$$\varepsilon = \varepsilon_1 + i\varepsilon_2$$

introduced. The integration over time can be performed to yield

$$[5] \quad L(\boldsymbol{R}) = \int_0^\infty \frac{\varepsilon_2(\omega)}{\varepsilon_1^2(\omega) + \varepsilon_2^2(\omega)} \boldsymbol{D}_\omega \cdot \boldsymbol{D}_\omega^* \omega d\omega$$

where the following symmetry in the Fourier transforms

$$[6] \quad \begin{aligned} \boldsymbol{D}_\omega &= \boldsymbol{D}_{-\omega}^* \\ \boldsymbol{E}_\omega &= \boldsymbol{E}_{-\omega}^* \\ \varepsilon_\omega &= \varepsilon_{-\omega}^* \end{aligned}$$

has been used (10, 26).

It is clear from [5] that the track enters the calculation only through the Fourier transform of the electric displacement. Magee and Helman (26) consider three kinds of tracks.

(*a*) A random track in which the electron starts at an initial position (on a molecule!) and then jumps to neighboring molecules in a random manner. A Monte Carlo routine is used to obtain such tracks.

(*b*) A random track in which the electron hesitates on 10% of the molecules for an average of five jump times. The significance of this type of track is an approximation of the effect of resonances which are believed to exist; in the energy region of subexcitation electrons most such resonances probably arise from the energy level structure of the electron in the disordered molecular system (27). This track is of course also obtained by a Monte Carlo procedure.

(*c*) A linear track in which the electron jumps from one molecule to the next along a line. The significance of this track is twofold. In the first place a check of the technique is desired and analytical calculations are available for the linear case. In the second place, the linear track provides an estimate of the minimum energy loss by the indirect mechanism; it is the lower limit for large mean free path.

The electric displacement is given by

$$[7] \quad \boldsymbol{D} = \frac{e}{|\boldsymbol{R}_n - \boldsymbol{R}|^3} (\boldsymbol{R}_n - \boldsymbol{R})$$

where $\boldsymbol{R}_n$ is the position of the electron at the nth jump in the track. A track is composed of N jumps and time is related to the jump so that zero time occurs in the middle of the track, *i.e.*

$$[8] \quad t = (n - N/2)\tau_J$$

where τ_J is the jump time.

Equation 5 shows that the spectrum $\omega \boldsymbol{D}_\omega(\boldsymbol{R}) \cdot \boldsymbol{D}_\omega^*(\boldsymbol{R})$ is the important quantity to determine. First this spectrum is obtained for particular tracks and then it is averaged over an ensemble; it is finally integrated over all $\boldsymbol{R}$ to obtain

$$[9] \quad \omega J_\omega = 4\pi \int_0^\infty R^2 \langle \omega \boldsymbol{D}_\omega(R) \cdot \boldsymbol{D}_\omega^*(R) \rangle dR$$

where J_ω is defined by the equation. Figure 1 shows ωJ_ω for ensembles of random tracks of 256 jumps for the three types *a*, *b*, and *c*.

Magee and Helman (26) considered the application of these results to the energy loss of electrons in water. Following Fröhlich and Platzman (10) they took

$$[10] \quad \varepsilon_1(\omega) = \varepsilon'(\omega) + \frac{\varepsilon_s - \varepsilon_{ir}}{1 + \omega^2\tau^2}$$

$$[11] \quad \varepsilon_2(\omega) = \varepsilon''(\omega) + \frac{(\varepsilon_s - \varepsilon_{ir})\omega\tau}{1 + \omega^2\tau^2}$$

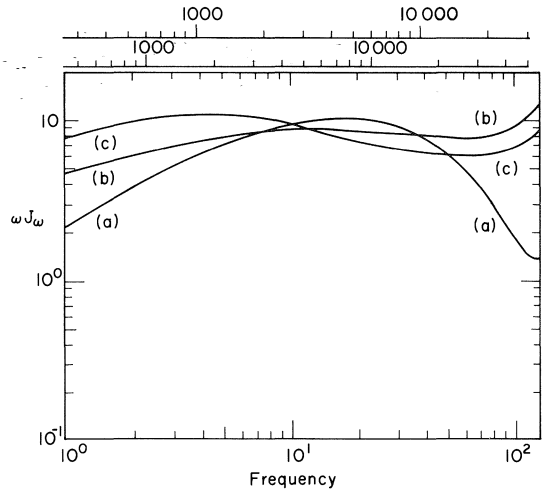

FIG. 1. The quantity ωJ_ω *vs.* frequency for tracks of 256 jumps normalized to an effect per jump. The abscissa is the frequency (*i.e.*, $\omega/2\pi$) in units of the smallest frequency calculated, $(256\ \tau_J)^{-1}$; three cases are shown: (*a*) linear trajectory; (*b*) simple random walk; (*c*) random walk with hesitation for an average of five jump times on 10% of sites. Two scales are shown above the plot which relate frequency to wave numbers for $\tau_J = 5 \times 10^{16}$ s, top scale, and for $\tau_J = 3 \times 10^{16}$ s, lower scale.

where τ is the relaxation time, ε_s is the static dielectric constant, and ε_{ir} is the dielectric constant at frequencies sufficiently lower than the lowest principal infrared absorption frequency ω_{ir}. The quantity $\varepsilon''(\omega)$ gives the absorption due to ionic oscillation in the infrared and any other resonant absorption processes at higher frequencies; $\varepsilon'(\omega)$ gives the corresponding dispersion.

These formulas have quite general validity for substances which have Debye-type relaxation. For water at 20°C, $\tau = 10^{-11}$ s. The frequency range of our calculation involves only $\omega\tau > 10^3$; thus we can take

$$[12] \qquad \varepsilon_1^2 + \varepsilon_2^2 \approx \varepsilon_1^2 \approx n^4$$

and

$$[13] \qquad \frac{(\varepsilon_s - \varepsilon_{ir})\omega\tau}{1 + \omega^2\tau^2} \approx \frac{\varepsilon_s - \varepsilon_{ir}}{\omega\tau}$$

The integrand of [7] when ensemble averaged and integrated over space becomes

$$[14] \qquad \frac{\varepsilon_s - \varepsilon_{ir}}{n^4\tau} J_\omega$$

The loss expression for Debye-type relaxation becomes

$$[15] \qquad W = \frac{\varepsilon_s - \varepsilon_{ir}}{n^4\tau} \int_0^\infty J_\omega d\omega$$

In order to get numerical values for the energy loss, explicit values for all quantities must be taken. We have used $\varepsilon_s - \varepsilon_{ir} = 75$, $n^4 = 3$; in the random walk $l = 3$ Å and the electron velocity 10^8 cm/s which gives $\tau_J = 3 \times 10^{-16}$ s.

Table 1 gives the values of W calculated for the three tracks whose spectra are shown in Fig. 1. According to the calculations the random track has a larger loss rate than the linear track and the track with hesitation has an even larger loss rate. The linear track as calculated by the approximate procedure has a loss rate somewhat larger than the loss rate given by the analytical calculation (about 15%). The value of the total loss in a track is found to vary with the track parameters as

TABLE 1. Energy loss rate to dipolar relaxation in H_2O

Track	Loss in eV per jump	Loss in eV/s
Random	0.0041	1.37×10^{13}
Random with hesitation	0.0049	1.63×10^{13}
Linear	0.0032	1.06×10^{13}

$$[16] \qquad W \propto \frac{\tau_J}{l}\Delta$$

where Δ is a dimensionless measure of the integral over J_ω; it is obtained numerically and is independent of the parameters. The average rate of energy loss is

$$[17] \qquad \frac{W}{256\tau_J} \propto \frac{\Delta}{256l}$$

and is *independent* of the velocity, in agreement with Fröhlich and Platzman (10).

Magee and Helman (26) also considered the indirect loss to infrared-active molecular vibrations. The problem of the frequency-dependent dielectric constant of a system which has resonance absorptions has been discussed by Van Vleck and Weisskopf (28) and Fröhlich (29, 30). The absorption in such resonances is expected to be less important than that to dipolar relaxation if the latter mechanism exists. Consider a system which has no dipolar relaxation; in a spectral region in which there are infrared absorptions at κ frequencies $\omega_1, \omega_2, \ldots, \omega_j, \ldots, \omega_\kappa$, the dielectric constant can be written as

$$[18] \qquad \varepsilon_1(\omega) - \varepsilon_{ir} = \sum_{j=1}^{\kappa} 2\pi\rho_j \frac{q_j^2}{M_j\omega_j^2}\left[\frac{1 + \omega_j(\omega + \omega_j)\tau_j^2}{1 + (\omega + \omega_j)^2\tau_j^2} + \frac{1 - \omega_j(\omega - \omega_j)\tau_j^2}{1 + (\omega - \omega_j)^2\tau_j^2}\right]$$

$$[19] \qquad \varepsilon_2(\omega) = \sum_{j=1}^{\kappa} 2\pi\rho_j \frac{q_j^2}{M_j\omega_j^2}\left[\frac{\omega\tau_j}{1 + (\omega + \omega_j)^2\tau_j^2} + \frac{\omega\tau_j}{1 + (\omega - \omega_j)^2\tau_j^2}\right]$$

where ρ_j is the number density of oscillators of the jth type which has an effective charge of q_j and a reduced mass of M_j; and τ_j is the effective collision time for the damping of the jth oscillator. The latter quantities are to be obtained from experiment; unfortunately the theory of infrared absorption is not developed far enough to be useful in predicting such parameters.

The energy loss is to be obtained from [5] and it is clear that all of the terms of the summations

TABLE 2. Infrared intensities and track absorptions in benzene for tracks of 256 jumps

Mode	Frequency (cm^{-1})	Γ (cm^2/mol)	Energy absorbed from track (eV)		
			Linear	Random	Random with hesitation
ν_{11} (A_{2u})	673	12 500	0.0284	0.0636	0.1001
ν_{18} (E_{1u})	1038	852	0.0034	0.0046	0.0066
ν_{19} (E_{1u})	1486	1 000	0.0049	0.0058	0.0081
ν_{20} (E_{1u})	3080	2 500	0.0166	0.0159	0.0168
Sum of line absorptions			0.063	0.089	0.1316
Rate of energy absorption (eV/s)			4.92×10^{11}	6.95×10^{11}	1.03×10^{12}

of [18] and [19] are involved in the integration. The fact that each term of ε_2 has a resonance allows a simplification; we assume that no other frequency dependence is important and the integration over the resonance term becomes

$$[20] \quad \int_0^\infty \frac{\omega\tau_j \boldsymbol{D}_\omega \cdot \boldsymbol{D}_\omega^* \omega d\omega}{1 + (\omega - \omega_j)^2\tau_j^2} \approx \pi\omega_j^2 \boldsymbol{D}_{\omega_j} \cdot \boldsymbol{D}_{\omega_j}^*$$

In most cases

$$\varepsilon_2(\varepsilon_1^2 + \varepsilon_2^2)^{-1} \approx \varepsilon_2/\varepsilon_{ir}^2$$

to a good approximation and we can write for the energy loss per unit volume at a molecule located at $\boldsymbol{R}$

$$[21] \quad W = \sum_{j=1}^{\kappa} W_j = \sum_{j=1}^{\kappa} \frac{2\pi^2\rho_j}{\varepsilon_{ir}^2} \frac{q_j}{M_j} J_{\omega_j}$$

Magee and Helman (26) show how q_j^2/M_j can be eliminated using experimentally determined absorption strengths. The energy loss is given by

$$[22] \quad w = \sum_j \left(\frac{\rho_j}{N}\right) \frac{\Gamma_j}{\varepsilon_{ir}^2} c\omega_j J_{\omega_j}$$

where Γ_j is the integrated absorption of the jth transition in cm^2/mol. Thus the energy absorption by infrared-active oscillators can be obtained from experimental data on integrated absorptions. Such experimental information is not readily available but data on the absorption in gas phase benzene have been published (31) and they have been used to obtain the estimates of electron loss given in Table 2. Absorption is stronger in the liquid. The calculated energy losses for the various tracks using gas phase data are perhaps minimal values.

Aliphatic hydrocarbons are of great interest in radiation chemistry but neither absorption intensities nor complete analysis of the vibrational spectra are available for these molecules. On the other hand, the vibrational spectrum of polyethylene is quite well understood and in some approximations it can be taken as a prototype for the aliphatic hydrocarbons. The basic unit is —CH_2—CH_2— which in the crystalline state is very symmetric, with a center of symmetry; there are 18 degrees of freedom and only six infrared-active frequencies (31) (one of these is strictly inactive in the crystal).

Table 3 shows the absorption of electrons in polyethylene as significantly larger than in benzene. One factor is that the mean free path, l, is taken to be 5 Å in benzene and 3 Å in polyethylene. The latter value was used because the calculation made for water used 3 Å and the unknown mean free path in polyethylene was taken to be the same.

The energy loss to a particular absorption line at ω_j over the entire track is found to vary as

$$[23] \quad W_j \propto \frac{1}{l}\tau_j^2\Delta_j'$$

where Δ_j' is a quantity proportional to the spectrum shown in Fig. 1. To a rough approximation it can be taken as independent of frequency for the random track; thus the contribution of the jth line to the *rate* of energy absorption is

$$[24] \quad \frac{W_j}{256\tau_j} \propto \frac{\tau_j}{l}\Delta'$$

where we take Δ' as a constant, and the absorption of the line varies *directly* as the jump time or *inversely* as the velocity. This dependence is approximately valid for all lines in the region 500 to 3500 cm^{-1}.

3. Theory of Energy Loss: Direct Processes

The theory of loss processes involving short-range interactions requires the use of wave

TABLE 3. Infrared intensities and track absorptions in polyethylene

Mode	Frequency (cm^{-1})	Γ (cm^2/mol)	Energy absorbed from track (eV) Linear	Random	Random with hesitation
ν_4 (a_u)[a]	1050	100	0.0013	0.0017	0.0027
ν_7 (b_{1u})	2919	1000	0.0211	0.0219	0.0276
ν_8 (b_{1u})	725	5000	0.0439	0.0782	0.1276
ν_{10} (b_{2u})	2851	1000	0.0211	0.0218	0.0276
ν_{11} (b_{2u})	1468	5000	0.0653	0.0925	0.1374
ν_{13} (b_{3u})	1176	300	0.0039	0.0054	0.0083
Sum of line absorptions			0.1566	0.2215	0.3312
Rate of energy absorption (eV/s)			2.03×10^{12}	2.88×10^{12}	4.31×10^{12}

[a]This mode is inactive in the crystal.

functions. The low-energy electrons are initially in extended states as they lose energy in the 1–6 eV region and we shall assume that the extended states can be made up of superpositions of negative ion states of the molecules; in other words, the tight-binding approximation is used. The electrons are in very low concentrations (in fact, we consider a system which only has *one* electron and N molecules with $N \sim 10^{22}$) and so the molecules vibrate in the potential function of the neutral ground state. The negative ion potential function is, of course, also important. As the electron moves about there is a tendency for the nuclei of the molecule which contains the electron to relax from the vibrational structure of the neutral molecule to that of the negative ion. The general theory of this process has not been worked out and we consider two limiting cases.

(*a*) The weak interaction limit in which no relaxation develops about the negative ion. The interaction produces excitation of vibrations in the neutral molecules.

(*b*) The strong interaction limit in which localization occurs in a single event and is followed by a large transfer of energy into vibrations.

It is likely that many loss processes can occur in molecular liquids in the spectrum between these two limiting cases. However, the most probable processes should be the special cases themselves.

According to the 'random phase model' (RPM) used in solid state physics (33, 34), under certain conditions the wave functions of extended states for electrons can be expanded in terms of localized functions (Wannier-like) centered on atoms, the latter having completely random phases. This type of model would seem to be in keeping with the requirements of subexcitation electrons in some of the molecular media of interest in radiation chemistry and we explore its use in the energy loss to phonons in the mechanism called (*a*). At the outset it should be stated that the RPM is not expected to be of universal validity for this problem and the range of applicability needs to be explored.[3]

Another matter of importance for subexcitation electrons is the spatial distribution as the energy approaches thermal. The use of a wave function is of course necessary for an adequate treatment and in this case we require a superposition of the extended wave functions to form a wave packet which spreads out as the energy is lost. This problem is also not considered at this time.

The electron wave function is assumed to be (34)

$$[25] \qquad |k\rangle = \sum_{n=1}^{N} a_{nk}\phi_n(\boldsymbol{r} - \boldsymbol{R}_n)$$

where the ϕ_n are located on the molecules and the a_{nk} have random phases.

The Hamiltonian of the system is taken as

$$[26] \qquad H = \sum_q \hbar\omega_q a_q^{+} a_q + H_{el} + H_{int}'$$

which consists of the Hamiltonian for the unperturbed phonon field of the neutral molecules, the electron Hamiltonian, and an interaction term between the phonons and the electron; a_q^{+} and a_q are creation and annihilation operators, respectively, and q goes over all phonon

[3]The Random Phase Model should be distinguished from the Random Phase Approximation also used in solid state theory. See ref. 35.

modes; the electron Hamiltonian operates on the wave function as follows:

$$[27] \qquad H_{el}|k\rangle = \varepsilon_k|k\rangle$$

The interaction Hamiltonian H_{int}' is taken to be of the deformation potential type (36, 37)

$$[28] \qquad H_{int}' = \sum_j E_{1j}\Delta \boldsymbol{u}_j$$

where E_{1j} is a constant with dimension energy which applies to the jth coordinate of the system and Δ is the dilation due to the phonons. It is the divergence of the local displacement $\boldsymbol{u}_j$ which is taken to be a continuous function for this purpose.

The system considered contains N molecules in a volume V. Most of the 'phonons' of interest are actually to a good approximation vibrations of individual molecules. Say that each molecule has p vibrations (three times the number of atoms minus six); we shall at first consider only the excitation of these vibrations, for the total system equal to Np. The other six degrees of freedom combine to form acoustical modes and a few additional 'optical' modes; these neglected modes are in fact active in the exchange of energy with thermal electrons and are certainly of importance in the latter stage of thermalization.

The excitations we consider are those of the normal vibrations of individual molecules; the $\boldsymbol{u}_j$ of [28], therefore, belongs to a single molecule and H_{int}' is composed of N terms each containing the p normal vibrations of one molecule.

The rate of energy loss is to be obtained through the use of the 'Golden Rule' and we need matrix elements of H_{int}' between arbitrary electron states k' and k. The phonon field is not explicitly involved in this consideration.

$$[29] \qquad \langle k'|H'|k\rangle = \sum_{n',n} a_{n'k'}{}^* a_{nk}\langle n'|H'|n\rangle$$

where

$$\langle k'|H'|n\rangle = \int \Phi_{n'k'}(\boldsymbol{r} - \boldsymbol{R}_{n'})H'\Phi_{nk}(\boldsymbol{r} - \boldsymbol{R}_n)\mathrm{d}\boldsymbol{r}$$

We assume that the Wannier-like states Φ_n are orthogonal and so we have the relationship (34)

$$[30] \qquad \sum_n a_{nk'}{}^* a_{nk} = \delta_{k'k}$$

We shall always assume that ensemble averages are to be used; we have from [30] for $k' = k$

$$[31] \qquad \begin{aligned} \sum |a_{nk}|^2 &= 1 \\ |a_{nk}|^2 &= 1/N = v/V \end{aligned}$$

where v is the volume of a molecule. We require the absolute values of the square of the matrix element

$$[32] \qquad |\langle k'|H'|k\rangle|^2 = \sum_{\substack{n',n \\ m',m}} a_{m'k'}{}^* a_{mk} a_{n'k'}{}^* a_{nk}\langle m'|H'|m\rangle\langle n'|H'|n\rangle$$

Because of the random phases, only terms which have $m' = n'$, and $m = n$ fail to vanish. Use of this fact and [31] allows us to write

$$[33] \qquad |\langle k'|H'|k\rangle|^2 = \left(\frac{v}{V}\right)^2 \sum_{n,n'} |\langle n'|H'|n\rangle|^2 = \left(\frac{v}{V}\right) \sum_{n'} |\langle n'|H'|n\rangle|^2$$

In our particular problem the 'phonons' are vibrations of individual molecules and so the matrix elements of the interaction Hamiltonian only involve single molecules. Thus we have

$$[34] \qquad |\langle k'|H'|k\rangle|^2 = \frac{v}{V}|\langle n|H'|n\rangle|^2$$

which means that the molecules of the medium all contribute equally and one only has to perform the calculation for one of them.

Let us now consider the energy loss to phonons. We require the matrix element

$$\langle k', n_q + 1|H_{int}'|k, n_q\rangle$$

where n_q is taken to represent all of the p modes and in general $n_{q'}$, the number of phonons initially present in a mode, can be taken as zero. The displacement of the nth molecule is (38)

$$[35] \qquad \boldsymbol{u}(n) = \sum_{j=1}^{p} \boldsymbol{u}_j(n)Q_j(n)$$

The internal condition of a molecule can be given in terms of the p normal modes and $\boldsymbol{u}_j$ are vectors in the directions of the modes; [35], therefore, has only a single sum

$$[36] \qquad Q_j = \left(\frac{\hbar}{2M_j\omega_j}\right)^{1/2}(a_j{}^+ + a_j)$$

Use of [35] and [36] with [28] gives

$$[37] \qquad |\langle k', n_q + 1|H'|k, n_q\rangle| = \sum_{j=1}^{p} \frac{(E_j q_j)^2 \hbar v}{2M_j\omega_j V}$$

where E_j has been substituted for E_{1j} and we have used

$$[38] \qquad |\langle n|\Delta u_j|n\rangle|^2 = q_j^2$$

for the matrix element of the dilation.

The rate of energy loss is given by

$$[39] \quad \left(\frac{\partial\varepsilon}{\partial t}\right) = \frac{2\pi}{\hbar}\frac{(E_j q_j)^2 \hbar v}{2M_j\omega_j}\hbar\omega_j\left[n_j\frac{\nu(\varepsilon_k + \hbar\omega_j)}{V} - (n_j + 1)\frac{\nu(\varepsilon_k - \hbar\omega_j)}{V}\right]$$

where $\nu(\varepsilon_k + \hbar\omega_j)$ is the number of states per unit energy interval for the electron with energy $\varepsilon_k + \hbar\omega_j$; it is proportional to V. The average numbers of vibrational quanta present initially can be taken as zero for almost all the molecular vibrational modes; the only surviving term is an energy loss term

$$[40] \quad \left(\frac{\partial\varepsilon}{\partial t}\right) = -\sum_{j=1}^{p}\frac{\pi\hbar}{\rho_j}(E_j q_j)^2\frac{\nu(\varepsilon_k - \hbar\omega_j)}{V}$$

where $\rho_j = M_j/v$ is a 'density', *i.e.*, mass per unit volume.

The difficulty with the use of [40] is the appearance of potential functions of both the neutral molecule and negative ion, the wave function for the electron and the density of states, quantities which are not known.

Consider a classical oscillator which is subjected to a transient force $-\partial U/\partial x$ for a short time τ. The momentum given the oscillator is

$$[41] \qquad P = -\int\left(\frac{\partial U}{\partial x}\right)dt \simeq -\left(\frac{\partial U}{\partial x}\right)\tau$$

and its energy increase is

$$[42] \qquad \Delta E = \frac{P^2}{2M} = \frac{1}{2M}\left(\frac{\partial U}{\partial x}\right)^2\tau^2$$

The *rate* of energy increase is

$$[43] \qquad \frac{\Delta E}{\tau} = \frac{1}{2M}\left(\frac{\partial U}{\partial x}\right)^2\tau$$

In [40] the quantity $E_j q_j$ is essentially $\partial U/\partial x$; the other terms of [40] can be identified with [43] as follows:

$$M = M_j$$

$$\tau = \frac{hv}{V}\nu(\varepsilon_k - \hbar\omega_j)$$

To some extent one can adopt the pictures of oscillators subject to excitation by transient negative ion fields.

Let us attempt to estimate the parameters involved in [40]. It has never been customary to attempt a calculation of a deformation potential when that model is used in solid state calculations; values of 1–10 eV are usually assumed and so let us take 1 eV; q_j has to be of the *order* of 10^8 (one reciprocal angström). The density ρ_j is smaller than the liquid density because M_j is one of the reduced masses; let us assume $\frac{1}{6}$ as a reasonable guess. The density of states is very uncertain but a number to assume is perhaps the free electron value, $\nu(\varepsilon_k - \hbar\omega_j) \simeq 7 \times 10^{21}$ if the argument is 3 eV. Use of these values gives

$$[44] \qquad \left(\frac{\partial\varepsilon}{\partial t}\right) = -1.4 \times 10^{12}\ \text{peV/s}$$

Although the uncertainties are great, [40] is not incompatible with an energy loss of 10^{14} eV/s. The dependence of the rate of energy loss on E_j is as the *square* and just one degree of freedom with $E_j \sim 10$ would give $\partial\varepsilon/\partial t \sim 10^{14}$ eV/s; the potential functions for H_2O^- calculated by Claydon, Segal, and Taylor (39) suggest that $E_j q_j \sim 10$ is reasonable. Because this mechanism involves essentially one molecule at a time, the gas phase data of Christophorou *et al.* (40) should be applicable. Use of their Fig. 3 and a linear correction for density allows an estimate of 5×10^{13} eV/s for the rate of loss of an electron in water at energy 1 eV.

For hydrocarbons in the hexane class, $p \sim 50$. Substitution of this value in [44] (which assumes $E_j q_j \sim 1$) gives a loss rate of 7×10^{13} eV/s.

The strong interaction limit (*b*) in which the negative ion state is actually attained is in many ways like the capture of the electron in a scavenger (41). Of course in this case the scavenger is a molecule of the principal component. 'Capture' means that a configuration is attained which prevents continued migration of the electron and all of the excess energy is transformed into vibrational excitation of one molecule. Such a molecule is very 'hot' and cools through loss of vibrational quanta to its immediate neighbors. The electron becomes thermalized at this point and only continues its migration as a thermal electron.

The initial state is the same as before with

the wave function of [25]. There are N final states, the N possible negative ions of the system. For the purpose of this treatment the fact that there is a weak resonance between these negative ion states can be ignored.

We are interested in the probability that the electron is captured per unit time, which can be written as:

$$[45] \qquad P = \frac{2\pi}{\hbar}|H_{if}'|^2\rho_E$$

where H_{if}' is the matrix element of the appropriate perturbation operator between the initial and final states and ρ_E is the density of final states. The transition is from the ground vibrational state of the neutral molecule to an excited vibrational state of the negative ions. Funabashi and Magee (41) have made an elementary consideration of the capture of an electron from an extended state in a liquid to a scavenger which dissociates. In that case the perturbation operator is shown to be the matrix element of the electron with respect to the electronic interaction with scavenger molecule, *i.e.*

$$[46] \qquad \beta_{21} = \langle\Phi_2 V_s \Phi_1\rangle$$

where Φ_2 is the negative ion wave function; Φ_1 is the extended state wave function; and V_s is the operator for the interaction of the electron with the scavenger. The matrix element in [45] for this case is

$$[47] \qquad H_{if}' = \langle\eta_2\beta_{21}\eta_1\rangle$$

where η_2 is the wave function for the nuclear motion of the negative ion and η_1 is that of the neutral scavenger molecule.

Funabashi and Magee (42) have shown that the same treatment can be applied approximately to the capture of electrons by the molecules in a homogeneous liquid. In this case there are many degrees of freedom and so wave functions for all of the vibrational modes of the system must be included; the term β_{12} is a function of all coordinates. In general the neutral molecule and the negative ion will have different potential functions and different normal modes. An analysis can be carried out in a formal manner (42) but it will not be presented at this time.

For the sake of orientation consider the magnitude of P given in [45] for the case of a dissociative capture by a molecule. It is probable that such a process is actually important as an energy loss mechanism for subexcitation electrons; the interpretation of experimental results of Hamill and co-workers (43) which bear on this point is discussed in the next section. The process considered is

$$e(k) + RX \rightarrow R + X^-$$

where RX is a hydrocarbon molecule, X^- is H^-, CH_3^-, etc., and k is a measure of the momentum. The value of the square of the matrix element of [45] is

$$[48] \qquad |H_{if}'|^2 \simeq E'^2 S^2 a/R$$

where E' is an electronic integral which is perhaps of the order of magnitude of an electronvolt; S is the overlap integral for all of the vibrational degrees of freedom which may be fairly small; a is a distance of the magnitude of a bond dissociation distance (10^{-8} cm), and R is a macroscopic distance arising out of the normalization of the dissociated state.

The density of states per unit energy interval is given by

$$[49] \qquad \rho_E = \left(\frac{2MR^2}{Eh^2}\right)^{1/2}$$

where M is the reduced mass for the dissociation and E is the relative kinetic energy in the dissociated state. It is clear that the constant R cancels from the calculation and if we take $E = 1$ eV and $M = 1$ atomic mass we obtain

$$[50] \qquad P \simeq 4 \times 10^{16} E'^2 S^2 a \text{ s}^{-1}$$

where a is to be taken in units of Å, and E' in eV.

This consideration does not establish the order of magnitude of P but it shows that the mechanism is not incompatible with a process which must have a specific rate of the general magnitude 10^{14} s^{-1}. It is reasonable to expect E' and a to be of the order of unity, and S^2 could easily be $(400)^{-1}$ or perhaps larger.

One thinks of dissociative processes as having large specific rates because of the high density of final states. A system of oscillators also has a high density of states which increases exponentially as the excitation increases. It is easily possible that there are polyatomic molecules for which the negative ion formation processes by the non-dissociative route dominate the energy loss mechanisms.

4. Discussion

This paper has been concerned only with theoretical aspects of the energy loss of subexcitation electrons. Unfortunately, the best understood mechanisms are the least important for systems of interest in radiation chemistry. The indirect loss mechanism described in section 2 can be developed in an elegant manner but there may be no cases in which it is the dominant process. All mechanisms act concurrently and so the more effective energy loss processes determine the experimentally observed phenomena. An entirely adequate theory would not consider the two mechanisms separately; they would both be contained within a single unified treatment.

Most subexcitation electrons probably have energies in the range below the threshold for dissociation processes and both mechanisms (*a*) and (*b*) of section 3 are effective. These are most probably the dominant subexcitation energy loss mechanisms in molecular media. Further development of the theory presented in section 3 requires quantum mechanical studies of the wave functions and energies of excess electrons in molecular systems.

There is a tendency for radiation chemists to think of energy loss in terms of one phonon at a time; this intuition leads to the process of section 2 and process (*a*) of section 3. On the other hand, many experimental results demand the type of process in which essentially all of the energy of a subexcitation electron is available for one purpose, such as a molecular dissociation (43, 44). Clearly the energy cannot be given up by the excitation of single phonons at a time. To be consistent with experimental results, mechanism (*b*) (of section 3) must compete favorably with mechanism (*a*). For the case of irradiated thin films of alkanes at 77 K, Hamill and co-workers (43) have made chemical studies of the products. The dissociation process which has the lowest threshold energy ($\sim$3.8 eV) is

$$e + RH \rightarrow R + H^-$$

and chemical products are observed at about this electron energy. Hamill[4] reports that the total observed product yield for electrons somewhat above threshold but below the energy required to excite the lowest electronic state requires that there is a G value for dissociation of 2 or 3. Say the electron energy is 5 eV, 20 electrons are required to give up 100 eV and 3 of these must produce dissociations. The effectiveness of an excited negative ion in dissociation as compared with energy loss to the environment without dissociation is unlikely to be as much as 50%; if there are 6 localized vibrationally-excited ions created per 20 electrons, this means that about one third of the loss processes proceed through route (*b*) as contrasted with (*a*). In any case, the two processes compete on something like an equal footing.

Other work by Hiraoka and Hamill (45, 46) on characteristic losses and luminescence indicates that energy of subexcitation electrons is available in larger quantities than single phonons at a time. On the other hand, in this same work a prominent energy loss occurs at about $\frac{1}{2}$ eV, and it is likely to be due to a single phonon.

In sections 2 and 3 the formal theory was developed in terms of a scattering mean free path explicitly or implicitly equal to a molecular diameter. The theory was developed so that the two mechanisms would be consistent. However, the transmission of the electrons through thin films depends upon the scattering mean free path and if the latter were as small as a molecular diameter, the transmission to backscattering ratio (T/B) would be very small for films as thick as 100 or 200 Å. Experimentally it is known (44, 46, 47) that the T/B ratios are the order of unity and not very sensitive to film thickness. These facts indicate that the mean free path for scattering is much larger than molecular dimensions. The results of Chang and Berry (47) give values of 'mean free path' which are 20–50 Å for a great many alkanes at 77 K; Huang and Magee (48) have shown that the results of Hamill are consistent with those of Chang and Berry.

Unfortunately the results of experiment are not well enough known so that the requirements of experiment on the theory presented here can be precisely stated at this time. In particular, the 'initial distributions' which are the most interesting to radiation chemists of all the experimental data are unknown quantities; uncertainties in subexcitation electron distribution, track entity distribution, etc., make them impossible to define precisely. In a general way, however, we know many things. Effective mean

[4]W. H. Hamill, private communication.

free paths for the electrons must be fairly large, 20–50 Å, and energy loss processes very efficient. Many results seem to indicate that the distribution is very broad (with a long tail), which might imply that a process such as 3(*b*) dominates but a significant fraction of loss is due to 3(*a*) and low-energy electrons have less efficient loss processes.

The principal defect of the theory as presented here is that the implied mean free path is too short. The theory can be restated in terms of the concept 'coherence length' for the wave function instead of requiring the wave function to be coherent only on each molecule. Relaxation processes may not be associated with single molecules, but may also involve intermolecular motions. Such processes arise naturally in a treatment which has a longer coherence length. Funabashi (49) has discussed this topic and the application to the present problem has been considered by Funabashi and Magee (42).

Phenomena resulting explicitly from disorder in molecular systems have also been neglected. Funabashi and Kajiwara (27) have shown that the effect of such disorder on electron scattering is important.

Acknowledgments

The author would like to acknowledge discussions of the material of this paper with his colleagues at Notre Dame. He would particularly like to thank Dr. K. Funabashi for reading the manuscript and making valuable suggestions.

1. J. L. MAGEE and M. BURTON. J. Am. Chem. Soc. **73**, 523 (1951).
2. H. A. KRAMERS. Philos. Mag. **46**, 836 (1923).
3. R. L. PLATZMAN. Radiat. Res. **2**, 1 (1955).
4. M. W. WILLIAMS, R. N. HAMM, E. T. ARAKAWA, L. R. PAINTER, and R. D. BIRKHOFF. Int. J. Radiat. Phys. Chem. **7**, 95 (1975).
5. R. H. RITCHIE, W. BRANDT, and V. N. NEELAVATHI. Int. J. Radiat. Phys. Chem. In press.
6. D. E. LEA. Actions of radiations on living cells. Cambridge University Press, London. 1947.
7. L. H. GRAY. J. Chim. Phys. **48**, 127 (1951).
8. L. H. GRAY. Br. J. Radiol. **26**, 609 (1953).
9. G. JAFFE. Ann. Phys. Leipzig, **42**, 303 (1913).
10. H. FRÖLICH and R. L. PLATZMAN. Phys. Rev. **92**, 1152 (1953).
11. A. H. SAMUEL and J. L. MAGEE. J. Chem. Phys. **21**, 1080 (1953).
12. H. A. SCHWARZ. J. Phys. Chem. **73**, 1928 (1969).
13. A. MOZUMDER and J. L. MAGEE. J. Chem. Phys. **47**, 939 (1967).
14. A. MOZUMDER. J. Chem. Phys. **55**, 3020 (1971); **55**, 3026 (1971).
15. G. C. ABELL, A. MOZUMDER, and J. L. MAGEE. J. Chem. Phys. **56**, 5422 (1972).
16. A. MOZUMDER. J. Chem. Phys. **60**, 4300 (1974); **60**, 4305 (1974); **61**, 780 (1975).
17. G. C. ABELL and K. FUNABASHI. J. Chem. Phys. **53**, 1079 (1973).
18. A. HUMMEL. Advances in radiation chemistry. Vol. 4. *Edited by* M. Burton and J. L. Magee. Wiley-Interscience, New York. 1974. Chapt. 1.
19. J.-P. DODELET, K. SHINSAKA, U. KORTSCH, and G. R. FREEMAN. J. Chem. Phys. **59**, 2376 (1973).
20. J.-P. DODELET, K. SHINSAKA, and G. R. FREEMAN. J. Chem. Phys. **59**, 1293 (1973).
21. M. G. ROBINSON and G. R. FREEMAN. Can. J. Chem. **51**, 1010 (1973); **52**, 440 (1974); **51**, 641 (1973).
22. K. SHINSAKA, J.-P. DODELET, and G. R. FREEMAN. Can. J. Chem. **53**, 2714 (1975).
23. R. A. HOLROYD, B. K. DIETRICH, and H. A. SCHWARZ. J. Phys. Chem. **76**, 3794 (1972).
24. S. S.-S. HUANG and G. R. FREEMAN. Can. J. Chem. This issue.
25. A. MOZUMDER. J. Chem. Phys. **55**, 3020 (1971); **55**, 3026 (1971).
26. J. L. MAGEE and W. P. HELMAN. J. Chem. Phys. **66**, 310 (1977).
27. K. FUNABASHI and T. KAJIWARA. J. Phys. Chem. **76**, 2726 (1972).
28. J. H. VAN VLECK and V. F. WEISSKOPF. Rev. Mod. Phys. **17**, 227 (1945).
29. H. FRÖHLICH. Theory of dielectrics. 2nd ed. Oxford University Press, Oxford. 1958.
30. H. FRÖHLICH. Nature, **157**, 487 (1946).
31. J. OVERAND and M. J. YOUNGQUIST. *In* Infrared spectroscopy and molecular structure. *Edited by* M. Davis. Elsevier, New York. 1963. p. 368.
32. T. SHIMANOUCHI. Tables of vibration frequencies. Consolidated Volume I, NSRDS-NBS 39. 1972. p. 156.
33. N. F. MOTT and E. A. DAVIS. Electronic processes in non-crystalline materials. Clarendon, Oxford. 1971. p. 102 ff.
34. N. K. HINDLEY. J. Non-Cryst. Solids, **5**, 17 (1970); **5**, 31 (1970).
35. D. PINES. Elementary excitations in solids. Benjamin, New York. 1974. p. 138.
36. J. BARDEEN and W. SHOCKLEY. Phys. Rev. **80**, 72 (1950).
37. W. HARRISON. Phys. Rev. **104**, 1281 (1956).
38. N. K. HINDEY. Phys. Rev. **153**, 952 (1967).
39. C. R. CLAYDON, G. A. SEGAL, and H. S. TAYLOR. J. Chem. Phys. **54**, 3799 (1971).
40. L. G. CHRISTOPHOROU, K. S. GANT, and J. K. BAIRD. Chem. Phys. Lett. **30**, 104 (1975).
41. K. FUNABASHI and J. L. MAGEE. J. Chem. Phys. **62**, 4428 (1975).
42. K. FUNABASHI and J. L. MAGEE. To be published.
43. L. M. HUNTER, T. MATSUSHIGE, and W. H. HAMILL. J. Phys. Chem. **74**, 1883 (1970); T. MATSUSHIGE and W. H. HAMILL. J. Phys. Chem. **76**, 1225 (1972).
44. P. B. MERKEL and W. H. HAMILL. J. Chem. Phys. **54**, 1695 (1971); **55**, 1409 (1971).
45. K. HIRAOKA and W. H. HAMILL. J. Chem. Phys. **57**, 3870 (1972); **57**, 3881 (1972); **59**, 5749 (1973).
46. K. HIRAOKA and W. H. HAMILL. J. Phys. Chem. **77**, 1616 (1973).

47. Y. C. CHANG and W. B. BERRY. J. Chem. Phys. **61**, 2727 (1974).
48. J. J. HUANG and J. L. MAGEE. J. Chem. Phys. **61**, 2736 (1974).
49. K. FUNABASHI. Advances in radiation chemistry. Vol. 4. *Edited by* M. Burton and J. L. Magee. Wiley-Interscience, New York. 1974. p. 103.

Discussion

G. R. Freeman: In calculations of the electric field effect on free ion yields, two electron–ion separation distance distributions are commonly assumed. One is a simple exponential function and the other is a Gaussian. Is the straight path assumed by Platzman associable with the exponential distribution (attenuation of a plane wave), and the random path assumed by you associable with the Gaussian?

J. L. Magee: The random path is of course compatible with a Gaussian distribution function. The straight line trajectory is a good approximation in any case where the mean free path is large. Simple exponential distributions are also obtained for some conditions of multiple scattering but the linear trajectory would probably be applicable.

G. R. Freeman: What is the mechanism of electron hesitation between jumps? Does it involve transient negative ion states?

J. L. Magee: Transient negative ion formation is the only physical mechanism I know which would cause a hesitation in the motion. The actual hesitation used (a delay of five jump times in 10% of the jumps) was chosen arbitrarily and does not actually mimic any known case of negative ion formation.

J. M. Warman: Over what range of electron energies are your calculations applicable?

J. L. Magee: The objective was to cover the entire subexcitation range from 6 eV or so to epithermal energies. However, there is no explicit use of energy in either consideration. The indirect loss mechanism employed a hopping of the electron from one molecule to another and the intermolecular distance combined with the jump time determine a kinetic energy. I think this calculation is reasonably consistent down to energies of 1 eV or so. The direct mechanism can be used for lower energies with an appropriate deformation potential. Of course it is understood that there are threshold energies for the molecular vibrations which must be treated properly.

G. R. Freeman: Did you consider processes that would be important below about 0.3 eV? They should be very important in hydrocarbons.

J. L. Magee: In principle the treatment of the direct effect can be used at low electron energies. The main excitations may not be the vibrations of individual molecules in this case, however, and a deformation potential for intermolecular vibrations must be used.

P. Delahay: The energy loss due to dielectric relaxation is inversely proportional to the relaxation time according to Platzman and Frohlich. This loss is $\sim 10^{13}$ eV s^{-1} for water, but it would be nearer to 10^{12} eV s^{-1} for other liquids (or even lower). Hence, the loss due to vibrational excitation would be dominant for other liquids than water for the indirect mechanism. Is this conclusion correct?

J. L. Magee: Yes, I think this is a correct conclusion. However, I think that in most cases the direct mechanism is actually responsible for the loss.

P. Delahay: Could you comment on the dependence of the energy loss on the kinetic energy for the *direct* mechanism?

J. L. Magee: There is no explicit dependence on the kinetic energy of the electron. In a general way the loss should be larger as the velocity decreases, but the perturbation Hamiltonian depends upon the details of the potential energy functions of the ion and neutral molecule. I don't think a generalized statement is possible.

U. Sowada: I would like to comment on the order of magnitude which you get out of your calculation about the rate of energy loss to nonpolar molecules (around 10^{12} eV/s) at liquid densities. There have been performed measurements in our laboratory concerning this topic (see this issue and Phys. Rev. A, **14**, 438 (1976)). For the case of methane the extrapolation to the liquid density is possible. For electron energies around 0.5 eV the product of the energy loss per drift distance (slightly above 10^5 eV/cm) with the thermal velocity for electrons of this energy (approximately 10^7 cm/s) the same order of magnitude as from your calculation is obtained.

J. L. Magee: This is an interesting result. Your electrons are just at the lower limit of validity of the calculation and at the moment I am not sure that my mechanism is responsible for your findings, although it may be.

J. Jortner: Concerning the inelastic electron scattering accompanied by excitation of intramolecular vibrations, let me point out that the process bears a close analogy to optical Raman scattering. In this context, let me inquire whether you have considered second-order contributions to this mechanism, which may be important.

J. L. Magee: I have not made a thorough study of this problem. A preliminary estimate of the effect seemed to indicate that it would be less important than the first order process, but a more careful examination should be carried out.

Photoelectric determination of V_0 values and electron ranges in some cryogenic liquids

WOLFGANG TAUCHERT, HELMUT JUNGBLUT, AND WERNER F. SCHMIDT

Bereich Strahlenchemie, Hahn-Meitner-Institut für Kernforschung Berlin GmbH, D 1000 Berlin 39, Germany

Received September 27, 1976

WOLFGANG TAUCHERT, HELMUT JUNGBLUT, and WERNER F. SCHMIDT. Can. J. Chem. **55**, 1860 (1977).

Conduction state energies V_0 were measured for liquid neon, argon, krypton, xenon, liquid nitrogen, liquid methane and ethane, and mixtures of methane and ethane by means of photoeffect on a metal electrode. A lower limit of V_0 for liquid hydrogen was estimated. From the dependence of the photocurrent on the electric field strength electron penetration ranges could be deduced.

WOLFGANG TAUCHERT, HELMUT JUNGBLUT et WERNER F. SCHMIDT. Can. J. Chem. **55**, 1860 (1977).

On a mesuré les énergies d'états de conductivité V_0 pour du néon, de l'argon, du krypton, du xénon liquide, pour de l'azote liquide, du méthane et de l'éthane liquide et pour des mélanges d'éthane et de méthane en faisant appel à l'effet photoélectrique sur une électrode métal. On a estimé la limite inférieure de V_0 pour l'hydrogène liquide. A partir de la dépendance du courant photoélectrique sur la force du champ électrique, on a pu déduire des limites pour la pénétration électronique.

[Traduit par le journal]

1. Introduction

Photoemission of electrons or holes into an insulator from a metal electrode can be employed for obtaining information on the electronic energy levels in the material. This technique has been used for the investigation of solid insulators and semiconductors (1–5) and in 1971 it was introduced for the study of electronic levels in non-polar liquids by Holroyd and Allen (6).

The experiment consists of the determination of the work function of a suitable metal electrode in a vacuum and in the liquid. The work function in the liquid ϕ_L is different from that in the vacuum ϕ_{vac} by a value V_0, the energy necessary to bring an electron from the vacuum into the liquid

$$[1] \qquad \phi_{liq} = \phi_{vac} + V_0$$

Negative V_0 values mean that energy is released.

Photoemission from a metal electrode in a vacuum was treated theoretically first by Fowler (7) who derived the dependence of the normalized photocurrent density j on the light frequency ν. Experimentally (6) and theoretically (8) it was shown that the Fowler formula can also be applied for the photoemission into an insulator with a low dielectric constant.

The work function is obtained from the experimental data either by numerical comparison with the Fowler function with the aid of a computer or simply by plotting $j^{1/2}$ as a function of ν which represents a straight line and yields $\nu_g = \phi/h$ at $j = 0$. The normalized photocurrent is obtained as i/I with i the measured photocurrent and I the light intensity measured with a calibrated photomultiplier.

If the measurements are carried out in a vacuum, saturation currents can be obtained. Injection into a liquid leads to thermalization of electrons near the cathode due to energy losses. Under the influence of the field of the image charge a certain fraction of the injected electrons returns to the cathode and the measured current is smaller than in vacuum at the corresponding wavelength where the same excess electron energy is obtained. The photo-response i_L/i_V ($i_{L,V}$ photocurrents in liquid and vacuum, respectively) depends on the applied electric field. Due to the image force a potential barrier is generated near the metal electrode and the escape probability for such a one-dimensional case has been derived by several authors (9–11). The photo-response is then given by

$$[2] \qquad i_L/i_V = \int_0^\infty P(x_0)D(x_0)\,dx$$

where

$$[3] \qquad P(x_0) = \frac{\int_0^{x_0} \exp\left(\frac{eV(x)}{k_B T}\right) dx}{\int_0^{\infty} \exp\left(\frac{eV(x)}{k_B T}\right) dx}$$

and

$$[4] \qquad V(x) = -Fx - \frac{e}{4\varepsilon x}$$

x_0 is the thermalization distance of the injected electron, F is the electric field strength, e electron charge, and ε the dielectric constant of the liquid. $D(x_0)$ is a range distribution and various distribution functions can be used in analogy to the treatment of ion yields in γ-irradiated liquids (12–14). It was found by Holroyd *et al.* (9) that with a one-dimensional Gaussian distribution

$$[5] \qquad D(x_0) = \frac{2}{b\sqrt{\pi}} e^{-x_0^2/b^2}$$

with a suitably chosen b the experimentally observed photo-response data in several hydrocarbons followed the field strength dependence given by [2].

Interest in V_0 values and ranges of low energy electrons exists from various problems of electron transport in liquids. In the theory of excess electron states in simple liquids by Springett *et al.* (15) a criterion of localization is derived in which the magnitude of V_0 determines whether an extended or a localized state of the electron in the liquid is energetically the most favorable one. Experimentally it was found that electrons in liquid helium (16) exhibited a low mobility in agreement with the V_0 value (17) which predicted a localized state. In liquid argon, krypton, and xenon high electron mobilities were observed (18) and the reported V_0 value for argon (19) favors the extended electron state. In liquid neon low electron mobilities have been reported (20–22) but V_0 values had not been measured. In liquid hydrocarbons many V_0 values and electron mobilities μ_{el} were reported by several groups and a relation was thought to exist between V_0 and μ_{el} (23–26).

The present experiments were carried out in order to obtain those V_0 values for liquefied rare gases and some other liquids which had not been measured yet and to obtain V_0 values for methane–ethane mixtures where electron mobilities as a function of composition had been measured previously in this laboratory (27).

2. Experimental

The set-up was essentially that of Holroyd and Allen (6). The measurement cell was placed in a cryostat. For the measurement of the light intensity a calibrated photomultiplier was used. The photocathode consisted of a brass base on which first a layer of gold and then a second layer of zinc were vacuum deposited.

Measurements were carried out on the following liquids: neon, argon, krypton, xenon, nitrogen, mixtures of methane and ethane for the whole range of composition, and liquid hydrogen.

The gases were high purity grades (99.95 vol.% minimum) and they were purified further by passage through columns of activated molecular sieve (Linde 3Å) and charcoal). The vacuum work function was measured before and after the measurement with the liquid and the vacuum work functions obtained this way agreed within ± 0.03 eV.

3. Results

The normalized photocurrents as a function of the light frequency (Fowler plot) for a zinc electrode in vacuum and in liquid methane, ethane, and neon are shown in Fig. 1. While the Fowler plots for vacuum and liquid ethane agree quite well with those published by Noda *et al.* (28) our plots for methane disagree with the results by Noda and Kevan (29). In their experiment the photocurrents at comparable excess energies above the work function were almost two orders of magnitude lower than the vacuum currents. The high excess electron mobility in liquid methane, however, favors escape from the electrode and leads to higher currents. We repeated the methane experiments also with a gold electrode and found the same relative magnitude of the Fowler plots for the vacuum and the liquid as with the zinc electrode. There was, however, a definite influence of the electrode material on the V_0 value which has been also reported by Holroyd and Allen (6). Gold gave more negative values. The vacuum work functions for zinc and gold were in the range of values reported in the literature. The temperature dependence of V_0 in liquid methane is shown in Fig. 2. Although the slope of the decrease of V_0 with increasing temperature is approximately the same for the different set of data, there is considerable discrepancy in absolute terms.

The temperature dependence of V_0 in liquid ethane is given in Fig. 3. The values for the methane–ethane mixtures were measured with a gold electrode at $T = 100 \pm 2$ K and are summarized in Table 1 together with the data for liquid neon, argon, krypton, and xenon, nitrogen,

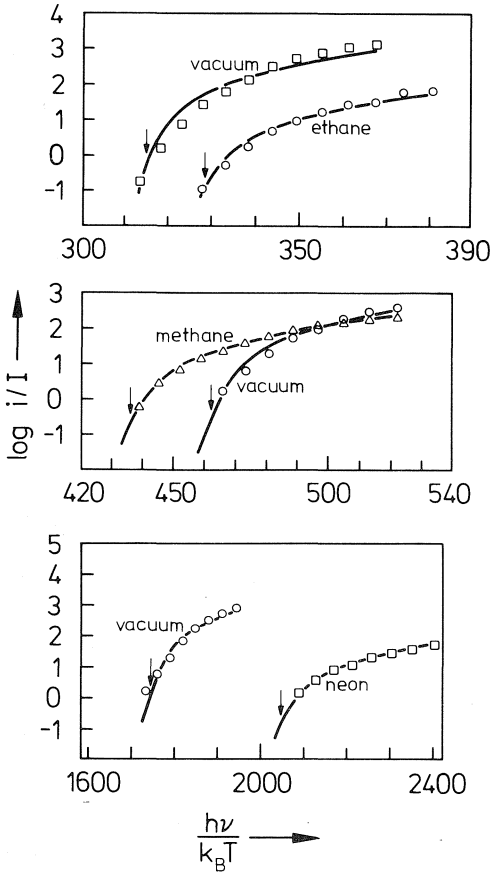

FIG. 1. Fowler plots for a zinc electrode in liquid ethane, methane, and neon. The arrows denote the work function.

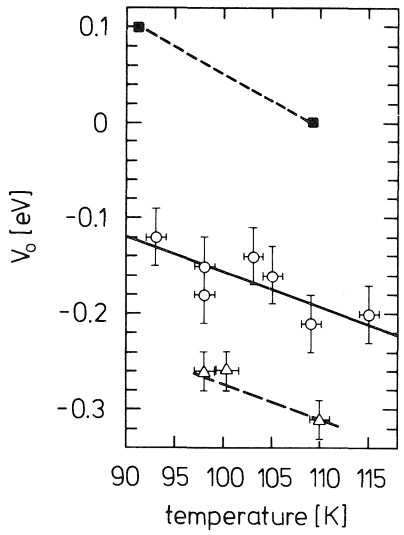

FIG. 2. Temperature dependence of V_0 values of liquid methane: ○ values measured with zinc electrode, △ values measured with gold electrode, ■ values by Noda and Kevan (29).

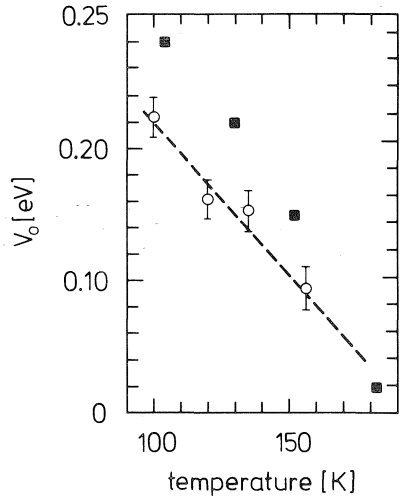

FIG. 3. Temperature dependence of V_0 values of liquid ethane: ○ values measured with zinc electrode, ■ values by Noda *et al.* (28).

and an estimate for hydrogen. In hydrogen no injection currents could be obtained with a zinc electrode and the lower limit given in Table 1 is the short wave limit of the lamp. Also with a sodium electrode no injection currents could be obtained in liquid hydrogen.

The photo-response of a gold electrode in the methane–ethane mixtures as a function of the electric field strength is shown in Fig. 4, while for the other liquids some data are compiled in Fig. 5. The photo-response i_L/i_V is determined by the distance b the electrons penetrate into the liquid. The solid lines in Fig. 4 represent i_L/i_V values obtained from [2] with the b values given in parentheses. The agreement is rather good.

No distribution function $D(x_0)$, however, could be found to fit the data of Fig. 5. The temperature dependence and the dependence on the electron energy of the b parameter in methane and ethane are shown in Figs. 6 and 7.

4. Discussion

Conduction state energies of excess electrons in liquefied rare gases have been calculated by Springett, Jortner, and Cohen (15) who adapted the Wigner–Seitz model by introducing a pseudo-

TABLE 1. V_0 values

Liquid	T (K)	V_0 (eV)	Electrode
Neon	25	$+0.67 \pm 0.05$	Zinc
Argon*	84	-0.2 ± 0.03	Zinc
	87.5	-0.21 ± 0.03	
Krypton*	116	-0.40 ± 0.05	Zinc
	123	-0.45 ± 0.05	
Xenon*	161	-0.67 ± 0.05	Zinc
	165	-0.61 ± 0.05	
Nitrogen	77	$+0.05 \pm 0.03$	Zinc
Hydrogen	15	$> +2.0$	Zinc
Methane	100 ± 2	-0.25 ± 0.03	Gold
Methane–ethane†			
0.81–0.19	100 ± 2	-0.1 ± 0.03	Gold
0.57–0.43	100 ± 2	± 0.0	Gold
Ethane	100 ± 2	$+0.2 \pm 0.03$	Gold

*These values have been published already in a short communication (30).
†Mole fractions.

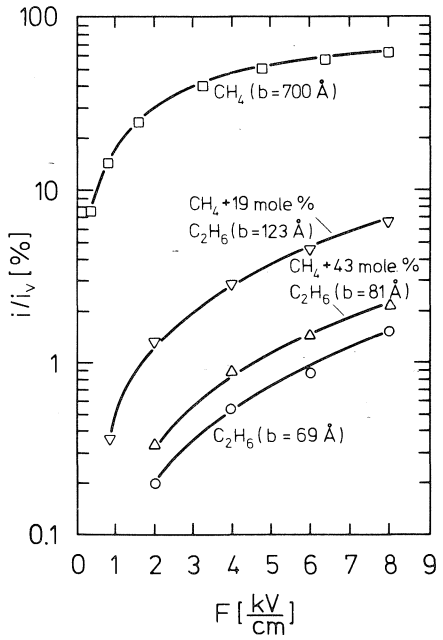

FIG. 4. Photo-response of gold electrode in liquid methane, ethane, and mixtures. Energy of injected electrons $\varepsilon = 0.5 \pm 0.02$ eV, $T = 100 \pm 2$ K.

potential which excludes the electrons from the hard core radius of the atoms. By applying their theory to our experimental V_0 values, hard core radii were obtained which are slightly smaller than the values from other physical experiments (30, 31). The positive V_0 value for neon predicts localized electron states to be stable (15) which is

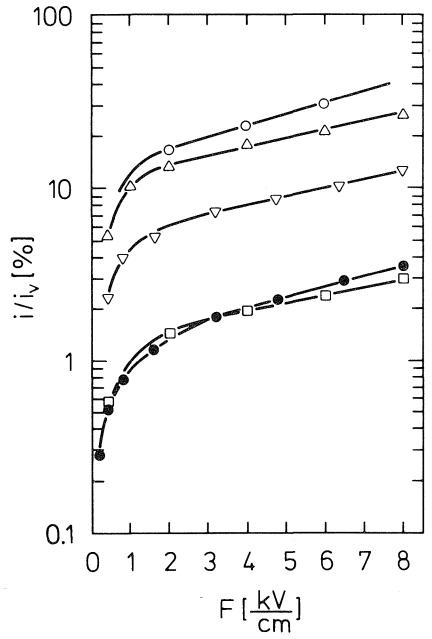

FIG. 5. Photo-response of zinc electrode in several liquids: ○ xenon, $T = 161$ K, $\varepsilon = 0.54$ eV; △ krypton, $T = 120$ K, $\varepsilon = 0.50$ eV; ▽ argon, $T = 85.5$ K, $\varepsilon = 0.54$ eV; ● nitrogen, $T = 77$ K, $\varepsilon = 0.49$ eV; □ neon, $T = 25$ K, $\varepsilon = 0.55$ eV.

supported by the low electron mobilities reported in the literature (20–22). The estimated lower limit for V_0 in liquid hydrogen and the low electron mobilities observed (32) indicate that the excess electron state is localized.

Miyakawa and Dexter (33) assumed localization of the electrons in liquid hydrogen and neon in bubbles and estimated for neon $V_0 = +0.45$ eV and for hydrogen $V_0 = +2$ eV.

Quantum field theory was applied by Tankersley (34) to the problem of the energy barrier for electron penetration into liquefied rare gases. V_0 is calculated in terms of the static structure factor of the liquid. Although his treatment is primarily concerned with liquid helium and treats the simultaneous interaction of two He atoms with the electron his results give also for neon and argon (where interaction with more than two atoms should be considered) V_0 values in fair agreement with our measured data.

Low electron mobilities were measured in liquid nitrogen (35) while the V_0 value would predict a delocalized state according to the localization criteria of Springett *et al.* (15) or

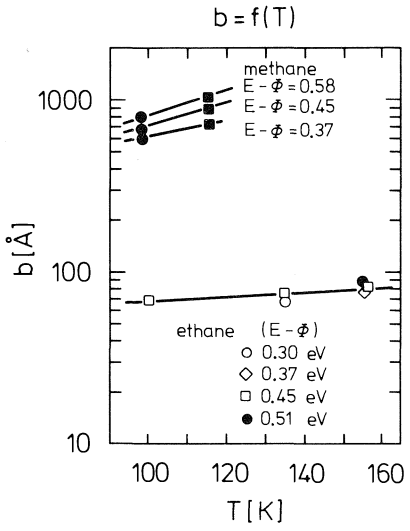

FIG. 6. Dependence of the electron range (parameter b of a Gaussian distribution) on the temperature ($E - \phi$ is the energy of the photoelectrons).

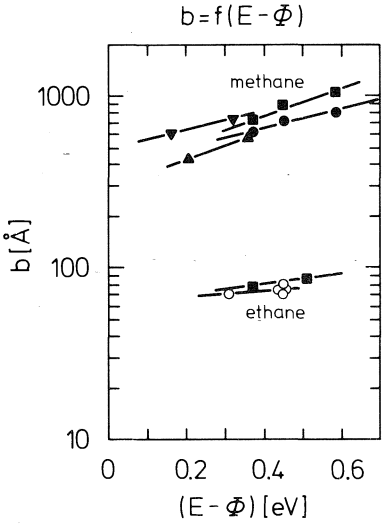

FIG. 7. Dependence of the electron range (parameter b of a Gaussian distribution) on the energy of the photoelectrons in liquid methane and ethane: ▼ methane, 110 K, Au electrode; ▲ methane, 98 K, Au electrode; ■ methane, 115 K, Zn electrode; ● methane, 98 K, Zn electrode; ■ ethane, 156 K, Zn electrode; ○ ethane, 135 K, Zn electrode.

Noda *et al.* (28). Mobility measurements with nitrogen, however, might suffer from contamination with oxygen. The measurements with the methane–ethane mixtures were carried out in order to test a μ_{el}–V_0 relationship proposed by Kestner and Jortner (26) based on percolation theory and by Schiller *et al.* (25) based on an equilibrium between localized and extended states. Electron mobilities had been measured previously for this system (27). It was not possible, however, to obtain agreement between experimental results and theory with any set of physically realistic parameters.

The ranges of photoelectrons estimated in these experiments should be compared with data obtained from the radiation induced conductivity. High free ion yields G_{fi} were observed in methane yielding a large separation distance between positive ion and electron while small G_{fi} values were reported for liquid ethane (36). The photoelectric ranges show the same influence of the molecular shape with ethane slowing down subexcitation electrons more efficiently than methane.

Application of the diffusion model (eqs. 2–5) on the photo-response data of the liquefied rare gases (Fig. 5) did not yield electron ranges since no agreement could be obtained with various distributions $D(x)$. It is possible, however, that the diffusion model does not apply for liquefied

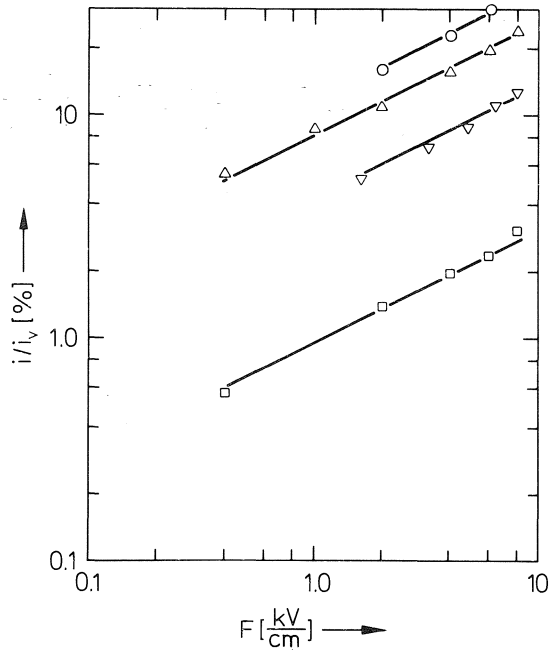

FIG. 8. Photo-response data of Fig. 5. The solid lines exhibit a slope of 0.5.

rare gases where the electrons lose energy very inefficiently in elastic collisions and travel large distances. Furthermore, at the field strengths applied here they do not reach thermal equilibrium with the liquid but the mean electron energy is greater than thermal. Electron loss from the conduction current can occur due to backscattering. Smejtek *et al.* (37) have discussed this mechanism for the injection of electrons into gaseous argon of high pressure. They found that the photo-response should be given approximately by

$$[6] \qquad \frac{i}{i_L} \approx \frac{1}{2}\pi^{1/2}\left(\frac{eF\lambda}{E_0}\right)^{1/2}$$

where E_0 is the energy of the injected electrons and λ is the mean free path for momentum transfer. The data of Fig. 5 follow this $F^{1/2}$ dependence quite well as is shown in Fig. 8. It may be concluded that in liquefied rare gases backscattering of electrons is the main factor which limits the photo-response. A more detailed evaluation would require more photo-response data at different electron energies E_0.

Acknowledgements

Financial support of this work by "Deutsche Forschungsgemeinschaft" is gratefully acknowledged. We wish to thank L. Tankersley for informative correspondence.

1. J. M. Caywood. Mol. Cryst. Liq. Cryst. **12**, 1 (1970).
2. J. Mort and A. I. Lakatos. J. Non-Cryst. Solids, **4**, 117 (1970).
3. R. Williams and J. Dresner. J. Chem. Phys. **46**, 2133 (1967).
4. R. Williams. Phys. Rev. **140**, 569 (1965).
5. A. M. Goodman. Phys. Rev. **144**, 588 (1966).
6. R. A. Holroyd and M. Allen. J. Chem. Phys. **54**, 5014 (1971).
7. R. H. Fowler. Phys. Rev. **38**, 45 (1931).
8. M. Brodskii and Yu. Ya. Gurevich. Sov. Phys. JETP, **27**, 114 (1968).
9. R. A. Holroyd, B. K. Dietrich, and H. A. Schwarz. J. Phys. Chem. **76**, 3791 (1972).
10. R. Haberkorn and M. E. Michel-Beyerle. Chem. Phys. Lett. **23**, 128 (1973).
11. D. F. Blossey. Phys. Rev. B, **9**, 5183 (1974).
12. W. F. Schmidt and A. O. Allen. J. Phys. Chem. **72**, 3730 (1968).
13. G. C. Abell and K. Funabashi. J. Chem. Phys. **58**, 1079 (1973).
14. J. P. Dodelet and G. R. Freeman. Can. J. Chem. **50**, 2667 (1972).
15. B. E. Springett, J. Jortner, and M. H. Cohen. J. Chem. Phys. **48**, 2720 (1968).
16. H. T. Davis, S. A. Rice, and L. Meyer. Phys. Rev. Lett. **9**, 81 (1962).
17. W. T. Sommer. Phys. Rev. Lett. **12**, 271 (1964).
18. L. S. Miller, S. Howe, and W. E. Spear. Phys. Rev. **166**, 871 (1968).
19. J. Lekner, B. Halpern, S. A. Rice, and R. Gomer. Phys. Rev. **156**, 351 (1967).
20. L. Bruschi, G. Mazzi, and M. Santini. Phys. Rev. Lett. **28**, 1504 (1972).
21. V. N. Lebedenko and B. U. Rodinov. JETP Lett. **16**, 411 (1972).
22. R. J. Loveland, P. G. LeComber, and W. E. Spear. Phys. Lett. A, **39**, 225 (1972).
23. R. A. Holroyd and R. L. Russel. J. Phys. Chem. **78**, 2128 (1974).
24. K. Fueki. Can. J. Chem. **50**, 3379 (1972).
25. R. Schiller, Sz. Vass, and J. Mandics. Int. J. Radiat. Phys. Chem. **5**, 491 (1973).
26. N. R. Kestner and J. Jortner. J. Chem. Phys. **59**, 26 (1973).
27. G. Bakale, W. Tauchert, and W. F. Schmidt. J. Chem. Phys. **63**, 4470 (1975).
28. S. Noda, L. Kevan, and K. Fueki. J. Phys. Chem. **79**, 2866 (1975).
29. S. Noda and L. Kevan. J. Chem. Phys. **61**, 2467 (1974).
30. W. Tauchert and W. F. Schmidt. Z. Naturforsch. Teil A, **30**, 1085 (1975).
31. W. Tauchert. Ph.D. thesis, Free University of Berlin, Berlin, Germany. 1975.
32. P. G. LeComber, J. B. Wilson, and R. J. Loveland. Solid State Commun. **18**, 377 (1976).
33. T. Miyakawa and D. L. Dexter. Phys. Rev. **184**, 166 (1969).
34. L. L. Tankersley. J. Low Temp. Phys. **11**, 451 (1973).
35. R. J. Loveland, P. G. LeComber, and W. E. Spear. Phys. Rev. B, **6**, 3121 (1972).
36. M. G. Robinson, P. G. Fuochi, and G. R. Freeman. Can. J. Chem. **49**, 3657 (1971).
37. P. Smejtek, M. Silver, and K. S. Dy. J. Chem. Phys. **59**, 1374 (1973).

Discussion

L. Kevan: Do you understand the difference in the magnitude of your V_0 values in methane obtained with zinc and with gold electrodes?

W. F. Schmidt: Not at this time. A detailed investigation should take into account the experimental conditions of the generation of the surface and the effect of impurities in the liquids.

L. Kevan: For your V_0 value in liquid nitrogen have you used the stability criterion that Noda, Fueki, and I (J. Phys. Chem. **79**, 2866 (1975)) suggested to see whether an extended or localized state is predicted.

W. F. Schmidt: Yes, your criterion as well as that of Springett, Cohen, and Jortner predict the extended state to be stable. Mobility measurements gave low values (in the range of 10^{-3} cm^2 V^{-1} s^{-1}). These experiments might have suffered from traces of oxygen, however.

P. Delahay: With reference to the effect of the electrode, it is to be noted that you measure the algebraic sum of V_0 and the surface potential. This potential undoubtedly varies from one metal to another, and consequently an electrode effect is not so surprising. This contribution from the surface potential renders values of V_0 somewhat approximate (independently of experimental errors).

W. F. Schmidt: This is correct, although the origin of this surface potential may be either an intrinsic property of the particular metal–liquid interface; it may, however, also be generated by impurities. On occasions it was observed that different V_0 values were obtained, when the purification of the liquid was carried out less vigorously.

P. Delahay: Did you examine the field effect in terms of backscattering of emitted electrons?

W. F. Schmidt: No, we did not, since good agreement was obtained in the case of hydrocarbons with the one-dimensional escape probability.

D. E. Brodie: Could the difficulty with electrodes be checked for a possible effect due to contamination by using two different inert metals for electrodes, say gold and platinum?

W. F. Schmidt: In the usual photoemission set-up a limitation arises from the absolute value of the work function which is ~5 eV for Pt. In order to determine V_0 it is desirable to follow the emission over a certain range of electron excess energy. The intensity of the xenon lamp decreases drastically below 250 nm making it difficult to get photocurrents with a Pt electrode.

Ion recombination processes in rigid solutions[1,2]

JOHN R. MILLER
Chemistry Division, Argonne National Laboratory, Argonne, IL, U.S.A. 60439
Received October 12, 1976

JOHN R. MILLER. Can. J. Chem. **55**, 1867 (1977).

It is known that the free ion yield is small in irradiated aromatic hydrocarbon liquids. This study uses pulse radiolysis to observe anions of aromatic solutes in matrices at 77 K. In aliphatic matrices, trapped electrons tunnel to aromatic solutes and the anion yield is observed to grow with time. If the concentration of aromatic solute is large (0.1 *M*) or if the matrix is aromatic, ion recombination via tunneling dominates the anion kinetics, and long lived triplet states are observed to grow in. These results and the effects of other charge scavengers indicate that just a few percent of added aromatic material can dramatically increase the probability of charge recombination in aliphatic media, and that this effect involves decreased charge separation distances. The same effect apparently also occurs in alkane liquids at room temperature.

JOHN R. MILLER. Can. J. Chem. **55**, 1867 (1977).

Il est bien connu que le rendement d'ions libres est petit dans les hydrocarbures aromatiques liquides irradiés. Cette étude utilise la radiolyse pulsée pour observer les anions des solutés aromatiques dans des matrices à 77 K. Dans des matrices aliphatiques, les électrons piégés sont transferés aux solutés aromatiques par un effet de tunnel et on observe que le rendement en anions augmente avec le temps. Si la concentration du soluté aromatique est grande (0.1 *M*) ou si la matrice est aromatique, la recombinaison ionique par un effet de tunnel domine la cinétique de l'anion et on observe que les états triplets de longue vie croissent. Ces résultats et les effets d'autres agents qui peuvent piéger des charges indiquent que l'addition de quelques pourcents de composés aromatiques peut produire une augmentation dramatique de la probabilité de recombinaison de charge dans un milieu aliphatique et que cet effet implique une diminution des distances de séparation des charges. Il semble que le même effet se produit aussi dans des alcanes liquides à la température de la pièce.

[Traduit par le journal]

Introduction

Ionizing radiation produces solvated electrons in liquids and trapped electrons in glasses. In most alkane liquids ion pairs are thermalized with a wide distribution of geminate ion separation distances. The ion separation distance distributions are thought to peak at about 75 Å (1–3). A few percent are thermalized beyond the Onsager distance (4), which is about 300 Å at room temperature, and become free ions. In rigid hydrocarbon glasses where diffusion is eliminated, electrons trapped within the coulomb field of the positive ion may still have very long lifetimes, because the only decay mechanism available is electron tunneling to the positive ion. The distance distributions in the glasses are thought to be roughly similar to those in liquids, but they may be shifted to slightly larger distances (2).

Electron acceptors added to the matrix capture trapped electrons by the tunneling mechanism (5). In this study it appears that high concentrations ($\approx 2\%$) of an aromatic solute prevent separation of charges to large distances. Most of the anion–cation pairs appear to be separated by less than 50 Å, and recombine by tunneling in the time range 10^{-7} to 10^{2} s.

Experimental

Aldrich 3-methylhexane (3-MHX) was allowed to stand over Linde 13X molecular sieve, which had been activated by heating at least 2 h at 250°C. Aldrich 3,3-dimethylbiphenyl, Eastman cumene, Phillips (research grade) 2-methylpent-1-ene, Fluka triethylamine, and Matheson Coleman and Bell 1-chloropropane were used as received. Samples were degassed in cells with silica windows, and sealed off under vacuum. Samples were frozen by immersion in liquid nitrogen and were subjected to 2 to 10 ns pulses of 12 ± 3 MeV electrons, which pass completely through the cell, leaving a trail of ionization events.

To prevent optical bleaching, analyzing light from a xenon arc-lamp passed through a monochromator and a

[1]Based on work performed under the auspices of the U.S. Energy Research and Development Administration.

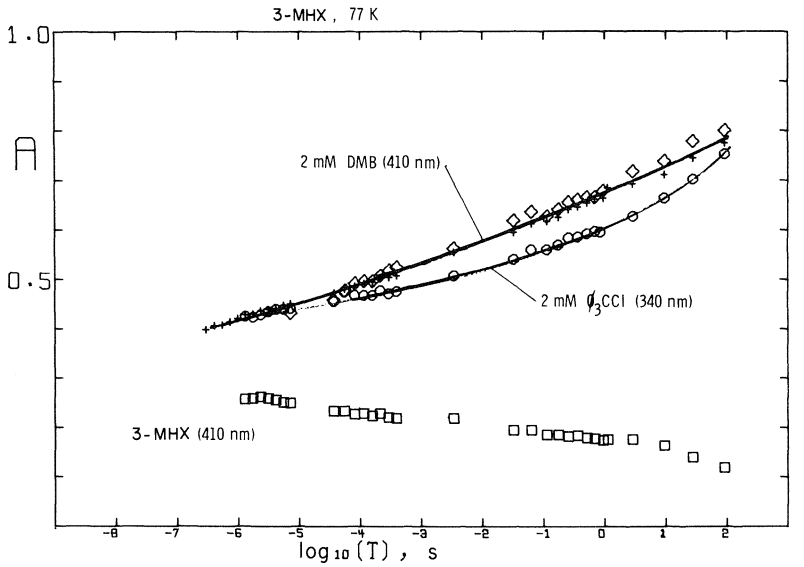

FIG. 1. The growth of absorbance (in arbitrary units) at 410 or 340 nm as trapped electrons in 3-methylhexane glass are captured to form dimethylbiphenyl anions (+ normal analyzing light intensity; ◇ analyzing light intensity on sample reduced by a factor of 15) or to form triphenylmethyl radicals (○). There is a background absorbance in the pulse irradiated 3-MHX matrix (□).

light chopper (open 5% of the time) before reaching the sample. The signal from an EMI 9781R photomultiplier was recorded by a computer-controlled Biomation 8100 transient recorder from 10^{-7} to 10^{2} s. Time resolution was often degraded to *ca.* 10^{-6} s by large amounts of fluorescence, especially if the sample contained cracks. More experimental details are given in ref. 6.[3]

The stated molar concentrations apply at 77 K, and are corrected for the fact that 3-MHX contracts by $\approx$17% as it is cooled from room temperature.

Results

Anion Growth by Electron Tunneling

Figure 1 shows the growth of absorbance of the 3,3′-dimethylbiphenyl (DMB) anion at 410 nm and the triphenylmethyl radical ($\phi_3C^{\bullet}$) at 340 nm, when 2 m*M* solutions of DMB or triphenylmethyl chloride in 3-MHX are pulse irradiated at 77 K. The growths of these products are the result of capture of trapped electrons by a tunneling mechanism (5). Slightly less than half of the trapped electrons are captured at 10^{2} s (5). It is possible for electrons captured by DMB to recombine by tunneling to the positive ion, but this is not possible in the case of a dissociative capture product such as $\phi_3C^{\bullet}$.

The similarities of the growth curves for DMB^{-} and $\phi_3C^{\bullet}$ suggest that there is little ion recombination. At higher concentrations of DMB we shall see much ion recombination.

A report by Kroh *et al.* (7) has indicated that there is no growth of the biphenyl anion under similar conditions. These authors claimed that biphenyl anion growth could only occur by bleaching of the trapped electron by the spectrometric analyzing light (7). But the growths in Fig. 1 are real and unaffected by the analyzing light, which was monochromatic (6 nm half height band width at the sample) and was chopped to reduce the average intensity by a factor of 20 (6). A further reduction of a factor of 15 by filters showed no effect on the kinetics of DMB^{-} growth (see Fig. 1). Further, the spaces between 0.5 and 3 ms and between 3 and 33 ms (Fig. 1) are times during which the chopper prevented any analyzing light from reaching the sample, but DMB^{-} growth continued unabated.

The apparent growth of DMB^{-} was reduced if the light passing through the sample was deliberately made more intense. The intense analyzing light bleached DMB^{-}. This probably is the explanation for the failure of Kroh *et al.* (7), to observe biphenyl^{-} growth. They did not use a monochromator before the sample, but used filters of 80 nm band width (7) *vs.* 6 nm in the present work. Because they did not use a monochromator before the sample to disperse

[3]Copies of the supplementary material for ref. 6 are available from the first author or from the journal.

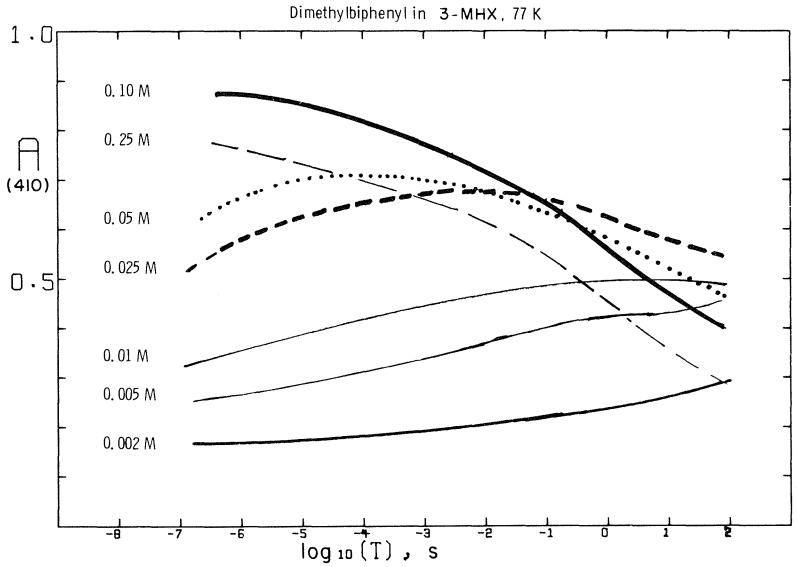

FIG. 2. The kinetics of DMB^- anions for DMB concentrations between 0.002 and 0.25 *M* in 3-MHX at 77 K.

the light, an image of the arc was probably formed in the sample, further aggravating the bleaching problem.

In the present work in 3-MHX at 77 K, anion growths have been observed for DMB, biphenyl, pyrene, and triphenylethylene. Similar anion growths have been reported by Klassen, Gillis, and Teather (8). Richards and Thomas (9) reported pulse radiolysis work at *ca.* 10^{-6} s which showed that a much greater fraction of trapped electrons survived capture by biphenyl at 10^{-6} s than at *ca.* 5 min after gamma irradiation. Because exposure to light was negligible in the gamma irradiation experiments (10, 11, 5), electron capture clearly cannot be due to bleaching as Kroh *et al.* (7) claim.

Ion Recombination at High Solute Concentrations

The growth of anions at low solute concentrations is well established. At higher concentrations, a remarkable behavior is observed: Instead of growing to a plateau, the anion yield decays with time (see Fig. 2). At the highest concentration, 0.25 *M*, almost all of the anions decay, giving the lowest final (10^2 s) absorbance at 410 nm of any of the concentrations used. The relative anion yield in 0.25 *M* DMB is probably even lower than apparent in Fig. 2, because no anion peak is seen in the spectrum at 100 s (see Fig. 3). Most of the final absorbance is probably

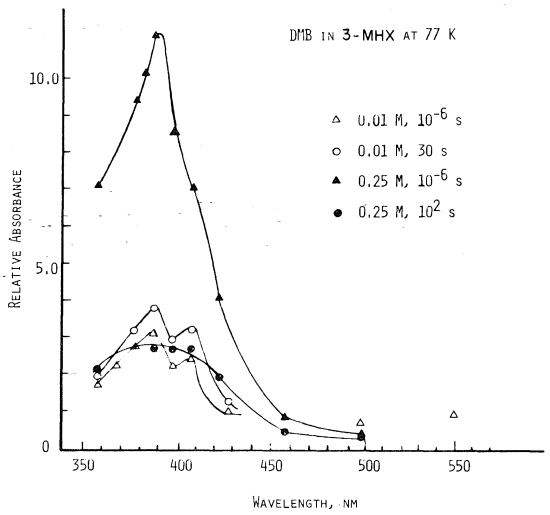

FIG. 3. Absorbance spectra for 0.01 and 0.25 *M* DMB at 10^{-6} and 10^2 s. After the triplet state (390 nm peak) in 0.25 *M* DMB has decayed out, it is still not possible to detect a 410 nm peak due to the anion.

due to various DMB and solvent radicals, which have not been identified here.

The yield of trapped electrons per 100 eV of absorbed energy (the *G* value) is 0.9 in 3-MHX glass (12). The yield of biphenyl anion (ϕ_2^-) is 1.6 if 0.015 *M* ϕ_2 is added to 3-MHX glass (12). Comparing these results with those in Fig. 2, and recalling that the final (10^2 s) absorbance in

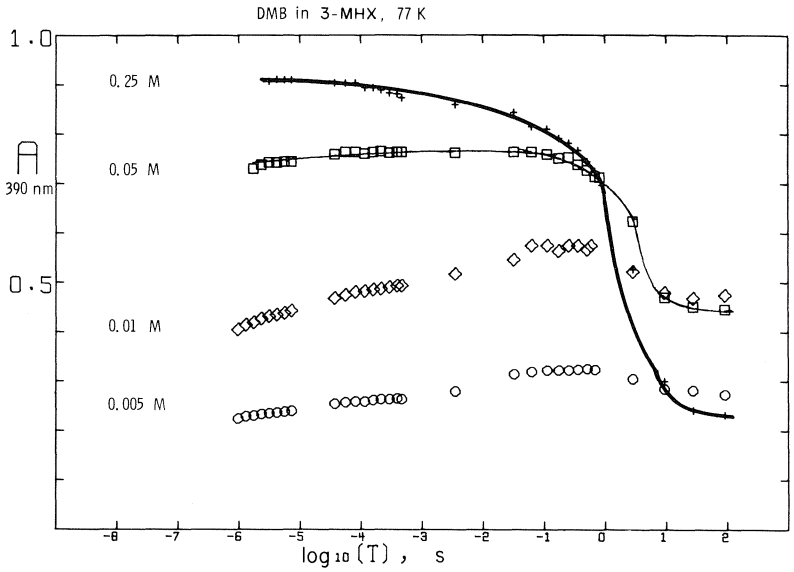

FIG. 4. Kinetics of the absorbance (in arbitrary units) at 390 nm, the peak of the triplet state absorption.

0.25 *M* DMB is due mainly to species other than DMB^-, we see that the final yield of DMB^- in 0.25 *M* DMB is much lower than the yield of trapped electrons in pure 3-MHX glass.

The disappearance of DMB^- in the more concentrated solutions of DMB appears to lead to substantial yields of triplet (T_1) states of DMB. The triplet absorption, peaking at 390 nm, dominates the spectrum at 10^{-6} s in 0.25 *M* DMB (Fig. 3). Unlike the anion which decays by the bimolecular process of ion recombination, the triplet decay is a unimolecular, first order process, which appears almost as a step function in log *t* (Fig. 4), with a triplet lifetime of about 3 s. This is quite similar to the phosphorescence lifetime of biphenyl, which is 3.7 s (13). The triplet state of biphenyl has an absorption peak at about 375 nm as measured in this work, and 367 nm as reported elsewhere (14, 15). So the DMB triplet has a slight red shift, as is usual for methyl substituted aromatics (15). The absorbance at 390 nm is not entirely due to the triplet, since by analogy to biphenyl, both DMB^+ and DMB^- are expected to absorb strongly at 390 nm (see ref. 16, Fig. 8). Because the absorbance at 410 nm (Fig. 2) shows little 'step function' behavior at 3 s, we may conclude that the triplet does not seriously interfere with measurement of DMB^- at 410 nm.

Effects of Charge Scavengers

Figure 5 shows the effect of a positive charge scavenger, triethylamine (TEA) and a negative charge scavenger 1-chloropropane on the DMB^- kinetics. The positive charge scavenger, TEA, appears to slightly increase the DMB^- yield, but does not slow its decay. Apparently ion recombination is almost as effective when TEA^+ is the cation.

The effect of the same scavengers on the triplet yield at *ca.* 3 s are given in Table 1. Both positive and negative ion scavengers reduce the triplet yield as expected if the triplets result from ion recombination. The triplet yield is

TABLE 1. Effect of additives on dimethylbiphenyl triplet yields* in 3-MHX at 77 K

Solute	Relative absorbance at 390 nm
0.25 *M* DMB	1.0
0.25 *M* DMB + 1.0 *M* TEA	0.6
0.25 *M* DMB + 1.0 *M* chloropropane	0.4
0.25 *M* DMB + 1.0 *M* TEA + 1.0 *M* chloropropane	0.4
0.025 *M* DMB + 1.0 *M* chloropropane	0.1

*Anions and cations of DMB also absorb at 390 nm and decay with the logarithm of time (Fig. 2). The first order (in time) decay of the triplet gives almost a 'step function' change of absorbance at 3 s on the log *t* plot, and is easily separated out from the DMB^- and DMB^+ absorbances.

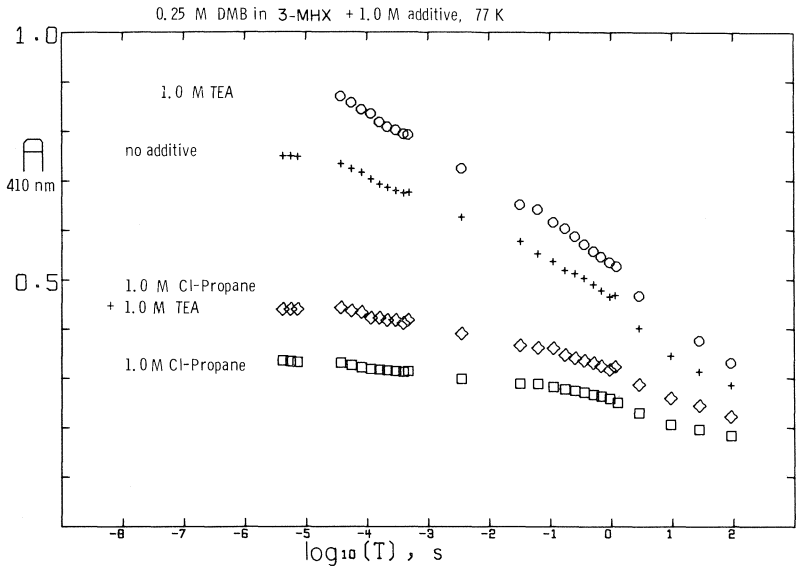

FIG. 5. Effects of 1.0 *M* concentrations of the positive charge scavenger triethylamine (TEA), and the electron scavenger 1-chloropropane on DMB^- kinetics in 0.25 *M* DMB solutions in 3-MHX at 77 K.

quite small in 0.025 *M* DMB + 1.0 *M* chloropropane. This result shows that production of triplet states by reabsorption of Cerenkov radiation is small. At 0.025 *M*, DMB will absorb almost all Cerenkov light within the DMB absorption band, so that little increase can be obtained by raising the DMB concentration. This assumes that the average light path for Cerenkov absorption is about 1 mm. It has been noted before (17) that internal absorption of Cerenkov light by solutes is essentially complete at low solute concentrations. This is true for the case of 0.025 *M* DMB because about 95% of the oscillator strength (>200 nm) is in regions where the molar absorption coefficient (18) $\varepsilon > 400\ M^{-1}\ cm^{-1}$.

Figure 6 shows that in 0.01 *M* biphenyl (ϕ_2) in 3-MHX at 77 K, the small yield of ϕ_2 triplets is decreased by addition of 2-methyl-1-pentene (2-MP-1), and is increased by addition of cumene (isopropylbenzene). Correspondingly, large concentrations of 2-MP-1 do not seem to increase the decay of ϕ_2^-, while cumene greatly increases ϕ_2^- decay. Cumene and 2-MP-1 both have lower ionization potentials than 3-MHX, so both are expected to capture positive charge. Both also have lower lying electronic states than 3-MHX. But cumene, unlike 2-MP-1, can capture electrons, as can benzene (11, 5). This may point to the role of electron capture in increasing ion recombination.

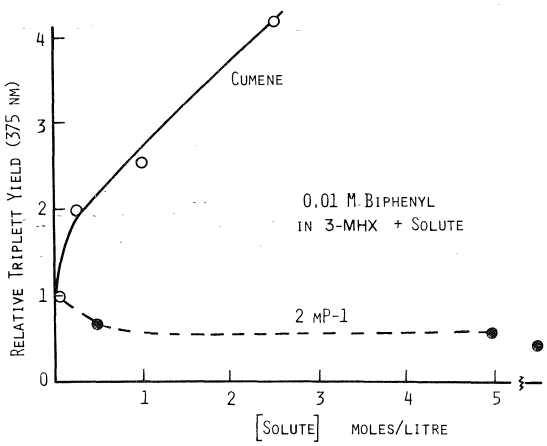

FIG. 6. The effects of 2-methyl-1-pentene and cumene on the absorbance step at 3 s (*e.g.*, see Fig. 4) due to the triplet state of biphenyl (ϕ_2) in 0.01 *M* ϕ_2 in 3-MHX at 77 K.

Figure 7 shows the ion recombination in cumene glass containing 0.1 *M* pyrene. Pyrene is very soluble in cumene, but sparingly soluble in 3-MHX. The anion, cation, and triplet state of pyrene can be observed almost independently.

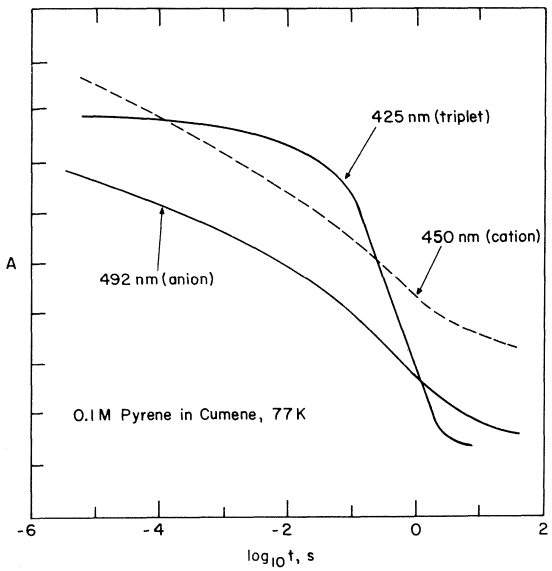

FIG. 7. Kinetics of the anion, cation, and triplet state of pyrene in cumene (isopropylbenzene) glass at 77 K.

Both the anion and cation decay with the log t kinetics typical of tunneling reactions over a range of distances. The pyrene triplet was observed to the red of its maximum, and is probably overlapped by cation absorption.

Pulse radiolysis of 0.15 M biphenyl in cumene glass seems to produce a large ϕ_2^+ absorption, which decays as does pyrene$^+$ in cumene. Substantial triplet yields are also obtained, but the yield of ϕ_2^- seems to be no more than one fifth as large as the yield of the cation. Perhaps ϕ_2^- can capture holes, but not electrons from the cumene matrix, which probably has a substantial electron affinity.

Discussion

General Conclusions: Ion Separation Shortening by Capture of Hot Electrons

The following tentative conclusions will be discussed: (*1*) Aromatic solutes capture trapped electrons in alkane glasses by electron tunneling. The anions which grow in show little decay at low solute concentrations ($\approx 10^{-3}$ M). (*2*) The probability of ion recombination (DMB^- + DMB^+) is dramatically enhanced at solute concentrations of 0.1 M ($\approx 1.5\%$) or greater. The triplet state of the solute is a major product. (*3*) The major reason for increased ion recombination appears to be shortening of ion separation distances so that most ion pairs are separated by less than 45 Å. (*4*) The solute molecules must act on the separating charges while they are 'hot'. (*5*) To enhance ion recombination, the solute molecule must be able to form a stable negative ion state.

The first two conclusions seem to be firmly established by the data, while the last three conclusions are tentative. These tentative conclusions are discussed below.

It was shown a few years ago that electron capture by solutes in hydrocarbon glasses could be accounted for by electron tunneling, which occurs after the electrons are thermalized and trapped (5). Inefficient processes for mobile electron capture (requiring solute concentrations substantially greater than 10^{-2} M) remained a possibility.

The rates of electron tunneling reactions depend exponentially on the distance between the electron donor and acceptor (19). A simple and useful expression for reasonably efficient tunneling reaction gives the distance a (in Å) over which the tunneling reaction can occur in a time t (in s)

$$[1] \quad a = a_0 + 2.26B^{-1/2}(15 + \log_{10} tF)$$

where B (in eV) is the binding energy of the electron on the electron donor and F is a nuclear overlap (Franck–Condon) factor for the reaction. We will assume that F is of the order of magnitude of unity. The quantity a_0 corrects for the finite size of the reactants and is about 5 Å. Equation 1 predicts that trapped electrons, which appear to be bound by about 0.5 eV in alkane glasses such as 3-MHX, can tunnel about 30 Å in 10^{-6} s and about 55 Å in 1 min. In a random distribution of distances, we expect growth kinetics to extend over many orders of magnitude in time, as observed in Fig. 1.

If ion recombination with DMB^- in rigid hydrocarbons proceeds by tunneling, we must use the binding energy of DMB^-. This is probably similar to the value of 1.6 eV found for the photobleaching threshold of biphenyl anion in 3-methylpentane glass (5). If we assume that the effect of the coulomb potential in the ion recombination reaction in hydrocarbons can be represented reasonably in the WKB approximation, then [1] will be a reasonable approximation for distances greater than 20 Å if we take a_0 to be about 12 Å. We then expect the ion recombination reaction of DMB^- + DMB^+ to

occur in about 10^{-6} s for ion pairs separated by 28 Å, and in about 10^{2} s for ion pairs separated by 43 Å.

Because the yield of DMB^- in 0.25 *M* DMB in 3-MHX is very small at 10^2 s, we conclude that almost all of the ion pairs are separated by less than about 45 Å.

This conclusion is tentative. If it is correct then DMB must have acted on the separating charges while they possessed energy in excess of thermal. Had the charges been thermalized at 45 Å in pure 3-MHX, they would not have been likely to separate further against the attractive coulomb potential. With a dielectic constant of 2.0, the energy required to increase the charge separation from 45 to 55 Å is 0.03 eV (= 0.17–0.14). This is more than four times thermal energy at 77 K.

The failure of large amounts of the positive charge scavenger 2-MP-1 to accelerate ion recombination pointed to the role of electron capture in the enhancement of ion recombination. Thus our tentative conclusion is that 'hot' (pre-thermal) electron capture is causing shortening of ion separation distances. This could involve a mobile, epithermal electron, or electron capture from an excited state which is a precursor to ionization. Both the concept of mobile, epithermal electron capture (20, 21), and reaction with an excited state which is a precursor to ionization (22, 23)[4] have been invoked to explain electron capture in irradiated condensed phases. Solid evidence has not been found for either concept.

Evidence for shorter ion pair separations in the presence of concentrated electron scavengers in neopentane has been seen by Schmidt and Allen (2), and in tetramethylsilane by Warman.[5] Neopentane and tetramethylsilane are unusual molecular liquids in that a very large fraction of ion pairs obtained separations greater than the Onsager distance at room temperature (300 Å) before thermalization.

Alternative Hypothesis

More Reactive Positive Ions

In the more concentrated solutions of DMB, probably most positive ions are converted to DMB^+, and DMB^+ might be more reactive toward DMB^- than is M^+, the matrix cation. This effect might explain the increased ion recombination without assuming a shortening of ion pair separations. But this effect should achieve its full impact once most positive charges (holes) have been captured by DMB. Because studies by Hamill and co-workers (10, 24, 25) have indicated that aromatic solutes such as DMB capture holes and electrons with very similar efficiencies, we would expect most holes to be captured at $\approx 10^{-2}$ *M*. Enhancement of ion recombination seems to grow most strongly at 10^{-1} *M* and above (Fig. 2). Furthermore, there is no *a priori* reason to expect DMB^+ to be more effective in ion recombination than M^+. DMB^+ and TEA^+ seem to be similar in effectiveness, since ion recombination was not appreciably slowed (Fig. 5) when about 40% of the cations were converted to TEA^+ (Table 1).

Tunneling Increases Ion Separation Distances at Low Concentrations

At low DMB concentrations, electrons are thermalized and trapped, and then tunnel tens of angströms to react with DMB. If the direction of this tunneling were completely random, the tunneling electrons would move, on the average, to farther distances from the hole. The DMB^- ions formed are probably at longer distances from the holes than were the trapped electrons from which they were formed. This effect is probably partly responsible for the fact that the ϕ_2^- yield in 0.015 *M* ϕ_2 in 3-MHX is 75% higher than the yield of trapped electrons in pure 3-MHX (12).

Two-step Tunneling

Enhanced ion recombination at high DMB concentrations might result from tunneling in two steps to the positive ion. For example, an electron on a DMB^- 60 Å from its geminate DMB^+ might tunnel 40 Å to reach another DMB, and then 35 Å to DMB^+. This two-step process would have essentially the same rate as the first (40 Å) step. Tunneling between two identical species (*e.g.* two DMB molecules) in a condensed medium is expected to be extremely slow (26), because relaxation of DMB^- and its surroundings will stabilize the anion. Were it not slow, $DMB^- \rightarrow DMB$ tunneling would set up a diffusive motion, contrary to experiment. Buxton and Kernsley, who advocate "trap to trap tunneling" (27) through a hierarchy (in increasing trap depth) of pre-existing solvent traps,

[4]H. B. Steen, unpublished results.
[5]J. Warman, private communication.

do not expect tunneling between identical species.[6]

However, the coulomb field would aid the DMB^- (60 Å) → DMB (35 Å) reaction by 0.1 eV. Simple calculations show that in 0.25 *M* DMB there is a sufficient probability of having a DMB molecule in the right region of space to allow such a two-step recombination process. There is presently not enough theoretical or experimental information to determine whether two-step (or multi-step) tunneling processes could play a significant role in the enhanced ion recombination observed here.

Even if the two-step tunneling processes do contribute to ion recombination, two pieces of experimental evidence suggest it is not the only effect: (*1*) Cumene enhances ion recombination (Figs. 6 and 7), although it has a much smaller electron affinity than DMB so that electrons could not tunnel from DMB^- to cumene. (*2*) Enhanced ion recombination also seems to occur in hydrocarbon liquids (see the following section) where ion recombination is not controlled by tunneling.

Evidence from Hydrocarbon Liquids

Thomas *et al.* (28) reported that the free ion yield for ϕ_2^- in cyclohexane at room temperature was nearly independent of ϕ_2 concentration from 10^{-3} to 3×10^{-1} *M*. On the basis of the present work, we would have expected the free ion yield to decrease almost to zero at 3×10^{-1} *M* ϕ_2. The work of Thomas *et al.* (28) may provide evidence against the conclusion that ion pair separation distances are greatly shortened by ≥ 0.1 *M* ϕ_2, at least for liquids at room temperature.

But the data of Thomas *et al.* (28) on ϕ_2^- free ion yields must be viewed with caution, because other species derived from ϕ_2 (radicals formed by H atom addition, the triplet state with $\varepsilon = 500$ at 620 nm (29)) may have been responsible for the absorbance Thomas *et al.* observed at about 600 nm. In concentrated solutions (≥ 0.1 *M*) of ϕ_2 Thomas *et al.* found a large, fast decaying ($t_{1/2} < 100$ ns) absorbance, attributed to geminate ϕ_2^-, and a much smaller absorbance, which decayed over many microseconds. At 10^{-3} *M* ϕ_2, only the small, slow decaying absorbance was present. It was shown by the use of scavengers and study of the spectrum to be predominantly due to ϕ_2^-. This same confirmation was not carried out at high ϕ_2 concentration.

I have performed this check for 0.25 *M* ϕ_2 in cyclohexane at room temperature. The small, slow decaying absorbance at $t \geq 1$ μs was not changed by adding 0.01 *M* ethyl bromide, which should have reacted with all ϕ_2^- before 1 μs. Also the spectrum at 1 μs did not correspond to the ϕ_2 spectrum, but was nearly flat between 575 and 675 nm.

The spectrum of the fast transient (about 50 ns half-life) did appear to be due to ϕ_2^-.

It thus appears that the free-ion yield in a 0.25 *M* solution of ϕ_2 in cyclohexane at room temperature is zero within experimental error. By comparison with the data of Thomas *et al.* (28), the free ion yield in 0.25 *M* ϕ_2 is no more than one fourth the yield in 10^{-3} *M* ϕ_2. This result tends to confirm the conclusion from the low temperature data that the aromatic additive shortens ion pair separations.

Closing Comments

About 2% of an aromatic solute in an alkane matrix dramatically increases the probability of ion recombination, apparently by preventing ions from separating to large distances. If this effect results from some efficient mechanism for moderation of hot electrons, then addition of a small amount of aromatic impurity to an aliphatic liquid or solid might help to prevent electrical breakdown at high voltages. Such a solution might also be more resistant to degradation by ionizing radiation, because most ions would recombine and produce excited states of aromatic solute, which usually decay without breaking bonds. Ion recombination is more probable in benzene than in aliphatic hydrocarbons. Liquid biphenyl and terphenyl are sufficiently stable toward radiation that they have been considered as working fluids in nuclear reactors (30).

[6]G. Buxton, private communication.

1. W. F. Schmidt and A. O. Allen. J. Phys. Chem. **72**, 3730 (1968).
2. W. F. Schmidt and A. O. Allen. J. Chem. Phys. **52**, 2345 (1970).
3. J. P. Dodelet. Can. J. Chem. This issue.
4. L. Onsager. Phys. Rev. **54**, 554 (1938).
5. J. R. Miller. J. Chem. Phys. **56**, 5173 (1972).
6. J. Miller, J. Hines, R. Runowski, and K. Johnson. J. Phys. Chem. **80**, 457 (1976).
7. J. Kroh, J. Mayer, E. Wojciechovska, and J. Grodkowski. J. Phys. Chem. **78**, 2696 (1974).

8. N. V. KLASSEN, H. A. GILLIS, and G. G. TEATHER. J. Phys. Chem. **76**, 3847 (1972).
9. J. T. RICHARDS and J. K. THOMAS. J. Chem. Phys. **53**, 218 (1970).
10. J. B. GALLIVAN and W. H. HAMILL. J. Chem. Phys. **44**, 1279 (1966).
11. W. H. HAMILL. *In* Radical ions. *Edited by* E. T. Kaiser and L. Kevan. Interscience, New York, NY. 1968. p. 321.
12. J. LIN, K. TSUJI, and F. WILLIAMS. J. Am. Chem. Soc. **90**, 2766 (1968).
13. V. L. ERMOLAEV. Uspekhi Fiz. Nauk. **80**, 3 (1963); Soviet Phys. Uspeki, **80**, 333 (1963).
14. J. S. BRINEN and M. K. ORLOFF. J. Chem. Phys. **51**, 527 (1969).
15. H. LABHAER and W. HEINZELMANN. *In* Organic molecular photophysics. Vol. I. *Edited by* J. Birks. Wiley-Interscience. 1973. p. 297.
16. J. B. GALLIVAN and W. H. HAMILL. J. Chem. Phys. **44**, 2378 (1966).
17. H. B. STEEN. Int. J. Radiat. Phys. Chem. **7**, 489 (1975).
18. I. B. BERLMAN. Handbook of fluorescence spectra of aromatic molecules. Academic Press. 1971. p. 183.
19. J. R. MILLER. J. Phys. Chem. **79**, 1070 (1975).
20. R. K. WOLF, M. J. BRONSKILL, and J. W. HUNT. J. Chem. Phys. **53**, 4211 (1970).
21. K. HARASA, M. IRIE, and H. YOSHIDA. In press.
22. J. J. WEISS. Ber. Bunsenges. Phys. Chem. **75**, 673 (1971).
23. (*a*) H. B. STEEN. J. Chem. Phys. **61**, 3997 (1974); (*b*) L. KEVAN and H. B. STEEN. Chem. Phys. Lett. **34**, 184 (1975).
24. D. W. SKELLY and W. H. HAMILL. J. Phys. Chem. **70**, 1630 (1966).
25. P. W. F. LOUWRIER and W. H. HAMILL. J. Phys. Chem. **72**, 3878 (1968).
26. (*a*) T. HOLSTEIN. Ann. Phys. **8**, 325 (1959); (*b*) J. J. HOPFIELD. Proc. Natl. Acad. Sci. U.S.A. **71**, 3640 (1974); (*c*) J. ULSTRUP and J. JORTNER. J. Chem. Phys. **63**, 4358 (1975); (*d*) J. JORTNER. J. Chem. Phys. **64**, 4860 (1976).
27. G. BUXTON and K. KEMSLEY. J. Chem. Soc. Faraday Trans. I, **72**, 466 (1976).
28. J. K. THOMAS, K. JOHNSON, T. KLIPPERT, and R. LOWERS. J. Chem. Phys. **48**, 1608 (1968).
29. Y. H. MEYER, R. ASTIER, and J. M. LECLERCQ. Chem. Phys. Lett. **4**, 587 (1970).
30. Organic nuclear reactors, an evaluation of current development programs. *ad hoc*. committee report, Argonne National Laboratory. Argonne, IL. 1961.

Discussion

J. Jortner: Electron – positive hole recombination will result in initial singlet and triplet yields in the ratio 1/3. This will result in a trivial mechanism for fluorescence. A more interesting mechanism for fluorescence involves triplet–triplet interaction resulting in the formation of an excited singlet state. Such a process was observed by McGlynn in rigid solutions doped with phenanthrene. I would like to inquire whether you have looked for fluorescence in your systems.

J. R. Miller: Fluorescence is definitely present in substantial amounts, but I have made no quantitative measurements.

Experimental evidence for the existence of a Ramsauer–Townsend minimum in liquid CH_4 and Ar (Kr and Xe) and in gaseous C_2H_6 and C_3H_8[1,2]

L. G. CHRISTOPHOROU[3] AND D. L. MCCORKLE[4]

Health Physics Division, Oak Ridge National Laboratory, Oak Ridge, TN, U.S.A. 37830

Received September 27, 1976

L. G. CHRISTOPHOROU and D. L. MCCORKLE. Can. J. Chem. **55**, 1876 (1977).

Experimental evidence for the existence of a Ramsauer–Townsend minimum in the electron scattering cross section for liquid CH_4 and liquid Ar (Kr and Xe) is presented and discussed. On the basis of evidence obtained from three sources: (*i*) comparisons of thermal electron mobilities in gases with those in liquids, (*ii*) changes in the electron mobility with gas density at high and very high gas pressures, and (*iii*) the dependence of the electron mobility on temperature for liquids whose V_0, the energy of the electron state in the liquid, is ≤ 0 eV, it is concluded that a Ramsauer–Townsend minimum is exhibited by the electron scattering cross section for CH_4, Ar (Kr and Xe) at all densities from a dilute gas to the liquid and that this minimum is shifted to lower energies (closer to thermal) with increasing density.

Additionally, it has been found that a Ramsauer–Townsend-type behavior is exhibited by gaseous ethane (C_2H_6) and propane (C_3H_8) with the cross section minimum located at lower energies than for methane (CH_4). For these latter molecules the measured mean scattering cross sections at thermal energies are comparable with the geometric cross sections.

L. G. CHRISTOPHOROU et D. L. MCCORKLE. Can. J. Chem. **55**, 1876 (1977).

On présente et on discute des données expérimentales supportant l'existence d'un minimum de Ramsauer–Townsend dans la section droite de la diffraction électronique du CH_4 liquide et de l'argon liquide (Kr et Xe). En se basant sur les données obtenues à partir de trois sources: (*i*) comparaisons des mobilités des électrons thermiques dans les gaz avec celles des liquides, (*ii*) changement dans la mobilité des électrons avec la densité gazeuse à haute et très haute pression de gaz et, (*iii*) la dépendance de la mobilité des électrons sur la température pour des liquides pour lesquels V_0, l'énergie de l'état de l'électron dans le liquide, ≤ 0 eV, on peut conclure qu'il existe un minimum Ramsauer–Townsend pour la section droite de la diffraction des électrons pour le CH_4, Ar (Kr et Xe) à toutes les densités (à partir d'un gaz dilué jusqu'au liquide) et que ce minimum est déplacé vers les basses énergies (plus près des énergies thermiques) lorsque la densité augmente.

De plus on a trouvé qu'un comportement de type Ramsauer–Townsend existe pour l'état gazeux de l'éthane (C_2H_6) et du propane (C_3H_8) avec une section droite minimale située à des énergies plus basses que celle du méthane (CH_4). Pour ces dernières molécules, les sections droites moyennes mesurées pour la diffraction à des énergies thermiques sont comparables avec les sections droites géométriques.

[Traduit par le journal]

I. Introduction

In this paper the experimental evidence supporting the existence of a Ramsauer–Townsend minimum in the scattering cross section for CH_4, Ar (Kr and Xe)[5] at all densities from the dilute gas to the liquid and the shifting of this minimum to lower energies (closer to thermal) with increasing density is presented and discussed. Experimental evidence is also presented showing that a Ramsauer–Townsend-type behavior is exhibited by gaseous ethane (C_2H_6) and propane (C_3H_8) with the cross section minimum located at lower energies than for methane (CH_4). For these latter molecules the measured mean scattering cross sections at thermal ener-

[1]Research sponsored by the Energy Research and Development Administration under contract with Union Carbide Corporation.

[2]By acceptance of this article, the publisher or recipient acknowledges the U.S. Government's right to retain a non-exclusive, royalty-free license in and to any copyright covering the article.

[3]Also Department of Physics, The University of Tennessee, Knoxville, TN, U.S.A. 37916.

[4]Present address: Department of Physics, The University of Tennessee, Knoxville, TN, U.S.A. 37916.

[5]Most of the experimental results for liquids presented in this paper are for CH_4 and Ar, but the conclusions drawn are expected to hold for Kr and Xe as well.

TABLE 1. μ_L/μ_G, V_0, P-dependence of μ, and existence of a Ramsauer–Townsend minimum in σ_m (or σ_T) at low pressures

Species	μ_L/μ_G[a,b]	Dependence of μ on P[b]	Ramsauer–Townsend minimum in σ_m (or σ_T) at low pressures[c]	V_0[d] (eV)	Reference
CH_4	>1	Increases with P	Yes	$-0.03(95)$	18
				$-0.15(111)$	19
$C(CH_3)_4$	>1	Increases with P	Yes(?)	$-0.4(296)$[e]	
Branched hydrocarbons	$\gtrsim 1$	—	—	<0	20–24
Other linear hydrocarbons	<1	Decreases with P^b	No(?)	>0	20–24
^4He	$\ll 1$	Decreases with P	No	$+1.05(4.2)$	25
Ne	$\ll 1$	Decreases with P[f]	No	$+0.5(22)$	25
Ar	>1	Increases with P	Yes	$-0.33(82)$	25
				$-0.45(82)$	25
				$-0.20(84)$	27
Kr	$\gg 1$	Increases with P(?)	Yes	$-0.78(117)$	25
				$-0.40(115)$	27
Xe	$\gg 1$	Increases with P(?)	Yes	$-0.63(163)$	25
				$-0.67(161)$	27
				$-0.61(165)$	27

[a]Reference 1.
[b]Reference 2.
[c]See ref. 6, chapt. 4.
[d]Values in parentheses refer to the temperature (in K) at which V_0 was measured.
[e]Average of values reported in refs. 20–24.
[f]Reference 26.

gies are comparable with the geometric cross sections.

II. Experimental Evidence from Studies of Thermal Electron Mobilities in Gases and Liquids

Christophorou *et al.* (1, 2) have performed such studies recently, and Table 1 summarizes those of their findings which are pertinent to the present discussion. The quantity μ_L is the thermal ('zero-field') electron mobility in the liquids, and μ_G is defined by (1, 2)

$$[1] \qquad \mu_G = S' N_{torr}/N_L$$

where $S' = \mu P$, $\mu = w/E$, P is the gas pressure in torr at the temperature T, N_{torr} is the number of molecules per cm^3 per torr at the specified gas temperature, $N(= PN_{torr})$ is the gas number density, N_L is the number density of the corresponding liquid at the temperature of the liquid measurement, w is the electron drift velocity, and E is the uniform electric field in volts per cm. μ_G may be regarded as the gaseous thermal electron mobility adjusted for the change in density between the gas and the liquid.

These studies (1, 2) suggest that $\mu_L/\mu_G > 1$ for CH_4 and the heavier rare gases for which $V_0 \leq 0$ eV.[6,7] Estimates of μ_L/μ_G are $\lesssim 16$, ~ 12, ~ 4, ~ 120, and ~ 730 for CH_4, $C(CH_3)_4$, Ar, Kr, and Xe, respectively. Although these values are considered approximate because of differences in the temperature at which μ_L and μ_G were determined, the conclusions drawn are not affected. For such systems, thermal electrons are more mobile in the liquid than in the corresponding low-pressure gas. Very importantly, also, the values of μ_L/μ_G increase in the order Ar, Kr, Xe, *i.e.*, in the direction the Ramsauer–Townsend cross section minimum becomes more pronounced in the low-pressure gas. Although

[6] $V_0 = \phi_L - \phi_V$, where ϕ_L and ϕ_V are, respectively, the work functions of a metal electrode in the liquid and in vacuum.

[7] In the case of liquids with $V_0 > 0$ eV (*e.g.*, C_2H_6 ($\mu_L/\mu_G = 0.026$)), μ_L/μ_G is <1 or $\ll 1$, and $1/\mu_{torr}$ increases with N (for the cases investigated so far; see discussion in ref. 2).

these changes may be partly attributed to changes in the structure factor $S(0)$ in the low ($\varepsilon \rightarrow 0$ eV) (3) energy limit, they also reflect the change (*decrease*) in the effective scattering cross section in the liquid as compared with the low-pressure gas.[8] The existence of a Ramsauer–Townsend minimum in the scattering cross section for liquid CH_4 and the heavier liquid rare-gas atoms *at lower energies* than in the corresponding gas can provide an explanation for this behavior. Evidence for such a minimum in the cross section and for a shift in its position to lower energies with increasing density is provided in section III.

III. Experimental Evidence from the Density Dependence of the Electron Mobility at High Gas Pressures

Christophorou (2) (see also Bartels (4*a*)) has reviewed the recent work on the dependence of the electron mobility on P (or N). Christophorou *et al.* (1, 2) also have defined the quantity

$$[2] \qquad \mu_{torr} = \frac{w}{E/P}\frac{1}{P_1}$$

where E/P is in units of V cm^{-1} torr^{-1} and $P_1 =$ 1 torr. The quantity μ_{torr} is basically the electron mobility normalized to 1 torr pressure. The inverse of the value of μ_{torr} is a measure of the effective frequency for elastic collisions ν_m, defined by (5, ref. 6, p. 275)

$$[3] \qquad \frac{\nu_m}{N} = \frac{e}{m}\frac{1}{w}\frac{E}{N}$$

where e and m are the electron charge and mass, respectively. The quantity $1/\mu_{torr}$ is proportional to a function of the mean cross section for momentum transfer $\langle\sigma_m\rangle$; actually, it is (roughly) proportional to it (see [5]).

In Fig. 1, $1/\mu_{torr}$ for CH_4 is plotted as a function of the mean electron energy $\langle\varepsilon\rangle_M$, taken equal to $\frac{3}{2}(eD_L/\mu)$, where D_L is the lateral electron diffusion coefficient. At near-thermal energies $1/\mu_{torr}$ goes through a minimum due to the well-known Ramsauer–Townsend effect in CH_4 (8). Also in Fig. 1 we have plotted $1/\mu_{torr}$ for CH_4 as determined from the w *vs.* E/P measurements of Lehning (9) at 32 800 torr. It is interesting to see that these data indicate a decrease of the cross section and a downward shift of the cross section minimum with increasing CH_4 density (7). These findings cannot be accounted for by changes in the structure factor $S(0)$ with gas density since, as has been discussed earlier (10), $S(0)$ increases with N in the density range covered by the data in Fig. 1, and thus $1/\mu_{torr}$ ought to have increased rather than decreased with N. This observation is consistent with the suggestion (2) that the increase in μ_{torr} for CH_4 and the heavier rare gases Ar, Kr, and Xe in going from the gas to the liquid is due to a decrease in σ_m, at least partially due to a downward shift of the Ramsauer–Townsend minimum exhibited by these species.

Consistent with the CH_4 data are those for Ar shown in Fig. 2. The minimum in the $1/\mu_{torr}$ *vs.* $\langle\varepsilon\rangle$ function in Fig. 2 appears at a much lower (mean) electron energy $\langle\varepsilon\rangle$ (see figure captions for sources of $\langle\varepsilon\rangle$) than does the low-pressure minimum of the momentum transfer cross section $\sigma_m(\varepsilon)$ (or the total scattering cross section $\sigma_T(\varepsilon)$). The latter occurs at an electron energy ε of $\sim$0.3 eV while the former appears at mean electron energies ranging from $\sim$0.17 to $\sim$0.02 eV, depending on density. Actually, the energy, $\langle\varepsilon\rangle_{min}$, at which the minimum of the $1/\mu_{torr}$ *vs.* $\langle\varepsilon\rangle$ occurs, shifts to lower energies with increasing N as is clearly shown by the data presented in Table 2. The broken function (identified by the formula) in Fig. 2 represents (see next section) an estimate of the e–atom scattering cross section in *liquid Ar* with the effect of the structure factor removed. It is very interesting to see (Table 2) that the position of the minimum of this cross section is quite consistent with the gaseous data.[9] Furthermore, as for the case of CH_4, the effective e–atom scattering cross section decreases (and the minimum becomes sharper) with increasing N. This behavior cannot be attributed to $S(0)$ since in the density range of the gaseous data in Fig. 2 the structure factor $S(0)$ increases with N (10).

IV. Experimental Evidence from Studies on the Dependence of μ_L on T for Liquids with $V_0 \leq 0$ eV

The temperature dependence of μ_L for liquids whose $V_0 \leq 0$ eV can be used to derive information on the electron scattering cross section σ_L

[8]We calculate that the structure factors $S(0)$ for liquid CH_4 and Ar at 111 and 90 K, respectively, are 0.05 and 0.06. If it is assumed that $\mu_L/\mu_G = S(0)_{gas}/S(0)_{liquid} = 1/S(0)_{liquid}$, one obtains for this ratio 20 and 16.6 for CH_4 and Ar, respectively.

[9]Unfortunately, we have not been able so far to unfold $\sigma_m(v)$ itself from the experimental data at high P due mainly to a lack of accurate electron transport coefficients at low E/P and high P.

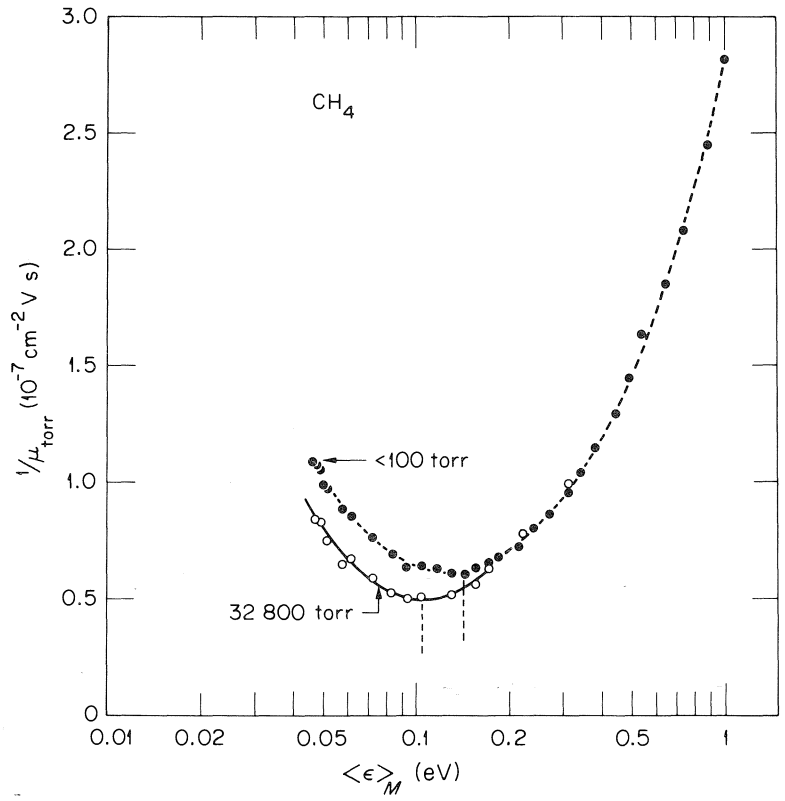

FIG. 1. $1/\mu_{torr}$ *vs.* $\langle\varepsilon\rangle_M$ for CH_4 at the indicated pressures; $T = 298$ K (from ref. 7). The vertical broken lines show the approximate position of the minima.

TABLE 2. Approximate values of $\langle\varepsilon\rangle_{min}$ for Ar at various densities $N^{a,b}$

N (10^{20} atoms/cm^3)	$\langle\varepsilon\rangle_{min}$ (eV)
0.24	0.170
5	0.128
7.5	0.120
10	0.110
12.2	0.100
15	0.090
17.5	0.085
20	0.080
22.5	0.072
25	0.066
121.5 (liquid at 151.8 K and 60.1 atm)	0.020

[a]Derived from plots such as Fig. 2 (see caption of Fig. 2 for original sources of data).
[b]The minimum in $\sigma_m(\varepsilon)$ is at $\varepsilon \simeq 0.3$ eV which is expected to be greater than the value of $\langle\varepsilon\rangle$ at which $1/\mu_{torr}$ possesses a minimum at low pressures.

in the liquid. Since when $V_0 \leq 0$ eV the electron is continuously in a quasi-free state (and not partly in it and partly in the captured (or trapped) state as in those cases where $V_0 > 0$ eV) the measured mobility μ_L is equal to the electron mobility in the quasi-free state. The temperature dependence of μ_L, therefore, reflects the changes with T of the overlap between the electron energy distribution function and $[\sigma_L(\varepsilon)]^{-1}$. Thus if the T-dependence of N_L and $S(0)$ are properly considered, the measurements of μ_L as a function of T can be employed to obtain information on $\sigma_L(\langle\varepsilon\rangle)$.

For low-pressure gas and elastic collisions (6)

$$[4] \quad w = -\frac{4\pi}{3}\frac{e}{m}\frac{1}{N_{torr}}\frac{E}{P}\int_0^\infty \frac{v^2}{\sigma_m(v)}\frac{df_0}{dv}\,dv$$

where f_0 is the spherically symmetric term in the expansion of the electron velocity distribution function, and v is the electron velocity. If we denote by $\langle\sigma\rangle$ an average of the electron scattering cross section over f_0 and assume f_0 to be Maxwellian

$$[5] \quad w \simeq \frac{2}{3}\left(\frac{2}{m\pi kT}\right)^{1/2}\frac{eE}{N}\frac{1}{\langle\sigma\rangle}$$

where k is the Boltzmann constant.

Under the assumption that [5] holds for thermal electrons drifting in a fluid with $V_0 \leq 0$ eV,

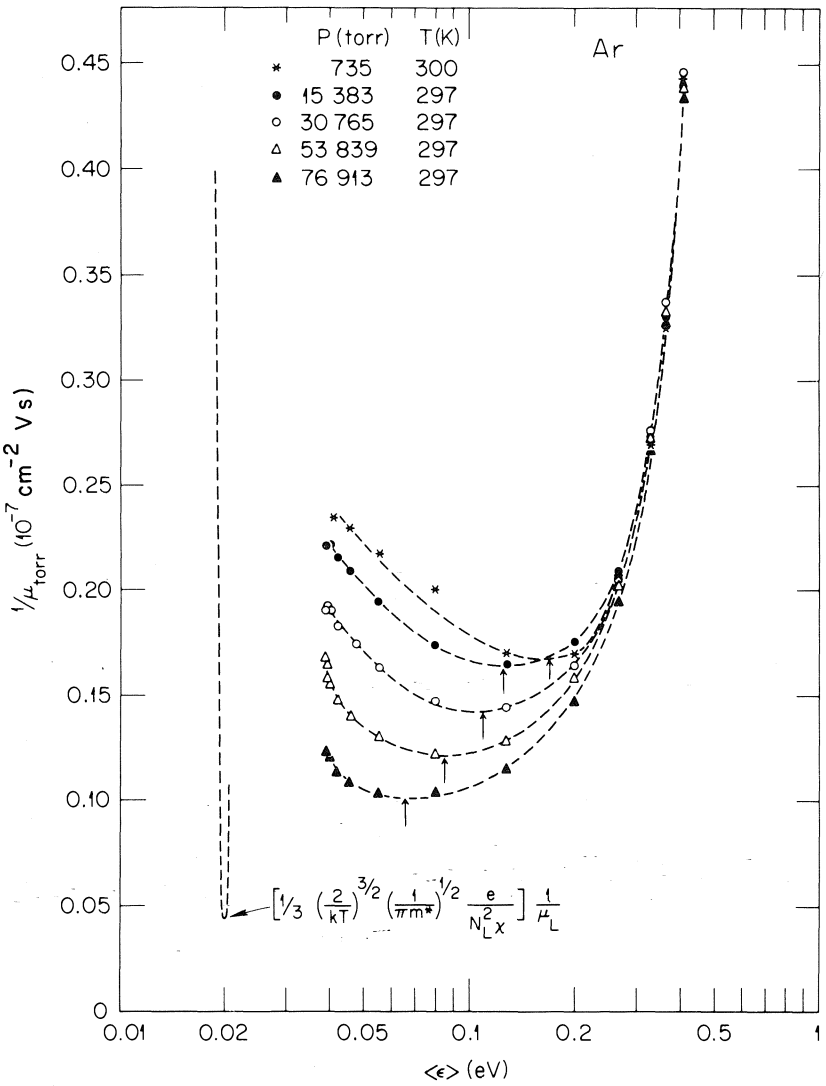

FIG. 2. $1/\mu_{torr}$ *vs.* $\langle\varepsilon\rangle$ for Ar at the indicated pressures and temperatures. Due to the low values of E/P at which the w *vs.* N measurements were made, we could not use the $\langle\varepsilon\rangle$ *vs.* E/P data listed by Christophorou (ref. 6, p. 431; see also ref. 30). Instead, we used the data on $\langle\varepsilon\rangle$ *vs.* E/P given by Frost and Phelps (31). The vertical lines indicate the approximate positions of the minima. The 735 torr data were deduced from the w *vs.* E/P measurements of Pack *et al.* (32) and the rest from the w *vs.* E/P measurements of Bartels (4*a*) at high densities. The broken line (identified by the formula) is the scattering cross section (in arbitrary units) for liquid Ar at 160 K (see text and Fig. 3).

we may express μ_L as

$$[6] \qquad \mu_L = \frac{2}{3}\left(\frac{2}{m^*\pi kT}\right)^{1/2}\frac{e}{N_L}\frac{1}{\langle\sigma\rangle_{eff}}$$

where m^* is the effective electron mass in the liquid and $\langle\sigma\rangle_{eff}$ is the mean effective scattering cross section in the liquid. Baldini (11) gives $m^* = 0.43m$ for solid argon at 20 K. In our calculation we used this value for m^* although we recognize that m^* may be density and/or temperature dependent. If we further assume that

$$[7] \qquad \langle\sigma\rangle_{eff} = S(0)\langle\sigma\rangle_L$$

and use for $S(0) = N_L kT\chi$, where χ is the isothermal compressibility, we have

$$[8] \qquad \mu_L = 0.532e[(kT)^{3/2}(m^*)^{1/2} \times (N_L)^2\chi\langle\sigma\rangle_L]^{-1}$$

For liquid Ar the quantities $\mu_L(T)$, $\chi(T)$, and

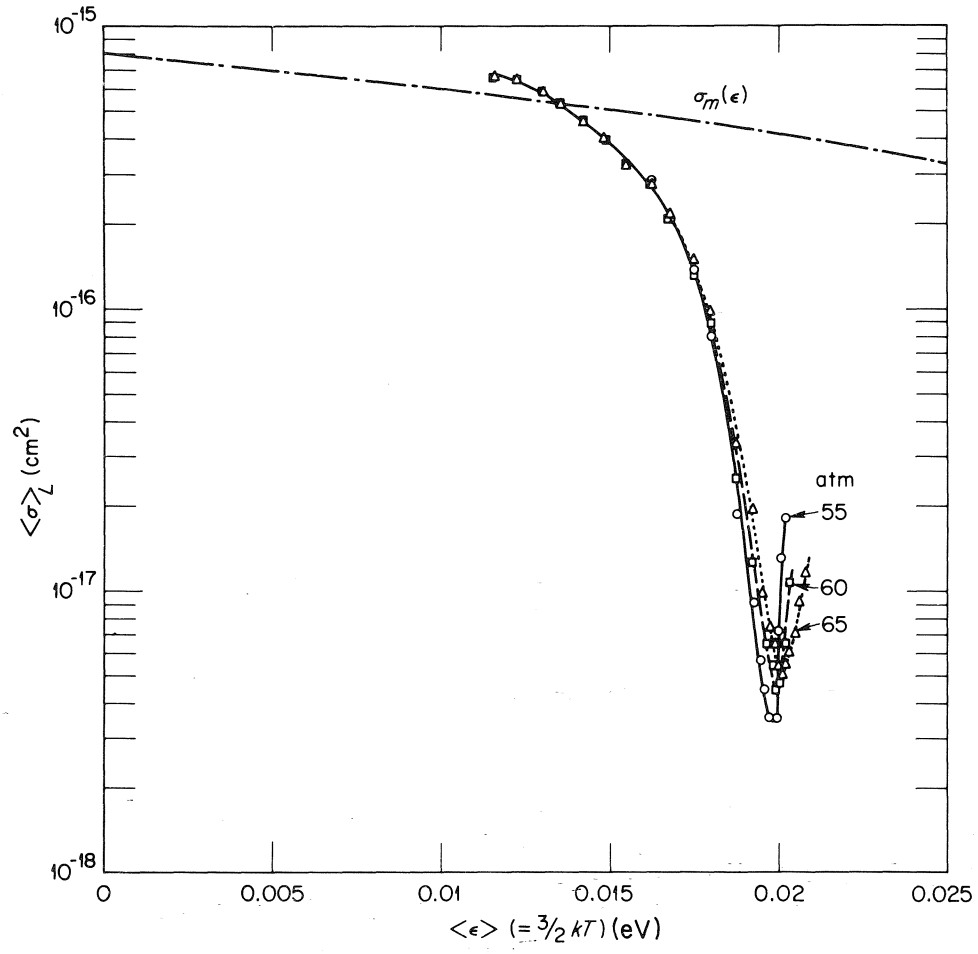

FIG. 3. $\langle\sigma\rangle_L$ *vs.* $\frac{3}{2}kT$ for liquid Ar ($90 \leq T \leq 161$ K) (see text). The broken curve is the swarm-determined momentum transfer cross section $\sigma_m(\varepsilon)$ (31). It should be noted that the $\sigma_m(\varepsilon)$ deduced (33) from recent electron beam data on Ar (34) exhibited a much sharper low-pressure Ramsauer–Townsend minimum compared with the $\sigma_m(\varepsilon)$ deduced from swarm data.

$N_L(T)$ are known (12) over the temperature range 90 to 161 K. Using these data we have determined (see Fig. 3) $\langle\sigma\rangle_L$ as a function of $\langle\varepsilon\rangle_M(\equiv \frac{3}{2}kT)$. For comparison, $\sigma_m(\varepsilon)$ for low-pressure argon has also been plotted in Fig. 3. The data in Fig. 3 clearly show the existence of a sharp minimum in $\langle\sigma\rangle_L$ at ~ 0.02 eV. This striking result is consistent with the high gas pressure behavior as can be seen from Fig. 2 and Table 2. Although the sharpness of the $\langle\sigma\rangle_L$ *vs.* $\langle\varepsilon\rangle$ function is not understood, it is not unreasonable since the electron energy distribution functions are very narrow at these low temperatures. In fact, over the temperature range 90 to 160 K the width of $\langle\sigma\rangle_L$ is comparable with the width of the electron energy distribution functions.

The results on argon are supported by the work of Bakale and Schmidt (13) on the temperature dependence of μ_L for liquid methane. In contrast to other hydrocarbon liquids for which μ_L increases with increasing T, μ_L for liquid CH_4 decreases with increasing T (13). This behavior is consistent with a cross section $\langle\sigma\rangle_L$ possessing a minimum at or below $\frac{3}{2}kT$ ($T = 90$ K; the lowest value of T for which μ_L was measured (13)), *i.e.*, far below the position of the low-pressure cross section minimum, and which increases in magnitude with increasing energy beyond $\frac{3}{2}kT$.

V. General Conclusion

From sections II to IV, it can be concluded that a Ramsauer–Townsend minimum is ex-

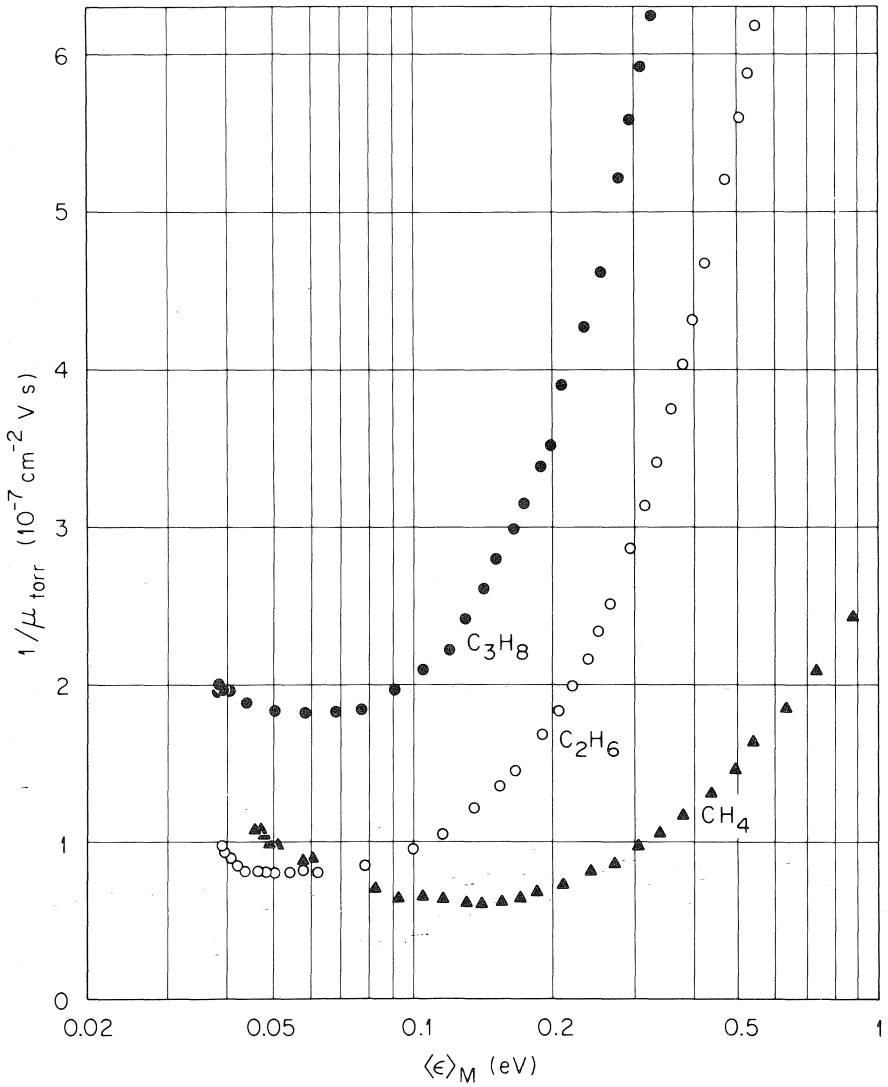

FIG. 4. $1/\mu_{torr}$ *vs.* $\langle\varepsilon\rangle_M$ for low-pressure (< 100 torr) C_2H_6, C_3H_8, and CH_4 (from ref. 7).

hibited by the electron scattering cross section for CH_4, Ar (Kr and Xe) at all densities from the dilute gas to the liquid, and that this minimum is shifted to lower energies with increasing density.

VI. Experimental Evidence for the Existence of a Ramsauer–Townsend Minimum in Gaseous C_2H_6 and C_3H_8

In Fig. 4, $1/\mu_{torr}$ for C_2H_6 and C_3H_8 is plotted (along with that for CH_4 for comparison) as a function of the mean electron energy $\langle\varepsilon\rangle_M$, taken equal to $\frac{3}{2}(eD_L/\mu)$, where D_L is the lateral electron diffusion coefficient. At near-thermal energies for all three molecules $1/\mu_{torr}$ goes through a minimum which shifts to lower energies in the order CH_4, C_2H_6, C_3H_8. This behavior would suggest that the well-known Ramsauer–Townsend minimum in CH_4 (8) is exhibited by C_2H_6 and C_3H_8 as well, but for the latter molecules it is located at energies considerably closer to thermal.

Contrary to the case of CH_4 where the mobility of slow electrons increases with increasing density of CH_4, the mobility of slow electrons in C_2H_6 and C_3H_8 decreases (14) with increasing density of C_2H_6 and C_3H_8. This behavior has been discussed recently by Christophorou (2) who argued that for C_2H_6 (also *n*-butane, *n*-pentane, and *n*-hexane) the decrease in electron

mobility with increasing density (including the liquid) results predominantly from the delaying effects of the electron capture-and-loss process.

Consistent with the behavior shown in Fig. 4 are the comparisons of mean scattering cross sections with the geometric cross sections for the *n*-alkanes reported by Christophorou *et al.* (7). Using [4], it can be shown that for thermal electrons in a low-pressure gas,

$$[9] \quad \langle\sigma_m\rangle_{exp} = 6.42 \times 10^{-9}/\mu_{torr} \quad (\text{for } T = 298 \text{ K})$$

when $\sigma_m(v)$ varies inversely with v and that

$$[10] \quad (\sigma_m)_{exp} = 4.28 \times 10^{-9}/\mu_{torr} \quad (\text{for } T = 298 \text{ K})$$

when σ_m is independent of v. The values of $\langle\sigma_m\rangle_{exp}$ and $(\sigma_m)_{exp}$ for the *n*-alkanes are listed in Table 3. Estimates of geometric cross sections for the same ten molecules are also given. These were determined from end-to-end molecular distances reported by two different sources (see ref. 7). They are seen to compare well with the experimental cross section data, and they imply that the effective range of the forces experienced by the electron is short, comparable with the mean molecular radius. A short-range and strong e–molecule interaction is required for a Ramsauer–Townsend-type behavior to be exhibited by the scattering cross section (10).

Finally, it should be noted that the existence of a Ramsauer–Townsend minimum in the scattering cross section, as well as the small magnitude of the scattering cross sections for CH_4, C_2H_6, and C_3H_8 are consistent with the relatively long electron thermalization times determined by Christophorou *et al.* (15) for these gases at low pressures. Estimates of the electron thermalization times at 1 torr pressure are given in Table 4 for CH_4, C_2H_6, C_3H_8 (and C_2H_4) where they are compared with electron ranges in the corresponding liquids (16). The longer the electron thermalization time, the longer is the electron range.

TABLE 3. $\langle\sigma_m\rangle_{exp}$ and σ_{geom} for *n*-alkanes

Molecule	$\langle\sigma_m\rangle_{exp}$ (10^{-15} cm^2) [9]	$\langle\sigma_m\rangle_{exp}$ (10^{-15} cm^2) [10]	σ_{geom} (10^{-15} cm^2) Ref. 7[a]	σ_{geom} (10^{-15} cm^2) Ref. 7[b]
Methane	0.69	0.46	0.28	0.30
Ethane	0.61	0.41	0.67	0.62
Propane	1.28	0.85	1.19	0.97
Butane	1.93	1.29	1.93	1.33
Pentane	2.52	1.68	2.57	1.69
Hexane	2.84	1.89	3.44	2.05
Heptane	3.45	2.30	4.37	2.41
Octane	4.4	2.93	5.31	2.77
Nonane	5.68	3.79	6.57	3.14
Decane	5.78	3.85	7.44	3.50

[a]Values determined from data on end-to-end molecular distances given in ref. 28.
[b]Values determined on the basis of data given in ref. 29.

TABLE 4. Comparison of electron thermalization times in hydrocarbon gases (P = 1 torr; T = 298 K) with electron ranges in the corresponding liquids

Molecule	Thermalization time[a] (μs)	Density-normalized range[b] (10^{-8} g cm^{-2})
CH_4	~1.5	224 (140 K)[c]
C_2H_6	~0.5	57 (200 K)
C_3H_8	~0.5	52 (238 K)
C_2H_4	~0.15	23 (170 K)

[a]The electron thermalization times were found (15) to increase slowly with $\langle\varepsilon\rangle$ above ~0.4 eV and to decline rapidly in the energy region corresponding to the vibrational excitation thresholds. The values listed in this table were estimated at the leveling-off portions of the thermalization time *vs.* $\langle\varepsilon\rangle$ functions reported in ref. 15.
[b]Reference 16.
[c]Values in parentheses refer to temperature.

VII. Concluding Remarks

A behavior similar to that exhibited by CH_4, Ar (Kr and Xe) may be exhibited by other molecules for which $V_0 < 0$ eV such as $C(CH_3)_4$ and $Si(CH_3)_4$. Additionally, the electron scattering cross section for higher members of the *n*-alkane series may possess a minimum which is located at thermal or subthermal energies.

The results of this study show the need for a better theoretical understanding of electron motion in dense gases and liquids. Present theoretical treatments (see, for example, ref. 17) fail to predict the existence of the Ramsauer–Townsend minimum in liquid Ar.

Acknowledgments

We wish to thank Dr. A. K. Bartels for kindly providing us with a copy of ref. 4*a* and Professor N. R. Kestner for useful discussions.

1. L. G. CHRISTOPHOROU, R. P. BLAUNSTEIN, and D. PITTMAN. Chem. Phys. Lett. **18**, 509 (1973).
2. L. G. CHRISTOPHOROU. Int. J. Radiat. Phys. Chem. **7**, 205 (1975).
3. M. H. COHEN and J. LEKNER. Phys. Rev. **158**, 305 (1967); C. A. CROXTON. Introduction to liquid state physics. John Wiley and Sons, New York. 1975.
4. (*a*) A. K. BARTELS. Ph.D. Dissertation, University of Hamburg, Hamburg, W. Germany. 1974; (*b*) Phys. Lett. A, **44**, 403 (1973).
5. L. S. FROST and A. V. PHELPS. Phys. Rev. **127**, 1621 (1962).
6. L. G. CHRISTOPHOROU. Atomic and molecular radiation physics. Wiley-Interscience, New York. 1971.

7. L. G. CHRISTOPHOROU, M. W. GRANT, and D. PITTMAN. Chem. Phys. Lett. **38**, 100 (1976).
8. C. RAMSAUER and R. KOLLATH. Ann. Phys. **4**, 91 (1930).
9. H. LEHNING. Phys. Lett. A, **29**, 719 (1969).
10. L. G. CHRISTOPHOROU and D. L. MCCORKLE. Chem. Phys. Lett. **42**, 533 (1976).
11. G. BALDINI. Phys. Rev. **128**, 1562 (1962).
12. J. A. JAHNKE, L. MEYER, and S. A. RICE. Phys. Rev. A, **3**, 734 (1971).
13. G. BAKALE and W. F. SCHMIDT. Z. Naturforsch. Teil A, **28**, 511 (1973).
14. B. HUBER. Z. Naturforsch. Teil A, **24**, 578 (1969).
15. L. G. CHRISTOPHOROU, K. S. GANT, and J. K. BAIRD. Chem. Phys. Lett. **30**, 104 (1975).
16. M. G. ROBINSON and G. R. FREEMAN. Can. J. Chem. **52**, 440 (1974).
17. J. LEKNER. Phys. Rev. **158**, 130 (1967).
18. W. TAUCHERT and W. F. SCHMIDT. Z. Naturforsch. Teil A, **29**, 1526 (1974).
19. U. SOWADA, G. BAKALE, K. YOSHINO, and W. F. SCHMIDT. Proc. 5th Int. Conf. Conduction Breakdown Dielectr. Liq. Noordwijkerhout, The Netherlands. July, 1975.
20. R. A. HOLROYD and C. O. ALLEN. J. Chem. Phys. **54**, 5014 (1971).
21. R. A. HOLROYD. J. Chem. Phys. **57**, 3007 (1972).
22. R. A. HOLROYD, B. K. DIETRICH, and H. A. SCHWARZ. J. Phys. Chem. **76**, 3794 (1972).
23. R. A. HOLROYD and R. L. RUSSELL. J. Phys. Chem. **78**, 2128 (1974).
24. R. SCHILLER, SZ. VASS, and J. MANDICS. Int. J. Radiat. Phys. Chem. **5**, 491 (1973).
25. B. RAZ and J. JORTNER. *In* Electrons in fluids. *Edited by* J. Jortner and N. R. Kestner. Springer-Verlag, New York. 1973. pp. 413–422.
26. L. BRUSCHI, G. MAZZI, and M. SANTINI. Phys. Rev. Lett. **28**, 1504 (1972).
27. W. TAUCHERT and W. F. SCHMIDT. Z. Naturforsch. Teil A, **30**, 1085 (1975).
28. P. J. FLORY. Statistical mechanics of chain molecules. Interscience, New York. 1969.
29. H. BENOIT and P. DOTY. J. Phys. Chem. **57**, 958 (1953).
30. A. A. CHRISTODOULIDES and L. G. CHRISTOPHOROU. J. Chem. Phys. **54**, 4691 (1971).
31. L. S. FROST and A. V. PHELPS. Westinghouse Scientific Paper 64-928-113-P6. 1964; Phys. Rev. **136**, A1538 (1964).
32. J. L. PACK, R. E. VOSHALL, and A. V. PHELPS. Westinghouse Research Laboratories, Research Report 62-928-113-R1. 1962.
33. D. E. GOLDEN. Phys. Rev. **151**, 48 (1966).
34. D. E. GOLDEN and H. W. BANDEL. Phys. Rev. **149**, 58 (1966).

Discussion

J. Jortner: You were right in pointing out the repeated failure of theoretical models in accounting for the mobility maximum (minimum in cross section) in dense Ar and other dense fluids. The reason may originate from adopting solid state models to the liquid. In particular, Lekner's calculations consider single scattering from a 'frozen' system. Such an approach may be reasonable for energetics, *i.e.* calculation of V_0, but not for dynamics of the excess electron. In the latter case the role of density fluctuations has to be incorporated.

L. Kevan: Although you do see evidence for a Ramsauer–Townsend minimum in gaseous C_2H_6, C_3H_8, and perhaps higher alkanes, you presumably do not predict that this would be observed in liquid C_2H_6 and higher alkanes, in contrast to liquid CH_4, because of the low electron mobility in liquid C_2H_6. It seems that it would be very important to directly measure the momentum transfer cross sections for electrons in liquid alkanes.

L. G. Christophorou: The data I have shown for C_2H_6 and C_3H_8 are for low pressures. At higher pressures and in the liquid although a similar behaviour to that for CH_4 may be exhibited with regard to the Ramsauer–Townsend minimum, the effect of this on the mobility must be overshadowed by the opposite one due to electron capture and loss; for both C_2H_6 and C_3H_8 the electron mobility decreases with increasing density (see L. G. Christophorou. Int. J. Radiat. Phys. Chem. **7**, 205 (1975)) and is quite low in the liquid, as you said. I agree that a direct measurement of the momentum transfer cross section in liquid alkanes is highly desirable.

G. R. Freeman: Was the increase in structure factor with density due to the increase in isothermal compressibility?

L. G. Christophorou: Yes.

G. R. Freeman: I question the use of the structure factor in this way. In the critical region the compressibility becomes very large, yet nothing much happens to the electron mobility. It seems that either the mobility model or the method of estimating the structure factor is not correct.

G. Ascarelli: The Ramsauer minimum is due to a quantum mechanical interference between the incident electron and the scatterer. The important parameter is the ratio of the electron wavelength and the size of scatterer. If the Ramsauer minimum shifts to lower energies shouldn't this imply that you have to consider some sort of a cluster rather than independent molecules?

L. G. Christophorou: Yes, perturbation by the surroundings, not necessarily a cluster.

J. W. Warman: We have also obtained evidence for Ramsauer minima in polyatomic gases by studying the absorption of microwaves in the nanosecond pulse irradiated gas at pressures where the thermalization of electrons is considerably longer than the pulse length. At the pressures used (several torr) the absorption signal is proportional to the electron collision frequency and it is found, for CH_4, C_2H_6, and C_6H_6, that the collision frequency initially decreases following the pulse as the electrons cool down, then passes through a minimum, eventually rising to a plateau value corresponding to the collision frequency for fully thermalized electrons. The importance of the Ramsauer minimum in the overall rate of thermalisation is shown by the rapid decrease of the collision frequency to the minimum value compared with the much slower subsequent increase to the thermal value.

The influence of nonelectronegative molecules on the mobility of excess electrons in liquefied rare gases and tetramethylsilane

ULRICH SOWADA AND WERNER F. SCHMIDT

Bereich Strahlenchemie, Hahn-Meitner-Institut für Kernforschung, Berlin GmbH, D 1000 Berlin 39, Germany

AND

GEORGE BAKALE

Department of Radiology, Case Western Reserve University, Cleveland, OH, U.S.A. 44106

Received September 27, 1976

ULRICH SOWADA, WERNER F. SCHMIDT, and GEORGE BAKALE. Can. J. Chem. **55**, 1885 (1977).

Addition of nonelectronegative molecules (*n*-alkanes, alkenes, CO, CO_2) to liquid argon, krypton, and xenon influences the drift velocity of excess electrons in an electric field. At high field strengths (10^4–10^5 V cm^{-1}), where the electrons have mean energies exceeding kT, inelastic collisions with solute molecules lead to an increase of the drift velocity above the value of the pure solvent. Analysis of this effect yields the energy dependent product of collision cross section and mean fractional energy loss per collision.

At low field strengths a decrease of the low field mobility with increasing solute concentration is observed from which the cross section for momentum transfer could be deduced. The influence of solutes on the low field mobility was also found in tetramethylsilane.

ULRICH SOWADA, WERNER F. SCHMIDT et GEORGE BAKALE. Can. J. Chem. **55**, 1885 (1977).

L'addition de molécules qui ne sont pas électronégatives (des alcanes, des alcènes, le CO et le CO_2) à de l'argon, du krypton ou du xénon liquide influencent la vitesse de déplacement des électrons en excès dans un champ électrique. A des forces de champ élevées (10^4–10^5 V cm^{-1}), où les électrons ont des énergies moyennes plus grandes que kT, des collisions inélastiques avec des molécules de soluté conduisent à une augmentation de la vitesse de déplacement au-dessus de la valeur observée pour le solvant pur. L'analyse de cet effet fournit le produit de la section droite collision, qui dépend de l'énergie, et la fraction moyenne de l'énergie perdue par collision. A des forces de champs faibles, on observe une diminution de la mobilité à champ faible avec une augmentation de la concentration du soluté à partir de laquelle des sections droites pour le transfert de moment peuvent être déduites. On a aussi trouvé l'influence des solutés sur la mobilité à champ faible dans le tétraméthylsilane.

[Traduit par le journal]

1. Introduction

The physico-chemical properties of excess electrons in liquefied rare gases have received continuing interest for more than 2 decades. On one hand electrons have served as probes for the investigation of the structure of these simple liquids, on the other hand liquefied argon and xenon have been applied in liquid ionization chambers and elementary particle detectors.

The electron transport in these liquids is understood relatively well although quantitative agreement between theory and experiment needs improvement. Cohen and Lekner (1, 2) analyzed theoretically the motion of electrons in liquid argon and found that the interaction between electrons and argon atoms could be described by two mean free paths: one related to momentum transfer Λ_P and a second one related to energy transfer Λ_0.

At low electric field strengths where the electrons are in thermal equilibrium with the argon atoms the mobility is determined by transfer of momentum while at higher field strength where the electrons are no longer in thermal equilibrium with the liquid the energy loss becomes important.

Molecular solutes in the liquefied rare gas represent additional centers for scattering and both mean free paths are influenced. The effect of some hydrocarbons on the electron drift velocity as a function of the electric field strength was investigated by Yoshino *et al.* (3) in this laboratory and the influence on the energy loss was analyzed. Changes in the low field mobility were observed but not evaluated quantitatively.

In mixtures of ethane and methane, Bakale *et al.* (4) found a decrease of the electron mobility with increasing ethane concentration.

We have extended these investigations and here we wish to report measurements on the in-

fluence of molecular solutes on the low field and high field electron mobility in liquid argon, xenon, and tetramethylsilane (TMS). The electron drift velocity as a function of the electric field strength was observed for the following solutions: (*a*) at 87 K liquid argon with methane, ethane, ethylene, propylene, carbon monoxide, and carbon dioxide, (*b*) at 165 K liquid xenon with butane, cyclopropane, and tetramethyl silane, and (*c*) in the temperature range 173 to 296 K TMS with propane, butane, pentane, octane, isooctane, cyclopropane, cyclopentane, and propylene.

2. Experimental

Measurement technique and cells have been described elsewhere (5). Argon (99.96 mol%), xenon (99.99 mol%), and methane (99.995 mol%) were passed over columns of activated molecular sieve (Linde 4 Å) and charcoal at 200 K and through a column with copper sponge at 650 K. The purified material was then condensed at 77 K in an evacuated bottle.

Ethane, ethylene, propylene, and cyclopropane (research grade quality) were degassed and purified as described above. All other hydrocarbons and TMS were passed through columns of activated silica gel and after degassing they were stored in contact with a fresh sodium mirror for at least 24 h.

Carbon monoxide was passed through columns of activated molecular sieve and charcoal and was purified further by trap-to-trap distillation in a vacuum. Carbon dioxide was condensed on activated silica gel in a vacuum and then degassed by trap-to-trap distillation.

The remaining impurity level in the purified solvents led to a lifetime of the electrons much greater than the longest drift time, which came close to 5 μs in cells with 1 mm electrode separation.

3. Results

The influence of a molecular solute on the electron drift velocity is twofold. At low solute concentration the drift velocity at low field strength remains the same as in the pure solvent while at higher field strength an increase of the drift velocity above the values of the pure solvent occurs. With increasing solute concentration a reduction of the drift velocity at low field strength occurs while at high field strength the drift velocity is increased further. Figure 1 shows as an example the data of the solution of CO in liquid argon. A stepwise increase of the drift velocity with field strength was found with ethylene and propylene as solutes. In Fig. 2 the data obtained in a solution of propylene in liquid argon are given. The increase of the drift velocity sets in above 300 V cm^{-1} and in this solution an additional steep increase occurs at 3×10^4 V cm^{-1}.

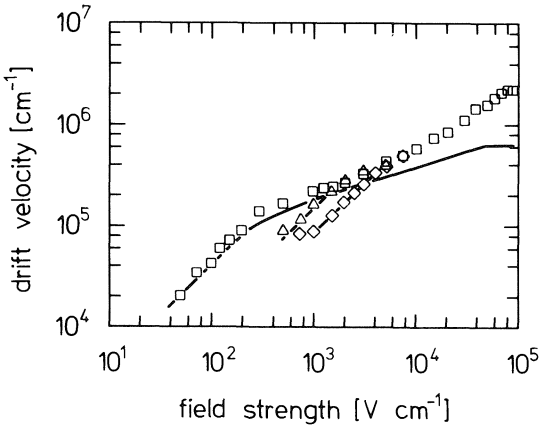

FIG. 1. The influence of carbon monoxide on the electron drift velocity in liquid argon at 87 K. CO concentration: □ 1.7×10^{19} cm^{-3}, ◇ 6.5×10^{20} cm^{-3}, △ 3.2×10^{20} cm^{-3}, — pure argon.

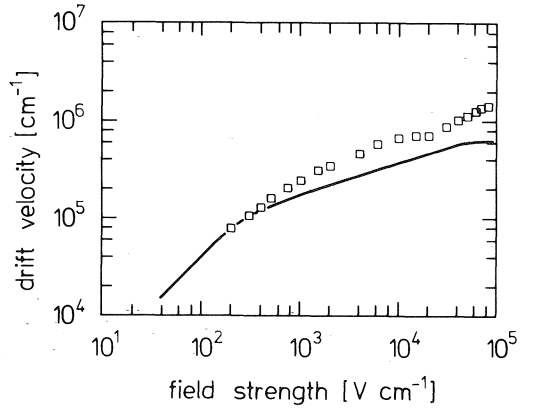

FIG. 2. The influence of propylene on the electron drift velocity in liquid argon. $T = 87$ K; 1.9×10^{19} cm^{-3}.

In solutions of methane and argon no decrease of the low field mobility with increasing methane concentration was observed. This may be due to the fact that the electron mobilities in the pure liquids are almost the same (2–4).

4. Discussion

4.1. Low Field Mobility

In pure argon, krypton, and xenon excess electrons exhibit large mobilities (Ar, 87 K, 450 cm^2 V^{-1} s^{-1}; Kr, 120 K, 1200 cm^2 V^{-1} s^{-1}; Xe, 165 K, 2000 cm^2 V^{-1} s^{-1}) and the electron is thought to move in an extended state or (in the terminology of solid state physics) in a con-

duction band (1, 2, 6, 7). The same picture may also be applied to TMS where the mobility is $\sim 100\ cm^2\ V^{-1}\ s^{-1}$.

The magnitude of the low field mobility is determined by scattering of the electron on single atoms while the scattering process is modified by the liquid structure around the scattering center (1, 2). The observed mobility μ_P is therefore correlated with a mean free path Λ_P by

$$[1] \qquad \mu_P = \frac{2}{3}\left(\frac{2}{\pi m k_B T}\right)^{1/2} e\Lambda_P$$

where m is the electron mass, e is the electronic charge, k_B is the Boltzmann constant, and T is the absolute temperature.

The addition of solutes introduces additional scattering centers and leads to a reduction of the mobility to a value μ_s. For small concentrations the scattering events are independent of each other and if the solvent structure is not changed the corresponding mean free path is given by

$$[2] \qquad \Lambda_s^{-1} = \Lambda_P^{-1} + n_s\sigma_m$$

with n_s the concentration of the solute and σ_m the cross section for momentum transfer to the solute. Combining [1] and [2] leads to an expression for σ_m

$$[3] \qquad \sigma_m = \frac{\mu_P/\mu_s - 1}{\Lambda_P n_s}$$

Plotting $\mu_P/\mu_s - 1$ as a function of n_s yields a straight line for low concentrations and σ_m is obtained from the slope. At higher solute concentrations the decrease of electron mobility with increasing concentration becomes steeper and the plot according to [3] bends upward. In Fig. 3, as an example, the reduction of the low field mobility in liquid argon at 87 K by small concentrations of ethane and carbon monoxide is given. The cross sections obtained from the various solutions are summarized in Table 1. For comparison cross sections obtained in the gas phase are also listed. σ_m(liq.) and σ_m(gas) exhibit the same order of magnitude. The embedding medium, apparently, has little influence on the scattering process. σ_m(liq.) is very small for molecules with no anisotropy of the electrical polarizability while σ_m(liq.) increases for the normal alkanes with increasing chain length. Introduction of a double bond seems to increase the cross section (*cf.* propane *vs.* propylene) while the branched isomer seems to show a

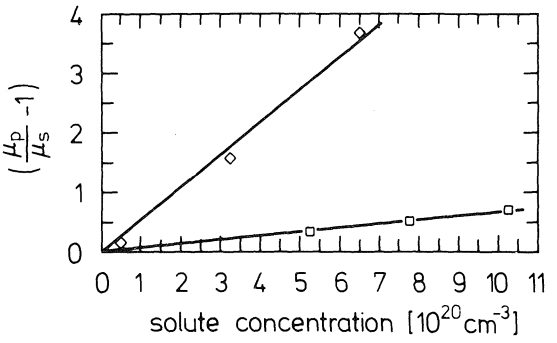

FIG. 3. Change of the low field electron mobility as a function of solute concentration; solvent: argon, 87 K; solutes: □ ethane, ◇ carbon monoxide.

smaller cross section in contrast to the gas phase, (*cf.* octane *vs.* isooctane). The carbon monoxide molecule is smaller than the ethane molecule but the permanent dipole moment of CO leads to a much greater cross section.

In general the cross section for momentum transfer seems to be correlated with the anisotropy of the polarizability (for instance, for *n*-octane $\delta^2 = 2.5 \times 10^{-2}$ while for isooctane $\delta^2 = 1.5 \times 10^{-2}$); however, other properties as, for instance, the size of the molecules may influence σ_m. Christophorou *et al.* (8) found satisfactory agreement between geometrical cross sections and σ_m(gas) for several *n*-alkanes.

4.2. High Field Mobility

At higher field strengths the drift velocity is no longer proportional to the field strength F. The electrons pick up more energy from the field between subsequent collisions than they can lose and a higher mean electron energy ε results. Addition of molecular solutes introduces new scattering centers where electrons can lose energy more efficiently than to the atoms of the solvent. In the pure liquid the rate of energy loss is determined by elastic collisions and given by

$$[4] \qquad ev_P F_P = \frac{\Delta W_{el}}{\Lambda_0/v_{el}}$$

where v_P is the drift velocity at the field strength F_P, v_{el} is the mean electron velocity, and ΔW_{el} the average energy transferred in an elastic collision.

In the solution the rate of energy loss is increased by inelastic collisions and given by

$$[5] \qquad ev_i F_i = \frac{\Delta W_{el}}{\Lambda_0/v_{el}} + \frac{\Delta W_{in}}{\Lambda_{in}/v_{el}}$$

TABLE 1. Cross section for thermal electron momentum transfer to solute molecules in liquefied rare gases and TMS

Solute	Solvent	T (K)	σ_m(liq.) $\times 10^{15}$ cm^2	σ_m(gas) $\times 10^{15}$ cm^2	References
Methane	Argon	87	—	0.43	†
				0.1	14
TMS	Xenon	165	<0.15	5.5	‡
Ethane	Argon	87	0.43	0.41	13
	Methane	111	0.9*		
n-Propane	TMS	296	0.8	0.79	
n-Butane	Xenon	165	1.0	1.2	13
	TMS	173–296	1.5		
n-Pentane	TMS	296	2.0	1.55	13
n-Octane	TMS	296	6.0	2.72	
Cyclopropane	Xenon	165	1.4		
	TMS	296	1.6		
Cyclopentane	TMS	296	1.0	2.66	13
Propylene	Argon	87	1.8		
	TMS	296	1.5		
Isooctane	TMS	173–296	2.2	7.1	13
Carbon monoxide	Argon	87	3.5	3.5	14
				0.6	13

*From ref. 4.
†Davis and Nelson, in ref. 13.
‡L. G. Christophorou, private communication.

where v_i is the drift velocity in the solution at the field strength F_i, ΔW_{in} the average inelastic energy loss, and Λ_{in} the mean free path

$$[6] \qquad \Lambda_{in} = (n_{in}\sigma_{in})^{-1}$$

with n_{in} the solute concentration and σ_{in} the cross section.

From the ratio of the loss rates follows

$$[7] \qquad \frac{v_i F_i}{v_P F_P} = 1 + \frac{\Delta W_{in}}{\Delta W_{el}} \Lambda_0 n_{in} \sigma_{in}$$

Introducing the mean fractional energy loss

$$[8] \qquad f = \Delta W/\varepsilon$$

(ε mean electron energy) we obtain from [7] for σ_{in}

$$[9] \qquad \sigma_{in} \frac{f_{in}}{f_{el}} = \left(\frac{v_i}{v_P}\frac{F_i}{F_P} - 1\right) \Big/ (\Lambda_0 n_{in})$$

From [9] the product $\sigma_{in} f_{in}/f_{el}$ as a function of the mean electron energy ε can be determined.

ε is the same in the solution and in the pure liquid at field strengths where

$$[10] \qquad v_i/F_i = v_P/F_P$$

Since the mean electron energy ε is correlated with the field strength F_P, $\sigma_{in}(F_P)$ can be converted into $\sigma_{in}(\varepsilon)$. The dependence $\varepsilon(F_P)$ was calculated from the field dependence of the electron drift velocity in the pure solvent by means of the Cohen–Lekner theory (1, 2).

The elastic losses are due to collisions with argon atoms and f_{el} is given by

$$[11] \qquad f_{el} = 2m/M$$

(m electron mass, M argon mass). $f_{in}(\varepsilon)$ is not known exactly and, therefore, from the drift velocity data (*e.g.* Fig. 1) $\sigma_{in} f_{in}$ as a function of the mean electron energy was determined. The results are shown in Fig. 4.

Measurements by Christophorou *et al.* (9) in the gas phase indicate that $f_{in}(\varepsilon)$ increases steeply with energy up to 0.1 eV and then levels off above this energy with values around 0.1 for hydrocarbons. A somewhat different analysis was carried out in our previous publication (3) where the product of the energy loss quantum ΔW_{in} and the cross section $\sigma_{in}(\varepsilon)$ was obtained. In Fig. 5 the data for propylene and ethylene obtained in the present study are compared with the data for ethane and propane. The values for TMS are also given in Fig. 5.

Cross sections for energy transfer to these molecules in the gas phase have been reported by Duncan and Walker (10, 11). With plausible values for f_{in} or ΔW_{in}, respectively, values for $\sigma_{in}(\varepsilon)$ of the same order of magnitude can be obtained from Figs. 4 and 5.

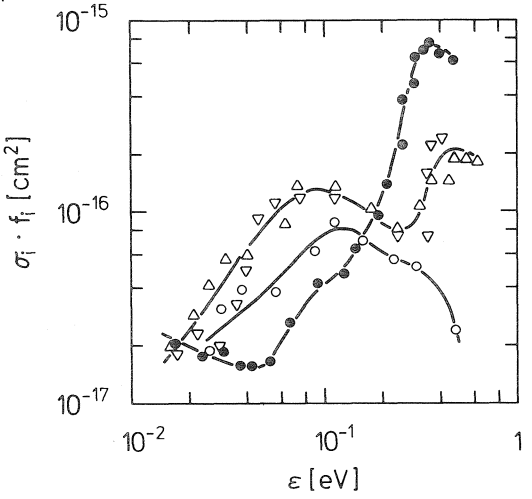

FIG. 4. Product of cross section for energy transfer and the ratio of the inelastic and elastic mean fractional energy losses as a function of the electron mean energy: ○ carbon dioxide, ● carbon monoxide, △ propylene, ▽ ethylene.

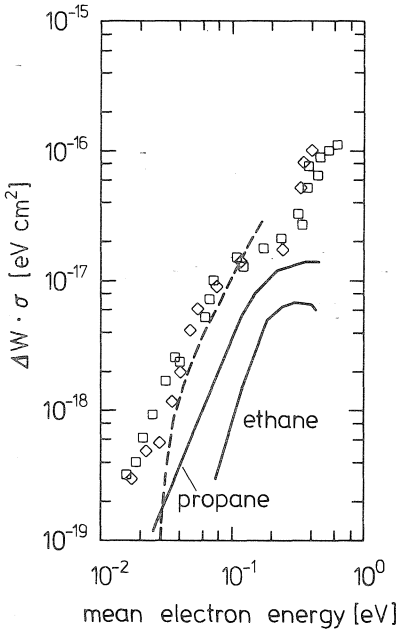

FIG. 5. Product of cross section for energy transfer and energy loss quantum as a function of the electron mean energy: □ propylene, ◇ ethylene, --- TMS; ethane and propane from ref. 3.

For TMS the energy loss as a function of the mean electron energy multiplied by the number density of the liquid at $T = 296$ K yields the energy loss per centimetre and this may be compared with the energy loss if only elastic losses given by $(2m/M)\varepsilon/\Lambda_0$ were active (M molecular mass of TMS). At thermal electron energies ($T = 296$ K) the ratio $f_{in}/f_{el} = 210$ is obtained in good agreement with the value of 230 deduced from the onset of the field strength dependence of the electron mobility in TMS (12).

Acknowledgment

Support by Deutsche Forschungsgemeinschaft is gratefully acknowledged.

1. M. H. COHEN and J. LEKNER. Phys. Rev. **158**, 305 (1967).
2. J. LEKNER. Phys. Rev. **158**, 130 (1967).
3. K. YOSHINO, U. SOWADA, and W. F. SCHMIDT. Phys. Rev. A, **14**, 438 (1976).
4. G. BAKALE, W. TAUCHERT, and W. F. SCHMIDT. J. Chem. Phys. **63**, 4470 (1975).
5. G. BAKALE and W. F. SCHMIDT. Z. Naturforsch. Teil A, **28**, 511 (1973).
6. L. S. MILLER, S. HOWE, and W. E. SPEAR. Phys. Rev. **166**, 871 (1968).
7. W. E. SPEAR and P. G. LECOMBER. Phys. Rev. **178**, 1454 (1969).
8. L. G. CHRISTOPHOROU, M. W. GRANT, and D. PITTMAN. Chem. Phys. Lett. **38**, 100 (1976).
9. L. G. CHRISTOPHOROU, K. S. GANT, and J. K. BAIRD. Chem. Phys. Lett. **30**, 104 (1975).
10. C. W. DUNCAN and I. C. WALKER. J. Chem. Soc. Faraday Trans. II, **68**, 1800 (1972).
11. C. W. DUNCAN and I. C. WALKER. J. Chem. Soc. Faraday Trans. II, **70**, 577 (1974).
12. U. SOWADA, G. BAKALE, K. YOSHINO, and W. F. SCHMIDT. Proc. 5th Int. Conf. Conduction Breakdown Dielectr. Liq. Delft University Press, 1975. p. 2.
13. L. G. CHRISTOPHOROU, R. P. BLAUNSTEIN, and D. PITTMAN. Chem. Phys. Lett. **18**, 509 (1973).
14. P. SMEJTEK and M. SILVER. J. Phys. Chem. **76**, 3890 (1972).

Discussion

L. G. Christophorou: Could you please elaborate on your assumption that the electron energies are the same when the electron mobilities are the same?

U. Sowada: To my knowledge there is no theoretical justification. A simple physical reason why this assumption is a good one is the following: if the electrons lose energy more efficiently, the electric field strength has to be higher to end up in the same mean energy of the extra electrons. Empirically the assumption seems to be suited to account for this physical effect.

G. R. Freeman: Was it only for dilute solutions that you assumed that the electron energies were the same if the mobilities were the same?

U. Sowada: Yes. There are empirical reasons, as *e.g.* the coincidence of the results from different dilute solutions, and others, which indicate it is a good assumption.

High-speed schlieren studies of electrical breakdown in liquid hydrocarbons

P. WONG AND E. O. FORSTER

Corporate Research Laboratories, Exxon Research and Engineering Company, Linden, NJ, U.S.A. 07076

Received September 27, 1976

P. WONG and E. O. FORSTER. Can. J. Chem. **55**, 1890 (1977).

High-speed schlieren studies have been carried out on the electrical breakdown of liquid hydrocarbons using a pulsed ruby laser. The development and propagation of charge carrier trajectories were recorded photographically on prebreakdown, breakdown, and postbreakdown events occurring in very pure, oxygen-free samples of hexane, benzene, toluene, and isooctane using a parallel plate electrode geometry. The initiation of breakdown was characterized by the growth of narrow streamers the creation of which was attributed to field injected electrons at local asperities of the cathode surface. Once the streamers reached the anode, large currents were found to flow through the gap leading to formation of a plasma column. Subsequent emissions occurring at the anode were attributed to field reversal. Details of the schlieren pictures have been interpreted in terms of classical electromagnetic theory.

P. WONG et E. O. FORSTER. Can. J. Chem. **55**, 1890 (1977).

On a effectué des études de schlieren à grande vitesse sur l'éclatage électrique des hydrocarbures liquides utilisant un laser de rubis pulsé. On a enregistré d'une manière photographique le développement et la propagation des trajectoires des transporteurs de charge pour des évènements avant l'éclatage, durant l'éclatage et après l'éclatage se produisant dans des échantillons très purs et sans oxygène, d'hexane, de benzène, de toluène et d'iso-octane utilisant une géométrie d'électrode plane et parallèle. L'initiation de la dégradation est caractérisée par une croissance de flèches dont la création est attribuée à des électrons injectés par le champ au niveau d'aspérités locales de la surface cathodique. Lorsque les flèches ont atteint l'anode, on a trouvé qu'il y a une circulation de grands courants à travers la trouée conduisant à la formation d'une colonne de plasma. Des émissions subséquentes se produisant à l'anode sont attribuées à un renversement de champ. On a interprété des détails des photos de schlieren en termes de la théorie électromagnétique classique.

[Traduit par le journal]

Introduction

An understanding of the phenomena associated with electrical breakdown occurring in dielectric liquids is very important because breakdown limits the high voltage level that can be applied to power equipment. Although numerous theories have been proposed to explain breakdown, a unified understanding of its origin is still missing because of a lack of data. Measurements related to breakdown are difficult because it is an ultrafast transient event, lasting only nanoseconds. Within that time, some quantities of interest such as conduction current can change from milliamperes to 10 000 A and higher. Moreover, even by taking the best precautions such as using isolation transformers and well-shielded cables, the electromagnetic radiation associated with breakdown has proved to strongly disturb electronic equipment. All these difficulties make an investigation of electrical breakdown events based on electrical measurements very difficult. In the present study, an optical method based on a laser schlieren system was used and the spatial development of electrical breakdown in liquid hydrocarbons was recorded photographically.

Early breakdown experiments using schlieren techniques were performed by Farazmand (1), Hakim and Higham (2), and Chaband and Wright (3). However, the electrode geometries used were of the point–point, point–plane, and sphere–sphere type, making the electrical field calculations very complicated. The work of these investigators was limited in temporal resolution by the use of conventional light sources which required rather prolonged exposures. Thomas (4) took advantage of the development of high intensity laser sources and he used a very fast laser pulse as light source for schlieren studies of prebreakdown events. (For a detailed description of the laser schlieren system see ref. 4.)

In the present study 15 ns pulses produced with a ruby laser were used to illuminate the space between two parallel plate electrodes. In

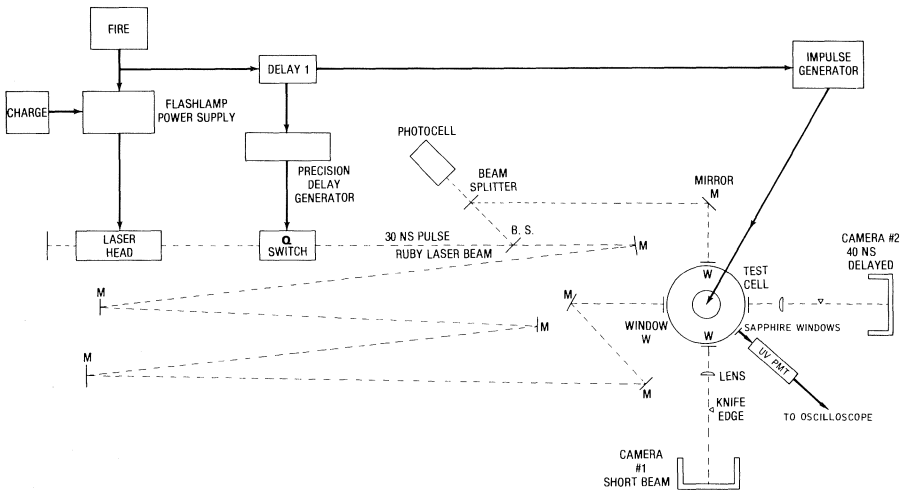

FIG. 1. Ultra high-speed electrooptical system for electrical prebreakdown in liquid hydrocarbons.

this manner it became possible to photograph density gradients produced in liquid hydrocarbons by the electronic charge carriers moving under the influence of a rapidly applied electrical stress. This paper presents some of the experimental results obtained and discusses their significance.

Experimental Technique

The experimental setup used in this investigation is basically the same as that described by Thomas (4). A simplified diagram of it is shown in Fig. 1. The *Q*-switched ruby laser was supplied by Holobeam, Inc. When the Pockel cell of the *Q*-switch is triggered, a laser pulse of 15 ns duration is generated. This pulse passes through a beam splitter and one beam is delayed with respect to the other by traversing a longer distance. The delay time can easily be adjusted by changing the optical path as defined by the mirror arrangements. The laser pulse shape is measured by using a high-speed photocell. When schlieren pictures were taken, the laser firing time is referenced to the breakdown time by displaying simultaneously the photocell output and the impulse voltage waveform on a Tektronix 556 dual-beam oscilloscope.

To produce the impulse voltage, a five stage Ferranti impulse generator was used. This instrument is of the Marx type and is capable of generating up to 275 kV. For the purpose of this study a rise time of about 1.4 μs was selected for the impulse waveform and the impulse decayed to 50% of its crest value in about 50 μs.

A parallel plane electrode system was used. The cylindrical brass electrodes had a 1 in. diameter and were spaced 6 mm apart. The edges of the electrodes were rounded (VDI type) and the surfaces were polished to a mirror finish. Since parallelism is extremely important in this plane–plane configuration, careful alignment is essential. In this setup, the upper electrode was fixed and the bottom electrode could be adjusted by means of a universal motion drive. The images of the electrodes were optically magnified onto a screen which permits monitoring of their positions for very fine adjustments.

The test liquids (toluene, benzene, *n*-hexane, isooctane) were Phillips research grade (99.9% purity). The liquids were first dried by contact with sodium ribbons for 2 days. Then they were subjected to repeated cryogenic distillations. A typical process would involve three such distillations. The liquid was then transferred to the test cell using pressurized nitrogen. Throughout the distillation and transfer process, the liquid was only in contact either with vacuum or nitrogen. The probability of having oxygen reabsorbed is estimated to be negligible.

In conjunction with the schlieren studies, a light detection system has recently been added. A RCA 4837 photomultiplier tube (PMT) was mounted just outside a sapphire window of the test cell. The latter permits the passage of uv light of wavelengths down to 200 nm. In the light emission experiment, the laser is not activated and the PMT is displayed simultaneously with the breakdown voltage waveform on the dual-beam scope. For low light-emission levels, an amplifier with an extremely fast rise time of about 1 ns was used to avoid distortion of the emitted light-pulse waveforms.

Experimental Results

The time for the collapse of the applied voltage, *i.e.* the time for the actual breakdown event, was deduced from voltage traces displayed on the oscilloscope such as the one shown in Fig. 2. From these traces it was decided that the breakdown event lasts less than 500 ns. The time lag between the instant the applied voltage reaches its crest value and the occurrence of breakdown is not reproducible in accordance with the well-known statistical nature of the breakdown mechanism. However, approximately half to one microsecond before breakdown, a sudden rise in uv light emission from the toluene

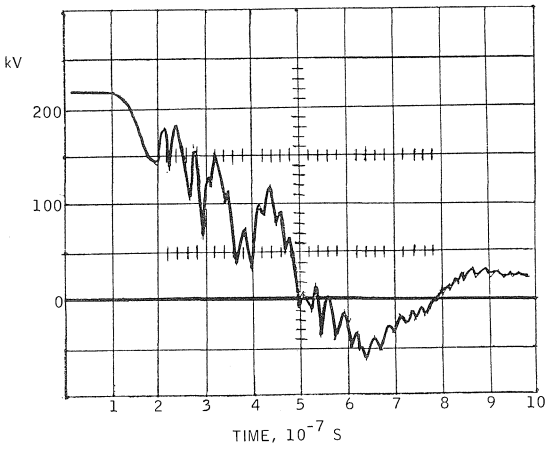

FIG. 2. Voltage trace of electrical breakdown, hexane.

sample can always be observed, as shown in Fig. 3*a*. The upper trace represents the temporal change in voltage, while the lower one represents the voltage output from the PMT. Most of the light emissions were identified as uv radiation because the light detection could be strongly attenuated if the optical window on the test cell was changed to ordinary pyrex glass (attenuation threshold at 300 nm and below). Light emission occurred as soon as the applied voltage started to increase (Figs. 3*b* and 3*c*), but a surge in intensity happened just before breakdown. This agrees very well with previous observations (5).

The schlieren photographs showed that electrical breakdown consists of three stages, which are labeled as: (*i*) prebreakdown; (*ii*) breakdown; and (*iii*) postbreakdown events. Figures 4*a* and 4*b* are a pair of photographs of the prebreakdown stage taken by the schlieren system in the crossed beam configuration. Figure 4*b* was recorded 40 ns after Fig. 4*a*. The initiation of breakdown is characterized by small, narrow cavitations near the cathode surface (see arrow in Fig. 4*a*). After 40 ns the tiny structure had developed into a well-defined streamer, propagating almost half-way between the electrodes. Hence, the velocity of the streamers is approximately 10^7 cm/s.

Typical breakdown pictures are shown in Figs. 5*a* and 5*b*. After the streamer had bridged the gap, rapid current discharge will flow through this conductive channel. By impact excitation and/or ionization, more ions will be produced and form a plasma column. It is interesting to note that the plasma columns were mostly

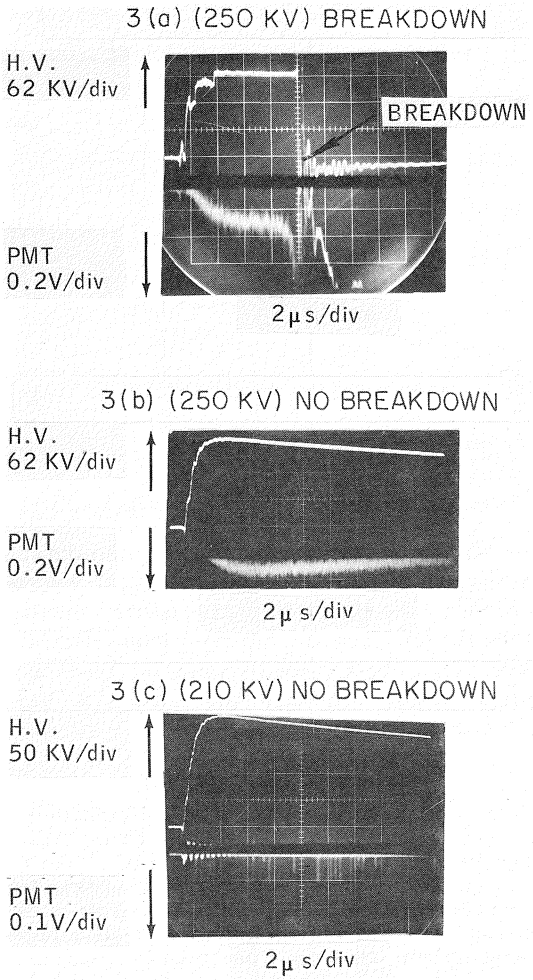

FIG. 3. Light emission from toluene.

crooked, suggesting they had been subjected to lateral forces.

In contrast to the breakdown events, the postbreakdown pictures (Figs. 6*a*, 6*b*, 6*c*, 6*d*) were marked by extensive propagation of shock waves from the plasma column. A very interesting feature was the carrier ejection from the anode electrode, moving in the cathodic direction. The structure never bridged the gap but became gradually more diffuse. (Compare Figs. 6*a* and 6*b* as well as Figs. 6*c* and 6*d*. The latter two pictures were taken more than 10 ns later with respect to the collapse of the electrical field than those shown in Figs. 6*a* and 6*b*.)

Discussion

The origin of micro-cavitation at the electrode–liquid interface has long been a topic of interest.

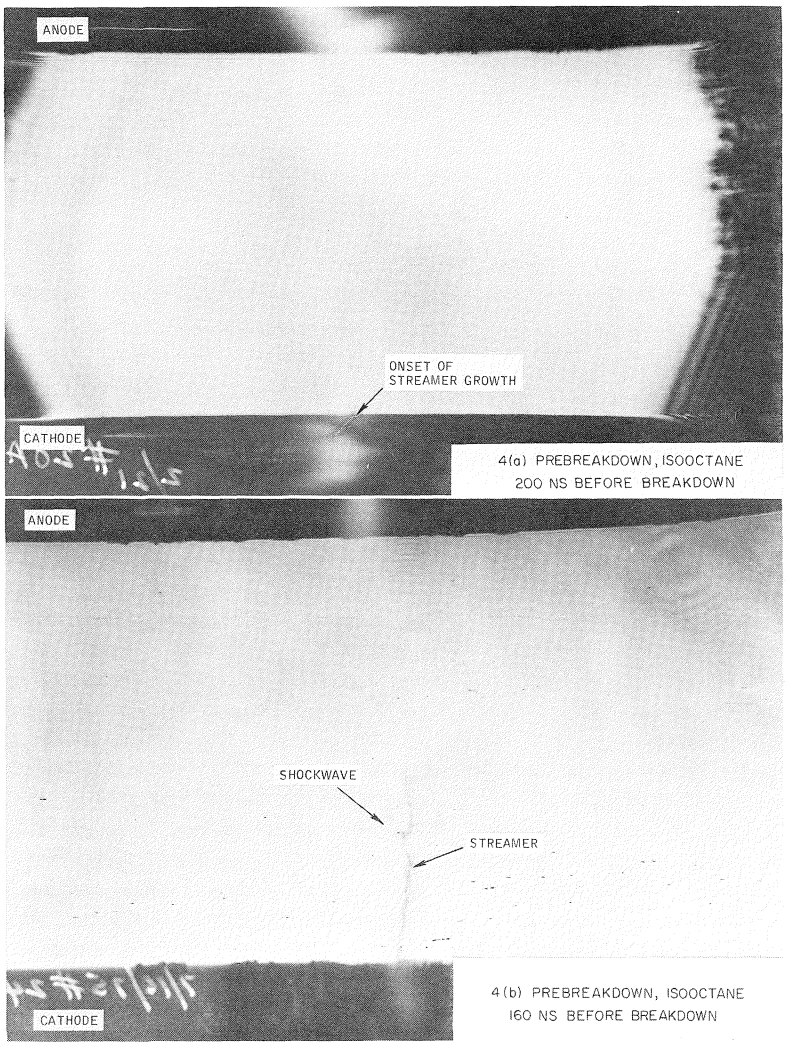

FIG. 4. Prebreakdown emission in isooctane.

Recently, a model for conduction and breakdown in liquids has been proposed by Thomas and Forster (6). The proposed scheme based on some two-dimensional calculations of Thomas (7) assumed that the electrons are being ejected from local asperities on the cathode surface by field enhancement. This agrees very well with the schlieren pictures that no streamer had been observed originating from within the liquid itself. Once the electron bombardment starts, the liquid will be heated locally. Together with an electron induced liquid motion, a region of low density will form and effectively increase the electron mean free path. The electrons, accelerated under the high electric field with fewer collisions, will gain more and more energy to cause impact excitation and/or ionization of the molecules. The excited molecules will emit light on decaying to lower energy quantum states. Within the low density region electron avalanche processes may develop leading to breakdown. The pattern of light emission will follow the growth or decay of these micro-cavities whose fate is determined by the flux of the ejected electrons.

The light emission data seem to support this growth–decay theory because the emitted light does show different degrees of intensities and occurrence rates, depending on the probability of having a breakdown. For the breakdown case,

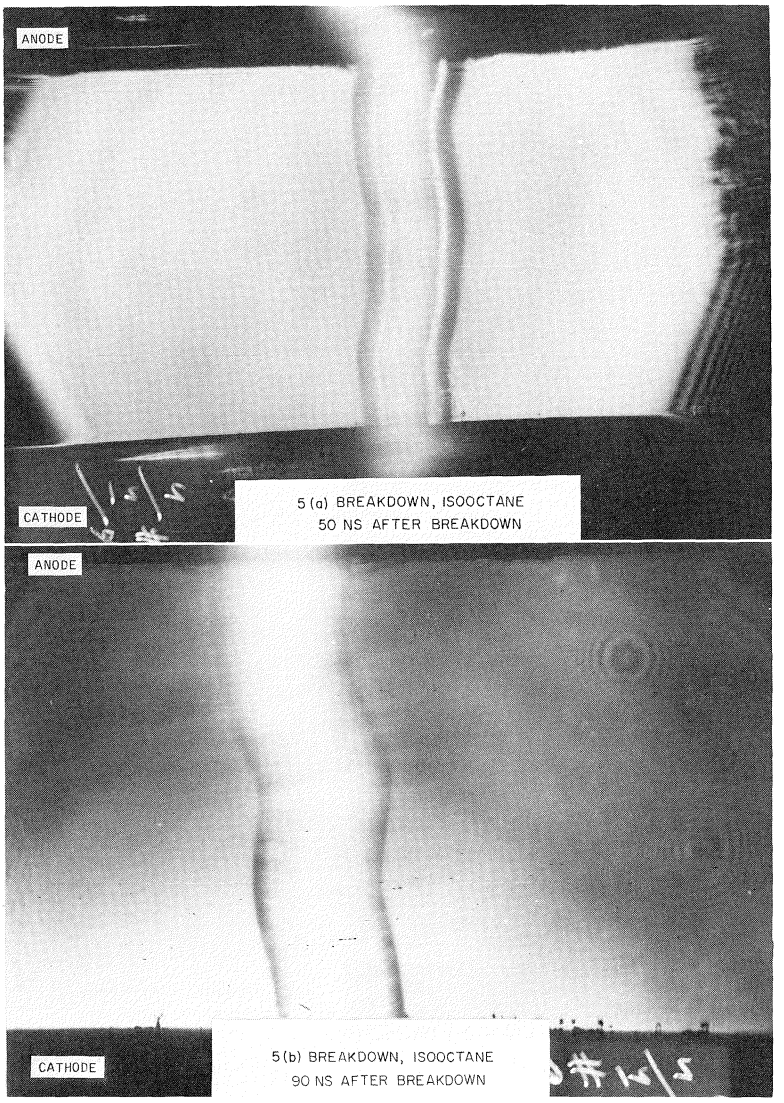

FIG. 5. Breakdown discharge in isooctane.

a rapid rise in light emission occurs just prior to breakdown. If there is no breakdown (applied voltage is the same), the light intensity will slowly decay, as shown in Fig. 3*b*. When the applied voltage is much below the breakdown strength, it is possible to observe isolated light pulses as shown in Fig. 3*c*. The last two cases indicate that the ejected electrons do not have enough energy to sustain cavitation growth long enough to create an avalanche.

When these cavities do grow, the high electric field will elongate the cavity into a streamer (a filamentary cavity with a plasma inside). Inspection of Fig. 4*b* reveals that small shock waves had already been created.

As the streamer bridges the gap and forms a highly conductive path between the electrodes, high currents will be dumped through it. The tremendous ionization and the associated energy release will expand the filament into a column as shown in Figs. 5*a* and 5*b*. The plasma columns had been distorted laterally in both cases, suggesting that the perturbing force most likely is the Lorentz force between the discharge

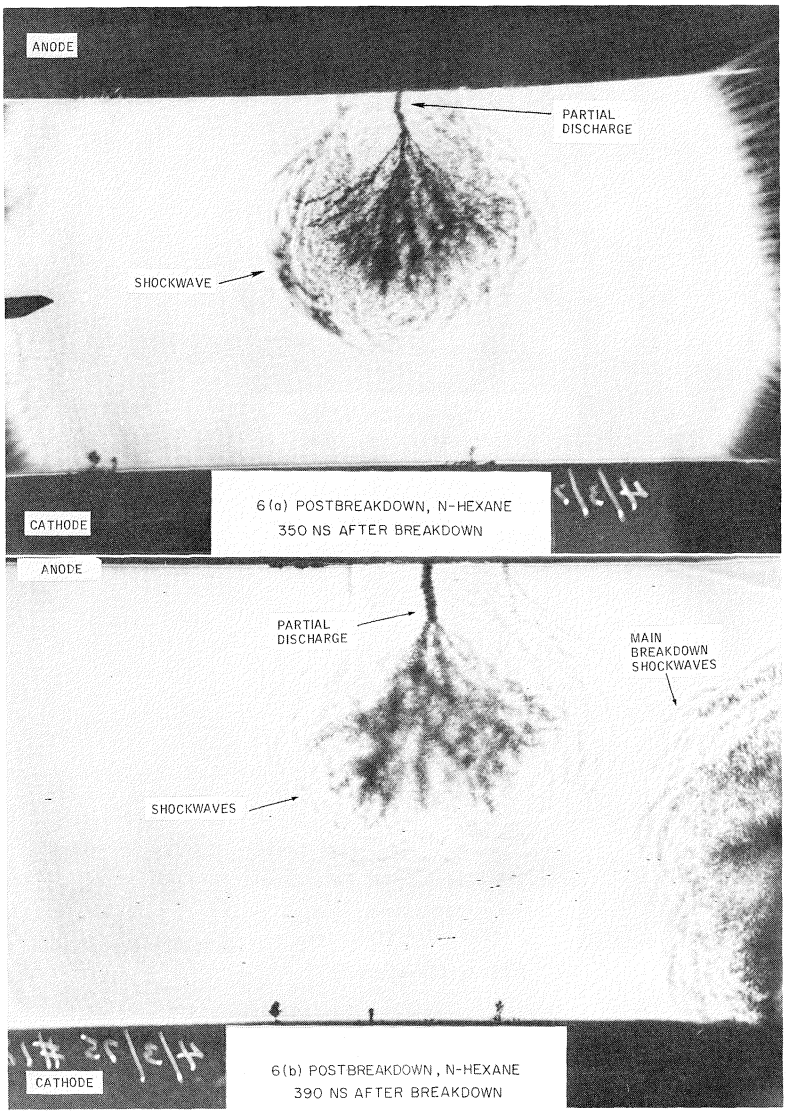

FIG. 6. Postbreakdown discharges and shock waves in *n*-hexane and in benzene.

current and the magnetic field induced by the current.

The current passing through such a column had experimentally been verified to be in excess of 5000 A. Using a diameter of 1 mm for the plasma column, the magnetic field at the column boundary was calculated to be in excess of 10 kG. The magnetic field distribution will be asymmetric if the column does not arc at the center of electrodes. The Lorentz force acting on the column will have a net force to push it outward and create a kink instability (8) in the plasma column. The physical explanation for the instability is illustrated in Fig. 7. The magnetic field is obviously stronger on the compressed side than on the stretched side, creating further asymmetry and the kink continues to grow. In the electrical breakdown case, the kink instability will eventually be limited by surface tension and hydrostatic pressure of the liquid.

The electrical breakdown is a high-power process, as evidenced by the postbreakdown photographs. By taking 3 pF as the electrode capacitance, an impulse breakdown of 250 kV

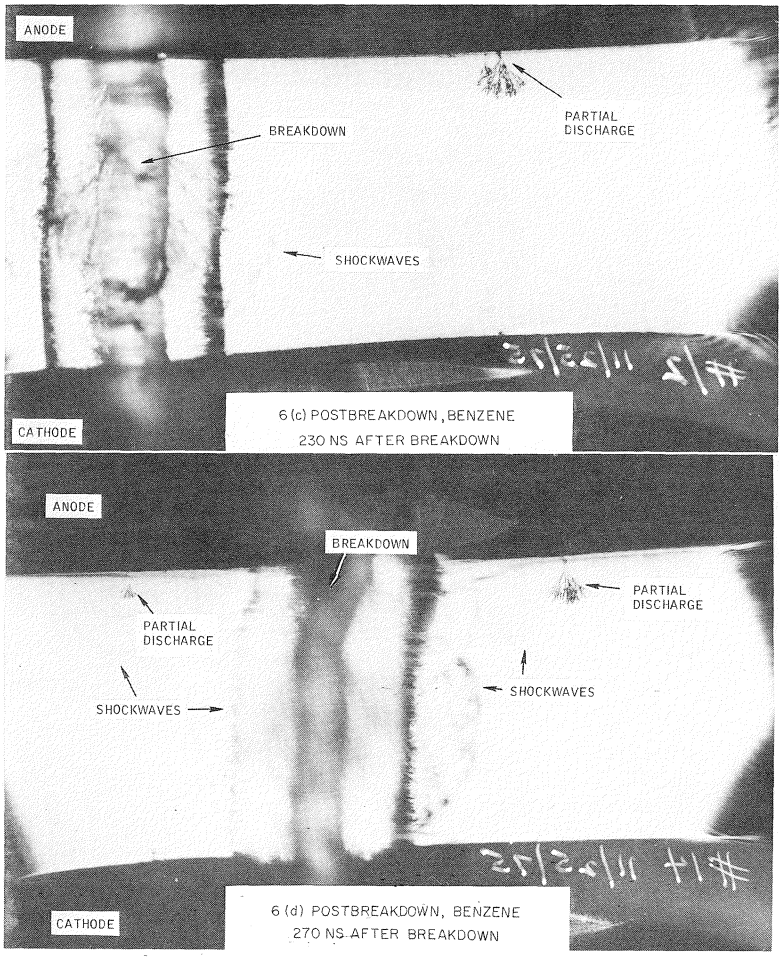

FIG. 6. (*Concluded*)

lasting 500 ns has associated with it a power of 2 MW. With that power being dissipated inside the 1 mm diameter plasma column, it is not surprising to observe significant shock waves. The Joule heating is probably extremely high. Graphitic structures had been identified by transmission electron microscopy of residues removed from the liquid after several breakdowns. This finding implies a spark temperature in excess of 1400°C.

Another noticeable feature of postbreakdown events is the electron ejection from the anode shown in Fig. 6. As shown in the Appendix, the field reversal caused by prebreakdown space charge distribution can turn the anode into a 'virtual cathode'. Curve *b* of Fig. 9 shows such a field profile. Since the negative field decreases gradually to zero at some distance away from

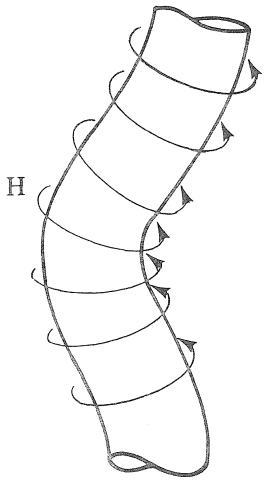

FIG. 7. Kink instability of plasma column.

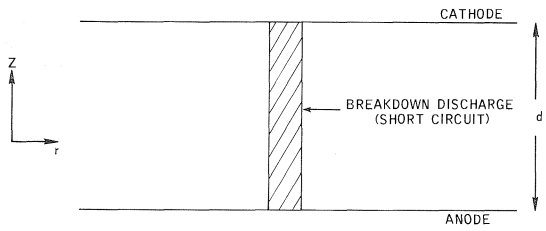

FIG. 8. Coordinate system for the plane–plane geometry.

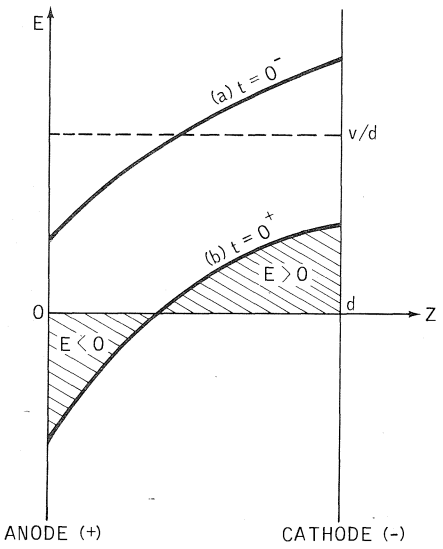

FIG. 9. Electric field distribution due to space change effects: (*a*) at $t = 0^-$, before breakdown; (*b*) at $t = 0^+$ after breakdown.

the anode, it explains very well why the propagation pattern of these ejected electrons is much slower and more diffuse than the streamers in the prebreakdown cases. Propagation of these electrons is further impeded by the decaying *E*-field because eventually $\boldsymbol{E}$ will be zero everywhere following redistribution of the space charges.

Conclusions

Although the available data are not extensive, they have shown convincingly the development of various stages of electrical breakdown in liquid hydrocarbons. While the overall patterns in these stages seem the same for the four liquids tested, it appears that there exist definite differences in the fine structures. These differences may well be due to the differences in molecular structures of the liquids. Fine details of the schlieren pictures have been explained in terms of classical electromagnetic theory. With improved instrumentation, which will include a self-triggering device based on the early light emission, it should become possible to test these explanations quantitatively.

1. B. FARAZMUND. Br. J. Appl. Phys. **12**, 251 (1961).
2. S. S. HAKIN and J. B. HINGHAM. Proc. Phys. Soc. **80**, 190 (1962).
3. W. G. CHABAND and G. T. WRIGHT. Br. J. Appl. Phys. **16**, 305 (1965).
4. W. R. L. THOMAS. 1973 annual report, conference on electrical insulation and dielectric phenomena. National Academy of Science, Washington, D.C. 1974. p. 130.
5. C. W. SMITH, K. C. KAO, J. H. CALDERWOOD, and J. D. MCGREE. Nature, **210**, 192 (1966).
6. W. R. L. THOMAS and E. O. FORSTER. Proceedings of the 5th International Conference on Conduction and Breakdown in Dielectric Liquids, Delft, Delft University Press, Netherlands. 1975. p. 49.
7. W. R. L. THOMAS. 1974 annual report, conference on electrical insulation and dielectric phenomena. National Academy of Science, Washington, D.C. 1975. p. 540.
8. S. GLASSTONE and R. H. LOVBERG. Controlled thermonuclear reactions. Van Nostrand, Princeton. 1960. p. 263.

Appendix. Field Reversal Due to Space Charge Effects

When a dielectric medium is under dc electric stress, the field strength inside the dielectric may no longer be uniform due to the pile-up of space charges. Such a nonuniform field configuration can be calculated by Poisson's equation if the charge distribution is known. For a plane–plane electrode geometry (Fig. 8), such a field distribution $\boldsymbol{E}^0(z)$ is drawn in Fig. 9 as curve *a*. Just after electrical breakdown, the applied voltage V is short-circuited by the discharge plasma column. If we denote the new electric field distribution as $\boldsymbol{E}(z)$, we arrive at the two relationships

$$[1] \qquad \int_0^d E^0(z)\,dz = V \qquad \text{at } t = 0^-$$

$$[2] \qquad \int_0^d E(z)\,dz = 0 \qquad \text{at } t = 0^+$$

Physically, it is reasonable to assume that space charges in the bulk liquid take time to redistribute themselves because of their finite mobility. Therefore, the charge distributions $q(r)$ are the same at $\tau = 0^-$ and $\tau = 0^+$. Since both $E^0(z)$ and $E(z)$ have to satisfy Poisson's equation, one obtains

[3] $$\partial E^0/\partial z = \partial E/\partial z = q(r)/\varepsilon$$

From [3], one can derive that

[4] $$E = E^0 + K$$

where K is a constant. Combining [4], [1], and [2], one obtains the final result:

[5] $$K = -V/d$$

Therefore, the new $\boldsymbol{E}(z)$ distribution will just have the same profile as $\boldsymbol{E}^0(z)$ except that it has been pulled *down* by an amount of V/d. This new distribution is plotted as curve *b* in Fig. 9. It is obvious from the curve that the condition

$$\int_0^d E\,\mathrm{d}z = 0$$

requires a negative E-field at the anode.

Discussion

P. K. Watson: The authors observe emission events at the anode, following breakdown; apparently this electrode is acting as a cathode during the post-breakdown period and this is due to field reversal in the gap. There are two possible reasons for field reversal: (*i*) internal space charge in the gap, and (*ii*) reversal of applied voltage following breakdown. There is undoubtedly a buildup of negative space charge in the gap due to the pre-breakdown electron emission, and when the applied voltage collapses at breakdown this internal space charge causes a field reversal; this is the process favoured by the authors. However, this space charge field will be very nonuniform and its effect will be most strongly felt in the vicinity of the breakdown channel; it is difficult to reconcile this with the authors' photograph which clearly shows back-discharge events occurring several millimetres away from the former breakdown channel. This suggests that the second reason for field reversal (*viz.* voltage reversal due to circuit transients) must also be included in the analysis.

G. R. Freeman: If you had a very efficient grounding of the anode, would the charge leak away fast enough that the field would not reverse?

E. O. Forster: This is a possibility. I doubt, however, whether the reversal can be reduced to zero. At present we are exploring this possibility by reducing all grounding connections to a minimum.

M. Pope: Since your electric field collapses during breakdown, what is the mechanism for the formation of additional breakdown figures during breakdown?

E. O. Forster: As discussed in the Appendix of our paper, the anode becomes a 'virtual' cathode at the surface of which electron emission occurs. Thus the mechanism of the formation of additional breakdown figures should be the same as that postulated to occur at the actual cathode in the pre-breakdown phase.

W. F. Schmidt: Why do these 'trees' have this short stem and then branch off? Why don't you see *e.g.* a bush-type?

E. O. Forster: The shape of the pre-breakdown and post-breakdown discharge channels, commonly referred to as 'trees', is a function of the electron emitting asperity (see ref. 4) as well as the molecular structure of the liquid (see ref. 5) and other parameters such as the local electrical field. For example the effect of molecular structure can be seen when comparing Figs. 6*a* and 6*b* with 6*c* and 6*d*. A closer look at the cathode surfaces shown in Fig. 6*a* and 6*b* reveal also a variety of 'tree-like' structures illustrating the influence of the structure of the emitting asperity.

L. Kevan: You showed the voltage reversing through several cycles in your initial slide. Can you see 'trees' growing from alternate electrodes with time?

E. O. Forster: No, our time resolution is inadequate for this purpose. The laser triggering technique is not, as yet, flexible enough to time in on these cycles.

L. G. Christophorou: How do electron scavengers affect the pictures you have presented?

E. O. Forster: So far we have been only concerned with very pure hydrocarbons to gain a basic understanding of the breakdown mechanism. Therefore we are unable to answer this question.

The role of electronic processes in the electrical breakdown of insulating liquids (Extended Abstract)

JOHN C. DEVINS, STEFAN J. RZAD, AND ROBERT J. SCHWABE
Corporate Research and Development, General Electric Co., Schenectady, NY, U.S.A. 12301
Received October 4, 1976

The present work has been aimed at revealing the particular electronic processes responsible for the sudden transition of an insulating liquid to a conductor under the influence of a sufficiently high electric field. This transient conducting state in the liquid can be observed by standard shadowgraphy or Schlieren optics (1–5) as a prebreakdown disturbance (streamer) with altered refractive index. We have measured, for point to plane geometries, the rate of streamer growth in a highly refined white mineral oil, Exxon Marcol 70. The voltage pulse (0.8/2500 μs) was supplied by a Marx generator and was chopped by a triggered spark gap. Observations were made between 0 to 150 μs. Steel needles were etched to a radius of approximately 1 μm. The plane was a polished stainless steel disk 10 cm in diameter with 1 cm radius edges. The electrodes were arranged in a 4 ℓ cylindrical Teflon cell provided with two optical windows, and the spacing was varied from 0.6 to 2.5 cm. The oil was generally degassed in the cell and measurements made under a 1 atm nitrogen blanket. Streamer velocities were the same with nitrogen-saturated and degassed oil (Fig. 4).

Positive and negative streamers are quite different as illustrated in Fig. 1 and Fig. 2. Typical propagation characteristics for these streamers are shown in Fig. 3, where we have plotted streamer length against time. The positive streamer velocity is remarkably constant during propagation across the gap for a given voltage suggesting a regulatory mechanism which maintains a constant field at its growing tip. On the other hand, as reported by Allan and Hizal (4), the negative streamers are much slower, and depending upon applied voltage, either develop to a constant length or speed up after crossing 50 to 60% of the gap. This is consistent with the picture proposed by Chadband and Wright (2) who approximate the negative streamer by a conducting plasma ball.

The effect of small amounts of a typical polyaromatic, 2-methylnaphthalene, is shown in Fig. 4. Both the positive and negative streamer velocities are increased with the largest concentration, *i.e.*, 7.3×10^{-2} *M*. With 7.3×10^{-3} *M*, the effect occurs only for the negative streamers.

Polyaromatics have two physical properties which may be relevant here, *i.e.*, low ionization potentials (6) and large electron trapping cross sections (7). To distinguish between these effects, we chose an additive which does not trap electrons (8), but which has an even lower ionization potential (6) than 2-methylnaphthalene (7.96 eV), *i.e.*, *N*,*N*′-dimethylaniline (DMA) (7.14 eV), and one which has a high ionization potential (9) (15.9 eV) and a large trapping cross section (7), sulfur hexafluoride. The results are shown in Fig. 5, where it is clear that the increase in negative streamer velocity is due to electron trapping. This was further substantiated using a second electron scavenger, ethyl chloride (7). It should be pointed out here that upon addition of the electron scavenger, the negative streamer becomes much more filamentary, resembling more the positive streamer. This is illustrated in Fig. 6. Neither of the electron scavengers had a measurable effect on the positive streamer velocity. The dimethylaniline, however, at concentrations above 7.9×10^{-2} *M*, accelerated the positive streamers to the same extent as did the 2-methylnaphthalene (up to a factor of *ca.* 2). Below the 7.9×10^{-2} *M* level, dimethylaniline, like 2-methylnaphthalene, did not alter the positive streamer velocity.

These results are difficult to explain in terms of the bubble mechanisms previously proposed for breakdown (10, 11), since small concentra-

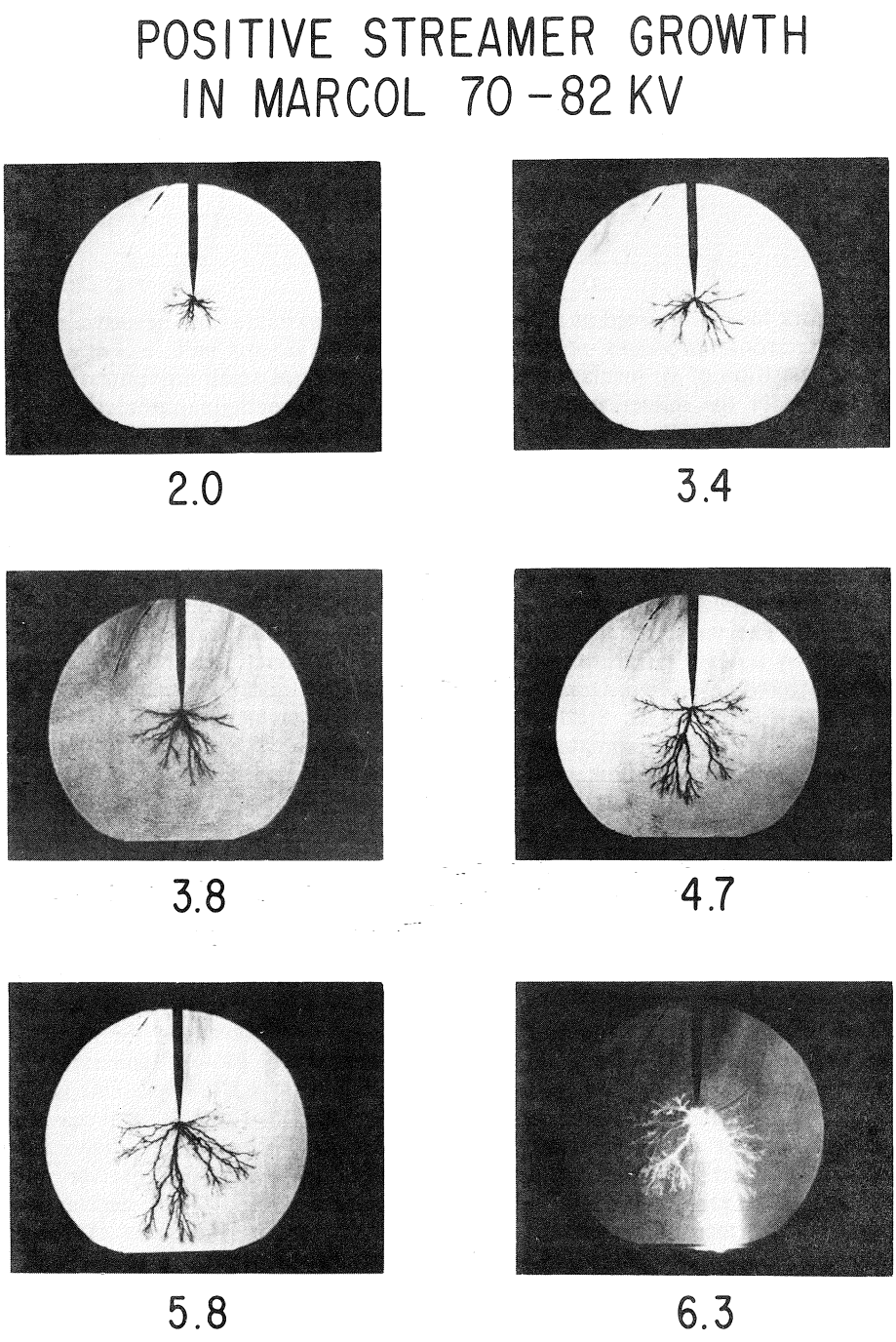

FIG. 1. Shadowgraphs of positive streamers in Marcol 70, time in microseconds.

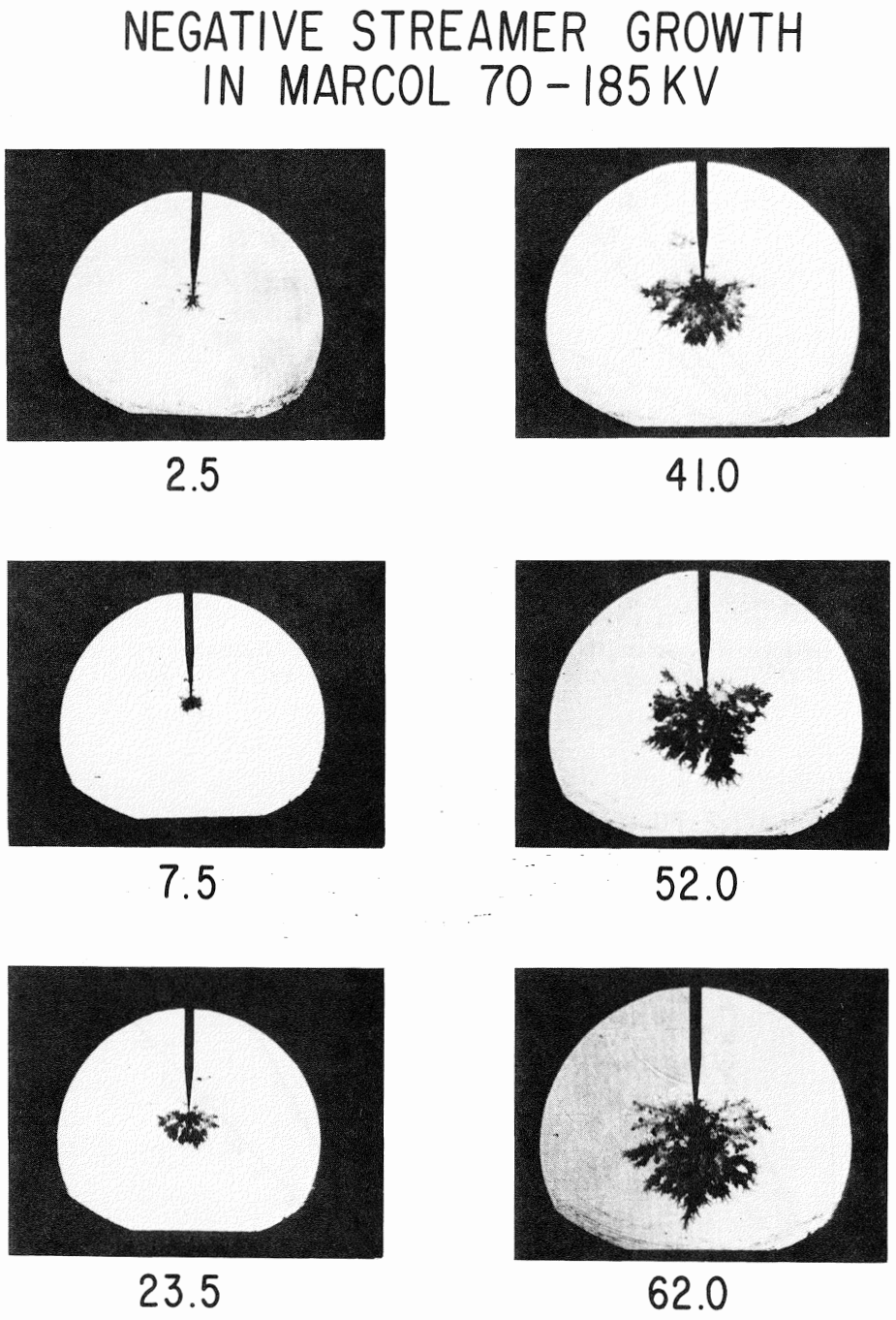

FIG. 2. Shadowgraphs of negative streamers in Marcol 70, time in microseconds.

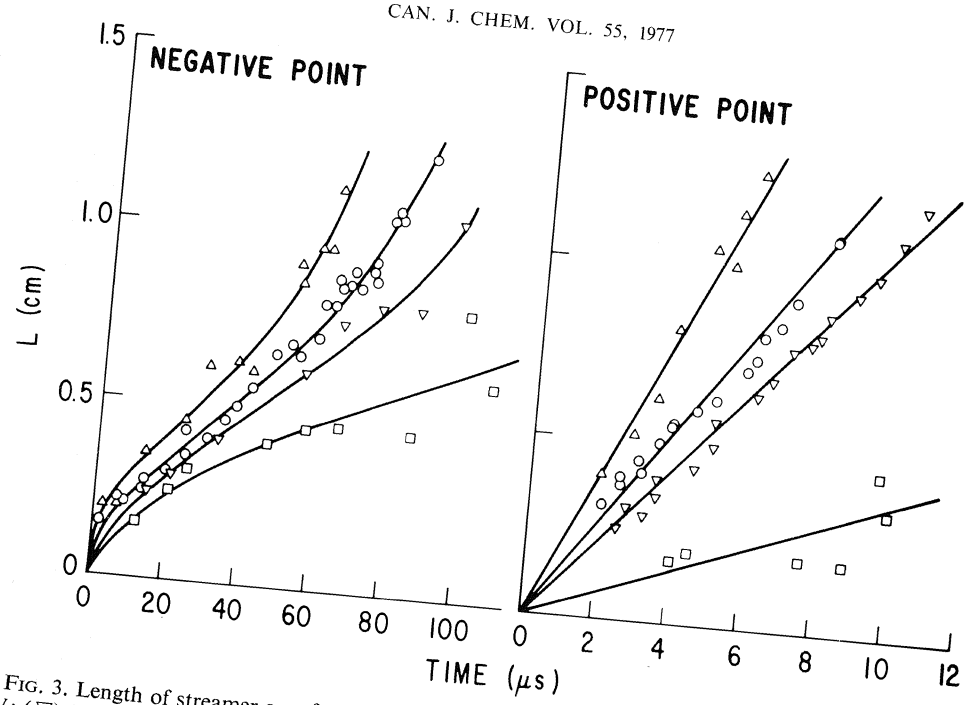

FIG. 3. Length of streamer as a function of time. Gap = 1.27 cm. Negative: (△) 185 kV; (○) 155 kV; (▽) 125 kV; (□) 100 kV. Positive: (△) 82 kV; (○) 60 kV; (▽) 45 kV; (□) 23 kV.

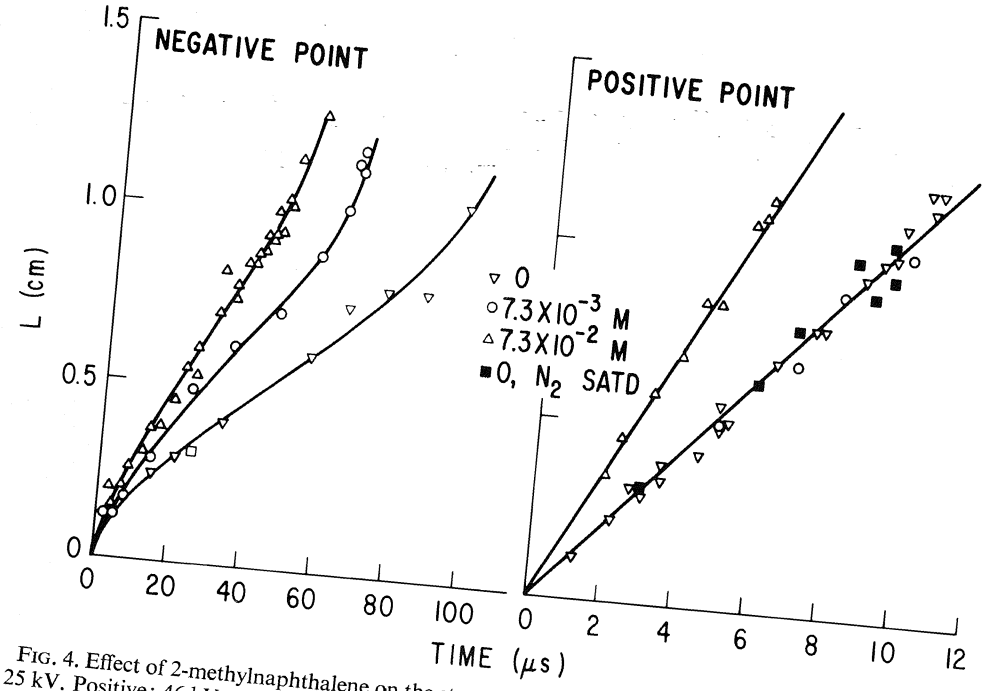

FIG. 4. Effect of 2-methylnaphthalene on the streamer propagation rates. Gap = 1.27 cm. Negative: 125 kV. Positive: 46 kV.

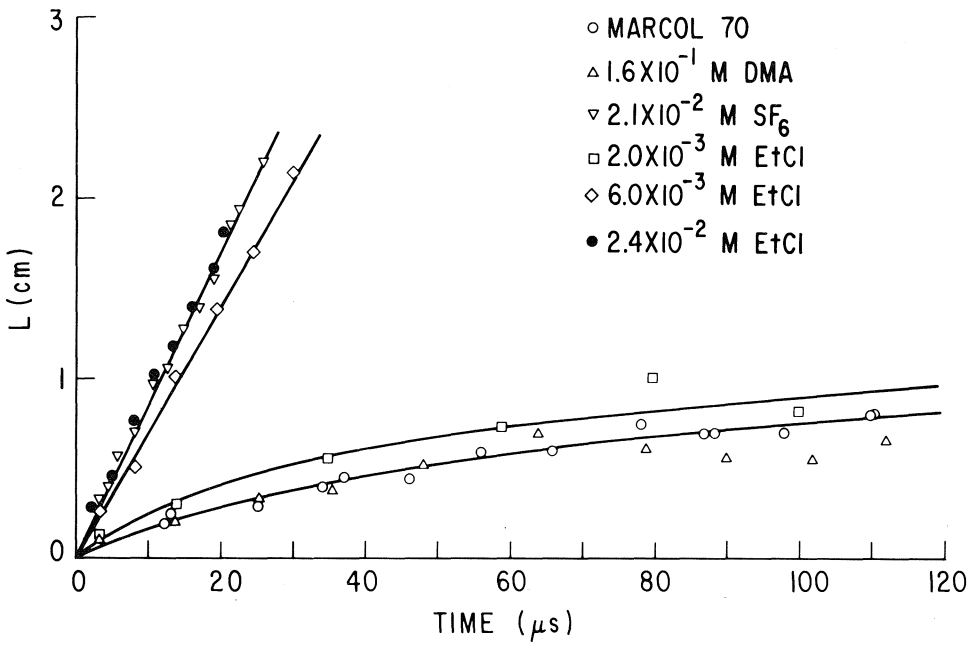

FIG. 5. Effect of several additives on the negative streamer propagation rates. Gap = 2.54 cm, 150 kV.

tions of our additives would not be expected to show such a large influence. Similarly, collisional ionization in the liquid is unlikely because of the lack of an effect of the electron scavengers, which should markedly decrease the avalanche size. However, the important role played by low ionization potential compounds in the development of the positive streamer could well be explained in terms of field ionization (12) at the propagating streamer tip. This phenomenon requires very large fields, 10^7–10^8 V cm^{-1}. Our measurements of the diameter of the tip of the growing positive streamer (15 μm) indicate that fields of this order of magnitude will occur if the potential at the tip is of the order of that applied to the needle.

For the negative streamer, we suggest a dual mechanism in which the velocity depends upon the time spent in two modes of propagation. The electrons injected from the cathode or the growing plasma become trapped at a certain distance depending upon the scavenger concentration. As the space charge builds up, the field at the space charge boundary increases while that at the emitter decreases. This will occur faster the greater the scavenger concentration, and will determine the fraction of time spent in this injection mode. When the field outside the boundary reaches a sufficiently high value, field ionization can occur and a positive-like streamer can develop locally. When the plasma density reaches a value sufficiently high to establish conductivity further injection of electrons will occur and the first mode will be reestablished. These processes will alternate as the streamer develops. Since high conductivity is established during field ionization, the current would be expected to be discontinuous. This was found to be the case experimentally, *i.e.*, the current consisted of a series of short (< 50 ns) pulses. This is quite different for the positive streamer where the current is continuous throughout its development.

The absence of an accelerating effect of dimethylaniline on the negative streamer development indicates that the velocity is determined primarily by the time spent in the injection mode. This suggests that the addition of an electron scavenger might reduce the latter time sufficiently so that the dimethylaniline effect could be observed. Such a synergistic effect of SF_6 and DMA is indeed observed. Thus, the addition of DMA to a solution of 2.1×10^{-2} *M* SF_6 in Marcol 70 produces no effect on the negative

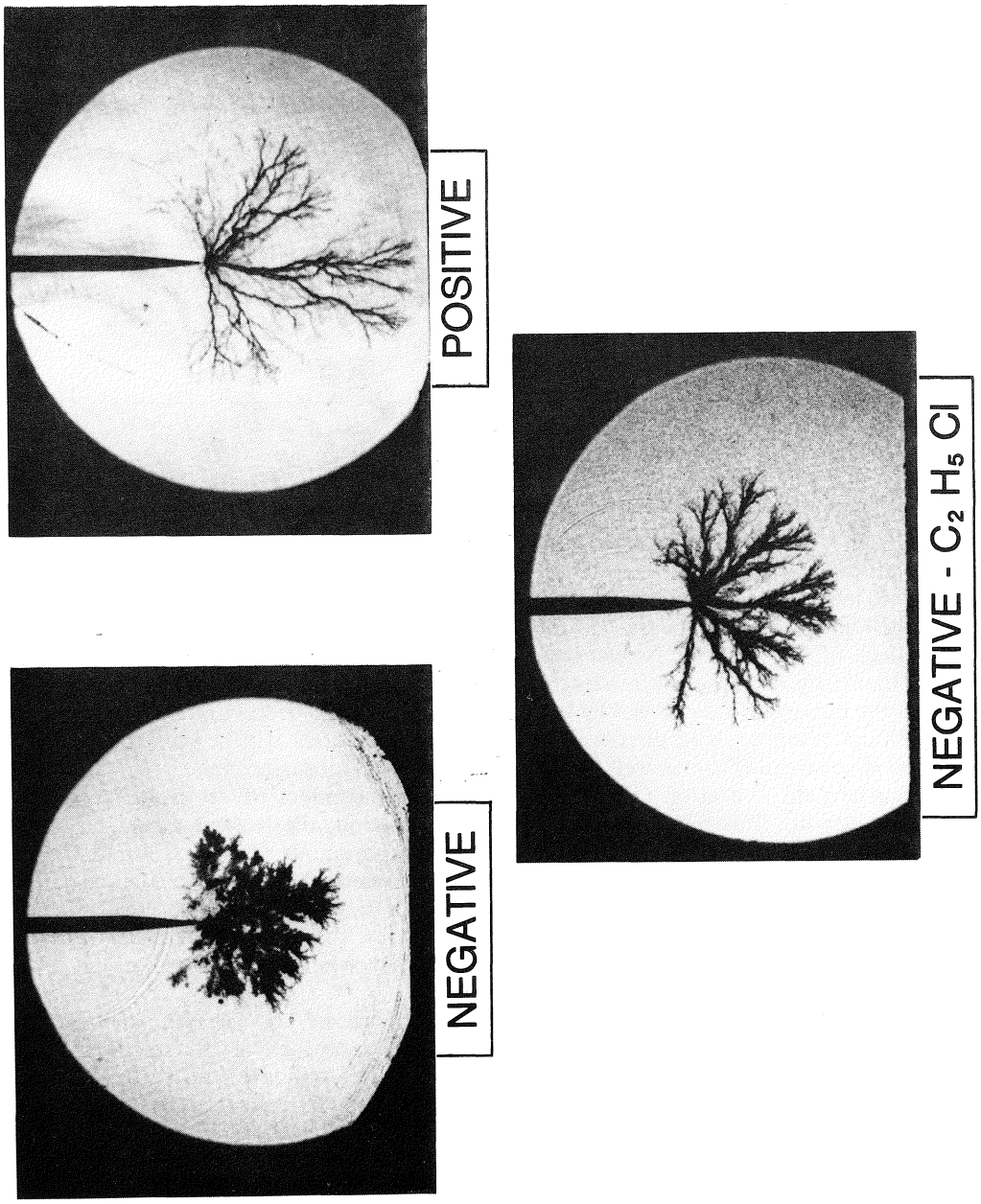

FIG. 6. Change of streamer pattern produced by ethyl chloride.

streamer velocity below 7.9×10^{-2}, and acceleration above this concentration, just as was observed with positive streamers.

1. B. FARAZMAND. Br. J. Appl. Phys. **12**, 251 (1961).
2. W. G. CHADBAND and G. T. WRIGHT. Br. J. Appl. Phys. **16**, 305 (1965).
3. E. MORIKAWA. Electr. Eng. Jpn. **92**, 11 (1972).
4. R. N. ALLAN and E. M. HIZAL. Proc. Inst. Electr. Eng. **121**, 227 (1974).
5. J. C. DEVINS, S. J. RZAD, and R. J. SCHWABE. J. Phys. D, **9**, 87 (1976).
6. R. P. BLAUNSTEIN and L. G. CHRISTOPHOROU. Radiat. Res. Rev. **3**, 69 (1971).
7. A. O. ALLEN, T. E. GANGWER, and R. A. HOLROYD. J. Phys. Chem. **79**, 25 (1975).
8. E. L. DAVIDS, J. M. WARMAN, and A. HUMMEL. J. Chem. Soc. Faraday Trans. I, **71**, 1252 (1975).
9. F. H. FIELD and J. L. FRANKLIN. Electron impact phenomena. Academic Press, New York. 1957.
10. Z. KRASUCKI. Proc. R. Soc. London Ser. A, **294**, 393 (1966).
11. A. H. SHARBAUGH and P. K. WATSON. Progr. Dielectr. **4**, 244 (1962).
12. H. C. ZENER. Proc. R. Soc. London, **145**, 523 (1934).

Discussion

L. G. Christophorou: I wish to point out that in breakdown work (both in liquids and gases) one should not only consider electron scavengers but also electron thermalizers. The latter are important in that by slowing down electrons make their scavenging more efficient, while the former should be such as to capture electrons over as wide an energy range as possible (0 to ~1.5 eV).

S. J. Rzad: If only thermalisation by SF_6 and C_2H_5Cl was occurring it is very difficult to understand why the negative streamer would accelerate. If thermalisation were affecting the rate of scavenging the end result would be the same as in our experiments.

W. F. Schmidt: Couldn't the enhancement of the negative streamer velocity by the addition of a scavenger be due to a more efficient momentum transfer from the ions to the liquid as compared to electrons?

S. J. Rzad: The fact that an order of magnitude change in viscosity hardly affects the streamer velocity suggests that momentum transfer from the ion does not play an important role in determining the streamer velocity.

Electrons in fluids: the role of disorder[1]

MORREL H. COHEN

Department of Physics and The James Franck Institute, The University of Chicago, Chicago, IL, U.S.A. 60637

Received October 18, 1976

MORREL H. COHEN. Can. J. Chem. **55**, 1906 (1977).

I review the present status of the theory of those aspects of the theory of disordered materials which are particularly relevant to the physics of electrons in fluids. First, however, I describe a general theory of the movement of slow electrons in fluids of arbitrary complexity in which the fluid is treated as a fluctuating medium. Coupling to the fluctuations is via a set of generalized deformation potentials. It is shown that this concept permits a way out of the impasse that has been reached in understanding the mobility of slow electrons in liquid argon via Lekner's theory. Assuming that molecular motion can be neglected on the electronic time scale permits taking over various relevant results from the theory of electrons in disordered solids, which is briefly reviewed. The effect of molecular motion is studied next. It is shown that strict localization does not occur and that the quasi-localized electrons diffuse with a characteristic correlation frequency depending on electron–molecule coupling and upon the characteristic frequencies of molecular motion as well as with a correlation length related to the localization length in static problems. Under easily reached conditions, this diffusion process is faster than that giving rise to the Stokes law mobility. Finally, a discussion is given of mobility transitions in which localization by disorder is distinguished from self-trapping.

MORREL H. COHEN. Can. J. Chem. **55**, 1906 (1977).

Je présente une revue de l'état actuel de la théorie des aspects de la théorie des matériaux désordonnés qui ont un intérêt particulier pour la physique des électrons dans les fluides. Je décris toutefois en premier lieu une théorie générale du mouvement des électrons lents dans les fluides de complexité arbitraire dans laquelle le fluide est considéré comme un milieu en fluctuation. Le couplage aux fluctuations se fait par l'intermédiaire de potentiels à déformation généralisés. On montre que ce concept permet de sortir de l'impasse qui a été atteinte lorsque l'on essaie de comprende la mobilité des électrons lents dans de l'argon liquide par l'intermédiaire de la théorie de Lekner. Faisant l'hypothèse que le mouvement moléculaire peut être négligé à l'échelle de temps électronique, il est permis d'utiliser divers résultats appropriés provenant de la théorie des électrons dans des solides désordonnés que l'on passe rapidement en revue. On étudie ensuite l'effet du mouvement moléculaire. On montre que la localisation stricte ne se produit pas et que les électrons pratiquement localisés se diffusent avec une fréquence de corrélation caractéristique dépendant du couplage électron–molécule et aussi des fréquences caractéristiques du mouvement moléculaire ainsi qu'avec une longueur de corrélation qui est reliée avec la longueur de la localisation dans les problèmes statiques. Utilisant des conditions qui sont facilement atteignables, ce processus de diffusion est plus rapide que celui donnant lieu à la loi de mobilité de Stokes. Finalement, on présente une discussion des transitions de mobilité dans laquelle la localisation par le désordre peut être distinguée de l'autopiégeage.

[Traduit par le journal]

I was asked to review for this conference the theory of electronic states in disordered materials. This subject has been extensively reviewed recently (1–4), and it seems more appropriate to confine my remarks to those aspects of it most relevant to electrons in fluids. States of electrons in liquid metals and liquid semiconductors will be discussed during the conference but much has been written elsewhere about the relevant theory. Accordingly, I shall concentrate on the role of disorder in determining the states of excess electrons in fluid insulators, in molecular fluids in particular. However, it is not possible to confine oneself to disorder. Other matters must be discussed for proper perspective to arise: behavior of quasi-free electrons, self-trapped electrons, and basic conceptual questions. Accordingly, in Section I we develop a general model for describing the movement of slow electrons in fluids of arbitrary complexity. In the model, the fluid is treated as a fluctuating medium and coupling to the fluctuations is via a set of generalized deformation potentials. The model provides the basic theore-

[1]Research supported by NSF DMR75-13343, The Louis Block Fund, and the Materials Research Laboratory of the National Science Foundation at The University of Chicago.

tical framework for discussion of the issues raised above. In Section II, it is shown that such a model provides a way out of the impasse that has been reached in understanding the mobility of slow electrons in liquid argon. The central purpose of this talk, a brief review of relevant results from the theory of disorder, is met in Section III, where it is supposed that molecular motion can be neglected on the electronic time scale. Such is not always the case for thermal electrons in molecular fluids, and the effect of molecular motion is discussed in Section IV. It is shown there that strict localization no longer occurs, and the diffusion of quasi-localized electrons is discussed semiquantitatively. This dynamical localization must be distinguished from self-trapping, and in Section V we give a discussion of the consequences of these two forms of localization for mobility transitions.

In preparing this review, I was struck repeatedly by how little we really know, and how many basic questions remain unnoticed or shunted aside and unanswered in either event. This point will be well illustrated in what follows.

I. Preliminaries

We consider the motion of an excess electron added to an insulating molecular fluid. The total Hamiltonian of the system fluid plus electron is

$$[1] \qquad \mathscr{H} = \frac{p^2}{2m} + V(\boldsymbol{r};\boldsymbol{r}_i,\boldsymbol{R}) + \mathscr{H}_{\text{FLUID}}$$

in which the first term is the electron's kinetic energy, the last term is the Hamiltonian of the fluid, which need not be specified, and the second term is the interaction potential V between electron and fluid. At the present *molecular level of description*, V depends on electron position, on the set of positions $\boldsymbol{r}_i$ of all electrons bound within the molecules, and on the set of all nuclear positions $\boldsymbol{R}$.

The structure of the problem can be simplified by introducing an adiabatic approximation which has two parts. First, the internal electrons move rapidly with respect to the excess electron. This permits replacement of the instantaneous interaction in [1] by one which has been averaged over the intramolecular motion of the internal electrons in the presence of an excess electron fixed at $\boldsymbol{r}$. Second, the excess electron moves rapidly with respect to the nuclei. This permits solution for the motion of the excess electron keeping the nuclei fixed. The problem splits into two parts. In the first part, the motion of the electron is determined from

$$[2] \qquad \mathscr{H}_e(\boldsymbol{R})\,\psi(\boldsymbol{r},\boldsymbol{R}) = E_e(\boldsymbol{R})\,\psi(\boldsymbol{r},\boldsymbol{R})$$

where

$$[3] \qquad \mathscr{H}_e(\boldsymbol{R}) = \frac{p^2}{2m} + V(\boldsymbol{r},\boldsymbol{R})$$

In [2] $\psi(\boldsymbol{r},\boldsymbol{R})$ is the wave function of the excess electron, and in [3] $V(\boldsymbol{r},\boldsymbol{R})$ is the average of the potential $V(\boldsymbol{r};\boldsymbol{r}_i,\boldsymbol{R})$ in [1] over internal electronic motion for fixed $\boldsymbol{r}$ and $\boldsymbol{R}$. The potential $V(\boldsymbol{r},\boldsymbol{R})$ is only statistically defined through the probability distribution $P(\boldsymbol{R})$ of the nuclear coordinates. It is at this point that the fluid can appear as a disordered material with regard to the motion of the electron. Whether disorder is important depends on the amplitudes of the important fluctuations in $V(\boldsymbol{r},\boldsymbol{R})$ and whether one can escape with neglect of the time dependence of the nuclear positions.

The probability distribution $P(\boldsymbol{R})$ can be obtained self-consistently from the Hamiltonian governing the nuclear motion in the adiabatic approximation

$$[4] \qquad \mathscr{H}'_{\text{FLUID}} = \bar{\mathscr{H}}_{\text{FLUID}} + E_e(\boldsymbol{R})$$

where the bar over $\mathscr{H}_{\text{FLUID}}$ on the right-hand side of [4] is meant to indicate that the motion of the internal electrons has been appropriately eliminated. There are two limiting cases commonly considered. The first is that $P(\boldsymbol{R})$ is largely unaffected by the presence of the excess electron. This is the case, for example, in high mobility fluids such as liquid argon (5, 6) or when the mobility transition occurs by Anderson–Mott localization (1–4, 7, 8). The other occurs when $P(\boldsymbol{R})$ is profoundly modified as, for example, in cavity formation (9) or, more generally, self-trapping.

Suppose now that we consider solution of [2] in a nuclear configuration not very different from those most probable in the unperturbed fluid for the ground state energy and wave function, *i.e.*

$$[5] \qquad \mathscr{H}_e\,\Psi_0(\boldsymbol{r},\boldsymbol{R}) = V_0(\boldsymbol{R})\,\Psi_0(\boldsymbol{r},\boldsymbol{R})$$

where $\Psi_0(\boldsymbol{r},\boldsymbol{R})$ is the excess electron's ground state for the configuration $\boldsymbol{R}$ and $V_0(\boldsymbol{R})$ is the corresponding position of the bottom of the conduction band. Ψ_0 and V_0 still depend implicitly on all the microscopic configurational coordinates $\boldsymbol{R}$. This is both inconvenient and unnecessarily complex. Accordingly, we state

without proof that only certain local configurational coordinates $X_i(\boldsymbol{r})$ derived from these are important in determining the features of Ψ_0, V_0, and other quantities of central interest in typical experiments. We choose, for example, for the $X_i(\boldsymbol{r})$ the molecular number density $n(\boldsymbol{r})$, a unit vector specifying the mean local molecular orientation $\hat{d}(\boldsymbol{r})$ (the directrix of liquid-crystal theory) for a fluid containing symmetric aspherical molecules or an appropriate tensorial generalization for totally asymmetric molecules, the local molecular polarization $\boldsymbol{P}_M(\boldsymbol{r}')$ for a fluid containing polar molecules, and finally the local electronic polarization $\boldsymbol{P}_e(\boldsymbol{r}')$. The set $X_i(\boldsymbol{r})$ may be extended or reduced according to the microscopic character of the particular fluid.

The short distance modulations of Ψ_0 which correspond to the details of motion between and into the molecules are not among the features of specific interest to us. Rather, we are interested in variations which occur on the scale of its de Broglie wavelength, many molecular separations, that is in the 'smooth' part of Ψ_0, smooth in the sense of pseudopotential theory (10). We once again state without proof that arguments akin to those of pseudopotential theory and effective-mass theory for crystals can be found which lead to an effective Hamiltonian

$$[6] \qquad \mathscr{H}_{\text{EFF}} = \frac{p^2}{2m^*} + V_0(\boldsymbol{r}, X_i(\boldsymbol{r}'))$$

for the 'smooth' part of the wave function.

The effective Hamiltonian [6] simplifies for the case of small fluctuations $\Delta X_i = X_i - \overline{X}_i$, where $\overline{X}_i$ is the thermodynamic average of X_i in the unperturbed fluid,

$$[7] \qquad \mathscr{H}_{\text{EFF}} = \frac{p^2}{2m^*} + \overline{V}_0 + \sum_i \int V_0{}^i(\boldsymbol{r},\boldsymbol{r}') \times \Delta X_i(\boldsymbol{r}')\, \mathrm{d}^3 r'$$

The nonlocal terms in [7] give the contribution of distant polarized regions. The contributions of density and orientation fluctuations can be taken as local. For example in a simple fluid in circumstances in which the long-range contributions of the electronic polarization are unimportant, the only relevant X_i is the density n so that

$$[8] \qquad \mathscr{H}_{\text{EFF}} = \frac{p^2}{2m^*} + \overline{V}_0 + \overline{V}_0'\Delta n(\boldsymbol{r})$$

This Hamiltonian has precisely the same form as that of an electron in a crystal interacting with density variations produced by longitudinal acoustic phonons. $\overline{V}_0'$ is thus a deformation potential coefficient, and the $V_0{}^i(\boldsymbol{r},\boldsymbol{r}')$ may be regarded as generalized deformation potential coefficients.

II. Excess Electron Mobility in Liquid Argon, a Test of the Medium Description

We have sketched in Fig. 1 the potential $V(\boldsymbol{r},\boldsymbol{R})$ entering [3] in a simple liquid such as argon. Between the atoms there is a local maximum in the potential which has the average value U_0. This background potential U_0 consists primarily of a superposition of screened polarization interactions of the electrons with the individual atoms. Subtracting U_0 leaves a superposition of potentials localized about each atom which can be regarded as scattering potentials and characterized by a scattering length a, *cf.* Lekner (11). The scattering length is positive as for a repulsive potential, which can easily be understood in terms of pseudopotential theory. The value of $\overline{V}_0$ can now be easily estimated by means of the Wigner–Seitz approximation (9)

$$[9] \qquad \overline{V}_0 \cong \frac{\hbar^2 k_0{}^2}{2m} + U_0$$

where the first term is the kinetic energy associated with avoiding the molecular interiors. In the low density limit, it reduces to the optical model (12)

$$[10] \qquad \frac{\hbar^2 k_0{}^2}{2m} \xrightarrow[n\to 0]{} \frac{\hbar^2}{2m} 4\pi n a$$

Using this physical picture, Lekner (11) treated each atom as a single, independent scatterer of cross section $4\pi a^2$ and obtained an excellent fit to the full field dependence of the drift velocity

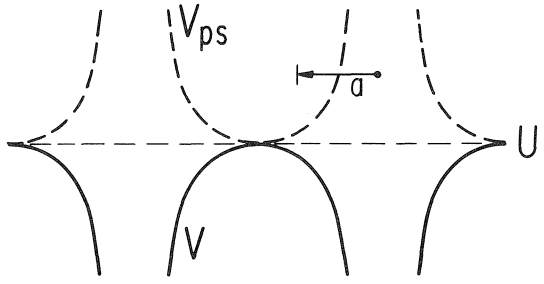

FIG. 1. The potential V within a simple liquid such as argon (schematic). U_0 is the background potential ($U_0 < 0$) above which a pseudopotential V_{ps} rises within each atom which defines a positive scattering length a for each atom in the liquid.

of excess electrons (13) in liquid argon at its triple point (84 K) (5). Jahnke *et al.* (6) extended the earlier mobility measurements of Schnyders *et al.* (5) to a wide range of densities at several pressures. They found a striking maximum in the mobility at 0.012 $Å^{-3}$. Lekner (14, 15) then proposed that a goes to zero at that density, a Ramsauer effect, and that fluctuations in a, $(\Delta a)^2$, kept the mobility finite. Jahnke *et al.* (16) searched for this effect, using Lekner's theory for the calculation of a. They found that a does not vanish in the observed range of densities and generally has the wrong density dependence to account for the data. Because this discrepancy can be interpreted as weakening the entire physical picture of electrons in fluids built up around the V_0 concept, now of central importance in the field, Basak and I have reexamined the matter.

We noted that in Lekner's theory of the scattering of an electron by the fluid (6, 13), the actual scattering occurred coherently from density fluctuations on the scale of the thermal wavelength of the electron. He therefore should have used the deformation potential in [8] as the scattering potential and not the potential associated with an individual atom; he coupled the electron incorrectly to the density fluctuations. Two errors are involved. The first is the neglect of multiple scattering included in the Wigner–Seitz energy $\hbar^2 k_0^2/2m$. The second is the neglect of the density dependence of the scattering length itself and of U_0. From the low density form of V_0, [9] and [10], we obtain

$$[11] \quad V_0' = \frac{\hbar^2}{2m} 4\pi a + \frac{\hbar^2}{2m} 4\pi n a' + U_0'$$

The first term alone, when used in the Born approximation for scattering, gives the Lekner theory. The remaining two terms are absent in the Lekner theory. In Fig. 2, the density dependence of the first term and of the total are shown. One sees that the first term is practically independent of density, whereas $|V_0'|$ has a minimum at a density equal to that of the observed mobility maximum. In calculating the terms of [11], we used the results of Jahnke *et al.* (16). Using the full Wigner–Seitz theory does not affect the conclusions.

These results give a simple physical explanation of the mobility maximum and provide the basis for a detailed semiphenomenological theory of the mobility which accounts well for the observed density dependence of the mobility. They provide an example of the utility of the medium description for long-wavelength, small-fluctuation phenomena.

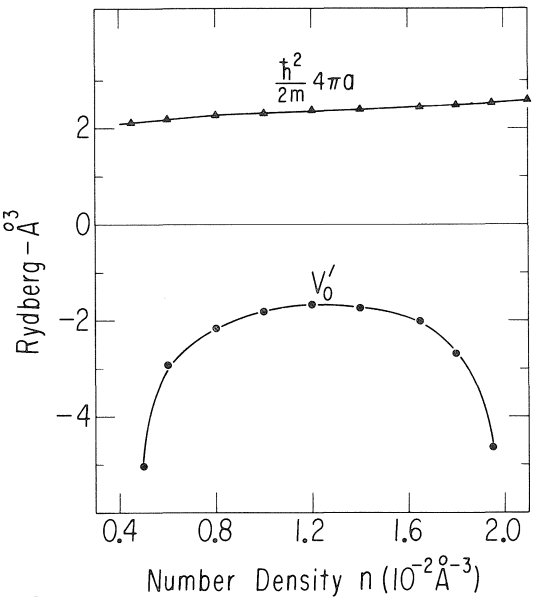

FIG. 2. Density dependence of V_0' in the optical model, [11], and of the first term, $(\hbar^2/2m)4\pi a$.

III. The Statically Disordered Medium

A. Semiclassical Theory

In the Hamiltonian [7], the $\Delta X_i(\boldsymbol{r})$ have a generalized Gaussian distribution and, as a consequence, so does the fluctuating potential. The detailed response of a long-wavelength, low-energy electron to such a fluctuating potential is unknown. However, one can make the following observations. The short-wavelength, positive fluctuations in $V_0(\boldsymbol{r})$ tend to be tunneled through, but with an amplitude reduction within the fluctuation. The kinetic energy required to follow the short-wavelength negative fluctuations tends to cancel the potential fluctuations. Thus the slow electron behaves, in effect, as though it moves within a potential which has been smoothed by averaging over some sampling length L (7, 8). Eggarter and I [2] have been able to construct explicitly for a fluid of nonoverlapping scatterers with a mean spacing significantly larger than the scattering length a smoothed wave function which satisfies a Schrödinger equation containing the smoothed

[2] T. P. Eggarter and M. H. Cohen, unpublished results.

potential. In Eggarter's original work (7, 8) he then went on to introduce a semiclassical treatment of the electron in the smoothed potential. We have been unable to justify this step explicitly. However, it is a simple matter to introduce and illustrate the basic concepts of electron motion in disordered materials via a semiclassical treatment, and we introduce one here.

The largest value of L which makes sense is one of the order of the de Broglie wavelength for an electron of a given energy. The fluctuations in the potential of shorter wavelength than L cause scattering, giving rise to a mean-free path ℓ_p for momentum transfer and one ℓ_E for energy transfer. It is the mean-free path for momentum transfer which determines the range of phase coherence of the wave function. Therefore, if $\ell_p \ll L$, we can regard the electronic properties and response functions as local on the scale of L. Similarly if $L \ll \ell_E$, we can regard the electronic motion as energy conserving on the scale of L. These are two requirements for a local, semiclassical treatment of the electronic states. The electron would then have an energy E given by

$$[12] \qquad E = \frac{p^2}{2m^*} + \mathscr{V}$$

within a given sampling region where the smoothed potential takes on the value $\mathscr{V}$. The probability distribution of $\mathscr{V}$ is Gaussian,

$$[13] \qquad P(\mathscr{V}) = \frac{\exp\left[-(\mathscr{V} - \bar{\mathscr{V}})^2/2\sigma_{\mathscr{V}}^2\right]}{(2\pi\sigma_{\mathscr{V}}^2)^{1/2}}$$

where $\sigma_{\mathscr{V}}$ relates to the corresponding quantities for the X_i, to the deformation potential coefficients, and to the sampling length L. The mobility μ takes on a local value determined by the value of $\mathscr{V}$.

If $\mathscr{V} < E$ at $\boldsymbol{r}$, then $\boldsymbol{r}$ is an allowed position, otherwise it is forbidden. Here we have supposed that L and $\sigma_{\mathscr{V}}$ are large enough that tunneling may be ignored. This defines a continuous three-dimensional percolation problem. The energy at which percolation ceases is the mobility edge E_c.

The density of states is readily calculated and sketched in Fig. 3. The position of the mobility edge is readily calculated from percolation considerations; one obtains[3]

$$[14] \qquad E_c = \bar{\mathscr{V}} - a\sigma_{\mathscr{V}} \qquad a = 1.0$$

as indicated in Fig. 3. If one ignores molecular movement, recent calculations (17) enable one to infer that the energy dependence of the mobility is

$$[15] \qquad \mu(E) = A(E - E_c)^{1.1}$$

as sketched in Fig. 4. However, molecular movement in the form of hydrodynamic drift of the localized regions, as proposed by Eggarter (8), leads to a finite mobility below the mobility edge (Fig. 5).

The mobility $\bar{\mu}$ observed in a typical experiment involves an average of $\mu(E)$ over energy:

$$[16] \qquad \bar{\mu} = \frac{\int dE n(E)\mu(E)f(E)}{\int dE n(E)f(E)}$$

The Boltzmann factor $f(E)$ decreases monotonically with energy; $n(E)$ and $\mu(E)$ both increase monotonically. Three distinct possibilities arise. First, there is a single maximum in the integrand $I(E)$ of the numerator of [16] which lies above the

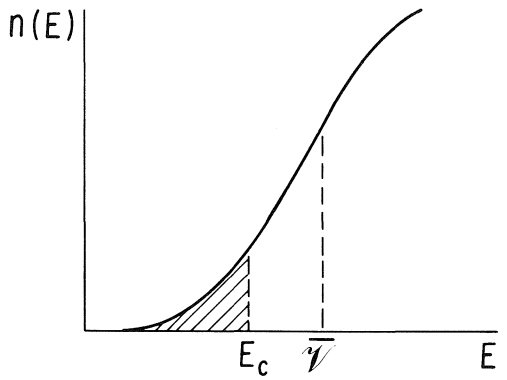

FIG. 3. Density of states in the semiclassical approximation for a Gaussian random potential, *cf.* [12] and [13]. Localized states below the mobility edge $E_c = \bar{\mathscr{V}} - \sigma_{\mathscr{V}}$ are shown shaded.

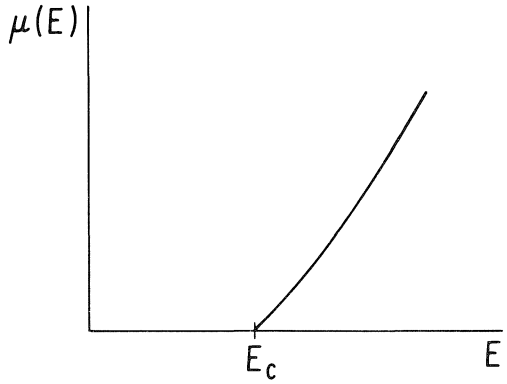

FIG. 4. Energy dependence of the mobility corresponding to Fig. 3 under the assumption of fixed nuclei.

[3]M. H. Cohen and D. Liccardello, unpublished results.

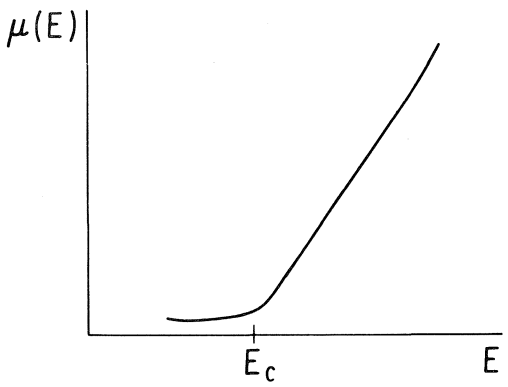

FIG. 5. Energy dependence of the mobility corresponding to Fig. 3 when hydrodynamic motion is allowed.

mobility edge. This corresponds to the case of quasi-free electrons. Second, $I(E)$ once again has a single peak but it lies well below E_c, in the region of localized states. This obviously corresponds to the case of localized electrons. Finally, there is the transitional case in which the contributions of the extended and localized states to $\bar{\mu}$ are of the same order. This can occur either as a gradual shift of a single peak in $I(E)$ from the extended to the localized states or, as occurs when the rise in $n(E)\,\mu(E)$ is large enough above E_c, there are two peaks, one in the localized region ($E < E_c$) and one in the extended region ($E > E_c$). This latter case would correspond to the simultaneous observations of a quasi-free and a slow electron by Schwarz and Prasad (18) within the mobility transition of He. These possibilities are depicted in Figs. 6 *a–c*. Thus, though oversimplified, the semiclassical model is very rich and illustrates clearly the way in which disorder affects the electronic states. Many of its features carry over into the general case.

B. Recent Developments in the General Theory

One of the major unresolved questions in the general theory of electronic states in disordered materials is the nature of the energy dependence of the conductivity or mobility in the vicinity of the mobility edge. Mott (19), in introducing his idea of the minimum metallic conductivity (20) had proposed that the mobility behaved in a step-like fashion at the edge, whereas I had proposed that it had percolation-like behavior (21, 22) as illustrated in Fig. 4. It now turns out that both are correct. Mott (23) has given an argument which shows that either can occur depending on the nature of the amplitude fluctuations in the wave functions. In the cases so far studied

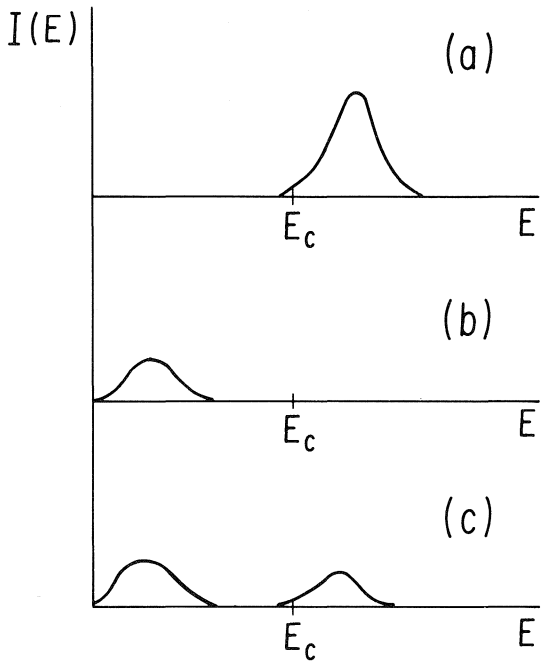

FIG. 6. The three types of weighting of the contributions of different energy ranges to the average mobility; $I(E)$ is the integrand in the numerator of [16]; (*a*) the quasi-free case, in which the weighting is above the mobility edge, (*b*) the localized case in which the weighting is below the mobility edge. A mobility transition can occur as a single such peak shifts continuously from case *a* to case *b*; or (*c*) a mobility transition occurs when the weighting splits up into two parts. Case *c* appears to occur in dense He vapor (18).

in detail experimentally, it is the step which appears to occur.[4] Wegner (24) has constructed a detailed scaling theory which provides a proof (within the limitations of a typical scaling theory) that either case can occur in three dimensions, but that only the step can occur in two.

Which case holds for slow electrons in fluids? The existing data (*e.g.* Levine and Sanders (12), Schwarz and Prasad (18)) are compatible with both. However, the existence of a step at E_c guarantees a double peak structure in $I(E)$.

IV. Dynamically Disordered Medium

In the preceding section, we treated the fluid as statically disordered. However, even in the adiabatic approximation the nuclear positions change with time, and the purely statistical approach described in Section I and used in Section III obscures some of the essential physics. Rather than use the standard Born–

[4] *Cf.* S. Pollit, work to be published.

Oppenheimer procedure which gives separate, though coupled, equations for the electronic and nuclear motion, for our present purposes it is more convenient to work in the interaction representation in which the nuclear coordinates are given their full, explicit time dependence. This can be done without making the adiabatic approximation. The electronic Hamiltonian then becomes

$$[17] \qquad \mathscr{H} = \frac{p^2}{2m^*} + V(\boldsymbol{r},t)$$

where the time dependence of the interaction V derives from the time dependence of the $X_i(\boldsymbol{r},t)$. One can show (25) that because one suppressed a large number of microscopic degrees of freedom in deriving equations of motion for the X_i, the latter undergoes a generalized Brownian motion, following a Gaussian random process in time. This last is completely characterized by the correlation functions,

$$[18] \quad \langle \Delta X_i(\boldsymbol{r},t)\, \Delta\, X_j(\boldsymbol{r}',t')\rangle \xrightarrow[\text{F.T.}]{} C_{ij}(q,\omega)$$

A frequency scale for the motion is readily established from the moments of the C_{ij},

$$[19] \qquad \omega_q{}^{ij} \equiv \frac{\int d\omega C_{ij}(q,\omega)|\omega|}{\int d\omega C_{ij}(q,\omega)}$$

Let ω_q be a typical value of the $\omega_q{}^{ij}$ for fixed q. It is an important fact that ω_q shows dispersion, *i.e.* a significant dependence on q. Let $\bar{\omega}$ be some appropriate mean value of ω_q. The phase of $V(\boldsymbol{r},t)$ will have changed irretrievably after a time $\bar{\omega}^{-1}$. Thus V remains correlated in time only for intervals $\lesssim \bar{\omega}_q{}^{-1}$.

Let us now recall the mobility theory done for the case of Fig. 6*b* where we are dealing only with localized states. We then considered that such states had a hydrodynamic (Stokes-law) mobility. However, a more chaotic mechanism, which we introduce here, can give rise to a larger mobility (26, 27). In the static picture an electron was localized in a region of spatial extent approximately equal to the localization length $L(E)$. However, the localizing potential changes in a time of order $\bar{\omega}^{-1}$. Therefore the region of localization randomly changes its position by distances at most of the order of the spatial extent of the wave function, *i.e.* $L(E)$, in times at most of order $\bar{\omega}^{-1}$. The electron thus undergoes a diffusion process. The mobility μ is related to the diffusion coefficient by the Einstein relation.

$$[20] \qquad \mu = eD/kT$$

and the diffusion coefficient has the standard form

$$[21] \qquad D = \tfrac{1}{6}\, \nu_c\, L_c{}^2$$

where the correlation frequency ν_c and correlation distance L_c can be roughly obtained from the above arguments:

$$[22] \qquad \nu_c \cong \bar{\omega} \qquad L_c \cong L$$

There results

$$[23] \qquad \mu \cong \tfrac{1}{6}\frac{e}{kT}\bar{\omega}L^2$$

Comparison of [23] with the Stokes law mobility (with slip at the boundary)

$$[24] \qquad \mu = e/4\pi\eta L$$

shows that [23] exceeds [24] whenever

$$[25] \qquad \bar{\omega}\, L^3 > 2kT/\eta$$

This condition is met if, for example, $\bar{\omega} > 10^{11}$ s^{-1}, $L > 5$ Å, $T < 300$ K, and $\eta > 1$ cP.

A consistency condition for the validity of [23] is that the time required to cross the region of localization is much less than the characteristic period, or

$$[26] \qquad \bar{v}/L \gg \bar{\omega}$$

where $\bar{v}$ is the mean speed in the localized state. If [26] is satisfied the localizing potential does not change before localization is established. If [26] is not satisfied, the mobility is that of a quasi-free electron with $\bar{\omega}$ replaced in [23] by the scattering rate τ^{-1}. As τ^{-1} is roughly equal to $\bar{v}/L$, one sees that the mobility of a dynamically localized electron as given by [23] is lower than that of a quasi-free electron by the factor $\bar{\omega}\tau$, which is $\ll 1$ whenever dynamical localization occurs.

These qualitative arguments for dynamical localization and thermal diffusion of electrons have been confirmed by a rigorous calculation for one dimension, carried out by Madhukar and Cohen (27).

There are thus two distinct processes for localized electrons, thermal diffusion and the Stokes mechanism. In developing the theory of static and dynamic localization, we here ignored the effect of the electron on the molecular configurations. When the electron–molecule interaction becomes strong enough to affect the dis-

tribution of molecular configurations significantly, the fluctuations responsible for the thermal diffusion mechanism are suppressed, and only the hydrodynamic mechanism remains.

V. Localization Versus Self-Trapping

Thus far in discussing electrons in localized states, we have had in mind only states that are localized by the disorder arising from fluctuations in the fluid, whether static (*i.e.* Anderson localization (1–4)) or dynamic. This process we call *localization*, which we distinguish from *self-trapping*. In localization, the distribution of molecular configurations can remain largely unchanged, whereas the distribution of the electron over different states associated with the various molecular configurations can change continuously. The electron can initially, before a mobility transition occurs, be found almost entirely in extended states. Then, as the mobility transition proceeds and is completed, it goes over to localized states associated with a narrow distribution of molecular configurations much like those with which a self-trapped electron is associated. In self-trapping, on the other hand, instead of a continuous change, there can be a gross change in molecular configuration to one of lower free energy. As the variable of state governing the mobility transition is changed, the self-trapped configuration can become locally stable and thereafter a mixture of the quasi-free state and the self-trapped state can occur, with relatively little probability of finding the states corresponding to intermediate stages of localization during the mobility transition. These are two alternative paths through the mobility transition. The first was emphasized by Eggarter and myself in discussing the mobility transition in He vapor, while the second was emphasized by Hernandez (28). Intermediate cases can of course occur as well.

In the preceding discussion of Anderson localization and its role in a mobility transition, we have found it convenient to use the generalized deformation-potential scheme. We have supposed both that the fluctuations are sufficiently small in amplitude that the electron–fluid interaction can be expanded to first order in the fluctuation amplitudes and that the resulting deformation potential is large enough to produce significant localization. The criterion for this is that $kT < \sigma_{\mathscr{V}}$, which can be met. This raises the question of whether the same scheme is adequate to the description of self-trapping, a convenient circumstance if so.

Jortner and I have examined self-trapping within the deformation-potential scheme by considering the configuration change illustrated in Fig. 7 for a simple liquid. A step-like increase Δn in n within a radius R is supposed to occur for negative V_0' (decrease for positive V_0'). The total energy E consists of

$$E = E_{el} + E_{dist} \qquad [27]$$

where the energy of distortion is

$$E_{dist} = \tfrac{1}{2}B\left(\frac{\Delta n}{\bar{n}}\right)^2 \frac{4\pi}{3}R^3 \qquad [28]$$

and the electronic energy is obtained as an eigenvalue of the Schrödinger equation,

$$\left[\frac{p^2}{2m^*} + (V_0'\bar{n})\frac{\Delta n}{\bar{n}}\right]\psi = E_{el}\psi \qquad r < R$$
$$\frac{p^2}{2m^*}\psi = E_{el}\psi \qquad r > R \qquad [29]$$

The surface energy is omitted from [28]; it does not change the conclusions. E_{el} was obtained in the weak-binding ($E_{el} \lesssim 0$) and strong-binding ($\psi \cong 0$, $r > R$) limits. E was then minimized with respect to the variational parameters Δn and R. The result in both cases was that the minimum value of E was positive; no stable self-trapped state could be found within the deformation-potential scheme.

Our conclusions from this study are first that self-trapping requires a large value of $\Delta n/\bar{n}$ for which the deformation-potential approximation and the simple distortion energy used above are inadequate. Second, the polarization energy is greatly modified for a bound state. It has to be

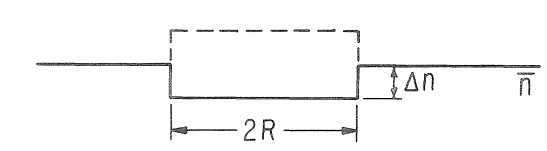

FIG. 7. Configuration change in a simple liquid employed by Jortner and Cohen to investigate self-trapping within the deformation potential approximation. A constant decrease in density of magnitude Δn (solid line) occurs within a spherical region of radius R for positive V_0'. An increase (dotted line) occurs for negative V_0'.

included explicitly into the calculation of the energy of self-trapping. Self-trapping can then occur for positive or negative V_0, positive or negative V_0', and it is important to find the explicit criteria.

The polarization energy also plays a very important role in Anderson localization, acting to provide extra stabilization of localized states in the tail of the conduction band. Thus the electron must be considered as interacting with the fluctuations and a self-induced polarization on an equal footing. The problem becomes that of a particular kind of polaron in a disordered material.

1. N. F. MOTT and E. A. DAVIS. Electronic processes in non-crystalline materials. Clarendon Press, Oxford. 1971.
2. R. J. ELLIOTT, J. A. KRUMHANSL, and P. L. LEATH. Rev. Mod. Phys. **46**, 465 (1974).
3. D. J. THOULESS. Phys. Rept. **136**, 93 (1974).
4. E. N. ECONOMOU, M. H. COHEN, K. F. FREED, and E. S. KIRKPATRICK. *In* Amorphous and liquid semiconductors. *Edited by* J. Tauc. Plenum Press, London. 1974. p. 101.
5. H. SHNYDERS, S. A. RICE, and L. MEYER. Phys. Rev. **150**, 127 (1966).
6. J. A. JAHNKE, L. MEYER, and S. A. RICE. Phys. Rev. A, **3**, 734 (1971).
7. T. P. EGGARTER and M. H. COHEN. Phys. Rev. Lett. **25**, 807 (1970); **27**, 129 (1971).
8. T. P. EGGARTER. Phys. Rev. A, **5**, 2496 (1972).
9. B. E. SPRINGETT, M. H. COHEN, and J. JORTNER. Phys. Rev. **159**, 183 (1967).
10. W. H. HARRISON. Pseudopotentials in the theory of metals. W. A. Benjamin, New York, NY. 1966.
11. J. LEKNER. Phys. Rev. **158**, 130 (1967).
12. L. L. FOLDY. Phys. Rev. **67**, 107 (1945); J. L. LEVINE and T. M. SANDERS. Phys. Rev. **154**, 138 (1967).
13. M. H. COHEN and J. LEKNER. Phys. Rev. **158**, 305 (1967).
14. J. LEKNER. Phys. Lett. A, **27**, 341 (1968).
15. J. LEKNER. Philos. Mag. **18**, 1281 (1968).
16. J. A. JAHNKE, N. A. W. HOLTZWARTH, and S. A. RICE. Phys. Rev. A, **5**, 463 (1971).
17. I. WEBMAN, J. JORTNER, and M. H. COHEN. Phys. Rev. In press.
18. K. SCHWARZ and B. PRASAD. Phys. Rev. Lett. **36**, 878 (1976); K. SCHWARZ. Unpublished. International Conference on Electrons in Fluids, Banff, Canada. Sept. 5–10, 1976.
19. N. F. MOTT. Philos. Mag. **17**, 1259 (1968); **22**, 7 (1970).
20. N. F. MOTT. Philos. Mag. **24**, 1 (1971).
21. M. H. COHEN. J. Non-Cryst. Solids, **4**, 391 (1970).
22. M. H. COHEN. *In* Electrons in fluids. *Edited by* J. Jortner and N. R. Kestner. Springer-Verlag, Berlin/Heidelberg, New York, NY. 1973. p. 257.
23. N. F. MOTT. Commun. Phys. **1**, 203 (1976).
24. F. WEGNER. Z. Phys. B, **25**, 327 (1976).
25. S. NORDHOLM and R. ZWANZIG. J. Stat. Phys. **13**, 347 (1975).
26. M. H. COHEN, J. A. HERTZ, P. M. HORN, and V. K. S. SHANTE. Int. J. Quantum Chem. Symp. **8**, 491 (1974).
27. A. MADHUKHAR and M. H. COHEN. Phys. Rev. Lett. **38**, 85 (1977).
28. J. P. HERNANDEZ. Phys. Rev. A, **7**, 1755 (1973).

Discussion

J. R. Miller: You stated in discussing percolation theory that localized states occur only below the mobility edge. Why don't localized states co-exist with conduction states above the mobility edge?

M. H. Cohen: In a purely classical theory, they do. However, as soon as the quantum mechanics is brought back into the problem, these localized states become resonances.

J. K. Baird: You have mentioned Lekner's theory of electron mobility in liquid argon. As I understand it, Lekner proceeded as follows: (*1*) Calculated the screening of the polarization potential for a condensed phase. (*2*) Averaged this potential over the structure of the fluid using the pair correlation function. (*3*) Calculated the maximum of this potential and subtracted this maximum from the average potential. (*4*) Calculated the electron scattering form factor from the resulting potential. (*5*) Concluded that the effective scattering cross section in the liquid is this form factor multiplied by the liquid structure factor. It would seem to me that steps *3* and *4* perhaps should be omitted. Instead, I would prefer to regard step *2* as being the correct calculation of the effective potential and calculate the form factor for electron scattering from it. Then I would proceed to step *5*. Also I might note that this proposition would seem more in accord with the spirit of pseudopotential theory. The analogy is the following: In a metal, the positive ionic cores are screened by the conduction electrons. In an insulator like liquid argon, however, a core is screened by valence electrons which react to the presence of an excess electron by distorting. As I understanded it, the effective potential is pseudopotential theory is the screened potential and hence it should also be considered in liquid Ar.

M. H. Cohen: Steps *3* and *4* can be omitted only when the total potential can be represented as a simple superposition of individual atomic potentials and when the Born approximation can be used for the scattering. In the present case, the scattering potential is enormous compared to the energy of the incident electron and the Born approximation cannot be used. A **t**-matrix approach cannot be used to replace the Born approximation because the potentials from different atoms overlap and a separation into single atom **t** matrices is not possible. By performing step *3*, a background potential is defined above which a separate scattering potential appears for each atom. Thus a scattering length and cross section can be defined for an atom in the liquid which are quite different from those in the solid because of the screening of the tails of the atomic potentials and the chopping them off at the background potential level. If one stopped at step *2*, an alternative scheme equivalent to steps *3* and *4* would have to be carried out. One such scheme is the muffin-tin potential scheme, commonly used for crystals and now for liquids. It is closely related to what Lekner did.

U. Sowada: What happens to a free electron (plane wave), if the mean free path for momentum exchange becomes smaller than the de Broglie wavelength?

M. H. Cohen: Then the motion of the electron becomes diffusive and the problem of determining the mobility becomes more complex, in general, but not in the present case. Because both the de Broglie wavelength and the mean free path are much larger than the intermolecular distance, the same long wavelength limit may be taken in both cases.

U. Sowada: You were talking about phonon–electron interaction in terms of just the displacements of the atoms in the liquid. Would you call the interaction between an electron and an optically anisotropic molecule also a phonon-exchange?

M. H. Cohen: I talked about phonons only in connection with examples drawn from crystals. In the present cases we are dealing with interaction between an electron and time-dependent configuration fluctuations. The physical picture is unaffected by the optical anisotropy of the molecules. One has only to use a sufficiently general configuration coordinate.

G. R. Freeman: Could you give a physical picture of the mobility maximum in liquid argon? Beginning at low density and increasing it, why does the mobility increase, and then why does it decrease?

M. H. Cohen: Part of the initial increase is associated with decreasing compressibility, *i.e.* decreasing amplitude of density fluctuation, and with changes in the effective mass with density. However, the dominant effect is the existence of a minimum in the coupling of the electron to the density fluctuations as measured by $|V_0'|$. The two contributions to V_0', that from the kinetic energy ($\hbar^2 k_0^2/2m^*$) and that from the background potential U_0, oppose and balance at the minimum.

Experimental detection of collective modes in a polar liquid: application to the case of the solvated electron in H_2O and NH_3[1]

GIANNI ASCARELLI

Physics Department, Purdue University, West Lafayette, IN, U.S.A. 47907

Received September 27, 1976

GIANNI ASCARELLI. Can. J. Chem. **55**, 1916 (1977).

We present experimental data that confirm the predicted existence of a collective mode in a liquid corresponding to the longitudinal optical mode in an ionic crystal. The experimental investigation was carried out in nitromethane, and the results bear out all the calculated properties of this collective mode: the dipolar plasmon. The calculated frequency of the dipolar plasmon, as well as the dielectric constant at high and low frequencies, are then used to calculate *without adjustable parameters* the polaron coupling constant of the solvated electron in NH_3 and H_2O. A comparison of the calculated and measured properties of the solvated electron indicates that in either case a polaron-like continuum theory can at most account for only a fraction of the energy of the observed optical absorption.

GIANNI ASCARELLI. Can. J. Chem. **55**, 1916 (1977).

On présente des données expérimentales qui confirment l'existence, dans un liquide, d'un mode collectif dont l'existence avait été prédite antérieurement et qui correspond au mode optique longitudinal présent dans un cristal ionique. L'étude expérimentale a été effectuée dans le nitrométhane et les résultats sont conformés avec toutes les propriétés calculées pour ce mode collectif: le plasmon dipolaire. On utilise alors la fréquence calculée du plasmon dipolaire de même que les constantes dielectriques à haute et à basse fréquence pour calculer, *sans paramètres ajustables*, la constante de couplage polaron de l'électron solvaté dans NH_3 et H_2O. Une comparaison des propriétés calculées et mesurées de l'électron solvaté indique dans chaque cas qu'une théorie continue ressemblant au polaron ne peut tenir compte que de seulement une fraction de l'énergie observée pour l'absorption optique.

[Traduit par le journal]

One expects an interaction of a charged carrier with a dipolar liquid via electrostatic forces (1–3). This interaction resembles the interaction of a charged carrier with a polarizable lattice: the polaron.

In the case of solids, polarons are characterized by a dimensionless constant α that measures the strength of the coupling of the electron with a polarizable continuum whose characteristic frequency ω is that of the longitudinal optical phonons. In the case of solids

$$[1] \quad \alpha = \frac{e^2}{\hbar}\left(\frac{1}{\varepsilon_\infty} - \frac{1}{\varepsilon_0}\right)\left(\frac{m_0}{2\hbar\omega}\right)^{1/2}\left(\frac{m}{m_0}\right)^{1/2}$$

In this expression ε_∞ and ε_0 are respectively the high and low frequency dielectric constants of the solid, m is the effective mass of the electron, and m_0 the free electron mass.

Two extreme cases are well known and experimentally confirmed: (*i*) when $\alpha \lesssim 4$ the electron is mobile and (*ii*) when α is large the electron is self-trapped. The first case is that of electrons in the alkali, silver, and thallium halides (4) while the second is the case of holes in alkali halides (V_K center) and AgCl.

When α is small, perturbation theory is valid and the energy of the electron is decreased an amount $\alpha\hbar\omega$ by the localized lattice distortion that is formed around it. When the value of α is very large the depth of the well where the electron is self-trapped is instead $\simeq 0.106\alpha^2\hbar\omega$. In the intermediate range a more complex treatment is used instead. It is, however, dubious that a continuum theory is valid for self-trapped carriers because the results of the calculation predict the electron to be localized within a distance smaller than the unit cell. Neither the concept of effective mass nor that of lattice dielectric constant remains valid in such a case.

We can investigate the validity of a polaron model for a polar liquid if a collective mode equivalent to a longitudinal optical phonon can be identified. In this paper we present experimental confirmation of the existence of such a mode and then apply the polaron theory to the case of the solvated electron in H_2O and NH_3. There are no adjustable parameters in the calculation.

Collective modes in the dipolar liquids have

[1]Supported in part by the National Science Foundation Grant DMR 73-02348A01.

been predicted by Lobo *et al.* (5). These authors studied the collective oscillations of a dipolar liquid where each dipole oscillates around a position of equilibrium determined by the instantaneous field created by all other dipoles that are in turn treated as a continuum. Two types of waves were predicted to exist: longitudinal (ω_p) and transverse (ω_t). The longitudinal wave arises on account of both the lag of the Onsager reaction field with respect to the instantaneous orientation of the individual dipoles and a random walk of the individual dipole orientations. The transverse mode instead depends only on the random walk of the dipole orientation.

The predicted frequency of the longitudinal wave (ω_p) is

$$\omega_p^2 \cong \omega_t^2 + \omega_0^2 \qquad [2]$$

where

$$\omega_0^2 = 4\pi \frac{N}{V} \frac{\mu_v^2}{I^*} \frac{(\varepsilon_\infty + 2)^2}{9\varepsilon_\infty} \qquad [3]$$

$$\omega_t^2 = \frac{kT}{I^*}\left(1 + 2\frac{\tau_0}{\tau}\right) \qquad [4]$$

N/V is the density of dipoles whose dipole moment, in vacuum, is μ_v, $I^{*-1} = \frac{1}{2}(I_1^{-1} + I_2^{-1})$ is the average moment of inertia for rotations perpendicular to the dipolar axis, and ε_∞ is the high frequency dielectric constant. All the factors appearing in ω_0 are known. By contrast, the relaxation time of the random torque (τ) is an unknown to be measured in units of a time (τ_0) of the order of the Debye relaxation time.

We have studied the far infrared absorption due to the dipolar plasmon in nitromethane (NM) and solutions of nitromethane in carbon tetrachloride. The NM concentration N/V can be changed over a reasonable range thus varying ω_0 while ω_t depends on temperature and may be expected to remain approximately fixed at constant temperature if the viscosity of the liquids being mixed is similar. NM and CCl_4 are miscible in all proportions above the critical solution temperature ($T_s \sim 0°C$).

In order to be able to couple an electromagnetic (em) wave to a longitudinal mode it is necessary to have oblique incidence. An em wave polarized in the plane of incidence will couple to both a longitudinal and a transverse wave in the liquid, while a wave polarized perpendicular to the plane of the incidence will couple only to a transverse collective mode. Coupling of the em radiation to the longitudinal wave in the liquid can be enhanced with respect to the coupling of the radiation to the transverse collective mode by studying the reflection of thin liquid films on a metallic backing. The films must be thin compared to the wavelength of the light (6).

Our measurements were carried out by substituting the plane mirror of the focusing optics of a Fourier spectrometer (Beckman, RIIC Mod. 720) with a metallic cell with a transparent cover containing the liquid under study. Plastics were preferred as covers, over *e.g.* either quartz or Si, because their transmission is larger than the latter materials. The plastics were also suitable for a vacuum tight seal of the sample cell. Among the plastics, Teflon was preferred because of its chemical inertness. TPX (polymethyl pentene) was also used. It is important to emphasize that these plastics must be well annealed before each measurement to assure the absence of triboelectric fields (7) that can give rise to inhomogeneities in the NM–CCl_4 solution (8[2]).

The resulting reflection spectra of various NM–CCl_4 solutions are shown in Fig. 1. The scale on the right hand of the figure corresponds to the spectrum of the pure NM solution obtained with light polarized in the plane of incidence. On account of the flexibility of the plastic the thicknesses of the liquid films were not in general either well known or uniform. They are estimated to be of the order of 30 μm. As can be seen in the figure, the reflection spectrum changes completely with changes of polarization, thus permitting the identification of the frequency corresponding to both a longitudinal and a transverse wave. The latter is in excellent agreement with the previous results of absorption measurements at normal incidence by Kroon and Van Der Elsken (9).

The positions of the reflection minima associated with ω_p for various values of N/V as measured by the volume concentration of NM in CCl_4 are given in Fig. 2. It is clearly seen that there is excellent agreement with the functional predictions of [2].

The concentration dependence of ω_p and the polarization dependence of the reflection spectra are two of the expected properties of a longitudinal wave like the dipolar plasmon. The slope

[2]A more extensive report of the dipolar plasmon measurements is given in this publication as well as a discussion of the effects of external electric fields on the homogeneity of the solution.

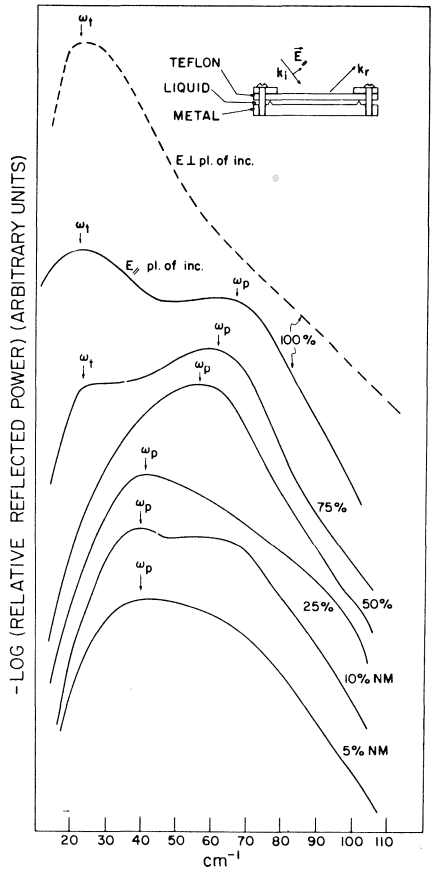

FIG. 1. Reflection spectra of solutions of nitromethane in CCl_4. The concentration of nitromethane in CCl_4 is expressed as a fraction of the total volume of the solution. R is the reflectivity of the solution. The solid line corresponds to spectra taken with radiation polarized in the plane of incidence while the broken line corresponds to a spectrum measured with light polarized perpendicular to the plane of incidence (reprinted with permission from ref. 8).

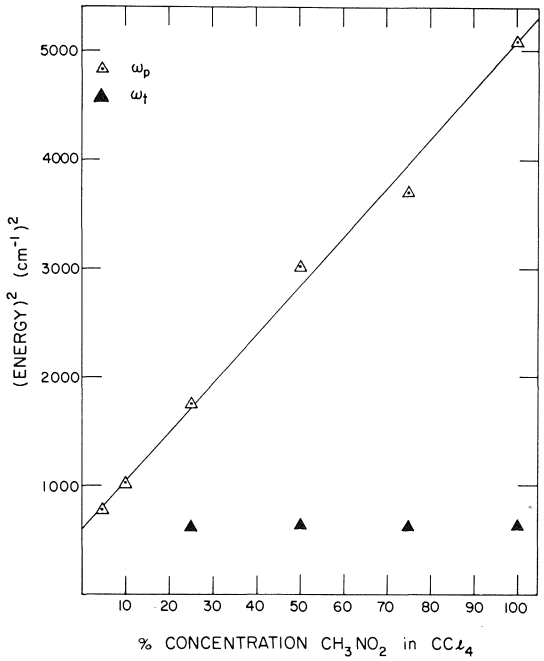

FIG. 2. Experimental relation between the square of the observed dipolar plasmon energy and the relative concentration of nitromethane in CCl_4.

of the line in Fig. 2 permits the calculation of ω_0 and a comparison with the value predicted on the basis of the known value of μ_v and I^* (10, 11). Agreement is excellent, thus confirming the calculated frequency of the dipolar plasmons.

Having demonstrated the existence of a dipolar plasmon we will apply the polaron theory (12–16) to the solvated electron problem. In order to compare the results with experiments we shall consider the case of water and NH_3. We shall use no adjustable parameters to adjust either the well depth or the well width.

We shall take $m/m_0 = 1$ in both cases and use the calculated values for ω_p (eqs. 2 and 3) to obtain α. The depth of the polaron well, *i.e.* the polaron self-energy E_p (Table 1), is obtained by interpolating between the results obtained by Shultz (14) who calculated it for several values of α using Feynman's path integral method. The extent of the electronic charge distribution (13), $\beta = 0.266\ (\hbar/2m\omega)^{1/2}$ (Table 1), corresponds to the strong coupling limit. If the solvated electron is to be described by a polaron picture the optical absorption of a polaron is an asymmetric line with a long tail toward high energies and a peak that approximately coincides with E_p (17). On the basis of a simplified configurational coordinate model the width of the optical absorption is (18)

$$[5] \qquad H_{\text{calcd}} \simeq 2.36\hbar\omega_p \frac{\alpha}{2}\left(\coth\frac{\hbar\omega_p}{2kT}\right)^{1/2}$$

A comparison of the properties of such a self-trapped electron with the experimental results (Table 1) indicates that the polaron continuum theory can at best account for half the energies of the optical absorption and of the linewidth in the case of NH_3. The agreement is even worse in the case of H_2O. In the case of NH_3 the region where the charge is concentrated agrees with the size of the cavity surrounding the solvated electron (3, 17).

The application of the polaron theory to the electron in H_2O is doubtful since the extent of the charge distribution is extremely close to the

TABLE 1. Calculated and measured properties of the solvated electron in H_2O and NH_3. The calculated values are obtained by the use of polaron theory assuming an effective mass equal to the free electron mass*

	H_2O	NH_3
ω_0	620 cm^{-1}	172 cm^{-1}
ω_p	630 cm^{-1}	200–250 cm^{-1}
α	7.9	12.3–11
E_p	0.58	0.41–0.46 eV
E_{max}	1.72 eV	0.83 eV
T	300 K	223 K
H_{calcd}	0.39 eV	0.18–0.2 eV
H_{meas}	0.92 eV	0.46 eV
β	1.8 Å	3.2–2.8 Å
$[(3/4\pi)(V/N)]^{1/3}$	1.92 Å	2.1 Å

*The meaning of the symbols ω_0, ω_p, α is discussed in the text. E_p and E_{max} are respectively the depth of the calculated polaron well and the maximum of the observed optical absorption of the solvated electron. T is the temperature at which the measurement is carried out. H_{calcd} and H_{meas} are respectively the calculated and measured width of the optical absorption. β is the polaron radius and V/N is the average volume/molecule in the solution.

intermolecular distance. In the case of NH_3 the validity of the polaron theory is not very justified either since $\beta \simeq [(3/4\pi)(V/N)]^{1/3}$. Attempts to fit the optical absorption data by introducing an effective mass $\sim 2\,m_0$ would produce an even larger discrepancy with the basic assumptions of the continuum theory, *i.e.* $\beta \gg [(3/4\pi)(V/N)]^{1/3}$.

From the above considerations it appears that the detailed description of a solvated electron in either H_2O or NH_3 will have to progress along the lines of the calculations for the V_K center in alkali halides (20, 21). Any continuum or semicontinuum theory will suffer from difficulties that are similar to those already found in the case of the F center in alkali halides (22) where there is a basic conflict between the idea of a continuum model and the calculated extent of the electronic charge distribution.

1. E. J. HART. The hydrated electron. Wiley Interscience, New York. 1970.
2. M. TACHIYA and A. MOZUNDER. J. Chem. Phys. **61**, 3890 (1974).
3. D. A. COPELAND, N. R. KESTER, and J. JORTNER. J. Chem. Phys. **53**, 1189 (1970).
4. E. KARTHEUSER. *In* Polarons in ionic crystals and semiconductors. *Edited by* J. T. Devreese. North Holland, Amsterdam. 1972. p. 717.
5. R. LOBO, J. E. ROBINSON, and S. RODRIGUEZ. J. Chem. Phys. **59**, 5992 (1972).
6. D. W. BERREMAN. Phys. Rev. **130**, 2193 (1963).
7. Keithley Instruments. Electrometer measurements. Cleveland, Ohio. 1972. p. 16.
8. G. ASCARELLI. Chem. Phys. Lett. **39**, 23 (1976).
9. S. G. KROON and J. VAN DER ELSKEN. Chem. Phys. Lett. **1**, 285 (1967).
10. N. HILL, W. E. VAUGHAN, A. H. PRICE, and M. DAVIES. Dielectric properties and molecular behaviour. Van Nostrand – Reinhold Co., London. 1967. p. 272.
11. D. C. SMITH, C. Y. PAN, and J. R. NIELSEN. J. Chem. Phys. **18**, 706 (1950).
12. H. FROHLICH. *In* Polarons and excitons. *Edited by* G. G. Kuper and G. D. Whitfield. Oliver and Boyd, Edinburgh. 1963. p. 1.
13. G. R. ALLCOCK. *In* Polarons and excitons. *Edited by* G. G. Kuper and G. D. Whitfield. Oliver and Boyd, Edinburgh. 1963. p. 45.
14. T. D. SCHULTZ. *In* Polarons and excitons. *Edited by* G. G. Kuper and G. D. Whitfield. Oliver and Boyd, Edinburgh. 1963. p. 71.
15. H. G. REIK. *In* Polarons in ionic crystals and semiconductors. *Edited by* J. T. Devreese. North Holland, Amsterdam. 1972. p. 673.
16. K. K. THORNBER. *In* Polarons in ionic crystals and semiconductors. *Edited by* J. T. Devreese. North Holland, Amsterdam. 1972. p. 361.
17. J. T. DEVREESE. *In* Polarons in ionic crystals and semiconductors. *Edited by* J. T. Devreese. North Holland, Amsterdam. 1972. p. 84.
18. D. B. FITCHEN. *In* Physics of color centers. *Edited by* W. Beal Fowler. Academic Press, New York. 1968. p. 294.
19. J. JORTNER. J. Chem. Phys. **30**, 839 (1959).
20. M. N. KABLER. *In* Point defects in solids. *Edited by* J. H. Crawford and L. M. Slifkin. Plenum Press, New York. 1972.
21. D. F. DALY and R. L. MIEHER. Phys. Rev. **183**, 368 (1969).
22. W. BEAL FOWLER and D. L. DEXTER. Phys. Status Solidi, **2**, 821 (1962).

Discussion

J. Jortner: You have resurrected the old continuum model for the solvated electron using some new and interesting input data. I would like to point out the danger in the transfer of solid state concepts to the liquid state because of two major differences between electron–fluid and electron–solid interactions. First, in the polar liquid large local orientational configurational changes are induced by the localized electron. Second, the crucial role of density fluctuations have to be considered in the liquid. You cannot get away by applying a continuum model for the short range electron–solvent interactions and these have to be handled and are currently treated by a molecular model. As far as the long range polaron-type interactions with the polar fluid are concerned, one has to consider the role of density fluctuations, as argued by Kestner.

G. Ascarelli: I agree that to some extent I have resurrected an old continuum model for the solvated electron. It differs however from what has usually been considered because there are no adjustable parameters. The point I would like to stress is that even at the level of a simple polaron-like theory there are inconsistencies because the polaron radius is smaller than the nearest neighbour distance. This aspect does not seem to have been appreciated in some of the previous semicontinuum calculations where the boundary between the core potential and the long range Coulomb potential described by an ionic polarization is taken to be at a distance smaller or equal to the nearest neighbour distance. The orientational configurational changes you mention are lumped into the polarization while the density fluctuations to which you refer have no correspondence in the polaron theory.

Localized electronic states in amorphous semiconductors[1]

DAVID ADLER

Department of Electrical Engineering and Computer Science and Center for Materials Science and Engineering, Massachusetts Institute of Technology, Cambridge, MA, U.S.A. 02139

AND

ELLEN J. YOFFA

Department of Physics, Center for Materials Science and Engineering, Massachusetts Institute of Technology, Cambridge, MA, U.S.A. 02139

Received September 27, 1976

DAVID ADLER and ELLEN J. YOFFA. Can. J. Chem. **55**, 1920 (1977).

The experimental results pertaining to the electronic structure of covalent amorphous semiconductors are briefly reviewed. It is found that three classes of materials exist, depending on the lowest-energy coordination of the predominant chemical component. In each case, the transport properties are ordinarily controlled by the localized states in the gap resulting from the minimum-energy *defect* sites, in which the local coordination is not optimal for certain atoms. These localized states are treated in terms of a Hubbard model, in which the effective repulsion between two electrons simultaneously present on the same center is taken as positive for tetrahedrally bonded solids and negative for chalcogenide and pnictide glasses. The electronic structure is discussed in detail. It is shown that even such a simple model can account for almost all of the experimental properties of the major classes of amorphous semiconductors.

DAVID ADLER et ELLEN J. YOFFA. Can. J. Chem. **55**, 1920 (1977).

On passe brièvement en revue les résultats expérimentaux se rapportant à la structure électronique de semiconducteurs amorphes covalents. On a trouvé qu'il existe trois classes de matériaux en fonction de l'énergie la plus basse de coordination pour le composé chimique prédominant. Dans chaque cas, les propriétés de transport sont ordinairement controlées par des états localisés dans le fossé résultant des sites de défauts d'énergie minimum dans lesquels la coordination locale n'est pas optimale pour certains atomes. On traite ces états localisés en termes du modèle de Hubbard dans lequel la répulsion effective entre deux électrons présents d'une façon simultanée sur le même centre est considérée comme positive pour les solides liés d'une façon tétraédrique et négative pour les verres chalcogénides et pnictides. On discute en détail de la structure électronique. On montre que même un modèle aussi simple peut rendre compte de pratiquement toutes les propriétés expérimentales des classes majeurs des semi conducteurs amorphes.

[Traduit par le journal]

I. Introduction

Although amorphous semiconductors have been studied intensively over the past 10 years, progress in understanding their electronic structure has come slowly. As is the case for the corresponding crystalline solids, both covalent and ionic amorphous semiconductors exist (1). Because only the former materials have been investigated sufficiently that their physical behavior can be understood in some detail, we shall concentrate on them in this paper.

Three major classes of covalent amorphous solids can be differentiated, depending on the chemical nature of the predominant constituent atoms. Perhaps the most intensively investigated materials are the *chalcogenides*, those materials which contain a large percentage of the chalcogen atoms, Te, Se, or S. On the other end of the spectrum are the *tetrahedral* amorphous solids. These include not only the Group IV atoms, such as Ge and Si, but also the Group III–V materials, such as GaAs, and more complex solids with an average valence of four, such as $CdGeAs_2$. Intermediate between these two major classes are the *pnictides*, which contain predominantly the Group V atoms, Sb, As, or P.

In this paper, we analyze the experimental results on these main groups of covalent amorphous semiconductors, and summarize a model for their electronic structure which appears to be in agreement with the available data. In Section II, we discuss the major observations and contrast the three sets of materials. Section III presents an analysis of the chemistry of the lowest-energy defect centers in these solids. A

[1]Research supported, in part, by the U.S. Army Research Office.

summary of an effective Hubbard model for the nature of the electronic states associated with these defect centers is given in Section IV.

II. Experimental Results on Covalent Amorphous Semiconductors

A. Optical Absorption

As is the case for all semiconductors, the optical absorption spectra of covalent amorphous semiconductors are dominated by sharp behavior in the region of the energy gap, E_g, which exists between the highest filled and lowest empty extended states (2). In most of the materials investigated, provided the short-range order is the same, the optical gap of the amorphous solid is strongly correlated with that of the corresponding crystalline solid, but many exceptions have been found, especially in the Group III–V's. There is a great deal of theoretical evidence (1, 3) that disorder should yield extensive band tails, which might be expected to manifest themselves in the optical absorption spectra, but the experimental evidence is generally ambiguous on this point. In Ge and Si, the optical absorption edge in apparently high-quality amorphous samples has been observed to be as sharp as in the crystals (4, 5), while in the chalcogenide and pnictide glasses, a comparison of the edges is masked by the so-called Urbach tails in both amorphous (6) and crystalline (7) systems. It is now believed that these tails are due to ionization of the band-edge excitons by the random electric fields present in these materials (8).

B. Electrical Conductivity

In tetrahedral amorphous semiconductors, conduction at room temperature and below is ordinarily dominated by variable-range hopping in the vicinity of the Fermi energy, ε_F (9). This indicates that there is a significant density of localized electronic states in the gap of these materials. Such a situation is not unique to amorphous semiconductors, but also characterizes partly compensated crystalline semiconductors. Conduction in such materials is generally insensitive to doping, since there are available electron and hole states at ε_F. For a particular class of amorphous Si, *viz.* that produced from silane gas (SiH_4) by an rf glow discharge, the density of localized states in the gap is relatively quite small, and conduction is dominated by thermally excited free electrons in the conduction band (10). For such material, it has proved possible to dope with ordinary donors and acceptors, and achieve extrinsic conduction (11).

The chalcogenide and pnictide glasses do not exhibit variable-range hopping near ε_F (1, 2). Conduction is predominated by thermally activated free holes in the valence band, and there is no direct evidence for a significant density of states at the Fermi energy. However, it has not yet proved possible to dope these materials to achieve extrinsic conduction.

C. Unpaired-spin Density

The tetrahedral amorphous semiconductors ordinarily exhibit an epr signal which indicates an unpaired-spin density in the range 10^{20}–10^{21} cm^{-3} (12). As the films are annealed below the crystallization temperature, the epr signal sharply decreases, although it does not disappear completely. On the other hand, no epr signal has been observed in amorphous Si prepared from glow-discharge decomposition of silane (13).

The situation is completely different for the chalcogenide glasses. No epr signal is observed at equilibrium (14) and no Curie term appears in the magnetic susceptibility (15). However, below 15 K, an epr signal can be induced by optical excitation with photons of frequency slightly below the band gap of the material (16). The resulting unpaired-spin density is of the order of 10^{16}–10^{18} cm^{-3}.

The pnictides appear to be intermediate between the other two classes. A weak epr signal, corresponding to a small spin density of the order of 10^{16} cm^{-3}, is obtained before exposure to light. This value is increased by an order of magnitude after optical excitation at very low temperatures (17).

D. Thermopower and Hall Coefficient

The tetrahedral amorphous semiconductors exhibit a nearly constant *n*-type thermopower at low temperatures, associated with the observed variable-range hopping conduction (18). At higher temperatures, more complex, history-dependent behavior is observed, although the results can be explained by superposing ambipolar band-like contributions onto the low-temperature hopping conduction. Hall-effect data has been inconsistent thus far, both *p*-type and *n*-type behavior having been obtained near room temperature (1). The existence of three parallel conduction mechanisms, as appears likely from the thermopower data, indicates the

need for controlled measurements on well-characterized samples, thus far lacking.

The chalcogenide glasses generally exhibit a nearly temperature independent, *n*-type Hall mobility (19). The discrepancy in sign between the Hall coefficient and the thermopower has received a great deal of attention (20), but it is not always observed; *e.g.* the Hall effect in $Tl_2Te{\cdot}As_2Te_3$ is *p*-type (21).

The pnictides are just beginning to be investigated, but an interesting result is that amorphous As has an *n*-type thermopower and a *p*-type Hall effect, the reverse anomaly as the chalcogenide glasses (22).

E. Photoluminescence

In tetrahedral amorphous semiconductors, photoluminescence is generally not observed (18), but, once again, glow-discharge-deposited samples behave differently. In the latter, strong photoluminescence has been found at low temperatures, with the photon energies emitted essentially equal to the exciting (band-gap) radiation (23). Any difference between the latter two quantities is ordinarily called a Stokes shift; it is small or nonexistent in glow-discharge-deposited Si.

In contrast, photoluminescence in chalcogenide glasses has been observed often (16, 24–26), although the exciting radiation is just slightly below the band gap. The luminescence appears only at low temperatures, and is significantly Stokes shifted, the emitted radiation peaking at about *half* the band gap. Initially, the luminescence is strong, and no epr signal is observed (16). As the exposure continues, the luminescence fatigues, while the epr signal grows and saturates. After exposure at low temperatures, there is also an additional optical absorption within the band gap.

F. Photostructural Changes

No photostructural effects appear to characterize the tetrahedral amorphous solids. However, chalcogenide glasses exhibit a wide range of optically induced transformations, both reversible and irreversible (27). A typical effect is photodarkening, apparently resulting from a broadening of the Urbach tail, but optically induced crystallization of the glass has also been observed (28).

G. Field-effect Measurements

The tetrahedral amorphous semiconductors prepared by ordinary techniques exhibit only a very small field effect (29), leading to the conclusion that the density of localized states in the gap is of the order of 10^{19} cm^{-3} or greater. However, the glow-discharge-deposited samples, especially those deposited on a high-temperature substrate, have a much larger field effect, providing evidence for a considerably smaller localized-state density, of the order of 10^{17} cm^{-3} (29, 30). There appear to be two peaks in the density of states in the gap, one 0.4 eV below the conduction-band edge and another about 0.4 eV above the valence-band edge (29).

Chalcogenide glasses exhibit only a small field effect (31–33), which can be interpreted to be due to a density of localized states of about 10^{18}–10^{20} cm^{-3}. The temperature dependence of the field effect is still unclear (32, 33), but there is evidence for two or more peaks in the localized-state density (32).

III. Chemistry of Defect States in Amorphous Semiconductors

Although it has been known for over 25 years that defect states control the transport properties of crystalline semiconductors, the importance of analogous states in amorphous semiconductors was not recognized until recently. This is because it was assumed that the intrinsic disorder of the amorphous state introduced a sufficiently large density of states in the gap to dominate any effects due to defect centers (3). It is now clear that this is not the case experimentally. The results on glow-discharge-deposited amorphous Si have shown that a tetrahedral amorphous solid can be prepared with a density of states in the gap sufficiently low that the Fermi level can be modulated by ordinary chemical doping (11). Consequently, the much larger localized-state density in evaporated and sputtered amorphous Si must be due to defects rather than intrinsic disorder (unless it is postulated that glow-discharge-deposited samples contain hydrogen impurities which remove intrinsic states from the gap). It is known that ordinary amorphous Si has a large density of voids, which result in dangling bonds (34). These produce what might be called *extrinsic* localized states in the gap. The fact that annealing the samples reduces the densities of both voids and localized states suggests that it is these extrinsic defects which control many of the physical properties of the material. As the defect density decreases, the epr

signal, the conductivity, and the tail of the optical absorption all decrease simultaneously.

Assuming the material is pure, the lowest-energy defects in the tetrahedral amorphous materials are vacancies and vacancy complexes (such as divacancies and larger voids). These defects lead to either strained bands or dangling bonds, the latter resulting in unpaired spins and an epr signal. Each dangling bond costs an energy E_b, depending on the bond strength, but a typical value is about 2 eV for Ge. Strained bonds cost somewhat less energy, depending on the actual configuration. Since evaporated or sputtered samples of these materials are condensed directly from the vapor phase, thermodynamic equilibrium is not reached, and a much greater density of these defects exists than would be estimated from a Boltzmann factor. Annealing the sample below its crystallization temperature does relieve some of the strains in the material, significantly reducing the defect density (perhaps by coalescing voids), but some always remain. It is evident that glow-discharge-deposited samples can have a much smaller density of defects.

In addition to increasing the ground-state energy of the sample, strained and dangling bonds also lead to localized states in the gap. In order to represent these states on a one-electron band diagram, we ask the following two questions. (*a*) How much energy does it take to remove an electron from the vicinity of the defect center and place it in the conduction (antibonding) band of the material? (*b*) How much energy does it take to remove an electron from the valence (bonding) band of the solid and place it in the vicinity of the defect? The first energy is called E_d, the second E_a. The electronic structure of the defects is then represented by placing the appropriate densities of *filled* localized states E_d below the conduction-band edge and of *empty* localized states E_a above the valence-band edge. The Fermi energy at $T = 0$ will always lie half way between the highest filled and lowest empty states; thus, ε_F will lie between the two sets of localized levels. The simplest situations, where only one type of defect exists, is shown in Fig. 1.

It might at first appear that $E_d + E_a$ should be equal to the energy gap of the semiconductor, $E_g = E_c - E_v$, in which case both sets of localized levels in Fig. 1 would coalesce. This is not the case because of the Coulomb repulsion between two electrons localized in the same

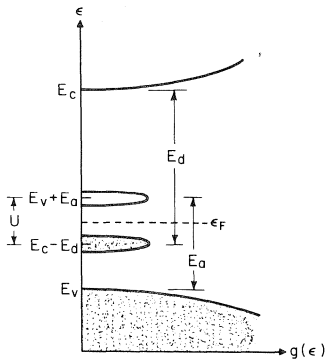

FIG. 1. Sketch of the density of electronic quasiparticle states for a semiconductor containing a single defect with effective positive correlation energy, U. Occupied states at $T = 0$ are shaded.

vicinity. When an electron is removed from the valence band and placed near a defect, it is repelled by the electron already present on that site. This repulsion is called U, the electronic *correlation* energy; thus, the two sets of localized levels are separated by an energy $U = E_d + E_a - E_g$.

If several types of defects exist or their density is very large, the defect bands can overlap, giving the situation sketched in Fig. 2. In such cases, a reoccupation of the localized states lowers the total energy, and this spontaneously occurs at low temperatures. (Any changes of correlation energy due to the effects of the redistribution of localized electrons must be taken into account in the final band diagram (35).)

It is clear that this type of approach can

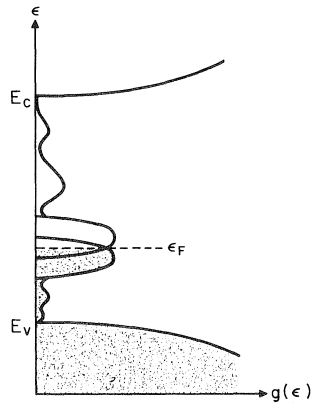

FIG. 2. Sketch of the density of electronic quasiparticle states for a semiconductor with several types of defects, in which the defect bands overlap. Occupied states at $T = 0$ are shaded.

account for all of the results thus far obtained on the tetrahedral amorphous semiconductors. The vapour-deposited samples have a large density of states at the Fermi energy resulting from the large defect densities. The dangling bonds produce a strong epr signal, while the large $g(\varepsilon_F)$ results in both the predominance of variable-range hopping at low temperatures and the lack of sensitivity of electrical conduction to doping with impurities. On the other hand, glow-discharge-deposited material can have a much smaller density of localized states in the gap. No epr signal is observable, ordinary band-like conduction can exist, and a field effect is obtained. The Fermi energy is not strongly pinned, and can be varied significantly by doping with heterovalent impurities.

The situation is entirely different in the chalcogenides (36). Since chalcogens possess lone-pair *p* electrons, the valence band of a chalcogenide glass is a nonbonding band (37). This also results in two sharp differences between chalcogenide and tetrahedral amorphous semiconductors. Firstly, since fewer bonds exist, a dangling bond tends to cost much more energy in a chalcogenide material than in a tetrahedral material; typical values are 4 eV for Se and 6 eV for S, compared to 2 eV for Ge and 3 eV for Si. Secondly, the possibility of converting a lone pair into a bonding–antibonding pair, with only a *small* loss in energy (*e.g.* 1.5 eV for Se), provides a degree of flexibility absent in other materials. These facts make the lowest-energy defect quite unique in chalcogenide glasses, and these defects control some of the major physical properties of the materials.

It is clear from the above discussion that the lowest-energy *neutral* defect in a chalcogenide glass is not a dangling bond (a singly coordinated chalcogen atom, which we call C_1°), but rather a threefold coordinated chalcogen (called C_3°). The former costs a bond energy, E_b, while the latter only costs the antibonding repulsive energy, which we call Δ. However, the lowest-energy defect is *not* neutral. As was shown by Kastner *et al.* (36), two C_3° centers are unstable towards the reaction

$$[1] \qquad 2C_3^\circ \rightarrow C_3^+ + C_1^- \qquad \text{Reaction 1}$$

is possible because a threefold coordinated chalcogen together with a neighboring twofold coordinated chalcogen can spontaneously transform to a neighboring singly and twofold coordinated center by breaking one of the bonds on C_3, leaving a C_1 neighbor. This is represented by

$$[2] \qquad C_3 + C_2 \rightarrow C_2 + C_1$$

The presence of an additional electron on an atomic site, as is the case with C_1^- requires an additional energy because of the Coulomb repulsion between two electrons on the same site, U_c. The approximate energies of all C_1, C_2, and C_3 states are shown in Fig. 3. It is clear that reaction 1 is exothermic, provided $2\Delta > U_c$, as appears to be the case (36). Furthermore, since positively and negatively charged centers attract one another via the Coulomb interaction, the defect centers with two oppositely charged chalcogens as nearest neighbors have the lowest energy of all. If we call the Coulomb attraction between nearest-neighboring, oppositely charged centers M, the energy of such a pair is

$$[3] \qquad U_c - M - U_p$$

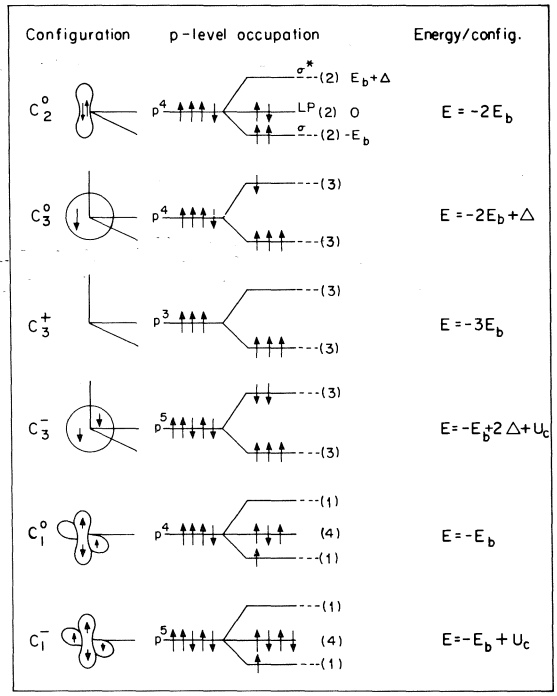

FIG. 3. Structure and energy of simple bonding configurations for chalcogen atoms in covalent amorphous semiconductors. Straight lines represent bonding (σ) orbitals, lobes represent lone-pair (nonbonding) orbitals, and large circles represent antibonding (σ*) orbitals. Each bonding electron is paired with another from a neighboring atom. The energy of a lone-pair electron is taken as the zero of energy (from ref. 36).

where U_p is the decrease in energy resulting from atomic relaxations. Reaction 1 is exothermic by an energy, $U \equiv 2\Delta - U_c + M + U_p$. Kastner *et al.* (36) called such nearest-neighboring pairs IVAP's (intimate valence-alternation pairs). Nonintimate pairs (NVAP's) are also possible, and have an energy M larger than IVAP's.

Chalcogenide glasses are made by cooling the material rapidly from the liquid state. Below the glass transition temperature, T_g, the long-range disorder is frozen in, and the amorphous state is stable. It is reasonable to estimate the density of IVAP's as

$$[4] \qquad n_I \sim n_0 \exp\left[-(U_c - M)/kT_g\right]$$

where $n_0 \sim 10^{23}\ cm^{-3}$ is the density of chalcogen atoms in the glass. For $U_c \simeq 0.55$ eV, $M \simeq 0.1$ eV, $T_g \simeq 600$ K, we obtain $n_I \sim 10^{19}\ cm^{-3}$. The density of NVAP's is then

$$[5] \qquad n_N \sim n_0 \exp\left[-U_c/kT_g\right]$$

For the same values of the parameters given above, [5] yields $n_N \sim 10^{18}\ cm^{-3}$.

For pnictides, the only lone-pair electrons are those in the lower s states. However, IVAP's become possible because of hybridization (a fourfold coordinated pnictide (P_4) can bond tetrahedrally via sp^3 orbitals). There is a slight additional cost of the s–p promotion energy and the relaxation energy, U_p, is likely to be smaller in the more rigid threefold-coordinated structure, so that relatively fewer IVAP's are present in pnictide as opposed to chalcogenide glasses. However, if the reaction

$$[6] \qquad 2P_4^{\circ} \rightarrow P_4^{+} + P_2^{-}$$

is still exothermic, IVAP's are the lowest-energy defect center.

In contrast, IVAP's are completely impossible for tetrahedrally bonded atoms, since fivefold coordination cannot occur with only s and p orbitals. This provides the explanation of why the chalcogenide and pnictide glasses have such strikingly different physical properties from the tetrahedral amorphous semiconductors.

Given the existence of about $10^{19}\ cm^{-3}$ IVAP's and $10^{18}\ cm^{-3}$ NVAP's in a typical chalcogenide glass, all of the experimental results summarized in Section II can be understood. For example, neither C_3^{+} or C_1^{-} contain any unpaired spins, so that the absence of any epr signal or Curie term in the magnetic susceptibility is clear. In addition, the existence of large densities of positively and negatively charged centers sets up strong internal electric fields which can account for the Urbach tail of the optical absorption. The photoluminescence is explained by the presence of the IVAP's, since the charged centers are efficient traps for photoexcited carriers and their spatial proximity then allows rapid luminescence. The difference between U and E_g is the observed Stokes shift.

Under nonequilibrium conditions, such as optical excitation at very low temperatures, the conversion from an IVAP to an NVAP is straightforward. Figure 4 shows how this process can occur for either chalcogenide or pnictide glasses. Upon photoexcitation and subsequent trapping of the free carriers by the charged centers, the IVAP's of Figs. 4(*a*) and 4(*c*) are transformed into the neutral, nonequilibrium configurations sketched in Figs. 4(*b*) and 4(*d*), respectively. In each case, only one bond shift occurs, at essentially no additional cost in energy. But now, since the trapped electron and hole are not sufficiently near one another, luminescence is not very probable. The centers such as C_1°, C_3°, and P_4° now have unpaired spins and thus

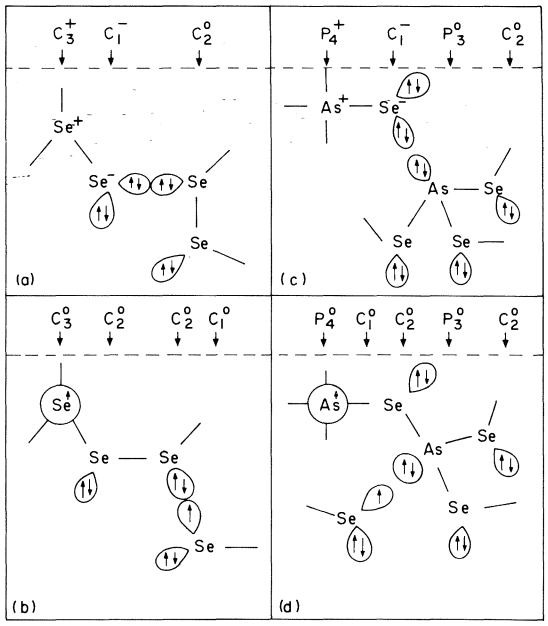

FIG. 4. Sketch of IVAP's and bond switching in Se and in As_2Se_3. C denotes a chalcogen and P denotes a pnictide atom. (*a*) An IVAP in Se. (*b*) Bond switching in photoexcited Se. (*c*) An IVAP in As_2Se_3. (*d*) Bond switching in photoexcited As_2Se_3 (from ref. 36).

yield epr signals. This further explains why the epr signal grows as the luminescence fatigues. Since only a small amount of atomic motion is involved in an NVAP → IVAP transition, the photoluminescence is restored at a relatively low annealing temperature. Even the photodarkening can be readily understood, by noting that non-radiative recombination in a material with localized optical absorption should yield intense local heating, leading to a larger density of frozen-in VAP's. In turn, the resulting increased internal electric field broadens the Urbach tail, thus darkening the sample.

Finally, we should note that the reversible electronic switching phenomena (38) which characterize chalcogenide glasses can also be a reflection of the equal densities of positively and negatively charged centers required by the VAP model (39).

IV. Effective Hubbard Model for Valence Alternation Pairs

In describing the electronic structure of localized states in a semiconductor, correlations are of vital importance and cannot be neglected. The simplest means for handling electronic correlations is the Hubbard model (40), in which only the Coulomb repulsion between electrons simultaneously localized on the same atom, U, is considered explicitly. When applying this model to localized states in the gap of a semiconductor resulting from a single type of defect, the narrow-band width limit is a good approximation (41). The Hamiltonian is then

$$[7] \qquad H = T_0 \sum_{i,\sigma} n_{i\sigma} + U \sum_i n_{i\uparrow} n_{i\downarrow}$$

where T_0 is the energy of a neutral (*i.e.* singly occupied) defect center, U is the effective electrostatic repulsion between two electrons simultaneously present in the vicinity of the same center, and $n_{i\sigma}$ is the operator which gives the number of electrons of spin σ localized on the defect i.

For the model discussed in Section III, because reaction 1 is exothermic, U is *negative*. Anderson (42) was the first to suggest that a negative U for chalcogenide glasses could account for the lack of any paramagnetism in these materials. Mott and co-workers (43, 44) showed how a single defect center, which they took as C_1, together with a negative U could also explain the photoluminescence results. We (45) previously showed that a negative U pins the Fermi energy as a function of both temperature and electronic density. The result for $kT \ll |U|$ is

$$[8] \qquad \varepsilon_F = T_0 - \tfrac{1}{2}|U| - \tfrac{1}{2} kT \ln (2n^{-1} - 1)$$

where n is the number of electrons present per defect center. A comparison of the motion of the Fermi energy with n for both positive and negative U is shown in Fig. 5. The corresponding densities of quasiparticle states are shown in Fig. 6.

In the valence-alternation-pair model of Section III, there are two types of defect pairs, IVAP's and NVAP's. (For simplicity, we are neglecting intermediate situations, when the pairs are near but not intimate.) This requires the introduction of two different values for U, with different possible densities. In the notation of Section III, the possible localized quasiparticle states are centered at $T_0 + M$, $T_0 - M$, $T_0 - |U| + M$, and $T_0 - |U| - M$. A straightforward calculation gives the results shown in Fig. 7. Only NVAP's are completely effective in pinning the Fermi energy. However, once the NVAP's are

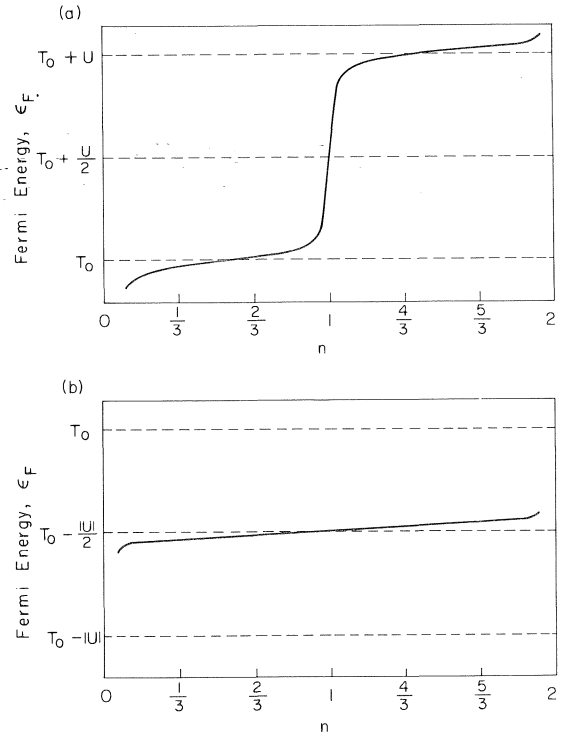

FIG. 5. Fermi energy, ε_F, as a function of localized electronic density, n, at a low but finite temperature. (*a*) $U > 0$. (*b*) $U < 0$.

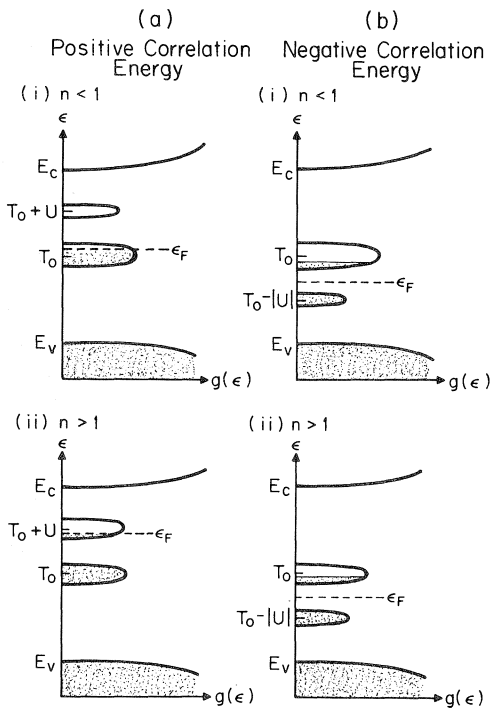

FIG. 6. Sketch of the density of electronic quasiparticle states for a semiconductor containing a single type of defect with effective correlation energy U either (*a*) positive or (*b*) negative. Occupied states at $T = 0$ are shaded.

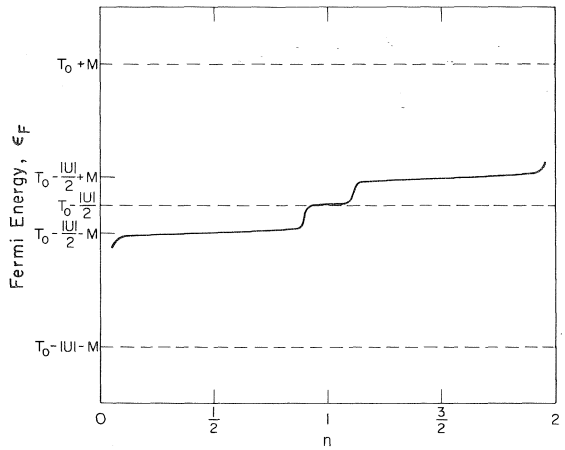

FIG. 7. Fermi energy, ε_F, as a function of localized electronic density, n, at a low but finite temperature, for a typical case where the density of IVAP's is 10 times that of NVAP's and $M = 0.1$ eV.

exhausted, as in a field-effect experiment, the considerably larger number of IVAP's pin ε_F to within a value $\pm M$ of its original value. If M is not too large, this quasi-pinning is quite effective in suppressing a sharp field effect, and, in any event, ε_F cannot be modulated nearly as much as it can when U is positive, as can be seen by contrasting Figs. 5(*a*) and 7. This explains the inability to dope chalcogenide glasses in the same way as doping of amorphous Si has proved possible. In addition, the field-effect experiments can be understood in the same way. Only after the NVAP's are saturated, will there be much modulation of the conductivity. Striking effects can be observed only after the much greater number of IVAP's are saturated.

When the effective correlation energy is negative, all transport coefficients have to be modified because of the unusual nature of the quasiparticle spectrum. In particular, the contribution to thermoelectric power from transport in the defect centers for $kT \ll |U|$ is

$$[9] \quad S = \frac{k}{e}\left[(n-1)\frac{|U|}{2kT} - \frac{1}{2}\ln\left(\frac{2}{n}-1\right)\right]$$

Thus, $S > 0$ for $n > 1$ and $S < 0$ for $n < 1$ at all temperatures. This is anomalous in the sense that for a positive effective correlation energy, S is negative for $0 < n < \frac{2}{3}$ and $1 < n < \frac{4}{3}$, while S is positive for $\frac{2}{3} < n < 1$ and $\frac{4}{3} < n < 2$ (46). Therefore, for the range $\frac{2}{3} < n < \frac{4}{3}$, S has the opposite sign from what might be expected. The Hall coefficient, R_H, for a square lattice, is negative for $n < 1$ and positive for $n > 1$, just as is the thermoelectric power. On the other hand, for a hexagonal lattice, Emin (47) has shown that anomalous signs exist for R_H, and a Hall-thermopower sign anomaly can occur. This result may be applicable to amorphous Si. However, for the chalcogenide glasses, it appears very likely that transport is predominantly band-like, in which case the pinned Fermi level required by the VAP model can account for the observed sign anomalies in a natural way (20).

V. Conclusions

The VAP model discussed in Section III makes use of the chemical nature of the atoms present in covalent amorphous semiconductors. It is simple to show that only glasses containing chalcogen or pnictide atoms are capable of exhibiting VAP's. However, when they are present, they are the most abundant defect in the material, and the fact that the centers exhibit an effective negative correlation energy leads to many unique physical properties. Among these

are the nearly complete absence of an unpaired-spin density, a pinned Fermi energy, and the lack of the ability to modulate the conductivity significantly by either doping or carrier injection. Furthermore, the model accounts for the lack of hopping conduction, the extensive Urbach edge in optical absorption, the photoluminescence and nonequilibrium epr experiments, the photostructural changes, and the switching properties of these materials. In no case are large structural rearrangements necessary for the creation of VAP's, and no large polarization energies are required beyond the electronic rearrangements implicit in the particular bond formations invoked.

1. D. ADLER. Amorphous semiconductors. Chemical Rubber Co., Cleveland, OH. 1971.
2. N. F. MOTT and E. A. DAVIS. Electronic processes in non-crystalline materials. Oxford University Press, Oxford. 1971.
3. M. H. COHEN, H. FRITZSCHE, and S. R. OVSHINSKY. Phys. Rev. Lett. **22**, 1065 (1969).
4. T. H. DONOVAN. *In* Tetrahedrally bonded amorphous semiconductors. *Edited by* N. H. Brodsky, S. Kirkpatrick, and D. Weaire. American Institute of Physics Conference Proceedings No. 20, New York, NY. 1974. p. 1.
5. D. ADLER and S. C. Moss. Comments Solid State Phys. **5**, 63 (1973).
6. E. A. DAVIS and N. F. MOTT. Philos. Mag. **22**, 903 (1970).
7. J. J. HOPFIELD. Comments Solid State Phys. **1**, 16 (1968).
8. J. D. DOW and D. REDFIELD. Phys. Rev. B, **5**, 594 (1972).
9. M. L. KNOTEK. Solid State Commun. **17**, 1431 (1975).
10. P. G. LE COMBER, A. MADAN, and W. E. SPEAR. J. Non-Cryst. Solids, **11**, 219 (1972).
11. W. E. SPEAR and P. G. LE COMBER. Philos. Mag. **33**, 935 (1976).
12. M. H. BRODSKY and R. S. TITLE. Phys. Rev. Lett. **23**, 581 (1969).
13. M. H. BRODSKY. J. Vac. Sci. Technol. **8**, 125 (1971).
14. S. C. AGARAWAL. Phys. Rev. B, **7**, 685 (1973).
15. F. J. DI SALVO, A. MENTH, J. B. WASZCZAK, and J. TAUC. Phys. Rev. B, **6**, 4574 (1972).
16. S. G. BISHOP, U. STROM, and P. C. TAYLOR. Phys. Rev. Lett. **34**, 1346 (1975).
17. S. G. BISHOP, U. STROM, and P. C. TAYLOR. Solid State Commun. **18**, 573 (1976).
18. W. BEYER and J. STUKE. *In* Amorphous and liquid semiconductors. *Edited by* J. Stuke and W. Brenig. Taylor and Francis, London. 1974. p. 251.
19. J. C. MALE. Br. J. Appl. Phys. **18**, 1543 (1967).
20. E. J. YOFFA and D. ADLER. Phys. Rev. B, In press.
21. P. NAGELS, R. CALLAERTS, M. DENAYER, and R. DE CONINCK. J. Non-Cryst. Solids, **4**, 295 (1970).
22. E. A. DAVIS. *In* Electronic phenomena in non-crystalline semiconductors. *Edited by* B. T. Kolomiets. Nauka, Leningrad. 1976. p. 212.
23. D. ENGEMANN and R. FISCHER. *In* Amorphous and liquid semiconductors. *Edited by* J. Stuke and W. Brenig. Taylor and Francis, London. 1974. p. 947.
24. R. FISCHER, U. HEIM, F. STERN, and K. WEISER. Phys. Rev. Lett. **26**, 1182 (1971).
25. J. MOLLOT, J. CERNOGORA, and C. BENOIT A LA GUILLAUME. Phys. Status Solidi A, **21**, 281 (1974).
26. R. A. STREET, T. M. SEARLE, and I. G. AUSTIN. Philos. Mag. **30**, 1181 (1974).
27. J. P. DE NEUFVILLE. *In* Optical properties – new developments. *Edited by* B. O. Seraphin. North-Holland, Amsterdam. 1975. p. 437.
28. D. ADLER and J. FEINLEIB. *In* Physics of opto-electronic materials. *Edited by* W. A. Albers. Plenum, New York, NY. 1971. p. 233.
29. A. MADAN, P. G. LE COMBER, and W. E. SPEAR. J. Non-Cryst. Solids, **20**, 239 (1976).
30. W. E. SPEAR and P. G. LE COMBER. J. Non-Cryst. Solids, **8–10**, 727 (1972).
31. R. F. EGERTON. Appl. Phys. Lett. **19**, 203 (1971).
32. J. M. MARSHALL and A. E. OWEN. Philos. Mag. **33**, 457 (1976).
33. J. E. MAHAN and R. H. BUBE. J. Non-Cryst. Solids, To be published.
34. S. C. Moss and D. ADLER. Comments Solid State Phys. **5**, 47 (1973).
35. D. ADLER and J. FEINLEIB. *In* Electronic density of states. *Edited by* L. H. Bennett. N.B.S. Special Publication 323, Washington, DC. 1971. p. 493.
36. M. KASTNER, D. ADLER, and H. FRITZSCHE. Phys. Rev. Lett. **37**, 1504 (1976).
37. M. KASTNER. Phys. Rev. Lett. **28**, 355 (1972).
38. S. R. OVSHINSKY. Phys. Rev. Lett. **21**, 1450 (1968).
39. D. ADLER, M. P. SHAW, and M. SILVER. To be published.
40. J. HUBBARD. Proc. R. Soc. London, Ser. A, **276**, 238 (1963).
41. D. ADLER. Solid State Phys. **21**, 1 (1968).
42. P. W. ANDERSON. Phys. Rev. Lett. **34**, 953 (1975).
43. R. A. STREET and N. F. MOTT. Phys. Rev. Lett. **35**, 1293 (1975).
44. N. F. MOTT, E. A. DAVIS, and R. A. STREET. Philos. Mag. **32**, 961 (1975).
45. D. ADLER and E. J. YOFFA. Phys. Rev. Lett. **36**, 1197 (1976). D. ADLER. *In* Proc. Int. Conf. Struct. Excitations Amorphous Semiconduct. *Edited by* G. Lucovsky and F. Galeener. American Institute of Physics Conference Proceedings. No. 31. 1976. p. 11.
46. E. J. YOFFA and D. ADLER. Phys. Rev. B, **12**, 2260 (1975).
47. D. EMIN. To be published.

Discussion

J. Noolandi: Can you estimate quantitatively the order of magnitude of the low energy states for sulphur?

D. Adler: The values of E_b, Δ, and V_c are larger for sulphur than for Se or Te. I would estimate that E_b is about 6 eV, Δ about 2.5 eV, and V_c about 1.5 eV, so that each NVAP has an energy of approximately 0.5–0.7 eV per atom above the ground state, depending on the polarization energy. For Se, E_b is about 4 eV, Δ about 1.5 eV, and V_c about 1.0 eV, reducing the additional energy per atom of an NVAP to

only 0.3–0.5 eV. For Te, these values are still further reduced. However, it is interesting to note that the glass transition temperature also decreases as we go from S to Te, so that the concentration of NVAP's may not vary much from material to material.

G. R. Freeman: You included elemental sulphur under the term chalcogenide. Does the term include both salts and the free elements of Group VI?

D. Adler: Current usage of the term 'chalcogenide glass' includes any amorphous alloy in which the major component is one or more of the chalcogen atoms, S, Se, and Te. For the purposes of this paper, I would add the requirement that the ground state of the chalcogen atoms in the glass be the twofold coordinated site, C_2°. This eliminates, for example, amorphous CdTe, which exhibits tetrahedral bonding.

M. Cutler: Why don't you allow for a Coulomb energy in the C_3^+ species? If the energy of C_3° is $-2E_b + \Delta$, it seems to me that the energy of C_3^+ would be decreased not only by $E_b + \Delta$ to give $-3E_b$ as you have it, but would also be increased by a Coulomb term to give $-3E_b$ + (Coulomb term) corresponding to the energy required to remove a charge from the neutral configuration.

D. Adler: This is a tricky point. We are really interested in the quasiparticle energy levels, in order to make contact with the one-electron density of states. In this case, the zero of energy must be set consistently. We are adopting a Hubbard model in which C_3^+ can be looked at as the ion core, and it is taken to be the zero of energy. The energy to add one electron, thus creating C_3°, is then T_0. this includes the bond energy and whatever Coulomb energy is involved. Adding a second electron, creating C_3^- then costs $T_0 + V_c$, where V_c is the *additional* Coulomb energy to place *two* electrons on the C_3^+ core. It is V_c which determines the Hubbard quasiparticle band separations. If we had broken T_0 or E_b into two components, say $E_b = E_b' + V'$, the individual terms would never be separable, and thus nothing would be gained from the decomposition except a more complicated notation. The important point is that the reaction $2C_3^\circ \rightarrow C_3^+ + C_3^-$ cost an energy V_c. This defines the separation of the quasiparticle bands.

J. Jortner: Once the chemical energetics works in your favor regarding charge separation, there are additional negative contributions to the correlation energy as V includes the polarization energy and the Coulomb interactions.

D. Adler: This is absolutely correct, and we have made it explicit in the paper. Unfortunately, I didn't have time to discuss it during my talk.

Bond equilibrium theory for Te-rich liquid Tl–Te alloys[1]

MELVIN CUTLER

Department of Physics, Oregon State University, Corvallis, OR, U.S.A. 97331

Received September 27, 1976

MELVIN CUTLER. Can. J. Chem. **55**, 1930 (1977).

Recent work has provided independent information about the behavior of the hole concentration c in Tl_xTe_{1-x} as a function of temperature T and composition x in the range $0.2 \leq x \leq 0.6$. This makes possible a critical reexamination of a molecular bond model for the structure of the alloy, in which holes are generated by broken Te—Te bonds. The earlier theory is revised to formulate an unrestricted independent bond model (ibm), for which the equations are simple and have obvious physical interpretations. This provides a good description of $c(T)$ but only a qualitatively correct $c(x)$. Using a Thomas–Fermi model for the screening interaction between holes and the acceptor ions, it is shown that the equilibrium constant can be expected to increase rapidly with c at large enough values. A modification in which the free energy of a dangling bond is decreased by proximity to a Tl—Te bond is found to significantly improve the result for $c(x)$. The thermochemical behavior is derived. The entropy of mixing is in fair agreement with experiment, but the enthalpy of mixing is grossly wrong. This reflects the neglect of intermolecular interactions in the theory, which, it seems, can easily account for the remaining discrepancies in the predicted behavior of c.

MELVIN CUTLER. Can. J. Chem. **55**, 1930 (1977).

Des travaux récents ont fourni des informations indépendantes concernant le comportement, en fonction de la température T et de la composition dans l'écart de x, $0.2 \leq x \leq 0.6$, de la concentration des trous c dans Tl_xTe_{1-x}. Ceci rend possible un réexamen critique du modèle de liaison moléculaire pour la structure de l'alliage dans lequel les trous sont générés par des liens Te—Te qui sont brisés. La théorie antérieure a été revisée de façon à formuler un modèle de liaison indépendante sans restrictions (ibm) pour lequel les équations sont simples et ont des interprétations physiques évidentes. Ceci fournit une bonne description de $c(T)$ mais seulement une valeur qualitativement correcte de $c(x)$. Utilisant un modèle Thomas–Fermi pour l'interaction d'écran entre les trous et les ions accepteurs, on montre que l'on peut s'attendre à ce que la constante d'équilibre augmente rapidement avec c pour des valeurs qui seront suffisamment grandes. On a trouvé qu'une modification dans laquelle l'énergie libre d'un lien suspendu décroît à la proximité d'un lien Tl—Te améliore d'une façon sensible le résultat pour $c(x)$. On en dérive le comportement thermochimique. L'entropie de mélange est en bon accord avec l'expérience mais l'enthalpie de mélange est très mauvaise. Ceci est un reflet du fait que l'on néglige les interactions intermoléculaires dans la théorie; il semble que ces interactions pourraient facilement tenir compte des disparités qui restent lorsque l'on prédit le comportement de c.

[Traduit par le journal]

Introduction

In the tellurium-rich range of compositions, the electronic properties of Tl–Te alloys change strongly with temperature T, as they do also in a number of other liquid chalcogenide alloys. Since the values of the electrical conductivity σ and the thermopower S indicate a semimetallic situation with the Fermi energy E_f within the valence band, the classical type of explanation for semiconductor behavior, *i.e.*, electronic excitations from states within or across a band gap, is not applicable, and the proper explanation is a question of broad interest. A molecular bonding model has been proposed for Tl_xTe_{1-x} with $x<2/3$, in which there are chain molecules of the form Tl—$(Te)_n$—Tl with variable n, and the thermal changes result from broken Te—Te bonds (refs. 1, 2, referred to, respectively, as I, II in the following text). The dangling bonds are assumed to give rise to negatively charged acceptor ions plus holes in the valence band. Critical evaluation of this model has been hampered by the absence of independent information about the structure of the valence band. This difficulty has been removed by a recent study of the thermoelectric behavior (3), in which it was shown that a rigid band model for the density of states is valid in the composition range $0.2 \lesssim x \lesssim 0.6$. Consequently it has been

[1]Work partially supported by a grant from the National Science Foundation.

possible to determine the hole concentration c^* (with an unknown constant factor) from experimental data on σ as a function of x and T in the range $x > 0.20$. This result is shown in Fig. 1.

The purpose of the present paper is to re-examine critically the molecular bonding theory introduced in II. To do this, a simplified version called the independent bond model (ibm) is derived whose equations have direct physical interpretations. The ibm is shown to reproduce the main features of the experimental results, but there are appreciable discrepancies. Complicating factors are considered, including the effect of the dangling bond concentration on the dangling bond energy (through screening), and effects of second order intramolecular and intermolecular interactions. These factors, or some combination of them, seem to be able to account for the discrepancies.

Effect of the Hole Concentration on the Energy of the Dangling Bond

The energy of formation of a dangling bond E_d can be separated into the energy E_b to break the bond (one half the energy per bond) to form a noninteracting dangling bond atom, and the energy C which results from the interaction with the valence band electrons to form a screened Te^- ion. At low concentrations, C is expected to be positive, and the extra electron is in a localized state above the band edge as shown in Fig. 2*a*. In this situation, Debye screening occurs, for which a satisfactory theory has been derived in the context of crystalline semiconductors (4). In the present problem, C is expected to be negative because of the high density of dangling bonds ($>10^{20}$ cm^{-3}), and the acceptor states are fully charged virtual impurity states below the Fermi energy as indicated in Fig. 2*b*. The negative value of C is caused by the kinetic energy necessary to keep the screening charge (holes) within the required volume. The screening particles obey Fermi–Dirac statistics, and because of the small impurity density (compared to typical metals), the screening is strongly nonlinear (5). The electronic configuration can be represented by a negative charge at the center of a spherically symmetrical 'Wigner-Seitz' (WS) cell of radius r_0 whose inverse volume is the average volume per acceptor state cN_a, where c is the hole concentration normalized to the atomic density $N_a(=2.7 \times 10^{22}$ cm$^{-3})$. The WS cell contains a distribution of positive charge (holes in the valence band) whose integrated value exactly cancels the negative charge at the center. If $\langle T \rangle$ is the average kinetic energy of the hole distribution in the WS cell and $\langle V \rangle$ is the average potential energy, $C = -\langle T \rangle - \langle V \rangle$.

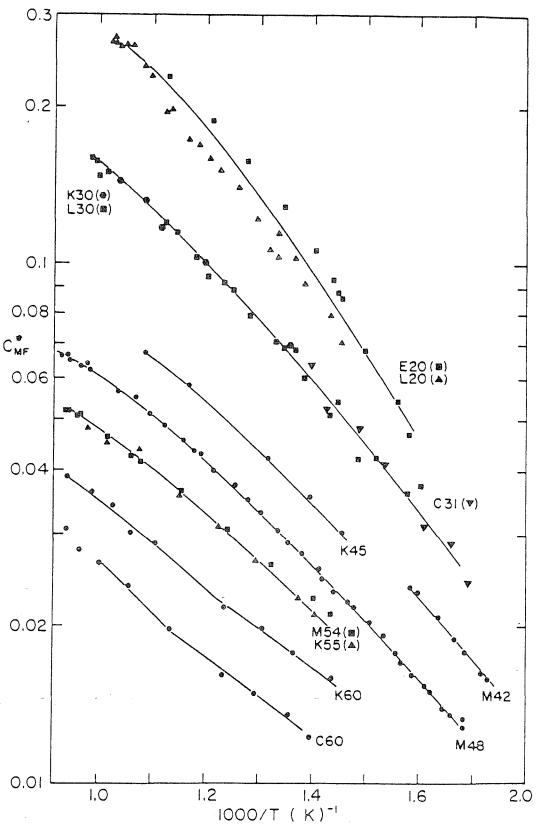

FIG. 1. Experimentally derived curves for the hole concentration c^* (to an unknown constant factor) *vs.* temperature for various compositions, indicated in at.% thallium (from ref. 3).

Useful physical insight is provided by a very rough model in which $\langle T \rangle$ is taken as the kinetic energy of a uniform free electron gas with density cN_a, and $\langle V \rangle$ is derived from a uniform positive charge distribution in the WS sphere with a dielectric constant κ. This gives

$$[1] \quad \langle T+V \rangle \cong (3\hbar^2/10m)(9\pi/4)^{2/3} r_0^{-2} - (3e^2/10\kappa) r_0^{-1}$$

As illustrated in Fig. 2*c*, this model predicts that $\langle V \rangle$ dominates at large r_0, but as r_0 decreases, the positive $\langle T \rangle$ term cancels the negative $\langle V \rangle$ term and becomes positive, causing an abrupt rise in $\langle T+V \rangle$.

The Thomas–Fermi model, which provides for

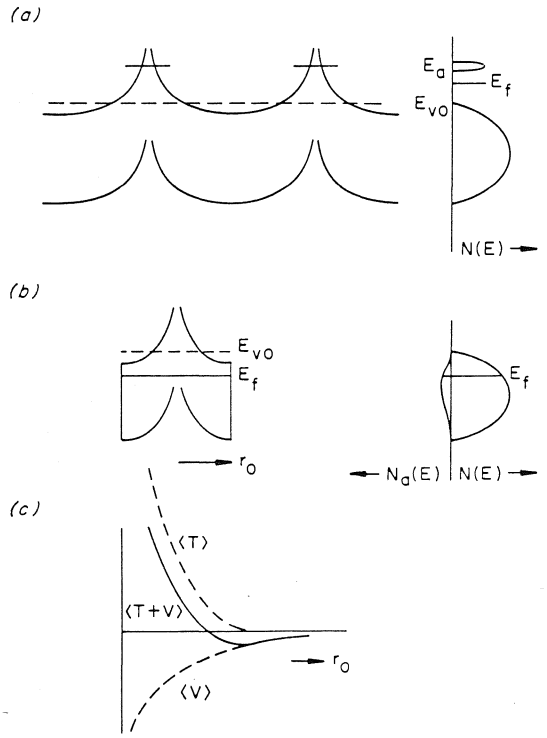

FIG. 2. Electronic behavior of acceptor impurity states due to dangling bonds. (*a*) Low hole densities. The spatial dependence of the band potential is shown on the left and the resulting density of states is on the right. The curved lines represent the local potentials of the top and bottom states of the valence band as affected by dangling bond atoms. Discrete acceptor states (E_a) are formed above the valence band edge E_{vo} (dashed line). (*b*) High hole densities. The charge and potential distribution is approximated by the Thomas–Fermi model, illustrated on the left, and the impurity state is a virtual level in the band, illustrated on the right. (*c*) Qualitative behavior of the kinetic energy $\langle T \rangle$ and the potential energy $\langle V \rangle$ and their sum as a function of r_0.

a self-consistent distribution of the screening charge, yields a better estimate for $\langle T+V \rangle$. Calculations made in previous work (5) were used to find solutions which are shown in Fig. 3, assuming $\kappa = 1$ and $\kappa = 3$. Since the equilibrium constant k_0 for broken bonds is proportional to $\exp(-C/kT)$, changes in C which are comparable to $kT(\sim 0.06$ eV) will cause large changes in k_0. The result in Fig. 3 indicates that this will occur at large enough values of c, and beyond this point k_0 will decrease rapidly with increasing c. Also, the range of c in which this occurs is sensitive to the choice of κ. The Thomas–Fermi model is still a relatively crude model since it neglects correlation and exchange

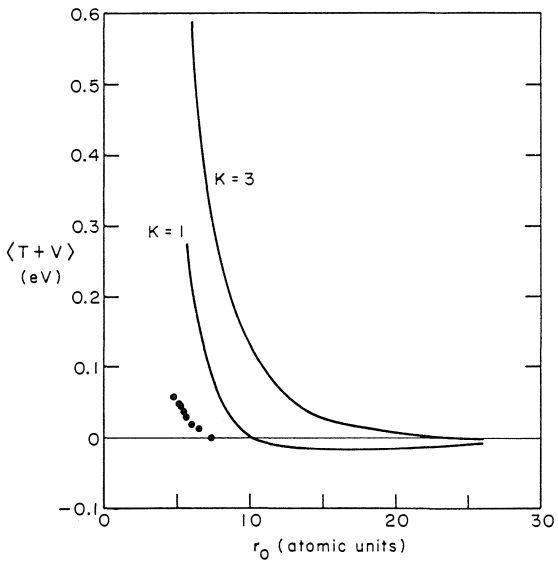

FIG. 3. Thomas–Fermi solutions for $\langle T+V \rangle$ *vs.* r_0 for $\kappa = 1$ and $\kappa = 3$. The points indicate the values of $-\Delta E_d$ required to reconcile the ibm and experimental curves for $c(x)$ in Fig. 4.

effects and it applies an electron gas approach for a relatively narrow valence band. Probably more important, the dielectric screening is treated in a very simplistic way in a range where complicated changes occur in that phenomenon. $\kappa \sim 1$ when E_f is well below the valence band edge (small r_0), but it becomes large when E_f approaches the valence band edge (large r_0) so that the true situation might be better represented by a combination of the curves shown in Fig. 2.

Bond Equilibrium Models

The Independent Bond Model

In II, equations of equilibrium were derived for a model in which there were certain constraints on what would otherwise be described as an independent bond model. The final relations are considerably simplified and their physical implications are clarified when these restrictions are removed. In what follows, parts of the original theory are repeated which are sufficient to indicate the basic assumptions and to define parameters which enter the discussion.

Three types of molecular species are assumed to be present: Tl—$(Te)_n$—Tl with concentration (per atom) a_n, Tl—$(Te)_n^-$ with concentration b_n, and $^-(Te)_n^-$ with concentration c_n. A basic assumption of the ibm is that aside from possible symmetry factors (2 or 1/2), the equilibrium con-

stant for the reaction

[2] $\text{X—Te—Te—Y} \overset{k}{=} \text{X—Te}^- + \text{Y—Te}^-$

is independent of whether X and Y is a dangling bond or any of the possible molecular groups. The second assumption is that the equilibrium constant K in

[3] $\frac{1}{2}\,\text{Te}_2 + \text{X—(Te)}_{n-1}\text{—Y} \overset{K}{=} \text{X—(Te)}_n\text{—Y}$

is also independent of X or Y, or the value of n. This immediately leads to

[4] $$a_n/a_{n-1} = b_n/b_{n-1} = c_n/c_{n-1} = y$$

where y is the product of K and the square root of the activity of Te_2. For most purposes, it is useful to think of y as a basic parameter instead of K since its value is ultimately determined from the tellurium concentration.

Application of [2] to some of the possible reactions leads to the results

[5] $$a_n = Ly^{n-1}$$
$$b_n = (2k_0Ly)^{1/2}y^{n-1}$$
$$c_n = (k_0y/2)y^{n-1}$$

where L is the concentration of Tl_2Te, and k_0 is the value of k when none of the species in [2] are symmetrical. (We are ignoring the distinction between activities and concentrations.) The constraints $x = \sum_n (2a_n + b_n)$ and $1 - x = \sum_n n \times (a_n + b_n + c_n)$ effectively determine L and y, respectively, and the total concentration of dangling bonds is $c = \sum_n (b_n + 2c_n)$, so that one obtains

[6] $$x = (2L + \sqrt{2k_0Ly})/(1-y)$$

[7] $$1-x = (\sqrt{L} + \sqrt{k_0y/2})^2/(1-y)^2$$

[8] $$c = (\sqrt{2k_0Ly} + k_0y)/(1-y)$$

From this, it is easy to derive the relations

[9] $$2k_0 = c^2/(1-\tfrac{3}{2}x - (c/2))$$

[10] $$y = 1 - (x+c)/2(1-x)$$

[11] $$L = x^2/2(1-x)$$

Since the concentration of Te—Te bonds is given by $1 - \frac{3}{2}x - (c/2)$, one can see that [9] is an expression of the law of mass action for the reaction

[12] $\text{(Te—Te bond)} \overset{2k_0}{=} \text{2(dangling bond)}$

Equation 9 is a simple quadratic equation in c which can be solved as a function of k_0 (or T) and x. Knowing this solution, [10] can be solved for y. It is interesting to note from [10] that y is equal to the fraction of Te—Te half-bonds which are neither tied to Tl atoms nor are dangling. It is also worth noting from [11] that the concentration of Tl_2Te is independent of temperature.

Comparison with Experiment

Using [8], ln c has been plotted in Fig. 4 for various values of x as a function of θ, which is defined by

[13] $$\theta = (E_d - TS_d)/kT = -\tfrac{1}{2}\ln k_0$$

These curves should correspond to those in Fig. 1 (aside from a vertical displacement determined by c^*/c) upon a linear transformation of the $1/T$ scale which fixes the values of the enthalpy (E_d) and entropy (S_d) of formation of a dangling bond. (No distinction is made here between the enthalpy and the internal energy.) As in Fig. 1, the curves in Fig. 4 are very nearly parallel,

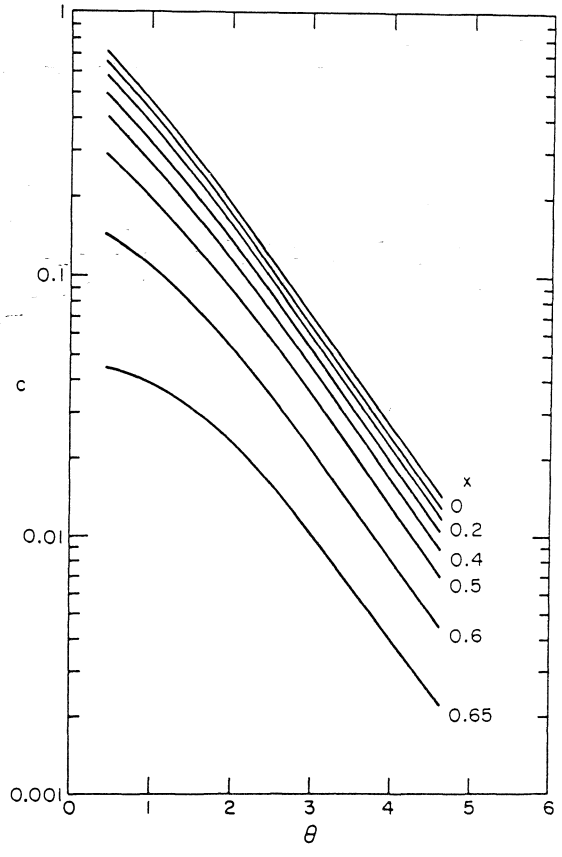

FIG. 4. Independent bond model solutions for ln c *vs.* θ for various values of x.

which indicates that values of E_d and S_d chosen to fit ln c *vs.* T^{-1} at one composition will be good at other compositions. (Actually, the experimental curves at $x \lesssim 0.30$ have a small but appreciable increase in slope not found in Fig. 4, which will be referred to later.)

A match of the theoretical and experimental curves for ln c *vs.* T^{-1} at $x \cong 0.5$ yields a very good fit (within experimental error) with $E_d = 0.23$ eV and $S_d = 2.0k$. These values don't differ much from the ones obtained previously in I. In Fig. 5, the experimental isotherm for ln c *vs.* x (marked exp) is compared with the theoretical curve (marked ibm), using the value $\theta = 1.39$ which corresponds to the experimental temperature 800 K. It is seen that there is only qualitative agreement, and the ibm curve, matched in the vicinity of $x = 0.5$ by setting $c/c^* = 3.9$, is $\sim 2x$ too small at $x = 0.20$.

The ibm is an extremely simplified model for molecular bonding, and one may ask whether reasonable modifications can improve the agreement with experiment. One reasonable modification is to allow the free energy of the dangling bond to be changed by proximity to a Te—Tl bond. This is done most simply by introducing a factor β^{-1} into the expression for b_1 in [5], which corresponds to increasing the free energy of the dangling bond in Tl—Te^- by kT ln β. This adds a term $(\beta^{-1} - 1)(2k_0yL)^{1/2}$ to the right side in [6], [7], and [8], which results in a much more complicated equation in place of [9]. If $\beta \ll 1$ over the range of temperature, the resulting curves for ln c *vs.* θ do not change much in slope, but the dependence of ln c on x is modified so that c decreases more strongly with x. In Fig. 5, the curve marked mibm was calculated with $E_d = 0.23$ eV, $S_d = 2.9k$, $E_{dl} = 0.46$ eV and $S_{dl} = -5.9\,k$, (the subscript l refers to dangling bonds on Tl—Te^- molecules), and it was fitted to the experimental curve by $c/c^* = 4.9$. It is seen that the discrepancy at low x is very much reduced.

A decrease in E_d at large c due to a change in C could also alter the shape of ln c *vs.* x in the right direction. The difference in the ibm and exp curves in Fig. 5 can be used to calculate the required change ΔE_d *vs.* c, and this result, plotted as $-\Delta E_d$ *vs.* r_0 is shown by the points in Fig. 3. It rises abruptly with decreasing r_0 as expected theoretically. But the magnitude of $-\Delta E_d$ becomes comparable to kT, and when this change is introduced into the predicted curve for

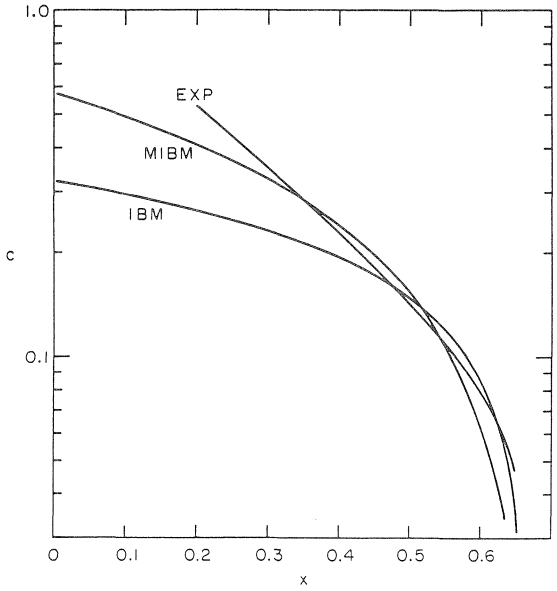

FIG. 5. Comparison of theoretical curves (ibm and mibm) for $c(x)$ with the experimental isotherm (exp).

ln c *vs.* T^{-1}, there is serious disagreement with experiment for $x = 0.30$ or 0.20. The theoretical curves rise much too fast with temperature. On the other hand the much smaller difference between the mibm and exp curves in Fig. 5 leads to much smaller values of $-\Delta E$, which actually improves the agreement with experiment for ln c *vs.* T^{-1} at $x = 0.20$.

Thermochemical Behavior

It is possible to derive the enthalpy and entropy of mixing from the ibm, and comparison with experimental results illustrates another limitation of the ibm. It will be convenient to use the entropy as ΔS_m^*, enthalpy ΔH_m^*, and Gibbs free energy ΔG_m^* of mixing of a pseudobinary alloy Te + Tl_2Te, defined by relations of the type

$$[14] \quad \Delta G_m^*(x) = G(x) - (1 - \tfrac{3}{2}x)G(0) - \tfrac{3}{2}xG(2/3)$$

The Gibbs potential $G(x)$ at composition x can be expressed in terms of the chemical potentials $\mu_i(x)$ at that composition, where i = Tl_2Te or Te, with the result

$$[15] \quad \Delta G_m^*(x) = (1 - \tfrac{3}{2}x)[\mu_{Te}(x) - \mu_{Te}(0)] + \frac{x}{2}[\mu_{Tl_2Te}(x) - \mu_{Tl_2Te}(\tfrac{2}{3})]$$

The ibm gives

[16] $\mu_{Te}(x) - \mu_{Te}(0) = RT \ln (y/y_0)$

where y_0 is evaluated at $x = 0$, and

[17] $\mu_{Tl_2Te}(x) - \mu_{Tl_2Te}(2/3) = RT \ln (L/L_0)$

where L_0 is evaluated at $x = 2/3$.

Equations 14–16 yield ΔG_m^* in terms of y and L, and ΔS_m^* and ΔH_m^* are calculated from ΔG_m^* and its temperature derivative. The results are shown in Fig. 6. The solid lines are the ibm curves and the points are from the experimental data of Nakamura and Shimoji (6). The calculated ibm values of ΔH_m^* are too small in magnitude to be distinguishable from the horizontal axis. The reason for this gross discrepancy is immediately apparent. The ibm ignores all interaction energies except those in breaking Te—Te bonds, and this is small compared to the enthalpy of mixing ($\sim RT$) caused by secondary nonbonding interactions. The result for ΔS_m^* is not so bad because the configurational entropy is taken into account, and the neglected contribution from secondary interactions is relatively small. The dashed curve in Fig. 6 represents ΔS_m^* calculated by the Flory formula (6) which also takes into account only the configurational entropy, assuming that Tl_2Te and Te are the only molecular species, and it is seen that it resembles the ibm result. The difference between theory and experiment for ΔG_m^* is simply the combined effect of the enthalpy and entropy contributions.

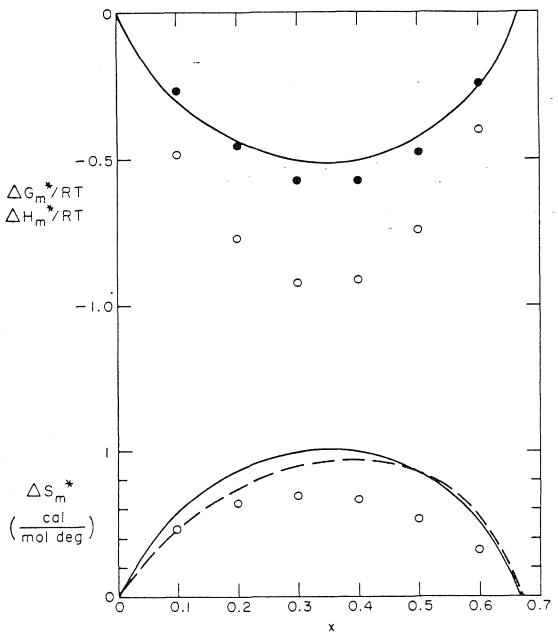

FIG. 6. Comparison of ibm theory (solid line) and experiment (open circles) for ΔG_m^* and ΔS_m^* for the pseudobinary mixture Tl_2Te + Te at 600°C. The closed circles are experimental data for ΔH_m^*. The dashed line is the theoretical curve for the ideal entropy of mixing, described by equations in ref. 6.

The neglect of intermolecular interactions undoubtedly causes an error in the calculation of $c(x,T)$. But since $E_d - TS_d$ depends on the difference between these interactions in bonded and dangling bond Te atoms, the error is much smaller than in ΔG_m^*. This effect is of course formally taken into account in chemical theory by the activity coefficients, and the discrepancies between the ibm (or mibm) and experiment seem to be well within the range to be expected from the usual variation of the activity coefficients in concentrated solutions. It is worth noting, however, that the alteration of $c(x)$ must occur largely through changes in S_d, since changes in E_d of the required magnitude would cause excessively large changes in the dependence of ln c on T^{-1}, as noted earlier.

Discussion

In II, it was noted that interactions between neighboring dangling bonds can be expected to be very strong in molecules such as $^-Te^-$ and $^-(Te)_2{}^-$, and in an effort to take these into account, constraints were introduced which led to much more complicated equations. These species play a significant role only at high T and when x is very small, so that their neglect is of little consequence in the experimental range considered here. For compositions approaching pure Te, there is evidence that configurations in which Te atoms have three bonds instead of two play an important role (7, 8). Since the ibm takes into account only twofold bonding, efforts to improve it in the range of small x are inappropriate.

A proximity effect in which $E_{dl} - E_d \gg kT$ seems to be consistent with the physical situation, since a dangling bond in a Tl—Te^- molecule places a negative charge onto a Te atom which has an extra negative charge due to the polar Te—Tl bond. Higher order proximity effects also seem to be reasonable possibilities, but their introduction into the model seems premature at the present time.

In summary, a simplified model for bond equilibrium has been considered together with

the complications which can be expected from changes in the equilibrium constant due to the electronic energy of the acceptor state, proximity of the dangling bond to Te—Tl bonds, and intermolecular interactions. The ibm provides a good explanation for the effect of temperature on c and a qualitatively correct description for the effect of composition. The deviations from experiment seem to be well within the range to be expected from the complicating factors. We therefore conclude that a molecular bond theory of the type described can account satisfactorily for the observed behavior of Tl—Te alloys in the range $0.2 < x < 0.6$, but the detailed form of it cannot as yet be ascertained.

1. M. CUTLER. Philos. Mag. **24**, 381 (1971).
2. M. CUTLER. Philos. Mag. **24**, 401 (1971).
3. M. CUTLER. Phys. Rev. B, **15**, 693 (1977).
4. W. W. HARVEY. Phys. Rev. **123**, 1666 (1961).
5. M. CUTLER. Phys. Rev. **181**, 1102 (1969).
6. Y. NAKAMURA and M. SHIMOJI. Trans. Faraday Soc. **67**, 1270 (1971).
7. B. CABANE and J. FRIEDEL. J. Phys. Paris, **32**, 73 (1971).
8. M. CUTLER. J. Non-cryst. Solids, **21**, 137 (1976).

Discussion

J. C. Thompson: What is the role of the threefold coordination of Te postulated by Adler for the chalcogenide glasses in the previous paper?

M. Cutler: Threefold bonding configurations are a possible species that can form once Te—Te bonds are broken, and they apparently occur in pure tellurium. In a recently published paper (8), I've presented arguments for believing that threefold configurations are inhibited at lower electrical conductivities because they have a large Coulomb energy, and this situation applies in Tl–Te alloys in contrast to tellurium. There are indications that the change to threefold bonding occurs between 20 and 0% thallium but the question is an open one, and needs further investigation.

An improved model of the localized electron in polar fluids

NEIL R. KESTNER
Chemistry Department, Louisiana State University, Baton Rouge, LA, U.S.A. 70803

Received September 27, 1976

NEIL R. KESTNER. Can. J. Chem. **55**, 1937 (1977).

A new model for the long range electron solvent interaction experienced by a trapped electron in a polar fluid is presented. It is an extension and modification of the work of Iguchi except that it includes a cutoff beyond which the orienting ability of the trapped electron is not strong enough to overcome other forces between the polar molecules. This potential is of finite range and supports only one bound *s* and *p* state, in contrast to the usual polaron form.

NEIL R. KESTNER. Can. J. Chem. **55**, 1937 (1977).

On présente un nouveau modèle pour l'interaction solvant électron à longue distance qui est ressentie par un électron piégé dans un liquide polaire. C'est une extension et une modification du travail d'Iguchi à l'exception de l'introduction d'une distance au-delà de laquelle la possibilité d'orientation de l'électron piégé n'est pas suffisamment forte pour surmonter d'autres forces entre les molécules polaires. Ce potentiel a des limites finies et ne supporte qu'un seul état *s* et *p* lié, ce qui est en opposition avec la forme usuelle du polaron.

[Traduit par le journal]

Introduction

In many recent papers the Copeland, Kestner, Jortner (CKS) model (1) as well as the semi-continuum model of Fueki and Kevan (see, for example ref. 2) has been observed to be incomplete especially as regards line shape and line width of the absorption spectrum of the solvated electron. For discussions on these points, see ref. 3. As Kestner and Logan (4) have pointed out the long range polaron potential in these models leads to an infinite number of bound states at quite high energy relative to the first excited state. Much experimental data such as photoelectron emission spectra suggest that the continuum is quite close to the first allowed transition (5). In this short paper we suggest a better, more molecular view of the long range electron solvent interaction which is short range and supports few bound states.

Model and Results

As stated earlier the long range electron solvent interaction used at present in almost all of the model calculations including the *a priori* work of Newton (6) becomes coulombic at large distances from the cavity center. We neglect in our discussion the obvious role of V_0, the energy of the quasi-free electron (see later comments). This term requires further study but it is not a major point of this paper. A coulombic potential means that an infinite number of bound states are supported by the potential. The estimates we have made of their location (4) and related experimental data mentioned earlier indicate that this cannot be reconciled with experimental data. Furthermore the polaron type of interaction assumes a continuum solid with no microscopic structure. Therefore our major goal must be to introduce a more molecular, microscopic approach to this electron solvent interaction.

In principle this could be done via a dielectric function approach (7) and the necessary formalism for this has been developed by Logan (8) but the dielectric function appropriate to a real polar liquid is not available even from molecular dynamics calculations in sufficient detail. Nevertheless we are continuing to explore the use of the dielectric function calculated by Lovett and Stillinger (9).

We now believe that we have a molecular model for the long range electron–solvent interaction which contains all of the essential microscopic ingredients. Basically our model is an extension and revision of the work of Iguchi (10). That work contained one major flaw and several weak points. The major flaw was in not correcting the electric field at a point far from the cavity for the standard dielectric constant screening, a fact observed previously by Gaathon (11) but never published. The weak points are its insistence on a continuum fluid at all distances from the cavity and its neglect of the importance of hydrogen bonding. The Iguchi model is

simple; it is simply the interaction of a charge distribution with a continuum dipolar fluid whose dipolar orientation is subject to thermal fluctuations via Langevin's formula. Each layer at a different distance from the cavity acts independently. The total potential at radius r is that due to all orientations beyond this.

We propose to use this model only beyond the first coordination shells. Furthermore we will cut off the interaction when the electric field is so weak that it does not have enough energy to break at least one hydrogen bond and therefore is too weak to orient the molecules. This latter point brings our thinking in line with the ideas of various people, in particular Funabashi (12). While we have arrived at that point from a totally different approach, the major philosophy is in agreement. Specifically this means that our long range potential is similar to formula [4] of Iguchi's 1968 paper (10) *i.e.*,

$$V(r)_{LR} = 4\Pi e\mu_0 n \int_r^{\infty} \left[\coth\left(\frac{\Sigma}{r^2}\right) - \frac{r^2}{\Sigma}\right] \times H\left(\frac{\Sigma kT}{r^2} - h\right) dr \quad \text{for } r > r_c$$

where μ_0 is the dipole moment of the solvent molecule, n is the number density of the solvent, r_c is the start of the continuum. The function in the integrand is

$$\Sigma = \mu_0 C_s(r)/(D_s kT)$$

where $C_s(r)$ is the charge enclosed within the radius r, and D_s is the static dielectric constant for liquid ammonia. Using a simple constant short range potential our model is (in atomic units)

$$\begin{aligned} V &= -0.039985 + V_{LR}(R = 4.25a_0) && r < 4.25a_0 \\ &= V_{LR}(R = 4.25a_0) && 4.25a_0 \leq r \leq 6.25a_0 \\ &= V_{LR}(r) && r > 6.25a_0 \end{aligned}$$

where we have set $C_s(r)$ equal to 1.0 for simplicity. The detailed potential is plotted in Fig. 1. In contrast, the potential using the polaron form of V_{LR} is $-0.523/r$ (Fig. 2). For liquid ammonia the value of Σ is 94 in atomic units, and h was selected as 0.2 kcal/mol.

In our calculations using numerical finite difference techniques we have found but one ground and one excited p-type state. The location of the states is indicated in Fig. 1. That we

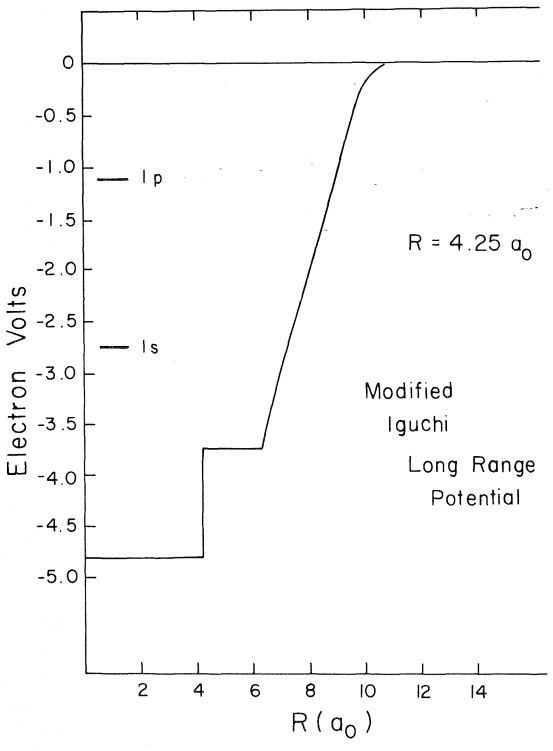

FIG. 1. Modified Iguchi long range potential for liquid ammonia. The two bound states are shown by solid lines on the left-hand side for this potential.

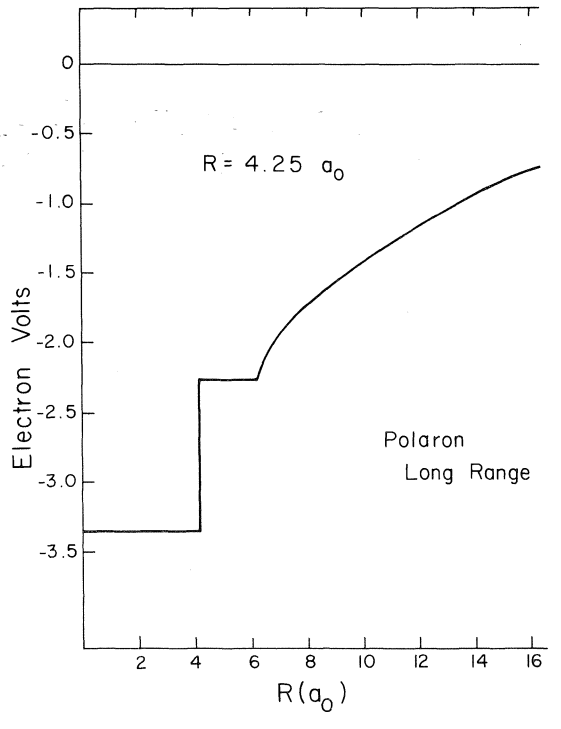

FIG. 2. Typical polaron long range potential for liquid ammonia. This potential has an infinite number of bound states.

only find one state of each type is in agreement with the rules for the number of states in a spherical box. In contrast, the polaron form would yield an infinite number of states. If V_0 were -0.5 eV in the case of ammonia, the p-type excited state would be near the ionization limit and one would expect a large contribution from the bound continuum transition in the observed line shape. Its energy should also be close to that of the bound–bound transition. The energy of the bound–bound transition is not greatly modified from our earlier model. In general a moderately negative V_0 value would bring the results of the new potential more in line with the polaron results with the only major difference being a loss of the higher excited states. We expect even less variation when the full potential is used with the proper charge enclosed, C_s. Such calculations are now underway along with the incorporation of this potential into the complete model for the calculation of the properties of electrons in fluids.

1. D. A. COPELAND, N. R. KESTNER, and J. JORTNER. J. Chem. Phys. **53**, 1189 (1970); A. GAATHON and J. JORTNER. *In* Electrons in fluids. *Edited by* J. Jortner and N. R. Kestner. Springer-Verlag, Heidelberg. 1973. pp. 429–446.
2. K. FUEKI, D.-F. FENG, and L. KEVAN. J. Am. Chem. Soc. **95**, 1398 (1973); J. Phys. Chem. **78**, 393 (1974).
3. N. R. KESTNER. *In* Electron–solvent and ion–solvent interactions. *Edited by* L. Kevan and B. Webster. Elsevier, Amsterdam. 1976. p. 1.
4. N. R. KESTNER and J. LOGAN. J. Phys. Chem. **79**, 2815 (1975).
5. L. NEMEC, L. CHIA, and P. DELAHAY. J. Phys. Chem. **79** (1975).
6. M. NEWTON. J. Phys. Chem. **79**, 2795 (1975).
7. R. R. DOGONADZE and A. A. KORNYSHEV. J. Chem. Soc. Faraday Trans. II, **70**, 1121 (1974).
8. J. LOGAN. Ph.D. Thesis, Louisiana State University, Baton Rouge, LA. 1976.
9. F. H. STILLINGER. Adv. Chem. Phys. **31**, 1 (1975).
10. K. IGUCHI. J. Chem. Phys. **48**, 1735 (1968); **51**, 3137 (1964).
11. A. GAATHON. Ph.D. Thesis, Hebrew University, Jerusalem, Israel. 1974.
12. K. FUNABASHI. Adv. Radiat. Chem. **4**, 103 (1974).

Discussion

P. Delahay: I would like to expand briefly on the evidence from photoelectron emission mentioned by Kestner with the help of Fig. 1. We have plotted the cross section for photoionization of solvated electrons in hexamethylphosphoric triamide as a function of photon energy. This result was published two years ago (J. Chem. Phys. 1974) and was discussed at the Colloque Weyl at Michigan State University last year. The main point I made at that time was that this spectrum could not be explained if one assumed a long-range Coulombic potential. I suggested that a square well, quite crudely, should be a better approximation, and I make the comparison with deuteron photodisintegration. It is interesting to note that you have come around to our point of view.

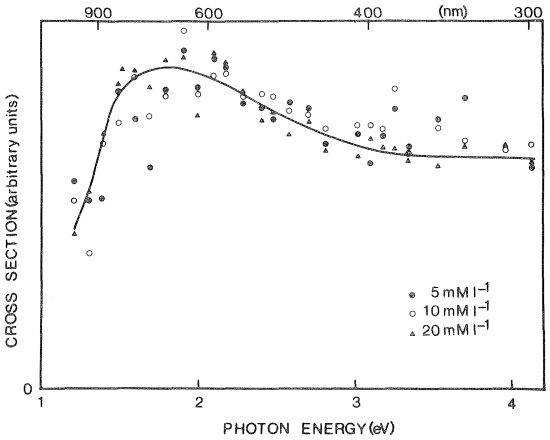

FIG. 1. Photoionization cross section of solvated electrons against photon energy for three sodium metal concentrations in hexamethylphosphoric triamide at approximately 10°C. Ordinates for the 5, 10, and 20 mM ℓ^{-1} solutions normalized in the ratios 1:1.57:2.63. Reprinted with permission from the Journal of Chemical Physics H. Aulich, L. Nemec, and P. Delahay. J. Chem. Phys. **61**, 4235 (1974). Copyright by the American Institute of Physics.

K. Funabashi: I would like to ask Professor Kestner about the possible role of *non-spherical* shape of trap potential on the line-shape of absorption spectrum of trapped electrons.

N. R. Kestner: In earlier work, especially the J. Phys. Chem. paper of 1975, we found that the role of nonspherical vibrations contributed little to the line shape. The role of permanent distortions was investigated somewhat in the same paper and found to contribute little to the line shape. However, this is a subject which should be given further attention.

J. R. Miller: In the glassy state we assume that only the polar molecules nearest the electron, which feel a large electric field strength, can reorient. Yet the absorption spectra of trapped electrons in polar glasses at 77 K are very similar to the spectra of solvated electrons in the same polar liquids (in alcohols and aqueous systems for example). This similarity may be explained by your assertion that a screened potential must be used so that polarization beyond the first or second coordination layer is only weakly operative even in the liquid.

N. R. Kestner: I agree, but one must also consider the effects of the smaller shifts in V_0 values.

A semicontinuum model with a structured first solvation shell for excess electrons in liquid and glassy alkanes

TOYOAKI KIMURA AND KENJI FUEKI

Department of Synthetic Chemistry, Faculty of Engineering, Nagoya University, Chikusa-ku, Nagoya, Japan

AND

P. A. NARAYANA AND LARRY KEVAN

Department of Chemistry, Wayne State University, Detroit, MI, U.S.A. 48202

Received September 27, 1976

TOYOAKI KIMURA, KENJI FUEKI, P. A. NARAYANA, and LARRY KEVAN. Can. J. Chem. **55**, 1940 (1977).

The microdipole model for excess electrons in alkanes seems inconsistent with recent electron spin echo data. We develop a new model for electron binding in alkanes based on a semicontinuum potential framework in which the electron-polarizability energy is dependent on molecular structure by considering the electron interaction with the polarizability of each C—C bond of the first solvation shell molecules rather than with point molecules. In addition we incorporate the effect of hydrogen–hydrogen repulsion between first solvation shell molecules. This model accounts well for the variety of experimental data known for localized electrons in 3-methylpentane glass at 77 K and for electron localization or nonlocalization in various liquid alkanes consistent with electron mobility data.

TOYOAKI KIMURA, KENJI FUEKI, P. A. NARAYANA et LARRY KEVAN. Can. J. Chem. **55**, 1940 (1977).

Le modèle de microdipole pour les électrons en excès dans les alcanes ne semble pas en accord avec les données récentes obtenues par la méthode de spin écho d'électrons. On a développé un nouveau modèle pour l'attachement d'un électron dans les alcanes qui est basé sur un potentiel semi-continu à l'intérieur duquel l'énergie de polarisabilité d'un électron est reliée avec la structure moléculaire en considérant l'interaction d'un électron avec la polarisibilité de chaque lien C—C des molécules de la première couche de solvatation plutôt que des molécules ponctuelles. De plus, on a incorporé l'effet de la répulsion hydrogène–hydrogène entre les molécules de la première couche de solvatation. Ce modèle tient bien compte des disparités dans les données expérimentales qui sont connues pour les électrons localisés dans des verres de méthyl-3 heptane à 77 K et pour la localisation et la non-localisation d'électrons dans divers alcanes liquides en accord avec les données de mobilité d'électron.

[Traduit par le journal]

Introduction

Excess electron localization in many liquid and glassy alkanes is demonstrable experimentally from mobility, optical absorption, and electron spin resonance (esr) studies (1), but the theoretical understanding of this phenomenon is still quite imperfect. When an electron is initially injected into a condensed phase alkane by ionizing radiation or by photoionization of a suitable solute it becomes localized if its initial interaction energy E_t^i (transient) is more negative than V_0, the conduction state energy of the electron in the alkane. When an electron is initially localized it has not necessarily reached an equilibrium configuration with the solvent molecules. This is attained through solvation in which the electron–solvent interaction causes rearrangement of the solvent molecules around an electron to reach an equilibrium configuration with localization energy E_t.

Electron solvation in a variety of polar matrices including water, alcohol, ether, and amines has been successfully treated theoretically by a semicontinuum model (2) which gives semiquantitative agreement with experimental values of the optical transition energy, the photoionization threshold, the number of first solvation shell molecules, and equilibrium cavity sizes although it does not account for the optical absorption linewidth. The semicontinuum model has been particularly useful in accounting for trends in the experimental observables with matrix polarity. A more detailed model which incorporates the explicit molecular structure of the first solvation shell in an *ab initio* molecular orbital framework has been developed and applied to aqueous

systems (3), but it currently appears too complex to readily apply to a series of large molecular systems.

The constraints on a successful theoretical model for solvated electrons in alkanes have been significantly increased by the recent geometrical information obtained about solvated electrons in 3-methylpentane glass at 77 K from an analysis of the modulation of the electron spin echo decay envelope (4). The results of the spin echo study give an electron solvation structure characterized by 18–21 equivalent nearest neighbor protons at a distance of 3.0–3.2 Å with an isotropic coupling constant of essentially zero. To these results we must add the previously known information about the optical absorption maximum (0.8 eV) and the photoionization threshold (1.0 eV) for solvated electrons in 3-methylpentane (3MP) glass (1). The totality of this geometrical and energy level structural data must be used to assess any theoretical model for electron solvation in alkane glasses.

The model developed to treat electron localization in alkanes was oriented toward explaining the magnitude of the optical absorption data (5). This model is termed the microdipole model. It is built on the semicontinuum model formalism and incorporates the effect of local CH bond dipoles into the potential. This model requires some assumption about the structure of the first solvation shell in order to calculate the electron dipole attractive interaction and the dipole–dipole repulsive interaction. It was found that two, four, or six CH_2 groups with the carbons located symmetrically about the electron and with the geometry of a methylene group do account for electron stabilization by about 0.1–0.4 eV. However, the amount of stability decreases as the number of CH_2 groups increases. This is a serious shortcoming since the electron spin echo data indicate that there are 18–21 equivalent nearest neighbor CH interactions. A microdipole model based on nine CH_2 groups would not show appreciable stability. We have also investigated a microdipole model based on four $-(CH_2)_3-$ groups arranged symmetrically around an electron, but this gives no electron stability due to large cancellation effects as a result of the $-(CH_2)_3-$ fragment structure.[1] It therefore appears that the CH dipoles are not the key to electron stability in alkanes because of this cancellation.

[1]D F. Feng and L. Kevan, unpublished results.

In order to develop a satisfactory model for electron localization in alkanes we are influenced by the fact that electron mobilities in alkanes vary widely with molecular structure (6). This suggests that a model be built that incorporates the explicit molecular structure. Our aim is to not only account for the structural aspects of electrons in alkane glasses, but also to at least semiquantitatively account for electron localization in those liquid alkanes which exhibit a low electron mobility ($\mu \leq 1$ cm^2 V^{-1} s^{-1}) and electron nonlocalization in those liquid alkanes which exhibit a high electron mobility ($\mu \geq 10$ cm^2 V^{-1} s^{-1}). In this work we develop a new model based on the semicontinuum potential framework in which the electron-polarizability energy is structured by considering the electron interaction with the polarizability of each C—C bond rather than with a point molecule. In addition we incorporate the effect of hydrogen–hydrogen repulsions because of the large number of equivalent nearest neighbor H atoms indicated by the electron spin echo results. This structured semicontinuum model appears to be remarkably successful.

Outline of Calculation

We assume a semicontinuum model (1, 2) in which the excess electron is considered to interact with a number N of structured and specifically arranged matrix molecules in the first coordination layer by short-range attractive and repulsive potentials and with the rest of the matrix molecules beyond the first coordination layer by a long-range polarization potential. The matrix molecules in the first coordination layer are considered to be symmetrically arranged around the electron with $N = 4$, 6, and 8. We approximate the molecular structure by the carbon atom framework and distribute the molecular polarizability, α, over all the carbon–carbon bonds in a molecule.

We first consider the short-range electronic energy for molecules with zero dipole moment. The polarization potential element of the jth C—C bond for the ith electronic state is given by [1].

$$[1] \quad dV_j(i) = -(\alpha e^2/2nl\cos\theta_j)C_i(r)\,dr/r^4$$

where n is the number of C—C bonds in the molecule, l is the C—C bond length, θ_j is the angle between the jth C—C bond and a specifically defined radial direction to be described later,

and $C_i(r)$ is the excess electronic charge enclosed within the distance r from the center of the cavity for the ith state. Integrating [1] from $r_{j(\min)}$ to $r_{j(\max)}$, we obtain [2] as the effective polarization potential due to the finite length jth bond.

$$[2] \quad V_j(i) = -(\alpha e^2/6nl\cos\theta_j)[r_{j(\min)}{}^{-3} - r_{j(\max)}{}^{-3}]C_i(r_{j0})$$

where $r_{j(\min)}$ and $r_{j(\max)}$ are the minimum and maximum radial distances of the projected jth bond, and $r_{j0} = [r_{j(\min)} + r_{j(\max)}]/2$. In deriving [2] an approximation has been made that the average electric field acting on the jth C—C bond is given by the charge enclosed within the distance r_{j0}.

The electronic energy of the ith bound state for short-range attractive interactions is then given by [3].

$$[3] \quad E_e{}^s(i) = \sum_j N V_j(i) C_i(r_{j0})$$

Equation 3 reduces to $-N\alpha e^2 C_i{}^2(r_d)/2r_d{}^4$ for the point molecule model ($l = 0$) where r_d is the center of the molecule. This is readily seen for the simple case of ethane aligned so that $\theta_j = 0$;

$$E_e{}^s(\text{ethane}) = (-e^2\alpha/6)(3r_d{}^2 + l^2/4) \times (r_d{}^2 - l^2/4)^{-3} C_i{}^2(r_d)$$

The short-range medium rearrangement energy due to induced dipole – induced dipole interaction is given by the semicontinuum model as $E_m{}^s = D_N\mu^2/r_d{}^3$ where $\mu = e\alpha C_i(r_d)/r_d{}^2$ and D_N is a numerical constant calculated from the number and geometrical arrangement of the molecules (1). Here we have assumed that a point induced dipole approximation is justified because this energy term is rather small.

The nonpolar medium beyond the first coordination layer beginning at $R = r_d + r_s$ is treated as a continuous dielectric characterized by an optical dielectric constant D_{op} so that only electronic polarization is considered. The sum of the long-range electronic and medium rearrangement energies is given by [4].

$$[4] \quad E_e{}^l(i) + E_m{}^l(i) = \frac{e}{2}\left(1 - \frac{1}{D_{op}}\right) \times \left[f_i(R)\int_{r\le R}\psi_i{}^2 d\tau + \int_{r\ge R} f_i(r)\psi_i{}^2 d\tau\right]$$

where f_i is a self-consistent field potential which is obtained from Poisson's equation (1, 2).

Two other medium rearrangement energy terms have been included in the semicontinuum model (1, 2). The short-range interaction of the excess electron with the medium electrons is approximated by $E_q = V_0[1 - C_i(r_d)]$ where V_0 is the quasi-free electron energy. The energy required to form a cavity in the medium is given by $E_v = 4\pi(r_d{}^2 - r_s{}^2)\gamma$ where γ is the surface energy and r_s is the radius of the molecule.

Because of the experimental evidence for a large number of equivalent nearest neighbor protons to the solvated electron in alkanes (4), we also include in this calculation repulsive interactions between the hydrogen atoms in the different methyl groups nearest to the center of the cavity in which the electron is localized. This medium rearrangement energy term has not been included in our previous semicontinuum model calculations. The H–H interaction energy is based on high velocity helium atom scattering data and an H atom van der Waals radius of 1.25 Å; it is given by [5] (7)

$$[5] \quad E_{HH}(ev) = \sum_h g_h \times 434\exp(-4.6r_h)$$

where g_h is the number of hydrogen atom pairs separated by a distance r_h (Å).

Each methyl group is presumed rotating and one average H–H interaction distance is considered between each pair of methyl groups. A summation is taken over all different classes of methyl pairs where each class corresponds to a different r_h. For example, if the methyl groups from six alkane molecules closest to the electron are located at the vertices of an octahedron there are two classes of pairs and g_h is 12 for the adjacent methyls and 3 for the methyls located at opposite vertices.

The total energy for the ith state is then given by [6].

$$[6] \quad E_t(i) = E_k(i) + E_e{}^s(i) + E_m{}^s(i) + E_e{}^l(i) + E_m{}^l(i) + E_q(i) + E_v + E_{HH}$$

where E_k is the kinetic energy of the excess electron. This E_t is formally the same as the semicontinuum model for polar molecules plus the addition of E_{HH}. Hydrogenic wave functions are used and the variational procedure is applied to the total energy of the system to obtain the minimum energy for a given r_d. The calculational details have been described previously (1, 2). The total energy is temperature dependent via E_q because V_0 is temperature dependent and via $E_e{}^l + E_m{}^l$ because D_{op} is temperature dependent.

TABLE 1. Geometrical constants used in the calculations

Matrix	Model	r_s (Å)	θ_1 (deg)	θ_2 (deg)	θ_3 (deg)	θ_4 (deg)	θ_5 (deg)	Remarks
Propane	1	2.11	0	70.5				Fig. 1
	2	2.00	54.75	54.75				Fig. 2
n-Pentane	1	2.92	0	70.5	70.5	0		
	2	2.11	0	70.5	109.5	70.5		
	3	2.11	0	70.5	141.1	70.5		Fig. 3
	4	3.65	0	70.5	0	70.5		
	5	3.91	35.3	35.3	35.3	35.3		
	6	2.62	54.75	54.75	15.8	15.8		
	7	2.62	54.75	54.75	15.8	90		Fig. 4
	8	1.54	54.75	54.75	90	90		
3MP	1	2.92	0	70.5	70.5	0	41.8	
	2	2.61	0	70.5	70.5	90	41.8	
	3	2.61	0	70.5	70.5	109.5	41.8	Fig. 5
	4	3.65	0	70.5	0	70.5	109.5	
	5	3.91	35.3	35.3	35.3	35.3	90	
	6	2.92	0	70.5	70.5	0	0	
	7	2.92	0	70.5	70.5	0	109.5	Fig. 6
	8	2.11	0	70.5	70.5	109.5	109.5	

The energy of the conduction state consistent with the ground-state medium arrangement is given by [7].

$$[7] \qquad E_t(\text{cond}) = V_0 + E_v + E_{HH}$$

The geometrical constants defining the various configurations are listed in Table 1. For ethane, propane, *n*-pentane, neopentane, and 3MP, α is 4.9, 6.2, 10, 10, and 11.8 Å^3, respectively; γ is 8.7, 11.1, 16, 16, and 37 erg cm^{-2}, respectively; and D_{op} is 1.92 (127 K), 1.80 (182 K), 1.77 (200 K); 1.91 (179 K), 1.87 (197 K), 1.84 (211 K), 1.81 (222 K); 1.84 (296 K); 1.78 (296 K); and 2.22 (77 K), respectively. The distance r_s is taken from the center of the molecule to the hydrogen atom furthermost in the radial direction to which the C—C bond angles are referred, plus 0.5 Å (about the Bohr radius of the hydrogen atom). The C—C and C—H bond lengths are taken as 1.54 and 1.10 Å, respectively. Values of V_0 (8–11) used in the calculations are given in Table 2.

Generalized structural models for the matrix molecule in the first coordination layer are shown in Figs. 1–6. The angle parameters involved in the structural models are given in Table 1 where both planar and non-planar conformations are included. In propane (model 1), *n*-pentane (models 1–4), and 3MP (models 1–4 and 6–8), the innermost C—C bond is directed to the center of the cavity and this direction is taken as a reference radial direction. In propane (model 2) and *n*-pentane (models 6–8), the line bisecting the central C—C—C angle is directed to the center of the cavity and this direction is taken as a reference radial direction. In *n*-pentane (model 5) and 3MP (model 5), a straight line passing through three carbon atoms and the center of the cavity is taken as a reference radial direction (see Figs. 3 and 5). In ethane the C—C bond is directed to the center of the cavity. In neopentane the molecule is arranged so that one of the C—C bonds points towards the center of the cavity.

Results and Discussion

The results of the calculations are given in Tables 2–9 and Figs. 7–9. Tables 7–9 and Fig. 9 may be obtained from the Depository of Unpublished Data.[2]

Liquid Ethane

Table 3 shows the calculated properties of localized excess electrons in liquid ethane. The cavity radius at the configurational minimum is r_d^0, $h\nu(1s \rightarrow 2p)$ and $f(1s \rightarrow 2p)$ are the optical transition energy and oscillator strength for the $1s \rightarrow 2p$ transition, respectively, I is the threshold energy for photoconductivity, $h\nu_{max}$ is the transition energy at the maximum of the bound-free transition probability (12), and ΔH is the heat of solution of the excess electron. The following trends are seen in Table 4: (*a*) r_d^0 increases with

[2]Tables 7–9 and Fig. 9 may be obtained free from the authors or at a nominal charge from the Depository of Unpublished Data, CISTI, National Research Council of Canada, Ottawa, Canada K1A 0S2.

TABLE 2. Stability of excess electrons in liquid and glassy hydrocarbons

Matrix	Model	T (K)	V_0 (eV)	$V_0 - E_t(1s)$ (eV) $N = 4$	$N = 6$	$N = 8$
Ethane		127	0.22*	0.440	0.420	0.373
		182	0.02*	0.282	0.266	0.223
		200	−0.13*	0.203	0.186	0.144
Propane	1	179	0.11†	0.254	0.263	0.219
		197	0.06†	0.214	0.220	0.176
		211	−0.01†	0.173	0.170	0.126
		222	−0.07†	0.141	0.128	0.084
	2	179	0.11	0.352	0.323	0.290
		197	0.06	0.312	0.285	0.252
		211	−0.01	0.289	0.264	0.229
		222	−0.07	0.234	0.209	0.173
n-Pentane	1	296	0.01†	0.123	0.107	0.046
		296	0.04‡	0.138	0.126	0.065
	2	296	0.01	0.216	0.182	0.111
		296	0.04	0.233	0.200	0.129
	3	296	0.01	0.250	0.187	0.129
		296	0.04	0.261	0.198	0.140
	4	296	0.01	0.151	0.121	0.062
		296	0.04	0.162	0.135	0.078
	5	296	0.01	0.090	0.055	0.000
		296	0.04	0.100	0.070	0.018
	6	296	0.01	0.382	0.217	0.159
		296	0.04	0.299	0.232	0.174
	7	296	0.01	0.358	0.255	0.186
		296	0.04	0.378	0.273	0.204
	8	296	0.01	0.579	0.368	0.253
		296	0.04	0.603	0.390	0.274
Neopentane		296	−0.43§	0.027	−0.024	−0.093
		296	−0.38†	0.036	−0.014	−0.084
		296	−0.35‡	0.041	−0.008	−0.077
3MP	1	77	1.0*	0.798	0.751	0.611
	2	77	1.0	0.811	0.762	0.619
	3	77	1.0	0.833	0.784	0.640
	4	77	1.0	0.904	0.863	0.724
	5	77	1.0	0.759	0.758	0.645
	6	77	1.0	0.796	0.698	0.585
	7	77	1.0	0.866	0.766	0.642
	8	77	1.0	0.915	0.791	0.647

*Reference 8.
†Reference 11.
‡Reference 10.
§Reference 9.

increasing N and it is nearly independent of temperature, (*b*) $h\nu(1s \rightarrow 2p)$ decreases with increasing N and temperature, (*c*) $f(1s \rightarrow 2p)$ increases with increasing N and temperature, (*d*) I and $h\nu_{max}$ decrease with increasing N and temperature, and (*e*) ΔH decreases with increasing N and decreasing temperature.

These trends are similar to those seen for polar matrices (2). The magnitudes of $h\nu(1s \rightarrow 2p)$ and $f(1s \rightarrow 2p)$ are much smaller than those calculated for solvated electrons in polar solvents and fit with the trend with decreasing matrix polarity established for polar solvents (2). The value of $I - h\nu(1s \rightarrow 2p)$ also decreases with decreasing matrix polarity in polar solvents and the small value of ~0.1 eV observed in liquid ethane also fits this trend. This means that the $2p$ level is close to the bottom of the conduction state for electrons in ethane and suggests that the optical absorption spectrum of the conduction state for electrons in ethane may not be mainly due to a bound–bound transition. This suggestion is

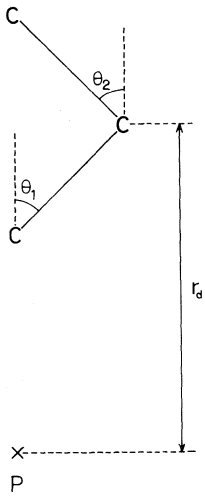

FIG. 1. Structural model for the propane molecule in the first coordination layer. Model 1 in Table 2. *P* indicates the center of a cavity.

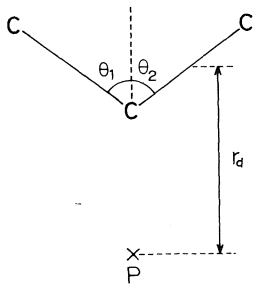

FIG. 2. Structural model for the propane molecule in the first coordination layer. Model 2 in Table 2.

reinforced by the relatively low values of $f(1s \rightarrow 2p)$, particularly at low temperature. The values of the bound–free transition energy $h\nu_{max}$ are about twice as large as those of $h\nu(1s \rightarrow 2p)$, and they fall in the near-infrared region. It is interesting to note that $h\nu(1s \rightarrow 2p)$, I, and $h\nu_{max}$ decrease significantly with increasing temperature over the temperature range studied. At present there are no experimental data available for comparison with these calculated optical properties. It would be interesting to carry out an optical absorption study of localized excess electrons in liquid ethane to test some of these predictions.

Figure 7 shows the configuration coordinate diagram for a localized excess electron in liquid ethane at 127 K. In the figure the 1*s* ground, 2*p* excited and continuum states are shown for $N = 4$, 6, and 8. The general features of the configuration coordinate curves are similar to

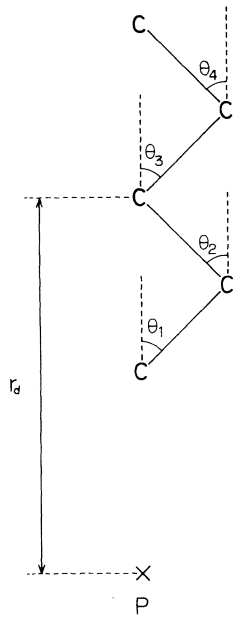

FIG. 3. Structural model for the *n*-pentane molecule in the first coordination layer. Models 1–5 in Table 2.

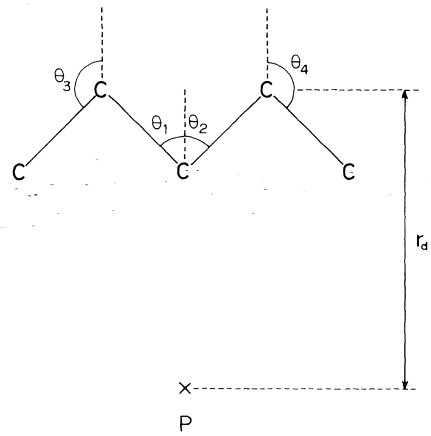

FIG. 4. Structural model for the *n*-pentane molecule in the first coordination layer. Models 6–8 in Table 2.

each other for cases of $N = 4$, 6, and 8. The ground-state energy becomes slightly higher with increasing N. The cavity radius, r_d^0, increases with increasing N. These trends are also observed in the theoretical results on solvated electrons in polar solvents (2).

Liquid Propane

Table 4 shows the properties of localized excess electrons in liquid propane calculated using the two structural models. The calculated properties and trends in Table 5 are similar to

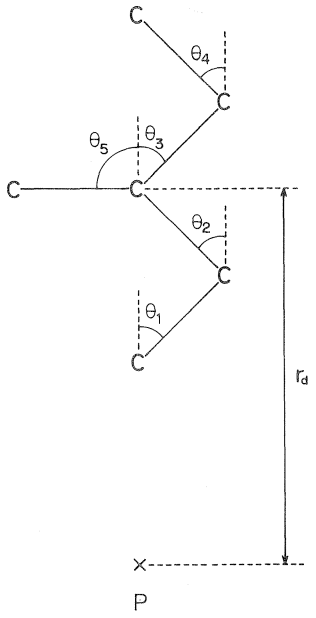

FIG. 5. Structural model for the 3MP molecule in the first coordination layer. Models 1–5 in Table 2.

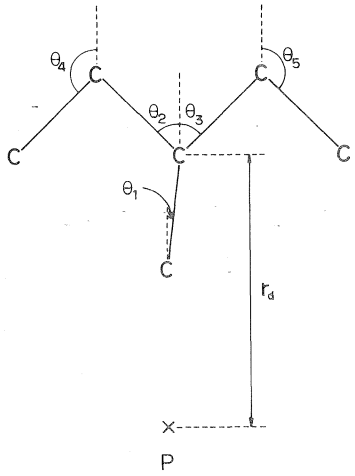

FIG. 6. Structural model for the 3MP molecule in the first coordination layer. Models 6–8 in Table 2.

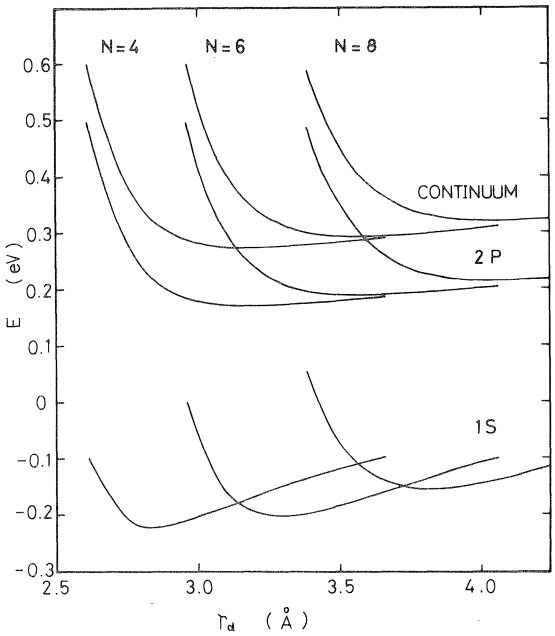

FIG. 7. Configuration coordinate diagram for the localized excess electron in liquid ethane at 127 K.

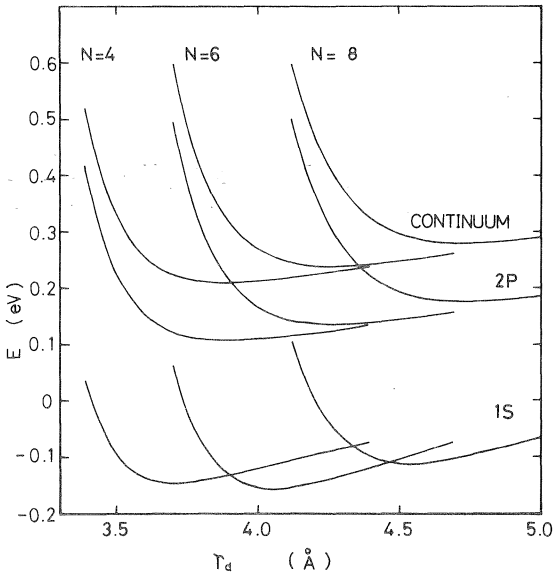

FIG. 8. Configuration coordinate diagram for the localized excess electron in liquid propane at 179 K (model 1).

those in Table 4. Model 2 with the central carbon of propane closest to the excess electron (Fig. 2) predicts $h\nu(1s \rightarrow 2p)$, I, $h\nu_{max}$, and ΔH somewhat greater than does model 1 with an end carbon of propane closest to the excess electron (Fig. 1). It is especially interesting that the ground-state energy at a given temperature shows a minimum for $N = 6$ compared to $N = 4$ and 8 in model 1 (see Fig. 8), but in model 2 the ground state is lowest for $N = 4$ as has been typically found. The optical absorption spectrum of localized excess electrons in liquid propane was observed at 88 K by pulse radiolysis techniques (13). The maximum absorption occurs at ≥ 2000 nm (≤ 0.6 eV) which is clearly higher than

TABLE 3. Properties of localized excess electrons in liquid ethane

T (K)	N	r_d^0 (Å)	$h\nu(1s \rightarrow 2p)$ (eV)	$f(1s \rightarrow 2p)$	I (eV)	$h\nu_{max}$ (eV)	ΔH (eV)
127	4	2.85	0.431	0.230	0.535	0.958	0.220
	6	3.25	0.418	0.268	0.522	0.861	0.200
	8	3.85	0.376	0.355	0.481	0.727	0.153
182	4	2.85	0.288	0.287	0.377	0.736	0.262
	6	3.35	0.261	0.371	0.350	0.602	0.246
	8	3.85	0.243	0.434	0.332	0.528	0.203
200	4	2.95	0.187	0.496	0.271	0.496	0.333
	6	3.35	0.185	0.521	0.270	0.466	0.316
	8	3.85	0.168	0.596	0.252	0.401	0.274

TABLE 4. Properties of localized excess electrons in liquid propane

T (K)	N	r_d^0 (Å)	$h\nu(1s \rightarrow 2p)$ (eV)	$f(1s \rightarrow 2p)$	I (eV)	$h\nu_{max}$ (eV)	ΔH (eV)
				Model 1			
179	4	3.7	0.268	0.451	0.370	0.623	0.144
	6	4.1	0.300	0.408	0.403	0.658	0.153
	8	4.5	0.304	0.422	0.408	0.634	0.109
197	4	3.7	0.233	0.485	0.330	0.559	0.154
	6	4.1	0.262	0.433	0.360	0.598	0.160
	8	4.6	0.253	0.482	0.351	0.544	0.116
211	4	3.8	0.183	0.636	0.276	0.431	0.183
	6	4.1	0.216	0.502	0.309	0.520	0.180
	8	4.6	0.208	0.541	0.301	0.472	0.136
222	4	3.8	0.155	0.728	0.244	0.366	0.211
	6	4.1	0.178	0.583	0.267	0.450	0.198
	8	4.6	0.171	0.625	0.259	0.409	0.154
				Model 2			
179	4	2.8	0.309	0.331	0.411	0.767	0.242
	6	3.3	0.292	0.406	0.394	0.650	0.213
	8	3.8	0.289	0.438	0.392	0.606	0.180
197	4	2.8	0.274	0.358	0.371	0.704	0.252
	6	3.3	0.259	0.431	0.356	0.594	0.225
	8	3.8	0.256	0.466	0.354	0.553	0.192
211	4	2.8	0.235	0.408	0.328	0.627	0.279
	6	3.3	0.221	0.490	0.315	0.526	0.254
	8	3.8	0.217	0.522	0.311	0.489	0.219
222	4	2.9	0.194	0.523	0.284	0.505	0.304
	6	3.3	0.190	0.554	0.280	0.464	0.279
	8	3.7	0.186	0.582	0.276	0.438	0.243

$h\nu(1s \rightarrow 2p)$ but rather close to the calculated $h\nu_{max}$. It is expected that the bound-free transition may significantly contribute to the observed absorption maximum, although the calculated $h\nu(1s \rightarrow 2p)$ and $h\nu_{max}$ are both temperature dependent. Such an interpretation is also supported by the fact that the calculated $f(1s \rightarrow 2p)$ is considerably lower than unity.

The cavity radius, r_d^0, for the same N is greater in the model 1 structure of propane than in ethane by about 0.8 Å, and it is about the same in the model 2 structure of propane and ethane. This simply reflects the geometry difference between models 1 and 2.

Figure 8 shows the configuration coordinate diagram for a localized excess electron in liquid propane at 179 K (model 1). The configuration coordinate curves in Fig. 8 are similar to those

TABLE 5. Properties of trapped electrons in 3MP glass at 77 K

Model	N	r_d^0 (Å)	$h\nu(1s \rightarrow 2p)$ (eV)	$f(1s \rightarrow 2p)$	I (eV)	ΔH (eV)
1	4	4.1	0.946	0.498	1.12	−0.202
	6	4.5	0.928	0.767	1.16	−0.249
	8	4.9	0.854	0.892	1.15	−0.389
2	4	4.1	1.00	0.527	1.18	−0.189
	6	4.5	0.974	0.801	1.22	−0.238
	8	4.9	0.890	0.912	1.21	−0.381
3	4	4.1	1.02	0.513	1.20	−0.167
	6	4.5	0.996	0.801	1.24	−0.216
	8	4.9	0.908	0.913	1.23	−0.360
4	4	4.1	0.940	0.367	1.11	−0.096
	6	4.5	0.938	0.615	1.14	−0.137
	8	5.0	0.840	0.864	1.12	−0.276
5	4	4.7	0.817	0.676	1.03	−0.241
	6	5.0	0.881	0.794	1.14	−0.242
	8	5.4	0.829	0.898	1.16	−0.355
6	4	3.7	0.823	0.384	0.981	−0.204
	6	4.1	0.784	0.675	0.969	−0.302
	8	4.6	0.726	0.876	0.979	−0.415
7	4	3.7	0.894	0.337	1.05	−0.134
	6	4.1	0.854	0.613	1.04	−0.234
	8	4.6	0.783	0.870	1.04	−0.358
8	4	3.6	1.08	0.285	1.24	−0.085
	6	4.0	1.00	0.636	1.19	−0.209
	8	4.5	0.884	0.895	1.16	−0.353

for liquid ethane (Fig. 7). However, the ground-state energy is a minimum for $N = 6$ in propane (model 1) as mentioned above.

3-Methylpentane Glass

Table 5 shows the calculated properties of trapped electrons in 3MP glass at 77 K, which includes results obtained using models 1–8 in Table 2. It is seen in Table 5 that (*a*) r_d^0 increases with increasing N, (*b*) $h\nu(1s \rightarrow 2p)$ decreases with increasing N with the exception of model 5, (*c*) $f(1s \rightarrow 2p)$ increases with increasing N and shows a relatively large increase between $N = 4$ and $N = 6$, (*d*) I is nearly independent of N, and (*e*) ΔH decreases with increasing N. The value of $h\nu(1s \rightarrow 2p)$ somewhat depends on the model used, but it is generally in reasonable agreement with the transition energy, 0.8 eV (1, 14) at the absorption maximum observed for trapped electrons in 3MP at 77 K. The relatively high value of $f(1s \rightarrow 2p)$ indicates that the $1s \rightarrow 2p$ transition significantly contributes to the absorption spectrum, although $f(1s \rightarrow 2p)$ is relatively low for $N = 4$ in some of the models. The energy difference between $h\nu(1s \rightarrow 2p)$ and I is about 0.2 eV, which is in good agreement with the experimental results on trapped electrons in 3-methylhexane glass at 77 K (1, 15). It is seen in Table 2 that the electron can be stably trapped in 3MP at 77 K and its binding energy is about 0.6 eV. The calculated value of ΔH has a negative sign for 3MP at 77 K in contrast to the positive ΔH for liquid ethane and propane. The distance of the nearest protons from the center of cavity, $r_{e^-\text{—H}}$, was calculated to be 1.9 ± 0.1, 2.3 ± 0.1, and 2.7 ± 0.1 Å for $N = 4$, 6, and 8, respectively, for all the models used for 3MP. These values are smaller than the experimental value, 3.0–3.2 Å, derived from electron spin echo data (4). However, semicontinuum models for solvated electrons in polar matrices have generally given smaller values of $r_{e^-\text{—H}}$ than observed. In order to further improve the theoretical results it would be necessary to treat short-range repulsive interactions between the excess electron and the medium electrons more adequately.

TABLE 6. Properties of trapped electrons in 3MP at 77 K for $V_0 = 0.6$ eV (model 4)

N	r_d^0 (Å)	$h\nu(1s \rightarrow 2p)$ (eV)	$f(1s \rightarrow 2p)$	I (eV)	ΔH (eV)	$V_0 - E_t(1s)$ (eV)
4	4.2	0.605	0.364	0.754	−0.012	0.588
6	4.5	0.659	0.394	0.815	−0.059	0.541
8	5.0	0.623	0.568	0.795	−0.198	0.402

	Ground state		Excited state	
N	$C_{1s}(r_d^0)$	$C_{1s}(R_0)$	$C_{2p}(r_d^0)$	$C_{2p}(R_0)$
4	0.756	0.979	0.038	0.259
6	0.789	0.982	0.060	0.330
8	0.785	0.975	0.132	0.492

Nevertheless, we consider the overall agreement between the variety of experimental data for trapped electrons in 3MP ($h\nu(1s \rightarrow 2p)$, I, $r_{e^-\text{–H}}$, and $N = 6$ depending on the configuration of the first solvation shell) and these calculations to be rather good.

Figure 9[2] shows the configuration coordinate diagram for a trapped electron in 3MP at 77 K (model 4). The general features of the configuration coordinate curves are similar to those for localized excess electrons in liquid ethane and propane.

If V_0 is decreased from 1.0 eV, which is probably an upper limit, used in Table 5, to 0.6 eV we obtain the results shown in Table 6. The main effect of making V_0 less positive is to decrease $h\nu(1s \rightarrow 2p)$ and I. This may give slightly better agreement with experiment.

Charge Distributions

The charge distributions of localized excess electrons in liquid ethane and propane were calculated *vs.* temperature. In ethane the ground state contains 0.82 of the charge within the first coordination layer at 127 K for $N = 6$. This fraction decreases to 0.67 as the temperature is increased to 200 K. The charge distribution of the excited state is much broader than that of the ground state and varies from 0.026 at 127 K to 0.018 at 200 K for $N = 6$. The charge distributions in liquid propane are similar for the various configurations considered. In 3MP at 77 K the charge is much more localized and has values of 0.97 for the ground state and 0.70 for the excited state within the first coordination layer for $N = 6$, model 1. The significant difference from ethane and propane is due in large part to the high value of V_0 for 3MP at 77 K. The narrow charge distribution of the excited state is responsible for the relatively high value of $f(1s \rightarrow 2p)$ found for 3MP at 77 K.

The detailed results for the charge distribution for all configurations are found in Tables 7–9.[2]

Criterion for Electron Localization

The criterion for excess electron localization is given by the quantity, $V_0 - E_t(1s)$; the localized electron state is stable for $V_0 - E_t(1s) > 0$ and the electron is not stably localized for $V_0 - E_t(1s) < 0$. The calculated values of $V_0 - E_t(1s)$ are given in Table 2. It can be seen that the excess electron in liquid ethane should be localized over the temperature range studied and for all cases of $N = 4$, 6, and 8. This conclusion is consistent with experiments that show a low electron mobility in liquid ethane (16, 17).

The stability of localized excess electrons in liquid propane is well established as seen in Table 2. It is interesting to note that the magnitude of the binding energy, $V_0 - E_t(1s)$, of the excess electron is comparable to the observed activation energy (~0.13 eV) (16) for the electron mobility, although the calculated binding energy is temperature dependent and somewhat higher at lower temperatures than the mobility activation energy. Since $V_0 - E_t(1s)$ contains $E_t(1s)$ which is obtained under the condition of energy minimization in the calculation while the mobility activation energy is probably associated with the energy of a transient trapped electron state, it is likely that $V_0 - E_t(1s)$ is somewhat greater than the mobility activation energy.

Calculations were also made of the stability of localized excess electrons in liquid *n*-pentane and

neopentane, in which the eight models and two values of V_0 were used for *n*-pentane and three values of V_0 were used for neopentane. The results of the calculations are given in Table 3. It can be seen that localized excess electrons are stable in *n*-pentane for almost all models. In neopentane the ground-state energy, $E_t(1s)$, of localized excess electrons is higher than V_0 for $N = 6$ and 8, and $V_0 - E_t(1s)$ is comparable in magnitude to the thermal energy kT for $N = 4$. These results indicate that in neopentane the localized excess electron is unstable and the excess electron exists as a delocalized quasi-free electron in accord with the electron mobility data (18–21).

Acknowledgment

This research was partially supported by the U.S. Energy Research and Development Administration under Contract E(11-1)-2086 and by the Computing Centers at Nagoya University and Wayne State University.

1. L. KEVAN. Adv. Radiat. Chem. **4**, 181 (1974).
2. K. FUEKI, D.-F. FENG, and L. KEVAN. J. Am. Chem. Soc. **95**, 1398 (1973).
3. M. NEWTON. J. Phys. Chem. **79**, 2795 (1975).
4. P. A. NARAYANA and L. KEVAN. J. Chem. Phys. **65**, 3379 (1976).
5. D.-F. FENG, H. YOSHIDA, and L. KEVAN. J. Chem. Phys. **61**, 4440 (1974).
6. W. SCHMIDT. *In* Electron–solvent and anion–solvent interactions. *Edited by* L. Kevan and B. Webster. Elsevier, Amsterdam. 1976. Chapt 7.
7. J. B. HENDRICKSON. J. Am. Chem. Soc. **83**, 4537 (1961).
8. S. NODA, L. KEVAN, and K. FUEKI. J. Phys. Chem. **79**, 2866 (1975).
9. R. A. HOLROYD and M. ALLEN. J. Chem. Phys. **54**, 5014 (1971).
10. R. A. HOLROYD, B. K. DIETRICH, and H. A. SCHWARZ. J. Phys. Chem. **76**, 3794 (1972).
11. R. A. HOLROYD and R. L. RUSSELL. J. Phys. Chem. **78**, 2128 (1974).
12. K. FUEKI, D.-F. FENG, and L. KEVAN. J. Chem. Phys. **59**, 6201 (1973).
13. H. A. GILLIS, N. V. KLASSEN, G. G. TEATHER, and K. H. LOKAN. Chem. Phys. Lett. **10**, 481 (1971).
14. W. H. HAMILL. *In* Radical ions. *Edited by* E. T. Kaiser and L. Kevan. Wiley-Interscience, New York. 1968. Chapt. 9.
15. T. HUANG and L. KEVAN. J. Am. Chem. Soc. **95**, 3122 (1973).
16. M. G. ROBINSON and G. R. FREEMAN. Can. J. Chem. **52**, 440 (1974).
17. W. F. SCHMIDT, G. BAKALE, and U. SOWADA. J. Chem. Phys. **61**, 5275 (1974).
18. R. M. MINDAY, L. D. SCHMIDT, and H. T. DAVIS. J. Phys. Chem. **76**, 442 (1972).
19. G. BAKALE and W. F. SCHMIDT. Chem. Phys. Lett. **22**, 164 (1973).
20. K. SHINSAKA and G. R. FREEMAN. Can. J. Chem. **52**, 3556 (1974).
21. A. O. ALLEN and R. A. HOLROYD. J. Phys. Chem. **78**, 796 (1974).

Discussion

K. Funabashi: This calculation uses a variational technique in which the ground-state wavefunction is a hydrogenic (1*s*)-function with one parameter. But this form is approximately suitable only when one knows the ground state is *localized* before the *calculation*.

L. Kevan: We calculate the ground state energy $E_t(1s)$ relative to the vacuum level. In the alkanes thus far investigated this energy is negative, indicating stability or localization relative to the vacuum level, so hydrogenic wavefunctions are appropriate. We then compare $E_t(1s)$ to V_0 to determine whether the electron is stable or localized relative to V_0.

J. Jortner: I would like to raise a question concerning an experimental criterion regarding electron localization in some hydrocarbons. You have stated that whenever your energetic data $(V_0 - E_t(1s)) > 0$ the electron is localized and the mobility is low. However, the 'low' electron mobilities in hydrocarbons are in the range 1.0–0.1 $cm^2 V^{-1} S^{-1}$. Such mobilities are too high for a hydrodynamic drag of a localized state. You may invoke thermal excitation from the bound state to the conduction band; however, the positive values of $V_0 - E_t(1s)$ calculated by you considerably exceed the experimental activation energies of the mobility. This points to a more complex picture for electronic structure and transport of excess electrons in hydrocarbons.

L. Kevan: Our localization criterion, $V_0 - E_t(1s) > 0$, contains $E_t(1s)$ which is obtained under the condition of energy minimization by varying a configurational coordinate. However, the mobility activation energy is probably associated with the energy of a *transient* localized electron state which is expected to be less than the energy $E_t(1s)$ of the equilibrium localized electron state that we calculate in this work. We have discussed transient localized electron states in alkanes earlier (J. Phys. Chem. **79**, 2866 (1975)). Thus in general, we expect $V_0 - E_t(1s)$ to be somewhat greater than the mobility activation energy. But in some cases such as propane at higher temperatures $V_0 - E_t(1s)$ is comparable to the mobility activation energy (0.13 eV). I certainly do agree that the transport of electrons in alkanes is complex and that we do not understand it at present. In the present work we have not yet attempted to treat the dynamics of this electron transport.

A. O. Allen: It would be interesting to study further the electron energy as a function of the orientations of the surrounding molecules. The single optimum state is one of a large number of states, produced by variation of the molecular positions and orientations, in which the electron exists in thermal equilibrium. Understanding the properties of the electron must therefore require an estimation of the density of states.

L. Kevan: We do hope to study the properties of electrons in alkanes for various nonequilibrium orientations of the first solvation shell molecules. However, in the framework of our calculation as described I don't believe we can readily estimate the density of states.

H. A. Gillis: You have carried out calculations for 3-methylpentane glass at 77 K which gives reasonable agreement with the observed E_{max} of about 0.8 eV. But in fact this E_{max} is for the blue-shifted spectrum found at long times. At shorter times we found a spectrum for this glass with $E_{max} \simeq 0.6$ eV (N. V. Klassen, H. A. Gillis, and G. G. Teather. J. Phys. Chem. **76**, 3847 (1972)). Presumably this spectrum corresponds to an electron solvated in a random mixture of configurations. Can your model explain this short-time spectrum?

L. Kevan: Our calculations are for various assumed *equilibrium* configurations for the solvated electron in alkanes in which a nearest C—C bond is oriented toward the electron. The optical absorption you see at early times in pulse radiolysis corresponds to an electron in a nonequilibrium configuration. I believe we can account for this red-shifted optical absorption by making calculations for nonequilibrium configurations with varying angles between a nearest C—C bond and the electron. This would be similar to our earlier calculations of this type on electrons in ethanol where we could well account for the time dependent spectral shift observed in pulse radiolysis.

Field-dependent electron mobility in methane–ethane liquid mixtures

BAPPANADU N. RAO, ROBERT L. BUSH, AND K. FUNABASHI

Department of Chemistry and Radiation Laboratory,[1] University of Notre Dame, Notre Dame, IN, U.S.A. 46556

Received September 27, 1976

BAPPANADU N. RAO, ROBERT L. BUSH, and K. FUNABASHI. Can. J. Chem. **55**, 1952 (1977).

Some aspects of the mobility of excess electrons in liquid hydrocarbons are discussed. Certain salient features of the experimental data on high-field mobility in ethane–methane mixtures are explained in terms of a hopping model, in which disorder plays an important role. The disorder is compositional, like that in a binary alloy, and enters the model in the form of two distinct jump distances for hopping motion. It is shown that decreasing the coherence length for a quasi-free electron increases the binding energy of a localized electron and hence affects the activation energy and rate of hopping. The effects of temperature and impurity concentration for high-mobility liquids are shown to be consistent with a scattering model.

BAPPANADU N. RAO, ROBERT L. BUSH et K. FUNABASHI. Can. J. Chem. **55**, 1952 (1977).

On discute de quelques aspects de la mobilité des électrons en excès dans les hydrocarbures liquides. On explique quelques caractéristiques importantes des données expérimentales concernant la mobilité à haut champ dans des mélanges d'éthane et de méthane en termes d'un modèle à sauts dans lequel le désordre joue un rôle important. Le désordre a trait à la composition, comme dans un alliage binaire, et apparait dans le modèle sous forme de deux distances distinctes pour le mouvement de saut. On montre que si l'on diminue la longueur de cohérence pour un électron pratiquement libre il y a augmentation de l'énergie de liaison d'un électron localisé et ainsi un effet sur l'énergie d'activation et la fréquence des sauts. On montre que les effets de la température et les concentrations d'impureté dans le cas des liquides de grande mobilité sont en accord avec un modèle de dispersion.

[Traduit par le journal]

Introduction

Electron transport in liquid hydrocarbons has been studied extensively in recent years (1–3). The magnitudes of electron drift mobilities in these liquids vary from $\sim 10^{-3}$ cm^2 V^{-1} s^{-1} in ethane to ~ 500 cm^2 V^{-1} s^{-1} in methane (see for example ref. 4). An apparent correlation between the magnitude of the mobility and the molecular geometry has also been found among larger hydrocarbons, such as *n*-pentane and neopentane (2, 3) and butene-1 and isobutene (5).

Davis, Schmidt, and Minday (6) proposed a transport mechanism which is now called the trapping mechanism. In their picture, the mobility of an electron in a hydrocarbon liquid depends only on the probability of finding the electron in a quasi-free state; this probability is determined by the average trap depth and the trapping frequency. The electron transport is assumed to take place only in the quasi-free state, in which the mobility is about 150 cm^2 V^{-1} s^{-1} or larger. Schiller (7) and Kestner and Jortner (8) have ascribed the differences among the mobilities of hydrocarbons to differences in V_0, the energy level of the quasi-free state (9).

All these proposed models are designed to explain the entire range (10^{-3} to 500 cm^2 V^{-1} s^{-1}) of magnitudes of mobility by a unified picture with few parameters, emphasizing the role of the quasi-free electrons even for low-mobility liquids. On the other hand, the conventional transport mechanism for the low-mobility ($< \sim 1$ cm^2 V^{-1} s^{-1}) liquids and solids is electron hopping, based upon the concept of the small polaron (10).

The correct transport mechanism for excess electrons in low-mobility hydrocarbons will depend on the details of the liquid structure and the electron–phonon interaction, which are not known at this time. In the absence of this information, a model theory which explains the low-field electron mobility may be judged by its ability to explain other observed properties of the excess electron in these systems.

The purpose of this article is to discuss a hopping model for the high-field electron mobility in low-mobility liquid hydrocarbons.

[1]The Radiation Laboratory of the University of Notre Dame is operated under contract with the U.S. Energy Research and Development Administration. This is ERDA Document No. COO-38-1055.

By a hopping model we mean a model which treats electrons as tightly bound, most likely by the electron–phonon interaction, and in which the motion is by hopping in random jumps whose length is of the order of the intermolecular separation. Specifically, we shall focus on the experimental results of Bakale, Tauchert, and Schmidt (4) on ethane–methane mixtures. We shall not attempt a quantitative explanation of the magnitude of the low-field mobility as a function of methane concentration. The high-field mobilities in the high-mobility methane-rich mixtures are also outside the scope of this article. Detailed theories to describe this latter behavior have been developed by Shockley (11) and Thornber and Feynman (12).

In the next section we review experimental results for field-dependent mobilities, and propose an explanation for certain qualitative features of these results in terms of a hopping model. Our hopping model is a modification of our earlier work (13). In the following section we present a calculation which exhibits the effect of the finite coherence length of the quasi-free electron on the binding energy of a localized electron in the same system, in order to understand the change in activation energy as a function of methane concentration. We shall also present a brief discussion of wave propagation with scattering as a transport mechanism for the high-mobility regime of methane–ethane mixtures.

Field-dependent Mobility

The electron drift mobility μ is defined by

$$[1] \qquad v_D = \mu F$$

where v_D is the drift velocity (cm/s) and F is the field strength (V/cm). It is known experimentally that for most materials the mobility μ is independent of F when F is sufficiently small. When log v_D is plotted against log F, the slope is unity as long as μ is independent of F. As the field strength increases, the relationship between log v_D and log F becomes non-linear. The trend and pattern of this non-linearity depends on the magnitude of the low-field electron mobility. Figure 1 represents the field-dependent drift velocity for ethane–methane mixtures, where the pattern of non-linearity is different for different values of the zero-field electron mobility $\mu(0)$ (4). We note the following three features of Fig. 1: (*1*) the onset of the non-linearity moves toward smaller field strengths as the zero-field mobility $\mu(0)$ increases, as shown in Fig. 1 by a dotted curve; (*2*) for $\mu(0) < 1\ \text{cm}^2\ \text{V}^{-1}\ \text{s}^{-1}$, the high-field mobility increases with increasing field strength, whereas for the high-mobility regime, the mobility decreases with increasing field strength (*i.e.*, the drift velocity increases but not in proportion to the field); (*3*) the non-linearity becomes less pronounced as $\mu(0)$ increases from the lowest value to $\sim 1\ \text{cm}^2\ \text{V}^{-1}\ \text{s}^{-1}$, at which point the non-linearity *apparently* disappears.

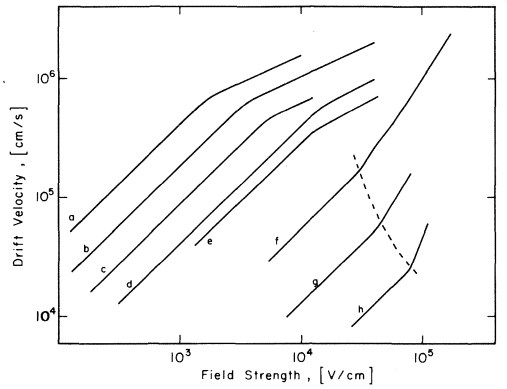

FIG. 1. Electron drift velocity v_D as a function of electron field F and concentration of ethane for ethane–methane mixtures at $T = 111$ K: (*a*) pure methane; (*b*) 4 mol% ethane; (*c*) 13 mol% ethane; (*d*) 24 mol% ethane; (*e*) 27.5 mol% ethane; (*f*) 50 mol% ethane; (*g*) 63 mol% ethane; (*h*) 74 mol% ethane.

The same three features are evident in the field-dependent electron mobility of helium as a function of pressure (14), and also in larger hydrocarbons (15), suggesting that these features may be the properties of some universal transport mechanism. We shall test the applicability of a hopping mechanism to these three features in the low-mobility regime.

The simplest theory for the non-linear mobility in the hopping model is the hyperbolic sine law (16–18):

$$[2] \qquad \mu(F) = \mu(0) \sinh\left(\frac{e\lambda F}{2kT}\right) \Big/ \left(\frac{e\lambda F}{2kT}\right)$$

where $\mu(F)$ is the electron drift mobility at the field strength F and λ is the jump distance for the hopping motion. The zero-field mobility $\mu(0)$ is given by the Einstein relationship

$$[3] \qquad \mu(0) = \frac{eD}{kT} = \frac{e\lambda^2\nu}{kT} \exp(-E/kT)$$

where ν is the jump frequency and E is the free energy barrier height for the hopping motion.

In order to explain the fact that the non-linearity sets in at smaller external fields with increasing methane concentration, the jump distance λ in [2] must increase with methane concentration. Bakale *et al.* (4) found that the jump distance increases from 10 Å for pure ethane to 50 Å for equimolar mixtures of ethane and methane. In addition to the fact that these jump distances are too large for a typical hopping motion, the increase in λ predicts that the mobility will rise more sharply with field as μ(0) increases, by [2], in qualitative contradiction to observation (*i.e.* our feature number (*3*)). In the following we present a hopping model containing disorder, which exhibits the observed behavior ((*1*)–(*3*), above) with a reasonable value for the jump distance.

The first step is to note that [2] is an approximation to the form:

$$[4]\quad \mu(F) = \mu(0)\exp\left[-(e\lambda F)^2/16EkT\right] \times \sinh\left(\frac{e\lambda F}{2kT}\right) \Big/ \left(\frac{e\lambda F}{2kT}\right)$$

which is valid for parabolic potentials, and where E is the barrier height as in [3]. Equation 4 can be derived quantum-mechanically (19, 20) or classically (21).

Let us assume for the moment that the barrier height E, which is a constant fraction of the binding energy of the polaron (22), decreases with increasing methane concentration, and both the jump frequency ν and the jump distance λ are independent of methane concentration. According to this model, the magnitude of the zero-field mobility μ(0), as given by [3], varies only as a function of E, while the high-field mobility, as given by [4], becomes more nearly constant with decreasing E. This is consistent with feature (*3*), above, but does not explain the fact that the non-linearity in v_D sets in at smaller field strengths as the methane concentration increases. In order to remedy this difficulty, we introduce some structural disorder into our model. Funabashi and Rao (13) have shown that any fluctuation in the barrier height lowers the threshold field for the non-linear drift velocity in comparison to that in a system with a constant barrier height. A similar observation has also been made by Austin and Sayer (21) and Böttger and Bryksin (23).

Before describing the nature of our specific 'disorder', we note that the lowering of the threshold field for the non-linear drift velocity as a function of the degree of disorder can be demonstrated in terms of several different models (13, 21, 23) and consequently is not a special phenomenon limited to a particular model.

In our model, we assume that all jumps in pure ethane are of length λ_1, and that adding methane introduces another jump distance λ_2, shorter than λ_1. A binary mixture of ethane and methane is therefore modeled as a linear chain of multiple barriers with jump distances λ_1 and λ_2. The fraction of jumps whose length is λ_2 is related to the concentration of methane. Clearly, there is no rigorous justification for choosing only two values for the jump distance, but we hope that this simple model may simulate some features of real binary mixtures.

The potential energy curve for hopping motion is drawn schematically in Fig. 2, where each potential is parabolic and the force constant for the potential is assumed to be the same throughout the chain. It is easy to show that the energy barrier E_i corresponding to the jump distance λ_i is given by

$$[5]\quad E_i = \alpha\lambda_i^2/8 \qquad i = 1, 2$$

where α is the force constant of the parabolic potential. Two jump distances therefore generate two values for the energy barrier.

The law of flux conservation requires

$$[6]\quad \lambda_1 \exp\left[-(ev_1)^2/16E_1kT\right]\sinh\left(ev_1/2kT\right) = \lambda_2 \exp\left[-(ev_2)^2/16E_2kT\right]\sinh\left(ev_2/2kT\right)$$

where v_1 and v_2 are the voltage drops across the jump distances λ_1 and λ_2, respectively. Because the total voltage drop across the entire system is fixed, v_1 and v_2 are related by

$$[7]\quad cv_1 + (1 - c)v_2 = [c\lambda_1 + (1 - c)\lambda_2]F$$

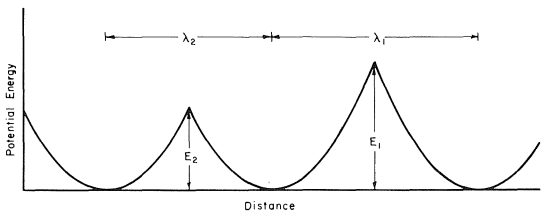

FIG. 2. Schematic diagram of potential energy *vs.* distance for a binary mixture. Note that two different barrier heights are associated with the two jump distances.

where c is the probability that a particular jump has length λ_1, and F is the external field strength as before.

The field-dependent mobility can be shown by methods analogous to those in ref. 13 to be

$$[8] \quad \mu(F) = \frac{e\lambda\lambda_1\nu}{kT}\exp\left[-\frac{E_1}{kT} - \frac{(ev_1)^2}{16E_1kT}\right] \times \frac{\sinh(ev_1/2kT)}{e\lambda F/2kT}$$

where

$$[9] \quad \lambda = c\lambda_1 + (1 - c)\lambda_2$$

For a fraction c, the voltage drop v_1 in [8] can be found from [6] and [7], and v_D can be plotted as a function of F. An example is shown in Fig. 3, where the ratio λ_2/λ_1 is taken to be 0.8 and the force constant α is assumed to decrease with a decrease in the fraction c, reflecting the physical situation that the binding energy of the small polaron decreases with the methane concentration. It can be seen in Fig. 3 that, unlike [4], [8] explains our three features ((*1*)–(*3*)) simultaneously. A comparison of Fig. 3 with the experimental results (Fig. 1) shows that the jump distance λ_1 in ethane–methane mixtures is about 10 Å, a reasonable value for the jump distance. This result implies that a hopping mechanism of electron transport properly designed is consistent with qualitative trends in the experimental results for non-linear mobility in low-mobility liquids.

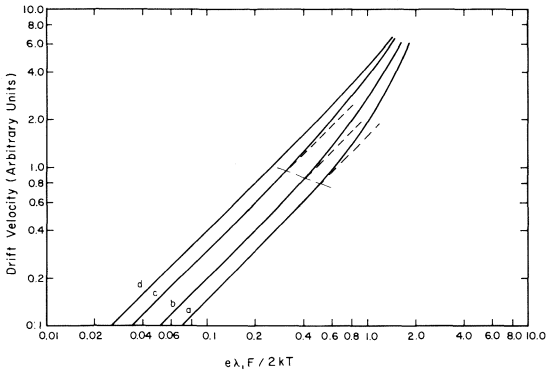

FIG. 3. Drift velocity v_D *vs.* field strength F for various concentrations c of λ_1 in a chain like that of Fig. 2, computed from eqs. 6–9. (*a*) $c = 0.64$, $\alpha = 80$ dyn/cm; (*b*) $c = 0.38$, $\alpha = 44.0$ dyn/cm; (*c*) $c = 0.15$, $\alpha = 36.8$ dyn/cm; (*d*) $c = 0.02$, $\alpha = 33.6$ dyn/cm. Here $\lambda_2/\lambda_1 = 0.8$. Comparison with Fig. 1 shows that $\lambda_1 \simeq 10$ Å in ethane–methane mixtures, a reasonable value for the jump distance.

Binding Energy of a Localized Electron

In order to provide some justification for our assumption that the binding energy of the small polaron decreases with an increase in methane concentration, we have examined the effect of a finite coherence length at the quasi-free state on the binding energy of a localized electron. Because basic information about the liquid structure and the nature of the electron–phonon interaction remains unknown, it is not possible to establish a quantitative relationship between the binding energy of a localized state and the concentration of methane. We have only investigated in a crude and qualitative way the effect of the finite coherence length on the binding energy of the localized electron and on the energy barrier for hopping motion; this finite coherence length is brought on by scattering, which varies monotonically with the concentration of methane.

Let us start with a simple tight-binding model for the electronic structure for an excess electron in molecular crystals. For example, if the crystal has a body-centered cubic (BCC) structure, the energy dispersion can be written as

$$[10] \quad E(k) = 8J\cos\theta_x\cos\theta_y\cos\theta_z$$

where the band center is chosen to be the zero of the energy scale, J is the nearest-neighbor transfer energy and

$$[11] \quad \theta_x = \tfrac{1}{2}a_l k_x \quad \text{etc.}$$

a_l being the lattice constant. When a defect potential is introduced at some site, a bound state can be realized (24) only if

$$[12] \quad V/8J > 0.722$$

where V is the diagonal matrix element of the defect potential. The situation is completely analogous to the localizability criterion for an excess electron in an attractive spherical potential; there is no bound state (25) unless $Ua^2 > \pi^2\hbar^2/8m$, where U and a are the depth and the radius of the potential, respectively. Electrons can also be localized by a sufficiently strong electron–phonon interaction (small polaron) (10). Although there is some question whether the transition from large to small polaron is continuous or sudden (26–28), the electron–phonon interaction energy must exceed one-half the band width in order for an electron to be localized as a small polaron. A finite

threshold strength for the defect or disorder potential or electron–phonon interaction is necessary to localize electrons.

In order to examine the effect of a finite coherence length, let us return to the BCC tight-binding model. For a perfect crystal all the energy levels, described by [10], correspond to completely coherent states and lie within a band of half-width $8J$. According to the general theory of electronic structure for disordered materials (29–31), fluctuation in the diagonal matrix elements, which is taken to be zero in [10], broadens the total band width, but narrows the region of extended states, so that the energy level for the lowest extended state goes up. When the energy fluctuation is sufficiently large, there are no extended states in the band (Anderson transition), as shown in Fig. 4. Since the energy fluctuation in the diagonal elements shortens the mean free path of scattering at the extended states, there is a correlation between the average binding energy of a localized electron and the finite coherence length at the quasi-free state.

Similarly, an electron–phonon interaction which is too weak to form a small polaron in the crystal could produce a small-polaron state in a highly disordered system, because of the narrowing of the band of extended states.

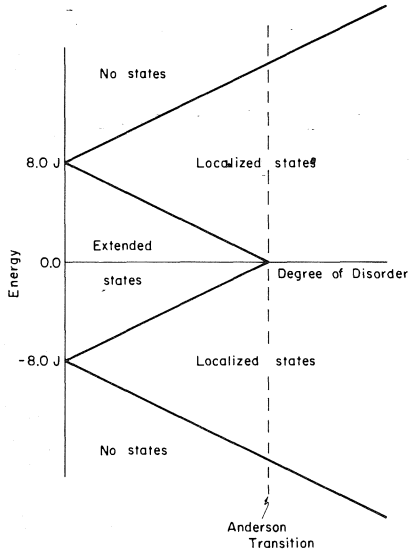

FIG. 4. Schematic diagram of the types of states which are present at various combinations of energy and randomness for a BCC lattice with nearest-neighbor interaction J and disorder in the diagonal terms of the Hamiltonian. The boundaries between the regions are not necessarily straight lines as we have drawn them. For degrees of disorder greater than that labelled 'Anderson Transition', all states are localized.

In order to show that the above argument is not restricted to the tight-binding model, let us consider the effect of a finite mean free path of scattering on the binding energy of a localized electron in a spherical potential well of depth $\hbar^2U_0/2ma^2$ and radius a. Such a potential well may be thought of as static or due to the electron–phonon interaction. We represent the fluctuating potential in the region outside the radius a by an imaginary potential $i\hbar^2U''/2ma^2$. This is a common substitution, and is used to represent such physical phenomena as widths of energy levels (optical potential for scattering) or attenuation (complex index of refraction). We expect that these features in the form of distributions of energy levels and finite mean free paths will be present in disordered systems. The presence of the imaginary potential implies, of course, that the eigenenergies will be complex. The imaginary part of the eigenenergy may be interpreted as an energy uncertainty or in terms of a mean free path.

The calculation of the binding energy proceeds as it does for the case of real potentials, except that all quantities are complex. For any complex energy ε (in units of $\hbar^2/2ma^2$) we define wavevectors p and q such that

$$[13] \qquad (p/2)^2 = \varepsilon + U_0$$

and

$$[14] \qquad (q/2)^2 = iU'' - \varepsilon$$

In terms of these, the wavefunction for the state at energy ε is

$$[15] \qquad \begin{aligned} \psi_\varepsilon(r) &= B \sin(pr/2a) && r < a \\ &= Ce^{-(qr/2a)} && r > a \end{aligned}$$

Equations 13 and 14 require a relation between p and q:

$$[16] \qquad \left(\frac{p}{2}\right)^2 - U_0 = iU'' - \left(\frac{q}{2}\right)^2$$

The requirements of continuity of the wavefunction and its first derivative at $r = a$ imply

$$[17] \qquad \frac{p}{2}\cot\frac{p}{2} = -\frac{q}{2}$$

Remembering that p and q are complex, and writing $p = p_1 + ip_2$, $q = q_1 + iq_2$, [16] and

[17] become

$$q_2^2 - q_1^2 = p_1^2 - p_2^2 - 4U_0$$
[18]
$$p_1p_2 + q_1q_2 = 2U''$$

and

$$q_1 = -\frac{p_1 \sin p_1 + p_2 \sinh p_2}{\cosh p_2 - \cos p_1}$$
[19]
$$q_2 = \frac{p_1 \sinh p_2 - p_2 \sin p_1}{\cosh p_2 - \cos p_1}$$

Equations 18 may be rewritten to show the explicit dependence of q on p:

$$q_1 = \{\tfrac{1}{2}(4U_0 - p_1^2 + p_2^2) + [\tfrac{1}{4}(4U_0 - p_1^2 + p_2^2)^2 + (2U'' - p_1p_2)^2]^{1/2}\}^{1/2}$$
[20]
$$q_2 = \{\tfrac{1}{2}(p_1^2 - p_2^2 - 4U_0) + [\tfrac{1}{4}(4U_0 - p_1^2 + p_2^2)^2 + (2U'' - p_1p_2)^2]^{1/2}\}^{1/2}$$

From this point on, the calculations to find the ground-state energy were done numerically: A value for p was chosen, and q was calculated both from [19] and [20]. Then the quantity $D \equiv (q_1(19) - q_1(20))^2 + (q_2(19) - q_2(20))^2$ was minimized by varying p_1 and p_2, using a principal axis technique (the algorithm used in a Fortran translation of procedure PRAXIS, taken from ref. 32). The initial values of p_1 and p_2 were chosen to be slightly greater than π and 0, respectively, to ensure that the eigenstate so found would be the ground state.

The result of this calculation is the ground-state energy as measured from the zero of potential. In random systems, however, a more useful number is the binding energy of the state measured with respect to the quasi-free level, the lowest conduction state. In order to satisfy the rule of Ioffe and Regel (33), that the real part of the wavevector must be greater than the imaginary part (reciprocal of mean free path), it is easy to convince oneself that the real part of the quasi-free energy must also be at least equal to the imaginary part of the potential.

The results of the calculation of the binding energy as measured from the quasi-free level are shown in Fig. 5, as a three-dimensional perspective plot. The general trend shown by this plot is that the binding energy increases with increasing U'', but not as fast as U''. That is, we observe that the energy of the ground state as measured from the zero of potential is becoming larger, but not as fast as the quasi-free level is rising. These results are also presented graphically in Fig. 6, where the separate terms are displayed for $U_0 = 2.50$ (in units of $\hbar^2/2ma^2$). There we see clearly that the term $\varepsilon_B(U_0,U'') - U''$, which is the negative of the ground-state energy measured from the zero of potential is monotonically decreasing as U'' increases. This calculation shows that a shorter coherence length at the quasi-free level increases the binding energy of localized states. As we have seen in the previous section (eq. 3), a decrease in binding energy leads to an increase in the low-field electron mobility in the hopping regime. Hence as more and more methane is added to ethane, the mean free path increases, and as a result the excess-electron mobility increases.

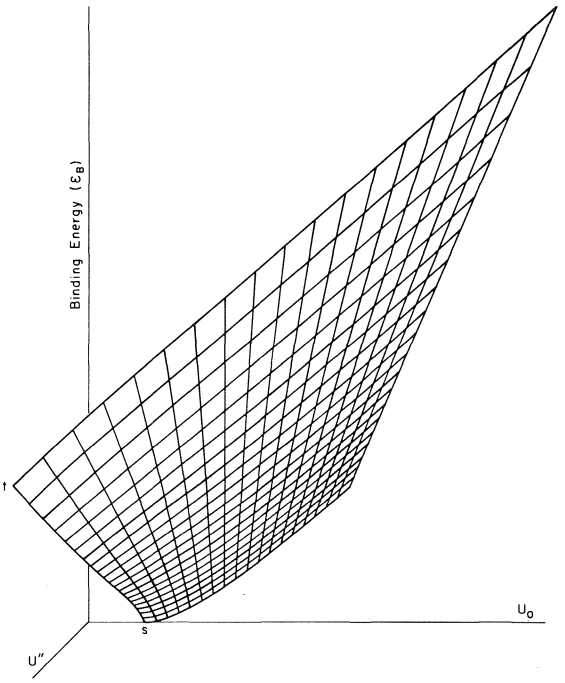

FIG. 5. Three-dimensional perspective plot of binding energy ε_B *vs.* real part of potential U_0 and imaginary part of potential U'', in the region $2.5 < U_0 < 11.5$, $0.0 < U'' < 5.0$. All energies are in units of $\hbar^2/2ma^2$ where a is the radius of the central well and m is the effective mass of the electron. Because this is the projection of a three-dimensional figure onto a two-dimensional surface, we have not shown the scales on the axes of this graph, for they would be misleading. As an example, line *st* is plotted in Fig. 6, where the scale is given.

The High-mobility Regime

We now examine briefly the high-mobility regime, and propose to show that it can be

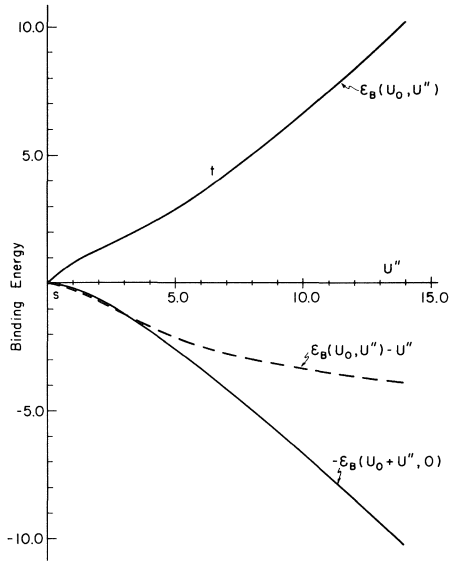

FIG. 6. Plot of the binding energy with respect to the quasi-free level $\varepsilon_B(U_0,U'')$ and the binding energy with respect to the zero of potential $\varepsilon_B(U_0,U'') - U''$ *vs.* U'' for $U_0 = 2.5$. $-\varepsilon_B(U_0 + U'',0)$ *vs.* U'' is also plotted for comparison. Here U_0 is the depth of the (real) potential well and U'' is the imaginary potential outside the well. (All energies are in units of $\hbar^2/2ma^2$ as in Fig. 5.) The line *st* corresponds to the line *st* in Fig. 5.

described adequately by a scattering model; a model containing traps and quasi-free states (6, 7) is *not* necessary in this regime. The usual argument is that the mobility is given by (34)

$$[21] \qquad \mu = \tfrac{4}{3}eL(2\pi mkT)^{-1/2}$$

where L is the mean free path. According to the proponents of the trapping model, [21] implies the mobility has a negative temperature dependence, so materials in which the mobility exhibits a positive temperature dependence cannot be described by a scattering model. This argument, however, ignores the possibility that L may be temperature-dependent. Funabashi and Kajiwara (35) have argued that L should be an increasing function of temperature in neopentane and other high-mobility hydrocarbon liquids. It is therefore possible that electron transport in high-mobility hydrocarbons may proceed via wave propagation with occasional scattering.

The scattering model also predicts the proper qualitative dependence of the mobility of ethane–methane mixtures on the ethane concentration in the high-mobility regime. For ethane concentrations of 0–20%, the mobility (4) is described by [21] with the mean free path given by

$$[22] \qquad L^{-1} = n_1\sigma_1 + n_2\sigma_2$$

where n_1 and n_2 are the numbers of molecules per unit volume for methane and ethane, respectively, and σ_1 and σ_2 are their respective cross sections. If more than 20% of the mixture is ethane, the combination of [21] and [22] no longer describes the concentration dependence of the mobility: L decreases faster than [22] predicts (4). There are two possible causes for this deviation from the simple single-scattering theory: the high density of scatterers may require a Lorentz correction such as that proposed by Landauer and Woo (36):

$$[23] \qquad L^{-1} = (n_1 + n_2)\sigma_1 + n_2(\sigma_2 - \sigma_1) \times (1 - 2n_2(\sigma_2 - \sigma_1)^{3/2})^{-1}$$

where we have assumed $\sigma_2 > \sigma_1$, and $n_2 \ll n_1$. The reason for this correction is most easily seen for hard sphere scatterers: if the incident electrons cannot penetrate into the interior of a sphere, there will be a higher current incident on other spheres. This is therefore a multiple-scattering effect, and is not restricted to hard spheres, but occurs in any medium in which the impurity cross section is larger than that of the host material. Equation 23 clearly predicts a faster decrease in the mean free path with increasing n_2 than [22] does. The second reason is that as more and more ethane molecules are added to the system they may tend to form clusters, and the cross section of a cluster of n ethane molecules may be greater than n times the cross section of a single ethane molecule. If the jth type of cluster occurs with density n_j' and the excess cross section referred to above is σ_j', then we may write

$$[24] \qquad L^{-1} = n_1\sigma_1 + n_2\sigma_2 + \sum_j n_j'\sigma_j'$$

This too will cause a more rapid decrease in L with increasing n_2. Both of these effects tend to decrease the mobility, in agreement with experiment.

Discussion

As with any model or theory, certain approximations have been made to make the mathematics tractable. The most important of these is that our model for the high-field mobility is inherently one-dimensional. A one-dimensional model gives correct results for a crystal or any other system which is uniform

or periodic in any plane perpendicular to the direction of motion. It is less clear that a one-dimensional model forms an acceptable description for disordered systems. The reason, of course, is that there is no way around a barrier in a one-dimensional system; the charge must 'go over' or tunnel through. In a three-dimensional system there may be other paths. The presence of the alternative paths reduces the effect of a small concentration of high barriers. Still, our one-dimensional model may be thought of as an idealization of the path of an individual electron through the sample in the presence of an external field, for even in a three-dimensional system, the electron's path will be over sites of randomly varying potentials. The effective width of the distribution of barrier heights may, however, be reduced. It is clear, then, that one must exercise caution when making *quantitative* comparisons between our model and experiment, although the predictions of our model should be qualitatively correct.

Although we have shown in the third section that shortening the mean free path at the quasi-free state has the effect of increasing the effective binding energy of a localized electron, we have not shown that a potential of arbitrarily small strength can bind an electron in a sufficiently highly disordered three-dimensional system. There may well be a range of values for potential strength and mean free path for which the wavefunction for an excess electron is neither localized nor extended. There is no adequate physical picture of electron transport in this regime. A number of physicists have denoted motion in this regime as electronic Brownian motion (see, for example, ref. 37) but have not provided any practical way of calculating transport properties for this intermediate range (1–10 $cm^2 V^{-1} s^{-1}$) of electron mobilities.

From what has been stated above, it is clear that the magnitude and temperature coefficient of the low-field dc mobility alone are not sufficient to determine the transport mechanism. Since other experiments such as ac conductivity, Hall effect, etc. have not yet been performed on alkane liquids, the only other available measurements of transport properties in these liquids are the high-field mobility measurements. It is on the basis of these measurements that the adequacy of models for transport must be decided.

These high-field results suggest that a simple trapping or two-state model would be difficult to apply to liquid alkanes. In the trapping model (6, 7) the observed mobility is expressed as

$$\mu = \mu_F P \qquad [25]$$

where μ_F is the mobility in the quasi-free state and P is the probability of finding the electron in the quasi-free state. The magnitude of μ_F is generally taken to be 100–150 $cm^2 V^{-1} s^{-1}$ or greater, and it is thought to be independent of the material in which the electrons are moving. The function P contains all of the information about the depth and density of the traps in a particular material. We note in passing that it is highly unlikely that a *universal* quasi-free mobility can be defined. The quasi-free mobility in a particular system depends on the amount by which electrons are scattered in the system. This in turn depends on the distribution of traps and scattering centers, a highly material-dependent quantity. Thus we expect the number and depth of traps to affect both factors in [25].

Aside from this, it appears unlikely that a reasonable functional form of P in terms of trap depth, field, temperature, etc. could be found which would predict the high-field behavior of the mobility in these liquid hydrocarbons. The functional form of μ_F can be inferred from the field dependence of the high-mobility materials: the mobility is independent of field up to $\sim 10^3$ V/cm, then decreases with increasing field. As the zero-field mobility decreases, however, the region in which the mobility is independent of field becomes larger (the lowest mobilities remain constant up to fields of $\sim 10^5$ V/cm), and the deviation changes sign: below ~ 1 $cm^2 V^{-1} s^{-1}$ the mobility *increases* with increasing field strength above the threshold. It would be difficult for the proponents of the trapping model to produce a function P which meets all these requirements and is still reasonable in terms of physical considerations such as its dependence on the trap depth and the external field. Instead of this, they could relax the requirement that the quasi-free mobility be independent of material, but then the model would be stripped of its most interesting feature.

In our model, on the other hand, we assume that transport in the high-mobility regime is by wave propagation with scattering, and in the low-mobility regime it is by hopping. In between is the uncharted region of electronic Brownian

motion. We have been able to show that the implications of these assumptions are in qualitative agreement with experimental results. It will be interesting to observe whether other experiments (ac conductivity, Hall coefficient, etc.) also produce results in agreement with our model.

A more complete treatment would be to combine the results of the trapping and hopping models, setting

$$[26] \qquad \mu = \mu_F P + \mu_H(1 - P)$$

where μ_H is the mobility due to hopping motion. The reason for this is that hopping and quasi-free motion are parallel channels for electron transport. To make such a model fit the high-field experiments, it is likely that μ_F and μ_H would have to depend on both the field strength and the choice of material, for reasons similar to those mentioned in our discussion of the trapping model above. For low-mobility materials, we would expect that P would be so small that the second term would dominate, so our treatment above would remain valid.

1. P. H. TEWARI and G. R. FREEMAN. J. Chem. Phys. **49**, 4394 (1968).
2. R. M. MINDAY, L. D. SCHMIDT, and H. T. DAVIS. J. Chem. Phys. **50**, 1473 (1969).
3. W. F. SCHMIDT and A. O. ALLEN. J. Chem. Phys. **50**, 5037 (1969).
4. G. BAKALE, W. TAUCHERT, and W. F. SCHMIDT. J. Chem. Phys. **63**, 4470 (1975).
5. J. P. DODELET, K. SHINSAKA, and G. R. FREEMAN. J. Chem. Phys. **59**, 1293 (1973).
6. H. T. DAVIS, L. D. SCHMIDT, and R. M. MINDAY. Chem. Phys. Lett. **13**, 413 (1972).
7. R. SCHILLER. J. Chem. Phys. **57**, 2222 (1972).
8. N. R. KESTNER and J. JORTNER. J. Chem. Phys. **59**, 26 (1973).
9. B. E. SPRINGETT, J. JORTNER, and M. H. COHEN. J. Chem. Phys. **48**, 2720 (1968).
10. T. HOLSTEIN. Ann. Phys. **8**, 325 (1959).
11. W. SHOCKLEY. Bell Syst. Tech. J. **30**, 990 (1951).
12. K. K. THORNBER and R. P. FEYNMAN. Phys. Rev. B, **1**, 4099 (1970).
13. K. FUNABASHI and B. N. RAO. J. Chem. Phys. **64**, 1561 (1976).
14. J. L. LEVINE and T. M. SANDERS, JR. Phys. Rev. **154**, 138 (1967).
15. G. BAKALE and W. F. SCHMIDT. Z. Naturforsch. Teil A, **28**, 511 (1973).
16. N. F. MOTT and R. W. GURNEY. Electronic processes in ionic crystals. 2nd ed. Dover Publications, Inc., New York. 1948. p. 43.
17. S. GLASSTONE, K. J. LAIDLER, and H. EYRING. The theory of rate processes. McGraw-Hill, New York. 1941. p. 563.
18. B. G. BAGLEY. Solid State Commun. **8**, 345 (1970).
19. A. L. EFROS. Sov. Phys. Solid State, **9**, 901 (1967).
20. H. G. REIK. Solid State Commun. **8**, 1737 (1970).
21. I. G. AUSTIN and M. SAYER. J. Phys. C, **7**, 905 (1974).
22. I. G. AUSTIN and N. F. MOTT. Adv. Phys. **18**, 41 (1969).
23. H. BÖTTGER and V. V. BRYKSIN. Phys. Status Solidi B, **68**, 285 (1975).
24. J. L. CALAIS and C. G. RIBBING. Phys. Rev. B, **4**, 376 (1971).
25. L. I. SCHIFF. Quantum mechanics. 1st ed. McGraw-Hill Book Company, Inc., New York and London. 1949. p. 77.
26. H. B. SHORE and L. M. SANDER. Phys. Rev. B, **7**, 4537 (1973).
27. D. EMIN and T. HOLSTEIN. Phys. Rev. Lett. **36**, 323 (1976).
28. Y. TOYOZAWA. Prog. Theor. Phys. **26**, 29 (1961).
29. P. W. ANDERSON. Phys. Rev. **109**, 1492 (1958).
30. M. H. COHEN, H. FRITZSCHE, and S. R. OVSHINSKY. Phys. Rev. Lett. **22**, 1065 (1969).
31. N. F. MOTT. Philos. Mag. **22**, 7 (1970).
32. R. P. BRENT. Algorithms for minimization without derivatives. Prentice-Hall, Englewood Cliffs, NJ. 1973. Chapt. 7.9.
33. A. F. IOFFE and A. R. REGEL. Prog. Semicond. **4**, 237 (1960).
34. H. MARGENAU. Phys. Rev. **85**, 621 (1946).
35. K. FUNABASHI and T. KAJIWARA. J. Phys. Chem. **76**, 2726 (1972).
36. R. LANDAUER and J. W. F. WOO. Phys. Rev. B, **5**, 1189 (1972).
37. L. FRIEDMAN. J. Non-Cryst. Solids, **6**, 329 (1971).

Discussion

G. R. Freeman: If one used a model involving an equilibrium between trapped states and a conduction band, could you estimate the field dependence of the retrapping rate from the conduction band?

K. Funabashi: If the field dependences for trapped states and conduction band are known separately, the observed field dependence should contain information on the field dependence of the retrapping rate and that of detrapping ('field-ionization').

J. M. Warman: The negative charge carrier mobility in liquid tetramethylsilane can be considerably reduced by the addition of low concentrations of a solute such as biphenyl which temporarily traps the otherwise quasifree electron. Such solutions correspond to a system in which a two state trapping mechanism is *known* to be responsible for the low mobility. A study of the field strength dependence of the mobility in such a system might therefore prove of interest with respect to the question of whether a two state trapping mechanism results in the observation of an increase or decrease in mobility at high field strengths.

W. F. Schmidt: With respect to the magnitude of the jump distance derived by us using the Bagley model we thought that the electron is not confined to say one ethane molecule but that it is spread out over a larger area and that the jump distance actually was comparable to the diameter of the trap. Values of this magnitude for trap diameters have been estimated also by Tachiya from the electron absorption spectrum of 3 MH and by Yakovlev from scavenging experiments in cyclohexane.

Experimental evidence from liquid semiconductors

J. E. ENDERBY

Department of Physics, University of Bristol, Bristol, England

Received September 27, 1976

J. E. ENDERBY. Can. J. Chem. **55**, 1961 (1977).

Two broad types of liquid semiconducting alloys will be discussed, namely those involving alkali metals (*e.g.*, the Li–Pb and the Cs–Au system) and those in which a chalcogen is involved (*e.g.*, Cu–Te or Ni–Te). It will be argued that relatively simple ionic bonding schemes in alkali metal systems must be replaced by more complicated ones in chalcogen based alloys. The close interaction between atomic structure on one hand, and the electronic structure on the other will be emphasized.

J. E. ENDERBY. Can. J. Chem. **55**, 1961 (1977).

On discutera de deux types généraux d'alliages liquides semiconducteurs soit ceux impliquant des métaux alcalins (par exemple le système Li–Pb et le système Cs–Au) et ceux dans lesquels un chalcogène est impliqué (par exemple Cu–Te ou Ni–Te). On croit que les schémas de liaisons ioniques relativement simples des systèmes métalliques alcalins doivent être remplacés par des systèmes plus compliqués dans les alliages basés sur les chalcogènes. On mettra en relief la grande interaction qui existe entre la structure atomique d'une part et la structure électronique d'autre part.

[Traduit par le journal]

Introduction

There exists a group of liquid conductors whose electronic properties are different from those of metals and are similar to those of semiconductors. Such liquids are usually referred to as 'liquid semiconductors'.[1] Two main types of liquid semiconductors have been identified, namely, those based on the *chalcogens* (for example, pure liquid Se or liquid Cu_2Te) and those liquids in which *metals* with large electronegativity differences (χ) are alloyed together (*e.g.*, liquid Mg_3Bi_2 or CsAu). Our basic understanding of these liquids is still in a very primitive state and progress continues to be painfully slow; the development of a comprehensive theoretical framework in which the various structural, electronic and thermodynamic properties of liquid semiconductors can be discussed, is now a matter of some urgency. One possible way of achieving this aim is to take some representative liquid alloy systems and to attempt, at an experimental level, to establish links between structural and electronic properties. We shall follow this course in this review.

[1]These should not be confused with the liquids formed by melting solid semiconductors. Such liquids are frequently metallic in character. A review of the electrical properties of liquid semiconductors has been given by Enderby (1).

Alkali Metal Based Semiconductors

Lithium Alloys

We first present results due to Nguyen and Enderby (2) for the resistivity, ρ, and thermoelectric power, S, for liquid lithium alloys of the type Li_xM_{1-x} where $1 < x < 0$ and M represents a metal whose valence, Z, is in the range $2 \leq Z \leq 5$. In addition, new data for the spin-flip cross-section, σ_s, for Pb and Bi in liquid lithium are given. These data were taken on dilute alloys ($x > 0.95$) so that interference effects between impurity atoms can be neglected. A summary of all the experimental results is given in Figs. 1–4.

We focus attention on the data contained in Fig. 1 which we interpret within the framework first suggested by Wignall, Enderby, Hahn, and Titman (3) and Asik, Ball, and Slichter (4). The magnitude of σ_s reflects the probability of a spin flip at an impurity site. This is dominated by the spin–orbit coupling and should, other things being equal, increase monotonically with Z. This indeed happens for $Z \leq 2$; however, as first noted by Asik *et al.* (3), for $Z \geq 3$ departures from the simple theory are evident and the new data reported here for the liquid state confirm the trend for Z values of 4 and 5.

We next consider the variation of the electronic transport parameters with composition. It is

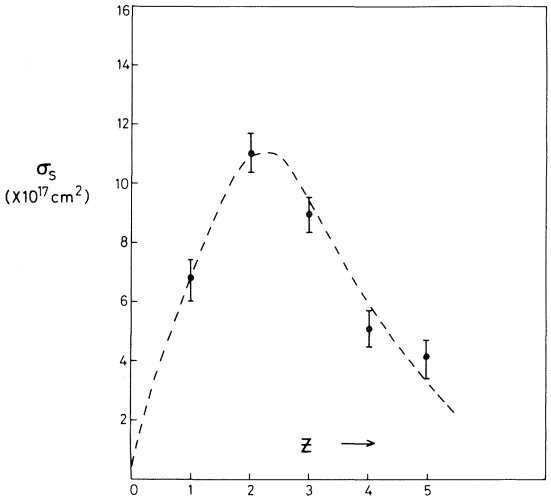

FIG. 1. Spin-flip scattering cross-sections as a function of impurity valence. The impurities were Au, Hg, Tl, Pb, and Bi.

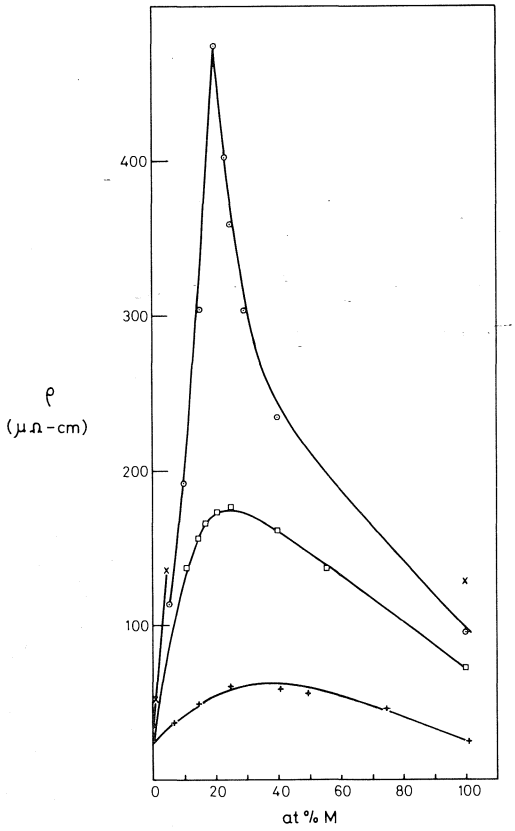

FIG. 2. Electrical resistivity of liquid Li alloys as a function of concentration: +, Li–Mg (Van Zytveld (15)); □, Li–Tl; ○, Li–Pb; ×, Li–Bi.

clear from Figs. 2–4 that this variation becomes increasingly less free electron like as $Z \geq 3$. The rapid variation in S with x around the composition Li_4Pb, for example, resembles behaviour found in other liquid alloy systems which are known to be liquid semiconductors (1).

We now assert that the anomalous electrical behaviour for $Z \geq 3$ and the reduction in σ_s which occurs at this value of Z have a common origin, namely, the formation of bound or virtually bound states at or below the bottom of the conduction band: and that for $Z \geq 3$ a progressive and actual reduction in the effective number of electrons occurs as the concentration of impurities increases. This arises first because the *s* electrons are bound to the impurity atoms and secondly because the impurity *p* orbitals fall and sharpen into virtual levels and finally, with high enough Z and χ, become bound orbitals below the bottom of the band. As noted by Flynn and Rigert (5), it is not possible, outside the one-electron approximation, to make a sharp distinction between bound and virtually bound states and the concept of an effective number of electrons is still a qualitative one. However, in this picture, it is unnecessary to invoke a pseudogap at E_F in order to explain the electrical properties for large x. Instead, attention shifts to the bottom of the conduction band. As the stoichiometric composition is approached, the density of states will fall and the possibility of localisation at E_F may then have to be considered.

The anomalies in ρ, S, and σ_s for $Z \geq 3$ are parallelled in the thermodynamic behaviour. Substantial heats of mixing develop for high (2) impurities and this reflects what is loosely called 'compound formation' at certain well-defined values of x. The most clear-cut examples are those of liquid Li–Pb (Li_4Pb) and liquid Li–Bi (Li_3Bi). We now make our second assertion, namely, that the bonding orbitals which give rise to the compound are precisely those referred to above; in asking questions about the nature of the compound, we are really asking about the spatial form of the *s* and the *p* orbitals.

The *ionic model* is one in which both the *s* and the *p* electrons are localised on the electronegative ion so that, for instance, liquid Li_3Bi consists of Li^+ and Bi^{3-} ions. In the *molecular model* the valence requirements are satisfied

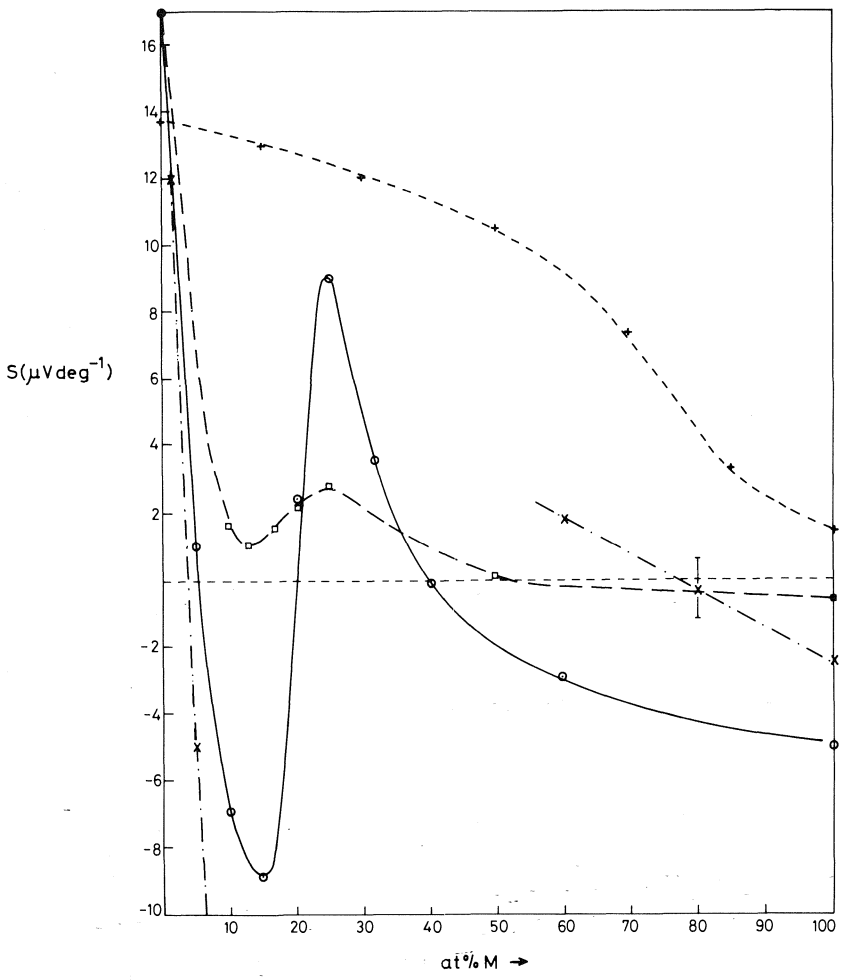

FIG. 3. Absolute thermoelectric power of liquid Li alloys as a function of concentration: +, Li–Mg (Van Zytveld (15)); □, Li–Tl; ○, Li–Pb; ×, Li–Bi.

within a molecule so that the liquid consists of electrically neutral molecules of Li_3Bi, the strong intra-molecular forces arising from *sp* hybridisation. Finally, in the *mixed bond model*, some fraction of the *s* and *p* electrons is localised on the electronegative ion and the rest are involved in an extended network of covalent bonds. We must emphasise that both Li_4Pb and Li_3Bi remain electronic conductors and that these models represent a zeroth order approximation to what is an exceedingly complex situation.

All of these models imply the presence of low-lying electron states; furthermore, the existence of ionic bonding in liquid NaCl (6) and molecular bonding in liquid $TiCl_4$ (7) is well established. Whether or not an extended network of covalent bonds can be maintained in the liquid state is not so clear, but the neutron diffraction evidence for liquid Te (8) favours this possibility.

Molecular liquids tend to be volatile and to have low freezing points. This behaviour is not at all characteristic of liquid Li_4Pb and Li_3Bi; furthermore, solid Li_4Pb is known not to be molecular and in agreement with the structural study of Ruppersberg and Egger (9) we tentatively conclude that molecules, as such, do not exist in these liquids. Of the two remaining models, the structural evidence points, albeit indirectly, to rather high co-ordination numbers (~10) for *unlike* atoms and near neighbour

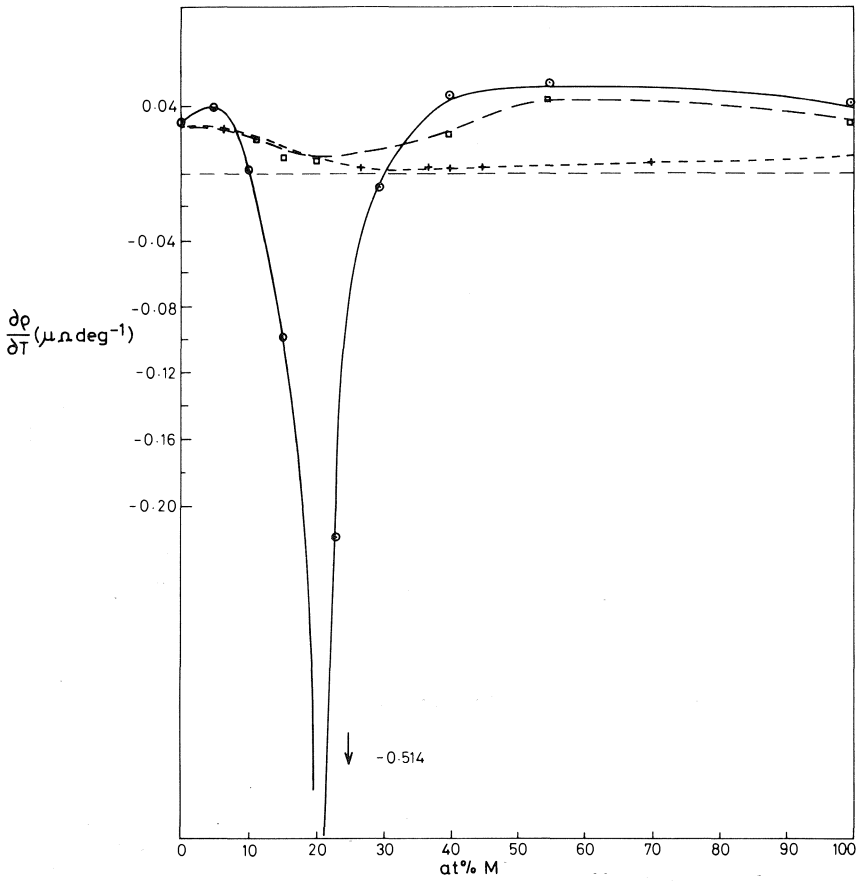

FIG. 4. $\partial\rho/\partial T$ as a function of concentration at temperatures just above the liquidus: +, Li–Mg (Van Zytveld (13)); □, Li–Tl; ⊙, Li–Pb.

distances considerably smaller than those predicted by hard sphere theory. This behaviour is consistent with the results of Edwards *et al.* (6) on molten NaCl and adds support to the ionic model.

Other Alkali Metal Systems

A detailed study of the Cs–Au system in the liquid state has recently been reported by Schmutzler, Hoshino, Fischer, and Hensel (10). Similar arguments based on electronegativitity differences used above should certainly hold for this case where χ is comparable with that of CsCl. It is found in practice that Cs–Au is indeed a liquid semiconductor, that there is a rapid increase in ρ as either Cs or Au is added to Au or Cs, and that at the stoichiometric composition, the conductivity is very low ($3\ \Omega^{-1}\ cm^{-1}$). Careful studies showed that this arises chiefly by ion-transport, that is to say, non-electronic effects. This work provides a convincing demonstration that a progressive reduction in the metallic characteristics of an alloy system can be understood in terms of increased ionicity.

Chalcogen Based Semiconductors

The electrical behaviour of these systems has been extensively studied and reviewed (see for example ref. 1). In systems like Cu–Te, Ni–Te, and Tl–Te, minima in the conductivity occur at Cu_2Te, $NiTe_2$, and Tl_2Te. A more detailed review of the present situation for Tl_2Te is given by Cutler (11). It remains, however, a matter of dispute which of the three structural models referred to above is appropriate for these cases where in general χ is less than for the alkali metal counterparts.

Let us now consider in detail the structure of

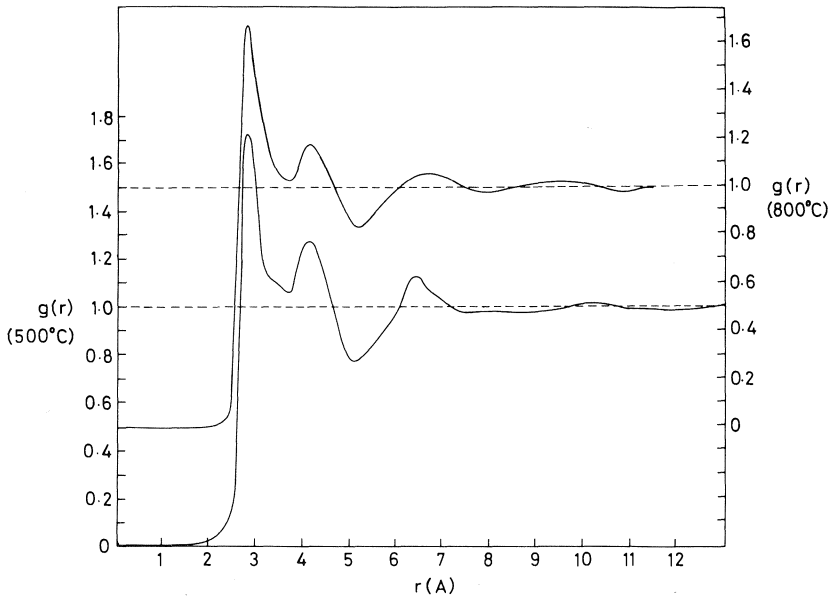

FIG. 5. The radial distribution function for pure liquid Te at 500 and 800°C.

these liquids. The quantity which can be extracted from a single diffraction experiment on a liquid containing two species, a, b is the *total structure factor* $F(Q)$ defined by

$$F(Q) = c_a^2 f_a^2 (S_{aa} - 1) + c_b^2 f_b^2 (S_{bb} - 1) + 2c_a c_b f_a f_b (S_{ab} - 1)$$

where c_a and c_b are the atomic concentrations of the two species, f_a and f_b are the neutron scattering lengths, and S_{aa}, S_{bb}, and S_{ab} are the *partial structure factors* which are related to the *radial distribution functions* $q_{\alpha\beta}$ for one atom type with respect to another atom type by

$$S_{\alpha\beta} = 1 + \frac{4\pi N}{V} \int (g_{\alpha\beta} - 1) r \sin Qr \, dr$$

α, β = a or b.

It is now accepted that the aim of structural analyses on binary systems should be to extract $S_{\alpha\beta}$ rather than $F(Q)$. This can be done by varying the scattering lengths of one or both components in such a way as to provide three total structure factors F_1, F_2, and F_3 which are sufficiently different to enable three linear equations to be solved for S_{aa}, S_{bb}, and S_{ab}. In recent experiments carried out by Nguyen[2] the variation in f was achieved by isotopic substitution since, in general, the neutron scattering length depends on the number of neutrons in the nucleus. A special study of Ni–Te was undertaken because by choosing a mixture of ^{58}Ni and ^{60}Ni, f_{Ni} could be made to be zero so that it becomes possible to study *directly* $S_{TeTe}(Q)$ as a function of concentration.

The radial distribution function for pure liquid Te at two temperatures is shown in Fig. 5. It differs from that for simple liquids in two characteristic ways: (*i*) the short range part of $g(r)$ is very hard; (*ii*) the co-ordination number is low ($\sim$4). These facts, together with other evidence of an electronic and thermodynamic character, point to the existence of an extended covalent network (8). If we now consider the Te–Te radial distribution function in the liquid semiconductor $NiTe_2$ (Fig. 6), both of these characteristic features have disappeared. Indeed, the observed $g(r)$ resembles comparable data for the Cl–Cl distribution in liquid $BaCl_2$, a liquid known to be essentially ionic in character. On the other hand, g_{TeTe} is quite different from the Cl–Cl distribution in the molecular liquid $TiCl_4$. We therefore conclude that the effect of Ni on liquid Te is to break down the extended covalent network and localise most of the charge on the Te and Ni ions. Similar experiments are in progress for the Cu–Te system and preliminary results, already reported in ref. 12

[2]V. T. Nguyen, private communication.

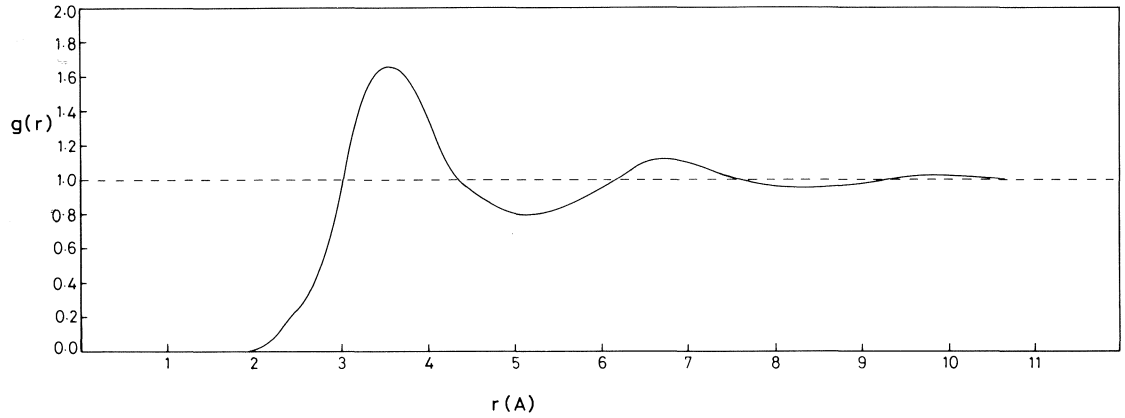

FIG. 6. The partial Te–Te radial distribution function in the liquid semiconductor $NiTe_2$ at 800°C (Nguyen, private communication).

have clearly demonstrated that substantial changes in g_{TeTe} occur with increased Cu content.

Future Developments

Apart from 'more of the same' (*i.e.* conventional electronic and structural investigations) several new techniques will need to be employed if a better understanding of these alloy systems is to be achieved. Extended X-ray absorption fine structure, EXAFS, a novel structural technique which employs synchrotron radiation, will be reviewed by Crozier *et al.* (13). Photoemission experiments will represent, when the technical problems of handling these awkward liquids are finally solved, a most powerful method of investigating core shifts and hence ionicity. Finally, nuclear spin–lattice relaxation measurements, as Warren (14) has convincingly demonstrated, yield unique information about the nature of the electron states close to the Fermi energy. Such experiments suggest, for example, that the relatively straightforward electron transfer model, though satisfactory for liquid CuTe, goes over to a mixed-bond model as the stoichiometric composition Cu_2Te is approached. This suggestion is strongly supported by the structural studies of Hawker *et al.* (12).

Acknowledgments

The work reported here was supported by the Science Research Council. The author is particularly grateful to Dr. V. T. Nguyen for allowing him access to a range of experimental data.

1. J. E. ENDERBY. Band structure spectroscopy of metals and alloys. Academic Press, London. 1973. p. 609.
2. V. T. NGUYEN and J. E. ENDERBY. Philos. Mag. In press.
3. G. D. WIGNALL, J. E. ENDERBY, C. E. W. HAHN, and J. M. TITMAN. Philos. Mag. **12**, 433 (1965).
4. J. R. ASIK, M. A. BALL, and C. P. SLICHTER. Phys. Rev. Lett. **16**, 740 (1966).
5. C. P. FLYNN and J. A. RIGERT. Phys. Rev. B, **7**, 3656 (1973).
6. F. C. EDWARDS, J. E. ENDERBY, R. A. HOWE, and D. I. PAGE. J. Phys. C, **8**, 3483 (1975).
7. F. C. EDWARDS, J. E. ENDERBY, R. A. HOWE, and D. I. PAGE. J. Phys. C, To be published.
8. G. TOURAND. Phys. Lett. A, **54**, 209 (1975).
9. H. RUPPERSBERG and H. EGGER. J. Chem. Phys. **63**, 4095 (1975).
10. R. W. SCHMUTZLER, H. HOSHINO, R. FISCHER, and F. HENSEL. Ber. Bunsenges. Phys. Chem. **80**, 107 (1976).
11. M. CUTLER. Can. J. Chem. This issue.
12. I. HAWKER, R. A. HOWE, and J. E. ENDERBY. Proc. Int. Conf. Liq. Met. Mexico, 1975. In press.
13. E. D. CROZIER, F. W. LYTLE, D. E. SAYERS, and E. A. STERN. Can. J. Chem. This issue.
14. W. W. WARREN. Properties of liquid metals. *Edited by* S. Takeuchi. Taylor and Francis, London. 1973. p. 395.
15. J. B. VAN ZYTVELD. J. Phys. F, **5**, 506 (1975).

Discussion

N. H. March: I have a comment on the structure factor of liquid Te that you showed. Mr. B. Bhuiyan and I have recently calculated the charged hard sphere structure factor in a classical system in which, with initially localized electrons, we delocalized a very small fraction. The height of the first peak in the hard sphere structure factor $S(Q)$ increases markedly as we delocalise electrons. We believe this is relevant to the atomic structure of liquid Te, in which

the number of conduction electrons increases with increasing temperature. It indicates a sensitive interrelation between electronic and atomic structure.

J. E. Enderby: Thank you for that comment which also seems to confirm the trends we have found for the Te—Te structure factor in the Te-based liquid alloys.

G. R. Freeman: If you made an Arrhenius plot of the temperature coefficient of conductivity for liquid Li_4Pb, approximately what activation energy would you get, and at roughly what temperature?

J. E. Enderby: I do not normally make such plots because they imply the existence of a well defined energy gap. However, an effective activation energy appropriate to liquid Li_4Pb is ~0.1 eV at temperatures around 800°C.

G. R. Freeman: How does that compare with values observed in other semiconductors?

J. E. Enderby: By solid state standards, such activation energies are rather low.

Structural determinations of liquid semiconductors using extended X-ray absorption fine structure

E. D. CROZIER
Physics Department, Simon Fraser University, Burnaby, B.C., Canada V5A 1S6
F. W. LYTLE
Boeing Aerospace Company, Seattle, WA, U.S.A. 981244
AND
D. E. SAYERS AND E. A. STERN
Physics Department, University of Washington, Seattle, WA, U.S.A. 98195

Received October 12, 1976

E. D. CROZIER, F. W. LYTLE, D. E. SAYERS, and E. A. STERN. Can. J. Chem. **55**, 1968 (1977).

The extended fine structure in the X-ray absorption coefficient is dominated by the interference of the photoelectron scattered by atoms in the immediate neighbourhood of the atom which absorbs the X-ray photon and thus can provide structural information about ordered or disordered systems. In this paper it is demonstrated that Extended X-Ray Absorption Fine Structure (EXAFS) measurements can be made on liquid systems at high temperatures. The technique is illustrated with results for As_2Se_3 in the liquid and amorphous states for temperatures between 100 and 773 K. A Fourier analysis of the EXAFS data reveals that a major structural rearrangement does not occur in the nearest neighbour shell when As_2Se_3 is melted. However, small structural changes do occur at the melting point which, within the limitations of the present data, suggest a slight increase in the nearest neighbour As–Se distance, a decrease in the number of nearest neighbours, and a decrease in the nearest neighbour disorder term σ_1^2.

E. D. CROZIER, F. W. LYTLE, D. E. SAYERS et E. A. STERN. Can. J. Chem. **55**, 1968 (1977).

La structure fine élargie dans le coefficient d'absorption de rayons-X est dominée par l'interférence du photoélectron dispersé par les atomes dans l'environnement immédiat de l'atome qui absorbe les photons de rayons-X et qui peut ainsi fournir de l'information structurale concernant les systèmes ordonnés ou désordonnés. Dans cette publication on démontre que des mesures de structure fine élargie d'absorption par rayons-X (EXAFS) peuvent être faites sur des systèmes liquides à haute température. On illustre la technique avec des résultats obtenus avec du As_2Se_3 à l'état liquide et dans un état amorphe à des températures allant de 100 à 773 K. Une analyse de Fourier des données EXAFS révèle qu'il ne se produit pas de réarrangement structural dans la couche voisine la plus près au moment de la fusion de As_2Se_3. Toutefois de petits changements de structure se produisent au point de fusion; à l'intérieur des limitations des données actuelles, il semble que ces changements impliquent une légère augmentation dans les distances As–Se les plus voisines, une diminution dans le nombre des voisins les plus près et une diminution dans le terme σ_1^2 de désordre des voisins les plus près.

[Traduit par le journal]

Introduction

An improved understanding of the electronic properties of liquid semiconductors requires knowledge of the fluid structure. In a disordered A–B binary system this structural information cannot be obtained from a single X-ray or neutron diffraction experiment. Enderby (16) reviewed how the partial radial distribution functions describing the A–A, A–B, and B–B correlations in a binary system can be determined from appropriate neutron diffraction experiments in alloys of different isotopic composition. In this paper we present structural data for amorphous and liquid As_2Se_3 obtained with the Extended X-Ray Absorption Fine Structure (EXAFS) technique, a technique, which it has only recently been realized, provides an important structural probe of disordered systems. In binary systems, under favourable conditions, the technique can yield the nearest neighbour distance, number, and type.

Fine structure is observed in the absorption coefficient on the high energy side of an X-ray absorption edge and in condensed phases may extend to 1000 eV beyond the edge. EXAFS refers to that fine structure in the extended range beyond ~30 eV above the edge. The structure below ~30 eV, while arising from the excitation

of a photoelectron, requires different considerations and is excluded from the discussion of EXAFS. The current theory of EXAFS for the K edge was developed and experimentally confirmed in a series of papers beginning in 1970 (1–7). The dominant absorption mechanism at usual X-ray energies is the photoelectric effect in which an X-ray with energy $h\nu$ is annihilated and a photoelectron is emitted from the atom with a kinetic energy E given by the conservation of energy as $E = h\nu - E_K$ where E_K is the initial binding energy of the electron. The photoelectron is scattered by the atoms surrounding the absorbing atom. A final state interference occurs at the origin of the absorbing atom between the outgoing part of the wavefunction of the photoelectron and the backward scattered part. This interference, which can be either constructive or destructive depending on the wavevector k of the photoelectron causes a modulation of the matrix element in which the initial state is dipole coupled to the final state. Thus the interference effect varies the photoelectric transition rate and causes the oscillation in the X-ray absorption coefficient which is referred to as the EXAFS.

Following the development of refs. 3, 4, and 5, neglecting multiple scattering effects and assuming that $kr_j \gg 1$ we write the normalized EXAFS interference term as (5)

$$[1]\quad \chi(k) = \frac{m}{4\pi\hbar^2 k}\sum_j t_j(2k)\int \frac{e^{-2r_j/\lambda}}{r_j^2} \times \sin 2(kr_j + \delta_j(k))p(r_j)\,dr_j$$

The sum is over the atoms at the distances r_j from the absorbing atom, $t_j(2k)$ is the magnitude of the amplitude for backscattering from the jth atom, λ is the meanfree path for inelastic scatterings of the photoelectron. The phase shift $\delta_j(k)$ in the sinusoidally varying term is energy dependent. It has two contributions; the phase shift produced by the absorbing atom and the phase shift produced when the photoelectron is backscattered by the jth atom. In a liquid it is convenient to specify the locations of the backscattering atoms by $p(r_j)$, the probability that the jth atom is at r_j. In a crystalline or amorphous solid it is reasonable to assume that

$$p(r_j) = \frac{1}{(2\pi)^{1/2}\sigma_j} e^{-(r-R_j)^2/2\sigma_j^2}$$

where R_j is the average position between the absorbing atom and the jth backscattering atom, and σ_j^2 is the mean square fluctuation in the interatomic distance between the origin atom and the jth atom. The fluctuation includes a dynamical term due to the thermal motion of the atoms and a static term due to structural disorder. A theoretical calculation of the structural disorder term has not yet been undertaken. In the case of the dynamical term there are two physically transparent limits. If the origin and jth atom are vibrating in phase then $\sigma_j^2 = 0$ and if they are vibrating independently then σ_j^2 is just the sum of the mean square displacements of the atoms from their equilibrium positions.

With the assumed Gaussian distribution of atoms [1] becomes

$$[2]\quad \chi(k) = \frac{m}{4\pi\hbar^2 k}\sum_j \frac{N_j}{R_j^2} t_j(2k)\, e^{-2R_j/\lambda} \times \sin 2(kR_j + \delta_j(k))\, e^{-2k^2\sigma_j^2}$$

where the sum is over the different shells of atoms whose average distance from the absorbing atom is R_j and which contains N_j atoms. In principle, by the appropriate combination of EXAFS measurements on suitable systems all the quantities in [2] can be determined for disordered solids. Analytical methods based on the Fourier transforms of the EXAFS function $\chi(k)$ are illustrated in refs. 5 and 8.

The experiments reported in this paper on As_2Se_3 were initiated to assess the feasibility of making EXAFS measurements on liquids at high temperatures. With increasing temperature the magnitude of σ_j^2 increases and the amplitude of $\chi(k)$ decreases. Utilizing the Bremsstrahlung radiation from a conventional X-ray source would necessitate taking data for a period in excess of two weeks to achieve a suitable signal-to-noise ratio in each EXAFS spectrum. Such experiments would be impractical. However the experiments were readily performed using the synchrotron radiation from SPEAR, Stanford's e^- e^+ storage ring which provides an X-ray intensity five or six orders of magnitude higher than that available from conventional X-ray sources. The As_2Se_3 system was chosen for preliminary investigations because the K edge EXAFS spectra of both the As and Se were accessible with the existing monochromator at the Stanford Synchrotron Radiation Project and because the local structure was known to remain

substantially unaltered at the melting point. Far-infrared measurements (9, 10) indicate that vibrational modes observed in the amorphous state persist into the liquid state. In this paper the EXAFS spectra are examined for changes in the first shell radii R_1 upon melting amorphous As_2Se_3 and the temperature dependence of ${\sigma_1}^2$ is determined between 100 and 773 K.

Experimental

The As_2Se_3 samples were prepared from 99.9% purity As_2Se_3 (Alfa Inorganics, Ventron, MA). The As_2Se_3 was evaporated in a vacuum of 5×10^{-5} torr from a Mo boat onto a boron nitride substrate which formed one side of the sample cell. The thickness of the As_2Se_3 films was monitored by a crystal oscillator and later determined to within 1 μm with a Reichert microscope of magnifying power 90. A film thickness of 22 μm provided suitable signal-to-noise ratio in the high k region of the EXAFS spectra. The sample cell was made from two rectangular slabs, $5.0 \times 2.5 \times 0.6$ cm, milled from BN (Union Carbide, Cleveland, OH). BN was selected as the material for the sample cell because it has a low X-ray absorption coefficient in the energy range of interest, does not react with As_2Se_3, is machinable, and does not undergo irreversible dimensional changes upon thermal cycling. To provide an X-ray window of low absorption the portion of the BN to be located in the X-ray beam was milled to a wall thickness of 0.7 mm. The loss of liquid As_2Se_3 from the cell was prevented by using a mica gasket cleaved to the same thickness as the evaporated As_2Se_3 film and by bolting the BN slabs together with BN bolts as indicated in Fig. 1. The temperature of the film was determined to within 5 K by chromel–alumel thermocouples embedded in the BN cell.

The EXAFS measurements were conducted in the symbiotic mode at the Stanford Synchrotron Radiation Project. In this mode radiation is incident on the sample cell for an uninterrupted period of approximately 3 h. The furnace indicated in Fig. 1 was designed to minimize the non-usage of available beam time. Up to three BN cells could be loaded on the translation stage indicated in the figure. One cell at a time could be heated by sliding it into a closely-fitting rectangular slot in the heating unit which consisted of BN wound with Kanthal A resistance wire. The X-ray beam passed through openings milled in the sides of the heater. The heating assembly was positioned in a cylindrical water-cooled vacuum chamber made of 304 stainless steel which was fitted with X-ray windows of 0.5 mil thick Kapton. To achieve rapid thermal cycling the chamber was evacuated and back-filled with 1 atm of helium. A cell could be heated from room temperature to 1000 K in $\frac{1}{2}$ h. In a separate assembly, which is not illustrated, low temperatures were achieved by securing the BN sample cells to a copper block which was cooled with liquid nitrogen.

A detailed description of the X-ray absorption apparatus is given elsewhere (11). Briefly, the high flux, broad band synchrotron radiation generated in the Stanford electron positron storage ring is incident on a monochromator which uses the (220) Bragg planes in a channel cut silicon crystal. The intensity I_0 of the monochromatized beam incident on the furnace housing is determined as it passes through a transmission ion chamber. After transmission through the sample the intensity I is detected by a second ion chamber. The ratio I_0/I of the digitized ion chamber currents are stored in a PDP-11/05 minicomputer. In our experiments the computer was programmed to take data in the energy range 11 450 to 14 150 eV from which could be extracted the EXAFS associated with the As and Se K edges at 11 867 and 12 658 eV, respectively. The resolution was the order of 1 eV. With the high photon flux available an integration time of 1 s per point was used for all energies. However, as will be indicated later this was insufficient for a good signal-to-noise ratio for energies 750 eV above the K edges of interest. Absorption data were taken at discrete temperatures in the range 100 to 773 K encompassing the amorphous and liquid states of As_2Se_3. One run on the absorption spectra of the As edge was taken at 867 K. Evaporation losses at this high temperature prevented our obtaining data on the Se edge.

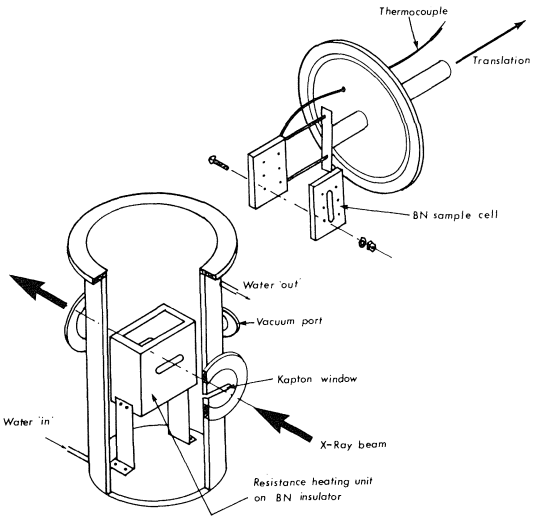

FIG. 1. Sketch of the high temperature sample cells and furnace.

The total absorption coefficient, obtained from the experimental ratio $\ln I_0/I$, contains background contributions from the furnace assembly, sample cell, and electrons in the sample as well as contributions from the K shell electrons of interest. The background contribution was found by fitting the data below the edge with a second order polynomial and extrapolating through the region of interest. This contribution was subtracted from the data leaving only $\mu(E)$, the K shell absorption coefficient (including EXAFS). The data were transformed to momentum space by taking the zero of the kinetic energy of the ejected K photoelectron to be at the K edge of interest. The EXAFS interference function $\chi(k)$ was determined by numerical procedures discussed in detail in ref. 5.

Results and Discussion

A representative plot of the EXAFS interference function $\chi(k)$ is shown in Fig. 2 for the

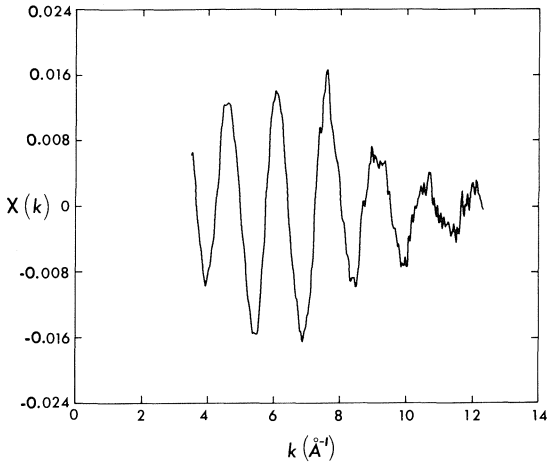

FIG. 2. The EXAFS interference function $\chi(k)$ as a function of k for the As K edge in liquid As_2Se_3 at 658 K.

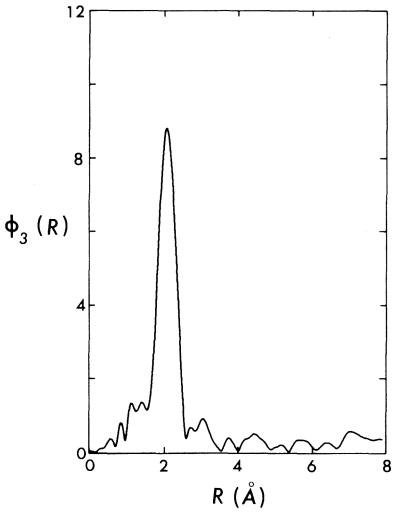

FIG. 3. The magnitude of the $\phi_3(r)$ transform as a function of r for liquid As_2Se_3 at 658 K. The absorbing As atom is located at $r = 0$. The plot was obtained by transforming the $\chi(k)$ shown in Fig. 2.

K edge of As in As_2Se_3 at 658 K (31 K above the melting point). The k-space data were truncated at 12.3 $Å^{-1}$, beyond this value the signal-to-noise ratio became unacceptable. The dominant low frequency oscillation in $\chi(k)$ is determined by interference of the photoelectrons backscattered from the nearest neighbours.

Interatomic distances are most readily obtained by taking the Fourier transform defined by

$$[3] \quad \phi_3(r) = \frac{1}{\sqrt{2\pi}} \int_{k\min}^{k\max} k^3\chi(k)\, e^{i2kr}\, dk$$

This transform is related to a pseudocharge density (3) and thus is useful for determining atom positions. The magnitude of the $\phi_3(r)$ transform obtained from the $\chi(k)$ of Fig. 2 is shown in Fig. 3 as a function of r. At the origin of the r-space is the absorbing As atom. The main peak, with a maximum value at $R_1 =$ 2.12 Å, is determined by the atoms in the nearest neighbour shell. In order to obtain the magnitude of the nearest neighbour interatomic distance R_1 must be corrected by the phase shift $\delta_1(k)$ introduced in [1]. The phase shift can be obtained (3–5) from EXAFS data in crystalline As_2Se_3. In this paper, where our interest is in structural changes at the melting point, we specify only the peak distance R_1. It is the R_1 peak which dominates the oscillations in $\chi(k)$. The shape of the R_1 peak is determined by a number of factors including the number and nature of the nearest neighbours, the disorder term σ^2, the nature of the $\phi_3(r)$ transform taken, and the finite range of the Fourier transform (which introduces a width $\Delta r \approx \pi/\Delta k = 0.36$ Å).

The magnitude of the $\phi_3(r)$ transform of amorphous As_2Se_3 at 619 K (8 K below the melting point) is shown in Fig. 4 with the absorbing As atom at the origin. A comparison of Figs. 3 and 4, and equivalent figures obtained with Se as the absorbing atom, indicates that major structural rearrangements do not occur in the nearest neighbour shells when the As_2Se_3 is melted. However some small structural changes are suggested. The mean peak in the solid at 619 K is shifted closer to the origin, the maximum value occurs at $R_1 = 2.10$ Å. This suggests that there is a slight increase in the nearest neighbour distance when the solid is melted. More extensive data with an improved signal-to-noise ratio at large k will be required to confirm this change in distance. The height of the R_1 peak in the liquid is less than that in the solid. Changes in peak heights can be attributed to changes in the number and nature of nearest neighbours and in the disorder term σ_j^2. In an earlier paper (12) the coordination numbers N_j were deduced for amorphous binary materials from an analysis of the nearest neighbour peak amplitude without including quantitatively the effect of the disorder term σ_j^2. More recent work (8) has shown that σ_j^2 can be determined separately for disordered systems. On the basis of the decrease in σ_j^2 calculated below, the

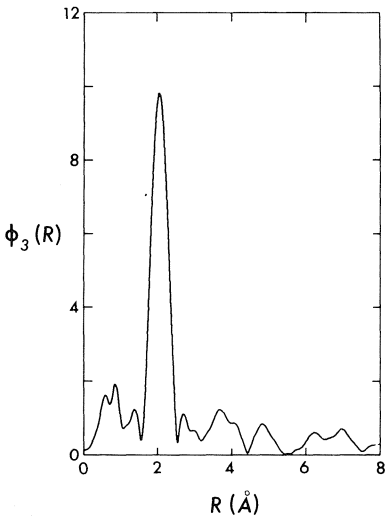

FIG. 4. The magnitude of the $\phi_3(r)$ transform as a function of r for amorphous As_2Se_3 at 619 K.

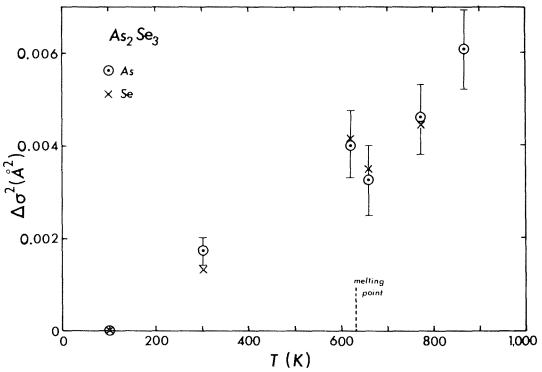

FIG. 5. $\Delta\sigma^2$ as a function of temperature. $\Delta\sigma^2$ represents the difference between σ_1^2 for amorphous or liquid As_2Se_3 at temperature T and σ_1^2 for a reference amorphous As_2Se_3 at 100 K. σ_1^2 is the mean square fluctuation in the distance between the origin atom and the nearest neighbour atoms. Data obtained with As and Se as the origin atoms are indicated by ⊙ and × respectively. For clarity error bars have been shown only for the As data. The error in the Se data is comparable.

decrease in the peak height implies a small decrease in N_j when the solid is melted.

With the present data it is not possible to distinguish unambiguously peaks arising from shells of higher radii from peaks introduced by the nature of the Fourier transform and the noise component. However a comparison of Figs. 3 and 4 does show that melting introduces differences in the peak structure at larger r. In subsequent experiments it will be determined if these differences are meaningful.

The dependence on temperature of the disorder term σ_1^2 for the first shell of atoms can be determined from a k-space analysis of the EXAFS data. With the assumptions that $\chi(k)$ is determined exclusively by the interference effect produced by backscattering from atoms in the nearest neighbour shell and that R_1 and N_1 are independent of temperature, [2] can be written as

$$[4] \qquad \chi(k, T) = \chi_1(k, 0)\, e^{-2k^2 \sigma_1^2(T)}$$

where $\chi_1(k, 0)$ is temperature independent. These assumptions must be examined more closely at the melting point (and above) where there are indications that N_1 (and possibly R_1) changes. By taking the ratio of χ at two different temperatures T_1 and T_2 we obtain

$$[5] \quad \ln\frac{\chi(k, T_1)}{(k, T_2)} = 2k^2(\sigma_1^2(T_2) - \sigma_1^2(T_1))$$

Plots of the logarithmic ratio *vs.* k^2 gave the difference $\Delta\sigma^2$ between $\sigma_1^2(T)$ for amorphous or liquid As_2Se_3 at temperature T and $\sigma_1^2(77\text{ K})$ for amorphous As_2Se_3 at 77 K. The temperature dependence of $\Delta\sigma^2$ is shown in Fig. 5 for both As and Se as the X-ray absorbing atoms.

It is seen that the disorder term σ_1^2 increases with temperature in both the amorphous and liquid states. This can be attributed to increased thermal motion increasing the dynamical contribution to σ_1^2 and a relaxation of the local structure towards a more disordered structure. It is known from conventional X-ray diffraction studies (13) that freshly deposited As_2Se_3 films of the thickness used in our EXAFS studies relax at higher temperatures to more disordered structures. Temperature dependent EXAFS studies on crystalline As_2Se_3 will assist in separating the different contributions to σ_1^2. An interesting feature of Fig. 5 is the possibility that the disorder term decreases at the melting point.

As_2Se_3 crystallizes into layer crystals. Within the layer the As and Se are covalently bonded, each As atom is threefold co-ordinated to Se atoms and each Se atom is twofold co-ordinated to As atoms. The bonding between layers is weak; the smallest interatomic separation between layers has been estimated to be 55% greater than the intra-layer As—Se bond length (14). Interpretations of optical measurements agree that the local order in amorphous and liquid As_2Se_3 is similar to that found in the crystal.

However different models have been proposed. Lucovsky and Martin (15) assume a molecular model for the amorphous state in which pyramidal $AsSe_3$ molecules are weakly coupled by bridging As—Se—As bonds. Taylor *et al.* (9) assume that the amorphous material and the liquid just above the melting point reflect the layer structure of the crystal. On the basis of either of these models, the main R_1 peak in the $\phi_3(r)$ transform measures the As—Se bond distance (when corrected for the phase shift $\delta(k)$ of [2]). Far infrared measurements (10) indicate that a band which peaks around 269 cm^{-1} in the amorphous material experiences a discontinuous decrease at the melting point of ~ 7 cm^{-1}. Arai *et al.* (10) attribute the band to a mode of the As—Se—As bridge connecting $AsSe_3$ molecules. The slight increase in R_1 at the melting point may correlate with the decrease in the frequency of the bridge mode. The decrease in σ_1^2 at the melting point may be due, in part, to changes in the bridge angles.

In conclusion, only small structural changes occur at the melting point. Within the limitations of the present data the nearest neighbour As–Se interatomic distance increases slightly, the number of nearest neighbours decreases, and the disorder term σ_1^2 decreases. Further EXAFS measurements on crystalline, amorphous, and liquid As_2Se_3 are in progress.

The number and type of nearest neighbours cannot be determined from the EXAFS data on As_2Se_3 without additional input about the assumed structure. Experiments will be undertaken on binary systems in which the backscattering amplitudes $t_j(2k)$ of the two species differ appreciably to assess if the differences in the $t_j(2k)$ will permit determination of the nearest neighbour number and type without the need for additional structural assumptions.

Acknowledgements

This work was partially supported by National Science Foundation Grant No. DMR 7307692, in cooperation with the Stanford Linear Accelerator and the U.S. Energy Research and Development Administration. The authors D.E.S. and E.A.S. wish to acknowledge support received from the National Science Foundation Grant No. DMR 7300251, F.W.L., from the National Science Foundation Grant No. DMR 74-24261-AO1, and E.D.C. wishes to acknowledge grants received from Simon Fraser University and the National Research Council of Canada.

1. D. E. Sayers, F. W. Lytle, and E. A. Stern. Advances in X-ray analysis. Vol. 13. Plenum, New York. 1970. p. 248.
2. D. E. Sayers, F. W. Lytle, and E. A. Stern. Phys. Rev. Lett. **27**, 1204 (1971).
3. E. A. Stern. Phys. Rev. B, **10**, 3027 (1974).
4. F. W. Lytle, D. E. Sayers, and E. A. Stern. Phys. Rev. B, **11**, 4825 (1975).
5. E. A. Stern, D. E. Sayers, and F. W. Lytle. Phys. Rev. B, **11**, 4836 (1975).
6. C. A. Ashley and S. Doniach. Phys. Rev. B, **11**, 1279 (1975).
7. P. A. Lee and J. B. Pendry. Phys. Rev. B, **11**, 2795 (1975).
8. D. E. Sayers, E. A. Stern, and F. W. Lytle. Phys. Rev. Lett. **35**, 584 (1975).
9. P. C. Taylor, S. G. Bishop, and D. L. Mitchell. Phys. Rev. Lett. **27**, 414 (1971).
10. T. Arai, S. Komiya, and K. Kudo. J. Non-Cryst. Solids, **18**, 289 (1975).
11. B. M. Kincaid, P. Eisenberger, and D. E. Sayers. Phys. Rev. In press.
12. D. E. Sayers, F. W. Lytle, and E. A. Stern. Amorphous and liquid semiconductors. Vol. 1. *Edited by* J. Stuke and W. Brenig. Taylor and Francis, London. 1974. p. 403.
13. A. J. Leadbetter, A. J. Apling, and M. F. Daniel. J. Non-Cryst. Solids, **21**, 47 (1976).
14. R. Zallen, M. L. Slade, and A. T. Ward. Phys. Rev. **3**, 4257 (1971).
15. G. Lucovsky and R. Martin. J. Non-Cryst. Solids, **8–10**, 185 (1972).
16. J. E. Enderby. Can. J. Chem. This issue.

Discussion

G. R. Freeman: How can the degree of disorder in a material decrease when it is melted?

E. D. Crozier: I believe that this question is adequately covered in the printed text.

G. R. Freeman: If it is a relaxation process, why doesn't the disorder decrease with increasing temperature in the solid?

E. D. Crozier: The disorder term σ_1^2 is temperature dependent because of a dynamical contribution due to the thermal motion of the atoms and a static contribution due to structural disorder. When temperature dependent EXAFS studies have been made on crystalline As_2Se it will be possible to estimate the static structural disorder term and to assess its temperature dependence for relaxation processes.

J. K. Baird: You have indicated that the structure in the X-ray absorption coefficient just beyond the K-edge is caused by the backscatter of photoelectrons from neighbouring atoms. Could a monochromatic beam of X-rays be used to produce photoelectrons having a fairly well defined energy of a fraction of an electronvolt? If these electrons were sufficiently monochromatic, they might be used to sample the effective electron scattering

cross sections in the condensed phase. For example, one might look for a Ramsauer minimum in the condensed phase cross section, evidence for which has been presented in L. G. Christophorou's analysis of the electron mobilities in the liquified rare gases.

E. D. Crozier: That portion of the fine structure in the X-ray absorption coefficient referred to as extended is assumed to begin about 30 eV above the edge. Below 30 eV the interpretation of the fine structure is complicated by many body interactions, the distortion of the excited state wave function by the Coulomb field of the excited atom and the density of final states. In principle a monochromatic beam of X-rays could be used to produce in the condensed phase of interest photoelectrons with a well-defined energy. However, I am unable to state at the moment whether the complexity of the absorption fine structure seen near the edge would obscure the Ramsauer minimum in something like liquid krypton.

D. E. Brodie: Is the structure between the origin and the first coordination peak real?

E. D. Crozier: The emphasis in the *r*-space analysis of the data presented in this paper was placed on the structure associated with the first shell of radius R_1 indicated by the main peak in the magnitude of the $\phi_3(r)$ transform. Some of the structure between the origin and R_1 is an artefact of the Fourier-transform taken. Some structure may result from the analytical procedures used to extract $x(k)$ from raw experimental data. However, there is a possibility that the peak for r less than 1 Å can be attributed to scattering from valence electrons in the chemical bond. This question is under study.

K. Ichikawa: Have you considered applying the EXAFS technique to simple ionic melts such as NaCl and to ionic melts which may have complex ionic species?

E. D. Crozier: The EXAFS technique can yield local structural information about ionic melts. The K edges of Na and Cl occur at low energies and thus it is currently not feasible to do the NaCl system. A system such as KBr would be feasible. The EXAFS technique has been applied recently by Lytle and Wong to a glass containing $ZnCl_2$. Measurements were made in both the glass and liquid states.

Electrical properties of some molten ternary semiconductors

YOSHIO NAKAMURA, MASAMITSU NAOI, AND MITSUO SHIMOJI

Department of Chemistry, Faculty of Science, Hokkaido University, Sapporo, Japan

Received September 27, 1976

YOSHIO NAKAMURA, MASAMITSU NAOI, and MITSUO SHIMOJI. Can. J. Chem. **55**, 1975 (1977).

The electrical conductivity and thermoelectric power of molten $AgTlSe_2$, AgTlSe, and Tl_2Se_3 have been measured as a function of temperature. The effect of doping with Ag, Tl, and Se on the electrical properties of molten AgTlSe has also been studied. The results are discussed in terms of the pseudogap model.

YOSHIO NAKAMURA, MASAMITSU NAOI et MITSUO SHIMOJI. Can. J. Chem. **55**, 1975 (1977).

On a mesuré, en fonction de la température, la conductivité électrique et le pouvoir thermoélectrique des $AgTlSe_2$, AgTlSe et Tl_2Se_3 à l'état fondu. On a aussi étudié l'effet de dopage avec Ag, Tl et Se sur les propriétés électriques du AgTlSe fondu. On discute des résultats en termes d'un modèle de "pseudogap".

[Traduit par le journal]

Introduction

In the previous paper (1), we have reported the electrical conductivity and thermoelectric power of some molten ternary semiconductors ABC_2 (A: Cu, Ag; B: Tl, Sb, Bi; C: Se, Te). The observed conductivity values of these compounds just above their respective melting points range from 2.5 to 2300 $ohm^{-1}\ cm^{-1}$. It has been shown that the compounds studied are classified into two groups: the electrical conduction of the one group with higher electrical conductivity can be interpreted in terms of the strong scattering model and that of the other group with lower electrical conductivity ($\lesssim 200\ ohm^{-1}\ cm^{-1}$) in terms of the pseudogap model due to Mott–CFO (2, 3).

In this study we have measured the electrical conductivity and thermoelectric power of molten $AgTlSe_2$, AgTlSe, and Tl_2Se_3. The effect of nonstoichiometric doping on the electrical properties of molten AgTlSe has also been investigated in order to test the validity of the pseudogap model.

Experimental

The experimental procedures are the same as those described elsewhere (1). The conductivity was measured by the dc four-probe method with tungsten electrodes sheathed with graphite rods. The thermoelectric power was determined from the emf's developed by temperature gradients between the two potential electrodes of the measuring cell. The purities of the elements used were 99.999% for Ag and Se and 99.95% for Tl.

Results and Discussion

Figure 1 shows the logarithm of the electric conductivity, σ, of molten $AgTlSe_2$, AgTlSe, and Tl_2Se_3 as a function of the reciprocal absolute temperature, $1/T$. The thermoelectric power, S, is also plotted as a function of $1/T$ in Fig. 2. The results fit in with the following relations:

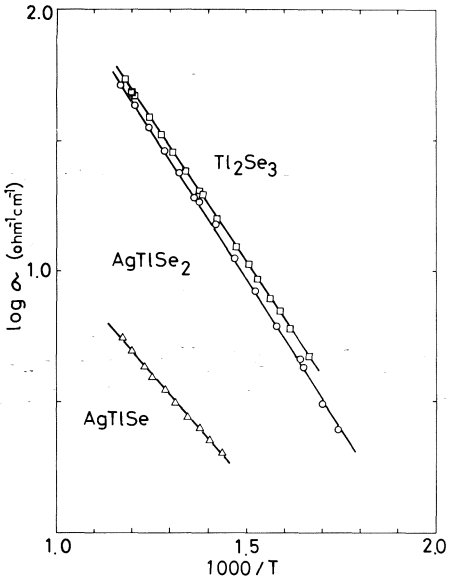

FIG. 1. The electrical conductivity of molten $AgTlSe_2$, AgTlSe, and Tl_2Se_3.

[1] $$\sigma = C \exp [- E_\sigma(0)/kT]$$

and

[2] $$S = (k/e)[E_S(0)/kT + B]$$

The observed positive sign of the thermoelectric power suggests that conduction may be dominated by holes in the extended states in the

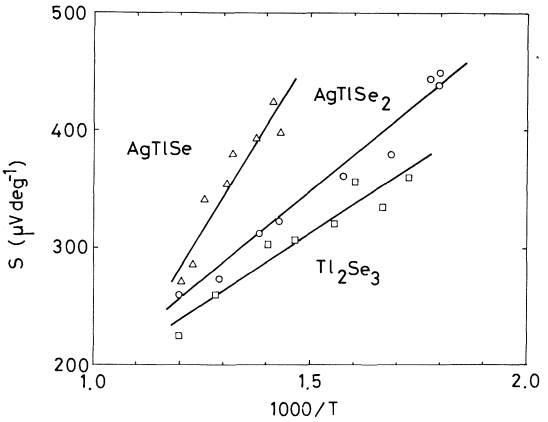

FIG. 2. The thermoelectric power of molten $AgTlSe_2$, AgTlSe, and Tl_2Se_3.

valence band. According to the pseudogap model, the hole conduction in the extended state gives rise to $E_\sigma(0) = E_S(0)$. The values of $E_\sigma(0)$ and $E_S(0)$ for $AgTlSe_2$, AgTlSe, and Tl_2Se_3 are shown in Table 1 together with those for $CuTlSe_2$, $AgTlTe_2$, and $CuSbSe_2$ reported earlier (1). We found $E_\sigma(0) > E_S(0)$, except for AgTlSe, in which $E_\sigma(0) < E_S(0)$. The inequality, $E_\sigma(0) > E_S(0)$, may be accounted for with an intrinsic two carrier model with a symmetric density of states (4). Though this may also be interpreted as originating with thermally assisted hopping conduction which has been suggested for amorphous semiconductors (5), it is reasonable to assume that conduction is dominated by carriers in extended states at such high temperatures as in the molten state. The result $E_\sigma(0) < E_S(0)$ for AgTlSe, which was also found for molten As–Se and As_2Se_3–As_2Te_3, can be explained on the basis of an intrinsic two carrier model with asymmetric density of states (6).

In the intrinsic two carrier model, the conductivity and thermoelectric power can be written as a sum of the respective contributions of electrons (subscript c) and holes (subscript v):

$$[3]\quad \sigma = \sigma_c + \sigma_v = \sigma_{0c} \exp\left[-(E_c - E_F)/kT\right] + \sigma_{0v} \exp\left[-(E_F - E_v)/kT\right]$$

and

$$[4]\quad S = \frac{\sigma_c}{\sigma} S_c + \frac{\sigma_v}{\sigma} S_v$$

S_c and S_v are given by (3):

$$[5]\quad S_c = -\frac{k}{e}\left[\frac{E_c - E_F}{kT} + A_c\right]$$

and

$$[6]\quad S_v = +\frac{k}{e}\left[\frac{E_F - E_v}{kT} + A_v\right]$$

where E_c and E_v are mobility edges of the conduction and valence bands, respectively, and E_F is the Fermi energy. The constants A_c and A_v depend on the scattering mechanism. In the symmetric density of states model (4), it is assumed that $E_c - E_F = E_F - E_v = (1/2)(E_c - E_v)$ (Fig. 3*a*). Then, if it is assumed that $E_c - E_v = E_0 - \beta T$, we have:

$$[7]\quad \sigma = (\sigma_{0c} + \sigma_{0v}) \exp\left[\frac{\beta}{2k}\right] \exp\left[-\frac{E_0}{2kT}\right]$$

and

$$[8]\quad S = \frac{\sigma_{0v} - \sigma_{0c}}{\sigma_{0c} + \sigma_{0v}} \frac{k}{e}\left[\frac{E_0}{2kT} - \frac{\beta}{2k} + A\right]$$

where $A = A_c = A_v$ is assumed. Comparing [1] and [2] with [7] and [8], respectively, we have $E_\sigma(0) = E_0/2$ and $E_S(0) = \{(\sigma_{0v} - \sigma_{0c})/(\sigma_{0c} +$

TABLE 1. Parameters of the pseudogap model

Substance	$E_\sigma(0)$ (eV)	$E_S(0)$ (eV)	σ_{0c}/σ_{0v}	$\beta \times 10^4$† (eV/deg)
$AgTlSe_2$	0.46	0.31	0.19	7
$AgTlSe_2$*	0.45	0.25	0.29	6
Tl_2Se_3	0.43	0.24	0.28	6
$CuTlSe_2$*	0.20	0.12	0.25	4
$AgTlTe_2$*	0.23	0.14	0.24	8
$CuSbSe_2$*	0.56	0.50	0.06	9
AgTlSe	0.33	0.42	—	—

*Reference 1.
†A is assumed to be unity.

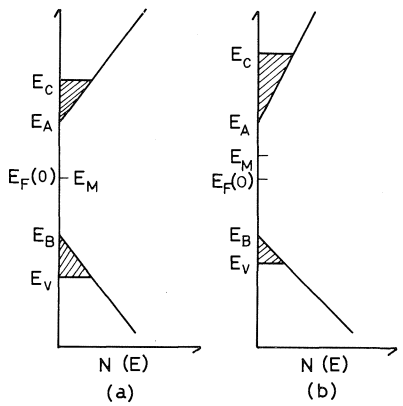

FIG. 3. (*a*) Symmetric density of states model and (*b*) asymmetric density of states model. Localized states are shown shaded. $E_M = (E_c + E_v)/2$, $E_F(0) = (E_A + E_B)/2$.

$\sigma_{0v})\}$ $(E_0/2)$. It is obvious that $E_\sigma(0) > E_S(0)$, since $(\sigma_{0v} - \sigma_{0c})/(\sigma_{0c} + \sigma_{0v}) < 1$. If A is assumed to be unity, the parameters $\sigma_{0c} + \sigma_{0v}$, σ_{0c}/σ_{0v}, and β can be determined from the experimental data (Table 1). The parameters σ_{0c} and σ_{0v} can be related to the mobility of carriers and density of states at the respective mobility edges (4).

In order to account for the inequality $E_\sigma(0) < E_S(0)$ found for molten AgTlSe, we adopt the asymmetric density of states model (6). In this model, the center of the density of states gap, $E_F(0) = (E_A + E_B)/2$, is different from the center of the mobility gap, $E_M = (E_c + E_v)/2$, as shown in Fig. 3*b*. From the observed sign of S, we assume that conduction by holes is dominant. This can be achieved, if $(E_c - E_F)$ is larger than $(E_F - E_v)$ by several kT as can be seen in [3]. The factor σ_c/σ in [4] is approximately given by

$$[9] \quad \sigma_c/\sigma \simeq \frac{\sigma_c}{\sigma_v} = \frac{\sigma_{0c}}{\sigma_{0v}} \exp\left[\frac{2(E_F - E_M)}{kT}\right]$$

which increases exponentially with temperature. This indicates that the negative term of S_c in [4] makes the positive total thermoelectric power decrease more rapidly at higher temperatures. Consequently, the obtained apparent activation energy of S, $E_S(0)$, is larger than that of the single S_v term which is equal to the conductivity activation energy, $E_\sigma(0)$. This may be the case for molten AgTlSe.

To confirm this interpretation, we have investigated the effect of the excess Tl, Ag, and Se on the electrical properties of molten AgTlSe. The results are shown in Figs. 4, 5, and 6. Ag and Tl behave quite similarly, indicating that the excess Tl acts as a monovalent metal as in molten Tl_2X (X: S, Se, Te) (7). The experimental results are summarized as follows: (*i*) the addition of Ag and Tl (up to 2 at.%) causes a slight change of the slope of ln σ *vs.* $1/T$, and a change of the sign of S (positive to negative), while the values of σ itself do not change considerably. (*ii*) the addition of Se (up to 2 at.%) causes an increase of σ by a factor of ~3–4 and decrease of the slope of S *vs.* $1/T$, while the slope of ln σ *vs.* $1/T$ and the values of S do not change significantly.

These results will be interpreted qualitatively in the framework of the asymmetric density of states model. The dissolved Ag and Tl atoms will behave as donor centers, giving valence electrons

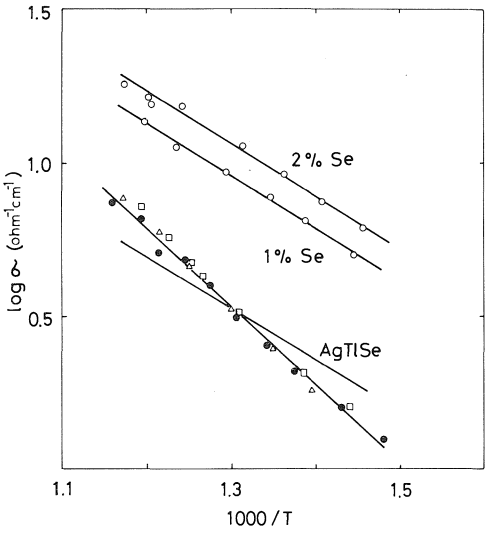

FIG. 4. The electrical conductivity of molten AgTlSe doped with Ag and Se. ●, 0.5 at.% Ag; △, 1.0 at.% Ag; □, 2.0 at.% Ag.

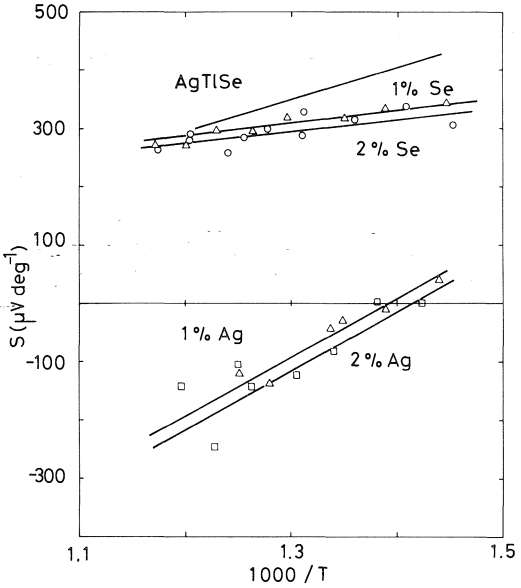

FIG. 5. The thermoelectric power of molten AgTlSe doped with Ag and Se.

to the conduction band. However, because of the localized region in the conduction band, not all of these electrons are in the extended states at lower temperatures. At the same time, the introduction of donor electrons reduces the number of holes through the well known mass-action law. Thus it appears reasonable to assume that σ_c and σ_v are compatible at the

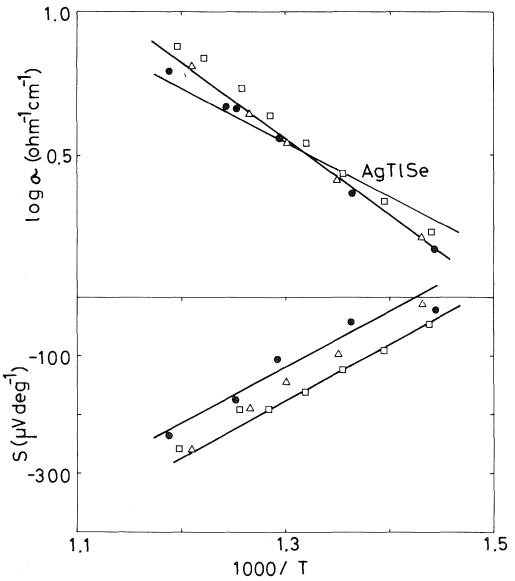

FIG. 6. The electrical conductivity and thermoelectric power of molten AgTlSe doped with Tl. ●, 0.5 at.% Tl; △, 1.0 at.% Tl; □, 2.0 at.% Tl.

lower end of the temperature range of the present study, and σ_c becomes larger than σ_v at higher temperatures. This is clearly seen from the curves of S in Fig. 5. The values of S are practically zero at lower temperatures and become large and negative at high temperatures. On the other hand, the excess Se may act as acceptor and create holes in the valence band. As these holes are in the extended states, the conductivity increases immediately. The suppression of the electron concentration by the introduction of holes would make the contribution of electrons to the thermoelectric power negligible even at higher temperatures. In consequence, the slope of S *vs.* $1/T$ becomes less steep and close to the slope of ln σ *vs.* $1/T$: for instance, we found $E_\sigma(0) = 0.33$ eV and $E_S(0) = 0.31$ eV for 1 at.% Se doped sample.

Though the arguments given above are still qualitative, we think that the present experimental data are well explained in the framework of the pseudogap model for amorphous semiconductors. For further quantitative arguments, it will be necessary to determine the contributions of both electrons and holes separately to the carrier density, mobility, etc. The determination of the band structure from optical measurements will also be needed.

1. Y. NINOMIYA, Y. NAKAMURA, and M. SHIMOJI. J. Non-Cryst. Solids, **17**, 231 (1975).
2. N. F. MOTT and E. A. DAVIS. Electronic processes in non-crystalline materials. Clarendon Press, Oxford. 1971.
3. H. FRITZSCHE. Amorphous and liquid semiconductors. *Edited by* J. Tauc. Plenum Press, London. 1974. Chapt. 5.
4. N. K. HINDLEY. J. Non-Cryst. Solids, **5**, 17 (1970).
5. A. J. GRANT, T. D. MOUSTAKAS, T. PENNEY, and K. WEISER. Proc. 5th Int. Conf. on Amorphous Liq. Semicond. Taylor and Francis, London. 1974. p. 325.
6. T.D. MOUSTAKAS, K. WEISER, and A. J. GRANT. Solid State Commun. **16**, 575 (1975).
7. Y. NAKAMURA, K. MATSUMURA, and M. SHIMOJI. J. Chem. Soc. Faraday Trans. I, **70**, 273 (1974).

Discussion

G. R. Freeman: How good is the approximation that the density of states in the band tail varies linearly with E?

M. Shimoji: It is now a very difficult task to derive accurately the density of states of real semiconducting liquids from first-principle methods, since it depends strongly on potentials, the distribution of which is highly fluctuating. Therefore, the density of states of such materials is sometimes conveniently written as a linear function of E to show schematically the relative positions of the Fermi energy, mobility edges, and band tails in an energy scale. Experimental information due to optical measurements, etc., is of course required for this problem (*cf.* N. F. Mott. Philos. Mag. **22**, 7 (1970); E. A. Davis and N. F. Mott. Philos. Mag. **22**, 903 (1970)).

L. Onsager: By common usage in solid state lore, 'electrons' are excess electrons in a conduction band, while 'holes' are unoccupied states in the valence band. In a semiconductor the proportion of such entities relative to the density of states is typically small everywhere (except for any states introduced by dopants).

M. Shimoji: Thank you very much for your pertinent comments. Because of large fluctuations of potentials the charge carriers excited to the extended states in noncrystalline semiconductors are supposed to correspond to those in a conduction (or valence) band of crystalline materials.

Electron spin resonance studies of preferential solvation in solutions of potassium in amines and ethers

R. CATTERALL

Department of Chemistry and Applied Chemistry, University of Salford, Salford M5 4WT, England

AND

J. SLATER AND M. C. R. SYMONS

Department of Chemistry, University of Leicester, Leicester 1E1 7RH, England

Received September 27, 1976

R. CATTERALL, J. SLATER, and M. C. R. SYMONS. Can. J. Chem. **55**, 1979 (1977).

Electron spin resonance spectra of solutions of potassium in tetrahydrofuran–ethylamine, tetrahydrofuran–diglyme, ethylamine–diglyme, and ethylamine–ethylenediamine mixtures are reported and compared with spectra obtained from the four pure solvents. Strong evidence for preferential solvation was observed in all mixtures, with the strength of solvation increasing in the order tetrahydrofuran < ethylamine < diglyme < ethylenediamine. Electron spin resonance spectra of mixtures containing ethylenediamine were used to investigate the nature of the single line spectrum obtained from solutions in ethylenediamine alone. It is concluded that this signal is an 'ammonia-like' time averaged spectrum arising from solvated electrons and ion-pairs.

R. CATTERALL, J. SLATER et M. C. R. SYMONS. Can. J. Chem. **55**, 1979 (1977).

On rapporte des spectres rpe de solutions de potassium dans des mélanges de tétrahydrofuranne–éthylamine, tétrahydrofuranne–diglyme, éthylamine–diglyme et éthylamine–éthylènediamine et on les compare avec les spectres obtenus à partir des quatre solvants purs. Il y a de fortes indications que l'on observe une solvatation préférentielle dans tous les mélanges alors que la force de solvatation augmente dans l'ordre tétrahydrofuranne < éthylamine < diglyme < éthylènediamine. On a utilisé les spectres rpe de mélanges contenant de l'éthylènediamine pour étudier la nature du spectre avec une seule ligne obtenu pour des solutions dans l'éthylènediamine seul. On en conclut que ce signal est un spectre moyenné dans le temps ressemblant à l'ammoniac et qui dérive d'électrons solvatés et de paires d'ions.

[Traduit par le journal]

Introduction

Although alkali metals dissolved in amine and ether solvents ionize completely in very dilute solutions, there is strong evidence that solvated cations and solvated electrons form neutral aggregates of stoichiometry M as the concentration of metal is increased.

[1] $$M^+ + e_{sol}^- \rightleftharpoons M^+e_{sol}^-$$

Considerable controversy (1–7) has surrounded the nature of these cation–electron aggregates. Electron spin resonance spectra include contributions from both paramagnetic species and the spectra observed can be divided into two groups: those for which two signals are observed, a hyperfine multiplet from cation–electron aggregates and a central singlet from isolated solvated electrons, and those for which only a single resonance line is seen. In the latter case the spectra are described as a time-average of the two possible environments for the unpaired electron. Examples of the first class are solutions of the higher alkali metals in ethylamine and tetrahydrofuran (THF), whilst solutions in ammonia and hexamethylphosphoramide belong to the second class. Spectra of solutions of potassium in ethylenediamine have been reported (8) to consist of a single line but it is not clear whether this line is a time-averaged signal ('ammonia-like') or an 'amine-like' signal in which the hyperfine lines are broad and weak as in 1,2-propylenediamine[1] and diglyme ($CH_3O(CH_2CH_2O)_2CH_3$) solutions.

In all instances where resolved hyperfine structure from alkali metal nuclei has been resolved, the hyperfine components show a progressive broadening towards the wings of the spectra. These line-width variations and also the temperature dependence of the splitting constants have generally been attributed either to a

[1]V. A. Nicely. Unpublished results.

TABLE 1. Percent atomic character for alkali metal species in amines and ethers

	$MeNH_2$	PDA	DlGL	$EtNH_2$	$PrNH_2$	*i*-$PrNH_2$	THF
Na				>8			
K		3.4	4.3	11.2	16.7	21.8	36.1
Rb	7.1	8.5		17.7	23.2	27.4	
Cs	6.8	8.2		15.7	20.9	29.4	

rapidly fluctuating hyperfine interaction involving time-dependent changes in the solvation shells surrounding the cations (10), or to an essentially static variation of the magnetic parameters with minor changes in solvation effects. Bar-Eli and Tuttle (4) refer to these as vibrational states, but their lifetimes would need to be in excess of $\sim 10^{-8}$ s to have any appreciable influence on the spectra. The importance of the solvent in a static sense is amply illustrated by the wide variation in the occupancy of metal *s*-orbital as gauged by the magnitude of the hyperfine coupling constant relative to that in the free atoms (Table 1).

Our approach to these systems has been to select a set of four solvents which differ widely in their ability to solvate cations. The four chosen were: ethylamine, tetrahydrofuran, ethylenediamine, and diglyme; two amines and two ethers. Of the two nitrogen-containing solvents, ethylenediamine is well known for its ability to chelate to metal cations, and we expect the entropy effect associated with coordination at two sites in the molecule to contribute markedly to the lifetime of solvent–metal interactions. Similarly, of the two oxygen-containing solvents, diglyme is known to be an efficient cation solvator because of its ability to chelate, whilst THF has a notoriously low solvating power. We have reported previously on solutions in ethylamine (7, 11) and THF (12, 13) and here we make a preliminary report of solutions in diglyme, ethylenediamine, and in the mixed solvent systems THF–ethylamine, THF–diglyme, ethylamine–diglyme, and ethylamine–ethylenediamine.

Experimental

High vacuum techniques were used as described elsewhere (14). Solvent mixture compositions were estimated volumetrically and converted to mole fractions using the appropriate densities and assuming no volume changes on mixing.

Electron spin resonance spectra were measured on a Varian E3 spectrometer. Temperature control was achieved using standard equipment, and field and frequency measurements were corrected by reference to standard samples.

Results and Discussion

Diglyme Solutions

Electron spin resonance spectra consisted of a quartet of broad lines which almost merged in the saturated solutions. In more dilute solutions an additional central feature was apparent which became progressively narrower at higher dilution until at the limit of detectability (no visible blue colour) the width was $\lesssim 0.1$ G. In contrast, the widths of the hyperfine lines were far less dependent upon concentration. The coupling constant varied from 2.0 to 5.0 G over the interval 15 to 35°C.

Ethylenediamine Solutions

For all metal concentrations only a single narrow line was observed. The width of this feature (~ 0.12 G at room temperature) decreased as temperature increased, but appeared to be independent of metal concentration.

Ethylamine and Tetrahydrofuran Solutions

The temperature dependence of the hyperfine coupling constants is compared with that for diglyme solutions in Fig. 1. Results for ethylamine are in good agreement with those reported in refs. 4 and 7 and we are again unable to reproduce the temperature dependence reported in ref. 10.

Mixed Solvent Systems

The dependence of the coupling constants upon solvent composition for the four systems studied is given in Figs. 2–5. In all cases the concentration of the more efficient solvating medium increases to the right and we note that A values always decrease as this solvent is added. Variations of coupling constants were always smooth functions of solvent composition and no trace of discontinuous or 'stepped' behaviour was ever observed. In all cases there was an initial rapid decrease in A value as the first few percent of the better solvating medium was added. In an early paper (7) we reported that the A value of solutions of potassium in a 1 : 1 mixture of ethylamine and butylamine was greater than that of either

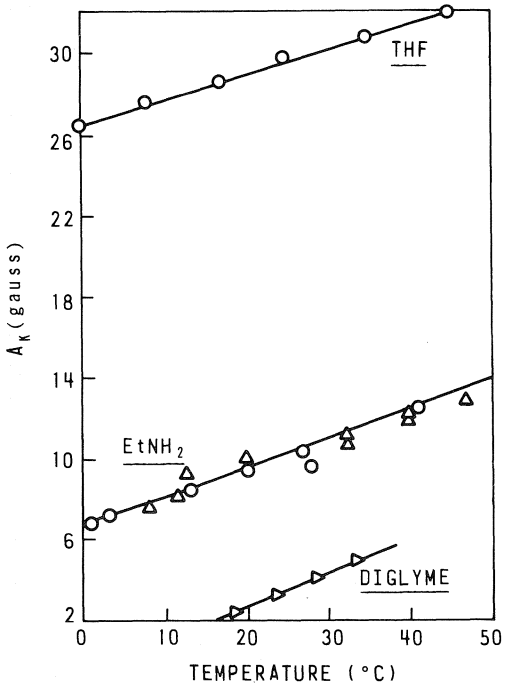

FIG. 1. The temperature dependence of the potassium hyperfine coupling constant (A_K) for solutions of potassium in tetrahydrofuran (THF), ethylamine ($EtNH_2$), and diglyme. $EtNH_2$ data: ○, this work; △, ref. 4.

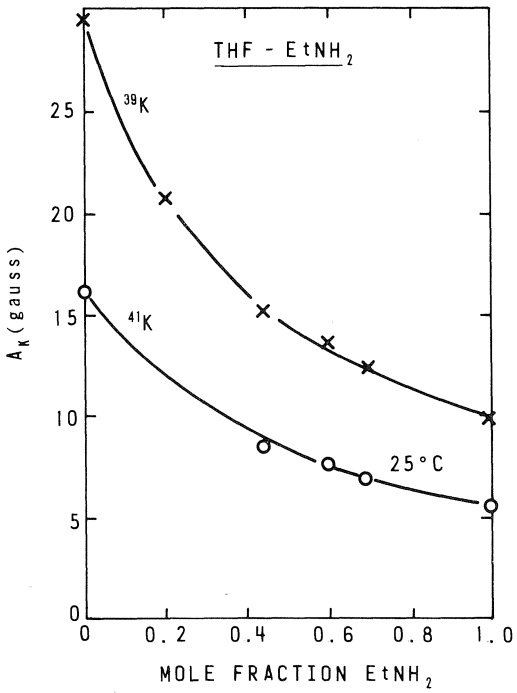

FIG. 2. The solvent dependence of the hyperfine coupling constant (A_K) to the two naturally occurring potassium isotopes in solutions of potassium in tetrahydrofuran–ethylamine mixtures.

pure solvent but approximately equal to the splitting in propylamine. No trace of this type of behaviour was observed in the present work.

For solutions in ethylamine–ethylenediamine mixtures hyperfine structure was only resolved for solutions containing less than about 20 mol% ethylenediamine (see below). Line widths of the hyperfine components were almost completely independent of metal concentration but increased rapidly with increasing concentration of ethylenediamine.

Line-widths and Time-dependent Processes

When small amounts of diglyme were added to solutions of potassium in THF, the width of the hyperfine lines increased. The rate of increase of line width was greatest for the outermost lines so that spectra with extreme linewidth variation were observed. For the outermost lines the widths in solutions containing more than 8 mol% diglyme were greater than those observed in either pure solvent. In contrast the A and g factors were always within the range of the pure solvent values. In marked contrast to these results, no significant changes in linewidths were observed when ethylamine, a solvent which cannot chelate to cations, was added to solutions of potassium in THF.

Preferential Solvation

The binary solvent systems shown in Figs. 2–5 have all been arranged so that the solvent giving rise to the highest hyperfine coupling constant is on the left. In all systems we observed an initial rapid decrease in the coupling constant as the second solvent was added, whilst the departures from linearity in the trends between the pure solvents indicate that the second solvent in each case is the more effective in determining the A value than would be expected for random solvent mixtures. A reduction in A value, indicating a lower unpaired electron spin density in the outer metal s orbital, is consistent with an increased population of the metal s orbital resulting from solvation effects such as the donation of oxygen or nitrogen lone pairs to the metal. Accordingly we attribute the observed changes in A value to a competition between different solvents for the metal cations (M^+) within the species of stoichiometry M which is responsible for the electron spin resonance spectra. The departures from linearity in Figs. 2–5 thus represent preferential

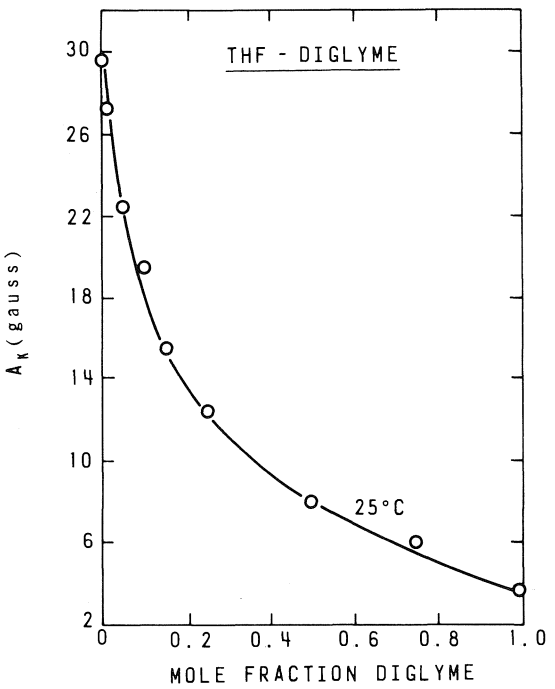

FIG. 3. The solvent dependence of the potassium hyperfine coupling constant (A_K) in solutions of potassium in tetrahydrofuran–diglyme mixtures.

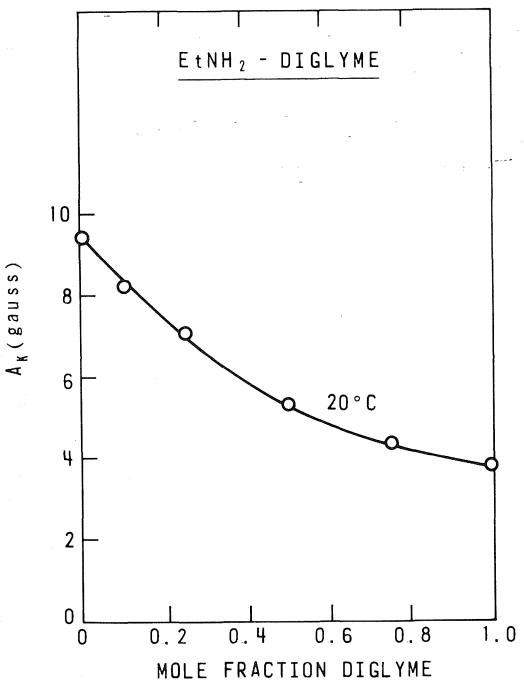

FIG. 4. The solvent dependence of the potassium hyperfine coupling constant (A_K) in solutions of potassium in ethylamine–diglyme mixtures.

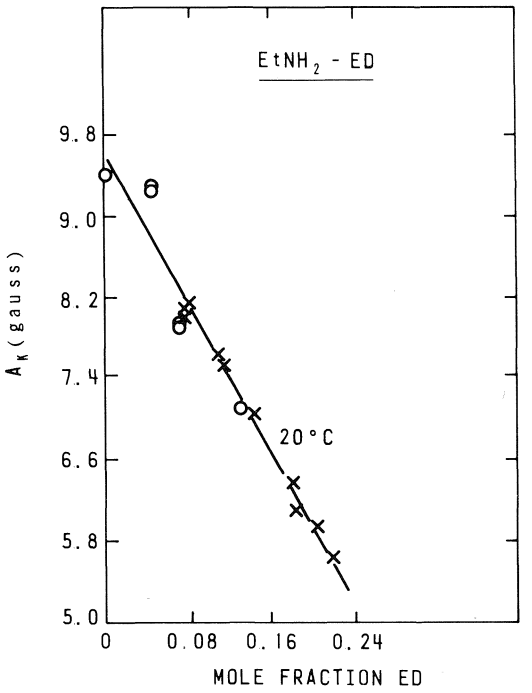

FIG. 5. The solvent dependence of the potassium hyperfine coupling constant (A_K) in solutions of potassium in ethylamine–ethylenediamine. ○, from individually prepared samples; ×, samples prepared successively by dilution techniques.

solvation of alkali metal cations. Preferential solvation as a cause of varying coupling constant was proposed for solutions of potassium in mixtures of ethylamine and methylamine (4).

The initial gradients in Figs. 2–5 can be used to establish an order of solvents reflecting the strength of the solvation forces: tetrahydrofuran < ethylamine < diglyme < ethylenediamine. As might be expected, solvents capable of forming chelate complexes with the metal ions are significantly more effective in reducing the A value than are monodentate ligands, whilst within this broad distinction, amines are more effective than ethers.

The linewidth effects observed when diglyme is added to tetrahydrofuran solutions are indicative of a slowing down of fluctuations of the hyperfine coupling constant, resulting from the tighter binding of solvent to metal in a chelate complex.

Ethylamine–Ethylenediamine Solutions

The esr spectra of solutions of potassium in mixtures of ethylamine with ethylenediamine and diglyme show significant differences. For mix-

tures with diglyme the spectra trended smoothly from one solvent to the other, but the behaviour of mixtures containing ethylenediamine was more complex and similar to that observed in solutions of potassium in mixtures of ethylamine and methylamine (4). The hyperfine coupling constant decreased rapidly (Fig. 5) as the diamine was added and all the lines broadened strongly and approximately equally until no trace of the hyperfine structure was observed at around 20 mol% ethylenediamine. Above this concentration the single line broadened and then sharpened up again over a very narrow concentration region. Since no dependence of linewidths of the hyperfine components on metal concentration was observed and no difference was observed between the broadening rates for the inner and outer lines, the fluctuation of the coupling constant to the metal nucleus cannot be the dominant electron relaxation mechanism in ethylamine–ethylenediamine mixtures. Instead we interpret these results in terms of [1]. If this equilibrium is governed by sufficiently high rate constants the coupling between the unpaired electron and the alkali metal nucleus will be randomized and as the rates increase the lines will broaden equally, coalesce, and finally sharpen up to a single line characteristic of a time averaged environment.

For this mechanism to be operative we require the rate constants governing [1] to be low in ethylamine and diglyme, but higher in ethylenediamine. The critical region is that which gives rise to effective lifetimes of the electron–cation aggregates of the order of the inverse of the hyperfine splitting constants. For ethylamine and diglyme these times are 0.36 and 1.2×10^{-7} s, respectively.

For [1], the mean lifetime (15) of the aggregates, τ_M is given by

$$[2] \qquad \tau_M^{-1} = k_1([K^+] + [e^-]) + k_1/K_{as}$$

where k_1 is the forward rate constant and K_{as} the association equilibrium constant (9):

$$[3] \qquad K_{as} = \exp(Z_e Z_M e^2/aD_s kT)$$

and k_1 is given by (15)

$$[4] \qquad k_1 = (4\pi L_0 Z_e Z_M e^2/D_s kT) \times (D_e + D_M)(K_{as}{}^{-1})^{-1}$$

where Z_e and Z_M are ionic charges, π, L_0, e, k, and T have their usual significance, D_s is the static dielectric constant of the medium, a is an ion separation parameter, and D_e and D_M are diffusion coefficients of e_{solv}^- and M^+ in the medium concerned.

We estimate D_e and D_M from values in ammonia (16) by correcting for viscosity changes. K_{as} for ethylamine we have estimated (17) from values of [e^-], [K], and total metal concentration, and reasonable estimates for K_{as} in diglyme and ethylenediamine were obtained from this value by correcting for changes in D_s. When this is done we find that the product $\tau_M A$ for ethylamine (~ 30) and diglyme (~ 7) are > 1 indicating that resolved hyperfine structure is to be expected, whilst for ethylenediamine (~ 0.04) $\tau_M A \ll 1$ indicating that a time-averaged signal is all we can hope to observe.

Acknowledgment

We thank the Science Research Council for a Research Studentship (J.S.).

1. E. Becker, R. H. Lindquist, and B. J. Alder. J. Chem. Phys. **25**, 971 (1956).
2. E. C. Evers. J. Chem. Phys. **33**, 618 (1960).
3. M. C. R. Symons. Q. Rev. Chem. Soc. London, **13**, 99 (1959).
4. (*a*) K. Bar-Eli and T. R. Tuttle, Jr. J. Chem. Phys. **40**, 2508 (1964); (*b*) T. R. Tuttle, Jr. J. Phys. Chem. **79**, 3071 (1975).
5. L. R. Dalton, J. D. Rynbrandt, E. M. Hansen, and J. L. Dye. J. Chem. Phys. **44**, 3969 (1966).
6. R. Catterall and M. C. R. Symons. J. Chem. Soc. 3763 (1965).
7. R. Catterall, M. C. R. Symons, and J. W. Tipping. J. Chem. Soc. A, 1529 (1966).
8. K. D. Vos and J. L. Dye. J. Chem. Phys. **38**, 2033 (1963).
9. R. A. Robinson and R. H. Stokes. Electrolyte solutions. Butterworth and Co. (Publishers) Ltd., London. 1959. Chapt. 14.
10. J. L. Dye and L. R. Dalton. J. Phys. Chem. **71**, 184 (1967).
11. R. Catterall and M. C. R. Symons. J. Chem. Soc. 6656 (1965).
12. R. Catterall, J. Slater, and M. C. R. Symons. J. Chem. Phys. **52**, 1003 (1970).
13. R. Catterall, J. Slater, and M. C. R. Symons. Pure Appl. Chem. (Colloque Weyl II), 329 (1970).
14. R. Catterall and M. C. R. Symons. J. Chem. Soc. 4342 (1964).
15. M. Eigen, W. Kruse, G. Maas, and L. de Maeyer. *In* Progress in reaction kinetics. Vol. 2. *Edited by* G. Porter. Pergamon Press Ltd., London. 1964. p. 285.
16. J. L. Dye, R. F. Sankuer, and G. E. Smith. J. Am. Chem. Soc. **82**, 4797 (1960).
17. J. Slater. Ph.D. Thesis, University of Leicester, Leicester, England. 1970.

Discussion

U. Schwindewolf: Is there a correlation between the esr spectra and optical spectra?

R. Catterall: In recent work carried out at the Chalk River Nuclear Laboratories in collaboration with Dr. W. A. Seddon we have attempted to correlate esr spectra with transient optical absorption bands produced after pulsed electron radiolysis of solutions of alkali metal salts. A general correlation is discussed in a later paper by Dr. Seddon, Dr. J. W. Fletcher, and myself (Can. J. Chem. This issue.). For the solutions of sodium tetraphenylboron in tetrahydrofuran–diglyme mixtures we observed two bands, one at 890 nm very similar to the one produced in $NaB\phi_4$–THF and another at ~1800 nm characteristic of $NaB\phi_4$–diglyme. The relative intensity of these bands varied with solvent composition and the spectra showed an isobestic point. This appears to be strong qualitative evidence for a two-state model for the paramagnetic monomer species in THF–diglyme mixtures. However, some of the 900 nm band is present in $NaB\phi_4$–diglyme without any THF.

S. A. Rice: Would you please comment on your esr measurements and pulse radiolysis of diglyme–THF mixtures in comparison to the flash photolysis experiments on sodium–diglyme solutions of Kloosterboer *et al.* (J. G. Kloosterboer, L. J. Giling, R. P. H. Rettschnick, and J. D. W. Van Voorst. Chem. Phys. Lett. **8**, 462 (1971)).

R. Catterall: Kloosterboer *et al.* flashed the band at ~700 nm assigned to Na^- anions in solutions of sodium metal in diglyme at −60°C, and observed the formation of a band in the infrared at ~1600 nm which they assigned to the solvated electron. As this band decayed they observed the growth of a new band at ~850 nm which then slowly decayed to regenerate the original band of Na^- at ~700 nm. They assigned the intermediate band at 850 nm to an aggregate of Na^+ and e^- by analogy with the band observed in THF solutions. However, the esr spectra of potassium in diglyme reveal a hyperfine coupling of only 3.7 G (23°C) whereas we correlate an absorption band at ~900 nm with a coupling constant of ~30 G (see Seddon *et al.* Can. J. Chem. This issue.). One possible explanation might be that the band at ~1600 nm observed by Kloosterboer *et al.* was the 'ion-pair' as we suppose, and that the band they observed at ~850 nm was in fact due to K^- (produced from potassium impurity) which then slowly converted to Na^- at 700 nm. A slow conversion of K^- to Na^- such as this has been observed after pulse radiolysis of mixed metal solutions (J. W. Fletcher and W. A. Seddon. J. Phys. Chem. **79**, 3055 (1975)).

J. L. Dye: The two types of ion-pairs, one with low hyperfine splitting and an infrared absorption band, and the other with high hyperfine splitting and an absorption band nearer the visible would be better described as solvent-shared ion-pairs and contact ion-pairs, respectively. In this way, you can have both present even in *a single solvent*.

R. Catterall: I'm quite happy to accept your nomenclature. Certainly we do see evidence for two types of ion-pairs between e_s^- and Na^+ after pulse radiolysis of $NaB\phi_4$ in diglyme. The dominant band, peaking at ~1800 nm is slightly blue-shifted from its position in pure diglyme, and this we attribute to the loose ion-pair formed between a *chelated* sodium cation and a solvated electron. The weaker band that we observe at ~900 nm (which is close to that observed in $NaB\phi_4$–THF) we also attribute to an ion-pair of a Na^+–diglyme cation with a solvated electron, but in this case we envisage the glyme as being attached to the cation as a monodentate ligand. The hyperfine coupling we observe by esr (~3.7 G) is then the weighted average of the two types of ion-pair, one (900 nm) with a coupling of ~30 G and the other (~1600 nm) with a much smaller splitting, possibly $\lesssim$0.3 G.

L. Onsager: How do the symptoms of hyperfine structure correlate with the dielectric constants?

R. Catterall: For solvents which can only coordinate to metal cations in a monodentate fashion, there is an approximate correlation with dielectric constant: propylene diamine ($D_s \sim 14$, $A_K \sim 3$ G), ethylamine ($D_s \sim 12$, $A_K \sim 10$ G), isopropylamine ($D_s \sim 10$, $A_K \sim 18$ G), and THF ($D_s \sim 7$, $A_K \sim 30$ G). However, when chelating solvents are included the correlation breaks down completely: THF and diglyme have the same dielectric constant (~7), but A_K(THF) ~ 30 G, whilst A_K(diglyme) ~ 3.7 G.

Thermal emission of excess electrons from liquid hydrocarbons (Extended Abstract)

A. A. Balakin, I. A. Boriev, and B. S. Yakovlev
Institute of Chemical Physics, Academy of Sciences USSR, 142432 Chernogolovka, USSR
Received November 22, 1976

An electrical conductivity due to a liquid-to-gas electron emission has been investigated in two-phase systems. The systems consisted of a liquid hydrocarbon in equilibrium with its own saturated vapour in vacuum. Excess electrons were generated in the system by 2×10^{-7} s X-ray pulse irradiation. The conductivity cell consisted of two electrodes which were 1.5 cm diameter nickel disks separated by the distance $d = 0.7$ cm. The excess electron current was measured for the three following conditions: *a*, the liquid filled the total volume between electrodes; *b* and *c*, the liquid level was between electrodes at the distance $d' = 0.2$ cm from the lower electrode, with the potential of that electrode being negative in the case *b*, but positive in the case *c*.

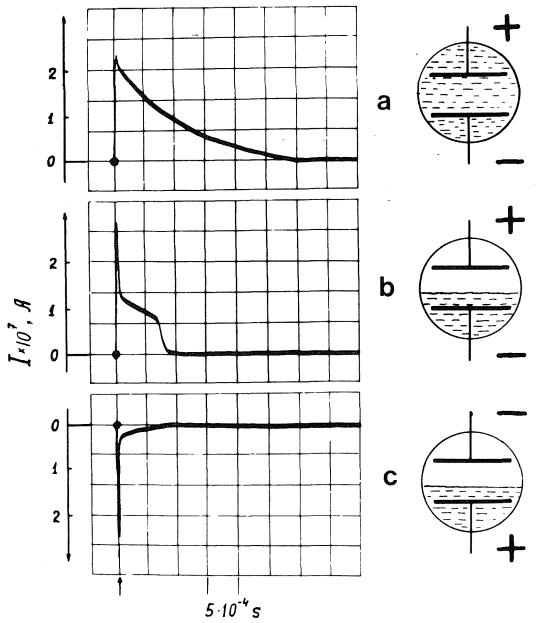

FIG. 1. Electron current *vs.* time observed in *n*-hexane at three conditions: *a* both electrodes immersed in liquid with lower electrode being negative; *b* and *c* liquid level is between electrodes, with lower electrode being negative in case *b* and positive in case *c*. Voltage between electrodes = 2000 V, $T = 296$ K.

Figures 1 and 2 show the current oscillograms for *n*-hexane and isooctane. In cases *a* and *c* the traces of current *vs.* time associated with the drift of electrons to the positive electrode in the liquid layer *d* (the case *a*) or *d'* (the case *c*), agrees with the known excess electron mobility, μ, in liquids (0.09 and 7 $cm^2\ V^{-1}\ s^{-1}$ in *n*-hexane and isooctane at 296 K). In the case *b* for isooctane and *n*-hexane the value of the current during the drift time, τ', for an excess electron to move the distance *d'* is significantly more than that in the case *c*. Corresponding measurements with tetramethylsilane (TMS) have shown that in the case *b* the current trace is the same as that in *c*.

The fact that the current value for *n*-hexane and isooctane in the case *b* was more than that in the case *c* can be connected with the transmission

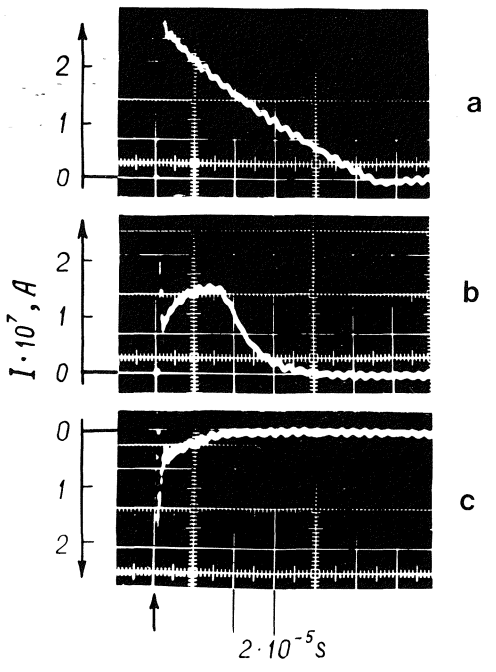

FIG. 2. Electron current *vs.* time observed in isooctane for the three conditions of Fig. 1. Voltage between electrodes = 600 V, $T = 296$ K.

of excess electrons into the vapour. (For *n*-hexane this conclusion agrees with data from ref. 1.) Comparison of the current integrals in cases *a*, *b*, and *c* showed that the bulk of electrons generated in the liquids were transferred to the vapour in a time about equal to τ'. The coincidence of currents in cases *b* and *c* for TMS is evidence of the absence of electron emission for these conditions.

The prompt increase of the current in case *b* for *n*-hexane immediately after the X-ray pulse, and its abrupt decrease at a time near τ', allowed an estimate of the delay time ($t_d < 5 \times 10^{-5}$ s) for the electron to cross the liquid surface. For isooctane the value t_d was sufficiently large to be recorded from current traces and it was inversely proportional to the electric field strength in the liquid, E, in the range 1.5×10^2 to 1.5×10^3 V/cm.

We have attempted to connect the dependence of $t_d(E)$ with the height of the surface barrier potential. The density of the emission current can be presented as $j(t) = vn_0(t)$, where $n_0(t)$ is the concentration of electrons in liquids near the liquid surface and v is the effective velocity of crossing the surface by electrons. At $t \geq d'/\mu E$ the electrons which have not yet escaped from the liquid are situated near its surface in a layer with the characteristic thickness $l = kT/eE$ (k is Boltzmann's constant, e is the electron charge), therefore

$$[1] \qquad t_d = \frac{l}{v} = \frac{kT}{eEv}$$

i.e. $t_d \sim E^{-1}$, in agreement with the experiments.

If we assume a conventional model of trap-limited transfer of excess electrons in liquid isooctane and a rectangular surface barrier potential with height V_0 for quasifree electrons then we obtain:

$$[2] \quad v = (1 - P) \int_{\sqrt{2mV_0}}^{\infty} \beta(p_z) f(p_z) \frac{p_z}{m} \, dp_z$$

Here the z axis is perpendicular to the liquid surface, β is the reflection coefficient of electrons from the barrier, $f(p_z)$ is the momentum distribution function, $P = 1 - \mu/\mu_0$ is the probability of electron localization, μ_0 is the quasifree electron mobility, and m is the effective mass of an electron. Using the experimental values of t_d, $\mu_0 = 150 \pm 50$ cm V^{-1} s^{-1}, the Maxwellian distribution function for $f(p)$ and m equal to the electron mass, we have from [1] and [2] $V_0 = -0.19 \pm 0.02$ eV for isooctane at 296 K. The measurements of t_d at 270 and 320 K allowed an estimate of $\partial V/\partial T = -8 \times 10^{-4}$ eV/deg. These values are in a fair agreement with the results obtained from metal-to-liquid electron photoemission data (2).

1. R. M. MINDAY, L. D. SCHMIDT, and H. T. DAVIS. J. Chem. Phys. **54**, 3112 (1971).
2. R. A. HOLROYD, S. TAMES, and A. KENNEDY. J. Phys. Chem. **79**, 2857 (1975).

Discussion

P. Delahay: Did you consider backscattering of electrons in the gas phase? This type of scattering depends on the vapor pressure and the electric field in the gas phase, and the fraction (per unit of time)

$$\frac{\text{number of collected electrons}}{\text{number of emitted electrons}}$$

can be considerably smaller than unity unless the ratio field/pressure is large enough. It would seem that this effect would affect your interpretation (particularly with regard to the distribution in the liquid).

E. L. Frankevich: We did not. Actually we had no need for that as all electrons reach the electrodes within a time which is much shorter than τ. This could be seen on the *i vs. t* curve for *n*-hexane where no delay current exists and the total area under the curve (or charge collected) is independent of the voltage applied. The only type of backscattering taken into account was that due to passing of electrons over the potential barrier.

L. G. Christophorou: You assumed that all electrons in the Maxwell distribution with energies greater than V_0 escape from the liquid into the vacuum. As Professor Delahay mentioned a large fraction of these should be backscattered and this fraction should vary depending on your E/N value. Shouldn't this be reflected in your current *vs.* time curves and also in the total charge you collect?

G. Freeman: Professor Frankevich is perhaps suggesting that electrons that are reflected back into the liquid by the gas may be re-emitted into the gas.

E. L. Frankevich: They certainly do this and it is demonstrated by the independence of the total electron charge collected by the electrodes of the voltage applied. The re-emittance seems to take a very short time as no delay could be seen for the case of *n*-hexane where V_0 is positive.

U. Sowada: If backscattering were important on the time-scale of these measurements, a delayed decay should have been observed for *n*-hexane too, which was not the case. The neglect of this effect seems to be justified.

Electron localisation: evolution of optical spectra

DAVID C. WALKER

Department of Chemistry, University of British Columbia, Vancouver, B.C., Canada V6T 1W5

Received September 27, 1976

DAVID C. WALKER. Can. J. Chem. **55**, 1987 (1977).

Attention is directed to experiments from several groups which bear on the origin of the electron's absorption band, particularly with regard to the spontaneous progression from metastable to equilibrated states and photoinduced spectral shifts. The absorption band is discussed as being heterogeneously broadened in both solid and liquid phases, the former being space-averaged and the latter time-averaged. This means that the proper extinction coefficients are higher than those currently in use which were evaluated on the presumption that the band was homogeneous. $E_{\lambda max}$ is seen as a generally useful measure of the solvating power of solvents.

DAVID C. WALKER. Can. J. Chem. **55**, 1987 (1977).

Cette publication permet d'orienter l'attention vers les expériences provenant de plusieurs groupes qui ont une incidence sur l'origine des bandes d'absorption d'électrons, particulièrement en ce qui a trait à la progression spontanée allant d'états métastables vers des états équilibrés et aux déplacements spectraux photoinduits. On discute de la bande d'absorption comme étant élargie d'une façon hétérogène à la fois dans les phases solides ainsi que liquides; il se produitrait une moyenne des espaces dans les premières et une moyenne dans le temps dans les dernières. Ceci implique que les coefficients d'extinction appropriés sont plus hauts que ceux utilisés actuellement et qui ont été évalués en faisant l'hypothèse que la bande était homogène. On considère que le $E_{\lambda max}$ est généralement une mesure utile du pouvoir de solvatation des solvants.

[Traduit par le journal]

1. Introduction

That the mere absence of crystalline order can, in itself, give rise to electron localisation is a notion which has emerged in the wake of extensive studies of two closely related phenomena: the trapping of electrons at vacancy or at impurity sites in crystals, and the solvating of ions in solution. It is now known that electrons may be localised (and thereby give rise to characteristic optical absorption spectra or electron spin resonance absorption) in a prodigious variety of media, including many polar and nonpolar liquids and amorphous solids, and in at least one fluid above its critical temperature. Naturally, the stability in a thermodynamic sense of the localised electron in these different environments varies considerably. Thus absorption bands are found to be centred from ~3500 to ~500 nm. Their stability with respect to chemical reaction is even more variable and is generally strongly temperature dependent at temperatures where the viscosity and diffusion coefficients change markedly. But the observed electron state, albeit often transient or metastable, also varies with temperature because of changes in the medium's relaxation and solvation rates.

There are several electron states to consider. I will use the following nomenclature: quasi-free (e_{qf}^-) for delocalised; infrared absorbing (e_{ir}^-) and weakly trapped or partially solvated for metastable states; and trapped (e_t^-) or solvated (e_s^-) for the fully equilibrated states.

2. Optical Absorption Bands of e_s^- and e_t^-

These are broad and structureless. In certain ordered solids they tend to be only ~0.2 eV wide at half height but generally range from 0.5 to 1.2 eV. In only one case (1), strongly disputed recently (2), has fine structure been reported for any of these bands. The photon energy at which the absorption band maximum occurs ($E_{\lambda max}$) for the equilibrated localised electron depends dramatically upon the composition of the chemical groups constituting the walls of the trap. Thus $E_{\lambda max}$ for monoethanolamine is the same as an equimolar mixture of monobutylamine and ethanol (1). The latter mixture, however, shows a much broader band, which suggests the broadness increases with the number of possible solvation energies that the medium can provide.

It was thought for some time that $E_{\lambda max}$ increased monotonically with the bulk dielectric

constant (D_s) of the solvating medium. Such a correlation was disproved, for instance, by the observation (3) that dimethylsulphoxide, with $D_s = 46$, had an electron absorption band in the near ir similar to that of a hydrocarbon having $D_s \sim 2$. In fact solvents like dimethylsulphoxide and hexamethylphosphorictriamide have well-defined negative stocks for strongly solvating positive ions, but the positive end of the molecular dipole is diffused over many weakly polar C—H bonds, with the result that negative ions (including solvated electrons, evidently) can be solvated to only a minor extent. $E_{\lambda max}$ is thus related to the solvation energy of the medium for negative ions. Perhaps $E_{\lambda max}$ will prove to be a more useful and broader-based factor with which to measure the relative solvating power of solvents for negative ions than the empirical parameters Y, a, Z, and E_T which are currently in use (4).

It is interesting to note that D_s was used as the principal guide to a solvent's solvating power until the dipolar aprotic solvents came to the fore (5). One of the advantages which would result from using $E_{\lambda max}$ as a measure of solvating power rather than, for instance, the pyridinium *N*-phenolbetaine anion (6) for this purpose, is that the electron's size is more flexible and therefore the correlation should apply better to small anions. Yet one finds that in liquid ammonia the electron creates, and resides in, a rather large cavity (equal to the displacement of about three ammonia molecules). On the other hand, in solvents with bulky secondary groups, steric interference among the molecules lining the walls of the trap cause the traps to be more cavernous than is found with molecules of the same basic solvating power but without bulky groups. Thus secondary and tertiary alcohols were found to have smaller values of $E_{\lambda max}$ than primary alcohols of comparable bond polarity (7).

At least two short-range factors are involved in determining $E_{\lambda max}$: The local structure and particularly the bond polarity at the walls of the trap (which in general will mean the protic character of the hydrogen atoms there) and the size of the cavity. To return momentarily to hexamethylphosphorictriamide, it has both weak polarity and an extended cavity of >8 Å diameter due to the confrontation of six methyl groups, from each of four nearest neighbour molecules (8).

Upon injecting electrons into a liquid which has been cooled to the glassy state, the absorption band is remarkably similar, though its maximum is generally shifted slightly to the blue and narrowed perceptibly when fully relaxed in the solid relative to that in the liquid phase. Electron absorption bands in solvent mixtures have also been extensively studied and seem to fall into two categories. When the solvents form relatively ideal solutions only a single absorption band is found and $E_{\lambda max}$ varies approximately linearly with volume composition between the pure components (9), even when they are of widely differing solvating power (10, 11). However, when the solutions are nonideal (as is the case for alcohol–hydrocarbon mixtures) then the equilibrated electron spectrum resembles that of the pure more-polar component over a disproportionately large range of composition in liquids (12–14); but the immediate, unrelaxed spectrum can be representative of the composition in cool viscous fluids (15), and can show two maxima in low temperature glasses (16). Small clusters of the more polar molecules seem to be acting as electron scavengers in these nonideal solutions.

3. Spontaneous Spectral Shifts

Several situations are known in which the electron absorption band is observed to change with the passage of time. Invariably the shift of the absorption band maximum is towards the blue, corresponding to a lowering of the mean energy state of the electron. The rate of transformation increases with temperature and the present extremes measured are $\sim 10^{12}\ s^{-1}$ in liquids at 295 K (17) and $<10^{-3}\ s^{-1}$ in solids at 4 K (18).

In cool liquid alcohols absorption in the near ir was observed to decay concurrently with a growth in the visible absorption band, the two bands being quite distinct (19). An absorption maximum has not yet been located for the ir band in the liquid but in solid ethanol it is at ~ 1300 nm (20). This shifting of the band from ir to visible wavelengths has also been observed in liquid alcohols at 295 K (21), in glasses at 77 K (20, 22), and in glasses which were warmed from 4 to 77 K (23). There was a significant rise-then-fall of absorption at the intermediate wavelengths in both solids and liquids (19, 20, 24). This suggests there is either (*i*) a progressive change in the overall distribu-

tion of trapped electrons or (*ii*) a sequential solvation through transient discrete, or continuously variable, states. The development of the fully solvated electron spectrum grew-in in the liquids with a single time constant which has been correlated with a relaxation time for molecular rotation over a range of temperatures (19, 21, 24, 25). This suggests electrons are digging deeper traps in the liquids. However, in glassy alcohols recent results on the effects of scavengers have been interpreted in terms of a hopping mechanism (26). As implied in Section 9, it may be more natural for electrons to be primarily 'seekers' in rigid low temperature glasses and 'diggers' in low viscosity liquids.

Spontaneous spectral shifts probably occur in most systems, the time required changing markedly with the viscosity. They have been observed in viscous hydrocarbons at low temperatures as a substantially faster decay of the infrared side of the absorption band compared to the decay rate on the visible side, which also resulted in $E_{\lambda max}$ increasing with time (27). In many aqueous glasses at 77 K a single band was observable immediately after a radiation pulse and subsequently the red edge of this band decayed (28).

But in certain other aqueous glassy systems (more on this later) a transient, separate, ir absorption band was also produced (29). In addition, there is reported to be a marked shift in absorbance from 1060 nm to 530 nm between 2 and 4 ps for electrons produced in aqueous solution at 295 K (17).

4. Origin of the Absorption Bands

It is natural for us to regard these spontaneous spectral shifts as direct observations of the electron localisation process, marking stages in the chronological development of the relaxed, equilibrated state. We can also disturb the equilibrated state photochemically and observe subsequent relaxations, or merely change the temperature and hope that we are just dilating the time scale. Eventually we focus our interpretations of these optical properties on several questions about the nature of the solvated electron.

(*i*) Is the optical transition to a bound excited state or to the quasi-free state or is some of both involved?

(*ii*) Why is the absorption band broad and structureless? Is it homogeneously broadened by phonon coupling of the excited state with a common ground state, or is it broadened through the ground state by variations in local dipoles and cavity sizes and is thus heterogeneous?

(*iii*) If it is heterogeneously broadened do we observe a time-averaged or a space-averaged spectrum?

(*iv*) Do spontaneous spectral changes to the blue arise because electrons are diggers or seekers of deeper traps?

(*v*) Is there a preferential chemical reactivity shown by electrons contributing predominantly to the red end of the band?

(*vi*) What influence does the electrolyte of aqueous glasses have?

Most of the information comes from electrons produced by radiolysis, where they start with a range of epithermal energies and are clustered together in spurs. So one should anticipate a somewhat different pattern of subsequent relaxation processes (both spontaneous and induced) for radiation-produced electrons as opposed to photochemically liberated ones. In this respect photobleaching studies of radiation-produced electrons are particularly complex.

5. Photoinduced Spectral Shifts

When a sample of trapped electrons in aqueous or alcohol glasses produced by γ irradiation at 77 K was partially bleached to rid it of trapped electrons which were close to potential reaction partners, photoinduced compensatory spectral shifts were observed (30). These were termed photoshuttling, or photoshuffling, since illumination with blue light caused loss of absorption in the blue edge of the band and a compensatory growth on the red side, and vice versa. These were permanent changes. Three significant inferences can be drawn from those observations. (*a*) One seems forced to accept the notion that the medium provides traps of different depth absorbing in different spectral regions, that is, that the band is heterogeneous. (*b*) Since it occurs equally from its blue as from its red extremities the same type of optical transition (be it bound–bound or bound–free) straddles the whole band. (*c*) The changes are permanent, so subsequent 'digging' to refurbish the original visible spectrum at 77 K did not occur. Furthermore, if refurbishing is normally accomplished by 'seeking' then photolysis must have permanently altered the distribution of available traps.

Unfortunately, photoshuttling does not directly aid in solving the bound–bound *vs.* bound–free issue. Shuttling would be a natural consequence if electrons were photobleached to the quasi-free state and then retrapped (merely by a forced net depopulation of blue traps by blue light, and of red traps by red light). But equally well, if the photoexcited state was bound, the photon energy should be dissipated, at least in part, by causing rotations of the molecules in the walls of the traps, thereby 'softening' those traps that absorbed light. The overall net effect of this would be for blue light to make deep (blue) traps shallower and red light to make shallow (red) traps deeper.

These photoinduced spectral shifts refer to rigid media at 77 K. Quite different results and inferences may be forthcoming in liquids or at higher temperatures.

6. The Visible Band in Aqueous Systems

Figure 1 shows solvated electron data from ref. 31 for aqueous 9.5 *M* LiCl pulse-irradiated at 298, 198, and 93 K and observed immediately after a 10 ns radiation pulse. Notice that the band is much narrower at the middle temperature, whereas the 298 and 93 K bands are very similar, except in intensity. At 298 K the whole band subsequently decayed without a measurable spectral shift. At 77 K a marked spectral shift occurred as indicated in Fig. 2. Absorbance was lost sequentially from the red end. The stable spectrum which was reached was similar to that found at 100 ns at 198 K. This loss was not compensated by growth elsewhere. So the questions arise: (*i*) does this represent preferential chemical reactivity by weakly trapped electrons or (*ii*) were these electrons caught in traps which were close to, and distorted by, the Coulomb field of the concomitant cation?

This loss of a short-lived red wing to the visible band is common to most aqueous glasses. But peculiar to some, including LiCl, is another transient electron absorption band much further in the ir, which will now be mentioned.

7. Infrared-absorbing Electron States in Certain Aqueous Glasses

An isolated and distinct absorption band in the ir has been found to arise in pulse-irradiated LiCl, $MgCl_2$, and ethylene glycol aqueous glasses and in D_2O ice at 77 K (29). If the lineshape is Lorentzian then the ir band maximum is indicated to be at ~3500 nm (0.35 eV) and its half-bandwidth to be ~0.38 eV. It has been shown to arise from a species with the characteristics of a weakly trapped electron. The species, designated e_{ir}^-, decays at 77 K but

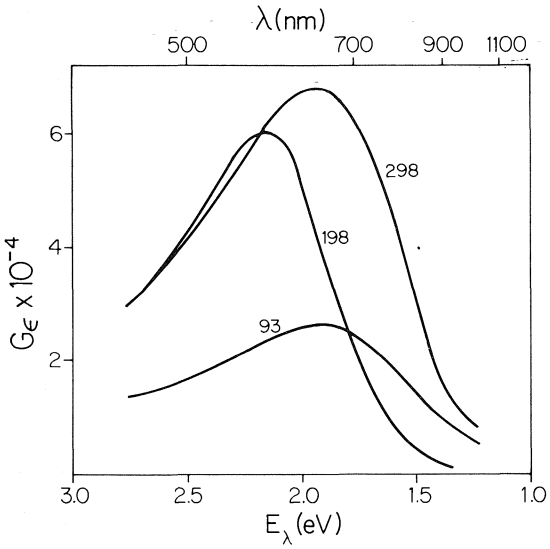

FIG. 1. Temperature dependence of the absorption spectrum of the electron in 9.5 *M* LiCl solution immediately following a 10 ns pulse at 298, 198, and 93 K (data taken from Buxton and Kemsley (31)).

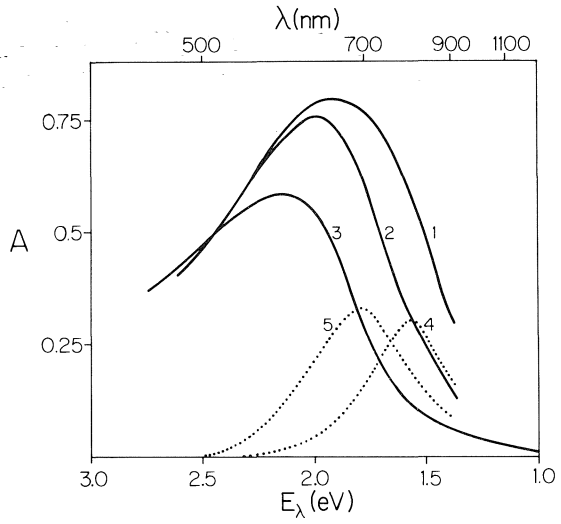

FIG. 2. Time dependence of the absorption spectrum of the electron in 9.5 *M* LiCl glass at 87 K. Curves 1, 2, and 3 were obtained 200 ns, 200 μs, and ~1 h respectively after the irradiation. Curve 4 shows the difference in absorbance between curves 1 and 2, curve 5 the difference between curves 2 and 3 (data from Buxton and Kemsley, private communication).

no compensatory absorption was observed in the visible. Instead luminescence was produced at a rate commensurate with e_{ir}^- tunneling to geminate reaction partners. e_{ir}^- was not observable under the same conditions in OH^-, K_2CO_3, $NaClO_4$, $CaCl_2$, HCOONa, $Mg(ClO_4)_2$, and $Mg(CH_3CO_2)_2$ glasses (29).

Evidently there are at least two spectral changes involved and two types of transient electron states to worry about in aqueous media at low temperatures, and at room temperature the picosecond changes (17) have to be fitted into the picture.

8. Photobleaching of e_t^- in Aqueous Glasses

Gillis and Walker (32) have recently shown that the same infrared-absorbing electron states (e_{ir}^-) as described above are produced with high quantum yield when trapped electrons in LiCl or $MgCl_2$ aqueous glasses at 77 K are subjected to 20 ns pulses of 694 nm light from a laser. These species also produce luminescence centred at ~410 nm as they decay, and are not found in K_2CO_3 or OH^- glasses. We inferred that optical excitation at 694 nm (130 nm on the red side of the band maximum) leads to quasi-free electrons (which then dispose themselves as in pulse radiolysis, but, according to the luminescence kinetics, still undergo geminate reactions). These results certainly support the view that the optical transition on the red side of the band maximum is of the bound–free type; but, as ever, it does not prove it because it is possible for the electron to be thermally released from a bound excited state, or for that state to be autoionising.

LiCl and $MgCl_2$ are the only two glasses of those studied which showed recovery of absorbance at 633 nm (8)[1] and rapid loss of absorbance at 1152 nm (34) when their stable trapped electrons were flash bleached at 694 nm. If we assume that (*a*) 1152 nm would monitor e_{ir}^- plus perhaps the short-lived red wing of the visible band which is formed during pulse radiolysis and maybe also during bleaching, while (*b*) 633 nm would also monitor this red wing plus the stable visible band and (*c*) 442 only the stable visible band, then the loss of 1152 nm absorbance concurrent with formation of 442 and 633 nm absorbance is consistent with some of the e_{ir}^- transforming spontaneously to the stable trapped electron e_t^-. This appears different from the pulse radiolysis situation (29) where growth was not seen at 633 nm as e_{ir}^- decayed; but in that situation part of the red end of the visible band was concurrently being lost.

Why should e_{ir}^- be formed in only 3 of the 10 aqueous glasses which have been studied? Is it a structural property of those particular glasses or does it have a chemical origin? Is it just a difference of time scales? What is the nature of e_{ir}^-? These are all issues currently being examined (35). It is curious that e_{ir}^- is a necessary precursor of the broad luminescence centred at ~410 nm. It is curious because one wonders why quasi-free electrons, or trapped electrons decaying from the red wing of the absorption band, or laser-bleached electrons in OH^- and K_2CO_3 glasses, or any of the melange of geminate electrons which decay during radiolysis, all do not produce luminescence in the visible or near uv which would be observable under similar conditions.

9. Heterogeneous Broadening in Liquid and Solid Phases

Whereas there is strong evidence that the absorption bands in glassy solids are heterogeneously broadened there is no such indication of this for the liquids. Consider the photobleaching results. Hydrated electrons in liquid water at 295 K showed no self-induced transparency or bleaching at 694 nm, and the time taken for the ground state to be repopulated after photoexcitation was estimated to be ≤ 5.5 ps (36). No photoinduced spectral shifts were observable either under those conditions (4). Likewise none were observed for the electron in liquid ammonia at ~220 K. When it was bleached at 610 nm the ground state was repopulated in <5 ps (37), and it was also found to be homogeneously bleached at 1060 nm with the relaxation time estimated to be $\sim 2 \times 10^{-13}$ s (38). Contrast this with various cold solid systems, where (*i*) hole-burning by monochromatic light was found in α-methyltetrahydrofuran (4, 39), ethanol (40), and various aqueous glasses (4) and (*ii*) photoinduced spectral shifts occur with the equilibrated electron spectra (30, 31, 41).

Yet it is striking how similar the electron spectra in the two phases are: as if the solid has a distribution of traps which is just the frozen-in, instantaneous distribution of polarised sites in the liquid. The initial spectra are nearly identical

[1]R. May. Unpublished data.

(see Figs. 1 and 2) and it is merely the loss of the red wing in the glass which results in the equilibrated spectra being different.

Heterogeneity in the solid implies that each electron is stabilised in a trap of a particular and relatively fixed energy. Each is thereby tinted with the characteristic absorption related to that particular energy and absorbs in only a limited region of the overall band. The overall spectrum is the envelope of this substructure. It shows the space-averaged population distribution of trapped electrons and thus parts of it may be selectively bleached.

If the liquid phase band was homogeneously broadened, in the strict sense of having a fine structure to its excited state but a single ground state, then its similarity with the solid phase would be largely fortuitous. So let us suppose the band in the liquid phase is heterogeneous also, but it is a time-averaged spectrum. That is, each electron in the liquid phase is continually and rapidly fluctuating in energy (by a factor of 2 or so) due to atomic and molecular motions of the solvent cage and due to its own wanderings. (By diffusion alone e_s^- in water is displaced, on average, a distance of $(4Dt)^{1/2}$, equal to ~ 0.4 nm, which is more than one solvent molecule away, in the time taken to rotate a solvent molecule.) The spectrum seen is thus the time-averaged, or instantaneous, distribution of these fluctuating electron energies. Since all electrons are alike and contribute equivalently to each part of the spectrum over a very short period of time, there is no possibility for hole-burning or spectral shifts, except during an exposure time which is shorter than the relaxation times of the vibrational and rotational motions which cause the fluctuations in the energy of the ground state. Only for exposure times of the order of 10^{-13} s or less could the band be observed to be heterogeneous in the liquid phase.

10. Extinction Coefficients

It has been pointed out before (4, 42) that when a band is heterogeneous because of a distribution of ground state energies, then only a fraction of the total number of species present will contribute significantly to absorption of light at any wavelength λ. Thus the real extinction coefficient at λ, ε^{hetero}, is greater than the value which is calculated on the basis of the band being homogeneous, ε^{homo}. This evidently should apply to trapped electrons in solids. It should also apply to electron bands in the liquid phase if the band is broadened through a fluctuating ground state electron energy as discussed above; for, although the excited state energy will also fluctuate, in general the transition probability will fluctuate with time, so that at any instant only a fraction of the species present will absorb significantly at λ.

If the substructure bands are narrow and essentially nonoverlapping then the overall band envelope merely shows the population distribution (4). A point on the side of the overall band then does not represent a lower ε than the peak, merely a smaller population density. The narrower the underlying bands are the larger ε^{hetero} becomes. Bleaching was found at 694 nm but not at 633 nm in aqueous and α-methyltetrahydrofuran glasses (4), so one infers substructure bands of less than 1400 cm^{-1} in a band of total width of $\sim 19\,000$ cm^{-1}. This suggests that $\varepsilon^{hetero}/\varepsilon^{homo}$ is greater than 14. Since ε^{homo} is typically evaluated to be 2×10^4 M^{-1} cm^{-1} or more at the band maximum, on the presumption that the band was homogeneous, it follows that the real values may be 3×10^5 M^{-1} cm^{-1} or more. An extinction coefficient of 3×10^5 M^{-1} cm^{-1} is equivalent to an absorption cross section of 5 $Å^2$ which, quite incidentally, is comparable to the cross-sectional area estimated for the charge distribution of the hydrated electron (33).

When should the real (ε^{hetero}) values of extinction coefficient be used? In theoretical calculations, when the oscillator strength is evaluated, ε is coupled with the bandwidth of the particular trap. In yield measurements C and ε are coupled through the $G\varepsilon$ value, so that until the concentration of a particular type of trap has been evaluated ε^{hetero} is not required. However, for photochemical processes (such as bleaching) the absolute value of ε is needed.

Acknowledgements

I am particularly grateful to Drs. H. A. Gillis, R. May, and G. V. Buxton for lengthy discussions I have had with them recently. The financial support of the National Research Council of Canada is appreciated.

1. A. V. Vannikov and V. S. Marevtsev. Int. J. Radiat. Phys. Chem. **5**, 453 (1973).
2. L. M. Dorfman and J. F. Gavlas. *In* Radiation re-

search. *Edited by* O. F. Nygaard, H. I. Adler, and W. K. Sinclair. Academic Press, NY. 1975. p. 326.
3. D. C. WALKER, N. V. KLASSEN, and H. A. GILLIS. Chem. Phys. Lett. **10**, 636 (1971).
4. D. C. WALKER and R. MAY. Int. J. Radiat. Phys. Chem. **6**, 345 (1974).
5. L. P. HAMMETT. *In* Physical organic chemistry. McGraw-Hill, N Y. 1970. p. 235.
6. K. DIMROTH, C. REICHARDT, T. SIEPMANN, and F. BOHLMANN. Ann. Chem. **661**, 1 (1963).
7. R. R. HENTZ and G. A. KENNEY-WALLACE. J. Phys. Chem. **76**, 2931 (1972); **78**, 514 (1974).
8. G. J. FLYNN. Ph.D. Thesis, University of British Columbia, Vancouver, B.C. 1975.
9. L. M. DORFMAN, F. Y. JOU, and R. WAGEMAN. Ber. Bunsenges. Phys. Chem. **75**, 681 (1971).
10. E. A. SHAEDE, L. M. DORFMAN, G. J. FLYNN, and D. C. WALKER. Can. J. Chem. **51**, 3905 (1973).
11. T. K. COOPER, D. C. WALKER, H. A. GILLIS, and N. V. KLASSEN. Can. J. Chem. **51**, 2195 (1973).
12. T. J. KEMP, G. A. SALMON, and P. WARDMAN. *In* Pulse radiolysis. *Edited by* M. Ebert *et al.* Academic Press, London. 1965. p. 247.
13. L. B. MAGNUSSON, J. T. RICHARDS, and J. K. THOMAS. Int. J. Radiat. Phys. Chem. **3**, 295 (1971).
14. B. J. BROWN, N. T. BARKER, and D. F. SANGSTER. J. Phys. Chem. **75**, 3639 (1971).
15. F. S. DAINTON and R. J. WHEWELL. J. Chem. Soc. Chem. Commun. 493 (1974).
16. T. SAWAI and W. H. HAMILL. J. Phys. Chem. **73**, 3452 (1969).
17. P. M. RENTZEPIS, R. P. JONES, and J. JORTNER. Chem. Phys. Lett. **15**, 480 (1972); J. Chem. Phys. **59**, 766 (1973).
18. T. HIGASHIMURA, M. NODA, T. WARASHINA, and H. YOSHIDA. J. Chem. Phys. **53**, 1152 (1970).
19. J. H. BAXENDALE and P. WARDMAN. Nature, **243**, 449 (1971); J. Chem. Soc. Faraday Trans. I, **69**, 584 (1973).
20. N. V. KLASSEN, H. A. GILLIS, G. G. TEATHER, and L. KEVAN. J. Chem. Phys. **62**, 2474 (1975).
21. W. J. CHASE and J. W. HUNT. J. Phys. Chem. **79**, 2835 (1975).
22. (*a*) J. T. RICHARDS and J. K. THOMAS. J. Chem. Phys. **53**, 218 (1970). (*b*) L. KEVAN. J. Chem. Phys. **56**, 838 (1972).
23. H. HASE, T. WARASHINA, M. NODA, A. NAMIKI, and T. HIGASHIMURA. J. Chem. Phys. **57**, 1039 (1972).
24. (*a*) L. GILLES, J. E. ALDRICH, and J. W. HUNT. Nature, **243**, 70 (1973). (*b*) R. S. DIXON, V. J. LOPATA, and C. R. ROY. Int. J. Radiat. Phys. Chem. In press.
25. G. A. KENNEY-WALLACE and C. D. JONAH. Chem. Phys. Lett. **39**, 596 (1976).
26. J. H. BAXENDALE and P. H. G. SHARPE. Chem. Phys. Lett. **41**, 440 (1976).
27. N. V. KLASSEN, H. A. GILLIS, and G. G. TEATHER. J. Phys. Chem. **76**, 3847 (1972).
28. G. V. BUXTON, F. C. R. CATTELL, and F. S. DAINTON. Trans. Faraday Soc. **67**, 687 (1971).
29. G. V. BUXTON, H. A. GILLIS, and N. V. KLASSEN. Chem. Phys. Lett. **32**, 533 (1975); Can. J. Chem. **54**, 367 (1976).
30. G. V. BUXTON, F. S. DAINTON, T. E. LANTZ, and R. P. SARGENT. Trans. Faraday Soc. **66**, 2962 (1970).
31. G. V. BUXTON and K. G. KEMSLEY. J. Chem. Soc. Faraday Trans. I, **71**, 568 (1975).
32. H. A. GILLIS and D. C. WALKER. J. Chem. Phys. **65**, 4590 (1976).
33. J. JORTNER. Radiat. Res. Suppl. **4**, 24 (1964).
34. R. MAY and D. C. WALKER. Chem. Phys. Lett. **30**, 69 (1974).
35. T. Q. NGUYEN and D. C. WALKER. To be published.
36. G. A. KENNEY-WALLACE and D. C. WALKER. J. Chem. Phys. **55**, 447 (1971).
37. J. BELLONI, M. CLERE, P. GOUJOU, and E. SAITO. J. Phys. Chem. **79**, 2848 (1975).
38. D. HUPPERT, P. M. RENTZEPIS, and W. S. STRUVE. J. Phys. Chem. **79**, 2850 (1975).
39. S. L. HAGER and J. E. WILLARD. J. Chem. Phys. **61**, 3244 (1974).
40. A. NAMIKI, M. NODA, and T. HIGASHIMURA. Chem. Phys. Lett. **23**, 402 (1973).
41. S. L. HAGER and J. E. WILLARD. Chem. Phys. Lett. **24**, 102 (1974).
42. D. C. WALKER. *In* Electron–solvent and anion–solvent interactions. *Edited by* L. Kevan and B. Webster. Elsevier, Amsterdam, Holland. 1976. p. 91.

Discussion

J. Jortner: I would like to comment on the problem of homogeneous *vs.* inhomogeneous (heterogeneous) line broadening. Adopting the wellknown concepts of solid state physics homogeneous broadening involves line width originating from optical absorption of a single type of absorbing centre. A Gaussian line shape does not necessarily imply evidence for inhomogeneous broadening. When a single type of centre interacts with lattice (or liquid) phonons two types of electron–phonon coupling should be distinguished. In the weak coupling limit a narrow zero-phonon line is exhibited, its width being determined by T_1 (level depletion via relaxation) process, T_2 type (line broadening) processes as well as by inhomogeneous broadening. The total line width is 10^{-2}–$1\ cm^{-1}$, depending on temperature. The second limit is the strong electron–phonon coupling, a situation which we will be concerned with here. In this case the line width is Gaussian, without invoking inhomogeneous broadening. Such situations are commonly encountered in solids, *e.g.* F centres, alkali halides, and rare-gas solids. To distinguish between homogeneous or inhomogeneous broadening one can use hole burning methods or the technique of photon echoes. Hole burning experiments on trapped electrons in solids provide conclusive evidence for inhomogeneous broadening. It should, however, be recalled that the hole burned by a narrow-band optical excitation is wide, ~ 0.1 eV, which corresponds to the occurrence of bleaching of a phonon-broadened single centre. In liquids the experimental evidence for the Bell group provides evidence for homogeneous broadening of the solvated electron band in NH_3 in the range 1.6 to 0.8 μm.

D. C. Walker: My point is that the bands in liquids at 295 K and glasses at 77 K are essentially the same; so if we accept that there are traps of different depths in the solids then a comparable distribution of ground state energies seems likely for the liquids.

J. Jortner: It is apparent that the uncertainty argument for the line broadening $\sim 10^{-2}$ eV of individual 'homogeneous bonds' does not apply for the situation of strong

phonon coupling. The absorption line widths shown by Kestner for a single trapping centre are ~ 0.2 eV broad.

D. C. Walker: I should have talked only about substructure bands whose width is seen to be < 0.17 eV from bleaching studies in glasses, rather than use the only relaxation time measurement (which refers to liquid) to make deductions about the possible band widths.

J. Jortner: Finally, I would like to comment on Walker's analysis of the oscillator strengths for the optical absorption. When phonon broadening prevails the intensity has to be summed over all vibronic transitions. The sum rule for Franck–Condon vibrational overlap factors will result in the electronic term which is extracted from experiment and corroborated with theoretical calculations.

D. C. Walker: Regarding the oscillator strengths, they are calculated for each trap and refer to the substructure band. Since their band width is much less than the overall band envelope the appropriate extinction coefficient is correspondingly larger. In the limit, if one bleaches away (or preferentially destroys by reaction) all trapped electrons except those few which dominate the absorbance at λ_1 then you still have nearly the same absorbance at λ_1 but the extinction coefficient evaluated from it is based on the small concentration of traps absorbing at λ_1.

A. C. Albrecht: The idea that the broad electron (statically trapped?) absorption band actually is 'heterogeneous' and reflects a distribution of traps seems to contradict the fact that the transient photoconductivity signals (from trapped electrons in nonpolar glasses), once generated by red (or far-red) excitation, are then fully removed in the visible and near ultraviolet. This is contrary to spectral hole burning. A view consistent with both observations is to say that those electrons primarily responsible for the absorption effects are not the ones giving the transient photoelectric signals.

D. C. Walker: However, hole burning of trapped electron bands has been seen under laser excitation in nonpolar (MTHF and 3MP) media in different regions of their spectra, including 694, 1338, and ~ 2300 nm.

A. C. Albrecht: Another point is that in explaining the energy distribution in absorption spectra a bias always seems to creep in which speaks in terms of environmental effects on the ground state of the trapped electron. In fact such effects are almost certainly actually dominant in the *excited* state of the electron, quasifree, perhaps, and it is there where one should seek the origin of the spectral shifts. If the spectrally significant shifts of the ground state are to be seen (not just of the order of kT) then significant entropy changes must accompany this as well, in order to justify a detectable population of species having a spectrally important difference in ground state energies. These comments of course refer only to spectra of an equilibrated sample, not one which is still developing in time.

D. C. Walker: Yes, I agree that one should consider fluctuations in the excited state energies too; but, since small (though significant) permanent shifts in the absorption spectrum can be caused by bleaching from either extreme of the band, it seems to be possible to permanently alter the distribution of occupied traps.

P. M. Rentzepis: In relation to homogeneity, it has been shown by Huppert *et al.* that bleaching at several positions of the band of methylamine–Na between 700 to 1400 nm shows homogeneous bleaching throughout the band.

D. C. Walker: A band will appear to be homogeneous, and bleach throughout, whenever the observation time is significantly greater than the inverse of the frequency of fluctuation of the ground state energy.

S. A. Rice: Photoconductance spectra of electrons in glasses implicate excited mobile states in a continuum. In most cases the photoconductance and optical spectra either approximately coincide or the former is blue-shifted (0.2–0.5 eV) and modified compared to the latter. Thus either bound–continuum or this and bound–bound (on the low energy tail) transitions seem to occur for electrons in glasses. Such a decomposition is in agreement with the qualitative details of the analysis by P. Delahay. However, the onset of photoconductance is at much lower energies than suggested by Delahay. He used a model based on hydrogenic photoionization in an infinite medium, which Huang and Ellison have questioned.

D. C. Walker: As you know, I have not been persuaded that your photoconductivity spectra, when computed on the basis of photoconduction electrons per *absorbed* photon, are coincident with the absorption spectrum or that they show maxima which are blue-shifted. However, one could imagine each substructure band to consist of a large bound–bound part with a long, low intensity, high energy tail which is a continuum in nature. These tails would give rise to photoconductivity, with low quantum yield, *throughout* the main absorption band and sum together for the overall high energy tail which Delahay has discussed.

S. A. Rice: The experiments which have been cited to justify a large variation of trap depths for the electron in glasses are not unequivocal. Indeed the postulate of bound–bound ($1s \rightarrow 2p$) transitions in glasses (where both states depend on trap depth) to explain the absorption spectrum in terms trap depth variations requires these to be ~ 2–4 eV. Tunnelling of the trapped electron to scavengers should give a measure of the binding energy for the electrons since less deeply trapped electrons tunnel faster. There seem to be no spectral changes (with different scavenger concentration or thus of different electron concentrations (Marshall, Pilling, and Rice). Finally, if trap depths do not vary by more than $\sim 10kT$, the trapped electron absorption spectrum must either arise from the nature of the excited state or from large fluctuations in the ground electron wavefunction due to structural variations of the electron trap walls. The latter would not necessarily have a marked effect on the electron trap depth. However, the different ground state electron wavefunctions should have very different transition probabilities to the continuum states, though not necessarily for transitions to the bound states.

D. C. Walker: Certainly, as the ground state energy changes in accordance with variations in the molecular configurations in the trap walls so will the energy of the excited state vary and this must be taken into account in deducing the absorption band.

R. S. Dixon: In discussing low temperature alcohols you rightly pointed out the three different absorption spectra of electrons measured at different times, that is the broad infrared absorption attributed to weakly solvated electrons, the final spectrum attributed to fully solvated electrons, and an intermediate spectrum peaking at ~ 700 nm. The evidence for the latter is good; it has been seen in work by Baxendale and Wardman and in our own laboratories. However, you seemed to imply that this was some intermediate state in the solvation process, *i.e.* that infrared electrons first decayed to this intermediate state before finally decaying to fully solvated electrons. Do you think this is what happens?

D. C. Walker: I did not mean to imply that there was direct evidence for all electrons to pass through an intermediate state whose absorption band was centred at 700 nm, only that the overall absorption band peaks there transiently.

A pulse radiolysis study of solvated electrons in dilute solutions of polar liquids in nonpolar solvents

J. H. BAXENDALE

Chemistry Department, University of Manchester, Manchester M13 9PL, England

Received September 27, 1976

J. H. BAXENDALE. Can. J. Chem. **55**, 1996 (1977).

Measurements of the conductivities following electron pulse irradiation of dilute solutions of ethanol, *n*-propanol, *tert*-butanol, or dimethyl sulphoxide in *n*-hexane, cyclohexane, or *i*-octane are quantitatively consistent with the existence of equilibria between electrons in the hydrocarbon and electrons solvated by dimers of the polar molecules. With dimethylformamide solutions in alkanes the equilibrium could be with the monomeric anion of the solute but this assignment is not unequivocal. Absorption spectra of e_s^- in *n*-hexane solutions of ethanol and of *tert*-butanol have been obtained.

J. H. BAXENDALE. Can. J. Chem. **55**, 1996 (1977).

Des mesures de conductivité à la suite de l'irradiation pulsée électronique de solutions diluées d'éthanol, *n*-propanol, *tert*-butanol ou diméthylsulfoxyde dans les *n*-hexane, cyclohexane ou *i*-octane, sont en accord quantitatifs avec l'existence d'un équilibre entre les électrons dans l'hydrocarbure et les électrons solvatés par les dimères des molécules polaires. Avec des solutions de diméthylformamide dans les alcanes, il est possible que l'équilibre existe avec l'anion monomère du soluté mais cette attribution n'est pas sans équivoque. On a obtenu des spectres d'absorption de e_s^- dans des solutions d'éthanol et de *tert*-butanol dans le *n*-hexane.

[Traduit par le journal]

Introduction

There is now a large body of information available on solvated electrons, e_s^-, in a wide variety of pure liquids from which it is clear that, in general, the polarity of the liquid is the major factor which determines the properties of e_s^-. Early observations (1) on mixtures of hydrocarbons and alcohols designed to produce liquids of intermediate polarity showed that as little as 4% v/v of methanol in cyclohexane gives an absorption spectrum similar to that of e_s^- in pure methanol and later work (2) showed that for e_s^- in *n*-hexane containing 2% methanol and in pure methanol the two spectra were almost indistinguishable. Most studies on such polar–nonpolar mixtures have been confined to high concentrations of alcohols in alkanes (3–5) but it has been shown in a detailed spectral examination (2) that changes in the far infrared absorption of e_s^- in *n*-hexane occur in the presence of a few tenths of 1% of *n*-propanol or of water. Simultaneously appreciable changes in ion mobility occur (6), both effects being attributed to electron solvation by the added polar molecules.

It is clear from the many thermodynamic and spectroscopic observations *on alkane–alcohol mixtures* that they do not give homogeneous liquids of intermediate polarities but that at low concentrations of the polar component, the latter forms aggregates the size of which is a function of the concentration.

The present report describes observations on the ion mobility and to a lesser extent the spectral changes occurring in the alkanes *n*-hexane, cyclohexane, and *i*-octane when small amounts of ethanol, *n*-propanol, *tert*-butanol, and several other polar materials are added. A preliminary report on some of this work has already been presented (7).

Experimental

The alkanes and alcohols were purified as described earlier (2). Dimethylformamide (DMF) was the quality 'for infrared spectroscopy' and was treated with molecular sieve 4A before use. Dimethyl sulfoxide (DMSO) was purified by distillation[1] and was shaken three times with five times its volume of alkane to give finally a saturated solution in the alkane which was used as a stock solution. The concentrations of these stock solutions were determined spectroscopically after dilution with ethanol, and for *n*-hexane, cyclohexane, and *i*-octane were found to be 34, 52, and 37 m*M* respectively at 20 ± 2°C.

The liquids were deaerated by purging and shaking with pure argon and introduced into the optical or conductivity cell by argon pressure. The apparatus and techniques for the optical and conductivity measurements

[1]Kindly supplied by Dr. A. M. Koulkes-Pujo.

have been described previously (2, 6). A 10 MeV linear accelerator introduced 5 or 10 ns pulses of radiation, electrons for *n*-hexane and cyclohexane, X rays from a tungsten target for *i*-octane. Doses of 1–2 krad were used for the optical and 0.1–0.5 krad for the conductivity measurements. All experiments were carried out at room temperature, 20 ± 2°C.

Results

Mobilities in Alcohol–Alkane Mixtures

Typical variations in the immediate post-pulse ion mobility sum as the alcohol concentration increases are shown for *n*-propanol in cyclohexane and in *n*-hexane in Fig. 1. The mobilities are calculated by extrapolating the CRO traces back to the middle of the pulse to give the immediate post-pulse conductivities. In constant experimental conditions (dose, cell geometry, and applied voltage) these conductivities are proportional to the mobility sum of the ions present and can be transformed into absolute mobilities using the known values in the pure hydrocarbons (8) as standards. The curves for ethanol and *tert*-butanol are similar, the only differences being in the effective concentration ranges. Thus to reduce the mobility sum to one half in cyclohexane requires *ca.* 45 m*M* *n*-propanol, 25 m*M* ethanol, and 100 m*M* *tert*-butanol. As previously reported (7) the behaviour of methanol is quite different. In *i*-octane little effect is produced by 40 m*M* but between 40 and 60 m*M* there is a precipitous fall in mobility to almost zero.

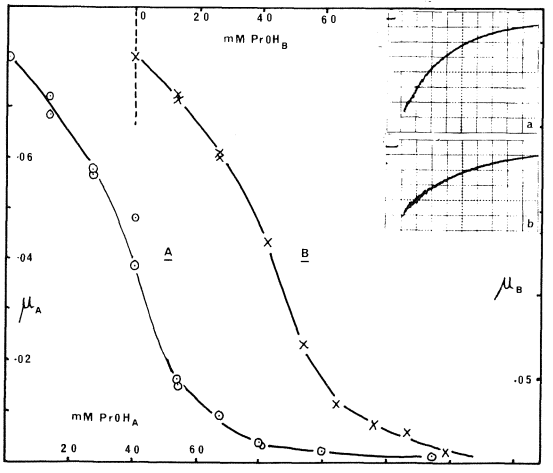

FIG. 1. Variation in mobility sum of ions, μ (cm^2 V^{-1} s^{-1}) in *n*-hexane (*A*) and cyclohexane (*B*) solutions of *n*-propanol. Inset: CRO traces on 10 mV and 100 ns/div.: (*a*) *n*-hexane + 27 m*M* propanol; (*b*) *n*-hexane + 40 m*M* propanol.

In the pure hydrocarbons it is well established that the mobility sum of the ions is determined almost entirely by the very high value of the electron mobility. When alcohols are added, the above decreases in conductivity are accompanied by changes in optical absorption (see below and ref. 2) which indicates that electron solvation by alcohol occurs. Such solvated electrons, would have the low mobility of normal ions, *i.e. ca.* 10^{-3} cm^2 V^{-1} s^{-1} compared with 0.1 to 10 for the electrons in the pure hydrocarbon. Hence even when the conductivity has been decreased to 10% of that of the pure hydrocarbon by the addition of alcohol, the contribution of the alcohol solvated electrons to this must be small. We conclude that in these conditions not all the electrons have been solvated by alcohol and the residual mobile 'hydrocarbon electrons' are still largely responsible for the conductivity. This conclusion is supported by the rates of decay of the conducting species in this range of alcohol concentrations, which are very much higher than expected from those of normal ions. The observations therefore suggest that there is an equilibrium established between electrons in the hydrocarbon and electrons associated with alcohol molecules.

Single molecules of alcohol are unlikely to be involved since the electron affinity is unfavourable and it is probable that the solvation process involves the diffusion of the electron to alcohol clusters (2). Calorimetric, infrared, and osmotic measurements (9–13) indicate that beyond *ca.* 100 m*M* alcohol tetramers are predominant. It is generally agreed that at lower concentrations more than one associated species may be present and there is specific evidence for the presence of dimers (12). Thus if solvation is by a cluster A_n we will have the equilibria

$$[1] \qquad nA \rightleftharpoons A_n \qquad K_n$$

$$[2] \qquad e_h^- + A_n \rightleftharpoons e_a^- \qquad K_e$$

where e_h^- and e_a^- are the hydrocarbon and alcohol solvated electrons. If the extent of cluster formation is small, these equations give

$$[3] \qquad [e_a^-]/[e_h^-] = K_e K_n [A]^n$$

Accepting the above conclusion that the measured mobilities at different alcohol concentrations are determined by only e_h^- and that the

reduction from μ_0 in pure hydrocarbon to μ_c at alcohol concentration c is due entirely to a reduction in $[e_h^-]$, then

$$[e_h^-]_0/[e_h^-]_c = \mu_0/\mu_c$$

From [3] above it follows that

$$[e_a^-]/[e_h^-] = (\mu_0 - \mu_c)/\mu_c = K_e K_n [A]^n$$

Figures 2, 3, and 4 and previous data (7) show that the measurements on ethanol, *n*-propanol, and *tert*-butanol in *n*-hexane or cyclohexane or *i*-octane are consistent with this interpretation for a value of $n = 2$ at least up to alcohol concentrations which reduce the mobility to one half of its original value and sometimes to higher concentrations. Deviations which occur at higher concentrations of ethanol and *n*-propanol may arise because of the increasing importance of larger clusters. Values of $K_e K_n$ derived from the lines in these figures are given in Table 1.

Although there is evidence for the presence of alcohol dimers at these low concentrations, unfortunately reliable values of K_n are not yet available because of experimental difficulties. However, it is generally agreed that the extent of dimer formation is small as required by the above analysis.

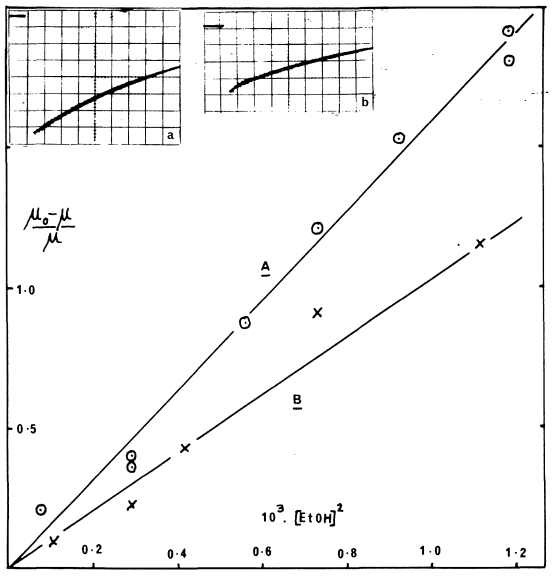

FIG. 2. Mobility – concentration relationship for cyclohexane (*A*) and *n*-hexane (*B*) solutions of ethanol. Inset: CRO traces on 50 ns, 20 mV/div.: (*a*) pure cyclohexane; (*b*) cyclohexane + 24 m*M* ethanol.

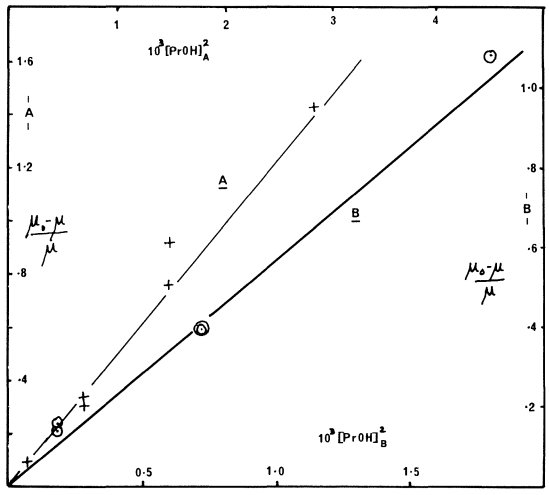

FIG. 3. Mobility – concentration relationship for cyclohexane (*A*) and *n*-hexane (*B*) solutions of *n*-propanol.

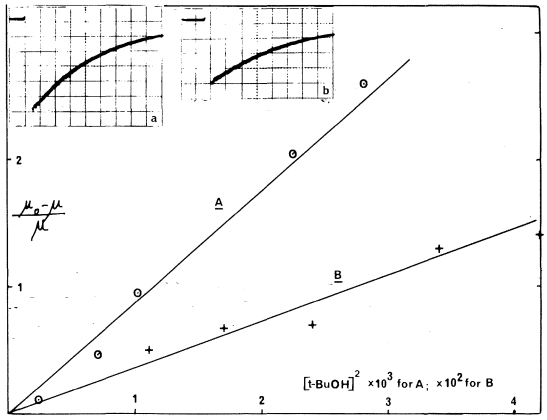

FIG. 4. Mobility – concentration relationship for *n*-hexane (*A*) and *i*-octane (*B*) solutions of *tert*-butanol. Inset: CRO traces on 20 mV and 50 ns/div.: (*a*) pure *n*-hexane; (*b*) *n*-hexane + 26 m*M* *tert*-butanol.

Spectra in Hexane–Alcohol Mixtures

The higher concentrations of e_s^- required to observe spectra in hydrocarbons reduce the lifetime of e_s^- because of their removal by the second order neutralisation reaction. With the limited response time of the present monitoring equipment, this short lifetime makes the observation of spectra difficult except for hydrocarbons such as *n*-hexane in which e^- has a relatively low mobility, and observations with alcohols have been limited to this solvent. Spectra of *n*-hexane + *n*-propanol and *n*-hexane + methanol mixtures have been reported previously (2, 7) and those of ethanol and *tert*-

TABLE 1. Values of K_eK_n for various hydrocarbon solutions

	Ethanol	*n*-Propanol	*tert*-Butanol	DMSO	DMF	H_2O
n-Hexane	1000	570	880	7.4×10^4	135	
Cyclohexane	1600	480	120	2.0×10^4	200	3.4×10^5
i-Octane	340	230	36	1.3×10^4	70	

NOTE: For DMF the values are for K_e assuming electron attachment to monomer. For H_2O the value of K_eK_n assumes the concentration is proportional to the water vapour pressure over the solution.

butanol are given in Figs. 5 and 6. The important point is that, assuming the present analysis in terms of alcohol dimers, for the concentration ranges in which solvation by the dimer is presumed to be considerable, *i.e.* where mobilities are appreciably less than those in the pure hydrocarbon, the important spectral changes occur beyond 1500 nm and are out of the range of the detection equipment. The much larger changes seen around 1000 nm must be due to solvation by larger clusters of alcohol.

Mobilities in Alkanes + DMSO

Much smaller quantities of DMSO are effective in reducing the mobility than is the case for alcohols. Thus about 7 m*M* is sufficient to halve it in cyclohexane. Again the data are consistent with solvation by a dimer of DMSO as is shown in Fig. 7 and the value of K_eK_n, which is much bigger, is listed in Table 1.

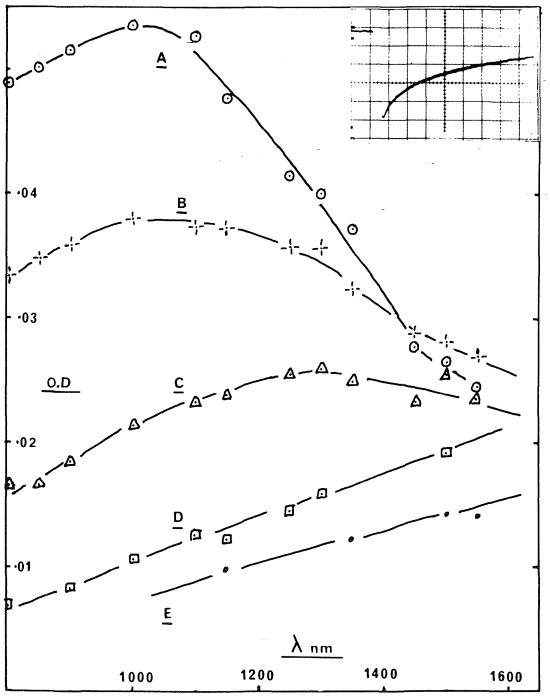

FIG. 5. Spectra of e_s^- in *n*-hexane solutions of ethanol. Inset: CRO trace at 1000 nm on 50 ns/div. for 66 m*M* ethanol.

Mobilities in Alkanes + DMF

DMF is also more effective than the alcohols as shown in Fig. 8 but in contrast to these and to DMSO the data do not fit the analysis in terms of a dimer. Figure 8 is consistent with electron capture by single molecules of DMF. Equilibrium between electrons in a hydrocarbon and electrons on a solute has been observed previously with CO_2 (14) and biphenyl (15) as solutes. However, in the present system this interpretation is not unequivocal since if for example almost all the DMF is present as a single type of cluster over the concentration range used (*i.e.* if K_n is high) then the same behaviour would be observed. Figure 8 gives the value of K_e and the value in Table 1 has been calculated assuming $n = 1$.

Water + Cyclohexane

We have previously reported (2) that appreciable spectral shifts occur in the e_s^- absorption when *n*-hexane is saturated with water even though the concentration of the latter is only *ca.* 4 m*M*. As can be seen from Fig. 9 the same is true for cyclohexane and the peak at *ca.* 1400 nm is similar to that in *n*-hexane.

Ion mobilities were also measured at various water concentrations, the latter being obtained by saturating the cyclohexane with argon containing water vapour at various water vapour pressures. The results are given in Fig. 10. It will be seen that in water saturated solution the mobility is decreased by a factor of about six. Assuming that the solution concentration is proportional to the partial pressure of water vapour and plotting as before, it will be seen that up to 60% of saturation, the data are again consistent with solvation by a dimer. However, the assumption is of doubtful validity and a reliable concentration – vapour pressure relationship is required for a more confident analysis. Data at present available are inconsistent.

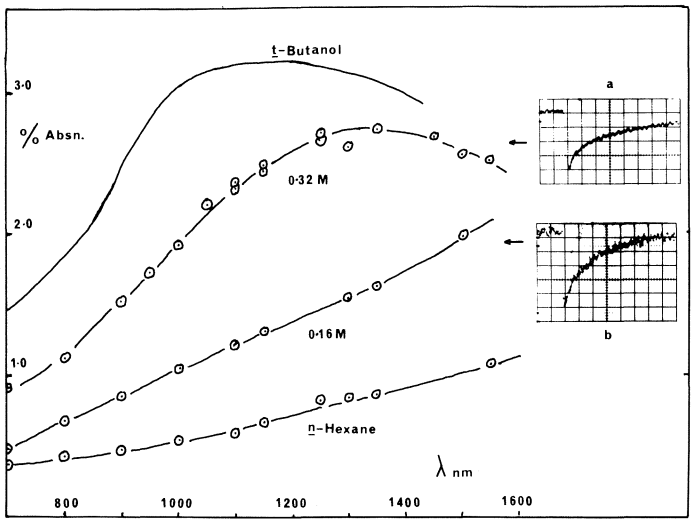

FIG. 6. Spectra of e_s^- in *n*-hexane solutions of *tert*-butanol. Inset: CRO traces at 1350 nm, 50 ns/div.: (*a*) 0.32 *M tert*-butanol, 50 mV/div.; (*b*) 0.16 *M tert*-butanol, 20 mV/div.

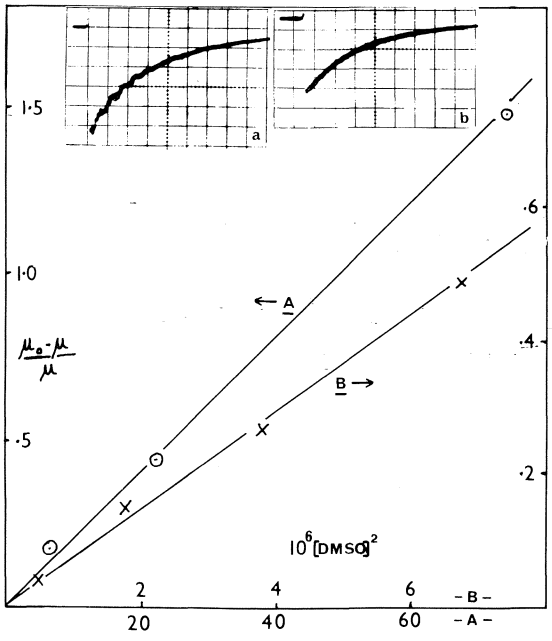

FIG. 7. Mobility – concentration relationship for DMSO in (*A*) cyclohexane and (*B*) *n*-hexane. Inset: CRO traces on 50 mV, 100 ns/div.: (*a*) pure *n*-hexane; (*b*) 2.5 m*M* DMSO in *n*-hexane.

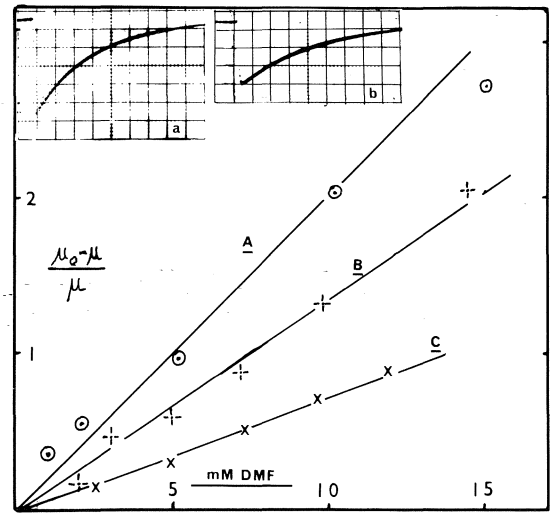

FIG. 8. Mobility – concentration relationship for solutions of DMF in (*A*) cyclohexane, (*B*) *n*-hexane, (*C*) *i*-octane. Inset: CRO traces on 100 ns/div.: (*a*) pure cyclohexane, 50 mV/div.; (*b*) 15 m*M* DMF in cyclohexane, 20 mV/div.

Other Solutes

Preliminary measurements indicate that ethyl acetate does not lower the measured mobility in cyclohexane up to *ca.* 100 m*M* while diethylamine at 1% v/v (137 m*M*) decreases the mobility to 57% of that in the pure hydrocarbon. If dimer solvation is again involved, this indicates a lower value of K_eK_n (*ca.* 40) than for any of the alcohols in cyclohexane.

Discussion

The present results strongly suggest that solvation of electrons by dimers of alcohols occurs in these dilute alkane alcohol mixtures. As mentioned above, thermodynamic and spectro-

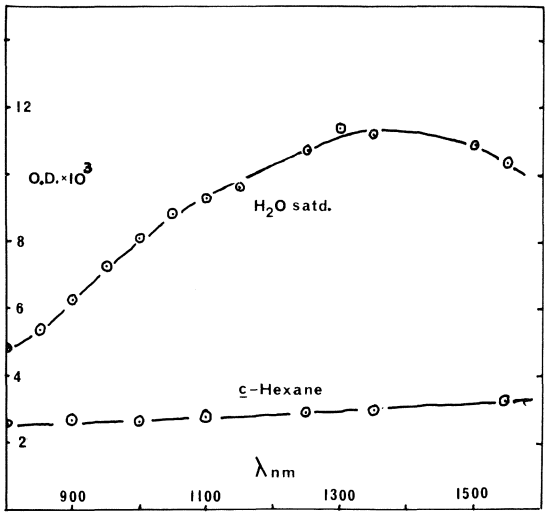

FIG. 9. Absorption spectra of e_s^- in cyclohexane and water saturated cyclohexane.

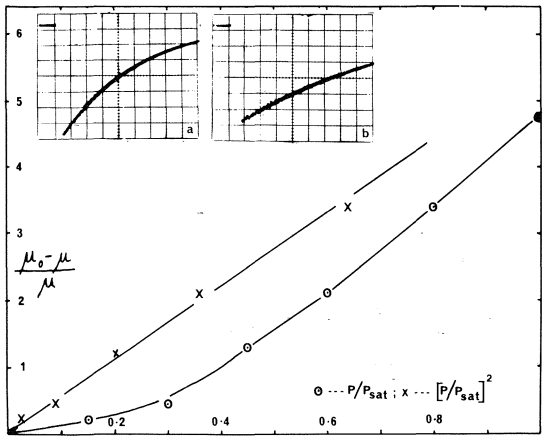

FIG. 10. Mobility variation for cyclohexane equilibrated with water vapour over a range of partial pressures P. P_{sat} is the saturated water vapour pressure. Inset: CRO traces on 50 ns/div. (*a*) pure cyclohexane, on 20 mV/div.; (*b*) cyclohexane equilibrated with 45% saturated water vapour, on 10 mV/div.

scopic investigations would support the presence of such dimers in mixtures of the concentrations used here, before the introduction of the electrons. In the spectral observations reported here the electron half-lives are at least *ca.* 100 ns in the mixtures and in this time there are no observable changes in the absorption spectra from those found immediately after the pulse. This is important since it indicates that the solvated state formed at the shortest time we can observe remains unchanged throughout the lifetime of the electron. Any subsequent aggregation of polar molecules would lead to a blue shift in the spectrum. As has been pointed out previously (2, 16) at diffusion controlled rates and concentrations of 10–100 mM of alcohol, the time required for further addition of alcohol is of the order 2–20 ns, so that the process is not restricted by the lifetime of the dimer solvated electron.

It appears (17) that theoretical calculations indicate that for water molecules in the gas phase electron solvation by four molecules would not give a stable species, and if this is the case it is very unlikely that solvation by an alcohol dimer would occur in the gas phase. Hence if the present analysis in terms of dimer solvation is correct, the stability in the hydrocarbons must derive from the interaction of the solvated species with the hydrocarbon continuum.

Although neither the alcohol dimer nor the tetramer solvated electron would appear to be stable entities in the gas phase, calculations on water (18) indicate that here the tetramer species could be more stable by *ca.* 1 eV. Hence once the dimer is formed it would be expected to acquire further alcohol molecules as envisaged by Mozumder (1b). However, it seems that this does not occur and a possible explanation is that the electron dissociation from the dimer is extremely rapid, *i.e.* the equilibrium solvated state has a short dynamic life, and the time required for aggregation is not available. Confirmation of this must await the determination of the values of K_n which will then allow K_e to be calculated and hence the electron dissociation rate.

It is interesting to note that the absorption spectrum of e_s^- in water saturated cyclohexane closely resembles that of e_s^- in D_2O vapour at 523 K when the gas density is 0.022 (17), in that it shows the same broad absorption with a peak at *ca.* 1400 nm.

In a recent treatment of the energetics of water clusters (19) the free energies of formation of various clusters have been derived from which the extent of dimer, trimer, etc. formation in the above D_2O vapour can be calculated. These data indicate that the concentrations of dimer, trimer, and tetramer present in these conditions are approximately 5 mM, 0.5 mM, and 0.01 mM respectively. It seems possible that, as suggested for cyclohexane (although still to be confirmed

by measurements of water concentrations), electrons in this vapour phase are also solvated by water dimers and that an equilibrium state exists between these and quasi-free electrons. Since at this density the bulk dielectric constant of the vapour will be of the same order as that of cyclohexane, very similar energetics and hence spectra would be expected.

It will be noted from Table 1 that with the exception of cyclohexane + ethanol the values of K_eK_n decrease in the order *n*-hexane, cyclohexane, *i*-octane, but the variation among the hydrocarbons for any one solvent except *tert*-butanol is at most a factor of six. It is to be expected that K_n will not change greatly with hydrocarbon and the same appears to be the case for K_e. A major factor determining K_e will be the free energy of solvation of the electron in the hydrocarbon (14) and it would seem that this varies little among these three hydrocarbons. The values of K_e for DMF are consistent with this conclusion.

Also, for any one hydrocarbon K_eK_n in general increases with increase in polarity of the solute which would be expected since this will increase K_e through increased electron solvation energy by the dimers, and K_n through increased association of the solute. The DMF system gives K_e directly and may lend itself to a detailed treatment such as has been carried out for CO_2 (8) to yield important thermodynamic information about the electron in these solvents.

1. T. J. KEMP, G. A. SALMON, and P. WARDMAN. Pulse radiolysis. Academic Press, New York. 1965. p. 247.
2. J. H. BAXENDALE and E. J. RASBURN. J. Chem. Soc. Faraday Trans. **70**, 705 (1974).
3. G. BECK and J. K. THOMAS. J. Chem. Phys. **57**, 3649 (1972).
4. B. J. BROWN, N. T. BARKER, and D. F. SANGSTER. Aust. J. Chem. **26**, 2089 (1973).
5. J. B. WEINSTEIN and R. F. FIRESTONE. J. Phys. Chem. **79**, 1322 (1975).
6. J. H. BAXENDALE, J. P. KEENE, and E. J. RASBURN. J. Chem. Soc. Faraday Trans. **70**, 718 (1974).
7. J. H. BAXENDALE and P. H. G. SHARPE. Chem. Phys. Lett. **41**, 440 (1976).
8. A. O. ALLEN and R. A. HOLROYD. J. Phys. Chem. **78**, 796 (1974).
9. B. D. ANDERSON, J. H. RYTTING, S. LINDENBAUM, and T. HIGUCHI. J. Phys. Chem. **9**, 2340 (1975).
10. A. N. FLETCHER. J. Phys. Chem. **76**, 2562 (1972) and earlier papers.
11. R. M. HAMMAKER, R. M. CLEGG, and L. K. PATTERSON. J. Phys. Chem. **76**, 1839 (1972).
12. T. S. S. R. MURTY. Can. J. Chem. **48**, 184 (1970).
13. R. AVEYARD, B. J. BRISCOE, and J. CHAPMAN. J. Chem. Soc. Faraday Trans. I, **69**, 1772 (1973).
14. R. A. HOLROYD, T. E. GANGWER, and A. O. ALLEN. Chem. Phys. Lett. **31**, 520 (1975).
15. J. M. WARMAN, M. P. DE MASS, E. ZADOR, and A. HUMMEL. Chem. Phys. Lett. **35**, 383 (1975).
16. A. MOZUMDER. J. Phys. Chem. **76**, 3824 (1972).
17. A. GAATHON, G. CZAPSKI, and J. JORTNER. J. Chem. Phys. **58**, 2648 (1973).
18. G. HOWAT and B. C. WEBSTER. J. Phys. Chem. **76**, 3714 (1972).
19. J. C. OWICKI, L. L. SHIPMAN, and H. A. SCHERAGA. J. Phys. Chem. **79**, 1794 (1975).

Discussion

J. M. Warman: Have you carried out a temperature study of the effect of alcohols on the mobility since this would provide firstly very interesting thermodynamic information about the trapping site and might also give an indication as to whether the nature of the site changes with concentration?

J. H. Baxendale: Not as yet. It is not so simple since to get the interesting information, the temperature dependence of the K_a are required, and even good values at room temperature are not yet available.

J. W. Chase: What is special about methanol? Why does it have a different power law than the other additives.

J. H. Baxendale: I think it is merely a matter of the values of K_a for the clusters of various sizes. These are such that the onset of larger clusters sets in suddenly over the critical concentration range.

W. F. Schmidt: How do you exclude any influence of the added alcohol on the initial charge carrier yield, especially in the higher yield liquid isooctane?

J. H. Baxendale: We have shown previously (2) that the free ion yield in *n*-hexane is changed little by 200 m*M* *n*-propanol. In view of the parallel behaviour of the other hydrocarbons, it seems unlikely to be an important factor, but I agree this requires confirmation.

Electron in cold alcohols: a pulse radiolysis study in ethanol

L. GILLES, M. R. BONO, AND M. SCHMIDT

Centre d'Etudes Nucleaires de Saclay, DRA/SRIRMA, B.P. No. 2, 91190 Gif-sur-Yvette, France

Received September 27, 1976

L. GILLES, M. R. BONO, and M. SCHMIDT. Can. J. Chem. **55**, 2003 (1977).

The pulse radiolysis of cold ethanol near its freezing point shows 'partly solvated' states of the electron with transient spectra whose maxima vary with time. It is shown that the determination of the solvation times of the electron can depend strongly on the wavelength considered; thus an explanation could be given for the different values obtained by Chase and Hunt at $\lambda = 1300$ and $\lambda = 1050$ nm.

L. GILLES, M. R. BONO et M. SCHMIDT. Can J. Chem. **55**, 2003 (1977).

La radiolyse pulsée de l'éthanol à basse température, près de son point de fusion, montre l'existence d'électrons 'partiellement solvatés' dont les spectres d'absorption varient avec le temps. La détermination des temps de solvatation de l'électron peut donc dépendre de la longueur d'onde choisie pour en effectuer la mesure: on expliquerait ainsi les différentes valeurs obtenues par Chase et Hunt aux longueurs d'onde de 1300 et 1050 nm.

Introduction

Fueki *et al.* (1) in their semicontinuum model have pointed out the importance of the microscopic viscosity in calculating the relaxation time for orientation of the dipoles of polar molecules such as alcohols. Even though the agreement between experimental (2) and calculated values was not perfect, the theoretical curves predicted the temperature dependence observed for the solvation times of the electron, $\tau(s)$, and it appeared that the macroscopic viscosity was a good approximation to the microscopic viscosity, at least for methyl, ethyl, and *n*-propyl alcohols.

In recent papers Chase and Hunt (3) on the one hand and Kenney-Wallace and Jonah (4) on the other have shown that in normal aliphatic alcohols, $\tau(s)$ measured at room temperature increased with increasing chain length. For each alcohol, they have correlated $\tau(s)$ with $\tau(2)$, the corresponding dielectric relaxation time associated with the rotation of the free molecules.

In this case since the rotational relaxation of the unassociated molecules depends, according to the Debye equation, on the viscosity of the medium one would expect that for a given alcohol $\tau(s)$ would vary with temperature in a similar way to the viscosity. This behaviour has been observed in the case of liquid *n*-propanol at low temperatures by Baxendale and Wardman (5).

On the same basis ($\tau(s)$ linked to $\tau(2)$) one can try to correlate the solvation times for different alcohols at a given viscosity with the chain length of these molecules: for linear aliphatic alcohols (the only ones considered here) the solvation times determined at a given viscosity should increase with the chain length.

The results of Chase and Hunt (3) for methanol, ethanol, *n*-propanol, and *n*-butanol obtained in the temperature range -65 to $+60°C$ and those of Kenney-Wallace and Jonah (4) measured at room temperature for alcohols having from 2 to 10 carbon atoms allow this comparison to be made. In Table 1 the values of $\tau(s)$ measured by Chase and Hunt are listed together with the viscosities reported by Komarenko *et al.* (6) for the same temperatures. The values of $\tau(s)$ were obtained from Arrhenius plots of the rate constants determined for the decay of absorption measured at 1300 nm (methanol, ethanol, *n*-propanol) or from the increase of absorption measured at 600 nm (*n*-butanol). When measured, values of $\tau(s)$ obtained by Chase and Hunt at both 600 and 1300 nm were roughly similar, but the values measured at 1050 nm were different (Table 1), a point which will be considered later.

The results given in Table 1 for 600 and 1300 nm merit two remarks.

(1) For viscosities between 1.1 and 2.2 cP the solvation times are the same within the limits of experimental error for the first three alcohols considered or, in other words, the relaxation time of these molecules is independent of their size.

(2) For values higher than 2.2 cP the results obtained for the four alcohols at the same

TABLE 1. Comparison of the solvation times τ(s) of the electron in methanol, ethanol, *n*-propanol, and *n*-butanol at different viscosities[a]

Viscosities (cP)	Methanol			Ethanol			*n*-Propanol			*n*-Butanol		
	T (°C)	τ(s) (ps) at 1300 nm	τ (ps) at 1050 nm	T (°C)	τ(s) (ps) at 1300 nm	τ (ps) at 1050 nm	T (°C)	τ(s) (ps) at 1300 nm	τ (ps) at 1050 nm	T (°C)	τ(s) (ps) at 600 nm	τ (ps) at 1050 nm
1.10	−19	19	24	25	21	28	45	23	26	—	—	—
1.16	−23	22	28	20	23	30	40	23	26	—	—	—
1.43	−33	25	35	10	27	36	35	26	30	—	—	—
1.77	−42	30	45	0	34	45	28	30	34	—	—	—
2.20	−52	38	62	−10	42	58	20	32	40	34	27	33
2.79	−60	47	81	−20	54	79	11	38	49	23	33	46
3.56	−67	56	—	−30	72	115	3	45	62	13	41	62
4.62	—	—	—	−40	98	170	−8	55	79	4	48	79
6.15	—	—	—	−50	141	275	−19	71	123	−5	63	112
8.44	—	—	—	−60	214	—	−27	87	162	−16	83	174

[a]Values of the viscosities are from ref. 6. Values of τ(s) are from ref. 3, measured from the decay of absorbance at λ = 1300 nm or the increase of absorbance at 600 nm.

viscosity are quite different. Furthermore, the case of methanol aside, it seems that for a given viscosity the solvation time is shorter the longer the molecule. The comparison of these results with those obtained at room temperature by Kenney-Wallace and Jonah (4) for the longer chain alcohols (pentanol, octanol, decanol) which have viscosities higher than 5 cP leads to the same conclusion.

In order to obtain more evidence on these points we chose first to study the solvation times of the electron in cold ethanol (near its freezing point), with a view to comparing our results with values previously obtained by Baxendale and Wardman (5) in cold *n*-propanol at similar viscosities.

Experimental

The irradiation source is a modified Febetron 707: the electron pulse from the Febetron tube window is dispersed by an electromagnet (7*a*) and only electrons in the range 1.7 to 1.8 MeV are selected. The total pulse length is thus reduced to 16 ns with a width at half-height of 8 ns. The experimental set up (irradiation, cooling, and detection systems) is described elsewhere (7*b*) and the spectra, measured between 300 and 830 nm, are determined by normalization of optical densities to an arbitrary dose of about 10 krad.

The ethanol is 'Merck zur Analyse' grade purified by distillation. It was verified that no traces of benzene or aldehyde and ketone remained after the distillation.

Results and Discussion

At −106°C, the spectra obtained immediately after the pulse (20 ns) and later are similar to those which Baxendale and Wardman (5) obtained at −110°C. However, the minimum observed by these authors in the wavelength region of 1000 nm seems to be in the region 700–750 nm in our case.

Figure 1 shows the results we obtained at −116°C where ethanol is still liquid (melting point −117.4°C). Spectra 1–5 were respectively measured 20, 30, 50, 90, and 140 ns after the beginning of the pulse from oscilloscope traces such as those given in the insets of this figure. Curve 5 corresponds to the solvated electron spectrum with λ_{max} ~600 nm slightly different from previous results (8).

At $\lambda \leq 650$ nm, solvation times measured from the rate of increase of absorption seem to depend upon the wavelength considered: τ(s) is about 40 ns at $\lambda = 550$ nm and about 30 ns at $\lambda = 450$ nm (as seen in the inset, it would be even smaller at 650 nm). At $\lambda > 650$ nm,

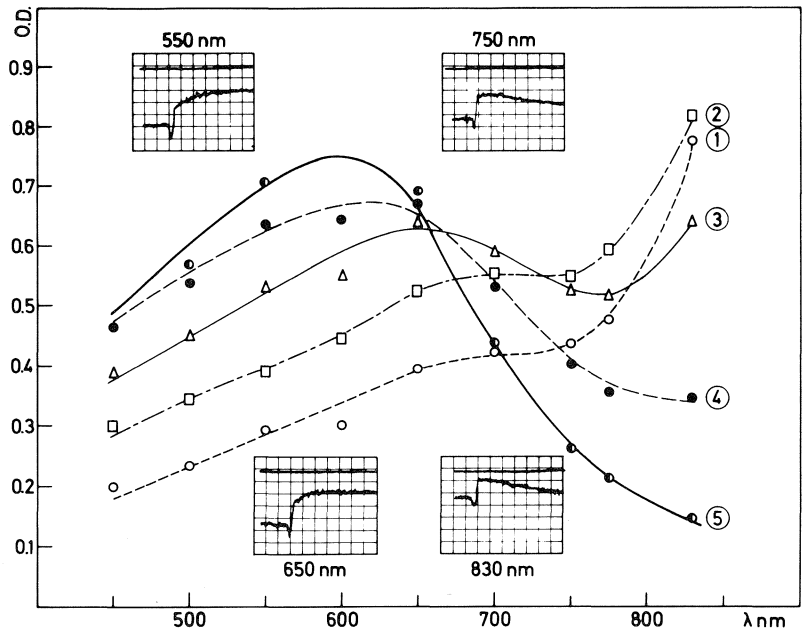

FIG. 1. Spectra observed in pulsed, Ar-purged, ethanol at −116°C. Spectra 1–5 have been obtained respectively 20, 30, 50, 90, and 140 ns after the beginning of the pulse. Optical densities were normalized to an arbitrary value of dose (~10 krad) from oscilloscope traces such as those given in the insets (20 ns/div.).

measurements become impossible as the first increase is followed by a decay of absorption.

Data obtained below the melting point at −123°C give the same kind of results with λ_{max} for e^-_{solv} at about 570 nm. At 450 nm and 600 nm $\tau(s) \approx 100$ ns whereas at $\lambda = 500$ nm and 550 nm $\tau(s) \approx 200$ ns.

These results lead to two remarks from which we will draw the necessary conclusions.

(1) Development of the Transient Spectra during the Solvation Process

Kenney-Wallace and Jonah (4) note that, at room temperature, their measured rates of increase of the absorption at 514 nm are similar to the rates measured by Chase and Hunt of decrease of absorption at 1300 nm in the cases of ethanol and *n*-propanol and of increase of absorption at 600 nm in the case of ethanol. This observation has led the authors to conclude that the passage from e^-_t to e^-_{solv} at room temperature occurs without the intervention of any intermediate solvated species of appreciable lifetime.

On the contrary, the increase in absorption followed by a decrease which we observe at both −116°C and at −123°C between 650 and 830 nm cannot be explained on the basis of only two configurations of the electron, one the trapped electron e^-_t and the other the solvated electron e^-_{solv}. In fact, if such were the case only an increase or a decrease in absorption, depending on the wavelength, should be observed (which suggests also an isosbestic point at a given wavelength). In the range of temperature which we have employed where ethanol is either liquid or glassy (−123°C) our results show the existence of transient absorption spectra of which the maxima move as a function of time.

These observations are in good agreement with previous results obtained for the glassy state (77 K) by Kevan (9) and Miller *et al.* (10). As at 77 K (10), the passage from one transient spectrum to another may be attributed to the variation with time of partly solvated states of the electron.

The response time of our detection system and the pulse length furnished by the electron gun do not allow us to make accurate measurements at higher temperatures (−106°C). But it should be noted that a detailed analysis of the results obtained at various wavelengths with *n*-propanol, irradiated at −12°C, led Chase and Hunt to suggest the possibility of a displacement of the

spectrum of e^-_t during the process of relaxation to a deeper trap. Thus the results obtained with ethanol at very low temperature (77 K) and these obtained above and below the freezing point (−116 and −123°C) are of the same type as those obtained with *n*-propanol at much higher temperature (−12°C). They indicate the existence of transient states which we assign to partly solvated states of the electron. If such a conclusion were valid at room temperature, it would imply the presence of intermediate states with very short lifetimes, and thus difficult to observe, as Kenney-Wallace and Jonah have suggested, but whose existence would have consequences for the measurement of the electron solvation time (defined now as a measurement of the time necessary for the passage of the spectrum of the first state of the electron observed immediately after a pulse to the spectrum of the fully solvated electron).

(2) Measurement of the Electron Solvation Time in Ethanol at −116°C and −123°C

In order to obtain a value for the solvation time of the electron from our results we have seen that different regions of wavelength have to be considered.

(a) $\lambda \leq \lambda_{max}\ (e^-_{solv})$

In this region of wavelength the situation appears relatively simple since one only observes an increase of absorption. However, errors may arise in the wavelength region (400–450 nm) where the final stage of variation of absorption is of the same order of magnitude as the noise level on the oscilloscope traces.

In our case the most accurate values of $\tau(s)$ which we can determine are obtained in the region where the difference between the initial and final absorption is the largest, that is to say at the wavelength corresponding to the maximum of the solvated electron spectrum at the temperature in question: at −116°C: $\tau(s) = 40 \pm 4$ ns (at λ = 550–600 nm); at −123°C: $\tau(s) = 200 \pm 15$ ns (at λ = 550 nm).

(b) $\lambda > \lambda_{max}\ (e^-_{solv})$

In this region of wavelength the various spectra overlap and confusing results are obtained. For instance, as noted previously, for wavelengths immediately above λ_{max} where only an increase of absorption is observed (650 nm at −116°C (Fig. 1) and 600 nm at −123°C) the values obtained are again lower than the values of $\tau(s)$ measured at λ_{max}.

(3) Consequences

The difficulties which we have pointed out in determining the solvation time of the electron in the range of wavelengths we have considered could suggest that it is preferable to study the phenomenon in the infrared region as did Baxendale and Wardman and Chase and Hunt. At first sight indeed both at low temperatures (5) and at higher temperatures (3), the solvation times measured at 1300 nm (decrease in absorption) appear essentially similar to those measured around 600 nm (increase in absorption). However, Chase and Hunt have clearly shown that the results measured at 1050 nm are very different and that the difference increases as the temperature is lowered. It thus appears that even in the infrared region the kinetics depend on the wavelengths used for the measurements. This difference is observed for all four alcohols considered and at all the temperatures employed by Chase and Hunt. We shall see that these results may be explained by the hypothesis of partly solvated states of the electron whose spectral contributions vary with time. In fact, in the infrared region where a decrease in absorption is measured, the change in absorption indicates the transition from the first spectrum detected immediately after the pulse to the last observable at these wavelengths: this last spectrum is not necessarily that of the solvated electron but rather of the last partly solvated state which absorbs at the wavelength considered. The spectra obtained at −12°C with *n*-propanol by Chase and Hunt are in agreement with this hypothesis: the solvated electron spectrum does not extend above 1100 nm. Under these conditions the apparent rate of solvation measured at 1300 nm will be faster than the true rate.

Furthermore it should be noted that as the temperature is lowered the spectrum of the solvated electron is shifted towards the blue and the difference between the results obtained at 1300 nm and 1050 nm increases in agreement with our hypothesis.

Finally the similarity between the results obtained at 600 and 1300 nm with ethanol ($\Theta \leq$ room temperature) and with *n*-propanol ($\Theta \leq -12$°C) can only be fortuitous, for depending on the temperature considered 600 nm falls on one side or the other of the maximum of the solvated electron spectrum. We have seen the results of such a situation in our study at

-116°C and -123°C. This is particularly noticeable in the case of *n*-propanol for which, at -12°C, the absorption maximum of the solvated electron is at 600 nm.

Conclusion

The solvation of the electron in alcohols is a complex process. The recent results reported by Miller *et al.* for ethanol irradiated at 77 K are similar to those we have obtained for the same alcohol irradiated at temperatures above and below its freezing point. The interpretation of the observations in terms of partly solvated states of the electron enables certain results of Chase and Hunt to be explained. If the hypothesis is correct a complete knowledge of the various spectra obtained after radiolysis is necessary and this for all alcohols and at all temperatures considered to obtain accurate values of τ(s).

It also appears that for measurements made in the infrared a contribution due to the solvated electron must be considered (stable residual absorption) in determining the solvation time. This is clearly shown in comparing values given in Table 1. Thus any correlation between τ(s) and η becomes impossible given the present state of knowledge.[1]

Acknowledgments

The authors wish to thank J. Potier for continuous assistance in the experiments and Dr. T. B. Truong for analysis of the purified ethanol. The authors wish also to thank J. Sutton for helpful discussions during the preparation of the final manuscript.

1. K. Fueki, D. F. Feng, and L. Kevan. J. Phys. Chem. **78**, 393 (1974).
2. L. Gilles, J. E. Aldrich, and J. W. Hunt. Nature London Phys. Sci. **243**, 70 (1973).
3. W. J. Chase and J. W. Hunt. J. Phys. Chem. **79**, 2835 (1975).
4. G. A. Kenney-Wallace and C. D. Jonah. Chem. Phys. Lett. **39**, 596 (1976).
5. J. H. Baxendale and P. Wardman. J. Chem. Soc. Faraday Trans. I, **69**, 584 (1973).
6. V. G. Komarenko, Y. G. Manzhelii, and A. V. Radtsig. Ukr. Fiz. Zh. **12**, 681 (1967).
7. (*a*) B. Lesigne and R. Sauneuf. Rev. Sci. Instrum. **47**, 1063 (1976); (*b*) L. Gilles and A. W. Boyd. Can. J. Chem. **54**, 531 (1976).
8. K. N. Jha, G. L. Bolton, and G. R. Freeman. J. Phys. Chem. **76**, 3876 (1972).
9. L. Kevan. J. Chem. Phys. **56**, 838 (1972).
10. J. R. Miller, B. E. Clifft, J. J. Hines, R. F. Runowski, and K. W. Johnson. J. Phys. Chem. **80**, 457 (1976).
11. G. A. Kenney-Wallace. Chem. Phys. Lett. **43**, 529 (1976).
12. J. H. Baxendale and P. H. G. Sharpe. Int. J. Radiat. Phys. Chem. **8**, 621 (1976).

[1]Two papers appeared after the Banff Conference. One by Kenney-Wallace (11) pointed out the importance of the polarizability and viscosity when considering the solvation times of the electron in alcohols. The other by Baxendale and Sharpe (12) gave three different rate constants for electron solvation, based on the absorption decay at 1300 nm and the absorption growth at 550 nm and 450 nm respectively for *n*-propanol irradiated at various temperatures between -119°C and -155°C. These results are in agreement with the idea we presented at the Conference and have developed in this article.

Discussion

J. W. Hunt: As discussed by Gilles and others, the changes of the absorption signals of the localized electron consist of a shift from infrared to visible wavelengths by complex decays and formations. Since the process is not one of a single jump from a shallow to a stabilized deep trap, I agree with Dr. Gilles that we must be careful in obtaining accurate values of the relaxation processes, although the values in the infrared wavelengths will probably be the best.

L. Gilles: The rate constants calculated from the decay of absorption at infrared wavelengths could appear easier to determine than those calculated from the increase of the absorption in the visible region, due to the difficulty in the latter case to determine precisely the time at which the final level is obtained. Nevertheless you will have to take care, that at the ir wavelength considered the solvated electron must absorb (*i.e.* a residual absorption must exist). Thus I don't know if the values measured at ir wavelengths will be better than those measured at the maximum of absorption of the solvated electron at the temperature considered.

L. Onsager: May I remind you again that on a simple-minded picture the pertinent dielectric relaxation time is not the Debye time τ_D, but the longitudinal relaxation time $\tau_L = \tau_D \, \varepsilon_\infty/\varepsilon_0$. This is not to assert that the concept of a simple hf dielectric constant is always appropriate. When not, then the concept represented by τ_L also must be picked apart. A good many radiation chemists do in fact know τ_L as the 'relaxation time at constant charge', as distinguished from the 'relaxation time in constant field' τ_D.

L. Gilles: In an earlier study I made with J. W. Hunt and J. E. Aldrich (2) using the stroboscopic pulse radiolysis system, we correlate the solvation times for methyl, ethyl, and *n*-propyl alcohols with τ_1', the relaxation time at *constant charge* for the breaking of hydrogen bonds. It appeared then from more recent results of Chase and Hunt on the one hand and Kenney-Wallace and Jonah on the other and also from the previous results of Baxendale and Wardman that a better relationship was found between τ(s) and τ(2) (the dielectric relaxation time of the free molecules in the liquid). As mentioned in ref. 4 modifying τ(2) to τ(2)′ would lead to times of

about 70% of $\tau(2)$ which would appear rather too fast. This observation would be even more striking in considering Baxendale's results.

L. Kevan: Your data show that the electron solvation times in methanol, ethanol, and 1-propanol are the same at the same viscosity *if* the viscosity is ≤ 2 cP. This is exactly what the simple model of Fueki, Feng, and Kevan (J. Phys. Chem. 1974 and 1976) predicts in which we equate the microscopic and macroscopic viscosities. The model does not depend on the size of the alcohol molecules. However, in glasses we know that our simple model for solvation time fails because the microscopic and macroscopic viscosities are presumably not the same. Your data seem to show that ~ 2 cP is the transition viscosity above which the microscopic and macroscopic viscosities are not equal. In this region the size of the solvent molecule becomes important. I would not be so pessimistic about defining a unique solvation time for electron solvation even though you have observed a wavelength dependence. Wouldn't you think that the solvation time determined at the farthest wavelength into the infrared is closest to the true solvation time? At shorter wavelengths the kinetics are complicated by the intermediate spectra formed during the process of solvation.

L. Gilles: I first should point out that the data reported in the table are from Chase and Hunt. From our results the wavelength dependence of the solvation time measurements could be partly due to experimental difficulties on determining a small change in the absorption level. I believe that I have shown that determination of the solvation times at the farthest wavelength into the infrared (where the fully solvated electron doesn't absorb) represents only a relaxation process towards the last partly solvated electron which absorbs at this wavelength. In that way I think that the results obtained by Chase and Hunt at 1050 nm are more representative of the solvation process than those at 1300 nm.

G. R. Freeman: The relaxation time observed at the long wavelength end of the spectrum might have a simpler interpretation than that observed at shorter wavelengths, because the former centers only decay, while the latter simultaneously grow and decay.

L. Gilles: Calculations are impossible in the region of wavelengths where the various transient spectra are overlapping. The results can be much more easily interpreted at longer wavelengths where there is only a decay of absorption.

Picosecond molecular relaxations: the role of the fluid in electron solvation

G. A. KENNEY-WALLACE

Department of Chemistry, University of Toronto, Toronto, Ont., Canada M5S 1A1

Received September 24, 1976

G. A. KENNEY-WALLACE. Can. J. Chem. **55**, 2009 (1977).

The role of the fluid is considered for a model of electron solvation in liquid alcohols. The events that lead to trapping and solvation of excess electrons are reconstructed from experimental data on the time and frequency-dependent electron absorptions (k_{mol}) and the appropriate molecular rotational relaxations (τ_2, τ_c), local liquid structure, viscosity (η), and orientational polarization (β) of the supporting fluid. The quasifree electron is captured at subpicosecond times in a preexisting trap in the liquid, which in alcohols is identified as an alcohol cluster whose local configurational fluctuations will be frozen in on this timescale. Rapid configurational relaxation of the cluster molecules, including multi-phonon processes, then occurs in the field of the excess electron at times $\leq 10^{-12}$ s. Finally, the molecules in the fluid layer adjacent to the initial trapping site align in the now screened field of the localized electron in a manner comparable to solvation of an ion embedded in a polar fluid. The relaxation may occur in competition with electron migration and reaction. The observed rate constant of the final step k_{mol} is shown to be proportional to $\beta\eta^{-1}$ for a range of alcohols at room temperature. The implications of this model for photobleaching experiments in liquids are briefly discussed.

G. A. KENNEY-WALLACE. Can. J. Chem. **55**, 2009 (1977).

On considère le rôle du fluide pour un modèle de la solvatation des électrons dans des alcools liquides. On reconstruit les évènements qui conduisent au piégeage et à la solvatation des électrons en excès à partir de données expérimentales sur l'absorption d'électrons (k_{mol}), qui dépend du temps et de la fréquence, et sur les relaxations rotationnelles moléculaires appropriées (τ_2, τ_c) ainsi que sur la structure locale du liquide, la viscosité (η) et la polarisation d'orientation (β) du fluide de support. L'électron pratiquement libre est capturé à des temps plus petits que la picoseconde dans un piège préexistant du liquide qui a été identifié, dans le cas des alcools, comme étant un agrégat d'alcool dont les fluctuations configurationnelles locales sont gelées sur cette échelle de temps. Il se produit alors une relaxation configurationnelle rapide des molécules agrégées, impliquant des processus multi-phonon, dans le champs de l'électron en excès à des temps $\leq 10^{-12}$ s. Finalement, les molécules dans la couche du fluide adjacente à celle du site du piégeage initial s'alignent dans le champs maintenant caché de l'électron localisé d'une façon comparable à la solvatation d'un ion imbriqué dans un fluide polaire. La relaxation peut se produire en compétition avec une migration d'électron et une réaction. On montre, pour plusieurs alcools à la température de la pièce, que la constante de vitesse observée pour l'étape finale, k_{mol}, est proportionnelle à $\beta\eta^{-1}$. On discute brièvement des implications de ce modèle pour des expériences de photodécoloration de liquides.

[Traduit par le journal]

Prologue

Accompanying Platzman's famous statement (1) postulating the existence of the hydrated electron e_{aq}^- and its optical absorption in the red, were remarks by Onsager (1) on the formation time of such a species, which would have to be on the timescale of dielectric relaxation of water, $\sim 10^{-11}$ s (2). The subsequent experimental developments that led to the discovery and characterization of e_{aq}^-, and the properties of electrons solvated or trapped in other media, have been extensively reviewed (3, 4). However, the precise sequence of events that leads to the formation of excess electron states in fluids, and the quantum mechanical description of these states, have been and continue to be a source of lively discussion over the years (3–5).

The picosecond timescale and wavelength dependence of the electron hydration process, as revealed in the experiments of Hunt and coworkers (6, 7) and Rentzepis, Jones, and Jortner (8) were qualitatively consistent with the expectations of the role of dielectric relaxation in electron solvation. It was further suggested (8) that the initial electron localization step was governed by the long range, dipolar interactions in the liquid, following which vibrational relaxation of the newly formed solvent sheath could take place

to leave the excess electron in a fully relaxed, ground electronic state. A similar process had been envisaged for relaxation following electronic excitation of e_s^- (9). However, the recent picosecond data on electron solvation in alcohols of Kenney-Wallace and Jonah (10) and Chase and Hunt (11), clearly indicate that the dipolar relaxation in liquids occurs *after* the initial electron localization step, the time-dependence of which has so far eluded present experimental observations (10–12).

Baxendale and Wardman (13) first observed electron solvation in liquid alcohols in low temperature *n*-propanol, and discussed the role of molecular relaxation vis-à-vis electron migration to account for the observed spectral shifts. Pulse radiolysis of cool and glassy alcohols has shown that molecular reorientation is the most probable mechanism in these systems (9, 13–17). However, new results (16) on ethanol at 77 K show that a significant degree of electron migration is taking place at these low temperatures, and suggest that the mechanism for electron solvation at low temperatures is quite different from that which governs room temperature events.

In order to explain the apparent correlation of electron solvation times τ_s with τ_2, the dielectric relaxation time normally assigned to the relaxation (18) of a single molecule in a weak, external electric field, Kenney-Wallace and Jonah (10) proposed that the quasifree electron was initially localized in a cluster of hydrogen-bonded alcohol molecules, and that the observable step in the solvation process reflected the formation of a second or third solvation shell. In their study of the temperature dependence of electron solvation times in small alcohols, Chase and Hunt (11) also observed the same correlation between solvation times and the dielectric relaxation time for molecular rotation τ_2. They concluded that molecular reorientation rather than migration mechanisms, such as hopping or tunnelling between traps, was responsible for electron solvation. In subsequent developments Kenney-Wallace (19) showed a direct correlation between the fluid dynamics and electron solvation in the same media, by considering the reorganization of the medium about the cluster as a function of $\beta\eta^{-1}$, where β represented the electrostatic field in which the dipolar molecules were reoriented and η the opposing frictional force in the fluid.

In this paper we present further details on the role of the fluid in the dynamics of electron solvation and in the fast radiationless transitions that follow photoexcitation and photobleaching of e_s^- at visible wavelengths.

Experimental

The electron solvation times τ_s were derived from the observed time evolution of the stable absorption spectra of e_s^- from 450 to 765 nm, following pulse irradiation of the alcohol at 298 K with single 30 ps electron pulses from the Argonne LINAC (20). The stroboscopic pulse radiolysis facility, sampling techniques, and treatment of data have been described in detail elsewhere (10, 20). Alcohols and alkanes were obtained from Burdick and Jackson (Distilled-in-Glass) where available or the highest purity from Fisher Scientific. The ^{13}C nmr measurements of T_1 relaxations were performed on a Varian CFT-20 Fourier transform spectrometer; full details of these and the viscosity measurements will be published elsewhere (21). Laser photobleaching experiments (22) employed the output from a Q-switched 100 MW, 20 ns ruby laser for both exciting and saturating laser pulses. Solvated electrons were generated in the alcohol via the two-photon photoionization of pyrene at 347 nm with a 100 mJ frequency-doubled ruby laser pulse, and photobleached some 30 ns later.

Results and Discussion

Electron Absorption and Dielectric Data

The evolution of the visible spectrum of e_s^- in the normal alcohols appeared as an initial rapid growth followed by a slower absorption component, the duration of which increased as the size of the alcohol molecule increased. Figure 1 shows typical absorption data, in this case recorded in *n*-decanol. When analyzed (10) the slower component fitted a single exponential growth and the rate constant k_{mol} (s^{-1}) and solvation times τ_s (ps) are listed in Table 1. Comparison of these solvation times τ_s with τ_2, the relaxation time assigned to single molecule rotation in dielectric dispersion measurements (18), reveals the similarity in each fluid between the experimentally observable electron solvation time and what is, in essence, the relaxation of dipoles into a preferred alignment under the influence of a weak external field. This correlation (10, 11) invites further investigation from the perspective of the fluid dynamics. Of the many variables that may be involved in determining the response of the nearby molecules to the sudden perturbation presented by the localized electron, the local frictional forces, dipolar energy in the field of the excess electron, dipole density (which reflects the local liquid structure), and dielectric relaxation times would appear to be the major ones of in-

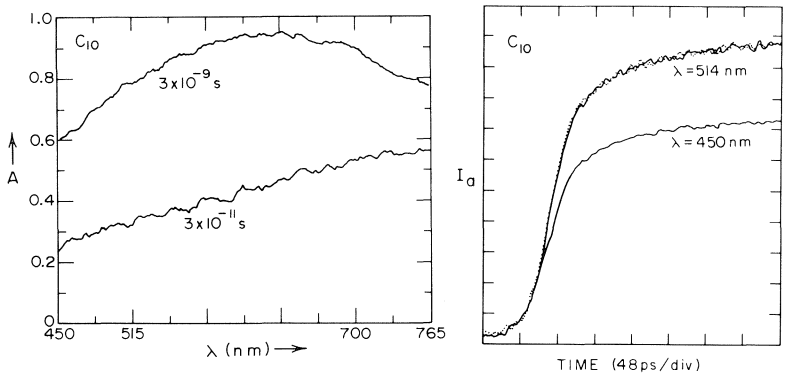

FIG. 1. The time-dependent absorption of e_s^- in *n*-decanol at 300 K: (*a*) showing the spectrum from 450 to 765 nm at 30 ps and 3 ns after the 30 ps electron pulse, where *A* is the relative absorbance; (*b*) showing the similarity in profile of the absorption signal I_a at two wavelengths by normalizing the data (10) at 450 nm to that at 514 nm.

TABLE 1. Electron solvation data

ROH	k_{mol} (10^{10} s^{-1})	τ_s (ps)	τ_2 (ps)
Methanol	9.34	10.7	12
Ethanol	5.55	18	20
Propanol	4.00	25	22
Butanol	3.33	30	27
Pentanol	2.94	34	28
Octanol	2.22	45	39
Decanol	1.96	51	48

terest. We will first consider the origin of the reaction field.

If we can envisage the initial localization step as capture of the quasifree electron by a preexisting trap due to fluctuations in the local molecular configurations in the liquid, then the subsequent step, which involves medium rearrangement about the trapped particle, can be thought of in terms of medium relaxation about an ion embedded in the fluid. The excess electronic charge will be distributed over the surface of the inner coordination shell and thus the field experienced by the dipolar molecules beyond this boundary will be much weaker than that felt by the molecules which comprise the initial trapping site. Of course the field experienced by the external dipoles will not remain constant during relaxation of the surrounding molecules. Calculations show that if the external field is kept constant, then the resulting dipole relaxation is slower than if the excess electronic charge distribution is conserved during medium relaxation (5, 23). The latter is thought to be a more appropriate basis for electron solvation and leads to the modification of the macroscopic dielectric relaxation times to $\tau' = \tau(D_{op}/D_s)$, where one is now considering a linear superposition of dielectric polarization from infinite past to the present time (23). When the τ_2' values are calculated this way there is only a 30% decrease on average from the macroscopically measured τ_2 values and thus the correlation between τ_s and τ_2 or τ_2' remains qualitatively the same (10). It is not unreasonable therefore to consider τ_s^{-1} or k_{mol} as the rate constant describing an orientational relaxation process which is the net effect of two counteracting torques: the electrostatic field and the opposing internal friction. An estimate of the distance at which the alcohol molecules no longer exhibit any preferred alignment with respect to this field shows that orientation of the dipoles is only significant up to 5 to 8 Å from the centre of the charged cluster. This is in accord with the spirit of the recent calculations of Kestner (24) whose long-range potential in fact only contributes to the stabilization energy of e_s^- at distances shorter than about 10 Å. We will approximate the field in which the external dipoles are relaxing by the orientational polarization of the alcohol molecules. Electronic polarization of these molecules has already been accomplished by the time angular rotation occurs. In Fig. 2 the rate constant k_{mol} is plotted against the reciprocal high frequency and static dielectric constants, which represent the electronic polarization α_e and the total polarization ($\alpha_e + \alpha_{or}$), respectively. By subtracting the two terms we obtain the orientational polarization α_{or}, and thus in the inset show the dependence of k_{mol} on β, where $\beta = 1/D_{op} - 1/D_s$, a familiar term for the long range potential in models of excess electron states (3–5).

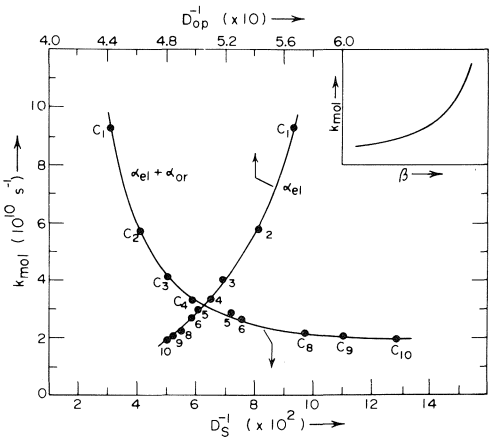

FIG. 2. The dependence of the solvation dynamics k_{mol} on the medium polarization for C_1 (methanol) to C_{10} (decanol) at 300 K (see text for discussion). Solvation data from ref. 10 except methanol (11).

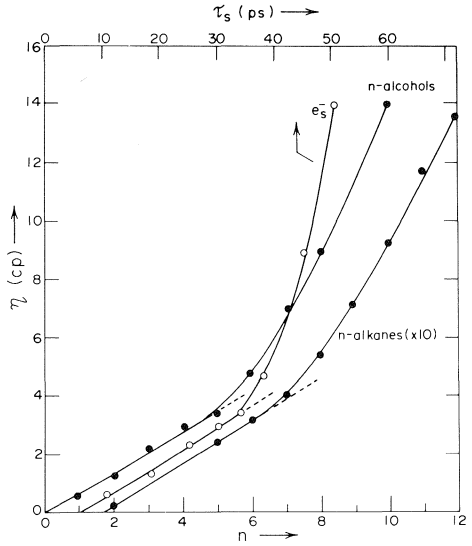

FIG. 3. ○ The dependence of the electron solvation time τ_s on η, the viscosity of the fluid; ● the viscosity as a function of carbon chain length, *n*, in *n*-alcohols and *n*-alkanes.

Viscosity Measurements

Opposing the electrostatic torque on the molecules is a frictional force which includes intermolecular forces, noticeably hydrogen-bonding in this case, and energy and momentum transfer during collisions of the rotating molecules. Clearly the motion of one molecule is coupled hydrodynamically to the motion of its neighbours in the fluid; the net angular velocity of a rotating, spherical molecule is described in the Debye–Stokes–Einstein model (2, 25) as

$$\tau_{or} = \eta V_m (kT)^{-1}$$

The orientational relaxation time τ_{or} is thus linearly proportional to the shear viscosity η, and to the hydrodynamic volume V_m swept out by the rotating molecules. To what extent do the solvation times τ_s reflect the local fluid dynamics? In Fig. 3 τ_s is plotted as a function of the fluid viscosities at 20°C for methanol to decanol. The τ_2 values exhibit the same profile, a linear dependence on viscosity up to hexanol and a sudden change in slope indicative of an additional component to the fluid viscosity. Since the alkyl end of these longer chain molecules is not a rigid extended chain but one capable of folding back over itself, it is tempting to assign the additional contribution to the viscosity to entanglement of neighbouring alkyl chains in the fluid. A plot of alcohol viscosity against chain length in Fig. 3 shows a break in the slope, again at hexanol. If the entanglement of the alkyl chains is largely responsible for this break and not the —OH bonded end of the molecule, then the viscosity of the parent alkanes should display a similar trend. The results are included on Fig. 3, and the break in slope again occurs between hexane and heptane. Subsequent ^{13}C nmr measurements of the T_1 spin–lattice relaxation times of the individual segments of the alkyl chains, in pure and alkane-diluted alcohols, confirmed the notion of chain entanglement and the inferred relationship between the autocorrelation times τ_c of each carbon moiety and the viscosity of the fluid. The full details of this work will be published elsewhere (21). All these results taken together not only add confidence to our claim that the τ_s values accurately reflect the trends in the local fluid properties, but also show that the dynamics of e_s^- may indeed be utilized in the future as a microscopic probe for local fluidity and liquid structure.

Finally, we must consider the validity of applying the Debye–Stokes–Einstein hydrodynamic model in these circumstances where the rotating molecules are probably far from spherical. In a series of picosecond laser experiments on induced dichroism, Einsenthal and Chwang (26) were able to show that the orientational relaxation time of rhodamine 6G, in the series of normal alcohols methanol to decanol, ranged from 2×10^{-10} s $< \tau_{or} <$ 2.2×10^{-9} s and scaled linearly with viscosity up to octanol. The relaxation times were apparently not influenced

by the significant changes in the hydrodynamic volume in the alcohols. The overall conclusion to be drawn from these data is that, during rotational relaxation, the solute molecule experiences a torque primarily arising from solvent–solvent interactions. Rentzepis, Struve, and Jortner (27), in their laser picosecond laser studies of solvent reorganization about a 'giant-dipole' molecule suddenly ($\leq 10^{-15}$ s) created in ethanol, also concluded that the observed orientational relaxation time reflected only the viscous rotational drag between adjacent alcohol molecules. Consequently their data could be described within the hydrodynamic model. Theoretical justification comes from recent microscopic calculations based on the generalized Langevin equation, in which orientation and angular-velocity correlation functions were calculated for a fluctuating molecular fluid (28). Expressions have been derived for rotational diffusion in which the inverse linear dependence on viscosity is retained although the formal expression is more complex than the Debye equation. Therefore we may conclude that bulk viscosity measurements do offer meaningful physical insight on the microscopic fluid interactions, and that the hydrodynamic model presents a valid framework within which to interpret these field-induced orientational relaxation times in polar fluids.

The Solvation Mechanism

The initial observation that τ_s and τ_2 were very similar raised the problem (10) of why the dipoles in the presence of a strong, inhomogeneous internal field should behave as though they were reorienting under the influence of a weak, homogeneous external field. In accepting that the correlation was not entirely coincidental, Kenney-Wallace and Jonah (10) proposed that the field of the excess electron, once trapped by a cluster, was screened by the layer of cluster molecules and that the induced-rotation of the dipoles outside of the cluster could be approximated by weak field conditions. If we assume that the rate of configurational relaxation of the molecules outside the initial trapping site is controlled by an accelerating electrostatic torque and the retarding viscous torque, and neglect affects due to variations in hydrodynamic volume (since they seem to be rather small for the alcohols in question), then we can plot k_{mol} *vs.* $\beta\eta^{-1}$ as shown in Fig. 4. The linearity of the relationship is convincing evidence that we have pinpointed the

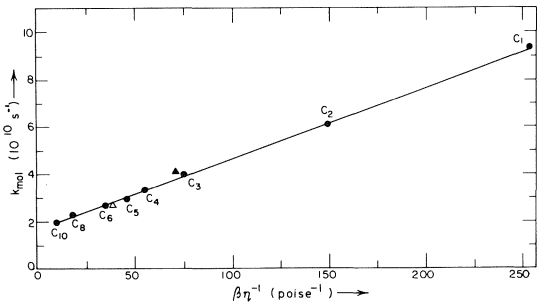

FIG. 4. The solvation dynamics k_{mol} as a function of both medium polarization β and fluidity η^{-1} for the *n*-alcohols ●, 2-propanol ▲, and 2-butanol △. Solvation data from ref. 10 except methanol (11), and normalized β values from ref. 40.

essential features of the hydrodynamic response of the fluid to the sudden perturbation in the local dipolar field and liquid structure provided by the excess electron in its initial localized state.

Although there are possibly other considerations which should be included, the most important part of this model of electron solvation which requires a quantitative time-dependence treatment is the internal field. In choosing β we have compromised between the initial and final polarizations. We are presently carrying out further experimental and theoretical work on this aspect, and on the temperature dependence of the observed solvation times for the $\beta\eta^{-1}$ correlation. Similarities in the τ_s values for small alcohols at varying temperatures but the same viscosity have been recently observed (29).

Contemporary models of electron solvation in polar liquids (30–32) have already considered the rotation of dipoles about an excess electron from different perspectives. Fueki, Feng, and Kevan (32, 33) have recently extended their semicontinuum model for solvated electrons into the time domain, and their new calculations on electron solvation explicitly incorporate dielectric relaxation of the medium beyond the first solvation layer. Their theoretical and ENDOR results imply that this relaxation must occur after the initial molecular trapping site has assumed an optimum configuration. In originally noting the $\beta\eta^{-1}$ relationship (19) we presented arguments which were used to evaluate the role of the long- and short-range interactions in determining the energetics of the solvated electron in polar fluids, and reached the same conclusion on the basis that rotational reorientation of the cluster dipoles must be accelerated in the strong

internal field of the electron due to the short-range, electron–medium interactions. Furthermore, these events probably occur on a subpicosecond timescale in liquids and may remain elusive to experimental observation. For the correlation of τ_s and τ_2 to be physically meaningful, a second relaxation process must be occurring.

Implications for Photobleaching Experiments

The nature of the electronic transition or transitions giving rise to the characteristically broad optical absorption spectrum of e_s^- remains a fruitful topic of experimental and theoretical debate (3–5). Measurements of the excited state lifetime of excess electrons in polar liquids via laser saturation (photobleaching) techniques have placed upper limits on these lifetimes ranging from 6 ps in water (34), 10 ps in several alcohols (22), 5 ps (35) and 0.2 ps (36) in ammonia to 0.2 ps in methylamine at 200 K (36). The interpretation of these values depends on both the saturating and observing wavelengths, and the degree of inhomogeneous broadening in the absorption band. A recent account of time-resolved photobleaching phenomena in solvated and trapped electrons by Walker and May (4, 37) contains a full discussion of this problem, with particular emphasis on the correct absorption coefficients ε. The latter have been recently determined (22) for our series of linear alcohols and within experimental error appear to be constant at $\varepsilon_{max} \sim 10^4\ M^{-1}\ cm^{-1}$.

Whether or not the excited state is a bound or continuum state, can in fact be examined in the context of the dynamics of electron solvation (9, 22, 34) as illustrated in Fig. 5. If, following injection of an electron into a polar fluid, the sequence of events leading to solvation can be described by an overall rate constant k_s, then the following comparison

$$e^-_{quasifree} \xrightarrow{k_s} e_s^-$$

can be made to photobleaching experiments in which the electron

$$e_s^- \xrightarrow{h\nu} e^{-*} \xrightarrow{k} e_s^-$$

is photoejected from its trap and subsequently undergoes the solvation process if chemical reaction does not occur (38).

The principle of the pulsed laser saturation technique (22, 34, 37) is to temporarily deplete the population of ground state absorbers and then to measure both the induced transparency of the system and the rate k at which the ground state acquires its normal population once more. The experimental variables are the photophysical parameters of the absorber and the amplitude and temporal profile of the transmitted laser pulse at varying incident proton fluxes, I. In a two level system, for excited state lifetimes much shorter than the laser pulse duration, it was shown that (34)

$$k = 2\varepsilon I(1 - 10^{-A})(A^0 - A)^{-1}$$

where A^0 is the linear absorption under low photon flux (Beer's law) and A is the high flux value. If following excitation and saturation of e_s^- with a photon of energy $h\nu_2$ the measured rate $k = k_2$ corresponded to the value of k_s at the same wavelength, then this would indeed be strong evidence for a continuum excited state. This is shown in Fig. 5. Excitation at lower incident photon energies ($h\nu_1$) to a bound state would lead to a rate constant k_1 where $k_1 \neq k_s$. However, if our model of electron solvation is essentially correct then it may be impossible to do such an unambiguous experiment because the initial localization step occurs on a timescale $\ll 10^{-12}$ s and is beyond direct experimental observation. Recent mobility data (39) show electrons are readily captured in alcohols by even dimers. The observed value of $k = k^*$ from photobleaching experiments will thus clearly depend on the time-window of the experiment, and the difference in absorbance will be given by the difference in the absorption coefficients of the electronically bound species in two localized states. Figure 1 suggests that this difference may not be very large, placing limitations on the sensitivity of the saturation technique. Nevertheless, one would still hope to see in k^* some contributions from orientational relaxation as indeed occur in k_s, whereas rapid vibronic relaxation k_1 from a bound photoexcited state, reached via $h\nu_1$, will not include such terms.

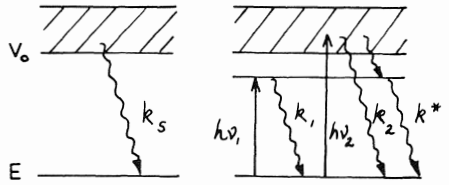

FIG. 5. Interpretations of optical photobleaching experiments (see text for discussion).

Acknowledgements

It is a pleasure to acknowledge the collaboration and valuable comments of Dr. C. D. Jonah on the solvation measurements, and the contributions from Dr. B. A. Garetz, G. Hall, K. Sarantidis, and R. Ling in my laboratory. We are grateful to the National Research Council of Canada, the Research Corporation, and Connaught Fund, University of Toronto, for financial support.

1. R. L. PLATZMAN. Energy transfer from secondary electrons to matter. N.A.S.–N.R.C. Reports, no. 305. 1953. pp. 22–50.
2. P. DEBYE. Polar molecules. Dover, London. 1929.
3. (*a*) E. J. HART and M. ANBAR (*Editors*). The hydrated electron. Wiley-Interscience, New York, NY. 1970; (*b*) G. A. KENNEY and D. C. WALKER. Hydrated electrons. Advances in electroanalytical chemistry. Vol. 5. *Edited by* A. J. Bard. Dekkar, New York, NY. 1971. pp. 1–66; (*c*) D. C. WALKER. Q. Rev. **21**, 79 (1967).
4. (*a*) L. KEVAN and B. WEBSTER (*Editors*). Electron–solvent and anion–solvent interactions. Elsevier Scientific Publishing Co., New York. 1976; (*b*) J. JORTNER and N. R. KESTNER (*Editors*). Electrons in fluids. Springer-Verlag, Berlin. 1973; (*c*) M. MATHESON. *In* Reactions in condensed phase. Physical chemistry. Vol. 5. Academic Press, New York, NY. 1975. Chapt. 10.
5. P. HELMAN, A. MOZUMDER, and A. ROSS (*Editors*). Proceedings of symposium on very early effects. Argentina. 1970. ERDA document C00-38-738.
6. R. K. WOLFF, M. J. BRONSKILL, and J. W. HUNT. J. Chem. Phys. **53**, 4201 (1970).
7. L. GILLES, J. E. ALDRICH, and J. W. HUNT. Nature Phys. Sci. **243**, 70 (1973).
8. P. RENTZEPIS, R. JONES, and J. JORTNER. J. Chem. Phys. **59**, 766 (1973).
9. G. A. KENNEY-WALLACE and D. C. WALKER. Ber. Bunsenges. Phys. Chem. **75**, 634 (1971).
10. G. A. KENNEY-WALLACE and C. D. JONAH. 58th Canadian chemical Congress. 1975; Chem. Phys. Lett. **39**, 596 (1976); To be published.
11. J. CHASE and J. HUNT. Colloq. Weyl IV, 1975; J. Phys. Chem. **79**, 2835 (1975).
12. D. HUPPERT, W. S. STRUVE, P. M. RENTZEPIS, and J. JORTNER. J. Chem. Phys. **63**, 1205 (1975).
13. J. H. BAXENDALE and P. WARDMAN. Nature, **230**, 449 (1971); J. Chem. Soc. Faraday Trans. 1, **69**, 584 (1973).
14. L. KEVAN. J. Chem. Phys. **56**, 838 (1972); Chem. Phys. Lett. **11**, 140 (1971).
15. J. T. RICHARDS and J. K. THOMAS. J. Chem. Phys. **53**, 218 (1970); G. BECK and J. K. THOMAS. J. Phys. Chem. **76**, 3856 (1972).
16. J. H. BAXENDALE and P. H. G. SHARPE. Chem. Phys. Lett. **39**, 401 (1976).
17. N. V. KLASSEN, H. A. GILLIS, G. G. TEATHER, and L. KEVAN. J. Chem. Phys. **62**, 2474 (1975).
18. S. K. GARG and C. P. SMYTH. J. Phys. Chem. **69**, 1294 (1965); G. JOHARI and C. P. SMYTH. J. Am. Chem. Soc. **91**, 6215 (1969).
19. G. A. KENNEY-WALLACE. Chem. Phys. Lett. **43**, 529 (1976).
20. C. D. JONAH. Rev. Sci. Instrum. **46**, 62 (1975).
21. R. LING, G. A. KENNEY-WALLACE, and W. R. REYNOLDS. To be published.
22. G. A. KENNEY-WALLACE. ERDA Document No. C00-2410-1; G. HALL, K. SARANTIDIS, and G. A. KENNEY-WALLACE. Unpublished data.
23. A. MOZUMDER. J. Chem. Phys. **50**, 3153 (1969).
24. N. R. KESTNER. Can. J. Chem. This issue.
25. F. K. FONG and D. DIESTLER. J. Chem. Phys. **57**, 4953 (1972).
26. T. J. CHWANG and K. B. EISENTHAL. Chem. Phys. Lett. **11**, 368 (1971); J. Chem. Phys. **57**, 5094 (1973).
27. P. M. RENTZEPIS, W. STRUVE, and J. JORTNER. J. Chem. Phys. **59**, 5014 (1973).
28. (*a*) D. BEDEAUX and P. MAZUR. Physica, **73**, 431 (1974); (*b*) F. GARISTO and R. KAPRAL. Phys. Rev. A, **10**, 309 (1974).
29. L. GILLES, M. R. BONO, and M. SCHMIDT. Can. J. Chem. This issue.
30. M. TACHIYA and A. MOZUMDER. J. Chem. Phys. **63**, 1959 (1975).
31. R. SCHILLER. Chem. Phys. Lett. **5**, 176 (1970); R. SCHILLER and S. VASS. Int. J. Radiat. Phys. Chem. **6**, 223 (1974).
32. K. FUEKI, D.-F. FENG, and L. KEVAN. J. Phys. Chem. **78**, 393 (1974).
33. K. FUEKI, D.-F. FENG, and L. KEVAN. J. Phys. Chem. **80**, 1381 (1976).
34. G. A. KENNEY-WALLACE and D. C. WALKER. J. Chem. Phys. **55**, 447 (1971).
35. J. BELLONI, M. CLERC, P. GOUJON, and E. SAITO. J. Phys. Chem. **79**, 2848 (1975).
36. D. HUPPERT, P. M. RENTZEPIS, and W. S. STRUVE. J. Phys. Chem. **79**, 2850 (1975).
37. D. C. WALKER and R. MAY. Int. J. Radiat. Phys. Chem. **6**, 345 (1974); D. C. WALKER. Can. J. Chem. This issue.
38. J. K. THOMAS and A. BROMBERG. J. Chem. Phys. **63**, 2124 (1975).
39. J. H. BAXENDALE and P. H. G. SHARPE. Chem. Phys. Lett. **41**, 440 (1976).
40. R. R. HENTZ and G. A. KENNEY-WALLACE. J. Phys. Chem. **76**, 2931 (1972); **78**, 514 (1974).

Discussion

K. Funabashi: Photo-bleaching of solvated electrons in ethanol is known to generate H from dissociation of the OH bond. If the major portion of energy relaxation arises from dipole rotation of the surrounding medium, photo-bleaching is not likely to generate H atoms. I feel that some *intra*molecular relaxation associated with the OH bond is more important in describing the solvation process than the dipole rotation mechanism.

G. A. Kenney-Wallace: The photo-bleaching effects in ethanol to which you refer have not been detected in laser saturation experiments from other groups. However, we are continuing to explore photo-bleaching in all the alcohols with picosecond laser pulses. Intramolecular relaxation of the molecules in the first solvation layer clearly occurs in times faster than we can resolve. This

was included when I stated that —OH dipole and configurational relaxation of the cluster itself occurred at times $< 10^{-12}$ s after electron localization.[1]

J. W. Chase: Your plot of k_{so1} *vs.* $\beta\eta^{-1}$ is very convincing, but have you tried this plot at different temperatures to see if this correlation still holds?

G. A. Kenney:Wallace: In order to do that we need good information on the behaviour of both β and η over a large temperature range. We have been investigating the change in fluidity of the alcohols via viscosity, and ^{13}C Fourier transform nmr measurements, at different temperatures. We are learning more about the relative degree of 'rigidity' of the carbon segments of the alkyl chain, and the origin of the initial dramatic viscosity change on dilution of alcohol in alkane. Ultimately we expect to characterize the degree of association via hydrogen bonding in the pure liquid and alcohol–alkane solutions. Once this work is completed I will be able to answer your question exactly. Over a small temperature range the correlation appears to hold.

J. Jortner: I would like to raise again the problem of the dynamics of electron localization in pure polar fluids. A few years ago Rentzepis and colleagues in their experiments on picosecond spectroscopy on electron localization in water proposed that the process occurs via the following consecutive steps: (*1*) relaxation of the long range dipolar field, (*2*) configurational changes in the vicinity of the trapping centre, reminiscent of molecular vibrational relaxation. Professor Onsager has pointed out that step (*1*) is determined by the longitudinal dielectric relaxation time which is shorter by 1 to 2 orders of magnitude (by the factor D_{op}/D_s) than the Debye relaxation time. This is an ultrashort timescale, which is on the verge of detection in some systems by the methods of picosecond spectroscopy. Recently an alternative physical picture was advanced replacing step (*1*) by trapping of the quasifree electron by 'pre-existing traps'. Evidence for such mechanism is available from Baxendale's experiments on alcohols–hydrocarbons mixture and from Gaathon's results on electron localization in supercritical polar vapors, but this evidence does not pertain directly to the pure polar solvents. I believe that crucial experiments regarding step (*1*) in the dynamics of electron localization were not yet performed.

G. A. Kenney-Wallace: I do not believe that there is any difficulty here with the points you raise, nor do they affect the correlation I reported. If you consider the case where the quasifree electron is initially localised in a pre-existing trap, such as would be created by favourable fluctuations in the local molecular configuration and, in the specific cases of the alcohols, is probably a hydrogen bonded cluster, then the rapid configurational changes in the cluster (your step *2*) must take place on a subpicosecond timescale in the strong Coulomb field. The subsequent dynamics (represented by my τ_s) appear to be governed by dipolar relaxation and the local fluidity. Certainly if τ_1 were the (Debye) relaxation time involved, the correct longitudinal dielectric relaxation time would be very much shorter, as you say. However, I am referring to τ_2 and the D_{op}/D_s modified value here is $\geq 70\%$ of the Debye time. Given the experimental uncertainties in the values of the dielectric constants, the difference between the τ_s and longitudinal dielectric relaxation time τ_2' becomes even less significant. We had already discussed this point (see Fig. 3 and text, Chem. Phys. Lett. **39**, 596 (1976)) and therefore the timescale over which the correlation is observed is the anticipated one. The order of our experimental events therefore shows that dipolar relaxation occurs as a second step, not as the initial one.

[1]NOTE ADDED IN PROOF: Recent laser saturation and photo-bleaching experiments in our laboratory clearly indicate that permanent and(or) transient photo-bleaching occurs in several alcohols at room temperature.

Correlation of optical and electron spin resonance spectra for metal–electron species in alkali metal solutions[1]

WILLIAM ARTHUR SEDDON, JOHN WALLACE FLETCHER, AND RON CATTERALL[2]

Physical Chemistry Branch, Chalk River Nuclear Laboratories, Atomic Energy of Canada Limited, Chalk River, Ont., Canada K0J 1J0

Received September 27, 1976

WILLIAM ARTHUR SEDDON, JOHN WALLACE FLETCHER, and RON CATTERALL. Can. J. Chem. **55**, 2017 (1977).

Pulse radiolysis of alkali metal cations (M^+) in amines and tetrahydrofuran has demonstrated the formation of transient optical absorption bands attributed to a species of stoichiometry M. Such bands exhibit a distinct blue shift from that of e_s^- observed in the same solvent. Comparisons with electron spin resonance (esr) spectra obtained in alkali metal solutions demonstrate that the blue shift can be correlated with the percent atomic character deduced for the species of the same stoichiometry. This correlation indicates that both the optical and esr spectra arise from the same species which, with decreasing solvent polarity, exhibits a continuous transition from well solvated ion-pairs to something approaching solvated atoms or tight ion-pairs.

WILLIAM ARTHUR SEDDON, JOHN WALLACE FLETCHER et RON CATTERALL. Can. J. Chem. **55**, 2017 (1977).

La radiolyse pulsée de cations métalliques alcalins (M^+) dans des amines et le tétrahydrofuranne a permis de démontrer la formation de bandes transitoires d'absorption optique attribuées à des espèces de stoechiométrie M. De telles bandes présentent un déplacement distinct vers le bleu par rapport à celle observée pour e_s^- dans les mêmes solvants. Une comparaison des spectres de résonance paramagnétique électronique obtenus dans des solutions de métaux alcalins démontre que le déplacement vers le bleu peut être relié avec le pourcentage de caractère atomique déduit pour les espèces de même stoechiométrie. Cette corrélation indique que les spectres optiques ainsi que les spectres rpe proviennent des mêmes espèces qui, lorsque l'on permet à la polarité du solvant de décroître, présentent une transition continue allant des paires d'ions bien solvatés vers quelque chose approchant des atomes solvatés ou des paires intimes d'ions.

[Traduit par le journal]

Extensive investigations (refs. 1–5 and references therein) of the optical, magnetic, and conductance properties of solutions of alkali metals in amines and ethers have revealed the presence of at least three species. There is now general agreement that two of these are best described as alkali metal anions M^- and solvated electrons e_s^-. The existence of a third species of stoichiometry M, composed of an alkali metal cation and e_s^-, has been demonstrated by both optical (6–12) and electron spin resonance (esr) spectroscopy (13–16). All three are considered to be solvated to some extent and in equilibrium according to a scheme of the form

$$[1] \qquad e_s^- + M^+ \rightleftharpoons M$$

$$[2] \qquad M + M \rightleftharpoons M^- + M^+$$

However, there is considerable discussion in the literature regarding the nature of M, and indeed, it is uncertain whether there are one, two, or more different species of this composition (3, 16–20).

In order to explain, firstly, the marked temperature dependence of the hyperfine splitting constant of the multiplet esr spectrum and, secondly, the dependence of esr line widths upon nuclear configuration, it has been proposed that the observed esr spectra are in fact a time average of spectra from two or more rapidly interconverting 'monomeric' species of stoichiometry M such as tight or loose ion pairs (21), or solvated atoms (16–20). Alternatively, Tuttle (22) has suggested that the ion-pair species does not contribute to the resolved hyperfine structure but has a single line esr spectrum identical with that of e_s^- whilst only

[1]AECL No. 5662.

[2]Visiting scientist, Chalk River Nuclear Laboratories, June–September 1976. Present address: Department of Chemistry, University of Salford, Salford, England M5 4WT.

a single 'monomer' species is responsible for the hyperfine multiplet. For clarity in presentation, we subsequently designate the species responsible for the hyperfine splitting as M_{esr}.

Steady state optical spectra in such alkali metal solutions are, in general, composed of two bands attributed to metal-dependent and metal-independent species. The former or 'visible' band occurs in the region 10 000–15 000 cm^{-1} and has been attributed to the diamagnetic species M^- whereas the latter band, which extends further into the infrared ($<7000\ cm^{-1}$), has generally been identified with e_s^-.

More recently, flash photolysis (6–9) and pulse radiolysis (5, 10–12, 23, 24) techniques have been used to investigate the approach to equilibrium and have demonstrated the existence of three distinct optical bands assigned to e_s^-, M^-, and M with the latter also referred to as an ion-pair (M^+, e_s^-). It is important to recognise, however, that the notation (M^+, e_s^-) is only a convenient symbol for the transient and that no definite evidence for this structure has been obtained (9).

For solvents such as ethylamine (EA) (10), isopropylamine (IPA) (24), and tetrahydrofuran (THF) (11, 12), it is evident that the M_{opt} absorption maxima occur at wavelengths intermediate to those of e_s^- and M^-. In this context it should be recognised that at equilibrium the monomer M_{esr} is a minor, but easily detectable constituent (3) whereas in the pulse or flash techniques M_{opt} is generated on the microsecond time scale and subsequently decays to the equilibrium condition.

Hitherto, because of spectral overlap and incorrect optical assignments, early attempts to correlate optical and esr spectra have not been successful (1, 16, 25). More recently, we have reported a linear correlation between the hyperfine splitting constant (hfs) observed in potassium/EA/THF solutions and the optical band maxima ($\nu_{max}\ cm^{-1}$) for Na_{opt} in similar solvent mixtures (26). Recognising the presence of different cations we nevertheless interpreted these results as evidence that the optical and esr hyperfine spectra arose from the same type species.

If we now compare the hfs in K solutions with values for the free atom then the atomic character decreases significantly from THF (36%) to EA (~12%) (27). This is accompanied by a distinct blue shift in $\nu_{max}(K_{opt})$ from that of $\nu_{max}(e_s^-)$, the magnitude of which decreases substantially for the corresponding change in solvent (10, 12). On the other hand, in methylamine (MA) (28), ethylenediamine (EDA) (28–31), or liquid ammonia (32–34) (see later) little or no change in optical spectrum from that of e_s^- is observed on M_{opt} formation. In these cases the percent atomic character observed by esr in alkali metal solutions is small and much less than observed in EA or THF (3, 13, 18, 27).

In view of this trend we have examined all the available data relative to M_{opt} and M_{esr}. These are shown in Table 1 listing ν_{max} for M_{opt}, e_s^-, M^-, and the gaseous atoms M_g (35), along with the percent atomic character for M_{esr} for different metal–solvent combinations. Because of strong solvent absorptions room temperature values for $\nu_{max}(e_s^-)$ in MA, EA, and IPA were obtained by pulse radiolysis via the temperature coefficient $-d\nu_{max}(e_s^-)/dT = 24.0$, 23.6, and 27.8 $cm^{-1}\ deg^{-1}$, respectively, determined at temperatures ranging from 193 to 253 K. These data are plotted in Fig. 1 expressing $\nu_{max}(M_{opt})$ as a percentage blue shift from that of $\nu_{max}(e_s^-)$ in the same solvent. The relative blue shift is defined by

$$[3]\quad (\nu_{max}(M_{opt}) - \nu_{max}(e_s^-))/(\nu_{max}(M^-) - \nu_{max}(e_s^-))$$

Since with respect to the free atom value, the shift in *g*-factor for M_{esr} is negative as the atomic character increases (27, 36, 37) we have not identified the optical transition energy for the 100% limit with that of the gaseous atoms ($\nu_{max}(M_g)$). Instead, in an attempt to allow for atom–solvent interactions we assume that the term $\nu_{max}(M^-)$ in the denominator gives an approximate representation of 100% atomic character.

It can be seen that a good correlation is obtained for all solvent and metal combinations indicating that the designation M_{opt} and M_{esr} refer to the same species. No attempt has been made to correct for the slight overestimation of atomic character for M_{esr}, especially when the hfs is small (18). However, the effect is systematic and any correction simply defines a slightly different line of correlation. Similarly, use of $\nu_{max}(M_g)$ in place of $\nu_{max}(M^-)$ in [3] does not invalidate the correlation but again would

TABLE 1. Optical and electron spin resonance parameters for alkali metal solutions at 298 K

Solvent	Metal	% atomic character from esr	ν_{max} (cm^{-1}) e_s^-	M_{opt}	M^-	M_g	% blue shift
MA			5405				
	K	<5.5		5882	11 173		8.2
	Cs	6.8		5882	9 090		12.9
EA			5348				
	Na	6.8*		7143	14 706		19.2
	K	11.2–12.4		7143	11 236		30.5
	Rb	12.3		7143	10 870		32.5 (39)
		17.7					
	Cs	15.6		6896	9 090		41.4
IPA			4717				
	K	21.8		7692	11 429		43.8
	Cs	30.0		7407	9 090		61.5
THF			4672				
	K	36.0		8888	11 111		65.0
1.1 NH_3†/EA	K		5348	6790	11 236		27.9
10 NH_3/EA		5.1	5348	6450	11 236		18.7
15 NH_3/EA		4.0	5376	6290	11 236		15.6
20 NH_3/EA		3.3	5394	6130	11 236		12.6
	Na					16 961	
	K					12 989	
	Rb					12 582	
	Cs					11 181	
NH_3	Na	<1.0	6250‡	~6250			0

*Extrapolated from Na/EA/NH_3 mixtures.
†Mol% NH_3.
‡268 K.

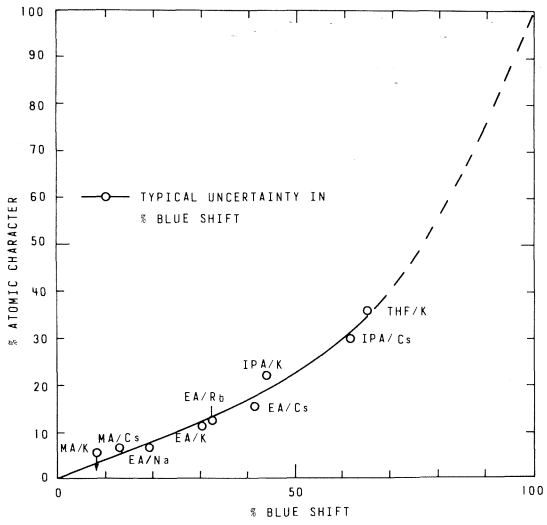

FIG. 1. Correlation of percent atomic character and percent blue shift (see text) for alkali metal solutions in amines and THF. Random errors in atomic character are expected to be small and ≤1–2%.

simply shift the curve. In no case do we attach any theoretical significance to a particular line.

Within experimental error an identical trend is observed for mixed solvents in K/NH_3/EA solutions with atomic character 3.3–11.3% (38) and blue shifts 12.6–30.5% from 20 mol% NH_3 to pure EA. For clarity these data are not shown in Fig. 1 but are listed in Table 1.

As outlined above the precise structure of the species responsible for the optical and esr spectra has been the source of much controversy and confusion in the literature (13–20, 21, 22). Thus, whilst species showing a small blue shift and low atomic character might be best described as loose ion-pairs, species such as those in K/THF having a large blue shift and high atomic character are probably better described as solvated atoms or tight ion-pairs. A significant point of Fig. 1 is the demonstration of a continuous transition between such ion-pairs and solvated atoms with decreasing polarity of

the solvent. We therefore conclude, that in agreement with Tuttle (22), a simple model involving a rapid equilibrium between a few relatively precise structures such as ion-pairs and solvated atoms (16–20, 36), is not sufficient to describe the range of species of stoichiometry M detected in these solutions. Instead we suggest that the correlation depicted in Fig. 1 illustrates a continuous desolvation process ranging from what might be regarded as well solvated dipolar ion-pairs to something approaching weakly solvated centrosymmetric alkali atoms or tight ion-pairs.

In support of this interpretation we have found that the optical band widths of the Na_{opt} species in EA–THF mixtures (26) are no broader than those in either pure solvent, whereas linear combinations of the corresponding bands from the pure solvent would show considerably greater widths.

As a final comment it is significant that in liquid ammonia the optical band attributed to the electron species shows a slight shift to the red, and not the blue, with increasing metal concentration from 10^{-3} to 10^{-2} M (40). No change in the band maximum is observed below $\sim 10^{-3}$ M and yet it is estimated from Knight shifts that $k(e_s^- + M^+) \sim 10^{12}\ M^{-1}\ s^{-1}$ (41). This is consistent with the suggestion that the spectra of e_s^- and (M^+, e_s^-) are indistinguishable and that the slight decrease in energy observed at higher concentrations represents the formation of an additional spin-paired species such as M_2 (40), rather than M^- (42). Evidence that the overall absorption band is composed of two components at equilibrium has been discussed elsewhere (34, 43, 44).

1. I. Hurley, T. R. Tuttle, Jr., and S. Golden. *In* Metal–ammonia solutions. I.U.P.A.C., Colloque Weyl II, Butterworth and Co., London. 1970. p. 449.
2. M. T. Lok, F. J. Tehan, and J. L. Dye. J. Phys. Chem. **76**, 2975 (1972).
3. J. L. Dye. Electrons in fluids. Colloque Weyl III, Springer-Verlag, West Berlin. 1973. p. 77.
4. J. L. Dye, C. W. Andrews, and S. E. Mathews. *In* Electrons in fluids – the nature of metal–ammonia solutions. Colloque Weyl IV; J. Phys. Chem. **79**, 3065 (1975).
5. J. W. Fletcher and W. A. Seddon. *In* Electrons in fluids – the nature of metal–ammonia solutions. Colloque Weyl IV; J. Phys. Chem. **79**, 3055 (1975).
6. L. J. Giling, J. G. Kloosterboer, R. P. H. Rettschnick, and J. D. W. Van Voorst. Chem. Phys. Lett. **8**, 457 (1971).
7. J. G. Kloosterboer, L. J. Giling, R. P. H. Rettschnick, and J. D. W. Van Voorst. Chem. Phys. Lett. **8**, 462 (1971).
8. M. Fisher, G. Rämme, S. Claesson, and M. Szwarc. Chem. Phys. Lett. **9**, 309 (1971).
9. M. Fisher, G. Rämme, S. Claesson, and M. Szwarc. Proc. R. Soc. London Ser. A, **327**, 481 (1972).
10. J. W. Fletcher, W. A. Seddon, and F. C. Sopchyshyn. Can. J. Chem. **51**, 2975 (1973).
11. B. Bockrath and L. M. Dorfman. J. Phys. Chem. **77**, 1002 (1973).
12. G. A. Salmon, W. A. Seddon, and J. W. Fletcher. Can. J. Chem. **52**, 3259 (1974).
13. K. D. Vos and J. L. Dye. J. Chem. Phys. **38**, 2033 (1963).
14. K. Bar-Eli and T. R. Tuttle, Jr. J. Chem. Phys. **40**, 2508 (1964).
15. R. Catterall and M. C. R. Symons. J. Chem. Soc. 6656 (1965).
16. L. R. Dalton, J. D. Rynbrandt, E. M. Hansen, and J. L. Dye. J. Chem. Phys. **44**, 3969 (1966).
17. J. L. Dye and L. R. Dalton. J. Phys. Chem. **71**, 184 (1967).
18. R. Catterall, M. C. R. Symons, and J. W. Tipping. J. Chem. Soc. A, 1529 (1966).
19. R. Catterall and P. P. Edwards. J. Chem. Soc. Chem. Commun. 96 (1975).
20. R. Catterall and P. P. Edwards. *In* Electrons in fluids – the nature of metal–ammonia solutions. Colloque Weyl IV; J. Phys. Chem. **79**, 3010 (1975).
21. M. Szwarc and J. J. Grodzinski. Ions and ion-pairs in organic reactions. Vol. 2. *Edited by* M. Szwarc. J. Wiley and Sons, New York. 1974. p. 133.
22. T. R. Tuttle, Jr. *In* Electrons in fluids – the nature of metal–ammonia solutions. Colloque Weyl IV; J. Phys. Chem. **79**, 3071 (1975).
23. J. W. Fletcher, W. A. Seddon, J. J. Jevcak, and F. C. Sopchyshyn. Can. J. Chem. **53**, 3571 (1975).
24. W. A. Seddon, J. W. Fletcher, and F. C. Sopchyshyn. Chem. Phys. **15**, 377 (1976).
25. M. Ottolenghi, K. Bar-Eli, H. Linschitz, and T. R. Tuttle, Jr. J. Chem. Phys. **40**, 3729 (1964).
26. R. Catterall, J. Slater, W. A. Seddon, and J. W. Fletcher. Can. J. Chem. **54**, 3110 (1976).
27. R. Catterall, J. Slater, and M. C. R. Symons. *In* Metal–ammonia solutions. I.U.P.A.C., Colloque Weyl II, Butterworth and Co., London. 1970. p. 329.
28. L. M. Dorfman, F. Y. Jou, and R. Wageman. Ber. Bunsenges. Phys. Chem. **75**, 681 (1971).
29. R. R. Dewald and J. L. Dye. J. Phys. Chem. **68**, 128 (1964).
30. J. L. Dye, M. G. DeBacker, and L. M. Dorfman. J. Chem. Phys. **52**, 6251 (1970).
31. J. L. Dye, M. G. DeBacker, J. A. Eyre, and L. M. Dorfman. J. Phys. Chem. **76**, 839 (1972).
32. R. Catterall, M. C. R. Symons, and J. W. Tipping. *In* Metal–ammonia solutions, I.U.P.A.C., Colloque Weyl II, Butterworth and Co., London. 1970. p. 317.
33. D. F. Burow and J. J. Lagowski. Adv. Chem. Ser. **50**, 125 (1965).
34. W. A. Seddon, J. W. Fletcher, J. Jevcak, and F. C. Sopchyshyn. Can. J. Chem. **51**, 3653 (1973).

35. W. WEYHMANN and F. M. PIPKIN. Phys. Rev. A, **137**, 490 (1965).
36. R. CATTERALL, M. C. R. SYMONS, and J. W. TIPPING. J. Chem. Soc. A, 1234 (1967).
37. K. BAR-ELI and T. R. TUTTLE, JR. J. Chem. Phys. **44**, 114 (1966).
38. R. CATTERALL, J. SLATER, M. C. R. SYMONS, and J. W. TIPPING. To be published.
39. W. A. SEDDON, J. W. FLETCHER, and F. C. SOPCHYSHYN. Can. J. Chem. **54**, 3110 (1976).
40. J. J. LAGOWSKI. Electrons in fluids. *Edited by* J. Jortner and N. R. Kestner. Springer-Verlag, Berlin. 1973. p. 29.
41. D. E. O'REILLY. J. Chem. Phys. **41**, 3729 (1964).
42. J. W. FLETCHER and W. A. SEDDON. Discuss. Faraday Soc. To be published.
43. T. R. TUTTLE, JR., G. RUBINSTEIN, and S. GOLDEN. J. Phys. Chem. **75**, 3635 (1971).
44. G. RUBINSTEIN, T. R. TUTTLE, JR., and S. GOLDEN. J. Phys. Chem. **77**, 2872 (1973).

Optical study of electrons and positive ions in pulse-irradiated liquid 3-methyloctane at low temperatures[1]

HUGH A. GILLIS, NORMAN V. KLASSEN, AND ROBERT J. WOODS[2]

Division of Physics, National Research Council of Canada, Ottawa, Canada K1A 0R6

Received September 23, 1976

HUGH A. GILLIS, NORMAN V. KLASSEN, and ROBERT J. WOODS. Can. J. Chem. **55**, 2022 (1977).

The spectrum of pulse-irradiated liquid 3-methyloctane at 127 K has maxima around 625 and 2100 nm. The latter is well-known as being due to the solvated electron (e_s^-). The former is attributed to a positive ion because it is eliminated by the addition of triethylamine, but remains in solutions of electron scavengers, and is very similar to bands observed earlier by Louwrier and Hamill in glassy solutions at 77 K of higher hydrocarbons in CCl_4 or CO_2-bubbled 3-methylpentane. At temperatures of 127 K and less the initial decay rate of e_s^- is greatly decreased by the addition of ~6 mol% triethylamine. The result is interpreted as indicating that at low temperatures the mobility of the initial hydrocarbon positive ion is much greater than that of either e_s^- or the positive ion in triethylamine solutions, and therefore the initial hydrocarbon positive ion must be the parent radical cation which moves by resonance charge transfer. As the temperature of pure 3-methyloctane is raised from 103 to 153 K, the initial $G\varepsilon_{650}$ decreases by about 30% while initial $G\varepsilon_{2100}$ almost doubles; because of these and other observations it is tentatively suggested that a second solvated electron is also produced.

HUGH A. GILLIS, NORMAN V. KLASSEN et ROBERT J. WOODS. Can. J. Chem. **55**, 2022 (1977).

Le spectre du méthyl-3 octane liquide irradié par pulsation à 127 K a deux maxima autour de 625 et 2100 nm. On sait que le dernier maximum est dû aux électrons solvatés (e_s^-). Le premier est attribué à un ion positif parce qu'il est éliminé par l'addition de triéthylamine mais demeure dans des solutions de piégeurs d'électron et est trés semblable à des bandes qui ont été observées antérieurement par Louwrier et Hamill dans des solutions d'hydrocarbures de poids moléculaires plus élevés dissous dans des verres de CCl_4 à 77 K ou de méthyl-3 pentane dans lequel on a fait barbotter du CO_2. A des températures de 127 K ou moins, le taux de décomposition initial de e_s^- diminue rapidement par addition ~6 mol% de triéthylamine. On interprète des résultats comme indiquant qu'à basse température la mobilité de l'ion positif de l'hydrocarbure initial est beaucoup plus grande que celle de soit e_s^- ou l'ion positif dans des solutions de triéthylamine et qu'ainsi l'ion positif de l'hydrocarbure initial doit être le cation radical parent qui se déplace par transfert de charge en résonance. A mesure que l'on augmente la température du méthyl-3 octane de 103 à 153 K, le $G\varepsilon_{650}$ initial diminue par environ 30% alors que le $G\varepsilon_{2100}$ initial double pratiquement; à cause de ces observations et d'autres, on suggère d'une façon non définitive qu'il y a aussi production d'une seconde espèce d'électron solvaté.

[Traduit par le journal]

Introduction

Electrons solvated or trapped in hydrocarbons have strong absorption bands with maxima in the near infrared and they have been the subject of many optical investigations in both glasses and liquids (1–3). In hydrocarbons, especially at low temperatures, an electron is usually thermalized at a distance from a positive ion in the same spur such that the coulombic energy between the pair is greater than the kinetic energy. The ion-pair is described as geminate and will undergo geminate recombination unless one or both members of the pair is scavenged by solute. Geminate recombination was demonstrated in liquid propane at 88 K (2) and in liquid 3-methylhexane at 126 K (3) by the observation that half-lives for electron decay are independent of initial concentration.

Studies of the positively charged species participating in the recombination reaction in hydrocarbons in the condensed phase have been relatively few. Louwrier and Hamill (4) found strong absorption in γ-irradiated glassy solutions of alkanes (RH) of seven or more carbon atoms in either CCl_4 or CO_2-saturated 3-methylpentane at 77 K. The bands had λ_{max} increasing with

[1]NRCC No. 15822.

[2]Visiting Research Officer at the National Research Council of Canada, June–August, 1975. Permanent address: Department of Chemistry and Chemical Engineering, University of Saskatchewan, Saskatoon, Sask., Canada S7N 0W0.

carbon number from 560 nm for C_7H_{16} to ~910 nm at $C_{15}H_{32}$ and higher, and were attributed to the parent radical ions, RH^+. The yield of this species was found to be a maximum around 0.5 mol% of the higher hydrocarbon in CO_2-saturated 3-methylpentane; smaller yields at higher concentrations were attributed to recombination of an appreciable fraction of all charge pairs by hole transfer of RH^+ along chains of RH. No RH^+ bands were observed in the pure hydrocarbons, presumably because recombination by hole transfer was fast enough to proceed to completion before the first observation period of some minutes after the irradiation.

Rate constants for charge transfer from solvent positive ions to solute can be calculated from the rate of formation of solute positive ions in pulse radiolysis studies. For some liquid hydrocarbons at room temperature these rate constants are more than an order of magnitude larger than expected for a diffusion controlled reaction of a molecular ion (5–8). More direct evidence for the formation of a very mobile positive ion was obtained in a recent study of pulse-irradiated liquid cyclohexane at room temperature in which electrical conductivity was studied by means of microwave absorption (9). The conductivity remaining after addition of SF_6 to convert electrons to SF_6^- or its decomposition products was more than an order of magnitude larger than expected for ions of normal mobility, and since it was greatly decreased by addition of the positive ion scavenger NH_3, was attributed mainly to the very mobile positive hole.

A functional description of the life-times of geminate electrons produced in the radiolysis of pure hydrocarbons has been derived by Rzad *et al.* (10) from the concentration dependence observed for electron scavenging. This description is

$$[1] \qquad G(t) = G_{gi} \exp(\lambda t) \operatorname{erfc}(\lambda t)^{1/2}$$

where $G(t)$ is the yield of electrons still present at time t, G_{gi} is the total yield of electrons, λ is a parameter with dimensions of frequency, and $\operatorname{erfc}(\lambda t)^{1/2}$ is the error function complement of $(\lambda t)^{1/2}$. Expression [1] was derived from experiments at room temperature, but it is not obvious that it should not also describe electron decay at low temperatures. However, in fact it is not a very good description of electron decay in 3-methylhexane at low temperatures (3).

In the present study of geminate neutralization reactions 3-methyloctane (3-MO) was chosen as the hydrocarbon medium because it was expected that reactions and yields of the positive ions as well as those of the electrons could be measured, and these should provide further information concerning the nature of these reactions. The temperature range of this work is 103–153 K. The viscosity of 3-MO has been measured between 107 and 114 K, and obeys a linear plot of log viscosity *vs.* T^{-1} over this range (11). The viscosities of other hydrocarbons give a linear plot between about 10^4 P and at least 10^{12} P (12). An extrapolation of the data for 3-MO gives a viscosity of 10^{12} P at 103 K, and indicates a viscosity of 10^4 P at 124 K. Since 153 K is in the region where linearity is no longer expected, we can say only that at this temperature the viscosity of 3-MO must be much less than 10^4 P.

Experimental

3-Methyloctane from Chemical Samples Co. was passed through a column of silica gel and Davison molecular sieve Type 4A which had been heated at 360°C for 12 h or more. The 3-MO was then degassed and stored over NaK. Triethylamine (TEA) from Matheson Coleman and Bell, CCl_4 (Fisher Spectranalysed), N_2O (Union Carbide), and SF_6 (Matheson) were used as received.

Samples were irradiated in high-purity quartz cells of 0.5 cm optical path with 35 MeV electrons from the National Research Council of Canada linac. Pulses were usually 40 ns long, and the dose per pulse was generally in the range 3–7 krad. Each sample was pulsed many times; effects due to repeated pulsing were looked for and not found. The cells were supported in a Dewar equipped with optical windows. Cold nitrogen gas was flowed through it at a rate required to give the desired temperature as measured by a thermocouple attached to the cell.

The dose per pulse was measured with a secondary emission monitor which was calibrated for each experiment by using an O_2-saturated 5 m*M* KSCN aqueous solution as a dosimeter. In correcting for differences in electron density between the 3-MO samples and the dosimeter solution, the density of 3-MO was taken to be 0.95 g ml^{-1} at all temperatures; 0.95 g ml^{-1} is the density calculated at 77 K by assuming that 3-MO shows the same percentage increase in density on cooling as 3-methylpentane does (13). Absorbance per unit energy absorbed is expressed as $G\varepsilon$ where G is the number of molecules of a particular species produced per 100 eV and ε is the decadic molar extinction coefficient in units of M^{-1} cm^{-1}.

In most experiments the intensity of the analyzing light, which was provided by a pulsed xenon lamp, was monitored simultaneously at two wavelengths. In determination of spectra one of these was fixed as the reference, usually at 650 nm, while the other was varied. The light detectors used were: for $410 \leq \lambda \leq 1000$ nm, an EG&G SHS-100 silicon photodiode; and for $\lambda > 900$ nm, a

Barnes A-100 room temperature InAs photodiode. The performance of these detectors has been described (14). The 0–98% response time of the oscilloscope–detector system was <40 ns with the silicon photodiode and <90 ns with the InAs photodiode for the conditions used in this work.

Results

Spectra of Solvated Electron and Positive Ion

The spectra of irradiated 3-MO at 127 K at different times after the start of a 40 ns pulse are shown in Fig. 1. The maximum around 2100 nm is attributed to the solvated electron (e_s^-) by comparison with our previous work (2, 15) and the maximum around 625 nm is attributed to RH^+ by comparison with the spectra of Louwrier and Hamill (4). A comparison of the three spectra of Fig. 1 indicates that at 127 K RH^+ decays somewhat faster than does e_s^-.

The spectra of an irradiated 5.7 mol% solution of TEA in 3-MO at 127 K at two times after a pulse are shown in Fig. 2. TEA is expected to scavenge RH^+ by accepting either the charge or a proton (16):

[2] $$RH^+ + (C_2H_5)_3N \rightarrow RH + (C_2H_5)_3N^+$$

[3] $$\rightarrow R + (C_2H_5)_3NH^+$$

As seen in Fig. 2 the ratio of absorption at 625 nm to that at 2100 nm is much smaller in the solution than in pure 3-MO at 100 ns, and this ratio becomes even smaller for the solution at 7 μs.

Spectra observed in solutions of known electron scavengers in 3-MO are shown in Fig. 3. Difficulties were encountered in dissolving enough scavenger in the cold 3-MO to completely remove e_s^-. Spectrum *A*, for a solution of SF_6 in 3-MO, shows a peak due to RH^+ around 625 nm and some residual absorption at longer wavelengths probably due to e_s^-. At 500 ns absorptions in this system at 2100 and 625 nm were 28% and 60%, respectively, of the corresponding absorptions at 100 ns, which is in accord with the assignment of absorption at 2100 nm to e_s^- which reacts rapidly with SF_6. Spectrum *B*, for a solution of N_2O in 3-MO,

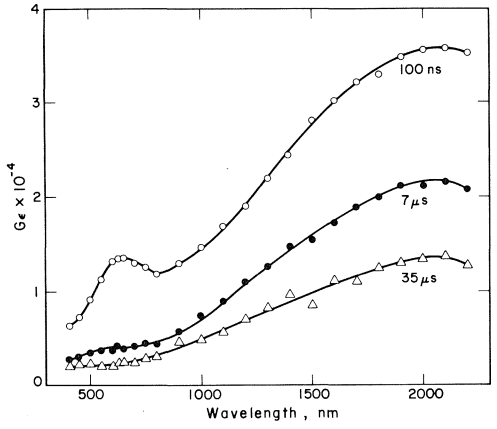

FIG. 1. Spectra observed at three times after the start of a 40 ns pulse in pure 3-methyloctane at 127 K.

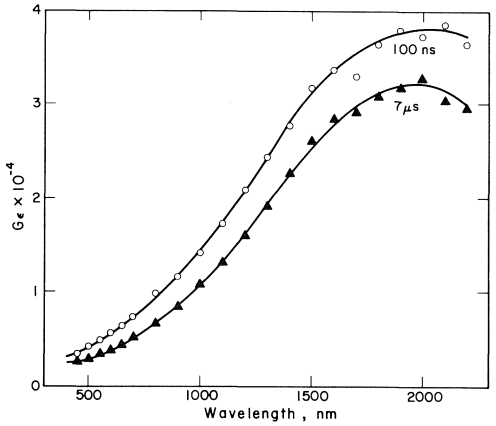

FIG. 2. Spectra observed at two times after the start of a 40 ns pulse in 3-methyloctane containing 5.7 mol% triethylamine at 127 K.

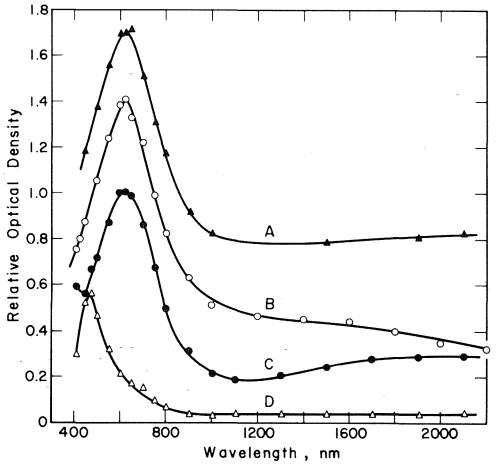

FIG. 3. Spectra observed after a 40 ns pulse in 3-methyloctane containing electron scavengers: (*A*) with 2.9 mol% SF_6, $T = 136$ K, 100 ns after start of the pulse; (*B*) saturated with N_2O at room temperature, $T = 127$ K, 60 ns after start of the pulse; (*C*) with 1.1 mol% CCl_4, $T = 127$ K, 100 ns after start of the pulse; (*D*) same as *C* except 7 μs after start of the pulse. Spectra *A* and *B* have been displaced upwards by 0.6 and 0.3 units, respectively. The magnitudes of *C* and *D* are relative to each other, but otherwise the magnitudes of the spectra are arbitrary.

shows the RH^+ peak around 625 nm and also absorption decreasing from 1000 to 2300 nm which cannot be due to e_s^-. At 7 μs, after RH^+ had largely decayed away, a peak around 425 nm remained. Spectrum *C*, for a solution of CCl_4 in 3-MO, shows the RH^+ peak around 625 nm, absorption increasing from 1000 to 2100 nm which is due to e_s^-, and an increase in absorption between 425 and 410 nm. This last feature may be due to the tail of a band assigned to CCl_4^+ and which is reported to have λ_{max} = 367 nm (17). The spectrum at 7 μs for this system, spectrum *D*, shows a peak around 470 nm which has been attributed to a charge-transfer complex, $CCl_4 \cdot Cl$, resulting from charge recombination of CCl_4^+ with Cl^- (17), though this assignment has been questioned (18). If the 470 peak is due to $CCl_4 \cdot Cl$, then it should grow in only as RH^+ decays and should not contribute significantly to spectrum *C*; in agreement with this, OD_{450}/OD_{650} for spectrum *C* is very similar to that for spectra *A* and *B*.

Effects of Solutes on e_s^- and RH^+

In Fig. 4*A* it is seen that the effect of a large concentration (6.2 mol%) of TEA on the initial yield of e_s^- in 3-MO at 109.5 K is negligible, but its initial decay rate is considerably decreased. Figure 5 shows the effect of the same concentration of TEA in 3-MO at 127 K over a greater extent of decay. At this temperature there is a small (3%) increase in concentration of e_s^- at short times in the presence of TEA. This increase is only about twice the experimental uncertainty for an individual trace but it was repeatable several times and for two different samples, and is probably not an artifact of the detector (14). However, at longer times e_s^- decays faster in the TEA solution, so that the time to reach 80% decay is the same as for pure 3-MO. Figure 6 gives results for electron decay at 141 K in the presence and absence of TEA. It is seen that at higher temperatures where electron decay is much faster in pure 3-MO, the effectiveness of TEA in decreasing the initial decay rate is much less.

The yields of trapped electrons in γ-irradiated 3-methylpentane at 77 K are increased by the addition of a few mol% TEA (1). Our work suggests that the reason is simply that the initial decay rate of the electrons is sufficiently fast in the pure hydrocarbon such that some of them disappear before the first measurement,

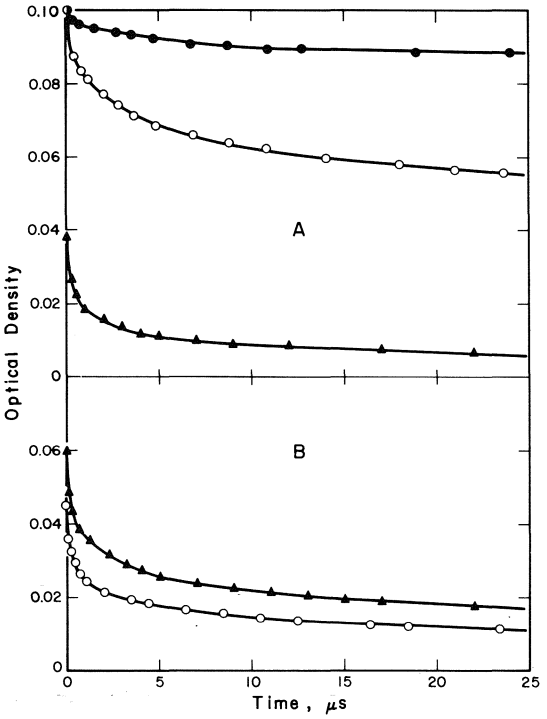

FIG. 4. Effects of solutes on electron and positive ion in 3-methyloctane at 109.5 K. Zero time refers to mid-pulse. (*A*) Optical density at 2100 nm, due to the electron, as a function of time; ○, no additives; ●, with 6.2 mol% triethylamine; ▲, with 1.22 mol% SF_6. (*B*) Optical density at 650 nm due to the positive ion (corrections have been made for electron absorption at this wavelength); ○, no additives; ▲, with 1.22 mol% SF_6.

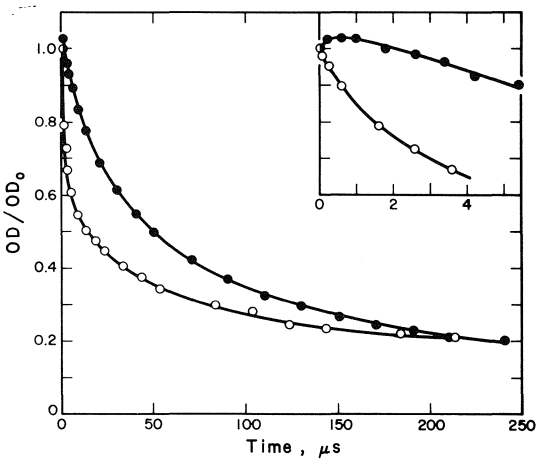

FIG. 5. Effects of triethylamine on electron decay in 3-methyloctane at 127 K: ○, pure 3-methyloctane; ●, with 6.2 mol% triethylamine. Measurements were made at 2100 nm. OD_0 is the optical density extrapolated to the middle of the 40 ns pulse. The inset shows the initial changes in optical density on an expanded time-scale.

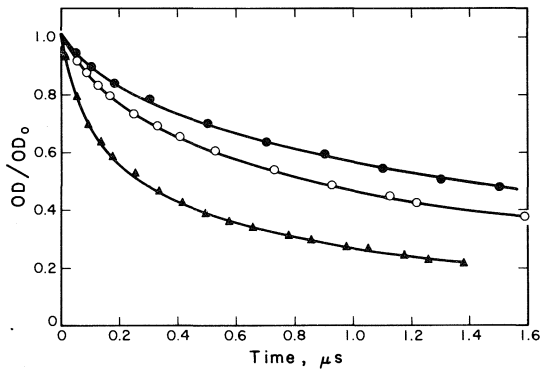

FIG. 6. Decay of electrons and positive ions in pure 3-methyloctane at 141 K, and electron decay in a 6.2 mol% triethylamine solution at 141 K. OD_0 is the optical density extrapolated to the middle of the 40 ns pulse. ●, λ = 2100 nm, triethylamine solution; ○, λ = 2100 nm, pure 3-methyloctane; ▲, λ = 650 nm, pure 3-methyloctane, corrected for electron absorption.

but the initial decay is much slower in the solutions so that fewer are lost.

Figure 4*A* shows that the effect of SF_6 on e_s^- is to considerably reduce the initial yield and greatly increase the decay rate. The effect of SF_6 on RH^+, as seen in Fig. 4*B*, is to increase the initial yield and slightly decrease the decay rate at short times. In Fig. 4*B* initial $t_{1/2}$'s for decay of RH^+ are approximately 1.7 μs in pure 3-MO and 2.8 μs in the 1.22 mol% SF_6 solution.

From a comparison of Figs. 4 *A* and *B* it is seen that in pure 3-MO at 109.5 K the decay rate of RH^+ is much faster than that of e_s^-, especially at short times. However, the fractional difference in rates becomes smaller with increase in temperature as shown by the results at 141 K given in Fig. 6.

Effect of Electron Scavengers on Yields of RH^+

The effects of SF_6 and CCl_4 on yields of RH^+ in 3-MO at two temperatures are shown in Table 1. In estimating the yields in CCl_4 solutions, it was assumed, as indicated above, that the species with λ_{max} around 470 nm found at long times makes no contribution to absorption at 650 nm at short times.

Effect of Temperature on Yields of e_s^- and RH^+

In Fig. 7 it is seen that the values of $G\varepsilon$ of e_s^- are the same in solutions of TEA as in pure 3-MO between 103 and 153 K, and the $G\varepsilon$'s almost double as the temperature is increased in this range. The $G\varepsilon$'s of RH^+ decrease by about 30% over the same temperature range. The values of $G\varepsilon$ given in Fig. 7 are those estimated

TABLE 1. Effect of electron scavengers on yields of positive ion in 3-methyloctane

T (K)	Solute	Mol%	$G\varepsilon_{650} \times 10^4$*
109.5	None	—	1.24†
109.5	SF_6	1.22	1.63†
127	None	—	1.09†
127	CCl_4	0.43	1.15†
127	CCl_4	3.61	1.24
127	CCl_4	6.51	1.35
127	SF_6	1.22	1.52†

*$G\varepsilon_{650}$ measured 100 ns after the start of a 40 ns pulse.
†After correction for electron absorption at 650 nm.

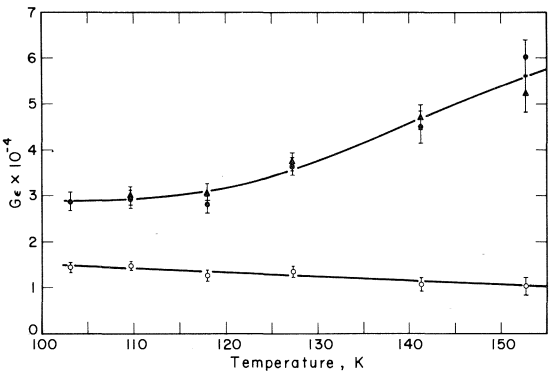

FIG. 7. Mid-pulse values of $G\varepsilon$ of electrons and positive ions as a function of temperature: ●, pure 3-methyloctane, λ = 2100; ▲, with 6.2 mol% triethylamine, λ = 2100; ○, positive ion contribution in pure 3-methyloctane at 650 nm (*i.e.* electron absorption at 650 nm has been subtracted).

from extrapolations to mid-pulse on plots of $1/OD$ *vs.* time. At the higher temperatures these extrapolations are large and therefore the uncertainties are considerable, as indicated by the error bars in Fig. 7. Thus at 153 K the estimated OD at mid-pulse (OD_0) for e_s^- is 2.3 times OD measured at 100 ns after the start of the pulse; by comparison, at 103 K OD_0 is 1.02 times OD at 100 ns.

Effect of Dose/Pulse and Light Intensity on Decay Rates

Variation of the dose per pulse and therefore OD_0 by a factor of 6.5 was found to have no effect on plots of OD/OD_0 against time at either 2100 or 650 nm for pure 3-MO at 127 K. This first order dependence on dose implies geminate reactions. Reduction of the intensity of the analyzing light by a factor of 10 also had no effect on the decay plots, so that the analyzing light was not inducing bleaching reactions.

Variation of the dose per pulse by a factor of 8.4 for a 1.22 mol% solution of SF_6 in 3-MO

at 127 K had some effect on plots of OD/OD_0 *vs.* time at 650 nm. At 1.3 μs OD/OD_0 was 0.60 and 0.50 for the low and high doses, respectively. An interpretation is that under these conditions a small part of RH^+ decays by a true second order reaction, and the rest by a reaction or reactions which are first order in dose.

Discussion

Spectra of e_s^- and RH^+

The spectra observed in irradiated pure 3-MO, Fig. 1, show maxima around 2100 and 625 nm which can be attributed confidently to the solvated electron and a positive ion, respectively. There is no indication in Fig. 1 of a shift with time in the spectrum of e_s^-. A shift with time in λ_{max} from 2000 to 1700 nm was found in 3-methylhexane glass at 76 K (15), but no such shift was found in liquid 3-methylhexane at temperatures above 112 K (3). The spectrum of the positive ion with $\lambda_{max} = 625$ nm is seen better in Fig. 3. Louwrier and Hamill (4) found $\lambda_{max} = 685$ nm for a γ-irradiated solution of 2-methyloctane in CCl_4 at 77 K and attributed it to the parent radical ion, RH^+. They also measured spectra of the parent radical ions of four methylnonanes at 77 K, and found a steady shift to the blue as the methyl group moved from the 2 to the 5 position. If it is assumed that the blue shift in going from 2-methyloctane to 3-MO is the same as in going from 2-methylnonane to 3-methylnonane, λ_{max} for 3-MO at 77 K would be expected at 650 nm. Comparison with our λ_{max} at 127 K indicates any shift with temperature is small.

Decay Kinetics for e_s^- and RH^+

The decay kinetics for e_s^- and RH^+ in pure 3-MO do not even approximately obey a log OD *vs.* time plot, but for both species the kinetics are first order in dose in that decay curves for different doses per pulse can be superimposed if normalized for dose. This demonstrates that these species are not decaying by second order reactions, and suggests that both species are undergoing geminate recombination. The decay kinetics for e_s^- in pure 3-MO are similar to those seen earlier in pure 3-methylhexane in that they happen to obey fairly well a plot of $1/OD$ against time (if the best line is drawn through the points for >50% decay, points for smaller percent decay fall below the line), but do not follow [1] (3).

However, a reaction or reactions other than recombination of e_s^- with RH^+ obviously occur also because RH^+ disappears much faster than e_s^-, as seen in Figs. 1, 4, and 6. The fractional difference in decay rates is greatest at the lowest temperature. One possibility is that, in addition to recombining with e_s^-, RH^+ dissociates or undergoes an ion–molecule reaction to form products that do not absorb in this region. However, such a reaction would be expected to obey a first order kinetics plot, and it is seen in Fig. 4*B* that successive $t_{1/2}$'s for RH^+ are very different in pure 3-MO. Instead we tentatively propose that RH^+ combines geminately with a second type of solvated electron (further evidence for this species is presented below) which presumably absorbs at $\lambda > 2200$ nm, as well as combining with e_s^-. Combination with this second type of solvated electron must be faster than with e_s^-. As well there seems to be a dissociation or ion–molecule reaction at longer times, to explain the almost complete disappearance of RH^+ by 35 μs in pure 3-MO at 127 K (Fig. 1).

In solutions of TEA where at short times the positive ion is mainly $(C_2H_5)_3NH^+$ or $(C_2H_5)_3N^+$ (16), the initial decay rate of e_s^- is very much slower than in pure 3-MO for $T < 127$ K, as indicated in Figs. 4 and 5. One possible reason is that the dominant positive ion in these solutions is $(C_2H_5)_3NH^+$ and the reaction

$$[4] \qquad e_s^- + (C_2H_5)_3NH^+ \rightarrow (C_2H_5)_3N + H$$

is very slow, just as the hydrated electron reacts slowly, if at all, with NH_4^+. However, this possibility is considered unlikely for three reasons: (*a*) if this were the case, initial electron decay would be expected to be much slower in TEA solutions than in pure 3-MO at all temperatures. In fact, as indicated in Fig. 6, the differences are smaller at the higher temperatures. (*b*) To explain why the effectiveness of TEA in increasing the yields of trapped electrons in 3-methylpentane glasses at 77 K goes through a maximum at a few percent, Hamill (1) has proposed that the decrease in effectiveness at higher concentrations is due to hole migration along chains of TEA molecules and therefore the dominant positive ion must be $(C_2H_5)_3N^+$ rather than $(C_2H_5)_3NH^+$. (*c*) If the proton affinity of $(C_2H_5)_3N$ is the same as that of NH_3, [4] is exothermic by about 110 kcal mol^{-1} in the gas phase. The energetics would be similar in a

hydrocarbon where the reactants are weakly solvated (as contrasted to the situation in water where solvation is strong) and therefore [4] would be expected to be fast in 3-MO.

A much more likely explanation for the slower initial decay of e_s^- in TEA solutions for $T \leq 127$ K is that RH^+ has a mobility which is much higher than that of $(C_2H_5)_3NH^+$ or $(C_2H_5)_3N^+$, and is also higher than the mobility of e_s^-. RH^+ must migrate by a resonance transfer of an electron from RH (hole transfer). However, at 141 K the mobilities of e_s^- and RH^+ are more similar, as indicated by the fact that TEA has a smaller effect on the decay rate of e_s^- (Fig. 6).

In pure 3-MO at 127 K, e_s^- decays more slowly at times >20 μs than in a TEA solution (Fig. 5). At these times only a small fraction of the original RH^+ remains (Fig. 1), and the remaining electrons must decay slowly with widely separated cations produced from RH^+ by dissociation or ion–molecule reactions.

A small growth of absorption at 2100 nm was seen in TEA solutions at temperatures around 127 K (inset of Fig. 5). This might be due to a conversion into e_s^- with $\lambda_{max} = 2100$ nm by a small percentage of a second type of solvated electron which was mentioned above and for which further evidence is given below.

In SF_6 solutions the decay of RH^+ is only slightly slower than in pure 3-MO (Fig. 4*B*). In these solutions the neutralization partner of RH^+ must be predominately SF_6^-. The mobility of SF_6^- has been measured in cyclohexane at room temperature, and is very much less than that of electrons in hydrocarbons like 3-MO at room temperature (19). Activation energies are not available, but at 109.5 K SF_6^- might still be expected to be less mobile than e_s^-. However, it was concluded above that at this temperature RH^+ moves much more than does e_s^- in the recombination process, so further decrease of the mobility of the negatively charged reactant is not expected to have much effect.

Yields of RH^+ and e_s^-

As the temperature is increased from 103 to 153 K, the initial $G\varepsilon$ of RH^+ decreases while that of e_s^- increases (Fig. 7). A referee has pointed out that these changes in $G\varepsilon$'s might simply reflect changes in ε at the chosen wavelengths. However, we have indicated above that any shift in λ_{max} for RH^+ between 77 and 127 K is small. A change in ε_{max} should be likewise small between 103 and 153 K since it would reflect an expected small change in band width. Earlier we found that the spectrum of e_s^- in liquid 3-methylhexane at 121 K is very similar to that of the glass at 76 K (3). Very recently small changes in λ_{max} with temperature have been reported for e_s^- in several ethers; ε_{max} was found to be practically constant with temperature (20). Therefore we cannot eliminate the possibility that the changes with temperature in $G\varepsilon$ seen in Fig. 7 are due to changes in ε, but we think they are more likely due to changes in G. A decrease in the yield of RH^+ while the yield of e_s^- increases could be explained by production of another type of initial positively charged species we have not observed, or another type of solvated electron we have not detected and which presumably absorbs at wavelengths >2200 nm. Since we have some other evidence for a second type of solvated electron, discussed above, we prefer the latter explanation. The yield of this second electron species would then decrease with increasing temperature to fulfill the presumed requirement that the yield of RH^+ equal the total yield of solvated electrons.

Only rough estimates of the extinction coefficients of e_s^- and RH^+ are available from the literature. For 3-methylpentane glass at 77 K, ε at λ_{max} ($\sim$1700 nm) has been estimated as $3 \times 10^4\ M^{-1}\,cm^{-1}$ (1). If we assume ε at λ_{max} is the same for electrons in liquid 3-MO, then $G(e_s^-)$ is 0.97 at 103 K and 1.87 at 153 K. The only estimate available for ε for RH^+ is for 2-methyldecane by Louwrier and Hamill (4), who noted that their results suggest that oscillator strengths increase markedly with carbon number. The ε_{max} for RH^+ from 2-methyldecane, $8.2 \times 10^3\ M^{-1}\,cm^{-1}$, may then be taken as an upper limit for ε_{max} for RH^+ from 3-MO. The lower limits of the initial G's for RH^+ are then calculated as 1.74 at 103 K and 1.27 at 153 K. These rough estimates suggest that if a second type of solvated electron is produced in 3-MO, its yield is appreciable at 103 K.

A second type of trapped electron with a clearly separated absorption band in the near infrared has been reported recently in a rather different type of system, three aqueous glasses and crystalline ice (21–23).

Effect of Electron Scavengers on Yields of RH^+

Our estimated initial yields of RH^+ and e_s^- are higher and lower, respectively, in the presence of SF_6 or CCl_4 than in pure 3-MO (Table 1). As indicated above, CCl_4^+ may also be produced in the CCl_4 solutions, and this may at least partly

account for the greater effectiveness of SF_6 than of CCl_4 in increasing the initial yield of RH^+. These effects can be explained by proposing that CCl_4 or SF_6 can scavenge an unsolvated, quasi-free electron (e_{qf}^-); in the absence of scavenger (S) this species can be solvated or can recombine with RH^+ very quickly, before our first observation:

[5] $$e_{qf}^- + \text{Trap} \rightarrow e_s^-$$

[6] $$e_{qf}^- + RH^+ \rightarrow RH$$

[7] $$e_{qf}^- + S \rightarrow S^-$$

Scavenging of the quasi-free electron, [7], increases the yield of RH^+ by decreasing the amount of [6], and of course decreases [5] also.

Another possible explanation is that in pure 3-MO some recombination between RH^+ and e_s^- takes place by tunnelling at very short times (24), such that our extrapolation procedure for estimating initial yields is not valid Added SF_6 or CCl_4 would interfere with this recombination by scavenging e_s^- and hence giving increased yields of RH^+ at our first observation times.

Relationship to Scavenging Experiments

If the neutralization reactions in cold hydrocarbons are as complicated as our experiments suggest and involve two types of solvated electron and a quasi-free electron, plus a mobile hole and cations produced from it by dissociation or ion–molecule reactions, then it is not surprising that decay of one type of solvated electron does not follow [1], the behaviour predicted from scavenging experiments at room temperature (10), since this prediction involves the implicit assumption that only one species reacts with electron scavengers. The situation in room temperature hydrocarbons might be much simpler in that perhaps only one electron species is important under these conditions, but at this time prediction of lifetimes of geminate electrons from scavenging experiments seems hazardous.

Acknowledgement

The authors gratefully acknowledge the very capable assistance of Mr. G. G. Teather in the experimental work, and helpful discussions with Professor W. H. Hamill and Dr. J. R. Miller.

1. W. H. Hamill. Radical ions. *Edited by* E. T. Kaiser and L. Kevan. Wiley-Interscience, New York, NY. 1968. Chapt. 9.
2. H. A. Gillis, N. V. Klassen, G. G. Teather, and K. H. Lokan. Chem. Phys. Lett. **10**, 481 (1971).
3. H. A. Gillis, N. V. Klassen, and G. G. Teather. Radiation research: biomedical, chemical and physical perspectives. *Edited by* O. F. Nygaard, H. I. Adler, and W. K. Sinclair. Academic Press, New York, NY. 1975. p. 443.
4. P. W. F. Louwrier and W. H. Hamill. J. Phys. Chem. **72**, 3878 (1968).
5. G. Beck and J. K. Thomas. J. Phys. Chem. **76**, 3856 (1972).
6. A. Hummel and L. H. Luthjens. J. Chem. Phys. **59**, 654 (1973).
7. E. Zador, J. M. Warman, and A. Hummel. Chem. Phys. Lett. **23**, 363 (1973).
8. O. Brede, W. Helmstreit, and R. Mehnert. Chem. Phys. Lett. **28**, 43 (1974).
9. M. P. De Haas, J. M. Warman, P. P. Infelta, and A. Hummel. Chem. Phys. Lett. **31**, 382 (1975).
10. S. J. Rzad, P. P. Infelta, J. M. Warman, and R. H. Schuler. J. Chem. Phys. **52**, 3971 (1970).
11. A. C. Ling and J. E. Willard. J. Phys. Chem. **72**, 3349 (1968).
12. A. C. Ling and J. E. Willard, J. Phys. Chem. **72**, 1918 (1968).
13. L. Kevan. Advances in radiation chemistry. Vol. 4. *Edited by* M. Burton and J. L. Magee. Wiley-Interscience, New York, NY. 1969. p. 188.
14. G. G. Teather, N. V. Klassen, and H. A. Gillis. Int. J. Radiat. Phys. Chem. **8**, 477 (1976).
15. N. V. Klassen, H. A. Gillis, and G. G. Teather. J. Phys. Chem. **76**, 3847 (1972).
16. J. B. Gallivan and W. H. Hamill. J. Chem. Phys. **44**, 2378 (1966).
17. P. W. F. Louwrier and W. H. Hamill. J. Phys. Chem. **73**, 1702 (1969).
18. R. E. Bühler. Radiat. Res. Rev. **4**, 233 (1972).
19. A. Hummel. Advances in radiation chemistry. Vol. 4. *Edited by* M. Burton and J. L. Magee. Wiley-Interscience, New York, NY. 1974. pp. 50, 51.
20. F.-Y. Jou and G. R. Freeman. Can. J. Chem. **54**, 3693 (1976).
21. G. V. Buxton, H. A. Gillis, and N. V. Klassen. Chem. Phys. Lett. **32**, 533 (1975).
22. G. V. Buxton, H. A. Gillis, and N. V. Klassen. Can. J. Chem. **54**, 367 (1976).
23. H. Hase and K. Kawabata. J. Chem. Phys. **65**, 64 (1976).
24. J. R. Miller. Chem. Phys. Lett. **22**, 180 (1973).

Discussion

R. S. Dixon: It is well-known from mass spectrometric studies that fragmentation can give rise to many different ions in the gas phase. Is it possible that you have more than one positive ion with a reasonable lifetime at low temperature in your system?

R. J. Woods: Ion fragmentation is less likely in liquid phase radiolysis than in the mass spectrometer because excitational energy of excited ions is rapidly dissipated in a condensed medium. However, we have suggested that ion fragmentation may contribute to the rapid disappearance of the positive ion which absorbs at 650 nm; carbonium ions formed by fragmentation would be expected to have a longer lifetime than the parent positive ion.

J. R. Miller: While you have shown that the positive ion in the cold liquid decays rapidly, have you studied its decay at a temperature low enough so that the system is rigid?

R. J. Woods: No. Studies have not been carried out below the glass transition point.

The yield and extinction coefficient of the solvated electron in methanol: pulse radiolysis of nitrobenzene and tetranitromethane solutions

DAVID W. JOHNSON AND G. ARTHUR SALMON

The University of Leeds, Cookridge Radiation Research Centre, Cookridge Hospital, Leeds LS16 6QB, U.K.

Received September 27, 1976

DAVID W. JOHNSON and G. ARTHUR SALMON. Can. J. Chem. **55**, 2030 (1977).

The radical anion $C_6H_5NO_2^{\cdot-}$, NB^-, which has a strong absorption spectrum from 250–500 nm, is formed by reaction of nitrobenzene with solvated electrons, e_s^-, and hydroxymethyl radical anions, $^{\cdot}CH_2O^-$, with $k_1 = (1.92 \pm 0.35) \times 10^{10}\ M^{-1}\ s^{-1}$ and $k_2 = (1.03 \pm 0.02) \times 10^{10}\ M^{-1}\ s^{-1}$.

[1] $$e_s^- + C_6H_5NO_2 \rightarrow C_6H_5NO_2^{\cdot-}$$

[2] $$^{\cdot}CH_2O^- + C_6H_5NO_2 \rightarrow C_6H_5NO_2^{\cdot-} + H_2CO$$

$G\varepsilon_\lambda$ is constant for NB^- over a wide range of nitrobenzene concentrations in basic solution. By assuming that the yields of scavengeable radicals are the same in neutral and basic solutions we obtain $\varepsilon(NB^-)_{300\ nm} = (1.66 \pm 0.02) \times 10^4\ M^{-1}\ cm^{-1}$. This value is used to evaluate the yield of e_s^- scavengeable by dilute solutions of solutes as $G(e_s^-)_{esc} = 1.20 \pm 0.03$. Extinction coefficients of e_s^-, hydroxymethyl radicals, $^{\cdot}CH_2OH$, and $^{\cdot}CH_2O^-$ and the oscillator strength of the e_s^- absorption are calculated.

The yields of e_s^- determined by previous workers are discussed in terms of dry, damp, geminate, free, spur, and escaped electrons. A model is constructed in terms of damp, spur, and escaped electrons which compares favourably with experimental scavenging results and direct measurements by optical pulse radiolysis.

DAVID W. JOHNSON et G. ARTHUR SALMON. Can. J. Chem. **55**, 2030 (1977).

Le radical anion $C_6H_5NO_2^{\cdot-}$, NB^-, qui a un spectre d'absorption très intense dans la région de 250–500 nm, se forme par réaction du nitrobenzène avec les électrons solvatés, e_s^-, et les anions radicaux hydroxyméthyles, $^{\cdot}CH_2O^-$, avec des constantes de vitesse $k_1 = (1.92 \pm 0.35) \times 10^{10}\ M^{-1}\ s^{-1}$ et $k_2 = (1.03 \pm 0.02) \times 10^{10}\ M^{-1}\ s^{-1}$.

[1] $$e_s^- + C_6H_5NO_2 \rightarrow C_6H_5NO_2^{\cdot-}$$

[2] $$^{\cdot}CH_2O^- + C_6H_5NO_2 \rightarrow C_6H_5NO_2^{\cdot-} + H_2CO$$

La valeur de $G\varepsilon_\lambda$ est constante pour NB^- à des concentrations de nitrobenzène très diverses lorsque l'on travaille en solution basique. En faisant l'hypothèse que les rendements des radicaux qui peuvent être piégés sont les mêmes en solutions neutres et basiques, on obtient la valeur $\varepsilon(NB^-)_{300\ nm} = (1.66 \pm 0.02) \times 10^4\ M^{-1}\ cm^{-1}$. On peut utiliser cette valeur pour évaluer le rendement en e_s^- piégeable pour des solutions diluées de solutés; alors $G(e_s^-)_{esc} = 1.20 \pm 0.03$. On a aussi calculé les coefficients d'extinction de e_s^-, des radicaux hydroxyméthyles, $^{\cdot}CH_2OH$, et $^{\cdot}CH_2O^-$ et la force d'oscillateur de l'absorption e_s^-.

On discute des rendements de e_s^- déterminés antérieurement par d'autres chercheurs en termes d'électrons secs, humides, géminés, libres, de grappe et qui se sont échappés. On construit un modèle en termes d'électrons humides, de grappe et qui se sont échappés qui se compare favorablement avec les résultats de piégeages expérimentaux et des mesures directes par radiolyse optique pulsée.

[Traduit par le journal]

Introduction

In a previous paper the overall scavengeable yield of solvated electrons, e_s^-, and hydroxymethyl radicals, $^{\cdot}CH_2OH$, was determined by pulse radiolysis of dilute solutions of tetranitromethane, TNM (1). Estimates of $G(e_s^-)_{esc}$,[1] the yield of e_s^- which escape from regions of high radical concentration (spurs) to become homogeneously distributed in solution, vary from 1.0–2.0 (2–14). Pulse radiolysis measurements of absorption spectra yield only the product $G\varepsilon_\lambda$,[2] thus uncertainty in $G(e_s^-)$ results in a correponding uncertainty in the extinction

[1] The G value of the designated product is the radiation chemical yield in molecules $(100\ eV)^{-1}$.

[2] $G\varepsilon(X)_\lambda$ is the product in units of $M^{-1}\ cm^{-1}$ of the radiation chemical yield and the molar decadic extinction coefficient of the light absorbing species, X, at wavelength λ.

coefficient of e_s^-. This work utilizes the strong absorption spectrum between 280 and 320 nm of $C_6H_5NO_2^{\cdot-}$, NB^- (15), generated by reaction of e_s^- and the hydroxymethyl radical anion, $^{\cdot}CH_2O^-$, with nitrobenzene by reactions 1 and 2 to obtain a more reliable value for $G(e_s^-)$ and hence determine the extinction coefficient of e_s^-.

[1] $$e_s^- + C_6H_5NO_2 \rightarrow C_6H_5NO_2^{\cdot-}$$

[2] $$^{\cdot}CH_2O^- + C_6H_5NO_2 \rightarrow C_6H_5NO_2^{\cdot-} + H_2CO$$

Experimental

Nitrobenzene (B.D.H. AnalaR) was washed three times with a threefold excess of triply distilled water, dried over anhydrous calcium chloride, and fractionally distilled in a nitrogen atmosphere, the middle fraction being collected at 211–214°C.

Nitrous oxide (B.O.C. 99.999%) was passed over potassium hydroxide pellets, through a trap at −80°C and either used directly or further purified by degassing at −130°C. This latter material was stored on a vacuum line and degassed again before use. Analysis by gas chromatography using a molecular sieve 5A (B.D.H.) column at 43°C with helium as a carrier gas showed no trace of any gaseous impurity.

Methanol (Wilkinson-Vickers A.R.), tetranitromethane (Koch Light, Puriss. A.R.), and argon (B.O.C. 99.995%) were purified as described previously (1).

Sodium metal (B.D.H., G.P.R. dry; or Hopkins and Williams, dry) was used as supplied.

Methods

The techniques of sample preparation, saturation with argon or nitrous oxide, and details of the pulse radiolysis apparatus have been described previously (16–18). Pulse lengths from 10 ns to 0.2 μs were chosen as appropriate.

Solutions for the determination of the reaction rate between N_2O and e_s^- were prepared by distillation *in vacuo* of a measured quantity of N_2O onto a sample of methanol which had been previously degassed at −80°C. The concentration of N_2O in solution at the temperature of the experiment was determined using values for the solubility of N_2O in methanol of 2.03×10^{-4}, 2.07×10^{-4}, and 2.99×10^{-4} M (mm Hg)$^{-1}$ at 25 (19), 20 (20), and 0°C (21), respectively. All experiments were performed at room temperature (20 ± 2°C). All errors quoted are one standard deviation of the mean (standard error).

Results

A. Nitrobenzene Solutions

I. Kinetic Studies

(a) Basic Solutions—The rate constant for reaction 1 between e_s^- and nitrobenzene was determined as $k_1 = (1.92 \pm 0.35) \times 10^{10}$ M^{-1} s^{-1} from the first order decays of the absorption of e_s^- at 580 nm in Ar saturated solutions containing $6 \times 10^{-5} \leq [C_6H_5NO_2] \leq 3 \times 10^{-3}$ M and $2 \times 10^{-2} \leq [CH_3ONa] \leq 2 \times 10^{-1}$ M. This value compares favourably with a previous measurement (5).

The rates of growth of absorption at 300 nm due to NB^- following 1.5–4.0 krad pulses measured for N_2O saturated solutions with $6 \times 10^{-5} \leq [C_6H_5NO_2] \leq 2 \times 10^{-2}$ M and $1 \times 10^{-2} \leq [CH_3ONa] \leq 1$ M conformed to first order kinetics in every case. In N_2O saturated solution the principal radical species, hydrogen atoms (H·), methoxy radicals ($CH_3O^{\cdot}$), and e_s^- are converted rapidly into $^{\cdot}CH_2OH$ with half-lives of <5 ns, 150 ns (16), and <1 ns, respectively, by reactions 3 to 5 and $^{\cdot}CH_2OH$ is in acid–base equilibrium 6 with $^{\cdot}CH_2O^-$ (22).

[3] $$H^{\cdot} + CH_3OH \rightarrow H_2 + {}^{\cdot}CH_2OH$$

[4] $$CH_3O^{\cdot} + CH_3OH \rightarrow CH_3OH + {}^{\cdot}CH_2OH$$

[5*a*] $$e_s^- + N_2O \rightarrow N_2 + {}^{\cdot}O^-$$

[5*b*] $$^{\cdot}O^- + 2CH_3OH \rightarrow H_2O + {}^{\cdot}CH_2OH + CH_3O^-$$

[6] $$^{\cdot}CH_2OH + CH_3O^- \rightleftharpoons {}^{\cdot}CH_2O^- + CH_3OH$$

Assuming that $^{\cdot}CH_2O^-$, but not $^{\cdot}CH_2OH$, reacts with nitrobenzene (as is observed in aqueous solution (15)) then the dependence of the observed first order rate constants for formation of NB^- on $[C_6H_5NO_2]$ and $[CH_3ONa]$ is given by [7]

[7] $$k_{obs} = \frac{k_2[C_6H_5NO_2]}{\left(1 + \frac{1}{K_6'[CH_3ONa]}\right)}$$

where $K_6' = K_6/[CH_3OH]$. This expression may be rearranged to [8]

[8] $$[C_6H_5NO_2]/k_{obs} = \frac{1}{k_2}\left(1 + \frac{1}{K_6'[CH_3ONa]}\right)$$

A graph of $[C_6H_5NO_2]/k_{obs}$ against $1/[CH_3ONa]$ shown in Fig. 1 gives $k_2 = (1.03 \pm 0.02) \times 10^9$ M^{-1} s^{-1} and $K_6 = 3440 \pm 250$. The latter value is to be compared with $K_6 = 2120 \pm 235$ determined previously (22). The reason for this discrepancy is not clear since under the experimental conditions employed the rate of formation of NB^- is not sufficiently rapid to be affected significantly by the rate of formation of $^{\cdot}CH_2O^-$ (22). However, the low degree of accuracy of reciprocal plots of the type employed may be responsible.

(b) Neutral Solutions—An attempt to measure the rate of reaction 9 of $^{\cdot}CH_2OH$ with nitrobenzene in N_2O saturated solutions by the increase in absorption at 300 nm was unsuccessful since no growth was observed over 20 μs

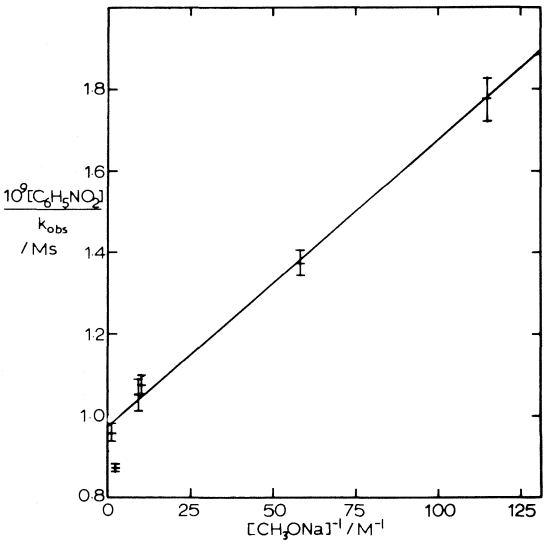

FIG. 1. Variation with $[C_6H_5NO_2]$ and $[CH_3ONa]$ of the observed first order rate constant, k_{obs}, for the formation of NB^- in N_2O saturated methanol.

at $[C_6H_5NO_2] = 3 \times 10^{-3}$ *M*. Furthermore the bimolecular decay of the

[9] $\cdot CH_2OH + C_6H_5NO_2 \rightarrow C_6H_5N(O\cdot)(O{-}CH_2OH)$

absorption of $\cdot CH_2OH$ at 320 nm (reaction 10) was unaffected by the presence of the solute. At higher concentrations of nitrobenzene absorption of light by the solute made observations

[10] $2\cdot CH_2OH \rightarrow (CH_2OH)_2$

impossible. A value for $k_9 = 3.3 \times 10^6$ M^{-1} s^{-1} has been determined in strongly acidic solutions of nitrobenzene (23). This value, and that for k_{10} (22), indicates that reaction 9 is too slow to be responsible for the disappearance of $\cdot CH_2OH$ in any solutions studied in this work.

In aqueous solution, H· and hydroxyl radicals, ·OH, react with nitrobenzene to form adducts to the aromatic ring by reaction 11 giving products which absorb strongly at 400 nm (24). There was

[11] $H(OH)\cdot + C_6H_5NO_2 \rightarrow H(OH)\cdot C_6H_5NO_2$

no evidence of any absorption at 400 nm on pulse radiolysis of an N_2O saturated solution containing 3×10^{-3} *M* nitrobenzene. It must be concluded that at this concentration of nitrobenzene reactions of H· and $CH_3O\cdot$ are too slow to compete with their reactions 3 and 4 with the solvent.

II. Spectra and Yields

(a) Basic Solutions—The spectra generated by 1.5 krad pulses in Ar and N_2O saturated solutions with $[C_6H_5NO_2] = 1$ m*M* and $[CH_3ONa] = 0.5$ *M* are identical within experimental error. The spectrum is shown in Fig. 2. This spectrum, with maxima at 295 and 420 nm, is similar to that attributed to NB^- in alkaline aqueous solution after allowance is made for the depletion of nitrobenzene (15). After the rapid formation of the absorption no decay was observed over 100 μs and only 50% of the absorption decayed over 2 min. This sets an upper limit to the decay since no allowance was made for the dilution of irradiated solution by unirradiated solution in the connecting tubing.

$G\varepsilon$ values for NB^- were determined at wavelengths from 290–320 nm for Ar saturated solutions with $6 \times 10^{-5} \leq [C_6H_5NO_2] \leq 3 \times 10^{-3}$ *M* and $1 \times 10^{-2} \leq [CH_3ONa] \leq 1.0$ *M*. The values, which were found to be independent of both $[C_6H_5NO_2]$ and $[CH_3ONa]$, are listed in Table 1. Also listed are the extinction coefficients of NB^- which were calculated on the assumption that the yield of radicals scavengeable by TNM in neutral Ar saturated solution, $G(NF^-)]_N^{Ar}$ (1), is equal to that scavenged by nitrobenzene in basic Ar saturated solution, *i.e.*,

$$[G(NF^-)]_N^{Ar} = [G(NB^-)]_B^{Ar} = [G(R\cdot)]^{Ar}$$

where the subscripts N and B refer to neutral and basic solutions and $[G(R\cdot)]^{Ar}$ is the yield of radicals scavengeable in neutral Ar saturated solutions (1). The basis for this assumption is considered in the discussion.

The variation of $G\varepsilon_{300\ nm}$ with $[CH_3ONa]$ was studied over a much larger range (1.36×10^{-4} to 1.0 *M*) for Ar and N_2O saturated solutions containing 8×10^{-4} *M* $C_6H_5NO_2$ at 3.5 krad/pulse. The large variation in yield (see Fig. 3) is due to reactions 10, 12, and 13 (22) which lead to the disappearance of $\cdot CH_2OH$ and $\cdot CH_2O^-$ in competition with their reaction with nitrobenzene.

[12] $\cdot CH_2OH + \cdot CH_2O^- \rightarrow$ } Products

[13] $2\cdot CH_2O^- \rightarrow$ }

The lines in Fig. 3 describing the dependence of the yield of NB^- on the concentration of base were calculated from [14].

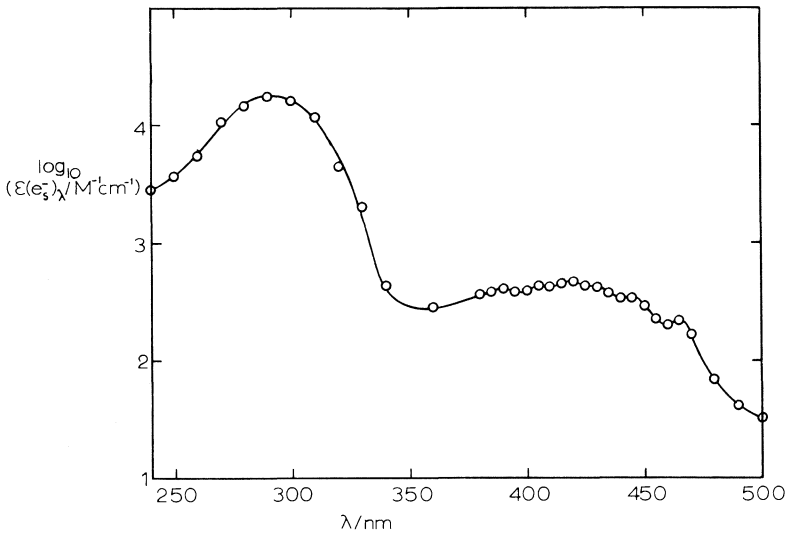

FIG. 2. Spectrum of NB^- produced by a 1.5 krad pulse in Ar saturated methanol containing 1 m*M* $C_6H_5NO_2$ and 0.5 *M* CH_3ONa.

$$[14] \qquad [G(NB^-)]_c = Z_c G(e_s^-)_0 + \frac{Yk_2[C_6H_5NO_2]}{AB} \log_e \left(1 + \frac{AB(G(R^\bullet) - Z_c G(e_s^-)_0)}{Yk_2[C_6H_5NO_2]}\right)$$

where

$$A = 2k_{10}\left(\frac{1}{1 + K_6'[CH_3ONa]}\right)^2 + \frac{2k_{12}}{B}\left(1 + \frac{1}{1 + K_6'[CH_3ONa]}\right) + \frac{2k_{13}}{B^2}$$

$$B = \left(\frac{1}{K_6'[CH_3ONa]}\right)$$

and $Y = 1.204 \times 10^6/D$. In [14], $[G(NB^-)]_c$ is the yield of NB^- at $[CH_3ONa] = c$ *M*, and $G(e_s^-)_0$ is the slowly decaying yield of e_s^- in neutral solution corrected for decay during the pulse (the 'initial' yield). Z_c is the experimentally determined ratio of the 'initial' yield of e_s^- in a solution with $[CH_3ONa] = c$ *M* to that in neutral solution and *D* is the dose delivered by the pulse in units of krads. Values of $[G(R^\bullet)]$ for Ar and N_2O saturated solutions were determined from $G\varepsilon_{300\,nm}$ at $[CH_3ONa] \geq 1 \times 10^{-2}$ *M* when scavenging of radicals by nitrobenzene is essentially complete. The results in Fig. 3 were obtained from a single experiment so that the agreement between the observed and calculated yields is good. The data used in this calculation are listed in Table 2.

(b) Neutral Solutions—On pulse radiolysis of Ar saturated solutions of methanol with $6 \times 10^{-5} \leq [C_6H_5NO_2] \leq 3 \times 10^{-3}$ *M* using 10 or 25 ns, 1–2 krad pulses an absorption spectrum with a maximum at 295 nm grew in after the pulse. The spectrum subsequently decayed rapidly over 25 μs and slowly over several hundred μs. The absorption is composed of contributions from NB^-, e_s^-, and $^\bullet CH_2OH$. In order to determine the yield of NB^-, which in neutral solution is generated by reaction between e_s^- and nitrobenzene (reaction 1), both the rate of formation and decay of NB^- must be known as well as the rate of decay of the absorption due to $^\bullet CH_2OH$. In aqueous solution NB^- is in equilibrium with the un-ionised radical $C_6H_5NO_2H^\bullet$,NBH, (equilibrium 15) (15). Although

$$[15] \qquad C_6H_5NO_2H^\bullet \rightleftharpoons C_6H_5NO_2^{\bullet-} + H^+$$

no value for K_{15} has been measured in methanol it is likely to be considerably less than its value in water ($K_{15} = 6.3 \times 10^{-4}$ *M* (15)) on account of the lower free energy of solvation of ions in

TABLE 1. Yields and extinction coefficients of NB^- in Ar saturated solution with $6 \times 10^{-5} \leq [C_6H_5NO_2] \leq 3 \times 10^{-3}$ M and $2 \times 10^{-2} \leq [CH_3ONa] \leq 1.0$ M

λ	10^{-4} $G\varepsilon_\lambda$	$10^{-3}\{\varepsilon(NB^-)_\lambda - \varepsilon(C_6H_5NO_2)_\lambda\}$*	10^{-3} $\varepsilon(NB^-)_\lambda$*
290	9.18±0.19	16.3±0.4	18.3±0.4
300	8.78±0.08	15.6±0.2	16.6±0.2
310	6.28±0.06	11.2±0.2	11.6±0.2
320	2.41±0.08	4.3±0.2	4.5±0.2

*Calculated assuming $[G(R\cdot)]_B^{Ar} = 5.63 \pm 0.05$.

methanol. However, in neutral methanol, for which $[H^+] = 1 \times 10^{-8}$ M, equilibrium 15 will lie towards the dissociated form. The relatively fast initial decay of absorption may be caused by reaction between H^+ formed during the pulse and NB^- forming the less strongly absorbing NBH (15).

The formation and decay of absorption can therefore be formulated in terms of [16]–[20].

$$[16] \qquad [e_s^-]_t = [e_s^-]_0 \exp(-[k_1' + k_{21}]t)$$

$$[17] \qquad [NB^-]_t = \frac{k_1[e_s^-]_0}{k_1' + k_{21} - k_{-15}'}(\exp(-k_{-15}'t) - \exp(-[k_1' + k_{21}]t))$$

$$[18] \qquad [NBH]_t = \frac{k_1'k_{-15}'[e_s^-]_0}{k_1' + k_{21} - k_{-15}'}\left(\frac{\exp(-[k_1' + k_{21}]t) - 1}{k_1' + k_{21}} - \frac{\exp(-k_{-15}'t) - 1}{k_{-15}'}\right)$$

$$[19] \qquad [C_6H_5NO_2]_t = [C_6H_5NO_2]_0 - k_1'[e_s^-]_0\left(\frac{1 - \exp([k_1' + k_{21}]t)}{(k_1' + k_{21})}\right)$$

$$[20] \qquad [\cdot CH_2OH]_t = \frac{[CH_2OH]_0}{(1 + 2k_{10}[\cdot CH_2OH]_0 t)}$$

where $[X]_0$ and $[X]_t$ are the concentrations of species X produced during the pulse and at time t after the middle of the pulse, respectively, and $k_1' = k_1[C_6H_5NO_2]$. It is assumed that the decay of NB^- by reaction with H^+ is first-order over the first few μs and that $k_{-15}' = k_{-15}[H^+]_0$. The decay of e_s^- other than by reaction with nitrobenzene is represented by reaction 21. In Ar saturated methanol it is found that the decay of e_s^- follows a first order rate law, but the observed first order rate constant, k_{21}, is dependent on the dose in the pulse (11). Hence values for k_{21} at the dose used in each experiment were determined from the decay of e_s^- in Ar saturated

$$[21] \quad e_s^- + 2CH_3OH \rightarrow \cdot CH_2OH + CH_3O^- + H_2$$

methanol. The sum of $[e_s^-]_0$ and $[\cdot CH_2OH]_0$ is calculated using $[G(R\cdot)]_N^{Ar} = 5.63 \pm 0.05$ (1).

The changes in absorption at 290 and 300 nm following a pulse were fitted to [16]–[20] at five different $[C_6H_5NO_2]$ using a linear least squares method with $G(e_s^-)_0$ and k_1 as independent variables. The extinction coefficient $\varepsilon(NBH)_\lambda$ was taken as its value in aqueous solution (15). The values for rate constants and extinction coefficients are taken from ref. 22 and elsewhere in the text. The calculated and observed absorption data were within experimental error at all concentrations of $C_6H_5NO_2$ and at both wavelengths studied. An example is shown in Fig. 4 which also shows contributions to the total absorption from each absorbing species. Since NB^- is the major component and decays only slowly, values used for the extinction coefficients of other species have little influence on $G(e_s^-)_0$. Values for $G(e_s^-)_0 = 1.20 \pm 0.03$ and $k_1 = (2.1 \pm 0.1) \times 10^{10}$ M^{-1} s^{-1} were obtained. The latter compares well with $k_1 = (1.92 \pm 0.35) \times 10^{10}$ M^{-1} s^{-1} determined in section A.*I.*(*a*) by direct observation of the decay of the absorption of e_s^-.

B. Nitrobenzene–Tetranitromethane Solutions

Pulse radiolysis of Ar saturated TNM solutions results in the formation by reactions 22 and 23 of NF^- which absorbs at 355 nm (1).

TABLE 2. Parameters employed in the calculation of the theoretical curves in Fig. 3

(*a*) Reactions

Reaction	10^{-9} k (M^{-1} s^{-1})	Reference
[2] $\cdot CH_2O^- + C_6H_5NO_2 \rightarrow C_6H_5NO_2^{\cdot -} + CH_2O$	1.02	This work
[6] $\cdot CH_2OH + CH_3O^- \rightleftharpoons \cdot CH_2O^- + CH_3OH$	(K_6 = 2120)	22
	(K_6 = 3440)	This work
[10] $2\cdot CH_2OH \rightarrow$	1.44	This work
[12] $\cdot CH_2OH + \cdot CH_2O^- \rightarrow$ products	2.25	This work, 22*
[13] $2\cdot CH_2O^- \rightarrow$	0.16	This work, 22*

(*b*) Yields

Species	Ar saturated	N_2O saturated
e_s^-	1.2	0
$\cdot CH_2OH$	4.6	5.92

*Calculated from k/ε_λ values from ref. 22 and ε_λ from this work (Fig. 6).

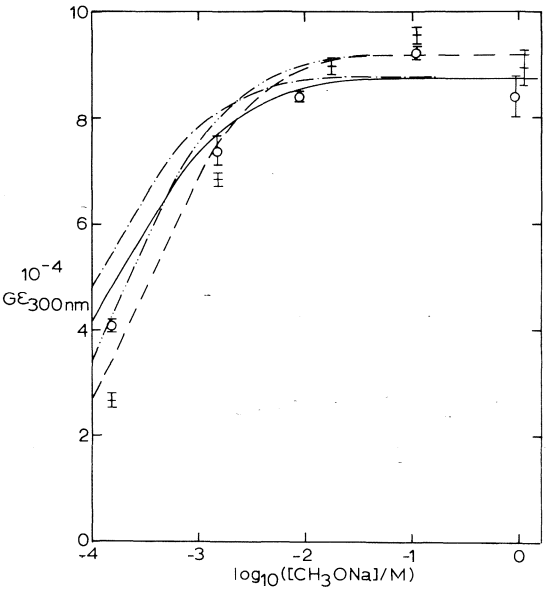

FIG. 3. Dependence of $G\varepsilon_{300\,nm}$ on the concentration of base in solutions containing 0.8 mM nitrobenzene. ○, Ar saturated; +, N_2O saturated. Curves calculated using [14] and data in Table 2. Ar saturated: K_6 = 2120, —; K_6 = 3440, -·-·-; N_2O saturated: K_6 = 2120, ---; K_6 = 3440, -·-·-·-.

Addition of nitrobenzene results in a decrease in $G\varepsilon_{355\,nm}$. This dependence of $G\varepsilon_{355\,nm}$ on $[C_6H_5NO_2]/[TNM]$ was studied in Ar saturated

[22] $e_s^- + C(NO_2)_4 \rightarrow C(NO_2)_3^- + NO_2$

[23] $\cdot CH_2OH + C(NO_2)_4 \rightarrow C(NO_2)_3^- + NO_2 + H_2CO + H^+$

solutions with $6 \times 10^{-5} \leq [TNM] \leq 3 \times 10^{-4}$

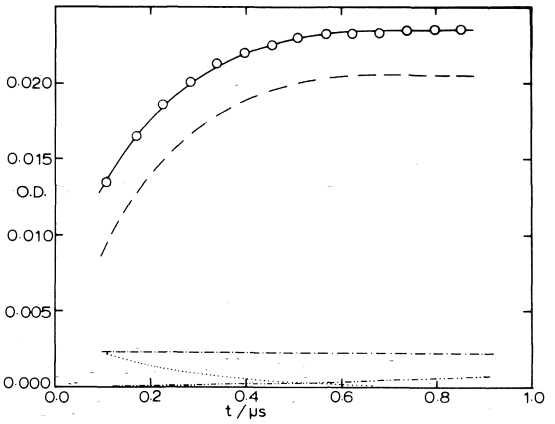

FIG. 4. Growth of absorption at 300 nm after a 10 ns, 1.6 krad pulse in an Ar saturated solution containing 3×10^{-4} M $C_6H_5NO_2$. Observed yield ○, solid line calculated from [16] to [20]. Time dependence of individual components: ---, NB^-; -·-·-·, $\cdot CH_2OH$; . . ., e_s^-; -·-·-·-, NBH.

M and $[C_6H_5NO_2]/[TNM] \geq 1$ and irradiated with 1.5–5.0 krad, 25 ns or 0.2 μs pulses. The 355 nm absorption grew in after the pulse to a plateau which was stable for at least 30 μs. The absorptions were not corrected for the absorption of NB^- since $\varepsilon(NB^-)_{355\,nm} \ll \varepsilon(NF^-)_{355\,nm}$. The dependence of $G(NF^-)$ on $[C_6H_5NO_2]/[TNM]$ is shown in Fig. 5. $G(NF^-)$ falls below its value in TMN solutions because nitrobenzene competes with TNM for e_s^- (reactions 1 and 22). Since $\cdot CH_2OH$ reacts only slowly with nitrobenzene the contribution to $G(NF^-)$ from reaction of $\cdot CH_2OH$ with TNM (reaction 23) is unaffected by nitrobenzene. Hence, at $[C_6H_5NO_2] \leq 1 \times 10^{-3}$ M, [24] applies where

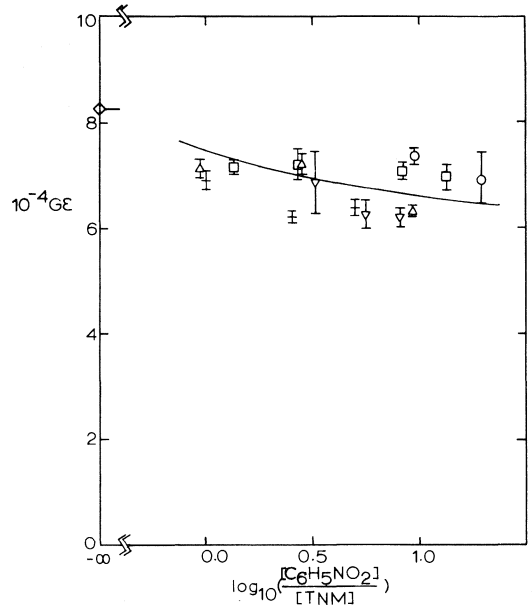

FIG. 5. Effect of nitrobenzene on $G\varepsilon_{355\text{ nm}}$ in Ar saturated solutions containing the following concentrations of TNM: ○, 6×10^{-5} *M*; □, 9.6×10^{-5} *M*; ▽, 1.15×10^{-4} *M*; +, 2.0×10^{-4} *M*; △, 2.15×10^{-4} *M*; and ◇, $3 \times 10^{-4}\ M < [\text{TNM}] < 3 \times 10^{-3}$ *M*. The solid line is calculated from [24] using $G(e_s^-)_0 = 1.38$.

$$[24]\quad [G(NF^-)]^{Ar}_{C_6H_5NO_2} = [G(NF^-)]^{Ar} - \left\{\frac{G(e_s^-)_0 k_1[C_6H_5NO_2]}{k_1[C_6H_5NO_2] + k_{22}[TNM]}\right\}$$

$[G(NF^-)]^{Ar}$ and $[G(NF^-)]^{Ar}_{C_6H_5NO_2}$ are the yields of NF^- in the absence and presence of nitrobenzene. The best value of $G(e_s^-)_0$ to fit the observed data for solutions with $[C_6H_5NO_2] \leq 1 \times 10^{-3}$ *M* is $G(e_s^-)_0 = 1.38 \pm 0.13$. Yields of NF^- calculated with this value in [24] are shown as the solid line in Fig. 5.

When the concentration of nitrobenzene is greater than 10^{-3} *M* $[G(NF^-)]^{Ar}_{C_6H_5NO_2}$ drops below the value predicted from [24] since nitrobenzene intercepts e_s^- inside spurs which would otherwise react with H^+ forming $\cdot CH_2OH$ by reactions 25 and 3.

$$[25]\qquad e_s^- + H^+ \rightarrow H\cdot$$

The absorption at 300 nm, which was corrected for the small NF^- absorption, exhibited a fast initial growth due to formation of NB^- by reaction 1 followed by a decay which was faster than found in the absence of TNM. The absence of a corresponding growth at 355 nm demonstrates that NB^- does not rapidly transfer an electron to TNM. The initial decay of NB^- may be due to reaction 26 involving nitrogen dioxide formed in reactions 22 and 23 since the electron affinities of NO_2 and $C_6H_5NO_2$, 3.10 and 0.51 eV, respectively (25), indicate that this process is energetically favoured.

$$[26]\quad NO_2 + C_6H_5NO_2^{\cdot -} \rightarrow NO_2^- + C_6H_5NO_2$$

C. Nitrous Oxide Solutions: Extinction Coefficients of $\cdot CH_2OH$ and $\cdot CH_2O^-$

The rate of reaction between e_s^- and N_2O (reaction 5*a*) was measured by following the kinetics of decay of e_s^- absorption at 630 nm following a pulse to solutions with $4 \times 10^{-4} \leq [N_2O] \leq 5 \times 10^{-3}$ *M*. The observed first order rate constants were independent of dose at each concentration of N_2O and from the variation of these rate constants with $[N_2O]$ we find $k_{5a} = (1.32 \pm 0.17) \times 10^{10}\ M^{-1}\ s^{-1}$. This value is in good agreement with those determined by Dainton *et al.* (19) and Seki and Imamura 6, 26).

The absorption spectra produced by 5–7.5 krad, 0.2 μs pulses in N_2O saturated neutral and basic ($[CH_3ONa] = 0.087$ *M*) solutions resembled those previously assigned to $\cdot CH_2OH$ and $\cdot CH_2O^-$ (19, 27) and are shown in Fig. 6. Extinction coefficients, calculated for these species using the radical yield $[G(R\cdot)]_N^{N_2O} = 6.45 \pm 0.05$ (1), are shown on the right hand ordinate of Fig. 6. In the calculation of $\varepsilon(\cdot CH_2O^-)_\lambda$, allowance was made for the incomplete dissociation of $\cdot CH_2OH$ to $\cdot CH_2O^-$ according to equilibrium 6.

The rate constant, $2k_{10}$, for disappearance of $\cdot CH_2OH$ in neutral N_2O saturated solution was determined at wavelengths from 250–320 nm from the values for $2k_{10}/\varepsilon(\cdot CH_2OH)_\lambda$ at each wavelength and the extinction coefficients taken from Fig. 6. The resultant $2k_{10}$ values were independent of wavelength within experimental error giving $2k_{10} = (2.89 \pm 0.05) \times 10^9\ M^{-1}\ s^{-1}$.

D. Argon Saturated Solutions: The Extinction Coefficient of e_s^-

The absorption spectrum produced at the end of a 0.2 μs, 5 krad pulse in neutral Ar saturated methanol is composed of contributions from e_s^- and $\cdot CH_2OH$. The absorption at $\lambda > 380$ nm due to e_s^- decayed rapidly and after 10 μs the spectrum in Ar saturated solution was normalizable to that of $\cdot CH_2OH$. At the doses

used e_s^- disappears predominantly by reaction

[27] $e_s^- + CH_3OH \rightarrow CH_3O^- + H^\cdot$

with either H^+ or methanol (reactions 25 and 27). In each case $^\cdot CH_2OH$ is formed by the rapid reaction of $H^\cdot$ with methanol (reaction 3). Therefore after complete decay of e_s^- the spectra should differ only according to the total yields of radicals which escape from the spurs in Ar and N_2O saturated solutions. In Ar saturated solutions the initial absorption at wavelength λ corrected graphically for decay during the pulse, $[G\varepsilon]_{N,\lambda}^{Ar}$, is composed of contributions from both e_s^- and $^\cdot CH_2OH$ and is given by [28].

[28] $$[G\varepsilon]_{N,\lambda}^{Ar} = G(e_s^-)_0\varepsilon(e_s^-)_\lambda + [G(^\cdot CH_2OH)]_N^{Ar}\,\varepsilon(^\cdot CH_2OH)_\lambda$$

Equation 32, for $\varepsilon(e_s^-)_\lambda$, is derived from [28]–[31].

[29] $$G(e_s^-)_0 + [G(^\cdot CH_2OH)]_N^{Ar} = [G(R^\cdot)]_N^{Ar}$$

[30] $$[G(^\cdot CH_2OH)]_N^{N_2O} = [G(R^\cdot)]_N^{N_2O}$$

[31] $$[G\varepsilon]_{N,\lambda}^{N_2O} = [G(^\cdot CH_2OH)]_N^{N_2O}\,\varepsilon(^\cdot CH_2OH)_\lambda$$

[32] $$\varepsilon(e_s^-)_\lambda = \frac{[G\varepsilon]_{N,\lambda}^{Ar} - \{[G(R^\cdot)]_N^{Ar} - G(e_s^-)_0\}[G\varepsilon]_{N,\lambda}^{N_2O}/[G(R^\cdot)]_\lambda^{N_2O}}{G(e_s^-)_0}$$

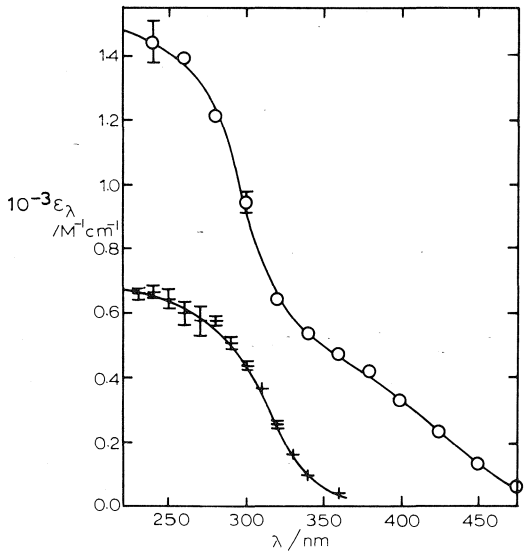

FIG. 6. Spectra of $^\cdot CH_2OH$ (+) and $^\cdot CH_2O^-$ (○) produced by 3.5–5 krad, 0.2 μs pulses of N_2O saturated solutions. +, neutral solution; ○, $[CH_3ONa] = 8.67 \times 10^{-2}$ *M*.

Values for $\varepsilon(e_s^-)_\lambda$ between 240 and 360 nm calculated using $G(e_s^-)_0 = 1.20 \pm 0.03$, $[G(R^\cdot)]_N^{Ar} = 5.63 \pm 0.05$, and $[G(R^\cdot)]_N^{N_2O} = 6.45 \pm 0.05$ are shown in Fig. 7.

Similar results were obtained in solutions containing 2.0×10^{-1} *M* CH_3ONa. Equations similar to those for neutral methanol were used to evaluate $\varepsilon(e_s^-)_\lambda$ except that $Z_cG(e_s^-)_0$ was used instead of $G(e_s^-)_0$. The values so obtained, which are also shown in Fig. 7, are slightly larger than those obtained in neutral solution. Large errors are expected for values of $\varepsilon(e_s^-)_\lambda$ computed from data for basic solutions since, especially at low wavelengths, $\varepsilon(^\cdot CH_2O^-)_\lambda \gg \varepsilon(e_s^-)_\lambda$.

The spectrum of e_s^- in neutral solution at wavelengths where $^\cdot CH_2OH$ does not absorb is in good agreement with previous determinations (10, 28, 29). The overall spectrum is shown in Fig. 7. The spectrum was extended to 850 nm

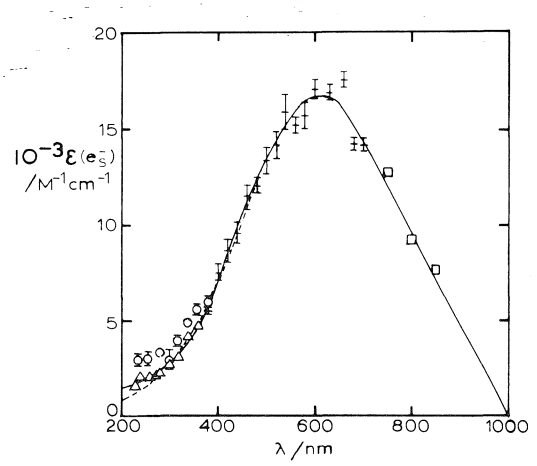

FIG. 7. Spectrum of e_s^- in neutral methanol: +, direct observation of absorption of e_s^-; △, calculated from [29] for neutral solutions; ○, calculated from [29] for solutions containing 8.7×10^{-2} *M* CH_3ONa; □, from ref. 29 normalized to 630 nm. The solid line (—) which is the best curve through the data is used for calculation of *f* (see text) and the broken line (---) a Lorentzian curve, normalized at 630 nm.

using data from ref. 29 and to longer wavelengths by graphical extrapolation. Jou and Dorfman (30) have shown that the high energy side of the spectra of e_s^- in a large number of solvents conform to Lorentzian curves. The broken line in Fig. 7 is the Lorentzian curve which fits best the data for methanol and is given by [33]. The oscillator strength of e_s^- is given by [34] (31) where $\bar{\nu}$ is in units of cm^{-1} and n_0 is the refractive index.

$$[33] \quad \varepsilon(e_s^-)_\lambda = \frac{\varepsilon(e_s^-)_{\lambda_{max}}}{1.82 \times 10^{-8}(\bar{\nu} - \bar{\nu}_{\lambda_{max}})^2 + 1}$$

$$[34] \quad f = 4.32 \times 10^{-9}[9n_0/(n_0^2 + 2)^2] \int_{\bar{\nu}_1}^{\nu_2} \varepsilon(\bar{\nu})\, d\bar{\nu}$$

A value of $f = 0.86$ was calculated from the solid line in Fig. 7, extrapolated to 200 nm, and $f = 0.90$ from the solid line at $\lambda > 630$ nm and the Lorentzian curve (to $\bar{\nu} = \infty\ cm^{-1}$) at $\lambda < 630$ nm. These values are larger than those calculated in refs. 10 and 28. In the former case $\varepsilon(e_s^-)$ at λ_{max} is similar to that obtained in this work, the higher value for f being due to the difference in shape of the spectrum at low wavelength. Any inaccuracy in the graphical extrapolation at long wavelengths will have little effect on f.

Discussion

(A) Validity of the Assumption that $[G(R^\bullet)]_N^{Ar} = [G(R^\bullet)]_B^{Ar}$

In the Results section the assumption was made that $[G(R^\bullet)]^{Ar}$ is identical in neutral and basic solutions as measured by TNM and nitrobenzene, respectively. This premise is central to our estimation of $\varepsilon(NB^-)_\lambda$ and hence $G(e_s^-)_0$. Figure 3 shows that within experimental error the yield of NB^- conforms to that expected for a constant $[G(R^\bullet)]^{Ar}$ in basic solutions with $[CH_3ONa] \geq 1.36 \times 10^{-4}$ *M*. Unfortunately the calculation of the yields of NB^- for solutions with $[CH_3ONa] = 1.36 \times 10^{-4}$ *M* is subject to large error due to their considerable dependence on the value chosen for K_6 and hence this data cannot be used to confirm the constancy of $[G(R^\bullet)]^{Ar}$ at $[CH_3ONa] < 1$ m*M*.

Further confirmation of this assumption can be drawn from the constancy of the glycol yield, which reflects the yield of radicals, between neutral and basic solutions with $[CH_3ONa] =$ 0.01 to 0.1 *M* (2, 32). It was proposed in an earlier paper (1) that the discrepancy between $[G(R^\bullet)]^{Ar}$ and $2G$(glycol) was due to the low reactivity of methyl radicals, $^\bullet CH_3$ (33), towards methanol (reaction 35) and TNM and their inability to react with TNM to form NF^-. The same arguments may be applied to the reaction

$$[35] \quad {}^\bullet CH_3 + CH_3OH \rightarrow CH_4 + {}^\bullet CH_2OH$$

of $^\bullet CH_3$ with nitrobenzene. This reaction is expected to be significantly slower than that of $^\bullet CH_2OH$ with nitrobenzene and hence can be ignored under the experimental conditions applied in this work.

The major effect of added base is to scavenge H^+ and hence to prevent geminate recombination reactions which convert e_s^- to $^\bullet CH_2OH$ (reactions 25 and 3); thus, the yield of e_s^- is increased at the expense of that of $^\bullet CH_2OH$ (11, 34, 35). This will only have an observable effect on the overall radical yield if the reactivities of e_s^- and $^\bullet CH_2OH$ in their radical–radical reactions differ. Except at the highest base concentrations it seems unlikely that the change in the overall yield of radicals escaping the spurs will be significant.

Hamill and co-workers (36–38) have proposed that base can scavenge the positive 'hole', ROH^+ (reaction 36), before this entity is stabilised by reaction with the solvent (reaction 37). The occurrence of reaction 36 may also prevent the recombination of presolvated, *i.e.* dry electrons, e^-, with ROH^+ (reaction 38) and

$$[36] \quad ROH^+ + RO^- \rightarrow ROH + RO^\bullet$$

$$[37] \quad ROH^+ + ROH \rightarrow ROH_2^+ + RO^\bullet$$

hence lead to an increase in the total radical yield. However the increase in $G(e_s^-)$ is small at

$$[38] \quad e^- + ROH^+ \rightarrow ROH$$

base concentrations where positive 'hole' scavenging is likely to be important (34) so this effect may be ignored for the base concentrations employed in this work.

(B) A Model for the Radiolysis of Methanol

Four methods have been employed to measure electron yields in methanol, namely, (*i*) the determination of the effects of solutes on the yield of hydrogen obtained by γ-irradiation (2–5), (*ii*) the measurement of the yields of species produced by dissociative electron capture by a solute (6–9), (*iii*) the determination by pulse radiolysis of $G\varepsilon$ values for radical anions produced by electron attachment to solutes (10–12),

and (*iv*) the observation of rapid conductivity changes induced by short pulses of radiation (13, 14). Following the formulation of the model by Freeman and Fayadh (39) it has become customary to associate the values given by each of the above methods with $G(e_s^-)_{fi}$, the yield of solvated electrons which escape geminate recombination. However, the disparity between the resultant values ($G(e_s^-)_{fi} = 1.0$–2.0) indicates the unsatisfactory nature of either the experimental methods employed, or the premise which suggests that each method yields $G(e_s^-)_{fi}$. We believe the latter to be the case and that the model of Freeman and Fayadh (39) is inapplicable to liquid methanol.

The probability, $P(r)$, that an electron thermalised at distance r from its counterion will escape geminate recombination with its partner is given by [39] (40),

$$[39] \qquad P(r) = e^{-r_c/r}$$

where $r_c = e^2/\varepsilon kT$, e is the electronic charge, ε the dielectric constant, k the Boltzmann constant, and T the absolute temperature. The value for r_c is dependent on the time dependence of the dielectric constant which is a function of the relaxation time of the solvent. However at times >5 ps the ordinary low frequency dielectric constant applies (41) giving $r_c = 1.7$ nm. The initial radius of a spur has been estimated as 2.3 nm (42) and is assumed to expand with time. Kevan and Chen (43) have measured a spur radius of 5.9 nm in glassy methanol at 77 K. Allowing for the greater thermalisation distances at 77 K compared to room temperature the expected spur radius is still greater than 4.0 nm so that there will be a considerable yield of e_s^- within regions of high radical concentration which do not recombine with geminate positive ions. It is proposed that these be defined as free solvated electrons, $(e_s^-)_{fi}$, whereas those combining geminately in the absence of radical–radical reactions be termed geminate solvated electrons, $(e_s^-)_{gi}$. A proportion of $G(e_s^-)_{fi}$ are expected to undergo reactions with other radicals (42, 44) and the remainder to escape into the bulk of the solution and to become homogeneously distributed. The latter category will be called 'escaped' solvated electrons, with a yield $G(e_s^-)_{esc}$, whereas the total number of electrons that undergo reactions in spurs (both geminate and free) will be termed 'spur' solvated electrons, $(e_s^-)_{spur}$. Hence, [40] applies and $G_{Tot} > G_{fi} > G_{esc}$.

$$[40] \qquad G_{Tot} = G(e_s^-)_{gi} + G(e_s^-)_{fi} = G(e_s^-)_{esc} + G(e_s^-)_{spur}$$

The existence of absorptions in the infrared region has recently been demonstrated for methanol (45) and other alcohols (45, 46). These absorptions have been assigned to partially solvated electrons. It seems necessary, therefore, to define two further types of electrons, the 'dry' electron, (e^-), and partially solvated 'damp' electron, e_{damp}^- (46). The lifetime of the former has been estimated to be about 10^{-15} s (47), *i.e.* the time taken for e^- to be thermalised, when it becomes trapped in the form e_{damp}^-. If trapping is immediate upon thermalisation it seems unlikely that e^- will participate significantly in reactions with solutes. The reactivity of e_{damp}^- with a large number of solutes has been shown to be parallel to, but greater than, that of e_s^- (45).

The total yield of fully solvated electrons at 30 ps has been measured by Lam and Hunt (48) as $G(e_s^-)_{30\ ps} = 2.0$ (based on the extinction coefficient obtained in this work). This was measured relative to $G(e_{aq}^-)_{30\ ps} = 4.0$ at 30 ps. However the stroboscopic pulse radiolysis technique does not lend itself to the accurate determination of absolute yields. Jonah *et al.* (49), using a single pulse technique enabling the observation of decays of species from 100 ps to several ns when dosimetry becomes very easy, have recently determined $G(e_{aq}^-) = 4.6$ at 100 ps. Since e_{aq}^- does not decay significantly over 300 ps (48) this value may be used for $G(e_{aq}^-)_{30\ ps}$ giving $G(e_s^-)_{30\ ps} = 2.3$ in methanol. Jha and Freeman (7) and Janovský (11) have measured scavengeable electron yields of at least 4.6 in methanol. Thus, there is a yield of electrons with $G \geq 2.3$ which do not become solvated and which presumably recombine geminately either in the form of e^- or e_{damp}^-.

(C) Comparison of the Model with Experiment

(I) Pulsed Conductivity Experiments

Fowles (13) and Busi and Ward (14) have determined $G(e_s^-)_{fi} = 2.0$ by observation of the conductivity change following a pulse of high energy radiation. Fowles concluded that the ionic conductances of e_s^- and CH_3O^- are identical so that the technique is not capable of differentiation between these species. Hence reactions of e_s^- with itself, $CH_3O^{\bullet}$, and $^{\bullet}CH_2OH$, which are known to occur in methanol (44, 50)

[41] $2e_s^- + 2CH_3OH \rightarrow 2CH_3O^- + H_2$

[42] $e_s^- + CH_3O^{\cdot} \rightarrow CH_3O^-$

[43] $e_s^- + {}^{\cdot}CH_2OH \rightarrow CH_3O^-$

to yield CH_3O^-, are not detected by this method. The method, therefore, possibly provides a measure of $G(e_s^-)_{fi}$ but not $G(e_s^-)_{esc}$. However, in the N_2O saturated solutions scavenging of dry electrons by N_2O may be expected to increase the yield of free ions, which would invalidate Fowles's conclusions.

(II) Radical-anion Formation

The reaction of e_s^- with a solute to form a radical anion may be represented by reaction 44. The yield of $X^{\cdot-}$ observed by microsecond pulse radiolysis depends on whether e_s^- originates from the $(e_s^-)_{spur}$

[44] $X + e_s^- \rightarrow X^{\cdot-}$

or $(e_s^-)_{esc}$ population. In the former case $X^{\cdot-}$ is protonated rapidly due to the high concentration of H^+ formed in spurs. This is demonstrated by the rapid decay over about 50 ns of the biphenyl anion, $C_{12}H_{10}^{\cdot-}$, absorption to a steady value (23). In contrast $X^{\cdot-}$ formed from $(e_s^-)_{esc}$ protonates by reaction with solvent or homogeneously distributed H^+ over a few μs and $G(X^{\cdot-})$ is therefore readily measurable by ns or μs pulse radiolysis. Thus the observed $G(X^{\cdot-})$ is equal to $G(e_s^-)_{esc}$ and is constant over a large concentration range of X (10, 11). Direct observation of the slowly decaying absorption of e_s^- yields $G(e_s^-)_{esc}\ \varepsilon(e_s^-)_\lambda$. Providing $\varepsilon(X^{\cdot-})_\lambda$ is known, $G(e_s^-)_{esc}$ and hence $\varepsilon(e_s^-)_\lambda$ may be calculated. Since $X^{\cdot-}$ can only be prepared by chemical methods in aprotic solvents, it has proved impossible to measure $\varepsilon(X^{\cdot-})_\lambda$ in methanol. In previous studies (10–12) $\varepsilon(X^{\cdot-})_\lambda$ has been assumed to be invariant from solvent to solvent. In this work $\varepsilon(NB^-)$ has been determined without recourse to this assumption. The agreement of the present result with those using biphenyl (10, 11) and pyrene (12) indicates that in these cases the values of $\varepsilon(X^{\cdot-})_\lambda$ do not change significantly in going from aprotic solvents (usually THF) to methanol.

(III) Dissociative Electron Capture and Reduction in Hydrogen Yields

Dissociative electron capture by N_2O (6, 7), SF_6 (8), and CH_3Br (8) has been employed to measure electron yields in γ-irradiated methanol while benzyl chloride has been used similarly in pulse radiolysis studies (9, 11). The reactions involved are of the general form of reaction 45 irrespective of whether the electrons reacting are

[45] $AB + e^- \rightarrow A^- + B^{\cdot}$

dry, damp, or solvated. More importantly, since the process is dissociative, an observable product results irrespective of whether the electrons are geminate, free, or escaped. Consequently the yield of product from reaction 45 varies continuously with [AB] and separation of the electron yield into its various components can only be achieved with prior knowledge of the reactivity and life-time distribution of each component. The effect of solutes such as nitrobenzene (5) in reducing the hydrogen yield is thought to be due to the scavenging of electrons and the interpretation of the data is therefore subject to the same complications. Jha and Freeman (5, 7) and Rzad and Fendler (8) have applied simplified treatments to their data. They have made the assumption that all geminate electrons recombine with H^+ and that free electrons all diffuse into the bulk solution and decay by a first order process. Freeman and Bolton (51) have since modified their treatment to allow for the scavenging of dry electron by the solute, but have not taken into account reaction of e_s^- with radicals. Furthermore if $\varepsilon(e_s^-)_{\lambda_{max}}$ has the value determined in the present work, it is necessary to take into account that only 50% of electrons become solvated.

We therefore propose a model which we believe to be consistent with all the known experimental observations and which, in view of the simplifications involved, provides as good a fit as can be expected to the measured yields.

The initial yield of e^- is set as $G(e^-) = 4.6$, *i.e.* equal to the maximum yield observed with high concentrations of N_2O (7). In the absence of a solute a yield, $G(e_s^-) = 2.3$ becomes solvated. It is assumed that once e^- are thermalised they can become trapped either as e_{damp}^- or e_s^-. The e_{damp}^- can undergo geminate recombination possibly by thermal excitation to the dry state. Thus the diffusion coefficient applicable to the geminate recombination is governed by the existence of shallow traps (e_{damp}^-) as is the case in hydrocarbons (52). Thus the competition between recombination (reaction 46) and solvation (reaction 47) can be expected to conform to the kinetics applied by Warman *et al.* (53) to

[46] $e^- + ROH(H)^+ \rightarrow$ Products

[47] $$e^- \rightarrow e_s^-$$

low polarity solvents. The yield of solvated electrons is given by [48]

[48] $$G(e_s^-) = G(e^-)\left(\frac{(\alpha_t)^{1/2}}{1 + (\alpha_t)^{1/2}}\right)$$

where α_t is a parameter which measures the solvation efficiency. A value for $\alpha_t = 1.0$ may be calculated from $G(e^-) = 4.6$ and $G(e_s^-) = 2.3$.

In the presence of a solute the additional reaction 49 must be considered. The yield of product, P, is then given by [50] (54)

[49] $$e^- + S \rightarrow P$$

[50] $$G(P) = G(e^-)\left\{\frac{(\alpha_t + \alpha_s[S])^{1/2}}{1 + (\alpha_t + \alpha_s[S])^{1/2}}\right\} \times \left\{\frac{\alpha_s[S]}{\alpha_s[S] + \alpha_t}\right\}$$

where α_s is the efficiency of reaction of e^- with S. The yield of e_s^- may be calculated from the corresponding equation for solvation. The assumption is made that the yield of $G(e_s^-)$ is divided into $G(e_s^-)_{spur}$ and $G(e_s^-)_{esc}$ in the same proportion as is observed in the absence of solute (*i.e.* 1.1:1.2). This approximation is not strictly valid since the electrons which travel further from the positive ion before trapping are more likely to be scavenged and also more likely to become part of the $G(e_s^-)_{esc}$ population in the absence of a solute. However, calculations show that the change in the ratio only becomes significant at values of $\alpha_s[S] > 1$ when the yield of electrons which become solvated is in any case much reduced by reaction of dry electrons with the solute (23). The rate constant for the decay of $G(e_s^-)_{esc}$ by reaction with solvent is $k_{21} = 2.2 \times 10^5\ s^{-1}$ in low dose rate γ-radiolysis experiments and is dependent on the dose rate (see section A.*II.*(*b*)) in pulse radiolysis experiments. The yield of product, P, from reaction of $(e_s^-)_{esc}$ with S (reaction 51) is given by [52].

[51] $$e_s^- + S \rightarrow P$$

[52] $$G(P) = G(e_s^-)_{esc}\left(\frac{k_{51}[S]}{k_{51}[S] + k_{21}}\right)$$

The spur decay of e_s^- has been shown both in water (49) and low temperature liquid methanol (55) to conform to [53] after an initial period, t_0, in which little decay is observed. Lam and Hunt (48) have observed that t_0 is about 350 ps for liquid methanol. Values for a and b may be determined from $G(e_s^-) = 2.3$ at t_0 and 1.65 at 7 ns (29) calculated using $\varepsilon(e_s^-)$ determined in this work.

[53] $$G(e_s^-)_{spur} = -a \log t + b$$

Thus, the rate equations for the disappearance of $(e_s^-)_{spur}$ and the formation of product are given by [54] and [55], which were integrated numerically to obtain the yield of product,

[54] $$\frac{dG(e_s^-)_{spur}}{dt} = -\frac{a}{t} - k_{51}[S]G(e_s^-)_{spur}$$

[55] $$\frac{dG(P)}{dt} = k_{51}[S]G(e_s^-)_{spur}$$

The sum of the product yields from each electron component may thus be determined. The total product yield $G(P)_{tot}$ is compared with experimental results and the one adjustable parameter α_s varied to give the best agreement between

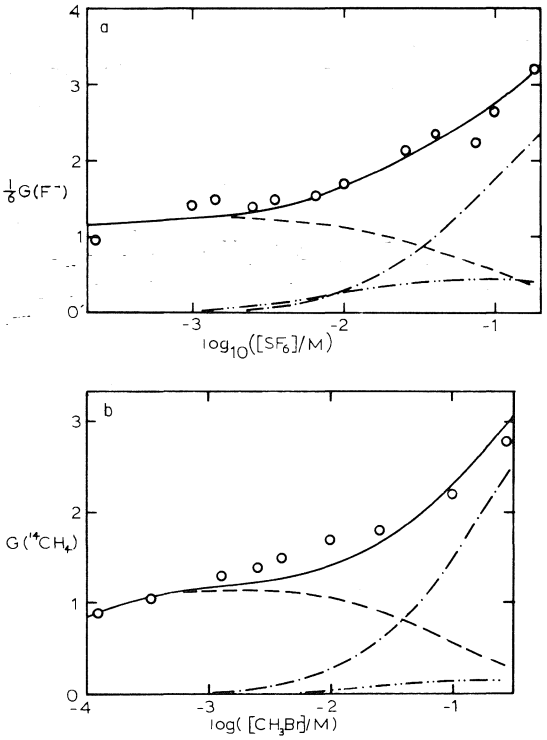

FIG. 8. Comparison between the observed dependence of product yield on solute concentration and that calculated from the model (see discussion). ○, observed data from ref. 8; —, calculated yield. Components of $G(P)$ from the various electron populations: ---, $G(P)_{esc}$ (from $(e_s^-)_{esc}$); -·-·-·-, $G(P)_{spur}$; ·····, $G(P)_{damp}$. (*a*) Sulphur hexafluoride, (*b*) methyl bromide.

TABLE 3. Values of α_s determined for dry electron reactions in methanol. Comparison with values for electron scavenging in hydrocarbons

Solute	In methanol		In cyclohexane	
	α_s (M^{-1})	Reference for scavenging data	α_s (M^{-1})	Reference
Benzyl chloride	100	9, 11, 23	39.5	57
Biphenyl	17	23	15	58
Methyl bromide	10.2	8	15.4	59
Nitrous oxide	82	7	19±2	57
Sulphur hexafluoride	17	8	6.8	60*

*Calculated from data in ref. 60.

theory and experiment. This calculation has been performed for scavenging results obtained for a number of solutes. In the case of biphenyl, the yields of $C_{12}H_{11}^{\bullet}$ measured (23) after protonation of $C_{12}H_{10}^{\bullet-}$ was complete, were used for the calculation. Data at $[S] > 3 \times 10^{-1}$ M were neglected in order to reduce any errors introduced by direct radiolysis of the solute. No allowance for encounter pair formation (56) was made since at the solute concentrations where they become important, scavenging of e_s^- is almost complete. The experimental and calculated scavenging dependences compare very well except for nitrous oxide. Figure 8 shows the results of these calculations for sulphur hexafluoride and methyl bromide. Values for α_s are listed in Table 3 where comparison is also made with the values obtained in the low polarity solvent cyclohexane where these are available. The treatment discussed here is semi-empirical but it serves to illustrate the essential features of the model.

Acknowledgments

We acknowledge helpful discussions with Dr. G. V. Buxton and one of us (D.W.J.) thanks the S.R.C. for the award of a Research Studentship.

1. D. W. JOHNSON and G. A. SALMON. J. Chem. Soc. Faraday Trans. I, **73**, 256 (1977).
2. J. H. BAXENDALE and F. W. MELLOWS. J. Am. Chem. Soc. **83**, 4720 (1961).
3. S. U. CHOI and N. N. LICHTIN. J. Am. Chem. Soc. **86**, 3948 (1964).
4. W. V. SHERMAN. J. Phys. Chem. **71**, 4245 (1967).
5. K. N. JHA and G. R. FREEMAN. J. Am. Chem. Soc. **95**, 5891 (1973).
6. H. SEKI and M. IMAMURA. J. Phys. Chem. **71**, 870 (1967).
7. K. N. JHA and G. R. FREEMAN. J. Chem. Phys. **48**, 5480 (1968).
8. S. J. RZAD and J. H. FENDLER. J. Chem. Phys. **52**, 5395 (1970).
9. J. LILIE, S. A. CHAUDHRI, A. MAMOU, M. GRÄTZEL, and J. RABANI. J. Phys. Chem. **77**, 597 (1973).
10. M. C. SAUER, S. ARAI, and L. M. DORFMAN. J. Chem. Phys. **42**, 708 (1965).
11. I. V. JANOVSKÝ. Ph.D. Thesis, University of Leeds, Leeds, England. 1969.
12. E. HAYON. J. Chem. Phys. **53**, 2353 (1970).
13. P. FOWLES. Trans. Faraday Soc. **67**, 428 (1971).
14. F. BUSI and M. D. WARD. Int. J. Radiat. Phys. Chem. **5**, 521 (1973).
15. K.-D. ASMUS, A. WIGGER, and A. HENGLEIN. Ber. Bunsenges. Phys. Chem. **70**, 862 (1966).
16. D. H. ELLISON, G. A. SALMON, and F. WILKINSON. Proc. R. Soc. London, Ser. A, **328**, 23 (1972).
17. T. J. KEMP, J. P. ROBERTS, G. A. SALMON, and G. F. THOMPSON. J. Phys. Chem. **72**, 1464 (1968).
18. F. S. DAINTON, E. A. ROBINSON, and G. A. SALMON. J. Phys. Chem. **76**, 3897 (1972).
19. F. S. DAINTON, G. A. SALMON, and P. WARDMAN. Proc. R. Soc. London, Ser. A, **313**, 1 (1969).
20. P. WARDMAN. Ph.D. Thesis, University of Leeds, Leeds, England. 1967. p. 69.
21. G. V. BUXTON, F. S. DAINTON, and M. HAMMERLI. Trans. Faraday Soc. **63**, 1191 (1967).
22. D. W. JOHNSON and G. A. SALMON. J. Chem. Soc. Faraday Trans. I, **71**, 583 (1975).
23. D. W. JOHNSON. Ph.D. Thesis, University of Leeds, Leeds, England. 1976.
24. K.-D. ASMUS, B. ČERČEK, M. EBERT, A. HENGLEIN, and A. WIGGER. Trans. Faraday Soc. **63**, 2435 (1967).
25. R. P. BLAUNSTEIN and L. G. CHRISTOPHOROU. Radiat. Res. Rev. **3**, 69 (1971).
26. H. SEKI and M. IMAMURA. Bull. Chem. Soc. Jpn. **44**, 1538 (1971).
27. M. SIMIC, P. NETA, and E. HAYON. J. Phys. Chem. **73**, 3794 (1969).
28. K. N. JHA, G. L. BOLTON, and G. R. FREEMAN. J. Phys. Chem. **76**, 3876 (1972).
29. R. R. HENTZ and G. A. KENNEY-WALLACE. J. Phys. Chem. **78**, 514 (1974).
30. F. Y. JOU and L. M. DORFMAN. J. Chem. Phys. **58**, 4715 (1973).
31. W. KAUZMANN. Quantum chemistry. Academic Press, New York, NY. 1957. p. 581.
32. L. M. THEARD and M. BURTON. J. Phys. Chem. **67**, 59 (1963).
33. J. K. THOMAS. J. Phys. Chem. **71**, 1919 (1967).
34. S. ARAI, A. KIRA, and M. IMAMURA. J. Phys. Chem. **74**, 2102 (1970).

35. A. K. PIKAEV, G. K. SIBIRSKAYA, and S. A. KABAKCHI. Proc. Tihany Symp. Radiat. Chem., Tihany, Hungary, 1971. 3rd, Vol. 2. *Edited by* J. Dobo and P. Hedvig. Akadémiai Kiado, Budapest. 1972. p. 1107.
36. W. H. HAMILL. J. Phys. Chem. **73**, 1341 (1969).
37. T. SAWAI and W. H. HAMILL. J. Chem. Phys. **52**, 3843 (1970).
38. P. L. T. BEVAN and W. H. HAMILL. Trans. Faraday Soc. **66**, 2533 (1970).
39. G. R. FREEMAN and J. M. FAYADH. J. Chem. Phys. **43**, 86 (1965).
40. L. ONSAGER. Phys. Rev. **54**, 554 (1938).
41. A. MOZUMDER. J. Chem. Phys. **50**, 3153 (1969).
42. H. A. SCHWARZ. J. Phys. Chem. **73**, 1928 (1969).
43. L. KEVAN and D. H. CHEN. J. Chem. Phys. **49**, 1970 (1968).
44. F. S. DAINTON, I. V. JANOVSKÝ, and G. A. SALMON. Proc. R. Soc. London, Ser. A, **327**, 305 (1972).
45. K. Y. LAM and J. W. HUNT. Int. J. Radiat. Phys. Chem. **7**, 317 (1975).
46. J. H. BAXENDALE and P. WARDMAN. J. Chem. Soc. Faraday Trans. I, **69**, 584 (1973).
47. A. MOZUMDER and J. L. MAGEE. Int. J. Radiat. Phys. Chem. **7**, 83 (1975).
48. K. Y. LAM and J. W. HUNT. J. Phys. Chem. **78**, 2414 (1974).
49. C. D. JONAH, M. S. MATHESON, J. R. MILLER, and E. J. HART. J. Phys. Chem. **80**, 1267 (1976).
50. D. W. JOHNSON and G. A. SALMON. Int. J. Rad. Phys. Chem. In press.
51. G. R. FREEMAN and G. L. BOLTON. Proc. 4th Symp. Radiat. Chem. Keszthely, Hungary. June, 1976.
52. R. M. MINDAY, L. D. SCHMIDT, and H. T. DAVIS. J. Chem. Phys. **50**, 1473 (1969).
53. J. M. WARMAN, K.-D. ASMUS, and R. H. SCHULER. Adv. Chem. Ser. **82**, 25 (1968).
54. J. M. WARMAN, K.-D. ASMUS, and R. H. SCHULER. J. Phys. Chem. **73**, 931 (1969).
55. J. H. BAXENDALE and P. WARDMAN. J. Chem. Soc., Chem. Commun. 429 (1971).
56. G. CZAPSKI and E. PELED. J. Phys. Chem. **77**, 893 (1973).
57. P. O'NEILL. Ph.D. Thesis, University of Leeds, Leeds, England. 1973.
58. S. J. RZAD, P. P. INFELTA, J. M. WARMAN, and R. H. SCHULER. J. Chem. Phys. **50**, 5034 (1969).
59. J. M. WARMAN and S. J. RZAD. J. Chem. Phys. **52**, 485 (1970).
60. S. SATO, T. TERAO, M. KONO, and S. SHIDA. Bull. Chem. Soc. Jpn. **40**, 1818 (1967).

Discussion

G. A. Kenney-Wallace: In a recent laser photolysis study of optical absorption coefficients for e_s^- in a series of alcohols, at the absorption maximum for electrons solvated in methanol we find a value of about 10 700 M^{-1} cm^{-1}, in agreement with Freeman's value of 10 200 M^{-1} cm^{-1}, Ward's value of 10 000 M^{-1} cm^{-1}, and the data of Dorfman *et al.* if the higher free ion value is used. Therefore your relatively high absorption coefficient implies to me that the free ion value you determine is possibly too low.

G. A. Salmon: The question of $G(e_s^-)_{fi}$ and $\varepsilon_{\lambda max}$ is, of course, intrinsically related since by pulse radiolysis one can only measure the product. Therefore, if you believe $G(e_s^-)_{esc} = 2.0$ you will of course obtain a lower ε. However, I should point out that the low values of ε (high $G(e_s^-)_{fi}$) imply very low values for the oscillator strength. Nevertheless, your approach using laser generation of e_s^- sounds interesting and I should be pleased to hear further details: for example, how you determine $\phi(e_s^-)$.

U. Schindewolf: In water and ammonia there is some evidence of increased light absorption in the near uv. Could you observe an increase of absorption below 230 nm?

G. A. Salmon: Our detection system does not allow us to make accurate measurements below 230 nm.

L. G. Christophorou: Why do you not consider the $C(NO_2)_4^-$ parent ion, but rather the fragment ion $C(NO_2)_3^-$?

G. A. Salmon: In water and alcohols the stable $C(NO_2)_3^-$ ion can be prepared by hydrolysis of $C(NO_2)_4$. The absorption spectrum of the product of reaction of e_s^- (and $^{\cdot}CH_2OH$) with TNM is compatible with that of $C(NO_2)_3^-$. This has been demonstrated by several groups of workers. For references, see our ref. 1.

J. W. Hunt: I would mention that we are also studying the yields of e_{sol}^- in water, alcohols, and mixtures at picosecond and microsecond times with test scavengers such as cadmium perchlorate, sodium salicylate, and biphenyl. The electron adducts were observed. Our results are consistent with a higher free ion yield of e_{solv}^- in methanol ($G(e_{sol})_{fi} \sim 1.9$), and total yields of electron adducts are at least 4.8 to 4.2 per 100 eV. I would like to have your comments.

G. A. Salmon: The high yields of product at high concentrations of solute and short times is compatible with our view that presolvated and spur electrons can be scavenged by high solute concentrations. However, the difficulty arises with the yields which you have observed on microsecond time scales. I can only say that to interpret microsecond yields it is necessary to know the chemistry of the radicals with the solute and of the radical anion. Your yields of biphenyl radical anion on microsecond time scale seem to be at variance with those measured by Sauer *et al.* (M. C. Sauer, S. Arai, and L. M. Dorfman. J. Chem. Phys. **42**, 708 (1965)) and Janovsky (I. V. Janovsky. Ph.D. Thesis. University of Leeds, Leeds, England. 1969).

J. H. Baxendale: Don't you have a problem with increases in the free ion yield due to spur scavenging by saturated N_2O?

G. A. Salmon: The total radical yield as measured by TNM increases from 5.63 for argon saturated solution to 6.45 in nitrous oxide solution (1). We have taken this increase in $G(R^{\cdot})$ into account in partitioning the uv absorption by addition of N_2O.

On the existence of H^- in γ-irradiated matrices at 77 K

A. BERNAS AND T. B. TRUONG

E. R. CNRS 98, Université Paris-Sud, 91405 Orsay, France

Received September 27, 1976

A. BERNAS and T. B. TRUONG. Can. J. Chem. **55**, 2044 (1977).

A band peaking around 1050 nm in the stimulated neutralization luminescence spectrum of γ-irradiated glassy EtOH, pure crystalline and alkaline glassy ices has recently been attributed to H^-. Further results on EtOH glass and on EtOH–H_2O mixtures are now presented which support our previous interpretation.

A shuttle of the electron from the presumed H^- to a matrix trapped state and back to H with restoration of the 1050 nm band can be induced in, and only in, alcohol–water mixtures where it has been shown that, contrary to either of the two pure solvents, H atoms can be trapped (H_t). Further, the intensity of the regenerated stimulated band is found to be maximum for the mixture composition which leads to the highest H_t yield.

It is noted that the red limit of the H^- stimulated band, which corresponds to a photodetachment energy threshold, is close to the electron affinity value of the isolated H atom. This observation seems to imply that, contrary to expectation, the solvation energy of H^- in these matrices is quite low.

A. BERNAS et T. B. TRUONG. Can. J. Chem. **55**, 2044 (1977).

La glace pure cristallisée, les glaces alcalines vitreuses, l'éthanol vitreux irradiés aux Rγ à 77 K donnent lieu à une luminescence de neutralisation dont le spectre d'excitation présente une bande centrée à 1050 nm. Il a été récemment suggéré que celle-ci était associée à H^-. De nouveaux résultats relatifs à EtOH vitreux et aux mélanges EtOH–H_2O sont maintenant présentés qui confirment cette interprétation.

Il est en effet observé qu'un transfert réversible des électrons de l'espèce X^- vers des pièges physiques puis vers X avec reconstitution de la bande X^- à 1050 nm n'est possible que dans les mélanges EtOH–H_2O où les atomes H sont stabilisés (H_t). L'intensité de la bande 1050 nm ainsi régénérée est trouvée maximale pour la composition du mélange qui conduit à un rendement maximum en H_t.

On note enfin que la limite vers le rouge de la bande de stimulation de H^- qui correspond à une énergie seuil de photodétachment est très voisine de la valeur de l'affinité électronique de H gazeux. Ceci semble impliquer que dans les matrices considérées l'énergie de solvatation de H^- est très faible.

Introduction

It is well known that after γ-irradiation of rigid matrices at low temperatures and stabilization of neutral and charged intermediates, solvated electrons may be detrapped or bleached by a suitable optical excitation. A deferred luminescence designated as 'stimulated' luminescence (SL) is then generally associated with the subsequent cation–electron neutralization (1, 2).

The emission spectrum, $I_{SL} = f(\lambda_{an})$, obtained upon bleaching the trapped electron at constant wavelength λ_b and recording the luminescence at variable wavelength $\lambda_{analysis}$, may give information on the neutralization mechanism, dissociative or not, and on the emitting electronic state (3).

On the other hand, the luminescence excitation spectrum or 'stimulation' spectrum, giving the neutralization luminescence intensity as a function of the bleaching wavelength, $I_{SL} = f(\lambda_b)$, characterizes the negative species, whether anions or solvated electrons (2–5).

This technique has recently been applied to γ-irradiated glassy ethanol and the results have led to the suggestion that H^- was present (6). The present study deals with γ-irradiated ethanol and ethanol–water mixtures at 77 K where hydrogen atoms are known to be stabilized, although trapped H (H_t) is not observed in either pure component (7).

Experimental Results and Discussion

The experimental set-up has been described elsewhere (4, 5). It mainly consists of a slightly modified commercial spectrofluorimeter in which the xenon source and excitation monochromator are used to release the trapped electrons in the pre-irradiated sample. The neutralization lumin-

escence is simultaneously recorded by a RCA IP 28 photomultiplier through the analyzing monochromator. The stimulation spectra have been corrected for the trapped electron consumption under successive bleachings and for the variation of the excitation light flux with bleaching wavelength λ_b.

EtOH

Emission Spectrum

For pure ethanol glasses γ-irradiated at 77 K, the observed neutralization emission spectrum is given in Fig. 1, curve *A*. The same emission spectrum peaking at 345 nm is recorded, whatever the bleaching wavelength: 500 or 1000 nm.

The nature of the emissive center has been much debated for irradiated alkane glasses, with no conclusive assignment, however, and the emitter is also unidentified in the alcohol case. For the former, Brocklehurst (8) has recently proposed a radiative tunneling mechanism so that there would be no emitter as such; the luminescence would be a property of the ion pair.

For alcohol, it can only be stated that neither alcohol impurities (curve *B*) nor stable radiolysis products (curve *C*) are responsible for the 345 nm emission band.

Stimulation Spectrum

However, whatever the origin of the emission, the luminescence excitation or stimulation spectrum provides an electron photodetachment efficiency curve. If $\lambda_{analysis}$ is fixed at 345 nm, the stimulation spectrum shown in Fig. 2 is obtained. The visible region of the spectrum appears quite similar to the previously reported (9, 10) bleaching efficiency curves relating the decrease in trapped electron optical density to the bleaching wavelength λ_b. An extra band, absent in the bleaching curves is, however, present in the stimulation spectrum peaking at about 1050 nm with a low energy threshold at about 1500 nm (0.86 eV). The intensity of the 1050 nm band decreases as the γ-dose increases as illustrated in Fig. 3.

An analogous band appears in the stimulation spectra of pure (11) or alkaline (12) ices. If present in the stimulation spectra of irradiated alkane glasses, it would be masked (6) by the

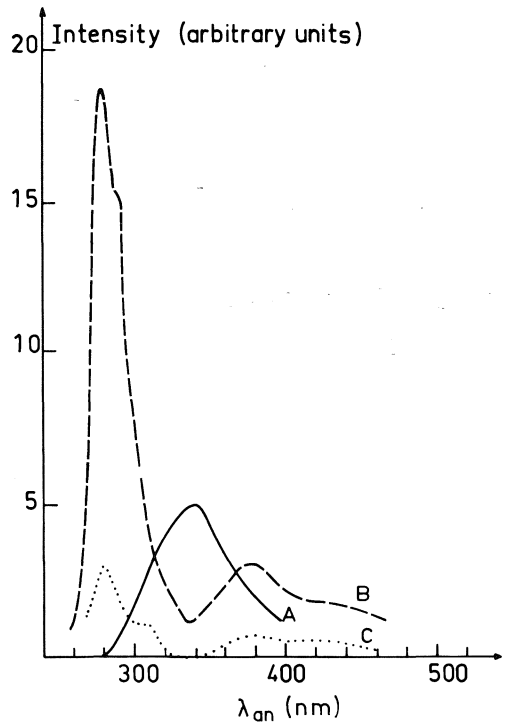

FIG. 1. Neutralization emission spectrum in γ-irradiated EtOH glass at 77 K. (*A*) Stimulated emission spectrum, $I_{SL} = f(\lambda_{an})$ of γ-irradiated EtOH glasses, (10^{19}eV g^{-1}), upon bleaching with λ_b = 1000 nm. (*B*) Emission spectrum of unpurified EtOH glass, upon excitation at λ_{exc} = 254 nm. (*C*) Emission spectrum of the γ-irradiated sample (10^{19} eV g^{-1}) subjected to one melting–freezing cycle, and excited with λ_{exc} = 254 nm.

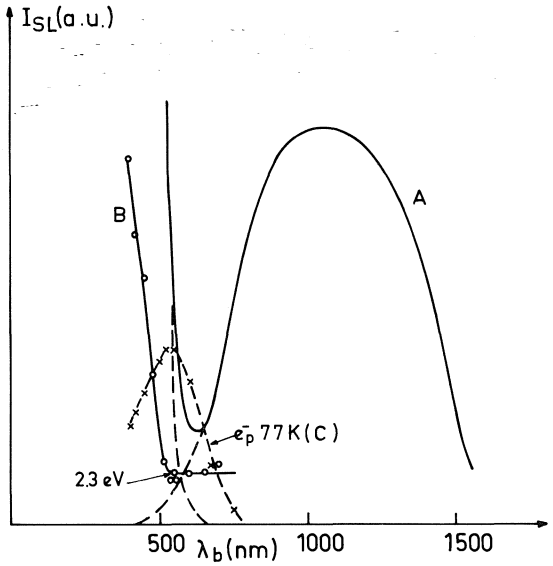

FIG. 2. Neutralization stimulation spectrum in γ-irradiated EtOH at 77 K. (*A*) Stimulation spectrum $I_{SL} = f(\lambda_b)$, λ_{an} = 345 nm. (*B*) Bleaching efficiency curve $(-D_{opt}) = f(\lambda_b)$ (9). (*C*) Absorption spectrum of solvated electrons in γ-irradiated EtOH glass (9).

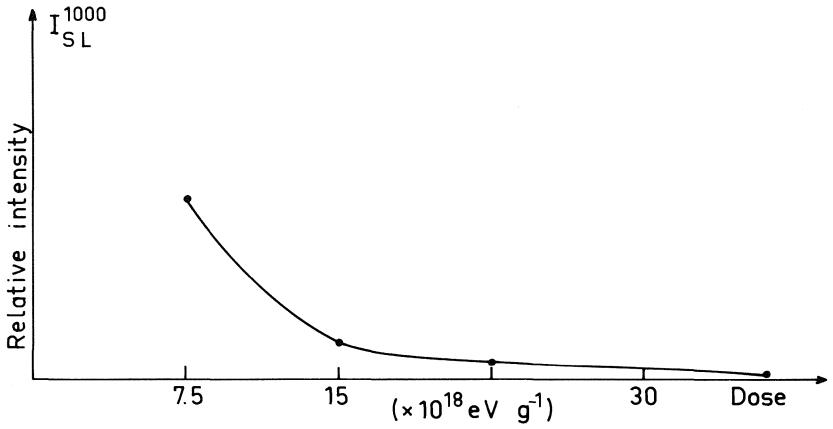

FIG. 3. Intensity of stimulated luminescence in γ-irradiated EtOH glass *vs.* γ-dose; λ_{an} = 345 nm, λ_b = 1000 nm.

broad trapped electron band peaking at 1600 nm. It has been observed (6), however, that the bleaching rate at 1600 nm for MCH or 3-MP glasses is much lower after large γ-doses ($>10^{20}$ eV g^{-1}), that is, when the trapped electron contribution is lower. Such a difference in the bleaching kinetics between physical and chemical electron traps has been pointed out before (13, 4). This observation would favour the conclusion that the 1050 nm band originates from an anion.

Absorption bands in the same spectral region have been reported previously.

In the case of alkaline aqueous glasses, the 1000 nm band has been attributed to dielectrons (14). In the case of ethanol irradiated and investigated at 4 (15) or 6 K (10), the ir band apparently originates from electrons located in shallow wells, non-relaxed traps. For *n*-propanol and higher aliphatic alcohols the shoulder observed in the near ir region would correspond to traps formed, at least partly, by alkyl groups (16).

None of these interpretations can apply to our experimental findings, however. A dielectron attribution cannot be considered since the 1050 nm band appears at low doses for irradiated ices (11) and since its intensity decreases as the γ-dose increases in the ethanol case (Fig. 3). As to the shallow traps, they are known to be stabilized at 4–6 K but to become fully relaxed as the temperature rises to 77 K (17) with a correlative shift of the absorption band maximum to higher energies. Besides, the 1050 nm band does not exist in the SL spectrum of photoionized tryptophane dispersed in ices or ethanol glasses (6). Electrons which would be solvated not only by OH dipoles but also by alkyl groupings might exist in alcohols but not in pure or alkaline ices. Again, we are led to suggest that the 1050 nm band is associated with an anion X^-.

OH radicals, and possibly OH^-, are stabilized in pure radiolyzed ice, O^- in alkaline ices, but the most plausible radiolysis product X^-, common to alcohols and ices, seems to be H^-.

EtOH–H_2O Mixtures

It is well known that no H atom signals have been recorded through esr in alcoholic matrices neither at 77 nor even at 4 K, even though much indirect evidence exists that hydrogen atoms are produced during radiolysis. In pure ice, H atoms are stable at 4 K but begin to diffuse and combine in the temperature range 20–50 K.

On the other hand, Hase and Kevan (*7a*) and Chandra (*7b*) have identified trapped hydrogen atoms through the characteristic esr doublet signal of H in irradiated MeOH–H_2O, EtOH–H_2O, and PrOH–H_2O mixtures at 77 K. Since the H_t yields as a function of the mixture composition show a striking correlation with the excess enthalpy of mixing of the alcohol–water mixtures, it was considered that both effects are related to alcohol–water complex formation, and that the simplest trapping site structure was a hydrogen bonded trimer of one alcohol and two water molecules (*7a*).

Neutralization luminescence has now been examined for these systems and the following observations have been made.

Emission Spectrum

For the EtOH–H_2O mixtures (10 to 50 mol% of EtOH), the stimulated emission spectrum

gives a λ_{max} at 360–365 nm under bleaching at 1000, 390, or 254 nm. This emission is red-shifted as compared with the stimulated emission of pure EtOH (λ_{max} = 345 nm) and blue-shifted with respect to the main neutralization luminescence band in pure irradiated ice (λ_{max} = 380 nm).

It is not clear at the present time whether the 365 nm emission is an envelope of the two pure solvents' emission bands or is due to a different emissive entity.

Stimulation Spectrum

The stimulation spectrum has the same shape as the EtOH stimulation spectrum (Curve *A*, Fig. 2) but, in the irradiated EtOH–H_2O mixtures, the 1050 nm band appears more intense than for either of the two pure solvents.

The 1050 nm band due to X^- can be completely bleached off under λ_b = 1000 nm. Then, by exciting the sample with a light frequency which is absorbed by the solvated electrons and not by X^-, *i.e.* at λ_b = 400 nm (6) the 1050 nm band is partially regenerated. This restoration of the X^- band is observed in the EtOH–H_2O mixtures but in neither one of the pure solvents. That is, the X^- band can be reproduced only in the systems where H atoms are stabilized, in which case one can induce the reversible electron transfer:

$$[1] \qquad e_{solv}^- + h\nu \rightarrow e_m^- \xrightarrow{H} X_t^-$$

$$[2] \qquad X_t^- + h\nu \rightarrow e_{solv}^-$$

Moreover, as shown in Fig. 4, the intensity of the regenerated X^- band appears maximum for a mixture containing 20 mol% EtOH. This is precisely the mixture composition which, from Hase and Kevan experiments (7*a*), leads to the maximum concentration of trapped hydrogen atoms, following γ-radiolysis or after a subsequent e_{solv}^- optical bleaching.

Similarly, the intensity of the regenerated X^- band increases with increasing γ-dose within a range where H_t concentration was found to be linear with dose: curve *A* (γ-dose = 0.6 Mrad) as compared with curve *B* (γ-dose = 0.32 Mrad).

The restored X^- band appears more intense for λ_b = 254 nm rather than λ_b = 390 nm which may reflect a higher e_{solv}^- photobleaching efficiency at shorter wavelengths (curves *B* and *C*).

These qualitative and quantitative features

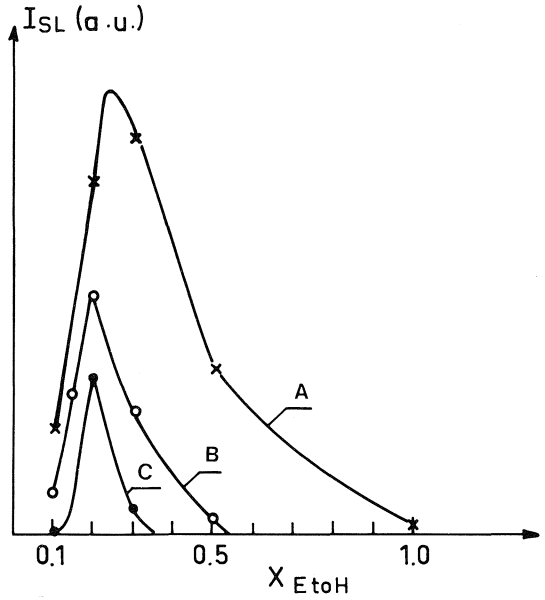

FIG. 4. Intensity of the regenerated 1050 nm band *vs.* EtOH mole fraction in EtOH–H_2O mixtures: (*A*) γ-dose = 0.6 Mrad, λ_b = 254 nm, (*B*) γ-dose = 0.32 Mrad, λ_b = 254 nm, (*C*) γ-dose = 0.32 Mrad, λ = 390 nm.

indicate that X^- anion is effectively the hydride ion, as previously suggested (6).

It is also worth mentioning that H^- has been detected in solar atmosphere (18) and that its calculated and observed absorption spectrum appears at the same spectral position, as illustrated in Fig. 5.

The decrease of the H^- stimulated band with increasing γ-dose for pure EtOH may be compared with the observed decrease with dose of the molecular hydrogen yield $G(H_2)$. It may be similarly explained by a competition between the H forming reactions 3 and 4

$$[3] \qquad e_m^- + C_2H_5OH_2^+ \rightarrow C_2H_5OH + H$$

$$[4] \qquad e_m^- + C_2H_5OH \rightarrow C_2H_5O^- + H$$

and the electron attachment on acetaldehyde, which is a good electron scavenger and whose concentration increases with dose (19).

$$[5] \qquad e_m^- + CH_3CHO \rightarrow CH_3CHO^-$$

A competition may also intervene between reactions 5 and 6:

$$[6] \qquad e_m^- + H \rightarrow H^-$$
$$R^\bullet \rightarrow R^-$$

where $R^\bullet$ is a radiation produced solvent radical.

Various modes for H^- formation may be envisaged depending on the matrix:

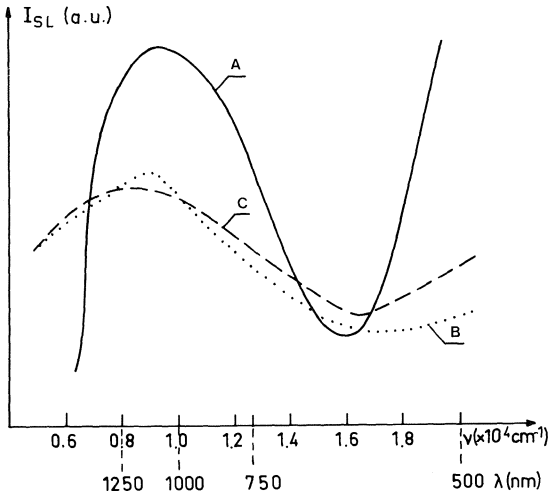

FIG. 5. Absorption spectrum of gaseous H^-: (*A*) Stimulation spectrum $I_{LS} = f(\lambda_b)$ of γ-irradiated EtOH glass, γ-dose = 10^{19} eV g^{-1}, λ_{an} = 345 nm, (*B*) Observed absorption spectrum of H^- (18), (*C*) Calculated absorption spectrum of H^- (18).

(*a*) In water vapor, the dissociative electron attachment [7] is well established (20)

[7] $$e^- + H_2O \rightarrow H^- + OH$$

Even though at higher pressures ion–molecule reaction 8

[8] $$H^- + H_2O \rightarrow OH^- + H_2$$

is known to occur, reaction 7 may be operative and H^- might be solvated and stabilized in condensed phase.

(*b*) In the EtOH–water mixtures, electron attachment may clearly occur on preformed, trapped hydrogen atoms

[9] $$e_m^- + H_t \rightarrow H_t^-$$

besides their possible formation during radiolysis through reaction 10.

(*c*) In pure radiolyzed solid alcohol, where hydrogen atoms are not trapped, the latter may diffuse toward the solvated immobile electrons and become trapped as H_t^-:

[10] $$H + e_{solv}^- \rightarrow H_t^-$$

Reaction 10 would thus provide another path for the decay of H atoms, besides the combination reaction 11

[11] $$H + H \rightarrow H_2$$

and the abstraction reaction 12:

[12] $$H + CH_3CH_2OH \rightarrow H_2 + CH_3CHOH$$

Reaction 10 has been previously suggested by Shirom and Willard (21) to account for the decrease in solvated electron concentration with increasing dose in hydrocarbon glasses. It was shown later (22) that reaction 10 was not responsible for the observed decrease in $G(e_{solv}^-)$; there is no indication, however, that reaction 10 does not take place in hydrocarbon glasses or other radiolyzed systems.

As to the occurrence of reaction 9, it is not easy to demonstrate. Electron spin resonance analyses of the γ-irradiated EtOH–H_2O mixtures have shown (7*a*) that, upon bleaching the solvated electrons, the H atom concentration increases due to H production through H_3O^+ (mostly) and $C_2H_5OH_2^+$ neutralization. Such an increase apparently overcomes the decrease which would be associated with electron attachment on H. The fact that the decrease in e_t^- is found to exceed the correlative increase in H (7*a*) indicates that some of the bleached electrons do not recombine with positive holes. This may be due to reaction 9 but also to electron attachment on other radiolysis products, attachment which, if dissociative, would not give rise to H.

Conclusion

We wish to conclude with two remarks.

The low energy limit of the H^- stimulated band, which corresponds to a photodetachment energy threshold, appears very close to the value of the electron affinity of the isolated H atom (0.7–0.8 eV). This observation is contrary to expectation. It would seem to imply that the influence of the matrix molecules, *i.e.* the solvation energy of H^- in these matrices, is quite low. As pointed out to us,[1] this could possibly be correlated to the helium-like, close-shell configuration of the hydride ion.

Finally, we want to stress again that recording the stimulation spectrum of the neutralization luminescence is a detection technique which is both sensitive and specific of negatively charged species. It may thus supplement optical absorption spectroscopy when the sensitivity of the latter is too low or when cations and anions have indistinguishable spectra. It may also replace esr spectroscopy in the search for nonparamagnetic anions.

1. E. DOLAN and A. C. ALBRECHT. J. Chem. Phys. **37**, 1149 (1962).
2. A. DEROULEDE. J. Lumin. **3**, 302 (1971).

[1]L. G. Christophorou, private communication.

3. A. BERNAS, J. BLAIS, M. GAUTHIER, D. GRAND, and T. B. TRUONG. Int. J. Radiat. Phys. Chem. **6**, 401 (1974).
4. T. B. TRUONG and A. BERNAS. J. Phys. Chem. **76**, 3894 (1972).
5. T. B. TRUONG, A. BERNAS, and J. RONCIN. J. Phys. Chem. **78**, 867 (1974).
6. T. B. TRUONG. Chem. Phys. Lett. **35**, 426 (1975).
7. (*a*) H. HASE and L. KEVAN. J. Phys. Chem. **74**, 3355 (1970); (*b*) R. CHANDRA. Int. J. Radiat. Biol. **17**, 497 (1970).
8. B. BROCKLEHURST. Chem. Phys. Lett. **39**, 61 (1976).
9. A. BERNAS, D. GRAND, and C. CHACHATY. J. Chem. Soc. Chem. Commun. 1667 (1970).
10. L. M. PERKEY, FARHATAZIZ, and R. R. HENTZ. Chem. Phys. Lett. **27**, 531 (1974).
11. A. BERNAS and T. B. TRUONG. C. R. Acad. Sci. Ser. B, **277**, 391 (1973).
12. T. B. TRUONG. J. Chem. Phys. In press.
13. K. FUNABASHI, C. HEBERT, and J. L. MAGEE. J. Phys. Chem. **75**, 3221 (1971).
14. L. KEVAN, D. RENNEKE, and R. J. FRIAUF. Solid State Commun. **6**, 469 (1968).
15. A. NAMIKI, M. NODA, and T. HIGASHIMURA. Chem. Phys. Lett. **23**, 402 (1973).
16. T. SHIDA, S. IWATA, and T. WATANABE. J. Phys. Chem. **76**, 3683 (1972).
17. J. TEPLY. Int. J. Radiat. Phys. Chem. **6**, 379 (1974).
18. H. S. W. MASSEY. Negative ions. Cambridge University Press, London. 1950. p. 128.
19. G. R. FREEMAN. *In* Actions chimiques et biologiques des radiations, 14e serie. Masson Ed. 1970. p. 128.
20. R. N. COMPTON and L. G. CHRISTOPHOROU. Phys. Rev. **154**, 110 (1967).
21. M. SHIROM and J. E. WILLARD. J. Am. Chem. Soc. **90**, 2184 (1968).
22. A. ECKSTROM, R. SUENRAM, and J. E. WILLARD. J. Phys. Chem. **74**, 1888 (1970).

Discussion

L. G. Christophorou: Could the fact that H^- is a closed-shell system explain the absence of a profound medium effect (on the photodetachment threshold)?

A. Bernas: This is indeed a very interesting comment and suggestion but before drawing such a conclusion I would prefer that our experimental work be extended to other anions, *e.g.* Cl^-.

R. S. Dixon: H^- is thought to react rapidly with H_2O in the gas and liquid phases. Would you expect reaction with neighboring water molecules in the glass?

A. Bernas: I agree that at high pressures the ion–molecule reaction $H^- + H_2O \rightarrow OH^- + H_2$ is known to occur. However, H^- may be formed in a trapped state through $H + e_{solv}^- \rightarrow H^-_{trapped}$.

N. K. Kestner: I am also concerned that the spectral shifts of the H^- spectrum are so small in the glass; H^- is a rather large system, compared to H. H^- is only stable relative to $H + e^-$ by 0.75 eV while the correlation energy is over 1 eV. In order for H^- to be stable the size of the orbitals in H expand. Thus I might expect larger spectral shifts for H^- than for H when present in condensed phases.

A. Bernas: As I just mentioned we were also puzzled that the photodetachment threshold in the glass appears close to the electron affinity of H in the gas, and so far we have no explanation to offer. As to the size of the H orbitals permitting H^- stability, it seems difficult to say anything in the case of condensed media.

R. Catterall: When the solvated electrons in γ-irradiated water–alcohol solutions are photobleached, the esr signal from e_{solv}^- disappears. Does the H atom esr signal also decrease?

A. Bernas: The experiment has been done but the data are not conclusive with regard to H^- formation. (*a*) The initial (*i.e.* before e_{solv}^- bleaching) H concentration is low as compared to that of e_{solv}^-. (*b*) Upon e_{solv}^- bleaching various reactions will modify the H concentration in opposite directions: neutralization of H_3O^+ or attachment on ethanol molecules will increase [H] whereas electron attachment on H will decrease it.

U. Schindewolf: Our attempts to dissolve alkali hydrides, *e.g.* in THF with the aid of crown-compounds, to complex the alkali ion failed. We hoped in this way to get H^- ions into solution. Has H^- even been observed in liquid solution as Na^-, K^-, etc. have been?

A. Bernas: Not to my knowledge, even though it has been suggested many times, in particular a long time ago by Platzman.

Low energy electron ranges in liquids: determination by nonhomogeneous kinetics[1]

J.-P. DODELET[2]

Chemistry Department, University of Alberta, Edmonton, Alta., Canada T6G 2G2

Received September 27, 1976

J.-P. DODELET. Can. J. Chem. **55**, 2050 (1977).

Free ion yields have been measured in four hydrocarbon liquids: *n*-pentane, cyclopentane, neopentane, and neohexane. Each liquid has been studied from room temperature or below up to the critical temperature. Theoretical curves have been calculated using the relation between the free ion yields and the external field strength derived by Terlecki and Fiutak on the basis of an equation by Onsager. Two popular electron range distribution functions, Gaussian and exponential, have been shown not to be an adequate representation of the reality as far as the model used for the calculations is concerned. In order to fit experimental points, both range distribution functions would require a drastic increase in the total ionization yield, G_{tot}, with temperature increase. This would mean an unrealistic decrease of the ionization potential of the molecule from the melting point up to the critical temperature.

It is possible to keep G_{tot} quite constant and within the range of values obtained by other techniques by extending the Gaussian range distribution function with a $(\text{range})^{-3}$ probability tail. The most probable range can be normalized for the liquid density. This parameter has been used to obtain information about the behaviour of epithermal electrons in the four alkane liquids from the melting point up to the critical temperature.

(*1*) Normalized penetration ranges of epithermal electrons are dependent on the structure of the molecule in the entire liquid range but differences are smaller at critical than at low temperatures.

(*2*) Normalized penetration ranges of epithermal electrons pass through a maximum in the liquid phase for neopentane, neohexane, and cyclopentane. No maximum is observed for *n*-pentane.

(*3*) There is no drastic change in the behaviour of epithermal electrons in these alkanes at the critical temperature.

J.-P. DODELET. Can. J. Chem. **55**, 2050 (1977).

Les rendements en ions libres ont été mesurés dans quatre hydrocarbures liquides: le *n*-pentane, le cyclopentane, le néopentane et le néohexane. Chaque hydrocarbure a été étudié depuis une température égale ou inférieure à celle du laboratoire jusqu'à la température critique. Les courbes théoriques ont été calculées en utilisant la relation, déduite par Terlecki et Fiutak d'après une équation d'Onsager, entre les rendements en ions libres et le champ électrique appliqué. Deux distributions des parcours électroniques, l'une de type gaussien, l'autre exponentiel, très populaires dans la littérature, ont été utilisées dans les calculs et n'ont pas donné satisfaction dans le cadre de ce modèle. En effet, pour ces deux distributions, une bonne coincidence entre les calculs et l'expérience requerrait, lorsque la température augmentait un accroissement considérable du rendement total en ions, G_{tot}, ce qui aurait signifié une diminution constante, très peu probable, du potentiel d'ionisation de la molécule à partir du point de fusion jusqu'à la température critique.

Il est possible de maintenir G_{tot} relativement constant et dans le domaine des valeurs obtenues par d'autres techniques, en prolongeant artificiellement la distribution gaussienne des parcours électroniques par une distribution du type $(\text{parcours})^{-3}$. Le parcours le plus probable peut alors être normalisé en tenant compte de la densité du liquide. Ce paramètre a été utilisé pour obtenir des renseignements sur le comportement des électrons épithermiques injectés dans les quatre alcanes liquides étudiés, depuis leur température de fusion jusqu'à leur température critique.

(*1*) Les parcours normalisés des électrons épithermiques dépendent de la structure des molécules sur l'ensemble de la phase liquide mais les différences, importantes à basse température, s'amenuisent en allant vers la température critique.

---

[1]Assisted financially by the National Research Council of Canada through grant No. A1285 (Freeman, G. R.).

[2]Present address: Département de Chimie-Biologie, Université du Québec à Trois Rivières, Case postale 500, Trois Rivières (Qué.), G9A 5H7.

(*2*) Les parcours normalisés des électrons épithermiques présentent un maximum dans la phase liquide pour le néopentane, le néohexane et le cyclopentane. Aucun maximum n'est observé pour le *n*-pentane.

(*3*) A la temperature critique il n'y a pas de changement brusque dans le comportement des électrons épithermiques injectés dans ces alcanes.

Introduction

Injection of low energy electrons into liquids can be done in various ways. The most popular methods are electron photoinjection (1, 2) and the use of pulsed ionizing radiation (3–5).

When an ionizing radiation like a pulse of X rays penetrates into a liquid, a random distribution of ionized atoms or molecules is produced. These primary electrons will generate a branching out of ionization events along their tracks. After the last ionization takes place, the liquid contains a number of low energy electrons and their parent positive ions. These epithermal electrons will become thermalized at some distance from their parent ions by transferring their surplus energy to the medium.

The important factors which govern the penetration ranges of low energy electrons are the energy loss processes when the electron energy is below the lowest electronic excitation potential of the medium (2, 6, 7). If their interactions with the medium at those energies are small, their penetration ranges will be large.

Once the electrons become thermalized, they become involved in reactions with the positive ions. These reactions can be described by nonhomogeneous kinetics. Nonhomogeneous qualifies the relative distribution of equal numbers of positive ions and electrons in the liquid. If a positive ion is chosen as a reference, there is a much larger probability to find an electron as its nearest charged neighbour than another positive ion, in contrast with homogeneous kinetics, where there is an approximately equal chance to find either a positive or a negative charge closest to the reference ion.

Once an electron is thermalized, at a distance designated y from its parent ion, it is submitted to the thermal agitation of the medium which tends to counteract the Coulombic attraction toward the parent ion. The probability that electrons escape geminate neutralization is given by the equation

$$[1] \qquad P_{fi} = \exp(-q^2/\varepsilon kTy)$$

where q is the charge of the electron, k is the Boltzmann constant, T is the absolute temperature, and ε is the dielectric constant of the medium. The derivation of this equation is due to Onsager (8).

The experimentally measurable quantity is G_{fi}, the number of pairs of free ions created by every 100 eV of energy absorbed by the liquid. It is related to the escape probability by the relation

$$[2] \qquad G_{fi} = P_{fi}G_{tot}$$

where G_{tot} is the total number of ion pairs created per 100 eV of energy absorbed by the liquid. G_{tot} depends among other things on the ionization potential of the medium.

The average energy, W, required to form an ion pair in the gas phase has been measured for rare gases and many organic molecules (9, 10). In the liquid phase, the W value is unknown and the gas phase value is often used.

However, recently Takahashi *et al.* (11) measured the average energy expended per ion pair in liquid Xe using ^{207}Bi as an internal source of electrons. They obtained W(liq. Xe) = 15.6 $\pm$ 0.3 eV, a value considerably smaller than the gas phase value (21.5–21.9). In earlier publications (12, 13) they reported W(liq. Ar) = 23.6 eV which is also lower than the gas phase value (26.4 eV). If this trend is confirmed with a molecular medium, it is possible that the total ionization yield in liquids is larger than the usually used gas phase value.

Experimental

Techniques

If some ions become free they can be collected on electrodes. In order to collect and integrate a current, a constant external voltage must be applied on the electrodes. Therefore, only dielectric liquids can be used with this technique.

A charge clearing technique is used (14). The ions are generated by a pulse of 1.7 MeV X rays. For a 1 μs pulse duration, the energy absorbed by the sample is of the order of 10^{10} eV/g. The transient current produced by the ion collection is integrated and the collected charge is measured. The radiation pulse intensity is also integrated.

[3] $$G_{fi} \propto \frac{\text{collected charge}}{\text{absorbed dose} \times \text{collection volume}}$$

The measurements are repeated at several electric field strengths E to obtain a series of values designated $G_{fi}{}^{E}$.

Material

The hydrocarbons used in this paper are three C_5 hydrocarbons (*n*-pentane, cyclopentane, neopentane) and neohexane. These Research Grade hydrocarbons were obtained from Phillips Petroleum Co. Their purity is > 99.9%.

In order to see an electron conductance transient in these liquids (15), further purification is required. The same purification technique was used for all four hydrocarbons. (*1*) 24 h shaking with sulfuric acid; (*2*) after separation, 1 h stirring with $BaCO_3$; (*3*) introduction in the vacuum system through a column of NaOH pellets; (*4*) degassing; (*5*) 24 h stirring on $LiAlH_4$ under their own vapor pressure; (*6*) at least 48 h stirring on Na–K alloy under their own vapor pressure; (*7*) introduction into the conductance cell under a remaining pressure of the order of 10^{-7} torr.

Conductance Cells

Two kinds of conductance cell were used for these experiments. The low pressure cell has been described in detail elsewhere (14). For high pressure experiments a cell able to support a pressure of 100 atm was used (15). In order to get good signals, the high pressure cell has to be baked at a temperature higher than the critical temperature of the hydrocarbon under investigation. Both cells were coated with carbon black. This provided an efficient grounding of the cell body. At high temperatures the high voltage source drives excessive current through glass coated with a conducting material and this may cause breakage. Because of this, the high voltage arm was not coated with carbon black.

Temperature Control

The low temperature system has been described earlier (14). For higher than room temperatures, the high pressure cell was positioned in a clear Dewar and air at the desired temperature was blown on the sample with a heat gun. One thermocouple was used to drive the temperature controller and another recorded the temperature. Both thermocouples were placed inside the guard electrode side-arm as close as possible to the body of the cell. The meniscus disappearance signified the critical point and this was observed through a window left uncoated on the cell body.

Physical Properties of the Liquids

Densities, d, for low temperature *n*-pentane and for neohexane from 0°C to 25°C have been obtained from Timmermans (16). Low temperature densities for neohexane were assumed to change linearly with temperature from 25°C to the melting point. Gallant (17) provided the densities for high temperature pentane and cyclopentane up to critical temperature. The density curve up to critical temperature is not available for neopentane or neohexane. For these alkanes the densities at 20°C and critical temperature are provided by Timmermans (16). The density variations of neopentane and neohexane were assumed to be similar to the density variations for *n*-butane and *n*-pentane respectively (17).

TABLE 1. Critical data

Liquid	T_c (°C)	d_c (g/cm³)
n-Pentane	197.2	0.2323
Cyclopentane	238.6	0.270
Neopentane	160.6	0.221
Neohexane	216.2	0.240

Critical temperatures and densities for the four hydrocarbons are given in Table 1.

The dielectric constants used for the various temperatures were calculated with the Debye formula using $\mu = 0.06$ D (18) for *n*-pentane and neohexane and $\mu = 0.0$ D for cyclopentane and neopentane. Refractive indices of these hydrocarbons were found in the Handbook of Chemistry and Physics (19). At 20°C the calculated values of ε are in good agreement with the literature values (19).

The Model

The field strength E produced by the external voltage is in competition with the field strength due to the Coulombic interaction. In other words the external field will help the ions to become free and this effect will be larger, the larger the voltage. The relation between the free ion yield and the external field strength is given by the relation calculated by Terlecki and Fiutak (20).

[4] $$G_{fi}{}^{E} = P_{fi}[1 + \psi(u_0, s)]G_{tot}$$

[5] $$\psi(u_0, s) = e^{-u_0} \sum_{n=1}^{\infty} \frac{{u_0}^n}{(n+1)!} \times \sum_{j=0}^{n-1} (n-j) \frac{s^{j+1}}{(j+1)!}$$

where $u_0 = Eqy/300kT$, $s = q^2/\varepsilon kTy$. This calculation is based on Onsager's escape probability in the presence of an external electric field (8).

This relation assumes a unique spur population: one positive ion and one electron only. It has been shown by Mozumder and Magee that a certain amount of energy deposition appears in the form of multiple ion spurs (21). However, the majority of spurs are single pair spurs when X radiation is used (21). Introduction of spurs with multiple ion population into the calculation highly complicates the problem, especially if the repulsion between the same charged species is to be taken into consideration.

The expressions [4] and [5] are derived for an electron penetration range y. It would be fortuitous if all the electrons would thermalize at the same distance y from the parent ion. A

distribution function of penetration ranges is more realistic but such a function is unknown and the problem is left for speculation.

Two distribution functions of penetration ranges have been used in many calculations. The first one is based on the random walk model (22) and is a three dimensional Gaussian (8, 23, 24). We will call it YG.

$$[6] \qquad F(y) = \frac{4y^2}{\pi^{1/2} b_G{}^3} \exp(-y^2/b_G{}^2)$$

where b_G is the Gaussian dispersion parameter. It is also the most probable value of y. The second range distribution function is a simple exponential (25), based on the wave nature of the electron motion (26). We will call it YE.

$$[7] \qquad \begin{aligned} F(y) &= 0 && y < y_0 \\ F(y) &= b_E{}^{-1} \exp -((y - y_0)/b_E) && y \geq y_0 \end{aligned}$$

where b_E is the exponential dispersion parameter and y_0 is an arbitrary truncation distance. It has been taken equal to 5 Å by Abell and Funabashi (25) as the distance at which neutralization occurs. The electron propagates through the liquid as a plane wave with $b_E{}^{-1}$ as attenuation coefficient. Both distributions are normalized and

$$\int_0^\infty F(y)\, dy = 1$$

With the use of a distribution function, [4] becomes

$$[8] \qquad G_{fi}{}^E = G_{tot} \int_{y=0}^{\infty} F(y) P_{fi}[1 + \psi(u_0, s)]\, dy$$

Results and Discussion

Model Calculations with YG and YE Range Distribution Functions

As stated previously, the exact value of the total ionization yield, G_{tot}, in the liquid phase is not known but it is a reasonable approximation that the ionization potential of a molecule in the liquid phase will remain constant when the temperature of the liquid varies. Therefore G_{tot} should remain approximately constant as well.

In order to test the model, the two range distribution functions YG and YE were used to fit the experimental free ion yields of *n*-pentane and neopentane at various temperatures, going from −123°C to 209°C for *n*-pentane and from 25°C to 174°C for neopentane. For each temperature G_{tot} was used as an adjustable parameter to fit the experimental free ion yields. For each value of G_{tot}, the value of b_G or b_E necessary to perform the calculation of $G_{fi}{}^E$ (eq. 8) was computed from the 'experimental' $G_{fi}{}^0$ using [1] and [2]. This 'experimental' $G_{fi}{}^0$ is obtained by extrapolation of the experimental $G_{fi}{}^E$ to 0 V. If this extrapolation is not obvious, a range of possible $G_{fi}{}^0$ is tested and the best value is chosen.

In the fitting process by computer, an error between calculated and experimental points is computed on the basis of the relation

$$[9] \qquad \text{error} = \frac{1}{n} \sum_{E=E_1}^{E_n} |G_{fi}{}^E{}_{calc} - G_{fi}{}^E{}_{exp}|$$

where n is the number of experimental points.

Figures 1 and 2 display the best fit obtained with YE and YG for the lowest and highest experimental temperatures of *n*-pentane and neopentane respectively. Using YE, the best fit value of G_{tot} goes from 4.3 at −123°C to 9.2 at 209°C for *n*-pentane and from 4.6 at 25°C to 8.2 at 174°C for neopentane. Using YG, the best fit value of G_{tot} goes from 1.2 at −123°C to 5.1 at 209°C for *n*-pentane and from 3.4 at 25°C to 5.5 at 174°C for neopentane.

The field strength dependence of $G_{fi}{}^E$ is never a straight line when the voltage range is large enough. Even in *n*-pentane at −123°C the curvature in the experimental and calculated lines are clearly visible (Fig. 1).

The best fit values of G_{tot} at intermediate temperatures are displayed in Fig. 3 for *n*-pentane and in Fig. 4 for neopentane. The credibility range of the best fit is given by 1.1 times the error on both sides of the best fit error curve.

For both distributions the best fit method would require an increase of G_{tot} when temperature increases. This would correspond to a decrease of the ionization potential. As we have made the reasonable assumption that the ionization potential remains constant when the liquid temperature varies, we can conclude that a pure Gaussian or exponential range distribution function is not an adequate representation of the reality as far as this model is concerned.

Amending the Distributions

The goal is to obtain by calculation a constant total ionization yield for the four alkanes for

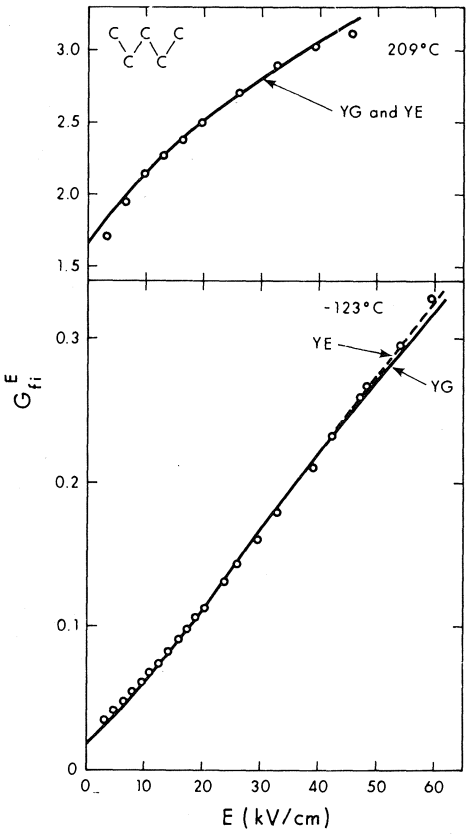

FIG. 1. Variation of the free ion yield $G_{fi}{}^{E}$ with field strength in *n*-pentane at −123°C and 209°C. The best fit lines are calculated using [8] with two range distribution functions, YE and YG. At −123°C, $G_{tot} = 4.3$ for YE and 1.2 for YG. At 209°C, $G_{tot} = 9.2$ for YE and 5.1 for YG.

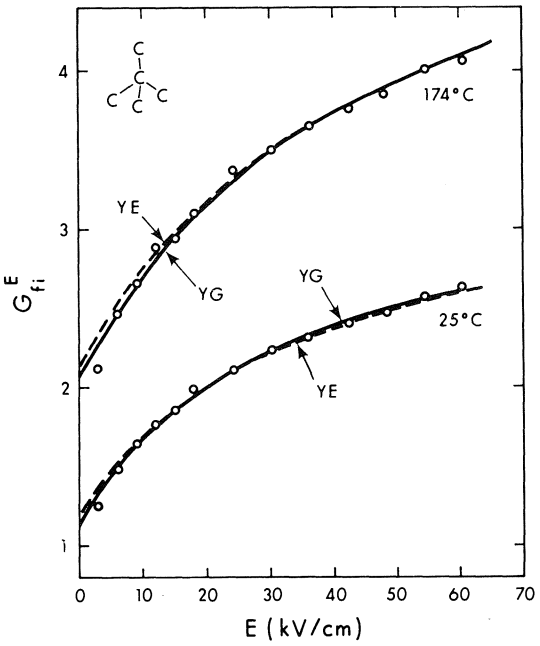

FIG. 2. Variation of the free ion yield $G_{fi}{}^{E}$ with field strength E in neopentane at 25°C and 174°C. The best fit lines are calculated using [8] with two range distribution functions YE and YG. At 25°C, $G_{tot} = 4.6$ for YE and 3.4 for YG. At 174°C, $G_{tot} = 8.2$ for YE and 5.5 for YG.

the entire range of temperatures. By using larger thermalization ranges than the ones allowed by YG or YE it is possible, when $G_{fi}{}^{0}$ is small, to increase the value of G_{tot} used to fit the experimental points.

Let us demonstrate why the best fit value of G_{tot} obtained with YG is small when $G_{fi}{}^{0}$ is small. At low temperature $G_{fi}{}^{0}$ in *n*-pentane, for example, is small. The only ions able to become free are the ones with large thermalization ranges. In order to provide large y values, the dispersion parameter of the Gaussian, b_G, which is also the most probable value of y, must be large. Equations 1 and 2 show that this is equivalent to saying that the escape probability is large. But $G_{fi}{}^{0}$ is given by extrapolation of experimental $G_{fi}{}^{E}$. A large escape probability requires therefore a small G_{tot} value.

To obtain larger thermalization ranges for a small portion of the electrons, we used a Gaussian tailed by a power probability function in y^{-3}. This combined function, called YGP, extends to much larger y values than YG. The tail contains the outermost 6% of the distribution function. It seemed to give quite good results in the past and has the following mathematical form (14).

$$F(y) = 0.96\text{YG} \qquad y < 2.4b_{GP}$$
$$F(y) = 0.96\text{YG} + 0.48(b_{GP}{}^{2}/y^{3}) \qquad y \geq 2.4b_{GP} \qquad [10]$$

The G_{tot} variation with temperature obtained with the YGP distribution function is displayed for *n*-pentane in Fig. 5 and the variation of G_{tot} with YG is displayed on the same graph for comparison. The curve obtained with YGP still shows some tendency to curve up, but it tends to make G_{tot} more constant on the entire temperature range. A value of $G_{tot} = 4 \pm 1$ could be accepted. A similar extension of the exponential range distribution function gave an apparent value around 7.5 for G_{tot}.

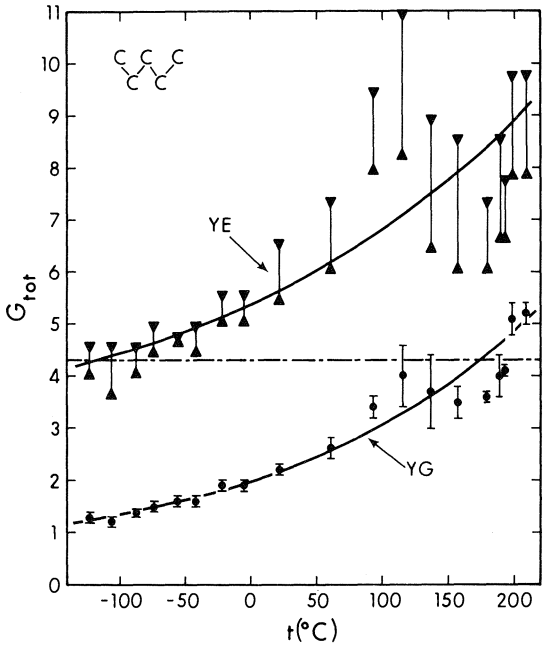

FIG. 3. Temperature variation of G_{tot} (with credibility gap) giving the best calculated fit for $G_{fi}{}^{E}$ *vs.* E in *n*-pentane for two range distribution functions YE (upper curve) and YG (lower curve). Increasing y_0 from 5 to 20 Å in YE did not shift the curve appreciably. The dotted line is the G_{tot} gas phase value.

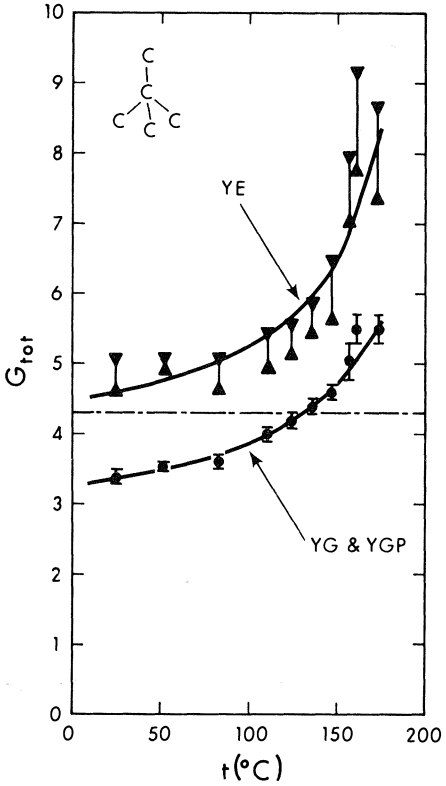

FIG. 4. Temperature variation of G_{tot} (with credibility gap) giving the best calculated fit for $G_{fi}{}^{E}$ *vs.* E in neopentane for three range distribution functions YE (upper curve), YG and YGP (lower curve). The dotted line is the G_{tot} gas phase value.

The adjunction of a power tail to both functions has nearly no effect when $G_{fi}{}^{0}$ and the escape probability are large. This can be seen in Fig. 5 for high temperature *n*-pentane and on Fig. 4 for neopentane on the entire temperature range studied. With these conditions the main contribution to the escape probability is from y values belonging to the Gaussian or exponential parts of the functions. The curvature observed on the variation of G_{tot} with temperature remains unchanged and suggestions are open for a better improvement on the range distribution functions.

It is possible to rationalize the existence of large thermalization ranges like the ones used in the tail of the YGP range distribution function. Some of the energy released by the primary electrons creates heavily populated spurs (21). After recombination of the inner electrons with parent positive ions, there would remain a single ion pair separated by a relatively large distance. The tail is an artifact inherent to a model treating only single ion pair spurs.

By assuming the generally accepted point that G_{tot} is almost independent of temperature over the entire liquid range, we have shown that conductivity results can be fit with a Gaussian type distribution function using $G_{tot} = 4 \pm 1$ *or* with an exponential type distribution function using $G_{tot} = 7.5 \pm 1$.

Previous attempts have been made (14, 25, 27) to decide whether an exponential or a Gaussian range distribution function better describes the reality. Another approach was used for these studies: G_{tot} was maintained constant at an arbitrary value (usually the gas phase value), different distribution functions were used, and their fit was compared. There are two approaches because there are two unknowns: the total ionization yield and the range distribution function. As long as the total ionization yield for these liquids remains unknown and until an adequate multipair spur model is devised, it will be impossible to chose by the conduction

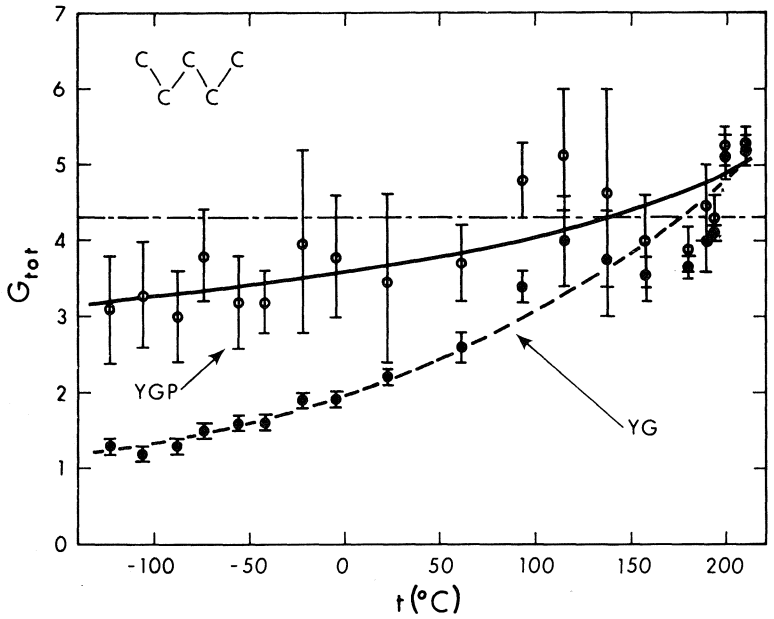

FIG. 5. Temperature variation of G_{tot} (with credibility gap) giving the best calculated fit for $G_{fi}{}^{E}$ *vs.* E in *n*-pentane for the YGP range distribution function (upper curve). YG (lower curve) is displayed for comparison. The dotted line is the G_{tot} gas phase value.

method alone between a Gaussian or an exponential type range distribution function. Even going to a very high field strength is not the answer, as has been shown by Mathieu and co-workers (28). The distinction between the two range distribution functions remains a problem.

Scavenging experiments are another way of getting information about the total ionization yield, but this technique also has its problems. For example: (*1*) A good scavenger should react with the electrons only. There should be no side reactions, as seems to be the case for all known scavengers. (*2*) In order to scavenge all the electrons produced by the irradiation the scavenger concentration must be high. Therefore, the liquid under investigation is far from being a single component system.

Having pointed out these limitations, scavenging experiments usually give values between 4 (29) and 6 (30) for the total ionization yield in the hydrocarbons. This would be consistent with the value of G_{tot} (4 ± 1) obtained from YGP ranges.

Deductions from Calculated Curves Performed with YGP

It seems that for hydrocarbons, the gas phase value can be used as an approximation for the liquid phase. Therefore, $G_{tot} = 4.3$ (9) was used for *n*-pentane, cyclopentane, neopentane, and neohexane. This value falls in the credibility gap of 4 ± 1 deduced earlier for a YGP range distribution function.

The voltage and temperature effects on the free ion yield are displayed in Figs. 6 and 7 for *n*-pentane at low and high temperatures respectively. Results for several temperatures are shown for cyclopentane in Fig. 8, neohexane in Fig. 9, and neopentane in Fig. 10. All calculations were done with a YGP range distribution function giving for each experimental temperature a most probable thermalization range, b_{GP}. At high temperatures, the calculated curves do not give a good fit to the data points in the low (<10 kV/cm) field strength region. This could be an artifact because the cell glass becomes slightly conducting at high temperatures, therefore allowing a voltage drop through the cell envelope. Fortunately this effect is not ohmic and seems not to affect higher voltages. In order to compare the ranges calculated for the four hydrocarbons, they must be multiplied by the density at the appropriate temperature.

A plot of the normalized most probable penetration ranges for the four compounds under

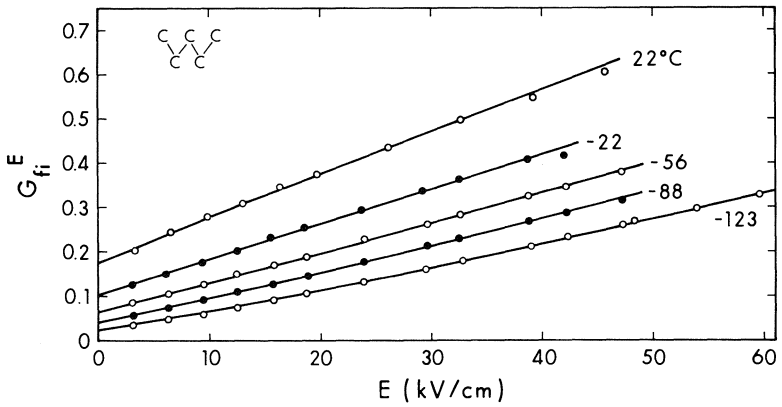

FIG. 6. Free ion yields at field strength E in liquid n-pentane at various temperatures. The lines are calculated using [8] with the YGP range distribution function and a total ionization yield, $G_{tot} = 4.3$.

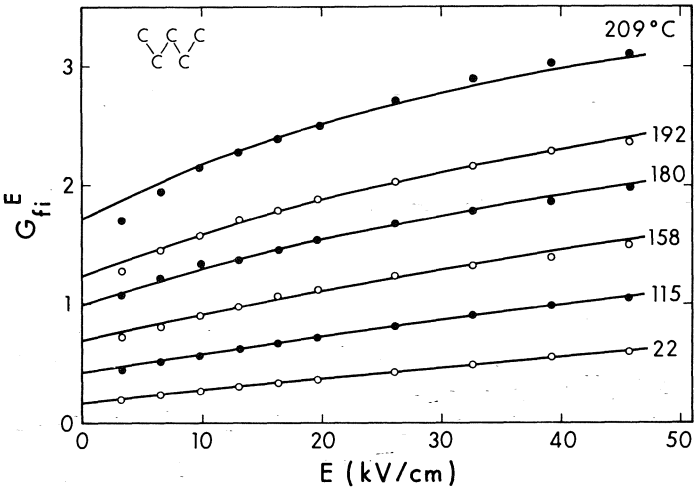

FIG. 7. Free ion yield $G_{fi}{}^{E}$ at field strength E in liquid at various temperatures and upper critical gas (209°C) in n-pentane. The lines are calculated using [8] with the YGP range distribution function and a total ionization yield, $G_{tot} = 4.3$.

investigation is displayed in Fig. 11. Three major conclusions can be deduced from this plot.

(*1*) The normalized mean penetration range is not the same for all hydrocarbons. It is dependent on the structure of the molecule. This has already been shown for part of the liquid range (23, 31). It remains true up to the critical temperature but differences are smaller at the critical than at lower temperatures.

(*2*) The normalized penetration range is not constant for the complete liquid range. Neopentane, neohexane, and cyclopentane curves go through a maximum. This maximum in the mean penetration range occurs at a temperature very close to the temperature where the mobility of thermal electrons in these liquids also goes through a maximum (15). The mean penetration ranges curve of n-pentane does not go through a maximum in the liquid phase. Nor is a maximum observed for the thermal electron mobility in n-pentane.

The observation of parallel behaviour between epithermal and thermal electrons is not new. It has already been pointed out (31) that the inelastic scattering cross sections of alkanes for both thermal and epithermal electrons are affected by the same factors, and only the relative magnitudes of the effects are different. The present work necessitates some elaboration

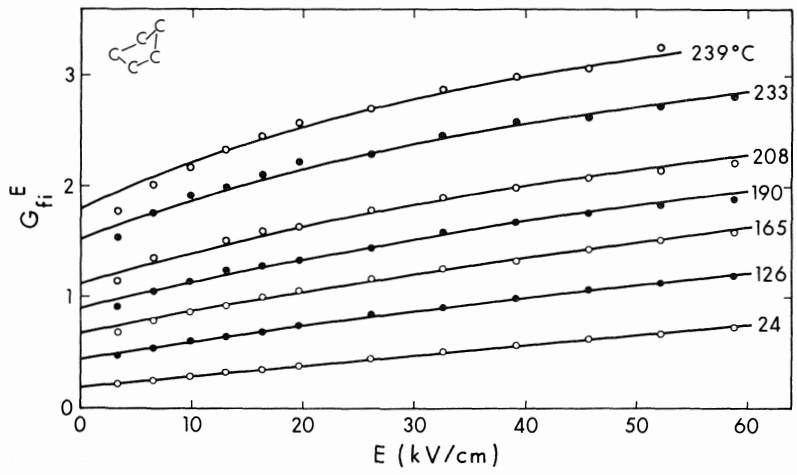

FIG. 8. Free ion yield $G_{fi}{}^{E}$ at field strength E in liquid at various temperatures and critical gas (239°C) in cyclopentane. The lines are calculated using [8] with a YGP range distribution function and a total ionization yield, $G_{tot} = 4.3$.

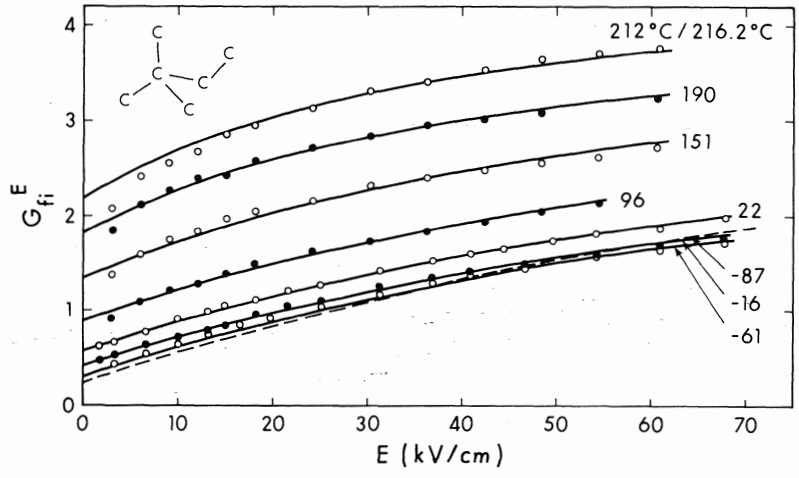

FIG. 9. Free ion yield at field strength E in liquid at various temperatures and critical gas (216.2°C) in neohexane. The lines are calculated using [8] with a YGP range distribution function and a total ionization yield, $G_{tot} = 4.3$. The experimental points are not plotted for −87°C and 216.2°C to avoid confusion.

of this point. The thermal electron mobility, in neopentane for example, first increases then decreases with an increase of temperature (15). This decrease in the mobility is interpreted by a breaking down of conduction bands resulting from a drastic decrease of the liquid density approaching the critical region. If the epithermal electron is also sensitive to the breaking of conduction bands, it seems logical to deduce that it has to travel in these conduction bands when its energy is very close to thermal. One can therefore suspect that the sensitivity of epithermal electron penetration ranges to molecular structure is due to the presence of well defined conduction bands in some liquids and their absence in others.

(*3*) At temperatures above critical, the density of the gas enclosed in the cell volume remains constant and an increase of temperature is associated with an increase of electron mean penetration range. This is shown in the present work for *n*-pentane and neopentane and has been measured for other hydrocarbons (32). At subcritical temperatures, a temperature in-

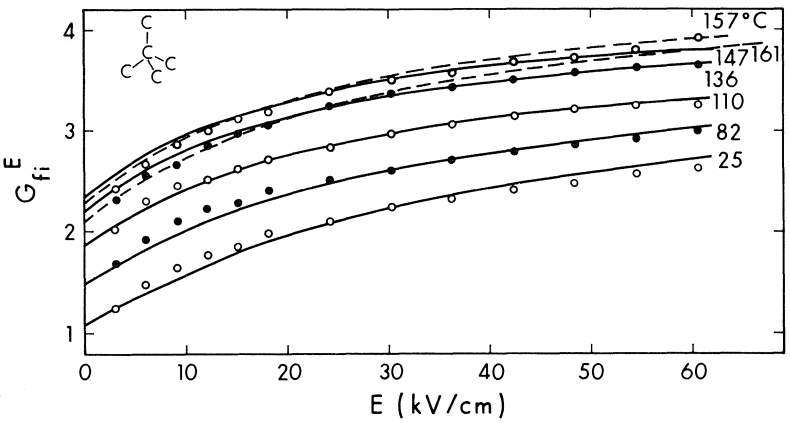

FIG. 10. Free ion yield $G_{fi}{}^{E}$ at field strength E in liquid at various temperatures and critical gas (161°C) in neopentane. The lines are calculated using [8] with a YGP range distribution function and a total ionization yield, $G_{tot} = 4.3$. The experimental points are not plotted for 157°C and 161°C to avoid confusion.

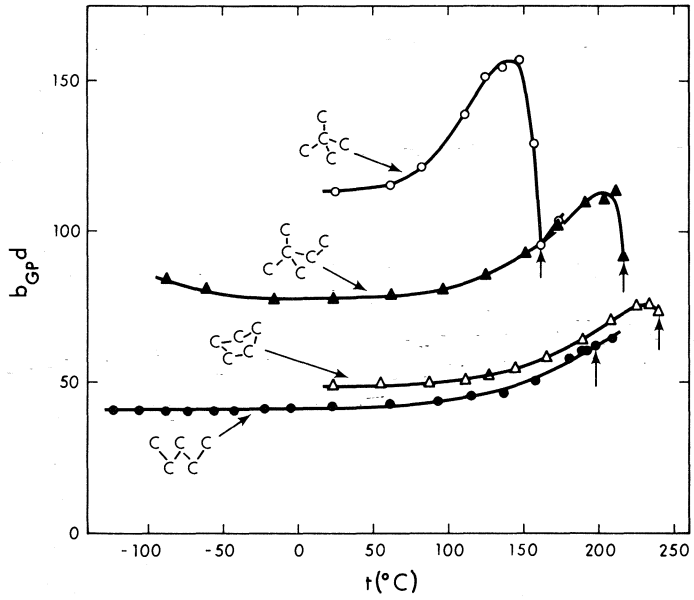

FIG. 11. Variation of normalized mean penetration ranges $b_{GP}d$ with temperature for *n*-pentane, cyclopentane, neohexane, and neopentane. The vertical arrows indicate the critical temperature of the alkanes.

crease goes with a density decrease. It is difficult to dissociate the relative effect of both factors on the electron mean penetration range. The maxima in the penetration ranges do not occur at the critical temperatures but at lower temperatures where the alkanes are still liquid and where the densities of neopentane, neohexane, and cyclopentane are about the same (0.390 g/cm^3). This tends to demonstrate that nothing special happens at the critical temperature, contrary to what had been anticipated from theory for electron mobilities (33). Consistent with the observations on electron ranges, the electron mobility in Xe did not undergo a transition in the critical region (34) nor in the four alkanes studied (15).

Acknowledgments

I wish to thank the staff of the Radiation Research Center for help with the electronics.

I am also grateful for discussions with Dr. G. R. Freeman and T. G. Ryan.

1. R. A. HOLROYD and M. ALLEN. J. Chem. Phys. **54**, 5014 (1971).
2. R. A. HOLROYD, B. K. DIETRICH, and H. A. SCHWARZ. J. Phys. Chem. **76**, 3794 (1972).
3. W. F. SCHMIDT and A. O. ALLEN. Science, **160**, 301 (1968).
4. W. F. SCHMIDT and A. O. ALLEN. J. Phys. Chem. **72**, 3730 (1968).
5. P. H. TEWARI and G. R. FREEMAN. J. Chem. Phys. **49**, 4394 (1968).
6. A. HUMMEL, A. O. ALLEN, and F. H. WATSON, JR. J. Chem. Phys. **44**, 3431 (1966).
7. A. MOZUMDER and J. L. MAGEE. J. Chem. Phys. **47**, 939 (1967).
8. L. ONSAGER. Phys. Rev. **54**, 554 (1938).
9. T. A. STONEHAM, D. R. ETHRIDGE, and G. G. MEISELS. J. Chem. Phys. **54**, 4054 (1971).
10. G. G. MEISELS and D. R. ETHRIDGE. J. Phys. Chem. **76**, 3842 (1972).
11. T. TAKAHASHI, S. KONNO, J. HAMADA, M. MIYAJIMA, S. KUBOTA, A. NAKAMOTO, A. HITACHI, E. SHIBAMURA, and T. DOKE. Phys. Rev. A, **12**, 1771 (1975).
12. M. MIYAJIMA, T. TAKAHASHI, S. KONNO, T. HAMADA, S. KUBOTA, H. SHIBAMURA, and T. DOKE. Phys. Rev. A, **9**, 1438 (1974).
13. M. MIYAJIMA, T. TAKAHASHI, S. KONNO, T. HAMADA, S. KUBOTA, H. SHIBAMURA, and T. DOKE. Phys. Rev. A, **10**, 1452 (1974).
14. J.-P. DODELET, K. SHINSAKA, U. KORTSCH, and G. R. FREEMAN. J. Chem. Phys. **59**, 2376 (1973).
15. J.-P. DODELET and G. R. FREEMAN. Can. J. Chem. This issue.
16. J. TIMMERMANS. Physico-chemical constants of pure organic compounds. Elsevier Publishing Company, England. Vol. 1. 1950; Vol. 2. 1965.
17. R. W. GALLANT. Physical properties of hydrocarbons. Vols. 1 and 2. Gulf Publishing Company, Houston, Texas. 1968.
18. R. D. NELSON, JR., D. R. LIDE, JR., and A. A. MARYOTT. Selected values of electric dipole moments for molecules in the gas phase. NSRDS-NBS 10, U.S. Department of Commerce, Washington, DC. 1967.
19. R. C. WEAST (*Editor*). Handbook of chemistry and physics. 49th ed. Chemical Rubber Co., Cleveland, Ohio. 1968.
20. J. TERLECKI and J. FIUTAK. Int. Radiat. Phys. Chem. **4**, 469 (1972).
21. A MOZUMDER and J. L. MAGEE. J. Chem. Phys. **45**, 3332 (1966).
22. S. CHANDRASEKHAR. Rev. Mod. Phys. **15**, 1 (1943).
23. W. F. SCHMIDT and A. O. ALLEN. J. Chem. Phys. **52**, 2345 (1970).
24. J.-P. DODELET, P. G. FUOCHI, and G. R. FREEMAN. Can. J. Chem. **50**, 1617 (1972).
25. G. C. ABELL and K. FUNABASHI. J. Chem. Phys. **58**, 1079 (1973).
26. M. LAX. Rev. Mod. Phys. **23**, 287 (1951).
27. A. MOZUMDER. J. Chem. Phys. **60**, 4305 (1974).
28. J. CASANOVAS, R. GROB, D. BLANC, G. BRUNET, and J. MATHIEU. J. Chem. Phys. **63**, 3673 (1975).
29. J. M. WARMAN, K. D. ASMUS, and R. H. SCHULLER. Adv. Chem. Ser. **82**, 25 (1968).
30. G. R. FREEMAN and T. E. M. SAMBROOK. J. Phys. Chem. **78**, 102 (1974).
31. J.-P. DODELET and G. R. FREEMAN. Can. J. Chem. **50**, 2667 (1972).
32. J.-P. DODELET and G. R. FREEMAN. In preparation.
33. J. LEKNER and A. R. BISHOP. Philos. Mag. **27**, 297 (1973).
34. T. KIMURA and G. R. FREEMAN. J. Chem. Phys. **60**, 4081 (1974).

Discussion

J. Jortner: An important mechanism for energy loss of electrons in liquid hydrocarbons may originate from inelastic electron–molecule scattering followed by vibrational excitation. Now, these hydrocarbons are characterized by low vibrational frequencies which may be thermally excited. Collision of an electron with a vibrationally excited molecule will provide a more effective energy loss mechanism than collision with a ground state molecule. It is possible that the maximum observed in the initial separation lengths b_{GP} *vs.* temperature originates from thermal vibrational excitations? This question will be settled by whether the maximum in b_{GP} originates essentially from a density effect or from a temperature effect. In the latter case the mechanism proposed herein may be relevant.

J.-P. Dodelet: The fact that a maximum appears in some liquids at about the same temperature for epithermal electron thermalization ranges and thermal electron mobilities indicates that the electron finds it difficult to lose energy when its energy is just above thermal. Therefore I do not think that vibrationally excited molecules provide a good explanation of the maximum appearing in thermalization lengths. A density effect seems to provide a better explanation. This is underlined by the fact that the density (g/cm^3) at the maximum thermalization length is the same for the three liquids in which this maximum appears.

G. R. Freeman: The data presented by Dodelet seem to indicate that the main part of the thermalization range in a liquid hydrocarbon is attained by the electrons when they are in the conduction bands not much above thermal energy. Scattering cross sections are relatively small in the conduction bands, so electron de-energization is inefficient in them. Conduction bands are less well defined in *n*-pentane than in neopentane, so electron scattering is greater and the range is shorter in the former than in the latter. Conduction bands seem to be more clearly defined in liquids that are made up of more spherelike molecules. The difference between density and temperature effects will be more clearly seen in our mobility paper in the last session of the conference.

L. G. Christophorou: In connection with Dr. Freeman's comment on the importance of the low-energy region in determining the size of the penetration range, I wish to point out that measurements of the rate of energy loss by subexcitation electrons for a number of polyatomic *gases*, including hydrocarbon vapors, (L. G. Christophorou, K. S. Gant, and J. K. Baird. Chem. Phys. Lett. **30**, 104 (1975)) show that the rate of energy loss varies greatly from one

compound to another in the region of vibrational excitation threshold ($\lesssim$0.5 eV), but it changes little for energies 1–2 eV. This clearly shows the importance of energy loss processes in the very low energy range ($\lesssim$0.5 eV) in determining the particle's range (or thermalization time).

G. R. Freeman: The effect is amplified in the liquid phase because conduction bands do not exist in low density gases. For example, the large difference between the ranges in neopentane and *n*-pentane in the liquids would not be expected in the gas phase.

K. Funabashi: The concept of 'thermalization' distance is sufficiently vague to warrant a detailed quantitative fit of experiment with any formula with more than one parameter. Energy loss for a subexcitation electron undoubtedly involves multiphonon processes besides single-phonon processes. In view of the fact that cross sections for elastic scattering in large alkane molecules are much (orders of magnitude) larger than those for inelastic processes, we have reason to believe that the so-called initial distribution is *mainly* determined by elastic scattering of the medium which is particularly important for very low-energy electrons.

G. R. Freeman: The difference in magnitude of the ranges in the liquids *n*-pentane and neopentane indicates that inelastic scattering is important. It appears to us that the range distributions are mainly determined by inelastic processes at electron energies not much above thermal.

E. O. Forster: What is the meaning of a "thermalized electron"?

J.-P. Dodelet: A "thermalized electron" is an electron having the same average kinetic energy as the molecules of the liquid.

E. O. Forster: Could one not readily associate the value of b_{GP} with the trap depth deduced from molecular structure? Neopentane has the most shallow trap and *n*-pentane is deepest. Hence a "thermalized" electron will be trapped more readily in a shorter distance in *n*-pentane than in neopentane.

J.-P. Dodelet: Yes. Alternatively, the magnitude of the thermalization length of epithermal electrons in liquids may be dependent upon the presence or absence of well-defined extended states. If the extended state is well defined it is because the trap depth is shallow.

E. O. Forster: How do you explain the decrease in b_{GP} near the critical point? Could the intense density fluctuations account for this phenomenon? Again, light scattering near the critical point suggests that such fluctuations might be worth considering.

J.-P. Dodelet: The decrease in b_{GP} near the critical point in some liquids is explained in terms of breaking down of extended states due to the density decrease. If the molecules become too far apart, their excited orbitals no longer overlap to produce an extended state.

J. L. Magee: I would like to congratulate Dr. Dodelet, Professor Freeman, and the Alberta group on the large amount of good work they have done on this problem. However, I have been thinking about this matter for a long time and I do not believe that we have a model which is ready for fine-tuning. There are several difficulties that are very troublesome, for example the multi-ion-pair neglect which Dr. Dodelet mentioned. Dr. Mozumder recently called my attention to another effect which may be of considerable importance, that the mobility of electrons in hydrocarbons is not constant, *i.e.*, the drift velocity is not proportional to the first power of the field strength. Mozumder has recalculated several free ion yields taking this effect into account and found that the initial distributions necessary to obtain given values are not those obtained from use of the Onsager equation. (He will publish a short paper on this topic.) There may be even other effects which have not been considered.

G. R. Freeman: Whether or not the electron mobility in a liquid hydrocarbon varies with the field strength depends on the hydrocarbon structure and density and on the field magnitude. It is up to the theoreticians to fine tune the model and up to the experimentalists to point the way. There are many shortcomings in our calculations, but we think that the similarities between the $b_{GP}d$ and mobility plots illustrate your early prediction that the electron ranges are attained mainly after the electrons have reached energies of a few tenths of an electronvolt.

J. M. Warman: We have calculated (J. M. Warman and M. C. Sauer. J. Chem. Phys. **62**, 1980 (1975)), from experimentally determined thermalization times in gases, the expected values of bd for neopentane and *n*-hexane (presumed similar to *n*-pentane). These values were 32 and 61 g Å cm^{-3}, respectively. The values of bd in the liquid phase at close to the critical temperature would therefore appear to be approaching the values expected in the gas phase. Secondly, since a decrease in mobility, as observed in neopentane, corresponds to a decrease in the scattering mean free path then this might be taken to directly indicate a decrease in the thermalization range as observed, if a random walk model is accepted. The correlation between μ and b has, however, been found to be rather weak when different liquids at normal densities are compared.

G. R. Freeman: We are now studying the gases at low and high densities. The density normalized ranges in the critical region are similar to, but not the same as, those in the low density gases. However, your estimated values are lower than ours. In answer to the second comment, although we have found fine structure in the correlation between μ and b_{GP} in different families of liquids (Can. J. Chem. **53**, 2714 (1975); **54**, 744 (1976)), I would not call the correlation weak. We must remember that μ in most liquids is strongly dependent upon three parameters (structure, density, and temperature), while b_{GP} depends mainly on the first two.

A. O. Allen: The many calculations on the subject of free ion yields which have appeared during the long period I have been interested in the subject, have in my opinion added little to our understanding. Looking at the data in a commonsense way, we see that those liquids which show thermally-activated mobilities have low free ion yields. This immediately suggests that the probability of an electron escaping the field of the positive ion depends on the

chance of its falling into a trap on the way out. A calculation made on this picture might provide a useful correlation between mobility and free ion yield.

J.-P. Dodelet: To my knowledge all fluid hydrocarbons display a thermally activated electron mobility if it is measured over a large enough temperature range. This includes neopentane and neohexane. The behavior of electron mobility in these hydrocarbons will be discussed in the last paper of this conference (Dodelet and Freeman). I agree that around room temperature and below, electron mobility in neopentane displays nearly no energy of activation, but at higher temperatures the mobility is quite sensitive to change of temperature. Furthermore, a high free ion yield is observed in *n*-pentane at temperatures close to critical and the electron mobility in *n*-pentane in the same temperature range is thermally activated. The picture is not simple.

G. R. Freeman: It is true that calculations are often more enlightening to those who make them than to others. I think that the large ranges in hydrocarbons are attained mainly by the epithermal electrons travelling in the conduction bands. Liquids comprised of less spherelike molecules are more efficient energy sinks (scatterers) and contain deeper traps. Dr. Allen's picture is qualitatively similar to ours.

L. Onsager: As we approach the critical point, fluctuations get large, which tends to reduce any benefit that the electron free path may obtain from Ramsauer effects.

G. R. Freeman: The density fluctuations characteristic of the critical region are long range. They appear to have little effect on the electron behavior. This was demonstrated for electrons in xenon by the work of Kimura (J. Chem. Phys. **60**, 4081 (1974)). However, I agree that the maxima observed in the range–density and mobility–density plots are related to Ramsauer effects.

Nonhomogeneous charge neutralization kinetics in nonpolar organic solids (Extended Abstract)

K. K. AMETOV, E. L. FRANKEVICH, G. F. NOVIKOV, AND B. S. YAKOVLEV
Institute of Chemical Physics, Academy of Sciences USSR, 142432 Chernogolovka, USSR

Received November 22, 1976

It is known that the bulk of electrons generated by ionizing radiation in organic nonpolar amorphous solids and liquids are thermalized in the vicinity of geminate positive ions, where the Coulomb energy is greater than the thermal energy. Such electrons form pairs correlated with positive ions and have a significant probability of recombination with 'their own' ions or ions of their track. This recombination process (so called 'geminate' recombination) cannot be described by applying homogeneous kinetics. Most of the theoretical approaches to geminate recombination in nonpolar liquids have been based on considerations of the diffusion of a classical charged particle. These approaches may prove to be unjustified for electron–ion geminate recombination in organic solids where electrons may be captured by structural traps for a time commensurable with the characteristic time of measurement.

To describe the kinetics of geminate recombination in this case we neglected a tunnelling mechanism of recombination and used a distribution function $Y(N)$ (1). This function gives the probability for an electron to recombine after N trapping events. The case was considered when a transition of an electron from one localized state, e_{tr}^-, to another can be characterized by a single relaxation time τ. Then the probability for the electron to undergo N captures by traps for the time t is the Poisson function

$$[1] \qquad \omega_N(t) = (t/\tau)^{N-1}\, e^{-t/\tau}/(N-1)!$$

and the rate of recombination is

$$[2] \qquad W(t) = \frac{1}{\tau}\sum_{N=1}^{\infty} Y(N)\omega_N(t)$$

This dependence was compared with experimental data on photo- and thermostimulated processes in 3-methylpentane (3-MP) glasses γ-irradiated at 77 K. For photostimulated recombination we used $\tau = (\sigma L)^{-1}$, where σ is the known photo-detrapping cross-section and L is the light intensity. For isothermal recombination at 77 K a good fit with experiment was obtained by using $\tau = 26$ min (1). A comparison of equation 2 with the decay of the photostimulated recombination luminescence of 3-MP at 77 K illustrated in Fig. 1 shows a satisfactory agreement for

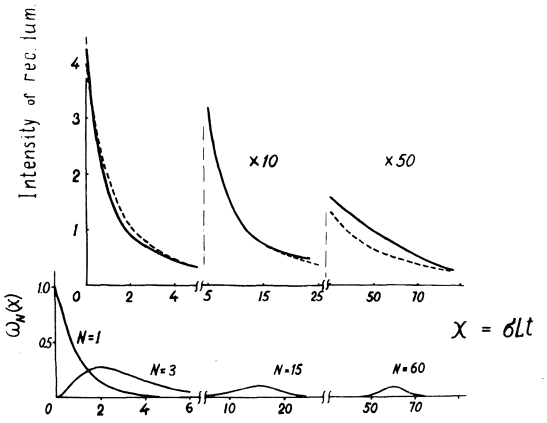

FIG. 1. Dependence of photostimulated luminescence in γ-irradiated 3-methylpentane at 77 K on ir-bleaching time; dose 3×10^4 rad; the ir light was switched on 36 min after e_{tr}^- generation. Dashed curve is calculated from [1]–[3]. The functions $\omega_N(x)$ are shown for $N = 1$, 3, 15, and 60.

$$[3] \qquad Y(N) = \begin{cases} 2.5 & \text{at } N = 1 \\ N^{-3/2} & \text{at } N > 1 \end{cases}$$

Such a distribution function has also been used to describe the decay of photoconductivity, isothermal recombination luminescence, quantum yield of e_{tr}^- bleaching (1), electric polarization of electron-ion pairs (2) in 3-MP at 77 K, and the radiothermoluminescence kinetics of 3-MP (3). For example, Fig. 2 shows the experimental (4) and calculated dependences of the quantum yield of e_{tr}^- bleaching, φ, on the optical density of e_{tr}^-, D. The latter was obtained from the equation:

$$[4] \qquad \varphi = \frac{1}{D}\frac{dD}{dx}$$

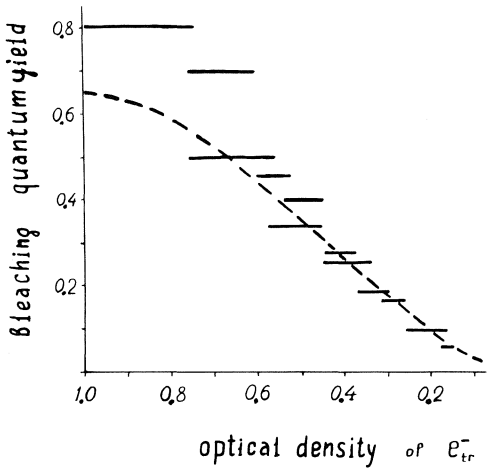

FIG. 2. Comparison of the calculated dependence of the quantum yield of bleaching of e_{tr}^- on the optical density of e_{tr}^- with experimental data (4) for 3-methylpentane: — Hamill's data; --- calculated.

where $x = \sigma Lt$, and

$$[5] \quad D \sim [e_{tr}^-] \sim \sum_{N=1}^{\infty} Y(N) \sum_{i=1}^{N} \omega_i(t)$$

At $t \gg \tau$, [5] may be written as

$$[6] \quad [e_{tr}^-] \sim (t)^{-1/2}$$

Such a relationship is known to be justified for geminate recombination of electrons in liquids and corresponds to the diffusion theory of recombination at longer times ($t \gg \lambda^{-1}$) (5). This result may be understood if one assumes the same space distribution of thermal electrons in both liquid and solid hydrocarbons because at $t \gg \tau$ the electron motion in solids may be described by a diffusion equation.

1. B. S. YAKOVLEV and G. F. NOVIKOV. Int. J. Radiat. Phys. Chem. **7**, 679 (1975).
2. K. K. AMETOV, G. F. NOVIKOV, and B. S. YAKOVLEV. Int. J. Radiat. Phys. Chem. In press.
3. K. K. AMETOV, G. F. NOVIKOV, and B. S. YAKOVLEV. Int. J. Radiat. Phys. Chem. In press.
4. D. W. SKELLY and W. H. HAMILL. J. Chem. Phys. **44**, 2891 (1966).
5. S. J. RZAD, P. P. INFELTA, J. M. WARMAN, and R. H. SCHULLER. J. Chem. Phys. **52**, 3971 (1970).

Discussion

A. C. Albrecht: (*1*) We have found that the decay of infrared stimulated recombination luminescence in 3-MP at 77 K can be fit to two exponentials and a second-order equation. The second order is interpreted through a simple distribution of unimolecular (one-jump) rate constants. The rate constant distribution is transformed to a radial distribution by making an assumption on how the rate constant depends on charge separation through the Coulomb field. Over 95% of the recombination events are accounted for in this way. As usual such a procedure represents simply another model which can be made to fit the data. The multiple hopping model seems to predict a polarization current which provides an interesting additional check on that model at least.

(*2*) A simple way of distinguishing polarization events from bulk transport is to see whether when electrodes are blocked the observed signal is altered. Polarization events within the Coulomb well should not be affected by blocking. Bulk current flow should be on an appropriate time scale. We have tried this for the 3-MP system at 77 K producing electrons photolytically. We found that blocking converts the normal ultraviolet dc photocurrents into polarization spikes, indicating that bulk flow is the major source of photocurrent in that system. However the photocurrent signals obtained when visible (or near infrared) light is used to excite previously produced electrons were not thus tested.

Electric field perturbed electron tunnelling in nonpolar organic glasses

A. J. DOHENY AND A. C. ALBRECHT

Department of Chemistry, Cornell University, Ithaca, NY, U.S.A. 14853

Received October 22, 1976

A. J. DOHENY and A. C. ALBRECHT. Can. J. Chem. **55**, 2065 (1977).

Isothermoluminescence (ITL) and electrophotoluminescence (EPL) resulting from electron–cation recombination are measured in a 2-methylpentane–methylcyclohexane glass. The ITL is more characteristic of quantum-mechanical tunnelling and the EPL signal is markedly stronger in this new glass than previous measurements in 3-methylpentane. Quantum-mechanical tunnelling theory is used to predict recombination rates of electrons in the potential field of a cation plus an applied field. Numerical integration of the nonhomogeneous kinetic equations resulting from a distribution of cation–electron separations leads to qualitative and quantitative predictions of the EPL signal that are observed experimentally. Fitting of the theory to experiment supports the conclusions that the angular distribution of the photoelectrons about the cations is close to isotropic, that the electrons active in ITL and EPL on the time scale of minutes are separated about 50 Å from their parent cation, and that the trap ionization potential in this nonpolar hydrocarbon glass is in the range of 0.5 to 0.7 eV.

A. J. DOHENY et A. C. ALBRECHT. Can. J. Chem. **55**, 2065 (1977).

On a mesuré l'isothermoluminescence (ITL) et l'électrophotoluminescence (EPL) qui se produit à partir de recombinaisons électron–cation dans des verres de méthyl-2 pentane et de méthylcyclohexane. L'ITL est plus caractéristique d'un tunnel de mécanique quantique et le signal EPL est beaucoup plus fort dans ce nouveau verre que ceux mesurés antérieurement dans le méthyl-3 pentane. On utilise la théorie des tunnels de mécanique quantique pour prédire les vitesses de recombinaison des électrons dans le champ potentiel d'un cation plus un champ appliqué. L'intégration numérique des équations cinétiques non-homogènes résultant des distributions des séparations cation–électron conduit à des prédictions qualitatives et quantitatives du signal EPL qui sont observées expérimentalement. L'ajustement de la théorie avec les expériences supporte les conclusions voulant que la distribution angulaire des photoélectrons autours de cations est près de l'isotropique, que les électrons actifs dans l'ITL et l'EPL sur une échelle de temps de minutes sont séparés par environ 50 Å de leur cation parent et finalement que le potentiel d'ionisation de piège dans ce verre hydrocarboné non-polaire est d'environ 0.5 à 0.7 eV.

[Traduit par le journal]

Introduction

When low temperature glasses are exposed to ionizing radiation, electrons are produced which subsequently may be chemically scavenged by other species of suitable electron affinity produced during the same irradiation (or added to the system before forming the glass). In many glasses, the electrons may be physically trapped in the medium for times much longer than the irradiation time, forming a trapped or solvated electron. In this temporary trapped state, they may be studied by conventional spectroscopies and over times ranging from nanoseconds to years depending on the natures of the glass and of the scavenging species.[1] In cases such as those described herein, where the scavenger is a radical cation, the neutralization of the charge pair can produce an electronically excited molecule; the intensity of the luminescent decay of this molecule is then a good measure of the rate of change of the trapped electron concentration. This isothermoluminescence (ITL) is a measure of the rate of charge neutralization only when this is slow compared to electronic relaxation times and is realizable only when it is fast enough to give a detectable flux of photons.

Quantum-mechanical tunnelling of an electron from its trapping site to the scavenger is thought to be the rate determining process in trapped-electron decay, at least in very hard ($\gtrsim 10^{12}$ P) glasses (2–4). However, ITL in 3-methylpentane (3MP) glasses at 77 K shows many effects not to be expected from a tunnelling process. The ITL is apparently quite temperature dependent (3, 5) and its fall-off with time is approximately $1/t^2$ at long times (3, 5), as compared with a $1/t$ law predicted and encountered in other cases of

[1] A general review of the subject with extensive reference is given in ref. 1.

ITL where tunnelling is the major mode of trapped-electron decay (3). In addition, strong electric fields (10^5 to 10^6 V/cm) applied to a 3MP glass which is undergoing ITL cause an enhancement of the electron decay rate, giving rise to a burst of light termed electrophotoluminescence (EPL) analogous to the Gudden–Pohl effect in inorganic phosphors (6). The EPL effect in 3MP was qualitatively and quantitatively explained (except at short times) by a one-parameter equation relating the EPL effect to the ITL. The parameter was found to be exponential in applied fields suggesting that the decay of any particular electron was governed thermally by a simple Arrhenius activation energy model (6).

Ott (5) and Bullot *et al.* (7) obtained an apparent activation energy for ITL in 3MP of about 0.67 eV, which corresponds to the activation energy of viscosity in 3MP obtained by Ling and Willard (8). Further, Ott (5) found that the temperature dependence of ITL in 3MP disappeared and that the ITL had a $1/t$ dependence below 72 K, consistent with the results of Kieffer *et al.* (3). This leads one to conclude that a mechanism similar to that of Pilling and Rice (9) is operative in the electron–cation recombination in 3MP at 77 K for times in the order of 10 min, *i.e.*, a trapped electron diffuses towards its parent cation at a viscosity-mediated rate until it reaches the point at which tunnelling becomes fast compared with further inward diffusional motion. Thus neither a pure tunnelling nor a pure thermal model can be adequate to explain the EPL phenomenon in 3MP at 77 K.

Instead of adapting a serial diffusion-tunnelling model to the EPL phenomenon, in the present work we report EPL in a hydrocarbon glass similar to but enough harder than 3MP so as to move the time scale of the viscosity-mediated effects beyond the time scale of the EPL experiment. Tunnelling theory is extended to the EPL experiment, whereupon it is found that the EPL effect in the harder glass is qualitatively predictable from a reasonable tunnelling model. Furthermore, it is found that the quantitative agreement between the model and the EPL experiment can be forced by variation of the parameters in the tunnelling calculations, but that only a limited range of trap depths is compatible with reasonable values of the other parameters and that a spherical distribution of electrons about their respective cations gives a significantly better fit to the experimental data than does an angularly anisotropic distribution.

Experimental Results

The experiments described herein have been carried out essentially as described previously by Bullot and Albrecht (6). *N,N,N′,N′*-Tetramethylparaphenylene diamine (TMPD) was obtained from Aldrich Chemical Company and purified by vacuum sublimation. Hydrocarbons were obtained from Phillips Petroleum Company. Hydrocarbon solutions of TMPD were frozen between two electrodes in a Dewar originally designed by Cadogan (10) for photoconductivity studies.

Exceptions to the method previously described (6) are that the back electrode is made of highly polished stainless steel, the irradiating light is passed through a filter consisting of two Corning 7-56 filters plus 2 cm of the hydrocarbon composing the glass, and the phototube is covered with a Corning 7-60 filter so that only the fluorescence of TMPD is monitored. Samples, once frozen between the electrodes, are allowed to relax at least 4 h before irradiation. Irradiation is for 1 min, following which the phototube is locked into place with the photomultiplier window approximately 5 cm from the window on the outside wall of the Dewar. Ott (5) found that the ITL in 3MP was apparently uncomplicated by viscosity for times up to 25 min at temperatures of 72 K or less. If we extrapolate the viscosity of 3MP below its glass transition using published data (8), we find that this temperature corresponds to a viscosity of about 3×10^{15} P. This figure is within an order of magnitude of that given by Hutzler *et al.* (11) for a 1:1 (v/v) mixture of 2-methylpentane (2MP) and methyl cyclohexane (MCH) at 77 K, which figure is also an extrapolation from measurements at higher temperatures.

Approximately millimolar solutions of TMPD in this solvent mixture were examined for the EPL effect. Most often the glasses cracked before attaining thermal equilibrium, but although they were thus unsuitable for the EPL experiment, ITL's determined with these cracked glasses exhibit ITL $\propto 1/t$ for times of 25 min or longer (Fig. 1).

One sample did resist cracking at 77 K, and sustained applied fields up to 5×10^5 V/cm. In this sample the EPL effect was measured at different fields in both polarities. In addition various sequences of field on and off and polarity reversals were tried. The qualitative results are summarized pictorially in Fig. 2. They are in every gross feature qualitatively

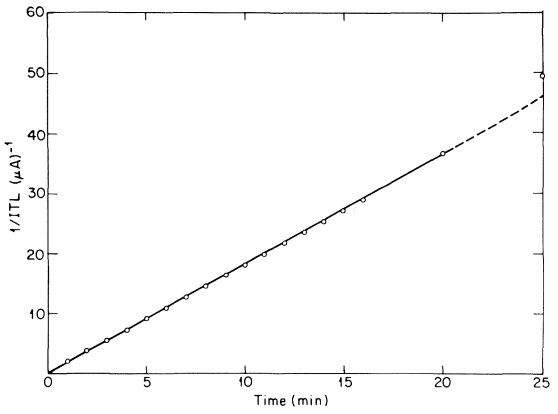

FIG. 1. Plot of $(ITL)^{-1}$ *vs.* time in 2MP/MCH (μA at anode of photomultiplier).

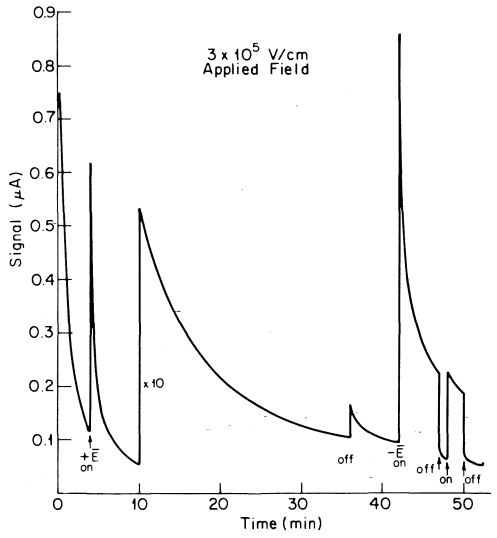

FIG. 2. Plot of EPL signals in 2MP/MCH.

identical with the EPL effects reported before for 3MP glasses (6). However, the relative height of the EPL spike and the time taken for the EPL signal to decay to the level of the ITL both appear to be about an order of magnitude larger in this glass than in the previous 3MP glasses. Further experiments established that the enhanced EPL effects in this glass could not be due to the infrared-stable, field-sensitive state of TMPD previously investigated in this laboratory (12) in 3MP glasses, for no evidence of this state was found in the harder glass of this work.

Theory

The recombination of a trapped electron with its geminate cation can be treated as a radiationless transition from an extreme charge-transfer state into an isoenergetic, near continuum of Rydberg-type states, the time dependence of which transition derives from the Fermi golden rule. The final state must be buried in a near continuum, since the total energy of the initial charge-transfer state in nonpolar glasses is at most only an electron volt or so below complete ionization in the nonpolar condensed phase, at which level molecular energy densities are quite large.

An apparently alternative approach is to treat the problem as the tunnelling of a trapped electron through a potential barrier from some trapping potential to the Coulomb well of the cation. This is not a real alternative, however, since in either view the recombination rate can be reduced to a frequency factor weighted by the probability that an electron initially trapped at a distance R from its parent cation can be found at the much shorter distance, r_0, from the cation where the electron emerges from the nonclassical into the classical region of the potential. These two approaches are distinguished only in their detailed interpretation of the frequency factor, which difference is related as much to the implicitly different choice of zeroth order states as to anything else.

The probability part of the recombination or transition rate must include tunnelling in the nuclear coordinates of the solvent cation system, *i.e.*, a Franck-Condon factor, as well as in electronic coordinates. For the present we will subsume this Franck–Condon factor as well as a geometric factor (13) into a generalized frequency ν; an appropriate and reasonable choice of this frequency, we intend to show, will theoretically duplicate the experimental EPL effect.

Theoretical Electron-tunnelling Rates

The electron space part of the probability can be derived from the semiclassical or WKBJ approximation to the electron wave function in the nonclassical region of the potential (14). Thus for the recombination rate of a cation–electron pair separated by a distance R we simply write

$$[1] \quad k(R) = \nu \exp\left[-2/\hbar \int_{r_0}^{r_1} (2m|U(r)|)^{1/2}\, dr\right]$$

In [1], m is the mass of the electron, r_0 and r_1 are the classical turning points of the motion, *i.e.*, the zeros of $U(r)$ which defines the energy

deficit of the electron below the top of the barrier, and the R dependence on the rhs is implicit. The frequency factor ν, in either approach to the transition rate, must have as an upper limit the frequency associated with a weakly bound electron or about 10^{14} to 10^{15} s^{-1}.

For the sake of concreteness, we may take the trapping potential of the electron to be a spherical square well of radius a and depth V_0. Then the barrier presented to a trapped electron in the Coulomb field of a monovalent cation in a medium of dielectric constant ε is shown in Fig. 3. V_0 and a determine the local binding energy or ionization potential of the electron, I_0, and the distance tunnelled by the electron to recombine with the cation is L^0. Figure 3 was drawn roughly to scale for a well of diameter 2.5 Å and ionization potential 0.5 eV, located at 47.5 Å from a cation in a medium of $\varepsilon = 2.3$. From the barrier potential of Fig. 3, we set $U(r)$ in the integrand of [1] to be simply $I_0 + (e^2/\varepsilon R) - (e^2/\varepsilon r)$.

Then [1] has the analytical result

$$[2]\quad k(R) = \nu \exp\left\{\frac{-2a}{\hbar}\sqrt{\frac{2me^2}{\varepsilon a}} \times \left[X_2\sqrt{\frac{1}{X_1}-\frac{1}{X_2}} - \frac{\sqrt{X_1}}{2} \times \ln\left(\frac{1+\sqrt{1-\frac{X_1}{X_2}}}{1-\sqrt{1-\frac{X_1}{X_2}}}\right)\right]\right\}$$

where

$$X_2 = \frac{r_1}{a} = \frac{R-a}{a}$$

and

$$X_1 = \frac{R}{a}\left(1 + \frac{RI_0\varepsilon}{e^2}\right)^{-1}$$

Equation 2 is similar to previously published results (3, 13, 15–17) the differences owing to the fact that the potential used includes a trap radius (18). Evaluation of [1] from its analytic form (eq. 2) and by numerical integration using a double-precision 32 point Gaussian quadrature give identical results, which in turn agree with Mikhailov's (16) numerical results when the same values of the parameters are used. Equation 2 predicts that to a good approximation,

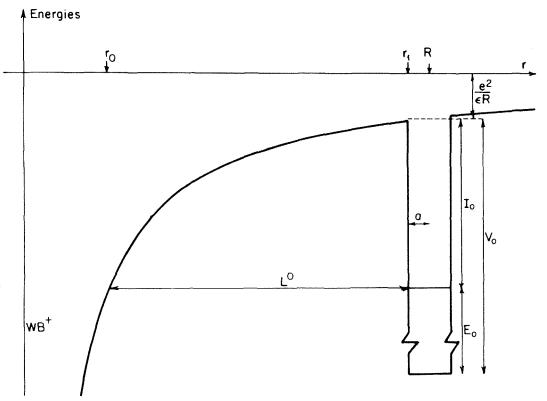

FIG. 3. Potential-barrier model for an electron in a spherical square well in the Coulomb field of a cation. WB^+ is Wurster's blue cation of TMPD. Symbols are defined in text.

$$[3]\quad \frac{\mathrm{d}\ln k(R)}{\mathrm{d}R} \simeq \frac{-2\sqrt{2mI_0}}{\hbar}$$

exactly as one would get from a square-barrier (*i.e.*, non-Coulomb) approximation to the integral. However, the square-barrier approximation introduces large absolute errors into $k(R)$ which can only be partially compensated by using L^0 or some other effective tunnelling length in a square-barrier formula. The major effect of the Coulomb field, as pointed out by Mikhailov (16), is that electrons decaying at a particular rate may be as much as 30% further from the cation in a low dielectric, small I_0 glass, than a square-barrier calculation would require them to be. This in turn has major ramifications on the theory of the EPL effect.

The shape of the potential when an applied electric field is superimposed on a Coulomb field is shown in Fig. 4. The energy scale is the same as in Fig. 3, but the horizontal scale has been halved to show the same trap as in Fig. 3 on both sides of the cation with respect to the internal field, which in the scale of the figure is 4×10^5 V/cm. When the potential barrier of Fig. 4 is used in [1], one obtains

$$[4]\quad k(R,\theta) = \nu \exp\left[\frac{-2}{\hbar}\sqrt{\frac{2me^2a}{\varepsilon}} \times \int_{X_1}^{X_2}\left(\frac{1}{X_1} - X_1\mathcal{E} - \frac{1}{Q} + Q\mathcal{E}\right)^{1/2}\mathrm{d}Q\right]$$

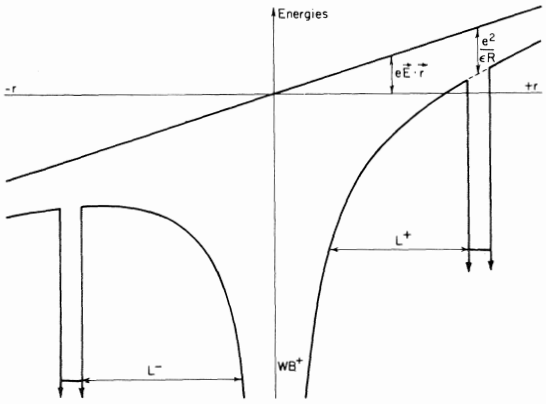

FIG. 4. Potential barriers resulting from application of an electric field to the potential of Fig. 3.

where $Q = r/a$, X_2 is defined as in [2], $\mathcal{E} = \varepsilon a^2 E \cos\theta/e$, and X_1 is the positive root of

$$X_1^2\left(\frac{\mathcal{E}R}{a}\right) + X_1\left\{1 + \frac{I_0\varepsilon R}{e^2} - \mathcal{E}\left(\frac{R}{a}\right)^2\right\} - \frac{R}{a} = 0$$

Fowler and Nordheim (19) encountered the tunnelling integral of [4] in a similar context, *i.e.*, the field emission of metals, and expressed the result as an elliptic integral. The same authors (19) and later Brocklehurst (2) evaluated [4] without including the angular dependence or the Coulomb field. Hagston (17) has derived an angle-dependent approximation to [4] when the field is so small as to give no experimentally observable effects. Instead, we employ the same numerical procedure that gives exact agreement with the analytical expression in the zero-field case. Qualitatively, the results of these calculations can be seen in graphs like Fig. 5 which shows $\log_{10} k(R, \theta)$ as a function of θ measured from the field vector. The internal field is 4.3×10^5 V/cm, $I_0 = 0.7$ eV, $\nu = 10^{15}$ s^{-1}, and $a = 1$ Å. The solid apple-shaped curves are for field-on conditions, with the more negative log scale in parentheses corresponding to the cation–trap separation of 60 Å. The dotted circles intersecting at 90° and 270° are the logs of the corresponding field-off rates which are of course angle independent. The field-off rate at 50 Å is approximately 3000 times faster than that at 60 Å. With the field on the recombination rate of an electron at 60 Å and directly upfield from the cation is increased by a factor of 250, while

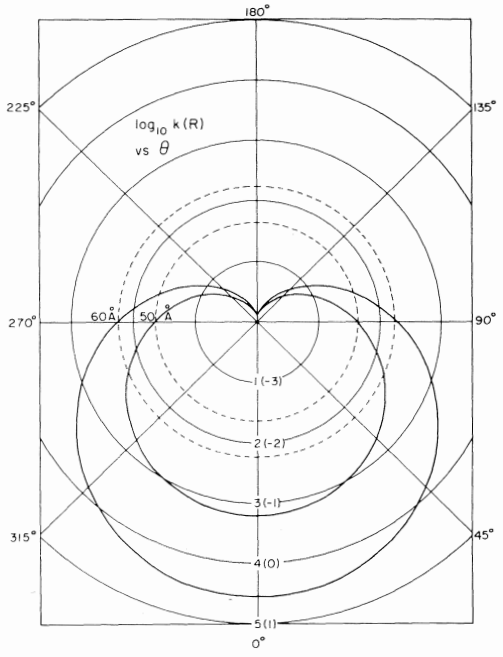

FIG. 5. Plot of log $k(R)$ *vs.* θ (measured from the positive field direction) for $I_0 = 0.7$ eV, $\nu = 10^{15}$ s^{-1}, $a = 1$ Å, and an internal field of 4.3×10^5 V/cm. The scales are explained in the text; but as an example, at 60 Å separation, the field-off rate is about 0.02 s^{-1} while with the field on the rate at 0° is about 5 s^{-1}.

an electron at 50 Å experiences a rate enhancement of only 30. In addition, Table 1 gives the ratio of the field-on rate to the field-off rate at different trap depths, internal fields, and cation–electron separations.

From consideration of Fig. 4, one can see that in the limit of large fields, shallow traps, or large cation–trap separations, all upfield electrons tunnel through virtually the same triangular barrier regardless of their distance from the cation. On the other hand, the tunnelling distance either downfield from the cation or even without the field is much more dependent on R. Therefore any comparison between field-on and field-off tunnelling rates will be highly R dependent. These observations give us warning that in calculating any EPL effect, we must exercise extreme caution in retaining any factors which affect the separation between the fastest remaining electrons and their cations at the instant the field is turned on.

Calculation of Isothermoluminescence and Electrophotoluminescence

Once we can predict field-dependent tunnelling

TABLE 1. $k_{\pm}/k$ for various I_0, E, and R (a = 1 Å)

		E (V/cm × 10^{-5})					
I_0 (eV)	R (Å)	−6	−4.3	−1.35	+1.35	+4.3	+6
0.7	40		~0.12	~0.53	~1.9	~9.0	
	50	0.0096	0.035	0.34	3.00	34.4	146
	60	0.0011	0.0070	0.02	5.18	212	1950

		E (V/cm × 10^{-5})			
I_0 (eV)	R (Å)	−4.3	−2.1	+2.1	+4.3
0.5	40	0.095	0.31	3.25	10.6
	50	0.022	0.15	7.07	50.8
	60	0.0039	0.060	18.5	363

rates at a particular cation–electron distance, we must apply them to the calculation of ITL and EPL effects. Since the tunnelling rate is such a strong function of the charge-pair separation, only a virtual δ-function distribution of separations (and of the other parameters) can lead to a simple exponential decay. Instead, even for a relatively narrow distribution of separations, say 10 Å wide, tunnelling rates varying over three to four orders of magnitude can be encountered. Hence we treat each electron–cation pair as a separate chemical species (which is valid up to ionic concentrations in the order of 10^{-2} M), each reacting at its own unimolecular rate, but all leading to the same product, and it is the rate of appearance of the product that we measure in ITL and EPL.

The development of the concentration, ITL, and EPL integrals where there exists a zero-time distribution of charge pairs having decay rates dependent upon the pair separation and orientation is standard in the recent literature (4, 17, 20, 21) and need not be repeated here. For our purposes a recapitulation of these integrals using the symbols of this work will suffice.[2]

If R is the charge-pair separation and θ the angle between the electron position vector (with origin at the cation) and the eventual field direction, then the number of pairs remaining at time t, $N(t)$, is given by

$$[5]\quad N(t) = \int_0^{\infty}\int_0^{\pi} n_0(R,\theta) \times e^{-k(R)t} \sin\theta\, d\theta\, dR$$

[2]Further details are to be found in the Ph.D. Thesis of Doheny (22) of which this work constitutes a part.

where $n_0(R,\theta)$ is a linear density of charge pairs and $k(R)$ is the zero-field tunnelling rate of [2]. The ITL signal is

$$[6]\quad \mathrm{ITL}(t) \propto \int_0^{\infty}\int_0^{\pi} n_0 k(R) \times e^{-k(R)t} \sin\theta\, d\theta\, dR$$

while the EPL signal resulting from applying an electric field at time t' to a sample undergoing ITL is

$$[7]\quad \mathrm{EPL}(t', t) \propto \int_0^{\infty}\int_0^{\pi} n_0\, e^{-k(R)t'} k_{\pm}(R,\theta) \times e^{-k_{\pm}(R,\theta)(t-t')} \sin\theta\, d\theta\, dR$$

where $k_{\pm}(R,\theta)$ is the angle-dependent field-on rate of [4]. One assumes that the proportionality in [6] and [7], involving instrumental and quantum-yield factors is field independent and hence identical for both ITL and EPL. The linear density $n_0(R,\theta)$ is motivated by the R^{-2} dependence of photoelectron flux in the limit of no electron scattering following isotropic photoionization.

Equations 6 and 7 have been integrated by various authors (4, 17, 20, 21) using the square-barrier approximation to $k(R)$, *i.e.*, $k = \nu e^{-AR}$. Most often used for n_0, where one has correlated charge pairs, is a constant distribution or a slowly decaying exponential. When a real experiment covers only a few, maybe up to four, orders of magnitude in time, the constant distribution assumption is not so restrictive. The rate constant k is such a strong function of R that only about 10 or 15 Å (not many molecular diameters) are being swept out in an experiment. Practically speaking n_0 must be constant only

over such a range. Since the field-on rates for the upfield electrons are less sensitive to their separation from the cation (than the field-off rates) the electric field will bring into the time domain of the experiment larger separations than are practically seen in ITL. Thus at long times the assumption of constancy of n_0 with R might fail in the field-on case. In any event any real distribution must be integrable on $R \subset (0, \infty)$, so that eventually the tail of the distribution must fall off at least as fast as e^{-R}.

Equation 6, when integrated with the square-barrier rate constant and a slowly decaying exponential distribution, e^{-BR}, where $B \ll A$, gives a simple power law decay at long times

$$[8] \qquad \mathrm{ITL}(t) \propto t^{-m}$$

where (20) $m = 1 + (B/A)$. For a constant distribution, one may take $B = 0$ in [8] or integrate [6] directly (17, 20, 21). In either case

$$[9] \qquad \mathrm{ITL}(t) = C_0/t$$

As already mentioned, the functional form of [9] has been observed in this work and in other glasses independently of temperature (3), but not in 3MP glasses at 77 K (3, 5). Of course, ITL at the experimental time zero is not infinite, but instead a plot of $1/\mathrm{ITL}(t)$ *vs.* experimental time will intersect the x axis sometime during the irradiation period.

In order to integrate [5]–[7] with the full form of the Coulomb well plus electric field barrier, a numerical integration procedure has been devised analogous to that used to perform the integral appearing in the rate constant. The logic of the numerical procedure is briefly outlined in the Appendix.[2] In every case investigated, the distribution $n_0(R,\theta)$ is assumed to be independent of R, but two types of angular distribution have been explored: isotropic and $\sin^2\theta$. The second distribution (in the coordinate system referred to the electric field) corresponds to that to be expected when the photoemissive state is spherically symmetric and the photoelectron ejection direction is governed by the electric field of the incoming photon with no subsequent angular scattering (23).

Theoretical Isothermoluminescence

In Fig. 6 are plotted the theoretical values of the inverse ITL *vs.* time for electrons tunnelling in the Coulomb field of a cation, for two different values of I_0 and an isotropic distribution of initial trapping sites. The integration method gives the same results for anisotropic distributions, which serves as a check on the numerical integration procedure. The differences between the curves are more an artifact of the normalization (*cf.* Appendix), for if the calculation were performed for the same density of traps in R space, the 0.7 eV curve would fall about 20% above the other.

As anticipated by Pilling and Rice (18), the inclusion of the Coulomb field has little effect on the observable ITL kinetics. The actual data for Fig. 6 show deviations from linearity of 0.5%/decade for $I_0 = 0.7$ eV and 1%/decade for $I_0 = 0.5$ eV, but these effects of the Coulomb field on ITL are so small as to be easily buried by the consequences of a nonconstant $n_0(R,\theta)$ (17). However, as noted previously the Coulomb field will determine both the R value whence virtually all the ITL originates at a given time, and, consequently, the magnitude of the EPL effect. Illustrating this are the numbers attached to the curves of Fig. 6, which are the separations in angstroms at times 1, 10, and 100 min where $n(R,\theta,t) = (1/e)n_0(R,\theta)$ for the case with the Coulomb field included and, in parentheses, without Coulomb distortion of the barrier.

Theoretical Electrophotoluminescence

The theoretical EPL effect was calculated for

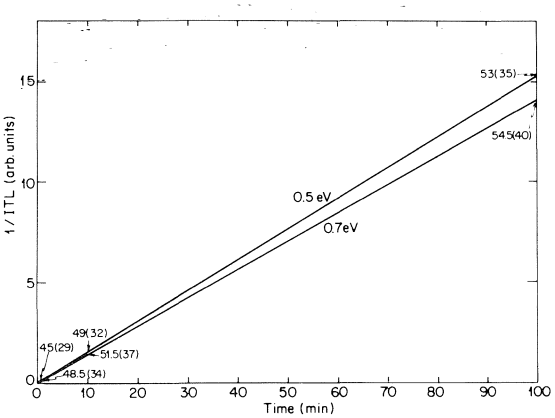

FIG. 6. Plot of $(\mathrm{ITL})^{-1}$ *vs.* time for two different values of ionization potential. For the 0.5 eV curve, $\nu = 3.6 \times 10^9\ s^{-1}$, and for the 0.7 eV curve, $\nu = 6 \times 10^{12}\ s^{-1}$. The numbers attached to the curves are the separations of the active electrons at the given time with and, in parentheses, without the Coulomb field. The fact these are smaller for 0.5 eV is the result of the smaller frequency factor. Note that the rate at which the active separation region increases with time is faster for a 0.5 eV ionization potential.

different fields, angular distributions, values of ν, and field-on times. The calculated EPL signal depends on the R value of the ITL active region and the number density of electrons in this region at the time the field is turned on. Both of these factors necessarily vary with the choice of parameters (the number density through our normalization protocol). However, to eliminate the proportionality in [6] and [7], we prefer to work with the ratio, $P_E(t)$, which we define as EPL(t)/ITL(t) where ITL(t) is the isothermoluminescence intensity which is theoretically predicted at time t in the absence of a field for the identical set of parameters. $P_E(t)$ is plotted *vs.* the logarithm of time, not for any theoretical reason, but simply because the values of this ratio vary dramatically at short times and much less so at longer times.

When plotted in this manner, all cases examined give remarkably similar curves, differing only in the height of the initial rise and their placement on the log (time) axis. Figure 7 is a plot of $P_E(t)$ *vs.* log t calculated for a trap with I_0 = 0.6 eV, when a 4.3 × 10^5 V/cm internal field is applied at 4 min. These curves in general can be described as consisting of an initial spike and then a slower decay until the ratio drops below 1 (*i.e.*, the signal in the presence of a field is eventually less than that expected had the field not been applied at all), reaches a minimum in the neighborhood of 0.9, and turns back toward 1.

Table 2 lists $P_E(t)$ information for traps having I_0 = 0.7 eV. If the field is turned on at

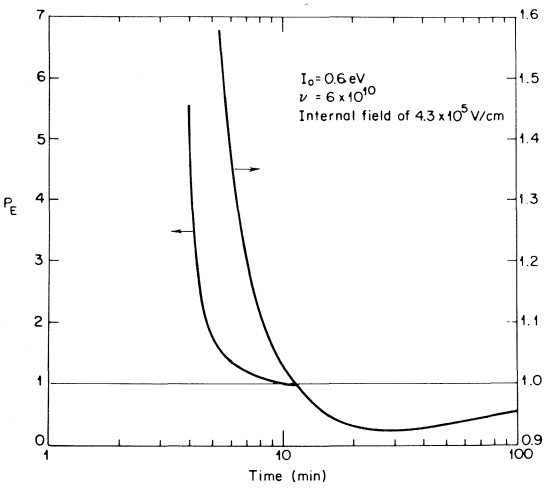

FIG. 7. Plot of $P_E(t)$ *vs.* log t for the indicated parameters. The field-on time, t', is 4 min and the crossing time, t_1, is about 11 min.

t', the initial peak value is $P_E(t')$ and is identified as P_E' in the table. To capture the sense of decay $P_E(1.1t')$ is also given, and thirdly the approximate time, t_1, at which $P_E(t)$ first reaches unity. Corresponding experimental data for two different experimentally applied fields are also given in Table 2. From Table 2 we see that as far as the peak ratio P_E' is concerned, an isotropic distribution is about as field sensitive as an anisotropic distribution having a 100-fold greater frequency factor. From additional calculations, it is established that the theoretical value of P_E' is an almost exponential function of field in this range. P_E' increases with greater values of t', *i.e.*, the later the field is turned on, reflecting the slightly greater cation–electron distance of the charge pairs which remain at the longer time.

Even though the P_E' values vary dramatically for the parameters in Table 2, the values of $P_E(1.1t')$ are fairly tightly grouped within each distribution, and are primarily affected by the internal field. In addition when a family of $P_E(t)$ curves differing only in field-on time are plotted as in Fig. 7, the curves are parallel from values of $P_E(t)$ between 2 and 1, but are displaced on the log-time axis. The curves coincide in this range of $P_E(t)$ if they are plotted as a function of their reduced time, t/t'. The implication is that whatever characteristic time is extracted from the slow decay of $P_E(t)$ from about 2 down to 1, it would be found that these times would then be a fairly linear function of the field-on time. The most remarkable example of this is simply the time t_1 defined by $P_E(t_1)$ = 1. From Table 2, we see that t_1 is very linear in field-on times, and only weakly affected by the applied field. Further calculations show that this crossing time is also insensitive to I_0.

The theoretical prediction that a simple t' scaling of time makes the family of curves coincide is somewhat understandable. The time at which the field is turned on selects the R value of the ITL-active electrons at that time. Accordingly, it determines the rate of decay and the electric field rate enhancement at the inside edge of the distribution of remaining electrons, which edge is receding from the cation as fast as log(t) is increasing. This is an area for further experimental testing of the model (22).

Discussion

We now wish to compare the theoretical EPL

TABLE 2. Calculated and experimental EPL signal characteristics

(*A*) Calculated EPL signal characteristics for $I_0 = 0.7$ eV, $a = 1$ Å at different values of ν and n_0

E (V/cm)	n_0 (R, θ)	ν(s^{-1})	t' (min)	P_E'	$P_E(1.1t')$	t_1 (min)
4×10^5	∝ const.	10^{12}	2	5.60	2.73	5.4
			4	6.20		10.7
			10	7.11	2.95	26.6
		10^{14}	2	11.54	3.37	5.3
			4	13.01		10.6
			10	15.31	3.58	26.6
	∝ $\sin^2$ θ	10^{12}	2	3.27	2.06	5.3
			4	3.53		10.3
			10	3.93	2.22	25.8
		10^{14}	2	5.74	2.53	5.2
			4	6.31		10.4
			10	7.19	2.70	25.5
6×10^5	∝ const.	10^{12}	2	25.96	4.15	6
			4	30.91		12
			10	39.18	4.40	31
		10^{14}	2	89.75	4.34	6.4
			4	109.97		12.7
			10	144.83	5.06	32.6
	∝ $\sin^2$ θ	10^{12}	2	11.06	3.11	5.5
			4	12.78		11
			10	15.57	3.33	27.5
		10^{14}	2	31.43	3.39	6
			4	37.42		12
			10	47.47	3.92	28

(*B*) Experimental EPL signal characteristics

E_{app} (V/cm)	t' (min)	P_E'	$P_E(1.1t')$	t_1 (min)
3×10^5	4	5.32	2.6	14
4×10^5	4	14.05	4.6	13.5

effect with that experimentally found in the 2MP/MCH glass. What we hope to find is an internally consistent set of parameters that can produce quantitative agreement with the measurable experimental facts of EPL.

Determination of the Angular Distribution

When an anisotropic distribution ($\sin^2$ θ), a frequency factor ν of 10^{12} s^{-1}, and an ionization potential I_0 of 0.7 eV are used in the calculations (Table 2), the theoretical P_E' values at internal fields of 4×10^5 and 6×10^5 V/cm are close to those determined at the experimentally applied fields of 3×10^5 and 4×10^5 V/cm (Table 2). However, with so few points in the parameter space explored, it cannot be said that these parameters are in any sense a best fit set of parameters to experiment. Now we have already mentioned that P_E' is exponential in the internal field in the range of fields we have used. This is confirmed experimentally when the logarithm of the experimental P_E' values is plotted as a function of the applied field (Fig. 8). This plot is linear over the range studied, although the slope must change at lower fields so that P_E' is 1 at zero field. The logarithm of the theoretical P_E' plotted *vs.* the applied field is also linear, but the slope of the line and the extrapolated intercept are both functions of the parameters ν, I_0, t', n_0, and $g(\varepsilon)$ which scales the applied field to the internal field. As an example, for Lorentz scaling

$$g(\varepsilon) = (2 + \varepsilon)/3 \qquad [10a]$$

$$\boldsymbol{E} = g(\varepsilon)\boldsymbol{E}_{app} \qquad [10b]$$

TABLE 3. Calculated and experimental field dependence of P_E' at different values of I_0, $n_0(R, \theta)$, and $g(\varepsilon)$

I_0 (eV)	$n_0(R, \theta)$	E_{app} (V/cm × 10^{-5})	$g(\varepsilon)$	ν (s^{-1})	R' (Å)	P_E'	$\frac{P_E'(4 \times 10^5)}{P_E'(3 \times 10^5)}$
0.7	∝ const.	3	1.43	10^{11}	50	5.47	2.65
0.7		4	1.43	10^{11}	50	14.48	
0.5		3	1.43	1.8×10^7	48	5.47	2.63
0.5		4	1.43	1.8×10^7	48	14.40	
0.5		3	1.00	3.6×10^9	55	5.32	2.62
0.5		4	1.00	3.6×10^9	55	13.93	
0.7	∝ $\sin^2 \theta$	3	1.43	6×10^{12}	56	5.33	2.87
0.7		4	1.43	6×10^{12}	56	15.28	
0.5		3	1.43	4×10^8	52	5.49	2.86
0.5		4	1.43	4×10^8	52	15.70	
0.5		3	1.00	1.8×10^{11}	62	5.41	2.87
0.5		4	1.00	1.8×10^{11}	62	15.53	

Experimental E_{app} (V/cm × 10^{-5})	P_E'	$\frac{P_E'(4 \times 10^5)}{P_E'(3 \times 10^5)}$
3	5.32	2.64
4	14.05	

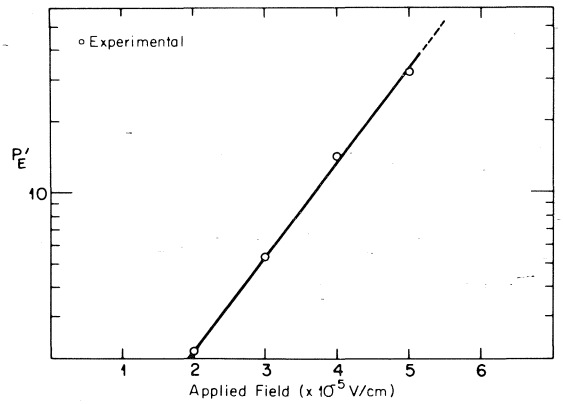

FIG. 8. Plot of log (P_E') *vs.* applied field.

In the laboratory only t' and E_{app} are under effective experimental control, and in this work, t' is fixed at 4 min while E_{app} ranges from 2×10^5 to 5×10^5 V/cm. What we seek, therefore, is a set of parameters which makes the theoretical and experimental curves for log P_E' *vs.* applied field coincide. In practice, we look for a set $\{\nu, I_0, n_0, g(\varepsilon)\}$ which forces coincidence between the experimental and theoretical values of P_E' at 3×10^5 V/cm and predicts P_E' at 4×10^5 V/cm. Such correspondence between theory and experiment is tested by the ratio $P_E'(4 \times 10^5$ V/cm$)/P_E'(3 \times 10^5)$, which is proportional to the slope of the log P_E' *vs.* E_{app} plot.

Variation of any parameters in our set will in general change both the slope and intercepts of these log P_E' *vs.* applied field curves. However, it quickly becomes apparent that one can fine-tune the calculated P_E' value at any applied field (in particular at 3×10^5 V/cm) to the experimental value by adjustment of the frequency factor ν. This is undestandable in that ν determines the R value of the closest remaining electrons at t'.

Table 3 gives the theoretical and experimental values of P_E' at two applied fields for different choices of I_0 and $g(\varepsilon)$ using both anisotropic and isotropic distribution. These are all for cases where adjustment of ν has forced coincidence at the lower of the two fields. The column labeled R' is the approximate cation–electron separation at which $n(R,\theta,t')$ has decayed to $(1/e)$ $n_0(R,\theta)$ at the time t'.

The data in Table 3 show that, for both kinds of angular distribution, the predicted value of P_E' at the higher field is independent of I_0 and $g(\varepsilon)$, once the frequency factor has been adjusted so that the calculated P_E' at the lower field matches experiment. The values of I_0 represented in Table 3 correspond to the probable extremes of those possible in this glass consistent with the tunnelling model of the EPL effect, as we discuss below. In addition the factor $g(\varepsilon)$ has been chosen to represent the extremes of no scaling and Lorentz scaling of the internal field (with $\varepsilon = 2.3$).

From Table 3 we see that the isotropic

distribution predicts correctly the observed P_E' at the high field while the anisotropic distribution is apparently incapable of doing so in the range of parameters explored. Further we may conclude that the electrons active in ITL and EPL in the time scale of minutes and at the chosen ionization potentials are in the order of 50 to 55 Å from the parent cation. Since the estimated uncertainty in the experimental ratio of the P_E' values at the two different applied fields is about 5%, a slight anisotropy in the angular distribution is not ruled out. Experiments conducted with the field applied obliquely to the ionizing radiation will be necessary to establish any small anisotropy in the angular distribution.

Figures 9 and 10 show the theoretical $P_E(t)$ for the parameters taken from the first two lines of Table 3. The circled points in Figs. 9 and 10 are experimental values of $P_E(t)$ for applied fields of 3×10^5 and 4×10^5 V/cm respectively. The fit, while good, suffers in that the experimental $P_E(t)$ goes through unity somewhat later than predicted and becomes smaller than predicted on the time scale of these experiments.

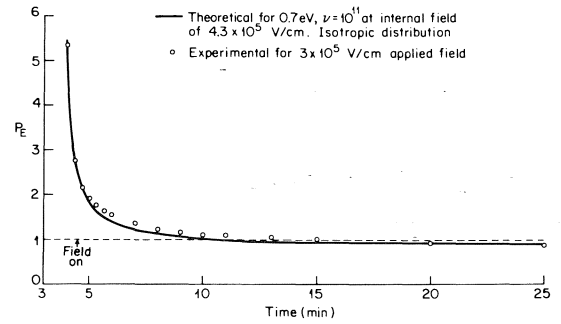

FIG. 9. Plot of P_E *vs.* time, experimental points and theoretical curve for 3×10^5 V/cm.

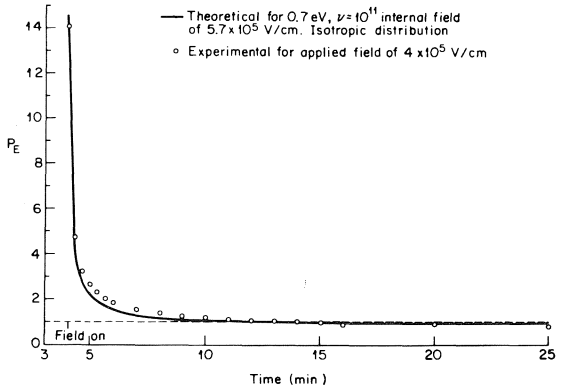

FIG. 10. Plot of P_E *vs.* time, experimental points and theoretical curve for 4×10^5 V/cm.

The model is apparently qualitatively predictive, and in some cases measurable experimental parameters are quantitatively predictable and indicate that the angular distribution of electrons is isotropic. Further, as Table 3 shows, the experimental facts about which the model is quantitatively accurate are insensitive to the other major unknown input parameters of the model, ionization potential and field scaling. The model at this point cannot be improved in any respect by changing these input parameters. Therefore the choice of the 'best' fit input parameters depends upon a discussion of the internal consistency of the set.

Reasonable Estimates of Internally Consistent I_0, ν, and $g(\varepsilon)$

So far we have been using the frequency factor ν as a totally free parameter, which for a given set of energy input parameters can be adjusted so that at a given field-on time, the inside edge of the distribution is far enough away from the cation as to produce a given field effect. In actuality, the factor ν, and for that matter the ionization potential I_0, ought to agree with the physical picture of the trapped electron derived from other sources.

The maximum in the trapped electron absorption spectrum in glassy hydrocarbons occurs at about 0.7 eV with a low energy onset of about 0.5 eV (24). In addition Miller and Willard (25) have reported photodetachment of the trapped electron at energies of 0.53 eV while Novikov and Yakovlev (26) estimate the photoionization threshold to be even as low as 0.4 to 0.44 eV. Hence, we have restricted ourselves to the investigation of trap ionization potentials in the range 0.5 to 0.7 eV.

However, there are some arguments to be made from the calculated EPL effect that place the barrier height, I_0, in the range we have been using. Previously we mentioned in passing that the frequency factor ν should not exceed the zero point frequency of a weakly bound electron. If, for definiteness, we use the zero point energy E_0 of a spherical square well trap to estimate the upper bound of ν, ν_{max}, we calculate from Funabashi's (27) parameterization of the ground state energy level that $\nu_{max} \simeq 6 \times 10^{14}\ s^{-1}$ for a trap radius of 2.5 Å, independently of the ionization potential (*i.e.*, E_0 in Figs. 3 and 4 is 2.5 eV no matter what V_0 and hence I_0 we use). For a trap of only 1 Å radius (which has been used throughout the kinetic calculation for

scaling convenience and to keep $R \simeq r$), ν_{max} becomes $3 \times 10^{15}\ s^{-1}$ and at $a = 5$ Å it is $2 \times 10^{14}\ s^{-1}$. Now the upper limit of ν should only apply for an electron completely surrounded by cations, but recalling that only a single direction of tunnelling can produce recombination, we ought really to reduce ν_{max} by a probability factor calculated from reasonable, if not rigorous, geometrical arguments (4, 9, 13, 21). We seek the fraction of all possible tunnelling directions that allow the electron to emerge into the Coulomb well without tunnelling a distance, $L^0 + \delta r$, much greater than the minimum tunnelling distance, L^0. If the radius r_0 of the Coulomb well at the emergence energy increases, the tunnelling rate falls off less drastically with the intra-pair separation, R. Hence, if we restrict ourselves to off-axis tunnelling directions that decrease the tunnelling rate by a small factor (less than 2) owing to an increase in the barrier width of approximately δr, we find that $\delta r/r_0$ is in the order of 5–10% and independent of I_0 and therefore r_0. The steric factor $P(R)$ is therefore the fractional solid angle subtended by a spherical lens with radius of curvature r_0 and thickness $\delta r \simeq 0.05 r_0$, at an electron a distance $L^0 \simeq R\text{-}r_0$ away. The result is simply (22)

$$[11] \qquad P(R) \simeq \frac{1}{2}\left(\frac{r_0}{L^0}\right)^2 \frac{\delta r}{r_0}$$

As an example, for $R = 50$ Å, $I_0 = 0.7$ eV, and $\delta r = 0.05 r_0$, we obtain a $P(R)$ of 8×10^{-4}.

We further estimate the Franck–Condon factor, which heretofore is also implicit in our use of ν and reflects the readjustment of the nuclei of the cation and all the intervening and surrounding solvent molecules, to be in the order of unity. This is because the transition, as mentioned previously, is essentially from charge-transfer to Rydberg-type states. In addition the initial and final states are surely degenerate within the band width of the final states for reasons previously discussed so that a lack of resonance should not further reduce ν_{max} to any extent. Thus we estimate that a reasonable effective frequency, ν, for these trap parameters is somewhere in the range of 5×10^{10} to 10^{12} s^{-1} ($\sim \nu_{max} P(R)$). Considering the oversimplifications in the model of the trapping potential, it is gratifying that such a rough estimate of the frequency factor is well within an order of magnitude of that needed to fit the experimental data at these trap parameters for an isotropic distribution.

If we ask now what would be the effect of a larger ionization potential, we can extrapolate from the data of Table 3 that it would require an effective frequency factor about two orders of magnitude larger to fit the experimental EPL effect for each 0.1 eV increase in I_0, yet the probability factor calculated as before would decrease since ν_{max} is insensitive to I_0 while the point at which the tunnelling electron emerges from the barrier is closer to the cation. These considerations enable us to put an upper limit of 0.7 eV on the trap ionization potential.

A lower limit to the ionization potential is not so easy to assign. Values of I_0 lower than 0.7 eV again lead to ν's about two orders of magnitude smaller for each 0.1 eV decrease in I_0 while $P(R)$ increases slightly. However, lower trap ionization potentials down to about 0.5 eV do fit the experimental EPL data slightly better in the 5 to 15 min range. In addition, there may be some as yet unexplored mechanisms involving the solvation sphere of the electron that could lower ν_{max} still further to fit the EPL data at a smaller I_0. For now we are content to accept a lower limit of about 0.5 eV to the trap ionization potential, consistent with the photoionization data. Given the limits on the trap ionization potential and more importantly the reasons for setting these limits, we can say little more about the appropriate internal field scaling except that Lorentz scaling appears to be favored at ionization potentials of 0.7 eV (since a $g(\varepsilon)$ of 1 would require $\nu \simeq 10^{13}$–$10^{14}\ s^{-1}$), but at smaller ionization potentials there is no clear choice. Kriebel (28) has determined that in low dielectric constant fluids there is no clear choice among various dielectric field-scaling models; in fact the magnitude of the internal field at a dielectric constant of about 2 varies little with the choice of the model. If we accept Lorentz scaling, or something of similar magnitude, as appropriate to the internal field, we are led to favor trap ionization potentials closer to 0.7 eV, since at lower I_0, Lorentz scaling leads to rather small values of ν (Table 3).

Prospects for Quantitative Improvement of the Model

Once we use a geometrical argument to rationalize the effective frequency factors obtained by a theoretical fit to the experiment, we

should re-examine some previous conclusions in light of this argument. In fact, qualitatively, the EPL effect arises predominantly from the up-field shortening of the tunnelling length which consequently increases the effective cation size. This means that there is a potentially significant field dependence in $P(R)$ as we have estimated it; and especially for the case of an isotropic angular distribution, this could alter the ratio of the P_E' values at two different fields, which is presently the main justification for assuming that the distribution is isotropic. We plan to re-calculate the EPL effect with a field-dependent $P(R)$, but preliminary estimates predict that the ratios previously calculated for the isotropic distribution may at worst be diminished by about 5%, not enough at present to reject the isotropic distribution. It is conceivable that including the field effect in $P(R)$ may also improve the match between theory and experiment at times between about 5 and 20 min.

The experimental fact that $P_E(t)$ becomes smaller than theoretically predicted may also be a result of not including field effects in $P(R)$. We must remember, however, that the assumption of a constant distribution in R may not be as harmless in calculating EPL as it is in ITL, for the field brings much larger R values into the purview of the experimental time scale. Since experimentally, the 1/ITL curves deviate from linearity at long times, there is some reason to suspect an effective limit on the R distribution and this should lower $P_E(t)$ at times greater than 20 min.

Conclusion

The calculations and experimental data on the EPL effect presented herein generally support the role of quantum-mechanical tunnelling in the decay of trapped electrons in very hard glassy hydrocarbons. From the field dependence of the EPL effect, the model indicates that the distribution of trapped photoelectrons about their parent cations is angularly isotropic. Furthermore reasonable quantum-mechanical limits on the largest possible frequency parameter of the tunnelling model put an upper limit of the trap ionization potential of about 0.7 eV, and at this value the magnitude of the EPL effect is consistent with Lorentz scaling of the internal field and electron–cation separations of about 50 to 55 Å. It is still a source of wonder to the authors that the model, which totally neglects the graininess of matter on the scale of angstroms and predicts order-of-magnitude effects on the scale of molecular diameters, is still qualitatively and even quantitatively in harmony with the observations. This is in all likelihood due to the statistical nature of the electron distribution. The success of the theory implicitly supports the notion of electrons trapped at distances from the cation great enough so that the radial correlation function of the solvent molecules has become constant on the same scale of separations.

Acknowledgments

Support from NIH Grant GM-10865 and the Materials Science Center at Cornell is gratefully acknowledged. One of us (A.C.A.) is indebted to Joshua Jortner and Stephen A. Rice for their helpful discussions of this material, and we are both grateful to Kiril Zamaraev for encouraging this investigation.

1. L. KEVAN. Trapped electrons in organic chemistry glasses. *In* Advances in radiation chemistry. Vol. 4. *Edited by* M. Burton and J. L. Magee. Wiley-Interscience, New York. 1974.
2. B. BROCKLEHURST. Chem. Phys. **2**, 6 (1973).
3. F. KIEFFER, C. MEYER, and J. RIGAUT. Chem. Phys. Lett. **11**, 359 (1971); Int. J. Radiat. Phys. Chem. **10**, 79 (1973).
4. F. S. DAINTON, M. J. PILLING, and S. A. RICE. J. Chem. Soc. Faraday Trans. II, **71**, 1311 (1975) and references therein.
5. R. OTT. Ph.D. Thesis, Cornell University, Ithaca, NY. 1972.
6. J. BULLOT and A. C. ALBRECHT. Acta Phys. Pol. **34**, 615 (1968); J. Chem. Phys. **51**, 2220 (1969).
7. J. BULLOT, D. CECCALDI, and H. SZWARC. Chem. Phys. Lett. **35**, 666 (1972).
8. A. C. LING and J. E. WILLARD. J. Phys. Chem. **72**, 1918 (1968).
9. M. J. PILLING and S. A. RICE. J. Chem. Soc. Faraday Trans. II, **71**, 1563 (1975); P. R. BUTLER, M. J. PILLING, S. A. RICE, and T. J. STONE. Can. J. Chem. This issue.
10. K. CADOGAN and A. C. ALBRECHT. J. Chem. Phys. **43**, 2550 (1965).
11. J. S. HUTZLER, R. J. COTTON, and A. C. LING. J. Chem. Eng. Data, **17**, 324 (1972).
12. R. DEVONSHIRE and A. C. ALBRECHT. Luminescence of crystals, molecules and solutions. *Edited by* F. Williams. Plenum Press, London. 1973. p. 304.
13. D. L. DEXTER. Phys. Rev. **95**, 985 (1954).
14. A. MESSIAH. Quantum mechanics. John Wiley and Sons, Inc., New York. 1968. p. 216, 231ff.
15. H. TSUJIKAWA, K. FUSKI, and Z. KURI. Bull. Chem. Soc. Jpn. **38**, 2210 (1965).
16. A. J. MIKHAILOV. Dokl. Phys. Chem. **197**, 223 (1971).
17. W. E. HAGSTON. J. Phys. C, **9**, 647 (1976).

18. M. J. PILLING and S. A. RICE. J. Phys. Chem. **79**, 3035 (1975).
19. R. H. FOWLER and L. W. NORDHEIM. Proc. R. Soc. London, Ser. A, **119**, 173 (1928); L. W. NORDHEIM. Proc. R. Soc. London, Ser. A, **121**, 626 (1928).
20. M. TACHIYA and A. MOZUMDER. Chem. Phys. Lett. **28**, 87 (1974); Chem. Phys. Lett. **34**, 77 (1975).
21. K. I. ZAMARAEV and R. F. KHAIRUTDINOV. Chem. Phys. **4**, 181 (1974).
22. A. J. DOHENY. Ph.D. Thesis, Cornell University, Ithaca, NY. 1977.
23. H. BETHE and E. E. SALPETER. Quantum mechanics of one- and two-electron systems. Springer-Verlag, Berlin. 1957. p. 300.
24. T. SHIDA, S. IWATA, and T. WATANABE. J. Phys. Chem. **76**, 3683 (1972).
25. J. R. MILLER and J. E. WILLARD. J. Phys. Chem. **76**, 2341 (1972).
26. G. F. NOVIKOV and B. S. YAKOVLEV. Opt. Spectrosc. USSR, **39**, 53 (1975).
27. K. FUNABASHI. Excess-electron processes in radiation chemistry. *In* Advances in radiation chemistry. Vol. 4. *Edited by* M. Burton and J. L. Magee. Wiley Interscience, New York. 1974. p. 116.
28. N. A. KRIEBEL. Ph.D. Thesis, University of Zurich, Zurich. 1974.

Appendix

A distribution which is constant in R space is set up between limits determined as follows: (*a*) at the first time point calculated, all the ITL from the region of the minimum R has ceased; (*b*) at the last time point calculated and at the highest internal fields expected, the concentration of electrons remaining near the maximum R is still greater than 90% of that specified by the starting distribution. It is desired to make this range as small as possible to minimize errors resulting from too coarse a grid in the integration, without introducing other errors resulting from time running off either distribution edge.

Once the distribution range of trapped electrons is decided it is possible to calculate the rate constants, both with and without field, for each of 2^{10} points in the range $R \subset (R_{min}, R_{max})$, $\theta \subset (0, \pi)$. The points are spaced in both directions according to the nonhomogeneous intervals appropriate to 32-point Gaussian integration. An additional 32 by 32 matrix is set up for the same points in R,θ space to contain the numerical value of the distribution $n_0(R,\theta)$. For convenience, these numbers are scaled so that $N(0) = 1$. At each value of t, Gaussian integration is carried out over $R \subset (R_{min}, R_{max})$ and the resulting number is used simply as a function value in a subsequent Gaussian integration over θ. In cases where an applied field effect is to be calculated, the distribution matrix is updated to the turn-on time, t', using $n(R,\theta,t') = n_0(R, \theta)e^{-k(R)t'}$ before calculating EPL from [7].

Confidence in the integration procedure is established by obtaining in every case the preselected normalization value of the integral [eq. 5] at zero time, independently of the angular distribution. In addition, the computer-generated ITL points are identical for isotropic and nonisotropic distributions when scaled for the R-distribution range, as long as other parameters remain unchanged. Finally, intermediate output can be compared with the analytic forms obtained in the square-barrier case, to see that local concentrations of electrons about cations are varying qualitatively as in the simpler cases (9, 17, 20).

Discussion

G. R. Freeman: You observed a rather narrow band of R in the vicinity of 50 Å. Could you estimate the fraction of the total number of electrons that was involved? Perhaps the light emitted prior to the EPL measurement could be integrated, and the sample could be warmed afterwards to measure the remaining emission. Measurement of the free ion yield in X irradiated liquid 3-methylpentane, as a function of applied electric field strength, indicates that only about 10% of the thermalized electron–ion pairs would have R values between 50 and 60 Å.

A. C. Albrecht: (*a*) The 'initial' distribution of geminate cation–electron pairs is inevitably complicated by the immense range of lifetimes of such pairs in rigid glasses. If charge pairs are generated by an energy pulse of duration τ s then, at the end of the pulse, those pairs having lifetimes, τ_p, much shorter than τ will have reached photostationary state concentrations, while the number of those pairs with τ_p much longer than τ will still be growing linearly with irradiation time. Thus, suppose the rate of generating geminate pairs having a separation R is $g(R)$ (s^{-1}). Then the distribution in R of pairs having $\tau_p \ll \tau$ is given by $g(R)\tau_p$ where, as we have seen, τ_p is an exponentially strongly increasing function of R, so that for such pairs the dominant factor in their distribution is $\tau_p(R)$ not (R). Furthermore in the context of rigid nonpolar organic systems this precludes finding geminate pairs having $R < 20$ Å even when viewing on the nanosecond time scale of the fluorescence process itself. On the other hand for $\tau_p \gg \tau$, the distribution of charge pairs goes as $g(R)\tau$ and will accurately reflect the function $g(R)$ itself. It must be remembered that τ_p represents the lifetime of the charge pair during irradiation. Particularly for charge pairs having very long dark lifetimes, their τ_p might well be governed by the radiative pathways for recombination. The competing time constant for such a path is just $I\sigma$, where I is the flux of incident radiation and σ is the cross section for an ion pair to absorb this energy and recombine. In summary, it is clear that no simple distribution function of geminate pairs in R space can be expected under practically any condition of excitation.
(*b*) What fraction of all geminate pairs is located in the

50 Å $\leq R \leq$ 60 Å range which is the active range in our experiments? In the Ph.D. Thesis of Robert Ott (ref. 5), the methods you suggest were employed, although not combined with an EPL measurement. The total photons received after various ITL periods were compared to the total possible recombination photons as measured in a separate experiment, where under otherwise identical conditions the sample was warmed about 4° above the glass point and the total *thermoluminescence* curve was collected. By this measure the first 30 min of ITL after 1 min irradiation (in 3-methylpentane) at 77.3 K corresponds to the collapse of about 80% of all geminate pairs. However, as we have emphasized, at 77 K in 3MP there is a considerable temperature component to the recombination process (it is not pure tunnelling). At 68 K in 3MP where only tunnelling is active, R. Ott finds that in 30 min of ITL about 29% of all possible recombination events are seen. This latter situation should presumably carry over to our tunnelling-only case in the hard MCH–2MP glass at 77 K, which we have used in our present paper. If so then a reasonable choice of parameters (in tunnelling calculation) tells us that geminate pairs having τ_p (dark) from 1 to 30 min will lie in the range 48 Å $< R <$ 53 Å, and to this range we we should assign 29% of all geminate pairs. If the radial distribution is assumed to be constant, it would then need to extend to about 65 Å to account for the total of possible recombination events. The same tunnelling calculations show that pairs with separations of 65 Å will have $\tau_p \simeq$ 30 min in the presence of 6×10^5 V/cm internal field. We conclude that in the distribution we prepare, the majority of geminate pairs will lie in the 50 Å $< R <$ 60 Å range. It is conceivable that X-ray produced electrons are distributed more broadly. Our experiment would still be sensitive only to the same small separation range corresponding to the 1 to 30 min time scale, but it would then constitute a smaller fraction of the total pair production.

G. R. Freeman: As you mentioned, the assumption that $n_0(R)$ = constant is acceptable for a narrow slice of the R distribution. An alternative to an exponential over-all distribution is a Gaussian. The latter might be the more probable in strongly scattering media such as 3-methylpentane and methylcyclohexane.

Temperature and solvent dependence of electron scavenging efficiency in polar liquids: water and alcohols

JOHN W. HUNT AND W. JOHN CHASE

The Ontario Cancer Institute and Department of Medical Biophysics, University of Toronto, 500 Sherbourne Street, Toronto, Ont., Canada M4X 1K9

Received October 18, 1976

JOHN W. HUNT and W. JOHN CHASE. Can. J. Chem. **55**, 2080 (1977).

High concentrations of electron scavengers reduce the initial yield of e_{sol}^- and its precursor, e_t^-. The scavenging efficiency of a solute is inversely proportional to its C_{37} value, the solute concentration required to reduce the initial electron yield to 37% of the yield with no scavenger present. Over a range of 40 to $-60°C$ the C_{37} value for a given scavenger is almost constant, and is the same for e_{sol}^- and e_t^-. In water and alcohols, the C_{37} value is not correlated with the time required for solvation of the electron, τ_s, or the static dielectric constant, ε_s, but rather with the concentration of oxygen atoms in the solvent. These results support the model in which the scavenging of a mobile electron occurs before the electron is trapped in the solvent.

JOHN W. HUNT et W. JOHN CHASE. Can. J. Chem. **55**, 2080 (1977).

Des grandes concentrations de pièges d'électrons réduisent le rendement initial de e_{sol}^- et de son précurseur e_t^-. L'efficacité d'un soluté comme piège est inversement proportionnelle à sa valeur C_{37}, la concentration de soluté requise pour réduire le rendement initial d'électron jusqu'à 37% du rendement obtenu en l'absence de piège. A des températures allant de 40 à $-60°C$, la valeur C_{37} d'un piège donné est pratiquement constante et est la même pour e_{sol}^- et e_t^-. Dans l'eau et les alcools, il n'y a pas de corrélation entre la valeur C_{37} et le temps requis pour la solvatation de l'électron, τ_s, ou la constante diélectrique statique, ε_s, mais plutôt avec la concentration des atomes d'oxygène dans le solvant. Ces résultats sont en accord avec le modèle dans lequel le piégeage d'un électron mobile se produit avant que l'électron soit piégé dans le solvant.

[Traduit par le journal]

Introduction

From the breakdown of the competition reaction between the scavenging of and formation of e_{aq}^- in concentrated solutions, Hamill and co-workers (1–3) suggested that the 'dry' electron, e^-, is chemically reactive. Picosecond pulse radiolysis experiments in our laboratory also support this conclusion. In aqueous and alcoholic solutions, high concentrations of electron scavengers reduce the initial yield of solvated electron, e_{sol}^-, (4–7) and its precursor, e_t^-, (7) an electron trapped in a shallow potential well. The initial electron yield, $[e_x^-]$, decreases as the scavenger concentration, [S], increases according to

$$[1] \qquad [e_x^-]/[e_x^-]_0 = \exp(-[S]/[C_{37}])$$

where e_x^- can be e_t^- or e_{sol}^-, $[e_x^-]_0$ is the initial electron yield with $[S] = 0$, and $[C_{37}]$ is the scavenger concentration which reduces the yield of e_x^- to 1/e (37%). The C_{37} value of a scavenger is thus inversely proportional to its scavenging efficiency.

Two general categories of models have been proposed to explain the reduction of the initial yield of electrons. In one category, as secondary electrons diffuse through the liquid they can react with neighboring scavenger molecules before they become localized (4, 5, 8). In the other category, the electron becomes localized and then reacts with scavenger molecules. The encounter-pair model of Czapski and Peled (9), the electron-tunnelling model of Miller (10), and the time-dependent rate constant theory of Schwarz (11) fall into this category. Although these models predict the exponential dependence of electron yield on the scavenger concentration of [1], Lam and Hunt (7) showed that they could not explain the magnitude of the observed effect.

Lam and Hunt (7) observed that, *for a given scavenger*, the C_{37} value was the same for e_{sol}^- and e_t^-, and the C_{37} value changed systematically with the polarity of the solvent. They noted an apparent correlation of the C_{37} values with the time for solvation of the electron, τ_{sol}, and with the static dielectric constant, ε_s. The reduced yield of e_{sol}^- could be explained by a tunnelling process, in which the rate of reaction

TABLE 1. Correlation of C_{37} values with parameters of solvent

Solvent	$[C_{37}]$ of acetone[a] (mol dm^{-3})	τ_{sol} (296 K)[b] (ps)	ε_s (298 K)[c]	[O] (mol dm^{-3})
H_2O	1.4	<2	78.5	55.5
Ethylene glycol	1.0	5	37.7	35.7
Methanol	0.5	10	32.6	24.7
Ethanol	0.3	21	24.3	17.1
1-Propanol	0.25	31	20.1	13.0
1-Butanol	0.25	34	17.1	10.9
1-Hexanol	0.3		13.3	8.0

[a]Reference 7.
[b]References 15, 16.
[c]Reference 27.

will be faster from a shallow than from a deep trap (10). Since τ_{sol} indicates the time spent by an electron in a shallow trap, the C_{37} value might decrease as τ_{sol} increases. Alternatively, the reduced initial yield of e_{sol}^- from solvent to solvent might be due to the different attractive forces between the electrons and the positive ions in the radiation spur. The attractive force between ions separated by a distance r is proportional to $1/(\varepsilon r^2)$ and this force could alter the range of the low energy electron as it diffuses through the media. The probability of an electron, and thus the C_{37} value might depend on ε_s.

This paper shows that the correlation of the C_{37} values with τ_{sol} and ε_s at room temperature is only fortuitous. However, a correlation with the concentration of oxygen, [O], in different solvents supports the model of a mobile electron.

Experimental

The reactions of e_{sol}^- and e_t^- in concentrated solutions of electron scavengers were observed using the stroboscopic pulse radiolysis (spr) system previously described (12–14). The spr system has been modified so that the temperature of the flowing liquid in the radiation cell can be varied from 40 to −60°C (15, 16). The initial electron yield was obtained from picosecond kinetic absorption traces by extrapolating back along the absorption curve to the middle of the pulse (for slow decays) or by using a computer convolution technique (15, 16) (for fast decays).

Results

Table 1 summarizes the C_{37} values of acetone in various polar solvents, at 298 K, with an attempt to correlate the C_{37} values with different parameters. As noted in the Introduction, there is a general relationship between the C_{37} value, τ_{sol}, and ε_s (7). A much more significant result is shown in the last column, where there is a correlation with the concentration of oxygen atoms in the solvent, [O]. For all of the solvents considered except ethylene glycol, [O] (or [OH]) is the same as the concentration of pure solvent, whereas for ethylene glycol, there are two oxygen atoms per molecule, and [O] is twice the concentration of pure solvent.

For acetone and carbon tetrachloride, as shown in Table 2, the C_{37} value is almost independent of temperature and is the same for e_{sol}^- and e_t^- within experimental error. This agrees with the preliminary results of Lam and Hunt (7). The fact that the C_{37} value is the same for e_{sol}^- and e_t^- over a wide range of temperature indicates that a precursor of e_{sol}^- and e_t^- is being scavenged.

In Table 3, τ_{sol} and ε_s are compared to the C_{37} values of carbon tetrachloride, acetone, and toluene in 1-propanol. At room temperature carbon tetrachloride and acetone are efficient scavengers while toluene is quite an inefficient scavenger. As was the case in ethanol, the C_{37} values for these first two scavengers are almost independent of temperature. The C_{37} value of toluene, on the other hand, shows a marked temperature dependence, decreasing by more than a factor of 10 from 25 to −123°C. We are not sure of the reason for this behavior, but it would appear that toluene scavenges

TABLE 2. Variation of C_{37} values with temperature in ethanol

T (°C)	$[C_{37}]$ of CCl_4[a] (mol dm^{-3})		$[C_{37}]$ of acetone[a] (mol dm^{-3})	
	For e_{sol}^-	For e_t^-	For e_{sol}^-	For e_t^-
25	0.14	0.15_5	0.3_1	0.3_1
−60	0.13	0.13_5	0.2_8	0.3_3

[a]This work. The values at 25 and −60°C are taken from a straight line drawn through at least four C_{37} values between 25 and −60°C.

TABLE 3. Variation of τ_{sol}, ε_s, and C_{37} values with temperature in 1-propanol

T (°C)	τ_{sol} (ps)	ε_s	$[C_{37}]$ of CCl_4 for e_t^- (mol dm^{-3})	$[C_{37}]$ of acetone for e_t^- (mol dm^{-3})	$[C_{37}]$ of toluene for e_t^- (mol dm^{-3})
25	31[a]	20[c]	0.14[d]	0.3_6[d]	2.6[d]
−60	250[a]	35[c]	0.12[d]	0.4_1[d]	1.0[d]
−123	26 000[b]	56[c]	0.065[e]	0.15[e]	0.23[e]

[a]References 15, 16.
[b]Private communication from J. H. Baxendale (see Fig. 8 of ref. 16).
[c]Reference 28.
[d]This work. The values at 25 and −60°C are taken from a straight line drawn through at least four C_{37} values between 25 and −60°C.
[e]Calculated from the data in ref. 29.

electrons by a different mechanism than the more efficient scavengers, such as carbon tetrachloride and acetone.

As shown in Table 3, as the temperature is changed from 25 to −123°C, τ_{sol} increases by a factor of 1000 while the C_{37} values for the *efficient* scavengers decrease by only a factor of two. While this change is in the same direction as in Table 1, the large size of the change in τ_{sol} seems to rule out a direct relationship between τ_{sol} and the C_{37} values, even for toluene. As the temperature is changed from 25 to −123°C, ε_s increases while C_{37} decreases, the opposite to what was found in Table 1. This certainly rules out any direct correlation between the C_{37} value and ε_s.

If the C_{37} value is related to the concentration of oxygen atoms in the solvent, [O], the C_{37} value should be independent of temperature. When the C_{37} values are corrected for the solvent density the values are almost constant over the range from 25 to −60°C. To further examine a possible correlation, various mixtures of water and ethanol were used for the solvent. As shown in Fig. 1, the C_{37} values are proportional to [O], although the proportionality is not exact, since the lines drawn through the points do not pass exactly through the origin. It is also striking that the C_{37} values of acetone and CCl_4 in viscous ethylene glycol are similar to those obtained in nonviscous H_2O–ethanol mixtures.

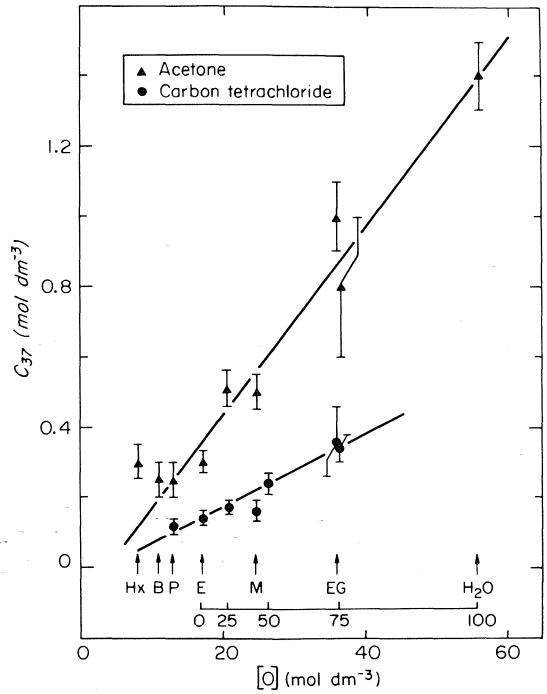

FIG. 1. C_{37} values for acetone (▲) and carbon tetrachloride (●) *vs.* the concentration of oxygen atoms in the solvent. The scales at the bottom identify the solvent used: H_2O, water; EG, ethylene glycol; M, methanol; E, ethanol; P, 1-propanol; B, 1-butanol; and Hx, 1-hexanol. The numbers are the mol% of water in the ethanol–water mixtures.

Discussion

Many models have been proposed to explain the reduction of the initial electron yield, such as dry or mobile electrons (1–5), encounter pairs (9), electron tunnelling (10), and time-dependent specific rates (11). These models have been considered in detail in previous papers (7, 17). For the solutions in this paper, a calculation shows that for the worst case (acetone in water)[1] the effect of the time dependence of the specific rates on the C_{37} values is about 10%, and that corrections for the time-dependent specific rates are much smaller in alcohols and cold solutions. The possible effect of electron tunnelling is

[1]At the concentrations and temperatures used, acetone in water has the highest rate of reaction with e_{sol}^-, and thus the time dependence of the specific rate will be largest for this reaction.

strongly dependent on the particular parameters used and competes with the time dependence of the specific rates (18), and thus it is difficult to estimate the contribution of electron tunnelling to the initial electron reactions. However, we feel that electron tunnelling is not *the* major factor in these reactions, since, as noted by Lam and Hunt (7), it cannot account for the systematic changes in the C_{37} values from solvent to solvent. Another attempt to explain the result is the encounter-pair concept of Czapski and Peled (9), in which the electron is localized very near a solute molecule. This encounter pair might react very quickly. This concept is difficult to evaluate, particularly in the case of nondiffusion-limited reactions such as e_{aq}^- + acetone. A calculation for this reaction shows that less than 20% of the prompt electron reactions are due to encounter pairs. As well, Lam and Hunt (7) showed that the encounter-pair concept does not explain the solvent-to-solvent variation of the C_{37} values for a given scavenger.

Because of the difficulties in making accurate corrections to the data, we have not attempted to do so. Instead, we have concentrated on the mobile electrons, which give the most lucid explanation of the prompt electron reactions.

Wolff *et al.* (4) and Aldrich *et al.* (5) obtained [1] by assuming that mobile electrons can react with scavenger molecules before the electrons reach thermal energies. In this model, the electron undergoes a random walk, colliding with solvent and solute molecules until it becomes thermalized. Bolton *et al.* (8) have proposed a similar model, although there are some differences (see below). The probability that the electron does *not* react with the scavenger molecule before it reaches thermal energies is given by

$$[2] \qquad [e_x^-]/[e_x^-]_0 = (1 - cP)^n$$

where c is the mole fraction of scavenger molecules (*i.e.* [S]/[solvent]), P is the probability of a mobile electron reacting with a scavenger, and n is the total number of collisions of the electron with solvent and scavenger molecules before the electron is thermalized. Since $cP < 1$ and, as noted by Aldrich *et al.* (5), $n \geq 150$ for efficient scavengers, [2] can be written as

$$[3] \qquad [e_x^-]/[e_x^-]_0 = \exp(-cPn)$$

Comparing this to [1], the terms in parentheses yield

$$[4] \qquad \frac{[S]}{[C_{37}]} = cPn = \frac{[S]}{[solvent]} Pn$$

and solving for $[C_{37}]$,

$$[5] \qquad [C_{37}] = [solvent]/Pn$$

This simple *theory* predicts that the C_{37} value is proportional to the solvent concentration, while *experimentally* the C_{37} value is proportional to [O]. For all of the solvents considered *except* ethylene glycol [O] = [solvent] and [5] can be written as

$$[6] \qquad [C_{37}] = [O]/Pn$$

For ethylene glycol, [O] = 2[solvent] and thus

$$[7] \quad [C_{37}] = \frac{[O]}{Pn} = \frac{2[solvent]}{Pn} = \frac{[solvent]}{Pn'}$$

where $n' = n/2$ is the actual number of electron–molecule collisions in ethylene glycol.

The mobile electron hypothesis implies that the energy loss per collision is inversely proportional to the number of collisions, n. For all of the solvents except ethylene glycol, a common value for n suggests that the energy loss per collision is the same, which in turn implies a common mechanism of energy loss, *i.e.* the oxygen atom (or the hydroxyl group) absorbs the energy. In ethylene glycol, the number of collisions is half that in the other solvents, suggesting that an ethylene glycol molecule either absorbs twice as much energy per collision or has two separate and independent modes of accepting energy (*i.e.* two oxygen atoms).

In a review article, Mozumder (19) noted that the range and the mechanism of energy loss of low energy electrons are only poorly known. Mozumder (19) considered mechanisms of energy loss in water, and Funabashi (20), several organic solids at 77 K, but no satisfactory theory for all solvents is available. Dodelet and Freeman (21) studied the effect of molecular structure of alkanes on the density-normalized range secondary electrons. They noted a correlation between the efficiency of energy loss and the relative inductive effect of the functional groups of the molecules, as indicated by the Taft coefficient, σ^* (22). The oxygen atom is highly electron affinic and the OH group has a much higher σ^* of 0.66 (23) than the methyl group with $\sigma^* = 0.0$. Thus, if our theory relating the slowing down of the mobile electron to the C_{37} values is correct, it is not surprising that

there is a good correlation between the C_{37} values and [O]. In solvents not containing oxygen, it may be possible to estimate the C_{37} value of a scavenger relative to that in other solvents by considering the Taft coefficient, σ^*, and the size of the solvent molecules.

The exponential function for the relative electron yield, derived using a fixed value of n (equation 3), describes the experimental data quite well. In reality, n does not have a single fixed value but a distribution of values. If a Gaussian distribution for n is assumed, with a mean value, $\bar{n}$, of 150 and a standard deviation, σ, as large as 50, the calculated electron yield fits an exponential function within our experimental error (5%). A minimum value for $\bar{n}$ can be obtained by considering the most efficient scavenger by assuming $P = 1$ and solving for n in [5]. Cd^{2+} has a C_{37} value of 0.39 mol dm^{-3} (5), yielding a value for n of 140. CrO_4^{2-} has a C_{37} value of 0.2 mol dm^{-3} (7), giving a value of 275 for n. Miller (10*c*) has shown that electrons tunnel to CrO_4^{2-} in NaOH glass. Because electron tunnelling (or time dependence of the specific rates, or encounter pairs) could contribute to electron scavenging, we estimate the minimum value of $\bar{n}$ to be 150. A Gaussian distribution for n implies that, although the electron can be scavenged at any time, it can only be localized when it has lost most of its energy.

Bolton *et al.* (8) described a different model than the one considered in our work, in which the probability of an electron being localized is constant along its path, or that scavenging is possible only "during the *last few* collisions of the epithermal electron prior to localization."[2] The resulting distribution function has a maximum value for n equal to 6 (the number of molecules in the solvation shell) and decreases slowly with increasing n. Bolton *et al.* (8) obtained good fits to their data using a value of 30 for $\bar{n}$, obtained from benzene, a relatively inefficient scavenger. However, we argue that the minimum value of $\bar{n}$ should be calculated from efficient scavengers. Using a value of 150 for $\bar{n}$, the relative electron yield calculated using the formulation of Bolton *et al.* (8) deviates considerably from an exponential function. Therefore, we feel that the formulation of Bolton *et al.* (8) disagrees with the picosecond studies, and that the electron can be scavenged before it can be localized.

The C_{37} value of toluene shows a marked temperature dependence, whereas those of carbon tetrachloride and acetone do not. Buxton *et al.* (24) and Hase and Kawabata (25) have recently observed an absorption at infrared wavelengths due to an electron in a very shallow trap. If the main mechanism of the initial yield reduction in toluene were tunnelling of the electrons from these very shallow traps at very short times (< 1 ps), rather than mobile electron scavenging, then the temperature dependence of the C_{37} value might be accounted for by assuming that either the number of electrons in these very shallow traps, or that the time spent there, is also temperature dependent. Another possibility is that the value of P in [3] is temperature dependent. Fueki *et al.* (26) calculated that the energy of the quasi-free electron state, V_0, decreases as the temperature increases. If the ground state of the toluene anion is near V_0, the temperature dependence of V_0 could change P in [2]. For carbon tetrachloride and acetone, the ground state of the anion might be sufficiently lower than V_0 that small changes in V_0 would not affect P.

Conclusion

For carbon tetrachloride and acetone, but not toluene, the C_{37} value is almost independent of temperature and is the same for e_{sol}^- and e_t^- in ethanol and propanol. In water and the alcohols, for a given scavenger the C_{37} value is proportional to [O], the concentration of oxygen atoms in the solvent. In the mobile electron hypothesis, the number of scavenger molecules that the electron collides with before solvation is determined by the electron range. The range is controlled by the efficiency of energy transfer from the mobile electron to the solvent molecules, which is in turn related to the electron affinity and the relative inductive effect of functional groups of the solvent molecules. In water and the alcohols, oxygen has the highest electron affinity and thus controls the range and therefore the C_{37} value.

Acknowledgements

D. Bazett-Jones, A. Worthington, and M. O'Loughlin performed some of the experimental

[2]Reference 8, our italics.

work in this paper. J. McLernon from Atmospheric Environment Services arranged the loan of a temperature measuring bridge (Rosemount Model 414L) for part of the experiments. Mr. W. B. Taylor and his staff provided excellent technical support. Mr. T. Horrigan and his staff kept the linear accelerator of the University of Toronto functioning smoothly. The National Research Council of Canada funded the operation of the linear accelerator. The Medical Research Council of Canada and the National Cancer Institute supported the experimental work. The Medical Research Council of Canada provided a studentship for one of us (W.J.C.).

1. W. H. HAMILL. J. Phys. Chem. **73**, 1341 (1969).
2. T. SAWAI and W. H. HAMILL. J. Phys. Chem. **74**, 3914 (1970).
3. P. L. T. BEVAN and W. H. HAMILL. Trans. Faraday Soc. **66**, 2533 (1970).
4. R. K. WOLFF, M. J. BRONSKILL, and J. W. HUNT. J. Chem. Phys. **53**, 4211 (1970).
5. J. E. ALDRICH, M. J. BRONSKILL, R. K. WOLFF, and J. W. HUNT. J. Chem. Phys. **55**, 530 (1971).
6. R. K. WOLFF, J. E. ALDRICH, T. L. PENNER, and J. W. HUNT. J. Phys. Chem. **79**, 210 (1975).
7. K. Y. LAM and J. W. HUNT. Int. J. Radiat. Phys. Chem. **7**, 317 (1975).
8. G. L. BOLTON, K. N. JHA, and G. R. FREEMAN. Can. J. Chem. **54**, 1497 (1976).
9. (*a*) G. CZAPSKI and E. PELED. J. Phys. Chem. **77**, 893 (1973); (*b*) G. CZAPSKI and E. PELED. *In* Radiation research, biomedical, chemical and physical perspectives. *Edited by* O. F. Nygaard, H. I. Adler, and W. K. Sinclair. Academic Press, New York. 1975. p. 356.
10. (*a*) J. R. MILLER. J. Chem. Phys. **56**, 5173 (1972); (*b*) J. R. MILLER. Chem. Phys. Lett. **22**, 180 (1973); (*c*) J. R. MILLER. J. Phys. Chem. **79**, 1070 (1975).
11. H. A. SCHWARZ. J. Chem. Phys. **55**, 3647 (1971).
12. M. J. BRONSKILL, W. B. TAYLOR, R. K. WOLFF, and J. W. HUNT. Rev. Sci. Instrum. **41**, 333 (1970).
13. M. J. BRONSKILL, R. K. WOLFF, and J. W. HUNT. J. Chem. Phys. **53**, 4201 (1970).
14. J. E. ALDRICH, P. FOLDVARY, J. W. HUNT, W. B. TAYLOR, and R. K. WOLFF. Rev. Sci. Instrum. **43**, 991 (1972).
15. W. J. CHASE. M.Sc. Thesis, University of Toronto, Toronto, Ontario. 1976.
16. W. J. CHASE and J. W. HUNT. J. Phys. Chem. **79**, 2835 (1975).
17. J. W. HUNT. *In* Advances in radiation chemistry. Vol. 5. *Edited by* M. Burton and J. L. Magee. Wiley-Interscience, New York. 1976. p. 185.
18. M. J. PILLING and S. A. RICE. J. Chem. Soc. Faraday Trans. II, **71**, 1563 (1975).
19. A. MOZUMDER. *In* Advances in radiation chemistry. Vol. 1. *Edited by* M. Burton and J. L. Magee. Wiley-Interscience, New York. 1969. p. 21.
20. K. FUNABASHI. *In* Advances in radiation chemistry. Vol. 4. *Edited by* M. Burton and J. L. Magee. Wiley-Interscience, New York. 1974. p. 133.
21. J.-P. DODELET and G. R. FREEMAN. Can. J. Chem. **50**, 2667 (1972).
22. J. TAFT. *In* Steric effects in organic chemistry. *Edited by* M. S. Newman. Wiley, New York. 1956. pp. 586–629.
23. I. MOCHIDA and Y. YONEDA. Bull. Chem. Soc. Jpn. **41**, 1479 (1968).
24. (*a*) G. V. BUXTON, H. A. GILLIS, and N. V. KLASSEN. Chem. Phys. Lett. **32**, 533 (1975); (*b*) G. V. BUXTON, H. A. GILLIS, and N. V. KLASSEN. Can. J. Chem. **54**, 367 (1976).
25. H. HASE and K. KAWABATA. J. Chem. Phys. **65**, 64 (1976).
26. K. FUEKI, D.-F. FENG, and L. KEVAN. J. Phys. Chem. **78**, 393 (1974).
27. R. C. WEAST (*Editor*). Handbook of chemistry and physics. 51st ed. The Chemical Rubber Co., Cleveland, Ohio. 1970.
28. D. W. DAVIDSON and R. H. COLE. J. Chem. Phys. **19**, 1489 (1951).
29. J. H. BAXENDALE and P. WARDMAN. J. Chem. Soc. Faraday Trans. I, **69**, 584 (1973).

Discussion

G. Czapski: The general scheme of the fate of e_{dry} is

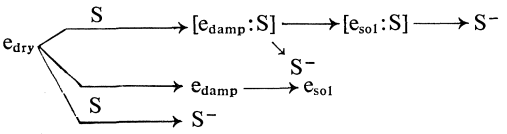

where $[e_{damp}:S]$ and $[e_{sol}:S]$ describe encounter pairs of e_{damp} and e_{sol} with S respectively, with an encounter radius R. In your studies the extrapolation of the yield of e_{sol} into the pulse assumes pseudo first order decay of $e_{sol} + S \rightarrow S^-$. This treatment neglected two essential corrections, the time dependence of the rate constant of the reaction $e_{sol} + S$ and the initial formation of encounter pairs. It was previously shown by Czapski and Peled (9) that by making the above-mentioned corrections for most of the solutes used in your earlier studies in water, the full initial yield of e_{sol} can be obtained by this procedure.

In the present studies you did not make these corrections and conclude from values of C_{37} for various solutes and solvents that e_{dry} reacts with the solutes. Even if this assumption would be true, you have to make these corrections, as $k_{e_{sol}+S}$ is time dependent and $[e_{sol}:S]$ are formed. Doing so at the concentration C_{37}, you would have found that the extrapolated yield of e_{sol} would be much larger than 37% and in some cases could give the full yield of e_{sol}, although in several systems there will still be a missing yield of e_{sol}. Even in the systems where with the appropriate corrections the initial yield is too low, it is not essential to assume the reaction of dry electrons with the solute.

Assuming electrons are 'trap diggers', the following solvation sequence occurs in the solvation site

$$e_{dry} \rightarrow e_{damp} \rightarrow e_{sol}$$

It is obvious that damp electrons also are partially formed as encounter pairs. It is reasonable to assume that the encounter radius, R, of damp electrons with S will exceed that of solvated electrons with S. With these assumptions the following behaviour is expected.

1. As the solvation time of the electron in H_2O is less than 10^{-12} s, the lifetime of the encounter pair of S with e_{damp} may be too short and e_{damp} may solvate prior to the formation of S^- from the encounter pair $[e_{damp}:S]$. This will not apply to the alcohols where the solvation times exceed by far the lifetime of $[e_{damp}:S]$.

2. For a given solute and solvent C_{37} will be temperature independent, as $R_{[e_{damp}:S]}$ and $R_{[e_{sol}:S]}$ should not vary with temperature. This is in accordance with your results.

3. You observed that C_{37} is the same for e_{damp} and e_{sol} in a given solvent. This is evident as the solvated electrons are formed from those damp electrons which did not disappear in $[e_{damp}:S]$.

4. You found that C_{37} for a given solute depends on the solvent and decreases the larger the solvation time in that solvent. This behaviour may be due to an additional correction which should be made. In these solvents some of e_{damp} disappear within $\sim 10^{-12}$ s in $[e_{damp}:S]$ while the rest are initially separated from S. The damp electron has a larger encounter radius than the solvated electron, and therefore it will also have a larger rate constant in the reaction with S. Therefore in addition to the usual time dependence of diffusion-controlled rate constants, another time dependence will occur. The longer the solvation time of e_{damp} is in a given solvent, the faster will S react. Therefore the lower values of C_{37} for solvents with longer solvation time is expected in accordance with your observations.

From this analysis it is concluded that for most systems you studied it is not necessary to postulate reactions of dry electrons. Benzene on the other hand appears to react with dry electrons.

W. J. Chase: I agree with Dr. Czapski that corrections for the time dependence of the specific rates and the formation of encounter pairs should be made to the C_{37} values. These corrections are difficult to assess but are not large for the solutions and experimental conditions that we used. In alcohols, the relaxation of the trapped electron, $e_t^- \rightarrow e_{sol}^-$, is faster than the reaction $e_t^- + S \rightarrow S^-$, and thus masks any time dependence of the latter specific rate. Both of these processes are slow in cold solutions; little extrapolation is needed to obtain the initial yield of e_t^- and thus time dependence of the specific rates is not important. For the solutions considered in this paper, time dependence of the specific rate will have its largest effect on the reaction of e_{aq}^- with acetone at room temperature. Using the same extrapolation technique as was used in the paper, and the formulation of Jonah *et al.* (J. Phys. Chem. **79**, 2705 (1975)), the correction to the C_{37} value for this nondiffusion-controlled reaction is only about 10%.

The correction for encounter pairs is more difficult to assess, since the encounter-pair concept is not well understood for nondiffusion-controlled reactions. For such reactions the top arm of Czapski's reaction scheme should include the escape of e_t^- from the encounter pairs, as in

$$e_{dry}^- \rightarrow [e_t^-:S] \rightarrow [e_{sol}^-:S] \rightarrow S$$
$$\swarrow \quad \searrow \qquad \swarrow \quad \searrow$$
$$S^- \quad e_t^- + S \qquad e_{sol}^- + S$$

$$(e_t^- \equiv e_{damp}^-)$$

Thus, nondiffusion-controlled reactions are explained if not every encounter pair forms S^-, but rather some leave e_t^- and S unreacted. Using an encounter radius of 0.5 nm, and the formulation of Jonah *et al.*, we estimate that the effect of the encounter pair is small (< 20%) in water, and smaller in alcohols. Thus, the total corrections due to time-dependent specific rates and encounter-pair formation does not account for the observed C_{37} values. Dr. Czapski also assumed that the encounter radius of e_t^- with S is larger than that of e_{sol}^- with S. However, esr measurements on electrons in ethanol glass of Hase *et al.* (J. Chem. Phys. **57**, 1039 (1972)) suggest that the radius of e_t^- is only 0.1 nm larger than that of e_{sol}^-, in general agreement with the theoretical work of Fueki *et al.* (J. Chem. Phys. **56**, 5351 (1972)).

Based on the assumption of a larger encounter radius for e_t^-, Dr. Czapski makes four predictions about the effect of scavengers, the last two of which I disagree with. Concerning point *3*, not all of the e_{sol}^- are formed from e_t^-. In fact, *some* are formed almost immediately, apparently because the electrons have become localized initially in a deep trap. Thus an immediate absorption is observed at short wavelengths (16, 29). Concerning point *4*, since we have measured the *initial* yield of e_t^-, the solvation time, as long as it is more than ~10 ps, should have very little to do with the reduction of the initial yield. And in fact it does not, since the C_{37} value remains the same when the solvation time is increased by lowering the temperature.

Lam and Hunt (7) and Hunt (17) showed that there is a serious inconsistency when the encounter-pair concept is used to explain the empirical relationship observed by Lam and Hunt (7),

$$[1] \qquad C_{37} = Q/k_{obs}$$

where Q is a constant for each scavenger. This equation can be explained, using the Smoluchowski equation as formulated by Jonah *et al.* and equation 6 from our paper. Thus we feel the C_{37} values obtained in various solutions can be explained best by changes in the rate of reaction of the mobile or dry electron.

G. R. Freeman: Scavenging of electrons prior to their solvation, mentioned by Chase, and scavenging in initial encounter pairs, mentioned by Czapski, are both treated in a recent article by Bolton, Jha, and myself (Can. J. Chem. **54**, 1497 (1976)).

W. J. Chase: As mentioned in the paper we agree that a stochastic model in the paper mentioned above might explain certain aspects of the precursors of the e_{solv}^-. However, we feel that our older approach (4) explains the results more accurately. That is, the subexcited electrons (the 'dry' electrons) lose energy relatively slowly and collide with solvent and solute molecules. In a pure solvent, a relatively constant number of collisions (~150) will occur before they reach energies low enough to be trapped. A low number and wide range of collisions, as

suggested by Bolton *et al.*, does not agree with the observed data. Of course, encounter-pair corrections must also be considered in a more accurate assessment as mentioned by Czapski, but they only account for a small part of the process.

G. R. Freeman: The basic stochastic model dates back to the mid-sixties and improves with time. In some systems the plots of log (initial absorbance) against solute concentration are not linear. The degree of linearity can be adjusted by choosing suitable values for the minimum number of encounters and the probability of localization per collision.

C. Jonah: I question the exponential dependence on solute using Freeman's model for scavenging *vs.* trapping.

W. J. Chase: I haven't looked at this myself, but I would expect that the departure from exponential behaviour would depend upon the particular distribution function used for n, the number of collisions. Qualitatively, I would expect that the sharper the distribution of n around a mean value, $\bar{n}$, the better the agreement with exponential behaviour. The experimental data do seem to follow the exponential behaviour quite well. In fact, Dr. Hunt looked at this years ago, and found that using a Gaussian distribution for n with a mean value, $\bar{n}$, of 150 and a width, α, of about 25 collisions there was little departure from linearity for the semilogarithmic plot.

Electron scavenging in the radiolysis of supercritical butenes[1]

MASARU NISHIKAWA AND YOH-ICHI YAMAGUCHI

Department of Pure and Applied Sciences, University of Tokyo, Komaba, Meguro-ku, Tokyo 153, Japan

Received September 27, 1976

MASARU NISHIKAWA and YOH-ICHI YAMAGUCHI. Can. J. Chem. **55**, 2088 (1977).

Electron scavenging reactions with N_2O have been studied in γ-irradiated supercritical butenes in the density range 0.25–0.48 g/cm^3 at 170 ± 1°C. Free ion yields were estimated as a function of density from the nitrogen yields by means of the 'square root' model. The estimated G_{fi} in butenes increased with the decrease in density, and were in the order *cis*-2-butene ≳ isobutene > *trans*-2-butene at a given density. The density-normalized range of electrons estimated from G_{fi} values was independent of density over the density range studied. The magnitude of the reactivity parameter A in *trans*-2-butene was much larger than that in other butenes studied, but it generally increased with a decrease in density. An analysis of the parameter on the basis of the Nernst–Einstein relationship indicates that the trend is related to the change in the encounter efficiency of the reaction $e^- + N_2O$.

MASARU NISHIKAWA et YOH-ICHI YAMAGUCHI. Can. J. Chem. **55**, 2088 (1977).

On a étudié des réactions de piégeage d'électrons par N_2O dans des butènes supercritiques irradiés par des radiations γ à des densités allant de 0.25–0.48 g/cm^3 à 170 ± 1°C. On a déterminé les rendements en ions libres en fonction de la densité à partir des rendements en azote en faisant appel à un modèle de "racine carré". Les G_{fi} évalués dans le butène augmentent avec une diminution de la densité et pour une densité donnée sont dans l'ordre de butène-2 *cis* ≳ isobutène > butène-2 *trans*. Les pénétrations d'électrons normalisées pour la densité, évaluées à partir de valeurs de G_{fi}, sont indépendantes de la densité à toutes les densités étudiées. La grandeur du paramètre de réactivité A du butène-2 *trans* est beaucoup plus grande que celle observée avec les autres butènes étudiés mais elle augmente d'une manière générale avec une diminution de la densité. L'analyse des paramètres sur la base d'une relation de Nernst–Einstein indique que la tendance est reliée au changement dans l'efficacité de la réaction $e^- + N_2O$.

[Traduit par le journal]

Introduction

Recent charge scavenging studies in supercritical hydrocarbons demonstrated that they are amenable to quantitative interpretation in terms of the 'square root' model (1, 2). The interpretation led to the estimation of free ion yields and the kinetic parameters for the reaction of electrons with N_2O in various hydrocarbons in the supercritical state. Freeman and coworkers (3, 4) found in the liquid phase that both the free ion yield and the electron mobility are anomalously low in *trans*-2-butene compared to those in other isomeric butenes. In the present study the observations are extended to the supercritical state in order to observe the resulting effects on the kinetics of electron scavenging.

Experimental

Phillips Research Grade *cis*-2-butene (99.98%), *trans*-2-butene (99.78%), and isobutene (99.9%) were purified further by circulating overnight through traps filled with KOH and NaK alloy by means of an electromagnetically operated pump. Takachiho Research Purity nitrous oxide (99.9%) was used after bulb-to-bulb distillation.

Methods of sample preparation, irradiation in a ^{60}Co source, and product analysis were described previously (1). The irradiation was carried out at 170 ± 1°C. The dose rate was 5.26×10^{18} eV g^{-1} h^{-1} in Fricke solution and appropriate corrections were made for the electron density ratios. Total dose per sample did not exceed 6×10^{18} eV/g.

The critical temperatures are *cis*-2-butene, 160.0°C; *trans*-2-butene, 155.0°C; isobutene, 144.73°C (5). Dielectric constants at different densities and 170°C were calculated by the Clausius–Mosotti equation from the data given in ref. 4.

Results and Discussion

Free Ion Yields

The yields of nitrogen from γ-radiolysis of *cis*-2-butene – nitrous oxide, *trans*-2-butene – nitrous oxide, and isobutene – nitrous oxide mixtures at 170 ± 1°C in the density range from 0.24 to 0.48 g/cm^3 exhibit features quite similar to those observed for other hydrocarbons in the supercritical state (1, 2). Firstly, they can be quantitatively described by the square root model, $G(N_2) = G(N_2)_{fi} + G(N_2)_{gi}(A[N_2O])^{1/2}$;

[1]Partially supported by a Grant-in-Aid from the Ministry of Education.

secondly, $G(N_2)_{fi}$ decreases with increase in density for each butene studied (Figs. 1–3). The values of $G(N_2)_{fi}$ obtained in the liquid phase agree quite well with those obtained by electrical measurements (4). It was previously argued that $G(N_2)_{fi}$ can be assumed to be equal to the free ion yields, G_{fi} (2). The G_{fi} values in the supercritical butenes in the density range studied are in the decreasing order *cis*-2-butene $\gtrsim$ isobutene > *trans*-2-butene (Table 1). The trend is in agreement with the finding that G_{fi} in liquid *trans*-2-butene is much smaller than in other isomer liquids (4).

Electron Ranges

By inserting the G_{fi} values into [1], electron ranges were estimated.

$$[1] \quad G_{fi} = G_{tot} \int_0^\infty f(r) \exp(-r_c/r)\, dr$$

where G_{tot} is the total ionization yield calculated from W values in the gas phase, $f(r)$ is the distribution function of ion–electron separation distances, and r_c is the Onsager distance ($e^2/\varepsilon kT$) (1, 2, 4). The distribution function $f(r)$ was taken to have the form composed of a Gaussian core and a power function tail (eq. 2):

$$f(r) = 0.96(4r^2/\pi^{1/2}b_{gp}^3) \exp(-r^2/b_{gp}^2) \qquad r < 2.4b_{gp}$$

$$[2] \quad f(r) = 0.96\{(4r^2/\pi^{1/2}b_{gp}^3) \exp(-r^2/b_{gp}^2) + 0.5(b_{gp}^2/r^3)\} \qquad r > 2.4b_{gp}$$

where b_{gp} is the most probable value of r. Although this form has been found to give an accurate description of electric field dependence of the free ion yields (4, 6, 7), the use of [2] in the present study is for the sake of comparison with values obtained by other methods (4) because it has not yet been possible to determine the most satisfactory form of $f(r)$ (6, 7). The value of b_{gp} has been found to be practically identical to that of the parameter b in the simple Gaussian form when $G_{fi} > 0.3$ (4). Thus most of the b_{gp} values in the present study are equal to b values; b_{gp} in butenes increased only gradually with decrease in density. The behavior is similar to that observed for C_3 and C_4 hydrocarbons in the supercritical state (1, 2).

The independence of the density-normalized electron ranges has been noted previously both in the liquid phase (4) and in the supercritical state (1, 2). This is again the case with the supercritical butenes. The values of $b_{gp}d$ in the present study agreed quite well with those obtained by electrical measurements in the corresponding liquids (4). The discussion based on the independence of the density-normalized ranges in the supercritical state may be premature before it can be confirmed by direct measurements. It might also be possible that the trend is susceptible to the form of $f(r)$ used in [1].

Scavenging Efficiency Parameter

The scavenging efficiency parameters, A, were evaluated from the slope of the square root plot in Figs. 1–3. They were found to increase regularly with decrease in density for each butene studied. This is different from the behavior observed in other C_3–C_4 hydrocarbons where they showed no definite trend (1, 2). A values in *cis*-2-butene and in isobutene were much smaller than those in *trans*-2-butene (Table 1).

It has been shown that the parameter A is given by

$$[3] \qquad A = k_s/\lambda$$

where k_s is the rate constant for charge scavenging, and λ is a constant for a given solvent and represents the rate of recombination of geminate ion-electron pairs (8). The Nernst–Einstein relationship has been found to be a good approximation for the geminate recombination (9), so that λ can be adequately expressed as (10)

$$[4] \quad \lambda = 3(D_e + D_+)r_c/b_{gp}^3 \simeq 3D_e r_c/b_{gp}^3$$

where D_e and D_+ are the diffusion coefficients

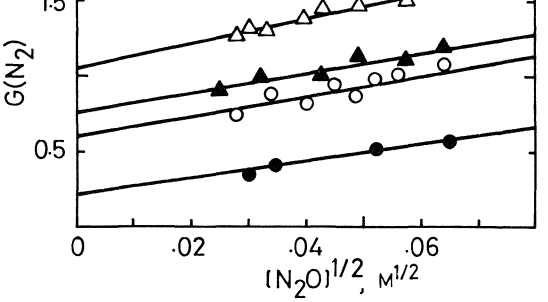

FIG. 1. Yields of nitrogen from *cis*-2-butene–N_2O mixtures as a function of the square root of the molar concentration of N_2O at various densities and 170°C. △, 0.25 ± 0.01 g/ml; ▲, 0.34 ± 0.01 g/ml; ○, 0.48 ± 0.01 g/ml; ●, 0.62 g/ml (liquid, 23°C).

TABLE 1. G_{fi}, electron ranges, and kinetic parameter values

Density (g/cm³)	G_{fi}	r_c (Å)	b_{gp} (Å)	$b_{gp}d$ (10^{-8} g/cm²)	A (M^{-1})
		cis-2-Butene			
0.24±0.01	1.06	286	190	48	6.8
0.34±0.01	0.75	255	134	46	3.6
0.48±0.01	0.60	226	100	48	3.3
0.62 (liq., 23°C)	0.22	288	72	45	1.8
		trans-2-Butene			
0.24±0.01	0.48	293	107	26	35
0.36±0.01	0.34	262	83	30	15
0.48±0.01	0.25	232	54	31	11
0.61 (liq., 23°C)	0.08	306	50	30	4.4
		Isobutene			
0.24±0.01	0.87	283	167	40	7.4
0.36±0.01	0.65	248	117	42	3.5
0.48±0.01	0.57	217	91	43	1.5
0.59 (liq., 23°C)	0.29	273	64	38	1.2

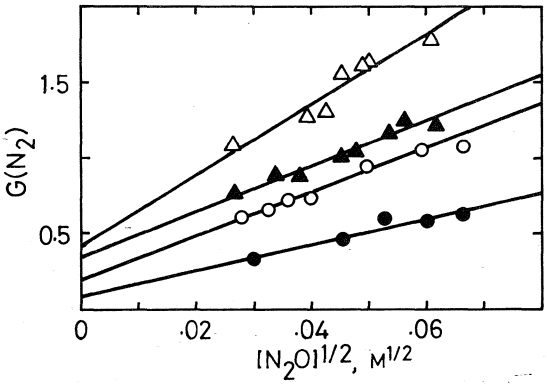

FIG. 2. Yields of nitrogen from *trans*-2-butene–N_2O mixtures as a function of the square root of the molar concentration of N_2O at various densities and 170°C. △, 0.24 ± 0.01 g/ml; ▲, 0.36 ± 0.01 g/ml; ○, 0.48 ± 0.01 g/ml; ●, 0.61 g/ml (liquid, 23°C).

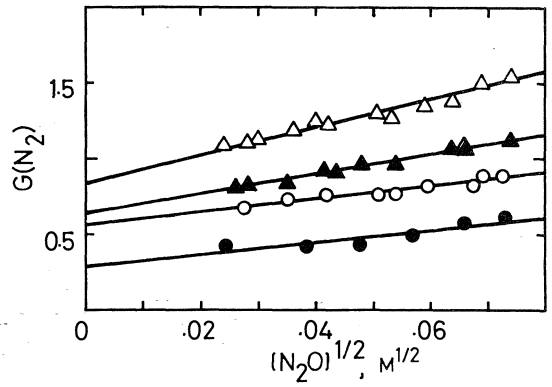

FIG. 3. Yields of nitrogen from isobutene–N_2O mixtures as a function of the square root of the molar concentration of N_2O at various densities and 170°C. △, 0.24 ± 0.01 g/ml; ▲, 0.36 ± 0.01 g/ml; ○, 0.48 ± 0.01 g/ml; ●, 0.59 g/ml (liquid, 23°C).

of the electrons and the positive ions, respectively. By combining [3] and [4], k_s is now given by

$$[5] \qquad k_s = 3D_e A r_c / b_{gp}^3$$

The encounter efficiency of a reaction is defined as the ratio of k_s to that in the diffusion-controlled case, *i.e.*, $4\pi R D_e$ in the present case. One notes that by using [5] the efficiency is quite generally given by

$$[6] \qquad f = \frac{3Ar_c}{4\pi R \cdot 6 \times 10^{20} b_{gp}^3}$$

where 6×10^{20} is the conversion factor from cm³ molecule^{-1} s^{-1} to l mol^{-1} s^{-1}. The values of f calculated by taking arbitrarily 5 Å for the reaction radius R are summarized in Table 2 where values for *n*-butane are included for comparison. Although there are some exceptions, f is generally seen to decrease with decrease in density. The large A values in *trans*-2-butene are apparently related to similarly large f values.

A correlation between the encounter efficiency for the reaction $e^- + N_2O$ and electron mobilities μ_e has been found in liquid rare gases and in several liquid hydrocarbons (11). This correlation also seems to exist in the liquid butenes

TABLE 2. Calculated values of V_0, electron mobilities, and encounter efficiencies in supercritical butenes

Density (g/cm³)	V_0 (eV)	$k_s \times 10^{-12}$ (M^{-1} s^{-1})	$\lambda \times 10^{-11}$ (s^{-1})	f	μ_e (cm² V^{-1} s^{-1})
		cis-2-Butene (a^* = 1.79 Å‡)			
0.25±0.01	−0.29	5	7	0.02	15
0.34±0.01	−0.36	2	6	0.03	5
0.48±0.01	−0.39	1	3	0.06	1
0.62 (liq., 23°C)	−0.26	0.8	46	0.11	2.2†
		trans-2-Butene (a = 1.89 Å§)			
0.24±0.01	−0.19	12	3	0.66	1.3
0.36±0.01	−0.20	12	8	0.55	1.5
0.48±0.01	−0.09	5	5	0.78	0.4
0.61 (liq., 23°C)	0.22	0.7	2	0.85	0.029†
		Isobutene (a = 1.89 Å§)			
0.24±0.01	−0.17	11	15	0.04	21
0.36±0.01	−0.18	11	32	0.04	18
0.48±0.01	−0.05	4	26	0.03	8
0.59 (liq., 23°C)	0.22	0.7	6	0.10	1.44†
		n-Butane (a = 1.89 Å‡)			
0.24±0.01	−0.19	12	4	0.03	24
0.36±0.01	−0.22	12	10	0.04	20
0.41±0.01	−0.20	12	10	0.06	13
0.58 (liq., 23°C)	0.06	1	0.7	0.83	0.27†

*Hard core radius.
†Experimentally obtained values from refs. 3 and 22.
‡Derived from experimental values of V_0 in refs. 18 and 23.
§Estimated from critical volumes in ref. 5.

when f values are compared with the measured values of electron mobilities taken from ref. 4. It would therefore be of some interest to see if this correlation extends into the supercritical state. Unfortunately, measurements of the mobilities have not been carried out in the gas phase in the density range of interest. Previously, a relationship $k_s \propto \mu_e^{1/2}$ observed in some hydrocarbon liquids (12, 13) was assumed for the estimation of μ_e in the supercritical state from scavenging data (2), but this relation appears to be of a more limited applicability than was originally thought (14–16). Instead, a correlation of apparently more fundamental nature has been noted recently between k_s and the energy of the electron in its conducting state V_0 in an assortment of hydrocarbon and rare gas liquids containing solutes including N_2O (15, 16). If one assumes the validity of the correlation in the supercritical state, then the problem is to find V_0 values.

The Springett *et al.* model (17) has been used to calculate V_0 in liquid hydrocarbons, and the agreement with experiment has been found to be remarkably good (18, 19). The calculation is based on the hard core radius a, the polarizability, and density. Since a is considered to be density- and temperature-independent within the framework of the present V_0 theory, it seems justifiable to employ the method for the calculation of V_0 in the supercritical hydrocarbons. The values of a to be used in the calculation were determined either from V_0's when experimental values were available in the corresponding liquid, or by the relationship $a = 0.305 V_{crit}^{1/3}$ where V_{crit} is the critical volume (20). Since V_0 is relatively sensitive to a, the V_0 values obtained by using the estimate of a from the relationship may be subject to large errors.

The values of a so obtained and V_0 calculated by the model are listed in Table 2. It is interesting to note that V_0 apparently passes through a minimum on going from the liquid to the low density region. This trend is quite reasonable, as V_0 must return to zero in low pressure gases, and seems to indicate the validity of the model for the calculation of V_0 in the supercritical state.

With the V_0 values one can find k_s from the

experimentally obtained relationship between V_0 and k_s (15), and thence μ_e by eq. 5 and $\mu_e = eD_e/kT$.[2] The μ_e values so estimated steadily increase with decreasing density (Table 2). Thus the decrease in the encounter efficiency is accompanied by the increase in electron mobilities. This is in keeping with observations in liquid hydrocarbons and rare gases (11). This behavior was accounted for in terms of the dependence of reaction probability on the electron–reactant interaction time per encounter (11).

Direct measurements of both k_s and μ_e in the supercritical state are desirable.

Acknowledgments

We wish to thank Dr. K. Fueki for valuable discussion, and Mr. Y. Kaneko for his assistance in a part of the study.

1. Y. Yamaguchi and M. Nishikawa. J. Chem. Phys. **59**, 1298 (1973).
2. M. Nishikawa, Y. Yamaguchi, and K. Fujita. J. Chem. Phys. **61**, 2356 (1974).
3. J.-P. Dodelet, K. Shinsaka, and G. R. Freeman. J. Chem. Phys. **59**, 1293 (1973).
4. J.-P. Dodelet, K. Shinsaka, U. Kortsch, and G. R. Freeman. J. Chem. Phys. **59**, 2376 (1973).
5. Landolt-Börnstein. Zahlenwerte und Funktionen. Vol. 2. Springer-Verlag, Berlin. 1971. Part 1.
6. J.-P. Dodelet and G. R. Freeman. J. Chem. Phys. **60**, 4657 (1974).
7. J. Casanovas, R. Grob, D. Blanc, G. Brunet, and J. Mathieu. J. Chem. Phys. **63**, 3673 (1975).
8. S. J. Rzad, P. P. Infelta, J. M. Warman, and R. H. Schuler. J. Chem. Phys. **52**, 3971 (1970).
9. K. Fueki. J. Chem. Phys. **63**, 4085 (1975).
10. S. J. Rzad and K. M. Bansal. J. Phys. Chem. **76**, 2374 (1972).
11. M. G. Robinson and G. R. Freeman. Can. J. Chem. **51**, 650 (1973).
12. G. Beck and J. K. Thomas. J. Chem. Phys. **57**, 3649 (1972).
13. A. O. Allen and R. A. Holroyd. J. Phys. Chem. **78**, 796 (1974).
14. G. Beck and J. K. Thomas. J. Chem. Phys. **60**, 1705 (1974).
15. A. O. Allen, T. E. Gangwer, and R. A. Holroyd. J. Phys. Chem. **79**, 25 (1975).
16. G. Bakale, U. S. Sowada, and W. F. Schmidt. J. Phys. Chem. **79**, 3041 (1975).
17. B. E. Springett, J. Jortner, and M. H. Cohen. J. Chem. Phys. **48**, 2720 (1968).
18. R. A. Holroyd, S. Tames, and A. Kennedy. J. Phys. Chem. **79**, 2857 (1975).
19. S. Noda, L. Kevan, and K. Fueki. J. Phys. Chem. **79**, 2866 (1975).
20. H. T. Davis and L. T. Schmidt. Can. J. Chem. **51**, 3443 (1973).
21. R. A. Holroyd and W. Tauchert. J. Chem. Phys. **60**, 3715 (1974).
22. M. G. Robinson and G. R. Freeman. Can. J. Chem. **52**, 440 (1974).
23. R. A. Holroyd and R. L. Russell. J. Phys. Chem. **78**, 2128 (1974).

[2]There is also an empirical relation that connects V_0 directly to μ_e noted for the neopentane–*n*-hexane mixture (21). μ_e's obtained by this relation are very much larger than those estimated by the method described in the text; moreover they begin to decrease in the intermediate density region.

Discussion

G. R. Freeman: The mobilities of electrons in the supercritical butenes at the critical density have been measured, but we haven't published them yet. They are about 10–20 cm^2 V^{-1} s^{-1}. How does this compare with the values you estimated?

M. Nishikawa: Our estimated values at $d \simeq 0.25$ g/ml and 170°C are 15 to 20 cm^2 V^{-1} s^{-1} for *cis*-2-butene and isobutene, in fair agreement with your values.

Effect of a magnetic field on the fluorescence produced in irradiated anthracene solutions[1]

R. S. DIXON, F. P. SARGENT, V. J. LOPATA, E. M. GARDY

Research Chemistry Branch, Atomic Energy of Canada Limited, Whiteshell Nuclear Research Establishment, Pinawa, Man., Canada R0E 1L0

AND

B. BROCKLEHURST

Department of Chemistry, University of Sheffield, Sheffield, U.K. S37HF

Received September 27, 1976

R. S. DIXON, F. P. SARGENT, V. J. LOPATA, E. M. GARDY, and B. BROCKLEHURST. Can. J. Chem. **55**, 2093 (1977).

The effect of an applied magnetic field on the fluorescence from radiolytic ion recombination has been studied for anthracene in some hydrocarbon solvents. In pulse-irradiated anthracene (10^{-2} mol dm^{-3}) in squalane, the fluorescence intensity following the pulse increases as a function of applied magnetic field in the range studied, 0 to 0.3 T (0 to 3000 G). At a constant magnetic field strength, the field-induced enhancement of the fluorescence intensity varies with time after the pulse. At high field strengths (0.3 T) the enhancement reaches a maximum of ~45% about 50 ns after the pulse. Similar effects are observed in cyclohexane but the enhancement is smaller than that in squalane. In benzene solutions the effect is extremely small. These findings are confirmed by observations in continuously gamma-irradiated solutions. In gamma-irradiated solutions of anthracene (10^{-2} mol dm^{-3}) in squalane, the fluorescence intensity increases with increasing magnetic field and approaches ~13% enhancement at high fields (>0.1 T). The enhancement is smaller (~3%) in cyclohexane and very small (<1%) in benzene solutions. 9,10-Dimethylanthracene gives a larger enhancement and anthracene-d_{10} a smaller enhancement than the parent anthracene at high fields. The results are in general agreement with recent theoretical predictions based on the effect of a magnetic field on the loss of spin correlation of geminate ions pairs prior to recombination.

R. S. DIXON, F. P. SARGENT, V. J. LOPATA, E. M. GARDY et B. BROCKLEHURST. Can. J. Chem. **55**, 2093 (1977).

On a étudié l'effet d'un champ magnétique appliqué sur la fluorescence provenant de la recombinaison ionique radiolytique de l'anthracène dans quelques solvants hydrocarbonés. Dans le cas de l'anthracène irradié par pulsation (10^{-2} mol dm^{-3}) dans le squalane, l'intensité de la fluorescence à la suite de la pulsation augmente en fonction du champ magnétique appliqué dans les intervalles étudiés soit de 0 à 0.3 T (0 à 3000 G). A une force constante du champ magnétique, l'augmentation, induite par le champ, de l'intensité de la fluorescence varie avec le temps après la pulsation. A des forces de champ plus élevées (0.3 T), l'augmentation atteint un maximum d'environ 45% environ 50 ns après la pulsation. On observe des effets similaires dans le cyclohexane mais l'augmentation est plus faible par rapport à celle observée dans le squalane. Dans des solutions benzéniques, l'effet est extrêmement faible. Ces découvertes sont confirmées par des observations dans des solutions irradiées d'une façon continue par des radiations gamma. Pour l'anthracène en solution dans le squalane (10^{-2} mol dm^{-3}) et irradié par des rayons gamma, l'intensité de la fluorescence augmente avec une augmentation du champ magnétique et atteint environ 13% d'augmentation en haut champ (>0.1 T). L'augmentation est plus faible (~3%) dans le cyclohexane et très faible (<1%) dans des solutions benzéniques. Comparé à l'anthracène, le diméthyl-9,10 anthracène donne des augmentations plus grandes alors que l'anthracène-d_{10} donne des augmentations plus faibles à des hauts champs. Ces résultats sont en accord général avec les prédictions théoriques récentes basées sur l'effet d'un champ magnétique sur la perte de corrélation de spin de paires d'ions géminés avant leur recombinaison.

[Traduit par le journal]

Introduction

Large yields of cations and electrons are produced following absorption of radiation by a liquid. In nonpolar liquids most of the electrons and parent cations recombine geminately (1), *i.e.* the separated charges remain coupled by electrostatic attraction and the electron recombines with its original counter ion. In

[1]Issued as AECL No. 5660.

solutions of an aromatic hydrocarbon in an alkane solvent, geminate recombination of solute radical ion pairs is thought to be a major source of solute excited state formation (2–6). Consequently much attention has focused on the ion recombination process and the production and yields of excited states in such systems (1–12).

For geminately recombining radical ions, the electron on the anion was initially paired in a singlet state with the odd electron in the cation. If the spins remain correlated (*i.e.* if the relative orientations and phase of the two electrons stay the same), excited singlet states will be produced, whereas if the correlation is lost, this will lead to the formation of triplet states. Statistically, ion recombination is expected to lead to a triplet:singlet (T/S) ratio of 3. However, measurements of triplet and singlet yields (9, 11, 12) show T/S ratios between 1 and 2, after correction for intersystem crossing. Although the picture may be complicated by energy transfer from excited singlet alkane molecules (10, 12) and excitation of solute triplet states by electrons with insufficient energy to excite the solvent (3), the experimental yields suggest that spin correlation may be partly, but not completely, lost.

The question of the mode and rate of loss of spin correlation was first discussed (13, 14) in terms of the spin relaxation times T_1 and T_2, as used in electron spin resonance (15). Since it was assumed that the loss of correlation would occur in times comparable with T_1 and T_2, it was predicted that a magnetic field would affect the loss of spin correlation when the ion recombination time T_G was longer than the spin–spin relaxation time T_2 but shorter than the spin–lattice relaxation time T_1. Since T_1 and T_2 occur in μs and T_G is ~1–100 ns in mobile liquids, no magnetic field effect would be expected under these conditions. However, if T_G could be increased by the use of viscous solvents, an effect might be seen.

On the basis of these arguments, solutions of fluorene in the viscous solvent squalane were pulse-irradiated and a magnetic field effect on the fluorescence intensity following the pulse was observed (16). The effect was confirmed in gamma-irradiated solutions (17). However, the pulse experiments showed the effect to develop on a shorter time scale than predicted and it was clear that a much more rapid process than spin relaxation was taking place. While the early arguments regarding T_1 and T_2 are still valid, it would be difficult experimentally to detect such an effect because of the low sensitivity.

Further developments in the theory led to predictions of a magnetic field effect on a nanosecond time scale (18, 19). It was shown that loss of spin correlation could occur because of the hyperfine interactions, a, between the unpaired electrons and the hydrogen nuclei of the ions M^+ and M^-. The rate of loss of correlation is mainly determined by the magnitude of a and the number of nuclei. The recent theory stresses the importance of the relative orientations of the spins of the two electrons on M^+ and M^-, which are in different nuclear spin environments. In a strong magnetic field, the electrons on M^+ and M^- precess at different rates about the total field. This difference in the rates of precession leads to conversion of the ion pair from a singlet to a triplet spin state. In principle, the probability of forming a singlet or triplet state should cycle between 1 and 0 but, in practice, it has been shown (18, 19) that the presence of several nuclei tends to mask this and a steady decay from singlet to a mixture of singlet and triplet is predicted. At zero field, the ion pair states S_0, T_0, T_+, and T_- are degenerate and mixing occurs between the singlet and all three triplet states. At high fields, T_+ and T_- have different energies because of the Zeeman splitting, hence mixing takes place only between S_0 and T_0 states. The latter is calculated to be slower and the limiting value for the ratio of singlet to triplet states to be larger than that at zero field. Thus the rate of loss of spin correlation is predicted to be lower in a strong magnetic field than at zero field. Further, the time scale for loss of spin correlation is predicted to correspond not to the esr line width (~100 kHz) but to the spectral width (~100 MHz). This leads to spin correlation changes on a nanosecond time scale.

The original experiments (16, 17) used fluorene because of its short fluorescence decay time (~10 ns) (20) and high fluorescence quantum yield (0.54) (21) and squalane because of its high viscosity. This paper describes the magnetic field effects found on anthracene fluorescence in both pulse-irradiated and continuously irradiated solutions in squalane, cyclohexane, and benzene and compares the results with theoretical predictions.

Experimental

The experimental arrangement for studying the magnetic field effect following pulse radiolysis is shown in Fig. 1. The electron beam flight tube of a 4 MV Van de Graaff accelerator was extended axially through the electromagnet of a Varian 4500 esr spectrometer by means of a hole which passed through the yoke, the pole piece, and the pole cap. The flight tube then passed into a pulse radiolysis cell block assembly at the centre of the electromagnet, and terminated in a 0.03 mm thick brass window located 1 mm from the face of the cell. The Suprasil cell was part of a flow system for ease of sample changing. The magnetic field strength was measured by a Hall effect probe. Since the field affected the beam focusing, the latter was adjusted to minimize this effect. Details of the effect of field strength on the dose per pulse measured by KCNS dosimetry are described elsewhere (22). In the present experiments, conditions were such that the magnetic field had no effect on the dose below 0.1 T and only ~5% at 0.3 T. The dose per pulse was $\sim 10^{-2}$ J. For experiments with the magnetic field off, a small residual field of $\sim 10^{-3}$ T (~10 G) remained when the magnet was turned off. To eliminate this, a small reverse dc current was applied to the magnet such that the magnetic field was a minimum in the direction of the Hall crystal. The field at the minimum was $< 10^{-4}$ T. A conventional optical detection system was used with a 1P28 photomultiplier tube and a Hewlett-Packard 183A oscilloscope. To facilitate measurements at long times after the pulse, a pulse generator with a variable delay was used to trigger the oscilloscope. Initially a Jarrell-Ash 0.25 m monochromator was used, but once the fluorescence spectrum was established, this was removed for greater sensitivity.

The experimental arrangement for studying the magnetic field effect on continuously irradiated solutions is shown in Fig. 2. Solutions were irradiated in a Suprasil cell, which was part of a flow system, by gamma rays from a movable Iridium-192 source. The dose rate was $\sim 6 \times 10^{-5}$ J g^{-1} s^{-1} ($\sim 4 \times 10^{14}$ eV g^{-1} s^{-1}) as measured by the Fricke dosimeter. A small electromagnet provided the magnetic field up to 0.5 T. A permanent magnet, used in a few experiments, gave the same results. Measurement of the field strength and zeroing of the field were as described for the pulse experiments. The magnetic field had no effect on the photomultiplier tube (RCA 1P28) or on the emission intensity from a cell containing solvent only. However, it was necessary to correct for the effect of the gamma rays on the photomultiplier tube. The light emitted from the cell was focused by a lens onto the photomultiplier tube and the level displayed on a recorder. The identity of the emitting species was assumed to be the same as that in the pulse radiolysis experiments.

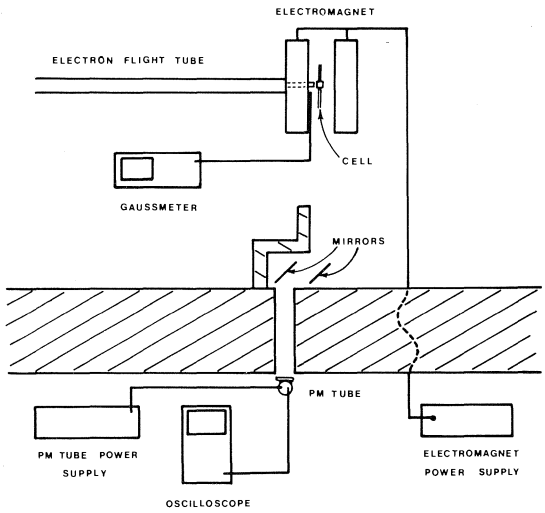

FIG. 1. Schematic of the apparatus for studying the effect of an applied magnetic field on the fluorescence from pulse-irradiated solutions.

Cyclohexane (Fisher or Matheson Spectroquality), benzene (Fisher certified), anthracene (Hinton, zone refined), anthracene-d_{10} (Merck, Sharpe, and Dohme 98% D), and dimethylanthracene (Aldrich) were used as received. Squalane was purified by repeated passes through a silica gel column until the absorption edge, measured spectrophotometrically, remained constant.

Results

(a) Pulse Radiolysis

The fluorescence from pulse-irradiated anthracene in squalane persists to hundreds of nanoseconds after the pulse, and the intensity increases in the presence of an applied magnetic field (Fig. 3). The field has little or no effect on the in-pulse intensity. The emission enhancement following the pulse was found to be both time and field strength dependent. The effect of field strength at ~100 ns following the pulse is shown in Fig. 4 for 10^{-2} mol dm^{-3} anthracene. The enhancement was found to increase rapidly with increasing field strength up to 0.1 T, followed by a much slower increase at higher fields. The behaviour was similar for times in the range 0–400 ns after the pulse. The time dependence of the enhancement at a field of 0.3 T is shown in Fig. 5 for 10^{-2} mol dm^{-3} anthracene. The enhancement increases rapidly with time, reaching a plateau of ~45% some 50 ns after the pulse. The enhancement may decrease slightly at longer times but the emission is small and the measurement less precise. Within the limits of experimental error, we saw no concentration effect in the range 10^{-3} to 10^{-2} *M* anthracene up to ~200 ns after the pulse, but at longer times the 10^{-2} *M* solution showed less enhancement than the 10^{-3} *M* solution.

Similar behaviour was seen in solutions of anthracene in cyclohexane but the magnetic

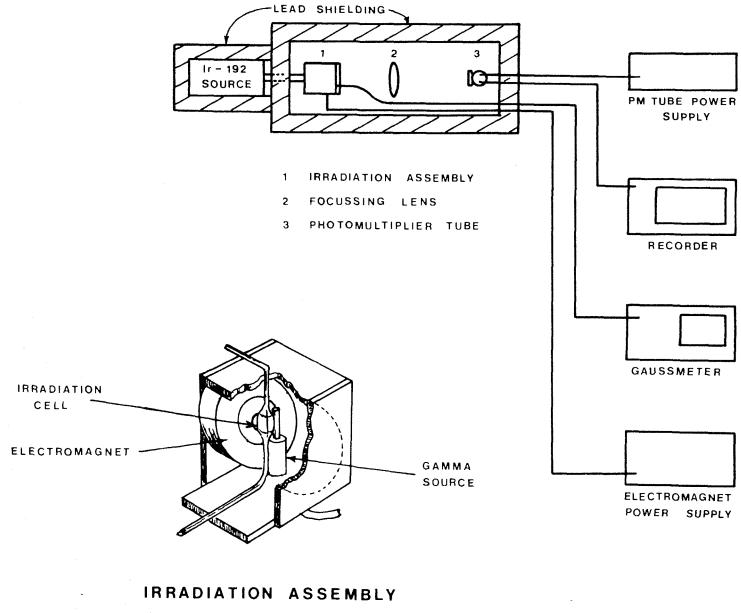

FIG. 2. Schematic of the apparatus for studying the effect of an applied magnetic field on the fluorescence from gamma-irradiated solutions.

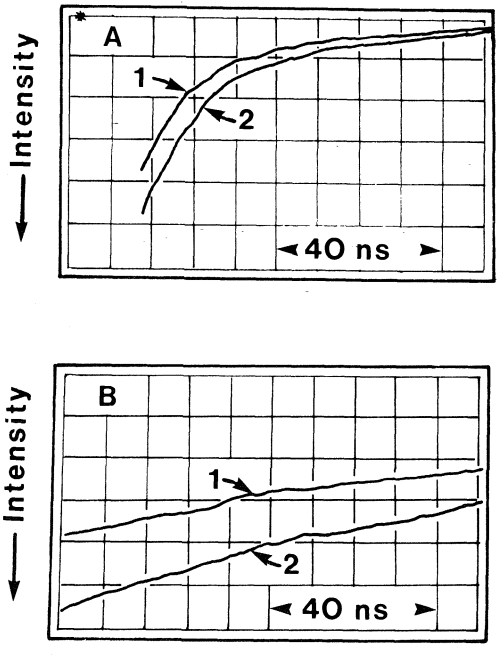

FIG. 3. Typical oscilloscope traces showing the effect of an applied magnetic field on the fluorescence intensity from 10^{-2} mol dm^{-3} anthracene in squalane following a 5 ns pulse: (*A*) $t = 0$ to 100 ns following start of pulse; (*B*) $t = 300$ to 400 ns following start of pulse (sensitivity × 150); curve *1*, no magnetic field; curve *2*, 0.3 T (3000 G).

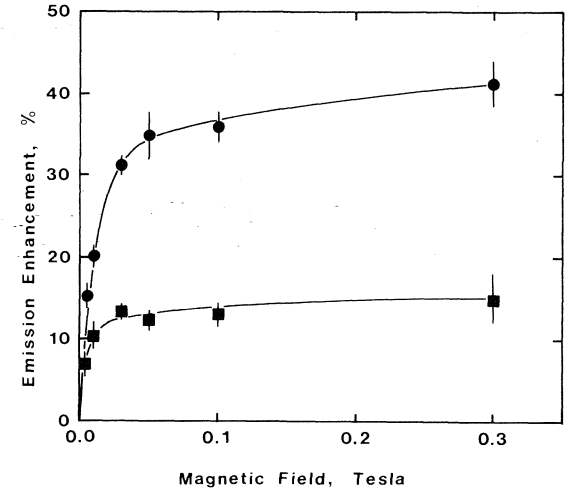

FIG. 4. Effect of applied magnetic field on the fluorescence intensity from 10^{-2} mol dm^{-3} anthracene in squalane (●) and cyclohexane (■): $t = 100$ ns following start of pulse.

field effect was smaller than in squalane (Figs. 4 and 5). For example, the maximum emission enhancement following the pulse was only ~20% at high fields (Fig. 5) at an anthracene concentration of 10^{-2} mol dm^{-3}.

In benzene the emission intensity was large but we found no measurable field effect up to ~100 ns following the pulse. However, there

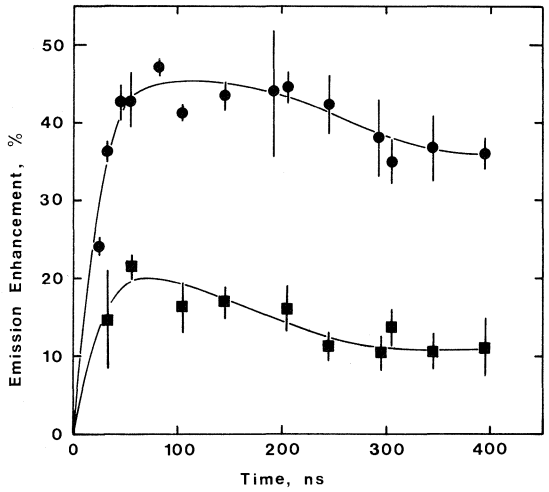

FIG. 5. Magnetic field induced increase in fluorescence intensity as a function of time following a 5 ns pulse for 10^{-2} mol dm^{-3} anthracene in squalane (●) and cyclohexane (■): magnetic field = 0.3 T.

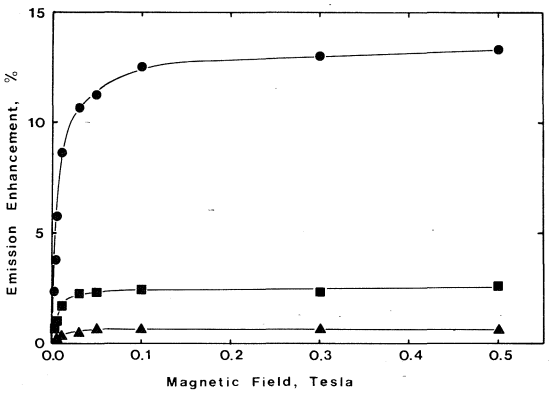

FIG. 6. Effect of applied magnetic field on the fluorescence intensity from gamma-irradiated 10^{-2} mol dm^{-3} anthracene in squalane (●), cyclohexane (■), and benzene (▲).

may be a small enhancement ($\leq 5\%$) in the range 100–200 ns following the pulse, but we could not make precise measurements because of lack of sensitivity.

(b) Continuous γ Radiolysis

The effect of solvent on the emission enhancement from anthracene solutions in an applied magnetic field is shown in Fig. 6. The enhancement is in the order squalane > cyclohexane > benzene, the effect being very small in benzene. In squalane solutions, the enhancement was also found to increase slightly with concentration in the range 5×10^{-4} *M* to 10^{-2} *M*, but

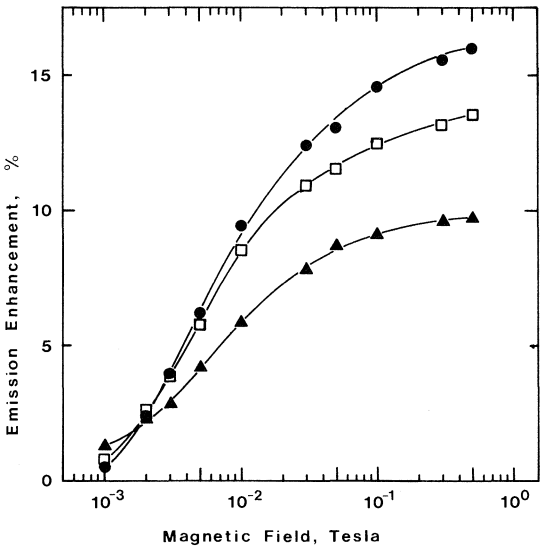

FIG. 7. Effect of applied magnetic field on the fluorescence intensity from some gamma-irradiated anthracenes (10^{-2} mol dm^{-3}) in squalane: (●) 9,10-dimethylanthracene; (□) anthracene; (▲) anthracene-d_{10}.

at higher concentrations it began to decrease slightly. The effect of magnetic field on the fluorescence from anthracene, perdeuteroanthracene, and 9,10-dimethylanthracene in squalane is shown in Fig. 7. Deuteration gives a smaller enhancement and methylation a larger enhancement than the parent anthracene at higher fields.

Discussion

(a) Pulse Radiolysis

Although there is still considerable debate on the possible mechanisms of excited state formation, their relative contributions, and the time scales over which they are important, ion recombination is thought to be a major source of excited states in irradiated systems. In nonpolar solvents, most of the ion pairs do not separate completely but undergo geminate recombination (1). The pertinent reactions occurring in solutions of an aromatic hydrocarbon, M, in an alkane, S, will be

[1] $$S \rightsquigarrow S^+ + e^-$$

[2] $$S^+ + M \rightarrow M^+ + S$$

[3] $$e^- + M \rightarrow M^-$$

[4] $$M^+ + e^- \rightarrow M^*$$

[5] $$S^+ + M^- \rightarrow M^* + S$$

[6] $$M^+ + M^- \rightarrow M^* + M$$

where M* can be an excited singlet or triplet state. At high solute concentrations, reaction 6, involving reaction of solute radical ions, will be the major process for ion recombination.

Figure 8 shows the decay of the fluorescence from 10^{-2} mol dm^{-3} anthracene in squalane following a 5 ns pulse. The fluorescence persists to longer times and decays much more slowly than would be expected from the photofluorescence decay time (4.9 ns in cyclohexane (20)), *i.e.* neglecting the effects of self-quenching, quenching by radiolysis products, etc. At short times following the pulse, a major fraction of the fluorescence arises from 'prompt' singlets (whether formed by energy transfer, ion recombinations, or other mechanisms) and the decay time is ~15 ns. At longer times the fluorescence arises mainly from slower ion recombinations, which explains the much slower fluorescence decay with increasing time.

The enhancement of the fluorescence intensity in the presence of a magnetic field increases with time following the pulse and reaches its maximum ~50 ns after the end of the pulse (Fig. 5). In his theory of magnetic field effects on excited singlet state formation, Brocklehurst describes approximate time regions following the pulse where different field effects are predicted (18, 19). At times <5 ns, there is no loss of spin correlation in the rapidly recombining ions and no magnetic field effect. At times >5 ns, loss of spin correlation occurs faster at zero field because the singlet can mix with all three degenerate triplets, whereas at high field only the singlet and T_0 states mix because of the Zeeman effect. At these times, the field effect is predicted to be large. On the basis of these predictions, we would expect no field effect during the pulse and a rapidly rising effect immediately following the pulse. The enhancement should reach a maximum when the 'prompt' fluorescence contribution has become negligible. These general features of the theory are found in our experimental results (Fig. 5).

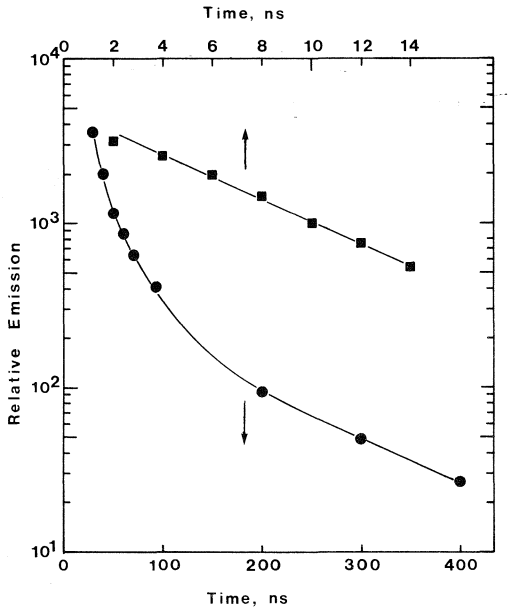

FIG. 8. Decay of the fluorescence from pulse-irradiated 10^{-2} mol dm^{-3} anthracene in squalane (●) and benzene (■).

The theoretical calculations predict a maximum in the field effect at ~10–20 ns after the pulse (18, 19). Maxima have been observed in this time region in studies of magnetic field effects on scintillations from geminate ion recombination (23, 24). We do not observe a maximum at this time but a somewhat longer time (~50 ns). However, our results are more complicated because of the width of the pulse and because of the fluorescence lifetime. The latter is particularly important since, at shorter times after the pulse, a considerable fraction of the total emission comes from 'prompt' fluorescence, which exhibits no magnetic field effect. If the prompt fluorescence contribution were subtracted from the total emission, the emission enhancement would reach its maximum in a shorter time. Qualitatively this has been shown to be the case for fluorene in squalane (22), assuming that the in-pulse emission is all prompt fluorescence and using the literature value for its decay time. This is not strictly true since the in-pulse emission includes Cerenkov emission, etc., but it does indicate that the field effect on ion recombination in the present system probably reaches its maximum at a time shorter than 50 ns after the pulse.

In cyclohexane solutions, ion recombination will be much faster than in squalane because of the lower viscosity. Thus a greater fraction of the geminately recombining ions will not be affected by a magnetic field, but the behaviour of the remaining ions should be similar to that in squalane. The overall decay of the fluorescence is similar to that found in squalane, but the magnetic field effect is smaller. In the simplest theoretical case, the magnetic field enhancement is calculated to reach a factor of 2 at longer

times (18, 19). The maximum enhancement which we have observed is about half of this, both in the present work and in other systems (16, 22). There are several possible reasons for the discrepancy. In discussing excited state yields, Magee and Huang (25) considered the formation of triplet ion pairs by cross-recombination in multiple ion pair spurs and by spin reversal of a secondary electron when it excites a solvent molecule to the triplet state. If these processes are significant in the present system, triplet ion pairs may reduce the extent of the magnetic field effect. In addition, the calculated limiting probabilities of 0.5 and 0.25 for singlet state formation in the presence and absence of a magnetic field may not be reached except at very long times (19). Finally the yields of excited states may depend not only on spin but on the energy level densities, *i.e.* Franck–Condon factors (14). Contributions from any of these factors may lead to an emission enhancement which is smaller than the maximum theoretical value. Nevertheless, it appears that some additional or alternative factor is involved in the case of cyclohexane solutions. A factor which is likely to be much more important in cyclohexane than in squalane is the effect of the prompt fluorescence decay. In cyclohexane the prompt fluorescence will be much larger and the emission from slower ion recombinations much smaller than in squalane. Consequently the prompt fluorescence contribution, which shows no magnetic field effect, will be larger and much more important than in squalane. This will lead to a smaller enhancement in cyclohexane than in squalane at short times after the pulse, though it appears doubtful that this can still be operative out to the longest times which we have measured.

Results in benzene are considerably different from those in squalane and cyclohexane since we see a large emission but no magnetic field effect during the first 100 ns after the pulse. Although excited state yields are high in benzene (2, 3), solute ions have not been observed. This implies that solute excited states arise from energy transfer from solvent excited states, fast ion recombination, or some other rapid process, none of which would be expected to exhibit a magnetic field effect, according to theory (18, 19). The fluorescence decay was found to be exponential (Fig. 8) with a lifetime of 6.4 ns, compared to the lifetime of 4.9 ns from photochemical measurements in cyclohexane (20). This comparison is reasonable since the lifetime under our experimental conditions may be increased by reabsorption and by any ion recombination contribution. At times in the range 100–200 ns after the pulse, we did observe a small magnetic field effect ($\leq 5\%$) at an applied field of 0.3 T. While measurements in this region were subject to large experimental uncertainty, they, together with the results from continuously irradiated benzene, do suggest a small contribution from slower ion recombinations and a small magnetic field effect.

(b) Continuous Radiolysis

The effects of a magnetic field on continuously gamma-irradiated solutions of anthracene in squalane, cyclohexane, and benzene are qualitatively similar to those found in pulse-irradiated solutions. Increasing the magnetic field intensity increases the fluorescence enhancement rapidly for fields up to 0.1 T but much more slowly at higher fields (Figs. 6 and 7). The enhancement is again larger in squalane than in cyclohexane and only a small enhancement ($< 1\%$) is seen in benzene solutions (Fig. 6). The enhancement in continuously irradiated solutions is smaller than that found in pulse-irradiated solutions, as expected. In the continuous radiolysis we are seeing the prompt emission, whether from energy transfer, fast ion recombination, or other processes, superimposed on the emission from slower ion recombinations. Since only the latter is expected to exhibit a magnetic field effect, the effect will be smaller than the maximum seen in pulse-irradiated solutions after most of the prompt emission has decayed. The enhancement in squalane solutions is expected to be larger than that in cyclohexane solutions because of the viscosity differences. In general, the range of ion recombination times in cyclohexane is smaller than in squalane, leading to a greater fraction of singlet excited states which exhibit no magnetic field effect. The enhancement is, however, smaller than expected on the basis of results from other solutes in cyclohexane (17, 22). This appears to be further evidence that some other process is contributing to the overall effects in both pulse-irradiated and continuously irradiated anthracene in cyclohexane. In benzene, excited state yields are high (2, 3) but solute ions have not been observed. This implies that the major mechanism of solute excited state formation in benzene involves energy transfer,

very fast ion recombination, or some other rapid process, none of which would be expected to show a magnetic field effect. This is confirmed by our experimental results (Fig. 6). Nevertheless, we do see a small, but positive, field effect which suggests that some solute excited states in benzene may be formed by slow ion recombinations.

The effect of deuteration and methylation at high field (Fig. 7) provides some support for the theory (18, 19). The ion recombination rate for the three anthracenes will be little affected by substitution and not at all by the magnetic field. The different effects of substitution must therefore be due to the effect on the rate of loss of spin correlation. A major reason for the decay of the spin correlation, *i.e.* the rate of conversion of singlet ion pairs to triplet pairs, is the electron–nuclear coupling in the respective radical ions. Decreasing the coupling constant should decrease the rate of loss of spin correlation, leading to an increase in excited singlet state formation, and vice versa. Anthracene-d_{10} has a smaller coupling constant than anthracene because of the smaller magnetic moment of the deuteron. Thus the rate of loss of spin correlation will be smaller for anthracene-d_{10}, resulting in a corresponding increase in the probability of excited singlet state formation and a smaller magnetic field effect. Conversely, 9,10-dimethylanthracene will have a larger coupling than anthracene because of the increased number of protons. This will lead to an increase in the rate of loss of spin correlation, *i.e.* a decrease in the probability of forming singlet excited states and a larger magnetic field effect, as is found (Fig. 7).

At low fields ($\sim 10^{-3}$ T) the reverse effect occurs, *i.e.* the enhancement is highest for anthracene-d_{10}. This is because, to be effective in preventing mixing between S_0 and $T_{\pm}$, the field must be $\gtrsim$ the spread of the hyperfine levels. This is smallest for anthracene-d_{10}, so a smaller field is required to give an enhancement.

(c) Other Considerations

We have attributed the magnetic field induced enhancement of the fluorescence to an increase in the fraction of geminate ion recombinations leading to excited singlet state formation. In principle, other mechanisms may be possible. We have ruled out a field effect on the fluorescence lifetime since, in benzene, the fluorescence is little affected by a magnetic field either in pulse-irradiated or continuously irradiated solutions. We assume the same to hold in squalane and cyclohexane. Studies on delayed fluorescence by triplet–triplet annihilation in both crystals (26–28) and fluid solutions (29, 30) and on electrochemically generated luminescence (31, 32) have shown the importance of magnetic field effects on this process. A magnetic field was found to decrease both the rate of the triplet–triplet reaction and the rate of triplet quenching by radical ions. However, we consider the contribution from these mechanisms to be small, if any, for several reasons. At the low dose rates used in our continuous radiolysis experiments, triplet–triplet annihilation is unlikely to be a major source of fluorescence, yet a large magnetic field effect can be seen. Conversely, in pulse-irradiated benzene solutions, we found little magnetic field effect even though triplet yields in benzene are high (2, 3). In our pulse radiolysis experiments, the dose rate is much higher than in the continuous radiolysis, but the results suggest that triplet–triplet annihilation is not of major importance in any solvent studied. In cyclohexane we found triplet anthracene to decay by a first order process with $k = 3.0 \times 10^4\ s^{-1}$, independent of magnetic field. Evidence from the literature shows similar triplet decays. In the pulse-irradiated viscous solvent liquid paraffin, biphenyl triplets were seen to decay by a first order process and little or no second order contribution was found (33). At the high doses used (0.15 J) the decay was attributed to quenching by radicals. In pulse-irradiated cyclohexane and benzene solutions (34), anthracene triplet decayed by a first order process for doses up to $0.02\ J\ g^{-1}$, which is similar to the doses used in the present work. Finally, the field effects on singlet state production from triplet–triplet annihilation should show no isotope effect since the processes depend on the fine structure of the triplet state (zero-field splitting) rather than the hyperfine interaction. Thus, although magnetic field effects on delayed fluorescence from triplet–triplet annihilation now appear well-established, our evidence suggests that their contribution in the present work is not of major importance.

Conclusions

An applied magnetic field increases the fluorescence intensity from pulse-irradiated and continuously irradiated solutions of anthracene

in squalane and cyclohexane. Only a small effect is seen in benzene solutions. The results are in qualitative agreement with theoretical predictions based on the effect of a magnetic field on the rate of loss of spin correlation of separated ion pairs prior to their geminate recombination. Both the effect of solvent and of substitution in the solute molecule support the theory. The results also provide evidence for the importance of geminate ion recombination in the formation of solute excited states in radiolysis.

1. A. HUMMEL. *In* Advances in radiation chemistry. Vol. 4. *Edited by* M. Burton and J. L. MAGEE. Wiley, New York. 1974. p. 1.
2. J. K. THOMAS. Ann. Rev. Phys. Chem. **21**, 17 (1970).
3. A. SINGH. Radiat. Res. Rev. **4**, 1 (1972).
4. J. K. THOMAS. Int. J. Radiat. Phys. Chem. **8**, 1 (1976).
5. G. A. SALMON. Int. J. Radiat. Phys. Chem. **8**, 13 (1976).
6. L. WALTER, F. HIRAYAMA, and S. LIPSKY. Int. J. Radiat. Phys. Chem. **8**, 237 (1976).
7. A. HUMMEL and W. F. SCHMIDT. Radiat. Res. Rev. **5**, 199 (1974).
8. A. HUMMEL and L. H. LUTHJENS. J. Chem. Phys. **59**, 654 (1973).
9. J. H. BAXENDALE and P. WARDMAN. Trans. Faraday Soc. **67**, 2997 (1971).
10. G. BECK and J. K. THOMAS. J. Phys. Chem. **76**, 3856 (1972).
11. F. S. DAINTON, M. B. LEDGER, R. MAY, and G. A. SALMON. J. Phys. Chem. **77**, 45 (1973).
12. P. O'NEILL, G. A. SALMON, and R. MAY. Proc. R. Soc. London, Ser. A, **347**, 61 (1975).
13. B. BROCKLEHURST. Nature, **221**, 921 (1969).
14. B. BROCKLEHURST. Chem. Phys. **2**, 6 (1973).
15. N. M. ATHERTON. Electron spin resonance. Ellis Horwood Ltd., Chichester. 1973.
16. B. BROCKLEHURST, R. S. DIXON, E. M. GARDY, V. J. LOPATA, M. J. QUINN, A. SINGH, and F. P. SARGENT. Chem. Phys. Lett. **28**, 361 (1974).
17. R. S. DIXON, E. M. GARDY, V. J. LOPATA, and F. P. SARGENT. Chem. Phys. Lett. **30**, 463 (1975).
18. B. BROCKLEHURST. Chem. Phys. Lett. **28**, 357 (1974); **29**, 635 (1974).
19. B. BROCKLEHURST. J. Chem. Soc. Faraday Trans. II, **72**, 1869 (1976).
20. I. B. BERLMAN. Handbook of fluorescence spectra of aromatic molecules. Academic Press, New York. 1965. p. 119.
21. J. G. CALVERT and J. N. PITTS. Photochemistry. J. Wiley and Sons Ltd., New York. 1966. p. 310.
22. F. P. SARGENT, R. S. DIXON, V. J. LOPATA, E. M. GARDY, and B. BROCKLEHURST. To be published.
23. B. BROCKLEHURST. Chem. Phys. Lett. **44**, 245 (1976).
24. J. KLEIN and R. VOLTZ. Phys. Rev. Lett. **36**, 1214 (1976).
25. J. L. MAGEE and J.-T. HUANG. J. Phys. Chem. **76**, 3801 (1972).
26. R. C. JOHNSON, R. E. MERRIFIELD, P. AVAKIAN, and R. B. FLIPPEN. Phys. Rev. Lett. **19**, 285 (1967).
27. V. ERN and R. E. MERRIFIELD. Phys. Rev. Lett. **21**, 609 (1968).
28. R. E. MERRIFIELD. J. Chem. Phys. **48**, 4318 (1968).
29. L. R. FAULKNER and A. J. BARD. J. Am. Chem. Soc. **91**, 6495 (1969); **91**, 6497 (1969).
30. H. TACHIKAWA and A. J. BARD. Chem. Phys. Lett. **26**, 10 (1974).
31. L. R. FAULKNER and A. J. BARD. J. Am. Chem. Soc. **91**, 208 (1969).
32. L. R. FAULKNER, H. TACHIKAWA, and A. J. BARD. J. Am. Chem. Soc. **94**, 691 (1972).
33. J. FULLER, N. PETELESKI, D. RUPPEL, and M. TOMLINSON. J. Phys. Chem. **74**, 3066 (1970).
34. F. S. DAINTON, T. MORROW, G. A. SALMON, and G. F. THOMPSON. Proc. R. Soc. London, Ser. A, **328**, 457 (1972).

Discussion

A. C. Albrecht: Can triplet–triplet annihilation be easily excluded in this work?

R. S. Dixon: Magnetic fields are known to decrease both the rate of triplet–triplet annihilation and the quenching of triplets by radical ions. The former would lead to a decrease in excited singlet formation and the latter to an increase. We cannot definitely exclude a contribution from these mechanisms but we consider it to be small for several reasons. Firstly, the field effect in benzene solutions is small even though triplet state yields in benzene are high. Secondly, at the low dose rates used in the continuous radiolysis, triplet–triplet annihilation is unlikely to be a major source of fluorescence. Thirdly, in pulse-irradiated anthracene in cyclohexane, we found a first order decay for the triplet with no measurable field effect. A first order triplet decay has been observed in similar studies in the literature. However, I should point out that, because of the long triplet lifetime, triplet decay measurements were necessarily made at much longer times (μs) than the fluorescence measurements.

Time resolved magnetic modulation of ion recombination in organic solutions: spin motion in radical ion pairs

JEAN KLEIN AND RENÉ VOLTZ

Centre de Recherches Nucléaires et Université Louis Pasteur, Laboratoire de Physique des Rayonnements et d'Electronique Nucléaire, F 67037, Strasbourg, Cedex, France

Received September 27, 1976

JEAN KLEIN and RENÉ VOLTZ. Can. J. Chem. **55**, 2102 (1977).

The evolution of the singlet character of correlated ion radical pairs, prepared by high energy impact (β particles) in organic liquid and solid solutions, is monitored by nanosecond time resolved solute recombination fluorescence. Results obtained show that the relative variations $[I^B(t) - I^0(t)]/I^0(t)$ of the luminescence intensity in presence $I^B(t)$ and in absence $I^0(t)$ of magnetic fields ($B \leq 5$ kG) decrease exponentially with time, according to a field and solute concentration dependent rate, in liquid but not in solid solutions; in the case of 2b PPD as solute, a damped oscillating component could be observed. The results are interpreted in terms of hyperfine interaction induced coherent singlet–triplet mixing and of field and solute concentration dependent spin–lattice relaxation.

JEAN KLEIN et RENÉ VOLTZ. Can. J. Chem. **55**, 2102 (1977).

L'évolution du caractère singulet de paires de radicaux-ions corrélés, créés dans des solutions organiques liquides et solides par une excitation brève (particule β), a pu être suivie dans le domaine de la nanoseconde par l'intermédiaire de la fluorescence de recombinaison résolue dans le temps. Les résultats obtenus montrent que les variations relatives $[I^B(t) - I^0(t)]/I^0(t)$ de l'intensité de la luminescence en présence $I^B(t)$ et en absence $I^0(t)$ de champs magnétiques ($B \leq 5$ kG) décroissent exponentiellement avec une constante de temps qui dépend du champ et de la concentration en soluté dans les solutions liquides mais non dans les solides; dans le cas de 2b PPD comme soluté, on observe de plus une composante oscillante. Ces résultats sont interprétés à l'aide d'un modèle impliquant d'une part un mélange cohérent entre états singulet et triplet induit par des interactions hyperfines, d'autre part des processus de relaxation spin–réseau dépendant du champ et de la concentration en soluté.

A radical ion pair model, where spin motion of the two unpaired electrons under the hyperfine structure and Zeeman interaction is responsible for time variations of the total spin state, has been used to describe a variety of phenomena in organic solutions, *e.g.*, (*i*) chemically induced dynamic nuclear and electronic polarization (1, 2); (*ii*) geminate ion pair recombination in polar and nonpolar solvents (3–8); (*iii*) hyperfine structure modulation of dye-sensitized fluorescence in organic crystals (9, 10).

In the present work, we analyse the time resolved magnetic field dependence of ion recombination luminescence in organic solutions excited by high energy radiation (11). The method allows one to follow in detail the behavior of the ion pair singlet character, on the nanosecond time scale, so that new and direct information on the general ion pair model is obtained (8). Here, special attention will be given to the influence of the phase of the solvent as well as the nature and concentration of the solutes on coherent motion and relaxation of the radical pair spin in liquid and solid solutions.

Experimental Set-up and Conditions

The block-diagram of the set-up is shown in Fig. 1. The sample (S) to be studied is placed between the poles of an electromagnet (M), supplying magnetic fields up to 5000 G. The fields are measured by placing the Hall effect probe of a gaussmeter at the position of the sample. In order to obtain 'zero field', a small reverse current in the electromagnet is used to cancel the residual (hysteresis and earth magnetic field) so that values less than 0.2 G are obtained. The luminescence of the solutions can be excited by light flashes or high energy particles. A photomultiplier (PM) detects a major part of the light emitted by the sample, and acts as a monitor giving the reference time t_0. The second photomultiplier (PEU) works under single photon counting conditions: per light pulse, it delivers at most one electric signal, corresponding to the extraction at a time t ($t \geq t_0$) of a single photoelectron from the cathode; at any time t, the probability of extraction of this electron is proportional to the light intensity $I(t)$ at the cathode (12). The time-to-amplitude converter (TAC) yields signals with amplitudes proportional to $\Delta t = t - t_0$, which are finally analysed by the multichannel analyser (MCA); the resulting counts in the

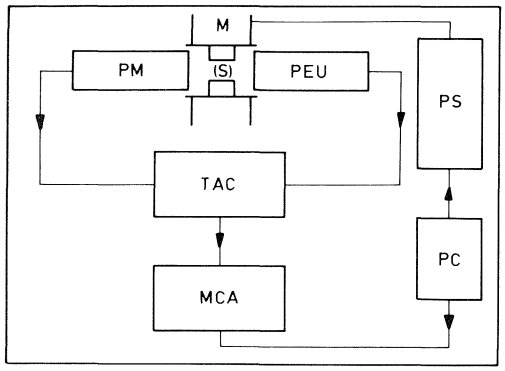

FIG. 1. Block-diagram of magnetic modulated time resolved luminescence measurement apparatus (S: sample; M: electromagnet and PS its power supply; PM and PEU: photomultipliers; TAC: time-to-amplitude converter; MCA: multichannel analyser; PC: periodic commutator).

memory of MCA are accumulated as long as necessary to get a histogram of Δt with a sufficient statistical precision.

To minimize eventual errors due to slow electronic jitter, the measurements with and without magnetic fields are performed successively, for a short time (10 s) by means of a periodic commutator (PC), switching alternatively on and off the magnetic power supply (MP) and the corresponding way-in of MCA; the results are stored in two separate parts of the MCA memory.

With this set-up, the luminescence intensity $I(t)$ can be followed between 0 and microseconds with a time resolution of 0.5 ns under very weak excitation intensity conditions. The results are similar to those previously published and discussed in detail (11).

In the present experiments, the luminescence is excited by β particles from a 0.1 μCi source of ^{90}Sr–^{90}Y plunged into the solutions. Samples are contained in cylindrical Pyrex cells and have been degassed by the usual freeze–pump–thaw technique. For the liquids, the solvents used are benzene, cyclohexane (Merck, "uvasol"), and methylcyclohexane (MCH) (Prolabo, "for spectroscopy"), with the following solutes which are used without special purification: *para*-terphenyl (*p*TP) (Progil), bis-2,5-(4-butylphenyl)-1,3,4-oxadiazole (2b PPD) (Ciba[1]), and 2,5-diphenyl-1,3-oxazole (PPO) (Nuclear Entreprise). The polystyrene solutions were prepared by thermal polymerization of styrene (Merck) purified by double distillation under vacuum. Solid glass solutions of MCH were obtained by freezing samples in liquid nitrogen in a dewar device having an optical tail which is placed in the magnetic field.

Results

If we denote respectively by $I^B(t)$ and $I^0(t)$ the luminescence intensities at time t measured in the presence and in the absence of an external magnetic field B, we can represent the relative field variation by the time dependent quantity $\Delta I/I = [I^B(t) - I^0(t)]/I^0(t)$. Figures 2*a* and 2*b* show the observed variations of $\Delta I/I$ with time, for various field strengths, in liquid cyclohexane solutions at room temperature (Fig. 2*a*) and solid MCH solutions at 77 K (Fig. 2*b*). Each of these two sets of curves may be taken as representative of the liquid and solid systems, since similar results were obtained in the other comparable cases.

We may first note that, on the time scale, each graph exhibits two regions where the magnetic field effect is different: the first time period, from 0 (maximum of the $I(t)$ curve) to about 30 ns, where the 'prompt' component radioluminescence is known to be dominant (11, 13); a second one, for times longer than 30 ns where only the 'delayed' component, due to ion recombination, is present (11).

In the case of the liquid solutions of 2b PPD in cyclohexane, the results of Fig. 2*a* suggest considering the time dependence of $\Delta I/I$ as the sum of a damped oscillatory term and a monotonic decreasing component. The former term exhibits an oscillation period of the order of 120 ns; but its observability strongly depends on the nature of the solute since no clear evidence for its occurrence could be found with other solutes like anthracene, *para*-terphenyl, and PPO (*cf.* Fig. 2*a*). On the other hand the second component was observed in all the liquid systems investigated: its decay is exponential with a rate constant k (s^{-1}) depending on the external field B and the solute concentration C_s as

$$[1] \qquad k = k' + k''(B, C_s)$$

where k' is constant, while k'' increases with C_s and decreases for increasing fields around $B \approx 10^2$ G. The results for the 2b PPD solutions in cyclohexane are represented in Fig. 3. In the case of the solid solutions, by contrast, no such variations could be observed on the time scale explored, where $\Delta I/I$ remained constant.

Discussion

We only consider the slow luminescence component arising from geminate recombination of solute ion pairs. Initially these pair states may be taken as prepared in a singlet spin state by high energy impact excitation. By recombination, these ion pairs produce fluorescing excited solutes

[1]2b PPD was kindly supplied by Ciba (Basel) as a specimen.

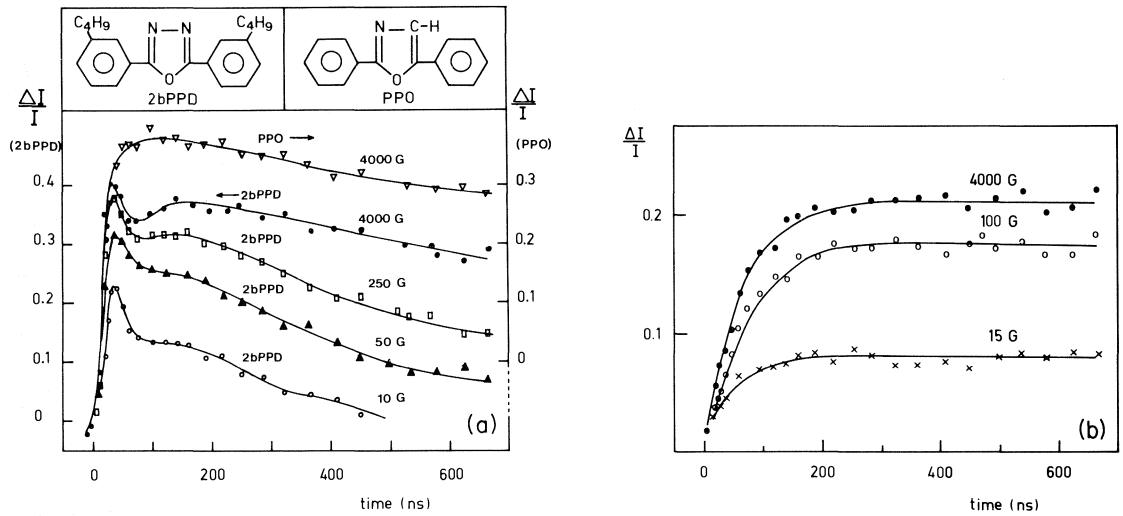

FIG. 2. Time dependence of relative fluorescence intensity $\Delta I/I$ upon application of magnetic fields B for (*a*) 1.5×10^{-3} M solutions of 2b PPD and PPO in cyclohexane at room temperature and (*b*) 10^{-3} M solution of *p*TP in methylcyclohexane glass at 77 K; excited by β rays from a 0.1 μCi ^{90}Sr–^{90}Y source.

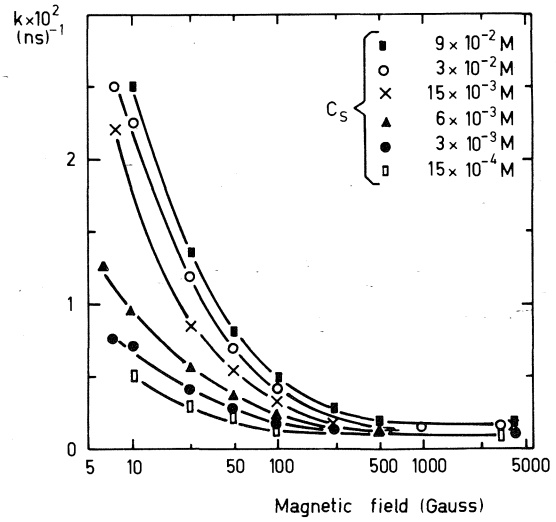

FIG. 3. Influence of the field strength B and the solute concentration C_s on the decay rate k of exponentially decreasing $\Delta I/I$ for 2b PPD solutions in cyclohexane at room temperature.

provided they are singlet at the neutralization time; recombination luminescence may thus be used to monitor the singlet character of the solute ion pair states between initial sudden preparation and final recombination. Denoting by $\rho_s(t)$ the probability of the correlated solute ion pair to be singlet at time t, one has

$$[2] \qquad \frac{\Delta I}{I} = \frac{\rho_s^B(t) - \rho_s^0(t)}{\rho_s^0(t)}$$

where $\rho_s^B(t)$ and $\rho_s^0(t)$ are the quantities in the presence and the absence of the magnetic field.

The time variations of $\rho_s^B(t)$ may be derived by taking for the unpaired electrons (1) and (2) a spin Hamiltonian involving a Zeeman and a hyperfine structure interaction term ($\hbar = 1$)

$$[3] \quad H = g\beta \boldsymbol{B}[\boldsymbol{S}(1) + \boldsymbol{S}(2)] + a(1)\boldsymbol{I}(1)\cdot\boldsymbol{S}(1) + a(2)\boldsymbol{I}(2)\cdot\boldsymbol{S}(2)$$

where $\boldsymbol{S}(i)$ and $\boldsymbol{I}(i)$ represent respectively the electronic and nuclear spins on the two radicals labelled $i = 1, 2$; $a(i)$ denotes the hyperfine isotropic coupling constant and β the Bohr magneton; nearly identical g values are assumed for the two ions. In order to define the representation in which the total spin $\boldsymbol{S} = \boldsymbol{S}(1) + \boldsymbol{S}(2)$ is diagonal, we split H into two terms which are symmetric and antisymmetric with respect to the interchange of the electronic spin indices on the two radicals:

$$[4] \quad H_0 = \left[g\beta \boldsymbol{B} + \tfrac{1}{2}\sum_i a(i)\boldsymbol{I}(i) \right][\boldsymbol{S}(1) + \boldsymbol{S}(2)]$$
$$H_1 = \tfrac{1}{2}[a(1)\boldsymbol{I}(1) - a(2)\boldsymbol{I}(2)][\boldsymbol{S}(1) - \boldsymbol{S}(2)]$$

The symmetric part H_0 defines the representation in which the total electronic spin $\boldsymbol{S}$ of the ion pair is diagonal. The basis eigenvectors are written as the direct products $|SM_s; n\rangle$ of electronic and nuclear spin eigenvectors: the former (SM_s) in-

clude the singlet S_0 and the triplet (T_0, T_{+1}, T_{-1}) eigenstates of $\boldsymbol{S}$; the nuclear spin states $|n\rangle$ are products of the eigenstates of $\boldsymbol{I}(1)$ and $\boldsymbol{I}(2)$: $|n\rangle = |I(1), M(1); I(2)M(2)\rangle$; their total number is $N = [2I(1) + 1][2I(2) + 1]$. The corresponding energy spectrum is (*cf.* Fig. 4)

$$E(S_0, n) = E(T_0, n) = 0$$

$$[5] \qquad E(T_\pm, n) = \pm \left[g\beta \boldsymbol{B} + \tfrac{1}{2} \sum_i a(i)M(i) \right]$$

The antisymmetric operator H_1 has only non-diagonal matrix elements, which couple the different $\boldsymbol{S}$ levels. For each nuclear $|n\rangle$ the two degenerate $|S_0 n\rangle$ and $|T_0 n\rangle$ states are hence submitted to resonance interaction, which gives rise to coherent oscillations between these $M = 0$ states (*cf.* Fig. 4), with a characteristic frequency

$$[6] \qquad \Omega_n = \langle T_0 n|H_1|S_0 n\rangle = \tfrac{1}{2}[a(1)M(1) - a(2)M(2)]$$

Damping is introduced by the spin-flip transitions between the ($M = 0$, n) states and the non-isoenergetic ($T_\pm$, $n \mp 1$) levels; these transitions are made possible by spin–lattice relaxation and are all assumed to have equal rate constants Γ.

Under these conditions the spin density matrix element $\langle S_0 n|\rho(t)|S_0 n\rangle$ representing the population of the $|S_0 n\rangle$ levels is given by (8)

$$\rho_s^{(n)}(t) = \langle S_0 n|\rho(t)|S_0 n\rangle$$

$$[7] \qquad \rho_s^{(n)}(t) = \frac{1}{2N} \cos(2\Omega_n t) \exp(-2\Gamma t) + \frac{1}{4N}[1 + \exp(-4\Gamma t)]$$

if one assumes that initially only the $|S_0 n\rangle$ states are formed with equal populations of the N possible nuclear states: $\rho_s^{(n)}(0) = N^{-1}$. From this, the quantity $\rho_s(t)$ which is the total population of the S_0 states, $\rho_s(t) = \sum_n \rho_s^{(n)}(t)$, is obtained as

$$[8] \qquad \rho_s^{B}(t) = \frac{1}{2N} \sum_n^N \cos(2\Omega_n t) \exp(-2\Gamma t) + \tfrac{1}{4}[1 + \exp(-4\Gamma t)]$$

The field dependence is due to the relaxation rates Γ which must be related to the experimental parameter k of [1]. For $B = 0$, this constant is maximum and equilibrium is attained after relaxation times ≤ 10 ns; under the present experimental conditions, we can hence take $\rho_s^0(t) = \frac{1}{4}$, so that one gets the expression

$$[9] \qquad \frac{\rho_s^B(t) - \rho_s^0(t)}{\rho_s^0(t)} = \frac{2}{N} \sum_n^N \cos(2\Omega_n t) \times \exp(-2\Gamma t) + \exp(-4\Gamma t)$$

which describes the principal features of the experimental data for $\Delta I/I$.

In Fig. 2*a*, the above-mentioned damped oscillatory part exhibited by the curves for the 2b PPD solutions is interpreted by the first term in expression [9]: a periodic behavior clearly appears, with a frequency of 8 MHz, which is indeed of the order of the isotropic hyperfine interaction in organic radicals (14) as expected from [6]. Periodicity requires that the various Ω_n values in [9] are multiples of a common frequency which implies following [6] that the hyperfine coupling constants $a(1)$ and $a(2)$ on the positive and negative ions are not too different. Also the spectrum of the sets of equivalent nuclei should be as simple as possible: this appears to be the case for 2b PPD where the two equivalent nitrogen nuclei form a single set which may be suspected to dominate hyperfine structure; in PPO, one of the nitrogen nuclei is replaced by a C—H group leading to a more complicated hyperfine structure spectrum, so that the time interference effects should be difficult to observe, in accord with the experiments (Fig. 2*a*).

The other monotonic decreasing component of $\Delta I/I$ in Fig. 2*a* is described by the second exponentially decaying term of expression [9]. The experimental quantities k of [1] are given by 4 Γ, with (8)

$$[1'] \qquad \Gamma = \Gamma' + \Gamma''(B, C_s)$$

i.e., two different contributions to spin–lattice relaxation. The first term Γ' is due to the rotational fluctuations of anisotropic magnetic interactions within the two radicals, and may be

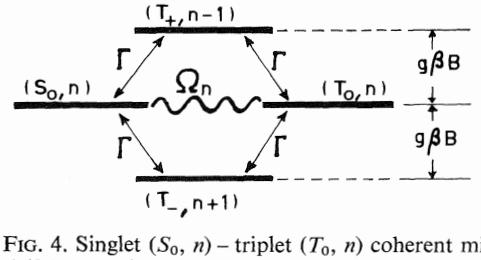

FIG. 4. Singlet (S_0, n) – triplet (T_0, n) coherent mixing and ($M_s = 0$, n) $\leftrightarrow$ ($M_s = \pm 1$, $n \mp 1$) states relaxation scheme for a radical ion pair in a magnetic field B (Ω_n frequency of the oscillations, Γ relaxation rate).

expected to be of the order of the $(T_1)^{-1}$ constants for the isolated radicals; indeed a value near 10^6 s^{-1}, in agreement with T_1 for organic radicals (15), is found in liquid solutions in the high field case (*cf.* Fig. 3). The second relaxation mechanism is attributed to time modulations of the isotropic hyperfine interactions by electron transfer from the radical ions to neutral solute molecules encountered during diffusion in the liquid (16). The field and solute concentration dependence of the corresponding rate constant Γ'' is justified with the help of the general expression (17, 18) $\Gamma'' = \alpha\langle\delta\omega\rangle^2 J(\Delta\omega)$, where $\langle\delta\omega\rangle$ is the interaction energy matrix element and $\Delta\omega$ the transition energy which according to [5] increases linearly with B; $J(\Delta\omega)$ represents the power spectrum of the fluctuating perturbation with correlation time τ_c: $J(\Delta\omega) = 2\tau_c/[1 + (\Delta\omega \cdot \tau_c)^2]$ decreases for increasing B in the 10^2 G range provided $\tau_c \approx 1$ ns, which is reasonable for intermolecular electron transfer (14). Finally α is the fraction of time during which the perturbation is operative: in terms of the mean times during (τ_1) and between (τ_2) the radical–neutral molecule encounters, α is of the form $\alpha = \tau_1/(\tau_1 + \tau_2)$ or, since τ_2 is proportional to ${C_s}^{-1}$, $\alpha = \tau_1\eta C_s/(1 + \tau_1\eta C_s)$ with $\tau_2 = (\eta C_s)^{-1}$, which shows that Γ'' increases with C_s. With data from Fig. 3 one can verify that $1/\Gamma''$ increases linearly with $1/C_s$ as predicted. In the solid solutions, no diffusion of radicals takes place so that only the field and concentration independent part Γ' may be important, which again agrees with experimental observations in Fig. 2*b*.[2]

As a concluding remark, we may note that the present experimental approach is particularly useful to focus attention on time development in spin subspace, independently from the kinetics of recombination luminescence itself, which has been considered elsewhere (11, 19).

1. R. KAPTEIN. J. Am. Chem. Soc. **94**, 6251 (1972).
2. J. H. FREED. Annu. Rev. Phys. Chem. **23**, 265 (1972).

[2]The authors are indebted to F. Heisel for the preparation of polystyrene solutions and to H. Gress for his technical assistance.

3. B. BROCKLEHURST. Chem. Phys. Lett. **28**, 357 (1974).
4. B. BROCKLEHURST, R. S. DIXON, E. M. GARDY, V. J. LOPATA, M. J. QUINN, A. SINGH, and F. P. SARGENT. Chem. Phys. Lett. **28**, 361 (1974).
5. R. S. DIXON, E. M. GARDY, V. J. LOPATA, and F. P. SARGENT. Chem. Phys. Lett. **30**, 463 (1975).
6. B. HABERKORN and M. E. MICHEL-BEYERLE. Z. Naturforsch. **31**a, 499 (1976).
7. K. SCHULTEN, H. STAERK, A. WELLER, H. J. WERNER, and B. NICKEL. Z. Phys. Chem. NF, **29**, 277 (1961).
8. J. KLEIN and R. VOLTZ. Phys. Rev. Lett. **36**, 1214 (1976).
9. R. P. GROFF, A. SUNA, P. AVAKIAN, and R. E. MERRIFIELD. Phys. Rev. B, **9**, 2655 (1974).
10. P. AVAKIAN. XIth European Congress on Molecular Spectroscopy, Tallinn, Estonia, USSR. 1973.
11. D. PALIGORIC and J. KLEIN. Int. J. Rad. Phys. Chem. **4**, 399 (1972); **7**, 731 (1975).
12. J. A. MIEHE, G. AMBARD, J. ZAMPACH, and A. COCHE. IEEE Trans. Nucl. Sci. **17**, 115 (1970).
13. R. VOLTZ. Actions chimiques et biologiques des radiations. Series 13. *Edited by* M. Haïssinsky. Masson, Paris. 1969. p. 1.
14. P. B. AYSCOUGH. Electron spin resonance in chemistry. Methuen & Co, London. 1968.
15. N. M. ATHERTON. Electron spin resonance. John Wiley, New York. 1973. Chapt. 8.
16. S. I. WEISSMAN. Z. Elektrochem. **64**, 47 (1960).
17. A. ABRAGAM. The principles of nuclear magnetism. Oxford University Press, London. 1961. Chapt. 8.
18. W. HAPPER. Rev. Mod. Phys. **44**, 169 (1972).
19. F. KIEFFER, C. LAPERSONNE-MEYER, and J. KLEIN. Chem. Phys. Lett. **40**, 492 (1976).

Discussion

R. S. Dixon: I want to point out that, in his calculations of ρ_s, the probability of forming a singlet state, Brocklehurst predicted a coherent oscillation of the overall wavefunction between singlet and triplet, which might be seen in some simple systems. In our system, the large number of protons on M^+ and M^- would smear out the oscillation effect. We concluded that relaxation was unimportant because it occurred on a longer time scale (μs) than that over which we observed the field effect (ns). Your work implies that relaxation is important on a nanosecond time scale. Is this the case?

J. Klein: Yes that is the case, but only in liquid solutions where, besides the usual spin–lattice relaxation processes (T_1) you have an additional relaxation process which we attributed to diffusion controlled electron transfer between ions and neutral solute molecules.

Field-assisted photo-stimulated charge transfer across photoconductor–dielectric liquid interfaces

C. C. YANG AND J. NOOLANDI

Xerox Research Centre of Canada Limited, 2480 Dunwin Drive, Mississauga, Ont., Canada L5L 1J9

Received October 25, 1976

C. C. YANG and J. NOOLANDI. Can. J. Chem. **55**, 2107 (1977).

Field-assisted photo-stimulated charge transfer across a photoconductor–dielectric liquid interface has been studied by a high sensitivity signal averaging transient measurement technique. The effects of both the temperature and electric field (below 2×10^5 V/cm) have been investigated. Experimental results were analyzed using an interface model developed earlier to describe the charge transfer kinetics. We have found evidence of direct and indirect transfer of charge across the interface and we have identified the controlling parameters for the desorption rate of charge carriers from the interface into the fluid.

C. C. YANG et J. NOOLANDI. Can. J. Chem. **55**, 2107 (1977).

On a étudié le transfert de charge photostimulé et assisté par le champ à travers l'interface entre un photoconducteur et une liquide diélectrique en faisant appel à une technique de grande sensibilité mesurant les phénomènes transitoires par une methode qui établit la moyenne des signaux. On a étudié les effets de la température ainsi que du champ électrique (en bas de 2×10^5 V/cm). On a analysé les résultats expérimentaux en faisant appel à un modèle d'interface qui a été développé antérieurement pour décrire la cinétique de transfert de charge. On a trouvé des preuves de transferts de charges directs et indirects à travers l'interface et on a identifié des paramètres qui contrôlent la vitesse de désorption des transporteurs de charges allant de l'interface vers le fluide.

[Traduit par le journal]

Introduction

The phenomenon of photo-assisted charge transfer across a photoconductor–dielectric liquid interface has been studied in this experiment. Evidence of charge transfer from a photoconductor into nonpurified dielectric liquids has been reported earlier (1) for high electric fields, and a phenomenological model was developed to describe this process. The experimentally observed transient current pulse was found to depend primarily on two important parameters; the release rate of charge from surface traps on the photoconductor into the lowest vacant state of a neutral impurity molecule adsorbed on the surface, and the desorption rate of the ions from the interface into the liquid. The electric field dependence of the two rates was examined previously for the range 2×10^5 to 10^6 V/cm. Here we investigated the validity of the charge-transfer model further by measuring the thermal activation energies of the rates, and by extending the measurements to lower electric fields (10^4–10^5 V/cm).

Experimental Approach and Charge Transfer Model

We used a typical capacitor cell arrangement for our experiment. The electrodes were SnO_2 coated glass, overcoated with a thin film of SiO (thickness 1000 Å) to prevent charge injection directly from the electrodes. Metal-free phthalocyanine was vacuum deposited (thickness 1300 Å) onto one of the SiO coated electrodes. The photoconductor was separated from the other electrode by a Teflon spacer, forming a cell which was filled with practical grade decane. The liquid was obtained directly from the supplier's container and was not further purified. The thickness of the liquid was 120 μm and the electrode area was 1 cm^2.

A Xenon flash lamp (3 μs duration), in conjunction with a band-pass filter (400–800 nm), was used to illuminate the cell. The photogenerated current pulse moved through the photoconductor layer in about 10^{-9} s (2), which was shorter than the response time of our instruments (2 μs). The charge then transferred into the liquid. The current in the liquid increased as the charge carriers desorbed from the photoconductor surface, and decreased as carriers began arriving at the other electrode. The peak of the current trace, shown in Fig. 1, corresponds to the average transient time τ for carriers to move through the liquid. A typical

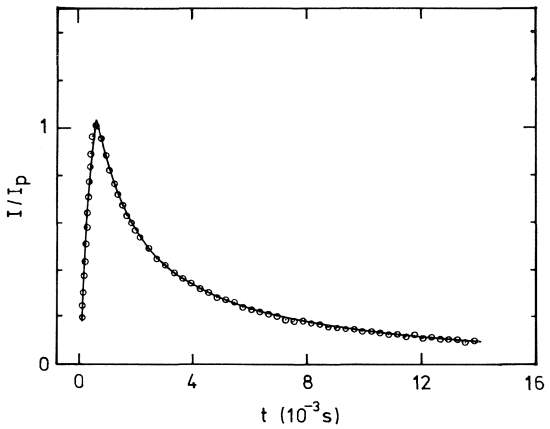

FIG. 1. The least squares fit (solid line) of the single surface trap interface model to a typical transient current pulse (circles) for negative charge transfer from phthalocyanine into decane. The current is normalized by the peak current I_p at $t = \tau$.

value of τ was 10^{-3} s. In terms of the drift mobility μ of the charge carrier, we have

$$[1] \qquad \tau = d/\mu E$$

where d is the fluid thickness and E is the electric field in the liquid. The magnitude of the carrier mobility as determined from [1] was of the order of 10^{-4} cm^2 V^{-1} s^{-1}, indicating that the carriers were ions (3).

As mentioned earlier, we restricted ourselves to the low field region between 4×10^4 and 2×10^5 V/cm. The signal in this field range was always below the noise level and the conventional single transient measurement technique was found to be inadequate for this case. We circumvented this problem by using a signal averaging technique. Each of our data points represents the average of a few hundred to a few thousand current traces taken at the same temperature and field. By using this technique, the signal-to-noise ratio is improved by a factor $\sqrt{n}$, where n is the number of current traces averaged. As a check, the average transit time obtained by this technique was plotted as a function of $1/E$, and good agreement with [1] was found.

The temperature in the cell was monitored by a micro-temperature sensor embedded in the dielectric liquid. The temperature was varied from 0 to 100°C and was stabilized to better than ± 1°C. At 100°C the sublimed phthalocyanine started to separate from the glass substrate, and the data points obtained at this temperature have only a qualitative significance.

According to the phenomenological model, the transfer of charge from the photoconductor into the liquid requires the presence of an unoccupied state whose energy (relative to the vacuum level) lies below the conduction band energy of the photoconductor. This state can be conveniently supplied by the lowest vacant state of an impurity molecule adsorbed on the photoconductor surface. Direct transfer into the liquid is unlikely because the energy level of the extended electronic state is a fraction of a volt (4), and is well above the conduction band energy of the photoconductor (3.2 eV). As shown in Fig. 2, charge in the photoconductor can either transfer to a neutral molecule directly or via surface traps at a release rate r_2. In the process of desorbing from the photoconductor, the ionized impurity molecule must overcome the potential barrier resulting from the image potential and the applied electric field in the liquid, *i.e.*

$$[2] \quad U(x) = -\frac{\alpha e}{x} - eEx \qquad \text{for } x \geq a$$

where a has the dimension of the ion radius, e is the electronic charge, and $\alpha = (3/16\pi\varepsilon_f)(\varepsilon_p - \varepsilon_f)/(\varepsilon_p + \varepsilon_f)$, where ε_p and ε_f are the dielectric constants of the photoconductor and fluid, respectively. The position and magnitude of the potential barrier can be evaluated from [2] for different fields.

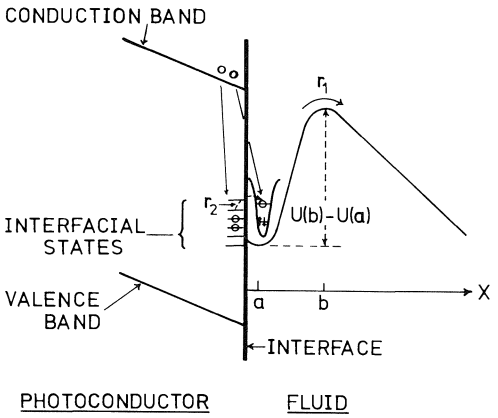

FIG. 2. Schematic of the kinetics of charge transfer from the photoconductor into the fluid. Energy levels of electrons are shown to the left of the interface and the potential well of the ionized impurity molecule in the fluid is shown to the right of the interface. r_1 is the desorption rate of ions from the interface into the liquid and r_2 is the release rate of charge from surface traps into the lowest unoccupied energy level of the molecule adsorbed onto the photoconductor surface.

The expression for the transient current pulse in the liquid has been shown to have the following form (1),

$$[3]\quad I(t) = \begin{cases} i(t) & t < \tau \\ i(t) - i(t-\tau) & t > \tau \end{cases}$$

where

$$[4]\quad i(t) = A[1 - \exp(-r_1 t)] + B[1 - \exp(-r_2 t)] + \frac{Br_2}{r_1 - r_2} \times [\exp(-r_1 t) - \exp(-r_2 t)]$$

Expressions for the constants A and B are given in ref. 1, and are not used in the present investigation. The desorption rate of carriers into the fluid is r_1, and r_2 is the release rate from surface traps. The functional dependence of r_1 on electric field and temperature is given by (1),

$$[5]\quad r_1 = CE^{3/4} \exp(-U_t/k_B T)$$

where C is a constant, k_B is Boltzmann's constant, and the total activation energy U_t consists of two parts; the potential barrier height $U(b) - U(a)$ (where $x = b$ corresponds to the potential maximum) and the ion mobility activation energy U_μ, *i.e.*,

$$[6]\quad U_t = U(b) - U(a) + U_\mu$$

The $E^{3/4}$ part of the prefactor in [5] arises from the change in the curvature at the maximum of the potential barrier as the field is varied.

The temperature and field dependence of the trap release rate r_2 have not been calculated because of lack of information about the physical nature of the surface traps.

Results and Discussion

The charge transfer model was checked by measuring the transient current as a function of the electric field and temperature, and comparing with [3]. The measured current traces were fitted to [3] by a nonlinear least squares computer routine. As mentioned earlier, each current trace used for comparison with the theory represented an average of many traces taken under identical conditions of electric field and temperature. Thus, the relative error of the data points depends primarily on the number of traces used for averaging, and is typically below 5% for most of our traces. The uncertainty in the temperature is less than $\pm 0.5\%$, and the uncertainty in the value of the electric field is $\pm 2\%$. Figure 1 shows an averaged current trace and the computer fit to [3]. It is evident that [3] describes the shape of the current pulse quite well.

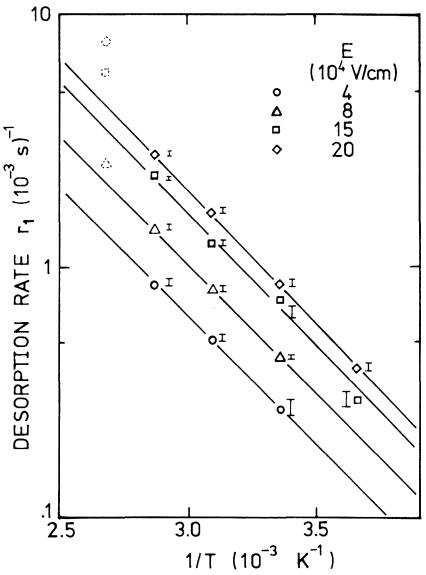

FIG. 3. Temperature dependence of the desorption rate r_1 for four different fields. The slopes at each field are almost identical and give a total activation energy of 0.21 ± 0.01 eV. Data points at 100°C are not very reliable because the photoconductor had partially separated from the substrate.

In Fig. 3 the logarithm of the desorption rate r_1 is plotted as an inverse function of temperature for four different electric fields. It should be noted that all data points for the same field lie on a straight line and the lines for the different fields are nearly parallel to one another. This implies that the desorption process of charge carriers is thermally activated, as described by the Boltzmann factor in [5], and the activation energy U_t is not very sensitive to the electric field for the low field range. The rate r_1 is shown in Fig. 4 as a function of the electric field. The data points for the different temperatures all follow the power law $E^{3/4}$ which is shown by the solid lines. This again indicates that the contribution to the field dependence of r_1 from the exponent in [5] is negligible. The experimental value of U_t, as deduced from the slope of the straight lines in Fig. 3, is 0.21 ± 0.01 eV. U_μ can be obtained from the temperature dependence of the charge carrier mobility, shown in Fig. 5. The slope of this line gives an activation energy of 0.17 ± 0.01 eV. The potential barrier height, $U(b) - U(a)$, is thus determined to be 0.04 ± 0.02 eV, with no measured field depen-

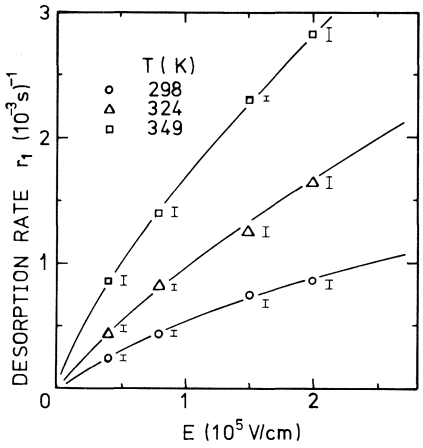

FIG. 4. Electric field dependence of the desorption rate r_1 for three different temperatures. The solid line is a fit to the theoretical expression given by [5].

dence. The value of $U(b)$ estimated from [2] for $E = 2 \times 10^5$ V/cm is about -0.02 eV, which cannot be resolved in our experiment. The barrier height is probably dominated by the ion binding energy at the interface, $U(a)$.

The trap release rate r_2 is plotted as an inverse function of temperature in Fig. 6. As one would expect, the detrapping of charge increases with increasing temperature. Unfortunately, the data for r_2 cannot distinguish whether the charge is released from surface traps or from bulk traps

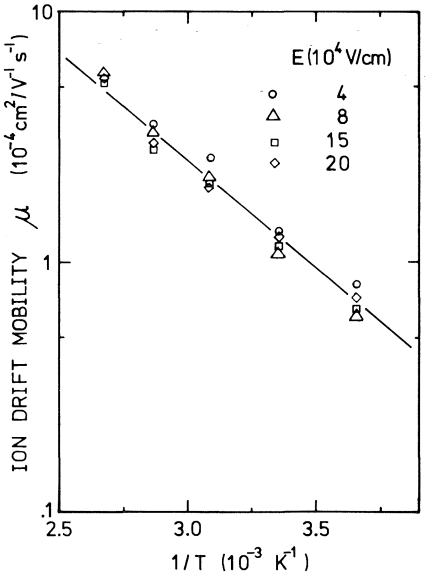

FIG. 5. Temperature dependence of ion mobility for four different fields. The mobility activation energy obtained from the slope is 0.17 ± 0.01 eV.

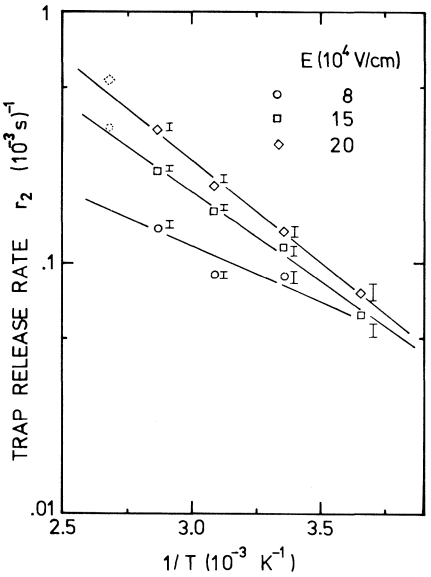

FIG. 6. Temperature dependence of the trap release rate r_2 for three different electric fields.

near the surface. However, we have observed that the charge transfer from different phthalocyanine thin films gives different values of r_2 for identical values of temperature and field. The reason for this variation could be that slightly different film evaporation conditions may result in different surface morphology and different surface states. A more precise control on the vacuum deposition conditions is required to study this effect. For consistency, all measurements presented here were performed on one sample. The field dependence of r_2 shown in Fig. 6 cannot be interpreted at this time because of insufficient knowledge about the physical nature of the traps.

Finally, the effective radius of the charge carrier, a, was determined by two different methods. The value calculated from [2], using the value of $U(a)$ estimated earlier from the activation energy of r_1, is $a \simeq 8$ Å. The corresponding value from Stokes' law, $\mu = e/6\pi\eta a$, where μ is obtained from the transit time data and $\eta = 0.88$ cp for decane at 25°C is $a \simeq 7.4$ Å. The agreement between these two methods of determining a indicates that the small value of the binding energy at the interface is indeed due to the large effective radius of the charge carrier.

In conclusion, we summarize our findings as follows: the phenomenological model proposed earlier (1) gives a good description of the transfer

of photogenerated charge from a photoconductor into a dielectric fluid under an applied electric field. The charge carriers in the fluid are ions, as indicated by the small value of the observed mobility, and charge transfer requires the presence of an impurity molecule with its lowest vacant energy level lower than the conduction band energy of the photoconductor. Both the desorption r_1 of ions from the interface and the release rate r_2 from surface traps are thermally activated. The rate r_1 has a power law field dependence which arises from the effect of the applied field on the curvature of the image potential barrier near its maximum. The variation of the height of the potential barrier with field is very small and is not observed for the low field range investigated. The origin of the field dependence of r_2 is not understood at present. An investigation of the effect of various impurity molecules on the charge transfer is presently in progress.

Acknowledgements

We would like to thank L. M. Marks for assistance with the computer work on the data reduction, and Drs. G. C. Hartmann and P. Cheng for valuable discussions and suggestions.

1. G. C. HARTMANN and J. NOOLANDI. J. Chem. Phys. To be published.
2. G. A. COX and P. C. KNIGHT. Phys. Status Solidi B, **50**, K135 (1972); Y. AOYAGI, K. MASUDA, and S. NAMBA. J. Phys. Soc. Jpn. **31**, 164 (1971); D. R. KEARNS, G. TOLLIN, and M. CALVIN. J. Chem. Phys. **32**, 1020 (1960).
3. I. ADAMCZEWSKI. Ionization, conductivity, and breakdown in dielectric liquids. Barness and Nobel, New York, NY. 1969.
4. R. A. HOLROYD and R. L. RUSSELL. J. Phys. Chem. **78**, 2128 (1974).

Discussion

A. C. Albrecht: We very much appreciate the nice analysis you have presented for the transfer of charge at a semiconductor–fluid interface. We have studied this very system with chlorophyll acting as the semiconducting film and see both the fast and the slow signal. Your model should be very useful in analyzing these results too. An interesting qualitative effect we have seen is that as we add chlorophyll monomer to the fluid phase the slow signal is greatly enhanced. Chlorophyll seems to mediate the discharge at the interface. The actual charge carrier in the fluid phase, though, is very likely a smaller molecule according to mobility estimates.

J. Noolandi: We would be very interested in applying the analysis to your experiment.

Electron reactivity as a function of phase

A. HENGLEIN

Hahn-Meitner-Institut für Kernforschung Berlin GmbH, Bereich Strahlenchemie, D 1000 Berlin 39, Germany

Received September 27, 1976

A. HENGLEIN. Can. J. Chem. **55**, 2112 (1977).

Reactions of free electrons in the gas phase, of quasi-free electrons and solvated electrons in dielectric liquids, of hydrated electrons in water, and of electrons originating from an electrode in contact with a solution are among the great variety of electronic processes in chemistry. It is the purpose of this paper to describe a few phase effects. Reactions of electrons in dielectric liquids will be discussed with respect to the corresponding processes in the gas phase. Furthermore, certain aspects in the transfer of an electron from a hydrocarbon phase into the aqueous phase will be dealt with. The processes will be described in terms of electronic redox level distributions of the acceptor redox systems.

A. HENGLEIN. Can. J. Chem. **55**, 2112 (1977).

Les réactions d'électrons libres en phase gazeuse, d'électrons pratiquement libres et d'électrons solvatés dans des liquides diélectriques, d'électrons hydratés dans l'eau et d'électrons ayant leur origine dans une électrode en contact avec une solution sont parmi la grande variété des processus électroniques de la chimie. Le but de ce travail est de décrire quelques effets de phases: on discutera des réactions des électrons dans des liquides diélectriques par rapport aux processus correspondants en phase gazeuse. De plus on examinera certains aspects du transfert d'un électron d'une phase hydrocarbonée à une phase aqueuse. On décrira les processus en termes des distributions des niveaux redox-électroniques des systèmes redox-accepteurs.

[Traduit par le journal]

I. Abnormal Kinetic Phenomena in the Reactions of Electrons in Dielectric Liquids

Excess electrons in dielectric liquids are very mobile and often react with dissolved substances with rate constants as high as 10^{12} to 10^{15} M^{-1} s^{-1}. However, unlike normal fast reactions their rate constants often do not bear a simple relationship to the diffusion characteristics of the reactants. This may be recognized from Figs. 1 and 2 which show the dependence of the bimolecular rate constant k on various variables such as the energy V_0 (energy of the delocalized electron in a solvent with respect to an electron in the gas phase), the nature of the acceptor molecule, the electron mobility, and the strength of a strong electric field across the solution.

Figure 1 shows how k varies with V_0 if the reaction of an acceptor molecule is studied in different solvents. V_0 is known to span the range from -0.6 to $+0.1$ eV for most of the dielectric liquids at room temperature. The mobility μ of the excess electron varies over several orders of magnitude in these solvents as can be seen from the upper abscissa in Fig. 1. In *n*-hexane which has a high V_0 value all acceptor molecules with the exception of molecular oxygen react with rate constants of the order of 10^{12} M^{-1} s^{-1}. For oxygen k is only 9.1×10^{10} M^{-1} s^{-1} at room temperature. In tetramethylsilane which has a low V_0 value some acceptors such as sulphur hexafluoride and carbon tetrachloride react extremely rapidly ($k \sim 10^{14}$ M^{-1} s^{-1}) while others such as nitrous oxide and ethyl bromide react even slower than in *n*-hexane. The two latter acceptors react fastest in solvents of intermediate V_0. Oxygen is a relatively poor acceptor in all these solvents (1)[1].

The activation energy of reaction has also been determined from the temperature dependence of the rate constant in various solvents. In *n*-hexane, many acceptors react with a positive activation energy (3). It amounts to 3.49 kcal mol^{-1} in the case of good acceptors, a value close to the activation energy of the mobility of the electron in *n*-hexane (4.30 kcal mol^{-1}). The reaction $e^- + O_2 \rightarrow O_2^-$, however, has a smaller activation energy of 2.29 kcal mol^{-1}, although this reaction is slower than those of the other acceptor molecules. In the case of the solvent 2,2,4-trimethylpentane, the activation energy can be positive (SF_6), almost zero (N_2O), or even switch from a positive value at low temperatures to a negative one at higher temperatures (C_2H_5Br) (1). In the case of tetramethylsilane, the reactions of N_2O and ethyl bromide occur

[1]R. A. Holroyd. Private communication.

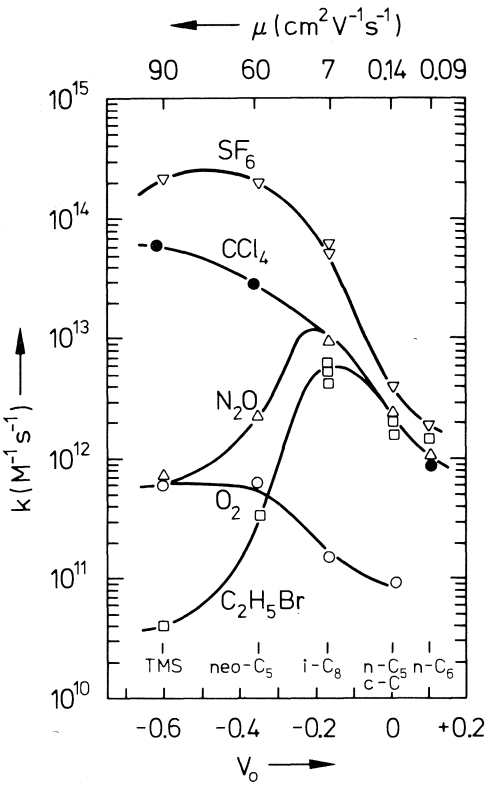

FIG. 1. Rate constants of the reactions of the electron with various acceptors in solvents of different V_0 at room temperature. Upper scale: mobility of the electron (experimental results from Allen *et al.* (1) and R. A. Holroyd, private communication. Reprinted with permission from the Journal of Physical Chemistry **79**, 25 (1975). Copyright by the American Chemical Society.

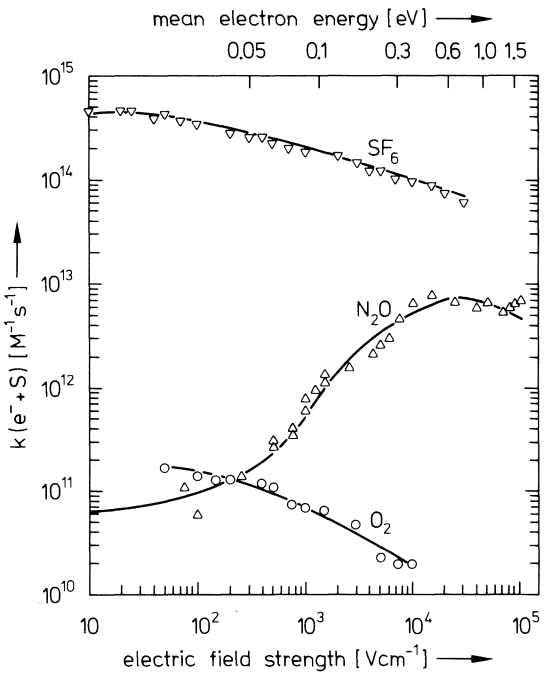

FIG. 2. Rate constants of electron–solute reactions in liquid xenon as a function of the electric field strength. Upper scale: mean electron energy (experimental results from Bakale *et al.* (4)). Reprinted with permission from the Journal of Physical Chemistry **80**, 2556 (1976). Copyright by the American Chemical Society.

with small negative activation energies, the reactions of oxygen and carbon tetrachloride with small positive activation energies (1). Figure 2 shows the dependence of the rate constant for various acceptors in liquid xenon as a function of the strength of a superimposed electric field. The mean kinetic energy with which excess electrons move under the influence of the electric field is given at the top of the figure. While the rate constant decreases for SF_6 and O_2 with increasing electron energy, that for N_2O goes through a maximum at about 0.6 eV of the mean kinetic energy (4).

II. Concepts from Ordinary Reaction Kinetics

The effects described above can be qualitatively explained by combining the concepts of ordinary reaction kinetics with data from electron impact on gas molecules and with concepts from the theories of electron transfer (7). A normal chemical reaction is said to be diffusion-controlled if the encounter time τ_e during which the two reactants are kept close together in the cage of the surrounding solvent molecules is longer than the time τ_r required for the reaction to occur after the reactants had come into this close contact. The bimolecular rate constant is given by the expression

$$[1] \quad k_d = \frac{4\pi N \Delta R}{10^3} M^{-1}\,s^{-1} \quad \text{for } \tau_e \gg \tau_r$$

where Δ is the total diffusion coefficient, R the collision diameter of the reactants, and $N = 6.02 \times 10^{23}$; τ_r may be expressed in terms of a frequency factor γ_r and a chemical activation energy E_r:

$$[2] \quad \tau_r = \frac{\exp(E_r/kT)}{\gamma_r}$$

τ_e may be written as

$$[3] \quad \tau_e \sim \tfrac{1}{2} R^2/\Delta$$

The activation energy of a diffusion-controlled reaction is given by that of the diffusion coefficient Δ.

On the other hand, if $\tau_e < \tau_r$, the probability p of the reaction per encounter is lower than unity and the bimolecular rate constant may now be expressed as

$$[4] \qquad k = k_d p$$

Putting p equal to τ_e/τ_r (for $\tau_e \ll \tau_r$) one obtains from [1], [2], and [4]

$$[5] \qquad k \propto \gamma_r \exp(-E_r/kT)$$

The measured activation energy of the reaction is now equal to the chemical activation energy E_r and the rate constant is independent of the rate of diffusion. In the case of the reaction of an electron, the movement of the acceptor molecule may be neglected and Δ is practically equal to the diffusion coefficient Δ_{el} of the electron

$$[6] \qquad \Delta_{el} = \mu kT/e$$

where μ is its mobility and e the amount of its charge. If the expression

$$[7] \qquad \mu = \mu_0 \exp(-E_\mu/kT)$$

describes the temperature dependence of the mobility of the electron, the rate constant of a diffusion-controlled reaction should be proportional to $T \exp(-E_\mu/kT)$. The measured activation energy of a diffusion-controlled reaction should therefore be slightly higher than E_μ, provided that R is not dependent on the temperature. The interaction radius R may be as large as the de Broglie wavelength λ of the electron. In a strong electric field the mean velocity $\bar{v}$ of the electron increases with field strength F and the interaction radius R may be expected to decrease. In liquid xenon, for example, $\bar{v}$ is proportional to $F^{0.32}$ and R should be proportional to $F^{-0.32}$ (5).

The time which an electron spends close to an acceptor molecule will become shorter with increasing mobility of the electron. We may thus talk in terms of an encounter time τ_e for reactions of electrons, although this concept which is based on a random-walk type of motion is very approximate for solvents of high electron mobility. Recent measurements of the rate constants for electron capture by sulphur hexafluoride in liquid rare gases indicate that R is close to $\lambda = \hbar/m\bar{v}$ (5, 6). The diffusion coefficient of the electron at room temperature amounts to 2.3×10^{-3} cm^2 s^{-1} in *n*-hexane and 2.3 cm^2 s^{-1} in tetramethylsilane. If R is of the order of 10^{-7} cm, the respective encounter times of [3] are of the order of 10^{-10} s (*n*-hexane), and 10^{-13} s (TMS). The rate constant k_d for diffusion-controlled processes in these solvents is of the order of 10^{12} M^{-1} s^{-1} (*n*-hexane) and 10^{15} M^{-1} s^{-1} (TMS) as calculated from [1]. The highest k values which have been measured in these solvents are indeed of this magnitude and the activation energies for such rapid reactions agree fairly well with those for the electron mobility (1, 3). τ_r is regarded as the time required for the acceptor molecule to reach a certain atomic configuration (including the solvation shell) at which the electron can be accepted.[2] In molecular photochemistry, Franck–Condon transitions to a higher electronic state of a molecule are associated with various transition energies depending on the actual interatomic distances in the molecule at the moment of light absorption. Similarly, the capture of an electron by a molecule can occur with a distribution of transition energies.

III. Concepts from Electron Impact in the Gas Phase and Electron Transfer Theories

Electron transfer reactions generally have a free energy of activation which is not zero even if the free energy of the reaction is negative. The activation of the reacting system has to occur in order to bring the reactants into the appropriate molecular configuration (including the solvation shells of the reactants). In this configuration, the energy of the system before the electron jumps is equal to that after the jump and the products are finally deactivated to their states of lowest energy. The theories of Marcus (8) and Levich (9) describe the properties of the activated states in electron transfer reactions in solution. We shall make use of the simpler treatment of Gurney (10) and Gerischer (11) in which the distributions of the electronic redox levels of the two redox systems involved in a transfer reaction are compared with each other. Although this treatment does not describe electron transfer reactions in the most exact manner, it readily leads to a semiquantitative explanation of the observed reaction rates. The density of states functions of the activated complexes are simply

[2]Since τ_r can hardly be shorter than 10^{-13} s, *i.e.* the encounter time in tetramethylsilane, the above-mentioned k_d value of 10^{15} M^{-1} s^{-1} for this solvent represents a general upper limit for the rate constant of reaction of e^- in solution (at room temperature).

substituted by those of the separated reactants (*i.e.* extremely weak interaction is assumed) and electron transfer is postulated to occur only from occupied electronic redox levels of the donor system to unoccupied ones of the acceptor system of equal energy. Such transitions are represented by vertical transitions between the potential curves of the systems $A + e^-$ and A^-.

Vertical transitions in reactions of electrons in dielectric liquids with solutes have been postulated in earlier papers (1, 7, 12). It is an intriguing feature of such considerations that reactions of electrons with molecules in the gas phase, where the kinetic energy of the electrons can be varied, may be compared with the reactions in dielectric solvents, where the total energy of the electrons can be varied by choosing solvents of different energy V_0 or by heating up the electrons in an electric field.

The energy of the electron in a liquid is characterized by the energy V_0 if the reaction of a delocalized electron is to be considered. We shall assume in the following treatment that the electron is in the V_0 level at the moment of reaction. This assumption is probably fulfilled in the case of liquids of high electron mobility where the electron spends most of its time in the delocalized state. It should, however, not be excluded that trapped electrons may also be able to react with a solute molecule before they are thermally released into the V_0 level. This may occur in liquids of low mobility in which the electron spends most of its time in the trap and where its optical absorption has even been observed (13, 14). Reactions of a localized electron may occur via tunneling to the acceptor molecule. The energy levels which are occupied by localized electrons lie below the level V_0. Trap depths of the order of 0.4–0.5 eV have recently been reported (15).

As the energy V_0 refers to that of an electron in the gas phase, one has to choose the same reference point for the energy ε with which the electron is bound in the acceptor molecule. ε is the energy which is liberated in the theoretical process $e^-(g) + A(s) \rightarrow A^-(s)$ where $e^-(g)$ is an electron in the gas phase and A(s) the acceptor molecule in solution. This energy liberated must be equal to V_0, if the reaction $e^-(s) + A(s) \rightarrow A^-(s)$ of an electron $e^-(s)$ in solution occurs as a vertical transition. Let us study the following cycle of processes in which all species are meant to be in their lowest state of internal energy:

$$[8] \qquad A(s) \rightarrow A(g) \quad -\Delta H_s(A)$$

$$[9] \qquad e^-(g) + A(g) \rightarrow A^-(g) \quad -EA(A)$$

$$[10] \qquad A^-(g) \rightarrow A^-(s) \quad \Delta H_s(A^-)$$

$$[11] \qquad e^-(g) + A(s) \rightarrow A^-(s)$$

$$\varepsilon_0 = -EA(A) + \Delta H_s(A^-) - \Delta H_s(A)$$

ΔH_s denotes the energy of solvation and EA the gas phase electron affinity. ε_0 is the energy liberated if all species are in thermodynamic equilibrium with their surroundings. $\varepsilon_0 - V_0$ is the energy of reaction ΔH_r of an electron in the V_0 level with an acceptor in solution.

In a vertical transition $e^-(g) + A(s) \rightarrow A^-(s)$, however, the anion $A^-(s)$ is generally not formed in its lowest state of internal energy but with a certain amount of excess energy. This excess energy has a distribution and consequently the transition energy ε has a distribution too. It will peak at some energy above ε_0. This distribution of transition energies may be called the density of unoccupied electronic levels $D_{unocc}(\varepsilon)$ of the redox system $A(s)/A^-(s)$.

The spontaneous ejection of an electron from the anion A^- into the V_0 level of the liquid may now be considered. If the electron is not to change its energy during the process, the energy for removal of the electron into the gas phase according to the theoretical process

$$[12] \qquad A^-(s) \rightarrow A(s) + e^-(g)$$

must be equal to $-V_0$. The energy for removal of the electron is equal to $-\varepsilon_0$ (eq. 11), if all particles are considered in their lowest states of internal energy (including their solvation shells), *i.e.* if the process occurs adiabatically. However, in a vertical transition, the product A(s) will generally be formed with excess energy. The energy for the removal of the electron into the gas phase will thus be larger than $-\varepsilon_0$. We may expect a distribution of energies for removal of the electron. The corresponding energies ε characterize the occupied electronic levels of the redox system $A(s)/A^-(s)$ and their distribution function may be designated $D_{occ}(\varepsilon)$. It will peak below ε_0.

The energies where the maxima of the functions D_{unocc} and D_{occ} are located differ more from ε_0 the more the atomic structures of A and A^- and their solvation shells differ from each other. In nonpolar solvents, solvation is mainly

due to electronic polarization of solvent molecules which is little dependent on their orientation. The width of the distribution functions will therefore mainly be determined by the changes in the equilibrium distances of the atoms in A and A^-.

Our model is the most simple-minded one: the solvent is regarded as a homogeneous dielectric medium. All processes are excluded in which part of the energy of reaction is channeled into internal degrees of freedom of the solvent. Furthermore, the effect of nuclear tunneling discussed in the theory of electron transfer (8) is disregarded. These processes, however, may play an important role in slow reactions of electrons, *i.e.* in reactions where the density of unoccupied levels of the acceptor system at the energy V_0 is low.

IV. Simple Acceptor Molecules

Potential functions of simple acceptor molecules such as N_2O, C_2H_5Br, CCl_4, and O_2 have been published in the literature (16–19). They are shown in the diagrams of Fig. 3. Consider diagram (*b*) for carbon tetrachloride: The curve for the system $CCl_4(s) + e^-(g)$ was obtained by shifting that for the system $CCl_4(g) + e^-(g)$ by the small amount of the solvation energy of carbon tetrachloride. Similarly, the curve for $CCl_4^-(g)$ was shifted downwards by the larger amount of the solvation energy of the anion to obtain the curve for $CCl_4^-(s)$. The upward pointing arrow indicates the most probable transition $e^-(g) + CCl_4(g) \rightarrow CCl_4^-(g)$ which requires an electron energy of 0.3 eV. Transitions with smaller and much higher energies are also possible in the Franck–Condon range. CCl_4^- immediately dissociates to form Cl^- whose ionization efficiency curve (cross section *vs.* electron energy) determined by mass spectrometry gives information about the spectrum of transition energies in the gas phase. The downward pointing arrow in Fig. 3*b* indicates the most probable transition of the theoretical process $e^-(g) + CCl_4(s) \rightarrow CCl_4^-(s)$. The energy ε of this transition differs from that of the corresponding gas phase process by $\Delta H_s(A^-) - \Delta H_s(A)$, provided that the anion is formed in its solvation state of lowest energy. In a vertical transition, this condition will generally not be fulfilled since the anion will be formed with the structure of the solvation shell of the neutral molecule. As mentioned before, this effect will

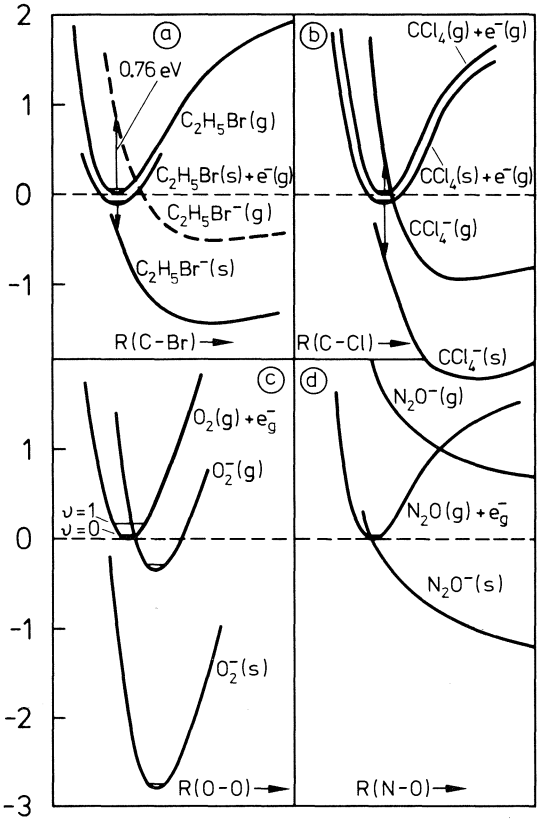

FIG. 3. Potential curves of various redox systems in the gas and liquid phase: (*a*) Christophorou *et al.* (16); (*b*, *d*) Wentworth *et al.* (17, 18); (*c*) Schultz (19).

not be too pronounced in dielectric liquids. We take this effect into account by adding only $0.8[\Delta H_s(A^-) - \Delta H_s(A)]$ to the transition energy in the gas phase to obtain that of the process $A(s) + e^-(g) \rightarrow A^-(s)$.

The problem lies in the calculation of the difference $\Delta H_s(A^-) - \Delta H_s(A)$. The free energy for charging a sphere of radius r with the elementary charge e in a medium of dielectric constant ϑ is (20)

$$[13] \qquad \Delta G_p = -\frac{e^2}{2r}\left(1 - \frac{1}{\vartheta}\right)$$

The free energy of solvation of an anion of radius r is then $\Delta G_p + \Delta G_s(A)$ where $\Delta G_s(A)$ is the free energy of solvation of the neutral molecule (21). The energy of polarization is

$$[14] \qquad \Delta H_p = -\frac{e^2}{2r}\left(1 - \frac{1}{\vartheta} - \frac{T}{\vartheta^2}\frac{d\vartheta}{dT}\right)$$

and the energy of solvation of an anion is

$\Delta H_p + \Delta H_s(A)$. The above-mentioned difference $\Delta H_s(A^-) - \Delta H_s(A)$ is therefore equal to ΔH_p.[3]

Since $d\vartheta/dT < 0$, $\Delta H_p < \Delta G_p$. ϑ has practically the same value for the various dielectric liquids, *i.e.* ΔG_p or ΔH_p can be regarded as independent of the nature of the solvent. The effective radius r is often calculated from the molar volume of the neutral molecule in its condensed state:

$$[15] \qquad \tfrac{4}{3}\pi r^3 = \frac{1}{N}\frac{M}{d}$$

where M = molecular weight, d = density of A (see, for example, ref. 23). This procedure yields reliable values of ΔG_p for large molecules. In the case of small molecules or molecules in which the charge is not uniformly distributed, too small amounts of the solvation energy are obtained. One must make a plausible estimate of r in these cases. The charge in the anion N_2O^-, for example, is strongly localized at the oxygen atom. The radius r calculated from the molar volume of liquid N_2O is certainly an upper limit, while a radius equal to half the sum of the NN and NO distances in this molecule can be taken as a lower limit.

The largest cross section for electron capture by ethyl bromide is observed at an electron energy of 0.76 eV in the gas phase. $0.8\Delta H_p$ is calculated as -1.06 eV for the anion. The energy of the electron in the most probable transition $e^-(g) + C_2H_5Br(s) \rightarrow C_2H_5Br^-(s)$ is obtained as $0.76 - 1.06 = -0.3$ eV. The function D_{unocc} drawn in Fig. 4 therefore peaks at $\varepsilon = -0.3$ eV. The shape of the curve roughly corresponds to that of the ionization efficiency curve of Br^- found in the gas phase reaction. The half width was broadened by 0.2 eV to account for the various reorganization energies of the solvation shell.

Similar functions are shown in Fig. 4 for the other systems in Fig. 3. Carbon tetrachloride is expected to have the highest density of unoccupied redox levels at $\varepsilon = -0.7$ eV. In the system $O_2(s)/O_2^-(s)$, the most probable transition energy is expected to be very negative, *i.e.* about -1.8 eV. This is due to the rather large value of the solvation energy of this small molecule. The energy ε_0 is calculated as about -2.8 eV.

[3]In earlier calculations of various authors (7, 22), small errors were introduced by regarding ΔG_p as equal to $\Delta G_s(A^-)$, and ΔH_p as equal to $\Delta H_s(A^-)$.

The system $N_2O(s)/N_2O^-(s)$ is characterized by a most probable transition energy of 2.2 eV in the gas phase. However, as mentioned before, the value of $0.8\Delta H_p$ is rather large in this case because of the concentration of the charge on the small oxygen atom. One can expect the function $D_{unocc}(\varepsilon)$ to peak at an ε value close to zero.

Figure 4 also shows the energies V_0 of the excess electron in various liquid hydrocarbons and in tetramethylsilane. The reaction of an electron–acceptor encounter pair will be fast, if the density of unoccupied electronic levels of the system $A(s)/A^-(s)$ is high at $\varepsilon = V_0$. With decreasing temperature, V_0 of most of the liquid hydrocarbons increases (24) while the increase in the dielectric constant causes the functions $D_{unocc}(\varepsilon)$ to shift downwards. Let us now discuss the experimental observations in Section I from these points of view.

(a) Dependence of the Rate Constant on V_0 or μ

Tetramethylsilane may first be regarded as a solvent of high electron mobility. Since $\tau_e \ll \tau_r$, only molecules where the distribution of unoccupied levels is peaking close to $V_0 = -0.6$ eV are expected to react rapidly with the electron in this solvent. Carbon tetrachloride is a typical example. Acceptor molecules whose distribution of unoccupied levels is peaking far above or far below $\varepsilon = -0.6$ eV are expected to react much slower. Ethyl bromide and nitrous oxide are examples of the first case and oxygen of the latter one.

In *n*-hexane, the condition $\tau_e > \tau_r$ is fulfilled

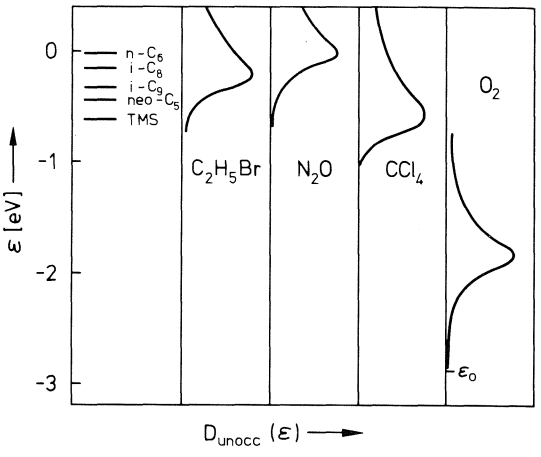

FIG. 4. Estimated distributions of unoccupied electronic redox levels of the system A/A^- of Fig. 3 and the energy levels V_0 of the electron in various hydrocarbons.

for many acceptor molecules even if their distribution of unoccupied levels does not peak close to $\varepsilon = 0$, *i.e.* close to V_0 in this solvent. One may thus understand why most of the solutes react with a diffusion-controlled rate constant in this solvent. Only in the case of oxygen, the density of unoccupied levels at $\varepsilon = 0$ is so low that the condition $\tau_e > \tau_r$ is no longer fulfilled. The reaction, therefore, is not diffusion-controlled.

That oxygen is able to react with a rate constant of about $10^{11}\ M^{-1}\ s^{-1}$ may be explained by one of the effects which we have excluded in the simple-minded model. (*1*) Reaction may occur at a suitable configuration of the solvent shell of the O_2 molecule which allows the flow of part of the energy of reaction into internal degrees of freedom of the solvent molecules. Such a configuration may be obtained during the thermal fluctuations of the system with little activation energy. (*2*) Reaction may occur via internal conversion of $O_2 + e^-$ into O_2^-. This process will be slow since internal conversion in diatomic molecules generally is not fast. Both explanations would be in agreement with the rapid attachment–detachment equilibrium $e^- + O_2 \rightleftharpoons O_2^{-*}$ postulated by Baxendale *et al.* (3).

The maxima for the rate constants of N_2O and C_2H_5Br in Fig. 1 can also be explained. In going from *n*-hexane to solvents of increased electron mobility such as neopentane, two opposing effects affect the rate of reaction. (*1*) The increased mobility causes an increase in the rate constant as long as $\tau_e > \tau_r$. (*2*) The density of unoccupied levels in these two acceptor molecules decreases with increasing μ (or decreasing V_0) for solvents of low V_0. This effect will lead to a decrease in the rate constant as soon as the condition $\tau_e > \tau_r$ is no longer valid.

In the case of oxygen, the reaction is slower in all the solvents than expected for a diffusion-controlled process. The increase in rate with decreasing V_0 (or increasing μ) of the solvent is not due to the increased mobility but to the increase of the density of unoccupied states at the V_0 level of the electron.

In tetramethylsilane, three cases may be distinguished.

(*1*) The acceptor system has a high density of unoccupied states at $\varepsilon = V_0 = -0.6$ eV. According to (a) the reaction is almost diffusion-controlled. A small positive activation energy almost equal to that of the mobility of the electron can be expected. A typical example is carbon tetrachloride.

(*2*) The acceptor system has its center of unoccupied levels at much lower ε values. A decrease in temperature leads to a smaller value of the function D_{unocc} at $\varepsilon = V_0$, *i.e.* to a lower rate. A positive activation energy will therefore be observed as well as a low rate of reaction. Oxygen is a typical example for this case.

(*3*) The acceptor system possesses a distribution of unoccupied levels far above -0.6 eV. The rate constant will again be low. A decrease in temperature leads to an increased value of $D_{\text{unocc}}(\varepsilon)$ at $\varepsilon = V_0$. The rate increases, *i.e.* a negative activation energy will be observed. Examples are nitrous oxide and ethyl bromide.

In solvents of intermediate V_0, such as 2,2,4-trimethylpentane, the condition $\tau_e > \tau_r$ will be fulfilled at low temperatures for almost all acceptors. Diffusion-controlled reactions with a positive activation energy will be observed. If the acceptor system has a high density of unoccupied levels at $\varepsilon = V_0$, the activation energy will still be positive at higher temperatures. However, if the density of states peaks at high ε values, the condition $\tau_e < \tau_r$ is reached at higher temperatures and the rate determined by the value of $D_{\text{unocc}}(\varepsilon)$ at $\varepsilon = V_0$. A negative activation energy will now be observed. This explains the maximum of the rate constant for C_2H_5Br in 2,2,4-trimethylpentane (1).

(c) Dependence of the Rate Constant on Electrical Field Strength

The electrons are mainly moving in a level with the energy $\varepsilon = V_0 + \bar{E}_K$, where $\bar{E}_K$ is the mean kinetic energy picked up by acceleration in the electric field. The decrease in ε with increasing field strength causes the interaction radius R to decrease. This effect will generally contribute to a decrease in the rate constant with increasing field strength. However, if the acceptor system possesses a distribution of unoccupied levels at energies higher than V_0, the increase in field strength will result in a higher value of the function $D_{\text{unocc}}(\varepsilon)$ at the energy $\varepsilon = V_0 + \bar{E}_K$. This effect may counterbalance or even surpass the decrease in the interaction radius and thus lead to an increase in the rate constant with increasing field strength. A typical example for this behavior is nitrous oxide. The rate constant passes through its maximum value with in-

TABLE 1. Thermodynamic and kinetic data on the equilibrium $A(s) + e^-(s) \rightleftharpoons A^-(s)$ for various acceptors in tetramethylsilane (22, 26) (all energies in kcal mol^{-1})

Acceptor	Electron affinity (gas phase)	Attachment reaction				Detachment reaction rate constant (s^{-1})
		ΔH_r	$298\Delta S_r$	ΔG_r	Rate constant ($M^{-1}\ s^{-1}$)	
Triphenylene	6.5	−17.6	−6.1	−11.5	$2.5\times10^{12}\exp(0.72/RT)$	$1.3\times10^{17}\exp(-16.9/RT)$
Phenanthrene	7.1	−16.8	−6.6	−10.2	$4.7\times10^{12}\exp(0.68/RT)$	$5.1\times10^{17}\exp(-16.1/RT)$
Naphthalene	3.5	−16.1	−8.5	−7.6	$2.6\times10^{12}\exp(0.78/RT)$	$4.7\times10^{18}\exp(-15.4/RT)$
Styrene	−0.2	−15.4	−9.6	−5.4	$4.6\times10^{12}\exp(0.77/RT)$	$1.2\times10^{18}\exp(-14.6/RT)$
α-Methylstyrene	−1.2	−16.0	−11.6	−3.9	$3.0\times10^{12}\exp(1.01/RT)$	$1.4\times10^{20}\exp(-15.0/RT)$
Carbon dioxide	−9.2	−21.1	−13.7	−7.4	$2.7\times10^{10}\exp(0.94/RT)$	$3.2\times10^{20}\exp(-20.2/RT)$

creasing field strength when the energy $\varepsilon = V_0 + \bar{E}_K$ of the electron is about equal to the energy at which the $D_{unocc}(\varepsilon)$ function of the acceptor peaks.

In the foregoing discussion, only those distributions of unoccupied electronic levels were considered which result from transitions from the vibrational ground state of the molecule to the anion. The influence of thermal activation of the acceptor molecule to higher vibrational states was neglected. Excitation of the O_2 molecule into the first vibrational excited state, for example, would enhance the probability of transitions which are accompanied by small transition energies, *i.e.* the function $D_{unocc}(\varepsilon)$ would become wider and larger at low ε values. However, this effect does not seem to play any role in *n*-hexane as the activation energy found by Baxendale *et al.* (3) is much lower than the energy of 4.6 kcal mol^{-1} of a vibrational quantum in oxygen. In the case of polyatomic molecules, thermal excitations may occur more frequently and influence the distribution of unoccupied electronic redox levels. Thermal fluctuations in the solvent shell are of great importance in electron reactions and slow electron transfer reactions in strongly polar media, and internal excitation of the reactants may play an important role in slow electron transfer reactions.

V. Aromatic Acceptor Molecules and Carbon Dioxide

The anions of aromatic compounds are stable with respect to atomic dissociation. They may, however, spontaneously lose the electron. Equilibria of the type

[16] $$A(s) + e^-(s) \rightleftharpoons A^-(s)$$

in tetramethylsilane have been studied (25, 26) by measuring the rate constant of the forward reaction as well as the constant of the equilibrium

[17] $$K = \frac{[A^-(s)]}{[e^-(s)][A(s)]}$$

at various temperatures. Table 1 shows thermodynamic data derived from the measurements as well as expressions for the temperature dependence of the rate constants.

All these aromatic acceptors react with about the same energy ΔH_r although they have different electron affinities in the gas phase. Small molecules have a low electron affinity but they are more strongly solvated. $\varepsilon_0 = -EA + \Delta H_p(A^-)$ is about 23 kcal mol^{-1} in all these cases. The differences in the free energy of reaction ΔG_r are caused by the reaction entropy ΔS_r which is the more negative for the smaller (*i.e.* more solvated) molecules.

Electron capture occurs with a small negative activation energy, which changes little for the various acceptor molecules. The preexponential factor of the rate constant has almost the same value in all the cases studied. The rate constant amounts to about $1 \times 10^{13}\ M^{-1}\ s^{-1}$ at room temperature. It is slightly smaller than the rate constants of sulfur hexafluoride and of carbon tetrachloride (Fig. 1). These findings suggest that the distribution of unoccupied redox levels of the aromatic acceptors is centered slightly above $V_0 = -0.6$ eV in tetramethylsilane.

The activation energy for electron detachment is slightly lower than $-\Delta H_r$, *i.e.* close to 21 kcal mol^{-1} for all the aromatic anions. The rate constant at room temperature generally amounts to 10^5 to $10^{10}\ s^{-1}$. That these detachment processes are so fast despite their large activation energy is due to the large preexponential factor of the rate constant which is of the order of 10^{17}

to $10^{20}\ s^{-1}$. Such large preexponential factors are known for a number of unimolecular reactions of polyatomic molecules in solution. They are observed if many internal degrees of freedom of the molecule participate in the process of activation and they are expressed by

$$10^{13}\left(\frac{E}{RT}\right)^{n-1}\frac{1}{(n-1)!}$$

where n is the number of active internal degrees of freedom and E the activation energy (see, for example, ref. 27).

The activated state of the detachment reaction is thought to be an activated molecular anion in which the energy ε of the electron (with respect to the energy of an electron in the gas phase) is equal to the energy V_0. It can thus readily escape into the solvent. The preexponential factor of the rate constant may be presented as the product $10^{13}\exp(\Delta S^*/R)$ where ΔS^* is the activation entropy ($10^{13}\ s^{-1}$: collision frequency). The ΔS^* values calculated from the preexponential factors of Table 1 are practically identical with the reaction entropy ΔS_r (26). Since the latter is equal to the entropy of polarization of the medium by the anion, one may suppose that the high entropy of the activated complex of the detachment reaction is due to little polarization of the solvent. If this supposition is correct, one must conclude that the electron is rather diffuse in the activated complex.

The electron attachment–detachment equilibrium of CO_2 has been studied in various solvents (22). The kinetic and thermodynamic data for tetramethylsilane are included in Table 1. The activation energy for detachment is clearly higher than that for the aromatic anions. The rate of detachment, however, is about the same as that of the aromatic anions, since the preexponential factor is correspondingly higher for CO_2^-. The high activation entropy for detachment is again explained by changes in the solvation shell of CO_2^-.

CO_2 is linear and CO_2^- is bent (134°) (28). Vertical electron attachment or detachment in the gas phase will lead to products with a lot of excess energy. It has recently been shown by *ab initio* calculations (29) that a series of extended Rydberg-like orbitals exist for an electron which is added to CO_2 in its linear configuration. The more extended the orbital, *i.e.* the higher its quantum number, the lower is the energy of the CO_2^- anion formed. On the other hand, the state of lowest energy of CO_2^- in its bent equilibrium configuration is the one in which the electron is located in the orbital of lowest quantum number. It is difficult to predict how the potential functions of these excited states will change upon dissolution of the molecules. It is, however, conceivable that these states play a role in both the attachment and detachment process.

VI. Heterogeneous Electron Transfer: Electronic States in Water

Electrons can be accepted by water from excited states of anions (30). Ultraviolet-light excitation of the ferrohexacyanide anion, for example, leads to a very rapid detachment of an electron. The dynamics of the later stages of its solvation have been studied using picosecond detection techniques (31). However, it could not be decided in this experiment whether the electron was initially injected into the conduction band of water or into a localized state below the level V_0. The excitation of ferrohexacyanide by 4.75 eV quanta leads to a state characterized by $\varepsilon = -0.1$ eV on our energy scale ($\varepsilon = 0$ for the electron in the gas phase). According to the present theoretical considerations, V_0 in water may lie somewhere between -0.5 and $+1.0$ eV.[4]

It has recently been found that molecules of low gas phase ionization energy (~ 6.5 eV) such as phenothiazine (33) and tetramethylbenzidine (34) can be ionized by 3.56 eV quanta (frequency doubled ruby laser) if they are irradiated in the lipoidic interior of anionic micelles in aqueous solution. Immediately after the 10 ns laser flash, the spectrum of the hydrated electron and that of the cation of the solubilized molecule could be seen. The interfacial potential of -0.5 V between the hydrocarbon-like part of the micelle and the aqueous phase facilitates the ejection of the electron from the first excited singlet state of the molecule formed by light absorption. The electron is transferred to the aqueous phase through the electric double layer at the surface of the micelle and the negative overall charge of the micelle prevents a fast neutralization of the ion pair produced.

The energetics of the process are shown in Fig. 5. The levels of the redox couples $P^+/P(S_0)$, $P^+/P(S_1)$, and $P^+(T_1)$ in the micelle are shown on the left side (S,T: singlet and triplet states of phenothiazine). Excitation by 3.56 eV quanta

[4]J. Jortner. Private communication.

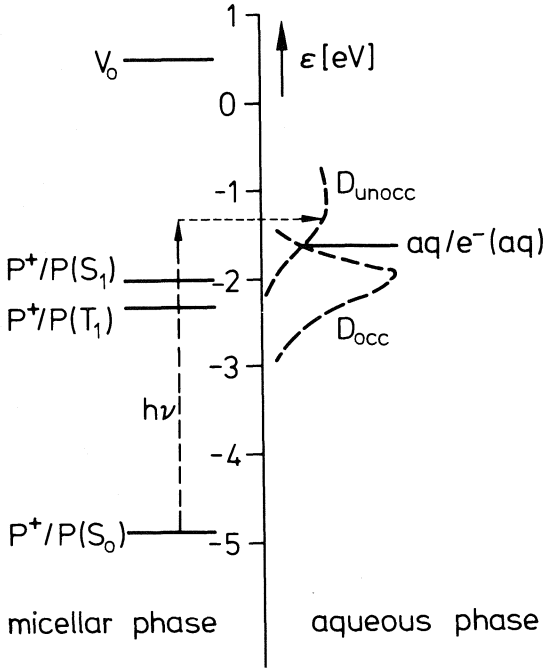

FIG. 5. ε^0 values of various redox systems of phenothiazine in anionic micelles and of the redox system aq./e_{aq}^-. The distribution functions of unoccupied and occupied electronic levels of the latter system are also indicated. Their exact shapes are not known.

leads to a vibrational level of the first excited singlet state at a position slightly above the thermodynamic level $\varepsilon^0 = -1.63$ eV of the hydrated electron (right side of Fig. 5). The electron can easily move into the aqueous phase at an energy ε which is far below the energies at which electrons are generally detached from CTTS states of anions.

Two explanations for this phenomenon may be given. The author prefers an explanation which is pictured by the functions D_{unocc} and D_{occ} on the right side of Fig. 5. The V_0 level is believed to be high (at about -0.2 eV (35)). Below this level, water may accept electrons into clusters of suitable structure present in the thermal fluctuations in the liquid. The electronic energies of these clusters(aq.) are characterized by the function $D_{unocc}(\varepsilon)$. After acceptance of the electron, reorganization of the solvent shell to reach the state of lowest energy will take place. The clusters(aq.) and the hydrated electron e_{aq}^- may thus be considered to be the oxidized and reduced forms of a redox couple. A function $D_{occ}(\varepsilon)$ below $\varepsilon^0 = -1.63$ eV must exist describing the distribution of occupied electronic levels of this redox system (*i.e.* the distribution of negative energies required to move the electron in a sudden process from e_{aq}^- into the gas phase). The shape of the two distribution functions is not known.

On the other hand, it has been shown in photoelectrochemical experiments that electrons can be ejected from a light irradiated electrode into water at energies $\varepsilon < -1.3$ eV (2, 32). The effects were explained by injection into the conduction band of water and thus V_0 should be equal to -1.3 eV. It should be mentioned that under these circumstances the maximum in the absorption spectrum of e_{aq}^- must be attributed to the transition to a bound state e_{aq}^{-*} which lies above the level V_0. No theoretical reasoning for the existence of such an excited state has yet been given. One may, however, also postulate that the electron can be transferred from an electrode into unoccupied electronic levels below V_0 as described above. A clear distinction between the two explanations does not seem possible at the present time.

Acknowledgment

The author wishes to thank Dr. R. A. Holroyd for helpful discussions.

1. A. O. ALLEN, T. E. GANGWER, and R. A. HOLROYD. J. Phys. Chem. **79**, 25 (1975).
2. G. C. BARKER. Ber. Bunsenges. Phys. Chem. **75**, 728 (1971).
3. J. H. BAXENDALE, B. P. H. M. GEELEN, and P. H. G. SHARPE. Int. J. Radiat. Phys. Chem. **8**, 371 (1976).
4. G. BAKALE, U. SOWADA, and W. F. SCHMIDT. J. Phys. Chem. **80**, 2556 (1976).
5. U. SOWADA, G. BAKALE, K. YOSHINO, and W. F. SCHMIDT. Chem. Phys. Lett. **34**, 466 (1975).
6. G. BAKALE, U. SOWADA, and W. F. SCHMIDT. J. Phys. Chem. **79**, 3041 (1975).
7. A. HENGLEIN. Ber. Bunsenges. Phys. Chem. **79**, 129 (1975).
8. R. A. MARCUS. Annu. Rev. Phys. Chem. **15**, 155 (1964).
9. V. G. LEVICH. *In* Physical chemistry, an advanced treatise. Vol. IXB. *Edited by* H. Eyring, D. Henderson, and W. Jost. Academic Press, New York. 1970. p. 985.
10. R. W. GURNEY. Proc. R. Soc. London Ser. A, **134**, 137 (1931).
11. H. GERISCHER. Z. Phys. Chem. N.F. **26**, 223 (1960).
12. K. FUNABASHI and J. L. MAGEE. J. Chem. Phys. **62**, 4428 (1975).
13. J. T. RICHARDS and J. K. THOMAS. Chem. Phys. Lett. **10**, 317 (1971).
14. J. H. BAXENDALE, C. BELL, and P. WARDMAN. Chem. Phys. Lett. **12**, 347 (1971).
15. L. NYIKOS, E. ZÁDOR, and R. SCHILLER. 4th International Symposium of Radiation Chemistry, Keszthely, Hungary, June 1976.
16. L. G. CHRISTOPHOROU, J. G. CARTER, P. M. COL-

LINS, and A. A. CHRISTODOULES. J. Chem. Phys. **54**, 4706 (1971).
17. W. E. WENTWORTH, R. GEORGE, and H. KEITH. J. Chem. Phys. **51**, 1791 (1969).
18. W. E. WENTWORTH, E. CHEN, and R. FREEMAN. J. Chem. Phys. **55**, 2075 (1971).
19. G. J. SCHULZ. Nat. Bur. Stand. (U.S.) Rep. NSRDS-NB 50. 1973.
20. M. BORN. Z. Phys. **1**, 45 (1920).
21. M. SZWARC and J. JAGUR-GRODZINSKI. *In* Ions and ion pairs in organic reactions. Vol. 2. *Edited by* M. Szwarc. John Wiley and Sons, New York. 1974. p. 32.
22. R. A. HOLROYD, T. E. GANGWER, and A. O. ALLEN. Chem. Phys. Lett. **31**, 520 (1975).
23. J. M. HALE. *In* Reactions of molecules at electrodes. *Edited by* N. S. Hush. Wiley Interscience, New York. 1971.
24. R. A. HOLROYD and R. L. RUSSELL. J. Phys. Chem. **78**, 2128 (1974).
25. J. M. WARMAN, M. P. DE HAAS, E. ZÁDOR, and A. HUMMEL. Chem. Phys. Lett. **35**, 383 (1975).
26. R. A. HOLROYD. Ber. Bunsenges. Phys. Chem. In press.
27. E. A. MOELWYN-HUGHES. The kinetics of reactions in solution. 2nd ed. Clarendon Press, Oxford. 1947. p. 281.
28. M. KRAUS and D. NEUMANN. Chem. Phys. Lett. **14**, 26 (1972).
29. P. J. BRUNA, S. D. PEYERIMHOFF, and R. J. BUENKER. Chem. Phys. Lett. **39**, 211 (1976).
30. G. STEIN. *In* Actions chimiques et biologiques des radiations. Vol. 13. *Edited by* M. Haissinsky. Masson et Cie., Paris. 1969. p. 119.
31. P. M. RENTZEPIS, R. P. JONES, and J. JORTNER. J. Chem. Phys. **59**, 766 (1973).
32. A. M. BRODSKY and Y. V. PLESKOV. Prog. Surf. Sci. **2**, 1 (1972).
33. S. A. ALKAITIS, M. GRÄTZEL, and A. HENGLEIN. Ber. Bunsenges. Phys. Chem. **79**, 541 (1975).
34. S. A. ALKAITIS and M. GRÄTZEL. J. Am. Chem. Soc. **98**, 3549 (1976).
35. A. HENGLEIN. Ber. Bunsenges. Phys. Chem. **78**, 1078 (1974).

Discussion

G. R. Freeman: Part of the high value of the apparent frequency factor (10^{20} s^{-1}) for detachment reactions in TMS might be due to a negative temperature coefficient of the enthalpy of activation $E_a \approx \Delta H^{\ddagger}(0) - \gamma T$, where $\Delta H^{\ddagger}(0)$ is the activation enthalpy extrapolated to zero Kelvin and γ is the temperature coefficient. We have observed a similar behavior for electron mobilities in olefins at low temperatures, where transient negative ions seem to form. It has also been observed in several semiconductors. A value of $\gamma \approx 10^{-3}$ eV/K will increase the apparent frequency factor by about 10^5.

$$k = A \exp(-E_a/RT) = A \exp(\gamma/R) \exp(-\Delta H^{\ddagger}(0)/RT)$$

The effect seems to be due to temperature dependence of the solvation free energy of the transient anion.

A. Henglein: I agree that this could be a contribution for the high preexponential factor. However, let me emphasize the fact that the calculated activation entropies always are equal to the energy of polarization of the anions. I do not think that this happens by chance.

G. R. Freeman: How accurately are the temperature dependences of the energies of polarization of anions known in TMS?

A. Henglein: Energies derived from the temperature dependence of the equilibrium constant can be regarded to be more accurate than 0.1 eV. Since equilibria of this type can only be observed within a relatively small temperature range, no data have been obtained for the temperature dependence of the energy of reaction.

A. C. Albrecht: The state from which you propose electron ejection appears to be an excited vibrational level of the first excited singlet state. The ejection or charge transfer process must therefore compete with picosecond type decay channels. The yield for transfer out of the micelle might for this reason be extremely low. How is this problem rationalized?

A. Henglein: The ejection should indeed be very rapid. However, the energy of the first excited state in phenothiazine is not known accurately. It might be higher by a few tenths of an electronvolt than shown in this figure. It could therefore be that the ejection of the electron occurs from the ground vibrational level of the first excited singlet. This question should be solved by looking at the process under conditions of picosecond time resolution.

Y. Hatano: Concerning the discussion of electron attachment to a molecule, *e.g.* O_2, in liquids based upon the knowledge of that in the gas phase, I would like to show some recent data on the effect of a third body on thermal electron attachment to O_2 in the gas phase, $e_{th}^- + O_2 + M \xrightarrow{k_M} O_2^- + M$, as studied by a microwave cavity technique combined with pulse radiolysis, where k_M is a three-body rate constant which is shown in the table for various medium gases (H. Shimamori and Y. Hatano Chem. Phys. Lett. **38**, 242 (1976); Chem. Phys. **12**, 439 (1976); Chem. Phys. To be published). The difference in these values is ascribed to the difference in the efficiency of collisional stabilization of vibrationally excited O_2^-*. This stabilization process may be classified into two cases depending on whether the vibrational relaxation is effected by V–T transitions or V–V transitions. Concerning the stability of a vibrationally excited negative ion, *i.e.*, an effective attachment rate of electrons in condensed media such as liquids or rigid matrices, it appears interesting now to take additionally into account V–phonon interactions.

M	k_M ($\times 10^{-30}$ cm^6/s)	M	k_M ($\times 10^{-30}$ cm^6/s)
He	0.033	C_2H_6	1.17
Ne	0.023	C_2H_4	~3
Ar	0.05	C_3H_8	3.3
Kr	0.05	n-C_4H_{10}	≃5
Xe	0.085	n-C_5H_{12}	7.9
H_2	4.8	neo-C_5H_{12}	8.0
D_2	1.4	n-C_6H_{14}	8.1
N_2	0.085	CH_3OH	11
O_2	2.3	C_2H_5OH	18
CH_4	0.34	H_2O	14

J. C. Thompson: What is the nature of D_{unocc} levels in H_2O into which e^- moves from the excited state of the micelle.

A. Henglein: These are configurations of water molecules which can localize an electron. They are characterized by the energy liberated if an electron is put into them in a sudden process from the gas phase. The distribution D_{unocc} is the distribution of these transition energies.

L. G. Christophorou: Negative ions, as neutrons, have a number of excited, higher states which often are closely spaced. In the gas phase a large number of molecules, such as the ones you considered, have two or three negative ion states within 0.5–1 eV of 0 eV. When such systems are placed in a liquid, especially when their electron affinity is large, there will be cases where two or more negative ion states will lie below 0 eV. In such cases, the electron can be captured in not only the lowest negative ion state as you described, but also in these higher states as well. Will this change your picture?

A. Henglein: They will complement the picture. I considered them at an earlier occasion (7).

Numerical investigation of tunnelling contributions to electron scavenging reactions in liquids at short times

P. Robin Butler, Michael J. Pilling,[1] Stephen A. Rice,[2] and Timothy J. Stone

Physical Chemistry Laboratory, South Parks Road, Oxford, England 0X1 3QZ

Received September 27, 1976

P. Robin Butler, Michael J. Pilling, Stephen A. Rice, and Timothy J. Stone. Can. J. Chem. **55**, 2124 (1977).

Fick's second diffusion equation, with an added exponential sink term, is integrated numerically to simulate the decay of electrons at short times in the presence of scavengers. The time dependence of the scavenger concentration profile, the scavenging rate constant, and the electron concentration are illustrated graphically. Using the experimental results of Buxton *et al.* and Jonah *et al.* It is shown that the Smoluchowski equation is valid within their experimental time ranges provided the cage encounter distance is replaced by R_{eff}, where R_{eff} can be evaluated explicitly in terms of reaction parameters. It is also shown that tunnelling from relaxed traps may make a significant contribution to ultra-short time electron scavenging.

P. Robin Butler, Michael J. Pilling, Stephen A. Rice et Timothy J. Stone. Can. J. Chem. **55**, 2124 (1977).

On intègre d'une façon numérique la deuxième équation de diffusion de Fick avec un terme de piège exponentiel afin de simuler la décroissance des électrons à des temps courts en présence de pièges. On illustre d'une façon graphique la relation qui existe entre le temps et la contribution du piège au profil ainsi que la constante de vitesse de piègeage et la concentration d'électrons. Utilisant les résultats expérimentaux de Buxton *et al.* et de Jonah *et al.*, on montre que l'équation de Smoluchowski est valide à l'intérieur des écarts de temps expérimentaux pourvu que l'on remplace la distance de rencontre en cage par R_{eff}, où R_{eff} peut être évalué explicitement en termes des paramètres de la réaction. On montre aussi que la réaction tunnel provenant de pièges relaxés peut apporter une contribution importante au piégeage d'électrons à des temps extrêmement courts.

[Traduit par le journal]

Introduction

The involvement of tunnelling in reactions of solvated electrons in rigid glasses is now well documented (1, 2) although there is some disagreement about the detailed mechanism of such reactions (3). Tunnelling has also been postulated in liquids, but the evidence is less convincing. Hart and Anbar (4) noted that the rate constants of some diffusion-controlled reactions of the hydrated electron are larger than would be expected on the basis of 'crystallographic' radii and the known diffusion coefficients of the reacting species. They suggested that the electrons react at large distances by a tunnelling mechanism. An analysis of the steady-state diffusion equation with an exponential sink term confirmed that the magnitude of the increase in the encounter distance is compatible with tunnelling parameters as derived from studies of glasses (5). Buxton *et al.* (6) and Jonah *et al.* (7) studied diffusion-controlled reactions in the time-dependent zone (8) prior to establishment of the steady state. They analysed their data using the time-dependent Smoluchowski equation or a variant which employs the so-called radiation boundary condition (8), neither of which takes account of any long range nature of the reaction. They were able to determine the effective encounter distance, R_{eff}, and the diffusion coefficient, D, independently. In both investigations reactive systems were found which gave R_{eff} greater than the 'crystallographic' values and a tunnelling mechanism was invoked.

The present paper presents a numerical integration of the time-dependent diffusion equation containing an exponential sink term and examines the validity of the conclusions of Buxton *et al.* (6) and Jonah *et al.* (7). A numerical analysis (9) of the same equation has been reported previously, but no specific application of the results was made.

Experimental studies have also been made of very short time (<30 ps) electron scavenging and various mechanisms, involving dry electrons

[1]To whom correspondence should be addressed.

[2]Present address: Department of Chemistry, Wayne State University, Detroit, MI, U.S.A. 48202.

or tunnelling, have been proposed (10–12). An analysis of the likely effects of tunnelling in this time regime is also presented.

Diffusion Equation

The rate of a fast reaction of the solvated electron depends on the mutual diffusion of the reactants. Provided the reaction occurs by a contact mechanism, the change in the ensemble averaged concentration of scavengers around electrons ($S(r,t)$) may be described by the diffusion equation derived from Fick's second law:

$$[1a] \qquad \frac{\partial S(r,t)}{\partial t} = \frac{D}{r}\frac{\partial^2 S(r,t)r}{\partial r^2}$$

Spherical symmetry is assumed and r is the electron scavenger distance, t is the time, and D is the relative diffusion coefficient of the reactants. If reaction occurs on every encounter of scavenger and electron, then the Smoluchowski boundary conditions may be applied

$$[2] \qquad S(r,t) = 0 \qquad r < R,\ t \geq 0$$

$$[3] \qquad S(r,t) = S_0 \qquad r > R,\ t = 0$$

$$[4] \qquad S(r,t) \rightarrow S_0 \qquad r \rightarrow \infty,\ t \geq 0$$

where R is the encounter (reaction) distance and S_0 is the bulk scavenger concentration. At zero time, the scavenger distribution is assumed random. The reaction depletes the region around $r = R$ of scavengers and provides a concentration gradient which promotes the diffusion of scavengers from larger distances. A steady-state concentration profile is eventually set up, with diffusive supply balancing reactive depletion and the equation becomes time independent. By evaluating the radial flux of scavengers, the steady-state rate constant for the reaction may be shown to be $4\pi RD$ (8). For reactions which are not quite so fast, the radiation boundary condition is introduced, modifying [2] and reducing the rate constant (8).

Pilling and Rice (5) modified [1a] in order to describe reactions, such as electron scavenging, which take place by a long range mechanism whose probability falls off exponentially with distance. They introduced an exponential sink term:

$$l_s(r) = \alpha' \exp\left[-\beta(r - R)\right]$$

into [1a], to give

$$[1b] \qquad \frac{\partial S(r,t)}{\partial t} = \frac{D}{r}\frac{\partial^2 S(r,t)r}{\partial r^2} - l_s(r)S(r,t)$$

and employed the boundary conditions [2]–[4]. $l_s(r)$ is the first order rate constant for reaction of an electron and scavenger held at a distance r, and may be derived from the Gamow equation (2). It describes tunnelling of an electron through the potential energy barrier separating it from the scavenger. α' is a frequency term and β is related to the height of the potential barrier (or, equivalently, to the depth of the electron trap). Alternatively, and more realistically, $l_s(r)$ may be derived using Fermi's golden rule; α' is now related to the electronic transition moment for the electron transfer process and to Franck–Condon factors, whilst β is determined by the radial dependence of the electron wavefunction. An analysis of electron scavenging in aqueous glasses showed that $\alpha' \sim 10^{14}\ s^{-1}$ and $\beta \sim 10^{10}\ m^{-1}$ (equivalent to a trap depth of 1 eV) (2).

Pilling and Rice (5) solved [1b] analytically and showed that the steady-state rate constant is given by

$$k = 4\pi R_{eff} D$$

where

$$[5] \qquad R_{eff} = R + \frac{1}{\beta}\left[2\gamma + \ln\frac{w_0^2}{4} + \frac{2K_0(w_0)}{I_0(w_0)}\right]$$

γ is Euler's constant (0.57721...), $w_0^2 = 4\alpha'/\beta^2 D$, and $I_0(w_0)$ and $K_0(w_0)$ are the modified first and second kind Bessel functions of zero order and argument w_0. They also derived steady-state concentration profiles ($S(r,\infty)$ *vs.* r) and showed that the reaction may be adequately described by placing an absorbing barrier at $r = R_{eff}$, which is greater than R for an efficient scavenger. They were unable to solve [1b] analytically in the time-dependent region; the present paper uses a numerical approach.

Numerical Solution

Equation 1b may be transformed into a reduced equation more suited to computation using the following substitutions:

$$x = \beta r/2 \qquad Y = xS(r,t)/S_0 \qquad \tau = \beta^2 Dt/4$$
$$\lambda = w_0^2 \exp(\beta R)$$

giving

$$[1c] \qquad \frac{\partial Y}{\partial \tau} = \frac{\partial^2 Y}{\partial x^2} - \lambda^2 Y \exp(-2x)$$

with suitably modified boundary conditions. Equation 1c was then solved numerically, using a modified Crank–Nicolson method (13) (see Appendix).

Scavenger Concentration Profiles

Figure 1 shows the computed scavenger profiles, $\rho(r,t) = S(r,t)/S_0$, as a function of time, for typical parameters:

(*a*) $\alpha' = 0$, $D = 10^{-8}$ m^2 s^{-1}, $R = 0.5$ nm, *i.e.*, for solution of the Smoluchowski equation with no tunnelling (eq. 1*a*).

(*b*) $\alpha' = 10^{14}$ s^{-1}, $\beta = 10^{10}$ m^{-1}, $D = 10^{-8}$ m^2 s^{-1}, $R = 0.5$ nm.

(*c*) $\alpha' = 10^{14}$ s^{-1}, $\beta = 10^{10}$ m^{-1}, $D = 0$, $R = 0.5$ nm, *i.e.*, the pure tunnelling case considered by Dainton *et al.* (2).

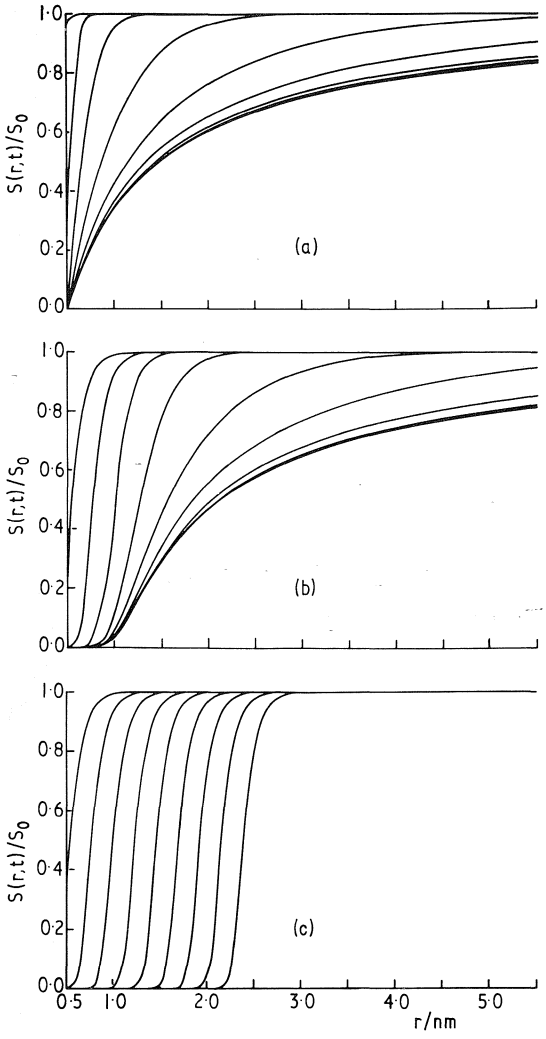

FIG. 1. Scavenger profiles (*a*) Smoluchowski: $\alpha' = 0$, $D = 10^{-8}$ m^2 s^{-1}, $R = 0.5$ nm; (*b*) tunnelling and diffusion: $\alpha' = 10^{14}$ s^{-1}, $\beta = 10^{10}$ m^{-1}, $D = 10^{-8}$ m^2 s^{-1}, $R = 0.5$ nm; (*c*) pure tunnelling $\alpha' = 10^{14}$ s^{-1}, $\beta = 10^{10}$ m^{-1}, $D = 0$, $R = 0.5$ nm. The profiles are shown at decadic time intervals from 10^{-14} to 10^{-6} s, with that for 10^{-14} s at the extreme left.

Figure 1*a* shows the relaxation of the scavenger distribution from a random form to the steady-state form, over a period of 10^{-7} s for case (*a*). Figure 1*c* shows the expansion of the volume depleted of scavengers when a tunnelling reaction takes place but diffusion is unable to replenish the local scavenger concentration (2). Figure 1*b* shows the time dependence most relevant to the present discussion. At short times ($t < 10^{-12}$ s) reaction occurs predominantly by static tunnelling and the quasi-steps in Fig. 1 *b* and *c* recede with time in a similar manner. At longer times diffusion makes good some of the local scavenger depletion and after $\sim 10^{-7}$ s the steady state is established. A comparison of Fig. 1 *a* and *b* shows, however, that the tunnelling reaction at small r occurs too rapidly for effective scavenger replenishment and $\rho(r,t)$ is small out to $r \sim R_{\text{eff}}$. The computed steady-state concentration profile agrees well with the analytical form given by Pilling and Rice (5). The same general conclusions could be made from the numerical results obtained with a range of diffusion and tunnelling parameters although the time regimes for pure tunnelling and steady-state behaviour are, of course, altered.

Rate Constants

Pilling and Rice (5) showed that the total scavenging rate constant, $k(t)$, is the sum of diffusive ($k_D(t)$) and tunnelling ($k_T(t)$) rate constants, where the former relates to reaction on encounter and the latter to reaction from all distances greater than R. They are given by:

$$[6] \qquad k_D(t) = 4\pi R^2 D \left.\frac{\partial \rho(r,t)}{\partial r}\right|_R$$

$$[7] \qquad k_T(t) = \int_R^\infty 4\pi r^2 \alpha' \rho(r,t) \times \exp[-\beta(r - R)]\, dr$$

$$[8] \qquad k(t) = k_D(t) + k_T(t)$$

The Appendix describes how $k_D(t)$ and $k_T(t)$ were obtained numerically from the computed scavenger concentration profiles.

Figure 2 shows computed rate constants, $k(t)$, for $\alpha' = 10^{14}$ s^{-1}, $\beta = 10^{10}$ m^{-1}, $D = 10^{-8}$ m^2 s^{-1}, and $R = 0.5$ nm, as a function of time. For all $t > 10^{-14}$ s, $k_T(t)$ is several orders

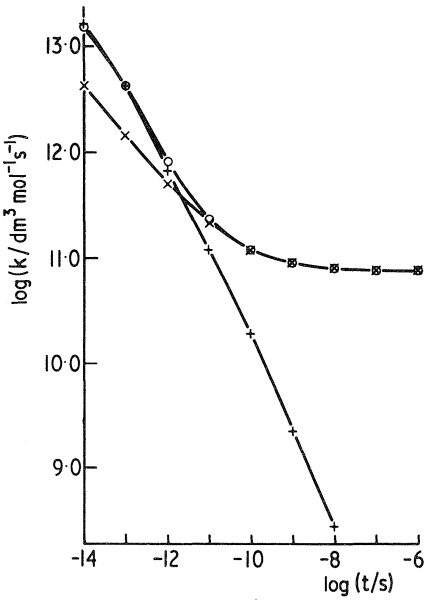

FIG. 2. Time dependence of rate constants: × Smoluchowski with R replaced by R_{eff}; ○ numerical results based on [1*b*], including both tunnelling and diffusion; + pure tunnelling. The parameters are: $\alpha' = 10^{14}$ s^{-1}, $\beta = 10^{10}$ nm^{-1}, $D = 10^{-8}$ m^2 s^{-1}, $R = 0.5$ nm.

of magnitude greater than $k_D(t)$, *i.e.*, $k(t) \simeq k_T(t)$. The origin of this effect may be illustrated by reference to Fig. 1*b*, which shows that the concentration gradient at $r = R$ is very small, even at short times: the exponential sink term at distances close to R is so large that this region is rapidly depleted of scavengers. In consequence only a very small fraction of the reaction occurs by the purely diffusive mechanism required by [7]; the majority of reactive events occurs with $r > R$.

Equation 1*a* may be solved analytically to give the Smoluchowski time-dependent rate constant, $k_S(t)$ (8):

$$[9] \qquad k_S(t) = 4\pi RD[1 + R/(\pi Dt)^{1/2}]$$

Buxton *et al.* (6) and Jonah *et al.* (7) assumed that [9] is applicable, with a suitably increased encounter distance, even when tunnelling takes place, *i.e.*, when [1*b*] applies. Figure 2 also shows $k_S(t)$, calculated from [9], but with R replaced by R_{eff} (eq. 5). The rate constant for pure tunnelling ($D = 0$) is shown in addition. This is defined by [7], with the profile derived from [1*b*] with $D = 0$.

At short times, the rate constant, $k(t)$, is close to the value obtained for pure tunnelling, as would be expected from Fig. 1 *b* and *c*; in this time region the concentration profiles recede in a similar manner and diffusion has little effect. For $t > 10^{-11}$ s, diffusion begins to play a part and the pure tunnelling rate constant falls below the composite value which in turn acquires good agreement with the Smoluchowski rate constant equation, [9], with R replaced with R_{eff}. This effect stems from the strong distance dependence of the sink term. It falls off so rapidly at longer distances that diffusive transport is more effective and scavengers approach R_{eff} with little reactive depletion: the system approximates closely one with an absorbing boundary at R_{eff} (*cf.* Fig. 1*b*).

The changeover from pure tunnelling to tunnelling/diffusion behaviour is in agreement with the perturbation treatment of Pilling and Rice (14) which predicts that the electrons react by static tunnelling for times less than t_D:

$$t_D = 1/\beta^2 D$$

At times longer than this they suggested that diffusion plays a role in electron transport. For the parameters considered in Fig. 2, $t_D \sim 10^{-12}$ s.

Figure 2 shows that [5] was applied down to times of 10^{-14} s, whilst the Brownian approximation, implicit in Fick's laws, is generally felt to fail for times less than 10^{-12} s. This failure is seen to be unimportant in the present system, since in this time regime the diffusive contribution is negligible.

At long times, the numerical results show the required approach to a steady-state value, which agrees well with the analytical value $4\pi R_{eff}D$.

Variable α'

Dainton *et al.* (2) suggested that α' is r-dependent and is given by $\alpha' = \alpha\sigma^2/4r^2$, where σ is the electron capture radius of the scavenger and α is an r-independent frequency term. In order to obtain an analytical solution to the diffusion equation in the steady state Pilling and Rice (2) set $\alpha' = \alpha\sigma^2/4\langle r\rangle^2$ where $\langle r\rangle$ is a 'mean' tunnelling distance. They suggested that in the steady state the exponential dependence of the sink term swamps any r-dependence of α' and they assumed $\langle r\rangle = R_{eff}$. Figure 3 shows a comparison of numerical rate constants for $\alpha' = 10^{14}$ s^{-1} and $\alpha' = (10^{-3}$ m$^2/4r^2)$ s^{-1}. The latter value of $\alpha\sigma^2$ was determined so that

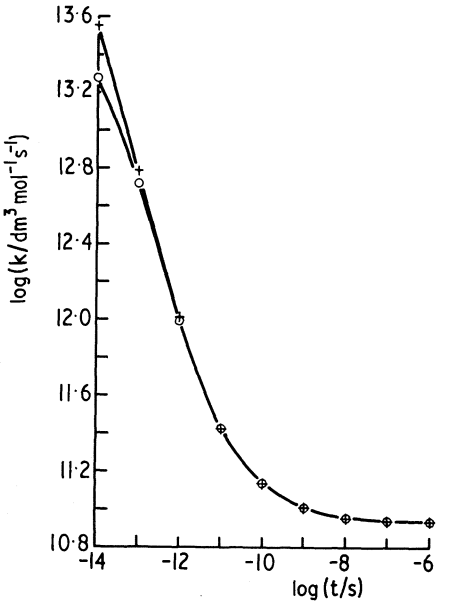

FIG. 3. A comparison between r-dependent and r-independent frequency factors: ○ $\alpha' = 10^{14}$ s^{-1}; + $\alpha' = (10^{-3}$ m$^2/4r^2)$ s^{-1}.

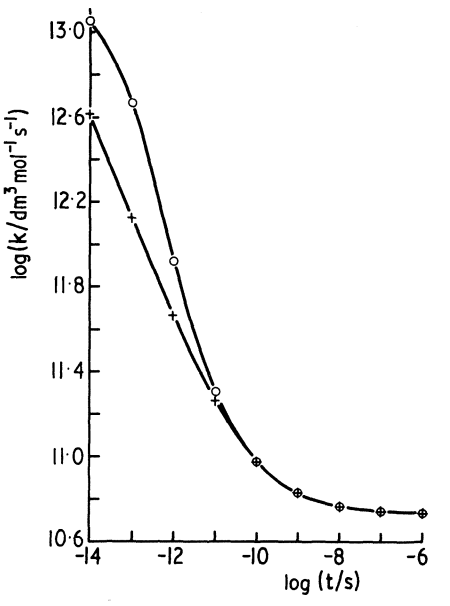

FIG. 4. A comparison of the numerically evaluated rate constant (○) and that calculated from the Smoluchowski equation with R replaced by R_{eff} (+), designed to simulate the data of Jonah *et al.* (7), for scavenging by IO_4^-. $\alpha' = 5.37 \times 10^{13}$ s^{-1}, $\beta = 10^{10}$ m^{-1}, $D = 6.5 \times 10^{-9}$ m^2 s^{-1}, $R = 0.5$ nm.

both forms gave the same computed steady-state solution. For $t > 10^{-12}$ s the results are identical, suggesting that the assumptions made by Pilling and Rice are at least operationally valid over the whole of the experimentally accessible time scale. The two forms for α' require $\langle r \rangle = 1.55$ nm, whilst $R_{eff} = 1.07$ nm.

Specific Fits to Experimental Data

(*i*) Jonah *et al.* (7) studied electron scavenging in water over the time scale 50–3500 ps. They were unable to analyse explicitly for time-dependent rate constants but instead determined the half-life, $t_{1/2}$, for electron decay. By varying the scavenger concentration they were able to vary the time scale of the reaction and so the mean rate constant, $\langle k \rangle$, for scavenging. For IO_4^- they found that $t_{1/2}$ and $\langle k \rangle$ could be adequately described by the Smoluchowski equation, with $R_{eff} = 1.06$ nm and $D = 6.5 \times 10^{-9}$ m^2 s^{-1}. Taking $\beta = 10^{10}$ m^{-1}, on the basis of low temperature studies, the data require $\alpha' = 5.37 \times 10^{13}$ s^{-1}. Figure 4 shows the numerically determined rate constant as a function of time; the time dependence of the Smoluchowski rate constant, $k_S(t)$, with R replaced by R_{eff} (*i.e.*, as used by Jonah *et al.*) is also shown. Significant differences occur only for $t < 10^{-11}$ s, which is outside the experimental time scale.

(*ii*) Buxton *et al.* (6) studied electron scavenging in 10 M aqueous hydroxide and 9.5 M aqueous LiCl solutions over the temperature range 190–240 K. The viscosity is so high at these temperatures that they were able to study the electron decay under non-steady-state conditions on a microsecond time scale and make a full analysis of the time dependence. They found several instances of large encounter distances and concluded that tunnelling is important. Before a numerical analysis is made, their data may be reinterpreted to obtain further confirmation of tunnelling. The steady-state model of Pilling and Rice (5) requires that the effective encounter distance increases as the diffusion coefficient falls, whilst Buxton *et al.* (6) reported no evidence for this. They obtained the temperature dependence of the steady-state rate constant

$$k(t \rightarrow \infty) = A \exp \{-B_k/(T - T_0)\}$$

where B_k is an experimental parameter and T_0 is the temperature of zero mobility of the glass forming solvents. They also determined the temperature dependence of the diffusion coefficient:

$$D = D_0 \exp \{-B_D/(T - T_0)\}$$

Since $k(t \rightarrow \infty) = 4\pi R_{eff} D$

$$R_{eff} = (A/4\pi D_0) \exp \{-(B_k - B_D)/(T - T_0)\}$$

There were large uncertainties in the values of B_D and B_k, but, with only two exceptions out of eight, $B_D > B_k$, suggesting that R_{eff} increases with decreasing temperature (*i.e.* with increasing viscosity) in line with the model of Pilling and Rice (5). For example, taking the mean values of B_D and B_k for CrO_4^{2-} in 10 *M* hydroxide, $R_{eff}(240\text{ K}) = 1.47$ nm and $R_{eff}(190\text{ K}) = 2.8$ nm. Using the CrO_4^{2-} values of R_{eff} and D, together with $\beta = 10^{10}\text{ m}^{-1}$, $R = 0.5$ nm requires $1.53 \times 10^{13} < \alpha' < 3.87 \times 10^{15}\text{ s}^{-1}$. Once again the Smoluchowski and numerical rate constants agree well for $t > 10^{-9}$ s at both 190 and 240 K. Figure 5 shows the computed and Smoluchowski time dependent rate constants at 240 K.

These numerical analyses show that, at both low and high viscosities, the Smoluchowski equation adequately represents a diffusion-controlled reaction with a tunnelling mechanism provided the encounter distance is replaced by R_{eff}. They thus confirm the validity of the conclusions reached by Jonah *et al.* (7) and Buxton *et al.* (6). It must be emphasized that the present treatment has been applied only to very efficient scavengers. A reduction in α' reduces R_{eff} and moderates the effect of tunnelling. For a sufficiently small α', reaction takes place only on encounter and the analytical form contained in the radiation boundary method (8) may be employed.

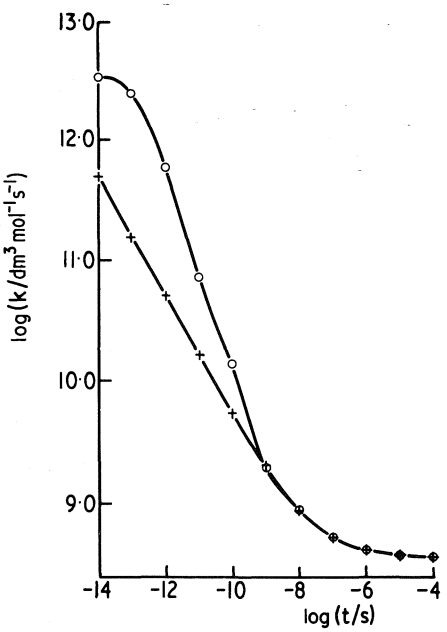

FIG. 5. A comparison of the numerically evaluated rate constant (○) and that calculated from the Smoluchowski equation with R replaced by R_{eff} (+), designed to simulate the data of Buxton *et al.* (6) for scavenging by CrO_4^{2-} in 10 *M* OH^- at 240 K. $\alpha' = 3.87 \times 10^{15}\text{ s}^{-1}$, $\beta = 10^{10}\text{ m}^{-1}$, $D = 3.08 \times 10^{-11}\text{ m}^2\text{ s}^{-1}$, $R = 0.5$ nm.

Short Time Studies

Hunt and co-workers (10–12) made a systematic study of short time ($t < 30$ ps) electron scavenging. They defined a parameter, S_{37} (in our notation), which is the scavenger concentration required to reduce the electron yield at zero time to $1/e$ of its value at the same time in the absence of a scavenger. The zero time yield was obtained by extrapolation of data obtained for $t > 30$ ps. They found a good correlation between S_{37} and the value of the rate constant, $\langle k \rangle$ measured at times greater than 30 ps (11).

$$[10] \qquad S_{37} \langle k \rangle = 10^{10}\text{ s}^{-1}$$

They did not specify the scavenger concentration at which $\langle k \rangle$ was determined and, since the rate constants are time dependent in this time regime, there is some uncertainty about the exact physical significance of $\langle k \rangle$.

Several mechanisms of short time scavenging have been proposed, including tunnelling from relaxed and partially relaxed traps and dry electron scavenging (10). The numerical technique allows us to examine the feasibility of the relaxed trap model.

The electron concentration at time t, $C(t)$, is obtained by integration of the pseudo-first-order equation:

$$dC(t)/dt = k(t)S_0C(t)$$

whence

$$[11] \quad C(t) = C_0 \exp\left[- \int_0^t k(t)S_0\, dt \right]$$

where C_0 is the true electron concentration at zero time. Because of the strong time dependence of the rate constant, extrapolation to zero time based on $\langle k \rangle$ underestimates C_0:

$$[12] \qquad C(t) = C_0' \exp(-\langle k \rangle S_0 t)$$

where C_0' is the extrapolated zero time electron concentration. Equating [11] and [12]

$$\frac{C_0}{C_0'} = \exp\left\{ S_0 \left[\int_0^t k(t)\, dt - \langle k \rangle t \right] \right\}$$

The parameter defined by Hunt *et al.* (11), S_{37}, is obtained when $C_0/C_0' = e$, whence

[13] $$S_{37} = \left[\int_0^t k(t)\,dt - \langle k \rangle t \right]^{-1}$$

where $t = 30$ ps.

CrO_4^{2-} was chosen as a model scavenger, since it has responded well to tunnelling treatments and also because it has the smallest S_{37} value and thus represents the most severe test. Using the tunnelling parameters derived from the short time rate data of Jonah *et al.* (7) ($4\pi R_{eff}D = 3 \times 10^{10}$ dm^3 mol^{-1} s^{-1}) together with $D = 5.5 \times 10^{-9}$ m^2 s^{-1} and $R = 0.5$ nm, and defining $\langle k \rangle$ by its 100 ps value, a value of 0.55 mol dm^{-3} was calculated for S_{37}. This is in fair agreement with the experimental value of 0.2 ± 0.05 mol dm^{-3}. The calculation is quite crude, however, and does not preclude the possibility of dry or damp electron scavenging. There is uncertainty in the value of $\langle k \rangle$ and charge effects (15) and trap relaxation have been neglected. The calculations do show, however, that tunnelling, even from fully relaxed traps, can account for a significant amount of scavenging at very short times. This observation applies only to the more efficient scavengers. The extreme dependence of the rate constant on time occurs only if α' is large.

If we assume that the short time scavenging may be ascribed exclusively to tunnelling, then [10] and [13] require that

$$\int_0^t \frac{k(t)\,dt}{\langle k \rangle} - t = 10^{-10} \text{ s}$$

for $t = 30$ ps. If we assumed that $\langle k \rangle$ is defined by its 100 ps value, and if we take the form shown in Fig. 2 for $k(t)$, then the left-hand side of this equation is equal to 5×10^{-11} s.

Charge Effects

The effect of scavenger charge and of ionic strength have been entirely neglected throughout the present calculations. Jonah *et al.* (7) showed that ionic strength had no effect on the scavenging of CrO_4^{2-} and IO_4^- and they ascribed this to the large effective encounter distance and to the consequently small Coulombic interaction. This argument will be even more valid at the low temperatures and high ionic strengths at which Buxton *et al.* (6) performed their experiments. The effects of scavenger charge in the time-dependent region and at the steady state have been considered by Butler and Pilling (16).

Conclusion

In fluid systems containing electrons in fully relaxed traps, the decay of the electrons can be divided into two well defined regions. For $t < t_D$ ($t_D = 1/\beta^2 D$), the electrons decay almost exclusively by static tunnelling (2). For $t \gtrsim 10t_D$ the decay occurs by combined diffusion and tunnelling with a rate constant:

$$k(t) = 4\pi R_{eff} D(1 + R_{eff}/(\pi Dt)^{1/2})$$

For electrons in water at 300 K, $t_D \sim 10^{-12}$ s.

1. J. R. Miller. J. Phys. Chem. **75**, 1070 (1975).
2. F. S. Dainton, M. J. Pilling, and S. A. Rice. J. Chem. Soc. Faraday Trans. II, **71**, 1333 (1975).
3. G. V. Buxton and K. Kemsley. J. Chem. Soc. Faraday Trans. I, **71**, 568 (1975).
4. E. J. Hart and M. Anbar. The hydrated electron. Wiley, New York, NY. 1970.
5. M. J. Pilling and S. A. Rice. J. Chem. Soc. Faraday Trans. II, **71**, 1563 (1975).
6. G. V. Buxton, F. C. R. Cattell, and F. S. Dainton. J. Chem. Soc. Faraday Trans. I, **71**, 115 (1975).
7. C. D. Jonah, J. R. Miller, E. J. Hart, and M. S. Matheson. J. Phys. Chem. **79**, 2705 (1975).
8. R. M. Noyes. Prog. React. Kinet. **1**, 129 (1961).
9. A. A. Gailitis and I. K. Vitol. Bull. Acad. Sci. USSR, Phys. Ser. **35**, 1188 (1971).
10. R. K. Wolff, J. E. Aldrich, T. L. Penner, and J. W. Hunt. J. Phys. Chem. **79**, 210 (1975).
11. K. Y. Lam and J. W. Hunt. Int. J. Radiat. Phys. Chem. 7, 317 (1975).
12. J. E. Aldrich, K. Y. Lam, P. C. Schragge, and J. W. Hunt. Radiat. Res. **63**, 42 (1975).
13. J. Crank and P. Nicolson. Proc. Cambridge Philos. Soc. **43**, 50 (1975).
14. M. J. Pilling and S. A. Rice. J. Chem. Soc. Faraday Trans. II, **72**, 792 (1976).
15. M. J. Pilling and S. A. Rice. J. Phys. Chem. **79**, 3035 (1975).
16. P. R. Butler and M. J. Pilling. Disc. Faraday Soc. To be published.
17. M. Abramowitz and I. A. Stegun. Handbook of mathematical functions. Dover, New York, NY. 1965. p. 887.

Appendix

The (x,τ) space (eq. 1*c*) was divided into a mesh of points separated by equal increments, δx and $\delta\tau$, and labelled by subscripts i and j, respectively. The $Y(i,0)$ array was defined from the boundary condition [3]. Condition [4] was redefined to give $Y(n,j) = x$; $i = n$ corresponds to the maximum value of the distance variable, defined by $x = \beta R_{max}/2$. $\partial Y(i,j)/\partial\tau$ was approximated by a forward difference relation and $\partial^2 Y(i,j)/\partial x^2$ by the mean of its finite difference approximations on the jth and $(j + 1)$th rows (13). The distance dependent sink term was

similarly averaged. This procedure allowed the $(j + 1)$th row of Y to be evaluated for all i from the predetermined values of $Y(i,j)$. It gave $(n - 1)$ simultaneous differential equations, which may be expressed in matrix form as:

$$\mathbf{D} \cdot \mathbf{Y} = \mathbf{K}$$

where $\mathbf{D}$ is a $(n - 1) \times (n + 1)$ matrix with elements

$$D_{l,k} = -1/2(\delta x)^2 \qquad k = l, l + 2$$
$$= 1/\delta\tau + 1/(\delta x)^2 + (\lambda^2/2) \exp(-2x_l) \qquad k = l + 1$$
$$= 0 \qquad k < l, k > l + 2$$

$\boldsymbol{Y}$ is an $(n + 1)$ dimensional column vector with elements $Y(i,j + 1)$ for $i = 0, 1, \ldots, n$ and $\boldsymbol{K}$ is an $(n - 1)$ dimensional column vector with elements

$$K(i) = Y(i + 1,j)/[2(\delta x)^2] + Y(i,j)(1/\delta\tau - 1/(\delta x)^2 - (\lambda^2/2) \exp(-2x_i)) + Y(i - 1,j)/[2(\delta x)^2]$$

for $i = 1, 2, \ldots, n - 1$. This generates $(n - 1)$ equations with $(n + 1)$ unknowns; the additional conditions $Y(0,j + 1) = 0$ and $Y(n,j + 1) = \beta R_{max}/2$ were employed and the equations solved by established computational techniques. Because of the large change in gradient at short times, the technique was modified to enable a change in the distance step, δx_1 to δx_2, to be made for integration at a given time. This required modifications in the equations defining $\partial^2 Y/\partial x^2$ at the changeover point from δx_1 to δx_2. Typically $\delta\tau$ was taken initially as 10^{-14} s and was then increased by a factor of 10 after 10 increments; this procedure was repeated until the profile became invariant (*i.e.* until the steady state was established). δx was taken as 0.2 nm for the first 25 steps in the space coordinate and then increased to 3.0 nm until R_{max} was reached. R_{max} was generally taken as 50.5 nm, although larger values were also used to test convergence. At very short times, some variation in δx was required to obviate oscillation.

The equations defining the rate constants ([6] and [7]) necessitated the generation of continuous profiles from the numerically evaluated mesh points. In order to avoid interpolations based on the extreme variations in $\rho(= S/S_0)$, a function Z was defined:

[A1] $$Z = \ln(\rho + 10^{-6})$$

which remains finite as $\rho \to 0$. The Z values at any distance between the mesh points were determined from a cubic fit. ρ was then found by inverting [A1]. Tunnelling rate constants were evaluated from [7] using Gauss's approximation (17), with an upper limit at R_{max}. Variation of the upper limit was used to check convergence. Gauss's approximation was also used to evaluate the electron decay. The diffusive rate constants were determined by evaluating the gradients of chords from the encounter distance to points on the concentration profile at decreasingly small distances from R. An approximate value of $\partial S/\partial r|_R$ was then obtained by extrapolation and hence $k_D(t)$ determined from [6].

Discussion

C. Jonah: What sort of change would one expect if one used the Waite or Noyes theory for reaction?

S. A. Rice: I do not know! I surmise that a good guess would be to replace the true (crystallographic) encounter distance by R_{eff}, for reactions which are only partially activation controlled. However, as the activation process becomes slower, so would I expect that electron tunnelling would also decrease in importance.

G. A. Salmon: Simple tunnelling models as applied to glassy systems have difficulties in accounting for differences between solutes. Does this present difficulties in computing rate constants for the fluid phase?

S. A. Rice: Providing this electron tunnelling model is treated as a phenomenological approach, the rigid glass and fluid regions are mutually consistent. Furthermore, the difficulties alluded to above refer, I believe, to comments of Buxton and Kemsley whose model of trap-to-trap tunnelling has very serious deficiencies. See also reply to J. Jortner.

P. K. Watson: A basic assumption in this work is that the motion of an electron diffusing towards a scavenger molecule is characterized by a constant diffusion coefficient. It is important to question whether a constant D is appropriate at molecular distances, where an electron will strongly polarize its environment, and nonhomogeneous surroundings will result in asymmetrical local fields. Presumably as an electron diffuses in the environment of a polarizable molecule there is an approach distance at which the self-induced field due to the electron will be large enough to complete with the motion due to kT, and in this case a biased random walk of the type discussed by Chandrasekhar will be appropriate. An extension of this idea is to consider the effect of local traps on the electron motion (one envisages this trap as being due to local polarization). Calculations by Scher and Montroll on stochastic hopping transport have described the motion of a charged particle in a trapping environment, with an applied electric field. They

show that carrier motion can be described by a diffusion-like process defined by a distribution of waiting time $\psi(t)$ between hops and in which the average jump distance $\bar{l}$ is field-dependent. This model has been very successful in describing, for example, the motion of a carrier packet moving in high fields in amorphous semiconductors.

S. A. Rice: The diffusion motion of charged species in water has been shown to be a reasonable approach for times of picoseconds or more. Polarization of solvent molecules and of scavenger by an electron is probably insignificant in highly ionic aqueous systems which have been alluded to above. Dainton studied the effect of ionic strength on electron – ionic scavenger reaction rates and found accord with the Bronsted–Bjerrum theory; for short times the electron can react without a relaxed ionic solvation shell and so is not so strongly screened. In ethers and alkanes solvent and scavenger polarization effects may have to be considered, I concede.

J. Jortner: I would like to comment on the interesting suggestion regarding the possible applicability of the Montroll–Scher theory to diffusion controlled reactions of the solvated electron. Montroll and Scher address themselves to electron–hole recombination in an amorphous semiconductor where the transport process involves thermal excitation to the mobility edge. In the case of the solvated electron transport occurs via a "hydrodynamic drag" and solvent short-range configurational charges. It is thus questionable whether the amorphous semiconductor recombination is directly applicable to the problem at hand.

There is, however, one analogy between the two systems which deserves serious consideration. The electron–hole recombination in amorphous semiconductors involves a multiphonon process. The same picture should be applied to describe the reactions of the solvated or trapped electron. The electron tunnelling picture applied by S. A. Rice, J. Miller, and A. C. Albrecht provides a grossly oversimplified picture for such reactions. As is well known, configurational nuclear charges have to be explicitly introduced in the electron transfer process and the electron follows adiabatically the motion of the nuclei. Such a picture for electron-transfer bears a close analogy to small polaron motion in solids. The Forster–Dexter intermolecular energy transfer and intramolecular radiationless transitions can be described within the framework of a unified approach which rests on the theory of multiphonon processes. The dependence of the electron transfer transition probability or the separation r of the solvated or trapped electron and of the electron acceptor is of the functional form $\exp(-\beta r)$, which is, of course, identical to that obtained from the tunnelling argument. However, the pre-exponential factor (and temperature dependent factors) in the general correct theory involve Franck–Condon vibrational overlap terms, which cannot and should not be disregarded in quantitative application.

S. A. Rice: While the approach of Kestner, Logan, and Jortner to electron transfer processes is elegant, it does not seem to reproduce the observed transfer probability as a function of electron-scavenger distance. The pre-exponential factor α' (containing information about Franck–Condon factor, density of states, and electronic coupling) does not appear to depend on the identity of the electron scavenger. Surprisingly, far better agreement between theory and experiment is obtained if β is dependent on the scavenger, and α is held constant at 10^{14} Hz (Rice and Pilling). Until this paradox is resolved advances in a quantitative description of the electron transfer probability are in danger of stagnating.

K. Funabashi: When the electronic energy separation between the initial and final states is much greater than their interaction energy, the electron transfer cannot be termed as 'tunnelling' which implies the driving force is essentially electronic. Apart from this semantic objection, long-range transfer process over 50 Å is not realistic in molecular solids. An alternative mechanism may involve some hopping motion of localized electrons in disordered or random lattice (Sher, Montroll, Ambegaoker, Halpern).

S. A. Rice: That an enhancement to the Smolchowski rate constant in liquids appears to correlate with electron tunnelling in glasses, suggests that the long-range (non-diffusive) motion of the electron is not associated with the thermally activated mobility of electrons discussed by Scher and Montroll.

Kinetics of electron capture by SF_6 in solution[1]

JAMES K. BAIRD

Health Physics Division, Oak Ridge National Laboratory, Oak Ridge, TN, U.S.A. 37830

Received September 27, 1976

JAMES K. BAIRD. Can. J. Chem. **55**, 2133 (1977).

We present a theory of the rate constant for electron capture by SF_6 when it is dissolved in liquid hydrocarbon and condensed rare gas solvents. The theory includes the effects of diffusion and solvation on the observed rate. Also included is the effect of the long-range polarization force acting between the electron and the SF_6 molecule. The role of the solvent molecules in modifying this force is taken into account by use of a dielectric screening function. The theory is applied with semiquantitative success to electron capture data in the solvents: methane, ethane, propane, butane, *n*-pentane, neopentane, *n*-hexane, cyclohexane, isooctane, tetramethylsilane, argon, and xenon.

JAMES K. BAIRD. Can. J. Chem. **55**, 2133 (1977).

On présente une théorie de la constante de vitesse de la capture de l'électron par SF_6 quand il est dissout dans un hydrocarbure liquide et dans des gas rares condensés agissant comme solvant. La théorie inclut les effets de diffusion et de solvatation sur les vitesses observées. On inclut aussi l'effet de la force de polarisation à longue distance agissant entre l'électron et la molécule de SF_6. On tient compte du rôle des molécules de solvant dans la modification de cette force en faisant appel à une fonction d'écran diélectrique. On a appliqué la théorie avec des succès semiquantitatifs pour des données de capture d'électron dans les solvants méthane, éthane, propane, butane, *n*-pentane, néopentane, *n*-hexanne, *c*-hexanne, isooctane, tétraméthylsilane, argon et xénon.

[Traduit par le journal]

Introduction

A number of measurements have recently been reported of the rate of electron capture by sulfur hexafluoride dissolved in various liquid hydrocarbons and condensed rare gases (1–3). Electrons were introduced into the solutions by the method of pulse radiolysis. In the experiments of Sowada *et al.* and Bakale *et al.*, for example, it was found that the electron current in the solutions decreased with time at a rate which was proportional to the sulfur hexafluoride concentration. The decay was taken to be evidence for a bimolecular reaction between an electron and a sulfur hexafluoride molecule. In discussion of these measurements, it is helpful to summarize first the relevant information which is known concerning the process whereby SF_6 captures electrons in the gas phase.

The often-proposed mechanism for the gas phase process is

$$[1a] \qquad e^- + SF_6 \underset{\tau^{-1}}{\overset{k}{\rightleftarrows}} SF_6^{-*}$$

$$[1b] \qquad SF_6^{-*} + M \xrightarrow{k_1} SF_6^- + M$$

$$[1c] \qquad SF_6^{-*} \xrightarrow{k_2} SF_5^- + F$$

where M is any third body, k is the rate constant for the formation of the compound negative ion SF_6^{-*}, τ is the autodetachment lifetime of SF_6^{-*}, k_1 is the rate constant for collisional stabilization, and k_2 is the rate constant for dissociative attachment. If the steady-state approximation $d[SF_6^{-*}]/dt = 0$ is applied, these equations give rise to an expression for the overall disappearance of the electrons

$$[2] \qquad \frac{1}{[e^-]}\frac{d[e^-]}{dt} = \frac{k(k_2 + k_1[M])[SF_6]}{\tau^{-1} + k_2 + k_1[M]}$$

The experimental value of the autodetachment lifetime, τ, of SF_6^{-*} is strongly dependent upon the conditions of measurement. Electron beam experiments, in which the electrons have an energy distribution with a width of about 0.1 eV, yield a lifetime of the order of 30 μs (4). Ion cyclotron resonance experiments where the electrons can have even lower energies, however, give a lifetime in the range 0.3–2 ms (5). The dissociative attachment rate constant k_2 is

[1] By acceptance of this article, the publisher or recipient acknowledges the U.S. Government's right to retain a non-exclusive, royalty-free license in and to any copyright covering the article.

characterized by an activation energy of approximately 0.43 eV (6) and is thus negligibly small for capture experiments carried out near room temperature. In experiments where a buffer gas M is present at a pressure of approximately 1 Torr or greater, the rate of collisional stabilization (eq. 1*b*) dominates the other rates leading to the destruction of SF_6^-*. Under this circumstance $k_1[M] + k_2 \gg \tau^{-1}$, so that

$$[3] \qquad d[e^-]/dt = -k[SF_6][e^-]$$

Thus, the forward reaction in [1*a*] is the rate-determining step, and the observed rate constant is equal to k. Experiment has shown that k is independent of temperature in the range 293 to 523 K (4, 6). The arithmetic mean of 23 reported experimental values is $k = (2.1 \pm 0.6) \times 10^{-7}$ cm^3/s (4, 6, 7). A careful analysis of the present state of our understanding of the SF_6 gas phase electron capture process has been given recently by Klots (8).

When the attachment experiment is run with sulfur hexafluoride dissolved in a liquid solvent, the solvent becomes the third body in the highest concentration capable of collisionally stabilizing the compound negative ion. Since collisions of SF_6^-* with the molecules of the solvent can be expected to be very frequent, the forward reaction in [1*a*] can be expected to remain the rate-determining step. This will be a basic assumption in what follows. Aside from this similarity between the gas and liquid phase attachment mechanisms, one can imagine at least two differences. (*1*) The rate of diffusion of electrons through the solvent may be slow enough to affect the observed values of the forward and backward rates in [1*a*]. (*2*) Assuming for the moment that the equilibrium constant of [1*a*] could be measured, the position of equilibrium will be shifted in the liquid phase toward the side of the reaction with the smaller Gibbs free energy of solution.

In the following sections of this paper, we will examine in detail these two effects.

Effect of Diffusion on Kinetics

The significance of diffusion may be seen by comparing (*a*) the electron velocity correlation length with (*b*) the distance which an electron travels before it meets a sulfur hexafluoride molecule. The velocity correlation length λ is the distance which an electron must travel in order to have suffered a sufficient number of collisions with the solvent molecules that its velocity is no longer correlated with its initial velocity. We let the correlation length serve as a measure of scale. A process which requires for its completion a dimension large compared with λ is considered to be macroscopic; otherwise, microscopic. An equation for λ is

$$[4] \qquad \lambda \approx (2\mu/e)(mk_BT)^{1/2}$$

where k_B is the Boltzmann constant, T the absolute temperature, and e, m, and μ are, respectively, the charge, the mass, and the mobility of the electron (9).

Calculation with measured values of the mobility (1, 2) shows that for ethane, propane, butane, *n*-pentane, *n*-hexane, and cyclohexane (hereafter called 'group 1 liquids'), λ is less than 1 Å. This distance is smaller than one molecular diameter and probably indicates that the electron spends part of its time in potential traps in these solvents as has often been postulated (10). For the solvents isooctane, neopentane, tetramethylsilane, methane, argon, and xenon (hereafter called 'group 2 liquids') under the conditions of the capture experiments (1, 2, 3), λ lies in the range 1.7 to 1074 Å. If we assume a uniform distribution of molecules in the solution, each SF_6 molecule finds itself at the center of spherical volume of solvent of radius $R = (3/4\pi[SF_6])^{1/3}$. In the experiments of Allen *et al.* (1) the SF_6 concentration varied little from 10^{-7} *M*. In the experiments of Bakale *et al.* (2) and Sowada *et al.* (3), the SF_6 concentration was adjusted so that in each solvent the electron current decayed with a characteristic time θ of approximately 30 ns. Hence, since $[SF_6] \gg [e^-]$, we have $k_s[SF_6] = \theta^{-1}$, where k_s is the observed rate constant. Numerical evaluation of R readily shows that $\lambda < R$ for all the experiments. We may conclude, therefore, that the capture of an electron takes place on a macroscopic scale and choose to describe its transport by use of diffusion theory.

Our analysis of diffusion follows the methods first introduced by Smoluchowski to treat the problem of coagulation of colloids and later extended by Debye to the problem of reaction kinetics in ionic solutions (11, 12).

Differential Equations

We begin by establishing a coordinate frame with center at the nucleus of the sulfur atom in SF_6. The SF_6 molecule is assumed to occupy

the spherical region $0 \leq r \leq \rho$, where r is the radial coordinate, and ρ is the SF_6 molecular radius. The region $\rho < r < \infty$ outside this sphere is assumed to be occupied by the solvent. An electron is regarded as being generated in the solvent at time $t = 0$ and diffusing toward the SF_6 molecule. Under the assumption that there are no sinks nor sources of electrons within the region $\rho < r < \infty$, Fick's laws of diffusion take the form

$$[5a] \qquad \frac{\partial c(\boldsymbol{r}, t)}{\partial t} + \nabla \cdot \phi(\boldsymbol{r}, t) = 0$$

$$[5b] \qquad \phi(\boldsymbol{r}, t) = -D\nabla c(\boldsymbol{r}, t) + c(\boldsymbol{r}, t)\boldsymbol{w}(\boldsymbol{r})$$

where $c(\boldsymbol{r}, t)$ is the electron concentration, $\phi(\boldsymbol{r}, t)$ is the electron flux, and $\boldsymbol{w}(\boldsymbol{r})$ is the electron drift velocity specified by

$$[6] \qquad \boldsymbol{w}(\boldsymbol{r}) = -\mu\nabla V(\boldsymbol{r})$$

In [6], $V(\boldsymbol{r})$ is the electrostatic potential of interaction of the electron with the SF_6 molecule. Since the center of coordinates lies at the center of the SF_6 molecule, the diffusion coefficient D in [5*b*] is given by

$$[7] \qquad D = D_{SF_6} + D_e$$

where D_{SF_6} is the coefficient for diffusion of a molecule of SF_6 through the solvent, and D_e is the coefficient for diffusion of an electron (13, see especially p. 61). For the solvents and temperatures we shall consider $D_{SF_6} \simeq 10^{-5}$ cm^2 s^{-1}, while $D_e > 10^{-4}$ cm^2 s^{-1}. Hence, we may conclude $D \simeq D_e$.

An analytical solution of [5] and [6] including both space and time dependence has yet to be obtained (11). However, a simplification can be achieved by reasoning as follows. Soon after the production of electrons by the pulse radiolysis, the initial electron concentration distribution dissipates, and the electron capture process reaches a steady state specified by $\partial c(\boldsymbol{r}, t)/\partial t = 0$. The time required for the approach to the steady state to be complete is of the order of $R^2/4D$ (11). Using experimental values for D (1, 2, 3), we find that in all experiments the steady state is achieved in times no longer than a few nanoseconds. These times are to be compared with $\theta = 1/k_s[SF_6]$. In the experiments of Bakale *et al.* (2) and Sowada *et al.* (3), for example, we noted previously that $\theta = 30$ ns. Since $\theta \gg R^2/4D$, we are fully justified in ignoring all explicit dependence on the time in [5]. In the steady state, substitution of [5*b*] into [5*a*] leads to

$$[8] \qquad \nabla^2 c(\boldsymbol{r}) + (1/k_B T)\nabla U(\boldsymbol{r}) \cdot \nabla c(\boldsymbol{r}) + (1/k_B T)c(\boldsymbol{r})\nabla^2 U(\boldsymbol{r}) = 0$$

which has been simplified by using the Nernst–Einstein relation

$$[9] \qquad \mu/D = e/k_B T$$

and by making the identification $U(\boldsymbol{r}) = e \cdot V(\boldsymbol{r})$. For the case of a sulfur hexafluoride molecule in the field of an electron, the leading term in the potential energy is

$$[10] \qquad U(r) = -\frac{1}{2}\frac{\alpha e^2}{r^4} f$$

where α is the SF_6 polarizability, and f is a screening function that expresses the diminution of the interaction between the SF_6 molecule and the electron due to the presence of the solvent (14, 15). The next lowest term in the potential energy is due to the interaction of the electron with the permanent hexadecapole moment of SF_6 and is the order of $1/r^5$ (16). This term, however, depends also upon the angular coordinates represented in $\boldsymbol{r}$ and leads to additional mathematical complications. Hence in what follows we shall ignore the hexadecapole term.

Inasmuch as $U(\boldsymbol{r})$ in [10] represents a central potential (depends only upon the magnitude of $\boldsymbol{r}$), eq. 8 simplifies to

$$[11] \qquad \frac{d}{dr}\left[r^2 \frac{dc(r)}{dr}\right] + \left(\frac{1}{k_B T}\right)\frac{d}{dr} \times \left[c(r)\left(r^2 \frac{dU(r)}{dr}\right)\right] = 0$$

Boundary Conditions

For the solution of [11], two boundary conditions are required. The first is

$$[12] \qquad \lim_{r \to \infty} c(r) = c(\infty)$$

where $c(\infty)$ is the bulk concentration of electrons, *i.e.*, that concentration measured at large distance from the SF_6 molecule. The second boundary condition is either of the two equations

$$[13a] \qquad 4\pi\rho^2\phi(\rho) = -k(\rho)c(\rho)$$

$$[13b] \qquad \lim_{r \to \infty} 4\pi r^2\phi(r) = -k(\infty)c(\infty)$$

where $k(\infty)$ is the scavenger rate constant observed at $r = \infty$, and $k(\rho)$ is a rate constant

determining the disappearance of electrons at $r = \rho$. Since there are no sources nor sinks of electrons within the region $\rho < r < \infty$, the quantity $4\pi r^2\phi(r)$ must be a constant independent of r. Hence,

$$[14] \qquad k(\rho)c(\rho) = k(\infty)c(\infty)$$

Relation Between $k(\rho)$ and $k(\infty)$

Subject to the above boundary conditions, the solution to [11] is

$$[15] \quad c(r) = c(\infty)\exp(-U(r)/k_BT) - \frac{k(\infty)c(\infty)}{4\pi D}\exp(-U(r)/k_BT) \times \int_r^\infty \exp(U(x)/k_BT)x^{-2}\,dx$$

We may use [14] and [15] to eliminate the ratio $c(\rho)/c(\infty)$ to obtain the relation

$$[16] \quad \frac{1}{k(\infty)} = \frac{1}{4\pi D\rho^*} + \frac{1}{k(\rho)\exp(-U(\rho)/k_BT)}$$

where ρ^* is the 'effective capture radius' (12) given by

$$[17] \quad \frac{1}{\rho^*} = \int_\rho^\infty \exp(U(x)/k_BT)x^{-2}\,dx$$

If in [10], $f > 0$, then $\rho > \rho^*$; if $f < 0$, then $\rho < \rho^*$.

In the limit that the reaction is diffusion controlled ($D \to 0$), $k(\infty)$ takes on the value k_d

$$[18] \qquad k_d = 4\pi D\rho^*$$

In the limit that the kinetics are homogeneous ($D \to \infty$), *i.e.*, the rate of reaction is determined by the rate of encounters between electrons and SF_6 molecules, $k(\infty)$ takes on the value k_h

$$[19] \qquad k_h = k(\rho)\exp(-U(\rho)/k_BT)$$

Condition of Equilibrium

The condition of equilibrium is attained when each separate elementary reaction in the mechanism is at equilibrium (17). Consider [1*a*] occurring in the liquid phase. We introduce lifetimes $\tau(\rho)$ and $\tau(\infty)$ to account for any difference between lifetimes evaluated at $r = \rho$ and at $r = \infty$, respectively. At equilibrium

$$[20a] \qquad k(\rho)\tau(\rho) = \frac{[SF_6^-{}^*]}{[SF_6]c(\rho)}$$

$$[20b] \qquad k(\infty)\tau(\infty) = \frac{[SF_6^-{}^*]}{[SF_6]c(\infty)}$$

At equilibrium there can be no net electron flux anywhere in the solution. Setting $\phi(r, t)$ to zero in [5*b*] and using the boundary condition [12], we find that

$$[21] \qquad c(r) = c(\infty)\exp(-U(r)/k_BT)$$

which is a Boltzmann distribution.

Combination of [16], [20], and [21] gives

$$[22] \quad \tau(\infty) = \tau(\rho)\left[1 + \frac{k(\rho)\exp(-U(\rho)/k_BT)}{4\pi D\rho^*}\right]$$

which is an expression relating the lifetimes, $\tau(\infty)$ and $\tau(\rho)$. Since the second term within the bracket in [22] is positive definite, we have $\tau(\infty) > \tau(\rho)$. Physically interpreted, this result means that the rate at which electrons appear at $r = \infty$ is much less than the rate at which they are produced at $r = \rho$ by autodetachment from $SF_6^-{}^*$. When an electron is emitted at $r = \rho$, there is a certain probability that it will be recaptured, since to reach $r = \infty$, it must diffuse against the action of the polarization potential $U(r)$. Hence, [22] evaluates the effect of 'secondary recombination' (32) on the decay of $SF_6^-{}^*$.

Effect of Solvation

By use of a thermodynamic cycle (29), one may show

$$[23] \quad \frac{k_h}{k} = \frac{\tau}{\tau_h}\exp[(\Delta G_s(e^-) + \Delta G_s(SF_6) - \Delta G_s(SF_6^-{}^*))/k_BT]$$

where we have defined

$$[24] \qquad \tau_h = \lim_{D\to\infty} \tau(\infty) = \tau(\rho)$$

as the lifetime for the case of homogeneous kinetics, and $\Delta G_s(e^-)$, $\Delta G_s(SF_6)$, and $\Delta G_s(SF_6^-{}^*)$ are the free energies for solution of e^-, SF_6, and $SF_6^-{}^*$, respectively. The gas phase quantities k and τ were previously defined by [1*a*]. Hence, we see that, the effects of diffusion aside, [1*a*] is shifted in the liquid phase toward the side of the reaction having the smaller Gibbs free energy of solution.

Comparison with Experiment

Calculation of ρ^* and k_h

To calculate ρ^* from [10] and [17], we need to establish the values of certain parameters. For ρ, the SF_6 radius, we take the value 2.92 Å, which is the sum of the S—F bond distance (1.57 Å) and the fluorine atom Van der Waal's radius (1.35 Å) (26, 27).

We may take for the polarizability of SF_6 either the static value $\alpha = 6.545$ Å^3 (28*a*) or the optical value $\alpha = 4.515$ Å^3 (28*b*) which was determined for electromagnetic radiation at 5460 Å. To establish the relevant value, we estimate the length of time during which the polarization interaction dominates the electron's motion through the solvent. The reciprocal of this time should be the order of magnitude of the natural frequencies of the sulfur hexafluoride molecule which are involved in interacting with the electron. The potential energy $U(r)$ becomes important when it equals the electron kinetic energy, $\frac{3}{2}k_BT$. From [10] we find that $|U(r)| = \frac{3}{2}k_BT$ at $r = r_c$, where

$$[25] \qquad r_c = \left(\frac{\alpha e^2 f}{3k_BT}\right)^{1/4}$$

The drift velocity of the electron is given by

$$[26] \qquad w = -\mu\frac{dV}{dr} = \frac{2\alpha e f}{r^5}\mu$$

The average drift velocity between r_c and ρ is

$$[27] \quad \bar{w} = 2\alpha e f\mu\left[\int_\rho^{r_c} r^{-5}\,dr\right]\left[\int_\rho^{r_c} dr\right]^{-1} = \frac{\alpha e f\mu}{2}\left(\frac{1}{r_c - \rho}\right)\left(\frac{1}{\rho^4} - \frac{1}{r_c^4}\right)$$

The time required for the electron to drift from $r = r_c$ to $r = \rho$ is

$$[28] \qquad t = \frac{r_c - \rho}{\bar{w}} = \frac{2\rho^2}{3D}\frac{[(r_c/\rho) - 1]^2}{[(r_c/\rho)^4 - 1]}$$

where we have used [9] to put μ in terms of D. For the temperatures we are considering (85–323 K) and either value of α, we find $r_c \sim 5$ to 7 Å. Taking $r_c \sim 6$ Å and applying [28], we find for group 1 liquids, $1/t \sim 10^{11}$ to 10^{13} s^{-1}. For these liquids, we choose to calculate ρ^* using the static value of α. For group 2 liquids, $1/t \sim 10^{14}$ to 10^{16} s^{-1}, so we choose the optical value of α.

To calculate ρ^*, we also need a formula for the electric dipole screening function, f. For a single component, nonpolar liquid without structure, Lekner has proposed the formula

$$[29] \qquad f = f_L = (1 + \tfrac{8}{3}\pi N_0\alpha_0)^{-1}$$

where α_0 and N_0 are, respectively, the electric dipole polarizability and number density of the molecules (14). In applying [29] to a solution, we assume that a solute molecule experiences the same dielectric screening as a solvent molecule. We identify the quantities N_0 and α_0 with the solvent molecules.

By use of the Clausius–Mossotti equation, the Lekner screening function may be put in the form

$$[30] \qquad f_L = (\varepsilon + 2)/3\varepsilon$$

where ε is the dielectric constant. We verified the validity of this substitution by testing the accuracy of the Clausius–Mosotti equation for the liquids under consideration. The densities of the liquids are known (18–20). Except for Ar and Xe, the electric dipole polarizabilities were calculated by addition of the appropriate atomic refractions (Landolt's rule) (21, 22). The polarizabilities of Ar and Xe are given in ref. 20. We used experimental values of the static dielectric constant ε or the sodium D line refractive index n_D ($n_D^2 = \varepsilon$, approximately for the hydrocarbons and the liquid rare gases) (23–25). We found that the Clausius–Mossotti equation was obeyed to within a few percent by all of the liquids except methane at 93 K where the error was 10%. Hence, we concluded that the replacement of $(8\pi/3)N_0\alpha_0$ in [29] by $(2\varepsilon - 2)/(\varepsilon + 2)$ was justified. For dilute solutions, the dielectric constant of the solution is very closely equal to the dielectric constant of the pure solvent; hence, in evaluating [30] for a solution, we identify ε with the dielectric constant of the solvent.

A screening function based upon a continuum dielectric model for a liquid has recently been proposed (15). It takes the form

$$[31] \quad f = f_1(u_1, \varepsilon) = \left(\frac{1}{u_1\varepsilon}\right) \times \left[\frac{u_1(\varepsilon + 2) - (\varepsilon - 1)}{(2\varepsilon + 1) - 2u_1(\varepsilon - 1)}\right]$$

This equation was also originally developed for a single component fluid. The parameter u_1 in that application referred to the properties of a single molecule, and the dielectric constant ε was taken to be that of the bulk fluid. In applying it to electron diffusion in solutions, we shall identify u_1 with the properties of the SF_6 molecule and take ε to be the dielectric constant of the pure solvent. We have $u_1 = \alpha/\rho^3$. The unit subscript was used in the original work to distinguish $f_1(u_1, \varepsilon)$ from the induced electric quadrupole screening function $f_2(u_2, \varepsilon)$, which was also derived, but which finds no immediate application here since the induced quadrupole potential is proportional to $1/r^6$.

The Lekner screening function, f_L, is positive definite, but $f_1(u_1, \varepsilon)$ is positive only for $\varepsilon < (1 + 2u_1)/(1 - u_1)$. When the screening function is positive, the integral in [17] can be related to the incomplete gamma function. When the screening function is negative, special techniques are required. The details of these calculations are given in the Appendix.

In [16], we identify $k(\infty)$ with the experimentally measured rate constant k_s and replace $k(\rho) \exp(-U(\rho)/k_B T)$ by k_h according to [19] to obtain

$$[32] \qquad \frac{1}{k_h} = \frac{1}{k_s} - \frac{1}{4\pi D\rho^*}$$

In what follows, we shall attempt to calculate k_h using experimental values of k_s and D in conjunction with values of ρ^* calculated on the basis of the Lekner and the continuum screening theories, respectively. We note that k_h, in contrast to k_s, contains none of the effects of diffusion.

Data Analysis Based on the Lekner Screening Function f_L

Our calculations based on the Lekner screening function (eq. 30) are summarized in Figs. 1 and 2.[2] For all liquids and conditions (1–3), we found that q defined by [A4] was greater than 10. Hence, ρ^* could be calculated to a high degree of accuracy from [A10*b*].

For the group 1 liquids (electron mobilities less than 1 $cm^2\ V^{-1}\ s^{-1}$), it was found that $4\pi D\rho^*$ was less than the experimental value of k_s. Hence, it made no sense to attempt to use [32] to calculate $1/k_h$, which must of necessity be positive definite. We assumed, instead, that in these liquids the reaction was diffusion controlled, *i.e.*, $k_s = k_d$. We calculated values of ρ^* from the experimental values of k_s and D using [18] and compared them with values of ρ^* calculated according to [A10*b*] as follows. From [A10*b*], it is clear that a plot of $\log_{10}(\rho^* f^{-1/4})$ as a function of $\log_{10} T$ forms a straight line of slope $-1/4$. For the liquids and range of temperatures under consideration (110 to 297 K), f as given by [30] is a weak function of ε, and hence T. Consequently, plots of $\log_{10} \rho^*$ *vs.* $\log_{10} T$ should also very nearly form straight lines. From Fig. 1, one may see that [A10*b*] reproduces the qualitative trend of the experimental data, but the calculated slope of $-1/4$ is smaller than the slope of the experimental data, which was determined by the method of least squares to be -1.2.

In Fig. 2, we have summarized our results for the group 2 liquids (electron mobility is greater than 1 $cm^2\ V^{-1}\ s^{-1}$). For these solvents we found that $4\pi D\rho^*$ was greater than k_s, so that it was possible to obtain a positive value for $1/k_h$ from [32]. The points are badly scattered, and the few trends that can be perceived are indicated by connecting the relevant points by curves.

Data Analysis Based on the Continuum Screening Function $f_1(u_1, \varepsilon)$

Our calculations based on the continuum screening function (eq. 31) are shown in Figs. 1 and 2.

Again, we found for the group 1 liquids that $4\pi D\rho^*$ was less than k_s. Hence, we chose to plot $\log_{10} \rho^*$ *vs.* $\log_{10} T$ under the assumption that the reaction was diffusion controlled. In most cases, we found q to be less than 3, so that ρ^* had to be calculated according to [A5] and [A7]. The theoretical points lie along straight lines because $I(q)$ is a rapidly converging series which is fairly well approximated by its first two terms only. A separate line is obtained for each liquid because $f_1(u_1, \varepsilon)$ is a much stronger function of ε than f_L (15), and the values of ε are different for different liquids. It is seen that the theoretical points derived from the continuum function lie along lines with positive slope while the experimental points show a trend characterized by a negative slope.

Our results for the group 2 liquids are shown in Fig. 2. In most cases, we found $f_1(u_1, \varepsilon) < 0$, and in a few cases were we able to determine a positive value for $1/k_h$. Because the continuum screening function in general predicts a less attractive polarization potential than does the Lekner screening function, we found that ρ^* was smaller when calculated from $f_1(u_1, \varepsilon)$ than when calculated from f_L. Hence, the values of k_h predicted by the continuum function are larger than those predicted by Lekner's function.

Discussion

We have seen that when we use the Lekner screening function, we are more often able to calculate a positive value of k_h than when we use the continuum screening function. Assuming

[2]A detailed summary of the relevant experimental data and all intermediate calculated quantities has been compiled in the form of tables. A complete set of tables is available, at a nominal charge, from the Depository of Unpublished Data, CISTI, National Research Council of Canada, Ottawa, Canada K1A 0S2.

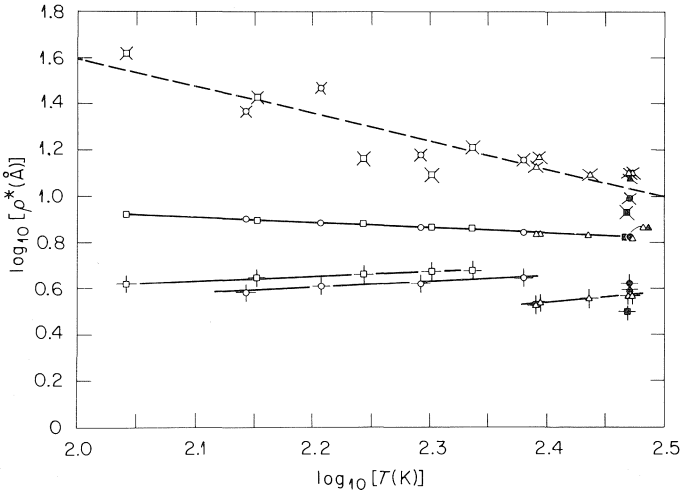

FIG. 1. Effective capture radius as a function of absolute temperature: □, ethane; ○, propane; ●, butane; ▲, *n*-pentane; △, *n*-hexane; and ■, cyclohexane. The plain symbols are points calculated from [A10*b*] with f given by the Lekner function (eq. 30). The symbols bearing crosses are points calculated from [A5] and [A7] with f given by the continuum function (eq. 31). In all calculations $\alpha = 6.545$ Å^3 and $\rho = 2.92$ Å. The symbols bearing the ×'s are based solely on experimental data (refs. 1–3) with ρ^* calculated from $\rho^* = k_s/4\pi D$.

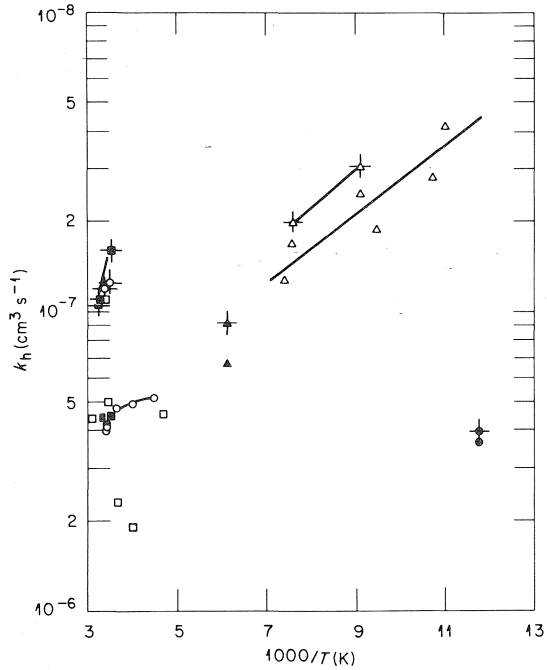

FIG. 2. Homogeneous rate constant as a function of absolute temperature: □, isooctane; ■, neopentane; ○, tetramethylsilane; △, methane; ●, argon; and ▲, xenon. All values of k_h were determined from [32] and experimental values of D and k_s (refs. 1–3). The plain symbols are points for which ρ^* was calculated using Lekner's screening function, while the symbols bearing the crosses are points calculated using the continuum screening function. In all calculations $\alpha = 4.515$ Å^3 and $\rho = 2.92$ Å.

that the capture rate is diffusion controlled in the group 1 liquids, we find that the Lekner screening function predicts a value of ρ^* which is uniformly too low, however. The values of ρ^* calculated on the basis of the continuum screening function are lower still. One may show that, even assuming the strongest attractive polarization potential possible ($f = 1$), eq. A10*b* gives values for ρ^* smaller than those observed experimentally. There are at least two possible causes. (*1*) The multipole expansion of the potential of interaction of the electron with the SF_6 molecule, of which $-\frac{1}{2}\alpha e^2 f/r^4$ is the leading term, may break down for values of r of the order of ρ; and (*2*) when the electron gets near the SF_6 molecule, it may tunnel through the solvent into the region $r < \rho$. Such a tunneling mechanism has already been proposed by Pilling and Rice (30). Until the role played by these two effects is examined, it would seem premature to rule in favor of the Lekner screening function.

Comparison of Different Scavengers

For the group 1 liquids, the electron mobility satisfies the empirical relation

$$[33] \qquad \mu = \mu_0 \exp(-E/k_B T)$$

where μ_0 is a constant independent of temperature and E is an activation energy (1). Assuming that the electron capture reaction is diffusion controlled, we may combine [A10*b*], [33], and

[9] to obtain for the case $q \geq 3$ the semiempirical equation

$$[34] \quad k_d = 4\pi D\rho^* = \frac{8\pi\sqrt[4]{8}}{\Gamma(1/4)}\mu_0 T^{3/4} \times (\alpha f_L k_B{}^3/e^2)^{1/4} \exp(-E/k_B T)$$

for k_d. For dilute solutions, the Lekner screening function depends upon properties of the solvent alone. Hence, if S_1 and S_2 are two different electron scavengers which interact with electrons at long range principally through the polarization force, one finds from [34] that for a given solvent and temperature

$$[35] \quad k_d(S_1)/k_d(S_2) = (\alpha(S_1)/\alpha(S_2))^{1/4}$$

where $k_d(S_1)$, $k_d(S_2)$, $\alpha(S_1)$, and $\alpha(S_2)$ are the respective polarizabilities and diffusion-controlled rate constants. Since $k_d(S_1)/k_d(S_2)$ depends upon the fourth root of $\alpha(S_1)/\alpha(S_2)$, one would expect to observe little difference in the scavenging power of S_1 and S_2.

Fluid Structure

For the case of liquid argon, Lekner's work provides us an opportunity to assess the role played by a fluid structure in determining ρ^*. Let us consider for the moment pure liquid argon and establish a coordinate system with origin at the nucleus of one of the atoms in the liquid. Call the radial distance from this atom to any other point in the fluid, r. Since the intermolecular force tends to attract a number of atoms into a coordination layer around any given atom in the fluid, the screening function will depend upon r. Lekner has shown that this screening function $f(r)$ satisfies an integral equation (eq. 11 of ref. 14) which involves the pair correlation function for the fluid. He took for his pair correlation function a form calculated from the Percus–Yevick equation for hard spheres. Lekner solved the integral equation for the screening function by numerical methods and obtained the plot shown in Fig. 3. Note that as r/β increases, where β is the Ar hard-core radius, that $f(r)$ approaches f_L (eq. 30). Remember that f_L is the screening function for a fluid without structure, *i.e.*, a fluid for which the pair correlation function $g(r)$ satisfies

$$[36] \quad g(r) = \begin{cases} 0, & r < 2\beta \\ 1, & r > 2\beta \end{cases}$$

The asymptotic relationship in Fig. 3 between $f(r)$ and f_L is due to the fact that there is no long-range order in the fluid.

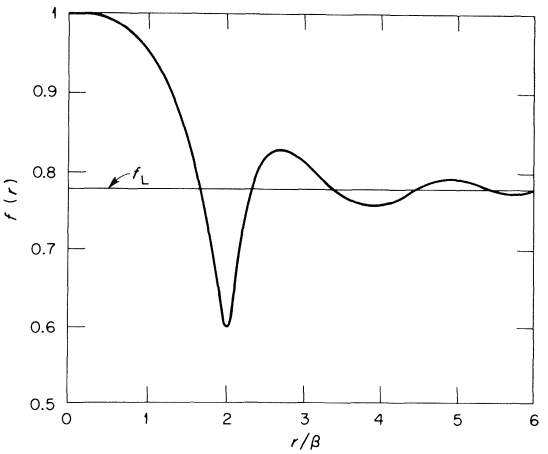

FIG. 3. Screening function $f(r)$ for liquid argon at 85 K. Hard-core radius $\beta = 1.72$ Å.

We now turn our attention to the case of sulfur hexafluoride dissolved in argon. The density of argon atoms in the vicinity of the SF_6 molecule is not known. In the absence of this information, we will make the following assumption. Although the SF_6 radius (2.92 Å) is significantly larger than the Ar hard-core radius (1.72 Å), we will assume that the radial distribution function which applies to an Ar atom in the pure liquid also applies to the SF_6 molecule. Consequently, we will assume that the screening function appropriate to an SF_6 molecule dissolved in liquid Ar is given by the $f(r)$ in Fig. 3 with $\beta = 2.92$ Å.

With this assumption, we have replaced f in [10] by $f(r)$ and evaluated the integral in [17] numerically. For comparison, we have plotted in Fig. 4 the integrand in [17] with f set equal to $f(r)$ and set equal to f_L, respectively. The small differences in these curves are due to the oscillations in $f(r)$. The areas under the two curves are nearly identical. When $f = f(r)$, we found $\rho^* = 8.42$ Å, while when $f = f_L$, we found from [A10*b*] $\rho^* = 8.45$ Å. Thus, we see that the liquid structure produces sizable oscillations in $f(r)$ which, however, tend to compensate each other in the calculation of ρ^* by [17]. Within the limitations of our assumption, we may conclude that the details of the liquid structure play no important role in determining the value of ρ^*.

Solvation

At this point it would be quite interesting to make a quantitative comparison between k_h and k using [23] and the results in Fig. 2. This comparison requires a knowledge of the free

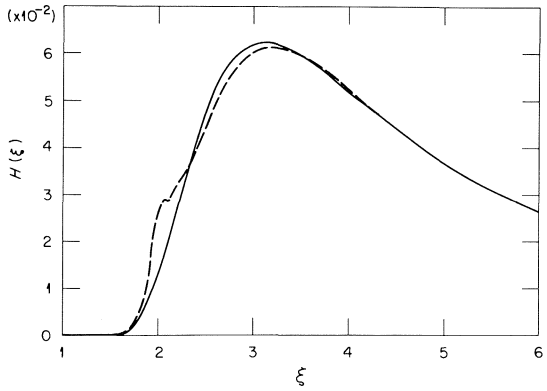

FIG. 4. Plot of the integrand of the ρ* integral (eq. 17) with potential given by [10]. The abscissa is $\xi = x/\rho$, and the ordinate is

$$H(\xi) = \xi^{-2} \exp(-p\xi^{-4} f(\xi))$$

where

$$\rho/\rho^* = \int_1^\infty H(\xi)\, d\xi, \quad p = (\alpha e^2/2k_B T\rho^4)$$

$\alpha = 4.515$ Å^3, $\rho = 2.92$ Å, and $T = 85$ K. Solid curve: $f(\xi) = f_L = (\varepsilon + 2)/3\varepsilon$ with $\varepsilon = 1.51$. Dashed curve: $f(\xi)$ is given by the curve in Fig. 3 with β set equal to ρ.

energies $\Delta G_s(SF_6)$, $\Delta G_s(SF_6^{-*})$, and $\Delta G_s(e^-)$. Methods of calculating these have been proposed recently by Henglein (33) and by Holroyd *et al.* (29). Quantitative evaluation of [23] is frustrated, however, because most of these estimates contain errors large compared with $k_B T$. Suffice it to say, however, that only k_h (not k_s) bears thermodynamic comparison with k. This is because diffusion is an inherently nonequilibrium process. According to [32], the effect of diffusion, which gives rise to the term $1/4\pi D\rho^*$, must be subtracted from $1/k_s$ before a result is obtained which depends only upon the equilibrium properties of solvent and solute.

Comparison with Other Theories

Henglein has given an electrochemical theory of electron capture in liquids (33). In this theory, the rate constant depends upon (*1*) the rate of encounters between the electrons and scavenger molecules, (*2*) the number of electrons per unit energy, and (*3*) the density of unoccupied electron acceptor levels in the scavenger. Henglein's rate constant most closely approximates k_h in the present theory.

Funabashi and Magee have used the Fermi golden rule of quantum mechanics to calculate the liquid phase rate constant for dissociative attachment of electrons to the solutes C_2H_5Br and CCl_4 (31). They have chosen to ignore the effects of diffusion on the rate constant and have thus limited their attention to solvents in which the electron mobility is much greater than 1 cm^2 V^{-1} s^{-1}. In cases where dissociative attachment is the rate-determining step, their calculation also represents an evaluation of a rate constant closely analogous to k_h in our theory. Both C_2H_5Br and CCl_4 interact with the electron through noncentral potentials, so that the treatment of diffusion we have used does not apply. It would be of interest, however, to combine the theory of Funabashi and Magee with a treatment of electron diffusion in a noncentral potential to give a general theory of dissociative attachment in the liquid phase.

Holroyd *et al.* (29) studied the kinetics of electron attachment to CO_2 in solution. In their theoretical analysis, they chose not to take into account the effect of the long-range interaction of the charge of the electron with the permanent quadrupole moment of the CO_2 molecule. They did, however, include the effect of the drift of the electron in an external electric field, a phenomenon not included by the present theory. A theory of electron diffusion combining the effects of the external field and the long-range electron–molecule forces is possible in principle. It would require, however, that noncentral potentials be dealt with as mentioned above.

Acknowledgements

The author would like to thank Dwight Russell for his help in preparing the tables and the figures. He would like to acknowledge some helpful discussions of the theory with C. E. Klots and V. E. Anderson.

1. A. O. ALLEN, T. E. GANGWER, and R. A. HOLROYD. J. Phys. Chem. **79**, 25 (1975).
2. G. BAKALE, U. SOWADA, and W. F. SCHMIDT. J. Phys. Chem. **79**, 3041 (1975).
3. U. SOWADA, G. BAKALE, K. YOSHINO, and W. F. SCHMIDT. Chem. Phys. Lett. **34**, 466 (1975).
4. R. N. COMPTON, L. G. CHRISTOPHOROU, G. S. HURST, and P. W. REINHARDT. J. Chem. Phys. **45**, 4634 (1966).
5. R. W. ODOM, D. L. SMITH, and J. H. FUTRELL. Chem. Phys. Lett. **24**, 227 (1974).
6. F. C. FEHSENFELD. J. Chem. Phys. **53**, 2000 (1970).
7. (*a*) F. J. DAVIS and D. R. NELSON. Chem. Phys. Lett. **6**, 277 (1970); (*b*) L. G. CHRISTOPHOROU, D. L. MCCORKLE, and J. G. CARTER. J. Chem. Phys. **54**, 253 (1971).
8. C. E. KLOTS. Chem. Phys. Lett. **38**, 61 (1976).
9. J. MATHEWS and M-A. NICOLET. Am. J. Phys. **44**, 448 (1976).
10. N. R. KESTNER and J. JORTNER. J. Chem. Phys. **59**, 26 (1973).
11. S. H. LIN, K. P. LI, and H. EYRING. Theory of reac-

tion rates in condensed phases. *In* Physical chemistry: an advanced treatise. Vol. 7. *Edited by* H. Eyring. Academic Press, New York. 1975. Chapt. 1.
12. R. M. Noyes. Prog. React. Kinet. **1**, 129 (1961).
13. S. Chandrasekhar. Rev. Mod. Phys. **15**, 1 (1943).
14. J. Lekner. Phys. Rev. **158**, 130 (1967).
15. J. K. Baird. J. Phys. Chem. **79**, 2862 (1975).
16. S. Kielich. General molecular theory and electric field effects in isotropic dielectrics. *In* Dielectric and related molecular processes: a specialist periodical report. *Edited by* M. Davies. The Chemical Society, London. 1972. Chapt. 7.
17. O. K. Rice. Statistical mechanics, thermodynamics, and kinetics. W. H. Freeman, San Francisco, Calif. 1967. p. 470.
18. F. D. Rossini, K. S. Pitzer, R. L. Arnett, R. H. Brown, and G. C. Pimental. Selected values of physical and thermodynamic properties of hydrocarbons and related compounds. American Petroleum Institute, Carnegie Press, Pittsburgh, Penn. 1953.
19. E. B. Baker, A. J. Barry, and M. J. Hunter. Ind. Eng. Chem. **38**, 1117 (1946).
20. R. L. Amey and R. H. Cole. J. Chem. Phys. **40**, 146 (1964).
21. R. C. Weast (*Editor*). Handbook of chemistry and physics. 54th ed. Chemical Rubber Company Press, Cleveland, Ohio. 1973–74. p. E221.
22. S. S. Batsanov. Refractometry and chemical structure. Translated by P. P. Sutton. Consultants Bureau, New York. 1961.
23. Landboldt-Bornstein. Zahlenwerte und funktionen aus physik, chemie, astronomie, geophysik und technik. II Band, 8 Teil. Optische Konstanten. Springer Verlag, Berlin, Sechste Auflage. 1962. p. 5-573.
24. A. P. Altshuller and L. Rosenblum. J. Am. Chem. Soc. **77**, 272 (1955).
25. R. C. Weast (*Editor*). Handbook of Chemistry and Physics. 54th ed. Chemical Rubber Company Press, Cleveland, Ohio. 1973–74. pp. E54–E57.
26. Gmelins handbuch der anorganishen chemie, Schwefel, Tiel B – Lieferung 3, System-Number 9. Verlag Chemie, GmbH, Weinheim/Bergstr. 1963. p. 1716.
27. J. C. Speakman. Molecules. McGraw-Hill, New York. 1966. p. 99.
28. (*a*) H. E. Watson, G. G. Rao, and K. L. Ramaswamy. Proc. R. Soc. London, **143**, 558 (1933–34); (*b*) Gmelins handbuch der anorganishen chemie, Schwefel, Tiel B – Lieferung 3, System-Number 9. Verlag Chemie, GmbH, Weinheim/Bergstr. 1963. p. 1720.
29. R. A. Holroyd, T. E. Gangwer, and A. O. Allen. Chem. Phys. Lett. **31**, 520 (1975).
30. (*a*) M. J. Pilling and S. A. Rice. J. Phys. Chem. **79**, 3035 (1975); (*b*) M. J. Pilling and S. A. Rice. J. Chem. Soc. Faraday Trans. II, **71**, 1563 (1975).
31. K. Funabashi and J. L. Magee. J. Chem. Phys. **62**, 4428 (1975).
32. W. Scheider. J. Phys. Chem. **76**, 349 (1972).
33. A. Henglein. Ber. Bunsenges. Phys. Chem. **79**, 129 (1975).

Appendix: Calculation of ρ^*

Case I, $f > 0$

In order to evaluate the integral

$$[A1] \quad \frac{1}{\rho^*} = \int_\rho^\infty \exp\left(U(x)/k_B T\right) x^{-2}\, dx$$

where

$$[A2] \quad U(x) = -\frac{1}{2}\frac{\alpha e^2}{x^4} f$$

we let

$$[A3] \quad y = \frac{\alpha e^2 f}{2k_B T x^4}$$

and

$$[A4] \quad q = \frac{\alpha e^2 f}{2k_B T \rho^4} = \frac{|U(\rho)|}{k_B T}$$

The result of making these substitutions in [A1] is

$$[A5] \quad \rho^*/\rho = 4q^{1/4}/I(q)$$

where

$$[A6] \quad I(q) = \int_0^q y^{-3/4} e^{-y}\, dy$$

is an integral related to the incomplete gamma function. Values of $I(q)$ may be readily generated, however, without reference to the incomplete gamma function by expanding the exponential in the integrand and integrating term by term. The resulting sum is

$$[A7] \quad I(q) = 4q^{1/4} \sum_{n=0}^{\infty} \frac{(-1)^n q^n}{(4n+1)n!}$$

For $q \lesssim 10$, this sum converges after the evaluation of a few dozen terms. However, for $q \gtrsim 3$, $I(q)$ differs insubstantially from $\Gamma(1/4) = 3.6256....$ Consider

$$[A8] \quad \Gamma(1/4) = \int_0^\infty y^{-3/4} e^{-y}\, dy = I(q) + \int_q^\infty y^{-3/4} e^{-y}\, dy$$

Now

$$[A9] \quad \int_q^\infty \frac{e^{-y}}{y^{3/4}}\, dy < \int_q^\infty \frac{e^{-y}}{q^{3/4}}\, dy = q^{-3/4} e^{-q}$$

For $q = 3$, $q^{-3/4} e^{-q}$ has the value 0.022. Hence, for most practical purposes, we may conclude that for $q \gtrsim 3$,

$$[A10a] \quad \rho^*/\rho = 4q^{1/4}/\Gamma(1/4) = 1.103q^{1/4}$$

By combining [A4] and [A10*a*], we find that ρ^* is in fact independent of ρ and given by

$$[A10b] \quad \rho^* = \frac{4}{\Gamma(1/4)}\left(\frac{\alpha e^2 f}{2k_B T}\right)^{1/4}$$

Case II, $f < 0$

For this case, we let

[A11] $$q = \frac{\alpha e^2 |f|}{2k_B T \rho^4}$$

and

[A12] $$\rho^*/\rho = 4q^{1/4}/J(q)$$

where

[A13] $$J(q) = \int_0^q y^{-3/4} e^y \, dy$$

which is no longer equal to a gamma function as q goes to infinity. Hence, we rely on the series representation

[A14] $$J(q) = 4q^{1/4} \sum_{n=0}^{\infty} \frac{q^n}{(4n+1)n!}$$

to calculate $J(q)$.

Discussion

G. R. Freeman: We have recently estimated that the reaction of electrons with SF_6 in alcohols is not quite diffusion controlled. Does that agree with what you would predict?

J. K. Baird: I have difficulty in answering the question in the affirmative, because alcohols belong to the class of polar solvents. The theories of dielectric screening presently available (see refs. 14 and 15) refer exclusively to nonpolar liquids. A theory of dielectric screening in a polar solvent is conceivable, however.

A. O. Allen: Would your treatment account for the very high rate of reaction of solvated electrons (in water or alcohol) with iodine (I_2), which corresponds to a reaction radius of the order of 10 Å?

J. K. Baird: No. The reason is that I_2 possesses a permanent electric quadrupole moment which would give rise to the leading term in its interaction with the electron. The quadrupole gives rise to a noncentral potential and consequently introduces an angle variable into the Debye–Smoluchowski equation. The angular and radial parts of this equation might not be separable in such cases, which of course would constitute a major obstacle in finding its solution. I have thought about this problem but as of yet not had the opportunity to investigate it in detail.

J. M. Warman: Have you looked at other spherical molecules such as CCl_4 which has an attachment rate constant similar to that for SF_6 in the gas phase but displays different temperature behaviour to SF_6 in both the gas and liquid (TMS) phases?

J. K. Baird: Carbon tetrachloride has a permanent electric octupole moment which would compete with the molecular polarizability in attracting the electron. The octupole moment is likely to raise the same difficulty in solving the Debye–Smoluchowski equation as was indicated in my answer to Dr. Allen's question. However, like you, it is clear to me that an attack on the problem of diffusion of electrons in multipolar fields (especially the field of a permanent dipole) is necessary if the theory is to be compared with the bulk of the experimentally known rate constant values.

Electron reactivity in liquid hydrocarbon mixtures

TOSHINORI WADA, KYOJI SHINSAKA, HIDEKI NAMBA, AND YOSHIHIKO HATANO

Laboratory of Physical Chemistry, Tokyo Institute of Technology, Meguro-ku, Tokyo 152, Japan

Received October 4, 1976

TOSHINORI WADA, KYOJI SHINSAKA, HIDEKI NAMBA, and YOSHIHIKO HATANO. Can J. Chem. **55**, 2144 (1977).

The electron current in neopentane–*n*-hexane mixtures, produced by a few nanoseconds X-ray pulse in the presence of external electric field, has been observed in the nanosecond–microsecond range. The form of the time dependence of the electron current has been shown to vary with dose per pulse and is analysed accordingly. The electron mobilities μ_e are thereby determined in the mixtures. The rate constant of electron–ion recombination, k_r, is proportional to the mobility over the wide range of μ_e. The rate constant for electron scavenging, k_s, by CCl_4 varies with $\sqrt{\mu_e}$; k_s for C_2H_5Br shows a maximum for a mixture with the mole fraction of *n*-hexane, $x_h = 0.48$. The results for k_s obtained for the mixtures agree with those by Allen and co-workers for various neat hydrocarbons. Further, the mechanism of electron transport in non-polar liquids is discussed. Using experimental results for V_0 and E_a for the mixtures (the energy of the electron in its quasifree state and the activation energy of μ_e, respectively) V_0 is expressed by a linear function of E_a: $V_0 = -0.42 + 2.6E_a$ at room temperature and μ_e is correlated with V_0 as an empirical formula $\mu_e = 125/[1 + 360 \exp(15V_0)]$ based on a trapping model.

TOSHINORI WADA, KYOJI SHINSAKA, HIDEKI NAMBA et YOSHIHIKO HATANO. Can. J. Chem. **55**, 2144 (1977).

On a observé le courant d'électrons qui se produit, dans l'écart de nanosecond–microsecond dans des mélanges de néopentane–*n*-hexane soumis à une pulsation de quelques nanoseconds de rayon-X en présence d'un champ électrique externe. On a démontré que la forme de la relation qui existe entre le temps et le courant d'électrons varie avec la dose par pulsation et on l'a analysée en conséquence. On a déterminé les mobilités électroniques, μ_e, des mélanges. La constante de vitesse de la recombinaison électron–ion, k_r, est proportionnelle à la mobilité sur un grand écart de μ_e. La variation de la constante de vitesse, k_s, pour le piégeage des électrons par CCl_4 est pratiquement proportionnelle à $\sqrt{\mu_e}$; k_s pour C_2H_5Br présente un maximum pour un mélange avec une fraction molaire de *n*-hexane $x_h = 0.48$. Les résultats obtenus pour k_s pour les mélanges sont en accord avec ceux de Allen et coll. pour divers hydrocarbures à l'état pur. De plus, on discute du mécanisme de transport d'électrons dans des liquides nonpolaires. Utilisant des résultats expérimentaux pour V_0 et E_a pour des mélanges, qui sont respectivement l'énergie de l'électron dans son état pratiquement libre et l'énergie d'activation de μ_e, on peut exprimer V_0 par une fonction linéaire de E_a: $V_0 = -0.42 + 2.6E_a$ à la température de la pièce et μ_e est relié avec V_0 par une formule empirique $\mu_e = 125/[1 + 360 \exp(15V_0)]$ qui est basée sur un modèle de piégeage.

[Traduit par le journal]

Introduction

Recently the behavior of electrons in non-polar liquids, especially in liquid hydrocarbons, has received great attention among radiation chemists, mainly with respect to electron transport phenomena (1–4) and electron reactivities (5–9).

The mobility μ_e has been measured for a large number of liquid hydrocarbons. It has been found that μ_e depends strongly upon the molecular structure of the solvent molecule: μ_e in neopentane is about three orders of magnitude greater than that in *n*-hexane. It has been suggested by Freeman and co-workers (4) that the electron mobility tends to be larger when the solvent molecule is more spherical. The temperature dependence of μ_e has also been investigated and it provides important information about the mechanism of electron transport in liquid hydrocarbons (1, 2). In addition the energy required to inject an electron from the vacuum into the liquid, V_0, has been measured by Holroyd *et al.* (10) for various hydrocarbons. The quantity V_0 is assumed to be the electron potential energy in the conducting state with respect to that *in vacuo* and it has been correlated with the electron mobility. It has generally been accepted that the mechanism of electron transport in liquid hydrocarbons can be explained in terms of two essentially different states for

electrons: a localized or trapped state and a delocalized or quasifree state. A suitable configuration of a group of molecules at a particular site in the liquid provides a region of low potential energy for an electron, where the electron is localized until it is thermally activated into the quasifree state. The electron transport takes place through a succession of migrations from one trap to another as a conduction electron. This mechanism has been referred to as a trapping model (1, 2).

The rates of electron scavenging and of electron–ion recombination have been measured in liquid hydrocarbons with different molecular structures. It has been found that the reactivity of the electron toward scavengers differs significantly from one solvent to another. In cyclohexane the absolute rate constants of free electron scavenging, k_s, as well as the efficiencies of geminate electron scavenging reported by Klein and Schuler (11), depend very little upon the nature of the scavengers (7, 8). In neopentane, on the other hand, a noticeable difference among the relative values of k_s was first observed by Hatano and co-workers (12) from experiments on the competitive free electron scavenging of N_2O with various scavengers. Allen and co-workers (8) have also pointed out that in neopentane and tetramethylsilane the value of k_s is largely dependent upon scavengers. Beck and Thomas (6*a*) have correlated k_s for biphenyl in several hydrocarbons with the electron mobility and found that k_s varies rather closely with the square root of μ_e. Allen *et al.* (8*b*) have correlated k_s for various scavengers in different hydrocarbons and tetramethylsilane with the quantity V_0, where CCl_4 and C_2H_5Br show the two typical correlations of k_s *vs.* V_0. The value of k_s for CCl_4 increases monotonically with decreasing V_0 (or increasing μ_e), while k_s for C_2H_5Br exhibits a maximum for a characteristic value of V_0. To elucidate theoretically these apparent anomalies Funabashi and Magee (13) have proposed a model where electron scavenging in high-mobility liquids is treated as an electron capture process which is completely analogous to the gas phase process.

In most experiments carried out so far the quantities μ_e, V_0, and k_s have been determined for various *neat* hydrocarbons with different molecular structures and correlated with each other as mentioned above. For hydrocarbon *mixtures*, on the other hand, the values of k_s are almost unknown, although the quantities μ_e (2*b*) and V_0 (10*d*) have already been determined as a function of the mole fraction of the component. In this work we have determined, using conductivity techniques, the values of k_s for CCl_4 and C_2H_5Br in neopentane–*n*-hexane mixtures, where μ_e and k_r, the rate constant of electron–ion recombination, are also measured. By mixing a suitable amount of the two hydrocarbons, one can obtain a solution adjusted to a desired μ_e or V_0. Further, the mechanism of electron transport in non-polar liquids is discussed on the basis of the experimental results obtained for the mixtures.

Experimental

Materials

Neopentane (>99.94 mol% pure) and *n*-hexane (>99.99 mol% pure) were Phillips Research Grade. These were used after further treatment as follows. Each hydrocarbon was stirred under vacuum with concentrated H_2SO_4 for 20 h, with NaOH pellets for 4 h, with $LiAlH_4$ powder for 4 h, and with Na–K alloy for 20 h, then transferred into a measuring cylinder with which the volume of the liquid was measured at room temperature. Known volumes of each hydrocarbon were transferred into a vessel and mixed together. After a final purification with Na–K alloy for 10 h, the mixture was introduced under high vacuum ($\sim 10^{-6}$ torr) into a conductance cell.

Carbon tetrachloride (Merck, 99.8%) and ethyl bromide (Tokyo Kasei, >99%) were used as solutes after the usual degassing.

Conductance Cell[1]

Circular plates of stainless steel were placed in parallel, having an interelectrode distance of 3.5 mm. The collecting electrode had an area of 7.8 cm^2 and was protected by a guard ring from edge effects. The electrodes were sealed in a glass envelope which had a reservoir of 50 ml and a side arm with several break-seals. The conductance cell was coated on the outside surface with Ag paint to shield it from electromagnetic effects.

Conductivity Measurements

The apparatus used for conductivity measurements is schematically shown in Fig. 1. The conductance cell containing a sample was set in the shielded box. A potential difference of -1000 V, unless otherwise mentioned, was supplied to the high voltage electrode by a FLUKE 415B high voltage power supply through a low pass filter (8 kHz). The sample between the electrodes was irradiated with a few nanosecond pulse of X-rays through a window surrounded by lead bricks of 5 cm thickness. The single pulse of X-rays was generated by an impinging pulse of 0.6 MeV electrons from a Febetron 706 accelerator on 0.1 mm tungsten foil (14). The electron current induced in the external circuit of the cell was observed by an oscilloscope (Tektronix 454A MOD 163D,

[1]The conductance cell used in this experiment is the same type as illustrated in ref. 4*c* except for some modification.

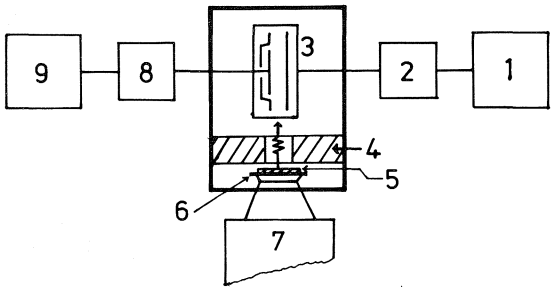

FIG. 1. Schematic representation of the apparatus: (*1*) high voltage power supply, (*2*) 8 kHz low pass filter, (*3*) conductance cell, (*4*) lead brick of 5 cm thickness, (*5*) lead plate of 0 to 8 mm thickness, (*6*) tungsten foil, (*7*) Febetron 706 accelerator, (*8*) 1 MHz amplifier, (*9*) 60 MHz oscilloscope.

150 MHz) through a signal filter (3 MHz) if necessary, or by an oscilloscope (Tektronix 5403-D44, 60 MHz) with an amplifier (Tektronix 5A26, 1 MHz) for measurements of the smaller current. The oscilloscope was connected to the collecting electrode by a coaxial cable with a 50 Ω termination. The conductivity measurements were carried out at room temperature (296 ± 3) K.

Dosimetry

The conductance cell was placed 11 cm from the tungsten foil. The dose absorbed by the sample was measured by a film-badge or a thermoluminescent dosimetry. Since the pulse intensity at a charging voltage of 25 kV varied from pulse to pulse with about ±10% fluctuation, the absorbed dose and the conductivity were determined by averaging the results of several runs. It should be noted that a single pulse of X-rays from Febetron 706 delivers a large dose to the sample in comparison with that from other accelerators. The highest pulse dose obtained in this experiment was 160 mrad. We could obtain any pulse dose desired by attaching a lead plate of 0 to 8 mm thickness to the tungsten foil (Fig. 1).

Addition of Solutes

A small space (1.24 ml) between two valves was filled with vapor (0.1 torr) of CCl_4 or C_2H_5Br. This small amount of the additive was transferred onto the frozen mixture in the conductance cell through the side arm. Then the cell was sealed off. After melting, the cell was inverted several times to dissolve the solute in the solvent. The method for additive transfer to the cell was checked by gas chromatography using a flame ionization detector. To prepare samples of various concentrations additional solute was added after each run to the mixture of 30 ml. It was assumed that the added solute dissolved completely in the liquid phase.

Results and Discussion

Rate Constants of Electron–Ion Recombination in Pure Neopentane and in Neopentane–n-Hexane Mixtures

The decay of the conductivity signal shown in Fig. 2 was observed when neopentane was irradiated with a pulse of X-rays at the highest pulse dose (160 mrad). Reducing the absorbed dose D, the initial half-life of decay $t_{1/2}$ becomes longer in proportion to log $(1/D)$, and at a pulse dose below 10 mrad it assumes a constant value (475 ± 15 ns) as shown in Fig. 3.

The electron current $I_e(t)$ observed following a pulse of X-rays is given by

$$[1] \qquad I_e(t) = \frac{eA\mu_e E}{d}\int_0^d n_e(x,t)\,dx$$

where e is the electron charge, A the area of the collecting electrode, d the distance between electrodes, E the applied field strength, and n_e the electron concentration at the distance x from the collecting electrode. The change in the electron concentration should be described by

$$[2] \quad -\left(\frac{\partial n_e}{\partial t}\right) = \mu_e E\left(\frac{\partial n_e}{\partial x}\right) + k_{tr}n_e + k_r n_e n_+ + k_s[S]n_e$$

The first term on the right hand side of [2] represents the contribution due to drifting of electrons to the collecting electrode in the presence of an external field. The second term is due to conversion of high-mobility electrons to negative charge carriers of lower mobility with the rate constant k_{tr}, possibly by attachment to residual impurities which might remain even after rigorous purification described in the Experimental section. The third is due to electron–ion recombination with the rate constant k_r, where n_+ is the concentration of positive ions. The last term is due to electron scavenging by a solute S with the rate constant k_s. In case of neopentane, the last term of [2] is eliminated. Reducing the pulse dose makes the contribution of the third term of [2] to the observed decay rate less important, because both n_+ and n_e become smaller in proportion to the absorbed dose. At the lower dose rate where $t_{1/2}$ assumes a constant value, the observed decay may be ascribed to only the first two terms of [2].

If only the first two terms of [2] contribute to the decay, the electron current is given by

$$[3] \quad I_e(t) = I_0\left(1 - \frac{\mu_e E t}{d}\right)\exp(-k_{tr}t)$$

where I_0, the peak current at the end of the pulse, is equal to $eA\mu_e E n_0$, where n_0 is the initial concentration of free electrons. The most suitable

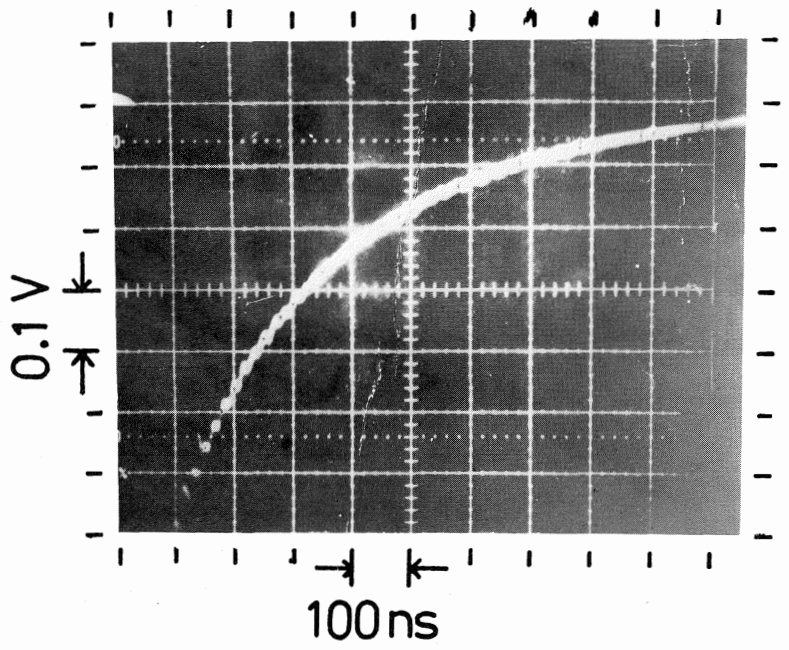

FIG. 2. Decay of the conductivity signal in neopentane: pulse dose = 160 mrad, E = 2.8 kV/cm.

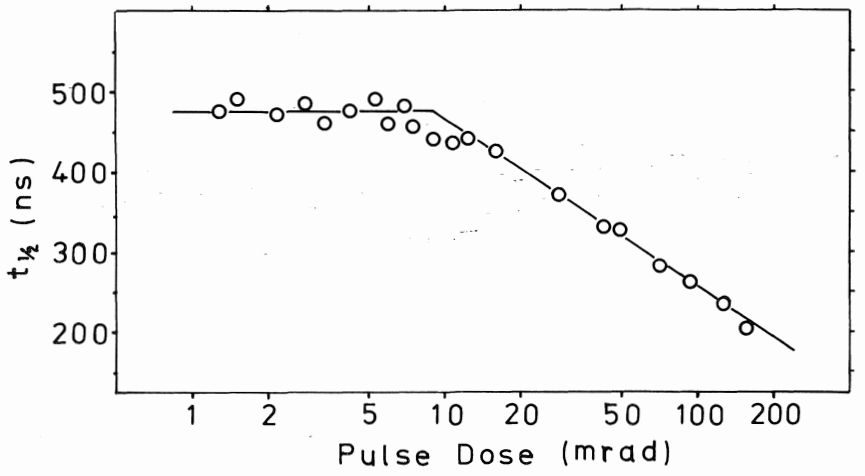

FIG. 3. Effect of dose rate on the initial half-life $t_{1/2}$ of the electron decay in neopentane.

value for μ_e is that in which the plot of $[I_e(t)/(1 - \mu_e Et/d)]$ is reduced to the exponential decay $I_0 \exp(-k_{tr}t)$. The electron mobility in neopentane is thus determined to be (60 ± 3) $cm^2\ V^{-1}\ s^{-1}$ from the analyses of decay plots at low pulse doses for several neopentane samples.

At the highest pulse dose, electron–ion recombination should compete with the first and the second processes of [2] and the electron current may be given approximately by

$$[4] \quad I_e(t) = I_0 \frac{(1 - \mu_e Et/d)}{(1 + n_0 k_r t)} \exp(-k_{tr}t)$$

The value of k_r can be so chosen as to fit [4] to the experimental result. In the actual calculation to find the value of k_r, [5], which is derived by combining [4] with [3], is used

$$[5] \quad 1 + (n_0)_h k_r t = \left(\frac{I_e(t)}{I_0}\right)_l \Big/ \left(\frac{I_e(t)}{I_0}\right)_h$$

where subscripts l and h represent the low and the high doses, respectively. Substituting two sets of $I_e(t)/I_0$ into [5], one can determine the value of $(n_0)_h k_r$ with an error of $\pm 10\%$. The initial concentration of free electrons at high pulse dose, $(n_0)_h$, is obtained from either the peak current I_0 using $\mu_e = 60\ cm^2\ V^{-1}\ s^{-1}$ or the absorbed dose using the field-enhanced free electron yields $G^E = 1.3$ (4*d*) at $E = 2.8$ kV/cm in neopentane. Thus the rate constant of electron–ion recombination in neopentane is determined to be $(2.8 \pm 0.3) \times 10^{16}\ M^{-1}\ s^{-1}$ at room temperature. In order to ensure that the drifting process is the only decay mechanism at low pulse doses, the external field strength is increased to 7.1 kV/cm. The electron current decays linearly with time and is given by

$$[6] \qquad I_e(t) = I_0\left(1 - \frac{\mu_e E t}{d}\right)$$

The signal decay time, t_d, corresponds to the time required for an electron to drift the distance between the electrodes. The electron mobility determined from t_d is 61 $cm^2\ V^{-1}\ s^{-1}$, which is in good agreement with that determined from the analysis of the decay plot at lower electric field. The value of μ_e also agrees well with those already reported (1–4, 8).

The mobilities of electrons in mixtures of neopentane–*n*-hexane have been determined from the peak current at the end of the pulse using the equation $I_0 = eA\mu_e E n_0$. The initial concentration of free electrons in the mixture is given by $n_0 = 6.25 \times 10^{11} D d_{mix} G_{mix}{}^E$, where D is the dose in rads and d_{mix} is the density of the mixture. The free electron yield in the mixture in the presence of the applied field E is calculated from [7] using a single-pair-spur model (4*c*, 15).

$$[7] \qquad G_{mix}{}^E = G_{tot} \int_0^\infty F(y)\phi(y,E)\ dy$$

where G_{tot} is the total ionization yield which is assumed to be 4.3, $\phi(y,E)$ is the probability that a thermalized electron–ion pair with initial inter-pair separation distance y will escape geminate recombination and become a free electron in the presence of the applied field E, and $F(y)$ is the initial separation distance distribution function. The escaping probability $\phi(y,E)$ is approximated by the initial four terms of a polynomial expression (4*c*). The distribution function $F(y)$ is given by the three dimensional Gaussian function

$$(4y^2/\pi^{1/2} b_{mix}{}^3) \exp(-y^2/b_{mix}{}^2)$$

where b_{mix} is the most probable value of y in the mixture. The value of b_{mix} is calculated using b values for neopentane and *n*-hexane from the relation found by Schmidt and Allen (16). The values of b_{neo} and b_h are determined so as to fit $G_{mix}{}^E$ calculated from [7] to the experimental plots of G^E *vs.* E reported by Freeman and co-workers (4*c*,*d*). The electron mobilities determined in this manner are plotted *vs.* the mole fraction of *n*-hexane, as shown in Fig. 4. For neopentane and a mixture of $x_h = 0.16$ the values of μ_e determined from the peak current are, respectively, in good agreement with those determined from the analysis of the decay plot within the experimental error. For *n*-hexane the peak current has not been accurately measured owing to the low ratio of signal to noise. The extrapolation of the curve in Fig. 4 to $x_h = 1$ gives 0.08 $cm^2\ V^{-1}\ s^{-1}$, which is in good agreement with that already reported (1, 2, 8).

The plot of log μ_e *vs.* x_h yields a straight line,

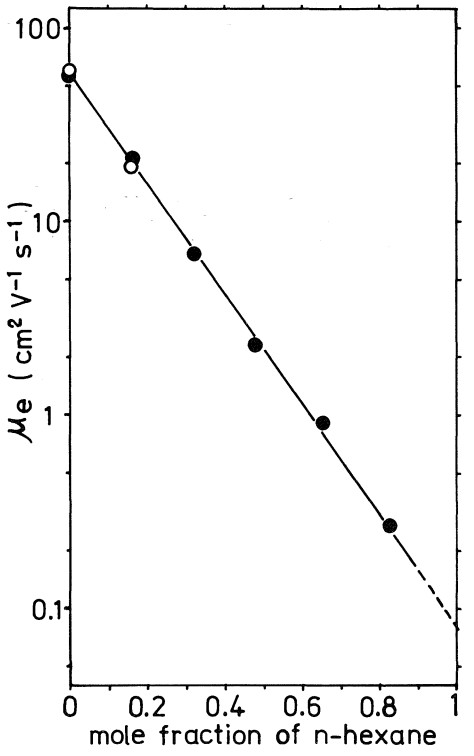

FIG. 4. The electron mobility μ_e as a function of mole fraction of *n*-hexane, x_h in the mixture. (○) determined from the analysis of the electron current decay; (●) determined from the peak current at the end of the pulse.

indicating that the electron mobility in the mixture μ_{mix} is expressed by

$$[8] \qquad \mu_{mix} = \mu_{neo}^{x_{neo}} \mu_h^{x_h}$$

where μ_{neo} and μ_h are the electron mobilities in neopentane and *n*-hexane, respectively, and x_{neo} is the mole fraction of neopentane in the mixtures. It is seen from [8] that by suitably mixing neopentane and *n*-hexane one can obtain a solvent of any desired electron mobility which lies between μ_{neo} and μ_h. The above relation has been found by Minday *et al.* (2*b*) for the same hydrocarbon mixtures using a time-of-flight method. They have also investigated the temperature dependence of μ_{mix} and found that the electron mobility in the mixtures, as in the cases of the pure components, can be expressed by the Arrhenius type expression,

$$[9] \qquad \mu_{mix} = \mu_f \exp(-E_{mix}/RT)$$

where μ_f is assumed to be the mobility of the electron in the quasifree state. The activation energy in the mixture, E_{mix}, increases with x_h and is given by a linear function of composition.

$$[10] \qquad E_{mix} = E_{neo}x_{neo} + E_h x_h$$

where E_{neo} and E_h are the activation energies in neopentane and *n*-hexane, respectively. It has been concluded (2*b*) that neopentane and *n*-hexane form an 'ideal' mixture in which the localized state or the trap for electrons is made up by a group of molecules which is weighted according to composition.

The rate constants for recombination of electrons with positive ions in the mixtures are determined in the same way as in the case of neat neopentane. A noticeable difference between the electron half-life at high pulse dose, $(t_{1/2})_h$ and that at low pulse dose, $(t_{1/2})_l$ has been observed in the mixtures. However, the electron current decay in the mixtures of large x_h exhibits pseudo-first-order behavior under both dose conditions. In this case [5] is reduced to

$$1 + (n_0)_h k_r t = \exp\{0.693[(t_{1/2})_h^{-1} - (t_{1/2})_l^{-1}]\}$$

Figure 5 shows a plot of the recombination rate constant k_r *vs.* the electron mobility. Our data obtained for the mixtures of $x_h = 0$, 0.16, 0.32, and 0.48 are represented together with those reported by Allen and Holroyd (8*a*) for *n*-hexane, *n*-pentane, and tetramethylsilane and by Baxendale and co-workers (7) for *n*-hexane and cyclohexane. All of these rate constants are proportional to the electron mobilities over a wide range of μ_e and lie on the straight line obtained from the reduced Debye equation

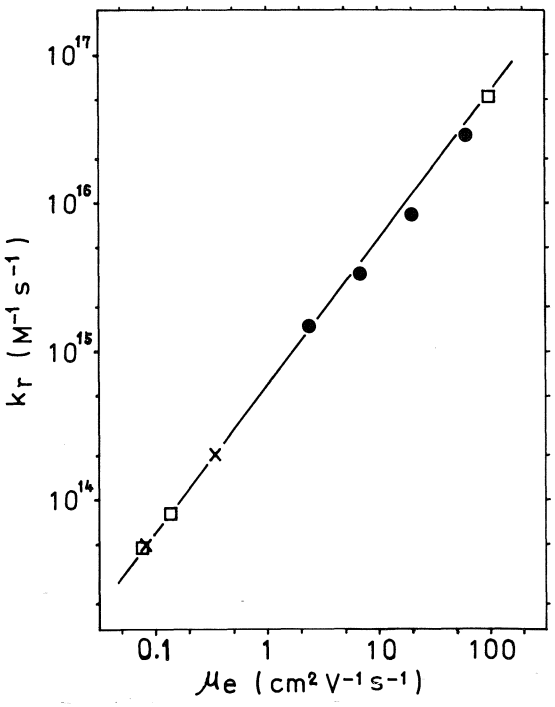

FIG. 5. The rate constants of electron–ion recombination, k_r, as a function of the electron mobilities, μ_e, in the mixtures (●) and in neat hydrocarbons (×) and tetramethylsilane (□) from refs. 7 and 8. The solid line is calculated from the reduced Debye equation [11].

$$[11] \qquad k_r = \frac{4\pi e}{\varepsilon}\mu_e$$

Figure 5 shows, therefore, that electron–ion recombination in non-polar liquids, where the electron mobility varies by three orders of magnitude, is a diffusion-controlled process.

It is generally considered that the reduced Debye equation, derived from the motion of ions which is essentially characterized by random diffusion, may be appropriate for low-mobility liquids such as *n*-hexane where the electron seems to reside in the spatially localized state for a long period of time and to move from one localized site to another as a conduction electron. In Fig. 5, however, [11] is also applicable for electron–ion recombination in high-mobility liquids such as neopentane where the electron seems to be extensively delocalized. Although the extent of delocalization of the electron in

high-mobility liquids seems not to have been estimated, it may be considerably smaller than the effective reaction radius of electron–ion recombination, ρ_r, which is close to 300 Å in liquids of low dielectric constant. The delocalized electron may stay in the vicinity of the positive ion for a time which is considerably longer than the vibrational period for nuclear motion and the recombination reaction may occur with a probability of unity whenever the electron enters into the effective reaction radius. If so, the rate constant of electron–ion recombination remains diffusion controlled even in high-mobility liquids.

Rate Constants of Electron Scavenging in the Mixtures

The time dependence of the electron current in the mixtures has exhibited pseudo-first-order behavior and the observed half-life $t_{1/2}$ is related to a rate constant, k_0. The exponential decay may be attributed to the relatively small contributions of electron drift and of electron–ion recombination processes in the mixtures. Addition of small amounts of CCl_4 or C_2H_5Br considerably increases the decay rate of the electron current, which still exhibits pseudo-first-order behavior with an effective rate constant k_e. The large increment in the decay rate caused by addition of solute may be exclusively attributed to electron scavenging by the solute. Then the effective decay constant k_e in the presence of the solute may be given by $k_e = k_0 + k_s[S]$, where k_s is the rate constant of electron scavenging by the solute. Typical examples are shown in Fig. 6 for a mixture of $x_h = 0.32$, where, as required in this treatment, k_e is linear with the solute concentration and the slopes of these lines yield k_s for CCl_4 and C_2H_5Br with errors of $\pm 10\%$.

The rate constants obtained in this way for electron scavenging in mixtures are plotted in Fig. 7. Data for *n*-hexane are those reported by Allen and Holroyd (8*a*). The mole fraction x_h is translated into the energy of the quasifree electron in the mixtures, $V_{0\,mix}$, using the relation found by Holroyd and Tauchert (10*d*),

$$[12] \qquad V_{0\,mix} = V_{0\,neo}x_{neo} + V_{0\,h}x_h$$

where $V_{0\,neo}$ and $V_{0\,h}$ are the energies of the quasifree electron in neopentane and *n*-hexane, respectively. The plot of log k_s for CCl_4 *vs.* x_h yields a straight line: k_s for CCl_4 is expressed

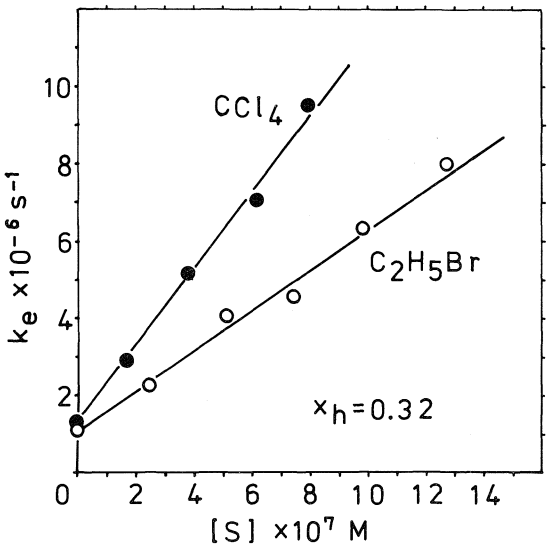

FIG. 6. The effective rate constants, k_e, of electron scavenging in the mixture of $x_h = 0.32$ as functions of the concentrations of CCl_4 (●) and C_2H_5Br (○).

fairly well by $4 \times 10^{12}\mu_e^{0.5}\ M^{-1}\,s^{-1}$. On the other hand, k_s for C_2H_5Br shows a maximum at $x_h = 0.48$ where $V_0 = -0.15$ eV. The results of k_s for CCl_4 and C_2H_5Br determined for the neopentane–*n*-hexane mixtures agree with those by Allen *et al.* (8*b*) for various neat hydrocarbons. The agreement of the results for neopentane–*n*-hexane mixtures and for various neat hydrocarbons indicates that the electron reaction with scavengers does not depend on the solvent molecular structure itself but only on the quantities μ_e and V_0 of the medium.

If electron scavenging is diffusion controlled, the rate constant should be proportional to the electron mobility and given by

$$[13] \qquad k_s = \frac{4\pi k T \rho_s}{e}\mu_e$$

where ρ_s is the effective reaction radius of electron scavenging. The broken line in Fig. 7 is the result of [13], assuming that ρ_s has a constant value of 5 Å in mixtures of any composition. In relatively low-mobility mixtures the reaction of electron scavenging appears to be a diffusion-controlled process. The data of k_s for a large number of scavengers in cyclohexane and *n*-hexane reported by Baxendale and co-workers (7) and Allen and co-workers (8) depend little on scavengers and agree closely with [13] for the respective solvents. In high-mobility mixtures,

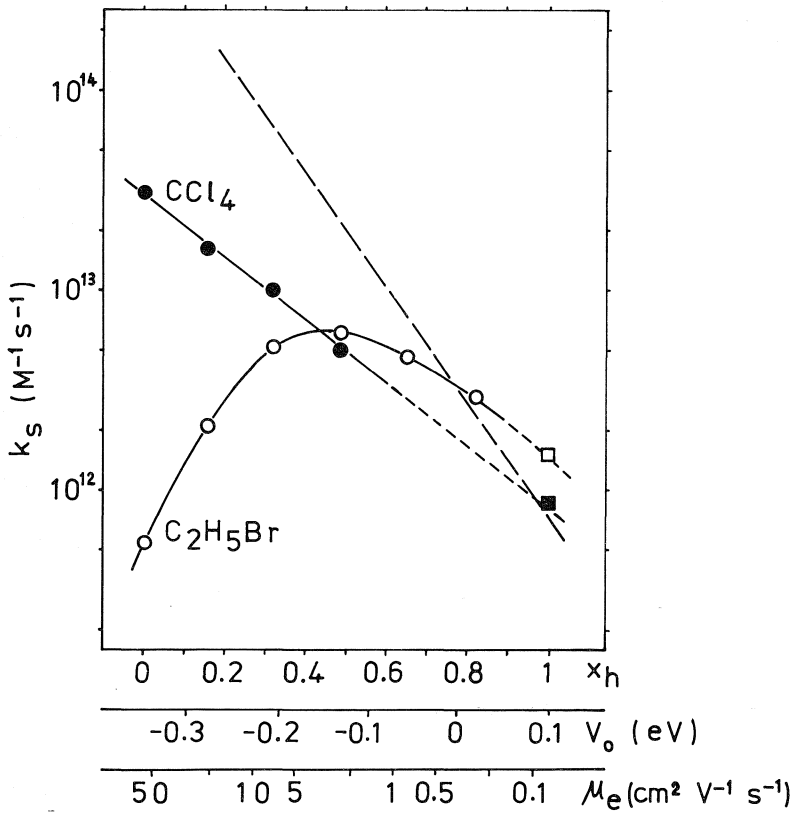

FIG. 7. The rate constants of electron scavenging, k_s by CCl_4 (●) and C_2H_5Br (○) as functions of x_h, V_0, and μ_e in the mixture. The data for neat *n*-hexane (■, □) are cited from ref. 8. The broken line is calculated from [13].

on the other hand, the rate constants k_s do not follow [13]. Electron scavenging in high-mobility mixtures is not diffusion controlled. This appears to hold particularly for the case of C_2H_5Br, since k_s decreases with increasing μ_e in the higher mobility region. For CCl_4, however, k_s might have something to do with [13], because its specific rate varies rather closely with the square root of the electron mobility over the wide range of μ_e.

It has been suggested that diffusion kinetics expressed by [13] is not necessarily valid for processes of electron scavenging in liquid hydrocarbons, especially in high-mobility liquids. In neopentane, Hatano and co-workers (12) have first indicated that the relative values of k_s are largely dependent upon scavengers and are correlated with the rate constants of thermal electron attachment in the gas phase, suggesting that a new theoretical approach taking account of 'gaseous character' (12) of liquid neopentane may be necessary instead of diffusion kinetics. Allen *et al.* (8*b*) have correlated k_s in various hydrocarbons and tetramethylsilane with the energy of the quasifree electron, V_0, and proposed that a characteristic value of V_0 at which k_s becomes a maximum can be predicted using the resonant energy maximum in the attachment cross section for electron reaction with the scavenger in the gas phase. For high-mobility liquids, Funabashi and Magee (13) have proposed a model where the process of electron scavenging is completely analogous to the gas phase process of electron attachment. Thus the 'gaseous character' (12) of the high-mobility liquid commonly has been emphasized to explain the non-diffusion-controlled behavior of k_s.

Let us here consider the situation in which diffusion kinetics is valid. When the following two requirements are satisfied, electron reactions in liquids may be described by diffusion

kinetics. The first is that the electron undergoes high-frequency diffusive displacements of the random walk type in a relatively small area compared with the effective reaction radius of interest, even if the electron wavefunction is somewhat extended over several solvent molecules. The second is that the electron reaction has a low or no activation energy: the rate is determined by the diffusion of the electron towards the reacting species rather than by the final reaction itself. The first requirement may be related to the electron mobility and the second to the quantity V_0. When either of the requirements is not satisfied, electron reactions in liquids may exhibit non-diffusion-controlled behavior.

In the high-mobility mixtures these requirements may not be met in the reactions of electrons with CCl_4 and C_2H_5Br shown in Fig. 7. For C_2H_5Br, in the high-mobility mixtures having V_0 lower than -0.15 eV, the final reaction of electron capture seems to require an activation energy, as suggested by Allen and co-workers (8), so it becomes the rate determining step. For CCl_4, on the other hand, the quasifree electron in the mixtures of any composition seems to have energies which are high compared with that required for the final reaction of electron capture. As μ_e becomes larger, the diffusive displacements of the electron become large compared with the effective reaction radius of electron scavenging, ρ_s. In other words, the more the electron wavefunction extends, the smaller its overlap with the orbitals of CCl_4 molecule becomes. For the reaction of electron scavenging, therefore, ρ_s may decrease with decreasing overlap (or increasing μ_e). Assuming that ρ_s for CCl_4 is tentatively equal to $r_s/\sqrt{\mu_e}$, where r_s is the geometrical radius of the CCl_4 molecule, [13] is reduced to $k_s = (4\pi kTr_s/e)\sqrt{\mu_e}$, which accounts for the result in Fig. 7.

Both μ_e and V_0 are important with respect to the rate of electron scavenging in liquid hydrocarbons. The details of the factors which determine the reaction rate k_s, however, still remain obscure. Further measurements of k_s for various scavengers in mixtures of hydrocarbons clearly are required.

Electron Transport in Non-polar Liquids

The mechanism of electron transport in non-polar liquids has been described in terms of three quantities: electron mobility, μ_e, its activation energy, E_a, and electron energy in its quasifree state, V_0. The temperature dependence of μ_e as is expressed by [9] may imply that the electron transport takes place through a succession of migrations from one trap to another as a conduction electron. This mechanism has generally been referred to as a trapping model (1, 2), which is *apparently* similar to a phonon-assisted hopping model proposed to explain the electron transport in amorphous semiconductors (17). The correlation between μ_e and V_0 received attention originally by Holroyd and Allen (10*a*). Recently Schiller and co-workers (18), Kestner and Jortner (19), and Freeman and co-workers (20) have theoretically calculated μ_e as a function of V_0 based on, respectively, a partial localization model, an effective medium model, and an activation model. The activation energy E_a has also been calculated from the theories. Then the experimental data of μ_e and E_a have been correlated with V_0 to test predictions from theories.

Turning to the experimental results on these three quantities for neopentane–*n*-hexane mixtures, which are expressed by [8], [10], and [12], it is seen that the correlations of μ_e *vs.* V_0 and V_0 *vs.* E_a can be expressed by simple formulae. The electron mobility, μ_{mix}, is expressed by a function of the mole fraction of components. Both $V_{0\,mix}$ and E_{mix} are linearly dependent on composition. Substituting [12] into [8], μ_{mix} is expressed by an exponential function of $V_{0\,mix}$,

$$[14] \qquad \mu_{mix} = 0.35 \exp(-15\, V_{0\,mix})$$

which is calculated using $\mu_{neo} = 60$, $\mu_h = 0.08$ $cm^2\ V^{-1}\ s^{-1}$, $V_{0\,neo} = -0.35$ (10*d*), and $V_{0\,h} = 0.10$ eV (10*d*). This relation was first reported by Holroyd and Tauchert (10*d*). Comparing [12] with [10], $V_{0\,mix}$ is expressed by a linear function of E_{mix}

$$[15] \qquad V_{0\,mix} = -0.42 + 2.6E_{mix}$$

at room temperature, which is calculated using $E_{neo} = 0.024$ (the average of refs. 4*a* and 2*b*) and $E_h = 0.20$ eV (the average of refs. 1, 2, and 8*b*). Equation 15 is an empirical formula derived from the experimental results on the mixtures and correlates the energy of the trapped state with that of the quasifree state quantitatively. Figure 8 shows a plot of V_0 *vs.* E_a for various hydrocarbons and tetramethylsilane for which both quantities have been reported. Equation 15, represented by the solid line, seems to hold for

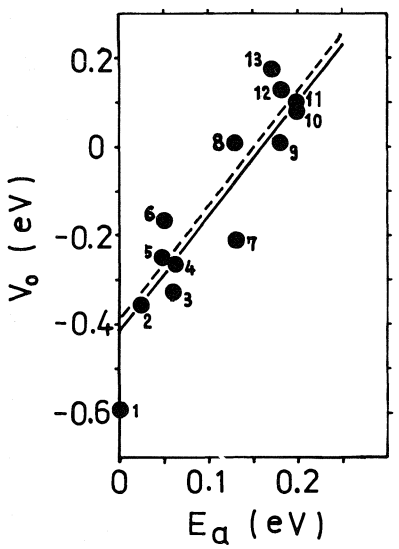

FIG. 8. Plot of V_0 *vs.* E_a in liquid hydrocarbons and tetramethylsilane. All values are experimental near 296 K. Values of V_0 are from ref. 10*e*. Values of E_a are the average of those in refs. 1, 2, 4, and 8. The solid and dotted lines are from [15] and its modification, respectively. The numbers labeling the points are: (*1*) tetramethylsilane, (*2*) neopentane, (*3*) 2,2,4,4-tetramethylpentane, (*4*) 2,2-dimethylbutane, (*5*) 2,3-dimethylbutene-2, (*6*) 2,2,4-trimethylpentane, (*7*) cyclopentane, (*8*) cyclohexane, (*9*) *n*-pentane, (*10*) methylcyclohexane, (*11*) *n*-hexane, (*12*) *n*-octane, (*13*) *n*-decane.

many hydrocarbons but not for tetramethylsilane. In order to elucidate the relationship more completely, it will be necessary to determine theoretically the composition dependence of E_{mix} as well as $V_{0\,mix}$ (21) in the mixtures.

The observed electron mobility is expressed by the mobility of the quasifree electron, μ_f, multiplied by the fraction of the time that the electron exists in the quasifree state. Using Frommhold's formula (22), the electron mobility is given by

$$[16] \qquad \mu_e = \frac{\mu_f}{1 + \nu\tau_t}$$

where ν is the frequency of trapping collisions of the quasifree electron and τ_t is the mean time that the electron resides in the trapped state. It was suggested by Davis and co-workers (2*a*) that τ_t depends on the activation process and so it can be expressed by $\tau_t = \tau_0 \exp(E_a/RT)$, where τ_0 is approximately the period of a vibrational oscillation. It is also assumed that $\nu\tau_0 \approx 1$ (23). The electron mobility is then expressed as

$$[17] \qquad \mu_e = \frac{\mu_f}{1 + \exp(E_a/RT)}$$

using the activation energy. Using [15] and taking 180 $cm^2\,V^{-1}\,s^{-1}$ for μ_f, the electron mobility can be expressed as

$$[18] \qquad \mu_e = \frac{180}{1 + 520\exp(15V_0)}$$

at room temperature. The value of μ_f is so determined that [18] is reduced to [14] for relatively high values of V_0. Figure 9 shows a plot of log μ_e *vs.* V_0 for various hydrocarbons

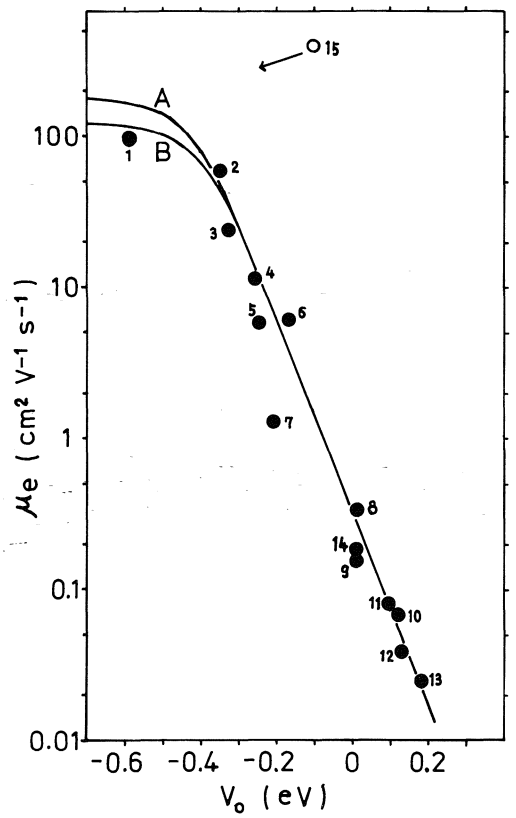

FIG. 9. Plot of μ_e *vs.* V_0 in liquid hydrocarbons and tetramethylsilane. All data are near 296 K except for liquid methane (○), near 110 K. Values of μ_e are the average of those in refs. 1–4, 8, 24, and 25. Values of V_0 are from refs. 10*e*, 24, and 26. The curves of *A* and *B* are calculated from [18] and [19], respectively. The numbers labeling the points are the same as in Fig. 8 except for: (*14*) 3-methylpentane, (*15*) methane. The arrow shows the expected direction of shift of the open circle with increasing temperature because μ_e in liquid methane has a negative temperature coefficient (24, 25) in the range of 90 to 140 K and V_0 may decrease with increasing temperature (10, 26).

and tetramethylsilane for which both quantities have been reported. It is seen that [18], denoted by curve *A*, expresses suitably the correlation between μ_e and V_0 for many hydrocarbons except tetramethylsilane, cyclopentane, and methane. Here, if [19] is used in place of [18],

$$[19] \qquad \mu_e = \frac{125}{1 + 360 \exp(15V_0)}$$

we can obtain curve *B* in Fig. 9, which passes near the point for tetramethylsilane. Equation 19 is obtained from the equation $V_0 = -0.39 + 2.6E_a$ (the dotted line in Fig. 8) in place of [15], which is a trivial modification. The value of μ_f results in 125 $cm^2\ V^{-1}\ s^{-1}$. The curve *B* in Fig. 9 appears to fit well to the theoretical curve obtained from Freeman's activation model (20) while not to those obtained from Schiller's (18) and Kestner and Jortner's models (19) over the entire mobility range.

As mentioned above, using the experimental results on the quantities μ_e, E_a, and V_0 for neopentane–*n*-hexane mixtures and a trapping model on electron transport, we have presented empirical formulae which express suitably the correlations of V_0 *vs.* E_a (eq. 15) and μ_e *vs.* V_0 (eq. 19) for many hydrocarbons and tetramethylsilane at room temperature. While [15] seems not to be valid for tetramethylsilane, [19] appears to hold for the highest mobility liquid such as neopentane and tetramethylsilane where the quasifree electron is considered to be dominant. A theoretical consideration of [15] clearly is required. It is also necessary to consider the connection between the empirical formula (eq. 19) and theoretical expressions (18–20).

It has been shown in this work that experiments using hydrocarbon mixtures give us a better understanding of behavior of electrons in non-polar liquids.

Acknowledgment

The authors wish to thank Dr. H. Hotta of the Japan Atomic Energy Research Institute for the use of his thermoluminescent dosimeter.

1. W. F. SCHMIDT and A. O. ALLEN. J. Chem. Phys. **52**, 4788 (1970) and references therein.
2. (*a*) R. M. MINDAY, L. D. SCHMIDT, and H. T. DAVIS. J. Chem. Phys. **54**, 3112 (1971); (*b*) R. M. MINDAY, L. D. SCHMIDT, and H. T. DAVIS. J. Phys. Chem. **76**, 442 (1972).
3. G. BAKALE and W. F. SCHMIDT. Chem. Phys. Lett. **22**, 164 (1973).
4. (*a*) J.-P. DODELET and G. R. FREEMAN. Can. J. Chem. **50**, 2667 (1972); (*b*) J.-P. DODELET, K. SHINSAKA, and G. R. FREEMAN. J. Chem. Phys. **59**, 1293 (1973); (*c*) J.-P. DODELET, K. SHINSAKA, U. KORTSCH, and G. R. FREEMAN. J. Chem. Phys. **59**, 2376 (1973); (*d*) K. SHINSAKA and G. R. FREEMAN. Can. J. Chem. **52**, 3556 (1974); (*e*) K. SHINSAKA, J.-P. DODELET, and G. R. FREEMAN. Can. J. Chem. **53**, 2714 (1975); (*f*) J.-P. DODELET, K. SHINSAKA, and G. R. FREEMAN. J. Chem. Phys. **63**, 2765 (1975).
5. G. BAKALE, E. C. GREGG, and R. D. MCCREARY. J. Chem. Phys. **57**, 4246 (1972).
6. (*a*) G. BECK and J. K. THOMAS. J. Chem. Phys. **57**, 3649 (1972); (*b*) G. BECK and J. K. THOMAS. J. Chem. Phys. **60**, 1705 (1974).
7. (*a*) J. H. BAXENDALE, C. BELL, and P. WARDMAN. J. Chem. Soc. Faraday Trans. I, **69**, 776 (1973); (*b*) J. H. BAXENDALE and E. J. RASBURN. J. Chem. Soc. Faraday Trans. I, **70**, 705 (1974); (*c*) J. H. BAXENDALE, J. P. KEENE, and E. J. RASBURN. J. Chem. Soc. Faraday Trans. I, **70**, 718 (1974).
8. (*a*) A. O. ALLEN and R. A. HOLROYD. J. Phys. Chem. **78**, 796 (1974); (*b*) A. O. ALLEN, T. E. GANGWER, and R. A. HOLROYD. J. Phys. Chem. **79**, 25 (1975); (*c*) A. O. ALLEN, T. E. GANGWER, and R. A. HOLROYD. Chem. Phys. Lett. **31**, 520 (1975).
9. G. BAKALE, U. SOWADA, and W. F. SCHMIDT. J. Phys. Chem. **79**, 3041 (1975).
10. (*a*) R. A. HOLROYD and M. ALLEN. J. Chem. Phys. **54**, 5014 (1971); (*b*) R. A. HOLROYD. J. Chem. Phys. **57**, 3007 (1972); (*c*) R. A. HOLROYD, B. K. DIETRICH, and H. A. SCHWARZ. J. Phys. Chem. **76**, 3794 (1972); (*d*) R. A. HOLROYD and W. TAUCHERT. J. Chem. Phys. **60**, 3715 (1974); (*e*) R. A. HOLROYD and R. L. RUSSEL. J. Phys. Chem. **78**, 2128 (1974); (*f*) R. A. HOLROYD, S. TAMES, and A. KENNEDY. J. Phys. Chem. **79**, 2857 (1975).
11. G. W. KLEIN and R. H. SCHULER. J. Phys. Chem. **77**, 978 (1973) and references therein.
12. (*a*) K. ITO and Y. HATANO. J. Phys. Chem. **78**, 853 (1974); (*b*) K. MORI, K. ITO, and Y. HATANO. J. Phys. Chem. **79**, 2093 (1975).
13. K. FUNABASHI and J. L. MAGEE. J. Chem. Phys. **62**, 4428 (1975).
14. (*a*) Y. HATANO, S. TAKAO, H. NAMBA, T. UENO, and S. SHIDA. Bull. Chem. Soc. Jpn. **47**, 741 (1974); (*b*) Y. HATANO, S. TAKAO, and T. UENO. Chem. Phys. Lett. **30**, 429 (1975); (*c*) H. SHIMAMORI and Y. HATANO. Chem. Phys. Lett. **38**, 242 (1976); (*d*) H. SHIMAMORI and Y. HATANO. Chem. Phys. **12**, 439 (1976); (*e*) T. UENO and Y. HATANO. Chem. Phys. Lett. **40**, 283 (1976).
15. J. TERLECKI and J. FIUTAK. Int. J. Radiat. Phys. Chem. **4**, 469 (1972).
16. W. F. SCHMIDT and A. O. ALLEN. J. Phys. Chem. **72**, 3730 (1968).
17. (*a*) M. CUTLER and N. F. MOTT. Phys. Rev. **181**, 1336 (1969); (*b*) M. H. COHEN. J. Non-Cryst. Solids, **4**, 391 (1970).
18. (*a*) R. SCHILLER. J. Chem. Phys. **57**, 2222 (1972); (*b*) R. SCHILLER, SZ. VASS, and J. MÁNDICS. Int. J. Radiat. Phys. Chem. **5**, 491 (1973); (*c*) L. NYIKOS and R. SCHILLER. Chem. Phys. Lett. **34**, 128 (1975).
19. N. R. KESTNER and J. JORTNER. J. Chem. Phys. **59**, 26 (1973).

20. (*a*) J.-P. DODELET and G. R. FREEMAN. Can. J. Chem. **53**, 1263 (1975); (*b*) J.-P. DODELET, K. SHINSAKA, and G. R. FREEMAN. J. Chem. Phys. **63**, 2765 (1975); (*c*) J.-P. DODELET, F.-Y. JOU, and G. R. FREEMAN. J. Phys. Chem. **79**, 2876 (1975).
21. R. G. BROWN and H. T. DAVIS. Chem. Phys. Lett. **27**, 78 (1974).
22. L. FROMMHOLD. Phys. Rev. **172**, 118 (1968).
23. H. T. DAVIS, L. D. SCHMIDT, and R. M. MINDAY. Chem. Phys. Lett. **13**, 413 (1972).
24. (*a*) W. F. SCHMIDT and G. BAKALE. Chem. Phys. Lett. **17**, 619 (1972); (*b*) G. BAKALE and W. F. SCHMIDT. Z. Naturforsch. Teil A, **28**, 511 (1973); (*c*) W. TAUCHERT and W. F. SCHMIDT. Z. Naturforsch. Teil A, **29**, 1526 (1974); (*d*) G. BAKALE, W. TAUCHERT, and W. F. SCHMIDT. J. Chem. Phys. **63**, 4470 (1975).
25. (*a*) P. G. FUOCHI and G. R. FREEMAN. J. Chem. Phys. **56**, 2333 (1972); (*b*) M. G. ROBINSON and G. R. FREEMAN. Can. J. Chem. **52**, 440 (1974).
26. (*a*) S. NODA and L. KEVAN. J. Chem. Phys. **61**, 2467 (1974); (*b*) S. NODA, L. KEVAN, and K. FUEKI. J. Phys. Chem. **79**, 2866 (1975).

Discussion

J. Jortner: Concerning the relations between μ_e and V_0, which many of us have been using, it appears now that the experimental data of Schmidt and colleagues on liquid ethane provide a striking exception to this rule.

Y. Hatano: I think so. But, the temperature effect of μ_e and V_0 should be noted as that indicated in Fig. 9 for liquid methane.

J. M. Warman: We have measured the temperature dependence of the mobility of the negative charge carrier(s) in liquid TMS containing low concentrations of the temporary electron trap biphenyl (J. M. Warman, M. P. DeHaas, and A. Hummel, Proc. 5th International Conference on Conduction and Breakdown in Dielectric Liquids, Noordwykerhout, The Netherlands, July 1975). Such a solution corresponds to a low mobility liquid in which the mobility is known to be controlled by equilibrium between a trapped and quasi-free state, of which the quasi-free mobility is known (100 $cm^2\ V^{-1}\ s^{-1}$). If the observed temperature dependence of the mobility in such a 'trap doped' solution is plotted in an Arrhenius fashion corresponding to $\mu = A \exp(-B/RT)$, then the value of B found from the slope (even up to mobilities quite close to the quasi-free mobility) is very close to the known (*i.e.* measured) value of ΔH for the trapping process. The preexponential parameter, A, determined from such a plot is, however, many orders of magnitude greater than the known quasi-free value of 100. These experiments were carried out deliberately to illustrate that the association of A with μ_0 is of dubious validity.

Scavenging of localized and quasifree electrons in liquid hydrocarbons (Extended Abstract)

A. A. BALAKIN, I. A. BORIEV, E. L. FRANKEVICH, L. V. LUKIN, AND B. S. YAKOVLEV
Institute of Chemical Physics, Academy of Sciences USSR, 142432 Chernogolovka, USSR
Received November 22, 1976

Excess electrons in liquid hydrocarbons are believed to be either in a localized or in a quasifree state. In what state are electrons which are scavenged by acceptor molecules? As an approach to this question we examined the values of rate constants k obtained for electron scavenging reactions in liquid hydrocarbons with highly different electron mobilities, μ. Scavenging by aromatic hydrocarbons and oxygen molecules has been studied.

The rate constant measured is a combination of partial rate constants for scavenging of localized and quasifree electrons. The contribution of the quasifree or localized state is assumed to be proportional to the time spent by electrons in this state, *i.e.*

$$k = k_1 P + k_f(1 - P) \qquad [1]$$

where k_f and k_1 are the rate constants for scavenging of a quasifree and localized electron; $1 - P$ is the fraction of time which an electron spends in a quasifree state and is equal to μ/μ_0 for the conventional model of trap-limited transfer of excess electrons; μ_0 is the mobility of the quasifree electron.

Figure 1 shows the dependence of k for pyrene molecules on the diffusion coefficient of excess electrons, D, obtained from Einstein's relationship by using μ.

For liquids with $D \lesssim 10^{-3}$ cm^2/s an assumption of the predominant capture of quasifree electrons leads to $k \lesssim k_0$, where k_0 is the maximum possible attachment rate constant for a thermal free electron at $\mu_0 \lesssim 20$ cm^2 V^{-1} s^{-1}. Such a value seems to be too low for quasifree electrons; therefore we suppose the localized electron scavenging process to be more adequate for liquids with small D. In this case a large effective radius of the reaction $R \approx 17$ Å obtained (1) for these liquids can be connected either with the localized electron radius (1) or with the electron transfer tunnelling mechanism

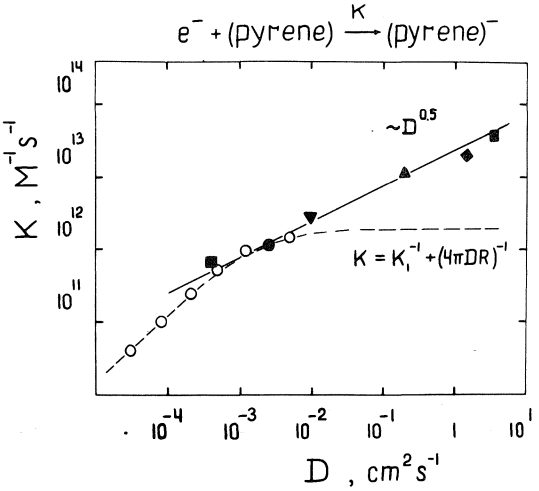

FIG. 1. The dependence of the rate constant of electron scavenging by pyrene in nonpolar dielectric liquids on the diffusion coefficient of excess electrons: pentadecane (■), *n*-hexane (●), cyclohexane (▼), isooctane (▲), neopentane (◆), and tetramethylsilane (■) at $T = 296$ K; *n*-hexane (○) at different temperatures (1).

(the latter gives $R \approx 17$ Å if we take the localized electron radius as 5 Å, the value usually used for the electron tunnelling theory parameter (2) $\alpha' \approx 10^{13}$ s^{-1}, and the parameter $\beta \approx 10^7$ cm^{-1} corresponding to a trap depth of 0.2 eV for localized electrons). Figure 1 illustrates the dependence $k(D)$ derived from the general expression of Noyes $k^{-1} = (4\pi DR)^{-1} + k_1^{-1}$, which agrees with the experiment for $D < 6 \times 10^{-3}$ cm^2 s^{-1}. For liquids with $D > 0.1$ cm^2 s^{-1} such a simple approach gives values of k lower than experimental. Two possible effects might lead to this result: (*1*) an increase of the 'genuine' rate constant, k_1, when going to liquids with larger D (for example, due to lowering of the tunnelling barrier); (*2*) an increase of a quasifree electron contribution.

For scavenging of excess electrons by oxygen molecules in liquid hydrocarbons with $\mu < 10$

$cm^2\ V^{-1}\ s^{-1}$ at $T = 296$ K the values of k proved to be about equal ($k \approx 5 \times 10^{10}\ M^{-1}\ s^{-1}$ (3)) though values of μ and, as expected, of $1 - P$ varied over a range of 10^2 in different liquids. These results permit, in view of [1], the description of scavenging as a capture of localized electrons. The rate constant k has been shown to increase when going to liquids with $\mu > 10\ cm^2\ V^{-1}\ s^{-1}$. This is believed to be due to a capture of quasifree electrons. On this assumption we obtained $k_f = 6 \times 10^{11}\ M^{-1}\ s^{-1}$ at 296 K and an activation energy $E_f \lesssim 0.01$ eV (3, 5) for scavenging quasifree electrons in neopentane and tetramethylsilane.

We compared the values of k_f and E_f with gas-phase data assuming a compound negative ion $(O_2^-)^*$ to be involved in the quasifree electron scavenging process, *i.e.*

$$e_f^- + O_2 \rightleftarrows (O_2^-)^* \rightarrow O_2^-$$

In gases the cross section of $(O_2^-)^*$ formation consists of series of spikes at energy values, $\varepsilon_{v'}$, corresponding to vibrational levels of O_2^- with the quantum number $v' \geq 4$ and $\Delta\varepsilon = \varepsilon_{v'+1} - \varepsilon_{v'} \approx 0.1$ eV (4). The formation of $(O_2^-)^*$ was proposed to proceed in liquids at kinetic energies of quasifree electrons of about

$$[2] \qquad \tilde{\varepsilon}_{v'} = \varepsilon_{v'} + V_p - V_0$$

where V_p is the polarization energy of the $(O_2^-)^*$ ion in the liquid and V_0 is the lowest level of e_f^-.

Aside from this one can imagine at least two differences between the gas and liquid phase attachment mechanisms: (*1*) different widths, $\Gamma_{in}^{v'}$, for decay into the ground state of O_2 plus a free electron, (*2*) because of a distribution of V_p in liquids, the quasifree electrons with a given energy can lead to the formation of $(O_2^-)^*$ with different vibrational levels. (As V_p is defined by the local density near an O_2 molecule just before electron attachment, then due to the density fluctuation one may expect a rather wide (~ 1 eV) distribution function $P(V_p)$ in liquid hydrocarbons (5). Therefore the thermal electron can form $(O_2^-)^*$ with v' from ~ 10 to ~ 20.)

In these circumstances we have

$$[3] \quad k_f = \sum_{v'} \int_{V_p^0}^{0} k_{v'}(V_p) w(\tilde{\varepsilon}_{v'}) P(V_p)\, dV_p$$

where V_p^0 is the lowest value of V_p and is about -2.1 eV for liquid isooctane (5); $w(\tilde{\varepsilon}_{v'}) = \tau_v^{-1}/(\tau_v^{-1} + \Gamma_{in}^{v'}/\hbar)$ is the stabilization probability of $(O_2^-)^*$ in a v' state; τ_v is the vibrational relaxation time for $(O_2^-)^*$ ions in liquids; $k_{v'}(V_p)$ is the rate constant of $(O_2^-)^*$ formation in the v' state if the polarization energy has a value V_p.

The relationship [3] may be simplified if we accept that, for the *d*-wave resonant scattering involved in the present reaction, as for a gas (6), $\Gamma_{in}^{v'} = B\tilde{\varepsilon}_{v'}^{5/2}$ and $\int \sigma_{v'} d\varepsilon = A\Gamma_{in}^{v'}/\tilde{\varepsilon}_{v'}$, where $A = (4/3)\pi^2(\hbar^2/2m)$, $\sigma_{v'}(\varepsilon, V_p)$ is the cross section for $(O_2^-)^*$ formation in the v' state, and m is the mass of the electron. Then for $B = 1.2 \times 10^{-1}\ eV^{-3/2}$ (the latter corresponds to $\hbar/\Gamma_{in}^4 = 2 \times 10^{-12}$ s (7) for the life time of $(O_2^-)^*$ with $v' = 4$ in the gas), we have $\hbar/\Gamma_{in}^{v'} \gtrsim 10^{-11}$ s for v' from ~ 10 to ~ 20 and consequently $w(\tilde{\varepsilon}_{v'}) \approx 1$ if $\tau_v \approx 10^{-13}$ s, and

$$[4] \quad k_f = \sum_{v'} P(V_0 - \tilde{\varepsilon}_{v'}) \int_0^\infty \frac{u}{\varepsilon} f(\varepsilon) A\Gamma_{in}^{v'}\, d\varepsilon \approx B(2\pi\hbar kT)^2/\Delta\varepsilon \cdot m^{3/2}$$

where u is the velocity of the quasifree electron with kinetic energy ε; $f(\varepsilon)$ is the Maxwellian energy distribution for excess electrons. The relationship [4] leads to $k_f = 3 \times 10^{11}\ M^{-1}\ s^{-1}$ and $E_f = 5 \times 10^{-2}$ eV at $T = 300$ K. These results are in rather good agreement with the experiment.

1. B. S. Yakovlev, I. A. Boriev, and A. A. Balakin. Int. J. Radiat. Phys. Chem. **6**, 23 (1971).
2. M. I. Pilling and S. A. Rice. J. Chem. Soc. Faraday Trans. II, **71**, 1311 (1975).
3. L. V. Lukin and B. S. Yakovlev. Dokl. Acad. Nauk SSSR, **224**, 381 (1975).
4. G. I. Shulz. Rev. Modern Phys. **45**, 423 (1973).
5. L. V. Lukin and B. S. Yakovlev. Khim. Vys. Energ. In press.
6. F. Koike and T. Watanabe. J. Phys. Soc. Jpn. **34**, 1022 (1973).
7. R. G. Goans and L. G. Christophorou. J. Chem. Phys. **60**, 1036 (1974).

Discussion

L. G. Christophorou: Your lifetime of 10^{-12} s for $(O_2^-)^*$ as well as your value of $4 \times 10^{11}\ M^{-1}\ s^{-1}$ or k_F are very consistent with our own values for $(O_2^-)^*$ derived from high-pressure electron attachment studies. We estimated (R. E. Goans and L. G. Christophorou, J. Chem. Phys. **60**, 1036 (1974)) a value of $\sim 2 \times 10^{-12}$ s for the lifetime of $(O_2^-)^*$ and a value for $k_F = 3.3 \times 10^{11}\ M^{-1}\ s^{-1}$ for the reaction $e_{thermal} + O_2 \rightarrow (O_2^-)^*$, when our data on the $e_{thermal}$, O_2 system in dense ethylene gas were extrapolated to liquid-ethylene density.

J. Jortner: You have estimated the rate constant for $O_2 + e$ reaction in solution in terms of a sum of Lorentzians involving the width $\hbar/\tau_{vib}$ where τ_{vib} is the $v \rightarrow v - 1$ medium induced vibrational relaxation time of O_2^-. This approach assumes sequential electronic coupling followed by vibrational relaxation. This approach is identical to the Robinson–Frosch theory of molecular radiationless transitions. An alternative physical picture involves the participation of medium phonons superimposed on the molecular vibrational levels v of the final state, which will provide a dissipative sink. Another modification of your theoretical rate constant should involve the vibrational nuclear overlap Franck–Condon factor between the appropriate states of O_2 and of O_2^-.

E. L. Frankevich: You are right but to date we have only approximate determinations of k_F (rate constant for reaction of quasifree electrons with O_2) in a liquid phase. This makes it impossible to compare the results of more advanced approaches and to choose the best one.

Comparison of solvated electron reaction rates in water and ammonia

U. SCHINDEWOLF AND P. WÜNSCHEL

Institut für Physikalische Chemie und Elektrochemie, Universität Karlsruhe, Germany

Received October 4, 1976

U. SCHINDEWOLF and P. WÜNSCHEL. Can. J. Chem. **55**, 2159 (1977).

New and literature data of solvated electron reactions in ammonia with some inorganic ions and organic neutral molecules are compared with corresponding data in water. In ammonia only a few reactions with aromatic molecules are diffusion controlled and therefore faster than in water ($k \approx 1 \times 10^{11}$ and 1×10^{10} M^{-1} s^{-1}, respectively). After correcting for the electrostatic contribution to the rate constant of the other reactions it is concluded that in general the reactivity of the solvated electron in ammonia is appreciably lower than in water. For the slow reactions of ammoniated electrons with acetonitrile and dimethylsulfoxide we find activation energies of 7 to 9 kcal/mol and activation volumes of -40 to -60 ml/mol. In these reactions it is suggested that the rate determining step is associated with the collapse of the large electron cavity in liquid ammonia.

U. SCHINDEWOLF et P. WÜNSCHEL. Can. J. Chem. **55**, 2159 (1977).

Des données nouvelles et des données trouvées dans la littérature concernant les réactions d'électrons solvatés dans l'ammoniac avec quelques ions inorganiques et des molécules organiques neutres sont comparées avec celles disponibles pour l'eau. Dans le cas de l'ammoniac, il n'y a que quelques réactions avec les molécules aromatiques qui sont contrôlées par la diffusion et qui sont donc plus rapides que dans l'eau ($k \approx 1 \times 10^{11}$ et 1×10^{10} M^{-1} s^{-1} respectivement). Si l'on fait la correction pour la contribution électrostatique à la constance de vitesse d'autres réactions, on peut conclure qu'en générale la réactivité des électrons solvatés dans l'ammoniac est beaucoup plus faible que celle dans l'eau. Pour des réactions lentes d'électrons solvatés dans l'ammoniac avec l'acétonitrile et le diméthylsulfoxyde, on trouve des énergies d'activation de 7 à 9 kcal/mol et des volumes d'activation de -40 à -60 ml/mol. Dans ces réactions, on suggère que l'étape déterminante de la réaction est associée avec la disparition de la grande cavité de l'electron dans l'ammoniac liquide.

[Traduit par le journal]

Introduction

Extensive studies of rates of solvated electron (e_s^-) reactions in water have been carried out (1). Little is known about their rates in ammonia, although a wealth of information about the physical properties of the ammoniated electrons is available (2–6). The most striking difference in kinetic behavior is the high stability of the ammoniated electron e_{am}^- in contrast to that of the hydrated electron e_{hyd}^-.

In 50 mol% water ammonia mixtures (7) the solvated electron lifetime is at least 10^3 times the value in pure water. Assuming the normal bimolecular rate law and a solvent independent rate constant the lifetime of the electron should only be increased by a factor of two, due to the twofold dilution of the reacting water. Considering the equilibrium $H_2O + NH_3 \rightleftarrows NH_4^+ + OH^-$ does not help to interpret the large observed lifetime increase. Neither does consideration of the electrostatic contribution to the rate constant (8) arising from the different dielectric constants of ammonia and water ($\varepsilon = 17$ and 78, respectively). This behavior should be contrasted with that in ethyl alcohol and water or their mixtures, where the observed small changes in rate constant with, for example, nitrate or zinc ions, can be solely explained by the electrostatic correction (9).

In this paper we demonstrate that after correcting for the electrostatic contribution (8) the reactivity of solvated electrons in ammonia is several powers of ten smaller than in water. The argument is based on published results (10) and new kinetic data of electron reactions in ammonia with inorganic anions, cations, and organic neutral molecules. The corresponding data in water were taken from literature (1). The experimental details, mainly concerning pulse radiolysis at high pressure, have been described before (7).

Results and Discussion

Inorganic Ions

Table 1 shows a comparison for water and ammonia of the experimental rate constants

TABLE 1. Kinetic data for the reaction of solvated electrons with inorganic ions in water and ammonia

Ion	Water*		Ammonia	
	Rate constant† (M^{-1} s^{-1})	Activation energy (kcal/mol)	Rate constant† (M^{-1} s^{-1})	Activation energy (kcal/mol)
NO_3^-	8.6×10^9	3.9	3.9×10^6	2.9
NO_2^-	2.7×10^9	3.4	1.7×10^5	3.3
BrO_3^-	1.6×10^9	4.5	7.5×10^4	2.3
CN^-	$<4 \times 10^6$	—	<1	—
CNO^-	$<1.0 \times 10^6$	—	<1	—
ClO_3^-	$<1.3 \times 10^6$	—	<1	—
Cd^{2+}	9.8×10^{10}	—	6.2×10^9	—
Ni^{2+}	3.9×10^{10}	—	3.5×10^{10}	—
Co^{2+}	2.0×10^{10}	—	4.2×10^{10}	—
Zn^{2+}	2.5×10^9	—	2.3×10^{10}	—
Mn^{2+}	7.7×10^7	—	5.5×10^9	—

*Reference 1.
†Extrapolated to zero ionic strength.

measured at 22°C and extrapolated to zero ionic strength (8) for the reaction of e_s^- with monovalent NO_3^-, NO_2^-, and BrO_3^- anions and the divalent Cd^{2+}, Ni^{2+}, Co^{2+}, Zn^{2+}, and Mn^{2+} cations. (At the substrate concentration $<10^{-4}$ M complete dissociation of the electrolytes even in ammonia can be assumed; the extrapolation yields half a power of ten decrease and one power of ten increase of the measured rate constants of anion and cation reactions, respectively; it is not decisive for the following discussion.) The anion rate constants in ammonia are three to four powers of ten lower than in water. On the other hand some cation rate constants (Mn^{2+}, Zn^{2+}, Co^{2+}) are increased whilst others (Cd^{2+}, Ni^{2+}) are decreased by up to a factor of ten in ammonia as compared to in water. These results can be separated into diffusion and nondiffusion controlled reactions.

Diffusion Controlled

In this case the calculated second order rate constant is given by the Debye equation [1] (8).

$$k_{\text{diff}} = \frac{4\pi a N_L D}{1000} \frac{Q}{\exp Q - 1} \qquad [1]$$

$$Q = \frac{N_L z_1 z_2 e_0^2}{\varepsilon a R T}$$

where N_L is Avogadro's number, R the gas constant, T the absolute temperature, D the diffusion coefficient $= D_1 + D_2$, z_1 and z_2 the charge number of e_s^- and the solute, respectively, ε the dielectric constant, e_0 the electronic charge, and a the collision diameter (distance of closest approach which leads to reaction). Q describes the electrostatic contribution of the ions to the rate of diffusion controlled reactions. In the limiting case for noncharged solutes where $z_2 \to 0$ the rate constant is given by the first term.

Figure 1 shows the diffusion controlled rate constant according to [1] as a function of the collision parameter between 1 and 9 Å for the electron reactions with divalent cations ($z_2 = 2$) and with monovalent anions ($z_2 = -1$) in ammonia and water. For reactions with cations k_{diff} is essentially independent of the collision diameter but with anions increases rapidly with increasing values of a. Diffusion coefficients $D = 5 \times 10^{-4}$ and 5×10^{-5} cm^2/s (22°C) were taken as averaged values for ammonia and for water, respectively, as computed from the known mobilities of the species in the two solvents (11, 12). The ratio of the diffusion coefficients in ammonia and water reflects the inverse ratio of the viscosity of the two solvents which is close to 9 at 25°C.

From the experimental data and theoretical curves of Fig. 1 it may be concluded that the e_s^- reactions with Cd^{2+}, Ni^{2+}, and Co^{2+} are diffusion controlled in water whereas this is not the case in ammonia. Of the anions only the NO_3^- ion might be diffusion controlled in water with a collision diameter around 5 Å. For the other two anions the collision diameter for a diffusion controlled reaction would be <3 Å, which hardly seems acceptable. As argued for the cations none of the anion reactions in ammonia are diffusion controlled, unless again

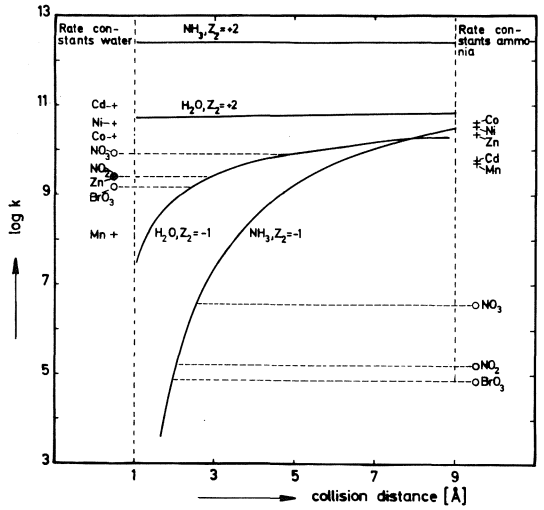

FIG. 1. Calculated rate constants for diffusion controlled reactions of solvated electrons with monovalent anions ($z_2 = -1$) and divalent cations ($z_2 = 2$) in water and ammonia; abscissa collision diameter. The experimental rate constants are given on the sides.

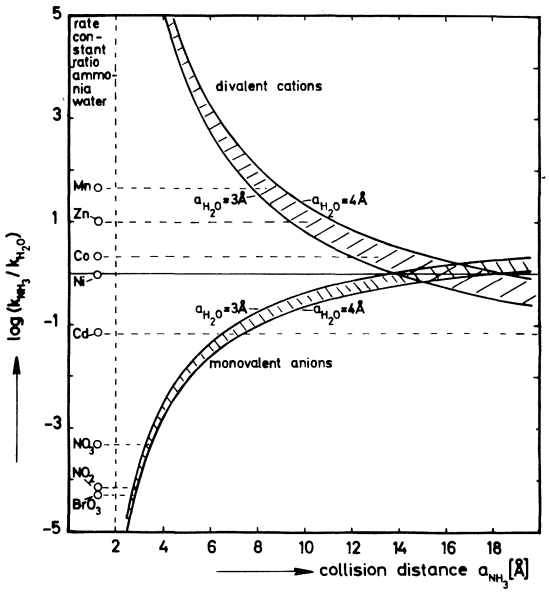

FIG. 2. Calculated ratio of the rate constants of electron reactions in ammonia and water with monovalent anions and divalent cations, considering the electrostatic contribution only (k_∞ independent of solvent); abscissa collision diameter in ammonia; collision diameter in water 3–4 Å. Experimental ratios are given on the side.

we assume an unreasonably small collision diameter (<2 Å). This is even less likely in ammonia than in water because of the larger effective radius r_e of the solvated electron cavity having values of 3.2 Å in ammonia (2–6) and <1.4 Å in water (13, 14).

Nondiffusion Controlled

If the ion reactions are not diffusion controlled, the rate constant can be calculated by the Brönsted–Christiansen–Scatchard equation (8)

$$[2] \qquad k = k_\infty \exp -Q$$

with Q from [1], describing the correction of the rate due to Coulomb interaction, and k_∞ being the rate constant in the absence of Coulomb forces ($\varepsilon \to \infty$). Assuming that the rate differences in the two solvents are caused only by the Coulomb term, *i.e.* k_∞ is solvent independent, then the ratio of rate constants in ammonia and water is given by

$$[3] \quad \ln\frac{k_{NH_3}}{k_{H_2O}} = \frac{N_L z_1 z_2 {e_0}^2}{RT} \times \left(\frac{1}{a_{H_2O}\varepsilon_{H_2O}} - \frac{1}{a_{NH_3}\varepsilon_{NH_3}}\right)$$

Figure 2 shows a plot of k_{NH_3}/k_{H_2O} according to [3] with a reasonable collision distance in water, a_{H_2O} = 3 to 4 Å (9), as a function of the collision distance in ammonia a_{NH_3}. The experimental rate ratios are given on the left hand side. For anions a fit is obtained only for a_{NH_3} of 2 to 3 Å, which appears too small considering the rather large effective radius of the ammoniated electron. For the cations, on the other hand, a_{NH_3} seems too large ranging from 8–20 Å. Varying a_{H_2O} does not yield a better value for a_{NH_3}. Therefore we conclude that k_∞ cannot be independent of the solvent.

Variations in k_∞ were computed from [2] using the experimental rate constants k and taking a_{H_2O} = 3–4 Å (9) and a_{NH_3} = 5–6 Å (because of the larger electron radius in ammonia). For both anions and cations it is found that k_∞ in ammonia is roughly three powers of ten smaller than in water. A smaller a_{NH_3}, or larger a_{H_2O}, gives smaller ratios of $k_{\infty H_2O}/k_{\infty NH_3}$ for anions and larger for cations and vice versa.

Therefore, excluding the electrostatic contribution to the rate constant, we conclude that the electron in ammonia has a lower reactivity than the electron in water. This may be due to the energy as well as the entropy factor determining the rate constant (8)

$$[4] \qquad k \propto \exp(\Delta S^{\ddagger}/R) \exp(-\Delta H^{\ddagger}/RT)$$

where $\Delta S^{\ddagger}$ = activation entropy and $\Delta H^{\ddagger}$ =

activation enthalpy. However, since we find activation energies for the three anions in ammonia only slightly smaller than those reported for water (Table 1) it must be the entropy factor which in this case is responsible for the decreased reactivity of e_{am}^-.

In contrast to the foregoing discussion it should be mentioned that in water, ethanol, or their mixtures the variation of the rate of the e_s^-–NO_3^- and of the e_s^-–Zn^{2+} reaction (9) can be explained solely on the basis of the Coulomb term of [2] with constant collision distance and constant k_∞.

Organic Molecules

Table 2 gives collected rate constants for the reaction of solvated electrons with organic molecules in water and ammonia. Again we can try to distinguish between reactions which are diffusion and which are nondiffusion controlled.

Diffusion Controlled

The bimolecular rate constant follows from [1] with $z_2 \rightarrow 0$ (8):

$$[5] \qquad k_{diff} = 4\pi a N_L D/1000$$

With the same diffusion constants and collision parameters as given before the diffusion controlled rate constants in water and ammonia should be $1.1\text{–}1.5 \times 10^{10}$ and $1.9\text{–}2.3 \times 10^{11}$ $M^{-1}\,s^{-1}$. It is seen that rate constants of this order of magnitude are obtained for the electron reactions with biphenyl, naphthalene, anthracene, and nitrobenzene. Consequently there is no doubt that these reactions are diffusion controlled in water as well as in ammonia.

Nondiffusion Controlled

All other reactions are slower in ammonia by two to seven powers of ten as compared to those in water, showing again that the electron in ammonia is less reactive than in water or alcohol (9). This is true even if the different electrostatic contributions to reactions of an ion with a neutral particle are included (8). This would account for a rate constant ratio in ammonia and water of 0.2 to 3 depending only on whether the radius of the solvated electron is smaller or larger than that of the activated complex.

TABLE 2. Rate constants for the reaction of solvated electrons with organic molecules in water and ammonia

Molecule	Water*	Ammonia
Benzene	$<7 \times 10^6$	<1
Toluene	1×10^7	<1
Biphenyl	7×10^9	8×10^{10}†
Naphthalene	5.4×10^9	1.1×10^{11}†
Anthracene	—	3.5×10^{11}†
Nitrobenzene	3×10^{10}	2.8×10^{11}†
Acetone	6×10^9	9×10^7
1-Bromopropane	8×10^9	8×10^6
1-Chloropropane	7×10^8	3×10^6
Acetonitrile	3×10^7	2
Dimethylsulfoxide	1.7×10^6	2.5×10^2

*Reference 1.
†Reference 10.

Activation Energy and Activation Volume

For further studies of the activation energy and activation volume of the solvated electron reactions (temperature- and pressure-dependence of reaction rate) we chose acetonitrile and dimethylsulfoxide, which react with solvated electrons in ammonia 10^7 and 10^4 times slower than in water. The large differences in rate constants definitely rule out a major contribution from the Coulomb effect. The activation energies and activation volumes of the electron reactions in ammonia are 7.0 and 9.0 kcal/mol and -60 and -45 ml/mol for acetonitrile and dimethylsulfoxide, respectively. The higher activation energies in ammonia as compared to those in water (which are around 5 kcal/mol (1)) cannot explain the differences in rate. Again it is concluded that the entropy factor of [4] is decisive for the slow electron reactions in ammonia.

The large negative activation volume in ammonia reflects the large molar volume of solvated electrons in ammonia as was found previously (7) ($\approx$65 ml/mol according to density measurements on metal ammonia solutions (2–6)). Together with the larger activation energy it proves that the rates of these two reactions in ammonia are controlled by a reaction step involving charge transfer to the substrate and collapse of the cavity of the ammoniated electron.

In pure water, however, where the molar volume of the electrons is small, the pressure effect on the rates also is small (13, 14).

Conclusions

After correction for the electrostatic contribution it is shown that (besides the few diffusion controlled reactions with neutral molecules) the electron reaction rates in ammonia are by several powers of ten slower than in water. This is

considered due to the entropy factor of the rate expression [4]; this includes that the entropy of the 'large' solvated electrons in ammonia is larger than that of the 'small' solvated electrons in water. A high molar entropy of the ammoniated electrons has been assumed before (15, 16) and also can be deduced from several e_s^--equilibrium reactions (*e.g.* $C_6H_6 + e_{am}^- \rightleftarrows C_6H_6^-$) (17) in ammonia which too exhibit pronounced pressure effects ($\Delta V = -60$ ml/mol). Therefore the high entropy of the ammoniated electron is associated with its large volume, so that all differences in rates of the electrons in water and in ammonia may be due to structural effects. They reflect the different interaction of the electron with an HN- or an HO-group of the solvent. Consequently there are no kinetic differences of the electron reactions in water and alcohol (after correction of the electrostatic contribution) since in alcohol the electron also is solvated by an HO-group.

NOTE ADDED IN PROOF

Very recently Farhataziz and Cordier (J. Phys. Chem. **80**, 2635 (1976)), working on a time scale 100 to 1000 times faster than we did, reported rate constants of ammoniated electron reactions with some inorganic ions which are 10 to 100 times larger than ours. It might be that Farhataziz data are too high because of interfering reactions of electrons with other radiation products like $H^\bullet$ or $NH_2^\bullet$ which Farhataziz did not remove but which we very effectively scavenged with methylate ions (electron half-times in our solutions with added scavengers but without substrates were far above 1 s). Another explanation could be given on the basis of an equilibrium reaction

$$e^- + M^{2+} \underset{k_2}{\overset{k_1}{\rightleftarrows}} M^+$$

followed by the slower reaction

$$M^+ \xrightarrow{k_3} \text{products}$$

Then on the fast time scale Farhataziz might have observed the rate constant of the electron attachment k_1, whereas we measured on the slow time scale a complex rate constant involving k_1, k_2, and k_3. Or, finally, the methylate scavenger might lead to complexed cations which are less reactive than the ammoniated cations. In the two latter cases some of our arguments have to be revised. Anyhow, it seems necessary to collect more data of solvated electron reactions in non-aqueous solutions to get to an understanding of their kinetics.

Acknowledgment

We are grateful to the Deutsche Forschungsgemeinschaft for financial support of these studies.

1. Selected specific rates of reactions of hydrated electrons. Document NSRDS-NBS 43. 1973.
2. Proceedings Colloque Weyl I, Lille, 1963; G. LEPOUTRE and M. J. SIENCO (*Editors*). Solution métal–ammoniac. Benjamin Inc., New York. 1964.
3. Proceedings Colloque Weyl II, Ithaka, 1968; J. J. LAGOWSKI and M. J. SIENCO (*Editors*). Metal–ammonia solutions. Butterworth, London. 1970.
4. Proceedings Internat. Conf. Solvated Electrons, Herrenalb, 1971; Ber. Bunsenges. Phys. Chem. **75**, 607 (1971).
5. Proceedings Colloque Weyl III, Tel Aviv, 1973; J. JORTNER and N. R. KESTNER (*Editors*). Electrons in fluids. Springer, Berlin. 1973.
6. Proceedings Colloque Weyl IV, East Lansing, 1975; J. Phys. Chem. **79**, 2789 (1975).
7. R. OLINGER and U. SCHINDEWOLF. Ber. Bunsenges. Phys. Chem. **75**, 693 (1971).
8. A. A. FROST and R. G. PEARSON. Kinetics and mechanism. J. Wiley Inc., New York. 1961; Verlag Chemie, Weinheim. 1964.
9. F. BARAT, L. GILLES, B. HICKEL, and B. LESIGNE. J. Phys. Chem. **77**, 1711 (1973).
10. FARHATAZIZ and L. M. PERKEY. J. Phys. Chem. **80**, 122 (1976); Private communication.
11. K. H. SCHMIDT and W. L. BUCH. Science, **151**, 70 (1966).
12. C. A. KRAUS and W. W. LUCASSE. J. Am. Chem. Soc. **43**, 2551 (1923).
13. R. R. HENTZ, FARHATAZIZ, and E. M. HANSEN. J. Chem. Phys. **56**, 4485 (1972); **57**, 2959 (1972).
14. U. SCHINDEWOLF, H. KOHRMANN, and G. LANG. Angew. Chem. Int. Ed. Engl. **8**, 512 (1969); Angew. Chem. **81**, 496 (1969).
15. G. LEPOUTRE and A. DEMORTIER. Ber. Bunsenges. Phys. Chem. **75**, 647 (1971).
16. J. JORTNER and R. M. NOYES. J. Phys. Chem. **70**, 770 (1966).
17. K. W. BÖDDEKER, G. LANG, and U. SCHINDEWOLF. Angew. Chem. Int. Ed. Engl. **8**, 138 (1969); Angew. Chem. **81**, 1181 (1969).

Discussion

G. R. Freeman: The reaction of inefficient scavengers such as acetonitrile with electrons in alcohols is followed by protonation.

[1, −1] $$e_{solv}^- + M \rightleftarrows M_{solv}^-$$

[2] $$M_{solv}^- + ROH \rightarrow MH + RO_{solv}^-$$

The activation volume of [2] is negative and contributes to the total observed activation volume of the electron capture reaction. Perhaps the protonation reaction also con-

tributes to the negative activation volume in liquid ammonia, and the low rate constant might be partly limited by the slowness of protonation of the anion by ammonia.

U. Schindewolf: I do not think that [2] would have the large negative activation volume we observed. However, it would contribute if [2] really is rate determining. But in the equilibrium reactions mentioned above the large pressure dependence definitely is to be attributed to volume change which is due to the large molar volume of the ammoniated electron disappearing in the reaction. In most cases people working in kinetics restrict themselves to the observation of the disappearing of the electrons. It seems now that the electron attachment–detachment equilibrium as you state it is to be considered in many cases, because it obscures the kinetics. The negative activation energy of the e_{am}^- + C_6H_5F reaction we observed in ammonia, and of many other reactions, is due to such an equilibrium.

W. Seddon: Would you care to comment or speculate on the magnitude of the rate constant for the ammoniated solvated electron with alkali metal cations?

U. Schindewolf: I am not sure about the evidence that e_{am}^- reacts with alkali cations. As we know the equilibrium $e^- + K^+ \rightleftarrows (K^+e^-)$, which might lead to an ion pair, in the low concentration solutions is far on the left side. I would suggest pulse radiolysis – conductivity experiments to find out whether the electron is 'trapped' this way. If the reaction occurs, it should be diffusion controlled.

Electron states in liquid metals: especially optical and magnetic properties

N. H. MARCH[1]

Department of Physics, The Blackett Laboratory, Imperial College, London, England SW7 2BZ

Received October 4, 1976

N. H. MARCH. Can. J. Chem. **55**, 2165 (1977).

The theory of optical absorption of the simple liquid metals (*e.g.* the alkalis) is outlined. At not too large frequencies, the Drude theory is regained. The relaxation time is that given by the weak scattering (Ziman) theory of electrical resistivity. For high frequencies, the relaxation time, however, becomes frequency dependent. Appreciable structure enters the theory, arising from collective excitations. The relation to recent ellipsometric measurements on liquid Na is briefly discussed. The optical conductivity and density of states in the divalent metals Hg and Be is then discussed, followed by the relation between photoemission and soft X-ray experiments and current electron theory. Specific attention is given to the evidence for a pseudo-gap in the divalent metals and to changes in the electron states which occur on melting the noble metals.

The second major area treated is concerned with the magnetic properties of liquid metals. The theory of orbital and spin magnetism in simple liquid metals is reviewed and confronted with experiment. It is clear that the electron–electron enhancement effects have a dominant influence on the trend of the spin susceptibility of simple liquid metals as a function of density. However, electron–ion interactions must be introduced as corrections to the interacting electron gas values and in a metal like Li the nearly free electron theory fails to do this adequately. Knight shift results are summarized, and some attention is given to a recent experiment on the Knight shift of expanded fluid Hg. Difficulties for the theory in relation to transport and the pseudo-gap are pointed out. Finally, new theoretical calculations are reported on the relation between the magnetic properties of the liquid rare earth metals and their electrical conductivity. Mathiessen's rule is shown to break down because of very strong potential scattering. A recent theory of this by Parrinello *et al.* shows that in the strong scattering limit the magnitude of the localized spin carried by the rare earth ion drops out of the transport theory, as required by the experiments of Güntherodt *et al.*

N. H. MARCH. Can. J. Chem. **55**, 2165 (1977).

On décrit la théorie de l'absorption optique des métaux liquides simples (par exemple les alcalis). A des fréquences qui ne sont pas trop grandes, on retrouve la théorie de Drude. Le temps de relaxation est celui prévu par la théorie (Ziman) de dispersion faible de la résistivité électrique. Pour des fréquences élevées, il existe toutefois une relation entre le temps de relaxation et la fréquence. Un degré appréciable de structure, provenant d'excitations collectives, entre dans la théorie. On discute de la relation qui existe avec les mesures ellipsométriques effectuées récemment sur du sodium liquide. On discute alors de la conductivité optique et de la densité d'états dans les métaux divalents Hg et Be; le tout est suivi par la relation qui existe entre les expériences de photoémission et de rayons-X doux et la théorie électronique prévaut actuellement. On porte une attention spéciale aux preuves concernant un pseudo-gap dans les métaux divalents et à un changement dans les états électroniques qui se produisent lorsque l'on fait fondre des métaux nobles.

La deuxième section importante qui sera traitée concerne les propriétés magnétiques des métaux liquides. On passe en revue la théorie des magnétismes orbital et de spin dans des métaux liquides simples et on la compare avec l'expérience. Il est évident que l'influence des effets de rehaussement électron–électron est dominante sur la tendance de la susceptibilité de spin des métaux liquides simples en fonction de la densité. Toutefois, des interactions électron–ion doivent être introduites pour corriger les valeurs des électrons interagissant en phase gazeuse; toutefois dans un métal comme le lithium la théorie d'électron presque libre ne parvient pas à l'expliquer d'une façon adéquate. On donne un sommaire des résultats de déplacement de Knight et on accorde une certaine attention à une expérience récente sur le déplacement de Knight par du Hg fluide gonflé. On met en relief les difficultés que la théorie rencontre pour expliquer le transport et le pseudo-gap. Finallement on rapporte de nouveaux calculs théoriques sur la relation qui existe entre les propriétés magnétiques des métaux de terres rares liquides et leur conductivité électrique. On montre que la règle de Mathiessen ne tient

---

[1]Permanent address from October 1, 1977: Department of Theoretical Chemistry, University of Oxford, 1 South Parks Rd., Oxford, England OX1 3TG.

pas à cause de la grande dispersion du potentiel. Une théorie récente à ce sujet par Parrinello et ses collaborateurs montre que dans la limite d'une forte dispersion, l'amplitude du spin localisé transporté par un ion de terre rare disparaît de la théorie du transport tel qu'il est requis par les expériences de Guntherodt et ses collaborateurs.

[Traduit par le journal]

Introduction

The theory of liquid metals divides usefully into two sections:

(*1*) Simple metals (*e.g.* Na, Al, Pb, etc.)

Here, almost free conduction electrons are scattered off ions by a weak electron–ion interaction. The basic ingredients in the theory are: (*a*) the liquid structure factor $S(k)$ and (*b*) a weak pseudopotential $U(k)$, representing the electron–ion interaction.

The nearly-free electron theory of transport (Ziman theory) then gives for the dc electrical resistivity the result (see, for example, ref. 1)

$$[1.1]\quad \rho = (3\pi^2/e^2\hbar v_f^2)\Omega \int_0^{2k_f} |U(k)|^2 S(k) k^3 \, dk = (ne^2\tau/m)^{-1}$$

where v_f and k_f are the Fermi velocity and wave number, respectively, while Ω is the atomic volume and τ the relaxation time. This formula can explain a lot of the general properties of transport in pure liquid metals. Valency is simple (Table 1) and the Hall effect confirms the number of free electrons per atom as equal to the valency (Na 1, Al 3, Pb 4, etc.).

(*2*) Strong scattering liquid metals (*e.g.* transition and rare earth metals: divalent metals, Be, Hg, Ba, etc.).

Here, theory to date generalizes [1.1] using again the measured structure factors but replacing $U(k)$ by the appropriate object (the so-called **t** matrix) describing the strong scattering off a single ion. Though this theory has had some successes (*e.g.* explaining why the dc resistivity of Ba is ~ 300 $\mu\Omega$ cm) the theory is less well based, because for strong scattering, higher order correlations between atoms enter the theory and we do not presently know how to either measure or calculate these with any certainty.

TABLE 1. Effective number of free electrons per atom in liquid metals

Metal	Valency	n^*
K	1	1.0
Ag	1	1.1
Cd	2	2.1
Ga	3	2.9
Sn	4	4.6
Pb	4	4.7
Sb	5	6.1
Bi	5	5.3

With this as background we turn to the first of the two major topics of this review, the optical properties of liquid metals. Subsequently, we shall deal with magnetic properties as the second topic. The link between the two is structure, both electronic and atomic.

(A) Optical Properties

2. *Theory of Optical Absorption of Simple Liquid Metals*

2.1. Drude Theory

The most elementary theory of high frequency conductivity, going back to Drude, writes the real part of the complex conductivity as

$$[2.1]\quad \sigma(\omega) = \frac{\sigma(0)}{1 + \omega^2\tau^2} = \frac{ne^2\tau}{m(1 + \omega^2\tau^2)}$$

where at $\omega = 0$ this reduces to the above formula [1.1], an explicit expression for τ resulting in terms of the structure factor and pseudo-potential.

Equation 2.1 adequately represents the ac conductivity of numerous liquid metals with $\omega\tau$ found to be ~ 1 in the visible, to be contrasted with the case of solids where $\omega\tau \sim 1$ lies in the far infrared. Equation 2.1 is, of course, the real part of the complex conductivity, the imaginary part being derivable from it, in principle, using the Kramers–Kronig relations.

The values obtained experimentally for n, the effective number of free electrons per unit volume, are shown in Table 1. The results are given per atom, for direct comparison with the valency.

The data available on the optical properties of liquid metals are seen to accord well with free-electron theory, a notable exception, however, being liquid Hg which does not obey the Drude formula [2.1].

We refer briefly at this point to two approaches to the basic theory, one of the principal aims being to get limits of validity for the Drude formula [2.1]. The first approach (see, for example, Sturm and Pajanne (2)) attempts to make direct contact with the Ziman theory, though it shows that, while τ in the denominator

of [2.1] can be correctly calculated from the Ziman theory for low frequencies, for high frequencies the relaxation time becomes frequency dependent. Appreciable structure then enters the theory, arising from collective excitations (see below for a short summary of the theory).

A second, more formal, approach is that of Parrinello and co-workers (3) who treat the liquid metal from the outset as a two-component system of positive ions and itinerant electrons, with correlation functions between each pair of particles. The connection of their approach with the Drude formula is also briefly referred to below.

2.2 Weak Scattering Theory of Optical Absorption

If one treats the simple liquid metals (*e.g.* the alkalis) in which it is appropriate to assume a weak effective electron–ion interaction, then the Drude formula results (see, for example, Sturm and Pajanne (2)) provided $\hbar\omega/E_f \ll 1$ but $\omega\tau \gg 1$. Furthermore the constant relaxation time is indeed given by the Ziman formula, as anticipated above.

The basic theory starts out from the general expression for the real part of the optical conductivity tensor, which, within linear response theory, is given by Pethick (4)

$$[2.2]\quad \mathrm{Re}\,\sigma^{\mu\nu}(\omega) = \frac{1}{2}\frac{e^2/m^2}{\hbar\omega^3}\int_{-\infty}^{\infty} dt(e^{-i\omega t} - e^{i\omega t})\frac{1}{N^2}\sum_{KK'} K^{\mu}K'^{\nu}U_K U_{K'} \times \langle \rho_K^{el}(0)\rho_{-K}^{ion}(0)\rho_{K'}^{el}(t)\rho_{-K'}^{ion}(t)\rangle$$

Here U_K is the Fourier component of the potential of a single ion, while the electronic and ionic density fluctuations are defined as

$$[2.3]\quad \rho_{\boldsymbol{K}}^{el}(t) = \sum_i e^{i\boldsymbol{K}\cdot\boldsymbol{r}_i(t)}$$

and

$$[2.4]\quad \rho_{\boldsymbol{K}}^{ion}(t) = \sum_j e^{i\boldsymbol{K}\cdot\boldsymbol{R}_j(t)}$$

$\boldsymbol{r}_i$ and $\boldsymbol{R}_j$ denoting electronic and ionic coordinates, respectively.

The important simplification which arises if we now calculate Re $\sigma^{\mu\nu}(\omega)$ to second-order in the potential is that the correlation function decouples to yield

$$[2.5]\quad \langle \rho_{\boldsymbol{K}}^{el}(0)\rho_{-\boldsymbol{K}}^{ion}(0)\rho_{\boldsymbol{K}'}^{el}(t)\rho_{-\boldsymbol{K}'}^{ion}(t)\rangle \simeq \langle \rho_{\boldsymbol{K}}^{el}(0)\rho_{\boldsymbol{K}'}^{el}(t)\rangle\langle \rho_{-\boldsymbol{K}}^{ion}(0)\rho_{-\boldsymbol{K}'}^{ion}(t)\rangle$$

In lowest order, $\langle \rho_{\boldsymbol{K}}^{el}(0)\rho_{\boldsymbol{K}'}^{el}(t)\rangle$ is the electronic density–density correlation function of jellium (Sommerfeld model of a metal). Therefore we have

$$[2.6]\quad \langle \rho_{\boldsymbol{K}}^{el}(0)\rho_{\boldsymbol{K}'}^{el}(t)\rangle \neq 0$$

only if $\boldsymbol{K}' = -\boldsymbol{K}$.

Furthermore, this is directly related to the frequency-dependent dielectric function $\varepsilon(K,\omega)$ of the electron gas by

$$[2.7]\quad \int_{-\infty}^{\infty} dt\langle \rho_{\boldsymbol{K}}^{el}(0)\rho_{-\boldsymbol{K}}^{el}(t)\rangle(e^{-i\omega t} - e^{i\omega t}) = \frac{\hbar^2K^2}{2\pi e^2}\,\mathrm{Im}\left(\frac{-1}{\varepsilon(K,\omega)}\right)$$

Also the (dynamic) structure factor is given by

$$[2.8]\quad S(\boldsymbol{K},t) = \frac{1}{N}\langle \rho_{-\boldsymbol{K}}^{ion}(0)\rho_{\boldsymbol{K}}^{ion}(t)\rangle$$

As the ions move slowly compared with the electronic motion we can put $t = 0$ since on the time scale defined by the frequency of the light, electrons see essentially a static distribution of ions.

Since $S(K)$ is isotropic for a liquid metal, we then obtain

$$[2.9]\quad \mathrm{Re}\,\sigma(\omega) = (24\pi^3 nm^2\omega^3)^{-1}\int dKK^6|U_K|^2S(K)\,\mathrm{Im}\,(-1/\varepsilon(K,\omega))$$

Introducing a formal definition of relaxation time through

$$[2.10]\quad \mathrm{Re}\,\sigma(\omega) = \frac{ne^2}{m}\frac{1}{\tau(\omega)\omega^2} \qquad \text{for } \omega\tau \gg 1$$

we obtain

$$[2.11] \qquad \frac{1}{\tau(\omega)} = (24\pi^3 n^2 m e^2 \omega)^{-1} \int dK K^6 |U_K|^2 S(K) \, \mathrm{Im}\,(-1/\varepsilon(K,\omega))$$

(a) Connection with Ziman Theory—Provided $\hbar\omega/E_f \ll 1$ we can write

$$[2.12] \qquad |U_K|^2 \, \mathrm{Im}\left(\frac{-1}{\varepsilon(K,\omega)}\right) \simeq \left|\frac{U_K}{\varepsilon(K,0)}\right|^2 \mathrm{Im}\,\varepsilon(K,\omega)$$

The Lindhard expression for Im $\varepsilon(K,\omega)$ for small frequencies is

$$[2.13] \qquad \mathrm{Im}\,\varepsilon(K,\omega) = \frac{3\pi}{2}\frac{\omega_p{}^2\omega}{K^3 v_f{}^3}$$

where ω_p is the plasma frequency and v_f the Fermi velocity.

Substituting this result in [2.11] we obtain the reciprocal relaxation time τ^{-1} as

$$[2.14] \qquad \tau^{-1} = \frac{m}{12\pi^3\hbar^3 n^2}\int_0^{2k_f} dK K^3 S(K)|U_K/\varepsilon(K,0)|^2$$

where U_K is normalized such that $U_{K=0}/\varepsilon(0,0) = -\frac{2}{3}E_f$. This is precisely the form given by the Ziman theory. Sturm and Pajanne (2) have made numerical calculations for Na at 100°C with the Ashcroft (5) empty core model potential

$$[2.15] \qquad U(r) = \begin{cases} -e^2/r & r > R_c \\ 0 & r < R_c \end{cases}$$

with $R_c = 1.66a_0$, a_0 being the Bohr radius. They use a hard sphere model for $S(K)$, with a hard sphere diameter 3.30 Å.

Figure 1 shows the real part of $\sigma(\omega)$ (full curve) from their calculations compared with the Drude (constant relaxation time) result (dashed curve). The most striking feature is the peak arising from the collective excitations (plasmons).

Comparison with experiment is still difficult, but it seems that for photon energies $\sim E_f$ the optical absorption is considerably greater than the Drude value, in general accord with theory. Measurements on liquid Al between about 0.8 and 4 eV (6) show essentially Drude behaviour. This is in agreement with theory, since for $\hbar\omega/E_f \ll 1$ the Drude formula should be valid.

(b) Ellipsometric Measurements on Na—Rather than attempt to survey earlier experiments (see, for example, Faber (7) for both experiment and theory), we shall conclude this discussion of optical absorption in the simple metals by referring to the accurate ellipsometric measurements on free surfaces of liquid Na at 120°C between 0.6 and 3.8 eV, recently reported by Inagaki *et al.* (8).

They find that the optical conductivity below 2.2 eV agrees well with the Drude formula [2.1]. Above 2.2 eV the optical conductivity exhibits a weak absorption, which they suggest is analogous to the interband absorption in the solid phase.

Their measurements of the optical conductivity, related to the imaginary part ε_2 of the dielectric constant by $\sigma = \omega\varepsilon_2/4\pi$, where ω is the angular frequency of the incident photons, are shown in Fig. 2, along with the Drude result. The free-carrier density of 2.405×10^{22} cm^{-3} at 120°C plus the measured dc conductivity $\sigma(0) = 8.607 \times 10^{16}$ s^{-1} lead to a relaxation time $\tau = 1.653 \times 10^{-14}$ s. This is obtained by taking an effective mass m^* of $1.17m$, which was deduced from the experimental values of the real part of the dielectric function in the infrared region.

The results for ε_1, the real part of the dielectric function, are plotted in Fig. 3, as a function of the square of the wavelength λ in μm. Inagaki *et al.* (8) analyzed these data by using the conventional form

$$[2.16] \qquad \varepsilon_1 = 1 + 4\pi n_0\alpha - ne^2\lambda^2/\pi m^* c^2$$

where n_0 is the atomic density and α is the ion-core polarizability. This gives $m^* = (1.17 \pm 0.01)m$ below 2.2 eV and $(1.10 \pm 0.01)m$ above 2.2 eV, a plasma energy, defined by $\varepsilon_1 = 0$, at 5.70 ± 0.05 eV, and $4\pi n_0\alpha = -0.05 \pm 0.05$. The result for m^* below 2.2 eV is comparable to that obtained by Mayer and Hietel (9) at 100°C, namely $m^* = 1.19m$, despite the substantial differences in σ recorded in Fig. 2.

3. Strong Scattering Liquid Metals

3.1. Summary of Two-component Theory

As remarked above, in ref. 3 an approach to liquid metals which treats them, from the outset,

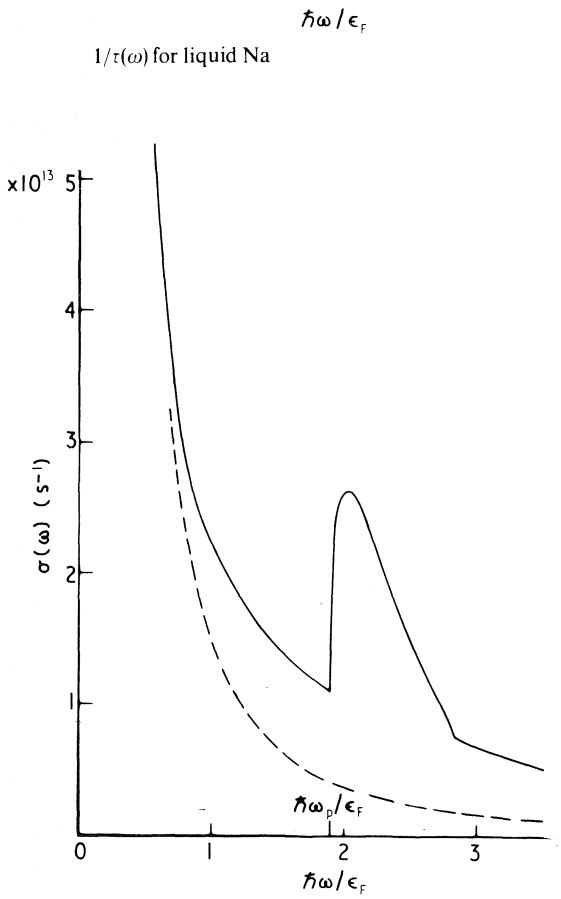

FIG. 1. High frequency conductivity of liquid Na: — calculated from [2.11], --- result of Drude theory. (Reprinted with permission from the Journal of Physics F: Metal Physics, **3**, 199 (1973). Copyright by The Institute of Physics.)

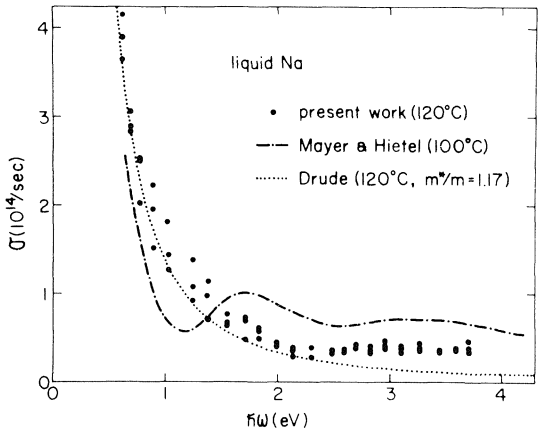

FIG. 2. High frequency conductivity of liquid Na. (Reprinted with permission from Physical Review Section B: Solid State, **13**, 5610 (1976). Copyright by The American Physical Society.)

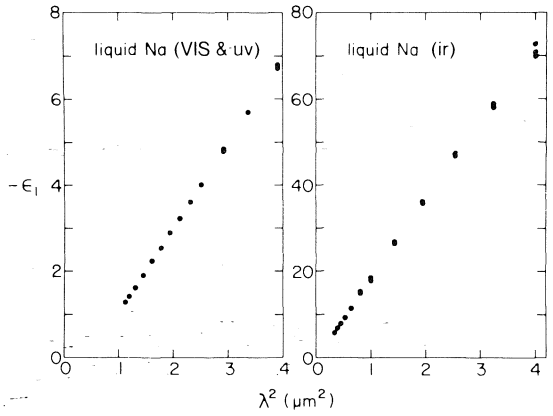

FIG. 3. Real part of dielectric constant for liquid Na. (Reprinted with permission from Physical Review Section B: Solid State, **13**, 5610 (1976). Copyright by The American Physical Society.)

as two-component systems, with three partial structure factors, has been developed, which may eventually afford a route to the strong scattering theory.

Optical properties are then described by a formula for the conductivity in the long wavelength limit $k \to 0$, namely

$$[3.1] \quad \sigma(k=0,\omega) = \frac{n_e e^2}{m_e} \times \frac{M/m_i}{-i\omega + M\gamma(\omega)/n_e m_i m_e}$$

where $M = m_i + Zm_e$, Z being the valence and e and i denoting electrons and ions, respectively.

The Drude theory, which, as we saw in section 2, is very useful for liquid metals, follows if $\gamma(\omega)$ in [3.1] is assumed to vary only slowly with frequency over the range of interest. Both theoretical predictions and empirically derived forms of $\gamma(\omega)$ for simple liquid metals are discussed in ref. 3. $\gamma(\omega)$ involves the electron–ion interaction and the functional derivative with respect to the electron current of the ion-density – electron-density correlations: to date no convincing approach to this object in the presence of strong scattering exists. Reference should also be made here to the work of Jones (10) on frequency-dependent conductivity.

In view of these difficulties in the theory for strong scattering, we shall restrict ourselves to a brief discussion of the optical properties of the divalent metals, Hg and Be, and the relation of these properties to the density of electronic states.

3.2. Optical Conductivity and Density of States in Divalent Metals

Divalent elements such as Be and Hg form metallic crystals below their melting temperatures because of band overlap. If this overlap is sufficiently small, it is evident that in the crystal the density of electronic states will pass through a minimum in the region where the bands overlap.

The question now arises, whether such a minimum in the density of states (often referred to as a pseudogap) will persist, when the long-range order in such a divalent metal is destroyed by melting.

(a) Liquid Mercury—Mott (11) has suggested that, if there is a pseudogap near the Fermi level, as depicted in the density of states $N(E)$ drawn in the lower part of Fig. 4, then the high frequency conductivity should have the form shown in curve *2* of the upper part of Fig. 4. The behaviour without a pseudogap should have the Drude form as in curve *1*. The reason why there should be a peak away from zero frequency in $\sigma(\omega)$, according to Mott's argument, is indicated by the available transitions for low and high frequency in the lower part of Fig. 4.

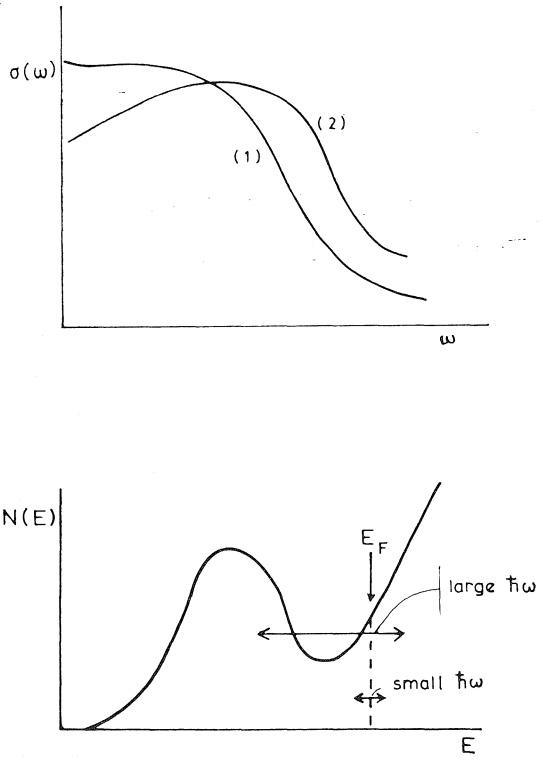

FIG. 4. Upper diagram: high frequency conductivity with (curve *2*) and without (curve *1*) a pseudogap. Lower diagram: density of states with pseudogap.

Subsequently, the optical conductivity and electronic density of states for liquid Hg have been discussed by Chan and Ballentine (12) using low-order perturbation theory. They found a dip near the Fermi energy in the density of states $N(E)$, which was less pronounced than that suggested by Mott, and which they found too small to alter the optical conductivity appreciably from Drude form.

Experimentally it is not clear that $\sigma(\omega)$ behaves like curve *2* of Fig. 4 (actually Hodgson (13) has found a shape like this for liquid Te). Thus, for liquid Hg, Guggenheim (14) finds such an effect, which disappears on alloying. Comins (15) comes to a similar conclusion, both these experiments being carried out using ellipsometric methods. In contrast, Boiani and Rice (16) get good accord with the Drude formula over a wide frequency range, using direct reflection methods. Bloch and Rice (17) maintain that the differences can be reconciled if a surface layer with different electrical properties from the bulk is assumed.

We shall return to the question of the existence of a pseudogap in liquid Hg several times. However, there has also been a small amount of work done on liquid and amorphous Be, another divalent metal, and we turn now to summarize the findings on this metal.

(b) Amorphous Beryllium—Rousseau *et al.* (18) have reported a calculation of the electronic density of states of liquid Be, in which the basic building block is the partition function of a single screened ion in a Fermi gas. This is treated by strong scattering, not by low-order Born approximation, and the partition function of the liquid metals is then built up from such screened ions (pseudoatoms) assuming independence, that is

$$[3.2] \qquad pf_{\text{liquid}} = \Pi pf_{\text{screened ions}}$$

The electronic density of states can be derived from, essentially, the inverse Laplace transform of the partition function. Rousseau *et al.* (18) conclude that there is considerable similarity between the liquid and the crystal and that some dip remains in the liquid density of states. It would, of course, be of considerable interest to apply the more modern methods of electronic structure calculations, briefly summarized in the Appendix, to this metal.

To our knowledge, there is no experiment as yet available relating to the optical properties of liquid Be. However, Hunderi and Myers (19) have measured the optical absorption of evaporated Be films, which they believe to be in a disordered state. They find, as can be seen from Fig. 5, that their data are quite similar to the spectrum obtained on bulk single crystal Be by Weaver *et al.* (20). Their findings are consistent with the view that the electronic structure of crystalline as well as disordered Be is governed largely by short-range order. The theoretical work of Rousseau *et al.* (18) supports this view. In particular, both experiment and theory lend some support to the view discussed above for Hg also, that a minimum in the density of electronic states near the Fermi level, known to exist in crystalline Be, will persist in the presence of disorder.

4. Soft X-Ray and Photoemission Experiments on Molten Metals

Within the general area of optical properties, we turn next to a class of experiments containing potentially much richer information on electronic states in liquid metals than ac conductivity.

Since the early days of the band theory of metals, it has been clear that experiments on soft X-ray emission, in which an electron falls from a conduction band state into a core hole (*e.g.* in Li from p states in the $2s$–p conduction band into the ($1s$) K shell state) must reflect the density of states in the conduction band. But, of course, matrix elements also come in, and only if these are slowly varying in energy can one extract the electronic density of states $N(E)$ from the intensity of the soft X-ray emission. Nevertheless, this class of experiment remains very important, and we shall discuss recent results by Hague (21) on the metals Fe, Ni, and Co. Passing reference will also be made to earlier work on Al.

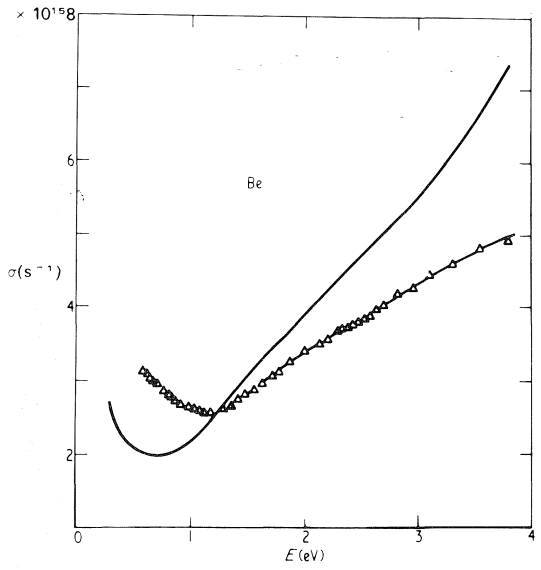

FIG. 5. Optical conductivity of crystalline Be (full curve) after Weaver *et al.* (20). Other results, conductivity of Be deposited and measured at 20 K. (Reprinted with permission from the Journal of Physics F: Metal Physics, **4**, 1088 (1974). Copyright by The Institute of Physics.)

The other very important approach to the experimental study of the electronic density of states is afforded by photoemission. We shall consider in some detail the experiments by Williams and Norris (22) on liquid noble metals as well as the work of Cotti *et al.* (23) on liquid Hg. Again, we make no claim to completeness. Theoretical approaches to the calculation of the electronic density of states in a liquid metal will be briefly referred to, and some of the principal conclusions confronted with the above experiments.

4.1. Photoemission and Electronic Band Structure

Williams and Norris (22) have observed ultraviolet photoemission (21.2 eV) from liquid Cu samples. Figure 6 shows their photoelectron energy distribution curves (EDC's) obtained for liquid Cu, and for comparison they show results from the same sample immediately after freezing and after being held for several days at 1000 K. The energy scale is such that the zero corresponds to the Fermi level.

The primary distribution of photoemitted electrons can be expressed as a sum over initial (i) and final (f) states, namely as

$$[4.1]\quad \mathcal{N}_{\text{primary}}(E,\hbar\omega) = \sum_{i,f} |\langle f|H'|i\rangle|^2 \times \delta(E_f - E_i - \hbar\omega)\delta(E - E_f)$$

where H' is the interaction describing both the probability of photoexcitation and escape into the vacuum.

For disordered systems such as liquids, in which non-direct transitions are possible, it may be argued that the matrix element is not a dominant function and can be removed from the summation to yield

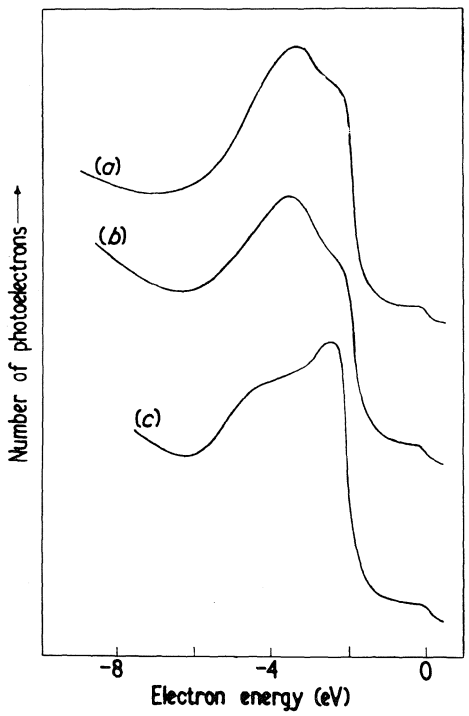

FIG. 6. Energy distribution curves for Cu (*a*) liquid, (*b*) solid immediately after freezing, and (*c*) solid after annealing. (Reprinted with permission from the Journal of Physics F: Metal Physics, **4**, L175 (1974). Copyright by The Institute of Physics.)

$$[4.2] \qquad \mathcal{N}(E,\hbar\omega) = BN(E - \hbar\omega)N(E)$$

as a product of initial and final density of states.[2]

Figure 7 shows a comparison between the measured result for liquid Cu and the result of a cluster calculation for liquid Cu by Keller *et al.* (25). Also plotted is the density of states computed by Mueller (26) for the face-centred cubic crystal.

There is substantial agreement between the shape of the 3*d* band and the cluster calculation. However, the agreement between the measured shape and the 3*d* band of the crystal is much poorer than was found for liquid and solid Au by Eastman (27). The explanation (*cf.* ref. 22) seems to lie in the fact that in Au there is greater *s–d* hybridization with correspondingly less sensitivity to the local order than is the case for Cu. The high energy peak at −2.5 eV in Cu is associated with an unhybridized level in the solid

[2]Refinements of this expression are discussed by Schaich and Ashcroft (24).

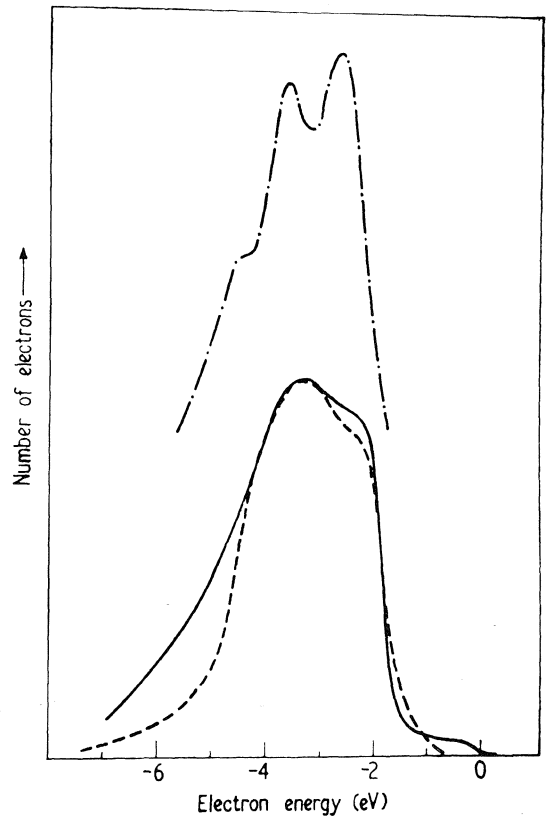

FIG. 7. Density of states of liquid Cu: -·-·- Mueller's calculation for fcc Cu, — experiment on liquid, --- cluster calculation. (Reprinted with permission from the Journal of Physics F: Metal Physics, **4**, L175 (1974). Copyright by The Institute of Physics.)

and would therefore be expected to weaken considerably, as Williams and Norris (22) observe, when the crystal melts and the long-range order is lost.

In connection with the above cluster calculation, it is of interest that House and Smith (28) found for crystalline Cu that a cluster calculation using only a single face-centred-cubic unit cell was in good agreement with the band structure result.

(a) Photoemission from Liquid Hg—Because of a possible pseudogap referred to previously, Hg has attracted considerable attention and Cotti *et al.* (23) have reported measurements of the energy distribution of photoemitted electrons from both the liquid and solid.

As remarked above, in connection with Cu, provided that $\boldsymbol{k}$-conservation is not an effective selection rule, as is the case for a liquid metal,

then the EDC's may be regarded as reflecting the density of states.

In Fig. 8, the EDC's show clearly that liquid and solid Hg exhibit the same general behaviour, though the solid curve has a little more structure, probably arising from direct transitions at critical points. Figure 9 shows a comparison of the liquid results with the predictions of nearly-free electron theory. The agreement is much poorer than for say potassium (23) and therefore Cotti *et al.* (23) claim that their results indicate the presence of a pseudogap (or minimum in the density of states) in liquid Hg, first suggested by Mott (11, 29). Such a minimum in the density of states was consistent with the experiments of Hunderi and Myers (19) discussed above for disordered divalent Be.

We have reproduced in Fig. 10 the density of states in a divalent liquid metal according to the proposal of Mott (ref. 29; compare $N(E)$ for Be from Rousseau *et al.* (18)). Part *a* would be the result of low order perturbation theory, curve *b* the suggested form for liquid Hg. Curve *c* is a form suggested for Hg at densities such that the conductivity lies in the range 300–2000 Ω^{-1} cm^{-1}, while *d* is the curve expected at low densities. Curve *d* is indeed what seems to be required by the low density experiments of Hensel and Franck (30) and Schmulzter (31). It is relevant in this context to refer to the work of Overhof *et al.* (32) who have attempted to explain the optical properties of expanded fluid Hg using a quasi-crystalline model with non-direct transitions. They also make a critical examination of discrepancies between optical and electrical transport data for fluid Hg but we must refer the reader to their paper for further details (see also refs. 36 and 39).

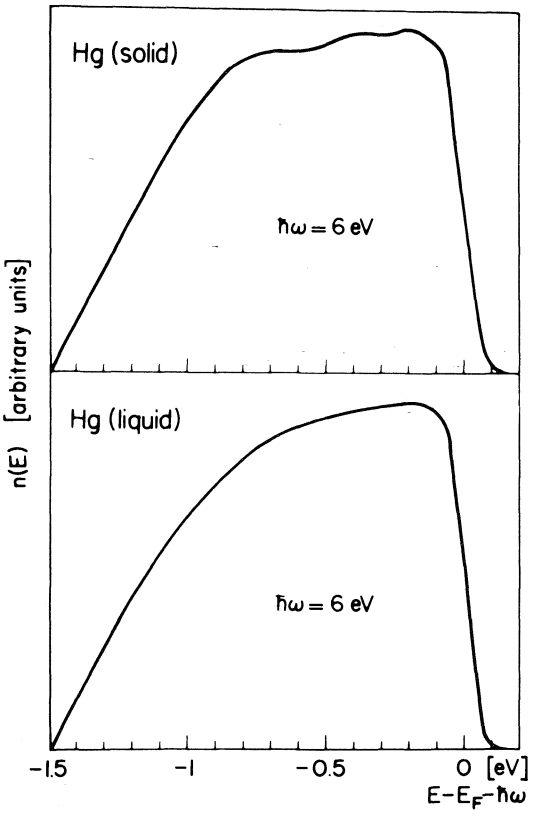

Comparison of EDC's for solid and liquid mercury.

FIG. 8. Energy distribution curves for liquid and solid Hg. (Reprinted with permission from Solid State Communications, **12**, 635 (1973). Copyright by Pergamon Press Ltd., Oxford.)

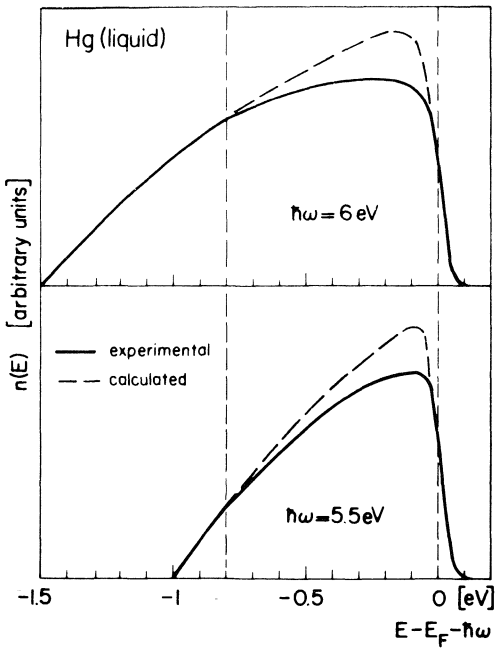

FIG. 9. Comparison of calculated and measured EDC's for liquid Hg. (Reprinted with permission from Solid State Communications, **12**, 635 (1973). Copyright by Pergamon Press Ltd., Oxford.)

(b) Other Results by Ultraviolet Photoemission Spectroscopy—Some other valence band results have been obtained by ultraviolet photoemission spectroscopy (ups). It seems that these techniques can provide a better resolution of the densities of states, if a sufficiently monochromatic excitation

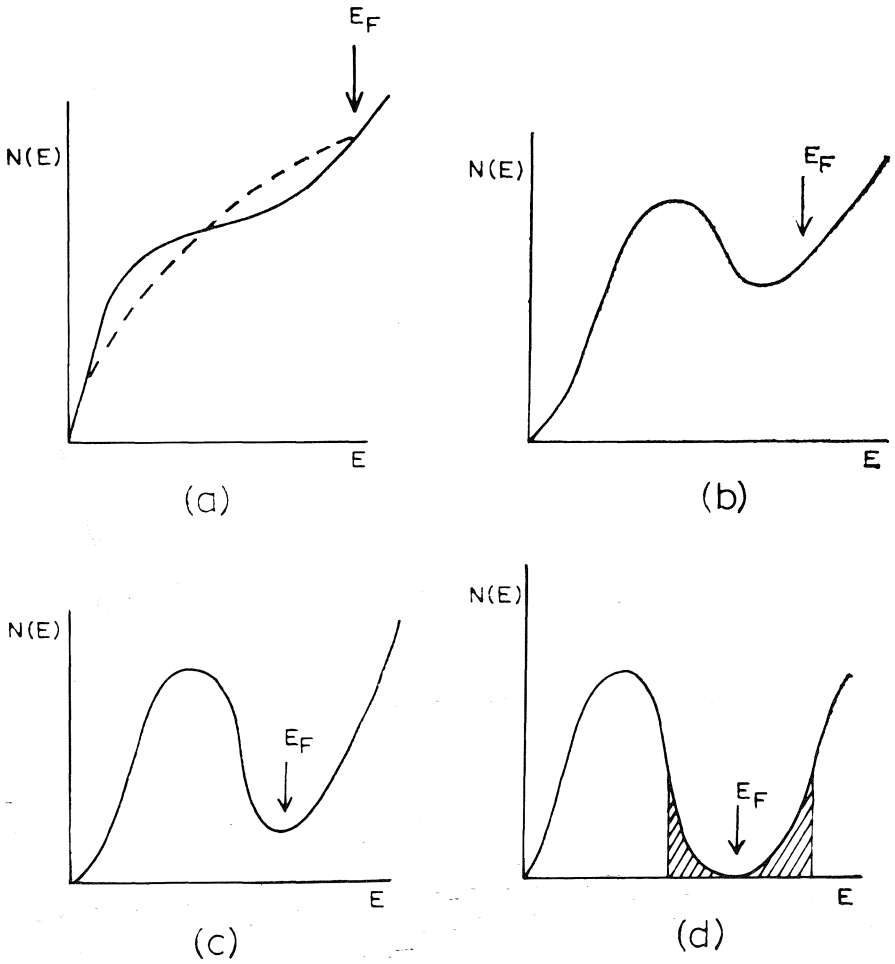

FIG. 10. Densities of states for liquid Hg at different densities: (*a*) high density, dashed curve is free electron result; (*b*) overlapping bands of divalent metal at intermediate density; (*c*) development of pseudogap at lower density; (*d*) shaded regions indicate localized states. Low density case. (Reprinted with permission from Philosophical Magazine, **26**, 505 (1972). Copyright by Taylor & Francis Ltd., London.)

radiation is employed (33, 27, 22, and 34). However, they are more subject to surface contamination and secondary effects than soft X-ray spectroscopy (sXs) (21).

Also, photoemission measurements, notably for Sn and In (Norris *et al.* (35); Norris and Rodway[3]) suggest considerably more structure in the electron density of states than calculations based on such a low-order approximation would imply (see Fig. 11).

The conclusion for the simpler metals, especially Sn, In, and Pb, is that the liquid density of states retains quite a few features in common with the crystalline phase, the nearly free electron approximation being almost always too crude.

Following this summary of photoemission results, we shall next consider what we can learn about electronic structure of liquid metals from soft X-ray experiments. We shall focus largely on the very recent work of Hague (21) on the iron group.

4.2. Soft X-Ray Band Spectra of Liquid Metals

Hague (21) has reported the L_3 emission and absorption spectra in liquid Fe, Co, and Ni and we shall briefly discuss his results and their qualitative interpretation.

(a) Emission Spectra—Hague (21) actually measured the L_3 emission curves at two excita-

[3]C. Norris and D. C. Rodway, private communication.

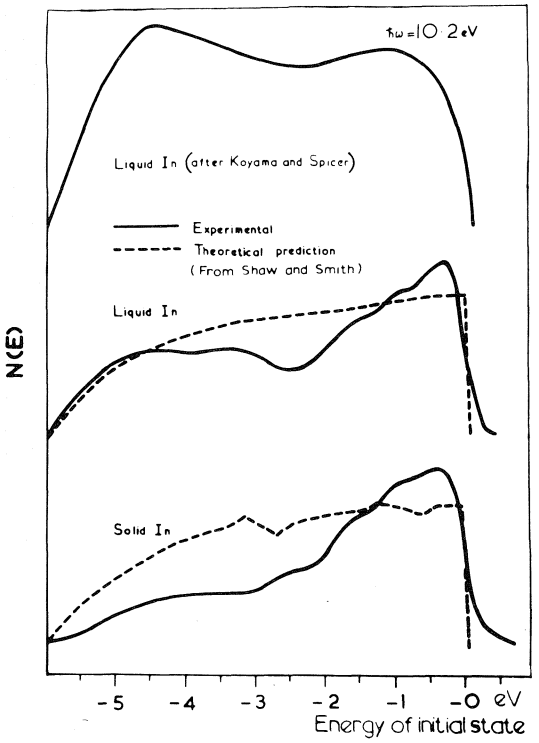

FIG. 11. Densities of states from photoemission for liquid In. (Reprinted with permission from ref. 35.)

tion voltages; only the curves for the 2.5 kV voltage are reproduced in Fig. 12. In Ni, comparison between solid and liquid results turns out to be difficult, because as Hague points out surface oxidation very probably exists in the solid phase (not in the liquid phase).

For Co the differences between solid and liquid emission spectra turn out to be small, though these may again be somewhat masked by some contamination in the solid. Finally, the Fe results are found by Hague to be slightly different from the other two liquid metals. Some modification in the electron states between liquid and solid Fe was observed by Hague in the data at 5 kV.

(b) Absorption Spectra for Fe, Co, and Ni— The experimental results shown in Fig. 12 are for the liquid phase. Curves for the solid phase are considered by Hague (21) to be unreliable because of self-absorption. Therefore, the absorption spectra from solid thin films are given for comparison purposes.

It can be seen that, for Ni, the resemblance between the self-absorption curve and the thin film result is close. Parratt (38) has shown that in

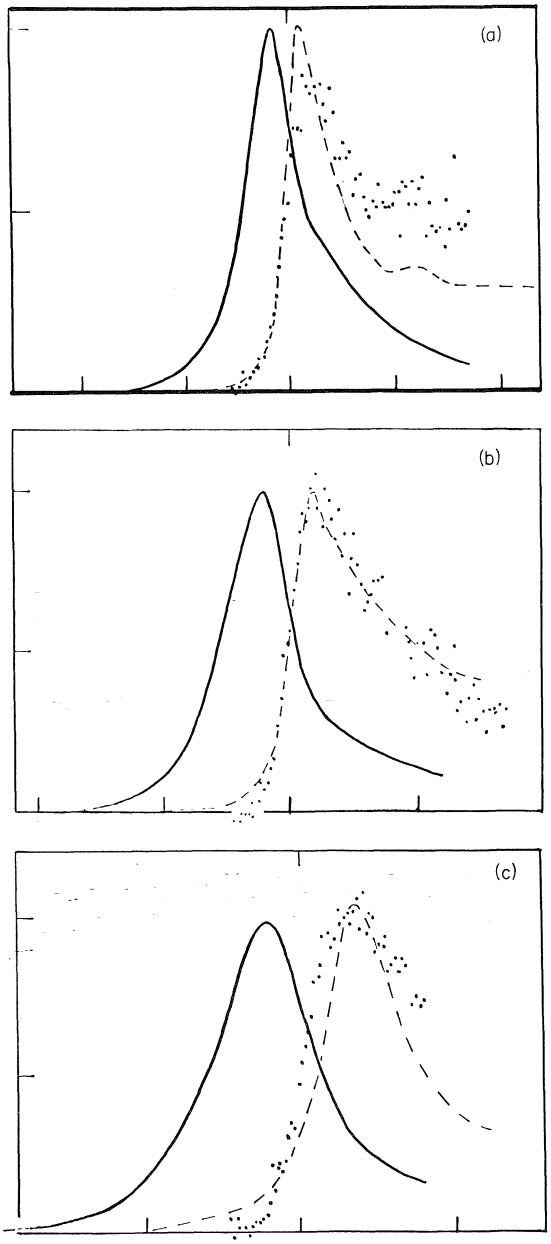

FIG. 12. L_3 emission curves of liquid metals at 2.5 kV—; L_3 self-absorption curves of liquid metals ···; and thin solid film L_3 absorption curves (*a*) Ni, (*b*) Co, (*c*) Fe. (From work of C. Hague; see also ref. 21.)

the case of a sharp peak representing the empty *d* states in the conduction band, as in this case, the amplitude of the maximum is very dependent on the thickness of the absorbant. Hague (21) suggests this as an explanation of the attenuation observed in the peak in the liquid spectrum.

For Co, in view of some arbitrariness in normalization of the absorption curves, the agreement between the liquid and solid thin film curves is good, and the small deviation occurring at high energy may not be significant.

Finally, for Fe, the absorption spectra show appreciable differences. However, the thin film spectrum, as Hague (21) points out, is most likely perturbed by an anomalous reflection in the analysing crystal containing Fe, which occurs close to the Fermi level. Hague (21) finds that the solid self-absorption curve follows closely that of the liquid result.

Summing up, it seems reasonable to expect that the L emission spectra in transition metals reflect somewhat closely the density of states $N(E)$ of the d states in the valence band. Also the peak in the absorption curve close to the Fermi level is characteristic of the unfilled d states in the conduction band.

Because there is little change in the interatomic distances or coordination number of these metals in the liquid state, modifications in the density of states can be expected to be small. The cluster calculations of House and Smith (28) referred to above, and perhaps also the hard sphere description of Gaspard[4] bear this out.

Hague's (21) soft X-ray spectra do not reveal the presence of any extra structure close to the Fermi level, and neither do the K spectra obtained by Garg and Kallne (40). This is in agreement with the theoretical work of Olsen (41).

Hague (21) stresses that, despite the blurring effect on fine structure due to inner level broadening, the soft X-ray band spectra should be capable of exposing quite small alterations in the electronic structure. Evidence exists, in his measurements, that the non-close-packed metal in the solid, namely Fe, already shows changes in the electronic states on melting.

(c) Soft X-Ray Spectra of Other Liquid Metals—Other measurements of similar type to those of Hague (21) were made on the L emission spectrum of liquid Al (42), its K emission spectrum (43, 44), and more recently on the K emission of liquid Cu and Fe (40).

In the X-ray region, the results for Al diverge for the K and L X-ray emission (44, 42). Catterall and Trotter (42) demonstrate that the L_{23} emission spectrum obtained from liquid Al shows some resemblance to the solid, though the peak characteristic of the zone overlaps is rather less pronounced. Again, the result shows that the short-range arrangement of atoms is playing a more important role than the long-range order. Fisher and Baun (44) find that near the melting point the K bands for solid and liquid differ only slightly. However, at a temperature several hundred degrees above the melting point, they find a markedly different result, which, they suggest, may be due to the liquid surface or to a dense vapour layer close to the liquid Al surface.

Garg and Kallne (40) study the K emission band (valence band $\rightarrow 1s$) and the emission lines $K\beta_{1,3}$ ($3p_{3/2,1/2} \rightarrow 1s$) for Fe and Cu. The main conclusion is that the K X-ray spectra of the transition metals Cu and Fe are unaffected by melting, within the accuracy of the experiment.

For Fe and Cu the density of states has been calculated by the cluster method (45). For liquid and solid Fe the calculation gives a broad $3d$ band almost split into two parts. For Cu, the $3d$ band is single and narrow, but with much fine structure. The band width predicted is the same for solid and liquid within 5%. Thus, the experiments agree in general terms with the calculations, although the experiment could not detect the splitting of the Fe $3d$ band due to limitations imposed by (*a*) the spectrograph and (*b*) the mode of detection.

Clearly, this is an area in which a good deal of effort is worthwhile, especially if the theoretical work on electron states could be brought to a state of refinement in which the observed intensities could be calculated, not just the electronic densities of states.

(B) Magnetic Properties

5. *Spin and Orbital Magnetism in Simple Liquid Metals*

We begin the discussion of magnetic properties by summarizing briefly the results of spin and orbital susceptibility, in a band theory framework, at first neglecting electron–electron correlations.[5]

If we start out from free electrons (certainly a good approximation for liquid sodium) then the Pauli spin paramagnetism is given by

$$[5.1] \qquad \chi_{\text{Pauli}} = \frac{3}{2} n_0 \mu_B{}^2 \frac{1}{E_f}$$

[4]J. Gaspard, private communication to C. F. Hague; see ref. 21.

[5]This neglect is not justified for quantitative work; see below.

where n_0 is the number of conduction electrons per unit volume, μ_B is the Bohr magneton, and E_f is the Fermi energy. Since $n_0 = k_f^3/3\pi^2$, where k_f is the Fermi wave number, then it follows from [5.1] that $\chi_{Pauli} \propto E_f^{1/2}$ since $E_f \propto k_f^2$. The rather obvious generalization of this to an energy band with density of states $N(E)$ is $\chi_{Pauli} \propto N(E_f)$, the free electron density of states being proportional to $E_f^{1/2}$.

For free electrons, as Landau first demonstrated, the orbital diamagnetism is the negative of $\frac{1}{3}\chi_{Pauli}$.

As already mentioned, the effect of electron–electron interactions on these formulae is important, χ_{Pauli} being relatively strongly enhanced by the interactions in the range of electron density appropriate to the simple liquid metals.

Formulae for liquid metals have been written down to second-order in the pseudopotential and we shall refer briefly to these. Naturally, as in the resistivity in the weak scattering regime, the liquid structure factor $S(q)$ enters the theory of both spin and orbital susceptibility. For liquid Na, the electron–ion interaction contribution to χ_{Pauli} appears to be small compared with the effects of electron–electron interaction, which we discuss below. For further references to pseudopotential work the reader may wish to consult the work of Borchi and De Gennaro (46). Some later references to pure liquid metal studies are given by Dupree and Sholl (47), though their main concern is with alloys.

5.1. Total and Spin Susceptibilities of Liquid Metals

Dupree and Seymour (48) have plotted values of the total volume susceptibility for liquid metals at their melting points against the mean interelectronic spacing r_s defined such that $\frac{4}{3}\pi r_s^3$ is the volume/conduction electron. Their results are shown in Fig. 13 in cgs volume units, r_s being measured in atomic units.

Writing the total susceptibility χ in the usual way as the sum of an ion-core contribution χ_i, an orbital susceptibility χ_d, and the spin susceptibility χ_p, namely

$$[5.2] \qquad \chi = \chi_i + \chi_p + \chi_d$$

Dupree and Seymour use χ_i from the work of Angus (49).[6] For χ_d they take the interacting

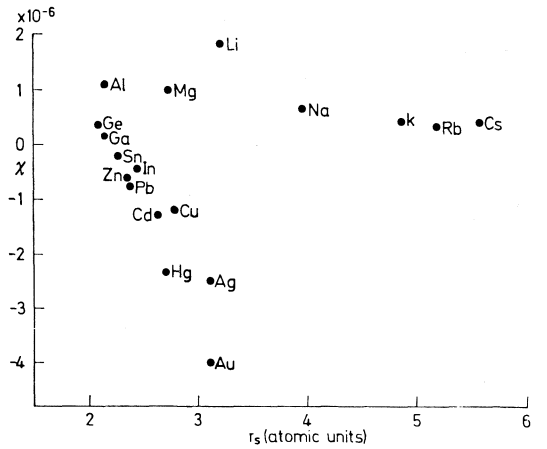

FIG. 13. Total volume susceptibilities of liquid metals. (Reprinted with permission from Physik der Kondensierten Materie, **12**, 97 (1970). Copyright by Springer-Verlag, Berlin.)

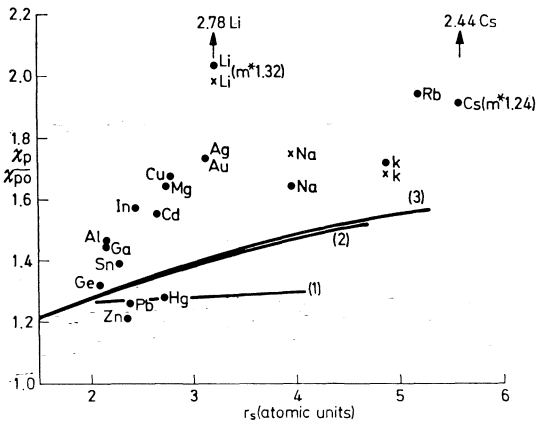

FIG. 14. Spin susceptibilities of liquid metals, extracted from experimental results of Fig. 13. Lines *1*, *2*, and *3* correspond to different choices of the Landau Fermi liquid parameters in [5.4]. (Reprinted with permission from Physik der Kondensierten Materie, **12** 97 (1970). Copyright by Springer-Verlag, Berlin.)

electron gas result of Kanazawa and Matsudaira (50; see also ref. 51), which, in units of the Landau free electron susceptibility χ_L may be written:

$$[5.3] \qquad \frac{\chi_d}{\chi_L} = 1 + \frac{\alpha r_s}{6\pi}\left[\ln r_s + 4 + \ln\left(\frac{\alpha}{2\pi}\right)\right]$$

where $\alpha = (4/9\pi)^{1/3}$.

Figure 14 gives the values of χ_p/χ_{Pauli} thus obtained. Here χ_{Pauli} is again the non-interacting free electron result, with effective mass $m^* = m$.

The following points are noteworthy (*cf.* 48):

(*i*) In spite of the large variation in χ in

[6]For the reasons for this choice, the reader may refer to Dupree and Seymour (48).

Fig. 13 all values of χ_p lie in the fairly narrow range 0.9 to 2.1 $\times$ 10^{-6}.

(*ii*) Direct determinations of χ_p, using conduction electron spin resonance techniques, are shown for Li, Na, and K (crosses). The measurements were made in each case for the solid metal: for Li and Na no significant change was found on melting and for K there is very little change in total susceptibility through the melting point. So it seems unlikely in that case that χ_p changes for K either. The direct measurements of χ_p are seen from Fig. 14 to be in good agreement with the values deduced from the total susceptibility. It is relevant here to refer to the very recent measurement of χ_p for Li through the melting point by Hanabusa *et al.* (52).

(*iii*) The curves *1–3* shown in Fig. 14 are from the theory of an interacting electron gas. In the Landau Fermi liquid theory, χ_p can be written in terms of the Landau parameters A_1 and B_0 (see, for example, Jones and March (53)) as

$$[5.4] \qquad \frac{\chi_p}{\chi_{Pauli}} = \frac{1 + A_1}{1 + B_0}$$

The different curves *1–3* in Fig. 14 correspond to different ways of approximating A_1 and B_0 in the many-electron problem (actually A_1 is considerably smaller in magnitude than B_0, which is negative). More refined theories for χ_p/χ_{Pauli} are given by Hamann and Overhauser (54) and Dupree and Geldart (55), the results being in reasonable overall agreement with the trends of χ_p/χ_{Pauli} shown in Fig. 14. If one wishes to do better and get quantitative results for individual metals, obviously electron–ion interaction and the liquid structure must be introduced, as we discuss briefly below.

(a) Possible Effects of Electron–Ion Interaction—Timbie and White (56), following early work of Baltensperger (57), have calculated the effect of electron–ion interaction on the orbital susceptibility χ_d, as also have later workers, *e.g.* Takahashi and Shimizu (58).

Whereas Baltensperger (57) estimates that for Na, χ_d increases (*i.e.* becomes less diamagnetic) by 20%, Timbie and White (56) estimate a correction smaller by an order of magnitude. The corrections found in no way alter the above conclusion that electron–electron interactions play a dominant role in the theory of the magnetic properties of the simple liquid metals.

Takahashi and Shimizu (58), as well as Timbie and White (56), also estimate the electron–ion corrections to the spin susceptibility. Though their expressions in terms of the liquid structure factor $S(k)$ and pseudopotential $U(k)$ agree, their numerical estimates differ somewhat. The results may be summarized by saying that electron–ion corrections cause only small deviations from electron gas values, when calculated by such a nearly free-electron approach.

While the above discussion indicates that, for the orbital diamagnetism, such corrections are indeed small, it does not seem possible for a metal like Li, which is not free-electron-like in the solid, to treat the electron–ion interaction in the spin susceptibility in the above manner. Presumably, because of the similarity of χ_p in solid and liquid, more structural information must go into the liquid theory than the pair correlation function. Thus, one should not use the nearly free-electron theory, without considerable caution, for correcting the electron gas results for the spin susceptibility, the similarity between liquid and solid results being a much better guideline.

6. Nuclear Magnetic Resonance

Nuclear magnetic resonance has been observed in some 20 liquid metals. Seymour (59) has reviewed the data on Knight shifts at the melting points in liquid metals, and Table 2 is taken from his paper.

6.1. Knight Shifts in Liquid Metals

Ignoring transition metals, one can write the Knight shift K in the usual way as

$$[6.1] \qquad K = (8\pi/3)\Omega P_F \chi_p$$

Here Ω is the atomic volume, P_F is the probability density at the nucleus for conduction electrons at the Fermi surface, while χ_p is the conduction electron (volume) spin susceptibility discussed extensively above.

For the electron contact density factor ΩP_F, expressions have been given by Faber (60), Cyrot-Lackmann (61), and Watabe *et al.* (62), with modifications given by Perdew and Wilkins (63). Unfortunately, the Knight shifts remain difficult to interpret in a really convincing way.

Seymour (59) also reviews the temperature coefficient of K and the change in the Knight shift on melting and we refer the reader to his paper for details, as well as (briefly) Knight shifts in alloys. Broadly, in alloys, one often finds that the shifts for both constituents of a binary alloy

TABLE 2. Experimental Knight shifts for liquid metals at their melting points (theoretical values shown are obtained from a single orthogonalized plane wave treatment)

	K (%)			K (%)	
Metal	Experimental	Theory	Metal	Experimental	Theory
Li	0.026	0.09	In	0.786	0.79
Na	0.116	0.15	Sn	0.73	0.75
Al	0.162	0.18	Sb	0.72	0.72
K	0.265	0.41	Te	0.38	0.70
Cu	0.264	0.52	Cs	1.44	1.63
Ga	0.449	0.53	Hg	2.42	1.45
As	0.32	0.52	Tl	1.48	1.31
Rb	0.662	0.82	Pb	1.49	1.34
Ag	0.575	0.74	Bi	1.41	1.32
Cd	0.795	0.77			

change roughly linearly with atomic concentration and in approximately parallel fashion (but a lot of exceptions occur). Fractional changes $\Delta K/K$ across the composition range are typically 5–20% except for alkali metal alloys where they are most often 20–50%: they are not very dependent on temperature except for transition metal solutes.

In concluding this discussion on Knight shifts, we return to the question of the existence of a pseudogap, and the change in electronic structure of liquid Hg as the density is varied.

(a) Knight Shift in Expanded Liquid Hg—El-Hahany and Warren (64) have reported measurements of the Knight shift in liquid Hg from the normal liquid density to less than 8 g/cm^3 at 1730 K and 1411 bar. An abrupt metal–nonmetal transition between 9 and 8 g/cm^3 is preceded by ranges of roughly linearly decreasing shift ($11 < \rho < 13.6$ g/cm^3) and constant shift ($9 < \rho < 11$ g/cm^3).

Theories by Mott (65) and Friedman (66) for conductivity and Hall coefficient would require that $N(E_f)$, the density of states at the Fermi level, would drop by a factor of 3 between 11 and 9 g/cm^3. The Knight shift remains constant as seen in Fig. 15 and it would appear at first sight that this could only be reconciled with the strong scattering model if a decrease in $N(E_f)$ is compensated almost precisely by a corresponding rise in ΩP_F in [6.1]. However, as demonstrated above, electron–electron interaction enhancement is so important that the above treatment of χ_p via $N(E_f)$ is obviously too primitive. For further discussion, the reader is referred to El-Hanany and Warren (64; see also Cohen and Jortner (67)). Obviously, the problem of the nature of the electronic states, and the transport processes, in liquid Hg is far from solved as yet.

6.2. Nuclear Quadrupole Relaxation

As Seymour (59) emphasizes, there is some interest in liquid metals in a relaxation rate T_{1Q}^{-1} involving coupling (for nuclei with $I > \frac{1}{2}$) of the nuclear electric quadrupole moment Q with the fluctuating electric field gradient produced by thermal motion of the ions. The effect can be isolated when there is a pair of isotopes with differing ratios of magnetic moments and of electric quadrupole moments (*e.g.* ^{69,71}Ga, ^{121,123}Sb, etc.).

An approximate relation for T_{1Q} is

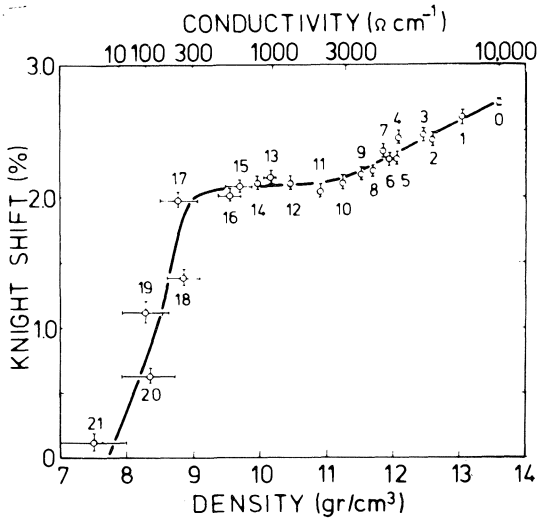

FIG. 15. Knight shift in liquid Hg as function of fluid density. (Reprinted with permission from Physical Review Letters, **34**, 1276 (1975). Copyright by The American Physical Society.)

$$[6.2]\quad \frac{1}{T_{1Q}} = \frac{3(2I+3)}{40I^2(2I-1)}\frac{e^4Q^2\overline{q^2}}{\hbar^2}\tau_i$$

where $\overline{q^2}$ is the mean square field gradient at a nucleus, and is assumed to be characterized by an autocorrelation function which decays exponentially with time constant τ_i. One might expect τ_i to vary inversely as the self-diffusion coefficient D. While this is qualitatively correct, the relationship to the diffusion constant is not as simple as that.

Coupling to the diffusional motion has been treated theoretically by Sholl (68) and extended to alloys by Claridge *et al.* (69) and by Jolly and Titman (70).

The three-body correlation function $g^{(3)}$ for the ions enters the theory, which is of some interest in view of the central position this function occupies in the statistical theories of liquids (see, for example, March (1)).

Sholl's (68) result for a metal is approximately (*cf.* Seymour (59))

$$[6.3]\qquad 1/T_{1Q} = (C/D)(I_1 + I_2)$$

and for species A in concentration c in an AB alloy

$$[6.4]\quad 1/T_{1Q} = (C/D)\{cI_1 + (1-c)a^2I_1 + c^2I_2 + a^2(1-c)^2I_2 + 2c(1-c)aI_2\}$$

Here a is the ratio of field gradients of A and B ions, D is assumed the same for A and B, and C has absorbed the constant terms. I_1 involves the nucleus interacting separately with the field gradients produced by other ions, while I_2 contains $g^{(3)}$. The equation shows the observed parabolic dependence for $I_2 \simeq -0.9I_1$; it is clear that such cancellation is going to occur on general grounds.

The conclusion here is that a large amount of nmr data for liquid metals can be understood in terms of a nearly free-electron model. We have not referred here to the Korringa relation, but this shows up the role of electron–electron interactions (see the discussion of Seymour (59)).

In conclusion, Gabriel and Schirmacher (71) have given a theory of nuclear quadrupole relaxation in liquid metals in terms of the usual effective ion–ion potential plus the van Hove function $S(k\omega = 0)$ for elastic scattering. This latter quantity is available from neutron experiments for some liquid metals (see, for example, Barker *et al.* (72)).

Rather than attempting a survey of a wide area of magnetic behaviour in other than the simpler liquid metals discussed above in detail, we shall focus most attention in the remainder of this article on one group, the liquid rare earth metals. Here, the basically new feature that appears is the existence of very localized magnetic moments on the ions. After surveying briefly their magnetic properties, we conclude by discussing the relation between dc conductivity and the magnetic moments.

7. Liquid Rare Earth Metals

We shall, therefore, first summarize the magnetic properties of liquid rare earth metals briefly (see also Güntherodt *et al.* (73)). The main point to be made immediately is that the magnetic susceptibility of liquid rare earths is rather similar to the solid state behaviour.

Below room temperature, the solid state susceptibility of Ce, Pr, and Nd obey a Curie–Weiss law. The effective magnetic moment is associated with localized $4f$ electrons, 1 for Ce, 2 for Pr, and 3 for Nd. At higher temperatures and beyond the melting point, a deviation to larger values of the magnetic susceptibility occurs. Figure 16 gives the magnetic susceptibility of Ce above room temperature and in the liquid state.

The deviations from the Curie–Weiss law can be explained as due to occupancy of low-lying $4f$ states above the ground state. This ionic contribution can be handled satisfactorily by the usual van Vleck theory.

At high temperatures, the ionic $4f$ contribution becomes small and the contribution from conduction electrons has to be taken into account. An estimate of this contribution can be made by considering the susceptibility of La, and χ^{-1} of Ce at high temperatures. La has no magnetic moment and one sees the Pauli paramagnetism, enhanced though by a factor of 10 compared with simple liquid metals. No change is observed at the temperature T_p of the fcc–bcc phase transition in Ce, whereas small changes have been detected at the melting point of Ce as well as at the melting point and the temperature T_p of the phase transition of La (see also Fig. 16).

7.1. Relation between Transport and Localized Spins

The electrical resistivity of some liquid rare earth metals, namely Dy, Ho, Gd, and Tb has been measured by Güntherodt *et al.* (74), samples of their results being shown in Fig. 17 for Ho, over the temperature range up to 1600°C.

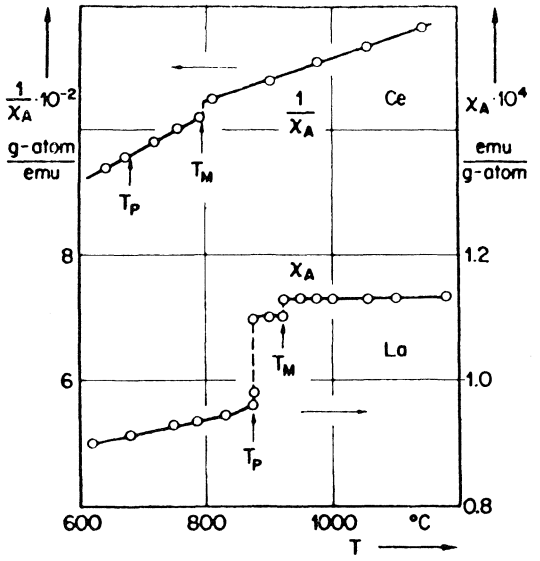

FIG. 16. Magnetic susceptibilities of Ce and La *vs.* *T*. (Reproduced from a preprint kindly supplied by Dr. H. U. Künzi; see also ref. 73.)

With regard to the comparison between the different materials, the electrical resistivities are about 10% higher for Dy and Ho than the values for the preceding rare earths, Gd and Tb. This is very different from the behaviour at room temperature, where Gd has the highest resistivity of all the rare-earth metals, as can be seen from data for all the rare earths, both solid and liquid, in Fig. 18.

As a function of temperature, the electrical resistivities for both Dy and Ho remain constant in the liquid state. The same temperature independence is found in Gd. However, for liquid Tb the electrical resistivity is found to increase by $1.5 \times 10^{-8}\ \Omega\,\text{cm}\ ^\circ\text{C}^{-1}$.

The absolute magnitude of the electrical resistivities is large compared with other liquid metals, *e.g.* for Gd 195 μΩ cm and Tb 190 μΩ cm, at their respective melting points. These values are 10 times larger than that for liquid Cu, though, for instance, as remarked above, liquid Ba has a resistivity of 300 μΩ cm.

The fact that the 4*f* states are far below the Fermi energy, as follows from recent XPS measurements by Bear and Busch (75; see Güntherodt *et al.* (74)), and have atomic character, suggests that the main contribution to the electrical resistivity is due to the 5*d* resonance scattering.

As Güntherodt *et al.* (74) point out, an additional contribution to the electrical resistivity due to spin disorder scattering which dominates at low temperatures is in question, since the resistivities of Dy and Ho at high temperatures and in the liquid state are larger than for Gd. It is to this point (*a*) plus (*b*) and (*c*) below that Parrinello *et al.* address themselves,[7] as we shall now discuss.

The main points on which this theoretical study focuses, stemming from the experiments of Güntherodt *et al.* (73, 74), are: (*a*) There is no obvious relation of the resistivity ρ at the freezing points of the liquid rare earth metals to the magnitude of the localized spins on the ions. Yet, as Fig. 18 shows, in the solid state at room temperature the resistivity has its maximum at Gd, with a spin of 7/2. (*b*) The resistivities are large, and for four of the heavy rare earths there is practically no temperature dependence. (*c*) As emphasized by Güntherodt *et al.* (73, 74), and shown in Fig. 19, there is a correlation between the resistivity ρ and θ_D^2, θ_D being the Debye temperature in the solid.

(a) Weak Scattering Theory—It is clear that, for weak scattering from an assembly of ions, each ion carrying a localized spin, we can invoke Mathiessen's rule to write the inverse of the total relaxation time τ as

$$[7.1] \qquad \frac{1}{\tau} = \frac{1}{\tau_d} + \frac{1}{\tau_m}$$

where τ_d^{-1} is the contribution from scattering off the ionic density fluctuations while τ_m^{-1} is the magnetic term. Following de Gennes and Friedel (76), for weak scattering $\tau_m^{-1} \propto S(S+1)$, where S is the spin (7/2 for Gd, etc). This explains the peaking of ρ in the solid at 25°C in Fig. 18, when the spin has its largest value, namely at Gd.

As the temperature is increased, the scattering increases for a strong ionic potential. Mathiessen's rule begins to break down, and therefore in the liquid rare-earths, Parrinello *et al.*[7] propose as the zeroth order theory the extreme strong scattering limit in which the single-centre scattering is so strong that the scattering off successive ions is incoherent. If the **t**-matrix for single-ion scattering is denoted by t, then the total scattering in this limit is given by Nt^2, N being the total number of scatterers.

(b) Strong Scattering Limit—It should be emphasized that, whereas when we transcend

[7]M. Parrinello, M. P. Tosi, and N. H. March, unpublished results.

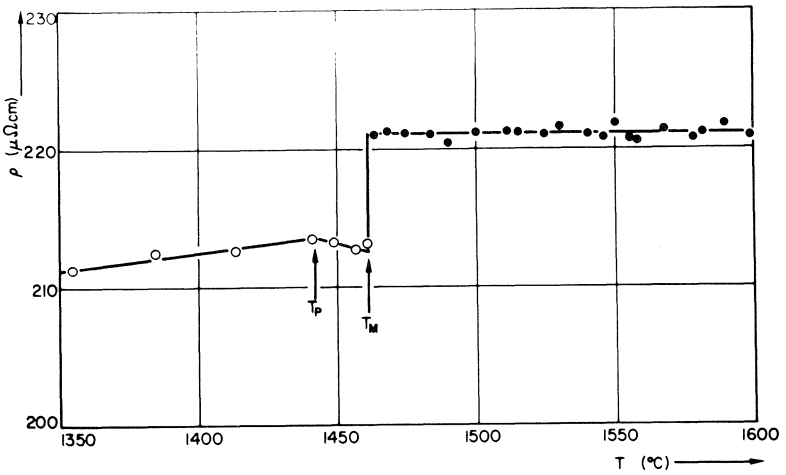

FIG. 17. Resistivity of liquid and solid Ho *vs. T.* (Reprinted with permission from ref. 74*b*; see also ref. 73.)

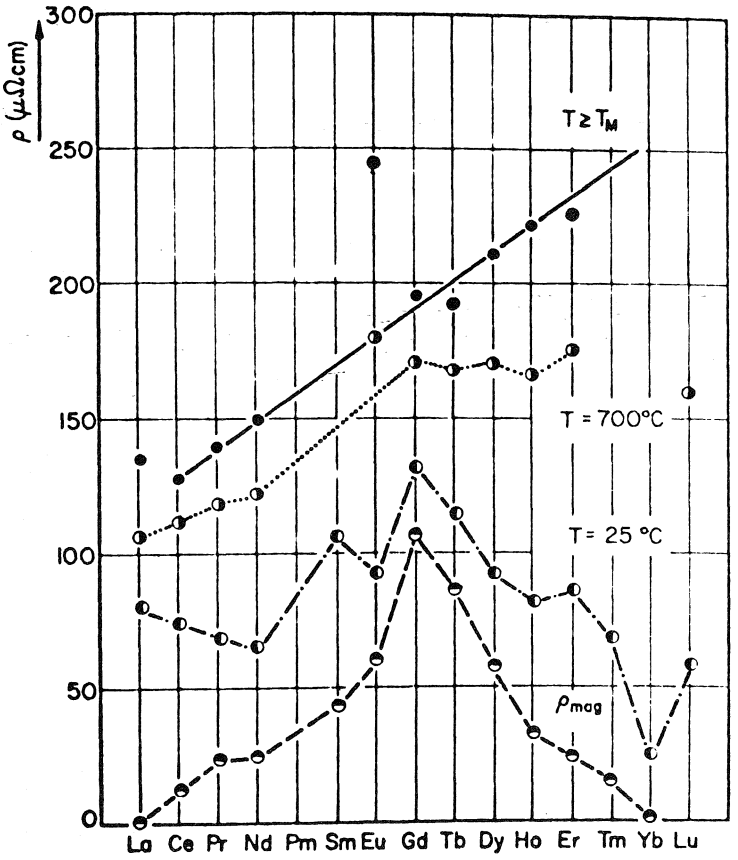

FIG. 18. Resistivities of rare earth metals at different temperatures in solid and liquid states. In the lowest curve labelled ρ_{mag} the spin disorder contribution to the resistivity has been separated from the total resistivity. (Reprinted with permission from Phys. Lett. A, **50**, 313 (1974); see also ref. 73.)

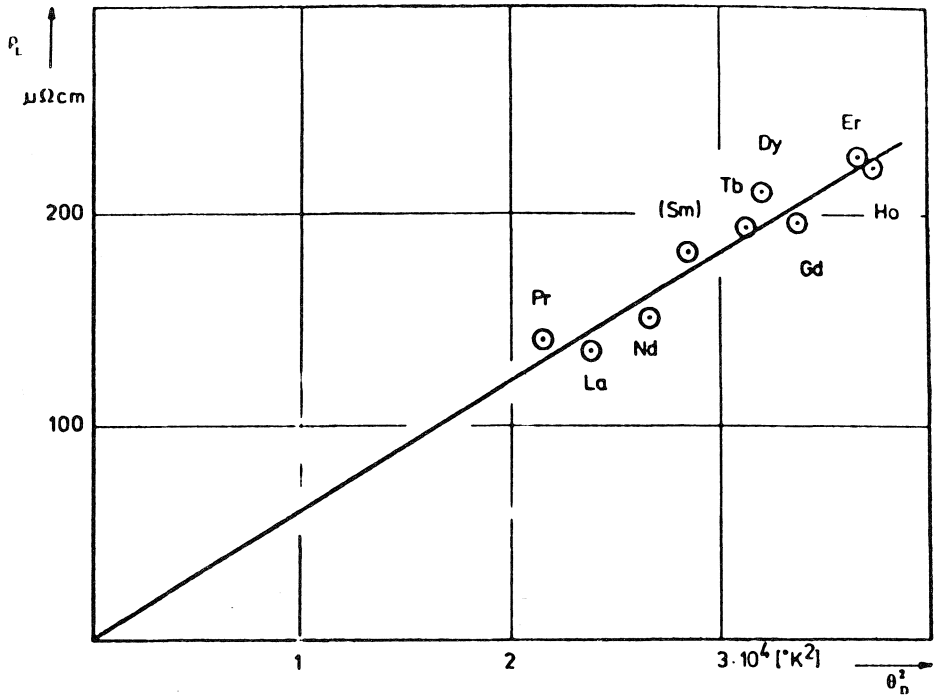

FIG. 19. Resistivities of liquid rare earth metals *vs.* square of Debye temperature. (Reprinted with permission from Phys. Lett. A, **50**, 313 (1974); see also ref. 73.)

the lowest order Born approximation, in which the radial distribution (pair) function only enters the theory through the static structure factor $S(k)$ (see [1.1]), higher order atomic correlation functions enter the theory (*e.g.* the three-body function $g^{(3)}$ referred to in section 6.2) of the resistivity, yet for sufficiently strong single-centre scattering the structure drops out of the theory, and with it the essential temperature dependence characteristic of weak scattering theory.

We can then utilize the well known result for the **t**-matrix for one ion in terms of phase shifts. Assuming that the *d*-wave phase shift is dominant, it is readily shown that the resistivity ρ is then

$$[7.2] \quad \rho = \frac{4\pi\hbar}{Ze^2k_f}\frac{5}{2S+1} \times [(S+1)\sin^2\eta_2^{+} + S\sin^2\eta_2^{-}]$$

where η_2^{+} and η_2^{-} are the *d*-wave phase shifts for the two spin directions. If we assume the conduction electron spin polarization round a single ion is small, then $\eta_2^{+} = \eta_2^{-}$ and equal to $\pi Z/10$ from the Friedel sum rule, Z being the valency. Then the spin S drops out of the theory and we find

$$[7.3] \quad \rho_0 = \frac{20\pi\hbar}{Ze^2k_f}\sin^2(\pi Z/10)$$

To refine this zeroth order result, we introduce *s* and *f* wave phase shifts. The resistance is substantially reduced by the interference between *d* and *f* phase shifts, the result being

$$[7.4] \quad \rho/\rho_0 = [\sin^2\eta_0 + 5\sin^2\eta_2 + \tfrac{1}{7}\alpha^2\sin^2\eta_3 - \tfrac{6}{7}\alpha\sin\eta_2\sin\eta_3 \times \cos(\eta_2 - \eta_3)]/[5\sin^2(\pi Z/10)]$$

with sum rule

$$[7.5] \quad \pi Z/2 \simeq \eta_0 + 5\eta_2 + \alpha\eta_3$$

We have written the multiplicity α, rather than 7, for Matthias and Zachariesen (77) have analyzed the melting points of the rare earths to conclude how much *f* contribution there is to the valence band charge density through the series. They conclude that $\alpha \doteqdot (14 - n_f)/2$, n_f being the number of *f* electrons and we find then an estimate of the *f* phase shift η_3 as $0.025\pi Z$. For two choices of η_0, zero and $0.2\pi Z/2$ (see

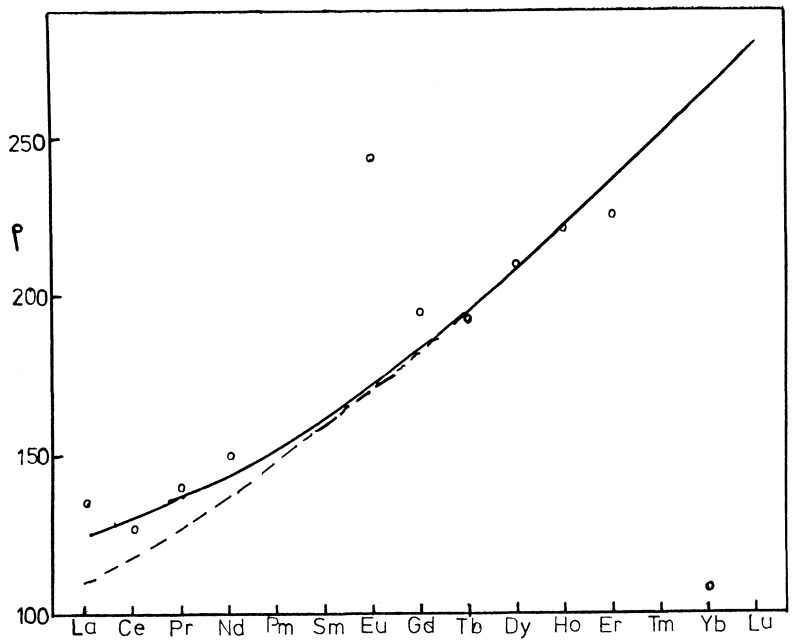

FIG. 20. Resistivities of rare earths at freezing point from theory and experiment.

Parrinello *et al.*[7]) we get the two curves shown in Fig. 20. There is a scale factor of 1.29 applied to the case $\eta_0 \neq 0$ to make the curve pass through the right value for Ho. This, we believe, is a manifestation of some residual liquid structure remaining in the theory, though the extreme incoherent limit is almost quantitative for the liquid rare earths.

The exceptions in Fig. 20, namely Eu and Yb, are easily explained as they are divalent, whereas the other rare earths in Fig. 20 are trivalent. In fact Eu and Yb are better compared with divalent Ba; the resistivities of these three elements then vary regularly. Here then, as emphasized in Parrinello *et al.*[7], we have a somewhat dramatic demonstration of the breakdown of Matthiessen's rule.

Finally, the relation of α, and the resistivity, to the number n_f of $4f$ electrons can be combined with the results of Matthias and Zachariesen (77) that the melting temperature T_m also is linearly dependent on n_f to get the correlation of resistivity with T_m shown in Fig. 21. Invoking Lindemann's law of melting, T_m is proportional to the square of the Debye temperature θ_D, and thus this is the origin of the correlation of the resistivity ρ with θ_D^2 shown in Fig. 19.

8. Concluding Comments on Magnetic Properties

The simple metals in the liquid state reflect the magnetic properties of a strongly interacting electron gas. The electron–electron interactions determine the general trend of the spin susceptibility with mean interelectronic separation. However, to get quantitative agreement for a liquid metal like Li, it is not adequate to include electron–ion interaction by nearly free-electron theory, the similarity with the solid indicating that higher order atomic correlation functions must come in.

Secondly, some of the features of the rare earth metals in the liquid state can be understood using a theory of strong potential scattering from ions carrying localized spins. Matthiessen's rule breaks down and it has been shown that the spin largely disappears from the electrical resistivity. The weak temperature dependence of the resistivity also follows naturally from the strong scattering limit.

It is interesting in this connection that the resistivity of liquid Fe, Co, and Ni have recently been measured by Güntherodt *et al.* (78). These resistivities are smaller than for the rare earths and it is satisfying that some contribution from spin disorder scattering is required.

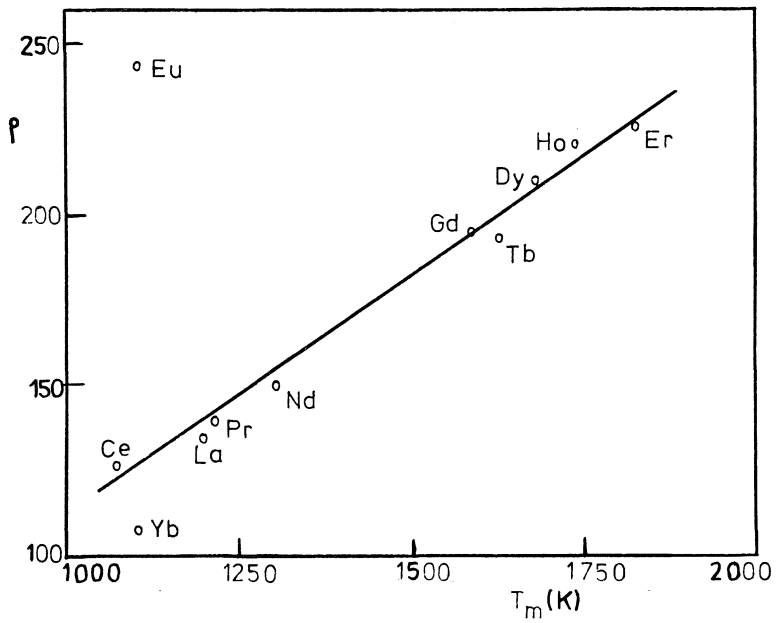

FIG. 21. Resistivities of liquid rare earths *vs.* melting temperature.

In connection with the magnetic moments in the liquid transition metals, it is worth remarking that neutron scattering has been recently studied from both Ni (79) and liquid Fe.[8] Whereas there is no marked spin disorder scattering contribution observed from liquid Ni, the results for liquid Fe show a significant component of magnetic scattering.

In the same context, a magnetic form factor for liquid Ce has recently been determined (80) by comparing the differential scattering cross section for thermal neutrons for liquid Ce with that for liquid La. The form factor is consistent with the dipole approximation and a $2F_{5/2}$ spectroscopic state for Ce^{3+}, roughly 20% of the Ce ions in the liquid state behaving as though they are instantaneously magnetically inactive. The coexistence in liquid Ce of two types of Ce ion, one of which has lost its f electron by a process associated with a resonating bond, is implicit in several qualitative discussions of the bonding properties of the lanthanides (81).

Progress, both experimental and theoretical, is to be expected in this general area in the fairly near future.

Acknowledgments

Many people, directly or indirectly, have helped in preparing this article. I want especially to thank my colleagues, Professor M. P. Tosi and Dr. M. Parrinello for many invaluable discussions on the whole area covered in this article. Thanks are also due to Drs. R. Dupree, P. J. Grout, B. L. Gyorffy, C. Hague, and C. Norris for supplying me with results and/or critical comments on their various areas of expertise. (Special thanks are due to Dr. Hague for supplying Fig. 12 prior to publication.) Needless to say, however, I alone am responsible for the final form and the point of view expressed here.

Finally, I wish to acknowledge support from the Science Research Council for the research programme on liquid metals at Imperial College, as well as partial contractual support from the US Army through its European Research Office.

[8]C. G. Windsor, private communciation.

1. N. H. MARCH. Liquid metals. Pergamon Press Ltd., Oxford. 1968.
2. K. STURM and E. PAJANNE. J. Phys. F, **3**, 199 (1973).
3. M. P. TOSI, M. PARRINELLO, and N. H. MARCH. Nuovo Cimento B, **23**, 135 (1974).
4. C. J. PETHICK. Phys. Rev. B, **2**, 1789 (1970).
5. N. W. ASHCROFT. J. Phys. C, **1**, 232 (1968).
6. J. C. MILLER. Philos. Mag. **20**, 1115 (1969).
7. T. E. FABER. An introduction to the theory of liquid metals. University Press, Cambridge. 1973.
8. T. INAGAKI, E. T. ARAKAWA, R. D. BIRKHOFF, and M. W. WILLIAMS. Phys. Rev. B, **13**, 5610 (1976).

9. H. MAYER and B. HIETEL. Optical properties and electronic structure of metals and alloys. *Edited by* F. Abeles. North-Holland Publishing Co., Amsterdam. 1966.
10. W. JONES. J. Phys. F, **4**, 1736 (1974).
11. N. F. MOTT. Philos. Mag. **13**, 989 (1966).
12. T. CHAN and L. E. BALLENTINE. Phys. Lett. A, **35**, 385 (1971).
13. J. M. HODGSON. Philos. Mag. **8**, 735 (1963).
14. J. GUGGENHEIM. Philos. Mag. **22**, 833 (1970).
15. N. R. COMINS. Philos. Mag. **25**, 817 (1972).
16. J. BOIANI and S. A. RICE. Phys. Rev. **185**, 931 (1969).
17. A. N. BLOCH and S. A. RICE. Phys. Rev. **185**, 933 (1969).
18. J. S. ROUSSEAU, J. C. STODDART, and N. H. MARCH. Proc. R. Soc. London Ser. A, **317**, 211 (1970).
19. O. HUNDERI and H. P. MYERS. J. Phys. F, **4**, 1088 (1974).
20. J. M. WEAVER, D. W. LYNCH, and R. ROSEI. Phys. Rev. B, **7**, 3537 (1973).
21. C. F. HAGUE. Proc. 3rd Int. Conf. Liquid Metals. Bristol. Institute of Physics. 1976.
22. G. P. WILLIAMS and C. NORRIS. J. Phys. F, **4**, L175 (1974); Proc. 3rd Int. Conf. Liquid Metals. Bristol. Institute of Physics. 1976.
23. P. COTTI, H. J. GUNTHERODT, P. MUNZ, P. OELHAFEN, and J. WULLSCHLEGER. Solid State Commun. **12**, 635 (1973).
24. W. SCHAICH and N. W. ASHCROFT. Solid State Commun. **8**, 1959 (1970).
25. J. KELLER, J. FRITZ, and A. GARRITZ. Proc. Conf. Disordered Metallic Systems, Strasbourg, Sept. 1973; Suppl. J. Phys. Paris, 1974.
26. F. M. MUELLER. Phys. Rev. **153**, 659 (1967).
27. D. E. EASTMAN. Phys. Rev. Lett. **26**, 1108 (1971).
28. E. HOUSE and P. V. SMITH. J. Phys. F, **3**, 753 (1973).
29. N. F. MOTT. Philos. Mag. **26**, 505 (1972).
30. F. HENSEL and E. U. FRANCK. Rev. Mod. Phys. **40**, 697 (1968).
31. R. SCHMULZTER. Dissertation, University of Karlsruhe, 1971.
32. H. OVERHOF, H. UCHTMANN, and F. HENSEL. J. Phys. F, **6**, 523 (1976).
33. R. Y. KOYAMA and W. E. SPICER. Phys. Rev. B, **4**, 4318 (1971).
34. H. PETERSON and C. KUNTZ. Proc. Int. Conf. VUV. Hamburg, Germany. Paper 28. 1974.
35. C. NORRIS, D. C. RODWAY, and G. P. WILLIAMS. The properties of liquid metals. Taylor and Francis, London. 1973. p. 181.
36. F. HENSEL. Can. J. Chem. This issue.
37. C. NORRIS and G. P. WILLIAMS. Proc. 3rd Int. Conf. Liquid Metals, Bristol. Institute of Physics. 1976.
38. L. G. PARRATT. Rev. Mod. Phys. **31**, 616 (1959).
39. F. YONEZAWA, S. ASANO, F. MARTINO, and Y. ISHIDA. International Conference on Electrons in Fluids. Banff, Canada. Sept. 5–10, 1976. Unpublished.
40. K. B. GARG and E. KALLNE. Phys. Status Solidi B, **70**, K121 (1975).
41. J. J. OLSEN. Phys. Rev. B, **12**, 2908 (1975).
42. J. A. CATTERALL and J. TROTTER. Philos. Mag. **8**, 697 (1963).
43. J. FARINEAU. Ann. Phys. Paris, **10**, 20 (1938).
44. D. W. FISCHER and W. L. BAUN. Phys. Rev. **138**, A1047 (1965).
45. J. KELLER and R. JONES. J. Phys. F, **5**, L33 (1971).
46. E. BORCHI and S. DE GENNARO. Phys. Rev. B, **5**, 4761 (1972).
47. R. DUPREE and C. A. SHOLL. Z. Phys. B, **20**, 275 (1975).
48. R. DUPREE and E. F. W. SEYMOUR. Phys. Kondens. Mater. **12**, 97 (1970).
49. W. R. ANGUS. Proc. R. Soc. London, Ser. A, **136**, 569 (1932).
50. H. KANAZAWA and N. MATSUDAIRA. Prog. Theor. Phys. **23**, 433 (1960).
51. N. H. MARCH and B. DONOVAN. Proc. Phys. Soc. London Sect. A, **67**, 464 (1954).
52. M. HANABUSA, T. KUSHIDA, and J. C. MURPHY. Phys. Rev. B, **13**, 5179 (1976).
53. W. JONES and N. H. MARCH. Theoretical solid state physics. Vol. 1. Wiley-Interscience, London. 1973.
54. D. R. HAMANN and A. W. OVERHAUSER. Phys. Rev. **143**, 183 (1966).
55. R. DUPREE and D. J. W. GELDART. Solid State Commun. **9**, 145 (1971).
56. J. P. TIMBIE and R. M. WHITE. Phys. Rev. B, **1**, 2409 (1970).
57. W. BALTENSPERGER. Phys. Kondens. Mater. **5**, 341 (1966).
58. Y. TAKAHASHI and M. SHIMIZU. J. Phys. Soc. Jpn. **34**, 942; **35**, 1046 (1973).
59. E. F. W. SEYMOUR. Pure Appl. Chem. **40**, 41 (1974).
60. T. E. FABER. Adv. Phys. **16**, 637 (1967).
61. F. CYROT-LACKMANN. Phys. Kondens. Mater. **3**, 75 (1964).
62. M. WATABE, M. TANAKA, H. ENDO, and B. K. JONS. Philos. Mag. **12**, 347 (1965).
63. J. P. PERDEW and J. W. WILKINS. Solid State Commun. **8**, 2041 (1970); Phys. Rev. B, **7**, 2461 (1973).
64. U. EL-HANANY and W. W. WARREN. Phys. Rev. Lett. **34**, 1276 (1975).
65. N. F. MOTT. Adv. Phys. **16**, 49 (1968); Phys. Rev. Lett. **31**, 446 (1974); Philos. Mag. **26**, 1241 (1972).
66. L. FRIEDMAN. Philos. Mag. **28**, 145 (1973).
67. M. H. COHEN and J. JORTNER. *In* Electrons in fluids. *Edited by* J. Jortner and N. R. Kestner. Springer, Berlin. 1973. p. 383.
68. C. A. SHOLL. Proc. Phys. Soc. **91**, 130 (1967).
69. E. CLARIDGE, D. S. MOORE, E. F. W. SEYMOUR, and C. A. SHOLL. J. Phys. F, **2**, 1162 (1972).
70. R. JOLLY and J. M. TITMAN. J. Phys. C, **5**, 1284 (1972).
71. H. GABRIEL and W. SCHIRMACHER. Proc. 18th Ampere Conf. on Magnetic Res. North-Holland Publishing Co., Amsterdam. 1975. p. 331.
72. M. BARKER, M. W. JOHNSON, N. H. MARCH, and D. I. PAGE. The properties of liquid metals. Taylor and Francis, London. 1973. p. 99.
73. H. J. GÜNTHERODT, E. HAUSER, and H. U. KÜNZI. Proc. Mexico Conf. 1973.
74. H. J. GÜNTHERODT, E. HAUSER, and H. U. KÜNZI. Phys. Lett. A, (*a*) **47**, 189 (1974); (*b*) **48**, 201 (1974).
75. Y. BEAR and G. BUSCH. 1974.
76. P. G. DE GENNES and J. FRIEDEL. J. Phys. Chem. Solids, **4**, 71 (1958).
77. B. T. MATTHIAS and W. H. ZACHARIESEN. Phys. Rev. Lett. **18**, 781 (1967).
78. H. J. GÜNTHERODT, E. HAUSER, H. U. KÜNZI, and R. MULLER. Phys. Lett, A, **54**, 291 (1975).
79. M. W. JOHNSON, B. MCCOY, N. H. MARCH, and D. I. PAGE. Phys. Chem. Liq. In press.

80. J. E. ENDERBY and V. T. NYUGEN. J. Phys. C, **8**, L112 (1975).
81. K. A. GSCHNEIDER. J. Less Common Met. **25**, 405 (1972).
82. L. M. ROTH. Phys. Rev. Lett. **28**, 1570 (1972); **29**, 142 (1972).
83. L. M. ROTH. Phys. Rev. B, **7**, 4321 (1973).
84. M. LAX. Phys. Rev. **85**, 621 (1952).
85. L. SCHWARTZ and H. EHRENREICH. Ann. Phys. **64**, 100 (1971).
86. L. M. ROTH. Phys. Rev. B, **9**, 2476 (1974).
87. J. S. FAULKNER. Phys. Rev. B, **1**, 934 (1970).
88. B. L. GYORFFY. Phys. Rev. B, **1**, 3290 (1970).
89. J. KORRINGA and R. L. MILLS. Phys. Rev. B, **5**, 1654 (1972).
90. F. YONEZAWA and M. WATABE. Phys. Rev. B, **11**, 4746 (1975).
91. M. WATABE and F. YONEZAWA. Phys. Rev. B, **11**, 4753 (1975).
92. M. WATABE and F. YONEZAWA. Proc. 3rd Int. Conf. Liquid Metals. Bristol. Institute of Physics. 1976.

Appendix

Electronic Structure of Liquid Metals: Strong Scattering Theories

We shall briefly summarize here without mathematical detail some recent work on the electronic structure of liquid metals, with strong scattering. The nearly free-electron theory has been discussed fully elsewhere and we shall omit that here.

Roth (82) used the tight-binding or linear combination of atomic orbitals (LCAO) methods to study electronic states in disordered systems. The work is restricted to a simple one-orbital model of a liquid metal.

Refinements of this approach are discussed by Roth (83). There, an equation is derived for a one-electron continuum Green function, from which the density of electron states can be obtained. Utilizing an analogy between this Green function and the **T** matrix of multiple scattering theory, Roth obtains approximations corresponding, respectively, to (*a*) the quasi-crystalline approximation (QCA) of Lax (84) and (*b*) the self-consistent approximation (SCA) of Schwartz and Ehrenreich (85).

What Roth (83) shows, by calculations using random and hard-sphere pair functions, is that the QCA is inadequate, while the SCA, though a considerable improvement, involves a questionable approximation to the three-body distribution function. Unfortunately, to date, direct comparison with experiment is hardly possible and will probably necessitate the generalization to more than one orbital.

In later work, an effective-medium approximation for liquid metals has been discussed by Roth (86) and a tight-binding version of this theory worked out. This follows the early work of Faulkner (87) on a random liquid, and a generalization by Gyorffy (88) (see also Korringa and Mills (89)) to include the liquid pair correlation function. These approaches have been taken further by Yonezawa and Watabe (90) (see also Watabe and Yonezawa (91)) and reviews are given by these workers in ref. 92, so that further details will not be given here. However, the reader interested in this area should be able to build up the full background by making use of the references given here.

It is obviously important that the progress in fundamental theory of strong scattering liquid metals in these papers should be turned into numerical calculations of densities of states which can then be confronted with the photoemission and soft X-ray experiments reviewed in the body of the text.

Discussion

E. D. Crozier: Regarding your calculation of $N(E)$ for liquid Be, would you comment on the main differences between your method and the weak scattering approach involving Green functions.

N. H. March: Our method calculates the single-centre scattering essentially exactly. Higher order atomic correlation functions come in and are approximated by a modification of the Kirkwood assumption. Weak scattering methods do not include $g^{(3)}$, etc.

E. D. Crozier: The slide for the $N(E)$ as deduced from pes for Hg did not show a dip close to E_F as indicated in the earlier work of Norris. Would you comment?

J. E. Enderby: The data of Norris *et al.* were taken under conditions of higher photon energy so that a better resolution of the spectra could be obtained.

J. K. Baird: From your partition function, how did you invert the required Laplace transform to obtain the density of states function?

N. H. March: As we had numerical values of the partition function as a function of $\beta = (k_B T)^{-1}$ only over a finite range of the real axis, it was necessary to parametrize the density of electronic states and to determine the parameters by fitting to the partition function.

J. C. Thompson: There are data on both susceptibility and optical constants of M—NH_3 solutions in the metallic regime, but at larger r_s values than even Cs which may be used to test the models you have discussed.

N. H. March: It would be interesting to try this. Difficulties could arise in interacting homogeneous electron gas theory at such low electron densities due to instabilities (*e.g.* spin density wave and(or) charge density wave states), which the metal–ammonia system would inhibit.

The far-infrared reflectivity of liquid Mg–Bi alloys (Extended Abstract)

E. D. Crozier, R. W. Ward, and B. P. Clayman
Department of Physics, Simon Fraser University, Burnaby, B.C., Canada V5A 1S6

Received November 22, 1976

The fluid and electronic structures of liquid binary alloys which display semiconducting behaviour are not well understood. The bulk of the experimental work has concentrated on measurement of thermodynamic and dc electron transport properties. Most of the alloys are characterized by a composition-dependent dc conductivity $\sigma(0)$ which displays a pronounced minimum near a stoichiometric composition. Taken together, the experimental results indicate that marked short range order exists near these critical stoichiometric compositions.

Mg–Bi is a representative system. The dc conductivity decreases from typical metallic values for the pure liquids Mg and Bi to a pronounced minimum of $\sim 45\ \text{ohm}^{-1}\ \text{cm}^{-1}$ at Mg_3Bi_2 (1, 2). In the narrow composition range about 60 at.% Mg the alloys display semiconducting behaviour. The thermoelectric power undergoes a change of sign (2) and the Hall coefficient[1] shows an increase at Mg_3Bi_2. These properties imply a decrease in the number of conduction electrons as the stoichiometric composition is reached. The concentration–concentration correlation function in the long wavelength limit $S_{cc}(0)$ shows a minimum near the composition 60 at.% Mg. Reasonable agreement with $S_{cc}(0)$ has been obtained in model calculations (3, 4) in which it was assumed that molecules of Mg_3Bi_2 existed with finite lifetimes. The molecules were assumed to be weakly bonded; the Gibbs free energy of formation was $\sim -15kT$/molecule.

The far-infrared reflectivity measurements discussed in this paper were initiated to test specifically for vibrational modes that could be associated with molecules of Mg_3Bi_2. In addition our reflectivity measurements, which span the range 3 to 300 cm^{-1} (9×10^{10} Hz to 9×10^{12} Hz), are in a frequency range where hopping processes may be important. According to the Mott pseudogap model when $\sigma(0) < 200\ \text{ohm}^{-1}\ \text{cm}^{-1}$ a dip develops in the density of electronic states near the Fermi energy E_F, states near E_F become localized, and electronic conduction occurs via thermally activated hopping processes.

Using high resolution Fourier transform spectroscopy the reflectivity of liquid Mg–Bi alloys was measured as a function of temperature and composition. Typical reflectivity results obtained with a resolution of $2.6\ \text{cm}^{-1}$ and normalized to the reflectivity of Cu at room temperature are shown in Fig. 1 for different compositions at temperatures slightly above the liquidus temperatures of the alloys. The normalized reflectivity is accurate to within 10%.

There is no evidence in the reflectivity spectra of absorption due to molecular vibrational modes. Within experimental error, for all compositions investigated the reflectivity decreases monotonically with increasing frequency.

Note that the reflectivity of 60 at.% Mg approaches unity. On the basis of the free electron model the reflectivity should be significantly less. The anomalous composition dependence of the reflectivity is emphasized in Fig. 2 which shows the reflectivity at the fixed frequency of 100 cm^{-1} as a function of at.% Mg.

The reflectivity data of Fig. 1 can be fitted using the Drude nearly free electron model wherein the ac conductivity is given by

$$\sigma(\omega) = \sigma(0)_{opt}/(1 - i\omega\tau)$$

provided the relaxation time τ and $\sigma(0)_{opt}$ are treated as adjustable parameters. The rapid increase of the reflectivity near Mg_3Bi_2 leads to a value of $\sigma(0)_{opt}$ which is enhanced by a factor of ~ 100 relative to the dc value of $\sim 45\ \text{ohm}^{-1}\ \text{cm}^{-1}$.

The reflectivity data of Fig. 1 can also be fitted by a simple Debye model with a single frequency of hopping between localized states. However, the parameters obtained in fitting the data are questionable. A physically plausible hopping frequency results in an anomalously high value of $\varepsilon_0 - \varepsilon_\infty$ the difference between the low and high frequency dielectric constants.

The reflectivity data imply the existence of localized states near the Fermi energy in a restricted composition range near 60 at.% Mg.

[1]U. Even. Private communication.

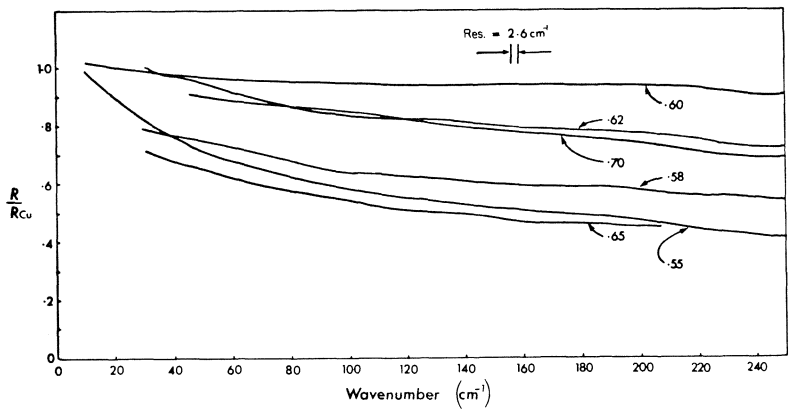

FIG. 1. The reflectivity of liquid Mg–Bi alloys. The reflectivity is normalized to the reflectivity of Cu at room temperature. The resolution is 2.6 cm^{-1}. The numbers represent the composition in at.% Mg. The temperature of the reflectivity curves are 832°C (60), 813°C (62), 790°C (58), 783°C (65), 770°C (70), 687°C (55).

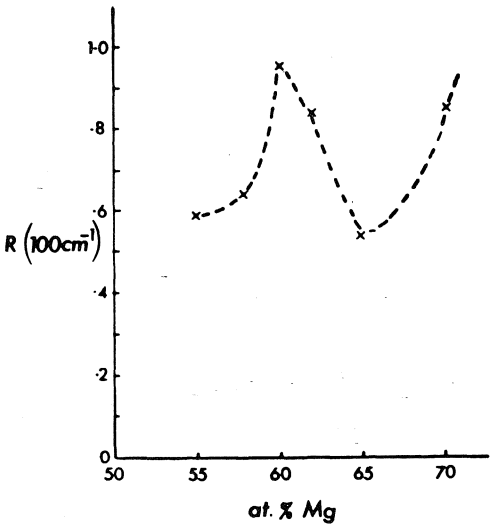

FIG. 2. Reflectivity of liquid Mg–Bi alloys at temperatures near the liquidus temperatures. The data were taken from Fig. 1 for the fixed frequency of 100 cm^{-1}.

However, the physical origin of the enhanced reflectivity is not understood.

1. B. R. ILSCHNER and C. WAGNER. Acta Metall. **6**, 712 (1958).
2. J. E. ENDERBY and E. W. COLLINGS. J. Non-Cryst. Solids, **4**, 161 (1970).
3. S. P. MCALISTER and E. D. CROZIER. J. Phys. C, **7**, 3509 (1974).
4. V. K. RATTI and A. B. BHATIA. J. Phys. F, **5**, 893 (1975).

Discussion

M. Cutler: In view of the large difference in electronegativity, one might expect a high degree of ionicity in Mg_3Bi_2. Have you considered the possibility of interpreting your reflectivity results in terms of an ionic structure?

E. D. Crozier: Yes. However, to my knowledge ionic liquids such as LiF have a reflectivity in the far infrared which is less than 0.75.

M. Cutler: The idea that hopping occurs when the conductivity $\sigma < 200$ ohm^{-1} cm^{-1} is a misleading concept which has frequently appeared in the literature. A more accurate description of the situation is as follows. The value 200 ohm^{-1} cm^{-1} characterizes the value of $\sigma(E)$ at the mobility edge E_c. For $E < E_c$, one has hopping transport with $\sigma_h(E) \lesssim 1$ ohm^{-1} cm^{-1}. The value of σ is obtained from

$$\sigma = -\int \sigma(E) \frac{\partial f}{\partial E} \, dE$$

where f is the Fermi–Dirac factor. When the Fermi energy $E_f > E_c$, $\sigma \gtrsim 200$ ohm^{-1} cm^{-1}. When $E_f < E_c$,

$$\sigma \cong \sigma_h(E_f) + \sigma(E_c) \exp\left[-(E_c - E_f)/kT\right]$$

the second term representing the contribution to transport by electrons excited thermally to the mobility edge. Therefore, in the range of σ between 1 and 200 ohm^{-1} cm^{-1}, the second term dominates. Only when $\sigma \lesssim 1$ ohm^{-1} cm^{-1} (below the minimum σ for Mg_3Bi_2) should one expect a major contribution by hopping.

J. C. Thompson: How does the reflectivity of the solid compare with that of the liquid?

E. D. Crozier: Reflectivity measurements were made on the solid alloys existing when the liquid alloys were cooled about 50 deg below their liquidus temperatures. In all cases the reflectivity of the liquid was greater than that of the solid (measurements were made on more than 30 alloys). For example at 60 at.% Mg at 100 cm^{-1} the reflectivity of the liquid was 16% higher than the solid.

Chemical potentials and fluctuations in indium–iodine solutions

KAZUHIKO ICHIKAWA

Department of Chemistry, Faculty of Science, Hokkaido University, Sapporo, Japan

Received September 22, 1976

KAZUHIKO ICHIKAWA. Can. J. Chem. **55**, 2190 (1977).

The composition dependence of the relative chemical potential of In in liquid In–I alloys was determined from emf data obtained over the range of composition from In to InI_3. Electrical conductivities were also measured for a limited number of concentrations. The specific conductance of the InI_3 composition differs from that of pure liquid In by almost five orders of magnitude; *i.e.*, at 600°C that for InI_3 is 0.104 while that for the pure metal is $2.16 \times 10^4\ \Omega^{-1}$ cm^{-1}. At the long-wavelength limit the concentration correlation function $S_{cc}(0)$, which was calculated from the chemical potential data, exhibits large composition fluctuations on the In-rich side and minimal compositional disorders in the vicinity of the intermediate compositions InI, InI_2, and InI_3. The mean square compositional fluctuation is developed to discuss the crude short range ordering, ΔN_α, and the role of charge transfer, Δe_α, in a general statistical mechanical theory of solutions. The large peak in $S_{cc}(0)$ at the indium-rich side provides crucial evidence of large concentration fluctuations, accompanied by microscopic inhomogeneities in the electronic structure, if a bimodal distribution is assumed. The limit $\Delta N_\alpha \rightarrow 1$ near the InI, InI_2, and InI_3 compositions shows that a preference exists for unlike nearest neighbors because of the ionic or covalent character in the chemical bonding. It is proposed that over the In–InI range there is the relationship between a gradual metal–nonmetal transition and the large concentration fluctuations which are associated with microscopic inhomogeneities in the electronic structure.

KAZUHIKO ICHIKAWA. Can. J. Chem. **55**, 2190 (1977).

On rapporte des données sur la relation qui existe entre la composition et le potentiel chimique relatif de l'indium dans des alliages liquides de In–I pour des compositions allant de In–InI_3; on a obtenu ces potentiels pour diverses compositions allant de In à InI_3 en faisant appel à des données de fem. On a aussi mesuré les conductivités électriques pour un nombre limité de concentrations. La conductivité spécifique de InI_3 diffère de celle de In par presque cinq ordres de grandeur; c'est-à-dire à 600°C celle de InI_3 est de 0.104 alors que celle de l'indium métallique à l'état pur est de $2.16 \times 10^4\ \Omega^{-1}\ cm^{-1}$. A la limite de longues longueurs d'onde, la fonction de corrélation de concentration $S_{cc}(0)$, qui a été calculée à partir de données de potentiel chimique de l'indium, démontre l'existence de grandes fluctuations dans la composition du côté riche en indium et des désordres au niveau de la composition qui sont minimes autour des compositions intermédiaires de InI, de InI_2 et InI_3. On a développé la fluctuation de composition quadratique moyenne afin de pouvoir discuter de l'arrangement brut à faible distance, ΔN_α, et le rôle du transfert de charge, Δe_α, par rapport à une théorie des solutions basée sur la mécanique statistique générale. Le pic important dans $S_{cc}(0)$ au niveau de la section riche en indium est une preuve critique des grandes fluctuations de concentration qui accompagnent les inhomogénéités microscopiques dans la structure électronique lorsque l'on fait l'hypothèse qu'il existe un mode de distribution bimodale. La limite $\Delta N_\alpha \rightarrow 1$ près des concentrations InI, InI_2 et InI_3 montre qu'il existe une préférence pour des voisins les plus près qui sont dissemblables à cause d'un caractère ionique ou covalent dans la liaison chimique. On propose qu'il existe dans la région In–InI une relation entre une transition graduelle métal–non-métal et les grandes fluctuations de concentration qui sont associées avec des inhomogénéités microscopiques dans la structure électronique.

[Traduit par le journal]

Introduction

A general statistical mechanical theory of solutions has been developed with the aid of the theory of composition fluctuations in the grand canonical ensemble (1). At temperatures above the Debye temperature and in the long-wavelength limit the concentration correlation function, $S_{cc}(0)$, represents the mean square fluctuations in concentration, and is linearly related to the partial structure factors, $a_{\alpha\beta}(q \rightarrow 0)$ (2). The values of $a_{\alpha\beta}(0)$ cannot be extracted from measurements at a finite wavevector because of the poor experimental resolution. The limits are, however, given in terms of measurable thermodynamic quantities, namely the density, compressibility, and chemical potential (2). Thus the long-wavelength partial structure factors provide a measure of detailed structure in the

binary mixtures such as $S_{cc}(0)$ and the crude short range ordering (3), ΔN_α.

A physical picture was recently advanced for the continuous metal–nonmetal (MNM) transition in a binary solution including a nonmetallic component such as metal–ammonia solutions. The concentration fluctuates locally about either of two well-defined regimes, a metallic propagation regime and a nonmetallic regime (4). Further, it was proposed that the large concentration fluctuations (5) near a consolute concentration of the metal–ammonia solutions originate from the microscopic inhomogeneities in bonding configurations which are distinct from critical fluctuations (4).

Nuclear magnetic resonance (nmr) provides information at the microscopic level on the electronic structure (6, 7). This is because the apparent Knight shift increases monotonically with increasing metal concentration for the metal–nonmetal solutions such as alkali metal – NH_3 (8, 9) and Bi–BiI_3 (10), while conductivity measurements demonstrate the continuous metal–nonmetal transition induced by a simple change in concentration (11, 12). A careful examination of the experimental data is required to discuss the MNM transition in view of microscopically inhomogeneity in electronic structure (7).

The present paper reports relative chemical potential and electrical conductivity measurements of the system indium–iodine. In the phase diagram of the In–I system (13, 14), a miscibility gap was assumed over the In–InI region and the exact consolute point is not yet known. The stoichiometric compounds of InI, InI_2, and InI_3 were examined at temperatures below their melting points. The mean square concentration fluctuations (or $S_{cc}(0)$) are determined from the concentration derivative of the chemical potential for indium and developed to estimate the terms ΔN_α and Δe_α which refer to crude short range atomic configuration and chemical bonding at the intermediate compositions of InI, InI_2, and InI_3, respectively. The relationship between a gradual metal–nonmetal transition and a large peak of $S_{cc}(0)$ resulting from a bimodal distribution is discussed for indium–iodine solutions.

Experimental

Electromotive force measurements are briefly reported, and are described in detail elsewhere. Determination of the activity of In has been carried out using a ZrO_2 (+CaO) solid electrolyte. A concentration cell without transference was employed:

$$W|In, InO||ZrO_2(+CaO)||In—I, InO|W$$

The emf, ε, of such a cell is related to the activity of In,

$$\varepsilon = -\frac{RT}{2F} \ln a_{In}$$

where O^{2-} transport can be regarded as the mechanism of conduction in the zirconia solid electrolyte. The emf of the cell was measured on a dc potentiometer. The electrical conductance measurements were made with the aid of a dc four-terminal potentiometric method for the indium-rich region and with an ac Jones type bridge (15) for the intermediate region.

Materials

The indium used was 99.999% pure. Guaranteed reagent grade InI_3 was purified by distillation *in vacuo*.

Results

Figure 1 shows the emf, ε, as a function of concentration at 600°C. The points shown in Fig. 1 are taken from the smoothed curves of the emf *vs.* the temperature at a given concentration. Some of the emf data in Fig. 1 are shown as a dotted line over the 70–90 at.% In region across a consolute concentration where the correct consolute point has not yet been determined. The specific conductance increases continuously and monotonically with increasing metal composition; *i.e.*, at 600°C, 0.104 Ω^{-1} cm^{-1} for the InI_3, 0.419 Ω^{-1} cm^{-1} near the InI_2, 2.17×10^4 Ω^{-1} cm^{-1} for 0.9985, 2.225×10^4 Ω^{-1} cm^{-1} for 0.9991, and 2.285×10^4 Ω^{-1} cm^{-1} for the pure In.

Discussion

Relationship among Metal–Nonmetal Transition and Concentration Fluctuations

In Fig. 2 the concentration fluctuations, $S_{cc}(0)$, directly determined from the emf data of Fig. 1 (2, 5, 16), show a large peak over the whole range of In–InI throughout which the conductivity, σ, can be expected to change by almost five orders of magnitude. It remains almost constant in the iodine-rich region between InI and InI_3 solutions. Thus the continuous metal–nonmetal transition induced by concentration changes takes place at the In-rich side where there are large composition fluctuations.

Bimodal and Unimodal Distributions

A bimodal distribution in an α–β liquid alloy occurs when one component, *e.g.* α, has two different electronic structures resulting from microscopic inhomogeneities. In the case of a

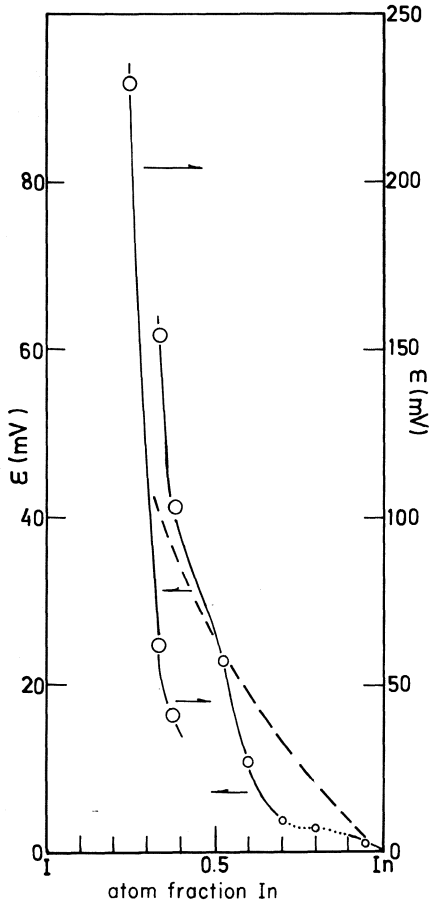

FIG. 1. The measured emf for In–I mixtures is shown by the open circle. All data were taken at 600°C. Ideal behaviour for ε is shown by the broken line.

unimodal distribution there is a single electronic state for each component. Whether the concentration fluctuations are bimodally or unimodally distributed should be experimentally determinable. The quantity

$$[1] \qquad \Delta N_\alpha \equiv x_\alpha[a_{\beta\alpha}(0) - a_{\alpha\alpha}(0)]$$

means the difference between the total number of α species surrounding a β species and the total number of α species surrounding an α species, and provides a crude measure of the short range ordering in a binary system (3). Here,

$$a_{\beta\alpha}(0) = 1 + \rho \int d\mathbf{r}[g_{\beta\alpha}(r) - 1]$$

From standard arguments of composition fluctuations in statistical thermodynamics (1) [1] can be expressed in terms of $S_{cc}(0)$ as follows (7),

$$[2] \qquad \Delta N_\alpha = 1 - (1+\delta x_\alpha)S_{cc}(0)/x_\alpha x_\beta$$

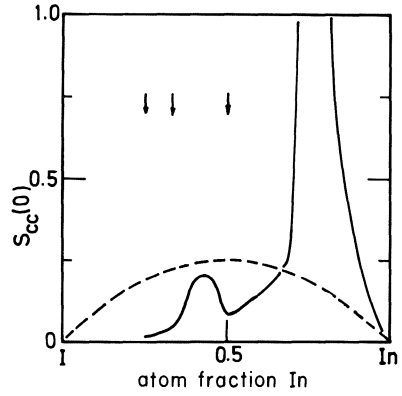

FIG. 2. The concentration correlation function $S_{cc}(0)$ for In–I mixtures at 600°C. The dashed curve is ideal.

where δ is a dilation factor defined by $v_m^{-1}\partial v_m/\partial x$ with a molar volume, v_m. The concentration dependences on ΔN_α for a variety of binary liquid alloys such as In–I, Na–NH_3, Ga–Bi, and Al–In are shown in Figs. 3–6. One can definitely classify them into the group in which $\Delta N_\alpha \neq \Delta N_\beta$ over a considerable range corresponding to the miscibility gap for the metal–nonmetal alloys such as In–I and Na–NH_3; in another group, $\Delta N_\alpha \simeq \Delta N_\beta$ for Ga–Bi and Al–In except for the range close to a consolute concentration. If microscopic inhomogeneities originate from ordinary critical fluctuations, that is, a unimodal distribution, the crude short range ordering, ΔN_α, for an α species can be expected roughly to equal ΔN_β for the other species β.

It is proposed that both bimodal distribution and $\Delta N_\alpha \neq \Delta N_\beta$ can occur in various metal–nonmetal liquid alloys. There are several experimental results to support this remark. Recent experiments on small-angle neutron scattering on K–KBr solutions (or K–Br) show that significant concentration fluctuations exist and that their large correlation length extends over a large temperature range above the immiscibility gap (17). It can be deduced from the determination of the three partial interference functions that nonmetal components cannot come in close contact in metal–nonmetal liquids or amorphous alloys. For amorphous Co–P, the experimental results show that a phosphorus atom cannot associate with other phosphorus atoms owing to electrical repulsion (18). For liquid Fe–P systems partial structure factors determined using anomalous scattering of X-rays (19) indicate not only that a phosphorus atom is surrounded by iron atoms but that

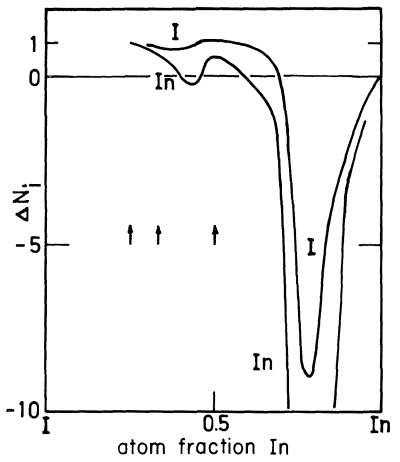

FIG. 3. The parameters ΔN_{In} and ΔN_I computed from [2] for In–I mixtures. For an ideal solution of the same atomic size this parameter is zero. The arrows mark the stoichiometric compositions of InI, InI_2, and InI_3.

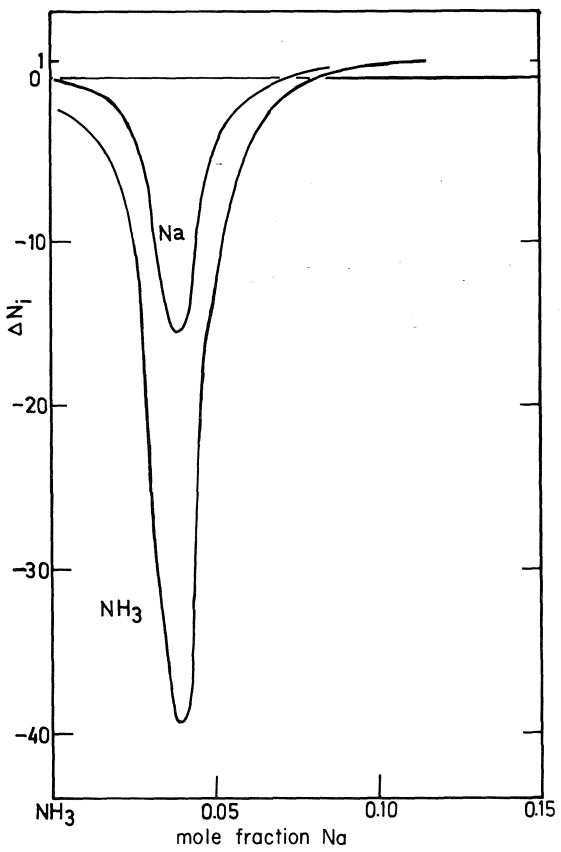

FIG. 4. The parameters ΔN_{Na} and ΔN_{NH_3} computed from [2] for Na–NH_3 solutions (ref. 5).

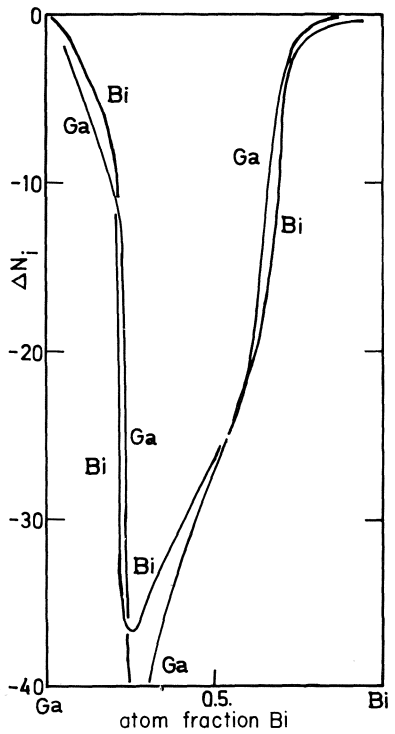

FIG. 5. The parameters ΔN_{Ga} and ΔN_{Bi} computed from [2] for Ga–Bi mixtures (ref. 28).

phosphorus atoms may not come in close contact. Thus, it is expected that in In–I solutions the iodine atoms cannot be brought into contact and that each of them is isolated by indium atoms. The fused salt-like local structure of the In–I pair may bring about aggregation of indium atoms in the indium-rich region. In view of the similarity between In–I (or In–InI) and K–Br (or K–KBr) systems the In–I solutions are also expected to have large amplitude concentration fluctuations which extend over large distances, as shown in Fig. 2. Therefore, the following remarks can be made: over the concentrations of In–InI (*i*) there exist two different local electron states for the indium component: a simple ionic fused salt-like electrostatic potential between In and I, and metallic cohesion among indium atoms, that is, a bimodal distribution; (*ii*) $\Delta N_I \neq \Delta N_{In}$ (in fact, $0 > \Delta N_I > \Delta N_{In}$ has been inferred from emf measurements and [2]). For Na–NH_3 solutions the fact that $0 > \Delta N_{Na} > \Delta N_{NH_3}$ is attributed to the following physical picture. The components may be viewed as positive sodium ions surrounded by a large group of oriented ammonia molecules and free-

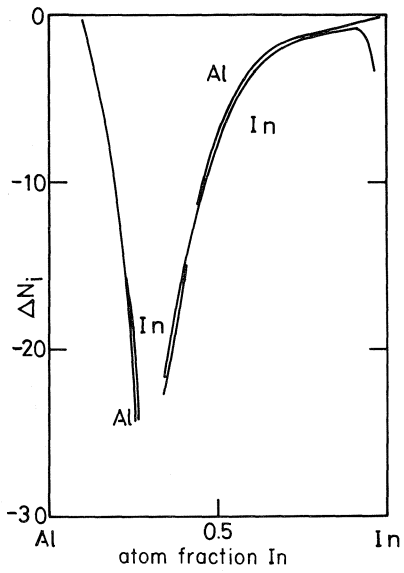

FIG. 6. The parameters ΔN_{Al} and ΔN_{In} computed from [2] for Al–In mixtures (ref. 29).

ammonia molecules which are not bound to a sodium ion (*e.g.* ref. 20). Two different dipoles can be considered for bound and unbound NH_3 molecules. Thus, the large fluctuations in concentration and their extension over large distances confirmed from chemical potential (5) and small-angle neutron scattering (21) studies on Na or Li–NH_3 and Li–ND_3 support the plausibility of a bimodal distribution.

It is proposed that over the In–InI range there is the relationship between metal–nonmetal transition and the large concentration fluctuations which are associated with a bimodal distribution and $0 > \Delta N_{In} \neq \Delta N_I$.

Minimal Compositional Disorder

S_{cc} (0) shows strong negative deviation from an ideal mixture at the InI, InI_2, and InI_3 concentrations for In–I (see Fig. 2). This result indicates minimal compositional disorder and stability at these compositions, which are apparently dominated by the chemical bonding (ionic or covalent) among the constituent atoms. It is worth noting that the values of ΔN_α approach unity at the stoichiometric compositions, InI, InI_2, and InI_3 (see Fig. 3). The facts that $\Delta N_\alpha = 1$ and $x_\alpha = 0.5$ in [1] lead to the conclusions which are quite satisfactory for a simple ionic melt of α^+–β^-, as follows: (*i*) $S_{\alpha\beta}(0) = S_{\alpha\alpha}(0) = S_{\beta\beta}(0)$ (22, 23), where their partial structure factors are defined by

$$S_{\alpha\beta}(0) \equiv (\rho_\alpha\rho_\beta)^{1/2} \int_0^\infty d\boldsymbol{r}\,[g_{\alpha\beta}(r) - 1] + \delta_{\alpha\beta}$$

(*ii*) the electrical neutrality condition (22, 24), and (*iii*) the limit $S_{cc}(0) \to 0$ (23). Therefore, the solutions at the intermediate concentration of InI or $x_{In} = x_I = 0.5$ have a fused salt-like configuration in view of preference for unlike nearest neighbors.

What is the kind of pair potential which brings about a fused salt-like configuration near the stoichiometric composition of InI? It is proposed that for metal–halogen alloys the minimal compositional disorder at this intermediate composition is attributed to a charging process. A new quantity, $(\partial\mu_\alpha/\partial\rho_\alpha)_{T,P}$ is introduced in addition to $S_{cc}(0)$ or $(\partial\mu_\alpha/\partial x_\alpha)_{T,P}^{-1}$ and ΔN_α. The theory of composition fluctuations is subsequently developed to evaluate thermodynamic parameters in terms of the partial correlation functions, $a_{\alpha\beta}(0)$, at the long-wave limits (1, 25). The thermodynamic relation for a binary α–β system at constant P and T

$$[3]\quad \left(\frac{\partial\mu_\alpha}{\partial\rho_\alpha}\right)_{T,P} = \frac{\rho_\beta(\partial\mu_\alpha/\partial\rho_\alpha)_{T,\mu_\beta}(\partial\mu_\beta/\partial\rho_\alpha)_{T,\mu_\alpha}}{\rho_\beta(\partial\mu_\beta/\partial\rho_\alpha)_{T,\mu_\alpha} - \rho_\alpha(\partial\mu_\alpha/\partial\rho_\alpha)_{T,\mu_\beta}}$$

can be expressed in terms of the $a_{\alpha\beta}(0)$ using

$$[4]\quad k_B T\left(\frac{\partial\rho_\alpha}{\partial\mu_\beta}\right)_{T,\mu_{\beta'}} = \frac{\rho_\alpha\rho_\beta}{\rho}[a_{\alpha\beta}(0) - 1] + \rho_\alpha\delta_{\alpha\beta}$$

In fact, substitution of [4] into [3] yields

$$[5]\quad \frac{1}{k_B T}\left(\frac{\partial\mu_\alpha}{\partial\rho_\alpha}\right)_{T,P} = \frac{1}{\rho_\alpha} - \frac{\frac{1}{\rho}[a_{\alpha\alpha}(0) - a_{\beta\alpha}(0)]}{1 + \frac{\rho_\alpha}{\rho}[a_{\alpha\alpha}(0) - a_{\beta\alpha}(0)]}$$

From the definition [1] of the local ordering, ΔN_α, [5] can be rewritten as

$$[6]\quad \left(\frac{\partial\mu_\alpha/k_B T}{\partial\log\rho_\alpha}\right)_{T,P} = 1 + \frac{\Delta N_\alpha}{1 - \Delta N_\alpha}$$

Here, $\Delta N_\alpha/(1 - \Delta N_\alpha)$ ($\equiv \Delta e_\alpha$) is the contribution to the deviation from the laws of ideal solutions. Figure 7 shows that Δe_I for the binary In–I solutions probably has two large peaks in the

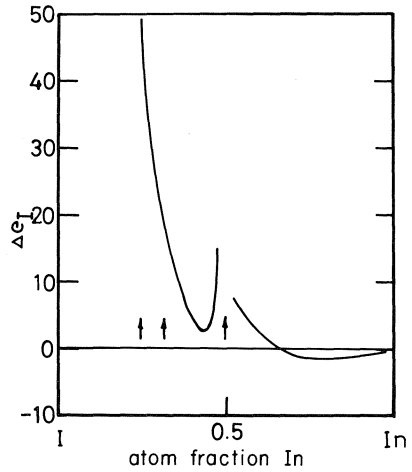

FIG. 7. The parameter Δe_I computed from [10] and [2] for In–I mixtures. For an ideal solution of the same atomic size, this parameter is zero. The arrows mark the stoichiometric composition of InI, InI_2, and InI_3.

vicinity of the intermediate compounds InI, InI_2, and InI_3, where each ΔN_α is close to unity and $S_{cc}(0)$ shows the probable and real minima in compositional disorder. Kirkwood and Buff (1) point out that [5] or Δe_α provides an alternative to the usual charging process encountered in electrolyte theory. According to Onsager (26) the electrostatic contribution, $\Delta F(\text{el})$, to the free energy of a concentrated electrolyte can be given by

$$[7] \qquad \Delta F(\text{el}) = \sum_{\gamma}^{2} \rho_\gamma \int_0^{Z_\gamma|e|} \phi(e_\gamma)\, de_\gamma$$

where $\phi(e_\gamma)$ is average potential due to other ions at the point of an ion with instantaneous charge, e_γ, and ρ_γ is the number density of a γ ion. The corresponding contribution to the chemical potential of an α ion is expressed as follows:

$$[8] \qquad \Delta\mu_\alpha(\text{el}) = \int_0^{Z_\alpha|e|} \phi(e_\alpha)\, de_\alpha + \rho_\alpha \frac{\partial \int_0^{Z_\alpha|e|} \phi(e_\alpha)\, de_\alpha}{\partial \rho_\alpha}$$

It is assumed that for the In–I liquid alloy the deviation from ideality can be attributed entirely to electrostatic forces between unlike ions, near the intermediate concentration, because the Coulomb energy, which is the main contribution to the internal potential in a simple ionic melt of α^+–β^-, is very large compared with the internal energy for a simple liquid metal (*e.g.*, liquid In) and the van der Waals energy for liquified inert gases. The contribution of the Coulomb energy to the deviation from the laws of ideal solutions may mask the contribution resulting from excess entropy and excess volume terms.

Therefore, near the stoichiometric composition of InI the form of $\Delta N_\alpha/(1 - \Delta N_\alpha)$ can be approximately expressed as

$$[9] \qquad \frac{\Delta N_\alpha}{1 - \Delta N_\alpha} = 2 \frac{\rho_\alpha}{k_B T} \frac{\partial \int_0^{Z_\alpha|e|} \phi(e_\alpha)\, de_\alpha}{\partial \rho_\alpha'}$$

by differentiation of [8] with respect to ρ_α and neglect of the second ρ_α derivative of the integrand in [8] for simplification only. Thus, the large positive value of Δe_α at this composition is directly related to the increment of the work of charging one α ion owing to its addition into a given concentration of an α–β alloy. For liquid Cs–Au it was proposed that, near equi-atomic concentration, ionic conduction plays an important role on the hypothesis of charge transfer, that is, the Cs atoms donate one valence electron to each Au atom (27). The system Cs–Au can be expected to have a peak of Δe_α near this equi-atomic concentration.

More detailed studies of the indium–iodine system, in particular, on its thermodynamic functions are clearly required.

Acknowledgments

I thank Professor J. C. Thompson for his encouraging discussions and for his critical reading, and Mr. T. Kiya for technical services.

1. J. G. KIRKWOOD and F. P. BUFF. J. Chem. Phys. **19**, 774 (1951).
2. A. B. BHATIA and D. E. THORNTON. Phys. Rev. B, **2**, 3004 (1970).
3. R. TURNER, E. D. CROZIER, and J. F. COCHRAN. J. Phys. C, **6**, 3359 (1973).
4. M. H. COHEN and J. JORTNER. Phys. Rev. B, **13**, 1548 (1974); M. H. COHEN and J. JORTNER. J. Phys. Chem. **79**, 2900 (1975); M. H. COHEN, I. WEBMAN, and J. JORTNER. J. Chem. Phys. **64**, 2013 (1976).
5. K. ICHIKAWA and J. C. THOMPSON. J. Chem. Phys. **59**, 1680 (1973); **62**, 4958 (1975).
6. W. W. WARREN. Phys. Rev. B, **3**, 3708 (1971); J. Non-Cryst. Solids, **8–10**, 241 (1972).
7. J. C. THOMPSON, K. ICHIKAWA, and S. M. GRANSTAFF, JR. Phys. Chem. Liq. **5**, 167 (1976).
8. E. DUVAL, P. RIGNY, and G. LEPOUTRE. Chem. Phys. Lett. **2**, 237 (1968).
9. J. P. LELIEUR and P. RIGNY. J. Chem. Phys. **59**, 1148 (1973).
10. R. DUPREE and W. W. WARREN. Preprint, 3rd Int. Conference on Liquid Metals. 1976.

11. M. H. COHEN and J. C. THOMPSON. Adv. Phys. **17**, 857 (1968).
12. L. F. GRANTHAM and S. J. YOSIM. J. Chem. Phys. **38**, 1671 (1963).
13. A. THIEL and H. KOELSCH. Z. Anorg. Allg. Chem. **66**, 317 (1910).
14. E. A. PERETTI. J. Am. Chem. Soc. **78**, 5745 (1956).
15. K. ICHIKAWA, T. OKUBO, and M. SHIMOJI. Trans. Faraday Soc. **67**, 1426 (1971).
16. K. ICHIKAWA, S. M. GRANSTAFF, JR., and J. C. THOMPSON. J. Chem. Phys. **61**, 4059 (1974).
17. J. F. JAL, P. CHIEUX, and J. DUPUY. Ber. Bunsenges. Phys. Chem. **80**, 820 (1976).
18. J. BLÉTRY and J. F. SADOC. J. Phys. F, **5**, L110 (1975).
19. Y. WASEDA. Met. Phys. Seminar Jpn. **1**, 305 (1976).
20. R. L. SCHROEDER and J. C. THOMPSON. J. Phys. Rev. **179**, 124 (1969).
21. P. CHIEUX. J. Phys. Chem. **18**, 2891 (1975).
22. M. C. ABRAMO, M. PARRINELLO, and M. P. TOSI. J. Nonmetals, **2**, 57 (1973).
23. P. J. DURHAM and D. A. GREENWOOD. Philos. Mag. **33**, 427 (1976).
24. M. WATABE and M. HASEGAWA. *In* The properties of liquid metals. *Edited by* S. Takeuchi. Taylor and Francis, London. 1973. p. 133; J. CHIHARA. *In* The properties of liquid metals. *Edited by* S. Takeuchi. Taylor and Francis, London. 1973. p. 137; N. H. MARCH, M. P. TOSI, and A. B. BHATIA. J. Phys. C, **6**, L59 (1973).
25. A. BEN-NAIM. Water and aqueous solutions – introduction to a molecular theory. Plenum Publishing Corporation, New York and London. 1974.
26. L. ONSAGER. Chem. Rev. **13**, 73 (1933).
27. R. W. SCHMUTZLER, H. HOSHINO, R. FISCHER, and F. HENSEL. Ber. Bunsenges. Phys. Chem. **80**, 107 (1976).
28. B. PREDEL. Z. Phys. Chem. Frankfurt am Main, **24**, 206 (1960).
29. A. YAZAWA and Y. K. LEE. J. Jpn. Inst. Metals, **33**, 318 (1969).

Electron mobility in nonpolar liquids: the effect of molecular structure, temperature, and electric field

WERNER F. SCHMIDT

Bereich Strahlenchemie, Hahn-Meitner-Institut für Kernforschung Berlin GmbH, D 1000 Berlin 39, Germany

Received October 4, 1976

WERNER F. SCHMIDT. Can. J. Chem. **55**, 2197 (1977).

A survey is given on the mobility of excess electrons in liquid hydrocarbons and related compounds. It was found that the mobility is strongly influenced by the molecular structure of the liquid, by the temperature, and by the electric field strength. The mobility in hydrocarbons increases as the shape of the molecule approaches a sphere. The temperature coefficient is positive in most liquids over a limited temperature although exceptions have been observed in liquid methane. The field dependence of the mobility in high mobility liquids (>10 cm^2 V^{-1} s^{-1}) showed a decrease of the mobility at higher field strengths while in low mobility liquids (<1 cm^2 V^{-1} s^{-1}) it showed an increase. These results are discussed on the basis of the extended and the localized electron models. The predictions of these theories are compared with the experimental results and conclusions on the validity of the underlying assumptions are drawn.

WERNER F. SCHMIDT. Can. J. Chem. **55**, 2197 (1977).

On présente une revue sur la mobilité des électrons en excès dans des hydrocarbures liquides et d'autres composés qui leur sont reliés. On a trouvé que la mobilité est grandement influencée par la structure moléculaire du liquide, par la température et par la force du champ électrique. La mobilité dans les hydrocarbures augmente à mesure que la forme de molécule approche celle d'une sphère. Le coefficient de température est positif dans la plupart des liquides à l'intérieur de faibles limites de température même si l'on a observé des exceptions dans le méthane liquide. La relation qui existe entre le champ et la mobilité dans des liquides de grande mobilité (>10 cm^2 V^{-1} s^{-1}) présente une diminution de mobilité à des forces de champ élevées alors que dans des liquides de basse mobilité (<1 cm^2 V^{-1} s^{-1}) elle présente une augmentation. On discute de ces résultats sur la base de modèles d'électrons étendus et localisés. On compare les prédictions de ces théories avec les résultats expérimentaux et on tire des conclusions sur la validité des hypothèses de base.

[Traduit par le journal]

Introduction

The electronic properties of nonpolar liquids have received increasing interest during recent years. From a fundamental point of view nonpolar liquids represent a class of non-crystalline materials; the physical properties and the chemical behavior of excess electrons can be studied since excess charge carries can be injected by various means (1). Radiation chemistry is interested in excess electrons since they represent one product of the interaction of high energy radiation with matter and since their chemical reactivity depends strongly on the liquid surrounding.

From a practical point of view nonpolar liquids have wide applications as insulators in electrical power equipment and the development of a cryogenic high voltage technology requires among other things the investigation of the conduction processes in cryogenic liquids (2).

The discovery of highly mobile electrons in certain nonpolar liquids has opened applications in fast nuclear radiation detectors and in fact right now huge liquid ionization chambers with effective volumes of 5000 ℓ are being built for the detection and the calorimetry of elementary particles in high energy physics (3, 4).

The subject of electron mobility in nonpolar liquids encompasses a wide field. Since over 20 years investigations have been carried out with liquefied rare gases and several reviews have appeared (5–7); this area will not be discussed here. Excess electrons in liquid hydrocarbons were observed first in 1969 independently by several groups (8–11) and since then a lot of experimental information has been gathered.

It is the purpose of this paper to review the experimental data and to discuss the salient features of the excess electron mobility in liquid hydrocarbons and related compounds. Emphasis will be placed on the effects of structure, temperature, and electric field strength. Com-

parison will be made with results from scattering studies of electrons and polyatomic molecules in liquefied rare gases.

Methods for Mobility Measurements

Measurements of excess electron mobility have been carried out mainly with two methods. Either the increase of the conductivity during a short pulse of high energy X rays or electrons is measured or the drift velocity is determined by a time of flight method. Excess charge carriers can also be produced by photoionization of a homogeneously distributed solute as for instance *N*,*N*,*N*′,*N*′-tetramethyl-*p*-phenylenediamine (TMPD) (12).

In the conductivity method use is made of the fact that the mobility of the excess electrons is usually much greater than the mobility of ions so that any change in the conductivity during the pulse is due to excess electrons. The conductivity σ is then given by

$$[1] \qquad \sigma = e_0 n(\mu_{e1} + \mu_+) \approx e_0 n \mu_{e1}$$

where n is the concentration of excess electrons/cm^3 and e_0 the electronic charge. The concentration n can be determined with the radiation yield of electrons $G_{e1}(F)$, which is a function of the applied electric field F and the absorbed dose D, from

$$[2] \qquad n = D \cdot G_{e1}(F) \times 10^{-2}$$

A necessary presumption is that no volume recombination between electrons and positive charge carriers occurs during the pulse. Usually a parallel plate measurement cell (area q, electrode distance l) is employed and the conductivity signal is converted into a voltage signal with a resistor R connected in series with the cell. If $R \ll (\sigma q/l)^{-1}$ than the signal voltage obtained with voltage U, $U_s = \sigma(q/l)UR$, is proportional to the conductivity.

In the time of flight method the drift of a spatial inhomogeneity of the charge carrier density in an electric field is observed. Neutralization of the charge carriers at their respective counter electrode leads to a discontinuity in the current–time signal. The drift time t_d is given by

$$[3] \qquad t_d = l^2/(\mu U)$$

Different methods for the production of this inhomogeneous density distribution are used. In the Hudson method the liquid in a parallel measurement cell is subjected to a step function of X rays and the time of flight is given by the time it takes those electrons generated near the cathode to reach the anode. In the pulse method the liquid volume is irradiated with a short pulse of X rays leading to a constant density of excess electrons. Under the influence of the electric field the electrons move to the anode, become neutralized, and a discontinuity travels across the gap leading to a linear decay. Other methods which have been applied to liquefied rare gases and ionic charge carriers in hydrocarbons were reviewed recently (1).

Both methods have advantages and disadvantages. While the time of flight method gives direct information on the mobility, it requires extremely pure liquids since only small concentrations of excess charge carriers can be generated if space charge effects are to be neglected.

In the conductivity method a higher level of impurities can be tolerated. The determination of the mobility, however, requires the independent determination of $G_{e1}(F)$ and measurement of the radiation dose; the accuracy of the mobility values is determined to a high degree by the accuracy of the dosimetry. Measurements in this laboratory were carried out with a time of flight method and the experimental set-up has been described repeatedly (13).

The Effect of Structure

One of the surprising features of excess electron mobilities in nonpolar liquids is the large variation with the structure of the molecules composing the liquid. This dependence is very much apparent in the liquid hydrocarbons where mobilities ranging from 400 cm^2 V^{-1} s^{-1} for methane at 111 K to 1.3×10^{-3} cm^2 V^{-1} s^{-1} for ethane and the same temperature have been measured. A sample collection of values is compiled in Table 1 where data for liquids at room temperature are given. Research on electron mobilities is being conducted in several laboratories all over the world and virtually hundreds of values have been reported. In order to show the salient features the data of Table 1 have been selected not for the sake of completeness but to give, for liquids where several values have been measured, a value which has been obtained recently and is in agreement with most of the other values.

Although it remains an open question whether comparison at an arbitrary temperature can give insight into the physics of the transport

TABLE 1. Excess electron mobilities at room temperature ($T = 296 \pm 2$ K) and activation energies in several hydrocarbons and related compounds

Liquid	μ_{el} (cm^2 V^{-1} s^{-1})	E_a (eV)	Refs.
n-Alkanes			
n-Butane	0.34	0.13	14
n-Pentane	0.15	0.2	12
n-Hexane	0.09	0.19	15
n-Heptane	0.046	0.17	12
n-Octane	0.040	0.18	16
n-Nonane	0.047	0.19	12
n-Decane	0.038	0.22	12
n-Dodecane	0.030	0.22	17
C_4 isomers			
n-Butane	0.34	0.13	13
2-Methylpropane	7.3	0.08	16
C_5 isomers			
n-Pentane	0.15	0.2	12
2,2-Dimethylpropane	70	~0	18
	55		19, 20
C_6 isomers			
n-Hexane	0.09	0.19	15
2-Methylpentane	0.29		16
3-Methylpentane	0.22	0.2	21
2,3-Dimethylbutane	1.1		16
2,2-Dimethylbutane	12	0.07	16, 18, 19
Cycloalkanes			
Cyclopentane	1.1	0.12	14, 19
Cyclohexane	0.35		19
	0.45	0.13	20
Cycloheptane	0.44		22
Cyclooctane	0.17		22
Double bonds			
2,2-Dimethylbutane	12	0.07	18, 16, 19
3,3-Dimethyl-1-butene	1.9	~0.13	16
2,3-Dimethylbutane	1.1		16
2,3-Dimethyl-2-butene	5.8	0.05, 0.09	16, 26
n-Butane	0.34		14
1-Butene	0.064		26
cis-2-Butene	2.2	0.16	26
trans-2-Butene	0.029	0.23	26
Cyclopentane	1.1	0.12	14, 19
Cyclopentene	1.3		22
Cyclohexane	0.35		19
	0.45	0.13	20
Benzene	0.6		23
	0.13		22
Cyclohexene	1.0		22
Cycloheptane	0.44		22
Cycloheptene	0.35		22
Spherical shape			
Tetramethylsilane	90	~0(200–300)	19
Tetramethylgermanium	90	~0(200–300)	14
Tetramethyltin	70		24
2,2-Dimethylpropane	70, 50	~0	18, 19, 20
2,2-Dimethylbutane	12	0.07	18, 19, 20
3,3-Dimethylpentane	2.3		16
3,3-Diethylpentane	0.76		16
2,2,4-Trimethylpentane	7	0.05	19, 25
2,2,4,4-Tetramethylpentane	24	0.06	20
2,2,3,3-Tetramethylpentane	5.2	0.06	20
2,2,5,5-Tetramethylhexane	12	0.05	20

process some general properties can be extracted by inspection of Table 1. In the normal alkanes we see a decrease of the electron mobility with increasing chain length which levels off at about 5×10^{-2} cm^2 V^{-1} s^{-1} for $C_n > C_6$. The electron obviously is 'myopic' (a description coined by Freeman and his co-workers (16)) being unable to look ahead for more than six CH_2 groups. Branching of the C_n chain leads to an increase of the mobility which is demonstrated by the comparison of the mobility in the isomers of C_4, C_5, and C_6. The greatest values are obtained for compounds which contain a quaternary carbon atom. As the mobility increases in these compounds the energy of activation decreases. The cycloalkanes exhibit higher mobilities than the corresponding *n*-alkanes. Introduction of double bonds into alkanes may lead to a decrease or an increase depending on the position of the double bond. In the case of 2,3-dimethylbutane/2,3-dimethyl-2-butene the double bond is shielded by the CH_3 groups and it may lead to a more compact molecule. A dramatic effect of the isomerization on the mobility is apparent for *cis*- and *trans*-2-butene.

In the cyclic compounds the influence of a double bond is not very clear.

In the aliphatic compounds there is a great influence of the shape of the molecule. The electron mobility is highest in spherical molecules (tetramethylsilane, tetramethylgermanium, tetramethyltin, neopentane) and it increases in the other liquids the more this shape is realized.

As with gas phase mobilities in these compounds (27) it is difficult to correlate the observed liquid values with any specific molecular property. The absence of a permanent dipole leads to short range interactions which are also influenced by the structure of the liquid or in other words by the simultaneous interaction of one electron with several molecules. This may be seen from measurements of the excess electron mobility in mixtures of liquid methane and ethane given in Fig. 1 (28).

While in pure methane at $T = 111$ K the mobility is 400 cm^2 V^{-1} s^{-1} it drops to 1.3×10^{-3} cm^2 V^{-1} s^{-1} in pure ethane at the same temperature. At low ethane concentrations the mobility is reduced due to single scattering while at higher ethane concentration collective interactions of an electron with a group of ethane molecules may take place leading to localization and a low mobility.

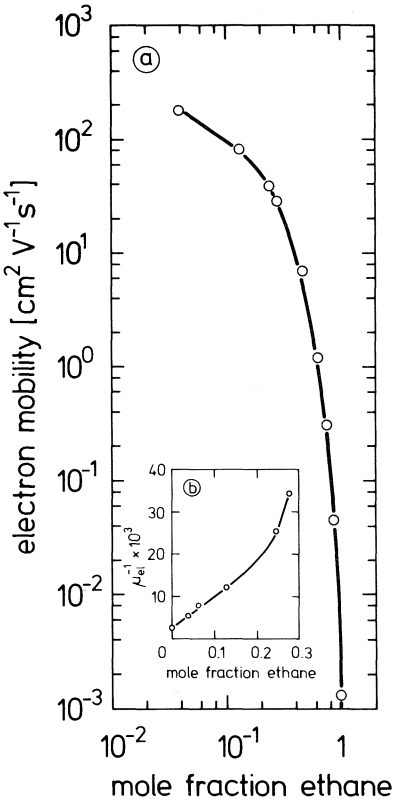

FIG. 1. Dependence of the electron mobility in liquid mixtures of methane and ethane on the ethane concentration (with permission, from ref. 28).

The Effect of Temperature

Electron mobilities in hydrocarbon liquids exhibit in general positive temperature coefficients. The only exception so far seems to be liquid methane where a decrease of the mobility with increasing temperature has been observed (Fig. 2). Very recently these temperature studies have been extended by Engels and van Kimmenade (30). A mobility minimum was found at 135 K and the mobility increased with increasing temperature to a maximum, as in the case of liquid argon (31). Most normal alkanes show an Arrhenius-type dependence of μ_{el} on T (Fig. 3) with activation energies between 0.1 and 0.2 eV. A decrease of the activation energy at higher temperature was obtained for ethane while the data for *n*-pentane show the opposite behavior. These two cases are also typical for a number of other liquids (16, 22, 26).

For the branched alkanes, as for example neohexane or isooctane, smaller activation

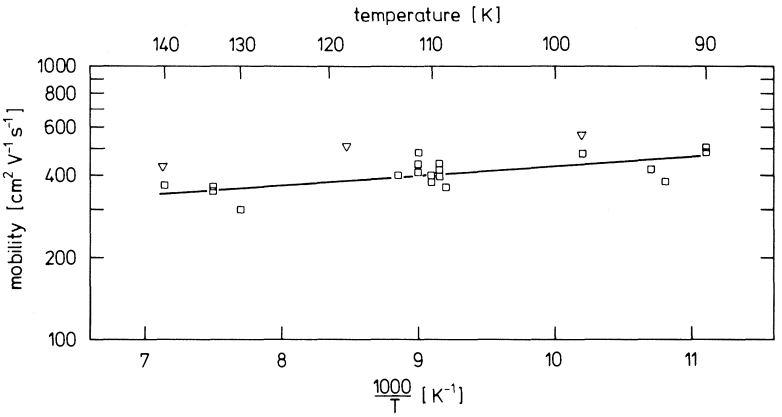

FIG. 2. Temperature dependence of electron mobility in liquid methane: □, from ref. 13; ▽, from ref. 29.

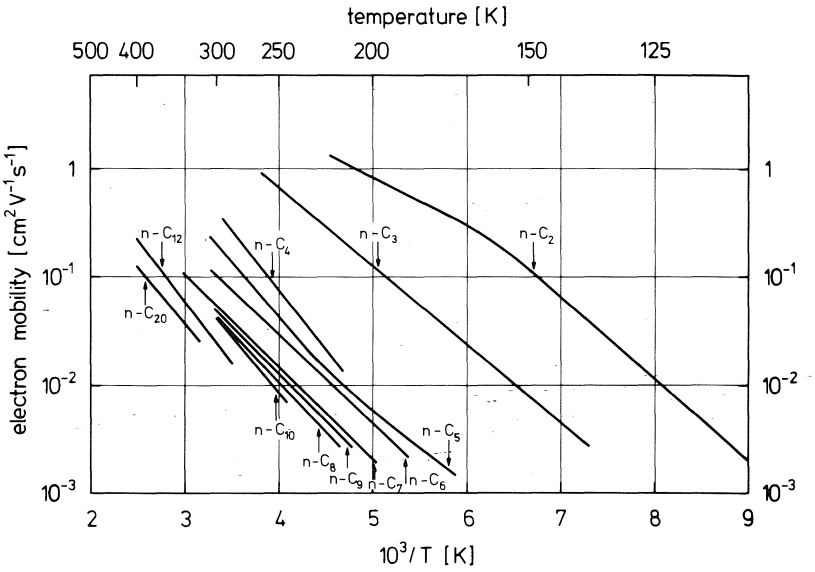

FIG. 3. Arrhenius plot of the electron mobility in *n*-alkanes. Data from refs. 12, 32, 29, 17.

energies were observed and the electron mobility in neopentane or tetramethylsilane was approximately independent of temperature in the range of temperature given in Table 1.

Expressing the dependence of $\mu(T)$ as

$$[4] \qquad \mu(T) = \mu_0 \exp(-E_a/kT)$$

gave values for μ_0 between 100 and 1000 $cm^2 V^{-1} s^{-1}$.

The Effect of an Electric Field

For the determination of the mobility μ_{el} measurements of the drift velocity v_d at different field strengths F are carried out and the usual mobility is the low field limit of the ratio v_d/F, *i.e.*

$$[5] \qquad \mu(T,0) = v_d/F$$

The proportionality between v_d and F extends over an interval of field strength which depends on the type of liquid. A further increase in field strength results in deviations from the proportionality and sublinear and superlinear dependencies have been observed. In Fig. 4 the electron drift velocity as a function of the field strength is shown for some liquids in which electron mobilities greater than 10 $cm^2 V^{-1} s^{-1}$ were observed. A characteristic field strength F_c

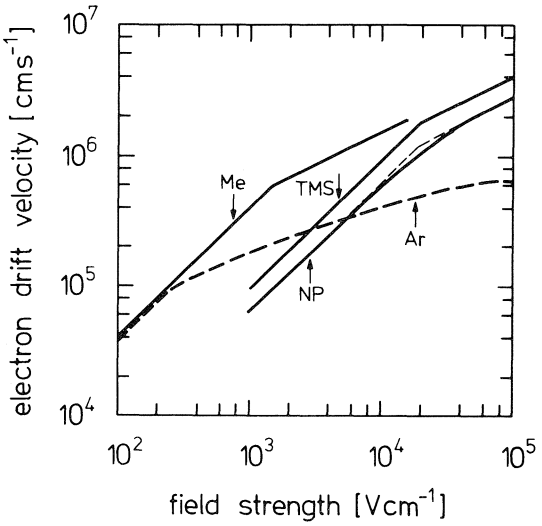

FIG. 4. Electron drift velocity as a function of the electric field strength in high mobility liquids: Me, methane, $T = 111$ K (ref. 13); TMS, tetramethylsilane, $T = 293$ K (ref. 34); NP, neopentane, $T = 295$ K (ref. 35); Ar, argon, $T = 87$ K (ref. 36).

can be found above which a sublinear dependence of v_d on F exists. In those liquids where the measurements have been carried out far enough into this sublinear region the data are consistent with a $v_d \propto F^{0.5}$ dependence which means that the mobility becomes a function of the field strength and decreases as $\mu \propto F^{-0.5}$. This sublinear dependence is generally interpreted as being due to an increase of the mean electron energy above $k_B T$.

Electrons pick up more energy from the field than they lose in subsequent collisions and a new stationary state results with a higher mean energy.

An interesting behavior is observed in methane/ethane mixtures of low ethane concentration where the low field mobility is decreasing with increasing ethane concentration (*cf.* Fig. 1) while the product $v_d = \mu_{el} F_c$ remains constant (*cf.* Fig. 5; the sublinearity sets in at a drift velocity of 5×10^5 cm s^{-1}).

A completely different field strength dependence of the drift velocity was found in hydrocarbons exhibiting a low electron mobility ($\mu_{el} < 1$ cm^2 V^{-1} s^{-1}). Here above a certain field strength a superlinear dependence was observed and data for ethane, propane, and pentane have been published already (32, 34). As examples for this type of behavior in Figs. 6 and 7 the electron drift velocities in liquid butane and cyclopentane are shown. It can be seen that the field strength at which the superlinearity sets in is shifted to lower values the higher the temperature.

A third type of field strength dependence was observed in isooctane at 221 K and in a 50/50 mixture of ethane and methane (Figs. 8 and 9), where the low field mobilities are 3 and 5 cm^2 V^{-1} s^{-1}, respectively.

Above a certain field strength a superlinear region is observed which is followed again at a still higher field strength by a linear region with a higher mobility. At 296 K in isooctane a sublinear dependence is found while at 195 K the drift velocity increases superlinearly with field.

Liquid Argon, Krypton, and Xenon: The Effect of Nonelectronegative Solutes

The interaction of thermal and superthermal electrons with alkane molecules in a condensed medium can be investigated by studying solutions of these compounds and liquefied rare gases (38). Use is being made of the experimental fact that in liquefied argon, krypton, or xenon electrons with mean energies above thermal can be obtained by the application of an electric field (36). Addition of hydrocarbon molecules influences the electron transport in a distinct way leading to a decrease of the low field mobility and to an increase of the high field mobility defined as

$$[6] \qquad v_d(F)/F = \mu(F)$$

at a fixed field strength F as compared to the pure solvent. As an example of this type of experiment in Fig. 10 the dependence of the excess electron drift velocity on the electric field strength is shown for liquid xenon and solution with *n*-butane. It is interesting to note that for low butane concentrations even a drift velocity maximum is obtained and at higher field strength the drift velocity approaches the value of the pure solvent again. Qualitatively these findings can be explained in the following way. At low field strength the electrons are in thermal equilibrium with the solvent and addition of butane molecules introduces new scattering centers for momentum transfer and a smaller mobility results. At the high field strengths the drift velocity is determined by elastic energy losses. Butane molecules act as energy sinks because a molecule can take up more energy

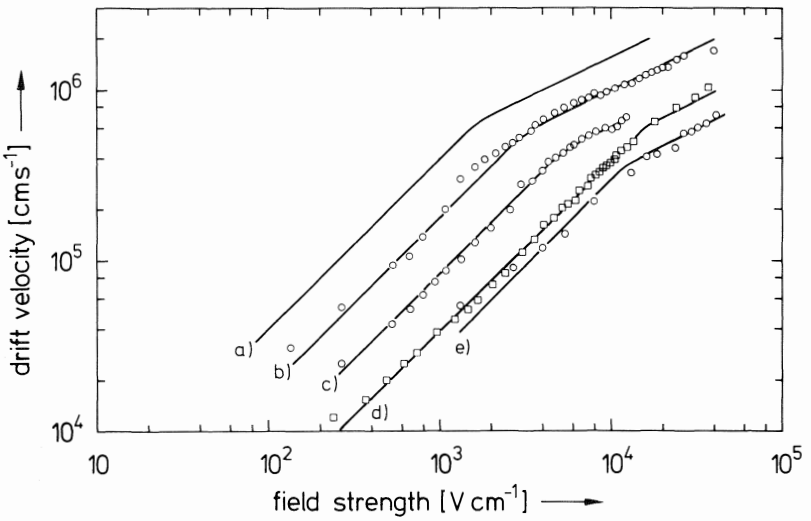

FIG. 5. Field strength dependence of electron drift velocity in methane–ethane mixtures at low ethane concentrations at $T = 111$ K: *a*, pure methane; *b*, 4 mol% ethane; *c*, 13 mol% ethane; *d*, 24 mol% ethane; *e*, 27 mol% ethane (with permission, from ref. 28).

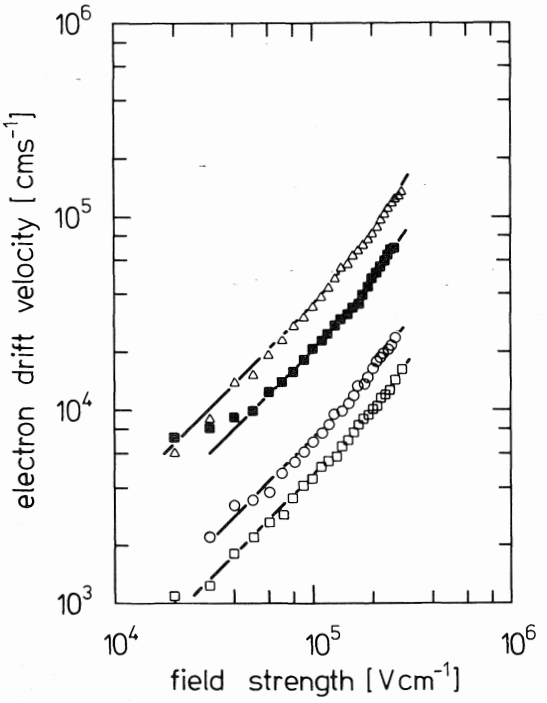

FIG. 6. Electron drift velocity as a function of the electric field strength in liquid butane: △, 297 K; ■, 278 K; ○, 250 K; □, 238 K (ref. 14).

from a colliding electron than a xenon atom. The drift velocity is then determined by the relative magnitude of the elastic loss rate to the inelastic loss rate. A simple analysis of these processes leads to a formula which gives the dependence of the drift velocity v_i on the solute concentration

$$[7] \quad v_i = \mu F_i = \left[\frac{\mu \Delta W \sigma(\varepsilon) N (2\varepsilon/m)^{1/2}}{e_0} + (\mu F_p)^2\right]^{1/2}$$

where F_i and F_p are the field strength in the solution and the pure solvent, respectively, where the same electron mobility μ (defined by eq. 6) exists. ΔW is the energy transferred to the molecule per collision, $\sigma(\varepsilon)$ the energy dependent cross section, N the solute concentration, ε the mean electron energy, m the electron mass, and e_0 the electronic charge. At high field strengths μF_p is constant (saturation velocity in the pure solvent) and for a certain solute concentration a drift velocity maximum occurs at an energy ε_{max} where $\mu\sigma(\varepsilon)\varepsilon^{1/2}$ shows a maximum.

By analyzing data as shown in Fig. 10 the product of $\Delta W\sigma(\varepsilon)$ can be obtained provided $\varepsilon = \varepsilon(F)$ is known. We applied the Cohen–Lekner theory (39, 40) and adjusted the mean free paths for momentum transfer Λ_1 to fit the theoretical dependence of electron drift velocity on field strengths for the pure solvents. Λ_0 values were obtained from V_0 measurements by means of the Springett–Jortner–Cohen theory (41).

Results of this type of analysis are shown in

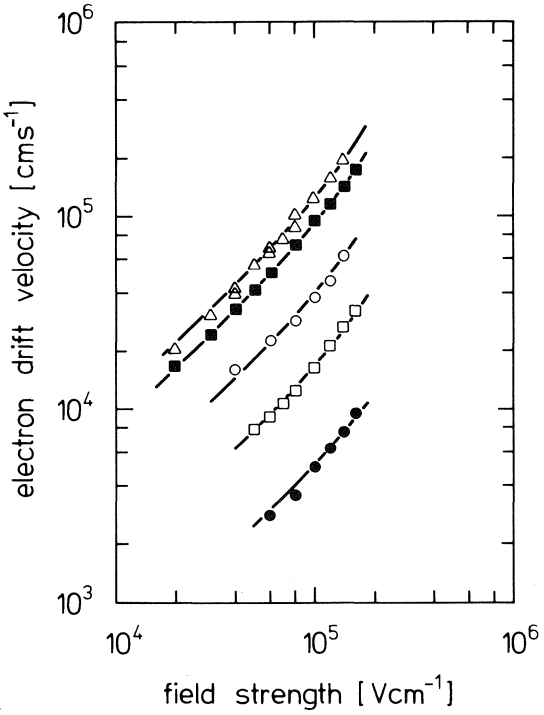

FIG. 7. Electron drift velocity as a function of the electric field strength in liquid cyclopentane: △, 296 K; ■, 278 K; ○, 251 K; □, 222 K; ●, 202 K (ref. 14).

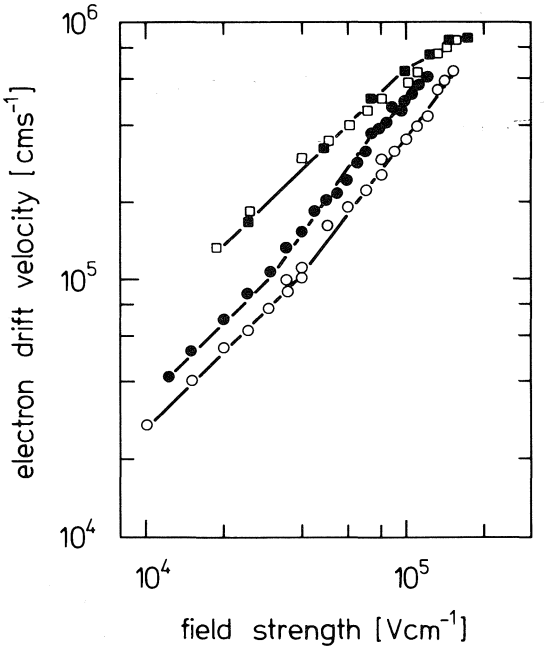

FIG. 8. Electron drift velocity as a function of the electric field strength in liquid 2,2,4-trimethylpentane (14, 24): □, 296 K; ●, 221 K; ○, 195 K. ■, 295 K (data from Balakin and Yakovlev (37)).

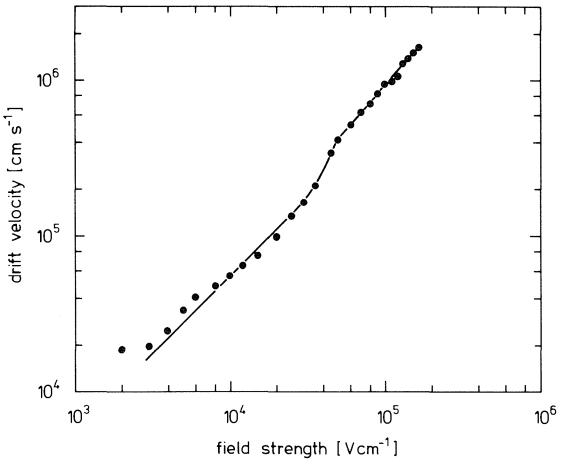

FIG. 9. Field strength dependence of electron drift velocity in an equimolar mixture of methane and ethane at $T = 111$ K (with permission, from ref. 28).

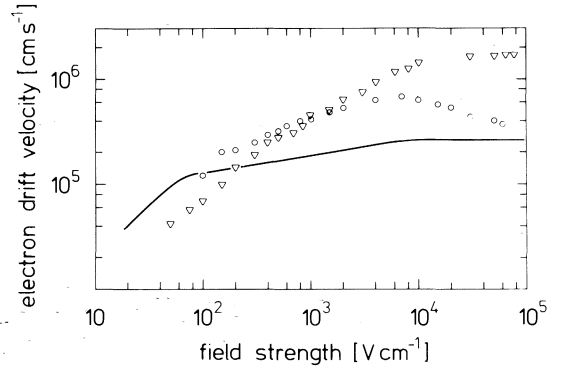

FIG. 10. Electron drift velocity as a function of the electric field strength in liquid xenon and the effect of butane. Butane concentration: ○, 1.26×10^{19} cm^{-3}; ▽, 1.9×10^{20} cm^{-3}; $T = 165$ K, solid line pure xenon (with permission, from ref. 38).

Fig. 11. With the mean electron energy approaching 0.1 eV a steep increase occurs and a maximum is reached between 0.3 and 0.5 eV. Butane is best in taking up energy since with increasing chain length the variety of possible vibrations increases. Hydrogen is effective at much higher energies.

Evaluation of the influence of solutes on the low field mobility has been reported by Sowada *et al.* in this symposium.

Mobility Models

Although no uniform theory exists which would describe all the dependencies mentioned in the foregoing sections some models have been proposed which take into account some of the properties and explain some of the data.

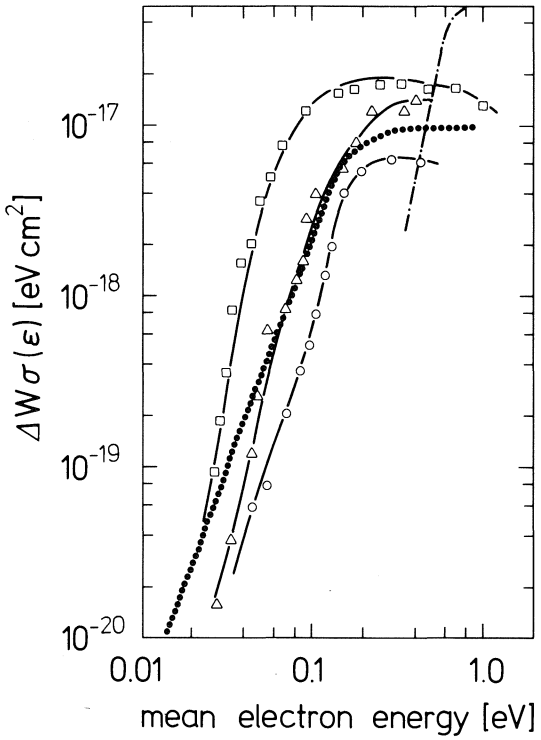

FIG. 11. Product of cross section for inelastic energy loss and loss quantum as a function of the electron mean energy: ●, methane; ○, ethane; △, propane; □, butane; ·-· hydrogen (38).

The simplest explanation for the exponential temperature dependence of the mobility is the trapping model first proposed by Minday *et al.* (42) for the electron mobility in *n*-hexane. The electrons are thought to be trapped by a molecule or a group of molecules for a time τ_t. Thermal activation would promote electrons from the traps into a conducting state with high mobility μ_{cb} where they travel for a time τ_f until retrapping occurs. The observed mobility μ_{el} is then given by

$$[8] \qquad \mu_{el} = \frac{\tau_f}{\tau_f + \tau_t}\mu_{cb} + \frac{\tau_f}{\tau_f + \tau_t}\mu_t$$

Here μ_t denotes the mobility of the trap which in liquid hydrocarbons is probably of the order of ionic mobilities. With the justifiable assumption that $\tau_f\mu_{cb} \gg \tau_t\mu_t$ then for μ_{el} one obtains

$$[9] \qquad \mu_{el} = \mu_{cb}\frac{1}{1 + \tau_t/\tau_f} \approx \mu_{cb}\frac{\tau_f}{\tau_t}$$

It is assumed that $\tau_f \ll \tau_t$ and that the residence time in the trap is temperature dependent

$$[10] \qquad \tau_t = \tau_0 \exp(E_a/k_BT)$$

which with eq. 9 leads to

$$[11] \qquad \mu_{el}(T) = \mu_{cb}(\tau_f/\tau_0) \exp(-E_a/k_BT)$$

The mobility in the extended state may also depend on temperature; however, over a limited temperature range the exponential dependence will be the dominating factor leading to a straight line in an Arrhenius plot. For the trapping model to be applicable it is required that the mean free path between trapping collisions Λ_t is greater than the relaxation length λ associated with the mobility in the extended state.

$$[12] \qquad \mu_{cb} = \frac{e_0}{m}\frac{\lambda}{v_{th}}$$

with v_{th} the thermal velocity of the electrons (e_0, m electronic charge and mass, respectively), or

$$[13] \qquad \tau_f \gg \lambda/v_{th}$$

From the measurement of the temperature dependence of the mobility alone no information on the different parameters of this model can be obtained. Application of a strong electric field leads to a voltage drop across the diameter of the trap a_t thus reducing the trapping energy. Considering classical processes only LeBlanc (43) found that the mobility should vary with field strength as

$$[14] \qquad \mu(F) = \mu_{cb} \exp\left(-\frac{(E_a - e_0a_tF)}{k_BT}\right)$$

or

$$[15] \qquad \frac{\mu(F)}{\mu(0)} = \exp\left(\frac{e_0a_tF}{k_BT}\right)$$

where $\mu(0)$ denotes the low field mobility. Sample calculations have shown that the dependence according to eq. 15 could not be fitted to the experimental data of butane with any value of a_t. Incorporation of quantum mechanical tunneling into the model might improve the situation.

While the trapping model actually requires the participation of extended states (or in the terminology of solid state physics a conduction band) the field strength and temperature dependences in low mobility hydrocarbons can also be described by the hopping model in which it is assumed that the electron moves by jumps from one localized state to another.

If Λ is the mean jump distance and ν_j the jump frequency then the diffusion coefficient is given by

[16] $$D = \Lambda^2 \nu_j$$

The low field mobility is obtained by the Nernst–Einstein relationship

[17] $$\mu(0,T) = \frac{e_0 D}{k_B T} = \frac{e_0}{k_B T} \Lambda^2 \nu_j$$

With the assumption that the transport is an activated process ν_j is

[18] $$\nu_j = \nu_0 \exp(-E_a/k_B T)$$

and the low field mobility becomes

[19] $$\mu(0,T) = \frac{e_0}{k_B T} \Lambda^2 \nu_0 \exp(-E_a/k_B T)$$

The application of an electric field leads to an increase of the mobility and Bagley (44) derived for $\mu(F,T)$

[20] $$\mu(F,T) = \mu(0,T) \frac{\sinh(e_0 \Lambda F/2k_B T)}{e_0 \Lambda F/2k_B T}$$

This equation has been used to analyze our temperature and field strength data by adjusting Λ. Temperature dependent values of Λ were obtained which are shown in Fig. 12. The other parameters of this model are given in Table 2. The temperature dependence of the jump frequency gave linear Arrhenius plots. With the parameters and $\Lambda(T)$, the temperature dependence of the mobility could also be reproduced.

A notable exception is propane, where Λ is independent of temperature and ν_0 is one order of magnitude greater. No reason for this behavior can be given at the present time. Funabashi and Rao (45) have extended the Bagley model for the case of statistically fluctuating barrier heights. Parameter fitting lead to smaller Λ values. A more detailed analysis, however, in three dimensions would be necessary. The temperature and field strength dependence of the mobility given by eq. 20 also follows from the theory of the small polaron (46–49).

An electron moving through a nonpolar liquid is surrounded by a cloud of induced polarization. In ionic crystals this can lead to self-trapping and the resulting entity is called a polaron. Polaron formation can also occur in molecular crystals and Holstein (46) has described the essential properties of this species. Depending on the temperature different modes of transport are thought to exist. At low temperatures a band-type motion is observed while at higher temperatures the polaron states are localized and the motion becomes thermally activated. The electron will jump from one site to another whenever the molecular configurations of the two sites are the same. This situation results from thermal fluctuations and its probability is proportional to $\exp(-E_a/k_B T)$. The jumps occur so rapidly that the polarization well due to molecular orientation remains behind and the electron ceases to exist as a localized polaron until it encounters the new site. The residence time in a trap Δt should be short compared to a tunneling time t_p but long compared to the jump time t_0. Estimates for these times given by Lang and Firsov (48) show that these conditions are indeed fulfilled for ethane and that the small polaron concept seems to be applicable.

Efros (49) derived a temperature and field strength dependence of the mobility as given by eq. 20. Different preexponential factors were obtained, however, for $\eta_2 < 1$ and $\eta_2 > 1$ where

[21] $$\eta_2 = J^2/\hbar w_0 (E_a k_B T)^{1/2}$$

with w_0 the vibration frequency of the molecules. The Efros equation can be written as

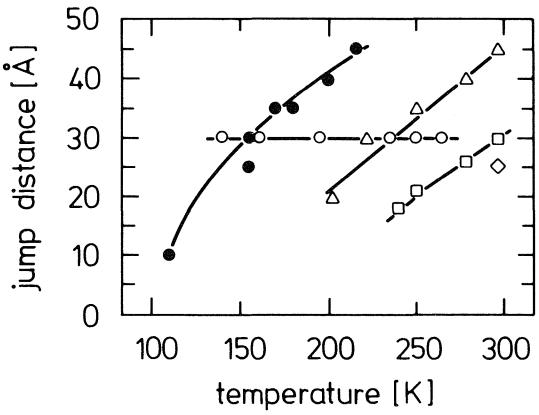

FIG. 12. Dependence of the mean jump distance (hopping model) on the temperature: ●, ethane; ○, propane; □, butane; ◇, pentane; △, cyclopentane (32, 34, 14).

TABLE 2. Parameters of the hopping model

Liquid	ν_0 (s^{-1})	E_a (eV)
Ethane	1.4×10^{13}	0.087
Propane	2×10^{14}	0.155
Butane	1.4×10^{13}	0.13
Cyclopentane	1.4×10^{13}	0.12

$$[22]\qquad \mu(T,F) = \underbrace{A(T)\Lambda^2(T)}_{f_1}\ \underbrace{\exp\left(-\frac{E_a}{k_B T}\right)}_{f_2}\ \underbrace{\frac{\sinh\left(\frac{e_0 F\Lambda}{2k_B T}\right)}{\frac{e_0 F\Lambda}{2k_B T}}}_{f_3}\ \underbrace{\exp\left(-\frac{(e_0 F\Lambda)^2}{16E_a k_B T}\right)}_{f_4}$$

At medium field strengths as applied in our experiments f_4 is negligible and the resulting $\mu(T, F)$ is the same as in the Bagley model.

The factor f_1 depends on η_2 and for $\eta_2 < 1$

$$[23]\qquad f_{11} = \frac{e_0\pi^{1/2}}{2\hbar}\frac{|J|^2}{(E_a k_B{}^3 T^3)^{1/2}}$$

while for $\eta_2 > 1$

$$[24]\qquad f_{12} = w_0 e_0/2\pi k_B T$$

If we take for $w_0 = 2\pi\nu_0$ then f_{12} coincides with the preexponential factor of eq. 19. Fitting our data for ethane and propane with f_{11} yields for the exchange integrals $J = 0.014$ eV and $J = 0.09$ eV, respectively. These values give $\eta_2 < 1$ and, furthermore, $J < E_a$ is fulfilled, the Holstein condition (46) for the small polaron model. A further test can be achieved with measurements at very high fields where f_4 becomes significant.

For liquids with high electron mobilities, notably liquid argon, the free electron theory developed by Cohen and Lekner (39, 40) can be applied. For the low field mobility they derive the Lorentz formula (52)

$$[25]\qquad \mu = \tfrac{2}{3}(2/\pi m k_B T)^{1/2} e_0\Lambda_1$$

with Λ_1 the mean free path for momentum transfer which is related to the structure of the liquid by

$$[26]\qquad \Lambda_1{}^{-1} = 4\pi\bar{a}^2 n S(0)$$

n is the number density of the liquid, $\bar{a}$ the scattering length, and $S(0)$ the structure factor for the limit of zero energy. From eq. 25 mean free paths Λ_1 obtained for the high mobility liquids mentioned in this paper are given in Table 3.

The observed field dependence of the mobility at higher field strengths is related to the way the electrons lose energy picked up from the field between subsequent collisions.

The Cohen–Lekner theory gives the critical field strength F_c at which this field dependence sets in as

$$[27]\qquad f \approx \tfrac{1}{3}(e_0 F_c\Lambda_1)(e_0 F_c\Lambda_0)/(k_B T)^2$$

Here Λ_0 is the mean free path for energy transfer and f the mean fractional energy loss per collision. Λ_0 values can be obtained from V_0 values by means of the Springett–Jortner–Cohen theory (41) and in Table 3 the ratio f/f_{el} derived for these liquids is given ($f_{el} = 2m/M$, with M the mass of an atom or molecule of the liquid). The strong influence of inelastic collisions on the mobility in the molecular liquids is apparent.

In the cases of neopentane and isooctane the applicability of the Cohen–Lekner theory may be doubtful since the necessary presumption that the de Broglie wavelength be smaller than Λ_1 is not fulfilled.

For liquid methane and tetramethylsilane the ratio f/f_{el} could also be derived from the scattering experiments in the liquefied rare gases (39) and similar ratios as given in Table 3 were obtained.

Attempts have been made to develop a general picture of the electron mobility in hydrocarbons. Schiller and co-workers (12, 52) and Dodelet *et al.* (16) extended the equilibrium model of Minday *et al.* (42) by introducing the concept of electron localization due to energy fluctuations in the liquid.

The probability of finding regions of the liquid capable of localizing electrons is given by

$$[28]\qquad P = (2\pi\Sigma^2)^{-1/2} \times \int_{\infty}^{V_0} \exp\left(-(E - E_t)^2/2\Sigma^2\right) dE$$

with E_t the energy of the localized state, V_0 the energy of the extended state, and Σ the energy fluctuation parameter. The observed mobility is then

$$[29]\qquad \mu_{el} = \mu_{cb}(1 - P)$$

Since P depends on V_0 a correlation between

TABLE 3. Critical field strength and velocity and mean fractional energy loss for high mobility liquids

Liquid	Experimental data					Cohen–Lekner theory			
	T (K)	μ (cm^2 V^{-1} s^{-1})	V_0* (eV)	F_c (V cm^{-1})	v_c (cm s^{-1})	v_{th}† (cm s^{-1})	Λ_1 (Å)	Λ_0 (Å)	f/f_{el}‡
Argon	87	400	−0.21	200	8×10^4	6.3×10^6	154	4.3	1.4
Krypton	121	1300	−0.40	80	1×10^5	7.4×10^6	595	4.0	0.4
Xenon	161	2000	−0.65	50	1×10^5	8.5×10^6	1100	3.6	0.2
Methane	111	400	−0.18	1500	6×10^5	7.1×10^6	175	2.7	5.7
Neopentane	296	65	−0.43	2×10^4	1.3×10^6	1.2×10^7	50	3.2	220
Tetramethylsilane	296	100	−0.6	2×10^4	2×10^6	1.2×10^7	72	1.8	230
2,2,4-Trimethylpentane	296	7	−0.18	9×10^4	6.3×10^5	1.2×10^7	5	4.0	862

*V_0 value from Tauchert, this symposium, and from ref. 51.
†$v_{th} = (3k_BT/m)^{1/2}$.
‡$f_{el} = 2m/M$.

μ_{el} and V_0 should exist. Some data follow the dependence while others do not (52, 54). Values for μ_{cb} between 100 and 400 cm^2 V^{-1} s^{-1} are obtained (12).

Percolation theory was invoked by Kestner and Jortner (53) and results similar to those of Schiller's were obtained. The experimental data, however, are not in general agreement with the predictions of the theory (54, 33).

Conclusion

Excess electrons in liquid hydrocarbons exhibit mobilities which range over several orders of magnitude.[1] Two limiting cases can be distinguished as seen from the dependence on the electric field strength. In liquids with a high mobility $\gtrsim$ 100 cm^2 V^{-1} s^{-1} the electrons move in an extended state and the magnitude of the mobility is determined by scattering processes. High electric field strength leads to an increase of the mean electron energy and a decrease of the mobility. In low mobility liquids $\lesssim$ 0.1 cm^2 V^{-1} s^{-1} the electrons spend most of their lifetime in localized states and the transport can be described either by a hopping process or a trap controlled band motion. High electric field strength increases changes of place thus leading to a higher mobility.

The further understanding of the electron transport process in nonpolar liquids will depend on the development and exploitation of other sources of physical information.

Acknowledgements

The author wishes to thank his colleagues Dr. Bakale, I. Kalinowski, Dr. J. G. Rabe, Dr. U. Sowada, Dr. W. Tauchert, and Prof. K. Yoshino for stimulating discussions. Financial support by Deutsche Forschungsgemeinschaft is gratefully acknowledged.

1. A. HUMMEL and W. F. SCHMIDT. Radiat. Res. Rev. **5**, 199 (1974).
2. M. RECHOWICZ. Electric power at low temperatures. Clarendon Press, Oxford. 1975.
3. J. ENGLER, W. HOFMANN, H. KEIM, B. FRIEND, W. SCHMIDT-PARZEFALL, D. WEGENER, K. WINTER, R. NICKSON, M. TYRRELL, T. WILLARD, and A. SEGAR. Nucl. Instrum. Methods, **120**, 157 (1974).
4. G. KNIES and D. NEUFFER. Nucl. Instrum. Methods, **120**, 1 (1974).
5. J. JORTNER. *In* Radiation chemistry of aqueous systems. *Edited by* G. Stein. Wiley-Interscience, New York. 1968. pp. 91–108.

[1]Many more values than given in Table 1 can be found in Allen's compilation of mobility data (55).

6. J. JORTNER. Actions Chim. Biol. Radiat. **14**, 7 (1970).
7. H. T. DAVIS and R. G. BROWN. Adv. Chem. Phys. **31**, 329 (1975).
8. P. H. TEWARI and G. R. FREEMAN. J. Chem. Phys. **49**, 4394 (1968).
9. R. M. MINDAY, L. D. SCHMIDT, and H. T. DAVIS. J. Chem. Phys. **50**, 1473 (1969).
10. W. F. SCHMIDT and A. O. ALLEN. J. Chem. Phys. **50**, 5037 (1969).
11. E. E. CONRAD and J. SILVERMAN. J. Chem. Phys. **51**, 450 (1969).
12. L. NYIKOS, E. ZADOR, and R. SCHILLER. 4th International Symposium of Radiation Chemistry, Keszthely, Hungary, June 1–6, 1976.
13. G. BAKALE and W. F. SCHMIDT. Z. Naturforsch. **28a**, 511 (1973).
14. U. SOWADA. Thesis, Free University of Berlin, Berlin, Germany. 1976.
15. A. O. ALLEN and R. A. HOLROYD. J. Phys. Chem. **78**, 796 (1974).
16. J. P. DODELET, K. SHINSAKA, and G. R. FREEMAN. Can. J. Chem. **54**, 744 (1976).
17. I. KALINOWSKI, J. G. RABE, and W. F. SCHMIDT. 1976. Tihany Conference on Radiation Chemistry.
18. G. BAKALE and W. F. SCHMIDT. Chem. Phys. Lett. **22**, 164 (1973).
19. W. F. SCHMIDT and A. O. ALLEN. J. Chem. Phys. **52**, 4788 (1970).
20. J. P. DODELET and G. R. FREEMAN. Can. J. Chem. **50**, 2667 (1972).
21. I. KALINOWSKI, J. G. RABE, and W. F. SCHMIDT. Z. Naturforsch. **30**, 568 (1975).
22. K. SHINSAKA, J. P. DODELET, and G. R. FREEMAN. Can. J. Chem. **53**, 2714 (1975).
23. R. M. MINDAY, L. D. SCHMIDT, and H. T. DAVIS. J. Phys. Chem. **76**, 442 (1972).
24. G. BAKALE. 1975. Unpublished.
25. B. S. YAKOVLEV, I. A. BORIEV, and A. A. BALAKIN. Int. J. Radiat. Phys. Chem. **6**, 23 (1974).
26. J. P. DODELET, K. SHINSAKA, and G. R. FREEMAN. J. Chem. Phys. **59**, 1293 (1973).
27. L. G. CHRISTOPHOROU. Int. J. Radiat. Phys. Chem. **7**, 205 (1975).
28. G. BAKALE, W. TAUCHERT, and W. F. SCHMIDT. J. Chem. Phys. **63**, 4470 (1975).
29. M. G. ROBINSON and G. R. FREEMAN. Can. J. Chem. **52**, 440 (1974).
30. J. M. L. ENGELS and A. J. M. VAN KIMMENADE. Chem. Phys. Lett. **42**, 250 (1976).
31. J. M. L. ENGELS and A. J. M. VAN KIMMENADE. Phys. Lett. A, **59**, 43 (1976).
32. W. F. SCHMIDT, G. BAKALE, and U. SOWADA. J. Chem. Phys. **61**, 5275 (1974).
33. J. P. DODELET, K. SHINSAKA, and G. R. FREEMAN. J. Chem. Phys. **63**, 2765 (1975).
34. U. SOWADA, G. BAKALE, and W. F. SCHMIDT. High Energy Chem. USSR, **10**, 323 (1976).
35. G. BAKALE and W. F. SCHMIDT. Chem. Phys. Lett. **22**, 164 (1973).
36. L. S. MILLER, S. HOWE, and W. E. SPEAR. Phys. Rev. **166**, 871 (1968).
37. A. A. BALAKIN and B. S. YAKOVLEV. High Energy Chem. USSR, **9**, 69 (1975).
38. K. YOSHINO, U. SOWADA, and W. F. SCHMIDT. Phys. Rev. A, **14**, 438 (1976).
39. M. H. COHEN and J. LEKNER. Phys. Rev. **158**, 305 (1967).
40. J. LEKNER. Phys. Rev. **158**, 130 (1967).
41. B. E. SPRINGETT, J. JORTNER, and M. H. COHEN. J. Chem. Phys. **48**, 2720 (1968).
42. R. M. MINDAY, L. D. SCHMIDT, and H. T. DAVIS. J. Chem. Phys. **54**, 3112 (1971).
43. O. LEBLANC. J. Chem. Phys. **30**, 1443 (1959).
44. B. G. BAGLEY. Solid State Commun. **8**, 345 (1970).
45. K. FUNABASHI and B. N. RAO. J. Chem. Phys. **64**, 1561 (1976).
46. T. HOLSTEIN. Ann. Phys. **8**, 343 (1959).
47. R. W. MUNN and W. SIEBRAND. J. Chem. Phys. **52**, 6391 (1970).
48. I. G. LANG and YU. A. FIRSOV. Sov. Phys. JETP, **16**, 1301 (1963).
49. A. L. EFROS. Sov. Phys. Solid State, **9**, 901 (1967).
50. H. A. LORENTZ. Proc. Amst. Acad. **7**, 438 (1905).
51. R. A. HOLROYD, S. TAMES, and A. KENNEDY. J. Phys. Chem. **79**, 2857 (1975).
52. R. SCHILLER, SZ. VASS, and J. MANDICS. Int. J. Radiat. Phys. Chem. **5**, 491 (1973).
53. N. R. KESTNER and J. JORTNER. J. Chem. Phys. **59**, 26 (1973).
54. W. TAUCHERT. Thesis, Free University of Berlin, Berlin, Germany. 1975.
55. A. O. ALLEN. Drift mobilities and conduction band energies. Natl. Stand. Ref. Data Ser. Natl. Bur. Stand. No. 58. 1976.

Discussion

P. K. Watson: The mechanism of hopping transport discussed by the author is described in terms of an attempt frequency and a mean hopping distance between traps. It seems likely however that in a liquid there will be a wide distribution of residence times in traps so that a model based on a single hopping frequency and a single jump distance is an oversimplification. A more appropriate model, which one might use to describe such a hopping process, is of the form described by Scher and Montroll in which the hopping transport is defined in terms of a distribution of waiting times in traps and a field-dependent asymmetry in the jump distance.

W. F. Schmidt: The Scher–Montroll model applies primarily to disordered solid material where a wide distribution of residence times exist. Electrons injected at one electrode travel into the material and get trapped in deeper traps. The current decay shows a long tail. In liquids we get out all electrons injected at almost the same time (only diffusion leads to a smearing out of the density distribution), therefore the application of a mean residence time seems to be justified.

J. Noolandi: I would like to point out that the decay time of the current for the experiments analyzed by the Scher–Montroll theory is typically of the order of milliseconds, not hours.

W. F. Schmidt: I think the important feature of these experiments is the long nonlinear decay of the current after the injection pulse as compared, for instance, to our liquid mobility work.

J. M. Warman: I don't wish to defend any particular mobility mechanism but I do think that the two-state trapping model was not given a fair chance since the effect of field

was considered only on the detrapping process. It is quite possible that the rate of the trapping process is (also?) dependent on field strength if the electron is 'heated up' by the field while residing in the quasifree state. If the trapping rate decreases with electron energy as might be suggested by your results on the attachment to SF_6 in liquid xenon then an increase in the residence time in the quasifree state will occur at high fields and hence an increase in mobility as observed for mobility liquids.

W. F. Schmidt: Your arguments are correct. Only at the present, to my knowledge, there is no theory describing the effect of field on the trapping model and I think besides the points you mentioned field assisted tunnelling out of the trap has to be included.

E. O. Forster: It appears that in discussing the various possible models for liquid hydrocarbons the liquid has been considered to be made up of individual molecules. Indeed the structure of these liquids is more complicated. How do the various models take into consideration (*a*) the clustering caused by induced dipole–dipole interactions and (*b*) the density fluctuations existing at constant temperature on the molecular level.

W. F. Schmidt: Structure of the liquid has been taken into account in the Cohen–Lekner theory of the extended excess electron state. In this conference L. Kevan has presented potential calculations for hydrocarbons with different orientations of the molecules towards the electron. It is clear that theoretical approaches have to include these effects you mention.

E. O. Forster: Have you looked at the values of E_a for viscous flow for the alkanes and alkenes you have studied? It might prove interesting to consider this parameter as a measure of structural effects.

W. F. Schmidt: There does not seem to exist a simple correlation between viscosity and any of the properties we measured. Sowada, in his thesis, has found, however, that the product of jumping distance and viscosity was constant for some liquids.

C. C. Yang: Could you elaborate the physics behind the structure influence on the electronic mobility?

W. F. Schmidt: Not really, since there is no model which could explain the difference in mobility in methane and ethane. From the high field measurements in high mobility liquids it is apparent that in the molecular liquid inelastic losses influence the mobility (see Table 3).

J.-P. Dodelet: (*a*) The activation energies you reported from the literature were often measured around room temperature. They could be very different at lower or higher temperatures as you have shown in ethane and methane. It could therefore be misleading to say that high mobility liquids are characterized by a very low energy of activation. This is true in only a small temperature range. (*b*) How do you explain the two activation energies you reported in ethane?

W. F. Schmidt: (*a*) The statements I made refer to the present status of the field, where, as you pointed out, measurements have been made only over a limited range of temperatures. Changes in activation energy or temperature dependence may indicate a change of the transport mechanism. (*b*) We actually have only one activation energy listed in Table 2. The variation of the mobility as a function of temperature is due to the temperature dependence of the jump distance derived from the Bagley model.

L. Onsager: Could Dr. M. H. Cohen tell us to what extent he looked at phonons, or time dependence of fluctuations, and similar aspects of the problem?

M. H. Cohen: With regard to interpretation of changes of activation energy with temperature, the obvious possibility is a change in mechanism. For example, at elevated temperatures the small polaron is unstable and the electron motion goes over to a diffusive mechanism similar to that I described in my talk which involves the time dependence of the fluctuations. With regard to the observed reduction in mobility caused by molecular asymmetry or by the introduction of double bonds, the obvious interpretation is that the possibility of orientational and polarization fluctuations is introduced, thereby introducing an increased tendency towards Anderson localization and increased possibilities for self-trapping. However optimistic one is about such mechanisms for interpreting the observations reported for drift velocities in complex molecules, the dramatic effect of ethane on mobilities, etc., in methane has to give one pause. There is no drastic increase in polarizability and the asymmetry of the molecule is not great, not nearly as large as in more complex liquids of higher mobilities. This raises the need of paying attention to quite specific properties of individual molecules.

G. R. Freeman: The jump from methane to ethane is enormous because methane is isotropically polarizable and ethane has an appreciable anisotropy.

L. G. Christophorou: Mobility is a gross, all-embracing quantity, *i.e.* the overall result of many processes, elastic, inelastic, capture, etc. I believe that, especially for the case of high field mobility, emphasis should be accorded to the detailed electron energy loss mechanisms, in a manner analogous to that in gases.

W. F. Schmidt: The overall picture has been established; measurements giving information on a microscopic level are necessary. First steps into this direction have been made by us in measuring the influence of molecular solutes on the electron drift velocity in liquid argon (K. Yoshino, U. Sowada, W. F. Schmidt. Phys. Rev. A, **14**, 438 (1976)).

J. Jortner: We have been talking about the role of density and orientational fluctuations of small amplitude configurational changes induced by the electron and of large configurational changes resulting in electron localization. I would like to draw attention to another effect which involves the coupling of the excess electron with a single vibrating solvent molecule. I am referring to the small polaron in the Holstein picture where the two-order picture involves the electron residing on a single molecule. Small polaron effects are exhibited in some diatomic molecular solids such as solid N_2, where the electron mobility studied by Spear is $\sim 10^{-2}$ cm^2 V^{-1} s^{-1}. Such small polaron effects may be responsible for the reduction of electron mobility upon the introduction of double bonds.

Equilibrium model for the interpretation of the conduction properties of metal–ammonia solutions

S. HAHNE, P. KREBS, AND U. SCHINDEWOLF

Institut für Physikalische Chemie und Elektrochemie, Universität Karlsruhe, Germany

Received October 19, 1976

S. HAHNE, P. KREBS, and U. SCHINDEWOLF. Can. J. Chem. **55**, 2211 (1977).

The electrical conductivity of metal–ammonia solutions can be described by an equilibrium of solvated electrons of low mobility and of free electrons of high mobility. With proper choice of the equilibrium constant and its temperature and pressure dependence and of the solvation number of the solvated species the experimental conductivities can be matched in the temperature and pressure range from 240 to 420 K and up to 1000 bar over the entire concentration range from 0.1 mol/ℓ to saturation, also fitting the extrema of the temperature and pressure coefficients of the conductivity around 1 mol/ℓ.

S. HAHNE, P. KREBS et U. SCHINDEWOLF. Can. J. Chem. **55**, 2211 (1977).

On peut décrire la conductivité électrique des solutions métal–ammoniac par un équilibre d'électrons solvatés de mobilité faible et d'électrons libres de grande mobilité. En faisant un choix approprié des constantes d'équilibres et de la dépendance sur la température et sur la pression ainsi que du nombre de solvatation des espèces solvatés, on peut trouver un bon accord avec les conductivités expérimentales à des températures et des pressions allant de 240 à 420 K et jusqu'à 1000 bar à toutes les concentrations allant de 0.1 mol/ℓ jusqu'à la saturation, et qui s'accordent aussi aux extrêmes des coefficients de température et de pression de la conductivité autour de 1 mol/ℓ.

[Traduit par le journal]

Recently we (1) presented experimental data about the electrical conductivity of metal–ammonia solutions (MAS) in the temperature and pressure range from 240 to 420 K and 200 to 1000 bar, respectively. As shown in Fig. 1, in which the equivalent conductance Λ at constant pressure ($\Lambda = \sigma/c$ (Ω^{-1} cm^2 mol^{-1}); σ specific conductivity (Ω^{-1} cm^{-1}), c molar concentration (mol/cm^3)) is plotted *vs.* molar concentration with temperature as parameter, the steep increase of the conductivity is shifted to smaller concentrations with increasing temperature; pressure increase on the other hand leads to a shift to higher concentrations.

No matter what the conduction mechanism in these solutions is and how the nonmetal–metal transition (NMT) is defined the data suggest that this transition is favoured by temperature increase and opposed by pressure increase.

For the interpretation of the NMT in MAS two contrasting theories were presented by Cohen and Jortner (2) and Mott (3), respectively, based on the percolation model and on the concept of the Anderson transition. Although the authors gave a series of arguments to support their concepts it seemed that no general agreement is obtained on the nature of the NMT and the conduction mechanism in moderate to high concentrated solutions. Only for the dilute range ($c < 0.05$ mol/ℓ or 0.1 mol% metal (mpm)) in which the equivalent conductance varies only slightly with concentration (Λ = 500–1000 Ω^{-1} cm^2 mol^{-1} at 240 K) is it not doubted that the electrical current is carried by individual moving solvated electrons and metal cations (4).

In the intermediate range (0.5–2 mol/ℓ or 1–4 mpm, depending on temperature) with the beginning steep conduction increase and the still unexplained maxima of the positive temperature coefficient (5) and the negative pressure coefficient (6) of the conductivity (see also Fig. 3), semiconduction is assumed. This is supported by the peculiar temperature dependence of the thermopower (7, 8) (see also Fig. 4) which in the intermediate range decreases with temperature as is to be expected for activated transport (3), whereas in lower and higher concentrated MAS it increases with temperature.

Besides a more or less quantitative description of the conduction behaviour of the MAS at normal temperature and pressure, no explanation was given or could be given on the basis of the percolation model or the Anderson concept for the observed shifts of the NMT with temperature and pressure.

Two experimental observations prompted us

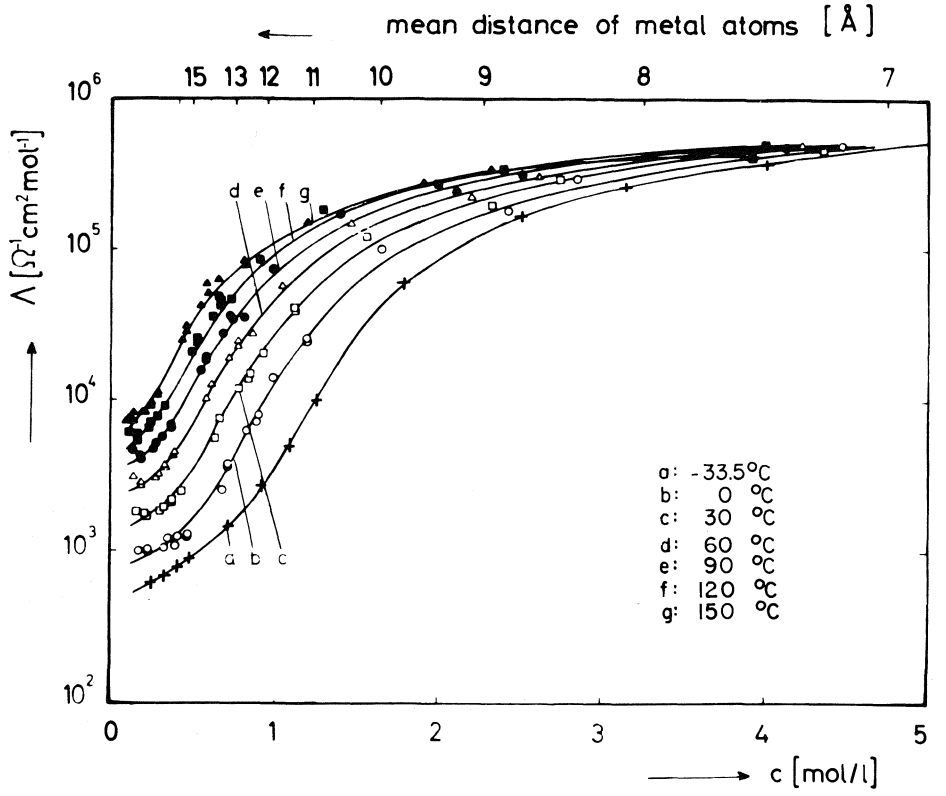

FIG. 1. Equivalent conduction Λ of sodium–ammonia solutions in the temperature and pressure range between 240 and 423 K at 200 bar. (Reprinted with permission from the Journal of Physical Chemistry, **79**, 2922 (1975). Copyright by the American Chemical Society.)

to propose an equilibrium model for the interpretation of the conduction behaviour of MAS, assuming a proper chemical equilibrium between solvated electrolytelike electrons e_s^- of low mobility and unsolvated free electrons e_f^- of high mobility. These observations are: (*1*) electrons photoinjected from a cathode into liquid ammonia exist in two different states, which exhibit low and high mobility (0.03 and 2000 $cm^2\ V^{-1}\ s^{-1}$) (9) and which might be characterized as solvated and free electrons, and (*2*) the absorption spectrum of solvated electrons persists still in higher concentrated solutions, *i.e.* that solvated electrons are present in solutions of metallic character (10). The assumed chemical equilibrium is written in the form

$$[1] \qquad e_s^-(iNH_3) \rightleftarrows e_f^- + iNH_3$$

with i the solvation number of the solvated electrons. The solvated metal cations $M^+(kNH_3)$ with solvation number k cancel in the equilibrium. The equilibrium constant is

$$[2] \qquad K = \frac{[e_f^-][NH_3]^i}{[e_s^-(iNH_3)]}$$

(squared brackets stand for concentration). The charge and material balance are

$$[3] \quad [e_s^-(iNH_3)] + [e_f^-] = [M^+(kNH_3)] = c_M$$

$$[4] \quad i[e_s^-(iNH_3)] + k[M^+(kNH_3)] + [NH_3] = c_A$$

c_M, the overall concentration of dissolved metal, is equal to the concentration of the solvated metal cations, providing complete dissociation; $[NH_3]$ is the concentration of unbound free ammonia, c_A its overall concentration. The combination of [2], [3], and [4] leads to a polynomial of i + 1st degree from which the concentration of solvated electron or free electrons can be obtained as a function of the concentration of dissolved metal.

The specific conductance of the MAS is given by the sum of the conduction of solvated and free

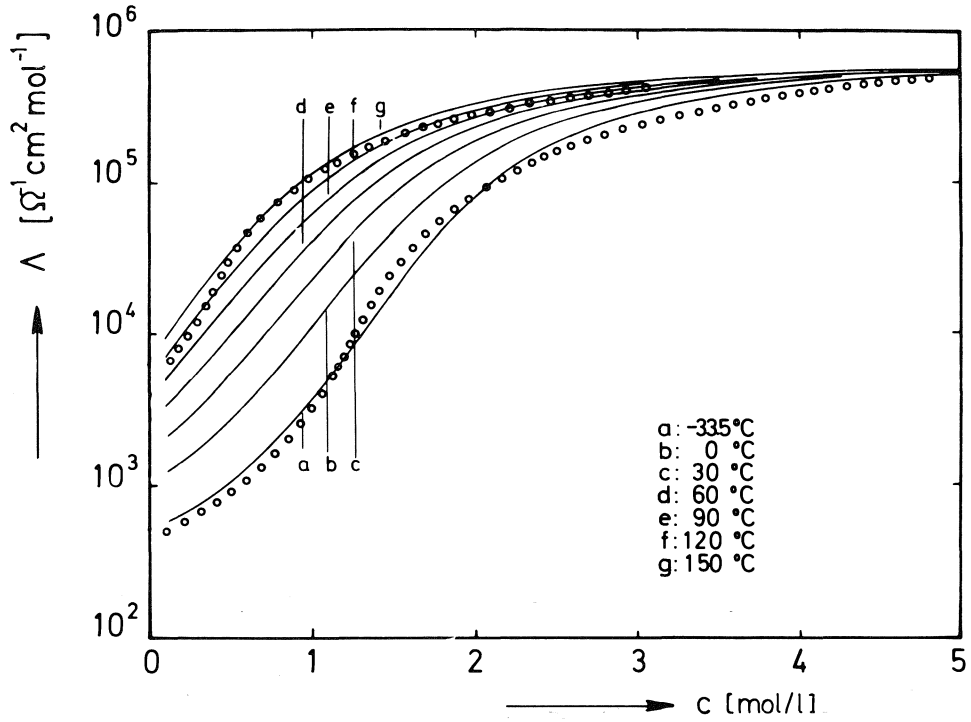

FIG. 2. Simulation of the equivalent conduction of metal–ammonia solutions in the temperature range from 240 to 423 K on the basis of the equilibrium model (experimental data at 240 and 423 K also shown).

electrons and of metal cations

$$\sigma = \sigma_s + \sigma_f + \sigma_{M^+} \quad [5]$$

The contribution of each species is taken as the product of its concentration and its concentration independent mobility (equivalent conduction)

$$\sigma_i = c_i \Lambda_i \quad [6]$$

The molar conduction of the solution follows from

$$\Lambda = \sigma / c_M = \sum c_i \Lambda_i / c_M \quad [7]$$

For evaluation of this concept, mobilities of solvated electrons and cations and of free electrons were taken from experimental conductivity data of very dilute MAS in which all electrons are solvated (electrolytic behaviour) and of saturated MAS, respectively, in which all electrons are assumed to be free (truly metallic solutions): $\Lambda_s + \Lambda_{M^+} \approx 500$, $\Lambda_f = 6 \times 10^5$ Ω^{-1} cm^2 mol^{-1} at 240 K and 200 bar (see lowest curve of Fig. 1). The solvation number of metal cations is taken as $k = 6$ on the basis that the solubility limit of sodium or potassium in ammonia is around 15 mol% metal (roughly 6 mol ammonia per mol of metal). After trial and error a rather good fit of experimental conduction data for 240 K and 200 bar in the concentration range from 0.1 mol/ℓ to saturation could be obtained by setting the solvation number of the solvated electrons $i = 6$ and the equilibrium constant $K = 2.5 \times 10^6$ (mol/ℓ as concentration units).

With the introduction of the normal temperature dependence of the equilibrium constant and of the mobility of the solvated electrons and metal cations

$$K = K_0 \exp\{-\Delta H/RT\}$$
$$\Lambda_s = \Lambda_{s0} \exp\{-E_a/RT\} \quad [8]$$

conductivity data at higher temperatures also could be matched (ΔH molar enthalpy difference between the free state and the solvated state of the electrons; E_a energy of activation of the mobility of the solvated particles; the mobility of the free electrons is in agreement with Fig. 1 taken independent of temperature). Figure 2 shows the results in which in addition

to the other constants given above ΔH was set at 5 kcal/mol and E_a to 2.8 kcal/mol, the latter taken from the literature (5). For comparison the experimental data for 240 and 423 K are also shown.

From Fig. 2, or from its comparison with Fig. 1, it is seen that the numerical evaluation of the proposed model gives a rather good approximation of the trend of the experimental conduction data which vary over three powers of 10 from low concentrated to saturated solutions in the wide temperature range covered by experiments.

Pressure dependences of the conductivity also can be evaluated by introducing the normal pressure dependence of the equilibrium constant and of the mobility

$$\frac{\mathrm{d} \ln K}{\mathrm{d}p} = -\frac{\Delta V}{RT}$$

$$\frac{\mathrm{d} \ln \sigma}{\mathrm{d}p} = -\frac{\Delta V^{\neq}}{RT}$$

(ΔV molar volume difference of the electrons in the free and solvated state, $\Delta V^{\neq}$ activation volume of the mobility of the solvated species). A good fit of the experimental data between 1 and 1000 bar in the temperature range up to 420 K is obtained with $\Delta V^{\neq} \simeq 2$ ml/mol, as taken from literature (6), and $\Delta V = 10$ ml/mol together with the other constants given above (the mobility of the free electrons is taken pressure independent).

In Fig. 3 we plot the calculated temperature and pressure coefficients $(\mathrm{d} \ln \sigma/\mathrm{d}T)_p$ and $(\mathrm{d} \ln \sigma/\mathrm{d}p)_T$ of the conductivity of MAS *vs.* concentration. Also these curves with the maxima of $(\mathrm{d} \ln \sigma/\mathrm{d}T)_p$ and the minimum of $(\mathrm{d} \ln \sigma/\mathrm{d}p)_T$ in the concentration range around 1 mol/ℓ or 2 mpm are in fair agreement with experimental data (dotted lines).

It should be stressed that the treatment given above is only an interpolation of the conduction behaviour of MAS between the two extrema, the electrolytic and the metallic state; only four parameters were chosen arbitrarily, *i.e.* the equilibrium constant K, its temperature and pressure dependence expressed by the reaction enthalpy ΔH and the reaction volume ΔV, and the solvation number i of the solvated electrons, to get a fit of the experimental data in a wide concentration, temperature and pressure range. The other necessary constants *i.e.*, the mobility

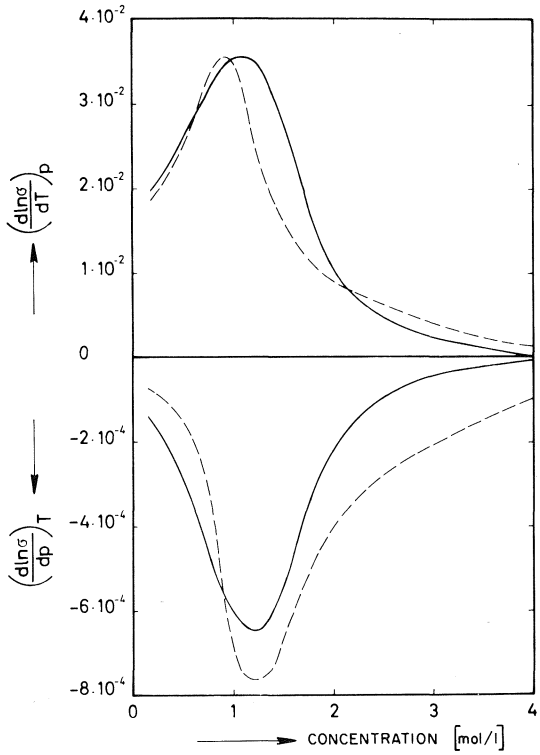

FIG. 3. Simulation of the temperature coefficient and the pressure coefficient of the conductivity of metal–ammonia solutions (240 K) on the basis of the equilibrium model (dotted lines experimental data).

and its temperature and pressure dependence of the solvated species and of the free electrons were taken from experimental data. For the choice of the solvation number of the cations a good argument was given.

Also, the arbitrarily chosen parameters are not unreasonable. The solvation number of solvated electrons $i = 6$ is also used by the theoreticians (11) to obtain a good fit between calculated and observed absorption spectra of solvated electrons in ammonia. The equilibrium constant $K = 2.5 \times 10^6$ at 240 K leads to a change of free energy of $\Delta G = -7$ kcal/mol and in combination with $\Delta H = 5$ kcal/mol to a change of entropy of 40 cal mol^{-1} K^{-1} associated with the transition from the nonmetallic to the metallic state. This entropy increase would not be surprising when a bound electron is converted into a free electron, releasing six ammonia molecules from its solvation shell. The positive ΔV also is not unrealistic, since an increase in the apparent molar volume of dissolved sodium in ammonia in the concentration range

of the NMT was found by density determinations (12) although this increase is not as large as that used here.

Of course one argument against the evaluation of the proposed model is that solutions were treated as ideal, not considering any interactions between particles which might be considerable but which presently are hard to estimate because as Mott (3) states "too many effects have a role for a quantitative theory to be possible". It has been the only aim of this paper to show that the rather simple concept of a chemical equilibrium, which might be more appealing to a chemist than the other theories, can describe the conduction phenomenon of MAS over a wide range of experimental conditions with a minimum number of parameters. Also the general trend of experimental data on thermopower (7, 8) and of the Hall coefficient (13) can be matched with this model.

The treatment given here is analoguous to that of Lelieur *et al.* (14) who also assume two different electronic states of different but strongly concentration dependent mobilities whereas we assumed the two states to have concentration independent mobilities. It also is analoguous to that of Arnold and Patterson (15) who, however, assume in addition for the intermediate concentration range electron jumping from F-centres (solvated electrons) to metal cations.

1. S. HAHNE and U. SCHINDEWOLF. J. Phys. Chem. **79**, 2922 (1975).
2. M. H. COHEN and J. JORTNER. J. Phys. Chem. **79**, 2900 (1975).
3. N. F. MOTT. J. Phys. Chem. **79**, 2915 (1975).
4. R. R. DEWALD and J. H. ROBERTS. J. Phys. Chem. **72**, 4224 (1968).
5. C. A. KRAUS. J. Am. Chem. Soc. **43**, 758 (1921); C. A. KRAUS and W. W. LUCASSE. J. Am. Chem. Soc. **44**, 1946 (1922).
6. U. SCHINDEWOLF, K. W. BÖDDEKER, and R. VOGELSGESANG. Ber. Bunsenges. Phys. Chem. **70**, 1161 (1966).
7. P. DAMAY, P. CHIEUX, and G. LEPOUTRE. Ber. Bunsenges. Phys. Chem. **75**, 642 (1971).
8. S. HAHNE, P. KREBS, and U. SCHINDEWOLF. Ber. Bunsenges. Phys. Chem. **80**, 804 (1976).
9. K. G. BREITSCHWERDT and H. RADSCHEIT. Can. J. Chem. This issue.
10. R. B. SAMOANS and J. C. THOMPSON. Phys. Rev. A, **1**, 376 (1970).
11. N. R. KESTNER and J. JORTNER. J. Phys. Chem. **77**, 1040 (1973).
12. C. A. KRAUS, E. S. CARNEY, and W. C. JOHNSON. J. Am. Chem. Soc. **49**, 2206 (1927); E. HUSTER. Ann. Phys. **33**, 477 (1938).
13. R. D. NASHBY and J. C. THOMPSON. J. Chem. Phys. **49**, 969 (1970).
14. J. P. LELIEUR, G. LEPOUTRE, and J. C. THOMPSON. Philos. Mag. **26**, 1205 (1972).
15. E. ARNOLD and A. PATTERSON. J. Chem. Phys. **41**, 3089 (1964); **41**, 3098 (1964).

Appendix: Pressure Dependence of Thermopower

In the preceding section we mentioned older data on MAS, according to which in the concentration range of the steep conduction change, temperature and pressure have an adverse, abnormally large effect on the conductivity. Also it was shown that the thermopower behaves abnormally: in the middle concentration range it decreases with temperature, whereas in the more dilute or more concentrated solutions it increases. We succeeded also in determining the effect of pressure on the thermopower with the following arrangement.

The solution was kept in a U-tube, the two sides of which were connected by a capillary to avoid thermal convection. Both sides of the tube could be heated separately by surrounding heating coils. Two identical thermocouples, each sealed without electrical contact in a thin steel mantel, were immersed in the solutions of the two sides of the U. The thermocouples were connected to the x-axis of an x,y-plotter to record the temperature differences of both solution sides. The steel mantels form together with the solution the thermocouple $(\text{steel/MAS})_{T_1}/(\text{MAS/steel})_{T_2}$, the voltage of which after suitable amplification was fed to the y-axis of the plotter. The absolute thermopower of the steel mantels, as measured against mercury was small enough ($<2\ \mu V/K$) to be neglected.

The assembly was housed in a thermostated autoclave (200–240 K) which was pressurised up to 800 bar with purified nitrogen. All electrical connections were passed in proper leads through the autoclave. For the measurements one side of the U was heated slowly by about 3 deg, and then allowed to cool again; then the other side was heated and cooled. This procedure required a period of 10 min. The plotter directly recorded the voltage of the MAS–steel thermocouple *vs.* the temperature differences of the solutions; the slope of the plot directly gives the thermopower of the solutions. Concentrations of the solutions were obtained by the usual analytical procedures and checked before and after an experiment by conductivity measurements directly in the cell

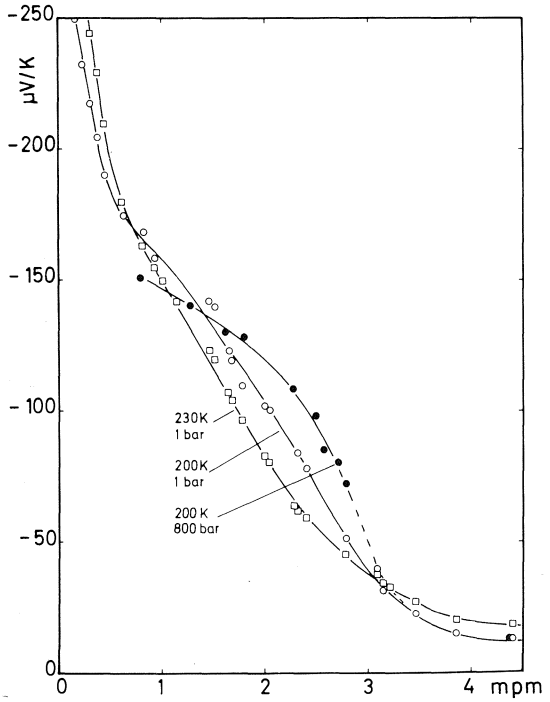

FIG. 4. Thermopower of potassium–ammonia solutions at 200 and 230 K, 1 bar, and 200 K and 800 bar, respectively.

with the two steel mantels as electrodes. The results are given in Fig. 4: the thermopower of the solutions is plotted *vs.* concentration for 1 bar and 800 bar at 200 K and 1 bar at 230 K.

In the intermediate concentration range pressure increases the thermopower very significantly whereas in the more dilute and concentrated ranges the pressure effect is small. It follows that in the intermediate range temperature and pressure also have an adverse effect on the thermopower as shown earlier for the conductivity.

Discussion

M. H. Cohen: All three models will have similar pressure and temperature behavior since all three involve mixtures of two kinds of configurations differing in free energy. All three models then would show temperature variations characterized by an activation energy and pressure variations characterized by an activation volume in roughly the same way. The main difficulty in this problem is that more than one thing is happening. In the theory of Jortner and myself, the metal–nonmetal transition starts at 2.3 mpm. The properties of the nonmetallic state, however, are strongly concentration dependent in the range 1–2.3 mpm, as evidenced by the conductivity, which is electronic and not ionic, and by your thermopower measurements, particularly with regard to the pressure dependence.

Finally, Ichikawa's interpretation of his concentration fluctuation data, reported yesterday, supports the hypothesis of Jortner and myself of bimodally distributed concentration fluctuations. Thus, it seems clear that one can construct a multiplicity of internally consistent models, all of which can be made to fit the data by adroit choice of parameters. What is needed is more microscopic structural data.

U. Schindewolf: I am aware that we can construct any number of models to describe this or another property of metal–ammonia solutions. As long as these models do not neglect the fundamentals of physics, each of them might have some truth in it, even if it considers the phenomena from a different and perhaps, as ours, unconventional point of view.

L. Onsager: Some parts of this I don't like. As long as the carriers interact by Coulomb forces the mobilities must vary with the concentration even when only one kind of electron is present This interaction together with some neutral atom formation and some dimerization of the trapped electrons might well account for the variation of the mobilities at concentrations well below that of the mobility minimum at about 0.03 mol/ℓ. Beyond that, through the concentration where the temperature coefficient peaks, the variation of mobility with concentration and temperature invites interpretation in terms of tunnelling between singly and doubly occupied cavities. More than a very small contribution from very mobile 'unsolvated' electrons at low concentrations can be ruled out on the grounds that their entropy must be large and yet they constitute only a small fraction of the total electron population, from which we must infer a large energy of liberation and a large temperature coefficient for the size of the free population. However, at low concentrations the temperature coefficient of conducitivity hardly differs from that of the fluidity, which now imposes a rather low ceiling on the proportion of the 'free' electrons.

U. Schindewolf: No effort was made to cover the range below 0.1 mol/ℓ where neutral atom formation or dimerization of electrons seems to occur. In this range the equivalent conductivity changes by a factor of two at the most, whereas here we deal with changes of three powers of 10. Of course tunnelling might be assumed as well as hopping and might, as Mott has shown, also explain the observed pressure changes of conductivity on the basis that the cavity has to increase in size when an electron tunnels or hops into it.

The fact that at low concentrations the T and P coefficients of conductivity correspond to that of fluidity of the solvent, implies that the concentration of very mobile unsolvated electrons is low in spite of their large entropy. The postulated equilibrium 'solvated–unsolvated electrons' is at low metal concentration far on the left side, because of the high concentration of the solvating ammonia. According to the model, the contribution of the unsolvated electrons to conductivity becomes important above 1 mol/ℓ only.

High field transport of excess electrons and holes in amorphous SiO_2 (Extended Abstract)[1]

R. C. HUGHES
Sandia Laboratories, Albuquerque, NM, U.S.A. 87115
Received November 22, 1976

High mobility, quasi-free electrons have been found to exist in very pure amorphous SiO_2 (1). Unlike hydrocarbon and inert gas liquids, and glasses, there is considerable ionic character in the bonding of SiO_2 glass. Consequently polar optical mode scattering of the electron controls the mobility, rather than acoustic mode scattering or interaction with other internal modes of the molecules. The mobility is found to be 21 ± 2 cm^2 V^{-1} s^{-1} at 300 K, which is in good agreement with the calculated value (no adjustable parameters) from theories of scattering from the known longitudinal optical (LO) modes in SiO_2. Above 300 K the mobility decreases with increasing temperature as predicted by theory. However, at lower temperatures the mobility becomes almost constant at about 40 cm^2 V^{-1} s^{-1}, which may be a consequence of the disorder in the glass; the mobility is not thermally activated at any temperature studied. At applied fields above 5×10^5 V/cm, the electrons become heated and the drift velocity *vs.* field curve indicates that the primary energy loss mechanism at high electron velocities (highest observed was 1.1×10^7 cm/s) is emission of optical phonons (2). In thin SiO_2 films, stable drift velocities for applied fields of 5×10^6 V/cm have been observed (*i.e.*, electron energy losses to the lattice are 0.05 eV/A) which explains the abnormally high attenuation of electrons passing through thin oxide films. The yield of electron–hole pairs in amorphous SiO_2 for excitation by high energy X-rays as a function of the applied field has also been measured. The short electron lifetime (longest observed was 15 ns) has prevented acquisition of accurate low field yield data which is normally used in testing for phenomena like geminate recombination. However, at the high fields which can be tolerated by SiO_2, the fairly strong field dependence of the yield can be fit approximately by the Onsager geminate recombination theory extended to high fields.

It is now known that the positive counterpart to the excess electron produced by ionization moves as a hole rather than an ion. The best picture that we can construct of the hole and its transport is that it is localized in the oxygen nonbonding $2p$ orbital (*i.e.*, a missing electron in that orbital) and that it hops as a small polaron to one of the six nearest neighbor oxygen $2p$ orbitals (2.6 Å away). It is known from bonding considerations that the nonbonding orbitals have a relatively small overlap with each other, and the band structure calculations which have been done for SiO_2 emphasize this fact by showing that the top of the valence band consists of a 'narrow' band formed mostly from the $2p$ nonbonding orbitals. The band structure calculation alone cannot tell us whether a small polaron forms or what is the origin of the temperature dependence of the mobility. The formation of a small polaron means that the localized hole distorts the equilibrium positions of nearby nuclei in such a way to lower its energy (the polaron binding energy). The main evidence that the hole is a small polaron comes from: (*1*) The fact that the mobility is less than about 1 cm^2 V^{-1} s^{-1} and (*2*) the mobility above 200 K is thermally activated by 0.16 eV, which is a reasonable magnitude for a polaron binding energy. A very strong piece of evidence is the non-Arrhenius temperature behavior, in which a break to lower activation energy is seen at about 200 K; the temperature dependence of the mobility is given by the solid line in Fig. 1. Emin (3) predicted recently that the small polaron should exhibit such behavior at about 1/3 the Debye temperature, which is close to 200 K for SiO_2. (*3*) The field dependence of the mobility was also predicted by Emin (3) for the small polaron at very high fields and for the parameters appropriate to SiO_2, no field dependence is expected up to 6×10^6 V/cm, and this is observed experimentally.

[1]Work supported by U.S. Energy Research and Development Administration.

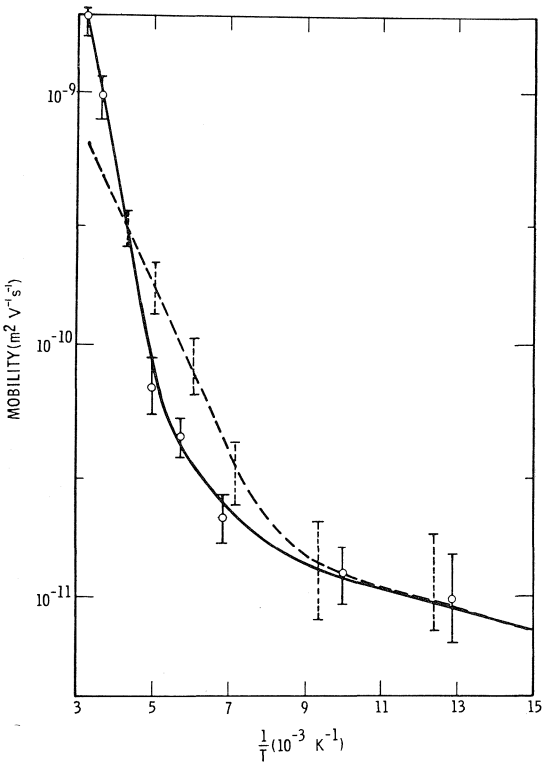

FIG. 1. The temperature dependence of the measured intrinsic hole mobility compared with a mobility calculated from the measured hopping rate of holes between nearest neighbor oxygens in the 'A' color center in quartz.

Another line of evidence concerning the hole transport in SiO_2 comes from detailed knowledge about the 'A' color center in single crystal SiO_2 (quartz). This optically active center is now known to be a hole trapped at an Al^{3+} substitutional (of which there are always a few ppm in quartz). The AlO_4 tetrahedron has the same electronic structure as the ordinary SiO_4 tetrahedron, with the only major difference being that it is negatively charged. Electron paramagnetic resonance studies (4) of the unpaired spin shows that it is localized in the oxygen $2p$ nonbonding orbital and that even at below 200 K the hole is hopping from one oxygen to the next in its own tetrahedron. The Coulomb attraction of the site prevents the hole from hopping to any of the other three nearest neighbor oxygens which are bonded to an Si^{4+}. The rate of hole hopping has been measured directly by dielectric relaxation techniques (4) and the dashed line in Fig. 1 gives the hopping rate with no adjustable parameters converted to a mobility (if v is the hopping rate and a is the hop distance the mobility of a simple random walker is $\mu = va^2/6kT\ m^2\ V^{-1}\ s^{-1}$). The agreement is very good, including the break in activation energy, which leads one to conclude that the hopping mechanism is the same for intrinsic hole transport in pure SiO_2 and the hole hopping within the color center.

In all samples of amorphous SiO_2 which have been studied, the defect concentration is very high, and the holes are trapped at defects after about 100 ns of hopping by the mechanism described above. However, the holes are not completely immobilized by the defects at room temperature and the drift of the holes from defect to defect in high applied fields has been measured (5). Because of the wide range of trapping and detrapping times, the transport of the holes becomes very dispersive, *i.e.*, some holes traverse the sample in times that are orders of magnitude shorter than others. The dispersive transport has been found to agree with the model of Scher and Montoll (6) so that the photocurrent *vs.* time data at any field, sample thickness, and temperature can be predicted from the two experimentally determined parameters of the model.

1. R. C. HUGHES. Radiat. Eff. **26**, 225 (1975).
2. R. C. HUGHES. Phys. Rev. Lett. **35**, 449 (1975).
3. D. EMIN. Adv. Phys. **24**, 307 (1975).
4. J. A. WEIL. Radiat. Eff. **26**, 267 (1975).
5. R. C. HUGHES. Phys. Rev. In press.
6. H. SCHER and E. W. MONTROLL. Phys. Rev. B, **12**, 2455 (1975).

Discussion

J. Noolandi: How do your experiments on the hole transport agree with the predictions of the stochastic hopping model of Scher and Montroll?

R. C. Hughes: We get good agreement with the Scher–Montroll theory for times long compared with the trapping time of the holes, which is about 100 ns at 300 K. The details will appear soon in Physical Review B.

P. K. Watson: Has the author observed electron trapping in his samples, and if so, what is the order of density of the traps, and can the electron be readily detrapped?

R. C. Hughes: The concentration of electron traps in pure amorphous SiO_2 varies with the method of preparation, but for good samples is about 10^{12}–10^{13} cm^{-3}. The electrons can be photodetrapped with visible light at longer wavelengths than those required for photoemission from the metal electrodes.

W. F. Schmidt: In your drift velocity measurements at higher fields, do the electrons have superthermal energies?

R. C. Hughes: At fields above 5×10^5 V/cm, the electrons are heated by the field so that optical phonons of energy 0.15 eV are emitted. Thus the average kinetic energy of the electrons approaches 0.15 eV as the field approaches 10^7 V/cm.

L. G. Christophorou: The SO_2 molecule has an electron affinity of ~1.1 eV and captures low-energy electrons to form SO_2^-. In SO_2^- the electron is binding with respect to the two oxygen atoms. Is it possible that this happens in your (amorphous) SiO_2?

R. C. Hughes: SiO_2 does not form a molecular solid like CO_2, but is polymerized in three dimensions with each O bonded to two Si. I know of no evidence for negative ion states of the polymer, and the mean free path of quasi-free electrons can be understood quantitatively by scattering from LO phonons; no additional scattering is needed to understand the mobility. However, the nature of electron traps in pure SiO_2 is not known, and may involve lattice bonding defects, like trivalent silicon, which have strong electron affinities.

Negative ion – molecule reactions in liquid argon following electron capture by N_2O

GEORGE BAKALE

Case Western Reserve University, Division of Radiation Biology, Department of Radiology, Cleveland, OH, U.S.A. 44106

AND

ULRICH SOWADA AND WERNER F. SCHMIDT

Hahn-Meitner Institut für Kernforschung Berlin Gmbh, Bereich Strahlenchemie, 1 Berlin 39, Germany

Received September 28, 1976

GEORGE BAKALE, ULRICH SOWADA, and WERNER F. SCHMIDT. Can. J. Chem. **55**, 2220 (1977).

Electrons produced in liquid argon by a short burst of X rays react readily with dissolved N_2O with a bimolecular rate constant of 5.8×10^{-10} cm^3/s or 3.5×10^{11} M^{-1} s^{-1}. The addition of H_2 or CO to the Ar/N_2O solution results in a fast and slower component in the decay of the electron current. We assume that O^- ions are formed in the reaction of electrons with N_2O and then react with H_2 to give

[11] $$O^- + H_2 \rightarrow H_2O + e^-$$

or with CO to give

[12] $$O^- + CO \rightarrow CO_2 + e^-$$

The addition of CH_4 does not regenerate electrons since the reaction

[13] $$O^- + CH_4 \rightarrow CH_3 + OH^-$$

is thought to occur. Reaction 12 is in agreement with the fact that CO_2 does not react with electrons in liquid argon.

GEORGE BAKALE, ULRICH SOWADA et WERNER F. SCHMIDT. Can. J. Chem. **55**, 2220 (1977).

Les électrons produits dans l'argon liquide par une courte émission de rayons-X réagissent facilement avec du N_2O dissout avec une constante de vitesse bimoléculaire de 5.8×10^{-10} cm^3/s ou 3.5×10^{11} M^{-1} s^{-1}. L'addition de H_2 ou de CO à la solution de Ar/N_2O conduit à des composantes rapides et plus lentes pour la décroissance du courant électrique. On fait l'hypothèse qu'il y a formation d'ions O^- lors de la réaction des électrons avec N_2O et qu'ils réagissent avec H_2 suivant l'équation

[11] $$O^- + H_2 \rightarrow H_2O + e^-$$

ou avec CO suivant l'équation

[12] $$O^- + CO \rightarrow CO_2 + e^-$$

L'addition de CH_4 ne regénère pas d'électrons puisque l'on croit que la réaction [13] se produit

[13] $$O^- + CH_4 \rightarrow CH_3 + OH^-$$

La réaction [12] est en accord avec le fait que le CO_2 ne réagit pas avec les électrons de l'argon liquide.

[Traduit par le journal]

Introduction

The growth of interest in excess electrons in nonpolar liquids during the last 8 years is best exemplified by the number of papers on this subject presented at this conference. Within this field of electrons in liquids, techniques have developed from simply measuring the mobilities of electrons (2–4) to measuring field effects on the electron drift velocity (5–7), electron recombination and attachment rates (8–13), and the energy dependence of electron attachment processes (1, 14). In this paper we add to this list of techniques of studying electron-related phenomena in liquids by reporting the first measurements of the rates of associative detachment reactions in nonpolar liquids.

An associative detachment reaction is a special form of an ion–molecule reaction which is characterized by the liberation of an electron from an anion A^- following collisional com-

bination with a molecule M; *i.e.*

[1] $$A^- + M \rightarrow AM + e^-$$

Such reactions are important to the chemistry of the upper atmosphere and have been intensively studied in the gas phase (15). Since most of these studies have been carried out with drift tube, ion cyclotron resonance, or flowing afterglow techniques at pressure below 1 torr, extrapolation of their results to liquid densities is highly questionable and the occurrence of associative detachment in liquid systems remained to be established. However, Warman *et al.* (16) used a microwave conductivity technique to study associative detachment reactions of O^- which was radiolytically generated by dissociative electron attachment to N_2O at pressures up to 260 torr. We employed a similar technique in this study to generate O^- in liquid argon and report upon associative detachment reactions in this liquid of O^- with H_2 and CO and the apparent abstraction of H by O^- from CH_4.

Experimental

The pulsed conductivity technique, in which a pulse of ~12 MeV bremsstrahlung from a linear accelerator irradiates the sample under study in a parallel-plate ion chamber and produces free electrons and positive ions in the solution, has been described previously (5). Oscillographically monitoring the dc current induced by the electrons drifting between the electrodes under the influence of an applied field provides a measure of the electron concentration and the decay of this current permits the evaluation of the electron velocity, attachment rate, and/or recombination rate (1).

Purification of Ar, N_2O, H_2, CO, and CH_4 has been described elsewhere (14, 17). Solutions were prepared by first admitting N_2O to a measured pressure P_1 into a cell of known volume and then adding the second solute (H_2, CO, or CH_4) at a pressure $P_2 \gg P_1$ to prevent escape of N_2O from the cell. The total solute pressure was then measured, the cell was cooled to 77 K, and argon was admitted to and condensed in the cell with the external argon pressure maintained at 800–1100 torr. The condensation at 77 K was continued until the cell was about half filled with the solution and the cell was then warmed to 87 K (liquid argon bath) until filled to a calibrated volume. All rate constant measurements were made at 87 K and with a sufficiently low external electric field to minimize heating of the electrons by the field.

Thermal energy electron attachment to N_2O in liquid argon had been found to occur with an overall rate constant of 5.8×10^{-10} cm^3 s^{-1} at 87 K (1). A typical oscillogram from which this rate constant was derived is shown in Fig. 1*A* for an N_2O concentration of 14 μM. Addition of H_2 to a similar N_2O/Ar solution results in the two-component decay illustrated in Fig. 1*B* in which H_2/N_2O is ~11. Similar two-component electron decays were observed when excess CO was substituted for H_2.

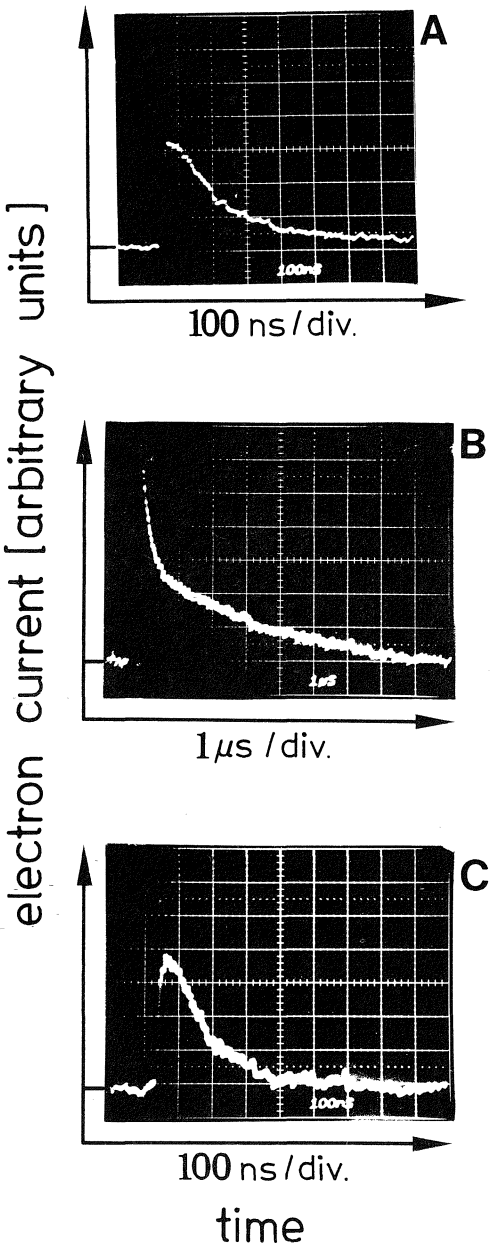

FIG. 1. (*A*) Decay of electron current due to electron attachment to N_2O in liquid argon at 87 K with $[N_2O]$ = 14 μM. (*B*) Decay of electron current due to electron attachment to N_2O (fast component, $t_{1/2} < 0.5$ μs) and electron detachment due to associative detachment of O^- with H_2 (slow component, $t_{1/2} > 2$ μs) in liquid argon at 87 K, $[N_2O]$ = 13.4 μM, $[H_2]$ = 0.15 mM. (*C*) Decay of electron current due to electron attachment to N_2O in liquid argon/methane solution at 87 K, $[N_2O]$ = 13.5 μM, $[CH_4]$ = 9.6 mol%.

With the addition of CH_4 to the N_2O/Ar solution, oscillograms typified by Fig. 1*C* were observed.

Before discussing analysis of the two-component electron decay curves to obtain detachment rate constants, we must first discuss the attachment/detachment mechanism in the next section.

Results and Discussion

Electron attachment to N_2O in the gas phase has recently been reviewed by Caledonia (18) who concludes that dissociative attachment by N_2O, *i.e.*

[2] $$e^- + N_2O \rightarrow N_2 + O^-$$

is followed by a sequence of reactions in which O^- acts as a chain carrier to produce NO^- by

[3] $$O^- + N_2O \rightarrow NO^- + NO$$

which regenerates the electron by the associative detachment reaction

[4] $$NO^- + N_2O \rightarrow NO + N_2O + e^-$$

In addition to these reactions, the chain terminating reactions

[5] $$NO^- + N_2O \rightarrow NO_2^- + N_2$$

[6] $$NO^- + 2N_2O \rightarrow N_3O_2^- + N_2O$$

[7] $$O^- + 2N_2O \rightarrow N_2O_2^- + N_2O$$

were proposed as being consistent with the mass-analyzed results (18).

In the present study as in the high pressure microwave conductivity studies of Warman *et al.* (16), the electron decay in reaction 2 and regeneration in [4] are the only reactions involving a monitorable species; consequently, having no mass analysis capability precludes our detailing the intermediates and products specified in [2]–[7]. Therefore, we are limited to a mechanism which involves only electrons, viz.

[8] $$e^- + N_2O \rightarrow P + X^-$$

[9] $$X^- + N_2O \dashrightarrow P' + e^-$$

[10] $$X^- + N_2O \rightarrow \text{no } e^-$$

where P and P′ are unspecified products and X^- an unidentified anion which may regenerate the electron through more than the one-step process indicated by [9] (*e.g.*, [3], [4]).

With the limitation of no mass analysis we utilized gas phase negative ion chemistry and propose a mechanism for electron attachment to N_2O in liquid argon in which attachment reaction 8 is identified with [2], detachment reaction 9 with [3] and [4], and chain termination [10] with reactions 5–7. Evidence for O^- being X^- in the above reaction sequence is based upon the effects of H_2, CO, and CH_4 on electron regeneration in liquid argon/N_2O solution and the known gas phase reactions

[11] $$O^- + H_2 \rightarrow H_2O + e^-$$

[12] $$O^- + CO \rightarrow CO_2 + e^-$$

[13] $$O^- + CH_4 \rightarrow CH_3 + OH^-$$

The rate constants of these reactions in the gas phase are listed in Table 1 and compared with the liquid phase rate constants which we determined as follows.

To obtain rate constants k_{11} and k_{12} from two-component electron decay oscillograms such as Fig. 1*B*, we assume at low electric field E that the electron current is proportional to the product of electron concentration n_e and electron mobility μ_e (8). We used low dose irradiations and maintained low fields to ensure that recombination and field effects on μ_e were negligible; consequently, any change in the electron current was due to a change in the electron concentration, n_e. Electrons attach to N_2O dissociatively (reactions 2 or 8) forming O^- which then reacts with excess H_2 or CO to regenerate electrons by [11] or [12], respectively. The net effect of this attachment is a reduction of the electron concentration as compared to the case of the pure argon. The electron concentration in the solution $(n_e)_S$ is given by

[14] $$(n_e)_S = (n_e)_{Ar}\, T_f/(T_f + T_a)$$

where $(n_e)_{Ar}$ is the electron concentration in pure argon and T_f and T_a are the electron residence times in the free and attached states respectively, and may be obtained from

[15] $$T_f = 1/k_2\,[N_2O]$$

[16] $$T_a = 1/k_{11,12}\,[S]$$

where $[N_2O]$ and [S] are the N_2O and H_2 or CO concentrations, respectively. Obviously, $(n_e)_{Ar} = (n_e)_S + [A^-]$. Combining [14]–[16] yields

[17] $$(n_e)_S = (n_e)_{Ar}\left(1 + \frac{k_2[N_2O]}{k_{11,12}[S]}\right)^{-1}$$

Since the observed current signal i is proportional to the temporary electron concentration, [17] may be rewritten as

TABLE 1. Liquid, gas, and limiting values of O^- attachment rate constants

Reaction	$k \times 10^{10}$ (cm^3/s) (ref.)			
	Liquid[a]		Gas	
	Obs.	Lim.[b]	Obs.	Lim.[c]
$O^- + H_2 \rightarrow H_2O + e^-$	0.17	0.096	7.5 (19) 8.0 (20) 7.0 (21)	16 (19)
$O^- + CO \rightarrow CO_2 + e$	0.21	0.10	7.5 (19) 7.3 (22)	10 (19)
$O^- + CH_4 \rightarrow CH_3 + OH^-$	—	—	1.1 (21) 1.0 (23) 0.8 (24)	13 (23)

[a]This work.
[b]Calculated using eq. 20, see text.
[c]Calculated using eq. 19, see text and ref. 25.

$$[18] \qquad \frac{i_{Ar}}{i_{eq}} = \left(1 + \frac{k_2[N_2O]}{k_{11,12}[S]}\right)$$

where i_{Ar} is the initial amplitude of the electron current in liquid argon at the end of the 5 ns X-ray pulse and i_{eq} is the amplitude at times where the attachment and detachment reactions are in equilibrium. Values of k_2 had been measured independently [1] and thus, from [18] k_{11} and k_{12} were obtained at known N_2O and H_2 or CO concentrations by extrapolating i_{eq} to $t = 0$, when the ionizing pulse was applied. (The decay of the slow component in Fig. 1*B* is due to electron neutralization at the electrodes.)

The limiting rate constants of the O^- reactions which we have listed in Table 1 are for a thermal ion colliding with a nonpolar molecule due to long range polarization interaction between the ion and molecule and were calculated (19, 23) using

$$[19] \qquad k = 2\pi e(\alpha/\mu)^{1/2}$$

where e is the electron charge, α the polarizability of the neutral molecule, and μ the reduced mass of the reactant (25). Whereas the measured gas phase values for O^- reacting via associative detachment with H_2 and CO are within a factor of two of the limiting values, the liquid phase values are ~50–100-fold less. This marked difference may result from an increase in the stability of the anion intermediate (H_2O^- or CO_2^-) in the liquid phase due to solvation effects opening a second reaction channel. This explanation seems implausible, however, due to the exceedingly low electron attachment rate of CO_2 in liquid argon of $<10^{-13}$ cm^3/s which we measured in Ar/CO_2 solutions.

An alternative explanation is the increased reduced mass in the liquid of the reactants due to solvation of O^-. This, too, seems unlikely since solvation of O^- by six argon atoms would decrease the limiting rate by only 6% for H_2 and 57% for CO.

Rather than these explanations, we attribute the observed difference in O^- reactivity to the lower diffusivity of O^- in the liquid phase. If we assume that the reactions in both phases are diffusion controlled as [19] implies for the gas phase, the limiting rate constant in the liquid phase may be calculated by application of the Smoluchowski equation (26). For a reactant of unit charge diffusing to a nonpolar molecule, the appropriate form of the Smoluchowski equation is

$$[20] \qquad k = 4\pi(R_A + R_S)(D_A + D_S)$$

where R is the effective encounter radius and D the diffusion coefficient of the reactant anion and solute denoted by the subscripts A and S, respectively. For the radius of O^- we use the radius of atomic oxygen of 0.6 Å (27) and use molecular radii determined from gas phase viscosity data of $R_{H_2} = 1.09$ Å and $R_{CO} = 1.9$ Å (28). Since diffusion coefficients of O^-, H_2, and CO in liquid argon are not available, we resort to the Loveland *et al.* (29) value of the anion mobility in liquid oxygen of 1.35×10^{-3} $cm^2/V\,s$ at 87 K, which is assumed to be O_2^-, and use

the Nernst–Einstein equation to convert this mobility to $D_{O_2^-} = 1.0 \times 10^{-5}$ cm^2/V s. We also assume that the ion (molecule) diffusion coefficient is inversely proportional to the radius of the diffusing species and using the above values of $D_{O_2^-}$ and $R_{O_2} = 1.49$ Å (28) approximate the diffusion coefficients to be $D_{O^-} = 2.5 \times 10^{-5}$, $D_{H_2} = 1.4 \times 10^{-5}$, and $D_{CO} = 0.78 \times 10^{-5}$ cm^2/s.

By substituting the above values of $R_{A,S}$ and $D_{A,S}$ in [20], we estimated the limiting liquid phase associative detachment rate constants listed in Table 1. Although we consider these limiting rate constants to be very approximate, the agreement within a factor of two between the measured and calculated values suggests that associative detachment reactions can occur in liquids at diffusion-controlled rates.

Acknowledgments

We thank Dr. R. A. Holroyd for stimulating discussions and are grateful to Fonds der chemischen Industrie and U.S. E.R.D.A. (Contract No. E[11-1]-2486) for support of this work.

1. G. Bakale, U. Sowada, and W. F. Schmidt. J. Phys. Chem. **80**, 2556 (1976).
2. P. H. Tewari and G. R. Freeman. J. Chem. Phys. **49**, 4394 (1968).
3. R. M. Minday, L. D. Schmidt, and H. T. Davis. J. Chem. Phys. **50**, 1473 (1969).
4. W. F. Schmidt and A. O. Allen. J. Chem. Phys. **52**, 4788 (1970).
5. G. Bakale and W. F. Schmidt. Z. Naturforsch. Teil A, **28**, 511 (1973).
6. W. F. Schmidt, G. Bakale, and U. Sowada. J. Chem. Phys. **61**, 5275 (1974).
7. G. Bakale, W. Tauchert, and W. F. Schmidt. J. Chem. Phys. **63**, 4470 (1975).
8. G. Bakale, E. C. Gregg, and R. D. McCreary. J. Chem. Phys. **57**, 4246 (1972).
9. J. H. Baxendale, J. P. Keene, and J. Rasburn. J. Chem. Soc. Faraday Trans. I, **70**, 718 (1974).
10. B. S. Yakovlev, I. A. Boriev, and A. A. Balakin. Int. J. Radiat. Phys. Chem. **6**, 23 (1974).
11. A. O. Allen and R. A. Holroyd. J. Phys. Chem. **78**, 796 (1974).
12. A. O. Allen, T. E. Gangwer, and R. A. Holroyd. J. Phys. Chem. **79**, 25 (1975).
13. G. Bakale, U. Sowada, and W. F. Schmidt. J. Phys. Chem. **79**, 3043 (1975).
14. U. Sowada, G. Bakale, K. Yoshino, and W. F. Schmidt. Chem. Phys. Lett. **34**, 466 (1975).
15. H. S. Massey. Negative ions. Cambridge Univ. Press, Cambridge, England. 1970.
16. J. M. Warman, R. W. Fessenden, and G. Bakale. J. Chem. Phys. **57**, 2702 (1972).
17. K. Yoshino, U. Sowada, and W. F. Schmidt. Phys. Rev. A, **14**, 438 (1976).
18. G. E. Caledonia. Chem. Rev. **75**, 333 (1975).
19. J. L. Moruzzi, J. W. Eakin, and A. V. Phelps. J. Chem. Phys. **48**, 3070 (1968).
20. F. C. Fehsenfeld and E. E. Ferguson. J. Chem. Phys. **51**, 3512 (1969).
21. D. A. Parkes. J. Chem. Soc. Faraday Trans. I, **68**, 613 (1972).
22. D. A. Parkes. J. Chem. Soc. Faraday. Trans. I, **68**, 627 (1972).
23. D. K. Bohme and F. C. Fehsenfeld. Can. J. Chem. **47**, 2717 (1969).
24. W. Lindinger, D. L. Albritton, F. C. Fehsenfeld, and E. E. Ferguson. J. Chem. Phys. **63**, 3238 (1975).
25. G. Gioumousis and D. P. Stevenson. J. Chem. Phys. **39**, 1413 (1963).
26. R. E. Weston and H. A. Schwartz. Chemical kinetics. Prentice Hall, Englewood Cliffs, NJ. 1972.
27. N. A. Lange (*Editor*). Handbook of chemistry. McGraw-Hill, New York. 1956. p. 109.
28. J. O. Hirschfelder, C. F. Curtiss, and R. B. Bird. Molecular theory of gases and liquids. John Wiley and Sons, New York. 1954.
29. R. J. Loveland, P. G. LeComber, and W. E. Spear. Phys. Rev. B, **6**, 3121 (1972).

Discussion

J. L. Magee: In the liquid your limiting rates were less than the observed rates. Why did you not reconsider the radii used in the calculations?

G. Bakale: The purpose of the calculated rate constants for the associative detachment reaction in liquid phase and comparison with our data was to illustrate that this process is nearly diffusion controlled. We recognize that the estimate of the limiting rate constant could have been improved by considering the induced dipole interaction but did not feel that this was warranted in view of the rough estimates of the diffusion coefficients that we had to make.

M. Nishikawa: Is your reaction mechanism independent of electron temperature? In other words, is there any evidence that you still get O^- in the presence of CH_4 with its cooling effect?

G. Bakale: Under the conditions of the experiments we observed no effect of electron temperature on the O^- reaction rate. At the lowest field strengths with either H_2 or CO present, we observed the two-component decay indicating that O^- was produced by thermal electron dissociative attachment to N_2O. We assume O^- was also produced in the presence of CH_4, but yielded single-component decay curves due to reaction 13.

Density-, temperature-, and concentration-induced metal–nonmetal transitions in fluids

F. HENSEL

Institute of Physical Chemistry, Philipps-University Marburg, D-3550 Marburg, Auf den Lahnbergen, Germany

Received November 1, 1976

F. HENSEL. Can. J. Chem. **55**, 2225 (1977).

A brief review is given of the continuous metal–nonmetal transition observed in different fluid systems, with special emphasis on recent work by the author and his colleagues. Selected results of a broad experimental survey of the electrical and magnetic properties of fluid binary semiconducting alloys, expanded fluid metals, and fluid selenium are reported. The results are discussed with special emphasis on their relationship to some theoretical areas of controversy, especially the importance of the amount of covalency and ionicity for the electrical and magnetic properties of semiconducting alloys, the role of chemical bond satisfaction in covalent selenium and tellurium for the temperature-induced nonmetal to metal transition, and some speculations concerning the importance of fluctuations and microscopic inhomogeneity for the metal–nonmetal transition in expanded fluid metals. It is concluded that no theory of the metal–nonmetal transition is available which is generally valid for all the fluid systems discussed. It is proposed that measurements of the structure factor and of thermodynamic data of the fluids are necessary to make it possible to formulate a theory which is tested experimentally. The first new results of the structure factor and the compressibility of fluid expanded rubidium are reported.

F. HENSEL. Can. J. Chem. **55**, 2225 (1977).

On présente une brève revue de la transition métal–nonmétal continue observée dans différents systèmes fluides en insistant d'une façon particulière sur les travaux récents de l'auteur et de ses collègues. On rapporte des résultats choisis sur un large éventail expérimental de propriétés électrique et magnétique d'alliages semiconducteurs binaires fluids, de métaux fluides gonflés et de sélénium fluide. On discute des résultats en tenant compte particulièrement de leur relation avec quelques sections théoriques controversées en particulier l'importance du degré de covalence et du caractère ionique sur les propriétés électrique et magnétique des alliages semiconducteurs, le rôle de la satisfaction du lien chimique dans le sélénium et le tellure covalent pour des transitions métal–nonmétal induites par la température et quelques spéculations concernant l'importance des fluctuations et de l'inhomogénéité microscopique pour la transition métal–nonmétal dans des métaux fluides déployés. On conclut qu'il n'y a aucune théorie disponible de la transition métal–nonmétal qui serait valide d'une façon générale pour tous les systèmes fluides discutés. On propose que des mesures de facteurs de structure et de données thermodynamiques des fluides sont nécessaires pour rendre possible la formulation d'une théorie qui pourrait être vérifiée expérimentalement. On rapporte les premiers nouveaux résultats de facteur de structure et de compressibilité d'un rubidium fluide gonflé.

[Traduit par le journal]

Introduction

Metal–nonmetal transitions (MNT) have been studied in a number of different fluid one-component and two-component systems including expanded liquid and gaseous metals (1–3), fluid selenium at high temperatures (4, 5), liquid Se–Te mixtures (6), solutions of alkali metals in fluid ammonia (7, 8), solutions of electropositive metals in their molten halides (9, 10), and semiconducting liquid alloys (11–15). All these fluids can transform from a metallic to a semiconducting or insulating state under changes of an appropriate thermodynamic parameter, *e.g.* temperature, pressure, density, and composition. The transition from a metallic to a nonmetallic fluid implies that the type of chemical binding or at least of the interatomic interaction changes from metallic to nonmetallic binding. Consequently, a successful model or theory of the MNT must explain not only the nature of the apparently continuous changes of electron transport properties during the course of the transition, but must also account for the changes of chemical bonds, the associated changes in the fluid structure, and changes of the more mechanical and thermodynamic properties, especially the thermal compressibility. Since there is an interdependence of electron–electron screening and the far reaching intermolecular forces, which control

the thermodynamic properties, it is interesting also to prove experimentally whether the thermodynamic critical points will coincide with the MNT.

The aim of the present paper is to review recent experimental results with an emphasis on work from the Institute of Physical Chemistry of the University of Marburg. Selected data will be discussed for all the fluid systems mentioned above except metal–ammonia and metal–molten salt solutions. Recent reviews on these systems are by Thompson (16), Schindewolf (7), and Nachtrieb (17).

Metal–Nonmetal Transition in Semiconducting Alloys

The group of fluid semiconducting alloys provides the most direct evidence that the formation of chemical bonds plays an important role for the MNT. Liquid Mg–Bi (11), Li–Bi (18), Cs–Au (13), Rb–Au (19), and Cs–Sb (20) represent some of the alloys which belong to this group. Although the pure metals Li, Mg, Cs, Rb, Au, and Sb are highly conducting liquid metals, in the neighbourhood of compositions satisfying simple chemical valence requirements the liquid mixtures have conductivities which are definitely outside the range typical for liquid metals. It seems to be clear from this observation that a large change in the bonding characteristics associated with changes in the liquid structure takes place as one proceeds from the pure metal to the stoichiometric concentration. Whereas the structural effect has been discussed in a large number of reviews (12, 21) and articles (22, 23) written mainly by Enderby, relatively little attention has been paid to how the properties of semiconducting alloys depend on the nature of the bonds, *i.e.* on the relative ionicity and covalency of the bonds. But the detailed electronic structure and the electrical transport properties of the molten alloys certainly depend on the character of the chemical bonds. In systems with predominantly ionic bonds ionic species must occur and they must be mobile in liquids, so that their effect may be considerably larger in the electrical transport properties, comparable to metal – molten salt solutions. In the following, recent experimental results for the Cs–Au and Cs–Sb system will be presented with particular emphasis on their relevance to the question raised above.

A rough measure of the relative ionic or covalent character of the bonds in CsAu and Cs_3Sb can be obtained from published tables of electronegativities. The electronegativity difference according to the Pauling scale leads to the suggestion that a high amount of covalent bonding exists in liquid Cs_3Sb, whereas liquid CsAu exhibits predominantly ionic bonding. In order to contrast the behaviour of these two systems the electrical conductivity σ and the molar magnetic susceptibility $\mathscr{H}_m$ of both Cs–Au and Cs–Sb are plotted as a function of the concentration in Fig. 1*a* and Fig. 1*b*. The concentration scale varies between the compound composition on the left and pure Cs on the right. It is obvious that there is a striking difference in the concentration dependence of σ and $\mathscr{H}_m$ for these two systems. σ of Cs_3Sb–Cs rises abruptly within a narrow concentration range of less than 5 at.% excess Cs, whereas σ of CsAu–Cs remains approximately constant up to about 15 at.% excess Cs. For the concentration dependence of $\mathscr{H}_m$, the slope of the curve gets steeper for the Cs–Au system when the compound composition is approached, whereas it is decreasing in the Cs–Sb system. It was recently shown by Freyland and Steinleitner (14, 20) that for liquid Cs_3Sb a logarithmic plot of the electrical conductivity *vs.* the reciprocal temperature gives a straight line over a temperature range of about 200°C. From the slope an activation energy $\Delta E = 0.44$ eV is determined. They concluded from the magnitude of ΔE and from the observed small absolute thermoelectric power of $S \approx -20$ μV K^{-1} that electronic conduction prevails in liquid Cs_3Sb. In addition they found this

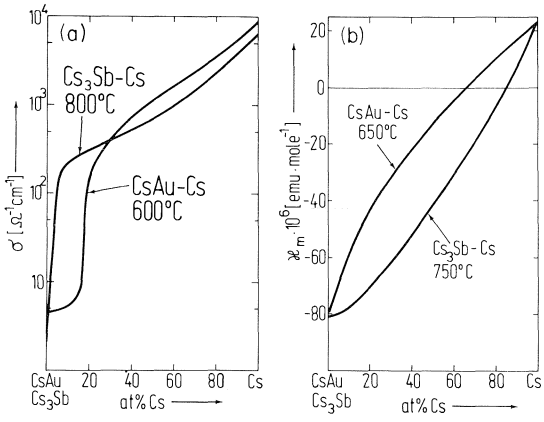

FIG. 1. Comparison of the electrical conductivity σ and the molar magnetic susceptibility $\mathscr{H}_m$ of Cs–Au and Cs–Sb alloys (data from refs. 14, 20, 13).

assumption in agreement with the observed positive temperature dependence of the magnetic gram susceptibility. Assuming that this positive temperature dependence is due to thermally excited electrons and holes and that the activation energy for the charge carrier contribution to the susceptibility $\mathscr{H}_g^c$ is the same as observed for the electrical conductivity, *i.e.* 0.44 eV, they were able to fit the experimental data. In contrast to the behaviour of liquid Cs_3Sb the temperature dependence of the liquid CsAu susceptibility is comparatively small and negative and the molar susceptibility of -81×10^{-6} cm^3 mol^{-1} is consistent with a description in which the liquid is assumed to consist of Cs^+ and Au^-. The latter is consistent with the observed temperature dependence of the conductivity σ of CsAu which is shown in Fig. 2. The 'apparent activation energy' of σ is about 4.5 kcal/mol (about 0.2 eV) for CsAu which is also of the order of the 'activation energies' of ion migration in salts. It must be pointed out, however, that the concept of 'apparent activation energies' of ion migration in liquid salts is based on theories developed for atomic transport in solids. And certainly it is necessary to prove by more accurate measurements over wider temperature intervals whether Arrhenius behaviour is the rule or the exception.

In addition the marked decrease of the conductivity of the alloys on melting (Fig. 3) indicates that the electrical behaviour in the liquid Cs–Au alloys is very different from that in solid Cs–Au alloys. One can contrast the behaviour of CsAu with that of other solid semiconductors, which mostly show a more or less large increase of σ on melting. Two main groups may be distinguished. In the first group of semiconductors, such as Ge, Si, InSb, etc., the coordination number increases on melting and the short range order and the nature of chemical binding drastically change. The conductivity becomes metallic, *i.e.* a semiconductor to metal transition is observed on melting. In the second group, to which semiconductors like Mg_3Bi_2, Se, In_2Se_3, etc. belong, the coordination number changes only slightly and the short range order of the crystal persists to a large extent on melting, *i.e.* a semiconductor to semiconductor transition is observed on melting. As the temperature is considerably increased, the short range order is possibly changed into a completely random atomic configuration which is typical of liquid metals at high temperatures, *i.e.* an abrupt

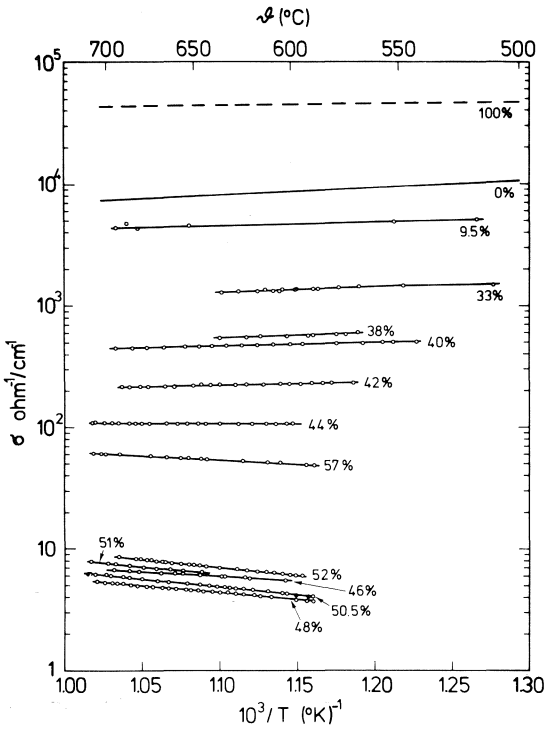

FIG. 2. Logarithm of the conductivity, σ, of liquid Cs–Au alloys as a function of the reciprocal temperature at different constant Au concentrations in at.% (from ref. 13).

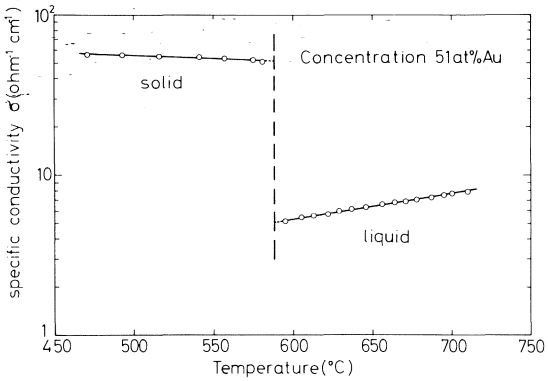

FIG. 3. Conductivity, σ, for a Cs–Au alloy with 51 at.% Au as a function of the temperature in the liquid and solid state (from ref. 13).

semiconductor to semiconductor and a gradual semiconductor to metal transition is observed. The latter was recently investigated for liquid Se (5). It is evident from the results in Fig. 3 that CsAu does not belong to one of the groups mentioned above. Therefore we make the assumption that a further type of solid–liquid

phase behaviour may be shown by semiconductors with a high degree of ionic binding. We believe that for these semiconductors the solid–liquid phase transition coincides with a transition from a solid semiconductor to a liquid mainly ionic conductor. CsAu was the first example of this type. In the meantime a similar behaviour has been observed for RbAu, whereas the system LiAu is metallic in its liquid state (19).

Further evidence for a mainly ionic structure of CsAu stems from the striking similarity in the concentration dependence of σ of the liquid Cs–CsAu system and solutions of electropositive metals in their molten salts as demonstrated by Fig. 4 for the K–KBr system. For comparison Fig. 4 includes also the concentration dependence of σ for the system Mg–Mg_3Bi_2 and Tl–Tl_2Te which in both cases is clearly different from that for the Cs–CsAu system. The poor correlation between the Mg–Mg_3Bi_2 and the Tl–Tl_2Te mixtures, which have both been classified as 'liquid-semiconductors', and the Cs–CsAu mixture and on the other hand the similarity between the K–KBr mixture and Cs–CsAu mixture are consistent with the conclusion that the conduction process in CsAu involves ionic transport.

This conclusion is supported qualitatively also by the relatively high value of the thermoelectric power S of liquid CsAu. As demonstrated by Fig. 5, S of liquid Cs–Au alloys is negative and larger than -1000 μV/K near the equiatomic composition. Probably, the presence of Cs^+ and Au^- ions precludes the n–p transition in S seen in systems with prevailing electronic conduction, *e.g.* Mg_3Bi_2 and Tl_2Te (15). Large values of S are typical for ionic conductors (24). However, it is very difficult to handle quantitatively the thermoelectric power near the equiatomic composition, since there exist different kinds of charge carriers, possibly electrons, cations, and anions, having similar mobilities and transference numbers. Therefore, again it is only possible to contrast the behaviour of the CsAu–Cs system with that of other systems, especially with that of metal – molten salts mixtures. Measurements of the thermoelectric power have been made for the systems $BiCl_3$–Bi, $BiBr_3$–Bi, and BiI_3–Bi (25–27). The results are qualitatively in accord with the observations on Cs–CsAu. When the metal excess is large and the current is mainly due to electrons the thermoelectric power

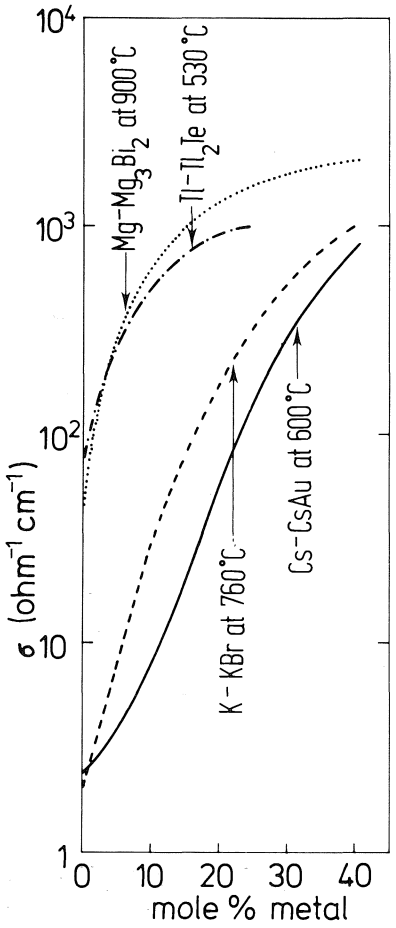

FIG. 4. Influence of excess metal on the conductivity of different compound forming alloys and salts (from ref. 13).

is relatively small, it increases rapidly with decreasing metal concentration, and reaches a maximum value near the pure salt concentration. Thus, the results are again consistent with the assumption that ions in liquid CsAu are movable and that conductivity and thermoelectric power are determined at small metal concentrations by ionic conduction superimposed by a contribution of electronic conduction. Finally there is evidence that enormous electromigration occurs in liquid CsAu. It was shown by Schmutzler and Krüger (28, 29) that Cs drifts to the cathode and Au drifts to the anode. One Cs^+ and one Au^- are transported per elementary charge to the electrodes within the experimental error. This is definitely the value required by Faraday's law for electrolysis in ionic conductors.

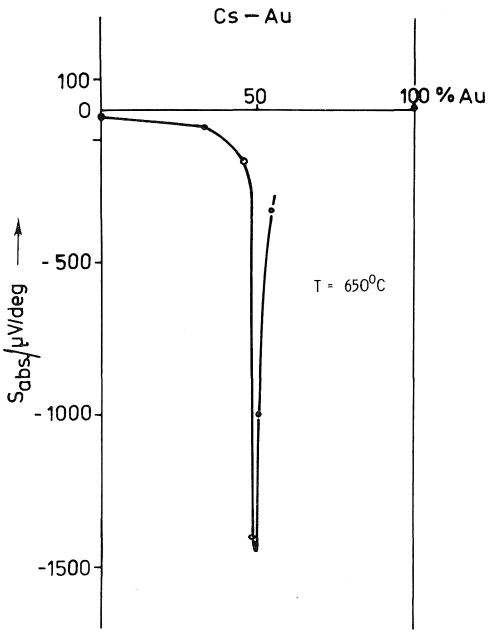

FIG. 5. The absolute thermoelectric power, S_{abs}, of liquid Cs–Au alloys at 650°C as a function of the concentration (from ref. 13).

The Metal–Nonmetal Transition in Elemental Liquid Semiconductors and Expanded Liquid Metals

The transition from metallic to semiconducting-like electronic properties in the alloys discussed above can be understood as a result of the formation of chemical bonds as one proceeds from the pure metal to the stoichiometric concentration. Other examples for the importance of chemical bonds are liquid Se and S which both are nonmetallic near the melting point where their liquid structures are dominated by the presence of molecular species as rings and relatively large chainlike units (30). However, the liquid structure including the local atomic coordination number can change markedly with temperature, pressure, or on alloying with more metallic elements. A gradual change toward a lower resistance liquid is observed due to the dissociation of the liquid chain structure induced by an increase in temperature or pressure (31). A very interesting element among the electronically conducting liquids is liquid selenium. It exhibits a relatively small strongly temperature-dependent electrical conductivity σ at its melting point. Since a logarithmic plot of σ *vs.* the reciprocal temperature shows a linear region in a not too extended temperature range, it is tempting to call selenium a 'liquid semiconductor' (32, 33). However various results suggest a tendency to a more metallic behaviour as the bonding arrangement is altered at very high temperatures (31) or pressures (34). Application of very high temperatures implies that the heating up of the liquid takes place at pressures greater than the liquid–vapour critical pressure p_c. A list of critical pressures p_c together with the corresponding critical temperatures T_c is assembled in Fig. 6 for those liquid chalcogenic and metallic elements which are of interest for the present discussion.

Experimental results are shown for Se (right side) and Hg (left side) in Fig. 7 in the form of conductivity isotherms plotted *vs.* pressure. It is only at temperatures close to the critical temperature that for both liquids the conductivity becomes strongly pressure dependent. This is certainly related to the strong pressure dependence of the density in this region. However, it is obvious from Fig. 7 that the conduction behaviour of selenium sharply differs from the behaviour of the metal mercury. The characteristic feature for Se is a very pronounced effect of the temperature on the conductivity at constant pressure. The conductivity isobars show a very large slope at subcritical conditions, giving a maximum conductivity near the critical temperature in the nearly metallic range 100–1000 ohm^{-1} cm^{-1}, many orders of magnitude larger than the conductivity near the melting point. Above the maximum the conductivity drops rapidly at the highest temperatures. The maximum in the 400 bar isobar lies at 1500°C,

Substance	T_c (K)	p_c (bar)
Hg	1760	1510
Cs	2020	110
Rb	2100	130
K	2200	155
Te	2500*	270*
Se	1760	380
S	1315	180

* estimated

FIG. 6. Thermodynamic critical points.

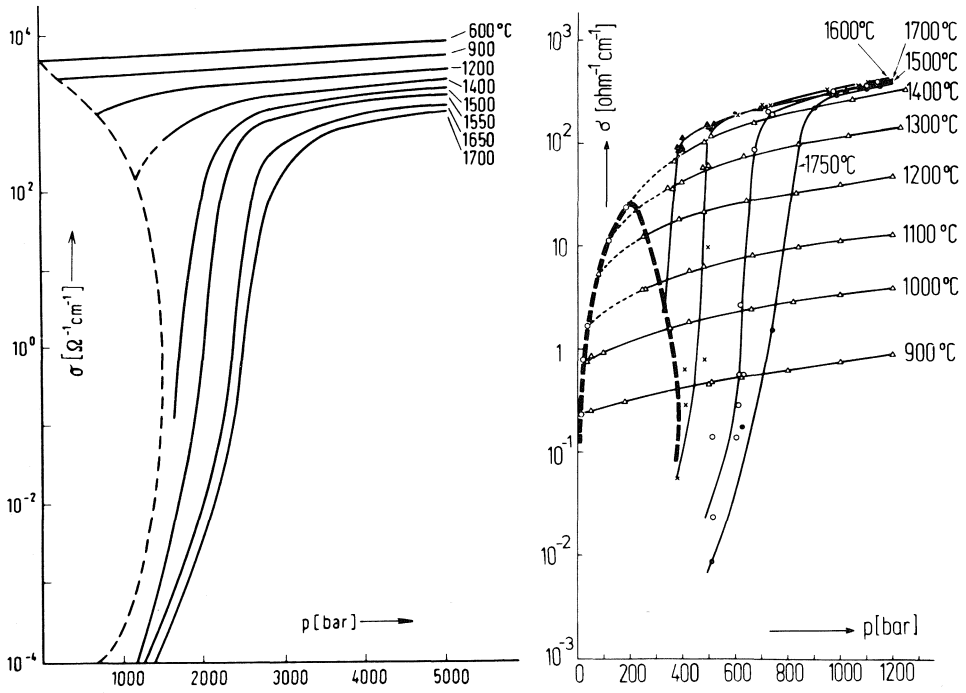

FIG. 7. The electrical conductivity of mercury and selenium at subcritical and supercritical temperatures as a function of pressure.

about 100°C lower than the critical temperature. This indicates that Se is semiconducting or insulating at the critical point (4). The conductivity of molten selenium throughout the entire liquid range at equilibrium pressure is given in Fig. 7 by the curve punctuated in heavy type. It reaches a maximum value of 25 ohm^{-1} cm^{-1} and decreases to a quite small value near the critical point. This small conductivity can be considered consistent with the result of an analysis of the vapour pressure curve of selenium in terms of 'correspondence state theory' which leads to the suggestion that selenium is essentially a molecular fluid in the vicinity of the critical point rather than a metallic one. The transformation to nearly-metallic conductivities can be induced either by increasing temperature in the liquid range (left hand side of the maximum) or by increasing pressure in the vapour (right hand side of the maximum). It is certainly a very complicated system. However, it seems reasonable to suppose that the temperature effect in the liquid results from the combined effects to thermal activation of carriers, increasing coordination number as Se chain- and ring-structure rupture, and decreasing density from thermal expansion. The former two effects should increase the conductivity while the density decrease should decrease the conductivity. The maxima in the isobars can then be understood. The decrease in density at high temperatures leads to a density-induced metal–insulator transition which is similar to those observed in supercritical fluid metals.

Liquid selenium near its melting point has been studied by many investigators both in regard to its electrical properties and its molecular and electronic structure (32). Its behaviour is consistent with the assumption that the chain-like structure, *i.e.* the covalent bonds between atoms in twofold coordination, of crystalline selenium persists to a large extent on melting. This assumption leads to a well-developed energy gap and semiconducting properties. However, if the temperature is increased, the chains rupture and the coordination number increases; the decrease of the chain length goes in the direction of a completely random atomic configuration which is typical for metals. The limitations of the 'semiconductor model' for liquid selenium become apparent at high temperatures. This is demonstrated by Fig. 8 where the logarithm of the conductivity is plotted *vs.* the reciprocal temperature. While it is possible to

identify an activation energy from the slopes below about 1300°C, these values depend on pressure at constant temperature. Moreover, at higher temperatures, the slopes increase and then decrease as the maxima are approached.

Further evidence for the limitations of the 'semiconductor model' for liquid selenium at very high temperatures stems from recent measurements of the absolute thermoelectric power (35). In the current picture of disordered semiconductors the band gap is replaced by a mobility gap (32, 36). Conduction at sufficiently high temperatures proceeds by thermal excitation of carriers across the mobility gap, *i.e.* σ and S are determined by electrons and holes thermally excited to the mobility edge probably for σ as low as about 1 ohm^{-1} cm^{-1}. When one band dominates, then σ and S are related by (32).

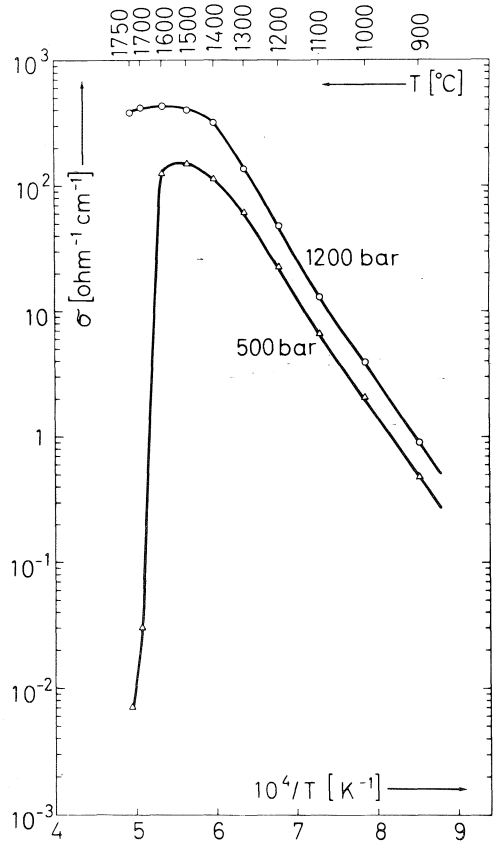

FIG. 8. Logarithmic plot of conductivity isobars of selenium *vs.* reciprocal temperature. Slopes in the range $10^4/T \geq 7.3$ K^{-1} yield 'activation energies' ΔE of roughly 1.8 eV. At higher temperatures, slopes increase to yield ΔE values of roughly 2.2 eV. In both ranges ΔE depends noticeably on pressure.

$$[1] \qquad \sigma = \sigma_0 \exp\left(-\frac{eS}{k} + 1\right)$$

An analysis of the thermoelectric power data shows that relation [1] is not obeyed for Se in the conductivity range between about 8 to 1000 ohm^{-1} cm^{-1}, *i.e.* at very high temperature, whereas it is consistent with the experimental results for smaller than 8 ohm^{-1} cm^{-1}. In respect to its electrical properties liquid tellurium is very different from liquid selenium. It provides an example of an electronically conducting liquid which exhibits some features of both metallic and semiconducting behaviour (37, 38). Its conductivity of about 1000 ohm^{-1} cm^{-1} at the melting point is relatively large and its Knight-shift value is in a range typically observed for liquid metals. On the other hand, the temperature coefficients of the conductivity and of the Knight shift are positive.

Neutron scattering data (39) indicate that the number of atoms in the first coordination shell is about two near the melting point and changes to about three at about 900°C. The twofold (binary) coordination is typical for the helical chainlike structure of selenium, while the threefold (ternary) coordination is similar to that of the arsenic crystal structure. Such a change of coordination was found to be consistent with the Knight-shift measurements (37) and velocity of sound measurements (40). Between the melting point and 900°C the existence of regions of twofold coordination which are semiconducting mixed with regions of threefold coordination which are metallic has been suggested by Cabane and Friedel (41). They assume that the number of free carriers increases with temperature due to the increase of ternary sites.

Since the first coordination number increases to a value larger than five at 1800°C (39), Cabane and Friedel (41) proposed that the local structure of liquid tellurium tends to a more metallic cubic structure like α-polonium with metallic character at high temperature (about 1700°C) or high pressure. This proposal is consistent with recent measurements of the electrical conductivity of liquid tellurium as a function of temperature at various pressures (42). Up to about 900°C the conductivity values along isobars increase and then decrease through broad maxima at about 1000°C. Above 1000°C the values of $(d\sigma/dT)_p$ are almost constant irrespective of pressure. The maxima shift slightly to

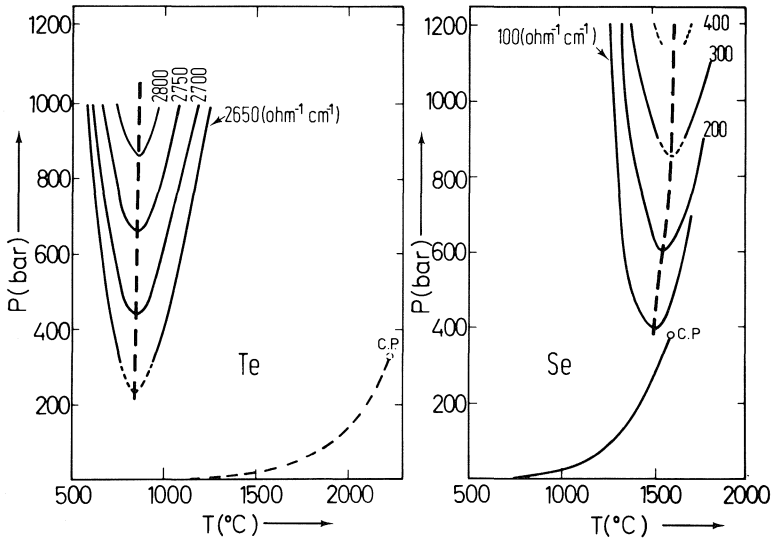

FIG. 9. Plots of pairs of temperature and pressure for constant conductivities for liquid selenium and tellurium. The numbers on the curves denote the value of the conductivity in ohm^{-1} cm^{-1}. The point C.P. is the critical point and terminates the vapour pressure curve.

higher temperatures with increasing pressure (42).

It seems reasonable to suppose that the effect of increasing temperature results from the combined effects of increasing coordination number and decreasing density from thermal expansion. The former effect should increase the conductivity while the latter should work in the opposite direction. A comparison of the temperature dependence of the electrical conductivity of liquid tellurium and liquid selenium both at moderate pressures shows that under the present experimental conditions the conductivity of liquid tellurium is always larger than that of liquid selenium. It is obvious that in both elements the conductivity varies through maxima and the change found in liquid tellurium is much smaller than that in selenium. This is certainly related to the larger stability of the bonds within the chain molecules in selenium. The difference in the pressure and temperature dependence of the conductivity between selenium and tellurium is shown in Fig. 9. It includes plots of pairs of temperature and pressure for constant conductivities. It is obvious from this figure that the maxima in the conductivities, *i.e.* the nearly-metallic conductivities, occur at much higher temperatures for selenium than for tellurium. For selenium the maximum conductivity is observed near the critical temperature of the liquid–vapour phase equilibrium, whereas for tellurium the maxima occur far beyond the critical temperature. The latter was determined by means of the corresponding states principle. In accordance with the rule (43) that any group of substances with effectively similar intermolecular forces should conform themselves to the principle of corresponding states, the correspondence between the vapour pressures of sulphur, selenium, and tellurium was used to determine the critical point of tellurium.

We turn next to the metal-nonmetal transition in low density metallic fluids. As can be seen from Fig. 7 the unavoidable critical temperatures and pressures of the metals are relatively high. Experiments for obtaining data under such extreme conditions are chiefly limited by the reduced strength and increased chemical reactivity of the sample containers at the high temperatures. It was only through the development of a special experimental technique favored by the rapid advances in the production of high-temperature construction materials during the past few years, that a number of experiments have been possible on Hg, Cs, Rb, and K which have critical temperatures lower than 2000°C. The fundamental thermodynamic and electronic properties, density, vapour pressure, critical data, viscosity, electrical conductivity, thermoelectric power, Hall effect, Knight shift, optical absorption, and structure factor, have been measured in some cases.

The metal that has been most intensively studied is mercury. Figure 7 (left side) shows the dc electrical conductivity measured by various groups of workers (44–47) as a function of the pressure for a number of subcritical and supercritical temperatures. The dotted line gives the densities or the conductivities of the coexisting liquid and vapour phases, respectively. Below the critical point, which was found at T_c = 1490°C and p_c = 1510 bar, a phase separation in a low density vapour with a relatively small conductivity and a highly conducting dense liquid is observed. The critical point must be the limit for observing the sharp transition between a highly conducting liquid and a lower conductance vapour, since at this point any distinction between liquid and vapour disappears. Above the critical temperature a steep but continuous increase of the conductivity with increasing pressure is observed. This behaviour of the electrical conductivity in the critical region is qualitatively typical for liquid metals and has been observed for mercury, cesium, and potassium. However, quantitatively a striking difference is observed in the critical behaviour of divalent mercury and monovalent cesium or potassium. Near the critical point the conductivity of mercury (σ_{Hg} is about 10^{-1} ohm^{-1} cm^{-1}) is three orders of magnitude smaller than the conductivity of cesium and potassium (σ_{Cs} is about 200 ohm^{-1} cm^{-1}). In addition the value of the absolute thermoelectric power of mercury, which is about -500 μV/K (47) at the critical point, is very large and certainly nonmetallic, whereas the value for cesium is -60 μV/K at the critical point (48). The latter is relatively small and not unreasonable for a metal. Thus, on the basis of this argument it is tempting to speculate that one observes two different types of critical points. For mercury close to the critical point a type of liquid–vapour phase transition similar to that in nonmetallic liquids is observed, *i.e.* liquid mercury exists in a high density metallic form and a low density nonmetallic form. For cesium (the same is true for potassium) it cannot be excluded that the liquid–vapour phase transition is associated with the metal–nonmetal transition. It must be pointed out, however, that it is not clear whether the existence of a relatively high conductivity at the critical point of cesium and potassium means that the state of these two elements can really be considered as metallic in the critical region, *i.e.* that the forces remain long range compared with an insulating liquid like argon.

For a divalent metal like mercury the Bloch–Wilson model of noninteracting electrons predicts a band-crossing transition. When the distance between the mercury atoms is continuously increased, the overlap between the s-valence band and the p-conduction band decreases, resulting in a metal–nonmetal transition. However, in a fluid the situation is more complicated; the atoms or ions are not rigidly held in position and fluctuations in density can be significant. Therefore in a fluid the singularities in the density-of-states function at the band edges are smeared out; the band edges exhibit tails in the energy region which is forbidden in the corresponding crystalline solid. Thus the gap separating the valence and the conduction band in the solid is replaced in fluid mercury by a minimum in the density of states near the Fermi energy. This is a suggested model, and it is very difficult to prove it experimentally. The difficulty arises because one of the most informative experiments used in crystal physics, optical absorption, disappoints us in fluid systems. In view of the uncertainties concerning the tails in the gap, it is necessary to ask whether it is possible to define an optical gap.

The spectral dependence of the absorption coefficient of mercury at the constant supercritical temperature of 1640°C and densities between 1 g/cm^3 and 4.8 g/cm^3 is shown in Fig. 10. The absorption edges exhibit the expected red shift with increasing density and are found to be exponential in form for values of K up to about 2×10^3 cm^{-1}.

At densities larger than 3 g/cm^3 the absorption curves flatten out to approximately constant values of the absorption coefficient at long wavelengths up to the infrared region. The level of these long wavelength tails increases very rapidly with increasing density and the density dependence is the same as observed for the dc conductivity. This equivalence of the density dependence for the dc conductivity and the optical frequency absorption coefficient is strong, if not conclusive, evidence that the mechanism of both have the same physical reason, *e.g.* free carrier conduction by thermally excited electrons in extended states.

At high enough values of the absorption coefficient ($K > 2 \times 10^3$ cm^{-1}) the linear dependence of log K on the photon energy is no longer observed and the absorption coefficient

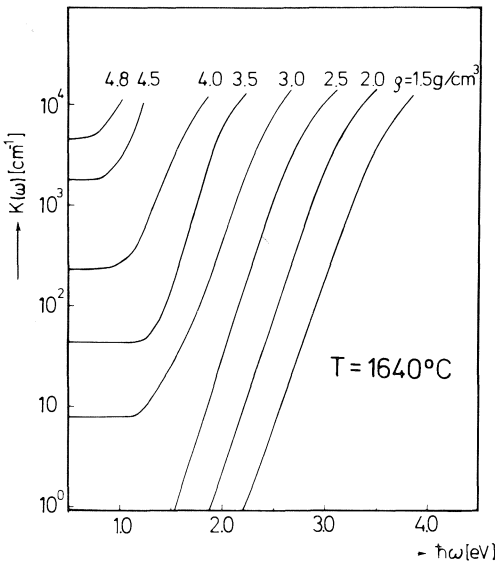

FIG. 10. Optical absorption edges in fluid mercury at different densities and the constant temperature of 1640°C (from ref. 1).

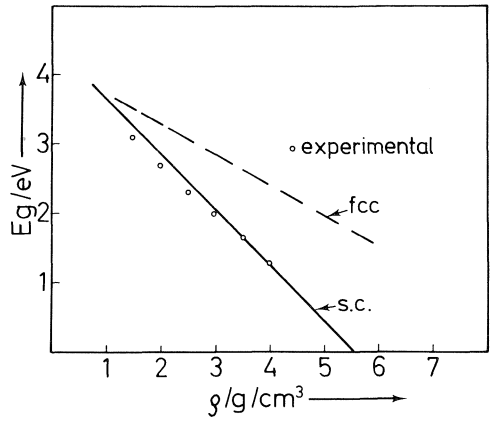

FIG. 11. Optical gap in mercury as a function of density at the constant temperature at 1640°C; the points are the experimental data. The curves give the calculated band edges for sc and fcc crystal structures (calculated values from ref. 50).

increases less steeply. In this region the absorption coefficient K can be described by the relation

$$[2] \qquad K\hbar\omega \propto (\hbar\omega - E_0)^2$$

This relation is of a form similar to that for indirect interband electronic transition in crystalline semiconductors and was derived by Tauc (49). He assumed that the density of states of the conduction and the valence bands not too close to the band edges is of a parabolic form and that the optical matrix element is constant in the energy range under consideration. Moreover the absorption in many semiconducting glasses at high enough absorption levels is observed to obey the relation [2], and the constant E_0 can be used to define an optical gap E_g. However, one fact should be emphasized. If the interpretation of the experimentally observed relation [2] given by Tauc is right then E_g is determined from an extrapolation of the densities of states deeper in the bands. Thus E_g may represent an extrapolated rather than a real zero in the density of states. The widths of the optical gaps E_g derived in this way for mercury at 1640°C as a function of the density are given in Fig. 11. The author feels that not too much physical significance should be given to E_g. Despite this fact, it is surely tempting to compare the density dependence of the optical gap defined in this way with the gap calculated for expanded mercury crystals (50–52). The main result of these calculations is that the energy gap is very sensitive to changes in structure. This is in accordance with the old empirical rule of chemistry that both density and coordination environment determine whether a fluid or amorphous material is metallic or not. In Fig. 11 the calculated band gaps as a function of density for fcc and sc structures are included. The absolute values, as well as the slopes of the curves, are different for each structure. The agreement between the measured gap and that calculated for the sc structure evident from Fig. 11 is extremely close and should be regarded as partly accidental. The plot in Fig. 11 demonstrates that the valence band (the 6s band) and the conduction band (the 6p band) cross at a density between 5 and 6 g/cm^3. At this density the dc conductivity is about 10^{-1} ohm^{-1} cm^{-1} and the thermoelectric power is about -500 μV/deg which are certainly nonmetallic values. This is quite consistent with the current picture of disordered semiconductors. As mentioned above in this picture the band gap of the crystalline solid is replaced by a mobility gap and all the states within the mobility gap are localized. Conduction at sufficiently high temperatures proceeds by thermal excitation of carriers across the mobility gap. The last mechanism leads for thermal excitation of electrons (32) to relation [1] between the thermoelectric power S and the electrical conductivity σ.

Schmutzler and Hensel (2) have shown that σ

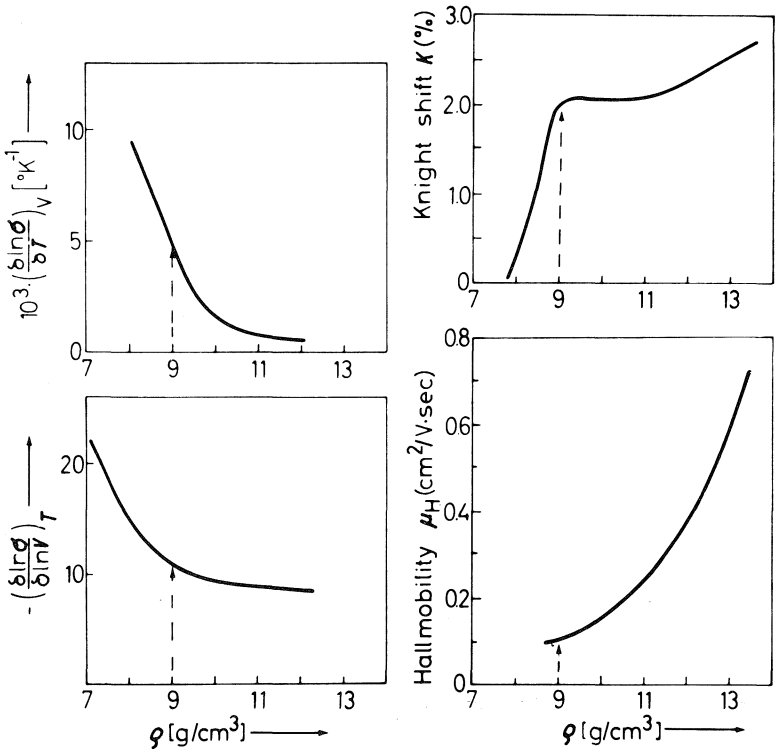

FIG. 12. Temperature and volume coefficient of the conductivity and the Knight shift and the Hall mobility of fluid mercury as a function of the density (from ref. 1).

and S for mercury in the density range between 8 g/cm^3 and 5 g/cm^3 are consistent with [1]; *i.e.* with an excitation of electrons from localized states at the Fermi energy to free states across the critical energy which divides ranges in which states are localized from those in which states are not. On the other hand $(\partial \ln \sigma/\partial \ln V)_T$ (47), $(\partial \ln \sigma/\partial T)_V$ (47), the Hall mobility (53, 54), and the Knight shift (55) indicate a change of the electronic state of mercury for densities around 9 g/cm^3, which is demonstrated by Fig. 12. Therefore, for the density range between 8 g/cm^3 and 9 g/cm^3 Cohen and Jortner (56, 57) have proposed an alternative explanation. They suggested the existence of an inhomogeneous transport regime in mercury between 9 g/cm^3 and 8 g/cm^3. They assumed that the microscopic inhomogeneities arise from density fluctuations. The metal–nonmetal transition in such a system with metallic and semiconducting clusters is then discussed within the framework of percolation theory. This matter is very controversial and up to now it is impossible to decide from the existing experimental results whether the Cohen–Jortner proposal is right. However, recent measurements of the isothermal compressibility χ_T and the thermal expansion coefficient α_p for expanded mercury as a function of the density from our laboratory (58) indicate an enormous increase of χ_T and α_p at densities smaller than 9 g/cm^3. It is certainly interesting to speculate on whether the mutual interdependence of electron–electron screening and interatomic forces necessarily leads to density fluctuations in the metal–nonmetal transition range.

At mercury densities larger than 9 g/cm^3 the analysis of the available electrical transport data, electrical conductivity, Hall effect, and thermoelectric power demonstrates the existence of two distinct regimes of electron transport in this one-component system. For densities between 9 and 11 g/cm^3 Even and Jortner (54) showed by combined conductivity σ and Hall effect R measurements that σ is proportional to $(R_{FE}/R)^2$, whereupon the Hall mobility μ_H follows $\mu_H \propto R_{FE}/R$. In these equations R_{FE} means the free electron value $R_{FE} \equiv (nec)^{-1}$. These experimental relations are in excellent agreement with

the theoretical predictions given by the strong scattering model (32) and Friedman's theory of the Hall effect (59, 60). However, it must be pointed out that expanded mercury is the only example for which the theory is in agreement with the experimental transport data. The recent measurements of the Knight shift by El-Hanany and Warren (55), however, seem inconsistent with the strong-scattering model. More accurate experimental and theoretical work on expanded mercury in the density range between 11 and 9 g/cm^3 is necessary to make it possible to formulate a theory which is in agreement with the experimental results.

For densities between 13.6 and 11 g/cm^3 it is found that the Hall coefficient has the free electron value $R_{FE} \equiv (nec)^{-1}$ and the conductivity exhibits no special relation to R. It is assumed that in this range, where the mean free path L of the conduction electrons exceeds the Fermi wavelength k_F^{-1}, σ is well represented by the nearly-free-electron (NFE) theory (61–63). The latter assumption, that the theory is valid when $L > k_F^{-1}$, has very recently been proved experimentally for fluid rubidium by measurements of the density (64, 65), the electrical conductivity (64, 65), and the structure factor (66, 67) as a function of temperature and pressure. It was found that the density dependence of the electrical conductivity can be well represented by the NFE theory even for an expansion of the fluid metal to a value of 65% of the density at the melting point (see Fig. 13). The experimental results agree satisfactorily with those calculated within the NFE theory using the measured structure factors of expanded rubidium. The latter is shown in Fig. 14 for different temperatures and pressures. Mainly three particular features may be distinguished in these curves. The first peak, which is relatively sharp at low temperatures, broadens appreciably with increasing temperature and its height decreases drastically. This fact illustrates that the 'shell of nearest neighbours' is less well defined and smears out with increasing temperature or decreasing density. At the same time the position of the first maximum is shifted by 10% to lower Q values between 450 K and 1400 K, which simply reflects the expansion of the liquid by about 30% within the above temperature limits. The main overall feature for Q values above 1 Å^{-1} is a considerable flattening of the structure factor.

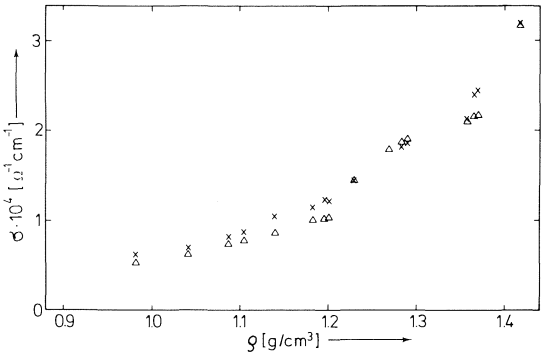

FIG. 13. The electrical conductivity of liquid rubidium: (×) calculated with the Ziman formula using a screened Ashcroft pseudopotential and experimental structure factors; (Δ) values recently reported in refs. 64–66.

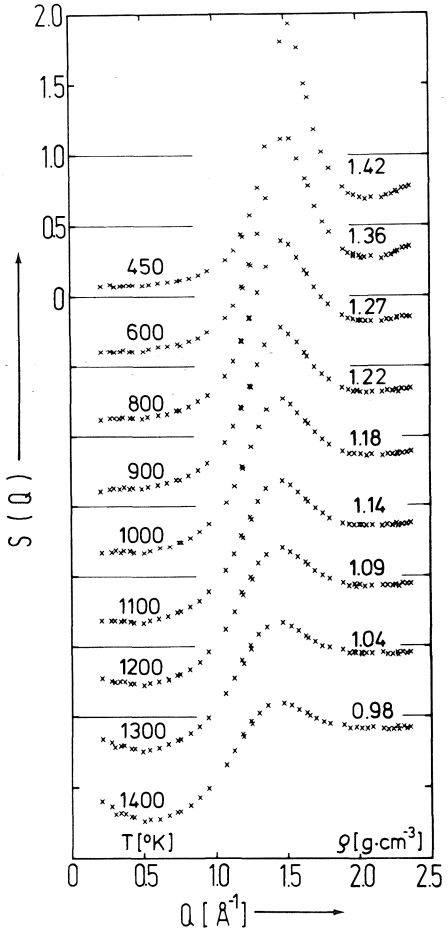

FIG. 14. Measured structure factors of liquid rubidium at nine different densities and temperatures for momentum transfers between 0.2 and 2.5 Å^{-1}.

At Q values below 0.5 $Å^{-1}$ two interesting observations can be made. Whereas for temperatures below 1100 K $S(Q)$ remains constant below $Q \leq 0.6$ $Å^{-1}$, a slight increase of $S(Q)$ with decreasing $Q \leq 0.4$ $Å^{-1}$ starts to show up at 1200 K, and is well pronounced at 1400 K. However, further measurements are necessary to establish this fact. The second interesting finding is that at the smallest Q reached in this experiment, $S(Q)$ increases by almost a factor of five between 450 K and 1400 K. This is consistent with the observed increase in the isothermal compressibility on expansion of fluid rubidium (Fig. 15) (64, 65) which is related to the structure factor at $Q = 0$ $Å^{-1}$ by the well-known equation

$$[3] \qquad S(0) = k_B T \chi_T n$$

where k_B is the Boltzmann constant and n the number density per cm^3. Since the compressibility is determined by the interatomic forces which are depending on the electron–electron screening, again one is tempted to speculate that the metal–nonmetal transition is probably connected with large fluctuations in the density. Further measurements of the structure factor of expanded metals at small wave vectors are necessary to prove this hypothesis. Possibly one can get better evidence by such an experiment for or against the various mechanisms proposed for the metal–nonmetal transition.

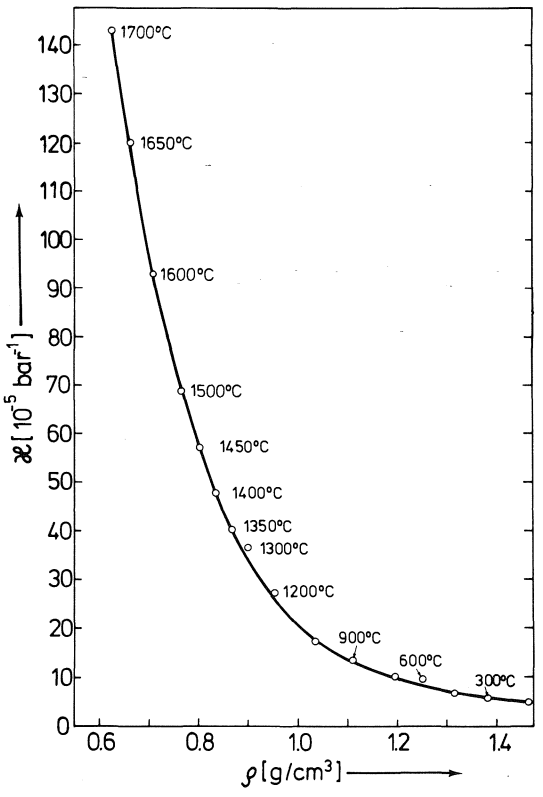

FIG. 15. Isothermal compressibility of expanded fluid rubidium as a function of the density (the points are measured at different temperatures) (data from refs. 64, 65).

1. F. HENSEL. Ber. Bunsenges. Phys. Chem. **80**, 786 (1976).
2. R. W. SCHMUTZLER and F. HENSEL. J. Non-Cryst. Solids, **8**, 718 (1972).
3. R. G. ROSS and D. A. GREENWOOD. Prog. Mater. Sci. **14**, 173 (1969).
4. H. HOSHINO, R. W. SCHMUTZLER, and F. HENSEL. Ber. Bunsenges. Phys. Chem. **79**, 1186 (1975).
5. H. HOSHINO, R. W. SCHMUTZLER, W. W. WARREN, and F. HENSEL. Philos. Mag. **33**, 255 (1975).
6. J. C. PERRON. Adv. Phys. **16**, 657 (1967).
7. U. SCHINDEWOLF. Angew. Chem. **80**, 165 (1968).
8. J. JORTNER and N. R. KESTNER (*Editors*). Electrons in fluids. Springer-Verlag, Heidelberg. 1973.
9. H. R. BRONSTEIN and M. BREDIG. J. Am. Chem. Soc. **80**, 2077 (1958).
10. R. H. ARENDT and N. H. NACHTRIEB. J. Chem. Phys. **53**, 3085 (1970).
11. B. R. ILSCHNER and C. N. WAGNER. Acta Metall. **6**, 712 (1953).
12. J. E. ENDERBY. *In* Amorphous and liquid semiconductors. *Edited by* J. Tauc. Plenum Press, London. 1974.
13. R. W. SCHMUTZLER, H. HOSHINO, R. FISCHER, and F. HENSEL. Ber. Bunsenges. Phys. Chem. **80**, 107 (1976).
14. W. FREYLAND and G. STEINLEITNER. Ber. Bunsenges. Phys. Chem. **80**, 810 (1976).
15. M. CUTLER and M. F. FIELD. Phys. Rev. **169**, 632 (1968).
16. J. C. THOMPSON. Rev. Mod. Phys. **40**, 704 (1968).
17. N. H. NACHTRIEB. J. Chem. Phys. 1976. To be published.
18. G. STEINLEITNER, W. FREYLAND, and F. HENSEL. Ber. Bunsenges. Phys. Chem. **79**, 1186 (1975).
19. N. NIKOLOSO. Diplomarbeit, University of Marburg, Marburg, Germany. 1976.
20. W. FREYLAND and G. STEINLEITNER. Proceedings of the Third International Conference on Liquid Metals, Bristol, 1976.
21. J. E. ENDERBY. Can. J. Chem. This issue.
22. J. E. ENDERBY. Proceedings of the Second International Conference on Liquid Metals. Taylor and Francis, London. p. 3.
23. J. HAWKER, R. A. HOWE, and J. E. ENDERBY. Proceedings of the Fifth International Conference on Amorphous and Liquid Semiconductors. *Edited by* J. Stuke and W. Bredig. Taylor and Francis, London. 1974.
24. J. GREENBERG. J. Electrochem. Soc. **113**, 937 (1966).
25. D. O. RALEIGH and L. E. TOPOL. J. Chem. Phys. **41**, 3179 (1964).

26. K. ICHIKAWA and M. SHIMOJI. Ber. Bunsenges. Phys. Chem. **71**, 1149 (1967).
27. K. ICHIKAWA and M. SHIMOJI. Ber. Bunsenges. Phys. Chem. **73**, 302 (1969).
28. K. D. KRÜGER and R. W. SCHMUTZLER. Ber. Bunsenges. Phys. Chem. **80**, 816 (1976).
29. K. D. KRÜGER, R. FISCHER, and R. W. SCHMUTZLER. Proceedings of the Third International Conference on Liquid Metals, Bristol, 1976.
30. A. EISENBERG and A. TOBOLSKY. J. Polym. Sci. **46**, 19 (1960).
31. G. C. VEZZOLI and R. J. ZETO. *In* Sulfur research trends. Advances in Chemistry Series. *Edited by* R. F. Gould. American Chemical Society, Washington, DC. 1972.
32. N. F. MOTT and E. A. DAVIS. Electronic processes in noncrystalline materials. Clarendon Press, Oxford. 1971.
33. H. GOBRECHT, D. GAWLIK, and F. MAHDJURI. Phys. Kondens. Mater. **13**, 156 (1971).
34. H. G. DRICKAMER and C. W. FRANK. Electronic transitions and the high pressure chemistry and physics of solids. Chapman and Hall, London. 1973.
35. H. HOSHINO, R. W. SCHMUTZLER, and F. HENSEL. Proceedings of the Third International Conference on Liquid Metals, Bristol, 1976.
36. M. H. COHEN, H. FRITZSCHE, and S. R. OVSHINSKY. Phys. Rev. Lett. **22**, 1065 (1969).
37. W. W. WARREN. Phys. Rev. B, **6**, 2522 (1972).
38. G. BUSCH and H. J. GÜNTHERODT. Phys. Kondens. Mater. **6**, 325 (1967).
39. G. TOURAND, B. CABANE, and M. BREUIL. J. Non-Cryst. Solids, **8–10**, 676 (1972).
40. M. B. GITIS and I. G. MIKHAILOV. Sov. Phys. Acoust. **12**, 17 (1966); **12**, 131 (1966).
41. B. CABANE and J. FRIEDEL. J. Phys. Paris, **32**, 73 (1971).
42. H. ENDO, H. HOSHINO, R. W. SCHMUTZLER, and F. HENSEL. Proceedings of the Third International Conference on Liquid Metals, Bristol, 1976.
43. K. S. PITZER. J. Am. Chem. Soc. **77**, 3427 (1955).
44. F. HENSEL and E. U. FRANCK. Ber. Bunsenges. Phys. Chem. **70**, 1154 (1966).
45. I. K. KIKOIN and A. R. SECHENKOV. Phys. Met. Metallogr. USSR, **24**, 5 (1967).
46. D. R. POSTILL, R. G. ROSS, and N. E. CUSACK. Adv. Phys. **16**, 493 (1967).
47. R. W. SCHMUTZLER and F. HENSEL. Ber. Bunsenges. Phys. Chem. **76**, 531 (1972).
48. W. FREYLAND, H. P. PFEIFER, and F. HENSEL. Proceedings of the Fifth International Conference on Amorphous and Liquid Semiconductors. *Edited by* J. Stuke and W. Bredig. Taylor and Francis, London. 1974.
49. J. TAUC. Amorphous and liquid semiconductors. Plenum Press, New York. 1974.
50. H. OVERHOF, H. UCHTMANN, and F. HENSEL. J. Phys. F, **6**, 523 (1976).
51. M. DEVILLERS and R. G. ROSS. J. Phys. F, **5**, 73 (1975).
52. F. YONEZAWA, Y. ISHIDA, F. MARTINO, and S. ASAMO. Proceedings of the Third International Conference on Liquid Metals, Bristol, 1976.
53. U. EVEN and J. JORTNER. Phys. Rev. Lett. **28**, 31 (1972).
54. U. EVEN and J. JORTNER. Philos. Mag. **25**, 715 (1972).
55. V. EL-HANANY and W. W. WARREN. Phys. Rev. Lett. **34**, 1276 (1975).
56. M. H. COHEN and J. JORTNER. Phys. Rev. Lett. **30**, 696 (1973).
57. M. H. COHEN and J. JORTNER. Proceedings of the Fifth International Conference on Amorphous and Liquid Semiconductors. *Edited by* J. Stuke and W. Bredig. Taylor and Francis, London. 1974.
58. G. SCHÖNHERR. Thesis, University of Marburg, Marburg, Germany. 1977.
59. L. FRIEDMAN. J. Non-Cryst. Solids, **6**, 329 (1971).
60. L. FRIEDMAN. Philos. Mag. **28**, 145 (1973).
61. J. M. ZIMAN. Philos. Mag. **6**, 1013 (1961).
62. J. M. ZIMAN. Adv. Phys. **16**, 578 (1967).
63. T. E. FABER. Adv. Phys. **15**, 547 (1966).
64. H. P. PFEIFER, W. FREYLAND, and F. HENSEL. Ber. Bunsenges. Phys. Chem. **80**, 716 (1976).
65. H. P. PFEIFER. Thesis, University of Marburg, Marburg, Germany. 1977.
66. R. BLOCK, J. B. SUCK, W. GLÄSER, W. FREYLAND, and F. HENSEL. Ber. Bunsenges. Phys. Chem. **80**, 718 (1976).
67. R. BLOCK, J. B. SUCK, W. GLÄSER, W. FREYLAND, and F. HENSEL. Proceedings of the Third International Conference on Liquid Metals, Bistol, 1976.

Discussion

G. R. Freeman: One may plot the conductances of cesium (Hensel and co-workers) and mercury (Jortner and co-workers) against the number of atoms/cm^3 instead of against temperature, and compare them with a similar plot of the mobility of electrons in liquid xenon against density. One finds the band–nonband transition in xenon sandwiched between the densities of the metal–nonmetal transitions in cesium and mercury. The approximate densities of the transitions are 1×10^{21} atom/cm^3 in cesium, 1.2×10^{22} atom/cm^3 in xenon, and 3×10^{22} atom/cm^3 in mercury. The transition in xenon occurs at a density far above the critical density, which is 5×10^{21} atom/cm^3, so is not associated with critical fluctuations. I suspect that the same is true for the transitions in the metals and other systems you mentioned.

F. Hensel: Your comment is certainly true for mercury, for which we believe the metal–nonmetal transition occurs at a density of 9 g/cm^3 which largely exceeds the thermodynamic critical density of 5.3 g/cm^3. But for the alkali metals the existing electrical and thermodynamic data do not exclude that the phase transition and the metal–nonmetal transition are correlated. If it is a Mott transition one really would expect a correlation between the critical point and the metal–nonmetal transition.

M. H. Cohen: I was intrigued by the rise in the structure factor of liquid Rb at small q for high temperatures. Jortner and I have proposed the existence of density fluctuations in liquid Hg at densities of 9 g/cm^3 and below with q of the order of 15 Å in radius. It has just now occurred to me that such density fluctuations may be a universal concomitance of metal–nonmetal transitions involving the development of a pseudogap and ultimately a gap as the density is decreased. The compressibility is determined by the interatomic in-

teractions which are screened by the electronic dielectric function. For small q, the pseudogap causes a screening reduction, nonmetallic forces, and an increased compressibility. For large q, electrons can be scattered across the pseudogap, and their dielectric response is little affected by it. Thus for larger q one has metallic forces and a smaller compressibility. The compressibility, dielectric function, and structure factor are all directly related in such a way that the physical effect described leads to long wavelength density fluctuations for only those densities in the range where a relatively small pseudogap exists. Thus I would welcome the improved experimental results you promised, and, in return, will attempt the relevant theoretical analysis.

F. Hensel: We are very much interested in these questions, and we certainly will try to measure the isothermal compressibility and the structure factor at lower densities (higher temperatures and pressures), especially in the density range of the metal–nonmetal transition. We are mainly interested in two questions, the role of long range fluctuations and the role of short range order, especially the formation of diatomic molecules of the alkali metals on the nonmetallic side.

Hall effect at the metal–nonmetal transition in metal–ammonia solutions[1]

U. EVEN, R. D. SWENUMSON,[2] AND J. C. THOMPSON
Physics Department, University of Texas at Austin, Austin, TX, U.S.A.

Received October 4, 1976

U. EVEN, R. D. SWENUMSON, and J. C. THOMPSON. Can. J. Chem. **55**, 2240 (1977).

The conductivity and Hall coefficient have been measured for solutions of Li, Na, K, and Cs in liquid NH_3 using a double ac method over a concentration range of 1–10 mol% metal (mpm). The conductivities vary from 10^{-1} to near $10^4\ \Omega^{-1}\ cm^{-1}$ and the Hall coefficients from 10^{-6} to $10^{-9}\ m^3\ C^{-1}$ over the 1–10 mpm range. Hall mobilities vary from 10^{-2} to $10^0\ cm^2\ V^{-1}\ s^{-1}$ over the same range. The mobility for Na–NH_3 solutions shows a maximum at 4 mpm while the others are monotonic. The mobility peak in Na–NH_3 solutions appears to be related to the presence of substantial composition fluctuations in that system.

U. EVEN, R. D. SWENUMSON et J. C. THOMPSON. Can. J. Chem. **55**, 2240 (1977).

Utilisant une méthode à double ca, on a mesuré la conductivité et le coefficient de Hall pour des solutions de Li, Na, K et Cs dans l'ammoniac liquide à des concentrations allant de 1 à 10 mol% de métal (mpm). Les conductivités varient de 10^{-1} jusqu'à près de $10^4\ \Omega^{-1}\ cm^{-1}$ et les coefficients de Hall de 10^{-6} à $10^{-9}\ m^3\ C^{-1}$ aux concentrations allant de 1–10 mpm. Aux mêmes concentrations, les mobilités de Hall varient de 10^{-2} à $10^0\ cm^2\ V^{-1}\ s^{-1}$. La mobilité, dans le cas des solutions Na–NH_3, présente un maximum à 4 mpm alors que dans les autres cas elle est monotonique. Il semble que le maximum dans la mobilité, dans le cas des solutions Na–NH_3, soit relié à la présence de fluctuations importantes dans la composition de ce système.

[Traduit par le journal]

1. Introduction

A measurement of the Hall coefficient R_H together with the electrical conductivity σ permits one to determine the carrier concentration ($R_H = (nec)^{-1}$, in the free electron approximation) and the Hall mobility ($\mu_H = \sigma R_H$) as well as Mott's g factor (the ratio of density of states to a free electronic density of states, both at the Fermi level, $g = R_H(\text{free})/R_H$). Such measurements are, therefore, central to any study of electronic transport processes and in particular to studies of the metal–nonmetal transition (1). However, there are ambiguities in interpretation of the Hall effect associated with low mobilities (2), and microscopic inhomogeneities (3–5) or fluctuations. One can relate R_H to the free carrier density only when the mean free path is long; should the free path be shortened by strong scattering processes or inhomogeneities then modifications of the conventional relationship ($R_H = (nec)^{-1}$) are required.

There are two current views of how the metal–nonmetal transition must proceed, one attributed primarily to Mott (1) and the other to Jortner and Cohen (3). We shall examine each in turn, though neither will turn out to be entirely satisfactory.

Mott (1) suggests that, in the strong scattering case, one replaces the usual relation by the Friedman (2) formula

$$R_H = C'/necg \qquad [1]$$

where C' is a constant with a value near unity (perhaps 0.7). Under the same circumstances the conductivity is given by

$$\sigma = \sigma_{min} g^2 C'' \qquad [2]$$

where σ_{min} is near $100\ \Omega^{-1}\ cm^{-1}$ and where C'' is a constant depending on the coordination number, with a value near 0.1. Under these circumstances, one expects $\sigma \propto R_H^{-2}$ or

$$\mu \propto R_H^{-1} \qquad [3]$$

Cutler (6) and also Fritzsche (7) have shown that one can write quite general formulae for the conductivity and thermoelectric power S which, in the case of semiconducting materials, reduce to

$$\sigma = \sigma_0 \exp -[(E_c - E_F)/kT] \qquad [4]$$

and

$$S = -(k/e)[(E_c - E_F)/kT + C'''] \qquad [5]$$

[1]Supported in part by the U.S. NSF under grant No. DMR 75-07828 and by the R. A. Welch Foundation of Texas.

[2]R. A. Welch Predoctoral Fellow.

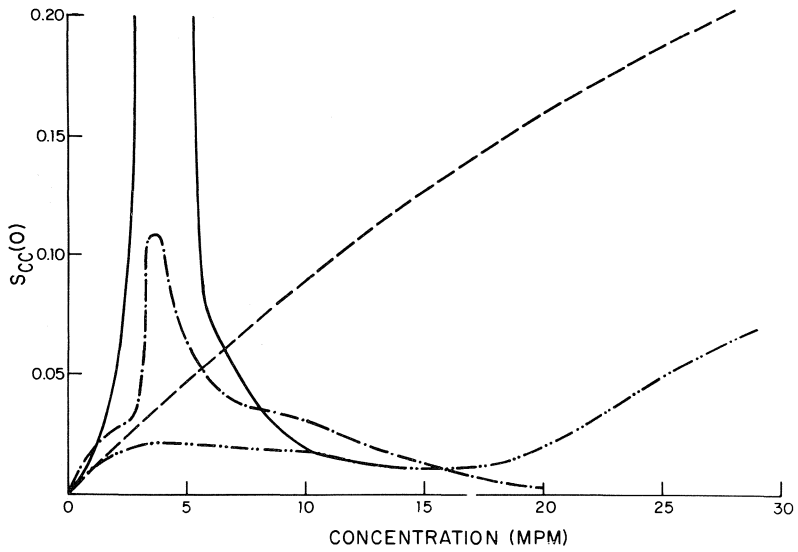

FIG. 1. The concentration correlation function for Li–NH_3 (---), Na–NH_3 (———), and Cs–NH_3 (-·-·-) solutions as a function of concentration is shown. The ideal value is also shown (---). (Reprinted with permission from the Journal of Chemical Physics, **59**, 1680 (1973).)

One therefore expects a model-independent relationship of the form

$$[6] \qquad \ln(\sigma/\sigma_0) = (e/k)S + C''' \qquad$$

where σ_0 and C''' are constants and k is Boltzmann's constant, whenever there is non-degenerate semiconducting behavior, in contrast to the small value of S and a wide variety of values of σ in metallic materials. One may therefore compare values of S and σ to fix the extremes of the metal–nonmetal (M–NM) transitions and use [1]–[3] to describe the transition regime.

If, however, there are microscopic inhomogeneities in the system then Jortner and Cohen (3, 4) suggest that quite a different approach is required. They believe that in many M–NM transitions a fraction C of the material is metallic in nature, containing free electrons in extended states, while the remainder $(1 - C)$ is non-metallic with localized electrons. The various regions are microscopic in size ($\sim$40 Å) and are mixed thoroughly. The problem then becomes one of determining whether a free electron can find a maze-like path from one metallic region to another and thence across the sample. Percolation theory (8) therefore enters. While results have been worked out for simple systems, using computer simulation in the main (4, 5), the problem is immensly complicated, particularly for transport parameters. One has as well to establish the origin of the inhomogeneities.

Since solutions of alkali metals in liquid ammonia (9) have often been used as subjects for the verification of each of the models described above (as well as others), it seems to be worthwhile to determine precisely how the M–NM transition affects σ and R_H in these materials so that a test of the two models can be made.

In Mott's model, we must look for the validity of [1]–[3]. In Cohen's model the test is more complex. If one looks at the phase diagrams of M–NH_3 solutions, it is immediately apparent that Cs–NH_3 solutions differ from the others in that there is no phase separation. This impression is confirmed by an analysis of the metal chemical potentials μ_M. One can calculate the mean square composition fluctuations $\langle(\Delta x)^2\rangle$ from [7],

$$[7] \qquad S_{cc}(0) = \langle(\Delta x)^2\rangle \propto (d\mu_{Na}/dx)^{-1}$$

where x is the metal concentration and $S_{cc}(0)$ is the long wave limit of the concentration correlation function (10). There is no sign in Cs–NH_3 solutions of the large fluctuations one commonly associates with phase separation as may be seen in Fig. 1. Note that there are stronger fluctuations in Na–NH_3 solutions than in the others. The data of Fig. 1 were taken at

$-33°C$ in each case; they are at larger values of $t = (T - T_c)/T_c$ for Li–NH_3 than for Na–NH_3 solutions, where T_c is the consolute temperature. Since fluctuations, and hence the peak in $S_{cc}(0)$, drop off as t increases one might expect the reduced values of $S_{cc}(0)$ for Li–NH_3 solutions. However, the temperature dependence of $S_{cc}(0)$ is not likely to be great enough to explain the total absence of fluctuations in the Cs–NH_3 solutions. This assertion is based on the assumption that the temperature dependence of $S_{cc}(0)$ does not grossly change with solute so that the observed behavior of Na–NH_3 solutions (10) may be taken as indicative of the behavior of solutions with other solutes as well. The absence of a phase separation in Cs–NH_3 solutions (9) is also an indicator of the relative weakness of concentration fluctuations in that system.

The fluctuations seen, say, in Na–NH_3 solutions might well be the origin of inhomogeneities in those solutions (3) while no inhomogeneities from this mechanism (phase separation) are to be expected in Cs–NH_3 solutions. If, indeed, fluctuations are important then clearly Cs–NH_3 solutions should not exhibit the same electrical transport properties in the 1–10 mol% metal (mpm) range as do solutions of the lighter alkalis.

The questions then to be answered by the experiments reported here are the following: (*a*) do all M–NH_3 solutions behave alike and (*b*) do they satisfy the Friedman relations? The next section contains a description of the experiments and the last a discussion of the results.

2. Experimental

The Hall cell was constructed from Pyrex glass plates with tungsten electrodes. A rectangular depression approximately 20 × 5 × 1 mm was ultrasonically milled into one glass plate which was in turn fused to a flat cover plate and the electrodes were then sealed into the edges. Platinum wires were spot-welded to the tungsten on the outside to permit easy soldering of the coaxial cable leads. Lead placement was designed to reduce pick-up. Geometrical constants for conductivity and Hall effect were determined using mercury as a standard. The inside part of the leads was electropolished with a sodium phosphate tribasic solution then electroplated with either gold or silver in a cyanide bath. The cell was rinsed with organic solvents and a dilute HF solution then baked for several hours at 250°C in a vacuum furnace at pressures below 10^{-6} torr. After baking, the cell was taken directly into the glove box to be loaded with metal, closed off, then taken out and attached to the ammonia still.

The lower part of the cell could be heated locally with a 3 W lamp to induce gentle boiling and thus mix the solution. A controlled flow of cold nitrogen vapor was used to maintain the desired low temperature. The nitrogen vapor was obtained as boiloff from a 25 ℓ Dewar containing a 30 W heater in the liquid. A platinum resistance thermometer, placed next to the sample cell, was used to feed a modified temperature controller which powered the heater. Temperature measurement was by a copper–constantan thermocouple attached to the cell; temperature stability and repeatability were ±0.2 K. The gas cooling system has a low heat capacity so that temperature could be changed conveniently.

The conductivity was measured by an ac four-probe method. Current was derived from an audio oscillator (HP 651A) and a 30 W power amplifier (McIntosh MI 75) at 5.2 kHz. The current was measured by a DVM (Keithley 171), and the voltage drop across the sample was measured through a tuned isolation transformer with the same DVM. The precision of the conductivity measurement was better than 2% over five decades of measurement. Accuracy, also near 2%, was limited by the calibration procedure.

The Hall coefficient measuring system uses the double ac method (11–13). The system can be subdivided into seven parts which are described in turn.

(*a*) The laminated iron-core, homebuilt magnet (14) had a field region of 40 × 100 × 100 mm. A series resonance for operation at about 200 Hz was achieved by connecting a 1 μF high-voltage capacitor. When fed by an audio oscillator and power amplifier (McIntosh MI 350) a highly stable (0.1%) 1 kG rms field was established. Stability and harmonic purity (0.1% total harmonic distortion) are essential for this method of measurement. Homogeneity of the field over the volume of the sample was about 1%. Normal air convection cooling of the magnet was sufficient.

(*b*) The sample current, at about 5.2 kHz, was produced as in the conductivity experiment. A 0.1 μF capacitor in series with the power output of the amplifier prevented the low frequency magnetic field pick-up from mixing with the current frequency at the output stage of the amplifier. Otherwise a false Hall signal would have been created.

(*c*) The Hall signal was stepped up by a 50:1 transformer wound on a 'pot-core' ferrite and tuned to resonate at the sum frequencies of field (0.2 kHz) and current (5.2 kHz). A capacitor at the input served as a high-pass filter. The preamplifier was an 'Ortec-Brookdeal 9452 precision ac amplifier' which has the necessary linearity (10 ppm), low noise, and band width needed at this stage.

(*d*) A ferrite-wound L–C circuit connected in a resonance-notch configuration passed the 5.4 kHz signal and attenuated the 0.2 kHz pick-up from the magnet, thus serving as an intermediate stage of filtering.

(*e*) A Brookdeal phase sensitive detector (9412a) referenced to the 5.2 kHz current frequency was used as a first stage demodulator. The Hall signal was thus transformed to 0.2 kHz, while the bothersome misalignment voltage at the current frequency was converted to easily filtered dc. This mode of operation allows large interference at the current frequency without necessitating special filtering or bucking signals. Nevertheless every

effort was made to position the Hall probes so that misalignment voltage was minimum.

(*f*) A PAR lock-in amplifier (128), referenced to the magnetic field frequency, was used as the final demodulator to convert the Hall signal to dc.

(*g*) A simple multiplier circuit, fed by the audio oscillators generating the current and magnetic field, was used to generate a signal of known level at the sum frequency of 5.4 kHz. This signal was injected through a step-down transformer in series with the cell to compensate for the wide variation in conductivity expected in this study.

System parameters and performance may be summarized as follows.

(*1*) sample impedance: 10^{-3}–10^{2} Ω;
(*2*) current at 5.2 kHz: 10^{-3}–10^{0} A (rms);
(*3*) field at 0.2 kHz: 10^{0}–10^{3} G (rms);
(*4*) equivalent noise at input: 0.1 nV at 10 s integration;
(*5*) precision of Hall voltage: 1%;
(*6*) dynamic range: 120 dB.

A portion of the dynamic response curve is given in Fig. 2.

Samples of the required alkali metal were cut from vacuum-packed ampoules (99.99%) inside a helium-filled glove box and loaded into the freshly baked cell. Ammonia gas, passed though a charcoal trap and condensed onto sodium, was then distilled into the cell after it was placed in the magnet. Concentrations were determined to within 0.1 mpm from the weight of the metal and the volume of gas transferred. Successive transfers of NH_3 varied the concentration. All solutions were stable throughout the measurement period with negligible evolution of hydrogen.

In common with previous investigators (11, 14, 15) we have encountered severe electrode problems at concentrations below 5 mpm and particularly below 3 mpm. We have employed a variety of electrodes: Au, W, Ag-plated W, Au-plated W, and Cs-plated W (the latter for solutions containing no Cs). None was satisfactory in every solution and it is abundantly clear that the 'chemistry' of the electrodes in M–NH_3 solutions is controlling. For example, clean W was sufficient in Cs–NH_3 solutions. We presume Cs to be sufficiently reactive to clean the electrode and the oxide (?) sufficiently soluble to be removed from the electrode region. Pure Au electrodes were noticeably reduced in size following an experiment in K–NH_3 solutions.

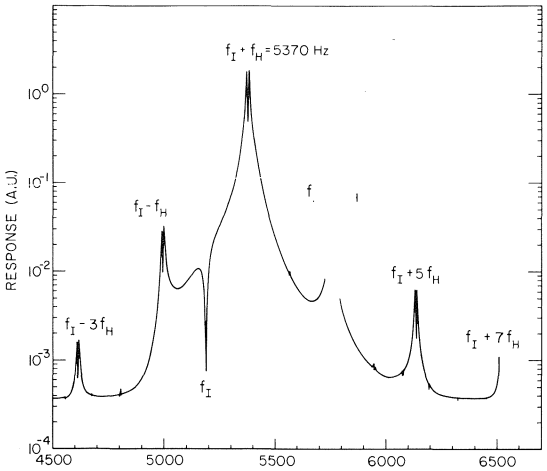

FIG. 2. The dynamic system response for the Hall measurement is shown. Hall data were taken at $f_I + f_H$ = 5370 Hz, where f_I = current frequency and f_H = magnetic field frequency.

In ac Hall effect measurements, the fundamental problem is that any nonlinearity in the electrode–solution interfacial resistance (or in the detection system, see above) can introduce a 'mixing' effect thereby producing a signal at the same frequency (though possibly a different phase) as the Hall voltage itself. The superposition of these two signals will then produce a false Hall voltage. Thus problems arise in measurement of R_H but not in the conductivity. In Li–NH_3 solutions the value of R_H decreases by two orders of magnitude as the electrode is changed from 'clean' W, to W coated with Cs, Ag, or Au. Furthermore, solutions of the lighter alkalis exhibit a reversal in the sign of R_H as the concentration is reduced below 2.5 mpm with noble-metal-coated W electrodes. With Ag-plated W electrodes, the application of a steady state (dc) current between one Hall (+) and one current electrode (−), of several mA for periods of several minutes would cause a further irreversible reduction of the Hall voltage V_H. We took this as an indication of a film coating (possibly oxide) on the Hall electrode and rejected data obtained with such electrodes. Pure Au electrodes were satisfactory in both Li–NH_3 and Na–NH_3 solutions, but were dissolved in K–NH_3 solutions where Ag-plated W was apparently successful.

The data reported here are regarded as 'true' on the basis of the following criteria. (*1*) These results were reproducible from run to run and cell to cell. (*2*) Values of V_H are linear in current and field. (*3*) Values of V_H do not change following prolonged operation of a cell with large dc currents between the Hall and other electrodes. (*4*) If a given concentration is reproduced during the course of a run, the same V_H was obtained. (*5*) Microscopic examination of the electrodes following an experiment failed to reveal any contamination or etching.

All data were taken at the consolute point plus 10 K, except with Cs where the temperature was −55°C.

3. Results and Discussion

We have obtained σ and R_H on solutions of Li, Na, K, and Cs in liquid NH_3 as well as density data for Cs–NH_3 solutions. Figures 3–6 display the measured values of σ and R_H for each solution and, in addition, the Hall mobility derived from the measured parameters. In each case the conductivities range from 10^{3}–10^{-1} Ω^{-1} cm^{-1} over the 10–1 mpm range of the M–NM transitions and are consistent with those of previous workers (9); R_H varies from 10^{3}–10^{0} in units of 10^{9} m^3/C except in Cs–NH_3 solutions where the maximum value is 10^{2}. These data

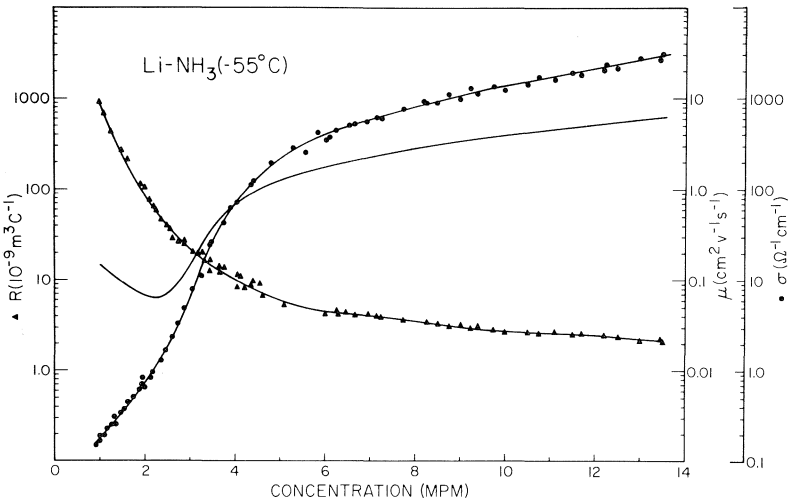

FIG. 3. The conductivity, mobility, and Hall coefficient for Li–NH_3 at −55°C are shown. The conductivity is denoted by ●, R_H by ▲, and μ_H by the solid line.

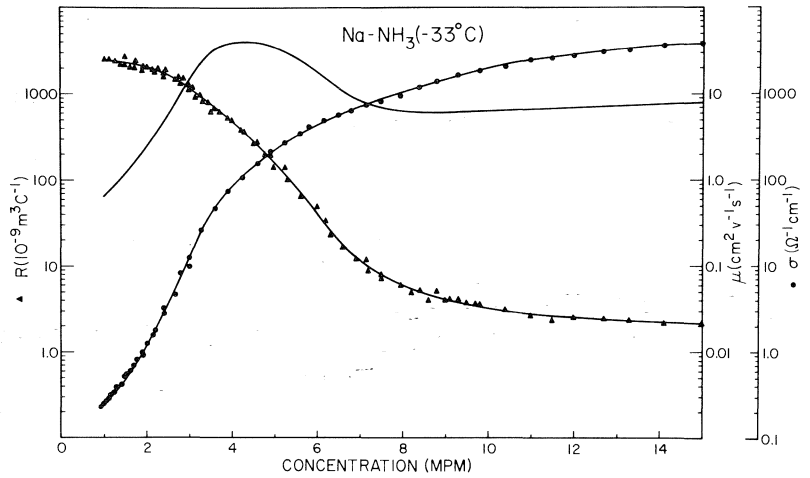

FIG. 4. The conductivity, mobility, and Hall coefficient for Na–NH_3 at −33°C are shown. Legend as in Fig. 3.

are not consistent with the meager data previously reported in the 1–5 mpm range, where electrode problems are most severe, but are in agreement with data reported at higher concentrations. The present data show less scatter and are considerably more extensive than those reported previously (9).

For concentrations above 6 mpm, *all* electrodes gave the same results within our precision of about 5% with no systematic differences. In addition these data are consistent with previous data (9). Below 6 mpm the precision of the data presented in Figs. 3–6 is near 10%. Inasmuch as the rejected data differed from those presented in both magnitude and sign it is difficult to assign absolute error bars. Since the data presented lie close to plausible extrapolations of the curves obtained above 6 mpm and, in particular, the high mobility of the Na–NH_3 solutions is observed above 6 mpm, we infer that the accuracy is also near 10%. Older data in the 1.5–6 mpm range are sufficiently sparse and scattered as to make comparison unrewarding.

The σ data are compared in Fig. 7, and may be seen to be essentially independent of solute.

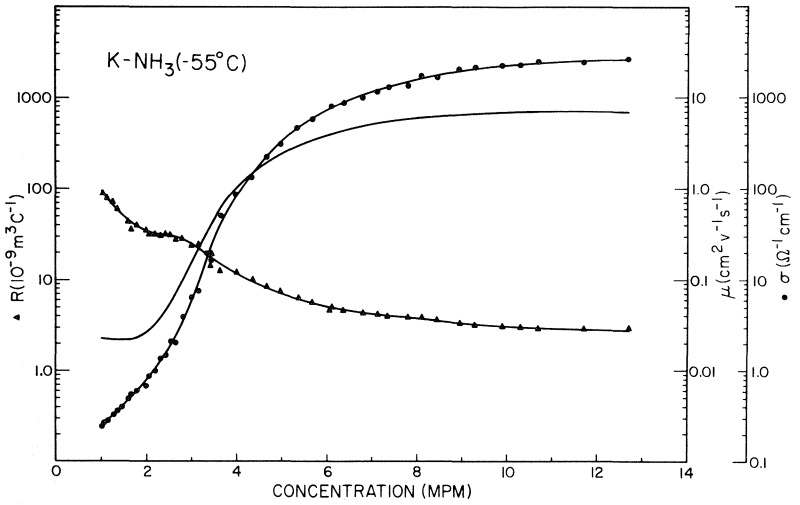

FIG. 5. The conductivity, mobility, and Hall coefficient for K–NH_3 at −55°C are shown. Legend as in Fig. 3.

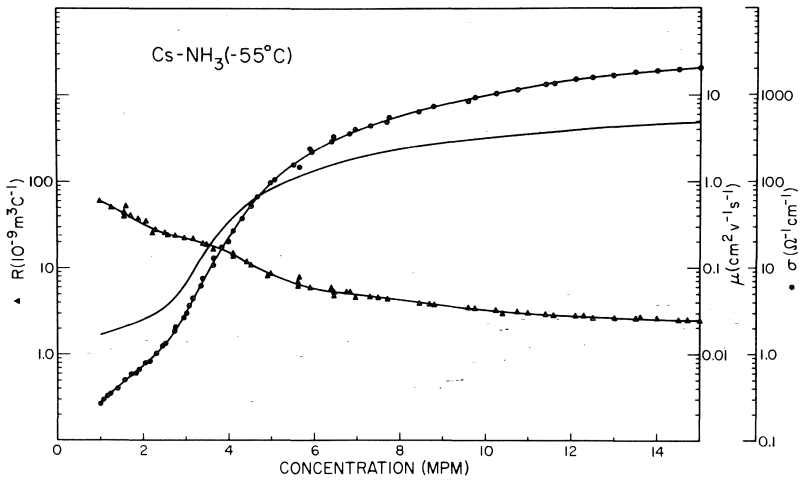

FIG. 6. The conductivity, mobility, and Hall coefficient for Cs–NH_3 at −55°C are shown. Legend as in Fig. 3.

The minimum metallic conductivity[3] σ_{min} of $100\ \Omega^{-1}\ cm^{-1}$ occurs near 4 mpm or at a solute number density of $10^{21}\ cm^{-3}$. Mobilities are compared in Fig. 8, where the Na–NH_3 data may be clearly seen to be different. Note that mobilities are near unity at the concentration for which $\sigma = \sigma_{min}$, except for Na–NH_3 solutions. There is a minimum mobility of $0.06\ cm^2\ V^{-1}\ s^{-1}$ in Li–NH_3 solutions.

If concentrations are normalized to that for which $\sigma = \sigma_{min}$, then the M–NH_3 solutions are even more alike as may be seen in Fig. 9 where σ data (13) for expanded Cs and Hg vapors are also displayed. The M–NH_3 solutions form a class of their own as might be expected from the different scattering mechanisms operative in the pure metal vapors. The nonmetallic states are different in the two (or three) sorts of material and the NH_3 molecules must also have an effect. The pure Cs conductivity is, however, strikingly close to that of the solutions.

Differences among the M–NH_3 solutions are

[3]The relevant concentrations are 10.5 mpm for Na–NH_3 and Cs–NH_3 and 5.4 and 6.2 mpm for Li–NH_3 and K–NH_3, respectively. For Hg, ρ_0 is 11 g cm^{-3}.

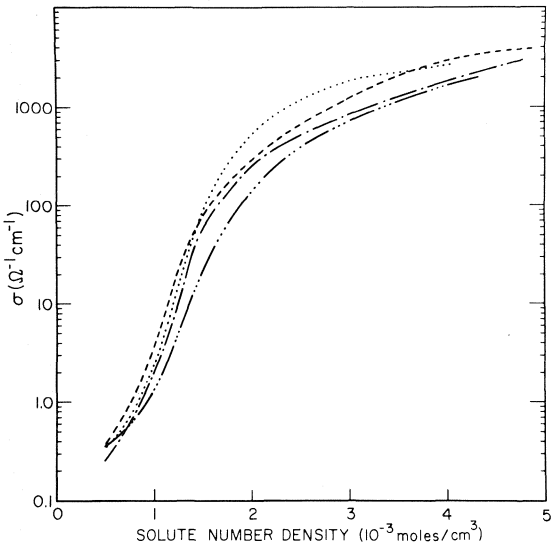

FIG. 7. The conductivities of Li–NH_3 (---), Na–NH_3 (---), K–NH_3 (···), and Cs–NH_3 (·····) solutions as a function of solute number density are shown.

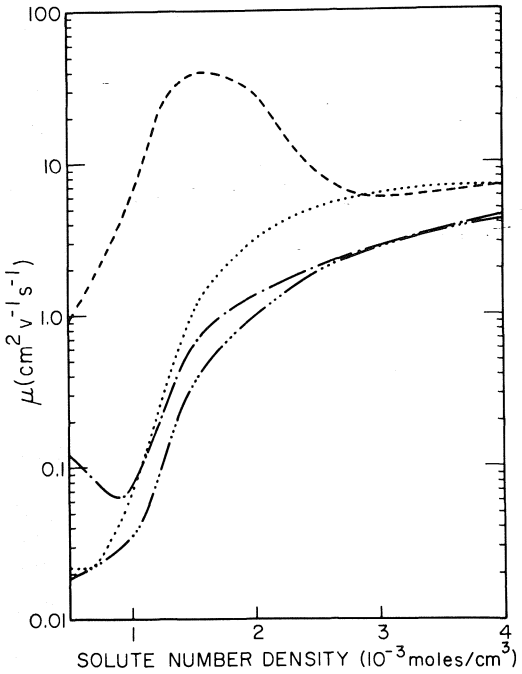

FIG. 8. The mobilities of Li–NH_3, Na–NH_3, K–NH_3, and Cs–NH_3 solutions as a function of solute number density (same notation as Fig. 1) are shown.

most apparent when the ratio of free-electron Hall coefficient to that measured (or the Mott g factor) is plotted against a concentration normalized to $\rho_0(\neq \rho_c)$. The density ρ_0 is defined by the intersection of the linear extension of that portion of the ratio (g) which lies below unity with the $g = 1.0$ line.[3] Here one finds a clear trend in that those solutions with larger fluctuations (as in Fig. 1) have a more rapid decrease of g as ρ/ρ_0 decreases below unity (see Fig. 10). The order is Na, Li, K, Cs. The pure Hg data show a drop-off even more rapid than any of the M–NH_3 solutions.

Mott suggests that the M–NM transition occurs when g falls to $\frac{1}{3}$. In the present instance g never quite reaches that value for the low-fluctuation, most homogeneous solutions of K and Cs. In Na–NH_3 solutions g is $\frac{1}{3}$ at 7 mpm where the conductivity is $700\ \Omega^{-1}\ cm^{-1}$ while in Li–NH_3 solutions the concentration is near 2.5 mpm and σ is only $4\ \Omega^{-1}\ cm^{-1}$. All attempts to reconcile these data with the Friedman formula, eq. 3, have also failed, as have similar efforts with the older data (1, 9).

Though Na–NH_3 solutions behave quite differently from the others so that it is possible to assign a role to the enhanced fluctuations seen in that system, it is nevertheless difficult to assess the details of that role. Certainly the straightforward application of percolation theory (3, 5) cannot reproduce the behavior of Na–NH_3 solutions though Li–NH_3 can be so described.

The mobility for electrons in Na–NH_3 solutions is shown in Fig. 11. Mobility maxima are also found for excess electrons in fluid Ar, Kr, and Xe (16). Those maxima occur at substantially higher *fluid* densities ($10^{22}\ cm^{-3}$) than the *solute* densities of the present experiments. The overall fluid densities are comparable. The maximum mobility in Xe is two orders of magnitude larger than that reported here. In the absence of any real theory of the maxima in the noble gases any relevance of the similarity to Na–NH_3 solutions must be questionable.

In summary our results must be regarded as inconsistent both with the Friedman formula and with the simple inhomogeneous model. The evidence for the importance of fluctuations may be regarded as strong but not yet conclusive. Efforts to confirm the effects of fluctuations are underway.

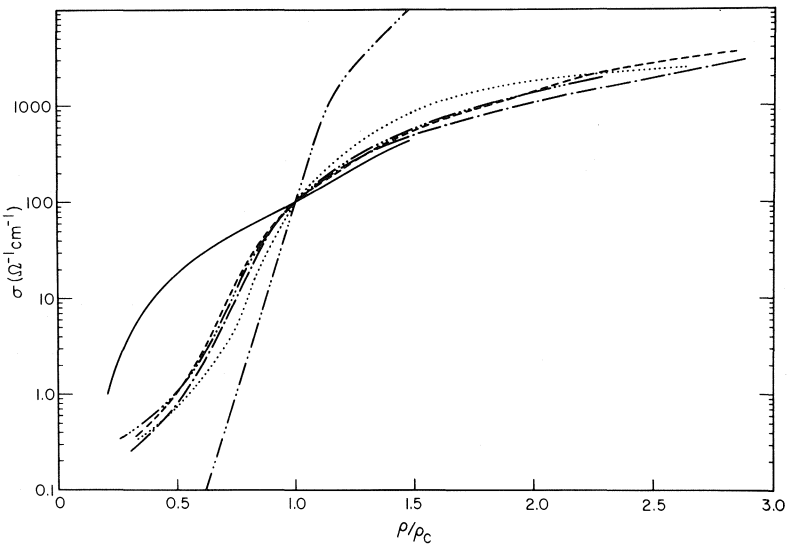

FIG. 9. The conductivities of Li–NH_3, Na–NH_3, K–NH_3, Cs–NH_3 solutions and expanded Cs (———) and Hg (····) systems *vs.* ρ normalized to the value of ρ where $\sigma = 100\,\Omega^{-1}\,cm^{-1}$ are shown.

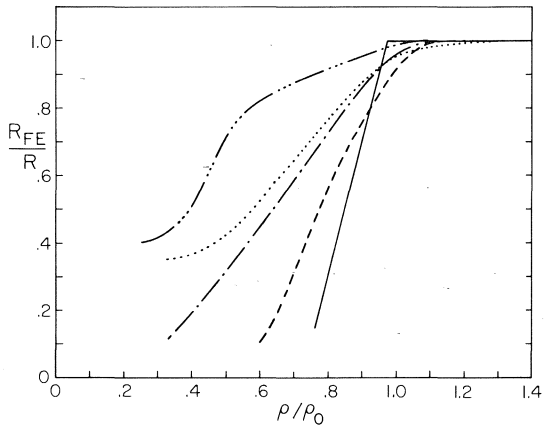

FIG. 10. R_H(free)/R_H for the systems Li–NH_3, Na–NH_3, K–NH_3, Cs–NH_3, and Hg(····) is shown. The value of ρ_0 is given in the text. The abscissa ρ/ρ_0 is defined in the text.

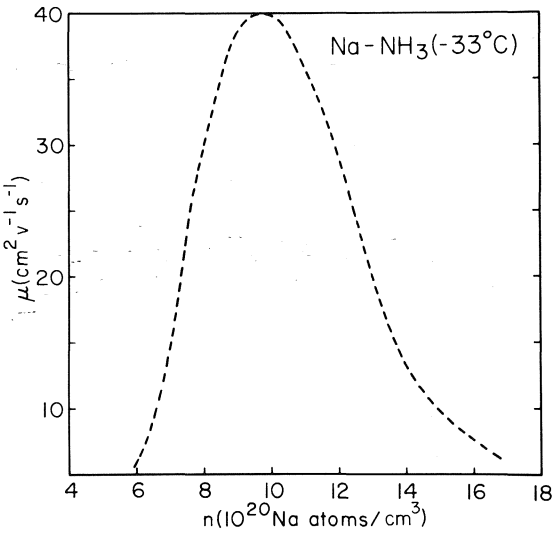

FIG. 11. The mobility of Na–NH_3 solutions at −33°C as a function of the Na number density is shown.

1. N. F. MOTT. Metal–insulator transitions. Taylor and Francis, London. 1974.
2. L. FRIEDMAN. J. Non-Cryst. Solids, **6**, 329 (1971).
3. J. JORTNER and M. H. COHEN. J. Phys. Chem. **79**, 2900 (1975).
4. I. WEBMAN, J. JORTNER, and M. H. COHEN. Phys. Rev. B, **11**, 2885 (1975).
5. R. D. SWENUMSON and J. C. THOMPSON. Phys. Rev. B, **14**, 5142 (1976).
6. M. CUTLER. Philos. Mag. **25**, 173 (1972).
7. H. FRITZSCHE. Solid State Commun. **9**, 1813 (1971).
8. S. KIRKPATRICK. Rev. Mod. Phys. **45**, 574 (1973).
9. J. C. THOMPSON. Electrons in liquid ammonia. Clarendon Press, Oxford. 1976.
10. K. ICHIKAWA and J. C. THOMPSON. J. Chem. Phys. **59**, 1680 (1973); **62**, 4958 (1975).
11. D. S. KYSER and J. C. THOMPSON. J. Chem. Phys. **42**, 3910 (1965).
12. H. L. MCKINZIE and D. S. TAUNHAUSER. J. Appl. Phys. **40**, 4954 (1969).
13. U. EVEN and J. JORTNER. *In* Electrons in fluids.

Edited by J. Jortner and N. R. Kestner. Springer-Verlag, Heidelberg. 1973. p. 363.
14. R. D. NASBY and J. C. THOMPSON. J. Chem. Phys. **53**, 109 (1970).
15. J. A. VANDERHOFF and J. C. THOMPSON. J. Chem. Phys. **55**, 105 (1971).
16. T. KIMURA and G. R. FREEMAN. Can. J. Phys. **52**, 2220 (1974).

Discussion

G. R. Freeman: Could the difference between the concentration dependences of the conductivities of cesium vapor and the metal–ammonia solutions, at low concentrations, be attributed to the dielectric constant of the ammonia?

J. C. Thompson: I think not. The scattering mechanisms are just too dissimilar to be treated the same way (with or without a dielectric constant) in the metal vapors as in $M–NH_3$ solutions.

G. R. Freeman: The greater slope of the conductance–density plot of liquid mercury might be associated with the fact that mercury atoms contain two paired valence electrons, whereas the alkali metal atoms contain only one valence electron.

J. C. Thompson: There is some evidence for Cs_2 in the vapor. A diatomic molecule is equivalent to a divalent atom. Hence a band-crossing basis for the M–NM transition is possible. Otherwise I would agree that the different valences of Cs and Hg are dominant.

The study of primary and secondary charge carriers in nanosecond pulse irradiated liquid dielectrics using a resonant microwave cavity

JOHN M. WARMAN, PIERRE P. INFELTA, MATTHIJS P. DE HAAS, AND ANDRIES HUMMEL

Interuniversity Reactor Institute, Mekelweg 15, Delft, The Netherlands

Received October 27, 1976

JOHN M. WARMAN, PIERRE P. INFELTA, MATTHIJS P. DE HAAS, and ANDRIES HUMMEL. Can. J. Chem. **55**, 2249 (1977).

A microwave resonant cavity technique for studying changes in conductivity of pulse irradiated dielectric liquids is presented. The sensitivity of the method is such that transient changes in conductivity of 5×10^{-9} ohm cm^{-1} can be measured with a signal to noise ratio of 10 and a response time of approximately 10 ns. The use of the technique is illustrated by a study of primary (excess electron, hole) and secondary (molecular ions derived from solutes) charge carriers in the saturated hydrocarbon liquid *trans*-decalin. The temperature dependences of the mobilities of the excess electron and hole are found to be described quite well by $\mu(-) = 25 \exp(-4500/RT)$ $cm^2\ V^{-1}\ s^{-1}$ and $\mu(+) = 4.0 \times 10^{-3} \exp(500/RT)$. The mobility of the hole is found to exceed that of the electron below approximately 10°C. The sum of the mobilities of the secondary ions at 22°C in a 5×10^{-3} *M* SF_6 plus 10^{-2} *M* benzene solution is 5.2×10^{-4} $cm^2\ V^{-1}\ s^{-1}$. In order to determine the mobilities of even the primary charge carriers consideration had to be given to the presence of geminate ion pairs on the time scale of the observations. The way in which corrections for geminate ion pairs were carried out is fully discussed.

JOHN M. WARMAN, PIERRE P. INFELTA, MATTHIJS P. DE HAAS et ANDRIES HUMMEL. Can. J. Chem. **55**, 2249 (1977).

On présente une technique de cavité résonante de microonde pour l'étude des changements dans la conductivité de liquides diélectriques irradiés par pulsation. La sensibilité de la méthode est telle que des changements temporaires dans la conductivité de l'ordre 5×10^{-9} ohm cm^{-1} peuvent être mesurés avec un rapport de signal à bruit de 10 et un temps de réponse approximatif de 10 ns. On illustre la technique par une étude des porteurs de charges primaires (excès d'électron et trou) et secondaire (ions moléculaires dérivés de solutés) dans la décaline-*trans* qui correspond à un hydrocarbure saturé/liquide. On a trouvé que les relations qui existent entre la température et la mobilité des électrons en excès et des trous peuvent être assez bien décrites par les relations $\mu(-) = 25 \exp(-4500/RT)$ $cm^2\ V^{-1}\ s^{-1}$ et $\mu(+) = 4.0 \times 10^{-3} \exp(500/RT)$. On a trouvé que la mobilité du trou excède celle de l'électron en dessous d'une température approximativement égale à 10°C. La somme des mobilités des ions secondaires à 22°C dans une solution de 5×10^{-3} *M* SF_6 plus 10^{-2} *M* de benzène est de 5.2×10^{-4} $cm^2\ V^{-1}\ s^{-1}$. Afin de déterminer les mobilités même des porteurs de charges primaires, on a dû faire entrer en considération la présence de paires d'ions géminés sur l'échelle de temps des observations. On discute de la manière par laquelle les corrections pour les paires d'ions géminés ont été effectuées.
[Traduit par le journal]

Introduction

The use of microwave techniques to study transient changes in the conductivity of pulse irradiated liquid hydrocarbons on a nanosecond time scale was reported by three of the present authors (1) in 1973. At that time the sensitivity of the apparatus was such that only signals due to relatively high mobility ($\mu \geq 1\ cm^2\ V^{-1}\ s^{-1}$) charge carriers could be detected. Subsequently, improvements in the components used and in the theoretical understanding and design of the experiment resulted in the use of this technique to observe primary positive ions with mobilities on the order of $10^{-2}\ cm^2\ V^{-1}\ s^{-1}$ in liquid cyclohexane and methylcyclohexane (2, 3).

A further increase in sensitivity has recently been achieved by the use of a low *Q* resonant cavity as the irradiation cell. It is the purpose of the present paper to demonstrate how this has resulted in the possibility of studying not only high mobility primary charge carriers but also secondary (molecular) ions on a nanosecond time scale. The use of the method will

be illustrated by results obtained in the saturated hydrocarbon liquid *trans*-decalin (*trans*-decahydronaphthalene).

Experimental

The *trans*-decalin (Merck) was distilled on a 90 theoretical plate column (Fisher "Spaltrohr-system"). The distilled solvent was passed through a column of activated silica gel, bubbled with N_2, degassed on a grease-free vacuum line, and distilled into a bulb containing sodium–potassium alloy (MSA Research Corp.) where it was allowed to stand several days before use. The liquid was transferred from the NaK bulb to a glass bulb attached to the microwave cell by distillation on a heated (*ca.* 60°C) vacuum line. The volume of liquid transferred (*ca.* 16 ml) was determined by weighing the cell before and after filling.

Known amounts of the solutes SF_6, NH_3, and benzene were added by distilling them from calibrated volumes into the cell bulb which was immersed in liquid nitrogen. The pressure of solute in the calibrated volume was measured using a capacitance manometer (MKS Instruments). The concentrations of SF_6 and NH_3 in the liquid phase were calculated using Ostwald solubility coefficients of 0.78 and 2.1 respectively which were measured in our laboratory.

The microwave cell used in the present experiments was designed as an iris coupled, rectangular resonant cavity. The cell consisted basically of a 4 cm length of X-band waveguide (internal dimensions 1 cm × 2.3 cm) which was completely closed at one end with a 1 mm thick copper plate. On the other end was fitted a 0.5 mm thick copper plate with a central coupling hole of 8 mm diameter which was sealed by a thin sheet of mica attached with epoxy cement. The cell was further fitted with a flange for attachment to the waveguide circuit and had a connecting hole in the 'upper' broadwall side to allow admission of liquid from the attached, via a metal–glass transition, glass bulb. The upper broadwall side was reduced to a thickness of 0.5 mm for a length of 3 cm from the completely closed end to allow transmission of the electron beam.

The cell was irradiated with 3 MeV electrons from a Van de Graaff accelerator using pulse widths of 20, 50, and 250 ns. The total charge in the pulse, Q nC, was measured by deflection of the beam onto a 50 ohm coaxial target and integration of the current using a Keithly model 616 electrometer. The dose absorbed by the liquid, under the present conditions, was $8.9 \times 10^{14} Q\rho$ eV cm^{-3} where ρ g cm^{-3} is the density of the liquid. For a 20 ns pulse the total dose absorbed was approximately 1.2×10^{16} eV cm^{-3} (*ca.* 200 rad). For a yield $G(100\text{ eV})^{-1}$ of ion pairs, for which the sum of the ion mobilities is μ, the change in conductivity of the medium will be

$$[1] \quad \Delta\sigma = Ne\mu$$

$$[2] \quad = 1.42 \times 10^{-6} Q\rho G\mu \text{ ohm cm}^{-1}$$

Changes in the microwave power reflected from the cell were measured using microwave circuitry almost identical to that published previously (1). The ac output of the detector diode (AEI 1502F, schottky barrier) was amplified × 100 by a Hewlett Packard 462A amplifier prior to being fed into a Tektronix 7904 transient digitizer and displayed on a Tektronix 604 monitor. The overall response time of the system of 10 to 15 ns was controlled principally by the response time of the cavity.

When filled with decalin ($\varepsilon_r = 2.159$) at 22°C the loaded quality factor, Q_L, of the cavity at its resonance frequency of 8.810 GHz was determined to be 467. At the minimum of the resonance the ratio, R_0, of the microwave power reflected by the cavity to the incident power level was 0.453. For such a cavity, it has been derived[1] that a small change in the conductivity of the medium within the cell, $\Delta\sigma$, will result in a change in the level of the reflected power, P_r, given by

$$[3] \quad \frac{\Delta P_r}{P_r} = \mp \frac{Q_L(1/\sqrt{R_0} \pm 1)}{\pi f_0 \varepsilon_0 \varepsilon_r} \Delta\sigma$$

In [3] f_0 is the resonance frequency, ε_0 is the permittivity of vacuum, and ε_r is the relative dielectric constant of the medium. As can be seen in [3] an increase in conductivity of the medium may result in a decrease in reflected power (absorption) or an increase in reflected power (emission). These two possibilities result from the fact that the cavity may be over or undercoupled respectively at resonance. If an absorption is observed the upper signs in [3] should be used, and for an emission signal the lower.

Equation [3] is based on irradiation of the total length, d, of liquid within the cavity. In most practical cases, including the present, a length d_i at the back of the cavity is irradiated. Taking this into account, the relationship between ΔP_r and the change in conductivity in the irradiated length becomes

$$[4] \quad \frac{\Delta P_r}{P_r} = \mp \frac{Q_L(1/\sqrt{R_0} \pm 1)}{\pi f_0 \varepsilon_0 \varepsilon_r} \times \frac{2\pi n d_i/d - \sin(2\pi n d_i/d)}{2\pi n} \Delta\sigma$$

where n is the number of half wavelengths in the cavity.

In the present case an absorption signal is found on irradiation of decalin within the cavity and substitution for the various parameters either known or measured in [4] gives

$$[5] \quad \Delta P_r/P_r = -1.53 \times 10^3 \Delta\sigma$$

for conductivity in units of ohm^{-1} m^{-1}. The conductivity change in units of ohm^{-1} cm^{-1} may be obtained from the observed change in reflected power using

$$[6] \quad \Delta\sigma = -6.54 \times 10^{-6} \Delta P_r/P_r \text{ ohm}^{-1} \text{ cm}^{-1}$$

From [2] and [6], the product of the ion pair yield and sum of the mobilities may then be obtained from

$$[7] \quad G\mu = -\frac{4.61}{Q\rho} \frac{\Delta P_r}{P_r}$$

[1]P. P. Infelta, M. P. de Haas, and J. M. Warman. Derivation to be published.

Using signal averaging of 16 pulses the noise level of the present system allows the measurement of a one part per thousand change in P_r with a signal to noise ratio of approximately 10. Conductivity changes of 5×10^{-9} ohm^{-1} cm^{-1} can therefore be accurately measured. This corresponds to a concentration of 3×10^{10} ions cm^{-3} or 5×10^{-11} M of a charge carrier of unit mobility (in cm^2 V^{-1} s^{-1}). Since doses up to 1 krad (50 ns, 1 A pulse) can be deposited in the liquid, values of the product $G\mu$ as low as 5×10^{-5} (100 eV)$^{-1}$ cm^2 V^{-1} s^{-1} can be readily measured.

Conventional dc conductivity methods are in theory two to three orders of magnitude more sensitive than the present method. However, in practice the ultimate sensitivity of dc methods is difficult to attain. This is due to problems of impedance matching of the cell to the transmission line which results in 'ringing' and to spurious transients resulting from 'pick-up' from the pulsed source of radiation. The latter is of considerable importance when the liquid is irradiated directly with electrons. Using microwave methods considerably diminishes this problem since the waveguide used has the effect of filtering out electromagnetic impulses with frequencies other than those which can propagate. The result is that, at least for electron irradiation, the present method is at least as sensitive as dc techniques presently in use.

Results and Discussion

Qualitative Considerations

One of the principal problems in the study of the conductivity of irradiated systems is the determination of the relative contributions to the conductivity of the positive and negative charge carriers. The method used in the present work is based on the knowledge, from radiation chemical studies, that certain compounds are capable of reacting specifically with one or other of the primary charge carriers formed in irradiated hydrocarbon liquids. These reactions lead to the formation of secondary molecular ions with corresponding changes in the total mobility as shown in the following scheme.

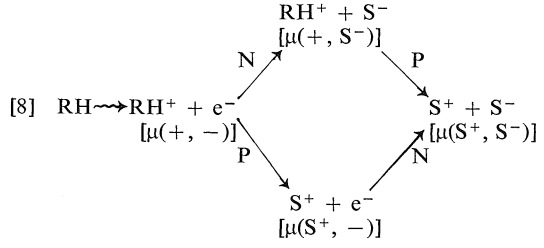

Of particular interest is whether or not a primary charge carrier, electron, or hole, has a mobility significantly larger than that of a molecular ion whose motion depends on molecular displacements within the medium. A qualitative answer to this question may be obtained from measurements of the conductivity induced by a given pulse under conditions of added solute(s) corresponding to the different stages in the above reaction scheme.

Such measurements are shown in Fig. 1 for the case of *trans*-decalin at 22°C to which 5×10^{-3} M SF_6 and 7×10^{-3} M NH_3 were added as electron and hole scavengers respectively. The conductivity signal in the case of the fully scavenged system, lowest trace, is seen to be considerably smaller than that in pure decalin, particularly at longer times, indicating that at least one of the primary charge carriers has a mobility considerably larger than that of a molecular ion. The initial rapid decay of the conductivity in the fully scavenged case, which is more fully discussed below, is due to the presence of a large yield of geminate ion pairs on a nanosecond time scale in such systems as is well known from optical pulse radiolysis studies (4, 5). Addition of either SF_6 or NH_3 singly to *trans*-decalin results in a decrease in the conductivity signal by a factor of approximately two in both cases, the remaining signal being considerably larger than that in the fully scavenged system. It may be argued, from these observations, that both of the primary ions in *trans*-decalin have mobilities considerably larger than those of molecular ions and that, at 22°C, the electron and hole mobilities are of the same order of magnitude.

In order to derive absolute values for the mobilities of primary and secondary ions from measured conductivities, it is necessary to know the total yield of ion pairs present at a given time following the pulse. In a previous publication (3), values of the mobilities of the primary charge carriers in some hydrocarbon liquids were estimated based on the assumption that all geminate ion pairs underwent recombination on a time scale much shorter than the pulse length and that therefore the yield of ion pairs present at the end of the pulse was equal to the free ion yield. As mentioned above, on the time scale of the present experiments, this is known not to be the case when both primary ions are scavenged and, even for the singly scavenged systems, the initial somewhat faster decay, shown by the traces in Fig. 1, is indicative of the presence of a significant yield of geminate ion pairs. An analysis of the possible con-

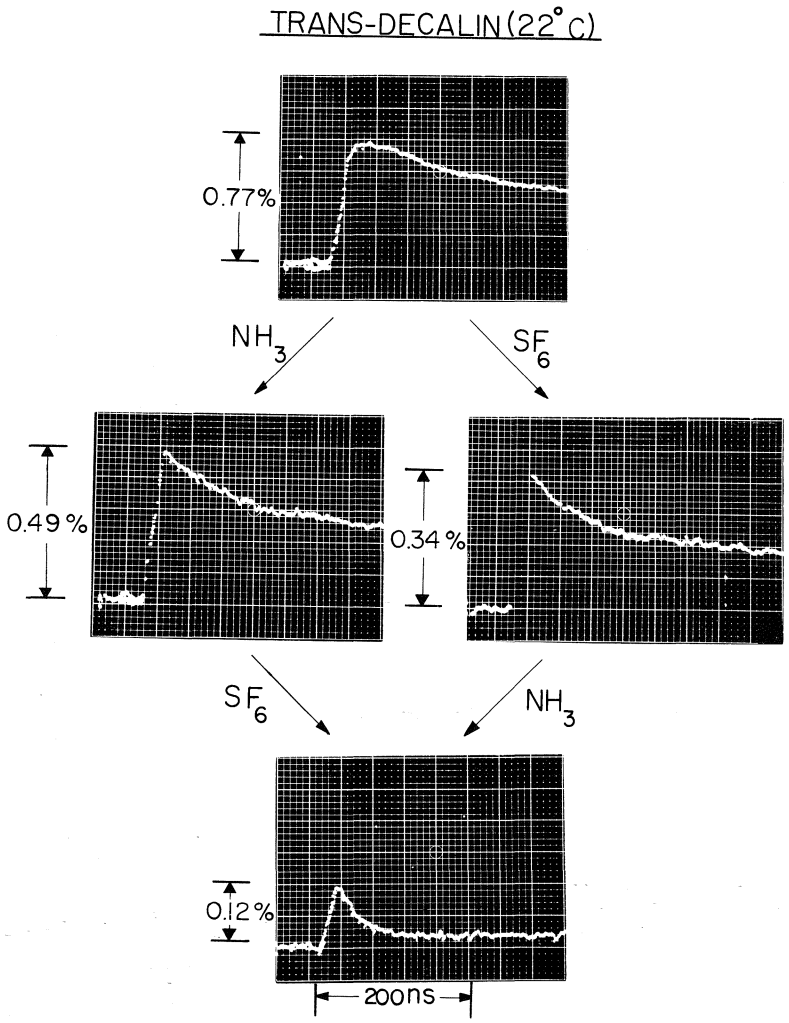

FIG. 1. Monitor traces of the absorption of microwave power resulting from pulse irradiation (20 ns, *ca.* 10 nC) of *trans*-decalin alone and containing 7×10^{-3} *M* NH_3 and 5×10^{-3} *M* SF_6 separately and combined, at 22°C.

tribution of geminate ions is therefore necessary and is presented below.

Decay Kinetics

(a) Pure Liquid

Estimates of the lifetime distribution of geminate ion pairs in irradiated liquid hydrocarbons have been derived from the concentration dependence of electron scavenging in these solvents using the Laplace transform method (6–9). If it is considered that one is dealing with single ion pairs then the WAS scavenging equation (10, 11) leads to the expression

$$[9] \quad F(t) = \exp [\lambda(+, -)t] \operatorname{erfc} [\lambda(+, -)t]^{1/2}$$

for the fraction of geminate ion pairs existing at a time t following an infinitely short pulse of irradiation. In [9], $\lambda(+, -)$ is a constant the reciprocal of which has the units of time and will subsequently be called the 'characteristic lifetime' of geminate ions. The value of $\lambda(+, -)$ can be determined if both the reactivity parameter α and the absolute rate constant k for scavenging of a primary ion by a given solute are known, via the relationship (8, 9)

$$[10] \quad \lambda(+, -) = k/\alpha$$

Based on [10], values of the characteristic lifetime in liquid cyclohexane of approximately 2×10^{-12} s (taking a geminate ion yield of 5.0 $(100\ \text{eV})^{-1}$) have recently been obtained

from measurements of the absolute rate constants of electron (12) and hole (13) scavenging together with the known reactivity values.

For times considerably longer than the characteristic lifetime [9] may be quite accurately approximated[2] by

$$[11] \qquad F(t) = [\pi\lambda(+, -)t]^{-1/2}$$

The observable yield of geminate ion pairs at a time t following a pulse of irradiation should therefore be $G_{gi}[\pi\lambda(+, -)t]^{-1/2}$, for $t \gg \lambda(+, -)^{-1}$. The parameter G_{gi} is an empirical constant in the WAS scavenging equation (10, 11) which, if this equation were known to be valid up to infinitely high solute concentrations, would be equal to the total yield of geminate ion pairs formed.

If the decay of free ions due to homogeneous recombination is negligible on the time scale of the observations then the time dependence of the total ion pair yield at long times following pulse irradiation will be given by

$$[12] \qquad G_i = G_{fi} + G_{gi}[\pi\lambda(+, -)t]^{-1/2}$$

(b) Secondary Ions

Equation [12] is the predicted time dependence of the ion pair yield in the pure solvent. It has been suggested (8, 9), however, that an equation of the same form as [12] may be applicable to recombination under conditions where either one or both of the primary ions has been converted into a secondary ion. This is based on the proposition that, for those ion pairs which have been scavenged, the time scale for geminate recombination will simply be extended compared with that in the pure liquid by a factor which is inversely proportional to the ratio of the total ion mobilities in the scavenged case to that in the pure liquid. For the case that both primary ions have been scavenged, $\lambda(+, -)$ in [12] should therefore be replaced by $\lambda(S^+, S^-)$ which is given by

$$[13] \qquad \lambda(S^+, S^-) = \frac{\mu(S^+, S^-)}{\mu(+, -)}\lambda(+, -)$$

from which the total yield of ion pairs is

$$[14] \qquad G_i = G_{fi} + G_{gi}[\pi\lambda(S^+, S^-)t]^{-1/2}$$

The assumptions on which the replacement of $\lambda(+, -)$ by $\lambda(S^+, S^-)$ are based are (*a*) the primary ion is scavenged on a time scale much shorter than its recombination time, (*b*) the initial separation distribution of the primary ions is not affected by the presence of the scavenger, and (*c*) the recombination time for both primary and secondary ions is dependent on the inverse first power of the mobility. These assumptions are at present being subjected to theoretical and experimental examination. The experimental results on the decay of secondary ions, obtained by optical pulse radiolysis studies (4, 5) and, as mentioned below, by the present method, are in fact found (9) to be described very well by a time dependence of the form given in [14].

For simplicity of presentation a parameter γ given by

$$[15] \qquad \gamma = (G_{gi}/G_{fi})^2/\lambda\pi$$

is introduced which on substitution in [14] leads to

$$[16] \qquad G_i = G_{fi}\{1 + [\gamma(S^+, S^-)/t]^{1/2}\}$$

As can be seen from [16], γ has the physical significance of being the time at which the contributions of free and geminate ion pairs to the total ion pair yield are equal, assuming no decay of free ions. This parameter will subsequently be called the 'equivalent lifetime' of geminate ion pairs.

Taking the sum of the mobilities of secondary ions to be independent of time[3] results in a predicted time dependence of the product of the yield of ion pairs and the total ion mobility given by

$$[17] \qquad G_i\mu = G_{fi}\mu(S^+, S^-)\{1 + [\gamma(S^+, S^-)/t]^{1/2}\}$$

According to [17], plots of $G_i\mu$ against $1/\sqrt{t}$ should be linear with an intercept equal to $G_{fi}\mu(S^+, S^-)$ and a slope to intercept ratio equal to the equivalent lifetime, $\gamma(S^+, S^-)$.

In Fig. 2 are shown plots of $G_i\mu$ *vs.* $t^{-1/2}$ for a solution containing 5×10^{-3} *M* SF_6 and 10^{-2} *M* benzene at -26, 38, and 108°C. The data

[2]The value of $F(t)$ calculated using [11] is larger than that obtained using [9] by 33%, 14%, and 4% for $\lambda t =$ 1, 3, and 10 respectively. Equation [11] is therefore accurate within 5% for $\lambda t > 10$.

[3]This assumption would appear to be reasonable in view of recent measurements (14) of secondary ion mobilities in isooctane and cyclohexane containing different solutes which showed the mobility to be independent of the solute present within the error limits of the measurements. This is taken to indicate that the mobility would remain unchanged even if the nature of a secondary ion should change due to further reactions occurring.

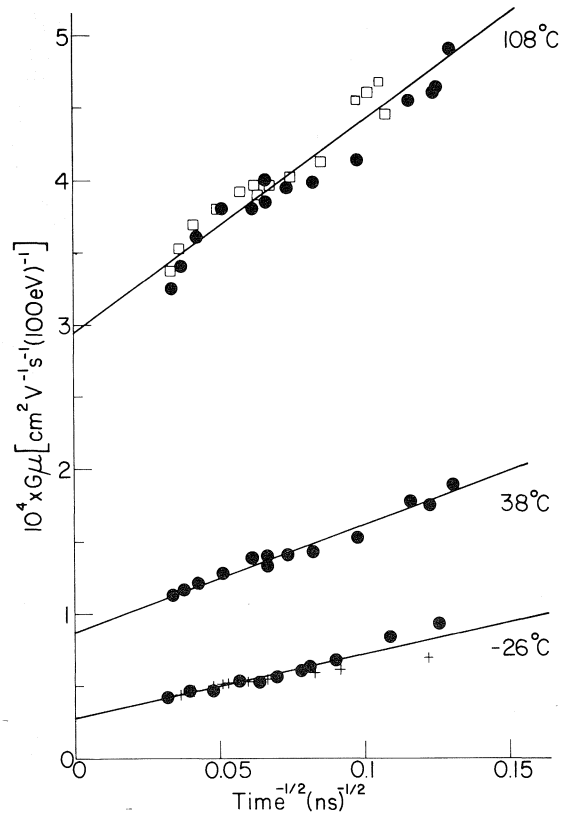

FIG. 2. Plots of the product of the ion pair yield, G (100 eV)$^{-1}$, and the total mobility, μ (cm^2 V^{-1} s^{-1}), against the reciprocal square root of the time for a solution of 1×10^{-2} M benzene plus 5×10^{-3} M SF_6 in *trans*-decalin at the temperatures shown. Pulse width used: □, 20 ns; ●, 50 ns; +, 250 ns.

plotted were taken over a time span from 50 ns to 1 μs from the end of the pulse and as can be seen obey the predicted reciprocal square root of time dependence very well. That no significant decay of free ions occurs over this time scale is shown by the independence of the $G_i\mu$ values on total dose (pulse length). The first half-life of free ions, for the results shown in Fig. 2, estimated using the Debye rate constant, is greater than 10 μs even for the highest conductivity measured.

The values of $\gamma(S^+, S^-)$ obtained from the plots in Fig. 2 and at other temperatures studied are listed in Table 1. Values of $\mu(S^+, S^-)$, obtained from the intercepts by dividing by the free ion yield (see below), are also listed in Table 1.

(c) High Mobility Primary Ions

The same treatment as that given above for secondary ions is usually not applicable to solutions containing a high mobility primary ion. This is due to a problem that frequently occurs which is that the primary ion reacts with impurities inadvertently present in the system. This results in a decrease in the total mobility as well as the yield of ion pairs with time.

In order to illustrate a data analysis procedure which may be carried out in such a case we take as an example the situation in which the electron is scavenged by a high concentration of SF_6 yielding a negative ion of mobility $\mu(S^-)$. If the hole which remains then reacts with an impurity to form a secondary ion of lower mobility, $\mu(S^+)$, the result will be a decrease in the total mobility of the charge carriers present with time according to

$$[18] \quad \mu = [\mu(+) - \mu(S^+)] \exp(-t/\tau) + \mu(S^+, S^-)$$

where τ is the mean lifetime for reaction with the impurity. If τ is considerably longer than the equivalent geminate ion lifetime $\gamma(+, S^-)$ then the total yield of ion pairs will be given by [16] with $\gamma(S^+, S^-)$ replaced by $\gamma(+, S^-)$, and hence the product $G_i\mu$ will be

$$[19] \quad G_i\mu = G_{fi}\{[\mu(+) - \mu(S^+)] \exp(-t/\tau) + \mu(S^+, S^-)\} \times \{1 + [\gamma(+, S^-)/t]^{1/2}\}$$

Rearrangement of [19] gives

$$[20] \quad \frac{G_i\mu}{1 + [\gamma(+, S^-)/t\,]^{1/2}} - G_{fi}\mu(S^+, S^-) = G_{fi}[\mu(+) - \mu(S^+)] \exp(-t/\tau)$$

If the correct value of $\gamma(+, S^-)$ is used then a linear dependence of the logarithm of the left-hand side of [20] on time should be observed with an intecept at $t = 0$ equal to the logarithm of $G_{fi}[\mu(+) - \mu(S^+)]$.

In order to arrive at the value of $\gamma(+, S^-)$ an iterative procedure is adopted. Thus, $\gamma(+, S^-)$ is initially taken to be equal to zero (corresponding to the assumption of the complete absence of geminate ions). A linear least-mean-squares fit to the variables ln $[G_i\mu - G_{fi}\mu(S^+, S^-)]$ and t, using the value of $G_{fi}\mu(S^+, S^-)$ determined as described above, is then carried out. This results in an initial (upper limit) value for $G_{fi}[\mu(+) - \mu(S^+)]$. This value may then be used to obtain a first estimate of $\gamma(+, S^-)$ from the value of $\gamma(S^+, S^-)$, determined as described above, using the relationship (derived from [13] and [15])

TABLE 1. The temperature dependence in liquid *trans*-decalin of the equivalent lifetime (see text for definition) of geminate ion pairs in a SF_6 benzene solution; the free ion yield; the total mobility in a SF_6 benzene solution; the hole mobility; and the excess electron mobility

T (°C)	$\gamma(S^+, S^-)$ (ns)	G_{fi} $(100\ eV)^{-1}$	$\mu(S^+, S^-)$ $(10^{-4}\ cm^2\ V^{-1}\ s^{-1})$	$\mu(+)$ $(10^{-3}\ cm^2\ V^{-1}\ s^{-1})$	$\mu(-)$ $(10^{-3}\ cm^2\ V^{-1}\ s^{-1})$
108	25	0.261	10.8	7.7	71
82	45	0.215	9.6	7.9	39
56	68	0.169	6.8	7.2	28
38	75	0.143	5.8	8.8	15
22	144	0.121	5.2	9.0	13
2	146	0.096	4.8	10.2	7
−15	174	0.076	3.8	8.2	3.2
−26	303	0.066	3.8	14.4	3.5

$$[21]\quad \gamma(+, S^-) = \gamma(S^+, S^-)\frac{\mu(S^+, S^-)}{\mu(+, S^-)}$$

$$[22]\quad = \frac{\gamma(S^+, S^-)}{1 + G_{fi}[\mu(+) - \mu(S^+)]/G_{fi}\mu(S^+, S^-)}$$

The value of $\gamma(+, S^-)$ so obtained is then used to obtain a second value of $G_{fi}[\mu(+) - \mu(S^+)]$ from a fit to the variables $\ln\{G_i\mu/(1 + [\gamma(+, S^-)/t]^{1/2}) - G_{fi}\mu(S^+, S^-)\}$ and t, and hence a second estimate of $\gamma(+, S^-)$. This iterative procedure was in the present case repeated until the value of $G_{fi}[\mu(+) - \mu(S^+)]$ obtained differed by less than 5% from the previous value. This required only three or four iterations in all cases. To illustrate the effects of this treatment on the raw data, in Fig. 3 are shown semilogarithmic plots against time of $G_i\mu$, $G_i\mu - G_{fi}\mu(S^+, S^-)$ and the left-hand side of [20] for a $5 \times 10^{-3}\ M$ SF_6 solution at 22°C. As can be seen, a good straight line semilogarithmic plot is found using the final value of $\gamma(+, S^-)$ obtained.

Values of the hole mobility were derived from the final value obtained for $G_{fi}[\mu(+) - \mu(S^+)]$ by dividing by the value of G_{fi} (see below) and then adding one half of the value determined for $\mu(S^+, S^-)$. The latter operation assumes that the mobilities of the secondary positive and negative ions are the same. This has, in fact, in certain cases been found (14) not to be so. However, since the correction is small, it is considered to be a satisfactory approximation for the present purposes. The values of $\mu(+)$ derived at different temperatures are listed in Table 1.

Of some interest is the magnitude of the value of $G_{fi}\mu(+)$ obtained after correction compared with the end-of-pulse value of $G_i\mu$. In the case of the $5 \times 10^{-3}\ M$ SF_6 solution the ratio of $G_i\mu$ at end-of-pulse to $G_{fi}\mu(+)$ was found to vary from 2.0 to 1.7 in going from −26°C to 108°C thus indicating an approximately equal yield of geminate and free ion pairs at end-of-pulse.

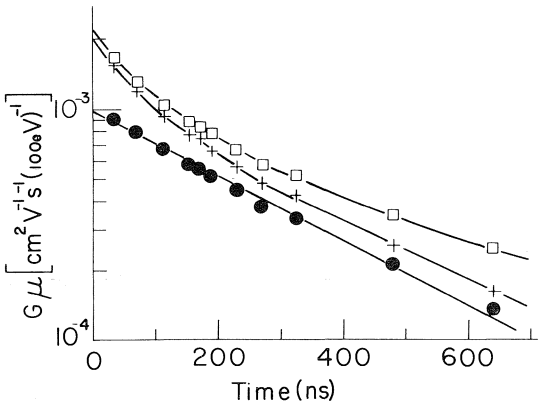

FIG. 3. Illustration of the effect on the raw data of corrections for the presence of secondary ions and geminate ion pairs following pulse irradiation (20 ns) of a $5 \times 10^{-3}\ M$ solution of SF_6 in *trans*-decalin at 22°C: □, experimental $G\mu$ values; +, $G\mu - G_{fi}\mu(S^+, S^-)$; ●, $[G\mu/(1 + [\gamma(+, S^-)/t]^{1/2}) - G_{fi}\mu(S^+, S^-)]$ calculated using the final value of $\gamma(+, S^-)$ obtained by the iterative procedure described in the text.

The same treatment as described above was carried out for solutions containing $7 \times 10^{-3}\ M$ NH_3 in which the excess electron is the primary charge carrier. The values of $\mu(-)$ so obtained are listed in Table 1. As opposed to the rather small change with temperature found for the ratio of $G_i\mu$ end-of-pulse to $G_{fi}\mu(+)$, in the case of the electron the equivalent ratio was found to decrease from 4.6 (*ca.* 80% contribution of geminate ions) at −26°C to 1.2 (*ca.* 20% geminate ion contribution) at 108°C.

The Free Ion Yield

A value of $G_{fi} = 0.04 \pm 0.01$ (100 eV)$^{-1}$ is to be found in the literature; however, in the same article the value of G_{fi} for cyclohexane is given as 0.06 (100 eV)$^{-1}$ which is much lower than the recent values in the range 0.15 to 0.2 (15–17). Since no recent values could be found for decalin we measured this quantity by the method (18, 19) of extrapolating to zero concentration a plot of the methane yield from a methylbromide solution against the square root of the methylbromide concentration. The value obtained was $G_{fi} = 0.12$ (100 eV)$^{-1}$. Using exactly the same method and apparatus we obtained a value of $G_{fi} = 0.15$ (100 eV)$^{-1}$ for cyclohexane which is in good agreement with recently reported values.

Taking a Gaussian form for the distribution function of ion pair separation distances results in the following relationship (15) between the free ion yield and the Gaussian distribution parameter b:

$$[23] \quad G_{fi} = G_{tot} \int_0^{\infty} \frac{4r^2}{\pi^{1/2}b^3} \times \exp\left(-\frac{r^2}{b^2} - \frac{r_c}{r}\right) dr$$

In [23], G_{tot} is the total ion pair yield, taken to be 4.3 (100 eV)$^{-1}$ (15), and $r_c = e^2/\varepsilon_r kT$ is the Onsager escape distance. From the measured free ion yield of 0.12, the value of the product $b\rho$ where ρ is the density of the liquid is found to be 50 Å g cm^{-3} for *trans*-decalin. It has been found (15–17), for the vast majority of liquids studied, that when free ion yield data are analysed using [23] with a constant (temperature independent) value for G_{tot}, then temperature independent values of $b\rho$ are derived, within the temperature range used in the present work. This finding may therefore be used quite empirically, independent of whether or not one accepts the constancy of G_{tot} or a Gaussian range distribution, to calculate G_{fi} values at different temperatures if the relevant value of $b\rho$ is known. The values of G_{fi} for *trans*-decalin at temperatures other than 22°C, listed in Table 1, were therefore calculated using [23] and the above value of $b\rho$ together with the known variation of ε_r and ρ with temperature (20).

Mobilities

As can be seen from the data in Table 1 the electron mobility in *trans*-decalin increases markedly with temperature. As has been found for other liquids, $\mu(-)$ is found to be quite well described by an equation of the form

$$[24] \quad \mu = A \exp(-B/RT)$$

with $A = 25$ cm^2 V^{-1} s^{-1} and $B = 4.5 \pm 0.3$ kcal mol^{-1}. The latter value is similar to that found for the activation energy of the excess electron mobility in other low (<0.1 cm^2 V^{-1} s^{-1}) mobility hydrocarbon liquids (16, 17).

As opposed to the strong temperature dependence of the electron mobility, that of the hole is seen to change very little over the almost 140°C temperature range studied. A slight decrease with increasing temperature is in fact indicated. In terms of [24] values of $A = 4.0 \times 10^{-3}$ cm^2 V^{-1} s^{-1} and $B = -0.5 \pm 0.3$ kcal mol^{-1} are found to give a best fit to the data. This lack of a significant temperature dependence of $\mu(+)$ has also been found in cyclohexane (3). The data previously reported for cyclohexane were not subjected to a correction for the presence of geminate ion pairs. When this is carried out the value of $\mu(+)$ at room temperature in cyclohexane is found to be 0.95×10^{-2} cm^2 V^{-1} s^{-1} (as opposed to the 1.6×10^{-2} cm^2 V^{-1} s^{-1} previously reported) which is close to that found in the present work for *trans*-decalin.

Of particular interest in the present results, as is shown by the data in Table 1, is that at low temperatures the mobility of the hole actually exceeds that of the electron. If the very low activation energies found for hole mobilities in cyclohexane and *trans*-decalin may be taken to represent the general case then a transition from the electron to the hole as major charge carrier would in fact be expected to occur in any liquid displaying a high hole mobility if the temperature could be lowered sufficiently.

The value of the sum of the slow ion mobilities of 5.2×10^{-4} cm^2 V^{-1} s^{-1} at 22°C is in the order of what would be expected for this liquid (viscosity 2.06 cP). Thus, from recent drift-time measurements (14) of secondary ion mobilities in cyclohexane (viscosity 0.93), the sum of the positive and negative ion mobilities has been found to be 7.8×10^{-4} cm^2 V^{-1} s^{-1}. If a simple linear dependence of mobility on fluidity (reciprocal viscosity) were assumed then from this result in cyclohexane a value of $\mu(S^+, S^-)$ of 3.5×10^{-4} cm^2 V^{-1} s^{-1} would be predicted for *trans*-decalin.

Further aspects of the present results such as the relevance of the parameter $\gamma(S^+, S^-)$ and the nature of displacement of the hole will be discussed in future publications.

1. J. M. WARMAN, M. P. DE HAAS, and A. HUMMEL. Chem. Phys. Lett. **22**, 480 (1973).
2. M. P. DE HAAS, J. M. WARMAN, P. P. INFELTA, and A. HUMMEL. Chem. Phys. Lett. **31**, 382 (1975).
3. M. P. DE HAAS, J. M. WARMAN, and A. HUMMEL. Proc. 5th Int. Conf. on Conduction and Breakdown in Dielectric Liquids, July 1975, Noordwijkerhout, The Netherlands. *Edited by* J. M. Goldschvartz. Delft University Press, Delft, The Netherlands.
4. J. K. THOMAS, K. JOHNSON, T. KLIPPERT, and R. LOWERS. J. Chem. Phys. **48**, 1608 (1968).
5. A. HUMMEL and L. H. LUTHJENS. J. Chem. Phys. **59**, 654 (1973).
6. A. HUMMEL. J. Chem. Phys. **49**, 4840 (1968).
7. A. HUMMEL. Adv. Radiat. Chem. **4**, 1 (1974).
8. S. J. RZAD, P. P. INFELTA, J. M. WARMAN, and R. H. SCHULER. J. Chem. Phys. **50**, 5034 (1969).
9. S. J. RZAD. P. P. INFELTA, J. M. WARMAN, and R. H. SCHULER. J. Chem. Phys. **52**, 3971 (1970).
10. J. M. WARMAN, K-D. ASMUS, and R. H. SCHULER. Adv. Chem. Ser. **82**, 25 (1968).
11. J. M. WARMAN, K-D. ASMUS, and R. H. SCHULER. J. Phys. Chem. **73**, 931 (1969).
12. A. O. ALLEN, T. E. GANGWER, and R. A. HOLROYD. J. Phys. Chem. **79**, 25 (1975).
13. J. M. WARMAN, P. P. INFELTA, M. P. DE HAAS, and A. HUMMEL. Chem. Phys. Lett. **43**, 321 (1976).
14. A. O. ALLEN, M. P. DE HAAS, and A. HUMMEL. J. Chem. Phys. **64**, 2587 (1976).
15. W. F. SCHMIDT and A. O. ALLEN. J. Chem. Phys. **52**, 2345 (1970).
16. J-P. DODELET and G. R. FREEMAN. Can. J. Chem. **50**, 2667 (1972).
17. K. SHINSAKA, J-P. DODELET, and G. R. FREEMAN. Can. J. Chem. **53**, 2714 (1975).
18. S. J. RZAD and J. M. WARMAN. J. Chem. Phys. **49**, 2861 (1968).
19. J. M. WARMAN and S. J. RZAD. J. Chem. Phys. **52**, 485 (1970).
20. J. TIMMERMANS. Physico-chemical constants of pure organic compounds. Elsevier, Amsterdam, The Netherlands. 1950. pp. 195, 209.

Discussion

L. G. Christophorou: Are the changes in your conductivity sensitive enough to the masses of the ions for your system to function, basically, as a liquid-state mass spectrometer?

J. M. Warman: We find, unfortunately perhaps, that the sum of the mobilities of molecular positive and negative ions in the liquids studied are very insensitive to the nature (including the mass) of the ions, *i.e.* that the total mobility of the ions is independent of the solutes used to scavenge the electron and hole.

G. R. Freeman: You referred to geminate neutralization in the solutions. Was the scavenger concentration high enough that you would not see the tail of the reaction of scavenger with the free ions?

J. M. Warman: Yes. For example in liquid cyclohexane the SF_6 concentration was 3×10^{-3} *M*, which using a rate constant for electron scavenging of 4×10^{12} M^{-1} s^{-1} corresponds to an electron lifetime of 0.1 ns. This is sufficiently short to ensure that no electrons are present within 10 ns following the pulse.

W. F. Schmidt: How do you correct for a dose rate drop in your sample since you are using 3 MeV electrons as ionizing agent?

J. M. Warman: We carried out our dosimetry by measuring the absorption of the solvated electron in a 10^{-2} *M* NaOH – 1 *M* EtOH solution in water using a He/Ne laser as light source. The cell used for dosimetry was identical to that used in the microwave experiments, but with optical (glass) windows at both ends. By use of the laser we measured the absorbed dose as a function of depth and breadth of the sample. The largest variation was an approximately 40% decrease in going from the top of the cell to the bottom for a 0.8 g cm^{-3} density medium. The absorbed dose was corrected for variations in dose within the cell by averaging over the field intensity of the microwave standing wave pattern.

W. F. Schmidt: Isn't there the possibility that more than one kind of positive charge carriers are formed?

J. M. Warman: This is a possibility which is often voiced. The principal evidence that in cyclohexane > 80% of the positive ions are the parent ions comes from optical absorption studies of the rapid formation of solute positive ions formed by the reaction, $RH^+ + S \rightarrow RH + S^+$. Thus the *G* values found for $TMPD^+$ formation immediately at the end of a 10 ns pulse, for a TMPD concentration of 10^{-4} *M*, is close to the value of the free ion yield in this liquid (0.16 $(100\,eV)^{-1}$), as would be expected if all positive ions were the parent.

Y. Hatano: Did you confirm experimentally the effect of the microwave power on the final signal intensity? I would like to know the input microwave power and the cavity *Q* value which you are using.

J. M. Warman: The microwave power levels we use are on the order of 100 mW, which in a medium of dielectric constant 2 corresponds to a field strength (maximum) of about 2 or 3 V/cm. The *Q*'s of the cavities we use are usually on the order of 400. In the cavity experiments the field strength is considerably larger than in normal reflection experiments, but we obtain identical results for $G\mu$ values where we have obtained them using both methods. This confirms the lack of a field strength (power) effect, as would be expected in molecular liquids for which field effects on electron mobilities are found to occur only above field strengths of 10^3 V/cm.

Metallic condensation of Wannier–Mott impurity states in lithium–hexamethylphosphoramide glasses

PETER P. EDWARDS[1,2]

Department of Chemistry, Cornell University, Ithaca, NY, U.S.A. 14853

AND

RON CATTERALL

Department of Chemistry and Applied Chemistry, University of Salford, Salford M54 4WT, England

Received October 4, 1976

PETER P. EDWARDS and RON CATTERALL. Can. J. Chem. **55**, 2258 (1977).

A metal to non-metal (MNM) transition observed in frozen solutions of lithium in hexamethylphosphoramide (HMPA) was tentatively interpreted as a Mott transition in which localized Wannier-type impurity states were the source of electrons in the metallic state. In this paper this assertion is examined in greater detail by calculating critical densities (n_c) on the basis of a scaled (variational) form of Mott's original criterion for the onset of localization in a dielectrically screened Coulomb potential, and also on the basis of the Hubbard tight-binding model. Mott's model for the transition is based upon the screening properties of a freely propagating gas of metallic electrons. In the Hubbard regime, however, the phenomenon is viewed from the tight-binding limit; the transition from localized to delocalized states occurs when the bandwidth (Δ) of a regular lattice of isolated centres exceeds the value of the intra-atomic Coulombic repulsion integral (U) associated with electron correlation.

Both electron-gas (Mott) and tight-binding (Hubbard) approaches give calculated critical densities (5.6×10^{18}, 3.2×10^{18} cm^{-3}, respectively) in good agreement with the experimental value ($\sim 3 \times 10^{18}$ cm^{-3}). These results therefore support the earlier suggestion that the MNM transition in frozen lithium–HMPA solutions is a Mott-transition associated with electron-interaction effects.

PETER P. EDWARDS et RON CATTERALL. Can. J. Chem. **55**, 2258 (1977).

On a interprété d'une façon non-définitive une transition métal à non-métal (MNM) observée dans des solutions congelées de lithium dans l'hexaméthylphosphoramide (HMPA) comme une transition de Mott dans laquelle des états d'impuretés du type Wannier localisés sont les sources d'électrons de l'état métallique. Dans cette communication on examine cette affirmation en détail en calculant les densités critiques (n_c) sur la base d'une forme échelonnée (variationnelle) du critère original de Mott pour le début de la localisation dans un potentiel de Coulomb qui est masqué d'une façon diélectrique et aussi sur la base du modèle d'attachement intime de Hubbard. Le modèle de Mott pour la transition est basé sur les propriétés de blindage d'un gaz d'électrons métalliques se propageant librement. Dans le régime de Hubbard, toutefois, on conçoit le phénomène à partir de la limite de l'attachement intime; la transition des états localisés vers les états délocalisés se produit quand la largeur de bande (Δ) d'un réseau régulier de centres isolés excède la valeur de l'intégrale de répulsion Coulombique intra-atomique (U) associée avec la corrélation d'électron.

Les approches d'électron-gaz (Mott) et d'association intime (Hubbard) conduisent respectivement à des densités critiques calculées de 5.6×10^{18} et 3.2×10^{18} cm^{-3}, en bon accord avec la valeur expérimentale qui est approximativement 3×10^{18} cm^{-3}. Ce résultat supporte donc la suggestion antérieure à l'effet que les transitions MNM dans des solutions congelées de lithium dans HMPA sont des transitions de Mott associées avec des effets d'interactions des électrons.

[Traduit par le journal]

Introduction

At the recent Colloque Weyl IV we have reported the observation of a metal–nonmetal (MNM) transition in frozen solutions of lithium in HMPA (1). The transition was found at a metal concentration of the order of $5 \times 10^{-3}\ M$ ($\sim 3 \times 10^{18}$ cm^{-3}). A cursory examination of the results suggested that the transition was of the Mott–Hubbard type, originating in electron-correlation effects. The purpose of this paper is to calculate explicitly the critical concentration for the MNM transi-

[1]This research sponsored by the National Science Foundation under Grant No. MPS 74-21480.

[2]British Fulbright Scholar, 1975–1977.

tion in this system using both the Mott and Hubbard models for the transition.

In the calculations to be outlined below, we have assumed that the system approximates a uniform, homogeneous material; that is, it is devoid of large (bimodal) concentration fluctuations and associated inhomogeneities (2, 3). We have previously reported the simultaneous observation of both delocalized (metallic) and localized (insulating) states in frozen solutions of potassium, rubidium, and cesium in HMPA (1), indicating large concentration inhomogeneities in these low-temperature glasses. In these systems (at least on the macroscopic scale[3]) the possibility of a Mott–Hubbard type transition would appear to be ruled out (4) and a realistic approach would presumably be to interpret the transition in terms of a threshold for continuous percolation (2, 3). However, in frozen lithium–HMPA solutions we have found no evidence for large scale inhomogeneities for the concentration range *ca.* 10^{-4} to 0.1 *M*. We suppose, therefore, that the concept of a Mott transition in this homogeneous system represents a good working hypothesis, and in this paper we calculate critical donor (lithium atom) concentrations.

A Scaled (Variational) Form of the Mott Criterion for the Homogeneous Regime

Mott (5–7) proposed that a MNM transition will take place when an itinerant (metallic) electron becomes localized on a specific centre. The model was originally developed with particular reference to (*i*) a dielectrically screened Coulomb potential for the long range electron–hole interaction and (*ii*) Thomas–Fermi screening by the free electrons. The critical concentration of donors (n_c) is then given (5–7) by

$$[1] \qquad n_c^{1/3} a_H \simeq 0.25$$

Here a_H is the ground state Bohr radius of the lowest localized state with a one-electron wavefunction

$$[2a] \qquad \psi(r) = \{1/(\pi a_H^3)^{1/2}\} \exp(-r/a_H)$$

where

$$[2b] \qquad a_H = \hbar^2 K_{st}/m^* e^2$$

and K_{st} is the static (low-frequency) dielectric constant of the host material and m^* the electron effective mass.

The idea of a *true* Coulomb potential is appropriate only for localized states in which there exists considerable overlap between the donor wavefunction and the electronic wavefunction of the surrounding matrix (8, 9). The electron – parent core interaction is then screened by the low-frequency dielectric constant and the resulting donor levels are truly hydrogenic (9).

Berggren and Lindell (10) have questioned the *direct* use of the Mott criterion in the form [1] for systems other than the high dielectric, large Bohr radius states (of which the doped group IV semiconductors are good examples). They (10) have proposed a modification to the Mott criterion in the form of a simple scaling relation;

$$[3] \qquad n_c^{1/3}(a_H/\gamma) = 0.25$$

where γ is a parameter defined such that the ratio ($a_H/\gamma = a^*$) defines an *appropriate* radius associated with a realistic wavefunction (not necessarily of the type [2*a*] for the isolated centres. Thus, the basis of the present approach is somewhat different from previous attempts at applying the Mott criterion to the MNM transition in metal–ammonia (11, 12) and related (13) systems.

One attractive feature of this scaled form of the Mott criterion is that it allows an independent determination of the radius a^* from *experimental* parameters which characterize the localized state.[4]

A possible criticism of this approach is that the constant in [3] will be sensitive to the particular nature of the donor wavefunction and the choice of the screening potential for the electron gas (14). One purpose of this paper is to show that the scaled criterion [3] may be applied to many experimental systems exhibiting a MNM transition; ranging from the tight binding (Frenkel) states in the rare gas solids (15) (with $a^* \sim 2$ Å) to shallow impurity states in germanium (16) (with $a^* \sim 46$ Å), with good agreement between calculated and experimental critical densities. In Table 1 we have assembled some representative experimental

[3]However, the arguments developed here could also be applied to regions in a microscopically inhomogeneous material which are smaller than the Debye correlation length for concentration fluctuations (2).

[4]In the past, it has been customary to attempt to apply the Mott criterion to non-Coulombic isolated donor states by replacing the low frequency dielectric constant by an arbitrary value reflecting some weighted average of high and low frequency values (see refs. 11–13).

TABLE 1. Critical densities for electron localization on the basis of scaled form of the Mott criterion

System	Nature of isolated centre	$\{a_H/\gamma\} = a^*/Å$	n_c/cm^{-3} Calculated (eq. 3)	n_c/cm^{-3} Observed
Sodium/argon (4 K)	Frenkel impurity state (8)	2.084[a]	1.73×10^{21}	3.67×10^{21} (15)
Lithium/methylamine (213 K)	Polaron state[b]	2.88[c]	6.55×10^{20}	$(1.79\pm0.3)\times10^{21}$ (13)
Lithium/HMPA glasses (77 K)	Wannier–Mott impurity state (1, 9)	14.1	5.6×10^{18}	$(3\pm1)\times10^{18}$ (This work)
Germanium (4 K)	Shallow impurity states (9, 18) (Wannier-like)			
	Sb	45.45 ± 0.95[d]	$(1.7\pm0.2)\times10^{17}$	0.95×10^{17} (16)
	P	38.7 ± 1.2	$(2.7\pm0.2)\times10^{17}$	2.5×10^{17} (16)
	As	36.95 ± 1.75	$(3.1\pm0.4)\times10^{17}$	3.5×10^{17} (16)

[a]Calculated from ref. 10.
[b]Reference 33.
[c]Obtained by fitting optical ($1s \rightarrow 2p$) transition of the isolated (localized) centre to Jortner's polaron model (33).
[d]Characteristic Bohr radii (a^*) for the doped group IV semiconductors were estimated from two approaches: (*a*) The Coulomb result $a^* = e^2/2K_{st}E_{expt}$ where E_{expt} is the experimental (18) ionization energy for the isolated donor state, and (*b*) the quantum defect approach (cited in ref. 25) $a^* = a_H(E_{EM}/E_{expt})$; where a_H and E_{EM} are taken from ref. 18. Values shown in the table are the average of these two values, together with associated error estimates.

values for characteristic Bohr radii (a^*), associated critical concentration (calculated from [3]), and corresponding experimental concentrations of a variety of systems showing a MNM transition. It appears, therefore, that the simple scaled form of the Mott criterion may be applicable to many experimental situations in which the isolated donor potential is not necessarily truly Coulombic.

For the lithium–HMPA system we can obtain an experimental estimate for a^* from the magnetic properties of the isolated centres (1). The isolated donor states in frozen lithium–HMPA solutions closely approximate (1) true Wannier–Mott impurity states in an amorphous medium (9). On the Kohn–Luttinger effective mass (EM) theory (17, 18) the wavefunction of the isolated donor states is constructed mainly from Bloch waves near the bottom of the (host) conduction band. The wavefunction for the lowest energy states is then

$$[4] \qquad \psi(\boldsymbol{r})_{EM} = \sum_{j=1}^{N} \alpha_j F_j(\boldsymbol{r})\phi_j(\boldsymbol{r})$$

where N is the number of conduction band minima in k-space, α_j are numerical coefficients of the appropriate linear combinations of $F_j(\boldsymbol{r})\phi_j(\boldsymbol{r})$, $\phi_j(\boldsymbol{r})$ is the Bloch wave at the jth minima, and the functions $F_j(\boldsymbol{r})$ are hydrogen-like envelope functions similar to those given previously (eq. 2*a*).

$$[5] \qquad F_j(\boldsymbol{r}) = 1/(\pi a_H^3)^{1/2} \exp(-r/a_H)$$

where a_H is given by [2*b*]. Setting $r = 0$ and squaring [5], we have an expression for the unpaired electron spin density at the donor (lithium) nucleus;

$$[6] \qquad |\psi(0)|_{EM}^2 = N|\phi_j(0)|^2|F_j(0)|^2$$

where

$$[7] \qquad |F_j(0)|^2 = 1/\pi a_H^3$$

A slightly different form of [6], first proposed by Kohn (18), allows for possible *minor* deviations from effective mass theory arising from the breakdown of the Coulomb potential in the vicinity of the impurity. On this 'corrected' effective mass (CEM) theory we have (18)

$$[8] \qquad |\psi(0)|_{CEM}^2 = |\psi(0)|_{EM}^2 K$$

where K, the Kohn enhancement factor, represents a measure of the deviation from effective mass formalism. Detailed discussions of K, and its estimation, are presented elsewhere (1, 18). For Li–HMPA we expect (9) negligible deviations from the effective mass theory.[5] For Wannier-type impurity states in lithium–HMPA glasses we have estimated (1) $K \simeq 1.4$ (*cf.* 9.8

[5]Observed unpaired electron spin densities at the alkali nucleus (9) for Wannier–Mott (alkali) impurity states in the M–HMPA glasses are independent of the donor atom. This invariance is predicted by the effective mass theory (eq. 6).

for P:Si (18)), and setting $|\phi_j(0)|^2 = 100$ and $|\psi(0)|^2$(observed) $= 0.061 \times 10^{24}$ cm^{-3} (1) we find $a_H = 14.1$ Å from [6] and [8].

In this particular instance, the form of the isolated donor potential approximates closely the Coulombic potential (1, 9) and we expect $\gamma \sim 1$ and $a^* \sim a_H$. Although the ground state wavefunction for Wannier-type impurity states (eq. 4) differs markedly from the single hydrogenic form over large distances [4], it is dominated by the hydrogenic terms F_j which have a characteristic radius of the magnitude of the Bohr radius a_H (eq. 2*b*).

Substituting for $a^* = 14.1$ Å in the scaled criterion [3] gives a critical donor concentration of 5.6×10^{18} cm^{-3}, in good agreement with the experimental value $\sim 3 \times 10^{18}$ cm^{-3}.

Critical Concentration from the Hubbard (Tight-binding) Model for the Homogeneous Regime

On Mott's model (5–7) the MNM transition occurs when a dielectrically-screened Coulomb (or other) potential starts to give rise to bound states. The Hubbard formulation (19), however, originates in the tight-binding (isolated-donor) limit. It prescribes a transition from the insulating to the metallic state when

$$[9] \qquad \{\Delta/U\} = \text{constant}$$

Here Δ is the unperturbed bandwidth of a regular array of centres and U is the intradonor repulsion energy associated with electron correlation. The magnitude of the constant in [9] depends upon the approximations inherent in any particular interpretation of the Hubbard model (20, 21), but typically it is of the order 1.0 to 1.5.

Berggren (21) has applied the Hubbard tight-binding model to an analysis of the MNM transition in shallow donor states in silicon and germanium. As in the lithium–HMPA system, the isolated donor states in these semiconductors are described by the Kohn–Luttinger effective mass theory (eqs. 4 to 8). When the host conduction band is isotropic,[6] the envelope function is given by [5] and the unperturbed bandwidth is then

$$[10] \qquad \Delta = 2z|T|$$

where z is a co-ordination number of donor states around a given centre and T is the hopping integral between two adjacent orbitals

$$[11] \quad T = \frac{e^2}{K_{st}a^*}\{-\tfrac{1}{2}S - [R/a^* + 1] \times \exp(-R/a^*)\}/\sqrt{N}$$

The overlap integral, S, is given by (21)

$$[12] \quad S = \{1 + (R/a^*) + \tfrac{1}{3}(R/a^*)^2\} \times \exp(-R/a^*)$$

where R is the distance between donors and N is the number of conduction band minima.

Utilising earlier results of Miller and Abrahams (23), Berggren (21) has obtained an expression for the intradonor repulsion energy,

$$[13] \qquad U = \tfrac{5}{8}(e^2/K_{st}a^*)$$

representing the electrostatic energy between two hydrogenic centres with orbital exponents $(1/a^*)$.

Hubbard's original estimate of the constant in [9] was 1.15, but more recent values range from 1.0 to 1.5 (20, 21). However, in the region of the MNM transition the bandwidth changes rapidly over a relatively narrow concentration range and the computed critical density is not particularly sensitive to the exact value of (Δ/U), *as long as it is close to unity* (21). We take Hubbard's value (19) of 1.15 for the value of (Δ/U) at the MNM transition, and for the particular case of Wannier-type donor states in Li–HMPA solutions, we estimate $n_c = 3.2 \times 10^{18}$ cm^{-3} in excellent agreement with the experimental value.

As yet, we have not specified what value of the dielectric constant is appropriate in [11] and [13]. In fact, having specified an appropriate (experimental) Bohr radius (a^*) for the donor state (see previous section), a particular choice of the dielectric constant is unnecessary. For a given value of the impurity Bohr radius, both the unperturbed bandwidth (Δ) and the repulsion energy (U) are inversely proportional to the dielectric constant (see [10] and [13]), but the Hubbard ratio (Δ/U), and therefore the critical donor concentration, is independent of the dielectric constant. This particular aspect gives some insight into the role played by the host matrix in the MNM transition.

[6]We feel this is a reasonable assumption for HMPA for the following reasons: (*i*) the experimental observation (9) of true Wannier–Mott impurity states in alkali metal – HMPA glasses requires that electrons in the host (HMPA) conduction band are free-electron-like (see ref. 31); (*ii*) the energy V_0 of the quasi-free electron state in HMPA has been estimated (22) as $-1.9 < V_0 < 0.3$ eV; based on the Wigner–Seitz model for the quasi-free electron state (32).

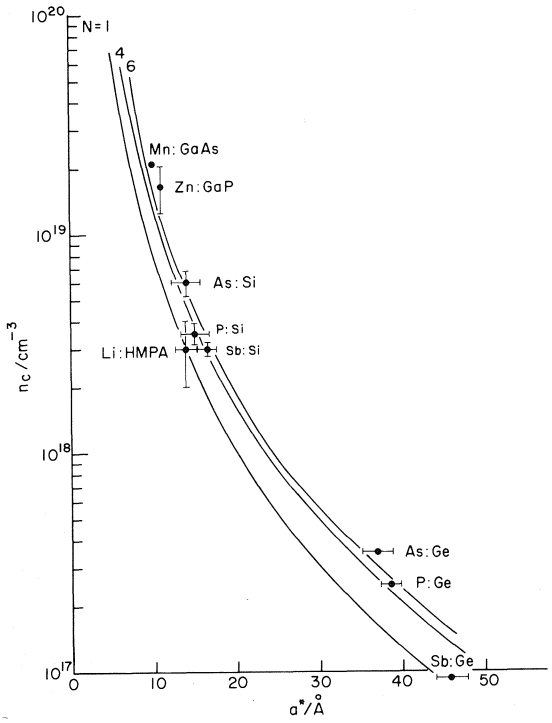

FIG. 1. The MNM transition in Wannier-like impurity states. The solid lines represent the predicted variation of n_c with a^* for Wannier-like states constructed predominantly of Bloch states from the host (matrix) conduction band. Curves are presented for conduction band with 1, 4, and 6 equivalent minima in k-space. The method of calculation based on Berggren's (21) interpretation of the Hubbard Hamiltonian (19), is described in the text. The points, and associated error bounds, are experimental values. No error estimates for n_c (experimental) are available for Mn:GaAs and for group V donors in germanium. For the group V donors in silicon and germanium characteristic radii were determined by the two methods described in the footnote [d] of Table 1. Experimental parameters for acceptor states in GaAs and GaP were taken from refs. 26 and 27.

Low dielectric systems (for example, the rare-gas solids (15)), produce only a small perturbation on the isolated (free) atom eigenstates of the donor, and the matrix-bound states have wavefunctions only slightly expanded relative to their gas-phase counterparts (8). On the other hand, high dielectric systems (for example, Si and Ge (16)) produce significant shielding of the electron – parent core interaction and a correspondingly large Bohr radius for the donor state (9). However, once these modifications to the donor state by the host matrix are taken into account, the subsequent phenomenon of the MNM transition (at finite donor concentrations) reduces to a hydrogen-like problem of competing kinetic and potential energy effects (24) *but with the reference (concentration) axis suitably 'displaced'*.

On this basis, we expect the expressions [9] to [13] to be directly applicable to all systems in which the localized (insulating) states are described in terms of the effective-mass theory.[7] We have computed critical densities for the MNM transition as a function of the Bohr radius (a^*) of the isolated donor states averaged over the three possible configurations of donors. The results of the numerical calculations are compared with experimentally determined values in Fig. 1 for both donor and acceptor states in various matrices.

For materials differing widely in dielectric properties we find good agreement between the experimental results and the predicted variation of n_c with a^*. The slight deviations from the predicted behavior probably arise from our use of an isotropic model for all the various systems; for silicon and germanium, in particular, this must be regarded as only a first approximation in view of the anisotropic nature of the conduction band in these materials (18).

Conclusions

In the preceding sections we have examined two particular models for the MNM transition in lithium–HMPA glasses. Both the Mott (electron-gas) and Hubbard (tight-binding) models predict similar critical concentrations in good agreement with the experimental values, arguing strongly that the transition is indeed driven by electron correlation effects (1) of the Mott–Hubbard type.

The general similarity in predictions for the two models has been recognised for some time (28, 29). In the present context, it follows naturally from the particular formulation (21) of the Hubbard model. The occurrence of a common factor $(e^2/K_{st}a^*)$ in the expressions for both the unperturbed bandwidth (via [11]) and the intradonor repulsion energy (eq. 13) requires that the critical concentration be determined by the dimensionless quantity

[7]In fact, these arguments could possibly be expanded to encompass all manner of matrix-bound states (from Frenkel to Wannier-like states) since the expressions derived by Berggren (21) are essentially hydrogenic (see also Brandow (24)), relating only to bandwidth and repulsion energies for s-like states.

$(R/a^*) \propto (1/n^{1/3}a^*)$, as in the scaled Mott criterion (eq. 3).

Jortner and Cohen (2) have recently proposed that in the absence of bimodal inhomogeneities (*i.e.* at temperatures sufficiently above the consolute temperature) the MNM transition in lithium– and sodium–ammonia solutions is a Mott transition. In addition, Toma *et al.* (13) have tentatively interpreted their recent transport measurements on fluid lithium–methylamine solutions in terms of electron-correlation effects of the Mott–Hubbard type. In the lithium–methylamine system there is experimental evidence (30) to suggest that microscopic inhomogeneities are negligible in the transition region.

It appears, therefore, that for metal solutions in which the only inhomogeneities are the normal, unimodally distributed fluctuations, the MNM transition is a Mott–Hubbard transition.

On a more general theme, we have indicated that both the scaled Mott criterion and the Hubbard model for the MNM transition possess a certain universality which allows their application to a wide range of experimental systems.

Acknowledgements

We would like to thank Professor M. J. Sienko of Cornell University for his cordial hospitality to one of us (P.P.E.) during the period when this report was prepared.

1. R. Catterall and P. P. Edwards. J. Phys. Chem. **79**, 3018 (1975).
2. J. Jortner and M. H. Cohen. Phys. Rev. **13**, 1548 (1976).
3. M. H. Cohen and J. Jortner. J. Phys. Chem. **79**, 2900 (1975); J. Phys. 35, C4-345 (1974).
4. M. H. Cohen. *Comments at* Colloque Weyl IV. *Following* R. Catterall and P. P. Edwards. J. Phys. Chem. **79**, 3018 (1975).
5. N. F. Mott. Proc. Phys. Soc. A, **62**, 416 (1949).
6. N. F. Mott. Can. J. Phys. **34**, 1356 (1956).
7. N. F. Mott. Philos. Mag. **6**, 287 (1961).
8. R. Catterall and P. P. Edwards. Chem. Phys. Lett. **42**, 540 (1976).
9. R. Catterall and P. P. Edwards. Chem. Phys. Lett. **43**, 122 (1976).
10. K.-F. Berggren and G. Lindell. Solid State Commun. **13**, 1589 (1973).
11. J. V. Acrivos and N. F. Mott. Philos. Mag. **24**, 19 (1971).
12. M. J. Sienko. *In* Solutions metal–ammoniac. Colloque Weyl 1, Lille. 1963. *Edited by* G. Lepoutre and M. J. Sienko. W. A. Benjamin Inc., New York, NY. 1964. p. 23.
13. T. Toma, Y. Nakamura, and M. Shimoji. Philos. Mag. **33**, 181 (1976).
14. F. Martino. G. Lindell, and K.-F. Berggren. Phys. Rev. **8**, 6030 (1973).
15. R. C. Cate, J. G. Wright, and N. E. Cusack. Phys. Lett. A, **32**, 467 (1970).
16. M. N. Alexander and D. F. Holcomb. Rev. Mod. Phys. **40**, 815 (1968).
17. W. Kohn and J. M. Luttinger. Phys. Rev. **97**, 883 (1955).
18. W. Kohn. *In* Solid state physics, Vol. 5. *Edited by* F. Seitz and D. Turnbull. Academic Press, New York, NY. 1957.
19. J. Hubbard. Proc. R. Soc. London Ser. A, **276**, 238 (1963); **281**, 401 (1964).
20. N. F. Mott and Z. Zinamon. Rep. Progr. Phys. **33**, 881 (1970).
21. K.-F. Berggren. Philos. Mag. **27**, 1027 (1973).
22. P. P. Edwards. Ph.D. Thesis, University of Salford, Salford, England. 1974.
23. N. F. Miller and E. Abrahams. Phys. Rev. **120**, 745 (1960).
24. B. H. Brandow. International symposium on quantum chemistry and solid state theory. Sanibel Island, Florida. Jan. 1976.
25. T. G. Castner, N. K. Lee, G. S. Cieloszyk, and G. L. Salinger. Phys. Rev. Lett. **34**, 1627 (1975).
26. D. A. Woodbury and J. S. Blakemore. Phys. Rev. **8**, 3803 (1973).
27. H. C. Casey, Jr., F. Ermanis, and K. B. Wolfstein. J. Appl. Phys. **40**, 2945 (1969).
28. N. F. Mott. Metal–insulator transitions. Taylor and Francis Ltd., London. 1974. Chapt. 4.
29. L. G. Caron and G. Kemeny. Phys. Rev. B, **3**, 3007 (1971).
30. Y. Nakamura, Y. Horie, and M. Shimoji. J. Chem. Soc. Faraday Trans. I, **70**, 1376 (1974).
31. S. A. Rice and J. Jortner. J. Chem. Phys. **44**, 4470 (1966).
32. B. E. Springett, J. Jortner, and M. H. Cohen. J. Chem. Phys. **48**, 2720 (1968).
33. J. Jortner. J. Chem. Phys. **30**, 839 (1959).

Discussion

M. H. Cohen: In the Hubbard criteria you used, the interaction should have been the intra-atomic Coulomb interaction between two electrons of opposite spin in the same 'hydrogenic' orbital. You used instead the Coulomb interaction between two electrons on neighboring sites. The criterion for the M–NM transition based on that interaction is not known in three dimensions. On dimensional grounds it must be of the same form ($T/U \propto$ constant) as that you used. However, the numerical value is unknown, and the coordination number may be associated with U as well as T. Nevertheless, your results are very interesting and quite impressive.

Electron mobilities in alkanes through the liquid and critical regions[1]

JEAN-POL DODELET AND GORDON R. FREEMAN
University of Alberta, Edmonton, Alta., Canada T6G 2G2

Received October 4, 1976

JEAN-POL DODELET and GORDON R. FREEMAN. Can. J. Chem. **55**, 2264 (1977).

Three properties of electrons in liquids are governed by scattering at low energies and show similar dependence upon liquid density and molecular shape. They are the mobility, the dependence of the mobility upon electric field strength, and the penetration range of low energy (< 10 eV) electrons. The scattering cross sections of hydrocarbons in the liquid phase (near or below the normal boiling point) are smaller when the molecules are more sphere-like. The degree of sphericity of the molecules in the present series decreases in the order 2,2-dimethylpropane (DMPr) > 2,2-dimethylbutane (DMB) > cyclopentane (cP) > *n*-pentane (nP).

Electron mobilities in DMPr and DMB measured as functions of the liquid density pass through maxima similar to those observed earlier in argon and xenon. The magnitudes of the maxima decrease in the order Xe > Ar > DMPr > DMB. The maxima occur at densities approximately double the critical density d_c. There is a small maximum for electrons in cP, but none for those in nP.

The mobilities in the supercritical gases are similar for the four compounds. The Arrhenius temperature coefficients are all 7–10 kcal/mol (0.3–0.4 eV/electron) for temperatures and densities near the critical values. This implies that electrons form localized states in the gases. The extent of localization in supercritical DMPr appears to be greater than that in the normal liquid. The localization is not the critical phenomenon predicted by Lekner.

The mobility in liquid DMPr decreases at high electric field strengths. The magnitude of the field dependence changes with the liquid density and passes through a maximum similar to that of the mobility itself. The field dependence in liquid DMB is smaller than that in DMPr, but it also passes through a maximum at a density about double d_c.

Equations are given that describe the mobility in nP at all temperatures from the triple point through to the supercritical gas. The electrons reside mainly in localized states over the entire temperature range, but transport occurs mainly in extended states to which the electrons are thermally excited.

The penetration range parameter b_{GP} of secondary electrons in these liquids is normalized for comparison by multiplying by the liquid density d. The values of $b_{GP}d$ plotted against d form curves similar in shape to the μ against d curves, but the relative variations in $b_{GP}d$ are much smaller.

JEAN-POL DODELET et GORDON R. FREEMAN. Can. J. Chem. **55**, 2264 (1977).

La mobilité des électrons dans un milieu constitue un outil très sensible pour déterminer la diffusion et le transfert d'énergie des électrons thermiques dans ce milieu. Les sections efficaces pour la diffusion et le transfert d'énergie des hydrocarbures en phase liquide (à proximité et en dessous de la température d'ébullition) sont d'autant moindres que la forme des molécules approche la forme sphérique. La sphéricité des molécules dans la présente série décroît dans l'ordre suivant: le diméthyle-2,2 propane (DMPr) > le diméthyle-2,2 butane (DMB) > le cyclopentane (cP) > le *n*-pentane (nP). Trois propriétes des électrons dans ces liquides à 295 K décroissent également dans cet ordre. Elles sont: la mobilité des électrons thermiques, la variation de cette mobilité en fonction du champ électrique et les distances de pénétration des électrons de 0.1 à 10 eV.

Les mobilités dans le DMPr et DMB, mesurées en fonction de la densité du liquide, passent par un maximum semblable à celui déjà observé dans l'argon et le xenon. Ce maximum apparait à une densité approximativement double de la densité critique d_c. L'amplitude de ce maximum décroît dans l'ordre suivant Xe > Ar > DMPr > DMB. Le maximum est peu visible pour le cP et inexistant pour le nP.

Les mobilités dans les gaz, au delà de la température critique, sont semblables pour les quatre hydrocarbures. Les coefficients de température d'Arrhénius sont tous de 7–10 kcal/mol (0.3–0.4 eV/électron) pour les températures et densités proches des valeurs critiques. Ceci implique que les électrons forment des états localisés dans les gaz et que la localisation au delà du point critique semble être plus importante que dans le liquide en dessous de la temperature d'ébullition. Cette localisation n'est pas le phénomene critique predit par Lekner.

---

[1]Assisted by the National Research Council of Canada.

La mobilité dans le DMPr liquide decroît aux champs électriques élevés. L'amplitude de cette dépendance en fonction du champ varie avec la densité du liquide et passe par un maximum similaire à celui de la mobilité. La dépendance en fonction du champ est plus petite pour le DMB liquide que pour le DMPr et le maximum de cette dépendance se situe également à une densité double environ de la densité critique.

Des équations decrivent la mobilité dans le nP à toutes températures depuis le point triple jusqu'au gaz supercritique. Les électrons resident principalement dans des états localisés mais le transport se fait par des états non localisés vers lesquels les électrons sont excités thermiquement.

Afin de comparer les parcours des électrons secondaires b_{GP} dans ces liquides, ils doivent être multipliés par la densité d. Les valeurs de $b_{GP}d$ portées en graphique en fonction de d présentent des courbes semblables aux courbes de μ en fonction de la densité. Toutefois, l'amplitude des variations de $b_{GP}d$ est de beaucoup inférieure à celle de μ.

Introduction

The mechanism of electron transport in materials undergoes a change when the density (1–9) temperature (10–12), or composition (10, 13, 14) of the material is varied over an appropriate range. Although density and temperature were usually varied together, the change of mechanism in a given system has been mainly attributable to one or the other of the properties.

Many different transport mechanisms have been proposed, each fitted to a certain type of system. A general understanding of electron transport has not been attained. For example electron behavior in amorphous solid silicon (15) is similar to that in liquid ethers (16); perhaps the 'ion-like' mechanism of electron transport in low temperature ethers is actually electron hopping between localized states on the edge of the conduction band as proposed for low temperature amorphous silicon. Results are needed from many more systems before a unified theory of electron transport can be formulated.

Experiments involving wide changes of density have involved monatomic fluids (1–9). The present work reports analogous studies with polyatomic molecules. The compounds were chosen to display a wide range of electron mobilities at room temperature.

Experimental

Materials

The hydrocarbons were Phillips Research Grade with initial purities $\geq 99.9\%$. They were further purified as follows: shake or stir 24 h with concentrated sulfuric acid; separate from acid and stir 1 h with solid barium carbonate; pass the vapor through a column of sodium hydroxide pellets; degas; stir 24 h with lithium aluminum hydride; degas; stir 48 h on sodium/potassium alloy; degas; distil into the conductance cell after the latter had been evacuated to 10^{-7} Torr.

Conductance Cells

Two kinds of conductance cells were used, one for low temperatures and pressures (17) and another for pressures up to 100 atm.

A sketch of the high pressure cell is shown in Fig. 1. The distance between the electrodes was determined by a spacer used during manufacture. The cell constant was determined conductiometrically, using standard potassium chloride solutions. The conductance bridge was designed to keep the guard and collector electrodes accurately at the same ac potential (Fig. 2). The cell constant was independent of frequency, 1–3 kHz.

The body of each cell was coated on the outside with Aqua Dag (GC Electronics TV Tube Coat), which was grounded to the copper braid that shielded the lead to the collector electrode. This minimized interference from conductance in the glass. The glass side arm over the high voltage lead was not covered with Aqua Dag or braid because the high fields thus formed in the glass created stresses in it and caused it to break more easily.

A vertical strip of wall on the front and back of the cell was left clean so that the liquid contents could be observed. It was important to note the occurrence of bubbling, the disappearance of the meniscus, and the appearance and disappearance of critical opalescence.

To degas the metal electrodes, the cells during evacuation were heated to a temperature 50 deg higher than that to which they would be raised when containing a sample.

Temperature Control

The low temperature system was the same as that described earlier (17).

For temperatures greater than ambient the cell was positioned on asbestos supports in a clear walled Dewar. A heat gun (Master Appliance Model H67518) was fitted to a 3 cm diameter glass pipe which passed through the asbestos lid, to the bottom of the Dewar. The fan motor and heating coil of the gun were connected to separate Variacs. The heating coil was connected to an LFE Corp. Model 226-A21 temperature controller. Two thermocouples were placed inside the side arm leading to the guard electrode, as near as possible to the body of the cell. One thermocouple was connected to the temperature controller and the other was used to record the temperature. The thermocouples were calibrated by the temperature at which the meniscus disappeared. During heating of the liquid the meniscus stayed in about the center of the cell, well above the electrodes.

The Dewar was placed in a grounded Faraday cage.

Determination of Mobility μ

Electron mobilities at low temperatures in nP were determined from the magnitudes of the electron conductance transients (ect) and the free ion yields (18). Amplifier model 4 (19), with a signal decay half-life of 75 ns and

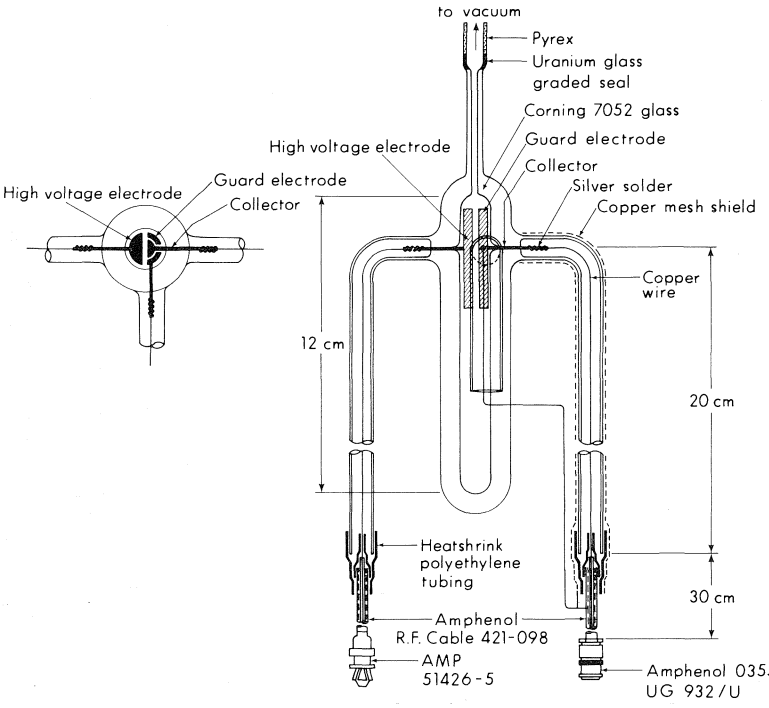

FIG. 1. Conductance cell for studying electrons in critical fluids. The walls were 12 mm thick Corning 7052 borosilicate glass. The electrodes were stainless steel and the pins Kovar. The distance between the electrodes was 3.2 mm and the cell constant 0.125 cm^{-1}.

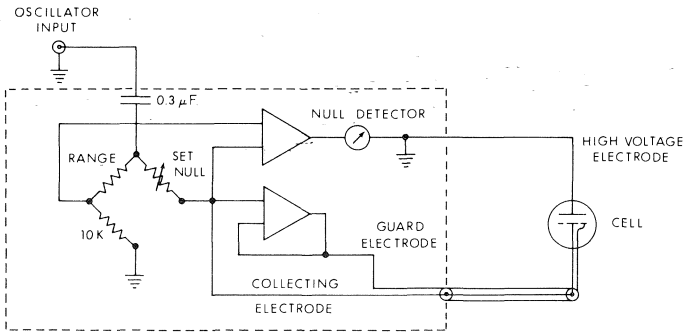

FIG. 2. Bridge circuit used to measure the cell constant. The dashed line represents a metal box which also contained the power supply.

3–97% response time of 200 ns, was used to measure the ect.

At high temperatures in nP and under all conditions in the other hydrocarbons, electron mobilities were obtained from the time of flight between the electrodes (eq. 1).

$$[1] \qquad \mu = l^2/Vt_d$$

where l is the distance between the electrodes, V is the applied voltage, and t_d is the time required for the charged particle to drift the distance l. An example oscilloscope trace for a time of flight measurement is shown in Fig. 3.

Under conditions where both methods could be used, the mobility values agreed within $< 10\%$.

Ion mobilities were determined using [1] and the circuit sketched in Fig. 4.

The radiation pulses were 0.1 or 1.0 μs of 1.7 MeV X rays delivering 0.1 or 1.0×10^{11} eV/g, respectively.

Physical Properties of the Liquids

The densities d for *n*-pentane (nP) and cyclopentane (cP) were obtained from refs. 20–22. Plots of d against T are not available for 2,2-dimethylpropane (DMPr) and 2,2-dimethylbutane (DMB), but the densities at 20°C and the critical temperature T_c are known (20, 21). The variation of d with T for DMPr and DMB were estimated by using the curves for *n*-butane, *n*-pentane, and *n*-hexane (22) as guidelines.

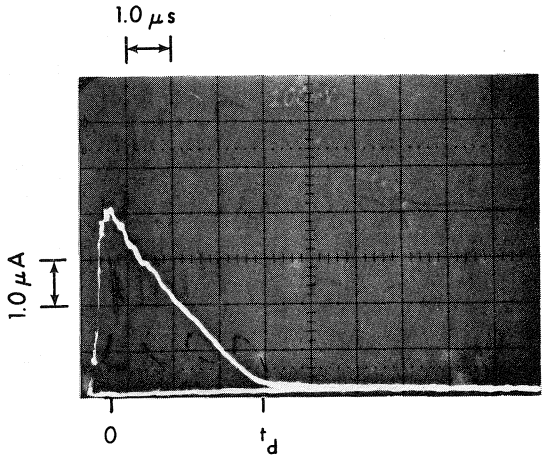

FIG. 3. Oscilloscope trace for an electron time of flight measurement in DMPr at 295 K. Applied voltage = 500 V.

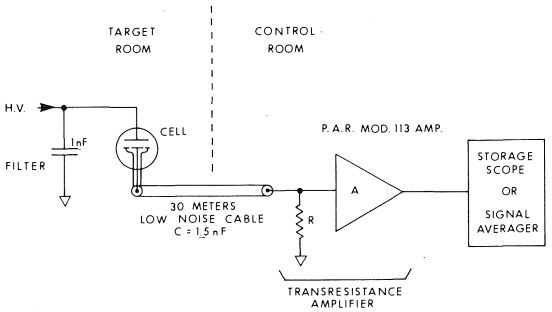

FIG. 4. Apparatus for measuring ion drift times. The 3–97% response time of the input network is $5.2 \times 10^{-9}R$ (s). The transresistance amplifier gain is $R \times A$ (ohm). Typical values of R and A are $10^4\ \Omega$ and 10^4, respectively.

The pressure on the liquid was always its vapor pressure.

The values of the dielectric constant ε at various temperatures were calculated using the Lorenz–Lorentz equation (23*a*) for cP and DMPr, and the Onsager relation (23*b*) for nP and DMB. A dipole moment $\mu = 0.06$ D (24) was used for the last two compounds, but it made $<1\%$ contribution to the dielectric constant even at the lowest temperature. Values of the refractive indices were obtained from refs. 20 and 21.

Results

Temperature Dependence at Low Field Strengths

Electron mobilities ($cm^2\ V^{-1}\ s^{-1}$) in the liquids at 296 K are: nP, 0.12; cP, 1.1; DMB, 11; DMPr, 61. The values for cP, DMB, and DMPr are within 10% of those listed in ref. 25, but there is a scatter of up to ±30% for reported mobilities of electrons in liquid hydrocarbons (11, 18, 25–30). The precision within a given series of experiments is usually <10%. Larger scatter may occur in results from the same laboratory over a period of years and the reason for it remains unknown. However, electron mobilities may differ by several orders of magnitude from one compound to another, so the 30% uncertainty in the absolute magnitudes does not seriously hinder progress in the investigation of electron behavior in liquids.

The mobility of electrons in nP increases continuously with temperature from 150 K through the critical temperature T_c and in the supercritical gas (Fig. 5). By contrast the mobility in DMPr goes through a maximum in the liquid phase at a temperature 29 deg below T_c, and through a minimum at T_c (Fig. 5).

The behaviors in cP and DMB are intermediate between those in nP and DMPr (Fig. 5). In all cases the curves undergo a change of slope at T_c. The validity of the change of behavior is illustrated in Fig. 6 by the error bars marking the upper and lower limits of the measured values at each temperature.

The mobilities in the four critical fluids all lie

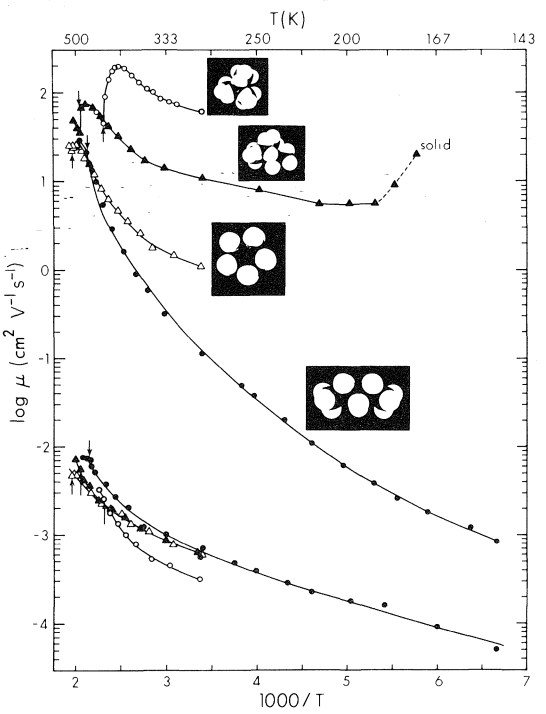

FIG. 5. Effect of temperature on the mobilities of electrons (upper set of curves) and positive ions (lower set) in fluid hydrocarbons. ○, DMPr; ▲, DMB; △, cP; ●, nP. The arrows mark the critical temperatures of the liquids. The curve through the nP points was calculated from eqs. 2–7.

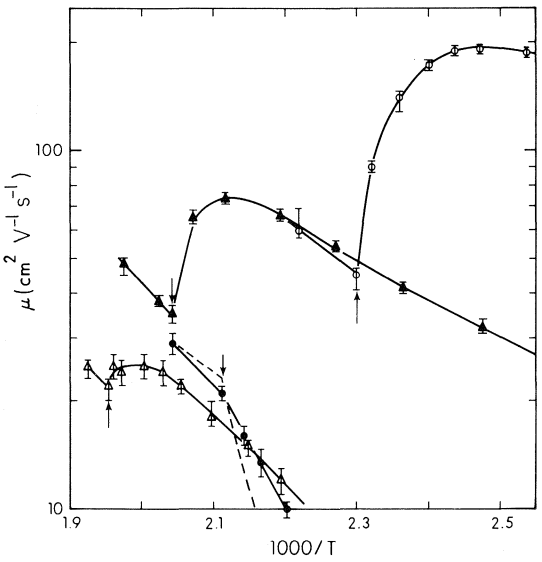

FIG. 6. Behavior of electron mobilities in the vicinity of the critical region in DMPr (○), DMB (▲), cP (△), and nP (●). The error bars mark the upper and lower limits of the measured values at each temperature. The dashed line represents the calculated curve for nP in this region.

within a factor of two of each other, while at 295 K the differences are up to 500-fold.

The mobilities of heavy positive ions increased monotonously with temperature in all the hydrocarbons (Fig. 5). Extrema are therefore characteristic of electron mobilities. The upward curvature of the ion mobility plots for high temperatures is similar to that in the electron mobility plots at temperatures below the mobility maxima.

Anion mobilities were usually not measured because under most conditions the electrons were swept out of the system before becoming attached to an impurity to form an anion. However, anions were obtained in cP and DMB at the lower temperatures. Compared to the positive ion mobilities in Fig. 5, $\mu_-/\mu_+ = 2.0 \pm 0.1$ in cP and 2.1 ± 0.1 in DMB. Similar values of the ratio have been obtained in many hydrocarbons (31–33).

In the high temperature sample of nP and in DMB, slower positive ions than those recorded in Fig. 5 were also observed. The ratio μ_+(fast)/μ_+(slow) had an average value of 2.3 ± 0.2 in nP and 1.9 ± 0.1 in DMB. The slower cations may have been mainly dimers to tetramers of product and impurity olefins.

Electric Field Dependence

In nP and cP the electron mobilities were independent of applied field strength over the range 3–20 kV/cm in liquids and 3–12 kV/cm in the supercritical gases. Experimental difficulties prevented measurements at higher fields at the highest temperatures. The difficulties included amplifier sensitivity and response time and field induced conductance switching in the hot glass (34).[2]

The electron mobility in DMPr at 295 K decreased gently with increasing field strength at $E > 4$ kV/cm. Upon raising the liquid temperature, the mobility and its field dependence increased (Fig. 7). Both the mobility and its field dependence passed through maxima at temperatures near 400 K (Figs. 7 and 8). For a given mobility, the field dependence was smaller on the high than on the low temperature side of the mobility maximum. A few degrees below T_c the field dependence became negligible up to 20 kV/cm and remained so in the supercritical gas (Fig. 8). The mobility passed through a minimum in this temperature region (Fig. 6).

The behavior was similar in DMB (Figs. 9 and 10), but the mobilities and their temperature dependences were smaller than in DMPr.

Cation mobilities were independent of applied field strength in the present region.

Discussion

Electrons in liquid alkanes are distributed among localized and extended states. The measured mobility is an appropriate average of the mobilities characteristic of the states, taken over the distribution of the electrons among the states. These things depend on the temperature and density of the liquid and on the nature of the molecules. The influences of all three factors are visible in Fig. 5.

Effect of the Nature of the Molecules at $T \ll T_c$

The molecules of the present liquids are nonpolar or only slightly polar, with gas phase dipole moments ≤ 0.1 D (24). The potential wells of the localized states of electrons in the liquids are at most a few tenths of an eV deep. The traps tend to be shallower when the molecules are more sphere-like (27). Electrons also appear to be less efficiently localized in traps the

[2]Field induced switching occurs in many amorphous materials such as boron-based glasses (34). Recently, most studies of the phenomenon have been made with chalcogenides (34–36).

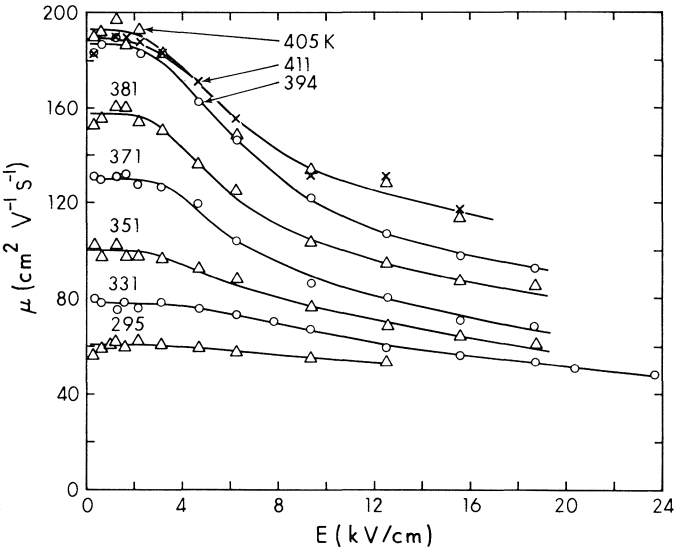

FIG. 7. Electric field dependence of electron mobilities in liquid DMPr at temperatures from 295 K through those at the mobility maximum.

more easily the molecules can rotate in the fluid (18).

The mobilities of electrons in extended states are several orders of magnitude greater than those in localized states. Thus the measured mobilities are greater in liquids of the more sphere-like molecules: nP < cP < DMB < DMPr (Fig. 5).

Effect of Temperature

In nP at the lowest temperature the electron mobility is eightfold greater than that of the anions, and the ratio increases with temperature. The contribution of an ion-like mechanism (12) to electron transport in liquid alkanes therefore appears to be negligible.[3] The mobility and its temperature dependence can be explained in terms of thermal partition of the electrons between localized and extended states, with transport occurring mainly in the latter (38).

The energy states are affected by local fluctuations in the molecular orientation and density of the fluid (39). It is assumed that the distribution of transition energies from localized to extended states is a Gaussian centered about a value E_0, with a distribution parameter σ.

$$[2] \quad N(E) = \pi^{-1/2}\sigma^{-1} \exp\left[-(E - E_0)^2/\sigma^2\right]$$

where $\pi^{-1/2}\sigma^{-1}$ is a normalization factor. The measured mobility μ_e is given by [3], where μ^0 is

$$[3] \quad \mu_e = \mu^0 \int_{-\infty}^{\infty} N(E)[1 + \exp(E/kT)]^{-1}\, dE$$

the mobility in the extended state. It is assumed that the entropy change is small for an electron going from a localized to an extended state and that the energy ranges of the localized and extended states overlap (12).

To calculate μ_e from [3] one requires values of μ^0, E_0, and σ. Unique values of the parameters in a given system are not available, but reasonable limitations can be put on them by comparison with other data. By analogy with the temperature dependences of the optical absorption parameters of solvated electrons (12), one may assume that $dE_0/dT \leq 0$ and $d\sigma/dT \geq 0$. Due to the Franck–Condon requirement of optical transitions and the probability that there are only one or two bound levels per electron trap in a liquid alkane, one may take $E_0 \leq E_{am}$, where E_{am} is the transition energy at the optical absorption maximum. The values of E_{am} in nP over the temperature range 150–

[3]The ion-like mechanism in liquid ethers is conceptually similar to thermally assisted tunnelling to nearest neighbor centers (35) and small polaron hopping (37). It does not involve migration of the solvation shell of the electron (12). The similarity between the activation energies of electron and ion mobilities in polar liquids had been rationalized in terms of the energy requirements of rotational–translational motions of the anisotropic solvent molecules (16). However, the striking resemblance between the behavior of electrons in a specimen of solid, amorphous silicon (37), and that in liquid ethers (16) is difficult to understand.

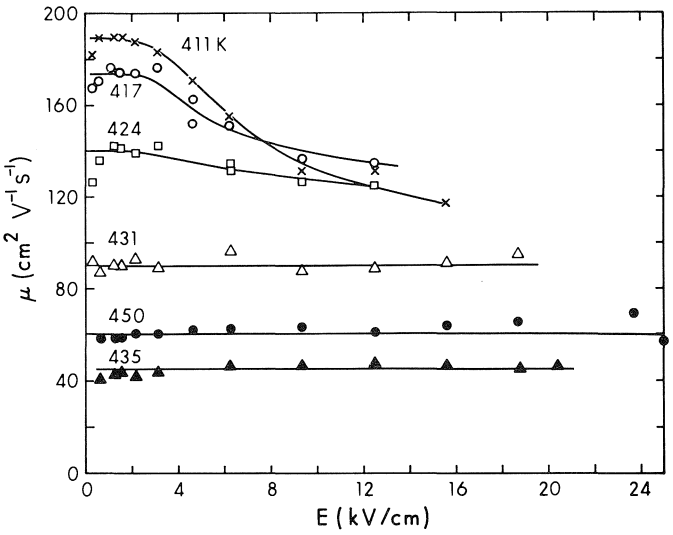

FIG. 8. Electric field dependence of electron mobilities in DMPr at temperatures above that of the mobility maximum. T_c = 434 K. The filled points refer to the gas at a density of 0.242 g/cm³.

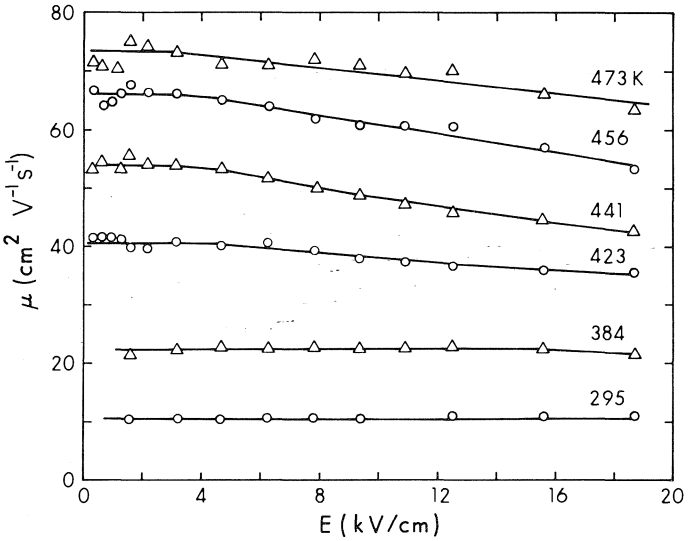

FIG. 9. Electric field dependence of electron mobilities in liquid DMB at temperatures from 295 K to that of the mobility maximum.

500 K are probably near 0.6–0.3 eV (12, 40). The value of $d\sigma/dT$ for the electron transitions is probably not greater than that of the thermal energy fluctuations in the liquid, so $d\sigma/dT \leq (2\ kC_p)^{1/2} \approx 5 \times 10^{-4}$ eV/K in nP at $T < 400$ K (22, 38).

In earlier studies over more limited temperature ranges μ^0 has usually been taken to be independent of temperature (12, 25, 28, 30). That approximation is inadequate for the wide ranges of temperature and fluid density in the present work. In particular, the rapid change of density at temperatures approaching T_c should be taken into account, although the way to do it is not straightforward. For electrons in nP it was assumed that the mean free path λ was inversely proportional to the density, and that μ^0 could be represented by [4] (12), where v^0 is the jump

$$\mu^0 = \lambda^2 v^0 e/2kT \qquad [4]$$

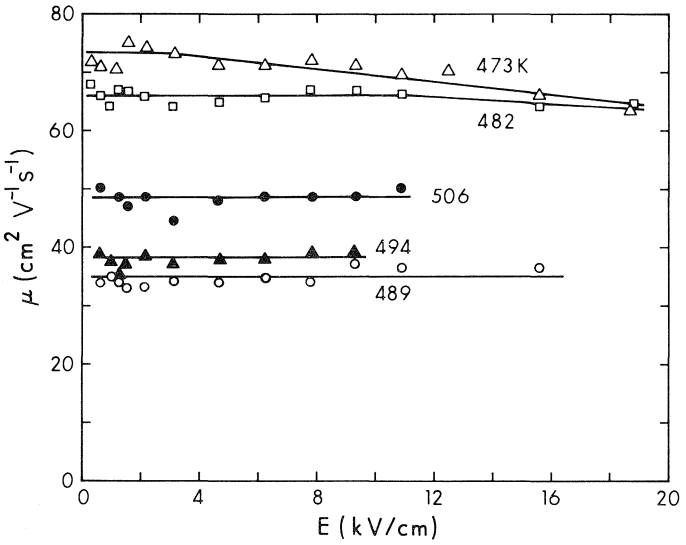

FIG. 10. Electric field dependence of electron mobilities in DMB at temperatures from the mobility maximum to the supercritical region. T_c = 489 K. The filled points refer to the gas at a density of 0.240 g/cm³.

attempt frequency and e is the unit electronic charge.

Within the above limitations we were able to fit the electron mobilities in nP over most of the liquid range and in the supercritical gas (Fig. 5) with the following parameter values.

$$[5] \qquad E_0\,(\text{eV}) = 0.64 - 7 \times 10^{-4}T$$

$$[6] \qquad \sigma\,(\text{eV}) = 0.15 + 8 \times 10^{-5}T$$

$$[7] \quad \mu^0\,(\text{cm}^2\,\text{V}^{-1}\,\text{s}^{-1}) = \mu^0{}_{\text{ref}}\left(\frac{d_{\text{ref}}}{d_T}\right)^2\left(\frac{T_{\text{ref}}}{T}\right) = 250\left(\frac{0.623}{d_T}\right)^2\left(\frac{295}{T}\right)$$

where $\mu^0{}_{\text{ref}}$ and the density d_{ref} are the values at the reference temperature T_{ref}. The fit is adequate over the entire 350 deg range of temperature except for a 30 deg region just below the critical temperature (Figs. 5 and 6). In this region the density changes rapidly and nonlinearly with temperature, so [5] and [6] become inadequate representations of E_0 and σ, respectively.

The transition energy E_0 is equal to $(V_0 - \overline{V})$, where V_0 is the energy of an electron in the lowest extended state relative to the vacuum level, and $\overline{V}$ is the mean energy of electrons in localized levels (38, 39, 41–43). Preliminary treatments of electron mobilities by fluctuation theories (39, 41) neglected the temperature dependence of E_0 and, based upon thermal energy fluctuations, assumed $d\sigma/dT$ = 6–11 × 10^{-4} eV/K for C_5 and C_6 hydrocarbons. However, to fit the temperature dependence of the mobilities using such large values of $d\sigma/dT$ would require that dE_0/dT be *positive* and of similar magnitude (38). Positive values of dE_0/dT are unlikely, so the temperature coefficient of σ must be much smaller than that of the dispersion parameter of thermal energy fluctuations.

Holroyd and co-workers (42, 43) have measured the photoinjection of electrons from metal surfaces into liquids and into a vacuum as functions of photon energy and applied electric field strength. From the difference between the injection energy into a liquid and into a vacuum they derived an energy that was equated to V_0. They obtained $dV_0/dT = -2.2 \times 10^{-3}$ eV/K for nP (43), which is much greater in magnitude than the temperature coefficient of E_0 in [5]. This implies that the energies of the localized and extended states in alkanes are affected similarly when the liquid temperature is changed. Thus V_0 and $\overline{V}$ in alkanes appear to be affected mainly by the changing density; $(dV_0/dd) \approx (d\overline{V}/dd)$ = positive, which multiplied by the negative (dd/dT) gives the observed results. There would be a positive contribution from $(d\overline{V}/dT)$ due to decreased orientational polarization at higher temperatures, but it would be relatively small in hydrocarbons.

The direct effect of density on electron energy

levels in liquids, distinct from its secondary effect through the dielectric constant, has also been detected through the influence of pressure on optical absorption energies in alcohols (44–46), and through the influence of temperature on V_0 in hydrocarbons (43).

Electron migration in nP remains in the thermally activated regime even in the supercritical gas. The mobility increases monotonously with temperature. By contrast, the mobility in DMPr goes through a maximum (Fig. 5). The maximum occurs at a temperature 29 deg below T_c, so the decrease in mobility at high temperatures is not a critical phenomenon. The behavior is reminiscent of that in argon (2) and xenon (5), where the electrons were presumed to normally reside in the lowest extended state (47). Changes in mobility would then reflect changes in μ^0. However, μ_e increases with temperature in the supercritical gas of DMPr at constant density, just as it does in nP (Fig. 6). It appears that electron transport in supercritical DMPr occurs by a two state mechanism and that the decrease of μ_e at $T > 405$ K is due to the formation of localized states. The Arrhenius activation energies of μ_e in all four of the present supercritical gases are 7–10 kcal/mol (0.3–0.4 eV/electron). They are about double that in liquid nP at room temperature, where the two state mechanism is generally accepted.

The mobilities and their temperature dependences in DMB and cP are intermediate between those in nP and DMPr (Fig. 5). Assuming that the values of σ are similar in the four hydrocarbons, the variations of μ_e with temperature indicate that the relative values of E_0 at a given temperature at $T \ll T_c$ decrease in the order nP > cP > DMB > DMPr. Measured values of V_0 at $\sim$296 K lie in the same order (42, 48).

An adequate interpretation of mobility maxima in fluids has not yet been found (2, 49), so theoretical curves are not offered for the DMPr, DMB, and cP results in Fig. 5.

Effect of Density

The mobilities are displayed as functions of the liquid densities in Fig. 11. Points for solid DMPr (29) and DMB are included.

The increase in mobility on going from the liquid to the crystalline solid is due to the smaller amount of scattering in the more ordered medium (represented by a smaller structure factor (50)). The continued increase of μ_e with increasing density of the solid is actually due to the decreasing temperature of the samples (29), and thereby reduced scattering of the electrons by phonons (51).

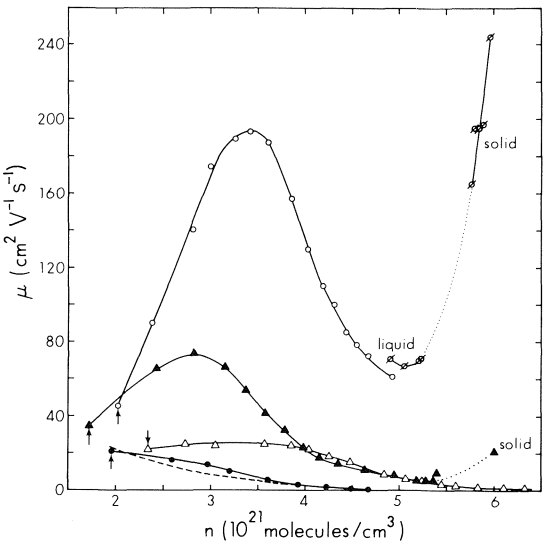

FIG. 11. Electron mobilities in DMPr (○), DMB (▲), cP (△), and nP (●) plotted against the molecular density of the medium. The arrows mark the critical fluids. The liquid and solid phase results for DMPr from ref. 29 are also included (ϕ). Dotted lines mark the liquid–solid transition. The dashed line for nP represents the mobilities calculated from eqs. 2–7. The densities were changed by changing the temperature of the samples under their vapor pressure.

Upon decreasing the density of liquid DMPr from that at the triple point, the mobility passes through a minimum. The increase of μ_e with decreasing density is attributed to a decreasing scattering length. The molecules in the normal liquid are so close together that an electron passing between them suffers mainly repulsion from the hard cores (Hartree fields) of the molecules (51). As the density decreases the molecules move farther apart and the electron experiences more of the attractive polarization interactions, which tend to counteract the hard core repulsions. The scattering length thereby decreases. The attractive interaction continues to increase with decreasing fluid density and at some point cancels the hard core repulsion, and the scattering cross section is a minimum. Upon further reducing the density the attractive polarization dominates the electron–molecule interaction, the scattering length becomes negative, and the scattering cross section increases again. The mobility therefore decreases. This model has been used to interpret the mobility maximum in

liquid argon (47). However, there are quantitative difficulties with the model (2, 49). Some other process contributes to limiting the mobility at the maximum and on the low density side of the peak. The present results from fluid hydrocarbons indicate that the other process is electron localization. Lekner and Bishop (4) proposed that localization would take place in simple fluids near the critical point. An effect that is peculiar to the critical region does not occur (5), but localization does take place over a broader range of densities.

The data in Table 1 and in Fig. 11 of ref. 2 indicate that electron migration in fluid argon gradually changes to a thermally activated two state mechanism at densities below 1.4×10^{22} atom/cm^3. The mobility maximum occurs at 1.2×10^{22} atom/cm^3. At 1.0 and 0.7×10^{22} atom/cm^3 the Arrhenius temperature coefficients of the mobilities are each 3 kcal/mol. Thus the formation of localized states could make a major contribution to limiting the mobility in this density region.

The maxima in DMB and DMPr occur at 2.8 and 3.4×10^{21} molecules/cm^3, which are 1.7 times the respective critical densities. The mobility maxima in argon and xenon occur at 12×10^{21} molecules/cm^3 (2, 5), which are respectively 1.5 and 2.4 times d_c.

The mobility in nP appears to be approaching a maximum at the critical point (Fig. 11). The complex behavior in all the hydrocarbons at densities $<4 \times 10^{21}$ molecules/cm^3 indicates why the simple calculations based on [2]–[7] gave poor agreement between calculated and observed mobilities for nP in this region (Fig. 11).

The electron mobility curve for each hydrocarbon in Fig. 5 changes slope abruptly at the critical temperature. The change of slope does not signify a change in electron behavior, but rather a discontinuity in dd/dT. As T_c is approached in the liquid phase the density decreases rapidly and the density effect dominates the change in μ_e. At $T > T_c$ the density remains constant, so the mobility is affected only by the change of T.

TABLE 1. Critical properties of the hydrocarbons

	T_c (K)	P_c (atm)	d_c (g/cm^3)	ε_c
Cyclopentane	512	44.6	0.270	1.29
2,2-Dimethylpropane	434	31.6	0.23	1.27
n-Pentane	470	33.3	0.232	1.27
2,2-Dimethylbutane	489	30.9	0.240	1.27

Ion Mobilities

The temperature dependences of ion mobilities in the liquid alkanes within 100 deg of their critical temperatures are non-Arrhenius (Fig. 5). The same is true of the temperature dependences of the viscosities (22) and self-diffusion coefficients (52). The non-Arrhenius behavior reflects the accelerating value of dV_f/dT in this temperature range, where V_f is the free volume.

The relationship between the positive ion mobility μ_+ (cm^2 V^{-1} s^{-1}) and the viscosity η (cP) for nP between 230 and 450 K is approximately given by [8], while that for cP between 300 and 420 K is [9]. The calculated and experimental results are displayed in Fig. 12. The mobility–viscosity relationship varies with the structure of the solvent molecules, but is similar for alkanes and ethers (16). Ions in cyclo-solvents have higher mobilities than those in *n*-alkyl solvents of the same viscosity. The mobilities do not fit Walden's rule; the viscosity exponents are -1.1 to -1.3 instead of the predicted -1.0.

$$[8] \qquad \mu_+ = 1.0 \times 10^{-4}\eta^{-1.3}$$

$$[9] \qquad \mu_+ = 2.2 \times 10^{-4}\eta^{-1.1}$$

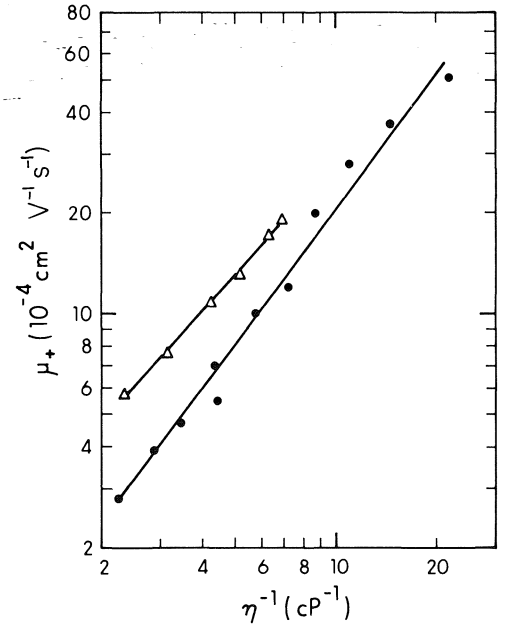

FIG. 12. Ion mobilities in cP (△) and nP (●) as functions of the inverse viscosity. The full lines represent [8] for nP and [9] for cP.

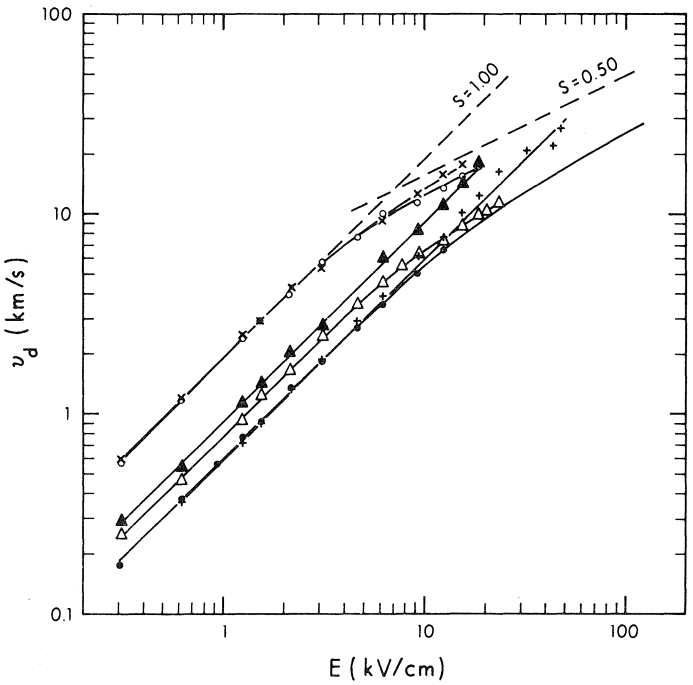

FIG. 13. Electron drift velocity v_d as a function of electric field strength in DMPr at different temperatures. ●, 295 K; △, 331 K; ○, 394 K; ×, 405 K; ▲, 431 K; +, 450 K (gas). T_c = 434 K. The curve beyond 13 kV/cm at 295 K represents results from ref. 56.

Rotational motions of the irregularly shaped solvent molecules are required to facilitate ion migration, to maintain the polarization energy at a reasonably low level while the ion moves. The temperature coefficient of rotational motion E_τ is often greater than that of shear viscosity E_η; for water and for diethyl ether $E_\tau/E_\eta = 1.2$ at 293 K (calculated from data in refs. 53 and 54). Equations 8 and 9 imply that $E_{\mu_+}/E_{\eta^{-1}} = 1.2 \pm 0.1$ in cP and nP, which indicates a correlation between μ_+ and τ^{-1}.

Walden's rule is an approximation, the validity of which stems from the interdependence of rotational and translational motions in these liquids. The rule would be expected to apply more accurately to liquids made up of spherical molecules.

Field Dependence

The electron mobilities in nP and cP are relatively low and they are independent of applied electric field strength up to 20 kV/cm. In DMB and DMPr the mobilities are relatively high and field dependent. The two properties tend to increase together (Figs. 7–10).

The usual way to display field dependence is to make a log–log plot of drift velocity v_d against field strength (Fig. 13). Field dependence occurs where the slope deviates from unity. It means that the energy acquired by the electron from the field is not dissipated efficiently enough, and the average electron energy increases above thermal. The lower the field at which deviation occurs, the less efficient are the energy loss processes.[4]

If deviation occurs when v_d is only about twice the speed of sound in the medium, the electron energy is dissipated mainly to acoustic phonons. At higher drift velocities more efficient processes are important (50, 55).

In DMPr at 295 K the mobility becomes field dependent when v_d exceeds about 3 km/s (Fig. 13). The present result agrees with that of Bakale and Schmidt (56). By extrapolation of data for other alkanes at the same temperature and at the same density (57), the velocity of sound in liquid DMPr at 295 K is 1.0 km/s. As the temperature of the liquid increases the velocity of sound de-

[4]This explains why the penetration ranges of epithermal electrons are greater in systems that show a greater field dependence of the mobility. Density normalized ranges tend to be greater when the energy loss processes are less efficient.

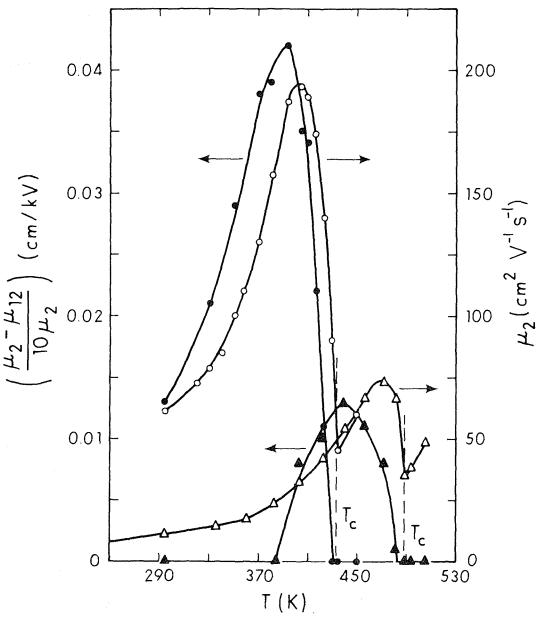

FIG. 14. Electric field dependence of the electron mobilities in DMPr (●) and DMB (▲) as functions of temperature. μ_2 and μ_{12} are the mobilities at 2 and 12 kV/cm, respectively. Values of μ_2 are also plotted so that the peaks can be compared.

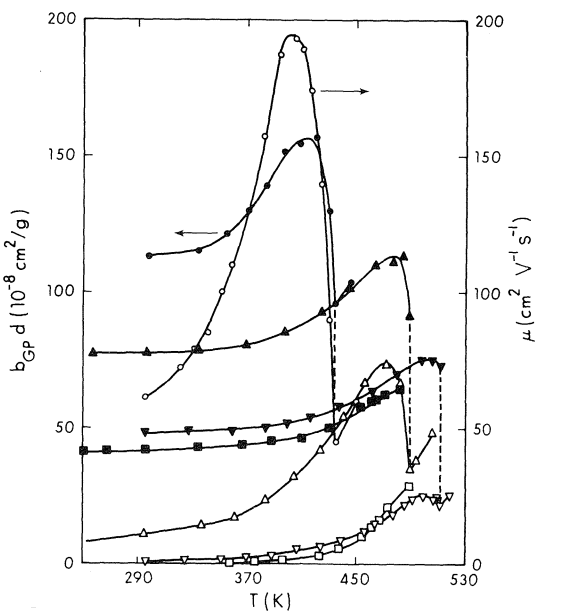

FIG. 15. Density normalized ranges ($b_{GP}d$) of secondary electrons in fluid hydrocarbons as functions of temperature. ●, DMPr; ▲, DMB; ▼, cP; ■, nP; data from ref. 58. The mobilities (open points) are plotted for comparison. The vertical dashed lines mark the critical temperature of each fluid.

creases (57), whereas the threshold drift velocity for field dependence goes in the opposite direction (Fig. 13). Electron thermalization in DMPr and the other hydrocarbons cannot be attributed to interactions with the collective motions of acoustic phonons. It must be due to more efficient interactions with motions of smaller groups of molecules.[5]

Simple theories (50) predict that at high fields the drift velocity will vary as $E^{1/2}$. For this reason it is usual to place reference lines with slopes $s = 1.00$ and 0.50 in graphs like Fig. 13. However, a survey of the literature provides little support for the existence of extended regions where $v_d \propto E^{1/2}$ in liquids. The slope simply becomes different from unity and can become as low as zero.

The field dependence varies with the temperature in a manner similar to the mobility itself. A comparative measure of the field dependence is $\mu^{-1}(d\mu/dE)$. In the present work it may conveniently be represented by $(\mu_2 - \mu_{12})/10\mu_2$, where the subscripts denote the field in kV/cm at which the mobility was measured and the units of the ratio are cm/kV. Values of this ratio peak about 10 deg below the temperature of the mobility maximum in DMPr and about 30 deg below the mobility maximum in DMB (Fig. 14). There is a remarkable coincidence between the relative sizes of the mobility and the field dependence peaks.

The density normalized penetration ranges of the secondary electrons in these liquids also pass through maxima (58). The range maxima occur at temperatures slightly higher than those of the mobility maxima (Fig. 15). The relative magnitudes of the range peaks are much smaller than those of the mobility and field dependence peaks. The major portion of the range is generated by electrons in a higher average energy state, probably a few tenths of an eV, while the mobility and its field dependence are properties of electrons having an average energy of a few hundredths of an eV.

The common factor that influences these three quantities is the electron energy transfer cross section. The cross section in liquids comprised of globular molecules first decreases, then increases as the density of the fluid decreases. The molecules of nP are distinctly nonsphere-like; the

[5]Terms for these motions in liquids are not well defined. They include optical phonons, rotational–translational oscillations, librations, lattice vibrations, and perhaps others.

scattering cross section in that liquid is relatively large and decreases monotonously with decreasing density at high temperatures.

Electron localization occurs when the scattering cross section is large. Localization apparently occurs in the supercritical gases near the critical region.

1. J. L. LEVINE and T. M. SANDERS, JR. Phys. Rev. **154**, 138 (1967).
2. J. A. JAHNKE, L. MEYER, and S. A. RICE. Phys. Rev. A, **3**, 734 (1971).
3. J. P. HERNANDEZ. Phys. Rev. A, **5**, 635 (1972).
4. J. LEKNER and A. R. BISHOP. Philos. Mag. **27**, 297 (1973).
5. T. KIMURA and G. R. FREEMAN. Can. J. Phys. **52**, 2220 (1974).
6. R. BOEHM. Phys. Rev. A, **12**, 2189 (1975).
7. F. HENSEL and E. U. FRANCK. Rev. Mod. Phys. **40**, 697 (1968).
8. F. HENSEL. Angew. Chem. Int. Ed. Engl. **13**, 446 (1974).
9. M. H. COHEN and J. JORTNER. Phys. Rev. A, **10**, 978 (1974).
10. N. F. MOTT and E. A. DAVIS. Electronic processes in noncrystalline materials. Clarendon Press, Oxford. 1971.
11. K. SHINSAKA, J.-P. DODELET, and G. R. FREEMAN. Can. J. Chem. **53**, 2714 (1975).
12. J.-P. DODELET, F.-Y. JOU, and G. R. FREEMAN. J. Phys. Chem. **79**, 3876 (1975).
13. C. A. KRAUS and W. W. LUCASSE. J. Am. Chem. Soc. **44**, 1941 (1922).
14. M. H. COHEN and J. C. THOMPSON. Adv. Phys. **17**, 857 (1968).
15. P. G. LE COMBER and W. E. SPEAR. Phys. Rev. Lett. **25**, 509 (1970).
16. J.-P. DODELET and G. R. FREEMAN. Can. J. Chem. **53**, 1263 (1975).
17. J.-P. DODELET, K. SHINSAKA, U. KORTSCH, and G. R. FREEMAN. J. Chem. Phys. **59**, 2376 (1973).
18. J.-P. DODELET, K. SHINSAKA, and G. R. FREEMAN. J. Chem. Phys. **59**, 1293 (1973).
19. M. G. ROBINSON and G. R. FREEMAN. Can. J. Chem. **52**, 440 (1974).
20. J. TIMMERMANS. Physico chemical constants of pure organic compounds. Elsevier Publishing Co., Amsterdam. Vol. 1, 1950; Vol. 2, 1965.
21. R. R. DREISBACH. Adv. Chem. Ser. **22** (1959).
22. R. W. GALLANT. Physical properties of hydrocarbons. Vols. 1 and 2. Gulf Publishing Co., Houston, Texas. 1968.
23. N. E. HILL, W. E. VAUGHAN, A. H. PRICE, and M. DAVIES. Dielectric properties and molecular behavior. Van Nostrand Reinhold Co., Toronto. 1969. (*a*) p. 191; (*b*) p. 23.
24. D. R. LIDE, JR. and A. A. MARYOTT. Selected values of electric dipole moments for molecules in the gas phase. NSRDS–NBS 10, U.S. Govt. Printing Office, Washington, DC. 1967.
25. W. F. SCHMIDT and A. O. ALLEN. J. Chem. Phys. **52**, 4788 (1970).
26. R. M. MINDAY, L. D. SCHMIDT, and H. T. DAVIS. J. Chem. Phys. **54**, 3112 (1971).
27. J.-P. DODELET and G. R. FREEMAN. Can. J. Chem. **50**, 2667 (1972).
28. R. M. MINDAY, L. D. SCHMIDT, and H. T. DAVIS. J. Phys. Chem. **76**, 442 (1972).
29. K. SHINSAKA and G. R. FREEMAN. Can. J. Chem. **52**, 3556 (1974).
30. A. O. ALLEN and R. A. HOLROYD. J. Phys. Chem. **78**, 796 (1974).
31. I. ADAMCZEWSKI. Acta Phys. Pol. **30**, 707 (1966).
32. A. HUMMEL and A. O. ALLEN. J. Chem. Phys. **44**, 3426 (1966).
33. P. H. TEWARI and G. R. FREEMAN. J. Chem. Phys. **49**, 4394 (1968).
34. S. R. OVSHINSKY. Phys. Rev. Lett. **21**, 1450 (1968).
35. J. FRITZCHE. *In* Amorphous and liquid semiconductors. *Edited by* J. Tauc. Plenum Press, London. 1975. Chapts. 5 and 6.
36. F. MAHDJURI. *In* Amorphous and liquid semiconductors. Vol. 2. *Edited by* J. Stuke and W. Brenig. Taylor and Francis, London. 1974. p. 1295.
37. W. E. SPEAR. Adv. Phys. **23**, 523 (1974).
38. J.-P. DODELET, K. SHINSAKA, and G. R. FREEMAN. Can. J. Chem. **54**, 744 (1976).
39. R. SCHILLER, SZ. VASS, and J. MANDICS. Int. J. Radiat. Phys. Chem. **5**, 491 (1973).
40. T. SHIDA, S. IWATA, and T. WATANABE. J. Phys. Chem. **76**, 3683 (1972); **76**, 3691 (1972).
41. N. R. KESTNER and J. JORTNER. J. Chem. Phys. **59**, 26 (1973).
42. R. A. HOLROYD, B. K. DIETRICH, and H. A. SCHWARZ. J. Phys. Chem. **76**, 3794 (1972).
43. R. A. HOLROYD, S. TAMES, and A. KENNEDY. J. Phys. Chem. **79**, 2857 (1975).
44. M. G. ROBINSON, K. N. JHA, G. L. BOLTON, and G. R. FREEMAN. Chemical Institute of Canada Pulse Radiolysis Symposium, Pinawa, Man., 1971.
45. K. N. JHA, G. L. BOLTON, and G. R. FREEMAN. J. Phys. Chem. **76**, 3876 (1972).
46. G. R. FREEMAN. J. Phys. Chem. **77**, 7 (1973).
47. J. LEKNER. Phys. Lett. A, **27**, 341 (1968).
48. R. A. HOLROYD and R. L. RUSSELL. J. Phys. Chem. **78**, 2128 (1974).
49. J. A. JAHNKE, N. A. W. HOLZWARTH, and S. A. RICE. Phys. Rev. A, **5**, 463 (1972).
50. L. S. MILLER, S. HOWE, and W. E. SPEAR. Phys. Rev. **166**, 871 (1968).
51. J. LEKNER. Phys. Rev. **158**, 130 (1967).
52. G. M. PANCHENKOV, N. N. BORISENKO, and V. V. ERCHENKOV. Russ. J. Phys. Chem. **43**, 1328 (1969).
53. F. BUCKLEY and A. A. MARYOTT. Tables of dielectric dispersion data for pure liquids and dilute solutions. NBS Circ. 589, U.S. Dept. of Commerce, Washington, DC. 1958.
54. R. C. WEAST (*Editor*). Handbook of chemistry and physics. 50th ed. Chemical Rubber Co., Cleveland, Ohio. 1969.
55. M. H. COHEN and J. LEKNER. Phys. Rev. **158**, 305 (1967).
56. G. BAKALE and W. F. SCHMIDT. Chem. Phys. Lett. **22**, 164 (1973).
57. V. F. NOZDREV. Applications of ultrasonics in molecular physics. Gordon and Breach, New York. 1963. Appendix.
58. J.-P. DODELET. Can. J. Chem. This issue.

Discussion

J. K. Baird: I wish to point out that I have integrated the Schrodinger equation numerically for argon with the following potential $V(r)$:

$$V(r) = V_{HF}(r) - \frac{1}{2}\frac{\alpha e^2 f}{(r^2 + r_c^2)^2}$$

where $V_{HF}(r)$ is the Hartree field, α is the polarizability, e the electron charge, f the screening function, and r_c is a cut-off radius. The screening function may be either that due to Lekner (Phys. Rev. **158**, 130 (1967)) or one based on the Onsager reaction field (J. K. Baird. J. Phys. Chem. **79**, 2862 (1975)). The difference is unimportant except to say that $f = 1$ at zero density and decreases toward zero as the density increases. The cut-off radius r_c was determined so that when $f = 1$, the potential predicted an energy dependence of the total scattering cross section in agreement with that observed in numerous experiments on the Ramsauer effect in low pressure gases. The result of using the above potential to calculate the scattering cross section as f decreased from unity was: (*1*) the Ramsauer minimum in the cross section persisted; (*2*) the energy at which the minimum occurred decreased; (*3*) the value of the cross section at the minimum decreased. It is my view that the above potential is the one from which the single atom cross section in the liquid should be calculated. To take into account diffraction effects, I believe that this cross section should be multiplied by the liquid structure factor, as in the Ziman weak scattering theory, to obtain the many atom scattering cross section in the liquid. Hence, since the single atom cross section appears to decrease with increasing density, one is tempted to conclude that the decrease in the screening function may account for the large electron mobility observed in liquid argon.

Y. Hatano: Do you have any experimental data on the hydrogen isotope effect of μ_e, such as μ_e's for CH_4, CH_3D, CH_2D_2, CHD_3, and CD_4, or μ_e's for C_2H_4, C_2H_3D, $C_2H_2D_2$ (*trans*-$C_2H_2D_2$, *cis*-$C_2H_2D_2$, asym-$C_2H_2D_2$), C_2HD_3, and C_2D_4? One may expect to get an interesting feature for the effect of molecular structure of μ_e.

G. R. Freeman: I agree that the isotope effect should exist. We tried to do measurements in the series of deuterated methanes several years ago, but failed due to impurity problems. We are going to try again soon. As a final comment, on several occasions during the conference experimentalists have presented evidence that behavior similar to the (gas phase) Ramsauer–Townsend effect can occur in simple liquids. The opinion of concerned theoreticians seems to be that the Ramsauer–Townsend effect cannot occur in liquids. At this point we must specify conditions more precisely. In mobility experiments the effect appears as a maximum in a plot of electron mobility against applied electric field strength. The mobility maximum occurs in both gaseous and liquid xenon. For the liquid phase, beginning at the critical density and proceeding towards higher densities, the low field mobility increases and the Ramsauer–Townsend maximum becomes less prominent (Kimura and Freeman. To be published). Thus, the Ramsauer–Townsend mobility maximum (scattering minimum) correlates with the density dependence of the mobility at low fields. What we lack is a formal theory that relates the two effects to common underlying properties of the fluid. Lekner's model for the density dependence of the scattering length (Phys. Lett. A, **27**, 341 (1968)) seems an appropriate place to start.

Canadian Journal of Chemistry

Journal canadien de chimie

Published by
THE NATIONAL RESEARCH COUNCIL OF CANADA

Publié par
LE CONSEIL NATIONAL DE RECHERCHES DU CANADA

Volume 55 Number 12 June 15, 1977

Volume 55 numéro 12 15 juin 1977

The photoinsertion of tin(II) chloride into the metal–metal bond of hexacarbonylbis(tri-*n*-butylphosphine)dicobalt[1]

PETER F. BARRETT, ARNOLD FOX, AND RAYMOND E. MARCH

Department of Chemistry, Trent University, Peterborough, Ont., Canada K9J 7B8

Received November 12, 1976

PETER F. BARRETT, ARNOLD FOX, and RAYMOND E. MARCH. Can. J. Chem. **55**, 2279 (1977).

The photochemical insertion reaction of $SnCl_2$ into the metal–metal bond of $[P(n\text{-}C_4H_9)_3Co(CO)_3]_2$ has been studied in THF at 23.0°C at the irradiating wavelengths 365 nm, 436 nm, and 546 nm. At 365 nm, the quantum yield for the reaction increases with increasing concentration of $SnCl_2$ and approaches a limiting value of 1.0. At 436 nm, however, the quantum yield increases above 1.0 and at 546 nm, quantum yields as high as 6 were measured. The uv–visible absorption spectrum of $[P(n\text{-}C_4H_9)_3Co(CO)_3]_2$ shows an intense band at 372 nm and a broad shoulder at about 440 nm. A simple mechanism is proposed to operate on irradiation at 365 nm due to absorption by the intense band, but a more complicated chain mechanism is suggested to operate at 546 nm as a result of absorption by the lower energy shoulder band. It appears that both mechanisms operate on irradiation at 436 nm due to the overlap of the two absorption bands at this wavelength.

PETER F. BARRETT, ARNOLD FOX et RAYMOND E. MARCH. Can. J. Chem. **55**, 2279 (1977).

On a étudié, dans le THF à 23.0°C et faisant appel à des longueurs d'irradiation de 365, 436 et 546 nm, la réaction d'insertion photochimique de $SnCl_2$ dans le lien métal–métal de $[P(n\text{-}C_4H_9)_3Co(CO)_3]_2$. A 365 nm, le rendement quantique de la réaction augmente avec une augmentation de la concentration de $SnCl_2$ et approche une valeur limite de 1.0. Toutefois à 436 nm, le rendement quantique augmente au-dessus de 1.0 et à 546 nm, des rendements quantiques aussi haut que 6 ont pu être mesurés. Le spectre d'absorption uv–visible de $[P(n\text{-}C_4H_9)_3Co(CO)_3]_2$ indique une bande intense à 372 nm et une épaule large autour de 440 nm. On propose un mécanisme simple qui s'appliquerait pour l'irradiation à 365 nm et qui serait dû à l'absorption par la bande intense; toutefois on suggère un mécanisme en chaîne beaucoup plus compliqué pour expliquer les résultats à 546 nm qui proviendraient d'une absorption par la bande existant sous forme d'épaule à une énergie plus basse. Il semble que les deux mécanismes agissent lors de l'irradiation à 436 nm dû à un recouvrement des deux bandes d'absorption à cette longueur d'onde.

[Traduit par le journal]

Introduction

There has been a recent surge of interest in the mechanisms of the photochemical reactions of transition metal carbonyl complexes containing metal–metal (M—M) bonds (1–7). The photochemistry of these complexes can be explained on the basis of the homolytic fission of the M—M bond (1), or in solvents of high donicity, on the heterolytic fission of this bond (2). Studies have shown that the lowest excited states of the M—M bonded species produced on absorption of radiation result from an electronic transition which weakens the M—M bond, either by an electron transition from the M—M σ bond orbital to a π* orbital of a ligand (1), or by a transition to the σ* orbital of the M—M bond from a π-*d* orbital

[1]Taken in part from the M.Sc. thesis of A.F., Trent University, 1975. Presented in part at the Canadian Chemical Conference of the Chemical Institute of Canada, Toronto, Ont., Canada, May 1975.

TABLE 1. Extinction coefficients in THF

λ (nm)	ε (M^{-1} cm^{-1})	
	$[P(n\text{-}C_4H_9)_3Co(CO)_3]_2$	$[P(n\text{-}C_4H_9)_3Co(CO)_3]_2SnCl_2$
365	28800	35000
436	3970	1950
500	1400	61.1
520	968	21.4
540	673	8.85
546	597	6.70
560	440	4.56

which is essentially non-bonding with respect to the M—M bond (5–7). Cleavage of the M—M bond to form two radicals appears to be the consequence either of these excitations, or of the higher energy process involving the transition of an electron from a σ orbital of the M—M bond to a σ* orbital associated with this bond.

In our studies of the thermal insertion of tin(II) halides into the M—M bonds of a number of complexes (8), we have noted that some of these reactions are greatly accelerated when performed in the presence of laboratory light (9, 10). A preliminary study of the photoinsertion of $SnCl_2$ into the M—M bond of $[P(n\text{-}C_4H_9)_3Co(CO)_3]_2$ has previously been reported (10), but we now present the results of a quantitative study of this reaction and discuss two mechanisms which are consistent with the variation in the observed quantum yields with changes in the reactant concentrations, and the intensity and wavelength of the radiation.

Experimental

Materials

Hexacarbonylbis(tri-*n*-butylphosphine)dicobalt and dichlorobis(tricarbonyltri-*n*-butylphosphinecobalt)tin were prepared by the methods outlined in the literature (11). Anhydrous tin(II) chloride was prepared by dehydration of the dihydrate as described previously (8) and stored under nitrogen. Tetrahydrofuran was refluxed over sodium wire and freshly distilled in an atmosphere of dry nitrogen immediately before use.

Determination of Extinction Coefficients

The extinction coefficients of $[P(n\text{-}C_4H_9)_3Co(CO)_3]_2$ and $[P(n\text{-}C_4H_9)_3Co(CO)_3]_2SnCl_2$ in THF were measured in the region 350 nm to 560 nm. A small amount of the complex was weighed on a microbalance, transferred to a volumetric flask, and dissolved up to the mark with THF under nitrogen. These solutions were exposed to light only from a 1A Kodak safelight filter, and other solutions of known concentration were prepared by accurate dilution of these stock samples. The absorption spectra were recorded at 23.0°C with a Unicam SP1800 Spectrophotometer using Teflon stoppered 1.0 cm path length cells. Figure 1 shows the spectra of $[P(n\text{-}C_4H_9)_3Co(CO)_3]_2$ and $[P(n\text{-}C_4H_9)_3Co(CO)_3]_2SnCl_2$ in THF, and Table 1 lists the extinction coefficients at several wavelengths.

Photolysis Procedures

$SnCl_2$ was weighed into a 25 ml volumetric flask and dissolved up to the mark with THF. Part of this solution was pressure-filtered through dried No. 42 filter paper (using a Sartorius pressure syringe) to fill two 1.0 cm cells to be used as blanks. Another 10 ml portion of the $SnCl_2$ solution was pressure-filtered into a 10 ml volumetric flask containing a weighed quantity of $[P(n\text{-}C_4H_9)_3Co(CO)_3]_2$. The weight of $[P(n\text{-}C_4H_9)_3Co(CO)_3]_2$ was relatively constant for a series of runs at a given wavelength of irradiation except when the effect of the concentration of this complex on the quantum yield was being studied. This reactant solution was used to completely fill two Teflon

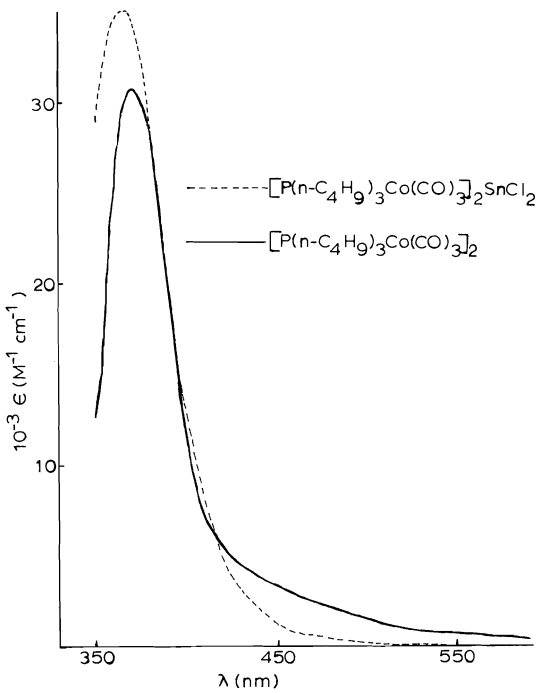

FIG. 1. Electronic absorption spectra of $[P(n\text{-}C_4H_9)_3Co(CO)_3]_2$ and $[P(n\text{-}C_4H_9)_3Co(CO)_3]_2SnCl_2$ in THF at 23.0°C.

stoppered 1.0 cm cells. One pair of cells (reactant solution plus blank) was used to study the photochemical reaction while the other was used to monitor any thermal reaction that might occur and whose contribution could therefore be subtracted from the reaction occuring during photolysis.

The cell to be photolyzed was placed in a thermostatted block at 23.0°C and was irradiated by a collimated beam of light which was contained entirely within the boundaries of the cell face. The beam was produced from the radiation of a 100 W medium pressure mercury lamp which had passed through a Heath scanning monochromator E. U. 700 with a slit width of 2.0 mm. The nominal band width resolution of the instrument was found to be 4 nm under these conditions. Controlled diminished light intensities in some runs were achieved either by inserting neutral density filters (Kodak) of known transmittance in front of the reaction cell, or by using different lamps of known intensity.

During illumination, the reaction cell (which contained a small glass bead) was removed from the illuminator at regular intervals and agitated in order to maintain homogeneity of the solution. Absorbances were recorded periodically at convenient monitoring wavelengths (540 nm or 560 nm) by transferring the cell to a Unicam SP1800 spectrophotometer. The irradiation time was stopped and started by using a manual shutter. The solutions were irradiated at 365 nm, 436 nm, and 546 nm, and the intensity of the radiation at these wavelengths was measured by the potassium ferrioxalate actinometric method (12).

The volumes of the reaction cells containing the small glass beads, which were required for the calculations, were calculated by determining the weight of distilled water that could be contained by each cell.

Determination of Quantum Yields

The rate of the photochemical reaction

$$M_2 \xrightarrow{h\nu} M_2^* \xrightarrow{L} MLM$$

is given by eq. 1 (13) when the path length of the reaction vessel is 1.0 cm and the only absorbing species are M_2 and MLM.

$$[1] \quad \frac{-d[M_2]}{dt} = \frac{\phi I_0}{V}(1-10^{-(\varepsilon_{M_2}[M_2]+\varepsilon_{MLM}[MLM])}) \times \frac{\varepsilon_{M_2}[M_2]}{\varepsilon_{M_2}[M_2] + \varepsilon_{MLM}[MLM]}$$

where $M_2 = [P(n\text{-}C_4H_9)_3Co(CO)_3]_2$, $L = SnCl_2$, which is virtually transparent to visible light used in this study, $MLM = [P(n\text{-}C_4H_9)_3Co(CO)_3]_2\text{-}SnCl_2$, ϕ = quantum yield, I_0 = incident light intensity in einsteins h^{-1}, V = volume of the reaction cell in ℓ, ε's are extinction coefficients for the species at the wavelength of the irradiation in M^{-1} cm^{-1}. Equation 1 can be simplified and integrated under two limiting conditions which are applicable in this study.

Condition A

If the solution is almost totally absorbing at the wavelength of irradiation, *i.e.* if

$$\varepsilon_{M_2}[M_2] + \varepsilon_{MLM}[MLM] \geq 2$$

eq. 1 can be simplified and integrated to give eq. 2.

$$[2] \quad (\varepsilon_{M_2} - \varepsilon_{MLM})([M_2]_0 - [M_2]) + \varepsilon_{MLM}[M_2]_0 \ln \frac{[M_2]_0}{[M_2]} = \frac{\phi I_0 \varepsilon_{M_2} t}{V}$$

If the progress of the reaction is monitored spectrophotometrically at a wavelength where absorbances are represented by A and extinction coefficients by ε', eq. 2 can be rearranged to give eq. 3.

$$[3] \quad f(A_t) = -\frac{\phi I_0 \varepsilon_{M_2} t}{V \varepsilon_{MLM}} + C$$

where

$$f(A_t) = \frac{(\varepsilon_{M_2} - \varepsilon_{MLM})A_t}{\varepsilon_{MLM}(\varepsilon_{M_2}' - \varepsilon_{MLM}')} + [M_2]_0 \ln (A_t - A_\infty)$$

and

$$C = \frac{(\varepsilon_{M_2} - \varepsilon_{MLM})A_0}{\varepsilon_{MLM}(\varepsilon_{M_2}' - \varepsilon_{MLM}')} + [M_2]_0 \ln (A_0 - A_\infty)$$

Condition B

If the solution is not totally absorbing at the wavelength of irradiation, but if

$$\varepsilon_{M_2}[M_2] \gg \varepsilon_{MLM}[MLM]$$

eq. 1 can be simplified and integrated to give eq. 4.

$$[4] \quad ([M_2]_0 - [M_2]) + \frac{1}{\varepsilon_{M_2}} \times \log \frac{(1 - 10^{-\varepsilon_{M_2}[M_2]_0})}{(1 - 10^{-\varepsilon_{M_2}[M_2]})} = \frac{\phi I_0 t}{V}$$

which in turn can be rearranged to give [5].

$$[5] \quad F(A_t) = \frac{\phi I_0 \varepsilon_{M_2} t}{V}$$

where

$$F(A_t) = A_0 - A_t + \log \frac{(1 - T_0)}{(1 - T)}$$

and A and T refer to the absorbance and transmittance of the solution at the monitoring wavelength.

According to eqs. 3 and 5, $f(A_t)$ and $F(A_t)$ should be linear functions of time, and quantum

yields can be determined from the slopes of plots of these functions against time.

In this study, the concentration of M_2 was such that condition *A* was applicable for runs at irradiating wavelengths 365 nm and 436 nm, while condition *B* was applicable for irradiation at 546 nm. Reactions were monitored for the first 20–25% of reaction.

Results and Discussion

Plots of $f(A_t)$ and $F(A_t)$ against time were indeed linear and from the slopes of these plots the quantum yields were determined. Figure 2 shows the variation of the quantum yield for the insertion of $SnCl_2$ into the Co—Co bond of $[P(n\text{-}C_4H_9)_3Co(CO)_3]_2$ to produce $[P(n\text{-}C_4H_9)_3Co(CO)_3]_2SnCl_2$, as a function of the concentration of $SnCl_2$ at the three wavelengths of irradiation 365 nm, 436 nm, and 546 nm.

Irradiation at 365 nm

Figure 2 indicates that for irradiation at 365 nm, the quantum yield increases with increasing $[SnCl_2]$ but begins to level off at high $[SnCl_2]$. A mechanism which is consistent with these data and which is similar to that proposed by Barrett and Poë (10) is as follows:

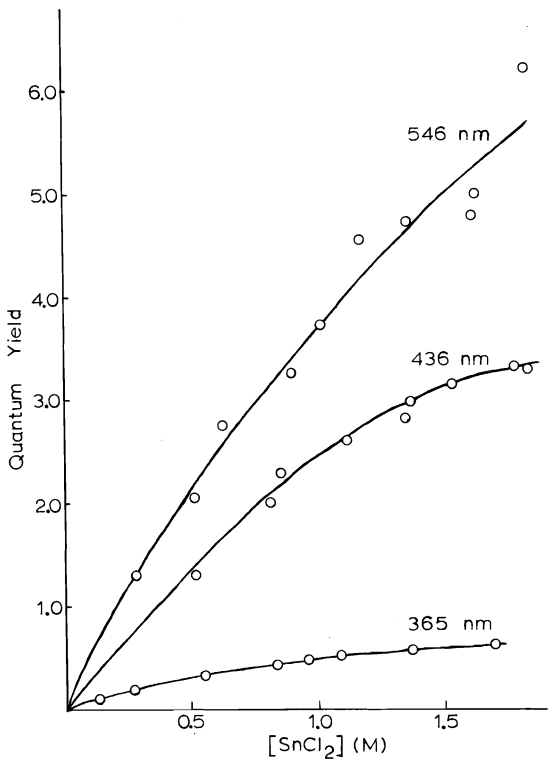

FIG. 2. Dependence of quantum yield on $[SnCl_2]$ for irradiation at 365 nm, 436 nm, and 546 nm.

Mechanism I

$$M_2 \xrightarrow{h\nu} M_2^*$$

$$M_2^* \xrightarrow{k_1} M_2$$

$$M_2^* + L \xrightarrow{k_2} MLM$$

The excited state produced directly on absorption of radiation due to the strong absorption band of $[P(n\text{-}C_4H_9)_3Co(CO)_3]_2$, which has a maximum absorption at 372 nm ($\varepsilon_{max} \sim 3.1 \times 10^4$) (Fig. 1), is assumed to be rapidly converted by radiationless processes having unitary efficiency to M_2^*, a lower energy, longer lived excited state which can undergo the chemistry indicated in the mechanism. Although the absorption spectrum also shows a broad shoulder around 440 nm, it is much weaker than the 372 nm band and therefore the bulk of the absorption of the 365 nm radiation would be due to the peak at 372 nm. Making a steady-state approximation for $[M_2^*]$ leads to the following expression for the quantum yield

$$\phi = \frac{k_2[L]}{k_1 + k_2[L]} \quad [6]$$

which can be rearranged to give

$$\frac{1}{\phi} = 1 + \frac{k_1}{k_2[L]} \quad [7]$$

Equation 7 predicts that a plot of ϕ^{-1} against $[L]^{-1}$ should be linear with an intercept of 1.0 and a slope of k_1/k_2. Figure 3 demonstrates the linearity of this plot and gives an intercept of 0.91 ± 0.05, *i.e.* a limiting ϕ at high [L] of 1.10 ± 0.06, and a value of k_1/k_2 of 1.18 ± 0.02. Equation 7 also implies that the quantum yield should be independent of both the intensity of the radiation and the concentration of $[P(n\text{-}C_4H_9)_3Co(CO)_3]_2$. Although there is a fair degree of scatter of the data points, Table 2 indicates that these criteria appear to be met.

Irradiation at 436 nm and 546 nm

Figure 1 indicates that photolysis at 546 nm will result in absorption due to the broad band centered at ~440 nm. Since overlap of this band with the strong band at 372 nm is negligible at the photolyzing wavelength of 546 nm, the

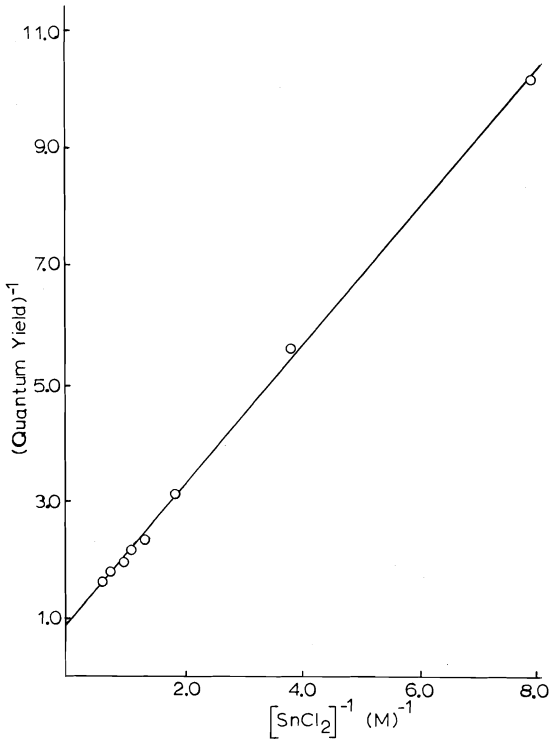

FIG. 3. Plot of ϕ^{-1} against $[SnCl_2]^{-1}$ for irradiation at 365 nm.

excited state produced, M_2*, will be electronically different from that formed from irradiation at 365 nm and could therefore give rise to an entirely different mechanism for the reaction. The fact that the quantum yields are greater than 1.0 (Fig. 2) implies that a chain mechanism is operating and the following scheme is consistent with the data:

Mechanism II

$$M_2 \xrightarrow{h\nu} M_2^*$$

$$M_2^* \xrightarrow{k_3} M_2$$

$$M_2^* + L \xrightarrow{k_4} MLM$$

$$M_2^* + L \xrightarrow{k_5} \cdot ML + \cdot M$$

$$\cdot ML + M_2 \xrightarrow{k_6} MLM + \cdot M$$

$$\cdot M + L \xrightarrow{k_7} \cdot ML$$

$$\cdot M + \cdot ML \xrightarrow{k_8} MLM$$

Applying the steady-state approximation to $[M_2^*]$, $[\cdot ML]$, and $[\cdot M]$, and if I_m = rate of absorption of radiation by M_2 in einsteins ℓ^{-1} h^{-1}, the following expression for the quantum yield can be derived:

$$[8] \quad \phi = \frac{(k_4 + k_5)[L]}{k_3 + (k_4 + k_5)[L]} + \left(\frac{[M_2]}{I_m}\right)^{1/2} \times \left(\frac{k_5 k_6 k_7}{k_3 k_8 + k_8(k_4 + k_5)[L]}\right)^{1/2} [L]$$

TABLE 2. Dependence of ϕ on $[M_2]$ and on the intensity of absorbed radiation I_m at 365 nm, $M_2 = [P(n\text{-}C_4H_9)_3Co(CO)_3]_2$

$[SnCl_2]$ (M)	$[M_2]$ (M)	$10^5 I_m$ (einsteins ℓ^{-1} h^{-1})	ϕ
1.50	4.19	1.93	0.560
1.50	4.07	3.26	0.540
1.50	4.62	5.10	0.681
1.50	3.55	6.85	0.585
1.50	3.25	5.10	0.708
1.50	8.76	5.10	0.766

Because irradiation at 436 nm occurs in a region of overlap of the two absorption bands at 372 nm and ~440 nm, presumably the insertion reaction can occur simultaneously by both mechanisms I and II. The quantum yields observed for irradiation at 436 nm would therefore be expected to fall between those observed for irradiation at 365 nm and 546 nm and this is borne out in Fig. 2. Equation 8 predicts that at constant $[M_2]$ and [L], the quantum yield should be inversely proportional to $I_m^{1/2}$, and that at constant [L] and I_m, ϕ should be directly proportional to $[M_2]^{1/2}$. Figures 4 and 5 show the plots which appear to verify these predictions. The intercept in both figures should lie between 0 and 1.0, but the accuracy of the intercepts is poor because the data points are so far removed from the intercept.

The nature of the excited states M_2* postulated in mechanisms I and II can be understood only if the electronic transitions involved in the two absorption bands in the uv–visible spectrum of $[P(n\text{-}C_4H_9)_3Co(CO)_3]_2$ are known. The intense absorption band between 350 nm and 400 nm for complexes of the type $[Co(CO)_3L]_2$, where L = phosphine or phosphite, has been assigned to a σ–σ* transition associated with the cobalt–cobalt bond (14). Although the broad shoulder on the lower energy side of the intense band in these complexes has not been unequivocally assigned, a similar shoulder band in $Mn_2(CO)_{10}$ adjacent to the band due to the

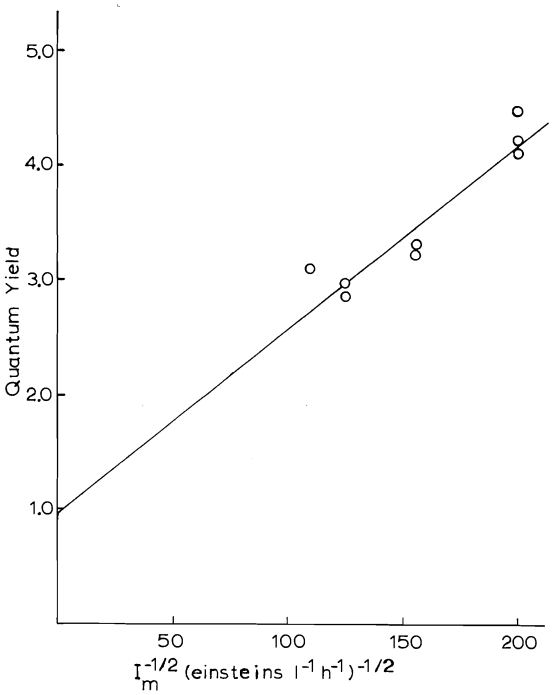

FIG. 4. Plot of ϕ against $I_m^{-1/2}$ for irradiation at 436 nm. $[SnCl_2] = 1.50\ M$.

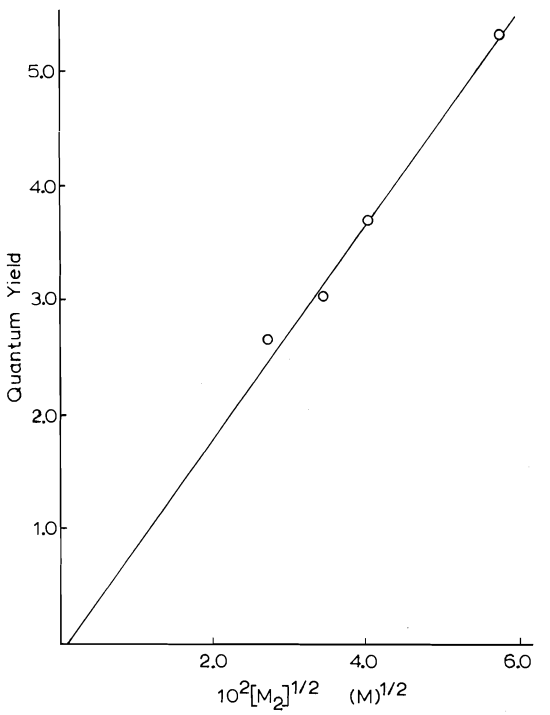

FIG. 5. Plot of ϕ against $[M_2]^{1/2}$ for irradiation at 436 nm. $[SnCl_2] = 1.50\ M$.

σ–σ^* transition has been assigned to a π–σ^* transition (15) and it would appear reasonable to make a similar assignment in the case of the cobalt complexes. Absorption of radiation at 365 nm therefore would result in an electronic transition from the M—M bonding σ orbital to a σ^* orbital. Such a transition would be expected to reduce to zero the bond order between the two halves of the dimeric complex and easily lead to the formation of radicals. No radicals could, however, be detected by esr in the range 3650 $\pm$ 250 G on irradiation of a solution of $[P(n\text{-}C_4H_9)_3Co(CO)_3]_2$ in THF with a 200 W high pressure mercury lamp. Irradiation of $Mn_2(CO)_{10}$ has been reported to result in the formation of Mn(O) radical species which are detectable by esr (16, 17), but these claims appear now to be unfounded (18, 19). Although the limiting quantum yield of 1.0 for irradiation at 365 nm, which is predicted by mechanism I and which is consistent with the data, rules out the possibility of a radical chain mechanism occurring, there still is the possibility that M_2^* could exist as two radicals trapped in a solvent cage.

Absorption of radiation due to the lower energy band at $\sim$440 nm does give rise to a chain mechanism as evidenced by the large quantum yields at 436 nm and 546 nm. The transition involved (π–σ^*) would result in the M—M bond order being reduced to one-half, but it is not clear why a radical propagation mechanism should be favoured here when there is no evidence for such a mechanism occurring with radiation corresponding to the σ–σ^* transition.

Acknowledgements

We are grateful to the National Research Council of Canada and Trent University for financial assistance, and to Dr. K. Wan of Queen's University for performing the esr work.

1. D. L. MORSE and M. S. WRIGHTON. J. Am. Chem. Soc. **98**, 3931 (1976).
2. D. M. ALLEN, A. COX, T. J. KEMP, Q. SULTANA, and R. B. PITTS. J. Chem. Soc. Dalton Trans. 1189 (1976).
3. C. GIANNOTTI and G. MERLE. J. Organomet. Chem. **105**, 97 (1976).
4. J. L. HUGHEY IV, C. R. BOCK, and T. J. MEYER. J. Am. Chem. Soc. **97**, 4400 (1975).
5. M. S. WRIGHTON and D. S. GINLEY. J. Am. Chem. Soc. **97**, 4246 (1975).
6. M. S. WRIGHTON and D. S. GINLEY. J. Am. Chem. Soc. **97**, 2065 (1975).
7. M. S. WRIGHTON and D. S. GINLEY. J. Am. Chem. Soc. **97**, 4908 (1975).

8. P. F. BARRETT. Can. J. Chem. **52**, 3773 (1974) and references therein.
9. P. F. BARRETT and K. K. W. SUN. Can. J. Chem. **48**, 3300 (1970).
10. P. F. BARRETT and A. J. POË. J. Chem. Soc. A, 429 (1968).
11. F. BONATI, S. CENINI, D. MORELLI, and R. UGO. J. Chem. Soc. A, 1052 (1966).
12. C. G. HATCHARD and C. A. PARKER. Proc. R. Soc. London, Ser. A, **235**, 518 (1956).
13. V. BALZANI and V. CARASSITI. Photochemistry of coordination compounds. Academic Press, London. 1970. p. 11.
14. T. E. BOYD. PH.D. Thesis. Dis. Abstr. Int. B, **34**(12), 5882 (1974).
15. R. A. LEVENSON, H. B. GRAY, and G. P. CEASAR. J. Am. Chem. Soc. **92**, 3653 (1970).
16. S. A. HALLOCK and A. WOJCICKI. J. Organomet. Chem. **54**, C27 (1973).
17. C. L. KWAN and J. K. KOCHI. J. Organomet. Chem. **101**, C9 (1975).
18. A. HUDSON, M. F. LAPPERT, and B. K. NICHOLSON. J. Organomet. Chem. **92**, C11 (1975).
19. A. HUDSON, M. F. LAPPERT, J. J. MACQUITTY, B. K. NICHOLSON, H. ZAINAL, G. R. LUCKHURST, C. CANNONI, S. W. BROTT, and M. R. S. SYMONS. J. Organomet. Chem. **110**, C5 (1976).

Substituent effects on the triplet–singlet energy separation in diphenylmethylene[1]

ROBERT W. R. HUMPHREYS AND DONALD R. ARNOLD[2]

Photochemistry Unit, Department of Chemistry, University of Western Ontario, London, Ont., Canada N6A 5B7

Received November 23, 1976

ROBERT W. R. HUMPHREYS and DONALD R. ARNOLD. Can. J. Chem. **55**, 2286 (1977).

The electron paramagnetic resonance (epr) spectra of the diarylmethylenes: diphenylmethylene, *p*-cyanodiphenylmethylene, *p*-methoxydiphenylmethylene, *p,p'*-dimethoxydiphenylmethylene, *p,p'*-dicyanodiphenylmethylene, *p*-cyano-*p'*-methoxydiphenylmethylene, have been studied. The zero-field splitting parameters have been determined. The signal intensity as a function of temperature (*ca.* 4–20 K) indicates these methylenes are ground state triplet species.

ROBERT W. R. HUMPHREYS et DONALD R. ARNOLD. Can. J. Chem. **55**, 2286 (1977).

On a déterminé les spectres de résonance paramagnétique électronique (rpe) des diarylméthylènes: diphénylméthylène, *p*-cyanodiphénylméthylène, *p*-méthoxydiphénylméthylène, *p,p'*-diméthoxydiphénylméthylène, *p,p'*-dicyanodiphénylméthylène, *p*-cyano-*p'*-méthoxydiphénylméthylène. On a déterminé les paramètres de couplage à champ zéro. L'intensité du signal en fonction de la température (environ de 4–20 K) indique que ces groupements méthylène existent sous forme d'espèces triplets dans l'état fondamental.

[Traduit par le journal]

Introduction

Diphenylmethylene has been extensively studied over the past fifteen years. In the process, a considerable amount of information about the structure and chemical reactivity of this molecule has been obtained.

Early reports of the electron paramagnetic resonance (epr) spectra of diphenylmethylene, both randomly-oriented in a rigid glass (3*a*) and oriented in a single-crystal matrix (3*b*), indicated that the triplet was the ground state of the molecule. Although one might expect such a triplet methylene to be linear, with the planes of the phenyl rings perpendicular (Fig. 1*a*) (4), the epr studies indicate that this is not the case. Hyperfine coupling data for diphenylmethylene oriented in single crystals of benzophenone, along with molecular orbital calculations (5), and ENDOR experiments on diphenylmethylene in single crystals of 1,1-diphenylethylene (6) suggest that the molecule is non-linear with a dihedral angle (*i.e.* the angle at the divalent carbon) of 140–155°. The ENDOR experiments also suggest that the phenyl rings deviate from coplanarity, but it is possible that the structure is altered somewhat by the crystal packing forces.[3]

The magnitude of the epr zero-field splitting parameter D for diphenylmethylene ($D = 0.4050$ cm^{-1}, $E = 0.0194$ cm^{-1}) (7) is considerably greater than that for the phosphorescent state of an aromatic hydrocarbon such as naphthalene ($D = 0.0992$ cm^{-1}, $E = 0.0143$ cm^{-1}). Thus the two unpaired electrons must be localized at the divalent carbon to a large extent. However, delocalization into the phenyl groups in diphenylmethylene is significant in comparison to phenylmethylene ($D = 0.5098$ cm^{-1}) (7) and methylene ($D = 0.95$ cm^{-1}) (8). It should also be

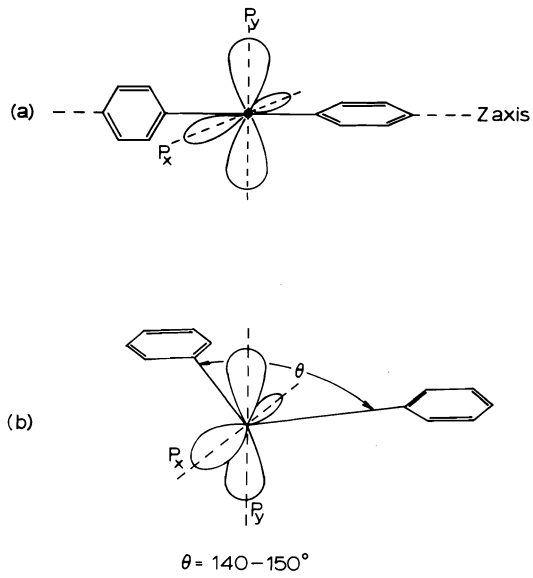

FIG. 1. Models for diphenylmethylene.

[1]Contribution No. 166.

[2]To whom correspondence should be addressed.

[3]The observed deviation from coplanarity of the phenyl rings in diphenylmethylene is very similar to that known for the host crystal diphenylene from X-ray analysis (6).

noted that E is not equal to zero. This was the first experimental indication that the linear model for diphenylmethylene with the phenyl planes perpendicular was incorrect, since one would expect such a triplet species to have $E = 0$.

The above results lead to a model for triplet diphenylmethylene in which the divalent carbon and phenyl rings are approximately coplanar (7, 9) (Fig. 1*b*). The two half-filled orbitals at the divalent carbon consist of a pure *p*-orbital perpendicular to the phenyl rings, and conjugated with the phenyl π-system, and an orbital occupying the plane of the molecule with considerable *s* character (referred to as the σ-orbital). The unpaired electron occupying the *p*-orbital is, thus, delocalized into the phenyl rings to a certain extent while the unpaired electron in the σ-orbital is localized at the divalent carbon atom.

There is one glaring problem still remaining in the understanding of diphenylmethylene. As has already been pointed out, it is well established that diphenylmethylene is a ground state triplet molecule. The stereospecificity of the addition of diphenylmethylene to *cis*- and *trans*-olefins at room temperature has led to the conclusion that both the singlet and the triplet were reacting and that these species are in thermal equilibrium at this temperature (10*a*). The actual energy gap between the ground triplet state and the first singlet state has been estimated, by a complex kinetic analysis of flash spectroscopic experiments, to be less than *ca.* 3.6 kcal mol^{-1} (10*b*).

Theoretical calculations of the energy separation between the triplet and singlet states of diphenylmethylene are very few due to the large size of the molecule. Extended Hückel calculations by Hoffmann, Zeiss, and Van Dine (11) led these authors to predict the ground state of diphenylmethylene to be the triplet state. However, no estimate of the energy separation between the ground triplet state and the first singlet state can be obtained from these calculations and in fact the prediction of the triplet ground state was based partially on empirical criteria.

It should be mentioned that the absorption and emission spectra of diphenylmethylene have also been studied (9, 12). Unfortunately, only fluorescence emission has been detected. Attempts to detect phosphorescence, which would give the triplet–singlet separation directly, were unsuccessful (9).

In a recent publication (13), we described the determination of the ground state multiplicity of a number of related phenylvinylmethylenes. Our interest centered on the effect of substituents on the ground state multiplicity of the species in question based on theoretical models for the parent vinylmethylene (12, 14). The problem associated with the triplet–singlet energy separation in diphenylmethylene led us to study the effect of substituents on this system.

The possible stabilization of singlet methylene with respect to the triplet has been discussed in some detail by other authors (11, 14*a*, 15, 16), and these concepts can be applied to diphenylmethylene. The basic problem involves removing the degeneracy of the singly occupied *p*-orbitals in linear triplet methylene to the point at which it is more favourable energetically for both electrons to occupy the same orbital. This, of course, involves overcoming the electron–electron repulsion which occurs when both electrons occupy the same orbital. Is it possible, with the proper choice of substituents, to remove the degeneracy of the two singly-occupied orbitals in triplet diphenylmethylene to such an extent that the singlet becomes the ground state?

It is not immediately obvious how the choice of substituents will affect the triplet–singlet energy gap in diphenylmethylene since it is clear that substituents will influence both the triplet and singlet states. Substituent stabilization of the triplet has been discussed by Closs and Goh in the case of *p*-nitrophenylcarbene (17). The zero-field splitting parameter D for *p*-nitrophenylcarbene (0.480 cm^{-1}) is smaller than that for phenylcarbene (0.512 cm^{-1}), indicating increased electron delocalization in the nitro derivative and, thus, some stabilization of the triplet state by the nitro group. However, the known substituent effects on the value of D are generally small and it is not apparent what relationship there is between the D-value and the actual energy of a triplet state, much less the energy separation between the triplet and singlet. We felt that the substituent effect on the triplet–singlet energy separation should be considerably larger than the substituent effect on the stability of the triplet state of diphenylmethylene. This assumption is supported by the very large Hammett ρ-value observed for the gas phase ionization of substituted benzyl radicals (18) and from the relatively small effect of substituents upon the epr spectra of substituted benzyl radicals (19) when con-

sidered with the accepted structure of diphenylmethylene (*i.e.* the triplet state, Fig. 1*b*).

Based on the above rationale, we prepared a series of *p*-cyano and *p*-methoxy substituted diphenylmethylenes (Table 1). We chose these substituents as examples of good resonance electron withdrawing and donating substituents, respectively. The diphenylmethylenes were easily obtained by irradiation of the corresponding diazo compounds in a rigid glass at very low temperatures. The diazo compounds were prepared from the corresponding hydrazones by oxidation with mercuric oxide in the presence of base using a method described in the Experimental section.

The experimental determination of the ground state multiplicity of these species and the attempts to observe the population of an upper state can be a relatively simple matter if the triplet methylene can be detected by epr spectroscopy. For a constant methylene concentration, the signal intensity should vary inversely with temperature. That is, the signal intensity should follow the Curie law. Deviation from this linear relationship indicates one of the following: (*1*) the triplet is reacting as the temperature is raised (this can easily be verified by repeating the temperature cycle on the same sample); (*2*) an upper singlet state is being populated as the temperature is raised, thus depleting the population of triplets; (*3*) the singlet state is the ground state and the triplet state is being populated as the temperature is raised.

The expected behaviour of the signal intensity under conditions (*2*) and (*3*) has been discussed in some detail previously (13). The temperature dependence of the signal intensity for various triplet species have been reported (1). These studies include several examples in which the triplet is the upper state which is thermally populated (1 *a–d*). Species examined by this technique which show singlet–triplet equilibrium behaviour include cyclic, symmetric 4n π-electron systems (1 *a, b*), aromatic dinegative ions (1*c*), and biradicals (1 *d, e*). This behaviour has never been observed for a methylene system.

There are no reported examples of the observation of temperature dependent signal intensity behaviour indicative of thermal population of an upper singlet from a lower energy triplet state (*i.e.* case *2*). This is perhaps not surprising in view of the limitations of this technique to detect this phenomenon (13).

TABLE 1. Series of *p*-cyano and *p*-methoxy substituted diphenylmethylenes studies

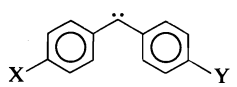

Compound	X	Y
1	H	H
2	H	CN
3	H	OMe
4	OMe	OMe
5	CN	CN
6	CN	OMe

Results

The diphenyldiazomethanes were characterized by ^{1}H nmr, ir, and visible spectroscopy. Examination of the visible absorption maxima for the series indicated a trend in the effect of substituents on the position of the maximum. A good correlation was found for the position of the visible absorption maximum as a function of the Hammett substituent parameter $\sum\sigma_p$. This correlation was useful to confirm the structure of the diphenyldiazomethanes, including other *para*-substituted diphenyldiazomethanes not described here.

Generation of the methylenes (**1–6**) at *ca.* 5 K in a rigid glass proved to be an easy matter. The diazo precursors were irradiated directly with a 1 kW high pressure mercury arc lamp. Once generated, the methylenes seemed to be stable to further irradiation. However, prolonged irradiation was avoided to prevent both excessive sample heating, thereby wasting liquid helium, and a significant increase in the signal due to free radicals in the $g = 2$ region.

The signals due to a triplet species were assigned in terms of the Hamiltonian $\mathcal{H} = g\beta H\cdot\hat{S} + D\hat{S}_z^2 + E(\hat{S}_x^2 - \hat{S}_y^2)$. The zero-field splitting parameters were obtained from the observed spectra by employing an iterative computer program and are summarized in Table 2. The spectral field positions were obtained accurately using an Alpha Scientific Model 675 Gaussmeter. In all cases, only four lines were observed: H_{z_1}; H_{x_2}; H_{y_2}; H_{z_2}.

The observed signal intensity (the peak-to-peak height of the H_{x_2} line was used in every case) as a function of temperature for two of the methylenes studied is shown in Fig. 2. As can be seen, the

TABLE 2. D and E values for diphenylmethylenes

Compound	p,p'-Substituents	D (cm^{-1})	E (cm^{-1})
1	H,H	0.4088(0.4050)[a]	0.0170(0.0194)[a]
2	H,CN	0.3906	0.0180
3	H,OCH_3	0.4043(0.4042)[a]	0.0191(0.0194)[a]
4	OCH_3,OCH_3	0.4022(0.4065)[a]	0.0189(0.0193)[a]
5	CN,CN	0.3879	0.0178
6	CN,OCH_3	0.3774	0.0172

[a]Previously reported values (7).

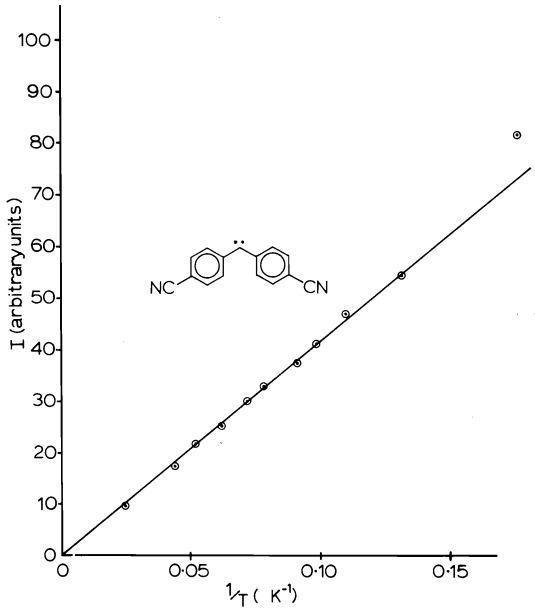

FIG. 2. Graph of I *vs.* $1/T$ for two diarylmethylenes.

plots are linear over the entire temperature range studied (5–20 K). These results were typical of all the diphenylmethylenes (**1–6**) listed in Table 1.

Discussion

On examining the D and E values in Table 2, it is, first of all, obvious that the effect of substituents is not large and, secondly, that there is no trend which is consistent with the Hammett substituent parameters (σ, σ^+, etc.). In general, the observed D value is somewhat lower than that of the parent species, indicating greater electron delocalization in the substituted diphenylmethylenes. This is predictable and has been observed previously (7).

The I *vs.* $1/T$ plots for diphenylmethylenes **1–6** indicate that all follow Curie law dependence over the temperature range studied. We interpret these results to mean that the diphenylmethylenes **1–6** are ground state triplets and the singlet state is not being populated to any discernible extent at the maximum temperature of the experiment. An alternative possibility is that the singlet is the ground state of the species and is separated by such a small energy (<5 cal mol^{-1}) from the upper triplet as to be in thermal equilibrium with this upper state even at the lowest temperatures used. We consider this unlikely for any of the diphenylmethylenes **1–6**.

The expected behaviour of the intensity *vs.* $(\text{temperature})^{-1}$ profile for an upper singlet state being populated from a lower triplet state can be calculated using the expression

$$I = \frac{a}{T}\frac{e^{-\Delta E/RT}}{3 + e^{-\Delta E/RT}}$$

Such calculations indicate that the practical limit for the observation of deviations from Curie law dependence, from a graphical standpoint, seems to be somewhat less than 100 cal mol^{-1} for the case in which the triplet is the ground state. This at least places a lower limit on the triplet–singlet energy separation in all diphenylmethylenes studied here

We conclude that the effects of the p-methoxy and cyano substituents in the derivatives **1–6** are not large enough to invert the order of states in diphenylmethylene. In view of the relatively small energy difference (<3.6 kcal mol^{-1} estimated) (10*b*) between these states in diphenylmethylene, we are reluctant to abandon the substituent effect approach to achieve this objective. We have, therefore, begun a study of the *p-N,N*-dimethylamino and nitro derivatives. Preliminary evidence indicates that the p,p'-bisdimethylamino and the p-dimethylamino derivatives are ground state triplets. Our results from this series will be reported in the near future.

TABLE 3. Spectral data for diphenyldiazomethane series

Compound	*p,p'*-Substituents	Nuclear magnetic resonance (δppm)	Infrared (μm)	Ultraviolet λ_{max}(nm)
1	CN,CN	7.46(m)	3.33(w), 4.49(m), 4.88(s), 6.23(m), 6.64(m), 8.49(w)	488
2	H,CN	7.24(m)	3.33(w), 4.50(m), 4.90(s), 6.24(s), 6.65(s), 8.48(m)	503
3	H,H	7.25(m)	3.32(m), 4.90(s), 6.27(s), 6.71(s), 7.92(m), 9.31(w)	523
4	H,OMe	3.80(s), 7.40(m)	3.32(w), 4.91(s), 6.23(m), 6.63(s), 8.04(s), 9.68(m)	529
5	OMe,OMe	3.72(s), 6.90(m)	3.35(m), 4.91(s), 6.20(m), 6.61(s), 8.01(s), 9.65(s)	543
6	CN,OMe	3.82(s), 7.42(m)	3.31(w), 4.39(m), 4.89(s), 6.23(s), 6.64(s), 8.00(s)	511

Experimental

General

Electron paramagnetic resonance spectra were obtained from and temperature dependence studies were performed on a Varian E-12 epr spectrometer equipped with an Air Products Model LTD-3-110 "Helitran" liquid helium Dewar and transfer system. Samples were placed in Supersil epr tubes and were irradiated with a Schoeffel 1 kW high pressure mercury arc lamp.

Electron paramagnetic resonance samples were generally prepared by dissolving approximately 6 mg of the appropriate diphenyldiazomethane in 1 ml 4:1 methylcyclohexane-isopentane (MCIP) followed by degassing by the freeze–pump–thaw technique. For samples used in the temperature dependence studies, approximately 6 mg phenylazide was added to the samples. The inclusion of the phenylazide provided an internal check on the temperature readings, since (triplet) signals from phenyl nitrene are known to follow the Curie law.

Temperature readings at liquid helium temperatures were obtained using two chromel *vs.* gold – 0.07% iron thermocouples, one imbedded in the liquid helium Dewar near the sample cavity and one used as a standard at ice–water temperature. The voltage readings were obtained from a Hewlett–Packard 3420B DC differential voltmeter.

Temperature Dependence Studies

The temperature dependence studies were performed in a manner essentially identical to that described in a previous paper (13) and will not be discussed here.

Preparation of Compounds

All diphenyldiazomethanes were prepared by the same method. The general procedure involved the preparation of the corresponding benzophenone hydrazone and subsequent oxidation with yellow mercuric oxide in the presence of base. The preparation of *p,p'*-dicyanodiphenyldiazomethane was typical, with the exception that dry THF was used as the solvent for the oxidation step due to the insolubility of *p,p'*-dicyanobenzophenone hydrazone in diethyl ether. For all of the other diphenyldiazomethanes, the oxidation step was carried out in diethyl ether.

Pertinent spectral data for the diazo compounds are summarized in Table 3.

The preparation of the hydrazones was generally carried out by a method described previously (2). For *p*-cyano- and *p,p'*-dicyanobenzophenone hydrozone, this method was found to produce considerable azine. Therefore, a different method was used for the preparation of the corresponding hydrazones of these ketones and will be described in detail for *p,p'*-dicyanobenzophenone hydrazone.

The preparation of *p,p'*-dicyanobenzophenone is also described due to the improved procedure used.

All ^{1}H nmr spectra were obtained on a Varian T-60 nmr spectrometer using TMS as an internal standard. All ir spectra were obtained on a Beckman IR-5A infrared spectrometer with polystyrene calibration. Visible spectra were obtained on a Cary 118C UV-Visible spectrometer.

p,p'-Dicyanobenzophenone

Dry *N,N*-dimethylformamide (20 ml), *p,p'*-dibromobenzophenone (20 g, 0.059 mol), and cuprous cyanide (12.7 g, 0.142 mol, 20% excess) were placed in a 50 ml round-bottom flask equipped with a magnetic stirring bar, reflux condenser, and drying tube. The mixture was heated to reflux using an oil bath and was allowed to heat for 9 h, at which time the hot, dark brown, granular mixture was poured into hot, 10% aqueous sodium cyanide (500 ml). The sodium cyanide solution was allowed to heat on a steambath for 30 min, at which time an orange solid had separated and come to the top. The sodium cyanide solution was extracted with benzene (3 × 250 ml), the orange solid dissolving in the benzene. The benzene solution was washed three times with water and dried over anhydrous magnesium sulfate.

In some cases, lumps of solid from the reaction mixture may appear and these should be broken up with a glass rod. Periodic manual stirring of the hot sodium cyanide solution also helps and the mixture may be left on the steambath for longer than 30 min. Some solid will remain

which cannot be dissolved in either the benzene or aqueous layers.

After filtration by gravity and removal of the benzene on the rotary evaporator, a yellow solid was obtained, the nmr and ir spectra of which indicated the presence of *p,p′*-dicyanobenzophenone. The crude yield was about 60% (8.2 g). Removal of the yellow colour required column chromatography on silica gel using 9:1 petroleum ether – diethyl ether elution and slowly changing to 6:4 petroleum ether – diethyl ether. Recrystallization of the pure product from chloroform – diethyl ether or benzene afforded needles, mp 159.5–160°C (uncorrected). *nmr (CDCl₃)*: δ 7.82(s); *ir (CHCl₃)*: 3.33(w), 4.47(m), 6.00(s), 7.86(s), 10.77(s).

p,p′-Dicyanobenzophenone Hydrazone

Hydrazine hydrate (3.5 g, 0.069 mol), absolute alcohol (50 ml), and anhydrous sodium sulfate (10 g) were placed in a 250 ml 3-neck round-bottom flask equipped with an addition funnel, stopper, condenser, and drying tube, and the mixture was heated to reflux using an oil bath. A solution of *p,p′*-dicyanobenzophenone (0.805 g, 3.47×10^{-3} mol) in ethanol (50 ml) and benzene (20 ml) was added through the addition funnel over a period of 8 h, at which point the reaction mixture was a light yellow colour. The mixture was allowed to heat at reflux overnight.

After cooling and filtering by gravity to remove the sodium sulfate, all solvent was distilled off under vacuum and the light yellow solid thus obtained was recrystallized from absolute alcohol. Very light yellow crystals of *p,p′*-dicyanobenzophenone hydrazone (0.445 g, 55%) were obtained after two recrystallizations from absolute alcohol. *nmr (CDCl₃)*: δ 5.7 (s, br, 2H), δ 7.74 (m, 6H); *ir (CHCl₃)*: 2.89(w), 3.33(w), 4.39(s), 6.36(m), 6.66(m), 11.90(s).

p,p′-Dicyanodiphenyldiazomethane

p,p′-Dicyanobenzophenone hydrazone (0.127 g, 5.16×10^{-4} mol) was placed in a 25 ml round-bottom flask equipped with a magnetic stirring bar and a drying tube. Spectral grade tetrahydrofuran (20 ml) was added and the hydrazone was allowed to dissolve. Anhydrous sodium sulfate (1.0 g), yellow mercuric oxide (0.450 g, 2.1×10^{-3} mol), and saturated ethanolic potassium hydroxide (0.5 ml) were added and the mixture was allowed to stir vigorously at room temperature in the dark overnight. The reaction mixture was filtered by gravity, with care being taken to exclude all light. The solution was a deep orange colour. Evaporation of the solvent on a rotary evaporator afforded an orange solid, the nmr and ir of which were consistent with the structure of the desired product, *p,p′*-dicyanodiphenyldiazomethane (Table 3).

Acknowledgement

This work was supported by the National Research Council of Canada.

1. (*a*) R. Breslow, H. W. Chang, and W. A. Yager. J. Am. Chem. Soc. **85**, 2033 (1963); (*b*) R. Breslow, R. Hill, and E. Wasserman. J. Am. Chem. Soc. **86**, 5349 (1964); (*c*) M. Glasbak, J. D. W. van Voorst, and G. J. Hoÿtink. J. Chem. Phys. **45**, 1852 (1966); (*d*) R. M. Pagni, C. R. Watson, Jr., J. E. Bloor, and J. R. Dodd. J. Am. Chem. Soc. **96**, 4064 (1974); (*e*) C. R. Watson, Jr., R. M. Pagni, J. R. Dodd, and J. E. Bloor. J. Am. Chem. Soc. **98**, 2551 (1976).
2. L. I. Smith and K. L. Howard. Org. Syn. Coll. Vol. 3. J. Wiley and Sons, Inc., New York. 1955. p. 352.
3. (*a*) R. W. Murray, A. M. Trozzolo, E. Wasserman, and W. A. Yager. J. Am. Chem. Soc. **84**, 3213 (1962); (*b*) R. W. Brandon, G. L. Closs, and C. A. Hutchison, Jr. J. Chem. Phys. **37**, 1878 (1962).
4. R. M. Etter, H. S. Skovronek, and P. S. Skell. J. Am. Chem. Soc. **81**, 1008 (1959).
5. R. W. Brandon, G. L. Closs, C. E. Davoust, C. A. Hutchison, Jr., B. E. Kohler, and R. Silbey. J. Chem. Phys. **43**, 2006 (1965).
6. C. A. Hutchison, Jr. and B. E. Kohler. J. Chem. Phys. **51**, 3327 (1969).
7. A. M. Trozzolo and E. Wasserman. *In* Carbenes. Vol. 2. *Edited by* M. Jones, Jr. and R. A. Moss. J. Wiley and Sons, Inc., New York. 1975.
8. E. Wasserman, V. J. Kuck, R. S. Hutton, and W. A. Yager. J. Am. Chem. Soc. **92**, 7491 (1970).
9. A. M. Trozzolo. Acc. Chem. Res. **1**, 329 (1968).
10. (*a*) G. L. Closs. Top. Stereochem. **3**, 193 (1968), and references cited therein; (*b*) G. L. Closs. *In* Carbenes. Vol. 2. *Edited by* M. Jones, Jr. and R. A. Moss. J. Wiley and Sons, Inc., New York. 1975.
11. R. Hoffmann, G. D. Zeiss, and G. W. Van Dine. J. Am. Chem. Soc. **90**, 1485 (1968).
12. (*a*) G. L. Closs, C. A. Hutchison, Jr., and B. E. Kohler. J. Chem. Phys. **44**, 413 (1966); (*b*) I. Moritani, S. Murihoshi, N. Nishino, K. Kimura, and H. Tsubimora. Tetrahedron Lett. 373 (1966); (*c*) W. A. Gibbons and A. M. Trozzolo. J. Am. Chem. Soc. **88**, 172 (1966).
13. D. R. Arnold, R. W. Humphreys, W. J. Leigh, and G. E. Palmer. J. Am. Chem. Soc. **98**, 6225 (1976).
14. (*a*) R. Gleiter and R. Hoffmann. J. Am. Chem. Soc. **90**, 5457 (1968); (*b*) L. Salem and R. Hoffmann. Angew. Chem. Int. Ed. Engl. **11**, 92 (1972); (*c*) L. Salem and W. D. Stohrer. Unpublished results; (*d*) J. H. Davis, W. A. Goddard III, and R. G. Bergman. J. Am. Chem. Soc. **98**, 4015 (1976).
15. R. Gleiter and R. Hoffmann. Tetrahedron, **24**, 5899 (1968).
16. N. C. Baird and K. Taylor. Pure Appl. Chem. In press.
17. G. L. Closs and S. H. Goh. J. Chem. Soc. Perkin I, 2103 (1972).
18. A. G. Harrison, P. Kenarle, and F. P. Lossing. J. Am. Chem. Soc. **83**, 777 (1961).
19. P. Neta and R. H. Schuler. J. Phys. Chem. **77**, 1368 (1973).

The internal coordinate Morse oscillator as a means to simplify the anharmonicity problem in the thermodynamics of systems of polyatomic molecules

JAN BRON AND R. WALLACE

Department of Chemistry, University of Manitoba, Winnipeg, Man., Canada R3T 2N2

Received November 15, 1976

JAN BRON and R. WALLACE. Can. J. Chem. **55**, 2292 (1977).

Two postulates simplify the evaluation and algebraic complexity of the expression for the anharmonic correction to the ground rotational–vibrational energy of a polyatomic molecule. The two postulates are: (*1*) anharmonicity of vibration is associated with bond stretching coordinates only; all other internal coordinates can be represented by harmonic potentials; (*2*) bonds vibrate according to a Morse potential. The result is the replacement of tedious computer calculations by a 'back of an envelope' type of computation. Relationships between anharmonic corrections to the ground state vibrational energies of isotopically different molecules are derived. Good agreement with exact results is obtained. Quantitative and qualitative applications are given.

JAN BRON et R. WALLACE. Can. J. Chem. **55**, 2292 (1977).

Deux postulats permettent de simplifier l'évaluation et la complexité algébrique de l'expression pour la correction anharmonique vers l'énergie rotationnelle vibrationnelle fondamentale d'une molécule polyatomique. Les deux postulats sont: (*1*) l'anharmonicité de la vibration est associée uniquement avec les coordonnées de vibration du lien; toutes les autres coordonnées internes peuvent être représentées par des potentiels harmoniques. (*2*) Les liens vibrent d'après un potentiel de Morse. Le résultat de cette simplification implique le remplacement de calculs complexes par ordinateur par un type de calcul qui peut se faire sur le "dos d'une enveloppe." On a pu dériver des relations entre les corrections anharmoniques vers les énergies vibrationnelles de l'état fondamental de molécules différentes du point de vue isotopique. On a obtenu un bon accord avec les résultats exacts. On donne des applications qualitatives et quantitatives.
[Traduit par le journal]

Introduction

The correction of partition functions and thermodynamic quantities for anharmonicity of vibration has been discussed in detail over the past few years (1–4). It has been found that thermodynamic quantities, calculated by means of the harmonic approximation, may be considerably changed when corrected for anharmonicity. This was especially found to be true for compounds containing hydrogen isotopes (5). Anharmonicity in the ground vibrational–rotational state seems to lead to the largest correction (5).

The anharmonic correction, a multiplicative factor, of the molecular canonical partition function, q, has the form

$$[1] \qquad \text{ANHC} = \exp\left[-(\text{AZPE})/kT\right]$$

The energy quantity, AZPE (5), is the difference between the anharmonic and harmonic vibrational zero-point energy. The expression for AZPE is complex and not easily evaluated (3). The calculation of AZPE requires the use of a large, modern computer. The time needed to calculate AZPE increases enormously when one atom is added to the molecule. For this reason it has proved impossible to study molecules with more than four atoms.

The time consuming part in calculations of AZPE is the transformation of cubic and quartic force constants in internal coordinates to those in dimensionless normal coordinates (6). In a recent paper (7) a theory of nuclear motion in polyatomic molecules based upon the Morse oscillator (bond stretches) has been developed. This theory can be used to evaluate AZPE, eliminating the tedious transformation mentioned above.

In this paper the Morse oscillator approach will be used to attempt to simplify the theory of anharmonicity. Since the anharmonicity correction, ANHC, is largest for compounds containing hydrogen isotopes, this discussion will mainly deal with H, D, and T containing molecules.

Theoretical Considerations

Perhaps the simplest way to evaluate the vibrational partition function, q_{vib}, is to sub-

stitute the harmonic frequencies, obtained by using the best available (harmonic) spectroscopic force field and Wilson's **F**, **G** matrix method (8), into the well known expression

$$[2] \quad q_{\text{vib}} = \prod_{i=1}^{3N-6(5)} e^{-hc\omega_i/2kT}(1 - e^{-hc\omega_i/kT})^{-1}$$

and then multiply q_{vib} by ANHC. In [2], ω_i (cm^{-1}) is the frequency of vibration of the ith normal mode and all other symbols have their usual meaning. It is proposed to estimate ANHC by assuming that the magnitude of AZPE is mainly determined by anharmonicity of vibration of the A—X bond (X = H, D, T; A is any other heavier element). Furthermore, it will be postulated that the bonds vibrate according to a Morse potential. An expression for AZPE can now be derived.

The vibrational Hamiltonian operator in terms of internal (stretching) coordinates, S_i, is (7)

$$[3] \quad \hat{H} = \sum_{i=1}^{m} \hat{H}_i^{(0)}(S_i) - \hbar^2 \sum\sum_{i<j} G_{ij}(\partial^2/\partial S_i \partial S_j)$$

There are m bonds in the molecule. The operator $\hat{H}_i^{(0)}(S_i)$ is defined as

$$[4] \quad \hat{H}_i^{(0)} = -\tfrac{1}{2}\hbar^2 G_{ii}(\partial^2/\partial S_i^2) + V_i(S_i)$$

and G_{ij} is a **G** matrix element defined by Wilson (8). The potential energy, $V_i(S_i)$, is given by the Morse expression

$$[5] \quad V_i(S_i) = D_i[\exp(-2a_iS_i) - 2\exp(-a_iS_i)]$$

where D_i and a_i are the usual Morse parameters for the ith bond. The approximate eigen values of the operator $\hat{H}$ in the vibration–rotational ground state can be found by (non-degenerate) perturbation theory.

Equation 3 can be written as

$$[6] \quad \hat{H} = \hat{H}_0 + \hat{H}^{(1)}$$

where

$$[7] \quad H_0 = \sum_{i=1}^{m} \hat{H}_i^{(0)}(S_i)$$

and the perturbation, $H^{(1)}$, is equal to

$$[8] \quad \hat{H}^{(1)} = -\hbar^2 \sum_{i<j}^{m}\sum^{m} G_{ij}(\partial^2/\partial S_i \partial S_j)$$

The zeroth-order wavefunction, $\psi_0^{(0)}$, is

$$[9] \quad \psi_0^{(0)} = \prod_{i=1}^{m} \phi_i^{(0)}(S_i)$$

The function $\phi_i^{(0)}(S_i)$ is the solution of the ith one-dimensional Morse oscillator problem and corresponds to the lowest eigenvalue (9):

$$[10] \quad E_i^{(0)} = -A_i^{-2}(K_i - \tfrac{1}{2})^2$$

In this equation the quantities A_i and K_i are defined as

$$[11] \quad A_i = (2\mu_i)^{1/2}/a_i\hbar; \quad K_i = A_i D_i^{1/2}$$

In [11], μ_i is the reduced mass of the atoms defining the ith bond. The solution, $E_0^{(0)}$, of the equation

$$[12] \quad H_0\psi_0^{(0)} = E_0^{(0)}\psi_0^{(0)} = \sum_{i=1}^{m} H_i^{(0)}\psi_0^{(0)}$$

is then

$$[13] \quad E_0^{(0)} = -\sum_{i=1}^{m} A_i^{-2}\left(K_i - \frac{1}{2}\right)^2$$

The first and second order contributions to the energy are more difficult to evaluate than for a set of m harmonic oscillators, because the matrix elements of the Morse oscillator do not have a set of well defined selection rules. By means of the eigen functions given in [9], the first order contribution, $E_0^{(1)}$, becomes

$$[14] \quad E_0^{(1)} = -\hbar^2 \sum_{i<j}^{m}\sum^{m} G_{ij}\langle 0|\partial/\partial S_i|0\rangle \times \langle 0|\partial/\partial S_j|0\rangle = -\tfrac{1}{4}\hbar^2 \sum_{i<j}^{m}\sum^{m} a_i a_j G_{ij}$$

The second order correction, $E_0^{(2)}$, to the ground state energy becomes

$$[15] \quad E_0^{(2)} = \sum_{k}' [\langle 0|\hat{H}^{(1)}|k\rangle^2/(E_0^{(0)} - E_k^{(0)})]$$

The prime near the summation sign indicates that the summation is over all states *except* the ground state. The energy $E_k^{(0)}$ is given by the expression (9)

$$[16] \quad E_k^{(0)} = -\sum_{i=1}^{m} A_i^{-2}(K_i - n_i - \tfrac{1}{2})^2$$

The subscript k is a symbol for the values of the quantum numbers n_i in the kth state.

For reasons given above, the summation in [15] will contain an infinite number of terms. However, by analogy with the harmonic oscillator, the term, V_{11}, in the sum that will be largest by far is

$$[17]\quad V_{11} = \hbar^4 \left[\sum_{i<j} \sum G_{ij} \langle 0|\partial/\partial S_i|1\rangle \times \langle 0|\partial/\partial S_j|1\rangle \right]^2 \Big/ \Delta E_{11}{}^{(0)}$$

The difference $\Delta E_{11}{}^{(0)}$ is defined as

$$[18]\quad \Delta E_{11}{}^{(0)} = -A_i{}^{-2}(K_i - \tfrac{1}{2})^2 - A_j{}^{-2} \times (K_j - \tfrac{1}{2})^2 + A_i{}^{-2}(K_i - \tfrac{3}{2}) + A_j{}^{-2}(K_j - \tfrac{3}{2})^2 = 2A_i{}^{-2}(1 - K_i) + 2A_j{}^{-2}(1 - K_j)$$

After evaluation of the matrix elements in [17], the expression for V_{11} becomes

$$[19]\quad V_{11} = (\hbar/2)^4 \left[\sum_{i<j} \sum a_i a_j G_{ij} (2K_i - 1)^{1/2} \times (2K_j - 1)^{1/2} \right]^2 \Big/ \Delta E_{11}{}^{(0)}$$

Expressions for the other terms in the sum can also be found.

Numerical values for [14] and the largest terms in [15] were obtained for several molecules, such as H_2O, HDO, D_2O, NH_3, NH_2D, . . . etc. It was found that they were extremely small compared to $E_0{}^{(0)}$. Therefore, considering the parametric character of the Morse oscillator, which shall be discussed below, $E_0{}^{(1)}$ and $E_0{}^{(2)}$ will be ignored. The ground state energy of the set of m oscillators in the molecule becomes then (*cf.* [13]):

$$[20]\quad E_0 = -\sum_{i=1}^{m} A_i{}^{-2}(K_i - \tfrac{1}{2})^2$$

Equation 20 is the ground state energy of a set of m *uncoupled* Morse oscillators and leads to important simplifications. Equation 20 can now be used to obtain an expression for AZPE in [1]:

$$[21]\quad \text{AZPE} = \sum(-A_i{}^{-2}(K_i - \tfrac{1}{2})^2 + D_i - \tfrac{1}{2}h\nu_i)$$

In [21] the Morse parameter D_i may be *roughly* identified with the depth of the potential well associated with the vibration of the ith bond. The harmonic part in E_0 is removed by subtracting $\frac{1}{2}\sum h\nu_i$. The frequency ν_i is defined as

$$[22]\quad \nu_i = (2\pi)^{-1}(F_i/\mu_i)^{1/2}$$

The force constant F_i can be expressed in terms of a_i and D_i, by differentiating [5] twice with respect to S_i and determining the value of the second derivative at $S_i = 0$. The result is

$$[23]\quad F_i = 2a_i{}^2 D_i \quad \text{or} \quad a_i = +(F_i/2D_i)^{1/2}$$

By means of [21], [22], and [23], AZPE becomes

$$[24]\quad \text{AZPE} = -\sum_{i=1}^{m} (2A_i)^{-2} = -\frac{\hbar^2}{16}\sum_{i=1}^{m} F_i/(\mu_i D_i)$$

It should be noted that [24] is easily evaluated if F_i and D_i are known. A reasonable value for F_i, the bond force constant, can be found in the literature (10) and an estimate for D_i can be obtained from Pauling's empirical formula (11). Results obtained from [24] can be compared with "exact" values (2, 3).

Discussion and Conclusions

The energy AZPE in [24] has been postulated to be a sum of contributions of m bonds in the molecule. It is convenient to define a quantity E(A—X) such that

$$[25]\quad \text{AZPE} = \sum E(\text{A—X})$$

where the summation is over all m bonds A—X. The bond anharmonic energy is then

$$[26]\quad E(\text{A—X}) = -(2A_i)^{-2} = -\hbar^2 F_i/(16\mu_i D_i)$$

Within the Born–Oppenheimer approximation F_i and D_i are the same for bonds differing only in isotopic substitution, therefore,

$$[27]\quad \frac{E(\text{A} - \text{X}')}{E(\text{A} - \text{X})} = \frac{\mu_i}{\mu_i'}$$

The prime denotes isotopic substitution. From [25] follows that AZPE for a molecule AX_mX_n' is

$$[28]\quad \text{AZPE}(AX_mX_n') = mE(\text{A—X}) + nE(\text{A—X}')$$

By means of [27], the above equation reduces to

$$[29]\quad \text{AZPE}(AX_mX_n') = E(\text{A—X}) \times [m + n\mu_i/\mu_i']$$

The relationship [28] has been observed (but not explained) previously (3) in exact calculations of AZPE for the NH_nD_{3-n}, NH_nT_{3-n}, AH_nD_{2-n}, and AH_nT_{2-n} (A = O, S, Se) molecules; also the reduced mass relationship, [27], holds. In the exact calculations, anharmonicity of the bending modes has been taken into account. Bending coordinates *probably*

cannot be related by equations of type [27] and [28]. The assumption that the magnitude of AZPE is mainly determined by anharmonic vibration of the A—X bonds, seems therefore reasonable.

A numerical example may be informative. The exact value for AZPE of NH_3 is -123.3 cm^{-1} (3). It took, by the way, about 50 min for a PDP-10 computer to obtain this number and the program used was the result of a year's work. From [28] follows that E(N—H) is equal to $-123.3/3$ or -41.1 cm^{-1}. By means of [27] and [29], AZPE for NH_2D, NHD_2, and ND_3 can be deduced. The results are -104.1, -85.0, and -65.8 cm^{-1} respectively. The exact values are -104.0, -84.9, and -66.1 cm^{-1}, so the agreement is excellent.

For molecules of the type AX_nX_m', the Morse oscillator approach reduces AZPE from a many to a *two* parameter equation. It may be useful to discuss these parameters, a_i and D_i, in greater detail. As pointed out above a_i and D_i are the same for chemical bonds differing only in isotopic substitution. The dissociation energy can approximately be identified with D_i, but a_i is a more abstract quantity. It is therefore suggested to use [23] and replace a_i by F_i. The force constant F_i is, of course, also the same for bonds only differing in isotopic substitution. The two (Morse) parameters are then only F_i and D_i. If F_i is obtained by spectroscopic means or from tables (10), AZPE depends on only *one* parameter. The remaining parameter D_i cannot be eliminated, since D_i and the bond dissociation energy are not the same. For example, for E(N—H) equal to -41.1 cm^{-1} and F_i equal to 8.454×10^5 dyn cm^{-1} (12) and [26] follows that D_i has the value of 278 kJ/mol. This compares poorly with 407 kJ/mol for the N—H bond (13). However, for molecules for which exact values for AZPE have not been obtained, the dissociation energy may serve as a first estimate of D_i.

Equations 25 and 27 are also useful for qualitative purposes. Recently a paper appeared (14) on *differences* in thermodynamic quantities of various $^x UF_6$ species (x = 238, 235, etc.). These differences are related to the partition function ratios of the $^x UF_6$ molecules. It was anticipated, by means of intuitive arguments, that the anharmonicity corrections for these partition function ratios are small. The equations in this paper can be used to prove this assertion. If, for example, the correction factor for the ratio $q(^{238}UF_6)/q(^{235}UF_6)$ is C, then

$$[30]\quad C = \mathrm{ANHC}(^{238}UF_6)/\mathrm{ANHC}(^{235}UF_6) = \exp\left[-\{\mathrm{AZPE}(^{238}UF_6) - \mathrm{AZPE}(^{235}UF_6)\}hc/kT\right]$$

It has been implied in [30] that the units of AZPE($^x UF_6$) are cm^{-1}. As mentioned above, there is no correction when C is equal to unity. By using [25] and [27], [30] becomes

$$[31]\quad C = \exp\left[-6E(^{238}U—F)(1 - \mu_{238}/\mu_{235}) \times hc/kT\right] = \exp\left[E(^{238}U—F)0.0057hc/kT\right]$$

If D_i(U—F) is equal to 517 kJ/mol (15) and F_i(U—F) is 3.85×10^5 dyn cm^{-1} (16), then C becomes 0.999985. Hence, anharmonicity is unimportant.

As has been implied above, two postulates simplify the evaluation and algebraic complexity of the expression for the anharmonic correction to the ground rotational–vibrational energy of polyatomic molecules. These two postulates are: (*1*) anharmonicity of vibration is primarily associated with bond stretching coordinates; all other internal coordinates can be represented by harmonic potentials: (*2*) bonds vibrate according to a Morse potential. The results obtained, eqs. 27 and 29, successfully relate AZPE for isotopic diatomic, triatomic, and tetratomic molecules (AX, AXY, AXYZ; X, Y, Z = H, D, T). Therefore, it is suggested that [27] and [29] may also be applied to suitable molecules of more than four atoms. It should be noted that [27] and [29] are essentially empirical in character.

The quantity ANHC, eq. 1, corrects only for anharmonicity of the ground state. A correction similar to ANHC can be defined for anharmonicity of the vibrational *excited* states, but it is expected that in that case simple expressions, such as [27] and [29], will not be obtained. However, detailed calculations have revealed (5) that corrections due to anharmonicity of the excited states are much smaller than ANHC at temperatures between 200 and 600 K. For higher temperatures the "local mode" method of Hayward and Henry (17, 18) shows promise to simplify the calculation of the correction for anharmonicity of excited states.

In this paper an attempt has been made to show how the values of AZPE for molecules

differing in isotopic substitution are related. Furthermore, a method has been presented to estimate AZPE, from the Morse parameters F_i (or a_i) and D_i. If precision is required and spectroscopic data are available it is best to calculate AZPE by the exact method and use the above formulae to determine AZPE for isotopic molecules. For larger molecules, containing more than four atoms, the exact method demands too much computer time, and the Morse oscillator approach can be used to gain an impression about the importance of anharmonicity of vibration. Equations 1, 25, and 27 can also be used in chemical kinetics (4).

1. M. WOLFSBERG. J. Chem. Phys. **50**, 1484 (1969).
2. M. WOLFSBERG, A. A. MASSA, and J. W. PYPER. J. Chem. Phys. **53**, 3138 (1970).
3. J. BRON and M. WOLFSBERG. J. Chem. Phys. **57**, 2862 (1972).
4. J. BRON. J. Chem. Soc. Faraday Trans. 2, **70**, 240 (1974).
5. M. WOLFSBERG, CHEN FEE CHANG, and J. BRON. Z. Naturforsch. **28**a, 129 (1973).
6. M. A. PARISEAU, I. SUZUKI, and J. OVEREND. J. Chem. Phys. **42**, 2335 (1965).
7. R. WALLACE. Chem. Phys. **11**, 189 (1975).
8. E. B. WILSON, J. C. DECIUS, and P. C. CROSS. Molecular vibrations. McGraw-Hill Book Company, Toronto, Ontario. 1955.
9. R. WALLACE. Chem. Phys. Lett. **37**, 115 (1976).
10. G. HERZBERG. Molecular spectra and molecular structure. II. Infrared and Raman spectra of polyatomic molecules. Van Nostrand Reinhold Company, New York. 1945.
11. L. PAULING. The nature of the chemical bond. 3rd ed. Cornell University Press. 1960.
12. W. S. BENEDICT, E. K. PLYLER, and E. D. TIDWELL. J. Chem. Phys. **32**, 32 (1960).
13. H. S. JOHNSTON. Gas phase reaction rate theory. Ronald Press Company, New York. 1966.
14. J. BRON. Can. J. Chem. **54**, 160 (1976).
15. T. L. COTTRELL. The strength of chemical bonds. 2nd ed. Butterworths, London. 1958.
16. R. S. MCDOWELL, L. B. ASPREY, and R. T. PAINE. J. Chem. Phys. **61**, 3571 (1974).
17. R. J. HAYWARD and B. R. HENRY. J. Mol. Spectrosc. **57**, 221 (1975).
18. B. R. HENRY. J. Phys. Chem. **80**, 2160 (1976).

Comments on "Librations around the C(S)–phenyl bond in *N*-thiobenzoylmorpholines observed by 220 MHz proton magnetic resonance spectroscopy"

ULF BERG

Division of Organic Chemistry 1, Chemical Center, University of Lund, P.O. Box 740, S-220 07 Lund 7, Sweden

Received December 21, 1976

ULF BERG. Can. J. Chem. **55**, 2297 (1977).

The interpretation of the temperature dependent nmr spectra of the three thiobenzmorpholides **1**–**3** in terms of torsional libration proposed in the title article is criticized. Pure samples of *cis*-**1** and *trans*-**1** have been prepared and studied by dynamic ^1H and ^{13}C nmr. A new interpretation is presented which involves the freezing of the passage over the steric barrier with a planar Ph—C(S)N transition state.

ULF BERG. Can. J. Chem. **55**, 2297 (1977).

On critique l'interprétation proposée dans l'article mentionné dans le titre pour expliquer la dépendance qui existe entre la température et les spectres rmn de trois thiobenzmorpholides **1** à **3** en termes de librations torsionnelles. On a préparé des échantillons purs de **1**-*cis* et de **1**-*trans* et on les a étudiés par rmn dynamique de ^1H et ^{13}C. On présente une nouvelle interprétation qui implique le blocage du passage au-dessus de la barrière stérique avec un état de transition Ph—C(S)N planaire.

[Traduit par le journal]

Recently an investigation of the temperature dependent ^1H nmr spectrum of the three thiobenzmorpholides **1**–**3** was communicated (1). The

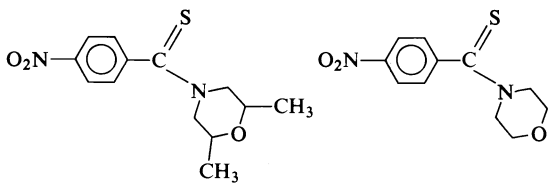

1

2

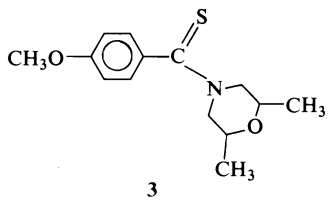

3

ortho-proton signals of **1** and **3** were reported to be temperature dependent in the region +40 – −50°C at 220 MHz in several solvents, whereas in **2** they remain unchanged under the same conditions.

Fulea and Krueger associate this phenomenon with the rotational process about the Ph—C(S) bond and suggest two energy maxima for this rotation, *i.e.* one steric barrier (E_{steric}) for the process by which *ortho*-protons would pass through the thioamide plane, and one electronic barrier (E_π) for the process by which the phenyl ring passes through a plane perpendicular to the thioamide plane. However, they do not attribute the observed spectral features to the freezing of any of these processes. Instead, the phenomenon is explained by "progressive freezing of the librations of the thioamide group around the Ph—C(S) bond as the temperature is lowered" and with the passages over both the E_{steric} and E_π barriers "frozen" in the relevant temperature region (0 – −50°C). This conclusion was based upon the existence of small sharp peaks in the neighbourhood of the coalescence temperature.

We question this interpretation and wish to present a critical analysis of their theory and a reinvestigation of the nmr spectrum of **1**.

In order to observe an effect on the nmr bandshape of the type shown in Fig. 1, ref. 1, of a set of nuclei interchanging between two (or more) sites, the condition has to be fulfilled that the lifetime of the nuclei in the different sites has to be much longer by far than what can be envisaged for the torsional levels around a local potential energy minimum (see, *e.g.*, ref. 2). In other words, the torsional states would have to be separated by barriers in the order of 11–14 kcal/mol in the present cases.[1] In the absence of such a high barrier, the nuclei in all populated

[1]This argument also contradicts the interpretations in terms of torsional librations in the other papers cited in ref. 1.

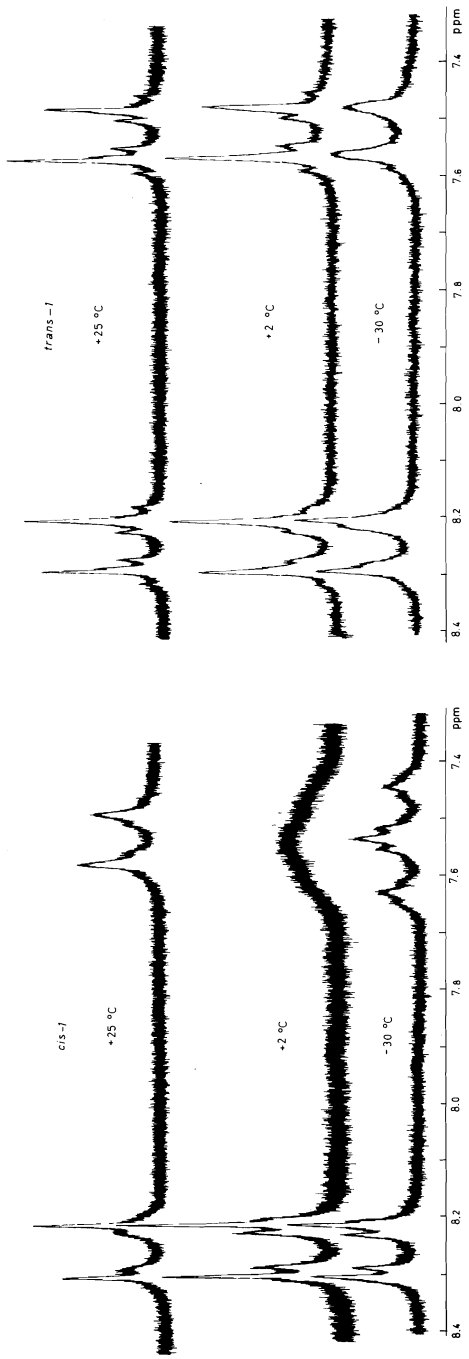

FIG. 1. ^{1}H nmr spectra of the aromatic protons of *cis*-**1** and *trans*-**1** in acetone-d_6 + $CDCl_3$ (1:1).

states give rise to only one chemical shift which is the weighted mean value of the chemical shifts in the different states. This, however, results in only "sharp" signals determined by this chemical shift and the coupling constants.

Furthermore, the statement in ref. 1 that passage over the E_π barrier, with a frozen E_{steric} rotation, will average the *ortho*-protons is erroneous in the case of **1** and **3** since the presence of the two methyl groups in the morpholine ring introduces anisochronism to the *ortho*-protons (in principle also to the *meta*-protons) even if the morpholine ring inversion is rapid, provided that the C(S)—N rotation is slow. This is true for both the *cis* and *trans* arrangements of the 2,6-dimethyl substituents.[2] In the absence of methyl substituents in the morpholine ring as in **2**, this anisochronism is lost if the inversion of this ring is rapid on the nmr time scale and the *ortho*-protons are indeed equalized by passage over the E_π barrier.

An analysis of the alternative possibility, *i.e.* that the E_π barrier is frozen, gives at hand that passage over the E_{steric} barrier does not equalize the *ortho*-protons in any of the compounds **1**–**3**. Though no barriers to rotation over the E_π maximum have so far been determined, a very low value for this barrier can be expected by an extrapolation from data on the Ph—C(O) system (3), taking into account the important barrier-lowering effect of the cross conjugation with the nitrogen lone pair as well as the destabilization of the ground state by non-bonded interactions (E_{steric}).

These remarks suggest an alternative interpretation which simply involves the freezing of the rotation about the E_{steric} barrier.

In a reinvestigation, authentic samples of *cis*-**1** and *trans*-**1** were prepared and examined by variable temperature ^{1}H and ^{13}C nmr. The 100

[2]The explanation in terms of torsional oscillations proposed in ref. 1 was just recently commented upon (8) and an interpretation, essentially concurring with ours, was suggested. In conflict with our analysis, however, the authors claimed (ref. 8, note 9) that the *ortho*-protons in the *trans* isomer are symmetrically equivalent. This is not the case as may be visualized by the following schematic formula. The non-equivalence is also verified by our ^{13}C nmr results.

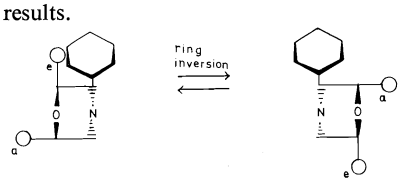

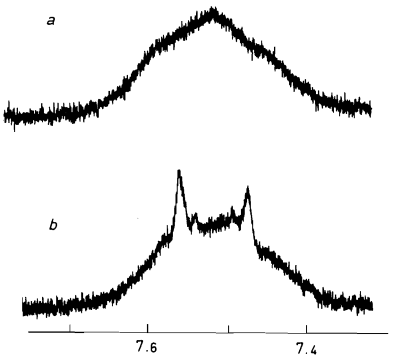

FIG. 2. ^{1}H nmr spectra of the *ortho*-protons at the coalescence temperature: *a*, pure *cis*-**1**; *b*, *cis*-**1** + *ca.* 10% of *trans*-**1**.

MHz ^{1}H nmr signal patterns for the aromatic and the methyl protons of the two isomers are very similar at ambient temperature. The spectra of the morpholine ring protons, however, differ substantially. *Cis*-**1** exhibits three groups of signals (δ 2.7–3.1, 3.5–3.9, 5.3–5.5), the low-field part of which integrates for one proton, which by double resonance was shown to be a N—CH_2 proton and, by analogy with earlier results, assigned to the *Z*-equatorial proton pointing in the direction of the strongly deshielding C=S group (4). In *trans*-**1**, on the other hand, all morpholine ring protons fall in one group of signals (δ 3.0–4.6).

On cooling, the *ortho*-proton part of *cis*-**1** undergoes broadening and at +2°C a decoalescence is observed, whereas for *trans*-**1** only a slight broadening is observed down to −60°C (Fig. 1). Furthermore, the spectrum of *cis*-**1** at +2°C does not contain the sharp peaks amidst the broad band reported in ref 1, but this pattern is perfectly reproduced when a small quantity of the *trans* isomer is added to the sample (Fig. 2). Thus, we conclude that Fulea and Krueger were studying a sample of *cis*-**1** containing a few percent of the *trans* isomer.

In order to acquire further information and to avoid the complication with badly resolved proton spectra a dynamic ^{13}C nmr study was also carried out. The ^{13}C chemical shifts are shown in Table 1. On lowering the temperature the signal assigned to the *ortho*-carbons showed exchange broadening and decoalesced to a symmetrical doublet. This phenomenon was observed for both *cis*-**1** and *trans*-**1**. The coalescence data are reported in Table 2.

So far we have considered the situation with rapid inversion of the morpholine ring. The study

TABLE 1. ^{13}C nmr chemical shifts for *cis*-**1** and *trans*-**1** in acetone-d_6/chloroform-*d* (1:1) at ambient temperature

	δ(ppm from TMS)	
Carbon	*Cis*-**1**	*Trans*-**1**
CH_3	18.5, 19.1	17.4, 17.9
CH_2	54.5, 57.9	53.7, 56.8
CH	71.8, 72.3	66.3, 66.9
C(*meta*)	124.4	124.1
C(*ortho*)	127.8	127.1
C(*quaternary*)	148.2, 149.6	147.2, 148.6
C=S	197.9	197.8

TABLE 2. Coalescence data from ^{13}C nmr for *cis*-**1** and *trans*-**1** in acetone-d_6/chloroform-*d* (1:1)

Compound	δν (Hz)	T_c (K)	$\Delta G^{\ddagger}$(kcal/mol)
Cis-**1**	18	282	14.4
Trans-**1**	9	253	13.2

of the nmr spectra of *cis*-**1** and *trans*-**1** at temperatures where this inversion is slow should give information about the *cis–trans* assignments of the isomers of **1**.

Cis-**1** exists in a single conformation with the methyls in diequatorial positions, this conformation being of *ca.* 5 kcal lower energy than the diaxial conformation (5), and one can expect no effect on the nmr spectrum of the freezing of the inversion of this ring.

Trans-**1** on the other hand, exists as an equilibrium between two rapidly interconverting conformations of comparable energy[3] with axial–equatorial methyls. Thus the *trans* isomer should be expected to give rise to decoalescence phenomena when the rate of ring inversion is slow. Accordingly, the ^{13}C nmr spectrum of *trans*-**1** below −80°C displayed exchange broadening of all the six signals from the morpholine carbons as well as those of the two *ortho*-carbons and the single signal of the *meta*-carbons, leaving only the three quaternary carbons (and those of the solvent) as sharp signals (Fig. 3). At −116°C, which unfortunately was the low temperature limit of the apparatus, the first decoalescence was reached corresponding to an upper limit of the barrier of 8.0 kcal/mol (with a δν of 10 Hz).

In previous work it has been found that *N*-

[3]Since the steric interactions between an axial *Z*-methyl and the sulfur might substantially differ in energy from that between an equatorial *Z*-methyl and the sulfur, unequal populations cannot be ruled out.

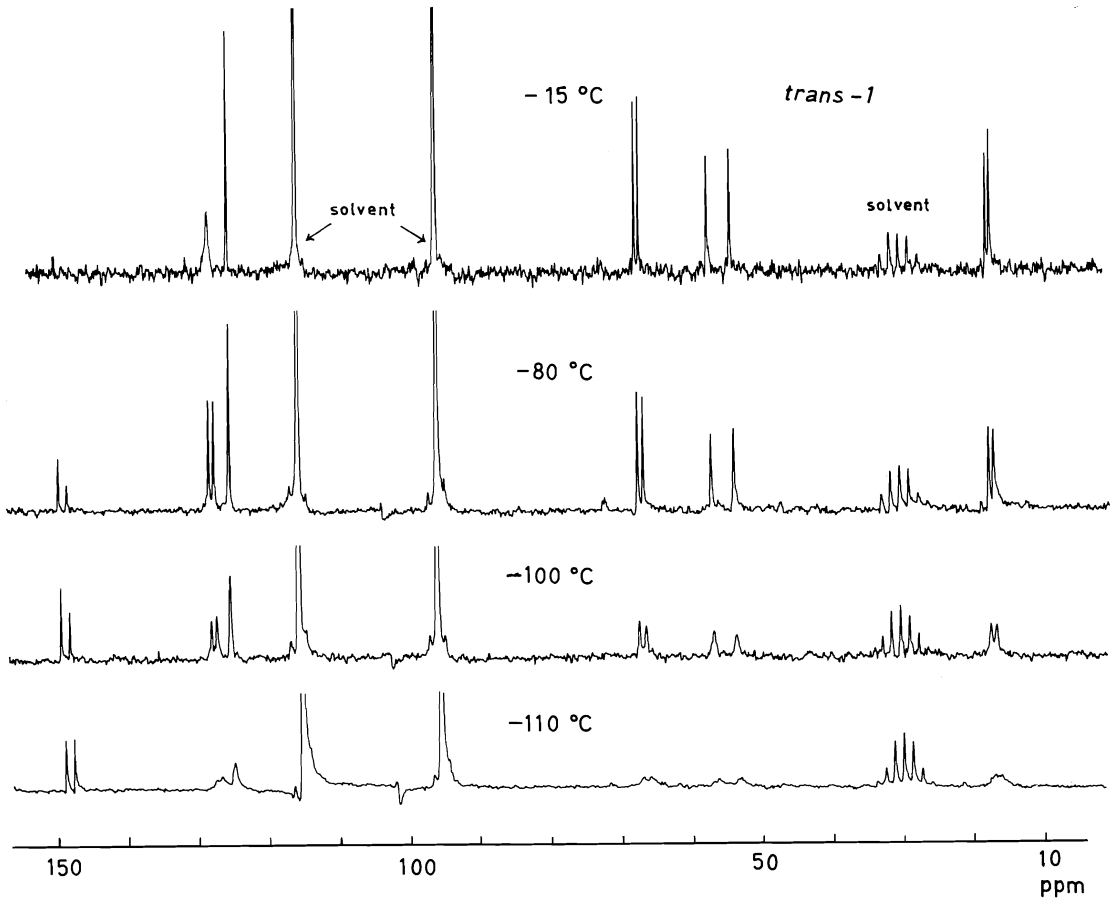

FIG. 3. Proton noise decoupled ^{13}C nmr spectra of *trans*-**1** in $CHCl_2F$ (+20% acetone-d_6).

acylation lowers the inversion barrier of morpholines by 2–3 kcal/mol (6). Thus, reduction of the thiocarbonyl group, giving the corresponding benzylmorpholine, should make the decoalescence accessible. On reaction with sodium borohydride it was found that both the thiocarbonyl group and the nitro group were reduced. The ^1H nmr spectrum of *N*-(*p*-aminobenzyl)-*trans*-2,6-dimethylmorpholine showed the expected decoalescence of the methyl signals as well as of the ring protons and the benzyl ($T_c = -80°C$, $\Delta G^{\ddagger} = 9.4$ kcal/mol), whereas the *cis* isomer remained unchanged at $-105°C$. This unambiguously clarifies the assignment of *cis* and *trans* configurations.

Experimental

Measurements

The ^1H nmr spectra were recorded on a Jeol MH-100 spectrometer utilizing an internal proton lock (TMS) and the ^{13}C nmr spectra on a Jeol FX-60 spectrometer working at 15.03 MHz. A flip angle of 60° was used, the number of data points was 8K and spectral widths were 5000, 2500, and 1000 Hz. The temperature was measured by means of the thermocouple fixed in the normal insert. This thermocouple was calibrated against a second thermocouple held inside the spinning nmr tube. Free energies of activation were estimated by the approximate formula appropriate for a coalescing doublet (7) and the Eyring equation in the form:

$$\Delta G^{\ddagger} = \frac{4.57 T_c}{1000}\left(9.97 + \log\frac{T_c}{\delta\nu}\right) \text{ kcal/mol}$$

Preparations

The *cis* and *trans* isomers of *p*-nitrothiobenz-2,6-dimethylmorpholide (**1**) were prepared by reaction of *p*-nitrobenzaldehyde (7 g), sulfur (4 g), and 2,6-dimethylmorpholine (15 ml, Aldrich, containing *ca.* 30% of the *trans* isomer) for 1.5 h under reflux conditions. The mixture was treated with ice water and extracted with chloroform. Analysis by tlc (silica, chloroform) gave rise to two yellow spots ($R_f = 0.64$; 0.54) in addition to by-products. The two products could be separated by re-

peated column chromatography (silica, Merck 70-230, chloroform) and by recrystallization of the different fractions from ethanol. The products were identified in the order that they were eluted: *cis*-**1**, 2.5 g, mp 165–166°C; *trans*-**1**, 0.5 g, mp 149–150°C. For identification see Discussion. In addition *p*-aminothiobenz-2,6-dimethylmorpholide (2.0 g, mp 135–159°C) was isolated, apparently formed by reduction of the nitro group by sulfide ions generated in the reaction. The *cis–trans* relation was not established for this compound but according to the large temperature interval of melting a mixture of the two isomers seems probable.

Reduction of 1

Each isomer of **1** (200 mg) was treated with sodium borohydride (excess) in ethanol at 50°C for 1 h. Dilute HCl was added to destroy the excess hydride and the solution was made basic with NaOH, extracted with ether, and evaporated. Analysis by gc–ms and nmr showed that the main component (80%) was *N*-(*p*-aminobenzyl)-2,6-dimethylmorpholine. Small amounts of recovered **1** and *p*-aminothiobenz-2,6-dimethylmorpholide could also be identified.

Elemental analyses, mass and nmr spectra were in agreement with the given structures.

Acknowledgements

I wish to thank Professor J. Sandström and Dr. T. Liljefors for valuable discussions and the Swedish Natural Science Research Council for financial support.

1. A. O. Fulea and P. J. Krueger. Can. J. Chem. **53**, 3315 (1975).
2. I. O. Sutherland. *In* Annual reports on nmr spectroscopy. *Edited by* E. F. Mooney. Academic Press, London and New York. 1971. Vol. 4. p. 71.
3. S. Sternhell. *In* Dynamic nuclear magnetic resonance spectroscopy. *Edited by* L. M. Jackman and F. A. Cotton. Academic Press, New York, NY. 1975. p. 182.
4. A. Lidén, C. Roussel, T. Liljefors, M. Chanon, R. E. Carter, J. Metzger, and J. Sandström. J. Am. Chem. Soc. **98**, 2853 (1976) and references therein.
5. E. L. Eliel, N. L. Allinger, S. J. Angyal, and G. A. Morrison. Conformational analysis. Wiley, New York, NY. 1965. p. 53.
6. P. Le Cam and J. Sandström. Chem. Scripta, **1**, 65 (1971).
7. H. S. Gutowsky and C. H. Holm. J. Chem. Phys. **25**, 1228 (1956).
8. R. R. Fraser and K. Taymaz. Tetrahedron Lett. 4573 (1976).

Etude expérimentale et théorique des spectres de vibration des dérivés di- et trisubstitués de l'isothiazole[1]

GILBERT MILLE, MICHEL GUILIANO ET JACQUES CHOUTEAU

Université de Droit, d'Economie et des Sciences d'Aix-Marseille, Centre de Spectrographie Infrarouge, Centre st. Charles, 3, Place V. Hugo, F. 13331, Marseille, Cédex 3 France

Reçu le 28 octobre 1976

GILBERT MILLE, MICHEL GUILIANO et JACQUES CHOUTEAU. Can. J. Chem. **55**, 2302 (1977).

Les spectres infrarouges sous différents états (liquide, solution, vapeur) et les spectres Raman en phases condensées d'une série de dérivés di- et trisubstitués de l'isothiazole ont été analysés. Pour certains composés une étude de modes normaux de vibration a également été faite. Une attribution des modes fondamentaux de vibration de ces molécules est proposée et discutée.

GILBERT MILLE, MICHEL GUILIANO, and JACQUES CHOUTEAU. Can. J. Chem. **55**, 2302 (1977).

The infrared absorption spectra in different physical states (liquid, solution, vapor) and the Raman spectra in the liquid or solid state of di- and trisubstituted isothiazole derivatives have been analyzed. For some compounds a study of the normal vibrations has also been done. An assignment of the fundamental modes of vibration of these molecules is given and discussed.

Introduction

Une analyse expérimentale et théorique des spectres de vibration de l'isothiazole (1–3) et de ses dérivés monosubstitués en position 3, 4 et 5 (4–7) vient de faire l'objet de plusieurs mémoires. Dans le prolongement de ces recherches en série isothiazolique, nous nous sommes proposés d'étendre ce travail aux composés di- et trisubstitués de l'isothiazole $C_3NSRR'R''$ (R = H, CH_3, Cl, R′ = H, D, CH_3, CN, NO_2, Br, I et R″ = H, D, CH_3, CD_3, Cl, Br, I) (fig. 1) afin, d'une part de compléter l'attribution fragmentaire existant pour les diméthyl- et triméthyl-isothiazoles (8) et d'autre part, de voir dans quelle mesure les résultats expérimentaux et théoriques relatifs aux dérivés monosubstitués pouvaient être utilisés pour l'interprétation des spectres de vibration des molécules polysubstituées.

Les spectres infrarouges ainsi que les spectres Raman de 14 composés disubstitués et de huit dérivés trisubstitués ont donc été examinés. De plus nous avons pour sept molécules complété l'étude expérimentale par un calcul de modes normaux de vibration.

Les attributions que nous proposons sont limitées aux oscillations propres du cycle isothiazole et des liaisons CX, CY et CZ.[2] Nous ne donnons pas ici une analyse détaillée des vibrations propres aux substituants polyatomiques; celle-ci est indiquée ailleurs (9).

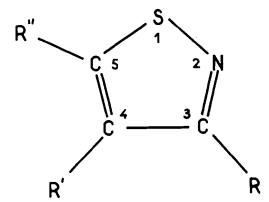

FIG. 1. Isothiazole $C_3NSRR'R''$.

Après le dénombrement et l'activité des vibrations nous donnerons les conditions expérimentales ainsi que les conditions de calcul. Nous indiquerons ensuite les résultats expérimentaux et théoriques qui seront discutés dans une dernière partie.

Dénombrement et activité des vibrations

Dans l'hypothèse où le squelette des dérivés di- et trisubstitués de l'isothiazole est plan, la

[1]Ce travail constitue une partie de la thèse de Doctorat d'Etat, n° d'ordre CNRS A0.10862, de M. Gilbert Mille, soutenue en 1975 à Marseille.

[2]X = R, Y = R′ et Z = R″, dans le cas où les substituants sont monoatomiques. X, Y, Z représente l'atome de carbone ou d'azote directement lié à l'hétérocycle dans le cas de substituants polyatomiques tels que CH_3, CD_3, CN et NO_2. Dans le cas des dérivés disubstitués X, Y ou Z = H, respectivement pour une substitution en position 4 et 5, 3 et 5 ou 3 et 4. Par convention X sera lié au carbone en position 3, Y au carbone en position 4 et Z au carbone en position 5.

symétrie est du type C_s. Dans ce groupe de symétrie les 18 vibrations fondamentales toutes actives en infrarouge et en Raman peuvent se décomposer en 13 mouvements ($7\omega + 1\nu CX + 1\nu CY + 1\nu CZ + 1\delta CX + 1\delta CY + 1\delta CZ$) de symétrie A' et 5 oscillations ($2\Gamma + 1\gamma CX + 1\gamma CY + 1\gamma CZ$) de type A''.[3]

Les vibrations de symétrie A' et A'' doivent pouvoir se caractériser de la même manière que dans les spectres de l'isothiazole (1). En particulier le grand axe d'inertie de ces molécules devant, si elles ont une structure plane, être normal au plan du noyau, on peut s'attendre à ce que dans les spectres infrarouges des composés à l'état vapeur les oscillations de classe A' et A'' donnent lieu à des bandes de vibration–rotation de type A, B ou hybride $A + B$, d'une part et de type C, d'autre part. Les séparations $\Delta\nu_{RP}$ des enveloppes de type A, B ou C doivent évidemment différer des écarts $\Delta\nu_{RP}$ des bandes de même type de l'isothiazole (1). De même que pour l'isothiazole, on doit trouver dans les spectres Raman des dérivés isothiazoliques des bandes de diffusion généralement fortes et polarisées pour les vibrations de symétrie A' et des bandes faibles et dépolarisées pour les modes de classe A''.

Conditions expérimentales

Synthèse

La synthèse des différents composés étudiés a été discutée ailleurs (8, 10).

Spectres infrarouges

Les spectres infrarouges ont été enregistrés sur spectrographes Perkin-Elmer, modèles 125 et 225.

Les composés solides ont été examinés sous forme de pastilles constituées de 2 mg de produit inclus dans 200 mg de bromure de potassium.

Les spectres infrarouges des composés à l'état vapeur ont été réalisés avec une cellule à gaz chauffante Perkin-Elmer de 5 cm d'épaisseur à fenêtres de bromure de potassium ou d'iodure de césium.

A l'état dissous les concentrations étaient voisines de 0.2 *M*. Le tétrachlorure de carbone a été employé dans les régions de 3000 cm^{-1} et de 1500 à 1300 cm^{-1}, le tétrachlorure d'éthylène, le sulfure de carbone et le cyclohexane ont respectivement été utilisés entre 2000 et 1400, 1350 et 450 et entre 450 et 200 cm^{-1}. Les coefficients d'extinction molaire apparents ont été mesurés aux maximums des bandes d'absorption.

Spectres Raman

Les échantillons à l'état liquide ou solide ont été examinés dans des tubes capillaires, avec un spectrographe Raman Coderg, type PH 1, équipé d'un laser He–Ne de 100 mW émettant à 6328 Å. Les facteurs de dépolarisation ont été corrigés d'après la méthode décrite par Bribes et Gaufres (11). Les intensités ont été chiffrées de 0 à 10 par comparaison avec la raie la plus forte de chacun des spectres. Dans les cas où il n'a pas été possible d'obtenir les spectres de diffusion de 3200 à 200 cm^{-1} sans changer les conditions d'enregistrement les intensités des raies Raman ont été estimées à l'aide des lettres F (forte); m (moyenne); f (faible) et ff (très faible). Pour les spectres infrarouges et Raman l'incertitude sur les fréquences est inférieure à 2 cm^{-1} dans la région de 4000 à 1000 cm^{-1} et d'environ 1 cm^{-1} de 1000 à 200 cm^{-1}.

Conditions de calcul

Le calcul des modes normaux de vibration des dérivés di- et trisubstitués de l'isothiazole a été entrepris par la méthode classique de Wilson *et al.* (12) dans l'hypothèse d'un champ de forces de valence du type GVFF. Le programme de calcul utilisé est celui écrit par Schachtschneider (13).

Structure géométrique

Les paramètres structuraux choisis pour les dérivés di- ou trisubstitués de l'isothiazole sont ceux adoptés pour les composés monosubstitués correspondants (7).

Coordonnées internes

Nous avons conservé les coordonnées internes[4] déjà utilisées pour l'isothiazole (3) et ses dérivés monosubstitués (7), pour décrire les différentes vibrations de symétrie A' (fig. 2).

Dans le cas des molécules méthylées, nous avons considéré le ou les substituants méthyle comme des groupements ponctuels de masse $M = 15.035$ g.

Champ de forces

L'analyse vibrationnelle a été menée en admettant qu'en première approximation le champ de forces des dérivés di- et trisubstitués de l'isothiazole résultait de la superposition des champs de forces trouvés pour les dérivés monosubstitués correspondants (7). Un premier calcul effectué dans ces conditions a donné des résultats très satisfaisants. Néanmoins pour améliorer certains écarts entre fréquences observées et fréquences calculées, nous avons introduit des constantes d'interaction du type: $f_{r_i r_{i+1}}$ ($i = 3$,

[3] ν, δ, γ désignant respectivement les vibrations de valence, de déformation dans le plan et hors du plan; ω et Γ les vibrations de déformation du noyau respectivement dans et hors du plan (*cf.* ref 4).

[4] Comme pour l'isothiazole et ses dérivés monosubstitués (3, 7) nous avons adopté pour les déformations angulaires des vibrateurs CX, CY ou CZ des coordonnées de groupe du type: $\beta_i = (\psi'_i - \psi_i)/\sqrt{2}$.

TABLEAU 1. Constantes de force* relatives aux vibrateurs CX, CY, CZ pour les dérivés di- et trisubstitués de l'isothiazole

R, R′, R″										
3	4	5	F_{r_3}	F_{r_4}	F_{r_5}	F_{β_3}	F_{β_4}	F_{β_5}	$f_{r_i r_{i+1}}$	$f_{\beta_i\beta_H}$
CH_3	CH_3	H	4.30	4.50	5.25	0.64	0.54	0.39	−0.49	—
CH_3	Br	H	4.30	3.17	5.25	0.64	0.56	0.39	−0.29	—
CH_3	H	CH_3	4.30	5.18	4.60	0.64	0.375	0.55	—	0.104
CH_3	H	Br	4.30	5.18	3.31	0.64	0.375	0.52	—	0.112
H	CH_3	CH_3	5.08	4.50	4.60	0.50	0.54	0.55	−0.34	
CH_3	CH_3	CH_3	4.30	4.50	4.60	0.64	0.54	0.55	−0.49 −0.34	—
Cl	CH_3	Cl	4.10	4.50	3.86	0.80	0.54	0.55	−0.29	—

*Elongation des liaisons (F_{r_i}) en 10^5 dyn cm^{-1}. Déformation des angles (F_{β_i}) en 10^{-11} erg rad^{-2}. Interactions (f) en 10^{-3} dyn rad^{-1}.

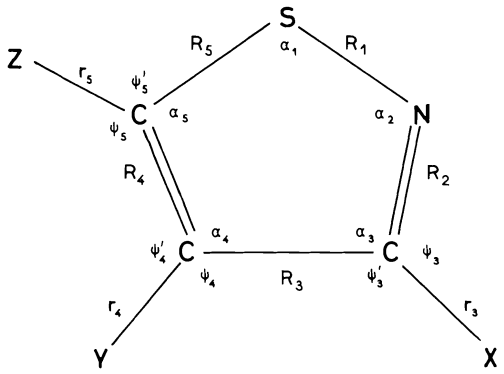

FIG. 2. Les différentes vibrations de symétrie A'.

4 ou 5) lorsque deux ou trois substituants étaient voisins et du type $f_{\beta_i\beta_H}$ (i = 3 et 5) dans le cas des dérivés disubstitués en position 3, 5. Nous indiquons dans le tableau 1 uniquement les constantes de force relatives aux vibrateurs CX, CY et CZ. Toutes les autres constantes de force concernant plus particulièrement le cycle sont identiques à celles de l'isothiazole et de ses dérivés monosubstitués et sont mentionnées dans les réfs 3 et 7.

Résultats expérimentaux et théoriques

Dans le tableau 2[5] sont indiquées les fréquences infrarouges, enregistrées à l'état dissous, des vibrations (ν, δ et γ) des liaisons CH (ou CD) des composés disubstitués de l'isothiazole. Le tableau 3[5] renferme sous forme de suites les fréquences infrarouges et Raman des vibrations fondamentales des hétérocycles C_3NSXYZ.[6] Dans ces deux tableaux les fréquences infrarouges mesurées à l'état dissous sont suivies du coefficient d'extinction molaire et lorsque les composés ont été examinés à l'état de vapeur elles sont précédées de la symétrie de vibration rotation (A, B ou C) des bandes. L'intensité des raies de diffusion, chiffrée de 0 à 10, succède aux fréquences Raman des composés en phase condensée.

Les résultats théoriques obtenus à partir du champ de forces défini précédemment (tableau 1 et réf. 3) sont comparés aux données expérimentales dans le cas des diméthyl isothiazoles (tableau 4), des méthyl-3 bromo-4 et méthyl-3 bromo-5 isothiazoles (tableau 5) des triméthyl 3,4,5 isothiazole et dichloro-3,5 méthyl-4 isothiazole (tableau 6). Dans ces tableaux sont indiquées également les attributions qu'il est possible de formuler d'après l'analyse de la distribution d'énergie potentielle (9).

Discussion des résultats

Nous examinerons en premier lieu, les vibrations des liaisons CH ou CD, puis celles de noyau en distinguant chaque fois les vibrations de type A' de celles de symétrie A''.

I. Vibrations des liaisons CH ou CD

(1) Vibrations de symétrie A′

(a) Vibrations de valence ν(CH ou CD)

Trois séries de fréquences vers 3102 ± 10, 3088 ± 7 et 3048 ± 11 cm^{-1} peuvent être constituées en examinant respectivement les spectres

[5]On peut obtenir les tableaux 2 et 3 à un prix nominal, en s'adressant au Dépôt de données non publiées, ICIST, Conseil national de recherches du Canada, Ottawa, Canada K1A 0S2.

[6]Les fréquences des maximums reliés à des oscillations des substituants ou à des vibrations harmoniques ou de combinaison, sont indiquées pour chacun des composés dans la réf 9.

TABLEAU 4. Diméthylisothiazoles: fréquences et attributions. L'attribution a été faite à partir de la distribution d'énergie potentielle (9)

Diméthyl-3,4 isothiazole			Diméthyl-3,5 isothiazole			Diméthyl-4,5 isothiazole		
Fréq. obs.	Fréq. calc.	Attributions	Fréq. obs.	Fréq. calc.	Attributions	Fréq. obs.	Fréq. calc.	Attributions
3092	3109	νC_5H	3085	3090	νC_4H	3039	3060	νC_3H
1537	1533	νN (νC=C)	1539	1532	νN (νC=C)	1556	1579	νN (νC=C)
1417	1416	νN (νC=N)	1402	1419	νN (νC=N)	1412	1402	νN (νC=N)
1347	1362	νN (νC—C)	1358	1328	νN (νC—C)	1325	1341	νN (νC—C)
1188	1136	δC_5H	1203	1190	νC—C*+νC—S	1229	1224	δC_3H
1116	1114	νC—C*+δN	1130	1097	δC_4H	1179	1167	νC—C*+νC—S
853	860	νN (νC—S)	956	932	νC—C*+δN	978	973	νC—C*+δN
817	841	νN (νS—N)	813	834	νN (νS—N)	792	801	νN (νS—N)
768	757	νC—C*+δN	700	698	νN+δN	725	729	νN+δN
588	572	νC—C*+δN	572	564	νC—C*+δN	630	604	νC—C*+νN
563	544	νC—C*+δN	559	556	νC—C*+δN	536	517	νC—C*+δN
392	397	δC—C*	367	359	δC—C*	355	377	δC—C*
268	244	δC—C*	254	263	δC—C*	242	239	δC—C*

C atome de carbone du groupement méthyle considéré comme ponctuel.

TABLEAU 5. Méthyl-3 bromo-4 et méthyl-3 bromo-5 isothiazoles. Fréquences et attributions (voir légende tableau 4)

Méthyl-3 bromo-4 isothiazole			Méthyl-3 bromo-5 isothiazole		
Fréq. obs.	Fréq. calc.	Attributions	Fréq. obs.	Fréq. calc.	Attributions
3112	3109	νC_5H	3092	3090	νC_4H
1500	1479	νN(νC=C)	1514	1491	νN(νC=C)
1395	1407	νN(νC=N)	1386	1406	νN(νC=N)
1336	1341	νN(νC—C)	1354	1323	νN(νC—C)
1163	1129	δC_5H	1170	1153	δC_4H
986	989	νC—C*+νC—Br+δN	975	968	νN+δN
845	858	νN(νC—S)	920	918	νC—C*+νC—Br
813	833	νN(νS—N)	807	833	νN(νS—N)
716	706	δN	699	682	δN+νN
582	568	νC—C*+δN	574	560	νC—C*+δN
400	407	δC—C*	382	370	δC—C*
301	297	νC—Br+δN	293	292	νC—Br
191	164	δC—Br	182	170	δC—Br

infrarouges des dérivés de l'isothiazole disubstitués en −3,4, −3,5 et −4,5. Les maximums composant ces suites donnent en Raman des raies faibles mais polarisées. Nous les relions respectivement aux vibrations νC_5H, νC_4H et νC_3H (tableau 2). On peut remarquer que les positions des modes νCH des composés disubstitués sont très proches de celles de l'isothiazole (1). La présence de substituants en position 3,4, 3,5 ou 4,5 a donc peu d'influence sur les mouvements νCH.

Dans le spectre infrarouge du diméthyl-3,5 deutério-4 isothiazole, on observe aucun maximum au-dessus de 3000 cm^{-1}, mais une absorption à 2287 cm^{-1} devant très certainement résulter du mode νC_5D.

(b) Vibrations de déformation δ(CH ou CD)

La fréquence de δC_3H a été situé à 1236 cm^{-1} dans l'isothiazole (1). Par analogie et en accord avec les résultats théoriques (tableau 4 et 5) nous relions les sommets infrarouges vers 1228 cm^{-1} relevés dans les spectres des composés disubstitués en position 4,5 à des mouvements analogues.

Dans les spectres de tous les dérivés substitués en 3,4 ou en 3,5, on observe entre 1200 et 1100 cm^{-1} une absorption forte pour les composés

TABLEAU 6. Dichloro-3,5 méthyl-4 et triméthyl-3,4,5 isothiazoles. Fréquences et attributions (voir légende tableau 4)

Dichloro-3-5 méthyl-4 isothiazole			Triméthyl-3,4,5 isothiazole		
Fréq. obs.	Fréq. calc.	Attributions	Fréq. obs.	Fréq. calc.	Attributions
1539	1543	νN(νC=C)	1560	1566	νN(νC=C)
1365	1382	νN(νC=N)	1418	1413	νN(νC=N)
1338	1356	νN(νC—C)	1369	1381	νN(νC—C)
1096	1103	δN+νC—C*+νC—Cl	1214	1214	νN+δN+νC—C*
979	989	νN+νC—Cl	1114	1065	νN+νC—C*
812	832	νN+(νS—N)	819	856	νN+νC—C*
792	803	νCC*+νCCl+δN	804	822	νN+δN
596	587	νCC*+νCCl+δN	633	622	νC—C*+νN+δN
508	503	δN+νC—Cl	585	567	νC—C*+δN
400	387	νC—Cl+δN	527	515	νC—C*+δN
362	371	δC—Cl+δC—C*	414	425	δC—C*
235	207	δC—C*+δC—Cl	265	259	δC—C*
194	171	δC—Cl	255	235	δC—C*

disubstitués en position 3 et 4 et moyenne pour ceux disubstitués en 3,5 (tableau 2). Ces bandes infrarouges disparaissant dans les spectres des molécules trisubstituées ou dans celui du diméthyl-3,5 deutério-4 isothiazole, doivent donc être rattachées à des vibrations δCH (tableau 2).

On peut noter que les fréquences des modes δC_4H ou δC_5H des dérivés disubstitués sont plus élevées que celles des composés monosubstitués correspondants, alors que la position de la bande δC_3H reste inchangée quel que soit le degré de substitution. Enfin on peut également remarquer que, pour un même type de substitution, la position des bandes dues à des oscillations δC_4H ou δC_5H diffère suivant la nature du substituant (tableau 2). Nous situons la fréquence de δC_4D du diméthyl-3,5 deutério-4 isothiazole à 840 cm^{-1} en raison de l'absence de maximum proche de cette fréquence dans les spectres infrarouge et Raman du diméthyl-3,5 isothiazole.

(2) Vibrations de symétrie A''

Vibrations de déformation γ(CH ou CD)

Les spectres infrarouges des méthyl-3 bromo-4, diméthyl-3,5 et méthyl-3 bromo-5 isothiazoles à l'état de vapeur (9) présentent respectivement à 776, 818 et 819 cm^{-1} des structures de vibration–rotation de type *C* qui doivent résulter d'oscillations γCH de symétrie *A''*. Nous rattachons donc les maximums rangés dans les suites vers 800 ± 21 et 807 ± 14 cm^{-1} respectivement aux mouvements γC_5H et γC_4H des dérivés disubstitués en position 3,4 et 3,5.

Par analogie avec l'attribution proposée pour le mouvement γC_3H du dideutério-4,5 isothiazole (1), on peut situer ce même mode dans les dérivés de l'isothiazole disubstitués en 4,5 vers 882 cm^{-1} (tableau 2). Notons que, dans les spectres Raman de ces composés, on n'observe aucune bande de diffusion dans cette région.

Remarquons enfin que les attributions antérieures proposées pour les mouvements γCH des diméthylisothiazoles (8) sont maintenues.

L'enveloppe de la bande de type *C* observée à 699 cm^{-1} uniquement dans le spectre infrarouge du diméthyl-3,5 deutério-4 isothiazole à l'état vapeur (9) indique que la vibration γC_4D doit être attribuée à cette fréquence pour ce composé. L'accord entre la valeur des produits de Teller–Redlich expérimental et théorique est satisfaisant pour les vibrations de type *A''* (9).

II. Vibrations des squelettes C_3NSXYZ

(1) Vibrations de symétrie A'

Nous examinerons les vibrations de noyau et de valence νC(X,Y ou Z), puis celles de déformation δC(X,Y ou Z).

(a) Vibrations de noyau et de valence νC(X, Y ou Z)

Les suites que nous allons discuter peuvent se décomposer comme pour les dérivés monosubstitués de l'isothiazole, en suites relativement fixes en position: I, II, III, V et VII et en suites variables suivant la nature et la position du substituant: IV, VI, VIII, VIII' et VIII''. Nous examinerons en premier lieu, les fréquences rangées dans les suites fixes, puis celles faisant l'objet des suites variables.

Suites fixes

Comme pour les dérivés monosubstitués de l'isothiazole, les cinq suites I, II, III, V et VII peuvent être rapprochées des vibrations ω_1, ω_2, ω_3, ω_5 et ω_7 de l'isothiazole. Pour les composés disubstitués en position 3,4, on retrouve une suite vers 840 cm^{-1} (tableau 3) pouvant être reliée à un mode de fréquence voisine du mouvement ω_4 de l'isothiazole. L'existence de cette suite avait déjà été mentionnée pour les dérivés monosubstitués soit en 3, soit en 4 (5, 7). Dans chacune des suites les fréquences les plus élevées sont observées dans les spectres des diméthyl et triméthyl isothiazoles et décroissent lorsque la masse du substituant augmente (tableau 3):

$$\nu_{\omega_i CH_3} > \nu_{\omega_i Cl} > \nu_{\omega_i NO_2} > \nu_{\omega_i Br} > \nu_{\omega_i I} \quad (i = 1,2,3,5 \text{ et } 7).$$

Comme pour les dérivés monosubstitués, ce sont les suites II et V qui regroupent les fréquences s'écartant respectivement le moins des fréquences des modes ω_2 à 1390 et ω_5 à 815 cm^{-1} de l'isothiazole. Dans chaque suite, les maximums les moins intenses sont relevés pour les molécules di- ou triméthylées. L'intensité des absorptions augmente généralement lorsqu'on remplace un groupement méthyle par un halogène (Cl, Br ou I) ou un groupement nitro (tableau 3). En Raman, les raies de diffusion correspondant aux maximums rangés dans les diverses suites sont très souvent assez intenses à l'exception toutefois, de celles faisant l'objet de la suite I qui sont généralement faibles et même parfois absentes. Comme pour les dérivés monosubstitués, certains modes de vibration mettent en jeu plus particulièrement, un vibrateur. C'est notamment le cas pour les trois oscillations entre 1500 et 1300 cm^{-1} et de la vibration vers 800 cm^{-1} qui font respectivement intervenir les élongations des liaisons C=C, C=N, C—C et S—N (*cf.* tableaux 4–6).

Les maximums formant la suite VII ont des fréquences plus élevées que ceux rangés dans la suite ayant la même notation pour les dérivés monosubstitués. Pour le diméthyl-3,4 isothiazole et les dérivés trisubstitués de l'isothiazole, les fréquences que nous avons choisies pour la suite VII sont particulièrement élevées. Cependant le fait qu'on observe en Raman vers ces fréquences une bande de diffusion forte et polarisée ne peut laisser de doute au sujet de cette interprétation. De plus, les résultats des calculs de modes normaux de vibration relatifs aux dérivés disubstitués indiquent que la fréquence la plus élevée de la suite VII est effectivement trouvée pour le diméthyl-3,4 isothiazole (tableau 4). Cette élévation de fréquence de la vibration de noyau ω_7 pourrait résulter d'un couplage partiel de cette vibration avec les oscillations $\nu C(X,Y,Z)$. Les résultats des calculs de modes normaux relatifs au triméthyl-3,4,5 isothiazole et au dichloro-3,5 méthyl-4 isothiazole sont en faveur de cette hypothèse (tableau 6).

Notons enfin, que l'attribution que nous avions proposée antérieurement pour les vibrations ω_1, ω_2, ω_3 et ω_5 des diméthylisothiazoles et du triméthylisothiazole est conservée (8).

Suites variables

Par analogie avec les composés de l'isothiazole monosubstitués en 3, 4 ou 5, on devrait retrouver, en analysant les spectres infrarouges et Raman des dérivés de l'isothiazole disubstitués en 3,5 ou 4,5, un premier couplage entre la vibration ω_6 et l'oscillation νC_3X ou νC_4Y et un deuxième couplage entre le mode ω_4 et le mouvement de valence νC_5Z.

Effectivement, les spectres infrarouges et Raman des dérivés disubstitués en position 3,5 ou 4,5 permettent de constituer quatre suites de fréquences variables: IV, VI, VIII et VIII′ qui peuvent s'interpréter suivant les déductions faites de l'analyse des spectres infrarouges et Raman des molécules monosubstituées (4–6). Les fréquences rangées dans ces suites sont proches de celles groupées dans les suites IV, VI et VIII des dérivés monosubstitués. Notons enfin, que pour le dideutério-4,5 isothiazole, où les fréquences νC_4D et νC_5D sont trop élevées par rapport à celles des vibrations de squelette pour que le couplage puisse avoir lieu, on retrouve, pour les mouvements de noyau ω_4 et ω_6, des fréquences proches de celles correspondantes dans l'isothiazole (1).

Les remarques relatives aux vibrations couplées dans les dérivés monosubstitués s'appliquant parfaitement aux composés disubstitués en 3,5 et 4,5, on devrait pour les molécules disubstituées en position 3,4 observer une interaction entre le mouvement de noyau ω_6 et les oscillations de valence νC_3X et νC_4Y. Nous avons déjà constaté pour ces dérivés l'existence de la suite IV formée de maximums ayant des positions voisines du mode ω_4 de l'isothiazole ou de la suite ayant la même notation dans les composés de l'isothiazole monosubstitués en 3 ou 4. De plus, l'examen des spectres infrarouges et Raman de ces hétéro-

cycles disubstitués en 3,4 révèle la présence de trois suites, l'une entre 1120 et 975 cm^{-1} et les deux autres entre 600 et 250 cm^{-1}. L'existence de ces suites ainsi que l'absence de maximum à des fréquences où l'on pourrait attendre les mouvements ω_6 et νC_3X et νC_4Y purs, indiquent effectivement que les résultats déduits de l'étude des dérivés monosubstitués en position 3 ou 4 sont totalement "transférables" aux composés disubstitués en 3,4. Comme dans les dérivés monosubstitués, la suite VI est formée d'absorptions infrarouges moyennes et de raies de diffusion faibles et les suites VIII et VIII′ regroupent des bandes faibles en infrarouge, mais souvent intenses en Raman. On peut également constater (tableau 3) que les fréquences de la suite VI pour un dérivé disubstitué, sont généralement plus élevées que celles choisies pour les composés monosubstitués correspondants. Notons que les résultats des calculs de modes normaux sont en parfait accord avec cette remarque. Ces calculs indiquent en outre que les couplages mettent principalement en jeu les oscillations de valence νC_3X ou νC_4Y et une vibration de déformation angulaire du noyau (δN) (tableaux 4 et 5). Si pour les composés trisubstitués il existe comme pour les dérivés mono- ou disubstitués de l'isothiazole des vibrations couplées on doit pouvoir former cinq suites de fréquences variables suivant la nature et la place du substituant. Effectivement cinq suites, notées IV, VI, VIII, VIII′ et VIII″ peuvent être décelées en examinant les spectres infrarouges et Raman des dérivés trisubstitués de l'isothiazole (tableau 3). Par analogie avec les composés mono- et disubstitués, deux de ces suites (IV et VIII″) résultent du couplage des mouvements ω_4 et νC_5Z et les trois autres (VI, VIII et VIII′) du couplage des oscillations ω_6, νC_3X et νC_4Y.

(b) Vibrations de déformation $\delta C(X,$ Y ou Z)

Les fréquences que nous proposons pour ces vibrations de type *A′* font l'objet de la suite notée $\delta C(X,$ Y ou Z) du tableau 3. Le choix des maximums de cette suite a été dicté par l'examen des spectres Raman au-dessous de 440 cm^{-1} dans lesquels on observe généralement deux bandes assez fortes et polarisées, puis par les fréquences théoriques calculées pour certains composés et enfin, par des comparaisons avec les fréquences reliées à des mouvements analogues dans les isothiazoles monosubstitués correspondants.

La fréquence δCI du méthyl-3 iodo-4 isothiazole doit vraisemblablement être située au-dessous de 200 cm^{-1}. N'ayant pas enregistré le spectre Raman de ce composé, il n'est pas possible de localiser cette vibration. Le méthyl-3 chloro-5 isothiazole n'ayant été examiné qu'à l'état liquide au-dessus de 400 cm^{-1}, nous n'avons pu proposer une attribution pour les oscillations δCC et δCCl de cette molécule.

(2) Vibrations de symétrie A″

Les vibrations de noyau et les mouvements $\gamma C(X,Y,Z)$ seront successivement traités.

(a) Vibrations de noyau

Les fréquences formant la suite IX peuvent être rapprochées de la vibration de noyau Γ_1 de l'isothiazole. Dans les spectres Raman, aucune raie n'apparaît à ces fréquences. Alors que pour le diméthyl-4,5 isothiazole les fréquences des modes ω_8 et Γ_1 étaient très proches, on ne relève pour le méthyl-4 trideutériométhyl-5 isothiazole qu'une seule absorption à 604 cm^{-1} ayant une intensité trop forte pour résulter uniquement du mode ω_8. L'intensité élevée de cette bande peut s'expliquer en admettant que les mouvements ω_8 et Γ_1 sont de même fréquence.

Nous relions à une vibration analogue à l'oscillation Γ_2 de l'isothiazole, les maximums de la suite X qui, lorsqu'ils apparaissent en Raman donnent des raies faibles et dépolarisées et qui possèdent, dans les spectres des composés examinés à l'état vapeur des structures de vibration–rotation de type *C*.

(b) Vibrations de déformation $\gamma C(X,Y,Z)$

Entre 400 et 200 cm^{-1} certains maximums ont déjà été reliés à des mouvements $\delta C(X,Y,Z)$. Nous rattachons dans les spectres des composés étudiés jusqu'à 200 cm^{-1}, les autres pics à des oscillations $\gamma C(X,Y,Z)$ par analogie avec les attributions faites pour des mouvements analogues dans les composés monosubstitués correspondants (4, 5). Les fréquences inférieures à 200 cm^{-1} que nous avons attribuées à des modes $\gamma C(X,Y,Z)$ ont été observées uniquement en diffusion. Notons enfin que certains maximums de la suite $\gamma C(X,Y,Z)$ peuvent résulter simultanément de modes δ et $\gamma C(X,Y,Z)$.

Conclusion

La validité de la "transférabilité" du champ de forces de l'isothiazole aux dérivés monosubstitués que nous avions montré dans le précédent mémoire (7) est à nouveau confirmée par notre

étude des dérivés di- et trisubstitués de l'isothiazole. Cette hypothèse est donc raisonnable et justifie par ailleurs la validité du champ de forces proposé. La nature des mouvements a pu être discutée grâce à l'analyse des distributions d'énergie potentielle. La diversité des composés examinés a permis de suivre l'influence de la nature, de la position et du nombre des substituants sur les vibrations fondamentales du cycle isothiazole. Pour les dérivés di- et trisubstitués de l'isothiazole le calcul des modes normaux de vibration a permis, comme pour les composés monosubstitués, d'apporter une justification et un complément théoriques à l'ensemble des attributions formulées d'après les résultats expérimentaux infrarouges et Raman. On peut noter que cette analyse vibrationnelle a été conduite en utilisant un nombre assez réduit de paramètres et que surtout, ces paramètres permettent de rendre compte de façon très satisfaisante des modes de vibration d'un nombre important de dérivés mono-, di- et trisubstitués de l'isothiazole.

Il est, enfin, remarquable de constater l'existence d'une loi additive, permettant à partir du champ de forces des molécules monosubstituées de préciser correctement la fréquence et la nature des vibrations fondamentales des composés di- et trisubstitués de l'isothiazole.

Remerciements

Nous remercions vivement MM. J. C. Poite et C. Perichaud d'avoir mis gracieusement à notre disposition l'ensemble des produits examinés.

1. J. L. Meyer, G. Davidovics, J. Chouteau, J. C. Poite et J. Roggero. Can. J. Chem. **49**, 2254 (1971).
2. G. Mille, S. Senez et J. Chouteau. C.R. Acad. Sci. Ser. B, **279**, 211 (1974).
3. G. Mille, J. Metzger, C. Pouchan et M. Chaillet. Spectrochim. Acta Part A, **31**, 1115 (1975).
4. G. Mille, G. Davidovics, J. C. Poite et M. Guiliano. C.R. Acad. Sci. **276**, 31 (1973).
5. G. Mille, J. Metzger et J. Chouteau. J. Chim. Phys. **72**, 31 (1975).
6. G. Mille, J. C. Poite, J. Chouteau et J. Metzger. Can. J. Chem. **53**, 1642 (1975).
7. G. Mille, J. Chouteau, T. Avignon et L. Bouscasse. Can. J. Chem. **54**, 3850 (1976).
8. A. Perichaud, J. C. Poite, G. Mille et J. Roggero. Bull. Soc. Chim. Fr. 3830 (1972).
9. G. Mille. Thèse Sciences, CNRS AO.10862, Marseille, France. 1975.
10. J. C. Poite. Thèse Sciences, CNRS AO.7292, Marseille, France. 1972.
11. J. L. Bribes et R. Gaufres. J. Chim. Phys. **67**, 1168 (1970).
12. E. B. Wilson Jr., J. C. Decius et P. Cross. Molecular vibrations. McGraw-Hill, New York, NY. 1955.
13. J. H. Schachtschneider. Shell Report No. 231-64.

Degenerate rearrangements in solvolytic studies with tri-*p*-tolylvinyl-2-^{13}C bromide

CHOI CHUCK LEE, ANTHONY J. PAINE, AND ERIC C. F. KO

Department of Chemistry and Chemical Engineering, University of Saskatchewan, Saskatoon, Sask., Canada S7N 0W0

Received October 12, 1976

CHOI CHUCK LEE, ANTHONY J. PAINE, and ERIC C. F. KO. Can. J. Chem. **55**, 2310 (1977).

The acetolysis in the presence of AgOAc of tri-*p*-tolylvinyl-2-^{13}C bromide (**3**-Br-2-^{13}C) gave about 14% scrambling of the label from C-2 to C-1 due to degenerate 1,2-tolyl shifts. This value is compared with the 7 and 20% scramblings previously observed for similar reactions with triphenylvinyl-2-^{13}C and trianisylvinyl-2-^{13}C bromides, and their mechanistic implications are discussed. The trifluoroacetolysis of **3**-Br-2-^{13}C in the presence of CF_3COOAg or CF_3COONa resulted in about 47% scrambling. In the absence of any added salt, the scrambling was found to increase with reaction time and in addition, solvent isotope effects of 1.6 and 2.6, respectively, were observed for $k_{CF_3COOH}/k_{CF_3COOD}$ at 100°C with or without added CF_3COONa. The role of electrophilic addition–elimination and the processes leading to the isotopic scrambling in the reaction with CF_3COOH, with or without added salt, are discussed.

CHOI CHUCK LEE, ANTHONY J. PAINE et ERIC C. F. KO. Can. J. Chem. **55**, 2310 (1977).

A cause de déplacements 1,2 dégénérés des groupes tolyles, l'acétolyse en présence de AgOAc, du bromure de tri-*p*-tolylvinyl-2-^{13}C (**3**-Br-2-^{13}C) conduit à une transposition d'environ 14% du marqueur de la position C-2 vers C-1. On compare cette valeur avec les valeurs de 7 et 20% observées antérieurement pour des réactions similaires des bromures de triphénylvinyl-2-^{13}C et de trianisylvinyl-2-^{13}C et on discute de leurs implications mécanistiques. La trifluoroacétolyse du **3**-Br-2-^{13}C en présence de $AgOCOCF_3$ ou de $NaOCOCF_3$ conduit à environ 47% de transposition. Lorsqu'il n'y a aucun sel d'additionné, on a trouvé que les transpositions augmentent avec le temps de réaction et de plus on a observé respectivement des effets isotopiques de solvant de 1.6 et 2.6 pour $k_{CF_3COOH}/k_{CF_3COOD}$ à 100°C avec ou sans addition de $NaOCOCF_3$. On discute du rôle du mécanisme d'addition–élimination électrophile et des processus conduisant aux mélanges isotopiques dans la réaction de CF_3COOH avec ou sans addition de sel.

[Traduit par le journal]

Reactions of vinyl cations, including rearrangements that gave rise to more stable from less stable cations via 1,2-shifts, have been extensively reviewed (1–3). Degenerate rearrangements arising from 1,2-aryl shifts across the double bond in a number of labeled triarylvinyl cations, with various combinations of phenyl and/or *p*-anisyl as the aryl groups, have been studied in this laboratory using the ^{14}C tracer technique or ^{13}C-labeling coupled with ^{13}C nmr analysis (4–8), and by Rappoport and coworkers using ^{2}H as label coupled with analysis by ^{1}H nmr and mass spectrometry (9–11). The reaction of triphenylvinyl-2-^{13}C bromide (**1**-Br-2-^{13}C) with HOAc in the presence of AgOAc was found to give 6–7% scrambling of the ^{13}C label from C-2 to C-1 (5), while similar studies with trianisylvinyl-2-^{13}C bromide (**2**-Br-2-^{13}C) gave 20 and 50% isotopic scrambling, respectively, for the acetolysis in the presence of AgOAc and trifluoroacetolysis in the presence of CF_3COOAg (6). As an extension of such studies, isotopic scramblings arising from 1,2-tolyl shifts in solvolytic reactions with tri-*p*-tolylvinyl-2-^{13}C bromide (**3**-Br-2-^{13}C) were investigated.

Analogous to the preparation of **1**-Br-2-^{13}C and **2**-Br-2-^{13}C (5, 6), **3**-Br-2-^{13}C was prepared by the following series of reactions:

$$\mathrm{TolCH_2MgCl} \xrightarrow{^{13}CO_2} \mathrm{TolCH_2{}^{13}COOH} \xrightarrow[H^+]{\mathrm{EtOH}}$$

$$\mathrm{TolCH_2{}^{13}COOEt} \xrightarrow{\mathrm{TolMgBr}} \mathrm{TolCH_2{}^{13}C(OH)(Tol)_2} + \mathrm{TolCH{=}{}^{13}C(Tol)_2}$$

$$\xrightarrow[\mathrm{HOAc}]{Br_2} \mathrm{(Tol)_2{}^{13}C{=}CBrTol}$$

3-Br-2-^{13}C

In the initial experiments, the solvolysis of **3**-Br-2-^{13}C was carried out in HOAc containing 1.1 equiv. of AgOAc or in CF_3COOH containing 1.1 equiv. of CF_3COOAg. The product obtained, **3**-OAc-*x*-^{13}C or **3**-$OOCCF_3$-*x*-^{13}C, was reduced twice successively with $LiAlH_4$ (6) to give 1,2,2-tri-*p*-tolylethanol-*x*-^{13}C (**4**-*x*-^{13}C), the ^{13}C nmr spectrum of which was utilized for the determination of the extent of isotopic scrambling from C-2 to C-1. The method, based on the measurement of relative intensities of the C-1 and C-2 absorptions using the CH_3 absorption containing ^{13}C in its natural abundance as an internal

reference standard, is the same as that described previously in the study with **2**-Br-*2*-^{13}C in which the CH_3O absorption served as internal reference standard (6). The ^{1}H-decoupled ^{13}C nmr spectrum of unenriched **4** and the chemical shifts are given in Fig. 1*A* and Table 1. A typical spectrum for **4**-*x*-^{13}C derived from one of the solvolysis experiments is shown in Fig. 1*B*. The relative intensities and the calculated extents of ^{13}C scrambling from C-2 to C-1 are summarized in Table 2. An illustration of the calculations is given in the Experimental section.

The reaction of **3**-Br-*2*-^{13}C with HOAc–AgOAc gave rise to 13–14% isotopic scrambling, a value that is intermediate between the 7 and 20% scrambling found, respectively, in similar reactions with triphenylvinyl-*2*-^{13}C bromide (**1**-Br-*2*-^{13}C) (5) and trianisylvinyl-*2*-^{13}C bromide (**2**-Br-*2*-^{13}C) (6). The relative extents of scrambling arising from degenerate 1,2-aryl shifts in reactions with HOAc–AgOAc for **1**-Br-*2*-^{13}C:**3**-Br-*2*-^{13}C:**2**-Br-*2*-^{13}C would be 7:14:20 or approximately 1:2:3. Another comparison of the scrambling data from the reactions in HOAc–AgOAc may be obtained from consideration of the mechanism shown in Scheme 1. Using the steady state treatment and a method analogous to that employed by Bonner and Collins (12), it can be shown (10) that after complete reaction, the following relationship holds:

$$[\mathbf{5}]/[\mathbf{5r}] = 1 + (k_{SOH}/k_r)$$

Thus when Ar = Ph, Tol, and An, respectively, in **5** and **5r**, k_{SOH}/k_r is calculated to be 12, 5.1, and 3.0.

It is well known that the migratory aptitude of aryl groups follows the order of An > Tol > Ph. From the classical work of Bachmann and Ferguson with symmetrical aromatic pinacols, the migratory aptitude for Ph:Tol:An was found to be 1:15.7:500 (13). Rappoport (11) has also concluded that for the Ph and An groups, the migratory aptitude in vinylic systems resembles that in saturated systems; for example, consideration of the rearrangement data from the 2-anisyl-1,2-diphenylvinyl and triphenylvinyl cations led to the value of 76–120 for the rearrangement ratio for An:Ph (9). If solvolyses of triphenylvinyl, tri-*p*-tolylvinyl, and trianisylvinyl systems were to proceed via classical vinyl cations **6***a*, **7***a*, and **8***a*, bridged structures **6***b*, **7***b*,

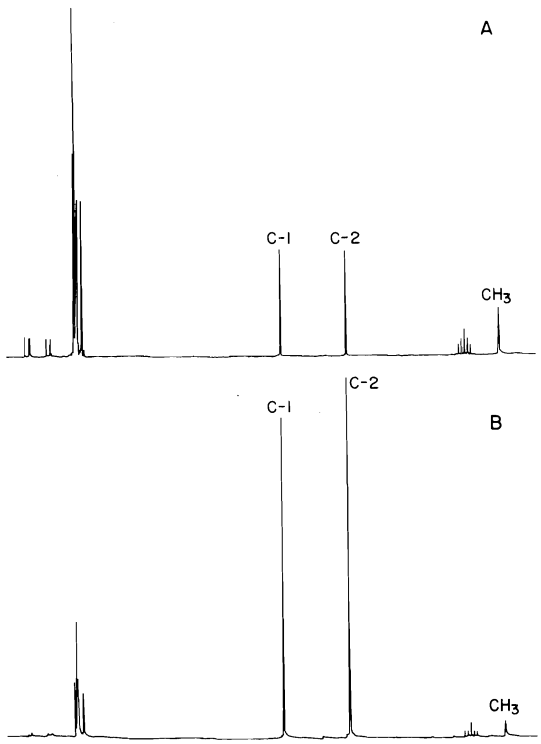

FIG. 1. ^{1}H-decoupled ^{13}C nmr spectra in acetone-d_6. A, unenriched 1,2,2-tri-*p*-tolylethanol (**4**); B, **4**-*x*-^{13}C derived from solvolysis of 19% enriched tri-*p*-tolylvinyl-*2*-^{13}C bromide (**3**-Br-^{13}C) in CF_3COOH–CF_3COOAg.

TABLE 1. Chemical shifts for the ^{1}H-decoupled ^{13}C nmr spectrum of 1,2,2-tri-*p*-tolylethanol (**4**) in $CDCl_3$ and acetone-d_6

	δ (ppm from TMS)	
Carbon	$CDCl_3$	acetone-d_6
C-1	76.6	76.6
C-2	59.4	59.9
CH_3	21.2, 21.9	20.9 (20.85, 20.95)
Aromatic	126.9, 128.1, 128.4	127.7, 128.8
	128.7, 128.9, 129.4	129.1, 129.6
Aromatic	135.6, 136.2, 136.9	135.5, 135.6, 136.5
quaternary	138.3, 138.9, 139.5	140.6, 140.9, 142.0

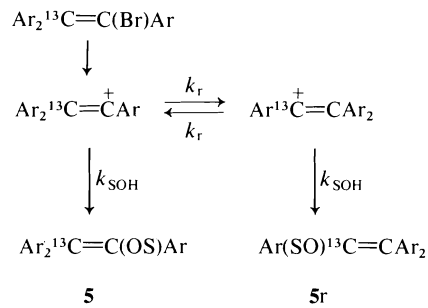

SCHEME 1

TABLE 2. Isotopic scrambling data from the ^{13}C nmr spectra of 1,2,2-tri-*p*-tolylethanol-*x*-^{13}C (**4**-*x*-^{13}C) derived from solvolyses of tri-*p*-tolylvinyl-*2*-^{13}C bromide (**3**-Br-*2*-^{13}C)

Solvent and added salt	Reaction time (min)	Reaction temp. (°C)	Relative intensity[a] I_1/I_s	Relative intensity[a] I_2/I_s	^{13}C enrichment (%)	^{13}C scrambling from C-2 to C-1 (%)
Unenriched 4			0.578	0.578		
			0.508[b]	0.525[b]		
HOAc–AgOAc	180	Reflux	2.93	15.1	32	14
			2.51[b]	14.2	33	13
CF_3COOH–CF_3COOAg	15	Room temp.	5.33	5.86	19	47
			6.15	6.60	23	46
CF_3COOH–CF_3COONa	20[c]	100	4.33	4.71	15	47
	50[d]	100	4.29	4.71	15	47
CFCOOH	25[c]	100	5.00	6.50	20	43
	60[d]	100	14.3	16.1	57	47
	180	100	4.57	4.57	15	50

[a]I_1, I_2, and I_s are, respectively, the integrated intensities for C-1, C-2, and the CH_3 internal standard.
[b]Spectra run in $CDCl_3$ as solvent; the other data were obtained in acetone-d_6.
[c]About 2 half-lifes.
[d]About 5 half-lifes.

and **8***b* may be regarded as models of the transition states for the degenerate 1,2-aryl shifts in these systems. In these three systems, not only the migrating group but also the migration origin and the migration terminus are different from

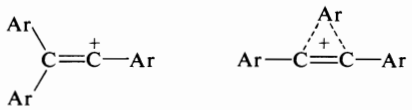

6*a*, Ar = Ph
7*a*, Ar = Tol
8*a*, Ar = An

6*b*, Ar = Ph
7*b*, Ar = Tol
8*b*, Ar = An

one system to another. Thus a direct comparison of the extents of scrambling or degenerate rearrangement[1] among these systems would reflect not only the effects of the migrating group, such as migratory aptitude, but also the effects of the different non-migrating aryl substituents at C-1 and C-2.

As indicated earlier, the scrambling ratio for the acetolysis of **1**-Br-*2*-^{13}C:**3**-Br-*2*-^{13}C:**2**-Br-*2*-^{13}C is only about 1:2:3. These values are much smaller than what one would expect if migratory aptitudes were the predominant factor. In going from cations **6***a*, **7***a*, and **8***a* to transition states **6***b*, **7***b*, and **8***b*, respectively, the stability of the cations apparently plays an important role. The greater stability of **7***a* over **6***a*, for example, would increase the activation energy for **7***a* → **7***b*, counterbalancing the higher migratory aptitude of the *p*-tolyl group. Thus the scrambling ratio for the acetolysis of **3**-Br-*2*-^{13}C:**1**-Br-*2*-^{13}C is only about 2:1, although the migratory aptitude of tolyl:phenyl in pinacol rearrangements was found to be 15.7:1. Another factor which could also counterbalance the greater migratory aptitudes of the tolyl and anisyl groups is the effect of the α-aryl substituent on the electrophilic character of the migration terminus. As suggested by Bonner and co-workers (14, 15), the delocalization of the positive charge in **7***a* or **8***a* by the α-tolyl or anisyl substituent would decrease the electrophilic character of the migration terminus, hence decreasing the tendency for the tolyl and anisyl migration.

The trifluoroacetolysis of **3**-Br-*2*-^{13}C in the presence of CF_3COOAg gave about 47% scrambling of the label from C-2 to C-1 (Table 2), and this corresponds to k_{SOH}/k_r (Scheme 1) of only 0.13. A similar reaction with **2**-Br-*2*-^{13}C was found to give rise to a complete scrambling of 50% (6). As pointed out previously (4, 6), the extremely low nucleophilicity of CF_3COOH (16, 17) allows the 1,2-aryl shift in the vinyl cation to compete favorably with product forming reaction with solvent, hence much greater extents of scrambling were observed in trifluoroacetolysis than in acetolysis.

In solvolytic studies with vinylic systems, under acidic conditions such as trifluoroacetolysis, there is the distinct possibility of an electrophilic addition followed by elimination to give the same product as that derived from an S_N1 reaction (18–21). In this laboratory, how-

[1]The percentage rearrangement used by Rappoport and co-workers (9–11) is equal to twice the percentage scrambling reported by us since complete rearrangement via 1,2-shifts in our systems would give rise to 50% scrambling.

ever, CF_3COOH has been used as solvent (4, 6) since the ester product derived from trifluoroacetolysis, for example as in the present work, may be readily converted to **4**-*x*-^{13}C for ^{13}C nmr examination. It has been pointed out that a solvent kinetic isotope effect is a good diagnostic test for electrophilic addition–elimination (20, 21). The rates of reaction of **3**-Br with HOAc or DOAc, and with CF_3COOH or CF_3COOD, without the presence of any Ag salt, were measured by the potentiometric titration of the liberated bromide ion (22). For acetolysis at 150°C, the rate constants in HOAc and DOAc, respectively, were 1.2×10^{-6} and 1.3×10^{-6} s^{-1}, indicating essentially no solvent kinetic isotope effect. Trifluoroacetolysis at 100°C in CF_3COOH and CF_3COOD, however, gave rate constants of 9.0×10^{-4} and 3.5×10^{-4} s^{-1}, respectively, corresponding to a solvent kinetic isotope effect, $k_{CF_3COOH}/k_{CF_3COOD}$, of 2.6.[2] Thus in the absence of Ag salt, electrophilic addition–elimination apparently plays an important part in the reaction of **3**-Br with CF_3COOH. In the presence of 1.1 equiv. of CF_3COOAg, however, the reaction, even at 0°C, was too fast for kinetic measurement by potentiometric titration. Presumably, the Ag salt catalyzes the formation of the vinyl cation via the S_N1 process, and the contribution from electrophilic addition–elimination may be negligible in the presence of Ag salt. When the trifluoroacetolysis was carried out in the presence of 2.5 equiv. of CF_3COONa, the rate constants observed at 100°C for CF_3COOH and CF_3COOD, respectively, were 1.1×10^{-3} and 7.1×10^{-4} s^{-1}, corresponding to $k_{CF_3COOH}/k_{CF_3COOD}$ of 1.6. It appears that for the trifluoroacetolysis in the presence of CF_3COONa, the contribution of the addition–elimination process is of much lesser importance than in the trifluoroacetolysis with no added salt.

Isotopic scrambling in the trifluoroacetolysis of **3**-Br-*2*-^{13}C with the presence of 2.5 equiv. of CF_3COONa or with no added salt were also carried out, and the results are included in Table 2. With added CF_3COONa, after a reaction time of about 2 or 5 half-lifes, the same extent of scrambling (47%), as was found in the reaction with CF_3COOH–CF_3COOAg, was observed. Moreover, the product apparently did not undergo further scrambling since the same result was noted after 2 or 5 half-lifes. Since both reactions with added Ag or Na salt involved capture of the tri-*p*-tolylvinyl cation by CF_3COOH–CF_3COO^-, the same extent of scrambling was observed.

In the reaction of **3**-Br-*2*-^{13}C with CF_3COOH with no added salt, the extent of scrambling was found to increase with increasing reaction time (Table 2), indicating that the initially formed product was unstable and could subsequently ionize and undergo further scrambling. Moreover, the solvent isotope effect of 2.6 for unbuffered CF_3COOH–CF_3COOD suggests a substantial contribution from electrophilic addition–elimination. Such an addition–elimination process would not give rise to any scrambling:

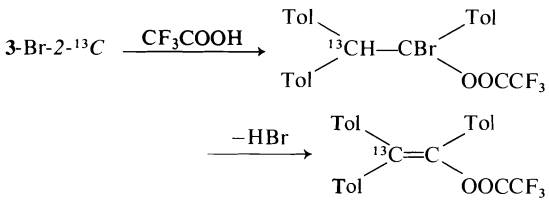

However, the trifluoroacetate product from addition–elimination could subsequently undergo ionization and 1,2-tolyl shift. Thus in CF_3COOH with no added salt, besides the possibility of S_N1 solvolysis with scrambling, addition–elimination also occurs giving rise to an unrearranged product which subsequently may undergo scrambling. A combination of these processes could, therefore, explain the observed scrambling results in the trifluoroacetolysis, with no added salt, of **3**-Br-*2*-^{13}C.

Experimental

*Ethyl p-Tolylacetate-carboxyl-^{13}C (**9**)*

Reaction of $TolCH_2MgCl$ with $^{13}CO_2$ (from $Ba^{13}CO_3$, 90% enriched) in a similar way as in the preparation of labeled *p*-anisylacetic acid (6, 23) gave a 62% yield of $TolCH_2{}^{13}COOH$, mp 91–92°C (lit. (24) mp 94°C), ^1H nmr δ($CDCl_3$) 2.30 (CH_3, s), 3.60 (CH_2, d, $J_{^{13}CCH_2} = 8.0$ Hz), 7.13 (arom, s), and 10.77 (COOH, s). The acid was esterified by the H_2SO_4 catalyzed reaction with absolute ethanol to give an 88% yield of $TolCH_2{}^{13}COOEt$ (**9**), bp 62–63°C/0.1 Torr (lit. (24) bp 240°C), ^1H nmr δ($CDCl_3$) 1.25 (ethyl CH_3, t), 2.35 (CH_3, s), 3.57 (CH_2, d, $J_{^{13}CCH_2} = 8.0$ Hz), 4.15 (ethyl CH_2, q of d's, $J_{^{13}COOCH_2} = 3.3$ Hz), and 7.15 (arom, s).

*Tri-p-tolylvinyl-2-^{13}C Bromide (**3**-Br-*2*-^{13}C)*

The reactions utilized in the synthesis of **3**-Br-*2*-^{13}C are the same as those previously described for the synthesis of **2**-Br-*2*-^{13}C (6). The following is a typical set of experimental procedures.

[2]Similarly, the solvent kinetic isotope effect in the reaction of *cis*- and *trans*-2-phenyl-1,2-di-*p*-tolylvinyl bromides with CF_3COOH and CF_3COOD was found to be 3.4–3.9 (to be published).

A solution of labeled ester **9** (70% enriched, 2.60 g, 14.5 mmol) in 45 ml of tetrahydrofuran (THF) was added dropwise over a period of 1 h to a solution of TolMgBr (from 20 g (120 mmol) of TolBr) in about 100 ml of THF. The mixture was heated under reflux for 48 h, cooled in an ice bath, decomposed with ice and 10% HCl, and then repeatedly extracted with 50-ml portions of ether. The combined extract was dried over $MgSO_4$ and the ether was removed under reduced pressure to give an oil consisting of about a 3:1 mixture (from ^1H nmr) of 1,1,2-tri-*p*-tolylethanol-*1*-^{13}C (**10**) and 1,1,2-tri-*p*-tolylethene-*1*-^{13}C (**11**).

In trials with unlabeled materials, the reaction mixture from the treatment of $TolCH_2COOEt$ with TolMgBr was decomposed with saturated NH_4Cl solution rather than with dilute HCl to minimize elimination. 1,1,2-Tri-*p*-tolylethanol was isolated from the oily product by recrystallization from absolute ethanol, mp 70–71°C (lit. (25) mp 72–73°C), ^1H nmr δ(acetone-d_6) 2.20, 2.23 (CH_3, s's), 3.58 (CH_2, s), 4.03 (OH, s), and 6.9–7.5 (arom, m). When a concentrated solution of this tertiary alcohol in HOAc–Ac_2O was stirred at room temperature for 1 h, the precipitated tri-*p*-tolylethene was collected and repeatedly recrystallized from HOAc–CH_3OH, mp 82–84°C (lit. (25) mp 89–90°C), ^1H nmr δ($CDCl_3$) 2.22, 2.38, 2.42 (CH_3, s's), 6.90 (olefinic H, s), and 7.0–7.3 (arom, m).

The 3:1 mixture of labeled alcohol **10** and olefin **11** obtained above was dissolved in 80 ml of HOAc and a solution of 4.0 g (25 mmol) of Br_2 in 30 ml of HOAc was added dropwise. The reaction mixture was stirred at room temperature for 10 h and the pale yellow product that precipitated was collected by filtration and the filtrate was concentrated under reduced pressure to give more product. The combined solid material was washed with $NaHCO_3$ solution and with water and then recrystallized from CH_3OH to give 2.45 g (45% based on ester **9**) of tri-*p*-tolylvinyl-*2*-^{13}C bromide (**3**-Br-*2*-^{13}C), mp 121–123°C, ^1H nmr δ($CDCl_3$) 2.38, 2.47, 2.55 (CH_3, three s's), and 7.0–7.5 (arom, m). *Anal.* calcd. for $C_{23}H_{21}Br$ (70% ^{13}C enrichment at C-2): C 73.25, H 5.61; found: C 73.82, H 5.68.

Solvolysis Reactions

The acetolysis of **3**-Br-*2*-^{13}C was carried out by heating the substrate under reflux and with stirring for 3 h in HOAc–Ac_2O containing 1.1 equiv. of AgOAc. The trifluoroacetolysis was effected by stirring a mixture of **3**-Br-*2*-^{13}C and 1.1 equiv. of CF_3COOAg in CF_3COOH–$(CF_3CO)_2O$ for 15 min at room temperature. The reaction of **3**-Br-*2*-^{13}C with CF_3COOH containing 2.5 equiv. of CF_3COONa or without the presence of any added salt was carried out at 100°C for different lengths of time as summarized in Table 2. A typical experiment is described below.

A mixture of 1.03 g (2.73 mmol) of **3**-Br-*2*-^{13}C (diluted with **3**-Br to about 33% enrichment) and 500 mg (3.00 mmol) of AgOAc in 16 ml of HOAc containing 2.2 ml of Ac_2O was heated under reflux for 3 h. The AgBr and excess AgOAc were removed by filtration and washed with warm HOAc. The combined filtrate was evaporated at 3–5 Torr to give the crude product, **3**-OAc-*x*-^{13}C as an oil which was directly utilized for two successive treatments with $LiAlH_4$ as described previously (6) to give 1,2,2-tri-*p*-tolylethanol-*x*-^{13}C (**4**-*x*-^{13}C) for ^{13}C nmr examination. The yield of 4-*x*-^{13}C, after recrystallization from EtOH–H_2O, mp 93–94°C, was 0.54 g (62% based on **3**-Br-*2*-^{13}C).

In preliminary trials with unlabeled materials, the crude product, tri-*p*-tolylvinyl acetate (**3**-OAc), was redissolved in ether, washed with 10% K_2CO_3 solution, and dried over $MgSO_4$. Removal of the ether and recrystallization from absolute ethanol gave the pure **3**-OAc, mp 128–130°C, ^1H nmr δ($CDCl_3$) 1.95 (CH_3CO, s) 2.35, 3.40 (CH_3, two s's), and 6.9–7.3 (arom, m). *Anal.* calcd. for $C_{25}H_{24}O_2$: C 84.24, H 6.79; found: C 84.05, H 6.58.

Similarly, the ester product from the trifluoroacetolysis, **3**-$OOCCF_3$, was isolated from trials with unlabeled **3**-Br. Recrystallized from ether–methanol, it melted at 112–113°C; ^1H nmr δ($CDCl_3$) 2.35, 2.40 (CH_3, two s's), and 7.0–7.4 (arom, m). *Anal.* calcd. for $C_{25}H_{21}O_2F_3$: C 73.16, H 5.16; found: C 73.24, H 5.35.

Reduction of **3**-OAc or **3**-$OOCCF_3$ once with $LiAlH_4$ gave an approximately 2:1 mixture of the ketone $(Tol)_2CHCOTol$ and the alcohol $(Tol)_2CHCH(OH)Tol$ (**4**), and after a second treatment with $LiAlH_4$, pure **4** was obtained, mp 93–94°C, ^1H nmr δ($CDCl_3$) 2.03 (OH, s), 2.18, 2.24, 2.28 (CH_3, three s's), 4.19 (C-2 H, d, J = 8.5 Hz), 5.29 (C-1 H, d), and 6.9–7.4 (arom, m). *Anal.* calcd. for $C_{23}H_{24}O$: C 87.30, H 7.64; found: C 86.90, H 7.55.

An illustration of the calculations using the data from **4**-*x*-^{13}C given in Table 2 is as follows.

Let I_1^0 and I_1^*, respectively, be the integrated intensities of the ^{13}C absorption due to the naturally abundant ^{13}C at C-1 and to the ^{13}C enrichment at C-1. Then, from the unenriched **4**, $I_1^0/I_s = 0.578$; from the **4**-*x*-^{13}C derived from one of the trifluoroacetolysis experiments (spectrum given in Fig. 1*B*), $I_1/I_s = (I_1^0 + I_1^*)/I_s = 5.33$. Hence

$$(I_1^0 + I_1^*)/I_1^0 = 5.33/0.578 = 9.22$$

Converting the intensities to percentage ^{13}C

$$(1.1 + I_1^*)/1.1 = 9.22$$

$$I_1^* = 9.0\%$$

Similarly,

$$I_2^0/I_s = 0.578$$

$$I_2/I_s = (I_2^0 + I_2^*)/I_s = 5.86$$

$$(I_2^0 + I_2^*)/I_2^0 = 5.86/0.578 = 10.14$$

$$(1.1 + I_2^*)/1.1 = 10.14$$

$$I_2^* = 10.0\%$$

Therefore, the total ^{13}C enrichment is 9.0 + 10.0 = 19.0% and the scrambling from C-2 to C-1 = (9.0/19.0)100 = 47%.

Kinetic Measurements

The rates of the reaction of **3**-Br with CH_3COOH or CH_3COOD at 150°C and with CF_3COOH or CF_3COOD at 100°C, with or without the presence of 2.5 equiv. of CF_3COONa, were followed by heating the reaction mixtures in sealed ampoules and measuring the liberated bromide ion by potentiometric titration as described in the literature (22).

Acknowledgment

The financial support given by the National Research Council of Canada and valuable

comments from Professors Z. Rappoport and P. J. Stang are sincerely acknowledged.

1. G. MODENA and U. TONELLATO. Adv. Phys. Org. Chem. **9**, 185 (1971).
2. P. J. STANG. Prog. Phys. Org. Chem. **10**, 205 (1973).
3. L. R. SUBRAMANIAN and M. HANACK. J. Chem. Educ. **52**, 80 (1975).
4. C. C. LEE, A. J. CESSNA, B. A. DAVIS, and M. OKA. Can. J. Chem. **52**, 2679 (1974).
5. F. H. A. RUMMENS, R. D. GREEN, A. J. CESSNA, M. OKA, and C. C. LEE. Can. J. Chem. **53**, 314 (1975).
6. M. OKA and C. C. LEE. Can. J. Chem. **53**, 320 (1975).
7. C. C. LEE and M. OKA. Can. J. Chem. **54**, 604 (1976).
8. C. C. LEE and E. C. F. KO. Can. J. Chem. **54**, 3041 (1976).
9. Z. RAPPOPORT, E. NOY, and Y. HOUMINER. J. Am. Chem. Soc. **98**, 2238 (1976).
10. Y. HOUMINER, E. NOY, and Z. RAPPOPORT. J. Am. Chem. Soc. **98**, 5632 (1976).
11. Z. RAPPOPORT. Acc. Chem. Res. **9**, 265 (1976).
12. W. A. BONNER and C. J. COLLINS. J. Am. Chem. Soc. **78**, 5587 (1956).
13. W. E. BACHMANN and J. W. FERGUSON. J. Am. Chem. Soc. **56**, 2081 (1934).
14. W. A. BONNER and T. A. PUTKEY. J. Org. Chem. **27**, 2348 (1962).
15. M. J. MCCALL, J. M. TOWNSEND, and W. A. BONNER. J. Am. Chem. Soc. **97**, 2743 (1975).
16. P. E. PETERSON and F. J. WALLER. J. Am. Chem. Soc. **94**, 991 (1972).
17. T. W. BENTLEY, F. L. SCHADT, and P. v. R. SCHLEYER. J. Am. Chem. Soc. **94**, 992 (1972).
18. P. E. PETERSON and J. M. INDELICATO. J. Am. Chem. Soc. **90**, 6515 (1968).
19. W. M. SCHUBERT and G. W. BARFKNECHT. J. Am. Chem. Soc. **92**, 207 (1970).
20. Z. RAPPOPORT, T. BASSLER, and M. HANACK. J. Am. Chem. Soc. **92**, 4985 (1970).
21. Z. RAPPOPORT and A. GAL. J. Chem. Soc. Perkin Trans. II, 301 (1973).
22. Z. RAPPOPORT and Y. HOUMINER. J. Chem. Soc. Perkin Trans. II, 1506 (1973).
23. C. C. LEE, D. NEWMAN, and D. P. THORNHILL. Can. J. Chem. **41**, 520 (1963).
24. J. R. A. POLLOCK and R. STEVENS (*Editors*). Dictionary of organic compounds. 4th ed. Eyre and Spottiswoode, London. 1965. p. 3080.
25. T. ANDO. YÛKI GÔSEI KAGAKU KYOKAI SHI, **17**, 339 (1959); Chem. Abstr. **53**, 17971 (1959).

The reactions of mercaptide anions with chlorinated sulfones

RICHARD F. LANGLER[1] AND JAMES A. PINCOCK

Chemistry Department, Dalhousie University, Halifax, N.S., Canada B3H 4J3

Received November 22, 1976

RICHARD F. LANGLER and JAMES A. PINCOCK. Can. J. Chem. **55**, 2316 (1977).

Mercaptide anions react with chlorinated sulfones in two modes, *i.e.* nucleophilic attack on carbon with chlorine as the leaving group and/or nucleophilic attack on chlorine with concomitant carbanion formation. Mercaptide anion pK_b, degree of chlorination of the sulfone substrate, and substituent effects are qualitatively assessed in terms of the propensity for nucleophilic attack at carbon or chlorine.

RICHARD F. LANGLER et JAMES A. PINCOCK. Can. J. Chem. **55**, 2316 (1977).

Les anions mercaptures réagissent avec les sulfones chlorées suivant deux voies: soit une attaque nucléophile sur le carbone impliquant le chlore comme nucléofuge et/ou une attaque nucléophile sur le chlore avec la formation concomitante d'un carbanion. On discute d'une façon qualitative des effets des paramètres suivants sur la facilité avec laquelle l'anion mercapture attaque d'une manière nucléophile au niveau soit du carbone soit du chlore: le pK_b de l'anion mercapture, le degré de chloration de la sulfone agissant comme substrat, et les effets de substituants.

[Traduit par le journal]

In recent papers (1–4), we have reported studies of the chlorination of a variety of sulfide substrates. The initial paper (1) detailed the fate of α-sulfonyl-sulfides upon chlorination in aqueous acetic acid. These α-sulfonyl-sulfides were prepared from the appropriate α-chlorosulfone and thiol anion; for example, from chloromethyl methyl sulfone (**1***a*) and phenylmethanethiol anion (Table 1). In contrast, a variety of non-sulfur nucleophiles do not displace the chlorine atom of an α-chlorosulfone (5–8). We have also shown that both sodium bisulfide and thiourea fail to react with **1***a* in refluxing ethanol (1). Based on these observations a more extensive study of this apparently unusual nucleophilic displacement was undertaken.

We began the study by examining the effect of variations in the structure of the chlorosulfone substrate in the preparation of the sulfone-sulfides **2***b* (R_1 = Ph) and **2***c* (R_1 = $ClCH_2$) (10).

Although both of these reactions were successful,[2] the yields of the sulfone-sulfides **2** obtained with phenylmethanethiol anion changed markedly as a function of the chlorosulfone (percentage yield); chloromethyl methyl, **1***a* (93%) (9), chloromethyl phenyl, **1***b* (22%), and bis-(chloromethyl), **1***c* (14.6%) (10). These results may well indicate a sensitivity to bulky groups in the sulfone substrate which is consistent with the S_N2 mechanism envisioned for this reaction. In contrast, the reaction appears to have little sensitivity to steric hindrance resulting from bulky groups in the mercaptide anion, *e.g.*, chloromethyl methyl sulfone (**1***a*) affords the corresponding sulfone-sulfide upon reaction with the following mercaptide anions (percentage yield); ethyl (55%); phenylmethyl (93%) (9), diphenylmethyl (81%) (1), and triphenylmethyl (43%) (1).

The next system chosen for study was the trichlorosulfone **1***d*. *A priori*, the preparation of the sulfone-sulfide **2***d* presented some points of interest. Firstly, there are two carbon sites for nucleophilic attack of the thiol anion and secondly, the steric and electronic effects of a third chlorine atom could not be easily predicted.

The products from the reaction of **1***d* with phenylmethanethiol anion in refluxing ethanol proved to be bis(chloromethyl) sulfone, dibenzyl disulfide, and unreacted **1***d*. Moreover, treatment of the tetrachlorosulfone **3** with benzyl mercaptide anion furnished the same products. These observations are nicely explained by nucleophilic attack of the mercaptide anion on chlorine rather than on carbon as outlined in Scheme 1. Three factors appear to contribute to the change in mechanism. First, the bulky di-

[1]Author to whom enquiries should be addressed.

[2]In agreement with the results (1) for the methyl analog **2***a* both sulfone-sulfides **2***b* and **2***c* were successfully converted to the corresponding, α,α-dichloro-α-sulfonyl sulfonyl chlorides and subsequently hydrolyzed to the corresponding dichloromethyl sulfones.

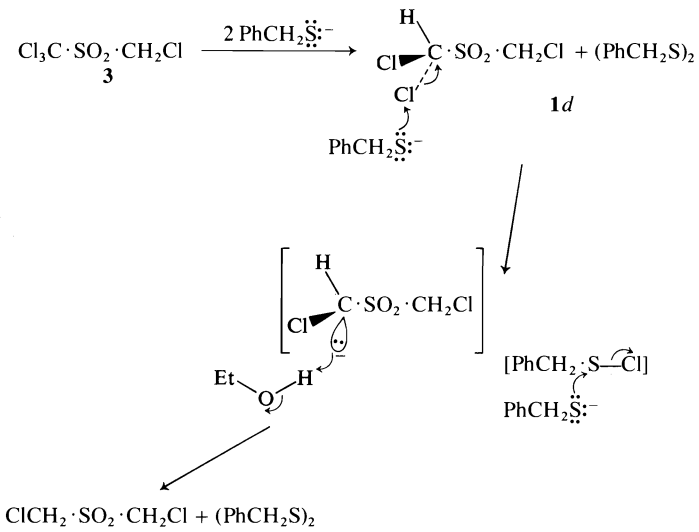

SCHEME 1

chloromethyl group hinders attack of the nucleophile at the chloromethyl carbon; second, the presence of a second chlorine atom on carbon hinders nucleophilic attack at the carbon of the dichloromethyl group; and third, the presence of the second chlorine atom on the carbon adjacent to the sulfonyl group enhances the stability of the departing carbanion.

At this point a reasonable alternate mechanism seemed possible for the 'normal' nucleophilic attack at carbon. These products could arise after attack by the nucleophilic mercaptide anion on chlorine as observed for **1***d* and **3**, if the resulting carbanion (*i*) displaced chlorine from the newly formed sulfenyl chloride or (*ii*) displaced thiol anion from disulfide formed from

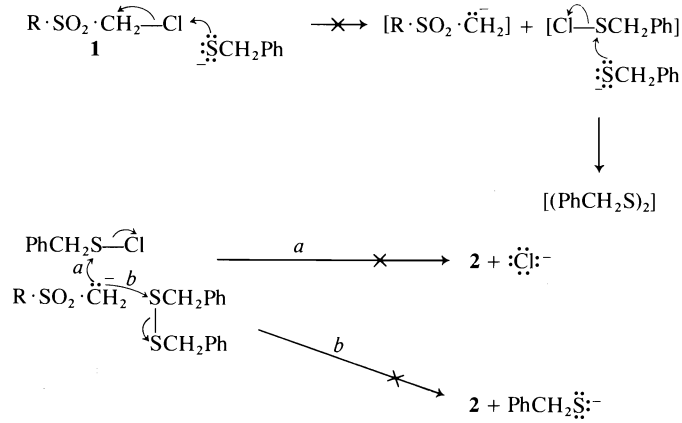

SCHEME 2

the reaction of the sulfenyl chloride and mercaptide anion. The net result as outlined in Scheme 2 would then appear to be nucleophilic attack of the mercaptide anion on carbon. We have examined these possibilities with three experiments. No sulfone-sulfide was obtained on treatment of dimethyl sulfone and benzenesulfenyl chloride with ethanol – sodium ethoxide, although methyl chloromethyl sulfone reacts with phenyl mercaptide anion under these conditions to furnish the corresponding sulfone-sulfide.[3] Therefore, sulfenyl chlorides do not function as intermediates in the formation of the

[3]D. Kay, R. F. Langler, and J. A. Pincock, unpublished results.

TABLE 1. Reactions of α-chlorosulfones with thiol anions

$$R_1—SO_2—CHCl—R_2 + R_3S^- \rightarrow \underset{\underset{SR_3}{|}}{R_1—SO_2—CH—R_2} \;(\mathbf{I}) + R_1—SO_2—CH_2—R_2 \;(\mathbf{II})$$

	R_1	R_2	R_3	I (% yield)	II (% yield)
1*a*	CH_3	H	$PhCH_2$	**2***a*(93)[a]	—(0)[a]
1*b*	Ph	H	$PhCH_2$	**2***b*(22)	—(0)
1*c*	CH_2Cl	H	$PhCH_2$	**2***c*(15)	—(0)
1*d*	CH_2Cl	Cl	$PhCH_2$	**2***d*(0)	**1***c*(62)
3	CCl_3	H	$PhCH_2$	—(0)	**1***c*(65)
4	CH_3	$PhCH_2S$	$PhCH_2$	—(0)	**5**(95)
6	PhO	H	$PhCH_2$	—(0)	**7**(22)
3	CCl_3	H	H	—(0)	**1***c*(95)
4	CH_3	$PhCH_2S$	H	—[b]	**5**(17)
8	CH_3	$PhCH_2SO_2$	H	—(0)	**9**(85)
4	CH_3	$PhCH_2S$	Ph	**11**(22)	**5**(43)

[a]Isolated yields. In cases where the yields are low (*i.e.* **2***c*) the remaining crude material was mainly starting material. Yields of 0% mean no such product was isolated.
[b]See Scheme 4 and discussion in text.

sulfone-sulfides **2**. Furthermore, dimethyl sulfone and dibenzyl disulfide in ethanol – sodium ethoxide failed to furnish any detectable amount of the corresponding sulfone-sulfide, although as shown in Table 1, chloromethyl methyl sulfone (**1***a*) furnishes **2***a* in 93% yield upon reaction with phenylmethanethiol anion. Finally, even the more acidic β-disulfone **9** and dibenzyl disulfide in ethanol – sodium ethoxide failed to give any substitution product. Therefore, disulfides do not function as intermediates in the formation of the sulfone-sulfides **2**. These results confirm our original formulation (1) of the substitution reactions as nucleophilic attack on carbon for **1***a*–**1***c* and the products obtained in the cases of **1***d* and **3** as nucleophilic attack on chlorine.

Nucleophilic displacements of carbon by attack on halogens have been observed previously with perhaps the most comparable example being the dechlorination reactions of α-halosulfones by phosphines (11, 12). However, they are sufficiently uncommon that an effort to examine the factors in the substrate and the nucleophile that lead to preferential nucleophilic attack at halogen, was undertaken.

Two cases of substrate variation are shown in Table 1 for **4** and **6**. The dechlorination of the chlorosulfone-sulfide **4** establishes that mercaptide anion nucleophilicity at chlorine can be induced by other groups which enhance the stability of the departing carbanion. The dechlorination of phenyl chloromethanesulfonate (**6**), establishes that the anion-stabilizing group need not be directly attached to the carbon atom involved. As an aside, the sulfonate **6** might have produced sulfene via nucleophilic attack on chlorine with concomitant ejection of phenoxide ion, although the absence of ethyl sulfonate products establishes that such a process did not occur. Clearly, now, from the reactivity of **6**, the preference for mercaptide anion attack at the chlorine of an α-chlorosulfone may be observed in substrates where carbanion stability is enhanced and where steric factors are not substantially different from α-chlorosulfone substrates which are attacked preferentially at carbon.

We subsequently examined variations in the nature of the sulfur nucleophile. As mentioned previously, simple α-chlorosulfones are inert to either substitution or dechlorination by bisulfide ion (1). However, substrates with enhanced carbon leaving group stability are dechlorinated as shown for the cases of **3**, **4**, and **8** (Table 1).

A cursory examination of these reactions would indicate that they appear to be following the pattern expected from the results obtained with the phenylmethanethiol anion. The key difference is the formation of dibenzyl disulfide in the reaction of the α-chloro-α-sulfonyl sulfide **4**. As outlined in Scheme 3, this would seem to require nucleophilic attack by the bisulfide ion on carbon with concomitant ejection of chloride ion resulting in the formation of the unstable intermediate **10**.

It now appears that there are two factors to consider in these nucleophilic reactions. The

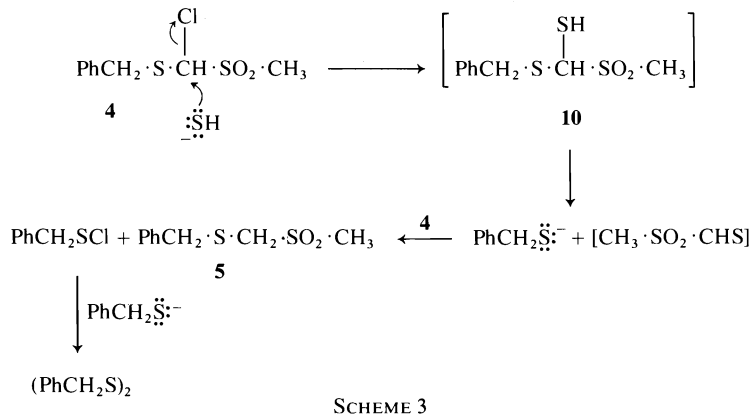

SCHEME 3

first is that the propensity for attack on carbon is changed to favour attack on chlorine when the stability of the departing anion is enhanced. The second is that increasing the pK_b of the mercaptide anion (pK_b $PhCH_2S^-$ < pK_bHS^-)[4] shifts the propensity back to nucleophilic attack at carbon. As a consequence of these conclusions we examined the reaction of **4** with a mercaptide anion whose pK_b is closer to that of bisulfide ion than that of phenylmethane thiol anion and

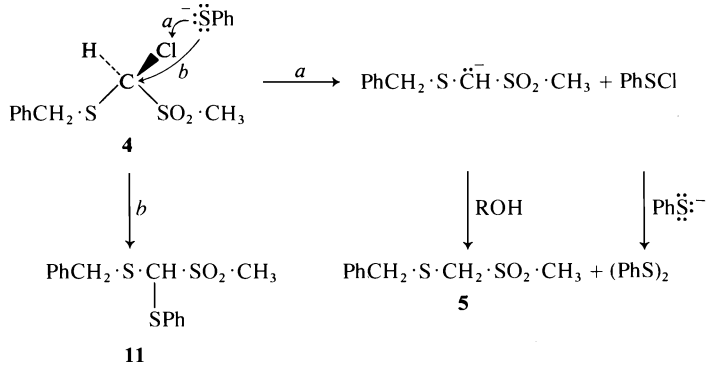

SCHEME 4

which would afford a stable carbon substitution product. Our choice was the phenyl mercaptide ion.[4]

It was with some satisfaction that we isolated from the reaction of **4** with phenyl mercaptide anion (see Scheme 4) both the dechlorinated sulfone-sulfide **5** (43%) along with diphenyl disulfide-sulfone **11** (22%) indicating nucleophilic attack on carbon. This reaction, therefore, represents an adjustment of the two factors which appear to dictate the course of nucleophilic attack of mercaptide anions on chlorosulfone substrates (*i.e.* dechlorinated carbanion stability and mercaptide anion pK_b) to the point where both pathways are observed in the same reaction. Such a system is highly advantageous in order to undertake a more quantitative mechanistic and kinetic study of these pathways which we hope to pursue shortly.

As a final comment on this type of dechlorination reaction, Pierce *et al.* (14) have recently reported the dechlorination of *N*-phenyl-2-chloro-3-oxobutyramide with sodium bisulfide. They proposed an S_N2 displacement of chlorine proceeding through the intermediacy of a thiol-keto-amide which they were unable to isolate. In view of our results it appears that this reaction might be better formulated as a direct attack on chlorine. Such a rationale can be advanced on the grounds that the pK_b of the dechlorinated keto-amide anion formed in this reaction would be expected to be comparable to that of the β-disulfone **9** (which forms via nucleophilic attack on chlorine by bisulfide ion) rather than that of the sulfone-sulfide **4** (which undergoes some

[4]The pK_a of H_2S, PhSH, and $PhCH_2SH$ are approximately 7.0, 8.0, and 12.0, respectively (13).

nucleophilic attack at carbon by bisulfide ion, *vide* Scheme 3).

In conclusion, we have found that α-chlorosulfones undergo nucleophilic attack by sulfur anions at both carbon and chlorine. Increasing the number of chlorine atoms adjacent to the sulfonyl group diverts the nucleophilic attack from carbon to chlorine. Rationales for this result may be found in the increased crowding of both centres adjacent to the sulfonyl group by the introduction of second and third chlorine atoms and in the enhanced stability of the departing carbanion conferred by the additional chlorine atom(s). The latter rationale permits one to anticipate the preferential nucleophilic attack of sulfur anions on chlorine in α-chlorosulfone-sulfides which was also observed. Finally, the preference for nucleophilic attack of sulfur anions at carbon is enhanced as the pK_a of the corresponding thiol decreases. Such an observation is consistent with the increasing polarizability (softness) of the sulfur nucleophile as the pK_a of the corresponding mercaptan diminishes leading to increased rate of reaction with increasing electron deficiency (hardness) at carbon in the substrates.

Experimental

General

The ir spectra were recorded on a Beckman IR-10 grating spectrophotometer and the nmr spectra were obtained on a Varian T-60 instrument using TMS as the internal standard. The mass spectra were recorded on a Dupont 21-490 instrument. Samples were directly introduced and the spectra run at 30 eV with a source temperature of 200°C. Melting points were determined on a Fisher-Johns melting point apparatus and are uncorrected. The tlc was carried out on 5 × 20 cm analytical plates (0.75 mm thickness) spread with silica gel HF-254 (A. G. Merck).

*Preparation of $PhSO_2CH_2SCH_2Ph$ (**2b**) (15)*

Sodium metal (0.67 g) was dissolved in absolute ethanol (100 ml), followed by the addition of phenylmethanethiol (3.6 ml). Phenyl chloromethyl sulfone (5.003 g) was added and the reaction mixture refluxed for 1 h. Water (100 ml) was added and the solution extracted with chloroform (three-100 ml aliquots). The chloroform layers were combined, dried ($MgSO_4$), filtered, and the chloroform rotary evaporated. The residue was crystallized from 95% ethanol furnishing the sulfone-sulfide **2b** (1.610 g, mp 107–109°C) (15). The product had R_F, 0.73 on tlc when developed with chloroform. The ir bands were present at 1320 and 1145 cm^{-1}. The nmr spectrum ($CDCl_3$) showed signals at τ 2.36 (10H, m) 6.06 (2H, s) and 6.26 (2H, s).

Preparation of $CH_3SO_2CH_2SCH_2CH_3$

Sodium metal (9.64 g) was dissolved in absolute ethanol (300 ml) and the solution cooled with ice water. Ethanethiol (9.630 g) and chloromethyl methyl sulfone (20.007 g) (9) were added and the solution refluxed for 1 h. Water (300 ml) was added and the resultant mixture extracted with chloroform (five-100 ml aliquots). The combined organic layers were dried ($MgSO_4$), filtered, and rotary evaporated. The residue was dissolved in $CHCl_3$ (300 ml), washed with 2.5% sodium hydroxide (ten-100 ml aliquots), dried ($MgSO_4$), filtered, and rotary evaporated. The residue was rectified at reduced pressure affording the sulfone-sulfide (13.441 g; bp 146°C/5 Torr). The ir bands were present ($CHCl_3$) at 1315 and 1150 cm^{-1}. The nmr spectrum ($CDCl_3$) showed signals at τ 6.06 (2H, s), 7.00 (3H, s), 7.06 (2H, q), and 8.73 (3H, t). The mass spectrum exhibited ions at *m/e* 154(M^+, 7.5%), 75(100%), and 47(73.5%). *Anal.* calcd. for $C_4H_{10}O_2S_2$: C 31.11, H 6.53; found: C 30.90, H 6.64.

*Reaction of $Cl_2CH{\cdot}SO_2{\cdot}CH_2Cl$ (**1d**) and $PhCH_2SH$*

Metallic sodium (0.680 g) was dissolved in absolute ethanol (100 ml). Phenylmethanethiol (3.5 ml) and 1,1,3-trichloro-2-thiapropane-2,2-dioxide (5.067 g) (16) were added and the solution refluxed for 1 h. Water (100 ml) was added and the resultant mixture washed with chloroform (three-100 ml aliquots). The combined chloroform layers were dried ($MgSO_4$), filtered, and rotary evaporated affording a residue composed of dibenzyl disulfide (3.6 g), 1,3-dichloro-2-thiapropane-2,2-dioxide (2.6 g), and unreacted trichlorosulfone (1.6 g) (composition determined by nmr). A portion of the residue crystallized. The crystals were filtered off and recrystallized from carbon tetrachloride. A portion of this recrystallized material (300 mgm) was chromatographed on preparative tlc plates (100 mgm/plate) using CCl_4 developer. The disulfide bands were detected (uv light) and scraped, washed with chloroform, and the chloroform concentrated to afford dibenzyl disulfide which was identical with authentic material by nmr, tlc, and ir. The remainder of the preparative plate from the lower edge of the disulfide band to the lower edge of the origin was scraped, washed with chloroform, and the chloroform concentrated to afford clean dichlorosulfone which was identical to authentic material by nmr, ir, mp, and mixture mp.

Reaction of $Cl_3C{\cdot}SO_2{\cdot}CH_2Cl$ (3) and $PhCH_2SH$

This experiment was virtually identical to the reaction of **1d** with phenylmethanethiol (detailed above) except that the amounts of Na and $PhCH_2SH$ were four fold molar excess as compared with the tetrachlorosulfone **3** (16).

*Reaction of $PhCH_2SCHClSO_2CH_3$ (**4**) and $PhCH_2SH$*

Sodium metal (0.213 g) was dissolved in absolute ethanol (50 ml). Phenylmethanethiol (1.2 ml) and the chlorosulfone-sulfide **4** (1.150 g) (1) were added and the reaction stirred at ambient temperature for 48 h. Water (100 ml) was added and the reaction mixture washed with chloroform (three-100 ml) aliquots. The combined chloroform layers were dried ($MgSO_4$), filtered, and rotary evaporated affording a crude residue (2.003 g). The residue was composed of the dechlorinated sulfone-sulfide **5** and dibenzyl disulfide (1:1 molar ratio) as confirmed by nmr and tlc.

*Reaction of $ClCH_2{\cdot}SO_2{\cdot}OPh$ (**6**) with $PhCH_2SH$*

Sodium metal (0.669 g) was dissolved in absolute ethanol (100 ml). Phenylmethanethiol (3 ml) and phenyl

chloromethanesulfonate (**6**) (4.999 g) (prepared from chloromethanesulfonyl chloride and phenol) were added and the reaction mixture refluxed for 48 h. Water (100 ml) was added and the resultant mixture washed with chloroform (three-100 ml aliquots). The combined chloroform layers were dried ($MgSO_4$), filtered, and rotary evaporated. The residue (10.9 g) contained phenyl methanesulfonate (7) (22% based on starting chloromethanesulfonate), unchanged phenyl chloromethanesulfonate (78%), and dibenzyl disulfide (22%).

A portion of the residue (0.5 g) was chromatographed on preparative tlc plates (100 mg/plate) using chloroform for development. Bands located (254 nm uv light) at R_F, 0.89 afforded dibenzyl disulfide (0.055 g) which was identical to authentic material by tlc, nmr, and ir. The band at R_F, 0.78 afforded unchanged phenyl chloromethanesulfonate (0.164 g) which was identical to starting material by tlc, nmr, and ir. The bands at R_F, 0.64 afforded phenyl methanesulfonate (0.035 g) which was identical to authentic material by tlc, nmr, and ir.

*Reaction of $Cl_3C{\cdot}SO_2{\cdot}CH_2Cl$ (**3**) with NaHS*

The tetrachlorosulfone **3** (1.001 g), and a solution of *p*-toluenesulfonic acid monohydrate (0.832 g) and sodium sulfide nonahydrate in water (15 ml) were mixed together in methanol (40 ml). The reaction was stirred at room temperature for 48 h. Water (100 ml) was added and the resultant mixture washed with chloroform (three-100 ml aliquots). The chloroform was evaporated yielding a crude solid (0.695 g). The solid was recrystallized and shown to be identical to authentic bis(chloromethyl) sulfone by nmr, ir, and mp.

*Preparation of $PhCH_2{\cdot}SO_2{\cdot}CHCl{\cdot}SO_2CH_3$ (**8**)*

The chlorosulfone-sulfide **4** (1.401 g) (1) was dissolved in glacial acetic acid (5 ml) and the resultant solution added dropwise (5 min) to a cooled mixture of chromium trioxide (1.490 g) in glacial acetic (50 ml). The resultant mixture was maintained between 90 and 100°C for 0.5 h. Water (50 ml) was added and the resultant solution washed with chloroform (four 50 ml aliquots). The combined chloroform layers were washed with 2.5% sodium hydroxide until the aqueous p*H* remained basic. The chloroform was washed with distilled water (50 ml), dried ($MgSO_4$), filtered, and rotary evaporated to yield a brownish oil (1.421 g). The oil was crystallized from 95% ethanol affording colorless crystals (1.084 g; mp 125–128°C). The ir bands were present ($CHCl_3$) at 1350, 1340, 1155 and 1130 cm^{-1}. The nmr spectrum ($CDCl_3$) displayed signals at τ 2.66 (5H, s), 4.80 (1H, s), 5.13 (1H, d, J = 14 Hz), 5.43 (1H, d, J = 14 Hz), 6.73 (3H, s). The mass spectrum[5] exhibited ions at *m/e* 140(2.6%), 138(7.9%) and 91(100%). *Anal.* calcd. for $C_9H_{11}ClO_4S_2$: C 38.22, H 3.92; found: C 38.53, H 3.72.

*Reaction of $PhCH_2SO_2CHCl{\cdot}SO_2CH_3$ (**8**) with NaHS*

A solution of the α-chloro-β-disulfone **8** (1.001 g) in methanol (40 ml) was added dropwise over 20 min to a solution of sodium sulfide nonahydrate (1.719 g) and *p*-toluenesulfonic acid monohydrate (0.820 g) in distilled water (15 ml). The reaction was stirred at ambient temperature for 18 h. Water (100 ml) was added and the solution extracted with chloroform (three-100 ml aliquots). The combined chloroform layers were dried ($MgSO_4$), filtered, and rotary evaporated affording the dechlorinated β-disulfone **9** (741 mgm). The dechlorinated material was recrystallized and shown to be identical to authentic material (9) by nmr, ir, and mp.

*Reaction of $PhCH_2SCHClSO_2CH_3$ (**4**) with NaHS*

A solution of the chlorosulfone-sulfide **4** (1.000 g) in methanol (40 ml) was added dropwise over 10 min to a solution of sodium sulfide nonahydrate (2.170 g) and *p*-toluenesulfonic acid monohydrate (0.964 g) in water (15 ml). The reaction mixture was stirred at ambient temperature for 48 h. Water (100 ml was added and the solution extracted with chloroform (three-100 ml aliquots). The combined chloroform layers were dried ($MgSO_4$), filtered, and rotary evaporated affording a crude residue (0.550 g). A portion of the crude residue (300 mgm) was developed on preparative tlc plates (100 mgm/plates) using carbon tetrachloride. The bands at R_F 0.65 were scraped and washed with chloroform furnishing dibenzyl disulfide (0.400 g) which was identical to authentic material by nmr, tlc, and ms. The bands at the origin were scraped and washed with chloroform yielding dechlorinated sulfone-sulfide **5** (0.150 g) which was identical with authentic material by nmr, tlc, and ms.

*Reaction of $PhCH_2SCHClSO_2CH_3$ (**4**) with PhSH*

Sodium metal (0.216 g) was dissolved in absolute ethanol (50 ml). Benzenethiol (1.018 g) and chlorosulfone-sulfide **4** (1.157 g) were added and the reaction mixture stirred at ambient temperature for 4 days. Water (100 ml) was added and the resultant mixture washed with chloroform (three-100 ml aliquots). The combined chloroform layers were dried ($MgSO_4$), filtered, and rotary evaporated affording a crude residue (1.566 g). A portion of the residue (1.051 g) was chromatographed on silica gel (100 g). The column was eluted with carbon tetrachloride (thirty-50 ml fractions) and then with chloroform (thirty-50 ml fractions). Fractions 6 and 7 were combined and concentrated which furnished diphenyl disulfide (0.196 g) which was identical with authentic material by tlc, nmr, and ms. Fractions 42–46 were combined and concentrated affording, as an oil, the sulfone-disulfide **11** (0.195 g). The sulfone-disulfide **11** exhibited ir bands ($CHCl_3$) 1325 and 1150 cm^{-1}. The nmr spectrum ($CDCl_3$) displayed signals at τ 2.80 (10H, pseudo-doublet), 5.45 (1H, s), 5.76 (1H, d, J = 13 Hz), 6.10 (1H, d, J = 13 Hz), 7.00 (3H, s). The mass spectrum showed ions at *m/e* 245(66.6%), 110(20.3%), 109(11.5%), and 91(100%). *Anal.* calcd. for $C_{15}H_{16}O_2S_3$: C 55.52, H 4.97; found: C 55.36, H 5.03. Fractions 47–51 were combined and concentrated affording the benzylic sulfone-sulfide **5** (0.347 g). The impure material obtained from these fractions was chromatographed on three preparative tlc plates employing chloroform development. The upper band furnished clean sulfone-sulfide **5** (0.260 g) which was identical with authentic material by tlc, nmr, and ms.

[5]The significance of the ions at *m/e* 140, 138 has been discussed in detail (9, 10).

Acknowledgements

It is a pleasure to acknowledge the kindness of Dr. T. T. Tidwell during the initial stages of this work which were carried out at the University of Toronto. The authors are indebted to Mr. D. Kay for technical assistance and to Dr. J. H. Kim

for running the mass spectra. We are grateful for some financial support from the University of Toronto and for financial support from the National Research Council of Canada.

1. W. R. HARDSTAFF, R. F. LANGLER, J. LEAHY, and M. J. NEWMAN. Can. J. Chem. **53**, 2664 (1975).
2. R. F. LANGLER. Can. J. Chem. **54**, 498 (1976).
3. J. S. GROSSERT, W. R. HARDSTAFF, and R. F. LANGLER. Can. J. Chem. **55**, 421 (1977).
4. J. S. GROSSERT and R. F. LANGLER. Can. J. Chem. **55**, 407 (1977).
5. F. G. BORDWELL and W. T. BRENNEN. J. Am. Chem. Soc. **86**, 4645 (1964).
6. L. A. PAQUETTE. J. Am. Chem. Soc. **86**, 4085 (1964).
7. F. G. BORDWELL and B. JARVIS. J. Org. Chem. **33**, 1182 (1968).
8. M. CINQUINI, D. LANDINI, and A. MAIA. Chem. Commun. 734 (1972).
9. W. R. HARDSTAFF and R. F. LANGLER. Org. Mass Spectrom. **10**, 215 (1975).
10. R. F. LANGLER, W. S. MANTLE, and M. J. NEWMAN. Org. Mass Spectrom. **10**, 1135 (1975).
11. B. B. JARVIS and B. A. MARIEN. J. Org. Chem. **40**, 2587 (1975).
12. B. B. JARVIS, R. L. HARPER, JR., and W. P. TONG. J. Org. Chem. **40**, 3778 (1975).
13. T. H. LOWRY and K. S. RICHARDSON. Mechanism and theory in organic chemistry. Harper and Row. 1976. p. 149.
14. J. B. PIERCE, R. J. FANNING, and R. A. DAVIS. Can. J. Chem. **53**, 1327 (1975).
15. W. G. PHILLIPS and K. W. RATTS. J. Org. Chem. **36**, 3145 (1971).
16. W. E. TRUCE, G. H. BIRUM, and E. T. MCBEE. J. Am. Chem. Soc. **74**, 3594 (1952).

Organic sulfur mechanisms. 20. Sulfenes from 1-haloalkanesulfinic acids: the 'abnormal route' [1,2]

JAMES FREDERICK KING, RODGER PETER BEATSON, AND JOSEPH MAX BUCHSHRIBER

Department of Chemistry, University of Western Ontario, London, Ont., Canada N6A 5B7

Received December 15, 1976

JAMES FREDERICK KING, RODGER PETER BEATSON, and JOSEPH MAX BUCHSHRIBER. Can. J. Chem. **55**, 2323 (1977).

1-Haloalkanesulfinic acids react with water, *p*-toluidine, or an enamine in the presence of added base to give products expected from an intermediate sulfene. It is concluded that sulfenes are formed, and hence may be presumed to react, via the 'abnormal route', *i.e.*, loss of a nucleophile from the *carbon* (rather than the sulfur) of the incipient sulfene, or, for the reverse process, addition of a nucleophile to the *carbon* (rather than the sulfur) of the sulfene. Since addition at the sulfur is well precedented, these conclusions indicate that sulfene is an 'ambifunctional' electrophile of a previously unknown kind. The mechanism of the sulfene formation is discussed in the light of deuterium labelling and kinetic experiments.

JAMES FREDERICK KING, RODGER PETER BEATSON et JOSEPH MAX BUCHSHRIBER. Can. J. Chem. **55**, 2323 (1977).

Mis en présence de base, les acides halo-1 alcanesulfiniques réagissent avec l'eau, la *p*-toluidine ou une énamine pour conduire aux produits attendus à partir d'un intermédiaire sulfène. On en conclut qu'il y a formation de sulfènes et qu'on peut donc supposer que ces acides réagissent par l'intermédiaire de la 'voie anormale' c'est à dire perte d'un nucléophile à partir du *carbone* (plutôt que du soufre) du sulfène qui se forme; pour les processus inverses, il y aurait addition d'un nucléophile sur le *carbone* (plutôt que sur le soufre) du sulfène. Puisque des réactions d'addition au niveau du soufre sont bien connues, ces conclusions indiquent que le sulfène est un électrophile 'ambifonctionnel' d'une sorte qui était inconnu jusqu'à maintenant. On discute du mécanisme de formation du sulfène à la lumière d'expériences de marquage au deutérium et de cinétique.

[Traduit par le journal]

Introduction

In all of their reactions known to date simple sulfenes apparently react as electrophiles, and usually the reaction occurs in such a way that an attacking nucleophile or nucleophilic component becomes attached to the sulfur atom, as in [1]. This mode which we call 'normal' addition is illustrated in its various forms by the formation of (*a*) sulfonic esters from reaction with alcohols,

[1] $RR'C{=}SO_2 + Nu^-(+E^+) \rightarrow RR'C(E){-}SO_2{-}Nu$

'Normal' addition

[2] $RR'C{=}SO_2 + Nu^-(+E^+) \rightarrow RR'C(Nu){-}SO_2(E)$

'Abnormal' addition

Nu = nucleophile, E = electrophile (not necessarily present)

where Nu = OR and E = H, (*b*) sulfonamides from ammonia or primary or secondary amines, where Nu = NR^2R^3 and E = H, (*c*) zwitterions from tertiary amines (3), where Nu = $\overset{+}{N}R^2R^3R^4$ and there is no electrophile E, and (*d*) 3-aminothietane 1,1-dioxides from enamines, where Nu = the nucleophilic carbon and E = the electrophilic (nitrogen bearing) carbon of the double bond.[3] As we have pointed out previously (6), there are certain reactions, however, in which it is reasonable to propose, at least formally, a nucleophilic attack on the *carbon* of the sulfene, as in [2]. The product of such an attack, instead of being an alkylsulfonyl compound, is an α-substituted sulfinic acid derivative. Such a mode of reaction, which we term 'abnormal' addition, is perhaps most easily depicted by the formation of α-chlorosulfinate anion, initially suggested (6*a*,*b*) as the second step in

[1]For part 19, see ref. 1.

[2]A preliminary account of this work has appeared; see ref. 2.

[3]For further examples see refs. 4 and 5, especially Table II of the latter. The only apparent anomaly in this list has recently been resolved (1), the reaction with chloral to give β-sultones having been shown to involve the sulfene in an orthodox manner.

the proposed mechanism for the formation of thiobenzoyl chloride *S*-oxides from phenylmethanesulfonyl chloride and tertiary amines as in [3].

[3] $PhCH_2SO_2Cl \xrightarrow{R_3N} PhCH{=}SO_2 \xrightarrow{Cl^-}$

$$PhCHSO_2^- \rightarrow \rightarrow PhC{=}SO$$
$$\quad\;\; | \qquad\qquad\quad\; |$$
$$\quad\;\; Cl \qquad\qquad\quad\; Cl$$

A number of what we regard as possible examples of 'abnormal' attack had been collected (6), but believing that the existence of this reaction was not adequately proved, we decided to attack the problem by examining the reverse process, *i.e.*, by seeing if it were possible to *form* a sulfene by the 'abnormal' route, for example, by simple loss of halide from a 1-haloalkanesulfinate anion.

Results and Discussion

Formation of Sulfenes by the 'Abnormal' Route

That such an approach might work was suggested by some observations reported by Müller and Raudenbusch in 1931 (7), who noted, without explanation, that 1-chloroethanesulfonyl chloride (**1**) gave the ethanesulfonate anion on treatment with zinc in the presence of water. This observation is readily explained if one assumes that the zinc effects the usual reduction (8) of the sulfonyl chloride to the sulfinate stage, **4** and (or) **5**, and that this is transformed by the 'abnormal' route to the sulfene **7** which then undergoes 'normal' addition of water to form **6**. We have verified the formation of ethanesulfonate from **1** with zinc and ethanol, though the yields were modest.

Further experiments which gave both better yields and a full confirmation of the existence of the 'abnormal' route are summarized in Scheme 1. Treatment of **1** with sodium sulfite followed by strong acid gave **5** as a colorless oil. Because a careful proof of the structure of this material is essential for the conclusions drawn in this paper, the following data were adduced. The nmr spectrum showed a doublet at 1.75 (3H), a quartet at 4.75 (1H, $J = 7$ Hz), and a singlet at 10.5 ppm (1H), and the infrared spectrum had strong bands at 2900 (broad, OH) and 1080 cm^{-1} (S=O stretch) (9). Redox titration gave a titre corresponding to essentially pure **5**. Potentiometric titration with sodium hydroxide showed **5** to be a strong acid ($pK_a < 2$). We know of no pK_a determinations of any alkanesulfinic acids but pK_a values in the range 1.8 to 2.16 have been reported for benzenesulfinic acid (10). The replacement of a phenyl by a 1-chloroethyl group in the sulfinic acid series might be expected to affect the pK_a in a manner at least roughly parallel to that found with carboxylic acids, *i.e.*, pK_a (benzoic acid) − pK_a (1-chloropropionic acid) = 4.20 − 2.88 = 1.32 (10); this would point to a pK_a of **5** of ~1, a value consistent with our (admittedly limited) observations. Attempts to determine the pK_a of **5** conductometrically also merely confirmed the strong acid character of **5**. Reaction of **4** with methyl iodide gave the crystalline sulfone **3** whereas treatment of **5** with thionyl chloride gave the sulfinyl chloride **2**. The infrared spectrum of **2** displayed the strong absorption at 1160 cm^{-1} characteristic of sulfinyl chlorides, and the nmr spectrum showed this material to be a mixture of diastereomers, having two doublets (respectively at 1.92 and 1.91, both $J = 6.5$) and two quartets (at 5.02 and 5.18 ppm) in the ratio 3:5. Because both chiral carbon and sulfur atoms are present in **2**, such a mixture of diastereomers is expected to be visible in the nmr spectrum, provided that the sulfur atom is capable of maintaining its chirality (on the nmr time scale at the temperature of the instrument). This observation was, in fact, the first reported experimental indication that this is indeed so; further examples have subsequently been described (11).

The formation of methylsulfene (**7**) from **5** is deduced from the following. Reaction of **5** with triethylamine and *p*-toluidine in refluxing acetonitrile gave ethanesulfon-*p*-toluidide (**9**). In refluxing benzene in the presence of the enamine 1-(2-methylpropenyl)pyrrolidine and triethylamine, **5** gave the characteristic enamine-sulfene cycloadduct **8** in 16% yield. Under similar conditions ethanesulfonyl chloride gave **8** in 23% yield (though better yields were obtained at lower temperatures). The structure of **8** follows from its formation from ethanesulfonyl chloride taken with its elemental analysis and spectroscopic properties; the coupling of 9 Hz between the ring hydrogens was suggested in similar examples to be evidence for a *trans* orientation of the substituents (12), though such assignments have subsequently been questioned (13). Reaction of **5** with an excess of aqueous NaOH under reflux for 30 min gave sodium ethanesulfonate. When this reaction was carried out in

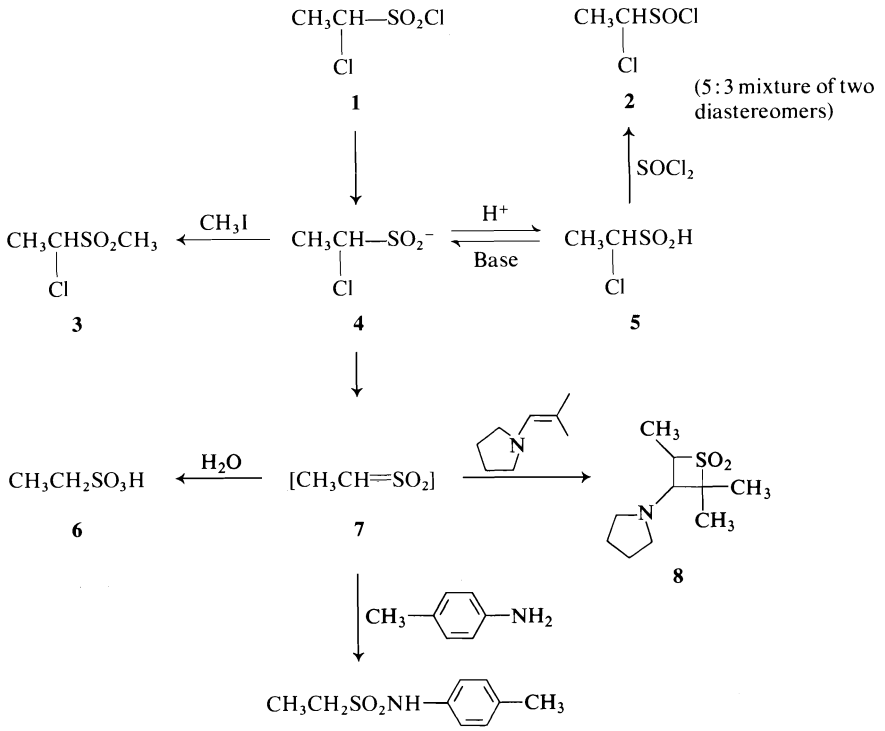

SCHEME 1

acetate buffer at 60°C, the pseudo first-order rate constants for p*H* values of 4.0, 5.0, and 5.9 were respectively 2.42, 2.67, and 2.53 × 10^{-5} s^{-1}. This insensitivity to change in p*H* taken with the previously mentioned strong acidity of **5**, fits with the proposal that **7**, **8**, and **9** are formed by unimolecular reaction of the anion **4**, as in Scheme 1. The nature of these products, especially **8**, points to the sulfene **7** as the only reasonable precursor for these materials.

The formation of the sulfene from 1-haloalkanesulfinic acids is presumably a general reaction. We found that 1-bromoethanesulfinic acid was rather unstable at room temperature and did not require heating to afford the *p*-toluidide **9**. Chloromethanesulfinic acid, on the other hand, needed extended refluxing in benzene to give methanesulfon-*p*-toluidide. Since the publication of our preliminary report, two reports of the abnormal route involving the trichloromethanesulfinate anion have appeared (14, 15). Dykman (14) postulated the transformation $Cl_3C—SO_2^- \rightarrow Cl_2C{=}SO_2$ as a step in a mechanism accounting for formation of the complex thiosulfonate ester $Cl_2CHSO_2SCCl_3$ on reaction of Cl_3CSCl with dilute base. Kempe and Norin (15) proposed both 'abnormal' addition and elimination processes, the former in the sequence

$$Cl_2CHSO_2Cl \xrightarrow{Et_3N} Cl_2C{=}SO_2 \xrightarrow{Cl^-} Cl_3CSO_2^-\,Et_3NH^+$$

and the latter to account for halogen exchange, $Cl_3CSO_2^- \rightarrow Cl_2BrCSO_2^-$, in the presence of $Et_3NH^+Br^-$.

Mechanism of 'Abnormal' Sulfene Formation

Although simple loss of chloride ion with direct formation of the sulfene is the most direct and the most likely route from the anion **4** to the sulfene **7**, there are less obvious routes which warrant some consideration here. One conceivable possibility, for example, is that the sulfinate anion **4** rearranges to the carbanion **10**, which then either loses chloride ion directly or picks up a proton to form ethanesulfonyl chloride which is transformed in the reaction medium to the sulfene **7** (either directly or via **10**). That ethanesulfonyl chloride cannot have been involved in the formation of **7**, however, is shown by an experiment in which 1-chloro-

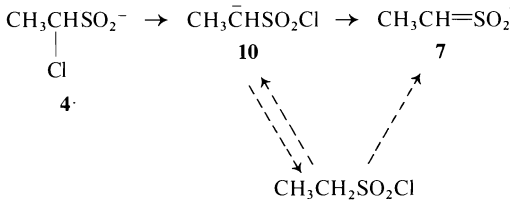

ethanesulfinic acid-*d* was treated with triethylamine in the presence of *p*-toluidine-d_2. In such a reaction mixture any ethanesulfonyl chloride formed (via the route **4** → **10** → ethanesulfonyl chloride) would necessarily have been mostly monodeuterated (*i.e.*, CH_3CHDSO_2Cl) since the only important sources of hydrogen ions for converting **10** to ethanesulfonyl chloride are the SO_2D and ND_2 groups. A control experiment with CH_3CHDSO_2Cl and triethylamine and *p*-toluidine-d_2 gave a substantial amount of the dideuterated *p*-toluidide ($CH_3CD_2SO_2NHC_6H_4$-CH_3, after normal work-up), and since there was no clear sign of any of the dideuterated sulfonamide in the reaction starting from **5**, we conclude that ethanesulfonyl chloride is not an intermediate for any significant portion of the reaction **5** → **7**.

Avoidance of formation of ethanesulfonyl chloride does not preclude involvement of **10**, but does require that the reaction **10** → **7** be very fast, since deuteration of **10** by $Et_3\overset{+}{N}D$ is probably diffusion-controlled (or close to it). In that event the reaction **4** → **10** is presumably rate determining. Our observation of simple first-order decomposition of **4** precludes bimolecular reactions of **4** either with itself or any other reagent not present at the same concentration in each of our experiments at three different p*H* values; this, in effect, would limit the reaction to a simple unimolecular reaction. Consideration of the stereochemistry of a unimolecular rearrangement, however, leads us to question its feasibility. The closest analogies for such a transfer of chlorine would appear to us to be the reaction of sulfinate anions with chlorine to form the sulfonyl chloride, or (in the reverse direction) the reaction of sulfonyl chlorides with carbanionic species such as acetylides (16) or enolates (17). These reactions may be regarded as S_N2 reactions at chlorine, and though the geometric requirements of nucleophilic displacements are not known, such 'endocyclic' S_N2 reactions at carbon are not observed, the preferred route being the intermolecular pathway (18).

One further point may be raised concerning the intermediacy of **10**. Williams and co-workers (19) have suggested that a carbanion of the type $PhCHSO_2Z$ where Z is a good leaving group (*e.g.*, 2,4-dinitrophenoxide) may be so short-lived as to be not a true intermediate but merely a point on the slope from the transition state to the sulfene. If this should be the case with **10**, then the *single* transition state for this reaction would look something like **11**, which differs from the presumed transition state **12** for the direct

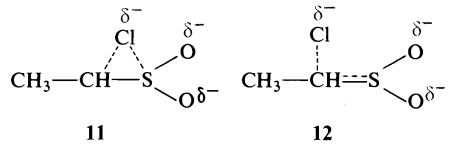

elimination from **4** only in that **11** has a partial bond from sulfur to chlorine rather than to carbon. An experimental distinction between **11** and **12** appears too subtle for us to attempt at present, and, in sum, the mechanism proceeding through **10**, to the extent that it is operationally distinguishable from the direct extrusion from **4**, remains a possible route, though in the face of the above points, a rather unlikely one.

A third conceivable route is the process **4** → **13** → **7**. The first step is analogous to the formation of α-lactones from carboxylate anions

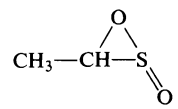

bearing a good leaving group in the α-position as proposed initially by Kenyon and Phillips (20). It has been suggested (21) that α-sultines, such as **13**, are intermediates in the formation of aldehydes or ketones from sulfenes on flash thermolysis above 800°C, but their implication in reactions in solution has not been demonstrated. Oxidation of sulfines is known to give ketones (22) and it is attractive to postulate that this reaction may take place via a transient α-sultine, which may be hydrolyzed to the α-hydroxyalkanesulfinic acid which in turn proceeds to the carbonyl product. Such a scheme would suggest that if **13** is an intermediate in the formation of **7** from **4** that one might well find some acetaldehyde (or derivative) also formed in the reaction; none has been observed in our experiments, however, and the possibility that the α-sultine may be formed in this system remains,

but without any basis other than the analogy to α-lactone formation.

The Ambifunctionality of Sulfene

From the above discussion it would appear that the simple direct elimination process is the most likely route for the formation of the sulfene, and it follows, of course, that the reverse reaction is similarly the most likely mechanism for the postulated abnormal addition. If this is so then sulfenes show the apparently hitherto unobserved property of being 'ambifunctional' (23) electrophiles in which the attacking nucleophile may form a bond by simple addition to either of two different nuclei, carbon or sulfur in this case. Ambifunctional electrophiles in which the electrophilic centres are atoms of the same kind are well known (*e.g.* allylic cations and α,β-unsaturated ketones), and, in addition, electrophilic behaviour involving attack at two different atoms in *displacement* (as opposed to addition) reactions is observed, for example, with sulfonyl chlorides, which may yield either a sulfonyl derivative and chloride ion or a chlorinated derivative and sulfinate ion by attack at either the sulfur or the chlorine atoms, respectively. We are unable to call to mind, however, any previously known examples of simple *addition* to either of two different nuclei. Though ambifunctionality often leads to an interesting interplay of kinetic and thermodynamic factors, we prefer not to discuss this aspect of the chemistry of sulfenes until we have more data.

Conclusion

The chief point that we make from these observations is that the transition state for the abnormal route is readily obtainable from an α-substituted alkanesulfinic acid (for 1-chloroethanesulfinate at 60% $\Delta G^{\ddagger} = 26.5$ kcal mol^{-1}) and hence must be regarded as a species which, under some circumstances at least, could be obtained from a sulfene and a nucleophile. To be sure, the normal reaction of a nucleophile in the presence of a proton donor is to form the sulfonic acid derivative, but the 'abnormal' process may be important in certain situations (*e.g.* when the normal route merely leads back to the starting material). The 'abnormal' route would appear to be the mode of reaction in the formation of the thioacyl chloride *S*-oxides (6*a*,*b*; see also ref. 1), and hence the singular 1,3-dipolar addition process suggested by Strating (24) is unnecessary.

A final comment on the synthetic limitations of the formation of sulfenes from α-haloalkanesulfinic acids seems in order. Though the present study provides a new route to sulfenes, it is likely that it will find only occasional synthetic use; neither the yields, which are at best unremarkable, nor the relative inaccessibility of starting materials (at least at present) recommends it for common use. It appears that sulfinic acids (or sulfinate anions) react with sulfenes (to give uncharacterized products) and it is likely that the yields of desired sulfene products obtainable from this route may be limited by the destructive tendency of the sulfene to be consumed by reaction with its precursor. The chief significance of this study lies not so much in its synthetic value but rather in the insight it provides into the mechanisms of sulfene reactions.

Experimental

Infrared spectra were obtained with Beckman IR-10 or IR-20 spectrometers; nuclear magnetic resonance spectra with Varian A-60, T-60, or HA-100 instruments using tetramethylsilane as internal standard. Potentiometric titrations and p*H* determinations were carried out with a Radiometer PHM 25 p*H* meter. Melting points were determined on a Kofler hot stage and are uncorrected. 1,2-Dimethoxyethane (DME) and triethylamine were reagent grade materials distilled from CaH_2.

*Reaction of 1-Chloroethanesulfonyl Chloride (**1**) with Zinc Dust*

1-Chloroethanesulfonyl chloride (**1**) was prepared from trithioacetaldehyde (25) by the method of Müller and Raudenbusch (7); bp 51–53°C/5 Torr, 50% yield; ir (film) ν_{max} 1380 (s), 1170 (s), and 690 (m) cm^{-1}; nmr, δ 2.06 (3H, d, $J = 7$ Hz) and 5.36 (1H, q). The sulfonyl chloride (**1**) (5.8 g, 35 mmol) was dissolved in 24 ml of absolute ethanol; zinc dust was added in small portions until no more heat was evolved. The mixture was filtered and the solvent removed from the filtrate by evaporation. Potassium carbonate solution was added to the liquid residue until it was alkaline and the water evaporated under reduced pressure. A solid was obtained which was dissolved in water and passed through a column of Dowex 50W-X8 (H^+) cation exchange resin, the column being eluted with water until the eluant was no longer acidic. Water was removed from the eluant by evaporation. The residue was refluxed with excess thionyl chloride and the product was distilled under reduced pressure. Ethanesulfonyl chloride (0.36 g, 2.7 mmol, 8%) was obtained. The ir (liquid film) showed peaks at 1500 (w), 1360 (s), and 1160 cm^{-1} (s); the nmr ($CDCl_3$) had peaks at δ 1.6 (3H, t, $J = 7.0$ Hz) and 3.7 (2H, q); both of the spectra matched those of a commercial sample of ethanesulfonyl chloride (Eastman).

*1-Chloroethanesulfinic Acid (**5**)*

1-Chloroethanesulfonyl chloride (3 g, 18.4 mmol) was stirred for 1 h with a solution of sodium sulfite (4.8 g,

38 mmol) in 50 ml of water. The solution was washed with methylene chloride. Sulfuric acid (2 *M*) was added to the aqueous layer and the acidic solution was extracted 6 times with 40 ml portions of ether. The ether extracts were combined, dried ($MgSO_4$), and the solvent evaporated at a low temperature (*ca.* 40°C) to yield 1-chloroethanesulfinic acid (1.8 g, 14 mmol, 60% yield); ir ($CHCl_3$) ν_{max} 2900 (br s), 1080 (s), and 830 cm^{-1} (m); nmr ($CDCl_3$) δ 1.75 (3H, d, J = 7 Hz), 4.75 (1H, q), and 10.5 (1H, s). A sample (0.132 g) was dissolved in 250 ml of water and a 5 ml aliquot pipetted into a beaker; the solution was diluted with 140 ml of distilled water plus 200 ml of 0.1 *M* sodium hydroxide, and titrated potentiometrically (glass and platinum electrodes and a salt bridge) with 0.0066 *M* potassium permanganate solution (26) to an end point of 3.17 ml. After correcting for a blank of 0.035 ml, the titre was 3.135 ml, corresponding to 0.0207 mmol (100.1%) of the acid. Potentiometric titration of 1-chloroethanesulfinic acid with 0.0428 *M* sodium hydroxide gave a titration curve indistinguishable from that given by perchloric acid.

Reaction of 1-Chloroethanesulfinic Acid (5) with p-Toluidine

p-Toluidine (4.28 g, 40 mmol) and triethylamine (1.2 g, 12 mmol) were dissolved in acetonitrile (30 ml) and the solution heated to reflux. 1-Chloroethanesulfinic acid (0.516 g, 4 mmol) dissolved in acetonitrile (20 ml) was added to the refluxing solution over a period of 5 min. Refluxing was continued for a further 30 min, and the acetonitrile solution was allowed to cool to room temperature. The solution was made acidic with 2 *M* hydrochloric acid, and most of the acetonitrile was removed by evaporation.

Extraction of the remaining solution with methylene chloride yielded, after drying ($MgSO_4$) and evaporation of the solvent, ethanesulfon-*p*-toluidide (617 mg, 3.09 mmol, 77.5%). Recrystallization from methylene chloride – petroleum ether gave the ethanesulfon-*p*-toluidide (532 mg, 2.67 mmol, 67% yield), mp 77–80°C. The mp and ir and nmr spectra were identical to those of an authentic specimen prepared (27) from ethanesulfonyl chloride (Eastman).

When the above reaction was carried out in benzene at 45°C the yield of ethanesulfon-*p*-toluidide was 10%, and at 65°C, 32%.

Reaction of 1-Chloroethanesulfinic Acid (5) with 1-(2-Methylpropenyl)pyrrolidine and Triethylamine

Triethylamine (2 g, 20 mmol) was dissolved in acetonitrile (20 ml) and the mixture heated to reflux. A solution of the enamine (28) (7.1 g, 56 mmol) in 10 ml of acetonitrile was added to the refluxing mixture. 1-Chloroethanesulfinic acid (**5**) (713 mg, 5.5 mmol) was dissolved in acetonitrile and added to the stirred, refluxing mixture over a period of 4 min. The reaction was refluxed for a further 35 min. The mixture was allowed to cool and then acidified with 2 *M* sulfuric acid. The acidic solution was washed with methylene chloride, made basic with potassium carbonate, and extracted with methylene chloride. The CH_2Cl_2 layer after drying ($MgSO_4$) and evaporation gave an oil, which after addition of MeOH gave the cycloadduct (**8**) (117 mg, 0.82 mmol, 15%), mp 79–83°C. Recrystallization from MeOH gave the analytical specimen, mp 83.5–85°C. *Anal.* calcd. for $C_{10}H_{19}NO_2S$: C 55.26, H 8.81, N 6.45, S 14.75; found: C 55.01, H 8.89, N 6.42, S 14.89.

Reaction of ethanesulfonyl chloride with the enamine under similar conditions gave **8** (23% yield), mp 83–84°C, mixture mp with the material obtained above, 82.5–83°C; the ir and nmr spectra were identical to those of the above material: ν_{max} ($CHCl_3$), 2970 (m), 2700 (m), 1460 (w), 1300 (s), 1100 cm^{-1} (s); δ ($CDCl_3$) 1.48 (3H, s), 1.58 (3H, d, J = 8 Hz), 1.60 (3H, s), 1.78 (4H, m), 2.50 (4H, m), 2.88 (1H, d, J = 8.7 Hz), and 4.03 (1H, dq, J = 8 and 8.7 Hz).

Preparation of Methyl 1-Chloroethyl Sulfone (3) from 1-Chloroethanesulfinic Acid (5)

Triethylamine (1.2 g, 12 mmol) was added to 1-chloroethanesulfinic acid (**5**) (690 mg, 5.4 mmol) and the mixture stirred while methyl iodide (17.5 ml, 38 g, 270 mmol) was added over a period of 12 min. The mixture was refluxed with continuous stirring for 23 min. Water was added and the mixture extracted with methylene chloride. The extracts were combined, washed with aqueous sodium thiosulfate, dried ($MgSO_4$), and the solvent evaporated leaving methyl 1-chloroethyl sulfone (**3**) (0.589 g, 4.1 mmol). Recrystallization from chloroform – petroleum ether gave white crystals of **3** (0.573 g, 4.0 mmol, 74% yield) mp 56–57°C; reported (29) mp 62°C. The nmr spectrum ($CDCl_3$) showed peaks at δ 1.85 (3H, d, J = 8 Hz), 2.98 (3H, s), and 4.68 (1H, q); ir ($CHCl_3$): ν_{max} 1322 (s), 1145 (s), and 960 cm^{-1} (m). *Anal.* calcd. for $C_3H_7ClSO_2$: C 25.27, H 4.95, Cl 24.86, S 22.48; found: C 25.26, H 5.02, Cl 24.66, S 22.65.

1-Chloroethanesulfinyl Chloride (2)

Thionyl chloride (8.3 g, 70 mmol) was slowly added to 1-chloroethanesulfinic acid (**5**) (1.22 g, 9.5 mmol) at 0°C, and the mixture stirred for 1 h at room temperature. The mixture was then refluxed for 1 h and the excess thionyl chloride distilled off at atmospheric pressure. The product was distilled under reduced pressure. A small amount of 1-chloroethanesulfinyl chloride was obtained as a colorless oil. The ir spectrum (liquid film): ν_{max} 1400 (m), 1375 (m), 1160 (s), and 1035 cm^{-1} (m). The nmr spectrum ($CDCl_3$, HA-100) showed quartets at δ 5.02 and 5.18 (J = 6.5 Hz) with relative areas of 3:5 and doublets at 1.92 and 1.91.

Reaction of 1-Chloroethanesulfinic Acid (5) with Aqueous Sodium Hydroxide

1-Chloroethanesulfinic acid (**5**) (0.73 g, 5.7 mmol) was added to a refluxing solution of sodium hydroxide (0.65 g, 16 mmol) in 20 ml of water. The mixture was stirred under reflux for 35 min and the water removed by evaporation under reduced pressure. The residue was suspended in methylene chloride and phosphorus pentachloride (8.5 g) was added in small portions while swirling the mixture at room temperature. The methylene chloride was decanted, washed with water, dried ($MgSO_4$), and evaporated leaving ethanesulfonyl chloride (0.48 g, 2.9 mmol, 52% yield). The identity of the product was determined by comparing the nmr and ir spectra with those of a commercial sample of ethanesulfonyl chloride (Eastman).

Rate of Release of Chloride Ion from 1-Chloroethanesulfinic Acid (5) in Aqueous Acetate Buffers

A solution of 1-chloroethanesulfinic acid (**5**) (*ca.*

4 mmol) in 0.2 *M* acetic acid – sodium acetate buffer (100 ml) was frozen in liquid N_2 and degassed, and then heated in a water bath at 60.0 ± 0.1°C. Argon was let into the flask which was then fitted with a serum cap. Aliquots (5.00 ml) were removed at intervals and quenched by diluting in cold water (40 ml). The chloride ion content was determined by potentiometric titration (silver and glass electrodes) with 0.01 *M* $AgNO_3$. Good first-order rate plots were obtained as far as the reactions were followed (to about 60% reaction). The rate constants (determined graphically) were as follows: p*H* 4.0, 2.42×10^{-5}; p*H* 5.0, 2.67×10^{-5}; p*H* 5.90, 2.53×10^{-5} s^{-1}.

Reaction of 1-Chloroethanesulfinic Acid-d with p-Toluidine-d_2

1-Chloroethanesulfinic acid (**5**) in ether was shaken with several portions of D_2O. The sulfinic acid obtained after drying ($MgSO_4$) and evaporation of the ether was found by nmr to contain >90% deuteration of the acidic hydrogen. *p*-Toluidine-d_2 was prepared as follows. *p*-Toluidine was recrystallized from ethanol–water and the crystals dissolved in CH_2Cl_2. The CH_2Cl_2 layer was removed from the aqueous layer which formed, dried ($MgSO_4$), and then shaken with several portions of D_2O and dried over anhydrous K_2CO_3. The product remaining upon removal of the solvent showed 96% incorporation of deuterium in the amino group.

Triethylamine (0.7 g, 7 mmol) and *p*-toluidine-d_2 (1.4 g, 13 mmol) were dissolved in 20 ml of acetonitrile and the solution heated to reflux. 1-Chloroethanesulfinic acid-*d* (0.18 g, 1.4 mmol) dissolved in acetonitrile (10 ml) was added to the stirred refluxing mixture over a period of 4 min, and the mixture was refluxed for 35 min. The reaction was cooled and dilute sulfuric acid was added. The acetonitrile was evaporated. The aqueous solution was extracted with methylene chloride. The methylene chloride was dried ($MgSO_4$) and evaporated yielding the toluidide (0.17 g, 0.86 mmol, 61% yield), which was recrystallized from methanol giving a product with mp 81–81.5°C. The nmr spectrum ($CDCl_3$) showed no detectable dideuterated toluidide. The mass spectrum analyzed for undeuterated 21 ± 2%, monodeuterated 77 ± 2%, and dideuterated 2 ± 2% products, corresponding to 6.18 atom % excess D; deuterium analysis gave 6.10 atom % excess D.

Reaction of Ethanesulfonyl-1-d Chloride with Triethylamine and p-Toluidine-d_2

Ethanesulfonyl-*1-d* chloride was prepared by reaction of ethanesulfonyl chloride in dioxane-D_2O with triethylamine and converting the resultant triethylammonium ethanesulfonate-*1-d* to the sulfonyl chloride with PCl_5 in CH_2Cl_2 as previously described (30); deuterium analysis gave 17.65 atom % excess D (calcd. for CH_3CHDSO_2Cl: 20.0 atom % excess D); nmr integration indicated 92% CH_3CHDSO_2Cl and 8% $CH_3CH_2SO_2Cl$. When this sulfonyl chloride was added to a refluxing mixture of triethylamine and *p*-toluidine-d_2 in acetonitrile as described for the experiment with $CH_3CHClSO_2D$, the toluidide (35% yield) was found by examination of the methyl signal at δ 0.9 to consist of 22 ± 5% of undeuterated, 44 ± 5% of monodeuterated, and 34 ± 5% dideuterated toluidide.

1-Bromoethanesulfinic Acid

1-Bromoethanesulfonyl chloride (31) (536 mg, 2.58 mmol) was stirred for 1 h with a solution of sodium sulfite (660 mg, 5.2 mmol) in water (10 ml). The work-up and isolation were performed at less than 10°C. The solution was acidified with sulfuric acid (2 *M*), then extracted with ether (4 × 10 ml). The combined ether extracts were dried ($MgSO_4$) and the solvent removed to give 1-bromoethanesulfinic acid (295 mg, 66%); nmr spectrum ($CDCl_3$): δ 9.3–6.0 (variable br s, combination of water and sulfinic acid proton), 4.41 (1H, q, J = 7 Hz), 1.84 (3H, d, J = 7 Hz). The acid was used within 2 h after isolation. An impurity with δ 3.66 (q, J = 7 Hz), 1.22 (t) was present in varying small amounts.

Reaction of 1-Bromoethanesulfinic Acid, p-Toluidine and Triethylamine

1-Bromoethanesulfinic acid (262 mg, 1.51 mmol) in acetonitrile (10 ml) was added during 5 min to a solution of *p*-toluidine (1.62 g, 15.1 mmol) and triethylamine (0.64 ml, 4.54 mmol) in acetonitrile (20 ml) at 0°C. The resulting pale yellow solution was stirred at room temperature for a further 55 min, then acidified (2 *M* HCl) and the solvent removed *in vacuo*. The acidic solution was extracted with ether (3 × 25 ml). The combined ether extracts were dried ($MgSO_4$) and the solvent removed to give the crude toluidide (**9**) (150 mg, 45%). The mp and nmr spectrum were identical to those of the toluidide prepared from ethanesulfonyl chloride, a mixture mp showed no depression. When the above reaction was carried out for 2 h and 19 h, the yields of ethanesulfon-*p*-toluidide were 50 and 74%, respectively; at 4°C for 10 min and 1 h the yields were 6 and 26%, respectively. Reaction of 1-chloroethanesulfinic acid (**5**) at room temperature for 1 h, as above, gave no toluidide (**9**) detectable by nmr.

Chloromethanesulfinic Acid and its Reaction with p-Toluidine

Chloromethanesulfonyl chloride (32) (3.4 g, 23 mmol) was stirred with an aqueous solution of sodium sulfite (4.8 g in 50 ml) containing $NaHCO_3$. The solution was washed with CH_2Cl_2 and then strongly acidified with 3 *M* H_2SO_4 and extracted with ether. The extracts were dried and the solvent evaporated leaving a pale yellow oil (1.6 g, 61%). *p*-Toluidine (2.0 g) and triethylamine (1.5 g) were dissolved in benzene (30 ml), added to chloromethanesulfinic acid (0.37 g, 3.2 mmol), and the mixture refluxed overnight. The precipitate ($Et_3NH^+Cl^-$) was removed by filtration and the benzene solution washed with dilute HCl, and the dried solvent evaporated leaving the crude methanesulfon-*p*-toluidide (0.3 g, 50%), which on recrystallization from ether – petroleum ether melted at 99–101°C; the infrared and nmr spectra were identical to those of authentic specimen (33) prepared from methanesulfonyl chloride.

Acknowledgments

We thank the National Research Council of Canada for financial support and Mr. S. K. Laurence Li for carrying out the experiment with chloromethanesulfonyl chloride.

1. J. F. KING and D. R. K. HARDING. Can. J. Chem. **54**, 2652 (1976).
2. J. F. KING and R. P. BEATSON. Chem. Commun. 663 (1970).

3. J. F. KING, E. A. LUINSTRA, and D. R. K. HARDING. J. Chem. Soc. Chem. Commun. 1313 (1972).
4. G. OPITZ. Angew. Chem. Int. Ed. Engl. **6**, 107 (1967).
5. J. F. KING. Acc. Chem. Res. **8**, 10 (1975).
6. (*a*) J. F. KING and T. DURST. Tetrahedron Lett. 585 (1963); (*b*) J. F. KING and T. DURST. Can. J. Chem. **44**, 819 (1966); (*c*) T. DURST and J. F. KING. Can. J. Chem. **44**, 1869 (1966); (*d*) J. F. KING, K. PIERS, D. J. H. SMITH, C. L. MCINTOSH, and P. DE MAYO. Chem. Commun. 31 (1969); (*e*) J. F. KING, A. HAWSON, D. M. DEAKEN, and J. KOMERY. Chem. Commun. 33 (1969).
7. E. MÜLLER and H. RAUDENBUSCH. Ber. **64**, 94 (1931).
8. R. SCHILLER and R. OTTO. Ber. **9**, 1584 (1876); C. PAULY. Ber. **10**, 941 (1877).
9. L. J. BELLAMY. *In* Organic sulfur compounds. Vol. 1. *Edited by* N. Kharasch. Pergamon Press, London. 1961. pp. 47–56.
10. R. K. BURKHARD, D. E. SELLERS, F. DECOU, and J. L. LAMBERT. J. Org. Chem. **24**, 767 (1959); G. KORTÜM, W. VOGEL, and K. ANDRUSSOW. Dissociation constants of organic acids in aqueous solutions. Butterworths, London. 1961.
11. G. CANALINI, G. MACCAGNANI, and F. TADDEI. Tetrahedron Lett. 3035 (1971); M. MIKOŁAJCZYK and J. DRABOWICZ. Z. Naturforsch. Teil B, **26**, 1372 (1971); A. MAJID and J. M. SHREEVE. Inorg. Chem. **13**, 2710 (1974); R. P. GUPTA, J. S. PIZEY, and K. SYMEONIDES. Tetrahedron, **32**, 1917 (1976).
12. L. A. PAQUETTE, J. P. FREEMAN, and R. W. HOUSER. J. Org. Chem. **34**, 2901 (1969).
13. V. N. DROZD, V. V. SERGEICHUK, and N. D. ANTONOVA. Zh. Org. Khim. **10**, 1498 (1974).
14. E. DYKMAN. Chem. Commun. 1400 (1971).
15. T. KEMPE and T. NORIN. Acta Chem. Scand. Ser. B, **28**, 609 (1974).
16. R. TRUCHET. Ann. Chim. **16**, 309 (1931).
17. E. P. KOHLER and M. B. MCDONALD. Am. Chem. J. **22**, 230 (1899); C. L. JACKSON and F. C. WHITMORE. J. Am. Chem. Soc. **37**, 1915 (1915).
18. L. TENUD, S. FAROOQ, J. SEIBL, and A. ESCHENMOSER. Helv. Chim. Acta, **53**, 2059 (1970).
19. K. T. DOUGLAS, A. STELTNER, and A. WILLIAMS. J. Chem. Soc. Chem. Commun. 353 (1975).
20. J. KENYON and H. PHILLIPS. Trans. Faraday Soc. **26**, 451 (1930); C. M. BEAN, J. KENYON, and H. PHILLIPS. J. Chem. Soc. 303 (1936).
21. C. L. MCINTOSH and P. DE MAYO. Chem. Commun. 32 (1969); J. F. KING, P. DE MAYO, C. L. MCINTOSH, K. PIERS, and D. J. H. SMITH. Can. J. Chem. **48**, 3704 (1970); H. HIRAOKA. J. Chem. Soc. Chem. Commun. 1014 (1974).
22. B. ZWANENBURG, L. THIJS, and J. STRATING. Recl. Trav. Chim. Pays-Bas, **86**, 577 (1967).
23. R. GOMPPER. Angew. Chem. Int. Ed. Engl. **3**, 560 (1964); R. GOMPPER and H. U. WAGNER. Angew. Chem. Int. Ed. Engl. **15**, 321 (1976).
24. J. STRATING. Recl. Trav. Chim. Pays-Bas, **83**, 94 (1964).
25. E. BAUMANN and E. FROMM. Ber. **22**, 2600 (1889).
26. P. ALLEN, JR. J. Org. Chem. **7**, 23 (1942).
27. N. N. MEL'NIKOV, E. M. SOKOLOVA, and P. P. TRUNOV. Zhur. Obshch. Khim. **29**, 529 (1959).
28. E. BENZING. Angew. Chem. **71**, 521 (1959).
29. H. BÖHME and H. J. GRAN. Ann. **577**, 68 (1952).
30. J. F. KING and T. DURST. J. Am. Chem. Soc. **87**, 5684 (1965).
31. L. A. CARPINO, L. V. MCADAMS III, R. H. RYNBRANDT, and J. W. SPIEWAK. J. Am. Chem. Soc. **93**, 476 (1971).
32. H. BRINTZINGER, H. KODDEBUSCH, K. E. KLING, and G. JUNG. Chem. Ber. **85**, 455 (1952).
33. I. B. DOUGLASS and B. S. FARAH. J. Org. Chem. **24**, 973 (1959).

Applicability of the H_T acidity function to the protonation of thioamides, thioureas, and thionesters

JOHN T. EDWARD, GARY D. DERDALL, AND SIN CHEONG WONG

Department of Chemistry, McGill University, P.O. Box 6070, Station A, Montreal, P.Q., Canada H3C 3G1

Received August 3, 1976[1]

JOHN T. EDWARD, GARY D. DERDALL, and SIN CHEONG WONG. Can. J. Chem. **55**, 2331 (1977).

The protonation of eleven thioamides, five thioureas, and four thionbenzoates in aqueous sulfuric acid has been found to follow the H_T acidity function with acceptable accuracy. Protonation constants pK_{TH^+} obtained by use of H_T agreed fairly well with pK_{TH^+} values obtained by the Bunnett–Olsen method, but less well with those obtained by the Marziano–Cimino–Passerini procedure. Linear free-energy relationships of pK_{TH^+} values are discussed.

JOHN T. EDWARD, GARY D. DERDALL et SIN CHEONG WONG. Can. J. Chem. **55**, 2331 (1977).

On a observé que la protonation d'onze thioamides, cinq thiourées et quatre thionbenzoates dans de l'acide sulfurique aqueux suit avec une précision convenable la fonction d'acidité H_T. Les constantes pK_{TH^+} établies par l'usage de H_T sont en assez bon accord avec les valeurs établies par la méthode de Bunnett et Olsen, mais pas avec les valeurs établies par la méthode de Marziano, Cimino et Passerini. On discute des relations linéaires de l'enthalpie libre des valeurs pK_{TH^+}.

In a recent paper (1), we have reported values of an acidity function H_T governing the conversion of thiocarbonyl compounds (T) into their conjugate acid forms (TH^+) in aqueous sulfuric acid. This function is defined by

$$[1] \quad H_T = -\log (a_{H^+} f_T / f_{TH^+}) = pK_{TH^+} - \log ([TH^+]/[T])$$

where all symbols have their customary definitions (2). In the present paper we test the applicability of this H_T function, developed by the classical Hammett–Deyrup (H.D.) overlap procedure (3), to the ionization behaviour of 20 other thiocarbonyl compounds, and compare pK_{TH^+} (H.D.) values obtained by its use with pK_{TH^+} values obtained by analysing the experimental data according to the procedures of Bunnett and Olsen (B.O.) (4) or Marziano, Cimino, and Passerini (M.C.P.) (5) which do not require a specific acidity function for each class of compounds.

Experimental

Materials

Thioacetamide (6), 2-phenylthioacetamide (6), thiocyclohexanecarboxamide (6), and 1-methyl-2-thiopyridone (7) were prepared by reaction of the corresponding amides with phosphorus pentasulfide. Their melting points were close to those reported in the literature. Thiopivalamide, a new compound, was similarly prepared: after crystallization from ethanol, it had the properties listed in Table 1.

All substituted thiobenzamides were prepared by reacting the appropriate nitriles with hydrogen sulfide in the presence of triethylamine (8, 9). Melting points and elemental analyses of two new compounds are given in Table 1.

All substituted thioureas were commercial products and were recrystallized to constant melting point.

Substituted thionbenzoates were prepared from the corresponding nitriles via benzimidate hydrochloride intermediates (1, 10). They were purified by chromatography in hexane solution over alumina, followed by distillation under reduced pressure.

Measurement of Ionization Ratios

Ionization ratios ($I = [TH^+]/[T]$) of thiocarbonyl compounds were measured spectrophotometrically, following general procedures already described (1) and are available as supplementary material.[2]

Results and Discussion

Applicability of H_T Function

From equation 1, it is evident that a plot of log I against H_T should give a straight line of unit slope. In practice, it is found that slopes often vary from unity, but their closeness to unity is an indication of the applicability of the acidity function to the particular compounds. Values in the range 0.95–1.05 are desirable, but

[1]Revision received March 1, 1977.

[2]A complete set of tabular data is available, at a nominal charge, from the Depository of Unpublished Data, CISTI, National Research Council of Canada, Ottawa, Canada K1A 0S2.

TABLE 1. Characterization of new compounds

Compound	mp (°C)	λ_{max} (nm) and ε_{max} (parentheses) in EtOH	Formula	Calcd.				Found			
				C	H	N	S	C	H	N	S
Thiopivalamide	116–119	340(55), 269.5(1020)	$C_5H_{11}NS$	51.2	9.5	12.0	27.3	51.2	9.5	12.1	26.9
3-Methoxythiobenzamide	102–103	384(240), 298(8530), 252(5630)	C_8H_9NOS	57.5	5.4	8.4	19.2	57.5	5.4	8.5	19.0
3-Methylthiobenzamide	90–91	384(230), 293(7080), 248(7250)	C_8H_9NS	63.5	6.0	9.3	21.2	63.4	6.0	9.3	21.4

those between 0.9–1.1 are considered acceptable (11).

Table 2 lists the 20 thiocarbonyl compounds investigated, along with the slopes of log I *vs.* H_T. All compounds have slopes within the range 0.9–1.1, with all of the thionesters and most of the thioamides having slopes between 0.95–1.05. The thioureas show a greater scatter in their slopes, probably because their spectra are subject to stronger medium shifts (1). If we include the 16 original H_T indicators (which obviously must have slopes close to unity), a total of 36 thiocarbonyl compounds are found to follow the H_T function, the average slope being 0.992 with a standard deviation of 0.037. The results are comparable to those obtained from the application of H_A to aromatic amides (11) (average slope 1.001, standard deviation 0.051) and of H_0 to substituted anilines (12) (average slope 0.995, standard deviation 0.040). This result is remarkable, considering the diversity of thiocarbonyl types tested, and indicates the H_T function to be generally applicable to the ionization behaviour of thiocarbonyl compounds.

pK_{TH^+} Values

With the applicability of [1] firmly established, the thermodynamic dissociation constant (pK_{TH^+}) of a thiocarbonyl compound may be calculated from either (*a*) the intercept of the plot of log I *vs.* H_T, or (*b*) the average pK_{TH^+} values obtained by application of [1] to log I data at various acid concentrations. The two methods proved to give essentially the same results within 0.02 logarithmic units. pK_{TH^+} (H.D.) values obtained by method *b* are reported in Table 2. The pK_{TH^+} of the strongest base, 1-methyl-2-thiopyridone, was also obtained by extrapolation to zero acid concentration of a plot of log I − log $[H^+]$ against $[H^+]$ for concentrations of perchloric acid between 0.7 and 2.5 M (13). The value of −1.56 agrees with the value obtained from [1], and gives a further proof that the H_T scale has been correctly anchored in dilute aqueous acid.

Also given in Table 2 are pK_{TH^+} values obtained by the B.O. and M.C.P. approaches. While the H.D. values obtained using H_T and [1] are in fair agreement with B.O. values, they are in much poorer agreement with M.C.P. values, obtained using M_C values for different concentrations of sulfuric acid (1) and the

TABLE 2. Protonation constants (pK_{TH^+}) of thiocarbonyl compounds obtained by different methods of analysing experimental data

Compound	H.D. slope of log I vs. $-H_T$	H.D. $-pK_{TH^+}$	B.O. $-\phi$[a]	B.O. $-pK_{TH^+}$	M.C.P. $-n^*$[a]	M.C.P. $-pK_{TH^+}$
Thioamides						
1-Methyl-2-thiopyridone	1.00	1.56±0.05	0.35	1.33	1.20	1.72
Thioacetamide	0.98	2.56±0.03	0.44	2.44[b]	1.47	3.15
Thiopivalamide	1.00	2.41±0.05	0.49	2.34	1.41	2.91
Thiocyclohexanecarboxamide	1.06	2.50±0.05	0.50	2.45	1.55	3.21
2-Phenylthioacetamide	1.07	3.16±0.04	0.47	3.10	1.50	3.83
3-Methoxythiobenzamide	0.93	3.44±0.07	0.41	3.32	1.28	3.65
3-Chlorothiobenzamide	0.97	3.78±0.05	0.26	3.37[c]	1.22	3.82
2-Methylthiobenzamide	1.02	3.52±0.05	0.40	3.36	1.36	3.90
3-Methylthiobenzamide	0.97	3.21±0.04	0.31	2.89	1.35	3.56
4-Methylthiobenzamide	0.94	3.14±0.04	0.29	2.79	1.29	3.38
2,6-Dimethylthiobenzamide	1.00	3.81±0.03	0.26	3.40	1.41	4.27
Thioureas						
1-Methylthiourea	0.94	1.67±0.05	0.22	1.37[d]	1.07	1.72
1-Phenylthiourea	0.92	2.20±0.06	0.28	1.92	1.22	2.42
1,1-Diphenylthiourea	1.07	2.54±0.08	0.51	2.52	1.60	3.34
1,3-Diphenylthiourea	0.94	2.73±0.05	0.41	2.58	1.36	3.13
1,3-Ethylenethiourea	1.02	2.59±0.04	0.48	2.52	1.50	3.23
Thionesters						
Ethyl 4-methylthionbenzoate	0.99	8.12±0.03	0.45	8.14	0.97	7.15
Ethyl 3-methylthionbenzoate	1.03	8.39±0.04	0.52	8.65	1.01	7.71
Ethyl 4-chlorothionbenzoate	0.99	8.99±0.04	0.43	8.92	0.95	7.90
Ethyl 4-bromothionbenzoate	1.00	9.12±0.03	0.44	9.07	0.96	8.05

[a]These symbols defined in ref. 1.
[b]Tissier and Tissier (14) report −2.53.
[c]−3.7 (14).
[d]−1.50 (14).

equation

$$[2]\quad pK_{TH^+} = n_T{}^*M_C - \log\frac{[T]}{[TH^+]} - \log[H^+]$$

However, the B.O. values of Table 2 are for the most part in excellent agreement with pK_{TH^+} values obtained by Professors K. Yates and R. A. Cox (private communication) using a more generalized M.C.P. procedure.

Hammett ρσ Relations

A referee has suggested that a comparison of LFER plots using pK_{TH^+} values obtained from H_T with plots using pK_{TH^+} values obtained by B.O. and M.C.P. methods "would give some idea of whether or not it is *necessary* to derive new acidity functions for new compounds".

A good linear correlation (linear regression correlation coefficient $r = 0.993$) was found between Hammett σ values (15) and pK_{TH^+} (H.D.) values of six *meta*- and *para*-substituted thiobenzamides (Fig. 1) which include 4-methoxythiobenzamide and 4-chlorothiobenzamide from the original H_T indicators (1). The correlation with σ^+ values (15) is poor ($r = 0.920$). The ρ value of −1.29 is close to the value of −0.92 for *meta*- and *para*-substituted benzamides, whose pK_{AH^+} values also correlate with σ rather than σ^+ (11). Correlation of σ with pK_{TH^+} (B.O.) ($r = 0.914$) and with pK_{TH^+} (M.C.P.) ($r = 0.827$) is very much poorer.

Similarly, a good correlation exists between pK_{TH^+} (H.D.) values of aliphatic thioamides and pK_a values of corresponding carboxylic acids (16), as shown in Fig. 2. The slope of the straight line is 1.09 ($r = 0.988$). Again, the correlation of pK_{TH^+} (B.O.) ($r = 0.964$) and of pK_{TH^+} (M.C.P.) ($r = 0.967$) with pK_a is much poorer.

Finally, a good linear correlation is found between σ and pK_{TH^+} (H.D.) for eight substituted thionbenzoates, four of them being H_T indicators (1), as shown in Fig. 3 ($\rho - 2.66$; $r = 0.995$). Correlation between σ and pK_{TH^+} (B.O.) ($r = 0.966$) and pK_{TH^+} (M.C.P.) ($r = 0.978$) is poorer. However, correlations of σ^+

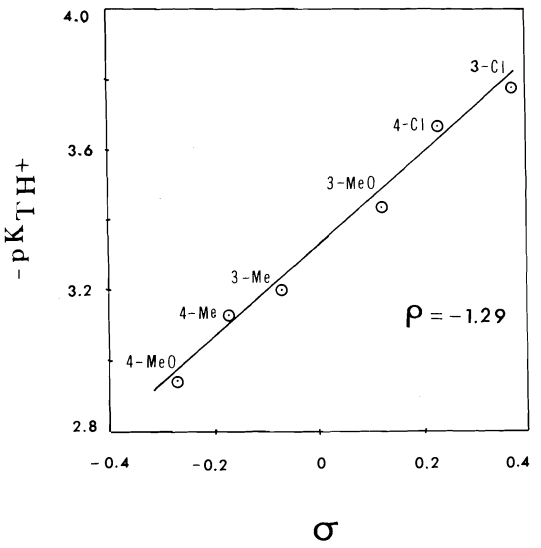

FIG. 1. Hammett ρσ plot for substituted thiobenzamides.

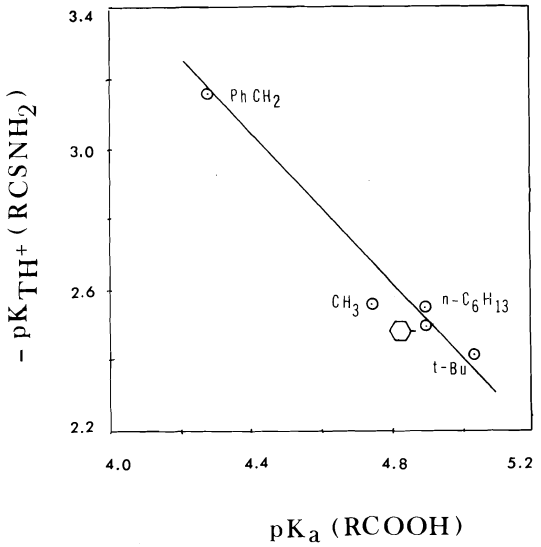

FIG. 2. Linear relation of pK's of carboxylic acids and thioamides.

with pK_{TH^+} (H.D.) (ρ − 2.33; r = 0.990), pK_{TH^+} (B.O.) (r = 0.996), and pK_{TH^+} (M.C.P.) (r = 0.995) are about equally good. (The *p*-methoxy compound was excluded because it is known to show gross deviation in $\rho\sigma^+$ plots for strong acid solutions (17).) The higher ρ values indicate that the ethoxy group of the thionesters is a weaker electron-releasing group than the amino group of the thiobenzamides, so that the extent of delocalization of the positive charge

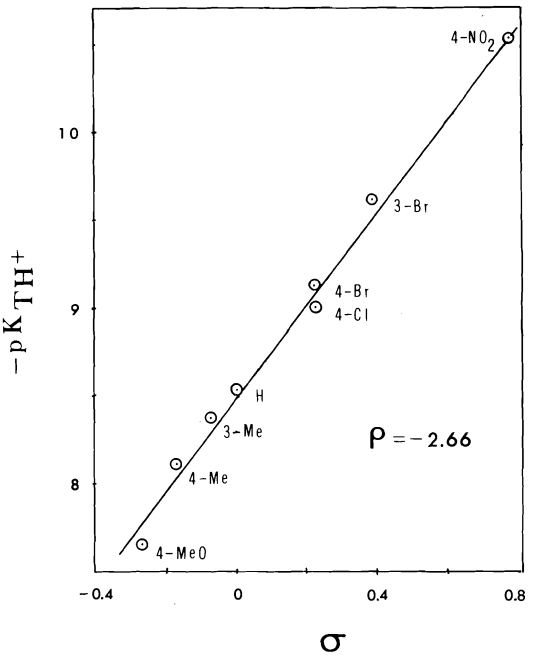

FIG. 3. Hammett ρσ plot for substituted ethyl thionbenzoates.

of the conjugate acid into the benzene ring is greater; this also explains the better correlation of pK_{TH^+} with σ^+.

These results with thionesters indicate that pK_{TH^+} values obtained by the Hammett–Deyrup acidity function method, applied to ionization data in concentrated sulfuric acid, have little or no superiority to pK_{TH^+} (B.O. and M.C.P.) obtained without use of a specific acidity function. However, for bases such as thioamides, ionizing in much more dilute sulfuric acid, the values obtained using H_T are definitely superior to the B.O. and M.C.P. values, as shown by the better correlation with σ and pK_a, and the better agreement with pK_{TH^+} values (ref. 1 and this paper) obtained by Paul's extrapolation procedure.

Acknowledgment

The continued financial support of the National Research Council of Canada is gratefully acknowledged.

1. J. T. EDWARD, I. LANTOS, G. D. DERDALL, and S. C. WONG. Can. J. Chem. **55**, 812 (1977).
2. M. A. PAUL and F. A. LONG. Chem. Rev. **57**, 1 (1957).
3. L. P. HAMMETT and A. J. DEYRUP. J. Am. Chem. Soc. **55**, 1901 (1933).

4. J. F. BUNNETT and F. P. OLSEN. Can. J. Chem. **44**, 1899 (1966).
5. N. C. MARZIANO, G. M. CIMINO, and R. C. PASSERINI. J. Chem. Soc. Perkin Trans. II, 1915 (1973).
6. W. WALTER and K. BODE. Angew. Chem. Int. Ed. Engl. **5**, 447 (1966).
7. A. GUTBIER. Ber. **33**, 3358 (1900).
8. J. L. CAVE and D. A. PEAK. J. Chem. Soc. 742 (1952).
9. G. A. BARAMKI, G. DERDALL, and J. T. EDWARD. Can. J. Spectrosc. **18**, 160 (1973).
10. M. RENSON and J. BIDAINE. Bull. Soc. Chim. Belg. **70**, 517 (1961).
11. K. YATES and J. B. STEVENS. Can. J. Chem. **43**, 529 (1965).
12. M. J. JORGENSON and D. R. HARTTER. J. Am. Chem. Soc. **85**, 878 (1963).
13. M. A. PAUL. J. Am. Chem. Soc. **76**, 3236 (1954).
14. C. TISSIER and M. TISSIER. Bull. Soc. Chim. Fr. 2109 (1972).
15. L. P. HAMMETT. Physical organic chemistry. 2nd ed. McGraw Hill, New York, NY. 1970. p. 356.
16. G. KORTÜM, W. VOGEL, and K. ANDRUSSOW. Dissociation constants of organic acids in aqueous solution. Butterworths, London. 1961.
17. R. STEWART and K. YATES. J. Am. Chem. Soc. **80**, 6355 (1958).

Studies in the usnic acid series. VII.[1] The biodegradation of (+)-usnic acid by a *Pseudomonas* species. Isolation, structure determination, and synthesis of (+)-6-desacetylusnic acid

JAMES P. KUTNEY, JEFFREY D. LEMAN, PHILLIP J. SALISBURY, IGNACIO H. SANCHEZ, AND TREVOR YEE

Department of Chemistry, University of British Columbia, 2075 Wesbrook Place, Vancouver, B.C., Canada V6T 1W5

AND

ROBERT J. BANDONI

Department of Botany, University of British Columbia, 2075 Wesbrook Place, Vancouver, B.C., Canada V6T 1W5

Received December 20, 1976

JAMES P. KUTNEY, JEFFREY D. LEMAN, PHILLIP J. SALISBURY, IGNACIO H. SANCHEZ, TREVOR YEE, and ROBERT J. BANDONI. Can. J. Chem. **55**, 2336 (1977).

Studies on the biodegradation of (+)-usnic acid (**1**) by a *Pseudomonas* species have revealed a novel aromatic deacylation process. The isolated metabolite, (+)-6-desacetylusnic acid (**2**) is crystalline and its structure is established by means of spectroscopic and chemical methods. The synthesis of **2** from usnic acid (**1**) is also reported and provides conclusive evidence for the structure of this metabolite.

JAMES P. KUTNEY, JEFFREY D. LEMAN, PHILLIP J. SALISBURY, IGNACIO H. SANCHEZ, TREVOR YEE et ROBERT J. BANDONI. Can. J. Chem. **55**, 2336 (1977).

Des études sur la biodégradation de l'acide (+) usnique (**1**) par les espèces *Pseudomonas* ont permis de mettre en évidence un nouveau processus de déacylation aromatique. Le métabolite qui a été isolé, l'acide (+) désacétyl-6 usnique (**2**), est cristallin et sa structure a été établie à l'aide de méthodes spectroscopique et chimique. On rapporte aussi la synthèse de **2** à partir de l'acide usnique (**1**); cette synthèse fournit une preuve concluante de la strucure de ce métabolite.

[Traduit par le journal]

The degradation of organic compounds by microorganisms, an essential biochemical step, has considerable chemical and ecological significance, as can be seen from the increased work in this area (1–8). Our interest in this field centers primarily on the study of the metabolic intermediates involved in the breakdown of various aromatic substrates as a means of elucidating the relevant biodegradation pathways involved (4–8).

In previous preliminary investigations (9) it was shown that various microorganisms have the ability to degrade the lichen antibiotic (+)-usnic acid (**1**) (10–12) and a more detailed study was now warranted. For this purpose a sample of *Pseudomonas* was obtained from surface soil samples collected in the Whistler mountain area of British Columbia and further experiments were undertaken.

The fermentation was carried out at room temperature on a rotary shaker in Erlenmeyer flasks containing an appropriate amount of nutrient medium (see Experimental) with 3–4 day old cultures of the purified bacterial isolate. After 7–10 days, work-up and purification of the crude extract produced a single component, isolated in 57% yield, as yellow crystals, mp 134.5–136°C, in addition to some recovered substrate (32%).

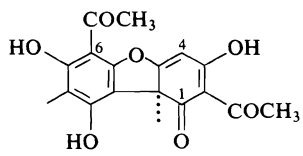

1

Pseudomonas sp. → $C_{16}H_{16}O_6$

2

This material possessed the molecular formula $C_{16}H_{16}O_6$ as shown by high resolution mass spectrometry and elemental analysis, and was optically active $[\alpha]_D^{27}$ +689° (CH_3OH). Its ultraviolet spectrum (λ_{max} (MeOH) 336, 266, 232 nm) showed a hypsochromic shift of the aromatic B band as compared to that of usnic acid

[1]Part VI, J. P. Kutney and I. H. Sanchez, ref. 36.

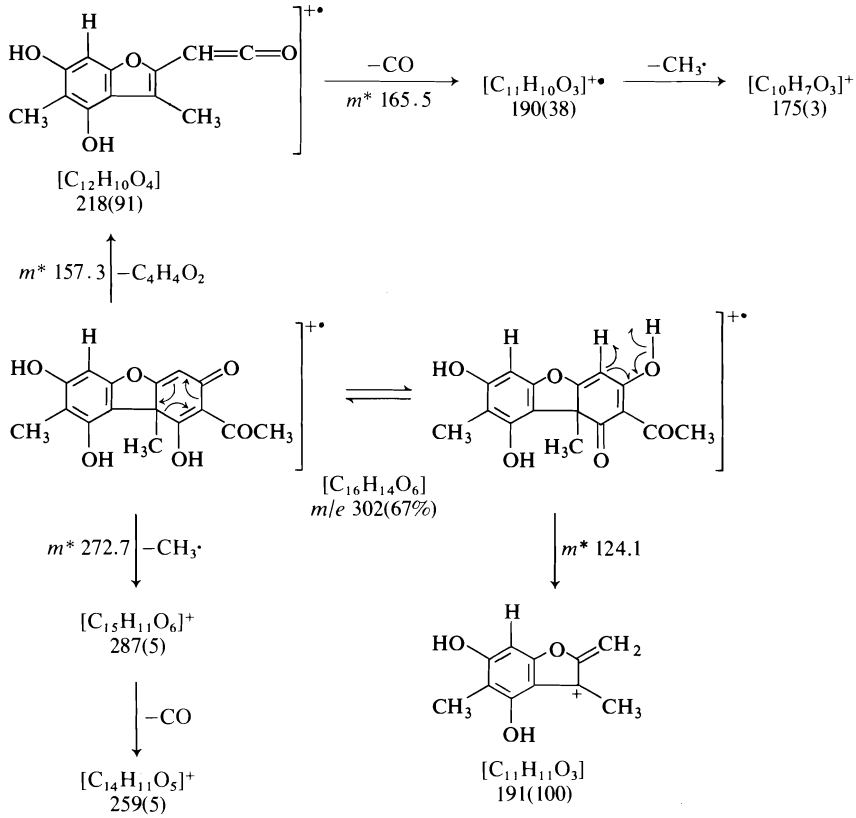

FIG. 1. The postulated fragmentation pattern of (+)-6-desacetylusnic acid in the mass spectrometer.

(285 to 266 nm), strongly suggesting that a change had occurred in the aromatic chromophore (13). Moreover, its infrared spectrum showed, in addition to the chelated hydroxyl groups (ν_{max} 3400–2800 cm^{-1}) similar to those of the parent molecule, the retention of the ring C chelated β-triketone system (14, 15) (1670, 1540 cm^{-1}). However, the reduction in intensity of the 1630 cm^{-1} band (as compared to that in (+)-usnic acid) assigned to the chelated aromatic methyl ketone (14, 15), coupled with a distinct band at 895 cm^{-1} that suggested the presence of a pentasubstituted aromatic ring (16), were strongly indicative of a ring A deacylated material.

The ^{1}Hmr spectrum of this product showed in addition to three three-proton singlets corresponding to the angular methyl group, the aromatic methyl group, and the ring C methyl ketone (δ 1.70, 2.11, and 2.61 ppm, respectively), characteristic signals for both the chelated enol (δ 18.64) and the C_4 olefinic proton (δ 5.79). However, while the C_9-phenolic absorption remained at its usual position (δ 10.23), two new absorptions were observed, and these could be readily assigned to an aromatic proton (δ 6.26) and a phenolic hydroxyl group (δ 5.67, reveals exchange with D_2O). The shift to higher field shown by the latter clearly indicates the loss of chelation as a result of bacterial deacylation of the aromatic ring.

In its mass spectrum this compound revealed a molecular ion at *m/e* 302 and significant fragments at *m/e* 287 ($M - 15$) and 218 ($M - 84$) characteristic of the usnic acid series (17, 18). The base peak observed at *m/e* 191 ($M - 111$) was again typical of this series. The latter two fragments, which show complete retention of the usnic ring system, appear at values corresponding to 42 mass units lower than the corresponding fragments observed for the parent compound and left no doubt about the absence of the aromatic acetyl side chain in the isolated product. Figure 1 summarizes the postulated fragmentation pattern.

On the basis of the above spectroscopic data,

the metabolite isolated was assigned the structure **2** and the name, (+)-6-desacetyl usnic acid.

Further evidence was obtained through the preparation of the corresponding diacetate **3**. This crystalline derivative, mp 208–209°C, $[\alpha]_D^{26}$ +121° (CH_3OH), showed the molecular formula $C_{20}H_{18}O_8$, and the expected infrared (1750 cm^{-1}) and ^{1}Hmr (δ 2.31 and 2.43 ppm) characteristics for an *O*-diacetyl derivative.

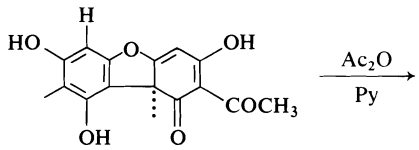

2

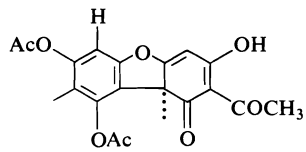

3

Having thus obtained all the required spectroscopic evidence in favor of structure **2**, it was decided to provide a firmer basis for our postulate by means of chemical transformations into known usnic acid derivatives. One of the few such derivatives lacking the aromatic acetyl group is pyrousnic acid (**4**), (19–22) obtained by heating (+)-usnic acid (**1**) to 210°C in 50% sodium or potassium hydroxide under a stream of hydrogen for 10 min (Fig. 2). Under somewhat milder conditions (23) (75% potassium hydroxide at 88–90°C for 1 h) usnetic acid (**6**), a derivative retaining the aromatic methyl ketone is obtained. Thus treatment of metabolite **2** under the latter conditions produced, in 35% yield, crystalline pyrousnic acid (**4**) which was shown to be identical with an authentic sample prepared directly from (+)-usnic acid.

It appeared clear that the biodegradation of (+)-usnic acid (**1**) by a *Pseudomonas* species had resulted in a novel and specific aromatic deacylation process. However, to provide a more conclusive proof for the structural assignment and to obtain synthetic intermediates which would be useful in subsequent studies, an investigation directed at the synthesis of (+)-6-desacetylusnic acid (**2**) was initiated.

In our initial synthetic studies it became clear that alkaline cleavage of the aromatic methyl ketone occurred with concomitant rearrangement (24–26) thus leading to the 'iso' series of usnic acid derivatives. It thus became necessary to investigate a suitable protection for the aromatic carbonyl system in ring A and it appeared that an amide function may satisfy such requirements. It is well known that amide hydrolysis can be accomplished under a variety of conditions (27, 28) and the resulting products, upon deamination (29–33), lead to the desired materials. Moreover, recent experiments on acylarylnitrosoamines (34, 35) have also shown that such transformations can be equally performed directly at the acetanilide stage. In view of these results, and the above mentioned difficulties encountered during our synthetic approaches, we decided to undertake a study of the preparation of ring aminated usnic acid derivatives.

Treatment of the racemic monoether **7** (36) under the conditions described by Chrochet and Kovacic for the conversion of *o*-hydroxyaldehydes and ketones into *o*-hydroxyanilides (37–39) produced selectively, in over 90% yield, the novel acetanilide derivative **8**. This crystalline compound, mp 118–119°C, exhibited in the infrared spectrum, the presence of an associated secondary amide group (3300, 1660, 1550, 1280 cm^{-1}) while its ^{1}Hmr spectrum confirmed the postulated rearrangement with signals at δ 2.34 and 7.70 ppm, assigned to the *N*-acetyl and N-H protons respectively. In the mass spectrometer this compound revealed fragmentations typical of the usnic acid series (40) with fragments containing the ring A amine function.

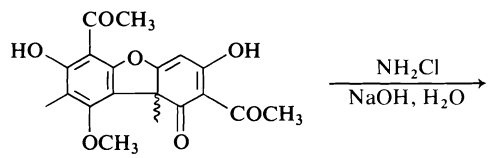

7

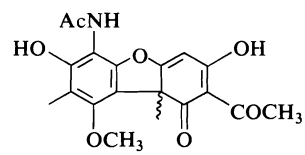

8

Attempted ether cleavage in **8** by means of boron tribromide (41, 42) produced in low yield (12%) the desired (±)-*N*-acetyl-6-aminousnic acid (**10**), mp 228–230°C, showing the expected spectral data (ir: 3460, 1685, 1520, 1260 cm^{-1}; ^{1}Hmr: δ 2.19, 9.97 ppm). The main component, isolated in 60% yield, possessed the amide group (ν_{max} 3280, 1655, 1550, 1270 cm^{-1}) but the methoxyl and angular methyl groups were absent.

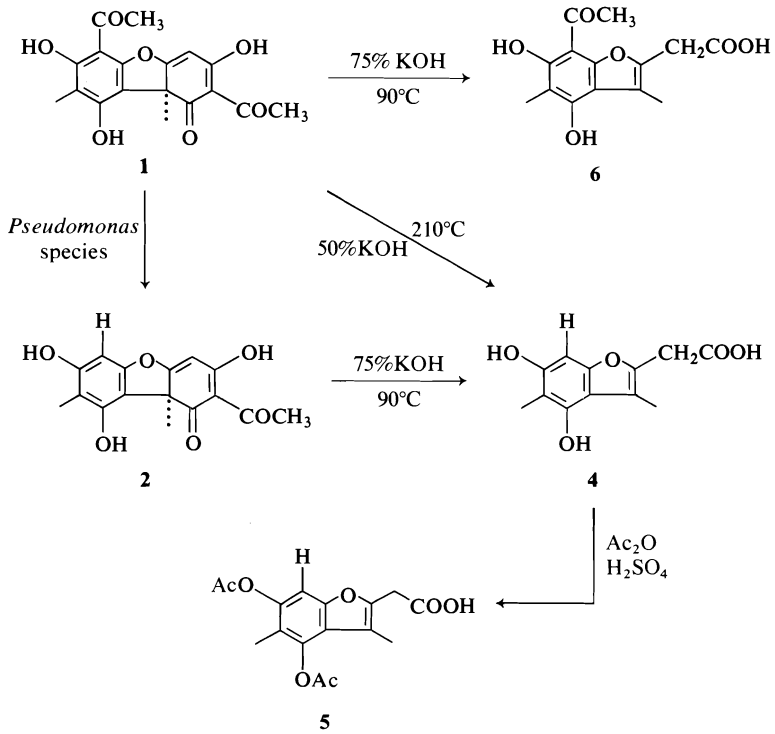

FIGURE 2

On the basis of spectral data this product was assigned the dibenzofuran structure **9**. Reaction of **8** with anhydrous aluminum trichloride (43, 44) permitted the isolation of **10** in 34% yield, whereas boron trichloride (45–48) in dry dichloromethane produced an 81% yield of the same component.

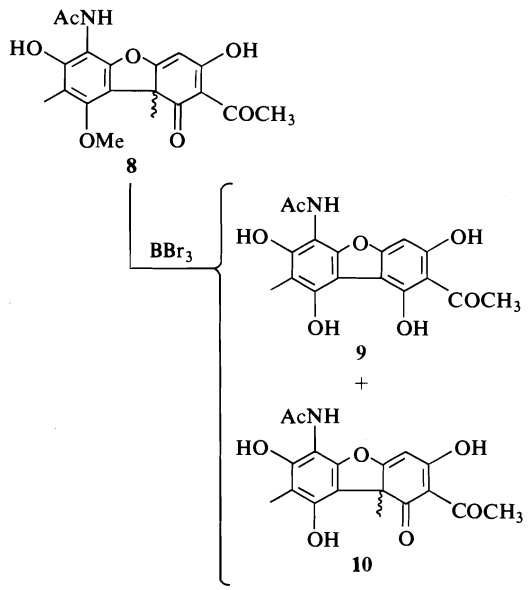

Having thus demonstrated the feasibility of introducing amide functionality into ring A of usnic acid derivatives, we decided to turn our attention to (+)-usnic acid itself. Although treatment of **1** under the conditions of the Schmidt reaction (49) resulted only in recovered starting material, the reaction with monochloramine in 2% methanolic sodium hydroxide or preferably 0.6% aqueous sodium hydroxide produced in 52% yield the optically active amide **11**, mp 230–232°C. This compound was further reacted with thionyl chloride (50) and the corresponding ring A oxazole derivative **12** was obtained in 52% yield.

Unfortunately complications arose when the triketone system (ring C) in the ring A aminated derivatives could not be converted to the isoxazole derivatives by the established procedures (51), a requirement for the synthetic approach envisaged for metabolite **2**.

Attempts to overcome this difficulty by performing the chloramine rearrangement on a preformed ring C isoxazole derivative bearing the C_6 acetyl side chain, similarly met with failure. However success was achieved in this area when the ring A ether derivatives were reacted with hydroxylamine and the resulting

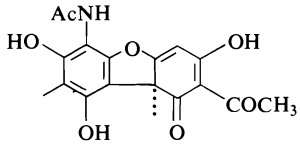

11

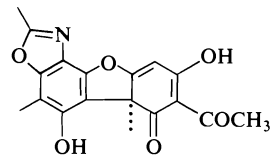

12

oximes exposed to Beckmann rearrangement conditions.

Treatment of the racemic dibenzyl ether **13** (36) with hydroxylamine hydrochloride in 5% methanolic potassium hydroxide – water (2:1) at 50°C resulted in good yields of the corresponding oxime intermediate **14**, which, without purification, was further treated with phosphorus pentachloride (52) in anhydrous ethyl ether at room temperature to produce in 48% yield the racemic dibenzylanilide derivative **15**, mp 168–170°C. Its infrared spectrum indicated clearly the presence of both an amide functionality (3430, 1680, 1520, 1250 cm^{-1}) and the

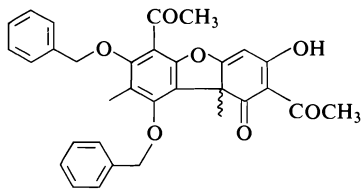

13

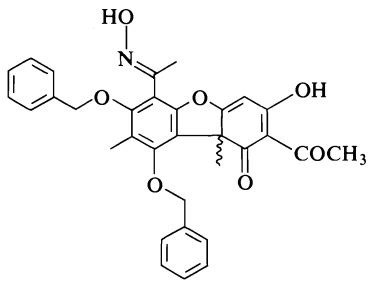

14

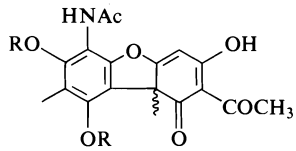

15

R = CH_2—C_6H_5

ring C β-triketone system (1680, 1540 cm^{-1}), both of which were confirmed by ^{1}Hmr spectroscopy, with signals at δ 2.27 and 6.87 ppm, assigned to the *N*-acetyl and the secondary amide protons, respectively. An improvement in yield (62%) could be achieved by a thionyl chloride catalyzed rearrangement (53) of the oxime **14**.

In similar fashion, the isoxazole derivative **16** (36) could be converted to the corresponding anilide derivative **17** (70% yield).

The necessary chemistry for the preparation of the required amino usnic acid derivatives was now developed and its utilization in the synthesis

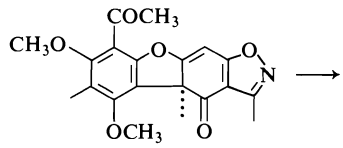

16

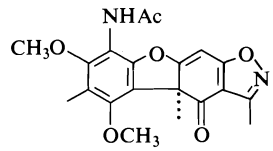

17

of the metabolite **2** is discussed presently. A summary of the successful synthetic pathway from usnic acid (**1**) is provided in Fig. 3.

Due to the severe difficulties encountered during the attempted hydrolytic cleavage of the amide C—N bond, it became necessary to find an alternative method for our synthetic objective. The use of acylarylnitrosoamines as intermediates came under serious consideration. Thus Bamberger (54) and Hey *et al.* (55) studied the use of acylarylnitrosoamines as arylating agents, while DeTar (56, 57) and White (58–60) and co-workers studied the decomposition of such compounds, both in the aromatic and aliphatic series, in a variety of solvents. Finally, Denney *et al.* (34) and Cadogan *et al.* (35) demonstrated that the relevant aryl radical formed upon decomposition of the intermediate diazonium cation is able to abstract hydrogen atoms from the solvent to generate the desired H-substituted materials in satisfactory yields.

The preparation of *N*-nitrosoacylaryl (alkyl) amines can be accomplished by a variety of methods (61–66) and the direct arylation of aromatic amines (67) and amides (68) has been performed as well by the use of alkyl nitrites in refluxing benzene or biphenyl, respectively.

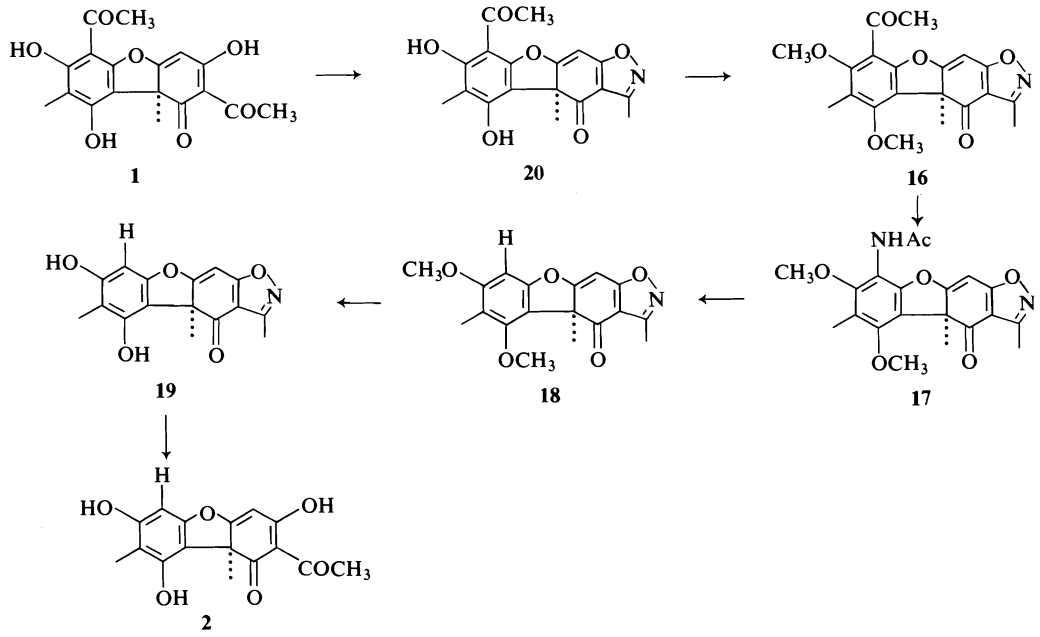

FIG. 3. The synthesis of (+)-6-desacetylusnic acid (**2**) from (+)-usnic acid (**1**).

Although all the attempts to prepare the desired *N*-nitroso intermediate by the usual methods (61–66) proved unsuccessful, treatment of the acetanilide **17** with isoamyl nitrite in anhydrous dioxane (32) at 88°C produced, in 78% yield, the crystalline (+)-6-desacetyl-7,9-di-*O*-methylisoxazolo[4,5-*b*]usnic acid (**18**), mp 156.5–158°C. This substance showed in its ^{1}Hmr spectrum, the retention of both ether functionalities (δ 3.78 and 3.96) as well as the new aromatic proton as a sharp singlet at δ 6.43. It must be mentioned, however, that this reaction could not be applied directly to either (+)-usnic acid (**1**) or its isoxazole derivative **20**.

The next step in our synthetic sequence required the removal of the various protecting groups. After several unsuccessful attempts using the normal reagents for cleavage of ether functions (32, 69–73) the use of boron tribromide (74, 75) at −50°C in dry dichloromethane furnished, in 98% yield, the crystalline monoether **21**, mp 167–168°C, arising from selective demethylation at the 9-position. The remaining methoxyl group appeared as a sharp three-proton singlet at δ3.76, while the phenolic proton (exchangeable with D_2O) was seen at δ 9.67. Further corroboration for this structure was obtained by the preparation of the monoacetyl ether **22**, molecular formula $C_{19}H_{17}O_6N$, mp 195–196°C, showing the expected infrared (1770 cm^{-1}) and ^{1}Hmr (δ 2.46, 3.85 ppm) absorptions.

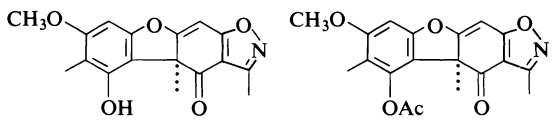

However, when the diether **18** was allowed to react at 10°C with boron tribromide, complete demethylation was observed and the product, (+)-6-desacetylisoxazolo[4,5-*b*]usnic acid (**19**), could be isolated in 87% yield. Acetylation of this material produced in good yield a mixture of the diacetate **24** and the 7-monoacetate **23** as highly crystalline materials, mp 168–170°C and 242–243°C, respectively.

Moreover, the phenol **19** and its diacetate **24** allowed the first direct comparison with the 'iso' series intermediates obtained previously (24, 51, 78). Some of the main differences arose from their infrared spectra, which showed that while the carbonyl group at the 1-position absorbs at 1675 cm^{-1} for the normal series isomer **19**, it appears at 1660 cm^{-1} for the isomer analogue **25**. As expected, ^{1}Hmr spectroscopy allows a facile differentiation between the two series, as seen from Table 1.

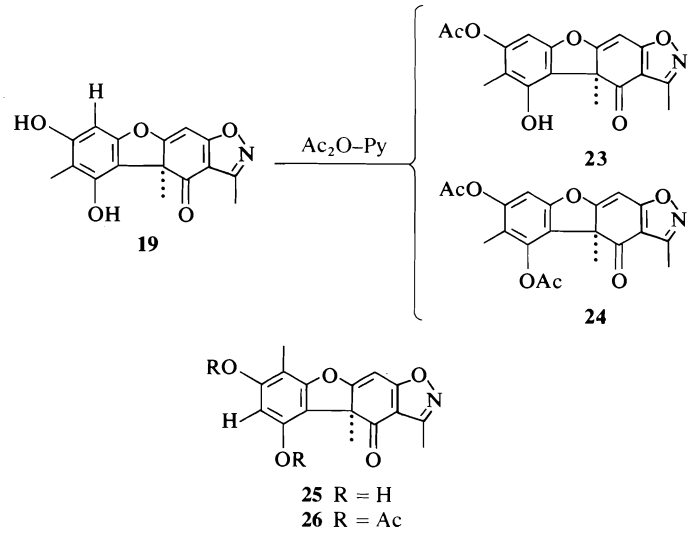

A minor product from the boron tribromide demethylation, isolated in 8% yield, was characterized as the bromophenol **27** resulting from the known (76) nuclear halogenation (bromination) of 1,3-diphenolic ethers upon treatment with Lewis acids.

The chemistry for the final steps in the sequence leading to the preparation of metabolite **2** had already been performed with the 'iso' series diacetate **26**, (24, 51, 78) and involved reductive cleavage (PtO_2/H_2) of the isoxazole N—O bond followed by immediate alkaline (1 *N* sodium hydroxide) regeneration of the ring C β-triketone system. Indeed treatment of the diacetate **24** under identical conditions furnished, in 97% yield, the desired (+)-6-desacetylusnic acid (**2**) mp 134.5–136°C, $[\alpha]_D^{26}$ +689° (CH_3OH), identical in all respects with the material isolated from the bacterial degradation. Table 2 indicates the circular dichroism data for the synthetic and natural compounds.

TABLE 1. Proton magnetic resonance data for (+)-6-desacetylisoxazolo[4,5-*b*]usnic acid (**19**) and (+)-6-desacetylisoxazolo[4,5-*b*]isousnic acid (**25**) and their corresponding acetates

	Compound, ppm (δ units)			
Functionality	(**19**)	(**24**)	(**25**)	(**26**)
C_{9b}-CH_3	1.70	1.77	1.80	1.83
C_8-CH_3	2.07	1.95	—	—
C_6-CH_3	—	—	2.14	2.16
C_7-OCOCH_3	—	2.29	—	2.32
C_9-OCOCH_3	—	2.41	—	2.49
C_{11}-CH_3	2.44	2.47	2.46	2.53
C_4-*H*	6.16	6.19	5.95	6.00
C_6-*H*	6.28	6.78	—	—
C_8-*H*	—	—	6.31	6.72
C_7-O*H*	8.63	—	8.59	—
C_9-O*H*	9.62	—	8.59	—

A further comparison of the natural and synthetic series was achieved on the corresponding diacetates (**28**).

Finally, the synthetic phenol **2** was converted via a one-step acetylation-aluminum trichloride-catalyzed Fries rearrangement (77) into synthetic (+)-usnic acid (**1**). The latter substance showed identical spectroscopic and chromato-

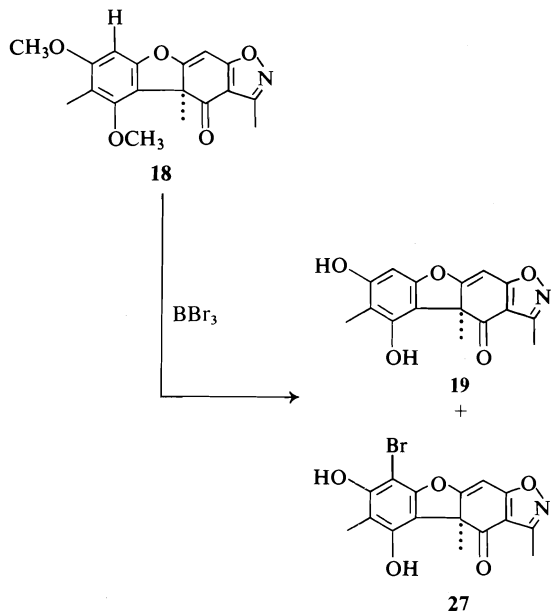

TABLE 2. Circular dichroism data λ_{max} ($\Delta\varepsilon$) for natural and synthetic (+)-6-desacetylusnic acid (**2**)

Natural		Synthetic	
CH_3OH	CH_3OH + KOH	CH_3OH	CH_3OH + KOH
328 (+9.99)	345 (+8.11)	328 (+9.42)	344 (+7.85)
284 (−6.66)	310 (+6.86)	283 (−6.06)	308 (+6.28)
262 (−3.53)	285 (+1.66)	260 (−3.59)	285 (+1.79)
241 (+13.11)	264 (−12.90)	239 (+13.24)	266 (−12.57)
	236 (+10.19)		238 (+9.87)

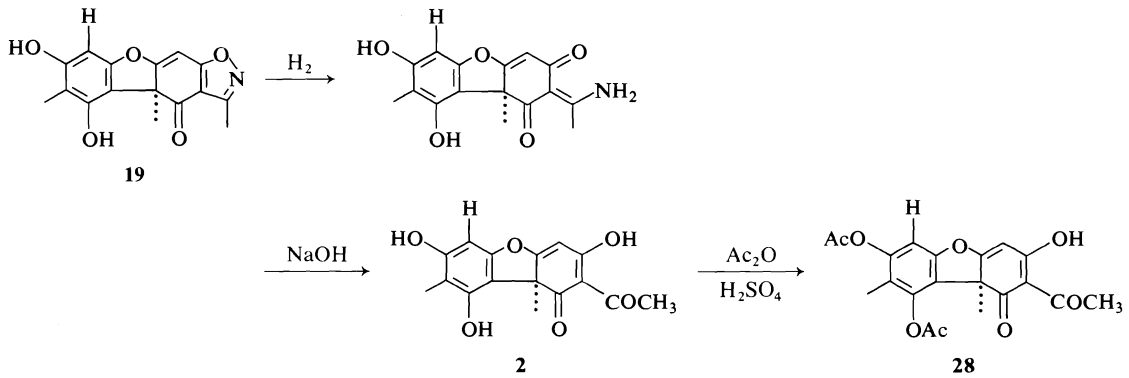

graphic properties to those of the naturally occurring optically active lichen substance.

In conclusion, it has been demonstrated that the biodegradation of (+)-usnic acid (**1**) by a *Pseudomonas* species results in a novel and specific aromatic deacylation process. Further studies are underway to provide a better understanding of this reaction.

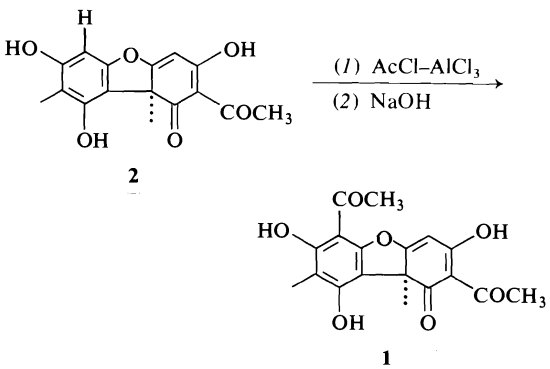

Experimental

Melting points were determined on a Kofler block and are uncorrected.

Ultraviolet (uv) spectra were recorded on a Cary 15 spectrophotometer in methanol solution (unless otherwise noted). The wavelength of the absorption maxima are reported in nanometers (nm).

Infrared (ir) spectra were measured routinely on a Perkin-Elmer model 710 spectrophotometer. Analytical or comparison spectra were recorded on a Perkin-Elmer model 457 spectrophotometer using matched cells with a cell path of 0.2 mm in chloroform solution. Calibration was achieved using the 1601 cm^{-1} absorption band of polystyrene. The absorption maxima are quoted in wave numbers (cm^{-1}).

Proton magnetic resonance (^{1}Hmr) spectra were measured in deuterochloroform ($CDCl_3$) solution (unless otherwise indicated) at room temperature. Routine spectra were recorded at 60 MHz on a Varian T-60 spectrometer, and analytical or comparison spectra at 100 MHz on either a Varian HA-100 or a Varian XL-100 spectrometer. Line positions are given in the δ (ppm) scale using tetramethylsilane (TMS) as internal standard. The integrated peak areas, multiplicity, and proton assignments are indicated in parentheses.

Low resolution mass (ms) spectra were determined on either an AEI MS 902 or an Atlas CH-4B mass spectrometer, with high resolution mass spectra being recorded exclusively on an AEI-MS-902 mass spectrometer.

Circular dichroism (cd) spectra were obtained on a Jasco model J-20 spectropolarimeter in methanol solution (unless otherwise indicated). The wavelength of the absorption maxima is reported in nanometers (nm). The differential molar extinction coefficient ($\Delta\varepsilon$) and the sign of the observed Cotton effect are indicated in parentheses.

Optical rotations ($[\alpha]_D$) were measured on a Perkin-Elmer model 141 polarimeter at the sodium D line in chloroform solution (unless otherwise noted) using cells with a 0.1 dm path.

Microanalyses were performed by Mr. P. Borda of the

Microanalytical Laboratory, University of British Columbia.

Merck silica gel G (acc. to Stahl) impregnated with oxalic acid (2%) and with 2% fluorescent indicator added, was used as adsorbent for thin layer chromatography (tlc), unless otherwise noted. The tlc plates were activated in an oven at 90°C for 4 h before use. For qualitative chromatography, layers of 0.3 mm thickness were used and the spots were visualized by viewing under ultraviolet (uv) light or spraying with a 1% ethanolic ferric chloride solution. For preparative (plc) chromatography, large (20 × 20 and 20 × 60 cm) plates with a thicker layer (0.7 mm) were used. The developing systems were *A*, petroleum ether (30–60°C) – acetone (4:1), and *B*, chloroform – ethyl acetate (3:2), unless otherwise indicated.

Column chromatography was performed on either Mackerey-Nagel (0.2–0.5 mm grain size) or Merck 60 (0.063–0.2 mm grain size) silica gel.

The usnic acid utilized throughout the course of this study was obtained from Koch-Light Laboratories, England, as the optically active dextrorotatory isomer, (+)-usnic acid, isolated from lichen sources (*Usnea barbata*).

The numbering system employed is that approved for the dibenzofuran series (79).

The bacterial isolate showing the ability to degrade (+)-usnic acid was obtained by serial dilution of soil in distilled water and plating on modified malt agar (malt–yeast–peptone agar) from surface soil samples collected in the Whistler Mountain area by Dr. J. Leman. The culture has since been purified and identified as a *Pseudomonas* species by one of us (R.J.B.).

Media and Stock Solutions

Constituents for malt–yeast–peptone agar: malt extract 7 g, soytone 1 g, yeast extract 0.5 g, agar 15 g, distilled water to 1000 ml.

Constituents for nutrient medium: dextrose 5 g, asparagine 2 g, KH_2PO_4 1 g, $MgSO_4 \cdot 7H_2O$ 0.5 g, vitamin stock solution 0.2 ml, minerals stock solution 0.2 ml, distilled water to 1000 ml.

Vitamin stock solution: biotin 25 μg, thiamine 500 μg, pyridoxine 500 μg, inositol 25 μg, ethyl alcohol (40%) to 100 ml.

Minerals stock solution: $FeCl_3 \cdot 6H_2O$ 98 mg, $CuSO_4 \cdot 5H_2O$ 78.5 mg, $MnSO_4 \cdot 4H_2O$ 40.5 mg, $ZnSO_4 \cdot 7H_2O$ 88 mg, distilled water to 250 ml.

Maintenance, Growth, and Fermentation Conditions

A 'stock culture' of the purified bacterial isolate was stored on modified malt agar in culture tubes placed in the refrigerator.

Before fermentation could be carried out, the culture was transferred to a fresh sterile plate (Petri dish) containing modified malt agar. Transfers were effected in a clean air station by means of an inoculating loop that had been sterilized by heating to redness in a burner flame, by scraping a few cells from the stock culture onto the *cool* loop, and then rubbing them off onto the fresh agar surface. In order to avoid contamination from air-borne micro-organisms, it is essential to observe all aseptic precautions, including the flaming of mouths of all containers. Prior to inoculation, the flasks and nutrient media were sterilized in an autoclave by heating at 121°C, 15 psi *steam* for about 20 min, and then allowed to cool down to room temperature.

The actual inoculation of *shake* culture flasks was carried out by transferring a small segment (about $\frac{1}{4}$ in. square) of active growth and agar from a recently inoculated Petri dish (not older than 2 weeks) to a sterile 500 ml Erlenmeyer flask equipped with a rubber foam stopper and containing an adequate nutrient medium (100 ml). To ensure proper aeration, the volume of the 'nutrient solution' should never exceed about two-fifths of the total volume of the flask.

Thus, the newly inoculated liquid culture was allowed to grow for 3–4 days before addition of the substrate (100 mg (+)-usnic acid (0.290 mmol) in 10 ml acetone).

Once the substrate had been incorporated, the flasks were agitated on a rotary shaker at room temperature for the required amount of time (7–10 days), after which the fermentation broth (p*H* 8–8.5) was acidified with tartaric acid to p*H* 4 and thoroughly extracted with ethyl acetate (3 × 30 ml). The organic extracts were then washed with water (2 × 20 ml), dried over anhydrous magnesium sulfate, and evaporated under reduced pressure. The residual broth was autoclaved before disposal.

The yellow residue (125 mg) was then purified by preparative layer chromatography (plc) on silica gel plates impregnated with oxalic acid (2%) using solvent mixture *A* to afford two main components.

*Component A: (+)-Usnic Acid (**1**) (2,6-Diacetyl-1,9b-dihydro-8,9bα-dimethyl-3,7,9-trihydroxy-1-oxodibenzofuran)*

Recrystallization of this material from chloroform–methanol produced bright yellow prisms of (+)-usnic acid (**1**, 32.1 mg, 0.093 mmol) identical in all respects (tlc, mixture mp, ir, ^{1}Hmr) with an authentic sample.

*Component B: (+)-6-Desacetyl Usnic Acid (**2**) (2-Acetyl-1,9b-dihydro-8,9bα-dimethyl-3,7,9-trihydroxy-1-oxodibenzofuran)*

Bright yellow needles (50.0 mg, 0.165 mmol; 57.0%) from chloroform – petroleum ether (30–60°C), mp 134.5–136°C; $[\alpha]_D^{27}$ +689° (*c* 0.1095); uv: λ_{max} 336 (3.15), 266 (3.87), 232 (4.07); ir: ν_{max} 3400–2800 (OH, chelated), 1670 (C=O, dienone system), 1630 (C=C, enol, enol ether and aromatic ring), 1540 (C=O, chelated carbonyl of the enolic triketone system), 895 (C—H, isolated Ar—H); ^{1}Hmr: δ 1.70 (3H, s, C_{9b}–C*H*$_3$), 2.11 (3H, s, C_8-C*H*$_3$), 2.61 (3H, s, C_2-COC*H*$_3$), 5.67 (1H, br s, C_7-O*H*), 5.79 (1H, s, C_4-*H*), 6.26 (1H, s, C_6-*H*), 10.23 (1H, s, C_9-O*H*), 18.64 ppm (1H, br s, C_3-O*H*); ms: *m/e* 302 (M^+), 287 ($M-15$), 218 ($M-84$), 191 ($M-111$, base peak), 161, 147, 135. *Anal.* calcd. for $C_{16}H_{14}O_6$: C 63.57, H 4.67; found: C 63.51, H 4.59. High resolution molecular weight determination calcd.: 302.079; found: 302.081; cd: λ_{max} (Δε) 328 (+9.99), 284 (−6.66), 262 (−3.53), 241 (+13.11); cd (CH_3OH + KOH): λ_{max} (Δε) 345 (+8.11), 310 (+6.86), 285 (+1.66), 264 (−12.90), 236 (+10.19).

*Preparation of (+)-6-Desacetylusnic Acid Diacetate (**3**) (2-Acetyl-7,9-diacetoxy-1,9b-dihydro-8,9b-dimethyl-3-hydroxy-1-oxodibenzofuran)*

(+)-6-Desacetylusnic acid (**2**) (50 mg, 0.165 mmol) was dissolved in a 1:1 mixture of acetic anhydride – pyridine (2 ml) and the solution allowed to stand at room temperature overnight. The reaction mixture was then poured over cracked ice (10 g) and extracted with ethyl ether (3 × 15 ml). The combined ethereal extracts were thoroughly washed with water (4 × 10 ml), dried over anhydrous magnesium sulfate, and evaporated under reduced pressure to yield an orange solid (60 mg) which

was purified by preparative chromatography (silica gel – oxalic acid plates, solvent system *A*) to produce pure (+)-6-desacetylusnic acid diacetate (**3**) (28 mg, 0.072 mmol; 44%), yellow crystals from chloroform – ethyl alcohol, mp 208–209°C; $[\alpha]_D^{26}$ +121 (*c* 0.06525); uv λ_{max} (log ε) 325 (3.26), 280 (3.73), 261 (3.85), 220 (4.00), ir: ν_{max} 1750 (C=O, acetates), 1685 (C=O, enone system), 1620, 1605 (C=C, enol ether, aromatic ring), 1540 (C=O, chelated acetyl of the triketone system); ^{1}Hmr: δ 1.78 (3H, s, C_{9b}-C*H*$_3$), 1.97 (3H, s, C_8-C*H*$_3$), 2.31 (3H, s, C_7-OCOC*H*$_3$), 2.43 (3H, s, C_9-OCOC*H*$_3$), 2.52 (3H, s, C_2-COC*H*$_3$), 5.81 (1H, s, C_4-*H*), 6.81 (1H, s, C_6-*H*), 18.41 ppm (1H, s, C_3-O*H*); ms: *m/e* 386 (M^+, base peak), 244 (*M* − 42), 302, 260, 233, 218, 191. *Anal.* calcd. for $C_{20}H_{18}O_8$: C 62.17, H 4.69; found: C 62.12, H 4.72. High resolution molecular weight determination calcd.: 386.100; found: 386.099.

*Preparation of Pyrousnic Acid (**4**) (2-Carboxymethyl-4,6-dihydroxy-3,5-dimethylbenzofuran)*

*I. From (+)-Usnic Acid (**1**)*

Usnic acid (**1**) (1 g, 2.90 mmol) was dissolved in 50% sodium hydroxide (4 ml) and heated to 210°C in an oil bath under a nitrogen atmosphere for 10 min. The reaction mixture was allowed to cool down to room temperature, poured into ice-cold 2 *N* sulfuric acid (50 ml), and extracted with ethyl acetate (3 × 50 ml). The combined extracts were dried over anhydrous magnesium sulfate and evaporated to yield a brown gum (421 mg). Repeated crystallizations from ethyl acetate – petroleum ether (light) afforded pure pyrousnic acid (**4**) (250 mg, 1.05 mmol; 36%) as tan needles mp 198–200°C (dec.) (lit. (22) mp 199–200°C); $[\alpha]_D^{26}$(CH$_3$OH) 0° (*c* 0.0875); uv: λ_{max} (log ε) 315 (3.03), 253 (3.51); ir (Nujol): ν_{max} 3500–2400 (OH, phenol, carboxylic acid), 1770, 1725, 1440 (C=O, carboxylic acid), 1640 (C=C); ^{1}Hmr (CD$_3$OD): δ 2.10 (3H, s, C_5-C*H*$_3$), 2.30 (3H, s, C_3-C*H*$_3$), 3.63 (2H, s, -C*H*$_2$COOH), 6.46 ppm (1H, s, C_7-H); ms: *m/e* 236 (M^+), 191, 44 (base peak). *Anal.* calcd. for $C_{12}H_{12}O_5$: C 61.01, H 5.12; found: C 61.05, H 5.03. High resolution molecular weight determination calcd.: 236.068; found: 236.068.

*II. From (+)-6-Desacetylusnic Acid (**2**)*

A solution of (+)-6-desacetylusnic acid (**2**) (363 mg, 1.20 mmol) in 75% aqueous potassium hydroxide (2 ml) was heated at 85–90°C under a nitrogen atmosphere for 40 min. After cooling, the reaction mixture was acidified with 1 *N* hydrochloric acid and then extracted with ethyl acetate (3 × 25 ml). The combined extracts were thoroughly washed with water (3 × 20 ml), dried over anhydrous sodium sulfate, and evaporated under reduced pressure to produce a brown oil (150 mg). Crystallization from ethyl acetate – petroleum ether (light) and ethyl alcohol gave pyrousnic acid (**4**) as a tan microcrystalline solid (100 mg, 0.42 mmol; 35%), mp 197–198°C; mixture mp with authentic pyrousnic acid 196–198°C. Chromatographic (silica gel – oxalic acid, solvent system *B*) and spectral (uv, ir, ^{1}Hmr) properties were also identical with those of authentic pyrousnic acid prepared from (+)-usnic acid.

*Preparation of Pyrousnic Acid Diacetate (**5**) (2-Carboxymethyl-4,6-diacetoxy-3,5-dimethylbenzofuran)*

A solution of pyrousnic acid (**4**) (40 mg, 0.169 mmol) in 0.5% concentrated sulfuric acid in acetic anhydride (1.5 ml) was allowed to stand at room temperature overnight. The resulting solution was poured into crushed ice (10 g), extracted with ethyl acetate (3 × 5 ml), and the combined extracts washed with water (2 × 5 ml), dried over anhydrous sodium sulfate, and evaporated under reduced pressure. The residue (59.2 mg) was directly crystallized from ethyl acetate – petroleum ether (30–60°C) to afford pure pyrousnic acid diacetate (48 mg, 0.150 mmol; 88%) as cream coloured needles, mp 206–208°C; mixture mp with authentic pyrousnic acid diacetate, 207–208°C; $[\alpha]_D$(CH$_3$OH) 0° (*c* 0.05725); uv: λ_{max} (log ε) 280 (3.33), 260 (3.79), 218 (4.04), 213 (4.06); ir (Nujol): ν_{max} 3000–2400 (OH, carboxylic acid), 1755 (C=O, acetates), 1705 (C=O, carboxylic acid), 1635, 1600 (C=C), 1420, 1220 (OH, C—O, carboxylic acid dimer); ^{1}Hmr (CDCl$_3$–DMSO-d_6): δ 1.95 (3H, s, C_4-C*H*$_3$), 2.14 (3H, s, C_6-OCOC*H*$_3$), 2.28 (3H, s, C_4-OCOC*H*$_3$), 2.34 (3H, s, C_3-C*H*$_3$), 3.65 (2H, s, C_2-C*H*$_2$-COOH), 5.95 (3H, br, COO*H*·H_2O), 7.03 ppm (1H, s, C_7-*H*); ms: *m/e* (M^+), 278, 236 (base peak), 191, 43. *Anal.* calcd. for $C_{16}H_{16}O_7$: C 59.99, H 5.03; found: C 60.06, H 5.10. High resolution molecular weight determination calcd.: 320.089; found: 320.088.

*Preparation of Usnetic Acid (**6**) (7-Acetyl-2-carboxymethyl-4,6-dihydroxy-3,5-dimethylbenzofuran)*

A solution of (+)-usnic acid (**1**) (1 g, 2.90 mmol) in 75% potassium hydroxide (3 ml) was heated at 88–90°C under nitrogen. After 1 h, when the bubbling had stopped, the reaction mixture was cooled to 10°C and acidified with 1 *N* hydrochloric acid. A solid precipitated and was allowed to stand overnight at 0°C. Water (10 ml) was then added and the mixture filtered to give a pale yellow solid (380 mg) which upon recrystallization from 70% acetic acid produced pure usnetic acid (**6**) (310 mg, 1.11 mmol; 38%), mp 207–208°C (lit. (23) mp 209–210°C); $[\alpha]_D$(CH$_3$OH) 0° (*c* 0.112); uv: λ_{max} 358 (4.20), 308 (3.81), 255 (3.94), 249 (4.00); ir (Nujol): ν_{max} 3605 (OH, free), 3300–2500 (OH, COOH, chelated), 1715 (C=O, carboxylic acid), 1625 (C=O, chelated acetyl grouping; C=C, aromatic ring); ^{1}Hmr (CDCl$_3$–DMSO-d_6): δ 2.06 (3H, s, C_5-C*H*$_3$), 2.26 (3H, s, C_3-C*H*$_3$), 2.67 (3H, s, C_7-COC*H*$_3$), 3.64 (2H, s, -C*H*$_2$-COOH), 6.00 (4H, br, C_4-COO*H*, H_2O), 13.71 ppm (1H, s, C_6-O*H*); ^{1}Hmr (CD$_3$OD): δ 2.09 (3H, s, C_5-C*H*$_3$), 2.31 (3H, s, C_3-C*H*$_3$), 2.68 (3H, s, C_7-COC*H*$_3$), 3.74 ppm (2H, s, -C*H*$_2$-COOH); ms: *m/e* 278 (M^+, base peak), 276, 263, 249, 234, 232, 215, 77, 43. *Anal.* calcd. for $C_{14}H_{14}O_6$: C 60.42, H 5.07; found: C 60.39, H 5.12. High resolution molecular weight determination calcd.: 278.079; found: 278.078.

*Preparation of (±)-N-Acetyl-6-amino-9-O-methylusnic Acid (**8**) (N-Acetyl-2-acetyl-6-amino-1,9b-dihydro-3,7-dihydroxy-8,9b-dimethyl-9-methoxy-1-oxodibenzofuran)*

A cold solution of (±)-9-*O*-methylusnic acid (**7**) (50 mg, 0.139 mmol) in 0.5 *N* sodium hydroxide (3 ml) was added dropwise to a cold freshly prepared stock solution of monochloramine[2] (2.24 ml; 10.75 mg monochloramine,

[2]The stock solution of monochloramine is prepared at 0°C (ice bath) by *carefully* adding an equal volume of a cold ammonium hydroxide solution, prepared by diluting concentrated ammonium hydroxide (7.4 *M*, 9.15 ml) with distilled water (90.85 ml), to cold 5% aqueous sodium hypochlorite solution (commercially available) with occasional shaking. The resulting solution contains 4.8 mg monochloramine/ml and is ready for immediate use.

0.208 mmol) and the resulting solution stirred at 0°C (ice bath) for 3 h. The reaction mixture was then neutralized with 1 *N* hydrochloric acid and extracted with ethyl acetate (3 × 3 ml). The combined extracts were washed with water, dried over anhydrous sodium sulfate, and evaporated under reduced pressure. The resulting yellow residue (56.2 mg) was purified by preparative layer chromatography (silica gel – oxalic acid plates, solvent *A*) to produce (±)-*N*-acetyl-6-amino-9-*O*-methylusnic acid (**8**) (47 mg, 0.1258 mmol; 90%), bright yellow prisms from chloroform – ethyl ether, mp 118–119°C; $[\alpha]_D$-($CHCl_3$) 0° (*c* 0.10); uv: λ_{max} (log ε) 305 (3.34), 262 (3.79), 221 (4.01); ir (Nujol): ν_{max} 3300 (NH, associated), 3200–2400 (OH, chelated), 1680 (C=O, enone system), 1660 (C=O, 'Amide I band', associated), 1610 (C=C), 1560 (C=O, chelated triketone system), 1550 (N—H, C—N, 'Amide II band', associated), 1280 (C—N, 'Amide III band', associated); ir: ν_{max} 3450 (NH, free), 3320 (NH, associated), 3200–2400 (OH, chelated), 1690 (C=O, enone system), 1680 (C=O, 'Amide I band', free), 1660 (C=O, 'Amide I band', associated), 1610 (C=C), 1560 (C=O, chelated triketone system), 1550 (N—H, C—N, 'Amide II band', associated), 1520 (N—H, C—N, 'Amide II band', free), 1280 (C—N, 'Amide II band', associated), 1260 (C—N, 'Amide III band', free); ^{1}Hmr: δ 1.78 (3H, s, C_{9b}-CH_3), 2.22 (3H, s, C_8-CH_3), 2.34 (3H, s, N-$COCH_3$), 2.54 (3H, s, C_2-$COCH_3$), 3.99 (3H, s, C_9-OCH_3), 5.62 (1H, s, C_4-*H*), 7.70 (1H, br, N-*H*), 9.43 (1H, br, C_7-O*H*), 18.07 ppm (1H, s, C_3-O*H*); ms: *m/e* 373 (M^+, base peak), 331, 316, 289, 262, 260, 247, 246, 245, 232, 220, 115, 83. *Anal.* calcd. for $C_{19}H_{19}O_7N$: C 61.12, H 5.13, N 3.73; found: C 61.50, H 5.25, N 3.59. High resolution molecular weight determination calcd.: 373.116; found: 373.117.

*Attempted Methyl Ether Cleavage on (±)-N-Acetyl-6-amino-9-O-methylusnic Acid (**8**). Experiment I. Isolation of N-Acetyl-2-acetyl-6-amino-8-methyl-1,3,7,9-tetrahydroxydibenzofuran (**9**)*

A solution of (±)-*N*-acetyl-6-amino-9-*O*-methylusnic acid (**8**) (67 mg, 0.179 mmol) in dry dichloromethane (6 ml) was cooled to −78°C (dry ice – acetone bath), treated with neat boron tribromide (415 mg, 1.62 mmol), and allowed to warm up to room temperature overnight. The resulting brown suspension was carefully poured into saturated sodium bicarbonate solution (10 ml), neutralized with 1 *N* hydrochloric acid and extracted with ethyl acetate (3 × 5 ml). The combined extracts were thoroughly washed with water, dried over anhydrous sodium sulfate, and evaporated under reduced pressure to produce a yellowish solid (11 mg). Repeated crystallization of the residue from methanol afforded *N*-acetyl-2-acetyl-6-amino-8-methyl-1,3,7,9-tetrahydroxydibenzofuran (**9**) (37 mg, 0.107 mmol; 59%), pale yellow crystals that decompose without melting at approximately 300°C; uv: λ_{max} (log ε) 305 sh (3.85), 290 (4.11), 280 (4.18), 271 (4.12), 237 (4.04); ir (Nujol): ν_{max} 3370 (OH), 3280, 3105 (N—H, associated), 2800–2500 (OH, chelated), 1655 (C=O, 'Amide I band', associated), 1630 (C=O, chelated ring C acetyl), 1620 (C=C), 1550 (N—H, C—N, 'Amide II band', associated), 1270 (C—N, 'Amide III band', associated); ^{1}Hmr ($CDCl_3$–DMSO-d_6): δ 2.07 (3H, s, C_8-CH_3), 2.18 (3H, s, C_6-NH-$COCH_3$), 2.64 (3H, s, C_2-$COCH_3$), 3.25 (4H, br, C_1-O*H*, C_9-O*H*, H_2O), 6.50 (1H, s, C_4-*H*), 8.95 (1H, s, C_6-N*H*-$COCH_3$), 9.71 (1H, s, C_7-O*H*), 11.55 ppm (1H, br, C_3-O*H*); ms: *m/e* 345 (M^+), 327, 303 (base peak), 302, 286, 285, 44, 43. *Anal.* calcd. for $C_{17}H_{15}O_7N\cdot\frac{1}{4}H_2O$: C 58.36, H 4.46, N 4.00; found: C 58.87, H 4.65, N 3.63. High resolution molecular weight determination calcd. for $C_{17}H_{15}O_7N$: 345.085; found: 345.085.

Preparative layer chromatography (silica gel – oxalic acid plates, petroleum ether (30–60°C) – acetone (3:1)) of the mother liquors afforded the desired product (±)-*N*-acetyl-6-aminousnic acid (**10**) (7.7 mg, 0.0215 mmol; 11%), yellow prisms from chloroform – petroleum ether, mp 227–228°C (dec.). Due to the small amount of sample available from this experiment, characterization was done at this point only by ^{1}Hmr and mass spectroscopy: ^{1}Hmr: δ 1.73 (3H, s, C_{9b}-CH_3), 2.18 (3H, s, C_8-CH_3), 2.31 (3H, s, C_6-NH-$COCH_3$), 2.65 (3H, s, C_2-$COCH_3$), 5.88 (1H, s, C_4-*H*), 9.18 (1H, br, C_2-N*H*-$COCH_3$), 9.93 (1H, s, C_7-O*H*), 10.61 (1H, s, C_9-O*H*), 19.43 ppm (1H, s, C_3-O*H*); ms: *m/e* 359 (M^+, base peak), 317, 275, 248, 233, 232, 206, 43. High resolution molecular weight determination calcd. for $C_{18}H_{17}O_7N$: 359.100; found: 359.103.

*Methyl Ether Cleavage of (±)-N-Acetyl-6-amino-9-O-methylusnic acid (**8**). Experiment II. Isolation of (±)-N-Acetyl-6-aminousnic Acid (**10**) (N-Acetyl-2-acetyl-6-amino-1,9b-dihydro-8,9b-dimethyl-3,7,9-trihydroxy-1-oxodibenzofuran)*

To a solution of (±)-*N*-acetyl-6-amino-9-*O*-methylusnic acid (**8**) (48 mg, 0.128 mmol) in dry dichloromethane (7 ml) was added anhydrous aluminum trichloride (99 mg, 0.745 mmol), and the reaction allowed to proceed at room temperature, under a nitrogen atmosphere for 2.5 h. The reaction mixture was then poured into cold 5% sodium bicarbonate solution (10 ml), neutralized with 1 *N* hydrochloric acid, and extracted with ethyl acetate (3 × 10 ml). The combined extracts were washed with water, dried over anhydrous sodium sulfate, and evaporated under reduced pressure to afford a yellow-brown glass (54 mg). Purification of the residue by preparative layer chromatography (silica gel – oxalic acid plates, petroleum ether – acetone (3:1)) produced (±)-*N*-acetyl-6-aminousnic acid (**10**) (15.6 mg, 0.0434 mmol; 33%), bright yellow prisms from methanol, mp 228–230°C (dec.); $[\alpha]_D$(CH_3CN) 0° (*c* 0.1075); uv: λ_{max} (log ε) 335 (3.33), 265 (3.90), 230 (4.27); ir: ν_{max} 3460 (N—H, free), 3400–2500 (OH, chelated), 1685 (C=O, 'Amide I band', free), 1660 (C=O, enone system), 1630, 1620 (C=C), 1540 (C=O, chelated triketone system), 1520 (N—H, C—N, 'Amide II band', free), 1260 (C—N, 'Amide III band', free); ^{1}Hmr ($CDCl_3$-DMSO-d_6): δ 1.72 (3H, s, C_{9b}-CH_3), 2.08 (3H, s, C_8-CH_3), 2.19 (3H, s, C_6-NH-$COCH_3$), 2.61 (3H, s, C_2-$COCH_3$), 5.90 (1H, s, C_4-*H*), 9.01 (1H, s, C_6-N*H*-$COCH_3$), 9.52 (1H, s, C_7-O*H*), 9.97 (1H, s, C_9-O*H*), 18.63 ppm (1H, s, C_3-O*H*); ms: *m/e* 359 (M^+, base peak), 317, 275, 248, 233, 232, 206, 43. *Anal.* calcd. for $C_{18}H_{17}O_7N$: C 60.16, H 4.77, N 3.90; found: C 60.45, H 4.91, N 3.92. High resolution molecular weight determination calcd.: 359.100; found: 359.105.

*Preparation of (±)-N-Acetyl-6-aminousnic Acid (**10**). Experiment III*

To a cold (−10°C) solution of (±)-*N*-acetyl-6-amino-9-*O*-methylusnic acid (**8**) (50 mg, 0.134 mmol) in dry dichloromethane (6 ml) was added boron trichloride

(147 mg, 1.257 mmol), obtained by condensing the gas at −78°C (dry ice – acetone bath). The reaction mixture was then stirred and under a nitrogen atmosphere allowed to warm up to room temperature over 4 h. The reaction mixture was then poured carefully into cold distilled water (15 ml) and extracted with ethyl acetate (3 × 5 ml). The combined extracts were washed with water, dried over anhydrous sodium sulfate, and evaporated under reduced pressure to afford a yellow glass (54.4 mg). Purification by preparative layer chromatography, (silica gel – oxalic acid plates, petroleum ether – acetone (3:1)) produced (±)-*N*-acetyl-6-aminousnic acid (**10**) (39 mg, 0.108 mmol; 81%), bright yellow prisms from methanol, mp 227–229°C; mixture mp with authentic material from previous experiments, 228–229°C. The spectroscopic and chromatographic properties of both samples are identical.

*Attempted Schmidt Reaction on (+)-Usnic Acid (**1**)*

A solution of (+)-usnic acid (**1**) (34.4 mg, 0.1 mmol) in chloroform (1 ml) and concentrated sulfuric acid (0.5 ml) was cooled to 0°C in an ice-bath. Crystalline sodium azide (7.5 mg, 0.115 mmol) was added over 0.25 h and stirring continued for 1 h. The crude reaction mixture was then poured onto crushed ice (10 g), extracted with chloroform (3 × 5 ml), and the combined extracts thoroughly washed with water, dried over anhydrous sodium sulfate, and evaporated under reduced pressure. The residue (37 mg) was directly crystallized from chloroform – ethyl alcohol to produce (+)-usnic acid (**1**) (32 mg, 0.093 mmol; 93%), mp 201–202°C; mixture mp with authentic (+)-usnic acid (**1**), 202–203°C. Both samples showed identical spectroscopic and chromatographic properties.

*Reaction of (+)-Usnic Acid (**1**) with Monochloramine. Experiment I. Isolation of (+)-N-Acetyl-6-aminousnic Acid (**11**)*

A cold solution of (+)-usnic acid (**1**) (2.5 g, 7.267 mmol) in 2% methanolic sodium hydroxide (40 ml) and distilled water (60 ml) was added dropwise to a cold (0°C) stock solution of monochloramine (4.8 mg monochloramine/ml, 120 ml; 576 mg NH_2Cl, 11.184 mmol), and the reaction allowed to proceed with external cooling (ice bath) for 4 h. The reaction mixture was then acidified with 1 *N* hydrochloric acid, extracted with ethyl acetate (3 × 25 ml), and the combined extracts washed with water, dried over anhydrous sodium sulfate, and evaporated under reduced pressure to produce a dark yellow residue (2.23 g). Purification by column chromatography on silica gel Merck (200 g) using 20% ethyl acetate in benzene as eluent afforded (+)-*N*-acetyl-6-aminousnic acid (**11**) (1.2219 g, 3.403 mmol; 46%), yellow prisms from methanol, mp 230–232°C; $[\alpha]_D^{26}$ (CH_3CN) +437° (*c* 0.17625); uv: λ_{max} (log ε) 335 (3.35), 265 (3.92), 230 (4.27); ir: ν_{max} 3455 (N—H, free), 3400–2400 (OH, chelated), 1685 (C=O, 'Amide I band', free), 1665 (C=O, enone system), 1630 (C=C), 1540 (C=O, chelated triketone system), 1520 (N—H, C—N, 'Amide II band', free), 2160 (C—N, 'Amide III band', free); ^{1}Hmr: δ 1.73 (3H, s, C_{9b}-CH_3), 2.16 (3H, s, C_8-CH_3), 2.30 (3H, s, C_6-NH-COCH_3), 2.65 (3H, s, C_2-COCH_3), 5.86 (1H, s, C_4-*H*), 9.15 (1H, br, C_6-NH-COCH_3), 9.90 (1H, s, C_7-O*H*), 10.62 (1H, s, C_9-O*H*), 19.43 ppm (1H, br, C_3-O*H*); ms: *m/e* 359 (M^+, base peak), 317, 275, 248, 233, 232, 206, 43. *Anal.* calcd. for $C_{18}H_{17}O_7N$: C 60.16, H 4.77, N 3.90; found: C 60.27, H 4.90, N 3.99. High resolution molecular weight determination calcd.: 359.100; found: 359.103.

*Reaction of (+)-Usnic Acid (**1**) with Monochloramine. Experiment II. Isolation of (+)-N-Acetyl-6-aminousnic Acid (**11**)*

A cold solution of (+)-usnic acid (**1**) (5 g, 14.534 mmol) in 0.6% aqueous sodium hydroxide (200 ml) was added dropwise to a cold (0°C) stock solution of monochloramine (4.8 mg NH_2Cl/ml, 240 ml; 1.152 g NH_2Cl, 22.368 mmol), and the reaction allowed to proceed with external cooling (ice bath) for 4 h. The reaction mixture was then acidified with 1 *N* hydrochloric acid, extracted with ethyl acetate (3 × 40 ml), and the combined extracts washed with water, dried over anhydrous sodium sulfate, and evaporated under reduced pressure. The residue (4.85 g) was purified by column chromatography on silica gel Merck (200 g) using 20% ethyl acetate in benzene as eluent to produce pure (+)-*N*-acetyl-6-aminousnic acid (**11**) (2.731 g, 7.607 mmol; 52%), yellow prisms from methanol, mp and mixture mp with authentic material, 230–232°C.

*Cyclization of (+)-N-Acetyl-6-aminousnic Acid (**11**). Isolation of (+)-Oxazolo[4,5-h]usnic Acid (**12**)*

A solution of (+)-*N*-acetyl-6-aminousnic acid (**11**) (50 mg, 0.139 mmol) in thionyl chloride (3 ml, freshly distilled) was heated at 55°C (oil bath temperature) under a nitrogen atmosphere for 0.5 h. Excess solvent was evaporated under reduced pressure, the residue taken up into ethyl acetate (8 ml), and the organic extract thoroughly washed with water, dried over anhydrous sodium sulfate, and evaporated under reduced pressure to yield a yellow glass (53 mg). Purification by preparative layer chromatography (silica gel – oxalic acid, petroleum ether – acetone (3:1)) produced (+)-oxazolo[4,5-*h*]usnic acid (**12**) (26.5 mg, 0.0777 mmol; 55%), yellow prisms from ethyl ether, mp 173–174°C; $[\alpha]_D^{26}$(CH_3CN) +538° (*c* 0.04); uv: λ_{max} (log ε) 335 (3.28), 268 (4.05), 218 (4.29); ir: λ_{max} 3300–2500 (OH, chelated), 1685 (C=O, enone system), 1635 (C=C), 1540 (C=O, chelated triketone system); ^{1}Hmr ($CDCl_3$–DMSO-d_6): δ 1.68 (3H, s, C_{9b}-CH_3), 2.34 (3H, s, C_8-CH_3), 2.60 (6H, s, C_2-COCH_3 and oxazole-CH_3), 5.98 (1H, br s, C_4-*H*), 10.54 (1H, br, C_9-O*H*), 18.72 ppm (1H, br, C_3-O*H*); ms: *m/e* 341 (M^+), 257 (base peak), 230, 229, 186, 43. *Anal.* calcd. for $C_{18}H_{15}O_6N$: C 63.34, H 4.43, N 4.10; found: C 63.39, H 4.52, N 4.01. High resolution molecular weight determination calcd.: 341.090; found: 341.089.

*Preparation of (±)-N-Acetyl-6-amino-7,9-di-O-benzylusnic Acid (**15**) (N-Acetyl-2-acetyl-6-amino-7,9-dibenzyloxy-1,9b-dihydro-8,9b-dimethyl-3-hydroxy-1-oxodibenzofuran). Experiment I*

A solution of (±)-7,9-di-*O*-benzylusnic acid (**13**) (52.4 mg, 0.1 mmol) and hydroxylamine hydrochloride (10.3 mg, 0.148 mmol) in 5% methanolic potassium hydroxide (2 ml) and distilled water (1 ml) was heated at 50°C (oil bath temperature) under a nitrogen atmosphere for 1.5 h. The resulting bright yellow solution was diluted with cold distilled water (10 ml), acidified with 1 *N* hydrochloric acid, and extracted with ethyl acetate (3 × 5 ml). The combined extracts were washed with water, dried over anhydrous sodium sulfate, and evaporated under reduced pressure to afford a bright yellow foam (54 mg). The

crude oxime was dissolved in anhydrous ethyl ether (5 ml), treated with phosphorous pentachloride (72.5 mg, 0.348 mmol) and stirred at room temperature for 1 h. The reaction mixture was then poured onto crushed ice (10 g), extracted with ethyl acetate (3 × 5 ml), and the combined extracts thoroughly washed with water, dried over anhydrous sodium sulfate, and evaporated under reduced pressure. The yellow residue (57.2 mg) was purified by preparative layer chromatography (silica gel – oxalic acid plates, petroleum ether – acetone (3:1)) to produce (+)-*N*-acetyl-6-amino-7,9-di-*O*-benzylusnic acid (**15**) (26 mg, 0.0482 mmol; 48%), fine yellow needles from ethyl ether, mp 168–170°C; $[\alpha]_D(CHCl_3)$ 0° (*c* 0.1052); uv: λ_{max} (log ε) 330 (3.19), 265 (3.93), 2.5 (4.30); ir: ν_{max} 3430 (N—H, free), 3400–3100 (OH, chelated), 1680 (C=O, 'Amide I band', free; enone system), 1610, 1590 (C=C), 1540 (C=O, chelated triketone system), 1520 (N—H, C—N, 'Amide II band', free), 1250 (C—N, 'Amide III band', free); ^{1}Hmr: δ 1.79 (3H, s, C_{9b}-CH_3), 2.01 (3H, s, C_8-CH_3), 2.27 (3H, s, C_6-NH-COCH_3), 2.46 (3H, s, C_2-COCH_3), 4.82 (2H, AB q, J = 10 Hz, C_7-O-CH_2-C_6H_5), 5.25 (2H, AB q, J = 10 Hz, C_9-O-CH_2-C_6H_5), 5.77 (1H, s, C_4-*H*), 6.87 (1H, br s, C_6-N*H*-COCH$_3$), 7.30–7.70 (10H, m, 2 × C_6H_5), 18.00 ppm (1H, s, C_3-O*H*); ms: *m/e* 539 (M^+), 449, 448, 422, 406 (base peak), 380, 364, 358, 338, 322, 316, 315, 306, 232, 205, 175, 91, 85, 65, 43. *Anal.* calcd. for $C_{32}H_{29}O_7N$: C 70.81, H 5.94, N 2.42; found: C 70.54, H 6.00, N 2.10. High resolution molecular weight determination calcd. for $C_{32}H_{29}O_7N$: 539.194; found: 539.191.

*Preparation of (±)-N-Acetyl-6-amino-7,9-di-O-benzylusnic Acid (**15**). Experiment II*

A solution of (±)-7,9-di-*O*-benzylusnic (**13**) (52.4 mg, 0.1 mmol) and hydroxylamine hydrochloride (10.3 mg, 0.148 mmol) in 5% methanolic potassium hydroxide (2 ml) and distilled water (1 ml) was heated at 50°C (oil bath temperature) under a nitrogen atmosphere for 1.5 h. The resulting solution was diluted with cold distilled water (10 ml), acidified with 1 *N* hydrochloric acid, and extracted with ethyl acetate (3 × 5 ml). The combined extracts were washed with distilled water, dried over anhydrous sodium sulfate, and evaporated under reduced pressure. The crude oxime (55 mg) was dissolved in dry ethyl ether (5 ml), treated with thionyl chloride (83.5 mg, 0.701 mmol), and stirred at room temperature for 20 min. To the resulting suspension was added a 1:1 mixture of ethyl acetate – water (10 ml), the reaction mixture transferred into a separatory funnel, the organic layer separated, and the aqueous mother liquors extracted with ethyl acetate (2 × 5 ml). The combined extracts were washed with water, dried over anhydrous sodium sulfate, and evaporated under reduced pressure. The crude residue (52.3 mg) was purified by preparative layer chromatography (silica gel – oxalic acid plates, petroleum ether – acetone (3:1)) to produce (±)-*N*-acetyl-6-amino-7,9-di-*O*-benzylusnic acid (**15**) (33.4 mg, 0.0619 mmol; 61%), pale yellow needles from ethyl ether, mp 169–170°C; mixture mp with authentic material from previous experiments, 169–170°C. Both samples showed identical spectroscopic and chromatographic properties.

*Preparation of (+)-N-Acetyl-6-amino-7,9-di-O-methylisoxazolo[4,5-b]usnic Acid (**17**) (N-Acetyl-10-amino-6,6a-dihydro-7,9-dimethoxy-5,6aα,8-trimethyl-6-oxoisoxazolo[4,5-b]dibenzofuran)*

A solution of (+)-7,9-di-*O*-methylisoxazolo[4,5-*b*]-usnic acid (**16**) (36) (2.0 g, 5.42 mmol) and hydroxylamine hydrochloride (1.13 g, 16.258 mmol) in dry pyridine (30 ml) was heated at 55°C (oil bath temperature) under a nitrogen atmosphere for 2.75 h. The reaction mixture was then diluted with cold distilled water (100 ml) and extracted with ethyl acetate (3 × 30 ml). The combined extracts were washed with 1 *N* hydrochloric acid, with water, dried over anhydrous sodium sulfate, and evaporated under reduced pressure. The crude oxime (2.1831 g) was dissolved in anhydrous ethyl ether (70 ml), treated with thionyl chloride (950 mg, 7.983 mmol), and the mild exothermic reaction allowed to proceed for 12 min. The reaction mixture was then quenched with a 1:1 mixture of ethyl acetate – water (100 ml), neutralized with 2.5% aqueous sodium bicarbonate solution, and extracted with ethyl acetate (3 × 20 ml). The combined extracts were washed with water, dried over anhydrous sodium sulfate, and evaporated under reduced pressure to afford a yellow-brown foam (2.36 g). Purification by column chromatography on silica gel Merck (150 g) using 20% acetone in benzene produced the following materials.

*Fraction I. (+)-7,9-di-O-methylisoxazolo[4,5-b]usnic Acid (**16**)*

Yellow foam that could not be induced to crystallize (208 mg, 0.563 mmol; 10%). This sample showed spectroscopic and chromatographic characteristics identical with those of the starting material.

*Fraction II. (+)-N-Acetyl-6-amino-7,9-di-O-methylisoxazolo[4,5-b]usnic Acid (**17**)*

Fine yellow needles from ethyl ether (1.302 g, 3.390 mmol; 69%) mp 188–189°C; $[\alpha]_D^{26}$ +354° (*c* 0.0395); uv: λ_{max} (log ε) 364 (3.06), 315 (2.84), 281 (3.15), 253 (3.71), 208 (4.48); ir: ν_{max} 3460 (N—H, free), 3320 (N—H, associated), 1685 (C=O, 'Amide I band', free), 1670 (C=O, enone system), 1650 (C=O, 'Amide I band', associated), 1610, 1590 (C=C), 1550 (N—H, C—N, 'Amide II band', associated), 1535 (N—H, C—N, 'Amide II band', free), 1300 (C—N, 'Amide III band', associated), 1265 (C—N, 'Amide III band', free); ^{1}Hmr: δ 1.78 (3H, s, C_{9b}-CH_3), 2.19 (6H, s, C_8-CH_3, and C_6-NH-COCH_3), 2.43 (3H, s, C_{11}-CH_3), 3.78 (3H, s, C_7-OCH_3), 3.96 (3H, s, C_9-OCH_3), 6.14 (1H, s, C_4-*H*), 7.28 ppm (1H, br s, C_6-N*H*-COCH$_3$); ms: *m/e* 384 (M^+, base peak), 369, 342, 341, 327, 316, 314, 301, 299, 284, 260, 259, 253, 246, 203, 43. *Anal.* calcd. for $C_{20}H_{20}O_6N_2$: C 62.49, H 5.18, N 7.29; found: C 61.98, H 5.18, N 6.77. High resolution molecular weight determination calcd.: 384.132; found: 384.127.

*Preparation of (+)-6-Desacetyl-7,9-di-O-methylisoxazolo-[4,5-b]usnic Acid (**18**) (6,6a-Dihydro-7,9-dimethoxy-5,6aα,8-trimethyl-6-oxoisoxazolo[4,5-b]-dibenzofuran)*

A solution of (+)-*N*-acetyl-6-amino-7,9-di-*O*-methylisoxazolo[4,5-*b*]usnic acid (**17**) (1.4 g, 3.645 mmol) in anhydrous dioxane (45 ml, freshly distilled from lithium aluminum hydride) was treated with excess isoamyl nitrite (10 ml) and heated at 88°C (oil bath temperature) under a nitrogen atmosphere for 8.5 h. The solvent was then evaporated under reduced pressure and the residue (1.32 g) purified by column chromatography on silica gel Merck (150 g) to produce the following component.

*Fraction I. (+)-6-Desacetyl-7,9-di-O-methylisoxazolo-[4,5-b]usnic Acid (**18**)*

Large bright yellow prisms from ethyl alcohol (812 mg, 2.483 mmol; 77%) mp 156.5–158°C; $[\alpha]_D^{26}$(CH_3CN)

+300° (*c* 0.07585); uv: λ_{max} (log ε) 368 (2.95), 305 (2.84), 281 (3.27), 254 (3.67), 211 (4.41); ir: ν_{max} 2940 (C—H, aromatic -OCH_3), 2850 (C—H, aromatic -OCH_3), 1630 (C=O, enone system), 1650 (isoxazole, trisubstituted), 1620, 1600 (C=C); ^{1}Hmr: δ 1.76 (3H, s, C_{9b}-CH_3), 2.12 (3H, s, C_8-CH_3), 2.44 (3H, s, C_{11}-CH_3), 3.78 (3H, s, C_7-OCH_3), 3.96 (3H, s, C_9-OCH_3), 6.12 (1H, s, C_4-*H*), 6.43 ppm (1H, s, C_6-*H*); ms: *m/e* 327 (M^+, base peak), 312, 299, 298, 284, 271, 259, 258, 246, 243, 231, 215, 203, 115. *Anal.* calcd. for $C_{18}H_{17}O_5N$: C 66.05, H 5.23, N 4.28; found: C 66.08, H 5.44, N 4.13. High resolution molecular weight determination calcd.: 327.111; found: 327.112.

*The Demethylation of (+)-6-Desacetyl-7,9-di-O-methylisoxazolo[4,5-b]usnic Acid (**18**). Isolation of (+)-6-Desacetyl-7-O-methylisoxazolo[4,5-b]usnic Acid (**21**) (6,6a-Dihydro-9-hydroxy-7-methoxy-5,6aα,8-trimethyl-6-oxoisoxazolo[4,5-b]dibenzofuran)*

A solution of (+)-6-desacetyl-7,9-di-*O*-methylisoxazolo[4,5-*b*]usnic acid (**18**) (50 mg, 0.1529 mmol) in dry dichloromethane (4 ml) was cooled to −50°C (dry ice – acetone bath) and treated with cold boron tribromide (383 mg, 1.530 mmol). The resulting deep red solution was allowed to warm-up to −30°C over 0.5 h and then poured into ethyl acetate (10 ml) and ice (10 g). The aqueous fraction was extracted once more with ethyl acetate (10 ml) and the combined extracts washed thoroughly with water, dried over anhydrous magnesium sulfate, and evaporated under reduced pressure. The residue (51 mg) was crystallized directly from ethyl alcohol to produce pale yellow prismatic needles of (+)-6-desacetyl-7-*O*-methylisoxazolo[4,5-*b*]usnic acid (**21**) (47 mg, 0.150 mmol; 98%), mp 167–168°C; $[\alpha]_D^{26}(CH_3CN)$ +250° (*c* 0.034); uv: λ_{max} (log ε) 372 (2.81), 304 (2.37), 256 (3.50), 214 (4.44); ir: ν_{max} 3500–3100 (OH, chelated), 1660 (C=O, enone system), 1620 (C=C); ^{1}Hmr: δ 1.71 (3H, s, C_{9b}-CH_3), 2.06 (3H, s, C_8-CH_3), 2.46 (3H, s, C_{11}-CH_3), 3.76 (3H, s, C_7-OCH_3), 6.18 (1H, s, C_4-*H*), 6.25 (1H, s, C_6-*H*), 9.67 ppm (1H, s, C_9-O*H*); ms: *m/e* 313 (M^+, base peak), 284, 270, 257, 245, 244, 229, 204, 201. *Anal.* calcd. for $C_{17}H_{15}O_5N$: C 65.17, H 4.83, N 4.47; found: C 65.59, H 4.71, N 4.75. High resolution molecular weight determination calcd.: 313.095; found: 313.094.

*Acetylation of (+)-6-Desacetyl-7-O-methylisoxazolo[4,5-b]usnic Acid (**21**). Preparation of (+)-6-Desacetyl-7-O-methylisoxazolo[4,5-b]usnic Acid Monoacetate (**22**) (9-Acetoxy-6,6a-dihydro-7-methoxy-5,6aα,8-trimethyl-6-oxoisoxazolo[4,5-b]-dibenzofuran)*

A solution of (+)-6-desacetyl-7-*O*-methylisoxazolo-[4,5-*b*]usnic acid (**21**) (115 mg, 0.367 mmol) in 0.5% concentrated sulfuric acid in acetic anhydride (2 ml) was allowed to stand at room temperature overnight. The resulting yellow-brown solution was poured onto crushed ice (10 g), extracted with ethyl acetate (3 × 5 ml), and the combined extracts thoroughly washed with water, dried over anhydrous magnesium sulfate, and evaporated under reduced pressure. The crude residue (90.8 mg) was purified by preparative layer chromatography (silica gel – oxalic acid plates, solvent *A*) to produce (+)-6-desacetyl-7-*O*-methylisoxazolo[4,5-*b*]usnic acid monoacetate (**22**) (42 mg, 0.181 mg; 32%), pale yellow plates from ethyl alcohol, mp 195–196°C; $[\alpha]_D^{26}(CH_3CN)$ +500° (*c* 0.064); uv: λ_{max} (log ε) 365 (3.01), 304 (2.90), 278 (3.44), 251 (3.70), 213 (4.39); ir: ν_{max} 2960, 2860 (C—H, aromatic -OCH_3), 1770 (C=O, acetate), 1690 (C=O, enone system), 1660 (isoxazole,t risubstituted), 1620, 1600 (C=C); ^{1}Hmr: δ 1.76 (3H, s, C_{9b}-CH_3), 2.01 (3H, s, C_8-CH_3), 2.46 (3H, s, C_9-$OCOCH_3$), 2.50 (3H, s, C_{11}-CH_3), 3.85 (3H, s, C_7-OCH_3), 6.20 (1H, s, C_4-*H*), 6.58 ppm (1H, s, C_6-*H*); ms: *m/e* 355 (M^+, base peak), 338, 312, 297, 286, 284, 273, 270, 269, 257, 244, 232, 229, 216, 204, 201. *Anal.* calcd. for $C_{19}H_{17}O_6N$: C 64.22, H 4.82, N 3.94; found: C 64.03, H 4.89, N 3.91. High resolution molecular weight determination calcd.: 355.105; found: 355.104.

*Preparation of (+)-6-Desacetyl-7-O-methylisoxazolo-[4,5-b]usnic Acid Monoacetate (**22**)*

A solution of (+)-6-desacetyl-7-*O*-methylisoxazolo-[4,5-*b*]usnic acid (**21**) (60 mg, 0.191 mmol) in a 1:1 mixture of dry pyridine – acetic anhydride (2 ml) was allowed to stand at room temperature overnight. The resulting yellow solution was poured onto crushed ice (10 g) and extracted with ethyl acetate (3 × 5 ml). The combined extracts were washed with water, dried over anhydrous sodium sulfate, and evaporated under reduced pressure. The crude residue (71 mg) was purified by preparative layer chromatography (silica gel – oxalic acid plates, solvent *A*) to produce (+)-6-desacetyl-7-*O*-methylisoxazolo[4,5-*b*]usnic acid monoacetate (**22**) (64.71 mg, 0.1822 mmol; 95%), pale yellow plates from ethyl alcohol, mp 195–196°C. Mixture mp with authentic material from the previous experiment, 195–197°C. Both samples showed identical spectroscopic and chromatographic properties.

*Preparation of (+)-6-Desacetylisoxazolo[4,5-b]usnic Acid (**19**) (6,6a-Dihydro-7,9-dihydroxy-5,6aα,8-trimethyl-6-oxoisoxazolo[4,5-b]dibenzofuran) I*

A solution of (+)-6-desacetyl-7,9-di-*O*-methylisoxazolo[4,5-*b*]usnic acid (**18**) (190 mg, 0.581 mmol) in dry dichloromethane (30 ml) was cooled to −78°C (dry ice – acetone bath) and treated with cold boron tribromide (1.483 g, 5.81 mmol). The resulting deep red solution was allowed to warm-up to 0°C over 1.5 h and then stirred at 10°C for 2.5 h. The reaction mixture was then poured into ethyl acetate (100 ml) – crushed ice (100 g), the organic extract separated and the aqueous phase extracted with ethyl acetate (2 × 30 ml). The combined extracts were washed with water, dried over anhydrous sodium sulfate, and evaporated under reduced pressure. The resulting residue was immediately purified by preparative layer chromatography (silica gel – oxalic acid plates, solvent *A*) to afford the diphenol **9** (136 mg, 0.4548 mmol) and a mixture (37 mg) consisting of the monophenol and another material of similar R_f. Recycling this mixture under identical experimental conditions and combining those fractions consisting of pure diphenol produced the following products.

*Compound I. (+)-6-Desacetylisoxazolo[4,5-b]usnic Acid (**19**)*

Pale yellow crystals from chloroform – petroleum ether (30–60°C) (151 mg, 0.505 mmol; 86%), mp 194.5–196°C (dec.); $[\alpha]_D^{26}(CH_3CN)$ +608° (*c* 0.0625); uv: λ_{max} (log ε) 370 (2.53), 319 (2.85), 258 (3.71), 210 (4.41); ir: ν_{max} 3610 (OH, free), 3500–3100 (OH, chelated), 1675 (C=O, enone system), 1640 (isoxazole), 1620 (C=C); ^{1}Hmr ($CDCl_3$-DMSO-d_6): δ 1.70 (3H, s, C_{9b}-CH_3), 2.07 (3H, s, C_8-CH_3), 2.44 (3H, s, C_{11}-CH_3), 6.16 (1H, s, C_4-*H*), 6.28 (1H, s, C_6-*H*), 8.63 (1H, br, C_7-O*H*), 9.62 ppm (1H, s,

C_9-O*H*); ms: *m/e* 299 (M^+, base peak), 284, 271, 270, 256, 243, 231, 230, 218, 202, 201, 190, 83. *Anal.* calcd. for $C_{16}H_{13}O_5N$: C 64.21, H 4.37, N 4.68; found: C 64.27, H 4.42, N 4.50. High resolution molecular weight determination calcd.: 299.079; found: 299.077.

*Compound II. (+)-6-Bromoisoxazolo[4,5-b]usnic Acid (**27**) (10-Bromo-6,6a-dihydro-7,9-dihydroxy-5,6aα,8-trimethyl-6-oxoisoxazolo[4,5-b]dibenzofuran)*

Pale yellow crystals from chloroform – petroleum ether (30–60°C) (17.12 mg, 0.0453 mmol; 7%), mp 209–211°C (dec.); $[\alpha]_D^{26}(CH_3CN)$ +593° (*c* 0.0455); uv: λ_{max} (log ε) 371 (3.01), 324 (2.59), 255 (3.57), 210 (4.53); ir: ν_{max} 3500–3100 (OH, chelated), 1675 (C=O, enone system), 1638 (isoxazole), 1625, 1600 (C=C); ^{1}Hmr ($CDCl_3$–DMSO-d_6): δ 1.72 (3H, s, C_{9b}-C*H*$_3$), 2.32 (3H, s, C_8-C*H*$_3$), 2.45 (3H, s, C_{11}-C*H*$_3$), 6.32 (1H, s, C_4-*H*), 7.96 (1H, br, C_7-O*H*), 9.68 ppm (1H, s, C_9-O*H*); ms: *m/e* 379 (M^+, ^{81}Br, base peak), 377 (M^+, ^{79}Br), 364, 362, 350, 348, 336, 334, 323, 321, 311, 309, 298, 296, 282, 280, 270, 268, 202, 200, 173. *Anal.* calcd. for $C_{16}H_{12}O_5Br$: C 50.80, H 3.20, N 3.70, Br 21.12; found: C 50.91, H 3.40, N 3.49, Br 21.29. High resolution molecular weight determination calcd. for $C_{16}H_{12}O_5N^{81}Br$: 378.988; found: 378.988; calcd. for $C_{16}H_{12}O_5N^{79}Br$: 376.990; found: 376.987.

*Acetylation of (+)-6-Desacetylisoxazolo[4,5-b]usnic Acid (**19**)*

A solution of (+)-6-desacetylisoxazolo[4,5-*b*]usnic acid (**19**) (32 mg, 0.107 mmol) in a 1:1 mixture of pyridine – acetic anhydride (2 ml) was allowed to stand at room temperature overnight. The resulting deep yellow solution was poured onto crushed ice (10 g) and extracted with ethyl acetate (3 × 5 ml). The combined extracts were washed with water, dried over anhydrous sodium sulfate, and evaporated under reduced pressure. The residue (39.7 mg) was purified by preparative chromatography (silica gel – oxalic acid plates, chloroform) to afford two main components.

*Fraction I. (+)-6-Desacetylisoxazolo[4,5-b]usnic Acid Monoacetate (**23**) (7-Acetoxy-6,6a-dihydro-9-hydroxy-5,6aα,8-trimethyl-6-oxoisoxazolo[4,5-b]-dibenzofuran)*

Pale yellow needles from ethyl alcohol (22.7 mg, 0.0665 mmol; 62%), mp 168–170°C; $[\alpha]_D^{26}(CH_3CN)$ +547° (*c* 0.03475): uv: λ_{max} (log ε) 365 (3.09), 315 (2.46), 264 (3.56), 255 (3.63), 214 (4.40); ir: ν_{max} 3300–3100 (OH, chelated), 1760 (C=O, acetate), 1675 (C=O, enone system), 1640 (isoxazole ring), 1620, 1610 (C=C); ^{1}Hmr: δ 1.77 (3H, s, C_{9b}-C*H*$_3$), 2.03 (3H, s, C_8-C*H*$_3$), 2.27 (3H, s, C_7-OCOC*H*$_3$), 2.46 (3H, s, C_{11}-C*H*$_3$), 6.22 (1H, s, C_4-*H*), 6.41 (1H, s, C_6-*H*), 9.99 ppm (1H, s, C_9-O*H*); ms: *m/e* 341 (M^+, base peak), 299, 284, 271, 270, 256, 243, 231, 230, 215, 202, 201, 190, 43. *Anal.* calcd. for $C_{18}H_{15}O_6N$: C 63.33, H 4.43, N 4.10; found: C 63.30, H 4.53, N 3.90. High resolution molecular weight determination calcd.: 341.090; found: 341.091.

*Fraction II. (+)-6-Desacetylisoxazolo[4,5-b]usnic Acid Diacetate (**24**) (7,9-diacetoxy-6,6a-dihydro-5,6aα,8-trimethyl-6-oxoisoxazolo[4,5-b]dibenzofuran)*

Colorless prisms from ethyl alcohol (13.6 mg, 0.0355 mmol; 33%) mp 242–243°C; $[\alpha]_D^{26}(CH_3CN)$ +368° (*c* 0.057); uv: λ_{max} (log ε) 361 (3.09), 310 (2.85), 280 (3.40), 250 (3.69), 210 (4.35); ir: ν_{max} 1765 (C=O, acetates) 1685 (C=O, enone system), 1650 (isoxazole ring), 1620, 1600 (C=C); ^{1}Hmr: δ 1.77 (3H, s, C_{9b}-C*H*$_3$), 1.95 (3H, s, C_8-C*H*$_3$), 2.29 (3H, s, C_7-OCOC*H*$_3$), 2.41 (3H, s, C_9-OCOC*H*$_3$), 2.47 (3H, s, C_{11}-C*H*$_3$), 6.19 (1H, s, C_4-*H*), 6.78 ppm (1H, s, C_6-*H*); ms: *m/e* 383 (M^+), 341, 326, 315, 299 (base peak), 284, 271, 260, 256, 243, 230, 218, 217, 202, 190, 43. *Anal.* calcd. for $C_{20}H_{17}O_7N$: C 62.65, H 4.47, N 3.65; found: C 62.50, H 4.57, N 3.49. High resolution molecular weight determination calcd.: 383.100; found: 383.099.

*Preparation of (+)-6-Desacetylusnic Acid (**2**)*

(+)-6-Desacetylisoxazolo[4,5-*b*]usnic acid (**19**) (56 mg, 0.187 mmol) in absolute ethyl alcohol (10 ml) was hydrogenated over platinum oxide (8 mg) at room temperature and atmospheric pressure. After the uptake of 1 mol equiv. hydrogen was observed (4.58 ml at 25°C) the reaction mixture was filtered through celite, the celite cake washed with absolute ethyl alcohol (3 × 5 ml), and the combined extracts evaporated under reduced pressure. The residue (56 mg) was dissolved in tetrahydrofuran (1 ml) and freshly prepared 1 *N* sodium hydroxide (5 ml) and stirred at room temperature under a nitrogen atmosphere for 1 h. The yellow brown solution was cooled down to 0°C (ice bath), acidified with 1 *N* hydrochloric acid, and extracted with ethyl acetate (3 × 5 ml). The combined extracts were washed with water, dried over anhydrous sodium sulfate, and evaporated under reduced pressure to afford a crystalline residue (57 mg). Recrystallization from chloroform – petroleum ether produced (+)-6-desacetylusnic acid (**2**) (55 mg, 0.182 mmol; 97%) mp 134.5–136°C; mixture mp with authentic (+)-6-desacetylusnic acid (**2**), 134.5–136°C; $[\alpha]_D^{26}$ +689° (*c* 0.06175); uv: λ_{max} (log ε) 335 (3.17), 265 (3.76), 233 (4.08); ir: ν_{max} 3400–2800 (OH, chelated), 1670 (C=O, enone system), 1630 (C=C), 1540 (C=O, chelated carbonyl of the triketone system); ^{1}Hmr: δ 1.67 (3H, s, C_{9b}-C*H*$_3$), 2.09 (3H, s, C_8-C*H*$_3$), 2.59 (3H, s, C_2-COC*H*$_3$), 5.28 (1H, s, C_7-O*H*), 5.78 (1H, br, C_4-*H*), 6.22 (1H, s, C_6-*H*), 10.22 (1H, s, C_9-O*H*), 18.65 ppm (1H, s, C_3-O*H*); ms: *m/e* 302 (M^+), 287, 218, 191 (base peak). *Anal.* calcd. for $C_{16}H_{14}O_6$: C 63.57, H 4.67; found: C 63.53, H 4.72. High resolution molecular weight determination calcd.: 302.079; found: 302.078; cd: λ_{max} (Δε) 328 (+9.42), 283 (−6.06), 260 (−3.59), 239 (+13.24); cd (CH_3OH + KOH): λ_{max} (Δε) 344 (+7.85), 208 (+6.28), 285 (+1.79), 266 (−12.57), 238 (+9.87).

*Acetylation of Synthetic (+)-6-Desacetylusnic Acid (**2**). Isolation of (+)-6-Desacetylusnic Acid Diacetate (**28**)*

A solution of (+)-6-desacetylusnic acid (**2**) (49 mg, 0.162 mmol) in 0.5% concentrated sulfuric acid in acetic anhydride (3 ml) was allowed to stand at room temperature overnight. The light brown reaction mixture was then poured onto ice (10 g) and extracted with ethyl acetate (3 × 5 ml). The combined extracts were thoroughly washed with water, dried over anhydrous magnesium sulfate, and evaporated under reduced pressure. The residue (47 mg) was purified by preparative layer chromatography (silica gel – oxalic acid plates, solvent *A*) to produce (+)-6-desacetylusnic acid diacetate (**28**) (25 mg, 0.0647 mmol; 39%), pale yellow fine needles from ethyl alcohol, mp 208–210°C, mixture mp with authentic (+)-6-desacetylusnic acid diacetate (**28**), 208–209°C; $[\alpha]_D^{26}$ +125° (*c* 0.1025); uv: λ_{max} (log ε) 325 (3.24), 280 (3.75), 261 (3.85), 220 (4.02); ir: ν_{max} 1755 (C=O, acetates), 1685

(C=O, enone system), 1620, 1600 (C=C), 1545 (C=O, chelated triketone system); ^{1}Hmr: δ 1.78 (3H, s, C_{9b}-CH_3), 1.98 (3H, s, C_8-CH_3), 2.33 (3H, s, C_7-OCOCH_3), 2.45 (3H, s, C_9-OCOCH_3), 2.55 (3H, s, C_2-COCH_3), 5.83 (1H, s, C_4-*H*), 6.82 (1H, s, C_6-*H*), 18.31 ppm (1H, br s, C_3-O*H*); ms: *m/e* 386 (M^+), 344, 302, 260, 233, 218 (base peak), 191, 190, 78, 43. *Anal.* calcd. for $C_{20}H_{18}O_8$: C 62.17, H 4.69; found: C 62.21, H 4.74. High resolution molecular weight determination calcd.: 386.100; found: 386.097.

Fries Rearrangement on (+)-6-Desacetylusnic Acid (2). Preparation of Synthetic (+)-Usnic Acid (1)

To a solution of anhydrous aluminum trichloride (41 mg, 0.307 mmol) and acetyl chloride (26 mg, 0.331 mmol) in dry nitrobenzene (0.8 ml, distilled from calcium hydride) was added crystalline (+)-6-desacetylusnic acid (**2**) (20 mg, 0.0661 mmol) and the resulting yellow-brown solution heated at 60°C (oil-bath temperature) under a nitrogen atmosphere for 1.5 h. The reaction mixture was cooled in an ice bath, diluted with chloroform (4 ml), and upon addition of freshly prepared 1 *N* sodium hydroxide (8 ml) stirred at room temperature for 0.5 h. The two layers were separated, and the chloroform–nitrobenzene fraction extracted with 1 *N* sodium hydroxide (2 × 3 ml). The combined aqueous extracts were *carefully* neutralized with 1 *N* hydrochloric acid, extracted with ethyl acetate (4 × 10 ml), and the combined extracts washed with water, dried over anhydrous magnesium sulfate, and evaporated under reduced pressure. The residue was immediately purified by preparative layer chromatography (silica gel – oxalic acid plates, solvent *A*) to produce (+)-usnic acid (**1**) (10.8 mg, 0.0314 mmol; 47%), yellow prisms from chloroform – ethyl alcohol, mp 201–203°C, mixture mp with authentic (+)-usnic acid (**1**), 202–203°C. The spectroscopic properties of both samples were identical.

Acknowledgement

Financial aid from the National Research Council of Canada is gratefully acknowledged. One of us (I.H.S.) wishes to thank NRCC for a scholarship during the period of this study. We would also like to acknowledge the efforts of Ms. I. B. Krizsan in preparing the illustrations.

1. W. C. Evans. J. Gen. Microbiol. **32**, 177 (1963).
2. W. C. Evans. Pfl. Physiol. **10**, 454 (1958).
3. W. C. Evans and B. S. W. Smith. Biochem. J. **49**, x (1951).
4. S. Dagley, W. C. Evans, and P. W. Ribbons. Nature, **188**, 560 (1960).
5. S. Dagley, P. J. Chapman, D. T. Gibson, and J. M. Wood. Nature, **202**, 775 (1964).
6. O. Hayaishi. Bacteriol. Rev. **30**, 720 (1966).
7. D. T. Gibson. Science, **161**, 1093 (1968).
8. M. H. Rogoff. Adv. Appl. Microbiol. **3**, 193 (1961).
9. R. J. Bandoni and G. H. N. Towers. Can. J. Biochem. **45**, 1197 (1967).
10. C. F. Culberson. Chemical and botanical guide to lichen products. The University of North Carolina Press, Chapel Hill, NC. 1969. p. 171.
11. C. F. Culberson. The Bryologist, **73**, 201 (1970).
12. Y. Asahina and S. Shibata. Chemistry of lichen substances. Japan Society for the Promotion of Science, Tokyo. 1954. p. 171.
13. R. M. Silverstein and G. C. Bassler. Spectrometric identification of organic compounds. John Wiley and Sons Inc., New York, NY. 1967. Chapt. 5.
14. S. Forsen, M. Nilsson, and C. A. Wachtmeister. Acta Chem. Scand. **16**, 583 (1962).
15. R. K. Sharma. Diss. Abstr. **24**, 4417 (1964).
16. K. Nakanishi. Infrared absorption spectroscopy. Holden-Day Inc., San Francisco, CA. 1966.
17. R. M. Letcher. Org. Mass Spectrom. **1**, 551 (1968).
18. J. P. Kutney, I. H. Sanchez, and T. Yee. Org. Mass. Spectrom. **8**, 129 (1974).
19. E. Paterno. Gazz. Chim. Ital. **6**, 113 (1876).
20. E. Paterno. Gazz. Chim. Ital. **12**, 231 (1882).
21. E. Paterno. Gazz. Chim. Ital. **30**, 97 (1900).
22. A. Robertson and F. H. Curd. J. Chem. Soc. 1173 (1933).
23. C. Schopf and K. Henck. Ann. **459**, 233 (1927).
24. J. P. Kutney, I. H. Sanchez, and T. Yee. Can. J. Chem. **54**, 3721 (1976).
25. J. P. Kutney, I. H. Sanchez, and T. Yee. Can. J. Chem. **54**, 1073 (1976).
26. J. P. Kutney and I. H. Sanchez. Can. J. Chem. **54**, 1079 (1976).
27. B. C. Challis and J. Challis. *In* The chemistry of amides. *Edited by* J. Zabicky. Interscience. 1970. p. 731.
28. C. O'Connor. Q. Rev. **24**, 553 (1970).
29. N. Kornblum. Org. React. **2**, 262 (1944).
30. R. A. Henry and N. G. Finnegan. J. Am. Chem. Soc. **76**, 290 (1954).
31. J. H. Ridd. Q. Rev. **15**, 418 (1961).
32. J. I. G. Cadogan and G. A. Molina. J. Chem. Soc. Perkin Trans. I, 541 (1973).
33. M. S. Newman and W. M. Hung. J. Org. Chem. **39**, 1317 (1974).
34. D. B. Denney, N. E. Gersham, and A. Appelbaum. J. Am. Chem. Soc. **86**, 3180 (1964).
35. J. I. G. Cadogan, R. M. Paton, and C. Thomson. Chem. Commun. 229 (1970).
36. J. P. Kutney and I. H. Sanchez. Can. J. Chem. **54**, 1085 (1976).
37. R. A. Crochet and P. Kovacic. Chem. Commun. 716 (1973).
38. W. Theilacker and E. Wegner. *In* Newer methods of preparative organic chemistry. Vol. III. *Edited by* W. Foerst. Academic Press, New York, NY. 1964. p. 303.
39. P. Kovacic, M. K. Lowery, and K. W. Field. Chem. Rev. **70**, 639 (1970).
40. J. P. Kutney, I. H. Sanchez, and T. Yee. Org. Mass Spectrom. **8**, 129 (1974).
41. J. F. W. McOmie, M. L. Watts, and D. E. West. Tetrahedron, **24**, 2289 (1968).
42. J. H. P. Tyman and A. A. Durami. Tetrahedron Lett. 4839 (1973).
43. R. G. Lange. J. Org. Chem. **27**, 2037 (1962).
44. R. H. Prager and Y. T. Tan. Tetrahedron Lett. 3661 (1967).
45. F. M. Dean, J. Goodchild, L. E. Houghton, J. A. Martin, R. B. Morton, B. Parton, A. W. Price, and N. Somvichien. Tetrahedron Lett. 4153 (1966).
46. D. Taub, N. N. Girotra, R. D. Hoffsommer, C. H. Kuo, H. L. Slates, S. Weber, and N. L. Wendler. Tetrahedron, **24**, 2443 (1968).

47. L. R. WORDEN, K. D. KAUFMAN, P. J. SMITH, and G. N. WIDIGER. J. Chem. Soc. C, 227 (1970).
48. R. J. MOLYNEUX. Chem. Commun. 318 (1974).
49. P. A. S. SMITH. *In* Molecular rearrangements. Vol. I. *Edited by* P. de Mayo. Interscience. 1963 pp. 507–527.
50. J. W. CORNFORTH. *In* Heterocyclic compounds. Vol. 5. *Edited by* R. C. Elderfield. J. Wiley and Sons Inc., New York, NY. 1957. pp. 418–450.
51. J. P. KUTNEY, I. H. SANCHEZ, and T. YEE. Can. J. Chem. **54**, 3713 (1976).
52. L. G. DONARUMA and W. Z. HELDT. Org. React. **11**, 1 (1960).
53. H. STEPHEN and W. BLELOCH. J. Chem. Soc. 886 (1931).
54. E. BAMBERGER. Ber. **30**, 366 (1897).
55. D. H. HEY, J. STUART-WEBB, and G. H. WILLIAMS. J. Chem. Soc. 4657 (1952).
56. D. F. DETAR and H. J. SCHEIFELE, JR. J. Am. Chem. Soc. **73**, 1442 (1951).
57. D. F. DETAR. J. Am. Chem. Soc. **73**, 1446 (1951).
58. E. H. WHITE. J. Am. Chem. Soc. **77**, 6011 (1955); **77**, 6014 (1955).
59. E. H. WHITE and C. A. AUFDERMASH, JR. J. Am. Chem. Soc. **83**, 1174 (1961); **83**, 1179 (1961).
60. E. H. WHITE and T. W. BACHELOR. Tetrahedron Lett. 77 (1965).
61. E. H. WHITE. J. Am. Chem. Soc. **77**, 6008 (1955).
62. W. A. SKINNER, H. F. GRAM, and B. R. BAKER. J. Org. Chem. **25**, 777 (1960).
63. Y. AHMAD, M. I. QURESHI, and I. BAIG. Can. J. Chem. **45**, 1539 (1967).
64. R. M. SCHRIBNER. J. Org. Chem. **29**, 3429 (1964).
65. G. A. OLAH and J. A. OLAH. J. Org. Chem. **30**, 2386 (1965).
66. G. A. OLAH, N. A. OVERCHUCK, and J. C. LAPIERRE. J. Am. Chem. Soc. **87**, 5785 (1965).
67. S. HUANG. Chem. Abstr. **54**, 4489h (1960).
68. E. B. MCCALL and E. J. BLACKMAN. Chem. Abstr. **59**, 12704d (1963).
69. I. J. HARRISON. Chem. Commun. 616 (1969).
70. V. ARKLEY, J. ATTENBURROW, G. I. GREGORY, and T. WALKER. J. Chem. Soc. 1260 (1962).
71. L. RENÉ, J. P. BUISSON, and R. ROYER. Bull. Soc. Chim. Fr. 475 (1974).
72. R. FILLER, B. T. KHAN, and C. W. MCMULLEN. J. Org. Chem. **27**, 4660 (1962).
73. F. W. BACHELOR, A. A. LOMAN, and L. R. SNOWDON. Can. J. Chem. **48**, 1554 (1970).
74. J. F. W. MCOMIE, M. L. WATTS, and D. E. WEST. Tetrahedron, **24**, 2289 (1968).
75. J. H. P. TYMAN and A. H. DURANI. Tetrahedron Lett. 4839 (1973).
76. L. R. WORDEN, K. D. KAUFMAN, P. J. SMITH, and G. N. WIDIGER. J. Chem. Soc. C, 227 (1970).
77. A. H. BLATT. Org. React. **1**, 342 (1942).
78. J. P. KUTNEY and I. H. SANCHEZ. Can. J. Chem. **54**, 2795 (1976).
79. A. M. PATTERSON, L. T. CAPELL, and D. F. WALKER. The Ring Index. 2nd ed. American Chemical Society, Washington, DC. 1960. p. 388.

Cationic rhodium(I) sulfoxide complexes. Synthesis and spectroscopic properties

BRIAN R. JAMES, ROBERT H. MORRIS, AND KENNETH J. REIMER

Department of Chemistry, University of British Columbia, Vancouver, B.C., Canada V6T 1W5

Received January 24, 1977

BRIAN R. JAMES, ROBERT H. MORRIS, and KENNETH J. REIMER. Can. J. Chem. **55**, 2353 (1977).

Displacement of the labile acetone ligand from [Rh(diene)(PPh_3)(acetone)]A (diene = 1,5-cyclooctadiene (COD), norbornadiene (NBD); A = PF_6^-, SbF_6^-) allows facile coordination of dialkyl or alkyl aryl sulfoxides, and [Rh(diene)(PPh_3)(sulfoxide)]$^+$ complexes have been synthesized using dimethyl sulfoxide (DMSO), tetramethylene sulfoxide (TMSO), di-*n*-propyl sulfoxide (NPSO), (*S*,*S*;*S*,*R*)-(+)-2-methylbutyl methyl sulfoxide (MBMSO), methyl phenyl sulfoxide (MPSO), (*R*)-(+)-methyl-*p*-tolyl sulfoxide (MPTSO), and (*R*)-*t*-butyl *p*-tolyl sulfoxide (TBPTSO).

Diaryl sulfoxides appear to coordinate in solution but no solid compounds could be isolated. The upfield shifts of the sulfoxide resonances (^1H nmr), reflecting shielding by the adjacent phenyl groups of PPh_3, and the decrease in ν(SO) on coordination, are indicative of O-bonding in all cases. Infrared data indicate that the frequency shift of ν(SO) upon O-coordination is roughly proportional to the strength of the metal–oxygen bond for a range of transition metal DMSO and TMSO complexes.

BRIAN R. JAMES, ROBERT H. MORRIS et KENNETH J. REIMER. Can. J. Chem. **55**, 2353 (1977).

Le déplacement du ligand acétone labile du [Rh(diène)(PPh_3)(acétone)]A {diène = cyclooctadiène-1,5 (COD), norbornadiène (NBD); A = PF^-_6, SbF^-_6} permet une coordination facile des dialkyl- et alkyl aryl sulfoxydes et on a synthétisé les complexes [Rh(diène)(PPh_3)(sulfoxyde)]$^+$ utilisant le diméthyle sulfoxyde (DMSO), le tétraméthylène sulfoxyde (TMSO) le di-*n*-propyl sulfoxyde (NPSO), le (*S*,*S*;*S*,*R*)-(+)(méthyl-2 butyl) méthyl sulfoxyde (MBMSO), le méthyl phényl sulfoxyde (MPSO) et le *R*-(+)-méthyl *p*-tolyl sulfoxyde (MPTSO) et le *R*-*tert*-butyl *p*-tolyl sulfoxyde (TBPTSO).

Il semble que le diaryl sulfoxyde se coordonne en solution mais on n'a pu isoler aucun composé solide. Les déplacements vers les hauts champs de résonances du sulfoxyde (rmn ^1H) suggèrent qu'il y a un blindage par les groupes phényles adjacents du PPh_3; par ailleurs la diminution de la valeur de ν(SO) par coordination indique qu'il y a formation de lien avec l'oxygène dans tous les cas. Des données infrarouges indiquent que le déplacement de la fréquence ν(SO) par coordination avec l'oxygène est approximativement proportionnel avec la force du lien métal/oxygène par un étendue de complexes de métaux de transition et de DMSO et TMSO.

[Traduit par le journal]

Introduction

Other studies from this group have recently described ruthenium complexes containing sulfoxide ligands, and the systems were found effective for homogeneous catalytic hydrogenation of olefins (1); use of a chiral sulfoxide ligand led to catalytic asymmetric synthesis (2). We then became especially interested in attaching sulfoxides, including chiral ones, to a rhodium(I) centre. The catalytic activity of rhodium(I) complexes, commonly with phosphines, is well-documented (3), but there is very little known about the catalytic potential of systems containing sulfoxides (4).

Catalysts derived from the complexes [Rh(diene)L_n]A, **1**, (diene = 1,5-cyclooctadiene (COD), norbornadiene (NBD); L = neutral donor ligand; A = anion) are known to be useful for the hydrogenation of a variety of unsaturated organic substrates (5). The selectivity and efficiency of such reactions (*e.g.*, hydrogenation *vs.* isomerization) is likely dependent on the nature of L, typically a tertiary phosphine or arsine, and suggests that catalytic selectivity might be further controlled by using mixed ligand precursors, [Rh(diene)L^1L^2]A, **2**. Compounds such as **1** are typically prepared (5) by the addition of excess L to [RhCl(diene)]$_2$, a procedure not applicable to the synthesis of **2**, but we have found that the latter are easily obtained from [Rh(diene)L^1(acetone)]A, **3**.

In view of our interest in rhodium sulfoxide complexes and the paucity of such complexes in general (6), and especially compounds of type **2**, we have initially investigated the utility of **3** as a synthetic precursor for [Rh(diene)(PPh_3)(sulfoxide)]A species. An appreciation of the electronic and steric requirements of the [Rh(diene)L^1L^2]$^+$ cation and the properties of sulfoxide derivatives (*e.g.*, O- *vs.* S-bonding) are essential

for an evaluation of such compounds as potential catalysts. During the course of this work, Crabtree (7) reported the use of $[Rh(COD)(PPh_3)(py)]^+$ for hydrogenation of 1-alkynes to 1-alkenes.

Experimental

Synthetic procedures and solution measurements were conducted under argon atmosphere. Spectral grade solvents were stored over molecular sieves (BDH, type 5A) and were vacuum-degassed before use.

Infrared spectra (accurate to $\pm 2\ cm^{-1}$) were recorded on a Perkin Elmer 457 grating spectrometer; solid samples were run as Nujol mulls between CsI plates, and for solutions 0.1 mm NaCl cells were used with $CHCl_3$, or CH_2Br_2, a solvent with a useful "window" from 1070–850 cm^{-1}. ^1H nmr spectra were run on a Varian T-60 spectrometer with tetramethylsilane as an internal reference. Conductivity measurements were made in nitromethane at 25°C using a Thomas Serfass conductivity bridge and cell.

Rhodium(III) trichloride was obtained as the trihydrate from Johnson, Matthey Limited. Silver salts were obtained from Alfa Inorganic and Cationics Inc. The chiral sulfoxides were kindly donated by R. S. McMillan of this group (2), and B. Bosnich and H. Boucher (University of Toronto). The other sulfoxides were obtained commercially (Aldrich, Fisher). Microanalyses were performed by Mr. P. Borda of this department.

Preparation of Complexes

Literature methods (8, 9) were used for the synthesis of $[RhCl(COD)]_2$ and $[RhCl(NBD)]_2$, but for the latter the reaction mixture was stirred at 40°C for 3 h under argon.

[Rh(diene)(PPh$_3$)(acetone)]A; diene = COD, NBD; A = PF$_6$, SbF$_6$

To a CH_2Cl_2 solution (15 ml) of PPh_3 (0.409 g, 1.56 mmol) and $[RhCl(COD)]_2$ (0.384 g, 0.774 mmol) was added dropwise with stirring $AgPF_6$ (0.395 g, 1.56 mmol) dissolved in acetone (10 ml); flocculent white AgCl precipitated. After 10 min the bright orange solution was filtered under argon and concentrated to 5 ml. Gradual addition of ether gave orange crystals which were collected, washed with ether, and dried. Additional product was obtained upon further concentration and addition of ether. The fractions were combined, dissolved in an equivolume acetone/dichloromethane mixture, and crystallized by the addition of ether (yield = 80%). Solvent of crystallization (CH_2Cl_2), usually found in samples so obtained, was removed by prolonged evacuation.

The NBD compound was prepared similarly.

[Rh(COD)(PPh$_3$)(DMSO)]PF$_6$

DMSO (21 μl, 0.29 mmol) and $[Rh(COD)(PPh_3)(acetone)]PF_6$ (0.20 g, 0.29 mmol) were dissolved in CH_2Cl_2 (3 ml) and stirred for 15 min. Addition of ether gave yellow crystals which were recrystallized from dichloromethane/ether, washed with ether, and dried *in vacuo* for several hours.

All of the mixed ligand species (Table 1) were similarly prepared from the appropriate acetone precursor. Yields were typically 80–90%.

Results and Discussion

Acetone Complexes

Facile cleavage (8–12) of the chloride bridge of $[RhCl(diene)]_2$ by a Lewis base, L^1, can give a monomeric derivative $[RhCl(diene)L^1]$, **4**, but excess reactant (especially where L^1 = phosphine or arsine) in a polar solvent may displace the labile chloride forming $[Rh(diene)L^1_n]^+$ (13, 14). The removal of chloride as a silver salt from **4** facilitates the coordination of acetone, a weak and easily displaced ligand (15); reactions 1 and 2.

$$[1] \quad [RhCl(diene)]_2 + 2L^1 \longrightarrow 2[RhCl(diene)L^1]$$

$$[2] \quad [RhCl(diene)L^1] + AgA \xrightarrow[CH_2Cl_2/acetone]{} [Rh(diene)L^1(acetone)]A + AgCl$$

(**4**; **3**)

Although a variety of ligands such as amines (10, 11), arsines (12), phosphines (8, 9), halides (8), etc., have been used to effect reaction 1, we have confined our initial investigation to triphenylphosphine derivatives. This provides a synthetic advantage, as crystalline samples of the acetone cation, **3**, are easily obtained when $L^1 = PPh_3$, as are the subsequently derived sulfoxide complexes. Table 1 gives the microanalytical data. The *in situ* synthesis of other reactive acetone complexes is readily accomplished.

Solid state infrared measurements on **3** show ν(CO) at $\sim 1660\ cm^{-1}$ (Table 2), consistent with a coordinated acetone moiety (15). The extreme lability of the acetone ligand is demonstrated by the replacement of this band by one of the free ligand at $1710\ cm^{-1}$ during the recording of solution infrared in CH_2Cl_2. Furthermore, only a singlet at δ 2.05 for free ligand is present in the ^1H nmr spectra (Table 3) and there is no evidence of coordinated acetone. In contrast, with the cationic complexes $[M(CO)(acetone)(PPh_3)_2]^+$, M = Rh, Ir, the coordinated acetone singlet appears at δ 1.6–1.8, due to diamagnetic shielding by the *cis* phosphines (13, 15, and see below), and free acetone is detected only after several hours (16). Accordingly, samples of **3** must be recrystallized in the presence of excess acetone.

The dissociation of acetone suggests the formation of formally three-coordinate species. Although such species are usually considered to be solvated four-coordinate square planar, evidence has been presented for three-coordinate

TABLE 1. Analytical data for the rhodium(I) complexes

Complex	Decomposition point (°C)[c]	Analysis %C Found	%C Calculated	%H Found	%H Calculated
$[Rh(COD)(PPh_3)(acetone)]PF_6$	148–150	51.53	51.49	4.89	4.92
$[Rh(NBD)(PPh_3)(acetone)]PF_6$	145–150	50.71	50.93	4.41	4.43
$[Rh(NBD)(PPh_3)(acetone)]SbF_6$	145–148	44.84	44.77	3.97	3.89
$[Rh(COD)(PPh_3)(DMSO)]PF_6$	179–180	48.67	48.28	4.80	4.77
$[Rh(NBD)(PPh_3)(DMSO)]SbF_6$	139–140	42.02	42.04	3.70	3.79
$[Rh(COD)(PPh_3)(TMSO)]PF_6$	173–175	49.46	49.87	4.66	4.88
$[Rh(COD)(PPh_3)(NPSO)]PF_6$[a]	119–121	48.43	48.37	5.22	5.26
$[Rh(COD)(PPh_3)(MBMSO)]PF_6$	57–59	50.75	51.07	5.50	5.49
$[Rh(COD)(PPh_3)(MPSO)]PF_6$[b]	96–98	50.58	50.62	4.68	4.50
$[Rh(COD)(PPh_3)(MPTSO)]PF_6$	137–139	52.56	52.85	5.00	4.83
$[Rh(COD)(PPh_3)(TBPTSO)]PF_6$	140–143	54.75	54.55	5.20	5.30

[a]The calculated analysis includes 0.7 CH_2Cl_2; nmr shows approx. 0.6 CH_2Cl_2.
[b]The calculated analysis includes 0.4 CH_2Cl_2; nmr shows approx. 0.5 CH_2Cl_2.
[c]Uncorrected, in air.

TABLE 2. Infrared data (cm^{-1}) for $[Rh(diene)(PPh_3)L]PF_6$ complexes[a]

L	ν(CO) or ν(SO)[b,c]	$\rho_r(CH_3)$[b,c]	Δν(SO)[d]
Acetone	1658 s,br		
Acetone (NBD)	1663 s,br		
DMSO	958 s,br (947 s,br)	992s (983s)	108
DMSO (NBD)	922 s,br (945 s,br)	983s (985s)	110
TMSO	935 s,br (938 s,br)		84
TBPTSO	947 s,br (940 s)		97
NPSO	942 s,br (947 s,br)		70

L	ν(900–1000 cm^{-1} bands)	Δν[e]
MBMSO	937m, 967s (965s,br)	65
MPSO	958s, 942s (959s, 945sh)	91, 105
MPTSO	957s, 939s (959s, 943sh)	88, 104

[a]Diene = COD, unless indicated otherwise.
[b]Nujol mulls; values in parentheses for CH_2Br_2 solutions.
[c]s = strong, br = broad, m = medium, sh = shoulder.
[d]Defined as (ν(SO) for free ligand − ν(SO) coordinated ligand) in CH_2Br_2.
[e]Defined as ν(SO) for free ligand − ν in solution.

intermediates in reactions of d^8 organometal systems (17). Unsymmetrical T- and Y-shaped configurations were favoured (17*b*) and the former, or solvated four-coordinate species, could account for the inequivalence of the COD olefinic protons in the present system. Two sets of resonances at δ 5.2 and 3.3 are observed in $CDCl_3$ solution (Table 3). A complex spectrum is observed for the NBD analogue in $CDCl_3$, but only a single olefinic signal at δ 4.4 is observed in acetone-d_6; intra- or intermolecular rearrangements are indicated and low temperature nmr studies should clarify the phenomenon. Previous studies (17*a*, 18) have demonstrated differences in the exchange reactions of rhodium(I) diene complexes depending on the nature of the diene, the NBD complexes undergoing rearrangements more readily than the COD analogues. Also relevant here is that for $[Rh(diene)L_n]^+$ complexes, *n* may be 3 for NBD, but only 2 for COD systems (13). The stronger π back-bonding properties of NBD have been invoked to rationalize the reactivity patterns (18).

Infrared data for all of the complexes reported here show that the anions are uncoordinated, since only the characteristic bands of PF_6^- and SbF_6^- are observed at 840 vs, 560 s, and 658 vs, 290 s cm^{-1}, respectively (19).

TABLE 3. ^{1}H nmr data[a] for [Rh(diene)(PPh_3)L]PF_6 complexes[b] at 30°C

L	δ diene (olefinic)[c] H_A	H_B	δ, coordinated L
Acetone	5.20	3.30	2.05 s (CH_3—)[d]
Acetone (NBD)	4.4[e]		2.05 s (CH_3—)
DMSO	5.15	3.15	2.20 s (S—CH_3)
DMSO (NBD)	[f]		2.45 s (S—CH_3)
NPSO	5.13	3.17	2.50 m (S—CH_2), 1.58 tq (—CH_2—), 0.90 t (CH_3—)
MPSO	5.18	3.18	2.38 s (S—CH_3)
MPTSO	5.17	3.17	2.38 s (S—CH_3), 2.38 s (*p*—CH_3—)
TBPTSO	5.18	3.15	0.98 s (S—$C(CH_3)_3$), 2.37 s (*p*—CH_3—)
MBMSO	5.15	3.17	2.22 s (S—CH_3),[g] 1.2 m (—$\overset{\displaystyle CH_3}{\underset{\displaystyle |}{CH}}$—), 0.80 m ($CH_3CH_2$—$\overset{\displaystyle CH_3}{\underset{\displaystyle |}{C}}$—)

[a]Measured in ppm (downfield positive) from TMS in $CDCl_3$, unless indicated otherwise; phenyl resonances omitted; s = singlet, m = multiplet, t = triplet, tq = triplet of quartets.
[b]Diene = COD, unless indicated otherwise; TMSO complex insufficiently soluble.
[c]Appear as broad singlets; H_A and H_B = olefinic protons *trans* to PPh_3 and L, respectively; methylene resonances appear as multiplets at δ 1.8–2.5.
[d]Free ligand signal observed.
[e]In acetone-d_6.
[f]Complex spectrum observed.
[g]S—CH_2 resonance obscured.

Sulfoxide Complexes

Despite the somewhat complex solution behaviour of **3**, such solutions react with an equivalent of a sulfoxide to give yellow (COD) or yellow-orange (NBD) crystalline products. Analytical data are presented in Table 1. The complexes are reasonably air-stable in the solid state. In solution the NBD derivatives are very air-sensitive, while the COD derivatives show reactivity only after several hours; the oxidation products are as yet uncharacterized but dioxygen intermediates are a possibility (20). Treatment of the complexes with dihydrogen at 20°C in solution gives metal, and dihydride complexes, readily formed and detected with the biphosphine cations (5, 13), seem likely intermediates. Of interest, a complex $[H_2Ir(diene)(PPh_3)_2]^+$ has recently been reported (21).

For [Rh(COD)(PPh_3)(DMSO)]A (A = PF_6, SbF_6) a molar conductance of 85 mho cm^{-2} is observed in nitromethane, identical to that for [Rh(COD)(PPh_3)$_2$]PF_6, a known 1:1 electrolyte (13). However, solution infrared spectra of these DMSO complexes in nitromethane show that the solution species is probably [Rh(COD)(PPh_3)($MeNO_2$)]$^+$: ν(SO) is detected at 1055 cm^{-1}, that of free DMSO.

The ^{1}H nmr spectra for the COD derivatives in $CDCl_3$ show two signals for the non-equivalent olefinic protons. The downfield resonance at δ ~ 5.2 is assigned to the protons (H_A) *trans* to PPh_3, consistent with previous assignments (22) for the neutral compounds [MCl(COD)PPh_3], M = Rh, Ir; in these, the signal due to the protons *trans* to chloride appears at δ ~ 3, similar to that found here for those (H_B) opposite the sulfoxide ligands.

The down- and up-field shifts of olefinic diene protons *trans* to PPh_3 and sulfoxide, respectively, are further supported by the respective positions of the equivalent olefinic protons at δ 4.6 and 3.9 for the cations [Rh(COD)(PPh_3)$_2$]$^+$ (13) and [Rh(COD)(DMSO)$_2$]$^+$ (18).

The methylene protons of the diene appear as a broad signal between δ 1.8–2.5. The ^{1}H nmr resonances of the olefinic and methine protons of the diene in the NBD–sulfoxide compounds are complex, as in the NBD–acetone complexes. This precludes definitive assignments, but there is no evidence for the dissociation of the sulfoxide ligands from either the NBD or COD complexes in dichloromethane or chloroform at room temperature. All the sulfoxide complexes contain O-bonded sulfoxide (see below).

DMSO and TMSO Complexes

A sharp ^{1}H nmr singlet due to the DMSO methyl protons of [Rh(COD)(PPh_3)(DMSO)]PF_6 appears at δ 2.2, compared to δ 2.6 for the free sulfoxide and δ 2.8 for [Rh(COD)(DMSO)$_2$]BF_4 (18). Downfield shifts of up to 1 ppm are usually characteristic of S-bonded DMSO, while the O-bonded complexes, in which the protons are further removed from the metal,

TABLE 4. Some infrared data[a] (cm^{-1}) for $[Rh(COD)(PPh_3)L]PF_6$, L = DMSO and DMSO-d_6

DMSO		DMSO-d_6		$\frac{\nu(H\ compound)}{\nu(D\ compound)}$
Frequency	Assignment	Frequency	Assignment	
[b]	ν(CH)	2260 m	ν(CD)	
[b]	ν(CH)	2125 m	ν(CD)	
1420 m	δ(CH)	1042 m	δ(CD)	
1327 m	δ(CH)	1020 s	δ(CD)	
1038 s	$\rho_r(CH_3)$	(831 s)[c]	$\rho_r(CD_3)$	(1.25)[c]
992 s (983)	$\rho_r(CH_3)$	[b]	$\rho_r(CD_3)$	
958 s,br (947)	ν(SO)	950 s,br (955)	ν(SO)	
450 m	ν(Rh—O)	430 m	ν(Rh—O)	1.046

[a]Nujol mulls; values in parentheses for CH_2Br_2 solutions; 4000–250 cm^{-1}.
[b]Obscured; other δ and ρ_r modes are also obscured in the 1450–950 cm^{-1} region, and thus the isotope ratios here cannot be assigned with certainty.
[c]From SbF_6^- complex, since obscured in the PF_6^- derivative.

show considerably less variation from the free values (23). The proximal phenyl rings of PPh_3 must be responsible for the upfield shifts observed here, and noted previously (24) for $[Ir(CO)(DMSO)(PPh_3)_2]ClO_4$ (δ 1.8). Indeed, space filling models suggest that the most favorable orientation is one where a phenyl group presents a ring centre to the adjacent sulfoxide ligand, and such a conformation will likely persist during the majority of rotational motion.

Addition of excess DMSO to a solution of $[Rh(COD)(PPh_3)(DMSO)]^+$ in $CDCl_3$ gives a sharp resonance at a weighted mean position of the free and coordinated ligand, suggesting that the exchange is fast on the nmr time scale. Interestingly, the COD(—CH=) resonances are not broadened. Facile exchange of O-bonded sulfoxides, less so for S-bonded (1), has been noted by others (23, 25), and this, together with the other nmr and infrared evidence (see below), is consistent with the O-bonded nature of DMSO in the present instance.

The position of the sulfur–oxygen stretching vibration in the infrared spectra of sulfoxide complexes is diagnostic of the bonding mode; S-bonding usually causes an increase of ν(SO) to about 1100 cm^{-1}, whereas a shift to a lower range (1000–900 cm^{-1}) is indicative of donation from oxygen (1, 6, 23, 26–29). However, assignments of ν(SO) for O-bonded sulfoxides with α-methyl groups, are complicated by the presence of methyl rocking vibrations which are similar in energy to the S—O stretch (26, 27, 30, 31).

Bands at 983 and 947 cm^{-1} are observed in the CH_2Br_2 solution infrared of $[Rh(COD)(PPh_3)(DMSO)]A$. The higher frequency band is absent in the spectrum of the DMSO-d_6 analogue (Table 4) indicating that the major contribution to this band is a methyl rocking mode.

By comparison of the infrared spectra of the present compounds with those of other rhodium diene species we have assigned ν(Rh—O) for the TMSO (432 cm^{-1}) and DMSO (450 cm^{-1}) compounds. The latter is shifted to 430 cm^{-1} in the DMSO-d_6 compound, and the frequency ratio 1.046 confirms this assignment and indicates that the vibrational modes are almost pure Rh—O stretches (32).

By means of a deuteration study, we have confirmed the O-bonded nature of the DMSO ligands in $[Rh(COD)(DMSO)_2]^+$; ν(SO) = 950 cm^{-1}, ν(Rh—O) = 473, 465 cm^{-1}. The Rh—O stretches again exhibit the expected deuterium shift of about 1.05 (32).

A correlation seems to exist between the bands assigned as ν(M—O) and the frequency reduction of ν(SO) on coordination of sulfoxide to metals. Data are given in Table 5 for O-bonded DMSO and TMSO in some transition metal complexes. There is sometimes ambiguity in the assignment of the O-bonded SO-stretch within certain of the DMSO complexes because of the methyl rocking modes (27, 31) (two Δν(SO) values are thus given), but nevertheless ν(M—O) increases generally with increasing Δν(S—O). Such a relationship has been suggested (37), but not previously documented. Figure 1 shows the data plotted for systems where there is thought to be no ambiguity. Except for the CrL_6^{3+} complexes (L = DMSO, TMSO), the data fall within a remarkably well-defined band for all the mono-, bi-, and trivalent species. Figure 1 unfortunately does not aid in establishing the

TABLE 5. Infrared data[a] for O-bonded DMSO and TMSO complexes

Complex[b]	Δν(SO)[c]	ν(MO)	Reference
1. $[Cr(DMSO)_6]^{3+}$	127	529	26, 32
2. *cis*-$[Pt(DMSO)_2(DMSO)_2]^{2+}$	176, 158	517	25
3. *cis*-$[Pd(DMSO)_2(DMSO)_2]^{2+}$	135, 150	493	25
4. *mer*-$RhCl_3(DMSO)(DMSO)_2$	120	491	33
5. *cis*-$RuCl_2(DMSO)(DMSO)_3$	140	480	1, 23
6. $[Fe(DMSO)_6]^{3+}$	115	475	26, 28*b*
7. $[Rh(COD)(DMSO)_2]^{+}$	105	473, 465	Present work
8. $[Rh(COD)(PPh_3)(DMSO)]^{+}$	97	450	Present work
$[Mn(DMSO)_6]^{2+}$	100 *or* 55	418	26, 29, 32
$[Fe(DMSO)_6]^{2+}$	105 *or* 70	438, 415	26, 29, 32
$[Co(DMSO)_6]^{2+}$	105 *or* 61	436	26, 27, 31, 32
$[Ni(DMSO)_6]^{2+}$	105 *or* 55	444	26, 29, 32
$[Cu(DMSO)_4]^{2+}$	115 *or* 67	467	26, 27, 34
trans-$CuCl_2(DMSO)_2$	132 *or* 75	496, 481	26, 35, 36
9. $[Cr(TMSO)_6]^{3+}$	90	484	28
10. *cis*-$[Pt(TMSO)_2(TMSO)_2]^{2+}$	143, 127	480, 469	25
11. *cis*-$[Pd(TMSO)_2(TMSO)_2]^{2+}$	121, 102	473, 458	25
12. $[Fe(TMSO)_6]^{3+}$	102	440	28
13. $[Rh(COD)(PPh_3)(TMSO)]^{+}$	87	432	Present work
14. $[Ni(TMSO)_6]^{2+}$	52	413	28
15. $[Co(TMSO)_6]^{2+}$	54	406	28
16. $[Fe(TMSO)_6]^{2+}$	55	397	28
17. $[Mn(TMSO)_6]^{2+}$	48	388	28

[a]Mulls; in cm^{-1}.
[b]DMSO and DMSO designate S- and O-bonded, respectively (and for TMSO).
[c]Frequency shift on O-coordination.

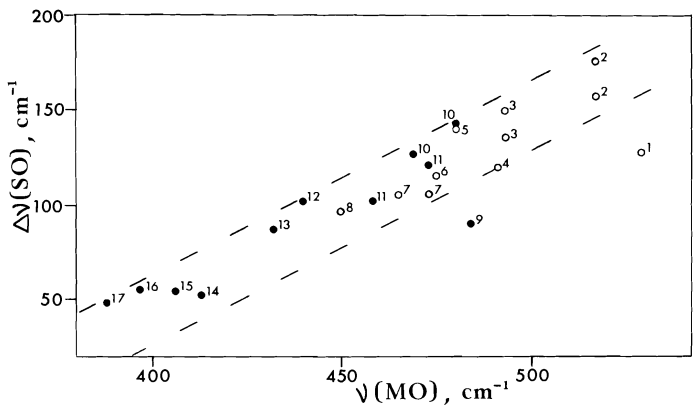

FIG. 1. Plot of frequency shift of ν(SO) on coordination of O-bonded sulfoxide *vs.* ν(MO); ○, dimethylsulfoxide complexes; ●, tetramethylene sulfoxide complexes. Numbers refer to complexes listed in Table 5.

correct assignments for ν(SO) and $\rho_r(CH_3)$ in the $M(DMSO)_6^{2+}$ species ($M = Mn^{II}$, Fe^{II}, Co^{II}, Ni^{II}). However, Fig. 1 likely resolves the corresponding ambiguity in the assignments for ν(SO) in $Cu(DMSO)_4^{2+}$ (940 or 988 cm^{-1}) and *trans*-$CuCl_2(DMSO)_2$ (923 or 980 cm^{-1}); in each case, the lower number giving Δν(SO) values of 115 and 132 cm^{-1}, respectively, is more consistent with the observed trend *vs.* ν(MO).

Other Sulfoxide Complexes

The ^1H nmr data of the other sulfoxide complexes (Table 3) show that, except for *p*-CH_3, all resonances are shifted upfield from the free ligand positions, indicating again a phenyl diamagnetic shielding of O-bonded sulfoxide ligands.

The infrared data in the 900–1000 cm^{-1} region for systems uncomplicated by the presence of α-methyl rocking modes (*i.e.*, for the DMSO-d_6, TMSO, TBPTSO, and NPSO systems) show that the SO stretch shifts by 70–110 cm^{-1} upon coordination to the metal (Table 2). This wide shift range precludes its use in helping assign

ν(SO) in the MBMSO, MPSO, and MPTSO systems which contain the methyl rocking modes; the shift of *both* bands in the region of interest is in the same 70–110 cm^{-1} range (Table 2). Nevertheless, the increased complexity in the 900–1000 cm^{-1} region upon coordination with the α-methyl-containing sulfoxides is consistent with O-bonding. Assignments of ν(Rh—O) were precluded by the multiplicity of infrared bands in the 400–500 cm^{-1} region.

Although diaryl sulfoxides appear to be O-bonded to rhodium (upfield nmr shifts) in solution, we have been unable to isolate discrete complexes, possibly due to unfavorable steric interactions in the solid state; the diaryl sulfoxide ligands studied were diphenylsulfoxide, and *S-o*-tolyl *p*-tolyl sulfoxide.

The choice of S- or O-coordination with a sulfoxide ligand has usually been rationalized in terms of steric effects (25, 38). However, considering that both the DMSO ligands are O-bonded in the unhindered $[Rh(COD)(DMSO)_2]^+$ complex, electronic factors must play a substantial role in the cationic rhodium(I) diene complexes. Attempts to force S-donation using different L^1 ligands, as well as investigation of the catalytic properties of these complexes, are in progress.

Acknowledgements

We acknowledge financial support from the National Research Council of Canada in terms of a research grant and a post graduate scholarship (R.H.M.), and from the Killam Foundation for a postdoctoral fellowship (K.J.R.). The $RhCl_3 \cdot 3H_2O$ was kindly loaned by Johnson, Matthey Ltd.

1. R. S. McMillan, A. Mercer, B. R. James, and J. Trotter. J. Chem. Soc. Dalton Trans. 1006 (1975).
2. B. R. James, R. S. McMillan, and K. J. Reimer. J. Mol. Catal. **1**, 439 (1976); R. S. McMillan. Ph.D. Thesis, University of British Columbia, Vancouver, British Columbia. 1976.
3. J. D. Morrison, W. F. Masler, and M. K. Neuberg. Adv. Catal. **25**, 81 (1976); B. R. James. Chem. Can. **27** (9), 27 (1975).
4. B. R. James, F. T. T. Ng, and G. L. Rempel. Can. J. Chem. **47**, 4521 (1969).
5. R. R. Schrock and J. A. Osborn. J. Am. Chem. Soc. **98**, 2134, 2143 (1976), and references therein.
6. W. L. Reynolds. Prog. Inorg. Chem. **12**, 1 (1970).
7. R. H. Crabtree. J. Chem. Soc. Chem. Commun. 647 (1975).
8. J. Chatt and L. M. Venanzi. J. Chem. Soc. 4735 (1957).
9. E. W. Abel, M. A. Bennett, and G. Wilkinson. J. Chem. Soc. 3178 (1959).
10. P. Fougeroux, B. Denise, R. Bonnaire, and G. Pannetier. J. Organomet. Chem. **60**, 375 (1973).
11. M. P. Li and R. S. Drago. J. Am. Chem. Soc. **98**, 5129 (1976).
12. K. Vrieze and H. C. Volger. J. Organomet. Chem. **11**, P17 (1968).
13. R. R. Schrock and J. A. Osborn. J. Am. Chem. Soc. **93**, 2397 (1971).
14. L. M. Haines. Inorg. Chem. **9**, 1517 (1970).
15. H. C. Clark and K. J. Reimer. Inorg. Chem. **14**, 2133 (1975).
16. H. C. Clark and K. J. Reimer. Unpublished results.
17. (*a*) K. Vrieze, H. C. Volger, and P. W. N. M. van Leeuwen. Inorg. Chim. Acta Rev. **3**, 109 (1969), and references therein; (*b*) S. Komiya, T. A. Albright, R. Hoffmann, and J. K. Kochi. J. Am. Chem. Soc. **98**, 7255 (1976).
18. M. Green and T. A. Kuc. J. Chem. Soc. Dalton Trans. 832 (1972).
19. H. C. Clark and R. J. O'Brien. Inorg. Chem. **2**, 1020 (1963); O. A. Serra, M. Perrier, V. K. L. Osorio, and Y. Kawano. Inorg. Chim. Acta, **17**, 135 (1976).
20. M. Laing, M. J. Nolte, and E. Singleton. J. Chem. Soc. Chem. Commun. 660 (1975).
21. R. H. Crabtree, H. Felkin, and G. E. Morris. J. Chem. Soc. Chem. Commun. 716 (1976).
22. K. Vrieze, H. C. Volger, and A. P. Praat. J. Organomet. Chem. **14**, 185 (1968).
23. I. P. Evans, A. Spencer, and G. Wilkinson. J. Chem. Soc. Dalton Trans. 204 (1973).
24. C. A. Reed and W. R. Roper. J. Chem. Soc. Dalton Trans. 1365 (1973).
25. J. H. Price, A. N. Williamson, R. F. Schramm, and B. B. Wayland. Inorg. Chem. **11**, 1280 (1972).
26. F. A. Cotton, R. Francis, and W. D. Horrocks, Jr. J. Phys. Chem. **64**, 1534 (1960).
27. R. S. Drago and D. Meek. J. Phys. Chem. **65**, 1446 (1961).
28. (*a*) C. V. Berney and J. H. Weber. Inorg. Chim. Acta, **5**, 375 (1971); (*b*) J. Reedijk, P. W. N. M. van Leeuwen, and W. L. Groeneveld. Rec. Trav. Chim. **87**, 1073 (1968).
29. W. F. Currier and J. H. Weber. Inorg. Chem. **6**, 1539 (1967).
30. M. T. Forel and M. Tranquille. Spectrochim. Acta, **26A**, 1023 (1970).
31. C. R. Piriz Mac-coll and L. Beyer. Inorg. Chem. **12**, 7 (1973).
32. C. V. Berney and J. H. Weber. Inorg. Chem. **7**, 283 (1968).
33. Yu V. Fadeev, Yu N. Kukushkin, and K. A. Khokhryakov. Russ. J. Inorg. **20**, 1519 (1975).
34. B. F. G. Johnson and R. A. Walton. Spectrochim. Acta, **22**, 1853 (1966).
35. D. M. Adams and W. R. Trumble. Inorg. Chem. **15**, 1968 (1976).
36. J. Selbin, W. E. Bull, and L. H. Holmes, Jr. J. Inorg. Nucl. Chem. **16**, 219 (1961).
37. D. W. Meek, D. K. Straub, and R. S. Drago. J. Am. Chem. Soc. **82**, 6013 (1960).
38. A. Mercer and J. Trotter. J. Chem. Soc. Dalton Trans. 2480 (1975).

Synthesis of 3,5-dihydroxy-2,2-dimethylchroman-4-one and its implications for the structure of the phytotoxin stemphylin[1]

A. N. STARRATT AND A. STOESSL

Agriculture Canada, Research Institute, University Sub Post Office, London, Ont., Canada N6A 5B7

Received February 21, 1977

A. N. STARRATT and A. STOESSL. Can. J. Chem. **55**, 2360 (1977).

3,5-Dihydroxy-2,2-dimethylchroman-4-one was prepared by an unambiguous synthesis. Its spectroscopic properties and those of its methyl ether are incompatible with its identity as the aglycone moiety of the fungal toxin stemphylin.

A. N. STARRATT et A. STOESSL. Can. J. Chem. **55**, 2360 (1977).

On a préparé la dihydroxy-3,5 diméthyl-2,2 chromanone-4 par une synthèse non-ambigue. Ses propriétés spectroscopiques et celles de son éther méthylique ne correspondent pas à celles de la fraction aglycone de la toxine fungale stemphyline.

[Traduit par le journal]

The phytotoxic compound stemphylin was recently isolated from the fungus *Stemphylium botryosum* (1). It was reported as a "chromone glucoside" and assigned structure **1** mainly on spectroscopic evidence (1), the interpretation of which appeared open to doubt. In order to clarify the situation, we prepared chromanone **2**, the aglycone of **1**, and report that its spectroscopic properties render **1** and related structural proposals for stemphylin untenable.

The synthesis of the acetate **3** of chromanone **2** was accomplished in one step by neutral permanganate oxidation of the known chromene acetate **4**. The latter was prepared from the corresponding chroman **5** essentially as described in the literature (2) but also, more conveniently and efficiently, by the oxidation of **5** with dichlorodicyanobenzoquinone.[2] The permanganate oxidation of **4** furnished **3** in 31% yield when 1.6 mol of reagent was used. The mechanism for the formation of ketols from olefins by oxidation with neutral permanganate has been discussed by Wiberg and Saegebarth (3). An oxidation of a chromene to an α-hydroxychromanone has also been reported with osmium tetroxide – sodium periodate (4).

Mild alkaline hydrolysis of acetate **3** gave the 3,5-dihydroxychromanone **2**, mp 61–62°C, whose structure was established by the usual criteria

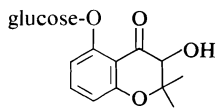

1

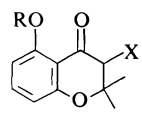

2 R = H, X = OH
3 R = Ac, X = OH
6 R = CH_3, X = OH
7 R = Ac, X = Br
8 R = H, X = H
9 R = Ac, X = H

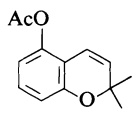

4

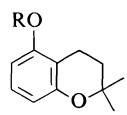

5 R = Ac
10 R = H

(see Experimental). This compound absorbs at λ_{max} 215, 275, and 349 nm (ε 11 860, 7900, and 2700) in ethanol as expected, since very similar values are reported in the literature for other 5-hydroxychromanones (5–7). In water at p*H* 5.5, **2** absorbs at λ_{max} 215, 274, and 346 nm (ε 12 300, 8300, and 2500). In contrast, stemphylin was reported (1) to absorb at λ_{max} 218 and 268 nm (ε 19 200 and 7330) in water at p*H* 5.5, with an additional weak maximum at 427.5 nm, but no mention was made of selective absorption near 350 nm. Methylation of **2** with diazomethane gave methyl ether **6** whose uv spectroscopic properties are similar to those of **2**, including an absorption maximum at 331 nm. This band, therefore, is not contingent on the presence of a free hydroxyl group at C-5. On the other hand, it should be noted that the bathochromic shift observed (1) for stemphylin at p*H* 8.9 suggests

[1]Contribution No. 676.

[2]In passing, we draw attention to the use of chlorobenzene as solvent for this oxidation. This refluxes at a temperature comparable to that of xylene but appears to be less subject to oxidation itself than the latter commonly used solvent.

that this substance does, in fact, possess a free phenolic hydroxyl, contrary to the suggested structure. No bathochromic shift was observed when alkali was added to the spectroscopic solution of the methyl ether **6**.

Other significant differences between the properties reported for stemphylin and those of the chromanone **2** are found in the nmr spectra. Particularly striking is the fact that the methyl groups of **2** are differentially shielded by the hydroxyl attached to C-3. This is observed both in chloroform and dimethyl sulfoxide solution and is also the case with acetate **3** and methyl ether **6**. The 3-bromochromanone **7**, prepared as a model, also exhibits this property which is, indeed, expected of any 3-substituted 2,2-dimethylchroman. Only in the absence of substitution at C-3 do the methyl groups at C-2 become equivalent and give rise to singlet absorption as observed in compounds **8** and **9**. Stemphylin shows only singlet absorption in the methyl region (1) and is therefore unlikely to be a 3-substituted 2,2-dimethyl chromanone, irrespective of the oxygenation pattern in the aromatic ring. Further, the low field absorption of stemphylin is broad and in the range δ 6.6–7.2 whereas the aromatic protons of chromanone **2** give rise to well-defined and fully analyzable bands in the noticeably wider range δ 6.3–7.5.

The substitution of glucosyloxy for a hydroxy or methoxy group at C-5 of **2** or **6**, respectively, will not alter their spectroscopic properties to any significant extent. Thus, the data reported in the present communication clearly indicate that the structure of stemphylin must be regarded as unknown. This conclusion is also in accord with the gross divergence between the figures calculated for the elementary composition of **1** and those determined experimentally for stemphylin (1).

Experimental

Melting points were determined on a Kofler hot stage and are uncorrected. Proton magnetic resonance spectra were measured with Varian A-60A or XL-100-12 spectrometers with tetramethylsilane as internal standard and $CDCl_3$ as solvent unless otherwise stated. Chemical shifts of multiplets were measured at the geometric centres and J represents observed splittings. Mass spectra were determined on a Varian MAT 311A mass spectrometer, infrared spectra were recorded using a Beckman IR-20A spectrophotometer, and ultraviolet spectra were recorded using a Beckman DK spectrophotometer. Silicic acid – celite (4:1) was used for column chromatography and separations were monitored by tlc on Kieselgel (Camag). Light petroleum, bp 35–60°C, was used for chromatography and bp 60–80°C for recrystallizations. Samples were sublimed for analysis (Dr. C. Daesslé, Montreal).

2,2-Dimethyl-5-acetoxychroman, **5**

2,2-Dimethyl-5-hydroxychroman (**10**) was synthesized by the method of Verhé *et al.* (8) with the exception that 1,3-cyclohexanedione was reacted with 1-chloro-3-methyl-2-butene for 4 h. The crude chroman was acetylated at room temperature with acetic anhydride – pyridine and the product was purified by column chromatography. Light petroleum – methylene chloride (9:1) eluted material which was recrystallized from ethanol to give chroman acetate **5**, mp 59–61°C (lit. (2) mp 63–63.5°C); nmr δ 1.31 (d, 6H, Me_2C), 1.75 (t, $J \simeq 6.5$ Hz, 2H, CH_2CMe_2), 2.58 (t, $J \simeq 6.5$ Hz, 2H, CH_2Ar), 2.28 (s, 3H, OAc), 6.59 (dd, $J \simeq 1.5$ and 8 Hz, 1H, H-6 or H-8), 6.70 (dd, $J \simeq 1.5$ and 8 Hz, 1H, H-8 or H-6), 7.12 (t, $J \simeq 8$ Hz, H-7).

2,2-Dimethyl-5-acetoxychromene, **4**

(*a*) Chroman acetate **5** (306 mg) was brominated with *N*-bromosuccinimide as described by Fukami and Nakajima (2). Best yields were obtained by monitoring each run by nmr. Typically the product was isolated after 30 min and dissolved in dry benzene (5 ml) containing 1,5-diazobicyclo[5.4.0]undec-5-ene (254 mg). After heating at reflux for 5 min, the solution was washed with dilute HCl and water and the product was purified by column chromatography. Elution with light petroleum – methylene chloride (19:1) gave chromene acetate **4** (146 mg), an oil; nmr δ 1.43 (s, 6H, Me_2C), 2.30 (s, 3H, OAc), 5.64 (d, $J \simeq 10$ Hz, 1H, $CHCMe_2$), 6.37 (d, $J \simeq 10$ Hz, 1H, CHAr), 6.60 (dd, $J \simeq 1.5$ and 8 Hz, 1H, H-6 or H-8), 6.68 (dd, $J \simeq 1.5$ and 8 Hz, 1H, H-8 or H-6), 7.12 (t, $J \simeq 8$ Hz, 1H, H-7).

(*b*) Chroman acetate **5** (220 mg, 1.0 mmol) in chlorobenzene (5 ml) was refluxed with dichlorodicyanobenzoquinone (253 mg, 1.1 mmol) until the reagent was consumed (tlc, 8 h). Column chromatography with light petroleum – methylene chloride (19:1) afforded pure chromene acetate **4** (105 mg; 48%). Ensuing fractions contained a little more chromene (12 mg, estimated by nmr) admixed with increasing amounts of starting material (48 mg). In similar experiments, with carefully purified xylene as solvent, only traces of the desired product were observed although the reagent was rapidly reduced (formation of precipitate).

2,2-Dimethyl-5-acetoxy-3-hydroxychroman-4-one, **3**

A solution of potassium permanganate (278 mg) and magnesium sulfate (211 mg) in water (8 ml) was added dropwise with stirring during 2.5 h to a solution of chromene acetate **4** (240 mg) in ethanol (7.2 ml) at −15 to −20°C. The precipitate was filtered off and washed thoroughly with boiling water. Extraction of the aqueous solution with ethyl acetate yielded the crude product (181 mg) which was purified by chromatography. Elution with light petroleum – methylene chloride (19:1) yielded a small quantity of starting material (tlc). Further elution with light petroleum – methylene chloride (9:1) gave the main product (84 mg) which was recrystallized from ether – light petroleum to yield chromanone acetate **3**, mp 68–70°C; uv (EtOH) λ_{max} 254 and 322 nm (log ε 3.81 and 3.47); ir ($CHCl_3$) 1762, 1687 (C=O) cm^{-1}; nmr δ 1.22 and 1.63 (s, 3H each, Me_2C), 2.38 (s, 3H, OAc), 4.36 (s, 1H, CHOH), 6.67 (dd, $J \simeq 1.5$ and 8 Hz, 1H,

H-6 or H-8), 6.84 (dd, $J \simeq 1.5$ and 8 Hz, 1H, H-8 or H-6), 7.49 (t, $J \simeq 8$ Hz, 1H, H-7) and in DMSO-d_6, 1.19 and 1.46 (s, 3H each, Me_2C), 2.29 (s, 3H, OAc), 4.20 (s, 1H, C*H*OH), 6.72 (dd, $J \simeq 1.5$ and 8 Hz, 1H, H-6 or H-8), 6.90 (dd, $J \simeq 1.5$ and 8 Hz, 1H, H-8 or H-6), 7.57 (t, $J \simeq 8$ Hz, 1H, H-7). *Anal.* calcd. for $C_{13}H_{14}O_5$: C 62.39, H 5.64; found: C 62.19, H 5.80.

2,2-Dimethyl-3,5-dihydroxychroman-4-one, **2**

Chromanone acetate **3** (18 mg) in ethanol (0.4 ml) was treated with a solution of KOH (15 mg) in 80% ethanol (3 ml). After standing under nitrogen at room temperature for 0.5 h, the solution was acidified with 0.1 *N* HCl and the product extracted into ethyl acetate. The product was chromatographed over a short column with light petroleum – methylene chloride (19:1) and recrystallized from light petroleum to give chromanone **2**, mp 61–62°C; uv (EtOH) λ_{max} 215, 275, and 349 nm (log ε 4.07, 3.90, and 3.43); uv (H_2O) λ_{max} 215, 274, and 346 nm (log ε 4.09, 3.92, and 3.40) and, after adjustment of p*H* to 9.5 with 0.1 *N* NaOH, λ_{max} 237, 280, and 372 nm (log ε 4.01, 3.77, and 3.66); ir ($CHCl_3$) 1652 (C=O) cm^{-1}; nmr δ 1.27 and 1.63 (s, 3H each, Me_2C), 4.43 (s, 1H, C*H*OH), 6.40 (dd, $J \simeq 1$ and 8 Hz, 1H, H-6 or H-8), 6.50 (dd, $J \simeq 1$ and 8 Hz, 1H, H-8 or H-6), 7.39 (t, $J \simeq 8$ Hz, 1H, H-7), and in DMSO-d_6, δ 1.26 and 1.48 (s, 3H each, Me_2C), 4.33 (s, 1H, C*H*OH), 6.40 (d, $J \simeq 8$ Hz, 1H, H-6 or H-8), 6.45 (d, $J \simeq 8$ Hz, 1H, H-8 or H-6), 7.40 (t, $J \simeq 8$ Hz, 1H, H-7), 11.27 (s, 1H, ArO*H*, D_2O exchangeable); ms *m/e* calcd. for $C_{11}H_{12}O_4$: 208.0734; found: 208.0733. *Anal.* calcd. for $C_{11}H_{12}O_4$: C 63.45, H 5.81; found: C 63.62, H 5.97.

2,2-Dimethyl-3-hydroxy-5-methoxychroman-4-one, **6**

Chromanone **2** (14 mg) was methylated with ethereal diazomethane and the product was purified by preparative tlc (chloroform–methanol, 99:1). Recrystallization from light petroleum yielded methyl ether **6**, mp 77–78°C; uv (EtOH) λ_{max} 269 and 331 nm (log ε 3.94 and 3.52); nmr δ 1.22 and 1.62 (s, 3H each, Me_2C), 3.93 (s, 3H, OMe), 4.31 (s, 1H, C*H*OH), 6.48 (d, $J \simeq 8$ Hz, 1H, H-6 or H-8), 6.52 (d, $J \simeq 8$ Hz, 1H, H-8 or H-6), 7.40 (t, $J \simeq 8$ Hz, 1H, H-7), and in DMSO-d_6, δ 1.19 and 1.44 (s, 3H each, Me_2C), 3.77 (s, 3H, OMe), 4.08 (d, $J \simeq 4$ Hz, 1H, C*H*OH, s after D_2O exchange), 5.54 (d, $J \simeq 4$ Hz, 1H, OH, D_2O exchangeable), 6.42 (d, $J \simeq 8$ Hz, 1H, H-6 or H-8), 6.54 (d, $J \simeq 8$ Hz, 1H, H-8 or H-6), 7.34 (t, $J \simeq 8$ Hz, 1H, H-7); ms *m/e* calcd. for $C_{12}H_{14}O_4$: 222.0891; found: 222.0888.

2,2-Dimethyl-5-hydroxychroman-4-one, **8**

2,6-Dihydroxyacetophenone (600 mg) in anhydrous ether (10 ml) was slowly added to sodium dispersion (1 g, 5 μm, 40% sodium – 60% xylene) in anhydrous ether (5 ml) under nitrogen. The mixture was then heated at reflux for 1.5 h. After cooling, dry acetone (5 ml) was added slowly and the mixture was stirred for 4 h at room temperature and then heated at reflux for 1 h. Water was added, the solution was acidified with acetic acid, and the product was extracted into ether. Chromatography with light petroleum – chloroform (3:1) yielded a mixture (524 mg) of chromanone and acetone condensation products. Extraction of an ether solution of this material with 1 *N* KOH and isolation of the alkali soluble material yielded chromanone **8** (131 mg), mp 73–74°C (lit. (2) mp 75.5–76°C); nmr δ 1.48 (s, 6H, Me_2C), 2.77 (s, 2H, CH_2), 6.43 (dd, $J \simeq 1$ and 8 Hz, 1H, H-6 or H-8), 6.53 (dd, $J \simeq 1$ and 8 Hz, 1H, H-8 or H-6), 7.42 (t, $J \simeq 8$ Hz, 1H, H-7); ms *m/e* calcd. for $C_{11}H_{12}O_3$: 192.0785; found: 192.0785.

Acetylation of chromanone **8** with acetic anhydride – pyridine yielded chromanone acetate **9**, an oil; nmr δ 1.44 (s, 6H, Me_2C), 2.34 (s, 3H, OAc), 2.65 (s, 2H, CH_2), 6.59 (dd, $J \simeq 1$ and 8 Hz, 1H, H-6 or H-8), 6.82 (dd, $J \simeq 1$ and 8 Hz, 1H, H-8 or H-6), 7.42 (t, $J \simeq 8$ Hz, H-7).

2,2-Dimethyl-5-acetoxy-3-bromochroman-4-one, **7**

2-Carboxyethyltriphenylphosphonium perbromide (9) (266 mg) was added to a stirred solution of chromanone acetate **9** (84 mg) in tetrahydrofuran (5 ml) at room temperature. After 9 h additional reagent (101 mg) was added. Stirring was continued for 3 days when reaction was essentially complete (tlc). The major product (98 mg) was isolated by chromatography with chloroform – light petroleum (1:1). Recrystallization from ether – light petroleum yielded bromochromanone **7**, mp 90–92°C; nmr δ 1.53 and 1.60 (s, 3H each, Me_2C), 2.37 (s, 3H, OAc), 4.32 (s, 1H, CHBr), 6.69 (dd, $J \simeq 1.5$ and 8 Hz, 1H, H-6 or H-8), 6.88 (dd, $J \simeq 1.5$ and 8 Hz, 1H, H-8 or H-6), 7.52 (t, $J \simeq 8$ Hz, 1H, H-7). *Anal.* calcd. for $C_{13}H_{13}O_4Br$: C 49.86, H 4.18; found: C 49.64, H 4.48.

Acknowledgments

We wish to thank Mrs. H. Schroeder for 100 MHz nmr spectra, Mr. D. Hairsine for mass spectra, and Mr. G. L. Rock and Mrs. M. E. Stevens for valuable technical assistance.

1. I. Barash, A. L. Karr, and G. A. Strobel. Plant Physiol. **55**, 646 (1975).
2. H. Fukami and M. Nakajima. Agr. Biol. Chem. **25**, 247 (1961).
3. K. B. Wiberg and K. A. Saegebarth. J. Am. Chem. Soc. **79**, 2822 (1957).
4. P. Cohen and P. Mamont. Bull. Soc. Chim. Fr. 1164 (1967).
5. D. C. Allport and J. D. Bu'lock. J. Chem. Soc. 654 (1960).
6. C. I. Jarowski and G. B. Hess. J. Am. Chem. Soc. **71**, 1711 (1949).
7. E. Guerreiro, G. Kunesch, and J. Polonsky. Phytochemistry, **12**, 185 (1973).
8. R. Verhé, N. Schamp, and L. de Buyck. Synthesis, 392 (1975); R. Verhé, N. Schamp, L. de Buyck, N. de Kimpe, and M. Sadones. Bull. Soc. Chim. Belg. **84**, 747 (1975).
9. V. W. Armstrong, N. H. Chishti, and R. Ramage. Tetrahedron Lett. 373 (1975).

Some reactions of ethyl azidoformate with quinones

MOHINDER S. CHAUHAN AND DAVID M. MCKINNON

Department of Chemistry, University of Manitoba, Winnipeg, Man., Canada R3T 2N2

AND

RAYMOND G. COOKE

Department of Chemistry, University of Melbourne, Melbourne, Australia

Received September 9, 1976

MOHINDER S. CHAUHAN, DAVID M. MCKINNON, and RAYMOND G. COOKE. Can. J. Chem. **55**, 2363 (1977).

Ethyl azidoformate has been allowed to react with 1,4-naphthoquinone, 1,2-naphthoquinone, and 2-methoxy-1,4-naphthoquinone under different thermolytic conditions. A variety of products involving addition, substitution, insertion, and molecular rearrangement have been observed. The nature and yields of these products under different conditions are discussed inrelation to the mechanisms proposed for these reactions.

MOHINDER S. CHAUHAN, DAVID M. MCKINNON et RAYMOND G. COOKE. Can. J. Chem. **55**, 2363 (1977).

On a permis à l'azidoformate d'éthyle de réagir avec les naphtoquinones-1,4, naphtoquinones-1,2 et méthoxy-2 naphtoquinones-1,4 dans diverses conditions de thermolyse. On a observé plusieurs produits impliquant des additions, des substitutions, des insertions et des réarrangements moléculaires. On discute de la nature et des rendements de ces produits sous diverses conditions en relation avec les mécanismes proposés pour ces réactions.

[Traduit par le journal]

Introduction

The reactions of azides with conjugated systems have been investigated by various workers (1–6). The addition of an azide moiety to the double bond initially forms a triazoline derivative which may be stable or undergo oxidation to a triazole (3). Loss of nitrogen to form an aziridine (4, 7–9) or subsequent rearrangement to form an anil (3) is possible. Various aziridines have been reported from the addition of nitrene species to the double bonds of various organic substrates without any isolation of triazoline derivatives (10, 11). The only difference between azide and nitrene mechanisms with respect to the aziridine formation is the time of loss of nitrogen in the reaction sequence. In some cases both mechanisms have been encountered (11) while in others a concerted mechanism involving simultaneous addition of the azide moiety and elimination of a nitrogen molecule has been encountered. Recently much interest has been shown in the reactions of ethyl azidoformate since it is a rigid azide and does not undergo Curtius Rearrangement and is a suitable reagent for the investigation of azide and/or nitrene mechanisms with many organic substrates (9–12). We have studied the reactions of this reagent with various quinones, firstly to elaborate previous findings (13), and secondly, as a method of preparation of azepinone derivatives required in a separate study. Also, aziridinoquinones have potential as anti-tumor agents (14).

Results

Reactions with 1,4-Naphthoquinone

Preliminary experiments on photolysis of ethyl azidoformate in the presence of 1,4-naphthoquinone, as monitored by nitrogen evolution, proceeded at a negligible rate, presumably because of the masking effect of the quinone ($\lambda_{max} < 400$ nm). Accordingly, thermolysis was investigated at various temperatures and times. While at 80°C the reaction proceeded smoothly and products **1***a–c*, **3***a*, and **4–10** were obtained along with some starting material and tar; at 60°C reaction was slow and only compounds **1***a* and **10** were isolated along with the starting material. At 100°C neither **1***a* nor **5** were isolated and relative yields changed considerably (Table 1). At higher temperatures increasing amounts of tar were obtained and at 114°C explosive decomposition was evident. Under a nitrogen atmosphere at 80°C, yields were essentially unchanged except that **5** was not obtained. Separa-

TABLE 1. Thermolysis of ethyl azidoformate with 1,4-naphthoquinone

(*a*) Experimental details*

Run	Conditions†	Reaction time (h)	Temperature (°C)	Naphthoquinone (g) Used	Recovered	Unrecovered
1	A	28	60–65	54	8.8	0.2
2	A	24	80	54	6.2	2.8
3	A	9	100–103	54	3.0	6
4	B	24	80	54	6.2	2.8

(*b*) Isolated yields in mg and percentage yields (in parentheses) of reaction products based on unrecovered 1,4-naphthoquinone

Run	**1***a*	**2**	**3***a*	**4**	**1***b*	**5**	**6**	**7**	**1***c*	**8**	**9**
1	30 (9.6)										100
2	130 (3)	1200 (28)	90 (2)	30 (0.6)	140 (3.4)	150 (3)	10 (0.28)	5 (0.18)	12 (0.39)	1000	300
3		900 (13.6)	150 (1.6)		250 (1.8)		36 (1)		7 (0.1)	12000	1500
4	150 (3.5)	1200 (28)	95 (2.1)	40 (0.8)	130 (3.1)		7 (0.2)	8 (0.3)	10 (0.32)	1000	340

*For each run the amount of ethyl azidoformate used was 54 g. Nine batches of 1 g each were used in each case.
†Conditions: A under atmospheric conditions, B under nitrogen.

tion of the various products was achieved by chromatographic and fractional crystallization techniques.

The structures of the products **1***c* and **8–10** were established from the identity of their spectral data with those of authentic specimens. The monooxime **1***c* was most probably derived from the oxazirane **3***a* during chromatography since pure oxazirane **3***a* when passed through a silica gel column under similar conditions afforded some **1***c*. The structure of the urethane **1***a* was established by spectroscopy and by base-catalyzed hydrolysis to the anticipated 2-hydroxy-1,4-naphthoquinone. The aziridine **2** exhibited a 2H singlet at δ 3.74 due to the protons at the saturated ring junction and a carbonyl absorption at 1689 cm^{-1} in the infrared, consistent with its structure. Although an azide mechanism shown in Scheme 1 could easily account for the formation of the aziridine, this is not entirely consistent with the yields of the products obtained at various temperatures. This will be discussed below. All attempts at ring expansion of **2** with acids were unsuccessful. Only urethane products were obtained, indicating that in **2**, the nitrogen atom, despite its association with the electron-withdrawing carbethoxy group, is much more basic than the oxygen of the carbonyl group. Thus treatment of **2** with various acids in all cases afforded **1***a*, sometimes along with other products, depending on the nature of the acids; **1***e* with concentrated sulfuric acid and 2-hydroxy-1,4-naphthoquinone with hydrochloric acid. Glacial acetic acid afforded only **1***a*. Attempts at thermal rearrangement in refluxing benzene, cyclohexene, or veratrole were unsuccessful.

The oxazirane structure of **3***a* was established from its nmr spectrum which exhibited two doublets due to the olefinic protons at δ 6.75 and 7.46. Also, heating under reflux with acetic acid yielded the nitrone **1***d* and the oxime **1***c* as expected. The nitrone **1***d* itself yielded the oxime **1***c* on heating with acetic acid. A possible mechanism for these conversions is shown in Scheme 2.

The structure of the urethane **4** was proved by alkaline hydrolysis which yielded the expected indan-1,3-dione-2-aldehyde, and that of the diurethane **1***b* was proved from its spectral data and alkaline hydrolysis to the expected 3-amino-2-hydroxy-1,4-naphthoquinone. That **1***b* arises from **1***a* is shown by the relative yield of **1***b* increasing with temperature while that of **1***a* decreases; also, **1***a* when treated with ethyl azidoformate afforded **1***b* as a major product.

The mass spectrum and analysis of **5** were consistent with a 1:1 adduct of carbethoxynitrene and 1,4-naphthoquinone, but with two additional atoms of oxygen. It exhibited carbonyl absorptions at 1751 and 1701 cm^{-1} in the

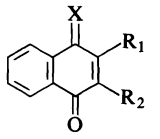

1

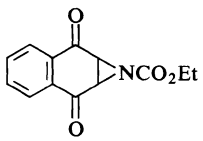

2

a $R_1 = NHCO_2Et$, $R_2 = H$, X = O
b $R_1 = R_2 = NHCO_2Et$, X = O
c $R_1 = R_2 = H$, X = NOH
d $R_1 = R_2 = H$, $X = \overset{+}{N}(O^-)—CO_2Et$
e $R_1 = OH$, $R_2 = NHCO_2Et$, X = O
f $R_1 = OMe$, $R_2 = NHCO_2Et$, X = O

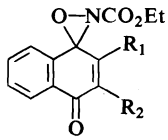

3

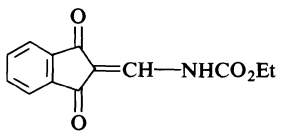

4

a $R_1 = R_2 = H$
b $R_1 = OMe$, $R_2 = NHCO_2Et$
c $R_1 = NHCO_2Et$, $R_2 = OMe$

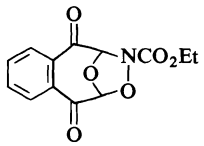

5

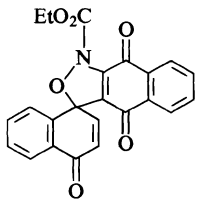

6

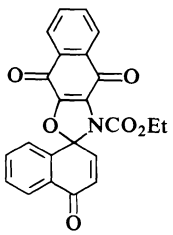

7

FIGURE 1

ir. The latter is higher than that for 1,4-naphthoquinone and suggested some alteration in the quinone ring. The nmr spectrum exhibited two 1H singlets at δ 5.75 and 6.34 as well as four A_2B_2 type aromatic protons. Thus the structure **5** is assigned to this compound. A possible mechanism for its formation is shown in Scheme 3. Treatment of **5** with dilute ethanolic hydrochloric acid afforded intractable tar, but when **5** was treated with water and zinc dust, a small amount of ethyl (2-hydroxy-1,4-naphthoquinone-3-yl)carbamate (**1***e*) was obtained, possibly by the mechanism shown in Scheme 4. The first reduction is analogous to the zinc dust reduction of an ozonide, while the formation of the new carbon–carbon bond in the second reduction stage is analogous to a pinacol formation (15). The oxidation at the final stage most probably occurs during work-up.

Either structure **6** or **7** is consistent with the properties of the last compound isolated. Elemental analysis indicated a 2:1 quinone:nitrene adduct; in addition, a molecular ion at 401.0898 was found in the mass spectrum. The nmr spectrum showed AB type two 1H doublets at δ 6.62 and 7.04 in addition to aromatic and ethyl signals. Attempted hydrolysis with dilute hydrochloric acid yielded only polymeric material. We were unable to detect any 3-amino-2-hydroxy-1,4-naphthoquinone or 1,4-naphthoquinone from it and are thus inclined to favor structure **6** over **7**. Further investigations were abandoned due to lack of material. The compound (**6** or **7**) is probably formed from a dihydro precursor by aerial oxidation during work-up, or reaction with diethyl azodicarboxylate.

Reactions with 1,2-Naphthoquinone

The reaction of 1,2-naphthoquinone with an excess of ethyl azidoformate at 92°C gave products **11***a–d* and **12** along with some **8**, **9**, and **1***e*. The structures of the urethanes **11***a* and **11***b* were established by spectral methods, and in addition, the treatment of the diurethane **11***b* with dilute base afforded the expected imidazolone **11***e*.

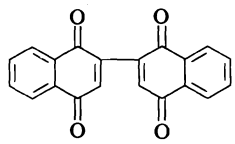

8

$N(COEt)_3$

9

$(NHCO_2Et)_2$

10

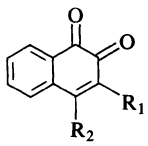

11

a $R_1 = NHCO_2Et$, $R_2 = H$,
b $R_1 = R_2 = NHCO_2Et$
c $R_1, R_2 = —N=C(OEt)—O—$
d $R_1, R_2 = —O—C(OEt)=N—$
e $R_1, R_2 = —NH—CO—NH—$
f $R_1 = H$, $R_2 = NH—CO_2Et$

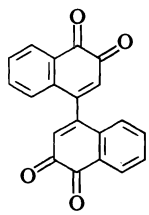

12

H_2NCO_2Et 13 $(NCO_2Et)_2$ 14

FIGURE 2

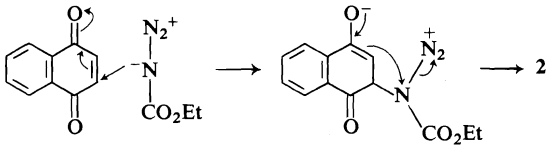

SCHEME 1

The nmr spectra of the two oxazole products **11***c* and **11***d* were rather similar. Treatment of **11***c* with dilute acid afforded ethyl (2-hydroxy-1,4-naphthoquinone-3-yl)carbamate (**1***e*) as expected. There was insufficient **11***d* to attempt this. While it is difficult to rationalize the formation of **1***e* in terms of reaction between 1,2-naphthoquinone and ethyl azidoformate, it may be explained by the decomposition of either **11***b* or **11***c* during chromatographic analysis of the reaction mixture over silica gel (Scheme 5).

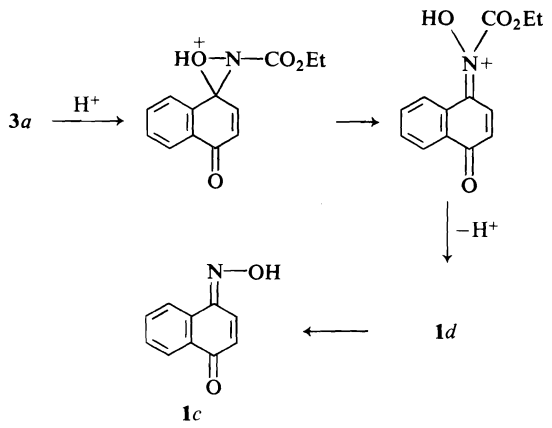

SCHEME 2

Reactions with 2-Methoxy-1,4-naphthoquinone

The reaction between 2-methoxy-1,4-naphthoquinone and ethyl azidoformate at 94°C yielded products **1***f*, **3***b*, and **11***f* along with **9**, **1***e*, and ethyl carbamate (**13**). The structure of the urethane **1***f* was established from its conversion to **1***e* by dilute base, and that of **11***f* by its identity with an authentic specimen. Its formation in the reaction may involve the mechanism shown in Scheme 6. The product **3***b* was a 2:1 adduct of carbethoxynitrene and 2-methoxy-1,4-naphthoquinone. Although the ir and the nmr spectra were consistent with either structures **3***b* or **3***c* the low frequency of the methoxy group (δ 4.48) compared with the corresponding peak in the urethane **1***f* (δ 4.17) favored structure **3***b*. The methoxy group shift in **3***c* would be expected to be closer to the value for that of the methoxy group in **1***f* as a result of their similar environments, whereas that in **3***b*, due to its proximity to the carbethoxy group of the oxaziridine ring would be expected to be shifted to a lower field.

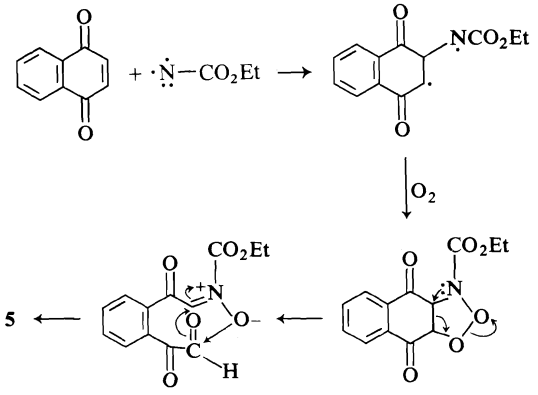

SCHEME 3

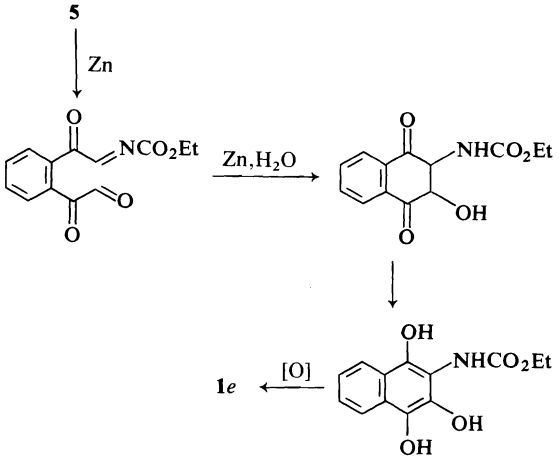

SCHEME 4

Compound **1***e* was formed by the demethylation of ethyl (2-methoxy-1,4-naphthoquinone-3-yl) carbamate on the silica gel column as some of it was also obtained by such treatment of the pure compound.

The formation of diethyl azodicarboxylate **14** in the thermolysis of ethyl azidoformate has been shown (16). This ester is a good dehydrogenating agent (17) and has been shown to dehydrogenate both alcohols and amines. Thus it is quite likely that the diurethane **10** may be formed from the hydrogenation of **14** during the reactions and/or chromatographic separation.

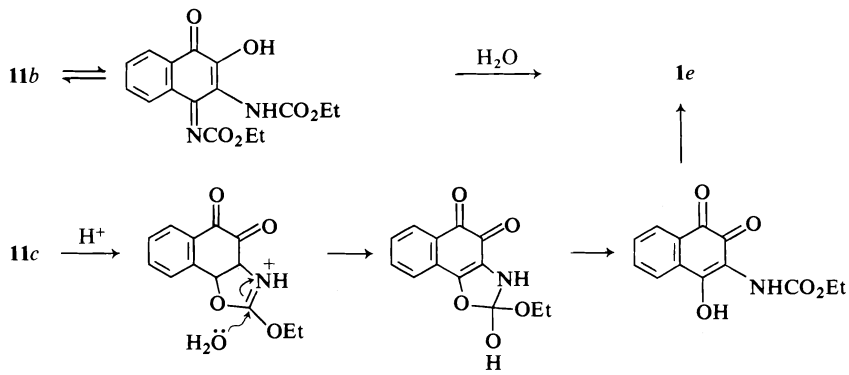

SCHEME 5

Indeed, some of the diurethane **10** was formed when pure diethyl azodicarboxylate was run through silica gel under conditions similar to those employed for the various reaction mixtures.

The possibility of the formation of the various urethanes from the reaction of ethyl carbamate with the naphthoquinones was eliminated as none of the products were obtained when these reagents were heated together. Furthermore, that diethyl azodicarboxylate was not involved in the formation of any of the products was shown by the lack of reaction between it and 1,4- and 1,2-naphthoquinone.

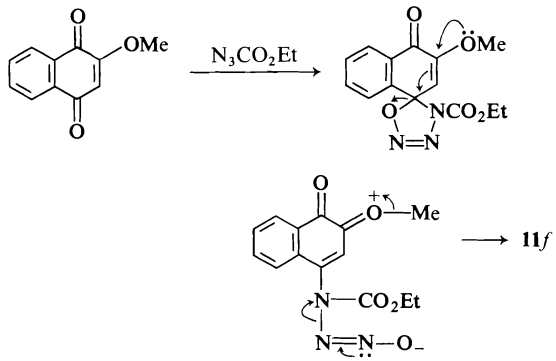

SCHEME 6

Discussion

Although the formation of the various products in the above reactions may be explained on the basis of the two electronic states of carbethoxynitrene a closer examination of the results suggests that the azidoester is also involved in the formation of some of the products. A comparison of the yields of **1***a* and the aziridine **2** obtained at 80°C or higher suggests that at these temperatures formation of **2** is favored over **1***a*. In contrast, at 60–65°C no aziridine **2** was observed and **1***a* was the major product. If the urethane had been formed by rearrangement of the aziridine, greater yields of the urethane than the aziridine would also have been expected at higher temperatures. The results suggest that the urethane and aziridine are formed either from different species or from the same species but by different mechanisms. The aziridine **2** may arise via a nitrene mechanism, since at the higher temperatures of its formation, decomposition of ethyl azidoformate will be enhanced, and in turn will lead to an increased rate of nitrene formation and a higher yield of aziridine. On the other hand, it appears unlikely that urethane formation, particularly at low temperatures, involves the participation of nitrenes. Alternatively, the urethane and the aziridine could both be formed from an intermediate triazoline formed by 1,3-dipolar cycloaddition of the azide followed by, because of different temperature coefficients for the two competing reactions, different modes of decomposition of the triazoline at different temperatures.[1]

The formation of the oxazole **11***c* may be explained in terms of a 1,3-dipolar addition of carbethoxynitrene to the quinone double bond to yield an oxazoline derivative and its subsequent dehydrogenation. Oxazole formation by [2 + 0] addition of carbethoxynitrene (1,2-addition) followed by a 1,3-shift is also a possibility. These suggest the need for the presence of a polarized double bond for the formation of oxazole or oxazoline derivatives by 1,3-dipolar

[1]We are grateful to the referees for helpful suggestions on triazoline mechanisms.

addition of carbethoxynitrene. Thus the absence of oxazoline or oxazole derivative in the reaction of 1,4-naphthoquinone may be due to the symmetrical nature of the quinone ring double bond which lacks the tendency to behave as a strong dipolarophile required for such 1,3-dipolar reactions. These results are in agreement with the facile formation of 1,3,4-oxadiazole from the aliphatic nitriles and carbethoxynitrenes (18) and the lack of formation of oxazoline or oxazole derivatives from cyclohexene (19). The reverse will be expected for the formation of the aziridine. This is indicated by the non-occurrence of aziridine in the 1,2-naphthoquinone reaction and it being a major product in the case of 1,4-naphthoquinone. A mechanism involving 1,3-dipolar addition of the azide to the quinone followed by loss of nitrogen and subsequent oxidation of the oxazoline derivative will also lead to oxazole formation, but it is difficult to differentiate between these mechanisms experimentally here.

Both ethyl carbamate and diethyl hydrazodicarboxylate require triplet carbethoxynitrene in their formation (19). The lack of formation of ethyl carbamate in the 1,2- and 1,4-naphthoquinone reactions suggests that the formation of diethyl hydrazodicarboxylate in these reactions did not involve triplet carbethoxynitrene, otherwise some ethyl carbamate formation would also have been observed as in the reaction of 2-methoxy-1,4-naphthoquinone.

Experimental

Melting points were observed with a Kofler block and are uncorrected. Analyses were performed by the Australian Microanalytical service, Melbourne, Australia. Infrared spectra were recorded on a Perkin-Elmer model 137E spectrophotometer using samples in potassium chloride discs. Nuclear magnetic resonance samples were obtained on Varian HR 60 and HA 100 spectrometers and mass measurements were obtained with the A.E.I. M59 spectrometer. Unless otherwise stated light petroleum ether refers to the boiling range 60–80°C fractions.

Thermolysis of Ethyl Azidoformate with 1,4-Naphthoquinone

A mixture of the quinone (1.0 g) and ethyl azidoformate (6.0 g) was heated at 80°C for 24 h. The products of nine such batches were combined and the excess ester removed by distillation under reduced pressure. The residue was dissolved in chloroform, and chromatography on silica gel, using elution with benzene, then benzene with greater concentrations of chloroform gave, in order of elution, 1,4-naphthoquinone, triethyl nitrilotricarboxylate (**8**), di-1,4-naphthoquinone-2-yl (**7**), compound **5**, ethyl (1,4-naphthoquinone-2-yl)carbamate (**1***a*); 3,4-benzo-7-ethoxycarbonyl-7-azabicyclo[4.1.0]-hept-3-ene-2,5-dione (**2**); 4,5-benzo-1-oxa-2-aza-2-ethoxycarbonylspiro[2.5]octa-4,7-diene-6-one (**3***a*); 1,4-naphthoquinone monooxime (**1***c*); 2-(*N*-ethoxycarbonylaminomethylene)indan-1,3-dione (**4**), diethyl 1,4-naphthoquinone-2,3-dicarbamate (**1***b*), compound **6**, and diethyl hydrazodicarboxylate (**10**).

The reaction was also investigated at 80°C under nitrogen, at 60–65°C and 100–103°C. Yields of the various products are shown in Table 1.

Triethyl nitrilotricarboxylate (**9**) was purified by distillation under reduced pressure (1 Torr) when the fraction distilling at 102–105°C was collected (lit. (20) bp 146–147°C/12 Torr). The infrared and nmr spectra of this compound were identical with those of an authentic specimen.

Di-1,4-naphthoquinone-2-yl (**8**) crystallized from ethanol in yellow plates, mp 270°C (lit. (21) mp 273–274°C). It was found to be identical in all respects with an authentic specimen.

Compound **5** crystallized first from a mixture of benzene and petroleum ether and then from ethanol in colourless needles, mp 108–108.5°C. *Anal.* calcd. for $C_{13}H_{11}NO_6$: C 56.32, H 4.00, N 5.05; found: C 56.25, H 4.16, N 5.11. Infrared ν_{max} (cm^{-1}): 1751, 1701, 1610 nmr ($CDCl_3$) δ 7.63–8.38 (m, 4H, A_2B_2 system), 6.34 (s, 1H), 5.75 (s, 1H), 1.37 (t, 3H, J = 7 Hz), 4.35 (q, 2H, J = 7 Hz).

Ethyl (1,4-naphthoquinone-2-yl)carbamate (**1***a*) crystallized from ethanol as yellow plates, mp 163.5°C. *Anal.* calcd. for $C_{13}H_{11}NO_4$: C 63.67, H 4.52, N 5.71; found: C 63.47, H 4.76, N 5.73. *Mol. Wt.* calcd. for $C_{13}H_{11}NO_4$: 245.0688; found: 245.0688. Infrared ν_{max} (cm^{-1}): 3300 (NH str), 1727, 1667 (C=O str), 1639; nmr ($CDCl_3$) δ 7.49 (s, 1H), 7.79 (s, NH), 7.64–8.16 (m, 4H), 1.35, (t, 3H, J = 7 Hz), 4.30 (q, 2H, J = 7 Hz).

3,4-Benzo-7-ethoxycarbonyl-7-azabicyclo[4.1.0]hept-3-ene-2,5-dione (**2**) crystallized first from a mixture of benzene and petroleum ether and then from aqueous ethanol to give pale yellow needles, mp 74°C. *Anal.* calcd. for $C_{13}H_{11}NO_4$: C 63.67, H 4.52, N 5.71; found: C 63.66, H 4.58, N 5.97. *Mol. Wt.* calcd. for $C_{13}H_{11}NO_4$: 245.0688; found: 245.06881. Infrared ν_{max} (cm^{-1}): 1721, 1689; nmr ($CDCl_3$): δ 3.74 (s, 2H), 7.66–8.09 (m, 4H, A_2B_2 system), 1.17 (t, 3H, J = 7 Hz), 4.05 (q, 2H, J = 7 Hz).

4,5-Benzo-1-oxa-2-aza-2-ethoxycarbonylspiro[2.5]octa-4,7-diene-6-one (**3***a*) crystallized from methanol as yellow needles, mp 145°C. *Anal.* calcd. for $C_{13}H_{11}NO_4$: C 63.67, H 4.52, N 5.71; found: C 63.96, H 4.52, N 5.84. Infrared ν_{max} (cm^{-1}): 1783, 1653, 1615; nmr ($CDCl_3$) δ 6.75 (d, 1H, J = 10 Hz), 7.46 (d, 1H, J = 10 Hz), 7.71 (m, 2H, aromatic), 8.25 (m, 1H, aromatic), 8.83 (m, 1H, aromatic), 1.46 (t, 3H, J = 7 Hz), 4.50 (q, 2H, J = 7 Hz).

1,4-Naphthoquinone monooxime (**1***c*) crystallized from benzene mp 189°C (dec.) (lit. (22) 193°C dec.). Its ir and nmr spectra were found to be identical with those of an authentic specimen. A mixture melting point with the authentic specimen was also undepressed.

2-(*N*-Carbethoxyaminomethylene)indan-1,3-dione (**4**) crystallized from a mixture of benzene and petroleum ether in pale yellow needles, mp 112°C. *Anal.* calcd. for $C_{13}H_{11}NO_4$: C 63.67, H 4.52, N 5.71; found: C 63.72, H 4.55, N 5.85. Infrared ν_{max} (cm^{-1}): 3268, 1748, 1715,

1667, 1613; nmr ($CDCl_3$) δ 7.70–8.11 (m, 4H), 8.27 (d, 1H, J = 12 Hz), 9.77 (d, NH, J = 12 Hz), 1.43 (t, 3H, J = 7 Hz), 4.46 (q, 2H, J = 7 Hz).

Diethyl 1,4-naphthoquinone-2,3-dicarbamate (**1***b*) crystallized from a mixture of benzene and petroleum ether as a yellow solid, mp 117°C. *Anal.* calcd. for $C_{16}H_{16}N_2O_6$: C 57.83, H 4.85, N 8.43; found: C 58.12, H 5.02, N 8.72. *Mol. Wt.* calcd. for $C_{16}H_{16}N_2O_6$: 332.100827; found: 332.10098. Infrared ν_{max} (cm^{-1}): 3300, 3247(sh), 1727, 1698, 1667, 1639; nmr ($CDCl_3$) δ 7.60–8.15 (m, 4H, A_2B_2 system), 7.86 (s, 2NH) 1.35 (t, 3H, J = 7 Hz), 4.22 (q, 2H, J = 7 Hz).

Compound **6** crystallized from methanol as yellow lustrous plates, mp 177–179°C (dec.). *Anal.* calcd. for $C_{23}H_{15}NO_6$: C 68.82, H 3.77, N 3.49; found: C 68.61, H 4.06, N 3.55. *Mol. Wt.* calcd. for $C_{23}H_{15}NO_6$: 401.0899; found: 401.0898. Infrared ν_{max} (cm^{-1}): 1770, 1667, 1639, 1592; nmr ($CDCl_3$) δ 7.43–8.36 (m, 8H), 7.04 (d, 1H, J = 10 Hz), 6.62 (d, 1H, J = 10 Hz), 1.04 (t, 3H, J = 7 Hz), 4.10 (q, 2H, J = 7 Hz).

Diethyl hydrazodicarboxylate (**10**) crystallized from benzene as colourless needles, mp 133°C (lit. (23) mp 133–134°C). The ir and nmr spectra of this compound were identical with those of an authentic specimen. A mixture melting point with the authentic specimen was undepressed.

Reaction of Compound 5 with Zinc Dust and Water

The compound (**5**) (100 mg) was refluxed with zinc dust (100 mg) and water (5 ml) for 30 min. After cooling, the filtrate was acidified with dilute hydrochloric acid and then extracted with ether (3 × 30 ml). The combined ether extracts were washed with water (2 × 30 ml) and dried overnight over anhydrous magnesium sulphate. Evaporation of the ether and crystallization of the residue from petroleum ether yielded ethyl (2-hydroxy-1,4-naphthoquinone-3-yl) carbamate (2 mg). The residue, after removal of ethyl (2-hydroxy-1,4-naphthoquinone-3-yl)carbamate was chromatographed over silica packed in benzene. Elution with benzene, benzene–chloroform (9:1, v:v), and chloroform yielded a yellow gum which could not be crystallized.

Hydrolysis of Ethyl (1,4-Naphthoquinone-2-yl)carbamate (1a) with Sodium Hydroxide

The urethane (100 mg) was heated with 10% sodium hydroxide solution (8 ml) on a steam bath for 30 min. The orange solution was cooled, acidified with dilute hydrochloric acid, and extracted with ether (4 × 40 ml). The yellow ether solution was washed with water (10 ml) and then dried over anhydrous magnesium sulphate. Evaporation yielded a yellow solid residue which crystallized from ethanol to give 2-hydroxy-1,4-naphthoquinone (65 mg), mp 192°C (lit. (24) mp 192°C).

Reaction of 3,4-Benzo-7-ethoxycarbonyl-7-azabicyclo-[4.1.0]hept-3-ene-2,5-dione (2) with Acetic Acid

The aziridine (100 mg) was refluxed with glacial acetic acid (10 ml) for 6 h on an oil bath. The acid was then evaporated and the residue was crystallized from ethanol to give ethyl (1,4-naphthoquinone-2-yl)carbamate (15 mg). Evaporation of the alcohol yielded starting material (75 mg).

When the above reaction was carried out over 15 h there was no change in the nature of the products, although the relative yields of the urethane (55 mg) to the aziridine (35 mg) were changed.

Reaction of 3,4-Benzo-7-ethoxycarbonyl-7-azabicyclo-[4.1.0]hept-3-ene-2,5-dione (2) with Concentrated Sulfuric Acid

Concentrated sulfuric acid (1 ml) was added slowly with shaking over 10 min to the aziridine (300 mg); the colour of the reaction mixture became reddish brown. The shaking was continued for another 30 min and then the reaction mixture was poured over ice. A yellow solid separated out on agitation. This was chromatographed over silica gel as usual to give ethyl (1,4-naphthoquinone-2-yl)carbamate (150 mg) and ethyl (2-hydroxy-1,4-naphthoquinone-2-yl)carbamate (30 mg). The latter was crystallized from ethanol mp 173–174°C. *Anal.* calcd. for $C_{13}H_{11}NO_5$: C 59.77, H 4.24, N 5.36; found: C 59.58, H 4.36, N 5.47. Infrared ν_{max} (cm^{-1}): 3247, 2564, 1669, 1616; nmr ($CDCl_3$): δ 7.41–8.30 (m, 4H), 7.79 (s, NH), 11.82 (s, OH), 1.37 (t, 3H, J = 7 Hz), 4.32 (q, 2H, J = 7 Hz).

Alkaline Hydrolysis of Ethyl (2-Hydroxy-1,4-naphthoquinone-3-yl)carbamate 1e

Ethyl (2-hydroxy-1,4-naphthoquinone-3-yl)carbamate (50 mg) was heated with 10% sodium hydroxide solution (5 ml) on a steam bath for 30 min. The colour of the solution became deep blue. The solution was cooled and acidified with dilute acetic acid to give a deep red solution. It was extracted with ether (3 × 40 ml) and the combined ether extracts were washed with water (2 × 20 ml) and then dried over anhydrous magnesium sulphate. The ether was evaporated on a rotary evaporator and the residue was crystallized from ethanol to give dark brown red needles of 3-amino-2-hydroxy-1,4-naphthoquinone (25 mg) darkening above 138°C (lit. (25) 130–140° dec.). *Mol. Wt.* calcd. for $C_{10}H_7NO_3$: 189.04258; found: 189.04228. Infrared ν_{max} (cm^{-1}): 3472, 3333, 1661 (sh), 1650, 1608; The nmr spectrum (100 MHz, DMSO-d_6) δ 9.48 (s, OH), 7.50–7.98 (m, 4H), 5.90 (s, 2NH).

Reaction of 3,4-Benzo-7-carbethoxy-7-azabicyclo[4.1.0]-hept-3-ene-2,5-dione (2) with Dilute Hydrochloric Acid

The aziridine (200 mg) was added to a 50 ml flask containing aqueous ethanolic hydrochloric acid solution (6 ml concentrated hydrochloric acid and 3 ml ethanol) and the mixture refluxed for 2 h. The solution was cooled and the yellow crystalline compound was collected. This was identified as ethyl (1,4-naphthoquinone-2-yl)carbamate from its melting point (161°C) and infrared spectrum. Yield 120 mg (60%).

The filtrate was concentrated on a rotary evaporator and the residue crystallized from ethanol to give 2-hydroxy-1,4-naphthoquinone (20 mg).

Reaction of 4,5-Benzo-1-oxa-2-aza-2-ethoxycarbonylspiro-[2,5]octa-4,7-diene-6-one (3a) with Acetic Acid

The oxazirane (100 mg) was refluxed with glacial acetic acid (6 ml) for 10 h. The acetic acid was then removed on a rotary evaporator. The residue was heated with petroleum ether (2 × 30 ml) and the solution filtered. The filtrate was cooled to give *N*-carbethoxy-1,4-naphthoquinone monoimine-*N*-oxide (**1***d*, 20 mg) in pale yellow needles, mp 104°C. *Anal.* calcd. for $C_{13}H_{11}NO_4$: C 63.67, H 4.52, N 5.71; found: C 63.51, H 4.90, N 5.65.

Infrared ν_{max} (cm^{-1}): 1786, 1667, 1592; nmr ($CDCl_3$) δ 7.92 (d, 1H, J = 10 Hz), 6.74 (d, 1H, J = 10 Hz), 7.57–7.73 (m, 2H), 8.40 (m, 1H), 8.17 (m, 1H), 1.46 (t, 3H, J = 7 Hz), 4.41 (q, 2H, J = 7 Hz).

The residue insoluble in petroleum was dissolved in benzene and filtered. 1,4-Naphthoquinone monooxime (10 mg), identified as above, crystallized from the cooled solution.

The solvent from the filtrate left after the crystallization of the oxime was evaporated on a rotary evaporator and the residue crystallized from methanol to give the starting material (30 mg).

*Chromatography of Pure 4,5-Benzo-1-oxa-2-aza-2-ethoxycarbonylspiro[2,5]octa-4,7-diene-6-one (**3a**)*

The oxazirane (50 mg) was dissolved in benzene and chromatographed over silica gel. Elution with benzene and benzene–chloroform (9:1, v:v) yielded 5 mg of 1,4-naphthoquinone monooxime along with the starting material.

*Reaction of N-Carbethoxy-1,4-naphthoquinone monoimine-N-oxide (**1d**) with Acetic Acid*

The nitrone (30 mg) was refluxed with glacial acetic acid (6 ml) for 10 h. The acetic acid was evaporated on a rotary evaporator and the residue was crystallized from benzene to give 1,4-naphthoquinone monooxime (15 mg).

*Alkaline Hydrolysis of 2-(N-Carbethoxyaminomethylene)indan-1,3-dione (**4**)*

2-(*N*-Carbethoxyaminomethylene)indan-1,3-dione (20 mg) was heated with 10% sodium hydroxide solution (5 ml) on a steam bath for 30 min. The reaction mixture was cooled, acidified with dilute hydrochloric acid, and extracted with ether (3 × 30 ml). The combined ether extracts were washed with water (2 × 30 ml) and dried over anhydrous magnesium sulphate. The ether was evaporated and the residue crystallized from petroleum ether to give indan-1,3-dione-2-aldehyde as pink crystals, mp 141°C (lit. (26) mp 141–142°C). The infrared and nmr spectra of this compound were identical with those of an authentic sample of indan-1,3-dione-2-aldehyde. A mixture melting point with the authentic specimen was also undepressed.

*Alkaline Hydrolysis of Diethyl-1,4-naphthoquinone-2,3-dicarbamate (**1b**)*

The diurethane (100 mg) was heated with 10% sodium hydroxide solution (5 ml) on a steam bath for 30 min. The colour of the solution became deep blue. The solution was cooled and then acidified with dilute acetic acid to give a deep red solution. It was extracted with ether (3 × 30 ml) and the combined ether extracts were washed with water (40 ml) and then dried over anhydrous magnesium sulphate. The ether was evaporated and the solid thus obtained was crystallized from ethanol to give 3-amino-2-hydroxy-1,4-naphthoquinone (35 mg).

*Attempted Thermal Isomerisation of 3,4-Benzo-7-ethoxycarbonyl-7-azabicyclo[4.1.0]hept-3-ene-2,5-dione (**2**)*

The aziridine (100 mg) was refluxed with benzene (50 ml) for 72 h. The benzene was evaporated and the residue chromatographed over a silica gel column in benzene to give the starting material. No urethane could be detected.

Similarly when the aziridine was refluxed in cyclohexene for 72 h or heated in veratrole to 130°C for 48 h, only starting material was obtained.

*Reaction of Ethyl (1,4-Naphthoquinone-2-yl)carbamate (**1a**) with Ethyl Azidoformate*

The urethane (400 mg) and ethyl azidoformate (5 g) were heated together at 85°C for 8½ h with occasional swirling. The unreacted ethyl azidoformate was removed by distillation under reduced pressure and the residue was chromatographed over silica gel. Elution of the column with benzene, benzene–chloroform (9:1, v:v), and chloroform afforded successively diethyl 1,4-naphthoquinone-2,3-dicarbamate (270 mg) and diethyl hydrazodicarboxylate (80 mg).

*Reaction of Diethylazodicarboxylate (**14**) with 1,4-Naphthoquinone*

Diethylazodicarboxylate (10 g) and 1,4-naphthoquinone (2 g) were heated together at 80°C for 24 h with occasional swirling. The reaction products were dissolved in chloroform and chromatographed over silica gel. Elution with benzene followed by a mixture of benzene–chloroform (9:1, v:v) and finally chloroform yielded successively diethylazodicarboxylate (8 g), 1,4-naphthoquinone (1.965 g) and diethyl hydrazodicarboxylate (150 mg).

When the above reaction was carried out at 60°C for 28 h and the reaction products chromatographed as before diethylazodicarboxylate (8.5 g), 1,4-naphthoquinone (1.97 g), and diethyl hydrazodicarboxylate (140 mg) were obtained.

*Chromatography of the Pure Diethylazodicarboxylate (**14**)*

Diethylazodicarboxylate (5 g) was dissolved in chloroform and then chromatographed over silica gel. Elution with benzene, benzene–chloroform (9:1, v:v), and chloroform afforded diethylazodicarboxylate (4.3 g), an unidentified pale yellow liquid (130 mg), and diethyl hydrazodicarboxylate (70 mg).

Thermolysis of Ethyl Azidoformate with 1,2-Naphthoquinone

Ethyl azidoformate (7.2 g) and 1,2-naphthoquinone (1.0 g) were heated together at 92°C for 8 h. The products of eight such batches were combined, the excess azido ester was removed as before, and the residue was boiled with chloroform (3 × 80 ml) and filtered to give di-1,2-naphthoquinone-4-yl. The chloroform solution was concentrated and chromatography on silica gel with elution by benzene, then benzene with increasing proportions of chloroform, gave successively triethyl nitrilotricarboxylate (**9**) (3.5 g), unchanged 1,2-naphthoquinone (700 mg), ethyl (1,2-naphthoquinone-3-yl)carbamate (**11***a*) (5 mg), ethyl (2-hydroxy-1,4-naphthoquinone-3-yl)carbamate (**1***c*) (20 mg), 2-ethoxynaphtho[1,2-*d*]oxazole-4,5-quinone (**11***c*) (20 mg), 2-ethoxynaphtho[1,2-*d*]oxazole-8,9-quinone (**11***d*) (5 mg), diethyl-1,2-naphthoquinone-3,4-dicarbamate (**11***b*) (120 mg), di-1,2-naphthoquinone-4-yl (**12**) (3 g), and diethyl hydrazodicarboxylate (**10**) (2.5 g).

Ethyl (1,2-naphthoquinone-3-yl)carbamate (**11***a*) crystallized first from a mixture of benzene and petroleum ether and then from ethanol to give violet needles, mp 148°C. *Anal.* calcd. for $C_{13}H_{11}NO_4$: C 63.67, H 4.52, N 5.71; found: C 63.82, H 4.57, N 5.59. Infrared ν_{max} (cm^{-1}): 3300, 1721, 1692(sh), 1672, 1623; nmr ($CDCl_3$)

δ 7.18–7.6 (m, 4H including NH at 7.21), 7.94 (s, 1H), 7.97 (q, 1H, J = 7 and 2 Hz), 1.33 (t, 3H, J = 7 Hz, 4.23 (q, 2H, J = 7 Hz).

2-Ethoxynaphtho[1,2-*d*]oxazole-4,5-quinone (**11***c*) crystallized first from benzene and then from ethanol, mp 195°C. *Anal.* calcd. for $C_{13}H_9NO_4$: C 64.20, H 3.73; found: C 63.92, H 4.06. Infrared ν_{max} (cm^{-1}): 1675, 1631, 1605; nmr ($CDCl_3$) δ 8.07 (q, 1H, J = 7 and 2 Hz), 7.33–7.74 (m, 3H), 1.51 (t, 3H, J = 7 Hz), 4.64 (q, 2H, J = 7 Hz).

2-Ethoxynaphtho[1,2-*d*]oxazole-8,9-quinone (**11***d*) crystallized from a mixture of benzene and chloroform to give violet rods, mp 235°C (dec.). *Anal.* calcd. for $C_{13}H_9NO_4$: C 64.20, H 3.73; found: C 64.08, H 3.99. Infrared ν_{max} (cm^{-1}): 1685, 1639; nmr (TFA) δ 7.59–7.99 (m, 3H), 8.31 (q, 1H, J = 7 and 2 Hz), 1.72 (t, 3H, J = 7 Hz), 4.93 (q, 2H, J = 7 Hz).

Diethyl 1,2-naphthoquinone-3,4-dicarbamate (**11***b*) crystallized first from benzene and then from ethanol to give orange needles mp 180–181°C. *Anal.* calcd. for $C_{16}H_{16}N_2O_6$: C 57.83, H 4.85, N 8.43; found: C 57.84, H 4.76, N 8.27. Infrared ν_{max} (cm^{-1}): 3205, 1698, 1689(sh), 1667, 1613, 1587; nmr ($CDCl_3$) δ 7.34–7.73 (m, 3H), 8.06 (q, 1H, J = 7 and 2 Hz), 8.68 (s, NH), 7.26 (s, NH), 1.32 (t, 3H, J = 7 Hz), 1.37 (t, 3H, J = 7 Hz), 4.26 (q, 2H, J = 7 Hz), 4.43 (q, 2H, J = 7 Hz).

Di-1,2-naphthoquinone-4-yl (**12**) crystallized twice from chloroform, then from dioxane, and finally from a mixture of chloroform and methanol to give an orange crystalline solid mp 290°C (dec.) (lit. (27) 289–290°C dec.). *Mol. Wt.* calcd. for $C_{20}H_{10}O_4$: 314.0579; found: 314.0580. Infrared ν_{max} (cm^{-1}): 1698, 1667; nmr spectrum (TFA) δ 6.80 (s, 2H), 8.30–8.55 (m, 2H), 7.40–7.96 (m, 6H).

Reaction of 2-Ethoxynaphtho[1,2-d]oxazole-4,5-quinone (11c) with Hydrochloric Acid

The oxazole (10 mg) was heated with 5% hydrochloric acid solution (3 ml) on a steam bath for 15 min and the solution filtered. The residue (2 mg) was found to be the starting material. On cooling the filtrate a yellow crystalline solid (2 mg) separated out which was found to be ethyl (2-hydroxy-1,4-naphthoquinone-3-yl)carbamate. The yellow filtrate on ether extraction yielded a further 2 mg of product.

Reaction of Diethyl 1,2-naphthoquinone-3,4-dicarbamate (11b) with Sodium Hydroxide

The diurethane (50 mg) was heated with 10% sodium hydroxide (2 ml) on a steam bath for 20 min. The reaction mixture immediately turned blue and a blue compound separated out after a few minutes. The solution was cooled and filtered leaving a blue residue. This was washed with water (30 ml) to remove any residual sodium hydroxide and crystallized from methanol to give naphtho[1,2-*d*]imidazolone-4,5-quinone (**11***e*) (30 mg). *Mol. Wt.* calcd. for $C_{11}H_6N_2O_3$: 214.03783; found: 214.03715. Infrared ν_{max} (cm^{-1}): 3145, 3205(sh), 3106(sh), 1678, 1623; nmr spectrum (100 MHz, TFA) δ 10.36 (s, 1H), 8.18 (m, 1H), 7.44–7.88 (m, 3H). The signal for the second NH proton was not observed probably due to the very rapid exchange with the strongly acidic solvent.

Reaction of Diethylazodicarboxylate (14) with 1,2-Naphthoquinone

1,2-Naphthoquinone (1 g) and diethylazodicarboxylate (6 g) were heated together at 90°C for 6 h with occasional swirling. The reaction products were dissolved in chloroform and chromatographed over silica gel. Elution with benzene, benzene–chloroform, and finally with chloroform yielded diethylazodicarboxylate (4.4 g), 1,2-naphthoquinone (0.5 g), and diethyl hydrazodicarboxylate (180 mg).

Thermolysis of Ethyl Azidoformate with 2-Methoxy-1,4-Naphthoquinone

Ethyl azidoformate (9.1 g) and 2-methoxy-1,4-naphthoquinone (1.0 g) were heated together at 94°C for 9 h. The combined products from eight batches were separated as before, by distillation of the unchanged azido ester and chromatography of the residue with elution by benzene, chloroform–benzene, chloroform, and finally chloroform–methanol (19:1, v:v) to give successively ethyl carbamate (**13**) (1.6 g), unchanged 2-methoxy-1,4-naphthoquinone (1.5 g), ethyl (2-methoxy-1,4-naphthoquinone-3-yl)carbamate (**1***f*) (5.0 g), (**3***b*) (480 mg), diethyl hydrazodicarboxylate (**10**) (1.5 g), ethyl (1,2-naphthoquinone-4-yl)carbamate (**14**) (120 mg), and ethyl (2-hydroxy-1,4-naphthoquinone-3-yl)carbamate (90 mg).

Ethyl carbamate (**13**) crystallized from petroleum ether as colourless needles, mp 48°C (lit. (28) mp 48–50°C). Its infrared and nmr spectra were found to be identical with those of an authentic specimen of ethyl carbamate. A mixture melting point with the authentic specimen was also undepressed.

Ethyl (2-methoxy-1,4-naphthoquinone-3-yl)carbamate (**1***f*) crystallized from ethanol in yellow needles, mp 140–141°C. *Anal.* calcd. for $C_{14}H_{13}NO_5$: C 61.09, H 4.76, N 5.09; found: C 60.83, H 4.90, N 5.24. Infrared ν_{max} (cm^{-1}): 3165, 2817(sh), 1718, 1689, 1664, 1618; nmr ($CDCl_3$) δ 7.59–8.14 (m, 4H), 6.84 (s, NH), 4.17 (s, 3H), 1.32 (t, 3H, J = 7 Hz), 4.23 (q, 2H, J = 7 Hz).

Compound **3***b* crystallized from ethanol as pale yellow rods, mp 131–132°C. *Anal.* calcd. for $C_{17}H_{18}N_2O_7$: C 56.35, H 5.01, N 7.73; found: C 56.08, H 4.99, N 7.95. Infrared ν_{max} (cm^{-1}): 3279, 1748, 1724, 1672, 1658, 1613; nmr ($CDCl_3$) δ 7.68–8.18 (m, 4H), 7.23 (s, NH), 4.48 (s, 3H), 1.28 (t, 6H, J = 7 Hz), 4.07–4.37 (m, 4H).

Ethyl (1,2-naphthoquinone-4-yl)carbamate (**11***f*) crystallized from chloroform as orange rectangular plates decomposing at 205°C. *Anal.* calcd. for $C_{13}H_{11}NO_4$: C 63.67, H 4.52, N 5.71; found: C 63.44, H 4.45, N 5.40. Infrared ν_{max} (cm^{-1}): 3257, 1727, 1686, 1629(sh), 1618; nmr (DMSO-d_6) δ 7.56–8.19 (m, 4H), 7.10 (s, 1H), 9.98 (s, NH), 1.34 (t, 3H, J = 7 Hz), 4.27 (q, 2H, J = 7 Hz).

Reaction of Ethyl (2-Methoxy-1,4-naphthoquinone-3-yl)carbamate (1f) with Sodium Carbonate

The urethane (20 mg) was heated with 10% sodium carbonate solution (10 ml) on a steam bath until the solution turned red. The solution was cooled and acidified with dilute hydrochloric acid to give ethyl (2-hydroxy-1,4-naphthoquinone-3-yl)carbamate (13 mg).

Alkaline Hydrolysis of Ethyl (1,2-Naphthoquinone-4-yl)carbamate (11f)

The urethane (20 mg) was heated with 10% sodium hydroxide (5 ml) on a steam bath for 15 min. The solution was cooled, acidified with dilute hydrochloric acid, and then extracted with ether (3 × 30 ml). The combined ether extracts were washed with water (10 ml) and then dried over anhydrous magnesium sulphate. The ether

was evaporated and the yellow residue crystallized from ethanol to give 2-hydroxy-1,4-naphthoquinone.

*Preparation of Ethyl (1,2-Naphthoquinone-4-yl)carbamate (**11f**)*

To a mixture of 4-amino-1,2-naphthoquinone (200 mg), pyridine (2 ml), and acetonitrile (70 ml) was added ethyl chloroformate (240 mg) dropwise with constant shaking over 15 min. The solution was shaken for a further 2 h and then refluxed on a steam bath for 1½ h. Cooling and filtration of the solution yielded a violet solid which was found to be unreacted 4-amino-1,2-naphthoquinone. The filtrate was evaporated to dryness and the solid residue from this crystallized from chloroform to give ethyl (1,2-naphthoquinone-4-yl)carbamate (160 mg) in 62% yield.

*Attempted Synthesis of Ethyl (2-Methoxy-1,4-naphthoquinone-3-yl)carbamate (**1f**) and Ethyl (1,2-Naphthoquinone-4-yl)carbamate (**11f**) from 2-Methoxy-1,4-naphthoquinone and Ethyl Carbamate*

2-Methoxy-1,4-naphthoquinone (2 g) and ethyl carbamate (1.5 g) were refluxed in toluene for 48 h. The solvent was evaporated on a rotary evaporator and the residue was dissolved in chloroform and chromatographed over silica gel. Elution with a mixture of benzene–chloroform (9:1, v:v), chloroform, and finally with chloroform–methanol (19:1, v:v), yielded only the starting materials.

*Chromatography of the pure Ethyl (2-Methoxy-1,4-naphthoquinone-3-yl)carbamate (**1f**)*

Ethyl (2-methoxy-1,4-naphthoquinone-3-yl)carbamate (2 g) was dissolved in chloroform and chromatographed over silica gel. Elution with a mixture of benzene–chloroform (9:1, v:v), followed by chloroform, and finally with a mixture of chloroform–methanol (19:1, v:v) yielded the starting material along with a small amount of ethyl (2-hydroxy-1,4-naphthoquinone-3-yl)carbamate (7 mg).

1. S. PATAI. The chemistry of the azido group. Interscience Publishers, John Wiley and Sons, New York, NY. 1971.
2. W. LWOWSKI. Nitrenes. Interscience Publishers, John Wiley and Sons, New York, NY. 1970.
3. L. WOLFF. Justus Liebigs Ann. Chem. **394**, 68 (1912); **399**, 274 (1913); **399**, 287 (1913).
4. F. D. CHATTAWAY and G. D. PARKES. J. Chem. Soc. 1307 (1925).
5. J. H. BOYER. J. Am. Chem. Soc. **73**, 5248 (1951).
6. W. I. AWAD, S. M. A. R. OMRAN, and F. NAGIEB. Tetrahedron, **19**, 1591 (1963).
7. R. HUISGEN. Angew. Chem. **72**, 359 (1960).
8. P. SCHEINER. J. Org. Chem. **30**, 7 (1965).
9. I. BROWN and O. E. EDWARD. Can. J. Chem. **43**, 1266 (1965).
10. L. HORNER and A. CHRISTMANN. Angew. Chem. Int. Ed. Engl. **2**, 599 (1963).
11. R. A. ABRAMOVITCH and B. A. DAVIS. Chem. Rev. **64**, 149 (1964).
12. W. LWOWSKI. Angew. Chem. Int. Ed. Engl. **6**, 897 (1967).
13. M. S. CHAUHAN and R. G. COOKE. Aust. J. Chem. **23**, 2133 (1970).
14. O. C. DERMER and G. E. HAM. Ethylenimine and other aziridines. Academic Press, New York, NY. 1969. p. 425.
15. J. B. BAPAT and D. ST. C. BLACK. Aust. J. Chem. **21**, 2497 (1968).
16. W. LWOWSKI, T. W. MATTINGLY, and J. MARICICH. Tetrahedron Lett. 1591 (1964).
17. G. O. SCHENCK and H. FORMANCK. Angew. Chem. **70**, 505 (1958); R. HUISGEN, F. JACOB, W. SIEGEL, and A. CADUS. Justus Liebigs Ann. Chem. **590**, 1 (1954); O. DIELS. Chem. Ber. **56**, 1933 (1923); O. DIELS and P. FRITZSCHE. Chem. Ber. **44**, 3018 (1911).
18. W. LWOWSKI and T. J. MARICICH. J. Am. Chem. Soc. **87**, 3630 (1965).
19. W. LWOWSKI and T. W. MATTINGLY. J. Am. Chem. Soc. **87**, 1947 (1965).
20. C. F. H. ALLEN and A. BELL. Org. Synth. Coll. Vol. III, 415 (1953).
21. E. ROSENHAVEN, F. BRAUN, R. PUMMERER, and R. RIEGELBAUER. Chem. Ber. **70**, 2281 (1937).
22. K. H. MEYER and S. LENHARDT. Justus Liebigs Ann. Chem. **398**, 79 (1913).
23. N. RABJOHN. Org. Synth. Coll. Vol. III, 375 (1953).
24. G. SOLIMAN and A. LATIF. J. Chem. Soc. 55 (1944).
25. G. CARRARA and G. BONACCI. Chemica e Industrie (Milan), **26**, 75 (1944).
26. G. ERRERA. Gazz. Chim. Ital. **32**, 330 (1902); **33**, 417 (1903).
27. E. ROSENHAVEN, F. BRAUN, R. PUMMERER, and G. RIEGELBAUER. Chem. Ber. **70**, 2281 (1937).
28. T. L. DAVIS and K. C. BLANCHARD. J. Am. Chem. Soc. **51**, 1808 (1929).

Synthesis and photochemistry of 4,4-diphenyl-γ-pyran. Di-π-methane rearrangement in a new chromophore

DENIS GRAVEL, CHRISTIAN LEBOEUF,[1] AND SERGE CARON

Département de Chimie, Université de Montréal, C.P. 6210, Montréal (Qué.), Canada H3C 3V1

Received January 10, 1977

DENIS GRAVEL, CHRISTIAN LEBOEUF, and SERGE CARON. Can. J. Chem. **55**, 2373 (1977).

A synthesis of 4,4-diphenyl-γ-pyran (**1**) was elaborated from diphenylmethane. Prolonged irradiation of pyran **1** in *tert*-butyl alcohol led to: *trans-endo*-5,6-diphenyl-2-oxabicyclo[3.1.0]-hexene (**18**), isomeric 3,5-diphenylpenta-2,4-dienals (**6**), *trans-tert*-butyl 3,5-diphenylpent-2-enoate (**7**), *cis-tert*-butyl 3,5-diphenylpent-2-enoate (**8**), and isomeric 3,5-diphenylpent-2-enoic acids (**9**). It was established that the photolysis of γ-pyran **1** yields only one primary photoproduct: the oxabicyclo[3.1.0]hexene derivative **18** via a di-π-methane rearrangement. The other compounds isolated result from further irradiation of the primary product. The results observed are discussed in the light of the di-π-methane rearrangement mechanism.

DENIS GRAVEL, CHRISTIAN LEBOEUF et SERGE CARON. Can. J. Chem. **55**, 2373 (1977).

Une synthèse du diphényl-4,4 γ-pyranne a été élaborée à partir du diphénylméthane. L'irradiation prolongée du pyranne **1**, en solution dans le *tert*-butanol, conduit au: diphényl-5,6-*trans-endo* 2-oxabicyclo[3.1.0]hexène (**18**), diphényl-3,5 pentadièn-2,4 als (**6**) isomères, diphényl-3,5 pentèn-2 oate de *tert*-butyle-*trans* (**7**), diphényl-3,5 pentèn-2 oate de *tert*-butyle-*cis* (**8**) et acides diphényl-3,5 pentènoïques (**9**) isomères. Il fut de plus établi que la photolyse du γ-pyranne **1** conduit à un seul photoproduit primaire: le dérivé oxabicyclo[3.1.0]hexène **18**, via un réarrangement di-π-méthane. Les autres produits isolés résultent tous de l'irradiation subséquente du photoproduit primaire. Les résultats observés sont discutés à la lumière du mécanisme du réarrangement di-π-méthane.

Introduction

Few photochemical reactions have been studied so extensively as the di-π-methane rearrangement (for the latest major contributions to appear in the field see ref. 1*a*,*b*; for a review see ref. 1*c*). This reaction which occurs on photolysis of compounds having two π moieties bonded to a single sp^3-hybridized carbon atom is an extremely general process. It formally involves the migration of one π moiety from the saturated carbon atom to the adjacent sp^2-hybridized carbon atom of the second π moiety with concomitant formation of a three-membered ring (1*c*). Zimmerman, who first named the rearrangement, noted that the skeletal change could be accounted for by one basic qualitative mechanism which is represented below (1*c*).[2]

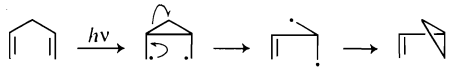

[1]Predoctoral Fellow, Ministère de l'éducation du Québec and National Research Council of Canada: 1973–1977.

[2]It is important to note that the π systems, here represented by vinyl groups, may alternatively include phenyl or carbonyl groups.

The great number of investigations of this rearrangement, largely due to Zimmerman and his co-workers, eventually led to a detailed understanding of (*i*) how the structure affects the excited state multiplicity by which the di-π-methane rearrangement proceeds; (*ii*) how the nature of the substituents on the π moieties controls the regiospecificity of the rearrangement; and (*iii*) the preferred rearrangement stereochemistry (1*c*).

In those cases where the di-π-methane system is comprised in a six-membered ring, the reaction leads to formation of a bicyclo[3.1.0] derivative as shown. When the sp^3-hybridized carbon

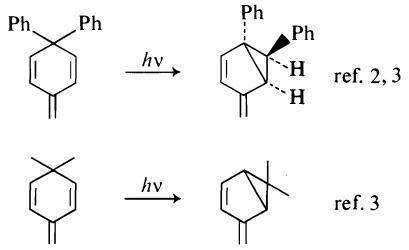

bears phenyl groups (which add additional di-π-methane arrangements to the system) the product is formed through phenyl–vinyl bonding

with concomitant phenyl migration, whereas in the case of *gem*-dimethyl substitution the product is formed through vinyl–vinyl bonding.

We were interested in studying some cyclic di-π-methane systems where the two π moieties in the ring would be joined by a heteroatom. Such models should provide further tests to the generality of the rearrangement, provide further insight into its mechanism, and also give access to new hetero bicyclo[3.1.0] systems and their chemistry. To our knowledge the photochemistry of 4,4-disubstituted γ-pyrans has been studied by two groups only (4, 5) and in both instances the compounds studied were of the 4-aryl-4-benzyl type and the sole behavior observed was the isomerization to the corresponding α-pyran with concomitant 1–3-benzyl migration by a probable sigmatropic mechanism. Specific examples are represented in Scheme 1.

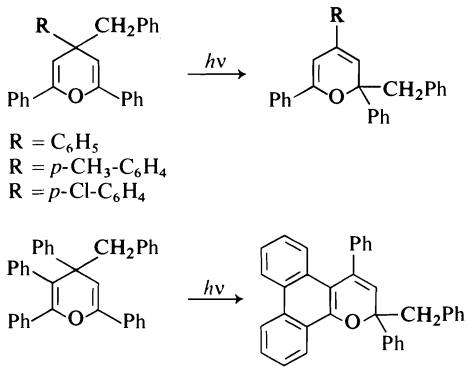

SCHEME 1. Photoisomerization of γ-pyrans to α-pyrans.

In our case, the first model chosen for study was 4,4-diphenyl-γ-pyran (**1**) which should not present the problem of 1–3 sigmatropic shifts.

Synthesis of the Title Compound 1

The synthesis of 4,4-diphenyl-γ-pyran (**1**) was devised starting from diphenylmethane as outlined in Scheme 2. A first alkylation (6) of the anion of diphenylmethane in liquid ammonia using 1,1-dimethoxy-2-chloroethane gave the corresponding 1,1-dimethoxy-3,3-diphenylpropane (**2**) in 67% yield. A second alkylation (6) using the same conditions afforded the tetramethoxy diacetal of 3,3-diphenylglutaraldehyde (**3**) in 50% yield. Hydrolysis of the diacetal **3** in 2 *N* sulfuric acid led to a quantitative yield of an insoluble white powder which appeared to be the hemihydrate of the desired 3,3-diphenylglutaraldehyde (**4**). Although the mass spectrum showed a molecular ion peak at *m/e* 252 which

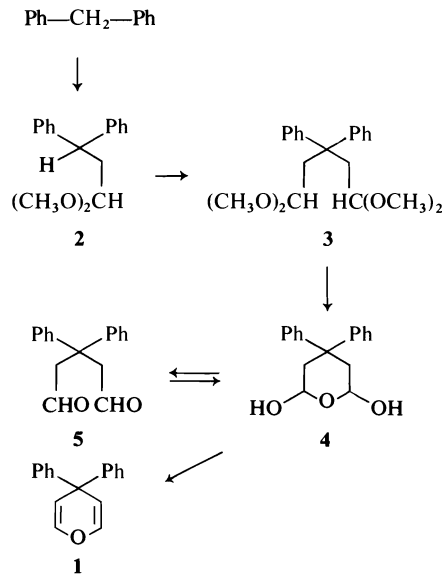

SCHEME 2. Synthesis of 4,4-diphenyl-γ-pyran (**1**).

corresponds to the dialdehyde, the ir showed hydrogen bonded hydroxyl absorption at 3190 and 3290 cm^{-1} and no carbonyl absorption. The nmr spectrum in DMSO-d_6 was also very revealing in that it showed a well resolved ABMX system where only the A proton showed appreciable coupling to the M proton. The A portion appeared as a pair of doublets centered at 1.68 ppm with J_{AB} = 12.5 Hz and J_{AM} = 10 Hz. The B portion appeared as a doublet at 2.91 ppm with J_{AB} = 12.5 Hz. The M portion of the system appeared as a doublet of doublets centered at 4.65 ppm with J_{AM} = 10 Hz and J_{MX} = 7.5 Hz, due to coupling with the hydroxylic proton. In fact, the addition of D_2O caused the doublet of doublets to collapse to a doublet with J_{AM} = 10 Hz. The X portion of the system, attributed to the hydroxylic proton, appeared as a doublet at 6.48 ppm with J_{MX} = 7.5 Hz; this signal disappeared upon addition of D_2O. Final verification of these assignments was obtained by irradiating the M portion of the system and observing the A proton doublet of doublets collapse to a doublet (J_{AB} = 12.5 Hz). Since the B proton was not appreciably coupled to the M proton the dihedral angle between the two must be close to 90° (7).

In order to chemically substantiate our proposal of the stable crystalline hemihydrate **4**, the compound was heated slightly above its melting point under vacuum for 10 min and the nmr spectrum of the resulting yellowish oil

recorded and shown to be in perfect accord with that expected of 3,3-diphenylglutaraldehyde (**5**). Furthermore, the reverse reaction, *ie* the addition of water, was easily accomplished when the dialdehyde **5** obtained above was heated at 100°C for 30 min in a mixture of DMSO and 10% HCl, 20:1, and the resulting solution diluted with cold water to give hemihydrate **4** as a precipitate whose physical and spectroscopic properties proved identical to those of the original hemihydrate.

Having demonstrated to a satisfactory degree of confidence the fact that dialdehyde **5** existed in the form of a hemihydrate (**4**) we proceeded to eliminate 2 mol of water from the compound by treating it with tosyl chloride in pyridine at 140°C (8). The product obtained in an 80% yield was shown unambiguously by ir, nmr, uv, and mass spectrometry to be the desired 4,4-diphenyl-γ-pyran (**1**) (see Experimental).

Preparative Scale Photolysis and Spectroscopic Characterization of Photoproducts

The ultraviolet irradiation during 20 h and at 254 nm of 500 ml of a 4.2×10^{-3} *M* solution of 4,4-diphenyl-γ-pyran (**1**) in anhydrous *tert*-butyl alcohol led to a mixture of at least five products as evidenced by thin layer chromatography (tlc). Separation of the mixture was carried out using preparative scale tlc on silica gel. In increasing order of polarity the products isolated were (see Scheme 3): starting material **1** (11%); 3,5-diphenylpentadienal (**6**) (7%), as a mixture of isomers which we did not attempt to separate; *tert*-butyl *trans*-3,5-diphenylpent-2-enoate (**7**) (15%); *tert*-butyl *cis*-3,5-diphenylpent-2-enoate (**8**) (9%) and 3,5-diphenylpent-2-enoic acid (**9**) (8%), as a mixture of *cis* and *trans* isomers. A 13% yield of a highly polar yellow oil was also isolated but not characterized.

The unsaturated aldehyde **6** was characterized by its mass spectrum which showed a molecular ion at *m/e* 234 (100%) and an important peak (62%) at *m/e* 205 for the loss of CHO, thus showing the product was an isomer of the starting material and was probably an aldehyde. In the ir the product showed the characteristic absorption of an unsaturated carbonyl at 1665 cm^{-1} along with vinyl and aryl absorption at 1610 cm^{-1}. The nmr spectrum showed complex absorption in the vinyl and aryl regions (13H), *i.e.* from 5.8 to 7.5 ppm and two doublets (1H) at 9.2 and 10.0 ppm ascribable to isomeric aldehydes in the mixture. Finally, the uv spectrum had a λ_{max} at 315 nm (ε 1200) with long wavelength absorption extending into the visible, characteristic of extended conjugation. These results, however, give no clue as to the relative position of the phenyl groups on the carbon chain, a point of vital importance in the rearrangement. A definitive and final proof of structure was therefore established by chemical correlation as will be shown below.

The *tert*-butyl ester **7**, on the other hand, could be characterized much more satisfactorily with spectroscopic techniques. The mass spectrum showed a molecular ion at *m/e* 308 indicating the product results from the addition of solvent to an isomer of the starting material, probably a ketene. Fragment ions at $M - 56$, $(M - 56) - 45$, and $(M - 56) - 17$ indicate, respectively, the loss of $(CH_3)_2C{=}CH_2$ by McLafferty rearrangement of a *tert*-butyl ester (9) followed by the loss of COOH or OH. The base peak at *m/e* 91 is characteristic of a $PhCH_2$— moiety in the structure. The ir spectrum showed an intense absorption at 1705 cm^{-1} indicating an α,β-unsaturated ester. In the nmr, a singlet (9H) at 1.55 ppm confirmed the presence of a *tert*-butyl group attached to an oxygen

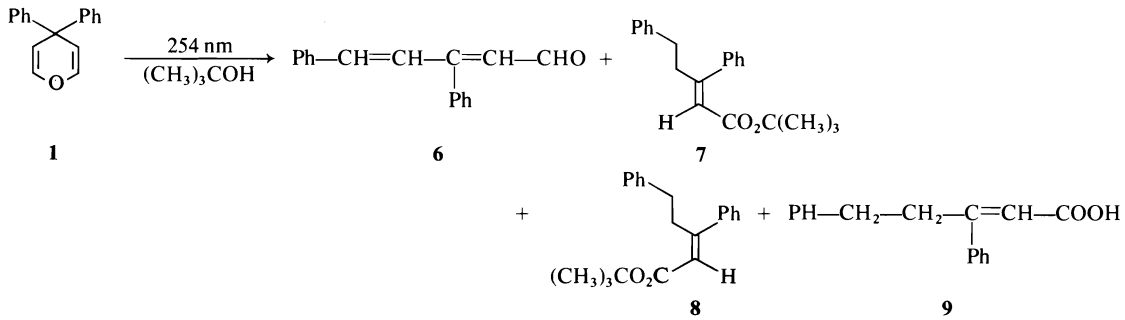

1 **6** **7** **8** **9**

SCHEME 3. Preparative scale photolysis of 4,4-diphenyl-γ-pyran (**1**).

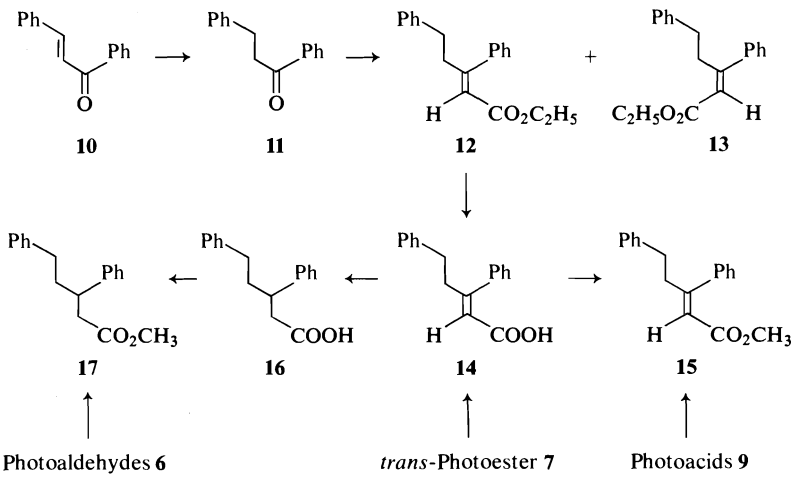

SCHEME 4. Synthesis of reference compounds and structure correlations.

atom. A symmetrical multiplet (5H) extending from 2.5 to 3.6 ppm could represent the AA′MM′ portion of an AA′MM′X system such as $PhCH_2CH_2—C(=CH—)$. A singlet (1H) at 6.0 ppm is characteristic of a vinyl proton. Finally, two broad singlets (10H) at 7.28 and 7.45 correspond to the aromatic protons. The stereochemical arrangement about the trisubstituted double bond was unambiguously established by nOe experiments (10): irradiation of the methylene signal at 3.37 (downfield portion of the AA′MM′ part of the AA′MM′X system) caused an increase in intensity of 11 to 13% of the vinyl proton signal at 6.00 ppm (X portion of the AA′MM′X system). As will be shown below the other stereoisomeric ester showed no noticeable nOe effect.

Complete characterization of *tert*-butyl ester **8** was also possible using spectroscopic techniques. The mass spectrum and the ir spectrum were characteristic and similar to those of ester **7** (see Experimental). The nmr spectrum on the other hand showed the *tert*-butyl group as a singlet at 1.28 ppm and the AA′MM′ portion of the AA′MM′X system as a deceptively simple widened singlet at 2.76 ppm. This hypothesis was substantiated by the progressive addition of small amounts of $Eu(fod)_3$ to the nmr sample solution (11) and the observation of the evolution from a deceptively simple singlet to a more complex pattern similar to that observed in the case of the other isomer. The vinyl proton appeared as a singlet at 5.93 ppm and the aromatic protons as a broad singlet at 7.34 ppm. Again in this case, nOe experiments (10) were conclusive in showing the stereochemistry about the double bond; indeed, irradiation of the deceptively simple signal at 2.76 ppm caused no noticeable increase in intensity of the singlet at 5.93 ppm while such experiments had caused an 11 to 13% increase in the intensity of the vinyl proton signal in the case of ester **7**.

The diphenylpentenoic acid (**9**) was isolated as a mixture of *cis* and *trans* isomers and was characterized as such. In the ir, characteristic absorptions appeared at 3500, 1725, and 1620 cm^{-1}. In the nmr, the allylic and benzylic methylenes appeared as a multiplet between 2.50 and 3.60 ppm, the vinyl proton as a singlet at 5.90, the aryl protons as a multiplet at 6.80 and 7.80 ppm, and finally the carboxyl proton as a singlet at 11.00 ppm.

Synthesis of Reference Compounds and Structure Correlations

In order to fully characterize the photoaldehydes isolated and also in order to corroborate the structures of the photoacids and esters obtained, the unambiguous synthesis of authentic reference compounds was carried out (see Scheme 4).

A mixture of authentic *trans*- and *cis*-ethyl 3,5-diphenylpent-2-enoate (**12** and **13**) was obtained from chalcone (**10**) by first reducing it to dihydrochalcone (**11**) (12) and then treating it with diethylcarbethoxymethylphosphonate in the presence of sodium hydride (13). Separation of the mixture by preparative tlc yielded samples

of authentic *trans*- and *cis*-ethyl 3,5-diphenylpent-2-enoate (**12** and **13**). Total yield of esters 35%.

Saponification of the *trans* ester **12** using potassium hydroxide in ethanol yielded 75% of recrystallized *trans* acid **14**. This authentic acid was used as reference material in all three chemical correlations to be described below.

Structure Correlation of the trans Photoester 7

Treatment of *tert*-butyl ester **7** with a catalytic amount of *p*-toluenesulfonic acid in refluxing benzene (14) yields a carboxylic acid which is identical in all respects with the authentic *trans* acid **14**.

Structure Correlation of the cis–trans Mixture of Photoacids 9

The reference acid **14** was first esterified with diazomethane (15) to yield authentic methyl ester **15** which was compared by vpc, using two different columns, to the mixture of methyl esters obtained by treating photoacids **9** with diazomethane.

Structure Correlation of Photoaldehydes 6

Authentic methyl 3,5-diphenylpentanoate (**17**) was first prepared from the unsaturated reference acid **14** by catalytic hydrogenation (16) followed by esterification with diazomethane (15). The mixture of photoaldehydes **6** was oxidized with nickel peroxide (17) to the corresponding mixture of acids which was hydrogenated (16) and then esterified with diazomethane (15) to yield a methyl ester identical to authentic methyl 3,5-diphenylpentanoate.[3]

Isolation and Characterization of the Primary Photoproduct 18

Consideration of the structures presented in Scheme 3 reveals that the expected primary photoproduct, a diphenyl-2-oxabicyclo[3.1.0]-hexene (**18** in Table 1), was not isolated from the photolysis. However, it also suggests that photoaldehyde **6** is possibly formed through thermal or photochemical ring opening of the unobserved primary photoproduct **18**. Finally, it is apparent that should the suggested primary photoproduct be formed it must involve the phenyl–vinyl bonding pathway since photoaldehyde **6** shows one of the phenyl groups migrated.

[3]The comparison was carried out on silica gel tlc plates using three different eluting mixtures and by vpc using two different columns.

TABLE 1. Comparison of nmr data of primary photoproduct **18** with those of pertinent models

Structure	Coupling constants	Reference
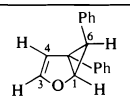 **18**	$J_{1,6} = 7$ $J_{3,4} = 2.5$	This work
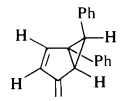	$J_{1,6} = 8.5$ $J_{3,4} = 5.5$	3
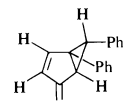	$J_{1,6} = 4$ $J_{3,4} = 5.0$	3
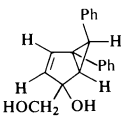	$J_{1,6} = 9.0$ $J_{3,4} = 5.5$	3
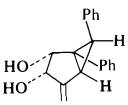	$J_{1,6} = 8.5$	3
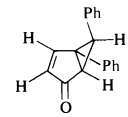	$J_{1,6} = 9$ $J_{3,4} = 5.50$	18
	$J_{2,3} = 2$	19, 20

This hypothesis was fully verified when a small scale photolysis of diphenylpyran **1** was carried out and the reaction monitored by tlc. It was then possible to isolate a 10% yield of a new product which was characterized as *trans-endo*-5,6-diphenyl-2-oxabicyclo[3.1.0]hexene (**18**). In the nmr this compound showed two typical AB systems, one for the cyclopropyl protons and one for the vinyl protons. The first of these is characterized by a doublet centered at 2.50 ppm ($J = 7$ Hz) for the cyclopropyl proton in the 6-position and a second doublet centered at 4.73 ppm ($J = 7$ Hz) for the cyclopropyl proton in the 1-position. This latter signal shows broadening probably due to long range W coupling with the 3-proton. The second AB system has a doublet centered at 5.10 ppm ($J = 2.5$ Hz) for the vinyl proton in the 4-position and a second doublet centered at

5.96 ppm (J = 2.5 Hz) for the vinyl proton in the 3-position. Again, this latter signal shows broadening most probably due to long range W coupling with the 1-proton.

In view of the fact that only one stereoisomer of the primary photoproduct could be isolated in sufficient amount for characterization[4] and also due to the great importance of the primary photoproduct structure and stereochemistry in establishing the intimate detail of the rearrangement (1*c*) we have included for comparison a table of nmr coupling constants for representative model substances (see Table 1).

It is readily apparent from the table that a typical value for $J_{1,6}$*cis* is of the order of 8.5–9 Hz and that a $J_{1,6}$*trans* is of the order of 4 Hz. The value of 7 Hz observed in the case of primary photoproduct **18** is in excellent agreement with a *cis* arrangement of protons 1 and 6 if one takes into consideration the fact that the oxygen in the 2-position should lower the value of the coupling constant between H-1 and H-6 due to an electronegativity effect not present in the other models included for comparison. The phenomenon of the lowering of vicinal coupling constants by electronegative substituents has been amply demonstrated in the case of substituted cyclopropanes (21) and is well documented in the literature generally (22, 23).

In the case of $J_{3,4}$, the value of 2.5 Hz observed for primary photoproduct **18** is considerably lower than that of 5.5 Hz reported for the carbocyclic model compounds. This lowering of the coupling constant is again attributable to the electronegativity effect of the oxygen atom. This assertion is supported by the value of 2 Hz reported for $J_{2,3}$ in 4,5-dihydrofuran (19, 20, 23).

The fact that the primary photoproduct **18** had not been observed in the original preparative scale photolysis is due in part to the fact that under the tlc conditions used to monitor the reaction and separate the products, the primary photoproduct **18** has the same R_f as the starting material, but mostly to the fact that it was present in very small amount since it is not stable under the conditions of photolysis and subsequent manipulations as we shall see below.

[4]Only once have we been able to observe a compound which is presumably the *cis-exo* isomer. It was isolated by preparative tlc in the usual manner but rearranged almost quantitatively to the known mixture of aldehydes **6** during extraction from the silica gel using a Soxhlet continuous extraction apparatus.

Interrelation Between the Products of Photolysis

In an effort to establish the relationship between the various products formed during photolysis and also to verify that the primary photoproduct **18** isolated was the sole primary product, we carried out the photolysis of each compound isolated (see Scheme 5)

In a first instance, the primary product **18** was applied to three tlc plates (silica gel) and the first plate irradiated for 1 h with 254 nm light; after elution the plate revealed extensive formation of the photoaldehyde **6** already characterized in the preparative scale photolysis, thus showing that aldehyde **6** is possibly formed by subsequent photochemical rearrangement of the bicyclic primary product **18**. The second plate when heated in an oven at 150°C for 10 min showed, after elution, a quantitative rearrangement of the primary product **18** to the photoaldehyde **6**, thus showing that the previously described rearrangement may also be brought about thermally. Finally, the primary product **18** spotted on the third plate showed partial rearrangement to the photoaldehyde **6** when a methanolic solution of *p*-toluenesulfonic acid was applied over the spot and the plate eluted after standing 30 min at room temperature. This result shows that rearrangement of the bicyclic primary product **18** to the aldehyde **6** can not only be initiated photochemically or thermally, but also by acid catalysis.

These findings are, in the end, not surprising in view of the fact that an examination of the literature revealed numerous examples of studies of carbenic additions to furans (24) which show that the 2-oxabicyclo[3.1.0]hex-3-ene initially formed is generally unstable thermally or in presence of acid or photochemically, when the compound has a chromophore with a significant absorption coefficient. In the present case it is therefore readily understandable that the primary photoproduct **18** be unstable and isomerize under the three different sets of conditions to the corresponding open-chain aldehyde **6** as depicted in Scheme 5.

The formation, on the other hand, of esters **7** and **8** during photolysis appears less trivial at first glance, but may be rationalized on the basis of two well known processes. Indeed, it is plausible to envisage that the *tert*-butyl ester is formed by reaction of the solvent on an intermediate ketene which would be formed by a [1,5] sigmatropic shift of the aldehydic hydrogen to the 5 position of the chain. Such photochemical

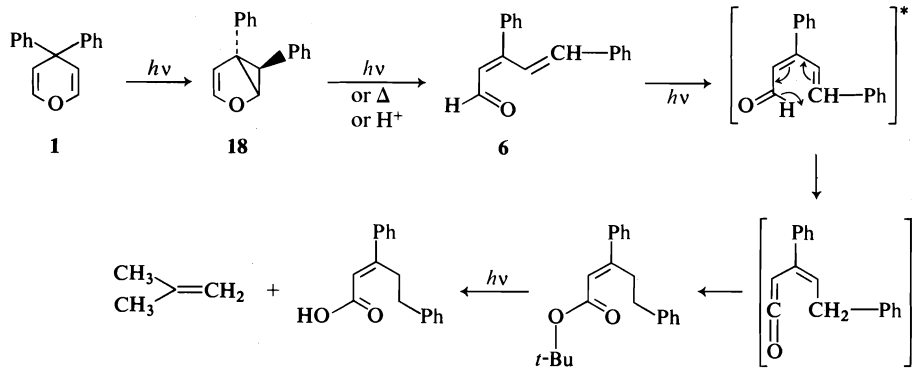

SCHEME 5. Interrelation between products formed in the photolysis of 4,4-diphenylpyran.

[1,5] shifts are well known in the case of aliphatic conjugated dienes (25*a*) but it appears that this could be the first example involving an unsaturated aldehyde.

It is interesting to point out that Pirkle *et al.* (25*b*) have observed analogous [1,5] hydrogen shifts in the intermediate unsaturated ketene aldehydes formed in the pyrolysis of 2-pyrone derivatives but these shifts did not take place when the intermediate was formed by photolysis.

In order to provide evidence to support our hypothesis of this two-step transformation a 50 mg sample of photoaldehyde **6** was irradiated in *tert*-butyl alcohol-*O-d* and the major *trans-tert*-butyl ester isolated. The mass spectrum showed a molecular ion at *m/e* 309 which indicates that the ester is formed by incorporation of the elements of one molecule of *tert*-butyl alcohol-*O-d* and that no deuterium is present at the 5-positions of the chain since the base peak of the spectrum appears at *m/e* 91 and not *m/e* 92. Unfortunately, the small amount available did not allow the recording of a useful nmr spectrum, Ft technique not being available to us at that time.

To circumvent this difficulty the starting 4,4-diphenylpyran (**1**) was irradiated in *tert*-butyl alcohol-*O-d* and the *trans* ester isolated and analyzed by both mass spectrometry and nmr. As expected, the mass spectrum proved identical to that obtained in the previous experiment. The nmr spectrum, on the other hand, provided supportive and conclusive evidence concerning the presence and the position of the incorporated deuterium atom. Indeed, whereas the undeuterated *trans* ester showed the vicinal 4- and 5-methylene groups as a multiplet for the AA′MM′ portion of an AA′MM′X system,the spectrum of the deuterated material showed a doublet ($J \simeq 7$ Hz) at 2.60 ppm for the 5-methylene group and a triplet ($J \simeq 7$ Hz) at 3.25 ppm, in excellent accord with a CHD group in the 4-position.

Finally, the relationship between the photoesters and the photoacids was easily established by carrying out the photolysis of a small sample of the *trans-tert*-butyl ester (**7**) and showing by tlc the progressive formation of the previously characterized photoacids (**9**). The photochemical Norrish type II decomposition of *tert*-butyl esters to yield the corresponding acids and isobutylene is well known (26) and the case reported herein is an additional example of this general reaction.

Discussion

Although sensitization and quenching results have not yet been obtained, the evidence thus gathered in the photolysis of 4,4-diphenyl-γ-pyran (**1**) clearly points to a di-π-methane rearrangement in the primary photochemical step. Indeed, the bicyclo[3.1.0] nature of the rearranged product and the *trans-endo* relationship of the phenyl groups are characteristic features of this rearrangement (1*c*). The stereochemistry observed in the phenyl migration is fully in accord with a concerted process involving inversion of configuration at the central ('methane') carbon and where rearrangement occurs in an *anti*-disrotatory mode as represented (1*c*).

Another observation which may be made pertains to the multiplicity of the reacting excited species. Zimmerman and co-workers have shown (1*c*) that di-π-methane systems having nonconstrained or free π moieties usually give an efficient rearrangement from the excited singlet state, because of an energy dissipation

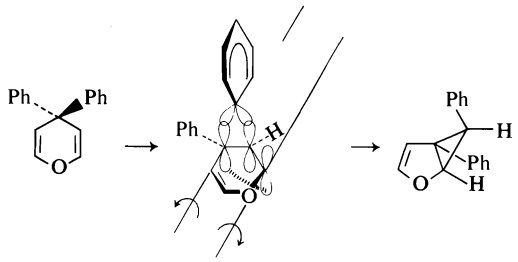

process available in the triplet state *i.e.* rotation about the excited π-bond or *cis–trans* isomerization. This deactivation process was named the "free rotor effect". In the case of compounds having constrained π-moieties the di-π-methane rearrangement usually proceeds efficiently from the triplet and inefficiently from the singlet, probably due to efficient alternative pathways.

The 4,4-diphenyl-γ-pyran (**1**) studied, being made up of constrained non-free π-moieties, the di-π-methane rearrangement observed should proceed more efficiently from the excited triplet state. However, since compound **1** did not show any primary photoreactivity other than di-π-methane rearrangement, it is possible that part of the rearrangement also originates from the singlet state.

Concerning the absolute regiospecificity observed *i.e.* rearrangement with phenyl–vinyl bridging (path *a* Scheme 6) totally preferred over vinyl–vinyl bridging (path *b*, Scheme 6), it appears, at first glance, that it could be due to the localization of the excitation energy mostly in the phenyl groups. Indeed, the divinyl ether chromophore (in a seven-membered ring) absorbs at 216 nm (ε 3720) and 231 nm (ε 2000) (27) while phenyl absorbs at 255 nm (ε 204) (28). However, it would be very surprising if both

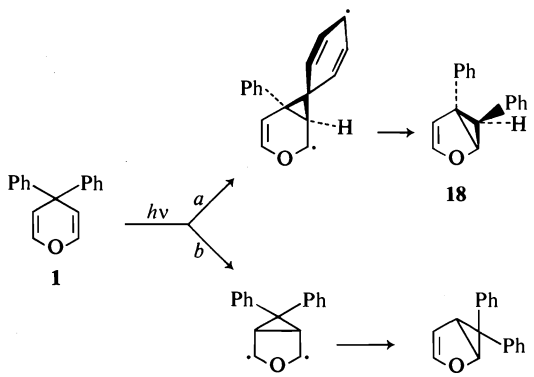

SCHEME 6. Odd-electron representation of *a priori* possible reaction pathways in the 4,4-diphenyl-γ-pyran system.

chromophores were not at least slightly coupled since they are homoconjugated and compound **1** has λ_{max} 240 nm (ε 1050). The excitation energy should then probably be distributed over the entire π system. The situation could, on the other hand, be quite different in the case of the triplet state where energy could be more or less localized in one of the π moieties. Unfortunately we have no data at this time to warrant any further discussion on that aspect.

A more plausible approach to explain the occurrence of path *a* over path *b* would be the relative ease of formation of the cyclopropyl–dicarbinyl-diradical species[5] where that in path *a* has more odd-electron stabilization relative to that in path *b*. Indeed, Zimmerman, in a study of substituent effects in the singlet di-π-methane rearrangement of an acyclic diene has concluded (29) that "bridging is the major process affecting the rate". In addition, one might point out that the diradical species in path *a* should also proceed to final product with greater ease due to the rearomatization of a phenyl ring which constitutes a very favorable driving force. In a comparative study of 1-methylene-4,4-dimethylcyclohexa-2,5-diene and the 4,4-diphenyl analog (*vide supra*), Zimmerman has commented (3) that the results "can be interpreted as an inherent preference for the phenyl participation process with intervention of phenyl migration whenever possible" and that vinyl migration seems to be abnormally inefficient compared to phenyl migration. In view of the present results it would appear that the above remarks apply equally well to the case of 4,4-diphenyl-γ-pyran (**1**).

Finally, if we compare the results reported for the photolysis of 4-phenyl-4-benzyl-γ-pyrans (4, 5) (see Scheme 1) which rearrange to the corresponding 4-phenyl-2-benzyl-α-pyrans via a [1,3] sigmatropic shift, with the results reported herein on 4,4-diphenyl-γ-pyran which gives only di-π-methane rearrangement, we have another remarkable example of the control of excited state processes by substituent effects.

Experimental

The silica gel used for preparative thin layer chroma-

[5]It is important to note here that this rationalization does not require a nonconcerted mechanism. As Zimmerman remarked (1*c*): "the diradical species may just be points on a potential energy surface and not represent minima". This argument has been given ample substance in Zimmerman's recent work (1*a*).

tography was GF-254 from Merck or G/UV 254 from Machery-Nagel. Melting points were taken on a Büchi apparatus and are uncorrected. The ir spectra were recorded on a Beckman model IR-8 apparatus. The nmr spectra were recorded on a Varian model A-60 apparatus or a JEOL model C60-H apparatus using TMS as internal reference. The nOe experiments herein described were performed on a JEOL model JNM-4H-100 apparatus. The letters s, d, t, q, m, meaning respectively singlet, doublet, triplet, quadruplet, and multiplet, are used in the description of the spectra. The uv spectra were recorded in ethanol on a Bausch and Lomb Spectronic 505 spectrophotometer. The mass spectra were obtained from AEI MS902 and Hitachi–Perkin-Elmer RMU6D mass spectrometers. Photolyses were carried out in a Rayonet photochemical reactor equipped with 254 nm lamps.

*1,1-Dimethoxy-3,3-diphenylpropane (**2**) (6)*

A solution of potassium amide in liquid anhydrous ammonia is first prepared by slowly distilling ammonia over anhydrous potassium hydroxide, and condensing it in a 1 ℓ, three necked flask mounted with an acetone – dry ice condenser and mechanical stirrer. When the volume of liquid ammonia has reached 400 ml, a catalytic amount of ferric nitrate (~150 mg) is added and 10.4 g (0.26 mol) of potassium are precautiously dissolved under continuous mechanical stirring. Diphenyl methane (35 g, 0.21 mol) in anhydrous ether (150 ml) is subsequently added over a period of 30 min, giving a dark red solution characteristic of the anion thus formed. A solution of chloroacetaldehyde dimethylacetal (25.8 g, 0.21 mol) is then slowly added to the reaction mixture.

The ammonia is evaporated overnight, the acetone – dry ice condenser having been removed. The remaining ether solution is washed with water, dried over anhydrous magnesium sulfate, and evaporated. The crude mixture is separated by distillation under reduced pressure (~0.3 Torr). Pure 1,1-dimethoxy-3,3-diphenylpropane (**2**) is thus obtained (35.8 g; 67%); bp 138°C/0.3 Torr; mp 58–59°C; ir 1600, 1120, and 1050 cm^{-1}; nmr ($CDCl_3$); δ 7.30 (s, 10H), 4.10 (m, 2H), 3.20 (s, 6H), 2.4 (dd, 2H).

*1,1,5,5-Tetramethoxy-3,3-diphenylpentane (**3**) (6)*

As previously described, 5.6 g of potassium (0.14 mol) are dissolved in 300 ml of anhydrous liquid ammonia, containing a catalytic amount of ferric nitrate (~75 mg) and 1,1-dimethoxy-3,3-diphenylpropane (**2**) (25.6 g, 0.1 mol) in anhydrous ether (150 ml) is slowly added. A solution of bromoacetaldehyde dimethylacetal (16.9 g, 0.1 mol) in anhydrous ether (150 ml) is then added and the reaction mixture allowed to stand overnight while the ammonia is evaporated. The ether solution is washed with water, dried over anhydrous magnesium sulfate, and evaporated. The title compound (**3**) is obtained (17.2 g; 50%) by reduced pressure fractional distillation on a Vigreux column (30 cm): bp 158°C/0.3 Torr; mp 68–69°C; ir ($CHCl_3$), 1050, 1120, and 1600 cm^{-1}; nmr ($CDCl_3$), δ 7.20 (s, 10H), 3.90 (t, 2H), 3.10 (s, 12H), 2.60 (d, 4H).

*2,6-Dihydroxy-4,4-diphenyltetrahydropyran (**4**)*

A fine suspension of 1,1,5,5-tetramethoxy-4,4-diphenylpentane (**3**) (3.0 g, 8.7 mmol) in 60 ml of a 2 *N* solution of sulfuric acid in water is heated under reflux over a period of 1 h. The precipitate thus formed is filtered, crushed, and washed with acetone, then anhydrous ether to yield pure 2,6-dihydroxy-4,4-diphenyltetrahydropyran (**4**); 2.23 g (95%); mp 138–140°C; ir (Nujol) 3290 and 3190 cm^{-1}; nmr (DMSO-d_6), δ 7.21 (complex signal, 10H), 6.48 (d, 2H, J = 7.5 Hz), 4.65 (dd, 2H, J = 10 Hz), 2.91 (d, 2H, J = 12.5 Hz, lowfield portion of the AB system), 1.68 (dd, 2H, J = 10 Hz, J = 12.5 Hz, highfield portion of the AB system). After exchange with D_2O, signal at δ 6.48 disappears (hydroxylic protons) and signal at δ 4.65 collapses to a doublet, J = 10 Hz. Decoupling experiment: signal irradiated at δ 4.65, signal observed at δ 1.68 collapses to a doublet, J = 12.5 Hz.

Further experimental proof to the proposed structure was obtained when a small amount of the title compound was heated for 10 min *in vacuo*, slightly above its melting point, and gave quantitatively the expected corresponding dialdehyde, 3,3-diphenylglutaraldehyde (**5**), as an oil: nmr (DMSO-d_6), δ 9.47 (t, 2H, $J \simeq$ 2.5 Hz), 7.27 (br s, 10H), 4.36 (d, 4H, $J \simeq$ 2.5 Hz). The above dialdehyde (**5**) was heated at 100°C for 30 min in DMSO containing a small volume of 10% HCl (20:1), then diluted with cold water. The precipitate thus formed was filtered, washed with water then acetone, and dried *in vacuo*. All physical and spectroscopic data were identical with the ones reported for the title compound (**4**).

*4,4-Diphenyl-γ-pyran (**1**)*

p-Toluenesulfonyl chloride (4.5 g, 24.7 mmol) is added to a solution of 2,6-dihydroxy-4,4-diphenyltetrahydropyran (**4**) (1.4 g, 5 mmol) in 50 ml of anhydrous freshly distilled pyridine and the mixture heated (8) at 140°C during 20 h under magnetic stirring. The reaction mixture is allowed to cool and is then diluted with ether. The ether solution, washed with a 10% aqueous solution of hydrochloric acid to remove the pyridine, is then washed with water, dried over anhydrous magnesium sulfate, and evaporated to give an oily residue which crystallizes on standing. Pure 4,4-diphenyl-γ-pyran (**1**) is obtained by sublimation *in vacuo* (100°C/0.2 Torr): 1.04 g (80%); mp 56–57°C; mass spectrum, calcd.: 234.1044; found: 234.1050; ir ($CHCl_3$), 1668, 1620, and 1590 cm^{-1}; nmr ($CDCl_3$) δ 7.20 (s, 10H), 5.90 (q, AB, 4H, J = 6 Hz); uv (ethanol), λ_{max} 240 nm (ε 1050).

Typical Irradiation Conditions and Characterization of Photoproducts

A solution of 500 mg of 4,4-diphenyl-γ-pyran (**1**) in 500 ml anhydrous *tert*-butyl alcohol (4.2×10^{-3} *M*) was irradiated for 20 h at 254 nm in a quartz vessel, using a Rayonet reactor. The photochemical products were then separated by preparative thin layer chromatography on silica gel plates (20 × 40 cm) eluted by a 20:80 ether–hexane mixture. Six products were thus obtained and are enumerated here in their increasing order of polarity.

(*a*) Unreacted starting material, γ-pyran (**1**): 55 mg (11%).

(*b*) *trans-tert*-Butyl 3,5-diphenylpent-2-enoate (**7**): 98 mg (15%); mp 55°C (ether–pentane); mass spectrum, molecular ion at *m/e* 308 (<1%), loss of isobutylene at *m/e* 252 (20%), followed by loss of CO_2H at *m/e* 207 (16.7%), and base peak at *m/e* 91 (100%); ir (CCl_4), 1705 and 1620 cm^{-1}; nmr ($CDCl_3$), δ 7.45 (br s, 5H), 7.28 (br s, 5H), 6.00 (s, 1H), 3.50 to 2.50 (m, AA′MM′X, 4H), 1.55 (s, 9H). nOe experiment: the product is dissolved in $CDCl_3$ and the solution degassed several times before sealing the tube. Irradiated signal at 3.37 ppm, lowfield

portion of the AA′MM′X system. Observed signal at 6.00 ppm, vinylic proton singlet shows an increase in intensity of 11 to 13% (10).

(*c*) *cis-tert*-Butyl 3,5-diphenylpent-2-enoate (**8**): 59 mg (9%); clear oil; mass spectrum, molecular ion at *m/e* 308 (1%), loss of isobutylene at *m/e* 252 (30%), followed by loss of CO_2H at *m/e* 207 (20%), base peak at *m/e* 91 (100%); ir ($CHCl_3$), 1700 and 1630 cm^{-1}; nmr ($CDCl_3$), δ 7.34 (m, 10H), 5.93 (s, 1H), 2.76 (br s, 4H), 1.28 (s, 9H). nOe experiment: (*vide supra*) irradiated signal at 2.76 ppm. Observed signal at 5.93 ppm, vinylic singlet, shows no noticeable increase in intensity (10). Contact shift reagent $Eu(fod)_3$: a qualitative study shows that when small amounts of $Eu(fod)_3$ are added to the solution in $CDCl_3$, there is a marked evolution from a deceptively simple singlet at 2.76 ppm, to a more complex AA′MM′X multiplet (10).

(*d*) Isomeric 3,5-diphenylpent-2,4-dienals (**6**): 33 mg (6.5%); yellow oil; mass spectrum, molecular ion at *m/e* 234 (100%), loss of CHO at *m/e* 205 (62%); ir ($CHCl_3$), 1665 and 1610 cm^{-1}; nmr ($CDCl_3$), δ 10.21, 9.47, 9.40 (d, 1H), 7.8 to 6.00 (m, 13H).

(*e*) Isomeric 3,5-diphenylpent-2-enoic acids (**9**): 43 mg (8%); ir ($CHCl_3$), 3500, 1725, and 1620 cm^{-1}; nmr ($CDCl_3$), δ 11.00 (s, 1H), 7.80 to 6.80 (m, 10H), 5.90 (br s, 1H), 3.60 to 2.50 (m, 4H).

(*f*) Unidentified organic polymers: yield measured as percentage starting material (13%).

*trans- and cis-Ethyl 3,5-Diphenylpent-2-enoate (**12** and **13**) (13)*

A solution of diethylcarbethoxymethylphosphonate (13) (2.25 g, 0.01 mol) in 5 ml DME is slowly added to a fine suspension of sodium hydride (0.4 g of a 51% suspension in oil; 8 mmol) in 15 ml of DME. Dihydrochalcone (**11**) (1 g, 4.8 mmol), previously obtained (12) by catalytic hydrogenation of chalcone (**10**), in 15 ml DME is subsequently added at room temperature and the resulting solution heated under reflux for 4 h. The reaction mixture is allowed to cool, 150 ml of water are then added, and both organic and water layers are filtered. The aqueous phase is extracted twice with ether and the organic extracts are combined, dried over anhydrous magnesium sulfate, and evaporated. A mixture (3.2 g) of *trans-* and *cis*-ethyl 3,5-diphenylpent-2-enoate (**12**, **13**) is thus obtained. The esters are separated by thin layer chromatography on silica gel plates (20 × 40 cm), eluted with a 30:70 ether–hexane mixture: total yield in esters, 35%.

trans-Ethyl 3,5-diphenylpent-2-enoate (**12**): mp 36–39°C; mass spectrum, molecular ion at *m/e* 280 (8%), base peak at *m/e* 91 (100%); ir ($CHCl_3$), 1700 and 1620 cm^{-1}; nmr ($CDCl_3$), δ 7.57 (s, 5H), 7.20 (s, 5H) 6.05 (s, 1H), 4.30 (q, 2H), 3.70 to 2.40 (m, AA′MM′X, 4H) 1.30 (t, 3H). nOe experiment: (*vide supra*), irradiated signal at 3.40 ppm, observed signal at 6.05 ppm, 13% increase in intensity (10).

cis-Ethyl 3,5-diphenylpent-2-enoate (**13**): clear oil; mass spectrum, molecular ion at *m/e* 280 (8%), base peak at *m/e* 91 (100%); ir ($CHCl_3$), 1705 and 1635 cm^{-1}; nmr ($CDCl_3$), δ 7.40 (m, 10H), 5.95 (s, 1H), 4.00 (q, 2H), 2.72 (s, 4H), 1.05 (t, 3H). nOe experiment: (*vide supra*), irradiated signal at 2.72 ppm, observed signal at 5.95 ppm, no appreciable increase in intensity (10).

*Authentic trans-3,5-Diphenylpent-2-enoic Acid (**14**)*

trans-Ethyl 3,5-diphenylpent-2-enoate (**12**) (100 mg, 0.4 mmol) is added to a solution of KOH (50 mg, 0.8 mmol) in 3 to 4 ml of 95% ethanol. The resulting mixture is heated to reflux during 75 min. The solution is then acidified by 2 *N* H_2SO_4 and extracted by two 20 ml portions of ether. The organic extracts are combined, washed with water, dried over anhydrous magnesium sulfate, and evaporated. The solid crude product (74 mg) is recrystallized from a pentane–ether mixture: yield 75%, mp 99–101°C; mass spectrum, molecular ion at *m/e* 252 (5%), loss of CO_2H at *m/e* 207 (8%), base peak at *m/e* 91 (100%); nmr ($CDCl_3$), δ 11.30 (s, 1H), 7.56 (s, 5H), 7.36 (s, 5H), 6.24 (s, 1H) 3.80 to 2.60 (m, AA′MM′X, 4H).

*Cleavage of trans-tert-Butyl 3,5-diphenylpent-2-enoate (**7**) (14)*

trans-tert-Butyl 3,5-diphenylpent-2-enoate (**7**) (75 mg, 0.24 mmol) and a catalytic amount of *p*-toluenesulfonic acid monohydrate are dissolved in 5 ml of benzene and the solution heated to reflux for 3 h. The benzene is evaporated and the crude product purified first by column chromatography on silica gel (5 × 15 cm) eluted with a 80:20 ether–hexane mixture, then by recrystallization from ether–pentane to yield *trans*-3,5-diphenylpent-2-enoic acid (**14**): mp 99–101°C. Mixture mp with authentic acid: 100–101°C. All the spectra were taken and are identical to those of the authentic acid **14**.

*3,5-Diphenylpentanoic acid (**16**)*

A solution of 3,5-diphenylpent-2-enoic acid (**14**) (210 mg, 0.8 mmol) in 30 ml of ethyl acetate containing 10 mg of PtO_2 is submitted to catalytic hydrogenation under a pressure of 3 atm for 5 h in Augustine's catalytic hydrogenator (16). After evaporation of the solvent, a yield of 200 mg (95%) of crude product is obtained; mp (ethyl ether – petroleum ether) 100–102°C; mass spectrum, molecular ion at *m/e* 254; nmr ($CDCl_3$); δ 10.90 (s, 1H), 7.20 (br signal, 10H), 3.50 to 1.50 (m, 7H).

*Authentic Methyl 3,5-Diphenylpentanoate (**17**)*

An ethereal solution of diazomethane prepared from Diazald (15) is added dropwise to 30 mg (0.12 mmol) of 3,5-diphenylpentanoic acid (**16**) in 20 ml ether until the evolution of nitrogen ceases and the solution remains yellow. The excess diazomethane is then eliminated by adding 1 to 2 drops of glacial acetic acid. The reaction mixture is washed with 15 ml $NaHCO_3$ (10%) and two portions of water. The solution is dried over magnesium sulfate and the solvent evaporated. Yield 30 mg (95%); colourless oil; nmr ($CDCl_3$), δ 7.00 (br signal, 10H), 3.40 (s, 3H), 3.40 to 1.50 (complex signal, 7H).

*Chemical Transformations of Photoaldehydes (**6**) and Structure Correlation*

A suspension of 50 mg (0.21 mmole) of the photoaldehydes (**6**) in 4 ml of water and 40 mg KOH is treated with nickel peroxide (17) (200 mg). The mixture is heated to reflux for 30 min and maintained at 50°C for 7 h. The reaction mixture is filtered, and extracted with ether. The aqueous layer is acidified and also extracted with ether. The latter ether extracts are dried and evaporated. The acids thus obtained are dissolved in 25 ml ethyl acetate and submitted to catalytic hydrogenation (*vide supra*) for 3 h (16). The solution is then filtered, the solvent evaporated, and the residue taken up in 30 ml of ether. The ethereal solution is treated with a solution of diazomethane in ether (*vide supra*) (15).

The resulting solution of methyl ester is compared to an authentic sample of previously prepared methyl 3,5-diphenylpentanoate (**17**) by tlc, using three different ether–hexane mixtures (10:90, 20:80, 40:60) and by gas chromatography, using the peak enhancement technique on two different columns (SE-30, 3%, 5 ft × 0.25 in. on Chromosorb W 60/80 and OV-1, 3%, 6 ft × 0.25 in. on Varaport).

*Correlation of Structure of the Photoacids (**9**)*

*Authentic trans-Methyl 3,5-Diphenylpent-2-enoate (**15**)*

The title compound is prepared by treating a solution of 50 mg of *trans*-3,5-diphenylpent-2-enoic acid (**14**) (0.2 mmol) in 2 ml of ether with ethereal diazomethane (*vide supra*). Yield 52 mg (100%); colourless oil; nmr ($CDCl_3$), δ 7.07 (br s, 5H), 6.90 (br s, 5H), 5.78 (s, 1H), 3.56 (s, 3H), 3.50 to 2.40 (m, AA′MM′X, 4H).

*Esterification of Photoacids (**9**)*

A mixture of photoacids (25 mg) is dissolved in 2 ml of ether and treated with ethereal diazomethane (15) (*vide supra*). The resulting mixture is compared to authentic *trans*-methyl 3,5-diphenylpent-2-enoate (**15**) by tlc on silica gel using three different ether–hexane mixtures (10:90, 20:80, 40:60) and by gas chromatography using the peak enhancement technique on two different columns (SE-30, 3%, 5 ft × 0.25 in. on Chromosorb W 60/80 and OV-1, 3%, 6 ft × 0.25 in. on Varaport).

*Isolation of the Primary Photoproduct, trans-endo-5,6-Diphenyl-2-oxabicyclo[3.1.0]hexene (**18**)*

Irradiation of 500 mg of 4,4-diphenyl-γ-pyran (**1**) in 100 ml of *tert*-butyl alcohol at 254 nm for 2 h gives 50 mg (10%) of *trans-endo*-5,6-diphenyl-2-oxabicyclo[3.1.0]hexene (**18**), along with all the other expected photoproducts. This product is isolated by preparative thin layer chromatography on silica gel plates (20 × 40 cm), eluted with a 3:97 ether–hexane mixture. The product was extracted from silica gel by washing several times with ether at room temperature. Continuous extraction with ether or chloroform using a Soxhlet yields an appreciable amount of isomeric aldehydes (**6**) by thermal rearrangement, nmr ($CDCl_3$) δ 7.40 (2 s, 10H), 5.96 (d, AB, $J_{AB} \simeq 2.5$ Hz), 5.10 (d, AB, $J_{AB} \simeq 2.5$ Hz), 4.73 (d, $J \simeq 7$ Hz), 2.50 (d, $J \simeq 7$ Hz); ir ($CHCl_3$), 3100, 3080, 3040, 2920, 1590, 1490, 1440, 1140, 690 cm^{-1}.

*Rearrangement of Primary Photoproduct (**18**) to Photoaldehydes (**6**)*

The primary photoproduct **18**, under various experimental conditions, leads to the formation of photoaldehydes (**6**), as evidenced by tlc on silica gel plates. A solution of 3 mg of **18** in 0.5 ml ether is spotted on three silica gel plates 2.5 × 7.5 cm. The first plate when irradiated for 1 h at 254 nm and then eluted by a 20:80 ether–hexane mixture showed extensive formation of aldehydes **6**. The second plate, when heated at approximately 150°C for 10 min showed quantitative rearrangement of **18** into the aldehydes **6** after eluting with a 20:80 ether–hexane mixture. The third plate showed partial rearrangement of the primary photoproduct **18** to the aldehydes **6** when a methanolic solution of *p*-toluenesulfonic acid was spotted over product **18** and the plate eluted by 20:80 ether–hexane mixture after standing 30 min at room temperature.

*Photolysis of 4,4-Diphenyl-γ-pyran (**1**) in tert-Butyl Alcohol-O-d*

Irradiation at 254 nm during 20 h of 500 mg of 4,4-diphenyl-γ-pyran (**1**) in 200 ml of *tert*-butyl alcohol-*O-d* leads to the formation of 11 mg (2.2%) of *trans-tert*-butyl-4-d_1 3,5-diphenylpent-2-enoate (**7**). Mass spectrum, molecular ion at *m/e* 309, loss of isobutylene at *m/e* 253, then loss of OH at *m/e* 236 or loss of CO_2H at *m/e* 208, base peak at *m/e* 91; nmr ($CDCl_3$), δ 7.25 (br s, 5H), 7.08 (br s, 5H), 5.83 (s, 1H), 3.25 (t, 1H), 2.60 (d, 2H), 1.30 (s, 9H).

*Photolysis of Aldehydes (**6**) in tert-Butyl Alcohol-O-d*

Irradiation at 254 nm during 5 h of a 50 mg solution of aldehydes **6** in 30 ml *tert*-butyl alcohol-*O-d* leads to the formation of 2 to 3 mg *trans-tert*-butyl 4-d_1 3,5-diphenylpent-2-enoate (**7**), identified by tlc. Mass spectrum, molecular ion at *m/e* 309 (≪1%), loss of isobutylene *m/e* 253, then loss of OH at *m/e* 236 or loss of CO_2H at *m/e* 208, base peak at *m/e* 91.

*Formation of Photoacids (**9**) from Photoester **7***

Irradiation at 254 nm during 5 h of 2 to 3 mg of *trans-tert*-butyl 2,5-diphenylpent-2-enoate (**7**) in solution in 1 ml *tert*-butyl alcohol leads to the formation of the photoacids, as evidenced by tlc on silica gel plates eluted by a 20:80 ether–hexane mixture.

Acknowledgements

Financial assistance from the National Research Council of Canada and le Ministère de l'Education du Quebec is gratefully acknowledged. The authors are also indebted to professor M. St-Jacques for directing their efforts during the nOe experiments and to R. Mayer for obtaining the spectra.

1. (*a*) H. E. Zimmerman, R. J. Boettcher, N. E. Buehler, G. E. Keck, and M. G. Steinmetz. J. Am. Chem. Soc. **98**, 7680 (1976); (*b*) C. Santiago, K. N. Houk, R. A. Snow, and L. A. Paquette. J. Am. Chem. Soc. **98**, 7443 (1976); (*c*) S. S. Hixson, P. S. Mariano, and H. E. Zimmerman. Chem. Rev. **73**, 531 (1973).
2. H. E. Zimmerman, P. Hackett, D. Juers, and B. Schröder. J. Am. Chem. Soc. **89**, 5973 (1967).
3. H. E. Zimmerman, P. Hackett, D. F. Juers, J. M. McCall, and B. Schröder. J. Am. Chem. Soc. **93**, 3653 (1971).
4. K. Dimroth, K. Wolf, and H. Kroke. Ann. Chem. **678**, 183 (1964).
5. (*a*) N. K. Cuong, F. Fournier, and J. J. Basselier. C. R. Acad. Sci. Paris, C, **271**, 1626 (1970); (*b*) N. K. Cuong, F. Fournier, and J. J. Basselier. Bull. Soc. Chim. Fr. 2117 (1974).
6. S. G. Kuznetsov and N. M. Libmann. Zh. Org. Khim. **1**, 1399 (1965); Chem. Abstr. **64**, 619b (1966).
7. M. Karplus. J. Am. Chem. Soc. **85**, 2870 (1963).
8. O. Wintersteiner and W. More. J. Am. Chem. Soc. **65**, 1507 (1943).
9. F. W. McLafferty. Interpretation of mass spectra: an introduction. Benjamin, New York, NY. 1966. p. 123.
10. (*a*) E. D. Becker. High resolution NMR. Academic Press, New York, NY. 1969. p. 187; (*b*) M. Ohtsuru, M. Teraoka, K. Tori, and K. Takeda. J. Chem. Soc. B, 1033 (1967).
11. (*a*) A. F. Cockerill, G. L. O. Davies, R. C. Har-

DEN, and D. M. ROCKHAM. Chem. Rev. **73**, 553 (1973); (*b*) O. CEDER and B. BEIJER. Acta Chim. Scand. **26**, 2977 (1972).
12. R. ADAMS, J. W. KERN, and R. L. SHRINER. Org. Synth. Coll. Vol. I, 101 (1941).
13. W. S. WADSWORTH and W. D. EMMONS. Org. Synth. **45**, 44 (1965).
14. D. S. BRESLOW, E. BAUMGARTEN, and C. R. HAUSER. J. Am. Chem. Soc. **66**, 1286 (1944).
15. D. J. DEBOER and M. J. BACKER. Recl. Trav. Chim. **73**, 229 (1954).
16. R. L. AUGUSTINE. Catalytic hydrogenation. Decker, New York, NY. 1965. p. 8.
17. K. NAKAGAWA, R. KONAKA, and T. NAKATA. J. Org. Chem. **27**, 1597 (1961).
18. H. E. ZIMMERMAN and R. L. MORSE. J. Am. Chem. Soc. **90**, 954 (1968).
19. P. K. KORVER, P. J. VAN DER HAAK, N. STEINBERG, and T. J. DE BOER. Recl. Trav. Chim. **84**, 129 (1965).
20. S. TOKI, K. SHIMA, and H. SAKURAI. Bull. Chem. Soc. Jpn. **38**, 760 (1965).
21. K. L. WILLIAMSON, C. A. LANFORD, and C. R. NICHOLSON. J. Am. Chem. Soc. **86**, 762 (1964).
22. L. M. JACKMAN and S. STERNHELL. Application of nuclear magnetic resonance spectroscopy in organic chemistry. 2nd ed. Pergamon Press, New York, NY. 1969.
23. P. LASZLO and P. R. SCHLEYER. Bull. Soc. Chim. Fr. 87 (1964).
24. (*a*) F. SORM and J. NOVAK. Chem. Listy, **51**, 1693 (1957); Chem. Abstr. **52**, 4480 (1958); (*b*) G. O. SCHENK and R. STEINMETZ. Angew. Chem. **70**, 504 (1958); (*c*) G. O. SCHENK and R. STEINMETZ. Ann. **668**, 19 (1963); (*d*) E. MULLER, H. KESSLER, H. FRICKE, and H. SUHR. Tetrahedron Lett. 1047 (1963); (*e*) L. JACKSON. Ph.D. Thesis, The Ohio State University, Columbus, OH. 1967.
25. (*a*) R. B. WOODWARD and R. HOFFMANN. The conservation of orbital symmetry. Academic Press, New York, NY. 1970; (*b*) W. H. PIRKLE, H. SETO, and W. V. TURNER. J. Am. Chem. Soc. **92**, 6984 (1970).
26. J. E. GANO. Tetrahedron Lett. 2549 (1969).
27. R. D. COCKROFT, E. E. WAALI, and S. J. RHOADS. Tetrahedron Lett. 3539 (1970).
28. C. N. R. RAO. Ultra-violet and visible spectroscopy, chemical applications. Butterworths, London. 1961. p. 39.
29. H. E. ZIMMERMAN and B. R. COTTER. J. Am. Chem. Soc. **96**, 7445 (1974).

Two types of localized excess electrons in crystalline D_2O ice[1]

GEORGE V. BUXTON,[2] HUGH A. GILLIS, AND NORMAN V. KLASSEN
Division of Physics, National Research Council of Canada, Ottawa, Ont., Canada K1A 0R6

Received January 28, 1977

GEORGE V. BUXTON, HUGH A. GILLIS, and NORMAN V. KLASSEN. Can. J. Chem. **55**, 2385 (1977).

In a pulse radiolysis study of crystalline D_2O ice, an intense infrared absorption band with $\lambda_{max} > 2350$ nm has been found at low temperatures, in addition to the well-known visible absorption band of the trapped electron. The infrared band is also attributed to trapped electrons, partly because of its similarity to the electron absorption band found recently in some D_2O glasses at low temperatures. The effects of temperature, dose per pulse, accumulated dose, and added NH_4F, HF, and ND_3 on the yields and decay kinetics of both bands have been investigated. It is concluded that the electron trap giving rise to the visible band is a vacancy which at low temperatures is radiation-produced by a two-step spur process. At temperatures close to the melting point the vacancy-trap probably exists before the radiation pulse at equilibrium concentration. The electron trap which gives rise to the infrared band is thought to be a cavity that occurs naturally in the perfect lattice. For previously unirradiated samples the infrared band decays by a second order process which is remarkably fast ($k \simeq 4 \times 10^{12}\ M^{-1}\ s^{-1}$ at 76 K). The decay reaction is probably neutralization by D_2O^+. Doping with NH_4F increases the yield of the infrared absorption and greatly decreases its decay rate. The total yield of localized electrons in irradiated crystalline D_2O is higher than has been generally recognized.

GEORGE V. BUXTON, HUGH A. GILLIS et NORMAN V. KLASSEN. Can. J. Chem. **55**, 2385 (1977).

En travaillant à basse température au cours d'une étude sur la radiolyse pulsée d'une glace de D_2O cristalline, on a trouvé une bande d'absorption infrarouge intense avec un $\lambda_{max} > 2350$ nm; cette bande est en surplus de la bande d'absorption visible bien connue pour les électrons piégés. On attribue aussi la bande infrarouge aux électrons piégés; cette conclusion est basée en partie sur sa similarité avec la bande d'absorption d'électrons trouvée récemment dans quelques verres de D_2O à basse température. On a étudié les effets de la température, des doses par pulsation, des doses accumulées et de l'addition de NH_4F, HF et ND_3 sur les rendements et la cinétique de disparition des deux bandes. On en conclut que le piège d'électron donnant lieu à la bande visible est un trou qui, à basse température, est produit par des radiations par un processus spontané à deux étapes dans les grappes. A des températures proches de celle du point de fusion, le piège trou existe probablement à la concentration d'équilibre avant la pulsation de radiation. On croit que le piège d'électron qui donne lieu à la bande infrarouge est une cavité qui se trouve naturellement dans un réseau parfait. Pour des échantillons qui n'ont pas été irradiés antérieurement, la bande infrarouge disparait suivant un processus du second ordre qui est remarquablement rapide ($k \simeq 4 \times 10^{12}\ M^{-1}\ s^{-1}$ à 76 K). La réaction de disparition est probablement une neutralisation par D_2O^+. Le dopage par NH_4F augmente le rendement de l'absorption infrarouge et diminue grandement sa vitesse de décroissance. Le rendement total d'électrons localisés dans du D_2O cristallin irradié est plus élevé que ce qui avait été habituellement observé.

[Traduit par le journal]

Introduction

Several studies of electrons localized in crystalline ice and absorbing in the visible have been reported (1–7). They have been especially concerned with the nature of the electron trap and the mechanism of trapping because self-trapping which occurs in liquid water is unlikely in ice at low temperatures due to its very long dielectric relaxation time. Several years ago it was concluded from the available experimental evidence that the visible band is probably due to an electron trapped in a vacancy in the crystal lattice (8). In one study it was concluded that the electron trap which gives rise to the visible band pre-exists (3). However, in a very recent study it was concluded that the trap involved is a radiation-produced lattice vacancy (7). In this paper we report some new observations on the

[1]NRCC No. 15899.

[2]This work was carried out while G.V.B. was a Visiting Research Officer at the National Research Council of Canada, June–September, 1974. Permanent address: University of Leeds, Cookridge Radiation Research Centre, Cookridge Hospital, Leeds LS16 6QB, England.

visible-absorbing electron in crystalline D_2O ice which enables us to say something further about the nature of the corresponding trap.

Recently we reported in a preliminary way on a radiation-produced infrared absorption band in crystalline D_2O and three kinds of D_2O glass at low temperatures (9). We assigned the band to a second type of trapped electron. Later we published a more extensive study of this band in the D_2O glasses (10), and here we describe further experiments concerning the infrared band in crystalline D_2O. Very recently the infrared band and an accompanying epr spectrum have been studied in crystalline D_2O at 4 K (11), and also assigned to trapped electrons.

Solids of D_2O, rather than H_2O, are used in these studies because of their greater transparency in the infrared; with samples of 5 mm optical path we can make measurements out to 2350 nm for crystalline D_2O, but only out to 1780 nm for crystalline H_2O.

Experimental

All crystals were made from D_2O (99.7 mol% D) from Merck, Sharp and Dohme which was used as received. The ND_3 was also from Merck, Sharp and Dohme, NH_4F and HF were analytical reagent grade and all three solutes were used without further purification.

Crystals were grown by lowering Pyrex tubes (19 mm id) containing degassed D_2O at a rate of 75 mm/day into a bath which was usually at −4°C. Each tube contained three or four round spacers with diameters slightly smaller than the inside diameter of the tube, which were attached perpendicularly to a rod at either 5 or 9.5 mm intervals. The rod and spacers were normally of brass, but were of Lucite for growing crystals doped with HF or ND_3. The samples were stored in the bath until used. Then an ice column was removed from its tube, an individual cylindrical sample of 5 or 9.5 mm thickness was pushed out from between its spacers, and slowly (in a period of about 5 min) lowered into liquid nitrogen in an irradiation Dewar. The samples were always clear and usually crack-free. We presume that each sample consisted of a few large crystals.

After NH_4F- and HF-doped samples were irradiated, they were melted and analyzed for F^- with an Orion fluoride electrode. Similarly ND_3-doped samples were analyzed with an ammonia electrode. These analyses indicated a somewhat more efficient incorporation of the solute into the crystal than found by Gross *et al.* (12). Thus they measured the distribution coefficient for NH_4F for unstirred systems as around 0.1, independent of concentration. However, we found that the concentration of NH_4F in a crystal was nearly as high as the concentration of the solution from which it was grown.

Samples were irradiated by single 30 or 40 ns pulses of 35 MeV electrons. The dose per pulse was generally in the range 4–9 krad. The irradiation Dewar, equipped with optical windows, was either filled with liquid nitrogen (bubbled with helium) or cold nitrogen gas was flowed through it to provide temperatures higher than 76 K. Temperature was measured with a copper–constantan thermocouple attached to the sample holder. Irradiation of the Dewar and liquid nitrogen but no sample showed that no blank corrections were required.

The dose per pulse was monitored with a secondary emission monitor which was calibrated for each experiment by using O_2-saturated 5 m*M* KSCN solution as a dosimeter. The irradiation cell with dosimeter solution was surrounded with methanol, which has an electron density similar to that of liquid nitrogen, and $G\varepsilon$ was taken as 2.2×10^4 molecules $(100\ \text{eV})^{-1}\ M^{-1}\ \text{cm}^{-1}$ at 475 nm.

In most experiments the light intensity was monitored simultaneously at two wavelengths. In determinations of spectra, one wavelength was fixed as the reference while the other was varied. The following light detectors were used: for $\lambda < 450$ nm, a Phillips XP-1003 photomultiplier; for 450 nm $\leq \lambda \leq$ 1000 nm, an EG & G SHS-100 silicon photodiode; and for $\lambda > 900$ nm a Barnes A-100 room temperature InAs photodiode. The 0–98% response time of the oscilloscope–detector system was < 30 ns for the first two detectors and ~ 60 ns for the last one. The performance of the silicon and InAs photodiodes has been described (13).

Results

(1) Spectrum of Trapped Electrons

The spectrum of trapped electrons (e_t^-) in pure crystalline D_2O at 76 K consists of two bands, as shown in Fig. 1. The low-energy side of the visible band decays much faster than the band as a whole; the band-width at half-height is 0.75 and 0.67 eV at 30 ns and 400 ns, respectively. The band-width following ^{60}Co

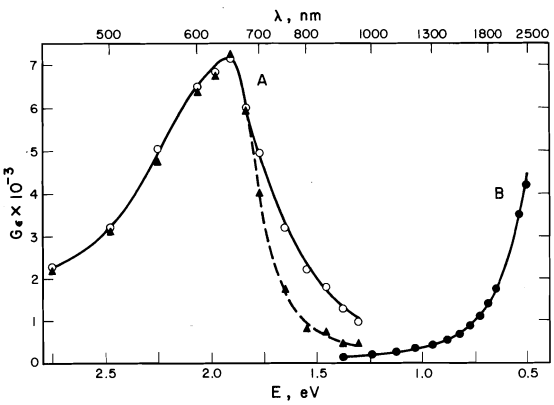

FIG. 1. Absorption spectra at 76 K in crystalline D_2O ice. For the visible band (*A*), points ○ were measured at the end of a 30 ns pulse. Points ▲ refer to measurements made 400 ns after the start of the pulse and multiplied by 1.90. For the infrared band (*B*), the line is a Lorentzian curve fitted to the experimental points ●, which refer to the end of a 30 ns pulse and were obtained by a short extrapolation from 100 ns. Points for both bands between 1.0 and 1.5 eV have been corrected for contributions from the other band (see text).

irradiation is about 0.58 eV (4), so presumably further narrowing occurs after 400 ns. For measurement of the visible band the reference wavelength was 650 nm and the points shown refer to samples which had received no more than 30 krad accumulated dose. This is relevant because not only do the yields for the visible and infrared bands have different dependences on dose (see below), but also in the visible band the ratio of absorption in the quickly-decaying red-edge to that in the main part of the band increases with accumulated dose. Thus it was found that the ratio of optical density at 800 nm to that at 650 nm changed from 0.31 for a previously unirradiated crystal to 0.48 for a crystal that had already received 80 krad.

For measurement of the infrared band of Fig. 1 the reference wavelength was 2300 nm and there was no evidence of a change in the band shape with accumulated dose. The spectrum of irradiated NH_4F-doped ($\sim 4 \times 10^{-3}$ *M*) crystalline-D_2O was found to be very similar to that shown in Fig. 1, but for the doped sample the life-time of the infrared band is much greater than that of the visible band. This permits resolution of the spectrum into the two bands, and the points in Fig. 1 in both bands for energies between 1.0 and 1.5 eV were obtained in this way.

The experimental points for the infrared band fit a Lorentzian function very well; the best fit, shown by the line for the band *B* in Fig. 1, predict $\lambda_{max} = 2950$ nm. By contrast the Lorentzian fit for the infrared band in a $MgCl_2$–D_2O glass at 76 K predicted a λ_{max} of 3600 nm (10). However the imprecision in this method of finding λ_{max} is considerable, so this difference between crystalline and glassy systems may not be experimentally significant. The visible band in the aqueous glasses was found to obey a Gaussian curve on the low-energy side, but this is not true for the visible band shown in Fig. 1.

We measured the spectrum of e_t^- in pure D_2O at 151 K and found that the infrared band has the same shape as band *B* of Fig. 1. The visible band at the end of the pulse at 151 K is intermediate between the 30 ns and 400 ns points of band *A* in Fig. 1, as expected because of the faster decay of the red-edge at the higher temperature.

(2) Decay of e_t^- in Pure Crystalline D_2O

The decay of absorption at 650 nm does not obey simple first or second-order kinetics. As shown in Fig. 2, the decay at 76 K in the pure crystal follows the same curve on a plot of $OD/(OD)_0$ against time for a four-fold variation of initial concentration. This strongly suggests that the species absorbing at 650 nm decays by reaction with a geminate partner.

Absorption in the infrared band for pure crystalline D_2O decays very differently in that the half-life for decay depends strongly on the dose. Figure 3 shows that for previously unirradiated samples the initial decay follows second-order kinetics although deviations from second-order decay occur at later times. What is much more significant is that the initial slopes for the second-order plots are the same within experimental error for a four-fold variation in initial concentration. This means that the decay is due to reaction of species which have a homogenous distribution.

(3) Effects of Accumulated Dose

The effect of repeated pulsing of a D_2O crystal at 76 K on the yields of both bands is shown in Fig. 4*A*. The yields reported here were measured 100 ns after the start of a 40 ns pulse. Accumulated dose also affects the decay rates for both bands. At 650 nm the decay rate increases somewhat with dose. At 2350 nm the initial decay becomes much faster with repeated pulsing but a long tail becomes increasingly significant (see trace *B* of the inset of Fig. 3). The faster initial decay could account for all of the apparent decrease in yield with dose indicated in Fig. 4*A*.

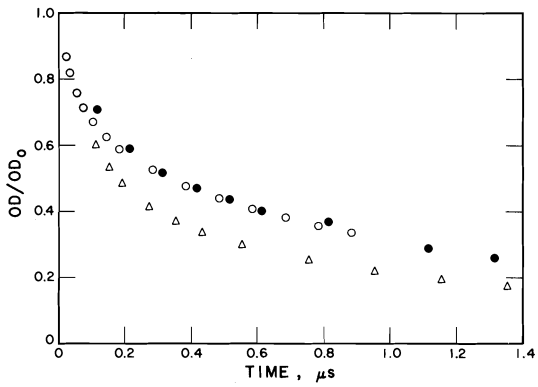

FIG. 2. Decay of absorption at 650 nm in crystalline D_2O ice at 76 K. $(OD)_0$ is OD at mid-pulse, obtained by extrapolation. For ○, no additive and $(OD)_0 = 28.6 \times 10^{-3}$; for ●, no additive and $(OD)_0 = 6.9 \times 10^{-3}$; for △, crystal doped with 9.6×10^{-4} *M* NH_4F, and $(OD)_0 = 25.0 \times 10^{-3}$. Each set of points refers to the first pulse for a sample.

TABLE 1. Electron yields for pure and doped crystalline D_2O at 76 K, for 0 and 50 krads previous dose

Additive	Concentration (M)	$G\varepsilon \times 10^{-3}$ 650 nm (0 krads)	650 nm (50 krads)	2350 nm (0 krads)	2350 nm (50 krads)
None	—	5.7	8.1	3.3	3.1
NH_4F	5.4×10^{-6}	6.2	7.0	4.1	4.4
NH_4F	9.0×10^{-5}	5.8	6.0	5.6	6.5
NH_4F	9.6×10^{-4}	6.4	6.1	9.0	14.5
NH_4F	1.51×10^{-2}	7.1	7.2	13.9	21.8
HF	2.31×10^{-2}	6.1	5.9	5.7	7.8
ND_3	9.8×10^{-5}	5.4	6.1	3.4	3.2
ND_3	1.3×10^{-4}	5.2	—	3.3	—

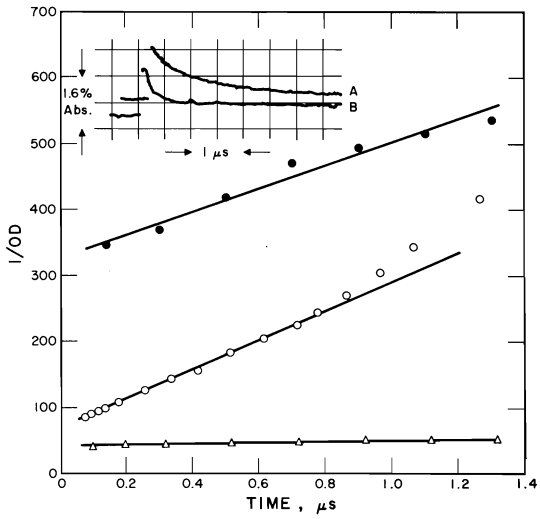

FIG. 3. Decay of absorption at 2350 nm in crystalline D_2O at 76 K, without additives (●) and (○), and doped with 9.6×10^{-4} M NH_4F (△). All three curves are for the first pulse for a sample. Inset: *A*, oscilloscope trace of absorption at 2350 nm for previously unirradiated crystal without additives at 76 K; *B*, oscilloscope trace of absorption at 2350 nm for pure crystal at 76 K that had received an accumulated dose of 100 krads.

(4) Effect of Dose/Pulse

$G\varepsilon$ for both the visible and infrared bands was constant within experimental error (±10%) for a variation of dose/pulse of a factor of 4.5 at a constant pulse width.

(5) Effects of Solutes

The yields of both electron bands for pure and doped crystalline D_2O at 76 K are given in Table 1, both for previously unirradiated samples and for samples that had already received 50 krads. All yields were determined 100 ns after the start of a 40 ns pulse. The yields given for pure D_2O represent the average of values obtained for several samples on different days. Because of uncertainties in positioning samples and dosimeter solutions, the uncertainty in each value given for $G\varepsilon$ is about ±10%, but the uncertainties in the ratio of $G\varepsilon$'s at 650 and 2350 nm and in the change in $G\varepsilon$ on pulsing are smaller.

The effect of 9.6×10^{-4} M NH_4F on electron decay rate for a previously unirradiated sample is shown in Figs. 2 and 3 for the visible and infrared bands, respectively. It is seen that NH_4F drastically decreases the decay rate of the infrared band, and decay was slowest for the most highly doped crystals. For a crystal doped with 6.7×10^{-4} M NH_4F the decay had a half-life of ~25 ms, as measured by using a bandpass filter at 1500 nm in front of the cell to minimize

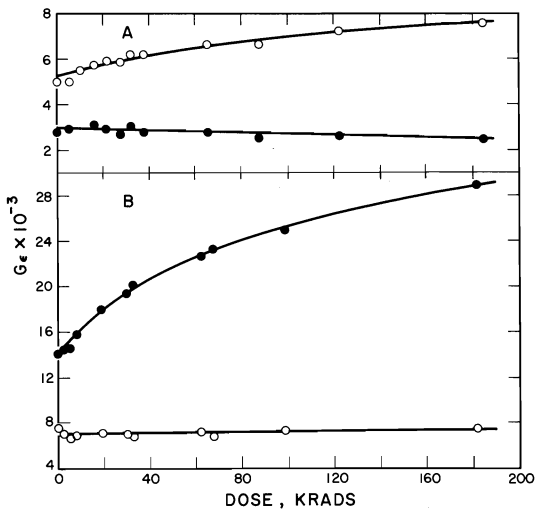

FIG. 4. Effect of accumulated dose on yields of both electron bands in crystalline D_2O at 76 K. *A*, no additives, ○, 650 nm; ●, 2350 nm. *B*, doped with 1.51×10^{-2} M NH_4F: ○, 650 nm; ●, 2350 nm.

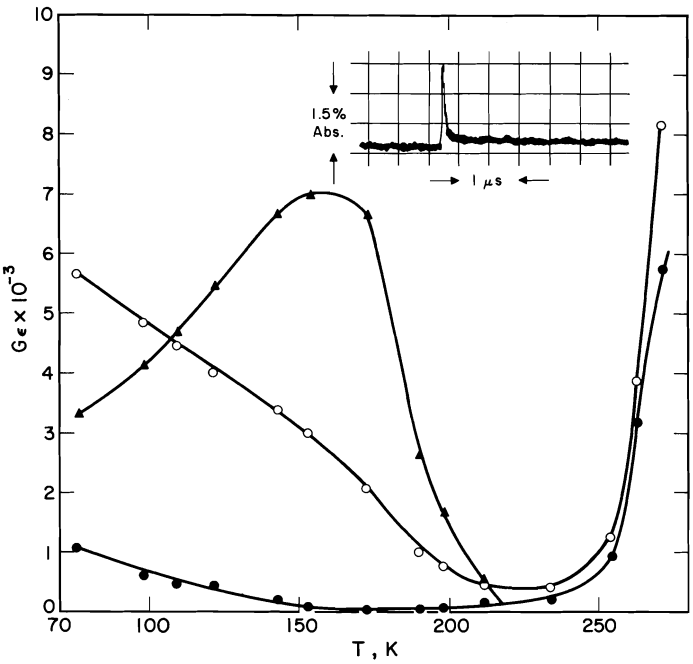

FIG. 5. Effect of temperature on absorption in pure crystalline D_2O. ▲, at 2350 nm, measured 100 ns after the start of a 40 ns pulse; ○, at 650 nm, measured 100 ns after the start of a 40 ns pulse; ●, at 650 nm, measured 3 μs after the start of a 40 ns pulse. Inset: oscilloscope trace showing decay of absorption at 650 nm in a crystal at 212 K.

photobleaching effects. The decay rate of the infrared band was also decreased by HF but not affected significantly by added ND_3.

The effect of dose on the most highly doped NH_4F crystal, 1.51×10^{-2} *M*, is shown in Fig. 4*B*. It is seen that for this sample the yield of infrared absorption doubles as the accumulated dose increases from 0 to 180 krads while the yield of the visible band remains practically constant.

(6) Effects of Temperature

The effect of temperature on yields in both absorption bands is shown in Fig. 5. The decay of absorption at 650 nm at higher temperatures appears to consist of a fast initial decay and a much slower second process, and the second process becomes increasingly important as the temperature is raised from 190 K. The inset to Fig. 5 shows the rapid initial decay and long tail at 212 K. In Fig. 5 the yields at 650 nm at 3 μs at the higher temperatures are roughly the yields of the long-lived absorption, but at temperatures <170 K this absorption at 3 μs appears to be simply the tail of the initial decay process. The effect of temperature on the decay half-life, measured from 100 ns after the start of a 40 ns pulse, is shown for both bands in Fig. 6. It is seen that the half-life for decay of infrared absorption becomes comparable to the detector response-time ($\sim$60 ns) around 180 K, so the decrease in yield at 2350 nm above 160 K, as seen in Fig. 5, is at least partially instrumental. The decay of the infrared band was studied carefully in previously unirradiated samples only at 76 K, but did not seem to obey good second-order kinetics at higher temperatures.

(7) Emission

We observed emission from irradiated crystalline D_2O and 76 K, and the spectrum of this emission is shown in Fig. 7. Corrections for change in the efficiency of the light-gathering system with wavelength have been applied to the points in Fig. 7. The reference wavelength used in determination of the spectrum was 400 nm. The intensity of emission increased considerably with accumulated dose up to a plateau. The intensity at 400 nm approximately tripled in going from an accumulated dose of 20 krads to $\sim$300 krads, and then remained approximately constant with dose up to $\sim$6000 krads. The effect

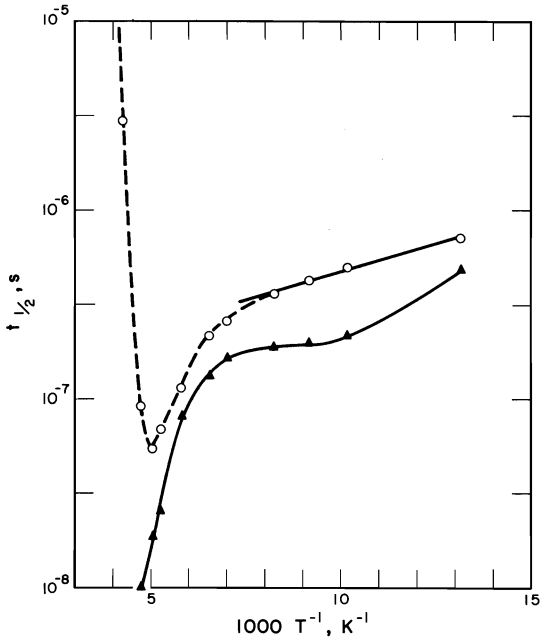

FIG. 6. Effect of temperature on $t_{1/2}$, measured from 100 ns after the start of a 40 ns pulse, for decay of absorption at 650 nm (○), and 2350 nm (▲) in pure crystalline D_2O.

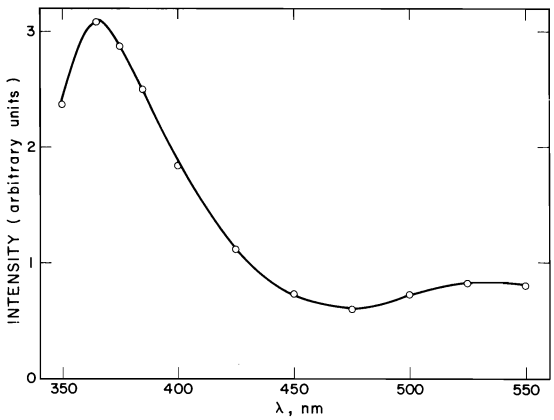

FIG. 7. Spectrum of luminescence from irradiated crystalline D_2O at 76 K, 200 ns after the start of a 400 ns pulse. Corrections for dependence of the efficiency of the light-gathering system on wavelength have been applied.

of dose on the second peak around 525 nm was not studied; in Fig. 7 the points at $\lambda > 450$ nm refer to a dose of ~ 50 krads.

Discussion

(1) Two Types of Excess Electron

The decay rates of the visible and infrared absorption in crystalline D_2O ice are different, and the effects of temperature, dose, and additives on the two bands are different, so they must be due to different species. The partial infrared band we see here is similar in shape and position to the partial infrared band we saw in several D_2O glasses (10), and we found fairly good evidence that the latter is due to a second type of trapped electron. By analogy then we conclude that in crystalline D_2O ice the infrared is also due to a shallowly trapped electron. At 4 K the infrared band decreased with time in the dark while the visible band grew (11); this is further evidence that the infrared band is due to a shallowly trapped electron. Significant infrared absorption was found in only 3 of the 11 D_2O glasses investigated (10), which raised the possibility that high concentrations of particular solutes are required for the production of this band. Finding a similar band in pure D_2O ice clearly removes this possibility.

We shall use the symbols e_{vis}^- and e_{ir}^- to indicate excess electrons which cause the visible and infrared absorption bands.

(2) Trap for e_{vis}^-

Our results can be interpreted on the basis that the visible band is due to an electron trapped in a vacancy in the crystal lattice, as concluded earlier (8). However, at 76 K this vacancy does not exist before a crystal has been irradiated, as indicated by the following calculation. The equilibrium concentration of vacancies at any temperature may be calculated from the Boltzmann equation if the energy required to form a vacancy is known. This energy is not well known but has been estimated as 0.5 eV (ref. 14, p. 162), and as 0.28 ± 0.07 eV (15) around 100 K. Since it is related to the energy of sublimation (14), it would not be expected to depend strongly on temperature. As a crystal is cooled down a temperature will be reached at which vacancies become frozen in, *i.e.* equilibrium is no longer attained. There is evidence that radiation-produced vacancies become mobile and disappear in the region of 100 K (15) or 120 K (11), and therefore equilibrium conditions must hold at higher temperatures. The maximum concentration of vacancies before the first pulse on a crystal at 76 K can then be calculated by using the lower limit of the lower estimate of the energy required to produce a vacancy, 0.21 eV, and by assuming that vacancies become frozen in at 120 K, and this concentration is 8×10^{-8} *M*. If

we assume ε_{650} is the same as ε_{max} in OH^- glasses at 76 K, *i.e.* $2.0 \times 10^4\ M^{-1}\ cm^{-1}$ (16), then for a pulse typical of those used to obtain the data of Fig. 1 the concentration of electrons at the end of the pulse was about $2 \times 10^{-6}\ M$. So the concentration of pre-existing cavities is not high enough to account for our results.

However, there is now fairly direct evidence for the production of vacancies by irradiation of ice (15, 17). We suggest that e_{vis}^- is produced at 76 K by the following mechanism:

$$[1] \qquad 2D_2O \rightsquigarrow (2D_2O^+ + 2e_{qf}^-)$$

$$[2a] \qquad (2D_2O^+ + 2e_{qf}^-) \rightarrow (D + OD + D_2O^+ + e_{qf}^- + \square)$$

$$[2b] \qquad \rightarrow 2D_2O^+ + 2e_{qf}^-$$

$$[3a] \qquad (e_{qf}^- + \square) \rightarrow e_{vis}^-$$

$$[3b] \qquad \rightarrow e_{qf}^- + \square$$

$$[4] \qquad e_{qf}^- + \square \rightarrow e_{vis}^-$$

Here parentheses around reactants are intended to indicate that the reaction takes place in a spur, $\square$ represents a vacancy and e_{qf}^- is the quasi-free electron. The major mechanism for producing e_{vis}^- is the two successive spur reactions 2*a* and 3*a*; the first is a neutralization reaction which produces the vacancy and the second is the trapping of a quasi-free electron in the same spur. A possible alternative to reaction 2*a* which could produce a vacancy in the same spur with e_{qf}^- is decomposition of an excited molecule. We consider that the non-spur reaction 4 is not an important source of e_{vis}^-, but does account for the slight increase in $G(e_{vis}^-)$ with increasing dose. From Fig. 4 it is seen that $G(e_{vis}^-)$ is only about 17% higher for the eighth pulse than for the first pulse for a crystal. It might be argued that most vacancies disappear between pulses (possibly most are destroyed when e_{vis}^- reacts) but that non-spur reactions between e_{qf}^- and vacancies produced in the same pulse are an important source of e_{vis}^-. However, in that case, since e_{qf}^- can undergo an alternative reaction with another kind of trap which is not radiation-produced (see below), one would expect the yield of e_{vis}^- to depend on dose per pulse. As indicated in the Results section, we find otherwise.

As discussed below, $G(e_{vis}^-) \simeq 0.4$ at 76 K, which means that roughly 10% of e_{qf}^- become e_{vis}^-. This seems plausible for the mechanism proposed since the percentage of spurs containing two or more ion pairs in which the successive reactions 2*a* and 3*a* would occur is expected to be rather low.

Kawabata (7) has shown that most of the traps for stable or slowly decaying e_{vis}^- in crystalline D_2O at low temperatures are produced by radiation previously received by a sample. However, he studied only a small percentage of total e_{vis}^-. Thus in pulse experiments he found $G(e_{vis}^-) \simeq 0.01$ in the ms region for the first pulse; our $G(e_{vis}^-)$ at 105 K at 100 ns is about 0.23 (Fig. 5).

The narrowing of the visible absorption band with time, as seen in Fig. 1, is easily explained in terms of a vacancy model. If one water molecule is removed from the tetrahedral structure of ice and an electron occupies this vacancy, then protons from only two of the four water molecules in the first shell point towards the electron. Natori and Watanabe (18) have calculated the optical transition energy for an electron in a vacancy in H_2O ice, and found agreement with experiment only by assuming that two of the molecules at the corners of the tetrahedron can rotate so that four OH bonds point to the center, and by assuming also that the OH bond length and the HOH angles can change from their values in the perfect crystal. Other models also require orientation of the dipoles around the electron in order to get agreement with the observed visible absorption (19, 20). The low-field dielectric relaxation time of water is very long at low temperatures (*e.g.* ~1 s at 165 K) (21). But it has been pointed out that the relaxation time in the high field close to the electron must be very much less than that at low fields (22, 23). Therefore the narrowing of the visible band seen in Fig. 1 is probably a reflection of the orientation of the OD dipoles so that they point towards the center of the vacancy. An increase in absorption at λ_{max} as this spectral shift occurs is not seen because of the rapid decay of e_{vis}^-.

If the vacancy sites for e_{vis}^- are formed by reactions 1–4, then the observed geminate decay of e_{vis}^- at low temperatures is easily explained as a spur reaction with OD or D_2O^+ which probably occurs by a tunnelling process:

$$[5] \qquad (e_{vis}^- + OD) \rightarrow OD^-$$

$$[6] \qquad (e_{vis}^- + D_2O^+) \rightarrow OD + D$$

In Fig. 6 the solid straight-line portion of the Arrhenius plot for e_{vis}^- gives an activation

energy of 0.27 kcal mol^{-1}; such a low activation energy is reasonable for a tunnelling reaction. Other features of the effect of temperature on lifetimes of e_{vis}^- are discussed below. Modest concentrations of solute such as NH_4F would not be expected to have an appreciable effect on the yield of e_{vis}^-, as observed. However, NF_4F seems to increase the decay rate of e_{vis}^- a little, and we cannot explain this. Also in ^{60}Co experiments it has been found that in samples doped with 10^{-2} *M* NH_4F, the yield of e_{vis}^- is about six times that in pure crystalline H_2O (4). However, again these yields refer to the very small fraction of electrons extant at very long times; in the sample doped with 10^{-2} *M* NH_4F, $G(e_{vis}^-)$ was estimated as 3.3×10^{-3}.

(3) Site for e_{ir}^-

In our preliminary account of this work (9) we suggested that an electron captured in a D-defect could give rise to the infrared band. However, this idea does not seem to be in accord with the results of our further studies on the effects of solutes on e_{ir}^- yields. Crystals doped with ND_3, HF, and NH_4F should have higher, lower, and approximately equal concentrations of D-defects, respectively, as compared to the pure crystals (ref. 14. chapt. 7), and one might expect corresponding effects on $G(e_{ir}^-)$ if e_{ir}^- is an electron trapped at a D-defect. Instead, as seen in Table 1, ND_3 has no effect and both HF and NH_4F increase the yields. If it is assumed that orientation of the dipoles surrounding an electron trapped in ice is not possible, then λ_{max} is predicted by the polaron model to be in the infrared (1, 19). This prompts us to suggest that the infrared band in crystalline D_2O is due to electrons trapped in cavities that are natural to the crystal structure and around which little orientational polarization takes place:

[7] $$e_{qf}^- + \text{trap} \rightarrow e_{ir}^-$$

In a crystal of ordinary ice (ice I_h) molecules form sheets of crinkled six-membered rings normal to the *c* axis. Rings from two adjacent sheets form dodecahedral cavities which are joined together along the *c* axis to form long open shafts (see Fig. 1 in ref. 23), and we suggest that electrons trapped in these cavities give rise to the infrared absorption. Fast orientational polarization around these electrons is less likely than around electrons in vacancies for two reasons: (*a*) It would have to work against the strong hydrogen bonding of the crystal, whereas broken hydrogen bonds surround a vacancy. (*b*) There are 12 molecules to be oriented in the first co-ordination shell of the natural cavity, compared to 4 molecules around a vacancy. However, before the infrared band was discovered, Nilsson (23) proposed that electrons trapped in these natural cavities absorb initially in the infrared, but the absorption shifts quickly to the visible as the dipoles of the first co-ordination shell line up with the electric field of the electron. He has developed an equation which enables one to calculate the microscopic relaxation time from the ordinary relaxation time. Use of this equation with data from reference 21 gives a microscopic relaxation time of about 10^{-7} s at 173 K, and of course at 76 K the time would be much longer. Thus Nilsson's treatment is not in accord with our observations that the visible band is present at 30 ns after the pulse and undergoes only a modest narrowing in the next 400 ns, nor with our findings that the effects of dose per pulse, accumulated dose, and solutes on the two bands are uncorrelated.

Earlier we reported finding an infrared absorption band in three D_2O glasses, but not in eight others. We suggest that in the three glasses which give the infrared band the arrangement of D_2O molecules around solute ions or molecules happens to be such that cavities similar to the natural cavities of the crystal are formed.

(4) Decay of e_{ir}^-

The decay of e_{ir}^- is essentially second-order at 76 K for previously unirradiated pure samples, as shown in Fig. 3, and remarkably fast. In order to calculate a rate constant from the slopes of Fig. 3, we estimate an extinction coefficient for e_{ir}^- at 2350 nm by assuming that ε_{1400} is the same for crystalline D_2O as it is for ethylene glycol – D_2O glass, 5.7×10^3 M^{-1} cm^{-1} (10), and by using the ratio of extinction coefficients at 2350 and 1400 nm from Fig. 1. From the estimated $\varepsilon_{2350} = 3.8 \times 10^4$ M^{-1} cm^{-1} and the straight line drawn through the points in Fig. 3, *k* is calculated as 4×10^{12} M^{-1} s^{-1} at 76 K. From this rate constant the sum of the mobilities of e_{ir}^- and its reaction partner can be calculated from the following expression for the rate constant of a diffusion-controlled reaction between particles A and B that are singly and oppositely charged (25):

$$k = \frac{4\pi e(\mu_A + \mu_B)N}{1000D}$$

where N is Avogadro's number, D is the dielectric constant, and μ is the mobility. If we take $D = 3$, the high-frequency dielectric constant of ice (26), then $k = 4 \times 10^{12}\ M^{-1}\ s^{-1}$ corresponds to $(\mu_A + \mu_B) = 1.1 \times 10^{-2}\ cm^2\ V^{-1}\ s^{-1}$. This sum of mobilities is somewhat higher than the sum of about $0.3 \times 10^{-2}\ cm^2\ V^{-1}\ s^{-1}$ expected for normal ions in liquids at room temperature.

We consider that the most likely decay reaction of e_{ir}^- which accounts for homogeneous second-order kinetics in previously unirradiated pure ice is neutralization by D_2O^+:

[8] $\quad e_{ir}^- + D_2O^+ \rightarrow D_2O \text{ or } D + OD + \square$

This requires that e_{qf}^-, the precursor of e_{ir}^-, is trapped sufficiently far from the site of ionization that e_{ir}^- has a homogeneous distribution with respect to D_2O^+. In view of the high mobility of e_{qf}^- and the probability that most spurs contain one ionized molecule, it does not seem unreasonable to expect this requirement to be satisfied in the D_2O crystal. Another possibility is neutralization by D_3O^+, formed from D_2O^+:

[9] $\quad D_2O^+ + D_2O \rightarrow D_3O^+ + OD$

[10] $\quad e_{ir}^- + D_3O^+ \rightarrow D + D_2O$

Reaction 8 seems more likely than reaction 10 for two reasons: (*a*) In aqueous glasses e_{ir}^- does not seem to react with acid (10); (*b*) If reaction 10 is the main decay reaction, e_{ir}^- must have a high mobility because the mobility of D_3O^+ has been measured as only $1 \times 10^{-3}\ cm^2\ V^{-1}\ s^{-1}$ at 95 K and should be rather similar at 76 K (27). (Earlier measurements which were interpreted as indicating a proton mobility so high it could only be explained by tunnelling, are now thought to be unreliable because of deficiencies in experimental technique (28).) However, if e_{ir}^- is very mobile then its long life-time ($t_{1/2} \simeq 25$ ms) in NH_4F-doped crystals is hard to understand; a mobile e_{ir}^- would be expected to react quickly with trapped OD radicals, for example. It seems more reasonable to propose that e_{ir}^- has a low mobility, at least at 76 K, and the large rate constant for decay of e_{ir}^- is due to the movement of D_2O^+ by a resonant charge transfer process. The long tail in the decay curves for e_{ir}^- in crystals that have already been heavily irradiated could be due to trapping of D_2O^+ at radiation-produced defects or impurities. The faster initial decay might be due to reaction of e_{ir}^- with a radiation product by tunnelling from the shallow trap.

(5) Effects of Solutes on e_{ir}^-

One effect of doping ice crystals with NH_4F is to considerably increase $G(e_{ir}^-)$ at 76 K both for previously unirradiated samples and especially for irradiated samples, as indicated in Table 1 and Fig. 4; at the highest concentration used, $1.51 \times 10^{-2}\ M$, a sample that had received 50 krads gave a $G(e_{ir}^-)$ 7 times as great as for a pure ice crystal at the same dose. Another effect of the added NH_4F is to slow down very markedly the decay rate of e_{ir}^- at 76 K, as seen in Fig. 3. The effects of doping with HF are qualitatively similar though not as large as those of NH_4F, and the low concentration of ND_3 that could be incorporated into the crystal had very little effect. To partly explain these effects we propose that D_2O^+, besides reacting with e_{ir}^- (reaction 8) and with e_{qf}^- in a spur (reaction 2*a*), can also react with e_{qf}^- in a non-spur reaction:

[11] $\quad D_2O^+ + e_{qf}^- \rightarrow D + OD + \square$

and can react with added F^-:

[12] $\quad D_2O^+ + F^- \rightarrow D_2O + F$

Removal of D_2O^+ by reaction 12 decreases the rates of reactions 8 and 11. The decrease of the rate of reaction 8 accounts for the longer life-time of e_{ir}^-, and the decrease of the rate of reaction 11 results in an increase in the fraction of e_{qf}^- which undergoes reaction 7 and hence $G(e_{ir}^-)$ is higher. However, we are not able to explain why $G(e_{ir}^-)$ increases with dose for doped crystals.

(6) Effects of Temperature

The dependence of $G(e_{vis}^-)$ on temperature shown in Fig. 5 is similar to that reported earlier (5) except that our yields are somewhat larger because of our shorter electron pulses. Kawabata (7) has argued that the decrease in $G(e_{vis}^-)$ as the temperature is raised from 76 K to 130 K or so is due to a faster recombination of e_{vis}^- or the vacancy with fragments such as D, D^+, and OD at the higher temperatures. However, this seems to account for only part of the temperature effect on yields; $G(e_{vis}^-)$ obtained by extrapolation to mid-pulse, though somewhat imprecise at higher temperatures, still shows a drop between 76 K and 140 K.

Use of estimated extinction coefficients indi-

cates that the sum $G(e_{vis}^-) + G(e_{ir}^-)$ is approximately constant (increases slightly) between 76 K and 140 K which suggests that the decrease in $G(e_{vis}^-)$ and increase in $G(e_{ir}^-)$ are connected mechanistically. One possibility is that reaction of D_2O^+ with D_2O to give D_3O^+, reaction 9, takes place and has a small activation energy. The greater importance of this reaction at higher temperatures would mean a smaller fraction of D_2O^+ available for reaction 2*a* and hence the yield of e_{vis}^- should be smaller. More e_{qf}^- would be available for reaction 7 and hence $G(e_{ir}^-)$ should be larger, as observed. In this argument it is assumed that e_{qf}^-, like e_{ir}^-, does not react efficiently with D_3O^+.

Above 155 K the measured yields of e_{ir}^- become decreasingly representative of the initial yields because of the very rapid decay indicated in Fig. 6. Measurements with a faster detector might reveal very high yields of e_{ir}^- at temperatures higher than 150 K, and possibly the same species exists in the liquid. Rentzepis *et al.* (29) have reported that in water absorption at 1.06 μm is observed within 2 ps after generation of the quasi-free electron, and then the absorption band shifts from lower to higher energies and the normal absorption of the hydrated electron is developed in 4 ps. We suggest that the absorption at 1.06 μm seen by Rentzepis *et al.* could be the same infrared band we see in crystalline ice at low temperatures, though alternatively it could be the rapidly-decaying red edge of the visible band.

At temperatures >140 K, $t_{1/2}$ for both e_{vis}^- and e_{ir}^- become very short (Fig. 6). As indicated above, there is evidence that radiation-produced vacancies become mobile in the region of 100 K (15) or 120 K (11). Therefore, it is possible that e_{vis}^- decays quickly at temperatures >140 K because of migration of their traps. However, in the references cited the time-periods involved were minutes (11) or days (15), whereas we are concerned with $t_{1/2} \simeq 100$ ns, and a high mobility of vacancies would be hard to reconcile with the relatively long-lived e_{vis}^- at temperatures slightly below 0°C. Also a high mobility of vacancies would not explain a rapid decay of e_{ir}^-. A better possibility is that OD radicals become very mobile at temperatures >140 K and react with both e_{vis}^- and e_{ir}^-. Taub and Eiben (3) have observed OH radicals decaying slowly at temperatures as high as 259 K, but at temperatures of 173 K and lower, a fast decay was seen in addition to the slow decay. The fast decay may well be due to reaction with e_{vis}^- and e_{ir}^-, with the slow decay occurring after they have been consumed.

As indicated in the Results section and as shown in the inset of Fig. 5, at temperatures of 212 K and higher the decay curve for e_{vis}^- consists of a spike and a long tail. The tail becomes relatively more important as the temperature is raised from 212 K and the yields also increase sharply with temperature. It seems reasonable to suggest that the spike is due to spur reaction (discussed above), and that the long tail is due to decay of free electrons. However, as pointed out earlier (30), the yield of free e_{vis}^- increases too quickly with temperature above 250 K to be explained directly by the Onsager (31) relation. We suggest that free e_{vis}^- results from e_{qf}^- being captured by pre-existing vacancies, the equilibrium concentration of which would be high enough to accommodate our observed concentrations of e_{vis}^- if 0.3 eV (15) is the correct energy of vacancy formation. On this basis the rapid increase in $G(e_{vis}^-)$ with temperature above 254 K would reflect the increase in equilibrium concentration of vacancies. A plot of log $G(e_{vis}^-)$ against $1/T$ for the three points above 250 K in Fig. 5 gives an energy of 0.6 eV, instead of 0.3 eV, but this determination is quite imprecise because the temperature measurements under our conditions could well have been in error by a few degrees.

At variance with our conclusion that there is an appreciable free electron yield in crystalline ice above 250 K is the conclusion of Schiller (32) based on experiments with polycrystalline H_2O ice doped with tetranitromethane. In neutral ice no nitroform anion (the expected product of electron scavenging) could be found and so it was concluded that free electrons are either absent or do not react with tetranitromethane in ice.

(7) Yields of e_t^-

It is often stated that the yields of trapped electrons in irradiated ice are very low, and it is sometimes said that the yields that are found are to be attributed to electrons trapped in glassy regions in the crystal. Of course the yields of very long-lived electrons that are measured in ^{60}Co experiments are low, but those measured in our experiments at short times are not insignificant. As indicated above, we assume

$\varepsilon_{650} = 2 \times 10^4\ M^{-1}\ cm^{-1}$ for e_{vis}^-, and $\varepsilon_{2350} = 3.8 \times 10^4\ M^{-1}\ cm^{-1}$. Then for a previously unirradiated sample of pure D_2O ice at 76 K, at mid-pulse $G(e_{vis}^-) = 0.41$ and $G(e_{ir}^-) = 0.11$, for a total $G(e_t^-) = 0.52$. For a sample doped with $1.51 \times 10^{-2}\ M$ NH_4F and previously irradiated to the extent of 180 krads, $G(e_{vis}^-) = 0.53$ and $G(e_{ir}^-) = 0.75$ for a total $G(e_t^-) = 1.28$.

(8) Emission

The emission spectrum from irradiated D_2O ice at 76 K is shown in Fig. 7. Steen and Holteng (33) recently reported a very similar spectrum for polycrystalline ice at 77 K, with band maxima at 373 and 534 nm. They found that the ratio of intensities of the two bands depends on dose.

In our study of irradiated deuterated aqueous glasses which show appreciable infrared absorption (10), we found that the emission decay kinetics correlate very well with the decay kinetics of the infrared band, and this led us to suggest that e_{ir}^- decays by reaction with an OD radical to give an OD^-* which fluoresces. In the present study we found no correlation between the decay of emission at 407 nm and the decay of absorption at either 600 nm or 2350 nm, and therefore conclude that emission from the crystal does not result from the same mechanism as in the glass. Bernas and Truong have concluded that OH^- is not responsible for the stimulated luminescence from γ-irradiated crystalline ice (24).

Acknowledgements

The authors are very grateful to Dr. G. J. Trudel for analyzing the doped crystals, and to him and Mr. G. G. Teather for very capable assistance in other aspects of the experimental work.

1. V. N. Shubin, V. A. Zhigunov, V. I. Zolotarevsky, and P. I. Dolin. Nature, **212**, 1002 (1966).
2. K. Eiben and I. A. Taub. Nature, **216**, 782 (1967).
3. I. A. Taub and K. Eiben. J. Chem. Phys. **49**, 2499 (1968).
4. K. Kawabata. J. Chem. Phys. **55**, 3672 (1971).
5. G. Nilsson, H. Christensen, P. Pagsberg, and S. O. Nielsen. J. Phys. Chem. **76**, 1000 (1972).
6. K. Kawabata, H. Horii, and S. Okabe. Chem. Phys. Lett. **14**, 223 (1972).
7. K. Kawabata. J. Chem. Phys. **65**, 2235 (1976).
8. L. Kevan. Radiation chemistry of aqueous systems. *Edited by* G. Stein. The Weizmann Science Press of Israel, Jerusalem. 1968. pp. 43–47.
9. G. V. Buxton, H. A. Gillis, and N. V. Klassen. Chem. Phys. Lett. **32**, 533 (1975).
10. G. V. Buxton, H. A. Gillis, and N. V. Klassen. Can. J. Chem. **54**, 367 (1976).
11. H. Hase and K. Kawabata. J. Chem. Phys. **65**, 64 (1976).
12. G. W. Gross, C. Wu, L. Bryant, and C. McKee. J. Chem. Phys. **62**, 3085 (1975).
13. G. G. Teather, N. V. Klassen, and H. A. Gillis. Int. J. Radiat. Phys. Chem. **8**, 477 (1976).
14. N. H. Fletcher. The chemical physics of ice. Cambridge University Press, London. 1970.
15. M. Eldrup. J. Chem. Phys. **64**, 5283 (1976).
16. H. Hase and L. Kevan. J. Chem. Phys. **54**, 908 (1971).
17. P. N. T. Unwin and J. Muguruma. Phys. Status Solidi A, **14**, 207 (1972).
18. (*a*) M. Natori and T. Watanabe. J. Phys. Soc. Jpn. **21**, 1573 (1966); (*b*) M. Natori. J. Phys. Soc. Jpn. **24**, 913 (1968); (*c*) M. Natori. J. Phys. Soc. Jpn. **27**, 1309 (1969).
19. P. S. Julienne and L. P. Gary. Mol. Cryst. **5**, 135 (1968).
20. K. Fueki, D.-F. Feng, and L. Kevan. J. Phys. Chem. **74**, 1976 (1970).
21. S. R. Gough and D. W. Davidson. J. Chem. Phys. **52**, 5442 (1970).
22. T. Sawai and W. H. Hamill. J. Phys. Chem. **73**, 3452 (1969).
23. G. Nilsson. J. Chem. Phys. **56**, 3427 (1972).
24. A. Bernas and T. B. Truong. Chem. Phys. Lett. **39**, 379 (1976).
25. R. E. Weston and H. A. Schwarz. Chemical kinetics. Prentice-Hall, New York. 1972. Chapt. 6; J. H. Baxendale, C. Bell, and P. Wardman. J. Chem. Soc. Faraday Trans. I, **4**, 776 (1973).
26. P. V. Hobbs. Ice physics. Clarendon Press, Oxford. 1974. p. 89.
27. U. Eckener, D. Helmreich, and H. Engelhardt. *In* Physics and chemistry of ice. *Edited by* E. Whalley, S. J. Jones, and L. W. Gold. Royal Society of Canada, Ottawa. 1973. p. 242.
28. A. Von Hippel, A. H. Runck, and W. B. Westphal. *In* Physics and chemistry of ice. *Edited by* E. Whalley, S. J. Jones, and L. W. Gold. Royal Society of Canada, Ottawa. 1973. p. 236.
29. P. M. Rentzepis, R. P. Jones, and J. Jortner. J. Chem. Phys. **59**, 766 (1973).
30. A. Mozumder. J. Chem. Phys. **50**, 3153 (1969).
31. L. Onsager. Phys. Rev. **54**, 554 (1938).
32. R. Schiller. J. Chem. Phys. **47**, 2281 (1967).
33. H. B. Steen and J. A. Holteng. J. Chem. Phys. **63**, 2690 (1975).

Studies of the behavior in magnetic fields of some lyomesophase systems with respect to electrolyte additions

DOUGLAS M. CHEN, FRED Y. FUJIWARA, AND LEONARD W. REEVES[1]

Department of Chemistry, University of Waterloo, Waterloo, Ont., Canada N2L 3G1 and Instituto de Química, Universidade de São Paulo, C.P. 20,780, São Paulo, Brazil

Received November 22, 1976

DOUGLAS M. CHEN, FRED. Y. FUJIWARA, and LEONARD W. REEVES. Can. J. Chem. **55**, 2396 (1977).

A systematic investigation has been made of some lyotropic mesophases (lyomesophases) which macroscopically orient in magnetic fields. These mesophases have been classified into type I which have a positive diamagnetic anisotropy ($\Delta\chi > 0$) and type II with $\Delta\chi < 0$. The mesophase behavior has been observed as a function mainly of electrolyte additions to binary and ternary systems. The electrolyte has a profound effect on the mesophase behavior at extremely low concentrations. It has the effect in the ternary system, sodium decylsulphate/decanol/water, of converting a type I to a type II mesophase with less than 1 wt.% electrolyte. The addition of electrolytes to binary surfactant/water systems had the effect of increasing the mesomorphic region to higher water concentrations. In the case of sodium and cesium decylsulphate, and potassium laurate, these ternary mesophases were of type I and for decylammonium chloride of type II. The method used to distinguish mesophases and determine the degrees of order of water and some hydrocarbon chain segments has been deuterium magnetic resonance.

DOUGLAS M. CHEN, FRED Y. FUJIWARA et LEONARD W. REEVES. Can. J. Chem. **55**, 2396 (1977).

On a fait une étude systématique de quelques mésophases lyotropes (lyomésophases) qui s'orientent d'une façon macroscopique dans les champs magnétiques. On a classifié ces mésophases en type I, celles qui ont une anisotropie diamagnétique positive ($\Delta\chi > 0$), et type II, pour celles où $\Delta\chi < 0$. On a principalement observé le comportement de la mésophase en fonction de l'addition d'électrolytes à des systèmes binaires et tertiaires. L'électrolyte a un effet considérable sur le comportement de la mésophase à des concentrations extrêmement basses. Sur le système tertiaire, décylsulphate de sodium/décanol/eau, l'électrolyte a comme effet de transformer une mésophase de type I en une mésophase de type II avec moins que 1% en poids d'électrolyte. L'effet de l'addition d'électrolytes à des systèmes binaires, agent actif à la surface/eau, est de déplacer la région mésomorphe vers des concentrations d'eau plus élevées. Dans le cas des décylsulphates de sodium et de césium et du laurate de potassium, les phases ternaires sont du type I alors que pour le chlorure de décylammonium elle est du type II. On utilise la résonance magnétique du deutérium comme méthode pour distinguer les mésophases et pour déterminer les degrés d'ordre de l'eau et de quelques segments de chaînes hydrocarbonés.

[Traduit par le journal]

Introduction

The complex superstructures of lyotropic mixtures of amphiphilic compounds, in water, formed in the regime of concentrated micellar systems, lead to liquid crystalline properties of the resulting fluids (1). These lyomesophases are important both with reference to basic structures of biological membranes and with respect to the aspects of colloid and interface science (2, 3). Phase diagrams have been an active area of study because they are so important in defining the number of liquid crystalline phases which occur in any given system (4–8). In the most thorough studies these mesophases are characterized by their low angle X-ray diffraction pattern. Lyomesophases which can be oriented either spontaneously or by other means offer exceptional advantages for study by any technique where the anisotropy of physical properties is accessible to measurement (9). The fact that a lyomesophase can be oriented in an applied magnetic field was first reported in 1967 (10). This very useful property opens up a research topic in which the chemical flexibility of such lyomesophases comes into question. Should such a variation of the chemistry of these spontaneously orienting lyomesophases be large, then many of

[1]Visiting Professor Universidade de São Paulo 1967–present.

the problems of colloid and interface science can be subjected to the full armament of the nuclear magnetic resonance (nmr) tool (11). In addition, these lyomesophases contain model aspects of the bilayer matrix of biological membranes (2–4).

In previous studies (12–15) the chemical variations which are possible have been investigated in some ternary and quaternary systems. The persistence of lyomesophases which can be oriented when counter ions are exchanged, partly or completely, for a complex ion has led to a new technique for investigating the structure of ions in fluid media (14–16). The behavior of alkali metal decylsulphates in mixtures with decanol and water (13) and the investigation of mixed alkali metal decylsulphates in similar mesophases leads to some important overall generalizations for these systems.

Two types of lyomesophases occur (12). One class, denoted type I, orients with the uniaxial direction (the director) parallel to the magnetic field. Therefore, the diamagnetic susceptibility along the director, $\chi_{\parallel}$, must be algebraically larger than that in the perpendicular direction, $\chi_{\perp}$, and the type I lyomesophases have a positive diamagnetic anisotropy, $\Delta\chi = \chi_{\parallel} - \chi_{\perp}$. In the second class of mesophases, denoted type II, the value of $\Delta\chi$ must be negative since the mesophase aligns with the director perpendicular to the magnetic field direction (12, 13). There is no implication that these lyomesophases can be assigned a single superstructure arrangement in order to achieve either type I or type II behavior. There appear to be several types of lyomesophases leading to the same behavior in magnetic fields.

In pure alkali metal decylsulphate/decanol/water systems the lithium salt has only a very narrow range of type I behavior, the sodium detergent leads to type I phases, while the cesium salt has broad ranges of type II mesophases (13). In lyomesophases of mixed alkali metal detergents, the change from type I to type II can be induced merely by changing lithium or sodium content in the counter ions. The addition of electrolytes to these lyomesophases has not been systematically studied with respect to the behavior of resulting uniaxial fluids in magnetic fields. The present study is an attempt to investigate the effect of added electrolytes in several mesophase systems. Such studies are important as the basis for using lyomesophases for all manner of physical measurements where bulk or molecular anisotropic properties are under scrutiny.

Experimental

Decylammonium chloride was prepared by neutralizing decylamine with hydrochloric acid. The crude product was recrystallized several times from ethanol – petroleum ether. The refined product was dried for several days under vacuum conditions and stored in an evacuated desiccator. Sodium decylsulphate was prepared by sulphation of *n*-decanol with either sulphuric acid in the manner previously reported by Radley *et al.* (12), or with chlorosulphuric acid (17). Recrystallization was repeated several times from 90% ethanol in water mixtures. Cesium decylsulphate was synthesized as previously reported (12) with recrystallization from ethanol – ethyl acetate mixtures. The sodium 3,3,4,4-tetradeuterodecylsulphate was prepared as described previously (18). The 1,1-dideuterodecylammonium chloride was prepared by reducing nonylnitrile with $LiAlD_4$. Purity was checked from the proton magnetic resonance spectra (Varian HA100) using the highest gains available to reveal impurities in aqueous isotropic solutions. Potassium laurate (Baker Chem. Co.) was recrystallized from ethanol. Electrolytes were analytical reagent grade and D_2O was > 99% deuterium from Merck Sharp and Dohme.

Various nmr spectrometers were used to study the various nuclei observed. These were Varian VF16, HA100, HR60, and XL-100 units.

Results

Sodium Decylsulphate/Decanol/Water System

A lyomesophase was prepared with the following composition: 1.53 g H_2O (0.1% D_2O added to give a deuterium nmr signal), 0.21 g decanol, and 1.05 g sodium decylsulphate (SDS). The sodium decylsulphate contained 19.00% of SDS-*3,3,4,4-d*$_4$ so as to provide a strong enough deuterium signal from the hydrophobic component. This lyomesophase falls into the region of type I properties (13). Spectra were taken at 23.7 $\pm$ 0.3°C on a Varian XL100 spectrometer for this series of experiments. The anhydrous sodium sulphate additions were performed with 0.098 to 7.03 wt.% of the total phase. The ^{23}Na and deuterium nmr signals were followed to show that partially averaged nuclear quadrupole splittings behave in a parallel manner. The deuterium doublets for the chain deuterium nuclei on carbon 3 and 4 were often not resolved in samples near the phase transition; the small amount of deuterium in the water appears as a separate doublet. A more complete study of the degree of order profile of the hydrocarbon chain by ^2H nmr has been previously reported (18).

In Fig. 1 the partially averaged quadrupole splittings (in the case of the chain an average for position 3 and 4) are plotted against the weight percent of sodium sulphate in the phases. The separation of two mesophases occurs after addition of 5.1% sodium sulphate.

The initial phase, before additions of sodium sulphate, is of type I and orients, somewhat slowly, in about an hour or so, with the mesophase director parallel to the magnetic field direction. On passing from initial powder pattern to fully oriented mesophase the separation of the quadrupole doublet increased by a factor of two, and when the oriented sample was turned in the magnetic field and a spectrum was obtained before the sample reoriented, the quadrupole splitting followed a $(3\cos^2\Omega - 1)$ dependence with the rotation angle. As shown in Fig. 1, an addition of only 0.272 wt.% sodium sulphate leads to a precipitous change in the deuterium quadrupole splittings which indicates a phase change induced by the addition of electrolyte. After this quantity of sodium sulphate has been added the new lyomesophase formed exhibits type II behavior. The change in the deuterium quadrupole splitting exactly at the critical concentration of the electrolyte for the phase transition is 1.64 for both water and chain deuterium signals. The values are: HOD 372 Hz type I to 227 Hz type II, and chain CD_2 groups 8.30 kHz type I to 5.06 kHz type II. The phase change is accompanied also by a characteristic change in the sign of the slope $(d(\Delta\nu)/dx)$; $\Delta\nu$ = quadrupole splitting and x = concentration of some component, in this case the electrolyte (12). With the assumption of an axially symmetric electric field gradient tensor for the C—D bond axis, the appropriate equation for the degree of order of this axis becomes:

$$[1] \qquad \Delta\nu_D = \tfrac{3}{4}QS_{CD}(3\cos^2\Omega - 1)$$

where $\Delta\nu_D$ is the deuterium quadrupole splitting, Q is the quadrupole coupling constant for deuterium in a C—D bond, Ω is the angle between the phase director and the magnetic field, and S_{CD} is the degree of order of the C—D bond axis.

Using the figure for the ratio at the phase transition, $\Delta\nu_D$(type I)/$\Delta\nu_D$(type II) = 1.64, in [1] gives 0.82 as the ratio S_{CD}(type I)/S_{CD}(type II). The degree of order of the C—D axes in the detergent are thus smaller with respect to the director in the type I phase by a small amount under equilibrium conditions between the two phases. A similar statement applies to all components of the lyomesophase.

The effect of electrolyte addition is more pronounced in producing phase transitions than the changes in the counter ion content investigated previously (12). An approximately 5 mol% substitution of cesium for sodium ion is necessary before the phase change type I to type II is induced.

The effect of adding lithium sulphate in the form $Li_2SO_4 \cdot H_2O$ to a lyomesophase of composition 0.35 g sodium decylsulphate, 0.07 g decanol, and 0.56 g D_2O was also studied. Very similar results were obtained to the sodium sulphate additions reported above. The transition type I to type II lyomesophase occurs at 0.65 wt.% added hydrated lithium sulphate. This concentration is considerably higher than in the case of sodium sulphate, but it is not surprising that the transition should depend on the nature of the added electrolyte. The phase change was followed using ^{23}Na, ^{7}Li, and ^{2}H resonance signals.

The effect of increasing the decanol content in the ternary type I mesophase was also investigated. A series of samples were prepared containing sodium decylsulphate and heavy

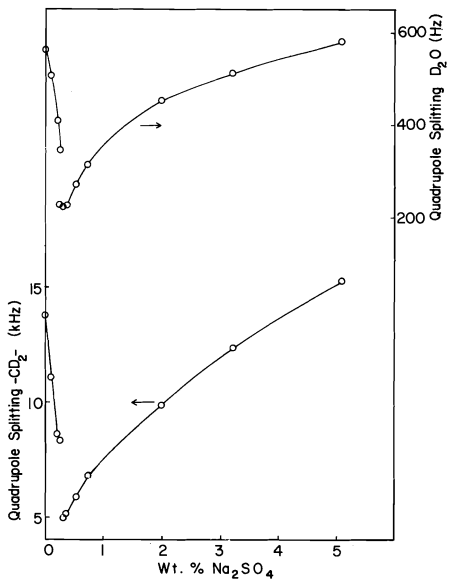

FIG. 1. Partially averaged deuterium quadrupole splittings in HOD and deuterated sodium decylsulphate-*3,3,4,4-d*$_4$ used as components of a lyomesophase described in the text. These splittings are plotted against added weight percent sodium sulphate.

water in the ratio 1:1.600 by weight and the decanol content was varied from 6.35 to 7.7 wt.% of the total sample. In Fig. 2 the sodium quadrupole splitting (measured as the total separation of the triplet) is plotted against the decanol concentration. The quadrupole splitting decreases slightly as the decanol content is increased up to 7.24 wt.% where a phase change occurs resulting in the formation of a second mesophase. This mesophase which is in equilibrium with the type I mesophase over a fairly extensive region does not orient in the magnetic field and results in a powder pattern spectrum. The second mesophase is less dense and samples in this region separate into two layers on standing. By comparison with the phase diagram of the corresponding sodium octylsulphate and sodium dodecylsulphate ternary systems (6), as well as those of similar ionic surfactants (6, 7) it is likely that the mesophase formed at high decanol content is a lamellar phase.

Decylammonium Chloride/Water Binary System

Simple binary mixtures of detergent and water do form birefringent uniaxial mesophases (4, 7), but these are not generally oriented in magnetic fields and the deuterium magnetic resonance spectra take on the powder diagram form (11). Decylammonium chloride/D_2O mixtures were studied between 29.9 wt.% D_2O to 53 wt.% D_2O. (The D_2O used contained 0.1 *N* HCl in order to decrease the rate of exchange of the labile deuteriums.) The temperature of the experiments was 27.8 $\pm$ 0.2°C and deuterium nmr powder signals were followed as a function of water content.

In Fig. 3 the water deuterium doublet splitting

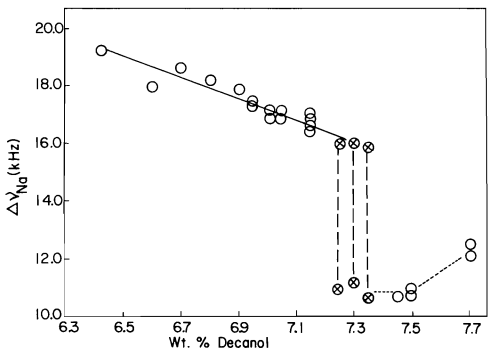

FIG. 2. Variation of the ^{23}Na quadrupole splitting with *n*-decanol content in a ternary SDS mesophase. The points ⊗ represent two splittings observed from the same sample.

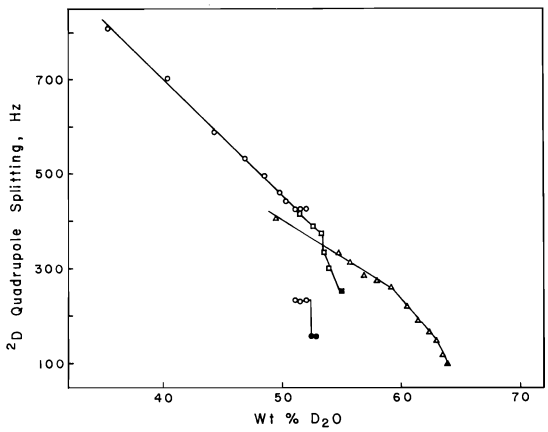

FIG. 3. The mesophase behavior of the binary system, decylammonium chloride/D_2O, with and without added ammonium chloride. The quadrupole splittings of the D_2O are plotted against the weight percent water: ○ the binary phase; □ the ternary system containing an ammonium chloride/decylammonium chloride ratio of 1:46.2; and △ the ternary system containing an ammonium chloride/decylammonium chloride ratio of 1:9.25. The filled points represent partly isotropic two phase samples.

is plotted against weight percent D_2O. Between 29.9 wt.% and 51.1% D_2O there is a linear decrease in D_2O quadrupole splittings with water content from 999 $\pm$ 10 Hz to 426 $\pm$ 1 Hz. The lyomesophases in this concentration range are known to be of lamellar form (4, 7). At 51.1 wt.% D_2O a separation of two birefringent phases occurs. Signals from both phases are doublets, but the new phase which appears in equilibrium with the original lamellar phase does orient in the magnet in a few seconds and appears as a sharp doublet. This second phase orients with the director perpendicular to the magnetic field direction. Fig. 4*A* is a spectrum of this two phase mixture in equilibrium. The co-existence concentration range is 51.1 to 52.3 wt.% D_2O. This appears to be a true equilibrium mixture of two mesophases because on warming to an isotropic medium and allowing the system to cool to 27.8°C again in the magnet, the two signals reappear in the same intensity ratio. When the samples near or in the two phase regions are allowed to cool from an isotropic solution in the magnetic field changes in the appearance of the signals assigned to the original lamellar phase occur. The powder pattern spectra from the lamellar phase become sharper doublets indicating that an orientation process has occurred. An almost completely oriented sample is shown in Fig. 4*B*. The doublet splitting

of the lamellar phase does not change on orientation which indicates that the mesophase directors orient perpendicular to the magnetic field. In the two phase region the ratio of the deuterium quadrupole splitting of the D_2O was 1.83 ± 0.01. Such a result clearly indicates that at least two different mesophases can lead to the same behaviour in a magnetic field.

At 52.3 wt.% D_2O and above a second two phase system occurs, but in this event only the upper one is birefringent. The upper phase is probably identical with the second type II phase indicated above. This upper phase orients in a few minutes and is type II while the lower phase is isotropic with a singlet deuterium spectrum. Above 53.0 wt.% only one isotropic solution remains.

The behavior in the absence of electrolyte is in complete contrast with the ternary system containing added salts. A mixture of ammonium chloride and decylammonium-*1,1-*d_2 chloride in the ratio by weight of 1:9.25 was weighed and to this mixture various percentages by weight of D_2O (containing 0.1 *N* HCl) were added so that composition variations were obtained between 48 and 64 wt.% water. The measurements of deuterium quadrupole splitting in the D_2O component are plotted in Fig. 3 against weight percent D_2O in the ternary mixture. The weight percent of electrolyte in the ternary system decreases somewhat between 48 and 64 wt.% D_2O, but the variation is not a strong one and for convenience of comparison it is included on a binary phase basis. At the lowest water contents the deuterium spectrum remains a powder pattern with no tendency to orientation in the magnetic field. Near 59 wt.% water there is a tendency for the mesophase to orient and at the highest water contents encountered the orientation process is rather rapid. At 59 wt.% there is a distinct break in the linear dependence of the quadrupole splitting of the type II phase on water content. Such a break indicates some structural change, perhaps a second-order type transition. We have obtained a similar subtle modification in a previous study of the same lyomesophase system with temperature (19). An isotropic phase in equilibrium with the type II lyomesophase occurs at 63.87 wt.% D_2O in the ternary mixture. The change in slope of the linear dependence of D_2O deuterium quadrupole splitting on water content was further probed by observing the $—ND_3^+$ and a α-d_2 deuterated chain segment. The $—ND_3^+$ and α-CD_2 deuterium doublets were obtained as a function of water content and this is plotted in Fig. 5. The corresponding subtle break in the linear dependence on water content is found at *ca.* 59% wt.% D_2O. The structural changes in the lyomesophase are transmitted to the degrees of order of both the hydrophilic and hydrophobic compartments. It is possible that interface water undergoes local rearrangements without producing a precipitous alteration of the mesophase superstructure. Low angle X-ray studies are suggested as a means of elucidating these modifications. At 63.87 wt.% water a second isotropic and more dense phase separates in equilibrium with the type II mesophase. At higher water contents the orientation is rapid. The ratio of α-CD_2 deuterium splitting to the $—ND_3^+$ value is constant at 2.33 ± 0.02 over the whole region investigated. The quadrupole couplings of the $—ND_3^+$ head group are linearly dependent on those of the D_2O component, but there is an intercept of 0.7 kHz, showing a discontinuity in extrapolated order between the hydrocarbon and aqueous regions. The experimental relationship found is:

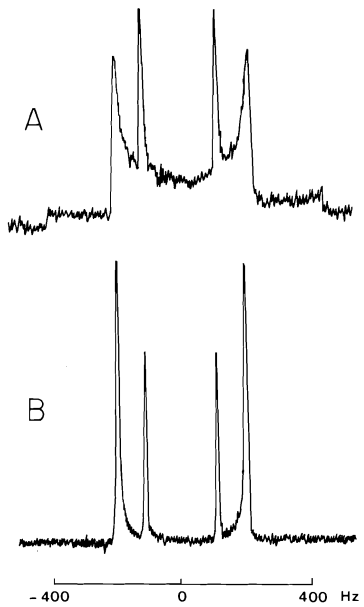

FIG. 4. ^2H spectrum of decylammonium chloride – D_2O samples in the two phase region. A: sample with 51.1% D_2O after leaving overnight in the magnetic field. B: sample with 51.4% D_2O after the sample was heated to an isotropic phase allowed to cool in the magnetic field. The mesophase with the largest splitting becomes almost completely oriented by this cycle.

[2] $$\Delta\nu_{D_2O} = 0.040\Delta\nu_{ND_3^+} - 29$$

where $\Delta\nu_{D_2O}$ and $\Delta\nu_{ND_3^+}$ are the quadrupole splittings in Hz of D_2O and $-ND_3^+$ groups, respectively. This effect has been reported earlier for both D_2O and Cl^- ion in the aqueous compartment (19).

To further investigate the effect of adding an electrolyte to the binary system, another series of samples containing a smaller amount of electrolyte was studied. These samples contained an ammonium chloride to decylammonium chloride ratio of 1:46.2 by weight (the electrolyte made up *ca.* 1% of the sample). The quadrupole splittings of the D_2O in these samples are also shown in Fig. 3.

There is a distinct change in the concentration dependence of the quadrupole splitting at 53.4% D_2O. Samples with D_2O concentrations higher than this amount rapidly orient macroscopically in the magnetic field with the director perpendicular to the field direction. Samples with slightly less than 53.4% D_2O tend to orient perpendicular to the field when they are allowed to cool from an isotropic solution in the magnetic field; the sample with the lowest amount of water (51.5%) showed no appreciable orientation.

Other Ternary Surfactant/Water/Electrolyte Systems

Some further investigations of new ternary systems which will spontaneously orient in magnetic fields have been implemented and the results, though not as comprehensive as those reported above, are worth recording as a guide to others who plan uses for lyomesophases. The ternary systems containing an electrolyte and the sodium or cesium decylsulphate or potassium laurate are in contrast with the corresponding ternary systems based on the decylamine salts described here and elsewhere (15, 19). Unlike the mesophases formed from the decylamine salts, these mesophases orient with the director parallel with the field; *i.e.*, type I behavior. These type I mesophases were found to orient homogeneously after several hours in the magnet.

Sodium decylsulphate/electrolyte/water was prepared in two mesophases of composition: (*a*) 55.7 wt.% D_2O, 39.8% sodium decylsulphate, and 4.5% anhydrous sodium sulphate; (*b*) 53.3% H_2O, 41.9% sodium decylsulphate, and 4.8% Na_2SO_4. Both mixtures formed single birefringent type I lyomesophases. The deuterium splitting in (*a*) at 35°C was 696 Hz and the

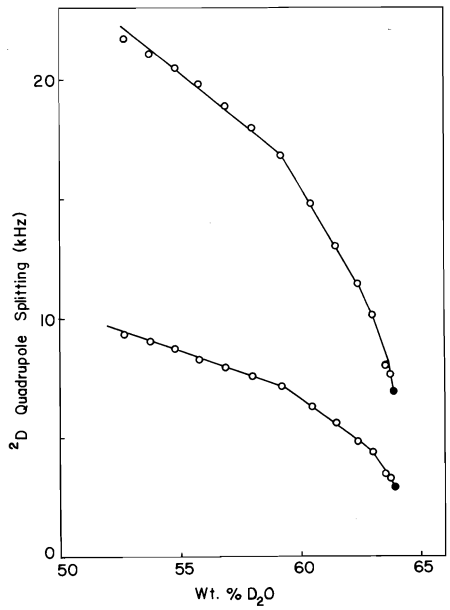

FIG. 5. Deuterium quadrupole splittings of the terminal $-ND_3^+$ group (lower curve) and α-CD_2 group for ternary mixtures ammonium chloride, decylammonium chloride, and D_2O as described in the text.

separation of adjacent peaks of the 3:4:3 triplet of ^{23}Na in mesophase (*b*) was 7.688 ± 0.005 kHz. The angularly dependent peaks were halved in separation on rotation 90° about an axis perpendicular to the magnetic field after sufficient time elapsed to homogeneously orient the sample.

Cesium decylsulphate/water/electrolyte systems were prepared as homogeneous lyomesophases of type I in the following proportions: (*c*) 44.3% D_2O, 52.2% cesium decylsulphate (CsDS), 3.5% Na_2SO_4; (*d*) 49.3% D_2O, 48.8% CsDS, 2.0% Na_2SO_4; (*e*) 49.7% H_2O (containing 0.5% D_2O), 46.6% CsDS, 3.7% $CsNO_3$. The mesophases gave D_2O deuterium splittings of 632 Hz, 545 Hz, and 458 Hz, respectively, at 35°C.

A ternary system potassium laurate (KL)/D_2O/potassium chloride with 65.1, 32.7, and 2.2 wt.%, respectively, with a deuterium (D_2O) doublet of 558 Hz at 35°C proved to be a type I lyomesophase.

Some comments can be added on these three new lyomesophase systems. Both the sodium decylsulphate and potassium laurate mesophases above form two phase mixtures in the absence of added electrolyte, an extremely viscous birefringent mesophase and an isotropic phase. The corresponding binary CsDS/water systems

form a single mesophase which is also extremely viscous. The ternary CsDS mesophases have the unusual physical property that they become extremely viscous on cooling and change into an isotropic phase.

Discussion

Compared to the large number of lyomesophases known, the number which will spontaneously orient in a magnetic field is relatively small. The mesophases which will macroscopically orient are characterized by a lower bulk viscosity. Presumably the forces exerted on these uniaxial liquids by the magnetic field due to their diamagnetic anisotropies are sufficient to overcome the internal viscous forces.

The binary surfactant/water systems containing sodium or cesium decylsulphate, or potassium laurate undergo a phase transition from an isotropic solution to an extremely viscous mesophase as the surfactant concentration is increased. In the case of the potassium laurate and the similar sodium octylsulphate and dodecylsulphate binary systems, these mesophases have been identified as a 'middle' or 'hexagonal' phase composed of cylindrical micelles packed in a hexagonal array (7, 20). These middle phases can incorporate up to *ca.* 10% decanol; at higher decanol concentrations lamellar phases are formed (7).

The addition of an electrolyte, decanol, or both to the binary CsDS, SDS, and KL systems has two marked effects. The liquid crystalline phase is extended to lower surfactant concentrations and there is a drastic reduction in the viscosity. In light of the difference in the behavior of the resulting mesophases, some of these changes must also be accompanied by a phase change. On the addition of only an electrolyte, all three systems form type I mesophases; on the addition of only decanol the SDS forms a type I phase, the CsDS forms a type II mesophase (12), and the KL system remains a viscous middle phase; and on the addition of both electrolyte and decanol all three systems form type II mesophases (21) which also have the most extensive mesomorphic region. However, a quaternary system containing anilinium decylsulphate has been found to be a type I phase (22).

Addition of less than 1 wt.% of electrolyte to the ternary lyomesophase system, sodium decylsulphate/decanol/water provokes a phase change from a uniaxial fluid (with $\Delta\chi > 0$) which orients with the director parallel to a magnetic field direction, to a mesophase (with $\Delta\chi < 0$) which orients with the phase director in all directions perpendicular to the field. It has been suggested that these ternary and quaternary phases are lamellar and hexagonal phases, respectively (23). However, the ratio of the degree of order parameter for the paraffinic chain and for D_2O of type I/type II $= 0.82$ observed at the phase transition is not consistent with such a phase change. A ratio of two would be expected as a result of the additional averaging motion in the hexagonal phase as a result of rapid diffusion around the cylindrical micelles. A factor of approximately two has been observed in the comparison of lamellar and hexagonal mesophases (19, 24). Also, the mesophase resulting from the phase change caused by increasing the decanol concentration of this type I mesophase can be assumed to be a lamellar phase by comparison with other similar surfactant systems (7).

The type II mesophases have been assumed to be of hexagonal type with a sufficiently low viscosity to allow the mesophase to orient in a magnetic field (12, 15, 16, 19). This assumption was mainly based on the fact that the hexagonal phase was the only mesophase which was usually found in the corresponding region of the phase diagrams of a large number of similar surfactants. The discovery of another class of type I mesophases, the surfactant/water/electrolyte system, in addition to the other ternary type I mesophases containing decanol which all have a similar surfactant/water concentration as the type II mesophase, makes comparisons with similar well characterized systems of little use. It is apparent that other data, in particular from low-angle X-ray diffraction studies, are necessary to elucidate the structure of these various mesophases.

The binary system decylammonium chloride/water has a large range of mesophase compositions but these liquid crystals do not spontaneously orient in a high magnetic field. The lamellar mesophase can be heated at the higher water contents to an isotropic fluid, which on cooling in the magnet slowly reforms a lamellar phase in a much more oriented state. This mesophase has a negative diamagnetic anisotropy and exhibits type II behavior with alignment of the director perpendicular to the field

direction. This alignment with the hydrocarbon chains perpendicular to the magnetic field is consistent with the diamagnetic anisotropy of paraffinic chains which is known to be negative (25). An extremely narrow co-existence range with a second type II mesophase occurs and at higher water contents this mesophase co-exists in equilibrium with an isotropic micellar solution. The behavior of this binary system is very similar to the octylammonium chloride systems in which the more extensive mesophase was assigned as lamellar and the other as hexagonal (7). A similar assignment of the mesophases formed with decylammonium chloride is consistent with the ratio of the quadrupole splittings observed; the ratio of 1.83 is close to the value of 2 expected for a lamellar to hexagonal transition. It should be noted that if this second phase is hexagonal, then it orients with the cylinder axis perpendicular to the field. Therefore, the diamagnetic anisotropy of the hydrocarbon chains cannot be the dominant contribution to the anisotropy of the mesophase.

Electrolyte additions provoke profound changes in the mesophase behavior. The presence of an electrolyte extends the mesophase region to much higher water concentrations, but in contrast to the other ternary systems discussed above, the resulting mesophases are of type II. On the addition of *ca.* 1% electrolyte, the mesophase with the lower degree of order has a larger composition range and there appears to be a subtle phase modification which reduces the difference between the two mesophases. At the higher electrolyte concentration (*ca.* 4%) the mesophase which will orient has a much more extensive region and the phase transition almost disappears. It is apparent that the addition of an electrolyte modifies the behavior of both lamellar and hexagonal phases.

Acknowledgments

The support of the Banco Nacional de Desenvolvemento Economico (BNDE) and Fundação de Amparo à Pesquisa do Estado de São Paulo (FAPESP) in a substantial equipment grant is gratefully acknowledged. Travel and local expenses (L.W.R.) were provided by the National Research Council of Canada (NRCC) and Consello Nacional de Perquisas (CNPq). F.Y.F. is indebted to BNDE and NRCC for financial support and D.M.C. to NRCC.

1. A. E. Skoulios and V. Luzzatti. Acta Crystallogr. **74**, 278 (1961).
2. M. S. Bretscher. Science, **181**, 622 (1943).
3. C. Tanford. The hydrophobic effect: formation of micelles and biological membranes. John Wiley and Sons, New York, NY. 1973.
4. P. A. Winsor. Chem. Rev. **68**, 1 (1968).
5. A. S. C. Lawrence. Discuss Faraday Soc. **25**, 51 (1958).
6. P. Ekwall, L. Mardell, and K. Fontell. Mol. Cryst. Liq. Cryst. **8**, 157 (1969).
7. P. Ekwall. *In* Advances in liquid crystals. *Edited by* G. H. Brown. Academic Press, New York, NY. 1975.
8. H. Cortopassi, Jr., V. R. Paoli, L. W. Reeves, R. R. Romano, and J. A. Vanin. Anais Acad. Bras. Cienc. **46**, 203 (1974).
9. A. Saupe. Angew. Chem. Int. Ed. Engl. **7**, 97 (1968).
10. K. D. Lawson and T. J. Flautt. J. Am. Chem. Soc. **89**, 5489 (1967).
11. A. Abragam. The principles of nuclear magnetism. Oxford University Press, London, U.K. 1961.
12. K. Radley, L. W. Reeves, and A. S. Tracey. J. Phys. Chem. **80**, 174 (1976).
13. K. Radley and L. W. Reeves. Can. J. Chem. **53**, 2998 (1975).
14. L. W. Reeves, J. Sanches de Cara, M. Suzuki, and A. S. Tracey. Mol. Phys. **25**, 1481 (1973).
15. L. W. Reeves, A. S. Tracey, and M. M. Tracey. J. Am. Chem. Soc. **95**, 3799 (1973).
16. A. S. Tracey and L. W. Reeves. J. Am. Chem. Soc. **96**, 1198 (1974).
17. E. E. Gilbert. Sulfonation and related reactions. Interscience, New York, NY. 1965.
18. L. W. Reeves and A. S. Tracey. J. Am. Chem. Soc. **97**, 5729 (1975).
19. F. Y. Fujiwara and L. W. Reeves. J. Am. Chem. Soc. **98**, 6790 (1976).
20. V. Luzzatti, H. Mustacchi, A. Skoulios, and F. Husson. Acta Crystallogr. **13**, 660 (1960); **13**, 668 (1960).
21. R. C. Long, Jr. J. Magn. Reson. **12**, 216 (1973).
22. P. Diehl and A. S. Tracey. Can. J. Chem. **53**, 2755 (1975).
23. A. S. Tracey and P. Diehl. Can. J. Chem. **54**, 2283 (1976).
24. M. J. Charvolin and P. Keller. Chem. Phys. Lipids, **15**, 161 (1975).
25. E. M. Weir and P. W. Selwood. J. Am. Chem. Soc. **73**, 3484 (1951).

Degrees of order of solubilized alkanes, alcohols, carboxylates, and carboxylic acids in oriented lyomesophases

DOUGLAS M. CHEN, FRED Y. FUJIWARA, AND LEONARD W. REEVES[1]

Department of Chemistry, University of Waterloo, Waterloo, Ont., Canada N2L 3G1 and Instituto de Química, Universidade de São Paulo, C.P. 20,780, São Paulo, Brazil

Received November 22, 1976

DOUGLAS M. CHEN, FRED Y. FUJIWARA, and LEONARD W. REEVES. Can. J. Chem. **55**, 2404 (1977).

The degree of order of solubilized molecules and ions in oriented lyomesophases has been determined at specifically deuterated C—D bond axes from the quadrupole splitting of the deuterium magnetic resonance. Mixtures at low concentration of specifically deuterated alkanes, alcohols, carboxylic acids, and carboxylates of different chain length have been observed in host cationic and anionic lyomesophases. The degree of order of a given C—D position in alcohols increases strongly with chain length up to a length comparable with the host detergent. A broad series of carboxylic acids and carboxylate ions from C_2 to C_{16} have been deuterated in the α position. The α-C—D bond axis in the solubilisate increases in order with chain length, the anion having lower order than the parent acid. An accurately *linear* increase in the degree of order of the α position is observed for intermediate chain lengths. At chain lengths approximately equal to the host chain lengths the α position reaches a limiting value in the degree of order and further segments do not influence the order. At short chain lengths the degree of order is *less* than that predicted from extrapolation of order in the linear region. This has been interpreted in terms of distribution into the aqueous compartment by the solubilisates of short chain length. Acetic acid and the acetate, propionate, butanoate, and pentanoate ions spend an appreciable amount of time in the aqueous region. An estimate has been made of these distributions based on reasonable assumptions.

DOUGLAS M. CHEN, FRED Y. FUJIWARA et LEONARD W. REEVES. Can. J. Chem. **55**, 2404 (1977).

On a déterminé le degré d'ordre des molécules et des ions solubilisés dans des lyomésophases orientées; ces études ont été effectuées par rapport à des axes de liaisons C—D deutérés d'une façon spécifique à partir des couplages quadrupolaires de la résonance magnétique du deutérium. On a observé, dans des lyomésophases cationique et anionique agissant comme hôtes, des mélanges contenant de faibles concentrations d'alkanes, d'alcools, d'acides carboxyliques et de carboxylates de longueurs de chaîne différentes et deutérés d'une façon spécifique. Le degré d'ordre pour une position C—D donnée dans les alcools augmente d'une façon très prononcée avec la longueur de la chaîne jusqu'à une longueur comparable à celle du détergent agissant comme hôte. On a deutéré en position α une grande série d'acides carboxyliques et d'ions carboxylates allant de C_2 à C_{16}. L'ordre de l'axe de liaison α-C—D des molécules solubilisées augmente avec la longueur de la chaîne; l'anion a un ordre plus bas que celui de l'acide qui lui a donné naissance. On observe une augmentation linéaire précise dans le degré d'ordre dans la position α pour des longueurs intermédiaires de la chaîne. A des longueurs de chaîne approximativement égales à celles des longueurs de chaîne de la molécule hôte, la position α atteint une valeur limite dans le degré d'ordre et des segments supplémentaires n'influencent pas l'ordre. Aux courtes longueurs de chaîne, le degré d'ordre est plus faible que celui prédit à partir de l'extrapolation de l'ordre dans la région linéaire. On a interprété ces résultats en termes de distribution dans la phase aqueuse par les molécules qui solubilisent et qui ont de courtes longueurs de chaîne. L'acide acétique et les ions acétate, propionate, butanoate et pentanoate passent une quantité appréciable de temps dans la région aqueuse. On a fait une évaluation de ces distributions qui est basée sur des hypothèses raisonables.

[Traduit par le journal]

Introduction

In aqueous micellar solutions of soaps and detergents (1, 2), the solubility of all manner of substances is greatly increased. This process of 'solubilization' is known to arise because of micelle formation (2) and the internal division of the stable colloidal dispersion into hydrophobic micelle interiors which are able to occlude organic substances in a similar manner to an organic solvent.

We have been engaged in a series of studies

[1]Visiting Professor, Universidade de São Paulo, 1967–present.

of concentrated micellar solutions which take on the form of uniaxial fluids (3). Many of these uniaxial media have the property of spontaneously orienting with the mesophase directors, either all parallel to a magnetic field direction or in all directions perpendicular to a large magnetic field (3). By using nuclear magnetic resonance methods the degree of order of axes in individual components of the mesophases can be determined with respect to the magnetic field direction (4). In general we may write

$$[1] \qquad S_a = \tfrac{1}{2}\langle 3\cos^2\theta_a - 1\rangle$$

where S_a = degree of order of an axis, θ_a = the angle between that axis and the mesophase symmetry axis (the director), and also

$$[2] \qquad \Delta\nu = \tfrac{3}{2}QS_a\tfrac{1}{2}(3\cos^2\Omega - 1)$$

where $\Delta\nu$ is the quadrupole splitting of the deuterium magnetic resonance doublet, S_a is the degree or order of the C—D, O—D, or N—D bond axis (assuming an axially symmetric nuclear quadrupole coupling tensor), Ω is the angle between the mesophase director and the magnetic field, and Q is the nuclear quadrupole coupling constant of the deuterium nucleus. In the case of parallel alignment of the phase director and the magnetic field the factor $(3\cos^2\Omega - 1)/2$ is $+1$ while with perpendicular direction of the symmetry axis of the mesophase this function has a value $-\frac{1}{2}$.

Being a fluid phase in which freedom of motion of molecules, ions, segments, and head groups is impeded only by uniaxial constraints, then S_a may be interpreted as a local measure of structure and order. Local symmetry must be sensibly used in these situations since the possibility of orientation of an axis about the magic angle $(3\cos^2\theta_a - 1)/2 = 0$ occurs. There is a great deal of heterogeneity of local order, the water O—D bond being almost isotropic in average motion, while the head group ionic region is the most highly ordered segment (4, 5). The degree of order in different parts of the lyomesophase tends to be imposed on any guest molecule or ion dissolved in the system and thus the location of a guest species can be investigated.

It is important to realize that the nuclear magnetic resonance (nmr) signals are averaged over all events which occur with smaller than $\sim 10^{-3}$ s correlation time. In the case of counter ions, added electrolytes, and water there is a rapid exchange between the actual interface and more distant localities in the water compartment and only an average degree of order for all sites is recorded (4).

The act of 'solubilization' implies inclusion in the hydrophobic region of the guest species. The extent to which this is true and what degree of local order is imposed upon a guest molecule or ion, is the object of this study of components solubilized in lyomesophases. The method used has been deuterium magnetic resonance of the guest and some host molecules and ions.

Experimental

Preparation of Deuterated Materials

Alcohols (*n*-propanol through *n*-decanol) deuterated at specific positions were prepared by deuteration of the corresponding alkynols over platinum oxide (Adam's catalyst), (6, 7) by a low pressure deuterogenation reaction. If a terminal acetylenic group was deuterogenated, this was preceded by exchange of the acidic acetylenic proton for deuterium. A typical exchange to form 5-deutero-4-pentyn-1-ol was achieved as follows: 0.4 g of sodium metal was slowly dissolved in 10 ml D_2O, followed by 10 g of 4-pentyn-1-ol. The mixture was stirred for 6 h and the organic layer separated, dried, and distilled (7). About 80% replacement of hydrogen was achieved in one exchange and this was deemed sufficient. In deuterogenation reactions about 90% deuteration was obtained but often a significant and detectable amount of deuterium wandered to the adjacent positions giving a bonus of easily assigned deuterium resonances. Similar procedures were used to deuterogenate alkynes.

A series of α-d_2-carboxylic acids were synthesized by heating the sodium or potassium salts with D_2O containing NaOD in a stainless steel bomb at 150°C (9). The deuterated carboxylic acids were fractionally distilled except those longer than lauric acid.

Spectrometers Used

The measurements in all cases were made at 15.36 MHz for deuterium signals with samples contained in 5 or 10 mm tubes on a Varian XL-100 spectrometer. For alkanes and alcohol solubilization the probe temperature was 26.6 to 26.8°C except where noted. The experiments on solubilization of carboxylic acids and carboxylates were carried out at 34°C. Proton noise decoupling was activated during the observation of deuterium nmr in some cases.

The deuterium nmr signals required accumulation of 6000 to 30 000 transients and in some cases high field and low field spectra were recorded separately because quadrupole couplings exceeded the 12.5 kHz spectral width limit imposed by the spectrometer. No difficulty was encountered in piecing together the two halves of the spectrum by use of the overlap region.

Methods Used to Compare Degrees of Order

In order to compare the degree of order of the components solubilized in a lyomesophase, it was found convenient to allocate in small amount each component to be studied to a single lyomesophase so as to compare them in the same phase at the same temperature. This finality was achieved in stages while taking care that the solubilized components did not appreciably change the

TABLE 1. Deuterium quadrupole splittings of specifically deuterated normal alkanes and alcohols in decylammonium chloride mesophases*

Sample	Solubilisates	Quadrupole splitting (kHz)	$\Delta\nu(CD_n)/\Delta\nu(HOD)$
1	Heptane-*3,3,4,4-d*$_4$	1.49	6.95
	Heptanol-*3,3,4,4-d*$_4$	9.3	43.0
2	Octane-*1,1,1,2,2-d*$_5$	0.310;†1.20	1.44;†5.58
	Octanol-*3,3,4,4-d*$_4$	11.0	50.2
3	Octane-*3,3,4,4-d*$_4$	1.17	5.44
	Octanol-*3,3,4,4-d*$_4$	10.8	51.2
4	Decane-*4,4,5,5-d*$_4$	0.503;0.780‡	2.22;3.44
	Decanol-*3,3,4,4-d*$_4$	12.0	53.0

*Where a single value for the quadrupole splittings is quoted the two doublets were not resolved.
†The smaller quadrupole splitting can be assigned to the CD_3 group on the basis of the difference in intensity.
‡Assignment uncertain.

host mesophase order. An example of this procedure is now given.

In order to compare the deuterium quadrupole couplings in the α-position for the acids, acetic to decanoic, a lyomesophase was prepared first containing all acids with an even number of carbons. The composition of this lyomesophase in our code denoted phase D28 was 50.95 wt.% H_2O (containing 0.1% D_2O and adjusted to p*H* 2), 5.45 wt.% decanol, 38.18 wt.% sodium decylsulphate (SDS), and 4.36% anhydrous sodium sulphate. The balance of mesophase D28 was made up of components of very low concentration, whose relative degree of order along the α-C—D bonds were to be compared. These were 0.11 wt.% C_2, 0.21% C_4, 0.35% C_6, and 0.38% C_8 using the notation C_2 as the 2 carbon acid, etc. The deuterium magnetic resonance spectra gave a series of doublets which could routinely be assigned to the α positions in the various acids and DOH. A second lyomesophase D29 of composition 50.83% H_2O (0.1% D_2O, p*H* = 2), 5.44% decanol, 38.11% SDS, 4.36% Na_2SO_4, 0.22% C_3, 0.24% C_5, 0.29% C_7, and 0.50% C_{10} was also prepared and the deuterium magnetic resonance spectrum of the oriented lyomesophase assigned as for D28. The two mesophases D28 and D29 were mixed to form a single lyomesophase with approximately equal weights of each. The resulting uniaxial fluid has the composition 50.89 wt.% H_2O, 5.45% decanol, 38.14% SDS, 4.36% Na_2SO_4, 0.05% C_2, 0.12% C_3, 0.09% C_4, 0.13% C_5, 0.16% C_6, 0.16% C_7, 0.16% C_8, and 0.28% C_{10}. The information gathered with respect to assignments of the deuterium spectra of D28 and D29 separately, served to assign completely the respective α-CD_2 doublets in the combined and oriented lyomesophase. A sample containing the C_9 to C_{12} acids and another containing the C_{10}, C_{14}, and C_{16} acids were prepared, with the same SDS/decanol/sodium sulfate ratio as in the samples described above, to study the longer chain acids.

The solubilization of the series of α deuterated carboxylate anions added as the sodium salts, was studied in a series of samples corresponding to those described above for the carboxylic acids but with water at p*H* = 10 to assure complete ionization of the carboxylic headgroups. The samples containing the long chain carboxylates were studied as a function of the water content in order to compare these quadrupole splittings with those observed in the samples containing the C_2 to C_{10} salts.

Solubilization studies of the alcohols were made in mesophases of decylammonium chloride/water/ammonium chloride. A typical lyomesophase was: 38.46 wt.% decylammonium chloride, 0.82% NH_4Cl, 56.94% H_2O (0.1% D_2O, p*H* 3), 0.15% methanol-d_3, 0.30% propanol-*2,2,3,3,3-d*$_5$, 1.12% pentanol-*3,3,4,4-d*$_4$, 1.12% heptanol-*3,3,4,4-d*$_4$, and 1.09% nonanol *3,3,4,4-d*$_4$. The alkanes and alcohols in Table 1 were prepared in similar lyomesophases.

The host lyomesophases based on the sodium decylsulphate and decylammonium chloride detergents used in this study macroscopically orient in the magnetic field with the director perpendicular to the field as a result of their negative diamagnetic anisotropy. It was necessary to keep the concentrations of the solubilized species sufficiently low since at higher concentrations a phase change occurs, which usually resulted in a mesophase which will not orient in the magnetic field. In several cases specifically deuterated decylsulphate ions were used and the degree of order profile of its hydrocarbon chain (7) was found to be unaffected by the presence of the small amounts of solubilized components employed.

Results and Discussion

The type II mesophases employed in this study have a fairly extensive liquid crystalline region and are probably 'middle' or 'hexagonal' phases composed of cylindrical micelles packed in a hexagonal array (12). Although the structure of these mesophases which have the ability to orient in magnetic fields have not been unambiguously established, a knowledge of the exact shape and packing of the micelles is not critical in this study of solubilization. Previous studies have indicated that the nature of the hydrocarbon core is not dependent on the shape, whether cylindrical or lamellar, of the micelle (5, 13, 14).

Solubilization of Alcohols and Alkanes in Decylammonium Chloride Mesophases

A typical deuterium nmr spectrum of the solubilized alcohols, methanol to nonanol, in the odd carbon series is present in Fig. 1. The extreme low field section is outside the spectral range but doublets can be discerned for water HOD (w), methanol (m), propanol (p) with a terminal CD_3 group of smaller splitting, pentanol-*3,3,4,4-d*$_4$ (pe) with the smaller doublet splitting associated with the 4,4 position, heptanol (h) with the 3,3 and 4,4 positions overlapping, and nonanol (n) also with the 3,3 and 4,4 positions superposed in the spectrum. The peaks become broader as the quadrupole splittings increase because there are small deviations in the homogeneity of the order and because dipole–dipole couplings between the deuterium nuclei and with adjacent protons (not completely decoupled) become larger as the order parameter increases.

Additional samples containing the same alcohols labelled in other positions were studied, as well as the corresponding samples containing the even carbon series of alcohols. The various samples were not directly comparable because of small differences in sample compositions. However it was observed that over the small range of compositions used the ratio of the deuterium quadrupole splitting of any labelled alcohol to that of the HOD was constant to within *ca.* 1%. In Fig. 2 these ratios for various deuterated positions are plotted against the length of the solubilized alcohol. The quadrupole splittings of the HOD were in the range from 221 to 246 Hz.

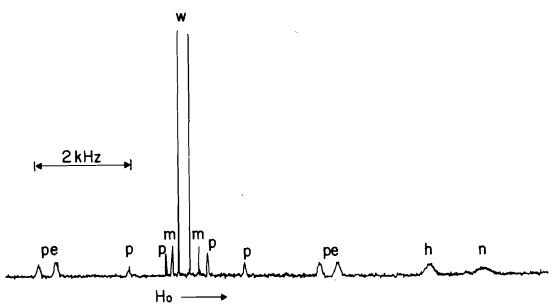

FIG. 1. Varian XL-100 F.t. spectrum of a decylammonium chloride mesophase containing: (*1*) methanol-d_3 (m), (*2*) propanol-*2,2,3,3,3-d*$_5$ (p), (*3*) pentanol-*3,3,4,4-d*$_4$ (pe), (*4*) heptanol-*3,3,4,4-d*$_4$ (h), (*5*) nonanol-*3,3,4,4-d*$_4$ (n). The sample composition is given in the experimental section. A total of 6000 transients were accumulated. Probe temperature was not determined accurately but was estimated to be around 32°C. Since the maximum spectral width was 12 kHz, and since this is in the range of the larger quadrupole splittings of the longer chain alcohols, the spectrum was offset so as to display only the high field peaks for splittings larger than 5 kHz.

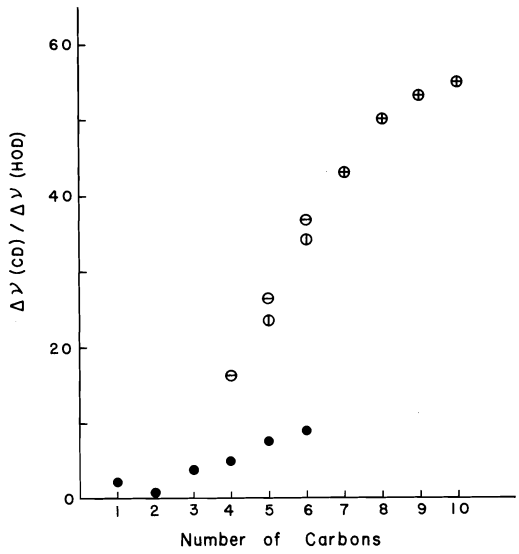

FIG. 2. The ratio of the deuterium quadrupole splitting of specifically deuterated alcohols to that of the HOD in the same mesophase plotted against the length of the alcohol chain. The following symbols indicate the position deuterated: ● terminal methyl group, ⊖ carbon 3, ⓘ carbon 4 and ⊕ average value for carbons 3 and 4.

Some general trends are noteworthy. The longer the chain the alcohol has, the larger the ratio for increase in degree of order over that of the water component, for any given —CD_2— in the chain. For example, factors for the 3,3-CD_2 position are 16.2 for butanol, 25.9 for pentanol, 37.0 for hexanol, 43.0 for heptanol, 50.1 for octanol, 53.0 for nonanol, and 57.5 for decanol. Terminal methyl CD_3— groups are always of lower degree of order than the —CD_2— segments of the chain. We have discussed in earlier papers the ratio of —CD_2— to —CD_3 couplings in terminal —CD_2—CD_3 groups (7, 10, 11). The ratios experimentally observed in this work are 13.2 ethanol, 2.8 propanol, 3.3 butanol, 3.0 pentanol, and 3.5 hexanol. The increase in degree of order at any segment with chain length could be connected with the exchange of the alcohol with the aqueous compartment in which its degree of order is expected to be low. In this case, the mean degree of order measured would be the time weighted average of the more and less ordered environment. Kinoshita *et al.* (15) mea-

sured the solubility of alcohols butanol to decanol in water. Using the degree of order ratios for the CD_2 3,3-position in decanol and butanol of 56.0 and 16.2, respectively, compared to the water, the butanol would appear to be largely in the water compartment. The solubility measurements (15) indicate a distribution of only ~2% of the butanol in water.

These results are, however, so disparate that it is clear the mean degrees of order measured at a given chain segment in this series, except for the very short chain alcohols, do not reflect in any way the distribution of the alcohol between aqueous and hydrocarbon chain regions. The change in degrees of order at a given position away from the head group in alcohol chains of increasing length embedded as guest molecules in a host bilayer probably reflect the increased freedom for conformational equilibria in the chain as it becomes shorter.

The data for deuterium quadrupole couplings on solubilized alkanes in the decylammonium chloride mesophase are summarized in Table 1. The table enables a comparison to be made with the solubilized alcohol of the same chain length in the same mesophase. For example, for heptane deuterated at 3,3,4,4 only one doublet was resolved and the degree of order in the corresponding alcohol positions is about six times larger. The head group thus seems to act as an anchor in the interface greatly restricting the motion of the chain at the 3,3,4,4 positions. The effect of the polar head group is evident even at the end of the hydrocarbon chain. The degree of order of the terminal CD_3 group of octane is much smaller than that expected (by extrapolating the results shown in Fig. 2) for the corresponding position of octanol.

Solubilization of Carboxylic Acids and the Carboxylate Ion

In this series of experiments, the α-CD_2 group of the solubilized components was observed. The host mesophases were always a water, sodium decylsulfate, decanol, and sodium sulfate system in which the ratio of the last three components was kept constant. Typical mesophase compositions are given in the experimental section. The solubilisates were studied in three groups; the carboxylic acids or carboxylates from C_2 to C_{10} with the exception of C_9 were studied in one sample and the longer chain solubilisates were studied in samples containing the C_9 to C_{12} or C_{10}, C_{14}, and C_{16} acids or carboxylates. Since the nature and amounts of added solubilisates does affect the average degree of order of the mesophase, the results from different samples were compared in the following manner. In the case of the carboxylic acids, the quadrupole doublet of the α-CD_2 signal of decanoic acid was found to be identical to those of the higher homologues. The line width of the overlapping peaks arising from the C_{10}, C_{11}, and C_{12} or C_{10}, C_{14}, and C_{16} acids were not significantly broader than the signal due only to C_{10} acid. The results for the carboxylic acids are shown in Fig. 3.

The α-CD_2 quadrupole doublets for the C_9 to C_{12} carboxylate anions were resolved. On varying only the water content the ratio of the quadrupole splittings, C_9:C_{10}:C_{11}:C_{12}, was found to be constant to within 0.5%. In the concentration range studied, the quadrupole splitting for lauric acid-α-d_2 varied from 17.64 to 10.96 kHz; the mesophase was stable on the addition of more water but the peaks could no longer be resolved. A similar behavior was observed in the samples containing the C_{10}, C_{14},

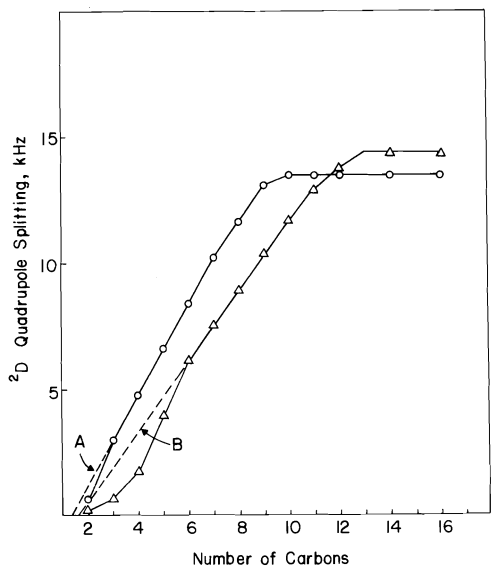

FIG. 3. Deuterium quadrupole splittings for the α-CD_2 position of solubilized carboxylic acids and carboxylates in a quaternary lyomesophase sodium decylsulphate, decanol, water, and sodium sulfate. These are plotted as a function of the chain length of the solubilisate. The carboxylic acids are denoted by ○ and carboxylates by △. In both cases linear portion of the dependence is extrapolated back to shorter chains by dotted curves A and B.

and C_{16} carboxylates. This constant ratio observed for the C_9 to C_{16} carboxylates was used to normalize these results to those observed in the sample containing the shorter homologues. In Fig. 3 the quadrupole splittings at the α-CD_2 positions are plotted against the length of the solubilized chain for both carboxylate and carboxyl systems.

The dependence of the degrees of order of a chain position with chain length for the carboxylic acids and the carboxylate anions appears to be very similar to that of the alcohols. There is an increase in the degree of order of the α-CD_2 group with chain length up to a length comparable to the host decylsulphate chain. This increase in degree of order with chain length reaches a saturation where additional —CH_2— groups have no effect. The carboxylic acids reach a maximum order at the α position at close to half the bilayer thickness of 10 carbon atoms, while the anionic carboxylate detergent ions reach a steady degree of order at the α position at a 13 or 14 carbon chain. A comparison between the degrees of order in the limiting regions cannot be made from these data because of differences in sample composition. Work is presently in progress to compare the degree of order of the α positions in these long chain carboxylic acids and anions with that of the host decylsulphate chains. However the results in Fig. 3 show that there is a considerable difference in order at the α-C—D bonds between anions and acids at all chain lengths below those in the limiting region, the carboxylate ion head group provoking the smaller degree of order.

The short chain carboxylates are much more soluble in water than the parent acids and low degrees of order are consequently observed for acetate and propionate ions because of a distribution into the water compartment of a significant fraction of the solubilized ion. Both the carboxylic acids and carboxylates from C_3 to C_9 and C_6 to C_{11}, respectively, increase in degree of order at the α position in a linear fashion. The linearity of the dependence of α position order on chain length is quite a precise one from C_3 to C_7 for the acids and C_6 to C_{10} for the detergent anions (Fig. 3). This experimental fact encourages an explanation of the degrees of order of the shorter chains in terms of an equilibrium distribution model. Linear extrapolations from the longer chains give the dashed lines A for acids and B for anions in Fig. 2. The degrees of order of shorter chain species always fall below the extrapolated linear dependence on chain length; furthermore, the extrapolations indicate a degree of order zero at a chain length approximately one carbon in length, this carbon being the carboxyl carbon. It is reasonable to assume therefore that for those acids or anions which are included completely in the bilayer the increase in order at the α-CD_2 position is a linear function of the chain length. The linear section of the degree of order dependence can be expressed:

$$[3] \qquad \Delta\nu_D = 1.401n_c - 2.294$$

for carboxylates, and

$$[4] \qquad \Delta\nu_D = 1.809n_c - 2.461$$

for carboxylic acids

The correlation coefficient for [3] is 0.9998 and for [4] 0.99996. '$\Delta\nu_D$' is the deuterium nuclear quadrupole splitting in the α-CD_2 positions in kHz and n_c is the number of carbons in the molecule or ion.

The experimental degree of orders measured for acetic acid-d_3, acetate-d_3, propionate-d_2, butanoate-d_2, and pentanoate-d_2 are smaller than those extrapolated from longer chains. Let us assume that there is a rapid exchange process which leads to this deviation from the above equations. The measured degree of order becomes:

$$[5] \qquad S_{obs} = x_D S_D + (1 - x_D)S_W$$

S_{obs} is the observed degree of order, S_D the degree of order while located in the hydrophobic bilayer, and S_W the value while located in the water compartment; x_D is the mole fraction of the solubilized component in the bilayer and thus $(1 - x_D)$ is that fraction in the aqueous region. Since degrees of order are proportional to the quadrupole splittings we may work with the latter. $\Delta\nu_{obs}$, $\Delta\nu_D$, and $\Delta\nu_W$ may be used to symbolize [3] and [4] in terms of quadrupole splittings. The value for $\Delta\nu_W$ must be very small compared to $\Delta\nu_D$. For example $\Delta\nu_W$ for the acetate ion must be less than 0.18 kHz. Let us assume that $\Delta\nu_W$ for both acids and ions is 0.15 kHz and that it has the same sign as $\Delta\nu_D$. The value of $\Delta\nu_D$ can be obtained from the extrapolated linear region with an appropriate n_c, while the value $\Delta\nu_{obs}$ is taken in each case from the values used for Fig. 3. The mole fractions x_D can be computed from [5]. The results obtained are the following: 0.298 for

propionate ion, 0.511 for butanoate ion, 0.831 for pentanoate ion, and 0.468 for acetic acid molecules. The uncertainty in the estimation of $\Delta\nu_W$ renders the calculations especially subject to large errors for acetic acid and consequently corrections for the difference between the methyl group methylene group motions was neglected. The mole fractions of these species calculated for the bilayer are in accord with the increasing hydrophobicity. The greater dispersion of carboxylate ions from the bilayer into the water is rational in terms of the existence of a counter ion and the aqueous solubility of the salts. The increase in order at the α position in the linear region per $-CH_2-$ segment is larger for a neutral carboxylic acid than the anion indicating a more effective packing of the neutral species in the host bilayer. Two types of chain motions can be identified which can account for the increase in the degree of order of the α position in the intermediate chain length region: (*1*) a decrease in the freedom of conformational motions as the chain becomes longer and (*2*) a decrease in the amplitude of the oscillations of the average chain axis about the normal to the interface. The second of these averaging motions could be expected to decrease and reach a limiting value with increasing chain length as a result of the increasing intermolecular interactions of the dilute guest hydrocarbon chain with host chain matrix. A quantitative analysis of the chain motions is needed to account for the observed linear dependence in the intermediate chain length region.

In the limiting region the degree of order of the chain segments near the head group appears to be dominated by conformational motions which are not affected by increased chain lengths. A study of the degree of order profile along the hydrocarbon chain of these solubilisates is currently in progress.

Acknowledgments

This work has been supported by operating grants from the National Research Council of Canada (NRCC) to L.W.R. The travel expenses were provided by NRCC and Couselho Nacional de Pesquisas do Brasil (CNPq) under an international exchange agreement. Equipment grants were provided by the Banco Nacional de Desenvolvemento Economico (BNDE) and Fundação de Amparo à Pesquisa do Estado de São Paulo (FAPESP). The financial support of NRCC and BNDE to F.Y.F. was also important.

1. J. W. McBain. Advances in colloid science. Vol. 1. Interscience Publishers Inc., New York, NY. 1942.
2. C. Tanford. The hydrophobic effect. J. Wiley-Interscience, New York, NY. 1973.
3. K. Radley, L. W. Reeves, and A. S. Tracey. J. Phys. Chem. **80**, 174 (1976) and references therein.
4. L. W. Reeves, F. Y. Fujiwara, and M. Suzuki. *In* Magnetic resonance in colloid and interface science. *Edited by* H. A. Resing and C. G. Wade. Am. Chem. Soc. Symp. Ser. 34. American Chemical Society, Washington, DC. 1976.
5. F. Y. Fujiwara and L. W. Reeves. J. Am. Chem. Soc. **98**, 6790 (1976).
6. A. F. Thomas. Deuterium labelling in organic chemistry. Appleton-Century-Crofts, Educational Division, New York, NY. 1971.
7. L. W. Reeves and A. S. Tracey. J. Am. Chem. Soc. **97**, 5729 (1975).
8. R. Ramonet and B. Wojtkowiak. Bull. Soc. Chim. Fr. 1500 (1960).
9. J. G. Atkinson, J. J. Csakuary, G. T. Herbert, and R. S. Stuart. J. Am. Chem. Soc. **90**, 498 (1968).
10. F. Fujiwara, L. W. Reeves, A. S. Tracey, and L. A. Wilson. J. Am. Chem. Soc. **96**, 5249 (1974).
11. D. M. Chen, L. W. Reeves, A. S. Tracey, and M. M. Tracey. J. Am. Chem. Soc. **96**, 5349 (1974).
12. (*a*) P. Ekwall. *In* Advances in liquid crystals. Vol. 1. *Edited by* G. H. Brown. Academic Press, New York, NY. 1975. p. 1; (*b*) P. A. Winsor. Chem. Rev. **68**, 1 (1968).
13. M. J. Carvolin and P. Keller. Chem. Phys. Lipids, **15**, 161 (1975).
14. A. S. Tracey and P. Diehl. Can. J. Chem. **54**, 2283 (1976).
15. K. Kinoshita, H. Isakawa, and K. Shinoda. Bull. Chem. Soc. Jpn. **31**, 1081 (1958).

Broad band absorption of solutes in liquid solutions and in polystyrene

C. K. McLellan and S. Walker

Department of Chemistry, Lakehead University, Thunder Bay, P, Ont., Canada P7B 5E1

Received December 23, 1976

C. K. McLellan and S. Walker. Can. J. Chem. **55,** 2411 (1977).

Broad band absorptions in the frequency range 20 to 100 cm^{-1} arising from four polar solutes in polystyrene matrices have been observed at 302 K and compared with those in liquid benzene or cyclohexane solutions. A broad band was also found for 1,4-diacetylbenzene in a polystyrene matrix at 124 K. The broad band absorption still occurs in the far-infrared region when group and/or molecular relaxation(s) occur in appreciably lower frequency regions. The significance of these absorptions is discussed in terms of some models which account for the origins of broad band absorptions.

C. K. McLellan et S. Walker. Can. J. Chem. **55,** 2411 (1977).

Travaillant à 302 K, on a observé de larges bandes d'absorption aux fréquences allant de 20 à 100 cm^{-1} et dérivant de quatre solutés polaires dans des matrices de polystyrène. On a comparé ces absorptions avec celles obtenues dans des solutions liquides de benzène ou de cyclohexane. On a aussi trouvé une bande large pour le diacétyl-1,4 benzène dans une matrice de polystyrène à 124 K. La bande d'absorption large existe encore dans la région de l'infrarouge lointain quand les relaxations du groupe et/ou de la molécule se produisent dans des régions de fréquence qui sont beaucoup plus faibles. On discute de l'importance de ces absorptions en termes de quelques modèles qui tiennent compte des origines des absorptions des bandes larges.

[Traduit par le journal]

Introduction

Broad band absorptions in the frequency range 10 to 100 cm^{-1} have been shown to exist for both polar and non-polar liquids (1–6). The effects of pressure, temperature, and solvents have been studied (7–11), and these bands have also been shown to exist in solid phases permitting molecular rotation (9, 10). Brot (12) has recently discussed the work on broad band absorption.

Hill (13) proposed a model in which a particular polar molecule in a liquid was temporarily confined to a "cage" of neighbours which provided potential energy wells encountered by the trapped molecule during its rotation. Rotation through large angles from one well to another corresponded to the well-known Debye dielectric relaxation process. Small-angle oscillations within one well in response to an applied field would account for the broad band absorption. Hill stated that the damping of this latter resonant process "cannot here be attributed to collisions. Instead the damping must arise from the lack of rigidity of the cage of neighbours, which allows a transfer of energy from the central molecule to the cage" (13).

Chantry and Gebbie felt that the experimentally-observed broad band might be composed of a number of overlapping absorption lines, the widths of which "would be determined by the lifetime of the pseudo-lattice state" (2) which they expected would be of the order of the dielectric relaxation time.

We have undertaken a study at room temperature of four polar solute molecules each dissolved in benzene and in polystyrene matrix. In the latter state the relaxation times of the molecules and of their substituent groups are very much longer than in liquid solutions. Studies of the dielectric relaxation processes of polar molecules in polystyrene matrices have been reported (14–17), and we have previously carried out such studies for the four solutes (acetophenone, 1,4-diacetylbenzene, 4-acetylbiphenyl, and 4-nitrobiphenyl) used in the present work (18).

Experimental

All far-infrared spectra have been recorded via Fourier transform interferometry by the use of a modular cube interferometer of the N.P.L. type for the frequency range 20 to 200 cm^{-1}. The details have been reported previously (5, 9, 11, 19, 20).

The polystyrene matrix samples were measured as disks without cell windows. No change of weight of the sample occurred as a result of the experiment.

For the polystyrene matrix containing 1,4-diacetylbenzene as solute we have also recorded spectra at 298 K

and 124 K using a cell which allowed temperatures to be controlled to within ±1 K anywhere in the range from 115 K to 340 K.

The absorption spectra of benzene and polystyrene are shown in Fig. 1. To obtain the absorption spectrum resulting from the presence of the solute a point-by-point subtraction of solvent from solution absorption was carried out. We have calculated from the solute absorption the maximum absorption cross-section σ_{max} (cm^2 mol^{-1}) via eq. 1 in which c is the solute concentration in mol ℓ^{-1} and α_{max} is the maximum value of the absorption coefficient.

$$[1] \qquad \sigma_{max} = \frac{\alpha_{max}}{c} \times 1000$$

A small difference between solution and solvent absorption curves means that a relatively large error must be associated with the difference. This applies particularly to the benzene solution of 4-acetylbiphenyl.

The error in the frequency of maximum absorption, $\bar{\nu}_{max}$, was typically ±4 cm^{-1} for the broad band absorption. The error estimate for the band width at half height, $\Delta\bar{\nu}_{1/2}$, was about ±10 cm^{-1} in most cases. Normally, we have found the error in α_{max} to be of the order of ±10%. However, when the absorption is weak the error could well be ±15% or worse, while the error in σ_{max} could be ±30% or even larger than this in cases where the difference is small compared to the absorptions of the solution and pure solvent.

Results

The far-infrared absorption spectra are presented as graphs of α (cm^{-1}) *vs.* $\bar{\nu}$ (cm^{-1}), with three curves representing solution, solvent, and difference spectra on each. In the case of acetophenone in cyclohexane only one curve is shown, since the solvent absorption is negligibly small in comparison with that of the solute (21). Parameters derived from these spectra are summarized in Table 1.

In polystyrene matrices at 302 K, the acetyl group relaxation times in the ketones investigated were: acetophenone, 9.8 × 10^{-10} s; 1,4-diacetylbenzene, 2.0 × 10^{-10} s; and 4-acetylbiphenyl, 4.0 × 10^{-10} s. Under these conditions the molecular relaxation time of 4-acetylbiphenyl also was 2.2 × 10^{-3} s, and that of 4-nitrobiphenyl was 3.7 × 10^{-4} s (18). This means that the frequency of maximum dielectric absorption due to acetyl group relaxation was lower than 2.6 × 10^{-2} cm^{-1}, and that dielectric absorption due to molecular relaxation of the two larger molecules was at frequencies lower than this by a factor of about 10^7. By contrast, the maximum absorption of the broad band in far-infrared spectra is usually observed at frequencies of about 50 cm^{-1}. Thus, there is a separation of dielectric absorption in the polystyrene matrix solutions from any absorption in the far-infrared region by a factor of 2 × 10^3 for group relaxation and about 10^9 for relaxation for the biphenyl molecules.

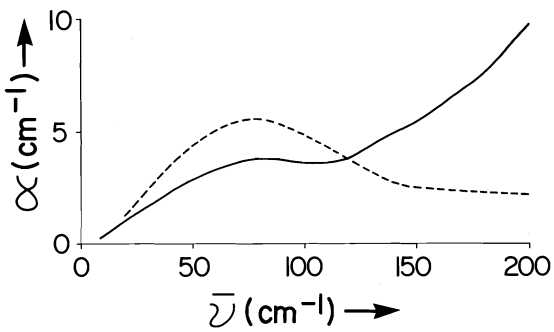

FIG. 1. Far-infrared spectra of pure benzene (- - -) and pure polystyrene (—) at 302 K.

Figures 2, 3, and 4 show the far-infrared absorption spectra of acetophenone as a 10% solution in cyclohexane, a 5% solution in benzene, and a 10% solution in polystyrene, respectively. The numerical data in Table 1 demonstrate that the peak frequencies and half-height widths are virtually the same in benzene and polystyrene solutions, with some reduction of maximum absorption cross-section in the polystyrene matrix solution. Solutions of 1,4-diacetylbenzene in benzene (Fig. 5) and polystyrene (Fig. 6) showed agreement of peak frequency, width, and absorption cross-section, both for the lower-frequency broad band and for the band around 160 cm^{-1}. This higher-frequency peak is not part of the broad band absorption, and infrared work by Varsányi (22) and Raman studies by Mross and Zundel (23) indicate that the C_{ar}—$COCH_3$ out-of-plane vibration occurs at this frequency.

Figures 7 and 8 give the spectra of solutions of 4-acetylbiphenyl in benzene and polystyrene, and there is very good agreement between the two spectra for the peak frequency, width, and maximum absorption cross-section of the low-frequency broad band (see Table 1). The 165 cm^{-1} band appeared to have a greater intensity in polystyrene than in benzene, and this could be related to the considerable overlap of the two peaks. As a result of the low solute concentration the intensity of this peak in the benzene solution is only slightly greater than that of benzene itself. Hence, the intensity of the difference may be in considerable error.

Thus, the broad band absorption spectra of

TABLE 1. Far-infrared absorption spectra parameters for pure solvents and for residual (solution–solvent) absorptions at 302 K except for one specified case

Solute	Solvent	Concentration (mol ℓ^{-1})	$\bar{\nu}_{max}$ (cm^{-1})	$\Delta\bar{\nu}_{1/2}$ (cm^{-1})	σ_{max} (cm^2 mol^{-1})
	Benzene	11.119	78	109	0.50×10^3
	Polystyrene	10.034	*		
Acetophenone	Cyclohexane	0.880	67	88	14×10^3
	Benzene	0.440	75	88	16×10^3
	Polystyrene	0.880	77	80	10×10^3
1,4-Diacetylbenzene	Benzene	0.123	85	70	22×10^3
			160	23	16×10^3
	Polystyrene (302 K)	0.652	90	70	27×10^3
			160	40	18×10^3
	Polystyrene (124 K)	0.652	93	66	30×10^3
			160	36	19×10^3
4-Acetylbiphenyl	Benzene	0.214	80	74	13×10^3
			166	13	4×10^3
	Polystyrene	0.533	82	80	14×10^3
			170	34	9×10^3
4-Nitrobiphenyl	Polystyrene	0.539	81	99	7×10^3
			185	11	9×10^3

*A rising tail up to $\bar{\nu} = 200$ cm^{-1}, see Fig. 1.

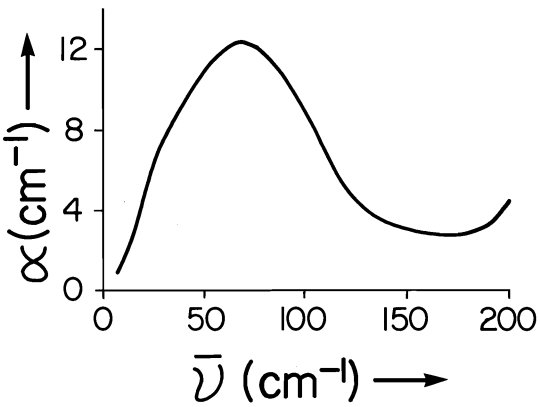

FIG. 2. Acetophenone (0.880 *M*) in cyclohexane at 302 K.

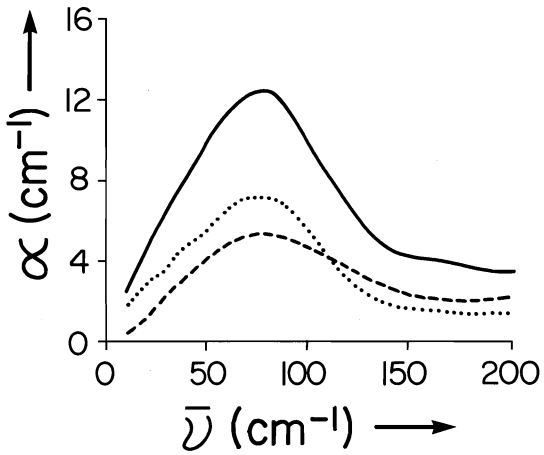

FIG. 3. Acetophenone (0.440 *M*) in benzene at 302 K. — solution, - - - solvent correction, . . . difference curve (*i.e.* — minus - - -).

acetophenone, 1,4-diacetylbenzene, and 4-acetylbiphenyl all appear not to have been altered appreciably by a change from benzene liquid solutions to polystyrene matrices. Yet, the molecular relaxation process would be very much slower in polystyrene than in benzene, and their molecular translational motions should also be substantially reduced.

It seems unlikely that the absorption may be due solely to the rotating acetyl groups since it is clear that the rates of rotation of the acetyl groups in polystyrene solutions are markedly slower than those in benzene solutions while the far-infrared absorptions appear unaffected by the change of solvent. For 4-nitrobiphenyl the group relaxation process would not be detectable, and this yielded broad band absorption in polystyrene (see Fig. 9) even though the molecular relaxation time was longer by a factor of about 10^7 than would be the case in liquid solutions.

The spectra of the matrix containing 1,4-diacetylbenzene as solute at two temperatures are shown in Fig. 10. The relaxation times for the acetyl group in a polystyrene matrix were about 10^{-10} s at 298 K and about 5×10^{-3} s at 124 K (18). In this solute molecule the dipole moments along the axis cancel so that in the absence of stable *cis* and *trans* forms the only relaxation process would be of the group type. A recent

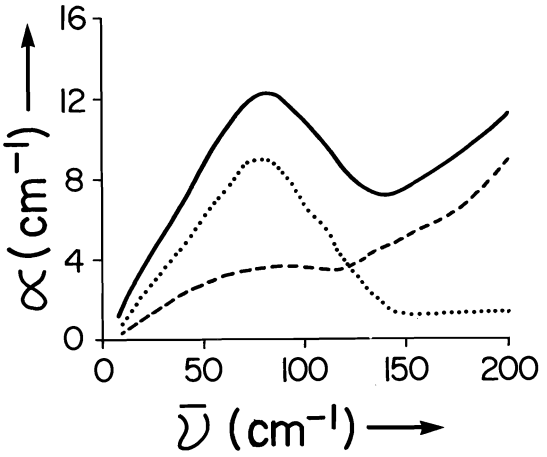

FIG. 4. Acetophenone (0.880 *M*) in polystyrene at 302 K. — matrix, - - - polystyrene correction, . . . matrix-polystyrene.

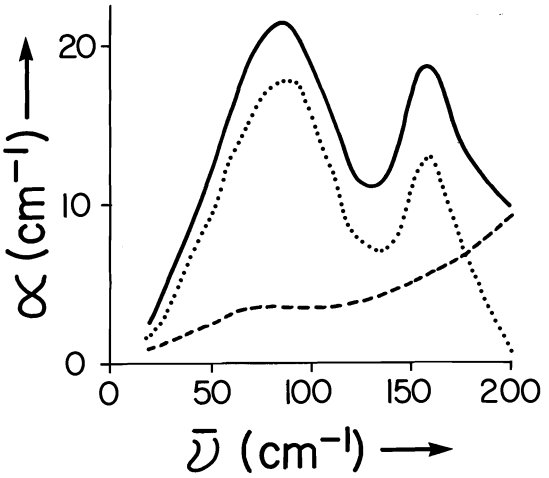

FIG. 6. 1,4-Diacetylbenzene (0.652 *M*) in polystyrene at 302 K. Key as for Fig. 4.

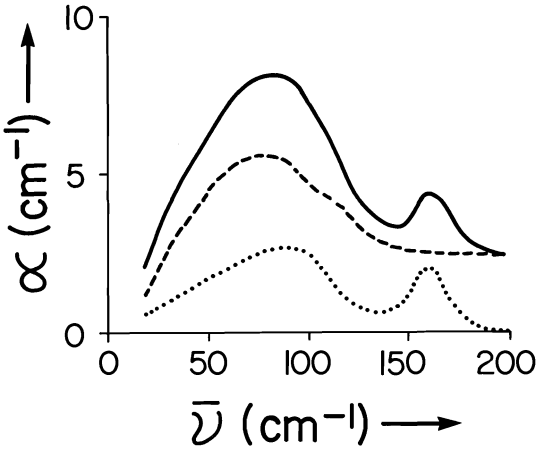

FIG. 5. 1,4-Diacetylbenzene (0.123 *M*) in benzene at 302 K. Key as for Fig. 3.

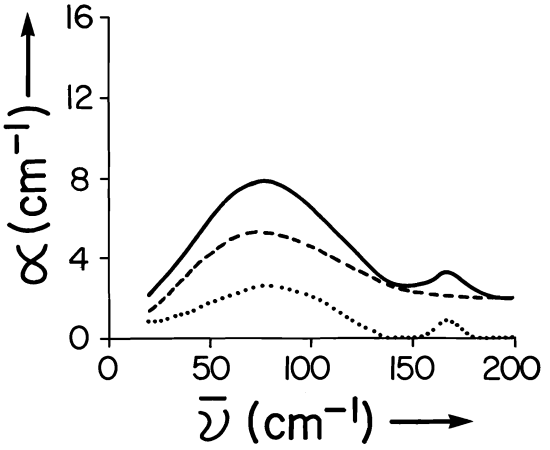

FIG. 7. 4-Acetylbiphenyl (0.214 *M*) in benzene at 302 K. Key as for Fig. 3.

study by McLellan and Walker has shown this to be the case (18). Thus, dielectric absorption due to the molecular relaxation process itself is not a factor which could be considered as a contributor to broad band absorption in this case at least. Further, for this molecule in a polystyrene matrix the rate of translational motion and therefore the resultant frequency of molecular collisions is expected to be considerably less at 124 K than at 298 K.

The spectra for 1,4-diacetylbenzene shown in Fig. 10 do not differ greatly. At the lower temperature, the broad band peak occurs at 93 cm^{-1} frequency compared to 90 cm^{-1} at 298 K. This difference is of the order of experimental error and is less than the resolution (approximately 7 cm^{-1}) at which the spectra have been recorded. The maximum intensity of the 93 cm^{-1} band is about 10% greater at the lower temperature, whereas very much larger changes of both peak height and frequency have been reported in pure liquid and rotator solid phases of other materials (5, 8–10). The dielectric absorption maximum has been shifted to lower frequency by a factor of about 10^7 at 124 K compared to 298 K, and yet the frequency, intensity, and shape of the far-infrared broad band do not appear to have been altered. Thus, the existence of this broad band absorption appears not to be due simply to the motion ascribed to acetyl group relaxation.

Discussion

Several procedures have been employed to increase molecular and intramolecular relaxation

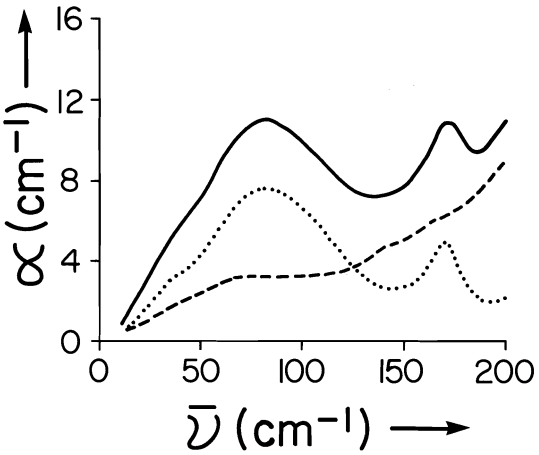

FIG. 8. 4-Acetylbiphenyl (0.533 *M*) in polystyrene at 302 K. Key as for Fig. 4.

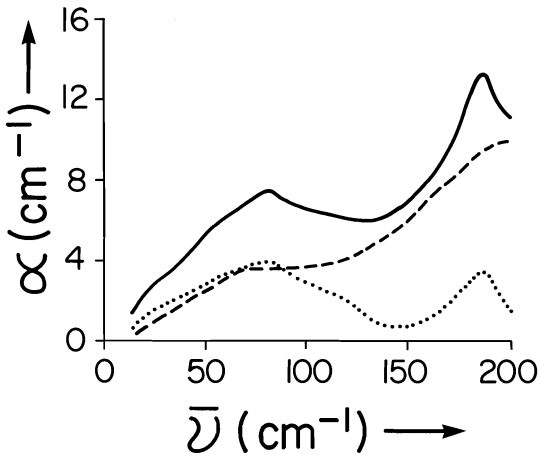

FIG. 9. 4-Nitrobiphenyl (0.539 *M*) in polystyrene at 302 K. Key as for Fig. 4.

times. Solid phases which allow some rotation of nearly spherical molecules have been examined (9, 10). Chantry *et al.* (24, 25) have reported the existence of a broad band absorption due to the presence of the slowly re-orienting polar acetate groups in vinyl acetate – ethylene copolymers. Thus, both in this work and our own in polystyrene broad band absorption has been found despite slow molecular relaxation and reduced translational motions. However, it has been shown (1, 2, 9, 10) that in solid phases lacking molecular rotational freedom one observes in the far-infrared region rather a different absorption spectrum consisting of intense narrow bands attributed to lattice modes.

It is apparent that the rates of molecular and substituent group relaxation are not critical for the existence of a broad absorption band in the

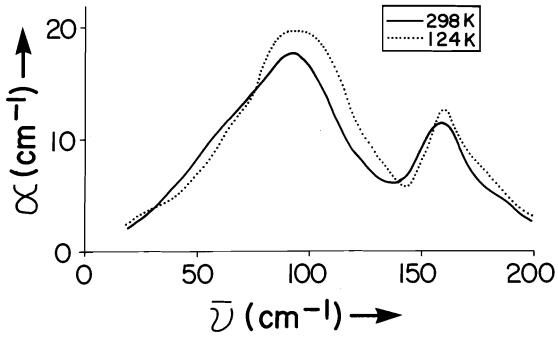

FIG. 10. 1,4-Diacetylbenzene (0.652 *M*) in polystyrene at two temperatures as indicated.

far-infrared region. Moreover, this absorption appears to arise from some process which is completely separate from that of dielectric absorption.

Haffmans and Larkin (10, 26), Minami and Ohno (27), and Higasi *et al.* (28) have considered the Hill model (13, 29, 30) and a square-well potential model, finding that the latter was more successful in fitting experimental data than a single resonant frequency of the Hill type subject to appreciable damping. However, Higasi *et al.* (28) pointed out that the fit of the Hill model would be improved if a distribution of resonant frequencies were employed.

In the square-well model the shape of the absorption band is influenced by time-dependent fluctuations of the surrounding cage. Since this model uses elastic librator-cage collisions, these cage fluctuations must arise from distortions of the cage produced by external collisions and/or by dielectric relaxation of the central molecule. The present work suggests that, even when the rate of collision-induced fluctuations of the cage is very much slower than in room-temperature liquid phase studies, a typical broad band absorption exists and is, furthermore, very much like that found in room-temperature studies in benzene solutions.

Conclusions

The polystyrene matrix solution technique offers a means of removing from the low-frequency side of the broad band possible contributions from dielectric relaxation processes (10, 26). In this regard it is interesting to note that on passing from benzene solutions to polystyrene matrices we have found no evidence of a decreased absorption intensity at frequencies down to 20 cm^{-1}, and the characteristic parameters of the broad band remain unchanged for

systems which are capable of the following types of relaxation (*a*) molecular, (*b*) group, (*c*) both molecular and group. It is apparent that the broad band absorption is not merely a higher-frequency band due solely to the molecular and intramolecular relaxation processes which give rise to dielectric absorptions at frequencies in the microwave region and lower. It would appear that the broad band absorption arises from some separate class of molecular motion such as has been proposed in theories involving a "cage" surrounding a central molecule which has at least some limited freedom to rotate. The rates of molecular and group relaxation processes and of translational motion do not appear critically important in the absorption process. It would seem likely that the relaxation time and the cage lifetime are not the dominant factors in governing the intensity of the broad band absorption for the systems reported here. Further, since the solutes are monomolecularly dispersed in the matrix (15), the concept that broad band absorption arises from lattice bands in local molecular structure would seem unlikely.

The main requirements for broad absorption would seem to be that the (solute) molecule is enclosed by other molecules or segments of them and that it is capable of limited rotation (oscillation) and possibly of translational motion. In such an environment the polar molecule could undergo small angle oscillations in response to the applied field leading to broad band absorption. In this Hill type process (13, 29, 30) it may well be that a distribution of resonant frequencies (28–30) is more important than time-dependent fluctuations of the surroundings of individual molecules in determining the appearance of the broad band. Certainly for these matrix systems the Fuoss–Kirkwood distribution parameter values ranging between 0.18 and 0.20 for the molecular relaxation processes of 4-nitro- and 4-acetylbiphenyl bear out that the solute molecules experience a wide variety of local environments and this could lead to a distribution of resonant frequencies.

Acknowledgements

We wish to thank Mr. B. K. Morgan for his technical assistance and the National Research Council of Canada for its financial support. This work forms part of the Ph.D. thesis of one of us (C.K.Mc.) submitted to the University of Manitoba, 1977.

1. G. W. Chantry, H. A. Gebbie, B. Lassier, and G. Wyllie. Nature, **214**, 163 (1967).
2. G. W. Chantry and H. A. Gebbie. Nature, **208**, 378 (1966).
3. M. Davies, G. W. F. Pardoe, J. Chamberlain, and H. A. Gebbie. Trans. Faraday Soc. **66**, 273 (1970).
4. M. Davies, G. W. G. Pardoe, J. Chamberlain, and H. A. Gebbie. Chem. Phys. Lett. **2**, 411 (1968).
5. S. R. Jain and S. Walker. J. Phys. Chem. **75**, 2942 (1971).
6. Y. Leroy, E. Constant, C. Abbar, and P. Desplanques. Adv. Mol. Relax. Processes, **1**, 273 (1967–68).
7. C. C. Bradley, H. A. Gebbie, A. C. Gilby, V. V. Kechin, and J. H. King. Nature, **211**, 839 (1966).
8. S. G. Kroon and J. van der Elsken. Chem. Phys. Lett. **1**, 285 (1967).
9. C. K. McLellan and S. Walker. J. Chem. Phys. **61**, 2412 (1974).
10. R. Haffmans and I. W. Larkin. J. Chem. Soc. Faraday II, **68**, 1729 (1972).
11. P. Hindle, S. Walker, and J. Warren. J. Chem. Soc. Faraday II, **71**, 756 (1975).
12. C. Brot. Dielectric and related molecular processes. Vol. 2. The Chemical Society. 1973.
13. N. E. Hill. Proc. Phys. Soc. **82**, 723 (1963).
14. M. Davies and A. Edwards. Trans. Faraday Soc. **63**, 2163 (1967).
15. M. Davies and J. Swain. Trans. Faraday Soc. **67**, 1637 (1971).
16. S. P. Tay and S. Walker. J. Chem. Phys. **63**, 1634 (1975).
17. S. P. Tay, J. Kraft, and S. Walker. J. Phys. Chem. **80**, 303 (1976).
18. C. K. McLellan and S. Walker. Can. J. Chem. **55**, 583 (1977).
19. M. Benson, G. D. Martin, S. Walker, J. Warren, and R. Wilson. Can. J. Chem. **50**, 2610 (1972).
20. M. S. Mathur and N. A. Weir. J. Mol. Struct. **19**, 309 (1973).
21. G. J. Davies, J. Chamberlain, and M. Davies. J. Chem. Soc. Faraday II, **69**, 1223 (1973).
22. G. Varsányi. Vibrational spectra of benzene derivatives. Academic Press, New York, NY, U.S.A. 1969. p. 319.
23. W. D. Mross and G. Zundel. Spectrochim. Acta, **26**A, 1097 (1970).
24. G. W. Chantry, J. W. Fleming, E. A. Nicol, H. A. Willis, and M. E. A. Cudby. Infrared Phys. **12**, 101 (1972).
25. G. W. Chantry, J. W. Fleming, R. J. Cook, D. G. Moss, and E. A. Cudby. Infrared Phys. **13**, 157 (1973).
26. I. W. Larkin. J. Chem. Soc. Faraday II, **69**, 1278 (1973).
27. R. Minami and A. Ohno. J. Phys. Soc. Jpn. **35**, 1730 (1973).
28. K. Higasi, R. Minami, H. Takahashi, and A. Ohno. J. Chem. Soc. Faraday II, **69**, 1579 (1973).
29. N. E. Hill. Chem. Phys. Lett. **2**, 5 (1968).
30. N. E. Hill. J. Phys. A, **2**, 398 (1969).

A relationship between correlation energies and sizes: the series of beryllium- and neon-like ions

FERNANDO BERNARDI
Istituto di Chimica Organica dell' Universita, Bologna, Italy
PAUL G. MEZEY AND IMRE G. CSIZMADIA
Chemistry Department, University of Toronto, Toronto, Ont., Canada M5S 1A1
Received January 20, 1977

FERNANDO BERNARDI, PAUL G. MEZEY, and IMRE G. CSIZMADIA. Can. J. Chem. **55**, 2417 (1977).

A simple empirical relation for the estimation of the correlation energy (E_{corr}) is found to be valid for the isoelectronic series of Be- and Ne-like ions to a very good accuracy. Although originally such a relation was proposed for the He-like ions, the present results indicate that it is applicable for layer systems as well. Thus the interelectron pair correlation in systems such as Be or Ne does not affect adversely the accuracy of the relation:

$$E_{corr} = \frac{K}{Z_{eff}^2 \langle r^2 \rangle}$$

where the denominator is the size $\langle r^2 \rangle$ weighted by the square of the effective nuclear charge Z_{eff}.

FERNANDO BERNARDI, PAUL G. MEZEY et IMRE G. CSIZMADIA. Can. J. Chem. **55**, 2417 (1977).

On a trouvé qu'une relation empirique simple permettant d'évaluer l'énergie de corrélation (E_{corr}) peut être appliquée pour des séries isoélectroniques d'ions du type Be et Ne avec une très bonne précision. Même si une telle corrélation avait été originalement proposée pour des ions du type He, les résultats actuels indiquent qu'elle peut être appliquée aussi bien pour des systèmes plus grands. Donc la corrélation de la paire interélectronique dans des systèmes tels que le Be ou le Ne n'affecte pas d'une façon adverse la précision de la relation:

$$E_{corr} = \frac{K}{Z_{eff}^2 \langle r^2 \rangle}$$

où le dénominateur est la grandeur $\langle r^2 \rangle$ pondérée par le carré de la charge nucléaire effective Z_{eff}.

[Traduit par le journal]

Introduction

It is of great importance to obtain reliable estimates for correlation energies of both atomic and molecular systems. Most of the previous attempts were based on estimating the correlation energies from Hartree–Fock density matrices (1). In this paper a conceptually simpler empirical relationship is proposed for multielectronic systems.

In earlier studies on helium and the helium-like ions (2) a simple empirical relationship was found between the correlation energy E_{corr}, effective nuclear charge Z_{eff}, and the size of the electron pair (3) as expressed by the expectation value of the spherical quadratic operator, $\langle r^2 \rangle$. It was observed that for the helium-like ions E_{corr} is inversely proportional to the product $Z_{eff}^2 \langle r^2 \rangle$ to a very good approximation. Since the correlation energy E_{corr} is expected to increase as the volume available for the electrons decreases, such a result may easily be interpreted in the qualitative sense.

The correlation energy E_{corr} may be expressed as the difference between the non-relativistic energy E_{NR} and the Hartree–Fock limit E_{HF} of the system:

$$[1] \qquad E_{corr} = E_{NR} - E_{HF}$$

Studies on a large number of isoelectronic systems (series of the He-, Be-, Ne-, and Mg-like ions) indicated that a relatively simple relation holds between the sizes and energies of localized orbitals (4):

[2] $$\frac{1}{e_i} = m\langle r^2\rangle^{\gamma} + \frac{1}{e_0}$$

where m, γ, and e_0 are adjustable parameters. The energy term for orbital i was defined as

[3] $$e_i = 2h_i + \sum_{j}^{\text{all pairs}} g_{ij}$$

As all these calculations were carried out using rather large gaussian basis sets, one may expect that the observed relations are valid at the Hartree–Fock limit, possibly with slightly different numerical parameters m, γ, and e_0. The essentially reciprocal dependence of the energy on $\langle r^2\rangle$ is expected to be retained for E_{HF}. If E_{corr} shows a similar dependence on $\langle r^2\rangle$, one should be able to express the 'size dependence' of E_{NR} on the basis of eq. 1. In the present study the functional relation of the size dependence of E_{corr} is analysed for polyelectronic atoms and a simple method proposed for the calculation of correlation energies that may possibly be extended to the molecular cases.

Results and Discussion

One may expect that in the family of isoelectronic series of atom-ions the Be- and Ne-like ions already exhibit some features related to electron pair – electron pair interactions that may result in a somewhat more general correlation energy-size relation. Therefore, in addition to the simplest series of He-like ions previously studied (2), in our present study we concentrate on the analysis of the Be- and Ne-like isoelectronic series of ions.

Earlier studies indicated that the calculated total size, $\langle r^2\rangle$, shows only insignificant change if instead of a correlated wavefunction a near Hartree–Fock wavefunction is used (2). Since in the Hartree–Fock framework the total size $\langle r^2\rangle_{HF}$ may be given in terms of orbital contributions,

$$\langle r^2\rangle_{HF} = \sum_i \langle r^2\rangle_i$$

the true expectation value $\langle r^2\rangle_{corr}$ may also be approximated by such a sum.

In Table 1 the Hartree–Fock energies, correlation energies, and total sizes are listed for the He-, Be-, and Ne-like ions. The rather large gaussian basis sets used in calculating total sizes are specified in an earlier paper (4).

For the helium-like ions the correlation energy E_{corr} may be approximated by the empirical formula (2),

[4] $$E_{corr} = \frac{K}{(Z-\sigma)^2\langle r^2\rangle}$$

that may be converted into a linear dependence between the nuclear charge Z and the quantity $(-E_{corr}\langle r^2\rangle)^{-1/2}$. Such a relation when plotted gives a straight line with slope $(-K)^{-1/2}$ and x-intercept σ, the screening constant.

In Table 2, the best fit K and σ values are given along with the calculated correlation coefficients. The results of Table 2 may be restated in terms of correlation energies calculated using empirical formula [4], the calculated total sizes and the optimized parameters K and σ. These calculated E_{corr} values are listed in Table 3. It is apparent from these values and the excellent correlation coefficients that eq. 4 is applicable for all three series to a very good approximation. Though the relative deviations are significantly larger for the second and third series, the inter-electron-pair correlation in the series of Be- and Ne-like ions does not affect adversely the fit to relation [4] originally proposed for the two-electron systems of the He-like ions.

TABLE 1. Hartree–Fock energies, correlation energies, and sizes of helium-, beryllium-, and neon-like ions

Ion	E_{HF}[a]	E_{corr}[a]	$\langle r^2\rangle$[b]
He	−2.8616799	−0.0421	1.18484
Li^+	−7.2364140	−0.0435	0.44535
Be^{2+}	−13.611256	−0.0443	0.23183
B^{3+}	−21.986189	−0.0448	0.14189
Be	−14.573021	−0.0944	8.65968
B^+	−24.237564	−0.1123	3.96840
C^{2+}	−36.408484	−0.1268	2.31087
N^{3+}	−51.082310	−0.1412	1.52021
Ne	−128.54705	−0.393	4.68844
Na^+	−161.67691	−0.396	3.20706
Mg^{2+}	−198.83051	−0.402	2.35931
Al^{3+}	−240.00001	−0.409	1.81775

[a]Reference 5.
[b]Reference 4.

TABLE 2. Linear correlation between nuclear charge Z and the quantity $(-E_{corr}\langle r^2\rangle)^{-1/2}$ for the He-, Be-, and Ne-like ions. Parameters σ and K are defined in eq. 4, ρ is the linear correlation coefficient

Series	σ	K	ρ
He series	0.330902	−0.138417	0.999996
Be series	0.800052	−8.089775	0.998671
Ne series	4.742590	−50.313386	0.999599

TABLE 3. Comparison of correlation energies calculated for the He-, Be-, and Ne-like ions

Ions	Correlation energies		
	Ref. 5	Empirical formula (present work)	Difference
He-like ions			
He	−0.0421	−0.041934	−0.0002
Li^+	−0.0435	−0.043627	0.0001
Be^{2+}	−0.0443	−0.044351	0.0001
B^{3+}	−0.0448	−0.044748	−0.0001
Be-like ions			
Be	−0.0944	−0.091232	−0.0032
B^+	−0.1123	−0.115567	0.0033
C^{2+}	−0.1268	−0.129468	0.0027
N^{3+}	−0.1412	−0.138438	−0.0028
Ne-like ions			
Ne	−0.393	−0.388250	−0.005
Na^+	−0.396	−0.400670	0.005
Mg^{2+}	−0.402	−0.404888	0.003
Al^{3+}	−0.409	−0.405940	−0.003

The present results indicate that the total size as weighted by Z_{eff} is the most important single factor in determining correlation energies for isoelectronic atom-ions. Regarding relation

$$E_{\text{corr}} = F(Z,\langle r^2\rangle)$$

this function does not contain essential terms depending on Z or $\langle r^2\rangle$ separately. This proposition is supported not only by the excellent fit to eq. 4, but also by the fact that the small deviations in all three series show a systematic slight 'bending'. This systematic pattern of deviations suggests that the small errors are mostly due to the simplicity of the relation

$$E_{\text{corr}} = F(Z_{\text{eff}}{}^2\langle r^2\rangle)$$

rather than the somewhat arbitrary pairing of variables Z_{eff} and $\langle r^2\rangle$. If correction terms depending on Z_{eff} and $\langle r^2\rangle$ separately would be important, then larger and less systematic deviations from eq. 4 could be expected.

The present results also lend hopes that in series of analogous molecules similar relationships may exist between sizes of molecular orbitals and correlation energies and may be utilized for approximate determination of molecular correlation energies.

Acknowledgements

The financial support of the National Research Council of Canada and the Italian C.N.R. is gratefully acknowledged.

1. E. CLEMENTI and H. POPKIE. J. Chem. Phys. **57**, 4870 (1972); G. C. LIE and E. CLEMENTI. J. Chem. Phys. **60**, 1275 (1974); **60**, 1288 (1974).
2. F. BERNARDI, I. G. CSIZMADIA, V. H. SMITH, JR., M. H. WHANGBO, and S. WOLFE. Theor. Chim. Acta, **37**, 171 (1975).
3. M. A. ROBB, W. J. HAINES, and I. G. CSIZMADIA. J. Am. Chem. Soc. **95**, 42 (1973).
4. R. DAUDEL, P. G. MEZEY, J. D. GODDARD, and I. G. CSIZMADIA. Can. J. Chem. **53**, 3739 (1975).
5. E. CLEMENTI. J. Chem. Phys. **38**, 2248 (1963).

Metal complex catalyzed reactions of anils. II. Transimination

A. R. BOATE AND D. R. EATON
Department of Chemistry, McMaster University, Hamilton, Ont., Canada L8S 4M1

Received August 19, 1976

A. R. BOATE and D. R. EATON. Can. J. Chem. **55**, 2426 (1977).

The exchange of aromatic residues between anilines and anils (transimination) has been shown to be efficiently catalyzed by metal complexes of thiourea. This reaction can be conveniently studied by nmr spin saturation transfer techniques. Experiments of this type using both CW and FT nmr spectrometers are reported. The rate of the reaction is about two orders of magnitude greater than the rates of reactions involving anil formation and hydrolysis with the same substrates and catalysts. The effectiveness of the catalysts vary in the same manner as they do for anil formation and the reaction is similarly subject to inhibition by competing ligands. The rate of exchange of the two inequivalent methyl groups in acetone anils is similarly catalyzed and may be studied by spin saturation transfer experiments. The lifetime of an anil molecule for methyl group exchange is approximately twice that for transimination suggesting that the rate determining process for transimination results in free rotation about the C—N bond so that the methyl groups have an equal probability of retaining or exchanging their environments.

A. R. BOATE et D. R. EATON. Can. J. Chem. **55**, 2426 (1977).

On a démontré que l'échange de résidus aromatiques entre des anilines et des anils (transimination) est catalysé d'une façon efficace par des complexes métalliques de la thiourée. Cette réaction peut être étudiée facilement par les techniques de transfert de saturation de spin en rmn. On rapporte des expériences de ce type faisant appel à des spectromètres rmn, CW et FT. La vitesse de la réaction est pratiquement deux ordres de grandeur plus grande que les vitesses de réactions impliquant la formation d'anil et l'hydrolyse avec les mêmes substrats et les mêmes catalyseurs. L'efficacité des catalyseurs varie de la même manière que pour la formation de l'anil et la réaction est aussi sujette à une inhibition par des ligands en compétition. La vitesse d'échange de deux groupes méthyles non-équivalents dans des anils de l'acétone est aussi catalysée d'une façon similaire et peut être étudiée par des expériences de transfert de saturation de spin. Le temps de vie d'une molécule d'anil par rapport à l'échange du groupe méthyle est approximativement deux fois plus grand que celui de la transimination; ces résultats suggèrent que le processus déterminant la vitesse pour les transiminations provient d'une rotation libre autour du lien C—N d'une façon telle que les groupes méthyles ont une probabilité égale de retenir ou d'échanger leur environnement.

[Traduit par le journal]

Introduction

The initial paper in this series (1) described experiments demonstrating the metal complex catalyzed formation and hydrolysis of anils, *e.g.*

[1] $C_6H_5NH_2 + (CH_3)_2CO \rightleftharpoons C_6H_5N{=}C(CH_3)_2 + H_2O$

Similar reactions occur with a variety of substituted anilines and aliphatic ketones and are very efficiently catalyzed by small concentrations of thiourea and substituted thiourea complexes of cobalt, nickel, and zinc. A subsequent paper will describe detailed studies of the kinetics and mechanisms of these reactions. There is, however, a second reaction occurring concurrently, namely, transimination. Transimination results in the exchange of aromatic residues between the aniline and the anil, *e.g.*

[2] 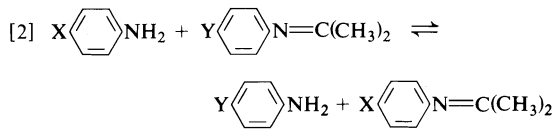

where X and Y may be different or identical substituents. It is very probable that the mechanisms for anil formation and for transimination are closely related. In the present paper we will therefore describe a number of experiments demonstrating catalyzed transimination before returning to a discussion of the mechanistic aspects of all of these reactions in the third paper of this series.

Most of the reactions to be discussed below are quite rapid. Typically the average lifetime of a reactant is a few seconds. A very useful tech-

nique for studying reactions on this timescale is provided by nmr experiments involving spin saturation transfer (SST). The theory involved in experiments of this type has been given by Forsen and Hoffman (2, 3) who used the method to measure keto–enol isomerization rates of acetylacetone. There have been relatively few quantitative applications. Van Leeuwen and Praat (4) have measured exchange rates in π allyl palladium complexes. Sherrod *et al.* (5) have studied kinetic isotope effects in metaparacyclophanes and Kabakoff and Namanworth (6) have used the method to measure a rotation barrier in the dimethylcyclopropylcarbinyl cation. Some interesting recent applications are provided by the work of Creelmore and Reilly (7) in determining the exchange rates for water with an ion exchange resin and that of Redfield and coworkers (8) in studying rates of electron transfer and ligand exchange for cytochrome *c* enzymes. A review by Faller (9) provides examples of more qualitative applications.

Briefly, the experiment involves choosing a pair of resonances (A and B) involved in an exchange process, saturating one (B) by applying a strong RF field and observing the effect on the second resonance A. When equilibrium has been reached the magnetization at site A ($M_\infty{}^A$) will be less than the value in the absence of the saturating field ($M_0{}^A$) since nuclei with their spin populations equalized will have been transferred from site B to site A. Forsen and Hoffman showed that:

$$M_\infty{}^A = M_0{}^A \frac{\tau_{1A}}{T_{1A}} \quad [3]$$

where

$$\frac{1}{\tau_{1A}} = \frac{1}{T_{1A}} + \frac{1}{\tau_A} \quad [4]$$

In these equations T_{1A} is the spin–lattice relaxation time and τ_A is the lifetime for chemical exchange of the A nuclei. If T_{1A} is known τ_A can be found and since

$$\frac{\tau_A}{\tau_B} = \frac{M_0{}^A}{M_0{}^B} \quad [5]$$

this leads to τ_B. In principle T_{1A} can be found either from the decay in the magnetization at A after applying the saturating field or from its recovery after removing the saturating field. In practice it is often more convenient to measure T_{1A} in an independent experiment. This is particularly the case if an FT instrument is available since T_1's for all nuclei in an exchanging system can be measured easily and routinely. It should be noted that T_2 is affected by chemical exchange but T_1 is not.

The utility of this technique to transimination reactions may be seen by reference to eq. 2. If X = Y in this equation, transimination will exchange the substituent between aniline and anil and spin saturation transfer effects may be anticipated if either the anil or the aniline resonance is irradiated and the other site observed. On the other hand the methyl peaks of the anil are in identical sites in the reactants and products. Only anil formation and hydrolysis will lead to exchange of methyl groups with the acetone present. A third process is however possible. The two CH_3 peaks are not equivalent, *e.g.*

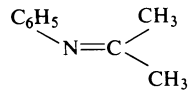

If the N=C bond is broken or weakened during the transimination reaction exchange between the methyl groups *cis* and *trans* to the aryl group may be anticipated.

^{19}F *Spin Saturation Transfer Experiments*

There are a number of practical limitations to the application of the spin saturation transfer technique. It is essential that there be no direct effect of the saturating field at frequency B on the observed resonance at frequency A. If A and B are too close together in frequency interference will occur. Experimentally it was found that a minimum separation of ~20 Hz is necessary if a CW instrument is used. Much smaller separations (3 or 4 Hz) are possible if an FT instrument is used. Initial experiments were therefore carried out on the ^{19}F resonances of *p*-fluoroaniline and its acetone anil. These resonances are separated by 400 Hz at 56.4 MHz and direct interference of the irradiating field is negligible. In the absence of catalyst, irradiation of either the aniline or anil peak produced no effect on the other peak. In the presence of either $Zntu_2Cl_2$ or $Zntu_4(ClO_4)_2$ spin saturation transfer was readily observed. The ^{19}F nuclei in both compounds are coupled to the aromatic protons. For quantitative work it is necessary to decouple

these protons by applying a strong RF field at 60 MHz.

It is necessary to position the observing frequency on the exact centre of one of the resonances and to observe the intensity at this frequency as the saturating field is switched on and off. An automatic device for switching the various fields was used and the results of a number of switching cycles accumulated in a Computer of Average Transients (CAT) to optimize the signal to noise ratio. The results of such an experiment involving *p*-F aniline and its acetone anil with $Zntu_4(ClO_4)_2$ as the catalyst and Freon 112 present for locking purposes are shown in Fig. 1. The *Y* axis represents intensity at the centre of the decoupled anil resonance (site A) and the *X* axis represents time. The time for one complete cycle was 100 s and this low noise level was achieved by accumulating 100 cycles. At point A the saturating field was switched off and the signal recovered to its full intensity at B. The observing signal was then switched off to obtain a base line reading. However, idiosyncrasies in the electronics results in a false base line reading and the true position was obtained by jumping the observing frequency (still at zero power) several hundred Hz off resonance at point C of Fig. 1. At point D the observing frequency reverted to the resonance position and was switched on. At point E the saturating frequency was switched on and the decay of the signal to its original value has occurred at point F. The value of $M_\infty{}^A/M_0{}^A$ can be obtained directly from this plot. From the decay of the magnetization commencing at point E a plot of $\ln [M_z{}^A(t) - M_\infty{}^A]$ against t has a slope of τ_{1A}. This information suffices to determine both T_{1A} and τ_A. If τ_A is relatively

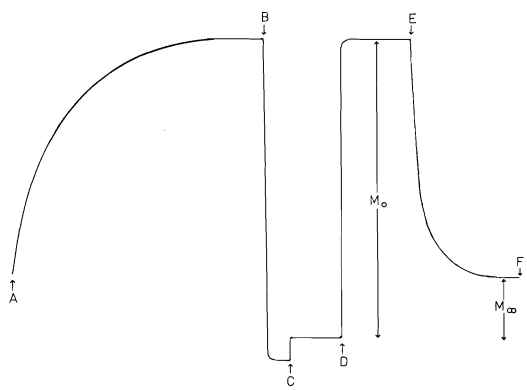

FIG. 1. Output from ^{19}F spin saturation transfer experiment. See text for explanation.

short compared to T_{1A} it is also possible to determine T_{1A} from the recovery curve commencing at point A. A third alternative is to measure $M_\infty{}^A/M_0{}^A$ and then find T_{1A} for *p*-F aniline independently using the saturation recovery technique. This last method has the inherent disadvantage that the environment of the *p*-F aniline in the reacting mixture is not the same as in a simple solution of *p*-F aniline and hence the T_1 obtained may not be appropriate.

In a typical experiment, values of τ_A (aniline) of 1.5 s, of τ_B (anil) of 0.5 s, of T_{1A} 9.5 s, and of T_{1B} 8.0 s were obtained. The T_1'*s* in this case were obtained from observation of the decay of magnetization. Although quite reproducible these T_1's agreed poorly with direct determinations of the T_{1A} for *p*-fluoroaniline. It must be concluded that T_{1A} is sensitive to the environment (probably water and catalyst concentrations are the determining factors) and that determination of T_1 in the reacting solution is necessary.

The experimental problems involved in these experiments, most notably the difficulty in maintaining ^{19}F and ^1H decoupling oscillators to the requisite 0.1 Hz frequency stability, limit the accuracy of quantitative data obtained using CW spectrometers. The results obtained with an FT instrument, described below, are much more reliable. However, a number of qualitative experiments served to better define the catalytic system. Thus it was shown that the metal salts and complexes, previously reported (1) to catalyze anil formation, also catalyze transimination. Using $Zntu_4(ClO_4)_2$ as a catalyst addition of excess thiourea decreased the spin saturation transfer showing inhibition by thiourea. In another experiment using $Ni(ClO_4)_2.6H_2O$ as a catalyst almost complete inhibition by ortho phenanthroline and terpyridine was demonstrated. The stability of the catalysts was also investigated. Thus a solution of $Zntu_4(ClO_4)_2$ lost approximately 8% of its catalytic activity as measured by the ratio $M_0{}^A/M_\infty{}^A$ in 6 h and transimination had ceased after the solution had stood for 1 week. In all these respects the catalysis of transimination shows essentially the same characteristics as does that of anil formation and hydrolysis.

^1H *Spin Saturation Transfer Experiments*

Using CW instruments it is difficult to examine transimination directly by proton nmr

since the aniline and anil peaks are usually not sufficiently separated. In these cases interference from the saturating field and Bloch-Seegert shifts of the observing resonance preclude spin saturation transfer experiments. However, it is possible to examine exchange between the two inequivalent methyl peaks since these are separated by 38 Hz at 100 MHz. It was noted that the addition of $Zntu_4(ClO_4)_2$ to a solution of the acetone anil of *p*-F anil caused a slight broadening of these methyl resonances suggesting that an exchange process might be occurring. Figure 2 illustrates SST experiments on this system. Trace A shows the methyl peaks of the anil together with a small peak due to acetone and solvent peaks (CD_2HCN). Irradiation of the high field CH_3 has no effect on either the low field CH_3 or the acetone (trace B). Addition of $Zntu_4(ClO_4)_2$ catalyst causes slight broadening (trace C). Irradiation of the low field CH_3 peak in the catalyst containing solution clearly causes spin saturation transfer to the low field CH_3 but not to acetone (trace D).

It is of interest to compare the rate of exchange of anil CH_3 peaks with the rate of transimination and with the rate of anil hydrolysis. For this purpose a sample containing an equilibrium mixture of *p*-F aniline and its acetone anil was first examined by both ^1H and ^{19}F SST. In both cases no effect was observed. $Zntu_4(ClO_4)_2$ was then added and the SST experiments repeated. Transfer of spin saturation was now observed and using the methods described above the ^{19}F experiment yielded lifetimes for the anil (τ_{anil}) of 0.72 s and for the aniline ($\tau_{aniline}$) 1.73 s. From the ^1H experiment we obtain $\tau_A = \tau_B = 1.55$ s. The lifetime of an anil molecule for interchange of the methyl groups is therefore greater than its lifetime for the transimination reaction by a factor of 2.1. The same sample was then split into two portions and the equilibrium for anil formation or hydrolysis displaced by adding acetone to one portion and water to the other portion. Return to equilibrium was monitored by measuring the change in intensity of the acetone and anil CH_3 peaks as a function of time. In the case of the sample with water added the reaction could be followed rather easily and the results are shown in Fig. 3. It may be noted that it took approximately 30 min to reach equilibrium so that anil hydrolysis is obviously considerably slower than transimination. From the slope of the curve in Fig. 3 an initial rate of 3×10^{-3} mol/ℓ s is obtained. This may be compared with the rate for transimination at equilibrium, *i.e.*

$$\text{Rate} = \frac{[\text{anil}]}{\tau_{anil}} = \frac{0.66}{0.74} = 0.9 \text{ mol}/\ell\text{ s}$$

Transimination is faster than anil hydrolysis by a factor of at least 10^2.

All of the experiments described above have involved transimination reactions in which the anil substituent and the aniline substituent are the same, *i.e.* X = Y in eq. 2 so that there is no net reaction. It seemed worthwhile to illustrate the generality of the reaction by demonstrating rapid transimination in a case where $X \neq Y$. The following experiment served this purpose. A sample of *p*-toluidine (0.2 *M*) in acetone was

FIG. 2. ^1H nmr spin saturation transfer experiment with the acetone anil of *p*-F aniline in CD_3CN. See text.

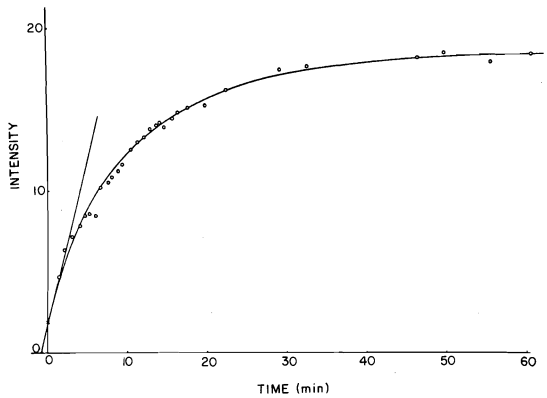

FIG. 3. Intensity of acetone peak as a function of time after addition of water to an equilibrium solution of *p*-F aniline and its acetone anil in CD_3CN. Catalyst $Zntu_4(ClO_4)_2$.

prepared, a little $Zntu_4(ClO_4)_2$ added and anil formation monitored by measuring the intensities of the p-CH_3 peaks of p-toluidine and its anil as a function of time. After 30 min the reaction had proceeded roughly 66% to completion. At this point sufficient aniline was added to the sample to make it 0.4 M in aniline. The first nmr sweep through the methyl region after the addition of aniline showed that the ratio

$$\frac{[p\text{-toluidine anil}]}{[p\text{-toluidine anil}] + [p\text{-toluidine}]}$$

had changed from 0.40 to 0.13. This occurred in less than 1 min. The added aniline has reacted with the p-toluidine anil by a transimination reaction, *i.e.*

[6] 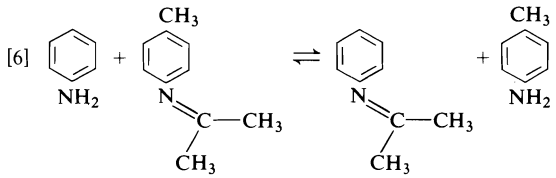

This has increased the concentration of p-toluidine and decreased that of p-toluidine anil to produce the change in the ratio noted above. Again the indication is that this reaction is faster than anil formation by a factor of at least 10^2. Reaction 6 does not occur in the absence of catalyst.

Fourier Transform Spin Saturation Transfer Experiments

There are two major advantages in using an FT instrument for SST experiments, namely, (*a*) a much smaller separation of peaks is necessary, and (*b*) the required T_1's can be measured directly in the presence of chemical exchange. This latter factor is of some significance. Thus the T_1 for the methyl group of p-toluidine changed from 3.0 s to 2.4 s as the concentration of $Zntu_2Cl_2$ was increased from 0.15 M to 0.45 M. Unfortunately an FT instrument was available only in the final stages of the present work. We report, however, some initial measurements on transimination reactions involving p-toluidine since this amine was used for many of the studies on anil formation and hydrolysis and a comparison with transimination is of interest. The p-CH_3 peaks of p-toluidine and its acetone anil are approximately 9 Hz apart at 90 MHz and it was shown that this separation was sufficient to allow SST experiments to be carried out on a Brucker WH 90 instrument. Some results are shown in Table 1. The $Zntu_2Cl_2$ used as a catalyst is a rather poor catalyst for anil formation and is also a relatively poor catalyst for transimination hence the rather high catalyst concentrations. The ratio R shown in the last column should be equal to 1 and provides a check on the experiment. An approximate comparison may be made between these lifetimes and the rate of anil formation with the same catalyst. For the same initial concentration of p-toluidine and for a catalyst concentration of 0.02 mol/ℓ the initial rate of anil formation was found to be 1.6×10^{-4} mol/ℓ s. This corresponds to an aniline lifetime of 1200 s. Since rate has been shown to be proportional to catalyst concentration this would give a lifetime of 120 s at 0.2 M compared to 4 s for transimination. A number of factors, however, make this comparison inaccurate. Thus the initial rate measurements were carried out at 35°C and the SST experiments at 27°C. The initial rate experiments used p-toluidine-d_2 and the SST experiments p-toluidine-h_2. The SST experiments refer to the rate at equilibrium rather than the initial rate. All three factors would tend to increase the difference between the rate of anil formation and that of transimination. The true ratio of rates is therefore most probably greater than the factor of 30 indicated and is likely to be of the order 10^2 as found for p-F aniline.

TABLE 1. FT spin saturation transfer experiments[a]

Concentration of catalyst (mol/ℓ)	T_1 (s)	τ_{anil} (s)	$\tau_{aniline}$ (s)	R^b
0.14	3.1	7.7	4.6	1.0
0.39	2.4	4.0	2.2	1.16

[a]Initial solution 0.2 M p-toluidine in acetone. Catalyst $Zntu_2Cl_2$. Temperature 28°C. Frequency 90 MHz.
[b]$R = (M_0^{anil}/M_0^{aniline})/(\tau_{anil}/\tau_{aniline})$.

Discussion

The spin saturation transfer experiments described above have clearly demonstrated a metal complex catalyzed reaction which exchanges aniline and anil substituents. This could be accomplished by reaction 1 involving the formation and hydrolysis of the anil. If this were so exchange between acetone and anil should occur at the same rate as between aniline and anil. Since the former exchange is approximately two orders of magnitude slower we conclude that the

exchange between aniline and anil proceeds by the transimination reaction 2. Except for its greater rate, the characteristics of this catalyzed reaction are very similar to those of the anil formation reaction. A catalyst which is effective for anil formation is effective for transimination and vice versa. Both reactions are inhibited by excess thiourea and by chelating ligands.

It has also been shown that the exchange of the non-equivalent anil methyl groups is metal complex catalyzed. It has been reported that the nmr spectrum of *N*-isopropylidene aniline shows coalescence of these methyl peaks at 126°C (10). In the absence of catalyst there is no indication of exchange at room temperature. The lifetime for methyl exchange is twice that for transimination. A hypothesis which satisfactorily accounts for these observations is that rotation about the C—N bond takes place during and only during transimination. If there were free rotation about this bond there would be an equal probability of a given CH_3 retaining or exchanging its environment in the product anil. Hence the lifetime for methyl exchange should be twice that for transimination. The agreement of the experimental ratio of 2.1 with this prediction is possibly fortuitous but it seems clear that the rate determining steps in both processes are closely related and that any proposed mechanism for these reactions must be consistent with this observation.

Experimental

The preparation and purification of the reagents and catalysts used in these studies have been described previously (1).

The nmr instruments used were a Varian HA 100 (probe temperature 34.5–35.0°C), a Varian DP 60 (probe temperature 27°C), and a Brucker WH 90 (probe temperature 26.5°C). The DP 60 operated at 56.4 MHz for ^{19}F studies and was modified for proton decoupling by supplying 60 MHz radiation from a crystal controlled frequency generator (General Radio Co.) amplified with an operational amplifier (Model 805, RF Communications Inc.) and fed into two specially tuned coils fitted in the spectrometer probe. The decoupled ^{19}F signal of *p*-F aniline had a line width of less than 0.5 Hz. An automatic device for switching the various fields required in the SST experiments and triggering the CAT was built. The main component of this device was an accurate variable speed electric motor driving a plastic disc to activate appropriate micro switches. On the WH 90 homonuclear decoupling may be accomplished using either a pulsed or gated decoupler. Both methods were used with the gated decoupling being rather more satisfactory since it produced less distortion near the decoupling frequency. A necessary condition for using this decoupling for SST experiments is that either $T_2^* \ll T_1$ or $\tau_A > T_{1A}$. These conditions were adhered to. Since the internal computer routines for intensity and area calculations are unreliable in the vicinity of the saturating frequency, intensities were measured directly from the spectra relative to a standard reference peak (usually TMS).

Acknowledgement

We are indebted to the National Research Council of Canada for financial support of this research.

1. A. R. Boate and D. R. Eaton. Can. J. Chem. **54**, 3895 (1976).
2. S. Forsen and R. A. Hoffman. J. Chem. Phys. **39**, 2892 (1963).
3. S. Forsen and R. A. Hoffman. J. Chem. Phys. **40**, 1189 (1964).
4. P. W. N. M. van Leeuwen and A. P. Praat. J. Organomet. Chem. **42**, 725 (1970).
5. S. A. Sherrod, R. L. da Costa, R. A. Barnes, and V. Boekelheide. J. Am. Chem. Soc. **96**, 1565 (1974).
6. D. S. Kabakoff and E. Namanworth. J. Am. Chem. Soc. **92**, 3234 (1970).
7. R. W. Creelmore and C. N. Reilley. Anal. Chem. **42**, 725 (1970).
8. R. K. Gupta, S. H. Koenig, and A. G. Redfield. J. Mag. Res. **7**, 66 (1972); R. K. Gupta and A. G. Redfield. Science, **169**, 1204 (1970).
9. J. W. Faller. *In* Determination of organic structures by physical methods. Vol. 5. *Edited by* F. C. Nachod and J. J. Zuckerman. Academic Press, New York. 1973. p. 75.
10. H. A. Staab. Ann. Chem. **708**, 36 (1967).

Metal complex catalyzed reactions of anils. III. Kinetic and mechanistic studies

A. R. BOATE AND D. R. EATON

Department of Chemistry, McMaster University, Hamilton, Ont., Canada L8S 4M1

Received October 4, 1976

A. R. BOATE and D. R. EATON. Can. J. Chem. **55**, 2432 (1977).

The kinetics of the homogeneously catalyzed formation and hydrolysis of anils in non-aqueous solution have been studied. The catalysts used are zinc complexes of thiourea. It is shown that all the evidence obtained, kinetic and otherwise, is consistent with a model in which the rate determining step for anil formation is nucleophilic attack by an aniline held in the second coordination sphere of the metal complex on an acetone molecule directly bound to the metal atom. Analogous mechanisms are suggested for anil hydrolysis and for transimination.

A. R. BOATE et D. R. EATON. Can. J. Chem. **55**, 2432 (1977).

On a étudié la cinétique de la formation, catalysée d'une façon homogène, et l'hydrolyse d'anils dans des solutions non-aqueuses. Les catalyseurs utilisés sont des complexes de zinc de la thiourée. On montre que toutes les données obtenues, soit cinétiques ou autres, sont en accord avec un modèle dans lequel l'étape déterminante de la réaction pour la formation de l'anil est une attaque nucléophile par une aniline maintenue dans la seconde sphère de coordination du complexe métallique d'une molécule d'acétone directement liée à l'atome métallique. On suggère des mécanismes analogues pour l'hydrolyse de l'anil et pour la transimination.

[Traduit par le journal]

Introduction

Previous papers (1) in this series have demonstrated that reactions involving anil formation, anil hydrolysis, and transimination are effectively catalyzed by a variety of metal complexes, particularly a series of thiourea and substituted thiourea complexes of cobalt, nickel, and zinc. The present paper describes kinetic and mechanistic studies of these reactions.

Anil Formation

(i) Dependence on Catalyst Concentration

The reaction of interest is the formation of an anil from an aniline, *e.g.*, *p*-toluidine and a ketone such as acetone, *i.e.*

[1] $p\text{-}CH_3C_6H_4NH_2 + (CH_3)_2CO \rightleftharpoons p\text{-}CH_3C_6H_4\cdot N{=}C(CH_3)_2 + H_2O$

At low concentrations of catalyst this reaction can be conveniently followed by repetitively scanning the methyl region of the ^1H nmr spectrum and observing the decrease of the $p\text{-}CH_3$ of the toluidine and the increase in intensity of the corresponding anil peak. A typical experimental trace is shown in Fig. 1. The fraction of anil formed, *i.e.* [Anil]/[Anil] + [Aniline]) can be found as a function of time from the measured intensities. The initial rate of the reaction can be obtained graphically. Alternatively since the reaction can be followed to equilibrium the complete reaction curve can be fitted to the equation:

$$\frac{d[Anil]}{dt} = k_1[Aniline] - k_2[Anil]$$

using a standard computer programme (2). The experimental data of Fig. 1 gave $k_1 = 0.136$ min^{-1} with a standard deviation of 0.0021 compared with the value $k_1 = 0.132$ min^{-1} obtained graphically. The plot of residuals from the computer fit was completely random. We estimate that rates obtained by this experimental method are accurate to at least $\pm 10\%$.

Table 1 presents data illustrating the dependence of rate on catalyst concentration. An excellent linear dependence is observed with the very small intercept showing that the rate of the uncatalyzed reaction is negligible. A plot of log (initial rate) against log (catalyst concentration) has a slope of 0.94 confirming that the reaction is indeed first order in catalyst.

(ii) Dependence on Aniline Concentration

The dependence of the initial rate on aniline concentration may be determined in essentially the same manner as described above. There is however one complication. The acetone-d_6 used contains D_2O as an impurity and this will rapidly exchange with the NH_2 protons. The

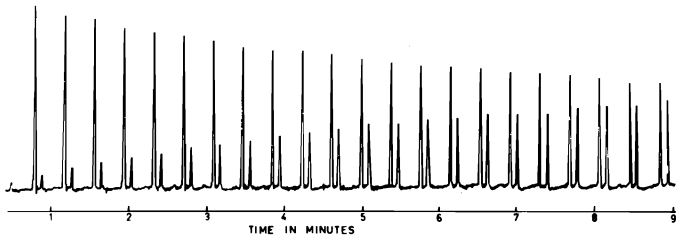

FIG. 1. Repeated scans of the methyl nmr peaks showing the diminution of the *p*-toluidine peak and the growth of the anil peak.

TABLE 1. Dependence of the initial rate of anil formation on catalyst concentration[a]

Catalyst concentration (mol/ℓ)	Initial rate (mol/ℓ s)
5.0×10^{-5}	5.8×10^{-5}
1.0×10^{-4}	1.14×10^{-4}
2.0×10^{-4}	2.10×10^{-4}
3.0×10^{-4}	3.05×10^{-4}
4.0×10^{-4}	4.20×10^{-4}

[a]Catalyst $Zntu_4(ClO_4)_2$, 0.19 *M* *p*-toluidine in acetone-d_6, $T = 35°C$.

extent of deuteration will vary with the concentration of *p*-toluidine used. If there is a significant kinetic isotope effect (see below) this factor will influence the apparent dependence of the rate on *p*-toluidine concentration. This problem was avoided by using *p*-toluidine-d_2 for the initial rate experiments. The results of a series of such measurements are shown in Table 2. The dependence on *p*-toluidine concentration is not linear as shown in Fig. 2*a*. The shape of this curve is reminiscent of the results obtained in many studies of enzyme kinetics in which there is a rapid pre-equilibrium between the enzyme and substrate followed by a rate determining reaction of the enzyme–substrate complex (Michaelis–Menton kinetics) (3). In such cases a linear plot is obtained by plotting the reciprocal of rate against the reciprocal of substrate concentration (a Lineweaver–Burk plot). Such a plot is indeed linear (Fig. 2*b*), suggesting a rapid pre-equilibrium leading to Michaelis–Menton kinetics or some more complex scheme which reduces to the same general mathematical form. The data in Table 2 show results for two catalysts. It may be noted that the catalyst concentrations differ by two orders of magnitude. In both cases the dependence of rate on substrate concentration was essentially the same.

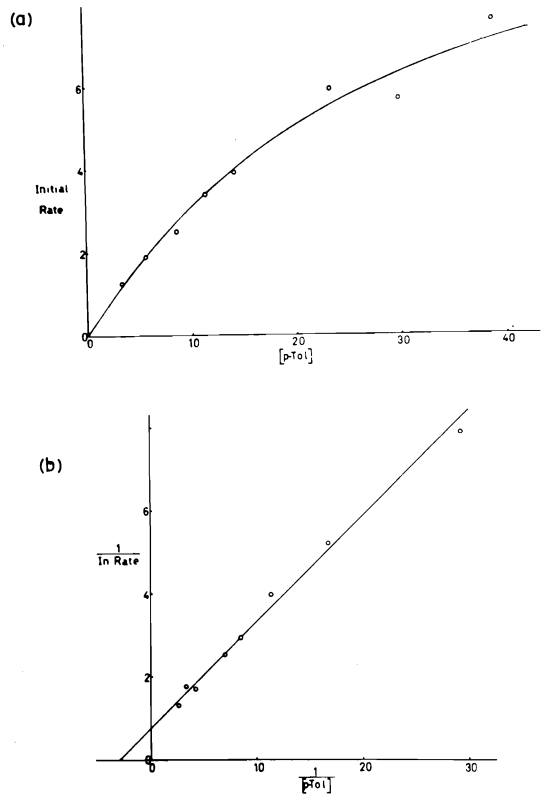

FIG. 2. (*a*) Dependence of initial rate of anil formation (mol/min × 10^6) on concentration of *p*-toluidine-d_2 (mol × 10^5); (*b*) double reciprocal plot of these data.

(iii) Overall Concentration Dependence

Since the anil formation reaction is carried out using acetone-d_6 as a solvent it is not feasible to directly examine the effect of varying the acetone concentration on the initial rate. An alternative experiment is to investigate the effect on the rate of dilution with an 'inert' solvent. In this context an 'inert' solvent is one which is incapable of functioning as a ligand in the metal complex. The concentrations of the various metal complex species in solution are controlled by equilibria

TABLE 2. Dependence of the initial rate of anil formation on *p*-toluidine concentration

Catalyst $Zntu_4(ClO_4)_2$[a]		Catalyst $Zntu_2Cl_2$[b]	
[*p*-Tol-d_2] (mol/ℓ)	Initial rate (mol/ℓ s)	[*p*-Tol-d_2] (mol/ℓ)	Initial rate (mol/ℓ s)
6.70×10^{-2}	4.23×10^{-5}	6.42×10^{-2}	7.43×10^{-5}
1.18×10^{-1}	6.40×10^{-5}	1.17×10^{-1}	1.21×10^{-4}
1.73×10^{-1}	8.38×10^{-5}	1.61×10^{-1}	1.44×10^{-4}
2.31×10^{-1}	1.15×10^{-4}	2.13×10^{-1}	1.67×10^{-4}
2.83×10^{-1}	1.31×10^{-4}	2.92×10^{-1}	2.24×10^{-4}
4.71×10^{-1}	1.96×10^{-4}	6.20×10^{-1}	3.31×10^{-4}
6.07×10^{-1}	1.86×10^{-4}		
7.80×10^{-1}	2.52×10^{-4}		

[a]Catalyst concentration 1.2×10^{-4} *M*, $T = 35°C$.
[b]Catalyst concentration 2.2×10^{-2} *M*.

TABLE 3. Dependence of initial rate of anil formation on dilution with carbon tetrachloride[a]

CCl_4 as fraction of sample volume	[Catalyst] (mol/ℓ)	[*p*-Toluidine] (mol/ℓ)	Initial rate (mol/ℓ s)
0	1.0×10^{-4}	2.38×10^{-1}	1.43×10^{-4}
0.2	1.0×10^{-4}	1.91×10^{-1}	1.44×10^{-4}
0.4	1.0×10^{-4}	1.43×10^{-1}	1.34×10^{-4}
0.6	1.0×10^{-4}	0.95×10^{-1}	1.45×10^{-4}

[a]Catalyst $Zntu_4(ClO_4)_2$, $T = 35°C$.

of the type:

$$ML_n + X \rightleftharpoons ML_{n-1}X + L$$

If a fraction α of ML_n has reacted, at equilibrium the concentrations of the various species will be determined by:

$$[2] \qquad \frac{m^2\alpha^2}{m(1-\alpha)(x-m\alpha)} = K$$

where m is the initial concentration of ML_n and x is the initial concentration of X. If the solution is now diluted by a factor V the initial concentration of ML_n becomes m/V and x becomes x/V. However, the fraction α is independent of V since there are an equal number of concentration terms in the numerator and denominator of eq. 2. It follows therefore that providing all metal complex species in solution have the same coordination number and providing the diluting solvent does not participate in any of the ligand exchange equilibria, dilution by a factor V will reduce the concentration of each species in solution by this factor but will not affect the relative concentrations of any of the species. In the present case carbon tetrachloride was used as a diluting solvent since it seems unlikely that it could function as a ligand. There is also evidence that both Co(II) and Zn(II) remain tetrahedral and four coordinate (4, 5) in all these systems so that the above conditions are met.

The results of such a dilution experiment are shown in Table 3. In this experiment the reacting mixture of *p*-toluidine and acetone was progressively diluted with carbon tetrachloride and a quantity of catalyst sufficient to make the solution 1.0×10^{-4} *M* in catalyst added to each sample. It is apparent that the initial rate of anil formation measured by the method described above is independent of dilution. The significance of this result will be discussed below.

(iv) Dependence on Thiourea Concentration

From the experiments described above and in a previous paper (1) it is very likely that these catalysts function by dissociation of thiourea and coordination of one or more of the substrate molecules to the metal ion. In this case excess thiourea should inhibit the reaction. This is indeed the case. Table 4 presents data showing the effect of excess thiourea on the initial rate of formation of *p*-toluidine anil. A plot of initial rate against the reciprocal of thiourea concentration passes through the origin showing that the complete repression of thiourea dissociation

TABLE 4. Dependence of initial rate of anil formation on thiourea concentration[a]

Thiourea added (mol/ℓ)	Initial rate (mol/ℓ s)
0	1.57×10^{-2}
4.08×10^{-3}	1.24×10^{-2}
9.08×10^{-3}	1.07×10^{-2}
1.65×10^{-2}	8.46×10^{-3}
2.58×10^{-2}	6.73×10^{-3}
5.61×10^{-2}	5.19×10^{-3}

[a]Catalyst 2.0×10^{-4} *M* $Zntu_4(ClO_4)_2$, 0.188 *M* *p*-toluidine, $T = 35°C$.

results in complete inhibition of the reaction. In these experiments the added thiourea ranges from ten to one hundred times the thiourea present in the $Zntu_4(ClO_4)_2$ catalyst so that total thiourea equals added thiourea to a good approximation. No catalysis attributable to thiourea itself rather than to a metal complex was noted in these experiments.

Anil Hydrolysis

(i) Dependence on Anil Concentration

The reverse reaction of [1] is anil hydrolysis. As it must be, this reaction is also catalyzed by thiourea complexes of zinc and cobalt. Since the anil can be prepared indirectly the kinetics of its catalyzed hydrolysis can also be studied using the nmr method described above. In this case, a double reciprocal plot of the data has a pronounced curvature. In enzyme kinetics such a curvature is often interpreted as arising from inhibition by the substrate itself (3). This is not unreasonable in the present case. The equilibrium constant for the formation of a metal anil complex is higher than for all other ligands except thiourea (1). At high anil concentrations the metal could therefore tend to become saturated with anil to the exclusion of the other substrate water. Inhibition would then result.

(ii) Dependence on Water Concentration

The dependence of the initial rate of anil hydrolysis on water concentration was also studied. D_2O was used for this study to avoid kinetic isotope effects. The amount of water present in the acetone-d_6 was found from the position of the final equilibrium. The double reciprocal plot for these data is linear.

(iii) Overall Concentration Dependence

The effect of dilution with an inert solvent (carbon tetrachloride) on the initial rate for anil hydrolysis has also been examined. This experiment was carried out in a slightly different manner to the corresponding experiment for anil formation. A stock solution of anil in acetone-d_6 with a little D_2O added was prepared and diluted with CCl_4 to make up five samples. Catalyst solution was added to each of these samples sufficient to keep the relative concentrations of anil and catalyst constant in each sample. This procedure differs from that used in the anil formation experiment in that the concentration of the catalyst as well as those of the substrates was progressively diminished. The results are shown in Table 5 in terms of the relative initial rates. It is apparent that the initial rate decreases in direct proportion to the fraction of carbon tetrachloride in the mixture. Since it has already been shown that the initial rate is proportional to catalyst concentration this result is exactly equivalent to the result obtained for anil formation, *i.e.* that initial rate was independent of dilution of the reactants.

The Kinetic Isotope Effect

In general isoptopically substituted molecules do not react at the same rates. The effect of substituting deuterium for hydrogen are particularly marked since the mass ratio of these two isotopes is greater than that of any other pair. The magnitude of the kinetic isotope effect depends on the nature of the rate determining step (6). If this step involves proton transfer a large primary kinetic isotope effect may be anticipated. If it does not involve proton transfer a smaller, secondary effect is predicted. We have already presented indirect evidence that proton transfer steps are too rapid to be rate determining in the present catalytic reactions (1). Since, however, this is a mechanistically impor-

TABLE 5. Dependence of initial rate of anil hydrolysis on dilution with carbon tetrachloride[a]

CCl_4 as fraction of sample volume	Relative concentrations of reagents	Relative initial rate
0	1.00	1.00
0.20	0.80	0.72
0.40	0.60	0.57
0.60	0.40	0.41
0.80	0.20	0.18

[a]Catalyst 1.13×10^{-3} *M* $Zntu_4(ClO_4)_2$, 0.27 *M* *p*-toluidine anil, $T = 35°C$.

tant conclusion it seemed worthwhile to obtain direct kinetic evidence on this point.

The experiment is somewhat complicated by the presence of D_2O in the acetone-d_6 used as solvent. As a result of this, as discussed previously, rapid exchange leads to partial deuteration of the NH_2 group of *p*-toluidine-h_2. The samples for this experiment were therefore made up in pairs, one containing *p*-toluidine-h_2 (A) and the other an equal concentration of *p*-toluidine-d_2 (B). The *p*-toluidine-d_2 was deuterated to the extent of 95% on the amino group. The initial rate of formation of anil was then measured over a range of *p*-toluidine concentrations. The ratios, rate A/rate B, increase steadily with concentration since the extent of deuteration of the *p*-toluidine-h_2 due to exchange with D_2O decreases with increasing *p*-toluidine concentration. At infinite *p*-toluidine concentration this effect would be negligible. To obtain the true kinetic isotope effect it is therefore necessary to extrapolate to infinite *p*-toluidine concentration. It may be shown that:

$$\ln \frac{X - X_\infty}{1 - X_\infty} = -kY$$

where X is the ratio of rates at a concentration of *p*-toluidine Y and X_∞ is the kinetic isotope effect at infinite *p*-toluidine concentration. The data were therefore fitted to this equation using a range of values for X_∞ and a least squares fitting procedure. The value of X_∞ chosen was that which led to a minimum in the standard deviation for the constant k. In this way we obtain a value for X_∞ (the kinetic isotope effect) of 1.55. This is probably a secondary effect and supports the conclusion that proton transfer is not involved in the rate determining step.

The Mechanism of Catalysis

It has been shown that anil formation, anil hydrolysis, and transimination are homogeneously catalyzed by metal complexes, specifically thiourea complexes of cobalt and nickel. The most effective catalysts are those which dissociate to the greatest extent in acetone (1). The rate of reaction is proportional to catalyst concentration and the reaction is inhibited by chelating ligands and by excess thiourea. All of this evidence suggests that one or more of the substrate molecules must be complexed to the metal for catalystis to occur. It is however possible to envisage mechanisms not involving substrate complexation. Thus for example one such possibility would be imine formation with thiourea followed by transimination, *i.e.*,

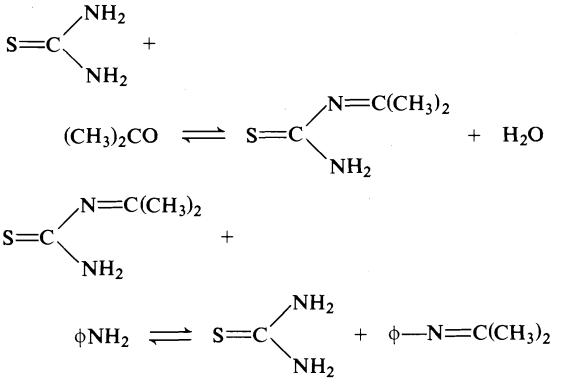

We reject this possibility on the grounds: (*a*) Thiourea alone is ineffective as a catalyst. (*b*) There is no evidence for imine formation between thiourea complexes and acetone in the absence of anilines. (*c*) Both $Zn(DMTu)_2Br_2$ and $Zn(TMTu)_2Br_2$ are very effective catalysts (DMTu $\equiv$ *N*,*N*′-dimethyl thiourea, TMTu $\equiv$ *N*,*N*,*N*′,*N*′-tetramethyl thiourea). In these cases the NH_2 groups necessary for imine formation are not present.

Given, then, the necessity for substrate complexation the question arises as to whether one or both substrates must be complexed. For the case of catalysis by metal ions in aqueous solution arguments have been advanced in favour of both these possibilities (7, 8). Our original interpretation of the results of the experiments involving dilution with carbon tetrachloride favoured the model with both substrates complexed.

The argument is as follows. For anil formation the rates of ligand exchange for both acetone and aniline are too rapid to allow complex formation to be a rate determining step. The observed rapid proton exchange and the measured kinetic isotope effect prelude proton transfer steps as being rate determining. Therefore the rate must be determined by the rate of attack of aniline on acetone. If both the substrates were complexed the rate would be proportional to the concentration of a binary complex, *i.e.*

$$\text{Rate} = k[\text{M.Ac.An}]$$

If only one of the substrates were complexed, then

$$\text{Rate} = k[\text{M.Ac}][\text{An}] \text{ or } k[\text{M.An}][\text{Ac}]$$

(An = aniline, Ac = acetone). However dilu-

TABLE 6. Comparison of calculated metal complex concentrations with experimental initial rates[a]

[*p*-Toluidine] (mol/ℓ)	[$MAnAcCl_2$] (mol/ℓ)	A^b	$B^{c,d}$	Initial rate (mol/ℓ s)
0.064	1.10×10^{-4}	3.74×10^{-5}	8.13×10^{-3}	7.45×10^{-5}
0.117	1.04×10^{-4}	4.84×10^{-5}	1.09×10^{-2}	1.28×10^{-4}
0.162	1.00×10^{-4}	5.55×10^{-5}	1.27×10^{-2}	1.44×10^{-4}
0.213	9.5×10^{-5}	6.97×10^{-5}	1.43×10^{-2}	1.67×10^{-4}
0.292	8.9×10^{-5}	6.97×10^{-5}	1.63×10^{-2}	2.24×10^{-4}
0.620	7.3×10^{-5}	9.09×10^{-5}	2.17×10^{-2}	3.31×10^{-4}

[a]Catalyst 0.0219 *M* $Zntu_2Cl_2$, acetone concentration 13.65 *M*, equilibrium constants K_1(tu) = 1.0, K_2(An) = 0.036, K_3(Ac) = 0.000107.
[b]A = ([$MtuAcCl_2$] + [$MAnAcCl_2$])[An].
[c]B = ([$MtuAnCl_2$] + 2[$MAnAnCl_2$] + [$MAnAcCl_2$]).
[d]It is only meaningful to correlate these concentrations with initial rates if it is assumed that An has not significantly displaced Ac in the second sphere.

tion with carbon tetrachloride reduces the concentration of all species in direct proportion to the degree of dilution (see above). Therefore in the first case dilution by a factor of two would half the rate and in the second case it would reduce it by a factor of four since both reactant concentrations are halved. The experimental results clearly favour the first alternative. The argument for the back reaction (anil hydrolysis) is exactly analogous and the experimental results are equally unambiguous.

However, more detailed analysis does not sustain this argument. Equilibrium constants are available for the complexation of each of the substrates with cobalt thiourea compounds. The above rate data have been obtained with zinc thiourea catalysts, hence we would not expect to be able to perform quantitative calculations using the equilibrium constants for the cobalt compounds. We would however expect correct qualitative predictions regarding the variation of rate with substrate concentrations. A set of equilibria of the type:

$$ML_jL_e + L_i \rightleftharpoons ML_jL_i + L_e$$

may be written involving Mtu_2X_2 catalysts in which L_i, L_j, and L_e are all possible combinations of thiourea, aniline, acetone, anil, and water. It may be shown that the concentration of any given species, say ML_2L_3 is given by the expression:

$$[ML_2L_3] = \frac{2mK_2K_3[L_2][L_3]}{(K_1[L_1] + K_2[L_2] + K_3[L_3])^2}$$

In this expression m is the total catalyst concentration and K_1, K_2, K_3 etc. are the equilibrium constants for the replacement of thiourea (L_1) by other ligands. The expressions for the case with four replacable ligands *e.g.*, $Mtu_4(ClO_4)_2$ are exactly the same except that the numerical factor is equal to 12 rather than 2. Knowing the equilibrium constants and the initial concentrations the set of equations of the above type may be solved by an iterative procedure. An appropriate computer programme was found to converge rapidly when m was small compared to any product $K_i[L_i]$. If complexed aniline reacts with complexed acetone then for a catalyst Mtu_2X_2:

$$\text{Rate} \propto [MAcAnX_2]$$

For a catalyst such as $Mtu_4(ClO_4)_2$ the rate will be proportional to the sum of the concentrations of all complexes containing both Ac and An. Some calculations giving the dependence of [$MAcAnX_2$] on aniline concentration are shown in Table 6 and compared with the experimental data for the rate of anil formation at the same aniline concentrations. The calculated concentrations of the binary complex decrease with increasing concentration, whereas the rates increase. The same result is obtained for $Mtu_4(ClO_4)_2$ catalysts. Examination of the calculations shows that the concentration [$MAnAcX_2$] will not increase with aniline concentration unless $K_3[Ac] \gg K_2[An]$. Although the equilibrium constants used for the replacement of thiourea by acetone (K_3) and by aniline (K_2) may not be accurate the above condition is clearly unrealistic and this model must be rejected.

It is therefore necessary to examine the significance of the experiments involving dilution with carbon tetrachloride more closely. The experimental results demand that both substrates be bound to the catalyst in such a manner that the addition of carbon tetrachloride will not dissociate the resulting adduct. It is not necessary

that they be both held in the first coordination sphere of the complex. It is recognized that ligands may be weakly held in the second coordination sphere of metal complexes (9) and that such entities may have kinetic significance. Thus in ligand exchange reactions associative (A) mechanisms may be distinguished from interchange (I_A) mechanisms in which the rate determining step involves interchange of a first sphere and a second sphere ligand (10). In the present case we may write a rapid pre-equilibrium involving the replacement of acetone by aniline in the second sphere: *i.e.*,

$$[3]\quad \mathrm{MtuAcCl_2{\cdot}(Ac)} + \mathrm{An} \overset{K'}{\rightleftharpoons} \mathrm{MtuAc{\cdot}Cl_2{\cdot}(An)} + \mathrm{Ac}$$

$MtuAcCl_2{\cdot}(An)$ is now the reactive species together with analogous complexes such as $MAnAc{\cdot}Cl_2{\cdot}(An)$ and $MAc_2Cl_2{\cdot}(An)$. The last term can be neglected since K_3 is small and the rate will be given by:

$$[4]\quad \text{Rate} \propto [\mathrm{MtuAcCl_2{\cdot}(An)}] + [\mathrm{MAnAc{\cdot}Cl_2{\cdot}(An)}]$$

By arguments analogous to those presented above the equilibrium 3 will not be affected by dilution with carbon tetrachloride providing CCl_4 does not compete with aniline or acetone for second sphere sites. Experimental evidence with other metal complexes does indeed indicate that CCl_4 is a very poor second sphere ligand (11). The rate expression 4 above will give the observed result in the dilution experiments.

Equations 3 and 4 predict that the initial rate be proportional to $([\mathrm{MtuAcCl_2{\cdot}(Ac)}]+[\mathrm{MAnAcCl_2{\cdot}(Ac)}][\mathrm{An}]$. Calculated values for this quantity are shown in column A of Table 6. They are plotted against the initial rate data in Fig. 3. A satisfactory linear dependence is obtained showing that this mechanism is consistent with experiment. There is another possibility, namely, that aniline be held in the first sphere and acetone in the second sphere. This is chemically less likely (see below) but cannot be entirely ruled out on kinetic grounds. The appropriate concentrations are shown in column B of Table 6. The hydrolysis of the anil would involve a mechanism in which anil is held in the first sphere and subject to nucleophilic attack by second sphere water. The kinetic implications of this mechanism are entirely analogous to those discussed above for anil formation.

It remains to be shown that the above model

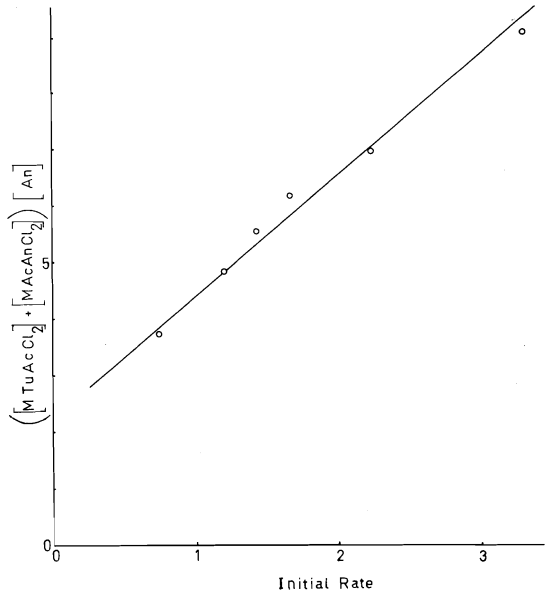

FIG. 3. Comparison of observed initial rate (mol/ℓ s $\times 10^4$) with calculated concentrations of reactants (mol^2/ℓ^2 $\times 10^5$).

satisfactorily accounts for the remaining kinetic data. All of the models predict a linear dependence of rate on catalyst concentration as is experimentally observed. It may be shown that for the Mtu_2X_2 catalysts to a good approximation:

$$\frac{1}{\text{Rate}} = \frac{\sqrt{K_2}}{2kK'K_3\sqrt{m}} \cdot \frac{1}{\sqrt{\text{An}}} + \frac{K_2}{2kmK'K_3}$$

Hence the reciprocal of rate should be linear with the reciprocal of the square root of aniline concentration. An appropriate plot is shown in Fig. 4 and is satisfactorily linear. A slight curvature is predicted in the Lineweaver–Burk double reciprocal plots but calculation of sample theoretical curves showed that the experimental scatter of the data is too great to reveal the curvature. The situation with $Mtu_4(ClO_4)_2$ catalysts is mathematically more complicated but numerical calculations confirm that 1/rate should be proportional to 1/[An] within the accuracy of the experiments. For the experiments involving inhibition with thiourea it is predicted that:

$$\frac{1}{\text{Rate}} = a[\mathrm{tu}] + b$$

Figure 5 shows an appropriate plot of the experimental data. It may be noted that the model involving the coordination of both acetone and

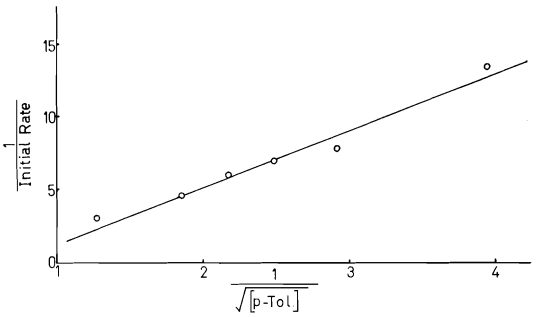

FIG. 4. Plot of (initial rate)$^{-1}$ (ℓ s/mol $\times 10^{-3}$) for anil formation against $[p\text{-tol}]^{-1/2}$ ($\ell^{1/2}$ mol$^{-1/2}$).

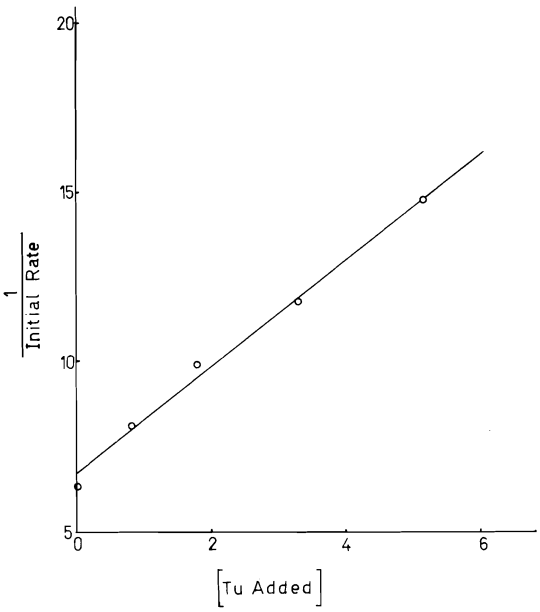

FIG. 5. Plot of (initial rate)$^{-1}$ (ℓ s/mol $\times 10^{-1}$) for anil formation against [tu] (mol/$\ell \times 10^2$) added.

aniline predicts that 1/rate will vary as $[tu]^2$ at high thiourea concentrations. Figure 5 shows no indication of this behaviour.

The Nature of the Rate Determining Step

On the basis of the evidence discussed above the reaction scheme shown in Fig. 6 is suggested. The steps shown are preceded by rapid pre-equilibria establishing the distribution of ligands in the first and second coordination spheres of the metal complex and are followed by further rapid equilibria re-establishing this distribution with the product anil and water molecules. Anil hydrolysis proceeds by the reverse of these reactions. A similar scheme for transimination may be readily written by replacing the acetone molecule with an anil.

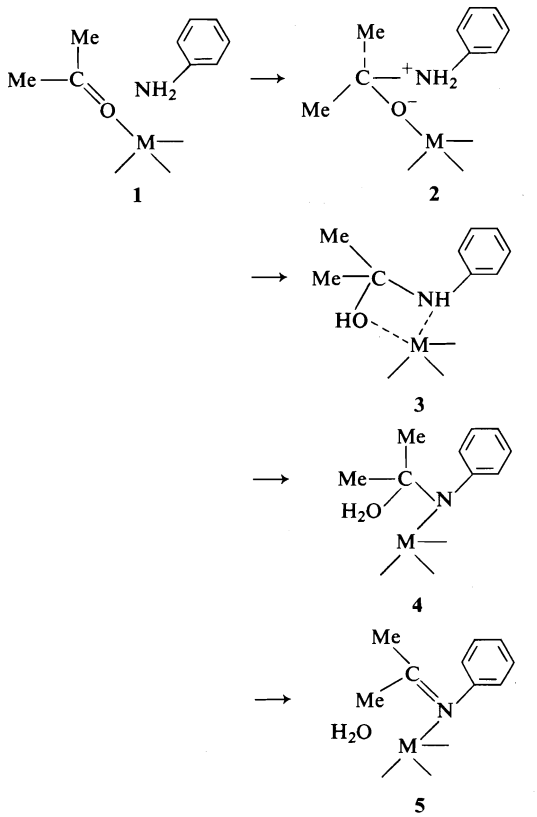

FIG. 6. Suggested mechanism for anil formation.

In this scheme steps **2** → **3** and **3** → **4** involve proton transfer. The observations of rapid exchange on the nmr time-scale and of a small kinetic isotope effect show that these steps are not rate determining. If step **4** → **5** were rate determining the carbinolimine should be a stable intermediate and as such observable by nmr. It is therefore suggested that step **1** → **2**, the nucleophilic attack of a second sphere aniline on a coordinated acetone molecule is the rate determining step in anil formation. For anil hydrolysis the rate determining step is the attack of second sphere water on coordinated anil.

For the transimination reaction the corresponding scheme has a higher symmetry since the forward and backward reactions are identical. Similar arguments suggest that attack of second sphere aniline on coordinated anil is rate determining. In this case nmr spin saturation transfer experiments provide additional evidence (1). The lifetime for exchange of *cis* and *trans* methyl groups is twice that for transimination indicating the two rates are determined by the

same process and suggesting facile rotation or inversion about the C—N bond during nucleophilic attack.

The above mechanism is also chemically attractive. Complexation of acetone or anil will withdraw negative charge from the molecule leaving the carbon more susceptible to nucleophilic attack (12) *e.g.*

On the other hand complexation of aniline or water involves utilization of the lone pair electrons and would make these molecules less effective nucleophiles (13). For this reason the above model with acetone in the first sphere and aniline in the second sphere is preferred over the kinetically similar model with aniline in the first sphere and acetone in the second sphere.

It cannot be unambiguously determined whether the aniline occupies a true second sphere site or is weakly bound to the metal to give a five coordinate complex. We prefer the first alternative. Binding to the metal would deactivate the nucleophile. There is no evidence for any stable five coordinate complexes with these ligands although such complexes may exist as intermediates in ligand exchange reactions. There is a fair amount of evidence for second sphere complexes involving anilines with binding energies of the order of 4 or 5 kcal/mol (14). If the aniline were primarily held by hydrogen bonding it would be activated as a nucleophile. There is a clear analogy between the mechanism suggested above and the I_A mechanism for ligand exchange. In an I_A mechanism a second sphere ligand is available for nucleophilic attack on the metal ion. In the reactions discussed above the nucleophilic attack is on a ligand atom.

Finally we summarize some of the factors which make these metal complexes particularly effective catalysts for the reactions discussed. The thiourea ligands are readily replaceable by substrate ligands but serve to prevent the precipitation of insoluble complexes. The availability of NH_2 groups on the periphery of the molecule may well serve a role in providing hydrogen bonding sites for second sphere coordination. The solubility in non-aqueous solvents implies that substrates such as acetone which could not compete with water as ligands in aqueous solution can complex the metal atom to a sufficient degree to react. Finally the role of the catalysts in bringing together the reactants should be mentioned. This has been referred to as the "promnastic" effect (15) and is undoubtedly a factor in any reaction which without catalysis would be bimolecular in nature.

Experimental

The preparation and purification of the chemicals used in this study has been described previously (1).

Initial rates were measured using a Varian HA 100 NMR spectrometer (probe temperature 35°C). The reaction was followed by using a voltage controlled frequency generator (Wavetek) to provide the sweep frequency so that the area of interest in the spectrum was repetitively scanned while the pen recorder was running. The sample containing the aniline or anil and a little TMS to provide a locking signal was placed in the probe and allowed to come to thermal equilibrium. The sample was then rapidly removed, catalyst solution injected with a syringe, a stopwatch started, and the tube shaken and replaced in the probe. The lock signal was relocated and the pen recorder started. This whole operation could be carried out in about 25 s and the first spectra were obtained about 30 s after the reaction had commenced. The fraction [Anil]/([Aniline] + [Anil]) is obtained from the measured intensities. Since the denominator is always constant, measurements of this quantity are insensitive to small changes in the homogeneity of the magnetic field or in the gain of the amplifier circuits. In the case of the measurements on the hydrolysis of anil the fraction [Aniline]/([Aniline] + [Anil]) was plotted against time, but the curve was extrapolated to meet the time axis where the concentration of aniline would be zero. This was necessary because the *p*-toluidine anil contained ~5% *p*-toluidine and the initial rate of formation of aniline must be determined where the aniline concentration is zero. Zinc thiourea complexes were used in these initial rate experiments to avoid complications arising from broadening of the nmr lines by the paramagnetic cobalt complexes.

p-Toluidine-d_2 was prepared by dissolving *p*-toluidine in diethyl ether and stirring together with successive portions of D_2O. The ether layer was dried with Na_2SO_4, the solvent removed on a vacuum line and the *p*-toluidine-d_2 sublimed *in vacuo*. It was kept in a glove bag under a dry nitrogen atmosphere. Integration of the nmr spectrum showed the material to be 95% deuterated.

Acknowledgement

We are indebted to the National Research Council of Canada for financial support of this research.

1. A. R. Boate and D. R. Eaton. Can. J. Chem. **54**, 3895 (1976); this issue.
2. A general non-linear curve fitting and equation solving programme. Programme Library, Michigan State University, Computer Laboratory.

3. K. J. LAIDLER. The chemical kinetics of enzyme action. Oxford. 1958.
4. D. R. EATON and K. ZAW. Can. J. Chem. **49**, 3315 (1971).
5. D. R. EATON and K. ZAW. J. Inorg. Nucl. Chem. **38**, 1007 (1976).
6. W. P. JENCKS. Catalysis in chemistry and enzymology. McGraw-Hill, New York. 1969.
7. K. S. BAI and D. L. LEUSSING. J. Am. Chem. Soc. **89**, 6126 (1967).
8. C. V. MCDONNELL, M. S. MICHAILIDIS, and R. B. MARTIN. J. Phys. Chem. **74**, 26 (1970).
9. M. T. BECK. Coord. Chem. Rev. **3**, 91 (1968).
10. C. H. LANGFORD and H. B. GRAY. Ligand substitution processes. Benjamin, New York. 1965.
11. D. R. EATON and K. L. CHUA. Can. J. Chem. **51**, 4137 (1973).
12. M. D. ALEXANDER and D. H. BUSCH. J. Am. Chem. Soc. **88**, 1130 (1966).
13. A. C. DASH and R. K. NANDA. J. Am. Chem. Soc. **91**, 6944 (1969).
14. D. R. EATON. Can. J. Chem. **47**, 2645 (1969).
15. B. E. LEACH and D. L. LEUSSING. J. Am. Chem. Soc. **93**, 3377 (1971).

Some methods for the preparation of α-alkylated vinylphosphonium salts and their use in 2,5-dihydrothiophene synthesis

JOHN M. MCINTOSH AND RICHARD S. STEEVENSZ

Department of Chemistry, University of Windsor, Windsor, Ont., Canada N9B 3P4

Received February 7, 1977

JOHN M. MCINTOSH and RICHARD S. STEEVENSZ. Can. J. Chem. **55**, 2442 (1977).

The preparation of a series of vinyltriphenylphosphonium salts, all of which bear a substituent on the carbon attached to phosphorus, is described. Yields are generally poor unless a symmetrical secondary allylic halide can be used. The use of these salts in the preparation of substituted 2,5-dihydrothiophenes has been examined. In general, reaction times are increased and product yields decreased relative to the reactions of the unsubstituted salts previously reported. This result is ascribed to steric inhibition of the intramolecular Wittig reaction.

JOHN M. MCINTOSH et RICHARD S. STEEVENSZ. Can. J. Chem. **55**, 2442 (1977).

On décrit la préparation d'une série de sels de vinyltriphénylphosphonium qui portent tous un substituant sur le carbone attaché au phosphore. Les rendements sont généralement mauvais à moins que l'on puisse utiliser un halogénure allylique secondaire symétrique. On a évalué les possibilités d'utiliser de tels sels pour la préparation de dihydro-2,5 thiophènes substitués. D'une façon générale, les temps de réaction augmentent et les rendements en produits diminuent par rapport aux réactions des sels non substitués qui avaient été rapportés antérieurement. On attribue ce résultat à une inhibition stérique de la réaction de Wittig intramoléculaire.

[Traduit par le journal]

In recent years, a number of research groups have demonstrated the usefulness of vinylphosphonium salts in the synthesis of a wide variety of acyclic (1), carbocyclic (2), polycyclic (3), and heterocyclic (4) compounds. Initially, most of the work was concerned with the use of vinyltriphenylphosphonium bromide because of its ready availability and unambiguous structure. Subsequently, we demonstrated (5) the simple conversion of primary allylic phosphonium salts **1** into their vinyl isomers (**2**), which allowed the use of the readily available **1** directly in the reactions and thereby provided facile formation of products derived from β-substituted salts (eq. 1).[1] Application of this technique to heterocyclic synthesis has afforded a wide range

[1] 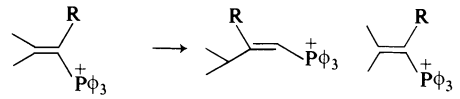

1 **2** **3**

of substituted dihydrothiophenes, (5, 6), dihydrothiopyrans (7), and products derived therefrom.

Reports of the synthesis and reactions of α-substituted vinyl salts (**3**) are much less frequent. Seyferth and Fogel (8) prepared **4** by a method which required initial quaternization of triphenylphosphine with an α-haloketone (eq. 2), a type of reaction well known to afford very low yields of phosphonium salts (see ref. 9 for a list of references). However, this route offers the possibility of complete generality if the alkylated salts **4** could be prepared more efficiently. Schweizer and co-workers (10) prepared several α-substituted salts **3** by routes which either did not appear to be general or afforded impure products or which led to substituents other than phenyl on the phosphorus atom. Another route, due to Vedejs *et al.* (11), also gives alkyl-substituted phosphorus atoms; difficulties encountered in the utilization of these compounds (10*b*) prompted us to develop other alternatives.

The importance of **3**, particularly those compounds bearing a functional group α to phosphorus, lies in their use in the synthesis of conjugated dienes by the route already outlined (5, 6) (eq. 3). The case of carboxy- or ether-substituted **3** would be particularly important in

[2] 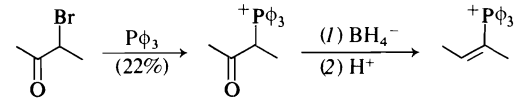

4

[1]The counterion for all salts in this paper is Br^- unless otherwise noted.

[3] 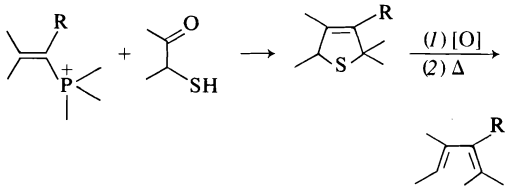

the preparation of rather inaccessible (12) dienes for use in the Diels–Alder reaction.

With these facts and ideas in mind, we set out to explore improved routes to **3** and their applications in synthesis.

Results and Discussion

Synthesis of α-Substituted Vinyl Salts

Considering our success in preparing simple vinyl salts **2** by the isomerization of **1**, we first investigated the feasibility of applying this technique to salts derived from secondary allylic halides. That the method was successful was shown by the isomerization of cyclohex-3-en-1-yl-triphenylphosphonium bromide to its vinyl isomer (**5**) using the usual pyridine–triethylamine system (5). However, a major difficulty frequently arises during the preparation of the allylic salts required as starting materials. This is illustrated in [4]. Identical phosphonium

[4] 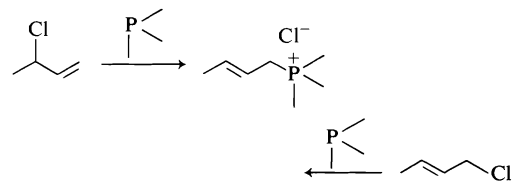

salts were obtained, starting with either 3-chloro-1-butene or 1-chloro-3-butene. In all cases of this type, the intervention of extensive allylic rearrangement during quaternization introduces ambiguity into the structure of both the allylic and vinyl salts and therefore into that of the products derived from them. Only in the case of primary or symmetrical halides can this possibility be discounted.

An alternative to quaternization for the preparation of the required secondary allylic salts involved the alkylation of primary allylic salts (eq. 5). Alkylation of both carbonyl-stabilized

[5] 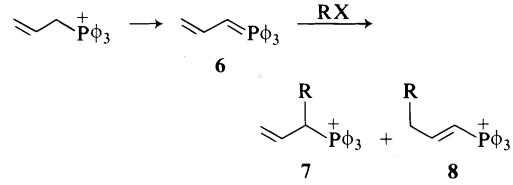

(13) and unstabilized phosphoranes (14) is a well-documented reaction. However, the use of **1** presents the possibility of both α- and γ-alkylation leading to **7** and **8**. While the ylide **6** is well known to react at the α-position in the Wittig reaction (15), it has been pointed out that γ-attack may well be an undetected reaction (γ-attack on **6** by ethyl chloroformate has been documented; see ref. 16). The observation of γ-attack on **6** in some specific instances (17) supports this possibility. However, we were confident that the α/γ alkylation ratio could be controlled by the use of the proper cation in the alkylation (see, for example, ref. 18). It should also be noted that the alkylation of the corresponding allyl phosphonate at the α-position has been reported (19).

When **6** was generated, either with *n*-butyllithium or under saltfree conditions (20), and mixed with a large excess of alkylating agent (methyl iodide, ethyl bromide etc.), no visible quenching of the red ylide colour could be detected, even upon addition of 10% HMPA as cosolvent. Addition of acid immediately quenched the colour and the allylic salt was reisolated in high yield. Also, addition of carbonyl compounds to the ylide solution led to a rapid Wittig reaction, confirming the presence of the ylide.

We are unable to offer an explanation for this result. However, it should be noted that the related sulfonium ylide is also very unreactive to alkylating agents, although it does react well with carbonyl compounds (21).

An alternative method for the preparation of the allylic salts **1** lay in the reported (22) addition of triphenylphosphine hydrobromide to conjugated dienes. Evidence is available that this addition proceeds well when the diene is symmetrical (eq. 6) or when a steric problem at one terminus of the diene system prevents attack of the bulky triphenylphosphine at that position (eq. 7) (6).

[6] 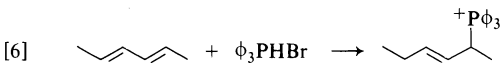

[7] 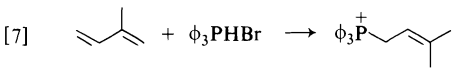

When the starting diene is readily available, this can be the method of choice for the preparation of **1**.

As previously mentioned, the work of Seyferth and Fogel (8) indicated that α-alkyl-β-keto-

phosphoranes **10** were a good source of vinyl salts. A possibly improved method for the preparation of **10** lay in the work of Bestmann (13) who had shown that simple phosphoranes could be acylated using thioesters (eq. 8).

[8]

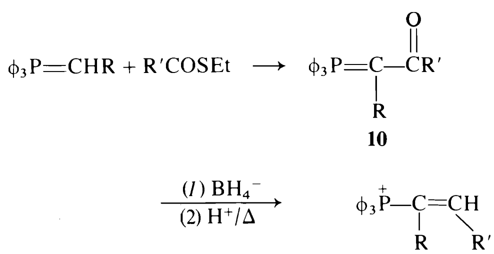

10

11 R = R′ = Me
12 R = Et, R′ = Me
13 R = Pr, R′ = Me

We were able to prepare **11–13** by this method, but both the yields (~20%) and the necessity of preparing the thiolesters detracted from this approach. However, it must be noted that, unlike the work described below, salts **11–13** were obtained as pure crystalline materials.

The major problem in the thioester approach lay in the formation of **10**. Therefore, an alternative appeared desirable and it occurred to us that interception of the betaine intermediate **14** of the normal Wittig reaction might overcome this difficulty and at the same time remove the necessity for reduction of **10**. It is well established (23) that the decomposition of **14** is slow at low temperature and by quenching the reaction with hydrobromic acid at 0°C, the oily β-hydroxyphosphonium salts **15** could be isolated (eq. 9). Unfortunately, **15** was contaminated with varying amounts of another product which we presume to be **16** derived by

[9]

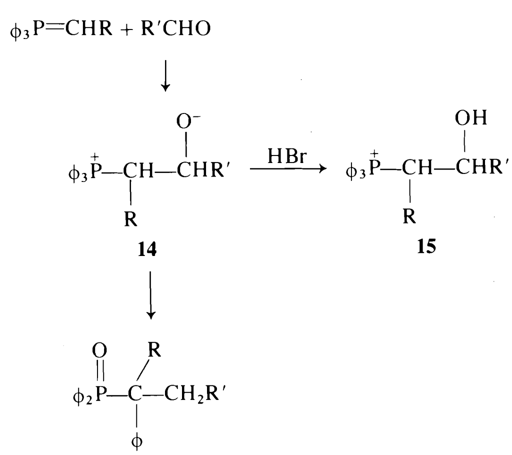

14 **15**

16

rearrangement (24) of either **14** or **15** which reduced the yields of **15** considerably. Its presence was inferred from the low-field region of the nmr spectrum and the infrared spectrum. Removal of **16** was accomplished by recrystallization.

Difficulties arose when the preparation of salt **15** bearing two bulky groups (R and R′) was attempted. In these cases little or none of the desired **15** could be obtained.

Dehydration of **15** in concentrated hydrobromic acid (8) led to the formation of the vinyl salt. Other methods for the dehydration did not prove effective. Thus, reaction of **15** with acetylchloride afforded the β-acetoxyphosphonium salt, but elimination of acetic acid using LDA gave only the olefin expected from normal Wittig reaction. Similarly untoward results were obtained when mesylation or tosylation of **15** was attempted. Finally, dehydration using phosphorous oxychloride or thionyl chloride also proved unsatisfactory.

The acid-catalyzed dehydration of **15** afforded material which was contaminated with up to 50% of another unidentified product. Separation using chromatographic techniques was unsuccessful and recrystallization led to large losses of material. Therefore, we decided to carry these impure materials on to the dihydrothiophene synthesis, as it was felt that the contaminants would be more easily removed at that stage.

The vinyl salts prepared are listed in Table 1. The yields for those prepared by method *D* are those of partially purified materials, whose purity is estimated (nmr) to be in excess of 65%. The nmr spectral data for new vinylphosphonium salts is given in Table 2.[2] These were obtained on small amounts of extensively purified material. The β-hydroxyphosphonium salts **15** were prepared and their nmr spectra are shown in Table 3. In addition to nmr analysis the presence of the desired salts was confirmed by the use of field-desorption mass spectrometry (25).

It should be noted that for the dehydration to be successful, a homogeneous acid phase must be attained while the solution is refluxing. Heterogeneous mixtures led to the formation of black tars.

[2]Tables 2 and 6 showing nmr and analytical data have been deposited in the Depository of Unpublished Data. Copies of these tables may be obtained, at a nominal charge, from the Depository of Unpublished Data, CISTI, National Research Council of Canada, Ottawa, Canada K1A 0S2.

TABLE 1. Vinylphosphonium salts prepared

Salt[a,b]	No.	Method[c]	Yield (%)[d]
	**5**[e]	*A*	Not isolated
	**9**	*A*	Not isolated
	**11**[f]	*C*	20
	**12**	*C*	18
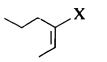	**13**	*C*	24
	**17**[g]	*B*	
	**18**	*D*	15
	**19**	*D*	8
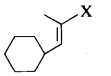	**20**	*D*	10
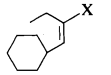	**21**	*D*	62
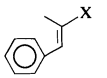	**22**	*D*	62
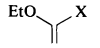	**23**	*h*	

[a]X = $\overset{+}{P}\phi_3$. [b]No stereochemistry implied. [c]*A*, isomerization of allylic salt; *B*, direct alkylation of triphenylphosphine; *C*, via β-ketophosphorane; *D*, via betaine method. [d]Assuming 100% purity. [e]See ref. 32. [f]See ref. 8. [g]See ref. 10*b*. [h]See ref. 28.

Synthesis of Dihydrothiophenes from α-Alkylvinylphosphonium Salts

The accepted mechanism for the formation of dihydrothiophenes is shown in [10]. The final step in this sequence is a Wittig reaction and as we have pointed out (5) we know of no examples of the formation of a tetrasubstituted double

[10] 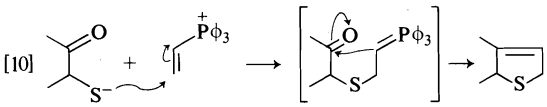

bond using this reaction. Also, Schlosser (26) has estimated that the presence of an α-alkyl substituent reduces the rate of betaine decomposition by a factor of ten. Therefore, our initial investigations utilized mercaptoaldehydes **24–26** (Table 4). Subsequently, ketones **27–29** were also included. While not all the salts listed in Table 1 were used, the reactions reported here illustrate the effects which determine the relative success of the method.

The reactants, products, yields, and reaction times are summarized in Table 4 and the spectral characteristics of the products in Table 6.[2] The yields indicated are based on an assumed 100% purity of the vinyl salts. As has already been pointed out, except for **5**, **9**, **12–14**, and **17**, this was known to be incorrect and therefore the yields indicated are minimum values.

As can be seen from Table 4, drastically reduced yields and increased reaction times are encountered relative to the simpler cases already reported (5, 6, 27). These were expected on the basis of earlier reports (7, 10) and the steric arguments mentioned above. In particular, the use of either acyclic ketones and α-substituted salts (products **46–48**, Table 4) or salts which have substituents larger than methyl at both the α- and β-positions (products **34**, **41**, **42**, Table 4) react very poorly. In some cases, the long reaction times caused the formation of some thiophene products derived from air oxidation of the dihydrothiophenes (7). Schweizer *et al.* have attributed the lower reactivity of the α-substituted vinyl salts to a steric inhibition of the initial conjugate addition reaction (10*b*). However, in view of the results of Schlosser and our previously demonstrated ability to form dihydrothiophenes from β,β-disubstituted vinyl salts, we prefer to attribute the results to inhibition of the Wittig cyclization.

The ability to form dihydrothiophenes from aldehydes and less hindered salts allows a degree of flexibility in synthetic planning as many can now be prepared from two different sets of reactants. For example, **37** can now be prepared as shown in [11].

[11] 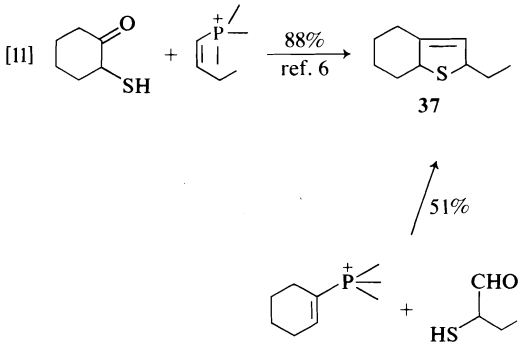

TABLE 3. New β-hydroxyphosphonium salts prepared ($R_1CH(OH)-CH(R_2)-\overset{+}{P}\phi_3$)

R_1	R_2	Method[a]	Yield (%)[c]	nmr spectral data[b]
CH_3	C_2H_5	*C*	67	7.68(m, 15), 5.45(m, 1), 4.7–3.2(m, 2), 3.0–3.2(m, 2), 1.3(m, 3), 1.3(t, 3, J = 6 Hz)
CH_3	n-C_3H_7	*C*	85	7.70(m, 15), 5.50(m, 1), 4.7–3.4(m, 2), 2.2–1.1(m, 7), 0.9(m, 3)
C_2H_5	CH_3	*D*	30	7.65(m, 15), 5.4–3.4(m, 3), 2.0–0.7 (m, 8)
Cyclo-C_6H_{11}	CH_3	*D*	25	7.75(m, 15), 5.20(m, 1), 3.6(m, 2) 2.4–0.7(m, 14)
Phenyl	CH_3	*D*	47	8.2–6.8(m, 20), 5.8(m, 1), 5.3(m, 1), 3.7(m, 1), 1.2(dd, 3, J = 22 and 7 Hz)
C_2H_5	C_2H_5	*D*	35	7.70(m, 15), 4.2–3.2(m, 3), 2.8–1.4 (m, 4), 1.1(t, 3, J = 7 Hz)
Cyclo C_6H_{11}	C_2H_5	*D*	27	7.6(m, 15), 4.6–2.5(m, 3), 2.5–0.6 (m, 16)

[a]See footnote *c*, Table 1.
[b]Tabulation follows the order chemical shift (δ), multiplicity, integrated intensity (protons), coupling constant. Spectra run in $CDCl_3$.
[c]Based on 100% purity (see text).

Reactions Using 1-Ethoxyvinyltriphenylphosphonium Bromide (23)

We have reported (28) the formation of **23** and the fact that it does function as a Michael acceptor. When this salt was utilized in the dihydrothiophene-forming reaction, unexpected results were obtained (eq. 12). In addition to the

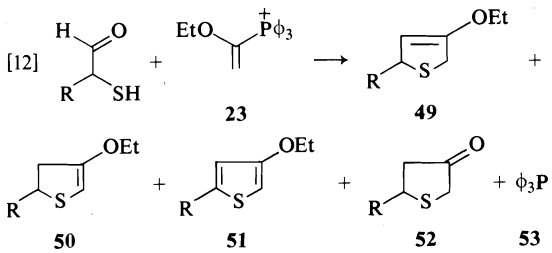

expected dihydrothiophene **49**, three other sulfur-containing products **50**–**52** were produced. The hydrolysis product **52** is unexceptional but the presence of thiophene **51** cannot be explained on the basis of air oxidation of **49** and **50**, since both of these are stable after isolation. The concomitant formation of triphenylphosphine (**53**) suggests another mechanism may be operating. We have previously noted (29) the formation of **53** and thiophene products in the reaction of butadienyltriphenylphosphonium salts and it appears possible that a mechanism similar to the one proposed in that case may be operating here (Scheme 1). The presence of an anion-destabilizing substituent might well favour the proton migration over the direct cyclization to **49** and account for the observed results.

Products of type **50** have not been observed previously by us. We presume they are formed by isomerization of **49**, a process which would be much more favourable in this case than in the alkyl-substituted dihydrothiophenes because of the increased ease of protonation of the double bond of the enol ether relative to the simple alkene. The products obtained from **23** are shown in Table 5 and their spectral characteristics are included in Table 6.[2]

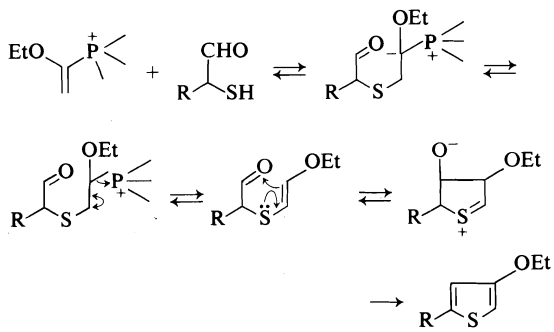

SCHEME 1

TABLE 4. New 2,5-dihydrothiophenes prepared 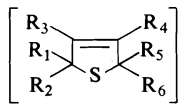

Mercaptan		Salt	Product No.	R_1	R_2	R_3	R_4	R_5	R_6	Time (h)	Yield (%)
	(24)	5	31	-$(CH_2)_5$-		H	-$(CH_2)_4$-		H	48	62
24		**17**	**32**	-$(CH_2)_5$-		H	Me	H	H	30	88
24		**18**	**33**	-$(CH_2)_5$-		H	Me	Et	H	60	60
24		**19**	**34**	-$(CH_2)_5$-		H	Et	Et	H	60	7
24		**20**	**35**	-$(CH_2)_5$-		H	Me	H	cyclo C_6H_{11}	60	11
24		**22**	**36**	-$(CH_2)_5$-		H	Me	Ph	H	72	31
	(25)	5	37[a]	Et	H	H	-$(CH_2)_4$-		H	30	51
25		**9**	**38**	Et	H	H	Me	H	Pr	48	37
25		**17**	**39**	Et	H	H	Me	H	H	18	31
25		**18**	**40**	Et	H	H	Me	Et	H	60	7
25		**19**	**41**	Et	H	H	Et	Et	H	43	27
25		**21**	**42**	Et	H	H	Et	H	cyclo C_6H_{11}	72	0
25		**22**	**43**	Et	H	H	Me	Ph	H	67	51
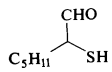	(26)	5	44	C_5H_{11}	H	H	-$(CH_2)_4$-		H	36	56
26		**17**	**45**	C_5H_{11}	H	H	Me	H	H	26	46
	(27)	17	46	H	-$(CH_2)_4$-		Me	H	H	264	36
	(28)	17	47	Me	H	Et	Me	H	H	168	36
	(29)	22	48	Me	Me	Me	Et	H	cyclo C_6H_{11}	72	0

[a] See ref. 6.

TABLE 5. Products and yields from reactions of salt **23**

Mercaptan	Products	Time (h)
24	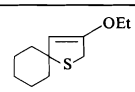 **54** (27%) + 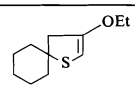 **55** (11%)	12
25	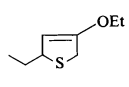 **56** (14%) + 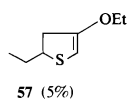 **57** (5%) + 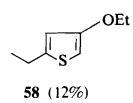 **58** (12%)	12
26	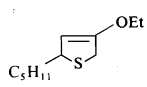 **59** (10%) + 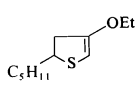 **60** (6%) + 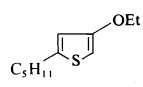 **61** (19%)	12

Conclusions

From the results, it is apparent that, except in some specific cases, we have not successfully solved the problems associated with the preparation of the α-substituted vinylphosphonium salts. Furthermore, the feasibility of using dihydrothiophenes bearing substituents at both the 3- and 4-positions as synthetic intermediates appears to be very limited and we do not plan any further investigations in this area.

Experimental

Nuclear magnetic resonance spectra were run on Varian EM 360 or JEOLCO C60HL instruments and are reported in ppm downfield from TMS as internal standard. Infrared spectra were obtained on a Beckmann IR 12 and mass spectra on a Varian-MATCH-5DF spectrometer under the control of an INCOS computer. Gas chromatography was performed on an F and M Model 720 instrument, utilizing the following columns: 6 ft × 0.25 in. 10% Carbowax 20M on Chromosorb W; 10 ft × 0.375 in. 10% Carbowax 20M on Chromosorb W.

Microanalyses were performed by A. B. Gygli, Microanalysis Laboratory, Toronto, Ontario.

Cyclohex-3-en-1-yltriphenylphosphonium Bromide

A mixture of 10 g (6.2 mmol) of 3-bromocyclohexene (30) and 16.3 g (6.2 mmol) of triphenylphosphine in 160 ml of acetonitrile was heated at reflux for 10 h. The cooled solution was reduced in volume to about 100 ml and poured into ether. After stirring for 0.5 h, the solution was filtered and the residue recrystallized from methylene chloride–ethyl acetate to give 18.0 g of product (69%), mp 222–224°C; nmr ($CDCl_3$) 8.1–7.4 (15H, m), 6.1–5.35 (3H, m), 2.1–1.25 (6H, m). *Anal.* calcd. for $C_{24}H_{24}BrP$: C 68.10, H 5.72, Br 18.89; found: C 68.01, H 5.64, Br 19.02.

Carrying out the reaction in ether solvent gave no reaction, whereas the use of benzene led to extensive decomposition. Dissolution of the salt in pyridine containing triethylamine (method *A*) led to complete isomerization to the vinyl isomer (**5**) as evidenced by the nmr spectrum.

Preparation of ***9***

To a solution of 7.0 g (0.02 mol) of triphenylphosphine hydrobromide (31) in 50 ml of acetonitrile was added 3.6 g of 2,4-hexadiene and the solution was refluxed for 18 h. The solvent was evaporated to afford a quantitative yield of the light yellow glassy allylic phosphonium salt which was quantitatively (nmr) isomerized to **9** by treatment with pyridine–triethylamine.

Preparation of Vinyl Salts via β-Ketophosphoranes (Method C)

To a toluene solution of the required phosphorane generated under salt-free conditions (20) was added 1.1 equiv. of the desired thioester. The mixture was refluxed for 18 h, filtered hot, and the α-alkyl-β-ketophosphorane isolated by filtration of the cooled solution. Recrystallization was effected from ethyl acetate – petroleum ether. Since borohydride reduction of these materials was difficult, they were converted to their phosphonium salts by reaction with gaseous hydrogen bromide in benzene solution.

To a solution of the phosphonium salt in methanol (25 ml per gram of salt) was added solid sodium borohydride (1.5 g per gram of salt) over a period of 2 h at 0°C. After 1 h, the excess hydride was decomposed with water. The methanol was evaporated and the aqueous phase extracted with chloroform. Evaporation of the dried extract gave the β-hydroxyphosphonium salt **15** which was recrystallized from ethyl acetate – chloroform. Yields and spectral data for the products can be found in Table 3.

The hydroxy salt was dissolved in 48% hydrobromic acid (15 ml per gram of salt) and heated at reflux for 3 weeks (shorter reaction times gave incomplete reaction). The cooled solution was diluted with an equal volume of water and extracted with methylene chloride. The combined organic extracts were washed with water, dried, and evaporated. The oil obtained was dissolved in the minimum amount of hot methylene chloride and ethyl acetate was added slowly to the cloud point. The cooled solution was filtered and the product recrystallized from methylene chloride – ethyl acetate. Products, yields, and spectral data are listed in Tables 1 and 2.[2]

Direct Formation of the β-Hydroxyphosphonium Salts (Method D)

To a suspension of the required phosphonium salt (0.05 mol) in 150 ml of dry ether under nitrogen was added 0.05 mol of *n*-butyllithium. After 1 h, the solution was cooled to 0°C and the desired aldehyde (0.07 mol) added slowly without stirring. A thick, white precipitate formed, to which was added 100 ml of 5% hydrobromic acid. This caused the formation of three layers. The upper ether layer was separated and the middle aqueous layer was extracted with methylene chloride. The combined organic layers were dried and evaporated. Precipitation of the product from methylene chloride solution using ethyl acetate afforded the β-hydroxyphosphonium salts **15** which crystallized over a 24 h period at 0°C. Using this method, salts **15** of about 90% purity could be obtained which were dehydrated using 48% hydrobromic acid as previously described.

Preparation of 2,5-Dihydrothiophenes

A solution of the vinyl salts (0.01 mol) and mercaptocarbonyl compound (0.015 mol) in 50 ml of pyridine containing 0.015 mol of triethyl amine was heated at reflux under a nitrogen atmosphere for the time indicated in Table 4. Water (600 ml) was added to the cooled solution and the mixture was extracted twice with 100 ml of ether and twice with 100 ml of pentane. The combined organic layers were washed with 10% hydrochloric acid until the washing was acidic, dried, and evaporated. The oil thus obtained was chromatographed on acidic alumina using pentane as the eluant. Evaporation afforded the dihydrothiophene in the yields shown in Tables 4 and 5 and it was shown to be at least 95% pure by glc. Analytical samples were collected from glc. The refractive indices and nmr spectral data are given in Table 6.[2] Except for the lack of carbonyl absorption, the ir spectra were uninformative.

By-products (thiophenes and positional isomers **53** and **54**) were also collected by glc where possible and the data for these are included in Table 6.[2]

Acknowledgments

The financial support of the National Research Council of Canada is most gratefully acknowledged.

1. E. E. SCHWEIZER, L. D. SMUCKER, and R. J. VOTRAL. J. Org. Chem. **31**, 467 (1966).
2. (*a*) E. E. SCHWEIZER. J. Am. Chem. Soc. **86**, 2744 (1964); (*b*) E. E. SCHWEIZER and G. J. O'NEILL. J. Org. Chem. **30**, 2082 (1965).
3. (*a*) R. M. CORY and D. M. T. CHAN. Tetrahedron Lett. 4441 (1975); (*b*) R. A. LUDEN and R. BONJOUKLIAN. Tetrahedron Lett. 2095 (1974).
4. (*a*) E. E. SCHWEIZER and J. G. LIEHR. J. Org. Chem. **33**, 583 (1968); (*b*) E. E. SCHWEIZER and C. S. KIM. J. Org. Chem. **36**, 4033 (1971); (*c*) E. E. SCHWEIZER, J. LIEHR, and D. J. MONACO. J. Org. Chem. **33**, 2416 (1968); (*d*) E. E. SCHWEIZER and L. D. SMUCKER. J. Org. Chem. **31**, 3146 (1966); E. E. SCHWEIZER and K. K. LIGHT. J. Am. Chem. Soc. **86**, 2963 (1964).
5. J. M. McINTOSH, H. B. GOODBRAND, and G. M. MASSE. J. Org. Chem. **39**, 202 (1974).
6. J. M. McINTOSH and G. M. MASSE. J. Org. Chem. **40**, 1294 (1975).
7. J. M. McINTOSH and H. KHALIL. Can. J. Chem. **54**, 1923 (1976).
8. D. SEYFERTH and J. FOGEL. J. Organometal. Chem. **6**, 205 (1966).
9. H. O. HOUSE. Modern synthetic reactions. 2nd ed. Benjamin, Menlo Park, CA. 1972. p. 698.
10. (*a*) E. E. SCHWEIZER and A. T. WEHMAN. J. Chem. Soc. C, 343 (1971); (*b*) E. E. SCHWEIZER, A. T. WEHMAN, and D. M. NYCZ. J. Org. Chem. **38**, 1583 (1973).
11. E. VEDEJS, K. A. J. SCHNOBLE, and P. L. FUCHS. J. Org. Chem. **38**, 1178 (1973).
12. S. DANISHEFSKY and T. KITAHARA. J. Am. Chem. Soc. **96**, 7807 (1974).
13. H. J. BESTMANN. Angew. Chem. Int. Ed. Engl. **4**, 645 (1965).
14. G. WITTIG and M. RIEBER. Justus Liebig's Ann. Chem. **562**, 177 (1949); H. J. BESTMANN. Bull. Soc. Chim. Fr. 1619 (1971).
15. E. VEDEJS, J. P. BERSHAS, and P. L. FUCHS. J. Org. Chem. **38**, 3625 (1973).
16. H. J. BESTMANN and H. SCHULZ. Angew. Chem. **73**, 27 (1961).
17. W. G. DAUBEN, D. J. HART, J. IPAKTSCHI, and A. P. KOZIKOWSKI. Tetrahedron Lett. 4425 (1973); W. G. DAUBEN and J. D. ROBBINS. Tetrahedron Lett. 151 (1975); G. BUCHI and H. WUEST. Helv. Chim. Acta, **54**, 1767 (1971).
18. J. A. KATZENELLENBOGEN and A. L. CRUMRINE. J. Am. Chem. Soc. **98**, 4925 (1976).
19. E. J. COREY and D. CAINE. J. Org. Chem. **34**, 3053 (1969); K. KONDO, A. NEGISHI, and D. TUNEMOTO. Angew. Chem. Int. Ed. Engl. **13**, 407 (1974).
20. H. J. BESTMANN. Angew. Chem. Int. Ed. Engl. **4**, 583 (1965).
21. R. W. LAROCHELLE, B. M. TROST, and L. KREPSKI. J. Org. Chem. **36**, 1126 (1971).
22. H. POMMER. Angew. Chem. **72**, 811 (1960).
23. M. SCHLOSSER and K. F. CHRISTMANN. Justus Liebig's Ann. Chem. **708**, 1 (1967).
24. E. M. RICHARDS and J. C. TEBBY. J. Chem. Soc. C, 1059 (1971).
25. G. W. WOOD, J. M. McINTOSH, and P.-Y. LAU. J. Org. Chem. **40**, 636 (1975).
26. M. SCHLOSSER. Topics Stereochem. **5**, 1 (1970).
27. J. M. McINTOSH and R. S. STEEVENSZ. Can. J. Chem. **52**, 1934 (1974).
28. J. M. McINTOSH and H. B. GOODBRAND. Synthesis, 862 (1974).
29. J. M. McINTOSH and F. P. SEGUIN. Can. J. Chem. **53**, 3526 (1975).
30. A. C. COPE and L. L. ESTES. J. Am. Chem. Soc. **72**, 1128 (1950).
31. S. D. SURMANTIS and A. OFNER. J. Org. Chem. **28**, 2735 (1963).
32. S. TRIPPETT and D. M. WALKER. J. Chem. Soc. 1266 (1961).

Use of ^{13}C in biosynthetic studies. Incorporation of ^{13}C-labeled acetate into chartreusin by *Streptomyces chartreusis*[1]

P. L. CANHAM AND L. C. VINING
Biology Department, Dalhousie University, Halifax, N.S., Canada B3H 4J1
AND
A. G. MCINNES, J. A. WALTER, AND J. L. C. WRIGHT
Atlantic Regional Laboratory, National Research Council of Canada, Halifax, N.S., Canada B3H 3Z1

Received October 29, 1976

P. L. CANHAM, L. C. VINING, A. G. MCINNES, J. A. WALTER, and J. L. C. WRIGHT. Can. J. Chem. **55**, 2450 (1977).

Examination by ^{13}C nuclear magnetic resonance spectroscopy of chartreusin produced in cultures of *Streptomyces chartreusis* supplemented with [1-^{13}C] and [2-^{13}C]acetate showed that the 19-carbon aglycone component was derived entirely from acetate. In the spectrum of chartreusin enriched from [1,2-^{13}C]acetate the signals for 16 of the carbon atoms were accompanied by satellites due to spin–spin coupling of intact ^{13}C—^{13}C units. The coupled pairs were matched with the aid of homonuclear single ^{13}C-frequency decoupling. Of the uncoupled carbon atoms, two were derived from methyl groups of acetate and the third came from an acetate carboxyl group. The arrangement of paired and unpaired ^{13}C atoms in chartreusin suggests that the aglycone is derived from a single 22-carbon polyketide chain. Cyclization to a benzpyrene-like intermediate followed by ring cleavage and loss of three carbon atoms provides a plausible route from the polyketide to the substituted isocoumarin structure of the aglycone.

P. L. CANHAM, L. C. VINING, A. G. MCINNES, J. A. WALTER et J. L. C. WRIGHT. Can. J. Chem. **55**, 2450 (1977).

L'examen des spectres rmn du ^{13}C de la chartreusine produite dans les cultures de *Streptomyces chartreusis* additionnées de [1-^{13}C] et [2-^{13}C]acétate montre que le composant aglycone contenant 19 atomes de carbone provient entièrement de l'acétate. Dans le spectre de la chartreusine enrichie à partir de [1,2-^{13}C]acétate, les signaux de 16 des atomes de carbone sont accompagnés par des satellites dus à un couplage spin–spin des unités ^{13}C–^{13}C intactes. On a pu comparer les paires couplées à l'aide d'un découplage de fréquence ^{13}C homonucléaire et simple. Des atomes de carbone non-couplés, deux proviennent des groupes méthyles de l'acétate et le troisième d'un groupe carboxyle de l'acétate. L'arrangement des atomes de carbone ^{13}C pairés et non-pairés dans la chartreusine, suggère que l'aglycone dérive d'une seule chaîne polykétide contenant 22 atomes de carbone. Une cyclisation conduisant à un intermédiaire ressemblant à du benzpyrène suivie par une fermeture de cycle et la perte de trois atomes de carbone fournit une route possible menant d'un polykétide à la structure isocoumarine substituée de l'aglycone.

[Traduit par le journal]

Introduction

Streptomyces chartreusis produces a glycosidic antibiotic, chartreusin, the aromatic dilactone component of which has been reported to originate from acetate (1, 2). Schmid located the carbon atoms derived from the methyl and carboxyl groups of acetate as shown in Fig. 1, but no experimental evidence was provided (1). Brown *et al.* (2) examined the distribution of ^{14}C-labeled carbon atoms in chartreusin enriched by growing cultures of *S. chartreusis* on diethyl [1-^{14}C] or [2-^{14}C]malonate. By chemical degradation of the aglycone they were able to confirm that C-3 and C-9 originated with the carboxyl and methylene carbons of malonate, and that the relative specific activities of substituted phthalic acids containing the carbon atoms of rings A and C were consistent with the distribution of label reported by Schmid. However, no complete chemical dissection of the labeled molecule has been described. Even if the proposed labeling pattern is assumed to be correct, the manner in which acetate and malonate units are assembled to generate chartreusin aglycone is not obvious. As observed by Brown and his colleagues, the carbon skeleton cannot be formed directly by the folding of a single polyketide chain; either an intermediate

[1]NRCC No. 15895.

of single-chain origin undergoes rearrangement or more than one polyketide chain is involved.

To obtain information on the assembly of two-carbon units in chartreusin we have prepared the antibiotic from cultures supplemented with ^{13}C-enriched acetate and measured the incorporation of isotopic label by ^{13}C nuclear magnetic resonance (^{13}C nmr) spectroscopy. A preliminary account of these experiments has already been reported (3). We present here the evidence supporting ^{13}C nmr assignments, biosynthetic labeling patterns, and our conclusion that chartreusin aglycone is derived from a single polyketide chain of 22 carbon atoms.

Biosynthetic Labeling

Of three isolates of *S. chartreusis* (strains K-180, ATCC 14922, and X-465) compared on defined (2) and complex (4) media for chartreusin production, strain X-465 gave the highest titre. Yields of 80–100 mg/ℓ were obtained at first, but deteriorated rapidly when the stock culture was transferred. To maintain good production we found it necessary to select a high-producing variant and prepare inocula for biosynthetic labeling experiments directly from stock cultures preserved by lyophilization. The culture medium favouring chartreusin formation was adapted from that of Berger *et al.* (4). An appropriate concentration of sodium acetate supplement, and suitable times for adding the supplement and harvesting the cultures to obtain optimum isotopic enrichment of the antibiotic, were selected in pilot experiments. Incorporation of radioactivity from sodium [2-^{14}C]acetate was used as a measure of isotopic enrichment.

The ^{13}C nmr spectra of chartreusin from cultures supplemented with sodium [1-^{13}C] acetate, [2-^{13}C]acetate, and [1,2-^{13}C]acetate are compared in Fig. 2 with the spectrum of the antibiotic at natural abundance. Signals at δ 15 (CH_3), 100 (anomeric carbon), and in the range 55–80 ppm (hydroxymethine carbons) could be assigned to the glycosidic moiety. They were enhanced to only a small extent in the spectra of samples enriched from ^{13}C-labeled acetate. Chartreusin derived from singly labeled acetate showed marked enhancement of a reciprocal series of signals, *i.e.* all of the non-glycosidic signals not intensified in the sample labeled from [1-^{13}C]-acetate were enhanced in the sample from [2-^{13}C]acetate. This result verifies the earlier deductions based on radiotracer studies that all of the aglycone carbon atoms are derived from acetate (1, 2). In the spectrum of the sample labeled from [1,2-^{13}C]acetate, signals for 16 of the 19 aglycone carbons were accompanied by satellites due to ^{13}C–^{13}C coupling between covalently bonded ^{13}C carbon atoms.

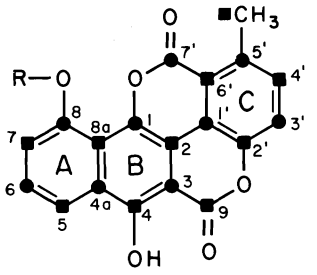

R= D-DIGITALOSE -D-FUCOSE

FIG. 1. Structure of chartreusin and labeling pattern proposed by Schmid (1) and Brown *et al.* (2).

Assignment of ^{13}C Resonances

Aglycone resonances in the ^{1}H broad-band decoupled pulse Fourier transform ^{13}C nmr spectrum of chartreusin were assigned from chemical shift trends (5), direct and long-range spin–spin couplings to hydrogen ($^{n}J_{CH}$, which were more easily measured in the high resolution (HR) spectra of samples labeled with [1-^{13}C] and [2-^{13}C]acetate), and unambiguous pairing of carbons that were spin–spin coupled ($^{1}J_{cc}$) in the spectrum of the [1,2-^{13}C]acetate-labeled metabolite. Values for chemical shifts and spin–spin coupling constants are presented in Table 1.

Chemical shift values and a characteristic one-bond ^{13}C–^{13}C coupling of 43.5 Hz identified the aglycone methyl carbon (δ_c 21.6 ppm) and the adjacent C-5′ quaternary aromatic carbon atom (δ_c 138.5 ppm). The HR signal for C-5′ was probably a doublet of quartets due to coupling with H-3′ and the methyl hydrogens ($^{2}J_{CH}$) but spectral resolution was insufficient to permit the small couplings to be measured. Signals for the five aromatic methine carbon atoms were easily recognized in the HR spectrum from the splitting due to one-bond ^{13}C–H couplings (5). Those for C-5 and C-7 could be distinguished by the additional splitting caused by three-bond ^{13}C–H coupling to H-7 and H-5. The carbon atom resonating at δ_c 116.2 ppm was assigned to C-5 because it was ^{13}C–^{13}C coupled ($^{1}J_{cc}$ 56.2 Hz) to a quaternary aromatic carbon (C-4a) at δ_c 126.0

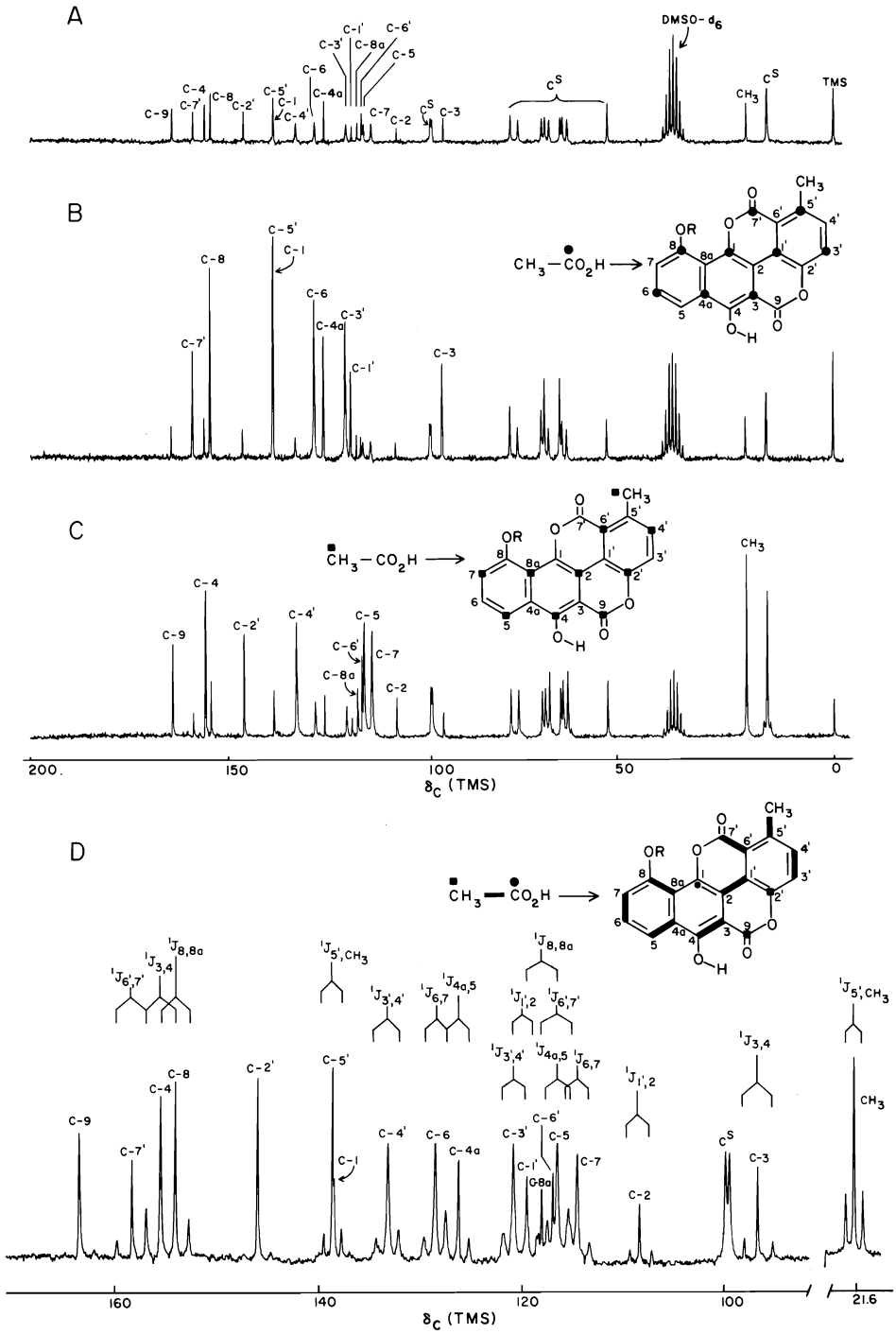

FIG. 2. ^{13}C nmr spectra (broadband (^1H)-decoupled) of chartreusin at natural abundance ^{13}C concentration (A), and from cultures supplemented with [1-^{13}C]acetate (B), [2-^{13}C]acetate (C), and [1,2-^{13}C]acetate (D). In D regions containing resonances of the aglycone carbon atoms are expanded and show satellites due to ^{13}C–^{13}C spin–spin coupling ($^1J_{cc}$). C^s denotes the glycosidic resonances.

TABLE 1. Assignments of resonances and ^{13}C–^{1}H spin–spin couplings in ^{13}C nmr spectra of ^{13}C-enriched chartreusin

δ (ppm)	Assignment	Multiplicity*	$^{1}J_{CH}$† (Hz)	$^{3}J_{CH}$† (Hz)	$^{n}J_{C(OH)}$† (Hz)
163.6	C-9	s	—	—	—
158.3	C-7′	s	—	—	—
155.4	C-4	dd→d‡	—	3.1	4.1
154.0	C-8	bd	—	6.3	—
145.8	C-2′	d	—	7.5	—
138.5	C-5′	dq	—	¶	—
138.4	C-1	s	—	—	—
133.1	C-4′	bdq	164.4	¶	—
128.3	C-6	d	165.0	—	—
126.0	C-4a	dd→d‡	—	8.7	6.9
120.6	C-3′	d	166.3	—	—
119.2	C-1′	bd	—	2.5	—
117.8	C-8a	dd	—	¶	—
116.7	C-6′	dq	—	¶	—
116.2	C-5	bdd	167.8	6.2	—
114.4	C-7	bdd	162±2	6.9	—
108.1	C-2	s	—	—	—
96.5	C-3	d→s‡	—	—	3.5
21.6	CH_3	q	129.7§	—	—

*s = singlet, d = doublet, q = quartet, b = broad.
†Error *ca.* ±0.5 Hz except where indicated; n = 2, 3, 3 for C-4, C-4a, C-3, respectively.
‡Multiplicity change caused by deuteration.
¶Accurate measurements of long-range coupling constants precluded by broadening or overlap of multiplets.

ppm which in turn was long-range coupled to an aromatic hydrogen (H-6, $^{3}J_{CH}$ 8.7 Hz) as well as to a hydroxyl hydrogen ($^{3}J_{C(OH)}$ 6.9 Hz). Replacing the hydroxyl hydrogen with deuterium removed the $^{13}C(OH)$ coupling. The signal at δ_c 114.4 ppm was allocated to C-7, since this carbon atom was ^{13}C–^{13}C coupled ($^{1}J_{cc}$ 53.9 Hz) to an aromatic methine carbon atom at δ_c 128.3 ppm which could only be C-6. The remaining carbons bearing hydrogen, namely C-3′ (δ_c 120.6 ppm) and C-4′ (δ_c 133.1 ppm), were also derived biosynthetically from an intact [1,2-^{13}C]acetate unit ($^{1}J_{cc}$ 54.5 Hz). The higher field resonance was assigned to C-3′ because the oxygen substituent at C-2′ would be expected to shield it, but not C-4′ (5). Consistent with those assignments the HR resonance attributed to C-4′ was a doublet of quartets due to coupling with H-4′ and the methyl hydrogens, whereas that for C-3′ was a sharp doublet due to coupling with H-3′ only. There was not sufficient spectral resolution to measure the small $^{3}J_{CH}$ values.

Resonances could be assigned to C-4 (δ_c 155.4 ppm, $^{2}J_{C(OH)}$ 4.1 Hz) and C-3 (δ_c 96.5 ppm, $^{3}J_{C(OH)}$ 3.5 Hz) because both carbon atoms (like C-4a) were spin–spin coupled to hydroxyl hydrogens, belonged to a ^{13}C–^{13}C unit ($^{1}J_{cc}$ 70.6 Hz), and possessed chemical shifts consistent with one (C-4) being deshielded and the other (C-3) being shielded by a hydroxyl substituent (5). Supporting these assignments, the resonance attributed to C-3 was enhanced in the spectrum of the metabolite enriched with [1-^{13}C]acetate, as predicted from the radiotracer study (2) which established that C-3 was derived from the carbonyl carbon of acetate. The long-range coupling ($^{3}J_{CH}$ 3.1 Hz) at C-4 must involve H-5.

Of the nine ^{13}C resonances still unassigned the five at lowest field were allocated to the two carbonyl carbon atoms (C-7′ and C-9) and the three aromatic carbon atoms bonded to oxygen (C-1, C-8, and C-2′). In HR spectra the signals at δ_c 154.0 and 145.8 ppm could be distinguished within this group as belonging to C-8 and C-2′ since they were present as doublets due to coupling with H-6 and H-4′, respectively. Of the three other resonances, those at δ_c 138.4 and δ_c 158.3 ppm were enhanced in the spectrum of chartreusin biosynthesized from [1-^{13}C]acetate whereas the carbon atom with a chemical shift of δ_c 163.6 ppm was derived from the methyl group of acetate. Since the earlier radiotracer study (2) established that C-9 was labeled by

[2-^{14}C]malonate the δ_c 163.6 ppm resonance was assigned to this carbon atom. Such an assignment is consistent with chemical shift expectations (5) and also with the absence of ^{13}C–^{13}C satellites at this resonance in the spectrum of chartreusin labeled by [1,2-^{13}C]acetate. Since C-3 and C-4 were incorporated as an intact two-carbon unit, C-9 is necessarily a product of acetate C—C bond fission. The signal at δ_c 158.3 ppm was attributed to C-7′, which should have a chemical shift similar to that of C-9. Moreover, it was ^{13}C–^{13}C coupled ($^1J_{cc}$ 74.1 Hz) to an aromatic quaternary carbon atom with δ_c 116.7 ppm, which should be C-6′ as it was also ^{13}C–H coupled to an aromatic hydrogen (H-4′) and to the hydrogens of the methyl group bonded to C-5′. The signal at δ_c 138.4 ppm was assigned to C-1, the only remaining carbon atom bonded to oxygen but not ^{13}C–H coupled; its chemical shift value is primarily accounted for by the shielding effect of substituents at C-4 and C-8 (6, 7).

The ^{13}C nmr spectrum of chartreusin labeled from [1,2-^{13}C]acetate showed that C-1, like C-9, was one of the three carbons in the aglycone not derived from an intact ^{13}C—^{13}C unit. The third such carbon atom resonated at δ_c 145.8 ppm and was one of the two low-field carbon atoms (C-2′ and C-8) that appeared as a doublet in HR spectra. The signal was assigned to C-2′, because C-8, with C-8a, comprised a ^{13}C—^{13}C pair ($^1J_{cc}$ 68.4 Hz) incorporated intact from [1,2-^{13}C]acetate. C-8 was assigned the resonance at δ_c 154.0 ppm and C-8a the one at δ_c 117.8 ppm. Confirming these assignments, HR spectra showed that the latter signal was coupled to two aromatic hydrogens (H-5 and H-7) as expected for C-8a, whereas signals attributed to C-8 and C-2′ were each coupled to one hydrogen (H-6 and H-4′, respectively). The carbon atoms at C-2 and C-1′, each shielded by lactone oxygens on adjacent carbons, were expected to resonate at high field. Of the two unassigned signals given by chartreusin, that at δ_c 119.2 ppm was a doublet ($^3J_{CH}$ 2.5 Hz) in HR spectra. It was assigned to C-1′ because this carbon should be spin–spin coupled with H-3′, whereas the other resonance, at δ_c 108.1 ppm, was a singlet and was more appropriately assigned to C-2. In samples labeled from [1,2-^{13}C]acetate the signals were coupled ($^1J_{cc}$ 53.9 Hz), confirming that the two carbon atoms to which they were assigned were adjacent.

Labeling Pattern

Inspection of the ^{13}C nmr spectra of chartreusin enriched from [1-^{13}C] and [2-^{13}C]acetate in the light of ^{13}C resonance assignments established the origin of the aglycone carbons (Table 2). Enrichments were approximately 6 and 3%, respectively, and were thus large enough to show the labeling pattern unequivocally. The distribution of carbon atoms derived from the carboxyl and methyl groups of the precursor was identical with that proposed earlier by Schmid (1) and partially confirmed by Brown and colleagues (2). However, evidence from ^{13}C–^{13}C coupling between carbons of chartreusin enriched from [1,2-^{13}C]acetate (Table 1) revealed that only eight two-carbon precursor units had been incorporated intact into the antibiotic. This result, together with the information on origin and location of the remaining three carbon atoms of chartreusin aglycone that were not coupled, exclude all previous biogenetic schemes based on a 20-carbon polyketide chain intermediate.

A plausible alternative, consistent with all of the ^{13}C nmr evidence for the labeling pattern as well as the arrangement of bonded and single carbon units, is shown in Fig. 3. In this a polyketide chain (**1**) with 22 carbon atoms derived by head-to-tail condensation of acetate and malonate units is condensed to a polycyclic aromatic intermediate (**2**) of the benzpyrene type. Oxidative cleavage of two rings, with elimination of three carbon atoms by decarboxylation, would generate the phenylnaphthalene dicarboxylic acid derivative (**3**). Rotation of the phenyl ring would orient the substituents to facilitate formation of the dilactone (**4**) with the labeling pattern observed in chartreusin aglycone. Attachment of sugars at the C-8 hydroxyl could take place at any stage after formation of the polyketide, but by analogy with the sequence of biosynthetic steps shown for other glycosidic antibiotics of *Streptomyces* species (8–10), it is probably a terminal step.

If chartreusin is derived from a single-chain 22-carbon polyketide as suggested, it is the first example of a metabolite in this biogenetic subgroup (11). Hitherto, the 24-carbon metabolite, siphulin (12), was the only compound of apparent polyketide derivation formed by participation of more than ten acetate units. Although the measurement of ^{13}C enrichment is subject to appreciable error the results obtained suggest that each precursor enriched uniformly those

TABLE 2. Isotopic enrichment (%) in chartreusin from cultures containing singly and doubly ^{13}C-labeled acetate

Aglycone carbon	$^1J_{cc}$ (Hz)	Position of label in precursor		
		1-^{13}C	2-^{13}C	1,2-^{13}C
CH_3	43.4		3.3	0.5†
C-5′	43.5	6.4‡		0.70
C-7	54.5		4.0	0.67
C-6	55±1	7.5		0.73
C-2	53.9		1.8	0.63
C-1′	54±2	6.8		0.54
C-4′	54.5		4.0	0.55
C-3	56±2	7.4		0.51
C-5	56.2		3.8	0.49
C-4a	56.7	4.4		0.7±0.1
C-8a	68±1		1.5	0.59
C-8	68.4	5.5		0.55
C-4	70.6		2.4	0.44±0.12
C-3	70±1	4.9		0.55±0.08
C-6′	74.0		2.0	0.45
C-7′	74.1	4.2		0.55
C-1	—	6.4‡		—
C-2′	—		2.2	—
C-9	—		1.6	—
Average ±SD		5.9±1.3	2.7±1.0	0.58±0.09
Measuring error	*ca.* ±0.5*	*ca.* ±1.3	*ca.* ±0.8	*ca.* ±0.07§

*Except those indicated in the Table.
†Inexact value due to peak overlap.
‡Average value for C-5′ and C-1, due to peak overlap in spectrum of sample from [1-^{13}C]acetate.
§Weighted average error. Individual errors were *ca.* ±0.05 where not shown.

chartreusin aglycone carbon atoms that it labeled. This is consistent with biosynthesis via a single-polyketide-chain intermediate, but it should be noted that the experimental conditions were not designed to test multichain alternatives. Precursors were added intermittently during growth of the cultures to produce a sustained isotopic enrichment of the acetate pool, the objective being to obtain maximum ^{13}C incorporation. To examine the possibility that chartreusin aglycone is formed from more than one polyketide chain a single-pulse addition of precursor would have been more informative, since it might have made it possible, from differences in enrichment at different positions in the molecule, to distinguish between chain-initiating units derived directly from acetate and chain-extending units derived via malonate. The limiting factor in such experiments is likely to be the accuracy with which small differences in enrichment can be detected and our results indicate that the use of doubly labeled acetate would be advantageous.

If chartreusin aglycone is derived from a single-chain-polyketide intermediate we see no reasonable alternative to the folding pattern and processing steps proposed in Fig. 3. In speculating about a multichain origin one might include a variation of this pathway in which the initial polyketide folding pattern is retained but the single-chain intermediate (**1**) is replaced by two or more shorter chains, assembled and condensed head-to-tail to form the same polycyclic aromatic intermediate (**2**). Clearly a large number of such short-chain variations can be entertained. Other routes, beginning with the condensation of two or more polyketide chains folded in different patterns, are conceivable. Since the presence in chartreusin aglycone of acetate-derived carbon atoms which are no longer part of bonded two-carbon units implies that processing reactions occur after the initial polyketide condensation, and since the nature of these reactions are not known at present, it is possible to construct and modify polyketide precursors with a variety of chain lengths and

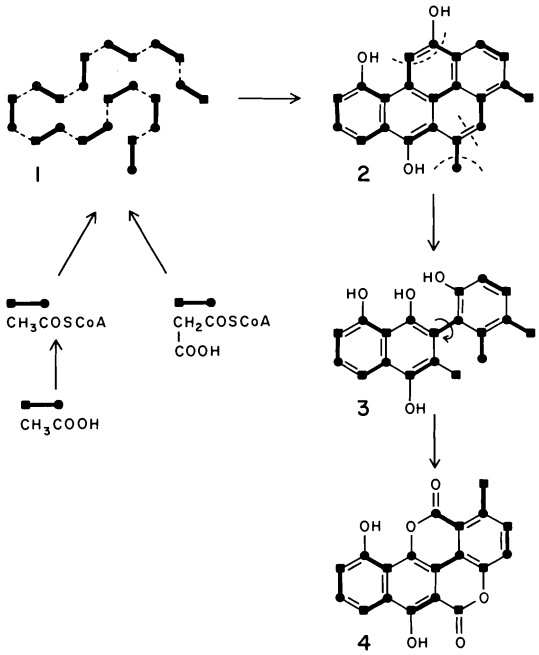

FIG. 3. Suggested biogenesis of chartreusin aglycone.

folding patterns to fit the labelling results. However, none of these alternatives appear to be more plausible than the route we have proposed.

Experimental

Labeled Compounds

Sodium [1-^{13}C]acetate, [2-^{13}C]acetate, and [1,2-^{13}C]acetate, all 90% enriched, were obtained from Merck, Sharp and Dohme, Pointe Claire, Quebec. An authentic sample of chartreusin was obtained from Dr. G. Whitfeld, the Upjohn Co., Kalamazoo, Mich.

Production, Extraction, and Purification of Chartreusin

In early experiments a sporulated slant of *S. chartreusis* X-465-4222 from Hoffmann-LaRoche, Nutley, NJ, maintained on a medium of Heinz Tomato Paste (2%), Heinz Baby Oatmeal (2%), and agar (1.5%), was used to seed 50-ml portions of a medium containing glucose (6%), soybean meal (2%), dipotassium hydrogen phosphate (0.1%), calcium carbonate (0.3%), zinc sulphate heptahydrate (0.001%), cupric sulphate pentahydrate (0.0002%), manganese sulphate tetrahydrate (0.0002%), and ferrous sulphate heptahydrate (0.001%) in 250-ml Erlenmeyer flasks. For later experiments it was necessary to plate spores of strain X-465-4222 and select a chartreusin-producing variant from the population. The variant was propagated on tomato paste – oatmeal agar and a spore suspension, subdivided into ampoules, was lyophilized and stored at −20°C. One of the lyophilized spore preparations was used to seed the liquid medium. Cultures seeded by either method were incubated in the dark for 2 days at 26°C on a shaker platform rotating at 220 rpm with an eccentricity of 3.8 cm, and used in 2-ml portions as a vegetative inoculum for chartreusin production medium. Cultures for producing chartreusin were grown under the same conditions as the vegetative inoculum.

In separate experiments, sterile solutions containing 10 mmol of sodium [1-^{13}C]acetate, sodium [2-^{13}C]acetate or sodium [1,2-^{13}C]acetate were added in aliquots to each of 20 flask cultures. The supplement was given in two portions, one on the fourth and one on the fifth day after inoculation. Cultures were harvested on the sixth day and extracted using the following adaption of previously described methods (4, 13). The broth was acidified to p*H* 5.5, centrifuged, and finally filtered through Whatman No. 5 paper to remove fine particles. Culture solids removed in this process were heated to boiling successively with three 100-ml portions of 80% aqueous acetone. The filtered extracts were combined with the culture filtrate and the mixture was extracted with an equal volume of acetone – methylene chloride (1:1) to completion. The combined extracts, evaporated and dried *in vacuo*, were redissolved in chloroform and applied to a column (2.6 × 25 cm) of silicic acid. The column was washed with acetone–chloroform (1:9) and chartreusin was eluted with acetone–chloroform (2:3). It was crystallized from methylene chloride and ethanol in yields ranging from 53 to 199 mg per litre of culture; the identity and purity of the samples was established by thin-layer chromatography (silica gel treated with citric acid, irrigated with chloroform–methanol, 9:1), ultraviolet absorption spectroscopy, and the absence of extraneous peaks in its ^{13}C nmr spectrum. Samples were compared with a reference specimen of chartreusin.

Spectra of chartreusin (50 to 120 mg samples dissolved in dimethyl sulfoxide-d_6) were obtained with a Varian XL-100/15 Fourier transform spectrometer under the following conditions: frequency 25.16 MHz, acquisition time 0.8 or 1.6 s (data accuracy ±0.6 or ±0.3 Hz), spectral width 5120 Hz, flip angle 40°, internal ^{2}H lock to solvent, temperature *ca.* 30°C, internal reference to tetramethylsilane. Broadband (^{1}H)-decoupling was achieved by phase modulation of the decoupling field ($\gamma H_2/2\pi$ 3800 Hz) from 0° to 180° at 150 Hz (14). During the acquisition of high-resolution spectra the nuclear Overhauser enhancement was maintained by applying this field for *ca.* 1.7 s between acquisition periods. For homonuclear (^{13}C) decoupling, a 25.12 MHz signal from a General Radio model 1061 frequency synthesizer was fed continuously via a tuned RF amplifier and BNC T connector to the transmitter coil of the probe. The higher frequency sideband of this signal, generated by the 40.96 KHz modulation field, was used to irradiate the resonance to be decoupled, the effective $\gamma H_2/2\pi$ being *ca.* 40 to 70 Hz. Coupled ^{13}C–^{13}C pairs of resonances were located from either direct irradiation of resonances or from the residual couplings caused by off-resonance decoupling effects.

The distribution of isotopic label in chartreusin from cultures supplemented with [1-^{13}C] or [2-^{13}C]acetate was determined by comparing ^{13}C nmr spectra of the enriched and natural abundance compounds recorded under identical experimental conditions. The ratio, *R*, of the intensity of each resonance to that of a reference peak known not to be enhanced was calculated for each spectrum. Spectra were compared via the ratio, *r*, for each peak, where $r = R$ (labeled compound)/R (natural

abundance compound). Thus $r \gg 1.0$ for peaks corresponding to enriched carbons; otherwise $r \simeq 1.0$. The percentage ^{13}C at each site was obtained by multiplying r for that carbon by the factor required to scale the average r for unenriched carbons to 1.108%. This procedure clearly distinguished enhanced peaks at the levels of enrichment encountered, and should detect enrichments $\geq 0.4\%$ above natural abundance. Errors stem mainly from the variation in r for unenhanced peaks, which places a limit on the accuracy of 'scaling' to natural abundance ^{13}C concentration. The measuring errors shown in the footnote to Table 2 are related to the standard deviation Δr in r for unenhanced peaks: error = $\Delta r/r \times$ average enrichment. In both cases the standard deviation (SD) of the enrichments is very similar to this error, showing that the relative variation in resonance intensity, due to factors other than enrichment, is almost the same for unenriched and enriched carbons. The method is independent of the choice of a reference peak for calculating R: if a peak enhanced by enrichment were chosen $r \ll 1$ for those peaks not enhanced. The percentage enrichment at labeled positions in chartreusin produced from doubly labeled acetate was calculated from the equation $1.1I_s/(I_c - fI_s)$, where I_s is the sum of the intensities of the two satellite resonances, I_c the intensity of the central peak, and f is the ratio of the concentrations of appropriate singly and doubly labeled precursors present in the doubly enriched acetate (15).

Acknowledgements

This work was supported by research operating grants (to L.C.V.) from the National Research Council of Canada and Merck Frosst Laboratories, Pointe Claire, Quebec, as well as by a graduate award (to P.L.C.) from Dalhousie University.

1. H. SCHMID. Angew. Chem. **75**, 347 (1963).
2. J. R. BROWN, M. S. SPRING, and J. R. STOKER. Phytochemistry, **10**, 2056 (1971).
3. P. L. CANHAM, L. C. VINING, A. G. MCINNES, J. A. WALTER, and J. L. C. WRIGHT. J. Chem. Soc. Chem. Commun. 319 (1976).
4. J. BERGER, L. H. STERNBACH, R. G. POLLOCK, E. R. LASALA, S. KAISER, and N. W. GOLDBERG. J. Am. Chem. Soc. **80**, 1636 (1958).
5. G. C. LEVY and G. L. NELSON. Carbon-13 nuclear magnetic resonance for organic chemists. Wiley Interscience, New York, NY. 1972.
6. P. GRANGER and M. MAUGRAS. Org. Magn. Reson. **7**, 598 (1975).
7. L. ERNST. Chem. Ber. **108**, 2030 (1975).
8. J. SPIZEK, M. CHICK, and J. W. CORCORAN. Antimicrob. Agents Chemother. 1965, 138 (1966).
9. T. FURUMAI, Y. SEKI, K. TAKEDA, A. KINUMAKI, and M. SUZUKI. J. Antibiot. **26**, 708 (1973).
10. T. HORI, I. MAEZAWA, N. NAGAHAMA, and M. SUZUKI. J. Chem. Soc. Chem. Commun. 304 (1971).
11. W. B. TURNER. Fungal metabolites. Academic Press, London. 1971. p. 191.
12. T. BRUUN. Acta Chem. Scand. **19**, 1677 (1965).
13. W. EISENHUTH, O. A. STAMM, and H. SCHMID. Helv. Chim. Acta, **47**, 1475 (1964).
14. J. B. GRUTZNER and R. E. SANTINI. J. Magn. Reson. **19**, 173 (1975).
15. A. G. MCINNES, D. G. SMITH, J. A. WALTER, L. C. VINING, and J. L. C. WRIGHT. J. Chem. Soc. Chem. Commun. 282 (1974).

Canadian Journal of Chemistry

Published by
THE NATIONAL RESEARCH COUNCIL OF CANADA

Journal canadien de chimie

Publié par
LE CONSEIL NATIONAL DE RECHERCHES DU CANADA

Volume 55 Number 13 July 1, 1977

Volume 55 numéro 13 1 juillet 1977

Fluorinated alkoxides. Part X. Template syntheses leading to fluorinated β-imino-alkoxy complexes of four- and five-coordinate nickel(II) and copper(II)

JOHN W. L. MARTIN AND CHRISTOPHER J. WILLIS

Chemistry Department, University of Western Ontario, London, Ont., Canada N6A 5B7

Received January 6, 1977

JOHN W. L. MARTIN and CHRISTOPHER J. WILLIS. Can. J. Chem. **55**, 2459 (1977).

Hexafluorodiacetonealcohol, HFDA, $HOC(CF_3)_2CH_2COCH_3$, is sufficiently acidic to coordinate to metal ions in an ionized form as a chelating, uninegative ligand. Complexes of Ni^{2+} and Cu^{2+} may be isolated, most conveniently by using a tridentate nitrogen-containing macrocycle as co-ligand so that five-coordinate unipositive compounds are produced.

In the presence of metal ions, HFDA readily undergoes template condensation reactions with diamino-ethane or -propane to give complexes of ionized β-imino alcohols, *e.g.* $^-OC(CF_3)_2$-$CH_2C(CH_3):N(CH_2)_2N:C(CH_3)CH_2C(CF_3)_2O^-$; these complexes are neutral and square planar but become five-coordinate by solvation in, *e.g.*, pyridine. The use of triamines H_2N-$(CH_2)_nNH(CH_2)_nNH_2$ (where $n = 2$ or 3) in template syntheses with HFDA gives complexes in which the metal ion is five-coordinate; these do not undergo solvation.

JOHN W. L. MARTIN et CHRISTOPHER J. WILLIS. Can. J. Chem. **55**, 2459 (1977).

L'hexafluorodiacétonealcool, HFDA, $HOC(CF_3)_2CH_2COCH_3$, est suffisamment acide pour se coordonner avec des ions métalliques sous une forme ionisée agissant comme ligand chélatant mononégatif. On a pu isoler les complexes du Ni^{2+} et du Cu^{2+}, particulièrement en faisant appel à des macrocycles tridentates contenant de l'azote comme co-ligand; de cette façon des composés monopositifs pentacoordonnés ont pu être obtenus.

En présence d'ions métalliques, HFDA subit facilement des réactions modèles de condensation avec les diamino éthane ou propane pour donner des complexes de β iminoalcools ionisés comme par exemple $^-OC(CF_3)_2CH_2C(CH_3):N(CH_2)_2N:C(CH_3)CH_2C(CF_3)_2O^-$; ces complexes sont neutres et sont plan-carrés mais deviennent pentacoordonnés par solvatation par exemple avec de la pyridine. L'utilisation de triamines $NH_2(CH_2)_nNH(CH_2)_nNH_2$ (où $n = 2$ ou 3) dans des synthèses modèles avec HFDA conduit à des complexes dans lesquels l'ion métallique est pentacoordonné; ceux-ci ne subissent pas de solvatation.

[Traduit par le journal]

Previous studies have shown that stable complexes of a variety of elements are given by highly fluorinated di-tertiary alcohols and related molecules, in which the enhanced acidity of the $-C(CF_3)_2OH$ group leads to coordination in the ionized form. The doubly ionized perfluoropinacolato ion, $^-OC(CF_3)_2C(CF_3)_2O^-$ (PFP^{2-}), has proved the most generally useful ligand, giving a variety of stable complexes with both main-group (1) and transition elements (2–4). Although anionic complexes such as $Ni(PFP)_2^{2-}$ are readily prepared, the more stable complexes are neutral compounds formed by the incorporation of one PFP^{2-} and neutral ligands containing nitrogen or phosphorus donor atoms, *e.g.* $L_2Ni(PFP)$. A further point of interest in the last type of complex is that, with a suitable choice of the ligand L, an additional ligand will coordinate in solution to give five-coordinate nickel species (4).

In the present study, we present several further instances of complexes in which an initially

square-planar, four-coordinate, nickel(II) ion, surrounded by two nitrogen and two oxygen donors, becomes five-coordinate by solvation. However, instead of mixing PFP^{2-} and nitrogen donor ligands to achieve the necessary environment, we have incorporated both the fluorinated tertiary alcohol grouping, $—C(CF_3)_2OH$, and the nitrogen donor sites into a number of polydentate ligands by template synthesis routes.

Results and Discussion

Preparation of Ligands and Complexes

The starting point for these syntheses was 5,5,5-trifluoro-4-trifluoromethyl-4-hydroxy-2-pentanone, more conveniently known as hexafluorodiacetonealcohol (HFDA), **1**, a known compound prepared by the reaction of hexafluoroacetone with acetone (5). The loss of a proton from this compound gives the anion (**2**) with the potential of acting as a bidentate, uninegative ligand:

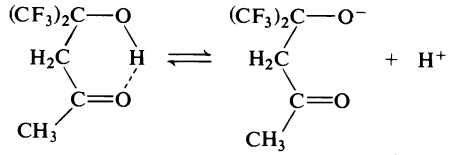

1 **2**

The carbonyl group is not a strong donor (in the absence of stabilization through delocalization of charge, as in acetylacetone complexes), and we have not yet been successful in preparing neutral complexes of the type $M^{2+}[CH_3COCH_2C(CF_3)_2O^-]_2$. However, through the use of the tridentate macrocycle **3** (abbreviated to [12]-ene-3) we have prepared the cationic, five-coordinate, nickel complex **4** and, for comparison in our assignment of this geometry to nickel, the neutral PFP^{2-} derivative **5***a*.

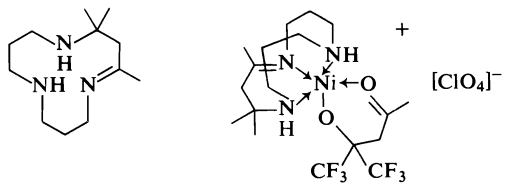

3 **4**

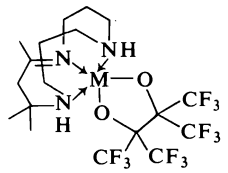

5*a*, M = Ni^{2+}
5*b*, M = Cu^{2+}

The greater utility of HFDA, however, was in the preparation of multidentate β-imino-alkoxy ligands, containing the $—C(CF_3)_2OH$ grouping, by its condensation with nitrogen bases in the presence of the metal ion. Template syntheses of this type are known to be successful in the case of the unfluorinated analogue, diacetonealcohol (6), but the ligands produced in that case coordinated by an un-ionized hydroxyl group because of the lower acidity found in the absence of fluorination. Our hope was that the fluorinated ligands would be dinegative through ionization and therefore more strongly coordinating ligands, and this proved to be the case.

In the presence of either Ni^{2+} or Cu^{2+}, HFDA underwent ready condensation with either 1,2- or 1,3-diamines, and neutral, square-planar complexes were formed of general structure:

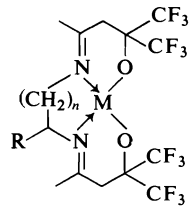

6 *n* = 1, R = H, M = Cu^{2+}
7 *n* = 1, R = H, M = Ni^{2+}
8 *n* = 1, R = CH_3, M = Ni^{2+}
9 *n* = 2, R = H, M = Ni^{2+}

A similar condensation reaction using dipropylenetriamine, $NH_2(CH_2)_3NH(CH_2)_3NH_2$, led to the formation of neutral, five-coordinate complexes of structure:

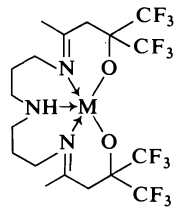

10 M = Ni^{2+}
11 M = Cu^{2+}

Previous workers (6) had found that, when diacetonealcohol was condensed with this triamine in the presence of nickel ions, an octahedral, cationic, hydrated complex formed.

The analogous condensation reaction of HFDA with diethylenetriamine, $NH_2CH_2CH_2NHCH_2CH_2NH_2$, also led to the formation of neutral, five-coordinate complexes, the structure being:

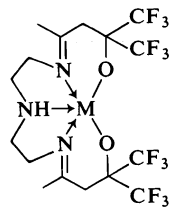

12 M = Ni^{2+}
13 M = Cu^{2+}

The ready condensation of this triamine with HFDA differs markedly from its behaviour towards unfluorinated diacetonealcohol, where no condensation was observed under these conditions (6).

Attempts to form any of the fluorinated β-imino alcohols by condensation reactions in the absence of metal ions were not successful, illustrating again the power of the template technique. The readier reactions undergone by HFDA, as opposed to the unfluorinated analogue, are clearly due to its much greater tendency to coordinate to the metal ion (in the ionized, anionic, form) simultaneously with the amine. It would seem unlikely that the ease of condensation of the carbonyl group is materially influenced by the fluorination of the two methyl groups, which are remote from it in the molecule.

Solvation Effects and Five-coordinate Nickel

In the solid state and in methanol solution, the nickel complexes **7**–**9** were four-coordinate, square planar, and diamagnetic, but more strongly coordinating solvents caused an increase in coordination. Water and other oxygen-containing donors were without effect, but adduct formation occurred with pyridine and amines. For example, **7**, an orange solid, gave an orange solution in methanol but a yellow-green solution in pyridine associated with the appearance of a strong absorption at 26 000 cm^{-1}. Spectra of **7**, **8**, and **9** in methanol–pyridine mixtures showed two isosbestic points, indicating the presence of only two species. Pronounced thermochroic behaviour was also noted for these solutions, *e.g.*, a solution of **7** in methanol/pyridine which was yellow at 25°C became green at −20°C and orange at +35°C; the absorption at 21 000 cm^{-1} characteristic of the square-planar complex diminished in intensity on cooling.

These visible spectra indicated the presence of five-coordinate nickel in solution. The ratio of solvated to unsolvated species in the methanol/pyridine solutions was found, from optical densities, to be directly proportional to the concentration of pyridine, as would be expected for 1:1 adducts. Strong support for five-coordinate nickel here was given by comparison with the spectra of the model compounds **4** and **5**, which showed characteristic absorption at 27 200 and 26 200 cm^{-1} respectively and other similarities in the lower frequency regions of their spectra (Table 1). Similarly, these spectra may be compared with those reported previously (4) and other instances where five-coordination has been unambiguously established (7, 8).

In the case of the PFP^{2-} complexes, we ascribed the formation of five-coordinate solvates (rather than the more common six-coordinate adducts) to the steric hindrance offered at the sixth coordination by the combination of the bulky PFP^{2-} ligand and a bulky substituted diamine. In the present work, it would appear that the approach of the fifth ligand caused some distortion of the essentially planar β-imino-alcohol complex giving an essentially square pyramidal structure which was not further solvated.

Concentration of pyridine solutions of **7** and **8** precipitated green crystals, presumably of the pyridine adducts, but removal of solvent led to rapid reversion to the orange, unsolvated, complexes.

None of the chelated five-coordinate nickel complexes prepared in this study (that is, **4**, **5***a*, **10**, or **12**) showed any evidence of accepting an additional donor molecule in the sixth coordination site, their spectra being unchanged in pyridine solution.

This is in sharp contrast to the unfluorinated analogue of **10**, which, as mentioned above, is only known as an octahedral hydrate. Although steric hindrance offered by the trifluoromethyl groups may be a contributing factor here, a major reason for this difference probably lies in the charge on each species. Since the weakly acidic unfluorinated $—C(CH_3)_2OH$ ligand coordinates without ionization, the resulting ligand is neutral overall and the nickel complex carries a 2+ charge. The complex as a whole, and the metal ion in particular, would therefore be much more likely to attract a nucleophilic water molecule than would be the case in the neutral fluorinated complex.

Solvation of Copper Complexes

The blue copper complex **6** showed a single, broad, intense absorption band (ε = 170) in both

TABLE 1. Visible spectra

Compound	Absorption maxima (cm^{-1}), (ε)	Solvent†
4	8500(17); 11000(8); 12800(9); 16100(46); 26900(102)	m
5a	~7300(16); 11800(9); 12700(9); 15800(26); 25000(sh); 27200(77)	m
	6900(19); 11800(10); 12700(10); 16100(26); 25400(sh); 27500(82)	py
7	20800(249)	m
	6300(17); 11700(23); 12600(23); 21500(33)*; 26200(sh)	py
8	20700(240)	m
	~6300(23); 6600(sh); 11800(25); 12900(27); 16300(29); 21700(sh)*; 26400(sh)	py
9	19500(157)	m
	6300(20); 11600(10); 12800(sh); 15700(33); 21000(37)*; 26300(sh)	py
10	8100(18); 10200(sh); 11800(6); 15700(31); 21500(sh); 26200(86)	m
	8200(7); 9700(sh); 10800(6); 16400(14); 27000(sh)	py
12	7800(9); 10200(12); 12200(12); 15600(49); 21100(55)	m
	~8500(sh); 9800(14); 11800(sh); 15300(38); 20800(41)	py
5b	10200(46); 15100(98)	m
6	15800(170)	d
	15800(163)	m
	~10400(sh); 15000(172)	py
11	~10200(sh); 14800(97)	m
	~10500(sh); 14800(85)	py
13, H_2O	12800(155)–15400(sh), br.	m
	13100(132)–14300(130), br, flat top	d

*Band expected for residual square-planar species.
†m = methanol, py = pyridine, d = dichloromethane.

dichloromethane and methanol solution (Table 1). In pyridine, a small shift of the band maximum to lower energy was observed, along with a considerable reinforcement (shoulder) on the low-energy side. The latter features were present in the spectrum of the complex **11** (expected to be five-coordinate on the basis of its known stoichiometry and analogy with the nickel complex **10**) in both methanol and pyridine solution, so we suggest that the initially four-coordinate **6** becomes five-coordinate in pyridine solution in the same way as its nickel analogue. However, the possible coordination of an additional solvent molecule at the sixth position cannot be excluded.

The model copper compound ***5b*** provided confirmation of the above suggestion. Use of the tridentate macrocyclic ligand **3** is known to produce many five-coordinate complexes (6) and the PFP^{2-} derivative showed a visible spectrum very similar to those of known examples. The band appearing as a shoulder in the pyridine solvates above was resolved in ***5b***, appearing as a discrete peak at 10 200 cm^{-1}.

The diethylenetriamine condensation complex of copper, **13**, showed slightly different properties from the other complexes. It crystallized as a stable hydrate, whereas other copper complexes were normally anhydrous, and the anhydrous material showed a very broad, almost flat-topped, visible absorption band in both methanol and dichloromethane solution. Because of the extended nature of this peak, the apparent shift in the absorption maximum (Table 1) may be misleading, but the geometry around copper does appear to be rather different from the very similar complex **11**. Some degree of solvent interaction at the sixth coordination site in **13** is possible, although this would be expected to be minimal in dichloromethane solution. Alternatively, the change in spectrum could arise from a distortion in the geometry caused by the decrease in size of two of the chelate rings between **11** and **13**.

Infrared Spectra

Important infrared absorption bands are shown in Table 2. All complexes of HFDA contained additional strong, characteristic, absorption in the region 1150–1250 cm^{-1} associated with the trifluoromethyl groups.

The absorption associated with the imino link appeared in the region 1640–1680 cm^{-1}, and additional confirmation that condensation of the primary amine had occurred was found in the absence of bands characteristic of the $—NH_2$ group.

The coordinated carbonyl group present in **4** gave rise to an absorption at 1690 cm^{-1}, which, as would be expected, is lower than that found in

TABLE 2. Infrared data (cm^{-1})*

Compound	ν(C=N)	ν(N—H)	Other
4	1664(s)	3239(s), 3260(m)	ν(C=O), 1690(s)
5*a*	1655(s)	3228(s), 3330(m)	
5*b*	1662(s)	3261(s), 3291(m)	
6	1666(m)		
7	1654(s)		
7, py adduct	1666(m)		
8	1664(s)		
9	1644(s)		
10	1670(s), 1659(m)	3278(w), 3230(w)	
11	1669(s), 1652(m)	3272(m)	
12	1678(s)	3210(s), 3295(sh)	
13	1672(s), 1658(m)	3320(m), 3332(m)	
13, H_2O	1677(s), 1663(m)	3290(m), 3370(sh)	ν(OH_2), 3560(m) δ(OH_2), 1608(w)

*Nujol mulls, s = strong, m = medium, w = weak, sh = shoulder.

TABLE 3. Analytical data and magnetic moments

		Carbon (%)		Hydrogen (%)		Nitrogen (%)			
Compound	Formula	Calcd.	Found	Calcd.	Found	Calcd.	Found	$\chi_g \times 10^6$ cgsu(294 K)	μ_{eff} (B.M.)
4	$C_{18}H_{30}ClF_6N_3NiO_6$	36.5	36.7	5.1	5.2	7.1	7.2	6.79	3.20
5*a*	$C_{18}H_{25}F_{12}N_3NiO_2$	35.9	35.9	4.2	4.3	7.0	6.9	6.24	3.10
5*b*	$C_{18}H_{25}CuF_{12}N_3O_2$	35.6	35.4	4.2	4.2	6.9	7.1	2.20	1.96
6	$C_{14}H_{14}CuF_{12}N_2O_2$	31.5	31.6	2.6	2.7	5.3	5.3	1.99	1.75
7	$C_{14}H_{14}F_{12}N_2NiO_2$	31.8	31.7	2.7	2.6	5.3	5.3	—	*
8	$C_{15}H_{16}F_{12}N_2NiO_2$	33.2	33.4	3.0	2.9	5.2	5.2	—	*
9	$C_{15}H_{16}F_{12}N_2NiO_2$	33.2	33.4	3.0	3.1	5.2	5.1	—	*
10	$C_{18}H_{23}F_{12}N_3NiO_2$	36.2	36.2	3.9	3.9	7.0	6.9	6.81	3.22
11	$C_{18}H_{23}CuF_{12}N_3O_2$	35.7	35.7	3.8	3.7	7.0	7.0	2.05	1.89
12	$C_{16}H_{19}F_{12}N_3NiO_2$	33.6	33.5	3.3	3.5	7.3	7.4	7.95	3.31
13, H_2O	$C_{16}H_{21}CuF_{12}N_3O_3$	32.3	32.3	3.6	3.6	7.1	7.2		

*Diamagnetic.

the free ligand **1** (1730 cm^{-1}) or the ion **2** (as the potassium salt, 1713 cm^{-1}).

Magnetic Data

As expected, the orange to red colored complexes **7**, **8**, and **9** were diamagnetic. The proposed five-coordinate nickel complexes had magnetic moments in the range 3.10–3.31 BM (Table 3), comparing well to the value for (DETA)Ni(PFP) (4), and in the range previously observed for five-coordinate nickel complexes (10). The copper complexes were paramagnetic as expected for one unpaired electron.

Conclusion

We conclude that the template condensation technique offers a valuable route to fluorinated complexes of a variety of metals because of the ready availability of a variety of carbonyl derivatives of the fluorinated alcohols. The production of metal complexes in which the steric requirements of the ligand are dominant leads to a well-defined geometry of coordination about the metal ion and, in particular, adds to recent accumulating evidence that five-coordination is by no means uncommon.

Experimental

General

Volatile compounds were handled in a conventional vacuum system. Infrared spectra were recorded on a Perkin-Elmer 621 instrument and visible spectra on Cary 14 and Cary 118 spectrometers. Microanalyses (Table 3) were performed by Alfred Bernhardt Laboratories, West Germany.

Hexafluorodiacetonealcohol (HFDA)

The preparation varied from that published (5) in that 20 g of hexafluoroacetone and 20 ml of dry acetone were allowed to react for 4 days in a sealed tube (100 ml) at 135°C. The distilled product had bp 150–153°C (lit. bp 150–151°C).

Nickel Complexes

The same general procedure was used for the five β-imino fluorinated alkoxy complexes prepared. In a typical preparation, nickel(II) chloride hexahydrate (2.37 g, 10 mmol) in warm ethanol was added to ethylenediamine (1.22 g, 20 mmol) in ethanol, followed by an ethanolic solution containing hexafluorodiacetonealcohol (4.48 g, 20 mmol) and potassium hydroxide (1.12 g, 20 mmol). The solution was cooled to 0°C and filtered to remove potassium chloride, refluxed for 4 h, then left at 25°C for 16 h. The resulting orange-red solution was filtered and concentrated to yield the solid product **7**; orange-red crystals from methanol.

The same method, using the appropriate amine, gave **8**, using 1,2-diaminopropane; orange needles from ethanol; **9**, using 1,3-diaminopropane; red needles from ethanol; **10**, using dipropylenetriamine; blue-green needles from ethanol.

Some **8** was produced by reaction of 1,2-diaminopropane present as impurity in the triamine; it was readily removed through its lower solubility. **12**, using diethylenetriamine; green crystals from 2-propanol/ether.

Copper Complexes

The same general route was used as described above for nickel, except that the ratio of metal chloride to amine was 1:1 rather than 1:2. Thus prepared were: **6**, using ethylenediamine; blue needles from ethanol; **11**, using dipropylenetriamine; blue plates from methanol; **13**, using diethylenetriamine; blue crystals of the hydrate from ethanol. Dehydrated by heating *in vacuo* 80°C/4 h.

Macrocyclic Ligand Complexes

The starting material for complexes incorporating the tridentate macrocycle **3** (abbreviated to [12]-ene-3) was the cationic hydroxo-complex $[M_2([12]\text{-ene-}3)_2(OH)_2](ClO_4)_2$ where $M = Cu^{2+}$ or Ni^{2+}. This was prepared as described previously (11); it should be noted that the postulated structure shown in that report has since been revised and bridging hydroxide ions and two 12-membered macrocyclic rings in a binuclear complex cation are now known to be present (6, 9).

The PFP^{2-} complexes, M([12]-ene-3)PFP, were prepared by the addition of perfluoropinacol, prepared as described previously (4), in methanol, to the appropriate hydroxo-complex in methanol, using a molar ratio of 2.02:1. Concentration of the solution yielded the products, which were recrystallized from ethanol to give the green nickel complex (**5***a*) and the blue copper complex (**5***b*).

The HFDA complex of nickel, **4**, was prepared by the same route, using HFDA in place of H_2PFP; green plates from ethanol.

Acknowledgments

We thank Professor N. F. Curtis for making available his results in advance of publication. Financial support of this work was provided by the National Research Council of Canada.

1. M. Allan, A. F. Janzen, and C. J. Willis. Can. J. Chem. **46**, 3671 (1968).
2. M. Allan and C. J. Willis. J. Am. Chem. Soc. **90**, 5343 (1968).
3. C. J. Willis. Chem. Commun. 944 (1972); 117 (1974).
4. W. S. Cripps and C. J. Willis. Can. J. Chem. **53**, 809 (1975).
5. L. A. Simonyan, N. P. Gambaryan, and I. L. Knunyants. Zh. Vses. Khim. Obshchestva. im D. I. Mendeleeva, **11**, 467 (1966); Chem. Abstr. **65**, 18489c (1966).
6. J. W. L. Martin and N. F. Curtis. J. Chem. Soc. Dalton, 87 (1975).
7. L. Sacconi, P. L. Orioli, and M. DiVaira. J. Am. Chem. Soc. **88**, 4383 (1966).
8. M. Ciampolini and N. Nardi. Inorg. Chem. **5**, 41 (1966).
9. J. W. L. Martin, J. H. Johnston, and N. F. Curtis. Unpublished observations.
10. J. S. Wood. Coord. Chem. Rev. **2**, 403 (1967).
11. N. F. Curtis and D. A. House. J. Chem. Soc. 5502 (1965).

Fluorinated alkoxides. Part XI. Studies on highly fluorinated amino-alcohols and their metal derivatives[1]

IN-SOON CHANG AND CHRISTOPHER J. WILLIS

Department of Chemistry, University of Western Ontario, London, Ont., Canada N6A 5B7

Received January 20, 1977

IN-SOON CHANG and CHRISTOPHER J. WILLIS. Can. J. Chem. **55**, 2465 (1977).

We describe the synthesis of a number of difunctional molecules in which the fluorinated tertiary alcohol grouping, $-C(CF_3)_2OH$, is combined with a nitrogen donor site such as an amino-group or a pyridine ring. In all cases, zwitterionic behaviour in solution is found resulting from intramolecular proton transfer from the acidic fluorinated alcohol to the nitrogen, and this sometimes persists in the solid state, *e.g.* $NH_2CH_2CH_2C(CF_3)_2OH$ exists as the dipolar ion $^+NH_3CH_2CH_2C(CF_3)_2O^-$. Measurements of p$K$ values suggest that the behaviour of the fluorinated amino-alcohols may be compared with that of the amino-acids, subject to changes to be expected from the lower acidity of the $-C(CF_3)_2OH$ group.

Metal complexes of the fluorinated amino-alcohols form readily; specifically, neutral complexes of Co^{2+}, Ni^{2+}, and Cu^{2+} of formula $M(L)_2$, where L is an ionized amino-alcohol chelating through the ionized hydroxy group and the nitrogen atom. Measurements of formation constants show that the six-membered chelate rings are the most stable, while a comparison of the stabilities of fluorinated amino-alkoxy complexes with those of analogous amino-acids shows that the former are less stable: this is attributed to the steric influence of the trifluoromethyl groups.

IN-SOON CHANG et CHRISTOPHER J. WILLIS. Can. J. Chem. **55**, 2465 (1977).

On décrit la synthèse d'un certain nombre de molécules difonctionnelles dans lesquelles le groupe alcool tertiaire fluoré $-C(CF_3)_2OH$ est combiné avec un azote agissant comme site donneur tel qu'un groupe aminé ou un cycle pyridine. Dans tous les cas, on trouve que le comportement zwitterionique en solution résulte d'un transfert de proton intramoléculaire provenant de l'alcool fluoré acide vers l'azote et que quelquefois ce transfert persiste à l'état solide; par exemple $NH_2CH_2CH_2C(CF_3)_2OH$ existe sous forme d'ion dipolaire $^+NH_3CH_2$-$CH_2C(CF_3)_2O^-$. Des mesures de valeur de pK suggèrent que le comportement des alcools aminés fluorés peuvent être comparé avec celui des acides aminés si l'on tient compte des changements auxquels on doit s'attendre à cause de l'acidité plus faible du groupe $-C(CF_3)_2OH$.

Les complexes des alcools aminés fluorés se forment rapidement; d'une façon spécifique, il y a formation des complexes neutres du Co^{2+}, Ni^{2+} et Cu^{2+} de formule $M(L)_2$ où L est un amino alcool ionisé chélatant par l'intermédiaire du groupe hydroxy ionisé et de l'atome d'azote. Des mesures sur les constantes de formation indiquent que les cycles chélatés à six chaînons sont les plus stables alors qu'une comparaison des stabilités des complexes amino alcool fluorés avec ceux des acides aminés analogues montrent que les premiers sont beaucoup moins stables; on attribue ce résultat à une influence stérique des groupes trifluorométhyles.

[Traduit par le journal]

We have previously shown (1) that metal complexes of highly fluorinated alkoxy ligands in which there is a second donor site (specifically, an imino nitrogen) in the molecule may be conveniently prepared by template synthesis routes. Although a powerful synthetic method, this approach has the disadvantage that the ligand molecule itself is not prepared and studied in the absence of the metal ion.

In the present work, we report the preparation of a number of molecules which contain the fluorinated tertiary alcohol grouping $-C(CF_3)_2$-OH in conjunction with a second potential donor site in the form of a primary amine, secondary amine, or pyridine group. These have been successfully used as ligands towards transition metal ions, chelation occurring by attachment of the amino-group and the ionized alkoxy group, $-C(CF_3)_2O^-$. The size of the chelate ring depends on the separation of these two sites in the ligand molecule, and we have prepared complexes having either five- or six-membered rings.

[1]Presented in part at the 8th International Symposium on Fluorine Chemistry, Kyoto, Japan, August 1976.

Results and Discussion

Preparation of Ligand Molecules

The easiest general route to the preparation of compounds containing the grouping $-C(CF_3)_2$-

OH is through the addition of hexafluoroacetone to an active hydrogen site (2).

$$R—H + (CF_3)_2CO \rightarrow RC(CF_3)_2OH$$

The addition across O—H or N—H is frequently reversible, while that across C—H is generally irreversible. In view of the excellent ligand properties of the pyridine ring system, we began this study by reacting hexafluoroacetone with 2-aminopyridine and with methyl-substituted 2-aminopyridines. Ready addition to give a stable product occurred in each case.

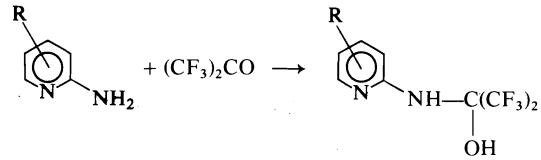

1 R = H
2 R = 3-methyl
3 R = 4-methyl
4 R = 5-methyl
5 R = 6-methyl

Ligands containing primary or secondary amino groups were prepared by two general methods, ring-opening reactions of fluoroepoxides with ammonia or amines, or catalytic reduction of fluorinated tertiary nitriles.

The addition of diazomethane to hexafluoroacetone gives the fluorinated epoxide **6** (3) and the ring may be broken across the $—CH_2—O—$ bond by ammonia or primary amines to yield fluorinated amino-alcohols

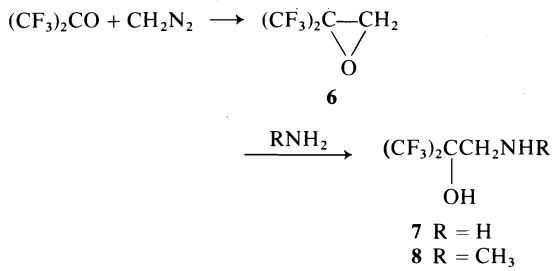

7 R = H
8 R = CH_3

This direction of ring opening is that which would be expected if reaction occurred by nucleophilic attack of the amine on the methylene group which, by attachment to the oxygen atom and the fluorocarbon residue, should be the most electrophilic point in the ring. To confirm this, we reacted the epoxide **6** with methylmagnesium iodide, when the product formed was $(CF_3)_2C(OH)C_2H_5$ by nucleophilic attack on the ring by the methyl group. A similar result has been reported with other partially fluorinated epoxides (4), although the reaction sequence is more complex when the ring is fully fluorinated (5).

The C—H bond in cyanoacetic acid is known (6) to be sufficiently reactive that ready addition to hexafluoroacetone occurs, followed by decarboxylation to give the fluorinated cyanoalcohol **9**. We have catalytically hydrogenated this to the amino-alcohol **10**.

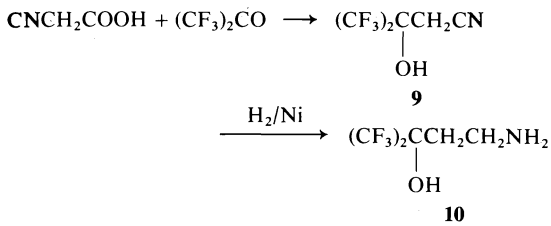

This reduction went readily in good yield, but the corresponding reduction of hexafluoroacetone cyanohydrin, $(CF_3)_2C(OH)CN$, giving the amino-alcohol **7**, required much more severe conditions and gave only poor yields.

Properties of the Ligands; Zwitterionic Behaviour

The four ligands studied in this work all have the potential for internal proton transfer to give zwitterions, in view of the acidity of the fluorinated tertiary alcohol group, and the fluorinated amino-alcohols may therefore be likened to amino-acids, *e.g.*

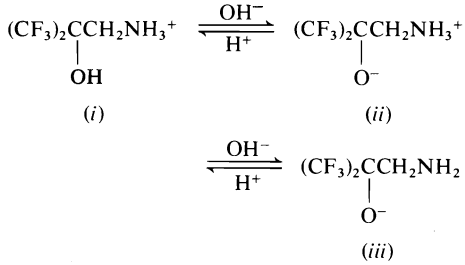

Titration of the compounds confirmed that this behaviour was occurring in solution in each case. Two pK_a values were determined, corresponding to the two steps in the above equilibrium, and these are recorded in Table 1, together with isoelectric point values; figures for glycine are added for comparative purposes. In comparing these figures with pK_a values for other fluorinated alcohols such as $(CF_3)_3COH$ (pK_a = 5.4 (7)) or $CH_3C(CF_3)_2OH$ (pK_a = 9.6 (8)) it should be remembered that, for the species studied in the present work, $pK_a(1)$ represents the ionization of the hydroxylic proton in the protonated species (*i*), whereas $pK_a(2)$ represents the ionization of the proton on the amine group in the

TABLE 1. pK_a and isoelectric point values for zwitterionic ligand molecules

Ligand	$pK_a(1)$	$pK_a(2)$	Isoelectric point
Glycine, NH_2CH_2COOH	2.34	9.60	5.97
1 	5.71	6.91	6.31
7 $(CF_3)_2CCH_2NH_2$ | OH	5.35	8.63	6.99
8 $(CF_3)_2CCH_2NHCH_3$ | OH	5.61	8.96	7.29
9 $(CF_3)_2CCH_2CH_2NH_2$ | OH	6.39	9.46	7.93

zwitterionic species (*ii*). This leads to an apparent enhancement of the acidity of the hydroxyl group in the fluorinated alcohol, just as the apparent acidity of the carboxylic acid in glycine is considerably greater than that of acetic acid ($pK_a = 4.74$).

The general features of this behaviour may be readily explained. All the fluorinated amino-alcohols have $pK_a(1)$ values 3–4 units greater than glycine, a difference similar to that found between fluorinated alcohols and carboxylic acids. The $pK_a(2)$ values of **7**, **8**, and **9**, which contain $—CH_2NH_2$ or $—CH_2NHR$, are similar to that of glycine, whereas that of the pyridine derivative **1** is notably less. This is consistent with the expected lower basicity of both the nitrogen atoms in **1**; that in the pyridine ring, and that in the side-chain, which is attached to the electronegative $—C(CF_3)_2O^-$ group.

In the solid state, infrared spectral studies showed a considerable difference between the compounds (Fig. 1). The γ-amino alcohol **10** showed neither O—H nor NH_2 absorptions, but very broad absorption in the region 2200–3000 cm^{-1} characteristic of $—NH_3^+$ and very similar to that of glycine. This alcohol would therefore appear to have the zwitterionic structure in the solid state and should be written $^-O—C(CF_3)_2-CH_2CH_2NH_3^+$. The β-amino alcohols, on the other hand, showed fairly sharp N—H absorptions at 3330 and 3400 cm^{-1} in $(CF_3)_2C(OH)-CH_2NH_2$ (**7**) and at 3380 cm^{-1} in $(CF_3)_2C(OH)-NH(C_5H_4N)$ (**1**), with much reduced absorption in the 2500–3000 cm^{-1} region. This suggests that the structures of these molecules in the solid state are not zwitterionic, but probably contain intramolecular hydrogen-bonding:

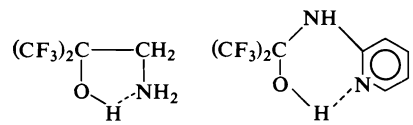

7 **1**

The marked difference between **7** and **9** in these solid-state structures is presumably associated with the different ring sizes required for internal hydrogen-bonding, the five-membered ring being more easily formed. However, this effect would not seem to operate in solution.

Metal Complexes of Amino-alcohols

In view of the resemblances between fluorinated amino-alcohols and amino-acids, noted above, we expected that chelation to metal ions as uninegative ligands would occur, and this proved to be correct. For each amino-alcohol ligand, neutral metal complexes of general formula $M(L)_2$ formed, where $M = Co^{2+}$, Ni^{2+}, or Cu^{2+}. In a square-planar environment, either a *cis*- or *trans*-configuration would be possible, as shown in Fig. 2.

The general environment of the metal in these complexes is very similar to that in complexes which we have previously studied (9) in which the

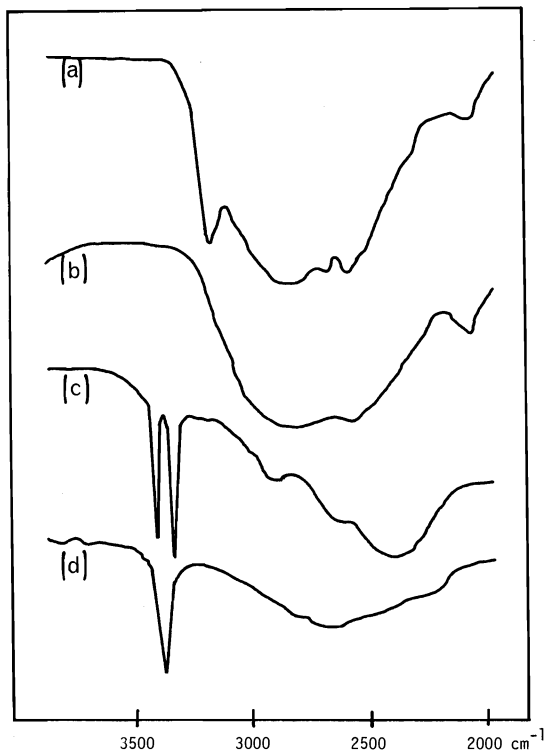

FIG. 1. The infrared spectra of some fluorinated amino-alcohols: (*a*) glycine, (*b*) ligand **9**, (*c*) ligand **7**, (*d*) ligand **1**.

ligands are a perfluoropinacolato dianion and a chelating diamine, so we would expect similar structures to prevail. This was the case, with the nickel complexes all being square-planar and diamagnetic.

With the substituted pyridine ligand **1**, the metal complexes both showed a strong sharp N—H absorption in the infrared spectrum at 3380 cm^{-1}, unchanged from its position in the free ligand. This shows that coordination is occurring from the nitrogen of the pyridine ring, rather than from the side-chain —NH— group; the latter would of course be most unlikely to form a chelate with oxygen, as a four-membered ring would be required. This result also shows that the —NH— nitrogen atom is not involved

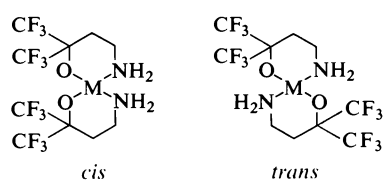

FIG. 2. *cis*- and *trans*-configuration of metal complexes of amino acids.

in zwitterion formation and supports the internally hydrogen-bonded model given above.

Present evidence does not allow us to distinguish between *cis*- and *trans*-configurations in these complexes. The local symmetry of the metal is C_{2v} for the *cis*- and C_{2h} for the *trans*-isomer, which should affect the infrared spectrum in the metal–oxygen and metal–nitrogen vibrational region (300–500 cm^{-1}) but the presence of other groups in the molecule complicates the spectrum and makes an unambiguous assignment impossible.

The magnetic moments and visible absorption spectra of most of the copper complexes were in the ranges previously found (9) for complexes of this type, to which we had assigned approximately square-planar geometry. However, the complex with ligand **5**, the derivative of 2-amino-6-methylpyridine, had a significantly higher magnetic moment of 2.12 BM, where the others were in the range 1.75–1.85 BM. The maximum in the visible absorption spectrum of this compound was also at slightly longer wavelength (626 nm against 550–610 nm) with a greater intensity ($\varepsilon = 142$ against $\varepsilon = 50$–70) than the other complexes. This behaviour is consistent with some degree of distortion from a square-planar arrangement being present in complexes of ligand **6**, associated with the steric hindrance offered by the methyl group in the 6-position on the pyridine ring.

Only restricted studies of cobalt(II) complexes of the fluorinated amino-alcohols were possible, since they had a very limited stability in solution. However, ligand **7** formed a cobalt complex, stable in the solid state, whose analysis corresponded to the dihydrate $Co[NH_2CH_2C(CF_3)_2O]_2(H_2O)_2$, which had a magnetic moment of 4.38 BM and a visible absorption spectrum with peaks at 480 and 570 nm (diffuse reflectance); properties consistent with octahedral cobalt(II). The water was easily removed *in vacuo*, but the properties of the compound were hardly changed at all. The magnetic moment was 4.36 BM, the visible absorption spectrum was almost identical, and the infrared spectrum was largely unchanged except for the loss of a sharp —OH absorption at 3860 cm^{-1}. It would appear, therefore, that the two water molecules are not coordinated to the cobalt ion but are simply present elsewhere in the lattice. The octahedral coordination of the cobalt is presumably achieved by extension of the coordination of the oxygen atoms

TABLE 2. Formation constants of metal complexes

Ligand	log K* Cu^{2+}	Ni^{2+}	Co^{2+}
1 	13.83	9.56	7.95
glycine, NH_2CH_2COOH (11, 12)	15.67	12.13	10.04
7 $(CF_3)_2CCH_2NH_2$ | OH	13.16	9.08	7.88
β-alanine, $NH_2CH_2CH_2COOH$ (13)	12.50	8.12	3.58†
9 $(CF_3)_2CCH_2CH_2NH_2$ | OH	10.09	8.11	4.21†

*$K = [M(L)_2]/[M^{2+}][L^-]^2$.
†K is for the formation of the 1:1 complex $M(L)^+$ only, due to the limited stability of the 1:2 amino-alcohol complex in solution.

in the ligand to form bridges between the cobalt ions and a polymeric structure, a tendency we have not previously observed with $-C(CF_3)_2O^-$ ligands, but the point cannot be definitely established without more detailed structural data.

The compound $(CH_3)_2NNHC(CF_3)_2OH$ was readily prepared by the addition of hexafluoroacetone to 1,1-dimethylhydrazine. Although this has the potential of acting as a chelating ligand, forming a five-membered ring similar to that in the amino-pyridine derivatives described above, we could find no indication of complex formation with metal ions. This is presumably due to steric hindrance from the relatively bulky dimethylamino group, whose coordination is less favourable than that of the pyridine ring.

Formation Constants

The isolation of a variety of metal complexes established that the fluorinated amino-alcohols were in all cases coordinating as the anionic form (*iii*). We were therefore able to determine overall formation constants for the reactions

$$M^{2+} + 2L^- \rightleftharpoons M(L)_2$$

for most of the amino-alcohols, by potentiometric titration in methanol/water mixtures (10). Solubility limitations prevented direct measurement in pure water, but values obtained in methanol/water were extrapolated to water in order to allow comparison with the known values of comparable constants for amino-acids; the results are summarized in Table 2.

In most cases where a direct comparison between similarly structured complexes is possible, that is, between **7** and glycine and between **9** and β-alanine, the amino-alcohol complex has the lower formation constant. This may be explained in terms of the greater steric crowding of the $-C(CF_3)_2O^-$ group, as compared with the carboxylate group. It is also clear by a comparison of **7** with **9** that the formation of complexes with 5-membered chelate rings is, as is usually found, more favourable that that of those with 6-membered rings. The pyridine derivative, **1**, gives the most stable complexes of any of the amino-alcohols studied, despite the formation of a 6-membered chelate ring; this may be ascribed to the greater donor strength of the pyridine nitrogen as compared with that of an amino-group.

Within a series of metal complexes of the same ligand, the stability in each case follows the usual Irving-Williams order $Cu^{2+} > Ni^{2+} > Co^{2+}$.

Solvate Formation

We have previously demonstrated (9) the existence of exclusively 5-coordinate solvate formation when complexes of nickel with PFP^{2-} and a bidentate diamine are dissolved in pyridine or a primary amine. In view of the similarity of the environment of the metal atom

TABLE 3. Analytical data

Compound	Formula	Carbon		Hydrogen		Fluorine		Nitrogen		Colour	$\chi_g \times 10^6$ cgsu(298 K)	μ_{eff} (BM)
		Calcd.	Found	Calcd.	Found	Calcd.	Found	Calcd.	Found			
$(C_5H_4N)NHC(CF_3)_2OH$ (1)	$C_8H_5F_6N_2O$	36.9	36.9	2.33	2.31	43.8	43.7	10.8	11.6	—	—	—
$Ni[(C_5H_4N)NHC(CF_3)_2O]_2$	$C_{16}H_{10}F_{12}N_4NiO_2$	33.3	33.2	1.75	1.52	39.5	39.4	9.7	9.9	red	—	diamag.
$Ni[(C_5H_4N)NHC(CF_3)_2O]_2(C_5H_5N)_2$	$C_{26}H_{20}F_{12}N_6NiO_2$	42.5	42.5	2.74	2.77			11.4	11.4	green	5.48	3.24
$Cu[(C_5H_4N)NHC(CF_3)_2O]_2$	$C_{16}H_{10}CuF_{12}N_4O_2$	33.0	33.2	1.73	1.82	39.2	40.5	9.6	9.8	purple	1.80	1.76
$NH_2CH_2C(CF_3)_2OH$ (7)	$C_4H_5F_6NO$	24.4	24.5	2.56	2.71			7.1	7.1	—	—	—
$Co[NH_2CH_2C(CF_3)_2O]_2(H_2O)_2$	$C_8H_{12}CoF_{12}N_2O_4$	19.7	19.7	2.48	2.27			5.7	5.9	purple	15.96	4.38
$Co[NH_2CH_2C(CF_3)_2O]_2$	$C_8H_8CoF_{12}N_2O_2$	21.3	21.4	1.79	1.73			6.2	6.3	purple	17.13	4.36
$Ni[NH_2CH_2C(CF_3)_2O]_2$	$C_8H_8F_{12}N_2NiO_2$	21.3	21.1	1.79	1.65			6.2	6.4	red	—	diamag.
$Cu[NH_2CH_2C(CF_3)_2O]_2$	$C_8H_8CuF_{12}N_2O_2$	21.1	21.1	1.77	1.66			6.1	6.2	purple	2.43	1.75
$CH_3NHCH_2C(CF_3)_2OLi$ (8)	$C_5H_6F_6LiNO$	27.7	27.9	2.79	2.77	52.5	52.9	6.5	6.4	—	—	—
$Cu[CH_3NHCH_2C(CF_3)_2O]_2$	$C_{10}H_{12}CuF_{12}N_2O_2$	24.8	25.0	2.50	2.55	47.1	47.3	5.8	5.9	purple	2.48	1.85
$NH_2CH_2CH_2C(CF_3)_2OH$ (9)	$C_5H_7F_6NO$	28.4	28.8	3.34	2.96	54.0	54.0	6.6	6.5	—	—	—
$Co[NH_2CH_2CH_2C(CF_3)_2O]_2$	$C_{10}H_{12}CoF_{12}N_2O_2$	25.1	24.9	2.52	2.69			5.8	5.8	purple	17.76	4.58
$Ni[NH_2CH_2CH_2C(CF_3)_2O]_2$	$C_{10}H_{12}F_{12}N_2NiO_2$	25.1	25.0	2.53	2.23	47.6	47.6	5.8	5.9	red	—	diamag.
$Cu[NH_2CH_2CH_2C(CF_3)_2O]_2$	$C_{10}H_{12}CuF_{12}N_2O_2$	24.8	24.8	2.50	2.03	47.1	47.2	5.8	5.7	purple	2.24	1.76
$(CH_3)_2NNHC(CF_3)_2OH$	$C_5H_8F_6N_2O$	26.5	26.6	3.57	3.71	50.4	50.3	12.4	12.1	—	—	—

in the compounds in the present study, particularly in respect of the steric hindrance presented by the four bulky trifluoromethyl groups, it is not surprising that these behave similarly. The nickel complexes, because of their characteristic visible spectra, show the effect best.

The nickel complex of the ligand **7**, initially square-planar and red, dissolved in pyridine to give a green solution from which a green solid solvate could be isolated. Analysis showed this to be a 1:2 adduct, $Ni[(C_5H_4N)NHC(CF_3)_2O]_2$-$(C_5H_5N)_2$, but it was clear from its visible spectrum that only one of the two solvent molecules had coordinated to the nickel. The strong sharp absorption near 380 nm with a weaker peak at 640 nm characteristic of 5-coordinate nickel(II) were present in both solid and solution spectra and a series of spectra run in methanol/pyridine mixtures gave two well-defined isosbestic points, similar to those found in our previous studies, confirming that only one solvate had formed. Furthermore, the spectrum of the solvate was virtually superimposable on that found for nickel(II) complexed by PFP^{2-} and the tridentate amine, diethylenetriamine (9). We conclude that the second pyridine molecule in the solid solvate is fortuitously included in the lattice without interacting with the metal ion.

With the other nickel(II) complexes of amino-alcohols, visible spectra in methanol/pyridine mixtures showed behaviour very similar to that noted above, showing that solvation to give 5-coordinate adducts was occurring, but no solid products could be isolated.

When the analogous copper complex of ligand **1**, in methanol, was treated with pyridine, it was clear that solvation was occurring, but no stable solid adduct could be isolated. The visible absorption maximum shifted from 550 to 600 nm with one isosbestic point, indicating that only one solvated species was present. That this was a 5-coordinate 1:1 adduct of the copper complex with pyridine may reasonably be suggested, by analogy with the nickel studies, but the visible spectra of copper in different environments are not sufficiently distinctive to allow a definite assignment to be made.

Conclusion

Our study of these difunctional molecules confirms that there is a valid analogy between the properties of a highly fluorinated tertiary

alcohol and a carboxylic acid. The acidity of the former is sufficient to undergo intramolecular proton transfer when a suitable basic site is present and to coordinate in an ionized form to a transition metal ion, giving isolable complexes. However, the greater bulk of the fluorinated alcohol results in steric hindrance around the metal, such that the coordination number of the metal appears to be limited to five.

Experimental

General

Volatile materials were handled by standard vacuum-line techniques. Infrared spectra were recorded on a Perkin-Elmer model 621 instrument and visible spectra on Cary model 14 and 118 spectrophotometers. A Corning model 12 p*H* meter was used for potentiometric titrations. Magnetic moments were determined by the Gouy method.

Microanalyses were performed by Alfred Bernhardt Laboratories, West Germany. All analytical data are given in Table 3.

Hexafluoroacetone (Matheson) was purified by trap-to-trap distillation. Other starting materials were reagent grade chemicals purified by standard methods.

*N-(2-Pyridyl)-2-aminohexafluoropropane-2-ol (**1**)*

2-Aminopyridine in dry benzene was maintained near 10°C while gaseous hexafluoroacetone was passed in through a bubbler below the surface with continuous stirring. Uptake was followed by weight gain to an equimolar ratio. The product crystallized on partial removal of solvent and was recrystallized from benzene. The yield was essentially quantitative; mp 122–124°C.

Use of the various methyl-substituted amino-pyridines in the same method gave the methyl-substituted products.

The copper complex was prepared by treating a methanolic solution of the ligand (30 mmol) and copper sulfate (10 mmol) with methanolic potassium hydroxide to p*H* 9. The solution was evaporated to dryness and extracted with tetrahydrofuran to remove potassium sulfate, then concentrated, and 30–60°C petroleum ether added to the cloud point. Crystals of the desired complex separated on cooling.

With nickel and cobalt, the method was very similar, with the metal nitrates used as a source of metal ions. The cobalt reaction was carried out using degassed solvents under a nitrogen atmosphere.

1,1,1-Trifluoro-2-trifluoromethyl-3-aminopropane-2-ol (7)

(a) By Ring Opening of an Epoxide

The known epoxide $(CF_3)_2\overline{CCH_2O}$ was made by the reaction of diazomethane with hexafluoroacetone as described previously (3), employing precautions usual to the handling of diazomethane. In a typical reaction, diazomethane was prepared from nitrosomethylurea (14) and distilled in ether into a cooled receiver containing ether over potassium hydroxide pellets. Based on the expected 65–70% yield, about 5.6 g (0.13 mol) diazomethane was present and hexafluoroacetone (33 g, 0.20 mol) was slowly passed in while maintaining the temperature at −10°C. Without separation of the epoxide, which has bp 39°C, the flask was fitted with a condenser at −78°C and excess gaseous ammonia bubbled through while the contents were slowly allowed to warm to reflux temperature. The final solution was filtered and evaporated and the solid product recrystallized from ether/hexane, mp 76–77°C.

(b) By Catalytic Hydrogenation

Hexafluoroacetone cyanohydrin (15) proved difficult to hydrogenate over Raney nickel, but pressures of 500 psi gave a satisfactory yield (75%) of product identical with that obtained by the ring-opening route.

Metal complexes were prepared by the method described above for ligand **1**. The nickel complex had very low solubility in all solvents tried, and was recrystallized from very dilute ether/hexane solution.

*1,1,1-Trifluoro-2-trifluoromethyl-3-(methylamino)-propane-2-ol (**8**)*

The ring-opening reaction on the epoxide, described above, was repeated with the substitution of methylamine for ammonia. Removal of solvent gave a white solid from which the product was isolated by recrystallization from ether/hexane, mp 73°C.

An alternative route to this compound is available through the reduction of the known dioxolane $(CF_3)_2\overline{COC(CF_3)_2OCNCH_3}$, made by the addition of hexafluoroacetone to methyl isocyanide (16). When 20 g of this compound was heated under reflux with lithium tetrahydridoaluminate (5 g) for 24 h, the mixture cooled and decomposed with water and aqueous alkali, the lithium salt of the *N*-methylamino alcohol was obtained in poor yield on evaporation. Previous workers reported that a similar reduction and workup procedure on the *N*-ethyl analogue gave the *N*-ethylamino alcohol, rather than its salt.

The copper complex of **8** was prepared by the same method used for **7**.

*1,1,1-Trifluoro-2-trifluoromethyl-4-aminobutane-2-ol (**9**)*

The hydroxy-nitrile $(CF_3)_2C(OH)CH_2CN$ was prepared by the addition of hexafluoroacetone to cyanoacetic acid (6). In the hydrogenation, 48 g (0.23 mol) of the purified hydroxy-nitrile was dissolved in anhydrous ether (250 ml) with 28 g of anhydrous sodium acetate and 10 g of Raney nickel, pre-treated with acetic anhydride. After shaking under an initial hydrogen pressure of 50 psi for 18 h, the mixture was filtered, the solvent removed, and the product recrystallized from ether/hexane, mp 82–83°C. The yield was essentially quantitative.

Complexes of cobalt, nickel, and copper were prepared by the same method described above for ligand **1**.

Acknowledgements

Financial support for this work was provided by the National Research Council of Canada.

We thank Dr. J. W. L. Martin for helpful discussions.

1. J. W. L. Martin and C. J. Willis. Can. J. Chem. This issue.
2. C. G. Krespan and W. S. Middleton. Fluorine Chem. Rev. **1**, 145 (1967).

3. R. E. A. DEAR and E. E. GILBERT. U.S. Patent 3,573,330 (1971); Chem. Abstr. **74**, 141498 (1971).
4. E. T. MCBEE, L. E. HATHAWAY, and C. W. ROBERTS. J. Am. Chem. Soc. **78**, 3851 (1956).
5. R. O. B. WATTS, C. G. ALLISON, K. P. BARTHOLD, and P. TARRANT. J. Fluorine Chem. **3**, 7 (1974).
6. Y. V. ZIEFMAN and N. P. GAMBARYAN. Izv. Akad. Nauk SSSR, Ser. Khim. 1687 (1964).
7. I. L. KNUNYANTS and B. L. DYATKIN. Izv. Akad. Nauk SSSR Ser. Khim. 923 (1964).
8. R. FILLER and R. M. SCHURE. J. Org. Chem. **32**, 1217 (1967).
9. W. S. CRIPPS and C. J. WILLIS. Can. J. Chem. **53**, 809 (1975).
10. C. B. MONK. Trans. Faraday Soc. **47**, 297 (1951).
11. J. R. BRANNAN, H. S. DUNSMORE, and G. H. NANCOLLAS. J. Chem. Soc. 304 (1964).
12. K. P. ANDERSON, W. O. GREENHALGH, and R. M. IZATT. Inorg. Chem. **5**, 2106 (1966).
13. V. S. SHARMA, H. B. MATHUR, and P. S. KILKARNI. Indian J. Chem. **3**, 146 (1965); **3**, 475 (1965).
14. J. HINE. J. Am. Chem. Soc. **85**, 3239 (1963).
15. T. MILL, J. O. RODIN, R. M. SILVERSTEIN, and C. WOOLF. J. Org. Chem. **29**, 3715 (1964).
16. W. J. MIDDLETON, D. C. ENGLAND, and A. G. KRESPAN. J. Org. Chem. **32**, 948 (1967).

Fluorosulfates of palladium

K. C. LEE AND F. AUBKE[1]

Department of Chemistry, The University of British Columbia, Vancouver, B.C., Canada V6T 1W5

Received February 1, 1977

K. C. LEE and F. AUBKE. Can. J. Chem. **55**, 2473 (1977).

The syntheses of $Pd(SO_3F)_2$ and $Pd(SO_3F)_3$ by the reactions of palladium with $BrOSO_2F$ and $S_2O_6F_2$ are described. Structural information on both compounds is based on infrared, Raman, diffuse reflectance, and electronic mull spectra as well as magnetic measurements from $\sim$300 to $\sim$100 K. Palladium bisfluorosulfate is found to have a polymeric structure with the fluorosulfate group acting as a tridentate ligand. As a consequence, an octahedral environment is found for Pd^{2+} with a $^3A_{2g}$ ground state, a μ_{eff}^{298} value of 3.39 BM and the ligand field parameter $Dq = 1177\ cm^{-1}$ and $B = 633\ cm^{-1}$. $Pd(SO_3F)_3$ is best regarded as $Pd^{II}[Pd^{IV}(SO_3F)_6]$.

K. C. LEE et F. AUBKE. Can. J. Chem. **55**, 2473 (1977).

On décrit la synthèse du $Pd(SO_3F)_2$ et du $Pd(SO_3F)_3$ par les réactions du palladium avec $BrOSO_2F$ et $S_2O_6F_2$. Les informations concernant la structure des deux composés sont basées sur les spectres infrarouges, Raman, de réflexions diffuses et électroniques de même que des mesures magnétiques de $\sim$300 à $\sim$100 K. On a trouvé que le bis(fluorosulfate) de palladium existe sous forme de polymère dans lequel un groupe fluorosulfate agit comme ligand tridentate. En conséquence on trouve un environnement octaédrique pour Pd^{2+} avec un état fondamental $^3A_{2g}$, une valeur de μ_{eff}^{298} de 3.39 BM et un paramètre de champ de ligand $Dq = 1177\ cm^{-1}$ et $B = 633\ cm^{-1}$. La meilleure façon de considérer $Pd(SO_3F)_3$ est $Pd^{II}[Pd^{IV}(SO_3F)_6]$.

[Traduit par le journal]

Introduction

Divalent palladium has a d^8 electronic configuration and is, much like divalent platinum, found in diamagnetic square planar, low spin complexes (1). The only notable exception is palladium difluoride (2) and some of its derivatives like $CsPdF_3$ (3) or $Pd^{II}[M^{IV}F_6]$ (4), with M = Ge, Sn, or Pd. The difluoride is found to have a rutile structure (5), and an octahedral environment is indicated for palladium also by the observed paramagnetism of the complex fluorides.

This study describes the syntheses of two new, strongly paramagnetic fluorosulfates of palladium, $Pd(SO_3F)_2$ and $Pd(SO_3F)_3$, and their structural characterisations by magnetic measurements, vibrational and electronic spectra.

Experimental

Chemicals

Peroxydisulfuryl difluoride, $S_2O_6F_2$ (6), and bromine(I)-fluorosulfate, $BrOSO_2F$ (7), were synthesised according to literature reports. Palladium powder of 60 mesh and of 99.95% purity was supplied by the Ventron Corp. Perfluoro-octyl sulfurylfluoride, $C_8F_{17}SO_2F$, was obtained as a gift from Dr. H. Niederpruem, Farbenfabriken Bayer, Leverkusen, W. Germany.

Instrumentation

Raman spectra were obtained with either a Cary 81 or a Spex Ramalog 5 spectrophotometer fitted with a He–Ne (635.5 nm) and an argon ion (514.5 nm) laser respectively. Solid samples were contained in Pyrex tubes. Infrared spectra were recorded on a Perkin-Elmer 457 spectrophotometer. Silver chloride or bromide was used as window material. Due to the reactivities of the palladium fluorosulfates, mulling agents such as Nujol and HCB could not be used and spectra were recorded on thin films of the solids. Electronic spectra were obtained on powdered samples using a Bausch and Lomb Spectronic 600 spectrophotometer (diffuse reflectance) and on samples mulled in $C_8F_{17}SO_2F$ (perfluoro-octyl sulfurylfluoride) using a Cary 14 spectrophotometer. Magnetic susceptibilities were measured using the Gouy apparatus described earlier (8). The coil current of the magnet was regulated to give a field of approximately 4500 G. The temperature of the sample was controlled by the rate of evaporation of N_2 around the chamber. Calibration was achieved using $HgCo(SCN)_4$ (9). Diamagnetic corrections of 25×10^{-6} for Pd^{2+}, 22×10^{-6} for Pd^{3+}, 18×10^{-6} for Pd^{4+}, and 40×10^{-6} for SO_3F^- were made (1, 10). All values are in cgs units.

All reactions were performed in Pyrex reaction vials of about 40 ml contents, fitted with Kontes Teflon stem valves. Volatile materials were handled using vacuum line techniques. Solids were handled in a Vacuum Atmospheres Corp. "Dri Lab" Model No. HE-43-2, filled with purified dry nitrogen and equipped with a "Dri-Train" Model No. HE-93-B circulating unit.

Preparations of $Pd(SO_3F)_2$

Palladium metal (508 mg, 4.77 mmol) was allowed to react at 110°C (oil bath) for about 14 days with a large excess (about 12 to 15 g) of $BrOSO_2F$. The completion of the reaction was indicated by the consumption of all metal and the appearance of an insoluble purple solid.

[1]To whom correspondence should be addressed.

Removal of all volatile material yielded 1437 mg (4.72 mmol) of palladium bisfluorosulfate. $Pd(SO_3F)_2$ is a light purple, hygroscopic solid, thermally stable up to +250°C. Above this temperature thermal decomposition according to

$$Pd(SO_3F)_2 \rightarrow PdF_2 + 2SO_3$$

was observed.

Synthesis of $Pd(SO_3F)_3$

A large excess of peroxydisulfuryl difluoride, $S_2O_6F_2$ (about 10 to 15 g), was added to 398 mg (1.31 mmol) of $Pd(SO_3F)_2$. An immediate reaction was noted, evidenced by the gradual darkening of the solid reactant. The mixture was heated overnight at 80°C. After removal of all volatiles, 518 mg (1.28 mmol) of $Pd(SO_3F)_3$ were obtained. $Pd(SO_3F)_3$ is a dark brown, hygroscopic solid, thermally stable up to 180°C at atmospheric pressure.

Analysis

Chemical analyses were performed by A. Bernhardt, Elbach, West Germany. The results are listed in %.

	Pd		S		F	
Compound	Calcd.	Found	Calcd.	Found	Calcd.	Found
$Pd(SO_3F)_2$	35.10	34.94	21.15	21.06	12.49	12.47
$Pd(SO_3F)_3$	26.36	26.54	23.83	23.68	14.12	14.01

Results and Discussion

Synthesis

The direct reaction of bromine-(I)-fluorosulfate with palladium powder according to:

$$[1]\quad Pd + 2BrOSO_2F \xrightarrow[14\ days]{+110°C} Pd(SO_3F)_2 + Br_2$$

was found to be a most convenient route to palladium(II) fluorosulfate. The formation reaction has two precedents: interaction of $BrOSO_2F$ with gold and platinum is reported to yield $Au(SO_3F)_3$ and $Pt(SO_3F)_4$ (11). However, there are some important differences. Palladium metal was far less reactive than either gold or platinum as indicated by the higher reaction temperature and the longer reaction time. The oxidation reaction proceeded exclusively to the +2 oxidation state and the resulting product was seemingly insoluble in excess $BrOSO_2F$ even at +110°C, whereas both $Au(SO_3F)_3$ and $Pt(SO_3F)_4$ dissolved readily in $BrOSO_2F$ and complete removal of the bromine-(I)-fluorosulfate required elevated temperatures. The purple $Pd(SO_3F)_2$ was also insoluble in HSO_3F and thermally stable up to 250°C. All these features are consistent with a polymeric structure for palladium bisfluorosulfate.

Oxidation to form palladium trisfluorosulfate was readily accomplished with peroxydisulfuryl difluoride. The resulting brown $Pd(SO_3F)_3$ decomposed quantitatively at +160°C *in vacuo* to yield $S_2O_6F_2$ and $Pd(SO_3F)_2$ in a reversal of the formation reaction:

$$[2]\quad 2Pd(SO_3F)_2 + S_2O_6F_2 \underset{+160°C}{\overset{+80°C/12\ h}{\rightleftharpoons}} 2Pd(SO_3F)_3$$

The formation of $S_2O_6F_2$ by pyrolysis of a metal fluorosulfate was unprecedented, but xenon bisfluorosulfate and the fluoride-fluorosulfates of $FXeSO_3F$ and F_5XeSO_3F have been reported to yield peroxydisulfuryl difluoride (12–14).

The direct reaction of $S_2O_6F_2$ with palladium powder proceeded extremely slowly, yielding only incompletely oxidised brown products. The successive oxidation by $BrOSO_2F$ and $S_2O_6F_2$ appeared to be a better route to $Pd(SO_3F)_3$.

The existence of $Pd(SO_3F)_3$ as a stable species with the metal in the +3 oxidation state would be rather surprising. Whereas both $Pd^{II}(d^8)$ and $Pd^{IV}(d^6)$ are rather common oxidation states for palladium, no evidence for $Pd^{III}(d^7)$ in stable binary compounds has been reported and PdF_3 is better regarded as $Pd^{II}[Pd^{IV}F_6]$ (4). A similar formulation may very well apply to the palladium trisfluorosulfate and both vibrational spectra and magnetic measurements should provide some structural insights.

Vibrational Spectra

The infrared and Raman data in cm^{-1} for $Pd(SO_3F)_2$ are found as follows, with Raman data in parentheses: 1240 s, b (1231 m); 1090 ms (1111 ms); 860 s (869 m); 610 s (612 w); 565 m (552 w, sh) and 421 m (430 m, 354 vw). The relatively simple spectrum with only six ir and Raman active vibrational modes indicates that the fluorosulfate group has C_{3v} symmetry.

Similar infrared spectra have been reported for a number of fluorosulfates of the type $M(SO_3F)_2$, with M = Mg, Ca, Zn, Cd, Hg, Fe, Co, and Ni, by Thompson and co-workers (10, 15). These authors have postulated a tridentate, oxygen bridged fluorosulfate group in these compounds rather than ionic groups, where the

TABLE 1. The Raman spectra of $Pd(SO_3F)_3$ and $K_2[Sn(SO_3F)_6]$*

$\Delta\nu$ (cm^{-1})		$\Delta\nu$ (cm^{-1})	
$Pd(SO_3F)_3$	$K_2[Sn(SO_3F)_6]$	$Pd(SO_3F)_3$	$K_2[Sn(SO_3F)_6]$
1412 w	1407 m	630 ms	
		612 s	625 s
1396 w	1390 w		
		578 w	582 w
1294 m	1278 ms		
		538 mw	560 m
1225 vs	1228 m		
1202 w,sh	1208 w	446 ms	435 m
1172 m	1190 m		
		420 m	416 m
1034 s	1096 s		
1001 m	1002 m	360 m, sh	
996 m,sh		335 m	360 m
860 w	859 m		
	836 m		266 w
822	823 m		

*Reference 19; vs = very strong, s = strong, m = medium, sh = shoulder.

point group C_{3v} would predict the same number and type of fundamental vibrations. The argument is based on frequency shifts, affecting all six fundamentals. In particular ν_2 the S—F stretch is found $\sim 100\ cm^{-1}$ higher than commonly observed for ionic fluorosulfates (16–18).

$Pd(SO_3F)_2$ also falls into this group. The fact that none of the degenerate modes appears to be split, leads one to expect a regular octahedral environment for palladium, rather than a distorted one as suggested for $Cu(SO_3F)_2$ (15, 16).

Vibrational information for $Pd(SO_3F)_3$ is obtained from the Raman spectrum using the He–Ne laser. The more powerful argon ion laser was found to cause decomposition of the sample evidenced by the appearance of lines due to $Pd(SO_3F)_2$. The extreme reactivity of the compound prevented us from recording any reliable infrared spectra.

The observed Raman shifts are tabulated in Table 1 and compared to previously reported data for $K_2[Sn(SO_3F)_6]$ (19). As can be seen from the table, a useful comparison between this complex and $Pd(SO_3F)_3$ can indeed be made, providing initial support for a formulation as $Pd^{II}[Pd^{IV}(SO_3F)_6]$. The SO_3 stretching frequencies are assigned to bands at 1400, 1220, and 1000 cm^{-1}, with all bands split into two or three components due to solid state splitting.

The similarities between $[Sn(SO_3F)_6]^{2-}$ and $[Pd(SO_3F)_6]^{2-}$ continue into the lower frequency range, suggesting approximately monodentate fluorosulfate groups with coordination via oxygen for both compounds. A more detailed vibrational assignment appears not very useful due to the observed complexity of the Raman spectrum.

Electronic Spectra

The vibrational spectrum had indicated a regular octahedral environment for palladium(II) in $Pd(SO_3F)_2$ and the magnetic results, to be discussed subsequently, support a high spin configuration and hence a $^3A_{2g}$ ground state. A three line ligand field spectrum is therefore expected and indeed observed. The mull spectrum shows bands at 850 and 575 nm and a shoulder at ~ 370 nm. The diffuse reflectance spectrum shows only bands at 575 nm and ~ 380 nm because the region beyond 700 nm was not accessible with the spectrometer used. The three bands are assigned as follows:

ν_1 at 850 nm (11 770 cm^{-1}), $^3A_{2g} \rightarrow {}^3T_{2g}$

ν_2 at 575 nm (17 400 cm^{-1}), $^3A_{2g} \rightarrow {}^3T_{1g}(F)$

ν_3 at 370 nm (27 000 cm^{-1}), $^3A_{2g} \rightarrow {}^3T_{1g}(P)$

Hence, 10 Dq is 11 770 cm^{-1}. The ligand field parameter, B, of 633 cm^{-1} is obtained from the measured ν_2/ν_1 ratio using Tanabe–Sugano diagrams as suggested by Lever (20). The position of ν_3 at 370 nm is confirmed by this method. Some pertinent ligand field parameters for $Pd(SO_3F)_2$, $Ni(SO_3F)_2$ (21), and $Co(SO_3F)_2$ (10) are listed in Table 2.

The comparison shows, that the three bands observed for $Pd(SO_3F)_2$ are best explained as

TABLE 2. Ligand field parameters for $Pd(SO_3F)_2$, $Ni(SO_3F)_2$, and $Co(SO_3F)_2$*

Compound	Dq (cm^{-1})	B (cm^{-1})	B^0 (cm^{-1})	B/B^0	Reference
$Pd(SO_3F)_2$	1177	633	830	0.763	This work
$Ni(SO_3F)_2$	734	905	1080	0.838	21
$Co(SO_3F)_2$	765	860	1120	0.768	10

*B^0 = free ion values for M^{2+} as tabulated in ref. 22.

TABLE 3. Magnetic behaviour of palladium fluorides and fluorosulfates and related compounds at room temperature*

Compounds	$\chi_M^{corr} \times 10^6$ (cgsu)	μ_{eff} (BM)	Temperature dependence of χ_M^{corr} and μ_{eff}	Reference
PdF_2	1284	1.74	Antiferromagn. coupling	24
$Pd(SO_3F)_2$†	4773	3.39	$\chi_M^{corr} = 1.38/(T - 13)$; μ_{eff}: 3.39–3.49 BM	This work
$Pd(SO_3F)_2$§	4620	3.34	Corrected for TIP	
$Ni(SO_3F)_2$§	5189	3.49	Curie–Weiss law is followed	23
PdF_3	1657	2.00	Curie–Weiss law is followed, $\theta = -28$ K	24
$Pd^{II}Pd^{IV}F_6$	3314	2.88	Curie–Weiss law is followed	24
$Pd(SO_3F)_3$‡	2463	2.49	Curie–Weiss law is followed, $\theta = 10 \pm 2$ K	This work
$Pd^{II}[Pd^{IV}(SO_3F)_6]$‡	4926	3.45	$\chi_M^{corr} = 1.44/(T - 10)$; μ_{eff}: 3.45–3.56 BM	This work

*χ_M^{corr} = corrected molar magnetic susceptibility; μ_{eff} = effective magnetic moment; TIP = temperature independent paramagnetism; θ = Weiss constant.
†Studied between 103 and 299 K.
‡Studied between 107 and 334 K.
§Denotes TIP corrected values using equation: TIP = $8N\beta^2/10Dq$.

ligand field bands for Pd^{2+} in a regular octahedral environment. The increase in Dq, and the decrease in B/B^0 when going from $Ni^{2+}(3d^8)$ to $Pd^{2+}(4d^8)$ are expected. Since the spectrum of PdF_2 seems not to have been investigated and all other palladium(II) compounds give spectra typical for square planar environments, no further meaningful comparisons can be made.

No useful electronic spectra could be obtained for $Pd(SO_3F)_3$. A very intense featureless band, presumed to be a charge transfer band, extended over most of the visible region. Any ligand field bands were most likely obscured.

Magnetic Measurements

Both $Pd(SO_3F)_2$ and $Pd(SO_3F)_3$ are paramagnetic. The observed magnetic moments for both compounds are listed in Table 3, together with magnetic information on related compounds. For $Pd(SO_3F)_2$, a μ_{eff} value of 3.39 BM at room temperature is observed, indicative of two unpaired electrons and in good agreement with the magnetic moment for $Ni(SO_3F)_2$ (21, 23). However, the μ_{eff} value for PdF_2 (2, 24) is considerably lower, obviously due to antiferromagnetic coupling via super exchange. The absence of such coupling for the fluorosulfate down to ~100 K is evident from the temperature dependent study.

The linear $1/\chi_M^{corr}$ *vs.* temperature plot indicates Curie–Weiss law behaviour with a Weiss constant of $\theta = +13 \pm 4$ K. Similar magnetic moments and negative Weiss constants are reported for numerous octahedral Ni^{2+} complexes (1), not altogether inconsistent with a $^3A_{2g}$ ground state. Some small variation of μ_{eff} with temperature is within the limit of experimental accuracy and probably not very significant.

The knowledge of 10 Dq for $Pd(SO_3F)_2$ allows one also to correct for contributions from the temperature independent paramagnetism (TIP) to the observed magnetic susceptibilities. The resulting TIP-corrected value of μ_{eff} is listed in Table 3, and the indication is that only a small TIP contribution is thus detected. Due to the

lack of spectroscopic data for $Pd(SO_3F)_3$ and the palladium fluorides, no such corrections are possible for these compounds.

The observed magnetic moment for Pd^{2+} in the fluorosulfate is noticeably higher than the 'spin-only' value of 2.83 BM. Since no orbital contribution is expected for an ion with a $^3A_{2g}$ ground state and the TIP contributions are rather small, the increase must be caused by spin–orbit coupling. The spin–orbit coupling constant, λ, for Pd^{2+} is unknown but is expected to be negative and hence should lead to a higher μ_{eff} value (22). It is also doubtful, whether spin–orbit coupling would follow the Russel Saunders coupling scheme for an ion as heavy as Pd^{2+} (22), and any further analysis of the magnetic data for $Pd(SO_3F)_2$ seems therefore not reasonable.

A reasonable interpretation of the magnetic results for $Pd(SO_3F)_3$ is possible when the formulation as $Pd^{II}[Pd^{IV}(SO_3F)_6]$ is used. Pd(IV) with a d^6 electron configuration should be diamagnetic, (*e.g.* in $K_2Pd^{IV}F_6$ (3)) and all paramagnetism should be due to the Pd^{2+} ion. The μ_{eff} value at room temperature now becomes 3.45 BM, and the $1/\chi_M^{corr}$ *vs.* T plot indicates a Weiss constant $\theta = +10 \pm 2$ K. Again the μ_{eff} values between 334 and 107 K show only a slight variation and it can be concluded that Pd^{2+} in both $Pd^{II}(SO_3F)_2$ and $Pd^{II}[Pd^{IV}(SO_3F)_6]$ must be in very similar environments. This would imply that the fluorosulfate group is coordinated strongly to Pd^{IV} and rather weakly to Pd^{II} with the metal in an octahedral environment each time. The noted complexity of the vibrational spectrum may be caused in part by such weak coordination to Pd^{II}.

The magnetic results are thus consistent with the conclusions reached earlier when analysing the vibrational spectrum, and the suggested formulation of PdF_3 as $Pd^{II}[Pd^{IV}F_6]$ (4, 24). The slightly lower μ_{eff} values for Pd^{2+} in the fluoride and the reported Weiss constant of $\theta = -28$ K indicate a different magnetic behaviour and perhaps some intermolecular antiferromagnetic interaction (25).

Conclusions

The investigation on palladium fluorosulfates has shown that an octahedral rather than a square planar environment for Pd^{II} is found in fluorosulfates as well as in fluorides, thus pointing to the similarities of SO_3F^- and F^- as weak field ligands. It is hoped that this analogy can be extended to other 4*d*- and 5*d*-block element fluorosulfates.

Acknowledgements

Financial support by the National Research Council of Canada is gratefully acknowledged. The authors are indebted to Dr. R. C. Thompson for practical advice, helpful discussion, and his permission to use unpublished results on $Ni(SO_3F)_2$.

1. Landolt-Börnstein. Numerical data and functional relationships in science and technology. Vol. 2. Magnetic properties of coordination and organometallic transition metal compounds. Springer Verlag, Berlin. 1966.
2. R. S. Nyholm and A. G. Sharpe. J. Chem. Soc. 3579 (1952).
3. N. Bartlett and J. W. Quail. J. Chem. Soc. 3728 (1961).
4. N. Bartlett and P. R. Rao. Chem. Soc. Proc. 393 (1964).
5. N. Bartlett and R. Maitland. Acta Crystallogr. **11**, 747 (1958).
6. G. H. Cady and J. M. Shreeve. Inorg. Synth. **7**, 116 (1963).
7. F. Aubke and R. J. Gillespie. Inorg. Chem. **7**, 599 (1968).
8. H. C. Clark and R. J. O'Brien. Can. J. Chem. **39**, 1030 (1961).
9. B. N. Figgis and R. S. Nyholm. J. Chem. Soc. 4190 (1958).
10. J. M. Taylor and R. C. Thompson. Can. J. Chem. **49**, 511 (1971).
11. W. M. Johnson, R. Dev, and G. H. Cady. Inorg. Chem. **11**, 2260 (1972).
12. M. Wechsberg, P. A. Bulliner, F. O. Sladky, R. Mews, and N. Bartlett. Inorg. Chem. **11**, 3063 (1972).
13. M. Eisenberg and D. D. DesMarteau. Inorg. Nucl. Chem. Lett. **6**, 29 (1970).
14. M. Eisenberg and D. D. DesMarteau. Inorg. Chem. **11**, 2641 (1972).
15. C. S. Alleyne, K. O'Sullivan-Mailer, and R. C. Thompson. Can. J. Chem. **52**, 336 (1974).
16. J. Goubeau and J. B. Milne. Can. J. Chem. **45**, 2321 (1967).
17. D. W. A. Sharp. J. Chem. Soc. 3761 (1957).
18. A. Ruoff, J. B. Milne, G. Kaufmann, and M. Leroy. Z. Anorg. Allg. Chem. **372**, 119 (1970).
19. P. A. Yeats, J. R. Sams, and F. Aubke. Inorg. Chem. **12**, 328 (1973).
20. A. B. P. Lever. Inorganic electronic spectroscopy. Elsevier Publ. Co. Inc., Amsterdam. 1968.
21. D. A. Edwards, M. J. Stiff, and A. A. Woolf. Inorg. Nucl. Chem. Lett. **3**, 427 (1967).
22. B. N. Figgis. Introduction to ligand fields. Interscience Publ. Co. Inc., New York. 1967.
23. R. C. Thompson. Unpublished results.
24. R. P. Rao. Ph.D. thesis, University of British Columbia, Vancouver, B.C. 1965.
25. A. Earnshaw. Introduction to magnetochemistry. Academic Press, London. 1968. p. 100.

Kinetics and mechanism of the decarboxylation of pyrimidine-2-carboxylic acid in aqueous solution

GERALD E. DUNN, EDWARD A. LAWLER, AND A. BRIAN YAMASHITA

Department of Chemistry, University of Manitoba, Winnipeg, Man., Canada R3T 2N2

Received January 17, 1977

GERALD E. DUNN, EDWARD A. LAWLER, and A. BRIAN YAMASHITA. Can. J. Chem. **55,** 2478 (1977).

Pseudo-first-order rate constants for the decarboxylation of pyrimidine-2-carboxylic acid have been determined at 65°C in aqueous solution over the acidity range pH = 2 to H_0 = −9.5. Rate constants increase rapidly from pH = 2 to H_0 = −3, then remain constant. This behaviour can be accounted for by a Hammick-type mechanism in which monoprotonated pyrimidine-2-carboxylic acid loses carbon dioxide to form an ylide (stabilized by the adjacent positively charged nitrogens) which rapidly converts to pyrimidine.

GERALD E. DUNN, EDWARD A. LAWLER et A. BRIAN YAMASHITA. Can. J. Chem. **55,** 2478 (1977).

Travaillant à 65°C, en solution aqueuse et à des acidités allant d'un pH = 2 jusqu'à H_0 = −9.5, on a déterminé les constantes de vitesse de pseudo premier ordre pour la décarboxylation de l'acide pyrimidinecarboxylique-2. Les constantes de vitesse augmentent rapidement du pH = 2 jusqu'à une valeur de H_0 = −3 et elles demeurent ensuite constantes. On peut expliquer ce comportement par un mécanisme du type Hammick dans lequel l'acide pyrimidinecarboxylique-2 monoprotoné perd une molécule de CO_2 pour conduire à un ylure (stabilisé par les azotes adjacents chargés positivement) qui se transforme rapidement en pyrimidine.

[Traduit par le journal]

Introduction

Earlier papers from this laboratory have reported on the decarboxylation of various substituted pyridine-2-carboxylic acids in aqueous solution (1, 2). They appear to decarboxylate by the Hammick mechanism, reaction 1, in which the developing carbanionic center at position 2

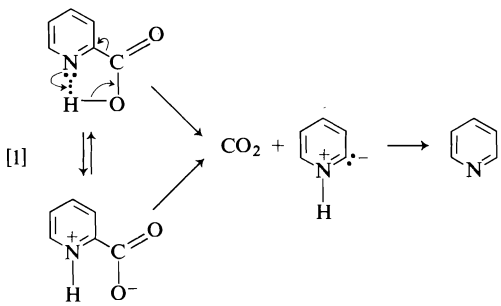

[1]

of the transition state is stabilized by the electron-withdrawing nitrogen at position 1 (3). Thus quaternization of the nitrogen increases the rate of decarboxylation by factors of about 100 in aqueous solution (1) and 700 in ethylene glycol (4). Substituents in the 3-position have a much larger effect on the rate than in the 4-, 5-, or 6-positions (1) and appear to exert their influence by a mixture of electronic and steric effects. Thus, a 3-methyl substituent increases the rate of decarboxylation by a factor of about 4, whereas 3-benzoyl, 3-carboxyl, and 3-nitro increase the rate by several orders of magnitude (2). It seemed, therefore, of interest to examine the effect of an electron-withdrawing 3-substituent of minimal steric requirements, such as the second ring nitrogen of pyrimidine-2-carboxylic acid. The decarboxylation of pyrimidine carboxylic acids is also of more general interest because it is sometimes involved in both the bio- and laboratory syntheses of pyrimidine-based nucleic acids (5).

Experimental

Pyrimidine-2-carboxylic Acid

4,6-Dihydroxy-2-methylpyrimidine (Aldrich) was converted to 4,6-dichloro-2-methylpyrimidine (6) which was dehalogenated to 2-methylpyrimidine (7). After several unsuccessful attempts to oxidize the methyl group with $KMnO_4$ or CrO_3, pyrimidine-2-carboxylic acid was obtained by selenium dioxide oxidation using a modification of the procedure developed by Jerchel *et al.* for oxidation of picolines (8).

2-Methylpyrimidine (1.5 g) and selenium dioxide (3.6 g) were heated for 2.5 h in 30 ml of refluxing pyridine. The deep red solution was filtered hot and the residue was washed with three 10 ml portions of pyridine, then with 20 ml of water. The filtrate was steam distilled to remove most of the pyridine, reduced to a volume of 70 ml on a rotary evaporator, and filtered into a solution of 5 g of cupric acetate in 50 ml of water. A blue-green pre-

cipitate was collected by filtration and combined with two additional crops obtained by further concentration and filtration over a period of several days. Hydrogen sulfide was passed into a suspension of the combined solids in 150 ml of water at 40°C for about 40 min, cupric sulfide was filtered off, and the pale blue filtrate was treated again with hydrogen sulfide. The final, colourless filtrate, taken to dryness on the rotary evaporator, left 350 mg of a brownish solid, mp 176–185°C. Vacuum sublimation yielded 250 mg (13%) of colourless crystals mp 193–197°C (lit. (9) mp 199°C); mass spectrum, *m/e*: 124, 107, 80.

Kinetic Measurements

The decarboxylation was followed spectrophotometrically by recording the decrease with time in the absorbance of pyrimidine-2-carboxylic acid at 220 nm using a Varian Techtron model 635 spectrophotometer.

For each kinetic run 3.5 ml of a stock solution of pyrimidine-2-carboxylic acid (8.8×10^{-2} *M*) was made up to 25 ml with the appropriate mineral acid. At p*H*'s greater than 1, the mineral acid was a buffer made from HCl, KCl, and NaH_2PO_4; at p*H*'s less than 1 it was a mixture of water and H_2SO_4. For buffer solutions the p*H* was measured on an Orion model 801, p*H* meter; for sulfuric acid solutions the density of the solution was determined in triplicate with a 5 ml pycnometer and from this the percent sulfuric acid and H_0 values were obtained (10). Ten 2-ml samples of this solution were sealed in ampoules and placed in the thermostat at 65 ± 0.01°C. At intervals samples were quenched in ice, diluted to 10 ml with distilled water, and analyzed in the spectrophotometer. In each case the uv spectrum of the product coincided precisely with that of pyrimidine. Reactions were carried to more than three half-lives of the faster runs; the very slow ones to only one half-life. The average standard deviation of experimental points from the first-order regression lines was 1.7%, and reproducibility of rate constants was ±2%. Results are shown in Table 1.

TABLE 1. First-order rate constants for decarboxylation of pyrimidine-2-carboxylic acid in aqueous acid at 65°C

p*H* (or H_0)	Acid	$k \times 10^4$
2.04	HCl	0.0023
1.07	HCl	0.025
0.92	H_2SO_4	0.025
−0.059	H_2SO_4	0.157
−1.01	H_2SO_4	0.821
−1.94	H_2SO_4	1.41
−2.61	H_2SO_4	2.12
−3.51	H_2SO_4	3.01
−4.83	H_2SO_4	3.45
−5.19	H_2SO_4	3.46
−5.87	H_2SO_4	3.76
−6.79	H_2SO_4	4.44
−7.78	H_2SO_4	4.15
−8.81	H_2SO_4	3.65
−9.48	H_2SO_4	3.60

Discussion

The ionization equilibria and Hammick mechanism for decarboxylation of pyrimidine-2-carboxylic acid are shown in reaction 2. In aqueous solution the anion and ylides shown as products would be rapidly converted to pyrimidine or its conjugate acid. Mason gives for pyrimidine-2-carboxylic acid $pK_2 = -1.13 \pm 0.05$ and $pK_3 = 2.85 \pm 0.02$ without specifying the temperature (11). Since the p*K*'s would probably change by less than one p*K* unit between room temperature and 65°C, one may conclude from the data in Table 1 that the species decarboxylating at $H_0 < -2$ is H_2A^+ and that its rate of decarboxylation is much greater than that of HA. Furthermore, since the rate does not decrease significantly at very high acidity, although previous experience suggests that the unionized carboxyl group does not decarboxylate easily (1, 12), it appears that very little H_3A^{2+} is present even at $H_0 = -9.5$ (~98% H_2SO_4), so that pK_1 is probably less than −10. This conclusion is perhaps not

[2]

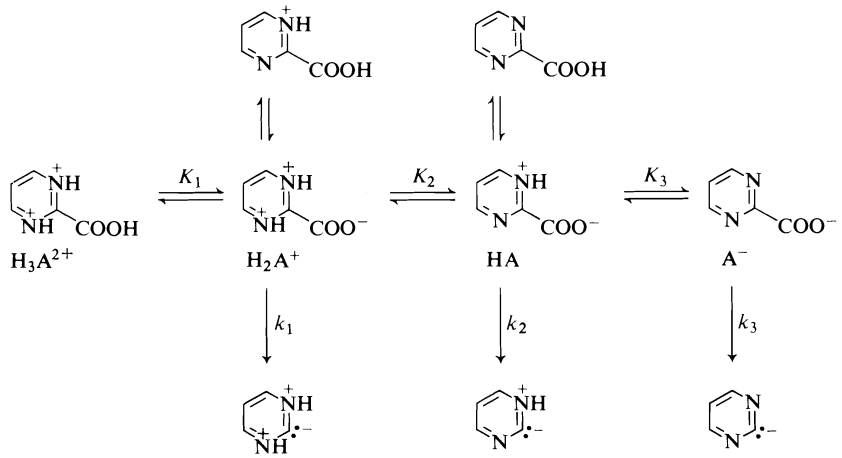

surprising since pK_1 for pyrimidine is *ca.* -6.3 (13), and it is reinforced by the observation that the ultraviolet spectrum of the acid does not change significantly from $H_0 = -2$ to $H_0 = -9.5$.

Accordingly, it may be assumed, at least as a first approximation, that, in the pH range studied, the only species present in significant concentration are H_2A^+ and HA, that the only important ionization constant is K_2, and that k_2 is negligible. These assumptions are expressed in [3], [4], and [5] which may be combined to give [6].

$$[3] \qquad [H_2A^+] + [HA] = [C]$$

$$[4] \qquad \frac{[H^+][HA]}{[H_2A^+]} = K_2$$

$$[5] \qquad \frac{d[CO_2]}{dt} = k_{obs}[C] = k_1[H_2A^+]$$

$$[6] \qquad k_{obs} = \frac{k_1[H^+]}{[H^+] + K_2}$$

At $H_0 < -4$, $[H^+] \gg K_2$, so that $k_{obs} = k_1$. The average value of k_{obs} at these high acidities is $3.8 \times 10^{-4}\ s^{-1}$, which may be taken as an estimate of k_1 at 65°C. At p$H > 0$, $[H^+] < K_2$ so that $k_{obs} = k_1[H^+]/K_2$. The first points of Table 1 give a value of $2.2 \times 10^{-5}\ s^{-1}$ for k_1/K_2, corresponding to a value of 17 for K_2 (p$K_2 = -1.23$) at 65°C, which may be compared with the literature value (11) of p$K_2 = -1.13$ (presumably at 25°C).

Figure 1 shows a plot of log k_{obs} *vs.* H_0 and pH. The solid line shows the rate constants calculated from [6] using the values of k_1 and K_2 estimated in the preceding paragraph. It is clear that the calculated k_{obs} are too large in the region where k_{obs} varies with H_0, which suggests that H_0 may not be the appropriate acidity function to represent the protonation of pyrimidine-2-carboxylic acid. Since most acidity functions are proportional to H_0 (14), one may plot log k_{obs} against nH_0. For this purpose [6] is modified to [7].

$$[7] \qquad k_{obs} = \frac{k_1 h_0^{\,n}}{h_0^{\,n} + K_2}$$

The optimum value for n is about 0.55, and the dotted line in Fig. 1 shows the rate constants calculated from [7] using $n = 0.55$ and the previously estimated values of k_1 and K_2. The fit is good, which suggests that the protonation

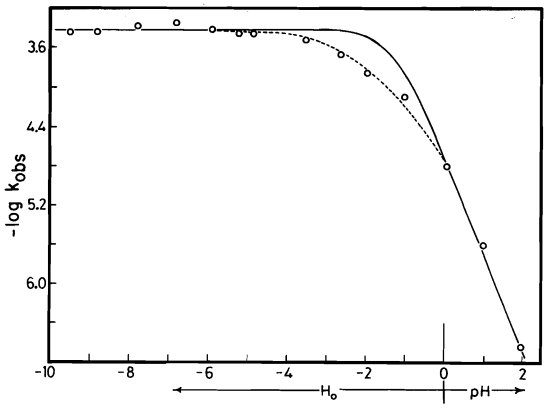

FIG. 1. The effect of changing acidity on the first-order rate constant for decarboxylation of pyrimidine-2-carboxylic acid in aqueous solution at 65°C. Circles represent experimental points, the solid and dotted lines represent [6] and [7], respectively, with $k_1 = 3.8 \times 10^{-4}\ s^{-1}$, $K_2 = 17$, and $n = 0.55$.

of pyrimidine-2-carboxylic acid follows an acidity function which increases about half as fast with acidity as does H_0. This description fits the amide acidity function, H_A (15) reasonably well, since a plot of H_A *vs.* H_0 has a slope of 0.53 (16). It is noteworthy in this connection that the second protonation of pyrimidine is reported to follow H_A (13).

Thus it is possible to account for the acidity dependence of the decarboxylation of pyrimidine-2-carboxylic acid by the Hammick mechanism using ionization constants and an acidity function in reasonable agreement with the literature. It is necessary, however, to assume that the rate constant for decarboxylation of protonated substrate (k_1) is at least a thousand times greater than that for the substrate itself (k_2). This emphasizes the importance of electronic (inductive and field) effects in stabilizing the transition state leading to ylide in the Hammick mechanism. In pyridine-2-carboxylic acids 3-substituents were found to have an accelerating effect that is at least partly steric (2), but in the present case steric effects should be negligible.

In the pyridine series 3-substituents inhibit the decarboxylation of pyridine-2-carboxylate ions, again by a steric effect, presumably (2). It would therefore be of particular interest to examine the decarboxylation of the pyrimidine-2-carboxylate ion (k_3), where steric effects are reduced but electronic effects should be favorable. Since k_2 is very small at 65°C and k_3 would be smaller still,

attempts were made to study the decarboxylation at 95°C. However, the product of decomposition at 95°C and pH = 5 (where the substrate should be over 99% in the form of A^-) had an ultraviolet spectrum quite different from that of pyrimidine. Pyrimidine itself behaved similarly, so it is apparent that the anion or its decarboxylation product undergoes some other reaction under conditions where A^- might be expected to decarboxylate.

Acknowledgments

The authors are grateful to the National Research Council of Canada for financial support and to Miss Jill Woodfield for the synthesis of some of the pyrimidine-2-carboxylic acid.

1. G. E. DUNN, G. K. J. LEE, AND H. THIMM. Can. J. Chem. **50**, 3017 (1972).
2. G. E. DUNN AND H. THIMM. Can. J. Chem. **55**, 1342 (1977).
3. P. DYSON and D. L. HAMMICK. J. Chem. Soc. 1724 (1937); M. F. R. ASHWORTH, R. P. DAFFERN, and D. L. HAMMICK. J. Chem. Soc. 809 (1939).
4. P. HAAKE and J. MANTECÓN. J. Am. Chem. Soc. **86**, 5230 (1964).
5. P. BEAK and B. SIEGEL. J. Am. Chem. Soc. **98**, 3601 (1976).
6. M. P. V. BOARLAND and J. F. W. MCOMIE. J. Chem. Soc. 3722 (1952).
7. V. H. SMITH and B. E. CHRISTENSEN. J. Org. Chem. **20**, 829 (1955).
8. D. JERCHEL, J. HEIDER, and H. WAGNER. Ann. **613**, 153 (1958).
9. A. HOLLAND. Chem. Ind. (London), 786 (1954).
10. P. TICKLE, A. G. BRIGGS, AND J. M. WILSON. J. Chem. Soc. B, 65 (1970); C. D. JOHNSON, A. R. KATRITZKY, and S. A. SHAPIRO. J. Am. Chem. Soc. **91**, 6654 (1968).
11. S. F. MASON. J. Chem. Soc. 1247 (1959).
12. G. E. DUNN and S. K. DAYAL. Can. J. Chem. **48**, 3349 (1970).
13. P. G. BRIGNELL, C. D. JOHNSON, A. R. KATRITZKY, N. SHAKIR, H. O. TARHAN, and G. WALKER. J. Chem. Soc. B, 1233 (1967).
14. K. YATES and R. A. MCCLELLAND. J. Am. Chem. Soc. **89**, 2686 (1967).
15. K. YATES, J. B. STEVENS, and A. R. KATRITZKY. Can. J. Chem. **42**, 1957 (1964).
16. R. I. ZALEWSKI and G. E. DUNN. Can. J. Chem. **47**, 2263 (1969).

Thermal and photochemical reactivity of cyclopropene derivatives: a semi-empirical molecular orbital study

J. A. PINCOCK AND R. J. BOYD

Department of Chemistry, Dalhousie University, Halifax, N.S., Canada B3H 4J3

Received December 23, 1976

J. A. PINCOCK and R. J. BOYD. Can. J. Chem. **55**, 2482 (1977).

The MINDO/3 semi-empirical MO method has been used to study the conversion of cyclopropene to vinyl carbene. In particular, the surfaces of the ground state and the first excited singlet and triplet states have been calculated. Additional calculations, including geometry optimization, have been carried out on vinyl substituted cyclopropenes. In general, the results are consistent with the known thermal and photochemical reactivities of cyclopropenes and the results of the few *ab initio* calculations on these species.

J. A. PINCOCK et R. J. BOYD. Can. J. Chem. **55**, 2482 (1977).

On a utilisé la méthode semi-empirique MINDO/3 MO pour étudier la conversion du cyclopropène en vinylcarbène. On a calculé en particulier les surfaces de l'état fondamental et des premiers états exités singulet et triplet. Des calculs additionnels incluant une optimisation de la géométrie ont été réalisés sur des cyclopropènes substitués par un groupe vinyle. D'une façon générale, ces résultats sont en accord avec les réactivités thermiques et photochimiques bien connues des cyclopropènes et les résultats des quelques calculs *ab initio* sur ces espèces.

[Traduit par le journal]

Introduction

The chemistry of cyclopropene derivatives has attracted considerable interest (1) mainly because of the high strain energy (~53 kcal/mol in the ground state (2)) associated with the unsaturated three-membered ring. Studies on their unimolecular behaviour in either the ground state (thermal chemistry) or the excited states (singlet and triplet photochemistry) have been used as an indirect method of gaining an understanding of the effect of bonding on reactivity. These results will be briefly summarized here.

The most extensive study of the thermal behaviour of cyclopropenes is the work of Bergman and co-workers (3) on the pyrolysis of racemic and optically active 1,3-diethylcyclopropene as shown in reaction 1. The formation of isomeric 2,4-heptadienes and 3-heptyne was nicely explained in terms of hydrogen migrations for the vinyl carbene intermediate **2**. The activation energy for this process (32.2 kcal/mol) agreed well with estimates made by the usual group equivalent and bond energy values for the heat of formation of **2**. Moreover, optically active **1** was shown to racemize (**1***S* ⇄ **1***R*) about nine times as fast as it was converted to products, making the case for the intervention of **2** even stronger. Note as well that the cyclopropene **1** has apparently reacted, as expected, by cleavage of the more highly substituted σ bond. However,

[1]

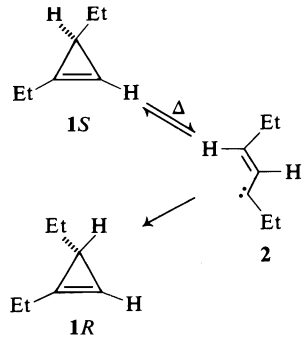

$CH_3CH{=}CH{-}CH{=}CH{-}Et$

3

+

$CH_3CH_2C{\equiv}CCH_2CH_2CH_2CH_3$

4

as Bergman points out, this type of substituent effect is not observed in all cases. Thus, tetraphenylcyclopropene, **5**, rearranges to the indene **6** (presumably via the isoindene), but the reported activation energy of 40 kcal/mol (4) is surprisingly high. Since the estimated value for the

[2]

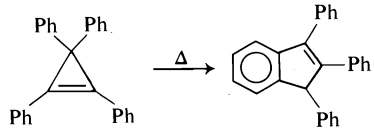

5 **6**

thermal cleavage of a σ bond in **5** is approximately 11 kcal/mol (3), the phenyl groups are clearly affecting the single bond energy in an unprecedented manner.

The photochemistry of cyclopropene derivatives has been shown to be remarkably dependent on the multiplicity of the excited state involved. As in thermal reactions, excited singlets give products also consistent with σ bond cleavage to vinyl carbenes (5) whereas triplet states dimerize by a $2\pi + 2\pi$ cycloaddition (6). For example (7), direct irradiation (excited singlet) of methyl 1-methyl-2-phenylcyclopropene-3-carboxylate, **7**, gives 2-methoxy-5-methyl-4-phenylfuran, **8**; in contrast, sensitized irradiation gives the tricyclic dimer **9** (reactions 3 and 4). Further,

[3] 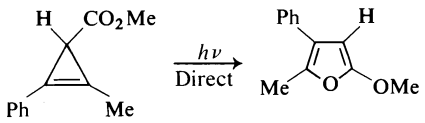

7 8

[4] 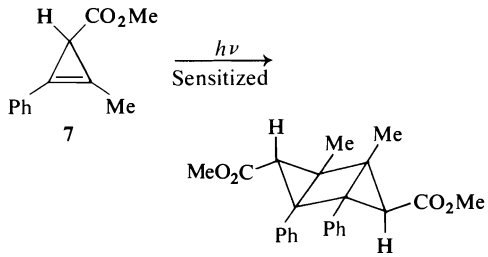

7 9

photolysis of optically active **7** demonstrated that racemization was occurring in the excited singlet state about four times as fast as conversion to **8**, whereas no racemization could be detected in the sensitized irradiations. Considering the high strain energy of the cyclopropene, plus the added energy from electronic excitation, the surprising feature of these observations is not that the excited singlet opens to a vinyl carbene but that the triplet state is long-lived enough as a three-membered ring to react by a bimolecular path.

This paper examines some of these properties of cyclopropene compounds by a quantum mechanical approach using the semi-empirical SCF–MO MINDO/3 method (8) on model systems. The particular features we wished to examine were the nature of the three surfaces (ground, excited singlet, and triplet) in the conversion of cyclopropene to vinyl carbene and the effect of substituents on the ground state surface. The choice of the MINDO/3 method was based on the fact that complete geometric minimizations along a reaction surface can be made for molecules of a reasonable size at a moderate cost. Further, although the technique has already been successful for a variety of thermal reactions (9), at least one experimental case (1,3-migration in vinyl cyclopropanes) is not predicted correctly (10). More tests of the method are therefore desirable before its general applicability to organic reactions is appreciated. Finally, for these systems, a limited number of *ab initio* calculations of both the valence bond (11) and the molecular orbital method (12)[1] have appeared and so comparison with the MINDO/3 approach is possible.

Results

Cyclopropene to Vinyl Carbene: Ground State

The conversion of **10** to **11** was studied taking the length of the σ bond as the reaction coordinate (C_1—C_3) and minimizing all other geometric variables. Initially, we reproduced Dewar's (13) previously reported result for the energy and equilibrium geometry of cyclopropene. As shown in Fig. 1 (circles), calculations using cyclopropene as the starting point and increasing the C_1—C_3 bond length gave a surface with the energy increasing continuously. (At C_1—C_3 greater than 2.4 Å the C_3H_4 system dropped in energy drastically by migrating a hydrogen atom and forming methyl acetylene.) There was no indication of rotation of the methylene group towards planarity and the intermediate **11**. In contrast, when the starting point for the calculations was a flat intermediate like

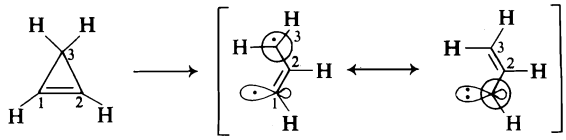

10 11

11 and the C_1—C_3 value was decreased, the points shown as triangles in Fig. 1 were obtained. At C_1—C_3 = 2.0 Å the two calculated structures coincided both in energy and geometry. This is an example of what Dewar calls "chemical hysteresis" (9) and results from the intersection of the surfaces of two states. As Salem *et al.* have discussed in considerable detail (14), the crossing

[1]L. Salem and W. D. Stohrer, private communication of unpublished results.

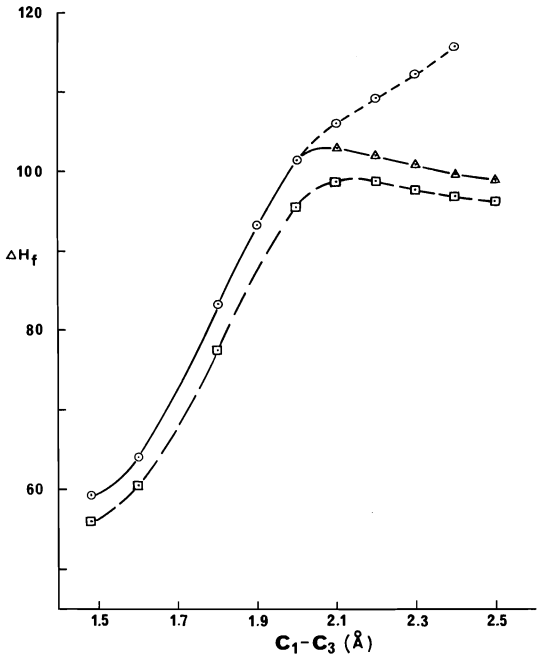

FIG. 1. Ground state surfaces for the conversion of **10** to **11**: starting point cyclopropene **10**, ⊙; starting point vinyl carbene **11**, △; including CI, ⊡.

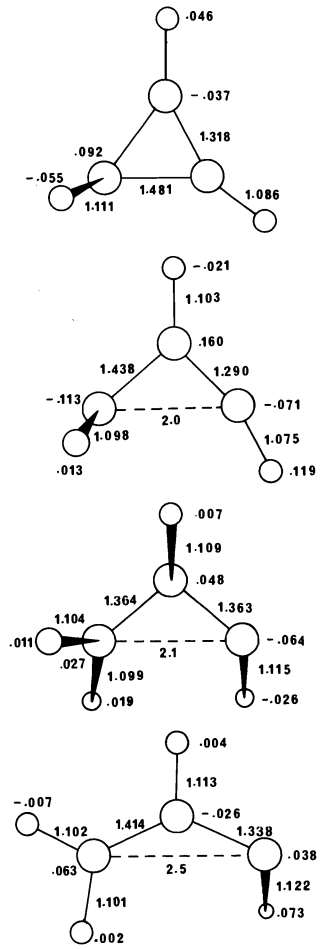

FIG. 2. Geometries and atomic charges of intermediates in the conversion of **10** to **11**: cyclopropene, minimized (59.3 kcal/mol); C_1—C_3 = 2.0 Å; C_1—C_3 = 2.10 Å; C_1—C_3 = 2.50 Å.

should be, but is not avoided because the crudeness of the method does not allow for mixing of the ionic and covalent configurations of each state. In our case the crossing is avoided in one direction (**11** → **10**) but not in the other (**10** → **11**). Despite these problems, we assume that the solid line in Fig. 1 represents an approximation to the true surface in the opening of cyclopropene to the vinyl carbene. Geometries including bond lengths and atomic charges for cyclopropene and three of the calculated points (C_1—C_3 = 2.0, 2.1, and 2.5 Å) are shown in Fig. 2. Comparison of charges in the two structures at 2.0 and 2.1 Å indicates the decrease in polarity as the crossing point is passed.

The MINDO/3 program has the option of including a limited CI with mixing of the first doubly excited configuration. As Dewar has pointed out (8), inclusion of CI should significantly lower heats of formation for species that are biradical in character and therefore a check must be made in bond dissociations of the type involved in the **10** → **11** conversion. As shown (squares in Fig. 1), inclusion of CI lowers the surface by an approximately constant amount independent of the bond length when compared with the results in the absence of CI. Since the CI option does make the calculations longer and since there seems to be no large improvement by its inclusion, we have elected to omit it for the remainder of our work in these systems.

A preliminary report of Generalized Valence Bond (GVB) calculations using assumed geometries has recently been published for several key intermediates on the **10** to **11** surface (11). These intermediates (**12**, **13**, and **14**) are shown

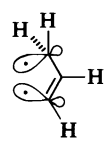

12
(42.6 kcal/mol)

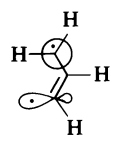

13
(38.9 kcal/mol)

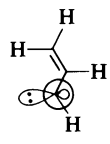

14
(36.6 kcal/mol)

with the calculated energies relative to cyclopropene as zero. Cyclopropene correlates through the open but non-planar biradical **12** to the planar vinyl carbene state represented by **13** ($^1A''$). (Note that **14** ($^1A'$) is the lowest singlet state of vinyl carbene.) Comparison of these GVB results with the MINDO/3 results indicates that the two are actually very similar.

Thus, the calculated barriers to ring openings of cyclopropene are: GVB 42.6 kcal/mol; MINDO/3 43.6 kcal/mol; MINDO/3 + CI 43.0 kcal/mol. The difference of ~11 kcal/mol from the experimental value of 32.2 kcal/mol (3) for 1,3-diethylcyclopropene is explained at least in part by alkyl group stabilization of a ring-opening transition state. A value of 35.2 kcal/mol has been reported for the conversion of cyclopropene to methyl acetylene (15). By MINDO/3 the ground state of cyclopropene does not correlate with the lowest energy state of **11** (note the crossing in Fig. 1), but remains as a non-planar diradical. The lowest singlet state of **11** is a near-planar structure (note C_1—C_3 = 2.5 Å in Fig. 2), the major deviation being the hydrogen at the carbene carbon.

Vinylcyclopropenes to Vinylcarbenes

Encouraged by the success of the MINDO/3 method in examining the conversion of cyclopropene **10** to vinyl carbene **11**, we next approached the larger problem of the effect of phenyl substituents on the barrier to ring opening. Despite the advantage the semi-empirical method has over the *ab initio* methods for large molecules, tetraphenylcyclopropene is too large even for MINDO/3. However, with the assumption that the effect of the phenyl groups would mainly be a result of conjugative interactions, we chose to examine vinyl cyclopropenes as analogues of phenylcyclopropenes.

Three substitution patterns are possible as shown in reactions 5, 6, and 7. These are: 1-vinylcyclopropene with cleavage of the C_1—C_3 bond (**15** → **16**); 1-vinylcyclopropene with cleavage of the C_2—C_3 bond (**15** → **17**); 3-vinylcyclopropene with cleavage of the C_1—C_3 bond (**18** → **19**). In order to minimize computation

[5] 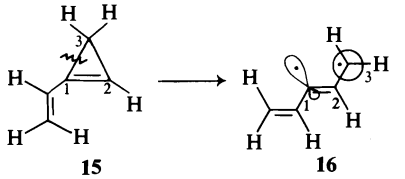

15 **16**

[6] 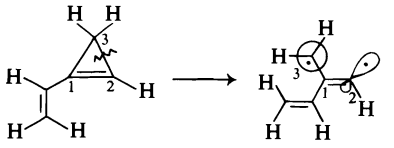

15 **17**

[7] 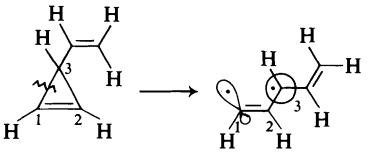

18 **19**

time, our first approach was to keep the vinyl group (—CH=CH_2) in a fixed geometry throughout the calculations (C=C = 1.33 Å; C—H = 1.10 Å; all angles 120°). All other geometric variables were minimized at each reaction coordinate value.

Here a comment on one problem associated with the conformations of these species is appropriate. In each case the vinyl group has freedom of rotation about the single bonds. If more than one minimum exists for the rotation of the vinyl groups, then the possibility arises that the barriers for ring opening of the cyclopropenes may be incorrectly calculated. This is true, despite the fact that the rotational angle is one of the geometric variables, since the MINDO/3 geometry optimization is based on an efficient steepest-descents approach rather than a more tedious search of the entire surface. Accordingly the optimized value for a rotational angle may depend on the starting point for the geometry search. For this reason additional calculations to determine whether or not a lower minimum exists are advisable.

We first checked these conformational aspects with the cyclopropenes **15** and **18**. The calculated results for rotation about the single bond are shown in Figs. 3 and 4. The main feature of these plots is the very small difference in energy between the various conformations; 0.3 kcal/mol between the most and least stable for **15** and 1.0 kcal/mol for **18**. As Dewar has demonstrated, MINDO/3 predicts conformational minima reasonably well but usually underestimates the barriers (13). Therefore these values may be somewhat too low but are probably of the right order of magnitude. We next examined conformational preferences in the open carbenes **16**, **17**, and **19** in all cases with a

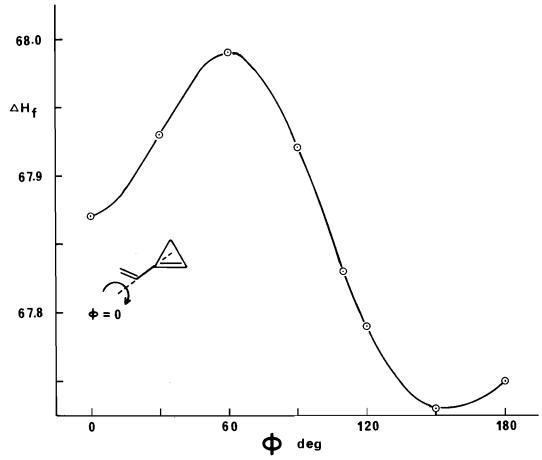

FIG. 3. Rotational surface for 1-vinylcyclopropene, **15**.

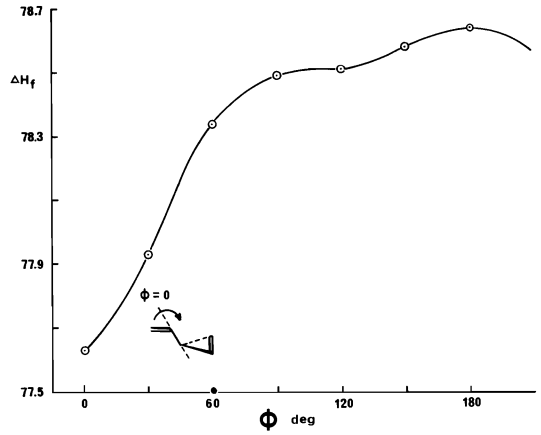

FIG. 4. Rotational surface for 3-vinylcyclopropene, **18**.

reaction coordinate C—C bond of 2.5 Å. Again, the energy differences between conformations were small, the largest being 0.81 kcal/mol between **19** and **20** as shown. Based on these

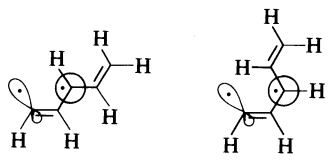

19 (112.81 kcal/mol) **20** (113.62 kcal/mol)

results, we felt confident that any errors that occurred because of incorrect conformational choices would be small and therefore not interfere with the general conclusions of the calculations.

Based on our experience with the cyclopropene to vinyl carbene conversion (*i.e.*, the crossing of states) we chose as starting points for these three sets of calculations the open carbenes **16**, **17**, and **19** in the conformations shown. The results are listed in Table 1 and plotted in Fig. 5. The geometries, including bond lengths and atomic charges, for some points along the surface are shown in Figs. 6, 7, and 8. No bond lengths are shown for the vinyl groups which are of fixed geometry.

The simplest feature to discuss in these results is the activation barrier for the three conversions: 41.1 kcal/mol (**15** → **16**); 51.8 kcal/mol (**15** → **17**) and 37.4 kcal/mol (**18** → **19**). In order to confirm that, despite the fixed vinyl group, these values were reasonable estimates of the activation energies, we repeated the calculations for both the starting vinylcyclopropenes and the transition states in the three cases, allowing complete geometric minimization. These results are shown in

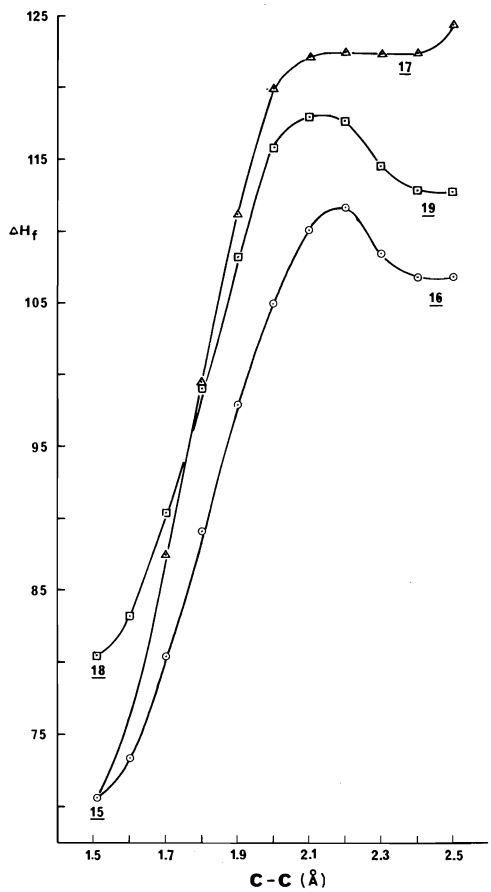

FIG. 5. Ground state surfaces for the thermal conversion of vinylcyclopropenes to vinylcarbenes.

TABLE 1. Calculated potential energy surfaces for the conversion of vinylcyclopropenes to vinylcarbenes

Bond length (Å)	Heats of formation ($\triangle H_f$) kcal/mol		
	15 → 16	**15 → 17**	**18 → 19**
1.51	70.63 (67.83)[a]	70.63 (67.83)[a]	80.46 (77.63)[a]
1.6	73.34	—	83.16
1.7	80.38	87.50	90.38
1.8	89.18	99.56	99.14
1.9	97.90	111.17	107.72
2.0	105.04	119.94	115.84
2.1	110.18	122.04	117.94 (115.72)[a]
2.2	111.67 (109.01)[a]	122.41 (120.09)[a]	117.71
2.3	108.51	122.34	114.58
2.4	106.79	122.40	112.87
2.5	106.80	124.43	112.81

[a]Complete geometric minimizations.

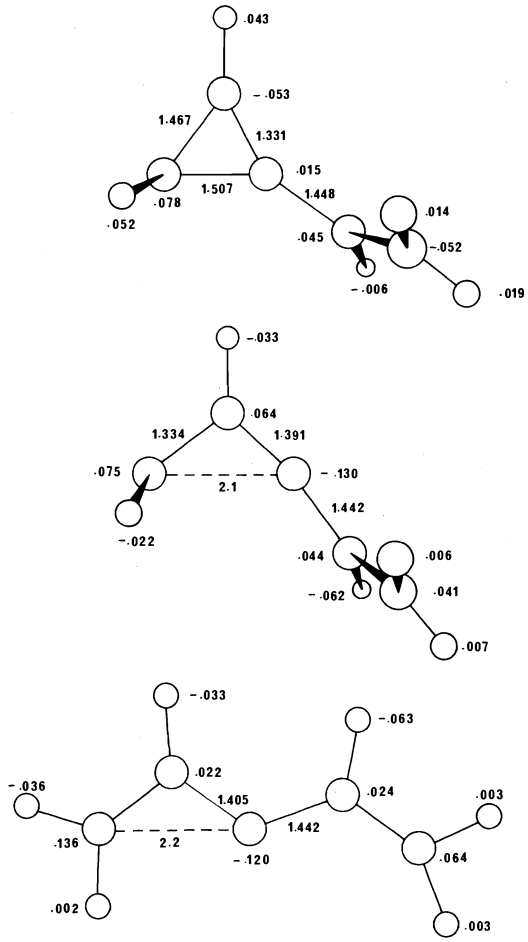

FIG. 6. Geometries and atomic charges of intermediates in the conversion of **15** to **16**: 1-vinylcyclopropene; C_1—C_3 = 2.1 Å; C_1—C_3 = 2.2 Å.

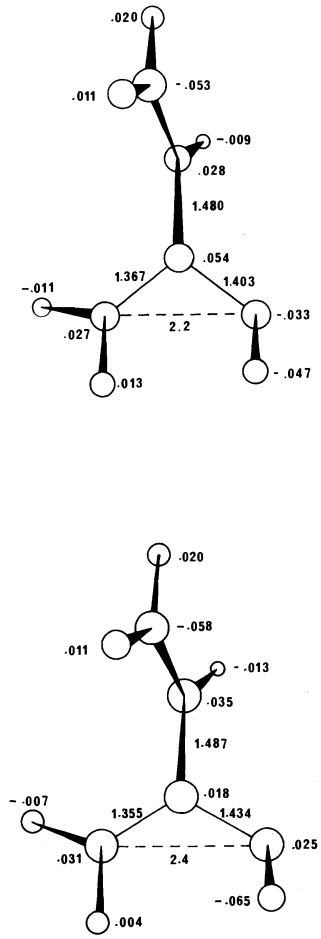

FIG. 7. Geometries and atomic charges of intermediates in the conversion of **15** to **17**: C_2—C_3 = 2.2 Å; C_2—C_3 = 2.4 Å.

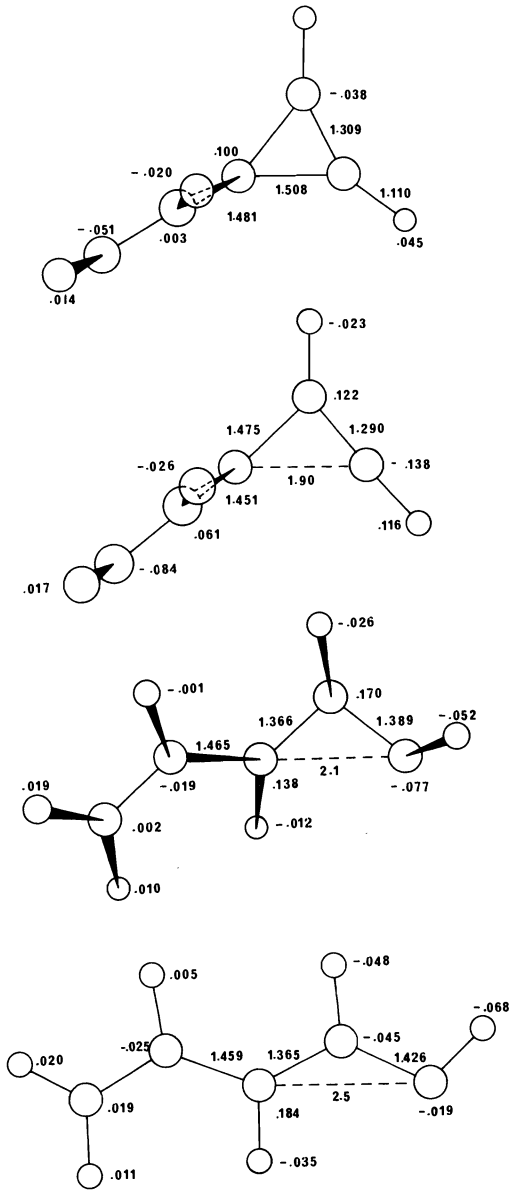

FIG. 8. Geometries and atomic charges of intermediates in the conversion of **18** to **19**: 3-vinylcyclopropene; C_1—C_3 = 1.9 Å; C_1—C_3 = 2.1 Å; C_1—C_3 = 2.5 Å.

parentheses in Table 1 and lead to the following activation energies: 41.2 kcal/mol (**15** → **16**); 52.3 kcal/mol (**15** → **17**) and 38.1 kcal/mol (**18** → **19**). Clearly, the differences are so small that restriction of the geometry of the vinyl group is unlikely to affect the general conclusions reached from a discussion of the results for these vinyl cyclopropenes.

On comparison with the value calculated for cyclopropene itself (43.6 kcal/mol) we note that the position of the vinyl group has a remarkable effect on the barrier to ring opening. As expected on the basis of conjugate effects with the developing radical center, a vinyl group on C-3 of cyclopropene lowers (by 6.2 kcal/mol) the activation barrier. A vinyl group at C-1 (C_1—C_3 bond breaking) also decreases (by 2.5 kcal/mol) the barrier. In contrast, a vinyl group at C-1 (C_2—C_3 bond breaking) actually raises the barrier by 8.2 kcal/mol. Qualitatively, an explanation is now available for the very high activation energy for tetraphenylcyclopropene pyrolysis (note reaction 2). The key feature is expected to be the presence of the phenyl group on the double bond carbon opposite to the σ bond that is breaking. In order to confirm that this destabilization of the transition state is still dominant when other stabilizing vinyl groups are present we have briefly examined divinyl cyclopropenes. Two point potential energy surfaces were obtained for 1,2-divinylcyclopropene (reaction 8) and 1,3-divinylcyclopropene (reaction 9) estimating the transition state energy by single calculations at a σ bond distance of 2.15 Å. This value was chosen based on the maxima in Fig. 5. In both cases the destabilizing effect of the vinyl group on the carbon opposite to the breaking σ bond is greater than any stabilizing effect that results from vinyl groups on the carbons of the bond involved. This

[8]

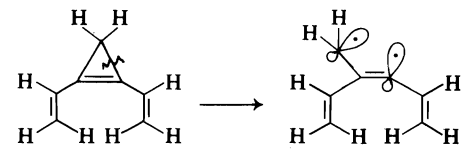

ΔH_f 81.90 kcal/mol ΔH_f 132.53 kcal/mol

ΔH_{act} 50.6 kcal/mol

[9]

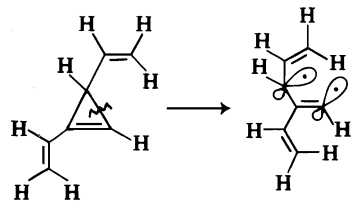

ΔH_f 94.14 kcal/mol ΔH_f 142.18 kcal/mol

ΔH_{act} 48.0 kcal/mol

destabilization, which should be enhanced even more by phenyl groups, could be checked experimentally by a systematic study of the pyrolysis of phenyl substituted cyclopropenes.

Although we feel these results indicate the main feature in the surprising stability of tetraphenylcyclopropene, the reason for this stabilizing effect is less obvious. An examination of the intermediate carbenes for the three systems suggests an explanation. In both cases where the effect of the vinyl group is stabilizing (*i.e.*, substituted on the bond breaking) the intermediate becomes almost planar (note Fig. 6, C_1—C_3 = 2.2 Å and Fig. 8, C_1—C_3 = 2.5 Å). Thus **16** is essentially divinyl carbene and **19** is butadienyl carbene. Moreover the electron density of the carbene carbons is concentrated almost exclusively in the plane of the molecule; the sum of the squares of the coefficients of the carbene carbon orbital in the HOMO is 0.685 and 0.923 with a π-contribution of 0.004 and 0.000 for **16** and **19** respectively. Therefore the π system itself is essentially cation-like. In contrast, **17** (the intermediate that is destabilized by vinyl substitution) never becomes planar (note Fig. 7, C_2—C_3 = 2.4 Å). In fact, the carbene center remains somewhat isolated from the π-system of the developing butadiene fragment. This carbene is then actually less stabilized than that formed from cyclopropene; that is, conjugation of the second vinyl group with the developing double bond of the vinyl carbene prevents stabilization of the carbene itself. This is seen clearly in the potential energy surface for conversion of **15** to **17** in Fig. 5 where lack of stabilization prevents the appearance of a true minimum.

This explanation raises the question as to why **17** does not become planar. A qualitative answer is suggested by examination of planar **17** which, by analogy to the other cases, would have a π-system similar to the 2-methylenebutadienyl cation. In contrast, planar **16** and **19** are similar to pentadienyl cation (see above). Cross con-

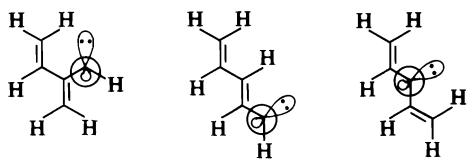

Planar **17** Planar **19** Planar **16**

jugated systems like **17** are less stable than linearly conjugated systems like **16** (**19**) as evidenced by the simple Hückel energy difference of 0.24β in favour of pentadienyl over 2-methylenebutadienyl. Therefore **17** is less stable than the intermediates from the other vinyl carbenes because its energy is not significantly decreased in a planar geometry.

Cyclopropene to Vinyl Carbene: Excited States

Our main objective in examining the excited state behaviour of these species was to find an explanation for the experimental observation that excited singlet states of cyclopropene derivatives open to vinyl carbene intermediates, whereas triplet states are surprisingly stable and long lived. Since, to our knowledge, no application of the MINDO/3 technique to excited state processes has appeared, this seemed an ideal small molecule to test the method.

Our initial calculations were simply of the excited singlet (182.5 kcal/mol) and triplet (125.0 kcal/mol) in the equilibrium ground state geometry of cyclopropene. The first value should give an estimate (182.5 − 59.2 = 123.3 kcal/mol) of the vertical excitation energy and therefore can be compared with the π–π* electronic absorption band at 58 000 cm^{-1} (166 kcal/mol) reported for cyclopropene (16). The comparison is rather poor and is certainly not as good as those obtained by *ab initio* SCF techniques: 173 kcal/mol (16) and 167 kcal/mol (12). No experimental value is known for the vertical ground state–triplet splitting (125.0 − 59.2 = 65.8 kcal/mol) but again results from *ab initio* calculations are considerably higher; 119.9 kcal/mol by the GVB technique (11) and 92.8 kcal/mol by an MO method (12). This poor agreement between MINDO/3 and *ab initio* results for excited state species suggests that attempts to obtain quantitative information on the cyclopropene to vinyl carbene surface may be difficult. However, hopefully the qualitative behaviour of the surfaces will still be acceptably reliable.

Thus in Fig. 9 the excited singlet and triplet surfaces are shown for the conversion of cyclopropene (**10**) to vinyl carbene (**11**) along with the ground state surface for comparison. Figures 10 and 11 show, respectively, geometries of some of the points along the excited singlet and triplet surfaces.

A problem was encountered obtaining the singlet surface. The solid line shown is drawn through the minimum calculated values at any given C_1—C_3 bond distance. Depending on the geometry used as the starting point to obtain the minimized structure, quite different energies and

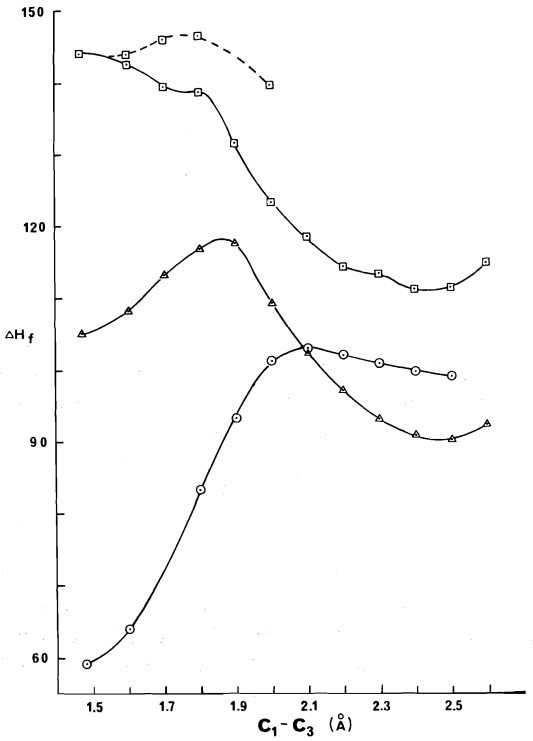

FIG. 9. Ground state, triplet state, and excited singlet state surfaces for the conversion of **10** to **11**: ground state ⊙; triplet state △; excited singlet state ⊡.

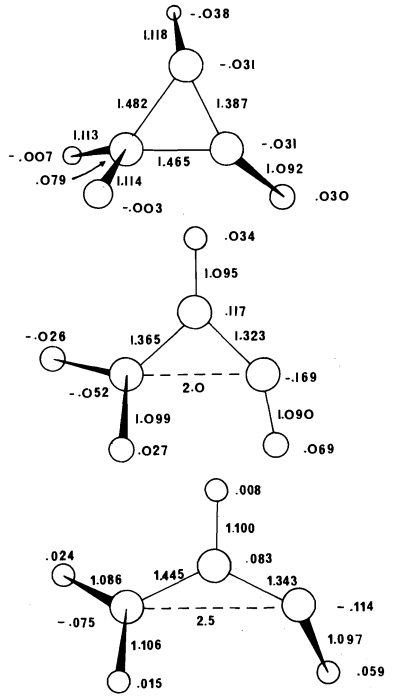

FIG. 10. Geometries and atomic charges of intermediates in the conversion of excited singlet **10** to **11**.

geometries were obtained. This may again reflect the inability of the MINDO/3 program to complete geometric minimizations adequately when there are intersecting surfaces for several states. (Note Fig. 2, ref. 12.) As an example, the points shown on the upper solid line in Fig. 9 were obtained starting at C_1—C_3 = 2.3 Å and shortening the C_1—C_3 distance. The points on the dotted line were obtained starting at C_1—C_3 = 1.48 Å and lengthening the bond. This same type of behaviour was previously encountered on the ground state surface (Fig. 1). The other irregularities in the excited singlet surface may again be a result of the inability of MINDO/3 to find a true minimum. Again we assumed that the solid lines shown on Fig. 9 are the best approximation that MINDO/3 can make for the excited state surfaces.

First, in agreement with previous calculations, we note that the most stable state of vinyl carbene is the triplet (11, 12). More interesting is the very different behaviour of the excited singlet and triplet surfaces. The singlet opens in an unactivated process whereas the triplet has a barrier of ~13 kcal/mol. This observation is,

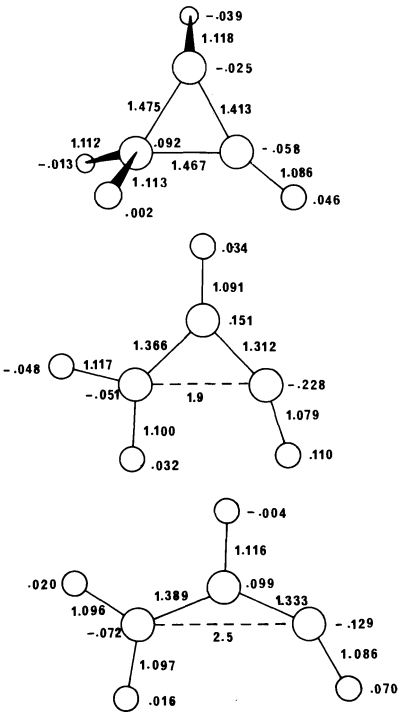

FIG. 11. Geometries and atomic charges of intermediates in the conversion of triplet **10** to **11**.

then, an explanation for the experimental results of cyclopropene photochemistry; the triplet states have a barrier to ring opening and are therefore long-lived enough to encounter another ground state molecule leading to dimerization. This also prevents photochemical racemization. The behaviour of the singlet state surface agrees well with the "funnel theory" of excited state to ground state conversions as outlined principally by Michl (17). Close approach of the two surfaces greatly enhances internal conversion and therefore gives a route for excited singlet cyclopropene to open to vinyl carbene and then return to ground state cyclopropene. Presumably there is a competition between this process leading to racemization of the cyclopropene and other processes leading to photoproducts.

Acknowledgements

We would like to thank the Computer Center at Dalhousie University for excellent service, Dr. L. Salem and Dr. W. D. Stohrer for helpful correspondence, and the National Research Council of Canada for financial assistance.

1. G. L. Closs. Adv. Alicyclic Chem. **1**, 53 (1966).
2. S. W. Benson. Thermochemical kinetics. Wiley, New York, NY. 1968. p. 179.
3. E. J. York, W. Dittmar, J. R. Stevenson, and R. G. Bergman. J. Am. Chem. Soc. **95**, 5680 (1973).
4. M. A. Battiste, B. Halton, and R. H. Grubbs. Chem. Commun. 907 (1967).
5. J. A. Pincock, R. Morchat, and D. R. Arnold. J. Am. Chem. Soc. **95**, 7536 (1973).
6. C. D. DeBoer, D. H. Wadsworth, and W. C. Perkins. J. Am. Chem. Soc. **95**, 861 (1973).
7. J. A. Pincock and A. Moutsokapas. Can. J. Chem. **55**, 979 (1977).
8. R. C. Bingham, M. J. S. Dewar, and D. H. Lo. J. Am. Chem. Soc. **97**, 1285 (1975).
9. M. J. S. Dewar, G. J. Fonken, J. Kirschner, and D. E. Minter. J. Am. Chem. Soc. **97**, 6750 (1975).
10. G. D. Andrews and J. E. Baldwin. J. Am. Chem. Soc. **98**, 6706 (1976).
11. J. H. Davis, W. A. Goddard III, and R. G. Bergman. J. Am. Chem. Soc. **98**, 4015 (1976).
12. J. D. Peyerimhoff and R. J. Buenker. Theor. Chim. Acta, **14**, 305 (1969).
13. R. C. Bingham, M. J. S. Dewar, and D. H. Lo. J. Am. Chem. Soc. **97**, 1294 (1975).
14. L. Salem, C. Leforestier, G. Segal, and R. Westmore. J. Am. Chem. Soc. **97**, 479 (1975).
15. M. R. Willcott, R. L. Cargill, and A. B. Sears. Prog. Phys. Org. Chem. **11**, 88 (1972).
16. M. B. Robin, H. Basch, N. A. Kuebler, K. B. Wiberg, and G. B. Ellison. J. Chem. Phys. **51**, 45 (1969).
17. J. Michl. J. Mol. Photochem. **4**, 243 (1972); **4**, 257 (1972).

Anchoring of the amide acidity function in dilute aqueous acid: a corrected H_A scale

JOHN T. EDWARD AND SIN CHEONG WONG

Department of Chemistry, McGill University, 801 Sherbrooke St. W., Montreal, P.Q., Canada H3A 2K6

Received February 10, 1977

JOHN T. EDWARD and SIN CHEONG WONG. Can. J. Chem. **55**, 2492 (1977).

Amide indicators ionizing over the range 0–30% sulfuric acid indicate that values of the H_A scale established by Yates *et al.* (Can. J. Chem. **42**, 1957 (1964)) should be corrected by +0.33 unit.

JOHN T. EDWARD et SIN CHEONG WONG. Can. J. Chem. **55**, 2492 (1977).

En utilisant trois amides comme indicateurs ionisant dans la région 0–30% H_2SO_4, on découvre que les valeurs de H_A de Yates *et al.* (Can. J. Chem. **42**, 1957 (1964)) doivent être corrigées par +0.33 unité.

Introduction

The various acidity functions H_R', H_0''', H_I, H_0, etc. all start out in dilute aqueous solution equal to pH (by definition), but diverge in sulfuric acid solutions more concentrated than about 1%. This shows up in a fanning out of curves for H_R', H_0''', and H_0 above $H_x \simeq 0.5$ in Fig. 1. The same behaviour might be expected (1) of the amide acidity function H_A of Yates *et al.* (2); however these authors, unable to find amide indicators ionizing over the range 0–16% sulfuric acid, chose to use 4-nitroaniline and 2-nitroaniline (indicators numbers 1 and 2 of Table 1), in effect making H_A coincident with H_0 over this concentration range. Bunnett and Olsen (3), on the basis of their LFER method of determining pK_{AH^+} values of amides, suggested that the H_A scale of Yates *et al.* was too negative by about 0.3 unit. This suggestion has the merit of lowering the H_A curve of Fig. 1 so that it diverges from the other curves at about the point to be expected. However, so far attempts to confirm the suggestion have been contradictory. Johnson *et al.* (4) claimed that pyridine-1-oxides followed the H_A acidity function, and used indicators 4, 5, and 6 of Table 1 to reassess the H_A scale in the lower acidity regions. They asserted that this investigation only confirmed the old scale. On the other hand, using the *N*-oxide indicators 7, 8, and 9 of Table 1, Homer and Johnson (1) changed the scale by 0.2 unit. However, none of these compounds are amides, and the parallelism between the logarithm of their ionization ratios with that of succeeding amide indicators is not very good. We have now investigated the ionization in 0–30% sulfuric acid of the amide indicators 10, 11, and 12 of Table 1 (2-hydroxynicotinic acid should exist preponderantly as the 2-pyridone tautomer (5)). We find that the H_A scale should indeed be shifted to the extent suggested by Bunnett and Olsen.

TABLE 1. Indicators used in attempts to establish the H_A scale in 0–25% aqueous sulfuric acid

Indicator (ref.)	$-\mathrm{d}\log I/\mathrm{d}H_0$
1. 4-Nitroaniline (2)	1.00
2. 2-Nitroaniline (2)	1.00
3. Pyrrole-2-carboxamide (2)	0.79
4. 3,5-Dimethyl-4-nitropyridine-1-oxide (4)	1.02
5. 3,5-Dichloropyridine-1-oxide (4)	0.77
6. 2,6-Dimethyl-4-nitropyridine-1-oxide (4)	0.82
7. 3-Chloropyridine-1-oxide (1)	0.91
8. 5-Nitroquinoline-1-oxide (1)	0.79
9. 8-Nitroquinoline-1-oxide (1)	0.79
10. 1-Methyl-2-pyridone (this work)	0.80
11. 5-Chloro-2-pyridone (this work)	0.78
12. 2-Hydroxynicotinic acid (this work) (2-pyridone-5-carboxylic acid)	0.77

Experimental

Materials

1-Methyl-2-pyridine, 5-chloro-2-pyridone, and 2-hydroxynicotinic acid (2-pyridone-5-carboxylic acid) were all commercial products.

Sulfuric acid and perchloric acid solutions were prepared by diluting commercial concentrated acids. Their final concentrations were determined by volumetric titration.

Ionization Measurements

Ionization ratios (I) of all three compounds (numbers 10, 11, and 12 of Table 1) in sulfuric acid, and of the first two compounds in perchloric acid were determined spectrophotometrically following standard procedures (6). Medium effects were corrected by characteristic vector analysis (7). Results are deposited as supplementary

TABLE 2. Ionization constants of 2-pyridone indicators

Compound	Δ log I	pK_{AH^+}	
1-Methyl-2-pyridone	—	0.38[a]	
5-Chloro-2-pyridone	0.35±0.04	0.03[b]	(−0.01)[a]
2-Hydroxynicotinic acid (2-pyridone-5-carboxylic acid)	0.67±0.03	−0.64[b]	
Pyrrole-2-carboxamide[c]	0.26±0.06	−0.90[b]	

[a]By extrapolation to zero acid concentration of plots of (log I − log [H+]) against [H+] in various concentrations of $HClO_4$ (8).
[b]pK_{AH^+} of the preceding compound − Δ log I.
[c]The most basic amide indicator of the original H_A function (2).

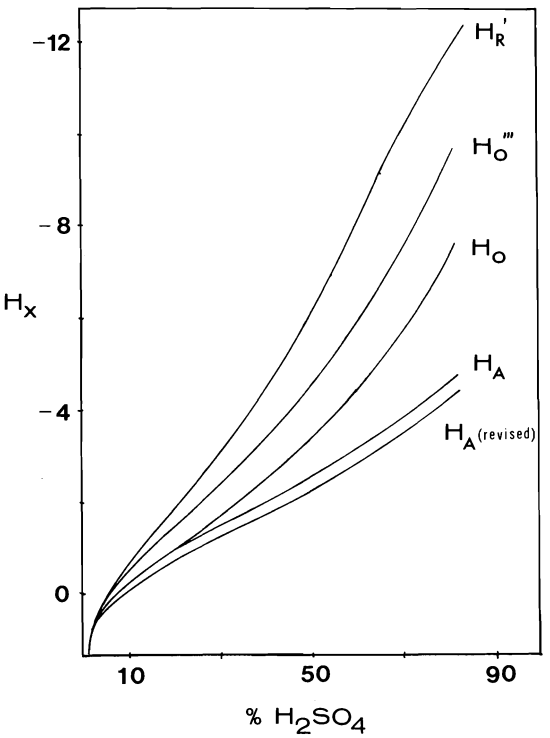

FIG. 1. Some representative acidity functions for aqueous sulfuric acid.

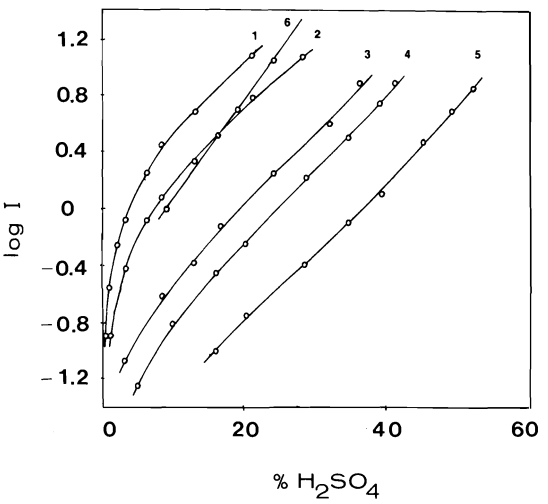

FIG. 2. Ionization of amide indicators in aqueous sulfuric acid: (*1*) 1-methyl-2-pyridone, (*2*) 5-chloro-2-pyridone, (*3*) 2-hydroxynicotinic acid, (*4*) pyrrole-2-carboxamide, (*5*) 3,4,5-trimethoxybenzamide, and (*6*) 2-nitroaniline.

material with the NRCC,[1] and were used to obtain the data of Table 1 and Fig. 2.

Results and Discussion

The parallelism in ionization ratios of the 2-pyridone indicators of Table 1 with those of the most basic amide indicators of Yates *et al.* (2), and hence their applicability in re-anchoring the H_A function, are shown by the plots of Fig. 2. The parallelism is good. Furthermore, indicators 10–12 have about the same slopes of log I against H_0 (Table 1) as pyrrole-2-carboxamide, the most basic indicator of Yates *et al.*, in contrast to some of the *N*-oxide indicators (numbers 4–9) used previously to anchor the H_A scale.

The pK_{AH^+} of the most basic amide, 1-methyl-2-pyridone, was obtained by a graphical method due to Paul (8). Examining [1]:

$$[1]\quad \log\frac{[AH^+]}{[A]} - \log[H^+] = pK_{AH^+} + \log f_A + \log\frac{f_{H^+}}{f_{AH^+}}$$

(the symbols being defined in ref. 2), since both log f_A (9) and log f_{H^+}/f_{AH^+} (8, 10, 11) can be expected to increase linearly with molar concentration of electrolyte, a plot of log I − log [H^+] against [H^+] should give a straight line with the intercept equal to pK_{AH^+} for a standard state of infinite dilution in water. In fact, 1-methyl-2-pyridone gave a straight line (linear regression

[1]The ionization data are available, at a nominal charge, from the Depository of Unpublished Data, CISTI, National Research Council of Canada, Ottawa, Canada K1A 0S2.

TABLE 3. Revised H_A scale

% H_2SO_4	H_A	% H_2SO_4	H_A
2.5	0.58	45	−1.91
5	0.25	50	−2.18
7.5	0.02	55	−2.44
10	−0.15	60	−2.77
12.5	−0.28	65	−3.05
15	−0.40	70	−3.41
20	−0.67	75	−3.82
25	−0.92	80	−4.29
30	−1.17	85	−4.69
35	−1.41	90	−5.24
40	−1.67		

correlation coefficient 0.998) indicating a pK_{AH^+} of 0.38 ± 0.01.

The pK_{AH^+} values of the other indicators were calculated according to the overlap procedure (12). They are reported in Table 2 along with the differences in log I values (Δ log I) used in calculating them. A pK_{AH^+} value of −0.90 is obtained for pyrrole-2-carboxamide, as opposed to the value of −1.23 reported by Yates *et al.* (2). Thus, the original H_A scale is 0.33 unit too negative for sulfuric acid concentrations from 16.1% up. For 0–16.1% H_2SO_4, H_A values have been calculated from pK_{AH^+} and log I values of the indicators, according to the equation: $H_A = pK_{AH^+} + \log I$. The revised H_A scale is given in Table 3.

Acknowledgments

We are grateful to the National Research Council of Canada for financial support.

1. R. B. HOMER and C. D. JOHNSON. *In* The chemistry of amides. *Edited by* J. Zabicky. Interscience, London. 1970. p. 187.
2. K. YATES, J. B. STEVENS, and A. R. KATRITZKY. Can. J. Chem. **42**, 1957 (1964).
3. J. F. BUNNETT and F. P. OLSEN. Can. J. Chem. **44**, 1899 (1966).
4. C. D. JOHNSON, A. R. KATRITZKY, and N. SHAKIR. J. Chem. Soc. B, 1235 (1967).
5. A. R. KATRITZKY and J. M. LAGOWSKI. *In* Advances in heterocyclic chemistry. Vol. I. *Edited by* A. R. Katritzky. Interscience, New York, NY. 1963. p. 339.
6. W. I. CONGDON and J. T. EDWARD. J. Am. Chem. Soc. **94**, 6096 (1972).
7. J. T. EDWARD and S. C. WONG. J. Am. Chem. Soc. In press.
8. M. A. PAUL. J. Am. Chem. Soc. **76**, 3236 (1954).
9. W. F. MCDEVIT and F. A. LONG. J. Am. Chem. Soc. **74**, 1773 (1952); M. A. PAUL. J. Am. Chem. Soc. **74**, 5274 (1952).
10. R. A. ROBINSON and R. H. STOKES. Electrolyte solutions. 2nd ed. Butterworths, London. 1959. p. 223 *et seq.*
11. L. M. SWEETING and K. YATES. Can. J. Chem. **44**, 2395 (1966).
12. L. P. HAMMETT and A. J. DEYRUP. J. Am. Chem. Soc. **54**, 2721 (1932).

Folded forms in tetrapeptides. Z-Val $(Ala)_3$-OEt[1]

ANTONIO MARIO TAMBURRO

Istituto di Chimica Analitica e Chimica Analitica Applicata, Universita' di Padova, Padova, Italy and Centro di Studio sulla Stabilita' e Reattivita' dei Composti di Coordinazione

AND

ANGELO SCATTURIN

Istituto di Chimica Organica, Universita' di Padova, Padova, Italy and Centro per lo Studio dei Biopolimeri, 35100 Padova, Italy

Received January 10, 1977

ANTONIO MARIO TAMBURRO and ANGELO SCATTURIN. Can. J. Chem. **55**, 2495 (1977).

The circular dichroism spectra of Z-Val-$(Ala)_3$-OEt in different solvents are reported. In dioxane the spectrum shows a negative band at 228–229 nm and a positive band at 212–213 nm, features which are consistent with the presence of some population of tetrapeptide molecules in a β-bend conformation. The infrared spectrum of Z-Val-$(Ala)_3$-OEt in KBr suggests an association of the molecules in an antiparallel β-structure in the solid state.

ANTONIO MARIO TAMBURRO et ANGELO SCATTURIN. Can. J. Chem. **55**, 2495 (1977).

On rapporte les spectres de dichroïsme circulaire de Z-Val-$(Ala)_3$-OEt dans différents solvants. Dans le dioxanne, le spectre montre une bande négative à 228–229 nm et une positive à 212–213 nm indiquant que des molécules du tétrapeptide existent dans la conformation β-bend. Le spectre infrarouge de Z-Val-$(Ala)_3$-OEt dans le KBr indique qu'à l'état solide il existe une association des molécules en structure β antiparallèle.

The so called β-bend folded conformation (1–4) is of paramount importance in the structure of small cyclic peptides (5) and it has also been found in some linear tetrapeptides (6, 7). Moreover, it has been suggested (2, 8) to play a particular role as a nucleation site in protein folding, although different points of view are possible (9, 10). Therefore we started with a wide-range project concerning structural investigations on linear tetrapeptides in order to elucidate the short-range forces responsible for the stabilization of this particular structure. In the present paper we report our results on the conformation of benzyloxycarbonyl-L-valyl-L-alanyl-L-alanyl-L-alanyl ethyl ester (Z-Val-$(Ala)_3$-OEt) which are of interest in connection with the recent finding of a β-bend type conformation in alanine tetrapeptide derivatives (6).

Experimental

The tetrapeptide was synthesized in a stepwise manner by the *p*-nitrophenyl ester method. The unprotected tripeptide L-alanyl-L-alanyl-L-alanine ethylester hydrobromide (11) was coupled with benzyloxycarbonyl-L-valine *p*-nitrophenylester (12) to give Z-Val$(Ala)_3$-OEt, mp 233°C. *Anal.* calcd. for $C_{24}H_{36}N_4O_7$: C 58.51, H 7.35, N 11.37; found: C 58.60, H 7.72, N 11.45. The cd spectra were recorded on a Cary 6002 dichrograph. The calibration was based upon $[\theta]_{290} = 7840$ deg cm^2 dmol^{-1} for a purified sample of *d*-10-camphosulfonic acid (Fluka, Bucks) in 0.1% aqueous solution (13). Samples were examined at concentrations ranging from 0.2 to 5 mg/ml using quartz cylindrical cells with optical paths of 0.01, 0.05, and 0.1 cm. The data are expressed in terms of $[\theta]_M$, the molar ellipticity in units of deg cm^2 dmol^{-1}. Infrared spectra were measured in the form of KBr pellets on a Perkin Elmer 21 spectrophotometer. Nujol spectra showed no significant variations.

Results and Discussion

Shown in Fig. 1 are the cd spectra of the protected tetrapeptide in TFE at three concentrations and in HFIP. Only minor concentration effects are found on both negative bands centered at 198 and 223–224 nm. Less polar solvents, such as water and ethylene glycol, induce a red shift and a decrease in the intensity of the bands (Fig. 2). As shown in Fig. 3, the alteration in the cd spectra, as a consequence of a change in solvent composition, could reflect a simple solvent effect and/or a conformational transition. However, when the apolar solvent dioxane is used (Fig. 4) a positive band appears around 212–213 nm. The spectrum under these

[1]Abbreviations used: cd, circular dichroism; ir, infrared; Z, benzyloxycarbonyl; Val, L-valine; Ala, L-alanine; OEt, ethyl ester; TFE, 2,2,2-trifluoroethanol; HFIP, 1,1,1,3,3,3-hexafluoropropan-2-ol; EG, ethylene glycol.

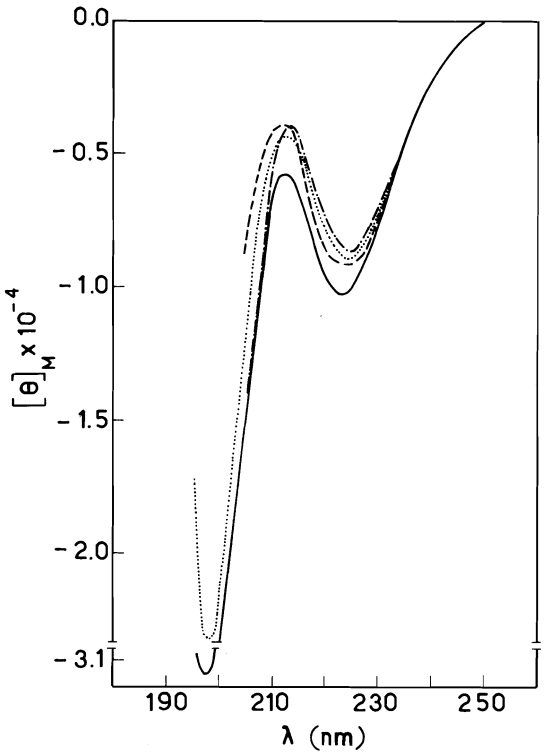

FIG. 1. Circular dichroism of Z-Val-$(Ala)_3$-OEt at 25°C in TFE at three concentrations and in HFIP: ··· HFIP, 0.2 mg/ml; --- 5 mg/ml; ·---· 0.5 mg/ml; — 0.2 mg/ml.

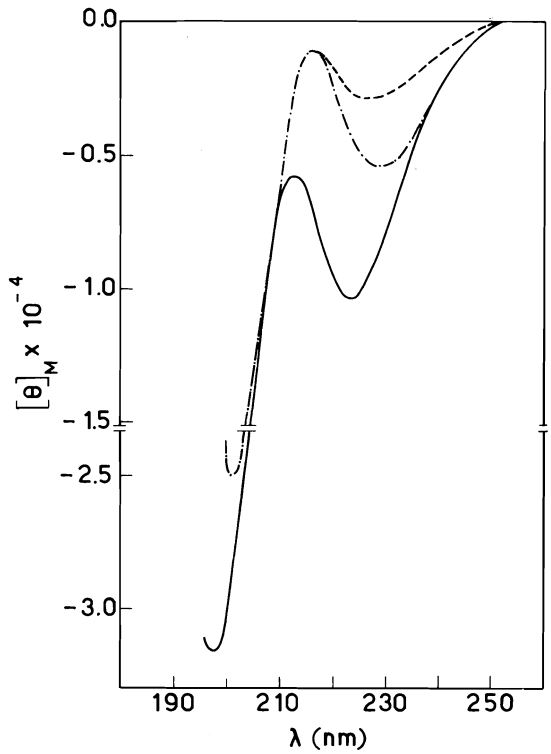

FIG. 2. Circular dichroism of Z-Val-$(Ala)_3$-OEt at 25°C in: — TFE; ·---· EG/TFE (90:10 v/v); --- H_2O/TFE (90:10 v/v). Peptide concentration was 0.2 mg/ml.

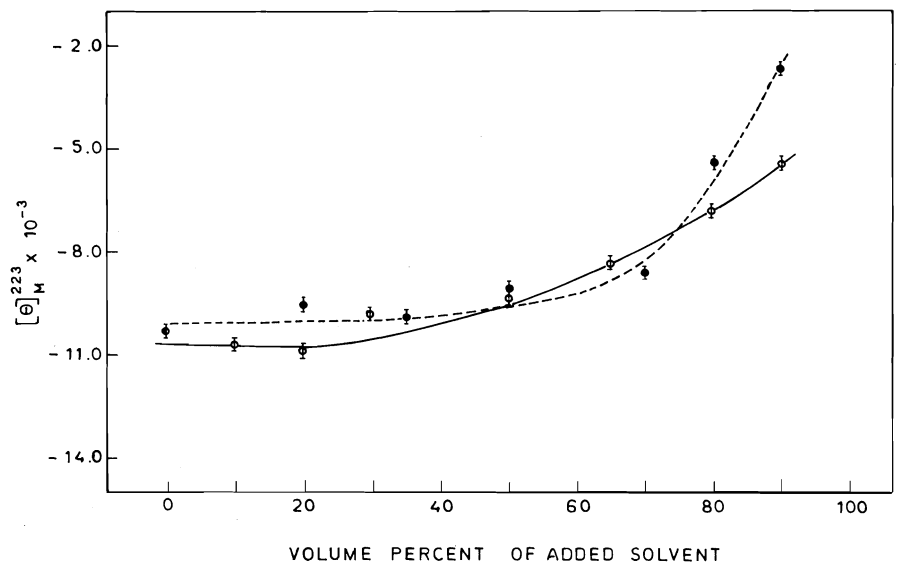

FIG. 3. Plot of $[\theta]_M$ at 223 nm of Z-Val-$(Ala)_3$-OEt at 25°C *vs.* percentage (v/v) of EG (○) in TFE and H_2O (●) in TFE. Peptide concentration was 0.2 mg/ml.

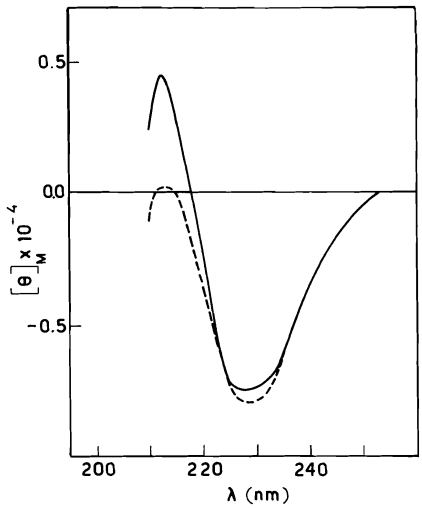

FIG. 4. Circular dichroism of Z-Val-$(Ala)_3$-OEt at 25°C in: — TFE/dioxane (30:70 v/v); --- TFE/dioxane (50:50 v/v). Peptide concentration was 0.2 mg/ml.

conditions looks similar to the one which is believed to be typical of β-bends (14). According to these results, we propose that on decreasing the solvent polarity, and therefore its hydrogen-bonding potential, the tetrapeptide is undergoing a conformational transition so that a significant fraction of the total population of its conformations exists in a chain-reversal (β-bend) conformation.

It is to be noted that, in principle, the presence of the phenyl ring in the protecting group could affect the 210 nm region of the cd spectrum. Therefore, we recorded cd spectra in TFE–dioxane mixtures in the region 250–300 nm in order to detect possible dichroic bands associated with the aromatic chromophore.

As a matter of fact, no such bands were observed even using long optical paths and sensitivities at the limit of the instrument adopted. Accordingly, we are confident that the cd changes observed in the far uv are not attributable to solvent-dependent aromatic bands.

The ir spectrum (Fig. 5) of the tetrapeptide in KBr shows the frequencies of Amide A, B, I, II, and V bands positioned at 3320, 3080, 1685 and 1630, 1530, and 690 cm^{-1}, respectively. All bands but one are fully consistent with the presence, in the solid state, of the antiparallel β-structure. The exception is represented by the Amide A frequency at 3320 cm^{-1} which is about 40 cm^{-1} higher than that observed for the anti-

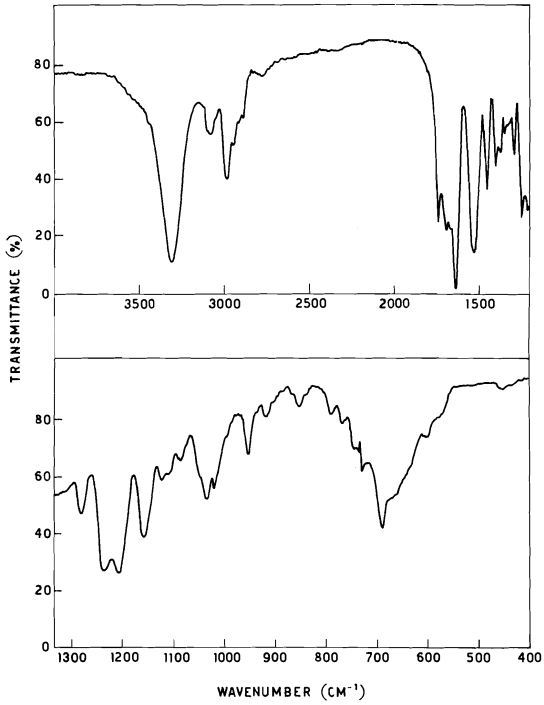

FIG. 5. Infrared spectrum of Z-Val-$(Ala)_3$-OEt in KBr pellets.

parallel β-form (15). In principle this higher NH-stretching frequency of hydrogen-bonded amides could arise from unusually long and/or very nonlinear hydrogen bonds. Peptides assuming 'bent' or 'folded' forms with intramolecular hydrogen bonds, show high Amide A frequencies (16, 17), probably because the groups involved are sterically prevented from adopting the optimal angles for hydrogen bond formation (15). In light of this, we suggest that for the Z-Val$(Ala)_3$-OEt chain folding is also occurring in the solid state with association of the molecules in an antiparallel fashion. A possible model would be the side-by-side aggregation postulated for protected tetraalanine at high concentrations in chloroform (6).

1. C. M. VENKATACHALAM. Biopolymers, **6**, 1425 (1968).
2. P. N. LEWIS, F. A. MOMANY, and H. A. SCHERAGA. Proc. Natl. Acad. Sci. U.S.A. **68**, 2293 (1971).
3. P. N. LEWIS, F. A. MOMANY, and H. A. SCHERAGA. Biochim. Biophys. Acta, **303**, 211 (1973).
4. J. L. CRAWFORD, W. N. LIPSCOMB, and C. G. SCHELLMAN. Proc. Natl. Acad. Sci. U.S.A. **70**, 538 (1973).

5. C. M. DEBER, V. MADISON, and E. R. BLOUT. Acc. Chem. Res. **9**, 106 (1976).
6. M. GOODMAN, N. UEYAMA, F. NAIDER, and C. GILON. Biopolymers, **14**, 915 (1975).
7. K. D. KOPPLE and A. GŌ. Biopolymers, **15**, 1701 (1976).
8. C. B. ANFINSEN and H. A. SCHERAGA. Adv. Protein Chem. **29**, 205 (1975).
9. D. B. WETLAUFER and S. RISTOW. Ann. Rev. Biochem. **42**, 151 (1973).
10. W. A. HILTNER and A. G. WALTON. J. Mol. Biol. **92**, 567 (1975).
11. F. MARCHIORI, R. ROCCHI, and E. SCOFFONE. Gazz. Chim. Ital. **93**, 834 (1963).
12. F. MARCHIORI, R. ROCCHI, and E. SCOFFONE. Ric. Sci. **32**, 647 (1962).
13. A. J. ADLER, N. J. GREENFIELD, and G. D. FASMAN. *In* Methods in enzymology. Vol. XXVII, Part D. *Edited by* C. H. W. Hirs and S. N. Timasheff. Academic Press, New York, NY. 1973. p. 675.
14. R. B. WOODY. *In* Peptides, polypeptides, and proteins. *Edited by* E. R. Blout, F. A. Bovey, and N. L. Lotan. Wiley, New York, NY. 1974. p. 338.
15. B. B. DOYLE, E. G. BENDIT, and E. R. BLOUT. Biopolymers, **14**, 937 (1975).
16. J. E. SHIELDS and S. T. MCDOWELL. J. Am. Chem. Soc. **89**, 2499 (1967).
17. J. E. SHIELDS, S. T. MCDOWELL, J. PAWLOS, and G. R. GRAY. J. Am. Chem. Soc. **90**, 3549 (1968).

Solubilities of the silver halides in propylene carbonate mixtures with bis(trifluoroethyl)sulfite

MARK SALOMON

Power Sources Technical Area, U.S. Army Electronics Technology and Devices Laboratory (ECOM), Fort Monmouth, NJ., U.S.A. 07703

Received January 5, 1977

MARK SALOMON. Can. J. Chem. **55**, 2499 (1977).

The complex solubilities of AgCl, AgBr, and AgI have been measured in several mixed solvents containing propylene carbonate and bis(trifluoroethyl)sulfite. The results indicate that a large inductive effect destabilizes the solvation of silver ions whereas the halide ions appear to be stabilized by coordination with the sulfinyl sulfur. Several physio-chemical properties of pure bis(trifluoroethyl)sulfite are reported.

MARK SALOMON. Can. J. Chem. **55**, 2499 (1977).

On a mesuré les solubilités de complexes de AgCl, AgBr et AgI dans plusieurs solvants mixtes contenant du carbonate de propylène et du sulfite de bis(trifluoroéthyle). Ces résultats indiquent qu'un effet inductif important déstabilise la solvatation des ions argent alors que les ions halogénures semblent être stabilisés par une coordination avec le soufre du groupe sulfinyle. On rapporte plusieurs propriétés physicochimiques du sulfite de bis(trifluoroéthyle) à l'état pur.

[Traduit par le journal]

Introduction

In previous papers (1) the complex solubilities of the silver halides, AgX (X = Cl, Br, I), were studied in a series of pure and mixed aprotic, sulfur-containing solvents. The reactions studied were

$$[1] \qquad AgX \rightleftharpoons Ag^+ + X^- \qquad K_{s0}$$

$$[2] \qquad Ag^+ + nX^- \rightleftharpoons AgX_n^{1-n} \qquad \beta_n$$

$$[3] \qquad AgX + X^- \rightleftharpoons AgX_2^- \qquad K_{s2}$$

The previous studies were concerned with the effect of solvent composition on the magnitudes of these equilibrium constants which, in turn, were used to interpret the nature of the ion–solvent interactions. For example, the magnitude of the solubility product, K_{s0}, is determined by the solvent interactions with Ag^+ and X^- whereas the magnitude of K_{s2} is governed by the relative interactions between the solvent and the ions X^- and AgX_2^-. In those solvents containing a sulfinyl, sulfonyl, and sulfenyl atom, the magnitude of K_{s2} was, in part, found to be dependent upon the electronic configuration at the sulfur which reflects the nature of the solvent–X^- interaction. The magnitudes of K_{s0} and K_{s2} could also be used to determine the specific solvent–Ag^+ interaction: *i.e.* whether Ag^+ interacts with a sulfur or with an oxygen atom.

The present paper is an extension of our related studies (1), being concerned with the solubilities of the silver halides in several mixed solvents composed of propylene carbonate (PC) and bis(trifluoroethyl)sulfite, $(CF_3CH_2O)_2SO$. One of the major aims of this study is to determine the effect of fluorine substitution on the above equilibria. Another objective is to determine some of the important physio-chemical properties of bis(trifluoroethyl)sulfite which shows promise as a new dipolar aprotic solvent for use in the study of medium effects.

Experimental Section

(a) Materials

Tetrapropylammonium perchlorate, chloride, bromide, and iodide (Pr_4NClO_4, Pr_4NCl, Pr_4NBr, and Pr_4NI) were purified by the methods described by Mann (2). Purified PC was used as received from Burdick and Jackson Laboratories. Bis(trifluoroethyl)sulfite was prepared by a method similar to that described by DeMarco *et al.* (3). A 1:1 alcohol:amine adduct was prepared at −10 to 0°C from 2,2,2-trifluoroethanol and triethyl amine. A stoichiometric quantity of $SOCl_2$ was condensed, under vacuum, onto the adduct at −196°C and the mixture was allowed to warm to room temperature overnight. The sulfite ester was distilled at ~1 Torr and 100–130°C and collected in an acetone/CO_2 bath. The middle 3/5 fraction was retained and placed over purified Hg and stirred for 24 h to insure that any monosubstituted sulfite, $CF_3CH_2OS(O)Cl$, had further reacted to yield the desired product (3, 4). The solvent was fractionated two more times from activated alumina and the middle 3/5 fraction retained in each step. A typical ele-

mental analysis, performed by PCR, Inc., gave the following. *Anal.* calcd.: C 19.52, H 1.64, S 13.00, F 46.30; found: C 19.91, H 1.98, S 13.05, F 46.52. All solvents and salts were stored in an argon-filled dry box (O_2 and H_2O content $\leq$ 1 ppm).

(b) Measurements of Dielectric Properties

The static dielectric constants of pure $(CF_3CH_2O)_2SO$ and its mixtures with PC were measured by the comparison method (5) at a fixed frequency of 2 MHz. The cell, provided by Payne (6), consisted of concentric brass electrodes threaded onto a Teflon base which also formed part of a water jacket. The cell capacitance was measured by a substitution method using a General Radio 1606-B bridge and Type 722-D and 1422-ME precision variable capacitors. The cell constants were determined from measurements made with air (7), benzene (8), PC (6), and dimethylsulfoxide (9). A least-squares fit gave

$$C = 5.626\varepsilon + 2.952 \ (15°C)$$
$$C = 5.634\varepsilon + 2.980 \ (25°C) \quad [4]$$
$$C = 5.657\varepsilon + 2.957 \ (35°C)$$

where C is the measured capacity and ε is the static dielectric constant.

The dipole moment of pure $(CF_3CH_2O)_2SO$ was determined at 25°C with the above apparatus by measuring the dielectric constants of five benzene solutions in which the mole fraction of $(CF_3CH_2O)_2SO$ was varied from 0.0028 to 0.2060. The dipole moment, μ_0, was calculated from the limiting molar polarization of the solute as described by Smyth (10). The Kirkwood "g" factor was calculated from the Kirkwood–Frölich equation (11)

$$[5] \quad g = \frac{9kT}{4\pi n_2 \mu_0} \times \frac{(2\varepsilon + \varepsilon_\infty)(\varepsilon + 2)}{3\varepsilon(\varepsilon_\infty + 2)} \times \left\{\frac{\varepsilon - 1}{\varepsilon + 2} - \frac{\varepsilon_\infty - 1}{\varepsilon_\infty + 2}\right\}$$

where all terms have their usual significance. The high frequency dielectric constant, ε_∞, was calculated from the optical index of refraction assuming a 10% increase in the total induced polarizability between optical and microwave frequencies (*e.g.* see ref. 12): *i.e.* $\varepsilon_\infty = 1.10n_D^2$. Refractive indices, n_D, were measured with a Bausch and Lomb model 8006 refractometer. Temperature control for all measurements was $\pm$0.1°C.

(c) Solubility Studies

The solubility and stability constants were obtained from potentiometric titration data as described previously (1). Three mixed solvents were studied in which the mole fractions of $(CF_3CH_2O)_2SO$, χ_{-so}, in PC were 0.3483, 0.6831, and 0.7960. Studies were not carried out in pure $(CF_3CH_2O)_2SO$ because $AgClO_4$ is not soluble to any appreciable extent in this solvent. $AgClO_4$ was only moderately soluble in the solution where χ_{-so} = 0.7960 and which therefore necessitated the reduction of its concentration. All solutions were of a constant ionic strength, μ: for χ_{-so} = 0.3483, 0.6831, and 0.7960, respectively, μ = 25.0, 10.0, and 5.0 mM (millimolar). The titrant was therefore either 25.0, 10.0, or 5.0 mM $AgClO_4$ in the respective solvent and the titrate was a solution of $Pr_4NX + Pr_4NClO_4$, the latter salt being used to maintain the required ionic strength. The titration cell is identical with the one described earlier (1) and consisted of an etched, coiled silver indicator electrode and a silver wire reference electrode in 25.0, 10.0, or 5.0 mM $AgClO_4$: the reference electrode was separated from the titrate by a salt-bridge. The cell and 10 ml of titrate was fitted with a Gilmont 2 ml microburet containing the titrant, removed from the dry box, and placed in a water bath at 25 $\pm$ 0.1°C. Magnetic stirring was maintained throughout the titration and all emf's were measured with a Fluke Model 8800A digital multimeter.

Results

Several physio-chemical properties of pure $(CF_3CH_2O)_2SO$ and its mixtures with PC are given in Table 1. The data for the χ_{-so} = 0.7960 solution were interpolated either graphically or by a power series least-squares fit. All other data are based upon experimental measurements. Although pure $(CF_3CH_2O)_2SO$ has a relatively low dielectric constant, it has a relatively large dipole moment ($\mu_0 = 2.55 \times 10^{-18}$ esu-cm) and a Kirkwood "g" value of 1.4 which indicate that the liquid is moderately associated and that the O—S(O)—O pyramidal angle is substantial. The temperature dependence of ε for pure $(CF_3CH_2O)_2SO$ is given by

$$[6] \quad \varepsilon = \frac{5070.89}{T} - 6.604(\pm 0.06)$$

where the temperature is in K.

The stability constant, β_2, was calculated by by an iterative least-squares technique (1) and the standard deviation of β_2 was calculated by Sillén's pit-mapping method (13). The K_{s0} values are averages calculated by a Newton–Raphson iteration for each point in the saturated solutions. Electromotive force values were generally stable to within $\pm$0.5–1.0 mV and formal potentials had standard deviations of $\pm$2–3 mV. Attempts to generate the equilibrium constants β_1 and β_3 by the least-squares method failed (*i.e.* convergence of the iterations was not achieved) and it was therefore assumed that they are of minor significance. The results for β_2, K_{s0}, and K_{s2} are given in Table 2. The equilibrium constants in Table 2 were adjusted to the state for zero ionic strength (Table 3) by using the Davies equation (14) to calculate the activity coefficients:

TABLE 1. Properties of PC/$(CF_3CH_2O)_2SO$ solutions at 25°C*

χ_{-SO}	M_{-SO}	n_D	d	ε	A
0.3483	3.1428	1.3782	1.3738	39.71	1.4165
0.6831	5.0640	1.3510	1.4861	21.52	3.5506
0.7960	(5.56)	(1.343)	(1.516)	(18.0)	(4.642)
1.0	6.3495	1.3308	1.5628	10.33	10.676

*χ_{-SO} and M_{-SO} are the mole fraction and molarity, respectively, of $(CF_3CH_2O)_2SO$ in solution; n_D is the optical refractive index measured at the sodium D line; d is the density in g/ml; A is the Debye–Hückel constant ($\ell^{1/2}$ mol$^{-1/2}$); data in parentheses are extrapolated values.

TABLE 2. Experimental equilibrium constants at 25°C (molar scale)

		Value*		
Salt	Parameter	$\chi_{-SO} = 0.3483^a$	$\chi_{-SO} = 0.6831^b$	$\chi_{-SO} = 0.7960^c$
AgCl	$\log \beta_2$	16.38±0.02	18.16±0.06	21.86±0.04
	$\log K_{s0}$	−18.24±0.02	−20.48±0.01	−22.96±0.01
	$\log K_{s2}$	−1.82±0.02	−2.32±0.06	−1.10±0.04
AgBr	$\log \beta_2$	18.60±0.01	20.30±0.02	22.93±0.07
	$\log K_{s0}$	−20.12±0.01	−22.188±0.003	−24.28±0.08
	$\log K_{s2}$	−1.52±0.01	−1.89±0.02	−1.35±0.11
AgI	$\log \beta_2$	21.73±0.02	23.24±0.02	
	$\log K_{s0}$	−22.37±0.08	−24.87±0.03	
	$\log K_{s2}$	−0.65±0.09	−1.64±0.03	

*a, b, c: ionic strength = 25.0, 10.0, and 5.0 mM, respectively.

TABLE 3. Standard equilibrium constants at 25°C (molar scale)

		Value for χ_{-SO} =				
Salt	Parameter	0.000	0.348	0.683	0.796	1.000
AgCl	$\log \beta_2^0$	21.2	16.7	18.8	22.5	30.9
	$\log K_{s0}^0$	−20.2	−18.6	−21.1	−23.6	−31.2
	$\log K_{s2}^0$	1.0	−1.8	−2.3	−1.1	−0.3
AgBr	$\log \beta_2^0$	20.9	19.0	20.9	23.5	30.4
	$\log K_{s0}^0$	−20.6	−20.5	−22.8	−24.9	−31.6
	$\log K_{s2}^0$	0.3	−1.5	−1.9	−1.4	−1.3
AgI	$\log \beta_2^0$	22.2	22.1	23.9		
	$\log K_{s0}^0$	−20.8	−22.7	−25.5		
	$\log K_{s2}^0$	1.3	−0.7	−1.6		

[7] $$\log y_{\pm} = \frac{-A\mu^{1/2}}{1 + \mu^{1/2}} + 0.3A\mu$$

Included in Table 3 are corresponding data for pure PC (16) and $(CF_3CH_2O)_2SO$, the latter obtained by a non-linear extrapolation. The standard deviations for the mixed solvents are not included in Table 2 but are expected to be about 10% higher than those in Table 2: the standard deviations in pure $(CF_3CH_2O)_2SO$ are however much larger (±2 log units), because of the non-linear extrapolations used to obtain these quantities.

In previous papers (1, 15), we have used the approximate extrathermodynamic assumption of

$$\Delta G_t^0(AgCl_2^-) = -\Delta G_t^0(AgBr_2^-)$$

to calculate the free energies of transfer of single ions from water to an organic solvent (ΔG_t^0(ion)). The ΔG_t^0(ion) values for the ions involved in the present study were calculated using this assump-

TABLE 4. Standard free energies of transfer of single ions from water to a nonaqueous solvent*

Solvent	ΔG_t^0(ion) (kcal/mol)					
	Ag^+	Cl^-	Br^-	I^-	$AgCl_2^-$	AgI_2^-
PC	5.5	8.7	5.9	1.0	1.3	−8.2
PC/$(R_fO)_2SO$ $\chi_{-SO} = 0.348$	7.5	4.6	3.7	1.6	1.0	−4.8
PC/$(R_fO)_2SO$ $\chi_{-SO} = 0.683$	10.9	4.6	3.5	1.9	1.6	−3.2
PC/$(R_fO)_2SO$ $\chi_{-SO} = 0.796$	13.2	5.6	4.0		1.0	
$(R_fO)_2SO$	22.5	6.8	4.0		1.0	
$(MeO)_2SO$	4.9	4.6	3.3	1.5	1.9	−5.3
DMSO	−8.9	10.0	6.6	2.8	1.7	−6.2
PC/THT $\chi_{THT} = 0.05$	−5.7	8.8	6.0	2.6	1.4	−5.0

*All data are based on molar units at 25°C. $(R_fO)_2SO$ = $(CF_3CH_2O)_2SO$; $(MeO)_2SO$ = dimethylsulfite; DMSO = dimethylsulfoxide; THT = tetrahydrothiophene.

tion and are presented in Table 4 along with those determined earlier (1).

Discussion

The data shown in Tables 3 and 4 reveal that the effects of $(CF_3CH_2O)_2SO$ additions to PC are to (*i*) greatly destabilize the energy of solvation of Ag^+ and (*ii*) to stabilize the energy of solvation of the X^- ions. In several solvents containing a sulfur atom, the Ag^+ ion – solvent interaction energy is often stabilized by π-bonding which is, in part, evident from the magnitude of $\Delta G_t^0(Ag^+)$: *e.g.* for the transfer from water to dimethylformthioamide, dimethylsulfoxide, PC/SO_2 mixtures, $\Delta G_t^0(Ag^+)$ has values of −23.8, −8.9, and −3.0 kcal/mol, respectively (1, 17). In those aprotic solvents containing only C, H, and O, $\Delta G_t^0(Ag^+)$ values are generally positive (~5 kcal/mol) which indicates that the soft Ag^+ coordinates with a hard oxygen atom. Since the alkyl sulfite esters are pyramidal, Ag^+ coordination might be expected to occur at the soft basic S-center. However, as shown earlier, the large positive values of $\Delta G_t^0(Ag^+)$ suggest that coordination occurs at an oxygen due to the high (positive) charge on the sulfur (1*c*). The value of 22.5 kcal/mol for $\Delta G_t^0(Ag^+)$ is unexpectedly large in view of the value of 5 kcal/mol found for the transfer from water to dimethyl- and ethylenesulfite, and because the transmission of electronic effects through two σ-bonds are usually small. The result of fluorine substitution appears to primarily affect the electronic structure at the oxygens (rather than the sulfur as discussed below). The decrease in basicity of the oxygen produced by fluorine substitution (separated by two σ-bonds) has previously been reported by Parker *et al.* (17) who determined that $\Delta G_t^0(Ag^+) = 11.7$ kcal/mol for the transfer from water to 2,2,2-trifluoroethanol.

Concerning the nature of anion solvation, the present results show little or negligible differences in the S—X^- interaction between $(CF_3CH_2O)_2SO$ and $(CH_3O)_2SO$ or $(CH_2O)_2SO$. The data for the mixed solvents clearly indicate this ($\log K_{s2} \simeq -1$) whereas the data for pure $(CF_3CH_2O)_2SO$ suggest a decreased interaction ($\log K_{s2} \simeq 0$). The data for pure $(CF_3CH_2O)_2SO$ are, however, less reliable owing to the large errors (±2 log units) in $\log K_{s2}$ which resulted from the non-linear extrapolations. It is concluded that the interaction of halide ions with $(CF_3CH_2O)_2SO$ is, essentially, the same as that with the unsubstituted alkyl sulfites: *i.e.* the halide ions' interaction with the sulfinyl sulfur is augmented by π-bonding (*cf.* 1*c*).

Acknowledgments

The author would like to thank Dr. R. DeMarco for his advice in the preparation of $(CF_3CH_2O)_2SO$, and Dr. R. Payne for providing the dielectric cell.

1. (*a*) M. SALOMON and B. K. STEVENSON. J. Phys. Chem. **77**, 3002 (1973); (*b*) M. SALOMON. J. Phys. Chem. **79**, 429 (1975); (*c*) **79**, 2000 (1975).

2. C. K. MANN. Adv. Electroanal. Chem. **3**, 57 (1969).
3. R. A. DEMARCO, T. A. KOVACINA, and W. B. FOX. J. Floru. Chem. **5**, 221 (1975).
4. R. A. DEMARCO, T. A. KOVACINA, and W. B. FOX. J. Floru. Chem. **6**, 93 (1975).
5. J. G. MILLER. J. Am. Chem. Soc. **60**, 42 (1938); **64**, 117 (1942).
6. R. PAYNE and I. E. THEODOROU. J. Phys. Chem. **76**, 2892 (1972).
7. C. G. MALMBERG and A. A. MARYOTT. J. Res. Nat. Bur. Stand. **56**, 1 (1956).
8. L. HARTSHORN and D. A. OLIVER. Proc. R. Soc. London, A**123**, 664 (1929).
9. R. GARNSEY and J. E. PRUE. Trans. Faraday Soc. **64**, 1206 (1968).
10. C. P. SMYTH. Technique of organic chemistry. Vol. I. Part III. *Edited by* A. Weissberger. Interscience, NY. 1959.
11. H. FRÖHLICH. Theory of dielectrics. Oxford, London. 1949.
12. C. P. SMYTH. Dielectric behavior and structure. McGraw-Hill, NY. 1955.
13. L. G. SILLÉN. Acta Chem. Scand. **16**, 159 (1962).
14. C. W. DAVIES. Ion association. Butterworths, London. 1962.
15. M. SALOMON. Can. J. Chem. **54**, 1487 (1976).
16. J. N. BUTLER. Anal. Chem. **39**, 1799 (1967).
17. D. A. OWENSBY, A. J. PARKER, and J. W. DIGGLE. J. Am. Chem. Soc. **96**, 2682 (1974).

The intramolecular hydrogen bond in some β-nitroalcohols. Chemistry of nitroalkanes. Part CXIX

E. LIPCZYŃSKA-KOCHANY AND T. URBAŃSKI

Chemical Faculty, Technical University (Politechnika), 00-662 Warszawa, Poland

Received December 29, 1976

E. LIPCZYŃSKA-KOCHANY and T. URBAŃSKI. Can. J. Chem. **55**, 2504 (1977).

New experimental evidence is given on the existence of an intramolecular hydrogen bond in β-nitroalcohols between the nitro and hydroxylic groups. The conclusion is based on examination of $n_a \rightarrow \pi^*$ and infrared absorption bands and nmr spectra.

E. LIPCZYŃSKA-KOCHANY et T. URBAŃSKI. Can. J. Chem. **55**, 2504 (1977).

Des nouvelles preuves sont fournis sur l'existence de la liaison hydrogène interne dans les β-nitroalcools entre les groupes nitrique et hydroxylique. La conclusion est basée sur l'examination de la bande d'absorption $n_a \rightarrow \pi^*$, spectres d'absorption infrarouge et spectres nmr.

Introduction

A suggestion on the existence of an intramolecular bond between the alcoholic and nitro groups in aliphatic β-nitroalcohols was given by one of the authors of the present paper and his co-workers between 1951 and 1959. The suggestion was based on the chemical reactivity of the compounds (1), on ultraviolet (2, 3, 6, 7) and infrared (4, 7) spectroscopy and on measurement of dipole moments (5). The latter substantiated the earlier work of Lumbroso and Lauransan (8).

At first the suggestion was met with sharp criticism (9). However a number of later papers (10–15) have supported the view of the existence of a weak hydrogen bond and the latter appears now to be accepted (16). In view of the weakness of the bond, it seemed desirable to collect more information by using different methods. A more detailed spectroscopic analysis is reported in the ultraviolet and infrared regions and by the nmr technique. We have examined 2-methyl-2-nitropropane-1-ol (**1**), its methyl ether (**8**), 2-alkyl-2-nitropropane-1,3-diols (**2–7**), and alcohols without the nitro group: 2-methylpropane-1-ol (**9**) and 2,2-dimethylpropane-1,3-diol (**10**).

Dipole moments were also measured and calculated and the results will be reported elsewhere (17).

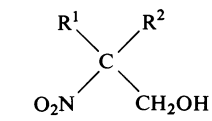

1: $R^1 = R^2 = CH_3$
2: $R^1 = CH_3$ $R^2 = CH_2OH$
3: $R^1 = C_2H_5$ $R^2 = CH_2OH$
4: $R^1 = C_3H_7$ $R^2 = CH_2OH$
5: $R^1 = CH_3(CH_2)_5$ $R^2 = CH_2OH$
6: $R^1 = CH_3(CH_2)_6$ $R^2 = CH_2OH$
7: $R^1 = CH_3(CH_2)_7$ $R^2 = CH_2OH$

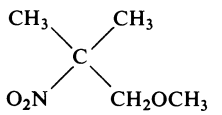

8

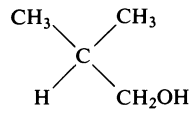

9

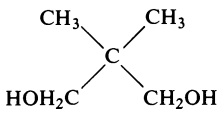

10

Experimental

2-Methyl-2-nitropropane-1-ol (**1**) and 2-alkyl-2-nitropropane-1,3-diols (**2–7**) were prepared from the corresponding nitroalkanes and formaldehyde by known procedures (18). The methyl ether of 2-methyl-2-nitropropane-1-ol was obtained by methylation of the alcohol by means of methyl sulphate (19). 2-Methylpropane-1-ol (**9**) from the Eastman Kodak Company, Rochester (Spectro Grade), was dried over $MgSO_4$ and distilled. 2,2-Dimethylpropane-1,3-diol was prepared from isobutyl aldehyde and formaldehyde by a known method (20).

Benzene and dioxane were of analytical grade from E. Merck, Darmstadt and Xenon, Łódź, Poland, respectively. They were purified by the method described previously (21). Their densities at 20°C were 0.8740 g/cm^3 and 1.0337 g/cm^3, respectively. Carbon tetrachloride for spectroscopy made by Chemapol, Prague, Czechoslovakia was dried over P_2O_5. Hexane for spectroscopy UCB, Bruxelles, Belgium was dried over $MgSO_4$. Methanol for spectroscopy made by Chemapol, Prague, was used.

Ultraviolet spectra were measured with a VSU-2P spectrometer, Carl Zeiss, Jena. A hydrogen lamp was used as the source of uv light; measurements were taken every 1 nm. Series of solutions of various concentrations were

TABLE 1. Ultraviolet spectra: the intensity* and the wavelength of the $n_a \rightarrow \pi^*$ band

	Compound	In hexane		In CCl_4		In methanol		In dioxane	
		λ_{max}	ε_{max}	λ_{max}	ε_{max}	λ_{max}	ε_{max}	λ_{max}	ε_{max}
1	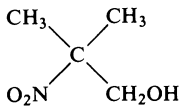	281.0	19	282	26.5	278	24.5	280	29.0
8	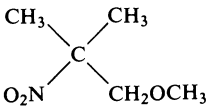	278.5	29	280	35.0	276	24.0	278	29.5
2–7	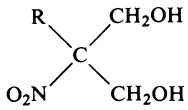	—	—	283	26.0	278	25.0	281.5	25.0

*Values of ε_{max} extrapolated to infinite dilution.

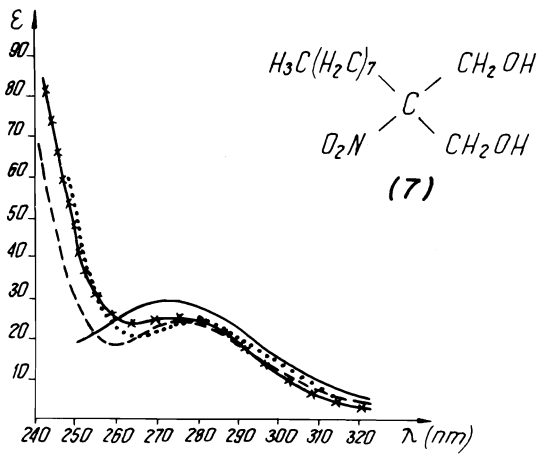

FIG. 1. Ultraviolet spectra of 2-octyl-2-nitropropane-1,3-diol (**7**): — in carbon tetrachloride, --- in methanol, ··· in dioxane, × × × in water.

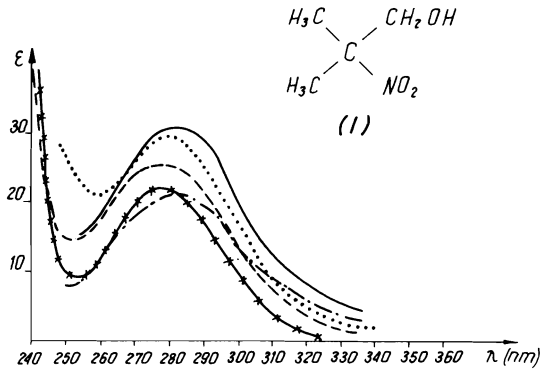

FIG. 2. Ultraviolet spectra of 2-methyl-2-nitropropane-1-ol (**1**): — in carbon tetrachloride, -·- in hexane, --- in methanol, ··· in dioxane, × × × in water.

prepared for each compound and solvent. The results were extrapolated to infinite dilutions (Table 1). All extrapolations show plots of ε_{max} as linear functions of concentrations with extrapolation to zero concentrations. The compound **8** does not show change of ε_{max} with the concentration. All other compounds show a fall of ε_{max} with decreasing concentration. The fall of ε_{max} is particularly prominent in diols (**2–7**), in non-polar solvents. The slope of the linear dependence of ε_{max} on concentration is 0.3640–0.4663 for diols in non-polar solvents. Typical absorption curves of diols and monols are presented in Figs. 1 and 2, respectively. The ether **8** gave a curve similar to that of the monol (Fig. 2).

Infrared spectra were taken with a Perkin-Elmer PE-577 spectrometer in cells of NaCl in the region of $\nu_{s(OH)}$. Solutions in carbon tetrachloride were made to concentrations 0.005–0.003 mol/ℓ. Sharp peaks, broader peaks, and shoulders could be determined to the accuracy of ± 1 cm^{-1}, ± 2 cm^{-1}, and ± 4 cm^{-1}, respectively. The data are collected in Table 2 and the typical absorption spectra at different concentrations are given in Figs. 3 and 4.

Nuclear magnetic resonance spectra were determined with a 100 MHz JEOL spectrometer in carbon tetrachloride using tetramethylsilane as internal reference. Solutions of various concentrations were the same as used in infrared spectroscopy. Values of frequencies were taken from the frequency meter with an accuracy of ± 0.05 Hz. The values of chemical shifts of OH protons were extrapolated to infinitive dilution by the method of least squares. The accuracy of the chemical shift measurements was of the order of 0.3 Hz. The data are collected in Table 2, some parts of the spectra are shown in Figs. 5, 6 and a diagram of the extrapolation of δ for compound **1** at various temperatures in Fig. 7. Similar linear dependence of δ on concentration were observed with compounds **2–7**. The spectral parameters were obtained from the experimental transitions using the iterative procedure of the LAOCOON program (22).

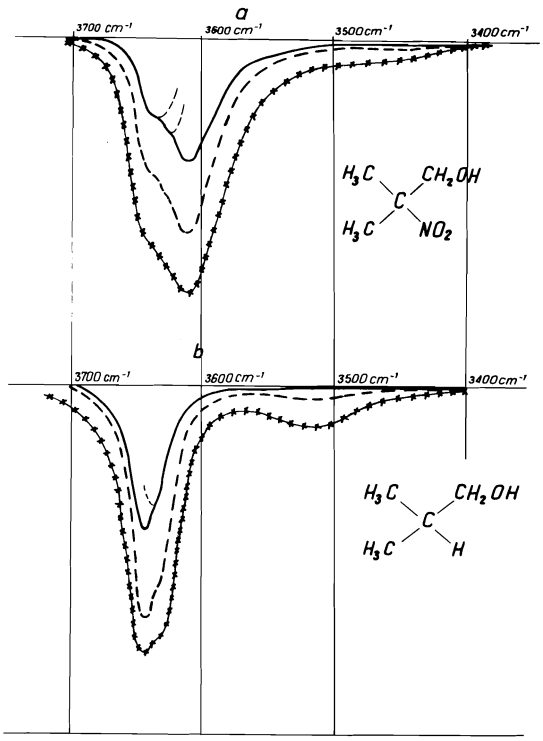

FIG. 3. Infrared spectra of 2-methyl-2-nitropropane-1-ol (**1**) and 2-methylpropane-1-ol in the $\nu_{S(OH)}$ regions; $d = 1$ cm. (*a*) — $c = 0.00428$ mol/ℓ, --- $c = 0.00925$ mol/ℓ, × × × $c = 0.0180$ mol/ℓ; (*b*) — $c = 0.00540$ mol/ℓ, --- $c = 0.01650$ mol/ℓ, × × × $c = 0.0256$ mol/ℓ.

Discussion

Ultraviolet Spectra

The previous finding (2, 6) on the shape of the curves of nitroalcohols in aqueous solutions is now confirmed: diols **2** to **7** do not show definite maxima (Fig. 1) but only well pronounced shoulders. On the contrary, the monol (**1**) (Fig. 2) shows a maximum. The spectra of the aqueous solution of its methyl ether (**7**) could not be taken owing to a very low solubility of the substance in water.

The molar absorption coefficients of the maxima in ethanol are approximately the same for all the compounds. The molar absorption coefficients for 2-methyl-2-nitropropane-1-ol (**1**) and its methyl ether (**7**) in dioxane are equal. If the hydrogen bond in this nitroalcohol exists, it seems to be weak and readily broken by dioxane and hence the shape of the absorption of both compounds is identical.

The absorption of nitrodiols (**2–7**) in dioxane is much lower compared to that of **1** and **8**, and approximately equal to the absorption of nitrodiols in methanol. No change in the intensity of the $n_a \rightarrow \pi^*$ absorption band in the spectra of these nitrodiols measured in CCl_4 and dioxane were observed. In carbon tetrachloride the absorption coefficients of nitrodiols (**2–7**) and of monol (**1**) were equal. Considerable weakness of the absorption band in the spectra of the 2-methyl-2-nitropropane-1-ol (**1**) and nitrodiols (**2–7**) in carbon tetrachloride as compared to that of the methyl ether (**8**) of 2-methyl-2-nitropropane-1-ol were observed. A comparison of the spectra of **1** and **8** in hexane also shows the weakness of the $n_a \rightarrow \pi^*$ absorption band of the alcohol **1**.

The presence of hydroxyl groups causes a bathochromic shift of the absorption band as compared to the spectra of the ether **8**. For all compounds examined we observed the following influence of the solvent on the wavelength of the $n_a \rightarrow \pi^*$ absorption band:

$$\lambda_{Methanol} < \lambda_{Dioxane} < \lambda_{Hexane} < \lambda_{CCl_4}$$

The change of the absorption coefficients of **1**

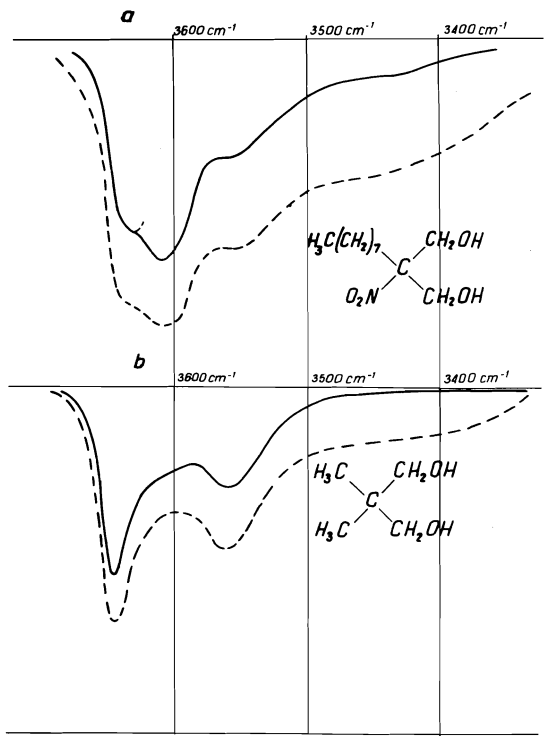

FIG. 4. Infrared spectra of 2-octyl-2-nitropropane-1,3-diol (**7**) and 2,2,-dimethylpropane-1,3-diol (**10**) in the $\nu_{S(OH)}$ regions; $d = 1$ cm. (*a*) — $c = 0.00563$ mol/ℓ, --- $c = 0.01150$ mol/ℓ; (*b*) — $c = 0.00570$ mol/ℓ, --- $c = 0.01350$ mol/ℓ.

TABLE 2. Infrared and nmr spectra: wave numbers $\nu_{s(OH)}$ and proton chemical shift $\delta_{(OH)}$

	Compound	Chemical shift* $\delta_{(OH)}$ (ppm) in TMS	Infrared wave numbers $\nu_{s(OH)}$ monomeric (cm^{-1})	
			Free	Bonded, intramolecular hydrogen bond
1	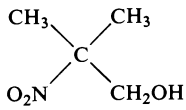	1.990	3640 sh 3632 sh	3612 —NO_2...HO—
2–7	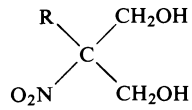	1.995	3636 sh	3606 —NO_2...HO— 3560 —OH....OH
9	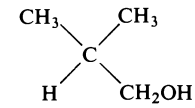	0.600 0.5–0.8†	3646 3636 sh	— —
10	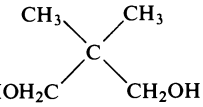	1.56	3642	3550

*Values of $\delta_{(OH)}$ extrapolated to infinite dilution.
†Values of $\delta_{(OH)}$ for primary alcohols, obtained by other authors (25).

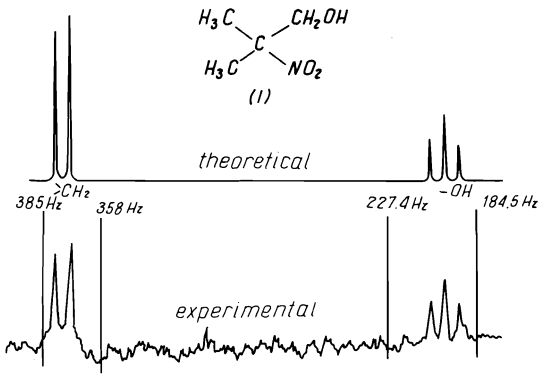

FIG. 5. Part of the nmr spectrum (experimental and theoretical) of 2-methyl-nitropropane-1-ol (**1**). c = 0.008 mol/ℓ; temperature +32°C. $\delta(1)$ = 376.42 Hz, $J(1,2)$ = 0.00 Hz; $\delta(2)$ = 376.42 Hz, $J(1,3)$ = 7.23 Hz; $\delta(3)$ = 200.00 Hz, $J(2,3)$ = 7.23 Hz.

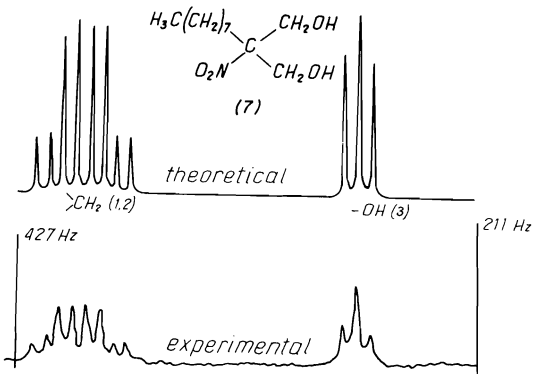

FIG. 6. Part of the nmr spectrum (experimental and theoretical) of 2-octyl-2-nitropropane-1,3-diol (**7**); c = 0.020 mol/ℓ, temperature +32°C. $\delta(1)$ = 408.00 Hz, $J(1,2)$ = −12.54 Hz; $\delta(2)$ = 385.38 Hz, $J(1,3)$ = +6.96 Hz; $\delta(3)$ = 230.50 Hz, $J(2,3)$ = +6.51 Hz.

and **8** with dilution gives an insight into the possible influence of the solvent upon the internal hydrogen bond. It seems that in polar solvents such as methanol and dioxane, the bond is broken whereas in non-polar solvents (carbon tetrachloride and hexane) the bond exists. This is particularly evident when comparing the ε_{max} values of the alcohol **1** with that of its ether **8**.

As noted above, the decrease of ε_{max} with dilution was particularly prominent in diols, when carbon tetrachloride and dioxane were used, whereas in methanol and water the decrease was less pronounced. This was probably due to a

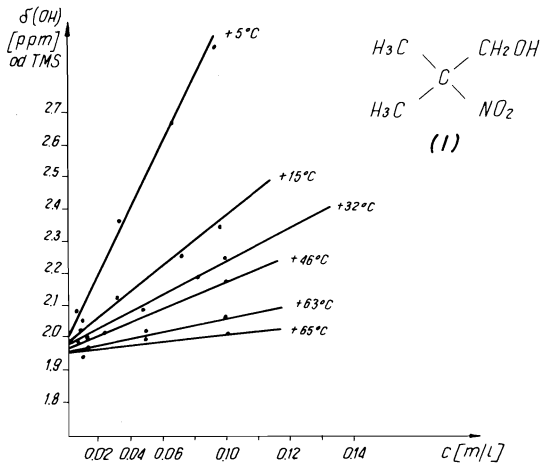

FIG. 7. Extrapolation of $\delta_{(OH)}$ of 2-methyl-2-nitropropane-1-ol (**1**) to infinite dilution at various temperatures.

competition between the intermolecular hydrogen bond in these solvents and the solute containing hydroxylic groups.

Infrared Spectra

All alcohols examined in solution show a band and a shoulder at frequencies between 3646 and 3628 cm^{-1}. This is in agreement with the fact already recorded in the literature for *all* primary and secondary alcohols in solutions with the exception of methanol. It is assigned to the existence of *two conformers* with "free" unbonded OH groups (23, 24).

With regard to the infrared spectra of β-nitroalcohols the existing data (4, 7, 9–16) are not fully consistent, although most of the authors admit the presence of the intramolecular hydrogen bond between the nitro and hydroxylic groups. Various conformations seem to be stabilized by internal hydrogen bonds as pointed out by Schleyer and co-workers (11) and Giguère and Tokiji (14).

Two series of experiments were carried out to elucidate the role played by the nitro group in the formation of the hydrogen bond: (*1*) Comparative examination of spectra of 2-methylpropane-1-ol (**9**) and its derivative containing the nitro group (**1**). (*2*) Examination of spectra of the diol (**10**) and its derivatives and homologues with a nitro group (**2** to **7**).

The spectrum of 2-methylpropane-1-ol shows a maximum at 3646 cm^{-1}, a shoulder at 3636 cm^{-1}, and a broad, low intensity band at 3520 cm^{-1} which disappeared on dilution. The latter is due to OH groups bonded through intermolecular hydrogen bonds. The former are two bands which should be assigned to two conformers of the monomer. The 2-nitroderivative (**1**) shows a main peak at 3612 cm^{-1} and two shoulders: 3640 and 3632 cm^{-1}. The former is probably produced by the OH group internally bonded to the NO_2 group and the latter by "free" (unbonded) OH groups. Both shoulders should be assigned to two conformers in agreement with existing views. An equilibrium is suggested between "bonded" and "unbonded" forms as shown on Scheme 1.

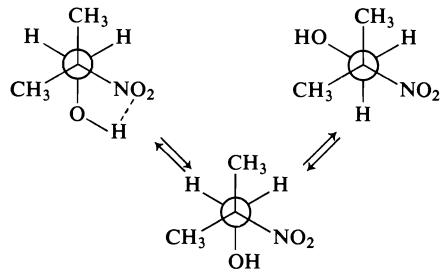

SCHEME 1

Comparison of the spectra of the diols gives a clearer picture. In Fig. 4 the difference can be seen in the spectra produced by the presence of the nitro group. Diol (**10**) shows two maxima 3642 and 3550 cm^{-1}, whereas all diols with the nitro group (**2–7**) give two maxima: at 3606 and 3560 cm^{-1} and a shoulder at 3636 cm^{-1}. The maxima at about 3550 cm^{-1} are clearly due to the internal hydrogen bonds between two OH groups, whereas the main peak at 3642 cm^{-1} and the shoulder at 3636 cm^{-1} in spectra of diol (**10**) and nitrodiols (**2–7**) respectively, are most likely produced by "free" (unbonded) OH groups. Consequently a broad maximum at 3606 cm^{-1} in (**2–7**) should be assigned to the hydroxyls bonded with the nitro group (Scheme 2).

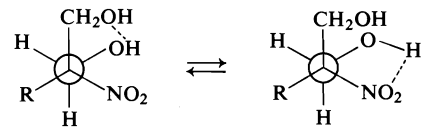

SCHEME 2

We did not examine the bands of the nitro group. It was shown earlier (4) that the frequencies of the nitro group are unchanged under the action of hydrogen bonds.

Nuclear Magnetic Resonance Spectra

There is a rather prominent influence of the presence of the NO_2 group in alcohols on the

chemical shift. The chemical shifts (δ) of protons of the hydroxyl groups of monohydroxylic alcohols and diol (**10**) are 0.5–0.8 and 1.56 ppm, respectively. The nitro group increases the value of $\delta_{(OH)}$ to 1.990 and 1.995 ppm in monohydroxylic nitroalcohols (**1**) and nitrodiols (**5–7**), respectively. This is in agreement with findings already published on the nmr spectra of nitrophenols (26–29) where the chemical shift of the OH proton was brought to considerably lower values of τ (ppm), *i.e.* higher values of δ (ppm) by virtue of the intramolecular hydrogen bond.

Acknowledgements

The authors are much indebted to Dr. M. Witanowski for a useful discussion of the nmr results and to Dr. P. Gluziński for his calculation of the theoretical nmr spectra.

1. S. Malinowski and T. Urbański. Rocz. Chem. **25**, 183 (1951).
2. T. Urbański. Bull. Acad. Pol. Sci. Cl. III, **1**, 239 (1953).
3. T. Urbański and D. Ciecierska. Rocz. Chem. **29**, 11 (1955).
4. T. Urbański. Bull. Acad. Pol. Sci. Cl. III, **4**, 87 (1976); **4**, 381 (1956); Rocz. Chem. **31**, 37 (1957).
5. H. Całus, H. Jankowska, H. Piotrowska, and T. Urbański. Chem. Ind. London, 1286 (1959).
6. T. Urbański. Tetrahedron, **6**, 1 (1959).
7. T. Urbański. *In* Hydrogen bonding (Symposium at Ljubliana, 1957). *Edited by* D. Hadži. Pergamon Press, Oxford. 1959. p. 143.
8. H. Lumbroso and D. Lauransan. Bull. Soc. Chim. Fr. 513 (1959).
9. H. E. Ungnade and L. W. Kissinger. Tetrahedron, **19**, Suppl. 121 (1963); H. E. Ungnade, E. D. Loughran, and L. W. Kissinger. J. Phys. Chem. **66**, 2643 (1962).
10. M. Kuhn, W. Lüttke, and R. Mecke. Z. Anal. Chem. **57**, 680 (1963).
11. W. F. Baitinger, P. von R. Schleyer, T. S. S. Murthy, and L. Robinson. Tetrahedron, **20**, 1634 (1964).
12. P. J. Krueger and H. D. Mettee. Can. J. Chem. **43**, 2888 (1965).
13. M. St. Flett. Spectrochim. Acta, **10**, 21 (1957).
14. P. A. Giguère and Kawamura Tokiji. Can. J. Chem. **49**, 3815 (1971).
15. A. O. Diallo. Spectrochim. Acta, **28**A, 1765 (1972).
16. C. N. R. Rao. *In* The chemistry of nitro and nitroso groups. Part I. *Edited by* H. Feuer. J. Wiley and Sons, London. 1969.
17. T. Urbański, E. Lipczyńska-Kochany, and W. Wacławek. Bull. Acad. Pol. Sci. In press.
18. T. Urbański and B. Chylińska. Rocz. Chem. **31**, 695 (1957).
19. P. E. Brumfield. Commercial Solvent Corp., Fr. Pat. 1,496,851 (1967); Chem. Abstr. **69**, 669000 (1968).
20. M. Apel and B. Tollens. Ber. **27**, 1088 (1894).
21. W. Wacławek, L. Skulski, B. Müller, and A. Szurowska. Bull. Acad. Pol. Sci. Sér. Sci. Chim. **17**, 321 (1969).
22. A. A. Bonner-By and S. Castellano. J. Chem. Phys. **41**, 3863 (1964).
23. (*a*) F. Dalton, G. D. Meakins, J. H. Robinson, and W. Zahara. J. Chem. Soc. 1566 (1962); (*b*) F. Dalton, G. D. Meakins, J. H. Robinson, and W. Zahara. J. Chem. Soc. 4068 (1963).
24. J. M. Bakke and G. B. Lorentzen. Acta Chem. Scand. B**28**, 650 (1974).
25. J. A. Pople. High resolution nuclear magnetic resonance. McGraw-Hill Book Company, New York. 1959.
26. L. W. Reeves. Can. J. Chem. **38**, 736 (1960).
27. L. W. Reeves, E. A. Allan, and K. O. Strømme. Can. J. Chem. **38**, 1249 (1960).
28. E. A. Allan and L. W. Reeves. J. Phys. Chem. **66**, 613 (1962).
29. U. Dabrowska, T. Urbański, W. Witanowski, and L. Stefaniak. Rocz. Chem. **38**, 1323 (1964).

3β-Azidoformate thermolysis as a method for functionalizing the 4α-methyl group of lanostan-3β-ol and similar systems[1]

PAUL FRANCIS ALEWOOD, MICHAEL BENN, AND JOHN WONG
Chemistry Department, The University of Calgary, Calgary, Alta., Canada T2N 1N4
AND
ALAN J. JONES
The National N.M.R. Centre, Australian National University, Canberra, A.C.T., Australia 2600

Received December 31, 1976

PAUL FRANCIS ALEWOOD, MICHAEL BENN, JOHN WONG, and ALAN J. JONES. Can. J. Chem. **55**, 2510 (1977).

Thermolyses of the azidoformate derivatives of 1,1,4a-trimethyl-*trans*-decalin-2β-ol, lanostanol-3β, and Δ^8-lanosten-3β-ol yield the perhydro-1,3-oxazin-2-one products of nitrene insertion into the adjacent α-oriented methyl groups, as well as oxazolidinones and ketones.

PAUL FRANCIS ALEWOOD, MICHAEL BENN, JOHN WONG et ALAN J. JONES. Can. J. Chem. **55**, 2510 (1977).

La thermolyse des dérivés azidoformates du triméthyl-1,1,4a décalinol-2β *trans*, du lanostanol-3β et du Δ^8-lanostenol-3β conduit à des produits perhydrooxazin-1,3 ones-2 provenant d'une insertion de nitrène dans les groupes méthyles adjacents orientés en α, ainsi qu'à des oxazolidinones et à des cétones.

[Traduit par le journal]

We describe here (1) the results of a study directed towards achieving the *in situ* functionalization of the 4α-methyl group in 4,4-dimethyl-3β-ol-5α-steroids, *i.e.* the transformation **1** → **2**.

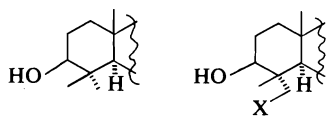

1 **2**

A reaction of this type is known to occur during the biosynthesis of cholesterol from lanosterol, where the oxidative removal of the geminal methyl groups from ring A involves an initial hydroxylation of the 4α-group (2). The same reaction is presumably also involved in the biosynthesis of such other triterpenes as 23-hydroxy betulin (3) from betulin, and hederagenin (4) from β-amyrin.

These biological oxidations might plausibly be considered to involve complexing of the substrate with a mixed-function oxidase through a 3β-hydroxy group – metal cation interaction, with the 4α-methyl group held in position for attack by an oxidant also complexed with the metal ion. However, some exploratory experiments directed along these lines, employing conditions similar to those recently described by Groves and van der Puy (5), were unpromising, so we decided to concentrate upon achieving the functionalization in a 'non-biological' way.

The bulk of functionalizations of 'remote', chemically unactivated sites have been achieved by intra-molecular[2] radical abstraction reactions: a radical is generated, abstracts a hydrogen atom from a geometrically favoured position, and thus produces a carbon radical which is functionalized in some trapping reaction (6).

The 3β-hydroxy function of **1** represents an obvious and attractive anchor-point for setting up a system to give an intramolecular attack on the C-4 methyls, but since the abstraction reactions are known to strongly favour attack on δ-located hydrogens (via a six-membered cyclic transition state) (6), this would require modification of **1** to set up a system like **3**.

We considered such possibilities, but were impressed by the observation that azidoformates could be decomposed thermally or photolytically to yield nitrenes, which could then un-

[1]A preliminary account of this work has been published in ref. 1*a*, and was presented, in part, at the 10th International Symposium on the Chemistry of Natural Products, IUPAC, Dunedin, N. Z., 1976. See also ref. 1*b*.

[2]Intermolecular radical abstraction reactions favour attack on tertiary sites and are thus in any case not suited to methyl group functionalization.

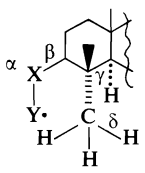

3

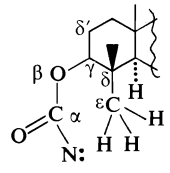

4

dergo intramolecular insertion reactions into accessible C_δ—H bonds to an extent that compared favourably with insertion into C_ε—H bonds. Indeed, as recounted earlier (7), we found that we could establish conditions for the thermolysis of acyclic azidoformates in which the yields of the tetrahydro-1,3-oxazin-2-ones (ε-insertion products) exceeded those of the oxazolidin-2-ones (δ-insertion products). Thus it appeared reasonable to expect the nitrene **4** to yield products arising from insertion into the methyl groups, as well as into the C(2)—H bonds (δ′-insertion). Furthermore it seemed likely that non-bonded interactions should disfavour conformations leading to attack on the 4β-methyl group (*cf.* **5** *vs.* **6**), and similarly (though less clearly) that insertion into the equatorial $C_{2\alpha}$—H bond should be preferred over the axial $C_{2\beta}$—H.

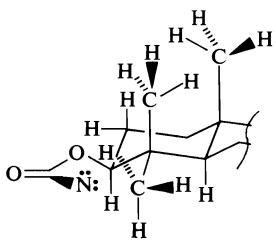

5

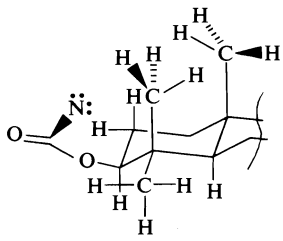

6

These considerations, together with the attractiveness of the ready preparation of azidoformates from alcohols via the corresponding chloroformates, induced us to investigate the thermolysis of **1**-azidoformates as a route to 4α-methyl functionalized products.

Thermolysis of 1,1,4a-trimethyl-*trans*-decalin-2β-yl azidoformate (**7**) in carbon tetrachloride, followed by column chromatography, yielded a trace of the carbamate **8**, some ketone (**9**), and two other products (homogeneous by tlc analysis) *A* and *B* which were identified as the oxazolidinone **10** and the tetrahydro-1,3-oxazin-2-one **11** on the basis of the following evidence.

The mass spectra of both compounds revealed an apparent molecular ion at *m/e* 237 amu which was proven to have composition $C_{14}H_{23}NO_2$ by high-resolution mass measurements. Among the differences in their mass spectra, that of *A* contained a prominent ion at *m/e* 178 amu, corresponding to the loss of $CHNO_2$, while instead of this in the spectrum of *B* there was an ion at 164 amu corresponding to the loss of $C_2H_3NO_2$. The infrared spectrum of *A* contained a strong absorption at 1750 cm^{-1}, while

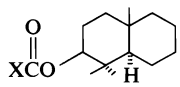

7 X = N_3
8 X = NH_2

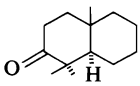

9

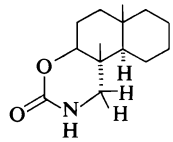

11

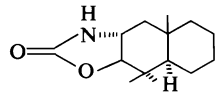

10

for *B* this appeared at 1700 cm^{-1}; and the ^{1}Hmr spectrum of *A* contained signals for three methyl groups, while that for *B* had only two. Thus we concluded that *A* was **10** and *B* was **11**. The ^{13}Cmr and 270 MHz ^{1}Hmr evidence which substantiated these conclusions and provided proof for the 4α-methyl functionalization, as well as the stereochemistry of the oxazolidinone – ring A fusion, is described below.

Similarly we thermolyzed lanostan-3β-yl azidoformate (**12**) and lanost-8-en-3β-yl azidoformate (**13**) and obtained from them products whose mass, infrared, and 100 MHz ^{1}Hmr spectra were consistent with their formulation as oxazolidin-2-ones (**14** and **16**) and tetrahydro-1,3-oxazin-2-ones (**15** and **17**). The 3-ketones analogous to **10** were also usually obtained, a matter to which we return later.

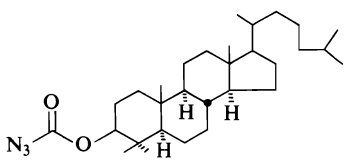

12
13 (Δ^8-**12**)

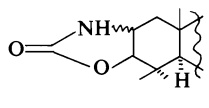

14
16 (Δ^8-**14**)

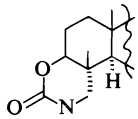

15
17 (Δ^8-**15**)

TABLE 1. ^{13}C chemical shifts in selected decalin and lanostanol derivatives

Carbon position	1,1,4a-Trimethyl-*trans*-decalin-2β-ol[a]	**10**[a]	**11**[a]	3β-Lanostanol	**12**	**14**	**15**
C-1	39.8_4	43.6_1	38.9_5	37.2_2	36.7_6	41.4_5	36.5_2
C-2	27.3_5	53.1_1	23.0_6	27.3_7	23.6_3	52.0_0	23.0_6
C-3	78.5_7	91.4_3	81.8_9	78.3_5	85.7_4	91.1_3	81.7_8
C-4	38.4_1	(36.5_2)	33.9_5	36.7_9	36.6_5	36.7_1	34.0_4
C-5	52.1_9	51.6_8	50.4_9	54.5_1	54.5_6	55.3_2	52.7_6
C-6	21.3_9	20.5_0	21.3_1	19.9_0	19.9_0	20.2_6	19.9_7
C-7	21.5_0	20.9_3	21.4_7	28.6_7	28.4_8	28.3_2	28.1_8
C-8	27.2_6	28.8_6	26.6_5	38.2_4	38.2_2	37.9_5	38.1_6
C-9	44.8_0	43.9_4	44.3_7	48.1_7	48.0_6	48.0_4	48.0_1
C-10	33.8_2	(36.0_0)	33.6_6	38.5_7	37.7_9	39.1_1	36.7_3
C-11	—	—	—	21.4_1	21.2_0	20.5_2	21.4_7
C-12	—	—	—	33.2_8	33.2_6	33.1_5	33.2_6
C-13	—	—	—	44.8_1	44.8_1	44.8_1	44.6_9
C-14	—	—	—	47.4_7	47.4_1	47.4_1	47.3_3
C-15	—	—	—	31.8_3	31.7_7	31.6_9	31.5_8
C-16	—	—	—	27.7_0	27.7_3	27.7_3	27.5_9
C-17	—	—	—	50.4_9	50.5_0	50.4_6	50.4_4
C-18	—	—	—	14.2_1	14.2_1	15.7_0	13.9_7
C-19	18.9_9	20.2_6	19.4_5	16.1_0	16.1_0	16.0_7	14.1_6
C-20	—	—	—	35.8_2	35.8_2	35.7_9	35.7_9
C-21	—	—	—	18.5_0	18.4_8	18.4_5	18.4_5
C-22	—	—	—	36.2_5	36.2_5	36.1_9	36.1_9
C-23	—	—	—	23.8_7	23.8_7	23.8_4	23.8_4
C-24	—	—	—	39.1_6	39.1_3	39.1_1	39.1_1
C-25	—	—	—	27.7_0	27.7_3	27.7_3	27.7_0
C-26	—	—	—	22.6_3	22.6_0	22.6_3	22.6_0
C-27	—	—	—	22.3_3	22.3_3	22.3_3	22.3_0
C-28	—	—	—	15.4_8	16.4_0	16.3_7	16.0_7
C-29	27.3_5	27.2_4	53.8_3	27.9_4	27.8_3	27.7_3	54.1_0
C-30	14.8_9	15.8_3	11.8_7	13.7_6	13.7_8	14.2_8	12.4_3
C=O	—	159.8_3	153.2_8	—	155.7_0	159.8_0	153.2_4

[a]The numbering system employed for these compounds in this table is analogous to that conventionally used for triterpenes.

In order to check these assignments and, in particular, to attempt to determine which methyl group has been functionalized, we turned to ^{13}Cmr (^{13}C magnetic resonance) investigations. The ^{13}C chemical shifts of 1,1,4α-trimethyl-*trans*-decalin-2β-ol, lanostan-3β-ol, and the compounds **10–12**, **14**, and **15** are given in Table 1. *Note that for the convenience of presentation in the table and intercomparison between the decalin and triterpenoid derivatives we have, in this table, numbered the carbon sites in the decalins to correspond with those of the analogous sites in the triterpenes.* The chemical shifts of lanostan-3β-ol have been assigned previously, though in the recent literature some uncertainty in the assignments given for the carbon atoms C-5 and C-9 and C-12, C-15, and C-16 has been implied (8–10). In the present work we have established the assignment of the carbons C-5 and C-9 and have followed the assignments recently determined by Lukacs and co-workers (9) for the carbons C-12, C-15 and C-16 in a series of cycloartenol derivatives in which simple monosubstituent effects facilitated identification. A variety of conventional techniques were used to assign individual carbon atoms to specific resonances in all the compounds studied, including gated decoupling (11) and modulated off-resonance (12) methods and chemical shift additivity relationships (8–10, 13) as particularly applied to structurally related compounds. The chemical shifts of some of the methyl groups (excluding C-29 and C-30) must remain tentative, though we have followed the order established by Knight (8) for these carbon atoms.

The methyl ^{13}C chemical shifts in 1,1,4α-trimethyl-*trans*-decalin-2β-ol and **10** help characterize the assignments in the more complex triterpenes. That is, the shift of the axial methyl group (C-30 ≡ 4β-CH_3) (14.5 ± 1 ppm) is

13 ppm to high field of the equatorial methyl group (C-29 ≡ 4α-CH_3) (27.6 ± 0.4 ppm), the consequence of the well-characterized 1,3-*syn*-axial or γ-steric effect (14). This shift difference was recently used most effectively in revising the structure of the related tetracyclic triterpenoid *Buxus* alkaloids (15). The methyl group functionalization in the oxazinones **11** and **15** is established by the observation that the equatorial C-29 resonance shifts to 54 ± 0.4 ppm now representing a substituted methylene group, while the slightly high field of the axial C-30 methyl carbon (12 ppm ± 0.4) is attributable to steric effects in both of these compounds. The *trans*-stereochemistry of the junction of the heterocyclic and A rings in **11** and **15** is also established by the high field shift (compared to the corresponding alcohols) of the C-4 carbon, −4.5 and −2.7 ppm, respectively, in these compounds (15). The γ-effect (−1.7 ppm) observed at C-5 in **11**, and **15** (−2.8 ppm) not only indicates substitution at the 4α-methyl site, but also confirms the assignment of the carbon C-5 in contrast to C-9 (8–10) in the triterpenoid systems. Note that formation of the tetrahydrooxazinone ring is also characterized by the down-field shift (3.4 ppm) at C-3 in both **11** and **15**.

The oxazolidinone structures **10** and **14** were further supported by the typical ^{13}C substituent shifts (compared to the precursor alcohols) at the α-carbon C-2 (25 ppm) and the β-carbons C-1 and C-3 (4 and 12.8 ppm).[3] The α-shift resembles that resulting from *exo*-amino substitution in norbornane (25.3 ppm) (16), but differs from that in the corresponding *endo*-derivative (23.3 ppm) (16). It is tempting to use this data to invoke the *trans*-stereochemistry at the junction of the heterocyclic and A rings. Particularly since if the alternative *cis*-stereochemistry were adopted, large γ-shieldings would be expected at C-4 and C-10 (*cf.* ref. 17): no such shifts are observed. Fortunately we did not need to rely on this argument for analysis of the 270 MHz proton spectrum of the oxazolidinone **10** established the *trans*-stereochemistry of the ring fusion: the H-3 proton signal exhibited a typical ABXX′ pattern at 3.82 ppm. Equivalent *trans*-couplings (10.8 Hz) (18) with the axial H-2 and H-4 protons, and a smaller *cis*-coupling (3.4 Hz) with the equatorial H-4 proton, give rise to this pattern. The magnitude of the coupling between H-3 and H-2 thus indicates the *trans*-stereochemistry of this oxazolidinone. Unfortunately, in the case of **14** and **16** overlapping C-2 and C-3 proton signals could not be resolved, even at 270 MHz, and thus our tentative assignment of a *trans* ring fusion of the heterocyclic system in these compounds rested on the assumption that it would be as in **10**. Vindication of this has been provided by a recent publication describing studies similar to ours in which chemical evidence was provided which established the *trans*-ring fusion in **16** (19).[4]

An aspect of the reaction which, in our hands, proved to be poorly reproducible, was the formation of ketonic side products. (In some thermolyses of lanostenyl azidoformate considerable amounts of the 3-ketone were formed while in other runs we did not obtain this compound.) Such by-products have not been commonly noted in the thermolysis or photolysis of azidoformates, perhaps because in simple alkyl systems the nitrogen-free carbonyl products are sufficiently volatile and non-polar to have escaped notice.

Interestingly Edwards and Paryzek observed ketone formation in the thermolysis of steroidal 7α- and 7β-azidoformates (20), and although Hora reported only carbamate arising from insertion into cyclohexane solvent when 3β-acetoxy-5-androsten-17β-yl azidoformate was photolyzed (21), we have found thermolysis of this substrate in methylene chloride to give substantial yields of the 17-one (together with products arising from intra-molecular nitrene cyclization).

It might be postulated that the ketones arise from fragmentation of the azidoformates or the nitrenes formed from them (20). We noted that in reactions where the ketones were formed in appreciable amount there was invariably accompanying formation of a high (but indistinctly) melting solid, insoluble in the thermolysis solvent, the infrared spectrum of which closely resembled that of cyanuric acid. We therefore write the reaction as one involving HNCO loss from the alkoxycarbonyl nitrene. A plausible

[3]A referee comments that the large downfield shift of C-3 in **10** (12.9 ppm) and **14** (12.8 ppm) resulting from two β-shifts is also diagnostic of the ring size.

[4]Since this paper was submitted for publication a report of the thermolysis of **7** has appeared (23). The conclusions were similar to ours, and confirmation of the structures of **10** (and **11**) was very nicely provided by chemical synthesis.

alternative is elimination of HNCO from an intermediate alkoxyisocyanate (19).

Conclusions

The thermolysis of the azidoformate derivatives of systems such as **1** provides a means for functionalizing the adjacent equatorial methyl group. In the steroid–triterpene field this procedure seems to complement the nitroxide photolysis procedure recently shown to functionalize the 4β-methyl group (21). It is clear that ^{13}Cmr spectroscopy provides the most facile route for establishing the stereochemistry of these reactions.

Experimental

Melting and boiling points are uncorrected. The proton magnetic resonance spectra were measured on 100 and 270 MHz instruments and chemical shifts are reported on the δ (ppm) scale downfield from an internal tetramethylsilane reference. Standard abbreviations are used to describe signal multiplicities. ^{13}C magnetic resonance spectra were measured on a Bruker HFX-270 instrument at 67.89 MHz in the Fourier mode and are similarly described.

All thin layer chromatography was performed on 0.2 mm thick Silica Gel G, with iodine vapour for spot detection. The solvent systems employed are as specified.

1,1,4α-Trimethyl-trans-decalin-2β-ol Chloroformate

A solution of 1,1,4α-trimethyl-*trans*-decalin-2β-ol[5] (3.09 g) in toluene (100 ml) containing pyridine (5.0 ml) was added dropwise over 1 h to an ice-cold solution of phosgene in toluene (100 ml of a 20% w/v solution). The reaction mixture was allowed to warm to room temperature and after 20 h was then shaken with ice water. The organic phase was separated, dried ($MgSO_4$), and the solvent removed under reduced pressure to yield a colourless oil (3.51 g, 90%), ν_{max} (film) 1770 cm^{-1}, and no OH stretch absorption. This material was immediately used for the preparation of the azidoformate.

1,1,4a-Trimethyl-trans-decalin-2β-yl Azidoformate

Dimethylformamide (200 ml) containing sodium azide (4.0 g) and the chloroformate from above was stirred magnetically and heated to 60°C. After 4 h the reaction mixture was diluted with cold water (400 ml) and extracted with diethyl ether (3 × 150 ml). The combined ether extracts were washed with water (5 × 100 ml) and then dried ($MgSO_4$). Removal of solvent left a residual light yellow oil (3.48 g), which crystallized on storage at 0°C. This material had mp 53–55°C, and was homogeneous by tlc (benzene–chloroform 2:1 v/v, R_F 0.60), ν_{max} (film) 2180, 2130, 1750, 1725, 1395, 1370, 1230, 980, and 750 cm^{-1}; δ ($CDCl_3$) 0.86 (3H, s), 0.93 (3H, s), 0.98 (3H, s), 1.0–2.0 (13H, br m), 4.52 (1H, dd, J_1 = 6.5 Hz, J_2 = 8 Hz); *cf.* data for **7** in ref. 23.

[5]This alcohol was prepared from 1,1,4a-trimethyl-Δ^8-2-decalone (22) by sequential reduction with sodium borohydride in 2-propanol and catalytic hydrogenation in ethanol over 10% palladium-on-charcoal.

Thermolysis of the Azidoformate (7)

A solution of the azidoformate **7** (1.02 g), in carbon tetrachloride (100 ml) under an atmosphere of nitrogen, was heated at 120°C in a thick-walled sealed tube for 24 h. Removal of solvent left a light yellow oil, $\nu_{max}(CCl_4)$ 3430, 3250, 1770 sh, 1755, 1710; tlc (diethyl ether) revealed six components R_F 0.1–0.8.

The mixture was chromatographed on silica gel (Merck for column chromatography) in ether and collected as *ca.* 5 ml fractions every 15 min. The individual fractions were evaporated, analyzed by tlc, and grouped accordingly. By this means six fractions were obtained. Fraction I (tubes 7 and 8) (79 mg) was a nearly colourless oil; R_F 0.68; >95% one component by glc; ν_{max} (film) 1700 cm^{-1}; δ 0.96 (3H, s), 1.01 (3H, s), 1.06 (3H, s); *m/e* 194 (70) ($M^{+\cdot}$), 137(45), 123(20), 109(90), 108(100) amu, all consistent with this being 1,1,4α-trimethyl-*trans*-decalin-2-one, from which it was indistinguishable by glc analysis.

Fraction II (tubes 13 and 14) (25 mg); mp 175–177°C; R_F 0.47; ν_{max} (KBr) 3540, 3430, 1715, 1245, 1050 cm^{-1}; δ 0.80 (3H, s), 0.88 (3H, s), 0.93 (3H, s), 4.2–4.9 (*ca.* 3H, br); *m/e* 178(75) (M − 61), 163(100); consistent with this material being 1,1,4a-trimethyl-*trans*-decalin-2-yl carbamate (**8**), and it proved to be identical with an authentic specimen prepared by treating the chloroformate with ammonia.

Fraction III (tubes 16–22); 381 mg; mp 187–187.5°C; R_F 0.35; ν_{max} (KBr) 3440 and 1750 cm^{-1}; δ 0.93 (3H, s), 1.04 (3H, s), 1.08 (3H, s), 1.81 (1H, m), 3.37–4.0 (2H, m), and 6.24 (1H); *m/e* calcd. for $C_{14}H_{23}NO_2$: 237.1729 ($M^{+\cdot}$); found: 237.1725, consistent with this being the oxazolidinone **10**.[6]

Fraction IV (tubes 26–37); 55 mg; mp 205–210°C; R_F 0.26; ν_{max} (KBr) 3440 and 1750 cm^{-1}; *m/e* 237(15), 178(12), 161(10), and 150(100), was apparently a mixture and was not investigated further.

Fraction V (tubes 40–55); 25 mg; mp 138–145°C; R_F 0.16; ν_{max} (KBr) 3460, 1745, and 1030 cm^{-1}; δ 1.05 (3H, s), 1.09 (3H, s), 1.13 (3H, s), 4.0–4.5 (2H, m), and 5.58 (1H, s); *m/e* 237; consistent with this being an oxazolidinone, however, and it was not investigated further.

Fraction VI (tubes 64–88); 184 mg; mp 185–188°C; R_F 0.05; ν_{max} (KBr) 3450, and 1700 cm^{-1}; δ 0.96 (3H, s), 1.0 (3H, s), 2.75–3.15 (2H, J_{AB} = 11 Hz, J_{ANH} = 4 Hz, J_{BNH} = 0 Hz), 6.16 (1H, dd, $J_{2\alpha,3}$ = 6 Hz, $J_{2\beta,3}$ = 6 Hz) and 6.5 (1H, br); *m/e* calcd. for $C_{14}H_{23}NO_2$: 237.1729; found: 237.1727(45), 164(95), 149(100), all consistent[6] with this being the tetrahydro-1,3-oxazin-2-one (**11**).

Lanostan-3β-yl Chloroformate

A solution of lanostan-3β-ol (1.6 g) in benzene (65 ml) containing pyridine (2.5 ml) was added over 1 h to an ice-cold solution of phosgene (10 g) in benzene (80 ml), and the reaction mixture was stirred overnight. Work-up was essentially as described for the preparation of the decalin system, but extracting with benzene gave a crystalline product which was recrystallized from acetone to yield colourless needles, mp 129–131°C (1.44 g, 78%); homogeneous by tlc analysis, *m/e* calcd. for $C_{31}H_{53}{}^{35}ClO_2$: 492.3734; found: 492.3732.

[6]See discussion for further analysis of this data and the ^{13}Cmr spectrum.

*Lanostan-3β-yl Azidoformate (**12**)*

The chloroformate (1.17 g) was added to a stirred solution of sodium azide (1.17 g) in dry dimethylformamide (100 ml). Benzene (15 ml) was added to give a homogeneous solution. After 4 h the reaction mixture was cooled, diluted with water (500 ml), and worked-up as described for **7** (benzene rather than diethyl ether being used for the extractions) to yield a colourless crystalline solid, which was recrystallized from acetone to yield lanostan-3β-yl azido formate mp 135–136°C (1.06 g, 89%); homogeneous by tlc analysis; *m/e* calcd. for $C_{31}H_{53}N_3O_2$: 499.41377; found: 499.41367.

*Thermolysis of Azidoformate **12***

The azidoformate **12** (1.0 g) was dissolved in methylene chloride (100 ml, purified by passage through a silica gel column), and the solution was thermolyzed at 125°C overnight as described for **7**. Some solid had separated from solution and after evaporating the reaction mixture to small volume, this was collected by filtration. Further concentration of the filtrate then yielded a pale yellow solid residue (971 mg) shown by tlc (chloroform) to contain two major, and at least seven minor, products. This mixture was chromatographed on Woelm Alumina grade III, 16 cm × 2.5 cm). Benzene eluted crystalline material (119 mg); R_F 0.45; mp 130–131°C; ν_{max} (KBr) 1695 cm^{-1}; *m/e* 428. This product was initially identified as 3-lanostanone from its ir spectrum and this was confirmed by comparison (ir and glc) with authentic material.

Benzene – diethyl ether (9:1 and 4:1 v/v) next eluted crystalline material (305 mg), R_F 0.08. Recrystallization from methylene chloride – methanol gave material mp 283–285°C; ν_{max} (KBr) 3450, 1780, and 1755 cm^{-1}; 0.7–1.1 (8 methyl signals), 3.55 (2H, br m), and 5.8 (1H, br s); *m/e* calcd. for $C_{31}H_{53}NO_2$: 471.40763; found: 471.40756, all consistent[6] with structure **14**.

Diethyl ether alone and with methanol (2% v/v) eluted the final major product as a colourless solid (392 mg) which was, however, amorphous. Attempts to crystallize this material from a variety of solvents gave solutions which gelled upon cooling, the gel yielding colourless solid upon drying, homogeneous on tlc; R_F 0.78 (MeOH–$CHCl_3$, 1:4); ν_{max}(KBr) 3450, 1725, and 1700; 0.7–0.9 (7 methyl groups), 2.85 (2H, m), 2.85 (1H, br m), and 6.12 (1H, d, J = 2 Hz) (the signal at 3.85 was an AB quartet J_{AB} = 12 Hz, with the low field pair of lines showing a second coupling of 2 Hz; addition of D_2O removed the 6.12 signal and converted the 2.85 absorption to a clean AB quartet); *m/e* calcd. for $C_{31}H_{53}NO_2$: 471.40763; found: 471.40679. This data is consistent with this substance being the perhydro-1,3-oxazin-2-one (**15**).

*Lanost-8-en-3β-yl Azidoformate (**13**)*

This compound was prepared from lanost-8(9)-en-3β-ol, via the chloroformate (mp 125–126°C) and obtained in 80% yield as a colourless crystalline solid mp 105–106°C (from methanol), ν_{max}(Nujol) 2200, 2140, 1740, and 1240 cm^{-1}; *m/e* 497, 482, 411, 395 (base). *Anal.* calcd. for $C_{31}H_{51}N_3O_2$: C 74.70, H 10.42; found: C 74.87, H 10.41.

Thermolysis of Lanostenyl Azidoformate

A solution of **13** (905 mg) in methylene chloride (120 ml) was thermolyzed in a sealed tube at 125°C/for 22 h. Removal of solvent left a pale yellow solid (845 mg) which was shown to contain at least four components by tlc analysis (benzene). Column chromatography on silica gel with benzene – ethyl acetate (4:1 v/v) as eluant yielded four substances.

The first (477 mg) was obtained as a crystalline solid mp 255–260°C (from methanol), ν_{max}($CHCl_3$) 3440 and 1755 cm^{-1}; *m/e* calcd. for $C_{31}H_{51}NO_2$: 469.3918; found: 469.3904; δ ($CDCl_3$) 0.8–1.20 (8 methyls), 3.7 (2H, br m), 5.3 (1H, br NH), all consistent[4] with this being the oxazolidinone **16**.

The second fraction (44 mg) was a colourless solid, mp 125–150°C, ν_{max}($CHCl_3$) 3440 and 1758 cm^{-1}, apparently impure oxazolidinone; while the third fraction (25 mg) similarly gave a colourless solid with an indistinct mp 140–150°C, ν_{max}($CHCl_3$) 3440, 1760, and 1705 cm^{-1} and was seemingly a mixture of oxazolidinone and tetrahydro-1,3-oxazinone. These materials were not investigated further.

The fourth fraction (140 mg) gave a colourless solid, mp 255–258°C, ν_{max}($CHCl_3$) 3440 and 1705 cm^{-1}; *m/e* calcd. for $C_{31}H_{51}NO_2$: 269.3918; found: 469.3909; δ 0.8–1.1 (7 methyl groups), 2.7–3.3 (2H, J_{gem} = 11 Hz, J_{He-NH} = 3 Hz), 3.85 (1H, dd, J = 7 and 3 Hz), 5.95 (NH, br, J = 3 Hz), all consistent[6] with this product being the tetrahydrooxazinone (**17**)

The Cyanuric Acid-like Side Product

In some thermolyses a highly insoluble white powder deposited on the walls of the sealed tube. This substance had mp > 300°C, essentially insoluble in water, ethanol, or chloroform, and had ν_{max}(KBr) 3450, 3420, 3330, 3150, 3050, 2730, 1720, 1650, and 1610 cm^{-1}, *m/e* 129(100) and 61(80) with no other major ions above 50 amu. Cyanuric acid (Eastman Chem. Co.) had a very similar but non-identical infrared, and mass spectrum.

Acknowledgements

This work was supported by an NRCC operating grant (to M.H.B.). Also, it is a pleasure to acknowledge helpful advice by Dr. O. E. Edwards of the Division of Biochemistry, NRCC, Ottawa.

1. (*a*) A. J. Jones, P. F. Alewood, M. Benn, and J. Wong. Tetrahedron Lett. 1655 (1976); (*b*) P. F. Alewood. Ph.D. Thesis, University of Calgary, Calgary, Alta. 1973.
2. R. Rahman, K. B. Sharpless, T. A. Spencer, and R. B. Clayton. J. Biol. Chem. **245**, 2667 (1970) and references therein.
3. W. Lawrie, J. MacLean, and G. R. Taylor. J. Chem. Soc. 4303 (1960).
4. J. Simonsen and W. C. J. Ross. The terpenes. Vol. 5. Cambridge University Press. 1957. p. 174.
5. J. T. Groves and M. van der Puy. J. Am. Chem. Soc. **96**, 5274 (1974).
6. K. Heusler and J. Kalvoda. Angew. Chem. Int. Ed. Engl. **3**, 525 (1964).
7. P. F. Alewood, M. Benn, and R. Reinfried. Can. J. Chem. **52**, 4083 (1974).
8. S. A. Knight. Tetrahedron Lett. 83 (1973); S. A. Knight. Org. Magn. Reson. **6**, 603 (1974).
9. G. Lukacs, F. Khuong-Huu, C. R. Bennett, B. L. Buckwalter, and E. Wenkert. Tetrahedron Lett. 3515 (1972); F. Khuong-Huu, M. Sangare, V. M.

CHARI, A. BAKAERT, M. DEVYS, M. BARBIER, and G. LUKACS. Tetrahedron Lett. 1787 (1975).
10. L. RADICS, M. KAJTAR-PEREDY, S. CORSANO, and L. STANDOLI. Tetrahedron Lett. 4287 (1975).
11. O. A. GANSOW and W. SCHITTENHELM. J. Am. Chem. Soc. **93**, 4294 (1971).
12. E. WENKERT, A. O. CLOUSE, D. W. COCHRAN, and D. DODDRELL. J. Am. Chem. Soc. **91**, 6879 (1969); A. J. JONES and M. H. BENN. Can. J. Chem. **51**, 486 (1973).
13. J. B. STOTHERS. Carbon-13 NMR spectroscopy. Academic Press, New York, NY. 1972.
14. A. J. JONES, C. P. BEEMAN, N. U. HASAN, A. F. CASY, and M. M. A. HASSAN. Can. J. Chem. **54**, 126 (1976) and references therein.
15. M. SANGARE, F. KHUONG-HUU, D. HERLEM, A. MILLIET, B. SEPTE, G. BERENGER, and G. LUKACS. Tetrahedron Lett. 1791 (1975).
16. J. B. GRUTZNER, M. JAUTELAT, J. B. DENCE, R. A. SMITH, and J. D. ROBERTS. J. Am. Chem. Soc. **92**, 7107 (1970).
17. S. H. GROVER and J. B. STOTHERS. Can. J. Chem. **52**, 870 (1974).
18. L. M. JACKMAN and S. STERNHELL. Applications of NMR spectroscopy in organic chemistry. Pergamon, Oxford. 1969.
19. J. J. WRIGHT and J. B. MORTON. J. Chem. Soc. Chem. Commun. 668 (1976).
20. O. E. EDWARDS and Z. PARYZEK. Can. J. Chem. **51**, 3866 (1973).
21. J. HORA. Coll. Czech. Chem. Commun. **29**, 1079 (1964).
22. Y. M. YANAGITA, M. HIRAKURA, and F. SEKI. J. Org. Chem. **23**, 841 (1958).
23. M. R. CZARNY, B. W. BENSON, and T. A. SPENCER. J. Org. Chem. **42**, 556 (1977).

Luminescence différée d'une solution organique vitreuse photoactivée et transition vitreuse

D. CECCALDI

Laboratoire de Physico-chimie des Rayonnements, associé au CNRS, Université de Paris-Sud, centre d'Orsay, 91 Orsay, France

Reçu le 17 juin 1976[1]

D. CECCALDI. Can. J. Chem. **55**, 2517 (1977).

Une théorie cinétique générale est utilisée pour interpréter la réponse d'un système luminescent à des sauts thermiques rapides ($\Delta T \sim 1$ K, $\Delta t \sim 1$ s). Les systèmes luminescents étudiés sont des solutions organiques vitreuses photoactivées de TMPD/MCH 10^{-3} *M* et TMPD/3-MP 10^{-3} *M*. L'étude est faite dans un domaine de température (63–91 K) situé de part et d'autre de la transition vitreuse. On montre qu'il y a diffusion lente des électrons piégés vers le cation et compétition entre dépiégeage thermique et dépiégeage par effet tunnel. La proportion d'effet tunnel Y est indépendante du temps au cours d'une cinétique de luminescence isotherme et dépend peu de la température lorsque $T \leq T_y$; T_y est très proche de la température de transition vitreuse. Pour $T > T_y$, Y décroit rapidement. L'énergie d'activation du dépiégeage thermique passe par un maximum à $T_m \simeq T_g$. On peut définir la température de transition vitreuse par:

$$T_g = \tfrac{1}{2}(T_y + T_m) \quad (\simeq T_y \simeq T_m)$$

Enfin on mesure un temps τ de relaxation de la matrice vitreuse. τ décroit avec la température.

D. CECCALDI. Can. J. Chem. **55**, 2517 (1977).

A general kinetic theory is used to explain the shapes of photoionized sample luminescence curves perturbed by thermal jumps ($\Delta T \sim 1$ K, rise time ~ 1 s). The samples studied are photoactivated organic vitreous solutions of TMPD/MCH 10^{-3} *M* and TMPD/3-MP 10^{-3} *M*. The experiments are performed within a temperature range (63–91 K) which includes the glass transition temperature T_g. It is shown that there is a slow diffusion of the trapped electrons towards the cation and competition between thermal detrapping and tunneling. The tunneling/thermal detrapping ratio Y is not time dependent during an isothermal luminescence and is only slowly temperature dependent if $T \leq T_y$. T_y is very close to T_g. For $T > T_y$, Y decreases rapidly with T. The activation energy for thermal detrapping shows a maximum when the temperature reaches $T_m \simeq T_g$. The glass transition temperature T_g may therefore be defined empirically as:

$$T_g = \tfrac{1}{2}(T_y + T_m) \quad (\simeq T_y \simeq T_m)$$

Finally we obtain a glassy matrix relaxation time, τ, which decreases with T.

Introduction

Dans un récent article (1), on a présenté une nouvelle méthode expérimentale pour étudier la luminescence de recombinaison électron–cation consécutive à la photoionisation d'une solution organique vitreuse. On applique, au cours de la luminescence isotherme (ITL), des sauts thermiques rapides ($\Delta T \sim 1$ K, $\Delta t \sim 1$ s) et on analyse la réponse du signal de luminescence à ces sauts thermiques en utilisant une théorie cinétique. Dans le cas du TMPD[2] piégé dans un verre de 3-MP[3] ou de MCH[4] à 77 K on a montré qu'il y a diffusion lente des électrons piégés vers le cation et compétition entre dépiégeage thermique et athermique (effet tunnel). On a mesuré l'énergie d'activation E du dépiégeage thermique et la proportion d'effet tunnel Y. La théorie cinétique permet en effet de montrer que, si on effectue un saut thermique rapide ΔT, la luminescence passe de I à I' et l'on a:

$$\frac{I'}{I} = \frac{\exp\left(\dfrac{\Delta T}{T}\dfrac{E}{kT}\right) + Y}{1 + Y}$$

Cette loi a été vérifiée expérimentalement en fonction de ΔT à 77 K. A cette température le verre est au point de transition vitreuse pour le 3-MP ($T_g = 77$ K) et en dessous de la transition vitreuse dans le cas du MCH ($T_g = 84$–89 K). Dans ce présent travail on poursuit cette étude

[1]Revision reçue le 21 mars 1977.

[2]TMPD = *N,N,N′,N′*-tétraméthyl *para*-phénylènediamine.

[3]3-MP = 3-méthylpentane.

[4]MCH = méthylcyclohéxane.

expérimentale en étendant la gamme de température de 63 à 91 K pour les verres de MCH et 3-MP. On explore donc un domaine de température de part et d'autre de la température de transition vitreuse (89 et 77 K) trouvée par calorimétrie (2, 3). On peut ainsi chercher à déterminer la variation de E et Y avec la température et à savoir s'il y a encore diffusion des électrons piégés. On peut aussi espérer caractériser la transition vitreuse comme par la mesure de la chaleur spécifique, du coefficient de dilatation thermique, du volume ou de la viscosité (4). On verra que ceci est possible et qu'on trouve aussi une méthode pour mesurer un temps τ de relaxation de la matrice vitreuse.

Rappels sur la théorie cinétique

On a défini précédemment (1) des états de configuration "j" pour l'ensemble "cation–électron piégé–solvant". L'ensemble évolue par une suite de transitions j–j'. Ces transitions sont des réarrangements moléculaires thermiques du solvant (avec en général diffusion de l'électron) ou des passages par effet tunnel de l'électron d'un site j à un site j' proche. On appelle $K_{jj'}$ la constante de vitesse correspondante. Pour chaque état j on a une vitesse de recombinaison avec le cation:

$$[1] \qquad k_j(T) = k_j{}^{\mathrm{th}}(T) + k_j{}^{\mathrm{tu}}$$

avec

$$[2] \qquad k_j{}^{\mathrm{th}}(T) = f_j(T)\exp(-E_j/kT)$$

(En général le dépiégeage thermique et le dépiégeage par effet tunnel sont en compétition.) Dans ces conditions, la vitesse d'évolution d'une population $N_j(t)$ est:

$$[3] \quad -\frac{\mathrm{d}N_j(t)}{\mathrm{d}t} = k_jN_j(t) + \sum_{j'} K_{jj'}N_j(t) - K_{j'j}N_{j'}(t)$$

La cinétique de luminescence, exprimée en nombre de recombinaisons par unité de temps s'écrit:

$$[4] \qquad I(t) = -\sum_j \frac{\mathrm{d}N_j(t)}{\mathrm{d}t} = \sum_j k_jN_j(t)$$

(Expérimentalement on observe la fluorescence de recombinaison de durée de vie 10^{-8} s.)

Saut thermique

Ecrivons la cinétique de luminescence $I(t)$ en décomposant la partie thermique et la partie tunnel:

$$[5] \qquad I(t) = I^{\mathrm{th}}(t) + I^{\mathrm{tu}}(t)$$

$$[6] \qquad I^{\mathrm{th}}(t) = \sum_j k_j{}^{\mathrm{th}}(T)N_j(t)$$

$$[6'] \qquad I^{\mathrm{tu}}(t) = \sum_j k_j{}^{\mathrm{tu}}N_j(t)$$

Si au cours d'une cinétique ITL on passe brusquement de la température T à la température $T + \Delta T$ la cinétique $I(t)$ devient $I'(t)$ et on montre que:

$$[7] \quad \frac{I'(t)}{I(t)} = X(t) = \frac{\left\langle \exp\left(\frac{\Delta T}{T}\frac{E_j}{kT}\right)\right\rangle + Y(t)}{1 + Y(t)}$$

La valeur moyenne est prise pour tous les électrons qui se recombinent au temps t. $Y(t)$ est la proportion d'effet tunnel:

$$[8] \qquad Y(t) = \frac{I^{\mathrm{tu}}(t)}{I^{\mathrm{th}}(t)}$$

Méthode expérimentale

Les systèmes étudiés sont des solutions (10^{-3} M) de TMPD dans MCH ou 3-MP. Les hydrocarbures saturés sont purifiés par ébullition sur tamis moléculaire (13X-5A) et distillation. La TMPD est photoionisée à basse température par irradiation uv (raie 313 nm, H_g HP). La cellule qui permet d'effectuer des sauts thermiques est formée de deux plaques de pyrex rectangulaires (40 × 50 × 4 mm^3) séparées de 0.4 mm par un joint de Mylar (rectangle ouvert). Les deux faces intérieures de la cellule sont rendues conductrices par un dépôt de SnO_2 transparent. Ce dépôt conducteur est traversé par un courant i qui dissipe une énergie calorifique par effet joule. La cellule contenant la solution étant immergée dans l'azote liquide, la solution devient un verre en contact avec les faces chauffantes de la cellule. La température est mesurée par un thermocouple Cu–constantan de 0.2 mm, isolé et piégé dans le verre. Avec une forme de signal convenable $i(t)$ on obtient une variation $T(t)$ désirée dans l'échantillon. Le temps d'équilibre thermique entre le thermocouple et l'échantillon est très rapide (si on effectue un pic δ de courant, le thermocouple et la luminescence répondent avec un décalage dans le temps inférieur à 1/10 s). L'homogénéité du dépôt de SnO_2 est contrôlée par une méthode de pont. On obtient la gamme de température 63–77 K en pompant sur l'azote liquide.

Diffusion lente des électrons et dépiégeage

Diffusion lente

Si on effectue des sauts thermiques identiques à différents temps t_n au cours d'une luminescence isotherme ITL à une température T donnée (63–91 K), le rapport $X(t_n) = I'(t_n)/I(t_n)$ est indépendant du temps t_n (figs 1*a* et

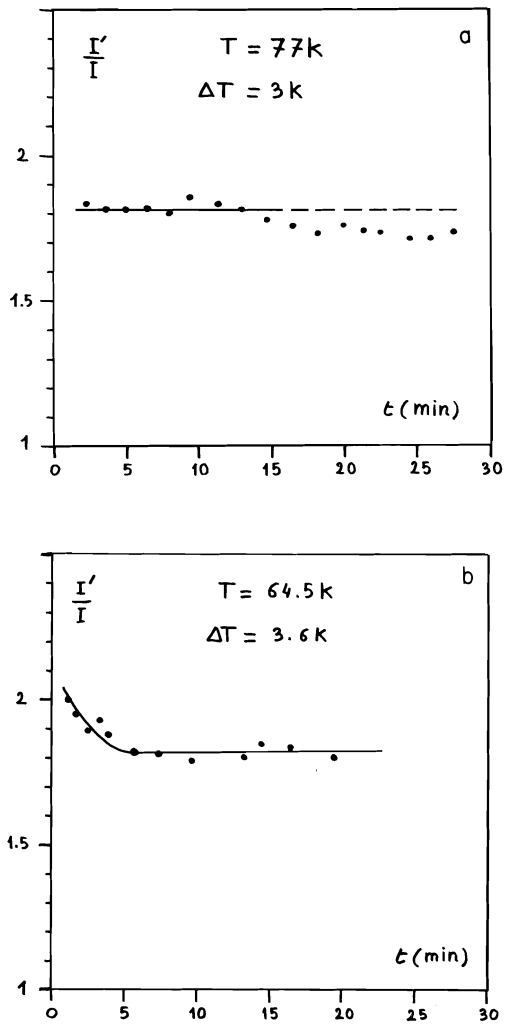

FIG. 1. Si on effectue des sauts thermiques rapides ΔT identiques au cours d'une ITL à la température T, le rapport I'/I est indépendant du temps à toute température T. Mais dans le MCH pour $T \lesssim 77$ K il y a décroissance légère pendant un temps $\tau_{uv} \gtrsim 5$ min. τ_{uv} décroit avec la température: (*a*) TMPD/MCH 10^{-3} M à 77 K; le léger écart des points à la droite horizontale peut être attribué à un phénomène secondaire (relaxation de la matrice); (*b*) TMPD/MCH 10^{-3} M à 64.5 K; le rapport I'/I décroit un peut pendant 5 min.

1*b*). En fait, dans le MCH pour $T \lesssim 77$ K, X décroit un peu pendant un temps $\tau_{uv} \lesssim 5$ min. Ce temps τ_{uv} diminue avec T et dépend de la dose d'irradiation. (On verra par la suite que c'est un temps d'équilibre d'état stationnaire dans la zône d'effet tunnel.)

D'après les formules [7] et [8] on doit avoir simultanement:

$$[9] \qquad \left\langle \exp\left(\frac{\Delta T}{T}\frac{E_j}{kT}\right)\right\rangle = \text{constante} = \exp\left(\frac{\Delta T}{T}\frac{E}{kT}\right)$$

$$[10] \qquad Y(t) = \text{constante} = Y$$

La deuxième égalité de [9] est légitime. En effet, en admettant une distribution gaussiènne pour les énergies d'activations E_j, centrée sur la valeur E, on montre par un calcul sur ordinateur que la formule [9] est correctement vérifiée si la gaussiènne a une largeur $\delta E/E \lesssim 1/7$ lorsque $E \leq 0.7$ eV et $\Delta T \lesssim 3$ K. D'après l'éq. 10 le dépiégeage thermique et le dépiégeage par effet tunnel donnent des intensités de luminescence dans un rapport constant. Ceci n'est possible que si la zône d'effet tunnel $\sum$ et la zône de dépiégeage thermique $\sum'$ sont constamment repeuplées avec la même vitesse. Il y a donc diffusion lente des électrons vers le cation. D'après les éqs 9 et 10 le rapport X de l'éq. 7 devient:

$$[11] \qquad X = \frac{\exp\left(\frac{\Delta T}{T}\frac{E}{kT}\right) + Y}{1 + Y}$$

Dépiégeage thermique. Effet tunnel

X et Y ne dépendent pas du temps au cours d'une ITL mais de la température T. A une température donnée T, on vérifie que la fonction:

$$[12] \qquad F(\Delta T) = X(\Delta T)(1 + Y) - Y$$

varie bien exponentiellement avec ΔT ou:

$$[13] \qquad kT^2 \ln(F) = E\Delta T$$

En fait il est plus pratique, au cours d'une cinétique isotherme d'effectuer des sauts thermiques ΔT_i ($i = 1, 2$, ou 3) croissants et de recommencer la séquence ΔT_i plusieurs fois, plutôt que d'effectuer une séquence ΔT_i longue ($i = 1, 2, \ldots, N$) unique. On prends alors la moyenne des X_i pour i donné (figs 2*a* et 2*b*). On montre expérimentalement que les deux méthodes sont équivalentes.

La variation de E et Y est donnée (figs 3*a* et 3*b*). L'énergie d'activation E passe par un maximum à une température T_m proche de la température de transition vitreuse T_g. La proportion d'effet tunnel Y dépend peu de la température et décroit brutalement à partir de $T_y \simeq T_g$. De 77 à 91 K, la vitesse de chauffage par paliers (entre deux cinétiques) est d'environ 2 K par

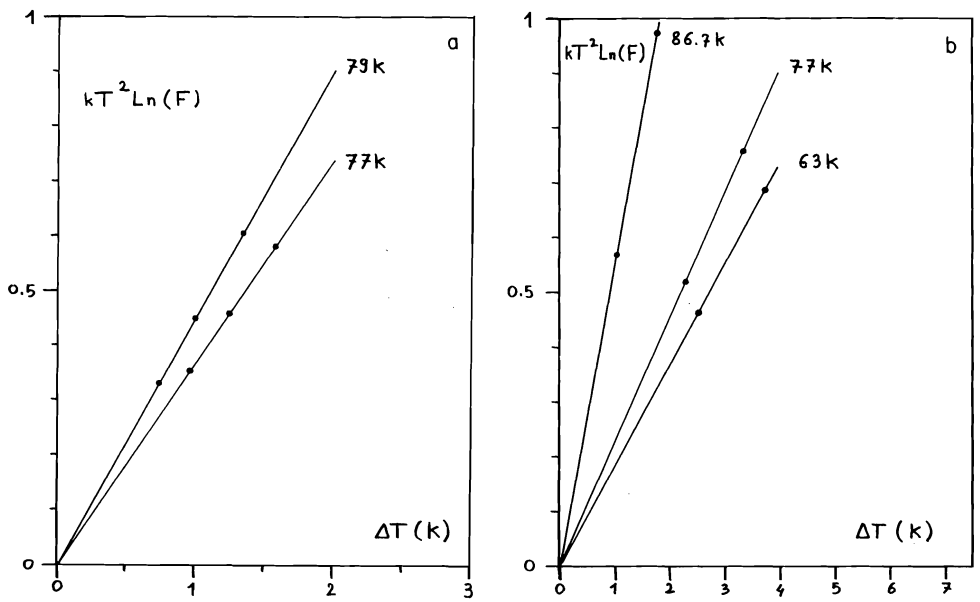

FIG. 2. La fonction F varie exponentiellement avec ΔT. La pente de la droite est l'énergie d'activation E du dépiégeage thermique. (*a*) TMPD/3-MP 10^{-3} *M*. (*b*) TMPD/MCH 10^{-3} *M*.

heure. La gamme de température 63 K $\leq T \leq$ 77 K est faite séparément.

Interprétation

Il existe une autre grandeur physique pour laquelle l'énergie d'activation passe par un maximum à la transition vitreuse. C'est la viscosité η. Prod'homme (5) pose:

$$\eta = AT \exp(E/kT)$$

L'énergie d'activation de la viscosité passe par un maximum à $T \simeq T_g$. Ceci a été vérifié sur différents types de verres (minéraux et organiques). D'autre part, à la transition vitreuse la chaleur spécifique passe aussi par un maximum lors du réchauffement (6); le maximum de C_p dans le MCH est situé vers 94 K. Dworkin (2), prenant le point d'inflection de C_p trouve T_g = 89 K. On sait qu'il est difficile de définir exactement T_g. Par notre méthode on peut poser:

$$T_g = \tfrac{1}{2}(T_m + T_y) = 88.5\ \text{K} \quad (\simeq T_m \simeq T_y)$$

Dans le MCH la proportion d'effet tunnel est pratiquement constante de T = 77 K à T_y = 87 K. On va voir que ceci est justifié s'il y a diffusion lente des électrons piégés. On a défini deux zônes sphèriques $\sum$ et $\sum'$ entourant le cation à l'intérieur desquelles il y a respectivement dépiégeage par effet tunnel et dépiégeage thermique; on appelera $\sum''$ la sphère de provenance des électrons qui, par une transition j''–j se trouvent dans un état j de $\sum$. Le nombre d'électrons piégés dans chacune de ces zônes est appelé respectivement $N_\Sigma(t)$, $N_{\Sigma'}(t)$, $N_{\Sigma''}(t)$.

Ecrivons l'approximation de l'etat stationnaire à la zône d'effet tunnel $\sum$ qui est constamment repeuplée par diffusion:

$$[14] \qquad \frac{dN_\Sigma(t)}{dt} \simeq 0$$

Or par définition:

$$[15] \qquad N_\Sigma(t) = \sum_{j\in\Sigma} N_j(t)$$

La notation $j \in \sum$ signifie que j est un état de piégeage dans la zône d'effet tunnel $\sum$. En tenant compte des éqs 3 et 15, la relation 14 devient:

$$[16] \qquad \frac{dN_\Sigma(t)}{dt} = -\sum_{j\in\Sigma}(k_j^{th}(T) + k_j^{tu} + K_j(T))N_j(t) + \sum_{j\in\Sigma, j''\in\Sigma''} K_{j''j}N_{j''}(t) = 0$$

On a posé $K_j(T) = \sum_{j'} K_{jj'}(T)$. Les éqs 5, 6, 6′ séparent la partie de la luminescence qui provient du dépiégeage thermique $I^{th}(t)$ de celle qui provient du dépiégeage par effet tunnel $I^{tu}(t)$.

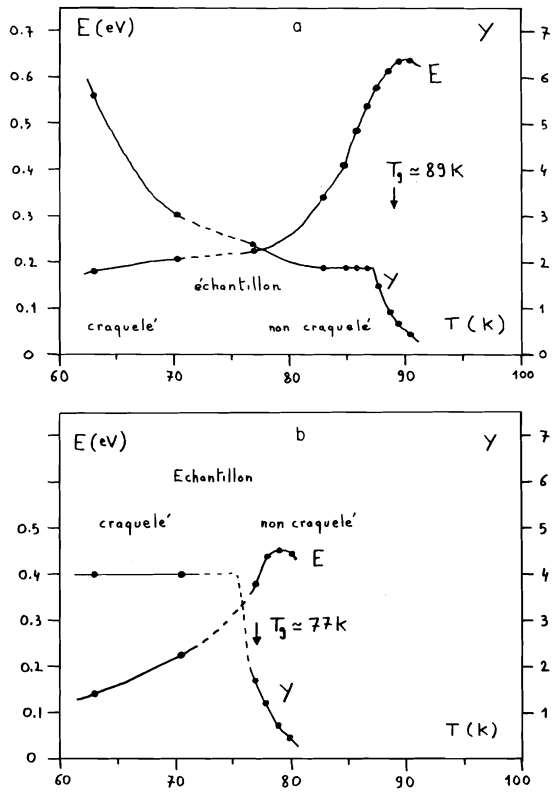

FIG. 3. L'énergie d'activation E du dépiégeage thermique passe par un maximum à T_m. La proportion d'effet tunnel Y décroit rapidement avec T à partir de T_y. On peut définir la température de transition vitreuse par: $T_g = \frac{1}{2}(T_y + T_m)$ ($\simeq T_y \simeq T_m$): (*a*) TMPD/MCH 10^{-3} *M*. (*b*) TMPD/3-MP 10^{-3} *M*.

Donc la relation [16] permet de calculer la proportion d'effet tunnel $Y(t) = I^{tu}(t)/I^{th}(t)$:

$$I^{tu}(t) = \sum_{j\in\Sigma, j''\in\Sigma''} K_{j''j}(T)N_{j''}(t) - \sum_{j\in\Sigma} (k_j^{th}(T) + K_j(T))N_j(t)$$

$$[17] \quad Y(t) = \frac{\langle K_{j''j}(T)\rangle N_{\Sigma''}(t)}{\langle k_j^{th}(T)\rangle N_{\Sigma'}(t)} - \frac{\langle k_j^{th}(T) + K_j(T)\rangle N_\Sigma(t)}{\langle k_j^{th}(T)\rangle N_{\Sigma'}(t)}$$

Il n'est donc pas illogique que Y soit indépendant de la température en dessous de la transition vitreuse. En effet, la température agit sur des constantes de diffusion et de dépiégeage thermique, mais elles apparaissent sous forme de rapport. On peut écrire Y de manière rigoureuse, en tenant compte des éqs 5, 6, 6′:

$$[18] \quad Y = \frac{\sum_j k_j^{tu} N_j(t)}{\sum_j k_j^{th}(T)N_j(t)} = \frac{\langle k_j^{tu}\rangle N_\Sigma(t)}{\langle k_j^{th}(T)\rangle N_{\Sigma'}(t)}$$

Y semble apparaitre sous forme d'une loi activée thermiquement et donc l'éq. 18 serait en contradiction avec le fait que Y est indépendant de T. Mais ce paradoxe s'explique facilement. Les électrons diffusent vers la zône d'effet tunnel $\sum$. Dans cette zône si un état j est tel que $k_j^{tu} \ll k_j^{th}(T)$, l'électron sera dépiégé par effet thermique. Si au contraire $k_j^{tu} \gg k_j^{th}(T)$, on aura, en appelant V_j la vitesse de peuplement de l'état j:

$$[19] \quad k_j^{tu} N_j(t) = V_j$$

Si la diffusion est thermique la vitesse V_j augmente avec la température comme k^{th}. Donc dans l'éq. 18, Y ne dépend pratiquement pas de la température.

Dans le MCH, $Y(T)$ décroit avec T de 63 à 77 K; cela peut provenir d'une diffusion par effet tunnel qui devient négligeable pour $T > 77$ K ($V_j = V_j^{th}(T) + V_j^{tu}$).

Lorsqu'on se rapproche de la température de transition vitreuse T_g, la proportion d'effet tunnel décroit brusquement pour $T \geq T_y$. L'augmentation de la mobilité moléculaire près de T_g doit modifier les processus thermiques et la zône de dépiégeage thermique doit s'agrandir de telle manière que le rapport $N_\Sigma(t)/N_{\Sigma'}(t)$ diminue avec T.

Décalage thermique et temps de relaxation de la matrice

On a vu que si on effectue des sauts thermiques ΔT au cours d'une ITL (à la température T), le rapport I'/I est constant (fig. 4*a*). Mais, si au cours d'une ITL on passe de la température T' à la température T au temps t_0, et si on effectue des sauts thermiques ΔT a la température T, ($t > t_0$), le rapport I'/I est plus grand et décroit vers sa valeur d'équilibre (fig. 4*b*). On mesure donc un temps τ (T', T) de relaxation de la matrice. Ce temps décroit avec la température (tableau 1).

On peut trouver une interpretation cinétique de ce phénomène. I'/I est donné par l'éq. 11; l'énergie E dépend un peu de la température; d'autre part la proportion d'effet tunnel Y (éq. 16) décroit brusquement quand on passe de T' à T. Y doit retrouver sa valeur d'équilibre $Y(T) \sim Y(T')$; il faut donc qu'il s'effectue une

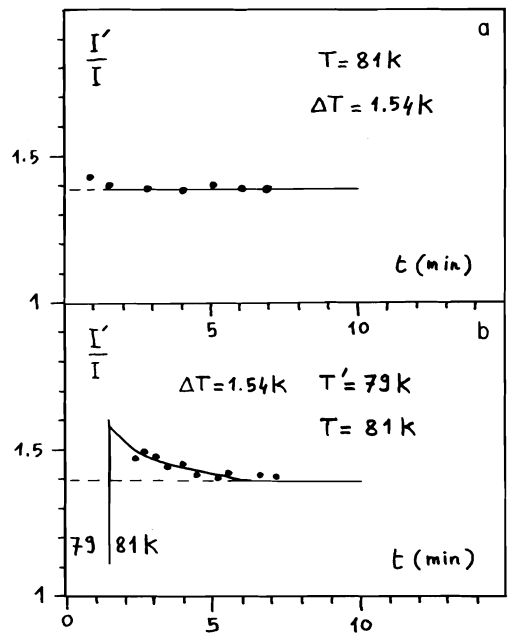

FIG. 4. (*a*) à $T = 81$ K le rapport I'/I est constant. (*b*) Le rapport I'/I n'est plus constant à $T = 81$ K si la photoionisation a été faite à $T' = 79$ K (avec décalage thermique 79–81 K au temps $t_0 = 1.4$ min). On mesure un temps $\tau(T',T)$ de retour à l'équilibre du système. Ici $\tau = 3.5$ min.

TABLEAU 1. La décroissance de τ avec la température

T' (K)	T (K)	τ (min)
70	77	7 ± 1
79	81	3.5 ± 0.5
81	83	1.2 ± 0.3
—	≥ 85	0 ± 0.5

nouvelle distribution des populations $N_j(t)$ qui s'obtient par relaxation thermique du système. On mesure donc un temps $\tau(T', T)$ de relaxation de la matrice; néanmoins ce temps n'est peut être pas un temps de relaxation pur de cette matrice car l'électron sélectionne des mouvements particuliers de la matrice et de plus il perturbe le milieu par sa présence (pression électronique, polarisation électrique).

1. D. CECCALDI. Int. J. Radiat. Phys. Chem. **8**, 539 (1976).
2. A. DWORKIN. 4ème journées nationnales de calorimètrie et d'A.T.D., Paris. 4–5 mai 1972.
3. D. HUFFMAN. J. Am. Chem. Soc. **68**, 1704 (1946).
4. A. J. KOVACS. Forts. Hochpolym. Forsch. Bd. 3, **5**, 394 (1963).
5. M. PROD'HOMME. Thèse d'état, Paris. 1960. Série A, no 3496.
6. S. I. KOMATU and T. HATA. Polymer J. **2**, 650 (1971).

5-Allyl-9-oxobenzomorphans. Part 4.[1] Synthesis of 3-hydroxy-8-oxyisomorphinans, 5-allyl-9α-hydroxy-6,7-benzomorphans, and related tetrahydrofuranobenzomorphans

YVON LAMBERT,[2] JEAN-PAUL DARIS, AND IVO MONKOVIĆ
Bristol Laboratories of Canada, Candiac, Quebec, P.Q., Canada J5R 1J1

Received January 17, 1977

YVON LAMBERT, JEAN-PAUL DARIS, and IVO MONKOVIĆ. Can. J. Chem. **55**, 2523 (1977).

A series of 3-hydroxy-8-oxyisomorphinans (**11**, **16**) has been synthesized from the corresponding 5-allyl-9β-hydroxy-6,7-benzomorphans (**7**, **12**) via a hydroboration, oxidation, mesylation, and cyclization sequence of reactions. Selective reduction of and methylmagnesium iodide addition to 5-allyl-2′-methoxy-2-methyl-9-oxo-6,7-benzomorphan (**1**) gave the respective 9α-hydroxy-6,7-benzomorphans (**17**). These were transformed to a number of 2-substituted-5-allyl-2′,9β-dihydroxy-6,7-benzomorphans (**22**) and corresponding methyltetrahydrofurano analogs (**24**).

YVON LAMBERT, JEAN-PAUL DARIS et IVO MONKOVIĆ. Can. J. Chem. **55**, 2523 (1977).

On a synthétisé une série d'hydroxy-3 oxy-8 isomorphanes (**11** et **16**) à partir des allyl-5 hydroxy-9β benzo-6,7 morphanes (**7**, **12**) correspondants par l'intermédiaire d'une hydroboration, d'une oxydation, d'une mésylation et d'une cyclisation. La réduction sélective et l'addition d'iodure de méthylmagnésium à l'allyl-5 méthoxy-2′ méthyl-2 oxo-9 benzo-6,7 morphane (**1**) conduisent respectivement aux hydroxy-9α benzo-6,7 morphanes (**17**) correspondants. Ceux-ci peuvent être transformés en un grand nombre d'allyl-5 dihydroxy-2′,9β benzo-6,7 morphanes (**22**) substitués en position 2 et de leurs analogues méthyltétrahydrofuranno correspondants (**24**).

[Traduit par le journal]

Introduction

In part 3 of this series (1) we have described the synthesis of a number of 5-propyl- and 5-allyl-2′,9β-dihydroxy-6,7-benzomorphans **2** as well as the corresponding tetrahydrofurano analogs **3**, via stereoselective reduction of, or organometallic addition to, 5-allyl-2′-methoxy-2-methyl-9-oxo-6,7-benzomorphan **1** (Scheme 1). In view of the fact that some of the compounds **2** have been found to possess high levels of analgesic and/or narcotic antagonist activities, comparable to reference agents in laboratory animal tests, we thought it desirable to explore the synthesis and pharmacological properties of isomeric 9-hydroxy-derivatives **5** in which orientation of the hydroxyl group is away from the nitrogen atom or α with respect to the aromatic ring. In addition, it was of interest to continue the investigation of C-ring oxygen-containing systems in both series, such as 8-oxyisomorphinans **4** and tetrahydrofuranobenzomorphans **6**.

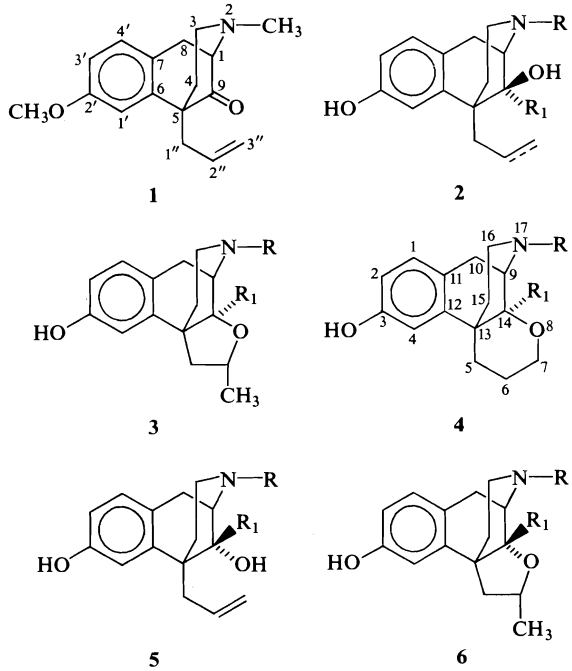

SCHEME 1

Results and Discussion

The synthesis of 8-oxyisomorphinans **11** is shown in Scheme 2. 5-Allyl-9β-hydroxybenzomorphans **7***a* and **7***b* were converted to the corresponding diols **8***a* and **8***b* in good yields via a hydroboration and oxidation reaction

[1]For part 3, see ref. 1.

[2]Present address: Veterinary School, St. Hyacinthe, P.Q.

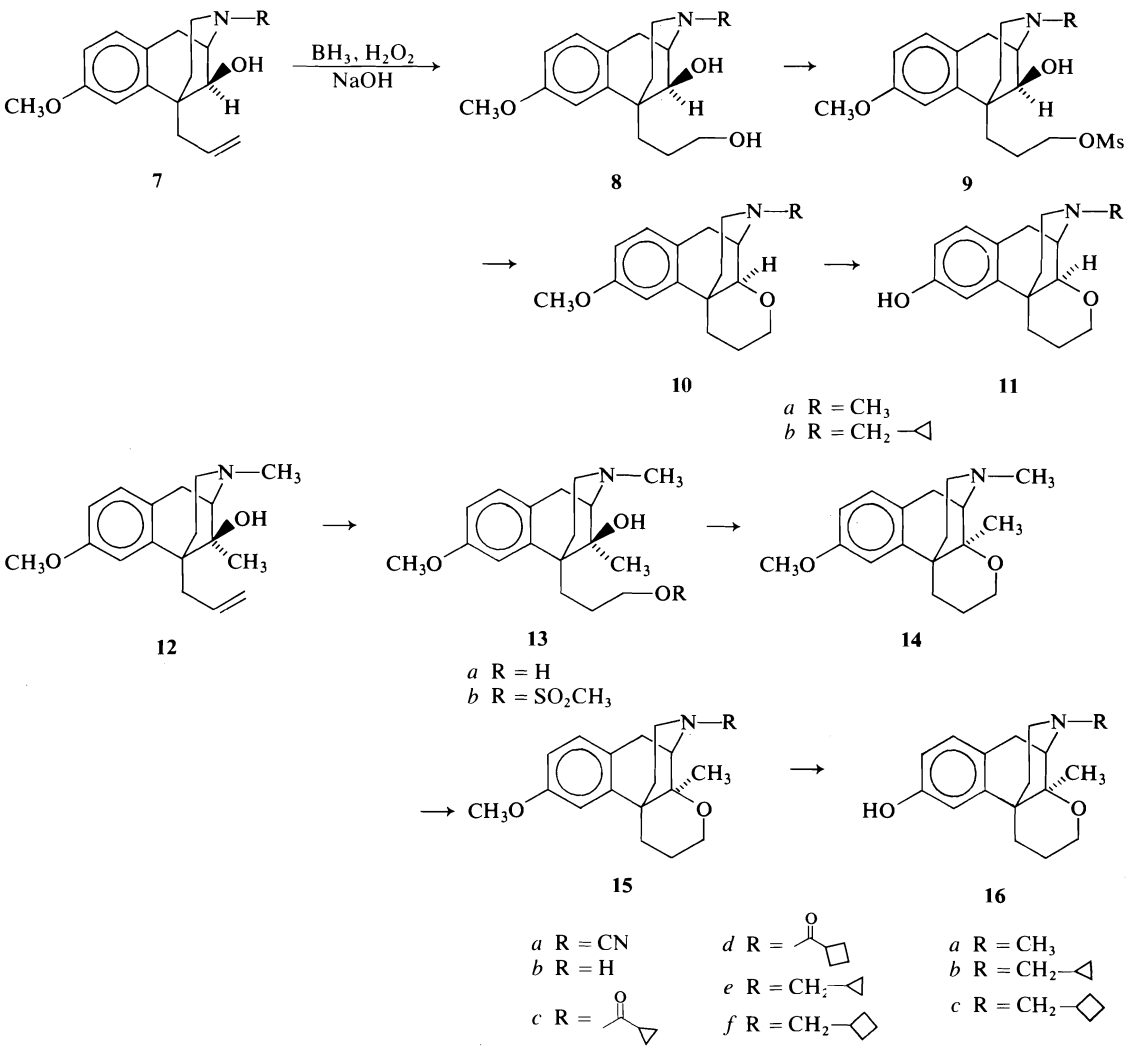

SCHEME 2

sequence. However the problem of formation of stable borane–nitrogen complexes required our attention. The complexed borane was decomposed thermolytically in a suitable hydroxylic solvent. The most convenient solvent was found to be ethylene glycol in which a reaction mixture was heated until hydrogen evolution ceased. The dihydroxy intermediates (**8***a* and **8***b*) were treated with methanesulfonyl chloride to give methanesulfonyl esters **9***a* and **9***b*, which were treated *in situ* with sodium hydride in DMF to give the respective 8-oxyisomorphinans **10***a* and **10***b*. These were demethylated by treatment with boron tribromide in dichloromethane to give **11***a* and **11***b*.

In a similar reaction sequence **12** was converted via **13***a* and **13***b* to the 3-methoxy-14-methyl-8-oxyisomorphinan **14**. A conversion of **14** to **15***e* and **15***f*, respectively, proceeded as expected via a well defined reaction sequence of von Braun demethylation, reduction, acylation, and again reduction. Demethylation of **14**, **15***e*, and **15***f* with boron tribromide gave poor yields of the corresponding phenolic products **16**, presumably due to opening of the tetrahydropyran ring. Better results were obtained with sodium thioethoxide in boiling DMF (2) or lithium diphenylphosphide in boiling THF (3).

Although a number of compounds in the 9α-hydroxy series have been prepared by May and

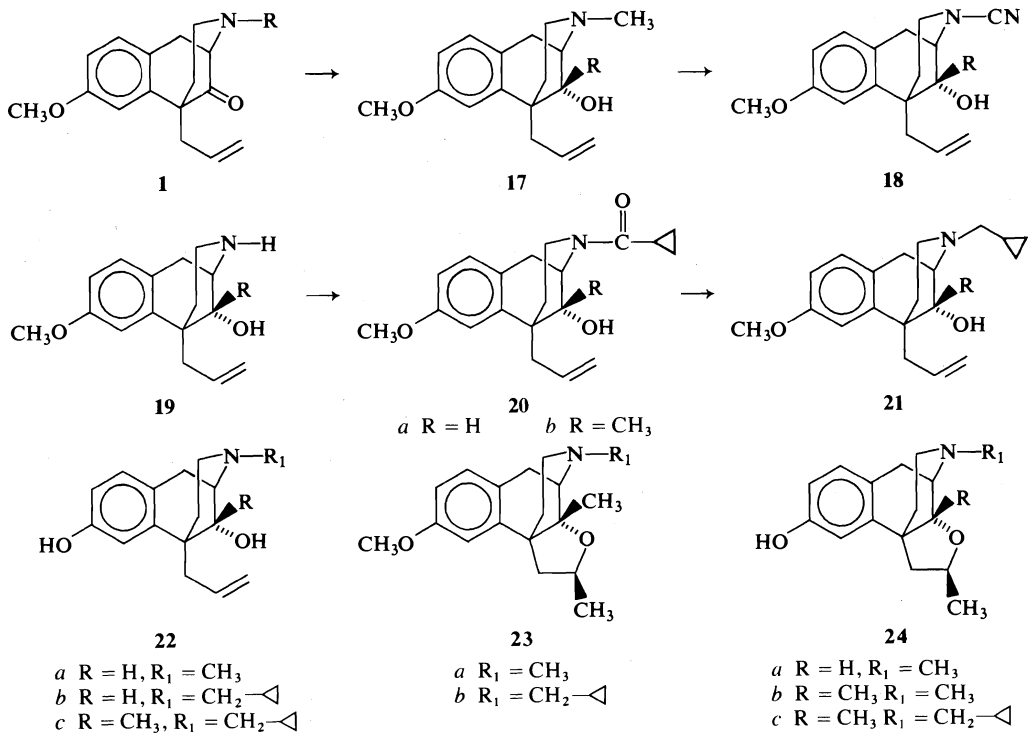

SCHEME 3

co-workers (4, 5) both by reduction and organometallic addition to tertiary amino ketones, from the start we were confronted with the following problems; firstly, catalytic reduction which is known to give α-alcohols could not be applied in our synthesis since it would be expected to reduce the double bond as well, which we need preserved. Secondly, addition of methyllithium to **1** has been demonstrated (1) to give selectively **12** instead of the expected **17***b* (Scheme 3). Consequently we had to investigate systematically these reactions in order to achieve the desired selectivity. We soon discovered that reduction of **1** with diisobutyl aluminum hydride does indeed give selectively **17***a* (better than 96% stereochemical purity) in quantitative yield.

While addition of methyllithium in ether to **1** gave selectively **12** (1) we observed that methylmagnesium iodide in the same solvent added to **1** to give a mixture of 45% **12** and 55% **17***b* as determined by nmr spectroscopy; in addition to a singlet at δ 1.1 due to **12**, a new singlet appeared at δ 1.58 due to **17***b*. Furthermore, the selectivity was lost when addition of methyllithium to **1** was conducted in a mixture of ether and petroleum ether (bp 30–60°C) 1:10, as observed by the product ratio of 60% **17***b* and 40% **12**, indicating, in addition to the observed large effect of the inorganic part of the organometallic reagent, a large solvent effect. These results also pointed a way in which further investigation should be directed; addition of the Grignard reagent in nonpolar solvent (petroleum ether) was expected and indeed found to give almost exclusively **17***b* (better than 95%).

In a recently published review article on the stereochemistry of organometallic compound addition to cyclic ketones Ashby and Laemmle (6) concluded that the stereochemical outcome of the addition is primarily a function of the entering groups and steric requirements of the particular ketone, which are controlled by steric and torsional strain in the transition state. Factors such as solvent, nature of the metal to which the entering group is attached, and others, result in only minor changes in overall observed stereochemistry. If this generalization is valid, it seems reasonable to assume that large metal and solvent effects observed by us must be related to the fact that our ketone is an amino ketone and therefore probably susceptible to a complexation with organometallic reagents via

a nitrogen lone electron pair. That such complexation would be more pronounced in a nonpolar solvent and consequently conducive to an intramolecular addition to give selectively *trans* amino alcohol (**17***b*) is not surprising, since a polar solvent could be expected to compete effectively with the bulky tertiary amine for the complexation of organometallic reagent. That complexation of a Grignard reagent is more effective than that of an organolithium compound is already known (7).

It is also conceivable that complex formation or lack of it plays an important role in the selective reduction of **1**. In a related study, Stevens *et al.* (8) concluded that primary and secondary 2-amino-2-phenylcyclohexanones form stable complexes with hydride reducing agents to give *trans* amino alcohols by an internal hydride transfer.

A conversion of **17***a* and **17***b* to **21***a* and **21***b* was accomplished by the standard reaction sequence shown in Scheme 3. Demethylation of **17***a*, **21***a*, and **21***b* (EtS^- or lithium diphenylphosphide) gave dihydroxybenzomorphans **22**. Compound **24***a* was obtained by hydrochloric acid-catalyzed cyclization of **22***a* (9) while **24***b* was obtained in two steps from **17***b*. Hydrochloric acid-catalyzed cyclization gave intermediate **23***a* which was demethylated to **24***b*. Similarly **24***c* was prepared from **21***b* via **23***b*.

Compounds **11**, **16**, **22**, and **24** were tested for analgesic and narcotic antagonist activities, and found to be considerably less active than corresponding compounds in the 9β-hydroxy series (1). Biological results will be discussed in more detail in another paper.

Experimental

The melting points were determined on Gallenkamp apparatus, and are uncorrected. The infrared (ir) spectra were recorded on a Unicam SP-200G grating ir spectrometer. The nmr spectra were recorded on a Varian A-60A spectrometer using deuterochloroform. The chemical shifts are expressed in δ values using tetramethylsilane as internal reference. Microanalyses were performed by Micro-Tech Laboratories Inc., Skokie, IL.

9β-Hydroxy-2′-methoxy-2-methyl-5-[3′′-(1′′-hydroxypropyl)]-6,7-benzomorphan ***8a***

To a cooled (ice–salt bath) stirred solution of 5-allyl-9β-hydroxy-2′-methoxy-2-methyl-6,7-benzomorphan (**7***a*) (1) (2.24 g, 8.2 mmol) in THF (12 ml) was added dropwise a 1 *M* borane solution in THF (30 ml) and the mixture allowed to stand for 3 h at −10°C followed by 16 h at room temperature. This was cautiously treated with water (5 ml), followed by 20% sodium hydroxide (5 ml, 30 mmol) and 30% hydrogen peroxide (0.92 g, 8 mmol). The whole was stirred for 3 h and then extracted with chloroform (3 × 20 ml). The extract was concentrated *in vacuo* and the residue was boiled briefly with ethylene glycol (10 ml) to decompose a borane complex, cooled, diluted with water, and made basic with sodium hydroxide. The product, an oil, was isolated by extraction with chloroform, drying, and concentration *in vacuo*. The oil crystallized from ether – petroleum ether to give 1.34 g (50%) of **8***a*, mp 96–98°C. Another 15% of **8***a* was obtained from mother liquors by chromatography (Al_2O_3, $CHCl_3$ – 10% CH_3OH). An analytical sample was obtained by recrystallization from ether, mp 98–100°C; nmr δ 6.6–7.2 (3H, m), 3.8 (3H, s, O—CH_3), 3.5–4.0 (3H, m, 9-H and 3′′-H_2), 2.7–3.5 (3H, m), 2.37 (3H, s, N—CH_3), 1.0–2.7 (8H, m). *Anal.* calcd. for $C_{17}H_{25}NO_2$: C 70.07, H 8.65, N 4.81; found: C 70.16, H 8.79, N 4.79.

2-Cyclopropylmethyl-9β-hydroxy-2′-methoxy-5-[3′′-(1′′-hydroxypropyl)]-6,7-benzomorphan ***8b***

The diol **8***b* (an oil) was similarly prepared from **7***b* in 62% yield isolated as a hydrochloride salt. An analytical sample crystallized with ½CH_3OH of crystallization from methanol–acetone; mp 202–203°C. *Anal.* calcd. for $C_{20}H_{29}NO_3 \cdot HCl \cdot \frac{1}{2}CH_3OH$: C 64.13, H 8.40, N 3.65; found: C 64.50, H 8.35, N 3.49.

3-Methoxy-17-methyl-8-oxyisomorphinan ***10a***

To a cooled (ice bath) solution of **8***a* (1.08 g, 3.7 mmol) in dry CH_2Cl_2 (5 ml) was added a 1 *M* solution of methanesulfonyl chloride in benzene (4 ml) and the whole allowed to stand at room temperature for 1 h. Then the reaction mixture was concentrated *in vacuo* and the residue was stirred with a suspension of sodium hydride (420 mg of 50%, 9 mmol, washed with benzene) in DMF (6 ml) for 16 h at room temperature and then for 30 min at 60–70°C. After the usual work-up the crude product was chromatographed on an alumina column. Elution with chloroform gave an oil, which crystallized from ether – petroleum ether to give 0.53 g (62%) of **10***a*, mp 104–105°C; nmr δ 6.7–7.3 (3H, m), 4.05–4.5 (1H, m), 3.84 (3H, s, O—CH_3), 2.5–4.0 (7H, m), 2.44 (3H, s, N—CH_3), 0.8–2.5 (6H, m). *Anal.* calcd. for $C_{17}H_{23}NO_2$: C 74.69, H 8.48, N 5.12; found: C 74.74, H 8.58, N 5.11.

17-Cyclopropylmethyl-3-methoxy-14-methyl-8-oxyisomorphinan ***10b***

This compound (an oil) was similarly prepared from **8***b* in 65% yield, isolated as its oxalate salt. An analytical sample crystallized from methanol–acetone with ½MeOH of crystallization, mp 181–183°C. *Anal.* calcd. for $C_{20}H_{27}NO_2 \cdot C_2H_2O_4 \cdot \frac{1}{2}CH_3OH$: C 64.42, H 7.44, N 3.34; found: C 64.47, H 7.57, N 3.22.

3-Hydroxy-17-methyl-8-oxyisomorphinan ***11a***

To a cooled (ice bath) solution of **10***a* (547 mg, 2 mmol) in dry CH_2Cl_2 (8 ml) was added a 1 *M* boron tribromide solution in CH_2Cl_2 (5 ml) and the mixture allowed to stand at room temperature for 3 h. The excess boron tribromide was carefully decomposed with water. The mixture was made basic with ammonium hydroxide and layers were separated. The water layer was extracted with CH_2Cl_2 and the combined organic phase was dried and concentrated *in vacuo*. The residual orange colored solid

was recrystallized from acetone–CH_2Cl_2 to give 370 mg (64%) of **11***a* as an almost colorless solid, mp 218–220°C; nmr δ 6.7–7.3 (3H, m), 4.0–4.3 (1H, m), 2.5–3.8 (7H, m), 2.44 (3H, s), 0.8–2.4 (6H, m). *Anal.* calcd. for $C_{16}H_{21}NO_2$: C 74.10, H 8.16, N 5.40; found: C 74.21, H 8.37, N 5.25.

17-Cyclopropylmethyl-3-hydroxy-8-oxyisomorphinan ***11b***

The oxyisomorphinan **11***b* (an oil) was similarly prepared from **10***b* in 65% yield, isolated as the oxalate salt with $\frac{1}{2}CH_3OH$ of crystallization; mp 178–180°C (from methanol–acetone). *Anal.* calcd. for $C_{20}H_{27}NO_2 \cdot C_2H_2O_4 \cdot \frac{1}{2}CH_3OH$: C 64.42, H 7.44, N 3.44; found: C 64.47, H 7.57, N 3.22.

2,9α-Dimethyl-9β-hydroxy-2′-methoxy-5-[3″-(1″-hydroxypropyl)]-6,7-benzomorphan ***13a***

The diol **13***a* was prepared from **12** in 69% yield by the procedure given for the preparation of **8***a*; mp 146–148°C from *i*-propanol; nmr δ 6.5–7.1 (3H, m), 3.76 (3H, s), 3.4–3.8 (2H, m), 2.4–3.3 (5H, m), 2.32 (3H, s), 1.12 (3H, s), 0.9–2.3 (6H, m). *Anal.* calcd. for $C_{18}H_{27}NO_3$: C 70.79, H 8.91, N 4.59; found: C 70.78, H 9.05, N 4.61.

14,17-Dimethyl-3-methoxy-8-oxyisomorphinan ***14***

This compound was prepared from **13***a* in 64% yield, by the method given for the preparation of **10***a*: The hydrochloride salt of **14** crystallized from methanol–acetone with 1 mol of methanol of crystallization, mp 229–231°C; nmr (free base) δ 6.6–7.2 (3H, m) 3.8–4.1 (2H, m, 7-H_2) 3.78 (3H, s, O—CH_3), 2.4–3.6 (5H, m), 2.39 (3H, s, N—CH_3), 1.27 (3H, s, 14-CH_3), 0.7–2.4 (6H). *Anal.* calcd. for $C_{18}H_{25}NO_2 \cdot HCl \cdot CH_3OH$: C 64.12, H 8.50, N 3.93; found: C 63.98, H 8.40, N 3.85.

17-Cyano-3-methoxy-8-oxyisomorphinan ***15a***

To a solution of **14** (7.2 g, 25 mmol) in dry benzene (40 ml) was added cyanogen bromide (5.3 g, 50 mmol) and the mixture heated under reflux for 2 h. This was concentrated *in vacuo* and the residual oil was dissolved in CH_2Cl_2, washed with aqueous hydrochloric acid, and water, dried, and concentrated *in vacuo*. The residue was chromatographed (silica gel, ether) to give 5.4 g (72%) of solid **15***a*, mp 143–145°C (from acetone–ether); nmr δ 6.5–7.2 (3H, m), 3.8–4.1 (2H, m), 3.73 (3H, s), 1.15 (3H, s), 0.7–3.6 (11H). *Anal.* calcd. for $C_{18}H_{22}N_2O_2$: C 72.45, H 7.43, N 9.39; found: C 72.43, H 7.43, N 9.41.

3-Methoxy-14-methyl-8-oxyisomorphinan ***15b***

A solution of **15***a* (5.0 g, 16.7 mmol) in anhydrous THF (20 ml) was added dropwise over a 15 min period to a boiling solution of lithium aluminum hydride (2.5 g) in THF (60 ml). The whole was heated under reflux for 2 h, cooled, and treated with 1 *N* NaOH (12.5 ml). A solid was removed by filtration and washed several times with ether. The combined filtrate and washings were concentrated *in vacuo* to give 4.57 g (quantitative yield) of crude **15***b* as an oil. An analytical sample was purified as the oxalate salt by recrystallization from 95% ethanol. It crystallized as neutral oxalate with ½ mol of water of crystallization; mp 145–148°C. *Anal.* calcd. for $C_{17}H_{23}NO_2 \cdot \frac{1}{2}C_2H_2O_4 \cdot \frac{1}{2}H_2O$: C 66.03, H 7.70, N 4.28; found: C 65.69, H 7.76, N 4.15.

17-Cyclopropylcarbonyl-3-methoxy-8-oxyisomorphinan ***15c***

To a cooled (ice bath), stirred solution of **15***b* (1.48 g, 5.4 mmol) in dry CH_2Cl_2 (15 ml) and triethylamine (1 ml, 7.2 mmol) was added a solution of cyclopropane carboxylic acid chloride (0.62 g, 6 mmol) in dry CH_2Cl_2 (5 ml). The mixture was stirred for 10 min, and then washed with water followed by dilute hydrochloric acid. Drying and evaporation of solvent gave 1.82 g (quantitative yield) of **15***c* as an oil. A sample for analysis was purified by distillation at 220–230°C/0.5 Torr. *Anal.* calcd. for $C_{21}H_{27}NO_3$: C 73.87, H 7.97, N 4.10; found: C 74.03, H 8.11, N 3.99.

17-Cyclobutylcarbonyl-3-methoxy-8-oxyisomorphinan ***15d***

The amide **15***d* was similarly prepared from **15***b* in quantitative yield. An analytical sample was distilled at 220–230°C/0.4 Torr. *Anal.* calcd. for $C_{22}H_{29}NO_3$: C 74.35, H 8.22, N 3.94; found: C 74.02, H 8.32, N 3.65.

17-Cyclopropylmethyl-3-methoxy-8-oxyisomorphinan ***15e***

This compound was obtained by reduction of amide **15***c* in a procedure similar to that described for the preparation of **15***b*. The product (an oil) was isolated by column chromatography (Al_2O_3, ether) in 75% yield. The oxalate salt was recrystallized from methanol–acetone; mp 195–197°C; nmr δ 6.4–7.1 (3H, m), 3.75–4.05 (2H, m), 3.7 (3H, s), 1.15 (3H, s), 0.0–3.4 (18H). *Anal.* calcd. for $C_{21}H_{29}NO_2 \cdot C_2H_2O_4$: C 66.17, H 7.48, N 3.36; found: C 66.04, H 7.40, N 3.26.

17-Cyclobutylmethyl-3-methoxy-8-oxyisomorphinan ***15f***

This compound (an oil) was prepared similarly from **15***d* in 77% yield and purified as the oxalate salt; mp 204–206°C (from methanol–acetone); nmr δ 6.5–7.2 (3H, m), 3.88 (3H, s), 1.15 (3H, s), 0.6–4.2 (22H). *Anal.* calcd. for $C_{22}H_{31}NO_2 \cdot C_2H_2O_4$: C 66.80, H 7.71, N 3.25; found: C 66.58, H 7.68, N 3.15.

14,17-Dimethyl-3-hydroxy-8-oxyisomorphinan ***16a***

To a solution of **14** (0.73 g, 2.54 mmol) in dry THF (5 ml) was added under a nitrogen atmosphere a 0.78 *M* solution of lithium diphenylphosphide in THF (14 ml) and the whole heated under reflux for 6 h. The reaction mixture was treated with 0.5 *N* hydrochloric acid (40 ml) and extracted with ether (2 × 50 ml). The ether extract was discarded and the aqueous phase was made basic with ammonium hydroxide and extracted with CH_2Cl_2, to give after drying and evaporation 0.65 g of an oil. The oil crystallized from acetone to give 0.34 g (49%) of **16***a* as a white solid; mp 261–263°C, nmr δ 6.4–7.0 (3H, m), 3.7–4.0 (2H, m), 2.36 (3H, s), 1.15 (3H, s), 0.6–3.3 (11H). *Anal.* calcd. for $C_{17}H_{23}NO_2$: C 74.69, H 8.48, N 5.12; found: C 74.35, H 8.47, N 5.05.

17-Cyclopropylmethyl-3-hydroxy-14-methyl-8-oxyisomorphinan ***16b***

To a cooled (ice bath), stirred slurry of sodium hydride (580 mg, 24 mmol) in dry DMF (15 ml) was added ethane thiol (1.5 g, 24 mmol) followed by a solution of **15***e* (0.79 g, 2.4 mmol) in DMF (2 ml). The cooling bath was removed and the whole was heated under reflux for 4 h. After cooling, the reaction mixture was partitioned between water and CH_2Cl_2. The organic phase was washed with water, dried, and concentrated *in vacuo* to give an oil. This was dissolved in acetone and treated with a solution of dry HCl in ether to give 0.51 g (49%) of the hydrochloride of **16***b* as white solid. Recrystallization from ethanol–acetone–ether gave an analytical sample

containing 1 mol of ethanol of crystallization; mp 235–238°C. *Anal.* calcd. for $C_{20}H_{27}NO_2 \cdot HCl \cdot C_2H_5OH$: C 67.63, H 8.38, N 3.76; found: C 67.48, H 8.47, N 3.56.

17-Cyclobutylmethyl-3-hydroxy-14-methyl-8-oxyisomorphinan **16***c*

This compound was prepared from **15***f* by the procedure given for the preparation of **16***a*. It crystallized from acetone in 53% yield; recrystallization from methanol–acetone gave an analytical sample; mp 203–205°C. *Anal.* calcd. for $C_{21}H_{29}NO_2$: C 77.02, H 8.93, N 4.28; found: C 77.39, H 9.16, N 4.09.

5-Allyl-9α-hydroxy-2′-methoxy-1-methyl-6,7-benzomorphan **17***a*

To a cooled (−50°C), stirred 25% solution of diisobutyl aluminum hydride in hexane (50 ml, 77 mmol) was added dry THF (25 ml) followed by a solution of ketone **1** (10.5 g, 38.7 mmol) in dry THF (30 ml) over a period of 20 min. The whole was kept for 15 min at −50°C, treated cautiously with methanol (8 ml), and then poured onto a mixture of ice (200 g) and concentrated hydrochloric acid (40 ml). The layers were separated and the organic layer was extracted with 1 *N* hydrochloric acid (60 ml). The combined aqueous phase was extracted with CH_2Cl_2 (3 × 50 ml), and the extract washed with 2 *N* ammonium hydroxide (50 ml), dried, and concentrated *in vacuo* to give 10.5 g (100%) of essentially pure **17***a* as an oil which crystallized on standing. An analytical sample was prepared by recrystallization from ether – petroleum ether; mp 74–78°C; nmr δ 6.5–7.1 (3H, m), 5.0–6.5 (3H, m), 3.9 (1H, d, J = 5 Hz, 9-H), 3.82 (3H, s), 2.35 (3H, s), 1.1–3.3 (9H). *Anal.* calcd. for $C_{17}H_{23}NO_2$: C 74.69, H 8.48, N 5.12; found: C 74.26, H 8.73, N 5.19.

5-Allyl-1,9β-dimethyl-9α-hydroxy-2′-methoxy-6,7-benzomorphan **17***b*

A Grignard reagent was prepared by addition of a solution of iodomethane (26 g, 0.184 mol) in dry ether (30 ml) to a stirred suspension of magnesium turnings (3.71 g, 0.159 mol) in dry ether (30 ml) over a period of 2 h. Then the ether was evaporated *in vacuo* under a stream of nitrogen. To the dry solid was added in one portion a solution of **1** (9.78 g, 0.036 mol) in petroleum ether (250 ml, bp 30–60°C) and the whole vigorously stirred for 18 h. This was treated cautiously with water (70 ml) and p*H* was adjusted to 8 by addition of diluted (1:1) hydrochloric acid. The emulsified mixture was cleared by the addition of ammonium hydroxide and the layers were separated. The water layer was extracted with ether and the combined organic phase was dried and concentrated *in vacuo* to give 9.4 g (91%) of essentially pure **17***b* as an oil; nmr δ 6.5–7.1 (3H, m), 4.8–6.4 (3H, m), 3.73 (3H, s), 2.6–3.0 (5H, m), 2.3 (3H, s), 1.58 (3H, s), 1.0–2.5 (4H, m). A sample for analysis was purified as the oxalate salt by recrystallization from methanol–ether; mp 208–209°C. *Anal.* calcd. for $C_{18}H_{25}NO_2 \cdot C_2H_2O_4$: C 63.65, H 7.21, N 3.71; found: C 63.78, H 7.41, N 3.92.

5-Allyl-1-cyano-9α-hydroxy-2′-methoxy-6,7-benzomorphan **18***a*

This compound was prepared from **11***a* by the method given for the preparation of **15***a*. It crystallized from ether – petroleum ether in 70% yield as a white solid; mp 92–93°C. *Anal.* calcd. for $C_{17}H_{20}N_2O_2$: C 71.81, H 7.09, N 9.83; found: C 71.69, H 7.15, N 9.87.

5-Allyl-1-cyano-9α-hydroxy-2′-methoxy-9β-methyl-6,7-benzomorphan **18***b*

This compound was similarly prepared in 73% yield from **17***b*; mp 103–104°C (from chloroform–ether). *Anal.* calcd. for $C_{18}H_{22}N_2O_2$: C 72.45, H 7.43, N 9.39; found: C 72.56, H 7.48, N 9.23.

5-Allyl-9α-hydroxy-2′-methoxy-6,7-benzomorphan **19***a*

This compound (an oil) was obtained in quantitative yield from **18***a* by the method given for the preparation of **15***b*, except that dioxane was used as solvent. An analytical sample was purified by molecular distillation at 150°C/0.01 Torr; nmr δ 6.5–7.1 (3H, m), 5–6.5 (3H, m), 3.87 (1H, d, J = 3.5 Hz, 9-H), 3.78 (3H, s), 1.1–3.5 (9H). *Anal.* calcd. for $C_{16}H_{21}NO_2$: C 74.10, H 8.16, N 5.40; found: C 73.92, H 8.27, N 5.36.

5-Allyl-9α-hydroxy-2′-methoxy-9β-methyl-6,7-benzomorphan **19***b*

This compound was prepared similarly by reduction of **18***b* in THF, and isolated by column chromatography (silica gel; ether – 5% methanol) in 62% yield as an oil. The hydrochloride salt was recrystallized from methanol–ether; nmr δ 6.5–7.1 (3H, m), 4.8–6.4 (3H, m), 7.8 (3H, s), 1.55 (3H, s), 1–3.5 (9H). *Anal.* calcd. for $C_{17}H_{23}NO_2 \cdot HCl$: C 65.90, H 7.81, N 4.52; found: C 65.60, H 7.76, N 4.40.

5-Allyl-17-cyclopropylcarbonyl-9α-hydroxy-2′-methoxy-6,7-benzomorphan **20***a*

The hydroxyamide **20***a* was prepared from **19***a* in 80% yield by the procedure given for the preparation of **15***c*; white solid; mp 146–147°C (from benzene–ether). *Anal.* calcd. for $C_{20}H_{25}NO_3$: C 73.37, H 7.70, N 4.28; found: C 73.53, H 7.71, N 4.32.

5-Allyl-17-cyclopropylcarbonyl-9α-hydroxy-2′-methoxy-9β-methyl-6,7-benzomorphan **20***b*

The hydroxy amide **20***b* was similarly prepared in 65% yield from crude **19***b*; mp 144–145°C (from acetone). *Anal.* calcd. for $C_{21}H_{27}NO_3$: C 73.87, H 7.97, N 4.10; found: C 73.80, H 8.00, N 4.01.

5-Allyl-1-cyclopropylmethyl-9α-hydroxy-2′-methoxy-6,7-benzomorphan **21***a*

Reduction of **20***a* with lithium aluminum hydride in boiling dioxane in a procedure similar to that given for the preparation of **15***b* gave **21***a* (an oil) in 86% yield. An analytical sample was purified by molecular distillation at 180°C/0.01 Torr; nmr δ 6.6–7.1 (3H, m), 4.5–6.5 (3H, m), 3.9 (1H, d, J = 4 Hz), 7.78 (3H, s), 0.0–3.5 (16H). *Anal.* calcd. for $C_{20}H_{27}NO_2$: C 76.64, H 8.68, N 4.47; found: C 76.77, H 7.78, N 4.43.

5-Allyl-1-cyclopropylmethyl-9α-hydroxy-2′-methoxy-9β-methyl-6,7-benzomorphan **21***b*

This compound (an oil) was similarly prepared in 96% yield from **20***b*. The hydrochloride salt was recrystallized from methanol–ether; mp 236–238°C; nmr δ 6.5–7 (3H, m), 4.8–6.4 (3H, m), 3.7 (3H, s), 1.6 (3H, s) 0.0–3.1 (16H). *Anal.* calcd. for $C_{21}H_{29}NO_2 \cdot HCl$: C 69.31, H 8.31, N 3.81; found: C 69.08, H 8.44, N 3.79.

5-Allyl-2′,9α-dihydroxy-1-methyl-6,7-benzomorphan ***22a***

The diol **22***a* was prepared in 58% yield from **17***a* by the method given for the preparation of **16***b* and purified by recrystallization first from methanol–benzene and then from toluene; mp 154–156°C, nmr δ 6.4–7.1 (3H, m), 4.8–6.4 (3H, m), 3.88 (1H, d, J = 3.5 Hz), 2.4 (3H, s), 1–3.3 (9H). *Anal.* calcd. for $C_{16}H_{21}NO_2$: C 74.10, H 8.16, N 5.40; found: C 74.45, H 8.20, N 5.01.

5-Allyl-1-cyclopropylmethyl-2′,9α-dihydroxy-6,7-benzomorphan ***22b***

The diol **22***b* was similarly prepared in 87% yield from **21***a*, as an amorphous solid. It was purified by recrystallization from methanol–ether; mp 171–174°C. An analytical sample was purified by molecular distillation at 160°C/0.01 Torr, nmr δ 6.4–7.0 (3H, m), 4.9–6.3 (3H, m), 3.75 (1H, t, J = 4 Hz, 9-H), 0.0–3.5 (16H). *Anal.* calcd. for $C_{19}H_{25}NO_2$: C 76.22, H 8.42, N 4.68; found: C 76.19, H 8.50, N 4.72.

5-Allyl-1-cyclopropylmethyl-2′,9α-dihydroxy-9β-methyl-6,7-benzomorphan ***22c***

The diol **22***c* was similarly prepared in 67% yield from **21***b* and purified by recrystallization of the hydrochloride salt from methanol–acetone; mp 220–223°C; nmr δ 6.4–7.0 (3H, m), 4.9–6.3 (3H, m), 1.62 (3H, s), 0.0–3.2 (16H). *Anal.* calcd. for $C_{20}H_{27}NO_2 \cdot HCl$: C 68.65, H 8.07, N 4.00; found: C 68.64, H 8.06, N 3.96.

Tetrahydrofuranobenzomorphan ***24a***

The diol **22***a* (0.50 g, 1.9 mmol) was treated with concentrated hydrochloric acid (10 ml) at reflux for 5 min. The reaction mixture was concentrated to *ca.* 5 ml, made basic with ammonium hydroxide, cooled, and filtered to give crude solid **24***a*. This was purified by recrystallization first from toluene and then from ethanol to give 160 mg of pure **24***a*; mp 207–208°C; nmr δ 6.5–7.1 (3H, m), 3.7–4.1 (2H, m), 3.3–3.6 (1H, m), 2.8–3.0 (2H, m), 2.46 (3H, s), 1.5–2.6 (6H, m), 1.25 (3H, d, J = 5 Hz). *Anal.* calcd. for $C_{16}H_{21}NO_2$: C 74.10, H 8.16, N 5.40; found: C 73.81, H 8.08, N 5.12.

Tetrahydrofuranobenzomorphan ***24b***

This compound was obtained in two steps from **17***b* as follows. A solution of **17***b* (820 mg, 2.85 mmol) in concentrated hydrochloric acid (10 ml) was heated under reflux for 5 min, cooled, made basic with sodium hydroxide, and extracted with ether, to give after drying and concentration 800 mg of crude **23***a* as an oil; nmr δ 6.4–7.1 (3H, m), 3.65 (3H, s, O—CH_3), 3.4–3.9 (1H, m, 2′′-H), 2.6–3.0 (3H, m), 2.3 (3H, s, N—CH_3), 1.5–2.7 (6H, m), 1.45 (3H, s, 9-CH_3), 1.22 (3H, d, J = 6 Hz, 3′′-H_3). This was demethylated without further purification by the procedure given for the preparation of **16***a* to give crude solid **24***b*. This was purified by recrystallization from ethanol–water to give 530 mg (68%) of the pure product; mp 217–219°C; nmr δ 6.4–7.1 (3H, m), 3.4–3.9 (1H, m) 1.2–3.2 (11H, m) 1.52 (3H, s, 9-CH_3), 1.3 (3H, d, J = 6 Hz, 3′′-H_3). *Anal.* calcd. for $C_{17}H_{23}NO_2$: C 74.69, H 8.43, N 5.12; found: C 74.52, H 8.41, N 5.06.

Tetrahydrofuranobenzomorphan ***24c***

This compound was similarly prepared in two steps (via **23***b*) in 78% yield from **21***b*, isolated as the hydrochloride salt from acetone. Recrystallization from methanol–acetone gave an analytical sample; mp 246–249°C; nmr δ 6.5–7.0 (3H, m), 3.4–3.9 (1H, m, 2′′-H), 3.1–3.3 (1H, m, 9-H), 1.5–2.9 (10H, m), 1.55 (3H, s, 9-CH_3), 1.32 (3H, d, J = 6 Hz, 3′′-H_3), 0.0–1.1 (5H, m, c-C_3H_5). *Anal.* calcd. for $C_{20}H_{27}NO_2 \cdot HCl$: C 68.65, H 8.07, N 4.00; found: C 68.68, H 8.06, N 3.87.

Acknowledgement

The financial support of the National Research Council of Canada is gratefully acknowledged.

1. M. Saucier, J. P. Daris, Y. Lambert, I. Monković, and A. W. Pircio. J. Med. Chem. **20**, 676 (1977).
2. (*a*) G. I. Feutrill and R. N. Mirrington. Tetrahedron Lett. 1327 (1970); (*b*) G. I. Feutrill and R. N. Mirrington. Aust. J. Chem. **26**, 357 (1973).
3. F. G. Mann and M. G. Pragnell. J. Chem. Soc. 4120 (1965).
4. E. L. May, H. Kugita, and J. H. Ager. J. Org. Chem. **26**, 1621 (1961).
5. S. Saito and E. L. May. J. Org. Chem. **26**, 4536 (1961).
6. A. C. Ashby and J. I. Laemmle. Chem. Rev. **75**, 521 (1975).
7. C. A. Buehler and D. E. Pearson. *In* Survey of organic synthesis. Wiley-Interscience, New York, NY. 1970. p. 226.
8. C. L. Stevens, K. J. Terbeek, and P. M. Pillai. J. Org. Chem. **39**, 3943 (1974).
9. I. Monković. Can. J. Chem. **53**, 1189 (1975).

Crystal and molecular structure of hexadecamethylcyclooctaphosphazene, $(NPMe_2)_8$

RICHARD T. OAKLEY, NORMAN L. PADDOCK, STEVEN J. RETTIG, AND JAMES TROTTER

Department of Chemistry, University of British Columbia, 2075 Wesbrook Mall, Vancouver, B.C., Canada V6T 1W5

Received December 23, 1976

RICHARD T. OAKLEY, NORMAN L. PADDOCK, STEVEN J. RETTIG, and JAMES TROTTER. Can. J. Chem. **55**, 2530 (1977).

Crystals of hexadecamethylcyclooctaphosphazene are tetragonal, $a = 13.637(1)$, $c = 8.215(1)$ Å, $Z = 2$, space group $P4/n$. The structure was solved by direct methods and was refined by full-matrix least-squares procedures to a final R of 0.033 and R_w of 0.032 for 1306 reflections with $I \geq 4\sigma(I)$. The molecule has crystallographic fourfold (C_4) symmetry with weighted mean bond lengths P—N, 1.590(13), P—C, 1.811(2), and C—H, 0.95(2) Å (those not involving hydrogen have been corrected for libration, rms deviations from the mean are given in parentheses). Angles in the 16-membered ring are 119.2(1) and 115.1(1)° at P and 131.5(1) and 148.2(1)° at N.

RICHARD T. OAKLEY, NORMAN L. PADDOCK, STEVEN J. RETTIG et JAMES TROTTER. Can. J. Chem. **55**, 2530 (1977).

Les cristaux de l'hexadécaméthylcyclooctaphosphazène sont tétragonaux, $a = 13.637(1)$, $c = 8.215(1)$ Å, $Z = 2$, groupe d'espace $P4/n$. On a résolu la structure par les méthodes directes et on l'a affinée par la méthode des moindres carrés (matrice complète) jusqu'à une valeur finale de R de 0.033 et R_w de 0.032 pour 1306 réflexions avec $I \geq 4\sigma(I)$. La molécule a une symétrie cristallographique quaternaire (C_4) avec des longueurs de liaison moyennes pondérées P—N, 1.590(13), P—C, 1.811(2) et C—H, 0.95(2) Å (les longueurs n'impliquant pas d'hydrogène ont été corrigées pour la libration; les déviations rms à partir des valeurs moyennes sont données entre parenthèses). Les angles dans le cycle à 16 chaînons sont 119.2(1) et 115.1(1)° au niveau du phosphore et 131.5(1) et 148.2(1)° au niveau de l'azote.

[Traduit par le journal]

Introduction

A method for preparing methylphosphazenes of large ring size ($n \geq 6$) has recently been described along with the crystal structure of the heptameric derivative $(NPMe_2)_7$ (1). We now report the crystal structure of the octamer $(NPMe_2)_8$. A detailed analysis of molecular geometry for the series $(NPMe_2)_{3-10}$ is planned upon completion of the structural work presently in progress. The structures of $(NPMe_2)_4$ (2) and $(NPMe_2)_5$ (3) have been determined.

Experimental

$(NPMe_2)_8$ was prepared as previously described (1). Crystals suitable for X-ray analysis were obtained by recrystallization from benzene. The crystal chosen for study was mounted with c parallel to the goniostat axis and had dimensions of *ca.* 0.2 × 0.2 × 0.4 mm. Unit-cell and space group data were obtained from film and diffractometer measurements. The unit-cell parameters were refined by a least-squares treatment of $\sin^2\theta$ values for 18 reflections measured on a diffractometer with Cu K_α radiation. Crystal data are:

$C_{16}H_{48}N_8P_8$ fw = 600.4

Tetragonal, $a = 13.637(1)$, $c = 8.215(1)$ Å, $V = 1527.7(2)$ Å^3, $Z = 2$, $\rho_c = 1.305$ g cm^{-3}, $F(000) = 640$ (22°C, Cu K_α, $\lambda = 1.5418$ Å, $\mu = 43.7$ cm^{-1}). Absent reflections: $hk0$, $h + k \neq 2n$. Space group $P4/n$ (C_{4h}^3, No. 85).

Intensities were measured with nickel-filtered Cu K_α radiation on a Datex-automated General Electric XRD-6 diffractometer. A θ–2θ scan at 2° min^{-1} over a range of (1.80 + 0.86 tan θ) degrees in 2θ was employed. Background counts (10 s) were measured at each end of the scan. Data were measured to $2\theta = 160°$. The intensity of the check reflection, measured every 40 reflections throughout the data collection, remained constant to within ±2%. The structure amplitudes were derived and an absorption correction was applied by a computer program using a Gaussian integration method (4, 5). Transmission factors ranged from 0.306 to 0.487. Of the 1678 independent reflections measured, 1312 had intensities greater than $4\sigma(I)$ above background where $\sigma^2(I) = S + B + (0.05S)^2$ with S = scan count and B = time-averaged background count. These reflections were used in the solution and refinement of the structure.

The structure was solved by direct methods with use of tangent formula refinement (6–8). An E-map calculated from the set of phases with the lowest value of R_k gave the positions of the eight non-hydrogen atoms among the 18 highest peaks. Two cycles of isotropic, followed by two cycles of anisotropic full-matrix least-squares refinement of the non-hydrogen atoms gave $R = 0.058$. The 12 highest peaks on a difference map calculated at this point accounted for the 12 hydrogen atoms. The entire structure (including hydrogen atoms with isotropic thermal parameters) was refined for four cycles giving a final R of 0.033 and R_w of 0.032 for 1306 reflections with $I \geq 4\sigma(I)$ (6 reflections which had $|F_o| - |F_c| > 3\sigma(F)$ were removed from the data set in the final stages of refinement; for all 1678 reflections $R = 0.048$ and $R_w = 0.039$).

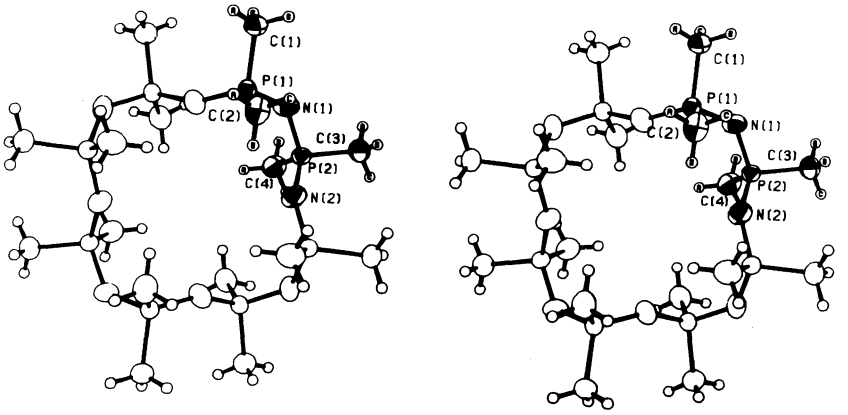

FIG. 1. A stereo view of the hexadecamethylcyclooctaphosphazene molecule. 50% ellipsoids are shown for the non-hydrogen atoms. Hydrogen atoms have been assigned artificially small temperature factors for the sake of clarity.

TABLE 1. Final positional parameters (fractional × 10^4, P × 10^5, H × 10^3, origin at $\bar{1}$) with estimated standard deviations in parentheses

Atom	x	y	z
P(1)	84284(3)	98171(3)	33326(6)
P(2)	97527(3)	85227(3)	16060(6)
N(1)	9339(1)	9551(1)	2223(3)
N(2)	9531(1)	7631(1)	2746(3)
C(1)	8539(2)	11120(2)	3647(4)
C(2)	8542(2)	9300(2)	5338(3)
C(3)	11045(2)	8699(2)	1287(3)
C(4)	9311(2)	8307(2)	−417(3)
H(1a)	804(2)	1134(2)	430(3)
H(1b)	917(2)	1129(2)	417(3)
H(1c)	853(2)	1148(3)	259(5)
H(2a)	803(2)	956(2)	597(4)
H(2b)	848(3)	861(3)	523(4)
H(2c)	913(2)	953(2)	577(4)
H(3a)	1118(2)	926(3)	65(4)
H(3b)	1131(2)	882(3)	235(5)
H(3c)	1135(2)	815(2)	83(4)
H(4a)	862(2)	821(2)	−39(4)
H(4b)	944(2)	890(3)	−102(4)
H(4c)	964(2)	775(3)	−85(4)

The least-squares refinement was based on the minimization of $\Sigma w[|F_o| - |F_c/(1 + gI)|]^2$ where g is the extinction parameter and I the uncorrected intensity. The final value of g was 6.8×10^{-7}. The scattering factors of ref. 9 were used for the non-hydrogen atoms and those of ref. 10 for the hydrogen atoms. Anomalous scattering factors from ref. 11 were used for the non-hydrogen atoms. The anisotropic thermal parameters employed in the refinement are U_{ij} in the expression:

$$f = f^0 \exp [-2\pi^2(U_{11}\, h^2a^{*2} + U_{22}\, k^2b^{*2} + U_{33}\, l^2c^{*2} + 2U_{12}\, hka^*b^* + 2U_{13}\, hla^*c^* + 2U_{23}\, klb^*c^*)]$$

where f^0 is the tabulated scattering factor and f is that corrected for thermal motion (for H atoms $f = f^0 \times \exp [-8\pi^2 U \sin^2 \theta/\lambda^2]$). The weighting scheme: $w = 1/[1.5360 - 0.12297|F_o| + 0.002314(|F_o|)^2 + 0.000020 \times (|F_o|)^3]$ gave uniform average values of $w(|F_o| - |F_c|)^2$ over ranges of $|F_o|$ and was employed in the final stages of refinement.

On the final cycle of refinement the mean parameter shift was 0.32σ, the largest shift, 1.8σ, being associated with a hydrogen atom. The mean error in an observation of unit weight was 1.059. The final positional and thermal parameters appear in Tables 1 and 2 respectively.[1] Measured and calculated structure factors have been placed in the Depository of Unpublished Data.[1]

The ellipsoids of thermal motion for the non-hydrogen atoms are shown in Fig. 1. The thermal motion has been analysed in terms of the rigid-body modes of translation (**T**), libration (**L**), and screw (**S**) motion (12) using the computer program MGTLS. The rms standard error in the temperature factors σU_{ij} (derived from the least-squares analysis) is 0.0011 Å^2. Analysis of the entire molecule as a rigid body was unsuccessful, but each of the phosphorus tetrahedra behaves as a rigid body (rms $\Delta U_{ij} = 0.0011$ Å^2 for P(1) and 0.0013 Å^2 for the P(2) group).

The appropriate bond distances have been corrected for libration (13, 14), using shape parameters q^2 of 0.08 for all atoms involved. Corrected bond lengths appear in Table 3 along with the uncorrected values.[1] Corrected angles differ from the uncorrected values in Table 4 by less than 1σ.[1]

Results and Discussion

Figure 1 shows the molecule viewed along the fourfold axis with the crystallographic numbering scheme and Fig. 2 shows the packing arrange-

[1]The structure factor table and Tables 2 (thermal parameters), 3(*b*), and 4(*b*) (individual bond lengths and angles involving hydrogen atoms) are available, at a nominal charge, from the Depository of Unpublished Data, CISTI, National Research Council of Canada, Ottawa, Canada K1A 0S2.

TABLE 3. Bond lengths (Å) with estimated standard deviations in parentheses

(*a*) Non-hydrogen atoms*

Bond	Length		Bond	Length	
	Uncorr.	Corr.		Uncorr.	Corr.
P(1)—N(2′)	1.572(2)	1.585	P(1)—C(1)	1.802(2)	1.812
P(1)—N(1)	1.582(2)	1.594	P(1)—C(2)	1.798(2)	1.812
P(2)—N(1)	1.594(2)	1.606	P(2)—C(3)	1.798(2)	1.810
P(2)—N(2)	1.564(2)	1.575	P(2)—C(4)	1.791(3)	1.807

*Primed atom is at $3/2-y, x, z$.

(*b*) Bonds involving hydrogen atoms

C—H 0.92(3)–1.00(4), weighted mean 0.95(2) Å

TABLE 4. Bond angles (deg) with estimated standard deviations in parentheses

(*a*) Non-hydrogen atoms*

Bonds	Angle (deg)	Bonds	Angle (deg)
N(2′)— P(1) —N(1)	119.2(1)	N(1) — P(2) —N(2)	115.1(1)
N(2′)— P(1) —C(1)	111.5(1)	N(1) — P(2) —C(3)	106.0(1)
N(2′)— P(1) —C(2)	105.2(1)	N(1) — P(2) —C(4)	108.7(1)
N(1) — P(1) —C(1)	104.0(1)	N(2) — P(2) —C(3)	112.4(1)
N(1) — P(1) —C(2)	111.7(1)	N(2) — P(2) —C(4)	111.3(1)
C(1) — P(1) —C(2)	104.4(1)	C(3) — P(2) —C(4)	102.5(1)
P(1) —N(1) — P(2)	131.5(1)	P(2) —N(2) — P(1″)	148.2(1)

*Primed atom is at $3/2-y, x, z$; doubled-primed atom is at $y, 3/2-x, z$.

(*b*) Angles involving hydrogen atoms

Bonds	Angle (deg)	Weighted mean
P—C—H	105(2)–112(2)	109(2)
H—C—H	106(3)–117(3)	110(3)

ment viewed along *c*. Bond angles are given in Table 4 and the unique intraannular torsion angles in the 16-membered ring in Table 5. The mean structural parameters for $(NPMe_2)_8$ are compared with those of related molecules $(NPMe_2)_4$ (2), $(NPMe_2)_5$ (3), and $(NPMe_2)_7$ (1) in Table 6.

The crystal structure (Fig. 2) consists of well-separated molecules of hexadecamethylcyclooctaphosphazene. All intermolecular nonbonded contacts correspond to normal van der Waals interactions. There are no intermolecular H. . .H separations shorter than 2.5 Å.

The molecule has crystallographic (exact) C_4 symmetry. Idealized local conformations (G = gauche, T = trans, ref. 15) at the phosphorus atoms are defined in terms of the intrannular torsion angles about the two P—N bonds. The ideal GG local conformation has both torsion angles 60° and the ideal GT local conformation has one torsion angle of 60° and one of 180°. In $(NPMe_2)_8$ P(1) has a GG and P(2) a GT local conformation, thus adjacent phosphorus atoms have alternately GG and GT local conformations around the ring. This arrangement is similar to that observed for the heptamer (1) in which the local conformations are alternately GG and GT except for one pair of adjacent phosphorus atoms which both have GT local conformations.

The mean structural parameters in Table 6 show that the mean P—N and P—C bond lengths are nearly the same in all three compounds. The

TABLE 5. Intraannular torsion angles (deg) 16-membered ring*

Bond	Value
N(2′)— P(1)	−76.8(2)
P(1) —N(1)	−61.3(2)
N(1) — P(2)	−27.8(2)
P(2) —N(2)	−156.5(3)

*Symmetry related torsion angles have the same signs as those listed above.

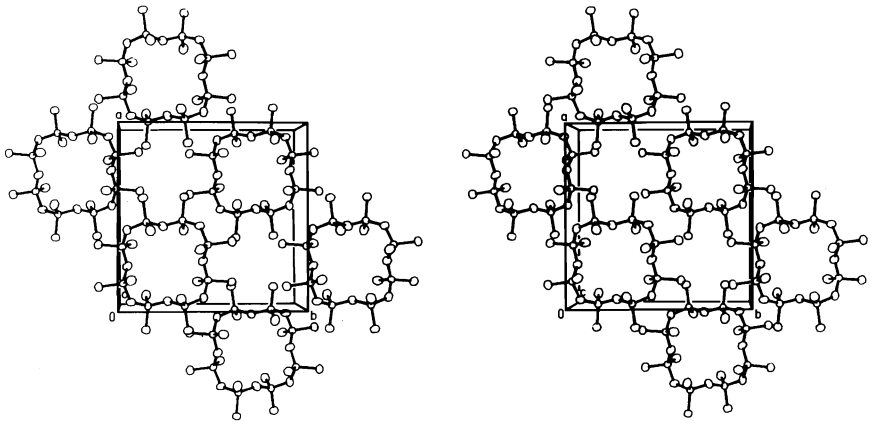

FIG. 2. The crystal structure of hexadecamethylcyclooctaphosphazene viewed along c (origin at $\bar{1}$).

TABLE 6. Mean structural parameters for $(NPMe_2)_n$ (n = 4, 5, 7, and 8) (distance in Å and angles in deg)*

	Length (Å) for n =			
Bond	4	5	7	8
P—C	1.804(3)	1.801(4)	1.804(11)	1.811(2)
P—N	1.596(5)	1.586(4)	1.592(6)	1.590(13)
	Angle (deg) for n =			
Bonds	4	5	7	8
N—P—N	119.8(2)	118.7(18)	117.1(16)	117.2(21)
P—N—P	132.0(2)	132.9(17)	132.9(20)	139.9(84)
C—P—C	104.1(2)	104.3(8)	103.9(5)	103.5(10)

*Root-mean-square deviations from the mean in parentheses.

N—P—N and C—P—C angles decrease slightly and the P—N—P angles increase with increasing ring size. In hexadecamethylcyclooctaphosphazene the corrected P—C bond lengths are equal within experimental error but the corrected P—N distances and the corresponding angles at both the P and N atoms differ significantly. This appears to result from differences in both local conformation and σ-hybridization between the unique P and N atoms in the structure.

Acknowledgments

We thank the National Research Council of Canada for financial support and the University of British Columbia Computing Centre for assistance.

1. K. D. GALLICANO, R. T. OAKLEY, N. L. PADDOCK, S. J. RETTIG, and J. TROTTER. Can. J. Chem. **55**, 304 (1977).
2. M. W. DOUGILL. J. Chem. Soc. 5471 (1961).
3. M. W. DOUGILL and B. SHELDRICK. Acta Crystallogr. Sect. B, **33**, 295 (1977).
4. P. COPPENS, L. LEISEROWITZ, and D. RABINOVITCH. Acta Crystallogr. **18**, 1035 (1965).
5. W. R. BUSING and H. A. LEVY. Acta Crystallogr. **10**, 180 (1957).
6. J. KARLE and H. HAUPTMAN. Acta Crystallogr. **9**, 635 (1956).
7. J. KARLE and I. L. KARLE. Acta Crystallogr. **21**, 849 (1966).
8. M. G. B. DREW. Private communication (1969); M. G. B. DREW, D. H. TEMPLETON, and A. ZALKIN. Acta Crystallogr. Sect. B, **25**, 261 (1969).
9. D. T. CROMER and J. B. MANN. Acta Crystallogr. Sect. A, **24**, 321 (1968).
10. R. F. STEWART, E. R. DAVIDSON, and W. T. SIMPSON. J. Chem. Phys. **42**, 3175 (1965).
11. D. T. CROMER and D. LIBERMAN. J. Chem. Phys. **53**, 1891 (1970).
12. V. SCHOMAKER and K. N. TRUEBLOOD. Acta Crystallogr. Sect. B, **24**, 63 (1969).
13. D. W. J. CRUICKSHANK. Acta Crystallogr. **9**, 747 (1956); **9**, 754 (1956).
14. D. W. J. CRUICKSHANK. Acta Crystallogr. **14**, 896 (1961).
15. S. MIZUSHIMA. Structure of molecules and internal rotation. Academic Press, New York. 1954.

Crystal and molecular structure of 2,2,4,6,6-pentamethyl-5-benzoyl-4-(*N*-methylbenzamido)-1,3-diaza-2,4,6(P^v)-triphosphorin

RICHARD T. OAKLEY, NORMAN L. PADDOCK, STEVEN J. RETTIG, AND JAMES TROTTER

Department of Chemistry, University of British Columbia, 2075 Wesbrook Mall, Vancouver, B.C., Canada V6T 1W5

Received January 4, 1977

RICHARD T. OAKLEY, NORMAN L. PADDOCK, STEVEN J. RETTIG, and JAMES TROTTER. Can. J. Chem. **55**, 2534 (1977).

Crystals of 2,2,4,6,6-pentamethyl-5-benzoyl-4-(*N*-methylbenzamido)-1,3-diaza-2,4,6(P^v)-triphosphorin are triclinic, $a = 13.375(1)$, $b = 11.313(1)$, $c = 7.925(1)$ Å, $\alpha = 107.72(1)$, $\beta = 98.23(1)$, $\gamma = 87.00(1)°$, $Z = 2$, space group $P\bar{1}$. The structure was solved by Patterson and Fourier syntheses and was refined by full-matrix least-squares procedures to a final R of 0.067 and R_w of 0.089 for 3954 reflections with $I \geq 3\sigma(I)$. The P_3N_2C ring is nearly planar and has a conformation corresponding to a flattened version of the chair – twist boat. Bond lengths in the azaphosphorin ring, P—N, 1.579–1.614(2), and P—C, 1.752(3) and 1.777(3) Å, indicate conjugation with the *C*-benzoyl group. The exocyclic P—N bond length, 1.742(3) Å, is longer than those in related compounds as a result of competitive electron withdrawal from the *N*-benzoyl group. Other bond lengths (corrected for libration) are: mean P—Me, 1.796(4); C=O, 1.242(3) and 1.247(4); C—N, 1.472(3) and 1.369(4); mean C—C(phenyl), 1.391(10); other $C(sp^2)$—$C(sp^2)$; 1.417–1.518(4) Å.

RICHARD T. OAKLEY, NORMAN L. PADDOCK, STEVEN J. RETTIG et JAMES TROTTER. Can. J. Chem. **55**, 2534 (1977).

Les cristaux de la pentaméthyl-2,2,4,6,6 benzoyl-5 (*N*-méthylbenzamido)-4 diaza-1,3 triphosphorine-2,4,6 (P^v) sont tricliniques $a = 13.375(1)$, $b = 11.313(1)$, $c = 7.925(1)$ Å, $\alpha = 107.72(1)$, $\beta = 98.23(1)$, $\gamma = 87.00(1)°$, $Z = 2$, groupe d'espace $P\bar{1}$. On a résolu la structure par la méthode des synthèses de Patterson et de Fourier et on l'a affinée par la méthode des moindres carrés (matrice complète) jusqu'à une valeur finale de $R = 0.067$ et $R_w = 0.089$ pour 3954 réflexions avec $I \geq 3\ \sigma(I)$. Le cycle P_3N_2C est pratiquement planaire et a une conformation correspondant à une version aplatie d'une chaise – bateau croisée. Les longueurs de liaison dans le cycle azaphosphorine, P—N, 1.579–1.614(2) et P—C, 1.752(3) et 1.777(3) Å, indiquent qu'il existe une conjugaison avec le groupe *C*-benzoyle. La longueur de liaison P—N exocyclique 1.742(3) Å est plus grande que celle observée dans des composés semblables et ceci est le résultat d'un enlèvement d'électron compétitif du groupe *N*-benzoyle. D'autres longueurs de liaison (corrigées pour la libration) sont: la moyenne P—Me, 1.796(4); C=O, 1.242(3) et 1.247(4); C—N, 1.472(3) et 1.369(4); moyenne C—C(phényle), 1.391(10); autre $C(sp^2)$—$C(sp^2)$; 1.417–1.518(4) Å.

[Traduit par le journal]

Introduction

In recent years, the molecular structures of many neutral and protonated phosphazene derivatives have been reported. The present paper represents a departure from these more well known compounds, and describes the crystal and molecular structure of the azaphosphorin derivative $Me_5(NMeCOPh)P_3N_2CCOPh$, **1**, in which a nitrogen atom of a P_3N_3 phosphazene ring has been replaced by a carbon atom (1).

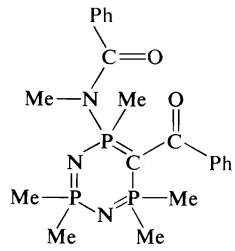

1

Experimental

Crystals suitable for X-ray analysis were obtained by recrystallization from benzene/octane. The crystal chosen for study was mounted with c^* parallel to the goniostat axis and had dimensions of *ca.* 0.35 × 0.40 × 0.60 mm. Unit-cell and space group data were obtained from film and diffractometer measurements. The unit-cell parameters were refined by a least-squares treatment of $\sin^2\theta$ values for 28 reflections measured on a diffractometer with Cu K_α radiation ($\lambda = 1.5418$ Å). Crystal data (at 22°C) are:

$C_{21}H_{28}N_3O_2P_3$ fw = 447.4

Triclinic, $a = 13.375(1)$, $b = 11.313(1)$, $c = 7.925(1)$ Å, $\alpha = 107.72(1)$, $\beta = 98.23(1)$, $\gamma = 87.00(1)°$, $V = 1130.4(2)$ Å^3, $Z = 2$, $\rho_c = 1.314$ g cm^{-3}, $F(000) = 472$, μ(Cu

K_α) = 25.7 cm^{-1}. Space group $P\bar{1}$ (C_i^1, No. 2) from structure analysis.

Intensities were measured with nickel-filtered Cu K_α radiation on a Datex-automated General Electric XRD-6 diffractometer. A θ–2θ scan at 2° min^{-1} over a range of (1.80 + 0.86 tan θ) degrees in 2θ was employed. Background counts (10 s) were measured at each end of the scan. Data were measured to 2θ = 146°. The intensity of the check reflection, measured every 40 reflections throughout the data collection, had an rms deviation of 6.5% from its mean value. Lorentz and polarization corrections and check reflection scaling were applied, and the structure amplitudes were derived. No absorption correction was made. Of the 4524 independent reflections measured, 3969 had intensities greater than 3σ(I) above background where $\sigma^2(I) = S + B + (0.06S)^2$ with S = scan count and B = time averaged background count. These reflections were used in the solution and refinement of the structure.

The analysis was carried out in the centrosymmetric space group $P\bar{1}$ on the basis of the $|E|$ statistics. The positions of the three phosphorus atoms were determined from the three-dimensional Patterson function. Two cycles of isotropic full-matrix least-squares refinement of the phosphorus atoms gave R = 0.468. The positions of the remaining non-hydrogen atoms were located on a difference map calculated at this point. The non-hydrogen atoms were then refined isotropically for two cycles and then anisotropically for two cycles giving R = 0.089. A subsequent difference map gave positions for all 28 hydrogen atoms which were included in later cycles of refinement with isotropic thermal parameters. The entire structure (375 variables) was refined for two cycles giving a final R of 0.067 and R_w of 0.089 for 3954 reflections with $I \geq 3\sigma(I)$ (15 reflections which had $|F_o| - |F_c| > 3\sigma(F)$ were removed from the data set in the final stages of refinement; for all 4524 reflections R = 0.073 and R_w = 0.092).

The least-squares refinement was based on the minimization of $\Sigma w[|F_o| - |F_c|/(1 + gI)|]^2$ where g is the extinction parameter and I the uncorrected intensity. The final value of g was 3.1 × 10^{-8}. The scattering factors of ref. 2 were used for the non-hydrogen atoms and those of ref. 3 for the hydrogen atoms. Anomalous scattering factors from ref. 4 were used for the non-hydrogen atoms. The anisotropic thermal parameters employed in the refinement are U_{ij} in the expression:

$$f = f^0 \exp\,[-2\pi^2(U_{11}\,h^2a^{*2} + U_{22}k^2b^{*2} + U_{33}\,l^2c^{*2} + 2U_{12}\,hka^*b^* + 2U_{13}\,hla^*c^* + 2U_{23}\,klb^*c^*)]$$

where f^0 is the tabulated scattering factor and f is that corrected for thermal motion (for H atoms $f = f^0 \exp[-8\pi^2 U \sin^2\theta/\lambda^2]$). The weighting scheme: $w = 1/\sigma^2(F)$ where $\sigma^2(F)$ is derived from the previously defined $\sigma^2(I)$ gave uniform average values of $w(|F_o| - |F_c|)^2$ over ranges of $|F_o|$ and was employed in the final stages of refinement.

On the final cycle of refinement the mean parameter shift was 0.37σ, the largest shift (1.8σ) being associated with a hydrogen atom. The mean error in an observation of unit weight was 2.238. The final positional and thermal parameters appear in Tables 1 and 2 respectively.

TABLE 1. Final positional parameters (fractional × 10^4, P × 10^5, H × 10^3), with estimated standard deviations in parentheses

Atom	x	y	z
P(1)	31342(5)	38124(6)	80867(9)
P(2)	37655(6)	27209(6)	44039(9)
P(3)	43369(6)	16281(6)	71943(10)
O(1)	2884(2)	5005(2)	3814(3)
O(2)	1950(2)	1811(2)	5997(3)
N(1)	1908(2)	3530(2)	8341(3)
N(2)	4249(2)	1650(2)	5181(3)
N(3)	3891(2)	2820(2)	8592(3)
C(1)	3181(2)	3936(2)	5955(4)
C(2)	3415(3)	5263(3)	9791(4)
C(3)	4735(3)	3315(4)	3542(6)
C(4)	2857(3)	2044(4)	2487(5)
C(5)	5635(3)	1467(4)	8018(7)
C(6)	3788(4)	227(3)	7232(6)
C(7)	2768(2)	4917(3)	5302(4)
C(8)	2110(2)	5907(3)	6380(4)
C(9)	1129(3)	5637(4)	6478(5)
C(10)	495(3)	6571(5)	7367(6)
C(11)	855(4)	7758(5)	8173(6)
C(12)	1817(4)	8030(4)	8075(6)
C(13)	2445(3)	7124(3)	7143(5)
C(14)	1435(3)	4268(4)	9899(4)
C(15)	1468(2)	2486(3)	7154(4)
C(16)	421(2)	2134(3)	7225(4)
C(17)	−414(2)	2908(3)	7129(4)
C(18)	−1383(3)	2481(4)	7012(5)
C(19)	−1512(3)	1276(4)	7003(5)
C(20)	−697(3)	506(4)	7117(6)
C(21)	267(3)	925(3)	7200(5)
H(2a)	405(3)	557(3)	963(5)
H(2b)	294(3)	585(4)	960(5)
H(2c)	351(3)	510(4)	96(6)
H(3a)	527(4)	357(4)	447(7)
H(3b)	452(4)	396(5)	294(7)
H(3c)	505(3)	262(4)	279(6)
H(4a)	247(4)	264(6)	203(8)
H(4b)	312(6)	128(7)	190(10)
H(4c)	241(5)	161(6)	262(9)
H(5a)	593(4)	215(5)	811(6)
H(5b)	587(3)	62(4)	740(6)
H(5c)	574(3)	143(4)	915(7)
H(6a)	388(4)	21(4)	844(7)
H(6b)	309(5)	19(5)	682(7)
H(6c)	415(4)	−49(5)	660(7)
H(9)	92(3)	483(4)	587(5)
H(10)	−16(3)	637(4)	734(5)
H(11)	57(5)	840(6)	863(8)
H(12)	209(4)	895(6)	860(8)
H(13)	314(3)	735(4)	709(6)
H(14a)	193(3)	455(3)	106(5)
H(14b)	113(4)	503(5)	967(7)
H(14c)	94(4)	372(5)	1013(7)
H(17)	−23(3)	386(4)	722(6)
H(18)	−195(3)	300(4)	684(6)
H(19)	−219(3)	83(4)	678(6)
H(20)	−82(4)	−36(5)	708(6)
H(21)	89(3)	31(4)	722(5)

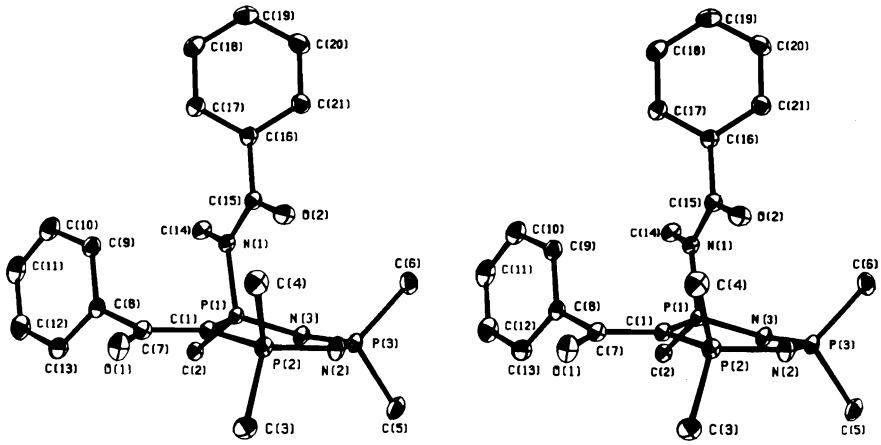

FIG. 1. A stereo view of the 2,2,4,6,6-pentamethyl-5-benzoyl-4-(*N*-methylbenzamido)-1,3-diaza-2,4,6(P^V)-triphosphorin molecule. 50% ellipsoids are shown. Hydrogen atoms have been omitted for the sake of clarity.

TABLE 3. Bond lengths (Å) with estimated standard deviations in parentheses

(*a*) Non-hydrogen atoms

Bond	Length		Bond	Length	
	Uncorr.	Corr.		Uncorr.	Corr.
P(1) —N(1)	1.738(2)	1.742	C(1) —C(7)	1.417(4)	1.419
P(1) —N(3)	1.577(2)	1.579	C(7) —C(8)	1.513(4)	1.518
P(2) —N(2)	1.589(3)	1.592	C(8) —C(9)	1.381(5)	1.391
P(3) —N(2)	1.590(3)	1.595	C(8) —C(13)	1.395(5)	1.404
P(3) —N(3)	1.611(2)	1.614	C(9) —C(10)	1.398(5)	1.403
P(1) —C(1)	1.748(3)	1.752	C(10)—C(11)	1.379(7)	1.389
P(1) —C(2)	1.797(3)	1.799	C(11)—C(12)	1.357(7)	1.365
P(2) —C(1)	1.773(3)	1.777	C(12)—C(13)	1.389(5)	1.394
P(2) —C(3)	1.796(4)	1.798	C(15)—C(16)	1.490(4)	1.494
P(2) —C(4)	1.797(4)	1.800	C(16)—C(17)	1.390(4)	1.398
P(3) —C(5)	1.786(4)	1.789	C(16)—C(21)	1.388(5)	1.396
P(3) —C(6)	1.792(4)	1.794	C(17)—C(18)	1.388(5)	1.391
O(1) —C(7)	1.244(4)	1.247	C(18)—C(19)	1.381(6)	1.389
O(2) —C(15)	1.237(3)	1.242	C(19)—C(20)	1.370(6)	1.376
N(1) —C(14)	1.470(3)	1.472	C(20)—C(21)	1.382(5)	1.386
N(1) —C(15)	1.365(4)	1.369			

(*b*) Bonds involving hydrogen atoms

Bond	Length	Mean
C(ar)—H	0.81(6)–1.10(5)	0.98(8)
C(Me)—H	0.84(7)–1.03(4)	0.95(5)

Measured and calculated structure factors have been placed in the Depository of Unpublished Data.[1]

The ellipsoids of thermal motion for the non-hydrogen atoms are shown in Fig. 1. The thermal motion has been analysed in terms of the rigid-body modes of translation (**T**), libration (**L**), and screw (**S**) motion (5) using the computer program MGTLS. The rms standard error in the temperature factors σU_{ij} (derived from the least-squares analysis) is 0.0016 Å^2. Analyses were successful for the two phenyl groups (rms ΔU_{ij} = 0.0021 Å^2 for C(7)—C(13) and 0.0017 Å^2 for C(16)—C(21)) and for the 13 atom group P(1)—P(3), N(1)—N(3), and C(1)—C(7) (rms ΔU_{ij} = 0.0040 Å^2).

[1]The structure factor table and Tables 2 (thermal parameters), 3(*b*), and 4(*b*) (individual bond lengths and angles involving hydrogen atoms), 6 and 7 are available, at a nominal charge, from the Depository of Unpublished Data, CISTI, National Research Council of Canada, Ottawa, Canada K1A 0S2.

TABLE 4. Bond angles (deg) with estimated standard deviations in parentheses

(*a*) Non-hydrogen atoms

Bonds	Angle (deg)	Bonds	Angle (deg)
N(1) —P(1) —N(3)	110.7(1)	P(1) —C(1) —C(7)	126.1(2)
N(1) —P(1) —C(1)	110.7(1)	P(2) —C(1) —C(7)	115.4(2)
N(1) —P(1) —C(2)	102.6(1)	O(1) —C(7) —C(1)	123.5(3)
N(3) —P(1) —C(1)	114.0(1)	O(1) —C(7) —C(8)	115.8(2)
N(3) —P(1) —C(2)	106.6(1)	C(1) —C(7) —C(8)	120.7(2)
C(1) —P(1) —C(2)	111.6(1)	C(7) —C(8) —C(9)	119.9(3)
N(2) —P(2) —C(1)	114.5(1)	C(7) —C(8) —C(13)	120.9(3)
N(2) —P(2) —C(3)	108.1(2)	C(9) —C(8) —C(13)	118.9(3)
N(2) —P(2) —C(4)	108.6(2)	C(8) —C(9) —C(10)	120.1(4)
C(1) —P(2) —C(3)	110.9(2)	C(9) —C(10)—C(11)	120.0(4)
C(1) —P(2) —C(4)	109.4(2)	C(10)—C(11)—C(12)	120.2(4)
C(3) —P(2) —C(4)	104.9(2)	C(11)—C(12)—C(13)	120.5(4)
N(2) —P(3) —N(3)	116.5(1)	C(8) —C(13)—C(12)	120.1(4)
N(2) —P(3) —C(5)	109.2(2)	O(2) —C(15)—N(1)	119.5(3)
N(2) —P(3) —C(6)	109.0(2)	O(2) —C(15)—C(16)	119.0(3)
N(3) —P(3) —C(5)	107.3(2)	N(1) —C(15)—C(16)	121.5(2)
N(3) —P(3) —C(6)	110.8(2)	C(15)—C(16)—C(17)	123.4(3)
C(5) —P(3) —C(6)	103.1(2)	C(15)—C(16)—C(21)	117.5(3)
P(1) —N(1) —C(14)	121.5(2)	C(17)—C(16)—C(21)	118.7(3)
P(1) —N(1) —C(15)	116.0(2)	C(16)—C(17)—C(18)	120.7(3)
C(14)—N(1) —C(15)	121.9(3)	C(17)—C(18)—C(19)	119.3(3)
P(2) —N(2) — P(3)	126.8(2)	C(18)—C(19)—C(20)	120.8(4)
P(1) —N(3) — P(3)	125.6(1)	C(19)—C(20)—C(21)	119.9(4)
P(1) —C(1) — P(2)	118.5(2)	C(16)—C(21)—C(20)	120.6(3)

(*b*) Angles involving hydrogen atoms

Bonds	Angle (deg)	Mean
C—C(ar)—H	109(5)–131(5)	120(5)
R—C(sp^3)—H	106(5)–117(5)	110(3)
H—C(sp^3)—H	83(5)–131(5)	108(11)

The appropriate bond distances have been corrected for libration (6, 7), using shape parameters q^2 of 0.08 for all atoms involved. Corrected bond lengths appear in Table 3[1] along with the uncorrected values.

Results and Discussion

The crystal structure (the first of a compound containing the P_3N_2C heterocycle) consists of discrete molecules of 2,2,4,6,6-pentamethyl-5-benzoyl-4-(*N*-methylbenzamido)-1,3-diaza-2,4,6-(P^v)-triphosphorin. A general view of the molecule with the crystallographic numbering scheme is shown in Fig. 1; Fig. 2 shows the packing arrangement viewed along *c**. The only intermolecular interaction is a possible C(14)—H-(14a). . .O(1) (x, y, $1 + z$) hydrogen bond (C. . .O = 3.309(4) Å); all other intermolecular contacts correspond to normal van der Waals interactions.

Bond angles are given in Table 4,[1] and intra-annular torsion angles in Table 5. Distances of atoms from weighted least-squares mean planes (Table 6) and non-bonded distances and details of the C—H. . .O interaction (Table 7) have been deposited.[1] Some of the key molecular dimensions are shown schematically in Fig. 3.

The P_3N_2C ring is slightly non-planar; the mean displacement from the mean plane is 0.075 Å, the maximum 0.226 Å (N(3)). The torsion angles in Table 5 indicate that the ring conformation corresponds closely to a flattened version of the chair – twist-boat transition (8). The bond angles are similar to those found in P_3N_3 rings (see *e.g.* ref. 9), but, in contrast to the marked alternation in bond lengths found in the structures of protonated phosphazenes (10–14), the P—N bonds vary only slightly in length. The averages of the P(1)—N(3), P(2)—N(2), and P(3)—N(2), P(3)—N(3) pairs are 1.586, 1.605 Å respectively, both close to the values found in $(NPMe_2)_{4,7,8}$ (1.596, 1.592, 1.590 Å (15–17)), indicating that the net effect of replacing a nitrogen atom by a carbon atom is small. The

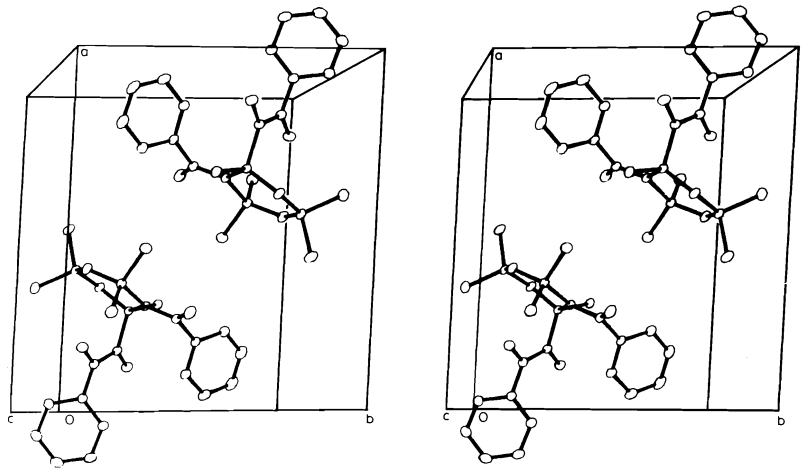

FIG. 2. The packing arrangement viewed along c^*.

TABLE 5. Intraannular torsion angles (deg), azaphosphorin ring

Bond	Value
P(1) —C(1)	16.9(2)
C(1) —P(2)	−3.1(2)
P(2) —N(2)	−5.6(2)
N(2) —P(3)	−0.1(2)
P(3) —N(3)	17.4(2)
N(3) —P(1)	−25.0(2)

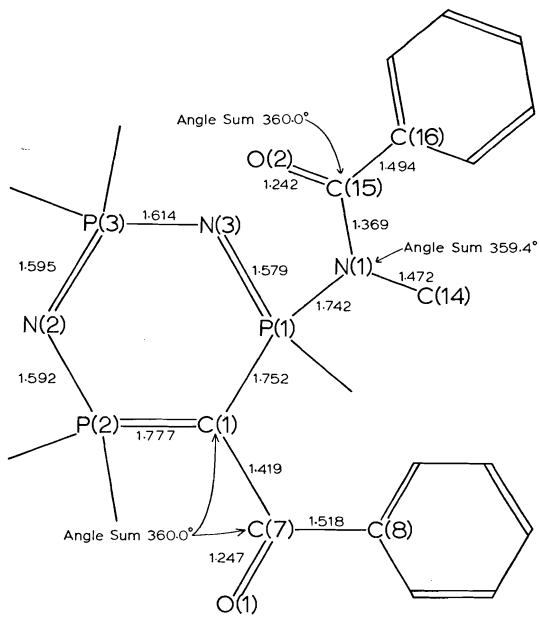

FIG. 3. Key molecular dimensions. The bond distances have been corrected for libration.

mean length[2] (1.765 Å) of the significantly different P(1)—C(1) and P(2)—C(1) bonds (1.752(3) and 1.777(3) Å) is somewhat greater than the mean of a single P—C bond (1.80 Å (18)) and a P=C bond found in a simple ylid (1.66 Å (19, 20)). The additional lengthening is probably the result of charge delocalization into the *C*-benzoyl group, as found in *C*-benzoyl ylids $Ph_3PCXCOPh$ (X = Cl, I) (21).[3] Conjugation with the *C*-benzoyl group is indicated by a lengthening of the C(7)=O(1) bond from 1.23 Å (18) to 1.247(4) Å, and a significant shortening of the C(1)—C(7) bond to 1.419(4) Å, compared to the 1.485 Å expected for a $C(sp^2)$—$C(sp^2)$ single bond (23). Because of the competing influence of the azaphosphorin ring, the extent of these effects is less marked than in the *C*-benzoyl ylids $Ph_3PCXCOPh$ (Table 8).

The coordination groups of the trigonal atoms C(1) and C(7) are significantly non-planar, though chemically the deviation is unimportant. Probably for steric reasons, the P—C(1)—C(7)-[O(1)]—C(8) unit is not planar. Torsion about the central C(1)—C(7) bond (7.7°) is small enough to allow conjugation between the P—C(1) and C(7)=O(1) bonds, but, consistently with the C(7)—C(8) distance of 1.518(4) Å, conjugation with the phenyl group is prohibited by a large torsion angle, as in $Ph_3PCXCOPh$ (Table 8). The geometry of the *N*-benzoyl group is somewhat different. The C(15) carbonyl group is planar within experimental error, and the co-

[2]Here and elsewhere in this paper when mean values are quoted they refer to weighted means with rms deviations from the mean in parentheses.

[3]For a recent summary of P=C bond lengths in substituted ylids $R_3PCR^1R^2$, see ref. 22.

TABLE 8. Bond lengths and torsion angles (τ) in *C*-benzoylated ylids

Compound	Length (Å)			Angle (deg)	
	P=C	C—C	C=O	τ(C—C)†	τ(C—Ph)†
$Ph_3P{=}CICOPh$*	1.71	1.35	1.28	12	52
$Ph_3P{=}CClCOPh$*	1.736	1.361	1.301	4.8	57.7
$Me_5(NMeCOPh)P_3N_2CCOPh$	1.765	1.431	1.244	7.7‡	73.5

*Reference 21.
†Mean value.
‡53.1° for the *N*-benzoyl group.

ordination group at N(1) is nearly so. The relative conjugative abilities of the azaphosphorin ring and the benzoyl group are indicated by the long P(1)—N(1) bond. At 1.742(3) Å, this bond is much longer than the exocyclic P—N bonds (1.651–1.678 Å) in the dimethylaminophosphazenes $(NP(NMe_2)_2)_{3,4,6,8}$ (9, 24–26), and approaches the value of 1.77 Å expected for a P—N single bond (27). It is similar to the unique exocyclic P—N bond length in $N_4P_4(NMe_2)_8 \cdot W(CO)_4$ (28), which is lengthened to 1.75 Å through the action of the metal as a competitive acceptor for the formally unshared electrons of a dimethylamino group. In both molecules, conjugation of the exocyclic nitrogen atom with the ring is reduced. Nevertheless, comparison of the N(1)—C(15) bond length (1.369(4) Å) with the corresponding distance in benzamide (1.342(3) Å) (29) offers direct evidence that some conjugation with the azaphosphorin ring still occurs.

Both phenyl groups are slightly but significantly non-planar. The mean phenyl C—C distance of 1.391(10) Å is as expected. The N—Me distance of 1.472(3) Å is significantly greater than the value of 1.446 Å expected for a $C(sp^3)$—$N(sp^2)$ single bond. The mean P—Me distance of 1.796(4) Å is somewhat less than the values of 1.804, 1.804, and 1.811 Å found in the methylphosphazenes $(NPMe_2)_{4,7,8}$ (15–17). The bond lengths involving hydrogen atoms (mean C(ar)—H, 0.98(8) and mean C(Me)—H, 0.95(5) Å) are as expected for X-ray data.

Acknowledgments

We thank the National Research Council of Canada for financial support and the University of British Columbia Computing Centre for assistance.

1. H. P. CALHOUN, R. T. OAKLEY, and N. L. PADDOCK. Chem. Commun. 454 (1975).
2. D. T. CROMER and J. B. MANN. Acta Crystallogr. Sect. A, **24**, 321 (1968).
3. R. F. STEWART, E. R. DAVIDSON, and W. T. SIMPSON. J. Chem. Phys. **42**, 3175 (1965).
4. D. T. CROMER and D. LIBERMAN. J. Chem. Phys. **53**, 1891 (1970).
5. V. SCHOMAKER and K. N. TRUEBLOOD. Acta Crystallogr. Sect. B, **24**, 63 (1969).
6. D. W. J. CRUICKSHANK. Acta Crystallogr. **9**, 747 (1956); **9**, 754 (1956).
7. D. W. J. CRUICKSHANK. Acta Crystallogr. **14**, 896 (1961).
8. J. B. HENDRICKSON. J. Am. Chem. Soc. **89**, 7036 (1967).
9. S. J. RETTIG and J. TROTTER. Can. J. Chem. **51**, 1295 (1973).
10. J. TROTTER and S. H. WHITLOW. J. Chem. Soc. (A), 455 (1970).
11. H. P. CALHOUN and J. TROTTER. J. Chem. Soc. Dalton Trans. 382 (1974).
12. H. R. ALLCOCK, E. C. BISSELL, and E. T. SHAWL. Inorg. Chem. **12**, 2963 (1973).
13. H. T. SEARLE, J. DYSON, N. L. PADDOCK, and T. N. RANGANATHAN. J. Chem. Soc. Dalton Trans. 203 (1975).
14. A. L. MACDONALD and J. TROTTER. Can. J. Chem. **52**, 734 (1974).
15. M. W. DOUGILL. J. Chem. Soc. 5471 (1961).
16. K. D. GALLICANO, R. T. OAKLEY, N. L. PADDOCK, S. J. RETTIG, and J. TROTTER. Can. J. Chem. **55**, 304 (1977).
17. R. T. OAKLEY, N. L. PADDOCK, S. J. RETTIG, and J. TROTTER. Can. J. Chem. This issue.
18. L. E. SUTTON (*Editor*). Interatomic distances and configurations in molecules and ions. Chem. Soc. Special Publication No. 11 (1958) and No. 18 (1965).
19. L. PAULING. The nature of the chemical bond. 3rd ed. Cornell University Press, Ithaca, NY. 1960. p. 224.
20. J. C. J. BART. J. Chem. Soc. (B), 350 (1969).
21. F. S. STEPHENS. J. Chem. Soc. 5640 (1965); 5658 (1965).
22. U. LINGER and H. BURZLAFF. Acta Crystallogr. Sect. B, **30**, 1715 (1974).
23. M. J. S. DEWAR and H. N. SCHMEISING. Tetrahedron, **11**, 96 (1960).
24. G. J. BULLEN. J. Chem. Soc. 3193 (1962).
25. A. J. WAGNER and A. VOS. Acta Crystallogr. Sect. B, **24**, 1423 (1968).
26. H. P. CALHOUN, N. L. PADDOCK, and J. TROTTER. J. Chem. Soc. Dalton Trans. 38 (1976).
27. E. HOBBS, D. E. C. CORBRIDGE, and B. RAISTRICK. Acta Crystallogr. **6**, 21 (1953); D. W. CRUICKSHANK. Acta Crystallogr. **17**, 671 (1964).
28. H. P. CALHOUN, N. L. PADDOCK, and J. TROTTER. J. Chem. Soc. Dalton Trans. 2708 (1973).
29. C. C. F. BLAKE and R. W. H. SMALL. Acta Crystallogr. Sect. B, **29**, 2201 (1972).

N,N-Ethylenebis(salicylideneimine) derivatives of gallium trimethyl: crystal and molecular structure of *N,N*-ethylenebis(salicylideneiminato)bis(dimethylgallium)

KENNETH S. CHONG, STEVEN J. RETTIG, ALAN STORR, AND JAMES TROTTER

Department of Chemistry, University of British Columbia, 2075 Wesbrook Mall, Vancouver, B.C., Canada V6T 1W5

Received January 13, 1977

KENNETH S. CHONG, STEVEN J. RETTIG, ALAN STORR, and JAMES TROTTER. Can. J. Chem. **55**, 2540 (1977).

Crystals of *N,N*-ethylenebis(salicylideneiminato)bis(dimethylgallium) are orthorhombic, $a = 22.781(1)$, $b = 9.4869(6)$, $c = 19.700(2)$ Å, $Z = 8$, space group *Pbca*. The structure was solved by direct methods and was refined by full-matrix least-squares procedures to a final R of 0.036 and R_w of 0.029 for 2248 reflections with $I \geq 3\sigma(I)$. Details of the preparation and physical properties of $(C_{16}H_{14}N_2O_2)(GaMe_2)_2$ and $(C_{16}H_{15}N_2O_2)(GaMe_2)$ are given. The $(C_{16}H_{14}N_2O_2)(GaMe_2)_2$ molecule is approximately centrosymmetric in the solid state. A "$GaMe_2$" unit is coordinated to each of the two salicylideneiminato moieties of the *N,N*-ethylenebis(salicylideneiminato) ligand. The gallium atoms have a distorted tetrahedral coordination geometry, with bond angles at gallium ranging from 92.7(1) to 124.6(3)°. Important bond lengths (corrected for libration) are: Ga—O, 1.886(2) and 1.884(2), Ga—N, 2.033(3) and 2.042(3), and weighted mean Ga—C, 1.959(9) Å.

KENNETH S. CHONG, STEVEN J. RETTIG, ALAN STORR et JAMES TROTTER. Can. J. Chem. **55**, 2540 (1977).

Les cristaux du *N,N*-éthylènebis(salicylidèneiminato)bis(diméthylgallium) sont orthorhombiques, $a = 22.781(1)$, $b = 9.4869(6)$, $c = 19.700(2)$ Å, $Z = 8$, groupe d'espace *Pbca*. On a résolu la structure par les méthodes directes et on l'a affinée par la méthode des moindres carrés (matrice complète) jusqu'à une valeur finale de R de 0.036 et R_w de 0.029 pour 2248 réflexions avec $I \geq 3\sigma(I)$. On donne les détails pour la préparation ainsi que les propriétés physiques de $(C_{16}H_{14}N_2O_2)(GaMe_2)_2$ et $(C_{16}H_{15}N_2O_2)(GaMe_2)$. La molécule $(C_{16}H_{14}N_2O_2)(GaMe_2)_2$ est approximativement centrosymétrique à l'état solide. Une unité "$GaMe_2$" est coordonnée à chacune des deux portions salicylidèneiminato du ligand *N,N*-éthylènebis(salicylidèneiminato). Les atomes de gallium possèdent une géométrie de coordination tétraédrique déformée avec des angles au niveau du gallium allant de 92.7(1) jusqu'à 124.6(3)°. Les longueurs de liaison importantes (corrigées pour la libration) sont: Ga—O, 1.886(2) et 1.884(2), Ga—N, 2.033(3) et 2.042(3) et la moyenne pondérée de Ga—C, 1.959(9) Å.

[Traduit par le journal]

Introduction

Gallium trimethyl reacts readily with compounds containing "active hydrogen", eliminating methane to yield products containing either four- or five-coordinate gallium (1–9). These products are often associated and frequently occur as dimers. The present study involves the reaction of gallium trimethyl with the "active hydrogen" compound *N,N*-ethylenebis(salicylideneimine), **1**. Two products have been isolated. The 1:1 complex, **2**, may contain an octahedrally coordinated gallium atom, but the material is polycrystalline and thus unsuitable for X-ray analysis. The crystal structure of the 2:1 complex, **3**, has been determined to discover if oligomerization *via* oxygen lone pair coordination to gallium occurs to give five-coordinate gallium.

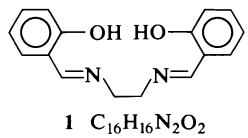

1 $C_{16}H_{16}N_2O_2$

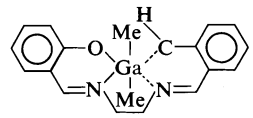

2 $(C_{16}H_{15}N_2O_2)GaMe_2$

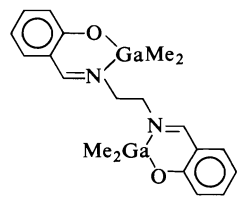

3 $(C_{16}H_{14}N_2O_2)(GaMe_2)_2$

Experimental

All solvents were dried and distilled before use and reactions involving gallium trimethyl were initiated in a glove box filled with dry nitrogen, with subsequent

handling occurring under a blanket of dry nitrogen or on a high vacuum line. Gallium trimethyl was prepared as described previously (10) and *N,N*-ethylenebis(salicylideneimine), **1**, was prepared from ethylenediamine and salicylaldehyde by standard methods.

*$(C_{16}H_{15}N_2O_2)(GaMe_2)$, **2***

This 1:1 compound was prepared by reacting **1** (3.57 g, 13.32 mmol) with gallium trimethyl (1.53 g, 13.34 mmol) in benzene solution at room temperature. Methane was briskly evolved and after completion of the reaction the solvent was removed to yield a yellow solid product. This was recrystallized from toluene to give an air-stable yellow material. *Anal.* calcd. for $(C_{16}H_{15}N_2O_2)(GaMe_2)$: C 58.9, H 5.7, N 7.6; found: C 58.6, H 5.6, N 7.59. Mass spectrum data (recorded on a Varian MAT CH4B mass spectrometer at 70 eV with an ion source temperature of approximately 70°C) are

m/e	Intensity	Assignment
353	36.0	$(C_{16}H_{15}N_2O_2)GaMe^+$
351	55.0	
338	38.0	$(C_{16}H_{15}N_2O_2)Ga^+$
336	57.0	
267	100	$(C_{16}H_{15}N_2O_2)^+$

^1H nmr (C_6D_6 soln.): τ_{GaMe_2} = 10.06 ppm singlet, τ_{OH} = 2.34 ppm singlet, $\tau_{"CH_2CH_2"}$ = 6.91 ppm "triplet" (J = 6 Hz), $\tau_{C_6H_6}$ = 2.84 ppm.

*$(C_{16}H_{14}N_2O_2)(GaMe_2)_2$, **3***

A stoichiometric 1:2 ratio of reactants, *N,N*-ethylenebis(salicylideneimine) and gallium trimethyl, failed to give the desired product, even under forcing conditions. It is necessary to react *N,N*-ethylenebis(salicylideneimine) with an excess of gallium trimethyl.

N,N-Ethylenebis(salicylideneimine) (0.41 g, 1.53 mmol) was dissolved in xylene and transferred quantitatively into a break–seal apparatus. Gallium trimethyl (1.6 g, 13.95 mmol) was condensed onto the frozen **1** solution at −196°C, and the apparatus evacuated and sealed. The reaction bulb was then maintained at 110°C for 48 h. The methane evolved was measured (calcd. 34.5 ml; found 41.0 ml at STP). The solvent was removed to yield a yellow powdery solid as product. This was recrystallized from benzene to yield an air-sensitive yellow crystalline material. Crystals suitable for X-ray study were positioned in capillary tubes which were subsequently sealed to prevent atmospheric interference. *Anal.* calcd. for *N,N*-ethylenebis(salicylideneiminato)bis(dimethylgallium): C 51.6, H 5.6, N 6.0; found: C 51.9, H 5.8, N 5.9. Mass spectrum data are

m/e	Intensity	Assignment
453	19.7	$(C_{16}H_{14}N_2O_2)Ga_2Me_3^+$
451	52.0	
449	40.6	
337	67.5	$(C_{16}H_{14}N_2O_2)Ga^+$
335	100.0	

^1H nmr (C_6D_6 soln.): τ_{GaMe_2} = 9.96 ppm singlet, $\tau_{"CH_2CH_2"}$ = 7.04 ppm singlet, $\tau_{C_6H_6}$ = 2.84 ppm.

*X-Ray Crystallographic Analysis of $(C_{16}H_{14}N_2O_2)(GaMe_2)_2$, **3***

The crystal chosen for study was mounted with c parallel to the goniostat axis and had dimensions of *ca.* 0.09 × 0.25 × 0.49 mm. Unit-cell and space group data were obtained from film and diffractometer measurements. The unit-cell parameters were refined by a least-squares on 2 sin θ/λ values for 20 reflections measured on a diffractometer with Cu K_α radiation (λ = 1.5418 Å). Crystal data (at 22°C) are:

$C_{20}H_{26}Ga_2N_2O_2$ fw = 465.9
Orthorhombic, a = 22.781(1), b = 9.4869(6), c = 19.700(2) Å, V = 4257.8(6) Å^3, Z = 8, ρ_c = 1.4535(2) g cm^{-3}, $F(000)$ = 1904, μ(Cu K_α) = 34.8 cm^{-1}. Absent reflections: $0kl$, $k \neq 2n$, $h0l$, $l \neq 2n$, and $hk0$, $h \neq 2n$ define uniquely the space group $Pbca$ (D_{2h}^{15}, No. 61).

Intensities were measured with nickel-filtered Cu K_α radiation on a Datex-automated General Electric XRD-6 diffractometer. A θ–2θ scan at 2° min^{-1} over a range of (1.80 + 0.86 tan θ) degrees in 2θ was employed. Background counts (10 s) were measured at each end of the scan. Data were measured to 2θ = 140°. The intensities of two check reflections, measured every 40 reflections throughout the data collection, remained constant to within ±5%. Lorentz and polarization corrections and batch check reflection scaling were applied, and the structure amplitudes were derived. An absorption correction was applied by a computer program using a Gaussian integration method (11, 12). Transmission factors ranged from 0.395 to 0.744. Of the 4046 independent reflections measured, 2263 (56%) had intensities greater than 3σ(I) above background where $\sigma^2(I) = S + B + (0.06S)^2$ with S = scan count and B = time averaged background count.

The solution and initial stages of refinement were carried out with 1443 observed reflections with 2θ ≤ 90°. The structure was solved by direct methods (13). The positions of the two gallium atoms were determined from an E-map calculated from the set of signs with the second highest consistency index (0.94). Two cycles of full-matrix least-squares refinement of the coordinates and isotropic thermal parameters of the gallium atoms gave R = 0.323. The positions of the remaining non-hydrogen atoms were given by a difference map calculated at this point. The non-hydrogen atoms were refined isotropically for two cycles and then anisotropically for two cycles reducing R to 0.056. The hydrogen atom positions were given by a subsequent difference synthesis. The entire structure (hydrogen atoms with isotropic thermal parameters) was refined using the full data set for six cycles giving a final R of 0.036 and R_w of 0.029 for 2248 reflections with $I \geq 3\sigma(I)$ (15 reflections which had $|F_o| - |F_c| > 3\sigma(F)$ were treated as unobserved in the final stages of refinement; for all 4046 reflections R = 0.088 and R_w = 0.030).

The least-squares refinement was based on the minimization of $\Sigma w[|F_o| - |F_c|/(1 + gI)]]^2$ where g is the extinction parameter and I the uncorrected intensity. The final value of g was 6.6 × 10^{-8}. The scattering factors of ref. 14 were used for the non-hydrogen atoms and those

of ref. 15 for the hydrogen atoms. Anomalous scattering factors from ref. 16 were used for the non-hydrogen atoms. The weighting scheme: $w = (|F_o|/55.0)^2$ for $|F_o| < 55.0$, $w = (55.0/|F_o|)^2$ for $|F_o| \geq 55.0$, and $w = 0.01$ for the unobserved reflections gave uniform average values of $w(|F_o| - |F_c|)^2$ over ranges of $|F_o|$ and was employed in the final stages of refinement.

On the final cycle of refinement the mean parameter shift was 0.11σ and the largest shift (0.94σ) was associated with the thermal parameter of H(4). The mean error in an observation of unit weight was 0.742. The final positional and thermal parameters appear in Tables 1 and 2 respectively.[1] Measured and calculated structure factors have been placed in the Depository of Unpublished Data.[1]

The ellipsoids of thermal motion for the non-hydrogen atoms are shown in Fig. 1. The thermal motion has been analysed in terms of the rigid-body modes of translation (**T**), libration (**L**), and screw (**S**) motion (17) using the computer program MGTLS. The rms standard error in the temperature factors σU_{ij} (derived from the least-squares analysis) is 0.0024 Å^2. Analyses were successful for the two Ga coordination groups (rms $\Delta U_{ij} =$ 0.0027 Å^2 for Ga(1), O(1), N(1), C(9), C(10) and 0.0032 Å^2 for Ga(2), O(2), N(2), C(19), C(20)), and for the two 11 atom groups Ga(1), O(1), N(1), C(1)–C(8) (rms $\Delta U_{ij} = 0.0051$ Å^2) and Ga(2), O(2), N(2), C(11)–C(18) (rms $\Delta U_{ij} = 0.0046$ Å^2).

The appropriate bond distances have been corrected for libration (18, 19), using shape parameters q^2 of 0.08 for all atoms involved. Corrected bond lengths appear in Table 3[1] along with the uncorrected values. Bond angles changed by less than one standard deviation in all cases, thus only the uncorrected values are reported in Table 4.[1]

Results and Discussion

$(C_{16}H_{15}N_2O_2)(GaMe_2)$, **2**, displays a broad ν_{OH} vibration in its infrared spectrum and a signal due to the OH group in its ^{1}H nmr spectrum with τ_{OH} at 2.34 ppm compared with τ_{OH} at 2.29 ppm in *N*,*N*-ethylenebis(salicylideneimine) itself. The unsymmetrical nature of compound **2** was demonstrated by the "triplet" signal in its ^{1}H nmr spectrum due to the "ethylene" protons, these protons giving a singlet in the ^{1}H nmr spectra of the symmetrical compounds **1** and **3**.

As expected, $(C_{16}H_{14}N_2O_2)(GaMe_2)_2$, **3**, displayed no ν_{OH} in its infrared spectrum and no τ_{OH} in its ^{1}H nmr spectrum. The forcing reaction conditions needed to introduce a second "$GaMe_2$" moiety into the $(C_{16}H_{15}N_2O_2)(GaMe_2)$ compound suggest that some type of interaction of the "$GaMe_2$" group already present in **2** with the OH group and/or the second N atom is already taking place. This is indicated by the dotted lines in **2**. The introduction of the second

TABLE 1. Final positional parameters (fractional × 10^4, Ga × 10^5, H × 10^3), with estimated standard deviations in parentheses

Atom	*x*	*y*	*z*
Ga(1)	58346(2)	46792(4)	25092(2)
Ga(2)	39048(2)	28823(4)	46979(2)
O(1)	6423(1)	3506(3)	2165(1)
O(2)	3556(1)	4121(2)	5319(1)
N(1)	5670(1)	3428(3)	3321(1)
N(2)	4254(1)	4486(3)	4143(1)
C(1)	6589(1)	2270(3)	2391(2)
C(2)	6361(1)	1617(3)	2970(2)
C(3)	6577(2)	298(4)	3163(2)
C(4)	7009(2)	−379(5)	2796(3)
C(5)	7233(2)	282(5)	2230(2)
C(6)	7031(2)	1548(5)	2037(2)
C(7)	5934(1)	2255(4)	3411(2)
C(8)	5270(2)	3921(5)	3857(2)
C(9)	6166(4)	6418(7)	2869(3)
C(10)	5183(3)	4589(11)	1868(3)
C(11)	3413(1)	5448(4)	5209(2)
C(12)	3656(1)	6285(4)	4690(2)
C(13)	3485(2)	7691(5)	4636(2)
C(14)	3083(2)	8262(5)	5060(2)
C(15)	2846(2)	7455(5)	5562(2)
C(16)	3006(2)	6089(5)	5641(2)
C(17)	4067(1)	5753(4)	4202(2)
C(18)	4657(1)	4145(5)	3586(2)
C(19)	3332(3)	2006(8)	4088(3)
C(20)	4504(3)	1841(7)	5183(3)
H(3)	641(1)	−13(4)	355(2)
H(4)	713(1)	−113(4)	295(2)
H(5)	753(2)	−21(4)	198(2)
H(6)	716(1)	199(3)	171(1)
H(7)	585(1)	168(4)	379(2)
H(8a)	538(1)	488(3)	399(1)
H(8b)	526(2)	334(4)	420(2)
H(9a)	633(2)	625(6)	326(3)
H(9b)	586(3)	663(8)	303(4)
H(9c)	627(2)	688(5)	254(2)
H(10a)	485(2)	501(5)	207(2)
H(10b)	515(2)	357(6)	181(3)
H(10c)	531(2)	480(5)	156(2)
H(13)	366(1)	814(3)	430(2)
H(14)	299(1)	912(3)	508(2)
H(15)	257(2)	773(4)	584(2)
H(16)	288(1)	557(3)	595(1)
H(17)	418(1)	646(3)	389(1)
H(18a)	455(1)	321(4)	341(2)
H(18b)	462(1)	486(4)	323(2)
H(19a)	358(3)	162(9)	388(4)
H(19b)	314(3)	274(6)	390(3)
H(19c)	304(2)	180(6)	430(3)
H(20a)	472(3)	131(6)	494(3)
H(20b)	481(2)	232(6)	539(3)
H(20c)	434(2)	142(6)	550(3)

[1]The structure factor table and Tables 2 (thermal parameters), 3(*b*) (bond lengths involving H), 4(*b*) (angles involving H), 6 (mean planes), and 7 (nonbonded distances) are available, at a nominal charge, from the Depository of Unpublished Data, CISTI, National Research Council of Canada, Ottawa, Canada K1A 0S2.

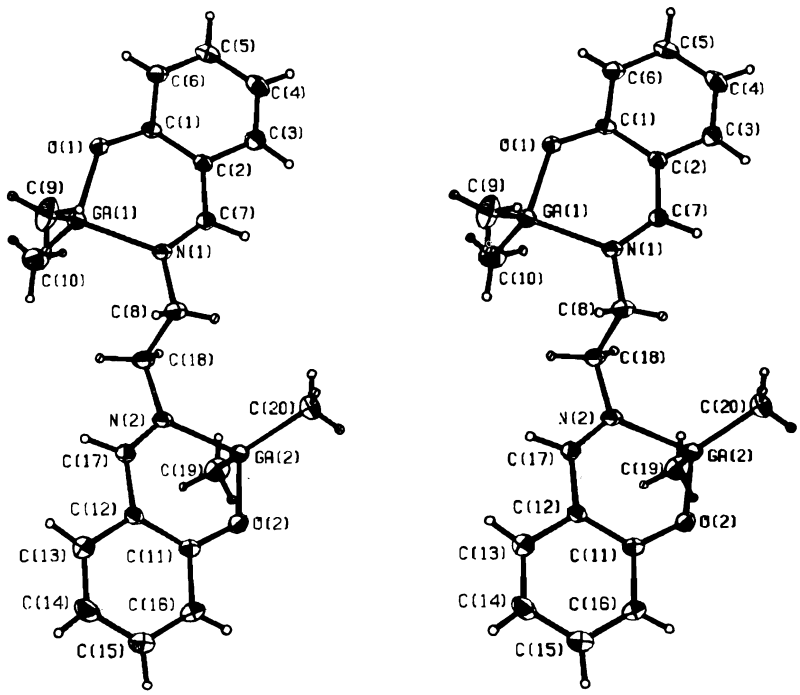

FIG. 1. A stereo view of the *N,N*-ethylenebis(salicylideneiminato)bis(dimethylgallium) molecule. 50% ellipsoids are shown for the non-hydrogen atoms. Hydrogen atoms have been given artifically small temperature factors for the sake of clarity. Hydrogen atoms labelled "b" and "c" in Table 1 are represented above by ⊘ and ⊗ respectively.

"$GaMe_2$" moiety necessitates a drastic ligand rearrangement in which any interaction of the type posulated in **2** must first be broken and then the molecule rearranged to accommodate the second "$GaMe_2$". In the arrangement illustrated by the X-ray structure of *N,N*-ethylenebis(salicylideneiminato)bis(dimethylgallium), **3** (see Fig. 1), steric crowding is reduced to a minimum and the gallium atoms are tetrahedrally coordinated, there being no evidence of association via O → Ga type linkages.

The mass spectra of the two compounds **2** and **3** displayed amongst their most intense peaks signals due to the parent ions minus one methyl group (see Experimental section) *viz.* $(C_{16}H_{15}N_2O_2)GaMe^+$ and $(C_{16}H_{14}N_2O_2)Ga_2Me_3^+$, respectively. The relative intensities of the peaks in the multiplet signals agree well with those predicted from the isotopic distribution of the metal atoms (^{69}Ga (60%); ^{71}Ga (40%)). The parent ions themselves were not detected, but this is not unusual in the mass spectra of this type of compound containing the dimethyl gallium moiety (1, 7).

The X-ray crystallographic analysis shows that the *N,N*-ethylenebis(salicylideneiminato)-bis(dimethylgallium) molecule (see Fig. 1) is somewhat distorted from C_i symmetry. This may be due to crystal packing forces, since the ^1H nmr spectrum in solution (Me and "CH_2-CH_2" singlets at $\tau = 9.96$ and 7.04 ppm respectively) requires the molecule to have at least C_i symmetry. The distortions from C_i symmetry are seen as differences between the two chelate rings (intraannular torsion angles are given in Table 5) and unequal torsion angles about the N(1)—C(8) and N(2)—C(18) bonds (C(7)[N(1)—C(8)]C(18) = −122.0(3) and C(17)-[N(2)—C(18)]C(8) = 107.0(3)°). The torsion angle about the central bond, N(1)[C(8)—C(18)]N(2), is 173.8(3)°, close to the value of 180° required by a centre of symmetry, but quite different from the value of ~30° expected for the quadridentate configuration of the *N,N*-ethylenebis(salicylideneimine) ligand postulated for **2**.

In the present structure, a "$GaMe_2$" unit is coordinated to each of the two salicylideneimine

TABLE 3. Bond lengths (Å) with estimated standard deviations in parentheses
(*a*) Non-hydrogen atoms

Bond	Length		Bond	Length	
	Uncorr.	Corr.		Uncorr.	Corr.
Ga(1)—O(1)	1.869(2)	1.886	Ga(2)—O(2)	1.874(2)	1.884
Ga(1)—N(1)	2.026(3)	2.033	Ga(2)—N(2)	2.035(3)	2.042
Ga(1)—C(9)	1.948(6)	1.957	Ga(2)—C(19)	1.959(5)	1.969
Ga(1)—C(10)	1.950(5)	1.962	Ga(2)—C(20)	1.938(5)	1.947
O(1) —C(1)	1.309(4)	1.315	O(2) —C(11)	1.318(4)	1.323
N(1) —C(7)	1.277(4)	1.280	N(2) —C(17)	1.280(4)	1.284
N(1) —C(8)	1.471(4)	1.473	N(2) —C(18)	1.469(4)	1.471
C(1) —C(2)	1.398(4)	1.411	C(11)—C(12)	1.407(4)	1.416
C(1) —C(6)	1.404(5)	1.406	C(11)—C(16)	1.398(5)	1.401
C(2) —C(3)	1.397(5)	1.400	C(12)—C(13)	1.395(5)	1.398
C(2) —C(7)	1.437(4)	1.441	C(12)—C(17)	1.434(4)	1.437
C(3) —C(4)	1.380(6)	1.382	C(13)—C(14)	1.350(6)	1.353
C(4) —C(5)	1.376(6)	1.387	C(14)—C(15)	1.363(6)	1.369
C(5) —C(6)	1.340(5)	1.344	C(15)—C(16)	1.355(6)	1.360
C(8) —C(18)	1.510(5)	1.514			

TABLE 4. Bond angles (deg) with estimated standard deviations in parentheses
(*a*) Non-hydrogen atoms

Bonds	Angle (deg)	Bonds	Angle (deg)
O(1) —Ga(1)—N(1)	94.0(1)	O(2) —Ga(2)—N(2)	92.7(1)
O(1) —Ga(1)—C(9)	111.0(3)	O(2) —Ga(2)—C(19)	112.6(2)
O(1) —Ga(1)—C(10)	106.5(3)	O(2) —Ga(2)—C(20)	107.3(2)
N(1) —Ga(1)—C(9)	106.3(2)	N(2) —Ga(2)—C(19)	104.4(2)
N(1) —Ga(1)—C(10)	110.2(3)	N(2) —Ga(2)—C(20)	111.8(2)
C(9) —Ga(1)—C(10)	124.6(4)	C(19)—Ga(2)—C(20)	123.8(3)
Ga(1)—O(1) —C(1)	128.1(2)	Ga(2)—O(2) —C(11)	126.6(2)
Ga(1)—N(1) —C(7)	122.2(2)	Ga(2)—N(2) —C(17)	121.6(2)
Ga(1)—N(1) —C(8)	119.6(3)	Ga(2)—N(2) —C(18)	118.8(3)
C(7) —N(1) —C(8)	118.0(3)	C(17)—N(2) —C(18)	118.8(3)
O(1) —C(1) —C(2)	124.5(3)	O(2) —C(11)—C(12)	124.1(3)
O(1) —C(1) —C(6)	118.4(3)	O(2) —C(11)—C(16)	118.6(3)
C(2) —C(1) —C(6)	117.0(3)	C(12)—C(11)—C(16)	117.3(3)
C(1) —C(2) —C(3)	119.2(3)	C(11)—C(12)—C(13)	119.0(3)
C(1) —C(2) —C(7)	123.8(3)	C(11)—C(12)—C(17)	123.1(3)
C(3) —C(2) —C(7)	116.8(3)	C(13)—C(12)—C(17)	117.9(3)
C(2) —C(3) —C(4)	121.7(4)	C(12)—C(13)—C(14)	121.8(4)
C(3) —C(4) —C(5)	118.4(4)	C(13)—C(14)—C(15)	119.5(4)
C(4) —C(5) —C(6)	120.7(4)	C(14)—C(15)—C(16)	120.9(4)
C(1) —C(6) —C(5)	122.8(4)	C(11)—C(16)—C(15)	121.6(4)
N(1) —C(7) —C(2)	127.0(3)	N(2) —C(17)—C(12)	127.4(3)
N(1) —C(8) —C(18)	111.4(3)	N(2) —C(18)—C(8)	110.2(3)

moieties of the *N,N*-ethylenebis(salicylideneimine) ligand. Both gallium atoms have distorted tetrahedral geometry, the bond angles (listed in Table 4) ranging from 94.0(2) to 124.6(3)° at Ga(1) and from 92.7(1) to 123.8(3)° at Ga(2). The mean[2] Ga—O (1.885(1) Å) and Ga—C (1.959(9) Å) bond lengths are close to the mean values observed for related structures containing tetrahedral gallium (Ga—O, 1.87 Å (20 and references therein), and Ga—C, 1.954(4) Å (7 and references therein)). The mean Ga—N bond length (2.038(5) Å) is significantly longer than the mean value of 1.998(1) Å for "long" Ga—N bonds in related molecules (7 and references therein). This lengthening is due, at least in part, to σ-hybridization effects (21). The mean angle at Ga involving N (103.2°)

[2]Here and elsewhere in this paper, mean values refer to weighted means with rms deviations from the mean in parentheses.

TABLE 5. Intraannular torsion angles (deg)

Bond	Observed	Bond	Observed
Ga(1)—O(1)	5.1(2)	Ga(2)—O(2)	23.7(2)
O(1) —C(1)	−2.9(3)	O(2) —C(11)	−20.8(3)
C(1) —C(2)	−3.2(4)	C(11)—C(12)	3.4(4)
C(2) —C(7)	5.7(4)	C(12)—C(17)	2.7(4)
C(7) —N(1)	−1.8(3)	C(17)—N(2)	7.7(3)
N(1) —Ga(1)	−2.7(2)	N(2) —Ga(2)	−17.0(2)

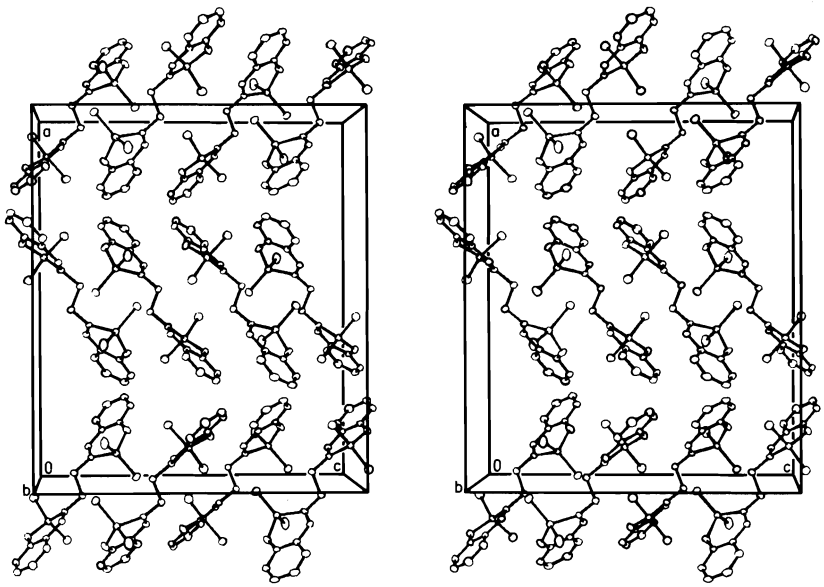

FIG. 2. The packing arrangement viewed along *b*.

implies that the bonding orbital of gallium (involved in the Ga—N bond) has a high degree of *p*-character which increases the bond length. The bond lengths in the remainder of the molecule are as expected.

The five atom OCCCN segments of both chelate rings are nearly planar (mean and maximum displacements from the OCCCN mean planes being 0.012 and 0.029 Å for the Ga(1) ring, 0.021 and 0.035 Å for the Ga(2) ring), with Ga(1) and Ga(2) displaced 0.0951 and −0.3887 Å respectively from the OCCCN mean planes. Both aromatic rings are planar within experimental error. The ring containing Ga(1) is more nearly planar (resembling the GaO_2C_3 chelate ring in the (salicylaldehydato)-dimethylgallium dimer (9)) than that containing Ga(2) (which has a conformation similar to that of the BO_2C_3 ring in (salicylaldehydato)-diphenylboron (22)). Torsion angles in the chelate rings are given in Table 5.

The crystal structure (Fig. 2) consists of well-separated molecules of *N,N*-ethylenebis(salicylideneiminato)bis(dimethylgallium). The shortest intermolecular distances (listed in Table 7[1]) correspond to normal van der Waals interactions.

Acknowledgments

We thank the National Research Council of Canada for financial support, the University of British Columbia Computing Centre for assistance, Mr. P. Borda for the C, H, and N analyses, and Mr. J. Nip for recording the mass spectra.

1. A. ARDUINI and A. STORR. J. Chem. Soc. Dalton Trans. 503 (1974).
2. D. F. RENDLE, A. STORR, and J. TROTTER. Can. J. Chem. **53**, 2930 (1975).
3. D. F. RENDLE, A. STORR, and J. TROTTER. Can. J. Chem. **53**, 2944 (1975).
4. K. R. BREAKELL, D. J. PATMORE, and A. STORR. J. Chem. Soc. Dalton Trans. 749 (1975).
5. D. F. RENDLE, A. STORR, and J. TROTTER. J. Chem. Soc. Dalton Trans. 176 (1975).

6. D. J. PATMORE, D. F. RENDLE, A. STORR, and J. TROTTER. J. Chem. Soc. Dalton Trans. 718 (1975).
7. R. T. BAKER, S. J. RETTIG, A. STORR, and J. TROTTER. Can. J. Chem. **54**, 343 (1976).
8. S. J. RETTIG, A. STORR, and J. TROTTER. Can. J. Chem. **53**, 58 (1975).
9. S. J. RETTIG, A. STORR, and J. TROTTER. Can. J. Chem. **54**, 1278 (1976).
10. A. STORR and B. S. THOMAS. Can. J. Chem. **48**, 3667 (1970).
11. P. COPPENS, L. LEISEROWITZ, and D. RABINOVICH. Acta Crystallogr. **18**, 1035 (1965).
12. W. R. BUSING and H. A. LEVY. Acta Crystallogr. **22**, 457 (1967).
13. R. E. LONG. Ph.D. Thesis. University of California at Los Angeles, Los Angeles, CA. 1965.
14. D. T. CROMER and J. B. MANN. Acta Crystallogr. Sect. A, **24**, 321 (1968).
15. R. F. STEWART, E. R. DAVIDSON, and W. T. SIMPSON. J. Chem. Phys. **42**, 3175 (1965).
16. D. T. CROMER and D. LIBERMAN. J. Chem. Phys. **53**, 1891 (1970).
17. V. SCHOMAKER and K. N. TRUEBLOOD. Acta Crystallogr. Sect. B, **24**, 63 (1969).
18. D. W. J. CRUICKSHANK. Acta Crystallogr. **9**, 747 (1956); **9**, 754 (1956).
19. D. W. J. CRUICKSHANK. Acta Crystallogr. **14**, 896 (1961).
20. S. J. RETTIG, A. STORR, and J. TROTTER. Can. J. Chem. **53**, 753 (1975).
21. S. J. RETTIG. Ph.D Thesis. University of British Columbia, Vancouver, British Columbia. 1974.
22. S. J. RETTIG AND J. TROTTER. Can. J. Chem. **54**, 1168 (1976).

Juvabione and its analogues. IV.[1] Isolation, identification, and occurrence of juvabione, juvabiol, and epijuvabiol from the whole wood of *Abies lasiocarpa*

JOHN F. MANVILLE AND CHARALYN D. KRIZ

Fisheries and Environment Canada, Western Forest Products Laboratory, 6620 N.W. Marine Drive, Vancouver, B.C., Canada V6T 1X2

Received January 26, 1977

JOHN F. MANVILLE and CHARALYN D. KRIZ. Can. J. Chem. **55**, 2547 (1977).

Juvabione (**1**), 1′*Z*-dehydrojuvabione (**10***a*), 1′*E*-dehydrojuvabione (**10***b*), juvabiol (**3**), epijuvabiol (**6**), and the epimeric 2′-dehydrojuvabi-1′-ols (**11**) occur in the whole wood of a number of North American *Abies lasiocarpa* trees. Wide variability of occurrence of these juvabione analogues and other previously characterized extractives is noted. The co-occurrence of **1** and **6**, with *opposite* configurations at C-1′, as shown by ^{13}C nmr indicates the necessity of accurately determining the *complete* structure of naturally occurring compounds *even* if isolated from the same source.

JOHN F. MANVILLE et CHARALYN D. KRIZ. Can. J. Chem. **55**, 2547 (1977).

Les composés suivants furent isolés du bois entier d'un certain nombre de Sapins subalpins (*Abies lasiocarpa*) nord-américains: le juvabione (**1**), le 1′*Z*-déhydrojuvabione (**10***a*), le 1′*E*-déhydrojuvabione (**10***b*), le juvabiol (**3**), l'épijuvabiol (**6**) et un mélange épimère de 2′-déhydrojuvabi-1′-ols (**11**). On remarque une grande variabilité de présence de ces composés analogues au juvabione. La co-présence de **1** et **6** avec les configurations opposées à C-1′, tel que démontré par ^{13}C rmn, indique la nécessité de déterminer avec précision la structure *complète* des composés qui apparaissent naturellement *lorsque* isolés d'une même source.

Introduction

The wood of balsam fir (*Abies balsamea* (L.) Mill.) contains compounds exhibiting juvenile hormone activity on the hemipteran bug *Pyrrhocoris apterus* L. (1, 2). To date five active insect juvenile hormone analogue (IJHA) components have been isolated and identified (3–5). They are juvabione (**1**), 4′-dehydrojuvabione (**2**), juvabiol (**3**), isojuvabiol (**4**), and 3′-dehydrojuvabi-5′-ol (**5**). These compounds and possibly others (5) present in the whole wood of balsam fir are responsible for the "paper factor" effect, first noted by Sláma and Williams (1).[2]

It is well known that balsam fir and alpine fir (*A. lasiocarpa* (Hook.) Nutt.) are two closely related fir species found across Canada (7). The balsam fir predominates in eastern Canada, whereas the alpine fir is found extensively in western Canada from the Pacific Coast to central Alberta. In view of the recently noted (4, 5) extensive occurrences of juvabione and related sesquiterpenoids in the whole wood of balsam fir, it was of interest to study the extractives of alpine fir wood to determine if similar compounds were present.

Alpine fir wood was previously shown to contain both the *Z*- and *E*-α-atlantones (**7**), manool (**8**), and lasiocarpenone (**9**); the occurrence of other sesquiterpene ketones, which were not fully characterized, was also reported (8–11).[3]

This paper reports the isolation and identification of juvabione (**1**) and an unresolved mixture of juvabiol (**3**) and epijuvabiol (**6**). Their variability of occurrence together with that for the atlantones (**7**), manool (**8**), lasiocarpenone (**9**), an isodehydrojuvabione (tentative structure 1′*E*-dehydrojuvabione (**10***b*)), and an unresolved mixture of tertiary alcohols (**11**) in the whole wood of alpine fir is noted.

Isolations

The petroleum ether extracts of the whole wood of nine alpine firs from three sites were pale yellow mobile oils. The individual tree extracts were examined by gas-liquid chromatographic (glc) analysis, which revealed the presence of at least seven major components which did not correspond to any of the common fatty

[1]For part III see ref. 13.

[2]Naturally occurring C-1′ epimers of **1** and **2** (epijuvabione and 4′-dehydroepijuvabione) have been isolated from a Czechoslovak fir (4, 6) growing in an arboretum in Czechoslovakia; both are active IJHAs.

[3]E. P. Swan, unpublished results.

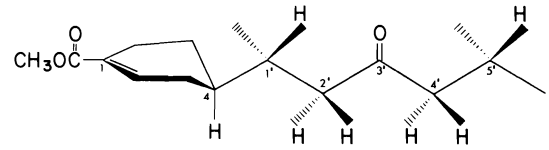

1

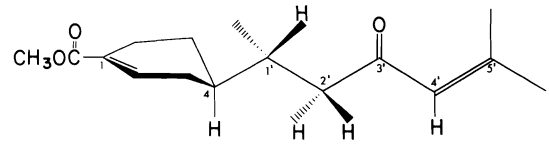

2

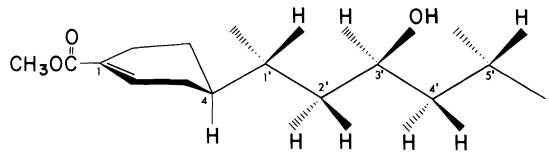

3

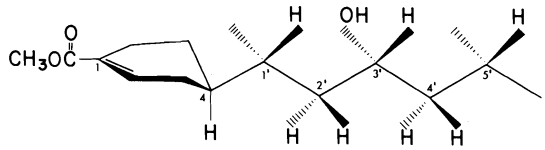

4

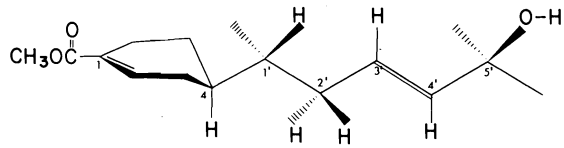

5

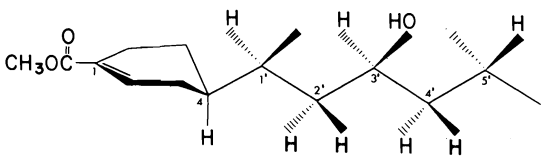

6

or resin acid methyl esters. A composite sample was obtained by combining wood from all nine trees and obtaining the petroleum ether extract which was used for isolation and identification of components. Using procedures given in the experimental section, silicic acid column chromatography effected separation of some of the major components from this extract mixture.

Results and Discussion

The first three major components were identified by glc retention times (r_t) (relative to internal **1**), thin-layer chromatogram (tlc) R_f values, and color reactions. They had been previously characterized as constituents of the wood of alpine fir (8–10) and balsam fir (4), and are the atlantones (**7**) r_t 0.24, manool (**8**) r_t 0.53, and lasiocarpenone (**9**) r_t 0.63.

Whereas previous studies (8–10) had identified these compounds as constituents of the wood of alpine fir, the present glc analyses (Table 1) indicated a considerable degree of variation in the amounts of these compounds in the nine trees sampled. Substantial, yet variable, amounts of the atlantones (**7**) (8–33%) were detected in all samples. Most wood samples contained only trace amounts of manool (**8**) and lasiocarpenone (**9**); in contrast tree 4 had 4.7% **8** and 8.0% **9** and in tree 1, from a different site, we found 0.4% **8** and 8.4% **9**. No other trees examined had more than trace amounts of **9**, while trees 5 and 6 contained substantial amounts of **8**. Site 2 (trees 4–6) had consistently large amounts of **8** in comparison with the other sites. The large degree of variation in the amounts of **9** supports the possibility of inconsistent or variable results in correctly identifying alpine fir wood as noted in the method proposed by Fraser and Swan (11).

The combined fractions 15–32, which gave rise to glc peaks at r_t 1.00 and 1.23 were studied next. Thin-layer chromatography indicated the presence of two ketones (yellow spots with 2,4-DNPH). Hydrogenation (4) of a portion of this mixture resulted in the formation of *cis* and *trans* dihydrojuvabiones, confirming only one monocyclic sesquiterpenoid skeleton to be present in this mixture (4). However, high performance liquid chromatography (hplc) of another portion of this mixture revealed the presence of three components by uv detection; one was juvabione (**1**) ($r_t' = 1.00$); the other two ($r_t' = 0.86$ and 0.94) absorbed much more strongly than did **1** (nmr indicated approximately 70% of the mixture

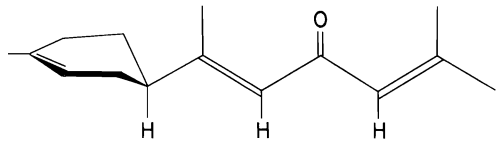

7 (E)

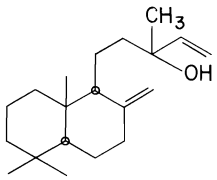

8

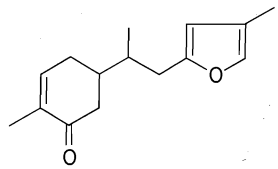

9

was **1**) indicating that they were α,β-unsaturated ketones, but neither was 4′-dehydrojuvabione (**2**) (r_t' = 0.80 (4)). A portion of this mixture was isolated in pure form by rechromatographing on a silicic acid column. This compound gave a glc peak at r_t 1.00 and had $[\alpha]_D$, ^{1}H nuclear magnetic resonance (nmr), infrared (ir), and mass spectra (ms) in accord with those reported for **1** (3, 4). The stereoconfigurations were proven by comparing the ^{13}C nmr chemical shifts observed for **1** with those obtained from samples of previous isolations (13). Juvabione (**1**) was a major component in all nine petroleum ether extracts and appeared to range in amounts from 16 to 65%.

However, further examination of some intermediate fractions from the above separation, which appeared to be pure **1** by glc, contained a second component when observed by hplc and ^{1}H nmr. This minor component had two ^{1}H nmr resonances distinct from those observed for **1**. A vinyl methyl resonance was observed at δ 1.82 (J = 1.6 Hz) (*cf.* δ 1.88 for *trans* methyl of **2** (4)) and an olefinic proton at δ 6.08 (br s, coupled to above methyl). These were assigned to the C-1′ methyl and C-2′ hydrogen of **10***a* respectively. This proposed structure (**10***a*) would account for the observations noted. Thus, reported (Table 1) amounts of **1** noted by glc may be due, in part (*ca.* 5%), to 1′*Z*-dehydrojuvabione (**10***a*).

A second (major) unsaturated ketone, responsible for the observation of a glc peak, at r_t 1.23 was isolated by silicic acid column chromatography together with **1** and was therefore only partly characterized. The ^{1}H nmr spectrum of this mixture revealed the presence of an additional olefinic resonance, at δ 6.08, and a

TABLE 1. *Abies lasiocarpa*, lithophilic extractives

Tree no.	Site*	Age (yr)	Height (m)	Yield (% o.d. wood) Benzene/ ethanol	Yield (% o.d. wood) Petroleum ether	% (glc) of petroleum ether solubles **7** r_t 0.24	**8** 0.53	**9** 0.63	**1** and **10***a* 1.0	**11** 1.11	**10***b* 1.23	**3** and **6** 1.37	— 1.57
1	1	90	14.6	2.44	2.20	9.4	<0.4	8.4	58.0	<0.4	15.2	6.9	<0.4
2	1	95	15.5	4.23	2.61	28.6	1.5	<0.5	20.3	6.5	25.5	15.6	<0.5
3	1	127	23.8	3.16	2.91	33.3	<0.5	<0.5	16.1	9.9	14.4	23.8	<0.5
4	2	155	27.4	2.25	1.76	12.4	4.7	8.0	50.8	<0.4	21.9	<0.4	<0.4
5	2	90	27.4	1.91	0.78	29.2	6.1	<1	39.8	<1	5.6	17.3	<1
6	2	126	26.5	2.22	1.18	13.3	5.1	<0.5	64.8	<0.5	10.6	4.2	<0.5
7	3	114	25.0	2.52	1.21	11.0	<0.3	<0.3	36.3	16.5	22.9	3.5	6.0
8	3	100	19.9	1.53	1.09	32.5	<0.5	<0.5	44.0	<0.5	5.5	15.9	<0.5
9	3	110	21.3	2.09	0.74	7.6	<0.6	<0.6	54.1	10.8	16.5	5.9	2.9

*Site locations: (*1*) McGregor River, 65 miles ENE of Prince George, B.C., (*2*) Blaeberry River drainage, N of Golden, B.C., (*3*) Lind Creek E of Greenwood, Kettle Valley, B.C.

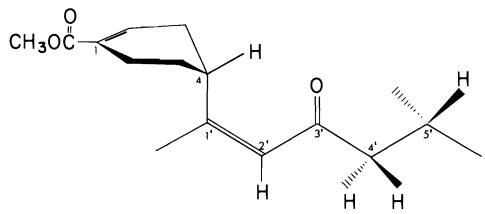

10 *a (Z)*

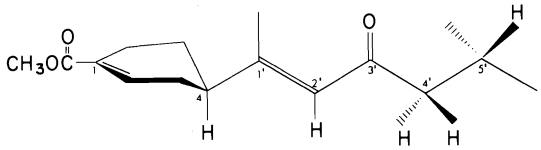

10 *b (E)*

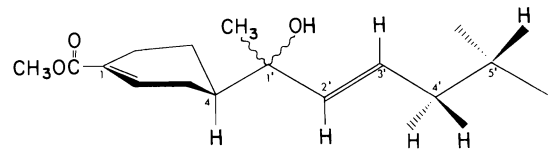

11

vinyl methyl resonance at δ 2.13 (J = 1.25 Hz) (*cf.* δ 2.14 for *cis* methyl of **2** (4)), which was coupled to this olefinic proton. The methyl ester protons were observed at δ 3.78 *vs.* δ 3.77 for **1**. This compound was tentatively assigned structure **10***b*, in accord with that proposed by Leach and Thakore (12). This 1′*E*-dehydrojuvabione (**10***b*) is a major constituent and accounts for from 5–25% of the petroleum ether soluble extract of alpine firs.

Next, the polar components (see isolations) were investigated and characterized by chromatographic and spectroscopic techniques. One portion was recovered unaltered by acetylation attempts. It gave rise to a glc peak at r_t 1.11 and proved to be identical with a mixture of tertiary alcohols (**11**) previously isolated by E. P. Swan[3] of this laboratory. The complete description of these alcohols, which account for up to 16% of the petroleum ether soluble material, will be reported separately. The acetylated portion was efficiently separated (5) into two major portions. The phytosterol acetates were isolated in the first portion and were not investigated further. The compounds present in the intermediate fractions had ^{1}H nmr, r_t, and R_f values which were indicative of juvabiol (**3**) and/or isojuvabiol (**4**) acetates except that $[\alpha]_D$ was different to that found previously (5).

The original alcohols were recovered by deacetylating a portion of the above acetates, the ^{1}H nmr, r_t, and R_f values were indicative of juvabiol and/or isojuvabiol (**3** and **4**) but the $[\alpha]_D$ was different (5). High performance liquid chromatographic analysis of this alcohol fraction showed that it was a mixture and that the ratio of isomers (1:10) was different than observed previously for balsam fir (approximately 1:1, (5)). The major alcohol corresponded with the 4*R*,1′*R*,3′*R* isomer (**4**) obtained previously from sodium borohydride reduction of **1** (5). The minor alcohol co-chromatographed with the 4*R*,1′*R*,3′*S* configurational product (**3**). However, ^{13}C nmr showed that the major alcohol or its acetate was identical with the 4*R*,1′*S*,3′*S* isomer (**6**) obtained from sodium borohydride reduction of epijuvabione (13). (Table 2 lists the ^{13}C nmr shifts for the epimeric alcohols and their acetates, obtained previously from sodium borohydride reduction of **1** and epijuvabione (5, 13).) The minor alcohol (this study) was identified as **3**. These alcohols can account for up to 24% of the petroleum ether soluble material isolated from alpine firwood.

The whole wood of alpine fir contains several juvabione-related compounds that are different from those found in balsam fir (3–5). Moreover, the fact that we observe both (*R* and *S*) C-1′ epimers, but only one C-3′ epimer (*S*), for this species, suggests a possible biosynthesis scheme as outlined in Scheme 1.

In order to rationalize the synthesis of **6**, the major alcohol isolated from alpine fir, one might postulate the stereoselective reduction of **10** to the allylic alcohol **12** with *S* stereochemistry at C-3′ (not isolated, but see below). The latter could then be reduced to either **6** or **3**. This scheme and the existence of **12** is supported by the isolation of the tertiary alcohols **11** (which could be formed in a manner analogous to that reported earlier for the formation of **5** (5)) and by the absence of any alcohols with the *R* configuration at C-3′.

The results of this study contrast those found previously (4, 5) for balsam fir in two important respects. First, both the *R* and *S* epimers at C-1′ were found in alpine fir, whereas only the *R*-epimer at C-1′ was found in balsam fir. Second, whereas the alcohols in balsam fir were epimeric at C-3′, only the *S* epimer at C-3′ was observed in alpine fir. These results suggest two different

biosynthetic pathways, for alpine fir and balsam fir, to the various juvabione-type products. No evidence of the occurrence, in alpine fir, of 4′-dehydrojuvabione (**2**) or 3′-dehydrojuvabi-5′-ol (**5**) was noted.

Experimental

The ^{1}H nmr spectra were determined on samples dissolved in deuteriochloroform containing tetramethylsilane as internal standard using a Varian XL-100 spectrometer. Mass spectra were recorded in the Department of Chemistry, University of British Columbia, using Atlas-4 and AEI-DS-50 spectrometers. Accurate mass measurements were made by reference to appropriate ions of the perfluorokerosene spectrum. Infrared spectra were recorded with a Perkin-Elmer 521 spectrophotometer. Samples were placed as liquid films on the surface of KBr discs. Optical rotations were recorded on a Perkin-Elmer 141 polarimeter made available by the Department of Chemistry, University of British Columbia. Gas–liquid chromatographic analyses were performed on a Hewlett Packard model 7620A equipped with flame-ionization detector. The column used was a 6 ft × $\frac{1}{8}$ in. o.d. stainless steel packed with 10% EGSS-X on 100–120 mesh Gas Chrom. P. The column was held isothermally at 185°C. The carrier-gas flow rate was 25 ml/min. The detector and injector ports were maintained at 270°C. All glc retention times (r_t) are relative to internal **1**.

The hplc analyses were performed on a Spectra-Physics 3500B liquid chromatograph equipped with their chromatronix Model 230 uv (280/254 nm) detector. The column used was 3 × 250 mm Spherisorb ODS (10 μm). The solvent system was water–acetonitrile; isocratic elution was used (40% acetonitrile); the flow rate was 1 ml/min at approximately 600 psi. All hplc retention times (r_t') are relative to internal **1**. Thin-layer chromatograms were performed on Mallinckrodt Chromar plates 7GF using petroleum ether – diethyl ether (3:1) as developer.

Extraction

In each case, debarked whole wood was air dried and ground in a Wiley mill to pass a 5-mm screen. Wood meal for each tree and a composite sample was first extracted over a 12-h period in an all-glass soxhlet apparatus with petroleum ether (bp 60–90°C) followed by benzene–ethanol extraction, prior to obtaining o.d. wood weights. The extracted yellow-brown oil was dried (Na_2SO_4) and the petroleum ether removed under reduced pressure. The petroleum ether soluble material obtained from a composite sample from all nine trees used for isolations of individual compounds contained 88% neutral components as determined by DEAE Sephadex A-25 chromatography using the method of Zinkel and Rowe (14).

Separation

Partial separation of the compounds present in the petroleum ether soluble material was achieved by repeated column chromatography using Woelm silicic acid and petroleum ether – diethyl ether (PE–DE) as eluent. A total of 6.71 g of extract was applied to column 1 (Table 3).

Fractions 33–52 were combined, concentrated to a syrup, and treated with acetic anhydride and pyridine, in

TABLE 2. ^{13}C nmr chemical shifts in $CDCl_3$ for alcohols and their acetates (acetates 170.4 ± 0.2 and 20.9 ± 0.1)†

Compound		Carbon 1	2	3	4	5	6	7	8	1′	2′	3′	4′	5′	CH_3-5′ 6′	CH_3-5′ 7′	CH_3-1′ 8′
Juvabiol (**3**)	(*R*,*R*,*S*)‡	129.9	139.7	29.6	37.2	23.8	24.8	167.7	51.3	33.3	42.3	68.1	46.7	24.4	21.7*	23.4*	16.2
Juvabiol acetate	(*R*,*R*,*S*)	130.0	139.3	29.5	37.3	24.0	24.6	167.5	51.1	33.3	38.8	71.3	43.2	24.4	21.9*	23.0*	15.9
Isojuvabiol (**4**)	(*R*,*R*,*R*)	129.9	139.6	29.6	38.3	24.4	24.7	167.7	51.3	32.7	42.0	67.2	47.7	24.5	22.0*	23.0*	15.6
Isojuvabiol acetate	(*R*,*R*,*R*)	130.0	139.2	29.4	38.1	24.5	24.7	167.5	51.1	32.9	39.1	70.7	44.3	24.5	22.2*	22.7*	15.9
Epijuvabiol (**6**)	(*R*,*S*,*S*)	129.8	139.7	28.1	38.2	25.7	24.7	167.8	51.1	32.7	42.0	67.3	47.5	24.3	21.9*	22.9*	15.2
Epijuvabiol acetate	(*R*,*S*,*S*)	129.9	139.2	28.0	37.8	25.8	24.7	167.5	51.1	32.9	39.2	70.5	44.2	24.5	22.1*	22.7*	15.5
Isoepijuvabiol	(*R*,*S*,*R*)	130.0	139.5	27.3	36.9	26.3	24.8	167.7	51.2	33.5	42.6	68.0	46.8	24.3	21.7*	23.4*	15.9
Isoepijuvabiol acetate	(*R*,*S*,*R*)	130.1	139.1	27.7	37.3	26.1	24.8	167.6	51.2	33.7	39.1	71.4	43.3	24.5	21.9*	23.1*	15.7

*Assignments may be interchanged.
†These compounds were available from earlier studies (refs. 4 and 5 and unpublished results (J. F. Manville and K. Bock)). ^{13}C nmr spectra were recorded in *ca.* 1 *M* $CDCl_3$ solutions on a Varian CFT-20 spectrometer at 20 MHz. Chemical shifts (± 0.1 ppm) are given with respect to Me_4Si using $CDCl_3$ (δ 76.9 ppm) as internal standard. Generally a pulse width of 10 μs (α = 45°), 8K data points and sweep width of 4000 Hz (digital resolution ± 0.98 Hz = ± 0.05 ppm) were used. All spectra were multiplied with an exponential function (sensitivity enhancement, *SE* = −0.4 s) prior to Fourier transformation.
‡Locants are 4, 1′, 3′, respectively.

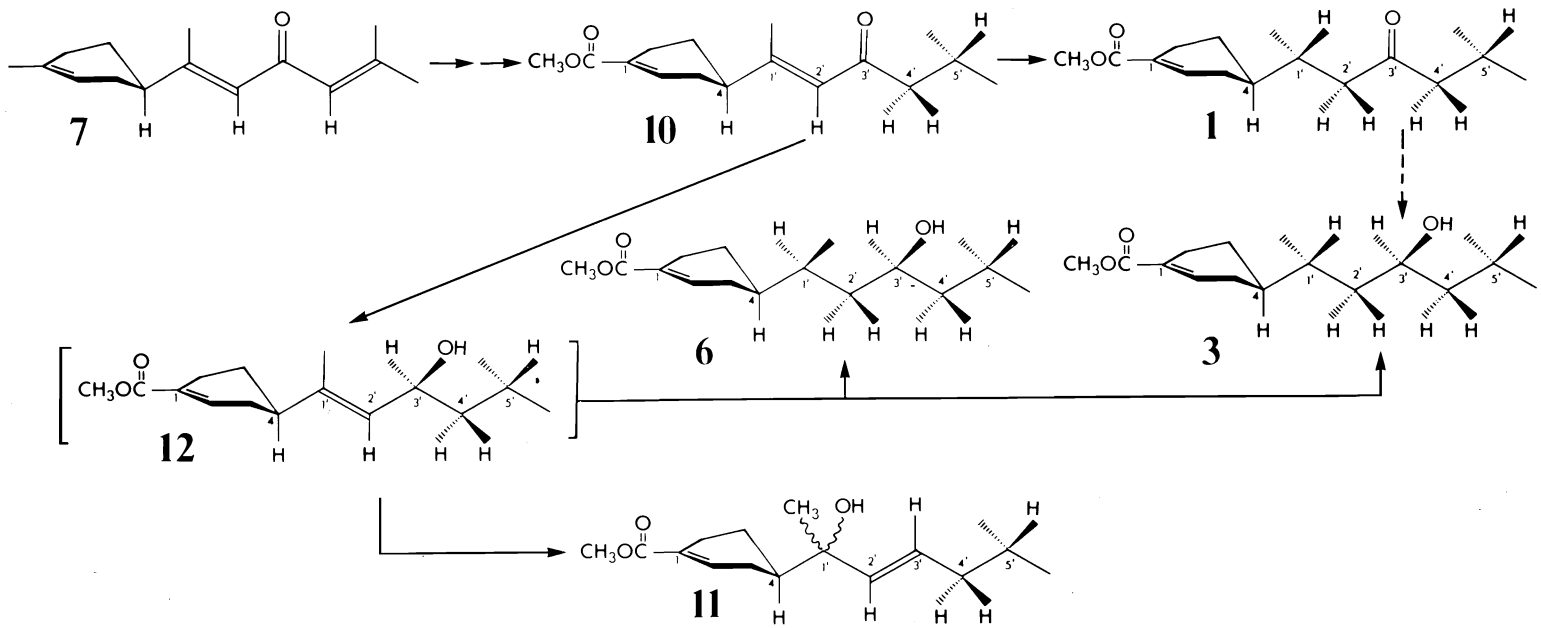

SCHEME 1. Postulated biosynthetic pathways for juvabione and its analogues in *Abies lasiocarpa*.

TABLE 3. Separation of compounds in the petroleum ether soluble fraction

Solvent ratio (PE:DE)	Volume (ml)	Fractions (19 ml)	Peak no. (glc)	Weight (g)
		Column 1		
3:1	400	1–7	—	—
—	—	8–14	I–III	1.89
3:2	375	15–32	IV, VI	1.79
1:1	300	33–52	V, VII	1.32
0:1	250	53–end	—	0.73
		Column 2		
3:1	600	1′–14′	—	—
—	—	15′–24′	New	0.63
1:1	300	42′–47′	V	0.19
0:1	300	48′–50′	V	0.11

the usual manner, to yield a syrup which was partly resolved by column chromatography (column 2) after most of the phystosterol acetates were removed by crystallization.

Deacetylation

Part (306 mg) of fractions 15′–24′ was dissolved in 25 ml of methanol, to which was added 108 mg of sodium methoxide. The solution was heated under reflux for 12 h; 90% of the acetate groups were removed (glc). The reaction mixture was diluted with H_2O, neutralized (H_2SO_4), and extracted with $CHCl_3$ (3 × 10 ml). The resulting syrup was re-chromatographed (column 2) to recover a colourless, viscous oil (139 mg).

*Compound **1** (Juvabione (4R, 1′R))*

Compound **1** was a colourless oil, which by glc was better than 90% pure; it had physical and spectral parameters in accord with those published (4). The ^{13}C nmr δ 209.8, 167.3, 138.9, 129.8, 52.1, 51.0, 47.4, 32.3, 29.4, 24.5, 24.2, 22.3, and 16.2 was identical to that found previously (13) for **1**.

*Compounds **3** and **6** (Juvabiol (4R,1′R,3′S) and Epijuvabiol (4R,1′S,3′S)*

Compounds **3** and **6**, isolated together as a colourless oil and characterized as an epimeric mixture (at C-1′), had most physical and spectral parameters in accord with those published (5) for the C-3′ epimeric mixture of juvabiol (**3**) and isojuvabiol (**4**). The $[\alpha]_D^{24}$ was +57.1° (*c* 0.92, CH_3OH) (*cf.* $[\alpha]_D^{23}$ +67.8° (5)). High performance liquid chromatographic analysis revealed a mixture of isomers (r_t′ 0.76 and 0.83) in a ratio of 1:10 (lit. 9:11 (5)). The ^{13}C nmr δ 167.8, 139.7, 129.8, 68.1, 67.2, 51.2, 47.5, 46.7, 42.3, 42.0, 38.2, 37.2, 33.3, 32.7, 29.6, 28.1, 25.7, 24.7, 24.3, 23.8, 23.4, 22.9, 21.8, 16.2, and 15.2. The observed intensities were consistent with a 1:10 ratio of **3** and **6** (see Table 2 for comparison). *Mol. Wt.* calcd. for $C_{16}H_{28}O_3$: 268.2038; found (high resolution mass spectrometry): 268.2023.

*Acetates of **3** and **6** [Juvabiol Acetate (4R,1′R,3′S) and Epijuvabiol Acetate (4R,1′S,3′S)]*

Acetates of **3** and **6**, isolated together as a colourless oil and characterized as an epimeric mixture (at C-1′), had most physical and spectral parameters in accord with those published (5) for the C-3′ epimeric mixture of juvabiol (**3**) acetate and isojuvabiol (**4**) acetate. Again, the $[\alpha]_D^{24}$ +68.6° (*c* 0.90, CH_3OH) was different from that observed previously ($[\alpha]_D^{23}$ +54.3°) (5). They had R_f 0.53 (incorrectly printed as 0.33 in ref. 5). The ^{13}C nmr δ 170.4, 167.4, 139.2, 129.9, 71.3, 70.4, 51.0, 44.1, 43.2, 39.2, 38.8, 37.8, 37.3, 33.3, 32.8, 29.5, 27.9, 25.7, 24.7, 24.4, 23.0, 22.6, 22.0, 20.8, and 15.5. The observed intensities were consistent with a 1:10 ratio of **3** and **6** acetates (see Table 2 for comparison). *Mol. Wt.* calcd. for $C_{18}H_{30}O_4$: 310.2143; found (high resolution mass spectrometry): 310.2144.

Acknowledgments

We wish to thank Mr. C. R. Daniels for obtaining the hplc results and Dr. K. Bock for help in determining the ^{13}C nmr assignments.

1. K. SLÁMA and C. M. WILLIAMS. Proc. Natl. Acad. Sci. U.S.A., **54**, 411 (1965).
2. A. MANSINGH, T. S. SAHOTA, and D. A. SHAW. Can. Entomol. **102**, 49 (1970).
3. W. S. BOWERS, H. M. FALES, M. J. THOMPSON, and E. C. UELBEL. Science, **154**, 1020 (1966).
4. J. F. MANVILLE. Can. J. Chem. **53**, 1579 (1975).
5. J. F. MANVILLE. Can. J. Chem. **54**, 2365 (1976).
6. V. ČERNÝ, L. DOLEJŠ, L. LÁBLER, F. ŠORM, and K. SLÁMA. Coll. Czech. Chem. Commun. **32**, 3926 (1967).
7. R. S. HUNT and E. VON RUDLOFF. Can. J. Bot. **52**, 477 (1974).
8. H. S. FRASER and E. P. SWAN. Bi-Mon. Res. Notes, Can. For. Serv. **29**, 13 (1973).
9. E. P. SWAN. Can. J. Chem. **45**, 1588 (1967).
10. H. S. FRASER and E. P. SWAN. Bi-Mon. Res. Notes, Can. For. Serv. **31**, 3 (1975).
11. H. S. FRASER and E. P. SWAN. Bi-Mon. Res. Notes, Can. For. Serv. **28**, 32 (1972).
12. J. M. LEACH and A. N. THAKORE. CPAR Rep. 149–2, Can. For. Serv. Ottawa, Ont. 1974.
13. J. F. MANVILLE and K. BOCK. J. Org. Magn. Reson. In press.
14. D. F. ZINKEL and J. W. ROWE. Anal. Chem. **36**, 1160 (1964).

The synthesis and thermal decomposition of bis(phenylthio)methyl derivatives of mercury

TRISTRAM CHIVERS AND RITCHWICK RAM

Department of Chemistry, The University of Calgary, Calgary, Alta., Canada T2N 1N4

Received February 7, 1977

TRISTRAM CHIVERS and RITCHWICK RAM. Can. J. Chem. **55**, 2554 (1977).

The mercurials, $[(PhS)_2CH]_2Hg$ and $PhHgCH(SPh)_2$, have been prepared from $(PhS)_2CHLi$ and $HgBr_2$ or PhHgCl, respectively. The unsymmetrical compound decomposes readily both in the solid state and in various solvents. The symmetrical compound is more stable but also undergoes decomposition in certain refluxing solvents. The identity of the products suggests that the major decomposition route involves homolytic fission of the Hg—$CH(SPh)_2$ bond and that PhS migration to mercury plays only a minor role.

TRISTRAM CHIVERS et RITCHWICK RAM. Can. J. Chem. **55**, 2554 (1977).

On a préparé les dérivés organomercuriques $[(PhS)_2CH]_2Hg$ et $PhHgCH(SPh)_2$ respectivement à partir de $(PhS)_2CHLi$ et $HgBr_2$ ou PhHgCl. Le composé non-symétrique se décompose facilement aussi bien à l'état solide que dans divers solvants. Le composé symétrique est plus stable mais il subit aussi une décomposition dans certains solvants à reflux. La nature des produits formés suggère que la principale route de décomposition implique une fission homolytique du lien Hg—$CH(SPh)_2$ et que la migration du PhS vers le mercure ne joue qu'un rôle mineur dans le mécanisme.

[Traduit par le journal]

Introduction

A number of investigations of organometallic derivatives containing β-sulfur substituents indicate that decomposition via the formation of M—SR bonds is a general feature of these compounds (1–4). By analogy with polyhalomethylmercurials (5), RS migration to mercury in derivatives of the type $PhHgCH_n(RS)_{3-n}$ (n = 1, 2) could provide a source of thio(alk)aryloxy carbenes. To test this idea we have prepared the mercurials $PhHgCH(SPh)_2$ and $Hg[CH(SPh)_2]_2$ and investigated their decomposition in various solvents. The synthesis of $Hg(CH_2SPh)_2$ and reactions with lithium and zinc to give $LiCH_2SPh$ and $Zn(CH_2SPh)_2$, respectively, have been briefly reported (3).

Experimental

General

All solvents were distilled from CaH_2 prior to use. Reactions involving lithium reagents were carried out under an atmosphere of dry, oxygen-free nitrogen.

The following instruments were used to obtain spectroscopic data: Infrared Spectra (Perkin Elmer Models 337 and 467), ^1H NMR Spectra (Varian HA 100), Mass Spectra (Varian CH5 operating at an ionising potential of 70 eV).

Microanalyses were performed by Alfred Bernhardt Mikroanalytisches Lab., W. Germany.

Synthesis of $[(PhS)_2CH]_2Hg$

$(PhS)_2CHLi$ (20 mmol) (6) in THF (20 ml) was added over 5 min to mercury(II) bromide (3.6 g; 10 mmol) in THF (15 ml) at 0°C. The turbidity of the initial suspension rapidly gave way to the final greenish mixture. Addition of ice-cold water (~200 ml) precipitated the product as white lumps which were collected, washed with water, and air dried. Analytically pure $Hg[CH(SPh)_2]_2$ was obtained as a white powder (mp 92–94°C) by slow precipitation from a solution in THF upon addition of pentane. (Yield = 4.97 g; 75%.) *Anal.* Calcd. for $C_{26}H_{22}HgS_4$: C 47.13, H 3.32, Hg 30.21, S 19.34. Found: C 46.99, H 3.33, Hg 30.21, S 19.17. The ^1H nmr spectrum (CS_2) exhibited signals at τ 2.58–3.03 (m, C_6H_5S) and τ 5.72 (s, $\diagdown CH—Hg\diagup$), $^2J_{^{199}Hg-^1H}$ = 129 Hz, with the appropriate intensity ratios.

The infrared spectrum showed a band at 462 cm^{-1} assigned to ν_{as} HgC_2. The mass spectral data are given in Table 1.

Synthesis of $PhHgCH(SPh)_2$

$(PhS)_2CHLi$ (15 mmol) in THF (25 ml) was added over 10 min to PhHgCl (4.7 g; 15 mmol) in THF (75 ml) at 0°C. The turbidity of the suspension rapidly gave way to a pale yellow-green mixture. The crude product was precipitated from this mixture by the addition of ice-cold water (200 ml). Slow addition of *n*-pentane to a toluene solution of the crude product (dried over $MgSO_4$) gave white crystals of analytically pure $PhHgCH(SPh)_2$; mp 107–108°C. Yield = 2.64 g; 43%. *Anal.* Calcd. for $C_{19}H_{16}HgS_2$: C 44.90, H 3.15, Hg 39.40, S 12.60. Found: C 44.93, H 3.08, Hg 39.30, S 12.54.

The ^1H nmr spectrum ($CDCl_3$) exhibited signals at τ 2.27–2.49 (m, Hg—C_6H_5, *m*- and *p*-), τ 2.49–2.97 (m, SC_6H_5), τ 2.97–3.14 ("d of d", Hg—C_6H_5, *o*-) and τ 5.30 (s, Hg—$CH\diagup\diagdown$), $^2J_{^{199}Hg-^1H}$ = 113 Hz, with the appro-

TABLE 1. Mass spectra at 70 eV of $PhHgCH(SPh)_2$ and $Hg[CH(SPh)_2]_2$[a]

Parent	Ion	Abundance (%)
$PhHgCH(SPh)_2$	$PhHgCH(SPh)_2$	1
	PhHgSPh	2
	Ph_2Hg	30
	$(PhS)_2CHPh$	4
	PhHg	19
	PhSCH=CHSPh	5
	$(PhS)_2CH$	100
	PhSSPh	4
	Hg	25
$Hg[CH(SPh)_2]_2$[b]	$(PhS)_2CHCH(SPh)_2$	<1
	$(PhS)_2CHCH(SPh)$	5
	PhSCH=CHSPh	96
	$(PhS)_2CH$	100
	Hg	56

[a]Ions in abundance above 1%; M^+(%) ($M > 200$).
[b]Parent ion not observed.

priate intensity ratios. In the infrared spectrum bands at 450 and 580 cm^{-1} are assigned to Hg—aryl and Hg—alkyl stretching frequencies, respectively. The mass spectral data are given in Table 1.

Decomposition of the Mercurials

The experimental results for the decomposition of $Hg[CH(SPh)_2]_2$ and $PhHgCH(SPh)_2$ in various solvents are summarized in Tables 2 and 3, respectively. A description of the general procedure for the work-up of reaction mixtures and the identification of products follows. After the decomposition, mercury metal was filtered off and weighed. Solvents were removed *in vacuo* and the decomposition products were isolated, where possible, and identified by comparison of their infrared spectra and mp with those of authentic samples. For comparison purposes, Ph_2Hg and PhHgCl were commercial samples (Alfa Inorganics). PhHgSPh and $Hg(SPh)_2$ (mp 150°C, *cf.* lit. 151–152°C) (7) were prepared by the reactions of benzenethiol with PhHgCl and HgO, respectively. $(PhS)_2CH_2$ was prepared from CH_2I_2 and PhSNa using the literature procedure (6). $(PhS)_3CH$, $[(PhS)_2CH]_2$, and $(PhS)_2C{=}C(SPh)_2$ were characterized by complete microanalytical data in addition to mp, infrared, ^1H nmr, and mass spectra (Table 4).

In cases where it was not possible to isolate pure organosulfur products, the molar composition of mixtures of $(PhS)_2CH_2$, $(PhS)_3CH$, and $[(PhS)_2CH]_2$ could be estimated from the integrated intensities of the aliphatic ≡CH signals in their ^1H nmr spectra. The progress of the decomposition was conveniently monitored by ^1H nmr spectroscopy.

Results and Discussion

The mercurials $Hg[CH(SPh)_2]_2$ and $PhHgCH(SPh)_2$ were obtained in fairly good yields from the readily available lithium reagent, $(PhS)_2CHLi$ (6), and $HgBr_2$ or PhHgCl, respectively. Two observations for the unsymmetrical mercurial prompted us to undertake a detailed investigation of the decomposition of these two compounds. First, solid samples darkened during several days at room temperature. Secondly, solutions in various solvents slowly deposited mercury. The results for the symmetrical mercurial are presented first.

Decomposition Pathways of $Hg[CH(SPh)_2]_2$

Table 2 summarizes the experimental results for the decomposition of $Hg[CH(SPh)_2]_2$ in various solvents and *in vacuo*. While the decomposition of the mercurial in low boiling-point solvents (*e.g.* $CHCl_3$, THF) is very slow, the mercurial is quantitatively converted to mercury metal in refluxing toluene or *in vacuo* at 150°C. By analogy with the extensive literature (10, ref. 11, pp. 403–421) on the thermal decomposition of R_2Hg compounds, the decomposition of $Hg[CH(SPh)_2]_2$ can be rationalised by postulating homolytic fission of the Hg—C bond in the initial rate-determining step.

$$[1]\quad Hg[CH(SPh)]_2 \xrightarrow{\text{slow}} (PhS)_2CH\cdot + \cdot HgCH(SPh)_2$$

$$[2]\quad \cdot HgCH(SPh)_2 \xrightarrow{\text{fast}} (PhS)_2CH\cdot + Hg$$

The decomposition products $(PhS)_2CH_2$ and $[(PhS)_2CH]_2$ can then be formed from the radicals produced in [1] and [2] by (*a*) abstraction of hydrogen from solvent or starting mercurial, or (*b*) dimerization, respectively. The detection of bibenzyl as a product in the decomposition in toluene solution provides support for the proposed radical mechanism (12).

$$[3]\quad (PhS)_2CH\cdot + C_6H_5CH_3 \rightarrow (PhS)_2CH_2 + C_6H_5CH_2\cdot \rightarrow (C_6H_5CH_2)_2$$

The formation of $[(PhS)_2CH]_2$ by a radical–molecule encounter, as in [4],

$$[4]\quad (PhS)_2CH\cdot + Hg[CH(SPh)_2]_2 \rightarrow [(PhS)_2CH]_2 + \cdot HgCH(SPh)_2$$

cannot, however, be ruled out on the basis of the available evidence.

The purple radical $(PhS)_2N\cdot$, isoelectronic with $(PhS)_2CH\cdot$, has recently been characterized by Barton and co-workers and shown to have unusual stability (13). In this work, no direct evidence, *e.g.* by esr, could be obtained for radical formation possibly because the steady state concentration of $(PhS)_2CH\cdot$ radicals was too low.

The origin of the predominant organosulfur product in the thermal decomposition of $Hg[CH(SPh)_2]_2$, *i.e.* $(PhS)_3CH$ is less certain. Seebach and co-workers have proposed the following sequence of reactions to explain the

TABLE 2. The decomposition of $Hg[CH(SPh)_2]_2$ in various solvents

Solvent	Conditions	Products identified[a]	Comments
In vacuo	150°C, 5 h	Hg, $(PhS)_3CH$ (6), $(PhS)_2CH_2$ (4), $[(PhS)_2CH]_2$* (1)	Quantitative decomposition to mercury metal
Toluene	110°C, 116 h	Hg, $(PhS)_3CH$* (12), $(PhS)_2CH_2$ (7), $[(PhS)_2CH]_2$* (3), $PhCH_2CH_2Ph$	Quantitative decomposition to mercury metal
Chloroform	61°C, 138 h	Hg, $(PhS)_3CH$ (2), $(PhS)_2CH_2$ (1)	>85% recovery of mercurial
Tetrahydrofuran	64°C, 264 h	Hg, $(PhS)_3CH$	Only 32% decomposition (based on Hg formation)
Cyclohexene	83°C, 117 h	—	No decomposition
Acetone	56°C, 24 h	Hg, $(PhS)_2C{=}C(SPh)_2$,* $(PhS)_3CH$	Almost quantitative decomp. to mercury. 15% yield of olefin

[a]Products marked with an asterisk were separated and identified by mp, elemental analyses, and mass spectra. The relative composition of other products was determined by nmr (see Table 4).

TABLE 3. The decomposition of $PhHgCH(SPh)_2$ in various solvents

Solvent	Conditions	Products identified[a]	Mol Hg/mol $PhHgCH(SPh)_2$
In vacuo	120°C, 39 h	Hg, Ph_2Hg,* $(PhS)_3CH$, $(PhS)_2CH_2$	0.404
Toluene	20°C, 66 days	Hg, Ph_2Hg,* PhHgSPh, $(PhS)_2Hg$,* $(PhS)_3CH$, $(PhS)_2CH_2$, $[(PhS)_2CH]_2$	0.607
Tetrahydrofuran	20°C, 40 days	Hg, Ph_2Hg, $(PhS)_3CH$, $(PhS)_2CH_2$	0.716
Methylene chloride	20°C, 36 days	Hg, Ph_2Hg, PhHgSPh,* $(PhS)_2Hg$,* PhHgCl,* $(PhS)_3CH$, $(PhS)_2CH_2$, $CHCl_3$	0.637
Cyclohexene	83°C, 161 days	Hg, $(PhS)_2Hg$,* PhHgSPh,* Unidentified PhHg-derivative	0.312

[a]Products marked with an asterisk were separated and identified by mp and ir spectra. Other products were determined by mass spectra (PhHg derivatives) or nmr (organosulfur compounds, see Table 4).

TABLE 4. Characterization of organosulfur products of decomposition of $Hg[CH(SPh)_2]_2$ and $PhHgCH(SPh)_2$

Compound[a]	Melting point (°C)	Analysis %[b] C	H	S	^{1}H nmr signals (τ)[c]
$(PhS)_2CH_2$	39.5–40.5	—	—	—	2.58–2.96(m); 5.80(s)
$(PhS)_3CH$	34–36 lit. 40–40.5 (8)	66.83 [67.10	4.64 4.71	28.45 28.22]	2.40–3.10(m); 4.77(s)
$[(PhS)_2CH]_2$	104–106	67.63 [67.50	4.79 4.76	27.48 27.70]	2.70–3.00(m); 5.52(s)
$(PhS)_2C{=}C(SPh)_2$	144–145 lit. 152–153 (9)	67.67 [67.95	4.50 4.39	27.92 27.82]	2.93(m)

[a]All compounds showed the expected parent ion peaks in their mass spectra.
[b]Calculated values in square brackets.
[c]In CCl_4.

products of thermolysis of $(PhS)_3C—C(SPh)_3$ (14) (R = SPh).

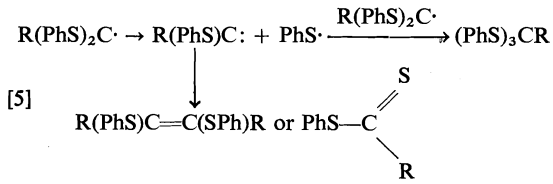

[5]

In the present work, reaction 5 (R = H) does not explain the formation of $(PhS)_3CH$ since no carbene ($PhS\ddot{C}H$) derived products have been detected. Direct abstraction of PhS from the starting mercurial by $(PhS)_2CH\cdot$ appears to be the most likely explanation for the formation of $(PhS)_3CH$.

[6] $(PhS)_2CH\cdot + Hg[CH(SPh)_2]_2 \rightarrow (PhS)_3CH + (PhS)_2CHHg\dot{C}H(SPh)$

Unexpectedly the decomposition of $Hg[CH(SPh)_2]_2$ in acetone produced the olefin $(PhS)_2C{=}C(SPh)_2$ in *ca.* 15% yield, in addition to $(PhS)_3CH$. Radical disproportionation followed by dimerization of the carbene formed would be a possible explanation, but the absence of $(PhS)_2CH_2$ among the products rules out this alternative.

[7] $2(PhS)_2CH\cdot \rightarrow (PhS)_2C: + (PhS)_2CH_2$

$\downarrow$

$\frac{1}{2}(PhS)_2C{=}C(SPh)_2$

A second possibility involves transfer of H atoms from $(PhS)_2CH\cdot$ *to the solvent* followed by dimerization of the carbene, $(PhS)_2C$:, but it was not possible to detect 2-propanol by nmr in the solvent after decomposition. Thus we do not have a satisfactory explanation for the formation of the olefin in acetone but not in other solvents.

Decomposition Pathways of $PhHgCH(SPh)_2$

Table 3 summarizes the experimental results for the decomposition of $PhHgCH(SPh)_2$ in various solvents. The decomposition of the unsymmetrical mercurial occurred more readily than the symmetrical mercurial and in most solvents took place at room temperature. The identification of the reaction products was considerably more difficult than in the case of the symmetrical mercurial due to the formation of PhHg— and PhSHg— derivatives, in addition to organosulfur compounds. In an attempt to rationalise the formation of the various products a number of competing decomposition pathways have been considered.

(a) Homolytic Fission

By analogy with previously reported studies of the thermal decomposition of $PhHgCH_2Ph$ (15) and related molecules, homolytic fission of the $Hg—CH(SPh)_2$ bond to give $(PhS)_2CH\cdot$ would explain the formation of $(PhS)_2CH_2$, $[(PhS)_2CH]_2$, and $(PhS)_3CH$ in the same way as for the symmetrical mercurial.

[8] $PhHgCH(SPh)_2 \xrightarrow{slow} PhHg\cdot + (PhS)_2CH\cdot$

The fate of the phenylmercury radical can be either as shown in [9] or [10].

[9] $2PhHg\cdot \rightarrow Ph_2Hg + Hg$

[10] $PhHg\cdot \rightarrow Ph\cdot + Hg$

Reaction 9 implies that equimolar amounts of diphenylmercury and mercury are formed and that the quotient mol Hg/mol $PhHgCH(SPh)_2$ = 0.5. This is true for PhHg radicals produced by the electrochemical reduction of dilute solutions of phenylmercury halides in ethereal solvents (16). In this work, the quotient was often >0.5 (see Table 3) and mol Ph_2Hg < mol Hg suggesting that reaction 10 is also an important route to metallic mercury.

A third possible reaction pathway for the phenylmercury radical is reaction with solvent, which would explain the formation of PhHgCl in methylene chloride. Similarly, PhHgSPh could result from abstraction of a PhS· radical from the starting mercurial by PhHg·.

[11] $PhHg\cdot + PhHgCH(SPh)_2 \rightarrow PhHgSPh + PhHg\dot{C}H(SPh)$

An alternative route to PhHgSPh *viz.* intramolecular PhS migration to mercury is discussed below.

(b) PhS Migration to Mercury

The migration of an RS substituent from α-carbon to a transition metal has been observed to occur readily (1–4) and, in the case of mercury derivatives, is a possible route to PhHgSPh.

[12] $PhHgCH(SPh)_2 \rightarrow PhHgSPh + PhS\ddot{C}H$

This intramolecular rearrangement invokes the formation of the carbene, $PhS\ddot{C}H$, previously trapped as an adduct with cyclohexene (17). When the decomposition of $PhHgCH(SPh)_2$ was carried out in refluxing cyclohexene or in benzene/cyclohexene none of the expected adduct, 7-phenylmercaptonorcarane, could be detected. It therefore appears that PhS migration to mercury plays an unimportant role in the de-

composition of $PhHgCH(SPh)_2$ and the formation of PhHgSPh is best explained by direct attack of PhHg· on the mercurial.

(c) Symmetrization of $PhHgCH(SPh)_2$

The formation of $(PhS)_2Hg$ is more difficult to rationalise. It is well known that unsymmetrical mercurials, RHgR′, have a strong tendency to symmetrize to give R_2Hg and $R_2'Hg$ (ref. 11, pp. 364–402). In the case of $PhHgCH(SPh)_2$, symmetrization followed by PhS migration to mercury is a possible source of $(PhS)_2Hg$.

[13] $2PhHgCH(SPh)_2 \rightarrow Ph_2Hg + Hg[CH(SPh)_2]_2$

[14] $Hg[CH(SPh)_2]_2 \rightarrow (PhS)_2Hg + 2PhS\ddot{C}H$

The unsymmetrical mercurial does not, however, form $(PhS)_2Hg$ even in refluxing solvents (Table 2) and thus this route to $(PhS)_2Hg$ can be discounted. Finally, it was shown in independent experiments that $(PhS)_2Hg$ is not formed by the disproportionation of PhHgSPh either in toluene or methylene chloride.

Conclusion

The products of the decomposition of the mercurials, $Hg[CH(SPh)_2]_2$ and $PhHgCH(SPh)_2$, in various solvents are best rationalised by postulating initial homolytic fission of a Hg—$CH(SPh)_2$ bond. In the case of the unsymmetrical derivative, the well-known affinity of mercury for sulphur is demonstrated, but the formation of Hg—S products apparently does not occur via intramolecular migration. Thus these mercurials, unlike the analogous haloalkyl compounds, are not useful as carbene transfer reagents.

Acknowledgements

We are grateful to the National Research Council of Canada for financial support in the form of an operating grant and to Dr. P. M. Boorman for helpful discussions.

1. R. B. KING and M. B. BISNETTE. J. Am. Chem. Soc. **86**, 1267 (1964); Inorg. Chem. **4**, 486 (1965).
2. T. CHIVERS and P. L. TIMMS. J. Organomet. Chem. **118**, C37 (1976).
3. R. TAUBE and D. STEINBORN. J. Organomet. Chem. **65**, C9 (1974).
4. E. W. ABEL and S. MOORHOUSE. Unpublished results.
5. D. SEYFERTH. Acc. Chem. Res. **5**, 65 (1972).
6. E. J. COREY and D. SEEBACH. J. Org. Chem. **31**, 4097 (1966).
7. H. C. Kaufman (*Editor*). Handbook of organometallic compounds. Van Nostrand Co. Inc., Princeton, NJ. 1961. pp. 61, 62.
8. D. SEEBACH, K-H. GEISS, A. K. BECK, B. GRAF, and H. DAUM. Chem. Ber. **105**, 3280 (1972).
9. D. SEEBACH. Chem. Ber. **105**, 487 (1972).
10. K. C. BASS. Organomet. Chem. Rev. **1**, 391 (1966).
11. L. G. MAKAROVA. *In* Organometallic reactions. Vol. 2. *Edited by* E. I. Becker and M. Tsutsui. Wiley-Interscience. 1971.
12. C. EABORN, R. A. JACKSON, and R. W. WALSINGHAM. Chem. Commun. 300 (1965).
13. D. H. R. BARTON, I. A. BLAIR, P. D. MAGNUS, and R. K. NORRIS. J. Chem. Soc. Perkin I, 1031 (1973).
14. D. SEEBACH and A. K. BECK. Chem. Ber. **105**, 3892 (1972).
15. G. A. RAZUVAEV and YU. A. OL'DEKOP. Zh. Obshch. Khim. **19**, 1483 (1949).
16. R. E. DESSY, W. KITCHING, T. PSARRAS, R. SALINGER, A. CHEN, and T. CHIVERS. J. Am. Chem. Soc. **88**, 460 (1966).
17. U. SCHÖLLOPF, G. H. LEHMAN, J. PAUST, and H. D. HÄRTH. Chem. Ber. **97**, 1527 (1964).

Vibrational spectra and normal coordinate analysis of crystalline lithium metasilicate

V. DEVARAJAN AND H. F. SHURVELL[1]

Department of Chemistry, Queen's University, Kingston, Ont., Canada K7L 3N6

Received January 12, 1977

V. DEVARAJAN and H. F. SHURVELL. Can. J. Chem. **55**, 2559 (1977).

Infrared and Raman spectra of polycrystalline lithium metasilicate have been recorded. A vibrational assignment in terms of the various symmetry species of the unit cell group, C_{2v}, has been made. A normal coordinate analysis of the unit cell vibrations at the centre of the Brillouin zone ($k = 0$) was carried out to support the assignment and provide descriptions of the vibrational modes. The results are discussed in the light of previous normal coordinate calculations on the isolated metasilicate chain.

V. DEVARAJAN et H. F. SHURVELL. Can. J. Chem. **55**, 2559 (1977).

On a enregistré les spectres infrarouges et Raman du métasilicate de lithium en phase polycristalline. Une analyse des coordonnées normales de vibration du cristal, dans l'approximation de $k = 0$, a permis de relier les bandes observées dans les spectres aux diverses espèces de symétrie du groupe de la maille élémentaire, tout en fournissant une description détaillée des modes normaux. Les résultats des calculs sont comparés à ceux obtenus précédemment pour une chaîne métasilicate isolée.

Introduction

The vibrational spectra of metasilicate (SiO_3) chains are of interest since they form the structural unit of many glasses, and studies of these chains give an indication of structural disorders in the glasses. Recently, Brawer and White (1, 2) recorded the Raman spectra of a number of meta and disilicates in both crystalline and glassy states. By comparing the spectra obtained from these two states and carrying out simple force field calculations on isolated silicate chains and sheets, they were able to study the structural disorders in several alkali silicate glasses. Although the conclusions reached by Brawer and White are qualitatively correct, there is a need for a more complete investigation of the vibrational spectra and force fields of crystalline meta and disilicates. We are not aware of any previous detailed study on lithium metasilicate.

In the present work, we have recorded the ir and Raman spectra of crystalline lithium metasilicate (Li_2SiO_3) and have carried out a normal coordinate analysis of the vibrations at the centre of the Brillouin zone ($k = 0$) in order to support the vibrational assignments, and give qualitative descriptions of the normal modes.

Crystal Structure and Vibrations

Lithium metasilicate, Li_2SiO_3, belongs to the orthorhombic system with four molecules per crystallographic unit cell. The space group is C_{2v}^{12} ($Cmc2_1$) (3–5). However, the primitive (Bravais) cell contains only two molecules. The structure contains double $(SiO_3)_n$ chains running parallel to the c_0 axis. The projection of the orthorhombic unit cell along its c_0 axis is shown in ref. 3. Figure 1 illustrates an $(SiO_3)_n$ chain.

There are twelve atoms per primitive unit cell giving rise to thirty-six vibrations including three acoustic modes. The factor group is C_{2v} and the distribution of the thirty-six vibrations into the various symmetry species can be made using the procedures of Adams and Newton (6) and Fateley *et al.* (7). The result of this analysis is

$$\Gamma_{vib}^{C_{2v}} = 10A_1 + 8A_2 + 8B_1 + 10B_2$$

Further division of the vibrations into internal and external vibrations of the SiO_3 double chain and the identification of their symmetry species can be made using the method due to Adams and Newton (6). The results are given below:

Motion	Species
Internal vibrations (chain)	$6A_1 + 4A_2 + 4B_1 + 6B_2$
Librations (chain)	$1A_2$
Translations (Li and chain)	$3A_1 + 3A_2 + 3B_1 + 3B_2$
Acoustic modes	$1A_1 + 1B_1 + 1B_2$
Total	$10A_1 + 8A_2 + 8B_1 + 10B_2$

[1]To whom all correspondence should be addressed.

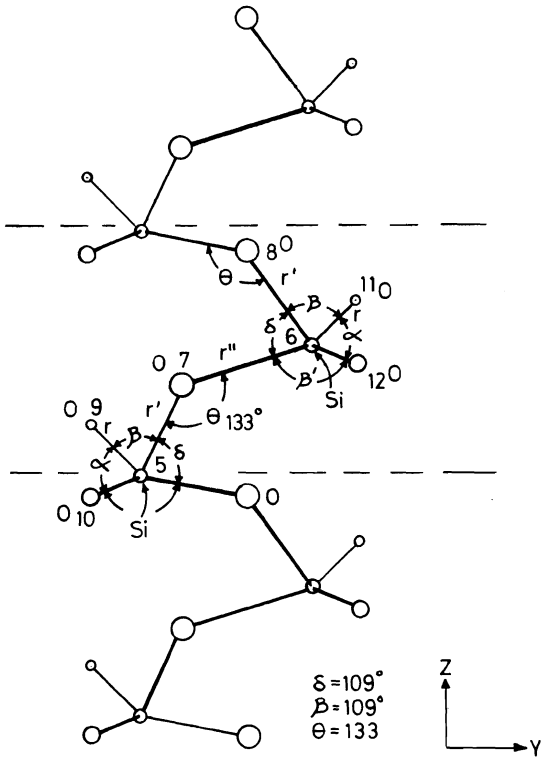

FIG. 1. An $(SiO_3)_n$ chain in the Li_2SiO_3 crystal.

Excluding the acoustic modes we should be able to observe $9A_1 + 8A_2 + 7B_1 + 9B_2$ vibrations in the spectra. All modes are Raman active, while the A_2 species modes are inactive in the infrared. Although longitudinal optical modes are allowed in the Raman spectrum of noncentrosymmetric crystals, it was not possible to identify any of these modes in the present work.

Experimental

Lithium metasilicate (Li_2SiO_3) was obtained in powder form from Alfa Products and used without further purification. The infrared spectra of the compound in Nujol mulls and KBr or CsI pellets were recorded using a Perkin-Elmer model 180 spectrometer. No important differences were observed between these spectra. The infrared spectrum is shown in Fig. 2.

Raman spectra were recorded in the polycrystalline form as a powder and as a solid formed from slowly cooling a melt. The Raman instrument consists of a Jarrell-Ash 25-100 monochromator, a cooled RCA C3103-02 photomultiplier, and photon counting electronics. The 514.5 nm line of an argon ion laser was used as the excitation line, at a power of 500 mW. A filter was not used, since plasma lines were not observed in the spectra. Although it was not possible to grow a single crystal of Li_2SiO_3, a Wollaston prism was mounted in front of the entrance slit of the monochromator to detect any polarization effects. In fact, some of the weaker bands did show some enhancement for certain orientations of the prism, or the solid sample formed from the melt. These intensity effects can be seen in Fig. 3. However, these partial depolarization measurements did not enable us to identify the A_1 modes. Table 1 contains a listing of the observed infrared and Raman wavenumbers. The selection of several very weak features for inclusion in Table 1 was based on their consistent appearance in a number of spectra obtained from different samples.

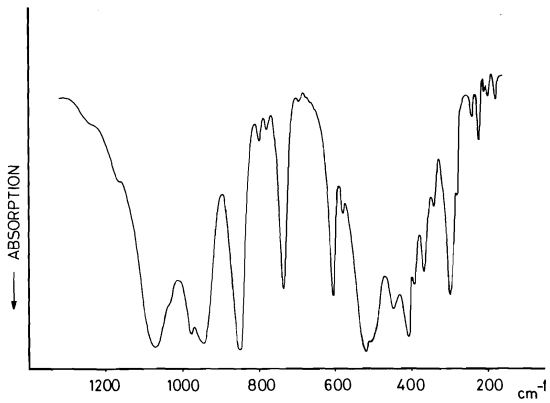

FIG. 2. The infrared spectrum of a CsI pellet of Li_2SiO_3.

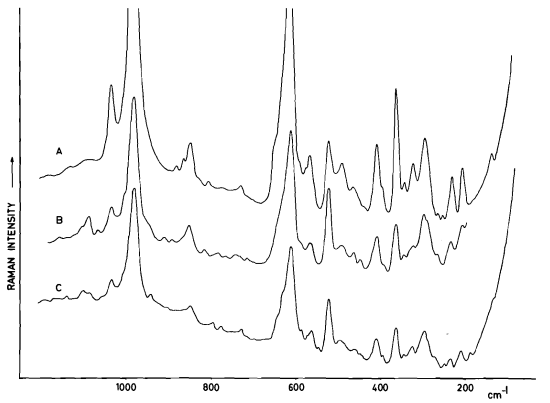

FIG. 3. Raman spectra of solid Li_2SiO_3 obtained by cooling a melt. Traces A and B were obtained by using parallel and perpendicular orientations, respectively, of a Wollaston prism analyser. Trace C was obtained using a different orientation of the sample with perpendicular orientation of the prism.

Vibrational Assignment

Lack of polarization measurements makes it difficult to assign the vibrational frequencies to specific symmetry species of the C_{2v} factor group. However, it is possible to identify the A_2 species as they are present in the Raman spectra, but absent in the infrared. A possible assignment can be made in terms of group frequencies of the

TABLE 1. Observed and calculated wavenumbers (cm^{-1}), descriptions of normal modes, and important contributing force constants for lithium metasilicate

Symmetry	Observed[a] Raman	Observed[a] Infrared	Calculated	Description	Important contributing force constants[b]
A_1	1087 w	1080 vs	1092	Si—O str	*7, 12*
	852 w	850 vs	870	Si—O str	*6*
	610 vs	604 s	601	O—Si—O bend	*9, 10, 12, 31*
	520 m	520 vs	540	Si—O str, Si—O—Si bend	*8, 11, 13*
	450 vw	450 ms	439	Li—O str	*1, 2*
	410 m	410 s	398	O—Si—O bend	*1, 3, 7, 10, 11, 30*
	273 vw	280 sh	290	Li—O str	*1, 3, 4, 13*
	210 w	214 vw	223	Li—O str	*3, 4, 10, 11, 30*
	186 w	196 w	180	O—Si—O bend	*9, 10, 12, 13, 31, 36*
A_2	1001 w.sh	—	994	Si—O str	*6*
	567 m	—	569	O—Si—O bend	*11, 12*
	465 w	—	448	Li—O str, O—Si—O bend	*2, 11*
	325 w	—	333	Li—O str	*1, 3*
	291 sh	—	304	O—Si—O bend, Li—O str	*1, 2, 6, 12*
	—	—	224	Li—O str, O—Si—O bend	*4, 11*
	—	—	187	Li—O str	*1, 2, 3, 4*
	—	—	58	Libration	*14, 15*
B_1	1034 w	1034 w.sh	1049	Si—O str, O—Si—O bend	*6, 11, 12*
	587 w.sh	580 vw	599	O—Si—O bend, Si—O str	*1, 2, 6, 11, 12*
	398 w.sh	398 w	398	Li—O str, O—Si—O bend	*2, 11*
	345 vw	345 w	342	Li—O str	*1, 3*
	297 m	305 s	302	O—Si—O bend, Li—O str	*3, 4, 11, 12*
	—	204 w	213	Li—O str	*1, 2, 3, 11*
	141 w	—	172	Li—O str, O—Si—O bend	*4, 11, 12*
B_2	983 vs	980 s.sh	985	Si—O str	*7, 9*
	945 w	950 vs	939	Si—O str, O—Si—O bend	*6, 7, 9*
	731 w	735 s	746	Si—O str	*6, 8, 11*
	645 w.sh	—	647	O—Si—O bend	*6, 9, 11, 12*
	496 w	505 s.sh	483	O—Si—O bend, Li—O str	*2, 3, 10, 12, 30, 31*
	398 w.sh	398 w	397	Li—O str	*1, 2, 10*
	258 vw	248 vw	275	O—Si—O bend, Li—O str	*1, 3, 10, 12, 31*
	234 w	230 w	259	Li—O str, O—Si—O bend	*4, 10, 11*
	141 w	—	169	O—Si—O bend, Li—O str	*3, 4, 7, 8, 9, 11*

[a]v = very, s = strong, m = medium, w = weak, and sh = shoulder.
[b]The numbering of force constants is given in Table 2.

metasilicate chain and the Li—O polyhedra. By using the concept of internal coordinates and the symmetry of the chain in the crystal, we can predict the distribution of stretching, bending, and torsional modes into various symmetry species of the factor group C_{2v}. It is more difficult to identify the frequencies and symmetry species corresponding to the external modes involving the motion of lithium atoms. However, some characteristic frequencies and force constants of the Li—O polyhedra are available in the literature (8, 9) and these may be used for assignment purposes.

General valence force constants for the SiO_4 tetrahedra and Li—O polyhedra were taken from the literature (9, 10) and a preliminary normal coordinate analysis (see next section) was carried out on the unit cell. It was then possible to associate the observed frequencies with the corresponding calculated frequencies. The calculated frequencies were evaluated according to the symmetry species and this enabled us to assign the observed frequencies. Although the above-mentioned process appears crude, it is unlikely to produce any large error in the internal vibration region for the following reasons: (*1*) Although the force constants were transferred from similar molecules they are unlikely to be changed in any drastic way in the new environment. (*2*) The change in geometry, which is included in the kinetic energy term, can account for the observed splitting and shifts in

the frequencies. (*3*) Because there is only one chain per primitive unit cell there are no complications of correlation splitting. The tentative assignments thus made are given in Table 1.

Normal Coordinate Analysis

The normal coordinate analysis of the crystal vibrations at the centre of the Brillouin zone ($k = 0$) was carried out following the Wilson **FG** matrix procedure adapted to crystals by Shimanouchi *et al.* (11). The internal coordinates used are based on the SiO_3 chain and the Li—O polyhedra. The SiO_3 chain coordinates are shown in Fig. 1. In the Li—O polyhedra, only Li—O stretching coordinates were used. The cartesian symmetry coordinates corresponding to the C_{2v} factor group, which help in reducing the dimensions of the secular equation to be solved, were constructed using the usual projection operator techniques (11).

The force constants used to set up the potential energy matrix were of the general valence type. As the SiO_3 chain is made up of SiO_4 tetrahedra, force constants for the SiO_4 group were taken from the work of Devarajan and Funck (10). The lithium atom is surrounded by five oxygen atoms. Of these, four lie at distances of approximately 2.0 Å from the lithium atom, whereas the fifth is at a distance of 2.6 Å. In the work of Jungerman (9), the value of the Li—O stretching force constant for a distance of 2.0 Å is given as 0.3 mdyn $Å^{-1}$. For 2.6 Å, the value is practically zero. A total of thirty-six force constants were used for the preliminary calculations which were used for the assignment of the observed frequencies. In the next step, the force constants were adjusted on a trial and error basis, allowing for the different Si—O bond lengths in the chain and the different Li—O distances. The Jacobian elements $\partial\nu/\partial f$ further aided the adjustment procedure by indicating the value and direction (positive or negative) by which the force constants should be changed. After several calculations, the agreement between the observed and calculated frequencies improved to a satisfactory level, without introducing unrealistic values for any force constants. Considering the approximations and uncertainties involved, it was felt that it would not be worthwhile attempting any further refinement of the force constants.

Potential energy distributions in terms of force constants were also calculated. All the above-mentioned calculations were carried out using the modified versions of computer programs AXSMZ and LSMX of Shimanouchi (12). The final set of force constants and their values are given in Table 2. The observed frequencies, calculated frequencies with descriptions of the normal modes and important contributing force constants are given in Table 1.

TABLE 2. General valence force constants for lithium metasilicate

Number	Description of force constant	Vaue[a]
1	f_{D1}(Li—O str, 2.02 Å)	0.35
2	f_{D2}(Li—O str, 1.96 Å)	0.45
3	f_{D3}(Li—O str, 2.03 Å)	0.25
4	f_{D4}(Li—O str, 2.11 Å)	0.15
5	f_{D5}(Li—O str, 2.60 Å)	0.01
6	f_r(Si—O str, 1.62 Å)	4.50
7	$f_{r'}$(Si—O str, 1.55 Å)	4.75
8	$f_{r''}$(Si—O str, 1.65 Å)	4.00
9	f_δ(O—Si—O bend)	2.00
10	f_α(O—Si—O bend)	2.00
11	f_β(O—Si—O bend)	1.80
12	$f_{\beta'}$(O—Si—O bend)	1.80
13	f_θ(Si—O—Si bend)	1.00
14	f_{τ_1}(Si—O torsion)	0.07
15	f_{τ_2}(O—Si torsion)	0.08
16	f_{rr}	0.50
17	$f_{rr'}$	0.25
18	$f_{rr''}$	0.50
19	$f_{r'r''}$(Si—O, Si—O)	0.70
20	$f_{r'r''}$(Si—O, O—Si)	0.40
21	$f_{r\alpha}$	0.30
22	$f_{r\beta}$	−0.30
23	$f_{r\beta'}$	−0.30
24	$f_{r'\beta}$	−0.30
25	$f_{r'\delta}$	0.30
26	$f_{r'\theta}$	−0.30
27	$f_{r''\beta}$	0.00
28	$f_{r''\delta}$	0.00
29	$f_{r''\theta}$	0.50
30	$f_{\alpha\beta}$	0.50
31	$f_{\alpha\beta'}$	0.40
32	$f_{\beta\beta}$	0.23
33	$f_{\beta\beta'}$	0.23
34	$f_{\delta\beta}$	0.40
35	$f_{\beta'\beta'}$	0.23
36	$f_{\delta\beta'}$	0.40

[a]Stretching and stretch–stretch interaction constants are in mdyn/Å; bending and bend–bend interaction constants are in mdyn-Å; stretch–bend interaction constants are in mdyn.

Discussion

In a recent paper, Brawer (1) calculated the frequencies and intensities in the Raman spectrum of the metasilicate chain in some alkali metasilicate glasses and crystals. He used a central Si—O stretching force constant $k =$ 5.0 mdyn $Å^{-1}$ and a non-central Si—O force

constant of $0.17k$. The Si—O—Si bending force constant was neglected. Bilton *et al.* (13) used $f_{Si-O} = 4.0$ mdyn Å^{-1}, $f_{O-Si-O} = 0.3$ mdyn Å^{-1}, and $f_{Si-O-Si} = 0.03$ mdyn Å^{-1} in a simplified calculation on the silicate chains in the pyroxene minerals enstatite and augite. Another normal coordinate calculation on silicate chains was carried out by Etchepare (14) using force constants taken from the earlier work of Siebert (15).

It is difficult to compare the results of the present complete unit cell calculation with the previous calculations on isolated chain models. However, it appears that our results do not agree at all well with this earlier work. There may be several reasons for this. The vibrational frequencies and assignments on which the previous workers based their calculations may not have been reliable. The simple force fields used are probably inadequate and the isolated metasilicate chain model may not be applicable to lithium metasilicate.

It can be seen in Table 1 that the frequencies assigned to Si—O stretching modes have contributions from bending force constants. This is expected in view of the chain structure. The Li—O stretching modes all lie below 500 cm^{-1} and couple with chain bending modes.

Conclusions

A fairly complete assignment of the unit cell vibrations of crystalline lithium metasilicate has been made. The observed coincidences between Raman and infrared wavenumbers for the normal modes is in agreement with the reported C_{2v} factor group. Although the results of the normal coordinate calculations reported here do not agree with previous calculations on isolated metasilicate chains, it is felt that the present results are more reliable, since they correlate well with experimentally observed frequencies and are based on a complete unit cell model.

The simple short range general valence force field used in this work appears to be adequate. However, the inclusion of additional long range forces would no doubt further improve the calculation. It is hoped that the more complete force field reported here for the metasilicate chain structure might be useful for further studies of glasses containing this structural unit.

Acknowledgement

This work was supported by a grant from the National Research Council of Canada.

1. S. Brawer. Phys. Rev. B**11**, 3173 (1975).
2. S. Brawer and W. B. White. J. Chem. Phys. **63**, 2421 (1975).
3. R. W. G. Wyckoff. Crystal structures. Vol. 4. Interscience, New York. 1968. p. 312.
4. G. Donnay and J. D. H. Donnay. Am. Mineral. J. **38**, 163 (1953).
5. H. J. Seemann. Acta Crystallogr. **9**, 251 (1956).
6. D. M. Adams and D. C. Newton. Tables for factor group and point group analysis. Beckman, U.K. 1970.
7. W. G. Fateley, F. R. Dollish, N. T. McDevitt, and F. F. Bentley. Infrared and Raman selection rules for molecular and lattice vibrations: the correlation method. Wiley-Interscience, New York. 1972.
8. S. Meshitsuka, H. Takahashi, and K. Higasi. Bull. Chem. Soc. Jpn. **44**, 3255 (1971).
9. A. Jungermann. Doctoral Thesis, University of Freiburg, Germany. 1974.
10. V. Devarajan and E. Funck. J. Chem. Phys. **62**, 3406 (1975).
11. T. Shimanouchi, M. Tsuboi, and T. Miyazawa. J. Chem. Phys. **35**, 1597 (1961).
12. T. Shimanouchi. Computer programmes for normal coordinate analysis of polyatomic molecules. University of Tokyo, Tokyo. 1968.
13. M. S. Bilton, T. R. Gilson, and M. Webster. Spectrochim. Acta, **28**A, 2113 (1972).
14. J. Etchepare. Spectrochim. Acta, **26**A, 2147 (1970).
15. H. Siebert. Z. Anorg. Allgem. Chem. **275**, 225 (1954).

Nuclear magnetic resonance spin–lattice relaxation and the rotation of adamantane and hexamethylenetetramine in solution

RODERICK E. WASYLISHEN

Department of Chemistry, University of Winnipeg, Winnipeg, Man., Canada R3B 2E9

AND

BRIAN A. PETTITT

Russell, Man., Canada R0J 1W0

Received February 24, 1977

RODERICK E. WASYLISHEN and BRIAN A. PETTITT. Can. J. Chem. **55**, 2564 (1977).

Deuterium nmr spin–lattice relaxation times have been measured for dilute solutions of adamantane-d_{16} in CH_2I_2, $CHBr_3$, CCl_4, $CHCl_3$, and CH_2Cl_2. The reorientation correlation times, τ_2, calculated from the experimental data are used to calculate τ_J, the angular momentum correlation times, assuming both the *J*-diffusion and Hubbard relations. The derived τ_J values suggest that adamantane executes small step diffusion in CH_2I_2 and $CHBr_3$, and large step diffusion in CCl_4, $CHCl_3$, and CH_2Cl_2. The calculated τ_J values do not appear to be related to the mean times between collisions calculated using a hard sphere model. Both variable solvent and variable temperature experiments indicate 1 ps/cP for the viscosity dependence of the adamantane reorientation time, about 1/36th the value predicted using the familiar Stokes–Einstein equation.

Carbon-13 and ^1H nmr T_1 data indicate that reorientation of hexamethylenetetramine in H_2O (28 ps/cP), $CHCl_3$ (27 ps/cP), and $CHBr_3$ (18 ps/cP) is severely hindered because of intermolecular hydrogen bonding.

RODERICK E. WASYLISHEN et BRIAN A. PETTITT. Can. J. Chem. **55**, 2564 (1977).

On a mesuré des temps de relaxation spin–réseau par rmn du deutérium pour des solutions diluées d'adamantane-d_{16} dans CH_2I_2, $CHBr_3$, CCl_4, $CHCl_3$ et CH_2Cl_2. On a utilisé les temps de corrélation de réorientation, τ_2, calculés à partir des données expérimentales, pour calculer, τ_J, les temps de corrélation de moment angulaire en utilisant à la fois les relations de diffusion *J* et de Hubbard. Les valeurs τ_J suggèrent que l'adamantane exécute de petits pas de diffusion dans le CH_2I_2 et le $CHBr_3$ et de grands pas de diffusion dans le CCl_4, le $CHCl_3$ et le CH_2Cl_2. Il ne semble pas qu'il y ait de relation entre les valeurs de τ_J calculées et les temps moyens entre les collisions calculés en utilisant un modèle de sphère dure. Des expériences où l'on a fait varier soit le solvant soit la température indiquent que la dépendance qui existe entre la viscosité et le temps de réorientation de l'adamantane est de 1 ps/cP soit environ 1/36ème de la valeur prédite utilisant l'équation bien connue de Stokes–Einstein.

Des données de T_1 obtenues par rmn du ^{13}C et du ^1H indiquent que la réorientation de l'hexaméthylènetétramine dans H_2O (28 ps/cP), $CHCl_3$ (27 ps/cP) et $CHBr_3$ (18 ps/cP) est très empêchée à cause de liaison hydrogène intramoléculaire.

[Traduit par le journal]

Introduction

Adamantane (Fig. 1*a*) and hexamethylenetetramine, HMTA, (Fig. 1*b*) belong to the molecular point group T_d, but their approximate sphericity makes them especially suitable for studies on molecular rotation. Rotational and translational motions in the solids have been studied (1, 2) and ^{13}C relaxation work on adamantane (3) in CS_2 at one temperature has been interpreted in terms of rotational diffusion. Results are presented here from experiments on the viscosity and temperature dependence of the spin–lattice relaxation times of these molecules, and interpreted in terms of some current theoretical ideas on molecular rotations in liquids.

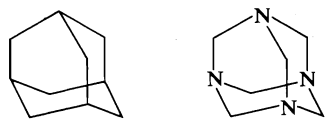

a *b*

FIG. 1. Structure of (*a*) adamantane, (*b*) hexamethylenetetramine.

Theory

The simplest model for the rotation of spherical molecules, beginning with the original work of Bloembergen, Purcell, and Pound (4),

assumes that the sphere is embedded in a continuous fluid medium and reorients in small, random jumps. A critical feature of the model is the boundary condition requiring that the fluid velocity at the surface of the sphere is equal to the velocity of the surface. The calculation can be repeated with the more general boundary condition requiring the fluid velocity at the surface to be some fraction, κ, of the surface velocity.

$$[1] \qquad \boldsymbol{v}(\boldsymbol{r}) = \kappa\boldsymbol{\omega} \times \boldsymbol{r}$$

where $\boldsymbol{r}$ is a vector from the centre of the sphere to an arbitrary point on its surface, $\boldsymbol{\omega}$ is the angular velocity of the sphere, $\boldsymbol{v}$ is the velocity of the fluid, and $\kappa \in [0,1]$. The rotational friction coefficient is then calculated by pretending that the angular velocity is $\kappa\boldsymbol{\omega}$, and the usual expression for the reorientation correlation time becomes

$$[2] \qquad \tau_2 = \frac{4}{3}\frac{\pi r^3 \kappa \eta}{kT}$$

where η is the shear viscosity.

The factor κ has been introduced in other ways. Gierer and Wirtz (5) argued that the molecule changes the viscosity of the fluid in its neighbourhood to $\eta' = \kappa\eta$ and give a procedure for calculating the 'microviscosity factor', κ, which is not very successful in practice (6). Kivelson *et al.* (7) have given the expression

$$[3] \qquad \kappa = \frac{3}{4}\frac{1}{r^2}\frac{\langle T^2\rangle}{\langle F^2\rangle}$$

relating κ to the mean-square torque, $\langle T^2\rangle$, and mean-square force, $\langle F^2\rangle$, on the molecule; which is as yet untested due to the difficulties in determining the latter two quantities from realistic potentials. It seems best at this stage to regard κ as an empirical parameter, with $\kappa = 1$ representing the usual 'stick' condition and $\kappa = 0$ the 'slip', or inertial, condition.

To determine whether or not a small step diffusion model is appropriate, Wallach and Huntress (8) examined the ratio of the observed to the inertial reorientation times. A variant of this idea is given here. The average (in a Maxwellian distribution of energies) of the time required for a spherical molecule to rotate through angle θ is

$$[4] \qquad \tau_{FR} = \theta\left(\frac{2I}{\pi kT}\right)^{1/2}$$

where I is the moment of inertia. In an unambiguous case of small step diffusion, $\tau_2 = 1/6R$, $R = \langle\Delta\theta^2\rangle/2\tau_2$, and $\langle\Delta\theta^2\rangle^{1/2} = \theta = \sqrt{3}/3$ radians is the root-mean-square angle diffused through in time τ_2. According to this argument, $\chi = \tau_2/\tau_{FR}$ must be substantially greater than unity for rotations slow enough to be small step diffusion; *i.e.*

$$[5] \qquad \chi = \left(\frac{3\pi}{2}\right)^{1/2}\tau_2^* \gg 1$$

where $\tau^* = \tau(kT/I)^{1/2}$ is a reduced time.

The work of Gordon (9) and McClung (10) extending the diffusion model to steps of arbitrary size appears to be quite successful for small molecules (11). In this theory, the molecule is assumed to rotate inertially in steps that are interrupted by instantaneous collisions that randomize the magnitude and direction of the angular momentum (J-diffusion), the time of a collision after the previous one being assumed to follow a Poisson distribution. The central feature of the J-diffusion model is a relationship between τ_2 and the angular momentum correlation time, τ_J, which for spheres is (10, 12)

$$[6] \qquad \tau_2^* = \tau_J^* X/(1 - X)$$

where

$$[7] \qquad X = \frac{1}{5}\left\{1 + 4\sum_{a=1}^{2} b^2[1 - F(b)]\right\}$$

$$[8] \qquad F(b) = \pi^{1/2} b \exp(b^2)\,\mathrm{erfc}\,(b)$$

$$[9] \qquad b = (2)^{-1/2}\tau_J^* a$$

and erfc (Z) is the complementary error function (13).

One clear virtue of this theory is that it includes the small step diffusion limit for $\tau_2^* \gg \tau_J^*$, in which case eq. 6 reduces to the Hubbard relation (14)

$$[10] \qquad \tau_2^*\,\tau_J^* = 1/6$$

In fact, it suggests placing the boundary between 'small' and 'large' step angular diffusion in the neighbourhood of $\tau_2^* = 2.5$ where the Hubbard and J-diffusion relations begin to diverge significantly (ref. 12, Fig. 1). Equation 5 shows that this is a stronger statement than the χ-test.

A model due to Ivanov (15, see also 16) allows for stochastic rotation in jumps of arbitrary size, but assumes that the time required to make a jump is small compared to the time between jumps; *i.e.* the rotation is severely hindered. The

TABLE 1. Characteristic times in the rotation of CCl_4 (ps)

Temperature (°C)	τ_2 (exp)	τ_J Exp.	τ_J *J*-diffusion	τ_J Hubbard	β^{-1}
−11	2.76	0.0857	0.085	0.0818	0.098
30	1.72	0.133	0.131	0.113	0.108
46	1.48	0.151	0.151	0.125	0.110

important relationship here is

$$[11] \qquad \tau_2 = \frac{\beta^{-1}}{1 - A_2}$$

where β is the jump rate and

$$[12] \qquad A_2 = \frac{1}{5}\left\langle \frac{\sin 5\theta/2}{\sin \theta/2} \right\rangle$$

an average over a distribution of jump angle θ. Steele (16) calculated

$$[13] \quad A_2 = \frac{1}{5}\{1 + 2[e^{-\langle\theta^2\rangle/2} + e^{-2\langle\theta^2\rangle}]\}$$

for a gaussian distribution of jump angle with rms value $\langle\theta^2\rangle^{1/2}$. This is a two parameter theory and thus a measured value of τ_2 must be accompanied by an assumed value of β or $\langle\theta^2\rangle^{1/2}$. β can be identified with the collision frequency, but this is a doubtful concept for hindered rotation.

The independent binary collision approximation for a rough sphere fluid (17) provides a theoretical means for determining β. Within the terms of the *J*-diffusion model, the identification $\tau_J = \beta^{-1}$, the mean time between collisions, can be made because collisions are responsible for changes in angular momentum. For collisions of molecules of type *b* on a molecule of type *a*, this theory gives

$$[14] \qquad \beta_{ab} = \left(\frac{8\pi kT}{\mu_{ab}}\right)^{1/2} n_b \sigma_{ab}^2 g(\sigma_{ab})$$

where μ_{ab} is the reduced mass of the (*a*,*b*) pair, n_b is the number density of *b*, $\sigma_{ab} = \frac{1}{2}(\sigma_a + \sigma_b)$ is the collision diameter, and $g(\sigma_{ab})$ is the radial distribution function for *b* on *a* at the point of contact.

Table 1 summarizes the work of Gillen *et al.* (11) on CCl_4 and includes values of β^{-1} for which $g(\sigma)$ was calculated in the Percus–Yevick approximation for the hard sphere model (18) with $\sigma = 5.46$ Å calculated from atomic volume increments (19). The agreement with the *J*-diffusion predictions of τ_J is excellent, and the comparison between τ_J and β^{-1} is quite reasonable considering the simplicity of the rough hard sphere model. For the continuous potentials of real fluids, a collision is not an instantaneous event and the correlated binary collisions are important (17).

Experimental

Adamantane (99+%, Gold Label) and HMTA (99+%) were obtained from Aldrich Chemical Company.

Adamantane-d_{16} was purchased from Merck, Sharp and Dohme.

All solvents were available commercially, and when available spectro-quality solvents were used.

All spin–lattice relaxation rates were measured using the inversion–recovery pulse sequence ($d - 180° - t - 90°$), where d is a delay time ($d > 5T_1$) and t is a variable time. T_1 values were calculated from the slope of a plot of $\ln(\langle M_z\rangle_0 - \langle M_z\rangle)$ *vs.* t (20). Deuterium relaxation rates of adamantane-d_{16} were measured at 10 MHz on a Bruker B-KR322 variable frequency spectrometer. Proton-decoupled ^{13}C nmr spectra were obtained on a Varian CFT-20 spectrometer (8 mm variable temperature probe). Full *n*0*e* factors were measured for the methylene carbons of adamantane and HMTA in all solutions using the gated proton decoupler on the CFT-20 with $d \simeq 10T_1$ (21).

Viscosities were measured using an Ostwald viscometer and density bottles.

Results and Discussion

In Table 2, the ^2H spin–lattice relaxation times of perdeuteroadamantane in five halomethanes at 23°C are listed. τ_2's were calculated from the usual expression (20, 22)

$$[15] \qquad \frac{1}{T_1} = \frac{3\pi^2}{2}\left(\frac{e^2qQ}{h}\right)^2 \tau_2$$

with $e^2qQ/h = 174$ kHz, the value for cyclohexane (23); and τ_J's were calculated from these according to the *J*-diffusion and Hubbard relations with $I = 373.7$ amu Å^2. These are accompanied by mean times between collisions, β^{-1}, calculated from eq. 14 using Lebowitz's solution of the Perkus–Yevick equation for mixtures of hard spheres (24). For comparison,

TABLE 2. Characteristic times of halomethanes and 0.1 M adamantane-d_{16} at 23°C

	0.1 M Adamantane-d_{16} (23°C)								
				τ_J (ps)			Pure solvents		
Solvent	Viscosity (cP)	T_1 (s)	τ_2 (ps)	J-diffusion	Hubbard	β^{-1} (ps)	τ_2 (ps)	τ_J (ps)	β^{-1} (ps)
CH_2I_2	2.647	0.532	4.19	0.060	0.060	0.049	4.3[a]		0.077
$CHBr_3$	1.903	0.693	3.22	0.081	0.078	0.063	4.2[b]		0.095
CCl_4	0.921	1.050	2.12	0.132	0.119	0.083	1.7[c]	0.13[c]	0.107
$CHCl_3$	0.547	1.047	2.13	0.132	0.119	0.066	1.6[d]	0.07[d]	0.088
CH_2Cl_2	0.416	1.190	1.88	0.150	0.135	0.049	0.7[e]		0.069

[a]25°C, ref. 30.
[b]30°C, ref. 31.
[c]30°C, ref. 11.
[d]28°C, ref. 32.
[e]25°C, refs. 6 and 33.

the corresponding quantities for the pure solvents are included. A plot of the adamantane τ_2's *vs.* viscosity gives a straight line with a slope of approximately 1 ps/cP, whereas eq. 2 with $\kappa = 1$ and $V = (4/3)\pi r^3 = 147.2$ Å^3 (19) gives 36 ps/cP.[1] This indicates that the reorientation of adamantane in these solvents is in a near 'slip' condition, *i.e.* essentially inertial. In general, the τ_2's of adamantane-d_{16} are similar to those of the solvents. It is a little slower than CH_2Cl_2, $CHCl_3$, and CCl_4, where it is only 1 to 1.5 Å larger in diameter and has a larger moment of inertia; whereas it is a little faster than $CHBr_3$ and CH_2I_2, which have larger moments of inertia.

The τ_J data and the success of the J-diffusion model with CCl_4 (11) suggest that adamantane executes large angle inertial steps in CH_2Cl_2, $CHCl_3$, and CCl_4; but crosses the boundary into small step diffusion in the much more viscous $CHBr_3$ and CH_2I_2. The β^{-1}'s, which are strongly affected by the number densities, do not follow the trend expected from the J-diffusion model for adamantane. The hard sphere and J-diffusion models have numerous assumptions that could produce this discrepancy, and it would be foolhardy to attach significance to it. If experimental τ_J's become more available in the literature, the general order of magnitude accuracy of β^{-1} should be encouragement to pursue better values of this quantity.

In Table 3 deuterium T_1 values for 0.2 M adamantane-d_{16} in CCl_4 are given at several different temperatures. Plotting τ_2 *vs.* η/T gives a slope of approximately 1 ps/cP when applied to a temperature of 23°C, in agreement with the result obtained by varying the viscosity at constant temperature (Fig. 2).

TABLE 3. Deuterium T_1 values for 0.2 M adamantane-d_{16} in CCl_4

Temperature (°C)	T_1[a] (s)	τ_2 (ps)
71.6	1.38	1.62
70.4	1.39	1.60
59.2	1.34	1.66
49.4	1.16	1.92
37.7	1.15	1.94
23.9	1.05	2.12

[a]Error in T_1 is less than 10%.

^{13}C spin–lattice relaxation times for ≤ 0.5 M solutions of adamantane and HMTA at 24.5 ± 2°C are given in Table 4. The τ_2's obtained for adamantane in $CDCl_3$ and $CHBr_3$ are slightly less than those obtained from the deuterium data (Table 2). Although there are several sources of error in the τ_2's (the experimental error in the T_1's, the assumed quadrupole coupling constant, and r_{CH}), the lower values for adamantane relative to adamantane-d_{16} are qualitatively consistent with the lower moment of inertia.

The temperature dependence of ^{13}C T_1's for 0.5 M solutions of HMTA in D_2O and 0.4 M solutions of HMTA in $CHBr_3$ were measured. From plots of τ_2 *vs.* η/T, straight lines were obtained and the slopes, when applied to 25°C, gave viscosity dependences of 27.8 ± 3 ps/cP and 18.3 ± 2 ps/cP, respectively. Atomic volume increments (19) gave $V = 130.8$ Å^3 for HMTA, which implies a viscosity dependence of 32

[1]In the disordered α-phase each adamantane molecule is in a cubic lattice (2, 25). If one assumes 74% of the available space in the cubic lattice is occupied by spheres, then $V = 150.5$ Å^3 from the measured density of α-adamantane (25).

TABLE 4. Carbon-13 spin–lattice relaxation times for ≤ 0.5 *M* solutions of adamantane and HMTA at 24.5 ± 2°C

Solute	Solvent	Solvent viscosity at 25°C (cP)	Approx. solution viscosity at 25°C (cP)	T_1[a] (s)	τ_2 (ps)
Adamantane	$CDCl_3$	0.542	0.62 (0.5 *M*)	13.0	2.0
HMTA	$CDCl_3$	0.542	0.68 (0.5 *M*)	1.89	12.3
Adamantane	$CHBr_3$	1.89	2.0 (0.4 *M*)	9.2	2.8
HMTA	$CHBr_3$	1.89	2.3 (0.4 *M*)	1.04	22.4

[a]Methylene carbon, error is less than 10%.

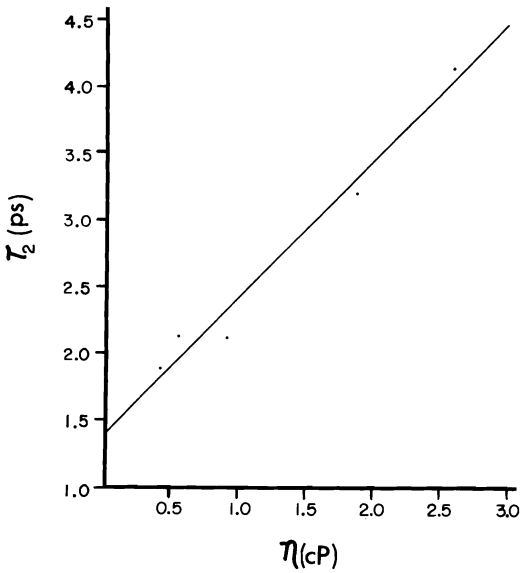

FIG. 2. Plot of the reorientational correlation time, τ_2, for 0.1 *M* adamantane *vs.* solvent viscosity at 23°C.

ps/cP.[2] A value of 27 ps/cP was calculated from the work of O'Reilly and Petersen (27) on HMTA in $CDCl_3$.

Thus, the observed τ_2's for HMTA in D_2O and $CDCl_3$ suggest that the rotation obeys a near stick condition; that is, it is consistent with the small step diffusion model. However, the well known complexities of hydrogen bonding (28) are not adequately represented by such a simplistic model of the boundary. The rotation may be within the scope of the Ivanov jump model, but no reasonable argument was found for choosing jump rates or rms jump angles.

The steeper slope observed for HMTA in chloroform compared to HMTA in bromoform suggests chloroform is a better proton donor than bromoform and hence forms stronger hydrogen bonds with HMTA. This suggestion is consistent with conclusions reached by Paterson and Cameron (29).

[2]HMTA crystallizes in the body centered cubic space group (2, 26); assuming 68% of the available space is occupied by spheres gives $V = 118.9$ Å^3, significantly smaller than the value calculated using the parameters of Edward (19). Using the above value of V, and eq. 2 with $\kappa = 1$ gives a viscosity dependence of 28.9 ps/cP.

Acknowledgements

We wish to thank Dr. Ronald Dong for carrying out the deuterium nmr measurements, Mr. Werner Danchura for the moment of inertia calculations, and Mr. Doug Durnin for the viscosity measurements.

Support of the National Research Council of Canada is gratefully acknowledged.

1. H. A. RESING. Mol. Cryst. Liq. Cryst. **9**, 101 (1969).
2. C. A. FYFE and D. HAROLD-SMITH. Can. J. Chem. **54**, 769 (1976); **54**, 783 (1976).
3. (*a*) K. F. KUHLMANN, D. M. GRANT, and R. K. HARRIS. J. Chem. Phys. **52**, 3439 (1970); (*b*) D. M. GRANT, R. J. PUGMIRE, E. P. BLACK, and K. A. CHRISTENSEN. J. Am. Chem. Soc. **95**, 8465 (1973).
4. N. BLOEMBERGEN, E. M. PURCELL, and R. V. POUND. Phys. Rev. **73**, 679 (1948).
5. A. GIERER and K. WIRTZ. Z. Naturforsch. **8a**, 532 (1953).
6. H. S. SANDHU. J. Am. Chem. Soc. **97**, 6284 (1975).
7. D. KIVELSON, M. G. KIVELSON, and I. OPPENHEIM. J. Chem. Phys. **52**, 1810 (1970).
8. D. WALLACH and W. T. HUNTRESS. J. Chem. Phys. **50**, 1219 (1969).
9. R. G. GORDON. J. Chem. Phys. **44**, 1830 (1966).
10. R. E. D. MCCLUNG. J. Chem. Phys. **51**, 3842 (1969); **54**, 3248 (1971), **57**, 5478 (1972); Chem. Phys. Lett. **19**, 304 (1973).
11. (*a*) K. T. GILLEN, J. H. NOGGLE, and T. K. LEIPERT. Chem. Phys. Lett. **17**, 505 (1972); (*b*) A. A. MARYOTT, M. S. MALMBERG, and K. T. GILLEN. Chem. Phys. Lett. **25**, 169 (1974).
12. T. C. FARRAR, A. A. MARYOTT, and M. S. MALMBERG. Ann. Rev. Phys. Chem. **23**, 193 (1972).
13. M. ABRAMOWITZ and I. A. STEGUN (*Editors*). 1964. Handbook of mathematical functions. Nat. Bur. Stand. Appl. Math. Ser. Washington, DC. **55**, 295–329 (1964).
14. P. S. HUBBARD. Phys. Rev. **131**, 1155 (1963).
15. E. N. IVANOV. Sov. Phys. (J.E.T.P.) **18**, 1041 (1964).

16. W. A. STEELE. The rotation of molecules in dense phases. Adv. Chem. Phys. To be published.
17. (*a*) B. J. BERNE and J. A. MONTGOMERY, JR. Mol. Phys. **32**, 363 (1976); (*b*) J. O'DELL and B. J. BERNE. J. Chem. Phys. **63**, 2376 (1975) and references therein.
18. M. S. WERTHEIM. Phys. Rev. Lett. **10**, 321 (1963).
19. J. T. EDWARD. J. Chem. Educ. **47**, 261 (1970).
20. T. C. FARRAR and E. D. BECKER. Pulse and Fourier transform nmr. Academic Press, NY. 1971.
21. (*a*) S. J. OPELLA, D. J. NELSON, and O. JARDETZKY. J. Chem. Phys. **64**, 2533 (1976); (*b*) D. CANET. J. Magn. Reson. **23**, 361 (1976); (*c*) R. K. HARRIS and R. H. NEWMAN. J. Magn. Reson. **24**, 449 (1976).
22. A. ABRAGAM. The principles of nuclear magnetism. Oxford University Press, London. 1961.
23. J. C. ROWELL, W. D. PHILLIPS, L. R. WHELBY, and M. PANAR. J. Chem. Phys. **43**, 3442 (1965).
24. J. L. LEBOWITZ. Phys. Rev. **133**, A895 (1974).
25. C. E. NORDMAN and D. L. SCHMITKONS. Acta Crystallogr. **18**, 764 (1965).
26. L. N. BECKA and D. W. J. CRUICKSHANK. Proc. R. Soc. London, Ser. A, **273**, 435 (1963).
27. D. E. O'REILLY and E. M. PETERSON. J. Chem. Phys. **59**, 1551 (1973).
28. E. E. TUCKER and E. LIPPERT. High resolution nmr studies of hydrogen bonding. *In* Recent advances in hydrogen bonding. Vol. II. *Edited by* P. Schuster, G. Zundel, and C. Sandorfy. North-Holland, Amsterdam. 1976. p. 793.
29. W. G. PATERSON and D. M. CAMERON. Can. J. Chem. **41**, 198 (1963).
30. H. S. SANHU and H. PEEMOELLER. J. Magn. Reson. **21**, 349 (1976).
31. T. C. FARRAR, S. J. DRUCK, R. R. SHOUP, and E. D. BECKER. J. Am. Chem. Soc. **94**, 699 (1972).
32. D. L. VANDERHART. J. Chem. Phys. **60**, 1858 (1974).
33. D. E. O'REILLY, E. M. PETERSON, and D. L. HOGENBOOM. J. Chem. Phys. **57**, 3969 (1972).

Motion of the SO_3^-NH radical trapped in potassium sulfamate. Electron spin resonance dipolar coupling tensors for the motionless radical

L. BONAZZOLA, J. P. MICHAUT, AND J. RONCIN

Laboratoire de Résonance Electronique et Ionique (Associé au CNRS), Université de Paris-Sud, 91405 Orsay, France

Received January 12, 1977

L. BONAZZOLA, J. P. MICHAUT, and J. RONCIN. Can. J. Chem. **55**, 2570 (1977).

The temperature dependence of the esr couplings in SO_3^-NH radical trapped in potassium sulfamate single crystals allows the study of the motion of this radical in the matrix and the determination of N and H dipolar tensors corresponding to the motionless radical. These values are compared with different theoretical calculations.

L. BONAZZOLA, J. P. MICHAUT et J. RONCIN. Can. J. Chem. **55**, 2570 (1977).

Les mouvements du radical SO_3^-NH piégé dans une matrice monocristalline de sulfamate de potassium sont étudiés à partir de la variation du couplage rpe avec la température. On détermine les tenseurs dipolaires des H et N relatifs au radical immobile et on les compare aux valeurs obtenues par différentes méthodes théoriques.

Introduction

It has been shown in a recent paper (1) on the study by epr of $SO_3^-NH_2^+$ radicals trapped in a single crystal of sulfamic acid, that the motion undergone by the radicals may be determined from the variations of the coupling tensors of H and N atoms as a function of temperature. The H and N tensors of the radical at rest may also be determined. A similar study on SO_3^-NH radicals trapped in a single crystal of potassium sulfamate is presented in this paper. The aim of this work was first to give another example of a coupling tensor for a radical at rest, for which the unpaired electron is borrowed by N atom. Secondly the knowledge of such coupling tensors from which contributions due to the motion of the radicals have been eliminated, making comparison between experimental and calculated hyperfine anisotropic coupling tensors possible.

Experimental

Potassium sulfamate was obtained from the neutralization of sulfamic acid by potassium hydroxide. Single crystals were grown from aqueous solutions by slow cooling. SO_3^-NH radicals are formed by irradiating potassium sulfamate crystals with a ^{60}CO source. The spectra were recorded on a JEOL ME IX spectrometer at five temperatures (4, 87, 156, 223, 293 K). Since the variations of the couplings as a function of temperature are weak, and since the accuracy in the determination of the coupling tensors depends strongly on the degree of orthogonality of the reference frame axes, the orientation of the crystal has to be exactly the same at all temperatures. Therefore, we first recorded the spectra at all temperatures for a rotation around one particular axis, then the spectra at all temperatures around a second axis, and so on. At 4 K, for technical reasons, the experiments were performed on a different single crystal, which was rotated about its crystallographic axes.

Results

Our results are reported in Tables 1 and 2. The signs of the principal values of the total hyperfine tensors have been assigned in the following way:

All H couplings have been taken to be negative as usual in the case of protons of π radicals.

It is generally assumed that the largest principal value (X) of the N tensor is positive. It is less obvious how to attribute the signs of the two other principal values Y and Z of the N tensor. It can be seen from Table 2 that the principal value Y does not vary significantly with temperature, within experimental errors. As shown previously (5), this indicates that torsional oscillations of the N—H group occur around an axis which is the principal direction corresponding to Y. This principal direction (0.900,0,0.435, Table 2) is parallel within 3° to the S—N bond of the undamaged molecule in the crystal (0.9202,0,0.3915, ref. 4). Let X_0 and Z_0 be the values of X and Z for a rotation angle $\theta = 0$ around the S—N bond. For a rotation angle θ, $Z = Z_0 \cos^2\theta + X_0 \sin^2\theta$, *i.e.* $Z = Z_0 + (X_0 - Z_0)\sin^2\theta$; $X_0 - Z_0$ is positive because $|Z_0| < |X_0|$ and $X_0 > 0$; when the temperature increases the experimental results show that $|Z|$ increases (Table 2). Consequently, Z has to be positive.

Let us now assume that the N tensor has a nearly cylindrical symmetry when the radical is at rest. Then, Z_0 and Y_0 (*i.e.* the values of Z and

TABLE 1. Experimental and calculated **H** hyperfine coupling tensors for SO_3^-NH radical trapped in single crystal of potassium sulfamate

T (K)	Principal values	Principal directions in a, b, c axes	Total coupling tensor	Isotopic coupling	Dipolar coupling tensor	Calculated dipolar coupling tensor
4	A	0.606 0 ±0.796	−38.7		−15.3	−15.1
	B	0 1 0	−23.0	−23.4	0.4	0.5
	C	0.796 0 ∓0.606	−8.5		14.9	14.6
87	A		−38.3		−15.1	−15.1
	B		−22.6	−23.2	0.6	0.6
	C		−8.8		14.4	14.5
156	A		−38.0		−15.0	−15.0
	B		−22.1	−23.0	0.9	0.9
	C		−8.9		14.1	14.1
223	A		−37.8		−14.9	−14.8
	B		−21.7	−22.9	1.2	1.2
	C		−9.2		13.7	13.6
293	A		−37.5		−14.7	−14.8
	B		−21.3	−22.9	1.6	1.6
	C		−9.8		13.1	13.2

TABLE 2. Experimental and calculated **N** hyperfine coupling tensors for SO_3^-NH radical trapped in a single crystal of potassium sulfamate

T (K)	Principal value	Principal directions in X, Y, Z axes	Total coupling tensor	Isotopic coupling	Dipolar coupling tensor	Calculated dipolar tensor
4	X	0 1 0	38.6		26.5	26.7
	Y	0.900 0 ∓0.435	−2.7	12.1	−14.8	−14.9
	Z	0.435 0 ±0.900	0.4		−11.7	−11.8
87	X		38.0		26.0	26.5
	Y		−2.8	12.0	−14.8	−14.9
	Z		0.7		−11.3	−11.6
156	X		37.3		25.3	25.4
	Y		−2.8	12.0	−14.8	−14.9
	Z		1.6		−10.4	−10.5
223	X		36.2		24.4	24.2
	Y		−3.0	11.8	−14.8	−14.9
	Z		2.1		−9.7	−9.3
293	X		34.6		22.8	22.9
	Y		−2.8	11.8	−14.7	−14.9
	Z		3.7		−8.1	−8.0

Y for the motionless radical) are equal. Since Y does not vary with temperature, $Y = Y_0$. It is seen from Table 2 that $|Z| < |Y|$; as Z is positive and decreases when the temperature decreases, Z_0 and consequently Y_0 have to be negative. With the present choice of the signs of X, Y, and Z, the N isotropic coupling (11.9 ± 0.15 G, Table 2) is smaller than the coupling found by Rowland (13.5 G, ref. 2) and Morton *et al.* (13.1 G, ref. 3) who postulated that the three principal values of the N tensor were positive.

Discussion

Structure and Position of the Radical SO_3^-NH in the Crystal

It is easy to determine the angle SNH in the SO_3^-NH radical from the directions of the S—N bond (*i.e.* the direction of the principal value Y of the N tensor), and the N—H bond

(*i.e.* the direction of the principal value C of the H tensor). The angle SNH is found to be 117°. As shown previously (6), the angle HNH of $\dot{N}H_2$ radical is 110° and the N isotropic coupling is 11.3 G. The spin density in the $2p_z$ orbital of SO_3^-NH is only about 0.9 and N isotropic coupling of SO_3^-NH (to be compared to NH_2) is 11.9/0.9 = 13.2 G. This result confirms that the N isotropic coupling increases with the angle XNY as predicted previously on the basis of an INDO calculation (6).

From crystallographic data (4) and esr results at 4 K, it can be shown that the H atom in the SO_3^-NH radical is in the plane determined by the S, N, and one O (say O_I) atoms of the parent molecule (Fig. 1). The S—N bond is a ternary symmetry axis for the SO_3 group in the molecule and hence, making the assumption that the skeleton of the molecule is not affected by the radiation process, there should be two other equivalent positions for the H atoms in the plane SNO_{II} or in the plane SNO_{III} (see Fig. 1) The esr spectra show that these two positions are not occupied. The reason for this is the existence of steric hindrance in the crystal as shown by Fig. 2, on which we have plotted the distance between H and its two closest neighbours in the crystal, an O atom of an adjacent molecule (O_{II}') and a K ion (K_I), as a function of the angle θ representing the rotation of the NH group around the S—N bond (θ = 0 being the equilibrium position found experimentally). Because of the symmetry in the crystal, only the region $0 < \theta < 180°$ is illustrated. The sum of van der Waals radii is 2.6 Å for the atoms O and H and 2.53 Å for the atom H and the K cation. From Fig. 2, it can be seen that both the conditions OH ≥ 2.6 Å and KH ≥ 2.53 Å are satisfied only when $-30° < \theta < 30°$. It is clear that the radical cannot have more than one equilibrium position in the crystal but that torsional oscillations around S—N are allowed.

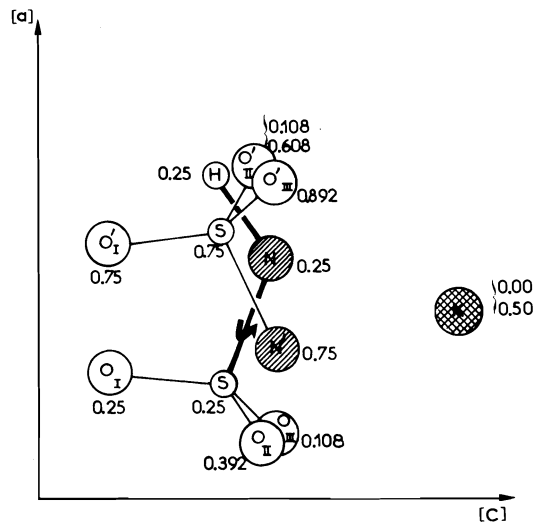

FIG. 1. Projection on the (010) plane of the SO_3^-NH free radical and its nearest neighbours in the *a*, *b*, *c* reference frame. The numbers correspond to the *b* coordinates of atoms. Steric hindrance occurs with O_{II}' and K.

Motions of SO_3^-NH in the Crystal

We have already remarked that esr results show that a torsional oscillation of N—H group occurs around the S—N bond, and that this N—H group has only one equilibrium position in the crystal. Therefore, the potential governing the oscillations of N—H around S—N may be represented by $V(\theta) = (V_0/2)(1 - \cos\theta)$, where V_0 is the maximum barrier height. Using the method already described (5), V_0 and the coupling tensor of the motionless radical may be determined. Very good agreement between experimental and calculated anisotropic tensor principal values is achieved (see Table 2) using the following parameters: V_0 = 6.5 kcal/mol; X_0 = 30.1 G (principal direction parallel to the orbital); Y_0 = 14.9 G (principal direction parallel to the S—N bond). In the same way, the proton dipolar coupling is influenced by the torsional oscillations of the N—H group (5). Thus, V_0 and the H dipolar tensor for the motionless radical may also be obtained from the data relative to the H tensor (Table 1): A_0 = −15.5 G (principal direction along the N—H bond); B_0 = 0.3 G (principal direction parallel to the π orbital). The maximum barrier height V_0 found from the data for the H tensor is slightly lower than from the N data. The first determination is very probably the more accurate because the variations of couplings with temperature are larger for N than for H.

The physical meaning of the barrier V_0 in the formula $V(\theta) = (V_0/2)(1 - \cos\theta)$ is questionable. As shown on Fig. 2, the torsional oscillations are not forbidden by steric hindrance for $-30° < \theta < 30°$. For small oscillations, the potential well has certainly an intramolecular origin. Because of the three possible equilibrium positions due to the symmetry of the radical, a better representation of the potential might be $V(\theta) = (V_0/2)(1 - 3\cos\theta)$. For small values of

TABLE 3. Comparison between calculated and experimental N and H dipolar coupling tensors relative to motionless radicals for a unit spin density

Dipolar tensor principal value (G)	Experimental		Calculated			
	$SO_3^-NH_2^+$*	SO_3^-NH	Ref. 7	Slater π orbital	STO orbital†	Ref. 10
N						
‖to orbital	34 to 36	32 to 34	34	26.5	34	29
H						
⊥NH bond	17 to 18	16.5 to 17.5		26.6	24	24.3
‖orbital	~0	~0		−8.0	−6.6	−5.6

*Reference 1.
†With coefficients of ref. 9.

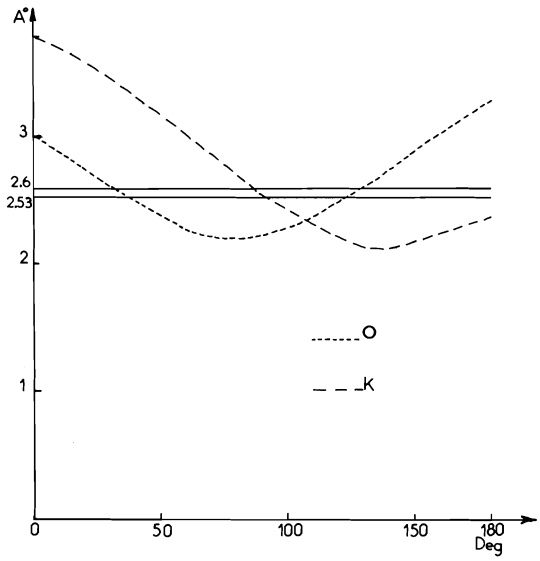

FIG. 2. Distances between the H atom of SO_3^-NH free radical and its two closest neighbours (O_{II}' atom of the adjacent molecule and the K ion of Fig. 1) as a function of the rotation angle θ around the N—S bond.

θ, the relation:

$$(V_0/2)(1 - \cos\theta) \simeq (V_0/2)(1/9)(1 - \cos 3\theta)$$

is approximately valid, and the physically meaningful barrier would be in fact 6.5/9 = 0.75 kcal/mol. This value is the height of the barrier which would hinder the free rotation of N—H bond if there were no steric hindrance in the trapping matrix.

Dipolar Coupling Tensors for the Radical at Rest

The N and H dipolar coupling tensors corresponding to motionless radicals have been derived from the temperature dependence of the couplings. They are respectively 30.1, −14.9, −15.2 G for N and −15.5, 0.3, 15.2 G for H. These tensors are given in Table 3 for $SO_3^-NH_2^+$ and SO_3^-NH radicals for a unit spin density. They may be compared to the calculated tensors.

(a) Nitrogen Coupling Tensor

Let us neglect the small π density in the bonds and consider the nitrogen tensor to be cylindrical. The theoretical principal values of N and H tensors given in Table 3 have been calculated by different methods: using Roothan and Clementi waves functions (7) (column 4, Table 3); the Mc Connel and Strathdee formula (8) using a Slater orbital (column 5, Table 3); by the same formula using a linear combination of Slater type orbitals (column 6, Table 3); in a spin unrestricted LCAO-MO-SCF approach using contracted gaussian-type functions for the expansion of molecular orbitals (10) (column 7, Table 3).

Good agreement between experiment and calculations is found only in the first and third cases. In the last calculation (column 7), the authors of ref. 10 claim to have found good agreement between experimental and theoretical tensors but, in fact, it is because the motion of the radical has not been accounted for.

(b) Proton Coupling Tensor

In the same way, the calculated H tensors are given in Table 3. Columns 5 and 6 concern $\dot{N}H_2$ radical, and column 7 concerns NH_3^+. Poor agreement is found between calculated and experimental tensors. This may be due to the poor accuracy of the wave function as soon as the distance from the N nucleus increases.

Conclusion

Measurements of the temperature dependence of the H and N couplings in SO_3^-NH radicals

trapped in a single crystal of potassium sulfamate allow the determination of the relative signs of the principal values of the N coupling tensor; the study of the torsional oscillations of the NH group around the S—N bond; the determination of the N and H dipolar coupling tensors corresponding to the radical at rest. These are the tensors that are to be compared to the theoretical calculations of the couplings. Let us note that these tensors, from which the contributions due to the motion of the radicals have been eliminated, may only be obtained in cases when there is a measurable temperature dependence of the couplings. As seen from Tables 1, 2 even measurements at 4 K do not give directly the tensor of the motionless radical because the zero point residual motions may give contributions of a few gauss (for N, $X_0 = 30.1$ G, $Y_0 = -14.9$ G, $Z_0 = -15.2$ G to be compared to the experimental values at 4 K, $X_0 = 26.7$ G, $Y_0 = -14.9$ G, $Z_0 = -11.8$ G).

1. J. P. MICHAUT, J. RONCIN, and K. LEIBLER. Chem. Phys. Lett. **40**, 28 (1976).
2. J. R. ROWLANDS. Mol. Phys. **5**, 565 (1962).
3. J. R. MORTON and D. R. SMITH. Can. J. Chem. **44**, 1951 (1966).
4. C. J. BROWN and E. G. COX. J. Chem. Soc. 1 (1940).
5. L. BONAZZOLA, C. HESSE-BEZOT, and J. RONCIN. Chem. Phys. **9**, 213 (1975).
6. J. P. MICHAUT, J. RONCIN, and R. MARX. Chem. Phys. Lett. **36**, 599 (1975).
7. J. R. MORTON, J. R. ROWLANDS, and D. H. WHIFFEN. Natl. Phys. L L. Gr. Brit. C No. BPR 13.
8. H. M. MCCONNELL and J. STRATHDEE. Mol. Phys. **2**, 129 (1959).
9. E. CLEMENTI. Tables of atomic functions, IBM Journal of Res. and Dev. **9**, 2 (1965).
10. J. ALMLOF, A. LUND, and K. A. THUOMAS. Chem. Phys. **7**, 465 (1975).

Ring currents, local anisotropy, and the problem of the out-of-plane protons: a reinvestigation of the nuclear magnetic resonance spectrum of [10]-paracyclophane

ARVIND AGARWAL, JOHN A. BARNES, JOHN L. FLETCHER, MICHAEL J. MCGLINCHEY,[1] AND BRIAN G. SAYER

Department of Chemistry, McMaster University, Hamilton, Ont., Canada L8S 4M1

Received July 28, 1976[2]

ARVIND AGARWAL, JOHN A. BARNES, JOHN L. FLETCHER, MICHAEL J. MCGLINCHEY, and BRIAN G. SAYER. Can. J. Chem. **55**, 2575 (1977).

The ^{1}H nmr spectrum of [10]-paracyclophane has been recorded at 220 MHz and the methylene protons assigned on the basis of homonuclear decoupled spectra. Local anisotropic contributions to chemical shifts for protons sited above or near the aromatic ring of [10]-paracyclophane have been calculated using a classical model previously proposed by Grant. The residual incremental shift was shown to follow the Waugh–Fessenden–Johnson–Bovey classical ring current model, but the loop separation originally invoked was shown to be unnecessary. These corrected ring current contributions also correlate very well with the quantum-mechanical approach of Haigh and Mallion.

ARVIND AGARWAL, JOHN A. BARNES, JOHN L. FLETCHER, MICHAEL J. MCGLINCHEY et BRIAN G. SAYER. Can. J. Chem. **55**, 2575 (1977).

On a enregistré le spectre rmn du proton du [10]paracyclophane à 220 MHz et on a attribué les protons méthylènes en se basant sur le spectre découplé d'une façon homonucléaire. Des contributions anisotropes locales aux déplacements chimiques des protons situés au-dessus ou près du cycle aromatique du [10]paracyclophane ont été calculées en faisant appel à un modèle classique proposé antérieurement par Grant. On a montré que l'augmentation résiduelle du déplacement suit le modèle classique de courant de cycle de Waugh–Fessenden–Johnson–Bovey mais on a trouvé qu'il n'est pas nécessaire de faire appel à la séparation de boucle qui avait été invoquée originalement. Ces contributions de courant de cycle corrigées offrent aussi une très bonne corrélation avec l'approche de mécanique quantique de Haigh et Mallion.

[Traduit par le journal]

Introduction

The deshielding of aromatic protons relative to olefinic protons has occupied the attention of nmr spectroscopists and theoreticians for almost 20 years, and the collective wisdom of these deliberations has been the subject of a number of reviews (1–3). Following the ideas of Pauling (4), the ring current concept was applied to benzene by Pople (5) who treated the system as possessing a point dipole located at the centre of the ring and showed that this would account for the downfield shift of benzene relative to ethylene. In a now classic paper, Waugh and Fessenden (6) developed their "Free Electron Model" in which the π-electrons were regarded as being analogous to a simple current loop and, using the well-established methods of classical electrodynamics (7), they were able to evaluate the induced field at any point whether in or out of the plane of the ring. The downfield shift of the benzene protons predicted by an in-plane current loop was 2.79 ppm and, in order to correlate with the then accepted shift of ~1.5 ppm (*i.e.*, the difference between benzene and the vinylic protons of 1,3-cyclohexadiene), Waugh and Fessenden separated the π current into two loops, one above and one below the ring plane; the separation between the loops was *empirically* adjusted to be 1.28 Å, and a very convenient tabulation of chemical shift increments calculated on this basis has been provided by Johnson and Bovey (8). Following the quantum mechanical treatment of McWeeny (9), Haigh and Mallion (10, 11) have presented a similar tabulation; both Johnson and Bovey (8) and Haigh and Mallion (11) approaches allow the evaluation of chemical shifts for out-of-plane protons.

In their original paper, Waugh and Fessenden (6) applied their theory to out-of-plane protons and they presented experimental and calculated nmr shift data on [10]-paracyclophane. Although

[1]To whom all correspondence should be addressed.
[2]Revision received March 23, 1977.

their 40 MHz spectrum clearly showed the presence of high field protons in the methylene chain, the resolution was insufficient to allow any definitive assignments to be made. We now present the 220 MHz spectrum of [10]-paracyclophane (Fig. 1) in which the five aliphatic resonances are clearly resolved. These data allow a critical and comparative evaluation of both Johnson–Bovey (8) and Haigh–Mallion (11) ring current theories.

Experimental

Proton spectra were obtained on a Varian HR 220 spectrometer operating at 220 MHz and 18°C. Proton homonuclear decoupled spectra were obtained on a Varian HA 100 spectrometer operating at 100 MHz at 35°C using standard techniques.

Concentrations of 0.1–0.2 *M* were used in $CDCl_3$ as solvent, and the peak positions were extrapolated to infinite dilution; TMS was used as an internal standard.

A section of the 220 MHz spectrum is shown in Fig. 1, and the data are listed in Tables 1 and 2.

Results and Discussion

1. The ^1H Nuclear Magnetic Resonance Spectrum of [10]-Paracyclophane

As previously mentioned, a number of models have been proposed to account for the shifts of aromatic protons. The now widely accepted free electron model was used in an attempt to rationalize the shifts of the out-of-plane protons in [10]-paracyclophane; however, the lack of resolution in the 40 MHz spectrum made quantitative verification of the theory somewhat hazardous. Nevertheless, constant application to a variety of aromatic systems has almost bestowed an imprimatur upon the theory. However, with the technological advances of two decades, a number of discrepancies are now apparent. Thus, in 1957 there was no method of reliably determining the structure of [10]-paracyclophane (or at least the most populated conformation in solution) and the authors had to estimate the proton positions relative to the aromatic ring by using Fisher–Hirschfelder models and trying to allow for the twisting motions of the decamethylene bridge. It is perhaps not surprising that the original assignment of the methylene protons as following the sequence: α, β, δ, γ, ε is incorrect. The 220 MHz spectrum, together with the homonuclear decoupling data, unequivocably established the order of the proton resonances as: α, β, γ, δ, ε with the ε protons at highest field.

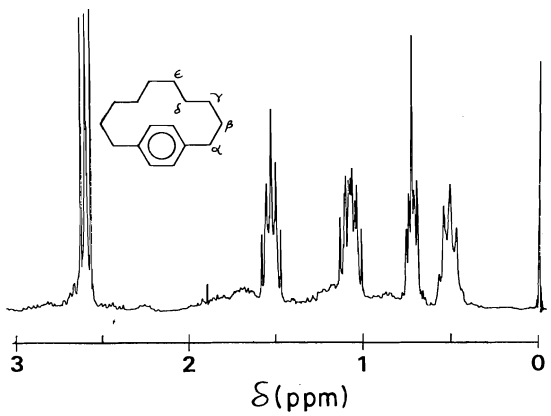

FIG. 1. 220 MHz ^1H nmr spectrum of high field resonances of [10]-paracyclophane.

TABLE 1. ^1H nmr data for [10]-paracyclophane

Position	δ values: Experimental 220 MHz	Calculated: Ref. 8 J–B	Calculated: Ref. 11 H–M
Ar	7.04		
α	2.62	1.66	1.60
β	1.54	1.55	1.36
γ	1.08	1.30	1.23
δ	0.73	0.82	1.13
ε	0.51	0.59	1.10

TABLE 2. Experimental vicinal coupling constants and calculated dihedral angles

Positions	*J* (Hz)	φ (Calculated, deg): Karplus	φ (Calculated, deg): Refined
Ring–α			155.5
α–β	6.2±0.1	62±3 or 112±3	62
β–γ	6.0±0.1	68±4 or 106±4	106
γ–δ	7.1±0.1	38±2 or 133±2	133
δ–ε	7.6±0.1	24±3 or 144±3	141.3

2. The Structure of [10]-Paracyclophane

The apparent inconsistency discussed above prompted us to direct our investigations toward a quantitative appraisal of the ring current tabulations (8, 11). Consequently, it was essential to know the structure of the molecule. In the absence of crystallographic data, it is necessary to calculate the molecular conformation of lowest energy, and for such systems a high degree of success has been achieved using Allinger's molecular mechanics calculations (12, 13). Thus, the correlation between the predicted and ob-

served structures of [8]-paracyclophane is very good and so one can confidently use this approach as the best available at present. Since the ^1H nmr spectrum shows only five methylene environments, the molecule is conformationally mobile on the nmr time scale; indeed Allinger calculated that the molecule would have a rather flat potential energy minimum allowing considerable amplitude of ring oscillation. The preferred conformation for [10]-paracyclophane was calculated to have a non-planar aromatic ring in which the *para*-carbons were displaced upwards through 8.4°, while the α-carbons were displaced downwards through 4.4° (13). The molecular mechanics method also predicted the conformation of the decamethylene chain, and an attempt to verify these predictions was undertaken using the Karplus theory (14, 15) relating vicinal coupling constants ($^3J_{HH}$) and dihedral angles which has been extensively used in structure determinations (16).

The dihedral angles of the most populated conformation were determined from the coupling constants obtained from the homonuclear decoupled spectra using the following relationship:

$$[1] \qquad J = A + B\cos\phi + C\cos 2\phi$$

where $A = 7$ Hz, $B = -1$ Hz, $C = 5$ Hz, a set of empirically derived parameters which refer to an H—C—C—H fragment in a carbon chain (17). The observed coupling constant is in fact an average of four coupling constants whose dihedral angles of interaction are ϕ, $120 + \phi$, ϕ, and $|120 - \phi|$. Then,

$$[2] \quad J_{obs} = 0.25(2J_{\phi} + J_{\phi+120} + J_{120-\phi})$$

with this consideration, eq. 1 becomes:

$$[3] \quad J_{obs} = 2.5\cos^2\phi - 0.25\cos\phi + 5.75$$

The calculated dihedral angles are listed in Table 2. In this analysis it was assumed that each $-CH_2-CH_2-$ unit could be regarded as an $[AX]_2$ system, since the chemical shifts of the protons in a given methylene group are dynamically averaged to give only one value and the chemical shift differences between adjacent methylene groups are relatively large. While this simplification is justifiable for the $J_{\alpha\beta}$, $J_{\beta\gamma}$, and $J_{\gamma\delta}$ couplings such is not the case for the $J_{\delta\varepsilon}$ case which is more correctly regarded as $[[AB]_2]_2$; consequently the dihedral angle predictions from $^3J_{H_\delta H_\varepsilon}$ are distinctly less reliable than are the others. Of course, the dihedral angle between the aromatic ring and the α-carbon—β-carbon bond is not evaluable directly as there is no appropriate coupling constant. This angle was approximated from a Fieser model and refined as outlined below. Now, accepting the values for the non-planarity of the ring and C_α atoms as calculated by Allinger (13), use of molecular models made it relatively easy to decide the unique combination of dihedral angles which allowed the construction of the decamethylene bridge. Finally, a molecular geometry programme (18) was used empirically to adjust not only the dihedral angles (within the calculated error limits) but also the aliphatic C—C—C bond angles (to parallel the behaviour of the corresponding angles in [8]-paracyclophane) such that the ε-carbon coordinates (x,y,z) corresponded to the ε′-carbon coordinates $(\bar{x},\bar{y},z)$ as required by C_2 symmetry. Throughout these calculations, the aromatic ring carbon–carbon bond lengths were taken as 1.39 Å, the exocyclic sp^2–sp^3 bond as 1.50 Å and the C—C and C—H bonds in the polymethylene chain as 1.54 and 1.08 Å respectively. Each H—C—H plane was positioned orthogonally to the appropriate C—C—C plane. It is gratifying that these experimental data, *viz.*, coupling constants, reinforce Allinger's theoretically predicted molecular geometry as shown by comparing Fig. 2 with Fig. 2 in ref. 13.

3. *Comparison of Ring Current Theories*

These structural data allow the evaluation of incremental shifts for the methylene protons lying out of the aromatic ring plane using both the semiclassical (8) and quantum mechanical (11) approaches. In order to predict chemical shifts relative to TMS it is necessary to select the "standard methylene shift" appropriate to the system. Typical values for large cycloalkanes average to 1.30 ppm (19), and this is the standard we have used. The chemical shifts thus predicted by the Johnson–Bovey (8) and Haigh–Mallion (11) tabulations for the α, β, γ, δ, and ε protons are presented in Table 1, and may be compared with the experimental values in the same table. It is apparent that, while both methods are qualitatively very useful, the quantitative agreement with the experimental shifts is not uniform throughout all positions which experience the effect of the ring current. The semi-classical method shows good agreement for protons held

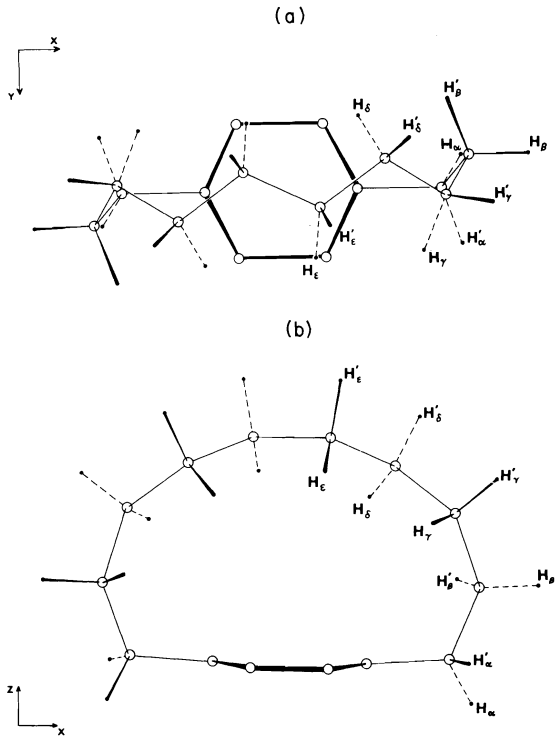

FIG. 2. Preferred conformations of [10]-paracyclophane: (*a*) plan, (*b*) elevation, the hydrogen atom positions are shown in perspective relative to the carbon atom to which they are attached.

over the centre of the ring, but becomes less reliable as the value of ρ increases and *z* decreases. However, the quantum mechanical approach gives adequate agreement in these latter regions but seriously underestimates the upfield shifts of the protons directly above the ring, as was originally inferred (10, 20). The work of Rose (21) on pyridylphenanthrenes also supports this generalization.

4. Local Anisotropic Contributions

It was apparent that the present ring current theories did not provide a complete rationale for the experimentally observed shifts and that some other important contribution had been overlooked. It had earlier been suggested by Pople (22, 23) that local anisotropic effects were a large contributing factor to the deshielding of the protons in benzene. Furthermore Barfield, Grant, and Ikenberry (24) have now successfully demonstrated that local anisotropic contributions to chemical shifts may be evaluated using the ^{13}C chemical shielding tensors so painstakingly obtained by Waugh and co-workers (25, 26) using proton-enhanced nuclear induction spectroscopy (27). Grant's data (24) clearly show that local anisotropic contributions cannot be ignored for in-plane protons in condensed aromatic systems,[3] and we now extend these calculations to out-of-plane protons.

Using the analogy of a current circulating in a loop of wire (24), the proton shielding component, σ_{ii}^{H}, is given by

$$[4]\quad \sigma_{ii}^{H} = \frac{a}{\pi}\frac{1}{[(a+\rho)^2 + z^2]^{1/2}} \times \left[K + \frac{a^2 - \rho^2 - z^2}{(a-\rho)^2 + z^2}\cdot E\right]\cdot \sigma_{ii}^{C}$$

where a is the radius of circulation about each carbon atom, taken as 0.47 Å (24), ρ and z are the usual cylindrical coordinates, and K and E are complete elliptical integrals of the first and second type with the argument

$$k^2 = \frac{4a\rho}{(a+\rho)^2 + z^2}$$

More simply, $\sigma_{ii}^{H} = G\sigma_{ii}^{C}$ where σ_{ii}^{H} and σ_{ii}^{C} are the proton and carbon shielding components and G is a geometric factor. The isotropic shielding, as measured in solution, is given by averaging the components

$$\langle\sigma^{H}\rangle = \tfrac{1}{3}[\sigma_{11}^{H} + \sigma_{22}^{H} + \sigma_{33}^{H}]$$

The ^{13}C shielding tensors used in this study are taken from refs. 25 and 26; values used for aromatic carbons bearing alkyl chains are those listed by Waugh for hexaethylbenzene, while those for aromatic carbons with hydrogen substituents are the average of the appropriate values from pentamethylbenzene and durene. To convert the values from shifts relative to benzene into absolute shifts, it is necessary to add 71 ppm to each ^{13}C shielding tensor (24). The local anisotropic contributions for each methylene proton brought about by circulations about each ring carbon in [10]-paracyclophane are presented in Table 3.

[3]A dipolar approximation presented in ref. 24 contains an algebraic error due to mis-evaluation of the elliptical integral power series. However, this does not materially affect the conclusions drawn previously, *i.e.*, it is unsafe to calculate chemical shifts for proximate protons using only a dipolar formula. For the situation in ref. 24, the correct dipolar formula is

$$\langle\sigma^{H}\rangle = \frac{a^2}{3r_{CH}^{\,2}}\left(\sigma_{11}^{C} + \frac{a}{r_{CH}}\cdot\sigma_{22}^{C} + \sigma_{33}^{C}\right)$$

5. Experimentally Determined Ring Currents

We can now define the ring current contribution (ΔRC) to the chemical shift as the difference between the experimental shift (δ) and that calculated by adding the local anisotropic contribution to the standard, *i.e.*,

$$[5] \quad (-\delta)_{\text{expt}} = -1.30 + \text{LA term} + \Delta\text{RC}_{\text{expt}}$$

These "experimentally determined ring current shifts" are listed in Table 3 together with ring current shifts calculated using the equation

$$[6] \quad \Delta = \frac{C}{[(a+\rho)^2 + z^2]^{1/2}} \times \left[K + \frac{a^2 - \rho^2 - z^2}{(a-\rho)^2 + z^2} \cdot E\right]$$

where $C = ne^2/6\pi M_e c^2 = 8.970$, where n is the number of circulating electrons of charge e and mass M_e, c is the velocity of light, ρ and z are the usual cylindrical coordinates, and a is the radius of circulation about the ring taken as 1.39 Å. In this case ρ and z are measured in Å rather than ring radii.

The quoted shifts are the average of two shifts Δ_1 and Δ_2 obtained by taking $z_1 = z + S/2$ and $z_2 = z - S/2$, where S is the separation of the current loops. It is necessary to accept that any ring current contribution calculated semi-classically must follow an equation of the type [6] where the only adjustable parameters are C and S. Waugh and Fessenden chose to adjust the separation of the loops, while Barfield, Grant, and Ikenberry adjusted both C and S. Our approach was to adjust the separation between the loops to get the best correlation between the "experimental ring current shifts" and the calculated shifts, and then to evaluate C empirically.

It is now apparent from our data that the arbitrary separation into two loops is not only unnecessary but is actually detrimental to the optimum fit. Now a plot (Fig. 3) of the $\Delta\text{RC}_{\text{expt}}$ values *vs.* calculated ring current by the Johnson–Bovey (8) method ($\Delta\text{RC}_{\text{J–B},S=0}$) provides a value for C, and follows the equation

$$[7] \quad \Delta\text{RC}_{\text{expt}} = 1.04\,\Delta\text{RC}_{\text{J–B},S=0} - 0.06$$

The correlation coefficient, $\bar{r}$, was found to be a maximum (0.9928) at $S = 0$; the correlation worsened very rapidly on invoking loop separation. Typically, $S = 1.0$ Å, $\bar{r} = 0.9461$; $S = 1.28$ Å (ref. 6), $\bar{r} = 0.8883$; $S = 1.63$ Å (ref. 24),

TABLE 3. Calculated and experimental ring current and local anisotropy incremental contributions to the shifts of protons in the decamethylene bridge of [10]-paracyclophane. H′ represents the proton of any given methylene pair having the larger positive z value

	Ring current increments[a]							
	Semi-classical theory				Quantum mechanical theory		Experimental	Local anisotropy increments
Atom	$S = 0$		$S = 1.28$[b]		$S = 1.63$[c]			
H_α	−0.729	−0.786	−0.379	−0.360	−0.228	−0.203	−0.278	−0.300	−0.905	−0.295	−0.415
H_α'	−0.842		−0.340		−0.178		−0.321			−0.535	
H_β	−0.173	−0.171	−0.171	−0.252	−0.161	−0.256	−0.069	−0.063	−0.155	−0.104	−0.086
H_β'	−0.169		−0.332		−0.351		−0.057			−0.067	
H_γ	0.265	0.177	−0.030	−0.002	−0.248	−0.132	0.102	0.068	0.095	0.193	0.125
H_γ'	0.088		0.026		−0.015		0.034			0.057	
H_δ	0.643	0.446	0.692	0.479	0.652	0.462	0.246	0.171	0.329	0.348	0.241
H_δ'	0.248		0.266		0.271		0.095			0.134	
H_ε	0.717	0.515	1.014	0.710	1.232	0.852	0.274	0.197	0.538	0.347	0.252
H_ε'	0.313		0.405		0.472		0.120			0.157	

[a]Units: ppm. A minus sign indicates a downfield effect.
[b]Johnson–Bovey separation (Å), ref. 8.
[c]Barfield–Grant–Ikenberry separation (Å), ref. 24.

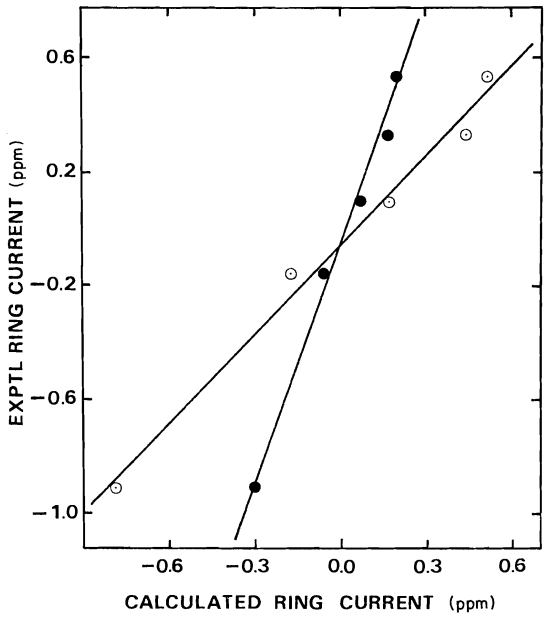

FIG. 3. Plot of experimental ring current (ΔRC_{expt}) *vs.* calculated ring current ($\Delta RC_{J-B,S=0}$, ○; and ΔRC_{H-M}, ●).

$\bar{r} = 0.7634$; $S = 2.0$ Å, $\bar{r} = 0.6161$. Therefore, the data force upon us the conclusion that the arbitary separation of the ring current into two loops is unnecessary; furthermore, the ring current increments derived by a semi-classical approach and those determined experimentally show good agreement.

A plot of measured chemical shift ($-\delta$) *vs.* calculated ring current ($\Delta RC_{J-B,S=0}$) also shows an interesting correlation, *viz.*,

$$[8] \quad (-\delta) = 1.57\,\Delta RC_{J-B,S=0} - 1.36 \qquad (\bar{r} = 0.9974)$$

Combining eqs. 5, 7, and 8, we see that

$$[9] \quad LA = 0.53\,\Delta RC_{J-B,S=0}$$

indicating that the ring current contribution to the incremental shift is of the order of 65%.

This whole postulate receives strong support from Dailey's work on magnetic anisotropy which showed that the ring current only contributes to the extent of ~60% to the chemical shifts of aromatic hydrocarbons (28).

Having shown that the experimental ring current shifts are readily rationalizable from the semi-classical viewpoint, it is of interest to determine whether any analogous correlation exists for the quantum mechanical theory. This latter theory has only one variable parameter which was obtained from a linear regression analysis of data for planar polycyclic aromatics.

A plot of our experimental ring current shifts against those predicted from the quantum mechanical approach shows excellent agreement ($\bar{r} = 0.9932$) and follows the equation

$$[10] \quad \Delta RC_{expt} = 2.73\,\Delta RC_{H-M} - 0.06$$

It will be noted that the predictions of the Johnson–Bovey (8) and Haigh–Mallion (11) tabulations differ by a factor of ~2.6 in the limit (11). Using our data (see Table 3) the following relationships were found

$$[11] \quad \Delta RC_{J-B,S=0} = 2.60\,\Delta RC_{H-M}$$

$$[12] \quad \Delta RC_{J-B,S=1.28} = 2.02\,\Delta RC_{H-M}$$

where $\bar{r} = 0.9998$ and 0.8938 respectively, thus reinforcing our earlier arguments dispelling the necessity for loop separation.

It is especially gratifying to see that the two entirely different models are compatible with the experimental data. Previous statements (11, 21) that the two theories are only applicable to specific spatial regions of the aromatic molecule are nullified when the correct ring current increments are evaluated. Thus previously published experimental ring currents which did not allow for the local anisotropic corrections would not be expected to fit either ring current model, except fortuitously.

One would have anticipated that eqs. 7 and 10 should have zero intercept since the overall chemical shift of any given methylenic proton is assumed to be a composite of only three terms *viz.*, LA and RC terms, which are of course position dependent, and the standard shift, which is the same for all protons in the chain. Since one obtains the identical non-zero intercept from both the semi-classical and quantum mechanical approaches, we propose that the standard methylene shift in chloroform be taken as 1.36 ppm rather than the initially chosen value of 1.30 ppm.

In the previous treatment of [10]-paracyclophane (6), the predicted shifts of the protons α to the ring gave such poor agreement that they were ignored, and these shifts were merely compared to the corresponding protons in ethylbenzene. However, the present approach adequately accounts for the α-CH_2 shift *without* invoking an inductive effect of the phenyl ring; that is, the inherent standard shift for the α-proton can still

be taken as 1.36 ppm. Thus, it would seem that the so-called inductive effect of the phenyl ring can be wholely attributed as being a manifestation of the anisotropic nature of the electron distribution within the ring.

In calculating incremental methylene proton shifts using a combination of local anisotropic and ring current contributions *from the aromatic ring*, we have assumed that local anisotropic contributions from atomic neighbours in the polymethylene chain are allowed for by suitable choice of a standard. One should point out[4] that whilst our determination of the local currents involves the use of the total carbon shielding tensor (the effect of the delocalised current being ignored), comparison of the isotropic ^{13}C shifts in benzene and for the C-2, C-3 resonances in cycloheptatriene shows that the delocalised effect must be relatively small.

We feel that this approach to the problem of the ring currents is valuable in that the investigation of the methylene protons is less hazardous than investigating the aromatic protons for which the choice of a standard shift is more difficult and controversial. An extension of the concepts developed here allows a study of ring currents in arene-metal π-complexes and this will be dealt with in a subsequent publication.

Conclusions

Present ring current tabulations do not allow for the local anisotropic contributions to the chemical shifts of protons in aromatic environments; independent calculation of these local anisotropic contributions allows the evaluation of corrected (experimental) ring current shifts. These corrected shifts were found to show simple relationships to both the quantum mechanical and semi-classical approaches; in each case, the correlation coefficients were excellent. However, the separation of the current loops in the semi-classical approach while aesthetically satisfying was shown to be unnecessary.

Acknowledgements

We wish to express our sincere gratitude to Professor Norman L. Allinger (University of Georgia) for his most generous gift of the sample of [10]-paracyclophane and for discussions on molecular geometry. We also wish to thank Dr. A. A. Grey for use of the 220 MHz spectrometer facilities (Ontario Research Foundation, Sheridan Park Research Centre, Mississauga, Ontario), Dr. F. G. Riddell (University of Stirling, Scotland) for helpful discussions, and our colleague Professor D. P. Santry for computational advice.

Financial assistance from the National Research Council of Canada is gratefully acknowledged.

[4]We thank a particularly diligent referee for this and other valuable comments on the manuscript.

1. A. J. Jones. Rev. Pure Appl. Chem. **18**, 253 (1968).
2. R. C. Haddon, V. R. Haddon, and L. M. Jackman. Top. Curr. Chem. **16**, 103 (1971).
3. J-F. Labarre and F. Crasnier. Top. Curr. Chem. **24**, 33 (1971).
4. L. Pauling. J. Chem. Phys. **4**, 673 (1936).
5. J. A. Pople. J. Chem. Phys. **24**, 1111 (1956).
6. J. S. Waugh and R. W. Fessenden. J. Am. Chem. Soc. **79**, 846 (1957); **80**, 6697 (1958).
7. W. R. Smythe. Static and dynamic electricity. 3rd ed. McGraw-Hill, New York, NY. 1968. pp. 290, 291.
8. C. E. Johnson, Jr. and F. A. Bovey. J. Chem. Phys. **29**, 1012 (1958).
9. R. McWeeny. Mol. Phys. **1**, 311 (1958).
10. C. W. Haigh and R. B. Mallion. Mol. Phys. **22**, 995 (1971).
11. C. W. Haigh and R. B. Mallion. Org. Magn. Reson. **4**, 203 (1972).
12. N. L. Allinger and J. T. Sprague. J. Am. Chem. Soc. **95**, 3893 (1973).
13. N. L. Allinger, J. T. Sprague, and T. Liljefors. J. Am. Chem. Soc. **96**, 5100 (1974).
14. M. Karplus. J. Chem. Phys. **30**, 11 (1959).
15. M. Karplus. J. Am. Chem. Soc. **85**, 2870 (1963).
16. H. Booth. *In* Progress in nuclear magnetic resonances spectroscopy. Vol. 5. *Edited by* J. W. Emsley, J. Feeney, and L. H. Sutcliffe. Pergamon Press, Oxford. 1969. p. 149.
17. A. A. Bothner-By. Adv. Magn. Reson. **1**, 195 (1965).
18. P. E. Stevenson and J. E. Merrill. Local version of COORD, Atomic Cartesian Coordinates for Molecules, Program 186, Quantum Chemistry Program Exchange, Indiana University, 1971.
19. J. J. Burke and P. C. Lauterbur. J. Am. Chem. Soc. **86**, 1870 (1964).
20. C. W. Haigh. Personal communication.
21. P. I. Rose. Org. Magn. Res. **5**, 187 (1973).
22. J. A. Pople. J. Chem. Phys. **41**, 2559 (1964).
23. A. F. Ferguson and J. A. Pople. J. Chem. Phys. **42**, 1560 (1965).
24. M. Barfield, D. M. Grant, and D. Ikenberry. J. Am. Chem. Soc. **97**, 6956 (1975).
25. S. Pausak, A. Pines, and J. S. Waugh. J. Chem. Phys. **59**, 591 (1973).
26. S. Pausak, J. Tegenfeldt, and J. S. Waugh. J. Chem. Phys. **61**, 1338 (1974).
27. A. Pines, M. G. Gibby, and J. S. Waugh. Chem. Phys. Lett. **15**, 373 (1972).
28. B. P. Dailey. J. Chem. Phys. **41**, 2304 (1964).

The hydrolysis of substituted cyclopropyl bromides in water. IV. The effect of vinyl and methyl substitution on $\Delta C_p^{\ddagger}$[1]

SURENDRA SINGH[2] AND ROSS ELMORE ROBERTSON[3]

Department of Chemistry, The University of Calgary, Calgary, Alta., Canada T2N 1N4

Received August 27, 1976[4]

SURENDRA SINGH and ROSS ELMORE ROBERTSON. Can. J. Chem. **55**, 2582 (1977).

In this study of the effect of vinyl and methyl substitution on the rates of hydrolysis of cyclopropyl bromides in water, we examine the changes in $\Delta C_p^{\ddagger}$ with substitution and configuration. The unusual values of $\Delta C_p^{\ddagger}$ found by Ong and Robertson (Can. J. Chem. **52**, 2660 (1974)) for the hydrolysis of 2-*cis*- and *trans*-vinylcyclopropyl bromide are shown to be characteristic of the vinyl substituent and reflect either a transition state which corresponds to a low degree of charge separation or to internal cancellation due to the formation of an extended dienylic cation. The 2,3-*cis*,*cis*-dimethylcyclopropyl bromide gave a value of $\Delta C_p^{\ddagger} = -145$ cal mol^{-1} deg^{-1}, comparable to limiting values obtained for hydrolysis of 1- and 2-adamantyl nitrate. The corresponding value of $\Delta C_p^{\ddagger}$ for 2,3-*cis*,*trans*-dimethylcyclopropyl bromide (-56 cal mol^{-1} deg^{-1}) was less negative than for the 2,3-*trans*,*trans* isomer (-75 cal mol^{-1} deg^{-1}). The mechanistic implications are discussed.

SURENDRA SINGH et ROSS ELMORE ROBERTSON. Can. J. Chem. **55**, 2582 (1977).

Dans cette étude sur l'effet des substituants vinyle et méthyle sur les vitesses d'hydrolyse de bromures de cyclopropane dans l'eau, on examine les changements dans les $\Delta C_p^{\ddagger}$ en fonction de la substitution et de la configuration. On a montré que les valeurs inusitées de $\Delta C_p^{\ddagger}$ trouvées par Ong et Robertson (Can. J. Chem. **52**, 2660 (1974)) pour l'hydrolyse des bromures de vinyl-2 cyclopropane *cis* et *trans* sont caractéristiques du substituant vinyle et sont un reflet soit d'un état de transition qui correspond à un très bas degré de séparation de charge ou à une annulation interne due à la formation d'un cation diènyle étendu. Le bromure de diméthyl-2,3 cyclopropane *cis-cis* a une valeur de $\Delta C_p^{\ddagger} = -145$ cal mol^{-1} deg^{-1} qui peut se comparer avec les valeurs limites obtenues pour l'hydrolyse des nitrates d'adamantyle-1 ou -2. La valeur correspondante du $\Delta C_p^{\ddagger}$ pour le bromure de diméthyl-2,3 cyclopropane *cis-trans* (-56 cal mol^{-1} deg^{-1}) est moins négative que pour l'isomère 2,3 *trans-trans* (-75 cal mol^{-1} deg^{-1}). On discute des implications mécanistiques de ces résultats.

[Traduit par le journal]

This report on the hydrolysis of substituted cyclopropyl bromides is an outgrowth of an earlier study of the hydrolysis of 2-vinylcyclopropyl bromides (1). In that study, the values of $\Delta C_p^{\ddagger}$ for the hydrolysis of the *cis* and *trans* isomers were found to be -27 and -35 cal mol^{-1} deg^{-1}, respectively. Values of $\Delta C_p^{\ddagger}$ in this range for displacement of a bromide ion (as opposed to displacement of tosylate or methanesulfonate (2)) have been associated with a minimal charge development at the transition state for hydrolysis in water and in the absence of other evidence this was the interpretation proposed by Ong and Robertson. Certain theoretical calculations were seen to lend support to this hypothesis (3, 4), even though results obtained in different solvents suggested that under other conditions a greater degree of charge development might be expected (5, 6). Thus in a previous study on the solvolysis of substituted cyclopropyl bromides in acetic acid, Schleyer *et al.* had concluded that there was "considerable" charge development at the transition state (7). That different degrees of charge development at the transition state will be found with different solvents is altogether reasonable unless the transition state corresponds to a limiting case (8). However, the unusually "low" value of $\Delta C_p^{\ddagger}$ for hydrolysis of the 2-vinylcyclopropyl bromides in water was unexpected, hence this earlier work was extended to include a study of the hydrolysis of other substituted cyclopropyl bromides. Some of these results have been published (9, 10) and these together with the results from the present study are collected in Table 1.

As in the past, rate data were determined by a conductance method (2). The limiting factor in such a study is frequently the limited solubility

[1]Based in part on the Ph.D. Thesis of S. Singh, University of Calgary, Calgary, Alta., 1975.

[2]Present address: Department of Chemical Engineering, McMaster University, Hamilton, Ont.

[3]Author to whom correspondence should be addressed.

[4]Revision received March 4, 1977.

TABLE 1. Pseudo-thermodynamic activation parameters for the aqueous solvolysis of substituted cyclopropyl bromides

Compound*	Temperature (°C)†	$\Delta F^{\ddagger}$ (cal/mol)	$\Delta H^{\ddagger}$ (cal/mol)	$\Delta S^{\ddagger}$ (cal deg^{-1} mol^{-1})	$-\Delta C_p^{\ddagger}$ (cal deg^{-1} mol^{-1})	References
2,2-DMCpBr(**1**)†	56	24962± 0.3	26805± 9	5.60±0.02	52±2	9
2,3-*cis*,*trans*-DMCpBr(**2**)	56	25051± 0.4	26816± 10	5.36±0.03	56±2	This work
2,3-*cis*,*cis*-DMCpBr(**3**)	56	28722± 9	32881±245	12.63±0.72	145±8	10
2,3-*cis*,*cis*-DMCpBr(**3**)	80	28543± 1.4	29388± 60	2.39±0.17	145±8	10
2,3-*trans*,*trans*-DMCpBr(**4**)	18	22533± 0.7	26670± 16	14.21±0.05	75±4	This work
2,3-*trans*,*trans*-DMCpBr(**4**)	56	22172±10	23797±163	4.94±0.53	75±4	This work
2,2-*cis*-Methyl,*trans*-vinyl-CpBr(**5**)	56	24817± 0.4	26271± 15	4.42±0.05	37±2	9
2,2-*cis*-Vinyl,*trans*-methyl-CpBr(**6**)	56	24871± 0.7	26068± 20	3.64±0.06	27±4	9
2,3-*cis*-Vinyl,*trans*-methyl-CpBr(**7**)	56	24174± 0.3	26080± 8.7	5.79±0.03	36±2	This work
2-*cis*-(1-Propenyl)CpBr(**8**)	56	25866± 0.3	26242± 14	1.14±0.04	36±1	This work
2-*cis*-Vinyl-CpBr(**9**)	75	27658± 0.4	27957± 28	0.85±0.08	27±4	1
2-*trans*-Vinyl-CpBr(**10**)	75	25912± 0.3	26363± 10	1.29±0.03	35±2	1

*Abbreviations: D di-, M methyl, Cp cyclopropyl.
†About the mid-point of temperature range over which rate measurements were made where errors are minimal.

TABLE 2. Empirical constants for the equation $\log_{10} k = A_1 + A_2/T + A_3 \log T$

Compound*	A_1	$-A_2$	$-A_3$
2,3-*cis*,*trans*-DMCpBr	94.5803	9884.5271	27.1499
2,3-*trans*,*trans*-DMCpBr	117.6657	10374.539	34.9677
2,3-*cis*-Vinyl,*trans*-methyl-CpBr	65.9033	8330.373	17.4027
2-*cis*-(1-Propenyl)CpBr	−42.6946	3155.675	−19.0450

*Abbreviations: D di-, M methyl, Cp cyclopropyl.

of the substituted compound. Our attempt to extend the study to *trans*-2,2,3-trimethylcyclopropyl bromide and *cis*-2,2,3-trimethylcyclopropyl bromide was thwarted by low solubility while the dimethyl substituted cyclopropyl bromides were found sufficiently soluble for our purpose.

The range of the temperature–rate study was about 30°C and the resulting data were fitted to the equation $\log k = A_1 + A_2/T + A_3 \log T$. The constants are collected in Table 2 and provide a means of interpolating rate constants and quasi-thermodynamic parameters.[5] Relative rates for hydrolysis in water are given in Table 3. We accept the hypothesis (5, 6, 11–14) that the activation process for the solvolysis of cyclopropyl halides in water as in other solvents involves anchimeric assistance from σ-bond interaction and electrocyclic ring opening (15, 16).

Substitution of carbonium ion stabilizing groups on the α-carbon of cyclopropyl bromide was known to have a relatively small effect on the rate of solvolysis (17, 18) and so was not investigated. In water, the relative effect of β-Me substitution on the rate of hydrolysis varied widely (Table 3). Such differences can be attributed to a combination of non-bonded interaction, facilitation of σ-bond participation, and variation in the probability of nucleophilic interaction (k_{2n}, ref. 8) as a consequence of the special configurational considerations imposed by the cyclopropyl structure and the requirement for opening of the ring. Dispersal of electron deficiency by substituents will have two effects on the observed rate: (*1*) to delay nucleophilic interaction and (*2*) to enhance the external effects of the charge of Br^-; the latter will result in more negative values of $\Delta C_p^{\ddagger}$, in water. Rate enhancement due to the vinyl group (280/3000)

[5]
$$A_1 = \frac{\Delta S_0^{\ddagger} - \Delta C_p^{\ddagger}}{2.303R} + \log\frac{k}{h}$$

$$A_2 = -\Delta H_0^{\ddagger}/2.303R$$

$$A_3 = \frac{\Delta C_p^{\ddagger}}{R} + 1$$

$$\Delta H_T^{\ddagger} = \Delta H_0^{\ddagger} + \int_0^T C_p^{\ddagger}\,dT$$

$$\Delta S_T^{\ddagger} = \Delta S_0^{\ddagger} + \int_0^T \frac{\Delta C_p^{\ddagger}}{T}\,dT$$

with T in Kelvins.

TABLE 3. Relative rates for the solvolysis of substituted cyclopropyl bromides at 100°C in H_2O

Compound*	k (s^{-1})	Relative rate
Cyclopropyl bromide	1.74×10^{-6}	1
2,2-DMCpBr(**1**)	0.0214	12300
2,3-*cis*,*cis*-DMCpBr(**3**)	0.000145	83
2,3-*cis*,*trans*-DMCpBr(**2**)	0.0185	10600
2,3-*trans*,*trans*-DMCpBr(**4**)	0.8573	492700
2,2-*cis*-Methyl,*trans*-vinyl-CpBr(**5**)	0.0257	14800
2,2-*cis*-Vinyl,*trans*-methyl-CpBr(**6**)	0.0228	13100
2-*cis*-Vinyl,3-*trans*-methyl-CpBr(**7**)	0.0664	38200
2-*cis*-Methyl,3-*trans*-vinyl-CpBr†	3.987×10^{-4} at 49.84°C	—
2-*cis*-(1-Propenyl)CpBr(**8**)	0.00674	3900
2-*cis*-Vinyl-CpBr(**9**)	0.000491	280
2-*trans*-Vinyl-CpBr(**10**)	0.00521	3000

*Abbreviations: D di-, M methyl, Cp cyclopropyl.
†Comparable value for 7 is 2.79×10^{-4} s^{-1}.

may be attributed to stabilization of the activated state by conjugation, but if the transition state resembled the extended ion:

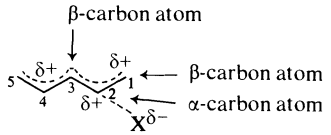

the substitution of a methyl would be expected to cause a much larger increase in the rate, whereas dispersal of electron deficiency would result in large negative values of $\Delta C_p^{\ddagger}$ (10). Neither expectation is found (Fig. 1 *A*–1*F* and Table 2). The simpler explanation is that the presence of a β-vinyl substituent facilitates nucleophilic attack by water. The relative rate ratios are higher in *C* and *D* where methyl substitution is on the other β-C but the difference is hardly remarkable. Methyl-substitution on the vinyl group (*E*, *F*) results in reduced ratios both here and by comparison with the allylic system.[6] Even in the latter where there is minimal steric hindrance to nucleophilic attack, substitution of Me in the α or γ position results in a rate enhancement of only 720 (*cis*) and 620 (*trans*), respectively (Table 4). We note also that the presence of a vinyl group *per se* does not result in abnormally 'low' $\Delta C_p^{\ddagger}$ values here as is the case for the cyclopropyl system, although the value for **16** is somewhat less than that for **11**. From Table 5, it is obvious that the relative effect of methyl substitution is virtually independent of the ionizing properties of the solvolyzing medium. This fact is consistent with a small degree of charge development at the transition state.

The kinetic α-deuterium isotope effects found (Table 6) appear to support the same conclusion. In general such isotope effects reflect changes in hybridization and to a lesser degree the nature of incoming and leaving groups (20). The k_H/k_D values for this series are small, but due to the fact that the exocyclic bond in the cyclopropyl system is already close to being sp^2 hybridized, no large effect is likely to accompany activation. Our limited results confirm this expectation and no attempt was made to determine this effect in every case, since it follows that in this series the α-deuterium isotope effect is unlikely to be a useful mechanistic indicator.

Attempts to attach physical significance to the negative temperature coefficient of $\Delta H^{\ddagger}$ for ionogenic reactions in water began with a recognition of the unique nature of solvation of weakly polar solutes in water and the effect of charge development and temperature on what has been termed the hydrophobic solvation shell (2). Initially it was assumed that charge development in the activation process modified the complete solvent shell to a greater or lesser degree, depending on the degree of charge separation at the transition state. Such an interpretation is deficient in several respects. We have noted that a value of $\Delta C_p^{\ddagger}$ of about -30 cal mol^{-1} deg^{-1} does not depend on water structure. Further, there is evidence that the major component of $\Delta C_p^{\ddagger}$ associated with modification of water structure is caused by charge development on the anion (9). There is the possibility, suggested by

[6]E. C. F. Ko, unpublished work (University of Calgary).

TABLE 4. Relative rates of solvolysis of substituted allylchlorides and the heat capacities of activation (19)

Compound	Relative rate in water at 40°C	$-\Delta C_p^{\ddagger}$ (cal deg^{-1} mol^{-1})
Allyl chloride(**11**)	1	50±1
β-Methylallyl chloride(**12**)	8.16	49±5
α-Methylallyl chloride(**13**)	720	92±3
cis-γ-Methylallyl chloride(**14**)	50	66±1
trans-γ-Methylallyl chloride(**15**)	620	82±3
Allyl nitrate*(**16**)		44±5

*log k = 73.6795 − 8519.276/T − 20.9060 log T (20).

Albery and Robinson (21), that ion-pair return could contribute a negative component to $\Delta C_p^{\ddagger}$, while partitioning between two possible mechanisms will make a positive contribution (22, 23). In spite of these possible complications this empirical coefficient is a useful indicator of mechanistic differences, particularly within a given series of related compounds (Table 2). While a value of $\Delta C_p^{\ddagger} \approx -80$ cal mol^{-1} deg^{-1} was considered limiting for displacement of a halide (2), and it was known that on destruction of the apparent water structure by the addition of >0.2 mole fraction of acetonitrile or ethanol, the corresponding $\Delta C_p^{\ddagger}$ now approached the 'base value' of −30 cal mol^{-1} deg^{-1}, large negative contributions to $\Delta C_p^{\ddagger}$ from ion-pair return, as postulated by Albery and Robinson, did not seem important. However with the discovery that 1- and 2-adamantyl nitrate gave a value of $\Delta C_p^{\ddagger}$ more negative than −130 cal mol^{-1} deg^{-1} (24) and 2,6-dimethylbenzyl nitrate gave a value of this coefficient in the same range compared to −101 cal mol^{-1} deg^{-1} found for 4-methylbenzyl nitrate (which we had previously regarded as reacting by an S_N1 mechanism (25)), the limiting value of $\Delta C_p^{\ddagger}$ for displacement in water was seen to be much more negative than previously suspected. Even making allowance for the unexplained −30 cal mol^{-1} deg^{-1} unrelated to water structure, these new large values of $\Delta C_p^{\ddagger}$ seemed far too large to be related to charge development on the anion, alone. While some contribution from ion-pair return could not be excluded and seemed plausible, this explanation is not without objection (24). If values of $\Delta C_p^{\ddagger}$ more negative than −130 cal mol^{-1} deg^{-1} be taken to signal front-side (*i.e.* limiting) displacement in water, then less negative values

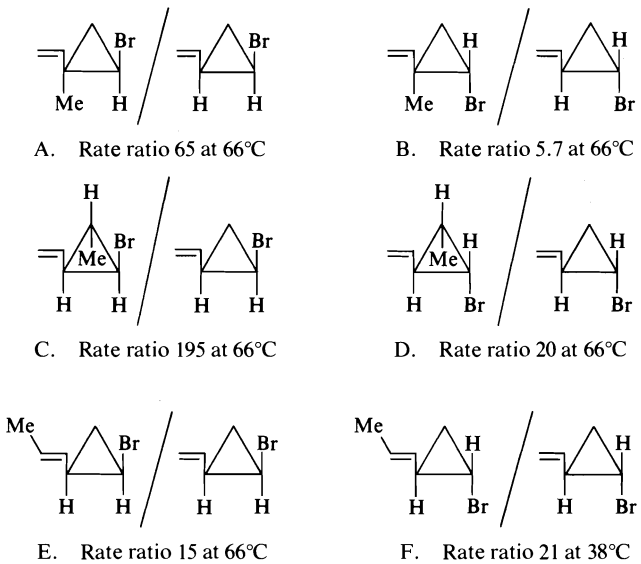

FIG. 1. Relative rates of hydrolysis for methyl substitution in a series of cyclopropyl bromides.

TABLE 5. Relative rates of solvolysis of the dimethylcyclopropyl derivatives in water and acetic acid with different leaving groups at 100°C

Solvent	Substituent X		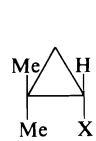	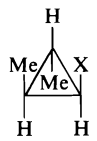	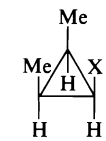	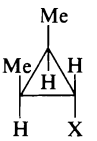
H_2O	Br*	1	12300	10630	83	492800
HOAc	Br (6)	1	—	9700	82	497000
HOAc	Cl (6)	1	—	20000	167	1330000
HOAc	OTs (5)	1	430	460	2.2	38000

*The rate for cyclopropyl bromide in water was estimated to be 1.74×10^{-6} s^{-1}. The observed value at 85°C is 0.83×10^{-6} s^{-1}.

TABLE 6. Kinetic α-deuterium isotope effects for the solvolysis of substituted cyclopropyl bromides

Compound*	Temp. (°C)	k_H (s^{-1})	k_D (s^{-1})	k_H/k_D
2,2-DMCpBr	60.00	0.000299	0.000298	1.003
	66.31	0.000643	0.000637	1.009
2,3-*cis,trans*-DMCpBr	54.07	0.0001245	0.0001239	1.005
	60.21	0.000271	0.000269	1.007
2,3-*cis,cis*-DMCpBr	78.48	0.0000129	0.0000217	1.016

*Abbreviations: D di-, M methyl, Cp cyclopropyl.

found in Table 2 for all save **3** are to be associated with a transition state where bond making has been initiated. In such cases there seems no reason to reject the hypothesis that the values of $\Delta C_p^{\ddagger}$ reflect the relative degree of charge development on the anion at the transition state. Thus **1** and **2** (Table 2) have values of $\Delta C_p^{\ddagger}$ about the same as found for MeBr (26) and hence reach the transition state at about the same degree of charge development while those reactants having a β-vinyl substituent (**5–10**) reach the transition state with a minimal charge separation. The 2,3-*trans,trans*-homologue with a value of $\Delta C_p^{\ddagger} = -75$ cal mol^{-1} deg^{-1} will have a charge development midway between **1**, **2**, and the 4-methylbenzyl nitrate which previously had been considered to react by an S_N1 mechanism.

As an alternative to this simple interpretation of the low $\Delta C_p^{\ddagger}$ values which characterize vinyl substitution, Singh has suggested (27) that the presence of a 2-vinyl substituent provides the possibility of approach to a dienylic cation of several forms depending on the stereochemistry at the 3–4 and 4–5 bonds. If there is 'considerable' charge development on Br^- at the transition state, it is conceivable that such an extended ion could shield or, through internal electrostatic interaction, largely reduce external effects. This balance between internal and external electrostatic effects contains a possible explanation for the difference in $\Delta C_p^{\ddagger}$ between *cis* and *trans* configurations for hydrolysis of crotyl (19) and cyclopropyl halides.

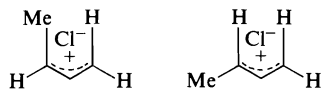

$\Delta C_p^{\ddagger} = -66$ $\Delta C_p^{\ddagger} = -82$

$k_t/k_c = 3.7$

Crotyl chloride

T.S. of **2** T.S. of **4**

$\Delta C_p^{\ddagger} = -56$ $\Delta C_p^{\ddagger} = -75$

$k_{tt}/k_{ct} = 46$

Dimethylcyclopropyl bromide

($\Delta C_p^{\ddagger}$ in cal mol^{-1} deg^{-1})

U-form Sickle-form W-form

Experimental

In this work the monobromides were prepared by reduction of dibromo derivatives with tri-*n*-butyltin hydride (28, 29). The dibromides were prepared by addition of dibromo carbene to the appropriate olefin (30).

1,1-Dibromo-trans-2,3-dimethylcyclopropane

trans-2-Butene (100 g, 1.78 mol, K & K) and potassium *tert*-butoxide (76 g, 0.68 mol, Ventron Alfa Products) were placed in a 2 ℓ three-necked flask. Distilled bromoform (130 g, 0.52 mol, Fisher Scientific Co.) was added dropwise at about −30°C under a nitrogen atmosphere.

The mixture was stirred for 2 h after addition was complete. The temperature was raised slowly overnight and then the addition complex was hydrolyzed with 250 ml of water. The organic layer was separated and the aqueous layer was extracted with two 50 ml portions of pentane. The combined organic extracts were dried over anhydrous Na_2SO_4. The solvent was removed with a rotary suction evaporator and then distilled to give the product: bp 55°C /9 Torr.

2,3-cis,trans-Dimethylcyclopropyl Bromide

1,1-Dibromo-*trans*-2,3-dimethylcyclopropane (17.1 g, 0.075 mol) was reduced with tri-*n*-butyltin hydride (21.6 g, 0.075 mol) to give 2,3-*cis*,*trans*-dimethylcyclopropyl bromide: bp 40°C/20 Torr. It was further purified by preparative glc using a 30% FFAP column (20 ft, $\frac{3}{8}$ in. on 60–80 Chromosorb W). For preparative glc work, in general, the following conditions were used: flow rates, carrier gas $N_2 \simeq 25$ ml/min, $H_2 \simeq 20$ ml/min; temperatures inlet ≃ 150°C, oven ≃ 90°C, collector ≃ 120°C, detector ≃ 250°C.

Spectral data: $nmr_{TMS}(CCl_4)$ δ 2.55–2.70 (m, 1H, CHBr), 1.04–1.22 (m, 6H, $2CH_3$), 0.55–0.85 (m, 2H, ring protons); ms parent peak at *m/e* 148, 150 (1:1), base peak at *m/e* 69 and significant peaks at *m/e* 133, 135 (1:1), 82, 81, 80, 79, 68, 67, 53, 41, 39.

1-Deuterium-2,3-cis,trans-dimethylcyclopropyl Bromide

Spectral data: $nmr_{TMS}(CCl_4)$ δ 1.05–1.22 (m, 6H, $2CH_3$), 0.55–0.85 (m, 2H, ring protons); ms parent peak at *m/e* 149, 151 (1:1), base peak at *m/e* 70 and significant fragments at *m/e* 134, 136 (1:1), 82, 81, 80, 79, 69, 68, 54.

1,1-Dibromo-cis-2,3-dimethylcyclopropane

cis-2-Butene (100 g, 1.78 mol, K & K) and potassium *tert*-butoxide (76 g, 0.68 mol, Ventron Alfa Products) were placed in a 2 ℓ three-necked flask. Distilled bromoform (130 g, 0.52 mol, Fisher Scientific Co.) was added dropwise at about −25°C under a nitrogen atmosphere. The mixture was stirred for 2 h after addition was complete. The temperature was raised slowly overnight and then hydrolyzed with 250 ml of water. The organic layer was separated and the aqueous layer was extracted with two 50 ml portions of pentane. The combined organic solution was then dried over anhydrous Na_2SO_4. The low boiling fraction was removed with a rotary suction evaporator and then the residual was distilled to give the product: bp 50–56°C/10 Torr.

2,3-trans,trans-Dimethylcyclopropyl Bromide

1,1-Dibromo-*cis*-2,3-dimethylcyclopropane (40 g, 0.17 mol) was reduced with tri-*n*-butyltin hydride (50.6 g, 0.17 mol) to give the isomeric monobromides. The *cis*:*trans* ratio was 5:1 (by glc) bp 34–36°C/30 Torr. These two isomeric monobromides were then purified and separated through preparative glc using a 30% FFAP column (20 ft × $\frac{3}{8}$ in. on Chromosorb 60–80).

2,3-trans,trans-Dimethylcyclopropyl Bromide

Spectral data: $nmr_{TMS}(CCl_4)$ δ 2.13 (m, 1H, CHBr), 1.05–1.21 (m, 2H, ring protons), 1.09 (s, 6H, $2CH_3$); ms parent peak at *m/e* 148, 150 (1:1), base peak at *m/e* 69 and significant fragments at *m/e* 133, 135 (1:1), 82, 81, 79, 68, 67, 53, 41.

1,1-Dibromo-trans-2,3-methylvinylcyclopropane and 1,1-Dibromo-2-(1-propenyl)cyclopropane

trans-Piperylene (93 g, 1.37 mol, Aldrich) and potassium *tert*-butoxide (100 g, 0.98 mol, Ventron Alfa Products) were placed in a 2 ℓ three-necked flask. Freshly distilled bromoform (170 g, 0.67 mol, Fisher Scientific Co.) was added dropwise at about −20 to −30°C under N_2 atmosphere. After complete addition of the bromoform, the reaction mixture was stirred for 2 h at about −25°C. The temperature was then raised slowly overnight and the addition product was hydrolyzed with water. The organic layer was separated and the aqueous layer extracted with two 50 ml portions of pentane. The combined organic layer was dried over anhydrous Na_2SO_4 and the solvent was then removed by a rotary suction evaporator and the residual distilled to give the product: bp 60°C/7 Torr. This distillate on reduction gave four isomeric monobromides: *(1) 2,3-cis-vinyl,trans-methylcyclopropyl bromide, (2) 2,3-cis-methyl,trans-vinylcyclopropyl bromide, (3) 2-cis-(1-propenyl)cyclopropyl bromide, (4) 2-trans-(1-propenyl)cyclopropyl bromide.*

1,1-Dibromo-*trans*-2,3-methylvinylcyclopropane and 1,1-dibromo-2-(1-propenyl)cyclopropane (23 g, 0.09 mol) were reduced with tri-*n*-butyltin hydride (27.0 g, 0.09 mol) to give the four isomeric monobromides: bp 40°C/8 Torr, which were then separated and purified through preparative glc using a QF_1 column (20 ft × $\frac{3}{8}$ in. on 45–60 Chromosorb W).

2,3-cis-Vinyl,trans-methylcyclopropyl Bromide

Spectral data: $nmr_{TMS}(CCl_4)$ δ 5.22–5.60 (m, 1H, —CH═), 4.79–5.08 (m, 2H, ═CH_2), 2.80–2.94 (m, 1H, CHBr), 1.24 (d, 3H, CH_3), 0.84–1.44 (m, 2H, ring protons); ms parent peak at *m/e* 160, 162 (1:1), base peak at *m/e* 79, 81 (1:1) significant fragments at *m/e* 80, 77, 66, 65, 53, 51, 41, 39.

2,3-cis-Methyl,trans-vinylcyclopropyl Bromide

Spectral data: $nmr_{TMS}(CCl_4)$ δ 5.30–5.68 (m, 1H, —CH═), 4.92–5.16 (m, 2H, ═CH_2), 2.66–2.82 (m, 1H, CHBr), 1.16 (s, 3H, CH_3), 1.00–1.46 (m, 2H, ring protons). The mass spectrum was almost identical to that of 2,3-*cis*-vinyl,*trans*-methylcyclopropyl bromide.

2-cis-(1-Propenyl)cyclopropyl Bromide

Spectral data: $nmr_{TMS}(CCl_4)$ δ 5.36–5.72 (m, 1H, ═CH—), 5.00–5.28 (m, 1H, ═CH—), 2.86–3.08 (m, 1H, CHBr), 1.56–1.82 (d, 3H, CH_3), 1.16–1.82 (d, 3H, ring protons). The mass spectra were almost identical to that of 2,3-*cis*-vinyl,*trans*-methylcyclopropyl bromide.

2-trans-(1-Propenyl)cyclopropyl Bromide

Spectral data: $nmr_{TMS}(CCl_4)$ δ 5.26–5.66 (m, 1H, ═CH—), 4.82–5.12 (m, 1H, ═CH—), 2.50–2.68 (m, 1H, CHBr), 1.56–1.82 (m, 4H, CH_3 and one ring proton), 0.92–1.24 (m, 2H, CH_2).

The mass spectrum was almost identical to that of 2,3-*cis*-vinyl,*trans*-methylcyclopropyl bromide.

Product Analysis

Approximately 0.05 g $CaCO_3$, 1 ml water, and a glass bead together with 5–6 μl of the pure substrate were added to a small test tube and stirred. About 1 μl of the aqueous solution was injected onto a glc (on FFAP column 6 ft × $\frac{3}{16}$ in.). The test tube was sealed and placed in a bath at the appropriate temperature. After 1–2 half-lives, 1 μl of the solution was again injected on the glc under the same conditions. The solution was allowed to react for a further time corresponding to several half-lives and a further chromatogram obtained. The reference allylic alcohols were synthesized by standard reactions of alkyllithium on the appropriate aldehyde or ketone, and the resulting alcohols checked by mass spectrometry.

2,3-Dimethylcyclopropyl Bromides

The only product from the solvolysis of three isomeric monobromides (*cis-cis*, *trans-trans*, *cis-trans*) was found to be *trans*-α,γ-dimethylallyl alcohol. *cis*-α,γ-Dimethylallyl alcohol was not detected.

The *trans* and *cis*-α,γ-dimethylallyl alcohols were prepared by adding methyllithium to a mixture of *cis*- and *trans*-crotonaldehyde. The commercially available α,γ-dimethylallyl alcohol had similar retention time to those prepared in the laboratory.

2,2-Methylvinylcyclopropyl Bromides

The only product from both of these 2,2-methylvinylcyclopropyl bromides was found to be 3-methyl-1,4-pentadien-3-ol. The corresponding primary alcohol was not detected.

3-Methyl-1,4-dipenten-3-ol was prepared by the reaction of vinyllithium on methylvinylketone.

2,3-cis-Vinyl,trans-methylcyclopropyl Bromide

The only product of solvolysis of 2,3-*cis*-vinyl,*trans*-methylcyclopropyl bromide was probably 3,5-hexadiene-2-ol.

cis-2-(1-Propenyl)cyclopropyl Bromide

The products of solvolysis of 2-*cis*-(1-propenyl)cyclopropyl bromide were 1,4-hexadiene-3-ol and probably 3,5-hexadiene-2-ol.

Before ending this section, it must be emphasized that in almost all the cases, only the corresponding allylic alcohols were observed.

Acknowledgments

We wish to acknowledge the useful criticism of Dr. G. D. Dyson. Part of this work was supported by an operational grant from NRCC.

1. J. H. Ong and R. E. Robertson. Can. J. Chem. **52**, 2660 (1974).
2. R. E. Robertson. Prog. Phys. Org. Chem. **5**, 121 (1967).
3. D. T. Clark and G. Smale. Tetrahedron, **25**, 13 (1969).
4. D. T. Clark and D. R. Armstrong. Theor. Chim. Acta, **13**, 365 (1969).
5. P. v. R. Schleyer, G. W. Van Dine, U. Schöllkopf, and J. Paust. J. Am. Chem. Soc. **88**, 2868 (1966).
6. U. Schöllkopf, K. Fellenberger, M. Patsch, P. v. R. Schleyer, T. Su, and G. W. Van Dine. Tetrahedron Lett. 3639 (1967).
7. P. v. R. Schleyer, W. F. Sliwinski, G. W. Van Dine, U. Schöllkopf, J. Paust, and K. Fellenberger. J. Am. Chem. Soc. **94**, 125 (1972).
8. S. Winstein, B. Appel, R. Baker, and A. Diaz. Chem. Soc. Spec. Publ. No. 19, 109 (1965).
9. S. Singh and R. E. Robertson. Can. J. Chem. **54**, 1246 (1976).
10. R. E. Robertson and S. Singh. Can. J. Chem. In press.
11. P. v. R. Schleyer and R. D. Nicholas. J. Am. Chem. Soc. **83**, 182 (1961).
12. C. H. De Puy, L. G. Schnack, and J. W. Hauser. J. Am. Chem. Soc. **88**, 3343 (1966).
13. J. A. Landgrebe and L. W. Becker. J. Org. Chem. **33**, 1173 (1968).
14. U. Schöllkopf. Angew Chem. Int. Ed. Engl. **7**, 588 (1968).
15. R. B. Woodward and R. Hoffmann. J. Am. Chem. Soc. **87**, 395 (1965).
16. H. C. Longuet-Higgins and E. W. Abrahamson. J. Am. Chem. Soc. **87**, 2045 (1965).
17. C. H. DePuy, L. G. Schnack, J. W. Hausser, and W. Wiedemann. J. Am. Chem. Soc. **87**, 4006 (1965).
18. E. F. Cox, M. C. Caserio, M. S. Silver, and J. D. Roberts. J. Am. Chem. Soc. **83**, 2719 (1961).
19. L. J. Brubacher, L. Treindl, and R. E. Robertson. J. Am. Chem. Soc. **90**, 4611 (1968).
20. V. J. Shiner, Jr. *In* Isotope effects in chemical reactions. *Edited by* C. J. Collins and N. S. Bowman. Van Nostrand-Reinhold Company, New York, NY. 1970. Chapt. 2.
21. W. J. Albery and B. H. Robinson. Trans. Faraday Soc. **65**, 980 (1969).
22. J. R. Hulett. Q. Rev. Chem. Soc. London, **18**, 227 (1964).
23. J. M. W. Scott and R. E. Robertson. Can. J. Chem. **50**, 167 (1972).
24. K. M. Koshy, R. K. Mohanty, and R. E. Robertson. Can. J. Chem. **55**, 1314 (1977).
25. K. M. Koshy and R. E. Robertson. Can. J. Chem. **52**, 2485 (1974).
26. R. L. Heppolette and R. E. Robertson. Proc. R. Soc. (London) A, **252**, 253 (1959).
27. S. Singh. Ph.D. Thesis, University of Calgary, Calgary, Alta. 1975.
28. D. Seyferth, H. Yamasaki, and D. L. Allerston. J. Org. Chem. **28**, 703 (1963).
29. G. J. M. Van Der Kerk, J. G. Nottes, and J. Luijten. J. Appl. Chem. **7**, 366 (1957).
30. W. Von E. Doering and A. K. Hoffmann. J. Am. Chem. Soc. **76**, 6162 (1954).

Studies of the rearrangements of aminoalkylsilanes to alkylaminosilanes

JAMES M. DUFF[1] AND ADRIAN G. BROOK[2]

Department of Chemistry, University of Toronto, Toronto, Ont., Canada M5S 1A1

Received January 10, 1977

JAMES M. DUFF and ADRIAN G. BROOK. Can. J. Chem. **55**, 2589 (1977).

A wide variety of aminoalkylsilanes (R_3SiCR_2NHR') are rearranged to the isomeric alkylaminosilanes ($R_3SiNR'CHR_2$) by traces of *n*-butyllithium. It is shown that an equilibrium exists between the isomeric amide ions (N^-) and carbanions (C^-) which are involved as intermediates in the rearrangement. The values of the equilibrium constants were determined for several systems and in one case the rates and activation parameters were obtained for both the forward and reverse directions. The overall kinetics were also investigated for several systems and kinetic parameters were obtained. In some cases anion isomerization was the rate-controlling step; in other cases the rate-controlling step was the proton transfer between the starting amine and the carbanion which leads to product.

JAMES M. DUFF et ADRIAN G. BROOK. Can. J. Chem. **55**, 2589 (1977).

On a montré qu'une grande variété d'aminoalkylsilanes (R_3SiCR_2NHR') se réarrangent en alkylaminosilanes isomères ($R_3SiNR'CHR_2$) sous l'influence de traces de *n*-butyllithium. On a montré qu'il existe un équilibre entre les ions amides isomères (N^-) et les carbanions (C^-) qui sont impliqués comme intermédiaires dans le réarrangement. On a déterminé les valeurs des constantes d'équilibre pour plusieurs systèmes et dans un cas on a pu obtenir les vitesses et les paramètres d'activation pour les deux directions de l'équilibre. On a aussi étudié les cinétiques globales de plusieurs systèmes et on a pu obtenir les paramètres cinétiques. Dans quelques cas, l'isomérisation de l'anion est l'étape déterminant la vitesse; dans d'autres cas, l'étape déterminante est le transfert du proton entre l'amine de départ et le carbanion qui conduit au produit.

[Traduit par le journal]

The rearrangement of silyl groups from carbon to more electronegative elements (O, S) is now well known, having been observed under thermal or photochemical conditions or where radical or anionic intermediates are involved (for general accounts of many of these reactions, see ref. 1). Following our investigations of the rearrangements of silylcarbinols to alkoxysilanes (2, 3) where isomeric oxyanions and carbanions have been shown to be intermediates, we turned

$$R_3SiCR_2(OH) \xrightarrow{:B} R_3SiCR_2(O^-) \rightleftarrows R_3SiO\bar{C}R_2 \xrightarrow{BH^+} R_3SiOCHR_2$$

our attention to the related nitrogen system and now wish to report on the rearrangement of aminomethylsilanes (silylmethylamines) to methylaminosilanes (for a preliminary report, see ref. 4).

Whereas traces of di- or trialkylamines were sufficient to effect the rearrangement of many silylcarbinols to their related alkoxysilanes (3), the very fact that aminomethylsilanes are isolable and survive distillation at elevated temperatures indicates that the Si—C—NH → Si—N—CH rearrangement occurs much less

$$R_3Si{-}CR_2(NHR') \longrightarrow R_3SiNCHR_2(R')$$

readily and is not effected by organic amines. However, it was found that 0.05 to 0.2 mol equiv. of *n*-butyllithium, added to a solution of the aminomethylsilane at 10–100°C led to a clean rearrangement at a convenient rate for many but not all of the compounds studied.

The catalyzed rearrangement can be described in terms of the sequence of steps shown in Scheme 1. Butyllithium reacts rapidly and completely with the parent amine, NH, to form a small amount of amide ion, N^-, which may isomerize (step *2*) to the isomeric carbanion, C^-, by migration of the silyl group from carbon to nitrogen. Finally, the carbanion, C^-, reacts with starting amine, NH, (step *3*) to yield product, CH, and regenerate amide ion which subsequently isomerizes, an overall chain process converting starting amine, NH, to product, CH (for studies of the migration of silicon from

[1]Present address: Xerox Research Centre of Canada, Ltd., Mississauga, Ont.

[2]Author to whom correspondence should be addressed.

TABLE 1. Rearrangements of secondary aminomethylsilanes catalyzed by *n*-butyllithium

Aminomethylsilane	Equivalents of *n*-BuLi	Reaction conditions[a]		Silylamines[b]
		Temp. (°C)	Time (h)	
1 $Me_3SiCH_2NHCH_2Ph$	0.10	100	40[c]	$Me_3SiNMeCH_2Ph$ (*A*)
2 $Me_3SiCH_2NHC_6H_{11}$	0.10	100	0.5[c]	$Me_3SiNMeC_6H_{11}$ (*A*)
3 $Ph_3SiCH_2NHCH_2Ph$	0.17	25	37	$Ph_3SiNMe(CH_2Ph)$ (*B*)
4 $Me_3SiCHPhNHMe$	0.10	25	1	$Me_3SiNMeCH_2Ph$
5 $Me_3SiCHPhNH$-*i*-Pr	0.10	25	36.5	$Me_3SiN(CH_2Ph)$-*i*-Pr (*B*)
6 $Me_3SiCHPhNHC_6H_{11}$	0.20	100	0.25[d]	$Me_3SiN(CH_2Ph)$-C_6H_{11} (*B*)
7 $Me_3SiCHPhNHCH_2Ph$	0.10	25	24	$Me_3SiN(CH_2Ph)_2$ (*B*)
8 Me_3SiCH_2NHPh	0.10	100	40	No rearrangement observed
9 $Me_3SiCHPhNHPh$	0.10	100	40	No rearrangement observed
10 Me_3SiCPh_2NHPh	0.10	25	20	Silylamine not isolated
11 $Me_3SiCPh_2NHCH_2Ph$	0.10	25	8	No rearrangement[e]

[a]Rearrangements carried out in benzene solution in nmr tubes sealed under nitrogen. If THF used as solvent, rearrangements were much faster.
[b]Method of alternative synthesis: *A*, $R_3SiCl + R'R''NH + Et_3N$; *B*, $R'R''NLi + R_3SiCl$.
[c]Very slow at room temperature.
[d]Rearrangement required many hours at 25°C.
[e]Hydrolysis gave 0.9 equiv. of starting material and 0.1 equiv. of rearrangement product.

nitrogen to nitrogen, see ref 5*a*; from oxygen to nitrogen, see ref. 5*b*).

As might be expected, the ease of this catalyzed rearrangement was found to be very dependent on structural features, as reference to Table 1, which lists the compounds studied, will show. *N*-Alkylaminomethyltrimethyl- (or triphenyl-) silanes such as **1**, **2**, **3** rearranged

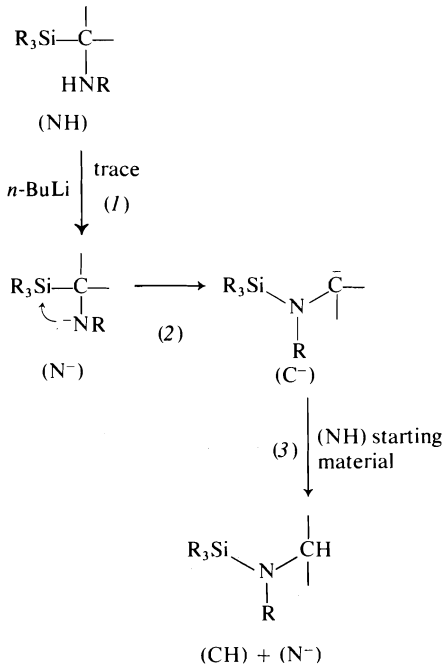

SCHEME 1

either at room temperature or at somewhat elevated temperatures on treatment with butyllithium in hexane or benzene. This infers that the nucleophilicity of N^- for silicon, the relative stabilities of N^- and C^-, and the basicity of C^- relative to N^- in the final proton abstraction step *3* were collectively compatible with the overall rearrangement process. When a phenyl group (which should effectively stabilize C^-) was attached to carbon as in the aminobenzyl compounds **4**, **5**, **6**, **7**, the rearrangement occurred more readily, in general. However, if the *N*-alkyl group was replaced by *N*-phenyl as in **8** and **9**, no rearrangement was observed, possibly because the N^- was now too weak a nucleophile toward silicon. However, if two phenyls were attached to carbon (thereby greatly stabilizing the C^- by delocalization as well as reducing its basicity) the *N*-phenyl compound **10** rearranged. In contrast, the *N*-alkylbenzhydryl compound **11** did not rearrange, probably because C^- was now too weak a base to be able to abstract a proton from NH, since it was subsequently shown that the anionic rearrangement $N^- \rightleftarrows C^-$ (step *2*) had occurred (*vide infra*) under the reaction conditions.

Fortunately, it was possible to cast further light on this behavior both by examining separately the anion equilibrium $N^- \rightleftarrows C^-$ (step *2*), including its kinetics in one case, and also by studying in detail the kinetics of the

catalyzed rearrangements of several of the *N*-alkylaminoalkyltrimethylsilanes.

These more detailed kinetic studies were interpreted on the basis of Scheme 2, with which all data acquired were consistent for the compounds studied. In all cases studied, step *3* appeared to be irreversible, a conclusion supported by the failure of either *N*-methyl or *N*-benzyl silylamines to undergo metallation.

$$NH \xrightarrow[\text{Fast}]{n\text{-BuLi, trace}} N^- \qquad \text{(step 1)}$$

$$N^- \underset{k_{-1}}{\overset{k_1}{\rightleftharpoons}} C^- \qquad \text{(step 2)}$$

$$C^- + NH \xrightarrow{k_2} CH + N^- \qquad \text{(step 3)}$$

SCHEME 2

The reaction of amine with butyllithium appears to be fast and complete. The $N^- \rightleftarrows C^-$ isomerization has been found to be a reversible equilibrium whose position varies markedly with the structure of the compound involved, and which is the rate-controlling step in some catalyzed rearrangements.

In other cases, step *3*, the protonation step has been found to be rate-controlling. Thus it is clear that quite different kinetic behavior can be anticipated from different aminoalkylsilanes. It is useful to describe the studies of the anionic equilibrium before discussing the kinetics of the catalyzed rearrangements.

The Anionic Equilibrium

The anionic equilibrium, step *2*, was studied for several compounds by treating them with a full equivalent (or excess) of *n*-butyllithium, and then observing the nmr spectrum of the system. Table 2 reports the data obtained.

TABLE 2. Equilibrium proportions of anions[a]

Compound	%N^-	%C^-
$Me_3SiCH_2NHC_6H_{11}$	>99	
$Me_3SiCH_2NHCH_2Ph$	>99	
$Me_3SiCHPhNHMe$	68	32[b]
	71.5	28.5[c]
$Me_3SiCHPhNHC_6H_{11}$	53	47
$Me_3SiCHPhNH$-*i*-Pr	50	50
$Me_3SiCPh_2NHCH_2Ph$	0	100

[a]General conditions involved addition of 1.0 to 1.2 equiv. of *n*-BuLi in hexane to 1 equiv. of amine in hexane and then determining anion proportions by nmr.
[b]25°C.
[c]19°C.

Under such conditions the nmr spectrum characteristic of $Me_3SiCH_2NHC_6H_{11}$, for example, immediately disappeared and was replaced by a similar spectrum attributable to the corresponding amide ion. No change in the latter spectrum occurred over 13 h at room temperature indicating that under these conditions the amide ion did not isomerize. Derivatization of the reaction mixture with methyl iodide gave essentially pure *N*-methyl derivative consistent with the exclusive presence of the amide ion. On the other hand the benzhydryl compound $Me_3SiCPh_2NHCH_2Ph$ when metallated existed completely as the carbanion $Me_3SiN(CH_2Ph)$-$\bar{C}Ph_2$ as judged by the change in the nmr spectrum with time and from derivatization studies with MeOD.

In contrast, aminobenzyl compounds Me_3-SiCHPhNHR′ (R′ = alkyl) when metallated formed equilibrium mixtures containing significant amounts of both N^- and C^-, whose proportions could be measured. Thus, when *N*-methylaminobenzyltrimethylsilane (Me_3Si-CHPhNHMe) was treated with an equimolar amount of *n*-butyllithium, a rapid reaction occurred to give an equilibrium mixture of amide ion and carbanion. The proportions of the

$$Me_3SiCHPhNHMe \xrightarrow{n\text{-BuLi}} PhCH(SiMe_3)\text{—}\bar{N}Me \rightleftarrows PhC^-(SiMe_3)\text{—}NMe$$

two anions could be measured by nmr techniques and were about 70% N^- to 30% C^- in hexane at room temperature. The proportions were approximately 50:50 for the *N*-cyclohexyl and *N*-isopropyl derivatives. Attempts to measure the rates of interconversion of the ions by variable temperature nmr techniques were unsuccessful since line broadening was observed up to 90°C by which temperature serious decomposition occurred. Attempts to study the equilibrium by C-metallation of *N*-methyl-*N*-benzylaminotrimethylsilane were inconclusive since reagents such as *tert*-butyllithium did not react at an appreciable rate.

However, it was found that if the *N*-methylaminobenzylsilane in hexane at −78°C was treated with 1 equiv. of *n*-butyllithium a nearly colourless solution was obtained whose nmr spectrum indicated that only the amide anion was present. On warming, the spectrum started to change, with absorption due to the isomeric

carbanion appearing. Concomitant with the appearance of the carbanion, the solution changed colour, becoming deep red-orange. The rearrangement continued until equilibrium was reached. The rate of attainment of equilibrium could be conveniently studied in the temperature range 10–40°C where $K_e = C^-/N^-$ was found to lie between 0.44 and 0.52. Analysis of the data from this study permitted the determination of the rate constants for both the forward and reverse reactions at various temperatures, and the activation parameters E_{act} and $\Delta S^{\neq}$. The value for E_{act} of 17.0 kcal/mol for the isomerization of the amide ion to carbanion, was slightly smaller than the E_{act} for conversion of carbanion to amide ion (17.4 kcal/mol) and the greater thermodynamic stability observed for the amide ion actually arose from small differences in $\Delta S^{\neq}$.

It was found that the $N^- \rightleftarrows C^-$ equilibrium was very sensitive to small amounts of reagents such as THF and TMEDA, and Table 6 shows how the percentage of C^- at 36°C changed from 23.5% C^- with no TMEDA present to 100% C^- with 1.12 mol equiv. of added TMEDA for the *N*-methylaminobenzylsilane. Similarly, in a different experiment at 18°C, the percentage of C^- changed irregularly with added THF, decreasing from 26.6% C^- (no THF) to about 18.7% C^- (with 1.23 mol equiv. of added THF) and then increasing to about 70% C^- with 2.45 mol equiv. added THF. It was also found that if excess THF was added to the equilibrium mixture of carbanion and amide anion in hexane at 0°C, and then after 30 min the reaction mixture was drowned in MeOD prior to aqueous work-up, the *N*-methylbenzylamine isolated was monodeuterated on the benzylic carbon. The almost 100% monodeuteration must have arisen from ionic precursors which were essentially 100% carbanion in composition.

It is clear that the $N^- \rightleftarrows C^-$ equilibrium is very sensitive to added basic reagents. Both THF and TMEDA are known to coordinate with lithium cations and such solvation evidently favours the Li^+C^- ion pair relative to the Li^+N^- pair. It follows that traces of amine (either starting material or product) are liable to play a similar role in affecting the position of the ionic equilibrium, which may account for the small erratic variations in the value of the equilibrium constant observed in otherwise identical runs. In this connection it was demonstrated that addition of 1 or 2 mol equiv. of triethylamine to the system accelerated the rate of anion isomerization, and altered somewhat the position of the equilibrium.

Kinetics of the Catalyzed Rearrangements of Aminoalkylsilanes to Alkylaminosilanes

It was found possible to observe the overall kinetics of rearrangement of several alkylaminoalkylsilanes ($R_3SiCHRNHR'$) to the isomeric dialkylaminosilanes ($R_3SiNR'CH_2R$) when catalyzed by small amounts of *n*-butyllithium. The kinetic scheme is not a simple one and interpretable results from a situation such as is given in Scheme 2 are only obtained if certain conditions concerning the relative magnitudes of the rate constants are fulfilled. In general, depending on the relative magnitudes of k_1, k_{-1}, and k_2 it is possible for the overall rearrangement to be either complex, *pseudo* first-order, or *pseudo* zero-order in starting amine. In the latter two categories at least four possible cases can be recognized and these are described in the Appendix, where the relevant rate equations are derived. Examples of rearrangements which appear to fit three of these situations have been observed, and will be described.

A. The Catalyzed Rearrangement of $Me_3SiCH_2NHC_6H_{11}$ in THF. Case 1

The rate of rearrangement of $Me_3SiCH_2NHC_6H_{11}$ could be followed by nmr spectroscopy using THF as solvent in the temperature range 30–50°C, but benzene or hexane could not be employed since unduly high temperatures (60–80°C) were required to obtain convenient rates. The concentrations of starting material and product were followed with time, and a plot of ln percentage amine with time was a good straight line for at least 3 half-lives indicative of a *pseudo* first-order reaction. Typical data are given in the Experimental section and in Table 10.

Since it was known from the anionic equilibrium studies that the $N^- \rightleftarrows C^-$ equilibrium lay strongly to the left (*vide supra*), then $k_{-1} \gg k_1$, and reference to the Appendix suggests that case *1* is applicable, with $k_{-1} \gg k_2[NH]$. Under these conditions proton transfer is the rate-determining step. A plot of $\ln k_2K_e$ *vs.* $1/T$ gave a good Arrhenius plot from which $E_{act} =$ 12.5 kcal/mol was obtained. $\Delta S^{\neq}$ cannot be obtained directly since it depends on K_e whose value is not known. If K_e is assumed to be

$< 10^{-2}$, which is consistent with the failure of the system to show any evidence in the nmr for the presence of C^- when the equilibrium was studied, then $\Delta S^{\ddagger} > -24$ eu.

B. The Catalyzed Rearrangement of Me_3SiCH_2NHMe. Case 2

With *N*-methylaminomethyltrimethylsilane difficulty was encountered in finding a solvent system that would give rearrangement at a reasonable rate and also yield reasonably separated nmr signals for the starting amine and rearrangement product. Thus rearrangement was virtually instantaneous in THF (<1 min at 20°C), and while THF–hexane (1:1) gave reasonable rates, the nmr signals (either Me_3Si or NMe) of both reagent and product were superimposed. In 1:3 THF–benzene rearrangement occurred at a reasonable rate at 30°C, and while the Me_3Si signals were superimposed, the N–Me signals of reagent and product were separated by about 6 Hz. This latter system was investigated.

The kinetics were in accord with a zero-order reaction since a plot of percentage amine *vs.* time gave a straight line. The data for various temperatures are given in the Experimental section where the slopes were determined using the least-squares method. The data fit case *2* (Appendix) where the anionic rearrangement of N^- to C^- is the rate determining step (*i.e.* $k_{-1} \gg k_1$, $k_2[NH] \gg k_{-1}$). Thus k_1 listed in Table 9 could be calculated directly from k_{obs}, and the Arrhenius plot of ln k_1 *vs.* $1/T$ gave a straight line yielding the parameters $E_{act} =$ 14.4 kcal/mol and $\Delta S^{\ddagger} = -26$ eu. The large negative $\Delta S^{\ddagger}$ is consistent with the proposed cyclic transition state arising from intramolecular nucleophilic attack of N^- on silicon.

C. The Catalyzed Rearrangement of $Me_3SiCHPhNHMe$. Case 4

When samples of *N*-methylaminobenzyltrimethylsilane in hexane were heated to 35–55°C with 0.05–0.15 mol equiv. of *n*-butyllithium the rearrangement could be conveniently followed by observing the trimethylsilyl peaks in the nmr spectrum of both the starting amine and the rearrangement product. The disappearance of starting material was first-order for up to about 2 half-lives, after which time the reaction speeded up. This effect may be due to changes in solvation effects with the changing medium or to the assumptions made in the solution of the kinetic equations not holding rather than to a change in mechanism. Similar linear plots of ln [amine] with time were obtained at other temperatures.

Since the study of the anionic equilibrium for this amine showed $k_1 \approx k_{-1}$ and since the observed kinetics are first order in amine, case *4* appears to apply where $k_2[NH] \ll k_1 \simeq k_{-1}$. Thus there is relatively fast equilibration of ions, followed by a rate-controlling proton transfer.

As appropriate to case *4*, a plot of ln $k_2/(1 + 1/K_e)$ derived from the k_{obs} at various temperatures *vs.* $1/T$ gave a reasonably straight line which yielded an E_{act} of 22.5 kcal/mol for the overall rearrangement. In the absence of knowledge about the actual values of K_e under the conditions of the catalyzed rearrangement it is not possible to calculate $\Delta S^{\ddagger}$. If K_e is assumed to be 0.5, then $\Delta S^{\ddagger} \simeq 1$ eu.

Summary

The above material has clearly demonstrated that the rearrangement of secondary alkylaminoalkylsilanes to dialkylaminosilanes is a complex reaction, sensitive to the medium and to the structure of the reagents. While all aspects of the reactions have not been investigated in depth, the data obtained are clearly consistent with the mechanism proposed by steps 1–3 depending on the structure of the reagents and the nature of the medium either the anionic rearrangement (eq. 2) or the protonation step (eq. 3) may be rate-controlling.

Because of the demonstrated sensitivity of the reaction and particularly the ionic equilibrium to solvent effects, it is probably not meaningful to compare the activation parameters obtained for the systems studied in detail, since each was done in a different solvent system; however, the data are summarized in Table 3. What is clear is that the expected electronic effects are observed as far as general ease of rearrangement of various amines is concerned. Thus *N*-phenyl compounds, which might be expected to be weak nucleophiles due to electron delocalization, generally fail to rearrange, whereas *N*-alkyl compounds generally do rearrange. Similarly, *C*-phenyl compounds, where stabilization of the intermediate carbanion can be expected, generally rearrange readily at room temperature, with protonation of the carbanion (step *3*) being the rate-determining step.

The results obtained clearly reveal that the

TABLE 3. Kinetic data for alkylaminoalkylsilane rearrangements

Compound	Kinetic order obsvd.	Rate constants	Rate determining step	K_e	E_{act} (kcal/mol)	$\Delta S^{\neq}$ (eu)
$Me_3SiCH_2NHC_6H_{11}$[a]	1st	$k_2[NH] \ll k_{-1} \gg k_1$	Proton transfer	$<10^{-2}$	12.5	>-24
Me_3SiCH_2NHMe[b]	Zero	$k_2[NH] \gg k_{-1} \gg k_1$	Anion isomerization	$<10^{-2}$	14.4	-26
$Me_3SiCHPhNHMe$[c]	1st	$k_1 \simeq k_{-1} \gg k_2[NH]$	Proton transfer	$\simeq 0.5$	22.5	≈ 1

[a]In THF from 32–56°C.
[b]In THF–benzene (1:3) from 20–50°C.
[c]In hexane from 25–55°C.

rearrangements of the aminomethylsilanes mechanistically generally follow the behavior previously described for the α-silylcarbinols. Major differences, resulting in the more complex mechanism are (*a*) the decreased nucleophilicity towards silicon of the amide ion *vs.* an oxyanion and (*b*) the decreased reactivity of the carbanion toward NH as compared to the more acidic OH of a silylcarbinol.

Experimental

Reactions involving organometallic reagents were carried out under nitrogen, using solvents dried over sodium. The *n*-butyllithium was a commercial product (Ventron). Nuclear magnetic resonance studies normally employed a Varian T-60 or A-60 instrument equipped with a variable temperature probe.

Synthesis of Silylmethylamines

Most compounds were prepared by the method of Speier and co-workers (6). The data for the compounds prepared are summarized in Table 4 which lists conditions, yields, and analysis for new compounds, and Table 5, which lists the nmr spectral details of new compounds. Two typical procedures are described below.

N-Methyl-N-cyclohexylaminomethyltrimethylsilane

A stirred solution of 16.7 g (0.10 mol) of bromomethyltrimethylsilane and 22.6 g (0.20 mol) of *N*-methylcyclohexylamine was heated in an oil bath at 140–150°C for 30 min. The resultant two-phase liquid was worked up with ether and 5% sodium hydroxide and the organic layer was dried and distilled to give 13.1 g (64%) of *N*-methyl-*N*-cyclohexylaminomethyltrimethylsilane, bp 216–218°C/760 Torr.

N-Methylaminobenzyltrimethylsilane

A. Anhydrous methylamine was bubbled through a sample of α-bromobenzyltrimethylsilane (12.15 g, 0.05 mol) stirred in an oil bath at 130°C. The entire system was maintained under a pressure of 100 Torr by bubbling the effluent gas through a mercury column. After 8 h a thick slurry was obtained. Work-up with ether and 5% sodium hydroxide gave a mixture (*ca.* 4:1, respectively) of the desired amine and starting bromobenzylsilane. The amine was separated by precipitation of its hydrochloride salt from ether. The salt was treated with base and the amine was distilled to give 4.8 g (42%) of *N*-methylaminobenzyltrimethylsilane, bp 44–45°C/0.1 Torr.

B. A solution of α-bromobenzyltrimethylsilane (12.15 g, 0.05 mol) in methylamine (15 ml, collected in a liquid nitrogen bath) in a sealed, thick-walled Pyrex tube was heated at 120°C for 1 h. The tube was cooled in liquid nitrogen before opening and the product was worked-up as above and distilled to give 7.55 g (79%) of product.

When a solution of bromomethyltrimethylsilane and methylamine was prepared in a sealed tube, the tube exploded violently before the sample had warmed to room temperature. A safety shield was damaged in the process. Although the possibility of a badly prepared tube cannot be ruled out (a thick-walled, annealed, Pyrex Carius tube was used) the low temperature at which the explosion occurred and the violence of the explosion implies that a rather vigorous exothermic reaction may have occurred.

Proportions of Equilibrated Anions

Solutions in hexane of various *N*-alkylaminoalkyltrimethylsilanes in an nmr tube were treated with a slight molar excess of *n*-butyllithium. After about 15 min, the proportions of species present, as observed by the intensity of the trimethylsilyl signal in the nmr spectra, were constant. Typical results are listed in Table 2.

Thus, a solution of 0.13 g (0.5 mmol) of *N*-methylaminobenzyltrimethylsilane in 0.25 ml dry hexane under N_2 in an nmr tube stoppered with a serum cap was treated with 0.25 ml (0.55 mmol) of *n*-butyllithium. The tube was shaken, and after the peak heights had ceased to change, the trimethylsilyl signals were recorded. A correction for the variation in peak widths was made since the signal from the nitrogen anion was broader than that of the carbanion signal ($W_{\frac{1}{2}}(N^-)/W_{\frac{1}{2}}(C^-) = 1.46$ in the above case). It was found that the proportions of anions at 19°C were $N^-:C^- = 71.5:28.5$.

Derivatization of the Equilibrating Anions

When solutions of lithiated $Me_3SiCHPhNHR$ (R = Me, C_6H_{11}) were treated with methyl iodide or trimethylchlorosilane only a slow reaction occurred as judged by the rate of disappearance of the deep red colour of the anion. Because of this slow reaction it was considered that the trapping of anions by these reagents would not provide a reliable measure of the equilibrium mixture. Addition of deuterated methanol (MeOD) to the anion solutions resulted in instantaneous

TABLE 4. Preparation, percentage yield, physical and analytical data for aminomethylsilanes

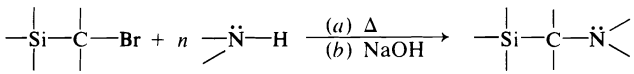

Amine	Reaction Conditions: n	Temp. (°C)	Time (h)	Yield (%)	bp/Torr or mp	Analytical data: Calculated C	H	N	Found C	H	N
Me_3SiCH_2NHMe	100[a]	60[b]	6	65[c]	96–98/760[d]						
$Me_3SiCH_2NHC_6H_{11}$	3[a]	140	8	74	201–203/760[e]						
$Me_3SiCH_2NHCH_2Ph$	3	190	1½	44	230–238/760	68.32	9.90	7.24	68.50	9.80	7.17
Me_3SiCH_2NHPh	2	155	¾	30	160/14[f]						
$Me_3SiCH_2NMeC_6H_{11}$	2	150	½	67	216–218/760	66.25	12.64	—	66.55	12.55	—
$Me_3SiCH_2NMeCH_2Ph$	4	190	¼	20	132–134/14	69.49	10.21	6.76	70.42	10.49	6.66
Me_3SiCH_2N⬠	5	90	7	79	157–158/760	61.07	12.17	8.90	61.24	12.21	8.76
$Me_3SiCHPhNHMe$	—[g]	120	10	72[c]	44–45/0.1	68.32	9.90	7.25	68.62	9.80	7.24
$Me_3SiCHPhNH$-*i*-Pr	15	40	340	46	120/13	70.52	10.47	6.33	71.21	10.62	6.43
$Me_3SiCHPhNHC_6H_{11}$	2	160	½	75	95–99/0.25	64.50	9.47[j]		64.39	9.24	
$Me_3SiCHPhNHCH_2Ph$	3	140	1	95	134–142/0.4	66.74	7.91[j]		66.74	8.33	
$Me_3SiCHPhNHPh$	3	135	1½	53	111–114/0.05	75.23	8.29		75.38	8.36	
$Me_3SiCHPhNMe_2$	3[h]	100	1	66	120–125/15	69.49	10.21	6.76	69.47	10.16	6.89
$Me_3SiCPh_2NHCH_2Ph$	3	160	⅓	63	90–91	79.94	7.88	4.05	80.20	8.04	4.09
Me_3SiCPh_2NHPh	3	135	½	68	102–103	79.70	7.60	4.23	79.91	7.67	4.11
$Ph_3SiCH_2NHCH_2Ph$	5	170	2¾	66[c]	—	82.27	6.64	3.69	82.01	6.28	3.85

[a]Chloride used instead of bromide. [b]A 40% solution of methylamine in methanol was used. [c]Isolated as the hydrochloride. [d]Lit. bp 101.6°C (6). [e]Lit. bp 211°C (6). [f]Lit. bp 242°C (6). [g]Gas passed over bromide under pressure. [h]Sealed tube. [j]Isolated and analyzed as hydrochloride salt.

TABLE 5. Data for aminomethylsilanes

Compound	Nmr data (δ in ppm)[a]
$Me_3SiCH_2NHCH_2Ph$	7.2 (s, Ph), 3.72 (s, PhCH_2), 2.00 (s, Si CH_2), 1.00 (br, NH), 0.01 (s, $SiMe_3$)
$Me_3SiCH_2NHC_6H_{11}$	2.5–0.5 (m, C_6H_{11}), 1.88 (s, SiCH_2), 0.03 (s, $SiMe_3$)
Me_3SiCH_2NHPh	7.4–6.4 (m, Ph), 3.13 (br, NH), 2.34 (s, SiCH_2), 0.10 (s, $SiMe_3$)
Me_3SiCH_2NMePh	7.37 (s, Ph), 3.53 (s, PhCH_2), 2.19 (s, NMe), 2.00 (s, SiCH_2), 0.17 (s, $SiMe_3$)
$Me_3SiCH_2NMeC_6H_{11}$	2.27 (s, NMe), 1.97 (s, SiCH_2), 2.3–0.8 (m, C_6H_{11}), 0.09 (s, $SiMe_3$)
Me_3SiCH_2N⬡	2.45 (m, N-CH_2), 1.97 (s, SiCH_2), 1.74 (m, N-CH_2CH_2), 0.07 (s, $SiMe_3$)
$Me_3SiCHPhNH$-*i*-Pr	7.15 (br, Ph), 3.37 (s, SiCH), 2.67 (septet, J = 6 Hz, C$H$$Me_2$), 1.14 (br, N$H$), 0.95, 0.93 (2d, J = 6 Hz, CHMe_2), −0.05 (s, $SiMe_3$)
$Me_3SiCHPhNHC_6H_{11}$	7.13 (br, Ph), 3.43 (s, SiCH), 2.5–0.8 (m, C_6H_{11}), −0.07 (s, SiMe_3)
$Me_3SiCHPhNHCH_2Ph$	7.22, 7.17 (2s, Ph), 3.62 (AB, J = 14 Hz, PhCH_2), 3.31 (s, SiCH), 1.62 (br, NH), −0.07 (s, $SiMe_3$)
$Me_3SiCHPhNHPh$	7.3–6.4 (m, Ph), 3.95 (br, NH), 3.90 (s, SiCH), 0.03 (s, $SiMe_3$)
$Ph_3SiCH_2NHCH_2Ph$	7.6–7.0 (m, Ph), 3.80 (s, PhCH_2), 2.84 (s, SiCH_2)
$Me_3SiCHPhNHMe$	7.13 (m, Ph), 3.12 (s, 1H, PhCH), 2.30 (s, 3H, MeN), 1.28 (br s, 1H, NH), 0.03 (s, 9H, Me_3Si)

[a]In $CDCl_3$, relative to internal TMS.

decolourization. The resulting deuterated product could be analyzed by nmr spectroscopy.

A. Lithiated $Me_3SiCHPhNHC_6H_{11}$ in Hexane

A solution of 0.52 g (2.0 mmol) of *N*-cyclohexylaminobenzyltrimethylsilane in 5 ml of hexane was allowed to react with 1.0 ml (2.2 mmol) of *n*-butyllithium in hexane (M = 2.2). After 30 min at room temperature the deep red solution was treated with 2 ml of MeOD. The solution was evaporated to dryness and the residue was extracted with water (1 ml) and deuterochloroform (1 ml). An nmr spectrum of the deuterochloroform solution indicated that three products, $Me_3SiCHPhNHC_6H_{11}$, $Me_3SiNC_6H_{11}$(CHDPh), and C_6H_{11}NHCHDPh in the ratio 3:2:1, respectively, were present. The mixture was stirred with methanol for 30 min to fully desilylate the aminosilane. Examination of the resultant product by nmr indicated that a 55:45 mixture, respectively, of the starting aminobenzylsilane, $Me_3SiCHPhNHC_6H_{11}$, and *N*-cyclohexyl-α-D-benzylamine, $PhCHDNHC_6H_{11}$, was present. The latter product showed a slightly distorted 1:1:1 triplet (J = 1.9 Hz) as expected for the benzyl proton split by the α-deuteron. Both products were also identified by comparison of their gc retention times with authentic samples. The result is in close agreement with the nmr study of the hexane solution of the anions which indicated a 53:47 ratio, respectively, of nitrogen anion and carbanion.

B. Lithiated $Me_3SiCHPhNHC_6H_{11}$ in Hexane–THF

In a similar experiment to the above, the red solution of anions prepared in hexane was cooled to 0°C and was diluted with an equal volume of dry THF. Addition of MeOD and work-up as above gave, as the only significant product (>90%), the deuterated amine, C_6H_{11}NHCHDPh.

C. Lithiated $Me_3SiCHPhNHMe$ in Hexane–THF

A solution of *N*-methylaminobenzyltrimethylsilane was metallated in hexane as above and the resultant deep red solution was cooled to 0°C and was treated with an equal volume of THF. After 30 min MeOD was added and the product was worked-up with ether and water. Removal of solvent at reduced pressure, with mild warming, gave a liquid which was shown by nmr and gc to contain only hexamethyldisiloxane and *N*-methyl-α-D-benzylamine.

D. Lithiated $Me_3SiCHPhNHMe$ in Hexane–THF; Isolation of the p-Toluenesulfonamide

In a similar procedure to the above the anionic solution from 0.97 g (5.0 mmol) of *N*-methylaminobenzyltrimethylsilane and 1 equiv. of *n*-butyllithium in hexane–THF was deuterated. Solvent was removed and the residue was treated with 10 ml of 5% sodium hydroxide solution and 1.90 g (10 mmol) of *p*-toluenesulfonyl chloride. An insoluble oil was obtained when the suspension was warmed to *ca.* 60°C and shaken. This oil was separated by decantation. Treatment with 10 ml of ethanol gave 0.52 g (38%) of fine white crystals of *N*-methyl-*N*-(α-D-benzyl)-*p*-toluenesulfonamide, mp 87–91°C. Recrystallization from ethanol gave mp 92–93°C (lit. (8) mp 95°C); nmr ($CDCl_3$) δ 7.7–8.2 (m, 9H, aryl), 4.88 (br t, $J \simeq$ 1.8 Hz, 1H, PhCHD) 2.55 (s, 3H, N–CH_3), 2.40 ppm (s, 3H, $ArCH_3$).

E. Lithiated N-Benzylaminobenzhydryltrimethylsilane

The title amine, in ether or benzene was treated with an equimolar (or excess) amount of *n*-butyllithium in hexane and a single, deeply coloured lithiated species was formed, as indicated by the nmr spectrum of the system. Hydrolysis followed by rapid work-up (to avoid cleavage of the Si—N bond) gave an almost quantitative yield of the rearrangement product *N*-benzyl-*N*-benzhydryltrimethylsilylamine.

Effects of TMEDA and THF on the Anionic Equilibrium

To a solution of $Me_3SiCHPhNHMe$ (96.5 mg, 105.5 μl, 0.50 mmol) in hexane (165 μl) at −78°C under nitrogen in an nmr tube fitted with a serum cap, was added 229 μl (0.55 mmol; M = 2.4) of a solution of *n*-butyllithium in hexane. The solution was mixed in the cold and then was allowed to warm to room temperature. After about 15 min, when the equilibrium composition had been reached, the relative amounts of carbanion and nitrogen anion were measured by scanning the two Me_3Si peaks at a sweep width of 100 Hz and a sweep time of 100 s.

(These conditions gave a reliable measurement of the peak widths which varied considerably with added THF or TMEDA and for which corrections were made.) The equilibrium mixture was similarly measured following the addition of small amounts of TMEDA (at 36°C) or THF at 18°C (the low temperature was necessary to minimize decomposition in the presence of THF). The results are summarized in Table 6. The measurements in THF were not highly reliable above 2 equiv. because the nitrogen anion peak became very broad and decomposition products had appeared at this stage.

Effect of Added Triethylamine on Rates of Anion Isomerization

Three nmr tubes were prepared as follows: tube *A*, 0.13 g (145 μl, 0.50 mmol) $Me_3SiCHPhNHMe$ and 0.25 ml hexane; tube *B*, 0.13 g of amine, 0.18 ml hexane, and 0.051 g (70 μl, 0.5 mmol) Et_3N; tube *C*, 0.13 g of amine, 0.11 ml hexane, and 0.102 g (141 μl, 1.0 mmol) of Et_3N. Each tube was cooled in liquid N_2, 0.30 ml (0.66 mmol) of *n*-butyllithium in hexane was added, and the kinetics were then determined at 15.6–18.5°C. Plots of ln ($\%N^- - \%N^-_\infty$) *vs.* time (9) gave linear plots from which the following data were obtained. *A*. (no Et_3N) $k_{obs} = 0.054\ min^{-1}$, $K_e = k_1/k_{-1} = 0.45$. *B*. (1 equiv. Et_3N) $k_{obs} = 0.088\ min^{-1}$, $K_e = 0.39$, *C*. (2 equiv. Et_3N) $k_{obs} = 0.153\ min^{-1}$, $K_e = 0.48$.

Studies of Catalyzed Systems

Catalyzed Rearrangement of $Me_3SiCHPhNH$-i-Pr.

A solution of 0.22 g (1.0 mmol) of the title amine in 0.5 ml of dry benzene was treated with 0.10 mmol (50 μl, $M = 2.0$) of *n*-butyllithium in hexane and tightly sealed in a vial. The colour rapidly turned red-orange. After 2 weeks the vial was opened and the solvent was removed under reduced pressure. The nmr spectrum of the residue was identical to that of a pure sample of $Me_3SiN(i\text{-}Pr)CH_2Ph$, bp 56–57°C/0.1 Torr, prepared from $PhCH_2NH$-*i*-Pr, PhLi, and Me_3SiCl in 60% yield. The glc retention times of the residue and of the authentic rearrangement product on a 20% SE 30 on Chromosorb G column were identical.

Similarly a solution of 0.166 g (0.50 mmol) of *N*-phenylaminobenzhydryltrimethylsilane in dry benzene (0.50 ml) in an nmr tube under nitrogen at room temperature was treated with 21 μl (0.05 mmol) of *n*-butyllithium in hexane. The rearrangement at room temperature was followed by nmr spectroscopy. A new peak at 10 Hz to low-field of the trimethylsilyl peak of the starting amine, attributed to rearranged product was observed to grow steadily. The rearrangement was 30% complete in 2 h and was 100% complete after 20 h at room temperature.

When *N*-benzylaminobenzhydryltrimethylsilane was treated with a catalytic amount (0.1 equiv.) of *n*-butyllithium in benzene or ether solvent a deep, dark-red solution was obtained. No evidence for extensive rearrangement could be obtained from spectroscopic studies of the solutions. Hydrolysis after several hours at room temperature gave mainly starting material along with approximately 0.1 equiv. of the rearrangement product, *N* - benzyl - *N* - benzhydryltrimethylsilylamine which likely arose from protonation of the intermediate benzhydryl anion.

Kinetics of the Anionic Equilibrium

A solution of 96.5 mg (105.5 μl, 0.050 mmol) of $Me_3SiCHPhNHMe$ in hexane (166 μl) under nitrogen in a serum capped nmr tube was cooled to −78°C and was treated with 229 μl (0.55 mmol; $M = 2.4$) of *n*-butyllithium in hexane. The solution was mixed and the tube was quickly inserted into the pretuned nmr probe set at a selected temperature. The trimethylsilyl peaks of the nitrogen anion and carbanion were scanned at ½ or 1 min intervals using a sweep width of 500 Hz and a sweep time of 500 s. Following completion of a run the sample was left in the probe for a sufficient time to ensure that equilibrium $[N^-_\infty]$ had been reached.

The final peak width ratio was determined using a sweep width of 100 Hz and a sweep time of 100 s. The relative peak heights of nitrogen anion and carbanion were corrected for peak width differences and the results were tabulated as relative percentage of each anion. For the system

$$N^- \underset{k_{-1}}{\overset{k_1}{\rightleftharpoons}} C^-$$

it is readily shown (9) that for a first order reaction the integrated rate expression has the form

$$\ln \frac{[N^-] - [N^-_\infty]}{[N^-_0] - [N^-_\infty]} = (k_1 + k_{-1})t = k_{obs}t$$

where $[N^-_\infty]$ is the concentration of the nitrogen anion at equilibrium. For the present case where identical initial concentrations were used, the denominator of the log term may be neglected. The plot of ln ($[N^-] - [N^-_\infty]$) *vs.* time was a good straight line and analysis by the least-squares method for the typical example shown in Fig. 1 at 9.4°C, gave $k_{obs} = (0.432 \pm 0.003) \times 10^{-3}\ s^{-1}$ with a correlation coefficient of 0.999.

Table 7 lists the results of similar runs at different temperatures. The values of k_1 and k_{-1} were obtained from the relationships $k_1/k_{-1} = C^-_\infty/N^-_\infty = K_e$ and $k_{obs} = k_1 + k_{-1}$.

The Arrhenius plots of ln k_1 and ln k_{-1} *vs.* $1/T$, were

TABLE 6. The effect of adding TMEDA and THF to a solution of metallated $Me_3SiCHPhNHMe$ (0.50 mmol) in hexane

TMEDA (36°C)		THF (18°C)	
mol equiv.	% carbanion	mol equiv.	% carbanion
0	23.5	0	26.6
0.066	29.4	0.25	28.5
0.132	36.2	0.49	29.8
0.198	44.0	0.74	25.1
0.330	50.2	0.99	20.6
0.462	56.5	1.23	18.7
0.594	65.6	1.48	27.4
0.726	81.3	1.73	35.4
0.856	95	1.97	47.8
1.12	100	2.22	59.4
		2.45	67.7
		2.96	~72[a]

[a]The nitrogen anion peak was too broad to measure accurately and considerable decomposition had occurred by this time.

TABLE 7. Kinetic data for the equilibration of metallated $Me_3SiCHPhNHMe$ in hexane[a]

Temp. (K)	$k_{obs} \times 10^3$ (s^{-1})	c.c.[b]	K_e	$k_1 \times 10^4$ (s^{-1})[c]	$k_{-1} \times 10^4$ (s^{-1})[c]
282.6	0.432 ± 0.003	0.999	0.475	1.39	2.93
292.0	1.39 ± 0.02	0.998	0.524	4.78	9.12
299.0	2.37 ± 0.08	0.990	0.482	7.70	16.0
305.2	4.01 ± 0.05	0.998	0.513	13.6	26.5
309.2	5.45 ± 0.34	0.976	0.477	17.6	36.9
313.1	10.76 ± 0.437	0.996	0.437	32.7	75.0

[a]Standard solution: 105.5 µl (96.5 mg, 0.50 mmol) amine; 166 µl hexane; 229 µl (0.55 mmol; $M = 2.4$) *n*-butyllithium in hexane.
[b]Correlation coefficient for least-squares analysis of data.
[c]From the relations, $k_{obs} = k_1 + k_{-1}$ and $K_e = k_1/k_{-1}$.

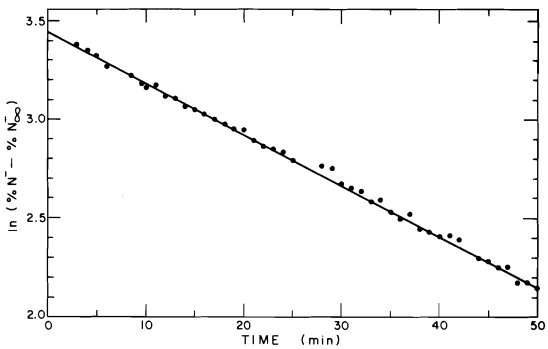

FIG. 1. Equilibration of metallated $Me_3SiCHPhNHMe$ in hexane at 9.4°C.

good straight lines (correlation coefficients 0.994 and 0.993, respectively). Analysis of the results yielded the following data (10)

$$N^- \xrightarrow{k_1} C^- \quad E_{act} - 17.0 \text{ kcal/mol}, \quad \Delta S^{\ddagger} = -17.8 \text{ eu}$$

$$C^- \xrightarrow{k_{-1}} N^- \quad E_{act} = 17.4 \text{ kcal/mol}, \quad \Delta S^{\ddagger} = -15.1 \text{ eu}$$

It was noted in this experiment (and similar experiments) that there were random variations in the values of K_e, from about 0.44–0.52, a range greater than that expected as a result of variations in temperature (if $\Delta G = 0.4$ kcal/mol, then K_e would range from 0.48 to 0.52). The variation is attributed to inaccuracies in the measurements and to the pronounced effects (*vide supra*) of traces of amines and other basic species on the position of the equilibrium.

Kinetics of the Rearrangement of $Me_3SiCHPhNHMe$

A solution of 145 µl (131 mg, 0.678 mmol) of $Me_3SiCHPhNHMe$ in hexane (419 µl) under nitrogen in an nmr tube stoppered with a serum cap was inserted in the nmr probe at a desired temperature. When the instrument had been tuned the sample was treated with 45.5 µl (0.10 mmol; $M = 2.2$) of a solution of *n*-butyllithium in hexane. The sample was quickly mixed and reinserted in the probe. The trimethylsilyl peaks of the starting amine and rearranged product, $Me_3SiNMe(CH_2Ph)$ were scanned at ½ or 1 min intervals.

TABLE 8. Kinetic data for the catalyzed rearrangement of $Me_3SiCHPhNHMe$ in hexane[a]

Temp. (K)	$k_{obs} \times 10^3$ (s^{-1})[b]	$\ln\left(\frac{k_2}{1 + 1/K_e}\right)$[c]
308.7	0.230 ± 0.001	−6.57
313.4	0.316 ± 0.002	−6.25
318.4	0.642 ± 0.003	−5.54
318.5	0.598 ± 0.007	−5.61
323.9	1.08 ± 0.006	−5.02
328.5	1.96 ± 0.03	−4.43
328.9	1.99 ± 0.03	−4.41

[a]Standard solution: 145 µl (131 mg, 0.678 mmol) amine; 419 µl hexane; 45.5 µl (0.10 mmol; $M = 2.2$) *n*-butyllithium in hexane. Molarity in amine (100%) = 0.949. Molarity in base [cat] = 0.164.
[b]Least-squares correlation coefficient 0.999 or better in all runs.
[c]From $k_{obs} = k_2[cat]/(1 + 1/K_e)$.

The results were tabulated as peak height *vs.* time; since both peaks were sharp and of equal width there was no need to apply a peak width correction. The data for several temperatures are given in Table 8. A plot of $\ln k_2/(1 + 1/K_e)$ *vs.* $1/T$ gave a straight line with a slope corresponding to $E_{act} = 22.5$ kcal/mol, as shown in Fig. 2.

Kinetics of the Rearrangement of Me_3SiCH_2NHMe

A solution of 78.2 µl (58.5 mg, 0.50 mmol) of Me_3SiCH_2NHMe in benzene (300 µl) – THF (100 µl) under nitrogen in a serum-capped nmr tube was treated with 20.9 µl (0.05 mmol; $M = 2.4$) of *n*-butyllithium solution in hexane. The kinetics were followed by measuring the heights of the *N*-methyl peaks of the starting amine and rearranged product (6 Hz separation) at ½ or 1 min intervals. A sweep width of 500 Hz and sweep time of 100 s were employed. A peak width correction factor was applied to correct for the wider peak of the rearranged product and the height of the product peak was divided by two to account for the mass balance (N—Me → NMe_2).

A plot of percentage amine *vs.* time was a good straight line over more than 90% of the reaction (zero-order kinetics), and the slope, k_{obs}, was obtained by the least-squares method. Data for various temperatures are given in Table 9, and an Arrhenius plot for this data gave $E_{act} = 14.4$ kcal/mol and $\Delta S^{\ddagger} = -26$ eu.

Kinetics of Rearrangement of $Me_3SiCH_2NHC_6H_{11}$

A solution of 109 µl (92.5 mg, 0.50 mmol) of Me_3-

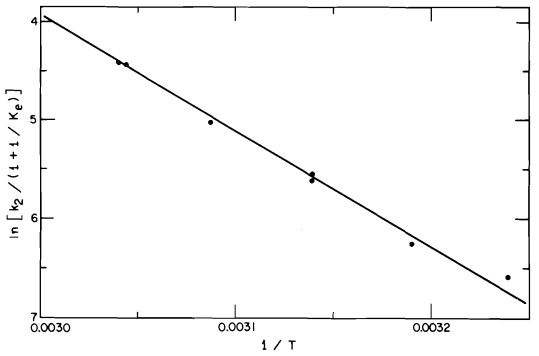

FIG. 2. Arrhenius plot for the catalyzed rearrangement of $Me_3SiCHPhNHMe$ in hexane.

TABLE 9. Kinetic data for the catalyzed rearrangement of Me_3SiCH_2NHMe in 1:3 THF–benzene[a]

Temp. (K)	k_{obs} (%/min)	c.c.[b]	$k_1 \times 10^4$ (s^{-1})[c]
293.6	0.4559 ± 0.0053	0.996	6.84
303.2	1.065 ± 0.011	0.995	16.0
311.0	1.956 ± 0.016	0.998	29.3
316.8	2.834 ± 0.018	0.999	42.5
322.0	4.256 ± 0.038	0.999	63.8
323.4	4.386 ± 0.033	0.999	65.8

[a]Standard solution: 78.2 μl (58.5 mg, 0.50 mmol) amine, 100 μl THF. 300 μl benzene + 20.9 μl (0.050 mmol) of *n*-butyllithium in hexane (M = 2.4); molarity in *n*-butyllithium = 0.10; initial molarity in amine (100%) = 0.90.
[b]Correlation coefficient from least-squares analysis of data.
[c]$k_1 = (k_{obs})(0.009)/([cat](60))$. (0.009 = factor to convert percentage amine to concentration in mol/ℓ.)

TABLE 10. Kinetic data for the catalyzed rearrangement of $Me_3SiCH_2NHC_6H_{11}$ in THF[a]

Temp. (K)	$k_{obs} \times 10^4$ (s^{-1})	c.c[b]	k_2K_e (s^{-1})[c]
305.4	1.12 ± 0.005	0.999	0.00112
311.8	1.59 ± 0.006	0.999	0.00159
316.9	2.02 ± 0.013	0.999	0.00202
323.2	2.96 ± 0.01	0.999	0.00296
331.6	5.71 ± 0.018	0.999	0.00571
337.9	7.65 ± 0.09	0.997	0.00765

[a]Standard solution: 109 μl (92.5 mg, 0.50 mmol) amine, 370 μl (0.050 mmol) *n*-butyllithium in hexane (M = 2.4). Concentration of catalyst, [cat] = 0.10 M.
[b]Correlation coefficient from least-squares analysis of data.
[c]From $k_{obs} = k_2K_e$ [cat].

$SiCH_2NHC_6H_{11}$ in dry THF (370 μl) under nitrogen in a stoppered, serum-capped nmr tube was used to pretune the nmr probe at a given temperature. The solution was then treated with *n*-butyllithium solution (20.9 μl, 0.050 mmol; M = 2.4). The reaction was followed kinetically by measuring the Me_3Si peaks using a sweep width of 250 Hz and a sweep time of 500 s. Although these peaks were very close together (1 Hz separation) they were well resolved. It was necessary, however, to use filtering (filter bandwidth 0.2–0.4) to suppress ringing of the product peak, which tended to perturb the starting material peak. A peak width correction factor was applied, the signal of the starting amine being slightly broader than that of the product. A plot of log percentage amine *vs.* time was a good straight line from which k_{obs} was derived. The data are given in Table 10. An Arrhenius plot of $\ln k_2K_e$ *vs.* $1/T$ gave a good straight line (c.c. 0.995) and the data gave E_{act} = 12.5 kcal/mol, and $\Delta S^{\ddagger} = -33.5 - 1.987 \ln K_e$. On the assumption that $K_e < 10^{-2}$, $\Delta S^{\ddagger} > -24$ eu.

Acknowledgements

The authors acknowledge the financial support of the National Research Council of Canada and of the Dow Corning Corporation, whose Post Doctoral Fellowship JMD held in 1973–1975.

1. A. G. BROOK. Acc. Chem. Res. **7**, 77 (1974); R. WEST. Advances in organometallic chemistry. In press.
2. A. G. BROOK and J. D. PASCOE. J. Am. Chem. Soc. **93**, 6224 (1971).
3. A. G. BROOK, G. E. LEGROW, and D. M. MACRAE. Can. J. Chem. **45**, 239 (1967).
4. A. G. BROOK and J. M. DUFF. J. Am. Chem. Soc. **96**, 4692 (1974).
5. (*a*) R. WEST. Pure Appl. Chem. **19**, 291 (1969); (*b*) P. BOUDJOUK and R. WEST. J. Am. Chem. Soc. **93**, 5901 (1971).
6. J. E. NOLL, J. L. SPEIER, and B. F. DAUBERT. J. Am. Chem. Soc. **73**, 3867 (1951).
7. V. R. SANDEL and H. H. FREEDMAN. J. Am. Chem. Soc. **85**, 2328 (1963).
8. R. L. SHRINER, R. G. FUSON, and D. Y. CURTIN. Systematic identification of organic compounds. 4th ed. J. Wiley and Sons, New York, NY. 1960. p. 288.
9. A. A. FROST and R. G. PEARSON. Kinetics and mechanism. 2nd ed. J. Wiley and Sons. New York, NY. 1961. p. 186.
10. J. F. BUNNETT. *In* Rates and mechanisms of reactions. Techniques of organic chemistry, Vol. VIII, Part. 1. *Edited by* A. Weissberger. Interscience, New York, NY. 1961.

Appendix

The following outlines the mathematical derivations of the equations used in the kinetic studies: NH = amine, N^- = amide ion, C^- = carbanion, CH = rearrangement product.

Solution of the Kinetic Scheme for the Catalyzed Rearrangement

For the system:

A $$NH + n\text{-BuLi} \xrightarrow[\text{fast}]{\text{very}} N^- + \text{butane}$$

B $$N^- \underset{k_{-1}}{\overset{k_1}{\rightleftharpoons}} C^-$$

C $\quad C^- + NH \xrightarrow{k_2} CH + N^-$

$$\text{Rate} = -d[NH]/dt = k_2[NH][C^-]$$

Neglecting reaction A, and using no assumptions, the scheme reduces to two differential equations.

$$[1] \qquad -\frac{d[NH]}{dt} = k_2[NH][C^-]$$

$$[2] \qquad -\frac{d[C^-]}{dt} = -k_1[N^-] + k_{-1}[C^-] + k_2[NH][C^-]$$

Substitute $[N^-] = [cat] - [C^-]$ in [2] ([cat] = [*n*-BuLi] added)

$$[3] \qquad -\frac{d[C^-]}{dt} = -k_1[cat] + k_1[C^-] - k_{-1}[C^-] + k_2[NH][C^-]$$

$$= k_2[NH][C^-] + (k_1 - k_{-1})[C^-] - k_1[cat]$$

Approximation I

If $k_{-1} \gg k_1$, the steady state approximation will hold. (This situation is known to apply for Me_3SiCH_2NHMe and $Me_3SiCH_2NHC_6H_{11}$.) Then,

$$-\frac{d[C^-]}{dt} = -k_1[N^-] + k_{-1}[C^-] + k_2[NH][C^-] = 0$$

Using $[N^-] = [cat] - [C^-]$ gives

$$k_1[C^-] - k_{-1}[cat] + k_{-1}[C^-] + k_2[NH][C^-] = 0$$

or

$$(k_1 + k_{-1} + k_2[NH])[C^-] = k_1[cat]$$

$$[4] \qquad [C^-] = \frac{k_1[cat]}{k_1 + k_{-1} + k_2[NH]}$$

or when $k_{-1} \gg k_1$, this reduces to

$$\frac{k_1[cat]}{k_{-1} + k_2[NH]}$$

Substituting for $[C^-]$ in the rate expression [1] gives

$$-\frac{d[NH]}{dt} = \frac{k_2[NH] \times k_1[cat]}{k_{-1} + k_2[NH]}$$

(*a*) Now, if $k_{-1} \gg k_2[NH]$, and since $K_e = k_1/k_{-1}$ then

$$-\frac{d[NH]}{dt} = k_2K_e[NH][cat] \qquad \text{Case } 1$$

i.e. pseudo first-order with $k_{obs} = k_2K_e[cat]$. This case involves proton transfer as the rate-determining step, and appears to apply to $Me_3SiCH_2NHC_6H_{11}$.

(*b*) If, however, $k_2[NH] \gg k_{-1}$ then

$$-\frac{d[NH]}{dt} = k_1[cat] \qquad \text{Case } 2$$

i.e. pseudo zero-order with $k_{obs} = k_1[cat]$, the kinetics tending to first order as [NH] becomes small. Case *2* is a situation where the rearrangement of the anion is the rate controlling step, and appears to apply to Me_3SiCH_2NHMe.

Approximation II

Instead of approximation I ($k_{-1} > k_1$), suppose $k_1 \approx k_{-1}$ as is known to be true for $Me_3SiCHPhNHMe$.

(*a*) Now, if $k_2[NH] \gg k_1, k_{-1}$ the steady state approximation will hold and the rate of the ionic equilibrium determines the overall rate and

$$\text{Rate} = -\frac{d[NH]}{dt} = \frac{k_2[NH]k_1[cat]}{k_1 + k_{-1} + k_2[NH]}$$

and substituting for $[C^-]$ from [4] above into [1]

$$-\frac{d[NH]}{dt} = k_1[cat] \qquad \text{Case } 3$$

i.e. pseudo zero-order with $k_{obs} = k_1[cat]$.

(*b*) Alternatively if $k_2[NH] \ll k_1, k_{-1}$, the pre-equilibrium assumption will be applicable (a case where protonation is the rate controlling step). Now

$$[C^-]/[N^-] = k_1/k_{-1} = K_e$$

Using $[N^-] = [cat] - [C^-]$ gives

$$[C^-] = K_e[cat] - K_e[C^-]$$

$$[C^-] = \frac{K_e[cat]}{1 + K_e} = \frac{[cat]}{1 + 1/K_e}$$

Substituting in the rate expression [1] gives

$$-\frac{d[NH]}{dt} = \frac{k_2[NH][cat]}{1 + 1/K_e} \qquad \text{Case } 4$$

i.e. pseudo first-order with $k_{obs} = k_2[cat]/(1 + 1/K_e)$. This case appears to apply to $Me_3SiCHPhNHMe$.

Reactions of the dipyrido[1,2-*a*:2′,1′-*c*]pyrazinium dication in basic solution

DONALD J. NORRIS,[1] JOHN W. BUNTING, AND WILLIAM G. MEATHREL[2]

Department of Chemistry, University of Toronto, Toronto, Ont., Canada M5S 1A1

Received January 24, 1977

DONALD J. NORRIS, JOHN W. BUNTING, and WILLIAM G. MEATHREL. Can. J. Chem. **55**, 2601 (1977).

The reactions of the dipyrido[1,2-*a*:2′,1′-*c*]pyrazinium dication (**1**) in basic solutions have been investigated. In aqueous base, this cation is involved in two rapid p*H*-dependent equilibration reactions associated with pK_a values of 9.9 ± 0.2 and 10.4 ± 0.2. Spectral studies indicate that pK_a 9.9 is associated with pseudobase formation by the addition of hydroxide ion at C-2 or C-4 of one of the pyridinium rings. The pK_a 10.4 is most probably attributable to the formation of a dipseudobase by addition of two hydroxide ions in the pyrazinium ring of **1**. The kinetics of these pseudobase formation reactions have been investigated by stopped-flow spectrophotometry over the range p*H* 9–13. Similar methoxide addition reactions occur in basic methanolic solutions.

The dication **1** also undergoes a slow decomposition reaction in aqueous base to initially form the 1-(formylmethyl)-2,2′-dipyridyl cation (**2**). The rate of this reaction, which has been measured as a function of p*H* at 25°C for p*H* 8–12, passes through a maximum in the vicinity of p*H* 10.2. The cation **2** undergoes a further decomposition reaction in these solutions to give an unidentified product.

DONALD J. NORRIS, JOHN W. BUNTING et WILLIAM G. MEATHREL. Can. J. Chem. **55**, 2601 (1977).

On a étudié les réactions du dication dipyrido[1,2-*a*:2′,1′-*c*]pyrazinium (**1**) en solutions basiques. Dans la base aqueuse, ce cation est impliqué dans deux réactions d'équilibration rapide qui dépendent du p*H* et qui sont associées avec des valeurs de pK_a de 9.9 ± 0.2 et de 10.4 ± 0.2. Des données spectrales indiquent que le pK_a de 9.9 est associé avec la formation de la pseudobase par addition de l'ion hydroxyde au niveau des atomes C-2 ou C-4 de l'un des cycles pyridinium. On doit probablement attribuer le pK_a de 10.4 à la formation de la dipseudobase par addition de deux ions hydroxydes au niveau du cycle pyrazinium de **1**. On a étudié la cinétique des réactions de formation de ces pseudobases par spectrophotométrie à flux stoppé à des p*H* allant de 9 à 13. Des réactions d'addition semblables impliquant le méthylate se produisent dans des solutions méthanoliques basiques.

Le dication **1** subit aussi une réaction de décomposition lente en solution aqueuse basique pour conduire au départ au cation (formylméthyl)-1 dipyridyl-2,2′ (**2**). La vitesse de cette réaction, que l'on a mesurée à 25°C à des p*H* allant de 8 jusqu'à 12, passe par un maximum autour de p*H* 10.2. Le cation **2** subit une réaction de décomposition subséquente dans ces solutions pour conduire à un produit non-identifié.

[Traduit par le journal]

In continuing our studies (1) of the reactions of heteroaromatic cations in basic solution, we have now investigated the dipyrido[1,2-*a*:2′,1′-*c*]-pyrazinium dication **1** (2, 3). This dication proved

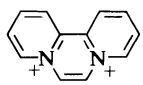

1

to be involved in two rapid p*H*-dependent equilibria in both aqueous and methanolic basic solutions, and also to slowly undergo decomposition reactions[3] in such solutions. We are not able at present to definitely identify all intermediates involved in these reactions from their spectral properties. However, we have established that in dilute aqueous base the dication **1** initially decomposes to **2** which in turn undergoes slow decomposition reactions in these solutions. We

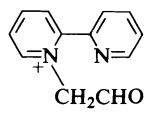

2

[1]National Research Council of Canada Postdoctoral Fellow, 1975–1977.

[2]Present address: Thomson Research Associates Ltd., Toronto, Ont.

[3]The term 'decomposition' is used in this work to conveniently distinguish slow irreversible reactions from rapid equilibration reactions.

have also determined the pH-dependence of the rates of conversion of **1** into **2**, and have measured rate and equilibrium constants for the pH-dependent equilibria in which **1** is involved.

Results

Rapid Equilibration Reactions

The uv spectra of fresh aqueous solutions of the dication **1** are pH-dependent above pH 8 (Fig. 1). Acidification of fresh solutions of pH < 12 readily regenerates the spectrum of **1** indicating that these pH-dependent equilibria are readily reversible. Further spectral changes occur at pH > 12. These changes appear to be the result of irreversible reactions since clean spectra of **1** are no longer obtained upon acidification of such solutions. The spectral changes in Fig. 1 are consistent with **1** being involved in acid–base equilibria having pK_a values of 9.9 ± 0.2 and 10.4 ± 0.2, respectively, for the interconversion of **1** and A and of A and B as indicated in Scheme 1. These pK_a values are

$$\mathbf{1} \underset{}{\overset{pK_a = 9.9}{\rightleftharpoons}} \mathrm{A} \overset{pK_a = 10.4}{\rightleftharpoons} \mathrm{B}$$

SCHEME 1

sufficiently close together that the spectrum of pure A, uncomplicated by the presence of significant amounts of either **1** or B, is not observable directly. We have therefore calculated the spectrum of pure A from the spectra of pH 9.34, 9.88, and 10.74 solutions by making use of the spectra of **1** (pH 7) and B (pH 11.76) and the pK_a values. This calculated spectrum is presented

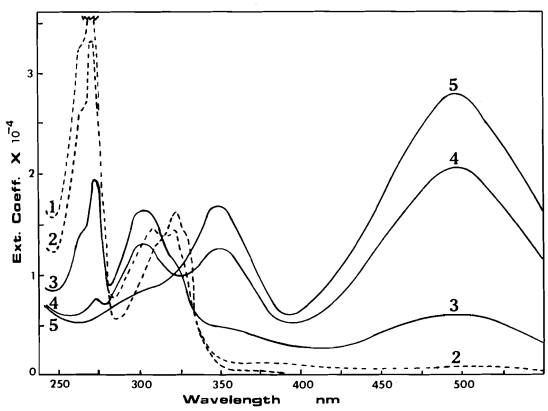

FIG. 1. The pH-dependence of the uv–visible spectra of fresh aqueous solutions of the dication **1**: Curve *1* pH 7.0; *2* pH 9.34; *3* pH 9.88; *4* pH 10.74; *5* pH 11.76.

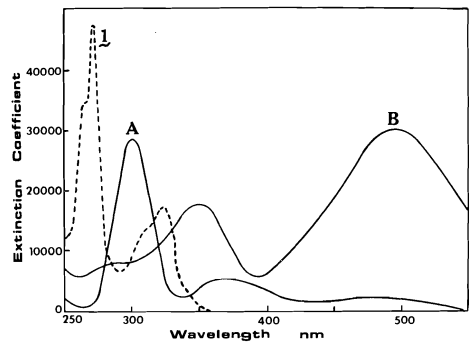

FIG. 2. Ultraviolet–visible spectra of **1** (pH 7), A calculated as described in text; and B pH 11.76.

in Fig. 2 along with the spectra of **1** and B for comparison.

Similar spectral changes were observed when **1** was dissolved in basic methanolic solutions. Thus, in neutral methanol the spectrum of **1**, essentially identical to that in water at pH 7, is observed; addition of 1 equiv. of $NaOCH_3$ gives a spectrum similar to that calculated for A; in more concentrated $NaOCH_3$ solutions (up to 1 M $NaOCH_3$) a spectrum is obtained which is similar to that observed for B at pH 11.7. The similarities of the spectra in aqueous and methanolic solutions indicate that very similar species are present in both basic media, and we designate the species in methanolic solutions as A′ and B′ to correspond to A and B, respectively, in aqueous solutions. Upon acidification of these fresh basic methanolic solutions, the spectrum of **1** is again regenerated, and so these reactions in basic methanol are also readily reversible.

The species A and B are not soluble in aqueous solutions at ^{1}Hmr spectral concentrations. However, ^{1}Hmr spectra are obtainable in basic methanol. The ^{1}Hmr spectra of **1** (*a*) in neutral CD_3OD, (*b*) in the presence of 1 equiv. of $NaOCD_3$, and (*c*) in the presence of 1 M $NaOCD_3$ are shown in Fig. 3. Acidification of solution *b* with DCl in D_2O regenerates the spectrum of **1**. In this initially acidified solution, the spectrum of **1** is superimposed on a broad envelope signal which slowly disappears over about 10 h to regenerate a clean spectrum of **1**. This two-phase regeneration of **1** upon acidification suggests that the basic ^{1}Hmr solution *b* actually contains a mixture of at least two species. One of these is presumably A′ which has been shown above at uv spectral concentrations to immedi-

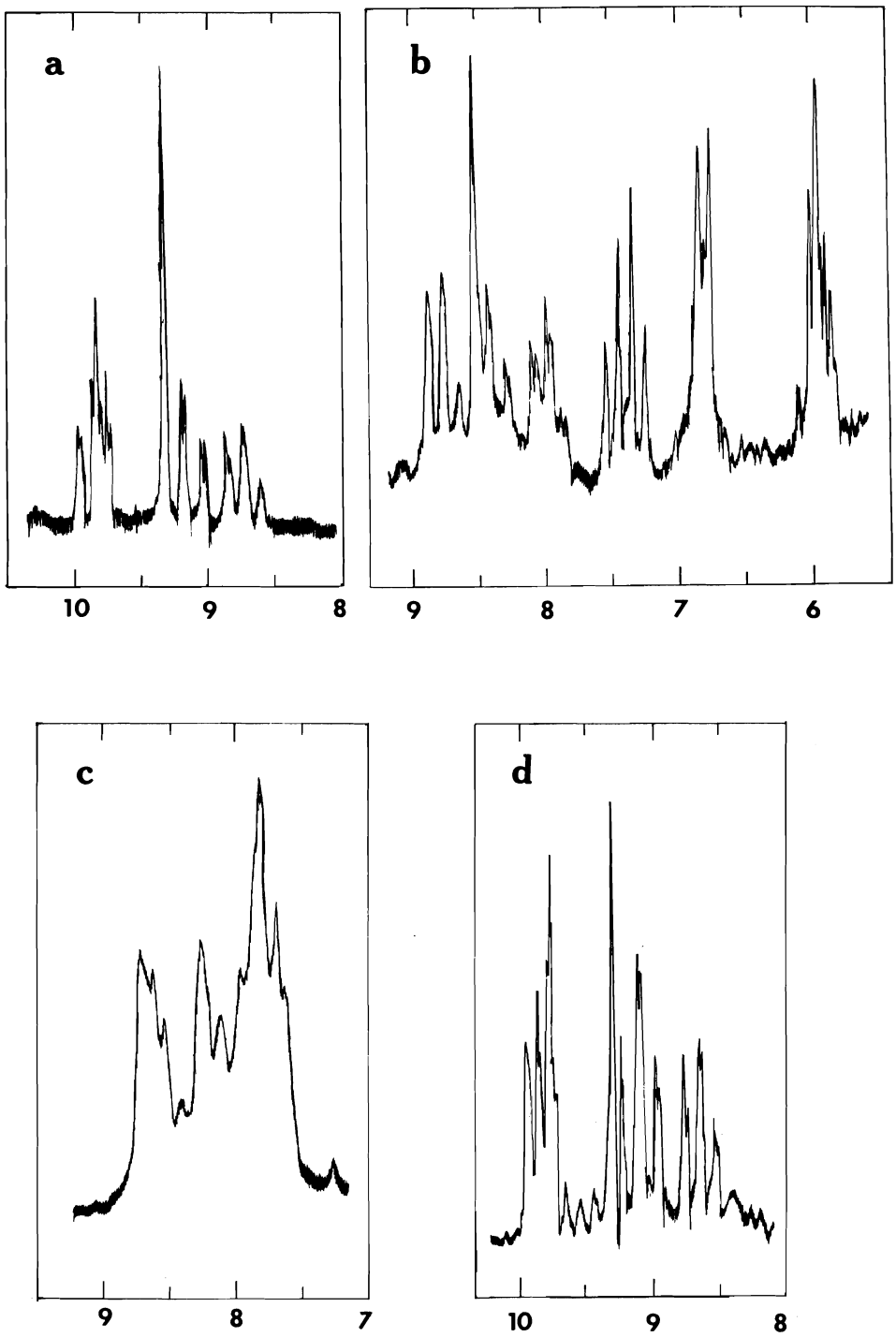

FIG. 3. ^{1}Hmr spectra of **1**: (*a*) in neutral CD_3OD; (*b*) in CD_3OD containing $NaOCD_3$ (1 equiv.); (*c*) in CD_3OD containing 1 *M* $NaOCD_3$; (*d*) solution *b* at 10 h after acidification with DCl in D_2O (all chemical shifts are δ ppm).

ately revert to **1** upon acidification. The other species is only slowly reconverted to **1** on acidification, and the fact that it is only apparently produced in the more concentrated ^{1}Hmr spectral solutions suggests the possibility that this latter species is a product of reaction between two or more heterocyclic molecules related to **1**. The broad, poorly defined, peaks in the spectrum of solution *c* (Fig. 3) also tend to suggest the presence of a mixture of two or more species.

Significantly, the complete ^{1}Hmr spectrum of **1** is regenerated upon acidification. This indicates that the acid–base equilibria involving A′ do not involve anion formation by removal of a ring hydrogen atom from **1**. If such were the case, this hydrogen atom would be replaced by deuterium upon acidification and would result in a modified spectrum for **1**.

The rate of equilibration of **1** with A and B was found to be amenable to investigation by stopped-flow spectrophotometry. When solutions of **1** are mixed with buffers in the range p*H* 9.0–9.8 a single reaction, which is first-order in heterocycle, is observable at 305 nm. However, at p*H* > 9.8 two absorbance changes are observed at 305 nm. These changes are consistent with the occurrence of two consecutive reactions (Fig. 4*a*). When this experiment is repeated at 500 nm, initially there is no change in absorbance but eventually a reaction, which is first-order in heterocycle, is observed (Fig. 4*b*). These observations are consistent with the rapid formation of A at all p*H* values, and then a subsequent slower equilibration to B at p*H* > 9.8 Pseudo first-order rate constants for the equilibration of **1** with A (k^{A}_{obs}) and of **1** and A with B (k^{B}_{obs}) are plotted as a function of p*H* in Fig. 5.

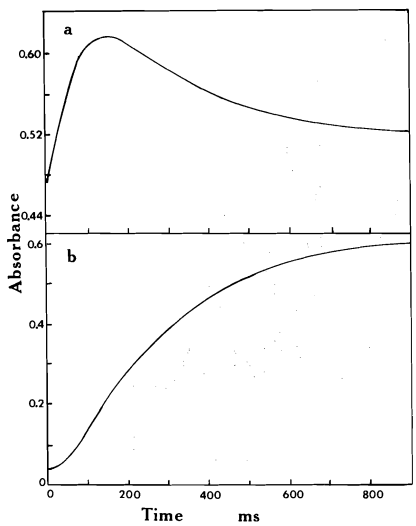

FIG. 4. Time-dependence of the absorbance of **1** (2.0×10^{-5} *M*) at p*H* 10.66 at 305 nm (*a*) and 500 nm (*b*). (Solutions of **1** in water were mixed on the stopped-flow apparatus with buffer p*H* 10.66.)

Slow Decomposition Reactions

Upon prolonged treatment of the dication **1** with aqueous base, the p*H*-dependent uv spectra discussed above undergo further changes. Examples of such time-dependent spectral changes are illustrated in Fig. 6 at p*H* 8.1 and 11.76. At both these p*H* values the final uv spectrum has a single maximum in the vicinity of 280 nm. A similar final spectrum is observed over the entire p*H* 7–13 range, although there appears to be a slight shift in the position of this peak from 281 nm in neutral solution to 277 nm in the most basic solutions. These spectral changes proved to be first-order in heterocycle, and the p*H*-dependence of the pseudo first-order rate constant (k^{1}_{dec}) for this reaction is indicated in Fig. 7. This p*H*-profile passes through a maximum in the vicinity of p*H* 10, and at lower and higher p*H* values k^{1}_{dec} appears to become linearly dependent on $[H^+]$ and $[OH^-]$, respectively (lines of slope +1 and −1 in Fig. 7). The line in Fig. 7 is of the form

$$k^{1}_{dec} = \frac{k}{1 + [H^+]/K_1 + K_2/[H^+]}$$

with $k = 1.04 \times 10^{-3}$ s^{-1}, pK_1 = 9.9 and pK_2 = 10.4, and appears to give a reasonable fit to the experimental data.

The uv spectrum of the decomposition product having λ_{max} in the vicinity of 280 nm is quite similar to the basic aqueous spectra of both

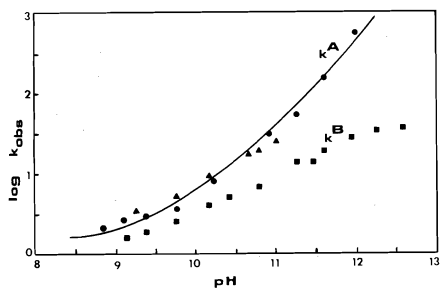

FIG. 5. p*H*-dependence of log k^{A}_{obs} (s^{-1}) for equilibration of **1** with A (● 272 nm; ▲ 305 nm) and of log k^{B}_{obs} (s^{-1}) for equilibration of A with B (■). All data at 25°C, ionic strength 0.1. Curve is calculated from: $k^{A}_{obs} = 1.3 \times 10^{4}[OH^-] + 1.4$.

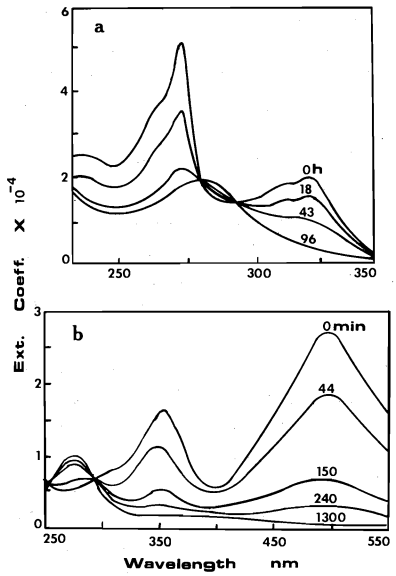

FIG. 6. Time-dependence of the uv–visible spectrum of solutions of **1** at p*H* 8.1 (*a*) and p*H* 11.76 (*b*). (25°C, ionic strength 0.1.)

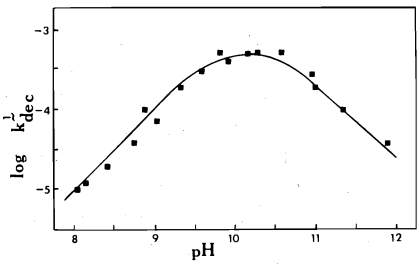

FIG. 7. p*H*-dependence of the rate of decomposition of **1** (k^1_{dec} s^{-1}) at 25°C, ionic strength 0.1. Curve is calculated from the equation given in the text.

2,2′-dipyridyl **3** (λ_{max} = 278 nm) and the cation **2** (λ_{max} = 277 nm), which is an intermediate in the synthesis of **1**. Both these species would seem to be reasonable products to which **1** might decompose in basic solution. Although **2** and **3** have quite similar spectra in basic solution, they are readily distinguishable on the basis of their uv spectra in acidic solution. Thus in aqueous acid **3** gives the protonated species **4** (λ_{max} = 302 nm; pK_a = 4.3 (4)) while **2** undergoes a rapid p*H*-dependent ring-closure (5) to give **5** (λ_{max} = 321 nm; pK_a = 4.35 ± 0.04) which is actually a covalent hydrate of **1**. Acidification to p*H* 0.5 of p*H* 9.3 solutions containing the decomposition product of **1** gave a spectrum that was almost completely superimposable on the spectrum of **2** in acidic solutions (*i.e.* **5**), and which was quite different from the spectrum of the 2,2′-dipyridyl cation **3**. However, similar acidification of p*H* 11.8 solutions containing the decomposition product of **1** gave only a slight shift to λ_{max} = 276 nm with no overall change in the shape of the spectrum.

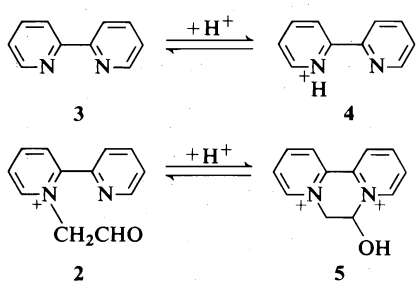

3 **4**

2 **5**

This apparent difference in the decomposition products of **1** at p*H* 9.3 and 11.8 was enlightened, when it was observed that the cation **2** also undergoes a slow decomposition in basic aqueous solutions. Thus when solutions of **2** were kept at p*H* 11.76 for about 30 min and then acidified, the spectrum of **5** was not regenerated; rather, the spectrum of a species of λ_{max} = 276 nm was obtained and this spectrum is similar to that observed upon acidification of a solution of **1** which had decomposed at p*H* 11.76. Similar acidification of a p*H* 9.3 solution of **2** after 30 min regenerated the spectrum of **5**, however after prolonged exposure (several days) of **2** to p*H* 9.3 the uv spectrum of acidified solutions tended towards that observed at p*H* 11.76. These observations suggest a p*H*-dependent decomposition of **2**, with the rate of decomposition increasing as the p*H* is increased. The rate of this decomposition was followed at 25°C at several p*H* values, and was found to be first-order in heterocycle. Pseudo first-order rate constants (k^2_{dec}) for this process are given in Table 1 at several p*H* values, and a comparison with k^1_{dec} for the rate of decomposition of the dication **1** at the same p*H* values is given. The rate of decom-

TABLE 1. Decomposition rates of the cations **1** and **2**[a]

p*H*	k^1_{dec} × 10^4 (s^{-1})	k^2_{dec} × 10^4 (s^{-1})
12.09	0.25	40.5
11.41	1.5	6.1
10.74	3.1	0.95
10.27	4.9	(0.47)[b]

[a]At 25°C, ionic strength 0.1.
[b]By extrapolation, assuming reaction is first-order in [OH^-].

position of **2** appears to be approximately first-order in hydroxide ion.

Although the above uv spectral studies rule out 2,2′-dipyridyl as a major product of the decomposition reaction of either **1** or **2**, it was found that small amounts of 2,2′-dipyridyl (~5% yields) could be obtained from the decomposed solutions of these two species. Thus chloroform extraction of a solution of **1** which had been kept at p*H* 10.95 for 2 days gave a small amount of a species that had uv and ^{1}Hmr spectral properties that were identical to those of an authentic sample of 2,2′-dipyridyl.

The dication **1** was also observed by uv spectrophotometry to undergo decomposition upon standing in basic methanolic solutions. This reaction has not been studied in detail, but it is clear from the uv spectral data that the decomposition product in methanol is not the same as the product in basic aqueous solution.

Discussion

Rapid Equilibration Reactions

Since the dication **1** has no readily ionizable hydrogen atoms, the pK_a = 9.9 associated with the conversion of **1** to A must presumably represent hydroxide ion addition to **1** to form a pseudobase species. Three such pseudobase species appear to be possible; these are **6**, **7**, and **8** which would be formed by hydroxide ion addition to **1** at a carbon atom in either the pyrazinium ring or at C-2 or C-4 of one of the pyridinium rings, respectively. By virtue of the

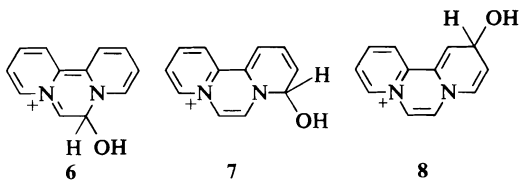

6 **7** **8**

proximity of the two positively charged nitrogen atoms, the carbon atoms of the pyrazinium ring would be expected to be more electron-deficient than the carbon atoms in the pyridinium rings. However, the formation of **6** by hydroxide ion addition in the pyrazinium ring results in disruption of the Kekulé resonance structures of all three rings of **1**, whereas in the formation of each of **7** and **8** one aromatic pyridinium ring is conserved. Consequently **7** and **8** would each be expected to be thermodynamically more stable than **6**.

The observed uv spectrum of A (λ_{max} = 302 nm) also tends to eliminate **6** as the structure of A. Thus, to a first approximation, one might consider a useful model for **6** to be six conjugated C=C double bonds with a terminal amino group (*i.e.* (—CH=CH)$_6$—NH$_2$). The spectrum of such a system would be expected to show absorption at much longer wavelengths than is observed for the major peaks of A (6). The intense peak in the vicinity of 302 nm for A is consistent with the presence of a substituted pyridinium cation as in **7** or **8**. It is difficult to predict the complete uv spectra of **7** and **8** since there seem to be no useful models to indicate the spectral consequences of the interaction of the pyridinium and dihydropyridine ring systems both via the 2,2′-bond of the dipyridyl moiety and the C=C bridging the two ring nitrogen atoms. The absorption peak in the vicinity of 370 nm may be indicative of the presence of a 1,2-dihydropyridine ring system since even simple 1,2-dihydropyridines lacking other chromophoric substituents have λ_{max} in the vicinity of 325 nm (7).

The ^{1}Hmr spectrum of A′ in Fig. 3*b* is also indicative of methoxide adducts analogous to **7** or **8** rather than the methoxide adduct related to **6**. Thus the signals in the region δ 8–9 in Fig. 3*b* are typical of protons on a pyridinium ring; *e.g.* for the *N*-methylpyridinium cation in D_2O: δ 8.93 H(2, 6); 8.61 H(4); 8.17 H(3, 5). In particular, the doublet in the vicinity of δ 8.9 in Fig. 3*b* is quite characteristic of the proton on the carbon atom adjacent to the pyridinium nitrogen atom. There does appear, however, to be an additional signal in this δ 8–9 region. This region integrates somewhat high for four protons relative to the rest of the spectrum. Possibly also located in this region is the signal from the proton on the bridge carbon atom adjacent to the positively charged nitrogen atom of the methoxide adducts related to **7** and/or **8**. The presence of this characteristic pyridinium spectrum also tends to rule out the methoxide adduct corresponding to **6**, since aromatic character is lacking in this latter structure. The signals in the region δ 6–8 are consistent with the presence of a dihydropyridine ring such as is present in **7** or **8**. A simple analysis of this region does not seem to be possible, however, and so suggests the possibility that a mixture of the methoxide adducts corresponding to **7** and **8** is actually present.

We therefore tentatively conclude that A is either **7** or **8** or a mixture of these two species.

The A′ species in methanol solution would then consist of the corresponding methoxide adduct(s).

The pH-dependence of k^{A}_{obs} in Fig. 5 is typical of that usually observed for cation–pseudobase equilibration reactions (11, 12). Separation of the pseudo first-order rate constants for formation (k_f) of A from **1** and decomposition (k_d) of A to **1** indicates that over the pH range investigated these rate constants can be represented by $k_f = 1.3 \times 10^4[OH^-]\ s^{-1}$ and $k_d = 1.4\ s^{-1}$. The line in Fig. 5 for k^{A}_{obs} is calculated from $k_f + k_d$ using these relationships and gives an acceptable fit to the experimental data. The terms in k_{H_2O} for k_f and in $k_1[H^+]$ for k_d, which are usually required (11, 12) for a complete description of the pH-dependence of the rates of cation–pseudobase equilibration, are not observable over the pH range that is amenable to investigation for **1** $\rightleftharpoons$ A.

The fact that the rate of formation of species B is readily observable on the stopped-flow spectrophotometer clearly indicates that B is not simply an alkoxide ion derived from A. Alkoxide ion formation is also not consistent with the occurrence of a similar reaction to generate B′ in methanolic solution, nor with the drastic spectral change associated with the conversion of A to B. The intense long-wavelength band of $\lambda_{max} = 498$ nm in the spectrum of B is suggestive of the presence of an extensively conjugated nonaromatic species. A number of such species can be generated by the addition of a second hydroxide ion to **7** or **8** (*e.g.* **9**). We feel that such

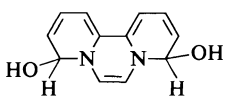

9

species can be ruled out since simple pyridinium ions do not generate significant amounts of pseudobase species even in quite strongly basic aqueous solutions (*e.g.* in aqueous 1 *M* KOH) (8–10). A more likely structure for B is **10** in which two hydroxide ions have added to the carbon atoms of the pyrazinium ring of **1**.

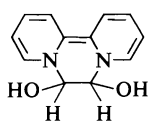

10

The pH-dependence of k^{B}_{obs} for the formation of B is also not consistent with simple hydroxide ion addition to A. Such a reaction would be expected to be first-order in $[OH^-]$, whereas in fact k^{B}_{obs} seems to depend on less than the first power of $[OH^-]$ even at p$H > 11.5$ where k^{B}_{obs} is not complicated by the rate constant for the reverse reaction. From Fig. 5 we estimate that k^{B}_{obs} is approximately linear in $[OH^-]^{0.5}$. Such a fractional order suggests that no single step in the reaction under observation is entirely rate-controlling. Presumably **10** would be formed by hydroxide ion addition to a small amount of **6** present in the equilibrium mixture A that is believed to be predominantly **7** and/or **8**. Such a situation is described in Scheme 2.

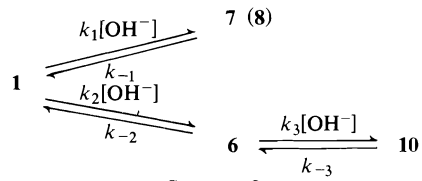

SCHEME 2

Slow Decomposition Reactions

The above data clearly indicate that the cations **1** and **2** both decompose to the same product in aqueous base. The formation of **2** as an intermediate in the decomposition of **1** is established at pH 9.3 from the uv spectra of acidified solutions of the initial decomposition product. At p$H > 11$ it is not possible to unequivocally establish the presence of **2** from spectral data because **2** decomposes faster than **1** in this region (Table 1). It seems likely, however, that **2** is an intermediate in the decomposition of **1** at all pH values since these two cations give identical decomposition products at all pH values as judged by the uv spectra of decomposed solutions. The nature of this final decomposition product has not been unequivocally established.[4] Although the uv spectrum of this product in basic solution ($\lambda_{max} = 276$ nm) is very similar to the spectrum of 2,2′-dipyridyl ($\lambda_{max} = 278$ nm), it does not undergo a bathochromic shift to $\lambda_{max} = 302$ nm upon acidification. Such a shift is typical of the monocation of 2,2′-dipyridyl. In fact the apparent pH-independence of the uv spectrum of the decomposition product suggests that it undergoes no protonation of a pyridine nitrogen atom in the range pH = 0–12. Since the spectrum seems to suggest that the dipyridyl

[4]Attempts to isolate this product at higher concentrations of **1**, produced brown oils which seemed to be complex mixtures.

unit is still intact in the decomposition product, the lack of a protonation in this region suggests that this dipyridyl unit already contains a pyridinium ring. In fact the similarity in the uv spectra of **2** and the decomposition product suggest that the decomposition of **2** in no way disrupts the electronic structure of the pyridylpyridinium moiety of **2**. The simplest structure for the decomposition product that is consistent with the above consideration is that of the dimeric aldol condensation product **11**.

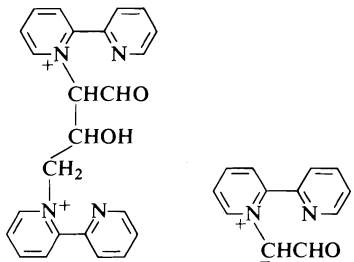

11 **12**

Since the conversion of **2** to **11** is kinetically first-order in **2** and also approximately first-order in hydroxide ion, the deprotonation of **2** to generate the carbanionic zwitterion **12** must be considered to be the rate-determining step in the formation of **11**.

The observed p*H*-dependence for the decomposition of **1** (Fig. 7) suggests that the conversion of **1** to **2** actually occurs via either A or else another species which is present in a rapid p*H*-independent equilibrium with A. As discussed above, the most likely structures for A are **7** and **8**. It is difficult to conceive of **7** or **8** as being intermediate in the formation of **2**, however, the structure **6** which has been ruled out for A clearly is a likely candidate for an intermediate between **1** or **2**. We therefore suggest that a small amount of **6** is present in solution in equilibrium with **7** and/or **8** and that decomposition of **1** to **2** proceeds through **6**. The presence of a small amount of **6** was also inferred above from the p*H*-dependence of the equilibration of **7** (or **8**) and **10**. The observed p*H*-dependence in Fig. 7 then requires a transition state in the same protonation state as **6** (*e.g.* **13** $\xrightarrow{k[H^+]}$ **2**). Of course, a kinetically equivalent mechanism would be rate-determining protonation prior to C—N bond-breaking, rather than the concerted reaction shown in **13**. In this case, the alkoxide ion derived from **5** would be a reaction intermediate.

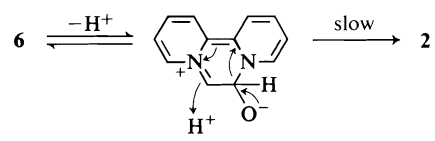

13

Experimental

The bromide salts of the cations **1** and **2** were synthesized as described by Calder and Sasse (2).

Determination of pK_a Values and Spectrum of A

Inspection of the p*H*-dependence of the spectra of fresh aqueous solutions of the dication **1** (25°C, ionic strength 0.1) indicates that the peak at 271 nm decreases in intensity with increasing p*H* whereas a new peak at 494 nm appears and increases in intensity with increasing p*H* (Fig. 1). This latter long wavelength absorption maximum results in high p*H* solutions being red in colour. Consideration of the differences between the spectra at p*H* 7 and p*H* 11.76 allows estimates that 50% of the change in intensity at 271 nm is complete at p*H* ~9.7 whereas 50% of the total increase in intensity at 494 nm is not complete until p*H* ~10.5. This suggests that these p*H*-dependent spectra do not merely reflect the equilibration between two species, but rather two successive p*H*-dependent equilibria are involved. The fact that unique isosbestic points are not observed over the entire p*H* range further confirms that complex equilibria are involved.

Assuming that the spectrum at p*H* 7.0 represented pure **1** and that the spectrum at p*H* 11.76 represented pure B, the above estimates of the two pK_a values were used to calculate an approximate spectrum for A from the observed spectra of each of p*H* 9.34, 9.88, and 10.74 solutions. These estimated spectra were averaged to give an approximate spectrum of A. These spectra were then used to calculate the concentrations of each of **1**, A, and B at each p*H*, and new pK_a values were thus estimated. These new estimates for the pK_a values were used to re-evaluate the spectra of A and B and the above procedure was repeated to give new pK_a values. After several cycles, the spectra calculated for A and B from the observed spectra at each of p*H* 9.34, 9.88, 10.74, and 11.76 were consistent to within 0.1 mM^{-1} cm^{-1} at all wavelengths. This self-consistency was attained with pK_a values of 9.9 and 10.4, respectively, for the equilibria in Scheme 1.

Equilibration Kinetics

The rates of equilibration of **1** with A and B were observed by mixing aqueous solutions of **1** (p*H* ~7) with buffers of ionic strength 0.2 at 25°C in a Durrum–Gibson stopped-flow spectrophotometer. The equilibration of **1** with A was followed at 272 and 305 nm. At 272 nm, the absorbances of A and B are approximately equal and are also approximately 10% of the absorbance of **1** at this wavelength. Plots of log $(A - A_\infty)$ against time were linear over more than three half-times at p*H* < 9.5 and were linear for 2–3 half-times at p*H* > 9.5. The deviations from strict first-order kinetics after 3 half-times at p*H* > 9.5 is presumably due to the equilibration of A with B. Pseudo first-order rate constants (k^A_{obs}) were calculated from the linear region of the log $(A - A_\infty)$ *vs.* time plot. At 305 nm, A_∞ could not be obtained directly at p*H* > 9.5 because of the large difference in absorbance

intensities of A and B at this wavelength. In this case, A_∞ was calculated from the estimated extinction coefficient of A at 305 nm based on the calculated spectrum in Fig. 2. Values of k^{A}_{obs} estimated in this way at 272 nm and 305 nm are in close agreement (Fig. 5).

Rates of equilibration of **1** and A with B were followed at 500 nm where neither **1** nor A has any significant absorbance. Values of the pseudo first-order rate constant k^{B}_{obs} were estimated from the slopes of log $(A_\infty - A)$ *vs.* time plots.

Decomposition Kinetics

Rates of decomposition of both **1** and **2** were determined spectrophotometrically at 25°C in buffer solutions of ionic strength 0.1. For **1**, the reaction was followed at 304 or 310 nm for pH < 11, and at 500 nm for pH > 11. Rates of decomposition of **2** were obtained at 390 nm, which is a peak in the pH-dependent spectrum of **2**. This decrease in absorbance at 390 nm in basic solution, closely parallels the spectral change of acidified solutions of partially decomposed **2**. Pseudo first-order rate constants (k_{dec}) were calculated for both **1** and **2** from the slopes of linear plots of log $(A - A_\infty)$ *vs.* time.

Acknowledgment

We appreciate the continued support of this work by the National Research Council of Canada.

1. J. W. BUNTING and W. G. MEATHREL. Can. J. Chem. **52**, 981 (1974).
2. I. C. CALDER and W. H. F. SASSE. Tetrahedron Lett. 1465 (1965).
3. D. H. CORR and E. E. GLOVER. Chem. Ind. 847 (1965); J. Chem. Soc. 5816 (1965).
4. P. KRUMHOLZ. J. Am. Chem. Soc. **71**, 3654 (1949).
5. I. C. CALDER and W. H. F. SASSE. Aust. J. Chem. **21**, 2951 (1968).
6. J. N. MURRELL. The theory of the electronic spectra of organic molecules. Methuen, London. 1963. p. 82.
7. U. EISNER and J. KUTHAN. Chem. Rev. **72**, 1 (1972).
8. A. HANTZSCH and M. KALB. Chem. Ber. **32**, 3109 (1889).
9. T. G. ASTON and P. A. LASELLE. J. Am. Chem. Soc. **56**, 426 (1934).
10. W. G. MEATHREL. M.Sc. Thesis, University of Toronto, Toronto, Ont. 1970.
11. J. W. BUNTING and W. G. MEATHREL. Can. J. Chem. **51**, 1965 (1973).
12. J. W. BUNTING and D. J. NORRIS. J. Am. Chem. Soc. **99**, 1189 (1977).

Structure and synthesis of a new cyclopentenone derivative from *Trichoderma album*

GEORGE M. STRUNZ,[1] WU-YUN REN, AND MERLYN A. STILLWELL
Canadian Forestry Service, P.O. Box 4000, Fredericton, N.B., Canada E3B 5P7
AND
ZDENEK VALENTA
Department of Chemistry, University of New Brunswick, Fredericton, N.B., Canada E3B 5A3

Received March 7, 1977

GEORGE M. STRUNZ, WU-YUN REN, MERLYN A. STILLWELL, and ZDENEK VALENTA. Can. J. Chem. **55**, 1610 (1977).

A dextrorotatory product isolated from cultures of *Trichoderma album* has been identified as 5-hydroxy-3-methoxy-5-vinyl-2-cyclopenten-1-one, and a synthesis of the latter in racemic form is described. The possibility that this compound might be an artifact produced during the isolation procedure, rather than a true metabolite, is not excluded.

GEORGE M. STRUNZ, WU-YUN REN, MERLYN A. STILLWELL et ZDENEK VALENTA. Can. J. Chem. **55**, 1610 (1977).

Un produit dextrogyre isolé des cultures du *Trichoderma album* s'avère etre l'hydroxy-5 méthoxy-3 vinyl-5 cyclopent-2 èn-1 one et on décrit la synthèse de celui-ci sous forme racémique. On n'a pas éliminé la possibilité que ce composé soit un artefact produit au cours d'isolement au lieu d'un vrai métabolite.

Trichoderma album, in plate culture, exhibits antagonism to a variety of microorganisms.[2] This prompted us to examine products extracted from the filtrates after growth of *T. album* in liquid-shake culture. From chromatography of extracted material, we have obtained, in low yield, a new optically active cyclopentenone derivative, $C_8H_{10}O_3$, the structure determination and synthesis of which are described herein.

The compound displays ir absorption ($CHCl_3$) at 1700 and 1592 cm^{-1} (strong), and a uv chromophore $\lambda_{max}(CH_3OH)$ at 243 nm (ε 15 600). These features, together with nmr signals corresponding to an olefinic hydrogen at δ 5.36 (poorly resolved doublet, $J \sim 1.5$ Hz), and methyl ether protons at δ 3.95 (3H, s) are readily interpreted in terms of a 3-methoxy-2-cyclopenten-1-one system (1–3). Infrared absorption at 3555 cm^{-1} indicates the presence of hydroxyl functionality: the latter is further manifested as an exchangeable one-proton signal at δ 3.19 in the nmr spectrum. A three-proton multiplet at δ 5.14–6.20 resembles closely the 11-peak pattern displayed by the vinyl hydrogens of 3-methyl-1-buten-3-ol (4), and the presence of a (tertiary) vinyl carbinol system can accordingly be inferred. The base peak in the mass spectrum, at *m/e* 55, corresponding to the ion $(C_3H_3O)^+$ provides support for this structural feature.

The combined spectral data can be accommodated by either of the isomeric structures **1** or **2**. (The geminal protons on the ring appear in the nmr spectrum as a two-proton doublet at δ 2.83 ($J \sim 1.5$ Hz).)

The remaining structural ambiguity was resolved by synthesis. Structure **2** was selected as the initial synthetic target since it appeared that it should be accessible by reaction of the known compound **3** with a vinyl Grignard reagent. Accordingly, **3** was prepared (5, 6), via 1,2,4-cyclopentane trione **4** (7), from diethyl acetonedicarboxylate and diethyl oxalate. Reaction of **3** with vinyl magnesium bromide in tetrahydrofuran (8) afforded a complex mixture of products, possibly as a result of anion formation at C-5 (5). The desired product **2** was, however, obtained in 32% yield (not optimized) on changing the solvent to ether, in which both reactants were but sparingly soluble.[3] That the compound obtained from the *T. album* fermentation was not **2** was immediately obvious on

[1]Author to whom correspondence should be addressed.
[2]J. L. Ricard: personal communication. We thank Dr. Ricard for providing a culture of *T. album*.
[3]The Grignard reagent was prepared in tetrahydrofuran in the normal manner (8): it was suspended in anhydrous ether after removal of the former solvent (nitrogen stream).

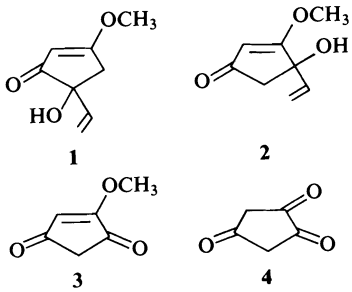

1 2

3 4

comparison of their spectra (see Experimental). Thus, for example, though the nmr spectra showed some similarities, significant differences were evident in the signals corresponding to the C-2 vinyl proton, and the methylene protons (for **2**, *singlets* at δ 5.33 and 2.68 ppm, respectively).

While **3**, derived from the more favorable enolic form of **4**, is the sole product (80%) reported from acid-catalyzed reaction of the latter with methanol (6), it appeared that similar treatment of **2** might give rise to an equilibrium mixture containing both **1** and **2**. In the event, when **2** was set aside at ambient temperature in methanol solution containing a catalytic quantity of sulfuric acid, tlc analysis revealed the gradual formation of a second, more polar product. After 4 h, 69 mg of **2** and 45 mg of **1** were recovered, starting from 150 mg of the former.

Comparison of solution spectra and tlc behavior of synthetic **1** thus prepared, with those of the *T. album* product established their identity. A biosynthetic pathway to **1** might comprise cyclization of a tetraketide precursor to a six-membered (orsellinic acid-type) intermediate, with subsequent loss of carboxyl, oxidation, and ring contraction.

The possibility that **1** could be an artifact produced from a metabolite during the isolation procedure was considered, on comparing its chromatographic characteristics with those of the crude extracts from which it was obtained. Since production of **1** has not been observed in subsequent fermentations, we have, as yet, no further evidence relating to the question of its authenticity as a 'true natural product'.

Bioassays, using the disc method, showed that **1** was devoid of antifungal activity against test organisms sensitive to the crude *T. album* extracts.

Experimental

Melting points were determined on a hot-stage apparatus and are uncorrected. Infrared and ultraviolet spectra were recorded on a Beckman Acculab 2 and a Perkin-Elmer 402 spectrophotometer, respectively. Nuclear magnetic resonance spectra were obtained for solutions in deuterochloroform using a Varian T-60 intrument, with tetramethylsilane as internal standard. Preparative thin layer chromatography was carried out on 0.5 mm layers of silica gel GF-254 (E. Merck); bands were detected by viewing under uv light (254 nm).

*Isolation of 5-Hydroxy-3-methoxy-5-vinyl-2-cyclopenten-1-one, **1***

Material extracted with chloroform from filtered culture medium[4] that had supported growth of *T. album* (liquid shake culture, temperature *ca.* 15°C) for 3 weeks, was passed through a short column of silica gel using chloroform as eluent. After removal of solvent *in vacuo*, the residue was chromatographed on preparative layer plates of silica gel (benzene–acetone, 4:1). A distinct band at R_F *ca.* 0.5 was isolated by extraction with methanol. On rechromatography using the same system, the principal band appeared to have shifted to lower R_F (artifact?). The yield of crystalline product, **1**, obtained from this band was less than 1 mg per litre culture medium. After crystallization from ether–*n*-hexane, **1** was sublimed at 0.1 Torr to give colorless crystals, mp 75–77°C; $[\alpha]_D$ +63° (*c* 0.741 g/100 ml methanol); cd (7.433 × 10^{-4} *M* in methanol, 1 mm cell) λ nm (Δε): 335(0), 281 (+2.36), 263 (0), 238 (+4.32), 219 (0), <219 (negative); ir (KBr) *inter alia* 3400 (br), 3080, 2990, 2940, 2850, 1695, 1575, 1355, 1250, 1190, 1110, and 975 cm^{-1}; ir ($CHCl_3$) 3555, 1700, 1592 (s), and 1362 cm^{-1}; uv λ_{max}(CH_3OH) 243 nm (ε 15 600); nmr spectrum described in text; ms (peaks of relative abundance greater than 20%) *m/e* 154.0631 (73) (calcd. for $C_8H_{10}O_3$: 154.0630), 125(48), 98(34), 97(26), and 55(100).

*Preparation of 4-Hydroxy-3-methoxy-4-vinyl-2-cyclopenten-1-one, **2***

Vinylmagnesium bromide was prepared in anhydrous tetrahydrofuran from magnesium turnings (300 mg; 12.3 × 10^{-3} g-atom) in the usual manner (8). The solvent was then removed with the aid of a stream of dry nitrogen, and the solid residue was suspended in anhydrous ether (50 ml). To the stirred suspension of vinyl Grignard reagent (ambient temperature, nitrogen atmosphere) was added in several portions from a dropping funnel, 2-methoxy-2-cyclopentene-1,4-dione, **3**, (1 g, 7.93 mmol) (5–7) suspended in ether (20 ml). The mixture was stirred under the same conditions for 4 h, after which saturated ammonium chloride solution was added. The material obtained on work-up (extraction with ethyl acetate etc.) was subjected to chromatography on preparative layer plates of silica gel (benzene–acetone 7:3), affording 98 mg of the cyclopentenedione starting material and 387 mg (32%) of **2**.

The product, **2**, was a colorless gum, ir (neat film) *inter alia* 3380 (br), 3100, 3020, 2990, 2950, 2850, 1690, 1600, 1332, 1252, 1206, and 1171 cm^{-1}; uv λ_{max}(CH_3OH) 238 nm; nmr δ 2.68 (2H, s), 3.73 (1H, br, exchangeable) 3.90 (3H, s), 5.33 (1H, s), and 5.14–6.23 (3H, m, *cf.* ref. 4); ms (peaks of relative abundance greater than 20%) *m/e*

[4]The culture medium was the basal synthetic medium of Jennison *et al.* (9), but with sucrose as carbon source. Nitrogen was provided by L-glutamic acid.

154.0626(79) (calcd. for $C_8H_{10}O_3$: 154.0630), 127(28), 125(24), 109(57), 108(25), 97(23), 96(87), 95(29), 57(25), and 55(100).

5-Hydroxy-3-methoxy-5-vinyl-2-cyclopenten-1-one, ***1***, *Synthetic*

The cyclopentenone vinyl carbinol, **2**, (150 mg, 0.97 mmol) was dissolved in anhydrous methanol (30 ml), and concentrated sulfuric acid (2 drops) was added. The pale yellow solution was stirred at 21°C for 4 h. It was then poured into dilute sodium carbonate solution, and extracted thoroughly with ethyl acetate. The extracts were washed with brine, dried over magnesium sulfate, and evaporated. Preparative layer chromatography of the residue on silica gel plates (benzene–acetone, 7:3) afforded starting material, **2**, (69 mg) and the isomer **1** (45 mg). After recrystallization from ether–*n*-hexane, **1** was obtained as colorless crystals, mp 65–67°C; ir ($CHCl_3$), uv (CH_3OH), and nmr ($CDCl_3$) spectra, as well as tlc behavior identical with those of the *Trichoderma* product; ir (KBr) *inter alia*, 3360 (br), 3100, 3025, 3005, 2980, 2950, 2850, 1680, 1575, 1355, 1250, 1195, 1150, 975, and 815 cm^{-1}; ms, *m/e* 154.0622; calcd. for $C_8H_{10}O_3$, 154.0630.

Acknowledgments

We thank Messrs A. I. Budd and J. Hoyle, University of Alberta, Edmonton, for the accurate mass measurements and circular dichroism measurements, respectively. Mrs. M. Austria, University of New Brunswick, kindly recorded other mass spectra.

1. K. NAKANISHI. Infrared absorption spectroscopy, practical. Holden-Day, Inc., San Francisco, CA. 1962.
2. A. I. SCOTT. Interpretation of the ultraviolet spectra of natural products. The Pergamon Press, Ltd., New York, NY. 1964.
3. J. M. LANDESBERG and D. KELLNER. J. Org. Chem. **33**, 3374 (1968).
4. High resolution NMR spectra catalogue. Vol. 2. Varian Associates. 1963. Spectrum No. 444.
5. C. F. SHELEY and H. SHECHTER. J. Org. Chem. **35**, 2367 (1970).
6. C. SAMARIAN and H. W. WANZLICK. Tetrahedron Lett. 2125 (1974).
7. J. S. CHICKOS. J. Org. Chem. **38**, 1231 (1973).
8. H. NORMANT. Bull. Soc. Chim. Fr. 728 (1956); H. NORMANT. *In* Advances in organic chemistry, methods and results. Vol. 2. Interscience Publishers, Inc., New York, NY. 1960. p. 1.
9. M. W. JENNISON, M. D. NEWCOMB, and R. HENDERSON. Mycologia, **47**, 275 (1955).

Erratum: Synthesis and characterization of Cu(I) complex compounds with methyl isonicotinate

MOHAMED A. S. GOHER

Department of Chemistry, Faculty of Science, Alexandria University, Alexandria, Egypt

Received March 29, 1977

(Ref.: Can. J. Chem. **53**, 2657 (1975))

In Table 1, the elements for which analyses are given should be in the order Cu, X, C, H, N.

Canadian Journal of Chemistry

Published by
THE NATIONAL RESEARCH COUNCIL OF CANADA

Journal canadien de chimie

Publié par
LE CONSEIL NATIONAL DE RECHERCHES DU CANADA

Volume 55 Number 14 July 15, 1977 Volume 55 numéro 14 15 juillet 1977

The affinity of aldehydic compounds to complex formation. Nickel(II) and cobalt(II) complexes with 2-pyridinecarboxaldehyde

M. S. El-Ezaby,[1] M. A. El-Dessouky, and N. M. Shuaib

Department of Chemistry, Kuwait University, Kuwait

Received August 10, 1976[2]

M. S. El-Ezaby, M. A. El-Dessouky, and N. M. Shuaib. Can. J. Chem. **55**, 2613 (1977).

The interactions of Ni(II) and Co(II) with 2-pyridinecarboxaldehyde have been investigated in aqueous solutions at $\mu = 0.10\ M\ (KNO_3)$ at 30°C. The stability constants of different complex equilibria have been determined using potentiometric methods. Spectrophotometric methods were also used in the case of the nickel(II) – 2-pyridinecarboxaldehyde system. It was concluded that nickel(II) and cobalt(II), analogous to copper(II), enhance hyrdation of 2-pyridinecarboxaldehyde prior to deprotonation of one of the geminal hydroxy groups. Complex species of 1:1 as well as 1:2 metal ion to ligand composition exist under the experimental conditions used.

M. S. El-Ezaby, M. A. El-Dessouky et N. M. Shuaib. Can. J. Chem. **55**, 2613 (1977).

On a étudié, en solutions aqueuses, à une valeur de $\mu = 0.10\ M$ de (KNO_3) et à 30°C, les interactions du nickel(II) et du cobalt(II) avec le pyridinecarboxaldéhyde-2. On a déterminé, faisant appel à des méthodes potentiométriques, les constantes de stabilité des équilibres des différents complexes. On a aussi utilisé des méthodes spectrophotométriques dans le cas du système nickel(II) pyridinecarboxaldéhyde-2. On en conclut que le nickel(II) et le cobalt(II), comme le cuivre(II), augmentent l'hydratation du pyridine – carboxaldéhyde-2 avant la déprotonation de l'un des groupes hydroxy géminés. Des espèces complexes de composition ion métallique/ligand de 1:1 de même que 1:2 existent dans les conditions expérimentales utilisées.

[Traduit par le journal]

Introduction

Although few reports discuss the complex formation of aldehydic compounds with metal ions, they are involved in Schiff bases metal complexes (1). Their importance cannot be overshadowed in many biological processes. Pyridoxal and pyridoxal phosphate, a well known 4-pyridinecarboxaldehyde derivative, in the presence of metal ions was shown to catalyze model reactions in vitro alone by enzymes in vivo (2).

In spite of the fact that some metal ions form quite stable complexes with some pyridinealdoximes (3), reports on the interaction of pyridinecarboxaldehydes with metal ions are scarce. The hydration of 2-pyridinecarboxaldehyde is facilitated in aqueous solutions by metal ions and, furthermore, one of the geminal hydroxy groups is easily deprotonated by forming a 5-membered chelate (4–6). In this work, we report the interaction of nickel(II) and cobalt(II) ions with 2-pyridinecarboxaldehyde.

Experimental

Materials

2-Pyridinecarboxaldehyde (2PA) was obtained from Fluka, and was redistilled under a reduced pressure of nitrogen and stored in dark at 0°C. Stock solutions of 1.0 *M* of the compound in 1.0 *M* HCl or 1.0 *M* HNO_3 were stored at 0°C in dark and were stable by uv spectral criteria (λ_{max} 235 nm ($\varepsilon_{max} = 6.1 \times 10^3$) for equilibrated aldehyde + hydrate, p*H* 6–10, $\mu = 0.5\ M$ KCl) over a

[1]To whom correspondence should be addressed.
[2]Revision received March 7, 1977.

TABLE 1. Protonation constants of 2-pyridinecarboxaldehyde and the stability constants of its complex reactions with Ni(II) and Co(II) metal ions, at 30°C, according to eq. 3 (s is the standard deviation)

Stoichiometric coefficients						
q	j	k	M^{2+}	log β	$\pm s$	Number of titration points
1	0	−1	—	−12.61[a,b]		
1	0	1	—	3.29	0.01	98
1	1	−1	Ni	−5.34	0.03	144
1	1	−2	Ni	−13.85	0.02	144
1	1	−3	Ni	−24.74	0.08	144
2	1	−2	Ni	−10.99	0.09	69
1	1	0	Ni	1.23[b]	0.14	60
2	1	0	Ni	1.73[b]	0.10	60
1	1	−1	Co	−6.02	0.01	230
1	1	−2	Co	−17.42	0.04	183
2	1	−2	Co	−14.28	0.02	230
1	1	−1	Cu[a]	−1.94		
1	1	−2	Cu[a]	−8.56		
2	1	−2	Cu[a]	−4.72		
1	1	0	Cu[a]	2.94		
2	1	0	Cu[a]	4.75		
3	1	0	Cu[a]	6.32		
4	1	0	Cu[a]	8.52		

[a]Reference 4.
[b]Values obtained from spectrophotometric methods.

period of a month. The concentration of the stock solutions of $NiCl_2$ or $Ni(NO_3)_2$ and $Co(NO_3)_2$ were checked complexometrically by EDTA titrations.

Radiometer pH meter model 63 (accurate to ±0.01 pH units) provided with combined glass electrode type GK (301 c) was used to record the hydrogen-ion concentration. The titrations were carried out in 25 ml thermostated cell. Sodium hydroxide carbonate-free titrant (0.102 M) was added in small increments through Metrohm Herisau Multi-Dosimat E 415 microburette accurate to ±0.005 ml. The pH meter was calibrated as previously reported (7).

Spectrophotometric measurements in the visible region (wavelength range 450–700 nm) were recorded on a Unicam SP 8000 double-beam spectrophotometer. The instrument was calibrated as described previously (7).

All pH metric and spectrophotometric measurements were taken at 30°C. The ionic strength was 0.10 M KNO_3 in potentiometric work and 0.5 M KCl in the case of spectrophotometric study. In potentiometric study, solutions of different metal ions and ligand concentrations were used in the pH range 2.75–11.00. The metal ions concentrations were in the range (1.0–4.0) × 10^{-3} M and that of the ligand in the range of (1.0–6.0) × 10^{-3} M. In spectrophotometric work, the range of concentrations of nickel(II) ions was (0.006–0.015 M) and that of ligand was (0.1–0.5 M).

Results

Pyridinecarboxaldehydes may exist in different forms in aqueous solutions at various pH values. The equilibrium reactions which involve these species and their corresponding protonation constants are represented as follows:

$$[1] \qquad POH^- + H^+ \rightleftharpoons P.H_2O \qquad K_P \left\uparrow \right. + H^+$$

$$[2] \qquad POH^- + 2H^+ \rightleftharpoons HP.H_2O^+$$

$$[1a] \qquad \beta_{101}' = \frac{[P{\cdot}H_2O]}{[POH^-][H^+]}$$

$$[2a] \qquad \beta_{102}' = \frac{[HP{\cdot}H_2O^+]}{[POH^-][H^+]^2}$$

where $HP.H_2O^+$, $P.H_2O$, and POH^- are the hydrated species of the protonated and deprotonated species and the deprotonated form of the hydrated species, respectively. The protonation constants β_{101}' and β_{102}' can be determined by spectrophotometric methods (4). The protonation constant K_p can also be determined by potentiometric methods (4). The values of the constants are listed in Table 1.

The titration curves of the 1:1 ligand to metal ion ratio show sharp inflection at $a = 1$ (pH range 5.0–7.0), Fig. 1, coinciding with that of ligand indicating that complex formation did not occur at pH values lower than ~7.0. An inflection point, however, occurs at $a \simeq 3.0$ in Ni system and 2.5 in Co system which may indicate that a 1:1 complex in addition to a hydrolysable complex species may exist. Titration curves of other mole ratios indicated that 1:2

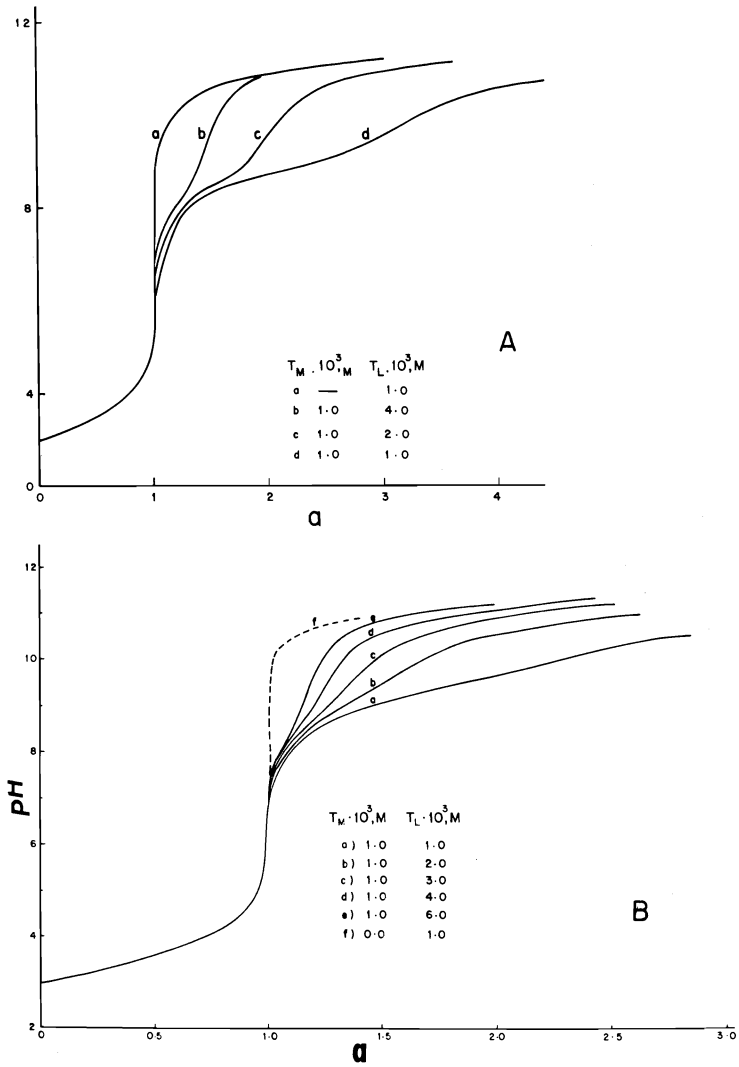

FIG. 1. The dependence of a (the ratio of moles of base to moles of ligand) on pH. (A) Ni(II)–2PA system; (B) Co(II)–2PA system.

complexes may occur with little possibilities of forming other higher complexes or even hydrolysable species, Fig. 1.

The color of the solutions of Ni(II)–2PA and Co(II)–2PA changed during titration from light green to light blue in the case of the former and purple to orange in the case of the latter. Slight precipitation occurs at pH values greater than 10.5, particularly in solutions of low ligand to metal ions ratios.

Titration data of the 1:1 ligand to metal ions ratio have been treated alone to describe different equilibria in solutions. Programme MINIQUAD and its modified versions MINIQUAD 75 have been used to test different models. Initially guessed values of stability constants β_{qjk} for the following generalized reaction are subjected to refinement

[3] $q\mathrm{P.H_2O} + j\mathrm{M^{2+}} + k\mathrm{H^+} \rightleftharpoons (\mathrm{P.H_2O})_q\,\mathrm{M}_j(\mathrm{H})_k^{2j+k}$

The model which gave the best fit is

[4] $\mathrm{P.H_2O} + \mathrm{M^{2+}} \rightleftharpoons (\mathrm{POH})\mathrm{M^+} + \mathrm{H^+}$

[5] $\mathrm{P.H_2O} + \mathrm{M^{2+}} + \mathrm{H_2O} \rightleftharpoons (\mathrm{POH})\mathrm{MOH} + 2\mathrm{H^+}$

[6] $\mathrm{P.H_2O} + \mathrm{M^{2+}} + 2\mathrm{H_2O} \rightleftharpoons (\mathrm{POH})\mathrm{M(OH)_2^-} + 3\mathrm{H^+}$

The MINIQUAD log β_{qjk}'s for the above model reactions are listed in Table 1. The

addition of one extra species or different model other than those shown above leads to an increase in the crystallographic R factor, greater X^2 value, or both. Equilibrium reactions 4, 5, and 6 have shown to occur only in Ni–2PA system while 4 and 5 only occur in Co–2PA system.

Titration data for other greater ligand to metal ions mole ratios indicated that only 2:1 complex species is further formed in solution. The equilibrium reaction which describes the experimental data is

$$[7] \quad 2P.H_2O + M^{2+} \rightleftharpoons (P.OH)_2M^0 + 2H^+$$

The MINIQUAD log β_{qjk}'s for Ni(II) and Co(II) systems are depicted in Table 1. The distribution diagram of the systems Ni(II)–2PA and Co(II)–2PA are shown in Fig. 2.

Ni(II)–2PA has been studied also by spectrophotometric methods. Figure 3 shows the spectra of Ni(II)–2PA system at different pH values in the wavelength range 450–700 nm. The band maxima shifted gradually to lower wavelengths as the pH increases. Isosbestic point is observed at λ 660 in the pH range 6.0–8.0. By using graphical methods (9), it was found that two absorbing species are present in the pH range 2.0–5.0 and 7.1–9.5. The pH dependence of absorbance (at a particular wavelength) on the initial concentrations of both metal ions and ligand is shown in Fig. 4. A unique formation curve was obtained when the average molar absorptivity ($= A_s/l\,T_M$) (where A_s, T_M, and l are the absorbance, total metal concentration, and light path length, respectively) was plotted against $-\log [P.H_2O]$ in the pH range 1.5–3.5, Fig. 5. The concentration of the free ligand, $P.H_2O$, was calculated by making use of the following equation

$$[8] \quad [P{\cdot}H_2O] = \frac{T_L[H^+]^{J-i}\prod_{l=0}^{i} k_l}{\sum_{j=0}^{J}[H^+]^{J-j}\prod_{l=0}^{j} k_l} \qquad T_L \gg T_M$$

Where k_l is the stepwise dissociation constant of the protonated ligand and T_L is the total ligand concentration. The absorbance data were analysed by the least-squares procedures. The sum of the squared deviations, s,

$$[9] \quad s = \sum_{1}^{N_p}(\bar{\varepsilon}_{obs} - \varepsilon_{calcd})^2 = \sum_{1}^{N_p}\left(\bar{\varepsilon}_{obs} - \frac{\sum_{0}^{N}\varepsilon_n\beta_n\,P{\cdot}H_2O}{\sum_{0}^{N}\beta_n\,P{\cdot}H_2O}\right)^2$$

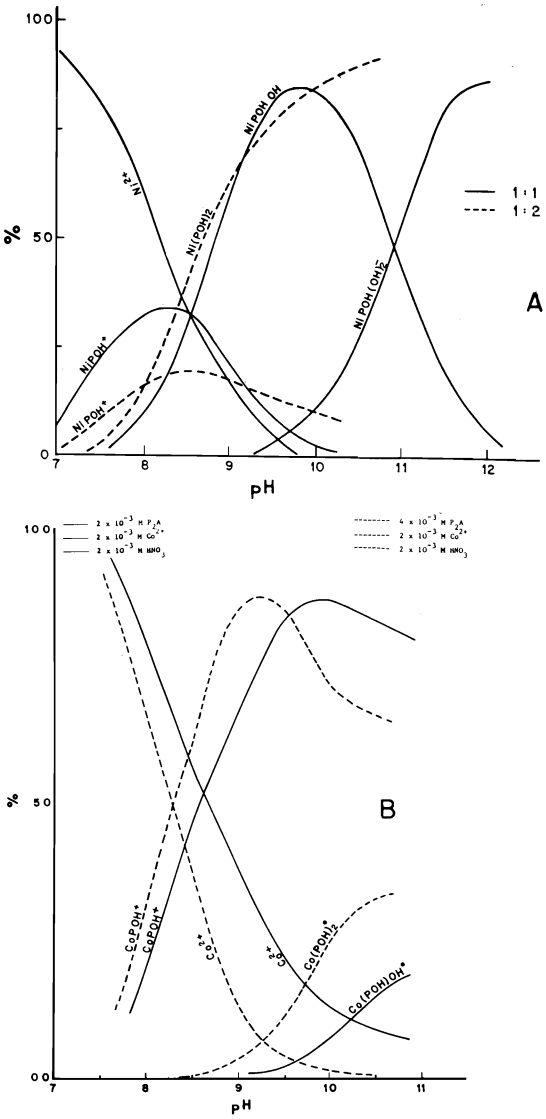

FIG. 2. Distribution of complex species. (*A*) Ni(II)–2PA system; (*B*) Co(II)–2PA system.

(where ε_n, β_n, N_p are the molar absorptivity of the nth species, the overall stability constant, and number of experimental points) is minimized with respect to the average molar absorptivity. Initially guessed values for the stability constants are usually made to solve for the $n + 1$ unknown by Gauss–Jordan elimination method. The method of steepest descents (10) is used to optimise the values of the stability constants to reduce s. The molar absorptivities and the sum of the squared residuals are then recalculated. The whole process may be repeated till refined β's could be obtained from the initial guesses. The plot of s *vs.* β_n or $\log \beta_n$ gives the optimum

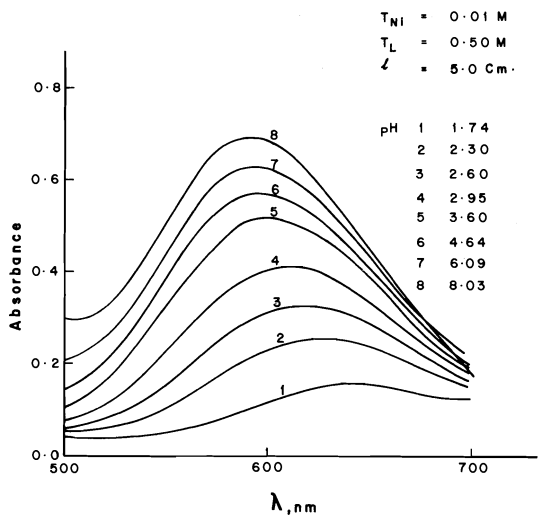

FIG. 3. The spectra of Ni(II)–2-pyridinecarboxaldehyde system at different pH values.

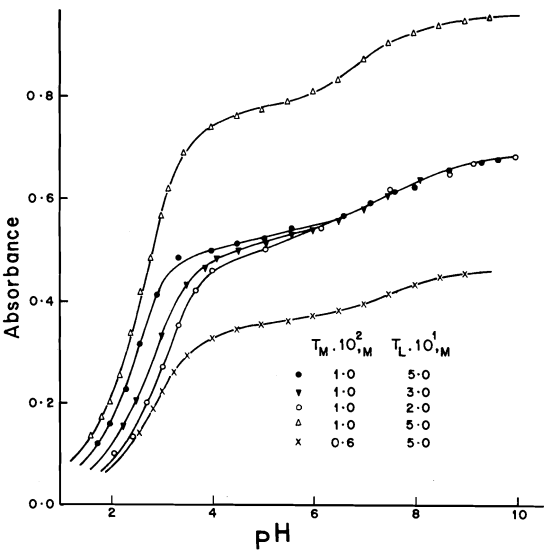

FIG. 4. The absorbance of Ni(II)–pyridinecarboxaldehyde system as functions of pH at λ 600 nm.

value of β_n which can be used to get β_m (7). Initial guesses for the stability constants of the following reactions

[10] $$Ni^{2+} + P.H_2O \rightleftharpoons NiP.H_2O^{2+}$$

$$\beta_{110} = \frac{[Ni\ P{\cdot}H_2O]}{[Ni^{2+}][P{\cdot}H_2O]}$$

[11] $$Ni^{2+} + 2P.H_2O \rightleftharpoons Ni(P.H_2O)_2{}^{2+}$$

$$\beta_{210} = \frac{[Ni(P{\cdot}H_2O)_2]}{[Ni^{2+}][P{\cdot}H_2O]^2}$$

have been subjected to refinement according to

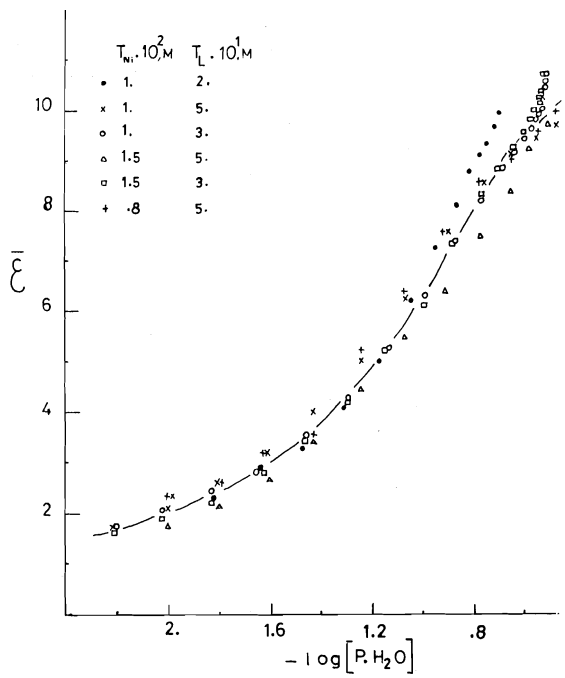

FIG. 5. The formations curve of Ni(II)–pyridinecarboxaldehyde system as functions of $P.H_2O$ species.

the above procedure using programme MONONUC (11). Table 2 shows the values of the refined β's. Back calculations of the $\bar{\varepsilon}$ from the obtained β's were in good agreement with the observed values within the allowed limits of experimental errors. At pH higher than 6 the absorbance is dependent upon pH when the metal concentration was kept constant while varying the initial concentration of the ligand, Fig. 4. This behaviour may be attributed to the deprotonation of the complex species $Ni(P.H_2O)_2{}^{2+}$ as the pH increases, *i.e.*,

[12] $$Ni(P.H_2O)_2{}^{2+} \rightleftharpoons Ni(P.H_2O)POH^+ + H^+$$

$$\beta_1 = \frac{[Ni(P{\cdot}H_2O)^{2+}]}{[Ni(P{\cdot}H_2O)POH^+][H^+]}$$

[13] $$Ni(P.H_2O)_2{}^{2+} \rightleftharpoons Ni(POH)_2 + 2H^+$$

$$\beta_2 = \frac{[Ni(P{\cdot}H_2O)_2{}^{2+}]}{[Ni(POH)_2][H^+]^2}$$

The protonation constants of the complex species $Ni(P.OH)_2$ can be calculated if first estimates of the β_1' and ε_0 can be determined at a given wavelength using eq. 14 (7).

[14] $$\bar{\varepsilon} = \frac{A_s}{lT_M} = \frac{\varepsilon_0 + \varepsilon_1\beta_1[H^+]}{1 + \beta_1[H^+]}$$

TABLE 2. Summary of the values of log β′ obtained from spectrophotometric methods for Ni(II)–2PA system at λ 600 nm

$T_M \times 10^2$	$T_L \times 10$	$\log \beta_{110}$	$\log \beta_{210}$	ε_1	ε_2
1.0	1.0	1.18	1.70	4.5	—
1.5	5.0	1.18	1.95	5.4	12.2
1.5	3.0	1.18	1.70	6.1	16.9
0.6	3.0	1.52	1.60	6.6	—
0.8	5.0	1.01	1.77	—	—
0.8	3.0	1.22	1.78	8.1	14.7
1.0	2.0	1.20	1.70	5.6	—
1.0	3.0	1.39	1.62	9.0	15.6
1.0	5.0	1.17	1.71	8.2	13.7

where ε_0 and ε_1 are the molar absorptivities of $Ni(POH)_2$ (they may be determined from the saturation value of absorbance in the pH range 9–10) and $Ni(P.H_2O)(POH)^+$ species. First approximations to ε_2 and β_2 at the same wavelength were evaluated using eq. 15.

$$[15] \quad \frac{\bar{\varepsilon} - \varepsilon_0}{[H^+]^2} + \beta_1 \frac{\bar{\varepsilon} - \varepsilon_1}{[H^+]} = \varepsilon_2\beta_2 - \bar{\varepsilon}\beta_2$$

where ε_2 is the molar absorptivity of $Ni(P.H_2O)_2$ which was employed to refine β_1 and ε_1 employing eq. 16.

$$[16] \quad \frac{\bar{\varepsilon} - \varepsilon_0}{[H^+]} + \beta_2[H^+](\bar{\varepsilon} - \varepsilon_2) = \varepsilon_1\beta_1 - \bar{\varepsilon}\beta_1$$

The results were found to converge by the third cycle of iteration. The values of log β_1' and log β_2' are 9.52 and 16.95, respectively.

Discussion

Complexes of Ni(II) and Co(II) with 2-pyridinecarboxaldehyde seem to be facilitated by the formation of the stable five-membered ring chelates through N and O atoms of the ligand. The chelates formation enhances deprotonation of the hydrated species of 2-pyridinecarboxaldehyde. The complex formation equilibria discussed in the forementioned results can be written in another form

$$[17a] \quad M^{2+} + POH^- \rightleftharpoons M(POH)^+$$

$$[17b] \quad M^{2+} + POH^- + OH^- \rightleftharpoons M(POH)(OH)$$

$$[17c] \quad M^{2+} + POH + 2OH^- \rightleftharpoons M(POH)(OH)_2$$

$$[17d] \quad M^{2+} + 2POH^- \rightleftharpoons M(POH)_2$$

Table 3 lists the calculated values of the stability constants of these equilibria including those reported for copper(II)–2PA system. It is clear that the order of complexing obeys the Irving–Williams series which, in turn, suggests high spin complexes in octahedral crystal field. However, the data cannot be interpreted in terms of the formation of more than bis complexes with 2PA. This conclusion strongly indicates that positive charge is essential for the complex species to attract another ligand species. In other words, neutral bis complex is incapable to deprotonate further a ligand species, $P.H_2O$, to form a tris chelated complex. However, the 5th and 6th coordination sites may be coordinated to the neutral ligand species, $P.H_2O$, or most probably to water molecules.

TABLE 3. Equilibrium constants for the equilibria 17

Parameter	Value		
	Co^{2+}	Ni^{2+}	Cu^{2+}
$\log \beta_{110}$	6.52	7.26	10.67
$\log \beta_{210}$	10.94	14.23	20.50
$\log \beta_{11-1}$	8.94	12.51	17.80
$\log \beta_{111}$	—	1.23	2.72
$\log \beta_{212}$	—	1.73	4.75

The enhanced deprotonation of hydrated species of 2-pyridinecarboxaldehyde may give the notion that metal complexes with pyridinic nitrogen can also facilitate deprotonation of one of the geminal diol of aldehyde group in either the meta or para position of pyridine. In current studies on the interaction of 4-pyridinecarboxaldehyde with amphetamine, it was found that metal ions, specially Cu(II), facilitate rapid condensation reactions at the ketone moiety at pH 5.0, a process which cannot be rapidly formed at pH's lower than 8 in the absence of metal ions (12). This kind of complex formation may raise the question of the possibility of other aldehydic compounds containing groups of complexing properties such as NH_2, OH . . . etc., to behave more or less in a similar manner.

1. D. L. LEUSSING. *In* Metal ions in biological systems. Vol. 5. *Edited by* H. Sigel. Marcel Dekker, New York. 1975. p. 1.
2. W. L. FELTY and D. L. LEUSSING. J. Inorg. Nucl. Chem. **36**, 617 (1974).
3. L. G. SILLEN and A. E. MARTELL. Stability constants of metal-ion complexes. The Chemical Society, London. Spec. Publ. No. 17 (1964) and Supplement No. 1, Spec. Publ. No. 25 (1971).
4. A. EL-HILALY and M. S. EL-EZABY. J. Inorg. Nucl. Chem. **38**, 1533 (1976).
5. P. HEMMERICH and S. FALLAB. Helv. Chim. Acta, **41**, 498 (1958).
6. R. W. GREEN and M. J. ROGERSON. Aust. J. Chem. **24**, 65 (1971).
7. M. S. EL-EZABY and N. GAYED. J. Inorg. Nucl. Chem. **37**, 1065 (1975).
8. A. SABATINI, A. VACCA, and P. GANS. Talanta, **21**, 53 (1974).
9. J. S. COLEMAN, L. P. VARGA, and S. H. MASTIN. Inorg. Chem. **9**, 1015 (1970).
10. W. E. GROVE. Brief numerical methods. Prentice-Hall, London. 1966.
11. N. GAYED. Master Dissertation. University of Alexandria. 1974.
12. M. S. EL-EZABY, N. M. MOUSSA, and S. FAREED. Unpublished results.

Ammonium fluorolanthanates: solid state synthesis, infrared spectral and X-ray diffraction data

KRISHNAN RAJESHWAR AND ETALO A. SECCO[1]

Department of Chemistry, St. Francis Xavier University, Antigonish, N.S., Canada B2G 1C0

Received March 4, 1977

KRISHNAN RAJESHWAR and ETALO A. SECCO. Can. J. Chem. **55**, 2620 (1977).

Solid state synthesis of thirteen ammonium fluorolanthanates is reported. Two main types of fluorolanthanates appeared in the primary synthesis reaction, *viz.* NH_4LnF_4 and $(NH_4)_3Ln_2F_9$.

The final decomposition product of the fluorolanthanates is LnF_3 with $NH_4Ln_2F_7$ appearing as an intermediate in $(NH_4)_3Ln_2F_9$ decomposition.

Infrared absorption spectra and X-ray diffraction data for the stable fluorolanthanates are presented.

KRISHNAN RAJESHWAR et ETALO A. SECCO. Can. J. Chem. **55**, 2620 (1977).

On rapporte la synthèse à l'état solide de 13 fluorolanthanates d'ammonium. Il semble qu'il y a deux types principaux de fluorolanthanates qui apparaissent dans la réaction primaire de synthèse soit NH_4LnF_4 et $(NH_4)_3Ln_2F_9$.

Le produit de décomposition final des fluorolanthanates est LnF_3 alors que $NH_4Ln_2F_7$ apparait comme un intermédiaire dans la décomposition de $(NH_4)_3Ln_2F_9$.

On présente des spectres d'absorption infrarouge et des données de diffraction de rayons-X pour les fluorolanthanates stables.

[Traduit par le journal]

Introduction

Ammonium fluorolanthanate is a stable source of anhydrous lanthanide fluoride (1); also it is a member of a family of compounds exhibiting the novel property of an "up-converter" phosphor (2).

The synthesis of ammonium fluorolanthanate in liquid medium has been reported (1, 3): aqueous solution precipitation yields the hydrate while attempts to obtain the anhydrous compounds in non-aqueous media have not been successful. Recently the feasibility of "dry method" synthesis of anhydrous fluorolanthanate, *viz.* solid state reaction of La_2O_3 and NH_4F had been shown (4). This paper is a more comprehensive report on the "dry method" synthesis of a new series of ammonium fluorolanthanates along with their physico-chemical and structural properties. An attempt is made to correlate the observed trends in behavior with lanthanide ion size.

Experimental

La_2O_3, Pr_2O_3, Sm_2O_3, Gd_2O_3, Dy_2O_3, and Yb_2O_3 were supplied by Alfa Inorganics Inc., MA, U.S.A. while Nd_2O_3, Eu_2O_3, Tb_2O_3, Ho_2O_3, Tm_2O_3, Lu_2O_3, and Y_2O_3 were obtained from American Potash and Chemical Corp., IL, U.S.A.; the stated purities ranged from 99.9% to 99.999%. Each oxide was ignited to 800°C before using; no thermal effect was observed up to 850°C in the DTA heating trace after ignition. NH_4F was Fisher Certified grade.

Each Ln_2O_3–NH_4F reaction mixture was thoroughly mixed and ground in a mortar. An excess of NH_4F, 15:1, was used to ensure the fluorolanthanate with the highest NH_4F:LnF_3 ratio expected. The mixture contained in a covered Pt crucible was heated in a sealed oven, whose temperature was controlled within ± 1°C, in the range 130–150°C for a period 1–3 days. The progress of the reaction was noted by monitoring the weight loss as a function of anneal time. Completion of reaction was indicated by a gravimetric arrest and the absence of any property (X ray, DTA, etc.) characteristic of the reactants. This gravimetric value was compared with the theoretical value from the expected reaction scheme. The validity of the reaction scheme was confirmed by the decomposition behavior of the isolated intermediate compounds and the internal consistency of the experimental results.

Thermal analyses (DTA, TG, DTG) were done with the instrumentation and platinum-ware already described (5, 6). X-Ray powder diffraction patterns were obtained according to the procedure reported (7). Infrared spectra of the samples were recorded on Perkin-Elmer Model-180 instrument using Nujol and fluorocarbons as mulling agents (8).

Results

The observed and theoretical quantitative results for the various fluorolanthanates are tabulated in Table 1.[2] From these results the

[1]To whom correspondence should be addressed.

[2]Photocopies of Tables 1, 2, and 3 may be obtained, at a nominal charge, from the Depository of Unpublished Data, CISTI, National Research Council of Canada, Ottawa, Canada K1A 0S2.

reactions may be classified into two groups:

Group A

[1] $Ln_2O_{3(s)} + nNH_4F_{(s)} \rightarrow 2NH_4LnF_{4(s)} + (n-2)NH_{3(g)} + (n-8)HF_{(g)} + 3H_2O_{(g)}$

where Ln = Pr, Nd, Sm, Eu, Gd, and Tb for $n \geq 8$;

Group B

[2] $Ln_2O_{3(s)} + nNH_4F_{(s)} \rightarrow (NH_4)_3Ln_2F_{9(s)} + (n-3)NH_{3(g)} + (n-9)HF_{(g)} + 3H_2O_{(g)}$

where Ln = Dy, Ho, Er, Tm, Yb, Lu, and Y for $n \geq 9$.

In addition to the above reaction equations, the unusual behavior of the La_2O_3–NH_4F reaction is to be noted where the stable solid product is a 1:1 mixture of NH_4LaF_4 and LaF_3 which results from the disproportionation of the unstable intermediate $NH_4La_2F_7$, *viz.*

[3*a*] $La_2O_{3(s)} + nNH_4F_{(s)} \rightarrow NH_4La_2F_{7(s)} + (n-1)NH_{3(g)} + (n-7)HF_{(g)} + 3H_2O_{(g)}$

for $n \geq 7$, and

[3*b*] $NH_4La_2F_{7(s)} \rightarrow NH_4LaF_{4(s)} + LaF_{3(s)}$

Thermal Analyses

Group A

The results on NH_4LnF_4 compounds, Table 2, are placed with the Depository of Unpublished Data.[2] NH_4PrF_4 is described below as a typical member.

DTA, TG, and DTG curves for NH_4PrF_4 are given in Fig. 1*A*, traces *a*, *b*, and *c*, respectively. A single step endothermic decomposition is observed, *i.e.*

[4] $NH_4PrF_{4(s)} \rightarrow PrF_{3(s)} + NH_{3(g)} + HF_{(g)}$

The calculated weight loss of 15.8% agrees with the observed 16.0%. The solid product PrF_3 was confirmed by its characteristic X-ray diffraction (9*a*).

DTA, TG, and DTG traces for the La compound are given in Fig. 1*B*. The DTA trace reveals two endothermic effects assigned to [3*b*] and [3*c*],

[3*c*] $NH_4LaF_{4(s)} \rightarrow LaF_{3(s)} + NH_{3(g)} + HF_{(g)}$

The TG heating curve of the unstable intermediate showed a single step [3*c*] since [3*b*] does not involve a weight change. The arrest in the isothermal–time gravimetric experiments corresponded to 38.7% weight loss which is consistent with the loss of 38.4% calculated for $n = 10$ according to [3*a*]. The observed weight loss of 8.2% agrees with the calculated loss of 8.6% from [3*c*].

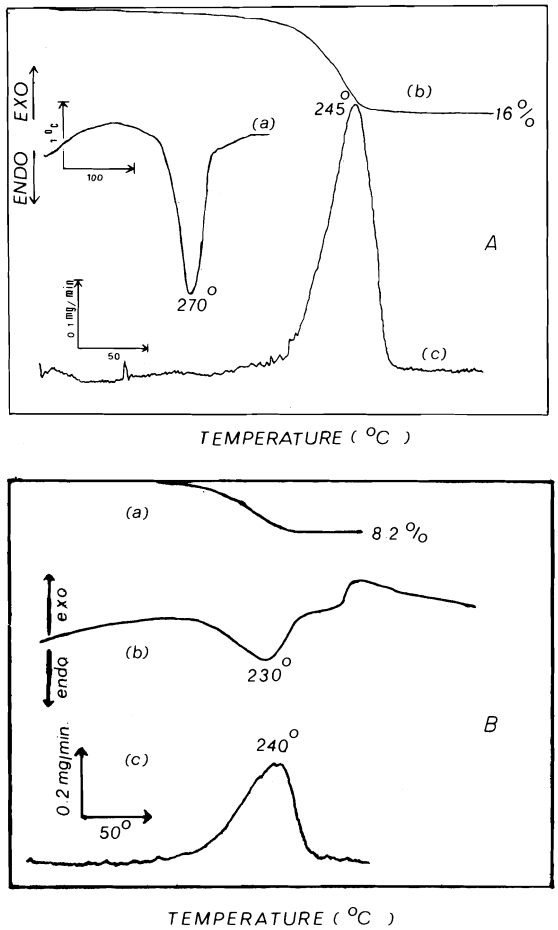

FIG. 1. (*A*) Thermal analyses traces for NH_4PrF_4; (*B*) thermal analyses traces for $NH_4LaF_4 \cdot LaF_3$.

Group B

The experimental data on $(NH_4)_3Ln_2F_9$ and $NH_4Ln_2F_7$ compounds, Table 3, are placed with the Depository of Unpublished Data.[2] The dysprosium compound is described below as representative of this group.

Figure 2*A* includes the DTA, trace *a*, TG, trace *b*, and DTG, trace *c* for $(NH_4)_3Dy_2F_9$. Two step decomposition is observed in accordance with [5*a*] and [5*b*],

[5*a*] $(NH_4)_3Dy_2F_{9(s)} \rightarrow NH_4Dy_2F_{7(s)} + 2NH_{3(g)} + 2HF_{(g)}$

[5*b*] $NH_4Dy_2F_{7(s)} \rightarrow 2DyF_{3(s)} + NH_{3(g)} + HF_{(g)}$

Heating $(NH_4)_3Dy_2F_9$ at 230°C permitted the

TABLE 4. Infrared absorption frequencies of NH_4LnF_4 compounds (cm^{-1})[a]

Compound	NH_4^+					LnF_6^{2-}	
	ν_4	$\nu_4 + \nu_6$	$2\nu_4$	$\nu_2 + \nu_4$	ν_3	ν_4	ν_3
NH_4LaF_4	1420(sp) 1455(sp) 1480(sp)	2100(w)	2890(sh)	3000(s)	3160(vs,b)	300(w)	350(m) 500(m)
NH_4PrF_4	1380(s) 1430(s) 1530(sp)	2320(m)	2960(vb)	3160(s)	3280(s)	280(sp)	520(w)
NH_4NdF_4	1380(s) 1440(s) 1520(sh)	2300(m)	2920(b)	3160(s)	3280(s)	280(sp)	420(sp) 500(sh)
NH_4SmF_4	1420(sp) 1430(sp) 1460(sp)	2300(m)	2940(s)	3180(s)	3230(vs)	270(w) 330(w)	530(sh)
NH_4EuF_4	1410(sp) 1435(sp) 1470(sp)	2080(w) 2300(m)	2900(s)	3040(s)	3180(s)	280(sp) 350(s)	500(sh)
NH_4GdF_4	1410(sp) 1430(sp) 1470(sp)	2100(w) 2300(m)	2920(s)	3040(s)	3180(s)	280(sp) 290(sp) 300(sp)	350(s) 400(s) 500(sh)
NH_4TbF_4	1410(sp) 1435(sp) 1470(sp)	2100(w) 2300(m)	2900(s)	3040(s)	3200(s)	280(sp) 290(sp) 300(sp)	350(s) 520(w)
NH_4BF_4[b]	1431	—	—	—	3332	—	—
NH_4FeF_4[c]	1425	1750	2850	3080	3195	500	575
NH_4AlF_4[c]	1435	1800	2905	3120	3230	537	610

[a]vs, very strong; s, strong; m, medium; w, weak; b, broad; sh, shoulder; sp, sharp.
[b]Data taken from ref. 12.
[c]Data taken from ref. 14.

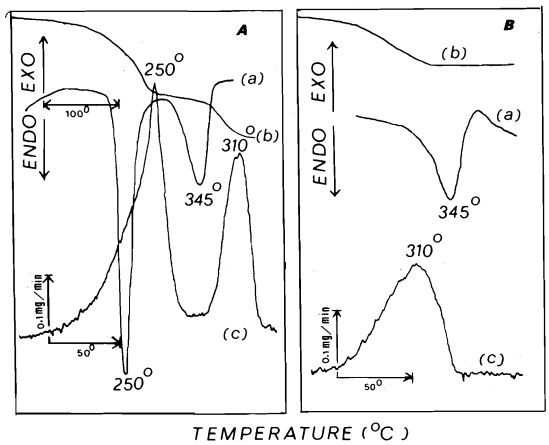

FIG. 2. (*A*) Thermal analyses traces for $(NH_4)_3Dy_2F_9$; (*B*) thermal analyses traces for $NH_4Dy_2F_7$.

isolation of $NH_4Dy_2F_7$. Thermal analyses traces on $NH_4Dy_2F_7$, Fig. 2*B*, confirm reaction [5*b*]. DyF_3 was confirmed by X-ray powder diffraction (9*b*).

There was no evidence for the postulated ammine intermediates (1), *viz.* $YF_3 \cdot \frac{1}{2}NH_3$ and $ErF_3 \cdot \frac{1}{2}NH_3$, during the thermal decomposition of $(NH_4)_3Y_2F_9$ and $(NH_4)_3Er_2F_9$, respectively.

Infrared Spectral Data

The infrared spectral results for NH_4LnF_4, $(NH_4)_3Ln_2F_9$, and $NH_4Ln_2F_7$ are presented in Tables 4, 5, and 6, respectively. The number of active modes and their absorption frequencies display an internal consistency within each series. The assignments are based on the data of known ammonium fluorometallates.

The sequence of spectra for each fluorolanthanate, on stepwise heating to its decomposition temperature, reveals the progressive disappearance of bands characteristic of NH_4^+ leading to the final spectrum of Ln—F band characteristic of LnF_3.

X-Ray Diffraction Data

The X-ray powder diffraction data for NH_4LnF_4, $(NH_4)_3Ln_2F_9$, and $NH_4Ln_2F_7$ are tabulated in Tables 7, 8, and 9, respectively. The

TABLE 5. Infrared absorption frequencies of $(NH_4)_3Ln_2F_9$ compounds (cm^{-1})[a]

	NH_4^+					LnF_6^{2-}	
Compound	ν_4	$\nu_4 + \nu_6$	$2\nu_4$	$\nu_2 + \nu_4$	ν_3	ν_4	ν_3
$(NH_4)_3Dy_2F_9$	1420(s) 1470(s)	2120(m)	2900(vb)	—	3200(vs)	270(w)	560(m)
$(NH_4)_3Ho_2F_9$	1370(s) 1450(sp)	2180(w) 2320(m)	2920(s)	3060(s)	3200(s)	270(w) 350(w)	540(w)
$(NH_4)_3Er_2F_9$	1390(s) 1460(s)	2300(m)	2920(s)	3060(s)	3200(s)	280(w) 330(m)	540(w)
$(NH_4)_3Tm_2F_9$	1400(b) 1450(m)	2140(w) 2300(w)	2900(s)	3060(s)	3200(s)	280(w) 330(w)	510(m) 550(m)
$(NH_4)_3Yb_2F_9$	1420(s) 1460(sp) 1480(sh)	2120(w) 2190(w) 2320(m)	2920(s)	3080(s)	3200(s)	280(w) 330(w)	550(vw)
$(NH_4)_3Lu_2F_9$	1400(sp) 1420(sp) 1460(sp) 1480(sh)	2300(s)	2490(s)	3080(vs)	3200(s)	280(w) 330(w) 370(m)	550(b)
$(NH_4)_3Y_2F_9$	1400(sp) 1445(sp) 1460(sp) 1475(sp)	2150(m) 2300(m)	2900(s)	3060(vs)	3200(s)	280(w) 330(w)	550(w)
$(NH_4)_3ZrF_7$[b]	1418(s)	2330(w)	2900(sh)	3077(sh)	3226(s)	—	—
$NH_4ZrF_5 \cdot H_2O$[c]	1408(sh) 1429(s)	—	2915(sh)	3106(sh)	3226(s)	—	—
$(NH_4)_3Y_2F_9 \cdot H_2O$[d]	1403(s) 1427(s) 1463(m) 1471(m)	—	2900(m)	3062(s)	3188(m,b)	292(s) 321(s) 354(s)	422(w) 451(w)

[a]vs, very strong; s, strong; m, medium; w, weak; b, broad; sh, shoulder; sp, sharp.
[b]Data taken from ref. 15.
[c]Data taken from ref. 16.
[d]Data taken from ref. 1.

TABLE 6. Infrared absorption frequencies of $NH_4Ln_2F_7$ compounds (cm^{-1})[a]

	NH_4^+					LnF_6^{2-}	
Compound	ν_4	$\nu_4 + \nu_6$	$2\nu_4$	$\nu_2 + \nu_4$	ν_3	ν_4	ν_3
$NH_4Dy_2F_7$	1400(s)	2300(s)	2860(sh)	3070(s)	3240(vs)	280(m) 360(m)	470(b) 550(s)
$NH_4Ho_2F_7$	1430(s)	2180(sh) 2300(s)	2860(sh)	3080(s)	3280(vs)	280(w) 370(m)	420(w) 520(m)
$NH_4Er_2F_7$	1370(sh) 1400(s)	2190(sh) 2300(s)	2840(sh)	3060(s)	3260(vs)	280(s) 370(s)	520(s)
$NH_4Tm_2F_7$	1420(s)	2320(s)	2840(s)	3080(b)	3260(vs)	280(s) 375(s)	530(s)
$NH_4Yb_2F_7$	1400(s)	2180(sh) 2300(s)	—	—	3240(m)	280(s) 360(s)	530(m)
$NH_4Lu_2F_7$	1420(s)	2100(sh) 2180(sh) 2320(s)	—	3080(sh)	3280(s)	290(s) 380(s)	530(s)
$NH_4Y_2F_7$	1420(s)	2320(m)	2850(sh)	3100(sh)	3150(vs)	285(s) 370(s)	520(s)

[a]vs, very strong; s, strong; m, medium; w, weak; b, broad; sh, shoulder; sp, sharp.

TABLE 7. X-Ray diffraction data for NH_4LnF_4 compounds[a]

NH_4PrF_4		NH_4NdF_4		NH_4SmF_4		NH_4EuF_4		NH_4GdF_4		NH_4TbF_4	
d(Å)	I/I_0	d(Å)	I/I_0	d(Å)	I/I_0	d(Å)	I/I_0	d(Å)	I/I_0	d(Å)	I/I_0
8.35	100	8.27	100	8.59	100	8.35	100	8.35	86	8.51	100
5.01	88	4.98	80	5.54	60	5.54	59	5.57	69	5.54	61
3.48	72	3.45	77	4.19	65	4.14	53	4.19	65	4.14	58
3.19	99	3.16	98	3.70	65	3.65	65	3.69	73	3.64	75
3.14	65	3.12	75	3.19	97	3.16	96	3.16	100	3.13	93
2.94	32	2.92	46	2.97	67	2.95	64	2.94	72	2.93	70
2.814	29	2.797	36	2.417	54	2.398	55	2.398	68	2.380	63
2.550	34	2.530	38	2.117	54	2.108	62	2.102	50	2.102	55
2.508	43	2.500	51	—	—	2.027	53	2.027	59	2.018	57
2.221	65	2.206	67	2.005	51	2.005	53	2.005	63	1.989	57
2.085	31	2.080	38	1.838	51	1.829	53	1.824	63	1.817	58
2.022	32	2.010	41	1.781	57	1.775	56	1.760	66		
1.961	51	1.949	57								
1.926	35	1.918	41								
1.911	40	1.888	43								
1.870	37	1.859	39								
1.824	43	1.811	48								
1.784	29	1.775	36								

[a]CuKα radiation.

TABLE 8. X-Ray diffraction data for $(NH_4)_3Ln_2F_9$ compounds[a]

$(NH_4)_3Dy_2F_9$		$(NH_4)_3Ho_2F_9$		$(NH_4)_3Er_2F_9$		$(NH_4)_3Tm_2F_9$		$(NH_4)_3Yb_2F_9$		$(NH_4)_3Lu_2F_9$		$(NH_4)_3Y_2F_9$	
d(Å)	I/I_0	d(Å)	I/I_0	d(Å)	I/I_0	d(Å)	I/I_0	d(Å)	I/I_0	d(Å)	I/I_0	d(Å)	I/I_0
7.25	100	7.25	100	7.25	100	7.14	100	7.19	100	7.19	100	7.20	100
6.42	37	6.38	31	6.30	32	6.24	25	6.24	24	6.24	18	6.34	12
5.80	42	5.83	31	5.83	31	5.76	25	5.76	24	5.76	19	5.92	10
5.10	57	5.10	47	5.10	54	5.04	44	5.10	38	5.04	57	5.10	34
—	—	3.98	20	3.98	18	3.93	18	3.95	13	3.91	15	—	—
3.62	32	3.60	25	3.62	27	3.60	25	3.60	22	3.60	40	3.62	12
—	—	3.51	27	3.48	30	3.47	26	3.47	22	3.44	22	3.48	15
3.40	52	3.40	50	3.41	50	3.38	44	3.39	43	3.39	68	3.40	30
3.31	81	3.30	78	3.29	79	3.26	75	3.26	72	3.25	82	3.29	75
3.15	51	3.14	47	3.13	45	3.11	44	3.11	40	3.10	50	3.13	25
3.08	37	3.08	28	3.07	28	3.06	25	3.05	21	3.04	27	3.07	9
3.02	49	3.01	36	3.00	40	2.98	38	2.98	36	2.96	59	2.99	25
2.89	36	2.89	25	2.875	27	2.857	23	2.857	21	2.849	22	—	—
2.780	40	2.780	28	2.771	29	2.747	26	2.747	25	2.747	32	2.774	9
2.691	30	2.675	19	2.675	19	2.667	18	2.660	15	2.660	19	2.675	7
2.600	39	2.592	25	2.592	22	2.571	20	2.571	19	2.564	21	2.592	9
2.410	40	2.417	28	2.410	29	2.392	25	2.398	23	2.398	34	2.360	9
—	—	—	—	2.338	21	2.332	21	2.327	18	2.332	19	—	—
2.309	39	2.309	27	2.309	33	2.298	25	2.298	24	2.292	32	2.309	20
—	—	2.275	23	2.270	22	2.259	19	2.259	17	2.253	18	2.276	6
—	—	—	—	2.191	22	2.181	18	2.171	16	2.171	13	—	—
2.151	42	2.151	34	2.142	32	2.132	30	2.132	24	2.128	19	2.148	24
2.067	37	2.067	20	2.062	26	2.058	24	2.054	22	2.054	22	2.067	17
2.005	42	1.997	33	1.993	35	1.977	30	1.969	23	1.965	29	1.996	24
1.934	34	—	—	1.918	23	1.907	20	1.899	18	1.895	24	1.920	8
1.838	49	—	—	1.838	37	1.829	36	1.828	33	1.824	49	1.839	24
—	—	—	—	—	—	1.771	25	1.768	21	—	—	1.780	9
—	—	—	—	—	—	1.743	23	1.743	19	1.734	25	1.750	9
—	—	—	—	—	—	—	—	1.698	20	1.698	22	—	—
—	—	—	—	—	—	—	—	1.642	19	—	—	—	—

[a]CuKα radiation.

TABLE 9. X-Ray diffraction data for $NH_4Ln_2F_7$ compounds[a]

$NH_4Dy_2F_7$		$NH_4Ho_2F_7$		$NH_4Er_2F_7$		$NH_4Tm_2F_7$		$NH_4Yb_2F_7$		$NH_4Lu_2F_7$		$NH_4Y_2F_7$	
d(Å)	I/I_0	d(Å)	I/I_0	d(Å)	I/I_0	d(Å)	I/I_0	d(Å)	I/I_0	d(Å)	I/I_0	d(Å)	I/I_0
6.71	72	6.71	63	6.71	59	6.71	53	6.71	47	6.71	35	6.71	58
5.99	90	5.99	88	5.95	82	5.91	74	5.87	76	5.83	81	5.97	82
4.48	63	4.48	49	4.46	45	4.46	36	4.44	37	4.44	36	4.47	35
3.44	58	3.45	39	3.42	37	3.42	40	3.40	33	3.40	32	3.43	31
3.26	100	3.26	100	3.25	100	3.24	100	3.22	100	3.22	100	3.26	100
3.00	66	3.00	49	2.99	45	2.98	45	2.97	43	2.97	46	2.99	40
2.94	63	2.96	45	2.92	46	2.91	47	2.90	49	2.89	50	2.93	24
2.739	55	2.739	31	2.731	27	2.715	25	2.715	24	2.707	21	2.739	15
2.578	66	2.571	45	2.564	45	2.557	44	2.550	40	2.543	36	2.576	24
2.287	50	2.287	28	2.287	22	2.281	18	2.270	15	2.264	14	2.297	13
2.227	54	2.227	26	2.216	21	2.201	21	2.197	15	2.191	13	2.210	13
2.108	59	2.104	39	2.094	37	2.085	36	2.080	33	2.071	32	2.100	31
1.956	79	1.953	73	1.949	71	1.937	71	1.933	68	1.926	65	1.950	78
		1.859	31	1.845	25	1.845	27	1.838	22	1.824	17	1.850	20
		1.781	31	1.775	32	1.768	27	1.762	24	1.759	28	1.784	22

[a]CuKα radiation.

number of active planes and their distances exhibit internal consistency within each series. However, the NH_4LnF_4 series reveals a distinction between Ln = Pr, Nd and Ln = Sm, Eu, Gd, Tb. Indexing the X-ray diffraction data by the Hesse–Lipson method (17, 18) shows a hexagonal system fit for NH_4NdF_4 and NH_4PrF_4 with unit cell dimensions a = 9.56 Å and c = 12.37 Å and a = 9.61 Å and 12.45 Å, respectively. On the other hand, NH_4SmF_4 and NH_4GdF_4 were indexed to the cubic system with a = 11.80 Å and 11.76 Å, respectively.

The close similarity of the diffraction data for the $(NH_4)_3Ln_2F_9$ series suggests these compounds to be isostructural. $(NH_4)_3Yb_2F_9$, selected as a representative member of this series, was indexed to the monoclinic system with unit cell dimensions a = 7.11 Å; b = 7.31 Å; and c = 12.54 Å.

The diffraction patterns for the $NH_4Ln_2F_7$ group of compounds also reveal an internal consistency associated with structural isotypes. The indexing of the diffraction data for $NH_4Dy_2F_7$, selected as representative of this group, showed the best fit for a cubic system with a = 13.40 Å.

Discussion

The members in the ionic radius range 1.35–1.55 Å, La—Tb, formed only NH_4LnF_4 compounds; the members from Dy to Y, ionic radius 1.58–1.69 Å, yielded $(NH_4)_3Ln_2F_9$ which in turn disproportionated to the corresponding $NH_4Ln_2F_7$. Our failure to detect certain $(NH_4)_3Ln_2F_9$ members, $(NH_4)_2Ln_2F_{11}$ and $NH_4Ln_3F_{10}$ series reported elsewhere (1, 10) may be explained in terms of (*i*) the higher solid synthesis temperature exceeded the compound stability temperature and (*ii*) the stabilizing effect of the solvent on specific compound formation in wet synthesis.

The known ammonium fluorolanthanates along with the ionic radius parameter ρ are listed in Table 10; ρ is defined as $r_{NH_4^+}/r_{M^{3+}}$, where $r_{NH_4^+}$ is the constant NH_4^+ radius and M^{3+} is the variable tervalent metal radius. The table reveals that lanthanides with ρ < 1.55 can form

TABLE 10. Correlation of cation size with formation of ammonium fluorolanthanates(III)

Ln^{3+}	$r_{NH_4^+}/r_{Ln^{3+}}$	$NH_4F:LnF_3$ ratio in compound
La	1.350	1:1,[a] 1:2,[b] 3:2[b]
Pr	1.412	1:1,[a] 3:2[b]
Nd	1.437	1:1[a]
Sm	1.483	1:1,[a] 1:2,[b] 3:2[b]
Eu	1.505	1:1[a]
Gd	1.525	1:1[a]
Tb	1.549	1:1[a]
Dy	1.575	1:2,[a] 2:3,[b] 3:2[a]
Ho	1.600	1:2,[a] 2:3,[b] 3:2,[a] 1:3[c]
Y	1.607	1:2,[a] 2:3,[b] 3:2,[a] 1:3[b]
Er	1.623	1:2,[a] 2:3,[b] 3:2,[a] 1:3[c]
Tm	1.646	1:2,[a] 3:2,[a] 1:3[c]
Yb	1.667	1:2,[a] 3:2[a]
Lu	1.686	1:2,[a] 3:2[a]

[a]This work.
[b]Reference 1.
[c]Reference 10.

TABLE 11. Correlation of cation size with formation of ammonium fluorometallates(III)

M^{3+}	$r_{NH_4^+}/r_{M^{3+}}$	$NH_4F:MF_3$ ratio in compound
Bi	1.490	1:1[a]
In	1.765	1:1, 1:2, 2:3, 5:3, 1:3[b]
Sc	1.959	1:1, 3:1[c]
Fe	2.234	1:1, 3:1[d]
Ga	2.307	1:1, 3:1[e]
Al	2.804	1:1, 3:1[d]
B	6.217	1:1[f]

[a]Reference 19.
[b]Reference 20.
[c]Reference 21.
[d]Reference 14.
[e]Reference 22.
[f]Reference 12.

$NH_4F:LnF_3$ compounds in ratios of 1:1, 1:2, and 3:2. For lanthanides with $1.55 < \rho < 1.69$, a wider range of compounds, excluding 1:1 ratio, is in evidence. Table 11 lists other ammonium fluorometallates for comparison purposes. In^{3+} with $\rho = 1.77$ exhibits the widest range of compounds including 1:1 type. Bi^{3+} and B^{3+} with ρ values of 1.49 and 6.22, respectively, form only 1:1 fluorometallate whereas the remaining M^{3+} elements with $1.96 < \rho < 2.81$ form 1:1 and 3:1 compounds. Two regions of stability for the 1:1 compound in NH_4F–MF_3 systems are noted, *viz.* $1.35 < \rho < 1.55$ and $\rho > 1.77$; the 3:1 compound is observed only for $\rho > 1.77$.

Thoma (11) predicted $ALnF_4$ formation for $1.40 > \rho > 0.77$ and A_3LnF_6 formation for $\rho > 1.43$ in AF_3–LnF_3 systems (A = alkali element). Obviously, the ammonium fluorometallates do not fit the simplified prediction by Thoma: hydrogen bonding from NH_4^+ could be the critical factor responsible for the extensive range of stable composition in ammonium fluorometallates.

The peak decomposition temperatures of the fluorolanthanates observed in this study along with NH_4ScF_4 and NH_4FeF_4 are plotted against corresponding ρ values in Fig. 3. The thermal stabilities of NH_4LnF_4 and $NH_4Ln_2F_7$ rise with increasing ρ value whereas $(NH_4)_3Ln_2F_9$ becomes less stable at higher ρ values. The higher stability of $NH_4Ln_2F_7$ relative to its parent $(NH_4)_3Ln_2F_9$ is evident. The results also support the failure to observe NH_4LnF_4 as a stable intermediate in the decomposition of its parent $NH_4Ln_2F_7$. However, extrapolation of the linear dependence of the $NH_4Ln_2F_7$ series to $NH_4La_2F_7$ suggests that NH_4LaF_4 can be a stable product of $NH_4La_2F_7$ decomposition as observed.

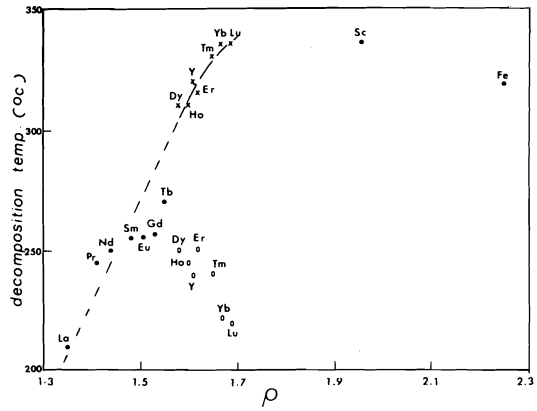

FIG. 3. Plot of peak decomposition temperatures of fluorolanthanates versus ρ, ionic radius parameter.

Hydrogen bonding in the ammonium fluorolanthanates is indicated in the infrared spectra by the splitting of the triply degenerate ν_4 of NH_4^+, the multiplicity of absorption peaks in 2900–3300 cm^{-1} regions and the appearance of the $(\nu_4 + \nu_6)$ combination band (12). By analogy with Fe and Al analogs (13, 14), the ammonium fluorolanthanate structure may be visualized as layers of LnF_6 octahedra (built up by mutual sharing of corners and edges) with interleaving layers of NH_4 groups. The splitting of ν_3 and ν_4 modes in the octahedral LnF_6^{3-} suggests a distorted configuration. It is to be noted that the triply degenerate ν_4 does not split in $NH_4Ln_2F_7$. A detailed discussion of these structures must await single-crystal structural data.

NOTE ADDED IN PROOF: The assignment of 2300 cm^{-1} frequency to the combination $\nu_4 + \nu_6$ was questioned by one referee. We suggest therefore the combination band is more likely $\nu_2 + \nu_6$, consistent with ref. 15.

Acknowledgments

The authors are grateful to the National Research Council of Canada for financial support, and to Dr. M. Natarajan, McMaster University for assistance in indexing the diffraction data.

1. R. C. RUSSO and H. M. HAENDLER. J. Inorg. Nucl. Chem. **36**, 763 (1974).
2. A. A. HEWES and J. F. SARVER. Phys. Rev. **182**, 427 (1969).
3. L. R. BATSANOVA. Izv. Sib. Otd. Akad. Nauk SSSR,

Ser. Khim. Nauk, 83 (1963); Chem. Abstr. **59**, 13578 (1963).
4. G. ADACHI, B. FRANCIS, K. RAJESHWAR, E. A. SECCO, and J. C-S. WONG. 8th International Symposium on Reactivity of Solids, Gothenburg (1976).
5. K. RAJESHWAR and E. A. SECCO. Can. J. Chem. **54**, 2509 (1976).
6. O. K. SRIVASTAVA and E. A. SECCO. Can. J. Chem. **45**, 579 (1967).
7. E. A. SECCO. Can. J. Chem. **42**, 2143 (1964).
8. K. C. PATIL and E. A. SECCO. Can. J. Chem. **53**, 2426 (1975).
9. X-Ray Powder Data File, Am. Soc. Testing Materials Index (*a*) No. 6-0325; (*b*) No. 5-0400.
10. A. ZALKIN and D. H. TEMPLETON. J. Am. Chem. Soc. **75**, 2453 (1953).
11. R. E. THOMA. Inorg. Chem. **1**, 220 (1962).
12. T. C. WADDINGTON. J. Chem. Soc. 4340 (1958).
13. A. TRESSAUD, J. PORTIER, R. DEPAPE, and P. HAGENMULLER. J. Solid State Chem. **2**, 269 (1970).
14. D. B. SHINN, D. S. CROCKET, and H. M. HAENDLER. Inorg. Chem. **5**, 1927 (1965).
15. P. W. SMITH, R. STOESSIGER, and A. G. TURNBULL. J. Chem. Soc. 3013 (1968).
16. H. HULL and A. G. TURNBULL. J. Inorg. Nucl. Chem. **29**, 2903 (1967).
17. R. HESSE. Acta Crystallogr. **1**, 200 (1948).
18. H. LIPSON. Acta Crystallogr. **2**, 43 (1949).
19. H. M. HAENDLER, F. A. JOHNSON, and D. S. CROCKETT. J. Am. Chem. Soc. **80**, 2662 (1958).
20. J. C. CHAMPARNAND-MESJAND, J. GRANNEC, and B. GAUDREAU. C. R. Acad. Sci., Ser. C. **278**, 171 (1974).
21. B. N. IVANOV-ERMIN, T. N. SUSANINA, and A. I. EZHOV. Zh. Neorg. Khim. **12**, 23 (1967).
22. I. V. TANANNEV and T. B. VOROTILINA. Russ. J. Inorg. Chem. **14**, 1354 (1969).

Study of NH_4EuF_4 in solid state reaction Eu_2O_3–NH_4F. Thermal analyses, calorimetry, and decomposition kinetics

KRISHNAN RAJESHWAR AND ETALO A. SECCO[1]

Department of Chemistry, St. Francis Xavier University, Antigonish, N.S., Canada B2G 1C0

Received March 4, 1977

KRISHNAN RAJESHWAR and ETALO A. SECCO. Can. J. Chem. **55**, 2628 (1977).

The solid state reaction Eu_2O_3–NH_4F leading to the formation of NH_4EuF_4 was studied by thermal analyses and X-ray diffraction.

The heat of decomposition of NH_4EuF_4 and the kinetics of thermal decomposition of NH_4EuF_4 are reported.

KRISHNAN RAJESHWAR et ETALO A. SECCO. Can. J. Chem. **55**, 2628 (1977).

On a étudié, à l'aide d'analyses thermiques et de diffraction de rayons-X, la réaction à l'état solide de Eu_2O_3–NH_4F conduisant à la formation de NH_4EuF_4.

On rapporte l'enthalpie de décomposition de NH_4EuF_4 et sa cinétique de décomposition thermique.

[Traduit par le journal]

Introduction

The formation of ammonium fluorolanthanate as a stable intermediate was reported in the solid state reaction of Ln_2O_3–NH_4F which yields LnF_3 as the final product (1, 2). No study has yet been reported on the steps leading to the fluorolanthanate formation and its subsequent mode of decomposition.

This paper contains the results of thermal analyses, calorimetry, and thermal decomposition kinetics on NH_4EuF_4, selected as a typical member of the NH_4LnF_4 series.

Experimental

The Eu_2O_3 used had a stated purity of 99.999% supplied by American Potash and Chemical Corp., West Chicago, IL, U.S.A. and the NH_4F was Fisher Certified grade.

The procedure followed for the synthesis of ammonium tetrafluoreuropiate(III) is described elsewhere (2).

Thermal analyses (DTA, TG, DTG) were done with the instrumentation and Pt-ware already described (2).

The heat of decomposition was determined using the DSC accessory to the duPont 990 Thermoanalyzer module; zinc fusion was used as standard. The specific heats of NH_4EuF_4 and EuF_3, at constant pressure, were determined as a function of temperature using a sapphire disc as standard. Gold sample pans were used in DSC measurements.

X-Ray powder diffraction patterns were obtained according to the procedure reported (3). Infrared spectra of the samples were recorded on Perkin-Elmer Model-180 instrument using Nujol and fluorocarbons as mulling agents (4).

Results and Discussion

The DTA heating trace for 1:10 molar ratio Eu_2O_3:NH_4F, Fig. 1, reveals three endothermic effects. The first endotherm is attributed to overlapping reactions, disproportionation of NH_4F as reported (1, 5), and fluorination of Eu_2O_3, *viz.*

[1*a*] $$n NH_4F_{(s)} \rightleftarrows (n/2)NH_4HF_{2(l)} + (n/2)NH_{3(g)}$$

and

[1*b*] $$Eu_2O_{3(s)} + nNH_4HF_{2(l)} \rightarrow 2NH_4EuF_{4(s)} + (n-2)NH_3 + (n-8)HF_{(g)} + 3H_2O_{(g)}$$

where the symbols *n*, s, l, and g assume their normal usage. The second thermal effect is due to volatilization of unreacted bifluoride, *i.e.*

[2] $$NH_4HF_{2(l)} \leftrightarrows NH_{3(g)} + 2HF_{(g)}$$

which is confirmed by its peak intensity depen-

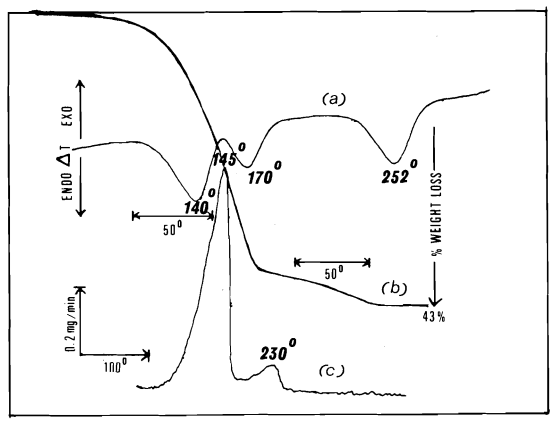

FIG. 1. Thermal analyses traces for 1:10 molar ratio Eu_2O_3:NH_4F mixture.

[1]To whom correspondence should be addressed.

dence on NH_4F excess in the mixture. TG and DTG traces, Fig. 1, exhibit the expected weight losses consistent with the assignments.

The X-ray powder diffraction pattern of the residue after the second endothermic peak, 180°C, is identified with the NH_4EuF_4 pattern (2). The diffraction pattern of the residue after the third endotherm is identified with EuF_3 in the orthorhombic modification (6). Infrared spectra of the residues are also consistent with the identification of NH_4EuF_4 and anhydrous EuF_3 (2) at the appropriate stages in heating. Accordingly, the third endotherm in DTA and the second peak in DTG traces are due to decomposition, *viz.*

[3] $$NH_4EuF_{4(s)} \rightarrow EuF_{3(s)} + NH_{3(g)} + HF_{(g)}$$

Figure 2 presents TG, DTA, and DTG heating traces a, b, and c, respectively, for NH_4EuF_4 prepared under isothermal conditions (2).

The ΔH of decomposition of NH_4EuF_4, reaction 3 in the range 235–265°C, is determined to be 21.82 ± 0.10 kcal/mol. Heat capacity measurements as a function of temperature indicate a heat capacity change of −0.004 kcal/mol deg associated with the decomposition, negligible within limits of the ΔH measurement. Using the literature values (7, 8) for ΔH_f^0 of $NH_{3(g)}$, $HF_{(g)}$, and $EuF_{3(s)}$, that is, −11.04 kcal/mol, −64.80 kcal/mol, and −429 kcal/mol, respectively, the ΔH_f^0 of $NH_4EuF_{4(s)}$ is computed as −526.6 kcal/mol.

The standard ΔH of reaction 1*c* is calculated,

[1*c*] $$Eu_2O_{3(s)} + 8\,NH_4F_{(s)} \rightarrow 2\,NH_4EuF_{4(s)} + 6\,NH_{3(g)} + 3\,H_2O_{(g)}$$

using literature data (9, 10) to be −12.44 kcal. The absence of any exothermic effect in the DTA trace is due to the greater endothermic effect generated by reaction 1*a* with $\Delta H = \sim +16$ kcal. The first endotherm represents, therefore, a net thermal effect. Previous studies on ammonium fluoride – metal fluoride complexes (11) have shown that thermal effects originating with NH_4HF_2 formation frequently overshadow the effect arising from the actual complex formation.

The standard enthalpy change for direct fluorination, reaction 1*d*, *viz.*

[1*d*] $$Eu_2O_{3(s)} + 8\,NH_4F_{(s)} \rightarrow 2\,EuF_{3(s)} + 8\,NH_{3(g)} + 2\,HF_{(g)} + 3\,H_2O_{(g)}$$

shows a large positive value. The standard entropy changes for both [1*c*] and [1*d*] are assumed to be sufficiently positive at the reaction temperature to yield a negative free energy term to favor reaction 1*c*, that is, formation of NH_4EuF_4 intermediate. This interpretation suggests that NH_4EuF_4 resulting from the secondary reaction between EuF_3 and excess NH_4F, *i.e.*

[4] $$EuF_{3(s)} + NH_4F_{(s)} \rightarrow NH_4EuF_{4(s)}$$

is energetically unfavorable.

Thermal Decomposition Kinetics

The isothermal decomposition of ammonium tetrafluoroeuropiate(III) was studied in the range 160–225°C. The experimental fractional decomposition *vs.* time ($\alpha - t$) data were processed through all the known kinetic rate expressions. The $\alpha - t$ data, $\alpha \geq 0.9$ and over the temperature range studied, show the best linear relationship with the contracting-sphere equation, Fig. 3.

[5] $$1 - (1 - \alpha)^{1/3} = kt$$

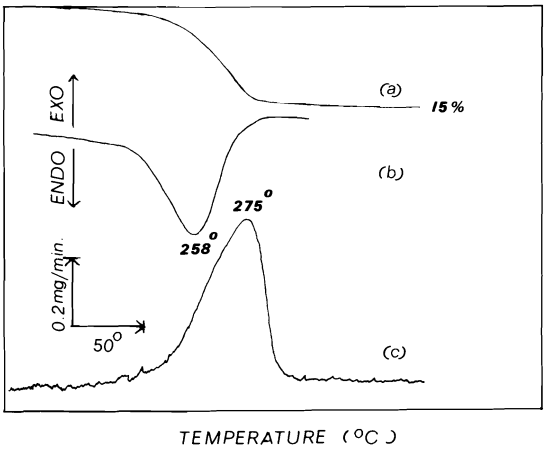

FIG. 2. Thermal analyses traces for NH_4EuF_4.

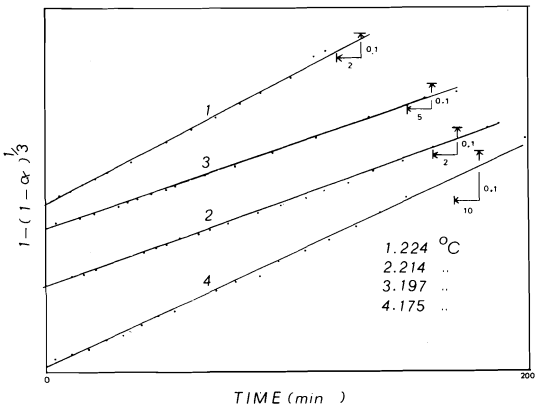

FIG. 3. Plot of $1 - (1 - \alpha)^{1/3}$ *vs.* time.

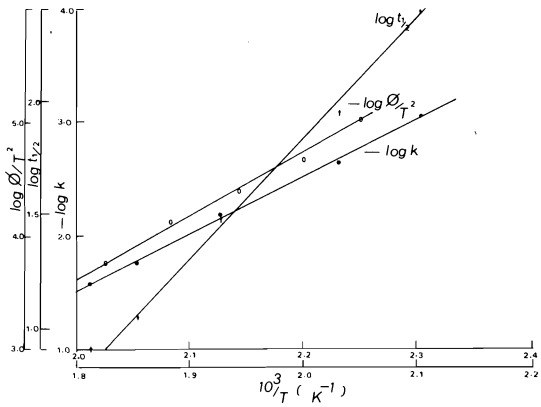

FIG. 4. Plots of log rate parameter *vs.* $10^3/T$ (K).

The activation energy, E_a, of 23 $\pm$ 1 kcal/mol is obtained from the slope of the Arrhenius plot, Fig. 4.

Two additional independent evaluations of E_a, Fig. 4, yield values of 24 $\pm$ 1 kcal/mol, from log $t_{1/2}$ ($t_{1/2}$ is half-life) *vs.* $10^3/T$(K) plot under isothermal conditions, and 26 $\pm$ 2 kcal/mol, from log ϕ/T^2 *vs.* $10^3/T$(K) plot under continuous, non-isothermal heating conditions where T is the peak temperature for the specific heating rate ϕ, 2–50°C/min. The reproducible value for E_a, within experimental limits, obtained by three independent analytical methods establishes a high confidence index for E_a.

The cubic crystal structure of NH_4EuF_4 may be compared with its analogues NH_4FeF_4 and NH_4AlF_4 (12, 13) where layers of EuF_6^- octahedra are interspersed with layers of NH_4^+ groups. The decomposition mode is postulated to proceed via proton-transfer from NH_4^+ to neighboring EuF_6^- resulting in the formation of NH_3 and HF, *i.e.*

[6] $NH_4EuF_{4(1/2\ c)} \rightarrow (NH_3 \ldots HF \ldots EuF_3)_{ad}$

where "1/2 c" refers to a "half-crystal" site on the surface and "ad" refers to surface adsorbed state. The subsequent growth of the product layer of EuF_3 in a three dimensional manner follows. Support for eq. 6 and the proton-transfer step is based on the close correspondence of E_a for NH_4EuF_4 and ammonium perchlorate (14) where it is accepted that a proton-transfer step is operative in the perchlorate.

Acknowledgment

The authors are grateful to the National Research Council of Canada for financial support.

1. G. ADACHI, B. FRANCIS, K. RAJESHWAR, E. A. SECCO, and J. C.-S. WONG. 8th International Symposium on Reactivity of Solids, Gothenberg. 1976.
2. K. RAJESHWAR and E. A. SECCO. Can. J. Chem. This issue.
3. E. A. SECCO. Can. J. Chem. **42**, 2143 (1964).
4. K. C. PATIL and E. A. SECCO. Can. J. Chem. **53**, 2426 (1975).
5. H. REMY. Treatise on inorganic chemistry. Vol. 1. Elsevier, London. 1956. p. 795.
6. X-Ray Powder Data File, Am. Soc. Testing Materials Index No. 5-0535.
7. M. A. MIKHAILOV, D. G. EPOV, V. I. SERGIENKO, E. G. RAKOV, and G. P. SHCHETININA. Russ. J. Inorg. Chem. **18**, 794 (1973).
8. G. I. NOVIKOV and O. G. POLYACHENCK. Russ. Chem. Rev. **33**, 342 (1964).
9. C. E. HOLLEY, JR., E. J. HARBER, JR., and F. B. BAKER. Progress in the science and technology of the rare earths. Vol. 3. *Edited by* L. Eyring. Pergamon Press. 1968. Chapt. 8, p. 389.
10. R. C. WEAST (*Editor*). Handbook of Chemistry and Physics. Chemical Rubber Co. Press, Cleveland, Ohio. 1972.
11. E. G. RAKOV, L. K. MARININA, B. V. GROMOV, and V. A. MINAEV. Russ. J. Inorg. Chem. **16**, 1085 (1971).
12. J. C. CHAMPARNARD-MESJAND, J. GRANNEC, and B. GAUDREAU. C.R. Acad. Sci. Ser. C, **278**, 171 (1974).
13. D. B. SHINN, D. S. CROCKET, and H. M. HAENDLER. Inorg. Chem. **5**, 1927 (1965).
14. P. W. M. JACOBS and H. M. WHITEHEAD. Chem. Rev. **69**, 551 (1969).

Simple electrochemical synthesis of vanadium(II) halides

JACOB J. HABEEB, LYNN NEILSON, AND DENNIS G. TUCK
Department of Chemistry, University of Windsor, Windsor, Ont., Canada N9B 3P4

Received February 28, 1977

JACOB J. HABEEB, LYNN NEILSON, and DENNIS G. TUCK. Can. J. Chem. **55**, 2631 (1977).

Vanadium metal dissolves rapidly in a cell Pt/X_2 in CH_3CN/V (anode) (X = Cl, Br, I) under applied voltages of 5–50 V. The solution phase yields crystalline $VCl_2.2CH_3CN$, $VBr_2.CH_3CN$, or VI_2; the acetonitrile adducts decompose to VX_2 on heating in vacuo. Overall yields of VX_2, based on weight of metal dissolved, are 80–90%.

JACOB J. HABEEB, LYNN NEILSON et DENNIS G. TUCK. Can. J. Chem. **55**, 2631 (1977).

Le vanadium métallique se dissout rapidement dans une cellule Pt/X_2 dans CH_3CN/V (anode) (X = Cl, Br, I) lorsque l'on applique des voltages de 5 à 50 V. De la phase liquide se forment le $VCl_2.2CH_3CN$, $VBr_2.CH_3CN$ ou VI_2 à l'état cristallin; les adduits avec l'acétonitrile se décomposent en VX_2 par chauffage sous vide. Dans chaque cas le rendement global de VX_2, basé sur le poids de métal dissous, est d'environ 80 à 90%.

[Traduit par le journal]

Introduction

Reviews of the chemistry of vanadium show that the lower oxidation states are the least accessible, and the chemistry of vanadium(II) in particular is relatively unexplored (1). Routes to this oxidation state is aqueous solution (2, 3) require the electrolytic or chemical reduction of V^V, V^{IV}, or V^{III}. A number of preparations of anhydrous VCl_2, VBr_2, and VI_2 have been reported (ref. 4, pp. 134–137); these have generally involved reduction of VX_3 with hydrogen at 500°C, the reaction of VX_3 and HX (X = Cl only) at 950°C, or the disproportionation of VX_3 at temperatures above 400°C. We now report that the acetonitrile adducts of VCl_2 and VBr_2 can be prepared in good yield at room temperature by the electrochemical oxidation of vanadium metal in the presence of halogen in acetonitrile solution. The adducts are easily decomposed *in vacuo* to yield the parent dihalides. In the case of iodine, the method yields VI_2 directly. The preparative method is similar to that reported previously for complexes of indium (5), for anionic halogeno complexes of transition metals (6), and for organo-cadmium compounds (7).

Experimental

Materials

Vanadium metal (99.7%) was supplied by Alfa Inorganics in the form of a rod, 5 mm diameter. Acetonitrile (reagent grade) was dried and redistilled before use. Halogens (reagent grade) were used as supplied.

Voltages between 5 and 50 V (dc) were supplied from a Coutant 50/50 power pack, delivering up to 50 V and 0.5 A; any dc unit satisfying these conditions can be used.

Electrochemical Procedure

In a typical experiment, 50 cm^3 acetonitrile containing 10 mg of tetraethylammonium perchlorate and 2–3 g bromine (or iodine) formed the solution phase, which was deoxygenated by bubbling with nitrogen before electrolysis. In the case of chlorine, a stream of gas (~25 cm^3 per min) was bubbled through the solution together with diluent nitrogen. The vanadium anode had a surface area (in contact with the solution) of 1.5 cm^2; the cathode was a coil of platinum wire (1 mm in diameter, 10 cm long). The electrodes were 1–2 cm apart. The voltage and current set out below are those actually observed in our experiments, and would no doubt be affected by changes in solution composition, etc. We have made no attempt to study the effect of such variables on the yield.

Analytical Procedures

Vanadium was determined by measuring the absorption at 450 nm following the addition of hydrogen peroxide (8). A standard solution was prepared by dissolving vanadium metal in acid.

Halogen was determined titrimetrically with potassium thiocyanate/silver nitrate, and by the Oakdale–Thompson method (9).

Results and Discussion

Vanadium(II) Chloride

Vanadium dissolved readily at a voltage of 28 V; the current was maintained at approximately 150 mA for 1 h. The green solution formed in the first 10 min gave way to a dark brown mixture. After expulsion of excess chlorine with nitrogen at the end of the electrolysis, dry ether was added to bring down a dark green precipitate which was dried *in vacuo* for 30 min at 230°C. This compound, $VCl_2.2CH_3CN$ (see Table 1), on further heating (15 min at 350°C) formed the dark brown – black VCl_2. The yield of $VCl_2.2CH_3CN$ (1.8 g) was 90%, based on

TABLE 1. Analytical results for vanadium(II) halides

Compound	Vanadium Found (%)	Vanadium Calcd. (%)	Halogen Found (%)	Halogen Calcd. (%)
$VCl_2.2CH_3CN$*	25.3	25.0	34.8	34.8
VCl_2	41.8	41.8	58.2	58.2
$VBr_2.CH_3CN$†	20.3	20.2	63.9	63.5
VBr_2	24.3	24.2	75.1	75.8
VI_2	16.5	16.7	82.7	83.3

*The presence of CH_3CN was confirmed by infrared absorptions (Nujol mull) at 2310 ($\nu(C\equiv N)$) 998, 903, and 725 cm^{-1}.
†CH_3CN vibrations (Nujol mull) at 2320, 980, and 730 cm^{-1}. Both acetonitrile adducts appear to react on grinding with alkali metal halides.

vanadium dissolved (0.51 g). The current efficiency is surprisingly high; a total of 700 coulomb (7.2×10^{-3} Faraday) caused 0.01 mol of vanadium to dissolve, to be compared with a quantity of 3.6×10^{-3} mol calculated on the assumption that the primary electrode process is $V_{(m)} \rightarrow V^{2+}{}_{(sol)} + 2e^-$. This efficiency ($\sim$275%) implies that substantial chemical reaction is occurring between vanadium and chlorine under the reaction conditions. Vanadium metal does not react with chlorine below 200–250°C, and in any case in such reactions the product (ref. 4, p. 120) is VCl_4 rather than VCl_2. Hathaway and Holah (10) have reported that vanadium reacts with elemental chlorine, bromine, and iodine in acetonitrile (= L), but in each the product is a vanadium(III) species, which in the case of chlorine is formulated by these authors as $[VCl_3L_3]L$. In the present case, the precipitation of $VCl_2.2CH_3CN$ from the reaction mixture establishes that the final product VCl_2 is not formed by thermal decomposition of some higher halide.

One obvious explanation of the present results would involve the chemical and electrolytic oxidation $V_{(m)} \rightarrow V^{3+}{}_{(sol)}$, followed by cathodic reduction to $V^{2+}{}_{(sol)}$. Against this, however, must be set the work of Suzuki (11), who showed that anodic dissolution of vanadium metal into a LiCl/KCl eutectic gave rise to $V^{2+}{}_{(sol)}$, both immediately after dissolution and in equilibrated melts. We tentatively conclude that the direct electrolytic production of vanadium(II) accounts for a fraction of the VCl_2 produced; the remainder, perhaps a substantial fraction, may result from electrolytic and/or chemical reduction in situ. Whatever the detailed mechanism, the method is a rapid and simple route to VCl_2 and $VCl_2.2CH_3CN$. The structure of these compounds is by no means established, and either one or both may involve metal cluster units. Little is known about the adducts of VCl_2, other than the hydrates (3, 12); the compounds $VCl_2.2EtOAc$ (13), $VCl_2.4py$ (13), and a series of ammines (14) and methylammines (15) have been reported, but no structural information is available. Further work on this topic is planned.

Vanadium(II) Bromide

A voltage of 5 V gave a current of 45 mA, which was maintained for 8 h, by which time 0.115 g of vanadium had dissolved. The black crystals which had deposited in the vessel were collected, crushed, and dried *in vacuo* at 120°C for 30 min. Analysis showed that this material was the adduct $VBr_2.CH_3CN$ which on further heating (230°C, 10 min) lost acetonitrile to give the black VBr_2. The yield of $VBr_2.CH_3CN$ (0.47 g) is 84%, based on the vanadium dissolved. The current efficiency, calculated as for the chloride, is 33%, suggesting that in this case there is no significant chemical process over and above the electrochemical reaction.

As in the chlorine system, there are previous reports in the literature on the direct reaction of vanadium metal and bromine. At high temperatures (ref. 4, p. 132) (400–550°C), the product is VBr_3, whereas the reaction in hot acetonitrile (10) produces $[VBr_2L_4](Br_3)$. The electrochemical process therefore is unique in stabilising the vanadium(II) state.

Vanadium(II) Iodide

Electrolysis for 2 h at 50 V and 40 mA caused 0.063 g of vanadium to dissolve (current efficiency 83%). Black crystals were deposited in the cell; these were collected, washed with petroleum ether, and dried *in vacuo* (25–80°C). This solid is vanadium(II) iodide (yield 100 mg; 26% based on vanadium consumption). We were not able to recover any further material from the reaction mixture.

Again we may note the sharp difference between the electrochemical product and that from direct reaction between vanadium and iodine in a sealed tube at 120–300°C (VI_3) (ref. 4, p. 133), or in hot acetonitrile (10) ($[VL_6](I_3)_3$).

General

The preparations described lead to vanadium(II) halides and their acetonitrile derivatives in good yield. The method is quick and simple, although the mechanism and processes involved

are not yet clear. The adducts of VCl_2 and VBr_2 present interesting problems which we plan to investigate further.

Acknowledgement

This work was supported in part by Operating Grants (to D. G. Tuck) from the National Research Council of Canada.

1. F. A. Cotton and G. Wilkinson. Advanced inorganic chemistry. 3rd ed. Interscience, New York. 1972. p. 828 et seq.
2. H. J. Seifert and T. Auel. Z. Anorg. Chem. **360**, 50 (1968).
3. L. F. Larkworthy, K. C. Patel, and D. J. Phillips. J. Chem. Soc. A, 1095 (1970).
4. R. Colton and J. H. Canterford. Halides of the first row transition metals. Wiley-Interscience, New York. 1969.
5. J. J. Habeeb and D. G. Tuck. Chem. Commun. 808 (1975).
6. J. J. Habeeb, L. Neilson, and D. G. Tuck. Synth. React. Inorg. Metal-org. Chem. **6**, 105 (1976).
7. J. J. Habeeb, A. Osman, and D. G. Tuck. Chem. Commun. 379 (1976).
8. N. H. Furman. Standard methods of chemical analysis. 6th ed. Van Nostrand, New York. 1966. p. 1215.
9. U. O. Oakdale and J. J. Thompson. J. Am. Chem. Soc. **52**, 1195 (1931).
10. B. J. Hathaway and D. G. Holah. J. Chem. Soc. 537 (1965).
11. T. Suzuki. Electrochim. Acta, **15**, 127 (1970).
12. H. J. Seifert and B. Gerstenberg. Angew. Chem. **73**, 657 (1961); Z. Anorg. Chem. **315**, 56 (1962).
13. H. Funk, G. Mohaupt, and H. Paul. Z. Anorg. Chem. **302**, 199 (1959).
14. F. Ephraim and E. Ammann. Helv. Chim. Acta, **16**, 1273 (1933).
15. G. W. A. Fowles and P. G. Lanigan. J. Less-Common Metals, **6**, 396 (1964).

The enthalpy of isomerisation of methyl isocyanide

MOHAMMAD H. BAGHAL-VAYJOOEE, JOHN L. COLLISTER, AND HUW O. PRITCHARD
Chemistry Department, York University, Downsview, Ont., Canada M3J 1P3

Received March 2, 1977

MOHAMMAD H. BAGHAL-VAYJOOEE, JOHN L. COLLISTER, and HUW O. PRITCHARD. Can. J. Chem. **55**, 2634 (1977).

A controlled thermal explosion in which methyl isocyanide isomerises quantitatively to methyl cyanide has been studied in a calorimeter at 300 K. The enthalpy of isomerisation $\Delta H = -23.70 \pm 0.14$ (2 sdm) kcal mol^{-1}, from which values of the enthalpies of formation of both gaseous and liquid methyl isocyanide are calculated.

Similar measurements for ethyl isocyanide yield $\Delta H = -21.5 \pm 1.0$ kcal mol^{-1}.

MOHAMMAD H. BAGHAL-VAYJOOEE, JOHN L. COLLISTER et HUW O. PRITCHARD. Can. J. Chem. **55**, 2634 (1977).

On a étudié une explosion thermique contrôlée dans laquelle l'isocyanure de méthyle s'isomérise quantitativement au cyanure de méthyle; cette étude a été effectuée dans un calorimètre à 300 K. L'enthalpie d'isomérisation $\Delta H = -23.70 \pm 0.14$ (2 sdm) kcal mol^{-1}; à partir de cette donnée, on a pu calculer les valeurs des enthalpies de formation de l'isocyanure de méthyle à l'état gazeux et à l'état liquide.

Des mesures semblables avec l'isocyanure d'éthyle conduisent à un $\Delta H = 21.5 \pm 1.0$ kcal mol^{-1}.

[Traduit par le journal]

Introduction

The currently accepted value for the enthalpy of isomerisation of methyl isocyanide to methyl cyanide is of the order of (minus) 15–16 kcal mol^{-1}, this being the difference between the heat of combustion for methyl isocyanide measured by Guillemard (1) and by Lemoult (2), and the heat of combustion for methyl cyanide measured by Lemoult (2). It has now become important to know this quantity with greater precision, particularly in the analysis of thermal explosion-limit data for methyl isocyanide (3), but also in an analysis of the unimolecular fall-off data for this isomerisation (4).

After some reflection, it will become clear to the reader that in this particular case, measurements of the high-temperature equilibrium for this isomerisation would be, to say the least, very difficult, and therefore a calorimetric technique would seem to be more tractable. Consequently, we undertook a study of the thermal isomerisation of gaseous methyl isocyanide induced by an electrically heated filament, on a scale consistent with an accurate calorimetric determination of the energy released: our principal constraint was the nature of the calorimeter available, a diphenyl-ether isothermal calorimeter (5) operating at 27°C, and the most severe limitation was the size of the reaction-vessel cavity, which was much too small for us to have exploited the full accuracy of this calorimeter in these measurements.

The Controlled Thermal Explosion of Methyl Isocyanide

The basic design constraints are as follows: the maximum reaction vessel size is 200 ml and the vapour pressure of the product at 27°C is 100 Torr; this corresponds to approximately 10^{-3} mol of the reactant, and an expected energy release of about 15 cal. The accuracy of the calorimeter is of the order of 0.01% for energy releases of the order of 350 cal.

Our initial experiments showed that if a platinum wire suspended on the axis of the vessel was heated to a temperature of about 375°C in the presence of about 100 Torr of methyl isocyanide, liquid condensed on the walls immediately, and a brown residue was produced. However, if the initial pressure of isocyanide was reduced to about 50 Torr, the pressure rise due to heating in the centre of the vessel was insufficient to cause condensation at the walls, and the isocyanide was converted cleanly and completely to the cyanide in about 4 min: using a 0.003 in. diameter platinum wire, the electrical energy release was of the order of 250 cal, compared with the chemical energy release of now, about 7

or 8 cal. On the other hand, if the wire was heated to 450°C, an explosion occurred after about 1 s: the isocyanide was completely consumed, the major product was methyl cyanide in about 98% yield, together with a small amount of non-condensable gas (about 0.2 Torr) and some slight discoloration of the vessel walls. Moderation of this explosion with about 50 Torr of carbon dioxide reduced the severity of the explosion somewhat, with the result that the conversion of isocyanide to cyanide was between 99.97 and 99.99% complete, and no non-condensable products were formed.

Experimental Details

As a result of this experimentation, the final experimental arrangement was as follows. A 35 cm length of 0.001 in. diameter platinum wire was suspended in the form of a V (using a small glass bead as a weight to keep it taut) down the centre of the cylindrical reaction vessel, 19 cm long and 4 cm in diameter. The reaction vessel was completed with a small-bore Teflon stopcock with FETFE sealing rings (Ace Glass 8195-03), appropriate current and potential leads for the platinum heating wire, and a pair of heat shields to prevent convection of heat up the main calorimeter tube (*cf.* Fig. 1 of ref. 5).

The vessel was pumped out on a vacuum line and filled with about 50 Torr of pure methyl isocyanide, the pressure being measured with a Texas Instrument quartz spiral gauge (calibrated by cathetometer against a wide-bore mercury manometer) and a Hewlett-Packard 2802A thermometer (calibrated at 0°C and 327°C): these observations were required to define the number of moles of reactant. Then about 50 Torr of inert gas, either carbon dioxide or argon, was added and the reaction vessel was isolated and placed in the calorimeter; great care was taken to ensure the rigorous exclusion of oxygen, since the heat of combustion of methyl isocyanide is of the order of 20 times the expected heat of isomerisation (1, 2).

The calorimeter was allowed to stand overnight and after a satisfactory fore-period had been established, the reaction was initiated using a 2 s dc pulse at about 37–38 V, supplied from a Hewlett-Packard 6289A power supply operating in constant voltage mode. The voltage across the heater and the current through the heater (measured as the voltage across a standard 10 ohm resistor in series) were displayed on a Hewlett-Packard 7100B two-channel recorder: the electrical energy input was calculated from these two traces by graphical integration; the time for which the heater was switched on was derived from the movement of the chart paper (calibrated by supplying 0.5 s pulses to an event marker on the recorder). Figure 1 shows a typical recorder trace for the current and voltage, from which it can be deduced that the temperature at the wire at the peak of the explosion was about 700°C. Following the recording of a satisfactory after-period, the reaction vessel was removed from the calorimeter and its contents analysed by gas chromatography to confirm the completeness of the reaction.

The sample of methyl isocyanide was one used previously (3) and was purified by preparative gas-phase chromatography: no impurities could be detected either using gas-phase chromatography or mass spectrometry.

Results

The results of four experiments, two using argon and two using carbon dioxide as the diluent, are shown in Table 1: the agreement between the results of the four experiments, calculated assuming that methyl isocyanide at 50 Torr is a perfect gas, is excellent. We may combine the final result for the enthalpy of isomerisation with (preliminary) results from a new heat of combustion study of methyl cyanide by Barnes and Pilcher (6) to give the following enthalpy of formation values for methyl isocyanide (where the errors quoted are now ±2 sdm).

Compound	ΔH_f (liquid) (kcal mol^{-1})	ΔH_{vap} (kcal mol^{-1})	ΔH_f (gas) (kcal mol^{-1})	Reference
CH_3CN	9.70 ± 0.18	7.92 ± 0.03	17.62 ± 0.19	6
CH_3NC	$33.9_5 \pm 0.3_5$	$7.3_7 \pm 0.2_5$*	41.32 ± 0.24	This work

*The value of the enthalpy of vaporisation of methyl isocyanide quoted here is derived from two measurements of the vapour pressure (66.59 Torr at 0°C and 207.10 Torr at 24.9°C).

These tentative results depend, of course, on our assumption that methyl isocyanide at 50 Torr and 35°C is a perfect gas. It is known that methyl cyanide is partly dimerised in the gas phase, and using the equilibrium constant of Rowlinson (7), we calculate that under these conditions, the compressibility factor (PV/nRT) for methyl cyanide would be between 0.993 and 0.995. We may surmise that methyl isocyanide is not so strongly dimerised from the observation that it has a much smaller pressure coefficient of thermal conductivity (8), by about a factor of 4. We attempted to measure the vapour density of methyl isocyanide, but at these low densities, with the equipment available to us, we were unable to do better than to show that the compressibility factor was within 0.5% of unity. A slightly more reliable indication comes from

TABLE 1. Calorimetric determination of the energy released in the explosive isomerisation of methyl isocyanide at 300.05 K

Number of moles of reactant*			Diluent	Energy released			
P (Torr)	T (°C)	n (μmol)	P (Torr)	Δl† (cm)	Electrical input (cal)	Net chemical energy (cal)	$-\Delta H$ (kcal mol^{-1})
56.08±0.01	35.60±0.02	576.4±0.1	54.0 (Ar)	2.131±0.002	3.278±0.040	13.65±0.04	23.68±0.07
58.46±0.01	37.02±0.02	598.1±0.1	53.7 (CO_2)	2.203±0.004	3.285±0.040	14.21±0.05	23.76±0.09
58.94±0.01	36.70±0.02	603.6±0.1	52.3 (Ar)	2.105±0.003	2.392±0.030	14.33±0.04	23.73±0.06
57.57±0.01	37.12±0.02	588.8±0.1	54.0 (CO_2)	2.081±0.006	2.657±0.035	13.87±0.06	23.56±0.10
						Mean‡	23.70±0.07

*Volume of vessel = 197.93±0.01 cm^3; ideal-gas molar volume at STP = 22.4174 ℓ (9).
†Calibration constant of calorimeter (5): number of calories = (7.9425±0.0006)Δl; 1 cal = 4.184 J.
‡The errors quoted in this table are calculated as follows: columns 1, 2, 5, 6: an estimate of the *maximum* possible uncertainty in each individual determination; columns 3, 7, 8: errors calculated by the normal rules for combining standard deviations; final mean value: mean calculated as a weighted mean of the four results listed in the final column.

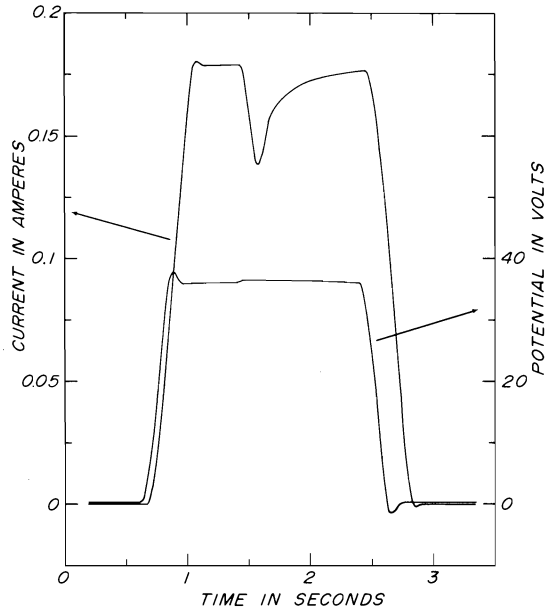

FIG. 1. Recorder traces of the current and voltage used to initiate the explosion, which occurs at about the 1.5 s marker. The attendant rise in the mean temperature of the wire to 691°C is shown by the marked drop in current (since the voltage is held constant). Apart from the slight voltage ripple when the explosion occurs, the applied voltage is a square-wave pulse; however the distortion of the traces due to pen lag and overshoot were so reproducible that no difficulty was encountered in performing the desired integration.

some auxiliary experiments in which we found that the reduction in pressure in the reaction vessel after isomerisation was usually of the order of 0.5 to 1% of the total initial isocyanide pressure.

We attempted to repeat these experiments for ethyl isocyanide, but because the vapour pressure of ethyl cyanide at 27°C is only 50 Torr, we chose to work with an initial isocyanide pressure of about 45 Torr. Under these conditions the explosive isomerisation was clean, but conversion was incomplete. The results of four experiments with carbon dioxide as diluent were −21.1, −21.6, −22.2, and −21.7 kcal mol^{-1} (where correction had been made for 1.5, 22, 6, and 2% of incomplete reaction respectively). It would seem reasonable to accept a tentative value of $\Delta H = -21.5 \pm 1.0$ kcal mol^{-1} for this isomerisation, and we also report an approximate enthalpy of vaporisation of about 7.9 kcal mol^{-1} (based on two vapour pressure measurements, 30.76 Torr at 0°C and 104.66 Torr at 25.2°C) for ethyl isocyanide.

Acknowledgement

This work was supported by the National Research Council of Canada.

1. H. GUILLEMARD. Ann. Chim. Phys. Ser. VIII, **14**, 408 (1908).
2. P. LEMOULT. C. R. Acad. Sci. Paris, **149**, 1602 (1909).
3. J. L. COLLISTER and H. O. PRITCHARD. Can. J. Chem. Submitted.
4. A. W. YAU and H. O. PRITCHARD. Can. J. Chem. To be submitted.
5. J. V. DAVIES and H. O. PRITCHARD. J. Chem. Thermodyn. **4**, 9 (1972).
6. D. S. BARNES and G. PILCHER. Personal communication.
7. J. S. ROWLINSON. Trans. Faraday Soc. **45**, 974 (1949).
8. H. O. PRITCHARD and B. J. TYLER. Can. J. Chem. **51**, 4001 (1973).
9. T. J. QUINN, A. R. COLCLOUGH, and T. R. D. CHANDLER. Phil. Trans. R. Soc. London, A**283**, 25 (1976).

Linear free energy relationships. VIII.[1] Ionization potentials of aliphatic compounds

HARRY W. GIBSON

Webster Research Center, Xerox Corporation, Webster, NY, U.S.A. 14580

Received January 28, 1977

HARRY W. GIBSON. Can J. Chem. **55**, 2637 (1977).

Ionization potentials (IP) of HX, CH_3X, C_2H_5X, and i-C_3H_7X, where X is a substituent with non-bonded electrons, are directly proportional to ionization potentials of 4-substituted quinuclidines. This is taken as evidence that in general the energy required to remove an electron from a substituent X, as is the case in HX, CH_3X, C_2H_5X, and i-C_3H_7X, is directly proportional to the energy required to remove an electron from a site remote from the substituent, as in the quinuclidines in which an electron is lost from the ring nitrogen. Furthermore, the IP's of the HX–i-C_3H_7X series are directly proportional to inductive substituent constants, σ_I, providing a valuable correlation between gas and solution phase behavior.

HARRY W. GIBSON. Can. J. Chem. **55**, 2637 (1977).

Les potentiels d'ionisation (IP) de HX, CH_3X, C_2H_5X et i-C_3H_7X, où X est un substituant comportant des électrons non-liés, sont directement proportionnels aux potentiels d'ionisation des quinuclidines substitués en position 4. On considère cette corrélation comme une indication que, d'une façon générale, l'énergie requise pour enlever un électron d'un substituant X, comme dans le cas de HX, CH_3X, C_2H_5X et i-C_3H_7X, est directement proportionnelle à l'énergie requise pour enlever un électron d'un site éloigné du substituant comme dans les quinuclidines dans lesquelles un électron est perdu par l'azote du cycle. De plus, les potentiels d'ionisation de la série HX à i-C_3H_7X sont directement proportionnels aux constantes inductives des substituants, σ_I, fournissant une corrélation très utile entre le comportement en phase gazeuse et en solution.

[Traduit par le journal]

Molecular orbital energy levels are determining factors both for chemical reactivity and many physical properties, especially spectral and electrical properties. Our previous work using linear free energy relationships (1–7), including the Hammett equation (8), was aimed at quantitatively relating these energy levels to molecular structure (1–4, 6, 7) and in turn to electrical properties (5) of aromatic compounds. In the first paper of this series it was shown that the ionization potentials (IP) of substituted benzenes are linearly related to the sums of the Hammett substituent constants. To understand and predict the properties of aliphatic series a similar linear free energy relationship would be most helpful.

A. Linear Free Energy Relationships

A number of correlations of ionization potentials of aliphatic compounds with Taft or inductive substituent constants have appeared (9). However, the substituents were restricted to hydrogen or alkyl groups. The only exception is the study of some quinuclidines (**1**) (10), in which substituents with non-bonded electrons were examined. It was our objective to determine if the ionization potentials of simple alkanes substituted with groups bearing non-bonded electrons could be correlated with the ionization potentials of series **1** and more generally with substituent constants.

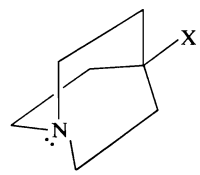

1

Table 1 contains the ionization potentials of such series of HX, CH_3X, C_2H_5X, and i-C_3H_7X compounds; most are adiabatic, derived by photoelectron spectroscopy. Figure 1 is a plot of the IP of CH_3X *vs.* the vertical IP of **1** for seven different X groups. As can be seen, with the exception of the point for X = NO_2 (see below), an excellent linear correlation exists.[2] Similar

[1]References 1–7 comprise parts I–VII of this series.

[2]The inadequacy of the correlation coefficient r for goodness of fit has been pointed out (11). In this case the conclusion is based on comparison of the average deviation of points from the line with the precision of the data (estimated to be 0.2–0.3 eV for the data of Table 1).

TABLE 1. Ionization potentials (eV)[a] of aliphatic compounds RX

Point No.	X	$\sigma_{I,X}$	Ionization potential HX	CH_3X	C_2H_5X	i-C_3H_7X
1	$N(CH_3)_2$	0.11	8.36	8.12	—	—
2	$NHCH_3$	0.11	9.18	8.36	—	—
3	NH_2	0.13	10.15	9.18	9.19	8.86
4	SCH_3	0.22	9.44	8.67[b]	8.55[c,d]	8.7[c,e]
5	$CONH_2$	0.27	10.13	9.80	—	—
6	SH	0.28	10.43	9.44[b]	9.29	9.05
7	OH	0.30	12.61	10.85	10.46	10.18
8	$COOC_2H_5$	0.30	10.62	10.24	10.00[c,d]	—
9	OCH_3	0.31	10.85	9.94	9.81[e,f]	—
10	COOH	0.34	11.33	10.37	10.24[c,d]	10.02[c,d]
11	$COCH_3$	0.34	10.20	9.68	9.53	9.30
12	$COOCH_3$	0.35	10.82	10.27	10.15[c,d]	9.98[c,d]
13	CHO	0.35	10.88	10.20	9.97	9.69
14	$OOCCH_3$	0.39	10.37	10.27	10.24	10.08
15	I[g]	0.43	10.75	9.86	9.64[b,h]	9.44
16	Br[g]	0.50	11.87	10.69	10.46	10.26
17	Cl[g]	0.51	12.80	11.33[h]	11.01[b]	10.78[c,d]
18	F	0.56	16.06	12.54	12.00	—
19	CN	0.61	13.60	12.21	11.85	11.6
20	NO_2	0.70	—	11.08	10.92	10.71

[a]Adiabatic, by photoelectron spectroscopy, from ref. 14, pp. 257ff unless otherwise indicated.
[b]Vertical.
[c]From ref. 15, pp. E-74ff.
[d]Photoionization data.
[e]Electron impact data.
[f]From ref. 16 p. 301.
[g]IP value given for these compounds is the average of the first two IP's which are due to spin-orbit coupling ($^2E_{3/2}$, $^2E_{1/2}$) of the non-bonding p-orbitals. The resultant splitting increases in the order Cl < Br < I and is not usually observed for F (see ref. 17).
[h]From ref. 17.

correlations exist for the data of HX, C_2H_5X, and i-C_3H_7X *vs.* those of **1**.

In series **1** the ionization process corresponds to loss of a non-bonded electron from the nitrogen atom; the energetics of the process are modified by the substituents X either through space or through bonds or both. In contrast, in the HX, CH_3X, C_2H_5X, i-C_3H_7X compounds it is generally loss of a non-bonded electron from the substituent itself that comprises the ionization process. This can be seen by reference to Fig. 2 in which the direct relationship[2] between IP's of CH_3X and HX is shown; the IP of HX is taken to be essentially that of X. (See below for discussion of point 18.) Thus variation of X involves a change in the site and nature of the ionization and not merely a substituent effect. The correlation of Fig. 1 therefore indicates that the energy required to remove an electron directly from a substituent is proportional to the energy required to remove an electron from a site remote from the substituent.

To substantiate this conclusion the dependence of IP for these series on the inductive substituent constant, $\sigma_{I,X}$, was determined. In Fig. 3

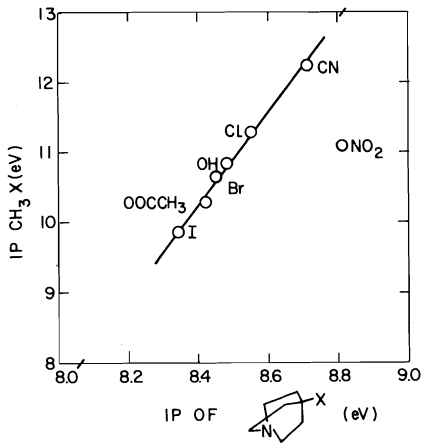

FIG. 1. Ionization potentials of substituted methanes (CH_3X) *vs.* ionization potentials of 4-substituted quinuclidines (**1**, QX). Linear least-squares line without X = NO_2: $IP_{CH_3X} = 6.61IP_{QX} - 45.30$; correlation coefficient, $r = 0.994$; average deviation of IP_{CH_3X} from the line = 0.08 eV.

the IP of CH_3X is plotted *vs.* $\sigma_{I,X}$ (8*a*). As can be seen, with the exception of points for X = NO_2, F, I, and OH (see below), a good linear relationship exists.[2] Similar relationships exist for the

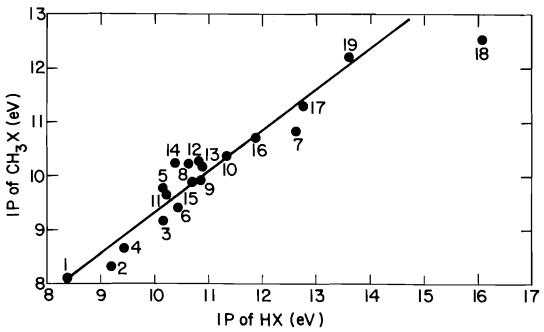

FIG. 2. Ionization potentials of substituted methanes (CH_3X) *vs.* ionization potentials of HX. Least-squares fit without X = F: $IP_{CH_3X} = 0.746\ IP_{HX} + 1.92$; correlation coefficient, $r = 0.957$; average deviation of IP_{CH_3X} from the line, 0.24 eV. For point code see Table 1.

HX, C_2H_5X, and *i*-C_3H_7X series. The fit parameters are given in Table 2. The linear relationships demonstrate that in general the energy required to remove an electron from non-bonding orbitals of a substituent X in the gas phase (IP) is directly proportional to the ability of the substituent to stabilize a charge in a remote part of a molecule in solution ($\sigma_{I,X}$).

B. Deviations

As we have seen in Figs. 1 and 3, the points for X = NO_2 are anomalous. In fact, the deviations in CH_3X, C_2H_5X, and *i*-C_3H_7X are systematic; NO_2 has an effective $\sigma_I = 0.50 \pm 0.01$. In other words, for these compounds the nitro group is not as electron poor as it normally appears to be. In correlations of IP with Hammett substituent constants, however, nitro compounds do not deviate (2). Nor does X = NO_2 ($\sigma_1 = 0.70$) deviate from the line (IP = $0.952\sigma_{I,X} + 8.07$; correlation coefficient, $r = 0.968$; standard deviation of points from the line 0.07 eV) for series **1** (X = C_6H_5, OH, $OOCCH_3$, Cl, Br, I, CN, NO_2, C≡CH, H, CH_3, C_2H_5, *i*-C_3H_7, and *tert*-C_4H_9) (10). Therefore, the deviation is not inherent to the gas phase. A possible explanation is that remote substituents, as involved in the IP of **1** and ArX and $\sigma_{I,X}$ in solution, are influenced predominantly by the positively charged nitrogen atom of the nitro group, whereas electrons within the NO_2 group which are involved in the IP of CH_3X, C_2H_5X, and *i*-C_3H_7X reside in a net neutral environment. This would lead to non-proportionalities between the energetics of the two situations, making X = NO_2 deviate below the line in correlations such as those of Figs. 1 and 3.

TABLE 2. Least-squares fits of ionization potential *vs.* inductive substituent constant[a]

$IP = m\sigma_{I,X} + b$

Series	*m*	*b* (eV)	*n*[b]	*r*[c]	AD[d] (eV)
HX	8.43	7.99	16	0.920	0.40
CH_3X	7.05	7.67	16	0.948	0.27
C_2H_5X	5.99	7.89	13	0.909	0.27
i-C_3H_7X	5.95	7.67	11	0.938	0.26

[a]Excluding points 7, 15, 18, and 20 in each series.
[b]Number of points.
[c]Correlation coefficient (see footnote 2).
[d]Average deviation of points from the line.

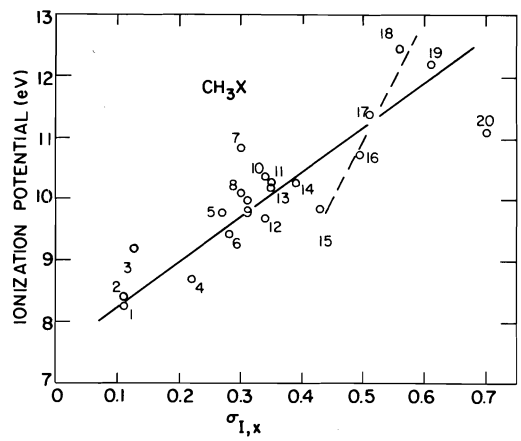

FIG. 3. Ionization potential *vs.* inductive substituent constant for CH_3X. Solid line, points 1–6, 8–14, 16, 17, 19. Dashed line, points 15–18. For point code see Table 1. For fit parameters see Table 2.

While the point for X = OH does not deviate significantly (less than the standard deviation) from the line of Fig. 1, X = OH is deviant in plots of IP *vs.* σ_I for HX, CH_3X (Fig. 3), C_2H_5X, *i*-C_3H_7X, and **1** by 2–4 standard deviations, the IP's being higher than expected. For series **1** the effective $\sigma_I = 0.43$; for the other four series the effective $\sigma_I = 0.46 \pm 0.05$. OH is thus effectively more electron withdrawing or less electron rich in the gas phase than in solution. This is also corroborated by the IP data for phenols which are up to 3.5 standard deviations higher than expected (2). Using the equation (8*b*) $\sigma^+ = 1.14\sigma_I + \sigma_R$, $\sigma_R{}^+ = -1.24$ (8*a*), and the effective σ_I value (0.46), for OH we calculate $\sigma^+ = -0.72$. This can be compared to the solution value of -0.92 (8*a*) and the value of -0.59 assigned on the basis of IP's of phenols (12). In fact, as has been pointed out (10), the solution-derived σ_I for OH is less than that of OCH_3 (8*a*); this seems incorrect in view of the relative gas phase values. There is apparently a solvent effect operative which reduces the solution σ_I of OH relative to the gas phase and to other substit-

TABLE 3. Assignment of inductive substituent constants on the basis of ionization potentials of aliphatic compounds RX

X	Ionization potential[a] (eV) HX	CH_3X	C_2H_5X	i-C_3H_7X	σ_I
$N(CH_3)C_6H_5$	7.32	7.12	7.37	—	-0.08 ± 0.01
NHC_6H_5	7.7	7.32	7.56	7.5[b]	-0.04 ± 0.01
OC_6H_5	8.51	8.21	8.13	—	$+0.06\pm0.02$
$OCH_2C_6H_5$	9.14	8.85	—	—	$+0.16\pm0.02$
$CON(CH_3)_2$	9.14	8.81[c]	—	—	$+0.15\pm0.01$
COC_6H_5	9.52	9.27	9.27	—	$+0.21\pm0.02$
NCS	9.94[d]	9.25	9.14[c]	—	$+0.22\pm0.01$
SCN	—	10.07	9.89[c]	—	$+0.34\pm0.01$
NCO	11.62	10.67	—	—	$+0.43\pm0.01$
ONO	—	10.53	—	10.23	$+0.42\pm0.01$

[a]Adiabatic, by photoelectron spectroscopy, from ref. 14, pp. 257ff unless otherwise indicated.
[b]From ref. 18.
[c]Photoionization data.
[d]Vertical.

uents; hydrogen bonding of the hydroxyl hydrogen with solvent would have this effect.

In the case of the halogens, a separate straight line may be drawn (see dashed line, Fig. 3). This indicates an internal consistency in the halogen family. Interestingly, in substituted benzenes the fluoro substituent with consistency leads to higher ionization potentials than expected on the basis of its substituent constant (2). The fewer examples of substituted iodobenzenes have lower ionization potentials than expected (2). This has led to assignment of a new σ^+ value for I (12). Also, **1**, X = I deviates below the correlation line for **1** by two standard deviations (10). Thus the deviations of F and I are systematic in the gas phase. For series **1** the effective σ_I of I is 0.29; for the other four series the effective $\sigma_I = 0.31 \pm 0.01$ for I. Thus I is more electron rich in the gas phase than in solution. This may be the consequence of its polarizability, which in solution would tend to lead to a more positive character by interaction with solvent. For F the effective $\sigma_I = 0.69 \pm 0.01$ from data for CH_3X and C_2H_5X. From Fig. 2 it is apparent that there is a difference between the effect of F on HX and CH_3X (point 18). From the data for HX the effective $\sigma_I = 0.96$ for F. This difference may be attributed to the inability of H to π-bond via hyperconjugation with F, in contrast to CH_3, C_2H_5, and i-C_3H_7 which can. It may be that π-bonding of F is more important in the gas phase than in solution, where it can hydrogen bond, leading to a difference in the effect of F in the two states. The different slope of the halogen line may then reflect a regular change in these two properties (polarizability and π-bonding) peculiar to the halogens.

Alternative rationalization of the deviations involves the size or 'hardness' of the X group. In small groups (OH, F) electron–electron repulsion is relaxed during ionization, allowing the relatively high nuclear charge to cling more tenaciously to the leaving electron than would be expected. Another way of stating this is that the small groups appear more electronegative (higher IP) than they should relative to large groups because they have no space to put the charge. The reverse is true for large soft groups (I, NO_2). In this vein in the gas phase ^-OH has been shown to be more basic (more electron releasing) than $^-OCH_3$ (13).

C. Assignment of Substituent Constants

Using the linear correlation equations it is also possible to assign new inductive substituent constants. A cogent argument can be made that the determination of all substituent constants, both aromatic and aliphatic, should be made from gas phase ionization potentials and that solvent effects then be treated as perturbations associated with either the main group or the substituent. Table 3 summarizes a number of inductive substituent constants estimated in this manner but not previously reported by other methods (8).

NOTE ADDED IN PROOF: A report which appeared after acceptance of this paper describes the relationship between IP's of HX and CH_3X in terms of orbital symmetry [$n(\pi)$, π, $n(\sigma)$] and hyperconjugative effects.

Conclusions

There is a general correlation of gas phase ionization potentials of substituted alkanes containing non-bonded electrons with ionization potentials of quinuclidines bearing these substituent and also with substituent constants derived from solution phase reactions. These relationships are of value both for estimation of such gas phase energy levels from substituent constants and vice versa.

Acknowledgment

The author wishes to thank Drs. Frank Saeva and Gerald Ceasar for helpful discussions and constructive criticism of this manuscript, Professor M. J. S. Dewar for encouraging discussions, and the referees for helpful comments.

1. H. W. GIBSON. Can. J. Chem. **51**, 3065 (1973).
2. H. W. GIBSON and F. C. BAILEY. Tetrahedron, **30**, 2043 (1974).
3. J. E. KUDER, H. W. GIBSON, and D. WYCHICK. J. Org. Chem. **40**, 875 (1975).
4. H. W. GIBSON and F. C. BAILEY. Can. J. Chem. **53**, 2162 (1975).
5. H. W. GIBSON. J. Am. Chem. Soc. **97**, 3832 (1975).
6. H. W. GIBSON and F. C. BAILEY. J. Chem. Soc. Perkin Trans. II, 196 (1976).
7. H. W. GIBSON and F. C. BAILEY. J. Chem. Soc. Perkin Trans. II, 1575 (1976).
8. N. B. CHAPMAN and J. SHORTER (*Editors*). Advances in linear free energy relationships. Plenum Press, New York, NY. 1972; (*a*) p. 37; (*b*) p. 38.
9. H. F. WIDING, B. W. LEVITT, and L. S. LEVITT. Israel J. Chem. **13**, 69 (1975) and references therein.
10. G. BIERI and E. HEILBRONNER. Helv. Chim. Acta, **57**, 546 (1974).
11. W. H. DAVIS, JR. and W. A. PRYOR. J. Chem. Educ. **53**, 285 (1976).
12. T. W. BENTLEY and R. A. W. JOHNSTONE. J. Chem. Soc. B, 263 (1971).
13. J. I. BRAUMAN and L. K. BLAIR. J. Am. Chem. Soc. **92**, 5986 (1970).
14. K. SIEGBAHN, D. S. ALLISON, and J. H. ALLISON. *In* Handbook of spectroscopy. *Edited by* J. W. Robinson. CRC Press, Cleveland, OH. 1974.
15. Handbook of chemistry and physics. 57th ed. CRC Press, Cleveland, OH. 1976–1977.
16. R. W. KISER. Introduction to mass spectrometry and its applications. Prentice-Hall, Englewood Cliffs, NJ. 1965.
17. K. KIMURA, S. KATSUMATO, Y. ACHIBA, H. MATSUMOTO, and S. NAGAKURA. Bull. Chem. Soc. Jpn. **46**, 373 (1973).
18. G. BRIEGLEB and J. CZEKALLA. Z. Elektrochem. **63**, 6 (1959).
19. K. N. HOUK, E. J. MCALDUFF, P. D. MOLLÉRE, R. W. STROZIER, and Y.-M. CHANG. J. Chem. Soc. Chem. Commun. 141 (1977).

The effect of substituents on geminal proton–proton coupling constants. III[1]

ROGER N. RENAUD AND JOHN W. BOVENKAMP[2]
Chemistry Division, National Research Council of Canada, Ottawa, Canada K1A 0R6

AND

ROBERT R. FRASER AND RAJ CAPOOR
Department of Chemistry, University of Ottawa, Ottawa, Canada K1N 6N5

Received February 8, 1977

ROGER N. RENAUD, JOHN W. BOVENKAMP, ROBERT R. FRASER, and RAJ CAPOOR. Can. J. Chem. **55**, 2642 (1977).

The effect of substituents at the 3-position in a series of *N*-methyl 5,6-dihydro-7*H*,12*H*-dibenzo[*c*,*f*]azocines on the geminal coupling constants of the C-12 methylene protons has been determined. The slope of the Hammett plot of ^2J *vs.* σ has been found to be $+0.20$. The orientation of the methylene protons with respect to the π orbitals of the benzene ring bearing the substituent is such that no hyperconjugative effect should be present. The value of $+0.20$ is in contrast to a previously measured slope of -1.9 for compounds having a geometry ideal for hyperconjugative effects and substantiates the predictions of theoretical MO calculations. As a result, the reliability of this conformational dependence of ρ for use in conformational analysis has been strengthened.

A comparison of the data for the azocines with those in the literature indicates the difference between the minimum and maximum effects of a phenyl substituent on a geminal coupling constant of an attached methylene group is 5.5 Hz.

ROGER N. RENAUD, JOHN W. BOVENKAMP, ROBERT R. FRASER et RAJ CAPOOR. Can. J. Chem. **55**, 2642 (1977).

On a déterminé l'effet des substituants en position 3 d'une série de *N*-méthyle dihydro-5,6 7*H*,12*H*-dibenzo[*c*,*f*]azocines sur les constantes de couplage géminales des protons méthyléniques en position C-12. La pente de la courbe de Hammett de ^2J en fonction de σ est de $+0.20$. L'orientation des protons méthyléniques par rapport aux orbitales π du noyau benzénique portant le substituant est telle qu'il ne devrait pas y avoir d'effet d'hyperconjugaison dans ce système. La valeur de $+0.20$ est en opposition avec la pente mesurée antérieurement de -1.9 pour des composés ayant une géométrie idéale pour des effets d'hyperconjugaison et apporte un support aux prédictions des calculs théoriques d'orbitales moléculaires. Ces résultats renforcent la crédibilité de la dépendance conformationnelle de ρ pour son utilisation en analyse conformationnelle.

Une comparaison des données pour les azocines avec celles rapportées dans la littérature indique que la différence entre les effets minimum et maximum d'un groupement phényle sur une constante de couplage géminale d'un groupe méthylène qui y est attaché est de 5.5 Hz.
[Traduit par le journal]

We have previously shown (1, 2) that the effect of *para* substituents on the geminal coupling constants of the methylene protons in several series of benzylic systems was proportional to the Hammett substituent constants and that the magnitude of change in ^2J, represented by ρ, the slope of the Hammett plot, depended upon the conformation of the methylene protons with respect to the adjacent aromatic ring. This angular dependence was attributed to the fact that hyperconjugation of a benzene ring with the adjacent methylene group causes a negative shift[3] in J which is itself angularly dependent. Both valence bond (VB) calculations (6) and molecular orbital (MO) calculations (7) predicted a maximum effect on ^2J when $\phi = 0°$ and no effect when $\phi = 90°$, where ϕ is defined using the conformers shown in Fig. 1. However, in the calculations, there was a discrepancy between the predictions of the VB and MO methods in the region of $\phi = 90°$. The former predicted a

[1]NRCC No. 15949.

[2]Present address: Defence Research Establishment Ottawa, Ottawa, Canada.

[3]Since the geminal coupling constants in benzylic systems have been shown to be negative (3), it is most convenient to describe the effect of, for example, the phenyl group in toluene ($^2J = -14.8$ Hz (4)) *vs.* methane ($^2J = -12.4$ (5)) as causing a negative shift in ^2J.

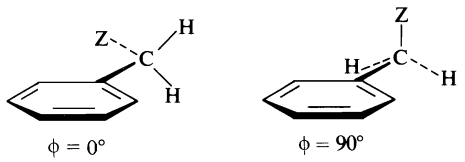

FIG. 1. The dihedral angle ϕ is the angle between the π orbital and an imaginary line passing through both protons of the methylene group (7). In refs. 6 and 8 the geometry is described by a different angle θ, where θ is the angle between the π orbital and a C—H bond.

small negative influence on ^2J, the latter predicted no effect. Since the previous studies on substituent effects were limited to several series of compounds having $\phi = 0°$ and one in which $\phi = 72°$ (2), it seemed desirable to examine an additional series of compounds having ϕ fixed in the region of 90°. The substituent effects on ^2J in such a series should provide a test of the contrasting theoretical predictions and thereby substantiate the explanation for the conformational dependence of ρ.[4]

Recently the conformational properties of several *N*-alkyl 5,6-dihydro-7*H*,12*H*-dibenzo[*c*,*f*]azocines (11, 12) were elucidated using proton nmr spectroscopy. The predominant conformation of the eight-membered ring was shown to be a rigid boat-chair form. Models indicated that the orientation of the methylene protons at C-12 with respect to each adjacent benzene ring was equivalent to $\phi \approx 90°$. An X-ray diffraction study on **1***a* where X = H and **1***d* where X = Br revealed that, in the solid, both molecules exist in a boat-chair conformation with the *N*-methyl group in a pseudo-axial position (13). The angles ϕ for **1***a* and **1***d* were found to be 87.5 ± 0.3° and 86.9 ± 1.2° (14), respectively. ^{1}H nmr spectroscopy has established for **1***a* the presence, in solution, of a rapidly interconverting equilibrium between a boat-chair (BC) and a flexible twist-boat (TB) conformation. In $CDCl_3$ at 10°C, at which temperature interconversion of conformers is slow in the nmr time scale, the ratio of BC to TB conformers was found to be 92:8 (11). The ^{1}H nmr spectrum of **1***d* also shows the molecule to prefer the rigid conformation with the *N*-methyl group in the same orientation.[5]

[4]This conformational dependence of ρ has already given information regarding the conformational properties of benzylic systems (9, 10).

[5]The chemical shifts of the methyl protons were shown to differ by 1.2 ppm with the axial methyl signal being to high field (11). Since the chemical shifts of the methyl groups remained constant (±0.02 ppm) throughout the series, its orientation is therefore constant.

Thus, in both the solid state and in solution, changing the substituent at C-3 does not affect the ring conformation nor the methyl groups orientation. Therefore, a series of 3-substituted *N*-methyl 5,6-dihydro-7*H*,12*H*-dibenzo[*c*,*f*]azocines **1** comprise an ideal system for the study of the π effect on the geminal coupling constant in the untested area of $\phi = 90°$.

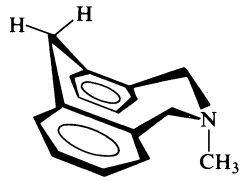

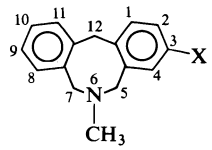

1

a X = H
b X = CH_3
c X = OCH_3
d X = Br
e X = CN
f X = CO_2CH_3
g X = $CONH_2$
h X = $NHCO_2CH_3$
i X = NH_2

The synthesis of the requisite compounds (**1***a* to **1***i*) was accomplished using the methods shown in Schemes 1 and 2. One specific aspect of interest is the synthesis of **1***i* from the amide **1***g*. The normal Hofmann rearrangement on the amide **1***g* was not successful (15). However, the method of Radlich and Brown (16) gave the desired amine in good yield. In this method the Hofmann rearrangement is carried out on the amide using a solution of bromine and sodium methoxide in methanol producing the carbamate **1***h*. Hydrolysis of **1***h* with refluxing hydrochloric acid gave the required amine **1***i*.

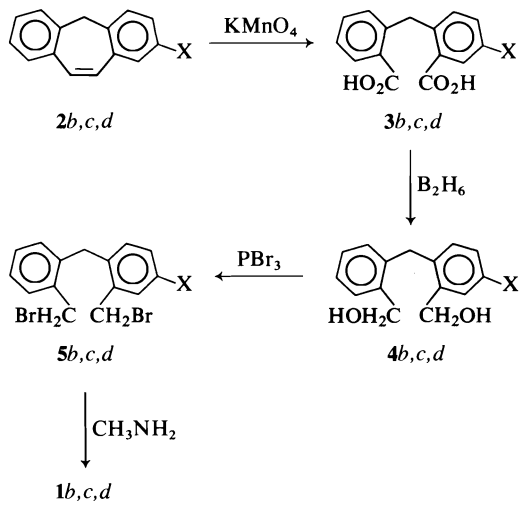

SCHEME 1

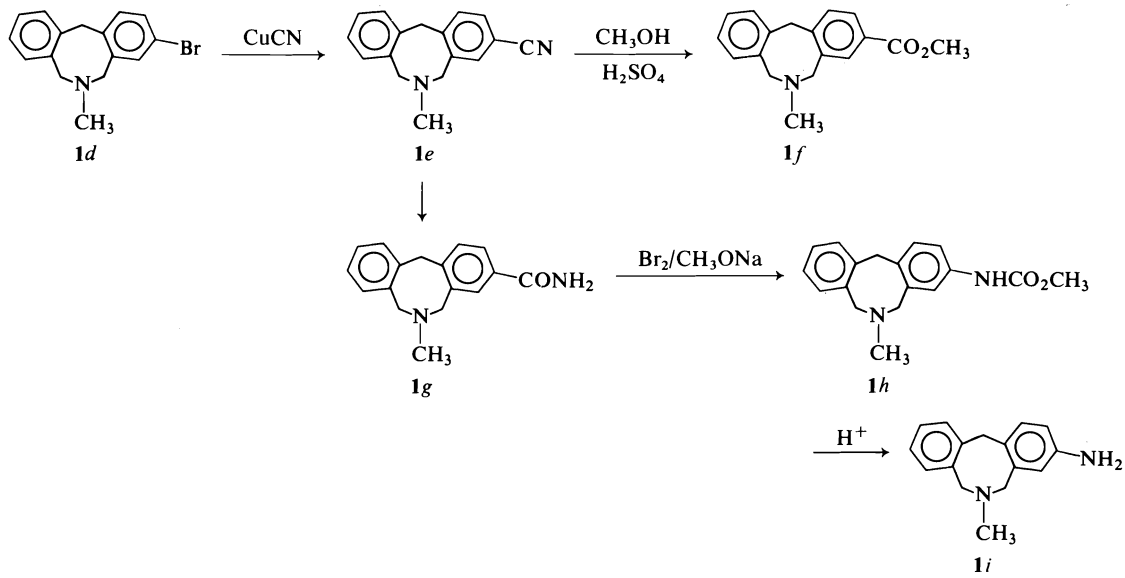

SCHEME 2

A typical ^{1}H nmr spectrum of the compounds studied is presented in Fig. 2 showing the methylene region of the spectrum of **1***i*. The spectrum is simplified by the fact that the signals of the strongly dominant BC conformation are well separated. In deuterochloroform at 10°C, the spectrum of **1***i* shows three well-defined AB quartets in the ratio of 1:1:1. They are centered at δ 3.92 ($^2J = -12.9$ Hz), 4.05 ($^2J = -14.8$ Hz), and 4.08 ($^2J = -14.8$ Hz). The quartet having a ^2J of -12.9 Hz corresponds to the protons on C-12 while the two quartets with a ^2J of -14.8 Hz are attributed to the protons on C-5 and C-7 (12). In two instances (**1***c* and **1***f*) problems occurred with the overlapping of peaks. The high field doublet due to the protons on C-12 was not resolved adequately from the peaks due to the protons on C-5 and C-7 in order for accurate geminal coupling constants to be measured. Fortunately, a complete set of geminal coupling constants could be obtained from the low field doublets of the C-12 protons for each of the azocines in Table 1.

The correlation between these geminal coupling constants and the Hammett σ values for the substituents (17) is graphically shown in Fig. 3. The slope of the best fitted line, calculated from a least-squares program (18), was +0.20 with a standard deviation of 0.085. From this slope, along with the values obtained before for the rigid systems 3-phenylphthalans ($\phi = 0°$; $\rho = -1.9$), 2-methyl-1-phenylisoindolines ($\phi = 0°$; $\rho = -1.7$) and 5*H*-dibenzo[*a*,*d*]cycloheptene-10,11-oxides ($\phi = 72°$; $\rho = +0.19$) (2), it can be concluded that the effect of the substituents on the geminal coupling constants at C-12 varies with the angle ϕ in accordance with the predictions of MO theory (7). As Fig. 4 shows the perturbation of the negative increment to ^2J follows a $\cos^2\phi$ relation (7) not the irregular double minimum curve predicted by VB calculations (6).

Another result of considerable significance is the value for ^2J in the unsubstituted azocine. The geminal coupling constant between the protons at C-12 (-12.7 Hz) is the least negative yet reported for a derivative of diphenylmethane. This is, of course, consistent with the fact that in this molecule ϕ is estimated to be 86° in which case there is essentially no hyperconjugative effect of either benzene ring on the geminal coupling constant.

It is now possible to reexamine the magnitude of the increment to ^2J due to the hyperconjugative interaction of a benzene ring. Previously Cookson *et al.* (19), from a variety of compounds having an unsaturated function (carbonyl, double bond or phenyl) adjacent to a CH_2, estimated the hyperconjugative effect to be about 6 Hz per adjacent unsaturated function group when $\phi = 0°$. The increment to ^2J for a CH_2 group α to a carbonyl has recently been estimated on the basis of further data (8), to be between +3 and -6 Hz depending on ϕ. Data

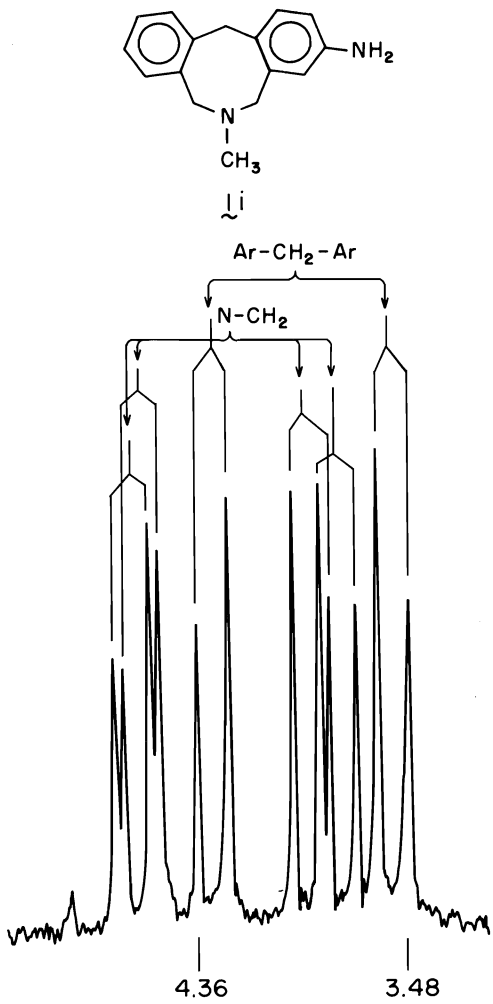

FIG. 2. The absorption of all methylene protons in the 100 MHz nmr spectrum of **1***i* in $CDCl_3$ at 10°C.

for estimating the effect of a phenyl group above was previously limited by (*a*) lack of a value for ^2J in the region of 90° and (*b*) inaccuracy in the measurement of ^2J (for $\phi = 0°$) at the 9-position of fluorene. The very careful study of Lehn and co-workers (4) showed that $^2J_{H-D}$ in fluorene, measured under conditions where quadrupolar relaxation effects were absent, was 3.5 Hz. Using the correction factor $^2J_{H-H} = 6.75$, $^2J_{H-D}$ as established earlier by one of us (9) and subsequently adopted by Bothner-By (20), the value for $^2J_{H-H}$ in fluorene is -23.6 Hz. Thus a comparison of this value ($\phi = 0°$) with that of the azocine and the carbocycle given in Table 2 for $\phi = 87°$, shows the difference between the minimum and maximum effects of the two aryl substituents on ^2J is 11 Hz. Two additional ^2J's measured in diaryl methanes whose conformations are known are also given in Table 2. All these data are consistent with the assignment of an angularly dependent increment to J. The value of this increment (per phenyl substituent) can be expressed as $\Delta J = -5.5 \cos^2 \phi$.

TABLE 1. The ^2J-values* for the benzylic methylene protons at C-12

	In $CDCl_3$ at 10°C	
X	Downfield ^2J	Upfield ^2J
NH_2	12.92	12.94
OCH_3	12.90	—
CH_3	12.69	12.65
H	12.66	12.67
Br	12.78	12.63
CO_2CH_3	12.61	—
CN	12.68	12.69

*The values reported are the average of ten readings.

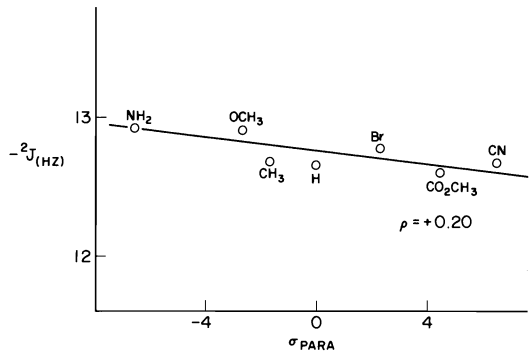

FIG. 3. A plot of ^2J *vs.* σ values.

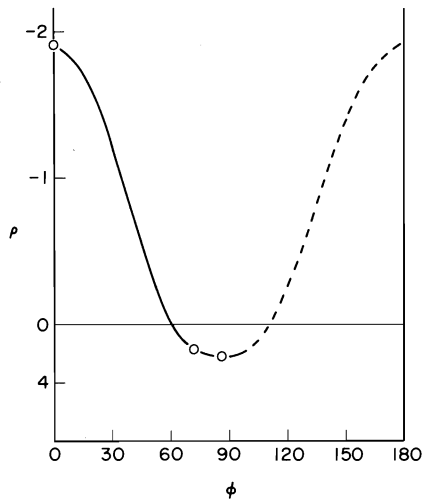

FIG. 4. A plot of the substituent effect *vs.* the angle φ.

TABLE 2. The dependence of ^2J on the angle ϕ

Compound	ϕ	$-^2J$(Hz)	Ref.
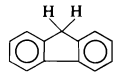	0	23.6	4
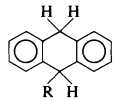 R = CH_3, C_6H_5 R = C_2H_5, C_3H_7 R = $C(CH_3)_3$	45*	18.1 18.3 18.8	21
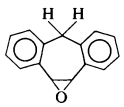	72	13.6	2
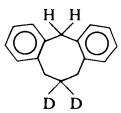	87	12.4	†
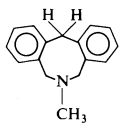	87	12.7	This work

*Although the angle may change with the nature of R (21), it has been determined for R = H by Ferrier and Iball (22).
†From a manuscript in preparation by R. R. Fraser, R. N. Renaud, and J. W. Bovenkamp.

Experimental

All melting points are uncorrected. Infrared spectra were observed on a Perkin-Elmer model 267 spectrophotometer and only characteristic bands are reported. Unless specified routine nmr spectra were taken in deuterochloroform solution on a Varian Associates spectrometer model E.M. 360 and the chemical shifts are reported on the δ scale. Precise coupling constant determinations were carried out using a Varian HA-100 spectrometer. All coupling constants were determined with 0.2 *M* solutions in deuterochloroform at 10°C. The spectral line positions were always determined from an average of at least ten measurements.

Preparation of ***1a***

This compound has been synthesized previously (11) starting from the commercially available dibenzsuberone.

Preparation of ***2b***, ***2c***, *and* ***2d***

The synthesis of **2***b*, **2***c*, and **2***d* has been described in ref. 23.

Preparation of ***3b***

Oxidation of **2***b* with potassium permanganate as described for the synthesis of **3***a* (11) gave a white solid (mp 213–217°C) in a yield of 58%. Upon recrystallization from methanol–water, a solid mp 224.5–225.5°C, was obtained; ^{1}H nmr (DMSO-d_6) 8.08–6.79 (9H, m, aromatic and carboxyl hydrogens), 4.65 (2H, s, methylene), 2.32 (3H, s, methyl).

The dimethyl ester derivative of **3***b* was prepared by methylating the diacid with an excess of diazomethane in ether. The viscous oil obtained was purified by a bulb to bulb distillation under reduced pressure. *Anal.* calcd. for $C_{18}H_{18}O_4$: C 72.46, H 6.08; found: C 72.64, H 6.17.

Preparation of ***3c***

The olefin **2***c* was oxidized in the same manner as **2***b*; however, a low overall yield of **3***c* was obtained because about one third of the crude oxidation product was the diacid with the bridgehead methylene group further oxidized to the ketone. After a careful fractional recrystallization from methanol–water, a 29% yield of the required white solid was obtained (mp 227–228°C); ^{1}H nmr (DMSO-d_6) 7.95–6.78 (9H, m, aromatic and carboxyl hydrogens), 4.60 (2H, s, methylene), 3.75 (3H, s, methoxyl).

Preparation of ***3d***

Oxidation of **2***d* (as described for **2***b*) gave a white solid which after recrystallization from methanol–water had an mp of 240.5–242°C (63%); ^{1}H nmr (DMSO-d_6) 8.11–6.74 (9H, m, aromatic and carboxyl hydrogens), 4.63 (2H, s, methylene).

The dimethyl ester derivative of **3***d*, obtained by methylation with diazomethane, had an mp of 40–42°C after a bulb to bulb distillation under reduced pressure. *Anal.* calcd. for $C_{17}H_{15}O_4Br$: C 56.22, H 4.16, Br 22.00; found: C 56.26, H 4.07, Br 22.07.

Preparation of ***4b***, ***4c***, *and* ***4d***

The diacids **3***b*, **3***c*, and **3***d* were reduced in near quantitative yields with diborane using the procedure of Schmitt *et al.* (24). A diagram of the apparatus used is given in ref. 25. Physical properties of: (*i*) **4***b*: mp 134–136°C; ^{1}H nmr: 7.59–6.63 (7H, m, aromatic), 5.09 and 5.05 (2H, two equal t (J = 5 Hz), two OH, exchange with D_2O), 4.48–4.43 (4H, two equal d (J = 5 Hz) two methylenes from the CH_2OH groups, two s in D_2O), 3.94 (2H, s, methylene), 2.30 (3H, s, methyl). (*ii*) **4***c*: mp 140.0–140.5°C; nmr: 7.51–6.01 (7H, m, aromatic), 5.10 and 5.07 (2H, two equal t (J = 5 Hz), two OH, exchange with D_2O), 4.46 and 4.41 (4H, two equal d, (J = 5 Hz), two methylenes of the CH_2OH groups, two s in D_2O), 3.86 (2H, s, methylene), 3.70 (3H, s, methoxyl). (*iii*) **4***d*: mp 142–144°C; ^{1}H nmr: 7.68–6.57 (7H, m, aromatic), 5.14 and 4.97 (2H, two equal t (J = 5 Hz), two OH, exchange with D_2O), 4.41 (4H, d (J = 5 Hz), two methylenes of the CH_2OH groups, two s in D_2O), 3.87 (2H, s, methylene).

Preparation of ***5b***, ***5c***, *and* ***5d***

The diols **4***b*, **4***c*, and **4***d* were converted to the corresponding dibromides with phosphorus tribromide using the same procedure used to obtain **5***a* (11). The yields of the crude products were nearly quantitative and analytical samples were obtained by recrystallization from a mixture of benzene and ethanol. Physical properties of: (*i*) **5***b*: mp 92–93°C; ^{1}H nmr: 7.52–6.76 (7H, m, aromatic), 4.50 and 4.48 (4H, two equal s, methylenes of the CH_2Br groups), 4.24 (2H, s, methylene), 2.34 (3H, s, methyl). *Anal.* calcd. for $C_{16}H_{16}Br_2$: C 52.20, H 4.38, Br 43.41; found: C 52.40, H 4.46, Br 43.27. (*ii*) **5***c*: mp 77.5–78.5°C; ^{1}H nmr: 7.37–6.71 (7H, m, aromatic), 4.47 and 4.40 (4H, two equal s, methylenes of the CH_2Br groups), 4.17 (2H, s, methylene), 3.77 (3H, s, methoxyl). *Anal.* calcd. for $C_{16}H_{16}Br_2O$: C 50.03, H 4.20, Br 41.61; found: C 50.20, H 4.23, Br 41.44. (*iii*) **5***d*: mp 118.5–119.5°C; ^{1}H nmr:

7.60–6.69 (7H, m, aromatic), 4.45 and 4.38 (4H, two equal s, methylenes of the CH_2Br groups), 4.20 (2H, s, methylene). *Anal.* calcd. for $C_{15}H_{13}Br_3$: C 41.61, H 3.03, Br 55.36; found: C 41.48, H 3.04, Br 55.21.

Preparation of 1b, 1c, and 1d

The ring closure reactions of the compounds **5***b*, **5***c*, and **5***d* were carried out with a 33% ethanolic solution of monomethylamine in 1-hexanol according to the procedure of Casadio *et al.* (26) (method *B*). Somewhat better yields were obtained if, during the work-up, the residue obtained on removal of the solvent is made strongly acidic with hydrobromic acid and heated for a short time at 60°C to make sure that all of the azocine has been taken up. The crude products were purified either by sublimation (**1***b* and **1***c*) or by recrystallization from 95% ethanol (**1***d*). Physical properties of: (*i*) **1***b*: mp 86–87.5°C; ^{1}H nmr: 7.42–6.82 (7H, m, aromatic), 4.89–3.48 (6H, m, methylenes at C-5, C-7, and C-12), 2.25 (3H, s, methyl at C-3), 1.95 (3H, s, *N*-methyl). *Anal.* calcd. for $C_{17}H_{19}N$: C 86.03, H 8.07, N 5.90; found: C 85.81, H 7.96, N 5.73. (*ii*) **1***c*: mp 101.5–102.5°C; ^{1}H nmr (CCl_4): 7.21–6.41 (7H, m, aromatic), 4.63–3.39 (6H, m, methylenes at C-5, C-7, and C-12), 3.63 (3H, s, methoxyl), 1.81 (3H, s, *N*-methyl). *Anal.* calcd. for $C_{17}H_{19}NO$: C 80.60, H 7.56, N 5.53; found: C 80.54, H 7.68, N 5.64. (*iii*) **1***d*: mp 142.5–143.5°C; ^{1}H nmr: 7.39–6.86 (7H, m, aromatic) 4.79–3.35 (6H, m, methylenes at C-5, C-7, and C-12), 1.92 (3H, s, *N*-methyl). *Anal.* calcd. for $C_{16}H_{16}NBr$: C 63.59, H 5.34, N 4.63, Br 26.44; found: C 63.44, H 5.22, N 4.65, Br 26.25.

Preparation of 1e

The compound **1***e* was prepared from **1***d* according to the method described by Newman and Boden (27) with some modification. A stirred mixture of **1***d* (1.00 g, 3.33 mmol), cuprous cyanide (0.685 g, 7.65 mmol), and freshly distilled *N*-methylpyrrolidone (35 ml) was refluxed for 3 h. The reaction mixture was cooled and then poured into a solution of ethylenediamine (20 ml) and water (60 ml). The complex was broken up by heating the mixture at 80°C for 1.5 h. The mixture was then twice extracted with benzene. The combined extracts were washed with 10% aqueous sodium cyanide and then water. The benzene solution was shaken twice with 24% aqueous hydrobromic acid. Upon neutralization with aqueous sodium hydroxide 0.700 g (mp 172–175°C) of white solid was obtained. This solid was sublimed to give 0.643 g (78%) of a white solid (mp 174.5–176°C); ^{1}H nmr: 7.47–6.87 (7H, m, aromatic), 4.85–3.50 (6H, m, methylenes at C-5, C-7, and C-12), 1.92 (3H, s, *N*-methyl). *Anal.* calcd. for $C_{17}H_{16}N_2$: C 82.22, H 6.49, N 11.28; found: C 82.23, H 6.54, N 11.33.

Preparation of 1f

The nitrile **1***e* (0.204 g, 0.823 mmol) and 5 ml of a mixture of concentrated sulfuric acid and methanol (33 wt.% concentrated sulfuric acid) were refluxed overnight. Water was added (20 ml) and the solution was neutralized with aqueous sodium hydroxide. The resultant white precipitate was collected (0.209 g, 91%) (mp 151–154°C). Recrystallization from a methanol–benzene mixture gave small white needles melting at 159–159.5°C; ^{1}H nmr: 8.03–7.02 (7H, m, aromatic), 4.89–3.59 (6H, m, methylenes at C-5, C-7, and C-12), 3.86 (3H, s, carbomethoxy), 1.95 (3H, s, *N*-methyl). *Anal.* calcd. for $C_{18}H_{19}NO_2$: C 76.84, H 6.81, N 4.98; found: C 77.01, H 6.81, N 5.10.

Preparation of 1g

The nitrile **1***e* (0.333 g, 1.34 mmol) was slowly added to 3.5 ml of a mixture of concentrated sulfuric acid and water (85 vol.% sulfuric acid) at 75°C. The solution was heated at 85–90°C for 1.5 h. After being cooled, the reaction solution was added to a mixture of concentrated ammonium hydroxide (16 ml), ice, and water (30 ml). The solid that precipitated out was collected and extracted with hot acetone several times. On removal of the acetone, 0.294 g (82%) of the amide **1***g* (mp 235.5–238°C) was obtained; ^{1}H nmr (DMSO-d_6) 8.04–6.96 (9H, m, aromatic and amide hydrogens), 4.90–3.53 (6H, m, methylenes at C-5, C-7, and C-12), 1.88 (3H, s, *N*-methyl).

Preparation of 1h

The compound **1***h* was prepared according to a modified procedure described by Radlich and Brown (16). A solution of sodium methoxide in methanol (8.5 ml) was prepared from sodium (0.38 g) in a three-necked flask equipped with a reflux condenser (protected by a drying tube) and a separatory funnel. The solution was cooled to −45°C with a dry ice – acetone bath and then bromine (0.93 g) was added dropwise with vigorous stirring. When the colour had discharged, the amide **1***g* (0.294 g, 1.11 mmol), dissolved in 3.5 ml of dioxane and 2.5 ml of methanol, was added slowly while maintaining the temperature at −40°C. After the addition, a further 2.5 ml of methanol was added. The temperature was then raised to 62°C for 1.25 h. The solution was cooled to 25°C. Water (30 ml) was added and the mixture was extracted twice with chloroform. The combined chloroform layers were washed with sodium chloride solution and then dried with anhydrous $MgSO_4$. On removal of the solvent 0.286 g (87%) of a white solid (mp 144–146°C) was obtained; ^{1}H nmr: 7.51–6.64 (8H, m, aromatic and NH hydrogens), 4.87–3.47 (6H, m, methylenes at C-5, C-7, and C-12), 3.75 (3H, s, carbamate methyl), 1.95 (3H, s, *N*-methyl).

Preparation of 1i

The carbamate **1***h* (0.286 g, 0.96 mmol) was added to 20 ml of 37% aqueous hydrochloric acid and the solution was refluxed for 17 h. At the end of the reflux period, the solution had become dark in colour. On neutralization with aqueous sodium hydroxide, a green precipitate was obtained which was collected by filtration and washed with water to leave 0.140 g (61%) of a solid melting at 144–146.5°C. An analytical sample was obtained by recrystallization from benzene and then sublimed to give a white solid melting at 151.5–152°C; ^{1}H nmr: 7.51–6.32 (7H, m, aromatic), 4.86–3.10 (8H, m, methylenes at C-5, C-7, and C-12 and amine hydrogens), 1.96 (3H, s, *N*-methyl). *Anal.* calcd. for $C_{16}H_{18}N_2$: C 80.63, H 7.61, N 11.76; found: C 80.51, H 7.49, N 11.59.

Acknowledgements

The authors are grateful to Mr. H. Séguin for elemental analyses. One of us (R.R.F) thanks the National Research Council of Canada for financial support.

1. R. R. Fraser, P. Hanbury, and C. Reyes-Zamora. Can. J. Chem. **45**, 2481 (1967).
2. R. R. Fraser, R. N. Renaud, C. Reyes-Zamora, and R. B. Swingle. Can. J. Chem. **47**, 2767 (1969); R. R. Fraser and R. N. Renaud. Can. J. Chem. **49**, 755 (1971).

3. R. R. FRASER. Can. J. Chem. **40**, 1483 (1962).
4. CH. BREVARD, J. P. KINTZINGER, and J. M. LEHN. Tetrahedron, **28**, 2429 (1972).
5. A. A. BOTHNER-BY. Adv. Magn. Reson. **1**, 197 (1965).
6. M. BARFIELD and D. M. GRANT. J. Am. Chem. Soc. **85**, 1899 (1963).
7. J. A. POPLE and A. A. BOTHNER-BY. J. Chem. Phys. **42**, 1339 (1965); G. E. MACIEL, J. W. MCIVER, N. S. OSTLUND, and J. A. POPLE. J. Am. Chem. Soc. **92**, 4151 (1970).
8. D. MONTECALVO and M. ST-JACQUES. J. Org. Chem. **40**, 940 (1975).
9. R. R. FRASER, M. A. PETIT, and M. A. MISKOW. J. Am. Chem. Soc. **94**, 3253 (1972).
10. Y. L. CHOW, S. BLACK, J. E. BLIER, and M. M. TRACEY. Can. J. Chem. **48**, 2134 (1970).
11. R. N. RENAUD, R. B. LAYTON, and R. R. FRASER. Can. J. Chem. **51**, 3380 (1973).
12. R. R. FRASER, M. A. RAZA, R. N. RENAUD, and R. B. LAYTON. Can. J. Chem. **53**, 167 (1975).
13. A. D. HARDY and F. R. AHMED. Acta Crystallogr. Sect. B, **30**, 1670 (1974).
14. F. R. AHMED. Acta Crystallogr. Sect. B, **31**, 26 (1975).
15. E. MAGNIEN and R. BALTZLY. J. Org. Chem. **23**, 2029 (1958).
16. P. RADLICH and L. R. BROWN. Synthesis, 290 (1974).
17. D. H. MCDANIEL and H. C. BROWN. J. Org. Chem. **23**, 420 (1958).
18. H. H. JAFFÉ. Chem. Rev. **53**, 191 (1953).
19. R. C. COOKSON, T. A. CRABB, J. J. FRANKEL, and J. HUDEC. Tetrahedron Suppl. **7**, 355 (1966).
20. M. RAMARAO and A. A. BOTHNER-BY. Org. Magn. Reson. **8**, 329 (1976).
21. A. W. BRINKMANN, M. GORDON, R. G. HARVEY, P. W. RABIDEAU, J. B. STOTHERS, and A. L. TERNAY, JR. J. Am. Chem. Soc. **92**, 5912 (1970).
22. W. G. FERRIER and J. IBALL. Chem. Ind. 1296 (1954).
23. R. R. FRASER and R. N. RENAUD. Can. J. Chem. **49**, 746 (1971).
24. J. SCHMITT, J. J. PANOUSE, A. HALBOT, H. PLUCHET, P. COMOY, and P.-J. CORNU. Bull. Soc. Chim. Fr. 816 (1963).
25. G. ZWEIFEL and H. C. BROWN. Organic reactions. Vol. 13. J. Wiley, New York, NY. 1963. p. 1.
26. S. CASADIO, G. PALA, E. CRESCENZI, E. MARAZZI-UBERTI, G. COPPI, and C. TURBA. J. Med. Chem. **11**, 97 (1968).
27. M. S. NEWMAN and H. BODEN. J. Org. Chem. **26**, 2525 (1961).

^1H and ^{13}C dynamic nuclear magnetic resonance study of hindered rotation in thiobenzoylpiperidines and thiobenzoylmorpholines. Correlation between barrier heights of amides and thioamides

CARLA PICCINNI-LEOPARDI, OMER FABRE, DANIEL ZIMMERMANN, AND JACQUES REISSE[1]

Chimie Organique E.P., Université Libre de Bruxelles, 50, avenue F. D. Roosevelt B 1050 Bruxelles, Belgium

AND

F. CORNEA AND C. FULEA

Faculty of Chemistry, University of Bucharest, Bucharest, Rumania

Received December 14, 1976

CARLA PICCINNI-LEOPARDI, OMER FABRE, DANIEL ZIMMERMANN, JACQUES REISSE, F. CORNEA, and C. FULEA. Can. J. Chem. **55**, 2649 (1977).

The free energies of activation for hindered rotation around the C—N bond have been determined for a series of *N*,*N*-disubstituted thioamides by means of ^{13}C and ^1H dynamic nmr. A comparison between barriers for 20 amides and the corresponding thioamides, studied under similar conditions, has been drawn up using both our results and data obtained from the literature. An excellent linear correlation has been obtained. The same correlation also holds for primary (thio)amides and seems to be of general significance. Substituent effects on the barrier heights of thioamides and amides are discussed in connection with some particular cases.

CARLA PICCINNI-LEOPARDI, OMER FABRE, DANIEL ZIMMERMANN, JACQUES REISSE, F. CORNEA et C. FULEA. Can. J. Chem. **55**, 2649 (1977).

L'energie libre d'activation associée à la rotation empechée autour du lien C—N a été déterminée pour une série de thioamides en utilisant la rmn dynamique de ^{13}C et ^1H. Une comparaison entre les barrières de 20 amides et des thioamides correspondants a été effectuée en se basant non seulement sur nos données mais aussi sur des valeurs fournies par la littérature. Une excellente corrélation linéaire a été obtenue. Cette corrélation est valable également pour des (thio)amides primaires et semble donc de portée générale. Les effets de substituants sur les hauteurs de barrière de quelques thioamides et amides sont discutés.

Introduction

Our study of the physical properties of thioamides and amides has led us to determine the barriers to rotation around the carbon–nitrogen bond of the thiobenzamides **1***a*–**1***f* and **2***b*, **2***d*, and **2***f*.

As usual, we had a choice of three possibilities

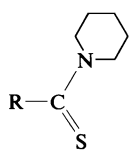

1

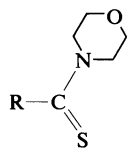

2

a R = C_6H_5—CH_2
b R = *p*-NO_2—C_6H_4
c R = *m*-NO_2—C_6H_4
d R = C_6H_5
e R = *p*-Cl—C_6H_4
f R = *p*-OCH_3—C_6H_4

b R = *p*-NO_2—C_6H_4
d R = C_6H_5
f R = *p*-OCH_3—C_6H_4

for obtaining the chemical exchange rates from the shape of nmr signals: the use of approximate equations (*i.e.* the single parameter methods), the total line shape (TLS) method, and the observation of coalescence phenomenon. The use of approximate equations, relating some features in the experimental nmr spectrum (such as line separation, linewidth, peak-to-valley ratio, or peak-to-peak ratio) to the exchange rate, may be the cause of appreciable errors at the level of $\Delta H^{\ddagger}$ and $\Delta S^{\ddagger}$, as has already been demonstrated (1, 2). It may thus appear desirable to determine exchange parameters using information taken from the complete spectral lineshape. It has been demonstrated by Drakenberg *et al.* (2) and Shoup *et al.* (3), however, that the use of the complete lineshape is, *per se*, not necessarily a guarantee of accurate activation parameters. $\Delta H^{\ddagger}$ and $\Delta S^{\ddagger}$ values can, in fact, be inaccurate because of unavoidable systematic errors due to $|\delta\nu|$ and T_2 temperature dependence ($|\delta\nu|$ is the chemical shift difference, in the

[1]Author to whom correspondence should be addressed.

absence of exchange, between the two exchanging sites and T_2 the transverse relaxation time, assumed to be the same for nuclei at either site). On the other hand, when evaluated near coalescence, the free energy of activation ($\Delta G^{\ddagger}$) is found to be quite insensitive to systematic errors on these two parameters, and, consequently, the error for $\Delta G^{\ddagger}$ may be assumed to be determined essentially by statistical random errors (if the accuracy of temperature measurement is optimized (4)). Accordingly, we preferred to determine the free energies of activation at the coalescence temperature ($\Delta G_c^{\ddagger}$). It may be objected that the determination of $\Delta G_c^{\ddagger}$ could preclude comparison between different thioamides and amides, because of the temperature dependence of this parameter. From this point of view $\Delta H^{\ddagger}$ would appear at first sight to be a better kinetical parameter. Nevertheless, as will be discussed later, $\Delta G_c^{\ddagger}$ may be considered to be a good measure of the intramolecular enthalpy contribution to the barrier.

Experimental

^{13}C chemical shifts have been reported previously for all the thiobenzamides studied (5), in $CDCl_3$ solutions, the only exception being derivative **1***a*. The ^{13}C chemical shifts for this compound are the following (in ppm, downfield from TMS as internal standard): (*i*) thiocarbonyl carbon 198.5; (*ii*) aromatic carbons: C-1 136.3, *ortho*, *meta*, and *para* carbons 126.9, 127.9, and 128.8; (*iii*) heterocyclic carbons: α-*N*-methylene carbons 51.1 and 51.6, β-*N*-methylene carbons 25.3 and 26.2, γ-*N*-methylene carbon 23.9.

The ^{13}C dnmr measurements were carried out on a Bruker HX-90 spectrometer equipped with a B-ST 100/700 variable temperature system and operating at 22.63 MHz in the Ft mode. The spectrometer was internally locked on a C_6F_6 sample contained in a coaxial capillary. The precision in $|\delta\nu|$ values is ± 1.5 Hz.

The ^1H dnmr spectra were recorded with a Varian A-60 spectrometer equipped with a variable temperature probe and a V-6040 variable temperature controller. Accurate frequency measurements of the ^1H nmr signals were performed by the audio sideband technique. Precision in $|\delta\nu|$ values can be estimated to ± 1 Hz, due to the shape of the signals.

Solutions were 1 *M* in *o*-dichlorobenzene, unless otherwise stated.

Temperatures, measured both before and after each spectrum, were determined from the temperature dependent chemical shift of ethylene glycol in the Varian A-60 probe and by mercury or alcohol thermometers in the Bruker HX-90 probe. All temperature sensors were calibrated independently by a melting point method (see ref. 4). The error for temperature measurements was estimated to be ± 0.5°C, including statistical and systematic errors such as those due to temperature gradients. The error in $\Delta G_c^{\ddagger}$ due to an error of 1°C in T_c is 50 cal mol^{-1}.

Results

By means of ^1H and ^{13}C dynamic nuclear magnetic resonance (dnmr) we have studied the hindered rotation around the C(S)—N bond in the molecules **1***a*–**1***f* and **2***b*, **2***d*, and **2***f*. The free energies of activation (which are listed in Table 1) have been calculated at coalescence from [1]:

$$[1] \quad \Delta G_c^{\ddagger} = 4.576T_c(10.32 + \log(T_c/k_c))$$

where k_c, the rate constant for rotation at the coalescence temperature (T_c), is given by [2]:

$$[2] \quad k_c = \pi|\delta\nu|/\sqrt{2}$$

$|\delta\nu|$ is the chemical shift difference in Hz between the two exchanging sites (in our case, the α-*N*-methylene protons or the α-*N*-methylene carbons) in the condition of infinitely slow exchange rate. Attention must be drawn to the fact that the $|\delta\nu|$ value which should be used in [2] is the $|\delta\nu|$ value at T_c. The $|\delta\nu|$ value we used in our calculations was the low temperature value measured for $T < T_c$. However, it must be noted that $|\delta\nu|$ is relatively temperature independent in the slow exchange region. Since $\Delta G_c^{\ddagger}$ is quasi-insensitive to small errors in $|\delta\nu|$, when the $|\delta\nu|$ value is high (which is the case), this approximation is therefore perfectly admissible. In fact, $\Delta G_c^{\ddagger}$ values are essentially affected by errors in T_c and we took care to minimize this kind of error by using a method already described (4).

Equation 2 is derived from the Gutowsky–Holm equation (6) describing exchange between two equally populated sites which are not coupled with each other or with other nuclei in the molecule. It holds for cases where, in the absence of exchange, lineshapes are Lorentzian and linewidths are smaller than the non-exchanging chemical shift. Gutowsky and Holm (6) have shown that the overlap of the components of the doublet is negligible when the linewidth is smaller than about $\frac{2}{3}$ of the true (*i.e.* assuming no exchange and no overlap) separation between the components. In cases where the linewidth is greater than $\frac{2}{3}|\delta\nu|$, the rate constant cannot be calculated from the simplified [2] and the observed coalescence temperature is not equal to the coalescence temperature which would have been observed in the absence of overlap.

α-*N*-Methylene carbons give well separated narrow signals with Lorentzian lineshapes in

TABLE 1. $|\delta\nu|$ (Hz), T_c (K) and $\Delta G_c^{\ddagger}$ (kcal mol^{-1}) for the restricted rotation around the C—N bond in some thiobenzamides (1 mol ℓ^{-1} in *o*-dichlorobenzene, unless otherwise stated)

Thioamide	Method*	$\lvert\delta\nu\rvert$‡	T_c	$\Delta G_c^{\ddagger}$
1*a*	A	50.5	$388._3$	19.3
1*b*†	A	57.0	$362._3$	17.9
1*c*	A	55.5	$355._5$	17.5
1*d*	A	58.0	$352._1$	17.3_3
1*d*	B	59.0	$353._1$	17.3_7
1*e*	A	55.5	$346._7$	17.1
1*f*	A	51.0	$324._0$	16.0
2*b*†	B	51.0	$347._5$	17.2
2*d*†	B	67.5	$338._4$	16.5
2*f*†	B	63.0	$312._4$	15.2

*A: ^{1}H dnmr at 60 MHz; B: ^{13}C dnmr at 22.63 MHz.
†Saturated solution.
‡These values are determined at about 250 K for ^{1}H nmr spectra and 280 K for ^{13}C nmr spectra.

the ^{13}C noise-decoupled spectrum. Therefore, all the conditions are fulfilled to use [1]–[2]. On the other hand, α-*N*-methylene protons give broadened triplets (because of the coupling with β-*N*-methylene groups). The lineshapes are not Lorentzian, but the linewidths remain smaller than $\frac{2}{3}|\delta\nu|$ and signals do not overlap. We were able to test the applicability of [2] in this particular case because, in the experimental conditions we used, and by chance, the $|\delta\nu|$ values observed in ^{1}H and in ^{13}C nmr were the same for unsubstituted thiobenzoylpiperidine, *i.e.* compound **1***d*. We were then able to compare the coalescence temperatures determined by ^{1}H and ^{13}C nmr. As is shown in Table 1, the two coalescence temperatures compare very well within the limits of experimental errors. We were then justified in making use of [2] when we evaluated by ^{1}H dnmr the rotational barriers of derivatives similar to **1***d*, which we did for compounds **1***a*–**1***f*.

We determined the $\Delta G_c^{\ddagger}$ of thiobenzoylmorpholines by ^{13}C dnmr. For these molecules, coalescence could not be accurately obtained by ^{1}H dnmr because of interference from other spectral lines.

Discussion

Before starting a discussion concerning the structural effect on $\Delta G^{\ddagger}$ values, it is necessary to consider the $\Delta H^{\ddagger}$, $\Delta S^{\ddagger}$ problem. As has been stated previously, it may be argued that $\Delta H^{\ddagger}$ (or E_a) is a better kinetic parameter than $\Delta G^{\ddagger}$, since $\Delta G^{\ddagger}$ is the sum of an enthalpy and an entropy factor. Nevertheless, it is well known that, because of the mutual compensating effect of the correlated errors on $\Delta H^{\ddagger}$ and $\Delta S^{\ddagger}$ (7), $\Delta G^{\ddagger}$ can be obtained with much greater accuracy than $\Delta H^{\ddagger}$ and $\Delta S^{\ddagger}$ (2, and see, for example, ref. 8). Moreover, $\Delta H^{\ddagger}$, like $\Delta S^{\ddagger}$ and $\Delta G^{\ddagger}$, can be described as the sum of an intermolecular contribution and an intramolecular contribution ($\Delta Y^{\ddagger} = \Delta Y^{\ddagger}_{\text{inter}} + \Delta Y^{\ddagger}_{\text{intra}}$, where $Y = G, H, S$). In some particular cases, it has been proved that the intermolecular contributions to $\Delta H^{\ddagger}$ and $\Delta S^{\ddagger}$, or ΔH^0 and ΔS^0, have a mutual compensating effect in a series of homologous systems (9). As Sandström noted (10), it is very difficult to prove that such a situation exists for the activation parameters of (thio)amides but this possibility cannot be ruled out. We can also say that the intermolecular contributions to $\Delta H^{\ddagger}$ and $\Delta S^{\ddagger}$, whatever they may be, must be similar for similar systems. We may finally observe that the intramolecular contribution to $\Delta S^{\ddagger}$ must be very small as is the case for all equilibria, or pseudo-equilibria, between two stereoisomers. This affirmation is based on an estimate of the difference between the partition functions of stereoisomers in the gas phase (11). The translational contribution to the entropy difference must be the same for two stereoisomers for obvious reasons, so the only possible differences arise from vibrational and rotational contributions. In our case, the symmetry number of the two molecular species (fundamental state and activated state) is equal to one, so the only difference between the two rotational partition functions is originated by the difference between the products of principal inertia moments. This contribution is known to be very small (<1 eu) in such systems (11).

Without any precise knowledge of the vibrational modes in the low frequency region, it is difficult to make an estimate of the vibrational contribution to the partition functions. Nevertheless, it seems safe to assume that the low frequency regions are similar for the two molecular species if we consider the thioamides and the corresponding amides as being roughly constituted of two independent moieties linked by the four-atom system C—C(X)—N which is the only system strongly modified by the $2\pi/4$ rotation around the C—N bond. It is clear that this group itself is characterized by some low frequency absorptions (torsional oscillation around the C—N bond in the fundamental state, out-of-plane and in-plane bending of the C(X) bond), but it is difficult to imagine that these contributions to the entropy of activation are larger than 2 or 3 eu and very different from compound to compound. This last point is the most important for a comparison of barriers obtained for various amides and thioamides.

Therefore, for the reasons previously discussed, we consider that $\Delta G^{\ddagger}$ is a good measure of the intramolecular contribution to the enthalpy of activation or, at least, that the variation of $\Delta G^{\ddagger}$ from one compound to another in a series of homologous molecules reflects the variation of the intramolecular contribution to $\Delta H^{\ddagger}$. We can then compare the $\Delta G^{\ddagger}$ values obtained for these two kinds of molecules in order to see if the intramolecular structural features have similar consequences on the barrier in the two series. This kind of approach has already been used by measuring the increments (in terms of $\delta\Delta G^{\ddagger}$) associated with the formal transformation *amide* → *thioamide* (12–14). We have preferred to use a slightly different approach based on a careful selection of many pairs of symmetrically disubstituted amides and thioamides recently studied in the literature. For each amide–thioamide pair we have selected barrier values determined in conditions which are as similar as possible (solvents, concentrations and temperatures). Our approach simply consists of the establishment of a linear correlation of the form

$$\Delta G^{\ddagger}(\text{thioamide}) = a + b\Delta G^{\ddagger}(\text{amide})$$

A least-squares linear regression analysis gives the following equation:

$$[3]\quad \Delta G^{\ddagger}(\text{thioamide}) = 1.13 + 1.11\Delta G^{\ddagger}(\text{amide})$$

Correlation coefficient, $r = 0.97$

Number of points: 20

represented in Fig. 1. The amide barriers chosen for this calculation are given in Table 2 and the corresponding values for thioamides are given in Table 3.

The average difference between values of the experimental barriers for thioamides (given in Table 3) and values of the barriers calculated by means of [3] is 0.54 kcal mol^{-1}, while the maximum and the minimum deviations are, respectively, equal to 1.73 and 0.09 kcal mol^{-1}. In 15 of the 20 cases, the difference in absolute value is smaller than 0.6 kcal mol^{-1}.

All the (thio)amides, except three, are formamides, alkyl-, or arylamides. The three exceptions in each series (entries 1, 4, 7 in Tables 2 and 3) correspond to derivatives with halogen or cyano substituents fixed on the (thio)carbonyl group. This small number of examples was selected in order to prove that even with such substituents the linear correlation holds very well. Moreover, and to test the generality of our relation, we added to the 20 points of the graph represented in Fig. 1 five further points corresponding to the barrier values of primary amides and thioamides studied by Walter *et al.* (24). Then the intercept and the slope become equal to 1.47 kcal mol^{-1} and 1.10, respectively, the correlation coefficient remaining equal to 0.97. It seems therefore that the same linear correlation holds for a great variety of primary and tertiary amides and thioamides.

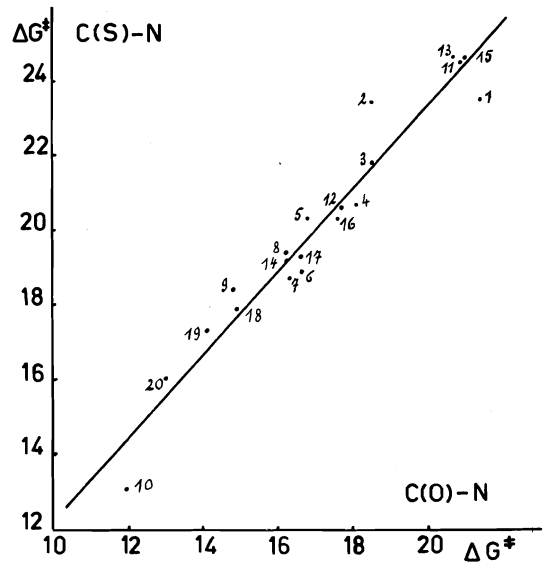

FIG. 1. The linear correlation between barriers of thioamides and amides ($\Delta G^{\ddagger}$, in kcal mol^{-1}; numbers refer to Tables 2 and 3).

TABLE 2. Free energies of activation for some *N,N*-disubstituted amides (kcal mol^{-1})

Entry	Amide	Method†	Solvent**	$\Delta G^*(T)$‡	Ref.
1.	$NC\text{-}C(O)\text{-}N(CH_3)_2$	TLS	TCE	21.4(298)	15
2.	$D_3C\text{-}C(O)\text{-}N(CH_3)_2$	TLS	DMSO-d_6	18.5(298)	16
3.	$H_3C\text{-}C(O)\text{-}N(CH_3)_2$	TLS	*o*-DCB	18.5(318)	12
4.	$F\text{-}C(O)\text{-}N(CH_3)_2$	TLS	CCl_4	18.1(298)	17
5.	$H_3C\text{-}C(O)\text{-}N(CH_3)_2$	T_c det.	Cyclohexane	16.8(311)*	18
6.		T_c det.	*o*-DCB	16.6(311.5)*	19
7.	$Cl\text{-}C(O)\text{-}N(CH_3)_2$	TLS	CCl_4	16.3(298)	20
8.	$(CH_3)_2CH\text{-}C(O)\text{-}N(CH_3)_2$	T_c det.	*o*-DCB	16.2(299)*	19
9.	$C_6H_5\text{-}C(O)\text{-}N(CH_3)_2$	T_c det.	*o*-DCB	14.8(286.5)*	§
10.	$(CH_3)_3C\text{-}C(O)\text{-}N(CH_3)_2$	T_c det.	$CDCl_3$	11.95(234)*	21
11.	$H\text{-}C(O)\text{-}N(C_2H_5)_2$	TLS	*o*-DCB	20.9(389)	12
12.	$H_3C\text{-}C(O)\text{-}N(C_2H_5)_2$	TLS	*o*-DCB	17.7(330)	12
13.	$H\text{-}C(O)\text{-}N[CH(CH_3)_2]_2$	TLS	*o*-DCB	20.7(378)	12
14.	$H_3C\text{-}C(O)\text{-}N[CH(CH_3)_2]_2$	TLS	*o*-DCB	16.2(322)	12
15.	$H\text{-}C(O)\text{-}N[CH_2CH(CH_3)_2]_2$	TLS	*o*-DCB	21.0(373)	12
16.	$H_3C\text{-}C(O)\text{-}N[CH_2CH(CH_3)_2]_2$	TLS	*o*-DCB	17.6(333)	12
17.		T_c det.	*o*-DCB	16.6(344.5)*	§
18.		T_c det.	*o*-DCB	14.9(297.5)*	§
19.		T_c det.	*o*-DCB	14.1(281)*	§
20.		T_c det.	*o*-DCB	13.0(256)*	§

**TCE: tetrachloroethane; DMSO: dimethyl sulfoxide; *o*-DCB: *o*-dichlorobenzene.
†TLS: total line shape analysis; T_c det.: coalescence temperature determination. For the amide of entry 6 only the ΔG^* value obtained by an approximate method was available. In this case, we preferred to calculate the barrier to rotation at coalescence by [1] from the $|\delta\nu|$ and T_c data furnished in the original paper.
‡Temperature, in Kelvin. A temperature marked with an asterisk is a coalescence temperature.
§C. Piccinni-Leopardi *et al.*, unpublished results.

It is difficult to decide whether the experimental value for the slope *b* is significantly different from unity or not. By the usual methods of correlation analysis, it is possible to calculate that the exact slope value is included, with a probability equal to 0.9, between the limits 1.0 and 1.2. The same treatment applied to the intercept proves without any doubt that this term is significantly different from zero. This conclusion reflects the fact that higher barrier values are generally observed for thioamides as opposed to amides. Both this problem and other problems like those concerning the substituent effects on the barriers of amides and thioamides have already been extensively discussed in the literature (see for example refs. 10, 12–14, 22 and the references cited therein). Electron donors have a lowering effect on the barrier when attached to the thiocarbonyl (or carbonyl) carbon. Such an effect can be observed both with alkyl and phenyl substituents, and with chlorine and fluorine atoms acting as π donors. On the other hand, electron acceptors like CN have virtually no effect on the barrier which remains similar to that for the unsubstituted system, *i.e. N,N*-dimethylthioformamide (12). Qualitatively, the electron donor effect can be justified in terms of the relative weight of the canonical structure I in the following scheme:

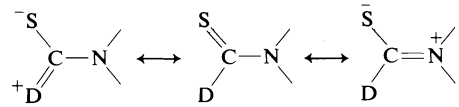

I II III

Any factor which increases the relative weight of I lowers the barrier. When D is a phenyl group, the donating effect can be increased or reduced by the substitution on the aromatic system. In the series of thiopiperidides and thiomorpholides studied during this work, we observed a decrease of the barrier for **1***f* (or **2***f*) but an increase for **1***b* (or **2***b*) relative to the unsubstituted derivative **1***d* (or **2***d*). We made

TABLE 3. Free energies of activation for some *N,N*-disubstituted thioamides (kcal mol^{-1})

Entry	Thioamide	Method†	Solvent**	$\Delta G^{\ddagger}$ (T)‡	Ref.
1.	$NC\text{-}C(S)\text{-}N(CH_3)_2$	TLS	TCE	23.5(298)	22
2.	$D_3C\text{-}C(S)\text{-}N(CH_3)_2$	TLS	DMSO-d_6	23.4(298)	16
3.	$H_3C\text{-}C(S)\text{-}N(CH_3)_2$	TLS	*o*-DCB	21.8(409)	12
4.	$F\text{-}C(S)\text{-}N(CH_3)_2$	TLS	TCE	20.7(298)	22
5.	$D_3C\text{-}C(S)\text{-}N(CH_3)_2$	TLS	Decalin	20.3(298)	23
6.		T_c det.	*o*-DCB	18.9(357)*	19
7.	$Cl\text{-}C(S)\text{-}N(CH_3)_2$	TLS	CCl_4	18.7(298)	22
8.	$(CH_3)_2CH\text{-}C(S)\text{-}N(CH_3)_2$	T_c det.	*o*-DCB	19.4(370)*	19
9.	$C_6H_5\text{-}C(S)\text{-}N(CH_3)_2$	T_c det.	*o*-DCB	18.4(365)*	10
10.	$(CH_3)_3C\text{-}C(S)\text{-}N(CH_3)_2$	T_c det.	$CDCl_3$	13.1(244)*	21
11.	$H\text{-}C(S)\text{-}N(C_2H_5)_2$	TLS	*o*-DCB	24.5(445)	12
12.	$H_3C\text{-}C(S)\text{-}N(C_2H_5)_2$	TLS	*o*-DCB	20.6(397)	12
13.	$H\text{-}C(S)\text{-}N[CH(CH_3)_2]_2$	TLS	*o*-DCB	24.6(427)	12
14.	$H_3C\text{-}C(S)\text{-}N[CH(CH_3)_2]_2$	TLS	*o*-DCB	19.2(387)	12
15.	$H\text{-}C(S)\text{-}N[CH_2CH(CH_3)_2]_2$	TLS	*o*-DCB	24.6(444)	12
16.	$H_3C\text{-}C(S)\text{-}N[CH_2CH(CH_3)_2]_2$	TLS	*o*-DCB	20.3(384)	12
17.		T_c det.	*o*-DCB	19.3(388)*	This work
18.		T_c det.	*o*-DCB	17.9(362)*	This work
19.		T_c det.	*o*-DCB	17.3(352)*	This work
20.		T_c det.	*o*-DCB	16.0(324)*	This work

**Abbreviations as in footnote **, Table 2.
†TLS: total line shape analysis; T_c det.: coalescence temperature determination. For the thioamides of entries 6 and 9 only the $\Delta G^{\ddagger}$ values obtained by approximate methods were available. In these cases we preferred to calculate the barriers to rotation at coalescence by [1] from the $|\delta\nu|$ and T_c data furnished in the original papers.
‡See the footnote ‡, Table 2.

the same observation in the case of the corresponding amides (C. Piccinni-Leopardi *et al.*, unpublished results). In the thiobenzoylpiperidines or -morpholines and in the corresponding amides, the phenyl ring in the preferred conformation is not in the plane of the thioamide group. An X-ray diffraction study (25) on thiocarbamoyl-4-pyridine has shown that the dihedral angle between the two planar moieties is 38°. Nevertheless, such an angle is not sufficient to completely suppress the conjugation between the two π systems (26) and the influence of the *para* substituents on the barrier is proof of the existence of an interaction between the two systems.

We will now point out the difference which exists between barriers of one thiopiperidide and the corresponding thiomorpholide (**1***b* compared to **2***b*, **1***d* to **2***d*, and **1***f* to **2***f*). Hirsch *et al.* (27), who observed the phenomenon in the case of benzoylpiperidine and benzoylmorpholine, considered the difference to be of no significance. We disagree with this conclusion since we have observed the same behaviour for three couples of thioamides and the analogous couples of amides. In all cases, the barrier in the (thio)morpholide is lower than the barrier in the corresponding (thio)piperidide. Considering the similarities between piperidine and morpholine it seems difficult to invoke a steric effect. It is therefore tempting to correlate the lower barrier in the (thio)morpholide series with a lower availability of the nitrogen lone pair electrons in morpholine compared to piperidine. A measure of this lower availability is given by the first ionization potentials of these two molecules, *i.e.* 8.91 eV for morpholine and 8.66 eV for piperidine (values obtained by photoelectron spectroscopy), since the first ionization potential may be safely assigned to the lone pair orbital on nitrogen (28).

Work is now in progress in order to see if the

barrier heights of amides and thioamides can be interpreted in terms of the electron-donating properties of the amine moiety and the electron-withdrawing properties of the acyl moiety as can be described in a HOMO–LUMO scheme (29).[2]

Acknowledgments

The investigation was supported by a grant from the Belgian "Fonds de la Recherche Fondamentale Collective". One author (C.P.-L.) is indebted to the Commission of the European Communities for a Euratom research grant.

1. A. ALLERHAND, H. S. GUTOWSKY, J. JONAS, and R. A. MEINZER. J. Am. Chem. Soc. **88**, 3185 (1966).
2. T. DRAKENBERG, K.-I. DAHLQVIST, and S. FORSÉN. Acta Chem. Scand. **24**, 694 (1970).
3. R. R. SHOUP, E. D. BECKER, and M. L. MCNEEL. J. Phys. Chem. **76**, 71 (1972).
4. C. PICCINNI-LEOPARDI, O. FABRE, and J. REISSE. Org. Magn. Reson. **8**, 233 (1976).
5. C. PICCINNI-LEOPARDI, O. FABRE, D. ZIMMERMANN, J. REISSE, F. CORNEA, and C. FULEA. Org. Magn. Reson. **8**, 536 (1976).
6. H. S. GUTOWSKY and C. H. HOLM. J. Chem. Phys. **25**, 1228 (1956).
7. (*a*) R. S. PETERSEN, J. H. MARKGRAF, and S. D. ROSS. J. Am. Chem. Soc. **83**, 3819 (1961); (*b*) K. B. WIBERG. Physical organic chemistry. Wiley, New York, NY. 1966; (*c*) R. R. KRUG, W. G. HUNTER, and R. A. GRIEGER. J. Phys. Chem. **80**, 2335 (1976); (*d*) R. R. KRUG, W. G. HUNTER, and R. A. GRIEGER. J. Phys. Chem. **80**, 2341 (1976).
8. H. KESSLER. Angew. Chem. Int. Ed. Engl. **9**, 219 (1970).
9. (*a*) K. J. LAIDLER. Trans. Faraday Soc. **55**, 1725 (1959); (*b*) L. G. HEPLER. J. Am. Chem. Soc. **85**, 3089 (1963).
10. J. SANDSTRÖM. J. Phys. Chem. **71**, 2318 (1967).
11. (*a*) G. J. JANZ. Thermodynamic properties of organic compounds. Academic Press, New York, NY. 1967; (*b*) S. W. BENSON. Thermochemical kinetics. Wiley, New York, NY. 1968; (*c*) J. REISSE. *In* Handbook of stereochemistry. Vol. II. *Edited by* H. Kagan. Georg Thieme Verlag, Stuttgart. In press.
12. T. H. SIDDALL III, W. E. STEWART, and F. D. KNIGHT. J. Phys. Chem. **74**, 3580 (1970).
13. W. E. STEWART and T. H. SIDDALL III. Chem. Rev. **70**, 517 (1970).
14. L. M. JACKMAN. *In* Dynamic nuclear magnetic resonance spectroscopy. *Edited by* L. M. Jackman and F. A. Cotton. Academic Press, New York, NY. 1975.
15. E. A. ALLAN, R. F. HOBSON, L. W. REEVES, and K. N. SHAW. J. Am. Chem. Soc. **94**, 6604 (1972).
16. R. C. NEUMAN, JR. and V. JONAS. J. Phys. Chem. **75**, 3532 (1971).
17. L. W. REEVES and K. N. SHAW. Can. J. Chem. **49**, 3671 (1971).
18. T. DRAKENBERG, K. J. DAHLQVIST, and S. FORSÉN. J. Phys. Chem. **76**, 2178 (1972).
19. G. ISAKSSON and J. SANDSTRÖM. Acta Chem. Scand. **21**, 1605 (1967).
20. R. C. NEUMAN, JR., D. N. ROARK, and V. JONAS. J. Am. Chem. Soc. **89**, 3412 (1967).
21. W. WALTER, E. SCHAUMANN, and H. PAULSEN. Justus Liebigs Ann. Chem. **727**, 61 (1969).
22. R. F. HOBSON, L. W. REEVES, and K. N. SHAW. J. Phys. Chem. **77**, 1228 (1973).
23. R. C. NEUMAN, JR. and V. JONAS. J. Org. Chem. **39**, 929 (1974).
24. W. WALTER, E. SCHAUMANN, and H. ROSE. Org. Magn. Reson. **5**, 191 (1973).
25. J.-C. COLLETER and M. GADRET. Bull. Soc. Chim. Fr. 3463 (1967).
26. I. FISCHER-HJALMARS. Tetrahedron, **19**, 1805 (1963) and references therein.
27. J. A. HIRSCH, R. L. AUGUSTINE, G. KOLETAR, and H. G. WOLF. J. Org. Chem. **40**, 3547 (1975).
28. F. P. COLONNA, G. DISTEFANO, S. PIGNATARO, G. PITACCO, and E. VALENTIN. J. Chem. Soc. Faraday Trans. II, **71**, 1572 (1975).
29. S. INAGAKI, H. FUJIMOTO, and K. FUKUI. J. Am. Chem. Soc. **98**, 4054 (1976).

[2]The authors would like to express their gratitude to Dr. Nguyen Trong Anh (Orsay) who, by his stimulating remarks, inspired their work in this direction.

Aromatic substitutions with carbanion nucleophiles. III. The kinetics of the reaction of picryl chloride with diethylmalonate anion[1]

KENNETH T. LEFFEK AND ANNA E. MATINOPOULOS-SCORDOU
Department of Chemistry, Dalhousie University, Halifax, N.S., Canada B3H 4J3

Received August 3, 1976[2]

KENNETH T. LEFFEK and ANNA E. MATINOPOULOS-SCORDOU. Can. J. Chem. **55**, 2656 (1977).

The reaction between 1-chloro-2,4,6-trinitrobenzene (picryl chloride) and diethylmalonate anion in benzene–DMSO 7:1 v/v solvent has been investigated by means of stopped-flow and uv–visible spectrophotometers. The results support a simple bimolecular aromatic substitution with a fast formation of a Meisenheimer-like coloured intermediate, followed by a slower decomposition to the picryl ester. The latter is rapidly deprotonated by the excess base. The steps of the reaction were followed separately and the rate constants and activation parameters have been measured.

KENNETH T. LEFFEK et ANNA E. MATINOPOULOS-SCORDOU. Can. J. Chem. **55**, 2656 (1977).

Travaillant dans un mélange de solvant formé de benzène et de DMSO 7:1 v/v et faisant appel à des spectrophotomètres à flux stoppé et uv–visible, on a étudié la réaction entre le chloro-1 trinitro-2,4,6 benzène (chlorure de picryle) et l'anion du malonate d'éthyle. Les résultats supportent un mécanisme de substitution aromatique bimoléculaire simple avec la formation rapide d'un intermédiaire coloré ressemblant à ceux de Meisenheimer qui est suivie par une décomposition plus lente conduisant à un ester de picryle. Ce dernier est rapidement déprotoné par un excès de base. On a suivi séparément les diverses étapes de la réaction et on en a mesuré les constantes de vitesse et les paramètres d'activation.

[Traduit par le journal]

Introduction

Except for the attack of bases derived from ketones on nitroaromatics, yielding mainly stable Janovsky or Zimmermann complexes (1–7), few reactions between carbanions and aromatic molecules have been reported (3–11). They all involve active methylene groups and, in contrast to ketones, usually lead to aromatic nucleophilic substitution products. Also, contrary to the case of oxygen nucleophiles where the kinetically controlled intermediate **1** is initially formed and is followed by the thermodynamically controlled **2**, with carbanion nucleophiles only one coloured intermediate has been observed in each reaction, which has been assumed to have the structure **2**. Direct observation by nmr has been reported only for the case of 2,4,6-trinitrocyclohexadienate with X = OCH_3 and Y = $CH(COCH_3)COOC_2H_5$ (12).

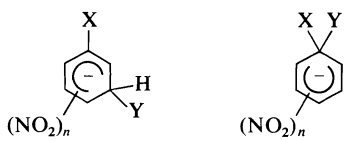

1 **2**

In the present study, a development of previous work on 1-fluoro-2,4-dinitrobenzene (13–14), the reaction between picryl chloride and diethylmalonate anion has been investigated using stopped-flow and uv–visible spectrophotometers. The results support the mechanism shown in reaction 1, with k_1, $k_3 \gg k_2$ and $k_{-1} \ll k_1$, $k_{-3} \ll k_3$.

Results and Discussion

Absorption Spectra

When solutions of picryl chloride and diethylmalonate sodium salt in DMSO are mixed, a red colour appears immediately which slowly changes to violet after about 4 h. This reaction cannot be studied kinetically because the formation of the red colour is too fast to be followed with a stopped-flow spectrophotometer. An additional inconvenience is that picryl chloride reacts slowly with DMSO to yield picric acid (15), so that stock solutions may not be used. The addition of benzene to the DMSO solvent decreases the rate of formation of the intermediate and increases its rate of decomposition. A mixture of benzene–DMSO of 7:1 v/v was found to be suitable for measurement of both the formation

[1]Presented at the 59th Annual Chemical Conference of the Chemical Institute of Canada, London, Ont., June 6–9, 1976.

[2]Revision received March 28, 1977.

[1]

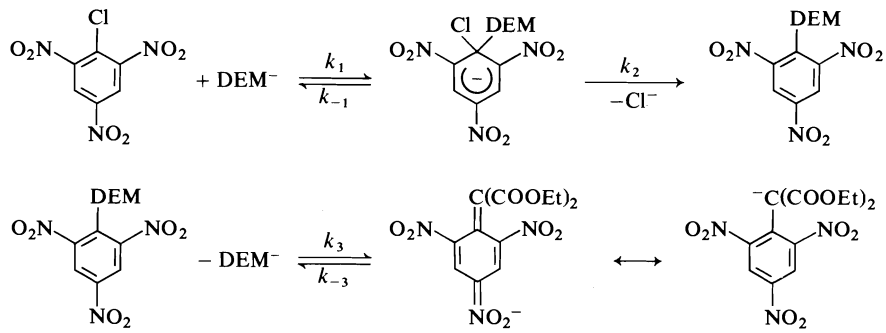

and decomposition rates. The spectra observed at various times after mixing are shown in Fig. 1. The decomposition of the initial intermediate to the final stable anion (λ_{max} 523 nm) goes through an isosbestic point, but is quite fast so that only part of the initial form can be scanned (curve 1).

With the excess of base, necessary to simplify the kinetic measurements, the reaction goes through to the final violet anion and if the conversion is assumed to be complete, the molar extinction coefficient of the peak at 523 nm is 9700 M^{-1} cm^{-1}. A sample of 2,4,6-trinitrophenyldiethylmalonate was isolated from the reaction carried out under preparative conditions and reacted with excess diethylmalonate anion in the same solvent. This gave a product peak at 523 nm, ε = 9600 M^{-1} cm^{-1}. The anion of the ester, which was isolated in reasonable purity and a solution made up by weight, gave λ_{max} 522 nm, ε = 9500 M^{-1} cm^{-1}. Thus, the reaction under study goes essentially to completion and is free from side reactions.

To obtain a spectrum of the initial intermediate a series of scans at fixed wavelengths and variable time were made on the stopped-flow spectrophotometer. From these, a series of spectra at definite times after mixing was obtained as shown in Fig. 2. It can be seen that there is an initial formation of an intermediate, essentially complete after about 20 ms, the spectrum of which closely resembles that of a Meisenheimer complex. A steady state exists from about 20 ms to about 2 s, after which decomposition of the intermediate takes place. Thus, by choosing the appropriate time base the rate constants for the formation and the decomposition of the intermediate of the reaction can be measured independently.

The final deprotonation step can be studied separately, using 2,4,6-trinitrophenyldiethylmalonate as substrate.

Kinetic Measurements

For an equilibrium in which the forward reaction is second order and the reverse reaction is first order, the integrated kinetic equation is

$$[2] \qquad \ln \frac{x_e}{x_e - x} = (k_1 b + k_{-1})t$$

where x_e and x are the product concentrations at equilibrium and at time t, respectively, k_1 is the second-order rate constant for the forward reaction and k_{-1} is the first-order rate constant for the reverse reaction and b is the reagent concentration, diethylmalonate anion in this case. If the concentration b is in excess of that of the substrate to the extent that it undergoes no significant change during the reaction, [2] yields a pseudo first-order rate constant k_{obs} equal to $(k_1 b + k_{-1})$. Thus, k_1 and k_{-1} can be obtained from the slope and intercept of a plot of k_{obs} *vs.* b.

The results for the formation of the intermediate are given in Table 1, for seven different temperatures. At two temperatures the rate constants were measured at the two wavelengths of 445 and 495 nm to check that the two peaks observed in Fig. 2 were, in fact, due to the same species. The second-order rate constants are the same within experimental error, showing that this is the case.

The half-lives for these runs ranged from 1 to 5 ms, *i.e.* at the limit of the capability of the stopped-flow spectrophotometer, and although satisfactory correlation coefficients of 0.995 to 0.999 were obtained for individual runs, the uncertainties in the observed rate constants were frequently large and the scatter in the second-order rate constants considerable. At all temperatures k_{-1} was approximately zero within experimental error.

Table 2 shows the rate constants for the decomposition of the intermediate at five tempera-

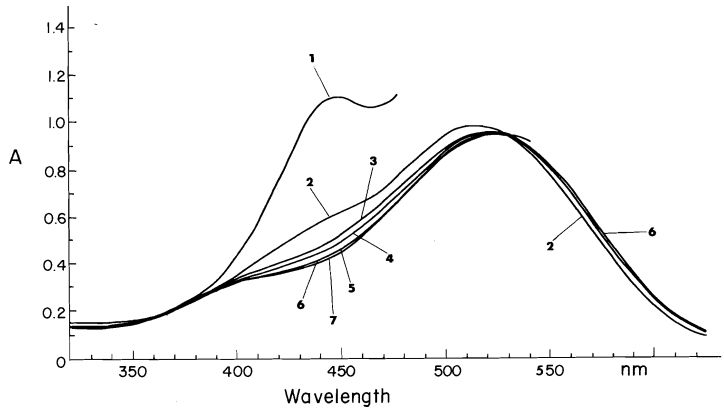

FIG. 1. Absorption spectra of the reaction mixture of picryl chloride and diethylmalonate anion in benzene–DMSO 7:1 v/v at times after mixing of *1*, 0.45 min; *2*, 1.8 min; *3*, 4.9 min; *4*, 6.2 min; *5*, 15 min; *6* and *7*, 29, 51, and 81 min.

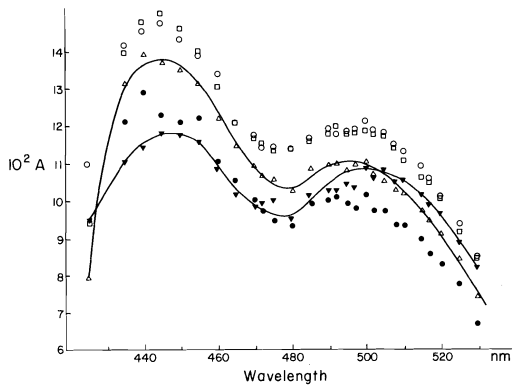

FIG. 2. Absorption spectra of the reaction mixture of picryl chloride and diethylmalonate anion in benzene–DMSO 7:1 v/v at times after mixing of ● 9.2 ms; △ 13.8 ms; □ 23.0, 184, 460, 920 ms and 1.8 s; ▼ 18.4 s.

tures, which were measured on a standard uv–visible spectrophotometer. The first-order rate constant is independent of base concentration, indicating that this step is first-order as written in the reaction scheme, with no base catalysis. The half-lives for these reactions varied between $\frac{1}{2}$ and 3 min.

The kinetics of the deprotonation step are shown in Table 3. This reaction was again very rapid, with half-lives of 1 to 5 ms and the plots of k_{obs} *vs.* b had intercepts of zero within experimental error.

The activation parameters for all three steps of the reaction are given in Table 4. These results indicate an almost irreversible formation of one coloured intermediate which decomposes to the substitution product and is finally converted to the anion of the product. The rate determining step is the decomposition of the intermediate to the product. The presence of an isosbestic point supports the absence of competing or sequential equilibria (16). The identity of the intermediate may be the C-1 complex **2** as shown in the reaction scheme [1], or it may be the C-3 complex **1**. If the latter is the case, then the C-1 complex is not observed at all, since we see only one coloured intermediate. The reaction would then follow the scheme in [3], where $k_0 \gg k_1$. Since C-1 complexes are generally thermodynamically more stable than C-3 complexes, k_{-1} must be small and k_2 large if the C-1 complex is not observed. Therefore, reaction schemes [1] and [3] are indistinguishable kinetically. However, the rate constant for the back reaction, which on the basis of [3] would be equal to $k_{-0}k_1/k_0$, is close to zero and if an upper limit of 1 s^{-1} is assumed, $K_0 = k_0^2/(k_{-0}k_1) = 5.8 \times 10^{-5}\ M^{-1}$ at 25°C for the C-3 complex. This represents the lower limit for K_0. Since C-1 complexes are generally much more stable, K_1 should be at least of the order of $10^7\ M^{-1}$ and a second coloured intermediate should be observed. This suggests that the coloured intermediate which we observe is not the C-3 complex.

Additional evidence may be obtained by examination of the reaction with trinitrobenzene. Under the conditions used in the reaction, diethylmalonate anion attacks trinitrobenzene to form a coloured complex at a rate which was too fast to measure with the stopped-flow spectrophotometer. Therefore, the attack on trinitrobenzene is considerably faster than that on picryl chloride. Since picryl chloride is activated

TABLE 1. Formation of the intermediate complex between picryl chloride and diethylmalonate anion

T (°C)	[Substrate] $\times 10^5$ (M)	[Base] $\times 10^4$ (M)	$k_{obs} \pm$ S.E.* (s^{-1}) 445 nm	$k_{obs} \pm$ S.E.* (s^{-1}) 495 nm	$k_1 \pm$ S.E.* $\times 10^{-4}$ ($s^{-1} M^{-1}$) 445 nm	$k_1 \pm$ S.E.* $\times 10^{-4}$ ($s^{-1} M^{-1}$) 495 nm	$k_{-1} \pm$ S.E.* (s^{-1}) 445 nm
14.6	1.0	2.2	96±1	99±2			
		4.4	204±7	219±3			
		6.6	287±4	321±7	52±3	56±3	−25±23
		7.4	381±5	378±7			
		8.7	406±7	423±7			
		11.0	556±5	606±11			
19.9	1.0	2.4	118±2	134±2			
		5.0	282±5	314±7			
		7.5	465±16	460±8	67±4	69±3	−47±31
		8.4	479±17	575±16			
		9.9	634±30	647±35			
20.2	1.1	2.9	130±1				
		5.9	363±9				
		8.9	525±8		61±3		−32±31
		10.4	583±6				
		11.9	665±8				
		14.8	896±36				
25.3	1.0	2.2	105±1				
		4.4	233±4				
		6.6	335±4		58±2		−24±18
		7.4	422±9				
		8.7	497±7				
		11.0	607±8				
30.3	1.0	2.4	113±3				
		5.0	298±8				
		7.4	581±23		90±6		−118±48
		8.4	601±22				
		9.9	785±16				
34.9	1.0	2.1	111±2				
		4.2	258±3				
		6.4	344±6		72±5		−55±38
		7.2	446±11				
		8.5	589±16				
		10.6	710±18				
39.9	1.0	2.1	117±5				
		4.2	292±4				
		6.4	449±5		79±2		−49±12
		7.2	506±8				
		8.5	637±14				
		10.6	790±22				

*Standard error.

towards nucleophilic attack relative to trinitrobenzene, and since the steric effect of the Cl on the NO_2 groups is not expected to be large, this is evidence supporting the formation of the C-1 rather than the C-3 complex.

The activation parameters of Table 4 are quite reasonable. The large activating power of the three nitro groups together with the strong nucleophilicity of the carbanion are expected to lead to a small enthalpy of activation for the formation of the intermediate. Its decomposition, involving the breaking of a carbon–chlorine bond, has a much greater enthalpy of activation. That both the formation and decomposition reactions should have negative entropies of activation would not have been predicted, since the latter would be expected to be much more positive, within the experimental error. However, negative entropies have been observed for other reactions (14, 18). The previously proposed explanations,

TABLE 2. Decomposition of the intermediate formed between picryl chloride and diethylmalonate anion

T (°C)	[Substrate] $\times 10^5$ (M)	[Base] $\times 10^4$ (M)	$k \pm$ S.E.* $\times 10^3$ (s^{-1})	$k_{av} \pm$ S.E.* $\times 10^3$ (s^{-1})
10.2	4.3	6.5	4.30±0.08	
		7.8	4.38±0.10	
		10.5	4.25±0.09	4.4±0.2
		19.6	4.77±0.12	
		26.2	4.35±0.10	
		32.8	4.18±0.09	
15.3	4.5	8.4	7.40±0.18	
		10.1	6.97±0.16	
		13.5	7.45±0.18	7.5±0.1
		25.3	7.12±0.17	
		33.8	7.17±0.16	
		42.2	6.58±0.15	
19.9	4.3	7.4	11.3±0.2	
		13.5	12.2±0.2	
		17.9	12.0±0.2	11.9±0.1
		22.4	12.1±0.2	
		29.9	11.8±0.2	
		37.4	12.1±0.2	
25.0	4.5	8.4	17.4±0.4	
		10.1	18.2±0.4	
		13.5	17.2±0.4	17.3±0.2
		25.3	17.2±0.4	
		33.8	17.3±0.4	
		42.2	16.6±0.3	
30.1	4.2	7.7	26.2±0.5	
		13.8	25.2±0.5	
		18.5	24.9±0.5	24.9±0.3
		23.1	24.5±0.6	
		30.7	24.1±0.5	
		38.4	24.8±0.5	

*Standard error.

that the incipient chloride ion enhances the solvation of the transition state of the decomposition reaction, fits, in a qualitative sense, the present results.

The activation parameters for the proton transfer step are quite reasonable for this carbon acid, the negative entropies are again consistent with many reports in the literature (19–24).

Experimental

Materials

Sodium diethylmalonate was prepared from sodium ethoxide and diethylmalonic ester. Sodium was dissolved

[3]

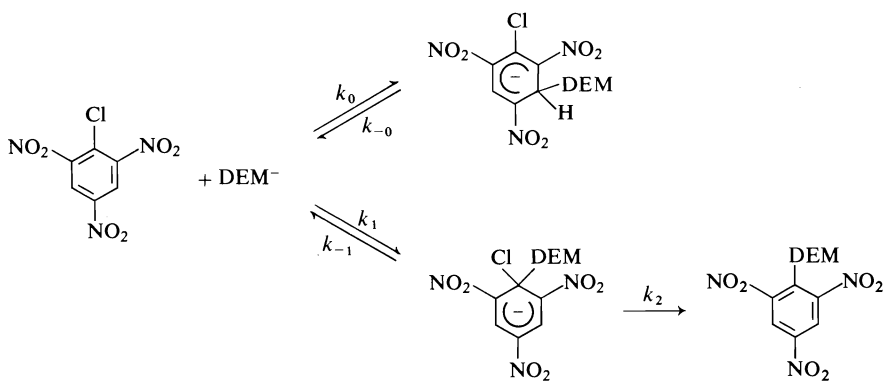

TABLE 3. Reaction of picrylmalonic ester with diethylmalonate anion

T (°C)	[Substrate] $\times 10^5$ (M)	[Base] $\times 10^4$ (M)	$k^1_{obs} \pm$ S.E.* (s^{-1})	$k_3 \pm$ S.E.* $\times 10^{-4}$ ($s^{-1}\ M^{-1}$)
15.1	0.8	1.5	89±4	
		2.9	166±6	
		4.4	241±12	49±1
		5.0	265±9	
		5.9	307±7	
19.9	0.8	1.5	78±1	
		2.9	203±5	
		4.4	248±11	50±8
		5.0	290±10	
		5.9	301±12	
24.9	1.1	1.9	134±4	
		2.6	223±5	
		4.0	264±5	64±8
		4.5	287±7	
		5.3	408±16	
		6.6	440±14	
29.9	1.1	1.9	138±2	
		2.6	167±4	
		4.0	290±7	68±4
		5.3	376±11	
		6.6	445±12	
35.2	0.8	1.5	126±4	
		2.9	209±6	73±3
		5.0	371±3	
		5.9	443±19	

*Standard error.

TABLE 4. Activation parameters for the separate steps of the reaction of picryl chloride with diethylmalonate anion

Reaction	$\Delta H^* \pm$ S.E.* (kcal/mol)	$\Delta S^* \pm$ S.E. (cal mol^{-1} deg^{-1})	$\Delta G^* \pm$ S.E. (kcal/mol)	$E_a \pm$ S.E. (kcal/mol)
Formation of complex (*1*)	2.2±1.3	−24.4±4.1	9.5±1.8	2.8±1.3
Decomposition of complex (*2*)	14.5±0.7	−18.0±2.3	19.8±1.0	15.1±0.7
Proton transfer step (*3*)	3.2±0.7	−21.3±2.4	9.5±1.0	3.8±0.7

*Standard error.

in absolute ethanol and then freshly redistilled diethylmalonic ester was added in a 1:1 molar ratio. After shaking the mixture overnight at room temperature, the alcohol was removed under vacuum and the white salt dried at room temperature (yield 87% on a 0.05 mol scale).

Picryl chloride (Matheson, Coleman & Bell) was recrystallized from chloroform (mp 82.5–83.5°C).

The sodium salt of picryldiethylmalonate (2,4,6-trinitrophenyldiethylmalonate) was prepared from sodium diethylmalonate and picryl chloride. Picryl chloride (0.02 mol) in DMSO was added slowly to the diethylmalonate salt (0.04 mol) in DMSO. The mixture was stirred overnight at room temperature, then poured into ice water and the dark purple precipitate was filtered, washed with cold water and petroleum ether, and then dried at room temperature (yield 72%).

For preparation of the ester, the salt was suspended in absolute ethanol, acidified with dilute sulfuric acid, heated to boiling, and filtered. The filtrate was allowed to cool slowly and colourless needle crystals were obtained (yield 50% on a 0.01 mol scale). The crystals were recrystallized from absolute alcohol, mp 57–58°C (lit. (25) mp 58°C).

Dimethyl sulfoxide was dried over 4A molecular sieve and then distilled over CaH_2 under nitrogen at reduced pressure. The middle fraction was collected (bp 48°C/3.0 Torr) and stored in a dark bottle under nitrogen.

Thiophene-free benzene was dried over $CaCl_2$ and then distilled over sodium (bp 80.5°C). For the kinetic runs, both solvents were used within 1 week after purification.

Kinetic Procedure

The absorption spectra were recorded on a SP800B spectrophotometer in cells of 1.0 cm path length. The same instrument, connected to an external recorder

TABLE 5

(*a*) Formation of intermediate from picryl chloride and diethylmalonate anion at 25.3°C; initial concentration picryl chloride = 1×10^{-5} *M*; initial concentration diethylmalonate anion = 4.4×10^{-4} *M*

	$10^2 \times$ Absorbance	
Time (ms)	Series *1*	Series *2*
0.0	2.27	4.02
0.92	2.65	4.08
1.85	2.97	4.11
2.77	3.21	4.14
3.70	3.40	4.16
4.62	3.58	4.17
5.55	3.70	4.19
6.47	3.81	4.20
7.40	3.91	4.21

Pseudo first-order rate constant = 236 ± 3 s^{-1}

(*b*) Decomposition of intermediate from picryl chloride and diethylmalonate anion at 19.9°C; initial concentration picryl chloride = 4.3×10^{-5} *M*; initial concentration diethylmalonate anion = 1.35×10^{-3} *M*

	Absorbance	
Time (min)	Series *1*	Series *2*
0.0	0.770	0.415
0.20	0.700	0.400
0.40	0.644	0.387
0.60	0.595	0.376
0.80	0.554	0.366
1.00	0.523	0.358
1.20	0.495	0.351
1.40	0.470	0.342
1.60	0.449	0.337
1.80	0.430	0.331

First-order rate constant = $(11.8 \pm 0.4) \times 10^{-3}$ s^{-1}

allowing for expansion of the signal and choice of any region of absorbance between 0–2, was used for the slow kinetic runs. The temperature was controlled within 0.05°C.

The fast reactions were followed on a Durrum–Gibson stopped-flow spectrophotometer fitted with a 2 mm light-path optical cell. The drive syringes, the mixing-jet, and the cell were kept within 0.05°C of the quoted temperature by means of an RTE-8 Neslab circulating bath. The dead time of the instrument was 1 ms checked by the standard reaction between $Fe(NO_3)_3$ and KCNS. In all the cases the solutions were prepared on the same day of measurement, the base in 3:1 v/v benzene–DMSO, the substrate in benzene. The solutions of the base were prepared and handled in a glove bag, under nitrogen. The weighed amount of base was dissolved in DMSO corresponding to $\frac{1}{4}$ of the volume required. Then, benzene was added to the mark in the volumetric flask. Dilutions were made by 3:1 v/v benzene–DMSO prepared in the same way.

For the stopped-flow, all the results reported correspond to at least three consecutive superimposed runs. The traces of percentage transmittance *vs.* time, stored on a Tektronix 564 oscilloscope were photographed, the transmittance converted to absorbance, and the pseudo first-order rate constants calculated by the Guggenheim method (26). A least-squares calculation provided the best line. Standard errors and correlation coefficients were calculated at the same time. Whenever possible scans were made at two or three time bases in which case the arithmetic mean of the rate constants was used. The errors reported refer to the standard error of the least-squares method. However, an error of 10%, estimated by duplicate runs, should be taken into account due to the fact that the instrument was being used at the limit of its capability with respect to the speed of the reaction.

For the slow kinetic runs, absorbance readings *vs.* time were obtained directly on the Unicam. The Guggenheim method was used again for the first order rates. Three runs were obtained for each base concentration and the arithmetic mean rate was calculated. This was repeated for various base concentrations and the average value obtained. Sample runs are given in Table 5.

Acknowledgments

The authors are grateful for financial assistance from the National Research Council of Canada and to the Killam Trust for a scholarship (to A.E.M-S.).

1. E. BUNCEL, A. R. NORRIS, and K. E. RUSSELL. Q. Rev. **22**, 123 (1968).
2. R. FOSTER and C. A. FYFE. Rev. Pure Appl. Chem. **16**, 61 (1966).
3. TH. J. DE BOER and I. P. DIRKX. *In* The chemistry of nitro- and nitroso-groups. Part I. *Edited by* H. Feuer. Interscience, New York, NY. 1969. Chapt. 8.
4. G. B. BARLIN. Aromatic and heteroaromatic chemistry. The Chem. Soc. **1**, 231 (1973).
5. G. B. BARLIN. Aromatic and heteroaromatic chemistry. The Chem. Soc. **2**, 271 (1974).
6. A. R. BUTLER. *In* Organic reaction mechanisms 1971. *Edited by* B. Capon and C. W. Rees. Interscience, New York, NY. 1972. p. 179.
7. A. R. BUTLER. Ann. Rep. Chem. Soc. B, **68**, 134 (1971).
8. A. R. BUTLER. Ann. Rep. Chem. Soc. B, **70**, 70 (1973).
9. M. ARIGA and E. MATSUMURA. Bull. Chem. Soc. Jpn. **46**, 3144 (1973).
10. M. R. CRAMPTON and H. A. KHAN. J. Chem. Soc. Perkin Trans. II, 1173 (1972).
11. E. ERK and C. TUZUN. Commun. Fac. Sci. Univ. Ankara B, **18**, 19 (1971).
12. M. J. STRAUSS. Chem. Commun. 76 (1970).
13. K. T. LEFFEK and P. H. TREMAINE. Can. J. Chem. **49**, 1979 (1971).
14. K. T. LEFFEK and P. H. TREMAINE. Can. J. Chem. **51**, 1659 (1973).

15. M. E. C. BIFFIN and D. B. PAUL. Aust. J. Chem. **27**, 777 (1974).
16. T. N. HALL and C. F. PORANSKI, JR. *In* The chemistry of the nitro- and nitroso-groups. Part II. *Edited by* H. Feuer. Interscience, New York, NY. 1970. Chapt. 6.
17. L. H. GAN and A. R. NORRIS. Can. J. Chem. **52**, 18 (1974).
18. C. F. BERNASCONI. J. Am. Chem. Soc. **90**, 4982 (1968).
19. E. F. CALDIN. J. Chem. Soc. 3345 (1959).
20. E. F. CALDIN and J. C. TRICKETT. Trans. Faraday Soc. 772 (1954).
21. E. F. CALDIN, A. JARCZEWSKI, and K. T. LEFFEK. Trans. Faraday Soc. 110 (1971).
22. A. JARCZEWSKI and K. T. LEFFEK. Can. J. Chem. **50**, 24 (1972).
23. J-H. KIM and K. T. LEFFEK. Can. J. Chem. **51**, 2805 (1973).
24. A. JARCZEWSKI, P. PRUSZYNSKI, and K . T. LEFFEK. Can. J. Chem. **53**, 1176 (1975).
25. I. REMSEN. Am. Chem. J. **18**, 134 (1896).
26. E. A. GUGGENHEIM. Philos. Mag. **2**, 538 (1926).

Aromatic substitutions with carbanion nucleophiles. IV. The kinetics and mechanism of the reaction of picryl bromide with diethylmalonate anion

KENNETH T. LEFFEK AND ANNA E. MATINOPOULOS-SCORDOU

Department of Chemistry, Dalhousie University, Halifax, N.S., Canada B3H 4J3

Received December 20, 1976

KENNETH T. LEFFEK and ANNA E. MATINOPOULOS-SCORDOU. Can. J. Chem. **55**, 2664 (1977).

The reaction of picryl bromide with sodium diethylmalonate has been studied in benzene–DMSO 7:1 v/v by means of stopped-flow and uv–visible spectrophotometers. A Meisenheimer-like intermediate was detected, decomposing to yield the stable violet anion of the substitution product. The rate constants of the individual steps have been measured and the activation parameters calculated. Comparison with those obtained for picryl chloride support a bimolecular substitution via the 1,1-complex. The reaction with 1,3,5-trinitrobenzene is too fast to be measured in the same solvent system. The equilibrium constant is estimated to be of the order of 10^4–10^5.

KENNETH T. LEFFEK et ANNA E. MATINOPOULOS-SCORDOU. Can. J. Chem. **55**, 2664 (1977).

Travaillant dans des solutions de benzène–DMSO 7:1 v/v et faisant appel à des spectrophotomètres à flux stoppé et uv–visible, on a étudié la réaction du bromure de picryle avec le sel de sodium du malonate d'éthyle. On a détecté un intermédiaire ressemblant à ceux de Meisenheimer qui se décompose pour conduire à l'anion violet stable du produit de substitution. On a mesuré les constantes de vitesse pour chacune des étapes et on en a calculé les paramètres d'activation. Une comparaison de ces données avec celles obtenues pour le chlorure de picryle supporte un mécanisme de substitution bimoléculaire par l'intermédiaire d'un complexe 1:1. La réaction avec le trinitro-1,3,5 benzène est tellement rapide que sa vitesse ne peut être mesurée dans le même système de solvant. On estime que la constante d'équilibre est de l'ordre de 10^4 jusqu'à 10^5.

[Traduit par le journal]

Introduction

The study of the reaction between picryl chloride and sodium diethylmalonate in benzene–DMSO 7:1 v/v (1) led to mechanism [1] for X = Cl with $k_1, k_3 \gg k_2$ and $k_{-1} \ll k_1$, $k_{-3} \ll k_3$.

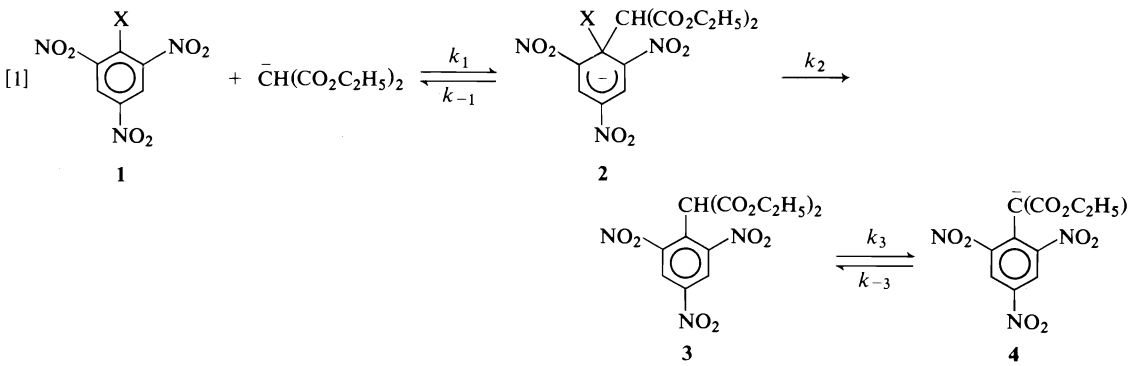

In the present study the similar reaction of picryl bromide is examined and the rate constants and activation parameters compared with those of the chloro-compound. The work of Gan and Norris (2) predicts that if the above mechanism is correct, the value of k_1 for picryl bromide will be clearly less than that of picryl chloride, whereas if we are actually observing the formation of the 1,3-complex **5**, the rate constant should be almost identical to that observed for picryl chloride.

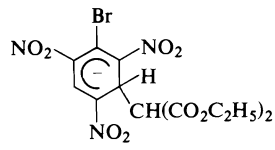

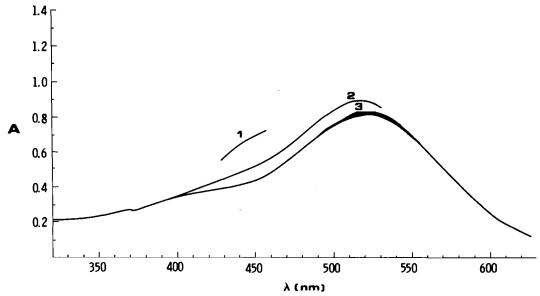

FIG. 1. Absorption spectra of the interaction of picryl bromide (0.75×10^{-4} *M*) and diethylmalonate anion (2.1×10^{-3} *M*) in benzene–DMSO 7:1 v/v at times after mixing of *1*, 0.43 min; *2*, 0.70 min; *3*, 1.37 min.

Results and Discussion

Picryl bromide in benzene, mixed in 1:1 v/v ratio with an excess of sodium diethylmalonate in benzene–DMSO 3:1 v/v gives rise to a red colour which changes very quickly to a violet stable product. The behaviour is similar to that of picryl chloride (1) with the difference that the decomposition is faster, so that observation of the visible spectrum on the conventional spectrophotometer shows only a shift towards higher wavelength, Fig. 1. The slow reaction of picryl bromide with DMSO does not interfere with the reaction under these conditions.

A check in either DMSO or DMSO–benzene 1:1 v/v, where the intermediate is more stable, shows the transition through an isosbestic point more clearly, as can be seen in Fig. 2, for the latter case.

The change of the spectrum at short times could be followed only by means of a stopped-flow spectrophotometer. Measurement at various wavelengths for different time bases showed that the two peaks initially formed at 447 and 492 nm increase up to a steady-state equilibrium after which the decomposition becomes dominant and the peak at the shorter wavelength gradually disappears whereas the other is shifted to higher wavelength due to the formation of the product as shown in Fig. 3. The product is similar in all respects with the one obtained from picryl chloride (1) and was thus identified as **4**. Because of the fast decomposition of the intermediate, the true extinction coefficients could not be measured. The assumption that the absorbance at equilibrium corresponds to the complete conversion of all the substrate gave good straight lines for $A = f(c)$ from which the approximate figures of $\varepsilon_{447} = 16\,700$ and $\varepsilon_{492} = 14\,800$ $cm^{-1}\,M^{-1}$ were calculated.

The formation of the intermediate was followed on a stopped-flow spectrophotometer at 447 nm for six temperatures. A check of the rate at 492 nm at 15.2°C gave the same rate constants as those obtained at 447 nm indicating that both peaks belong to a single intermediate. The second-order reaction was reduced by use of an excess of base, to pseudo first-order, the rate constant of which, k_{obs}, plotted against the base, [2], gave as slope k_1, the second-order rate constant for complex formation.

$$[2] \qquad k_{obs} = k_1 b + k_{-1}$$

The results are given in Table 1 and all the kinetic runs correspond to correlation coefficients of 0.995–0.999. The rate constant for the decomposition to reactants (k_{-1}) could not be obtained from the intercept but was very small and assumed to be approximately zero.

The decomposition of the same complex, followed on a conventional spectrophotometer at

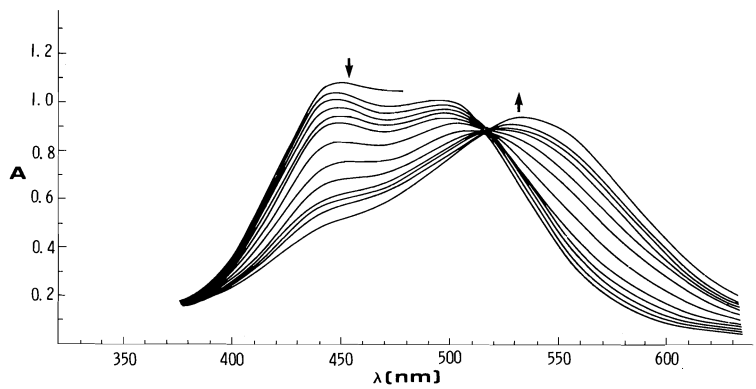

FIG. 2. Absorption spectra of the interaction of picryl bromide (0.63×10^{-4} *M*) and diethylmalonate anion (2.2×10^{-3} *M*) in benzene–DMSO 1:1 v/v at times after mixing of 0.3 to 97 min.

TABLE 1. Formation of the intermediate complex in the reaction of picryl bromide with diethylmalonate anion

Temp. (°C)	[Substrate] $\times 10^5$ (M)	[Base] $\times 10^4$ (M)	$k_{obs} \pm$ S.E.† (s^{-1})	$k_1 \pm$ S.E.† $\times 10^{-4}$ ($s^{-1} M^{-1}$)	$k_{-1} \pm$ S.E.* (s^{-1})
15.2	1.0	2.4	39±1		
		5.0	78±2		
		7.4	131±1	20±1	−14±8
		8.5	161±3		
		10.0	188±3		
15.2*	1.0	2.4	37±1		
		5.0	81±1		
		7.4	151±4	21±2	−15±11
		8.5	156±4		
		10.0	193±8		
19.9	1.0	2.3	37±1		
		4.7	73±1		
		6.9	137±2	22±2	−17±2
		7.9	148±2		
		9.3	201±4		
		11.6	224±5		
25.5	1.0	2.4	45±1		
		5.0	107±2		
		7.4	172±2	25±4	−17±2
		8.5	199±3		
		10.0	237±7		
30.4	1.0	2.3	47±1		
		4.7	105±1		
		6.9	150±3	23±5	−5±3
		7.9	180±3		
		9.3	214±5		
		11.6	261±4		
35.1	1.0	2.9	60±1		
		4.1	96±1		
		6.1	166±2	26±2	6±13
		6.9	185±3		
		8.2	205±6		
		10.2	249±7		
40.0	1.0	2.9	66±1		
		4.1	111±2		
		6.1	172±2		
		6.9	199±3	30±1	−13±7
		8.2	234±4		
		10.2	284±5		

*λ = 492 nm.
†Standard error.

447 nm, was independent of the base concentration. The results given in Table 2 are in accord with [3] in which K_1 is the equilibrium constant for the formation of the intermediate. This step

$$[3] \quad k_{dec} = k_2\left(\frac{K_1 b}{1 + K_1 b}\right) \simeq k_2 \text{ if } K_1 b \gg 1$$

is much slower than the formation of the intermediate and since the last deprotonation step has a second-order rate constant of $k_3 = (64 \pm 8) \times 10^4\ s^{-1}\ M^{-1}$ at 25°C (1), the decomposition is the rate-determining step of the overall reaction. The activation parameters for both the formation and decomposition of the intermediate are given in Table 3. These parameters are quite similar to those obtained for picryl chloride and may be rationalized in the same manner (1).

An attempt was made to study the reaction of trinitrobenzene with the same carbanion under identical conditions. A complex with λ_{max} at 460 (ε 29 400) and 564 (ε 14 100) was observed. However, the rate of formation was too fast for the stopped-flow method. For [TNB] = 0.2×10^{-5} M and [DEM] = 0.11×10^{-3} M, the reaction is over at approximately 4 ms. An attempt to

TABLE 2. Decomposition of the intermediate formed between picryl bromide and sodium diethylmalonate

Temp. (°C)	[Substrate] $\times 10^4$ (M)	[Base] $\times 10^3$ (M)	$k_{obs} \pm$ S.E.* $\times 10^3$ (s^{-1}) (average of 3 runs)	$k_{obs} \pm$ S.E.* $\times 10^3$ (s^{-1}) (average)
10.0	0.49	1.0	7.9±0.2	
		1.8	7.3±0.1	
		2.4	8.3±0.2	7.8±0.2
		3.0	8.1±0.2	
		4.0	8.1±0.2	
		5.1	7.3±0.2	
15.2	0.60	2.2	12.7±0.2	
		3.0	13.0±0.3	
		3.7	12.7±0.2	12.5±0.2
		4.9	12.0±0.2	
		6.2	12.1±0.2	
20.0	0.42	0.9	16.4±0.3	
		1.7	15.7±0.3	
		2.2	15.9±0.3	16.0±0.2
		2.8	16.8±0.3	
		3.7	16.1±0.3	
		4.4	15.2±0.4	
24.9	0.47	0.8	25.0±0.5	
		1.4	24.3±0.4	
		1.9	24.6±0.4	24.1±0.4
		2.3	23.6±0.4	
		3.1	22.6±0.3	
		3.9	24.4±0.4	
30.0	0.44	0.7	35.0±0.7	
		1.3	36.5±0.7	
		1.7	34.8±0.7	35.3±0.3
		2.2	34.2±0.6	
		2.9	35.3±0.6	
		3.7	36.0±0.6	

*Standard error.

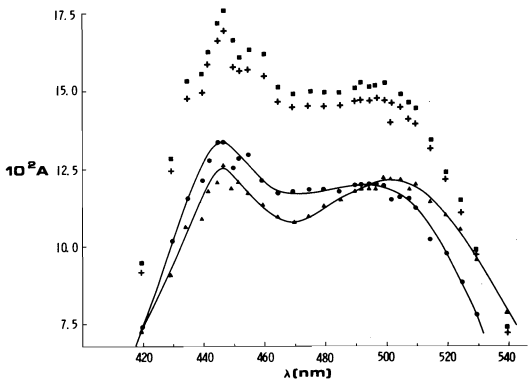

FIG. 3. Change of absorption spectrum during the reaction of picryl bromide and diethylmalonate anion in benzene–DMSO 7:1 v/v at times after mixing of ● 9.2 ms, + 23.1 ms, ■ 69.4 ms, ▲ 18.5 s.

calculate the equilibrium constant (K_{eq}) using the Benesi–Hildebrand method (3) was equally unsuccessful because the ratio $[TNB]_0/A_{eq}$ where $[TNB]_0$ = initial concentration of substrate, A_{eq} = absorbance at equilibrium, was essentially constant. The slope of $[TNB]_0/A_{eq} = f(1/b)$, where b = base concentration, was estimated to be of the order of 10^{-8}–10^{-9} which gives a K_{eq} of the order of 10^4–10^5 M^{-1}. The only conclusion which could be drawn from this reaction was the useful observation that the unsubstituted substrate reacts faster than the chloro- or bromo-substituted ones. The only visible spectrum of a diethylmalonate anion addition product reported is that of **6** which in DMF shows λ_{max} at 460 and 568 nm (4).

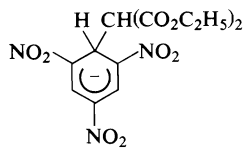

6

In the present work, the trinitrobenzene reaction shows λ_{max} at 459, 562 nm in pure DMSO;

TABLE 3. Activation parameters for the reaction of picryl bromide with diethylmalonate anion

Step	ΔH^{+} ± S.E. (kcal/mol)	ΔS^{+} ± S.E. (cal mol^{-1} deg^{-1})
Formation of intermediate	1.9±0.6	−27.5±1.8
Decomposition to products	12.0±0.5	−25.6±1.8

TABLE 4. Summary of results regarding the intermediate formed in the reaction 1-X-2,3,5-trinitrobenzene and diethylmalonate anion in benzene–DMSO 7:1 v/v

Intermediate		k_{form} × 10^{-4} at 25°C	ΔH^{+}_{form}	ΔS^{+}_{form}	k_{dec} × 10^{3} at 25°C	ΔH^{+}_{dec}	ΔS^{+}_{dec}
X	λ_{max} (nm)	($s^{-1} M^{-1}$)	(kcal/mol)	(cal mol^{-1} deg^{-1})	($s^{-1} M^{-1}$)	(kcal/mol)	(cal mol^{-1} deg^{-1})
H	460 564						
Cl	445 495	58±2	2.2±1.3	−24.4±4.1	17.3±0.2	14.5±0.7	−18.0±2.3
Br	447 492	25±0.5	1.9±0.6	−27.5±1.8	24.1±0.3	12.0±0.5	−25.6±1.8

458, 562 nm in benzene–DMSO 1:1 v/v; and 460, 564 nm in benzene–DMSO 7:1 v/v. This suggests strongly that the product is actually the anionic complex **6**. The ratio of the extinction coefficients at the two wavelengths is approximately 2:1 as expected from such complexes.

A summary of the results in Table 4 shows that between the two halo-substrates picryl chloride forms the intermediate 2.3 times faster than the picryl bromide at 25°C, whereas the rate of decomposition of the same intermediate is slower by a factor of 1.4 than that of the bromo-complex. Gan and Norris (2) found that the rate constants for the formation of **7** and **8** in methanol differed by a factor of about 2 at 25°C, with that for **7** being the greater. In contrast they observed identical rate constants, within experimental error, for the formation of **9** and **10**.

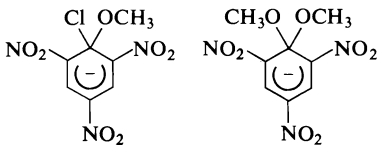

7 **8**

Thus, for both picryl chloride and bromide, the assignment of the observed attack of the carbanion to the halo-substituted position of the substrate, yielding **2**, gives the most satisfactory rationalization of the results, since it presents an interpretation of these reactions and those of Gan and Norris (2) on a common set of criteria even though these criteria indicate a C-1 attack in the present case, whereas they fit a C-3 attack for the reaction of picryl chloride with methoxide (2). If the observed colour is accepted as the C-1 complex, the main factor on which the reactivity

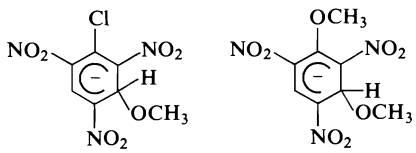

9 **10**

depends would be the electronegativity of the substituent present (5), the difference in the steric requirements of the chlorine and bromine not being large enough to account for such a difference in rate (6). Chlorine being more electronegative, facilitates the attack and leads to faster formation of the intermediate. The decomposition depends mainly on the ease with which the bond between carbon and the substituent is broken, and since bromine is the better leaving group, the faster decomposition of the bromo-complex is expected, as observed. Another factor supporting the mechanism shown in [1] is the fast reaction of trinitrobenzene. Since so far in aromatic nucleophilic substitutions, attack at unsubstituted positions has always been faster mainly because of steric reasons (7), the formation of **11** would be expected to be faster than that of **6**.

Finally, for the overall rate represented by k_2, the ratio $k_{Cl}/k_{Br} = 0.7$ is obtained. The result agrees with the previous range of $k_{Cl}/k_{Br} = 0.5$–

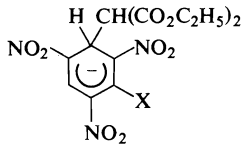

11

0.8 obtained for the reaction between sodium phenoxide and **12** (6).

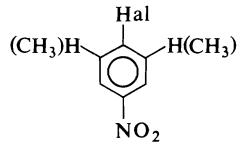

12

Experimental

Picryl bromide was prepared according to the method of Sygden and Willis (8) using 1-bromo-2,4-dinitrobenzene as starting material. The yield of crude material was only 29%. The product was recrystallized from absolute ethanol (mp 123–124°C).

Purification of the other chemicals used, as well as the procedure followed during the experiments, were described previously (1).

Acknowledgments

The authors are grateful for financial assistance from the National Research Council of Canada and to the Killam Trust for a scholarship to A.E.M-S.

1. K. T. Leffek and A. E. Matinopoulos-Scordou. Can. J. Chem. Preceding paper.
2. L. H. Gan and A. R. Norris. Can. J. Chem. **52**, 18 (1974).
3. H. A. Benesi and H. H. Hildebrand. J. Am. Chem. Soc. **71**, 2703 (1943).
4. R. J. Pollitt and B. C. Saunders. J. Chem. Soc. 4615 (1965).
5. J. Miller. Aromatic nucleophilic substitution. Elsevier Publishing Co. Amsterdam, The Netherlands. 1968.
6. G. Bartoli, G. Ciminale, and P. E. Todesco. J. Org. Chem. **40**, 872 (1975).
7. M. J. Strauss. Chem. Rev. **70**, 667 (1970).
8. S. Sygden and J. B. Willis. J. Chem. Soc. 1360 (1951).

Reactions of some 2,5-dialkylpyridines with aldehydes and phenyllithium

JOHN A. FINDLAY AND GREG C. LONERGAN

Department of Chemistry, University of New Brunswick, Fredericton, N.B., Canada E3B 5A3

Received June 21, 1976[1]

JOHN A. FINDLAY and GREG C. LONERGAN. Can. J. Chem. **55**, 2670 (1977).

The structure chemistry and stereochemistry of novel and complex adducts of type **3** obtained by reactions of 2,5-dialkylpyridines with aliphatic aldehydes and phenyllithium is discussed. A mechanism of formation is proposed.

JOHN A. FINDLAY et GREG C. LONERGAN. Can. J. Chem. **55**, 2670 (1977).

On discute de la chimie et de la stéréochimie de la structure de nouveaux adduits complexes de type **3** obtenus par des réactions de dialkyl-2,5 pyridines avec des aldéhydes aliphatiques et du phényllithium. Un mécanisme pour la formation de ces composés est proposé.

[Traduit par le journal]

In the course of preparing 4-methyl-1-(5-methyl-2-pyridyl)pentan-2-ol, **2***a* (1) by phenyllithium catalyzed condensation of 2,5-dimethylpyridine **1***a* with isopentanal an unanticipated and remarkable by-product was recovered in 18% yield. The structure **3***a*, 2,5-dimethyl-2-(5′-methyl-2′-picolyl)-3-(1′′-hydroxy-4′′-methylbutyl)-6-phenyl-4,5-didehydropiperidine dihydrochloride, is assigned to it on the basis of chemical and spectroscopic evidence.

Treatment of bromobenzene in ether with 2 equiv. of lithium gave a solution containing phenyllithium which turned red-brown upon addition of 1 equiv. of 2,5-dimethylpyridine **1***a*. Subsequent addition of isopentanal followed by acidic (HCl) work-up afforded an organic layer from which the white crystalline adduct separated. The elemental composition, $C_{25}H_{34}ON_2 \cdot 2HCl$, ascertained by microanalysis and supported by mass spectral data, is consistent with a dihydrochloride adduct derived from two molecules of 2,5-dimethylpyridine, one of benzene, and one isopentanal and possessing a total of ten sites of unsaturation. The presence of phenyl and 5-methyl-2-picolyl features was learned from the nmr ($CDCl_3$) spectrum which shows a total of eight protons in the aromatic region, two of which display chemical shifts and couplings appropriate for a 2,5-dialkyl substituted pyridinium moiety (2), δ 7.99 (s, 1H, $W_{1/2}$ = 4 Hz, C6H) and 7.12 (d, J = 8 Hz, C3H), while signals corresponding to five phenyl hydrogens plus a C4 pyridinium proton are accommodated in a complex multiplet centred near δ 7.5. Furthermore,

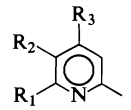

1

a $R_1,R_3 = H; R_2 = CH_3$
b $R_1,R_2,R_3 = H$
c $R_1,R_2 = H; R_3 = CH_3$
d $R_1,R_3 = CH_3; R_2 = H$
e $R_1,R_3 = H; R_2 = C_2H_5$

$C_6H_5Li \mid R_4CHO$

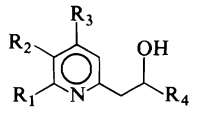

2

a $R_1,R_3 = H; R_2 = CH_3; R_4 = (CH_3)_2CHCH_2$
b $R_1,R_2,R_3 = H; R_4 = (CH_3)_2CHCH_2$
c $R_1,R_3 = H; R_2 = CH_3; R_4 = C_6H_5$
d $R_1,R_2 = H; R_3 = CH_3; R_4 = (CH_3)_2CHCH_2$
e $R_1,R_3 = CH_3; R_2 = H; R_4 = (CH_3)_2CHCH_2$

the mass spectrum corroborates the 5-methyl-2-picolyl feature in displaying a strong ion *m/e* 272 ($M - 2HCl - C_7H_8N$). In addition, nmr signals at δ 2.32 (3H, s) and an AB quartet at δ 3.63, 3.48 (J = 18 Hz) are consistent with the 5-methyl-2-methylene pyridinium substituent attached via the 2-methylene group to a fully substituted carbon. The presence of a secondary hydroxyl is confirmed by the broad singlet at δ 4.00 (1H) transformed to a doublet of doublets after addition of D_2O. This signal is displaced to δ 5.15 in a monoacetate derivative **3***b* (*vide infra*). Additional methyl singlets are located at δ 1.81

[1]Publication was delayed 6 months at the authors' request.

and 1.55 while a pair of doublets at δ 0.80 (3H, J = 6 Hz) and 0.76 (3H, J = 6 Hz) are ascribed to an isopropyl feature. Furthermore, double irradiation near δ 1.5 ppm causes collapse of the δ 4.00 signal to a broad singlet ($W_{1/2}$ = 10 Hz) and the isopropyl methyl doublets to singlets thus confirming the sequence $(CH_3)_2$-$CHCH_2CHOH$-.

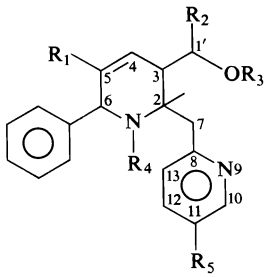

3

a ·2HCl $R_1,R_5 = CH_3$; $R_2 = (CH_3)_2CHCH_2$; R_3,R_4 = H
b ·2HCl $R_1,R_5 = CH_3$; $R_2 = (CH_3)_2CHCH_2$; $R_3 = COCH_3$; R_4 = H
c $R_1,R_5 = CH_3$; $R_2 = (CH_3)_2CHCH_2$; R_3,R_4 = H
d $R_1,R_5 = CH_3$; $R_2 = (CH_3)_2CHCH_2$; $R_3 = COCH_3$; R_4 = H
e $R_1,R_5 = CH_3$; $R_2 = (CH_3)_2CHCH_2$; $R_3,R_4 = COCH_3$
f ·2HCl $R_1,R_5 = C_2H_5$; $R_2 = (CH_3)_2CHCH_2$; R_3,R_4 = H
g ·2HCl $R_1,R_5 = C_2H_5$; $R_2 = (CH_3)_2CHCH_2$; $R_3 = COCH_3$; R_4 = H
h $R_1,R_5 = C_2H_5$; $R_2 = (CH_3)_2CHCH_2$; R_3,R_4 = H
i ·2HCl $R_1,R_5 = CH_3$; $R_2 = (CH_3)_2CH$; R_3,R_4 = H
j $R_1,R_5 = CH_3$; $R_2 = (CH_3)_2CH$; R_3,R_4 = H

Thus the adduct comprises four structural units; namely, phenyl, 5-methyl-2-picolyl, and 1-isopentanol groups attached to a nitrogen containing framework originating from a second 2,5-dimethylpyridine molecule. Assuming that this latter is an intact six-membered nitrogen containing ring, it remains to place the above identified appendages on a didehydro-2,5-dimethylpiperidinium nucleus. Initial difficulty in arriving at a unique structural conclusion based on spectral data was due to the fact that the nmr signals for the hydrogens attached to the presumed didehydropiperidinium system could not be assigned unambiguously. Thus, the relevant signals are displayed as broad singlets at δ 2.45 (1H, $W_{1/2}$ = 8 Hz), 4.82 (1H, $W_{1/2}$ = 8 Hz), and 5.91 (1H, $W_{1/2}$ = 6 Hz). Decoupling experiments did not provide any useful information. Hence, apart from structure **3***a*, alternates such as **4**, **5***a*, and **5***b* could not readily be excluded.

The nmr ($CDCl_3$) spectrum of the monoacetate **3***b* of the dihydrochloride **3***a* shows new features consistent with a secondary acetoxyl function at δ 5.15 (1H, apparent triplet, $J \simeq 6$ Hz, -C*H*OCOCH$_3$) and δ 2.06 (3H, s, CH_3COO-) while other non aromatic downfield hydrogens again appear as broad singlets and are located at δ 2.93 ($W_{1/2}$ = 7 Hz), 4.89 ($W_{1/2}$ = 7 Hz), and 5.88 ($W_{1/2}$ = 6 Hz) and defy unique assignments.

Dehydration of the adduct **3***a* was readily accomplished using thionyl chloride and gave an anhydrodihydrochloride. Its nmr ($CDCl_3$) spectrum shows a δ 5.25 triplet (1H, J = 6.5 Hz) ascribed to the A part of a new AX_2 system while other downfield signal patterns remain essentially unchanged. The ultraviolet spectrum (EtOH) λ_{max} 250 (ε 15 000) is reasonably consistent with a tetrasubstituted conjugated diene possessing an exocyclic double bond (calculated λ_{max} 242).

The only structure for the adduct in agreement with the foregoing is **3***a* in which the double bond is located between carbons 4 and 5 of the piperidinium moiety, thus allowing for the generation of the tetraalkyl substituted diene **6**[2] upon dehydration. Alternative structures, for example **4**, **5***a*, or **5***b* capable of featuring a new chromophore after dehydration would necessarily give rise to dienamine systems with quite different uv chromophores. Furthermore, structure **3***a* is fully supported by a detailed analysis of nmr spectral data.

The free base **3***c* is readily obtained from **3***a* by

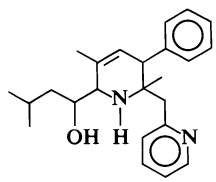

4·2HCl

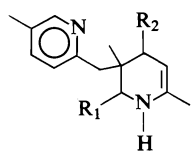

5

a ·2HCl $R_1 = C_6H_5$; $R_2 = (CH_3)_2CHCH_2CHOH$
b ·2HCl $R_1 = (CH_3)_2CHCH_2CHOH$; $R_2 = C_6H_5$

[2]For stereochemical assignments, *vide infra*.

treatment with dilute sodium hydroxide solution at room temperature and can be converted back to the dihydrochloride by hydrochloric acid. Thionyl chloride converts the free base **3***c* directly to the anhydrodihydrochloride **6**. Acetylation of the free base **3***c* with acetic anhydride – pyridine affords the monoacetate **3***d* and the *O*,*N*-diacetate **3***e* both of which can be hydrolyzed back to **3***c*. The monoacetate dihydrochloride obtainable by treatment of **3***a* with acetic anhydride – pyridine is now formulated as **3***b*. The structures of these transformation products are fully supported in detail by spectroscopic and analytical data.

Attempts at selective hydrogenation of **3***a* and **3***c* under a variety of catalytic conditions were unsuccessful and it was apparent from incomplete reductions that the isolated double bond and the phenyl group are reduced simultaneously. Catalytic hydrogenation of **3***a* at room temperature under pressure (40 psi) using Adam's catalyst gave in 75% yield a crystalline (mp 138–141°C) product devoid of ultraviolet absorption and displaying a molecular ion *m*/*e* 392 (*M* − 2HCl) in its mass spectrum, corresponding to a tetradecahydro derivative formulated as **7**.[2]

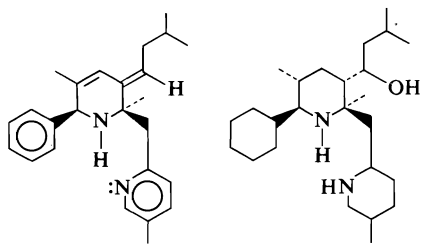

6·2HCl **7**·2HCl

Consistent with our structural assignment, **3***a* is the preparation of the homolog **3***f*, $C_{27}H_{38}ON_2 \cdot 2HCl$ by parallel reaction of 5-ethyl-2-methylpyridine with phenyllithium and isopentanal. As anticipated, this adduct shows nmr ($CDCl_3$) signals for two additional vinylic methylene groups, one at δ 1.85 (2H, q, J = 8 Hz) and 2.59 (2H, q, J = 8 Hz). The corresponding acetate **3***g* and free base **3***h* of this homolog were prepared and characterized and displayed the expected spectral features.

When isobutanal was treated with a benzene solution of 2,5-dimethylpyridine in the presence of phenyllithium, the crystalline adduct **3***j* was obtained, isolated as the dihydrochloride **3***i*.

No adduct of the type **3** could be isolated following parallel reaction involving 2-picoline **1***b* or 2,4-dimethylpyridine **1***c* and the alcohols **2***b* (60%) and **2***d* (25%), respectively, were recovered. Similarly, the reaction of 2,5-dimethylpyridine **1***a* with benzaldehyde in the presence of phenyllithium gave the expected compound **2***c* in 25% yield and no novel adduct was detected. Product **2***e* was obtained in 75% yield in the same reaction system, employing 2,4,6-trimethylpyridine **1***d* and isopentanal. Thus the ready formation of novel adducts of type **3** occurs with 2,5-dialkylpyridines and aliphatic aldehydes.

While no firm conclusion can yet be reached concerning the complete stereochemistry of the system **3**, the configuration contained in structure **3** is suggested by the following considerations. Throughout the series **3***a*–**3***h*, the C3H appears as a broad singlet indicating a dihedral angle near to 80° with its neighbours at C4 and C1′. Thus the hydrogen at C3 is probably quasiaxial allowing the bulky alkanol side chain to be quasi equatorial. To best accommodate the sterically encumbered C2 the larger methylpicolyl substituent is placed equatorial and *trans* to the large C3 substituent while the smaller methyl group occupies the axial site. To avoid serious steric crowding from the C2 axial substituent the C6 phenyl group should be disposed in the quasi equatorial position.

The low nmr field position of the C2 methyl throughout the series **3***a*–**3***h* is explained by its position β to the amine (or ammonium) nitrogen and its possible orientation with respect to the deshielding zone of the pyridine (or pyridinium) nucleus. Thus in the three ammonium salts (**3***a*, **3***i*, **3***f*) this methyl's signal is found near δ 1.8 while in the corresponding free bases it is located near δ 1.25 ± 0.1. In all cases the chemical shifts are lower than anticipated (3) for the effect of a β-nitrogen alone, no doubt due to the deshielding by the appropriately oriented heteroaromatic nucleus.

Support for the assignment of configuration at C1′ comes from the ready dehydration of **3***a* to **6** allowed by the easy attainment of a *trans* antiparallel relationship of the C3 hydrogen and the C1′ hydroxyl, together with the observation that such a configuration will lead, on dehydration, to the sterically feasible geometry at C1′ in which the vinylic hydrogen is *cis* to the bulky C2 substituents as in structure **6**.

Additional support for the stereochemical assignment **3** can be derived from mechanistic

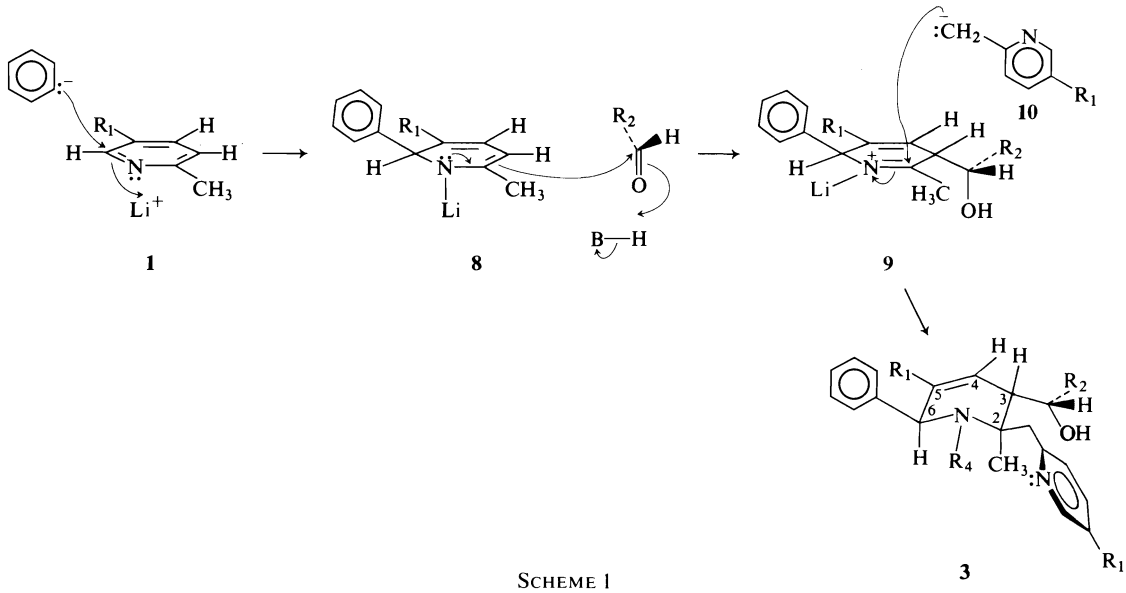

SCHEME 1

considerations (see Scheme 1). The generation of the 1-lithio-2-phenyl-1,2-dihydropyridine system **8** is well precedented (4). The dienamine **8** is visualized as attacking an aldehyde molecule via a transition state which for steric reasons requires orientation of the aldehyde alkyl group away from the C2 methyl and the formation of the intermediate quaternary lithioimmonium ion **9** in which the substituents at C3 and C6 have the preferred *trans* relationship. Discharge of the cation **9** via least hindered approach of the anion **10** at C2 would result in the unique stereochemistry **3** for the adducts. Thus mechanistic considerations indicate why a single stereoisomer results in a process in which four chiral centres are developed.

Some support for the initial phase of this mechanism is found in the observations of Giam *et al.* (4) who obtained the unexpected product **13** in 33% yield when a solution of 2-phenylpyridine **11** was treated with 1-lithio-2-phenyl-1,2-dihydropyridine **8**. These authors suggest the intermediacy of **12** which undergoes further transformation to **13** (Scheme 2). Thus the nucleophilicity of **8** at position 5 is precedented. In addition it is also known that 1-lithio-2-substituted-1,2-dihydropyridines react with alkyl halides to produce 2,5-disubstituted pyridines (5, 6).

A variation of the mechanism proposed in Scheme 1 in which the anion **10** makes initial attack at the 2 position of the pyridine **1** can also be considered and could be expected to lead to product and stereochemistry **3**; however, it seems to be less likely in view of the above precedents.

The reluctance of **3***a* to undergo selective reduction at the 4,5-double bond can be explained on the basis of the stereochemistry **3**. Steric impedance on the one side from the axial methyl and quasi equatorial isopentanol side chain and on the other from the presence and orientation of the phenyl ring. Once the phenyl ring is reduced, the isolated double bond becomes more accessible to the catalyst from the β side (to give stereochemistry **6**) which accords with the experience that the double bond is apparently reduced at approximately the same rate as the phenyl ring.

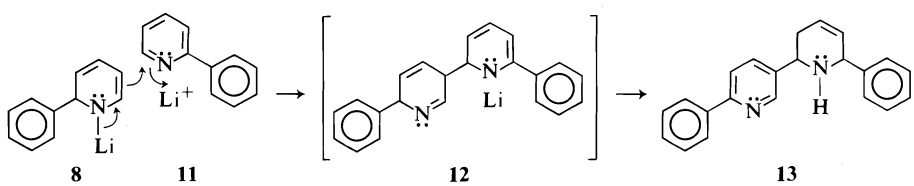

SCHEME 2

TABLE 1. Proton magnetic resonance parameters for adducts and derivatives

Compound (MHz)	Chemical shifts (ppm), apparent multiplicity and coupling constants (Hz)*																			
	NH, OH	2-Me	3-H	4-H	5-Me	6-H	7-Ha	7-Hb	10-H	11-Me	Ar-H 12-H	13-H	1′-H	2′-H_2	3′-H	3′-Me_a	3′-Me_b	N-Ac O-Ac	5-Et	11-Et
3*a* (220)	10.6, 3.5	1.81s	2.45bs $W_{1/2}$ 8	5.91s $W_{1/2}$ 6	1.55s $W_{1/2}$ 5	4.82bs $W_{1/2}$ 8	3.63d *J* 18	3.48d *J* 18	7.99d *J* 2	2.32s	~7.5m	7.12d *J* 8	4.00dd *J* 8 *J* 4	~1.5m by irr at 4.0	~1.5m by irr at 4.0	0.80d *J* 6	0.76d *J* 6			
3*b* (60)	10.9	1.64s	2.93bs $W_{1/2}$ 8	5.88bs $W_{1/2}$ 8	1.64s $W_{1/2}$ 5	4.89bs $W_{1/2}$ 8	3.88d *J* 18	3.27d *J* 18	8.0bs $W_{1/2}$ 5	2.30s	~7.5m	7.10d *J* 8	5.15t *J* 6	~1.4m	~1.4m	0.78bs $W_{1/2}$ 8 (coalesced	0.78bs $W_{1/2}$ 8 doublets)	2.06s		
3*c* (220)		1.27s	2.41s $W_{1/2}$ 10	5.55s $W_{1/2}$ 6	1.50s $W_{1/2}$ 5	4.37bs $W_{1/2}$ 7	2.97d *J* 14	3.10d *J* 14	8.25d *J* 1.5	2.28s	~7.3m	6.95d *J* 8	4.02dq *J* 6 *J* 4 *J* 2	1.15m 1.60m	1.75m by irr at 4.0	0.94d *J* 6	0.94d *J* 6			
3*d* (220)	3.8	1.15s	2.51bs $W_{1/2}$ 9	5.80bs $W_{1/2}$ 5	1.44s $W_{1/2}$ 5	4.37bs $W_{1/2}$ 9	3.18d *J* 14	3.06d *J* 14	8.24d *J* 1.5	2.28s	~7.4m	7.08d *J* 8	5.45t *J* 6	~1.3m	~1.6m	0.90d *J* 6	0.95d *J* 6	2.05s		
3*e* (220)		1.35s	2.96bs $W_{1/2}$ 9	5.89q *J* 2	1.91s $W_{1/2}$ 5	4.84s $W_{1/2}$ 3	4.52d *J* 14	3.27d *J* 14	8.20d *J* 2	2.32s	6.9–7.4ms	7.19d *J* 8	5.97q *J* 4	~1.56m	~1.56m	0.94d *J* 7	0.98d *J* 7	2.05s 1.97s		
3*f* (220)	10.5	1.80s	2.58bs $W_{1/2}$ 9	5.84bs $W_{1/2}$ 6		4.95bs $W_{1/2}$ 7	3.74d *J* 17	3.34d *J* 17	7.99d *J* 2		~7.5m	7.11d *J* 8	3.96dd *J* 10 *J* 5	~1.56m ~1.85m	~1.39m	0.77d *J* 6	0.81d *J* 6		1.85q 0.98t *J* 8	2.59q 1.19t *J* 8
3*g* (60)	10	1.58s	2.98bs $W_{1/2}$ 9	5.92bs $W_{1/2}$ 6		5.01bs $W_{1/2}$ 9	3.89d *J* 18	3.38d *J* 18	8.10d *J* 2		~7.5m	7.15d *J* 8	5.22t *J* 6	·1.3–2.0m	1.3–2.0m	0.80bs $W_{1/2}$ 8 (coalesced	0.80bs $W_{1/2}$ 8 doublets)	2.05s	2.02q 1.00t *J* 7	2.64q 1.20t *J* 7
3*h* (220)		1.28s	2.42bs $W_{1/2}$ 9	5.53bs $W_{1/2}$ 6		4.43bs $W_{1/2}$ 8	3.14d *J* 17	2.97d *J* 17	8.32d *J* 2		~7.5m	6.96d *J* 8	4.03dq *J* 6 *J* 4 *J* 2	~1.7m ~1.6m	~1.25m	0.95d *J* 6	0.95d *J* 6		1.77q 0.96t	2.59q 1.2t
3*i* (60)	11, 3.4	1.78s	2.87bs $W_{1/2}$ 9	5.85bs $W_{1/2}$ 8	1.55s $W_{1/2}$ 5	4.83bs *J* 9	3.66d *J* 18	3.30d *J* 18	8.00d *J* 2		~7.5m	7.10d *J* 8	3.3m	2′-H ~1.5		2′-Me_a 0.35d *J* 7	2′-Me_b 0.85d *J* 7			
3*j* (60)	2.8	1.15s	2.65bs (on 7Hb)	5.84bs $W_{1/2}$ 8	1.50s $W_{1/2}$ 5	4.35bs *J* 8	3.15d *J* 17	2.68d *J* 17	8.30d *J* 2		~7.3m	6.92d *J* 8	3.5d *J* 8	2′-H ~1.8		2′-Me_a 0.85 *J* 6	2′-Me_b 1.05 *J* 6			

*Abbreviations: s singlet, t triplet, q quartet, m(s) multiplet(s), dt doublet of triplets, dd doublet of doublets, dq doublet of quartets.

Experimental

Melting points were determined on a Kofler hot stage apparatus and are uncorrected. High resolution mass spectra were obtained from the Mass Spectrometry Laboratory, University of Alberta. Other mass spectra were obtained with an Hitachi–Perkin-Elmer RMU-6D spectrometer. The 60 MHz spectra were recorded with a Varian T-60 instrument and 220 MHz spectra were recorded with a Varian HR 220 instrument. Line positions are reported in ppm from tetramethylsilane which was used as internal standard. The ir spectra were recorded with a Perkin-Elmer 457 grating infrared spectrophotometer. The uv spectra were obtained with a Perkin-Elmer model 467 spectrophotometer.

Adduct 3a

Under nitrogen atmosphere, bromobenzene (39.5 g, 0.25 mol) in absolute ether (50 ml) was added to a stirred suspension of lithium (3.45 g, 0.5 mol) in ether (200 ml) at a rate to maintain steady refluxing. After 4 h the metal had all dissolved and 2,5-dimethylpyridine (27 g, 0.25 mol) was added over 2 h. The flask was then cooled to 0°C and isopentanal (23 g, 0.25 mol) in ether (25 ml) was added over 1½ h at 0–+5°C. Then water (50 ml) was added followed by 12 *N* HCl (50 ml). The aqueous layer was separated and treated with anhydrous sodium carbonate (55 g in H_2O, 100 ml). Chloroform extraction gave a crude brown oil (45 g) which yielded crystals upon heating. Filtration and recrystallization from CCl_4–CH_2Cl_2 (4:1) gave adduct **3***a* (9.9 g, 18.3%) as white needles, homogeneous on tlc, mp 178–190°C. *Anal.* calcd. for $C_{25}H_{36}ON_2Cl_2$: C 66.52, H 7.98, O 3.55, N 6.21; found: C 66.04, H 7.71, O 4.10, N 6.17. Mass spectrum: *m/e* 378.26737(4) (*M* − 2HCl, calcd. 378.26711), 291(7), 272(17), 230(26), 194(6), 186(33), 185(6), 184(13), 173(9), 170(5), 150(7), 149(68), 145(8), 144(6), 139(6), 131(8), 129(11), 128(8), 117(5), 115(5), 108(26), 107(27), 106(11), 105(6), 91(23), 86(6), 85(100), 79(5), 77(5), 57(31), 43(12), 42(5), 41(9). Zerevitinov active hydrogen determination: calcd. for 4 active H: 0.88%; found: 0.81%. The ir spectrum ν_{max} ($CHCl_3$) 3400 cm^{-1} (hydroxyl). The uv spectrum ν_{max} (EtOH) 218, 279, 277 nm (ε 14 000, 3500, 3100).

From the mother liquors of **3***a* the expected amino alcohol **2***a* was recovered in 16% yield by preparative plate silica gel chromatography ($CHCl_3$–MeOH, 9:1) as a yellow solid, mp 53–54°C, identical with an authentic sample of **2***a* characterized earlier (1).

Monoacetate Dihydrochloride 3b

A solution of **3***a* (0.2 g), pyridine (5 ml), and acetic anhydride (8 ml) was stirred at room temperature for 22 h. Excess reagent and solvent were evaporated yielding a crude solid (0.18 g). Recrystallization from CCl_4–CH_2Cl_2 (4:1) gave product **3***b* (0.15 g, 77%), homogeneous on tlc, mp 175–183°C. Mass spectrum: *m/e* 420.27739(18) (M^+ − 2HCl, calcd. 420.27768), 361(6) (420 − C_4H_9), 272(33), 254(72), 230(31), 229(19), 212(41), 184(19), 173(18), 170(21), 169(72), 157(29), 156(57), 155(56), 149(64), 143(27), 129(25), 108(35), 107(34), 106(20), 91(39), 85(100), 57(41), 43(89). The ir spectrum ν_{max} ($CHCl_3$) 1740 cm^{-1} (ester). The uv spectrum λ_{max} (EtOH) 214, 270, 277 nm (ε 11 000, 3200, 2700).

Free Base 3c

A solution of **3***a* (1.1 g) in ethanol (60 ml) and 2 *N* NaOH (10 ml) was stirred at room temperature for 22 h. Solvent evaporation, water (20 ml) addition, and extraction with chloroform afforded a crude product (1.1 g), which on recrystallization from CCl_4–hexane (2:1) gave product **3***c* (1.0 g), homogeneous on tlc, mp 143–143.5°C. *Anal.* calcd. for $C_{25}H_{34}ON_2$: C 79.36, H 9.00, O 4.31, N 7.41; found: C 78.80, H 9.12, O 4.51, N 7.28. Zerevitinov active hydrogen determination calcd. for 2 active H: 0.53%; found: 0.45%. The ir spectrum ν_{max}(CCl_4) 3300 cm^{-1} (hydroxy/NH). The uv spectrum λ_{max} (EtOH) 217, 270, 277 nm (ε 11 500, 3500, 3100). Mass spectrum: *m/e* 378(52) (M^+), 320(9) (M^+ − C_5H_{11}), 307(32), 291(33), 272(93) (378 − C_7H_9N), 253(57), 252(58), 230(78), 212(76), 210(32), 186(91), 184(67), 183(40), 180(100), 108(41), 107(85) ($C_7H_9N^+$), 106(42), 91(21).

Monoacetate 3d and O,N-Diacetate 3e

A solution of the free base **3***c* (0.14 g) in pyridine (5 ml) and acetic anhydride (8 ml) was stirred at room temperature for 40 h. Evaporation of solvent gave a crude mixture (0.13 g) which was separated by preparative tlc on silica gel ($CHCl_3$–CH_3OH, 20:1) and afforded two major compounds; namely, monoacetate **3***d* (0.028 g) an oil, homogeneous on tlc and diacetate **3***e*, homogeneous on tlc, mp 128–130°C.

Compound **3***e*: *Anal.* calcd. for $C_{29}H_{38}O_3N_2$: C 75.29, H 8.28, O 10.38, N 6.06; found: C 75.24, H 8.08, O 10.72, N 5.71. Mass spectrum: *m/e* 462.28809(1) (M^+, calcd. 462.28824), 345(10), 296(16), 255(7), 254(31), 184(5), 108(19), 107(100), 106(7), 91(5), 43(32). The ir spectrum ν_{max} ($CHCl_3$) 1735 cm^{-1} (ester), 1635 cm^{-1} (amide). The uv spectrum λ_{max} (EtOH) 218, 270, 276 nm (ε 13 600, 3000, 2800). No active H (Zerevitinov).

Compound **3***d*: Mass spectrum *m/e* 420(49) (M^+), 361(21), 360(22), 343(23), 314(25), 272(78), 254(98), 253(48), 252(49), 250(32), 230(52), 212(78), 210(49), 196(63), 184(40), 182(41), 169(95), 157(39), 156(44), 155(61), 143(42), 129(46), 108(50), 107(100), 106(50), 91(57), 85(40). The ir spectrum ν_{max} ($CHCl_3$) 1730 (ester), 1640 cm^{-1} (aromatic). The uv spectrum λ_{max} (EtOH) 218, 279, 275 nm (ε 13 000, 3100, 2800).

Adducts 3f and 3i

The adducts **3***f* and **3***i* were prepared in 6.4 and 4% yield from **1***e* and **1***a*, respectively, via the same procedure employed for preparation of **3***a* and replacing isopentanal for isobutanal for **3***i*.

Compound **3***f*: mp 177–186°C. *Anal.* calcd. for $C_{27}H_{40}ON_2Cl_2$: C 67.64, H 8.35, O 3.34, N 5.84; found: C 67.53, H 8.30, O 3.65, N 5.93. Mass spectrum *m/e* 406(24) (M^+ − 2HCl), 319(21), 286(35), 245(20), 244(50), 200(60), 199(27), 198(30), 197(27), 196(75), 182(51), 170(40), 163(95), 158(25), 153(46), 130(30), 129(60), 128(30), 123(29), 122(91), 121(91), 120(22), 117(21), 115(20), 107(31), 106(100), 105(20), 93(25), 91(71), 85(79), 84(70), 79(40), 77(43). The ir spectrum ν_{max} ($CHCl_3$) 3400 cm^{-1} (OH/NH). The uv spectrum λ_{max} (EtOH) 217, 270, 277 nm (ε 13 000, 5000, 3900).

Compound **3***i*: mp 185–198°C. Mass spectrum *m/e* 364(31) (M^+ − 2HCl), 291(29), 258(91), 224(22), 187(34), 186(92), 185(58), 184(86), 183(45), 182(90), 174(33), 173(100), 170(32), 150(31), 129(67), 128(25), 125(20), 117(22), 115(100), 108(67), 107(85), 106(66), 105(20), 92(25), 91(46), 79(32), 77(30), 71(40). The ir spectrum ν_{max} ($CHCl_3$) 3370 cm^{-1} (OH/NH). The uv spectrum λ_{max} (EtOH) 215, 270, 276 nm (ε 11 600, 3700, 3070).

Free Bases 3h and 3j

The free bases **3***h* and **3***j* were prepared from **3***f* and **3***i* in 95% and 93% yield, respectively, via the same procedure used to prepare free base **3***c* from the dihydrochloride adduct **3***a*.

Compound **3***h*: mp 141–142°C. Mass spectrum *m/e* 406(29) (M^+), 320(27), 319(60), 287(21), 286(100), 285(22), 284(22), 268(20), 267(43), 266(44), 265(18), 251(35), 245(45), 244(72), 238(35), 227(34), 226(60), 224(43), 215(20), 213(21), 210(28), 208(65), 201(20), 200(75), 199(46), 198(65), 197(58), 196(70), 194(30), 187(42), 183(42), 182(75), 181(41), 172(34), 171(35), 170(38), 169(68), 164(31), 163(85), 162(29), 161(26), 159(26), 158(28), 157(26), 154(20), 153(75), 144(22), 143(22), 141(25), 131(32), 130(33), 129(68), 128(32), 123(40), 122(40), 121(76), 120(65), 117(60), 115(62), 107(64), 106(90), 105(60), 104(47), 84(72). The ir spectrum ν_{max} ($CHCl_3$) 3300 cm^{-1} (OH/NH). The uv spectrum λ_{max} (EtOH) 218, 270, 276 nm (ε 14 000, 4900, 4000)

Compound **3***j*: mp 144–145°C. Mass spectrum *m/e* 364(26) (M^+), 331(29), 321(30), 291(41), 264(51), 259(44), 258(76), 253(36), 225(60), 224(33), 216(22), 215(29), 214(35), 187(55), 186(57), 185(40), 184(75), 182(100), 181(41), 174(28), 173(86), 170(46), 158(21), 153(63), 130(71), 129(30), 128(50), 108(60), 107(86), 106(41), 91(36). The ir spectrum ν_{max} ($CHCl_3$) 3300 cm^{-1} (OH/NH). The uv spectrum λ_{max} (EtOH) 217, 270, 277 nm (ε 11 300, 4900, 3300).

Monoacetate 3g

The monoacetate **3***g* was prepared from the dihydrochloride adduct **3***f* in 63% yield via the same procedure used to prepare **3***b* from **3***a* and showed mp 175–185°C. Mass spectrum *m/e* 448(40) (M^+ − 2HCl), 370(25), 269(26), 268(80), 267(27), 266(32), 250(23), 226(43) 224(41), 198(23), 183(64), 182(90), 170(49), 169(48), 163(48), 157(22), 156(21), 155(22), 141(30), 129(36), 128(35), 122(85), 121(85), 120(39), 112(23), 106(88). The ir spectrum ν_{max} ($CHCl_3$) 1730 cm^{-1} (ester). The uv spectrum λ_{max} (EtOH) 215, 270, 276 nm (ε 13 800, 4420, 3650).

Hydrolysis of O,N-Diacetate 3e

A solution of *O,N*-diacetate **3***e* (0.06 g) in ethanol (20 ml) and 20% NaOH (2 ml) was refluxed gently for 24 h. After solvent evaporation, addition of water (10 ml), and chloroform extraction, a crystalline product (0.055 g) was obtained on evaporation, homogeneous on tlc, mp 142–143.5°C, identical in all respects (including mixture mp) with free base **3***c*.

Catalytic Hydrogenation of Adduct 3a to 7

A solution of **3***a* (0.1 g) in ethanol (25 ml) containing PtO_2 (0.018 g) was shaken in a Parr apparatus under H_2 at 40 psi at room temperature for 30 h. Filtration and evaporation gave 0.08 g of crystalline product, homogeneous on tlc, mp 138–141°C. The mass spectrum *m/e* 392(10) (M^+ − 2HCl), 310(30), 309(100), 305(36), 280(91), 218(22), 212(23), 198(80), 194(68), 192(22), 179(21), 160(20), 152(42), 113(45), 112(21), 111(40), 110(38), 98(51). The ir spectrum ν_{max} ($CHCl_3$) 3400 cm^{-1} (OH/NH). No uv chromophore.

Compounds 2b, 2c, 2d, and 2e

The compounds **2***b*, **2***c*, **2***d*, and **2***e* were obtained from experiments performed as for the preparation of **3***a* in which the substituted pyridines employed were **1***b*, **1***a*, **1***c*, and **1***d*, respectively, and in the case of **2***c* benzaldehyde was used instead of isopentanal. All were isolated by preparative layer chromatography on silica gel ($CHCl_3$–CH_3OH, 20:1). All except **2***c* (mp 76–83°C) were obtained as oils and all showed the expected (1) M^+ and ir, uv, and nmr characteristics.

Anhydro Adduct 6a

A solution of **3***a* (0.2 g), pyridine (3 ml), and thionyl chloride (1 ml) was stirred at 0–5°C for 4 h. Careful evaporation of volatile materials gave a crude product (0.18 g). Purification by preparative tlc and subsequent recrystallization (CCl_4–CH_2Cl_2, 1:1) gave compound **6***a* (0.06 g, 33%), homogeneous on tlc, mp 142–144°C. *Anal.* calcd. for $C_{25}H_{34}N_2Cl_2$: C 69.27, H 7.91, N 6.46; found: C 68.94, H 7.95, N 6.60. Mass spectrum *m/e* 360(8) (M − 2HCl), 254(43), 253(60), 252(100), 251(46), 250(65), 238(53), 236(43), 210(89), 197(48), 196(87), 182(79), 155(71), 154(23), 153(22), 152(24), 141(20), 107(50), 106(33). The nmr (60 MHz) spectrum ($CDCl_3$ δ_{TMS}: 0.60 (d, J = 7 Hz, 3H, C3′Me_a), 0.70 (d, J = 7 Hz, 3H, C3′Me_b), 1.30 (m, 1H, C3H), 1.54 (bs, $W_{1/2}$ = 4 Hz, C5Me), 1.63 (s, 3H, C2Me), 1.9 (m, 2H, 2′HaHb), 2.23 (s, 3H, C11Me), 3.27 (d, J = 18 Hz, 1H, C7Ha), 3.60 (d, J = 18 Hz, 1H, C7Hb), 4.74 (bs, $W_{1/2}$ = 6 Hz, 1H, C6H), 5.26 (t, J = 7 Hz, 1H, C1′H), 7.015 (d, J = 7 Hz, 1H, C13H), 7.4 (m, 6H, phenyl H's plus C12H), 8.10 (bs, $W_{1/2}$ = 5 Hz, 1H, C10H), 7.8 (bs, deuterium exchangeable 2H, $—\overset{+}{N}H_2—$), 3.4 (bs, deuterium exchangeable pyridinium $—\overset{+}{N}H—$). The uv spectrum λ_{max} (EtOH) 220 (s), 250 nm (ε 10 000, 15 000).

Acknowledgments

This work was supported in part by financial assistance from the National Research Council of Canada. The 220 MHz spectra were obtained by courtesy of Canadian 220 MHz NMR Centre, University of Toronto. Thanks are due to Z. Valenta (Chemistry Department, University of New Brunswick) for helpful discussion on the stereochemistry.

1. J. A. Findlay and D. Kwan. J. Chem. Soc. Perkin Trans. I, 2962 (1972).
2. J. A. Findlay and L. Radics. J. Chem. Soc. Perkin Trans. I, 2071 (1972).
3. R. M. Silverstein and G. C. Bassler. Spectrometric identification of organic compounds. 2nd ed. Wiley. 1967. p. 136.
4. C. S. Giam, E. E. Knaus, R. A. Lockhart, and I. G. Keener. Can. J. Chem. **53**, 2305 (1975).
5. P. Doyle and R. Yates. Tetrahedron Lett. 3371 (1970).
6. R. Levine and W. Kadunce. Chem. Commun. 921 (1970).

On the induced decomposition of α-phenylethylhydroperoxide by peroxy radicals

I. P. HAJDU, I. NEMES, AND D. GÁL
Central Research Institute for Chemistry, Budapest, Hungary
AND
V. L. RUBAYLO AND N. M. EMANUEL
Institute for Chemical Physics, Moscow, USSR

Received October 14, 1976

I. P. HAJDU, I. NEMES, D. GÁL, V. L. RUBAYLO, and N. M. EMANUEL. Can. J. Chem. **55**, 2677 (1977).

The induced decomposition of α-phenylethylhydroperoxide (HROOH) has been investigated in three different systems: hydroperoxide + cyclohexene + AIBN + O_2 (I); cyclohexene substituted by isooctane (II), and cyclohexene substituted by chlorobenzene (III). The decomposition products of the HROOH were in all cases acetophenone (RO) and methylphenylcarbinol (HROH).

It was established that peroxy radicals induced the decomposition. The considerable material balance deficit in I is due to the addition of the peroxy radicals to cyclohexene the rate constant of which was estimated from the experimental data. No material balance deficit was observed with II. Experiments supported the assumption that both RO and HROH were formed simultaneously in the interaction between peroxy radicals and HROOH.

The rate constant of the reaction $HRO_2^{\cdot} + HROOH \rightarrow HROH + O_2 + HRO^{\cdot}$ was measured as $k = 1.03 \times 10^9 \exp(-13\,100/RT)$. It is suggested that in the autoxidation of ethylbenzene the induced decomposition of HROOH is fast enough to be the main source of RO and HROH.

I. P. HAJDU, I. NEMES, D. GÁL, V. L. RUBAYLO et N. M. EMANUEL. Can. J. Chem. **55**, 2677 (1977).

On a étudié la décomposition induite de l'hydroperoxyde d'α-phényléthyle (HROOH) dans trois systèmes différents: l'hydroperoxyde + le cyclohexène + AIBN + O_2 (I); on substitue le cyclohexène par de l'iso-octane (II) et le cyclohexène par du chlorobenzène (III). On a trouvé que les produits de décomposition de HROOH sont, dans tous les cas, l'acétophénone (RO) et le méthylphénylcarbinol (HROH).

On a établi que la décomposition est induite par les radicaux peroxy. Le fait que la balance des matériaux est considérablement déficitaire dans I est dû á l'addition de radicaux peroxy au cyclohexène, réaction pour laquelle on a mesuré la constante de vitesse. On n'a observé aucun déficit dans la balance des matériaux avec le système II. Les expériences supportent l'hypothèse que les produits RO et HROH se forment simultanément lors de l'interaction entre les radicaux peroxy et HROOH.

La constante de vitesse de la réaction $HRO_2^{\cdot} + HROOH \rightarrow HROH + O_2 + HRO^{\cdot}$ est $k = 1.03 \times 10^9 \exp(-13\,100/RT)$. On suggère que lors de l'autooxydation de l'éthylbenzène, la décomposition induite de HROOH est suffisamment rapide pour être la source principale de RO et de HROH.

[Traduit par le journal]

Hydroperoxides are primary products of hydrocarbon oxidation processes. The kinetics and routes by which they are decomposed to other products are of general interest. As indicated by Hiatt *et al.* (1), the difficulty of measuring true rates for the decomposition can be attested by several attempts referred to in the literature.

Recently, we have shown by direct tracer experiments (2) that in the oxidation of ethylbenzene the thermal homolysis of α-phenylethylhydroperoxide, though very important as the degenerate branching process, cannot provide the amounts of products formed from the hydroperoxide and observed experimentally. Since hydroperoxides are very labile toward attack by free radicals, we assumed that their decomposition, induced by peroxy radicals, was the main route for the formation of secondary products.

In the case of secondary hydroperoxides, reaction 1 was suggested as an interaction between peroxy radicals and hydroperoxides (3):

[1] $HRO_2^{\cdot} + HROOH \rightarrow HROOH + {}^{\cdot}ROOH$

(where $HRO_2^{\cdot}$, HROOH, and ·ROOH mean

peroxy radical, hydroperoxide molecule, and hydroperoxide radical, respectively) followed by the instantaneous decomposition of ROOH into ketone and an ·OH radical. Similar reactions were suggested by Robertson and Waters (4), Benson (5), and Martan *et al.* (6) for alkoxy and hydroxyl radicals. However, it is known that the alcohol is formed also.

According to Dean and Skirrow (7), the induced decomposition might proceed by the following route:

[2] $HRO_2\cdot + HROOH \rightarrow HRO\cdot + O_2 + HROH$

(HRO· and HROH are alkoxy radicals and alcohol, respectively). Skibida *et al.* (8) and Ingold (9) suggest different possibilities for the detailed mechanism of reaction 2.[1] The importance of processes [1] and [2] becomes especially striking if we take into account that the oxidation intermediates possess higher reactivity toward peroxy radicals than the parent hydrocarbon (10, 11).

The possibility of an O—H bond rupture also cannot be excluded. This type of reaction was studied thoroughly by Howard, Schwalm, and Ingold (3) as well as by Niki *et al.* (12) who determined the rate constants of the following hydrogen transfer reaction:

[3] $R'O_2\cdot + ROOH \rightarrow R'OOH + RO_2\cdot$

Naturally, parallel to the induced decomposition, the termination reaction of the peroxy radicals yields alcohol and ketone molecules according to a Russell-type combination (13):

[4] $HRO_2\cdot + HRO_2\cdot \rightarrow RO + O_2 + HROH$

where RO means ketone. This latter process, however, becomes decisive *as a source of products* only at high initiation rates.

Consequently we studied the reactions between α-phenylethylhydroperoxide and different peroxy radicals, generated *in situ* by the initiated oxidation of two hydrocarbons. The choice of cyclohexene and isooctane as hydrocarbons was motivated by two reasons: (*i*) both can be oxidized at temperatures where the thermal decomposition of the α-phenylethylhydroperoxide can be neglected, and (*ii*) by their comparison we can obtain information with respect to the interaction of the peroxy radicals with double bonds. In addition, peroxy radicals were generated also by the hydrogen transfer between radicals from the decomposition of an initiator and α-phenylethylhydroperoxide.

[1]One of the referees suggested a third possibility via a four centered transition state which seems acceptable to the authors.

Experimental

Materials

Commercial cyclohexene (purity higher than 99%) was distilled twice from metallic sodium, bp, 82.5°C. α-Phenylethylhydroperoxide (HROOH) was prepared in our laboratory as described elsewhere (14). 2,2,4-Trimethylpentane (purity 99.2%) was used without further purification. Azobisizobutyronitrile (AIBN) was "Fluka" product and has been recrystallized four times from chloroform, mp, 101–101.5°C. Acetophenone (RO) and phenylmethylcarbinol (HROH) ("Fluka") were used without further purification. Cyanopropylhydroperoxide (CPH) was prepared by the AIBN-initiated oxidation of ethylbenzene according to Buligin *et al.* (15).

2,6-Di-*tert*-butyl-4-methylphenol (ionol) and 2,4,6-tri-*tert*-butylphenol were used as commercial products ("Fluka").

Analysis

Molecular products were analyzed by glc as described earlier (16).

Procedure

Experiments have been carried out at atmospheric pressure in a glass reactor using an oxygen stream of 1.8–3.0 $dm^3\ h^{-1}$ between 70–90°C. Neat cyclohexene was used while chlorobenzene was the solvent for studies with isooctane.

Experimental Results

Thermal Decomposition of HROOH

A chlorobenzene solution of HROOH (0.2 mol dm^{-3}) was kept at 110°C for 7 h. Measurable quantities of products were not detected during this time and thus the thermal decomposition of the HROOH in the temperature range of 70–90°C can be neglected. Neither HROH nor RO added in amounts 0.1 mol dm^{-3} at 90°C affected these results. A chlorobenzene solution of HROOH (0.2 mol dm^{-3}) and AIBN (0.03 mol dm^{-3}) was kept at 70–90°C in argon atmosphere; no decomposition of the HROOH was detected.

Study of the System HROOH + Cyclohexene + AIBN + O_2

The accumulated amounts of phenylmethylcarbinol and acetophenone formed from the induced decomposition of α-phenylethylhydroperoxide in the course of the initiated oxidation of cyclohexene *vs.* time are shown in Figs. 1 and 2. Separate experiments done with up to 0.5 mol dm^{-3} HROOH content have shown that the addition of the hydroperoxide to the system

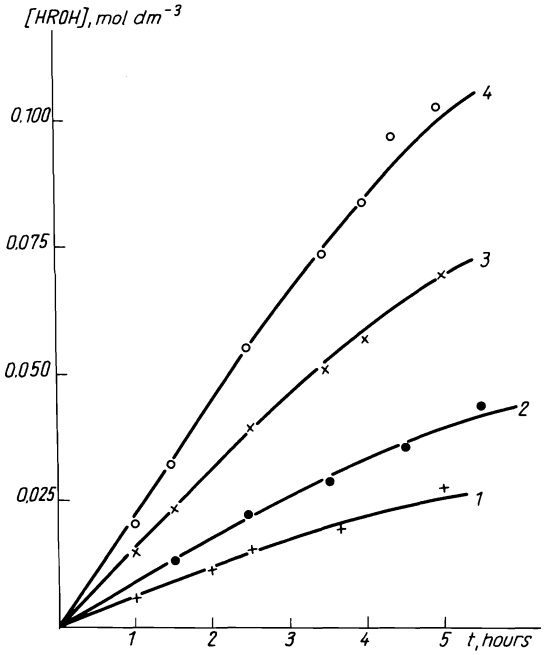

FIG. 1. Accumulation of HROH during the decomposition of α-phenylethylhydroperoxide induced by cyclohexenylperoxy radicals at 70°C. Initial HROOH concentrations were *1*, 0.25; *2*, 0.50; *3*, 0.75; and *4*, 1.00 mol dm^{-3}.

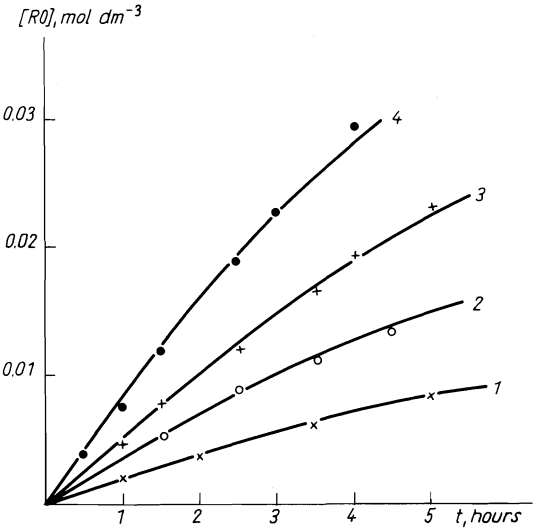

FIG. 2. The same as Fig. 1 for the accumulation of acetophenone.

cyclohexene + oxygen does not affect the kinetics of the accumulation of cyclohexenylhydroperoxide and the kinetic parameters of the oxidation. Thus, *e.g.*, at an initiation rate of 1.6×10^{-6} mol dm^{-3} s^{-1} the kinetic chain length of the cyclohexene oxidation is about 70 which remains unchanged in the presence of α-phenylethylhydroperoxide.

Figure 3 shows the consumption of the HROOH (its initial concentrations were 0.75 and 0.50 mol dm^{-3}, respectively). The dashed lines refer to the consumed amounts of [HROOH] calculated from the product accumulation [HROH] + [RO]. It is evident that, in the system AIBN + cyclohexene + HROOH + O_2, a material balance deficit exceeding 60% was observed.

Study of the System HROOH + Isooctane + AIBN + O_2

Figure 4 shows the accumulation of both RO and HROH for an initial concentration of HROOH of 0.50 mol dm^{-3}, as well as the consumption of the HROOH obtained in two different ways: (*i*) by measuring it directly, and (*ii*) calculated from the product accumula-

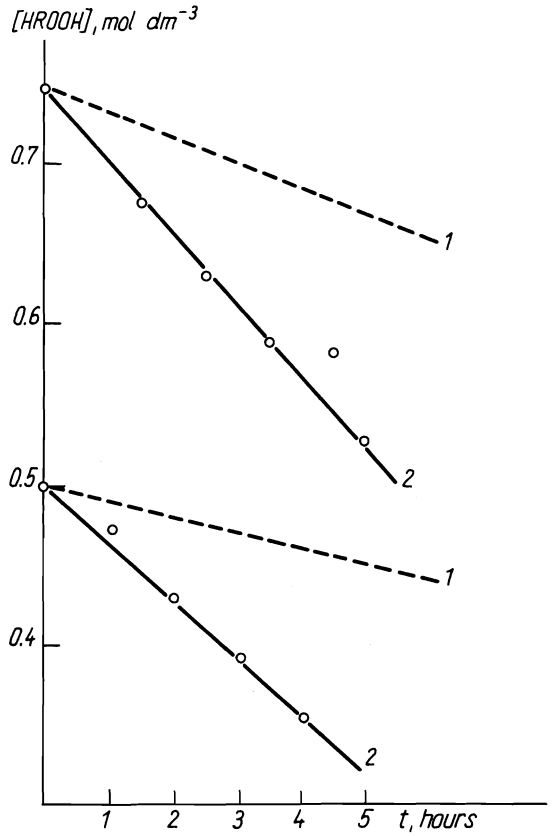

FIG. 3. Consumption of HROOH at its two different initial concentrations at 70°C. *1*, calculated from the accumulation of products; *2*, experimental data.

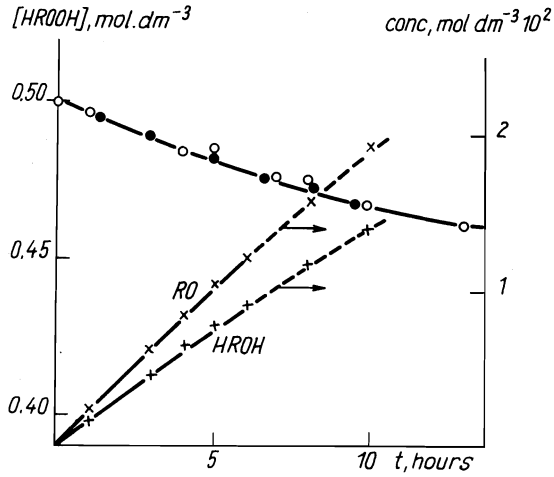

FIG. 4. Accumulation of RO and HROH during the decomposition of HROOH induced by isooctylperoxy radicals at 70°C. Consumption of HROOH in the same system. Full circles, experimental data; open circles, calculated from the accumulation of products.

tion. It can be seen that the material balance is satisfactory, that is, amounts of HROOH decomposed are recovered exclusively in the form of RO and HROH. In this case the amount of RO accumulated exceeds that of the HROH while with cyclohexene as substrate the reverse was found.

Decomposition of HROOH in the Presence of AIBN and Oxygen

Three main products have been found: RO, HROH, and CPH. In order to determine the reaction order with respect to both HROOH and AIBN two series of runs were performed at 80°C: (*i*) at constant $[HROOH]_0 = 0.2$ mol dm^{-3}, $[AIBN]_0$ has been varied between 0.015–0.060 mol dm^{-3}, and (*ii*) at constant $[AIBN]_0 = 0.060$ mol dm^{-3}, $[HROOH]_0$ has been varied between 0.020 and 0.35 mol dm^{-3}. The partial reaction order was 1 with respect to AIBN and zero with respect to HROOH.

The temperature-dependence of the decomposition was studied between 70 and 90°C at $[HROOH]_0 = 0.20$ mol dm^{-3} and $[AIBN]_0 = 0.030$ mol dm^{-3}. Experimental data for the accumulation of HROH are given in Fig. 5.

The separate determination of the accumulation of CPH was vital. Corresponding experimental data are plotted in Fig. 6. Unfortunately, curves in Fig. 6 should be regarded only as approximate, because of impurities in the CPH-standard.

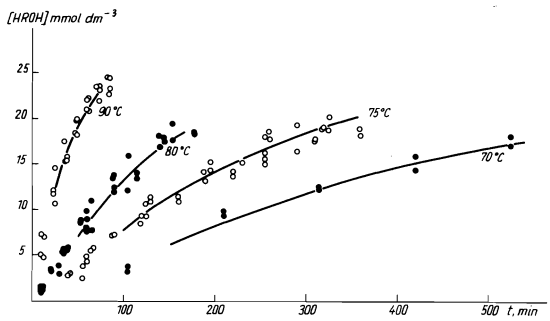

FIG. 5. Accumulation of HROH *vs.* time at different temperatures, $[AIBN]_0 = 0.030$; $[HROOH]_0 = 0.20$ mol dm^{-3}. Points correspond to experimental values; curves are calculated.

Using the decomposition rate constant and radical yield of the AIBN we have calculated the amounts of CPH expected theoretically assuming that all the 'escaped radicals' lead to CPH, and compared them to the experimental values. The agreement was satisfactory.

Determination of the Radical Yield (f) of the Decomposition of AIBN

There are several data in the literature for chlorobenzene solvent, but they are contradictory and we could not exclude *a priori* that the addition of HROOH affecting the viscosity and the dielectric constant of the solution might affect the value of *f*. Therefore, the value of *f* has been determined at 80°C in an oxygen atmosphere in the presence of 0.20 mol dm^{-3} HROOH, and using 2,6-di-*tert*-butyl-4-methylphenol as inhibitor.[2] We obtained $f = 0.6$, in good agreement with some literature values and this indicated that neither oxygen nor HROOH affected *f*.

Discussion

The material balance deficit observed during the decomposition of HROOH 'induced' by the oxidation of cyclohexene, and its absence if isooctane was used, can be easily explained by taking into account the addition of peroxy radicals to double bonds observed in the course of olefin oxidations (17).

The existence of the balance deficit may be regarded as an indirect proof of the occurrence

[2]In this case the conditions for the gas chromatography were changed. Carrier: Chromosorb W; stationary phase, 10% Apiezon L; length of column, 80 cm; temperature, 150°C; internal standard, 2,4,6-tri-*tert*-butylphenol.

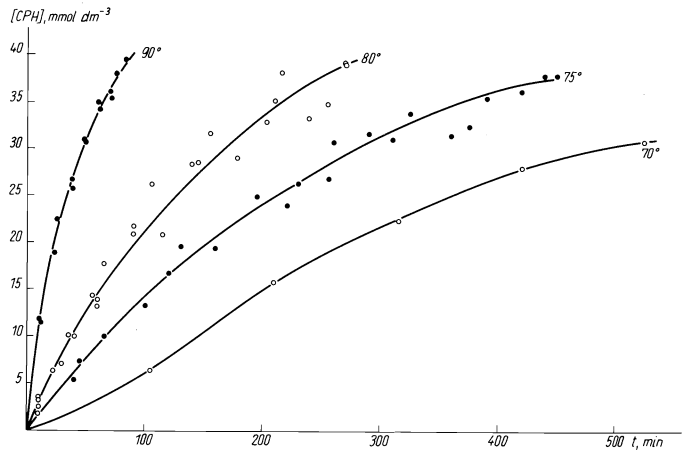

FIG. 6. Accumulation of CPH *vs.* time at different temperatures; $[AIBN]_0 = 0.030$; $[HROOH]_0 = 0.20$ mol dm^{-3}.

of transfer process [3]. Namely, it must be assumed that the cyclohexenylperoxy radicals react with α-phenylethylhydroperoxide:

[5] $HR'O_2\cdot + HROOH \rightarrow HR'OOH + HRO_2\cdot$

that is, the chain carrier radicals of the oxidation are exchanged for α-phenylethyl peroxy radicals and consequently:

[6] $HRO_2\cdot + R'H_2 \xrightarrow{O_2} DO_2\cdot$

where D is a radical formed by the addition of $HRO_2\cdot$ to cyclohexene. The consumption of cyclohexene in process [6] is:

$$[7] \quad -\left(\frac{d[R'H_2]}{dt}\right)_6 = k_6[HRO_2\cdot][R'H_2]$$

The left side of [7] can be easily obtained from Fig. 3, since

$$[8] \quad -\left(\frac{d[R'H_2]}{dt}\right)_6 = w_1 - w_2 \equiv \Delta W$$

where

$$[9] \quad w_1 = -\left(\frac{d[HROOH]}{dt}\right)$$

and

$$[10] \quad w_2 = \frac{d([RO] + [HROH])}{dt}$$

From [7] and [8]

$$[11] \quad k_6 = \frac{\Delta W}{[HRO_2\cdot][R'H_2]}$$

In eq. 11 $[HRO_2\cdot]$ is not known. However, it can be assumed that the rate determining termination occurs between α-phenylethylperoxy radicals. This assumption yields the maximal steady state concentration of $[HRO_2\cdot]_{st}^{max}$ from $w_i = k_t([HRO_2\cdot]_{st}^{max})^2$. Thus the minimal value of k_6 can be computed:

$$[12] \quad k_6^{min} = 2.8 \text{ dm}^3 \text{ mol}^{-1} \text{ s}^{-1}$$

in good agreement with literature data (18), giving 2.5 dm^3 mol^{-1} s^{-1}.

Figure 7 shows the initial accumulation rates of acetophenone and phenylmethylcarbinol *vs.* the initial concentration of the α-phenylethylhydroperoxide. Two important conclusions can be drawn: (*i*) the initial rates of the product accumulations exceed essentially the rates of initiation for both products, and (*ii*) the initial rates of the accumulation depend linearly on $[HROOH]_0$. These experimental facts indicate that both products are formed primarily in the induced decomposition. The ratio of the slopes of the two straight lines shows that the rate of the accumulation of alcohol exceeds by approximately 2.5 times that of the ketone formation.

Since with isooctane as substrate the accumulation rates of both acetophenone and phenylmethylcarbinol are considerably lower than the rate of initiation, it is obvious that in this case the $HRO_2\cdot$ radicals cannot be considered the main chain carriers *and* that they react faster with HROOH than do the isooctylperoxy radicals.

The calculations of the rate constants of reactions 1 and 2 were carried out from the experimental results obtained for the system HROOH + AIBN + O_2. Since the kinetic chain length, expressed as the ratio of the accumulation rates

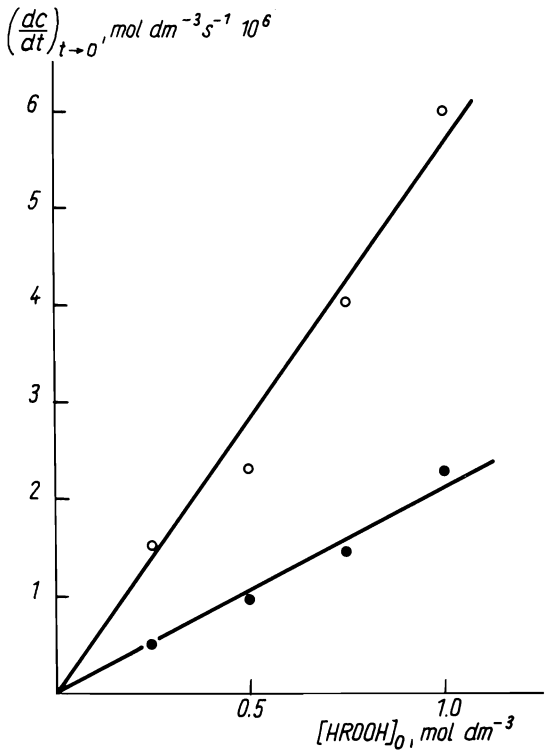

FIG. 7. The initial rates of accumulation of the HROH (open circles) and RO (full circles) *vs.* initial concentration of HROOH at 70°C during the oxidation of cyclohexene.

of the products to the initiation rate (w_i), is larger than unity:

$$[13] \quad \nu = \frac{d([RO] + [HROH])}{dt} \cdot \frac{1}{w_i} > 1$$

ketone and alcohol are formed also in reactions 1 and 2. The values of ν found in the range under investigation are: 70°C, ν = 1.57; 75°C, ν = 1.54; 80°C, ν = 1.59; 90°C, ν = 1.59. By knowing the rate of initiation, we can distinguish the two pathways of product formation (radical combination and induced decomposition). This is shown for one run in Fig. 8.

$HRO_2\cdot$ radicals are generated in the interaction between cyanopropylperoxy radical ($rO_2\cdot$) and HROOH in a hydrogen transfer process:

$$[14] \quad rO_2\cdot + HROOH \rightarrow rOOH + HRO_2\cdot$$

According to literature data, HROH molecules yield ketone in the presence of oxygen (19, 20). Therefore, in order to obtain the actual formation rates of ketone and alcohol, the experimental rate values must be corrected by the

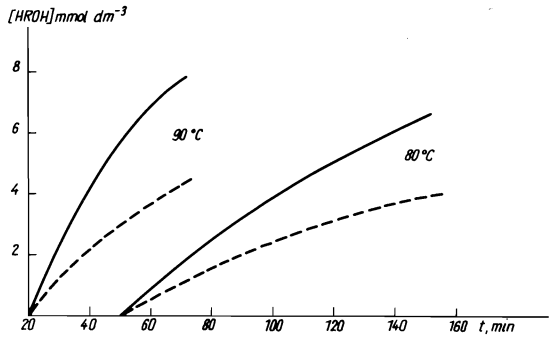

FIG. 8. Formation of HROH in radical combination and in induced decomposition (dotted line) at different temperatures.

consumption rate of the HROH. (Calculations of these corrections are deposited as supplementary material.[3])

The requirements to be fulfilled by the mechanism are as follows. Both RO and HROH should be formed by two different pathways, partly from the combination of $HRO_2\cdot$ (the validity of the Russell mechanism for the radical combination process (13) has been accepted) and partly in decomposition induced by $HRO_2\cdot$. New radicals formed in the induced decomposition are consumed by their reactions with HROOH.

Consequently the mechanism suggested for the induced decomposition of HROOH besides reactions 1, 2, 4, and 14 includes the following processes:

$$[15] \quad AIBN \xrightarrow{O_2} 2frO_2\cdot$$

$$[16] \quad HRO\cdot + HROOH \rightarrow HROH + HRO_2\cdot$$

$$[17] \quad \cdot OH + HROOH \rightarrow H_2O + HRO_2\cdot$$

$$[18] \quad \cdot OH + HROOH \rightarrow H_2O + RO + \cdot OH$$

$$[19] \quad HRO\cdot + HROOH \rightarrow HROH + RO + \cdot OH$$

Cross combination reactions between $rO_2\cdot$ and $HRO_2\cdot$ have been neglected because the CPH concentrations found experimentally were in good agreement with their expected values.

With respect to the H-transfer reaction [16] Benson estimated $k_{16} = 10^{8.0} \exp(-7\,500/RT)$ for *tert*-butylhydroperoxide and the corresponding alkoxy radicals (5). Since the reactivities of alkoxy radicals and ·OH do not differ greatly,

[3]Photocopies of Table 1 may be obtained upon request, at a nominal charge, from the Depository of Unpublished Data, CISTI, National Research Council of Canada, Ottawa, Canada K1A 0S2.

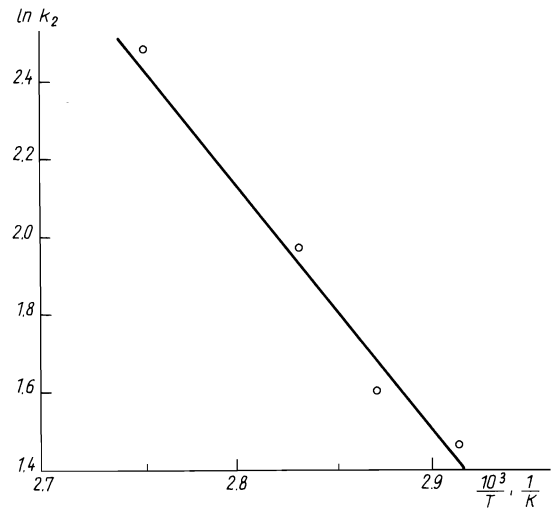

FIG. 9. The Arrhenius plot of the rate constant k_2.

it can be assumed that reaction 17 is also fast. Since peroxy radicals are capable of abstracting tertiary hydrogen from the hydroperoxide molecules (reaction 1), it was assumed that hydroxyl and alkoxy radicals (reactions 18 and 19) reacted in a similar way.

Assuming steady state concentrations for the radicals we obtain the following rates of formation of the products:

$$[20]\quad w_{\mathrm{HROH}} \equiv \frac{\mathrm{d[HROH]}}{\mathrm{d}t} = 2k_2[\mathrm{HROOH}](w_i/k_4)^{1/2} + \tfrac{1}{2}w_i$$

and

$$[21]\quad w_{\mathrm{RO}} \equiv \frac{\mathrm{d[RO]}}{\mathrm{d}t} = K[\mathrm{HROOH}](w_i/k_4)^{1/2} + \tfrac{1}{2}w_i$$

where

$$[22]\quad K = \left(1 + \frac{k_{18}}{k_{17}}\right)\left(k_1 + \frac{k_2k_{19}}{k_{16} + k_{19}}\right)$$

and

$$[23]\quad w_i = 2fk_{15}[\mathrm{AIBN}]$$

Using our experimental data we have determined w_{HROH} and w_{RO} by the parabolic method and the corresponding constants:

$$[24]\quad k_2 = \frac{w_{\mathrm{HROH}} - \frac{1}{2}w_i}{2[\mathrm{HROOH}](w_i/k_4)^{1/2}}$$

and

$$[25]\quad K = \frac{w_{\mathrm{RO}} - \frac{1}{2}w_i}{[\mathrm{HROOH}](w_i/k_4)^{1/2}}$$

Calculations have been carried out for runs performed at $[\mathrm{HROOH}]_0 = 0.20$ mol dm^{-3}; results are given in Table 1.[3]

Corrections for the radical-initiated oxidative transformation of the alcohol to ketone were calculated in the following way.

The rate of the transformation can be expressed as

$$-\frac{\mathrm{d[HROH]}}{\mathrm{d}t} = k^{\mathrm{HROH}}[\mathrm{HROH}][\mathrm{HRO_2}\cdot] = k^{\mathrm{HROH}}[\mathrm{HROH}](w_i/k_4)^{1/2}$$

Earlier we have reported (21) the value of the ratio $k^{\mathrm{HROH}}/k^{\mathrm{RH_2}}$ where k^{HROH} and $k^{\mathrm{RH_2}}$ are the rate constants of the hydrogen abstraction from alcohol and ethylbenzene molecules by α-phenylethylperoxy radicals, respectively. According to literature data (22) $k^{\mathrm{RH_2}} = 9.6 \times 10^5 \exp(-8\,500/RT)$ dm^3 mol^{-1} s^{-1} and consequently the values of k^{HROH} are: 70°C, 32.2; 75°C, 36.3; 80°C, 39.6; 90°C, 47.4 dm^3 mol^{-1} s^{-1}. The calculations are correct only if the ratio of the formation rates of alcohol and ketone remains constant during one run (assuming that the mechanism remains unchanged). The ratios of the formation rates are given separately in Table 1.

After taking into account these corrections for the alcohol–ketone transformation, we obtain the Arrhenius plot of k_2 given in Fig. 9.

$$[26]\quad k_2 = 1.03 \times 10^9\, \mathrm{e}^{-13100/RT}\ \mathrm{dm^3\ mol^{-1}\ s^{-1}}$$

The following rate constants were used: $k_{15} = 1.737 \times 10^{15} \exp(-30\,800/\mathrm{RT})$ s^{-1} and $k_4 = 1.9 \times 10^7$ dm^3 mol^{-1} s^{-1} (23).

Knowing k_2, w_i, [HROOH], and the corrections to w_{HROH} we can calculate $[\mathrm{HROH}] = f(t)$ by graphical integration. The comparison with the experimental values gives satisfactory agreement as shown in Fig. 5.

Acknowledgements

We acknowledge the help of Dr. T. Vidóczy in determining the rate of initiation and the assistance of Mrs. Kerepesi in the experimental work.

1. R. HIATT, T. MILL, and F. R. MAYO. J. Org. Chem. **33**, 1416 (1969).
2. É. DANÓCZY, I. NEMES, and D. GÁL. J. Chem. Soc. Faraday Trans. I, **73**, 135 (1977).

3. J. A. HOWARD, W. J. SCHWALM, and K. U. INGOLD. Adv. Chem. Ser. **75**, 6 (1968).
4. A. ROBERTSON and W. A. WATERS. J. Chem. Soc. 1578 (1948).
5. S. W. BENSON. J. Chem. Phys. **40**, 1007 (1964).
6. M. MARTAN, J. MENASSEN, and D. VOFSI. Tetrahedron Lett. **26**, 3815 (1970).
7. M. H. DEAN and G. SKIRROW. Trans. Faraday Soc. **54**, 849 (1958).
8. I. P. SKIBIDA, Z. K. MAIZUS, and N. M. EMANUEL. Dokl. Akad. Nauk, SSSR, **149**, 1111 (1963).
9. K. U. INGOLD. Chem. Rev. **61**, 563 (1961).
10. D. GÁL, É. DANÓCZY, I. NEMES, T. VIDÓCZY, and P. HAJDU. Ann. New York Acad. Sci. **213**, 51 (1973).
11. I. P. SKIBIDA, Z. K. MAIZUS, and N. M. EMANUEL. Neftekhimiya, **4**, 82 (1964).
12. E. NIKI, K. OKAYASU, and Y. KAMIYA. Int. J. Chem. Kinet. **6**, 279 (1974).
13. G. A. RUSSELL. J. Am. Chem. Soc. **79**, 3871 (1957).
14. L. SÜMEGI, I. KENDE, A. NÉMETH, and D. GÁL. Magy. Kém. Folyóirat. **77**, 571 (1971).
15. M. G. BULIGIN, T. VIDÓCZY, and É. DANÓCZY. Neftekhimiya, **14**, 78 (1974).
16. P. HAJDU and D. GÁL. Magy. Kém. Folyóirat. **82**, 455 (1976).
17. D. E. VAN SICKLE, F. R. MAYO, and R. M. ARLUCK. J. Am. Chem. Soc. **87**, 4824 (1965); **87**, 4832 (1965).
18. V. A. RUBAYLO, A. B. GAGARINA, and N. M. EMANUEL. Kinet. Katal. **15**, 891 (1974).
19. C. PARLANT, I. SERÉE DE ROCHE, and J. CH. BALACEANU. Bull. Soc. Chim. Fr. 2452 (1963).
20. T. VIDÓCZY, É. DANÓCZY, and D. GÁL. J. Phys. Chem. **78**, 828 (1974).
21. É. DANÓCZY, I. NEMES, T. VIDÓCZY, and D. GÁL. J. Chem. Soc. Faraday Trans. I. **71**, 841 (1975).
22. V. F. TSEPALOV and V. YA. SHLYAPINTOKH. Kinet. Katal. **3**, 870 (1962).

Regiospecific horse liver alcohol dehydrogenase-catalyzed oxidations of some bishydroxycyclohexanes

J. Bryan Jones and H. Bruce Goodbrand

Department of Chemistry, University of Toronto, Toronto, Ont., Canada M5S 1A1

Received February 7, 1977

J. Bryan Jones and H. Bruce Goodbrand. Can. J. Chem. **55**, 2685 (1977).

Horse liver alcohol dehydrogenase has been shown to be effective in catalyzing regiospecific oxidations of only the primary alcohol functions of several cyclohexane substrates possessing both primary and secondary alcohol substituents. The reactions, which were all performed on a preparative scale, were also enantioselective in some cases.

J. Bryan Jones et H. Bruce Goodbrand. Can. J. Chem. **55**, 2685 (1977).

On a montré que la déhydrogénase d'alcool provenant du foie de cheval est efficace pour catalyser les oxydations régiospécifiques des fonctions alcool primaire uniquement dans plusieurs substrats de cyclohexane possédant à la fois des substituants alcool primaire et secondaire. Les réactions qui ont toutes été effectuées sur une base préparative sont aussi quelquefois énantiosélectives.

[Traduit par le journal]

One of the consequences of the current high level of sophistication in organic synthesis has been an increased demand for reagents capable of effecting a transformation in a rigidly controlled manner. As a result of their individual specificities, many enzymes are uniquely suited to meeting the most exacting requirements in this regard, including catalysis of highly regiospecific and selective reactions which would otherwise involve several operations with traditional reagents (1).

Selective oxidation of one specified hydroxyl group only in a polyhydroxylated molecule is an example of the control that can be achieved. Oxidations of this type, whose synthetic value is self-evident, are catalyzed by the nicotinamide coenzyme-dependent alcohol dehydrogenases (1). The commercially available NAD^+/NADH-dependent enzyme from horse liver, HLADH, is currently the alcohol dehydrogenase of the most general preparative utility (1, 2).[1] Recently, it was demonstrated that HLADH possessed the ability to mediate regiospecific, and often highly enantioselective, oxidation of only one alcohol function of chiral bishydroxycyclopentanes (2*b*).

We have now extended our investigation of this aspect of HLADH catalysis to some cyclohexyldiol substrates. Synthetically viable regiospecific oxidations were observed with each substrate evaluated and, as in the cyclopentyl series (2*b*), the results were in accord with diamond lattice analysis predictions.

Results

The substituted cyclohexanes **1**–**5** were examined. They, or their immediate precursors, were synthesized in good yields largely by

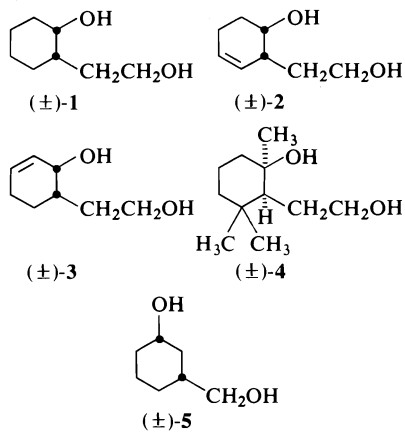

application of literature procedures. The racemates **1**–**5** were all found to be substrates of HLADH; the results are summarized in Table 1. In each case, the rate of oxidation was sufficiently rapid for preparative-scale reactions to be carried out. Accordingly, (±)-**1**–**5** were subjected to HLADH-catalyzed oxidations with

[1]Abbreviations used: NAD^+ and NADH, oxidized and reduced forms, respectively, of nicotinamide adenine dinucleotide; HLADH, horse liver alcohol dehydrogenase; FMN, flavin mononucleotide (riboflavin phosphate).

TABLE 1. Relative rates of HLADH - catalyzed oxidation of (±)-**1–5***

Substrate	V_{rel}
Cyclohexanol	1.0
(±)-**1**	0.39
(±)-**2**	0.43
(±)-**3**	0.30
(±)-**4**	0.09
(±)-**5**	~0.05

*Relative velocities were measured at 25°C in 0.05 *M* glycine–NaOH buffer, p*H* 9.0.

FMN being employed to effect *in situ* recycling (3) of catalytic amounts of the expensive NAD^+ coenzyme required.

HLADH-mediated oxidation of (±)-**1** proceeded as shown in Scheme 1. Oxidation was

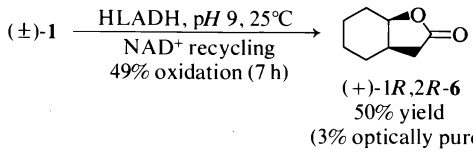

SCHEME 1

totally regiospecific for the primary hydroxyl group, with the aldehyde initially formed undergoing subsequent enzyme catalyzed oxidation (2*b*,*c*) to give the observed product **6** directly. Some enantioselectivity was also manifest during the reaction but the preference for the previously characterized (4) 1*R*,2*R*-enantiomer of **6** was marginal only.

Complete regiospecificity for primary hydroxyl oxidation was also observed with the unsaturated diols (±)-**2** and -**3** as substrates (Scheme 2). An encouraging degree of enantioselectivity occurred during the oxidation of (±)-**2**, whereas for the isomeric substrate **3**, the product lactone **8** was almost racemic.

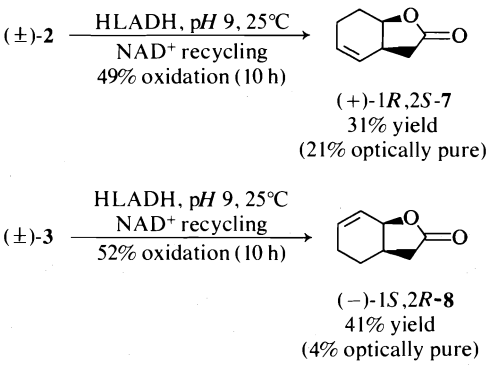

SCHEME 2

The absolute configurations and optical purities of the Scheme 2 lactones were assigned using the literature data available (4*a*).

Although the more highly substituted cyclohexyldiol (±)-**4** underwent HLADH-catalyzed transformation rather slowly, relatively efficient oxidation of the hydroxyethyl function was again observed.[2] The lactone **9**, enriched in the 1*R*,2*S*-enantiomer (5), was formed as shown in Scheme 3.

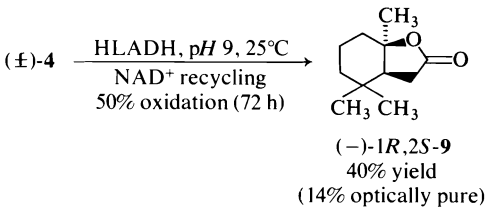

SCHEME 3

Attention was then directed towards the 1,3-disubstituted diol (±)-**5**. HLADH-catalyzed oxidation was very slow for this substrate but once more was completely specific for the primary alcohol, with *cis*-3-hydroxycyclohexane carboxylic acid (**10**) being the only product. As Scheme 4 indicates, the acid **10** was devoid of optical activity.

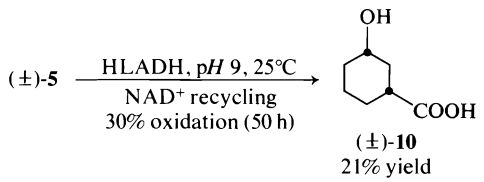

SCHEME 4

Discussion

The selection of structures **1–5** for evaluating the ability of HLADH to discriminate between unhindered primary and secondary alcohol groups attached to cyclohexane moieties was governed by several factors. A major consideration was our desire to choose compounds which were clearly of organic chemical interest. For example, the diols **1–3** lead to lactones **6–8**, which are of prostaglandin synthon value (4), while **4** is a precursor of *cis*-tetrahydroactinodiolide **9**, a member of a group of potent cat and beetle attractants (5, 6). In addition, structures **1–3** and **5** are cyclohexyl analogues of the cyclopentyldiols studied previously (2*b*).

[2]In this case it cannot be claimed that the process is a truly selective one in the chemical sense, since the hydroxyethyl group is the only oxidizable function present.

Each of **1–5** was a substrate of HLADH (Table 1). While the rates of oxidation of **4** and **5** were low, they were still marginally above the level (1% of V_{rel} of cyclohexanol (1)) required for synthetic-scale reactions to remain viable. Each practical-mode enzymic oxidation was performed on preparatively-significant (0.6–0.8 g) amounts of **1–5**. All reactions were terminated as close to the 50% oxidation stage as was practical since, for enzyme-mediated transformations of racemates, this is the point at which pure enantiomers will be obtained if the stereospecificity is absolute. The course of each oxidation was monitored by glc and the reactions were conveniently worked-up using simple continuous solvent extraction procedures. The percentage yields cited in the schemes are of the purified isolated products and were calculated taking the extent of oxidation into account. No attempt was made to optimize the yields in this initial survey. As the experimental details indicate, much higher yields should be obtainable using modified work-up procedures. Recrystallization of optically-active products was avoided in order to preclude the possibility of optical fractionation and all optical purities were determined from the specific rotations reported for the pure enantiomers.[3]

From analyses of the structures of **1–4** using the diamond lattice section (see below for details) it was predicted that HLADH would catalyze oxidation of the primary alcohol function exclusively. The results obtained (Schemes 1–3) are in complete accord with this projection. The hydroxyaldehydes, such as **11**, formed in the initial step were not detected

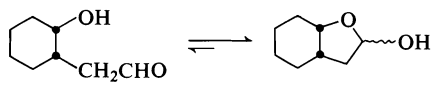

11 **12**

in the final reaction mixtures owing to the facility with which their hemiacetals, *e.g.*, **12**, undergo HLADH-catalyzed oxidation (2*b*,*c*) to the lactones **6–9**. The regiospecificities of these reactions parallel those observed for HLADH-mediated oxidation of the related *cis*-2-hydroxyethylcyclopentyl alcohols (2*b*).

[3]Attempts to measure enantiomeric excesses directly using glc or hplc analyses of diastereomeric derivatives or by nmr in the presence of shift reagents were unsuccessful.

In principle, selective enzymic oxidations of the above type could be accompanied by high enantioselectivity. However, the diamond lattice analyses of (+)- and (−)-**1–4** gave no indication that any significant enantiomeric preferences should manifest themselves. The very low to modest levels of enantiomeric enrichments observed in the Scheme 1–3 reactions were therefore not unexpected.[4] As with the analogous cyclopentyl substrates (2*b*), the degree of enantiomeric enrichment is influenced by the presence and/or position of a double bond in the ring. Although no dramatic stereospecificity was evident with (±)-**1–4** as substrates, it is interesting to note that in each case, the lactone products **6–9** are of the same absolute configuration type. Furthermore, in keeping with the apparent proclivity of HLADH to favour 'unnatural' configurations (1, 2), the enzymically-preferred configurations of the prostaglandin synthons **6–8** and the actinolide **9** are opposite to those of the 'natural' series.

HLADH-catalyzed oxidation of the 1,3-diol **5** was also completely regiospecific for the primary alcohol function, with the aldehyde product produced first being further transformed into the corresponding acid **10**. The latter reaction is presumably due to the aldehyde dehydrogenase content of HLADH (1). The hydroxymethyl specificity of the HLADH-catalyzed transformation of (±)-**5**, the sluggish nature of the reaction, and the racemic nature of the product are in accord with the diamond lattice analysis detailed below. The course of the enzymic oxidation of **5** contrasts sharply with that of the related *cis*-3-hydroxyethylcyclopentanol substrate. In the latter case, the process was highly enantioselective, with oxidation of the secondary hydroxyl group predominating (2*b*).

Diamond Lattice Section Analyses

The diamond lattice (7) section used is an updated model (1, 2*a*) based on those formulated previously (7, 8).

The behaviours of **1–4** are interpretable in terms of one basic lattice analysis. This is depicted in Fig. 1 using the enantiomers of

[4]No literature data on the individual enantiomers of **1–4** are available. Accordingly, since the optical purities of the lactone products **6–9** were so low, no attempt was made to establish the absolute configurations and optical purities of the diols **1–4** recovered from the Scheme 1–3 reactions.

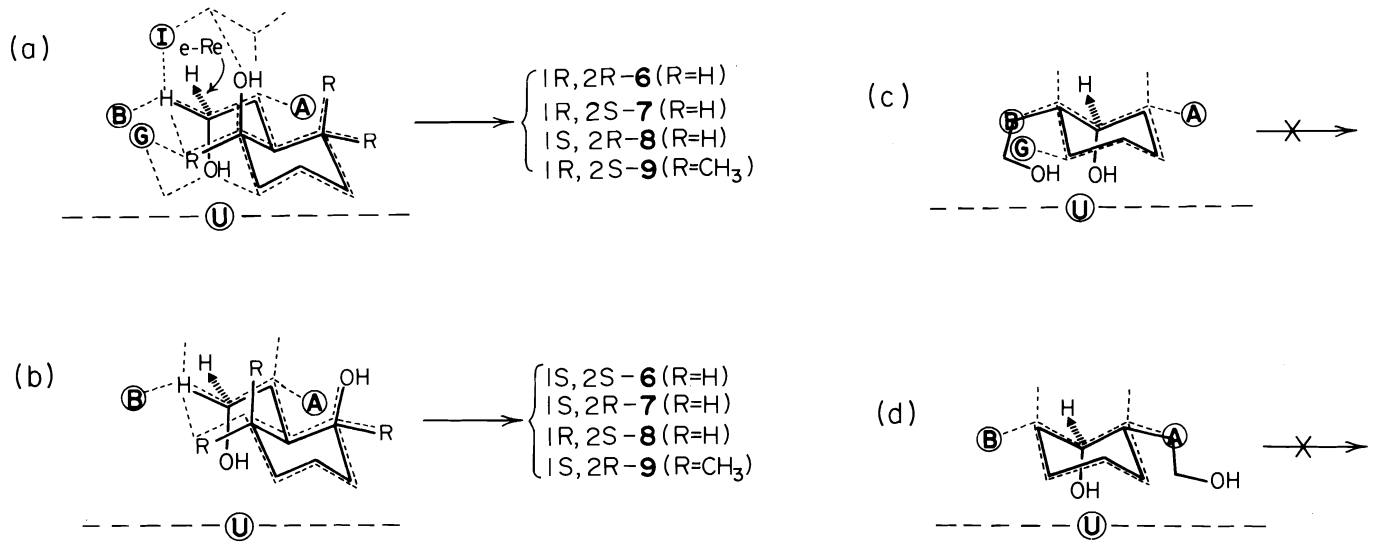

FIG. 1. Diamond lattice analysis of the regiospecificity of HLADH with respect to diols **1**–**4**. The relevant portions of the lattice (described in detail in refs. 1 and 2*a*), including the forbidden or unfavourable positions **A**, **B**, **G**, **I**, and **U**, are indicated by the dashed lines. The enantiomers of **1** (R = H) and **4** (R = Me) are used as the representative structures in the diagrams. When, as in (*a*) and (*b*), the hydroxyethyl groups of either enantiomer of **1** or **4** are oriented such that removal of the *pro-R*-hydrogen from the *e-Re* direction can occur as required by the model (1), there are no unfavourable lattice interactions. Oxidation of the primary alcohol group is thus an allowed process. Neither of the orientations in (*a*) and (*b*) appears more favoured than the other. There is thus no reason to expect any significant enantiomeric discrimination. On the other hand, oxidation of the secondary alcohol moiety is not allowed. Positioning of either enantiomer to permit hydride removal at C-1 in the required *e-Re* direction, as in (*c*) and (*d*), results in violation of forbidden position **A** (and possibly **G**), or **B**, by the respective hydroxyethyl groups. The introduction of double bonds into the cyclohexane ring, as for **2** and **3**, does not alter the analysis in any significant manner.

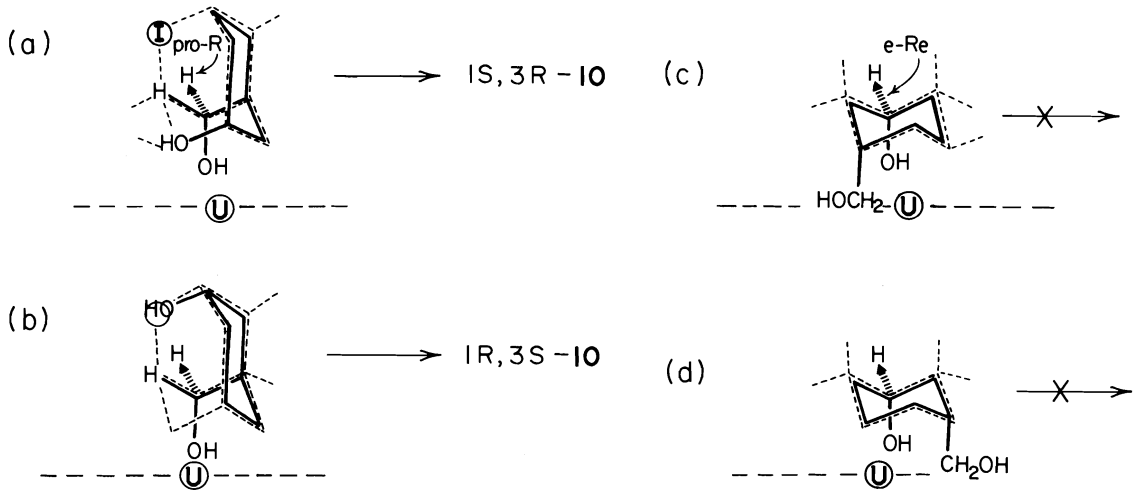

FIG. 2. Diamond lattice analysis of the regiospecificity of HLADH towards (±)-**5**. Oxidation of the primary alcohol function via removal of the *pro-R* hydrogen from the *e-Re* direction as shown in (*a*) and (*b*) are allowed processes since no forbidden positions are violated (position **I** is merely somewhat unfavoured relative to the other allowed lattice locations (1)). In contrast, oxidations of the secondary alcohol functions of either (+) or (−)-**5** are not preferred processes. These would require axial orientation of the C-1 hydroxyl group in order to permit hydride removal from the required (1) *e-Re* direction. Such orientations of the substrate are disfavoured since they force the hydroxymethyl substituents into the highly forbidden **U** region of the lattice as shown in (*c*) and (*d*).

1 and **4** for illustrative purposes. As Fig. 1 indicates, HLADH-catalyzed oxidation is a permitted process when the hydroxyethyl group of each enantiomer of **1**–**4** is positioned in the lattice in accordance with the known stereochemical requirements of the hydride removal step (1). Comparisons of the Fig. 1*a* and *b* orientations of each pair of enantiomers do not provide any reason to expect significant enantioselectivity during the hydroxyethyl group oxidation process. In contrast, when the secondary alcohol functions of (+)- and (−)-**1**–**4** are in the transition state-like orientation required for oxidation, the hydroxyethyl substituents interact adversely with at least one forbidden lattice position, as shown in Fig. 1*c* and *d*. Accordingly, oxidation at C-1 is precluded. The experimental results of Schemes 1–3 are in total accord with this analysis.

For the 1,3-diol **5**, the lattice analysis also unambiguously predicts preferred oxidation of the hydroxymethyl groups (Fig. 2). The oxidation is, however, a slow process because both enantiomers of **5** are required to be in their thermodynamically disfavoured diaxial conformations in order for *pro-R*, *e-Re*-hydride removal (1) to take place. Position **I** is only a moderately unfavourable lattice location (1) and its violation as indicated in Fig. 2*b* is evidently not serious enough to result in the Fig. 2*a* orientation being preferred to a sufficient degree for enantiomeric distinctions to be manifest.

Oxidation of the secondary alcohol function of **5** would require the C-1 hydroxyl group to be axially oriented (1). As shown in Fig. 2*c* and *d*, oxidation in such orientations is precluded for both enantiomers since, in each case, the hydroxymethyl group is required to project into the highly forbidden **U** region of the lattice.[5]

Conclusions

From the current and previous (2*b*) results, it is now clear that HLADH can be used with confidence to effect regiospecific and selective oxidation of one only of two or more hydroxyl groups within the same substrate molecule. Such selectivity in a single step reaction can very rarely be achieved using chemical oxidizing agents (9, 11). Furthermore, the course of the enzymic oxidation is predictable and may also be enantioselective to a greater or lesser degree. However, it is clear that small structural changes in the substrate can have large influences on both regiospecificity and enantio-

[5]The reader is urged to use molecular models to confirm the analyses of both Figs. 1 and 2.

selectivity which cannot yet be explained. Further work on this aspect is in progress.

Experimental

Melting points were determined on a Fisher–Johns apparatus and are uncorrected. Nuclear magnetic resonance spectra were recorded in C^2HCl_3 on a Varian T-60 instrument and ir data were obtained on liquid films (unless specified otherwise) using a Perkin-Elmer 237 spectrometer. Gas–liquid chromatographic analyses were made on 3% QF-1 on Chromosorb G columns with an F & M 400 unit. NAD^+ and FMN were purchased from Sigma and HLADH (EC 1.1.1.1, 3× crystallized) from Worthington.

*cis-2-Hydroxyethylcyclohexanol ((±)-**1**)*

cis-2-Hydroxycyclohexylacetic acid lactone ((±)-**6**) bp 130°C/15 Torr (lit. (12*a*) bp 140–145°C/25 Torr); ir, 1775 cm^{-1}; nmr δ 1.0–2.8 (11H, m) and 4.55 (1H, m) ppm was prepared in three steps from cyclohexanone by the method of Klein (12). The lactone (±)-**6** (10 g, 0.071 mol) was added to a cooled (0°C), stirred, suspension of lithium aluminum hydride (2.71 g, 0.77 mol) in dry ether (200 ml). The mixture was then kept at 20°C for 2 days. Water (10 ml), followed by an excess of 15% aqueous sodium hydroxide, was then added cautiously. The dried ($MgSO_4$) ether solution was evaporated and the residual oil distilled to give the diol (±)-**1** (13) (7.5 g) bp 108°C/0.2 Torr; ir 3600 cm^{-1}; nmr δ 1.6 (11H, m) and 3.75 (5H, m) ppm.

*cis-2-Hydroxyethylcyclohex-3-enol ((±)-**2**)*

cis-6-Hydroxycyclohex-2-enylacetic acid lactone ((±)-**7**) was prepared (three steps) from cyclohexa-1,3-diene by the procedure of Corey and Ravindranathan (4*c*). It had bp 105°C/0.15 Torr; ir 1775 cm^{-1}; nmr δ 1.6–3.3 (7H, m), 4.95 (1H, m), and 5.8 (2H, m) ppm. Lactone (±)-**7** (5.0 g, 3.6 mmol) was added with stirring to lithium aluminum hydride (1.37 g, 3.6 mmol) in dry ether (50 ml). The mixture was refluxed for 1 h and then worked-up with saturated aqueous ammonium chloride. The dried ($MgSO_4$) solution was evaporated and distilled to yield the diol (±)-**2** (1.4 g) bp 105°C/0.15 Torr; ir 3600, 3000, and 1645 cm^{-1}; nmr δ 1.4–2.5 (7H, m), 3.7 (2H, s, OH), 3.8 (3H, m), and 5.5 (2H, m) ppm. *Anal.* calcd. for $C_8H_{14}O_2$: C 67.63, H 9.85, O 22.52; found: C 67.80, H 9.83, O 22.37.

*cis-6-Hydroxyethylcyclohex-2-enol ((±)-**3**)*

Cyclohexene was converted in four steps to cyclohex-2-enylacetic acid bp 116°C/1 Torr (lit. (14) bp 109–112°C/4 Torr); nmr δ 1.2–2.9 (9H, m) and 5.7 (2H, m) ppm as described by Youssef and Sharaf (14). This material was then converted via iodolactonization (12*b*) to *cis*-2-hydroxycyclohex-3-enylacetic acid lactone ((±)-**8**) bp 87–89°C/0.4 Torr (lit. (12*b*) bp 140–145°C/20 Torr); ir 1770, 1660, and 1620 cm^{-1}; nmr δ 1.2–3.0 (7H, m), 4.85 (1H, m), and 6.0 (2H, m) ppm. The lactone (±)-**8** (4.03 g, 0.029 mol) was added with stirring to lithium aluminum hydride (1.11 g, 0.029 mol) in dry ether (50 ml). After being stirred at 20°C for 14 h, the mixture was worked-up by the cautious addition of water and the ether layer dried ($MgSO_4$) and evaporated. Distillation yielded the diol (±)-**3** (4.0 g) bp 101°C/0.4 Torr; ir 3600 cm^{-1}; nmr δ 1.3–1.9 (5H, m), 1.9–2.2 (2H, m), 2.85 (2H, s, OH), 3.8 (2H, t), 4.15 (1H, m), and 5.85 (2H, m) ppm. *Anal.* calcd. for $C_8H_{14}O_2$: C 67.63, H 9.85, O 22.52; found: C 67.81, H 9.86, O 22.33.

*cis-2-Hydroxyethyl-1,3,3-trimethylcyclohexanol ((±)-**4**)*

cis-Tetrahydroactinodiolide ((±)-**9**) was prepared from cyclohexanone in eight steps according to the procedure of Sakan *et al.* (5*b*); it had ir ($CHCl_3$) 1770 cm^{-1}; nmr δ 0.9 (3H, s), 1.05 (3H, s), 1.53 (3H, s), and 1.0–2.5 (9H, m) ppm.

The lactone (±)-**9** (5.0 g, 27.4 mmol) was added to lithium aluminum hydride (1.04 g, 27.4 mmol) in dry ether (200 ml) and the mixture refluxed for 1 day. The reaction mixture was then quenched cautiously with a little water and anhydrous Na_2SO_4 added. The filtered, dried ($MgSO_4$), ether solution was evaporated and the resulting solid recrystallized from ether to give the diol (±)-**4** (3.0 g) mp 96–97°C; ir ($CHCl_3$) 3600 cm^{-1}; nmr δ 0.8–2.2 (9H, m), 0.9 (3H, s), 1.0 (3H, s), 1.2 (3H, s), and 3.7 (2H, t) ppm. *Anal.* calcd. for $C_{11}H_{22}O_2$: C 70.94, H 12.09, O 16.97; found: C 70.90, H 11.93, O 17.17.

*cis-3-Hydroxymethylcyclohexanol ((±)-**5**)*

Cyclohex-3-ene carboxylic acid was converted by the method of Grave and Heinke (14) into *cis*-3-hydroxy-*trans*-4-iodocyclohexane carboxylic acid lactone mp 134°C (lit. (15) mp 134°C). This iodolactone (15.2 g, 0.06 mol) was then added slowly over 30 min at 0°C to a solution of tri-*n*-butyltin hydride (20.34 g, 0.07 mol) in dry benzene. The reaction mixture was stirred at 20°C overnight, and was then evaporated and distilled *in vacuo*. The crude lactone obtained was saponified directly with aqueous sodium hydroxide (7 g, 0.15 mol NaOH) at 20°C for 4 h followed by 2 h under reflux. The cooled solution was washed with ether, then acidified with concentrated hydrochloric acid and extracted with ethyl acetate. Evaporation of the dried ($MgSO_4$) extract gave the hydroxy acid (±)-**10** (2.5 g) mp 131–132°C (lit. (16) mp 131–132°C). The *cis*-acid (±)-**10** was reduced as described by Noyce and Denny (16) to give the diol (±)-**5**, bp 89°C/0.1 Torr (lit. (16) bp 132–134°C/4 Torr); nmr δ 0.8–2.4 (9H, m), 3.0 (2H, s), and 3.4 (3H, m) ppm.

*Determination of Rates of HLADH-catalyzed Oxidations of **1–5***

The assay method used was as described previously (2*a*, 8) employing the following stock solutions: HLADH, 0.5 mg/ml in 0.05 *M* tris–HCl buffer, p*H* 7.4; NAD^+, 10 mg/ml of 0.05 *M* glycine–NaOH buffer, p*H* 9.0. Substrates, 2×10^{-2} *M* solutions in 0.05 *M* glycine–NaOH buffer, p*H* 9.0.

*HLADH-catalyzed Oxidation of (±)-**1***

The diol (±)-**1** (600 mg, 4.16 mmol) was dissolved at 20°C in 0.05 *M* glycine–NaOH buffer (300 ml, p*H* 9.0) and NAD^+ (235 mg, 0.35 mmol) and FMN (3.11 g, 6.5 mmol) added. The reaction was initiated by adding HLADH (45 mg) and the p*H* periodically readjusted to 9. The oxidation was terminated after 7 h (glc showed 49% conversion) and the p*H* brought to 12 with 1 *M* aqueous sodium hydroxide. Continuous chloroform extraction yielded unchanged diol (287 mg). The aqueous reaction mixture was then acidified to p*H* 3 with

1 *M* aqueous hydrochloric acid and reextracted with chloroform for 20 h. Evaporation of the dried ($MgSO_4$), decolourized (Norite) chloroform extract gave the lactone **6** (146 mg), identical with the sample prepared previously. It had $[\alpha]_D^{27}$ +1.5° (*c* 2.2, MeOH) (lit. (4*a*) for 1*R*,2*R*-**6**, +45.5° (*c* 0.43, MeOH).

HLADH-catalyzed Oxidation of (±)-2

The diol (±)-**2** (700 mg, 4.9 mmol) was oxidized as described above for 10 h after which time glc analysis indicated 50% oxidation. Continuous chloroform extraction of the p*H* 13 solution gave unchanged diol (429 mg) containing some lactone and hemiacetal. The p*H* 3 reaction mixture was then reextracted for 10 h as before to give the lactone **7**, which after chromatography on Woelm alumina (activity I, ether elution) gave material, spectrally identical with the racemate prepared above, $[\alpha]_D^{27}$ +5.78° (*c* 1.07, MeOH) (lit. (4*a*) for 1*R*,2*S*-**7** $[\alpha]_D$ +28° (*c*, 0.6, MeOH).

HLADH-catalyzed Oxidation of (±)-3

This experiment was performed using the general procedure described above with diol (±)-**3** (630 mg, 4.4 mmol). After 10 h, when glc showed 52% oxidation, the reaction was worked-up as described above to give recovered diol (400 mg, containing some lactone and hemiacetal) and lactone **8** (130 mg), $[\alpha]_D^{27}$ −0.033° (*c* 0.23, MeOH). The lactone in ethyl acetate (50 ml) was hydrogenated in the presence of 10% Pd-on-C. Work-up gave the saturated lactone **6** (107 mg), identical with (±)-**6** except that it had $[\alpha]_D^{27}$ +1.96° (*c* 1.07, MeOH) (lit. (4*a*) for 1*R*,2*R*-**6**, $[\alpha]_D$ +45.5° (*c* 0.43, MeOH).

HLADH-catalyzed Oxidation of (±)-4

The diol (±)-**4** (700 mg, 3.7 mmol) was oxidized at 20°C in the usual way. After 48 h (33% oxidation) a further quantity of HLADH (15 mg) was added. After a total reaction time of 72 h (51% oxidation) the mixture was basified (p*H* 13) and continuously extracted with chloroform to give a mixture of recovered diol and lactone **9** (520 mg). The acidified (p*H* 3) mixture was then continuously reextracted to give an oil (140 mg) which, after chromatography on a short column of acidic alumina (ether elution), gave *cis*-tetrahydroactinodiolide **9** mp 80–81°C $[\alpha]_D^{22}$ −8.8° (*c* 1.34, $CHCl_3$) (lit. (6) for 1*S*,2*R*-**9**, mp 81–82°C, $[\alpha]_D^{22}$ +64.5° ($CHCl_3$)).

HLADH-catalyzed Oxidation of (±)-5

Oxidation of the 1,3-diol (±)-**5** (700 mg, 5.4 mmol) was performed as described above, with additional HLADH (30 mg) added after 24 h. The reaction was terminated after 50 h (30% oxidation). Continuous chloroform extraction at p*H* 13 for 3 days gave mainly unchanged **5** (511 mg). Subsequent continuous ethyl acetate extraction at p*H* 3 yielded the racemic hydroxy acid (±)-**10** mp 131–132°C (lit. (16) and previous mp 131–132°C).

Acknowledgement

The work was supported by the National Research Council of Canada and was performed during the tenure of an NRCC Postdoctoral Fellowship awarded to H.B.G.

1. J. B. Jones and J. F. Beck. Applications of biochemical systems in organic chemistry. Part 1. *Edited by* J. B. Jones, C. J. Sih, and D. Perlman. J. Wiley and Sons, Inc., New York, N.Y. 1976. Chapt. 4.
2. (*a*) A. J. Irwin and J. B. Jones. J. Am. Chem. Soc. **98**, 8476 (1976); (*b*) J. Am. Chem. Soc. **99**, 1625 (1977); (*c*) J. Am. Chem. Soc. **99**, 556 (1977).
3. J. B. Jones and K. E. Taylor. Can. J. Chem. **54**, 2969 (1976).
4. (*a*) E. J. Corey and B. B. Snider. J. Org. Chem. **39**, 256 (1974); (*b*) E. J. Corey and P. A. Grieco. Tetrahedron Lett. 107 (1972); (*c*) E. J. Corey and T. Ravindranathan. Tetrahedron Lett. 4753 (1971).
5. (*a*) T. Sakan, A. Fujino, F. Murai, A. Suzui, and Y. Butsugan. Bull. Chem. Soc. Jpn. **32**, 1155 (1959); (*b*) T. Sakan, S. Isoe, and S. B. Hyeon. Tetrahedron Lett. 1623 (1967).
6. M. Ribi and C. H. Eugster. Helv. Chim. Acta, **52**, 1732 (1969).
7. V. Prelog. Pure Appl. Chem. **9**, 119 (1964).
8. J. M. H. Graves, A. Clark, and H. J. Ringold. Biochemistry, **4**, 2655 (1965).
9. J. Fried and J. C. Sih. Tetrahedron Lett. 3899 (1973).
10. J. Wicha and A. Zarechi. Tetrahedron Lett. 3059 (1974).
11. M. E. Jung and L. M. Speltz. J. Am. Chem. Soc. **98** 7882 (1976).
12. (*a*) J. Klein. Isr. J. Chem. **1**, 385 (1963); (*b*) J. Am. Chem. Soc. **81**, 3611 (1959).
13. M. Fetizon, M. Golfier, M. T. Montaufier, and J. Reno. Tetrahedron, **34**, 987 (1975).
14. A. A. Youssef and S. M. Sharaf. J. Org. Chem. **33**, 2581 (1968).
15. R. Grewe and A. Heinke. Chem. Ber. **89**, 1978 (1956).
16. D. S. Noyce and D. B. Denney. J. Am. Chem. Soc. **74**, 5912 (1952).

The conformation of a ten-membered ring: the crystal and molecular structure of *trans-syn-trans*-4,5:9,10-biscyclohexano-1,3,6,8-tetraoxecane

ARIS TERZIS,[1] T. BRUCE GRINDLEY,[1] AND J. BRIAN FAUGHT

Department of Chemistry, Dalhousie University, Halifax, N.S., Canada B3H 4J3

Received December 13, 1976

ARIS TERZIS, T. BRUCE GRINDLEY, and J. BRIAN FAUGHT. Can. J. Chem. **55**, 2692 (1977).

The crystal structure of *trans-syn-trans*-4,5:9,10-biscyclohexano-1,3,6,8-tetraoxecane (**1**) has been determined by X-ray diffraction. The crystals are monoclinic, $a = 10.995(2)$, $b = 5.291(1)$, $c = 12.241(2)$ Å, $\beta = 114.68(1)°$, $P2_1/c$, with $Z = 2$. The structure was solved by the application of symbolic addition procedures and refined with anisotropic thermal parameters for all atoms to a final R value of 0.039 (R_w 0.062) for 1135 independent reflections.

The ten-membered tetraoxecane ring is present in the crystal in a boat–chair–boat (BCB) conformation, which is somewhat different in geometry than the BCB conformations observed for cyclodecane derivatives. The causes of these differences are discussed. Intramolecular non-bonded interactions cause one CH_2 group to be significantly distorted from local C_{2v} symmetry.

ARIS TERZIS, T. BRUCE GRINDLEY et J. BRIAN FAUGHT. Can. J. Chem. **55**, 2692 (1977).

On a déterminé la structure cristalline du *trans-syn-trans*-biscyclohexano-4,5:9,10 tétraoxécane-1,3,6,8 (**1**) par diffraction de rayons-x. Les cristaux sont monocliniques $a = 10.995(2)$, $b = 5.291(1)$, $c = 12.241(2)$ Å, $\beta = 114.68(1)°$, groupe d'espace $P2_1/c$ et $Z = 2$. On a résolu la structure par l'application des méthodes d'addition symbolique et on l'a affinée avec des paramètres thermiques anisotropiques pour tous les atomes jusqu'à une valeur finale de R de 0.039 ($R_w = 0.062$) pour 1135 réflexions indépendantes.

Le cycle tétraoxécane à dix chaînons existe dans le cristal sous la conformation bateau–chaise–bateau (BCB) qui est quelque peu différente, de par sa géométrie, des conformations BCB observées pour les dérivés du cyclodécane. On discute des causes de ces différences. Des interactions non-liées intramoléculaires font que des groupes CH_2 sont passablement déformés de la symétrie C_{2v} au niveau local.

[Traduit par le journal]

Introduction

Strain minimization calculations on cyclodecane, carried out by a large number of workers (1–4), have shown that there are a number of conformations which may be of comparable energy in the gas phase. An electron diffraction study (1) at 130° suggested that the following conformations were present: the boat–chair–boat[2] (BCB, 49%); the twist–boat–chair (TBC, 35%); the twist–boat–chair–chair (TBCC, 8%), and the boat–chair–chair (BCC, 8%), although some possibilities including the conformation calculated to be the most stable by Engler *et al.* (4), the twist–chair–chair–chair (TCCC), were not considered. In view of the above results, it is not surprising that there is little known about the conformational preference of cyclodecane itself in solution.

In the solid state, the conformation suggested to be most stable in the gas phase by the electron diffraction study (1), the BCB, is strongly preferred (5, 6) for cyclodecane derivatives. The BCB conformation has C_{2h} symmetry which results in three different types of carbon atoms, termed I, II, and III. Other conformations have been observed only for derivatives (7, 8) with substituents which strongly disfavor this conformation. 1,3,5,7,9-Pentaoxecane (8), the only ten-membered ring previously examined which contained a number of oxygen atoms, is one of the exceptions and it adopted the twist–chair–boat–chair (TCBC) conformation. Interestingly, nmr spectral evidence suggests that a sugar derivative which has a 1,3,6,8-tetraoxecane ring fused to two tetrahydropyran rings also adopts this TCBC conformation (9) in solution.

A dynamic nmr study showed (10) that the 10-membered ring in *trans-syn-trans*-4,5:9,10-biscyclohexano-1,3,6,8-tetraoxecane (**1**) exists in solution in two degenerate sets of two diastereomeric BCB conformations termed BCB1 and BCB2 (see Fig. 1) which are formally neighbours (2) on the BCB pseudorotation itinerary. BCB1

[1]To whom correspondence should be addressed.

[2]The nomenclature used is that devised by Hendrickson (2).

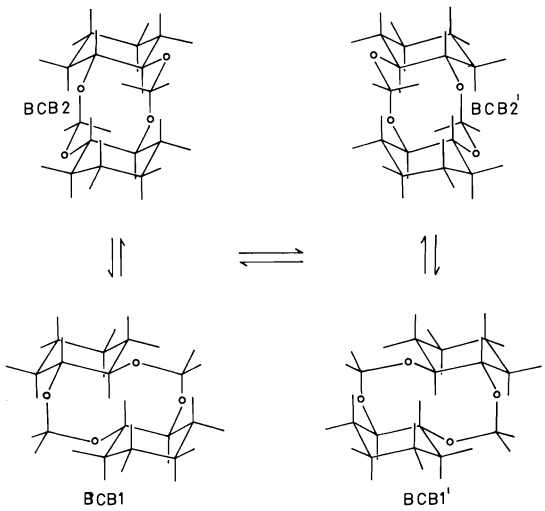

FIG. 1. The conformations observed for *trans-syn-trans*-4,5:9,10-biscyclohexano-1,3,6,8-tetraoxecane in solution.

is dominant at low temperatures in solution (below −30°C), while BCB2 is favoured at room temperature. Recently there has been considerable interest in the effects of the interactions between polar groups on conformations (11, 12) and BCB's 1 and 2 differ in the stereochemical relationships between their polar groups. In BCB1, models suggest that the two COCO torsional angles in each COCOC group are both 60° and equal in sign whereas in BCB2, the torsional angles in each COCOC group are 180° and 60°. Jeffrey *et al.* (11) have calculated that the latter arrangement would be 4.4 kcal/mol less stable than the former and have made predictions about bond length distortions expected in the two arrangements. In this publication we report the structure of *trans-syn-trans*-4,5:9,10-biscyclohexano-1,3,6,8-tetraoxecane in the solid state.

Experimental

trans-syn-trans-4,5:9,10-Biscyclohexano-1,3,6,8-tetraoxecane (**1**) was prepared according to the procedure of Brimacombe *et al.* (13). Crystals suitable for study were obtained by recrystallization from ethanol and had mp 167–168°C (lit. (13) mp 166–167.5°C). Crystal data are

$C_{14}H_{24}O_4$ fw = 256.35

Monoclinic, $a = 10.995(2)$, $b = 5.291(1)$, $c = 12.421(2)$ Å, $\beta = 114.68(1)°$, $V = 656.51$ Å^3, $Z = 2$, $\rho_{calcd} = 1.296$ g cm^{-3}, $\rho_{obs} = 1.28$ g cm^{-3} (18°C, CuK$_\alpha$, $\lambda = 1.54051$ Å).

Preliminary photographic data showed the crystals to be monoclinic with the following systematic absences: $h0l$, $l = 2n + 1$; $0k0$, $k = 2n + 1$, which indicated that the space group was $P2_1/c$.

A crystal (0.33 × 0.41 × 0.45 mm) was mounted with the *b* axis nearly parallel to the φ axis of a Picker FACS-1 automatic diffractometer with a graphite monochromator. Data were collected by the θ–2θ scan technique from a point 0.95° below the calculated 2θ position for CuK$_{\alpha 1}$ to 0.95° above the position calculated for CuK$_{\alpha 2}$ at a rate of 1° min^{-1}. Stationary-crystal stationary-counter background counts of 20 s were recorded at each limit of the scan range. During the data collection, three standard reflections were measured at a period of 30 reflections. Their intensities decreased uniformly by 4%. A total of 1170 intensity measurements were made in the form $\pm h, k, l$ in the region $2\theta < 127°$ and reduced to a set of 1135 independent reflections. The integrated intensity was calculated as

$$I(\text{net}) = I(\text{scan}) - 0.5\frac{t_T}{t_B}(B_1 + B_2)$$

where I(scan) is the number of counts over the scan range, t_T is the scan time, t_B is the time for each background count B_1 and B_2. The standard deviations $\sigma(I)$ were calculated according to the expression

$$\sigma_{(I)} = [N_T + 0.25t_T/t_B(B_1 + B_2) + C(I)^2 + 0.03^2(I - I_c)^2]^{1/2}$$

where N_T is the total net integrated scan count obtained in time t_T, C is a factor to account, among other things, for instrumental instability during data collection (for this structure, C was 0.04), I is the net intensity, and I_c is I corrected for absorption. The last term in the expression is a factor accounting for errors in the absorption correction.

An absorption correction[3] (9) was applied and the calculated transmission coefficients based on a linear absorption coefficient of 7.7 cm^{-1} for CuK$_\alpha$ radiation ranged from 0.698 to 0.802. Lorentz and polarization corrections were applied. 1098 reflections with $I > 2\sigma(I)$ were used in the refinement of the structure.

Solution and Refinement

The structure was determined by the application of symbolic addition procedures (18). The 9 non-hydrogen atoms were found in the *E*-map and a structure factor calculation based on this model gave a conventional *R* factor 0.276 where $R = (\Sigma||F_o| - |F_c||)/\Sigma|F_o|$. Temperature and scale factors were taken from the Wilson plot. Four cycles of block-diagonal least-squares refinement with unit weights and isotropic thermal parameters for the non-hydrogen atoms converged at $R = 0.116$. The twelve hydrogen atoms were located in a difference Fourier synthesis calculated at this point. Block diagonal refinement was continued with anisotropic thermal parameters for the non-hydrogen atoms and isotropic parameters for the hydrogens. A weighting scheme was introduced ($w = 1/[\sigma^2(F_o)]$) as well as a secondary extinction correction (19). The *R* factor at convergence

[3]The computer programs used were locally modified versions of the following: F. R. Ahmed and C. P. Huber, NRC-2 (data reduction) (14); F. R. Ahmed and B. Singh, NRC-3 (absorption correction) (14); A. Zalkin, FORDAP (Fourier, Paterson maps) (15); R. V. Doedens and J. A. Ibers, NUCLS (least-squares refinement with black-diagonal option introduced by J. Sygusch) (16); C. K. Johnson, ORTEP (drawings) (17).

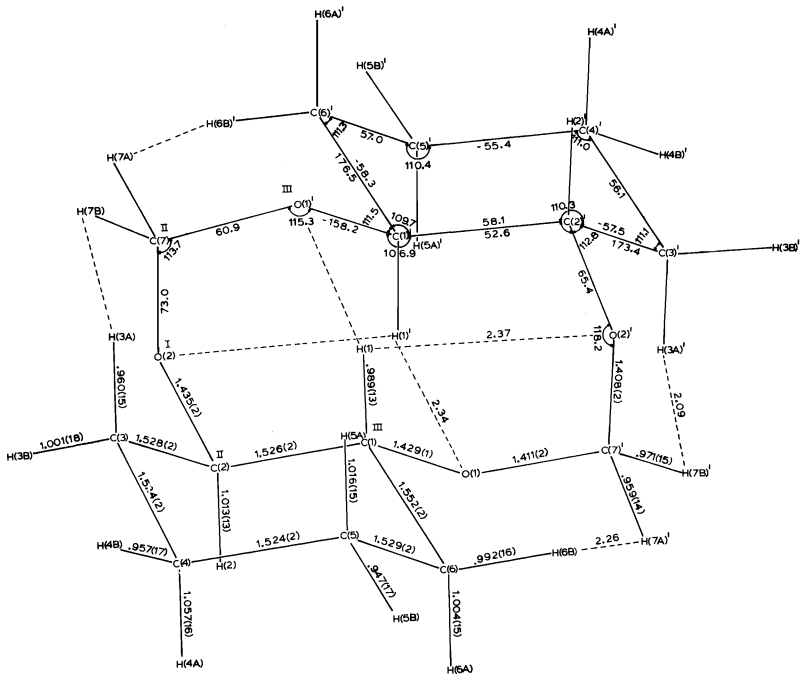

FIG. 2. Numbering and structural parameters for *trans-syn-trans*-4,5:9,10-biscyclohexano-1,3,6,8-tetraoxecane. Bond lengths (Å), with their errors in parentheses (10^3 Å), and the more significant calculated short intramolecular distances (- - -) are shown on the bottom half of the diagram. Bond angles (deg) and torsional angles (deg) between heavy atoms are shown on the top half. All errors in angles were 0.1°. Roman numerals indicate the locations of the three different types of BCB positions on the structure.

was 0.041. Inclusion of anisotropic thermal parameters for the hydrogen atoms reduced R to 0.039 after 4 cycles of refinement and $R_2 = ([\Sigma(w|F_o| - |F_c|)^2]/[\Sigma w|F_o|^2])^{1/2}$ to 0.062 for observed and unobserved data. The maximum shifts in the final least-squares refinement were 0.4 σ. The final 'goodness of fit', defined as $([\Sigma w(|F_o| - |F_c|)^2]/(m - n))^{1/2}$ was 2.88, where m = number of observations and n = number of refined parameters. The scattering factors for all atoms were from Cromer and Mann (20).

Results and Discussion

Atomic positions and thermal parameters for **1** are given in Table 1. The structure factor table and Table 2, which contains the bond angles involving hydrogen were put on deposit.[4] Numbering, bond lengths, bond angles, torsional angles, and short intramolecular distances are shown in Fig. 2. To facilitate comparison with results from strain minimization calculations, the short intramolecular distances involving H were recalculated using a C—H bond length of 1.1 Å.

[4]This information can be obtained, at a nominal charge, from the Depository of Unpublished Data, CISTI, National Research Council of Canada, Ottawa, Canada KIA 0S2.

Figure 3 shows an ORTEP diagram of the crystal structure of **1**.

Since compound **1** is centrosymmetric, the *syn* configuration previously (21) assigned for the relative orientations of the cyclohexane rings in **1** on the basis of its nmr spectrum is correct. In the solid state, **1** adopts the BCB conformation referred to as BCB1 in the Introduction and this conformation appears to have similar geometry to the average BCB conformation of cyclodecane derivatives (4, 6) although there are a number of important differences which will be discussed below.

Bond Angles and Torsional Angles

Bond angles in cyclodecane derivatives are normally large (see Table 3) presumably to relieve transannular non-bonded interactions between opposing hydrogen atoms. Since in this conformation of compound **1**, all of the transannular non-bonded CH–CH interactions have been replaced by CH–O interactions, the angles at all carbons but particularly those at BCB type I and II carbons in **1** should be smaller than in

TABLE 1. Positional and thermal parameters (e.s.d.'s)* for *trans-syn-trans*-4,5:9,10-biscyclohexano-1,3,6,8-tetraoxecane

Atom	x	y	z	U_{11}†	U_{22}	U_{33}	U_{12}	U_{13}	U_{23}
O(1)	0.9198(1)	0.7204(2)	0.5230(1)	349(4)	342(4)	393(4)	−30(3)	148(3)	−17(3)
O(2)	0.8811(1)	0.4295(2)	0.3234(1)	377(4)	488(5)	315(4)	−47(4)	143(3)	12(3)
C(1)	0.8440(1)	0.4920(2)	0.5063(1)	308(5)	310(5)	344(5)	−3(4)	125(4)	14(4)
C(2)	0.7852(1)	0.4332(2)	0.3749(1)	304(5)	371(5)	312(5)	−9(4)	94(4)	37(4)
C(3)	0.7010(1)	0.1925(2)	0.3479(1)	378(6)	440(6)	358(6)	−92(5)	132(5)	−37(5)
C(4)	0.5900(1)	0.2162(3)	0.3906(1)	329(6)	502(7)	432(7)	−76(5)	122(5)	14(5)
C(5)	0.6473(1)	0.2809(3)	0.5221(1)	367(6)	504(7)	435(7)	−53(5)	191(5)	29(6)
C(6)	0.7326(1)	0.5204(2)	0.5472(1)	374(6)	446(6)	431(6)	−31(5)	202(5)	−34(5)
C(7)	0.9804(1)	0.2407(2)	0.3614(1)	355(6)	449(6)	382(6)	−52(5)	170(5)	−116(5)
H(1)	0.909(1)	0.357(2)	0.550(1)	24(7)	28(7)	31(7)	−12(5)	16(5)	−9(6)
H(2)	0.726(1)	0.580(2)	0.329(1)	24(7)	31(7)	47(8)	8(6)	13(6)	13(6)
H(3A)	0.758(1)	0.054(3)	0.388(1)	29(7)	41(8)	70(10)	11(7)	28(7)	16(8)
H(3B)	0.667(2)	0.157(3)	0.261(2)	89(14)	61(12)	52(11)	−49(10)	15(10)	−23(9)
H(4A)	0.522(1)	0.361(3)	0.344(1)	31(7)	72(11)	42(9)	5(8)	10(7)	11(9)
H(4B)	0.543(2)	0.059(3)	0.376(1)	63(10)	59(10)	58(10)	−10(8)	43(8)	−11(8)
H(5A)	0.701(1)	0.133(3)	0.572(2)	40(8)	32(8)	70(11)	−5(7)	16(7)	−3(8)
H(5B)	0.578(1)	0.311(3)	0.547(1)	34(8)	76(11)	54(10)	−12(8)	29(7)	−6(8)
H(6A)	0.675(1)	0.666(3)	0.503(1)	37(8)	36(8)	66(11)	−7(7)	32(8)	1(7)
H(6B)	0.766(2)	0.567(3)	0.632(1)	64(10)	90(13)	48(10)	−43(10)	31(8)	−8(9)
H(7A)	1.019(1)	0.251(3)	0.305(1)	28(7)	71(10)	42(9)	17(7)	26(7)	−5(7)
H(7B)	0.948(1)	0.070(3)	0.362(2)	26(7)	31(8)	90(12)	−14(6)	12(8)	−21(8)

*The form of the anisotropic vibration is exp $[-2\pi^2(a^{*2}h^2U_{11} + \ldots 2a^*b^*hkU_{12} + \ldots)]$.
†$U_{ij} \times 10^4$ for non-hydrogen atoms and $U_{ij} \times 10^3$ for hydrogen atoms.

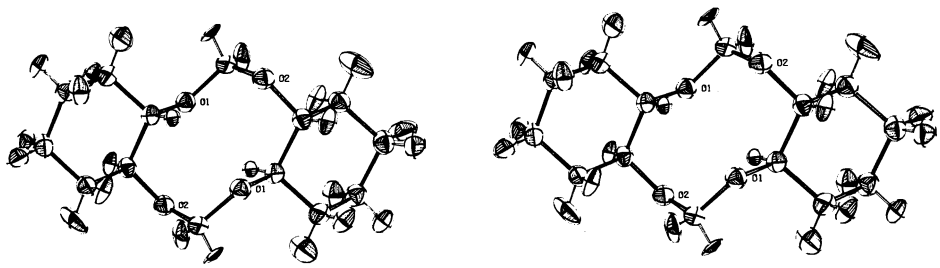

FIG. 3. Stereoscopic view of the solid state conformation of *trans-syn-trans*-4,5:9,10-biscyclohexano-1,3,6,8-tetraoxecane.

TABLE 3. Comparison of bond angles and torsional angles between **1** and cyclodecane derivatives

BCB position type	Atoms involved	Angle (deg)		
		Compound **1**	Average value in cyclodecane*	Difference
Bond angles				
I	COC	118.2	118.6 (±2)	−0.4
II	OCC	113.7	117.7 (±4)	−4.0
III	COC	115.3	114.5 (±3)	+0.8
III	OCC	106.9	114.5 (±3)	−7.6
II	CCO	114.3	117.7 (±4)	−3.4
Torsional angles				
I and II	COCO	73.0	65.8 (±6)	+7.2
II and III	OCOC	60.9	55.5 (±4)†	+5.4
III and III	COCC	−158.2	−152.4 (±1.6)	−5.8
III and II	OCCO	52.6	55.5 (±4)†	−2.9
II and I	CCOC	65.4	65.8 (±6)	−0.4

*Average of values from refs. 5 and 6.
†Two values were observed outside this range in an intramolecularly H-bonded molecule (6).

cyclodecane. Table 3 compares the bond angles in **1** to those of cyclodecane and the observed bond angles at type II positions in **1** are both smaller, as predicted above. Although the COC angle at the type I carbon is not smaller, in compound **1** there is an intramolecular non-bonded interaction between C(7) and C(3) similar to the type between an axial methyl and the —OCH_2O— groups in 4-methyl-1,3-dioxane (evaluated at 2.8 or 2.9 kcal/mol (22)) and this interaction presumably maintains the size of this angle at approximately the value observed in cyclodecane. In a closely related compound where this interaction is not present, the bond angle decreased in magnitude by 1.7° to 116.5° (23).

The most notable difference between **1** and cyclodecane is the CCO bond angle of 106.9° at a BCB type III position. CCO bond angles are often small. For instance, in diethyl ether (24), CCO bond angles vary from 107.8° to 108.3°, in 1,5,9,13-tetraoxacyclooctadecane four CCO bond angles are below 109.6° with the smallest being 106.4° (25). In the present case, intramolecular non-bonded interactions appear to be the main cause of the small bond angle, since a decrease in bond angle allows increase of both of the short intramolecular distances, H(7A)—H(6B)′ and H(7B)—H(3A).

The torsional angles of **1** are compared to those of cyclodecane in Table 3 and all of the *gauche* torsional angles fall within the ranges observed for cyclodecane derivatives or are just outside. The one *anti* torsional angle (−158.21°), about the two BCB type III carbons, is considerably outside the observed range. The larger size of this angle contributes to the general narrowing of this tetraoxecane ring as compared to cyclodecane and is caused by the relief of transannular non-bonded interactions, particularly between hydrogens on opposing type III carbons.

TABLE 4. Extraannular intramolecular non-bonded interactions

Atoms	Involved	Distance (Å)†	Distance (Å)‡	E (kcal/mol)*
C(7)	C(6)′	3.138 (0.002)		0.02
C(7)	H(6B)′	2.937 (0.017)	2.934	−0.03
H(7A)	C(6)′	2.848 (0.015)	2.830	0.02
H(7A)	H(6B)′	2.365 (0.024)	2.263	0.28
	Total interactions between $C(7)H_2$ and $C(6)'H_2$			0.29
C(7)	C(3)	3.018 (0.002)		0.14
C(7)	H(3A)	2.780 (0.016)	2.772	0.07
H(7B)	C(3)	2.729 (0.017)	2.715	0.13
H(7B)	H(3A)	2.245 (0.023)	2.093	0.71
	Total interactions between $C(7)H_2$ and $C(3)H_2$			1.05

*Calculated using the force field of Hilderbrandt *et al.* (1).
†From the X-ray structural determination.
‡Calculated using observed C positions and CCH or OCH bond angles but with the C–H distance assumed to be 1.10 Å.

Intramolecular Interactions

The shortest intramolecular transannular interactions are shown in Fig. 2. Since no force fields are available with parameters for oxygen, the interactions shown in Fig. 2 have been evaluated qualitatively by consideration of the van der Waals radii of Pauling. The van der Waals radii are 2.0, 1.4,[5] and 1.2 Å,[5] for CH_3, O, and H respectively. The shortest O—O transannular distances are about equal to the sum of their van der Waals radii so non-bonded interactions between oxygens should not make a large contribution to the energy. The shortest O—H distances are somewhat less (~0.2 Å) than the sum of their van der Waals radii. Dale (27) has suggested that this latter type of interaction is not repulsive and is perhaps attractive where the hydrogen is on a carbon adjacent to oxygen and therefore acidic. However, recent evidence (28) shows that hydrogens geminal to methoxy groups on a carbon are only very slightly more acidic than those geminal to methyl groups. It therefore appears more likely that the conformational effects observed by Dale (27) who compared ethers to alkanes are simply a consequence of the change of the sum of the van der Waals radii from 4.0 to 3.4 Å when CH–CH interactions were replaced by CH–O interactions. Accordingly, it is likely that the O–H interaction in **1** is slightly repulsive; a H–H interaction 0.2 Å less than the sum of the van der Waals radii can be evaluated at 0.4 kcal/mol using the force field of Hilderbrandt *et al.* (1) and this O–H interaction is probably also small. The sum of the van der Waals radii of CH_3 and O is 3.4 Å, while the short C—O distances observed in **1** are ~2.9 and 3.0 Å. However, here the oxygen is staggered between the atoms on the carbon, so this interaction is probably also only slightly repulsive.

Compound **1** also possesses intramolecular extraannular non-bonded interactions between each OCH_2O group in the ring (*i.e.* C(7)) and one methylene group on each cyclohexane ring (*i.e.* C(3) and C(6)′). Table 4 gives the distances between the atoms in these groups and the corresponding repulsive energies calculated using the force field of Hilderbrandt *et al.* (1). The larger part of the non-bonded repulsion arises from interaction between the hydrogen atoms on C(3) and C(6)′ and different hydrogen atoms on C(7). Since the interactions are with different hydrogen atoms, the effect of the resulting torque should be observable in distortion of the CH_2 group from local C_{2v} symmetry. Distortion of this sort can be conveniently discussed (6) in terms of the following linear combinations of the four HCO-angles, α_1, α_2, α_3, α_4, where m, w, r, and t stand for mean, wag, rock, and twist.

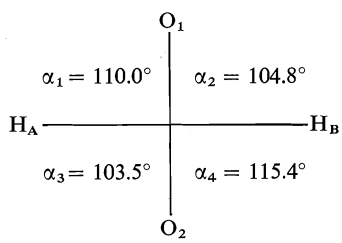

$$m = (1/4)(\alpha_1 + \alpha_2 + \alpha_3 + \alpha_4)$$
$$w = (1/2)(\alpha_1 + \alpha_2 - \alpha_3 - \alpha_4)$$
$$r = (1/2)(\alpha_1 - \alpha_2 + \alpha_3 - \alpha_4)$$
$$t = (1/2)(\alpha_1 - \alpha_2 - \alpha_3 + \alpha_4)$$

[5]Other values have been suggested including shorter (11) and longer (26) values for hydrogen and longer (11) values for oxygen.

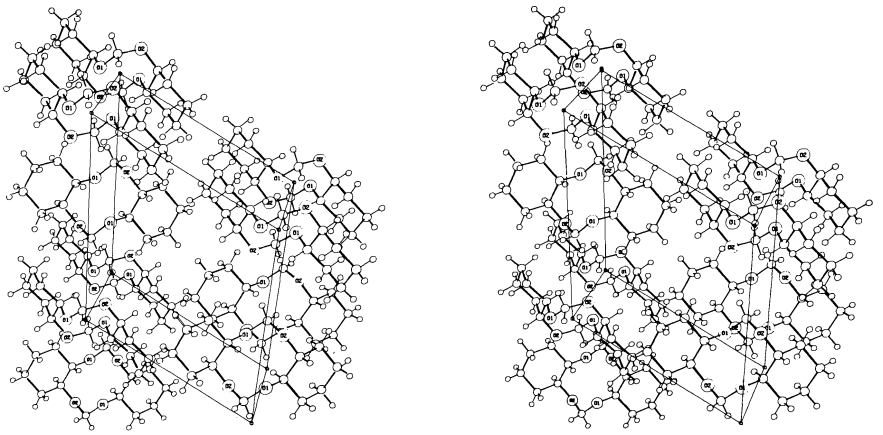

FIG. 4. Stereoscopic view of the molecular packing.

The four angles of α_1, α_2, α_3, and α_4 have values as shown and yield m, w, r, and t values of 108.4°, −2.0°, −3.4°, and 8.6° respectively. For other cyclodecane derivatives, wagging and rocking distortions (but only slight twisting) of up to 4° at types I and III positions are common (6) to relieve non-bonded interactions but little distortion of any type has been observed at the relatively unhindered type II carbons. This observation of the distortion of the $C(7)H_2$ groups (primarily twisting) confirms the importance of these extraannular interactions. It suggests that OCH_2O groups are fairly easily distorted and that force field calculations which assume local C_{2v} symmetry in CH_2 groups will give erroneous results. Each of the interactions of these hydrogens is also similar to that between the OCH_2O group and an axial methyl in 4-methyl-1,3-dioxane.

Polar Effects

The conformation adopted by compound **1** is the BCB conformation (BCB1) in which both torsional angles about C—O bonds in each OCH_2O group are *gauche* and of the same sign; an arrangement calculated (11) to be 4.4 kcal/mol more stable than the *gauche*, *anti* relationship in the other BCB conformation observed in solution (BCB2). The C—O bond lengths observed for this arrangement (1.411 and 1.408 Å) are, as predicted (11), significantly shorter than normal C—O bonds (1.429 and 1.435 Å in this molecule) and approximately equal in length.

Intermolecular Interactions

The packing diagram for compound **1** is shown in Fig. 4. It is unlikely that intermolecular interactions affected the observed conformation to a large extent since there are only 5 intermolecular distances shorter than the sum of the van der Waals radii, none of which are H–H interactions and none of which are energetically important (>0.1 kcal/mol) when the energy is calculated by the force field of Hilderbrandt *et al.* (1).

Acknowledgement

This work was supported by the National Research Council of Canada.

1. R. L. HILDERBRANDT, J. D. WIESER, and L. K. MONTGOMERY. J. Am. Chem. Soc. **95**, 8598 (1973).
2. J. B. HENDRICKSON. J. Am. Chem. Soc. **89**, 7036 (1967); **89**, 7043 (1967); **89**, 7047 (1967).
3. K. B. WIBERG. J. Am. Chem. Soc. **87**, 1070 (1965); M. BIXON and S. LIFSON. Tetrahedron, **23**, 769 (1967).
4. E. M. ENGLER, J. D. ANDOSE, and P. V. R. SCHLEYER. J. Am. Chem. Soc. **95**, 8005 (1973).
5. J. D. DUNITZ. *In* Perspectives in structural chemistry. Vol. 2. *Edited by* J. D. Dunitz and J. A. Ibers. John Wiley and Sons, Inc., New York. 1968. p. 1; G. SAMUEL and R. WEISS. Tetrahedron, **26**, 3005 (1970).
6. O. ERMER, J. D. DUNITZ, and I. BERNAL. Acta Crystallogr. B**29**, 2778 (1973).
7. J. D. DUNITZ, H. ESER, M. BIXON, and S. LIBSON. Helv. Chim. Acta, **50**, 1572 (1967).
8. Y. CHATANI and K. KITAHAMA. Bull. Chem. Soc. Jpn. **46**, 2300 (1973).
9. D. GAGNAIRE, V. TRAN, and M. VIGNON. J. Chem. Soc. Chem. Commun. 6 (1976).
10. T. B. GRINDLEY and W. A. SZAREK. Can. J. Chem. **52**, 2566 (1974).
11. G. A. JEFFREY, J. A. POPLE, and L. RADOM. Carbohyd. Res. **25**, 117 (1972).
12. S. WOLFE, A. RAUK, L. M. TEL, and I. G. CSIZMADIA. J. Chem. Soc. B, 136 (1971); S. DAVID, O. EISENSTEIN, W. J. HEHRE, L. SALEM, and R. HOFFMAN. J. Am. Chem. Soc. **95**, 3806 (1973).
13. J. S. BRIMACOMBE, A. B. FOSTER, B. D. JONES, and J. J. WILLARD. J. Chem. Soc. C, 2404 (1967).

14. F. R. AHMEN, S. R. HALL, M. E. PIPPY, and C. P. HUBER. NRC-Crystallographic programs of the IBM/360 System. National Research Council of Canada, Ottawa, 1970.
15. A. ZALKIN. FORDAP, A Fortran Program for Fourier Calculations. University of California, Berkeley, CA. 1965.
16. J. SYGUSCH, F. R. BRISSE, and S. HANESSIAN. Acta Crystallogr. B**30**, 40 (1974).
17. C. K. JOHNSON. ORTEP, Report ORNL-3794. Oak Ridge National Laboratory, Oak Ridge, Tennessee, 1965.
18. J. KARLE and I. L. KARLE. Acta Crystallogr. **21**, 849 (1966).
19. P. COPPENS and W. C. HAMILTON. Acta Crystallogr. A**26**, 71 (1970).
20. D. T. CROMER and A. MANN. Acta Crystallogr. A**24**, 321 (1968).
21. T. B. GRINDLEY, J. F. STODDART, and W. A. SZAREK. J. Am. Chem. Soc. **91**, 4722 (1969).
22. E. L. ELIEL. Acc. Chem. Res. **3**, 1 (1970); K. PIHLAJA and S. LUOMA. Acta Chem. Scand. **22**, 2401 (1968).
23. A. TERZIS, J. B. FAUGHT, and T. B. GRINDLEY. Can. J. Chem. To be published.
24. D. ANDRE, R. FOURME, and K. ZECHMEISTER. Acta Crystallogr. B**28**, 2389 (1972).
25. P. GROTH. Acta. Chem. Scand. **25**, 725 (1971).
26. D. H. WERTZ and N. L. ALLINGER. Tetrahedron, **30**, 1579 (1974).
27. J. DALE. Tetrahedron, **30**, 1683 (1974).
28. F. G. BORDWELL, M. V. D. PUY, and N. R. VANIER. J. Org. Chem. **41**, 1885 (1976); J. HINE and P. D. DALSIN. J. Am Chem. Soc. **94**, 6998 (1972).

Nuclear analogs of β-lactam antibiotics. III. Synthesis of 1,3-dimethyl-Δ^3-*O*-2-isocephems[1]

TERRENCE WILLIAM DOYLE,[2] BING-YU LUH, AND ALAIN MARTEL[3]

Bristol Laboratories of Canada, 100 Industrial Boulevard, Candiac, P.Q., Canada J5R 1J1

Received February 16, 1977

TERRENCE WILLIAM DOYLE, BING-YU LUH, and ALAIN MARTEL. Can. J. Chem. **55**, 2700 (1977).

The synthesis of 1-α-methyl and 1-β-methyl isomers of 7-β-phenoxyacetamido-1,3-dimethyl-Δ^3-*O*-2-isocephem-4-carboxylic acids (**14***a* and **14***b*) is described. Treatment of amine **2** with methacrolein followed by cycloaddition gave **4** which was ozonolyzed to yield the methyl ketones **6**. Upon reduction of **6** there was obtained a mixture of isomeric alcohols **8** which were resolved by column chromatography, converted to their mesylates **9**, and hydrolyzed to yield **10***a* and **10***b*. Conversion of each isomer to the corresponding *O*-2-isocephems **11***a* and **11***b* followed by azide reduction, coupling of the amines to phenoxyacetic acid, and removal of the ester blocking groups gave **14***a* and **14***b*. An attempt to prepare the *gem*-dimethyl compound failed. The structural assignments to **14***a* and **14***b* are discussed.

TERRENCE WILLIAM DOYLE, BING-YU LUH et ALAIN MARTEL. Can. J. Chem. **55**, 2700 (1977).

On décrit la synthèse des acides isomères méthyl-1 α et méthyl-1 β des acides phénoxyacétamido-7 β diméthyl-1,3-Δ^3 isocéphem-*O*-2 carboxyliques 4 (**14***a* et **14***b*). La réaction de l'amine **2** avec de l'aldéhyde méthacrylique, suivie par une cycloaddition, conduit à **4** qui peut être ozonolysé pour conduire aux méthyl-cétones **6**. La réduction de **6** fournit un mélange d'alcools isomères **8** qui peut être résolu par chromatographie sur colonne et chacun des alcools peut alors être transformé dans son mésylate **9** et hydrolysé pour conduire à **10***a* et **10***b*. On fait suivre la conversion de chacun des isomères en isocéphem-*O*-2 correspondants **11***a* et **11***b* par une réduction de l'azide, un couplage des amines avec l'acide de phénoxyacétique et l'enlèvement des groupes esters bloqueurs pour donner **14***a* et **14***b*. Un essai en vue de préparer le composé *gem*-diméthylé n'a pas réussi. On discute des attributions de structure de **14***a* et de **14***b*.
[Traduit par le journal]

In the previous paper of this series the syntheses of a number of *O*-2-isocephem systems (Fig. 1, wherein $R_1 = R_2 = H$ and $R_3 = H$,

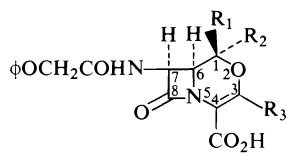

1

$R_1 = R_2 = H$ $R_3 = H, CH_3, CH_2\phi, CH_2CH_2\phi$
$R_1 = H$ $R_2 = R_3 = CH_3$
$R_2 = H$ $R_1 = R_3 = CH_3$

FIGURE 1

Me, $CH_2\phi$, $CH_2CH_2\phi$) were described (1). Encouraged by the promising biological activity of these systems the synthesis of 1-substituted *O*-2-isocephems was attempted next. In this paper we report the synthesis of the 1-α,3-dimethyl- and 1-β,3-dimethyl-*O*-2-isocephems **1** ($R_1 = H$, $R_2 = R_3 = CH_3$ and $R_2 = H$, $R_1 = R_3 = CH_3$).[4]

Treatment of amine **2** (Scheme 1) (1) with an excess of methacrolein in the presence of a catalytic amount of the hydrochloride of **2** gave the Schiff base **3** in 90% yield. The catalysis was necessary to ensure rapid formation of **3**. Compound **3** was then treated with azidoacetyl chloride followed by triethylamine to yield β-lactam **4** (82.5%) as a mixture of diastereoisomers (epimeric about the $N—\overset{*}{C}(CO_2Bz)$-center). The isomers could be partially separated by column chromatography on silica gel using benzene as eluent. The nmr spectra of the two isomers (Table 1) indicated that the azido and isopro-

[1]For part II of this series see ref. 1.

[2]Author to whom correspondence concerning this paper may be addresssed c/o Bristol Laboratories, P.O. Box 657, Syracuse, NY, U.S.A. 13201.

[3]Holder of an NRCC Industrial Postdoctoral Fellowship, 1972–1974.

[4]For an explanation of the trivial nomenclature used throughout this series of papers and a review of the literature pertaining to the syntheses of nuclear analogs of β-lactam antibiotics see ref. 2.

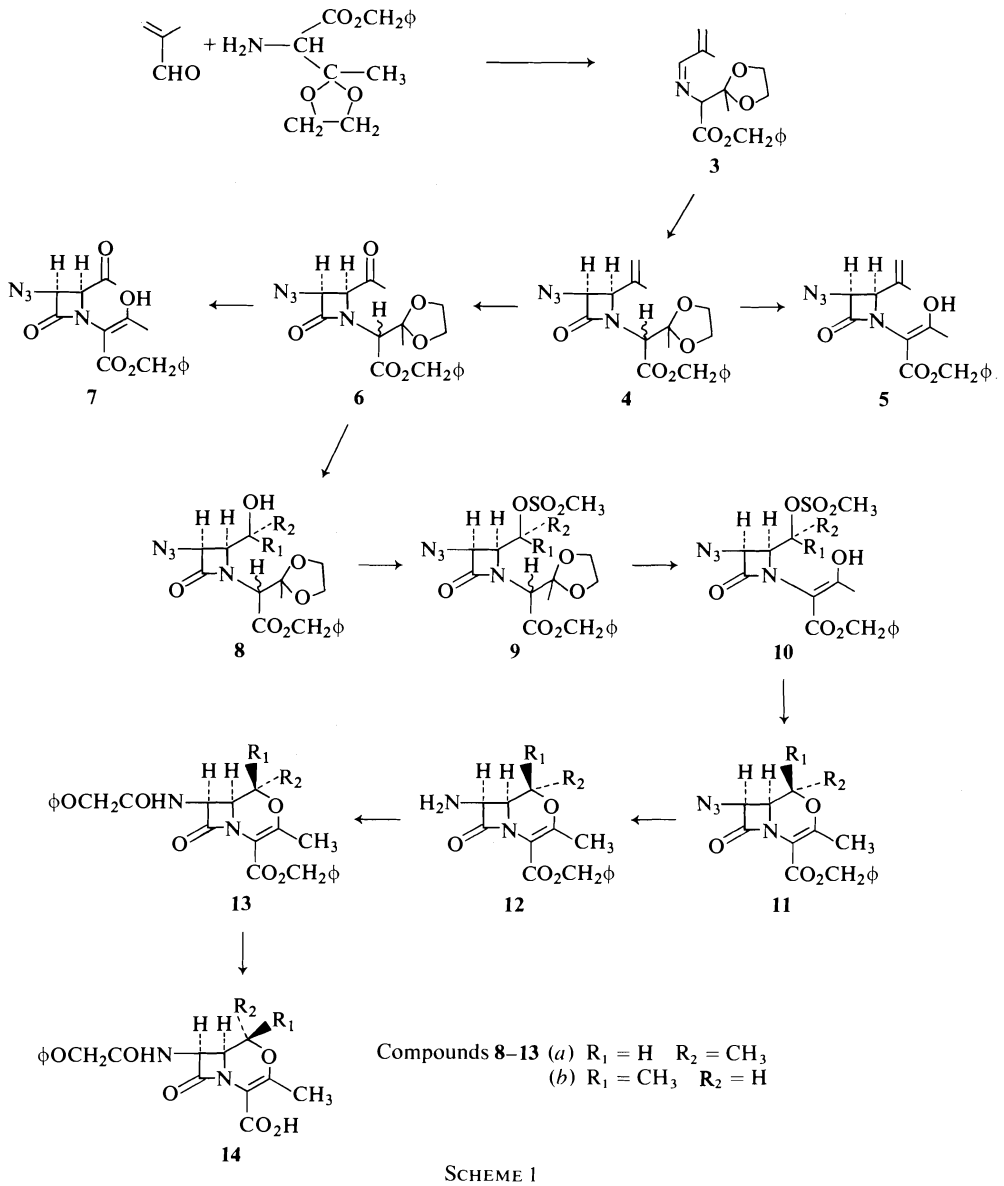

SCHEME I

penyl groups were *cis* to one another as shown by the coupling constants for the protons at C_3 and C_4 in the azetidinone ring (3) J = 5.3 Hz.[5] Hydrolysis of either isomer of **4** gave a single enol **5** (82%). No trace of the *trans* isomer of **5** could be detected by nmr spectroscopy.

Ozonolysis of **4** (1:1 isomer mixture) and decomposition of the ozonide gave a mixture of methyl ketones **6** in 95% yield. The product was chromatographed on silica gel with chloroform as eluent to give each isomer as a crystalline solid. When the isomer of **4** which was eluted first from the column was ozonized a single methyl ketone corresponding to the ketone which eluted second from the column was isolated. The stereochemistry of the isomers of **4** and **6** about the chiral center in the side chain attached to the nitrogen has not been deter-

[5]The order of addition of azidoacetyl chloride and triethylamine to the Schiff base **3** had no effect on the stereochemistry of the products. The procedure described was found to be cleaner (4).

TABLE 1. Nuclear magnetic resonance spectra[a]

Compd.	Aromatic and olefinic	$CH_2\phi$	CH_3	$O(CH_2)_2O$		Other
3	7.21(s, 5H) 5.54(m, 1H)[b] 5.33(bs, 1H)[b]	5.12(s)	1.52(s)[c] 1.93(m)[d,b]	3.90(s)		7.66(s, 1H, C*H*=N) 3.98(s, 1H)[e]
4[f]	7.27(s, 5H) 5.00(m, 1H)[b] 5.13(m, 1H)[b]	5.09(s)	1.43(s)[c] 1.69(m)[d,b]	3.89(s)	4.69(d) $J = 5.3$	4.48(d, 1H, $J = 5.3$)[h] 4.49(s, 1H)[e]
4[g]	7.25(s, 5H) 5.04(m, 1H)[b] 5.14(m, 1H)[b]	5.14(s)	1.50(s)[c] 1.75(m)[d,b]	3.89(s)	4.62(d) $J = 5.3$	4.47(s, 1H)[e] 4.41(d, 1H, $J = 5.3$)[h]
5	7.34(s, 5H) 5.08(m)[b] 4.93(m)[b]	5.35(d, 1H)[i] 5.08(d, 1H)[i] $J = 12.5$	1.73(m)[d,b] 2.17(s)[j]		4.64(d) $J = 6.0$	4.57(d, $J = 6.0$)[h] 12.30(s, 1H, O*H*)
6[f]	7.36(s, 5H)	5.18(s)	1.45(s)[c] 2.22(s)[k]	3.80(m)	4.78[l] 4.56(d)[m] $J = 5.0$	4.47(s, 1H)[e] 4.40(d, 1H, $J = 5.0$)[m,n]
6[g]	7.32(s, 5H)	5.08(s)	1.35(s)[c] 2.14(s)[k]	3.84(s)	4.82[l] 4.64(d)[m] $J = 6.0$	4.67(s, 1H)[e] 4.45(d, 1H, $J = 6.0$)[m,n]
7	7.28(s, 5H)	5.27(d, 1H)[i] 5.04(d, 1H)[i] $J = 12.0$	2.10(s) 2.31(s)		4.79(d) $J = 6.0$	4.55(d, 1H, $J = 6.0$)[m] 12.05(s, 1H, O*H*)
8*b*	7.32(s, 5H)	5.18(s)	1.50(s) 1.20(d)[q] $J = 5.0$	3.92(m, 7H)[o]	4.54(d) $J = 5.0$	
9*b*	7.32(s, 5H)	5.17(s)	2.92(s)[p] 1.52(s)[c] 1.53(d, $J = 6.0$)[q]	3.92(s)	4.82(d) $J = 5.5$	4.10(dd, 1H, $J_1 = 5.5$, $J_2 = 7.8$)[r] 4.26(s, 1H)[e] 5.00(m, 1H)[q]
10*a*	7.25(s, 5H)	5.10(m)	1.27(d, $J = 6.0$)[q] 1.98(s)[i] 2.87(s)[p]		4.60(d) $J = 5.5$	4.75(m, 1H)[q] 3.95(dd, 1H, $J_1 = 5.5$, $J_2 = 6.5$)[r] 12.0(s, 1H, OH)
10*b*	7.31(s, 5H)	5.36(d, 1H)[i] 5.05(d, 1H)[i] $J = 12.0$	1.40(d, $J = 6.0$)[q] 2.13(s)[j] 2.79(s)[p]		4.72(d) $J = 5.5$	4.92(m, 1H)[q] 4.03(dd, 1H, $J_1 = 8.3$, $J_2 = 5.5$)[r] 12.0(s, 1H, OH)
11*a*	7.32(m, 5H)	5.20(s)	2.24(s)[u] 1.38(d)[s] $J = 6.0$		5.07(d) $J = 5.0$	3.25(dd, 1H, $J_1 = 8.5$, $J_2 = 5.0$)[t] 3.94(dq, 1H, $J_1 = 6.0$, $J_2 = 8.5$)[s]
11*b*	7.38(m, 5H)	5.24(s)	2.23(s)[u] 1.32(d)[v] $J = 6.5$		5.15(d) $J = 5.5$	4.72(dq, 1H, $J_1 = 6.5$, $J_2 = 3.7$)[v] 3.73(dd, 1H, $J_1 = 5.5$, $J_2 = 3.7$)[t]

TABLE 1 (*Concluded*)

Compd.	Aromatic and olefinic	$CH_2\phi$	CH_3	$O(CH_2)_2O$		Other
12*a*	7.34(m, 5H)	5.22(s)	2.24(s)[u] 1.42(d)[s] $J = 6.5$		4.62(d) $J = 5.5$	3.92(dq, 1H, $J_1 = 6.5$, $J_2 = 8.5$)[s] 3.14(dd, 1H, $J_1 = 8.5$, $J_2 = 5.0$)[t] 1.60(s, 2H, NH_2)
12*b*	7.34(m, 5H)	5.24(s)	2.22(s)[u] 1.30(d)[v] $J = 6.5$		4.68(d) $J = 5.5$	4.70(dq, 1H, $J_1 = 6.5$, $J_2 = 3.7$)[v] 3.61(dd, 1H, $J_1 = 5.5$, $J_2 = 3.7$)[t] 1.70(s, 2H, NH_2)
13*a*	7.26(m, 5H) 6.7–7.5 (m, 5H)	5.17(s)	2.24(s)[u] 1.14(d)[s] $J = 6.4$		5.56(dd) $J_1 = 8.0$ $J_2 = 4.5$	4.43(s, 2H)[w] 4.06(dq, 1H, $J_1 = 6.4$, $J_2 = 8.5$)[s] 3.27(dd, 1H, $J_1 = 4.5$, $J_2 = 8.5$)[t] 8.06(d, 1H, $J = 8.0$, N*H*)
13*b*	7.31(m, 5H) 6.7–7.5(m, 6H)	5.24(s)	2.24(s)[u] 1.16(d)[v] $J = 6.5$		5.50(dd) $J_1 = 4.7$ $J_2 = 6.0$	4.50(s, 2H)[w] 4.65(dq, 1H, $J_1 = 6.5$, $J_2 = 3.7$)[v] 3.90(dd, 1H, $J_1 = 4.7$, $J_2 = 3.7$)[t]
14*a*[x]	6.7–7.5(m, 5H)		2.22(s)[u] 1.17(d)[s] $J = 6.4$		4.50(s, 2H)[w] 4.11(dq, 1H, $J_1 = 8.5$, $J_2 = 6.4$)[s] $J_1 = 5.0$ $J_2 = 8.5$	3.29(dd, 1H, $J_1 = 8.5$, $J_2 = 5.0$)[t] 8.31(d, 1H, $J = 8.5$, N*H*)
14*b*[x,y]	6.7–7.4(m, 5H)		2.21(s)[u] 1.15(d)[v] $J = 6.3$		5.48(d) $J = 5.0$	4.51(s, 2H)[w] 3.90(dd, 1H, $J_1 = 5.0$, $J_2 = 3.9$)[t] 4.63(dq, 1H, $J_1 = 6.3$, $J_2 = 3.9$)[v]
15	7.35(m, 5H)	5.21(s)	2.22(s)[u] 1.34(s)		5.22(d) $J = 5.5$	3.42(d, 1H, $J = 5.50$)[t] 2.0–2.5(m, 2H, CH_2 HgCl)

[a]Recorded at 60 MHz on a Varian A-60A spectrometer in $CDCl_3$ using tetramethylsilane as internal standard unless otherwise noted. The chemical shifts are in δ (ppm) and the *J*'s in Hz. [b]Exhibited allylic coupling. [c]Assigned to  . [d]Assigned to  . [e]Assigned to C*H*—CO_2R. [f]Isomer 1. [g]Isomer 2. [h]Assigned to C*H*—$C(CH_3)$=CH_2. [i]Arms of AB quartet. [j]Assigned to =C(OH)CH_3. [k]Assigned to COCH_3. [l]Signals for 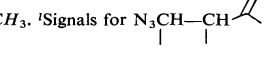 overlap as singlet. [m]On addition of benzene–ASIS. [n]Assigned to C*H*COMe. [o]The protons C*H*—C*H*OHCH_3 are obscured under the ketal resonance. [p]Assigned to O—SO_2CH_3. [q]Assigned to C*H*OMesCH_3. [r]Assigned to C*H*—CHOMesCH_3. [s]Assigned to C_1-α-CH_3 and C_1-β-*H*. [t]Assigned to C_6-H. [u]Assigned to C_3-CH_3. [v]Assigned to C_1-β-CH_3 and C_1-α-*H*. [w]Assigned to φOCH_2. [x]Recorded in $CDCl_3$–DMSO-d_6. [y]After D_2O exchange.

mined. Hydrolysis of either isomer of **6** with 95% trifluoroacetic acid gave a single enol **7** as a crystalline solid in 97% yield.

Reduction of **6** (either as single isomers or isomer mixtures) with sodium borohydride led to complex mixtures of alcohols. Invariably the reduction of ketone isomer 2 was more sluggish than that of isomer 1.[6] Reduction of a 1:1 mixture of ketone isomers **6** gave, after chromatography, a recovery of ~10% ketone isomer 2, a mixture of alcohols **8***a* in 43% yield, and a single isomer **8***b* as a crystalline solid in 9.8% yield. The assignment of configuration to the alcohol mixture **8***a* and the single isomer **8***b* was made retrospectively on the basis of the subsequent reactions of **8***a* and **8***b*. Reduction of the isomeric ketones **6** separately also gave complex mixtures, presumably due to epimerization under the reaction conditions.

Treatment of **8***a* with methane sulfonyl chloride and triethylamine gave **9***a* as a mixture of diastereoisomers in 89% yield. Hydrolysis of the ketal with 95% trifluoroacetic acid gave **10** (65%) as a mixture of **10***a* and **10***b* (9:1). Similarly **8***b* was converted to **9***b* (99%) and hydrolyzed to yield **10***b* exclusively in 96% yield.

Treatment of **10***a* with sodium hydride in dimethyl sulfoxide gave **11***a* (38%) contaminated with ~10% **11***b*. Recrystallization from ether gave pure **11***a* (33%). When **10***b* was refluxed with 1 equiv. of triethylamine in chloroform there was obtained **11***b* in 80% yield. The assignments of configuration to **11***a* and **11***b* have been made on the basis of their nmr spectra (Table 1). Compound **11***a* exhibits a coupling constant of 8.5 Hz between the C_6 and C_1 protons. The only configuration which would be predicted to show such a *J* value is that illustrated in Fig. 2

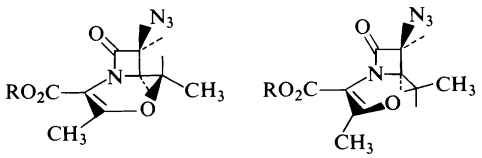

FIGURE 2

for **11***a* in the conformation shown. The coupling constant for compound **11***b* was J_{16} = 3.7 Hz which could be accommodated by either of the two possible conformations for the Δ^3-*O*-2-isocephem system (illustrated in Fig. 2). It is more probable, however, that **11***b* adopts the conformation shown in Fig. 2 as this would relieve the steric interaction between the azido group at C_7 and the 1-β-methyl group.

Reduction of the azido function in **11***a* with hydrogen sulfide – triethylamine (2) followed by coupling of the amine **12***a* to phenoxyacetic acid using *N*-ethoxycarbonyl-2-ethoxy-1,2-dihydroquinoline (EEDQ) (5) gave the amide **13***a* in 60% yield from **11***a*. Similarly compound **11***b* was reduced to the amine **12***b* (74%) and coupled with phenoxy acetic acid to give **13***b* in quantitative yield.

Hydrogenolysis of the benzylesters **13***a* and **13***b* over 20% $Pd(OH)_2/C$ in ethyl acetate gave the corresponding acids **14***a* and **14***b* in 84 and 73% yields, respectively. Both **14***a* and **14***b* exhibited antibacterial activity the details of which will be published separately.

The synthesis of the 1,1,3-trimethyl-Δ^3-*O*-2-isocephem was attempted next via oxymercuration of compound **5** (Scheme 2). Treatment of **5**

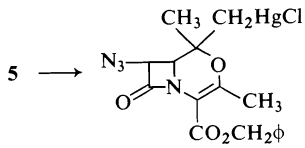

15

SCHEME 2

with mercuric acetate in tetrahydrofuran (6) gave **15** in 66% yield. All attempts to reduce **15** to the desired 1,1,3-trimethyl-Δ^3-*O*-2-isocephem failed, compound **5** being isolated in its stead.

Experimental

The infrared spectra were recorded on a Unicam SP-200G grating, ir spectrometer. The nmr spectra were determined on a Varian A60-A spectrometer using tetramethylsilane as an internal standard. Melting points are uncorrected and were determined on a Gallenkamp melting point apparatus. The analyses were performed by Micro-Tech Laboratories, Skokie, IL.

cis-N-(α-Carbobenzyloxy-β,β-ethylene ketal propyl)-3-azido-4-isopropenyl-2-azetidinone ***4***

(A) Preparation of Schiff Base ***3***

To a mixture of 50.0 g (0.20 mol) aminoketal **2** and 35.0 g (0.5 mol) freshly distilled methacrolein in 300 ml methylene chloride was added 1.0 g of the amine hydrochloride. To this was added a large excess of anhydrous sodium sulfate (100 g) and the whole vigorously stirred with a magnetic stirrer. After 45 min an aliquot was removed and evaporated to dryness. The nmr spectrum of the residual oil indicated complete formation of the desired Schiff base. The remaining solution was filtered and the filtrate

[6]The terms isomer 1 and isomer 2 refer to their order of elution on chromatography.

passed through a pad of activity III silica gel (Woelm, 50–100 g) to remove the amine hydrochloride. The filtrate was evaporated to dryness to yield 54.90 g (90.5%) of pale yellow oil, the nmr spectrum of which was consistent with the assigned structure; ir (film): 1740, 1640, 1617 cm^{-1}.

(B) β-Lactam Formation

The freshly prepared Schiff base **3** (54.90 g, 0.182 mol) in 500 ml dry methylene chloride was cooled to −15°C (in a methanol–ice bath). To this was added 21.60 g (0.182 mol) azidoacetyl chloride over 5 min. Following this 18.2 g (0.182 mol) TEA in 125 ml dry methylene chloride was added dropwise over 1 h while the temperature was maintained at 0–5°C for 18 h and then evaporated at reduced pressure. The residual oil was triturated with 300 ml ether and the TEA hydrochloride removed by filtration. The filtrate was washed successively with 10% hydrochloric acid (100 ml), saturated sodium bicarbonate (100 ml), and brine (100 ml), dried over sodium sulfate, and filtered. This filtrate was in turn filtered through a pad of 150 g silica gel. The filtrate was evaporated to yield 57.8 g (82.5%) of the desired β-lactam **4** as a mixture of diastereoisomers. A sample of the crude **4** was chromatographed on silica gel (15% water, w/w) using benzene as the eluting solvent to give each of the isomers ~90% pure; ir ($CHCl_3$): 2110, 1773, 1750 cm^{-1}. *Anal.* calcd. for $C_{19}H_{22}N_4O_5$: C 59.06, H 5.74, N 14.50; found: C 59.20, H 5.84, N 14.23.

cis-N-(α-Carbobenzyloxy-β,β-ethyleneketalpropyl)-3-azido-4-acetyl-2-azetidinone ***6***

A solution of 15.18 g (0.0394 mol) β-lactam **4** in 100 ml of methanol was prepared and cooled to −78°C in an acetone – dry ice bath. Ozone was passed through the solution until a distinct blue color due to excess ozone was observed. The solution was purged of excess ozone with a stream of dry nitrogen and 15 ml of dimethyl sulfide (large excess) were added. The solution was allowed to come to ambient temperature (~22°C) and evaporated at reduced pressure. The residue was taken up in ether and washed with water (50 ml) and brine (200 ml in 4 portions). The organic layer was dried over Na_2SO_4, filtered, and evaporated to yield 14.5 g of an oil (95%), the nmr spectrum of which indicated that a mixture of two diastereoisomeric ketones **6** had been obtained. Trituration of this oil with ether induced solidification of the mixture.

A small sample of the mixture was chromatographed on silica gel (15% water, w/w) using chloroform as the eluting solvent. Each of the ketones was isolated as a crystalline solid. Isomer 1 (eluted first) had mp 96–96.5°C after recrystallization from chloroform–ether; ir ($CHCl_3$): 2105, 1780, 1740, 1733(s) cm^{-1}. Isomer 2 had mp 91–91.5°C after recrystallization from benzene–ether, ir ($CHCl_3$): 2110, 1775, 1740, 1735(s) cm^{-1}. *Anal.* calcd. for $C_{18}H_{20}N_4O_6$: C 55.66, H 5.19, N 14.43; found (for isomer 1): C 55.47, H 5.25, N 14.44; found (for isomer 2): C 55.76, H 5.23, N 14.53.

Hydrolysis of Compound ***4***

To 3.70 g (10 mmol) of compound **4** (either isomer) was added 20 ml of 95% trifluoroacetic acid at 25°C. The solution was let stand 45 min at 25°C and poured into brine (100 ml). The solution was extracted with methylene chloride (3 × 50 ml), the extracts washed with water (2 × 50 ml) and brine (50 ml), and dried over sodium sulfate. The extracts were evaporated and the residual oil taken up in 200 ml of ether. The organic layer was then extracted with 2% sodium hydroxide (3 × 25 ml) and the aqueous layer acidified to p*H* ~ 3 with 10% hydrochloric acid. The solution was extracted into ether (3 × 50 ml), the extracts dried over sodium sulfate, filtered, and evaporated to dryness. Trituration of the residual oil with ether – petroleum ether induced crystallization of the oil and gave 2.73 g (82%) of **5**, mp 74–75°C. ir: 2115, 1780, 1740, 1665, 1615 cm^{-1}. *Anal.* calcd. for $C_{17}H_{18}N_4O_4$: C 59.64, H 5.30, N 16.37; found: C 59.53, H 5.15, N 16.14.

Hydrolysis of Compound ***6***

To 1.75 g (4.7 mmol) of **6** (1:1 isomer mixture) was added 10 ml 95% trifluoroacetic acid at 25°C. The solution was stirred 20 min at 25°C and worked-up as in the above example to yield 1.495 g (97%) of compound **7**, mp 108–110°C after recrystallization from benzene – petroleum ether (30–60°C); ir ($CHCl_3$): 2120, 1782, 1738, 1660, 1615 cm^{-1}. *Anal.* calcd. for $C_{16}H_{16}N_4O_5$: C 55.81, H 4.68, N 16.27; found: C 55.77, H 4.72, N 16.17.

Reduction of Compound ***6***

To a solution of 11.16 g (0.0288 mol) of ketone mixture **6** (~1:1) in 100 ml THF (4% H_2O) at 22°C was added 0.450 g (0.0118 mol, 0.047 *N* in hydride) sodium borohydride and the solution was stirred 35 min. To the solution was added 10% HCl to p*H* 4 and the solution was evaporated to dryness. The residue was taken up in ether, washed with 10% HCl and brine, and dried over Na_2SO_4. Evaporation of the filtrate gave 10.0 g of an oil, the nmr spectrum of which indicated that the oil contained ~15% of ketone isomer **2**. Thin layer chromatography of the mixture (on silica gel using φH–EtOAc, 3:2) showed 4 spots at R_f's 0.22, 0.29, 0.44, and 0.51 the first and last of which were minor. The sample was coated on 50 g silica gel and chromatographed on 1 kg silica gel (preequilibrated with 100 ml φH–EtOAc, 3:2) via dry column technique (7) using φH–EtOAc, 3:2 as eluent. The column was eluted, 5 ml fractions being taken. The fractions corresponding to the R_f 0.51 spot (1.33 g) consisted of ketone isomer **2** and benzyl alcohol. The fractions corresponding to the R_f 0.44 spot (4.80 g) consisted of a mixture of alcohols epimeric about the ester —CH linkage, the relative configuration of which about the secondary alcohol was subsequently shown to be as in **8*a***. The yield of mixture **8*a*** was 43%. An intermediate fraction consisting of the spots R_f 0.44 and 0.29 (0.75 g) was collected. Finally, 1.10 g (10%) of crystalline alcohol R_f 0.22 was collected, the configuration of which corresponded to **8*b***. A total of 8 g was eluted from the column.

The ir and nmr spectra of the crystalline alcohol were compatible with a single isomer, **8*b***. The configuration about the secondary alcohol was shown by subsequent reactions although the ester function's relative configuration is unknown. Compound **8*b*** was recrystallized from φH–ether, mp 105–106°C. *Anal.* calcd. for $C_{18}H_{24}N_4O_6$: C 55.38, H 5.68, N 14.38; found: C 55.45, H 5.76, N 14.21. The ir and nmr spectra of **8*a*** were compatible with a mixture of isomeric alcohols. The subsequent reactions of **8*a*** indicate it to have the configuration about the secondary alcohol shown. This mixture was not analyzed but was used as such in the next reaction.

Preparation of ***9a***

To a solution of 4.80 g (0.0123 mol) of **8*a*** in 50 ml

CH_2Cl_2 at 0–5°C was added 2.10 ml (0.015 mol) of TEA followed by 1.77 g (0.0156 mol) of methane sulfonyl chloride in 15 ml CH_2Cl_2 over 15 min. The solution was allowed to stand 5 h at room temperature (~22°C), washed once with 10% HCl once with brine, dried over Na_2SO_4, filtered, and evaporated to yield 5.15 g (89%) of crude mesylate **9***a*. The ir and nmr spectra of **9***a* were compatible with the assigned structure. The oil was used as such in the next step without further purification.

Preparation of **9***b*

To a solution of 370 mg (0.00095 mol) of crystalline alcohol **5***b* in 10 ml CH_2Cl_2 at 0–5°C was added 0.154 ml (0.0011 mol) TEA followed by 0.125 g (0.0011 mol) methane sulfonyl chloride. The solution was allowed to stand 18 h at 22°C, washed with 10% HCl and brine, dried over Na_2SO_4, filtered, and evaporated to yield an oil which crystallized on trituration with ether to give 445 mg (99%) pure mesylate **9***b*. A small sample was recrystallized from benzene–ether, mp 89–90°C. *Anal.* calcd. for $C_{19}H_{24}N_4O_8S$: C 48.71, H 5.16, N 11.96, S 6.84; found: C 48.79, H 5.17, N 11.93, S 6.65.

Hydrolysis of **9***a*

Compound **9***a* (5.15 g, 0.011 mol) was hydrolyzed with 95% trifluoroacetic acid as in the procedure given for the hydrolysis of **4** to yield 3.05 g (65%) of **10***a* contaminated with ~10% **10***b*; ir ($CHCl_3$): 2115, 1780, 1660, 1620 cm^{-1}. The oil was not purified further but was used as such in the next step.

Hydrolysis of **9***b*

From 570 mg (1.21 mmol) of **9***b* was obtained 510 mg (96%) of the enol **10***b* upon hydrolysis with trifluoroacetic acid; ir ($CHCl_3$): 2110, 1781, 1670, 1620 cm^{-1}. The oil was used as such in the subsequent experiment.

Benzyl 1-α,3-Dimethyl-7-β-azido-Δ³-O-2-isocephem-4-carboxylate ***11a***

To a suspension of 0.33 g sodium hydride (55% mineral oil dispersion washed three times with petroleum ether) in 25 ml DMSO was added 3.05 g (0.0072 mol) of enol **10***a*. The solution was stirred for 1 h at 22°C at the end of which time all gas evolution had ceased. To this a solution of 10 ml 10% HCl in 100 ml brine was added with cooling (exothermic). The solution was extracted with 200 ml CH_2Cl_2 in four portions and the extracts washed twice with brine. The extracts were dried over Na_2SO_4 and concentrated to yield an oily residue, which on chromatography on silica gel (20 g) with benzene yielded 900 mg (38%) of crystalline **11**. A sample was recrystallized from ether, mp 121–122°C; ir ($CHCl_3$): 2120, 1782, 1715, 1615 cm^{-1}; uv (EtOH, 3.5 mg/125 ml) λ_{max} 268 nm (ε 11 100). *Anal.* calcd. for $C_{16}H_{16}N_4O_4$: C 58.53, H 4.91, N 17.06; found: C 58.64, H 5.01, N 17.14.

Benzyl 1-β,3-Dimethyl-7-β-azido-Δ³-O-2-isocephem-4-carboxylate ***11b***

To a solution of 852 mg (0.002 mol) enol mesylate **10***b* in 25 ml $CHCl_3$ was added 202 mg (0.002 mol) TEA. The solution was refluxed 3 h and let stand 18 h at 22°C. The solution was washed with 10% HCl and brine, dried over Na_2SO_4, filtered, and evaporated. The residue was filtered through 3 g silica gel with benzene and the eluent evaporated to yield 520 mg (80%) of crystalline **11***b*. A sample was recrystallized from ether, mp 119–120°C; ir ($CHCl_3$): 2115, 1780, 1715, 1613 cm^{-1}; uv (EtOH, 3.4 mg/125 ml) λ_{max} 266 nm (ε 13 900). *Anal.* calcd. for $C_{16}H_{16}N_4O_4$: C 58.53, H 4.91, N 17.06; found: C 58.50, H 4.91, N 17.02.

Benzyl 1-α,3-Dimethyl-7-β-(aminophenoxyacetoyl)-Δ³-O-2-isocephem-4-carboxylate ***13a***

To a solution of 470 mg (0.00143 mol) of **11***a* in 20 ml CH_2Cl_2 was added 0.5 ml TEA. A stream of H_2S gas was bubbled in over 5 min and the solution let stand 30 min at 22°C. The solution was washed with water (100 ml) and $NaHCO_3$ (saturated) (3 × 20 ml portions), dried over Na_2SO_4, and concentrated to give 430 mg (100%) crude amine. The ir and nmr spectra of **12***a* were compatible with the assigned structure. Compound **12***a* was used as such in the next step.

To a solution of the above oil in 25 ml CH_2Cl_2 was added 220 mg (0.00143 mol) phenoxyacetic acid and 360 mg (0.00143 mol) EEDQ. The solution was allowed to stand 18 h at 0–5°C, washed with 10% HCl, dried over Na_2SO_4, and evaporated to yield an oil. The oil was chromatographed on 10 g silica gel using benzene – ethyl acetate (3:2) as eluent to yield 372 mg (59.5%) of **13***a*, mp 120–121°C recrystallized from ether–cyclohexane; ir ($CHCl_3$): 3430, 1778, 1770(s), 1703(s), 1695, 1615, 1604, 1522, 1495 cm^{-1}; uv (EtOH, 1.6 mg/50 ml) λ_{max} 269 (ε 11 100), 275 nm (ε 10 800). *Anal.* calcd. for $C_{24}H_{24}N_2O_6$: C 66.04, H 5.54, N 6.42; found: C 65.87, H 5.57, N 6.40.

Benzyl 1-β,3-Dimethyl-7-β-amino-Δ³-O-2-isocephem-4-carboxylate ***12b***

To a solution of 590 mg (0.0018 mol) of **11***b* in 25 ml CH_2Cl_2 was added 0.5 ml TEA. A stream of H_2S gas was passed through the solution for 2 min. Vigorous nitrogen evolution was observed. The solution was let stand 10 min at 22°C and evaporated to dryness. The residue was partitioned between CH_2Cl_2 and 10% HCl. The aqueous layer was neutralized with Na_2CO_3 and extracted into CH_2Cl_2. The extracts were dried and evaporated to yield 392 mg (74%) of a water white oil which crystallized on trituration with ether, mp 96–97°C; ir ($CHCl_3$): 3430, 1770, 1712, 1615 cm^{-1}. *Anal.* calcd. for $C_{16}H_{18}N_2O_4$: C 63.56, H 6.00, N 9.27; found: C 63.40, H 6.05, N 9.31.

Benzyl 1-β,3-Dimethyl-7-β-(aminophenoxyacetoyl)-Δ³-O-2-isocephem-4-carboxylate ***13b***

To a solution of 370 mg (0.00123 mol) of **12***b* in 25 ml CH_2Cl was added 185 mg (0.00123 mol) phenoxyacetic acid and 302 mg (0.00123 mol) EEDQ. The solution was let stand at 25°C and monitored by tlc (silica gel – ether) every 15 min. The reaction was complete in 45 min. After 1 h the solution was washed once with 20 ml 10% HCl, dried over Na_2SO_4, and concentrated to yield 535 mg (100%) crystalline amide **13***b*, mp 129–130°C recrystallized from benzene–cyclohexane; ir ($CHCl_3$): 3440, 1780, 1770, 1715, 1695, 1615, 1600, 1520, 1500 cm^{-1}; uv (EtOH, 1.5 mg/50 ml) λ_{max} 270 (ε 12 300), 275(s) nm (ε 11 600). *Anal.* calcd. for $C_{24}H_{24}N_2O_6$: C 66.04, H 5.54, N 6.42; found: C 66.02, H 5.43, N 6.45.

1-α,3-Dimethyl-7-β-(aminophenoxyacetoyl)-Δ³-O-2-isocephem-4-carboxylic Acid ***14a***

A suspension of 332 mg (0.00076 mol) of **13***a* and 300 mg 20% $Pd(OH)_2/C$ in 40 ml ethyl acetate was shaken under hydrogen at 50 psi for 54 min. The suspension was

filtered through Celite and evaporated. The residue crystallized on trituration with ether. Filtration of the solid gave 220 mg (84%) of **14***a*, mp 220°C (with decomposition) recrystallized from $CHCl_3$; ir ($CHCl_3$): 3440, 1780, 1695, 1600, 1525, 1495 cm^{-1}. *Anal.* calcd. for $C_{17}H_{18}N_2O_6$: C 58.95, H 5.24, N 8.09; found: C 58.85, H 5.32, N 8.01.

1-β,3-Dimethyl-7-β-(aminophenoxyacetoyl)-Δ^3-O-2-isocephem-4-carboxylic Acid ***14b***

A suspension of 500 mg (0.00115 mol) of **13***b* and 400 mg 20% $Pd(OH)_2/C$ in 50 ml ethyl acetate was shaken under hydrogen at 60 psi for 45 min. The suspension was filtered through Celite and evaporated to yield an oily residue which crystallized on trituration with ether to which a few drops of CH_2Cl_2 had been added. Filtration gave 282 mg (73.5%) acid **14***b*, mp 154–155°C (with decomposition) recrystallized from CH_2Cl_2–Et_2O; ir ($CHCl_3$): 3440, 1775, 1695, 1600, 1520, 1495 cm^{-1}. *Anal.* calcd. for $C_{17}H_{18}N_2O_6$: C 58.95, H 5.24, N 8.09; found: C 59.10, H 5.25, N 8.03.

Preparation of ***15***

To a solution of 102 mg (0.3 mmol) of **5** in 2 ml tetrahydrofuran was added 104 mg (0.3 mmol) mercuric acetate in 2 ml of water at 0–5°C. The cooling was removed and the solution stirred at 25°C for 3.5 h. The solution was poured into 30 ml of brine and extracted with chloroform (5 × 15 ml). The extracts were washed with water (10 ml) and brine (25 ml), dried over magnesium sulfate and concentrated to give 115 mg (66%) of an oil which crystallized from chloroform–ether, mp 130–132°C; ir (Nujol): 2110, 1785, 1715, 1600 cm^{-1}. *Anal.* calcd. for $C_{17}H_{17}ClHgN_4O_4$: C 35.36, H 2.96, N 9.70; found: C 35.24, H 3.02, N 9.55.

Acknowledgements

The financial support of this work of the National Research Council of Canada through its Industrial Research Assistance Program is gratefully acknowledged. We also thank Dr. Bernard Belleau of McGill University for numerous consultations in the course of this work as well as Dr. V. DiTullio, Dr. Y. Lambert, Mr. Jacques Chapuis, and Mr. J. Lajeunesse for technical assistance.

1. T. W. Doyle, B. Belleau, B.-y. Luh, T. T. Conway, M. Menard, J. L. Douglas, D. T. Chu, G. Lim, L. R. Morris, P. Rivest, and M. Casey. Can. J. Chem. **55**, 484 (1977).
2. T. W. Doyle, B. Belleau, B.-y. Luh, C. F. Ferrari, and M. P. Cunningham. Can. J. Chem. **55**, 468 (1977).
3. (*a*) D. A. Nelson. Tetrahedron Lett. 2543 (1970); (*b*) J. Decazes, J. L. Luche, and H. B. Kagan. Tetrahedron Lett. 3661 (1970); (*c*) K. D. Barrow and T. M. Spotswood. Tetrahedron Lett. 3325 (1965).
4. A. K. Bose *et al.* Tetrahedron, **23**, 4769 (1967); Tetrahedron Lett. 3167 (1971).
5. B. Belleau and G. Malek. J. Am. Chem. Soc. **90**, 1651 (1968).
6. H. C. Brown and W. J. Hammar. J. Am. Chem. Soc. **89**, 1524 (1967).
7. B. Loev and M. M. Goodman. Intra-Science Chem. Rep. **4**, 283 (1970).

Nuclear analogs of β-lactam antibiotics. IV. Synthesis of 1-oxo-Δ^3-*O*-2-isocephems[1]

TERRENCE WILLIAM DOYLE,[2] ALAIN MARTEL,[3] AND BING-YU LUH

Bristol Laboratories of Canada, 100 Industrial Boulevard, Candiac, P.Q., Canada J5R 1J1

Received February 16, 1977

TERRENCE WILLIAM DOYLE, ALAIN MARTEL, and BING-YU LUH. Can. J. Chem. **55**, 2708 (1977).

The synthesis of 7-β-phenoxyacetamido-3-methyl-1-oxo-Δ^3-O-2-isocephem-4-carboxylic acid **14** is described. Condensation of amine **2** followed by β-lactam formation and ozonolysis gave the acid **5**. This was converted to its trichloroethyl ester **8** and the ketal was hydrolyzed to give **9**. Reduction of the azido function followed by amide formation gave **11**. The trichloroethyl group was removed and the enol acid **12** closed to yield **13**. Hydrogenolysis of the benzyl ester gave **14**. The structural assignments to the compounds are discussed.

TERRENCE WILLIAM DOYLE, ALAIN MARTEL et BING-YU LUH. Can. J. Chem. **55**, 2708 (1977).

On décrit la synthèse de l'acide phénoxyacétamido-7 β méthyl-3 oxo-1 Δ^3 isocéphem-*O*-2 carboxylique-4 **14**. La condensation de l'amine **2** suivie par la formation d'un β lactame et d'une ozonolyse, conduit à l'acide **5**. Celui-ci peut être transformé en ester trichloroéthylé **8** et le groupement cétal peut être hydrolysé pour conduire à **9**. La réduction du groupe azido, suivie par la formation de l'amide, donne **11**. On a éliminé le groupe trichloroéthyle et on a cyclisé l'anol acide **12** pour fournir **13**. L'hydrogénolyse de l'ester benzylique conduit à **14**. On discute des attributions de structure de ces composés.

[Traduit par le journal]

In the previous paper of this series the syntheses of the 1-α and 1-β isomers of the 1,3-dimethyl-Δ^3-*O*-2-isocephem systems (Fig. 1, wherein R_2 = H, R_1 = Me and R_1 = H, R_2 = Me) were described. In order to further explore the effect of substituents at C_1 on the biological activities of the *O*-2-isocephem system the synthesis of the lactone, 1-oxo-Δ^3-*O*-2-isocephem ($R_1 = R_2 = O$), was examined next.[4] In addition to any purely steric effects of substituting the one position by a carbonyl, considerable enhancement of β-lactam reactivity due both to ring strain and electronic (conjugative) effects is to be expected.

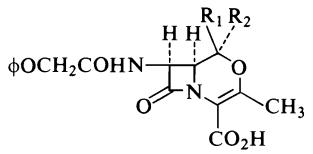

R_1 = H R_2 = CH_3
R_1 = CH_3 R_2 = H
$R_1 = R_2 = O$

FIGURE 1

Condensation of amine **2** (Scheme 1) (3) with a slight excess of furfural gave the Schiff base **3** in quantitative yield. Treatment of compound **3** with an excess of azidoacetyl chloride and triethylamine gave *cis*-β-lactam **4** in 93% yield as a mixture of diastereoisomers.[5] The nmr spectrum of the isomer mixture indicated that no detectable amounts of *trans* isomer had been formed in the cycloaddition. Silica gel chromatography of the mixture using benzene as eluent gave partial separation of the two isomers, the nmr spectra of which are recorded in Table 1.

Ozonolysis of **4** in acetic acid at 20–25°C gave, after work-up, the carboxylic acid **5** as a mixture of diastereoisomers (1:1) in 63.5% yield (9). Hydrolysis of **5** using 95% trifluoroacetic acid gave compound **6** in 94% yield as the enol, as was shown by the singlet in the nmr spectrum at δ 8.90 integrating for one proton. A number of attempts to convert enol acid **6** to the lactone via the mixed anhydride of the acid failed; *e.g.* treatment of **6** with 1 equiv. of triethylamine and either methyl or isobutyl chloroformate gave the methyl and isobutyl esters of **6** respectively, rather than the desired lactone **7**. Attempted ring closure via reaction of the acid with dicyclohexylcarbodiimide in pyridine also failed (4) as

[1]For part III of this series see ref. 1.

[2]Author to whom correspondence concerning this paper may be addressed c/o Bristol Laboratories, P.O. Box 657, Syracuse, NY, U.S.A. 13201.

[3]Holder of an NRCC Industrial Postdoctoral Fellowship, 1972–1974.

[4]For an explanation of the trivial nomenclature used throughout this series of papers and a review of the literature pertaining to the syntheses of nuclear analogs of β-lactam antibiotics see ref. 2.

[5]While the compounds are illustrated as single entities they are, of course, racemic mixtures.

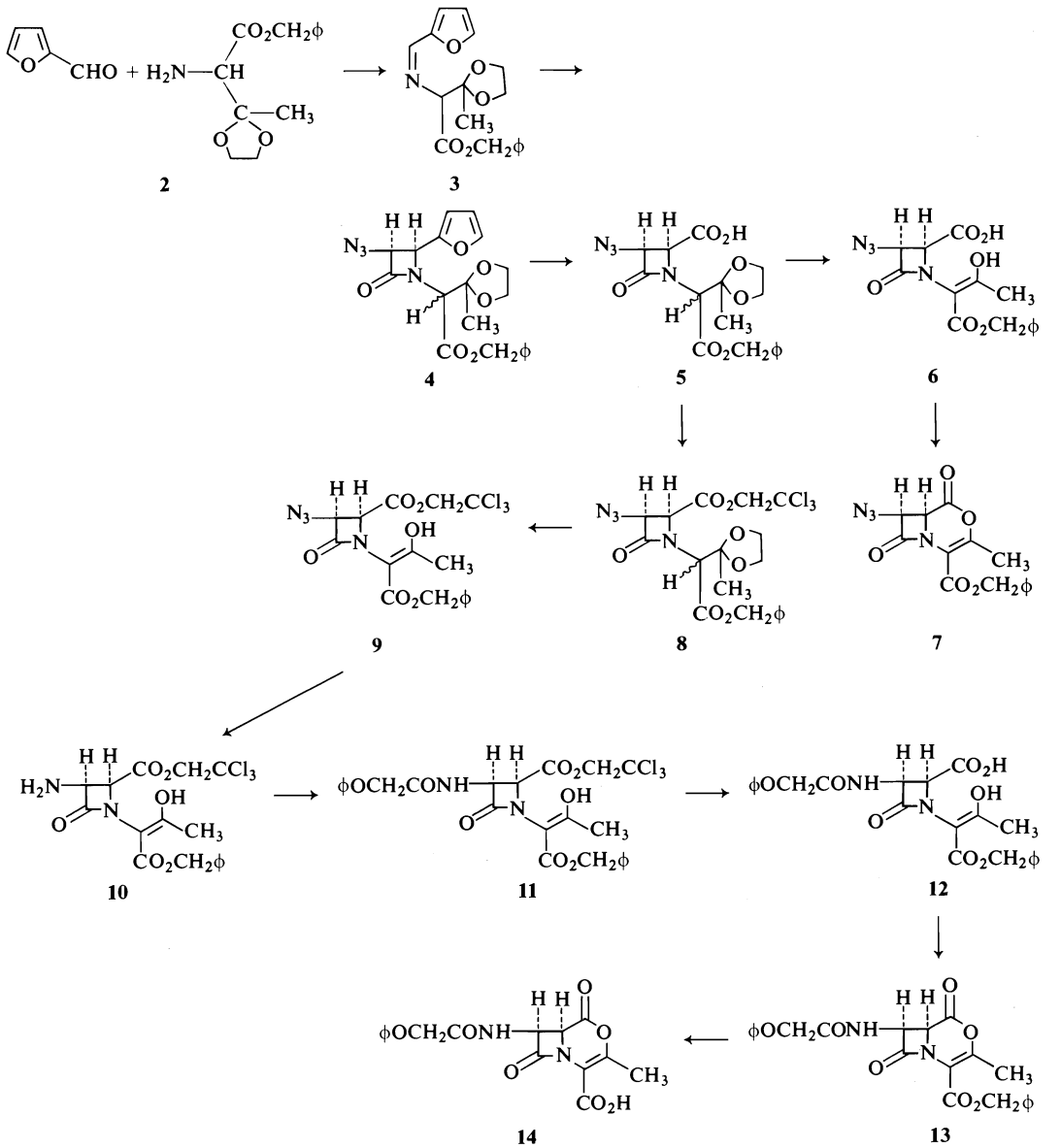

SCHEME 1

did refluxing **6** in benzene with a catalytic amount of *p*-toluene sulfonic acid. The cyclization of **6** to **7** was finally achieved via conversion of **6** to its acid chloride using thionyl chloride. Treatment of the acid chloride with 1 equiv. of triethylamine gave the desired lactone **7** as an oil. That compound **7** was indeed the lactone was shown by its infrared and nmr spectra. In the ir there were two high frequency carbonyl bands at 1785 and 1800 cm^{-1} which we assign to the lactone and β-lactam, respectively, although these might conceivably be reversed. As a model for the position of the lactone carbonyl resonance we have used the lactone (Fig. 2) 1-dehydro-10-deoxy-7,8-dihydrogenepin. This lactone is reported to have the lactone carbonyl resonance at 1773 cm^{-1} (5). A shift to

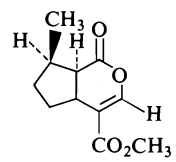

FIGURE 2

TABLE 1. Nuclear magnetic resonance spectra[a]

Compd.	Aromatic protons	H H / N—R		CH_3	$CH_2\phi$	Other
3	7.36(s, 5H) 7.53(d, 1H, J=2.0) 6.88(d, 1H, J=3.5) 6.48(dd, 1H) J_1=3.5, J_2=2.0			1.55(s)	5.22(s)	3.98(s, 4H)[b] 4.15(s, 1H)[c] 8.11(s, 1H, C*H*=N)
4[d]	7.40(s, 5H) 6.48(m, 2H) 7.51(m, 1H)	5.26(d) J=5.5	4.77(d) J=5.5	1.33(s)	5.20(s)	4.26(s, 1H)[c] 3.70(m, 4H)[b]
4[e]	7.30(m, 5H) 7.38(d, 1H) J=2.0 6.40(m, 2H)	5.20(d) J=5.5	4.80(d) J=5.5	1.43(s)	4.91(s)	4.58(s, 1H)[c] 3.88(s, 4H)[b]
5[f]	7.25(s)	5.20(m, 2H)		1.33(s) 1.46(s)	5.08(m)	3.90(m, 4H)[b] 4.50, 4.65(s, 1H)[c]
6	7.24(s, 5H)	4.84(d) J=5.5	4.53(d) J=5.5	2.20(s)	5.14(s)	8.90(s, 1H, O*H*)
7	7.28(s, 5H)	5.22(d) J=5.0	4.25(d) J=5.0	2.34(s)	5.20(s)	
8[d]	7.38(s, 5H)	4.75(m, 3H)[g]		1.36(s)	5.17(s)	3.94(s, 4H)[b] 4.99(s, 2H)[h]
8[e]	7.38(s, 5H)	4.60(s, 2H)		1.48(s)	5.30(d, 1H)[i] 5.14(d, 1H)[i] J=8	3.78(m, 4H)[c] 4.86(s, 2H)[h]
9	7.30(s, 5H)	4.88(d) J=5.5	4.68(d) J=5.5	2.28(s)	5.30(d, 1H)[i] 5.06(d, 1H)[i] J=12.0	12.2(s, 1H, OH) 4.78(s, 2H)[h]
11	7.24(s, 5H) 6.7–7.4(m, 5H)	5.45(dd) J_1=9.0 J_2=5.5	4.70(d) J=5.5	2.37(s)	5.04(d, 1H)[i] 5.27(d, 1H)[i] J=12.0	12.0(s, 1H, OH) 4.39(s, 2H)[j] 4.51(s, 2H)[h]
12[k]	7.43(s, 5H) 6.7–7.4(m, 5H)	5.42(dd) J_1=10 J_2=6.0	4.81(d) J=6.0	2.37(s)	5.39(s)	4.61(s, 2H)[j] 8.17(m, 1H, NH) 6.10(bs, 2H, O*H*, CO_2H)
13	7.38(s, 5H) 6.7–7.4(m, 5H)	5.06(dd) J_1=7.5 J_2=5.5	4.16(d) J=5.5	2.42(s)	5.26(s)	4.46(s, 2H)[j]
14[l]	6.7–7.4(m, 5H)	5.21(dd) J_1=7.0 J_2=5.5	4.48(d) J=5.5	2.31(s)		4.47(s, 2H)[j] 8.96(d, 1H, J=7.0, NH)

[a]Recorded at 60 MHz on a Varian A-60A spectrometer in $CDCl_3$ using tetramethylsilane as internal standard unless otherwise noted. The chemical shifts are recorded in δ (ppm) and the J's in Hz. [b]Assigned to ketal protons O—C*H*$_2$—C*H*$_2$—O. [c]Assigned to C*H*—CO_2R. [d]Isomer 1. [e]Isomer 2. [f]1:1 isomer mixture. [g]Assigned to N_3C*H*—C*H* and C*H*CO_2Bz. [h]Assigned to C*H*$_2$$CCl_3$. [i]Arms of AB quartet. [j]Assigned to φOC*H*$_2$. [k]Recorded in acetone-d_6. [l]Recorded in DMSO-d_6.

higher frequency of 10–12 cm^{-1} for this resonance in compound **7** due to ring strain imparted to **7** by the fused β-lactam would not be unexpected. Similarly the β-lactam carbonyl resonance would be expected to be shifted to higher frequency than in the parent *O*-2-isocephem. We have previously reported (3) the β-lactam carbonyl resonance in the parent system to come at 1780 cm^{-1}. The shift to 1800 cm^{-1} with the substitution of the polar carbonyl group for the methylene at C_1 is as would be expected on the basis of electronic and steric grounds.[6] The nmr spectrum of compound **7** showed doublets at 5.22 and 4.25 δ (J = 5.0 Hz) which we assign to H_7 and H_6, respectively. The coupling constant of 5 Hz is diagnostic of *cis* stereochemistry (6). Examination of the data in Table 1 shows that the proton α to the azido function underwent a shift of +0.38 δ on ring closure (compare **6** and **7**). Similar shifts to lower fields were observed for the proton α to

[6]For a discussion of factors influencing β-lactam carbonyl resonance positions see ref. 7.

TABLE 2. Chemical shift changes for N_3—C*H* upon ring closure[a]

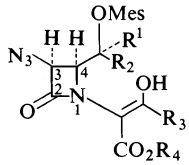

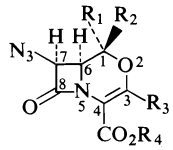

R_1	R_2	R_3	R_4	C_3	C_7	$\Delta\delta$	Ref.
H	H	H	Et	5.01	5.34	+0.33	3
H	H	H	Bz	4.86	5.25	+0.39	3
H	H	CH_3	Bz	4.84	5.05	+0.21	3
H	CH_3	CH_3	Bz	4.60	5.07	+0.47	1
CH_3	H	CH_3	Bz	4.70	5.15	+0.45	1

[a]All spectra were recorded in $CDCl_3$ at 60 MHz using TMS as an internal standard.

the azido function upon ring closure in our earlier work (Table 2).

Compound **7** proved to be somewhat unstable, extensive decomposition occurring upon standing at ambient temperature for a week. Attempts were made to reduce the azido function in **7** to no avail; instead polymerization occurred. In view of these problems it was decided to couple the eventual 7-side chain prior to ring closure.

Treatment of **5** with thionyl chloride gave the corresponding acid chloride which was then converted to its 2,2,2-trichloroethyl ester as a mixture of diastereoisomers. The yield of **8** from **5** was 99%. Hydrolysis of the ketal gave the enol **9** as a crystalline solid in 89% yield. The reduction of the azido function in **9** was carried out using hydrogen sulfide – triethylamine. In view of the potential amphoteric nature of the amino compound **10** only catalytic amounts of the base were used along with extended reaction times (2). The crude amine **10** was coupled to phenoxyacetic acid using *N*-ethoxycarbonyl-2-ethoxy-1,2-dihydroquinoline (EEDQ) (7) to give the amide **11** in 70% overall yield from **9**. Cleavage of the 2,2,2-trichloroethyl ester **11** using zinc in acetic acid gave **12** as a crystalline solid in quantitative yield (8). The conversion of enol acid **12** to the lactone **13** proceeded in 63% yield via the acid chloride. In view of the instability demonstrated by **7**, compound **13** was characterized by its ir and nmr spectrum and its subsequent conversion to **14**. Hydrogenolysis of the benzyl ester in **13** using 20% $Pd(OH)_2/C$ in ethyl acetate gave the acid **14** in 56% yield as a crystalline solid. The structure of **14** was shown via its ir, nmr, and uv spectra.

As was expected compound **14** showed enhanced β-lactam reactivity as was indicated by the high β-lactam carbonyl at 1800 cm^{-1}. This could also be seen from the uv spectrum in ethanol. The characteristic bands at 268 (ε 5500) and 275 nm (ε 5300) disappeared rapidly with time indicating a half life of approximately 1 h for **14** in ethanol. That the decomposition of **14** did not involve primary lactone ring opening was shown by the fact that appearance of a uv absorption at 257–262 nm did not occur concomitantly with loss of the absorptions at 268 and 273 nm as would have been expected if **14** were decomposing by lactone ring opening.

The nmr spectrum of **14** was also in accord with assigned structure (Table 1).

Experimental

The infrared spectra were recorded on a Unicam SP-200G grating ir spectrophotometer. The uv spectra were determined on a Unicam SP-800 uv spectrophotometer. The nmr spectra were determined on a Varian A60-A spectrometer using tetramethylsilane as an internal standard. Melting points are uncorrected except where noted and were determined on a Gallenkamp melting point apparatus. The analyses were performed by Micro-Tech Laboratories, Skokie, IL.

cis-N-(α-Carbobenzyloxy-β,β-ethyleneketalpropyl)-3-azido-4(-2'-furyl)-2-azetidinone ***4***

A. Preparation of Schiff Base

A mixture of 28.0 g (0.113 mol) of amine **2** and 11.6 g (0.12 mol) furfural in 150 ml methylene chloride was boiled at reflux for 5 min. After the initial reflux period, 500 ml of methylene chloride was distilled (with the simultaneous addition of 500 ml methylene chloride) over 1.5 h (azeotrope with water). The residue was dried over Na_2SO_4, filtered, and evaporated to dryness. The oil was heated at 40°C at 0.1 Torr pressure. The solid residue was used in the next step without further purification. The

nmr spectrum of **3** indicated that Schiff base formation was quantitative; ir ($CHCl_3$): 1743, 1643, 1495 cm^{-1}.

B. β-Lactam Formation

A solution of Schiff base (0.113 mol) in 300 ml methylene chloride was cooled to 0–5°C in an ice bath. To this was added 13.3 g (0.131 mol) TEA. A solution of 14.4 g (0.12 mol) azidoacetyl chloride in 100 ml methylene chloride was added over 1 h. An aliquot was removed, washed with water, dried over Na_2SO_4, and concentrated. The nmr spectrum of the residual oil indicated that the reaction was incomplete. To the reaction mixture was added a second equivalent of TEA followed by 12.0 g (0.10 mol) azidoacetyl chloride in 100 ml methylene chloride as before. After the addition was complete, the solution was evaporated to near dryness and the residue triturated with 300 ml ether. The TEA hydrochloride was removed by filtration. The filtrate was treated with 2 g activated charcoal, filtered, washed with water (twice) and brine (twice), and dried over Na_2SO_4.

The suspension was filtered and the solvent removed at reduced pressure to yield 42.6 g (93%) of β-lactam **4** as a mixture of diastereoisomers. The material was sufficiently pure to be used as such in the subsequent steps. A small sample was chromatographed on silica gel (deactivated with 15% w/w water) using benzene as an eluent to give a pale yellow oil; ir ($CHCl_3$): 2120, 1775, 1748, 1640, 1625 cm^{-1}. *Anal.* calcd. for $C_{20}H_{20}N_4O_6$: C 58.25, H 4.89, N 13.59; found: C 58.07, H 4.82, N 13.51.

cis-N-(α-Carbobenzyloxy-β,β-ethyleneketalpropyl)-3-azido-2-azetidinone-4-carboxylic Acid ***5***

A solution of 17.0 g (0.0422 mol) β-lactam **4** in 200 ml glacial acetic acid was prepared. A stream of ozone was passed through the solution for 2 h, while maintaining the temperature between 20–25°C. The solution was evaporated at reduced pressure, and the residue taken up in ether and extracted with 10% sodium bicarbonate. The aqueous layer was acidified with 10% hydrochloric acid and extracted several times with ether. The ethereal extracts were dried over Na_2SO_4 and concentrated to give 10.2 g (63.5%) of a heavy oil which crystallized on scratching with a little ether. An analytical sample was recrystallized from ether, mp 114–115°C. This material was a 1:1 mixture of diastereoisomers; ir ($CHCl_3$): 2800–3600, 2120, 1782, 1742 cm^{-1}. *Anal.* calcd. for $C_{17}H_{18}N_4O_7$: C 52.31, H 4.65, N 14.35; found: C 52.29, H 4.74, N 14.62.

Hydrolysis of ***5***

Ketal **5** (3.5 g) was treated with 95% TFA for 0.5 h at room temperature. The mixture was cooled to 0°C and diluted with brine. It was extracted with CH_2Cl_2 (3 × 30 ml). The methylene chloride extracts were combined, washed with brine (2 × 20 ml), dried over Na_2SO_4, and evaporated to give the desired enol **6** in 94% yield (2.9 g); ir ($CHCl_3$): 2500–3600, 2120, 1780, 1745, 1660, 1620 cm^{-1}.

Benzyl 1-Keto-3-methyl-7-β-azido-Δ³-O-2-isocephem-4-carboxylate ***7***

To a solution of 377 mg enol acid **6** in 25 ml dry CH_2Cl_2 at 0–5°C was added dropwise 0.152 ml TEA in 3 ml CH_2Cl_2. The mixture was stirred at room temperature for 60 min, then treated dropwise with a solution of 0.079 ml $SOCl_2$ in 5 ml CH_2Cl_2. It was stirred at 0°C for 1 h and refluxed for 5 h. After cooling to 0°C, 0.152 ml TEA in 10 ml CH_2Cl_2 was added over a 20 min period. The mixture was allowed to warm slowly to room temperature and stirred for 18 h. The solvent was partially evaporated and the residue was diluted with ether. TEA·HCl was removed by filtration and the solvent was evaporated to give the desired lactone in 63% yield (225 mg) as an oil; ir (film): 2120, 1800, 1785, 1725 (s 1715), 1645 cm^{-1}.

2,2,2-Trichloroethyl-cis-N-(α-carbobenzyloxy-β,β-ethyleneketalpropyl)-3-azido-2-azetidinone-4-carboxylate ***8***

A solution of 10.0 g (0.0256 mol) acid **5** and 10 ml thionyl chloride in 200 ml methylene chloride was refluxed 3 h. The solution was evaporated to dryness. The last traces of thionyl chloride were removed by pumping the residue at 0.1 Torr pressure, for 15 min; ir (film): 1790, 1780(s), 1740 cm^{-1}.

The residue was taken up in 200 ml dry methylene chloride and 5.0 g (0.033 mol) trichloroethanol was added at 0–5°C. To this was added a solution of 5 ml TEA in 25 ml methylene chloride over 0.5 h. The reaction was allowed to stand 60 h at 0–5°C, washed twice with 10% HCl and twice with 10% $NaHCO_3$ brine, and dried over Na_2SO_4. Evaporation of the filtrate gave 13.30 g (99%) of **8** as a mixture of diastereoisomers. An analytical sample was purified by chromatography on silica gel using benzene as the eluent; ir (neat): 2120, 1785 (1770s), 1745 cm^{-1}. *Anal.* calcd. for $C_{19}H_{19}Cl_3N_4O_7$: C 43.74, H 3.67, N 10.74, Cl 20.38; found: C 43.61, H 3.57, N 10.65, Cl 20.24.

Hydrolysis of ***8***

A solution of 13.0 g (0.0249 mol) of ketal **8** in 50 ml of 95% trifluoroacetic acid was let stand 1 h at room temperature. The solution was diluted with 500 ml brine and extracted three times with ether. The organic phase was washed several times with 10% $NaHCO_3$ and once with brine, dried over Na_2SO_4, and evaporated to give 10.60 g (89%) of crystalline enol **9**. An analytical sample was recrystallized from ether, mp 81.5–82.5°C; ir ($CHCl_3$): 2120, 1780, 1663, 1618 cm^{-1}; uv (EtOH) λ_{max} 258 nm (ε 5800). *Anal.* calcd. for $C_{17}H_{15}Cl_3N_4O_6$: C 42.74, H 3.16, N 11.73, Cl 22.27; found: C 42.61, H 3.07, N 11.89, Cl 22.09.

Preparation of ***11***

A. Azide Reduction

A solution of 2.46 g (0.00515 mol) of azide **9** in dry CH_2Cl_2 (50 ml) was treated with a stream of H_2S gas for 20 min at 0–5°C. To this was added 3 drops TEA and the mixture was allowed to stand 3 h at room temperature. The above process was repeated and the mixture allowed to stand an additional 3 h. The solution was evaporated to give an oil which showed no azide absorption in the ir and exhibited an absorption band for NH_2; ir (neat) 3340, 1770(b), 1660, 1615.

B. Side Chain Coupling

To the crude amine in 50 ml CH_2Cl_2 was added 0.88 g (0.0058 mol) phenoxyacetic acid and 1.40 g (0.0057 mol) EEDQ at 0–5°C. The solution was allowed to stand 16 h at 4°C, washed once with 10% HCl, 10% $NaHCO_3$, and brine, and dried over Na_2SO_4. The residue obtained on evaporation of the solvent was chromatographed on

silica gel (20 g, 15% w/w, water) using benzene as eluent to give 2.18 g (70%) of amide **11**; mp 140–140.5°C recrystallized from ether; uv (EtOH), λ_{max} 222 (ε 8900), 262 nm (ε 10 000); ir ($CHCl_3$): 3410, 1780, 1770s, 1695, 1663, 1620, 1600, 1530, 1500 cm^{-1}. *Anal.* calcd. for $C_{25}H_{23}Cl_3N_2O_8$: C 51.26, H 3.96, N 4.78, Cl 18.16; found: C 51.03, H 3.92, N 4.71, Cl 18.06.

Preparation of ***12***

To a solution of 200 mg (0.352 mmol) of **11** in 10 ml of 90% acetic acid was added 1 g activated zinc dust at 5°C. The suspension was stirred 4 h, filtered through Celite, and diluted with 40 ml ether. The solution was washed seven times with 10 ml portions of brine and dried over Na_2SO_4. Evaporation gave 170 mg (100%) of crystalline **12**. An analytical sample was recrystallized from acetone–ether; mp 142–143°C; uv (EtOH) λ_{max} 219 (ε 8500) 257 nm (ε 7400); ir ($CHCl_3$): 3410, 3600–2500, 1780 (s 1770), 1745, 1695, 1665, 1620, 1605, 1535, 1500 cm^{-1}. *Anal.* calcd. for $C_{23}H_{22}N_2O_8$: C 60.79, H 4.88, N 6.16; found: C 60.54, H 4.85, N 6.10.

Benzyl 1-Keto-3-methyl-7-(β-phenoxyacetamido)-Δ³-O-2-isocephem-4-carboxylate ***13***

To a solution of 380 mg (0.838 mmol) enol acid **12** in 80 ml dry CH_2Cl_2 was added 80 mg (0.802 mmol) TEA at 0°C. The solution was let stand 1 h. A solution of 0.12 ml (1.676 mmol) thionyl chloride in 3 ml CH_2Cl_2 was added dropwise over 15 min. The solution was stirred 2 h at 0°C then refluxed 15 min. The solution was cooled to 0°C and a solution of 0.140 ml (1.0 mmol) TEA in 5 ml CH_2Cl_2 was added dropwise over 20–30 min until the color of the solution darkened. The solution was stirred 17 h at room temperature, partially evaporated to 5–10 ml volume, and diluted with 50 ml dry ether. The suspension was stirred 15 min with 200 mg charcoal, filtered through Celite, and evaporated to yield an oily residue. The residue was chromatographed on silica gel (activity I) (200 mg) using dry CH_2Cl_2 as eluent to yield 230 mg (63.3%) of lactone **13** as an oil. No further attempts to purify **13** were made and it was used as such in the next step; ir ($CHCl_3$): 3410, 1805, 1790, 1725, 1690, 1650, 1609, 1525, 1495 cm^{-1}.

1-Keto-3-methyl-7-(β-phenoxyacetamido)-Δ³-O-2-isocephem-4-carboxylic Acid ***14***

Compound **13** (230 mg, 0.528 mmol) and 400 mg 20% $Pd(OH)_2/C$ in 50 ml ethyl acetate were shaken under H_2 for 45 min at 50 psi. The suspension was filtered through Celite and evaporated to dryness. The residue crystallized from CH_2Cl_2–Et_2O (1:1) to yield 100 mg (56%) of acid **14**. An analytical sample was recrystallized from acetone–ether, mp 161–161.5°C; uv (EtOH) λ_{max} 268 (ε 5500), 275 nm (ε 5300); ir (Nujol): 3360, 1800, 1785, 1705, 1690, 1625, 1598, 1515, 1495 cm^{-1}. *Anal.* calcd. for $C_{16}H_{14}N_2O_7$: C 55.49, H 4.08, N 8.09; found: C 55.58, H 4.09, N 8.20.

Acknowledgements

Partial financial support of this work by the National Research Council of Canada through its Industrial Research Assistance Plan is gratefully acknowledged. We also thank Dr. Bernard Belleau of McGill University for helpful discussions during the course of this work.

1. T. W. Doyle, B.-y. Luh, and A. Martel. Can. J. Chem. **55**, 2700 (1977).
2. T. W. Doyle, B. Belleau, B.-y. Luh, C. F. Ferrari, and M. P. Cunningham. Can. J. Chem. **55**, 468 (1977).
3. T. W. Doyle, B. Belleau, B.-y. Luh, T. T. Conway, M. Menard, J. L. Douglas, D. T. Chu, G. Lim, L. R. Morris, P. Rivest, and M. Casey. Can. J. Chem. **55**, 484 (1977).
4. R. B. Woodward, F. E. Bader, H. Bickel, A. J. Frey, and R. W. Kierstead. Tetrahedron, **2**, 1 (1958).
5. C. Djerassi, T. Nakano, A. N. James, L. H. Zalkow, E. J. Eisenbraun, and J. N. Shoolery. J. Org. Chem. **26**, 1192 (1961).
6. E. H. Flynn (*Editor*). Cephalosporins and penicillins chemistry and biology. Academic Press, New York and London. 1972.
7. B. Belleau and G. Malek. J. Am. Chem. Soc. **90**, 1651 (1968).
8. R. B. Woodward, K. Heusler, J. Gosteli, P. Naegeli, W. Oppolzer, R. Ramage, S. Ranganathan, and H. Vorbruggen. J. Am. Chem. Soc. **88**, 852 (1966).
9. R. Lattrell and G. Lohaus. Ger. Offen 2 046 822, 2 046 823, 2 046 824 (1970).

Nuclear analogs of β-lactam antibiotics. V. Synthesis of a benzo[3,4]-*O*-2-isocephem[1]

TERRENCE WILLIAM DOYLE[2]

Bristol Laboratories of Canada, 100 Industrial Boulevard, Candiac, P.Q., Canada J5R 1J1

Received February 16, 1977

TERRENCE WILLIAM DOYLE. Can. J. Chem. **55**, 2714 (1977).

The synthesis of 7-β-phenoxyacetamido-4′-hydroxybenzo[3,4]-*O*-2-isocephem **14** is described. Condensation of **5** with cinnamaldehyde gave **6** which was converted to the 3-azido-4-styrrylazetidinone **7**. Ozonolysis and reduction of the resulting aldehyde **8** gave **9**. Compound **9** was converted to the mesylate **12** by reduction of the azide to the amine **10**, coupling of **10** with phenoxyacetic acid to give **11**, and mesylation of **11**. Removal of the benzyl groups of **12** by hydrogenolysis and base catalyzed ring closure of the phenol gave **14**.

TERRENCE WILLIAM DOYLE. Can. J. Chem. **55**, 2714 (1977).

On décrit la synthèse du phénoxyacétamido-7 β hydroxy-4′ benzo[3,4]isocéphem-*O*-2 **14**. La condensation de **5** avec le cinnamaldéhyde conduit à **6** qui peut être transformé en azido-3 styrryl-4 azétidinone **7**. L'ozonolyse et la réduction de l'aldéhyde **8** qui en résulte donne **9**. On peut tranformer le composé **9** en son mésylate **12** par réduction de l'azide conduisant à l'amine **10**, le couplage de **10** avec l'acide phénoxyacétique qui donne **11** et par mésylation de **11**. L'enlèvement des groupes benzyles de **12** par hydrogénolyse et la cyclisation, catalysée par les bases du phénol conduit à **14**.

[Traduit par le journal]

The previous papers of this series have described the syntheses of a number of *O*-2-isocephem systems (Fig. 1). In order to further explore structure activity relationships in this series the synthesis of a [3,4]benzo fused cephalosporin analog was carried out.[3]

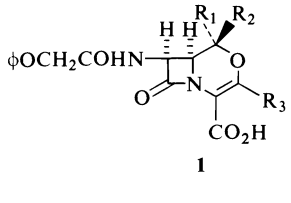

1

R_1	R_2	R_3
H	H	H
H	H	CH_3
H	H	$CH_2\phi$
H	H	$(CH_2)_2\phi$
H	Me	CH_3
Me	H	CH_3
O		CH_3

FIGURE 1

Thus nitration of dibenzylhydroquinone **3** according to the procedure of Burton and Praill (3) gave the desired nitro derivative **4** in 98% yield. Reduction of the nitro group to the amine was accomplished in 93% yield using aluminum amalgam in tetrahydrofuran. The efficient conversion of the amine **5** to the Schiff base **6** required the use of a sixfold excess of cinnamaldehyde. Trituration of the reaction mixture with petroleum ether induced crystallization of the Schiff base and led to recovery of the excess aldehyde. The yield of compound **6** was 80%.

Treatment of Schiff base **6** with azidoacetyl chloride in the presence of triethylamine gave **7** in 70% yield. The nmr spectrum of **7** did not permit an assignment of stereochemistry due to overlap of the signals of the protons on the azetidinone. The assignment of *cis* stereochemistry was made retrospectively. Thus ozonolysis of compound **7** followed by treatment of the ozonide with dimethyl sulfide gave the aldehyde **8** as a crystalline solid in 60% yield. Compound **8** had carbonyl bands in the infrared spectrum at 1770 and 1740 cm^{-1}. The nmr spectrum of **8** (Table 1) indicated the stereochemistry of the 3-azido and 4-formyl functions to be *cis* inasmuch as the proton α to the azido function appeared as a doublet with a coupling constant of 6 Hz (4). By inference, therefore, the stereochemistry of compound **7** was also *cis*.

Compound **9** was prepared directly from compound **7** without isolation of the intermediate aldehyde **8**. Ozonolysis of **7** in methylene chloride – methanol followed by removal of the solvent, redissolution of the residual oil in ethanol, and reduction using sodium borohydride gave the desired alcohol **9** in 65% overall yield. As we contemplated removal of the benzyl groups by

[1]For part IV of this series see ref. 1.

[2]Present Address, Bristol Laboratories, P.O. Box 657, Syracuse, NY, U.S.A. 13201

[3]For an explanation of the trivial nomenclature used throughout this series of papers and a review of the literature pertaining to the syntheses of nuclear analogs of β-lactam antibiotics see ref. 2.

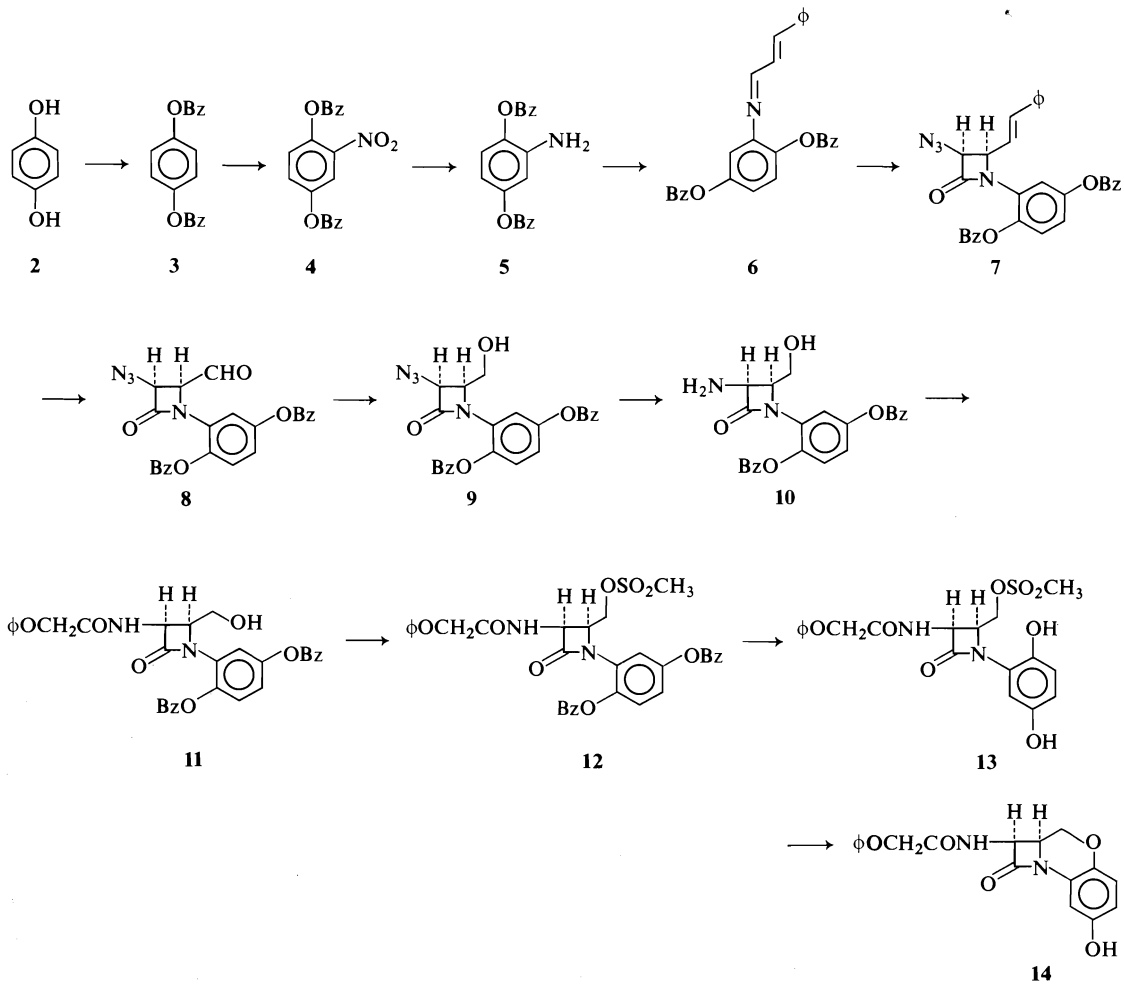

SCHEME 1

hydrogenolysis it was decided to introduce the amido side chain at this time. Accordingly the azido function in **9** was reduced using triethylamine – hydrogen sulfide (2) to give the amine **10** in 91.5% yield. Coupling of the amine **10** with phenoxyacetic acid was achieved using *N*-ethoxycarbonyl-2-ethoxy-1,2-dihydroquinoline(EEDQ) in 65% yield (5). Mesylation of alcohol **11** proceeded in 82% yield to give **12**. Hydrogenolysis of **12** using palladium hydroxide on carbon in acetic acid gave the substituted hydroquinone **13** in 78% yield. Finally treatment of **13** with 1,5-diazobicyclo[4.3.0]non-5-ene (DBN) in dimethyl sulfoxide followed by silica gel chromatography afforded 7-β-phenoxyacetamido-4′-hydroxybenzo[3,4]-*O*-2-isocephem **14** in 47% yield.

Compound **14** was only weakly biologically active.

Experimental

The infrared spectra were recorded on a Unicam SP-200 G grating ir spectrophotometer. The nmr spectra were determined on a Varian A60-A spectrometer using tetramethylsilane as an internal standard. Melting points are uncorrected except where noted and were determined on a Gallenkamp melting point apparatus. The analyses were performed by Micro-Tech Laboratories, Skokie, IL.

Dibenzyl 2-Nitrohydroquinone **4**

(*A*) To a solution of 110 g hydroquinone (1 mol) and 280 ml benzyl chloride (2.05 mol) in 1 ℓ of ethanol at reflux was added 80 g sodium hydroxide in 600 ml water. Reflux was continued for 4 h and the solution was allowed to stand at 25°C for 18 h. The suspension was filtered and the filter cake washed with benzene. The filtrate was evaporated to a volume of 1 ℓ at reduced pressure and extracted with ether (5 × 100 ml). The extracts were dried over sodium sulfate and concentrated to give a white solid. The combined solids from filtration and ex-

TABLE 1. Nuclear magnetic resonance spectra[a]

Compd	C_6H_5—	Other aromatic protons	ϕ—CH_2—	H H N—C—C—R	Other
3	7.91(s, 10H)	7.40(s, 4H)	5.35(s, 4H)		
4	7.46(bs, 10H)	7.46(m, 1H) 7.01(m, 2H)	5.05(s, 2H) 5.16(s, 2H)		
5	7.33(s, 10H)	6.72(d, 1H, J=8.5) 6.37(d, 1H, J=2.75) 6.23(dd, 1H, J_1=8.5 J_2=2.75)	4.92(s, 2H) 4.95(s, 2H)		5.60(bs, 2H, NH_2)
6		6.5–7.7(m, 20H)	5.03(s, 2H) 4.93(s, 2H)		8.22(dd, 1H, J_1=2.2, J_2=5.4, C*H*=N)
7	7.70(s, 10H) 7.55(s, 5H)	7.91(d, 1H, J=3) 7.01(d, 1H, J=9.5) 6.92(dd, 1H, J_1=9.5 J_2=3)	5.20(s, 2H) 5.15(s, 2H)	5.15(m, 2H)	6.50(m, 2H, ϕC*H*=C*H*)
8	7.60(s, 10H)	8.08(d, 1H, J=3) 7.08(d, 1H, J=9) 6.90(dd, 1H, J_1=9 J_2=3)	5.18(s, 2H) 5.08(s, 2H)	5.15(d) 4.90(dd) J=6 J_1=6 J_2=3	9.80(d, 1H, J=3, C*H*O)
9	7.36(s, 10H)	7.58(d, 1H, J=3) 6.88(d, 1H, J=9) 6.66(dd, 1H, J_1=9 J_2=3)	4.96(s, 2H) 4.92(s, 2H)	4.75(d) 4.35(dt) J=5.5 J_1=5.5 J_2=4.0	3.80(d, 2H, J=4.0, CH_2—OH) 2.0(s, 1H, O*H*)
10	7.31(s, 10H)	7.60(d, 1H, J=3) 6.85(d, 1H, J=9) 6.61(dd, 1H, J_1=9 J_2=3)	4.97(s, 4H)	4.25(m, 2H)	3.83(m, 2H, CH_2—OH) 2.33(s, 3H, NH_2, O*H*)
11	7.33(s, 10H)	7.66(d, 1H, J=3) 6.6–7.4(m, 7H)	4.97(s, 4H)	5.76(dd) 4.47(m) J_1=10 J_2=5.5	8.25(d, 1H, J=10, N*H*) 4.48(s, 2H, ϕOCH_2) 3.96(dd, 1H, J_1=13, J_2=3)[b] 3.47(d, 1H, J_1=13)[b]
12	7.40(s, 10H)	7.70(d, 1H, J=3) 6.6–7.5(m, 7H)	4.97(s, 4H)	5.57(dd) J_1=10 J_2=6	7.55(d, 1H, NH, J=10) 2.55(s, 3H, SO_2CH_3) 4.0–4.5(m, 3H, C*H*—CH_2—OMes)
13[c]	6.8–7.5 (m, 6H)	6.68(d, 1H, J=9) 6.40(dd, 1H, J_1=9 J_2=3)		5.52(dd) J_1=10 J_2=5	3.08(s, 3H, SO_2CH_3) 4.5–5.0(m, 3H, C*H*, CH_2OMes) 4.64(s, 2H, ϕOCH_2) 9.15(bs, 2H, O*H*)
14[c]	6.8–7.5 (m, 7H)	6.42(dd, 1H, J_1=9 J_2=3)		5.66(m)	9.0(d, 1H, J=10, N*H*) 4.59(s, 2H, ϕOCH_2) 3.9–4.4(m, 3H) 9.15(s, 1H, OH) 8.91(d, 1H, J=9, NH)

[a]Recorded at 60 MHz in $CDCl_3$ unless otherwise noted. The splitting constants are recorded in Hz.
[b]Assigned to the two protons —CH_2—OH.
[c]Recorded in DMSO-d_6.

traction were taken up in 1 ℓ of hot benzene and decanted from the residual sodium chloride. The benzene solution was reduced to 800 ml in volume by evaporation at reduced pressure. Following this, the solution was brought to reflux and 300 ml petroleum ether (60–90°C boiling range) added slowly. On cooling white plates crystallized out of solution to give 230 g (68%) pure dibenzyl ether, mp 127.5–128°C (lit. (6) mp 128–129°C).

(*B*) To a suspension of 38.7 g dibenzyl ether **2** (0.1145 mol) in 400 ml glacial acetic acid at 18°C was added 39 ml concentrated nitric acid (sg = 1.42 g/ml) dropwise over 15 min. The temperature was maintained below 20°C with ice cooling.

The solution was stirred 45 min, diluted to 1.5 ℓ with water, and extracted into methylene chloride (5 × 100 ml). The extracts were washed with water (4 × 100 ml), brine (2 × 100 ml), dried over sodium sulfate, filtered, and concentrated to give a yellow solid. The solid was triturated with 200 ml ether and 50 ml petroleum ether (30–60°C boiling range) and filtered to give 43.1 g (98%) of the desired 2-nitro-1,4-dibenzyloxy benzene **4**, mp 81–82.5°C; ir ($CHCl_3$): 1540, 1508, 1463, 1390, 1360 cm^{-1}. *Anal.* calcd. for $C_{20}H_{17}NO_4$: C 71.63, H 5.11, N 4.18; found: C 71.81, H 5.09, N 4.16.

2-Amino-1,4-dibenzyloxybenzene ***5***

Aluminum amalgam was prepared from 14.0 g aluminum foil according to Vogel (see ref. 2). The amalgam was layered with 150 ml tetrahydrofuran and 20.0 g nitro compound **3** (60 mmol) added in 450 ml THF. After an induction period of 20 min, a vigorous reflux ensued which abated somewhat after 30 min. The suspension was stirred an additional hour and filtered. The filtrate was dried over sodium sulfate, filtered, and evaporated to yield 16.6 g (93%) crystalline amine **5** as white plates, mp 101.5–102°C (on trituration with ether); ir ($CHCl_3$): 3460, 3380, 1670, 1680, 1520, 1460, 1387 cm^{-1}. *Anal.* calcd. for $C_{20}H_{19}NO_2$: C 78.66, H 6.27, N 4.59; found: C 78.76, H 6.27, N 4.64.

cis-N-(2′,5′-Dibenzyloxyphenyl)-3-azido-4-styryl-2-azetidinone ***7***

To 46.0 g (151 mmol) crystalline amine **5** dissolved in 500 ml methylene chloride was added 93.0 ml cinnamaldehyde. To this was added 50 g magnesium sulfate (not sodium sulfate!) and the suspension was stirred 1.5 h at 25 °C. The suspension was filtered and the filtrate was evaporated. To the oil was added 1 ℓ petroleum ether (30–60°C) with vigorous stirring in two portions. The layers were separated and the petroleum ether fraction set aside for recovery of the excess cinnamaldehyde. The residue was slurried with petroleum ether (500 ml) which induced crystallization. The suspension was filtered and following pressing of the filter cake it was washed once with 50 ml of petroleum ether – ether (4:1). Pure crystalline Schiff base **6** (45.4 g) was obtained. An additional 5.1 g was obtained from the mother liquors. The combined yield was 80%.

To a solution of 23.5 g (0.0505 mol) of Schiff base **6** in 200 ml dry methylene chloride at −10°C was added 7 ml triethylamine (0.096 mol). To this was added a solution of 6.0 g (0.0504 mol) azidoacetyl chloride in 100 ml methylene chloride dropwise over 30 min. The solution was allowed to come to 25°C over 30 min and evaporated. The residue was taken up in methylene chloride – ether, washed with water (3 × 100 ml), dried over sodium sulfate, and evaporated. The residual oil was taken up in 250 ml benzene and filtered through a pad of silica gel (activity III, 200 g). The residue after evaporation of the filtrate was triturated with 50–100 ml of ether and filtered to give 17.0 g (63.5%) pure **7**, mp 105–106°C. The mother liquors from trituration were chromatographed on silica gel (100 g, activity III) with chloroform as eluent to yield an additional 1.71 g (6.4%) of **7**; ir ($CHCl_3$): 2110, 1760, 1595, 1515 cm^{-1}. *Anal.* calcd. for $C_{31}H_{26}N_4O_3$: C 74.09, H 5.21, N 11.15; found: C 74.28, H 5.29, N 11.13.

cis-N-(2′,5′-Dibenzyloxyphenyl)-3-azido-4-formyl-2-azetidinone ***8***

A solution of 275 mg (0.55 mmol) of **7** in 25 ml methylene chloride was cooled to −78°C in a dry ice – acetone bath and an excess of ozone bubbled in over 3 min. To the solution was added 1 ml dimethyl sulfide. The solution was evaporated to dryness and the residue taken up in 10 ml ether. On standing 18 h at room temperature, the aldehyde crystallized out. Filtration gave 140 mg tan crystals, mp 137–138°C (with decomposition); ir ($CHCl_3$): 2110, 1770, 1740 cm^{-1}. *Anal.* calcd. for $C_{24}H_{20}N_2O_4$: C 67.27, H 4.71, N 13.08; found: C 67.38, H 4.91, N 12.80.

cis-N-(2′,5′-Dibenzyloxyphenyl)-3-azido-4-hydroxymethyl-2-azetidinone ***9***

A solution of 5.38 g (10.7 mmol) of **7** in 50 ml methylene chloride – 2 ml methanol was ozonized at −78°C (excess of ozone). The solution was evaporated to dryness and the residual oil taken up in 100 ml ethanol and cooled to 0–5°C in an ice bath. To this was added 400 mg sodium borohydride. The solution was stirred for 1 h. To the solution was added 10 ml 10% hydrochloric acid. The solution was evaporated to dryness and the residue partitioned between water and methylene chloride. The organic layer was dried over sodium sulfate, filtered, and passed through a pad of silica gel (activity III, 25 g). The filtrate was evaporated and the residual oil triturated with 10 ml ether. Filtration gave 3.0 g (65%) crystalline alcohol, mp 114–115°C, recrystallized from benzene – petroleum ether; ir ($CHCl_3$): 2115, 1760 cm^{-1}. *Anal.* calcd. for $C_{24}H_{22}N_4O_4$: C 66.96, H 5.15, N 13.02; found: C 67.09, H 5.16, N 12.90.

cis-N-(2′,5′-Dibenzyloxyphenyl)-3-amino-4-hydroxymethyl-2-azetidinone ***10***

To a solution of 430 mg (1.0 mmol) azide **9** in 20 ml methylene chloride was added 0.20 ml triethylamine. Hydrogen sulfide gas was passed through this solution for 2 min and a vigorous gas evolution was observed. The orange solution was let stand for 20 min (gas evolution ceased) and then was evaporated to dryness at reduced pressure. The residue was taken up in 50 ml of methylene chloride and washed with water (1 × 50 ml) then brine (2 × 50 ml). The organic layer was dried over sodium sulfate, filtered, and evaporated to yield 370 mg (91.5%) solid amine on trituration with ether, mp 136–137°C; ir ($CHCl_3$): 3400, 1750 cm^{-1}. *Anal.* calcd. for $C_{24}H_{24}N_2O_4$: C 71.27, H 5.98, N 6.93; found: C 70.78, H 6.01, N 6.65.

cis-N-(2′,5′-Dibenzyloxyphenyl)-3-phenoxyacetamido-4-hydroxymethyl-2-azetidinone ***11***

To 370 mg (0.915 mmol) amine **10** in 20 ml methylene chloride was added 139 mg (0.915 mmol) phenoxyacetic acid followed by 226 mg (0.915 mmol) EEDQ. The solu-

tion was let stand for 2 h at 25°C following which it was washed with 10% hydrochloric acid (10 ml), saturated sodium bicarbonate (10 ml), and brine (25 ml). The organic layer was dried over sodium sulfate, filtered, and passed through a pad of silica gel (activity III, 5 g). The solution was evaporated and the residue triturated with ether. Filtration gave 320 mg (65%) of **11**, mp 155–156°C, recrystallized from benzene; ir ($CHCl_3$): 3380, 1760, 1685, 1600, 1520, 1500 cm^{-1}. *Anal.* calcd. for $C_{32}H_{30}N_2O_6$: C 71.36, H 5.61, N 5.20; found: C 71.20, H 5.58, N 5.07.

cis-N-(2′,5′-Dibenzyloxyphenyl)-3-phenoxyacetamido-4-mesyloxymethyl-2-azetidone ***12***

To 2.45 g alcohol **11** (4.55 mmol) in 100 ml methylene chloride was added 0.75 ml TEA. To this 0.40 ml (5.0 mmol) mesyl chloride was added. The solution was allowed to stand 18 h at 25°C. The solution was washed with 10% hydrochloric acid, saturated sodium bicarbonate, and brine. It was dried over sodium sulfate, filtered, and evaporated. The residue was triturated with 15 ml ether and the resulting crystals filtered to yield 2.30 g (82%) of **12**, mp 125–126°C after recrystallization from ethanol; ir ($CHCl_3$): 3420, 1760, 1690, 1600, 1520, 1500 cm^{-1}. *Anal.* calcd. for $C_{33}H_{32}N_2O_8S \cdot H_2O$: C 62.44, H 5.39, N 4.42, S 5.05; found: C 62.10, H 5.04, N 4.35, S 4.80.

cis-N-(2′,5′-Dihydroxyphenyl)-3-phenoxyacetamido-4-mesyloxymethyl-2-azetidinone ***13***

A suspension of 1.70 g (2.76 mmol) dibenzyl ether **12** and 0.50 g 20% Pd $(OH)_2$/C in 50 ml acetic acid was hydrogenated at 25°C and atmospheric pressure for 1 h. The suspension was filtered and evaporated. The residual gum was triturated with ethyl acetate and the crystals filtered to give 0.94 g (78%) of the desired material **13**, mp 155–156°C (with decomposition). *Anal.* calcd. for $C_{19}H_{20}N_2O_8S$: C 52.28, H 4.62, N 6.42, S 7.35; found: C 52.23, H 4.76, N 6.68, S 7.24.

7-β-Phenoxyacetamido-4′-hydroxybenzo[3,4]-O-2-isocephem ***14***

To a solution of 436 mg (1 mmol) of **13** in 5 ml dry dimethyl sulfoxide at 25°C was added 124 mg (1 mmol) 1,5-diazobicyclo[4.3.0]non-5-ene in 1 ml dimethyl sulfoxide. The solution was stirred 1.5 h and diluted to 50 ml with water. The solution was extracted into methylene chloride. The organic phase was washed with brine and dried over sodium sulfate. The residue obtained on evaporation was chromatographed on 5 g silica gel (activity III) using methylene chloride as eluent followed by acetonitrile. The desired material eluted in the methylene chloride fraction. The residue on evaporation was recrystallized from acetonitrile–ether to give 160 mg (47%) of **14**, mp 212–213°C; ir (CH_3CN): 3380, 1780, 1695, 1604, 1540, 1515 cm^{-1}. *Anal.* calcd. for $C_{18}H_{16}N_2O_5$: C 63.52, H 4.73, N 8.23; found: C 63.37, H 4.79, N 8.24.

Acknowledgements

Partial financial support of this work by the National Research Council of Canada through its Industrial Research Assistance Plan is gratefully acknowledged. We also thank Dr. Bernard Belleau of McGill University for helpful discussions during the course of this work.

1. T. W. Doyle, A. Martel, and B.-y. Luh, Can. J. Chem. **55**, 2708 (1977).
2. T. W. Doyle, B. Belleau, B.-y. Luh, C. F. Ferrari, and M. P. Cunningham, Can. J. Chem. **55**, 468 (1977).
3. H. Burton and P. F. G. Praill. J. Chem. Soc. 522 (1951).
4. (*a*) D. A. Nelson. Tetrahedron Lett. 2543 (1970); (*b*) J. Decazes, J. L. Luche, and H. B. Kagan. Tetrahedron Lett. 3661 (1970); (*c*) K. D. Barrow and T. M. Spotswood. Tetrahedron Lett. 3325 (1965).
5. B. Belleau and G. Malek. J. Am. Chem. Soc. **90** 1651 (1968).
6. J. Druey. Bull. Soc. Chim. Fr. **2**, 1737 (1935).

Nuclear analogs of β-lactam antibiotics. VI. Synthesis of *N*-2-isocephems[1]

TERRENCE WILLIAM DOYLE,[2] BING-YU LUH, DANIEL TIM-WU CHU,[3] AND BERNARD BELLEAU

Bristol Laboratories of Canada, 100 Industrial Boulevard, Candiac, P.Q., Canada J5R 1J1

Received February 16, 1977

TERRENCE WILLIAM DOYLE, BING-YU LUH, DANIEL TIM-WU CHU, and BERNARD BELLEAU. Can. J. Chem. **55**, 2719 (1977).

The syntheses of *N*-methyl and *N*-carboethoxy-7-β-phenoxyacetamido-Δ^3-*N*-2-isocephem-4-carboxylic acids **17***a* and **17***b* are reported. Treatment of aldehyde **3***c* with methylamine followed by reduction of the Schiff base gave **4***d* which was converted to its trifluoroacetamide **5***c*. Acid catalyzed elimination of a mole of ethanol from **5***c*, gave **8***b* which was converted to the enol **10***b* via the vinylogous pyrrolidino amide **9***b*. Reductive removal of the trifluoroacetamide function led to spontaneous ring closure to give **11***b*. Alternatively treatment of bis-mesylate **12***b* with ammonia or methylamine gave **13***a* and **13***b*, respectively. Treatment of **13***b* with sodium hydride in DMSO gave **11***b*. Attempted acylation of **13***a* gave **14**. Reduction of the azido functions in **11***b* and **14** followed by coupling of the amines to phenoxyacetic acid and reductive removal of the benzyl esters gave **17***a* and **17***b*, respectively. The structural assignments are discussed.

TERRENCE WILLIAM DOYLE, BING-YU LUH, DANIEL TIM-WU CHU et BERNARD BELLEAU. Can. J. Chem. **55**, 2719 (1977).

On rapporte la synthèse des acides *N*-méthyl et *N*-carboéthoxy phénoxyacétamido-7 β Δ^3 isocéphem-*N*-2 carboxyliques-4 **17***a* et **17***b*. Le traitement de l'aldéhyde **3***c* avec la méthylamine, suivi par une réduction de la base de Schiff, donne **4***d* qui est transformé en trifluoroacétamide **5***c*. L'élimination acido-catalysée d'une mole d'éthanol de **5***c* donne **8***b* qui est transformé en énol **10***b* par l'intermédiaire de la pyrrolidino amide vinylogue **9***b*. L'enlèvement réducteur de la fonction trifluoroacétamide conduit à la fermeture spontanée de cycle pour donner **11***b*. On peut aussi traiter le bis-mésylate **12***b* avec de l'ammoniac ou de la méthylamine pour obtenir respectivement **13***a* et **13***b*. Le traitement de **13***b* avec de l'hydrure de sodium dans le DMSO donne **11***b*. Lorsque l'on à essayé d'acyler **13***a*, on a obtenu **14**. Les réductions des fonctions azido de **11***b* et **14** suivi par un couplage des amines avec l'acide de phénoxyacétique et l'enlèvement réducteur des groupes benzyles, conduisent respectivement à **17***a* et **17***b*. On discute des attributions de structures.

[Traduit par le journal]

The preceding papers of this series have described the preparation by total synthesis of a number of *O*-2-isocephem systems (1, 2).[4] The high level of antibiotic activity in these systems encouraged us to explore the extension of this work to other systems in which the oxygen atom is replaced by another heteroatom. In this paper we wish to report the synthesis of the *N*-2-isocephem systems **1***h* and **1***i* (Fig. 1).

Our first approach to the syntheses of these compounds involved conversion of the aldehydes **3***a–c* (2*a*, *b*) to the appropriate 4-aminomethyl-2-azetidinones **4** followed by ring closure of these

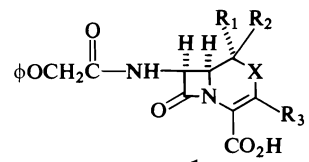

1

	R_1	R_2	R_3	X
a	H	H	H	O
b	H	H	CH_3	O
c	H	H	$CH_2\phi$	O
d	H	H	$(CH_2)_2\phi$	O
e	CH_3	H	CH_3	O
f	H	CH_3	CH_3	O
g	—O—		CH_3	O
h	H	H	H	N—CH_3
i	H	H	H	N—CO_2Et

FIGURE 1

derivatives to the desired compounds. Thus treatment of **3***a* with aniline to form the Schiff base **3***d* followed by reduction of the imine with sodium borohydride gave the amine **4***a* in 49.5% yield. Similarly, treatment of **3***a* with benzyla-

[1]For part V of this series see ref. 1.

[2]Author to whom correspondence concerning this paper should be addressed. c/o Bristol Laboratories, P.O. Box 657, Syracuse, NY, U.S.A. 13201.

[3]Holder of an NRCC Industrial Postdoctoral Fellowship 1971–1972.

[4]For an explanation of the trivial nomenclature used throughout this series and a resume of the literature on nuclear analogs of β-lactam antibiotics see ref. 2*a*.

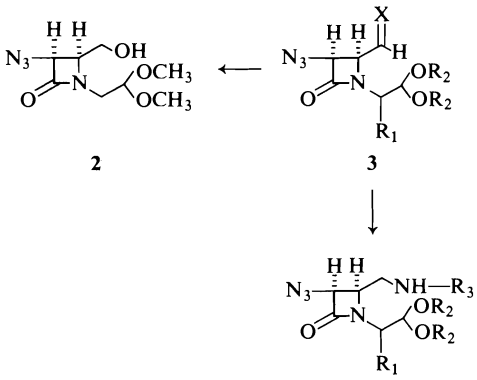

	R_1	R_2	R_3	X
3*a*	H	Me	—	O
b	CO_2Et	Et	—	O
c	CO_2Bz	Et	—	O
d	H	Me	ϕ	NR_3
e	H	Me	$CH_2\phi$	NR_3
f	CO_2Et	Et	Me	NR_3
g	CO_2Bz	Et	Me	NR_3
4*a*	H	Me	ϕ	—
b	H	Me	$CH_2\phi$	—
c	CO_2Et	Et	Me	—
d	CO_2Bz	Et	Me	—

SCHEME 1

mine followed by reduction gave **4***b* in 55.5% yield. Attempts to prepare the primary amine (R_3 = H) via displacement of the mesylate or tosylates of **2** with azide ion followed by reduction failed.

A number of attempts were made to convert compounds **4***a* and **4***b* to the cyclic enamines **7** by direct hydrolysis of the acetal followed by ring closure. In the case of **4***a* either complete decomposition of starting material occurred with no isolable product being produced or the starting material was recovered unchanged. Treatment of **4***b* with 70% trifluoroacetic acid gave a new product in approximately 10% yield which proved to be very unstable. Attempts to improve the yield or to isolate the material in a pure state led to extensive decomposition. We have tentatively assigned structure **7** to this material based on its ir and nmr spectra. The ir spectrum of **7** showed bands at 2110, 1755, and a weak band at 1620 cm^{-1}. The nmr spectrum of **7** (Table 1) showed the proton α to the azide as a doublet (J = 5.0 Hz). If rupture of the β-lactam had occurred the coupling constant for this proton as well as its chemical shift would be expected to be considerably different. In addition the appearance of a pair of protons in the olefinic region as doublets (J = 6.0 Hz) with loss of the signals in **4***b* for the $CH_2CH(OCH_3)_2$ side chain and a shift of the signal of the benzyl group to lower field are all supportive of the assignment of structure **7** to the compound.

In view of the low yield of **7** from **4***b* an attempt to prepare **7** via an alternate sequence was made. Treatment of **4***b* with trifluoroacetic anhydride gave the trifluoroacetamide **5***a* in 84% yield. Hydrolysis of **5***a* using 90% trifluoroacetic acid gave the aldehyde **6** which proved to be rather unstable. Attempts to prepare **7** via base catalyzed hydrolysis of the trifluoroacetamide in **6** with concommitant ring closure gave only tars. Attempts to introduce functionality at C_4 via enamine condensation reactions of **7** led only to decomposition of **7** with no isolable product being formed.[5] Consequently, this approach was abandoned.

Our second approach was to start with the eventual 4-carboxyl group incorporated into the nitrogen side chain of the azetidinone. As in the case of **4***a* and **4***b* the desired amines **4***c* and **4***d* were prepared via the aldehydes **3***b* and **3***c* (*2a*, *b*). Thus condensation of either **3***b* or **3***c* with methylamine followed by reduction of the Schiff

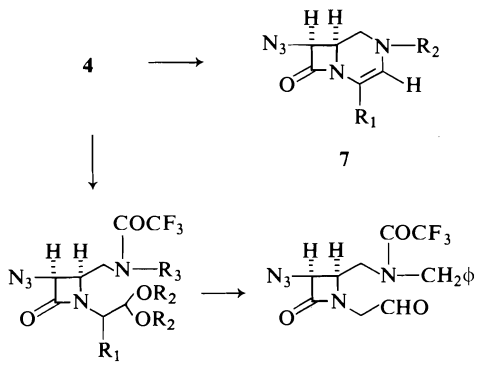

	R_1	R_2	R_3
5*a*	H	Me	$CH_2\phi$
b	CO_2Et	Et	Me
c	CO_2Bz	Et	Me
7	H	$CH_2\phi$	—

SCHEME 2

bases **3***f* or **3***g* with sodium borohydride gave **4***c* or **4***d* in 59 and 43% yield, respectively.

Treatment of **4***c* with a suspension of zinc chloride in trifluoroacetic anhydride gave the

[5] *e.g.* The condensation of crude **7** with ethyl chloroformate failed to give any of the 4-carboethoxy-*N*-2-isocephem.

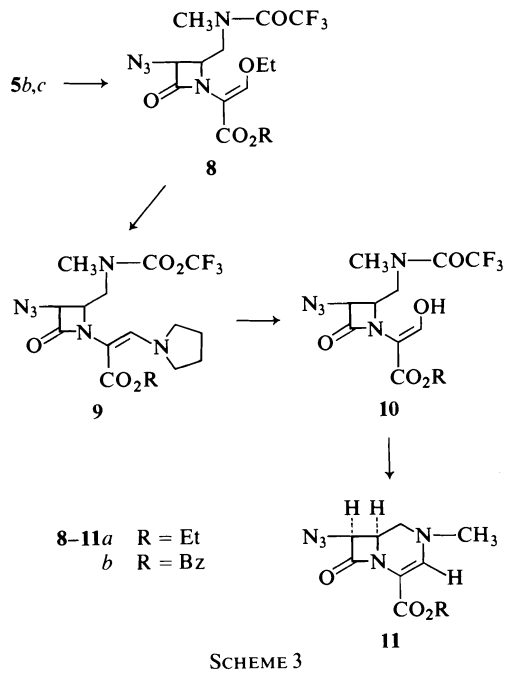

SCHEME 3

amide **8***a* presumably via the acetal **5***b*. The yield of **8***a* from **4***c* was 66.5%. On treatment of **4***d* with zinc chloride – trifluoroacetic anhydride the reaction stopped at the intermediate stage giving **5***c* in 82.5% yield. Prolonged reaction times gave **8***b* from **5***c* in 76% yield.

Our earlier work (2*b*) had shown that the β-ethoxy acrylate system in compounds similar to **8** could be readily converted to the β-hydroxy acrylates via the pyrrolidine derivatives. Thus treatment of **8***a* with pyrrolidine acetate in refluxing benzene gave **9***a* in 97% yield. Similarly **8***b* was converted to **9***b* in 90% yield. Hydrolysis of **9***a* with acetone – 10% hydrochloric acid gave the enol **10***a* in 60% yield. Attempted removal of the *N*-trifluoroacetyl group using the methods of Newman and Wolfrom and Bhat (3) failed, the starting material being recovered unchanged. Accordingly the reductive cleavage of the *N*-trifluoroacetyl group with sodium borohydride according to Weygand was used (4). Treatment of **10***a* with sodium borohydride in ethanol gave **11***a* upon work-up. Similarly hydrolysis of **9***b* to **10***b* (53%) followed by reductive cleavage of the amide gave **11***b*. The yield in this latter case was only 14% and could not be improved upon.

In view of the poor yield of **11***b* and our desire to prepare an analog of **11***b* unsubstituted on the nitrogen atom a third approach to the synthesis of these molecules was made (Scheme 4).

We had available to us a number of useful intermediates from our earlier work (2*b*). The enol mesylate **12***c* was converted to the bismesylate **12***b* in 81% yield by treatment with mesyl chloride and triethylamine. Alternatively **12***b* could be prepared in 80% yield from the diol **12***a* by the same procedure. Treatment of **12***b* with ammonia in dimethyl sulfoxide gave the amine **13***a* in 92% yield. Alternatively compound **13***a* could be prepared from **12***d* (2*b*) by treatment with ammonium acetate in chloroform in 57% yield. The nmr spectrum of **13***a* indicated it to consist of a single isomer the geometry of which has not been determined. Treatment of **12***d* with monomethyl ammonium acetate in benzene gave **13***b* in 81% yield as a mixture of geometrical isomers in the ratio of ~1:1. The isomers were separated by silica gel chromatography. We have tentatively made assignments to each of these isomers on the basis of their spectral characteristics. A comparison of the positions of the vinyl and amino protons between **13***a* and isomer 2 of **13***b* indicate that these compounds very likely have the same configuration.[6] We have assigned the configurations shown in Fig. 2 to each of these isomers of **13***b* on the basis of the following evidence. In the nmr spectra of isomer 1 the vinyl proton appears at δ 6.96 while the nitrogen proton is at δ 7.69. In contrast the vinyl protons of **13***b* isomer 2 and **13***a* appear at δ 7.40 and 7.54, respectively, while the nitrogen protons appear at δ 5.68 and 5.52 respectively. One would predict that the vinyl proton in the *Z* configuration would appear at higher field than that in the *E* configuration. In addition, one would also predict that the nitrogen protons in the *Z* configuration would appear at lower field than those in the *E* configuration (5). Thus, compounds **13***a* and **13***b* isomer 2 are assigned the *E* configuration while **13***b* isomer 1 is assigned the *Z* configuration. The ir spectra of compounds **13***a* and the 2 isomers of **13***b* support this assignment. While **13***a* and isomer 2 of **13***b* show both free and hydrogen bonded NH bands (at 3500 and 3330 cm^{-1} for **13***a* and at 3415 and 3335 cm^{-1} for isomer 2 of **13***b*) isomer 1 of **13***b* exhibited only hydrogen bonded NH bands in the ir (at 3340 cm^{-1}).

[6]The terms isomer 1 and isomer 2 with reference to **13***b* indicate their order of elution from a silica gel column.

TABLE 1. Nuclear magnetic resonance spectra[a]

Compd.	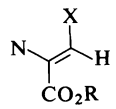	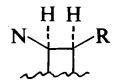		CH_3	$CH_2\phi$	Other
4*a*	6.75(m, 3H) 7.30(m, 2H)	4.75(d) J=5.0	4.02(m)	3.40(s, 6H)		4.44(t, 1H, J=5.0)[b] 3.58(dd, 1H, J_1=16, J_2=4.7)[c] 3.18(dd, 1H, J_1=16, J_2=5.5)[c] ~3.40(m, 2H)[d] 4.10(s, 1H, N*H*)
4*b*	7.40(s, 5H)	4.73(d) J=5.0	3.92(m)	3.38(s, 6H)	3.85(s)	2.92(d, 2H, J=6.0)[e] 4.50(t, 1H, J=5.0)[b] 3.56(dd, 1H, J_1=15, J_2=5.0)[c] 3.18(dd, 1H, J_1=15, J_2=5.5)[c] 1.80(s, 1H, N*H*)
4*c*[f]		4.87(d) 4.91(d) J=5.0		2.43(s, 3H)[j] 1.20(m, 9H)		2.92, 2.95(d, 2H, J=5.0)[e] 3.58(m, 5H)[g] 4.19(q, 3H, J=7.0)[h] 4.62(m, 1H)[i] 1.55(s, 1H, NH)
4*d*[f]	7.28(s, 5H)	4.93(d) 4.89(d) J=5.0	4.14(m)	2.39(s)[j] 2.36(s)[j] 1.14(m, 6H)	5.14(s)	3.57(m, 5H)[g] 2.87(d, J=5.5)[e] 4.61, 4.64(d, 1H, J=5.0)[i] 1.60(s, 1H, N*H*)
5*a*	7.42(m, 5H)	4.75(d) J=5.0	4.17(dt) J_1=7.0 J_2=5.0	3.39(s) 3.43(s)	4.82(s)	3.50(m, 2H)[d] 3.82(dd, 1H, J_1=15, J_2=4.5)[c] 3.10(dd, 1H, J_1=15, J_2=5.0)[c] 4.54(t, 1H, J=5.0)[b]
7	7.40(s, 5H)	5.08(d) J=5.0	3.70(m)[k]		4.18(s)	3.20(m, 2H)[k] 6.00(d, 1H, J=6.0)[l] 5.77(d, 1H, J=6.0)[l]
8*a*	7.60(s, 1H)[m]	5.0(d) J=5.0	4.62(m)	3.21(s)[j] 3.23(s)[j] 1.3(t, J=7) 1.4(t, J=7)		4.27(q, 4H, J=7.0)[n] 3.80(m, 2H)[e]
8*b*	7.42(s, 5H) 7.53(s, 1H)[m]	4.88(d) J=5.4	4.55(m)	1.37(t, J=7.0) 3.10(m, 3H)[j]	5.22(s)	3.70(m, 2H)[e] 4.20(q, 2H, J=7.0)[o]
9*a*	7.50(bs)	4.83(d) J=5	~4.6(m)	1.20(t, J=7.0) 3.08(bs, 3H)[j]		1.85(m, 4H, ) 3.45(m, 6H,  + CH_2N) 4.08(q, 2H, J=7.0)
9*b*	7.60(bs, 1H) 7.34(s, 5H)	4.80(m)	4.50(m)	3.0(bs, 3H)[j]	5.14(s)	3.5 (m, 8H, ) 1.95
10*a*[p]	7.40(s) 7.43(s)	4.90(m)	4.50(m)	1.26, 1.31 (t, J=7.0) 3.14(m, 3H)[j]		4.14, 4.27(q, 2H, J=7.0) 3.70(m, 2H)[e]
10*b*[p]	7.65, 7.53 (s, 1H) 7.42(s, 5H	4.90(m)	4.50(m)	3.15(m, 3H)[j]	5.20, 5.30(s)	3.75(m, 2H)[e]
11*a*	6.99(s, 1H)	5.10(d) J=5.0		3.04(s)[j] 1.26(t, J=7.0)		4.17(q, 2H, J=7.0) 3.60(m, 1H) 3.27(m, 2H)
11*b*	7.33(s, 5H) 7.07(s, 1H)	5.10(d) J=5.0		3.02(s)	5.20(s)	3.57(m, 1H) 3.23(m, 2H)

TABLE 1 (*Concluded*)

Compd.	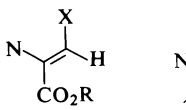	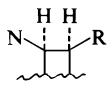		CH_3	$CH_2\phi$	Other
12*b*	7.52(s, 5H) 7.95(s, 1H)	5.04(d) J=5.0		2.96(s) 3.32(s)	5.34(s)	4.50(m, 3H, $CHCH_2OSO_2Me$)
13*a*	7.41(s, 5H) 7.54(t, 1H) J=12.0	4.96(d) J=5.0		3.0(s, 3H)	5.17(s)	5.52(d, 2H, J=12.0, NH_2) 4.45(m, 3H, $CHCH_2OMes$)
13*b* isomer 1	7.33(s, 5H) 6.96(d, 1H) J=14.5	4.76(d) J=5.0		2.92(s) 2.94(d)[j] J=6.0	5.14(s)	7.69(m, 1H, N*H*) 4.3(m, 3H)
13*b* isomer 2	7.38(s, 5H) 7.40(d, 1H) J=13.0	4.93(d) J=5.0		2.97(s) 2.97(d) J=7.5	5.17(s)	4.40(m, 3H) 5.68(m, 1H, N*H*)
14	7.38(s, 5H) 7.78(s, 1HO)	5.18(d) J=5.0	3.69(ddd) J_1=10.0 J_2=5.0 J_3=3.5	1.33(t) J=7.0	5.26(s)	4.30(q, 2H, J=7.0) 4.51(dd, 1H, J_1=13.0, J_2=3.5) 3.14(dd, 1H, J_1=13.0, J_2=10.0)
16*a*	6.7–7.7(m, 11H)	5.43(dd) J_1=5.0 J_2=7.0	3.67(m)	2.85(s)	5.0(d) 5.26(d) J=13.0	8.10(d, 1H, J=7.0, N*H*) 4.28(q, 2H, ϕOCH_2) 3.05(m, 2H)
16*b*	7.40(s, 5H) 6.7–7.4(m, 5H) 7.77(s, 1H)	5.53(dd) J_1=5.0 J_2=7.0	3.85(m)	1.32(t) J=7.0	5.28(s)	4.52(s, 2H, ϕOCH_2) 4.28(q, 2H, J=7.0) 8.15(d, 1H, J=7.0, N*H*) 3.0(dd, 1H, J_1=13.0, J_2=10.0) ~3.5(m, 1H) obsc.
17*b*	6.7–7.4(m, 5H) 7.70(s, 1H)	5.50(m)	3.75(m)	1.30(t) J=7.0		4.48(s, 2H, ϕOCH_2) 4.23(q, 2H, J=7.0) 3.0(m, 1H)

[a]Spectra were recorded at 60 MHz in $CDCl_3$ unless otherwise noted. [b]$CH(OCH_3)_2$. [c]Arms of AB quartet for CH_2—$CH(OR)_2$. Partially obscured by O*Me*. [d]Obscured, assigned CH_2—N—ϕ. [e]CH_2—N—R. [f]Mixture of diastereoisomers. [g]$CH(OCH_2CH_3)$ + $CHCO_2R$. [h]CO_2CH_2-CH_3 + CH—CH—N_3. [i]$CH(OEt)_2$. [j]N—CH_3. [k]Assigned to CH—CH_2—N. [l]Assigned to  [m]Assigned to . [n]Assigned to —$C(CO_2Et)$=CHOEt. [o]Assigned to =$CHOCH_2$—CH_3. [p]Two isomers.

Treatment of **13***b* (as a 1:1 mixture of isomers) with sodium hydride in dimethyl sulfoxide gave **11***b* in 7.65% yield after chromatography. In a second experiment the yield was 16.7%. The material obtained by this method was identical in all respects with that obtained earlier. All attempts to improve the yields beyond the low levels reported failed. An attempt to ring close **13***a* to give the corresponding *N*-demethyl *N*-2-isocephems also failed.

In order to increase the acidity of the NH bond and presumably improve the chances of obtaining the ring closure an attempt was made to acylate **13***a* with ethyl chloroformate and triethylamine in chloroform. The only isolable product proved to be the *N*-carboethoxy *N*-2-isocephem **14** which was formed in 26.8% yield.

Presumably compound **14** arose via formation of the intermediate urethane and subsequent ring closure of this urethane to **14** (Fig. 3). Attempts to isolate the intermediate have failed.

The structures of compounds **11***a*, **11***b*, and **14** were assigned on the basis of their mode of preparation, elemental analyses, and spectral characteristics. Formation of **11***b* from both **10***b* and **13***b*, the shift of the proton α to the azido group from δ ~4.90 to 5.10, and the bathochromic shift in the uv from 280 to 307 nm on ring closure establish the structure of **11***b* as benzyl *N*-methyl-7-β-azido-*N*-2-isocephem-4-carboxylate. Earlier we have shown in the case of the *O*-2-isocephems that ring closure invariably led to a shift of from 20–50 Hz to lower field for the proton α to the azido function (2*d*).

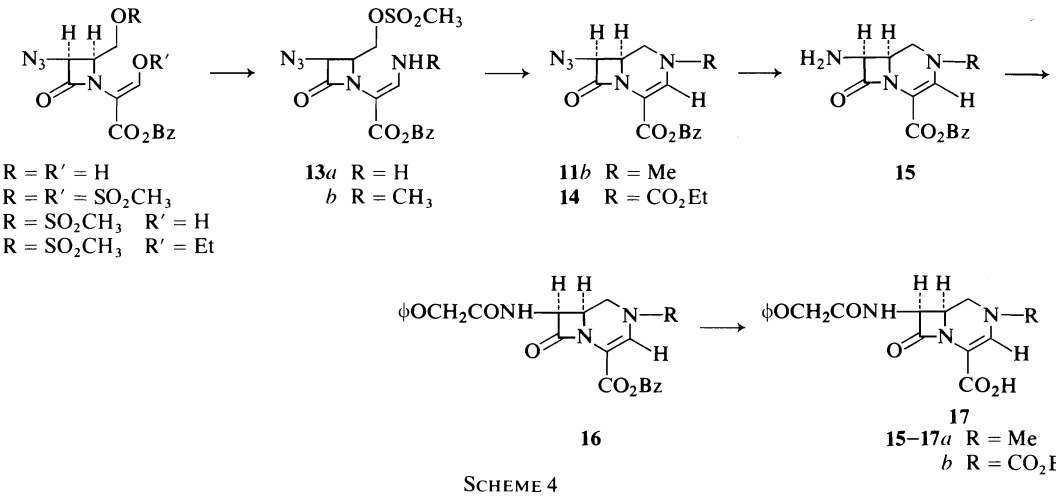

12*a* R = R′ = H
b R = R′ = SO_2CH_3
c R = SO_2CH_3 R′ = H
d R = SO_2CH_3 R′ = Et

13*a* R = H
b R = CH_3

11*b* R = Me
14 R = CO_2Et

15

16

17
15–17*a* R = Me
b R = CO_2Et

SCHEME 4

Similarly ring closure leads to a bathochromic shift of ~30 nm in the *O*-2-isocephem series (2*b*). While the nmr spectra of **11***a* and **11***b* do not permit a conformational assignment to the *N*-2-isocephem ring system (due to overlap of the C_1 and C_6 protons), the nmr spectrum of **14** was first order and permits one to assign the 'A'

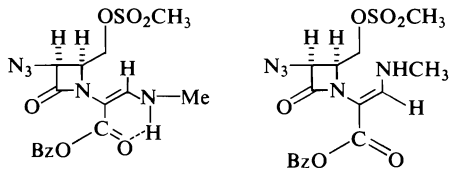

Z configuration *E* configuration

13*b*

FIGURE 2

conformation to this molecule (Fig. 4). The pattern of coupling constants for $C_{1\alpha}$, and $C_{1\beta}$ and C_6 protons (Table 1) is consistent with that predicted from the Karplus relationship for conformer A (6).[7]

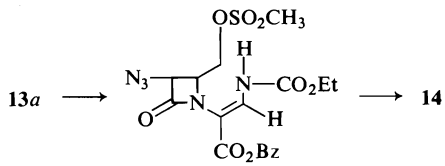

FIGURE 3

The conversion of **11***b* to the appropriately substituted cephalosporin analog was carried out in the following manner. Reduction of the azido group in **11***b* was accomplished using 10% palladium-on-carbon as catalyst. This gave **15***a* in 76% yield. The amine was converted to the phenoxyacetamide **16***a* using *N*-ethoxycarbonyl-2-ethoxy-1,2-dihydroquinoline (EEDG) and phenoxyacetic acid in 60.5% yield. On reduction of **16***a* with 20% palladium hydroxide on carbon there was obtained a 36% yield of **17***a* as an unstable solid. The spectral characteristics of **17***a* were in accord with the assigned structure. Attempts to purify **17***a* led to decomposition The sample was screened for antibiotic activity as such even though it was estimated (by the extinction coefficient of the band at 308 nm) to be only 30–40% pure. The compound exhibited only a low order of antibiotic activity.

The conversion of **14** to **17***b* was carried out analogously. Thus reduction of the azide gave **15***b* in 90% yield. Coupling of **15***b* with phenoxyacetic acid using EEDQ gave the amide **16***b* as an oil in 37% yield after chromatography. Reduction of **16***b* using 20% palladium hydroxide on carbon gave **17***b* as a solid in 58% yield. Compound **17***b* proved to be relatively stable, nevertheless attempts to recrystallize **17***b* to obtain a sharp melting solid failed. The ir, nmr, and uv spectra of **17***b* were in accord with the assigned structure. Compound **17***b* was active as an antibiotic. Details of the antibiotic spectrum will be published separately.

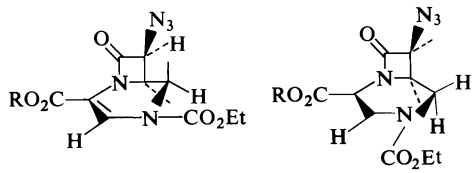

A B

FIGURE 4

[7]For a detailed assignment in the case of the *O*-2-isocephem systems see refs. 2*b* and 2*c*.

The instability of compounds **17***a* and **17***b* (to a lesser extent) may be due to a greater tendency towards decarboxylation inasmuch as these compounds are vinylogous carbamates.

Experimental

The infrared spectra were recorded on a Unicam SP-200G grating, ir spectrometer. The nmr spectra were determined on a Varian A60-A spectrometer using tetramethylsilane as an internal standard. Melting points are uncorrected and were determined on a Gallenkamp melting point apparatus. The analyses were performed by Micro-Tech Laboratories, Skokie, IL.

cis-N-(β,β-Dimethoxyethyl)-3-azido-4-anilinomethyl-2-azetidinone **4***a*

To a solution of 400 mg (1.75 mmol) of **3***a* in 20 ml benzene was added 0.5 ml of aniline. The solution was boiled at reflux and the water formed in the reaction was collected in a Dean–Stark trap. After 2.5 h the solution was evaporated to dryness to yield **3***d* as an oil. The oil was taken up in 15 ml of dioxane and 200 mg sodium borohydride added at 15°C. The solution was stirred for 1 h and an aqueous ammonium chloride solution was added. The solution was partitioned between water and methylene chloride and the methylene chloride was dried over sodium sulfate. Evaporation of the organic extracts gave an oil which was chromatographed on 10 g alumina (activity III) with chloroform as eluent. There was obtained 287 mg (49.5%) of an oil which crystallized on standing, mp 54.5°C; ir ($CHCl_3$): 3420, 2120, 1765, 1601 cm^{-1}. *Anal.* calcd. for $C_{14}H_{19}N_5O_3$: C 55.07, H 6.27, N 22.94; found: C 55.13, H 6.30, N 23.02.

cis-N-(β,β-Dimethoxyethyl)-3-azido-4-benzylamino-methyl-2-azetidinone **4***b*

In a manner analogous to that given for **4***a* treatment of **3***a* (300 mg, 1.31 mmol) with benzylamine (0.30 ml) followed by reduction of the intermediate **3***e* with sodium borohydride (100 mg) gave 244 mg (55.5%) of **4***b* after chromatography; ir (neat): 2120, 1710 cm^{-1}. *Anal.* calcd. for $C_{15}H_{21}N_5O_3$: C 56.42, H 6.62, N 21.94; found: C 56.26, H 6.65, N 21.75.

Preparation of **5***a*

A solution of 82 mg (0.257 mmol) of **4***b* in 1.5 ml trifluoroacetic anhydride was let stand 15 min at room temperature. The excess trifluoroacetic anhydride was removed at reduced pressure to give 95 mg of crude amide. The amide was filtered through a pad of alumina (activity III) in CH_2Cl_2 and evaporated to yield 90 mg of **5***a* as an oil; ir ($CHCl_3$): 3520, 3420, 2120, 1780, 1770 1700 cm^{-1}. *Anal.* calcd. for $C_{17}H_{20}F_3N_5O_4$: C 49.17, H 4.85, N 16.86, F 13.72; found: C 48.68, H 4.71, N 16.73, F 13.82.

cis-N-(α-Carboethoxy-β,β-diethoxyethyl)-3-azido-4-methylaminomethyl-2-azetidinone **4***c*

A mixture of 11.5 g (34.6 mmol) of **3***b* and 120 mmol of anhydrous methylamine in 60 ml benzene was stirred 18 h over 10 g magnesium sulfate. The suspension was filtered and evaporated to dryness to yield 12.4 g of crude **3***f* as an oil.

The crude Schiff base was taken up in 50 ml absolute ethanol and 1.31 g sodium borohydride added. The solution was stirred for 0–5 h at 0.5°C followed by 0.5 h at 25°C. To this was added 10 ml 10% hydrochloric acid, following which the solvent was evaporated at reduced pressure. The oily aqueous residue was adjusted to pH 8 with sodium bicarbonate and extracted with chloroform (5 × 25 ml). The extracts were dried (sodium sulfate) and evaporated to give an oil which was chromatographed on 100 g alumina (activity III) using chloroform as the eluting solvent. A total of 7.1 g (59%) of the desired **4***c* was obtained as an oil; ir ($CHCl_3$): 2120, 1770 cm^{-1}. *Anal.* calcd. for $C_{14}H_{25}N_5O_5$: C 48.97, H 7.33, N 20.40; found: C 49.50, H 7.03, N 21.70.

cis-N-(α-Carbobenzoxy-β,β-diethoxy)-3-azido-4-methylaminomethyl-2-azetidinone **4***d*

A mixture of 4.0 g (10.02 mmol) crude compound **3***c* and 80 mmol anhydrous methylamine in 80 ml dry benzene was stirred with 10 g anhydrous magnesium sulfate at 25°C for 2 h. The drying agent was removed by filtration and the filtrate was evaporated to dryness to yield 4.0 g (98%) crude Schiff base, **3***g*. To a solution of 4.0 g (9.8 mmol) of **3***g* in 50 ml absolute ethanol at 0–5°C was added 500 mg (13.13 mmol) sodium borohydride. The solution was stirred 1 h and acidified to p*H* 4 with 10% HCl. The solution was then adjusted to p*H* 8 with saturated sodium bicarbonate and solid sodium chloride added to saturation. The solution was extracted with chloroform (3 × 30 ml). The chloroform extracts were washed with brine, dried over $MgSO_4$, filtered, and evaporated to give 3.7 g of an oil which was chromatographed on 80 g silica gel (15% water) with chloroform then chloroform – 5% methanol as eluent to yield 600 mg of pure amine **4***d* (15%); ir ($CHCl_3$): 2120, 1770 cm^{-1}. An additional 1.4 g of amine contaminated with an unidentified impurity was also obtained. This material contained ~80% of **4***d*. The total yield was 43%.

Preparation of **8***a*

A suspension of 2.45 g (7.4 mmol) of **4***c* and 1.2 g zinc chloride in 10 ml trifluoroacetic anhydride was refluxed for 1 h. The solvent was removed at reduced pressure and the residual oil taken up in chloroform (40 ml). The solution was washed with water (10 ml) and brine (3 × 20 ml) and the organic phase was dried (sodium sulfate) and evaporated. The residue was filtered through a pad of Florisil (5 g) and the filtrate (CH_2Cl_2 solution) evaporated to give 1.9 g (66.5%) of **8***a* as an oil; ir ($CHCl_3$): 2110, 1777, 1698, 1647 cm^{-1}.

Preparation of **8***b*

Upon treatment of 600 mg (1.46 mmol) of **4***d* with 0.245 g zinc chloride in 8 ml trifluoroacetic anhydride as in the above example there was obtained 618 mg (82.5%) of **5***c*; ir ($CHCl_3$): 2110, 1770, 1695 cm^{-1}.

The oil was taken up in 6 ml trifluoroacetic anhydride and treated with 310 mg zinc chloride for an additional 72 h at 25°C. Work-up as in the previous example and chromatography of the resultant oil gave 427 mg (76%) of **8***b* as an oil; ir ($CHCl_3$): 2120, 1780, 1700, 1645 cm^{-1}. *Anal.* calcd. for $C_{19}H_{20}F_3N_5O_5$: C 50.11, H 4.43, N 15.38; found: C 49.74, H 4.47, N 14.98.

Preparation of **9***a*

A solution of 1.45 g (3.75 mmol) of **8***a*, 293 mg (4.13 mmol) pyrrolidine and 248 mg (4.13 mmol) acetic acid in 30 ml benzene was refluxed for 18 h. The solution was washed with water (25 ml) and brine (25 ml) and dried over magnesium sulfate. On evaporation there

was obtained 1.50 g of **9***a* (97%) as an oil; ir ($CHCl_3$): 2400, 2110, 1770, 1695, 1630, 1610 cm^{-1}.

Preparation of ***9b***

A solution of 427 mg (0.93 mmol) compound **8***b*, 110 mg (1.5 mmol) pyrrolidine and 100 mg (1.5 mmol) glacial acetic acid was refluxed in 20 ml benzene for 18 h. The solvent was evaporated and the residue partitioned between chloroform (30 ml) – water (5 ml). The chloroform solution was washed with water (5 ml) and brine (5 ml), dried over Na_2SO_4, filtered, and evaporated to give an oil which was filtered through 3 g silica gel (15% water) with chloroform to yield 347 mg (90%) compound **9***b*; ir ($CHCl_3$): 2110, 1770, 1695, 1625 (s, 1612) cm^{-1}.

Ethyl N-Methyl-7-β-azido-Δ³-N-2-isocephem-4-carboxylate ***11a***

A solution of 1.50 g (3.65 mmol) of **9***a* in 10 ml acetone – 5 ml 10% hydrochloric acid was boiled at reflux for 15 min. The acetone was evaporated at reduced pressure and the oily aqueous residue extracted with chloroform (3 × 20 ml). The organic extracts were washed with water (20 ml) and brine (2 × 20 ml), dried over sodium sulfate, and evaporated. The residual oil was taken up in 30 ml of ether and the ethereal solution was extracted with saturated sodium bicarbonate solution (3 × 10 ml). The basic extracts were adjusted to p*H* 5 with 10% hydrochloric acid and extracted with chloroform (5 × 20 ml). The extracts were dried over magnesium sulfate, filtered, and evaporated to yield 788 mg (60%) of **10***a*; ir ($CHCl_3$): 2110, 1778, 1695, 1630(w) cm^{-1}.

To a solution of 447 mg (1.28 mmol) of **10***a* in 7 ml ethanol – 0.5 ml water was added 110 mg sodium borohydride at 25°C. The solution was warmed to 40–45°C for 1.5 h following which the p*H* was adjusted to 4 with 10% HCl to decompose the excess sodium borohydride. After 10 min, the solution was adjusted to p*H* 8 with sodium bicarbonate and diluted to 50 ml with brine. The solution was extracted with chloroform (4 × 10 ml). The extracts were dried over magnesium sulfate and evaporated to yield 247 mg of an oil which was chromatographed on 2 g of silica gel (15% water, w/w) using chloroform. There were obtained 120 mg (40%) of **11***a* as a crystalline solid, mp 147–148.5°C after recrystallization from chloroform–ether; ir ($CHCl_3$): 2110, 1778(s), 1768, 1690, 1680, 1618 cm^{-1}. *Anal.* calcd. for $C_{10}H_{13}N_5O_3$: C 47.80, H 5.22, N 27.88; found: C 47.71, H 5.17, N 28.13.

Benzyl N-Methyl-7-β-azido-Δ³-N-2-isocephem-4-carboxylate ***11b***

A solution of 347 mg (0.78 mmol) compound **9***b* was refluxed for 15 min in 3 ml acetone – 3 ml 10% HCl. The reaction mixture was treated with 20 ml salt solution and extracted with chloroform (3 × 15 ml). The chloroform layer was washed with water and evaporated to dryness. The residual oil was dissolved into 10 ml ethyl ether. The ethyl ether solution was then extracted with saturated sodium bicarbonate solution (4 × 5 ml). Finally, the bicarbonate extract was acidified to p*H* ~ 5 with 10% hydrochloric acid. Extracted with chloroform (3 × 10 ml), dried over $MgSO_4$, the drying agent was filtered off, and the filtrate was evaporated to dryness to yield 175 mg (0.41 mmol) (53%) of compound **10***b* as an oil; ir ($CHCl_3$): 2110, 1775, 1695, 1630(w) cm^{-1}. *Anal.* calcd. for $C_{17}H_{16}F_3N_5O_5 \cdot \frac{1}{2}H_2O$: C 46.79, H 3.93, N 16.05; found: C 46.56, H 3.82, N 15.63.

To 174 mg (0.41 mmol) of compound **10***b* in 4 ml ethanol – 0.25 ml water was added 60 mg (1.58 mmol) of sodium borohydride at 25°C with stirring. After 5 min, the solution was placed into a warm water bath (45–54°C) for 1 h. The solution was acidified with 10% HCl to p*H* ~ 4, rebasified with sodium bicarbonate to p*H* ~ 8, diluted with water (25 ml), and extracted with chloroform (3 × 10 ml). The chloroform layer was washed with water and brine, dried over magnesium sulfate, filtered, and evaporated to yield 18 mg crystalline material (14%).

The solid was recrystallized from ether–chloroform, mp 166–168°C; ir (CH_3Cl_3): 2115, 1775, 1695, 1615 cm^{-1}; uv (EtOH, 0.3 mg/12.5 ml) λ_{max} 307 nm (ε 12 850). *Anal.* calcd. for $C_{15}H_{15}N_5O_3$: C 57.50, H 4.83, N 22.35; found: C 57.40, H 4.95, N 22.21.

From ***13b***

A solution of 2.80 g (6.85 mmol) of **13***b* (as a mixture of isomers) in 10 ml dimethyl sulfoxide was added to a suspension of 165 mg sodium hydride (6.85 mmol). The solution was stirred at 25°C for 1 h at the end of which time all of the sodium hydride had reacted. The mixture was poured into a 1% hydrochloric acid solution (50 ml at 0°C) and the whole extracted with chloroform (3 × 30 ml). The extracts were washed with brine (50 ml) and dried over magnesium sulfate. The solvent was evaporated to yield a dark red oil which was chromatographed on 15 g of silica gel (15% water w/w) to yield 162 mg (7.65%) of **11***b* identical in all respects with that obtained from **10***b*. In another experiment on smaller scale, the yield was 16.7%.

Preparation of ***12b***

From ***12a***

To a solution of 2.40 g (7.55 mmol) of **12***a* in 50 ml of methylene chloride was added 3.14 ml triethylamine (22.65 mmol) at 0–5°C. To this was added 2.58 g (22.65 mmol) mesyl chloride in 5 ml methylene chloride over 10 min. The solution was stirred 20 min at 25°C. The solution was diluted to 150 ml with ether and washed with 10% hydrochloric acid and brine. The solution was dried over sodium sulfate and evaporated. The residual oil was chromatographed on silica gel (15% water w/w) (50 g) using benzene (200 ml) then ether as eluent. The ethereal fractions from the column contained 2.85 g (80%) of **12***b* as a mixture of two isomers; ir (film): 2110, 1780, 1620, 1640 cm^{-1}; uv (EtOH, 7.0 mg/50 ml) λ_{max} 242 nm (ε 6300).

From ***12c***

Treatment of 13.37 g (33.7 mmol) of **12***c* with 11.1 ml triethylamine (66 mmol) and 7.50 g (66 mmol) of methane sulfonyl chloride as in the above example furnished 12.80 g (81%) of **12***b*.

Preparation of ***13a***

From ***12d***

A solution of 201 mg (0.475 mmol) of **12***d*, 30 mg glacial acetic acid, and 20 mg ammonia in 10 ml of chloroform was heated in a Parr pressure vessel at 48–52°C for 18 h. The solution was washed with water (10 ml) and brine (10 ml), dried over magnesium sulfate, and evaporated to yield an oil which was taken up in methylene chloride and filtered through a pad of silica gel to give 107 mg (57%) of **13***a*; ir ($CHCl_3$): 3500, 3330, 2110, 1770, 1760, 1695, 1650 cm^{-1}.

*From **12b***

To a solution of 2.30 g (4.85 mmol) of **12*b*** in 30 ml of DMSO was added a stream of dry ammonia for 10 min at 25°C. The solution was let stand 30 min at 25°C, poured into brine (100 ml) and extracted with chloroform (5 × 20 ml). The extracts were washed with water (2 × 20 ml) and brine (2 × 20 ml). The extracts were dried over magnesium sulfate and evaporated to yield 1.75 g (92%) of **13*a***.

*Preparation of **13b***

A solution of 5.25 g (12.4 mmol) of **12*d***, 560 mg (18.6 mmol) monomethylamine, and 110 mg acetic acid in 50 ml benzene was heated to 46°C for 18 h in a Parr pressure vessel. Work-up as in the previous example (preparation of **13*a***) gave an oil which was chromatographed on 30 g of silica gel (5% water, w/w) using chloroform as the eluting solvent. A total of 4.1 g (81%) of **13*b*** was obtained in three fractions, 1.3 g of isomer 1 (elutes first), 1.0 g of isomer 2, and 1.8 g mixed fraction (~1:1). Isomer 1: ir ($CHCl_3$): 3340, 2110, 1777, 1769, 1680, 1649, 1625 cm^{-1}; uv (EtOH, 0.3 mg/10 ml) λ_{max} 284 nm (ε 21 100); isomer 2: ir ($CHCl_3$): 3415, 3335, 2110, 1770 (1777sh), 1682, 1650, 1630 cm^{-1}; uv (EtOH, 0.3 mg/10 ml) λ_{max} 280 nm (ε 16 200).

*Benzyl N-Carboethoxy-7-β-azido-Δ³-N-2-isocephem-4-carboxylate **14***

To a solution of 1.75 g (4.43 mmol) of **13*a*** in 40 ml of chloroform was added 1.50 g (13.8 mmol) of ethyl chloroformate followed by 2.02 g (20 mmol) of triethylamine in 5 ml chloroform over 5 min at 25°C. An exothermic reaction was observed. The reaction mixture was let stand at 25°C for 18 h, following which it was washed with water (25 ml) and brine (25 ml). The solution was dried (magnesium sulfate) and evaporated. The oil which resulted was chromatographed on 30 g silica gel using chloroform as eluent to give 440 mg (26.8%) of **14** as a crystalline solid, mp 133.5–134.5°C; ir ($CHCl_3$): 2110, 1780, 1727, 1710, 1625 cm^{-1}; uv (EtOH, 1.4 mg/50 ml) λ_{max} 288 nm (ε 14 600). *Anal.* calcd. for $C_{17}H_{17}N_5O_5$: C 54.98, H 4.61, N 18.86; found: C 54.74, H 4.64, N 18.85.

*Benzyl 7-β-(Aminophenoxyacetoyl)-N-methyl-Δ³-N-2-isocephem-4-carboxylate **16a***

A suspension of 313 mg (1 mmol) of **11*b*** and 100 mg 10% Pd/C in 50 ml ethyl acetate was shaken under hydrogen at 55 psi and 25°C for 1.5 h. Filtration of the suspension through diatomaceous earth and evaporation of the filtrate gave an oil which was filtered through a pad of silica gel (5% water, w/w) (2.0 g) in methylene chloride. Evaporation of the filtrate gave 220 mg (76.5%) of **15*a*** as an oil; ir ($CHCl_3$): 1764, 1685, 1615 cm^{-1}.

Treatment of 204 mg (0.71 mmol) of **15*a*** with 178.2 mg (0.75 mmol) EEDQ and 110 mg (0.75 mmol) phenoxyacetic acid in 30 ml methylene chloride gave after work-up (2*a*) 181 mg (60.5%) of **16*a***, mp 180–182°C, recrystallized from chloroform–ether; ir ($CHCl_3$): 3410, 1767, 1695, 1685, 1615 cm^{-1}; uv (EtOH, 0.9 mg/50 ml) λ_{max} 308 nm (ε 18 300). *Anal.* calcd. for $C_{23}H_{23}N_3O_5$·0.05$CHCl_3$: C 64.77, H 5.43, N 9.83; found: C 64.82, H 5.44, N 9.92.

*Benzyl 7-β-(Aminophenoxyacetoyl)-N-carboethoxy-Δ³-N-2-isocephem-4-carboxylate **16b***

Reduction of 420 mg (1.13 mmol) of **14** with 200 mg 10% Pd/C in 40 ml ethyl acetate at 25°C at 57 psi and for 1.5 h gave 350 mg (90%) of **15*b*** as an oil; ir ($CHCl_3$): 3000–3500b, 1777, 1725, 1712, 1625 cm^{-1}.

Treatment of 315 mg (0.92 mmol) of **15*b*** with 242 mg (0.92 mmol) EEDQ and 140 mg (0.92 mmol) phenoxyacetic acid in 10 ml methylene chloride gave after work-up (2*a*) **16*b*** as an oil. This oil was chromatographed on silica gel using chloroform – 3% acetone as eluent to give 164 mg pure **16*b*** as an oil; ir ($CHCl_3$): 3410, 3330, 1782, 1728, 1712, 1692, 1625, 1602, 1505 cm^{-1}.

*7-β-(Aminophenoxyacetoyl)-N-methyl-Δ³-N-2-isocephem-4-carboxylic Acid **17a***

A suspension of 158 mg (0.38 mmol) of **16*a*** and 290 mg 20% $Pd(OH)_2$/C in 50 ml ethyl acetate was shaken under hydrogen (58 psi) at 20°C for 3 h. The suspension was filtered through diatomaceous earth and the filtrate evaporated to yield an oil. Trituration of the oil with methyl isobutyl ketone gave 45 mg of a tan solid which decomposed above 158°C; ir ($CHCl_3$): 3420, 2500–3600(CO_2H), 1757, 1680, 1613, 1530, 1495 cm^{-1}; uv (EtOH, 0.4 mg/10 ml) λ_{max} 302 (ε 6200), 275 (ε 5700), 268 nm (ε 5600).

The material proved to be unstable, darkening rapidly on standing.

*7-β-(Aminophenoxyacetoyl)-N-carboethoxy-Δ³-N-2-isocephem-4-carboxylic Acid **17b***

A suspension of 158 mg (0.33 mmol) of **16*b*** and 390 mg 20% $Pd(OH)_2$/C in 40 ml ethyl acetate was shaken under hydrogen (57 psi) at 25°C for 1.5 h. Work-up as in the above example yielded an oil which upon trituration with ether solidified, 74 mg. The solid failed to give a sharp melting point decomposing over the range 107–134°C; ir ($CHCl_3$): 3410, 2500–3600b CO_2H, 1780, 1728, 1710, 1694, 1628, 1600, 1520, 1495 cm^{-1}; uv (EtOH, 1.7 mg/50 ml) λ_{max} 284 nm (ε 17 750). *Anal.* calcd. for $C_{18}H_{19}N_3O_7$: C 55.52, H 4.92, N 10.79; found: C 55.45, H 5.21, N 10.64.

Acknowledgements

Partial financial support of this work by the National Research Council of Canada through its Industrial Research Assistance Plan is gratefully acknowledged.

1. T. W. Doyle. Can. J. Chem. **55**, 2714 (1977).
2. (*a*) T. W. Doyle, B. Belleau, B.-Y. Luh, C. F. Ferrari, and M. P. Cunningham. Can. J. Chem. **55**, 468 (1977); (*b*) T. W. Doyle, B. Belleau, B.-Y. Luh, T. T. Conway, M. Menard, J. L. Douglas, D. T. Chu, G. Lim, L. R. Morris, P. Rivest, and M. Casey. Can. J. Chem. **55**, 484 (1977); (*c*) T. W. Doyle, B.-Y. Luh, and A. Martel. Can. J. Chem. **55**, 2700 (1977); (*d*) T. W. Doyle, A. Martel, and B.-Y. Luh. Can. J. Chem. **55**, 2708 (1977).
3. H. Newman. J. Org. Chem. **30**, 1287 (1965); M. Wolfrom and H. B. Bhat. Chem. Commun. 146 (1966).
4. (*a*) I. Monkovic, H. Wong, A. W. Pircio, Y. G. Perron, I. J. Pachter, and B. Belleau. Can. J. Chem. **53**, 3094 (1975); (*b*) F. Weygand and E. Frauendorfer. Chem. Ber. **103**, 2437 (1970).
5. F. A. Bovey (*Editor*). Nuclear magnetic resonance spectroscopy. Academic Press, New York and London. 1969.
6. M. Karplus. J. Am. Chem. Soc. **85**, 2870 (1963).

Characterization of the triplet state of aromatic esters and nitriles. Evaluation of the steric effect on the triplet of methyl mesitoate[1]

D. R. ARNOLD, J. R. BOLTON, G. E. PALMER,[2] AND K. V. PRABHU[3]

Photochemistry Unit, Department of Chemistry, The University of Western Ontario, London, Ont., Canada N6A 5B7

Received January 4, 1977

D. R. ARNOLD, J. R. BOLTON, G. E. PALMER, and K. V. PRABHU. Can. J. Chem. **55**, 2728 (1977).

The phosphorescence emission and electron spin resonance spectra of methyl mesitoate (**1**) and mesitonitrile (**2**) have been studied in order to assess the steric effect (inhibition of resonance) in the former. The triplet energy of **1** (80.5 kcal mol^{-1}) is considerably higher than that of **2** (74.2 kcal mol^{-1}) while the zero-field splitting parameters are very similar (**1**, D/hc = 0.127 cm^{-1}, E/hc = 0.013 cm^{-1}; **2**, D/hc = 0.127 cm^{-1}, E/hc = 0.006 cm^{-1}). The triplet energy and zero-field splitting parameters of *o*-, *m*-, and *p*-methyl toluate and *o*-, *m*-, and *p*-tolunitrile are also reported.

D. R. ARNOLD, J. R. BOLTON, G. E. PALMER et K. V. PRABHU. Can. J. Chem. **55**, 2728 (1977).

On a étudié les spectres d'émission phosphorescence et de résonance paramagnétique électronique du mésitoate de méthyle (**1**) et du mésitonitrile (**2**) afin de déterminer l'effet stérique (inhibition à la résonance) dans le premier. L'énergie de l'état triplet de **1** (80.5 kcal mol^{-1}) est beaucoup plus élevée que celle de **2** (74.2 kcal mol^{-1}) alors que les paramètres de couplage à champ zéro sont très similaires (**1**, D/hc = 0.127 cm^{-1}, E/hc = 0.013 cm^{-1}; **2**, D/hc = 0.127 cm^{-1}, E/hc = 0.006 cm^{-1}). On rapporte aussi l'énergie de l'état triplet et les paramètres de couplage à champ zéro pour les *ortho*-, *méta*- et *para*-toluates de méthyle et les *ortho*, *méta* et *para*-tolunitriles.

[Traduit par le journal]

Introduction

Electron spin resonance (esr) spectroscopy can give useful information about the effects (steric and electronic) of substituents on electronically excited triplet states (1). The zero-field splitting parameters (D and E) obtained from the esr spectrum are intrinsic properties of the triplet. Furthermore, in the best of cases, hyperfine splitting may be discernible in which case information about the unpaired electron distribution can be obtained. In contrast, other sources of information, for example, singlet–triplet absorption, phosphorescence emission, and triplet–triplet absorption, of course, involve transitions between two states and substituent effects on these spectra result from perturbations of both initial and final states. The usefulness of esr for providing information on the effect of substituents on stable (ground state) triplet molecules is also well established (2).

We have reported (1*c*) results of a study on the esr and phosphorescence emission spectra of methyl benzoates with electron-withdrawing substituents (cyano- and carbomethoxy-) from which it was possible to conclude that the lowest triplet of these compounds has π,π^* character. It was also clear, from the relatively small value of D (compared with that for benzene for example) that considerable spin density was distributed onto the carbomethoxy and cyano groups. We have now extended this study to include methyl mesitoate and mesitonitrile in an attempt to assess the steric-effect (inhibition of resonance) on the zero-field splitting parameters and triplet energy.

It is well known that the carboxyl carbonyl of methyl mesitoate cannot be coplanar with the phenyl ring in the ground state and therefore resonance interaction is reduced.[4] On the other hand, the nitrile function, being linear, is not prevented from being planar with the ring in mesitonitrile and resonance and inductive interaction with the ring are uninhibited. This classic concept, established over thirty-five years ago, has

[1]Contribution No. 167 from the Photochemistry Unit.

[2]On leave (1973) from Department of Chemistry, University of Prince Edward Island, Charlottetown, P.E.I.

[3]Present address: Solar Laboratories, Inc., Costa Mesa, CA.

[4]X-Ray analysis of mesitoic acid (hydrogen-bonded dimer) indicates the carboxyl group is twisted out of plane of the ring by 48.4° (3) while *o*-toluic acid (hydrogen-bonded dimer) is almost planar (4).

been used to explore the importance of steric effects in several diverse systems (5).

An example of the difference in steric interaction in methyl mesitoate and mesitonitrile which is most pertinent to the present discussion is the comparison of the ultraviolet absorption spectra of these compounds, first reported by Fehnel and Wepster (6). These spectra are shown in Figs. 1 and 2. Figures 1*a* and 1*b* allow a comparison of the absorption spectra of methyl benzoate and cyanobenzene

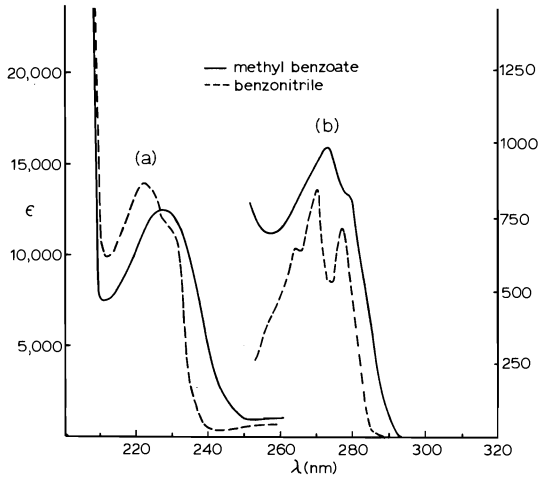

FIG. 1. The primary band (*a*, left axis of ordinates) and secondary band (*b*, right axis of ordinates) of the ultraviolet absorption spectra of methyl benzoate and benzonitrile in ethanol solution.

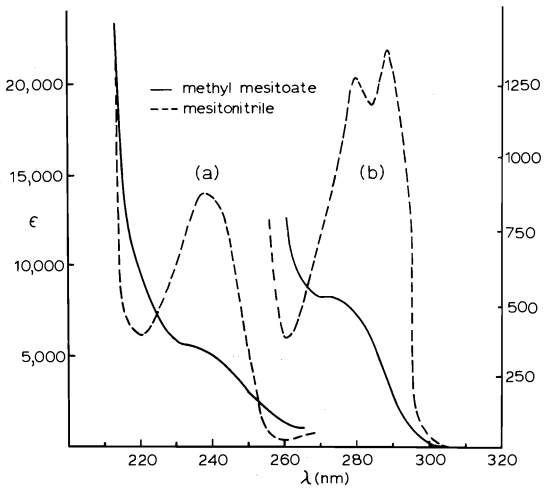

FIG. 2. The primary band (*a*, left axis of ordinates) and secondary band (*b*, right axis of ordinates) of the ultraviolet absorption spectra of methyl mesitoate and mesitonitrile in ethanol solution.

in the primary (^1L_a) and secondary (^1L_b) absorption band regions. The similarity of the spectra indicates a resonance interaction involving the carbomethoxy and cyano substituents in both compounds. Figures 2*a* and 2*b* show the same absorption regions for methyl mesitoate and mesitonitrile. While the spectrum of mesitonitrile still indicates the strong resonance interaction between the cyano group and the phenyl ring, the spectrum of methyl mesitoate is very different from that of methyl benzoate and reflects the diminished resonance interaction. The lowest triplet has the ^1L_a configuration; therefore, the steric effect on the corresponding singlet evident in Fig. 2*a* should be compared with that on the triplet (7).

Results and Discussion

The spectral (electron spin resonance and phosphorescence emission) characteristics of the triplet states of the substituted methyl benzoate esters and cyanobenzenes studied here are summarized in Table 1.

It is apparent, from the overall similarity of the data, that a π,π^* triplet is involved in every case. In particular, the phosphorescence lifetime which varies between 1 and 5 s is too long for an n,π^* state. We assume, therefore, that the differences that do exist can be considered as substituent effects on the ^3L_a (or $^3B_{1u}$) state (7).

Since the triplet energy of methyl benzoate (77.9 kcal mol^{-1}) and cyanobenzene (77.0 kcal mol^{-1}) are similar, the difference in the triplet energy of methyl mesitoate (80.5 kcal mol^{-1}) and mesitonitrile (74.2 kcal mol^{-1}), that is, 6.3 kcal mol^{-1}, can be attributed to the steric effect in the former. The triplet energy of methyl mesitoate is in fact comparable to that of mesitylene (79.8 kcal mol^{-1}) or isodurene (79.6 kcal mol^{-1}) (8).

The observed steric effect upon the absorption and emission spectra are, of course, the combined influence on both the ground state and on the excited singlet and triplet states, respectively. The increase in triplet energy of methyl mesitoate relative to mesitonitrile and methyl benzoate is interpreted to mean that while the ground state energy of methyl mesitoate may be raised by the lack of resonance interaction, the excited state energy is raised even more and the result is a net increase in the transition energy.

TABLE 1. Zero-field splitting parameters and phosphorescence energies for the triplet of some substituted methyl benzoates and cyanobenzenes

Compound	τ_{Phos} (s)	E_T (kcal mol^{-1})	D/hc (cm^{-1})	E/hc (cm^{-1})	D^*/hc (cm^{-1})[a]	Reference
Methyl benzoate	2.7	77.9	0.133	0.011	0.134	[b]
Methyl-*o*-toluate	2.2	77.5	0.120	0.023	0.126	[c]
Methyl-*m*-toluate	4.2	75.9	0.120	0.035	0.134	[c]
Methyl-*p*-toluate	3.8	76.4	0.123	0.009	0.124	[c]
Methyl mesitoate	1.2	80.5	0.127	0.013	0.129	[c]
Cyanobenzene	3.7	77.0	0.135	0.005	0.135	[c]
	0.04	76.7	0.137	0.007	0.138	[d, e]
	—	—	0.134	0.019	0.138	[f, g]
	—	—	0.136	0.006	0.139	[h, i]
o-Tolunitrile	3.9	75.9	0.133	0.014	0.135	[c]
m-Tolunitrile	4.7	75.3	0.130	0.022	0.135	[c]
p-Tolunitrile	3.9	75.8	0.131	0.006	0.131	[c]
	—	76.1	0.136	0.005	0.136	[d, e]
	—	—	0.134	0.022	0.139	[f, g]
Mesitonitrile	—	74.2	0.127	0.006	0.127	[c]
	—	—	0.127	0.019	0.132	[f, g]

[a]Calculated $[D^* + (D^2 + 3E^2)^{1/2}]$.
[b]Reference 1*a*.
[c]This work.
[d]In 1,4-dibromobenzene crystals at 77 K.
[e]References 1*g*, 1*h*.
[f]In 2-methyltetrahydrofuran at 77 K.
[g]References 1*i*, 1*j*.
[h]Reference 1*e*.
[i]In ethanol at 77 K.

We look next to the zero-field splitting parameters for direct evidence on the structure of the triplet.

The decrease in the D value from that for benzene (0.158 cm^{-1} (9)) to that for methyl benzoate (0.133 cm^{-1}) is taken as an indication of the greater average separation of the electrons in the triplet of methyl benzoate. Assuming the point dipole approximation, the D value of benzene is equivalent to an average separation of the electrons of 2.02 Å; while that of methyl benzoate is equivalent to 2.14 Å.[5] The same increase in the average separation of the electrons is observed with cyanobenzene. The trend to lower D values continues with mesitonitrile indicative of the ability of a methyl substituent to take on spin density.

If the carbomethoxy moiety is prevented from becoming coplanar with the phenyl ring in the triplet of methyl mesitoate, the D value should increase relative to that of mesitonitrile and approach that of mesitylene itself. Such is not the case; methyl mesitoate has the same D value as mesitonitrile (within experimental error) and the value is considerably smaller than that for mesitylene ($D/hc = 0.140$ cm^{-1} (10)).

[5]The average separation of the electrons in the triplet was estimated using the equation $D = (3/4)g^2\beta^2 \times (1/r^3)$ (ref. 1*a*).

There are several possible explanations for this result; one is that in the triplet the carbomethoxy moiety is able to twist enough toward the plane of the phenyl ring so that electron delocalization can occur. That is, the steric interactions may not be severe enough to prevent the triplet of methyl mesitoate from becoming planar enough to allow delocalization of the electrons to an extent similar to that of mesitonitrile. This, of course, would be at the expense of energy reflected in the increased triplet energy. To test this possibility we attempted to obtain the esr spectrum from the triplet of methyl 1,3,5-tri-*tert*-butylbenzoate. However, the esr spectrum and the phosphorescence emission spectrum of this compound indicate that more than one species is present; we believe this ester to be photochemically reactive, and have thus far been unable to characterize the triplet.

Experimental

The procedure and apparatus used have been described previously (1*c*, 2*c*).

Acknowledgements

This work was supported by the National Research Council of Canada.

1. (*a*) J. E. WERTZ and J. R. BOLTON. Electron spin resonance. McGraw-Hill Co., New York. 1972. Chapt. 10. (*b*) M. GUÉRON. Creation and detection of

the excited state. Vol. 1*A*. *Edited by* A. A. Lamola. M. Dekker, Inc., New York. 1971. Chapt. 6. (*c*) D. R. ARNOLD, J. R. BOLTON, and J. A. PEDERSEN. J. Am. Chem. Soc. **94**, 2872 (1972). (*d*) B. J. SCHEVE and P. J. WAGNER. Chem. Phys. Lett. **25**, 324 (1974). (*e*) P. J. WAGNER and M. J. MAY. Chem. Phys. Lett. **39**, 350 (1976). (*f*) E. WASSERMAN, R. S. HUTTON, and F. B. BRAMWELL. J. Am. Chem. Soc. **98**, 7429 (1976). (*g*) S. W. MAO, T. C. WONG, and N. HIROTA. Chem. Phys. Lett. **13**, 199 (1972). (*h*) E. T. HARRIGAN, T. C. WONG, and N. HIROTA. Chem. Phys. Lett. **14**, 549 (1972). (*i*) J. DE JONG and C. MACLEAN. J. Magn. Reson. **11**, 373 (1973). (*j*) J. DE JONG. Thesis. Vrije Universiteit, Amsterdam. 1970.

2. (*a*) A. M. TROZZOLO and E. WASSERMAN. Carbenes. Vol. 2. *Edited by* R. A. Moss and M. Jones, Jr. Wiley-Interscience, New York. 1975. Chapt. 5. (*b*) W. KIRMSE. Carbene chemistry. Academic Press, New York. 1971. Chapt. 6. (*c*) D. R. ARNOLD, R. W. HUMPHREYS, W. J. LEIGH, and G. E. PALMER. J. Am. Chem. Soc. **98**, 6225 (1976). (*d*) R. W. HUMPHREYS and D. R. ARNOLD. Can. J. Chem. **55**, 2286 (1977). (*e*) R. S. HUTTON, M. L. MORRISON, H. D. ROTH, and E. WASSERMAN. J. Am. Chem. Soc. **96**, 4680 (1974).
3. V. BENGHIAT and L. LEISEROWITZ. J. Chem. Soc. Perkin II, 1778 (1972).
4. C. KATAYAMA, A. FURUSAKI, and I. NITTA. Bull. Chem. Soc. Jpn. **40**, 1293 (1967).
5. W. C. SPITZER and G. W. WHELAND. J. Am. Chem. Soc. **62**, 2995 (1940).
6. (*a*) E. A. FEHNEL. J. Am. Chem. Soc. **72**, 1404 (1950). (*b*) B. M. WEPSTER. Recueil, **76**, 335 (1957).
7. (*a*) H. B. KLEVENS and J. R. PLATT. J. Chem. Phys. **17**, 470 (1949). (*b*) S. P. MCGLYNN, T. AZUMI, and M. KINOSHITA. Molecular spectroscopy of the triplet state. Prentice-Hall, Inc., Englewood Cliffs, NJ. 1969. pp. 92–97.
8. R. V. NAUMAN. Ph.D. Thesis, University of California, Berkeley. 1947. p. 60.
9. M. S. DE GROOT, I. A. M. HESSELMANN, and J. H. VAN DER WAALS. Mol. Phys. **16**, 45 (1969).
10. M. S. DE GROOT, I. A. M. HESSELMANN, and J. H. VAN DER WAALS. Mol. Phys. **16**, 61 (1969).

La pyrolyse de poly(adipate de butylène-1,4)

FRANÇOIS MESSIER ET DON C. DEJONGH[1]

Département de Chimie, Université de Montréal, C.P. 6210, Succ. A, Montréal, (Qué.), Canada H3C 3V1

Reçu le 29 novembre 1976

FRANÇOIS MESSIER et DON C. DEJONGH. Can. J. Chem. **55**, 2732 (1977).

Le poly(adipate de butylène-1,4) (**1**) a été pyrolysé dans un bateau de porcelaine placé à l'intérieur d'un tube de quartz chauffé à l'aide d'un four externe. Les produits volatils ont été entraînés dans un courant d'azote et conduits à l'extérieur de la zone chauffée. Le polyester **1** fut pyrolysé près de l'entrée de la zone chauffée ainsi que près de la sortie de la zone chauffée à des températures de 500 et 700°C avec ou sans vide. L'acide adipique (**2**) et la cyclopentanone (**4**) ainsi qu'un mélange de mono (**5**) et diesters (**6**) du monomère, du dimère et du trimère furent isolés comme produits de pyrolyse.

La pyrolyse de **1** à 500°C près de la sortie de la zone chauffée à la pression atmosphérique, a donné un rendement de 14% de **2**, 10% de **4**, 40% de **5** et 18% de **6**; **5** était constitué de 26% du monoester du monomère et 74% du monoester du dimère, tandis que **6** était constitué de 63% du diester du monomère et 37% du diester du dimère. Par contre, à 700°C sous vide (0.2–0.3 Torr) avec le polymère **1** près de l'entrée de la zone chauffée, le rendement de **2** était plus élevé (~35%), et les trimères étaient trouvés dans les monoesters **5** et les diesters **6**, avec les dimères et monomères.

FRANÇOIS MESSIER and DON C. DEJONGH. Can. J. Chem. **55**, 2732 (1977).

Poly(1,4-butylene adipate) (**1**) was pyrolyzed in a porcelain boat placed in a quartz tube heated by a furnace. Volatile products were carried out of the heated zone into traps by a flow of nitrogen. Polyester **1** was pyrolyzed both near the entrance and near the exit of the heated zone, at 500 and 700°C with and without a vacuum. Adipic acid (**2**), cyclopentanone (**4**), and a mixture of mono (**5**) and diesters (**6**) of the monomer, dimer, and trimer, were isolated as products of the pyrolyses.

The pyrolyses of **1** at 500°C near the exit of the heated zone at atmospheric pressure gave 14% of **2**, 10% of **4**, 40% of **5**, and 18% of **6**; **5** consisted of 26% monoester of monomer and 74% monoester of dimer, whereas **6** consisted of 63% diester of monomer and 37% diester of dimer. At 700°C, 0.2–0.3 Torr, with **1** near the entrance of the heated zone, the yield of **2** was higher (~35%), and trimers were found in the monoesters **5** and diesters **6**, along with dimers and monomers.

Introduction

Plusieurs méthodes existent pour caractériser des polymères (1); par exemple, on peut citer la spectroscopie infrarouge, qui est une des principales techniques pour connaître la structure physique et chimique du polymère, et la spectroscopie de résonance magnétique nucléaire (rmn), qui permet de déterminer la tacticité du polymère ainsi que sa distribution séquentielle. Il existe également des méthodes de caractérisation en solution telles que la mesure de la viscosité, ainsi que l'osmométrie, qui permettent de connaître la masse moléculaire moyenne ($\overline{M}_n$) des polymères (2). On peut aussi faire l'étude de polymères à l'état solide à l'aide de la diffraction des rayons-X (1), méthode qui donne un aperçu de la cristallinité des polymères. Une autre méthode permettant de caractériser un polymère et d'avoir une idée sur sa stabilité thermique est la thermogravimétrie (1).

Une méthode apparentée à la thermogravimétrie existe pour déterminer la stabilité thermique d'un polymère, la pyrolyse. Dans ce cas, on étudie les produits formés lors de la pyrolyse, contrairement à ce qui se passe pour la thermogravimétrie. Avec cette dernière méthode, l'étude se porte sur le résidu, c'est-à-dire la perte de poids en fonction de l'augmentation de température.

Depuis quelques années, on se sert du patron obtenu lors de la pyrolyse d'un polymère pour l'identifier. En couplant un chromatographe en phase gazeuse (cpg) au pyrolyseur, les produits de la pyrolyse sont séparés et analysés par cpg. La distribution des produits vue sur le chromatogramme devient une caractéristique du produit de départ (3, 4). Il existe de nombreuses références impliquant cette méthode d'analyse

[1]A qui toute demande d'information devra être adressée.

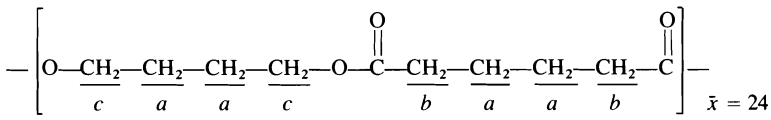

1

a(δ 1.8,m,2H), *b*(δ 2.5,m,1H), *c*(δ 4.2,m,1H)

de polymères. On peut citer, à propos de ce présent travail, l'analyse par cpg des produits de la pyrolyse du poly(éthylacrylate d'éthylène), du poly(vinylacétate d'éthylène) (5), du poly(méthacrylate de *n*-butyle) (6) et du poly(méthacrylate de méthyle) (7). Nombreuses autres références concernant la pyrolyse de polymères se trouvent dans la littérature (8).[2]

Dans nos laboratoires on possède une vaste expérience de la pyrolyse en phase gazeuse de molécules aromatiques et volatiles (9, 10). Nous voulions acquérir de l'expérience dans la pyrolyse de polymères, et, à cette fin, nous avons décidé de mettre au point la pyrolyse de polymères avec nos appareils en effectuant la pyrolyse du poly(adipate de butylène-1,4) (**1**). En général, la pyrolyse d'ester donne lieu à la formation d'acide carboxylique et d'oléfine via l'intermédiaire d'un cycle à six membres (11). Par exemple, la dégradation thermique du poly(oxycarbonyléthylène) donne en premier lieu la formation de deux fragments, un contenant un site d'insaturation et l'autre une fonction acide en bout de chaîne (12). La partie portant la fonction acide en bout de chaîne se fragmente à nouveau, toujours par le même mécanisme, pour donner lieu à la formation de l'acide acrylique.

Des dégradations thermiques de polyesters aromatiques et aliphatiques ont été effectuées aussi directement dans la source d'ionisation d'un spectromètre de masse (13), sans passer par la cpg. Les polyesters de l'acide téréphtalique et diols aliphatiques se dégradent par une élimination-*cis*, ce qui donne l'acide téréphtalique. Dans le cas des polyesters des acides dicarboxyliques aliphatiques, ce sont les liaisons O—CO et CO—CH_2 qui se brisent. De plus, une petite quantité de trimère cyclique a été trouvée dans un échantillon commercial de poly(téréphtalate d'éthylène) (14); ce trimère se volatilise à 190°C, tandis que la pyrolyse du polyester commence vers 300°C.

Aux différents exemples cités où la pyrolyse se fait dans un pyrolyseur, l'appareil admet une quantité d'un microgramme à un milligramme de produits, et est directement couplé à un appareil de cpg. Au contraire, dans notre cas, on isole le mélange de produits. Puis, on les identifie et on en détermine le rendement, ce qui demande une quantité de polymères au départ d'environ $\frac{1}{2}$ g à 1 g.

Partie théorique

Caractérisation du poly(adipate de butylène-1,4) (1)

Nous avons déterminé la masse moléculaire moyenne ($\overline{M}_n$) du poly(adipate de butylène-1,4) (**1**) par la tonnométrie (15). Une masse moyenne de 4700 g/mol a été trouvée, correspondant à 24 pour le nombre moyen d'unités de répétition ($\bar{x}$). Il faut préciser que la tonnométrie ne donne aucune indication sur la courbe de distribution des molécules de différentes masses présentes dans le polymère. Le spectre rmn du polymère **1** ne révèle que trois pics, c'est-à-dire qu'il n'y a pas de pics provenant d'un groupe hydroxyle ou d'impuretés.

Méthode de pyrolyse

Dans les cas des produits de départ volatils, il s'agit d'abord de les sublimer, et, puis, à l'aide d'un courant d'azote de les amener dans un four pour y être pyrolysés (9, 10). Dans le cas de **1**, au lieu de sublimer l'échantillon dans un courant d'azote, on le place dans un bateau de porcelaine, et puis, il est amené dans la zone chauffée à l'aide d'un déplacement manuel (voir la fig. 1), ou d'une tige de fer et d'aimants. Par cette méthode, le polymère sera pyrolysé en phase

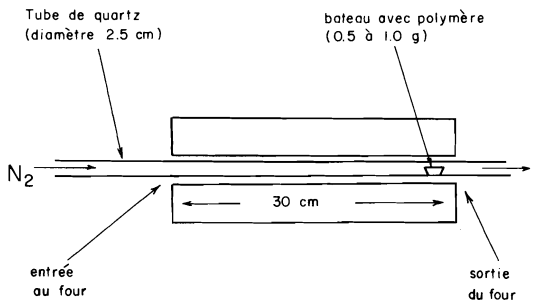

FIG. 1 L'introduction du polymère dans la zone chauffée.

[2]N.B.: cette dernière référence contient au-delà de 500 références.

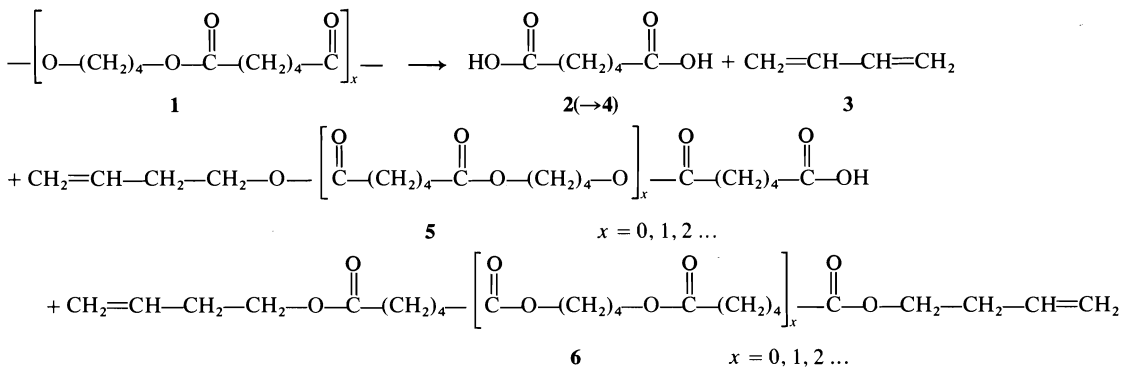

SCHÉMA 1

solide, mais dès qu'il y aura formation de produits volatils, ceux-ci seront entraînés dans le courant d'azote et amenés à l'extérieur de la zone chauffée. Si les produits primaires sont pyrolysés en route, on obtiendra des produits primaires, secondaires, etc, de pyrolyse.

Il y a plusieurs paramètres pouvant influencer la formation et la distribution des produits, tels que la pression, la température et le débit d'azote. En plus, il y a l'endroit où est placé le bateau dans la zone chauffée. Lorsque la pyrolyse est effectuée près de l'entrée, la zone chauffée parcourue par les produits dans le courant d'azote est beaucoup plus longue, environ 30 cm, que lorsque cette pyrolyse est effectuée près de la sortie (environ 10 cm). De ce fait, dans les mêmes conditions de température, de pression et de débit d'azote, la pyrolyse est plus complète lorsque celle-ci est effectuée près de l'entrée plutôt que près de la sortie de la zone chauffée.

*Pyrolyse du polymère **1** près de la sortie de la zone chauffée*

Le polyester **1** est amené dans la zone chauffée pour y être pyrolysé à une température de 700°C à la pression atmosphérique. Un léger débit d'azote permet aux produits formés d'être balayés de la zone chauffée et récupérés dans une série de trappes. Le mélange de produits obtenu est formé de l'acide adipique (**2**), du butadiène-1,3 (**3**), de la cyclopentanone (**4**), ainsi que de deux groupes d'esters, soit les monoesters **5** et les diesters **6** de butène-3 (schéma 1). La cyclopentanone (**4**) se forme de la pyrolyse de l'acide adipique (16).

En injectant ce mélange brut de produits sur un chromatographe en phase gazeuse, nous avons pu isoler le monomère du monoester (**5** où $x = 0$). Sa formule et ses fragmentations caractéristiques ont été déterminées à l'aide de ses spectres de masse à haute et basse résolution (tableau 1).

Le spectre rmn permettait également l'élucidation de la structure du monomère **5** ($x = 0$).

De plus, nous avons pu isoler le monomère du diester (**6** où $x = 0$) par cpg. La structure du diester **6** fut élucidée à l'aide de son spectre de masse ainsi que par son spectre rmn. Cette fois-ci, l'ion moléculaire est présent à *m/e* 254, mais en faible abondance relative, et les fragmentations sont les mêmes que celles du monoester **5** (tableau 1): *m/e* 254(1%), 183(57%), 129(50%), 111(52%), 101(15%), 83(13%), 55(100%) et 54(77%).

Nous avons pris aussi le spectre rmn du mélange brut obtenu de la pyrolyse, après l'élimination de l'acide adipique par précipitation. Ce spectre rmn était identique à la superposition de ceux des monomères, sauf que la valeur de l'intégration obtenue était beaucoup plus élevée que celle attendue pour la présence des monomères seuls. Le spectre de masse de ce

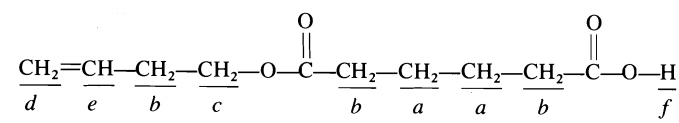

5 ($x = 0$)

a(δ 1.7,m,4H), *b*(δ 2.4,m,6H), *c*(δ 4.2,t,2H), *d*(δ 5.2,m,2H), *e*(δ 5.7,m,1H), *f*(δ 10.3,m,1H)

TABLEAU 1. Spectres de masse du monoester **5** ($x = 0$)

m/e[a]	Int. rel.[b]	Formule[c]	Interprétation[d]
200	0	[e]	Ion moléculaire
183	8	$C_{10}H_{15}O_3$	Perte de OH·
182	15	$C_{10}H_{14}O_3$	Perte de H_2O
129	38	$C_6H_9O_3$	Perte de ·OR
111	21	$C_6H_7O_2$	m/e 129 − H_2O, m*
101	19	$C_5H_9O_2$	m/e 129 − CO
83	17	C_5H_7O	m/e 101 − H_2O, m*
55	69	C_4H_7	R^+
54	100	C_4H_6	Réarrangement d'hydrogène-γ

[a]Les pics les plus importants.
[b]Intensités relatives à 70 eV.
[c]Obtenues à haute résolution.
[d]La présence de pics métastables est notée par "m*".
[e]Cette formule n'était pas déterminée.

mélange brut contenait des pics correspondant aux monomères, et, de plus, des pics indiquant le même genre de fragmentations observées dans le cas des monomères, mais à des masses plus élevées de 200 unités. Ces pics devaient être dûs à un mélange du monomère ($x = 0$), du dimère ($x = 1$), du trimère ($x = 2$), etc., de structures **5** et **6**.

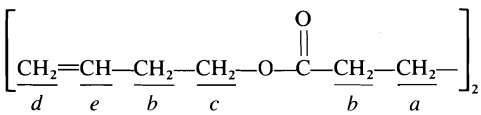

6 ($x = 0$)

a(δ 1.7,m,2H), *b*(δ 2.4,m,4H), *c*(δ 4.2,t,2H), *d*(δ 5.2,m,2H), *e*(δ 5.7,m,1H)

Vu que rien de plus grand que les monomères (**5** et **6**, $x = 0$) ne sortait du chromatographe en phase gazeuse, nous avons décidé de séparer par extraction les monoesters **5** des diesters **6** et d'en déterminer les masses moyennes. Les rendements de l'acide adipique (**2**), de la cyclopentanone (**4**) et des esters **5** et **6**, ainsi que la valeur de la masse moyenne des monoesters **5** et des diesters **6**, sont présentés au tableau 2.

Les valeurs obtenues pour les masses moyennes indiquent que les monoesters et les diesters **5** et **6** consistent surtout en monomère et en dimère, car ces valeurs se situent entre la masse du monomère, qui est de 200 (**5**, $x = 0$) ou 254 g/mol (**6**, $x = 0$), et celle du dimère, qui est de 400 (**5**, $x = 1$) ou 454 g/mol (**6**, $x = 1$). De plus, les valeurs d'intégration des protons apparaissant sur les spectres rmn ne correspondent pas au monomère ou au dimère simplement et sont trop faibles pour correspondre au trimère. Les valeurs d'intégration se situent entre celle du monomère et celle du dimère, confirmant l'énoncé que les esters **5** et **6** consistent d'un mélange monomère–dimère dans ce cas.

Le partage en monomère et en dimère dans les mélanges de **5** et **6** fut déterminé par la méthode de tâtonnement à partir de la masse moyenne trouvée expérimentalement. Pour commencer, on choisissait un pourcentage du monomère et le pourcentage complémentaire en dimère, d'une façon arbitraire. En multipliant le pourcentage par la masse moléculaire du monomère ou du dimère selon le cas, on obtenait alors une masse moléculaire moyenne que l'on comparait à celle obtenue expérimentalement. On procédait ainsi jusqu'à ce que la masse moyenne correspondant aux pourcentages de monomère et dimère soit égale à celle obtenue expérimentalement. Les différents pourcentages en monomère ($x = 0$) et dimère ($x = 1$) des mélanges de **5** et de **6** déterminés de cette façon sont également présentés dans le tableau 2.

Nous avons alors pris les spectres rmn des monoesters **5** et des diesters **6**. D'après les pourcentages en monomère et dimère des esters **5** et **6**, tels que présentés dans le tableau 2, l'intégration des protons correspondant à chacun des pics devant apparaître sur les spectres rmn pouvait être prédite. Il s'agissait de multiplier les pourcentages de $x = 0$ et de $x = 1$ par le nombre de protons présents dans le monomère et le dimère et de les additionner. Les intégrations trouvées dans ces spectres rmn étaient très voisines de celles déduites des pourcentages de monomère et dimère.

Une autre pyrolyse du polyester **1** fut effectuée mais à une température de 500°C et avec un léger débit d'azote. Les resultats obtenus pour cette

TABLEAU 2. Pyrolyse de **1** à la sortie à la pression atmosphérique

Composé	A 700°C[d] Rendt (%)	A 700°C[d] $\overline{M}_n$ [monomère / dimère]	A 500°C[d] Rendt (%)	A 500°C[d] $\overline{M}_n$ [monomère / dimère]
2[a]	17±0.6		14±0.6	
4[a]	7±0.6		10±0.5	
5[b]	37±6	343±17[c] [$x = 0$, 28% / $x = 1$, 72%]	40±2	349±18[c] [$x = 0$, 26% / $x = 1$, 74%]
6[b]	13±2	323±15[c] [$x = 0$, 65% / $x = 1$, 35%]	18±1	327±2[c] [$x = 0$, 63% / $x = 1$, 37%]

[a]Ce rendement est calculé en supposant que tout le polymère est transformé en ce produit.
[b]Ce rendement est calculé en faisant le rapport de la quantité de **5** et **6**, selon le cas, sur la quantité de polymère de départ.
[c]Les masses moyennes ($\overline{M}_n$) sont déterminées par tonnométrie; g/mol.
[d]Ces résultats sont les moyennes déterminées de trois pyrolyses; les erreurs indiquées représentent les écarts types.

température sont pratiquement les mêmes que ceux obtenus à 700°C. Les rendements sont présentés au tableau 2 et sont reproductibles.

Lorsque la pyrolyse est effectuée sous vide (0.2–0.3 Torr) à une température de 700°C, la formation de l'acide adipique est pratiquement nulle et on ne remarque que la formation des mono et diesters **5** et **6**. En prenant le spectre rmn du mélange de la pyrolyse, nous avons constaté que les abondances des pics dûs aux protons oléfiniques (*d* et *e*) étaient très faibles. La masse moyenne de ce mélange était déterminée sans au préalable séparer les monoesters **5** des diesters **6**. La valeur de la masse moyenne obtenue est de 733 g/mol, ce qui indiquerait une dominance de trimères ($x = 2$) et de tétramères ($x = 3$) dans le mélange de la pyrolyse.

En effectuant la pyrolyse sous vide (0.2–0.3 Torr) à 500°C, nous avons remarqué que les résultats sont les mêmes que pour la pyrolyse précédente. La masse moyenne du mélange des monoesters et des diesters **5** et **6**, sans au préalable avoir été séparé, est de 702 g/mol comparativement à 733 g/mol pour la pyrolyse sous vide à 700°C.

Les résultats sont reproductibles. Il semble que la différence de température n'ait pas un effet très grand sur les rendements des produits. Par contre, la pression joue un rôle très important sur la grosseur des molécules formées. Sous vide, les molécules de plus haute masse sont rendues volatiles, et, la nécessité d'une repyrolyse des grosses molécules, afin de former des plus petites molécules volatiles, est éliminée.

*Pyrolyse du polyester **1** près de l'entrée de la zone chauffée*

Après avoir constaté l'effet que la pression à laquelle la pyrolyse est effectuée peut avoir sur la formation des produits, nous voulions ensuite connaître l'effet de la longueur de la zone chauffée. Par conséquent, la pyrolyse du poly(adipate de butylène-1,4) (**1**) était refaite dans les mêmes conditions de température et de pression que précédemment, mais cette fois-ci près de l'entrée de la zone chauffée. Encore, les produits volatils étaient entraînés dans les trappes par un courant d'azote. Nous avons donc amené le polymère à 700°C à la pression atmosphérique, et le seul produit que nous avons pu récupérer est la cyclopentanone, dans un rendement de 32%. A une température de 500°C à la pression atmosphérique, il n'y avait pas d'esters **5** et **6** formés non plus, mais, contrairement à la pyrolyse précédente (à 700°C), nous avons noté la formation de l'acide adipique avec un rendement de 32%, en plus de la cyclopentanone dont le rendement a baissé à 18%.

Ensuite, la pyrolyse a été faite dans les conditions d'une température de 700°C sous vide (0.2–0.3 Torr) avec un courant d'azote. Les produits récupérés à la fin de cette pyrolyse sont les mêmes que ceux trouvés lorsque la pyrolyse est effectuée près de la sortie de la zone chauffée et à la pression atmosphérique (voir le schéma 1). Les masses moyennes, ainsi que les rendements de l'acide adipique, de la cyclopentanone et des esters **5** et **6** sont présentés au tableau 3 pour quatre pyrolyses.

Les rendements de l'acide adipique et de la cyclopentanone sont reproductibles. Le rendement de l'acide adipique est important dans ces conditions-ci, alors qu'il était nul lorsque la pyrolyse était effectuée près de la sortie et sous vide. Il y a des variations d'une expérience à l'autre dans les masses moyennes des monoesters

TABLEAU 3. Résultats de la pyrolyse de **1** près de l'entrée de la zone chauffée à 700°C sous vide (0.2–0.3 Torr)

Composé	Pyrolyse	Rendt (%)	$\overline{M}_n$[c] [monomère, dimère, trimère]
2	1	37[a]	
	2	36	
	3	40	
	4	29	
4	1	7[a]	
	2	7	
	3	8	
	4	5	
5	1	31[b]	482(x = 1, 59%; x = 2, 41%)
	2	19	343(x = 0, 29%; x = 1, 71%)
	3	17	321(x = 0, 40%; x = 1, 60%)
	4	33	468(x = 1, 66%; x = 2, 34%)
6	1	9[b]	511(x = 1, 71%; x = 2, 29%)
	2	29	562(x = 1, 46%; x = 2, 54%)
	3	19	514(x = 1, 70%; x = 2, 30%)
	4	12	483(x = 1, 85%; x = 2, 15%)

[a]Ces rendements sont calculés en supposant que tout le polymère est transformé en ce produit.
[b]Ces rendements sont calculés en faisant le rapport de la quantité de **5** et **6** selon le cas sur la quantité de polymère au départ.
[c]Les masses moyennes sont déterminées par tonnométrie, g/mol.

5 et des diesters **6** ainsi que dans leurs rendements.

Dans ces cas aussi, nous avons déterminé les différents pourcentages de monomère (x = 0), de dimère (x = 1) et de trimère (x = 2) pour les esters **5** et **6** en procédant de la même façon que décrite pour les résultats présentés dans le tableau 2. Dû aux valeurs de ces masses moyennes qui sont assez élevées, nous avons calculé les pourcentages en termes du dimère et du trimère excepté pour la formation des monoesters **5** dans les pyrolyses 2 et 3 où nous avons déterminé les pourcentages en termes du monomère et du dimère. Ces résultats sont également présentés au tableau 3. En prenant les spectres rmn de ces esters **5** et **6**, nous étions capables de vérifier les pourcentages en monomère, dimère et trimère déterminés à partir des masses moyennes.

A une température de 500°C, sous vide (0.2–0.3 Torr), nous avons isolé de l'acide adipique (7%), de la cyclopentanone (9%), ainsi que les esters **5** et **6**. La détermination de la masse moyenne du mélange des monoesters et des diesters donne une valeur de $\overline{M}_n$, de 518 g/mol. Ce résultat laisse supposer la présence surtout de trimères. Aussi, si on regarde le spectre rmn de ce mélange, on constate que les abondances des pics *d* et *e* sont très faibles devant les pics *c*, *b* et *a*.

Discussion

On peut expliquer l'origine des différents produits lors de la pyrolyse du poly(adipate de butylène-1,4) (**1**) par la transposition de l'hydrogène-γ. Ce mécanisme très bien connu lors de la pyrolyse d'esters a permis l'explication de la formation de l'acide acrylique lors de la dégradation thermique du poly(oxycarbonyléthylène) (12). Le mécanisme de la formation des produits lors de la pyrolyse du composé **1** est donné au schéma 2.

Le groupe carbonyle active les atomes d'hydrogènes adjacents, ce qui permet de passer par un état de transition quasi-cyclique à six membres. Par la suite, l'hydrogène-γ est transposé sur l'oxygène du groupe carbonyle pour donner lieu à la formation de deux fragments: l'un comportant un site d'insaturation à la fin de la chaîne et l'autre fragment portant un groupement carboxyle en fin de chaîne. Ce mécanisme explique très bien la formation de l'acide adipique (**2**), ainsi que celle des monoesters **5** et des diesters **6**, et également, celle du butadiène-1,3 (**3**). La cyclopentanone (**4**) proviendrait de la cyclisation de l'acide adipique (**2**).

Dans les publications sur la pyrolyse de polymères à l'aide d'un pyrolyseur directement couplé au chromatographe en phase gazeuse, on ne note que la présence de monomères (6, 7, 17). Si les oligomères ne sortent pas de la

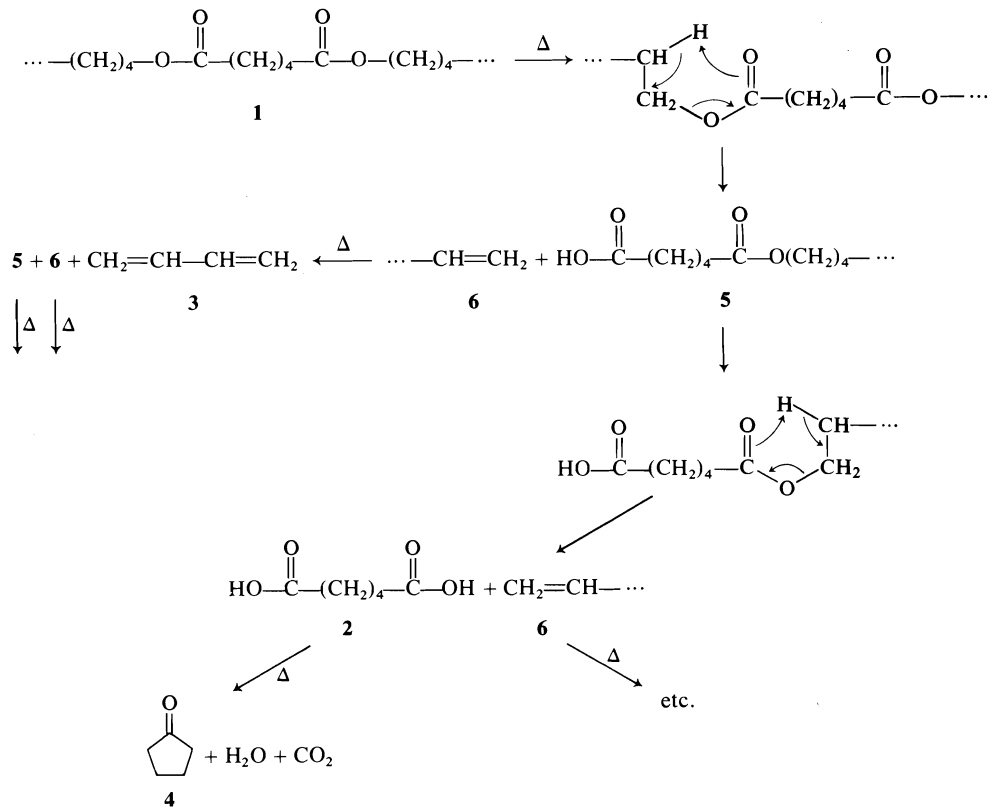

SCHÉMA 2

colonne, ou se dégradent sur la colonne, il devient impossible de savoir s'ils se sont formés. Par contre, un avantage de notre méthode est la mise en évidence de grosses molécules par les spectres rmn et de masse, ainsi que par les déterminations des masses moyennes.

Dans nos interprétations des spectres et des masses moyennes, nous avons présumé que la distribution des oligomères soit déterminée par leurs volatilités, c'est-à-dire, par leurs masses. Il serait également possible d'interpréter ces résultats en proposant la formation de monomère et de trimère, ou même de tétramère, mais au détriment, par exemple, du dimère. D'après le mécanisme de pyrolyse d'esters, nous n'avons pas de raison de préférer cette dernière interprétation et nous pensons que la première est plus probable. De toute façon, nous voulons souligner que les oligomères se forment avec notre méthode et ne sont pas perdus dans le traitement. Il serait possible de les étudier en détail si on le désirait.

La quantité du polymère employée est très petite (~50 μg) avec un pyrolyseur couplé au chromatographe, alors que nous pouvons faire la pyrolyse sur des quantités pouvant aller jusqu'à 1 g de polymère. Ce paramètre est très important surtout si on avait l'intention de se servir de la pyrolyse pour la préparation d'oligomères. Par contre, cet avantage peut devenir un dèsavantage lorsqu'il n'y a qu'une petite quantité du polymère disponible. Une autre comparaison que l'on peut faire de notre méthode par rapport à celle où le pyrolyseur est directement couplé au chromatographe concerne le temps nécessaire pour faire une pyrolyse et pour analyser les produits. Alors que dans notre cas ceci prend plusieurs heures, avec le pyrolyseur cela ne prend que quelques minutes. Donc, si on fait la pyrolyse de polymères dans le but de former et d'étudier les grosses molécules obtenues de la pyrolyse, la méthode mise au point dans ce laboratoire est beaucoup plus avantageuse dû à la quantité du polymère que l'on peut pyrolyser à la fois.

Partie expérimentale

Le point de fusion a été déterminé à l'aide d'un appareil Buchi: la valeur rapportée n'est pas corrigée. Le spectre infrarouge a été enregistré sur un spectrophotomètre

Beckmann modèle IR-8 à double faisceau. Les spectres de résonance magnétique nucléaire ont été pris sur des spectromètres de 60 MHz Varian modèle T-60-A et JEOL modèle C-60-H. Les déplacements chimiques rapportés sont exprimés en ppm, le tétraméthylsilane étant utilisé comme référence interne. Ces spectres furent pris dans le $CDCl_3$. Les spectres de masse ont été pris sur un spectromètre AEI modèle MS-902 et/ou Hitachi–Perkin-Elmer modèle RMU-6-D selon le cas. Les analyses par chromatographie en phase gazeuse ont été faites sur un chromatographe analytique modèle Hewlett-Packard 5750 muni d'un détecteur à conductivité thermique. Les mesures des masses moyennes en nombre ($\overline{M}_n$) par tonométrie (15) ont été faites à l'aide de l'appareil 301A vapor pressure osmometer de la compagnie Hewlett-Packard. Le poly(adipate de butylène-1,4) provient de la compagnie Eastman Kodak.

Méthode de pyrolyse

(a) Pyrolyse près de l'entrée de la zone chauffée

Le polymère (environ 900 mg) est placé dans un bateau de porcelaine (8.5 × 1 × 0.8 cm) et gardé sous un courant d'azote à l'intérieur d'un tube de quartz non-garni (60 cm de long et 2.5 cm de diamètre interne) qui est placé dans un four. Lorsque le four, de marque Linberg Hevi-Duty SB Type 167, a atteint la température désirée pour la pyrolyse, le bateau est amené à l'intérieur de la zone chauffée à l'aide d'une tige de fer et d'aimants. A la sortie de la zone chauffée par le four, il y a trois trappes afin de récupérer les produits de la pyrolyse; la première est refroidie à l'air ambiant alors que les deux autres sont refroidies à l'azote liquide. Lorsque la pyrolyse est faite sous vide, il y a une pompe à vide et une jauge McLeod placées à la suite des trois trappes. Le débit d'azote est réglé à l'aide d'un régulateur placé au début du système. D'habitude, le débit d'azote est ajusté à 0.2 ℓ/min.

En faisant la pyrolyse de cette façon, les produits ont une longueur d'environ 30 cm de la zone chauffée par le four à parcourir.

(b) Pyrolyse près de la sortie de la zone chauffée

Cette fois-ci, le bateau est placé à l'extérieur du four dans le tube de quartz (voir la fig. 1). Lorsque la température désirée du four est atteinte, le tube de quartz est poussé de façon à ce que le bateau de porcelaine contenant le polymère se retrouve maintenant à l'intérieur de la zone chauffée par le four, mais cette fois-ci, près de la sortie. Dans ce cas, le polymère dans le bateau est placé environ 10 cm à l'intérieur de la zone chauffée, ceci étant par conséquent la distance maximum parcourue par les produits volatils de pyrolyse.

(c) Traitement des produits de la pyrolyse

Lorsque la pyrolyse est terminée et que la température du four est en deçà de 100°C, les produits se trouvant dans le tube de quartz à la sortie du four ainsi que dans les trappes sont recueuillis à l'aide de solvants appropriés. La colonne ainsi que les trois trappes sont lavées avec du $CHCl_3$. Le $CHCl_3$ est par la suite évaporé mais pas complètement. Déjà l'acide adipique commence à précipiter; ce précipité est filtré et la solution mère est placée au réfrigérateur afin de continuer la précipitation de l'acide adipique qui demeure en solution. Après avoir filtré à nouveau l'acide adipique, la solution restante est amenée à 10 ml en ajoutant du $CHCl_3$. Cette solution est, par la suite, analysée sur un chromatographe en phase gazeuse contenant une colonne de 9 pied × 0.25 po. de SE-54 10% sur Chromosorb W et programmée de 80 à 260°C à un taux de 10°C par min. La température est maintenue à 260°C durant 10 min environ. La température d'injection est de 260°C alors que celle du détecteur est de 300°C; le débit d'hélium est de 100 ml/min.

Analyse des produits

(a) Cyclopentanone

L'analyse quantitative de la cyclopentanone est effectuée en injectant une quantité connue d'une solution standard de cyclopentanone, et en comparant la surface enregistrée pour ce composé sur le chromatogramme à celle obtenue en injectant une quantité connue de la solution de pyrolyse.

(b) Butadiène-1,3

Pour mettre en évidence la présence du butadiène-1,3, la troisième trappe est refroidie à l'azote liquide afin d'isoler ce produit. La première trappe est toujours refroidie à l'air alors que la seconde trappe est refroidie à l'aide d'un mélange acétone – glace sèche qui laisse passer le butadiène-1,3. Le butadiène-1,3 était identifié par son spectre de masse qui correspond bien avec celui dans la littérature (18).

(c) Acide adipique

L'acide adipique est obtenu sous forme de cristaux blancs: pf 152–153°C (litt. (19) pf 153°C) (recristallisé dans l'eau). Le spectre infrarouge pris dans une suspension de KBr révèle une bande s'échelonnant entre 3300 et 2500 cm^{-1} caractéristique des acides carboxyliques. Une bande C=O à 1700 cm^{-1} est notée également. Le spectre rmn fut pris dans la pyridine-d_6, et il est similaire à celui donné dans la littérature (20). Le spectre de masse, qui montre un pic de base à m/e 100 ($C_5H_8O_2^{+\cdot}$), concorde bien avec celui donné dans la littérature (18).

*(d) Esters **5** et **6***

Lorsque l'acide adipique est enlevé par précipitation, le $CHCl_3$ est évaporé autant que possible, ainsi que la cyclopentanone. Le résidu, environ 500 mg, contenant les esters **5** et **6** est dissous dans 20 ml d'éther. Après l'avoir extraite trois fois avec 5 ml d'une solution de $NaHCO_3$ saturée, la phase organique est séchée sur du $MgSO_4$, puis évaporée pour donner le mélange de diesters **6**. La phase aqueuse est acidifiée, puis extraite au $CHCl_3$, afin de récupérer le mélange de monoesters **5**.

Nous présentons aux tableaux 2 et 3 les pourcentages de produits récupérés. Comme il nous a fallu déterminer les masses moyennes des esters **5** et **6**, nous présentons ces valeurs pour chacune des pyrolyses.

Remerciements

Les auteurs remercient vivement le Conseil National de Recherches du Canada (CNRC) pour l'aide financière accordée. F. Messier est reconnaissant des bourses d'étude du CNRC et du Ministère de l'Education du Québec.

1. J. Mitchell et J. Chiu. Anal. Chem. **47**, 289R (1975).
2. G. Champetier et L. Monnerie. Introduction à la chimie macromoléculaire. Masson et Cie, Paris. 1969.
3. R. L. Levy. Chromatogr. Rev. **8**, 49 (1966).
4. J. D. Kelly et C. J. Wolf. J. Chromatogr. Sci. **8**, 583 (1970).
5. E. M. Barral, R. S. Porter et J. F. Johnson. Anal. Chem. **35**, 73 (1963).

6. K. ETTRE et P. F. VARADI. Anal. Chem. **35**, 69 (1963).
7. F. A. LEHMANN et G. M. BRAUER. Anal. Chem. **33**, 673 (1961).
8. A bibliography on solids pyrolysis with selected references to vapor phase pyrolysis. Technical Paper 110672, Chemical Data Systems, Inc., Oxford, PA, U.S.A.
9. D. C. K. LIN, M. L. THOMSON et D. C. DEJONGH. Can. J. Chem. **52**, 2359 (1974).
10. D. C. K. LIN, M. L. THOMSON et D. C. DEJONGH. Can. J. Chem. **53**, 2293 (1975).
11. R. C. FUSON. Reactions of organic compounds. John Wiley and Sons, New York, NY. 1964. p. 678.
12. S. IWABUCHI, V. JAACKS, F. GABIL et W. KERN. Makromol. Chem. **165**, 59 (1973); S. IWABUCHI, V. JAACKS et W. KERN. Makromol. Chem. **177**, 2675 (1976).
13. I. LÜDERWALD et H. URRUTIA. Makromol. Chem. **177**, 2093 (1976).
14. I. LÜDERWALD, H. URRUTIA, H. HERLINGER et P. HIRT. Angew. Makromol. Chem. **50**, 163 (1976).
15. G. CHAMPETIER et L. MONNERIE. Introduction à la chimie macromoléculaire. Masson et Cie, Paris. 1969. p. 211.
16. R. C. FUSON. Reactions of organic compounds. John Wiley and Sons, New York, NY. 1962. p. 670.
17. N. IGLAUER et F. DENTLEY. J. Chromatogr. Sci. **12**, 23 (1974).
18. A. CORNU et R. MASSOT. Compilation of mass spectral data. Heydon and Son, London. 1966.
19. Handbook of chemistry and physics. 50ème ed. The Chemical Rubber Co., Cleveland. 1969–1970. p. C-329.
20. The Sadtler standard spectra. Sadtler Research Laboratories. 1972. Spectre No 4406 M.

Hydride transfer reactions. Oxidation of *N*-methylacridan by π acceptors[1]

ALLAN K. COLTER, GUNZI SAITO, AND FRANCES J. SHAROM

Guelph–Waterloo Centre for Graduate Work in Chemistry, University of Guelph, Guelph, Ont., Canada N1G 2W1

Received February 25, 1977

ALLAN K. COLTER, GUNZI SAITO, and FRANCES J. SHAROM. Can. J. Chem. **55**, 2741 (1977).

The oxidation of *N*-methylacridan (**1**) to *N*-methylacridinium ion (**2**) by the π acceptors *p*-benzoquinone (BQ), 7,7,8,8-tetracyanoquinodimethane (TCNQ), *p*-chloranil (CA), tetracyanoethylene (TCNE), and 2,3-dicyano-1,4-benzoquinone (DCBQ) has been investigated. Second-order rate constants in acetonitrile (AN) vary by a factor of more than 10^7 for this series. The rate of reaction of **1** with BQ increases 45-fold as the solvent composition is varied from AN to 50% (v/v) AN–water, but is insensitive to changes in buffer ratio or concentration in 75% AN. Spectroscopic evidence for charge-transfer complexing between the reactants was obtained with BQ and CA, and kinetic evidence for complexing was obtained with BQ in 75% AN. The primary isotope effect, p, calculated from the rates of oxidation of **1**, **1**-*9-d*, and **1**-*9,9-d*$_2$ (**1**(HH), **1**(HD), and **1**(DD)) in AN varied from 4.5 (TCNE) to 13 (BQ), while the secondary isotope effect, s, was approximately constant (~1.1). Values of the isotope partitioning ratio, *ipr* (the ratio of **2**(D) to **2**(H) formed in reaction of **1**(HD)) were determined for BQ in three AN–water mixtures and for CA, TCNE, and DCBQ in AN. For all systems studied, except BQ in 90% AN, where determination of the *ipr* is complicated by isotopic exchange between unreacted **1** and product (**2**), the *ipr* agrees with p/s from the kinetic measurements. These results are discussed in terms of mechanism and compared with those of other hydride transfer reactions involving dihydronicotinamide donors.

ALLAN K. COLTER, GUNZI SAITO et FRANCES J. SHAROM. Can. J. Chem. **55**, 2741 (1977).

On a étudié l'oxydation du *N*-méthylacridane (**1**) en ion *N*-méthylacridinium (**2**) par des accepteurs π comme la *p*-benzoquinone (BQ), le tétracyano-7,7,8,8 quinodiméthane (TCNQ), le *p*-chloranil (CA), le tétracyanoéthylène (TCNE) et le dicyano-2,3 benzoquinone-1,4 (DCBQ). Les constantes de vitesse du deuxième ordre dans l'acétonitrile (AN) varient par un facteur de plus de 10^7 pour cette série. La vitesse de réaction de **1** avec le BQ augmente par 45 fois lorsque l'on fait varier la composition de solvant de AN jusqu'à un mélange de 50% (v/v) de AN–eau; toutefois cette vitesse de réaction est insensible à des changements dans des rapports de tampons ou de concentrations dans AN à 75%. On a pu obtenir des données spectroscopiques indiquant qu'il y a une complexation de transfert de charge entre les réactifs avec BQ et CA et des données cinétiques suggérant qu'il s'effectue une complexation avec BQ dans AN à 75%. L'effet isotopique primaire, p, calculé à partir des vitesses d'oxydation de **1**, **1**-*9-d*, et de **1**-*9,9-d*$_2$ (**1**(HH), **1**(HD) et **1**(DD)) dans AN varie de 4.5 (TCNE) jusqu'à 13 (BQ) alors que l'effet isotopique secondaire, s, est approximativement constant (~1.1). On a déterminé les valeurs de rapport de partition d'isotopes (*ipr*) (le rapport de **2**(D) à **2**(H) formé lors de la réaction de **1**(HD)) pour BQ dans trois mélanges de AN–eau et pour CA, TCNE et DCBQ dans AN. Dans tous les systèmes étudiés, excepté BQ dans AN à 90% où la détermination de *ipr* est compliquée par un échange isotopique entre le composé **1** qui n'a pas réagit et le produit **2**, les valeurs de *ipr* sont en accord avec les valeurs de p/s obtenues à partir de mesures cinétiques. On discute de ces résultats en termes de mécanisme et on les compare avec ceux d'autres réactions de transfert d'hydrure impliquant la dihydronicotinamide comme donneur.

[Traduit par le journal]

Oxidations of dihydropyridines and related compounds by hydride acceptors are of interest as models for biological oxidation–reduction reactions involving the pyridine nucleotide coenzymes (2), and as reactions of π donors with π acceptors (3). Although generally viewed as one-step hydride transfers, several mechanisms involving sequential transfer of one or two electrons and a hydrogen atom or proton are possible in theory. In fact, arguments for a mechanism involving electron transfer followed by hydrogen atom transfer have been made (4), and evidence for free radical (5) and free radical chain (6) mechanisms has been reported for certain systems. More recently, isotope effects requiring one or more intermediates in the oxidation of N-substituted-1,4-dihydronicotinamides by trifluoroacetophenone (7), *N*-methylacridinium ion

[1]For a preliminary account of a portion of these results, see ref. 1.

(8), and the Zn^{2+} complex of 1,10-phenanthroline-2-carboxaldehyde (9) have been reported. The kinetic deuterium isotope effect in these reactions is substantially smaller than that demanded by the isotope partitioning ratio (*ipr*) (*i.e.*, the ratio of hydrogen to deuterium transferred in reaction of the 4-*d*-dihydronicotinamide) for a one-step mechanism.

While it is clear that oxidation of dihydropyridines by compounds capable of reacting as either hydride or electron acceptors sometimes occurs by a stepwise mechanism, we know of no reaction where all of the evidence *requires* a synchronous transfer of a proton and two electrons. For example, kinetic deuterium isotope effects which establish C—H bond breaking in the rate-determining step (1, 7–10) are equally consistent with hydrogen atom transfer within a reversibly-formed radical ion pair. We have undertaken a systematic study of the oxidation of dihydropyridine analogs with π acceptors with the aim of elucidating the mechanisms of these reactions and the dependence of the mechanism on structural and environmental variables.

For our initial studies we have chosen *N*-methylacridan (**1**) as hydride donor. This choice

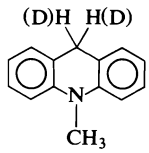

1(HH), **1**(HD), **1**(DD)

was based on several considerations. It is experimentally much simpler than the more extensively studied dihydronicotinamides, which are chemically more labile and in which there is a possibility of concurrent scrambling of deuterium between the 2-, 4-, and 6-positions (11). More importantly, both the lower ionization potential of **1** (below) and the smaller gain in resonance energy accompanying loss of hydride (compared to the dihydropyridines) (12) was expected to increase the lifetime of a radical ion pair intermediate. This paper describes an investigation of the products and stoichiometry, kinetics, solvent effects, and deuterium isotope effects in reaction of **1** with the acceptors *p*-benzoquinone (BQ), 7,7,8,8-tetracyanoquinodimethane (TCNQ), *p*-chloranil (CA), tetracyanoethylene (TCNE), and 2,3-dicyano-1,4-benzoquinone (DCBQ). An

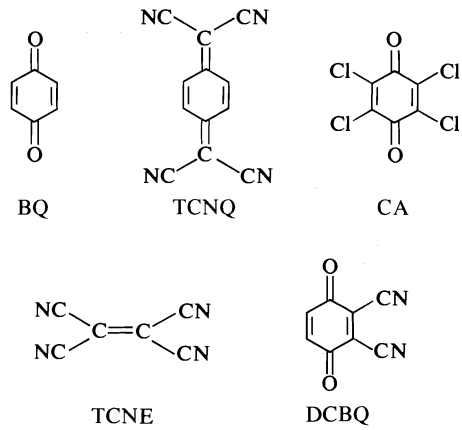

BQ TCNQ CA

TCNE DCBQ

earlier kinetic study of the oxidation of **1** with 2,6-dichloroindophenol has appeared (13).

Results

The products of oxidation of **1** by the five acceptors were identified by direct spectral examination of reaction mixtures under conditions similar to those of the kinetic studies (below), and by spectral and elemental analysis of isolated crystalline products. In agreement with earlier work (13, 14), the oxidation product in all cases is the *N*-methylacridinium ion (**2**), identi-

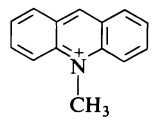

2

fied by spectral comparison with authentic *N*-methylacridinium salts (λ_{max} = 359 nm), and by isolation as the chloride or perchlorate salt. Reaction of 1:1 molar quantities of **1** and BQ in buffered 90% (v/v) acetonitrile–water (90% AN) followed by addition of hydrochloric acid afforded $\mathbf{2}^+Cl^-$, along with hydroquinone, as the only isolable products. Reaction of **1** (2×10^{-4} *M*) with TCNQ (1.5×10^{-2} *M*) in AN was accompanied by the appearance of absorption maxima at 670 and 740 nm characteristic of the radical anion $TCNQ^{\cdot-}$ (15). The spectra (above 400 nm) of solutions of the products of reaction of **1** with excess CA are consistent with those expected for mixtures of CA and its hydroquinone monoanion, CAH^- in equilibrium with the radical anion $CA^{\cdot-}$ (λ_{max} 415–420, 435–440 nm) (16). With TCNE and DCBQ the principal reduction products as indi-

cated by uv–visible spectra are the corresponding radical anions $TCNE^{\cdot-}$ (17), and $DCBQ^{\cdot-}$ (18), respectively. Similar results have been reported by Wallenfels *et al.* (19) in reaction of dihydropyridines with TCNE. In the reactions of **1** with TCNQ, TCNE, and DCBQ the corresponding crystalline radical ion salts of **2** can be isolated in high yield, however the $DCBQ^{\cdot-}$ salt rapidly decomposes on exposure to air. Details of the application of this method to the preparation of radical anion salts of quaternary heterocyclic cations will be published separately.

Based on these observations, the stoichiometry of these reactions is best represented by [1] for

[1] $$\mathbf{1} + A \rightarrow \mathbf{2}^{+} + AH^{-}$$

BQ; with the other four acceptors the equilibrium represented by [2] (16, 20) occurs to vary-

[2] $$2AH^{-} + A \rightleftharpoons 2A^{\cdot-} + AH_2$$

ing extents. With TCNQ, TCNE, and DCBQ the complete oxidation of 1 mol of **1** requires approximately 1.5 mol of acceptor.

Hydroquinone isolated from reaction of **1**(HD) with BQ in 90% AN contained no excess deuterium (mass spectral analysis) indicating that the hydrogen is transferred to an oxygen rather than to a carbon. Intermediate formation of **3**, as might be expected by analogy with other

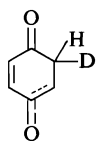

3

nucleophilic additions to quinones (21) would, in isomerizing to the hydroquinone monoanion, retain some excess deuterium bound to carbon. A second control experiment in which **1**(DD) was oxidized by BQ in 90% AN led to **2**(D) having no detectable H in the 9-position, demonstrating the absence of any exchange of the hydrogens at this position with solvent during the course of the oxidation. This result rules out mechanisms in which the hydrogen is transferred as a proton from any intermediate of reasonable lifetime.

Mixing of separate solutions of BQ and **1** in benzene, chloroform, ether, or AN is accompanied by instantaneous appearance of a new broad long wavelength absorption band (λ_{max} in benzene 505 nm) which disappears as the components react. A transient long wavelength absorption could be observed for several other acceptors as well, but measurement of its position becomes increasingly difficult with increasing acceptor reactivity. In benzene solvent, in which the subsequent reaction is slowest, measurement of λ_{max} was possible with CA and less reactive acceptors. With acceptors more reactive than CA, the band was masked by absorption due to the rapidly-formed acceptor radical anion.

In order to confirm that the new maxima were charge-transfer absorptions, λ_{max} was measured for a series of five acceptors with the donors **1**, pyrene, and perylene (Table 1). Plots of the absorption frequencies for **1** *vs.* those for the corresponding pyrene and perylene complexes describe reasonably good straight lines with slopes of 0.95 ± 0.07 (pyrene) and 0.97 ± 0.07 (perylene).

It is noteworthy that the donor strength of **1** (as measured by charge-transfer frequencies) is much closer to that of 10-methylphenothiazine (**4**) and phenoxazine (**5**) than diphenylamine. For example, the charge-transfer frequencies for complexes of **4**, **5**, and diphenylamine with CA

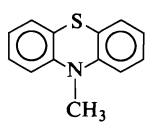

4

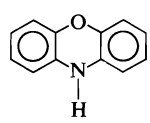

5

are, respectively, 14.4×10^3 cm^{-1} (AN) (22), 13.7×10^3 cm^{-1} (AN) (22), and 15.4×10^3 cm^{-1} (chloroform) (23), compared to 13.7×10^3 cm^{-1} (benzene) for **1**.

Spectroscopic evidence for charge-transfer complexing between the reactants in hydride transfer reactions involving dihydropyridine donors has been reported previously (10*c*, 10*e*, 24). While no quantitative comparison of the donor strengths of **1** and *N*-alkyl-1,4-dihydronicotinamides is presently available, *N*-2,4,6-trimethylbenzyl-1,4-dihydronicotinamide was shown to be a weaker donor than **1**. Mixtures of TNB and **1** in chloroform showed a well-defined maximum at 515 nm, while chloroform solutions of the dihydronicotinamide and TNB showed no evidence for charge-transfer absorption above 500 nm.

TABLE 1. Charge-transfer absorption maxima for complexes of π acceptors with *N*-methylacridan (**1**), pyrene, and perylene

Acceptor	$10^{-3} \times \bar{\nu}_{max}$ (cm^{-1})		
	1[a]	Pyrene[b]	Perylene[b]
BQ	19.8	22.6	19.0
1,3,5-Trinitrobenzene	19.5	22.2	19.6
2,3-Dichloro-1,4-naphthoquinone	17.9	19.5	16.8
2,3-Dichloro-5-nitro-1,4-naphthoquinone	15.0	17.5	14.5
CA	13.7	16.2	13.2

[a]Benzene solvent.
[b]Chloroform solvent.

TABLE 2. Rates of oxidation of *N*-methylacridan (**1**) by BQ in buffered aqueous AN[a]

Run No.	%AN[b]	$10^2 \times$ [HOAc] (*M*)	$10^2 \times$ [NaOAc] (*M*)	$10^3 \times k$ (M^{-1} s^{-1})[c]
1	75.12	1.02	1.02	6.35 ± 0.03(6.41)[d]
2	75.24	2.03	2.03	6.07 ± 0.09(6.17)
3	75.40	4.06	4.06	5.51 ± 0.02(5.66)
4	75.15	2.03	1.02	6.27 ± 0.01(6.33)
5	75.09	0.508	1.02	5.96 ± 0.09(6.00)
6	75.12	0.979	0.979	42.2 ± 1.1[e]

[a]Concentrations: **1**, $1.0–1.3 \times 10^{-4}$ *M*; BQ, $1.01–1.09 \times 10^{-2}$ *M*. Temperature, 25.07°C unless otherwise indicated.
[b]Percentage acetonitrile (v/v, 25°C).
[c]Pseudo first-order rate constant ÷ stoichiometric BQ concentration. Averages of two rate runs with average deviation.
[d]Values in parentheses corrected to exactly 75% (v/v) acetonitrile–water.
[e]Temperature, 54.95°C.

All rate measurements were carried out under pseudo first-order conditions using a large excess of acceptor. The progress of the reaction was followed spectrophotometrically utilizing the acridinium absorption at 359 nm (BQ, TCNE) or 420 nm (CA, DCBQ) or that of the radical anion (TCNQ, 680 nm). The TCNE and DCBQ rates were measured using stopped flow spectrophotometry. The kinetics are first-order in each reactant within experimental error at sufficiently low acceptor concentrations, with small deviations from strict second-order behaviour at higher acceptor concentrations (below).

The first kinetic studies with BQ were carried out in buffered AN–water mixtures. Because of the possibility of general acid catalysis, the influence of small changes in buffer ratio and concentration was examined with acetic acid – sodium acetate buffers. Within the limited ranges studied, second-order rate constants (Table 2) vary only slightly with buffer ratio or concentration. A similar insensitivity to p*H* and ionic strength has been observed in oxidations of *N*-alkyl-1,4-dihydronicotinamides with thiobenzophenone (10*a*), BQ (25), and trifluoroacetophenone (26), all in mixed aqueous solvents. The difficulty in demonstrating general acid catalysis in mixed aqueous solvents has been noted (27) and our limited investigation does not exclude the possibility of a very small contribution from acid catalysis. The small decrease in second-order rate constant with increasing buffer concentration is most likely a result of a salt-induced medium effect (28). The activation parameters for reaction of **1** with BQ in 75.12% AN, calculated from runs *1* and *6*, are $\Delta H^{\ddagger} = 11.7 \pm 0.3$ kcal mol^{-1} and $\Delta S^{\ddagger} = -29.4 \pm 1.2$ cal deg^{-1} mol^{-1}.

The rate measurements with BQ are complicated by its photochemical instability, which becomes more serious with decreasing ratio of acetic acid to sodium acetate and increasing percent AN (slower rates). In the absence of a proton source the kinetic behaviour in 100% AN is complex. For these reasons, most of the subsequent rate measurements were carried out in the presence of 0.01 *M* acetic acid.

Because of the expectation of molecular complexing between the reactants, second order rate constants (pseudo first-order rate constant ÷ stoichiometric acceptor concentration) were measured at several concentrations of BQ in

75% AN (Table 3). The reproducibility of independently-determined rate constants is about ±2% (*e.g.*, compare runs *11* and *12*). Nevertheless, a fairly regular decrease in k with increasing BQ concentration is clearly discernible. Similar results have been observed in the oxidation of *N*-alkyl-1,4-dihydronicotinamides with flavins (10*c*, 24*c*) and *N*-methylacridinium ion (24*d*).

The data are consistent with any of several mechanisms involving equilibrium complexation of the reactants, *e.g.*, [3], where DH is the

$$\text{DH} + \text{A} \underset{}{\overset{K}{\rightleftharpoons}} \text{DH}\cdot\text{A} \xrightarrow{k_c} \text{Products} \qquad [3]$$

donor and A the acceptor. Under conditions where the acceptor is in large excess, this mechanism leads to [4] (3), where k is the

$$1/k = 1/k_cK + c_A/k_c \qquad [4]$$

observed second-order rate constant at a stoichiometric concentration of A = c_A. A plot of the kinetic data in Table 3 according to [4] leads, by least-squares analysis, to $K = 0.19\ M^{-1}$ (standard deviation 0.03) and k_cK (the true second-order rate constant based on uncomplexed reactants) = $5.88 \pm 0.05 \times 10^{-3}\ M^{-1}\ s^{-1}$. Exclusion of the point for run *13*, which lies furthest from the best fit straight line, leads to $K = 0.20 \pm 0.02\ M^{-1}$ and $k_cK = 5.88 \pm 0.04 \times 10^{-3}\ M^{-1}\ s^{-1}$.

While the kinetic results are consistent with 1:1 complex formation between the reactants with an association constant of *ca.* $0.20\ M^{-1}$, this interpretation must be viewed with some caution because of the very small decreases in k. Nonspecific medium effects resulting from 0.5 *M* BQ might easily produce changes in k comparable to those observed.

TABLE 3. Rates of oxidation of *N*-methylacridan (**1**) by BQ as a function of BQ concentration[a]

Run No.	c_{BQ} (M)[b]	$10^3 \times k$ ($M^{-1}\ s^{-1}$)[c]
7	0.0118	5.841±0.003
8	0.0236	5.80 ±0.03
9	0.0986	5.76 ±0.04
10	0.1033	5.81 ±0.05[d]
11	0.1845	5.76 ±0.01[d]
12	0.1967	5.57 ±0.04
13	0.2984	5.76 ±0.05
14	0.3931	5.51 ±0.04
15	0.5001	5.28 ±0.05

[a]Solvent 75:25 (v/v, 25°C) acetonitrile–water, 0.01 *M* acetic acid. Temperature, 25.0°C. Concentration of **1**, $0.5–1.4 \times 10^{-4}$ *M*.
[b]Stoichiometric BQ concentration.
[c]See footnote *c*, Table 2. Averages of three measurements, except as noted, listed with standard deviations.
[d]Average of two measurements.

TABLE 4. Solvent effect on the rate of oxidation of *N*-methylacridan (**1**) by BQ in AN–water mixtures[a]

Run No.	%AN[b]	Z (kcal mol^{-1})[c]	$10^3 \times k$ ($M^{-1}\ s^{-1}$)
16	100	71.8	0.567±0.001
17	90	80.1	1.80 ±0.02
18	80	83.6	4.26 ±0.04
9	75	83.9	5.76 ±0.04
19	70	86.1	8.08 ±0.02
20	60	—	14.2 ±0.02
21	50	—	25.4 ±0.02

[a]Temperature, 25.0°C. Concentrations: **1**, $0.7–1.2 \times 10^{-4}$ *M*; BQ, 0.0986 *M*.
[b]Percentage AN (v/v, 25°C), 0.01 *M* acetic acid.
[c]Energy of the interionic charge-transfer band of 1-ethyl-4-carbomethoxypyridinium iodide, 25°C (29).

The effect of solvent on the rate of reaction of **1** with BQ was examined in AN–water mixtures covering the range 50 to 100% AN (Table 4). In order to obtain a more quantitative measure of the sensitivity of the rate to changes in ion-solvating ability, Z values (29) were measured for five of the seven solvents. Direct measurement of Z is not possible for AN–water mixtures containing more than about 30% water (29). A plot of log k *vs.* Z is reasonably linear; least-squares analysis leads to [5] (corr. coef. 0.985),

$$\log k = 8.11 \pm 0.64 \times 10^{-2}\, Z - 9.12 \pm 0.52 \qquad [5]$$

where the stated uncertainties are standard deviations.

An increase in rate with increasing ion-solvating ability has been noted previously in reactions of various 1,4-dihydropyridines with thiobenzophenone (10*a*), riboflavin (10*b*), pyridoxal (30), and hexachloroacetone (10*e*). The most extensive study of solvent effects is that of van Eikeren and Grier (26) who found that the rate of oxidation of *N*-propyl-1,4-dihydronicotinamide by trifluoroacetophenone in dimethyl sulfoxide – water and 2-propanol–water mixtures depended only on the mole fraction of water. If the same is true of AN–water mixtures (AN and dimethyl sulfoxide have almost identical Z values) then log k for the reaction of **1** with BQ is about 0.7 times as sensitive to solvent changes as log k for the reaction of van Eikeren and Grier, between $X_{H_2O} = 0.50$ to 0.75. In contrast, solvent effects in the oxidation of *N*-propyl-1,4-dihydronicotinamide with BQ in AN–water mixtures at 23.5°C[2] are practically identical to those found in the present work.

[2]F. J. Sharom, unpublished work.

TABLE 5. Rates of oxidation of **1**(HH), **1**(HD), and **1**(DD) with various π acceptors[a]

Acceptor	Solvent	[Acceptor] (M)	k (M^{-1} s^{-1}) **1**(HH)	**1**(HD)	**1**(DD)
BQ	60% AN[b]	9.87×10^{-2}	1.42×10^{-2}	7.40×10^{-3}	1.48×10^{-3}
BQ	75% AN[b]	3.93×10^{-1}	5.51×10^{-3}	2.90×10^{-3}	4.80×10^{-4}
BQ	90% AN[b]	5.00×10^{-1}	1.86×10^{-3}	9.92×10^{-4}	1.55×10^{-4}
BQ	AN[b]	5.00×10^{-1}	5.79×10^{-4}	2.96×10^{-4}	4.11×10^{-5}
TCNQ	AN	1.54×10^{-2}	2.32×10^{-1}	1.18×10^{-1}	3.21×10^{-2}
TCNQ	AN[b]	1.37×10^{-2}	2.33×10^{-1}	1.16×10^{-1}	3.16×10^{-2}
CA	AN	4.18×10^{-3}	1.17×10	5.91	1.34
TCNE	AN	2.08×10^{-3}	1.01×10^{2}	5.67×10	1.94×10
DCBQ	AN	2.02×10^{-3}	8.67×10^{3}	4.80×10^{3}	1.49×10^{3}

[a]Temperature, 25.0°C. Concentration of **1**, $0.8–2.0\times10^{-4}$ M. Rate constants reproducible to ±1% with BQ, TCNQ, and CA; ±3% with TCNE and DCBQ.
[b]Containing 0.01 M acetic acid.

We next carried out a less detailed investigation of the kinetics of reaction of **1** with the four stronger π acceptors in AN. Under the conditions studied, the five acceptors cover a 1.5 × 10^7-fold range of reactivity (Table 5). With TCNQ, CA, TCNE, and DCBQ a proton source is not required for good pseudo first-order kinetics, however the presence of 0.01 M acetic acid was shown to have no significant effect on the observed rate with TCNQ (Table 5). Spectroscopic evidence for complexing between the reactants was observed with CA and complexing is expected for the other acceptors as well. However, at the low concentrations of acceptor used in the rate measurements, the calculated second-order rate constants were shown to be very close to the true second-order rate constants for uncomplexed reactants. For example, k for reaction of **1**(HH) with 5.0×10^{-3} M TCNQ is 2.38×10^{-1} M^{-1} s^{-1}, close to the value observed with 1.5×10^{-2} M TCNQ (Table 5). Similarly, a tenfold increase in TCNE concentration led to no significant change in k.

Also listed in Table 5 are rate constants for reaction of **1**(HD) and **1**(DD) with BQ in three AN–water mixtures and with all five acceptors in AN.

Any mechanism in which the hydrogen is transferred in a rate-determining step involving the reactants or an intermediate in equilibrium with reactants leads to the relationships summarized in [6]. The rate constants k_{HH}, k_{HD}, and k_{DD} are the experimental rate constants for **1**(HH), **1**(HD), and **1**(DD), respectively; k_H, k_H', k_D, and k_D' are the corresponding rate constants for transfer of the four types of hydrogen and deuterium. The primary isotope effect, p, and the secondary isotope effect, s, defined by [7] and [8], are related to the experimental rate

[6]

$$\mathbf{1}(HH) \xrightarrow{2k_H} \mathbf{2}(H) \qquad k_{HH} = 2k_H$$

$$\mathbf{1}(HD) \xrightarrow{k_H'} \mathbf{2}(D) \qquad \mathbf{1}(HD) \xrightarrow{k_D} \mathbf{2}(H) \qquad k_{HD} = k_H' + k_D$$

$$\mathbf{1}(DD) \xrightarrow{2k_D'} \mathbf{2}(D) \qquad k_{DD} = 2k_D'$$

[7] $$p = k_H/k_D = k_H'/k_D'$$

[8] $$s = k_H/k_H' = k_D/k_D'$$

[9] $$k_{HH}/k_{DD} = p \times s$$

[10] $$k_{HD}/k_{DD} = (p + s)/2$$

constants by [9] and [10]. Primary and secondary isotope effects, calculated from the data in Table 5 using [9] and [10], are listed in Table 6. With BQ, the experimental rate constants are slightly smaller than the true second-order rate constants (above). However, barring extraordinarily large secondary isotope effects on the complexation constants, K, such corrections will have a negligible effect on the calculated values of p and s.

For any of the mechanisms for which the relationships in [6] hold, the isotope partitioning ratio (*ipr*) that is, the ratio of **2**(D) to **2**(H) formed from reaction of **1**(HD), is given by k_H'/k_D, or p/s. Values of the *ipr* were determined for four of the acceptors by mass spectral analysis of isolated *N*-methylacridinium chloride (**2**$^+$Cl$^-$) and are listed for comparison with the kinetically-determined values of p/s in Table 6.

TABLE 6. Kinetic isotope effects and isotope partitioning ratios

Acceptor	Solvent	Kinetic isotope effects[a]			
		p	*s*	*p*/*s*	*ipr*[c]
BQ	60% AN[b]	8.95±0.41	1.08±0.06	8.3±0.6	8.1±1.4
BQ	75% AN[b]	11.0 ±0.5	1.04±0.05	10.6±0.7	9.1±1.9
BQ	90% AN[b]	11.8 ±0.5	1.02±0.05	11.6±0.8	9.4±2.0
BQ	AN[b]	13.3 ±0.6	1.06±0.05	12.6±0.8	—
TCNQ	AN	6.20±0.32	1.16±0.07	5.3±0.4	—
CA	AN	7.66±0.37	1.14±0.06	6.7±0.7	6.2±0.7
TCNE	AN	4.76±0.33	1.10±0.09	4.4±0.5	4.5±1.4
DCBQ	AN	5.37±0.35	1.09±0.08	4.9±0.5	4.7±0.1

[a]Calculated from the data in Table 5 using [9] and [10]; errors based on ±1% uncertainties in k_{HH}, ±3% in k_{HD}, and ±2% in k_{DD} for BQ, TCNQ, and CA, and ±3% in all rate constants for TCNE and DCBQ (See Experimental).
[b]Containing 0.01 *M* acetic acid.
[c]Ratios of acceptor to **1** were 1000 with BQ, 50 with CA, 20 with TCNE and DCBQ. Averages of two to nine determinations, listed with standard deviations. The *ipr*'s are corrected for contamination of **1**(HD) by **1**(HH).

With BQ the measured *ipr* was found to increase toward an upper limit as the ratio of BQ to **1** was increased. For example, in 90% AN the *ipr* increased from 2.9 at 1:1 BQ–**1**, to approximately 9.4 at 1000:1 BQ–**1**. This variation is believed to be a result of isotopic exchange involving unreacted *N*-methylacridan, **1**, and the *N*-methylacridinium ion, **2**, produced in the reaction, *e.g.*, [11].

$$\mathbf{1}(HD) + \mathbf{2}(D) \rightleftharpoons \mathbf{1}(DD) + \mathbf{2}(H)$$
$$\mathbf{1}(HD) + \mathbf{2}(H) \rightleftharpoons \mathbf{1}(HH) + \mathbf{2}(D) \quad [11]$$

Reactions of this type provide a mechanism for conversion of unreacted **1**(HD) to a mixture of **1**(HH), **1**(HD), and **1**(DD). Such scrambling of deuterium will have the effect of reducing the measured *ipr*, and if the true *ipr* is large even a very small amount of scrambling will cause a large error. The *N*-methylacridinium ion is expected to be a much more reactive acceptor than BQ.[3] The occurrence of rapid exchange was directly confirmed by nmr spectroscopic monitoring of solutions containing isotopically labelled **1** and **2**. Complications due to isotopic scrambling are expected to become more serious with increasing percent AN since the rates of the exchange reactions should be less sensitive to solvent ion-solvating ability than that of the BQ reaction. In fact, it was not possible to completely suppress scrambling in 90 and 100% AN, even at a 1000 to 1 ratio of BQ to **1**. Higher ratios are impractical because of the consequent difficulty of isolating the product. Lower ratios of acceptor to **1** were required with the more reactive acceptors. In theory, exchange reactions [11] leading to isotopic scrambling should lead to curvature in the first-order rate plots for **1**(HD). However, under the conditions of the rate measurements no significant curvature was observed.

The most significant results of the isotope effect studies are the uniformly high primary isotope effects and the agreement between *p*/*s* derived from kinetic measurements and product analyses. Both results stand in striking contrast to those for the dihydronicotinamide oxidations cited earlier (7–9). Dittmer *et al.* (10*e*) also found approximate agreement between kinetic and product isotope effects in oxidation of *N*-benzyl-1,4-dihydronicotinamide with hexachloroacetone, pentachloroacetone, and *s*-tetrachloroacetone. Significantly, the agreement between kinetic and product isotope effects in the present work holds for acceptors covering a 1.5×10^7-fold range in reactivity, and in spite of considerable variation in the primary isotope effect. The very high primary isotope effects observed with BQ suggest a contribution from quantum mechanical tunneling (32). This possibility is under investigation. Secondary isotope effects are normal, and approximately constant. Although *s* appears to be somewhat smaller with BQ than with the more reactive acceptors, the difference may well be less than the combined experimental uncertainties.

Discussion

The kinetic isotope effects observed in the

[3]For example, Hajdu and Sigman (31) found CA to be only 29 times as reactive as **2** in oxidation of *N*-benzyl-1,4-dihydronicotinamide in AN, while the reactivity of CA relative to BQ observed in the present work is approximately 2×10^4.

present work require a mechanism in which the C—H bond is broken in a step which is both rate- and product-determining. Two such mechanisms, which we will describe as one-step hydride transfer and sequential electron–hydrogen atom transfer mechanisms, are represented by [12] and [13]. DH represents hydride

$$[12]\quad DH + A \underset{}{\overset{\text{Rapid}}{\rightleftharpoons}} \underset{\text{Charge-transfer complex}}{DH\cdot A} \xrightarrow[\text{of } H:^-]{\text{Slow transfer}} D^+ + AH^-$$

$$[13]\quad DH + A \overset{\text{Rapid}}{\rightleftharpoons} DH\cdot A \underset{k_{-1}}{\overset{k_1}{\rightleftharpoons}} \underset{\text{Radical-ion pair}}{DH^{\ddagger}A^{\mp}} \xrightarrow[\text{Slow transfer of H}\cdot]{k_2} D^+ + AH^-$$

donor and A the hydride (or π) acceptor. Since some dihydronicotinamide oxidations require an intermediate such as $DH^{\ddagger}A^{\mp}$ (7–9) it is of interest to examine the extent to which the present results can be accomodated by a mechanism such as [13].[4]

The reactants are in rapid equilibrium with a charge-transfer complex and it is at least reasonable to assume that subsequent electron or hydride transfer proceeds by way of a transition state resembling the complex in relative orientation of the donor and acceptor. Substantial donor–acceptor interaction is expected between the two reactants (**6**) and the products of either electron (**7**) or hydride (**8**) transfer, the donor

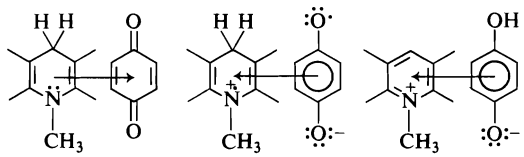

6 **7** **8**

and acceptor roles reversing in the process. Although any charge-transfer interaction may be weaker in the transition state than in the reactants (**6**) or products (**7** or **8**), a face-to-face orientation will also be favored by electrostatic interaction between the developing positive and negative charges. However, further work is required to establish the orientation of the donor and acceptor in the transition state.

The somewhat smaller solvent effects in the oxidation of *N*-propyl-1,4-dihydronicotinamide[2] (or **1**) with BQ than with trifluoroacetophenone (26) may be a result of greater delocalization of the developing negative charge, or to donor–acceptor or electrostatic interaction in the transition state for the BQ reaction. It is instructive to compare our solvent effects with those in the anchimerically-assisted ionization of *p*-methoxyneophyl *p*-toluenesulfonate at 75°C (k_{ion}) (33). Using the extensive comparisons of the common solvent polarity parameters published by Reichardt and Dimroth (34), we can estimate that

$$[14]\quad \log k\ (\mathbf{1} + BQ, 25°C) \approx 0.58 \log k_{ion} + \text{constant}$$

The observation that log k for reaction of **1** with BQ is less sensitive to ion-solvating ability than log k_{ion} seems more consistent with partially developed charges in the rate-determining transition state (as in [12]) than with fully developed positive and negative charges (as in [13]).

The isotope effects observed in the present work and those reported by Chipman and Sigman and their co-workers in oxidations of *N*-alkyl-1,4-dihydronicotinamides (7–9) can both be accomodated by mechanism [13] ($k = k_1k_2/(k_{-1} + k_2)$) provided that $k_{-1} \gg k_2$ for oxidation of **1** but that $k_{-1} \approx k_2$ for the dihydronicotinamide oxidations. *A priori* we expect both k_{-1} and k_2 to be smaller, and k_1 to be larger, for the oxidation of **1** than for oxidation of a dihydronicotinamide with the same acceptor under similar conditions. This prediction follows from the lower ionization potential of **1** and the smaller gain in resonance energy accompanying aromatization. More specific comparisons of the present systems with those of Chipman and Sigman are difficult because of the different acceptors and solvents used. However, the reactivity of *N*-propyl-1,4-dihydronicotinamide is approximately 10^3 times that of **1** for reaction with BQ in aqueous AN.[2] If both reactions proceed according to [13], then given the relative magnitudes of k_1 and $(k_{-1} + k_2)$ for the two systems (above), this difference in reactivity must reflect a *greater* than 10^3-fold difference in k_2 in the expected direction.

It is more difficult to understand the large variation in p on the basis of [13]. The acceptors studied are of two types: those in which hydro-

[4]While it is convenient to picture [12] and [13] as discrete mechanisms for the purposes of this discussion, a continuous spectrum of mechanisms intermediate between [12] and [13] is possible.

gen is transferred to oxygen (BQ, CA, DCBQ) and those in which hydrogen is presumably transferred to carbon (TCNQ, TCNE). Within each group, p decreases with increasing reactivity. To reconcile these results with [13] the transition state for the hydrogen transfer step must vary substantially from $BQ^{\bullet-}$ to $DCBQ^{\bullet-}$. Specifically, since the hydrogen transfer step in [13] would have to be highly favorable energetically, the observed trends in p seem to require that k_2 increase in the order $BQ^{\bullet-} < CA^{\bullet-} < DCBQ^{\bullet-}$. While the observed dependence of the rate on acceptor and solvent are in line with expected changes in k_1/k_{-1}, there is less reason to expect k_2 to be greatly different for $BQ^{\bullet-}$, $CA^{\bullet-}$, and $DCBQ^{\bullet-}$, or for $BQ^{\bullet-}$ in the four solvents investigated. However, a more complete understanding of the dependence of the rate on acceptor structure is required before we can comment further. On the other hand, the variation in p is easily accomodated by [12], where the large differences in reactivity result from differences in the rate of the step in which the C—H bond is broken.

Either mechanism predicts a correlation of acceptor reactivity with the stability of AH^- relative to A. Unfortunately, no independent measure of hydride acceptor strength is presently available. Acceptor reactivity parallels the ease of one-electron reduction (as measured, for example, by the polarographic half-wave potentials, $\varepsilon_{1/2}$ (red), for reversible one-electron reduction) within each group but not necessarily when comparing a cyanocarbon to a quinone. For example, the reactivities of CA and TCNQ are in the opposite order to that predicted by their ease of one-electron reduction ($\varepsilon_{1/2}$ (red) = +0.01 and 0.19 V, respectively, *vs.* S.C.E. in AN) (35). A more extensive investigation of reactivity as a function of acceptor structure is in progress.

In summary, the results of the present investigation are completely consistent with a one-step hydride transfer mechanism [12]. While the results do not conclusively exclude a sequential electron–hydrogen atom transfer mechanism such as [13], solvent effects and trends in primary isotope effects are less easily accomodated with such a mechanism.

Experimental

Reagents and Solvents

N-Methylacridan, **1**(HH), was prepared by reduction of *N*-methylacridinium chloride, iodide, or perchlorate with sodium borohydride. In a typical reaction, a solution of 0.386 g (0.01 mol) of sodium borohydride (98%) in 15 ml of water was added dropwise to a stirred, cooled (0°C), solution of 2.30 g (0.01 mol) of $\mathbf{2}^+Cl^-$ in 25 ml of methanol. After stirring for 1 h at 0°C and 3 h at room temperature, the methanol was evaporated under reduced pressure and the product extracted into ether. The combined extracts were dried over K_2CO_3, filtered, and the ether evaporated to yield **1** in quantitative yield. The product was purified by crystallization from absolute ethanol or methanol and sublimation, to give colourless crystals, mp 89–91°C (lit. (36) mp 95°C). The *p*-toluenesulfonate and iodide salts of **2** were prepared by standard methods (37). The chloride salt was prepared by heating an aqueous solution of $\mathbf{2}^+I^-$ with an excess of AgCl in suspension, filtration, and evaporation to dryness under reduced pressure. The residue was dissolved in ethanol, precipitated by addition of ether, and recrystallized from 80:20 ethyl acetate – ethanol, mp 165–168°C. The perchlorate salt was obtained by dropwise addition of 70% perchloric acid to a solution of 5 g of the *p*-toluenesulfonate salt in 30 ml of ethanol until precipitation was complete, filtration and crystallization from methanol, mp 243–247°C (dec.).

N-Methylacridan-*9-d*, **1**(HD), was prepared and purified as described for **1**(HH) using $NaBD_4$ (> 98% isotopic purity). The product ordinarily contained about 5% **1**(HH) (nmr).

N-Methylacridan-*9,9-d*$_2$ was prepared from **1**(HD) by oxidation with 2,3-dichloro-5,6-dicyano-1,4-benzoquinone (DDQ), isolation as $\mathbf{2}^+ClO_4^-$, re-reduction with $NaBD_4$, and so on. In a typical oxidation, a solution of 1.71 g (7.5×10^{-3} mol) of DDQ in 125 ml of ether was added dropwise to a stirred solution of 1.42 g (7.2×10^{-3} mol) of **1** in 25 ml of ether, at room temperature. Addition of 2 ml of 70% perchloric acid resulted in precipitation of $\mathbf{2}^+ClO_4^-$, which was filtered, washed with ether, and dried. Yield, 2.14 g (100%). Starting from 7.03 g of **1**(HD), six oxidations and six reductions, followed by crystallization from methanol, led to **1** in 26% overall yield, containing 98.8% D at the 9-position, *i.e.*, 97.6% **1**(DD). The product was sublimed before use.

BQ, TCNQ, CA, and TCNE were obtained from commercial sources and were carefully purified before use. BQ was purified by repeated crystallization from CCl_4 and sublimation, TCNQ was crystallized three times from AN and once from tetrahydrofuran, CA was crystallized four times from benzene, and TCNE was sublimed twice. DCBQ was prepared as described by Brook (38) and purified by sublimation, mp 177–179°C (lit. (38) mp 178–180°C).

Pyrene, perylene, 1,3,5-trinitrobenzene, and 2,3-dichloro-1,4-naphthoquinone were obtained from commercial sources and, where necessary, purified by crystallization and/or sublimation until their melting points agreed with published values. 2,3-Dichloro-5-nitro-1,4-naphthoquinone was prepared by nitration of 2,3-dichloro-1,4-naphthoquinone following the procedure of Wilbur and Day (39), and purified by crystallization from $CHCl_3$, mp 175.5–176°C (lit. (39) mp 174–175°C). 1-Ethyl-4-carbomethoxypyridinium iodide was prepared by refluxing a benzene solution of methyl isonicotinate and ethyl iodide in 1:4 molar ratio, filtration, and crystallization from acetone, mp 109–110°C (lit. (29) mp 111–112°C).

Reagent grade acetonitrile was purified by successive

distillations over sodium hydride, concentrated sulfuric acid, phosphorus pentoxide, and anhydrous potassium carbonate, and stored over a molecular sieve (40). Water and reagent grade acetic acid were further purified by distillation over potassium permanganate.

Tracer Studies

A solution containing **1**(HD) (0.100 g, 5.1×10^{-4} mol) and BQ (0.0554 g, 5.1×10^{-4} mol) in 20 ml of 90% AN, 0.01 *M* in acetic acid and sodium acetate, was allowed to stand at room temperature, protected from light, for approximately 24 h. The AN was evaporated under reduced pressure, 5.1 ml of 0.1 *M* hydrochloric acid and 5 ml of water added, and the resulting mixture extracted several times with ether. The combined ether extracts were washed with aqueous bicarbonate, dried, filtered, and the ether evaporated off. The solid residue was dissolved in 20 ml of 0.1 *M* aqueous NaOH and the alkaline mixture washed several times with ether to remove unreacted **1** and BQ. After acidification with hydrochloric acid, the hydroquinone was isolated by extraction into ether, drying, filtration, and evaporation. The solid residue was sublimed yielding about 10 mg of pure hydroquinone. Mass spectral analysis (comparison with hydroquinone) revealed no excess deuterium. As a control, a sample of hydroquinone containing 67.1% of the hydrogen replaced by deuterium was taken through the reaction and isolation procedure. Mass spectral analysis showed no loss of deuterium.

In a similar reaction of equimolar amounts of **1**(DD) and BQ in buffered 90% AN, the aqueous solution remaining after the first ether extraction was evaporated to dryness under reduced pressure, and the residue dissolved in the minimum amount of 95% ethanol and cooled to deposit yellow crystals of $\mathbf{2}^+Cl^-$ which were washed with ether and dried. The product contained no detectable hydrogen at the 9-position (nmr, D_2O).

Spectroscopic Measurements

Charge-transfer maxima were measured using a Cary model 116 recording spectrophotometer. *Z* values were determined from the average of four or five successive measurements of the wavelengths of the absorption maxima of freshly prepared solutions of 1-ethyl-4-carbomethoxypyridinium iodide (1.66×10^{-2} *M*) in the appropriate solvent. Standard deviations in λ_{max} measurements were 0.4 nm or less.

Kinetic Measurements

Kinetic measurements utilized Guilford model 200 and Cary model 116 spectrophotometers, with thermostatted cell compartments, for the BQ, TCNQ, and CA rates, and a Durrum stopped flow spectrophotometer for the TCNE and DCBQ rates. The progress of the reaction was followed at 359 nm (BQ, TCNE), 420 nm (CA, DCBQ), or 680 nm (TCNQ). Measurements were carried out under pseudo first-order conditions using a 20 to 5000-fold molar excess of acceptor (Table 5). First-order rate plots were linear through at least 3 half-lives and pseudo first-order rate constants were determined both graphically and by computer. Duplicate rate measurements utilizing the same stock solutions of **1** and acceptor were reproducible to $\pm 1\%$ (BQ, TCNQ, CA) or $\pm 3\%$ (TCNE, DCBQ), while completely independently-determined rate constants were reproducible to ± 2–3%. Errors in k_{HD} and k_{DD} due to contamination of **1**(HD) and **1**(DD) by **1**(HH) and **1**(HD), respectively, were minimized by calculation of the rate constant from the limiting slopes after at least one half-life. Such errors are most serious for k_{HD}, where, for example, the rate constant calculated from the average slope between 50 and 75% reaction would be approximately 1.9% high. In calculation of the uncertainties in *p* and *s*, uncertainties in k_{HD} and k_{DD} were therefore taken as $\pm 3\%$ and $\pm 2\%$, respectively, for BQ, TCNQ, and CA.

Isotope Partitioning Ratios

Isolation of $\mathbf{2}^+Cl^-$ was carried out as follows. The reaction mixture was evaporated under reduced pressure in a flask protected from light. The acridinium salt was dissolved by addition of hydrochloric acid and the unreacted quinone removed by repeated ether extractions. The $\mathbf{2}^+Cl^-$ was isolated by evaporation and purified by repeated solution in methanol followed by addition of ether. The proportions of **2**(D) and **2**(H) were determined by mass spectral analysis of $\mathbf{2}^+Cl^-$ at 40 and 70 eV, utilizing the relative intensities of the *m/e* 194 and 195 peaks and the *m/e* 179 and 180 peaks, by comparison with the mass spectra of a series of known mixtures containing 0 to 25% $\mathbf{2}(H)^+Cl^-$. The measured ratios of **2**(D) to **2**(H) were corrected for contamination of the **1**(HD) starting material by **1**(HH).

Acknowledgements

Financial support by the National Research Council of Canada is gratefully acknowledged. We wish to thank M. Snider for technical assistance. One of the authors (A.K.C.) wishes to thank the Department of Chemistry, University of California, San Diego, for its hospitality during the period in which this manuscript was written.

1. A. K. COLTER, G. SAITO, F. J. SHAROM, and A. P. HONG. J. Am. Chem. Soc. **98**, 7833 (1976).
2. (*a*) T. C. BRUICE and S. J. BENKOVIC. Bioorganic mechanisms. Vol. 2. W. A. Benjamin, New York, NY. 1966. pp. 343–349; (*b*) H. SUND. *In* Biological oxidations. *Edited by* T. P. Singer. Wiley-Interscience, New York, NY. 1968. pp. 603–639.
3. A. K. COLTER and M. R. J. DACK. *In* Molecular complexes. Vol. 2. *Edited by* R. Foster. Crane Russak, New York, NY. 1974. pp. 1–61.
4. E. M. KOSOWER. *In* Progress in physical-organic chemistry. Vol. 3. *Edited by* S. Cohen, A. Streitwieser, and R. W. Taft. Wiley-Interscience, New York, NY. 1965. p. 81.
5. (*a*) K. A. SCHELLENBERG and L. HELLERMAN. J. Biol. Chem. **231**, 547 (1958); (*b*) D. C. DITTMER and R. A. FOUTY. J. Am. Chem. Soc. **86**, 91 (1964); (*c*) L. A. NEGIEVICH, O. M. GRISHIN, V. D. PODHODENKO, and A. A. YASNIKOW. Ukr. Khim. Zh. **33**, 756 (1967); Chem. Abstr. **67**, 107922 (1967); (*d*) A. OHNO and N. KITO. Chem. Lett. 369 (1972); (*e*) R. J. KILL and D. A. WIDDOWSON. J. Chem. Soc. Chem. Commun. 755 (1976).
6. (*a*) J. L. KURZ, R. HUTTON, and F. J. WESTHEIMER. J. Am. Chem. Soc. **83**, 584 (1961); (*b*) K. A. SCHELLENBERG and F. H. WESTHEIMER. J. Org. Chem. **30**, 1859 (1965).

7. J. J. STEFFENS and D. M. CHIPMAN. J. Am. Chem. Soc. **93**, 6694 (1971).
8. D. J. CREIGHTON, J. HAJDU, G. MOOSER, and D. S. SIGMAN. J. Am. Chem. Soc. **95**, 6855 (1973).
9. D. J. CREIGHTON, J. HAJDU, and D. S. SIGMAN. J. Am. Chem. Soc. **98**, 4619 (1976).
10. (*a*) R. H. ABELES, R. F. HUTTON, and F. H. WESTHEIMER. J. Am. Chem. Soc. **79**, 712 (1957); (*b*) C. H. SUELTER and D. E. METZLER. Biochim. Biophys. Acta, **44**, 23 (1960); (*c*) D. J. T. PORTER, G. BLANKENHORN, and L. L. INGRAHAM. Biochem. Biophys. Res. Commun. **52**, 447 (1973); (*d*) J. W. JACOBS, J. T. MCFARLAND, I. WAINER, D. JEANMAIER, C. HAM, K. HAMM, M. WNUK, and M. LAM. Biochemistry, **13**, 60 (1974); (*e*) D. C. DITTMER, A. LOMBARDO, F. BATZOLD, and C. S. GREEN. J. Org. Chem. **41**, 2976 (1976); (*f*) A. BROWN and H. F. FISHER. J. Am. Chem. Soc. **98**, 5682 (1976); (*g*) J. B. JONES and K. E. TAYLOR. Can. J. Chem. **54**, 2974 (1976).
11. T. J. VAN BERGEN, T. MULDER, and R. M. KELLOG. J. Am. Chem. Soc. **98**, 1960 (1976).
12. E. A. BRAUDE, J. HANNAH, and R. LINSTEAD. J. Chem. Soc. 3268 (1960).
13. S. J. LEACH, J. H. BAXENDALE, and M. G. EVANS. Aust. J. Chem. **6**, 409 (1953).
14. L. M. JACKMAN. *In* Advances in chemistry: methods and results. Vol. 2. *Edited by* R. A. Raphael, E. C. Taylor, and H. Wynberg. Interscience, New York, NY. 1960. p. 340.
15. L. R. MELBY, R. J. HARDER, W. R. HERTLER, W. MAHLER, R. E. BENSON, and W. E. MOCHEL. J. Am. Chem. Soc. **84**, 3374 (1964).
16. S. CARTER, J. N. MURRELL, E. J. ROSCH, N. TRINAJSTIĆ, and P. A. H. WYATT. J. Chem. Soc. B, 477 (1967).
17. O. W. WEBSTER, W. MAHLER, and R. E. BENSON. J. Am. Chem. Soc. **84**, 3678 (1962).
18. Y. IIDA. Bull. Chem. Soc. Jpn. **44**, 1777 (1971).
19. K. WALLENFELS, G. BACHMANN, H. DIEKMANN, K. FRIEDRICH, D. HOFMANN, and R. KERN. Angew. Chem. Int. Ed. Engl. **3**, 241 (1964).
20. J. H. BAXENDALE and H. R. HARDY. Trans. Faraday Soc. **49**, 1433 (1953).
21. K. T. FINLEY. *In* The chemistry of the quinoid compounds. *Edited by* S. Patai. Wiley-Interscience, New York, NY. 1974. Chapt. 17.
22. R. FOSTER and P. HANSON. Biochim. Biophys. Acta, **112**, 482 (1966).
23. R. BEUKERS and A. SZENT-GYORGYI. Recl. Trav. Chim. Pays-Bas, **81**, 255 (1962).
24. (*a*) G. CILENTO and S. SCHREIER. Arch. Biochem. Biophys. **107**, 102 (1964); (*b*) J. LUDOWIEG and A. LEVY. Biochemistry, **3**, 373 (1964); (*c*) G. BLANKENHORN. Biochemistry, **14**, 3172 (1975); (*d*) J. HAJDU and D. S. SIGMAN. J. Am. Chem. Soc. **98**, 6060 (1976).
25. K. WALLENFELS and M. GELLRICH. Ann. **621**, 149 (1959).
26. P. VAN EIKEREN and D. L. GRIER. J. Am. Chem. Soc. **98**, 4655 (1976).
27. P. SALOMAA, A. KANKAANPERA, and M. LAHTI. J. Am. Chem. Soc. **93**, 2084 (1971).
28. (*a*) E. GRUNWALD and A. F. BUTLER. J. Am. Chem. Soc. **82**, 5647 (1960); (*b*) E. F. J. DUYNSTEE, E. GRUNWALD, and M. L. KAPLAN. J. Am. Chem. Soc. **82**, 5654 (1960).
29. E. M. KOSOWER. J. Am. Chem. Soc. **80**, 3253 (1956).
30. S. SHINKAI and T. C. BRUICE. Biochemistry, **12**, 1750 (1973).
31. J. HAJDU and D. S. SIGMAN. J. Am. Chem. Soc. **97**, 3524 (1975).
32. E. F. CALDIN. Chem. Rev. **69**, 135 (1969).
33. S. G. SMITH, A. H. FAINBERG, and S. WINSTEIN. J. Am. Chem. Soc. **83**, 618 (1961).
34. C. REICHARDT and K. DIMROTH. Fortschr. Chem. Forsch. **11**, 1 (1968).
35. (*a*) M. E. PEOVER. J. Chem. Soc. 4540 (1962); (*b*) M. E. PEOVER. Trans. Faraday Soc. **58**, 2370 (1962).
36. R. A. REED. J. Chem. Soc. 679 (1944).
37. A. ALBERT. The acridines. St. Martin's Press, New York, NY. 1966. p. 330.
38. A. G. BROOK, J. Chem. Soc. 5040 (1952).
39. J. M. WILBUR and A. R. DAY. J. Org. Chem. **25**, 753 (1960).
40. G. A. FORCIER and J. W. OLVER. Anal. Chem. **37**, 1447 (1965).

The crystal structure of *tert*-butyl ethyldiazoacetate mercury(II)

R. A. SMITH, M. TORRES, AND O. P. STRAUSZ

Department of Chemistry, University of Alberta, Edmonton, Alta, Canada T6G 2G2

Received January 12, 1977

R. A. SMITH, M. TORRES, and O. P. STRAUSZ. Can. J. Chem. **55**, 2752 (1977).

tert-Butyl ethyldiazoacetate mercury(II) is monoclinic with the following unit cell data at 20°C: $P2_1/n$, $a = 8.089(3)$, $b = 18.720(10)$, $c = 7.893(3)$ Å, $\beta = 93.20(3)°$, $V = 1193.3$ Å^3, $\rho_o = 2.09(1)$, $\rho_c = 2.06$, $Z = 4$. The structure was solved by heavy atom methods and refined to $R = 6.6\%$ for 1003 reflections. The diazoacetate portion is planar; the CN_2 portion is linear.

R. A. SMITH, M. TORRES et O. P. STRAUSZ. Can. J. Chem. **55**, 2752 (1977).

Le *tert*-butyle diazoacétate d'éthyle mercure(II) est monoclinique et les paramètres de la maille à 20°C sont: $P2_1/n$, $a = 8.089(3)$, $b = 18.720(10)$, $c = 7.893(3)$ Å, $\beta = 93.20(3)°$, $V = 1193.3$ Å^3, $\rho_o = 2.09(1)$, $\rho_c = 2.06$, $Z = 4$. On a résolu la structure par la méthode des atomes lourds et on l'a affinée jusqu'à une valeur de $R = 6.6\%$ pour 1003 réflexions. La portion diazoacétate est planaire; la portion CN_2 est linéaire.

[Traduit par le journal]

Introduction

Photolysis of $Hg(CN_2CO_2Et)_2$, **1**, has been reported to be a usable source of the novel carbon radical carbethoxymethyne and detailed mechanistic studies have been reported for the photolysis of **1** in olefins and paraffins (1), chloroalkanes (2), and pentacarbonyl manganese bromide (3).

Recently, the photolysis of the source compound *tert*-butyl ethyldiazoacetate mercury(II), **2**, has been investigated (4). The ir spectrum of **2** in CCl_4 solution exhibits bathochromic shifts of *ca.* 75 cm^{-1} in the diazo and carbonyl stretching regions of the spectrum, relative to ethyldiazoacetate. Similar shifts are observed in mercurybis-(α-diazoketones) (5), indicative of large electron delocalization in these portions of the molecule.

Little is known about the crystal structures, molecular geometries, or the nature of the bonds in these diazomercurials. This kind of information, apart from its inherent interest, would be helpful in the elucidation and interpretation of the chemical reactivity of this class of molecules. For this reason an X-ray diffraction study of **2** has been undertaken, the details of which are reported here.

Experimental

The title compound was prepared following the method reported for the methyl analog (6). The resulting prismatic yellow crystals were suitable in terms of size and shape for an X-ray study.

$C_8H_{14}HgN_2O_2$ fw = 370.8

Monoclinic, $P2_1/n$, $a = 8.089(3)$, $b = 18.720(10)$, $c = 7.893(3)$ Å, $\beta = 93.20(3)°$, $V = 1193.3$ Å^3, $\rho_o = 2.09(1)$, $Z = 4$, $\rho_c = 2.06$ (20°C; $MoK_{\alpha 1}$ $\lambda = 0.7093$ Å).

Preliminary photographs showed systematic absences, $h0l$, $h + l = 2n + 1$, $0k0$, $k = 2n + 1$, the non-standard space group was maintained since the standard setting had a β value close to 60°. Twelve high angle reflections were carefully centered on a Picker FACS 1 diffractometer ($MoK_{\alpha 1}$ radiation, no monochromator) and accurate cell constants were derived.

A unique set of data with $0 < 2\theta \leq 47°$ (MoK_α radiation, graphite (002) monochromator) was collected by the coupled $\theta/2\theta$ scan method. The crystals decomposed rapidly under the experimental conditions and three separate crystals were necessary to collect all the data. Decomposition was monitored by measurement of standards every 100 reflections. A total of 1840 reflections were measured and corrected for Lorentz-polarisation, decomposition, and absorption (7) (μ, $MoK_\alpha = 121$ cm^{-1}; crystal *1*, 0.13 × 0.06 × 0.06 mm; crystal *2*, 0.13 × 0.10 × 0.06 mm; crystal *3*, 0.10 × 0.08 × 0.06 mm) and then merged to one data set on the basis of common reflections. The data were reduced to F, $\sigma(F)$, and $\sigma(I)$ using a p value of 0.06 (8). Using an acceptance criterion $I \geq 3\sigma(I)$, 1003 reflections had significant intensity and were used in subsequent calculations.

Conventional heavy atom methods were used to locate the mercury atom. A difference Fourier map for data of the form $h + k + l = 2n$ showed the expected molecule and one related to it by a two-fold axis along b and passing through the mercury atom, but none of the peaks overlapped and an immediate distinction between real peaks and their symmetry-related ones was possible for all non-H atoms. Using full-matrix least-squares procedures on all 1003 reflections, R was reduced to 6.6% with anisotropic thermal parameters for all atoms. A weight of $4F^2/\sigma^2(F^2)$ was applied to every reflection. Scattering

TABLE 1. Final parameters (esd's) (Hg × 10^4; others × 10^3)

$\pm |x,y,z; 1/2 + x, 1/2 - y, 1/2 + z|$

t.f. = $\exp(-2\pi^2\{a^{*2}h^2U_{11} + \ldots + 2a^*b^*hkU_{12} + \ldots\}$

Atom	x	y	z	U_{11}	U_{22}	U_{33}	U_{12}	U_{13}	U_{23}
Hg	146(1)	1504(1)	141(2)	411(10)	506(8)	548(9)	19(8)	16(4)	17(1)
O(1)	−234(3)	155(1)	−307(3)	89(15)	59(16)	63(15)	39(14)	−19(13)	−34(15)
O(2)	−424(2)	236(1)	−247(3)	33(11)	70(17)	86(17)	10(10)	−19(11)	14(15)
N(1)	−260(3)	250(2)	53(4)	38(16)	82(25)	61(20)	4(15)	8(14)	−1(20)
N(2)	−310(5)	287(3)	153(7)	79(26)	139(43)	152(47)	20(26)	−5(28)	−41(36)
C(1)	233(5)	87(2)	61(6)	63(22)	53(25)	111(35)	27(19)	−48(24)	−7(24)
C(2)	377(4)	142(3)	81(6)	48(19)	129(41)	94(29)	3(24)	5(19)	67(32)
C(3)	226(6)	49(4)	234(7)	108(36)	213(63)	100(39)	96(45)	35(30)	62(48)
C(4)	248(6)	37(3)	−72(9)	106(34)	107(41)	272(73)	73(32)	−25(41)	−139(48)
C(5)	−207(3)	207(2)	−54(4)	36(14)	35(18)	42(19)	22(13)	9(14)	11(15)
C(6)	−300(4)	203(2)	−207(5)	44(18)	45(21)	67(26)	−2(15)	−25(18)	21(18)
C(7)	−314(6)	144(3)	−473(5)	129(37)	140(46)	49(25)	37(37)	−22(27)	−16(33)
C(8)	−205(6)	106(3)	−577(6)	97(34)	206(68)	60(31)	−32(37)	−37(29)	10(37)

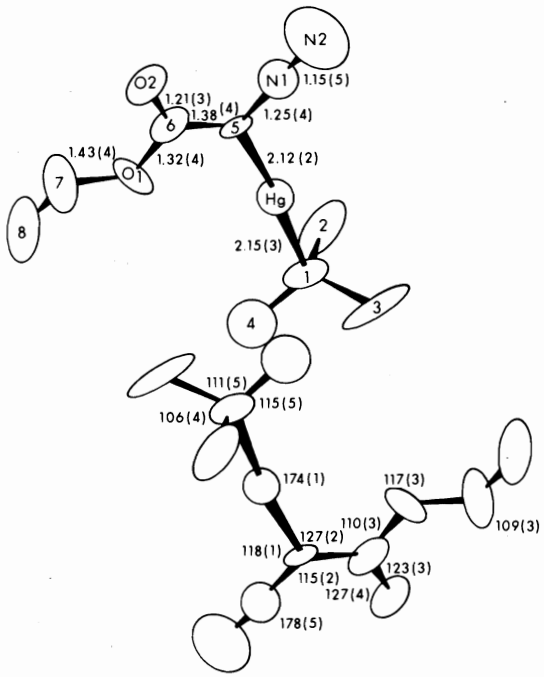

FIG. 1. Atomic numbering, bond angles, and distances in *tert*-butyl ethyldiazoacetate mercury(II).

factors for neutral atoms were used (9) and anomalous dispersion corrections were applied to the mercury atom (10). A final difference Fourier map was calculated and contained peaks of the order of 1.0 e/Å^3 in the vicinity of the mercury atom and up to 0.75 e/Å^3 elsewhere. Consequently no attempt was made to determine the hydrogen atom positions.

Results and Discussion

The atomic numbering scheme and important bond angles and distances are given in Fig. 1. Final atom parameters are given in Table 1 and the table of structure factors has been placed in the Depository of Unpublished Data.[1]

It is interesting to note the planar *cis* structure with respect to the carbonyl and azo groups of the diazoacetate because this configuration which is generally more stable than the *trans* (11), has been claimed for diazoketones which are capable of undergoing the Wolff rearrangement (12) yet mercury diazo compounds do not isomerize to ketenes (13). All 7 atoms of the $HgCN_2CO_2$ portion of the molecule lie within 0.02 Å of the mean plane. The standard deviations for the observed bond lengths and angles are, as expected, nearly twice as large as those for similar molecules reported recently (14) because the data from three separate crystals had to be merged. This precludes detailed discussion of the bonding scheme, but it is probably a resonance hybrid of the structures shown below.

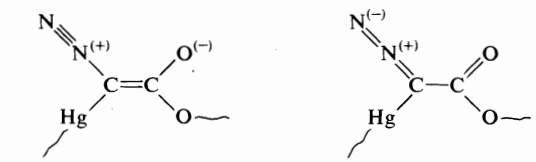

[1]The Structure Factor Table is available, at a nominal charge, from the Depository of Unpublished Data, CISTI, National Research Council of Canada, Ottawa, Canada K1A 0S2.

Bis(ethyldiazoacetate) mercury(II) is currently under investigation, it will be interesting to compare the azocarbonyl moiety in this compound to that found in the title compound.

Acknowledgements

We thank the National Research Council of Canada for financial support and Dr. E. M. Lown for reading the manuscript.

1. T. Do Minh, H. E. Gunning, and O. P. Strausz. J. Am. Chem. Soc. **89**, 6785 (1967); O. P. Strausz, T. Do Minh, and J. Font. J. Am. Chem. Soc. **90**, 1930 (1968); G. Kennepohl. Ph.D. Thesis, University of Alberta, 1973; O. P. Strausz, G. Kennepohl, F. X. Garneau, T. Do Minh, B. Kim, S. Valenty, and P. S. Skell. J. Am. Chem. Soc. **96**, 5723 (1974).
2. T. B. Patrick and G. H. Kovitch. J. Org. Chem. **40**, 1527 (1975).
3. W. A. Herrmann. Angew. Chem. Internat. Ed. **13**, 812 (1974).
4. M. Torres and O. P. Strausz. Presented at Symposium on Interdisciplinary Aspects of Photochemistry, Barcelona, Spain, July 25–30, 1976.
5. P. Yates, F. X. Garneau, and J. P. Lokensgard. Tetrahedron, **31**, 1979 (1975).
6. S. J. Valenty and P. S. Skell. J. Org. Chem. **38**, 3937 (1973).
7. P. Coppens, L. Leiserowitz, and D. Rabinovich. Acta Crystallogr. **18**, 1035 (1965).
8. R. J. Doedens and J. A. Ibers. Inorg. Chem. **6**, 204 (1967).
9. D. T. Cromer and J. B. Mann. Acta Crystallogr. A**24**, 321 (1968).
10. International Tables for X-ray Crystallography. Vol. III. Kynoch Press, Birmingham, England. 1962.
11. I. G. Csizmadia, H. E. Gunning, R. K. Gosavi, and O. P. Strausz. J. Am. Chem. Soc. **95**, 133 (1973).
12. S. Sorriso and A. Foffani. J. Chem. Soc. Perkin II, 2142 (1973).
13. P. S. Skell and S. J. Valenty. J. Am. Chem. Soc. **95**, 5042 (1973).
14. C. Chieh and L. P. C. Leung. Can. J. Chem. **54**, 3077 (1976).

Theoretical studies of the chemistry of singlet and triplet species. II. Cycloaddition reaction[1]

R. F. W. BADER, M. E. STEPHENS,[2] AND R. A. GANGI[3]

Department of Chemistry, McMaster University, Hamilton, Ont., Canada L8S 4M1

Received February 11, 1977

R. F. W. BADER, M. E. STEPHENS, and R. A. GANGI. Can. J. Chem. **55**, 2755 (1977).

Ab initio SCF potential energy surfaces for the cycloaddition reactions $C_2H_4(^1A_{1g}) + O(^1D, ^3P)$ are reported. The lowest energy singlet path corresponds to the symmetric, concerted addition reaction yielding ethylene oxide. The lowest energy triplet path corresponds to an asymmetric approach of the reactants to form an open ring adduct ($\angle CCO = 105°$). The spatial distribution of the spin density in this adduct conforms to that expected for a diradical. The barrier to internal rotation of the terminal methylene is calculated to be ~ 5 kcal mol^{-1}. The lowest intersystem crossing from the triplet to the singlet surface, as required for ring closure to yield ground state product, is found to occur ~ 36 kcal mol^{-1} above the energy of the triplet reactants.

The differences in singlet and triplet charge distributions and energies for similar approach geometries may be rationalized in terms of the additional restraints imposed on the course of the triplet reaction by the Pauli principle, restraints which are made evident by the spatial distribution of the spin density. Two principal mechanisms of spin polarization, spin unpairing and spin decoupling, are found to provide a rationale for the observed differences of singlet and triplet reactants in abstraction, insertion and addition reactions. The favoured course of a triplet reaction is found to be governed by the axiom that localized distributions of spin density are to be maximally separated in space.

R. F. W. BADER, M. E. STEPHENS et R. A. GANGI. Can. J. Chem. **55**, 2755 (1977).

On rapporte des surfaces d'énergie potentielle calculées par la méthode SCF *ab initio* pour les réactions de cycloaddition de $C_2H_4(^1A_{1g}) + O(^1D,^3P)$. Le chemin singulet d'énergie la plus basse correspond à la réaction d'addition concertée symétrique conduisant à l'oxyde d'éthylène. Le chemin triplet de plus basse énergie correspond à une approche asymétrique des réactifs pour former un adduit à cycle ouvert ($\angle CCO = 105°$). La distribution spatiale des densités de spin dans cet adduit est en conformité avec celle attendue pour un diradical. On a calculé que la barrière à la rotation interne du méthylène terminal est d'environ 5 kcal mol^{-1}. La conversion intersystème la plus basse entre la surface triplet et la surface singulet, telle que requise pour la fermeture du cycle conduisant à un produit dans l'état fondamental, se produirait environ 36 kcal mol^{-1} au dessus de l'énergie des réactifs triplets.

On peut rationaliser les différences dans les distributions de charge des états singulet et triplet et les énergies pour les géométries d'approches similaires en termes de contraintes additionnelles imposées sur l'évolution de la réaction triplet par le principe de Pauli, restrictions qui sont rendues évidentes par la distribution spatiale des densités de spin. On a trouvé que deux mécanismes principaux de polarisation de spin, de dépairage de spin et de découplage de spin peuvent fournir une explication rationnelle pour les différences observées dans les réactions d'enlèvement d'insertion et d'addition des réactifs singulet et triplet. On a trouvé que le chemin favorisé pour une réaction à l'état triplet est gouverné par l'axiome voulant que les distributions localisées de densité de spin doivent être séparées au maximum dans l'espace.

[Traduit par le journal]

Introduction

This paper presents a theoretical study and comparison of the mechanisms of the addition of singlet and triplet states of a reactant to a double bond. *Ab initio* SCF potential surfaces are reported for the cycloaddition reactions of $O(^1D, ^3P)$ with $C_2H_4(^1A_{1g})$. In a previous publication (1) we obtained a qualitative interpretation of the differing tendencies of singlet and triplet species to undergo insertion and abstraction reactions in terms of the spatial distributions of the electronic charge density $\rho(r)$, and spin density $\sigma(r)$. It was observed that the spin density of a triplet adduct is spatially localized in separate

[1]For paper I, see ref. 1.

[2]Centre de Mecanique Ondulatoire Appliquee, 23, rue du Maroc, 75019 Paris, France.

[3]Gloucester County College, Sewell P.O., NJ, U.S.A. 08080.

distributions on neighbouring nuclei in a manner dictated by the molecular geometry. There is a characteristic pattern for the polarization and localization of $\sigma(\boldsymbol{r})$ induced by the approach of a triplet species along the bisector of a singlet, bonded pair of atoms (insertion approach), a pattern which is different from that obtained when the triplet species approaches one atom of the bonded pair to yield an abstraction reaction. The present study shows that the same two patterns of polarization and localization of the spin density are operative for the corresponding geometries of approach of a triplet species to a doubly bonded pair of atoms. The differences in singlet and triplet charge distributions and energies for motion along reaction paths of identical nuclear geometries may be rationalized in terms of the additional restraints imposed on the course of the triplet reaction by the Pauli principle, restraints which are made evident by the spatial distribution of the spin density. The favoured course of a triplet reaction is found to be dictated by the simple axiom that localized distributions of spin density (of the same sign) are to be maximally separated in space.

Since the studies of Skell *et al.* (2) on methylene addition of olefins, much debate has ensued over the relationship between the reaction mechanisms and the spin-multiplicity of open-shell reactants (3, 4).

It has been experimentally established, for instance, that $O(^1D)$ (5), $S(^1D)$ (6), and $CH_2(^1A_1)$ (7) insert into paraffinic CH bonds, while $O(^3P)$ (8) and $CH_2(^3\Sigma_g^-)$ only abstract H atoms and $S(^3P)$ is unreactive with paraffins under the same conditions. The three singlet species add stereospecifically to olefin double bonds (7, 9–11), whereas triplet oxygen or methylene addition results in some loss of the reactant's geometrical isomeric purity. Thus studies on olefin–oxygen reactions in gas (12), liquid (13), and solid (14) phases indicate an electrophilic character (12) of triplet oxygen and temperature-dependent stereospecificity of triplet addition (15). Addition to *cis*-2-butene is non-stereospecific at 77 K and 300 K, but addition to *trans*-2-butene produces *trans*- and *cis*-1,2-dimethyloxirane in the ratio of 17:1 at 77 K (liquid phase) but only 2:1 at 300 K (gas phase).

The most detailed theoretical studies of the potential surfaces for the reactions of CH_2 (3), S (16), and NH (17) all indicate clearly differentiable energetically preferred symmetric lowest singlet and asymmetric lowest triplet paths (with a barrier to rotation of the terminal methylene in the sulphur case sufficient to preserve reactant stereochemistry).

The qualitative interpretation of the CH_2 results originally proposed by Skell (2) has been extended to the other cases as well (8, 12). Briefly, his description is as follows. The singlet species insert into paraffinic CH bonds through concerted formation of CX and XH bonds (X = ^1O, ^1S, or $^1CH_2$), and add to olefinic double bonds through concerted formation of two CX bonds. The triplet species, on the other hand, cannot undergo such a 'spin-forbidden' concerted formation of two bonds in either case, and instead initially forms only one bond to an exposed paraffinic hydrogen or to an olefinic carbon (forming an open-ring diradical capable of internal rotation around the now formally 'single' carbon–carbon bond). The result is H-atom abstraction from paraffins and non-stereospecific cycloaddition to olefins (after intersystem crossing from the triplet to singlet surface).

These mechanisms have been criticized (4) and an alternate, symmetric path for the triplet cycloaddition reaction proposed on several theoretical grounds (18–20). The existence of an open-ring triplet diradical in the cycloaddition reactions has been proposed (12) to account for the loss of stereospecificity, to provide paths to the other reaction products observed, and as an explanation for the observed increased production of addition at the expense of fragmentation products for larger substituted olefins (9, 13).

Pauli Principle and Localization of Spin and Charge Densities

The Hamiltonian used in the calculation of molecular energies (in the absence of external magnetic fields or spin–orbit coupling) is independent of the spin variables of the electrons. Yet the energy so calculated is dependent upon the spin multiplicity of the system. The reason for this result is, of course, a consequence of the antisymmetry requirements imposed on the wave function of the system by the Pauli exclusion principle. The Pauli principle exerts a strong influence on the allowable charge and spin (21) distributions for states of a molecule. One may interpret the effect of the Pauli principle on a system as being one which imposes a correlation

on the motions of electrons with identical spins, the so-called Fermi correlation.

In particular it has been shown that the extent to which some number of electrons $N(\Omega)$ are localized in a well-defined region of real space Ω is determined by the fraction of the total Fermi correlation contained in this same region of space (22). One finds the degree of localization of the charge density to be significantly greater along the triplet than along the corresponding singlet reaction paths. The increased localization of the total charge density of the triplet is reflected in the even more localized nature of the density of the unpaired electrons, *i.e.*, of the spin density. Since the course of a triplet reaction may be rationalized in terms of the extent and separation of localized regions of spin density, it is necessary to understand fully the origin of the localization and its effect upon the energy of a system.

An oft-quoted statement of the Pauli principle is that no electron can occupy the same spatial point as that of another electron with the same spin. However, the restrictions of the exclusion principle are not confined to the single point in space occupied by a given electron. Rather, the probability of finding other electrons with the same spin as that of the reference electron is decreased from the uncorrelated distribution by varying amounts throughout all of space. When this decreased probability is expressed in terms of a decrease in the value of the corresponding pair density referenced to the position of a single electron, it is called the Fermi hole. As the reference electron moves through space, the Fermi hole changes in shape and spatial extent. However, the magnitude of the hole (*i.e.*, the total reduction in the number of pairs over all space) remains equal to one. Thus by its definition, the net effect of the Fermi correlation is to correct for the pairing of an electron with itself. The Fermi hole integrated over all space therefore, equals -1 per electron or $-N$ for a system containing N electrons.

The antisymmetry requirement on the wave function corrects for this self-pairing of the electrons in a very special and nontrivial manner. What one finds is that in certain systems, the Fermi hole is very localized around the position of the reference electron and it remains so for motion of the reference electron throughout a given region (Ω) of space (22). If the Fermi hole for an electron is so localized that it integrates to -1 over just the region (Ω), rather than over all space, for any position of the reference electron within the region (Ω), then this electron is totally localized within the region (Ω). Thus an electron has a doppelgänger, its Fermi hole, which goes wherever the electron goes. Conversely, the electron may go only to regions of space in which its Fermi hole is non-vanishing. If the Fermi hole is localized to a given region of space, so is the electron (22).

In summary, if we label the magnitude of the total Fermi correlation (or Fermi hole) of a region (Ω) as $|F(\Omega,\Omega)|$, then $L(\Omega)$, the percentage localization of the $N(\Omega)$ electrons in (Ω), is given by (22)

$$L(\Omega) = 100 \times |F(\Omega,\Omega)|/N(\Omega)$$

corresponding to 100% localization of the $N(\Omega)$ electrons in (Ω) when $|F(\Omega,\Omega)|$ obtains its maximum value of $N(\Omega)$.

Consider the ethylene molecule, in its $^1A_{1g}$ ground and $^3B_{3u}$ excited states, to be bisected by a planar surface at the bond midpoint to yield two methylene fragments, each with an average population of 8 electrons. An integration of the Fermi hole over such a CH_2 fragment in the ground state molecule indicates that the charge in each fragment is 86% localized. If there were no Fermi correlation (over and above the simple statistical correction for self-pairing) then the charge would be equally localized in each fragment, *i.e.*, there would be no preferred spatial localization.

The localization of the charge in a CH_2 fragment increases to 92% when the molecule is excited to its triplet state, retaining the planar geometry, and undergoes a further increase to 94% when the triplet molecule is twisted into its lowest energy geometry of D_{2d} symmetry. This increase in the localization of the electronic charge in each of the CH_2 fragments on excitation from a singlet state of one electronic configuration to the triplet state of another is the result of the very localized nature of the distributions of the unpaired electrons.

The spin density at a point $\boldsymbol{r}$ in positional space is equal to the excess density of the α or β electrons at that point

$$\sigma(\boldsymbol{r}) = \rho^{\alpha}(\boldsymbol{r}) - \rho^{\beta}(\boldsymbol{r})$$

When $\sigma(\boldsymbol{r}) > 0$, there is an excess of α spins at $\boldsymbol{r}$

and when $\sigma(r) < 0$, there is an excess of β spins at r. The integral of $\sigma(r)$ over all space yields the total number of unpaired α electrons N^{α}, or minus the total number of unpaired β electrons N^{β}, in the molecule.

$$\int \sigma(r)\, dr = N^{\alpha} \text{ (or } -N^{\beta})$$

The spin densities portrayed in this paper are obtained from (spin) unrestricted SCF wave functions, wave functions which allow different orbitals for different spins. This extra variational flexibility is necessary to obtain good representations of $\sigma(r)$, and is essential for a prediction of the polarizations within the spin distribution. In a restricted SCF calculation, $\sigma(r)$ for the $M_s = 1$ component of a triplet reduces to the sum of the densities of the two singly occupied orbitals which describe the excess α electrons. In this approximation $\sigma(r)$ is everywhere greater than zero for a $M_s = 1$ state. In a spin unrestricted calculation, all of the orbital densities contribute to $\sigma(r)$, from both the α and β sets of electrons, and $\sigma(r)$ may exhibit negative values, corresponding to a local predominance of β spin density in a system with a net excess of α spins, *i.e.*, there is a polarization of $\sigma(r)$.

The difference in the descriptions provided by the restricted and unrestricted methods of calculation are illustrated by the example of the lowest triplet ($^3B_{3u}$) state of ethylene. Figures 1 *d* and *e* portray the spin density distributions for this molecule from an unrestricted calculation for the $M_s = 1$ component. The spin density distribution contains significant differences from that obtained from a RHF calculation.

This state of ethylene may, in simplest terms, be considered to result from a simple $\pi^* \leftarrow \pi$ excitation from the $^1A_{1g}$ ground state of the molecule. To a first approximation, the unpaired spin density is due to the occupation of the π and π* molecular orbitals by one α-electron each. Considering the spin density map Fig. 1*d*, one sees a distribution which is an apparent sum of such orbital densities. However, considering the second plot, Fig. 1*e*, that of the spin density in the plane of the nuclei, other features are seen. Surrounding each hydrogen nucleus is a region of excess β-density, and this in a molecule constrained to have a net spin excess of two α-electrons. Integration over the regions of excess α-density would yield a total of more than two α-electrons. There has been a 'polarization' of the molecular spin density with excess α-density being localized on the two carbons and excess β-density on the four hydrogens (and to a small extent along the line joining the two carbon nuclei). The polarization effects predicted by UHF functions have been shown (1) in several examples to agree qualitatively with the results of more detailed calculations. The maps reported here may be expected to faithfully reproduce the pattern of the primary spin polarizations operative in the system studied. Since the spin distributions for the levels of an electronic term differ only by a multiplicative constant (23), M_s/S, we base our interpretation on the properties of the distribution for the (computationally convenient) level of highest M_s value (= 1 for the triplet term).

The excess α spin density is very localized in the region about each carbon nucleus (Fig. 1*d*). In the plane perpendicular to the plane of the nuclei, only contours of relatively low value (less than 0.02 au) encompass both nuclei. For comparison with a related but delocalized two-electron system, one finds that contours with values in excess of 0.04 au encompass both nuclei in the density distribution derived from the π orbital of ground state ethylene. Thus the increase in the degree of localization of the charge in each (CH_2) fragment upon excitation of ethylene to its triplet state may be explained in terms of the mutual avoidance of the two α spin distributions, as shown by the separate localization of the spin density on each of the two carbon atoms. The mutual avoidance of the two localized α spin distributions is maximized, as is the extent of localization of the total charge in each CH_2 fragment, when the triplet molecule is twisted into its lowest energy geometry of D_{2d} symmetry (Fig. 1*f*). The behaviour of the spin density in the twisting motion of ethylene illustrates the axiom that the geometry of lowest energy is the one which maximizes the spatial separation of localized spin distributions of like sign.

The increased localization of the Fermi correlation on excitation to a triplet is reflected in a corresponding increase in the spatial localization of the charge density. Figure 1*a* shows a wide belt of density, defined by the 0.2 au contour, encompassing the carbon nuclei in ground state ethylene. This same contour is very much reduced in width between the same nuclei in the triplet state in both planar (Fig. 1*b*) and twisted (Fig. 1*c*) geometries, indicating a significant re-

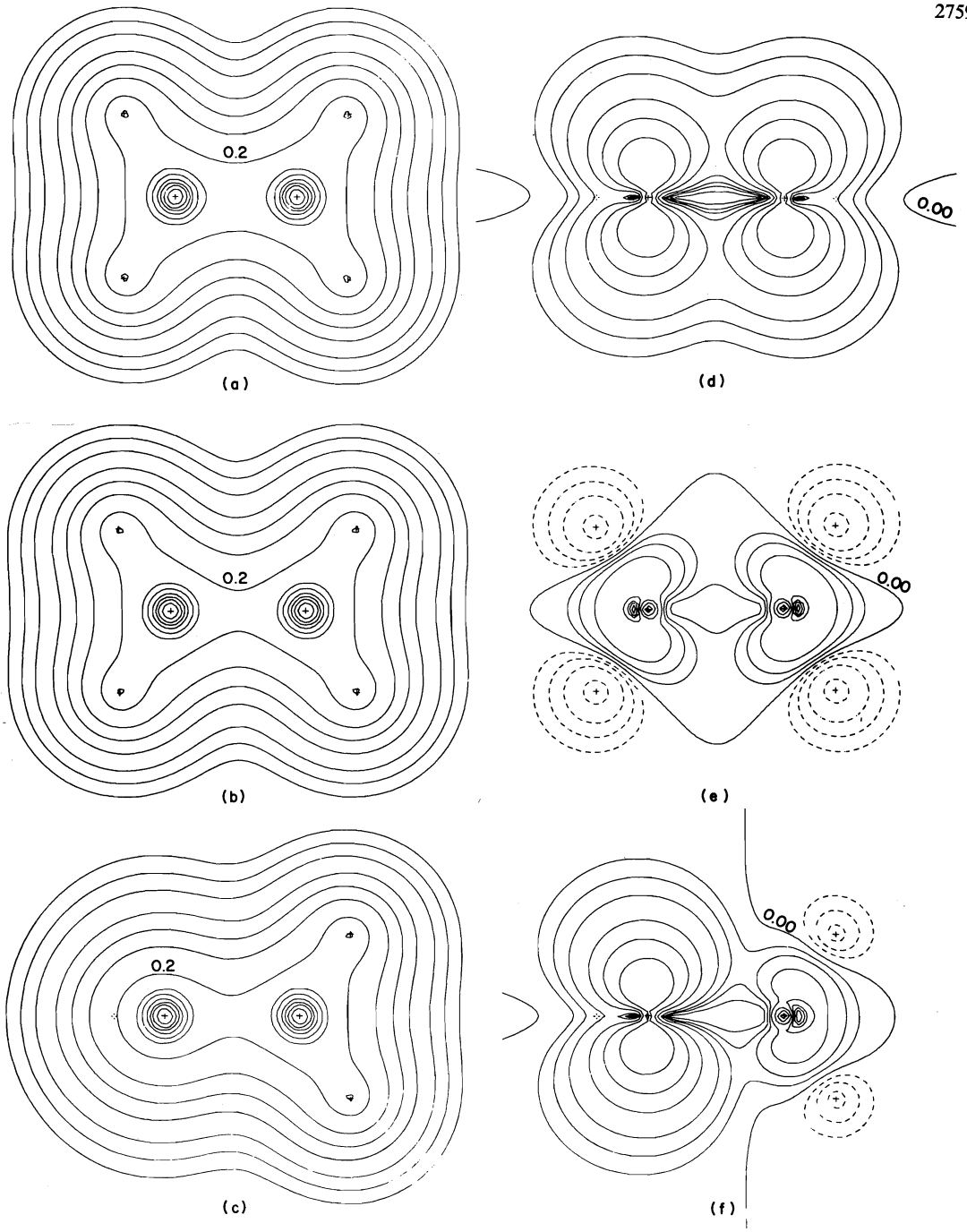

FIG. 1. Total electronic charge, $\rho(\boldsymbol{r})$, and spin, $\sigma(\boldsymbol{r})$, distributions for ethylene. (*a*) $\rho(\boldsymbol{r})$ for ground state ($^1A_{1g}$) in plane containing protons. R(C—C) = 2.5304 au. (*b*) $\rho(\boldsymbol{r})$ for lowest triplet state ($^3B_{3u}$) in plane containing protons. R(C—C) = 2.8346 au, the calculated equilibrium separation. (*c*) $\rho(\boldsymbol{r})$ for lowest energy (twisted) geometry of triplet state ($^3A_{2u}$). R(C—C) = 2.8346 au. (*d*) $\sigma(\boldsymbol{r})$ for $^3B_{3u}$ in plane containing C—C, perpendicular to plane of protons. (*e*) $\sigma(\boldsymbol{r})$ for $^3B_{3u}$ in plane containing protons. (*f*) $\sigma(\boldsymbol{r})$ for $^3A_{2u}$. In all charge density maps, the contours increase in value from the outer contour, in steps of 2×10^n, 4×10^n, 8×10^n au for increasing integer n starting at $n = -3$. In all spin density maps, the contours vary similarly, regions of excess α-density being denoted by solid contours and excess β-density by dashed contours. The first solid contour adjacent to a dashed one is the zero contour line.

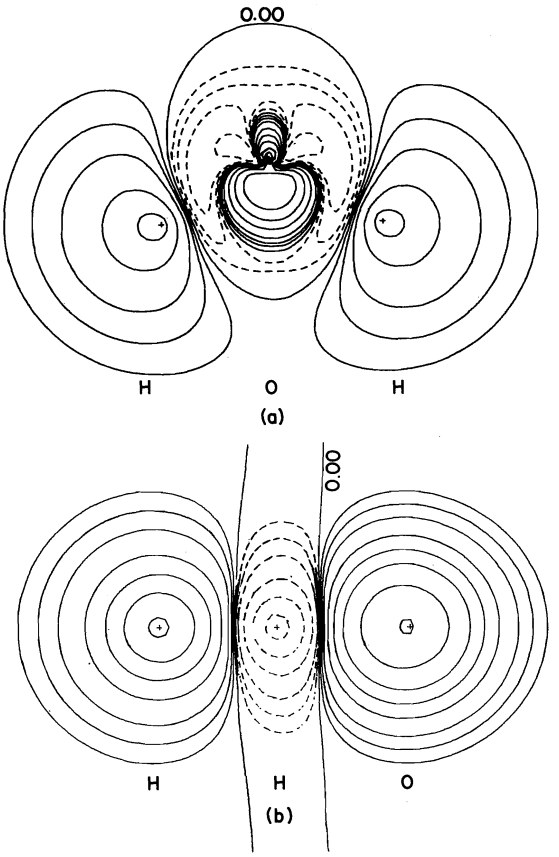

FIG. 2. Spin density maps for the $O(^3P) + H_2(^1\Sigma_g^+)$ system (1). (*a*) Illustrative of the spin unpairing mechanism, is for the symmetric insertion approach at a point where the separation between oxygen and the mid-point of H—H equals 1.11 au, the separation in ground state water. (*b*) Illustrative of the spin uncoupling mechanism, is for the abstraction approach.

duction in charge density and in binding between them. In the $^1A_{1g}$ ground state the value of the charge density at the midpoint of the C—C internuclear axis (the point of maximum $\rho(\boldsymbol{r})$ in the partitioning surface) is 0.3187 au. In the $^3B_{3u}$ excited state this value decreases to 0.2350 au and in the twisted equilibrium geometry, it decreases further to 0.2345 au. *Thus the localization of identical net spin densities on two neighbouring nuclei in a molecule leads to a decrease in the density accumulation, and hence to a decrease in the binding, between them.*

The same axiom and associated observations on the behaviour of the total charge density apply to the determination of the geometries of lowest energy which define the triplet reaction path. This is illustrated by the spin distributions in Fig. 2 for the reaction of $O(^3P)$ with $H_2(^1\Sigma_g^+)$. They illustrate the two basic patterns of spin polarization which characterize triplet reaction paths (1). Figure 2*a* is representative of the spin polarization obtained for triplet insertion, the *spin unpairing mechanism*. The spin density is for a point on the symmetric reaction path for insertion of $O(^3P)$ into $H_2(^1\Sigma_g^+)$. The approach of the oxygen causes an unpairing of the initially paired electrons binding the hydrogen nuclei. As the reaction proceeds the degree of unpairing increases and the resulting spin density becomes increasingly separately localized in the region about each proton. In effect, the spin polarization caused by the approach of $O(^3P)$ corresponds to a quasi-excitation of H_2 from its singlet ground state to its unbound $^3\Sigma_u^+$ state, a state characterized by a localization of $\rho(\boldsymbol{r})$ on each nucleus and to a depletion of the charge density in the region between the nuclei. Indeed $\sigma(\boldsymbol{r}) > 0$ in the regions of all three nuclei, and the electronic charge is depleted in all three internuclear regions (relative to the singlet state in the same geometry) corresponding to an intermediate in which the substrate bond has been broken and no new bonds to the oxygen have been formed. Thus the triplet insertion approach is one of rapidly increasing energy, the energy rising monotonically to a value 124 kcal mol^{-1} above that of singlet ground state water at the equilibrium position of the latter.

The second spin polarization is that characteristic of triplet abstraction, the spin *uncoupling mechanism*. In this case the initial (α,β) substrate bonding pair is polarized so as to localize separate α and β spin distributions on the two centres of the substrate; the spins are uncoupled. Because of the alternation in the sign of the localized spin distributions, increased binding between O and the adjacent H proceeds simultaneously with the decrease in binding in the substrate and the reaction proceeds with a much smaller energy of activation. Thus the spin uncoupling mechanism is the preferred mechanism of spin polarization for the approach of a triplet reactant to a singlet substrate. The same mechanisms of spin polarization with the same energetic consequences are found to apply to the approach of $O(^3P)$ to a doubly bonded system in cycloaddition reactions.

SCF Calculations

The HF method requires three determinants to provide a limiting description of $O(^1D)$ of cor-

TABLE 1. Final atomic basis set

Atom	Type	Basis function expansion in primitive gaussians[a]
H	S	0.817238(0.65341) + 0.231208(2.89915) + 0.032828(19.24060)
	S	1.000000(0.17758)
C	S	0.904751(159.62740) + 0.121599(781.64950) + 0.029314(2548.72600)
	S	1.053375(0.47350) − 0.146302(4.93440)
	S	1.000000(0.14800)
	S	1.000000(0.045)
	S	1.000000(0.014)
	S	1.000000(0.00426)
	P	0.640080(0.35945) + 0.386200(1.14293) + 0.115440(3.98040) + 0.018533(18.15570)
	P	1.000000(0.037)
O	S	0.243991(31.31660) + 0.458240(12.86070) + 0.264438(4.60370) + 0.152763(76.23200)
	S	0.0904785(290.78500) + 0.121603(1424.06430) + 0.029225(4643.44850)
	S	1.051534(0.92110) − 0.140314(9.70440)
	S	1.000000(0.28250)
	S	1.000000(0.089)
	S	1.000000(0.0028)
	S	1.000000(0.00882)
	P	0.627380(0.71706) + 0.394730(2.30512) + 0.124190(7.90403) + 0.019580(35.18320)
	P	1.000000(0.064)

[a]Each basis expansion is written as $C_1(\alpha_1) + C_2(\alpha_2) + \ldots + C_N(\alpha_N)$ where C_i is the expansion coefficient of the gaussian function $\exp(-\alpha_i R^2)$.

rect spatial symmetry (1, 24), but only one determinant for the final product, ethylene oxide in its ground state. In this study, a limited three-state configuration (CI) was included wherever technically possible to take this into account.

The $O(^3P)$ reaction species can be consistently described by one determinant throughout the paths (1). However, because of the UHF approximation used, there is a possibility of 'contamination' of the triplet wavefunction by states of higher multiplicity. The degree of contamination was monitored by evaluation of $\langle S^2 \rangle$ for all points computed on the surface. For the symmetric cycloaddition path, $\langle S^2 \rangle$ is approximately 2.023 for all points, and for the asymmetric path, $\langle S^2 \rangle$ decreases from 2.43 at long range to approximately 2.08 for geometries approaching the equilibrium bond lengths of the ground state ethylene oxide product. The unwanted contributions from quintet, etc., states are thus negligible for the compact geometries of most interest.

The LCAO-SCF wavefunctions were calculated in a basis set derived from the *sp*-gaussian set used by Basch *et al.* (25) in studies of the low-lying electronic states of several small molecules. The basis is of best-atom double-zeta quality. Preliminary studies indicated that the addition of more diffuse orbitals to the basis was necessary to satisfactorily describe the highest occupied molecular orbitals of the three lowest-lying excited triplet states of possible interest. This was accomplished by the addition of three *s*- and one set of three *p*-type functions (left uncontracted) per heavy nucleus, continuing the trend in the ratio of the orbital exponents in the original set. The final basis set used for the surfaces is reported in Table 1. The net contraction is (13 6/4) → [7 3/2] yielding a 56-function set. A basis of this size may be expected to reproduce rotational barriers to within 1 kcal mol^{-1} (26) and charge densities to $\pm 10\%$ (27).

The Potential Surfaces

The energy hypersurfaces for the seven-nucleus C_2H_4 + O system are functions of 15 internal coordinates. Accordingly, a complete geometry search could not be contemplated. Instead, restricted searches were made to answer several specific questions. The first was whether or not the energetically preferred singlet and/or triplet cycloaddition paths are symmetric with respect to the carbon nuclei of the substrate olefin. An alternative is an unsymmetrical binding to one carbon only. In the former case a symmetric ring product may be expected, and in the latter an open-ring product or intermediate. The second question was the height of the energy barrier to rotation of the terminal methylene for open-ring geometries, as this may determine the degree of retention of stereochemistry of a final closed-ring product. Finally, the minimum energy barrier (assumed to be rate-determining) leading to

TABLE 2. Experimental bond lengths and bond angles of ground state ethylene (28) and ethylene oxide (29)

	Value	
Parameter (au or deg)	Ethylene	Ethylene oxide
$R_{CO}(=R2)$	—	2.7164
$R_{CC}(=R1)$	2.5304	2.7817
R_{CH}	2.052	2.045
$\angle CCO(=\alpha)$	—	59.2
$\angle HCH$	117.6	116.7

a transition or intermediate state on the singlet and triplet paths was to be determined.

Each of these questions necessitated a geometry search with respect to variation of one or more of four independent nuclear geometry parameters of the C_2H_4 + O adduct: $R1$, the carbon–carbon distance; $R2$, the shorter of the two carbon–oxygen distances; α, the angle between $R1$ and $R2$; and γ, the torsion angle of the terminal methylene group. For a symmetric oxygen approach (along the bisector of the carbon–carbon axis), it was useful to further define $R3$, the distance between the oxygen nucleus and midpoint of the carbon–carbon axis. The geometries of the two methylene groups were assumed to vary between the (very similar) limiting geometries of reactant ground state ethylene (28) and product ground state ethylene oxide (29). (See Table 2.) The difference in energy caused by this assumption is less than 5 kcal mol^{-1}.

Symmetric Path

The variations in total singlet and triplet energies versus $R3$ were followed for oxygen approaching the olefin in the plane perpendicular to that of the ethylene nuclei and equidistant from the carbons (C_{2v} approach).

The paths computed are presented in Fig. 3 and define the following symmetric cycloaddition reactions:

[1] $C_2H_4(^1A_{1g}) + O(^1D) \rightarrow C_2H_4O(^1A_1)$
$\Delta E = -55$ kcal mol^{-1}

[2] $C_2H_4(^1A_{1g}) + O(^3P) \rightarrow C_2H_4O(^3B_1)$
$\Delta E = +145$ kcal mol^{-1}

The singlet surface is seen to be strongly 'downhill' attractive leading to the potential well around the ground state equilibrium geometry. The triplet surface is purely repulsive. The energy increase quoted for reaction 2 is for the formation of the (unstable) triplet adduct with the equilibrium geometry of the singlet adduct, C_2H_4O. This differing behaviour of the singlet and triplet potential energy curves for the symmetric addition of oxygen is the same as that obtained for the corresponding symmetric insertion of $O(^1D)$ and $O(^3P)$ into $H_2(^1\Sigma_g^+)$; the singlet curve being monotonically decreasing, leading to the formation of stable ground state water and the triplet being repulsive, crossing the singlet curve at a value of $R3$ greater than its equilibrium value in the ground state (1, 24). For several values of $R3$, the singlet energy was optimized with respect to $R1$. A smooth increase from the limiting value of 2.53 au (for reactant ethylene) to 2.78 au (for product ethylene oxide) was found for decreasing $R3$, reflecting the weakening of the carbon–carbon binding with approach of the oxygen. The singlet path is accurate to better than ± 5 kcal mol^{-1} with respect to $R1$ variation along the complete range of $R3$ values.

The effects of the configuration interaction correction to the singlet is also shown in Fig. 3. For the extended geometry with $R3 = 10$ au, wavefunctions for the lowest singlet state were computed by three methods. The lowest single determinantal energy is -152.68075 au. A CI was performed using as a basis the three lowest individually converged SCF closed-shell functions at this geometry. The lowest CI energy was found to be -152.72013 au, only 0.08 kcal mol^{-1} less than the sum of the energies of separated $C_2H_4(^1A_{1g})$ (-78.00643 au) and $O(^1D)$ (-74.71357 au) when the $O(^1D)$ energy is itself obtained from a separate three-state CI. The $O(^1D)$ energy is from a basis of reconverged SCF functions, yielding an $O(^1D) - O(^3P)$ energy difference of 53 kcal mol^{-1}. The spectroscopic energy difference between the oxygen ^1D and ^3P terms is 45 kcal mol^{-1}. Finally, a CI was performed using a virtual orbital (VO) description of the first and second excited closed-shell states. This yielded a lowest singlet energy of -152.68888 au, 18 kcal mol^{-1} above the previous CI result and recovering only 6 kcal mol^{-1} of the 24 kcal mol^{-1} error incurred by the description of $O(^1D)$ by a single determinantal function.

The importance of configurational mixing is expected to decrease as the nuclear structure closes to that of the equilibrium ground state of ethylene oxide. (There the energies of two of the three determinants diverge from that of the low-

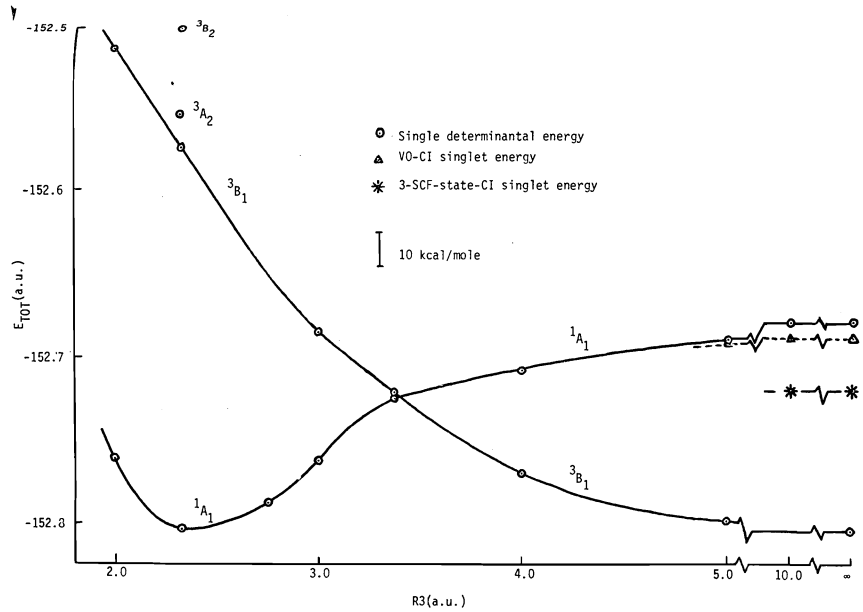

FIG. 3. Symmetric singlet and triplet potential energy paths.

est determinantal function and thus become unimportant contributors to the description of the lowest state.) At $R3 = 5$ au, a VO-CI calculation yielded an energy decrease of 1.3 kcal mol^{-1}. Assuming a roughly proportional relationship of the energy corrections recovered by the VO and reconverged-function basis CI's, there may thus exist an activation barrier to the singlet reaction of the order of 10 kcal mol^{-1} at $R3 = 5$ au.

The symmetric triplet path consists of a smooth energy increase on approach of the reactants. For each value of $R3$, the UHF triplet function was computed for the optimal $R1$ value of the singlet.

Figure 4 displays the singlet and triplet charge distributions for three points on the symmetric surfaces. For $R3 = 4.0$ au, the charge distributions for both states show apparently similar overlap of the reactant charge densities. At $R3 = 3.0$ au, while the regions of high density in the binding regions of the ethylene moiety in the two states are still almost superimposable, the charge density of this fragment in the triplet state has extended into its nonbonded region in the form of a diffuse distribution. For $R3 = 2.31$ au (ground state equilibrium geometry), the singlet distribution contains wide belts of high (>0.2 au) density in the binding regions between the three heavy nuclei indicative of the strong ring binding of the conventional bond description. In contrast, the triplet density plot shows much lower charge between the nuclei. The 0.2 au contours are still separately localized around the oxygen and ethylene fragments indicating the lack of any significant binding between oxygen and the carbons of ethylene. Furthermore, the 0.2 au contour encompassing the carbon nuclei at this geometry has contracted indicating a substantial decrease in the charge density in the C—C internuclear region and hence a decrease in the C—C binding. These observations regarding the charge distributions of the symmetrical singlet and triplet adducts apply equally to the corresponding insertion reactions of oxygen with H_2 (1).

The potential energy and molecular charge distribution exhibit the same characteristic properties along the singlet path for both the insertion and addition reactions, and both differ from the corresponding triplet paths in identical ways with regards to the behaviour of the potential energy and charge density distributions. The differences between the singlet and triplet paths may in each case be related to a common cause, the *added restrictions* placed on a system with two or more unpaired electrons. In the description of a singlet pair of electrons, the antisymmetry requirement is imposed in spin space. For a triplet pair, the spin function is symmetric and the consequences of the antisymmetry are

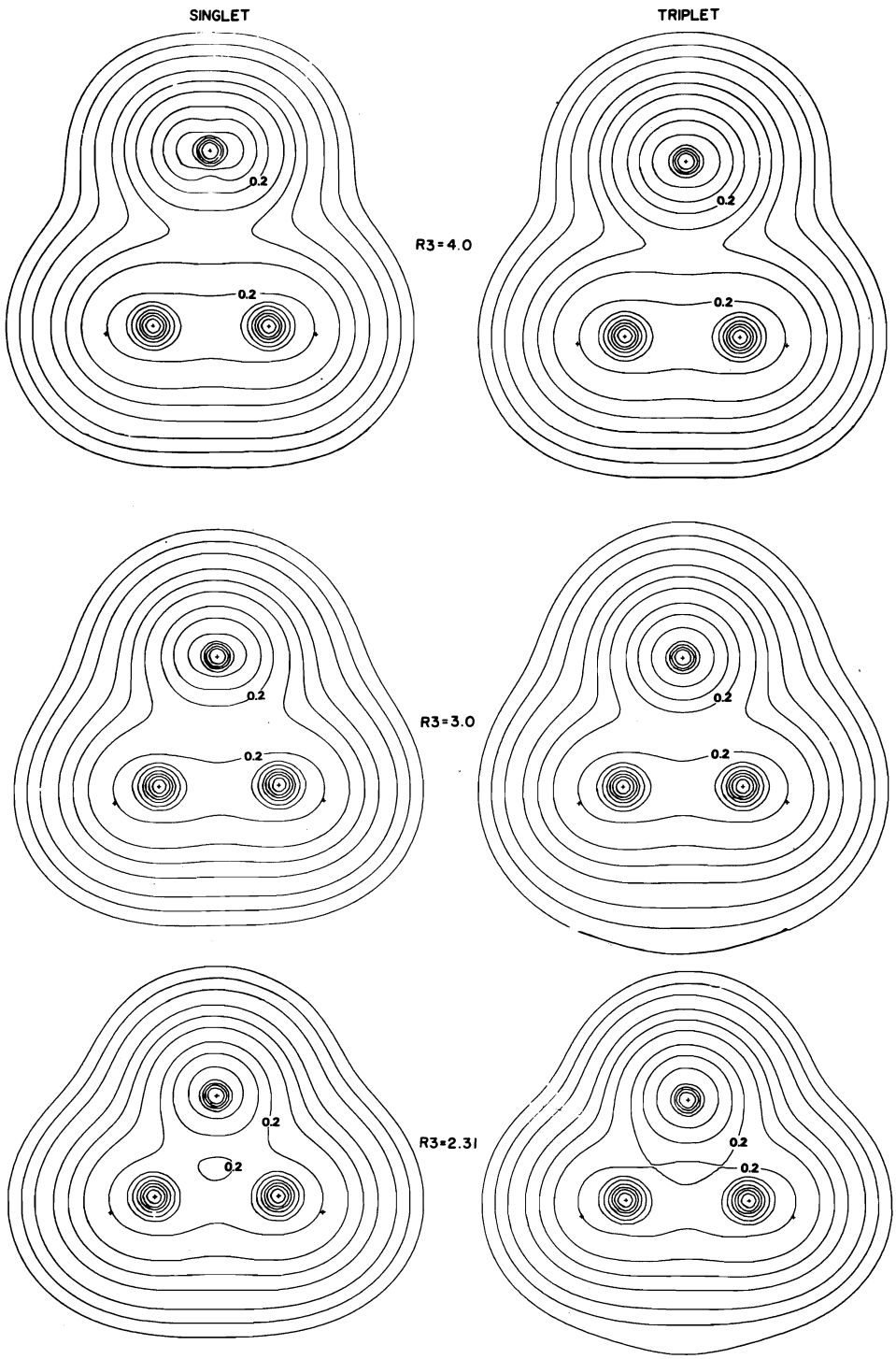

FIG. 4. Total singlet and triplet charge distributions (in the plane of the heavy nuclei) for the symmetric path.

made manifest in real space. Its effect on the energy and charge distribution may be understood and predicted in terms of the spin density, the spatial distribution of which provides a direct display of the consequences of the antisymmetry requirement in real space.

Figure 5 contains plots of $\sigma(r)$ for the first two points of Fig. 4, based on the $M_s = 1$ UHF wavefunctions. One of two unpaired electron distributions remains largely localized on the oxygen, in the plane perpendicular to the plane illustrated. At $R3 = 4.0$ au, a spin 'polarization' is already apparent. There is a π-like distribution of α-density on the ethylene carbons and small regions of excess β-density near the oxygen. For $R3 = 3.0$ au, these effects are more pronounced, and in addition a small region of excess β-density appears between the carbons. A large α-density excess has been localized in the carbon π-regions. The polarization pattern is strongly reminiscent of that of the triplet ethylene molecule (Fig. 1*d*) modified, of course, by the presence of the oxygen. Thus, as in the insertion approach of $O(^3P)$ into $H_2(^1\Sigma_g^+)$, the spin polarization obtained in the symmetric addition approach of triplet oxygen corresponds to the quasi-excitation of the singlet substrate to its lowest triplet, with the related consequences on its charge density and energy. The spin polarization at $R3 = 3.0$ au is characteristic of the spin unpairing mechanism illustrated in Fig. 2*a* for the symmetrical triplet insertion. They differ only in the spatial nature of the electron pair so affected, a σ pair in one case, a π pair in the other.

Thus a symmetric approach to a pair of bonded 'π' electrons results in a localization of spin density of like sign on each nucleus, with the consequence that charge density cannot be accumulated in any of the internuclear regions. The binding between the carbon atoms arising from the charge density in the π-like distribution is reduced and no new binding with the approaching oxygen is possible. The symmetric approach is an energetically unfavourable one for both triplet addition and triplet insertion.

As the angle of approach of the oxygen as measured by β is increased, the spin polarization changes smoothly from that characteristic of a spin unpairing (for $\beta = 90°$) to that characteristic of a spin decoupling. The latter polarization, since it yields an alternation in the signs of the localized spin distributions, in this case C(α)—C(β)—O(2α), allows for simultaneous binding between all three nuclei. Thus one finds a CCO angle such that an uncoupling, that is, a spatial separation of the spin densities of the α,β bonded pair is obtained. This occurs at an angle $\alpha(= \angle CCO)$ equal approximately to the tetrahedral angle (Fig. 8).

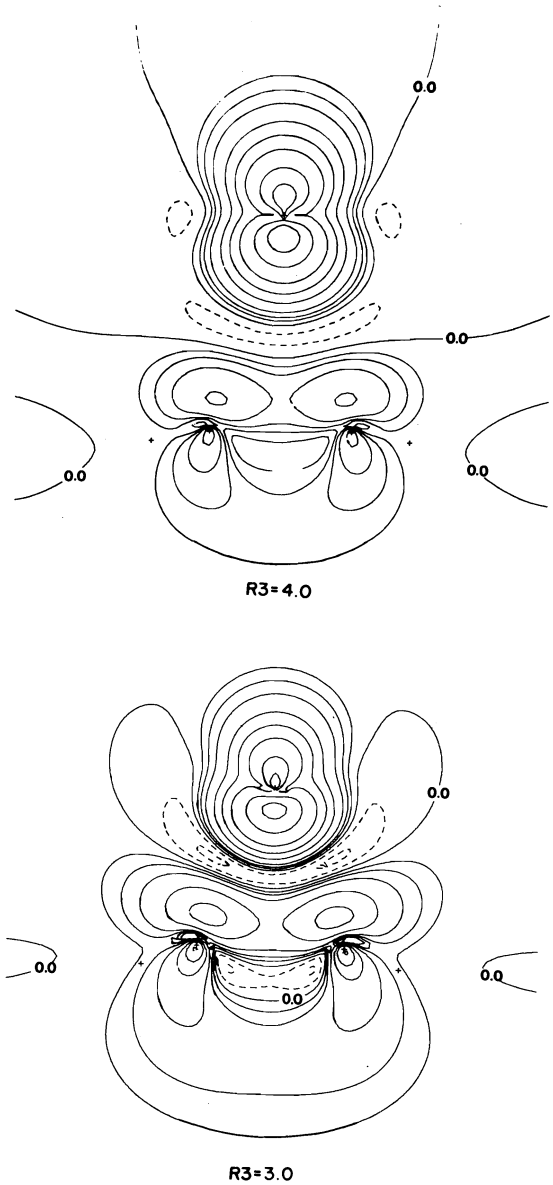

FIG. 5. Triplet spin density distributions (in the plane of the heavy nuclei) for the symmetric oxygen approach points of Fig. 4.

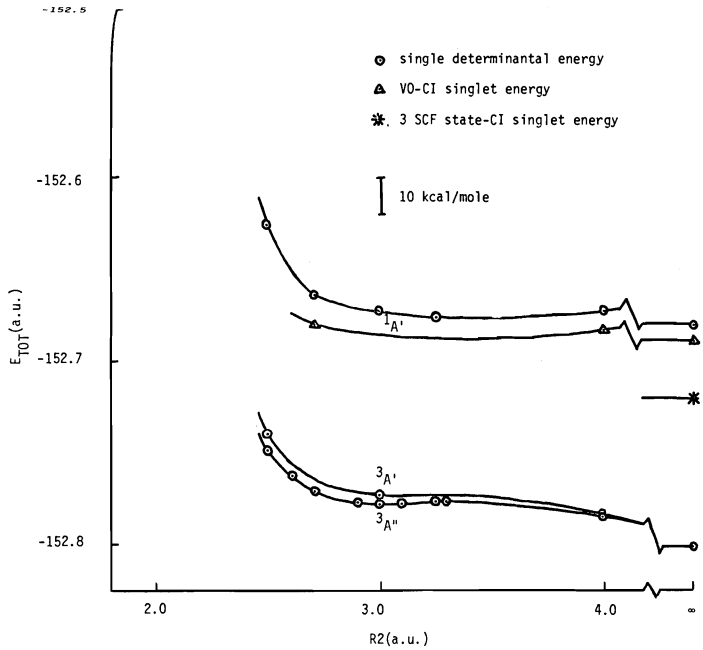

FIG. 6. C_s ($\alpha = 109.47°$) singlet and triplet potential energy paths.

Asymmetric Path and Spin Transfer

To define the energetics of unsymmetrical oxygen approach, which has been variously (2, 8, 30) suggested to be a particularly likely path for the triplet reaction, computations of the singlet and triplet energy variation versus $R2$ were made for α fixed at 109.47° (tetrahedral C—C—O angle). The oxygen was constrained to lie in the plane containing the carbon–carbon axis perpendicular to that of the ethylene nuclei. The terminal methylene was fixed in its planar geometry in ethylene, and the internal methylene given the almost tetrahedral geometry of the ground state ethylene oxide equilibrium geometry. For such molecular geometries, the point group is C_s and the lowest singlet and triplet states are now $^1A'$ and $^3A''$ respectively.

The paths computed are shown in Fig. 6. The lowest (closed-shell) singlet state is repulsive to the extent of 30 kcal mol^{-1} at ground state ethylene oxide equilibrium bond lengths, 25 kcal mol^{-1} with inclusion of VO-CI. For $R2 =$ 2.814 au, the energy of the lowest open-shell $^1A'$ state was computed (by addition of the 2K energy difference to the lowest $^3A'$ RHF state (24, 25)) to be 18 kcal mol^{-1} above that of the lowest single-determinantal closed-shell $^1A'$ state. A VO-CI calculation (including the lowest open-shell $^1A'$ state as well as the lowest three closed-shell determinants) showed only negligible contributions to the single-determinantal description of the lowest singlet, and left the singlet path still repulsive to the extent of 20 kcal mol^{-1} at the ground state equilibrium bond lengths. (This is equivalent to finding the lowest singlet state to have no significant diradical character at such geometries.)

There are two triplet states, slightly repulsive (15 kcal mol^{-1} at the ground state equilibrium bond lengths) and designated $^3A'$ and $^3A''$ (the latter lower by 1–3 kcal mol^{-1} over the whole path). Because of the shallow minimum found at $R2 = 3.0$ au, the path in that region of the surface was optimized with respect to α, then with respect to $R1$ for fixed α at $R2 = 3.5$ and 3.0 au. The originally observed dip, less than 1 kcal mol^{-1}, is not meaningful in itself because of the approximations and constraints imposed by the method of calculation used. However, the α- and $R1$-optimizations defined the lowest energy approach angle to be $104 \pm 2°$ and $R1 = 2.75 \pm 0.05$ au, respectively, in this $R2$ range with the remainder of the molecular geometry rigid. The full curves are possibly within 2 kcal mol^{-1}, and

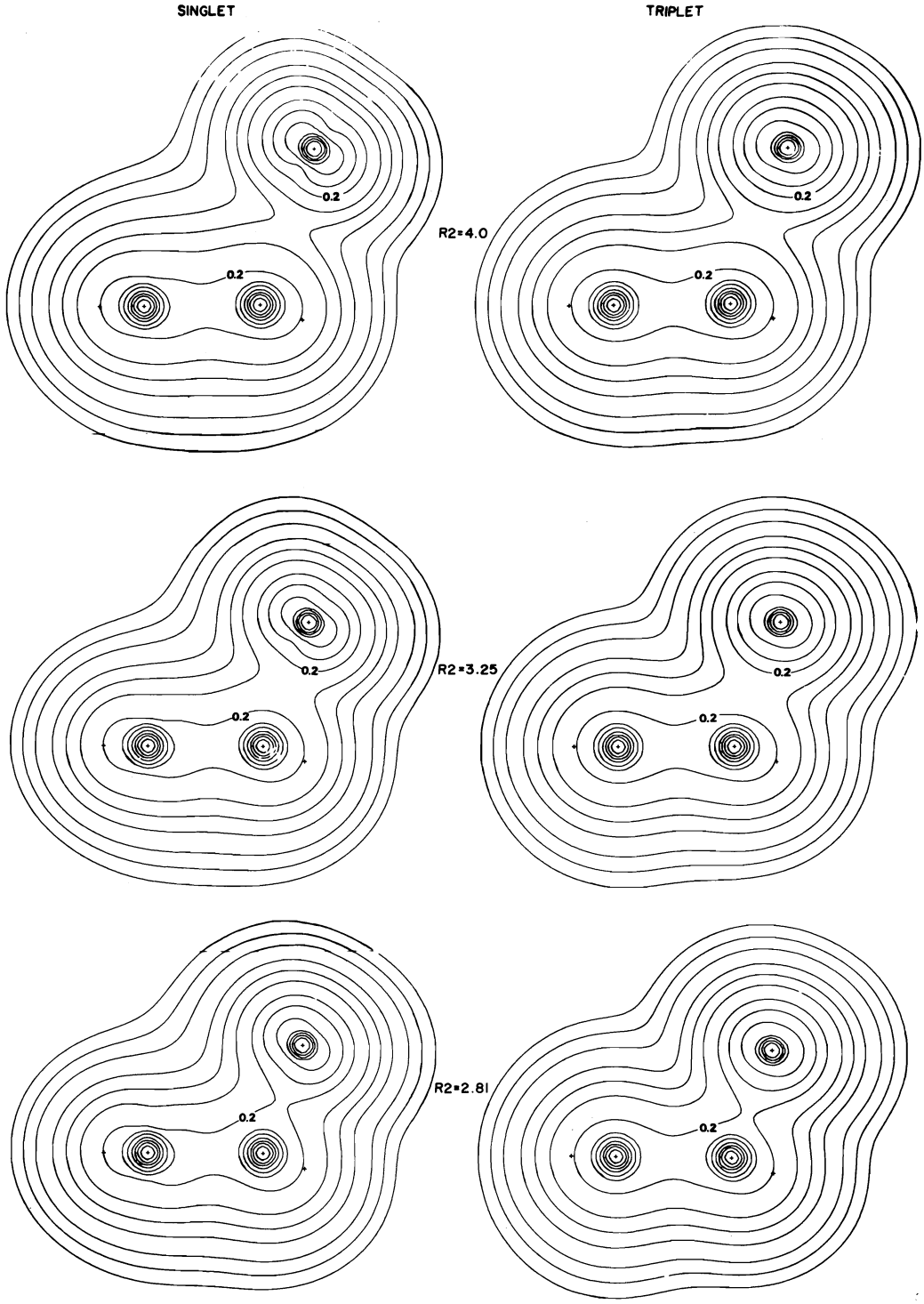

FIG. 7. Total singlet and triplet charge distributions (in the plane of the heavy nuclei) for asymmetric ($\alpha = 109.47°$) oxygen approach to C_2H_4.

certainly 10 kcal mol^{-1}, of the unconstrained path. The singlet asymmetric surface is energetically downhill to the symmetric path for all $R2 <$ 4.0 au. In contrast, the triplet surface is uphill for α both higher and lower than 105° all along the path.

The singlet and triplet charge distributions for three points on this unsymmetric path are shown in Fig. 7. For $R2 = 4.0$ au the oxygen and ethylene fragment distributions are still clearly identifiable. For $R2 = 2.81$ au the 0.2 au contour encircles all the heavy nuclei in both the singlet and triplet adducts, indicating some degree of CO bonding. However, not only is there binding between just one carbon and the oxygen in this region of the singlet surface, the binding which is present is very weak. This is reflected in the ellipsoidal nature of the distribution of charge along the C—O axis.[4] In the triplet plot for $R2 =$ 2.81 au the charge distribution in the region of the terminal methylene is essentially superimposable on that of triplet ethylene (Fig. 1*c*).

Figure 8 shows the spin density for three points along the triplet surface; in the CCO plane (first column) and in the plane perpendicular to this one along the C—O axis. Even for $R2 = 4.0$ au, a spin polarization is strongly in evidence. In addition to the (slightly perturbed) oxygen atom containing an α-density torus (around the CO axis) there are large $p\pi$-like accumulations of excess α- and β-density on the terminal and internal methylene carbons, respectively. The approach of oxygen is accompanied by an 'uncoupling' of the α,β-density of the ethylene. The mechanism of spin polarization is the same as that for the linear abstraction reaction (1) (Fig. 2*b*). Throughout the path there is less β-density induced on the internal carbon than α-density on the terminal carbon. Thus there has also been a net transfer of α-spin from oxygen to terminal methylene. The transfer effect increases along the reaction path until for $R2 = 2.81$ au, the excess α-spin distribution near the terminal methylene is essentially superimposable on that of the ethylene triplet state (Fig. 1*d*).

By referring as well to the second column of plots in Fig. 8 one sees that for large C—O separations the distribution of spin density on oxygen has a directional character (*p*-like) directed along the C—O axis and near spherical character in the perpendicular plane. As the C—O separation is decreased the amount of α spin density in the nuclear plane and its directed nature along the C—O axis are decreased and the spin distribution becomes increasingly localized and directed in the perpendicular plane. Clearly, as the localization of excess α spin density on the terminal carbon increases, the remaining spin density on oxygen is increasingly localized along an axis which is perpendicular to the axis of localization on the terminal carbon. In this manner the two localized distributions of α spin density are maximally separated in space.

The first two columns of Fig. 9 contain the triplet charge and spin density maps for three planes of an asymmetric geometry with $R2$ further reduced to 2.71 au. At this geometry, the triplet has an energy only 22 kcal mol^{-1} above that of the separated reactants (compared to 148 kcal mol^{-1} for the corresponding symmetrical geometry). There is a charge accumulation between the oxygen and internal methylene almost as great as for the singlet equilibrium geometry (Fig. 4), indicative of strong CO bonding. The three planes illustrate the localization of alternating regions of excess α- or β-density on all the nuclei in the incipient molecule. Thus there has been a spin polarization of the σ-bonding density of the reactant ethylene. The amounts of β-density induced on the internal carbon and of α-density remaining on the oxygen in the C—C—O plane are smaller than at long range (*cf.* Fig. 8) corresponding to a short-range spin 'recoupling' and formation of paired CO binding density. The dominant spin structure in the resulting molecule consists of two

[4]The three states of the $O(^1D)$ term which describe the state of oxygen which interacts with ethylene, yield an ellipsoidal charge distribution with its major axis perpendicular to the axis of approach (see Figs. 4 and 7); there is a deficit of charge along the direction of approach. In an orbital description of this 'prepared' state, there are one and two-third orbital vacancies in the plane containing the carbon and oxygen nuclei and one-third of a vacancy in the oxygen orbital perpendicular to this plane. In the symmetric approach, these vacancies are filled by the π electrons of ethylene and the deficit in charge density along the C_2 symmetry axis is not present in the equilibrium geometry. However, in a corresponding close approach in an asymmetric geometry, the ellipsoidal nature of the charge distribution on oxygen is still very much in evidence, indicating that the orbital vacancies in this plane are not filled and that considerably less density is accumulated along one C—O axis than in the symmetric geometry.

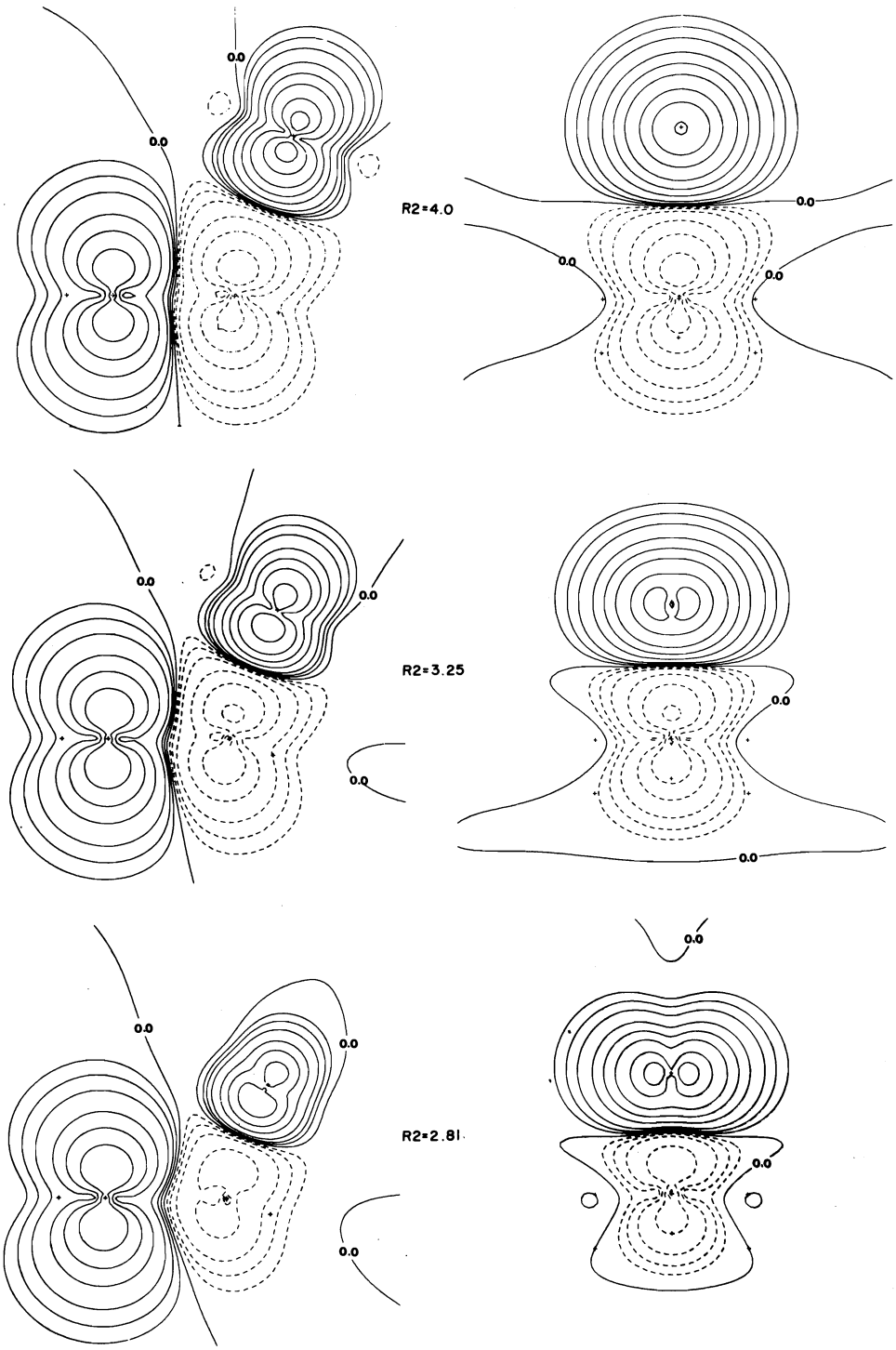

FIG. 8. Triplet spin density distributions; (*a*) in the plane of the heavy nuclei and (*b*) the plane perpendicular to (*a*) and also containing the CO axis, for the points on the triplet asymmetric path in Fig. 7.

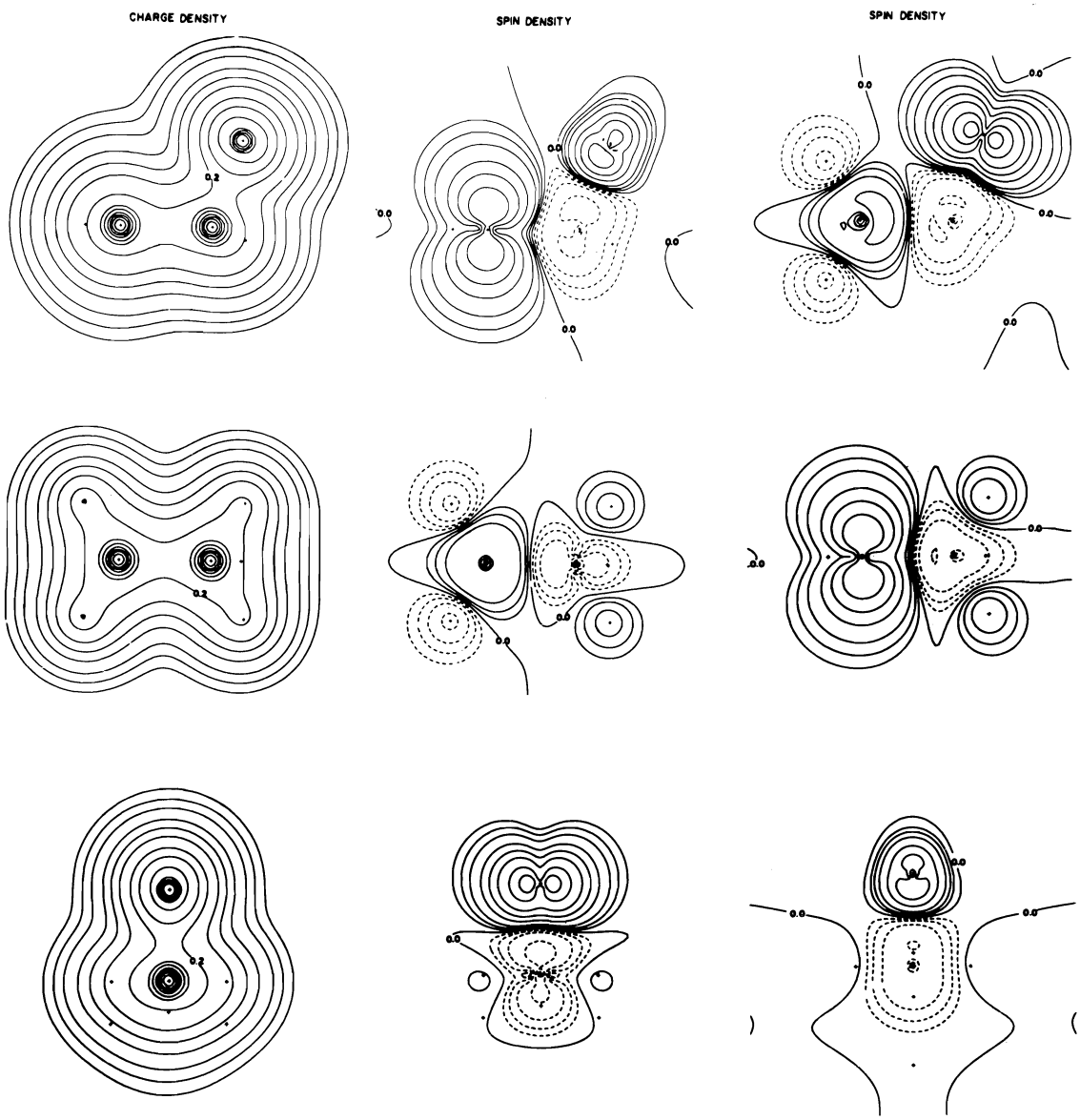

FIG. 9. Total charge and spin density distributions for ethylene oxide $^3A''$ state at $R2 = 2.71$ au. The first column contains charge plots for (from top to bottom) the plane containing the three heavy nuclei, the plane containing the carbons and terminal hydrogen nuclei, and the plane containing the internal carbon–oxygen bond and also perpendicular to the first plane. The second column contains the corresponding spin distributions. The third column contains the spin density plots in the same three planes for the same state and geometry, except that the terminal methylene group is rotated into the plane of the heavy nuclei.

separate distributions of excess α-spin with the axes of their maxima mutually perpendicular; a $p\pi$-like distribution on the terminal methylene and another such distribution on the oxygen directed along an axis perpendicular to that of the former. Also shown, in the third column of Fig. 9, are the spin distributions for the same three planes of the molecule with the same geometry, except that the terminal methylene has been rotated 90°. It can be seen that the perpendicularity

of the two terminal α-density distributions persists. That is, *the rotation of the terminal methylene group induces a rotation of the localized spin distribution on oxygen, such that the mutual avoidance of the two localized α spin distributions is maintained.* Recalling that the distribution of charge and spin density localized on the terminal methylene is essentially superimposable on that for the same fragment of triplet ethylene, the triplet adduct described here has the characteristics of a diradical of the form $CH_2(\alpha)$—C—O(α) with the added understanding that the localized α spin distributions are localized in mutually orthogonal directions.

For these open-ring structures, the barrier to rotation of the terminal methylene around the carbon–carbon axis (*i.e.* variable γ) was computed to be 6 kcal mol^{-1} for $\alpha = 109.47°$ and 5 kcal mol^{-1} for $\alpha = 90°$, a maximum for $\gamma = 90°$ in both cases.[5] This barrier is nearly twice the value for rotation about the C—C bond in ethane.

The spin polarization accompanying an asymmetric triplet reaction path can be described as proceeding in the following manner; (*i*) initial uncoupling of the olefin π-bonding density and counter-migrations of the α- and β-components to the two carbon nuclei, accompanied by a decrease in the carbon–carbon binding density and thus weakening of the carbon–carbon bonding; (*ii*) recoupling of the β-density on the internal carbon to the α-distribution on the oxygen nucleus, associated with accumulation of carbon–oxygen binding density, hence bonding; (*iii*) localization of the two excess α-spins in two mutually perpendicular distributions of one α-spin each at opposite ends of the structure; (*iv*) simultaneous counterpolarization of the σ-binding density on adjacent nuclei throughout the resultant open-chain structure similar to that of the triplet state of ethylene itself. Thus the decrease in the extent of carbon–carbon binding occurs simultaneously with an increase in the extent of carbon–oxygen binding, thereby accounting for the much lower energy barrier to asymmetric rather than symmetric triplet attack.

[5]The rotation barrier for ethylene in its lowest triplet state was computed to be 15 kcal mol^{-1} (for $R1 = 2.961$ au) in the basis set used, the energy for $\gamma = 90°$ being a minimum. The experimental (28) barriers for singlet and triplet ethylene are respectively 66 kcal mol^{-1} (minimum for coplanar methylenes) and 31 kcal mol^{-1} (minimum for perpendicular methylenes).

The lowest energy triplet reaction path is the one which allows for a polarization of the spin density corresponding to the spin uncoupling mechanism: abstraction or ring-opened adduct.

All along the asymmetric path the incipient molecule is unstable to redissociation into $C_2H_4 + O$; it is thus not a chemical intermediate. This path is the lowest triplet reactive channel found. To reach the (dilute, gas-phase) product of interest, ethylene oxide in its ground state, the triplet species must at some point undergo a radiationless transition to the singlet surface. To obtain an estimate of the triplet activation barrier, it suffices to find the geometry of lowest energy at which the singlet and triplet surfaces cross. The singlet surface lies below that of the triplet for symmetric geometries for $R2 < 3.6$ au (Fig. 3); for the asymmetric path ($\alpha = 109.47°$, Fig. 6), the triplet surface lies below that of the singlet for all values of $R2$. Thus the surfaces must cross at intermediate α-values and at $R2 < 3.6$ au, linking the surfaces at a lower crossing energy than on the symmetric path. Optimization of the crossover energy (31) with respect to $R2$ (with the remainder of the molecule fixed in the geometry of Fig. 9) yielded an energy barrier of 36 ± 2 kcal mol^{-1} above the energy of the separated reactants for $R2 = 2.9$ au and $\alpha = 83°$. In comparison, for the symmetric approach, the triplet encounters a barrier of 49 ± 5 kcal mol^{-1} (Fig. 3) before intersecting the singlet surface.

Conclusions

The potential energy surfaces computed for the singlet cycloaddition reaction are in accord with the suggestions of Cvetanović (32); that singlet oxygen undergoes a symmetric, concerted reaction to form an ethylene oxide ring product. The conclusions that the triplet reaction proceeds via the formation of an open-ring diradical with concurrent rotation of the terminal methylene followed by a ring-closing cross-over to the singlet surface are also in agreement with the experimentally based suggestions of Cvetanović (32, 33). We do not find a potential minimum on the triplet surface which would correspond to the formation of an intermediate π-complex as postulated by Cvetanović (34). Our calculated results for the triplet path differ from the experimental findings in one important aspect. The experimental results are interpreted as indicating that $O(^3P)$ adds

to olefins with small (<2 kcal mol^{-1}) energies of activation (12, 33, 34), while the lowest crossover from the triplet to singlet surfaces to yield ground state ethylene oxide is calculated to occur at an energy $\sim$36 kcal mol^{-1} above the energy of the reactants. Thus while the geometry, behaviour, and properties of the theoretically determined triplet adduct agree well with the experimentally based proposals regarding the mechanism of triplet addition, theoretical and experimental proposals of the activation energies are in serious disagreement. In both the $O(^3P) + H_2(^1\Sigma_g^+)$ (1) and $O(^3P) + C_2H_4(^1A_{1g})$ calculations, we did not find an approach geometry which was not repulsive with regards to energy.

It is the principal purpose of this investigation to draw attention to the potential use of the spin density in the understanding of the mechanisms of reactions involving unpaired electrons. A more complete knowledge of the manner in which the spatial localization of the spin density varies with nuclear geometry in systems of experimental interest would provide a theoretical and physical basis for predicting the course of a reaction for a system with a net spin angular momentum.

1. R. F. W. Bader and R. A. Gangi. J. Am. Chem. Soc. **93**, 1831 (1971).
2. R. C. Woodworth and P. S. Skell. J. Am. Chem. Soc. **81**, 3383 (1953) and references therein.
3. R. Hoffmann. J. Am. Chem. Soc. **90**, 1475 (1968) and references therein; H. Fujimoto, S. Yamabe, and K. Fukui. Bull. Chem. Soc. Jpn. **45**, 2424 (1972).
4. P. G. Gaspar and G. S. Hammond. Carbene chemistry. *Edited by* W. Kirmse. Academic Press, New York, NY. 1964. Chapt. 12.
5. G. Paraskevopoulos and R. J. Cvetanović. J. Chem. Phys. **50**, 590 (1969).
6. A. R. Knight, O. P. Strausz, and H. E. Gunning. J. Am. Chem. Soc. **85**, 2349 (1963).
7. R. F. W. Bader and J. I. Generosa. Can. J. Chem. **43**, 1631 (1965).
8. H. Yamasaki and R. J. Cvetanović. J. Chem. Phys. **41**, 3703 (1964).
9. R. J. Cvetanović. Can. J. Chem. **36**, 623 (1958).
10. K. S. Sidhu, E. M. Lown, O. P. Strausz, and H. E. Gunning. J. Am. Chem. Soc. **88**, 254 (1966).
11. F. A. L. Anet, R. F. W. Bader, and A. M. Van der Awera. J. Am. Chem. Soc. **82**, 3217 (1960).
12. R. J. Cvetanović. Adv. Photochem. **1**, 115 (1963).
13. S. Hirokami and R. J. Cvetanović. Can. J. Chem. **51**, 373 (1973).
14. E. E. Kasmovskaya and A. N. Ponomarev. Kinet. Katal. **9**, 687 (1968).
15. M. D. Sheer and R. Klein. J. Phys. Chem. **73**, 597 (1968).
16. O. P. Strausz, H. E. Gunning, and I. G. Csizmadia. J. Am. Chem. Soc. **94**, 8317 (1972); H. E. Gunning and O. P. Strausz. Adv. Photochem. **4**, 143 (1966).
17. W. J. Haines and I. G. Csizmadia. Theor. Chim. Acta, Berlin, **31**, 283 (1973).
18. W. B. Demore and S. W. Benson. Adv. Photochem. **2**, 219 (1964).
19. R. Hoffmann, C. C. Wan, and V. Neagu. Mol. Phys. **19**, 113 (1970).
20. E. Leppin and K. Gollnik. Tetrahedron Lett. **43**, 3819 (1969).
21. F. A. Matsen and A. A. Cantu. J. Phys. Chem. **72**, 21 (1968).
22. R. F. W. Bader and M. E. Stephens. J. Am. Chem. Soc. **97**, 7391 (1975).
23. R. McWeeny and B. T. Sutcliffe. Methods of molecular quantum mechanics. Vol. 2. Academic Press, New York, NY. 1969. p. 104.
24. R. A. Gangi and R. F. W. Bader. J. Chem. Phys. **55**, 5369 (1971).
25. H. Basch, M. B. Robin, and N. A. Keubler. J. Chem. Phys. **47**, 1201 (1967); **49**, 5007 (1968); J. R. Lombardi, W. Klemperer, M. B. Robin, H. Basch, and N. A. Keubler. J. Chem. Phys. **51**, 33 (1969).
26. R. F. W. Bader and R. A. Gangi. *Ab initio* calculation of potential surfaces. *Edited by* R. N. Dixon. Specialist Reports of the Chemical Society, Theoretical Chemistry, Vol. I. 1975. p. 1.
27. R. F. W. Bader. Molecular charge distributions, their display and use. *Edited by* C. A. Coulson and D. A. Buckingham. M.T.P. International Series on Science, Theoretical Chemistry, Vol. II, Butterworths. 1975. p. 43.
28. M. H. Wood. Chem. Phys. Lett. **24**, 239 (1974).
29. G. L. Cunningham, Jr., A. W. Boyd, R. J. Meyers, W. D. Gwinn, and W. I. LeVan. J. Chem. Phys. **19**, 676 (1951).
30. S. Weiss and G. E. Leroi. J. Chem. Phys. **48**, 962 (1968).
31. M. E. Stephens. Ph.D. Thesis, McMaster University, Hamilton, Ont. 1975.
32. R. J. Cvetanović. J. Phys. Chem. **74**, 2730 (1970).
33. S. Hirokami and R. J. Cvetanović. J. Am. Chem. Soc. **96**, 3738 (1972).
34. W. B. Demore. Chem. Phys. Lett. **16**, 608 (1972).

Canadian Journal of Chemistry

Published by
THE NATIONAL RESEARCH COUNCIL OF CANADA

Journal canadien de chimie

Publié par
LE CONSEIL NATIONAL DE RECHERCHES DU CANADA

Volume 55 Number 15 August 1, 1977

Volume 55 numéro 15 1 août 1977

Enumeration of structural isomers in alicyclic hydrocarbons and in porphyrins

BRIAN ALSPACH

Department of Mathematics, Simon Fraser University, Burnaby, B.C., Canada V5A 1S6

AND

S. ARONOFF

Department of Chemistry, Simon Fraser University, Burnaby, B.C., Canada V5A 1S6

Received October 25, 1976

BRIAN ALSPACH and S. ARONOFF. Can. J. Chem. **55**, 2773 (1977).

The number of structural isomers obtainable from all possible substitutions in an alicyclic hydrocarbon is found by the use of Burnside's Lemma. Four classes of compounds exist according to the number of vertices of the ring, and the number and type of substituents on the carbons. The theory is also applicable to other types of compounds in which paired substituents occur, *e.g.* in the biologically-synthesisable porphyrins. Where the pairing is not mandatory, Polya's Theorem is utilized for enumeration. Examples are provided for each of the classes of compounds.

BRIAN ALSPACH et S. ARONOFF. Can. J. Chem. **55**, 2773 (1977).

Le nombre d'isomères de structure que l'on peut obtenir par toutes les substitutions possibles dans un hydrocarbure alicyclique peut être obtenu en utilisant le Lemma de Burnside. Il existe quatre classes de composés suivant le nombre de sommets du cycle et le nombre et le type de substituants sur les carbones. On peut aussi appliquer la théorie à d'autres types de composés dans lesquels des substituants existent sous forme de paires, par exemple dans des porphyrines, qui peuvent être synthétisés d'une façon biologique. Quand l'existence sous forme de paires n'est pas obligatoire, le théorême de Polya peut être utilisé pour l'énumération. On fournit des exemples pour chacune des classes des composés.

[Traduit par le journal]

For purposes of stereoisomer calculations, alicyclic hydrocarbons may be considered as polygons analyzable by graph theory (1). The use of graph theory has been employed in chemical enumeration (2, 3), using exhaustive techniques to produce all possible isomers with a given generic formula. These are then searched (*e.g.*, by computer) to find those with certain prescribed properties. In this paper we count directly the number of isomers with prescribed properties.

Let the polygon have n vertices. Then the carbon at each vertex will be homo- or heterosubstituted (=CXX or =CXY, respectively). Each n-gon will then have m_i homosubstitutents (*e.g.* m_1 of =CXX, m_2 of =CYY, and m_s of =CZZ. Similarly, among the heterosubstituents, there will be k_1 of =CXY (or its enantiomer, =CYX), k_2 of =CXZ (or its enantiomer, =CZX), etc. Then, if $K = k_1 + ... + k_r$, $n = K + m_1 + ... + m_8$, the n-gons may be described by the notation $(k_i,k_j; m_i,m_j)$, so that chlorobromocyclohexane would be (1,1;4), and 1,1-dimethylcyclopentane would be (0;1,4).

Equation 1 is based on Burnside's Lemma (4) (*cf.* below) involving the number of elements in a permutation group and the number of configurations left fixed on making all possible permutations.

It can be shown (see the Appendix) that the number of isomers, F, is given by

$$[1] \qquad F = \frac{1}{2n}\left(\sum_{d|g} \frac{\phi(d)(n/d)!2^{K/d}}{(k_1/d)! \ldots (k_r/d)!(m_1/d)! \ldots m_s/d)!} + L\right)$$

where the following definitions stand. $\phi(n)$ is the number of positive integers *relatively prime* to n in the interval (1, ..., n). In the set (1,2,3,4,5,6), the integers 1 and 5 are prime to 6 so that $\phi(6) = 2$. g is the *greatest common divisor (gcd)* of the set of integers (a_1, ..., a_m). The *gcd*(2,6) is 2 (2 divides 2 and 6), while that of (3,6) is 3 (3 divides 3 and 6). d is a divisor of g. If $g = 6$, $d = 1$, 2, 3, and 6.

The residual term, L, has values depending upon whether n, k, and m are even or odd. Four categories may be distinguished:

Category 1

n is odd; one of the m_i's (say m_j) is odd; all the other m_i's and k_i's are even.

In this case,

$$L = \frac{n[(n-1)/2]!2^{K/2}}{(k_1/2)! \ldots (k_r/2)!(m_1/d)! \ldots (m_{j-1}/2)!(m_{j+1}/2)! \ldots (m_s/2)!}$$

Category 2

n is even; all of the k_i's are even; two of the m_i's (say m_h, m_j) are odd.

In this case, the value of the numerator is identical with that of category 1, but the denominator has the value

$$(k_1/2)! \ldots (k_r/2)!(m_1/2)! \ldots (m_{h-1}/2)!(m_h/2)!(m_{h+1}/2)! \ldots (m_{j-1}/2)!(m_j/2)!(m_{j+1}/2)! \ldots (m_s/2)!$$

Category 3

n is even; all k's and m's are even.

In this case the value of the denominator is identical with that of category 1, but the numerator has the value

$$(n/2)(n/2)!2^{K/2} + (n/2)[(n-2)/2)!(n/2) - (K/2)]2^{K/2}$$

Category 4

In all other cases, $L = 0$.

In the above, where m's are absent by virtue of the generic description of the molecule or its formal deletion (*e.g.*, if $m_j = 1$, then $m_{j-1} = 0$), the formulae are abbreviated accordingly, *i.e.*, the m's are not formal zeros.

The following examples illustrate the application of this equation.

Example 1

Find the number of isomers of hexahydroinositol, i.e., 1,2,3,4,5,6-hexahydroxyhexane. The isomerism arises, of course, from the axial or equatorial position of the substituent on each carbon.

The molecule is described generically as $F(6,0;0)$ or simply as $F(6;0)$, as the k's are single-valued and the m's are vacant. Then as *n and k are even*, we are in category 3. The *gcd* is 6 and the divisors, d, of 6 are 1, 2, 3, and 6. The numerical equivalence of n and K results in the existence of only a single numerator for L. Then

$$\text{For } d = 1, \phi(1) = 1, F_1 = \frac{(1)(6/1)!2^{6/1}}{(6/1)!} = 2^6 = 64$$

$$\text{For } d = 2, \phi(2) = 1, F_2 = \frac{(1)(6/2)!2^{6/2}}{(6/2)!} = 2^3 = 8$$

$$\text{For } d = 3, \phi(3) = 2, F_3 = \frac{(2)(6/3)!2^{6/3}}{(6/3)!} = 2 \times 2^2 = 8$$

$$\text{For } d = 6, \phi(6) = 2, F_6 = \frac{(2)(6/6)!2^{6/6}}{(6/6)!} = 2 \times 2^1 = 4$$

and

$$L = \frac{(6/2)(6/2)!2^{6/2}}{(6/2)!} = 3 \times 2^3 = 24$$

Consequently,

$$F(6;0) = (1/2 \times 6)(64 + 8 + 8 + 4 + 24) = 108/12 = 9$$

Example 2

Find the number of stereoisomers of the myoinositols, i.e., the trihydroxycyclohexanes. The molecule is $F(3;3)$, $g = 3$, and L is category 4.

$$F(3;3) = (1/2 \times 6)\left[\frac{(1)(6/1)!(2^{3/1})}{(3/1)!(3/1)!} + \frac{(2)(6/3)!(2^{3/3})}{(3/3)!(3/3)!}\right] = 14$$

Example 3

Find the number of stereoisomers of 1,2,3,4,5-pentachlorocyclopentane. Here, $L = 0$, $g = 5$, and $d = 1, 5$.

$$F(5;0) = (1/2 \times 5)\left[\frac{(1)(5/1)!(2^{5/1})}{(5/1)!} + \frac{(4)(5/5)!(2^{5/5})}{(5/5)!}\right] = 4$$

Example 4

Find the number of isomers of tetrachlorocyclopentane. In this case, $n = 5$, $k = 4$, *and* $m = 1$, so that the generic description is $F(4;1)$ and L is category 1. Then,

$$F(4;1) = (1/2 \times 5)\left[\frac{(1)(5/1)!(2^{4/1})}{(4/1)!(1/1)!} + \frac{(5)(4/2)!(2^{4/2})}{(4/2)!}\right] = 10$$

Example 5

Find the number of stereoisomers of 1,1-dimethyltetrachlorocyclohexane. In this case, the generic description is $F(4;1,1)$, and where $g = 1$, $d = 1$, L is category 2. Consequently,

$$F(4;1,1) = (1/2 \times 6)\left[\frac{(1)(6/1)!(2^{4/1})}{(4/1)!(1/1)!(1/1)!} + \frac{(6)(4/2)!(2^{4/2})}{(4/2)!}\right] = 42$$

Example 6

Find the number of stereoisomers of mesoporphyrin. The mesoporphyrins are tetramethyl, diethyl, dipropionic acid porphines. In this example we distinguish between two possible classes, (*a*) those in which the substituents are not constrained with regard to pairing at the β,β′-positions, and (*b*) those where, as in mesoporphyrins of possible biologic origin, the ethyls and propionic acids are each accompanied by methyl groups. In all of the 15 known isomers of this class (5, 6), each pyrrole ring is substituted by either a methyl (*m*), ethyl (*e*), or a methyl, propionic acid (*p*). If the porphyrin is thought of as a square plane, then there is formal substitution at the vertices of a rectangle. The isomerism arises from the position of substitution of *m*, *e*, and *p*, recognizing that the order of substitution must be considered, *i.e.* that $m,e \neq e,m$.

We first consider the porphyrins of possible biological origin. The generic description is $F(2,2;0)$, with L in category 3, $g = 2$ and $d = 1$. Then,

$$F(2,2;0) = (1/2 \times 4)\left[\frac{(1)(4/1)!(2^{4/1})}{(2/1)!(2/1)!} + \frac{(2)(2/1)!(2^{4/2})}{(2/2)!(2/2)!} + \frac{(4/2)(2/2)!(4/2 - 4/2)(2^{4/2})}{(2/2)!(2/2)!} + \frac{(1)(4/2)!(2^{4/2})}{(2/2)!(2/2)!}\right]$$

$$= (1/8)(96 + 16 + 0 + 8) = 15$$

In contrast with the biologically-possible mesoporphyrins, the chemically-possible mesoporphyrins involve no constraint of the *m*, *e*, and *p* substituents. In this case there are 60 isomers (5), a result which can be derived from Polya's Theorem as follows.

If the cyclic decomposition of a permutation is the product of α_k cycles of length k, then the term $x_1^{\alpha_1}, x_2^{\alpha_2}, \ldots x_m^{\alpha_m}$ corresponds to the permutation. The corresponding terms for all the permutations are added together and divided by the order of the group, to form what is called the *cycle index* (7) of the group. For example, the cycle index of a square (P_4) is $(1/8)(x_1^8 + 5x_2^4 + 2x_4^2)$. Thus, the four 2-cycles (x_2^4) may undergo four reflections and one 90° rotation, providing the coefficient, 5. Similar reasoning leads to the coefficients of x_1^8 and x_4^2.

Assume that the porphyrin is such a square, with the β,β′ substituents meeting at each of the four

vertices. At each vertex we may substitute *any* pair of methyl, ethyl, or propionic acid. We may have, as an extreme, octamethylporphine or, less extremely, tetramethyl, tetraethylporphine. We want to know how many exist as tetramethyl, diethyl, dipropionic acid-substituted. According to Polya's Theorem, this number is the coefficient of the $m^4e^2p^2$ term in the expansion of the cycle index polynomial where $(m + e + p)$ is substituted for x_1, $(m^2 + e^2 + p^2)$ for x_2, and $(m^4 + e^4 + p^4)$ for x_4, to give

$$(1/8)[(m + e + p)^8 + 5(m^2 + e^2 + p^2) + 2(m^4 + e^4 + p^4)]$$

Obviously, the term $m^4e^2p^2$ cannot arise from the last term. The number arising from the second term is 4!/2!, and from the first is 8!/4!2!2!. The coefficient of $m^4e^2p^2$ is then

$$(1/8)[(8!/4!2!2!) + 5(4!/2!)] = 60$$

as noted earlier (5).

Acknowledgement

We are pleased to acknowledge the support, in part, of the National Research Council of Canada.

1. J. K. SENIOR. Am. J. Math. **73**, 663 (1951); G. POLYA. Acta Math. **68**, 145 (1937); A. CAYLEY. Collect. Math. Pap. **3**, 242; **9**, 202; **9**, 427; **11**, 365; **13**, 26 (1889–1897).
2. A. T. BALABAN. Rev. Roum. Chem. **18**, 635 (1973).
3. L. M. MASINTER, N. S. SRIDHARAN, J. LEDERBERG, and D. H. SMITH. J. Am. Chem. Soc. **96**, 7702 (1974).
4. J. ROTMAN. *In* The theory of groups; and introduction. Allyn and Bacon, Boston. 1965. p. 49.
5. S. ARONOFF. Ann. N.Y. Acad. Sci. **244**, 327 (1975).
6. R. L. C. PILGRIM. J. Chem. Educ. **51**, 316 (1974).
7. N. G. DE BRUIJN. *In* Applied combinatorial mathematics. *Edited by* E. Beckenbach. Wiley, New York, NY. 1964. Chapt. 5, pp. 144–184.

Appendix

When discussing permutations we have used the so-called *cyclic* notation. For example, (1 3 4 5)(2 6)(7) denotes the permutation in which 1 goes to 3, 3 goes to 4, 4 goes to 5, 5 goes to 1, 2 goes to 6, 6 goes to 2, and 7 goes to itself. We say that this permutation is a product of a 4-cycle, a 2-cycle, and a 1-cycle (a 1-cycle is also called a *fixed-point*). We are particularly interested in the cycle structure of the powers of a given permutation σ when σ is an n-cycle. For example, in cyclohexane, where σ = (1 2 3 4 5 6), then σ^2 = (1 3 5)(2 4 6), σ^3 = (1 4)(2 5)(3 6), etc. Notice that $gcd\{2,6\} = 2$ and σ^2 is a product of two 3-cycles while $gcd\{3,6\} = 3$ and σ^3 is a product of three 2-cycles. This pattern holds in general. If σ is an n-cycle, then σ^r is a product of g (n/g)-cycles if $g = gcd\{r,n\}$.

Let P_n denote a regular n-gon. At each of the vertices of P_n we shall substitute one of the ordered pairs a_1A_1, A_1a_1, a_2A_2, A_2a_2, ..., a_rA_r, A_ra_r, x_1x_1, x_2x_2, ..., x_sx_s. The resulting structure will be called a *configuration*. Arbitrarily label the vertices of P_n as 1, 2, ..., n in a clockwise manner.

Consider the group D_n on P_n consisting of σ = (1 2 ... n) and its distinct powers and the n reflections of P_n about the central axes. D_n is commonly called the *dihedral group of degree n* and contains $2n$ permutations. We shall say two configurations are *equivalent* if one can be obtained from the other under the action of D_n. By an *isomer* we shall mean a collection of configurations all of which are equivalent to each other and none of which are equivalent to any configuration not in the collection. In terms of permutation groups an isomer is an orbit of D_n acting on the set of all configurations.

Under a power of σ the order of an ordered pair is not altered; however, a reflection sends an ordered pair of the form aA to Aa. For example, 1-*aA*,2-*bB*,3-*XX*,4-*bB*cyclobutane, under the reflection (1)(3)(2 4) goes to 1-*Aa*,2-*Bb*,3-*XX*,4-*Bb*cyclobutane. Under the rotation (1 3)(2 4), it goes to 1-*XX*,2-*bB*,3-*aA*,4-*bB*cyclobutane. A further restriction placed on the configurations relates to the number of paired substituents. We specify that altogether there must be k_1 of a_1A_1, k_2 of a_2A_2, ..., k_r of a_rA_r and A_ra_r, m_1 of x_1x_1, m_2 of x_2x_2, ..., and m_s of x_sx_s, appearing on the n-gon with k_1, k_2, ..., k_r, m_1, ..., m_s each at least one.

The proof of the theorem is based on a counting result known as Burnside's Lemma [4], which states that if G is a permutation group, the number of orbits of G is given by the formula

$$\frac{1}{|G|}\sum_{\sigma \in G} f(\sigma)$$

$|G|$ denotes the number of elements in G, $f(\sigma)$ is the number of objects left fixed by the permutation

σ, and the summation is taken over all σ in G. Since the order of D_n is $2n$, the $1/2n$ is accounted for in the formula (1). It now remains to count the number of configurations left fixed by each of the $2n$ permutations.

Let $\sigma = (1\ 2\ 3\ \ldots\ n)$, that is, σ is the rotation of the n-gon through an angle of $2\pi/n$. We saw earlier that any power of σ is a product of n/d d-cycles for some divisor d of n. Such a permutation will leave a configuration fixed if, and only if, each substitution in a given d-cycle is the same. Hence, d must divide each of $k_1, \ldots, k_r, m_1, \ldots, m_s$, that is, d must divide g. Now we need to choose k_1/d d-cycles to give us k_1 of a_1A_1 and A_1a_1, k_2/d d-cycles to give us k_2 of a_2A_2 and A_2a_2, etc. Thus we can choose the d-cycles to fill up with a_iA_i's or A_ia_i's and X_jX_j's in

$$\begin{bmatrix} \frac{n}{d} \\ \frac{k_1}{d} \end{bmatrix}\begin{bmatrix} \frac{n}{d} - \frac{k_1}{d} \\ \frac{k_2}{d} \end{bmatrix}\cdots\begin{bmatrix} \frac{n}{d} - \frac{k_1}{d} - \cdots - \frac{m_{s-1}}{d} \\ \frac{m_s}{d} \end{bmatrix} = \frac{\left(\frac{n}{d}\right)!}{\left(\frac{k_1}{d}\right)!\cdots\left(\frac{k_r}{d}\right)!\left(\frac{m_1}{d}\right)!\cdots\left(\frac{m_s}{d}\right)!}$$

ways. But for each choice of k_1/d d-cycles we can put either all a_1A_1 or all A_1a_1 in each d-cycle. This can be done in $2^{k_1/d}$ ways. Similarly for a_2A_2 or A_2a_2 through a_rA_r or A_ra_r. Thus there are

$$2^{k_1/d} \times 2^{k_2/d} \cdots 2^{k_r/d} = 2^{K/d}$$

ways of filling up any selection of d-cycles. Moreover, there are exactly $\phi(d)$ powers of σ that are products of d-cycles. Therefore, the first term in formula 1 is accounted for and the n permutations that are powers of σ have been considered.

We now consider the n reflections of P_n. If n is odd, then every reflection has its axis passing through a single vertex, that is, the cycle structure is $(n-1)/2$ 2-cycles and a fixed vertex. So a reflection leaves a configuration fixed if, and only if, there is a substitution of the form XX at the fixed vertex, aA is substituted at one vertex of a 2-cycle when Aa is substituted at the other, and YY is substituted at one vertex of a 2-cycle when YY is substituted at the other. First of all we see that exactly one of the m_i's is odd (say m_j) and all other m_i's as well as all k_i's are even if $L \neq 0$ is to be possible. If all except m_j are even, then there are

$$\begin{bmatrix} \frac{n-1}{2} \\ \frac{k_1}{2} \end{bmatrix}$$

ways of choosing 2-cycles for the substitution of a_1A_1 and A_1a_1. Moreover, the a_1A_1 and A_1a_1 can be put into the $k_1/2$ 2-cycles in 2 ways. Similarly, there are

$$\begin{bmatrix} \frac{n-1}{2} - \frac{k_1}{2} \\ \frac{k_2}{2} \end{bmatrix}$$

ways of choosing 2-cycles for a_2A_2 and A_2a_2 and $2^{k_2/2}$ ways of putting them into the 2-cycles. Continuing in this way we find that any reflection fixes

$$\frac{\left(\frac{n-1}{2}\right)!2^{K/2}}{\left(\frac{k_1}{2}\right)!\cdots\left(\frac{k_r}{2}\right)!\left(\frac{m_1}{2}\right)!\cdots\left(\frac{m_{j-1}}{2}\right)!\left(\frac{m_j}{2}\right)!\left(\frac{m_{j+1}}{2}\right)!\cdots\left(\frac{m_s}{2}\right)!}$$

configurations. As there are n such reflections, the formula for L in category 1 follows.

The formulas for L in categories 2 and 3 follow from the fact that, when n is even, half of the reflections have an axis passing through no vertices and the remaining reflections have an axis passing through two opposite vertices. The rest of the calculations are similar to the above.

Molecular orbitals from group orbitals. IV. Quantitative perturbational molecular orbital analysis of the methyl rotational barriers in $(CH_3)_2X$ molecules. Effect of the fragmentation mode upon the results of the analysis

MYUNG-HWAN WHANGBO[1] AND SAUL WOLFE

Department of Chemistry, Queen's University, Kingston, Ont., Canada K7L 3N6

Received February 21, 1977

MYUNG-HWAN WHANGBO and SAUL WOLFE. Can. J. Chem. **55**, 2778 (1977).

A quantitative perturbational molecular orbital (PMO) analysis has been performed on *ab initio* SCF-MO wavefunctions associated with the rotation of the methyl groups in a series of $(CH_3)_2X$ molecules (X = CH_2, O, S, C=O, C=CH_2). Two fragmentation modes have been investigated: Method *a*, in which the system is dissected into X and $(CH_3)_2$; and Method *b*, in which the system is dissected into CH_3X and CH_3. Both fragmentation modes reproduce the principal property of these molecules, viz., that the more crowded *SS* conformation is preferred. However, whether this conformational preference is controlled by two-electron stabilizing effects or four-electron destabilizing effects is found to depend upon both the mode of fragmentation and the nature of the substituent X. The quantitative results are supplemented by a detailed qualitative description of the nature of the group orbitals associated with the two fragmentation modes and the various types of orbital interactions. It is shown that orbital energy differences control the qualitative discussion of Method *a*, and overlap effects control that of Method *b*. Although the final result, i.e., the preference for the *SS* conformation, and the behaviour of individual orbital interactions are anticipated correctly by the qualitative arguments, these are unable to assess the relative contributions of the stabilizing and destabilizing interactions.

MYUNG-HWAN WHANGBO et SAUL WOLFE. Can. J. Chem. **55**, 2778 (1977).

On a effectué une analyse quantitative d'orbitale moléculaire perturbationnelle (OMP) à l'aide de fonctions d'onde SCF-MO *ab initio* associées avec la rotation des groupes méthyles dans une série de molécules $(CH_3)_2X$ (X = CH_2, O, S, C=O, C=CH_2). On a étudié deux modes de fragmentation: méthode *a*, dans laquelle le système est divisé en X et $(CH_3)_2$; la méthode *b* dans laquelle le système est divisé en CH_3X et CH_3. Les deux modes de fragmentation reproduisent la propriété principale de ces molécules à savoir que la conformation *SS* la plus empêchée est celle qui est préférée. Toutefois, on trouve que la conformation préférentielle qu'elle soit contrôlée par des effets stabilisants dus à deux électrons ou des effets déstabilisants dus à quatre électrons dépend à la fois du mode de fragmentation et de la nature du substituant X. On a ajouté un complément aux résultats quantitatifs en faisant une description qualitative détaillée de la nature des groupes d'orbitales associés avec les deux modes de fragmentation et les divers types d'interaction entre orbitales. On a montré que les différences d'énergie entre les orbitales contrôlent la discussion qualitative de la méthode *a* et que les effets de recouvrement contrôlent celle de la méthode *b*. Quoique les résultats finals, à savoir la préférence de la conformation *SS* et le comportement des interactions orbitales individuelles, peuvent être anticipés d'une façon correcte par des arguments qualitatifs, ces derniers ne permettent pas de déterminer les contributions relatives des interactions stabilisantes et déstabilisantes.

[Traduit par le journal]

Introduction

In Part III of this series (1), a method was developed for the quantitative perturbational molecular orbital (PMO) analysis of *ab initio* SCF-MO wavefunctions. This PMO method reproduces rather well the total energy rotational behaviour of the small hydrocarbon molecules ethane and propylene.

Regardless of the details of the procedure employed, any PMO analysis of a conformational effect begins with a dissection of the molecule into fragments. Although there is, in principle, no restriction concerning the specific fragmentation scheme which should be used, in practice it is customary to work within the framework of chemically 'reasonable' functional groups. Thus, for example, it is 'reasonable' to dissect ethane into two methyl fragments, and to dissect propylene into methyl and vinyl fragments. However, for larger molecules, more than one 'reasonable' fragmentation scheme can

[1]Present address: Department of Chemistry, Cornell University, Ithaca, NY, U.S.A. 14853.

often be conceived. In such a case, it is important to know whether the results of the PMO analysis depend upon the mode of fragmentation of the system. The purpose of the present paper is to examine this problem by a consideration of the rotational behaviour of systems $(CH_3)_2X$ (X = CH_2, O, S, C=O, C=CH_2). A detailed examination of four of these compounds at the 4-31G level has been presented by Pople and co-workers (2). To rationalize their results, these workers have suggested that a π-electron or hyperconjugative effect is operative in these molecules and leads to aromatic stabilization involving bonding between methyl groups when the central atom is a π-donor (as in dimethyl ether), and to a corresponding antiaromatic destabilization when the central atom is a π-acceptor (as in acetone). These qualitative ideas have been developed further by Epiotis and Yates (3), in the course of a study of overlap repulsion as a contributor to aromaticity.

The present quantitative PMO analysis has been performed using two different fragmentation modes: Method *a*, in which the system is dissected into X and $(CH_3)_2$; this is the method employed by Epiotis and Yates (3). In Method *b* the system is dissected into CH_3X and CH_3. The first objective of the work is to determine whether both methods lead to the same conclusions concerning the total energy behaviour of $(CH_3)_2X$ molecules. Since this behaviour is calculated by a summation of the contributions of stabilizing and destabilizing π-type orbital interactions, a second objective of the work is to determine whether one or the other of these is the major contributor to the total energy. A third and most important objective is to demonstrate that the quantitative results can be understood in terms of simple qualitative arguments. Such a demonstration would generate considerable confidence in the use of such arguments for the discussion of conformational effects.

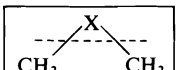

a

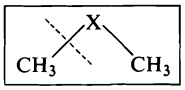

b

It is known (ref. 2 and references cited therein) that $(CH_3)_2X$ molecules exist in the more crowded *SS* conformation, and that the observed rotational barriers refer to the process $SS \rightleftarrows SE$.

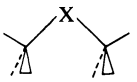

SS

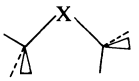

SE

The present discussion has, therefore, been restricted to these two conformations.

Results and Discussion

Ab initio SCF-MO calculations were performed using the STO-3G basis set (4) of Gaussian 70 (5). The methyl rotational barriers of the various $(CH_3)_2X$ molecules refer to the process $SS \rightarrow SE$, and were obtained by rigid rotation of one methyl group. The PMO analysis was performed after each SCF-MO calculation by evaluation of the two-electron stabilizing and four-electron destabilizing interaction energies. These energy terms are defined by eqs. 1 and 2 respectively (1).

$$[1] \quad \Delta e_{ij} = 2(\Delta_{ij} - e_i^0 \tilde{S}_{ij})^2/(e_i^0 - e_j^0)$$

$$[2] \quad \Delta e_{ij} = \frac{2\tilde{S}_{ij}\,[-2\Delta_{ij} + (e_i^0 + e_j^0)\tilde{S}_{ij}]}{(1 - \tilde{S}_{ij}^2)}$$

where Δ_{ij} is the interaction matrix element between the fragment orbitals ϕ_i^0 and ϕ_j^0, and $\tilde{S}_{ij}$ is the overlap integral between them. In the discussion which follows, only interactions between π-type fragment orbitals have been taken into account.

Table 1 summarizes the results of the present SCF-MO calculations. The experimental values for the rotational barriers of these systems and the results of Pople's 4-31G computations (2) are included for comparison. The agreement between calculated and experimental barriers is reasonable. In particular, variations in the barrier as X is varied are reproduced by the computations.

Quantitative Analysis by Method a

The results of the PMO analysis based upon Method *a* are summarized in Tables 2–4. The π-type fragment orbitals of X and $(CH_3)_2$ on which the analysis is based are shown schematically in Fig. 1. The butadiene-like character of the $(CH_3)_2$ group orbitals is clearly evident, and their nodal properties can be regarded as the result of in-phase (leading to π_+ and π_+*) and out-of-phase (leading to π_- and π_-*) combinations of methyl π and π* group orbitals.

The orbital energies e_i^0 collected in Table 2 reveal that the energy gap between π_+ and π_-

TABLE 1. Computed total energies and methyl rotational barriers of $(CH_3)_2X$ molecules[a]

X	Total energy (au)		Rotational barrier (kcal/mol)	
	SS	*SE*	Calculated	Experimental
CH_2	−116.88502	−116.87904	3.75 (3.70)[b]	3.33[c], 3.68[d]
O	−152.13125	−152.12651	2.98 (2.98)	2.71[e]
S	−471.48129	−471.47843	1.80	2.13[f]
C═O	−189.53445	−189.53240	1.29 (0.75)	1.01[g]
C═CH_2	−154.24325	−154.24031	1.85 (1.93)	2.17[h]

[a]In each molecule, the geometrical parameters adopted for the methyl groups are r_{CH} = 1.09 Å and ∠HCH = 109.5°. Other geometrical parameters are as follows: X = CH_2: r_{CC} = 1.526 Å, ∠CCC = 112.4°. For the methylene group, r_{CH} = 1.09 Å, ∠HCH = 109.5°. X = O: r_{CO} = 1.417 Å, ∠COC = 111.5°. X = S: r_{CS} = 1.802 Å, ∠CSC = 99°. X = CO: r_{CC} = 1.515 Å, r_{CO} = 1.215 Å, ∠CCC = 116°. X = C═CH_2: r_{CC}(single bond) = 1.507 Å, r_{CC}(double bond) = 1.330 Å, ∠CCC = 115.3°. For the methylene group, r_{CH} = 1.09 Å, ∠HCH = 120°.
[b]Numbers in parentheses refer to the results of 4-31G computations (see text).
[c]Reference 6.
[d]Reference 7.
[e]Reference 8.
[f]Reference 9.
[g]Reference 10.
[h]Reference 11.

and between π_+* and π_-* is greater in the *SS* conformation, as expected (3) from a recognition that the overlap between the methyl groups is greater in the *SS* conformation. A comparison of the e_i^0 values of π_X and π_X* reveals that the X fragment orbitals are nearly transferable from one conformation to the other within the same molecule.

The gross populations Q_i collected in Table 3 are consistent with the assumption that, prior to orbital interaction, the fragment orbitals π_+, π_-, and π_X are doubly occupied, and π_+*, π_-*, and π_X* are unoccupied. With this assignment of electron occupancies, the orbital interaction energies Δe_{ij} can be calculated, using eqs. 1 and 2, to give the results summarized in Table 4.

In the *SS* conformations, interactions ($\pi_X - \pi_-$), ($\pi_X - \pi_-$*) and (π_X* − π_-) are zero by symmetry. Although this symmetry restriction is removed in the *SE* conformations, these three interactions remain small. In each molecule, the sum of the four-electron destabilizing interactions is more positive, and the sum of the two-electron stabilizing interactions is less negative in the *SE* conformation. This is in harmony with the qualitative prediction by Epiotis and Yates (3) that the *SS* conformation will be more stable because it is stabilized more by the two-electron interaction and destabilized less by the four-electron interactions. For X = CH_2, C═O, and C═CH_2, the four-electron factor is greater than the two-electron factor. In dimethyl sulfide, the two effects are almost the same; however, in dimethyl ether, the two-electron effect is greater.

The differences in the total orbital interaction energies, $\sum\Delta e_{ij}$, of the *SS* and *SE* conformations are 2.68, 2.14, 0.80, 1.20, and 2.18 kcal/mol, for X = CH_2, O, S, C═O, and C═CH_2, respectively. The corresponding methyl rotational barriers obtained from the total energies of the SCF-MO computations are 3.75, 2.98, 1.80, 1.20, and 2.18 kcal/mol, respectively.

Qualitative Analysis by Method a

Our calculations reveal that, for a given interaction, $-\Delta_{ij}$ and $\tilde{S}_{ij}$ vary in the same way.[2] Therefore, it is valid to approximate Δ_{ij} by $k\tilde{S}_{ij}$, with k a negative constant. It then follows, from eqs. 1 and 2, that the magnitude of an interaction energy Δe_{ij} increases as S_{ij}^2 increases, regardless of whether such an interaction is stabilizing or destabilizing. On the other hand, the orbital energy dependence of an interaction energy depends upon the nature of the interaction. A two-electron stabilizing interaction increases as the orbital energy difference ($e_i^0 - e_j^0$) decreases; and a four-electron destabilizing interaction increases as the absolute value of the orbital energy sum ($e_i^0 + e_j^0$) decreases. These qualitative simplifications are, of course, well known (3).

Since π_+ and π_+* lie lower in the *SS* conformation than in the *SE* conformation, an argument based upon orbital energies predicts that the destabilizing interaction ($\pi_+ - \pi_X$) will

[2]More detailed data concerning Δ_{ij}, $\tilde{S}_{ij}$, and other quantities generated in the quantitative PMO analysis, are available from the authors.

be smaller, and the stabilizing interaction ($\pi_X - \pi_+^*$) will be larger in the *SS* conformation. This is confirmed for all X. When X is CH_2, C═O, or C═CH_2, there is also a ($\pi_+ - \pi_X$) stabilizing interaction; the orbital energy argument now predicts greater stabilization in the *SE* conformation. This is observed when X is C═O and C═CH_2, but not when X is CH_2.

The discrepancy is caused by the (secondary) overlap effect, which is difficult to assess qualitatively when X is a single atom, but cannot be ignored when X is a group. As shown in Fig. 2, the ($\pi_+ - \pi_X$) overlap is smaller in the *SS* conformation, but the ($\pi_X - \pi_+^*$) and the ($\pi_+ - \pi_X^*$) overlap is smaller in the *SE* conformation.[3] An overlap argument would, therefore, predict more stabilization and less destabilization in the *SS* conformation. Thus, for the destabilizing ($\pi_+ - \pi_X$) and the stabilizing ($\pi_X - \pi_+^*$) interactions, the overlap and the energy gap arguments operate in the same direction. However, in the case of the stabilizing ($\pi_+ - \pi_X^*$) interaction, they lead to different predictions, and qualitative arguments alone cannot determine which of the two effects should be dominant. Nevertheless, it can be predicted that the conformational dependence of this ($\pi_+ - \pi_X^*$) interaction should be small, as is observed.

It follows from the discussion just presented that the most appropriate qualitative rationalization of the *total energy* behaviour of $(CH_3)_2X$ molecules within the framework of fragmentation Method *a* is the one that emphasizes the energy gap argument (3), because this approach encompasses all X. However, it is not possible with such a procedure to probe the relative contributions of the stabilizing and destabilizing interactions.

Quantitative Analysis by Method b

The orbital interaction energies Δe_{ij} calculated by Method *b* are summarized in Table 5. The π-type fragment orbitals of CH_3X and CH_3 that are employed in this analysis are shown schematically in Fig. 3.

[3]A possible conceptual problem arises at this point, since one might reasonably ask why a repulsive $CH_3 \ldots CH_3$ interaction, greater in the *SS* conformation than in the *SE* conformation, can be ignored. The reason for this is that Method *a* treats $CH_3 \ldots CH_3$ as a single unit (group), and only interactions *between* the $(CH_3)_2$ and X groups are meaningful in the PMO analysis. Furthermore, the $CH_3 \ldots CH_3$ interaction has already been taken into account in the energy gap argument.

TABLE 2. The orbital energies e_i^0 of the X and $(CH_3)_2$ fragment orbitals in $(CH_3)_2X$[a]

	e_i^0									
	CH_2		O		S		C═O		C═CH_2	
ϕ_i^0	*SS*	*SE*	*SS*	*SE*	*SS*	*SE*	*SS*	*SE*	*SS*	*SE*
π_+	−0.5383	−0.5331	−0.5693	−0.5612	−0.5469	−0.5418	−0.5553	−0.5503	−0.5425	−0.5377
π_-	−0.5065	−0.5117	−0.5241	−0.5309	−0.5224	−0.5268	−0.5269	−0.5307	−0.5126	−0.5172
π_+^*	0.6858	0.7028	0.6389	0.6627	0.6757	0.6927	0.6680	0.6821	0.6787	0.6937
π_-^*	0.7265	0.7114	0.7062	0.6841	0.7123	0.6958	0.7032	0.6907	0.7175	0.7037
π_X	−0.5290	−0.5286	−0.3998	−0.3990	−0.2764	−0.2760	−0.4379	−0.4377	−0.3312	−0.3308
π_X^*	0.6985	0.7001					0.2698	0.2689	0.3013	0.3020

[a]In atomic units.

TABLE 3. The gross populations Q_i of the X and $(CH_3)_2$ fragment orbitals in $(CH_3)_2X$

	Q_i									
	CH_2		O		S		C=O		$C{=}CH_2$	
ϕ_i^0	*SS*	*SE*	*SS*	*SE*	*SS*	*SE*	*SS*	*SE*	*SS*	*SE*
π_+	1.989	1.990	1.998	1.998	1.999	1.999	1.961	1.960	1.966	1.966
π_-	2.000	2.000	2.000	2.000	2.000	2.000	2.000	2.000	2.000	2.000
π_+^*	0.013	0.011	0.059	0.055	0.025	0.021	0.012	0.010	0.020	0.016
π_-^*	0.000	0.000	0.000	0.000	0.000	0.000	0.000	0.000	0.000	0.000
π_X	1.987	1.989	1.943	1.948	1.975	1.977	1.985	1.987	1.977	1.980
π_X^*	0.011	0.010					0.042	0.043	0.037	0.038

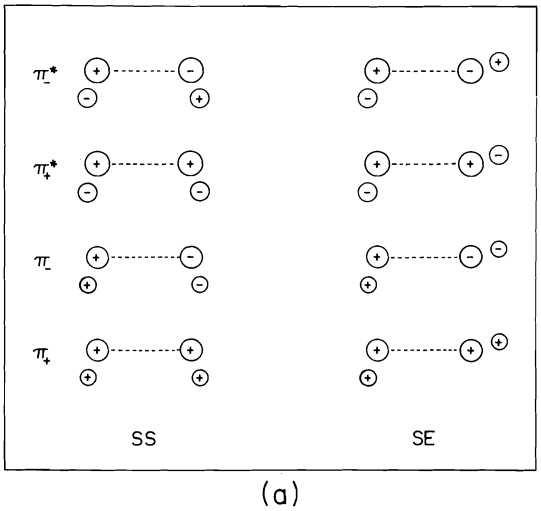

FIG. 1. The π-type fragment orbitals in $(CH_3)_2X$ molecules which correspond to fragmentation Method *a*: (*a*) the $CH_3 \ldots CH_3$ group; (*b*) the X group.

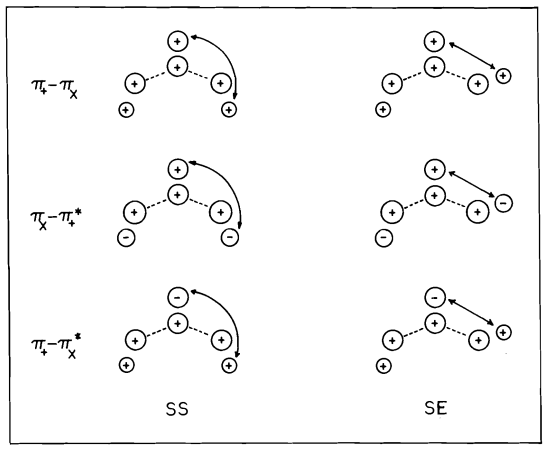

FIG. 2. The overlap between the $(CH_3)_2$ and X groups in the *SS* and *SE* conformations. Several stabilizing and destabilizing interactions are shown. The primary overlap between the fragments is shown as a dotted line. Secondary overlap is indicated by a double-headed arrow.

The nature of the CH_3X group orbitals requires comment. When X is oxygen or sulfur, the nodal property of the CH_3X group is like that of the allyl system, because the two methyl hydrogens, the methyl carbon, and X each contribute one *p*-type atomic orbital. The lowest-lying CH_3X group orbital (π_α) is the in-phase combination of π_{CH_3} and p_X, and the highest occupied CH_3X group orbital (π_β) is the out-of-phase combination of π_{CH_3} and p_X. Since π_{CH_3} lies lower than p_X, it has greater weight in π_α, and p_X has greater weight in π_β. The unoccupied CH_3X group orbital, designated π_γ^*, is mainly the out-of-phase combination of $\pi_{CH_3}^*$ and p_X, and is, therefore, weighted heavily on carbon and hydrogen.

When X is CH_2, C=O, or $C{=}CH_2$, the nodal property of CH_3X is like that of butadiene, because four *p*-type atomic orbitals are used to form the group. The two occupied CH_3X orbitals (π_α and π_β) result mainly from the in-phase and out-of-phase combinations of π_{CH_3} and π_X; the two unoccupied CH_3X orbitals (π_γ^* and π_δ^*) result mainly from the in-phase and out-of-phase combinations of $\pi_{CH_3}^*$ and π_X^*.

TABLE 4. The orbital interaction energies Δe_{ij} (kcal/mol) between the π-type orbitals in $(CH_3)_2X$, according to fragmentation Method *a*

Interaction $(\phi_i^o - \phi_j^o)$	Δe_{ij}									
	CH_2		O		S		C=O		$C{=}CH_2$	
	SS	*SE*	*SS*	*SE*	*SS*	*SE*	*SS*	*SE*	*SS*	*SE*
$\pi_X - \pi_+$	34.88	37.10	44.68	45.64	30.86	31.12	25.48	26.40	31.62	33.08
$\pi_X - \pi_-$	0.00	0.00	0.00	0.06	0.00	0.16	0.00	0.04	0.00	0.04
$\pi_X - \pi_+^*$	−2.12	−1.78	−16.36	−15.06	−5.98	−5.08	−2.50	−2.08	−4.32	−3.58
$\pi_X - \pi_-^*$	0.00	0.00	0.00	−0.06	0.00	−0.52	0.00	0.00	0.00	0.00
$\pi_X^* - \pi_+$	−1.82	−1.70					−6.68	−6.86	−5.52	−5.58
$\pi_X^* - \pi_-$	0.00	0.00					0.00	0.00	0.00	0.00

TABLE 5. The orbital interaction energies Δe_{ij} (kcal/mol) between the π-type orbitals in $(CH_3)_2X$, according to fragmentation Method *b*

Interaction $(\phi_i^o - \phi_j^o)$	Δe_{ij}									
	CH_2		O		S		C=O		$C{=}CH_2$	
	SS	*SE*	*SS*	*SE*	*SS*	*SE*	*SS*	*SE*	*SS*	*SE*
$\pi - \pi_\alpha$	12.64	11.60	9.78	6.68	1.98	1.08	4.92	3.72	3.76	2.52
$\pi - \pi_\beta$	5.14	7.56	13.16	15.84	13.48	14.36	8.06	9.48	12.04	13.90
$\pi - \pi_\gamma^*$	−0.36	−0.30	−0.16	−0.12	−0.06	−0.04	−3.34	−3.36	−2.78	−2.72
$\pi - \pi_\delta^*$	−0.64	−0.52					−0.16	−0.14	−0.16	−0.14
$\pi^* - \pi_\alpha$	−0.38	−0.46	−0.64	−1.10	−0.02	−0.10	−0.10	−0.20	−0.04	−0.16
$\pi^* - \pi_\beta$	−0.82	−0.32	−8.06	−6.40	−3.06	−2.72	−1.20	−0.68	−2.20	−1.34

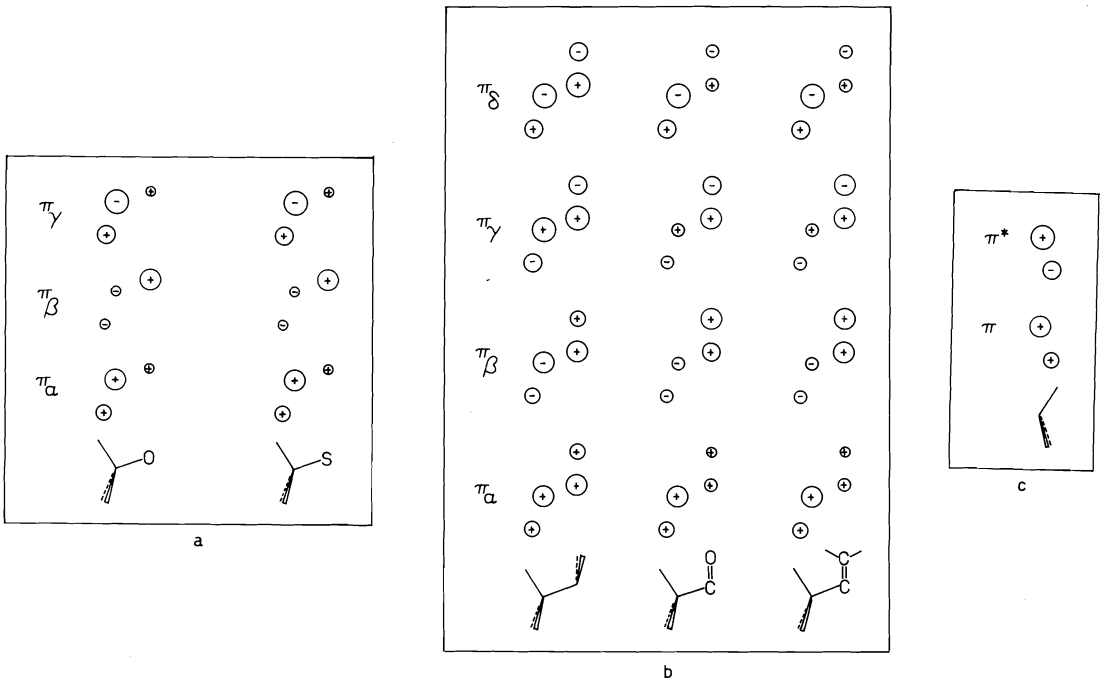

FIG. 3. The π-type fragment orbitals in the CH_3X and CH_3 groups of $(CH_3)_2X$ molecules: (*a*) the CH_3X group, when X = O, S; (*b*) the CH_3X group, when X = CH_2, CO, and C=CH_2; (*c*) the CH_3 group.

Since the energies of π_{CH_3} and $\pi_{CH_3}{}^*$ are not very different from those of π_{CH_2} and $\pi_{CH_2}{}^*$, respectively, the weights on CH_3 and CH_2 in the four CH_3CH_2 group orbitals are all about the same. However, when X is C=O or C=CH_2, π_X lies higher than π_{CH_3} and $\pi_X{}^*$ lies lower than $\pi_{CH_3}{}^*$. Consequently, π_α and $\pi_\delta{}^*$ are weighted in favour of CH_3, and π_β and $\pi_\gamma{}^*$ are weighted in favour of X.

In each molecule, the sum of the two-electron stabilizing interactions is less negative in the *SE* conformation, as in the analysis by Method *a*. However, in contrast to the analysis by Method *a*, the sum of the four-electron destabilizing interactions is more positive *in the SS conformation* in dimethyl ether and dimethyl sulfide. The differences in the total orbital interaction energies of the *SS* and *SE* conformations indicate that the *SS* is more stable by 1.98, 0.82, 0.26, 0.64, and 1.64 kcal/mol for X = CH_2, O, S, C=O, and C=CH_2, respectively.

Qualitative Analysis by Method b

We begin this discussion with the observation that the methyl group orbitals (π and π* of Fig. 3 and Table 5) are almost quantitatively transferable from *SS* to *SE* in each of the five molecules, since the $e_j{}^0$ values calculated for these two orbitals are almost exactly the same in the two conformations.[2] Therefore, the qualitative description of fragmentation Method *b* will be based upon overlap considerations.

The ($\pi - \pi_\alpha$) Interaction

This interaction is shown in Fig. 4. Figure 4 *a* and *b* indicates that the overlap **1** is large in *SS*, and the overlap **2** is large in *SE*. A prediction requires knowledge of which of these two overlaps is larger. This is not possible in the case of X = CH_2 without quantitative results. However, for X = CO and C=CH_2, overlap **2** in *SS* will be greater than overlap **1** in *SE*, because the π_α orbital is more heavily weighted on the methyl group of CH_3X. Figure 4*c* also shows that the overlap is greater in the *SS* conformation. Four of the five molecules are therefore predicted to exhibit greater destabilization in the *SS* conformation in terms of the ($\pi - \pi_\alpha$) interaction.

The ($\pi - \pi_\beta$) Interaction

This interaction is shown in Fig. 5. In this case, Fig. 5 *a* and *b* leads to the same prediction, viz., that the overlap in *SS* is less than that in *SE*, because overlap **2** in *SS* is negative, and

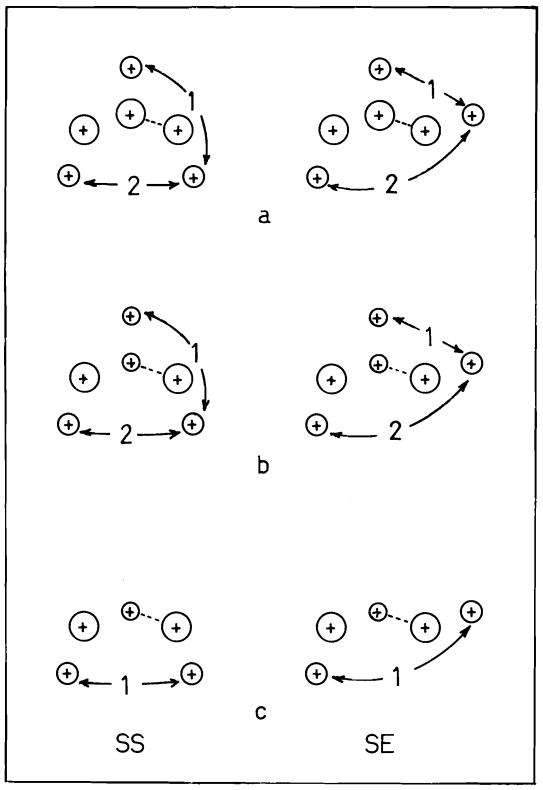

FIG. 4. The phase relationships between the CH_3X and CH_3 fragment orbitals in the *SS* and *SE* conformations for the $(\pi - \pi_\alpha)$ interaction: (*a*) X = CH_2; (*b*) X = CO, C=CH_2; (*c*) X = O, S. The primary overlap between the fragments is shown as a dotted line. Secondary overlap is indicated by a double-headed arrow.

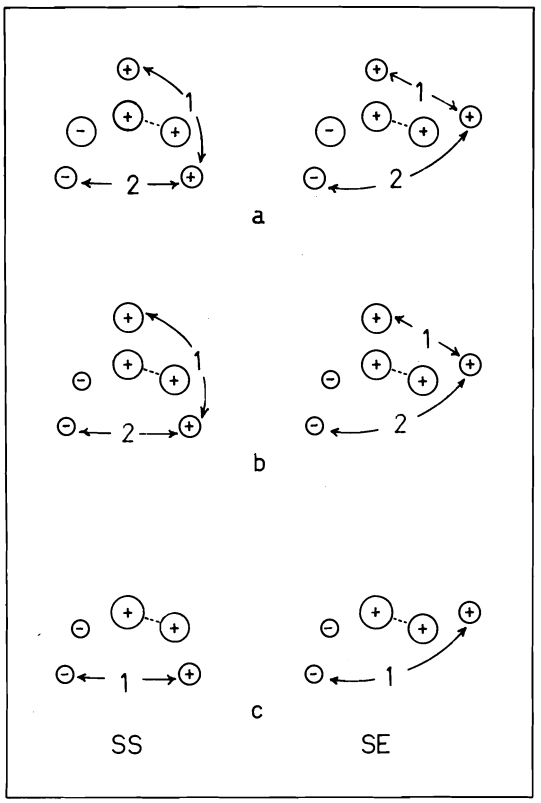

FIG. 5. The phase relationships between the CH_3X and CH_3 fragment orbitals in the *SS* and *SE* conformations for the $(\pi - \pi_\beta)$ interaction: (*a*) X = CH_2; (*b*) X = CO, C=CH_2; (*c*) X = O, S. The primary overlap between the fragments is shown as a dotted line. Secondary overlap is indicated by a double-headed arrow.

overlap **1** in *SE* is positive. Figure 5*c* also shows a more negative contribution from overlap **1** in the *SS* conformation. In terms of the $(\pi - \pi_\beta)$ interaction, all five molecules are predicted to exhibit greater destabilization in the *SE* conformation. In the cases of CH_3O and CH_3S, the $(\pi - \pi_\alpha)$ interaction outweighs the $(\pi - \pi_\beta)$ interaction because the methyl group of CH_3O and CH_3S is more heavily weighted in π_α than in π_β. Thus, the net destabilization is greater in the *SS* conformation in these two molecules, even though the higher orbital energy of π_β would lead to the opposite prediction, as is found in the other three molecules.

The $(\pi - \pi_\gamma^*)$ Interaction

This interaction is shown in Fig. 6. Figure 6 *a* and *b* shows that the overlap **2** is smaller in *SS*, and the overlap **1** is smaller in *SE*. As with the $(\pi - \pi_\alpha)$ interaction, no qualitative prediction is possible in the case of X = CH_2. However, for X = CO and C=CH_2, the negative overlap in *SS* will be less than that in *SE*, i.e., the total overlap will be larger in *SS*, because the π_γ^* orbital is more heavily weighted on the X group of CH_3X. Figure 6*c* also shows that the overlap is greater in the *SS* conformation. Thus, four of the five molecules are predicted to show greater stabilization in the *SS* conformation.

The $(\pi_\beta - \pi^*)$ Interaction

This interaction is shown in Fig. 7. In all cases, the overlap is greater in the *SS* conformation. The $(\pi_\beta - \pi^*)$ interaction therefore predicts greater stabilization in the *SS* conformation.

The $(\pi_\alpha - \pi^*)$ and $(\pi - \pi_\delta^*)$ Interactions

These interactions can be depicted and analysed in an analogous manner, but it is already clear that the qualitative PMO analysis based

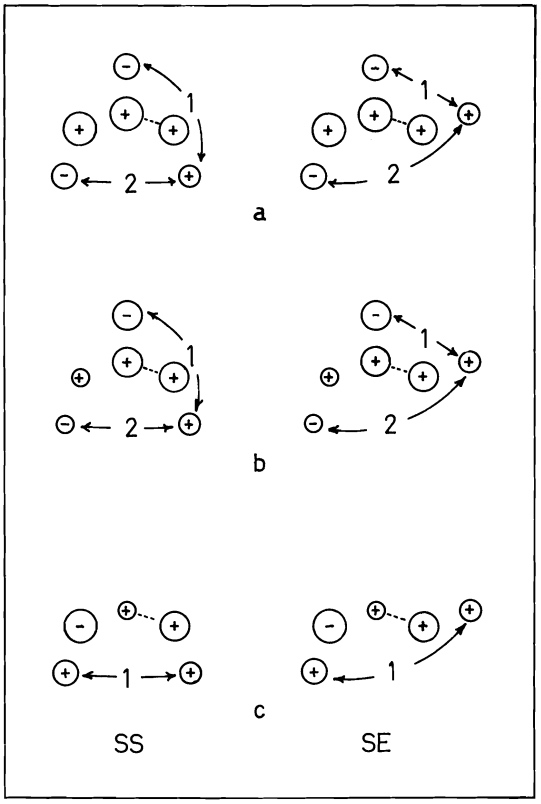

FIG. 6. The phase relationships between the CH_3X and CH_3 fragment orbitals in the *SS* and *SE* conformations for the $(\pi - \pi_\gamma)$ interaction: (*a*) X = CH_2; (*b*) X = CO, C=CH_2; (*c*) X = O, S. The primary overlap between the fragments is shown as a dotted line. Secondary overlap is indicated by a double-headed arrow.

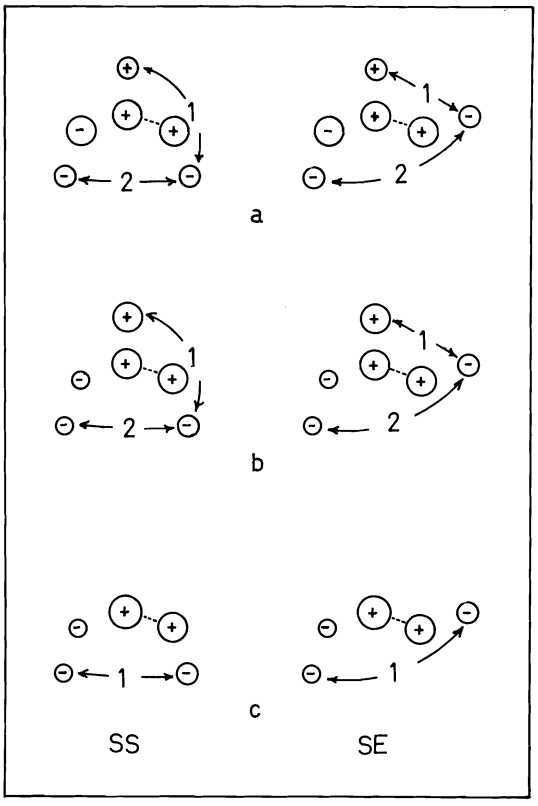

FIG. 7. The phase relationships between the CH_3X and CH_3 fragment orbitals in the *SS* and *SE* conformations for the $(\pi_\beta - \pi^*)$ interaction: (*a*) X = CH_2; (*b*) X = CO, C=CH_2; (*c*) X = O, S. The primary overlap between the fragments is shown as a dotted line. Secondary overlap is indicated by a double-headed arrow.

upon Method *b* is much more cumbersome than that based upon Method *a*. A simplifying assumption seems to be necessary for Method *b* to be useful as a qualitative procedure. A reasonable simplifying assumption is that only interactions associated with the frontier orbitals be considered, i.e., interactions $(\pi - \pi_\beta)$, $(\pi_\beta - \pi^*)$, and $(\pi - \pi_\gamma^*)$. With this simplification it is readily shown that the *SS* conformation is more stable than the *SE* conformation for all X. However, as with Method *a*, it is not possible using qualitative arguments alone to state the relative contributions of the stabilizing and destabilizing interactions to the overall result.

Conclusions

Both fragmentation modes reproduce the principal fact, that the SS conformation is more stable than the SE conformation in $(CH_3)_2X$ molecules. In terms of the orbital interaction energies, the total energy behaviour of these molecules is reproduced more closely by Method *a*. However, neither mode of analysis supports the notion (3) that overlap repulsion effects play a dominant role in deciding the conformational behaviour of dimethyl ether and dimethyl sulfide.

Regardless of the mode of fragmentation, the sum of the gross populations Q_i of all π-type fragment orbitals in a $(CH_3)_2X$ system is 6. It is understandable, therefore, that an analogy has been drawn (2, 3) between the greater stability of an *SS* conformation and the aromaticity of cyclic 6π-electron systems. However, as has been noted, whether such 'aromaticity' is caused by a minimization of repulsive effects or a maximization of attractive effects depends on X.

Acknowledgement

This research was supported by the National Research Council of Canada.

1. M. H. WHANGBO, H. B. SCHLEGEL, and S. WOLFE. J. Am. Chem. Soc. **99**, 1296 (1977).
2. D. CREMER, J. S. BINKLEY, and J. A. POPLE. J. Am. Chem. Soc. **96**, 6900 (1974).
3. N. D. EPIOTIS and R. L. YATES. J. Am. Chem. Soc. **98**, 461 (1976).
4. W. J. HEHRE, R. F. STEWART, and J. A. POPLE. J. Chem. Phys. **51**, 2657 (1969).
5. W. J. HEHRE, W. A. LATHAN, R. DITCHFIELD, M. D. NEWTON, and J. A. POPLE. Gaussian 70: Quantum Chemistry Program Exchange, Indiana University, Bloomington, Indiana, No. 236.
6. E. HIROTA, C. MATSUMARA, and Y. MORINO. Bull. Chem. Soc. Jpn. **40**, 1124 (1972).
7. D. M. GRANT, R. J. PUGMIRE, R. C. LIVINGSTON, K. A. STRONG, H. MCMURRY, and R. BRUGGER. J. Chem. Phys. **52**, 4424 (1970).
8. E. C. TUAZON and W. G. FATELEY. J. Chem. Phys. **54**, 4450 (1971).
9. L. PRIERCE and M. HAYASHI. J. Chem. Phys. **35**, 479 (1961).
10. W. C. HARRIS and I. W. LEVIN. J. Mol. Spectrosc. **43**, 117 (1972).
11. J. DEMAISON and H. D. RUDOLPH. J. Mol. Struct. **24**, 325 (1975).

On the blue complexes of ruthenium. Part II. The structure of *fac*-trichlorotriammineruthenium(III)

FRANK BOTTOMLEY

Department of Chemistry, University of New Brunswick, P. O. Box 4400, Fredericton, N.B., Canada E3B 5A3

Received December 21, 1976

FRANK BOTTOMLEY. Can. J. Chem. **55**, 2788 (1977).

The structure of $[RuCl_3(NH_3)_3]$ prepared from the blue chloro-ammine complex of ruthenium is described. The crystals are orthorhombic, $a = 9.933(3)$, $b = 6.522(2)$, $c = 5.475(2)$ Å, $Z = 2$, space group $Pmn2_1$. The structure analysis used 283 observed reflections, whose intensity was measured on a Picker FACS-1 diffractometer. The structure was refined (full-matrix) to $R = 0.029$. The crystal is composed of chains of *fac*-$[RuCl_3(NH_3)_3]$, and is disordered, approximately 10% of the chains being reversed in direction and displaced one-half in z. The Ru–ligand distances and angles are normal.

FRANK BOTTOMLEY. Can. J. Chem. **55**, 2788 (1977).

On décrit la structure du $[RuCl_3(NH_3)_3]$ préparé à partir du complexe bleu de chloreammine du ruthénium. Les cristaux sont orthorhombiques $a = 9.933(3)$, $b = 6.522(2)$, $c = 5.475(2)$ Å, $Z = 2$ groupe d'espace $Pmn2_1$. L'analyse structurale a fait appel aux 283 réflexions observées dont l'intensité a été mesurée sur un diffractomètre Picker FACS-1. On a affiné la structure par la méthode des moindres carrés (matrice complète) jusqu'à une valeur de $R = 0.029$. Le cristal est composé de chaînes de *fac*-$[RuCl_3(NH_3)_3]$ et est désordonné; environ 10% des chaînes sont dans une direction renversée et déplacée de moitié suivant l'axe des z. Les distances et les angles du ruthénium avec le ligand sont normaux.

[Traduit par le journal]

Introduction

In a previous paper we outlined our investigations of the blue species obtained by treating hexaammineruthenium(II) with hydrohalic acids (1). We found that the blue complexes were ruthenium(II)–ruthenium(III) dimers of empirical formula $Ru_2X_5(NH_3)_6H_2O$ (X = Cl, Br), and suggested the dimeric cation contained a single halo-bridge, *i.e.* had a formula $[Cl_2(NH_3)_3RuClRu(H_2O)(NH_3)_3Cl]^+$. Later work by Mercer and Gray on the chloro-complex confirmed the dimeric Ru(II)–Ru(III) nature of the cation, and suggested a triply chloro-bridged structure, *i.e.* a formula $[(NH_3)_3RuCl_3Ru(NH_3)_3]^{2+}$ (2). To finally confirm the structure we repeatedly attempted to obtain crystals of the blue cation with various anions but obtained microcrystalline material at best. In the absence of these crystals we turned our attention to $[RuCl_3(NH_3)_3]$, which was the product obtained when the blue chloro-complex was treated with HCl. Our tentative conclusion, on the basis of the infrared spectrum, was that this product had the *mer*-configuration, a structure incompatible with a triple chloro-bridge (1). Mercer and Gray concluded $[RuCl_3(NH_3)_3]$ was *cis*- (*fac*-), which geometry, while compatible with either bridging structure, is clearly more probable from reaction of a triply chloro-bridged cation (2). Hence the structure of $[RuCl_3(NH_3)_3]$ provides good evidence for the structure of the blue complex. We were also interested in this structure in connection with our studies of the *trans*-influence in octahedral complexes of this type (3, 4).

Experimental

$[RuCl_3(NH_3)_3]$ was obtained, as long needles, from $Ru_2Cl_5(NH_3)_6H_2O$ by the method described previously (1). Crystal data are as follows

$[RuCl_3(NH_3)_3]$ mw = 258.5
Orthorhombic, $a = 9.933(3)$, $b = 6.522(2)$, $c = 5.475(2)$ Å, $U = 354.7$ Å^3, $D_c = 2.49$ for $Z = 2$, $D_m = 2.46$ g cm^{-3} (by flotation in $CHCl_3/C_2H_2Br_4$); Zr-filtered Mo-K_α radiation, $\lambda = 0.70926$ Å; μ (Mo-K_α) = 31.7 cm^{-1}. $h0$-$2l$ Weissenberg and 0–$2kl$ and hk0–2 precession photographs showed systematic absences compatible with space groups $Pmn2_1$, $P2_1nm$, or $Pmnm$. The first is correct from the refinement.

The crystal used for the intensity determination was the tip cut from a long needle, and had dimensions 0.08 × 0.35 × 0.15 mm. It was mounted with shellac in a glass tube with the b axis deliberately mis-set with respect to the ϕ axis of the Picker FACS 1 diffractometer. Cell dimensions were determined from 12 accurately centered reflections of $2\theta > 30°$. Data were collected using the following instrumental settings: Zr-filtered Mo-K_α

radiation; 2.0° scan, corrected for $K_{\alpha 1}$–$K_{\alpha 2}$ dispersion; ω–2θ scan of rate 1° min^{-1} in 2θ in the range $2 < 2\theta < 50°$; stationary 20 s background counts on either side of the peak; take-off angle 2.0°; pulse-height analyser set for 97% of the Mo-K_α window; no attenuators needed since count rate was always less than 1×10^4 s^{-1}; the 121 reflection was monitored every 20 reflections as standard; its intensity varied by about 6% during data collection, and this was corrected for in processing. A group of reflections of high h could not be measured because of the position of the crystal in the tube; their presence or absence (less than minimum observable intensity), was established from the photographic record, but they were treated as unobserved and not used in the refinement. In processing, the data reflections having a net count less than 20 or less than 0.05 times the background count were considered unobserved. The processing, including Lorentz and polarisation corrections, gave 88 unobserved and 283 observed reflections. A trial absorption calculation showed the transmission factors varied from 68 to 76%, and hence no absorption correction was applied. In the refinement, which minimized $\Sigma w(|F_o| - |F_c|)^2$, scattering factor curves for Ru(3+), Cl^-, and N were taken from refs. 5 and 6 and were corrected for both the real and imaginary parts of the anomalous dispersion. A weighting scheme of the form given earlier (7) with $A = 35$, $B = 0.02$, and $C = 1.0 \times 10^{-5}$ was used. All calculations used the XRAY 76 package (8).

Results and Discussion

A Patterson function was readily interpretable in terms of Ru^{3+} and three Cl^- ions in space group $Pmn2_1$. Because of the short c axis no solution in $P2_1nm$ was chemically reasonable (there was no room for the Cl^- ions along z). The Patterson solution was confirmed by a Fourier phased on Ru^{3+} alone; this showed the three Cl^- ions and four light atoms, three of which, with the Cl^-, completed a *facial* octahedral co-ordination around the Ru^{3+}. The fourth was sandwiched between the three Cl^- ligands of one $[RuCl_3(NH_3)_3]$ molecule and the three NH_3 of the next. Neither microanalysis (Found: Cl 40.2, N 16.1. Calcd. for $Cl_3H_9N_3Ru$: Cl 41.1, N 16.2) nor the infrared spectrum of the crystals indicated the presence of water of crystallization, but as a preliminary model the additional atom was assumed to be oxygen. Full matrix refinement of this model with all atoms having isotropic temperature factors proceeded to $R = 0.12$. At this stage it was clear that the additional atom was apparently octahedrally coordinated by the three Cl^- and three NH_3, with a co-ordination geometry very similar to that of the ruthenium. The atom was approx. 2.7 Å from the ruthenium. The only reasonable explanation for this unlikely geometry was a disordered crystal. A large number of disordered models were tested, reasonableness of the thermal parameters, R value, bond distances, and chemical sense being used to evaluate the results. The model finally adopted may be visualised, with the aid of Fig. 1, as chains whose *fac*-$[RuCl_3(NH_3)_3]$ links are connected together by hydrogen bonds (because of the disorder no attempt was made to find the hydrogen atoms in the structure analysis, but the intermolecular N. . .Cl distances within the chains are 3.25 (N(1). . .$Cl(1_1)$); 3.53 (N(1′). . .$Cl(2_1)$); and 3.56 (N(2). . .$Cl(1_1)$) Å (for numbering scheme see Fig. 1) indicative of hydrogen bonding (9). There are two almost linear chains running through the unit cell with the idealized threefold axis of *fac*-$[RuCl_3(NH_3)_3]$ (which passes through the midpoints of the trichloro and triammine faces) parallel to c, one chain at $x = 0$, $y = 0.2773$ and the other at $x = 0.5$, $y = 0.7227$. The two chains are held together by hydrogen bonds (the interchain N. . .Cl distances are 3.39 (N(2). . . Cl(1)); 3.51 (N(1). . .Cl(2)); and 3.54 (N(1). . . Cl(1)) Å. For both chains the vector running along the threefold axis from Cl through Ru to NH_3 points in the direction $-z$ to $+z$. The disorder arises because about 10% of the chains are displaced 0.5 in z (the ruthenium, Ru(2), now being at position A in Fig. 1), and they run in the opposite direction (the vector points from $+z$ to $-z$), so that the NH_3 and Cl^- ligands are approximately coincident in position with the NH_3 and Cl^- of the 90% of 'undisordered' chains. The 10% figure was arrived at after refining models with various percentages of the displaced chains, and allowing them to run in both directions. The site occupancy of the Ru^{3+} of the 'undisordered' chains (Ru(1)) was held invariant at 0.9, and of the Ru^{3+} of the 'disordered' chains (Ru(2)) invariant at 0.1. This model, with anistropic thermal parameters for Ru(1) and the three Cl^- ions, and isotropic thermal parameter for the N and Ru(2) atoms refined to a final R of 0.029 ($R_2 = 0.044$). Finally, since $Pmn2_1$ is a polar space group refinement of a model using the data in the $\bar{h}k\bar{l}$ form was tried. This made no significant difference, as would be expected since the Ru(3+) ions are extremely close to being centric, and the same applies to the Cl(2) atom in the special position. A final difference Fourier synthesis showed nothing unusual, neither did statistical tests on R and R_2. The final parameters are listed in

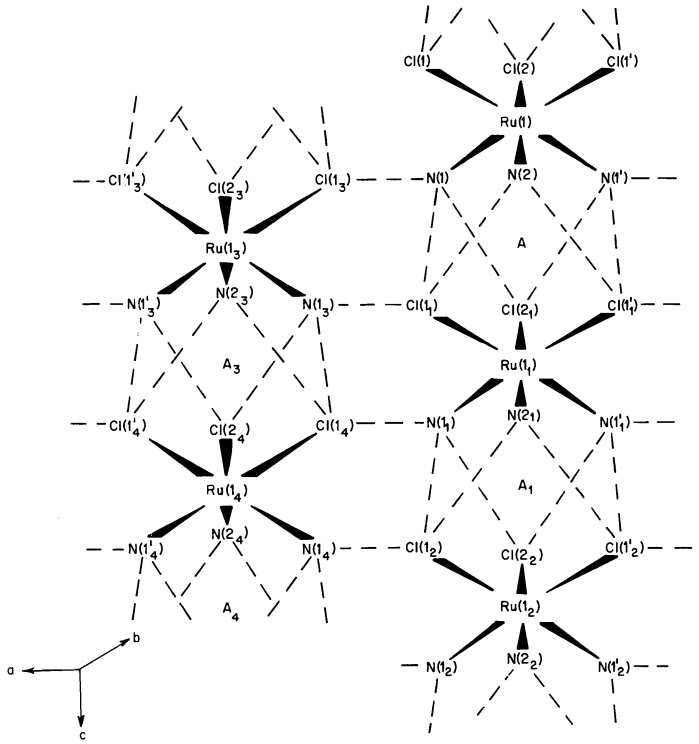

FIG. 1. The chains of *fac*-$[RuCl_3(NH_3)_3]$ projected onto a plane normal to *b* containing Ru(1). Dashed lines indicate hydrogen bonding. The asymmetric unit is the *fac*-$[RuCl_3(NH_3)]$ (containing 9/10 Ru) and the 1/10 Ru at position A. Subscripted atoms belong to repeat asymmetric units (*e.g.* Cl(1) and $Cl(1_1)$). Superscripted atoms are related to the corresponding non-superscripted ones by space group symmetry (*e.g.* (Cl(1) and Cl(1′)).

Table 1, and the final table of F_o and F_c (Table 2) has been deposited.[1]

The results show definitively that the product of the reaction of HCl with $Ru_2Cl_5(NH_3)_6H_2O$ is *fac*-$[RuCl_3(NH_3)_3]$, and not the *mer*-isomer. While this is compatible with from one to three bridging Cl^- in the blue complex, it tends to support the triply chloro-bridged structure proposed by Mercer and Gray rather than the other possibilities. We also note that we have now prepared the blue salts $[Ru_2Cl_3(NH_3)_6]I_2 \cdot H_2O$ and $[Ru_2Cl_3(NH_3)_6]ZnCl_4$, characterised by conductivity, analysis, spectroscopy, and reactions, which provide further and almost conclusive evidence for a triple chloro-bridge (10).

The intramolecular dimensions in $[RuCl_3(NH_3)_3]$ are listed in Table 3. Because of the disorder only the distances and angles around Ru(1) can be compared to those in other ruthenium complexes, and even then no detailed comparison is worthwhile. The ruthenium ion is octahedrally co-ordinated, with angles acceptably close to 90°, by the three Cl^- and three NH_3 groups. The Ru—N distances (2.10(1) and 2.13(1) Å) are similar to those observed in $[Ru(NH_3)_6](BF_4)_3$ (2.104(4) Å (11)) and $[Ru(en)_3]Cl_3 \cdot 3H_2O$ (en = ethylenediamine; 2.10(2) and 2.12(2) Å (12)), and the Ru—Cl distances (2.37(1) and 2.39(1) Å) are in the same region (2.34–2.38 Å (13)) as observed previously for such bond distances.

It is interesting to speculate briefly on the reason for the disorder. The intramolecular distance between the trichloro and triammine faces of the *fac*-$[RuCl_3(NH_3)_3]$ unit (2.5 Å) is similar to the intermolecular distance between the same faces (2.9 Å). This must be the consequence of the strong $NH_3 \ldots Cl$ hydrogen bonding. The disorder arises because the initial orientation of a *fac*-$[RuCl_3(NH_3)_3]$ is determined

[1]Photocopies of Table 2 are available upon request, at a nominal charge, from the Depository of Unpublished Data, CISTI, National Research Council of Canada, Ottawa, Canada K1A 0S2.

TABLE 1. Final positional and thermal parameters for *fac*-$[RuCl_3(NH_3)_3]$*

Atom	Site occupancy	x	y	z	U
Ru(1)	0.9	0.0	0.2773	0.0	
Cl(1)	1.0	0.1720(4)	0.1397(4)	−0.2510(12)	
Cl(2)	1.0	0.0	0.5931	−0.2225(13)	
N(1)	1.0	0.1469(12)	0.3928(14)	0.2405(29)	3.30(26)
N(2)	1.0	0.0	−0.0003(21)	0.2038(29)	2.93(36)
Ru(2)	0.1	0.0	0.2760(17)	0.512(9)	2.71(34)

Anisotropic thermal parameters†

Atom	$U_{11} \times 10^4$	$U_{22} \times 10^4$	$U_{33} \times 10^4$	$U_{12} \times 10^4$	$U_{13} \times 10^4$	$U_{23} \times 10^4$
Ru(1)	184(10)	226(6)	166(6)	0	0	3(11)
Cl(1)	301(25)	444(18)	272(15)	77(14)	−70(15)	−5(14)
Cl(2)	359(34)	320(22)	467(33)	0	0	−66(23)

*Standard deviations, relating to the least significant figures, are given in parentheses.
†The form of the thermal ellipsoid is $\exp[2\pi^2(U_{11}h^2a^{*2} + U_{22}k^2b^{*2} + U_{33}l^2c^{*2} + U_{12}hka^*b^* + U_{13}hla^*c^* + U_{23}klb^*c^*)]$.

TABLE 3. Distances (Å) and angles (deg) in *fac*-$[RuCl_3(NH_3)_3]$*

Bond	Length (Å)	Bonds	Angle (deg)
Around Ru(1)			
Ru—Cl(1)	2.369(5)	N(1)—Ru—Cl(1)	89.93(38)
Ru—Cl(2)	2.392(5)	N(1)—Ru—Cl(1′)	176.71(44)
Ru—N(1)	2.105(13)	N(1)—Ru—Cl(2)	90.60(34)
Ru—N(2)	2.127(15)	N(2)—Ru—Cl(1)	88.96(31)
N(1)—Ru—N(1′)	87.76(52)	N(2)—Ru—Cl(2)	178.96(67)
N(1)—Ru—N(2)	88.65(43)	Cl(1)—Ru—Cl(1′)	92.29(17)
		Cl(1)—Ru—Cl(2)	91.76(15)
Around Ru(2)			
Ru(2)—Cl(1)	2.323(28)	N(1)—Ru(2)—Cl(1)	91.3(4)
Ru(2)—Cl(2)	2.529(30)	N(1)—Ru(2)—Cl(1′)	172.0(2.0)
Ru(2)—N(1)	2.216(36)	N(1)—Ru(2)—Cl(2)	96.0(5)
Ru(2)—N(2)	2.467(38)	N(1)—Ru(2)—Cl(1)	95.9(5)
N(1)—Ru(2)—N(1′)	82.3(1.6)	N(2)—Ru(2)—Cl(2)	172.1(1.8)
N(1)—Ru(2)—N(2)	78.1(1.4)	Cl(1)—Ru(2)—Cl(1′)	94.7(1.5)
		Cl(1)—Ru(2)—Cl(2)	89.5(1.3)

*Standard deviations, relating to the least significant figures in parentheses.

only by the direction in which the hydrogen bonds form; the strength of the bonds is the same whichever direction is adopted.

Acknowledgements

I thank the National Research Council of Canada for financial support, Drs. S.-B. Tong and P. H. White for helpful discussions, Johnson Matthey for a generous loan of ruthenium trichloride, and a referee for interesting comments on the nature of the disorder.

1. F. BOTTOMLEY and S. B. TONG. Can. J. Chem. **49**, 3739 (1971).
2. E. E. MERCER and L. W. GRAY. J. Am. Chem. Soc. **94**, 6426 (1972).
3. F. BOTTOMLEY. J. Chem. Soc. Dalton, 1600 (1974).
4. F. BOTTOMLEY. J. Chem. Soc. Dalton, 2148 (1972).
5. L. H. THOMAS and K. UMEDA. J. Chem. Phys. **26**, 293 (1957).
6. International tables for X-ray crystallography. Kynoch Press, Birmingham. 1968 and 1974.
7. F. BOTTOMLEY. J. Chem. Soc. Dalton, 2538 (1975).
8. J. M. STEWART (*Editor*). The XRAY System - Version of 1976. Technical Report TR-446 of the Computer Science Center, University of Maryland, College Park, MD, U.S.A.
9. W. C. HAMILTON and J. A. IBERS. Hydrogen bonding in solids. Benjamin, New York. 1968.
10. S. B. TONG. Ph.D. Thesis. University of New Brunswick, Federicton, N.B. 1973.
11. H. C. STYNES and J. A. IBERS. Inorg. Chem. **10**, 2304 (1971).
12. H. J. PERSIE and J. A. STANKO. Chem. Commun. 1674 (1970).
13. T. E. HOPKINS, A. ZALKIN, D. H. TEMPLETON, and M. G. ADAMSON. Inorg. Chem. **5**, 1427 (1966); **5**, 1431 (1966); **8**, 2421 (1969).

Double salts of indium trichloride with the alkali chlorides, with ammonium chloride, and with indium sulfate

ELINOR M. KARTZMARK

Department of Chemistry, University of Manitoba, Winnipeg, Man., Canada R3T 2N2

Received January 31, 1977

ELINOR M. KARTZMARK. Can. J. Chem. **55**, 2792 (1977).

From a determination of the phase diagrams, at 25°C, the following double salts were shown to exist: $3LiCl{\cdot}InCl_3{\cdot}8H_2O$ in the system LiCl–$InCl_3$–H_2O, $2KCl{\cdot}InCl_3{\cdot}H_2O$ and $3KCl{\cdot}InCl_3{\cdot}2H_2O$ in the system KCl–$InCl_3$–H_2O, $2RbCl{\cdot}InCl_3{\cdot}H_2O$ in the system RbCl–$InCl_3$–H_2O, $2CsCl{\cdot}InCl_3{\cdot}H_2O$ in the system CsCl–$InCl_3$–H_2O, $2NH_4Cl{\cdot}InCl_3{\cdot}H_2O$ in the system NH_4Cl–$InCl_3$–H_2O, $In_2(SO_4)_3{\cdot}InCl_3{\cdot}(17 \pm 1)H_2O$ in the system $In_2(SO_4)_3$–$InCl_3$–H_2O. No double salt was found in the system NaCl–$InCl_3$–H_2O, studied previously (1). All the double salts except the two involving potassium chloride are congruently saturating at 25°C.

ELINOR M. KARTZMARK. Can. J. Chem. **55**, 2792 (1977).

A partir de déterminations de diagrammes de phase à 25°C, on a démontré que les sels doubles suivants existent: $3LiCl{\cdot}InCl_3{\cdot}8H_2O$ dans le système LiCl–$InCl_3$–H_2O, $2KCl{\cdot}InCl_3{\cdot}H_2O$ et $3KCl{\cdot}InCl_3{\cdot}2H_2O$ dans le système KCl–$InCl_3$–H_2O, $2RbCl{\cdot}InCl_3{\cdot}H_2O$ dans le système RbCl–$InCl_3$–H_2O, $2CsCl{\cdot}InCl_3{\cdot}H_2O$ dans le système CsCl–$InCl_3$–H_2O, $2NH_4Cl{\cdot}InCl_3{\cdot}H_2O$ dans le système NH_4Cl–$InCl_3$–H_2O, $In_2(SO_4)_3{\cdot}InCl_3{\cdot}(17 \pm 1)H_2O$ dans le système $In_2(SO_4)_3$–$InCl_3$–H_2O. On n'a trouvé aucun sel double dans le système NaCl–$InCl_3$–H_2O qui avait été étudié antérieurement (1). Tous les sels doubles à l'exception des deux impliquants le chlorure de potassium se saturent d'une façon congruente à 25°C.

[Traduit par le journal]

Introduction

Many double salts between indium trichloride and the alkali metal halides were reported in the early literature but no systematic study of the aqueous systems has been undertaken. Only a systematic phase rule study can prove the existence or non-existence of compounds in a given system and this is the reason for the present work.

Two of the binary salt systems were studied by Kley (2) using a microscopic technique which did not involve a proper analysis: the double salts Rb_3InCl_6 and Cs_3InCl_6 were reported. An analogous compound K_3InCl_6 was found by Fedorov (3) who did a thermal analysis which also showed the existence of a double salt, K_2InCl_5.

Meyer (4) reported a compound between lithium chloride and indium trichloride, but did not determine its composition. Ensslin *et al.* (5) gave this double salt the formula $3LiCl{\cdot}InCl_3{\cdot}9H_2O$. An incongruently saturating compound of formula $K_3InCl_6{\cdot}2H_2O$ was found by Wallace (6). He also studied the rubidium chloride, cesium chloride, and ammonium chloride systems with indium trichloride and water and reported compounds of formulae $M_2InCl_5{\cdot}H_2O$. He failed to find an analogous compound with potassium chloride which in the present study has been found to occur with an excess of indium trichloride. It is incongruently saturating and decomposes with addition of water to form the compound $K_3InCl_6{\cdot}2H_2O$, found by Wallace. The compound $(NH_4)_2InCl_5{\cdot}H_2O$ was also reported by Klug, Kummer, and Alexander (7).

In the earlier papers by this author on the double salts of indium trichloride the assumption was made that the stable hydrate of indium trichloride, at 25°C, was the trihydrate, since it was reported as such on the label from the BDH supplier. A paper by Ensslin *et al.* (5), which gave the formula $InCl_3{\cdot}4H_2O$ was discounted because of their experimental method: they refer to removing the solid phase by filtration, pressing it dry with filter paper, and analysing. Recently, however, Wignacourt (8) gave the formula as the tetrahydrate and based a Raman study on that formula. This caused the author of this paper to pay more particular attention to this matter. The problem arises because the invariant point on the indium trichloride side of the ternary

systems usually has less than 5% of the second salt and the tie-lines through the "wet residue" do not have sufficient slope to distinguish between three and four moles of water on a total molecular weight near 300. The system: indium trichloride – indium sulfate – water, was chosen in the hope that the invariant point would lie nearer to the middle of the diagram. This system has not previously been studied but Seward (9) gave the formula $In_2(SO_4)_3 \cdot 9H_2O$ to the hydrate of indium sulphate.

Experimental

Materials

Indium trichloride was obtained from Cominco in the form of a concentrated solution in water. To study the indium-rich regions, anhydrous indium trichloride obtained from J. T. Baker was used. The alkali chlorides and ammonium chloride were reagent grade and used without further purification. Anhydrous indium sulfate was obtained from Alfa Inorganics of Beverly, MA.

Analysis

Systems were equilibrated by stirring at 25.00°C for a period of 2 to 3 days. The indium-rich solutions were very viscous and required lengthy stirring to ensure equilibrium. The phases were separated by filtration through sintered glass and were analysed for chloride by precipitation as silver chloride and for alkali halide using a Perkin-Elmer flame photometer, Model 146, which gave an accuracy of ±1%. The presence of indium trichloride affects this estimation, so the indium trichloride was removed by adding ammonia and centrifuging to settle the indium hydroxide. Ammonium ion was estimated to ±1% by distillation from strong sodium hydroxide solution and absorption in boric acid solution, followed by conductimetric titration with standard hydrochloric acid. Indium chloride was determined by difference.

The technique of separation of the phases in the indium trichloride – indium sulfate – water system had to be changed because filtration proved to be impossible. The saturated solution together with solid phase was transferred to a closed centrifuge tube and rotated for from 5 to 6 h. The clear solution was decanted and the remaining wet residue treated as described below. The centrifuging was done at room temperature, 24 ± 1°C. Sulfate was determined as barium sulfate, with an accuracy of ±1%.

The composition of the compounds was obtained by the method of the 'wet rest'. This method requires that the solid phase and the adhering mother liquor be as dry as possible, without preferential loss of water. The simple procedure of placing it, after filtration, between pads of filter paper and submitting it to hydraulic pressure produced a 'wet rest' whose composition was so close to that of the compound, that error in extrapolation was minimized. This is important in high molecular weight compounds containing water if the true degree of hydration is to be obtained.

The experimental data are summarized in Table 1 which gives the composition of invariant solutions and nature of the solid phases for the six systems. The complete solubility data are to be found in the Depository.[1] The data are plotted in Figs. 1 to 6.

Discussion

The system indium trichloride – lithium chloride – water shows the existence of a congruently saturating double salt containing 3 mol of lithium chloride to 1 mol of indium trichloride (Table 1*a*). This salt was reported by Ensslin to have 9 mol of water of hydration but none of the compressed wet solids with compound as solid phase contained this amount of water (31.8%). The six pairs of points containing compound as solid phases were plotted on a triangular diagram, 55 cm to a side, using a width of tie-line equal to ±1%. The intersections of the six tie-lines enclosed a circle of 3 percentage points in diameter, centred at 29.5% water. The salt ratio is undoubtedly 3LiCl to $1In(Cl)_3$: the water content of the circle corresponds to 7 to 9 mol of water. The formula $3LiCl \cdot InCl_3 \cdot 8H_2O$ represents 29.2% water and in all probability is the correct formula of the double salt.

A second interesting feature of this phase diagram (Fig. 1) is the appearance of anhydrous lithium chloride in equilibrium with solution of very high indium trichloride content. This dehydration of a salt hydrate by a second salt is not uncommon. (Under normal laboratory conditions lithium chloride monohydrate loses its water of hydration around 98°C.)

The three systems of indium trichloride with ammonium chloride, rubidium chloride, and cesium chloride present very similar phase diagrams (Figs. 2, 3, 4): the congruently saturating double salts $2RbCl \cdot InCl_3 \cdot H_2O$ and $2CsCl \cdot InCl_3 \cdot H_2O$ occupy the major area of the diagrams, the invariant points lying very close to the water-salt edges and the solubilities being quite small. The double salt $2NH_4Cl \cdot InCl_3 \cdot H_2O$ is also congruently saturating but the solubility is much greater. Thus the double salts first reported by Wallace are the only ones to be found in these systems.

The potassium chloride – indium trichloride – water system (Fig. 5) features two double salts. The first, of formula analogous to those above,

[1]Complete set of data may be obtained at a nominal charge, upon request, from the Depository of Unpublished Data, CISTI, National Research Council of Canada, Ottawa, Canada K1A 0S2.

TABLE 1. Compositions of invariant solutions at 25.00°C and nature of the solid phases

(*a*) System $LiCl–InCl_3–H_2O$

Wt% LiCl	Wt% $InCl_3$	Nature of solid phase
45.40	—	$LiCl·H_2O$
42.35	6.47	$LiCl·H_2O + 3LiCl·InCl_3·8H_2O$
10.42	59.82	$3LiCl·InCl_3·8H_2O + LiCl_{(s)}$
—	67.60	$InCl_3·4H_2O$

(*b*) System $NH_4Cl–InCl_3–H_2O$

Wt% NH_4Cl	Wt% $InCl_3$	Nature of solid phase
28.63	—	$NH_4Cl_{(s)}$
24.66	28.80	$NH_4Cl_{(s)} + 2NH_4Cl·InCl_3·H_2O$
—	67.60	$InCl_3·4H_2O$

(*c*) System $RbCl–InCl_3–H_2O$

Wt% RbCl	Wt% $InCl_3$	Nature of solid phase
47.92	—	$RbCl_{(s)}$
48.98	0.56	$RbCl_{(s)} + 2RbCl·InCl_3·H_2O$
1.44	67.78	$2RbCl·InCl_3·H_2O + InCl_3·4H_2O$
—	67.60	$InCl_3·4H_2O$

(*d*) System $CsCl–InCl_3–H_2O$

Wt% CsCl	Wt% $InCl_3$	Nature of solid phase
65.67	—	$CsCl_{(s)}$
67.21	1.62	$CsCl + 2CsCl·InCl_3·H_2O$
—	67.60	$InCl_3·4H_2O$

(*e*) System $KCl–InCl_3–H_2O$

Wt% KCl	Wt% $InCl_3$	Nature of solid phase
26.72	—	$KCl_{(s)}$
24.00	28.03	$KCl_{(s)} + 3KCl·InCl_3·H_2O$
14.1*	50.7	$3KCl·InCl_3·H_2O + 2KCl·InCl_3·H_2O$
6.20	62.96	$2KCl·InCl_3·H_2O + InCl_3·4H_2O$
—	67.60	$InCl_3·4H_2O$

(*f*) System $In_2(SO_4)_3–InCl_3–H_2O$

Wt% $In_2(SO_4)_3$	Wt% $InCl_3$	Nature of solid phase
7.92	65.30	$InCl_3·4H_2O + InCl_3·In_2(SO_4)_3(17 \pm 1)H_2O$
49.91	10.25	$In_2(SO_4)_3·9H_2O + InCl_3·In_2(SO_4)_3(17 \pm 1)H_2O$

*Estimated from rectangular graph.

i.e. $2KCl·InCl_3·H_2O$, occurs in equilibrium with indium trichloride-rich solution and is incongruently saturating: on addition of water it reverts to a second incongruently saturating compound of formula $3KCl·InCl_3·2H_2O$ which in turn on addition of water decomposes to give KCl. The composition of the invariant solution in equilibrium with both double salts was estimated by plotting the solubility data on rectangular co-ordinates as g KCl per 100 g

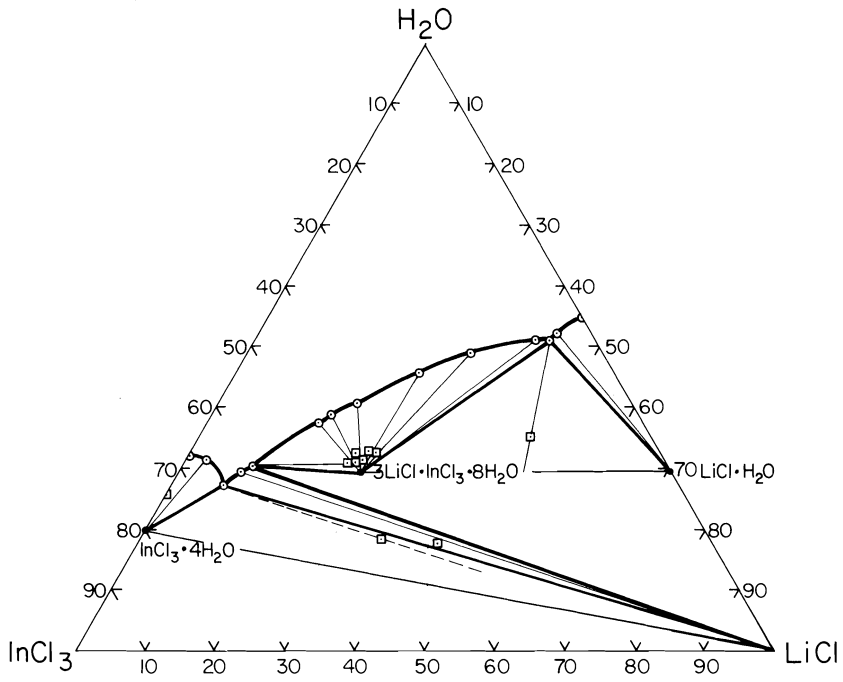

FIG. 1. System $LiCl–InCl_3–H_2O$ at 25.00°C.

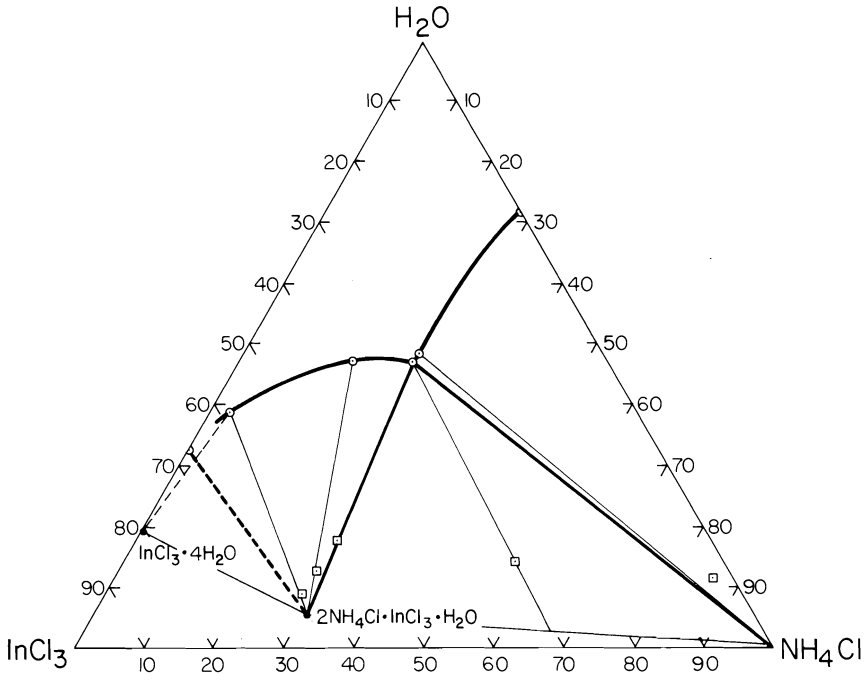

FIG. 2. System $NH_4Cl–InCl_3–H_2O$ at 25.00°C.

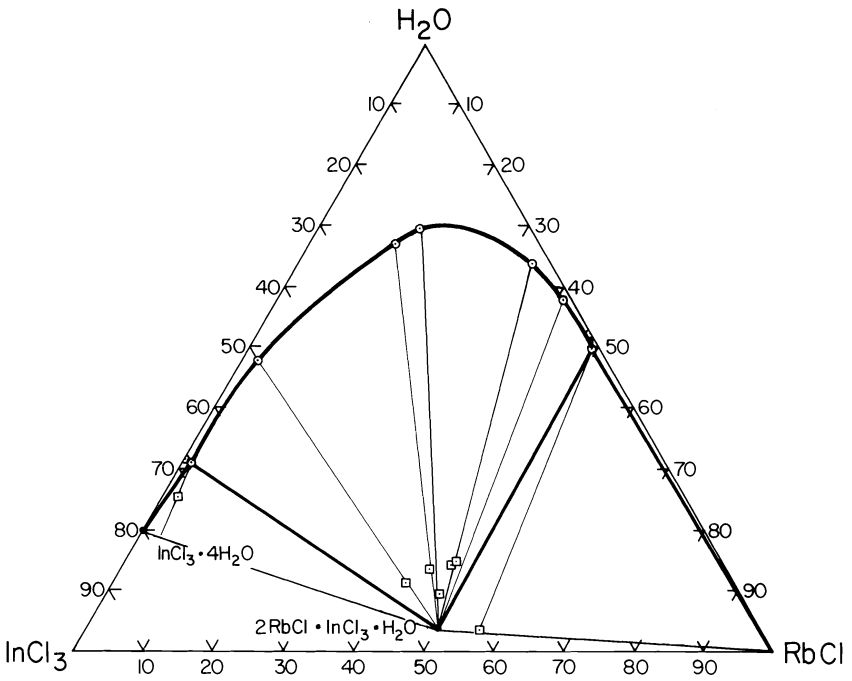

FIG. 3. System RbCl–$InCl_3$–H_2O at 25.00°C.

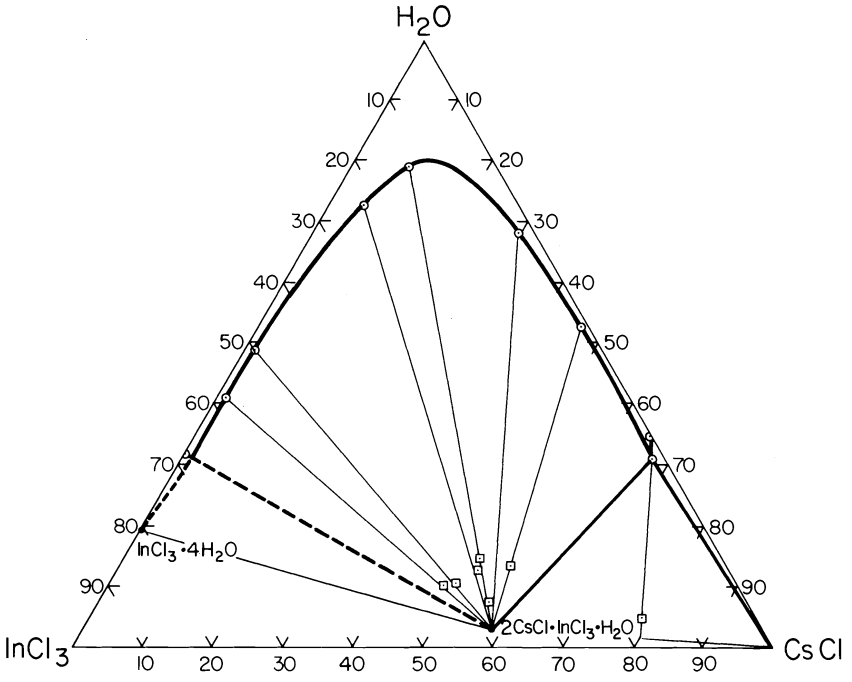

FIG. 4. System CsCl–$InCl_3$–H_2O at 25.00°C.

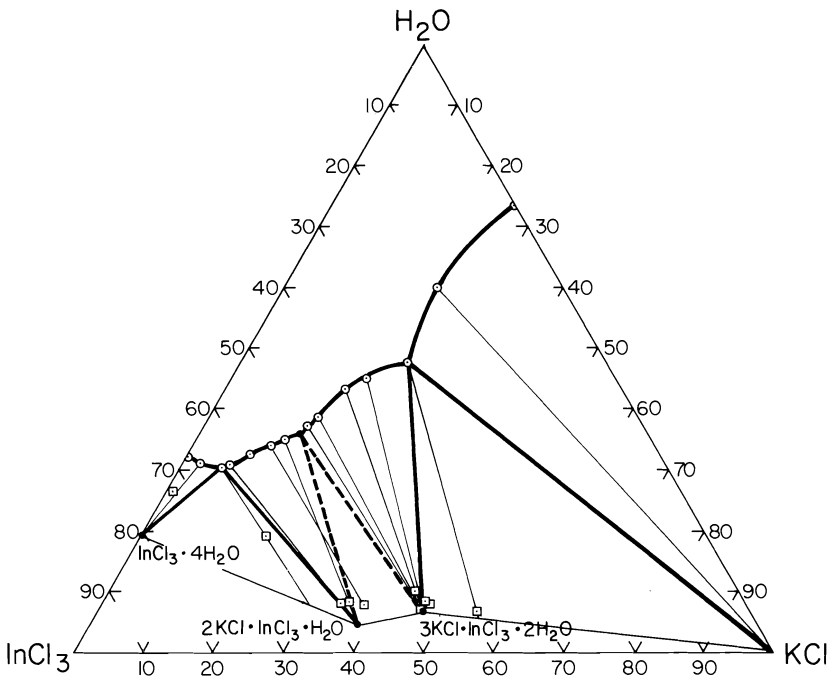

FIG. 5. System KCl–$InCl_3$–H_2O at 25.00°C.

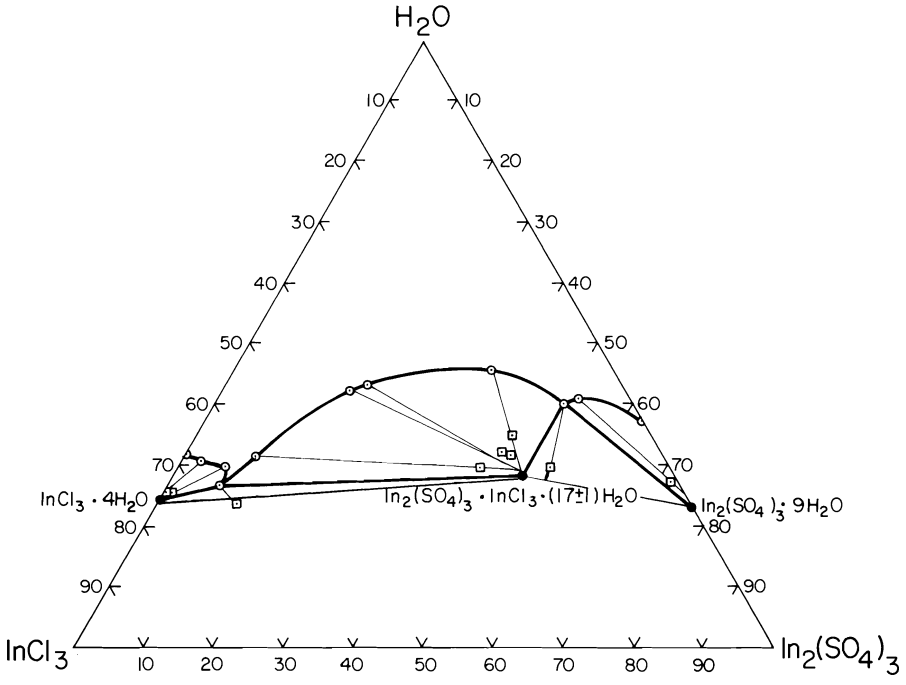

FIG. 6. System $InCl_3$–$In_2(SO_4)_3$–H_2O at 24 ± 1°C.

water and g $InCl_3$ per 100 g water. This treatment may be found in the Depository of Unpublished Data.[1]

This system has recently been studied by Wignacourt (8) who also finds the two double salts from a phase rule study at 21°C. He gives the formula $InCl_3 \cdot 4H_2O$ to hydrated indium trichloride and draws an analogy between it and thallium trichloride tetrahydrate. The tie-lines in his phase diagram are not conclusive as to the degree of hydration of indium trichloride, because the wet residue contained a large amount of mother liquor.

Figure 6, which gives the phase diagram at 24 ± 1°C, for the system indium trichloride – indium sulfate – water, shows without doubt that the formula of the hydrate of indium trichloride is $InCl_3 \cdot 4H_2O$. This system also shows the existence of a hydrated double salt of indium trichloride and indium sulfate, in the molar ratio of 1:1. The exact degree of hydration of the double salt cannot be obtained by this method, because the molecular weight is so high; it has been estimated as $17 \pm 1H_2O$. The indium sulfate side of the diagram has been taken from Seward (9) because, as with the double salt, the hydration of indium sulfate cannot be firmly established by the wet residue method.

In conclusion, indium trichloride forms at least one double salt with all of the alkali metal chlorides (except sodium chloride) and with ammonium chloride. Also, the stable hydrate at 25°C, of indium trichloride is $InCl_3 \cdot 4H_2O$.

1. E. M. KARTZMARK. Can. J. Chem. **52**, 3457 (1974).
2. P. KLEY. Ch. Ztg. **25**, 563 (1901).
3. P. I. FEDOROV and N. I. IL'INA. Zh. Neorg. Khim. **9**, 1207 (1964).
4. R. E. MEYER. Lieb. Ann. **150**, 152 (1869).
5. F. ENSSLIN, B. ZIEMECK, and L. DE SCHAEPDRYVER. Z. Anorg. Chem. **254**, 305 (1947).
6. R. C. WALLACE. Z. Krystallogr. **49**, 424 (1911).
7. H. P. KLUG, E. KUMMER, and L. ALEXANDER. J. Am. Chem. Soc. **70**, 3064 (1948).
8. J. P. WIGNACOURT. M.Sc. Thesis, University of Lille, France. 1974.
9. R. P. SEWARD. J. Am. Chem. Soc. **55**, 2741 (1933).

Mechanism of L-ascorbic acid oxidation and dehydro-L-ascorbic acid reduction on a mercury electrode. I. Acid medium

JUAN JOSÉ RUIZ, ANTONIO ALDAZ,[1] AND MANUEL DOMÍNGUEZ
Departamento de Química Física, Facultad de Ciencias, Universidad de Sevilla, Spain

Received January 21, 1977

JUAN JOSÉ RUIZ, ANTONIO ALDAZ, and MANUEL DOMÍNGUEZ. Can. J. Chem. **55**, 2799 (1977).

A polarographic study of the oxidation mechanism of L-ascorbic acid and of the reduction mechanism of dehydro-L-ascorbic acid was carried out in an acid medium.

For L-ascorbic acid, the oxidation process involves a two electron transfer and obeys the overall reaction

$$AH_2 \rightarrow B + 2e + 2H^+$$

The polarographic curve shows that the limiting current is governed by diffusion. On the rising portion of the wave, the two electron oxidation process consists of two consecutive one electron transfers, the second being the rate determining step (rds). The reaction orders, together with the Tafel slopes, were calculated.

The reduction of dehydro-L-ascorbic acid at the limiting current is kinetically controlled and involves a two electron transfer. The reaction kinetic pathways were studied and the reaction orders and Tafel slope were calculated. It is deduced that, for low overvoltages, the second one electron transfer is the rate determining step.

JUAN JOSÉ RUIZ, ANTONIO ALDAZ et MANUEL DOMÍNGUEZ. Can. J. Chem. **55**, 2799 (1977).

On a effectué, dans un milieu acide, une étude polarographique du mécanisme d'oxydation de l'acide L-ascorbique et du mécanisme de réduction de l'acide déhydro-L-ascorbique.

Pour l'acide L-ascorbique, le processus d'oxydation implique un transfert de deux électrons et est soumis à la réaction générale

$$AH_2 \rightarrow B + 2e + 2H^+$$

La courbe polarographique montre que le courant limitant est gouverné par la diffusion. Sur la portion montante de la vague, le processus d'oxydation à deux électrons implique deux transferts successifs d'un électron, le deuxième étant l'étape déterminante de la vitesse de la réaction. Les ordres de la réaction ainsi que les pentes de Tafel ont été calculés.

La réduction de l'acide déhydro-L-ascorbique, à courant limitant, est contrôlée cinétiquement et implique un transfert de deux électrons. On a étudié les chemins réactionnels cinétiques et on a calculé les ordres de la réaction et la pente de Tafel. On en déduit qu'à de bas survoltages, le deuxième transfert d'un électron est l'étape déterminante de la vitesse de la réaction.

[Traduit par le journal]

Introduction

Several studies have been carried out (1–4) on the electrochemical oxidation of L-ascorbic and dehydro-L-ascorbic acids on a mercury electrode.

However, as far as we know, there exists no detailed study on the mechanism of these reactions. The aim of this study is, therefore, to determine the reaction mechanism for the two acids using direct current polarography.

Experimental

Apparatus

The *i–E* curves were registered either automatically or traced point by point using a PO4 Radiometer with the damping circuit completely suppressed. The potentials were measured vs. s.c.e. with a Beckman Research potentiometer, which was also used as a p*H*-meter.

Electrolysis was carried out with an Amel potentiostat, model 541.

Cells and Electrodes

The polarographic measurements were carried out using a thermostated Radiometer V519 cell. A saturated calomel reference electrode was used. The working electrode was a mercury capillary with the following characteristics: $m = 2.005$ mg/s, $t = 4.32$ s, open circuit, in our buffered solution at pH 1.80 and $h = 40$ cm.

Electrolysis was carried out using a mercury electrode as a working electrode and a platinum auxiliary electrode.

Solutions, Products, and Measurements

All reagents used were Merck p.a. grade. As a supporting electrolyte solution, a buffered solution was used with the following components and concentrations: 0.04 *M* acetic acid, 0.04 *M* phosphoric acid, 0.04 *M*

[1]Present address: Departamento de Investigaciones Químicas, Centro Coordinado del C.S.I.C., Universidad Autónoma, Canto Blanco, Madrid 34, Spain.

ammonium nitrate, and 0.2 *M* NaOH which were mixed in varying proportions according to the p*H* desired. The ionic strength was adjusted with $NaNO_3$ to 0.2 *M* for the ascorbic acid study and to 0.5 *M* for the dehydro-L-ascorbic acid study.

All measurements were carried out in an atmosphere of nitrogen and at a temperature of 25 ± 0.05°C.

The Mapson and Partridge technique (5) was used to identify products by paper chromatography.

The Tafel curves were taken on the rising portion of the polarographic wave ($i/i_{lim} < 0.2$) and, to avoid depleting the solution, the maximum current for plotting the polarographic curve point by point was taken with each first drop (6).

Results

General Behaviour

The L-ascorbic acid oxidizes over the DME producing either one or two polarographic waves depending on the p*H* of the solution. The first wave is visible throughout the p*H* range 2–14, whilst the second is only visible from p*H* 8. Only the first wave was studied to p*H* 7.

The dehydro-L-ascorbic acid gives a stable reduction in an acid medium (p*H* 0.5–6), Fig. 2, only for solutions much more concentrated than those normally used in polarography; *e.g.* for a concentration of 4×10^{-2} *M* currents of less than 1 μA are obtained. This is due to the fact that the acid in solution forms a polarographically active hydrate (1).

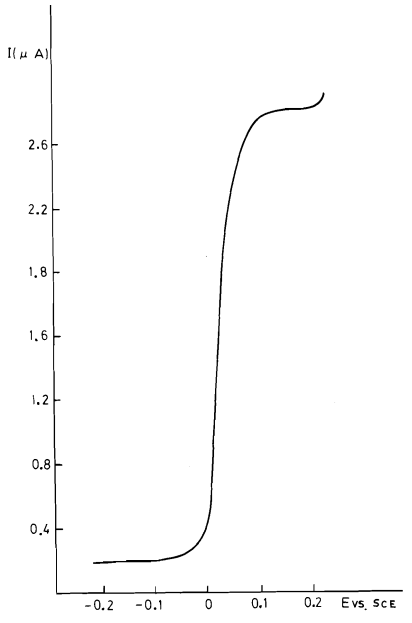

FIG. 1. First wave of L-ascorbic acid. Concentration 5×10^{-4} *M*. p*H* = 5.24.

Microcoulometric Measurements

The number of electrons taking part in the overall reaction was calculated from the decrease of the limiting current with the time of electrolysis (7). The average value obtained was 1.8.

Polarographic Behaviour

In the case of L-ascorbic acid, the limiting current is independent of the p*H* whilst $E_{1/2}$ varies with the p*H*. The values of the slopes of the linear sections were −59 and −27 mV/H^+ decade.

$E_{1/2}$ is independent of the concentration of the L-ascorbic acid. The logarithmic analysis of the polarographic wave gave straight lines with a slope of 30 mV per decade that are practically independent of the p*H*.

The limiting current is controlled by diffusion as: log i_{lim} vs. log *h* (corrected for the back pressure) is linear with a slope of 0.5; i_{lim} has a temperature coefficient of 1.1% per °C, and is proportional to the concentration of the L-ascorbic acid in the bulk of the solution.

In the case of dehydro-L-ascorbic acid, the limiting current is independent of the p*H* and the variation of $E_{1/2}$ with the p*H* is shown in Fig. 4. The values of the slopes were −44 and −72 mV/H^+ decade.

The limiting current is controlled kinetically (i_{lim} independent of *h* and with an elevated temperature coefficient).

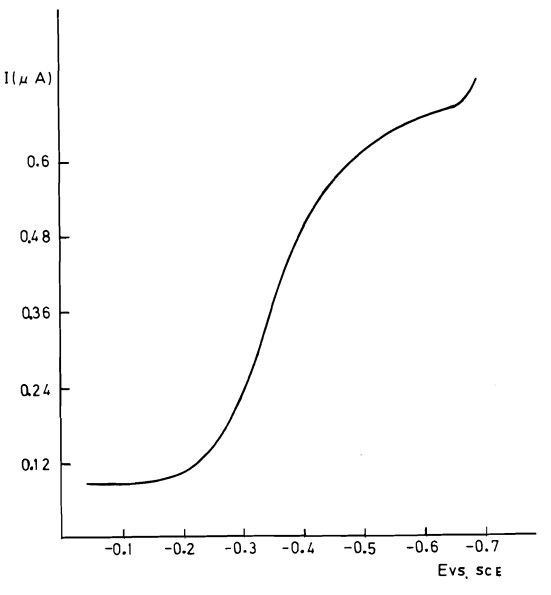

FIG. 2. Wave of dehydro-L-ascorbic acid. Concentration 4×10^{-2} *M*. p*H* = 2.81.

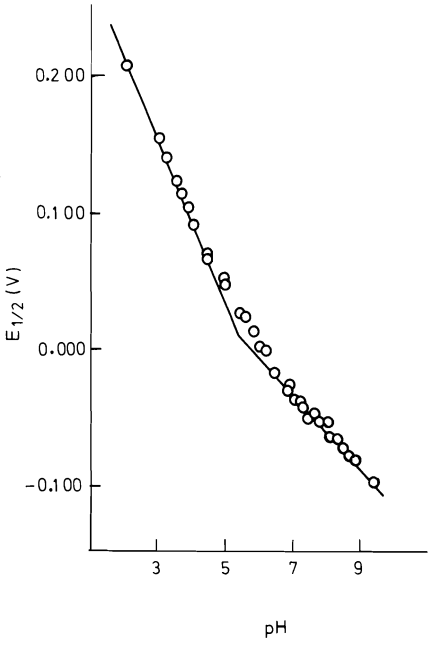

FIG. 3. L-Ascorbic acid. Variation of $E_{1/2}$ with pH.

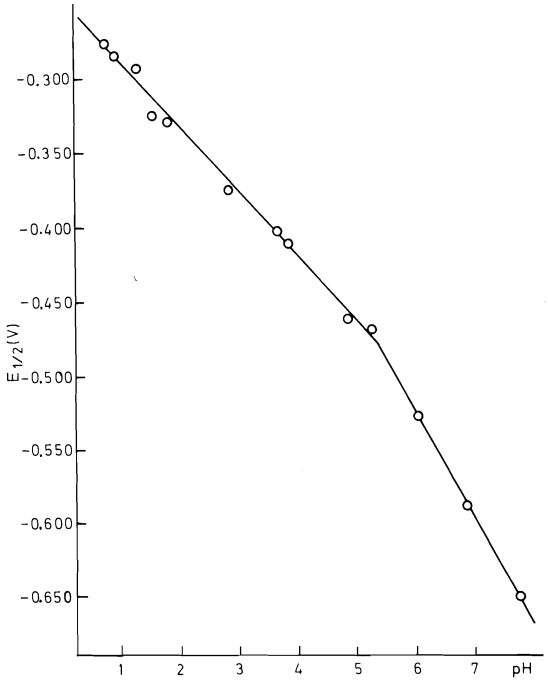

FIG. 4. Dehydro-L-ascorbic acid: variation of $E_{1/2}$ with pH.

Tafel Curves and Reaction Orders

(*a*) Influence of pH. With L-ascorbic acid, the Tafel curves are independent of the pH and their slopes have an average value of 34 mV per decade.

The reaction orders with respect to the H^+ concentration are:

pH	$\left(\frac{\partial \log i_j}{\partial \log H^+}\right)_{E,T,C_{i\neq j}}$
2–3	−1.9
7–8	−0.9

The order is independent of the potential in the area where Tafel's law is obeyed.

For dehydro-L-ascorbic acid, the Tafel slopes are equally independent of the pH with a mean value of 43 mV. The reaction orders with respect to the H^+ concentration are:

pH	$\left(\frac{\partial \log i_j}{\partial \log H^+}\right)_{E,T,C_{i\neq j}}$
0.5–5	1.1
5–7	2.0

(*b*) Influence of the concentration. The reaction order with respect to the concentration of the depolarizing agent was 1 in the case of both acids and was independent of the potential at which measurements were taken.

Electrolysis and Identification of Products

The first product of the oxidation of L-ascorbic acid was identified by paper chromatography of a solution of L-ascorbic acid at pH 4 which had undergone electrolysis at a controlled potential.

From the chromatogram, two zones were observed with the R_f characteristics (0.07 weak and 0.49 strong) of dehydro-L-ascorbic acid. As the position of the weak zone coincides exactly with that assigned to 2,3-diketogulonic acid, it can be assumed that there is a rupture of the lactone ring of the dehydro-L-ascorbic acid during the period of the electrolysis or during the chromatography.

Conclusion

In previous papers (2–4) it appeared to be established that the overall oxidation mechanism of L-ascorbic acid takes place through a reversible transfer of charge followed by a rapid chemical reaction of the product formed with water to form a very stable hydrate.

Our polarographic results confirm that the first

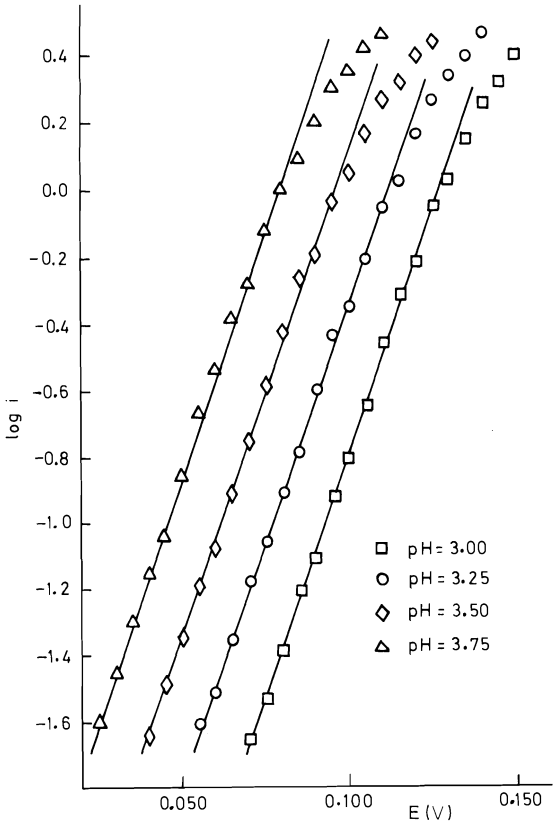

FIG. 5. L-Ascorbic acid: representation of Tafel's law.

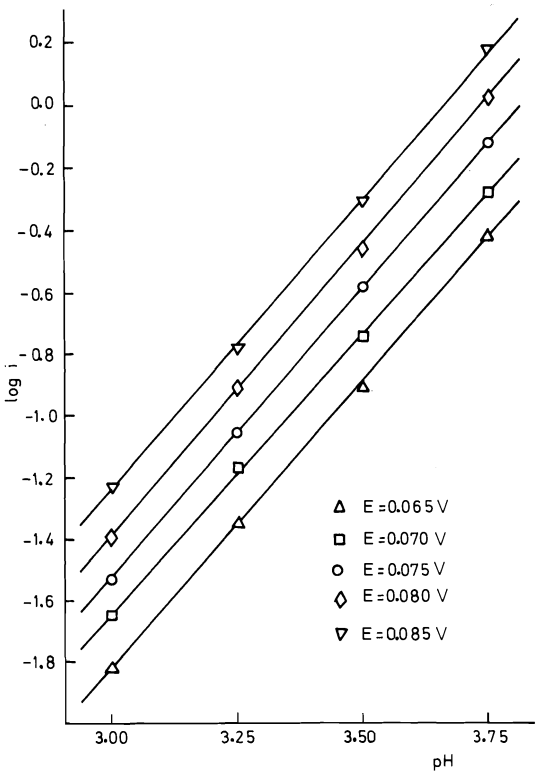

FIG. 6. L-Ascorbic acid: reaction orders.

wave of L-ascorbic acid is produced by a polarographically reversible two electron transfer (Tomes slope 30 mV/H^+ decade) in which two protons intervene in the interval pH 2–5 (slope -59 mV/H^+ decade) and another between pH 5–9 (slope -27 mV/H^+ decade). Thus, the overall reaction in the pH 2–9 interval would be:

$$AH_2 \rightleftarrows B + 2H^+ + 2e$$
$$\downarrow$$
$$C$$

substituting AH_2 by AH^- for pH's larger than the pK_1 of L-ascorbic acid.

The presence of a free radical (8) in the oxidation process of L-ascorbic acid clearly indicates that the transfer of two electrons is realized electron by electron.

With the aforementioned conclusions, the mechanism can be represented by the following reaction kinetic pathways, as shown in Fig. 7 where reaction 1 represents the dissociation of H^+ from the carbon 3, reactions 2 and 3 represent the one electron transfers with the formation of a free radical. Reactions 4 and 5 represent the normal hydration mechanism of carbonyl groups (9).

Assuming reaction 3 as being the rds and applying the approximation of equilibrium state, the value of the anodic current intensity on the rising portion of the wave can be expressed as (taking the electrokinetic potential to be negligible):

$$[1] \quad i = 2Fk_3K_1K_2 \times \frac{C_T}{K_1C_H + C_H^2} \exp((2 - \beta)FE/RT)$$

where C_T is the total concentration of L-ascorbic acid in the bulk of the solution; C_H is the concentration of the H^+ ions; K_1 and K_2 are the equilibrium constants of reactions 1 and 2; k_3 is the rate constant of the rate controlling step. Table 1 gives a comparison between the theoretical values deduced in the aforementioned reaction kinetic pathways and the experimental

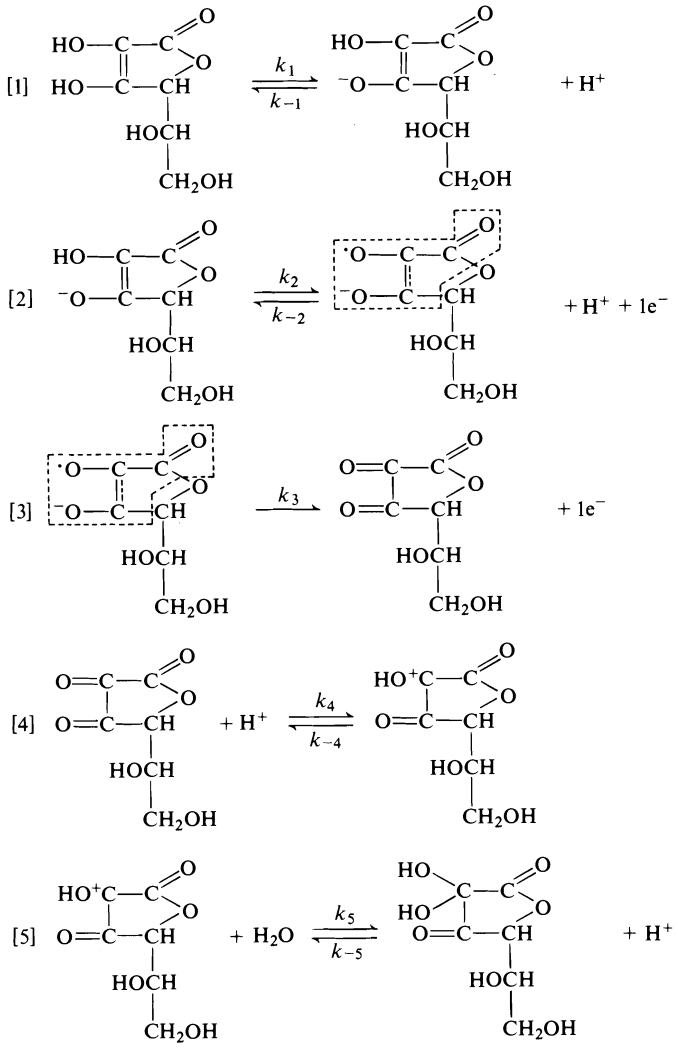

FIG. 7. L-Ascorbic acid: reaction kinetic pathways.

TABLE 1. Comparison between theoretical values (based on mechanisms in Fig. 7) and experimental results

Parameter	Value	
	Theoretical ($\beta \simeq 0.5$)	Experimental
Tafel slope	39 mV	34 mV
Order with respect to L-ascorbic acid concentration	1	1
Order with respect to H^+ ion	-2 for $K_1 \ll C_H$ -1 for $K_1 \gg C_H$	-1.9 (pH 2–4) -0.9 (pH 6–9)

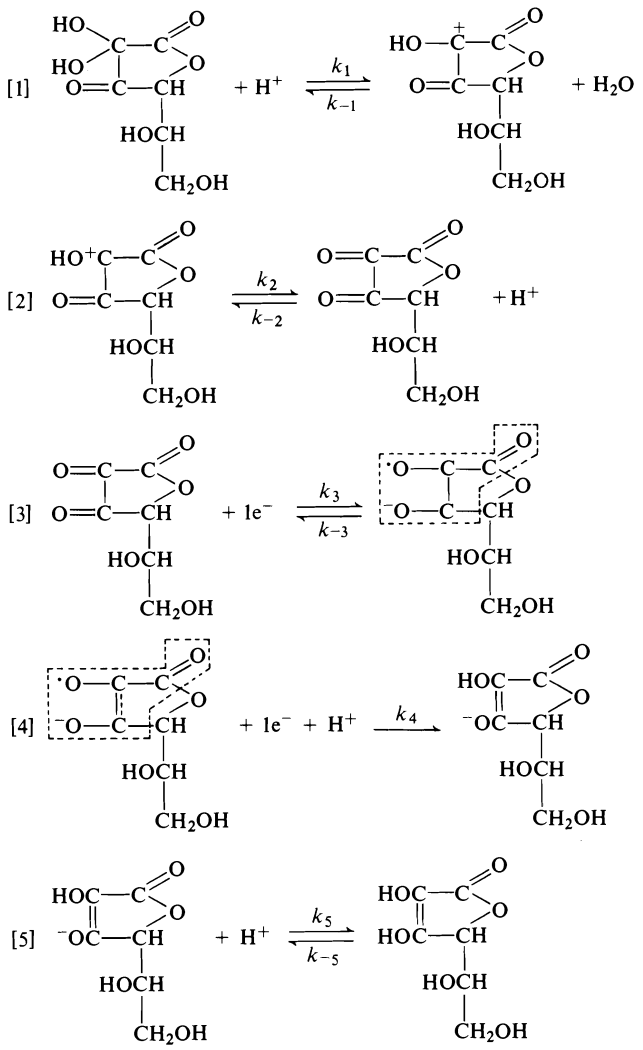

FIG. 8. Dehydro-L-ascorbic acid: reaction kinetic pathways.

results (where β is assumed to have a value of 0.5).

As is logical, in the case where pK_1 is less than the pH of the medium, the reaction:

$$AH_2 \rightleftarrows AH^- + H^+$$

should not be taken into account.

The close agreement between the experimental and theoretical results clearly indicates that the oxidation process takes place as shown in Fig. 7.

Dehydro-L-ascorbic Acid

The polarographic study shows that the reduction process includes a chemical stage which precedes the electron transfer and which controls the reaction rate at those potentials corresponding to the limiting current.

The electron transfer is not a reversible process as no linearity is observed in the plot E vs. log $i/(i_L - i)$.

The low value of i_L (<1 μA) compared with the dehydroascorbic acid concentration (4×10^{-2} M) indicates that the preceding reaction is shifted towards the formation of an electrochemically inactive substance. This substance could be the compound produced during the hydration of one of the two carbonyl groups of the dehydroascorbic acid (1, 2).

From these results and granted that, in this case, it is virtually impossible for a simultaneous

TABLE 2. Comparison between theoretical values (based on mechanisms in Fig. 8) and experimental results

Parameter	Value	
	Theoretical	Experimental
Tafel slope	−39 mV	−43 mV
Order with respect to dehydro-L-ascorbic acid concentration	1	1
Order with respect to H^+ ion	1 for $1 \gg K_1C_H$ 0 for $1 \ll K_1C_H$	1.1 (pH 0.5–5)

TABLE 3. Comparison between theoretical values (based on mechanism in Fig. 9) and experimental results

Parameter	Value	
	Theoretical	Experimental
Tafel slope	−39 mV	−43 mV
Order with respect to dehydro-L-ascorbic acid concentration	1	1
Order with respect to H^+ ion	2 for $1 \gg (1+K_2K_3)K_1C_H$	2

two electron transfer to take place by the tunnel effect (the probabilities being extremely low), reduction mechanism is proposed as shown in Fig. 8, where reactions 1 and 2 represent the dehydration of the carbonyl group, 3 and 4 the one electron transfers, and 5 the recombination with the H^+ ion to form L-ascorbic acid.

Assuming reaction 4 as the rds, the function $i = f(E)$ in the rising portion of the wave would be:

$$[2] \quad i = 2Fk_4K_1K_2K_3 \frac{C_TC_H}{1 + K_1K_2 + K_1C_H} \times \exp(-(1 + \beta)FE/RT)$$

where C_T = total concentration of L-ascorbic acid, C_H = concentration of hydrogen ions, K_1, K_2, K_3 = equilibrium constants, k_3 = rate constant.

Table 2 shows the close agreement between the theoretical and experimental results and permits us to assume that our mechanism is correct.

Near pH 5 a variation in the slope of the $E_{1/2}$ vs. pH plot (Fig. 2) is observed together with a change in reaction order with respect to the H^+ ion which varies from 1.1 to 2. A potentiometric titration of dehydro-L-ascorbic acid gives a first point of complete neutralization at pH 5.3. It is assumed that this is caused by the rupture of the lactone ring of the dehydro-L-ascorbic acid and produces the 2,3-diketogulonate anion according to (9). Therefore, after this pH, the dehydro-L-ascorbic acid in solution is in the form of the 2,3-diketogulonate and the first reaction of the reduction mechanism would be as shown in Fig. 9.

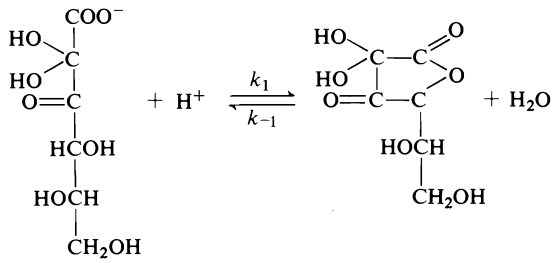

FIG. 9. First reaction on the reduction mechanism of the dehydro-L-ascorbic acid for pH > 5.

Once the dehydro-L-ascorbic acid is formed, the subsequent reactions will occur as before.

Assuming, once again, the last transfer reaction to be the rds, the i–E function is now expressed by:

$$[3] \quad i = 2Fk_5K_1K_2K_3K_4 \times \frac{C_TC_H^2}{K_1K_2C_H^2 + (K_2K_3 + 1)K_1C_H + 1} \times \exp(-(1 + \beta)FE/RT)$$

Table 3 shows the complete agreement between the theoretical and experimental results.

Acknowledgements

This study was supported by the Comisión Asesora de Investigación Científica y Técnica, Madrid.

1. D. H. M. KERN. J. Am. Chem. Soc. **76**, 1011 (1954); **75**, 2473 (1953).
2. S. ONO, M. TAKAGI, and T. WASA. Bull. Chem. Soc. Jpn. **31**, 356 (1958).
3. A. ALDAZ, R. JIMENEZ, C. PIAZZA, and J. L. VAZQUEZ. Anales R.S.E.F.Q. (Química), **70**, 410 (1974).
4. C. CATTANEO and G. SARTORI. Gazz. Chim. Ital. **72**, 351 (1942).
5. L. W. MAPSON and S. M. PARTRIDGE. Nature, **164**, 479 (1949).
6. E. KIROWA-EISNER and E. GILEADI. J. Electroanal. Chem. **38**, 191 (1972).
7. G. A. GILBERT and L. K. RIDEAL. Trans. Faraday Soc. **47**, 396 (1951).
8. A. ALDAZ and A. M. ALQUIE. J. Electroanal. Chem. **47**, 532 (1973).
9. C. K. INGOLD. Structure and mechanism in organic chemistry. 2nd ed. Cornell Univ. Press, Ithaca. 1969. p. 1014.

Complex formation between sulfur dioxide and halide ions

ETELA MILANOVA AND ROBERT L. BENOIT

Département de chimie, Université de Montréal, C.P. 6210, Montréal (Qué), Canada H3C 3V1

Received February 28, 1977

ETELA MILANOVA and ROBERT L. BENOIT. Can J. Chem. **55**, 2807 (1977).

Complex formation between sulfur dioxide and iodide ions in acetonitrile (AN) has been studied by vapour pressure measurements. The enthalpy changes ΔH^0 for 1:1 association reactions between SO_2 and halide (X^-) ions in AN and between SO_2 and Cl^- in dimethylsulfoxide (DMSO) have been determined at 25°C by calorimetry. The ΔH^0 values (kcal mol^{-1}) are respectively -4.1 (Cl^-), -3.4 (Br^-), -3.0 (I^-) in AN and -0.7 (Cl^-) in DMSO. In contrast to previous literature data there is a linear relationship between these ΔH^0 and reported ΔG^0 values for the formation of the SO_2X^- complexes in AN. The difference between the ΔH^0 values for SO_2Cl^- in the solvents AN and DMSO is accounted for by the more exothermic enthalpy of solution of SO_2 in DMSO which is the more basic solvent, and by the expected minor difference in the enthalpies of transfer of Cl^- and SO_2Cl^- from AN to DMSO, both dipolar aprotic solvents. Some of the problems connected with the stability order of the SO_2X^- complexes are discussed in relation to solvent effects and properties of X^-.

ETELA MILANOVA et ROBERT L. BENOIT. Can. J. Chem. **55**, 2807 (1977).

On a étudié par mesure de pression de vapeur la formation de complexes entre l'anhydride sulfureux et les ions iodures dans l'acétonitrile (AN). On a déterminé par calorimétrie à 25°C les changements d'enthalpie ΔH^0 des réactions d'association 1:1 entre SO_2 et les ions halogénures X^- dans l'AN et entre SO_2 et Cl^- dans le diméthylsulfoxyde (DMSO). Les valeurs de ΔH^0 (kcal mol^{-1}) sont respectivement -4.1 (Cl^-), -3.4 (Br^-), -3.0 (I^-) dans l'AN et -0.7 (Cl^-) dans le DMSO. Contrairement aux données publiées, on observe une relation linéaire entre ces valeurs de ΔH^0 et les valeurs connues de ΔG^0 pour la formation des complexes SO_2X^- dans l'AN. La différence entre les valeurs de ΔH^0 pour SO_2Cl^- dans les solvents AN et DMSO s'explique par une chaleur de solution de SO_2 plus exothermique dans le DMSO, le solvent le plus basique, et une faible différence, comme prévu, des enthalpies de transfert de Cl^- et SO_2Cl^- entre l'AN et le DMSO, tous deux des solvants dipolaires aprotoniques. On examine quelques uns des problèmes liés à l'ordre de stabilité des complexes SO_2X^- en relation avec l'effet de solvant et les propriétés de X^-.

Early studies on sulfur dioxide solvates of salts, and data on solubility of salts in liquid sulfur dioxide (refs. 1, 2 and references cited therein) suggested specific interactions between SO_2, a Lewis acid, and basic inorganic anions. Complex formation between SO_2 and halide ions X^- in non-aqueous solvents is also evidenced in the presence of a strong uv absorption band which, in turn, is indicative of the charge transfer nature of the $SO_2 - X^-$ interaction. Spectrophotometric data were used to determine formation constants K for some SO_2X^- complexes in acetonitrile (AN) (3, 4) and in dimethylsulfoxide (DMSO) (4). The corresponding enthalpies of complex formation ΔH^0 in AN were also derived from values of K between 15 and 35°C (3, 4).[1] The rather poor agreement between both sets of reported ΔH values in AN is not too surprising in view of first, the difficulties involved in the use of the Benesi–Hildebrand equation to interpret the spectral data and second, the propagation of experimental errors from K to ΔH^0 in the narrow temperature range used. A direct calorimetric method should give more reliable ΔH^0 values.

We are therefore presenting here the results of a calorimetric determination of the enthalpy change $\Delta H^0(s)$ for reaction 1 in two dipolar aprotic (dpa) solvents s.

$$[1] \qquad SO_2(s) + X^-(s) \rightleftharpoons SO_2X^-(s)$$

where X = Cl, Br, I with s = AN, and X = Cl with s = DMSO. This work is of further interest because it extends our current study of the solvent influence on anion–molecule type reactions. We have recently discussed the effect of solvent on two related reactions, namely that between HR, Brønsted acids, and Cl^- (5), and that between I_2, a Lewis acid, and I^- (6). Although in principle calorimetric data on a reaction such as [1] could yield simultaneously ΔH^0 and K (7, 8), this was not the case here as the volatility

[1]The ΔH^0 values reported are not corrected for thermal expansion of the solvent (20).

TABLE 1. Vapor pressure data for acetonitrile solutions at 25°C

C_{salt} ($M\ell^{-1}$)	Salt	C_{SO_2} ($M\ell^{-1}$)	Total pressure P (mm Hg)	SO_2 partial pressure P_{SO_2} (mm Hg)	K ($M^{-1}\ell$)
0.09860	NEt_4I	—	88.19	—	—
0.2168	NBu_4I	—	86.97	—	—
0.4108	NBu_4I	—	85.75	—	—
		0.2822	108.49	21.17	
		0.6115	132.60	46.82	
		0.6401	134.90	49.25	
		0.9437	160.20	75.97	
		1.112	169.66	86.21	
		1.283	183.78	101.14	
0.1070	NEt_4ClO_4	1.387	192.04	110.0	—
0.1940	NEt_4ClO_4	1.355	190.00	108.1	—
0.6245	NBu_4I	0.3853	88.34	2.48	43
0.4345	NBu_4I	0.2847	90.05	3.47	29
0.6123	NBu_4I	0.5472	92.30	6.65	40
0.4411	NBu_4I	0.4337	95.75	9.44	21
0.4113	NBu_4I	0.5844	101.44	15.52	91
0.5550	NBu_4I	1.338	138.89	56.70	(—)

of SO_2 made it difficult to vary the SO_2/X^- ratio over a wide range, a condition necessary to get meaningful ΔH^0 and K values. The values of K needed to obtain ΔH^0 were taken from Norris *et al.* (3). We also estimated K from SO_2 vapour pressure measurements in the case of SO_2I^- in AN as a check on conflicting reported values.

Experimental

Materials

Tetraalkylammonium halides and tetraethylammonium perchlorate were Eastman Kodak white label products. The salts were dried under vacuum in presence of phosphorus pentoxide for several weeks. The solutions were prepared by weighing. The solvents were reagent grade acetonitrile (Fisher) and dimethylsulfoxide (BDH). Both solvents were dried and stored over activated 4A molecular sieves. Concentrated solutions of SO_2 in AN and DMSO were prepared by bubbling anhydrous (99.98%) gas (Canadian Liquid Air). The stock solutions were then diluted as required.

Apparatus and Procedure

The LKB Model 8725-2 isoperibol calorimeter and the calorimetric procedure have been described previously (8). The heats of mixing of 0.2–3.0 M SO_2 solutions with 27 ml of 0.1–0.2 M halide solutions were determined at 25°C. The volume of SO_2 solution (0.3–0.8 ml) in the glass ampoules was obtained from the density of the solvent and the weight of solution. The concentration of these SO_2 solutions was determined by addition of a known volume dispensed from a Gilmont micropipette to an excess of aqueous standard iodine solution, and back titration with standard thiosulfate. The SO_2 concentration was checked at the end of the calorimetric runs and the runs were discarded if the final SO_2 concentration was more than 3% lower than the calculated 'initial' concentrations.

Total vapor pressures were measured with a quartz spiral (Texas Instruments). The apparatus and procedure used have been described elsewhere (9).

Results

The vapor pressure data for acetonitrile solutions containing SO_2 and/or electrolytes at 25°C are given in Table 1. The SO_2 partial pressures P_{SO_2} are calculated from the experimental total pressures P by subtracting the solvent partial pressures P_{AN}. These latter pressures are derived from the pure solvent vapor pressure P_{AN} = 88.63 mm Hg by assuming that Raoult's law applies for the solute mole fractions used ($x \leq 0.033$). The P_{AN} data for 0.2–0.4 M NBu_4I solutions in absence of SO_2 do not support fully this assumption. However, looking at the solutions containing 0.1 M or 0.2 M NEt_4ClO_4 and SO_2, when we subtract P_{AN} calculated by using Raoult's law, we obtain P_{SO_2} values such that the corresponding Henry's law constant $H = P_{SO_2}/(SO_2)$ (atm/$M\ell^{-1}$) agrees within 1% with the same constant (0.104) determined for six (0.3–1.5 M) SO_2 solutions in absence of electrolyte. This result brings some justification to our method of calculation of P_{AN} and also implies that the salting effect of 0.1–0.2 M NEt_4ClO_4 on solute SO_2 is negligible. We have then assumed that these conclusions could be extended to NBu_4I solutions containing SO_2 so that we attributed the observed lowering of P_{SO_2} in these latter solutions to complex formation between SO_2 and I^-. Values of K, the formation constant of SO_2I^-, given in Table 1, are calculated from the known total concentrations

TABLE 2. Calorimetric data for the systems $SO_2(s) + X^-(s) \rightleftharpoons SO_2X^-(s)$

Total volume (ml)	Final SO_2 concentration ($M\ell^{-1}$) $\times 10^2$	Final X^- concentration ($M\ell^{-1}$)	$-Q_{exp}$ (cal)	$-Q_{dil}$ (cal)	$-\Delta H^0$ (kcal mol^{-1})
		(*a*) X = Cl, solvent: acetonitrile			
27.39	0.3870	0.10	0.454	0.037	4.05
27.39	0.5984	0.10	0.720	0.043	4.39
27.40	0.9055	0.10	1.039	0.051	4.10
27.72	1.066	0.10	1.295	0.070	4.36
27.38	1.352	0.10	1.529	0.067	4.26
27.68	1.558	0.10	1.770	0.083	4.03
27.51	1.769	0.10	2.005	0.084	4.07
27.29	2.062	0.10	2.322	0.077	4.11
27.37	1.282	0.20	1.420	0.073	3.9
27.48	1.698	0.20	1.936	0.082	4.0
27.71	3.916	0.20	4.306	0.182	3.9
		(*b*) X = Br, solvent: acetonitrile			
27.40	0.2809	0.09584	0.249	0.035	3.06
27.69	0.4325	0.09751	0.416	0.055	3.35
27.67	0.4377	0.09758	0.400	0.053	3.13
27.53	0.6701	0.09807	0.650	0.051	3.59
27.52	1.318	0.09811	1.263	0.068	3.66
27.51	1.558	0.09815	1.435	0.076	3.54
27.68	2.452	0.09754	2.189	0.071	3.45
27.65	2.105	0.1953	1.992	0.100	3.43
27.37	2.331	0.1973	2.200	0.109	3.46
27.38	2.418	0.1972	2.344	0.133	3.56
27.43	3.546	0.1969	3.274	0.176	3.37
27.64	4.009	0.1954	3.819	0.233	3.44
		(*c*) X = I, solvent: acetonitrile			
27.75	0.7637	0.09565	0.479	0.041	3.18
27.25	0.9592	0.09564	0.576	0.048	2.93
27.36	1.361	0.09523	0.803	0.067	3.04
27.61	1.856	0.09440	1.109	0.090	3.11
27.59	2.231	0.09446	1.271	0.105	3.00
27.72	2.730	0.09440	1.569	0.127	3.05
		(*d*) X = Cl, solvent: dimethylsulfoxide			
27.44	1.254	0.08551	0.208	0.081	0.55
27.56	1.604	0.08513	0.258	0.103	0.53
27.45	2.004	0.08546	0.342	0.103	0.66
27.56	2.468	0.08513	0.347	0.161	0.42
27.41	4.323	0.08559	0.862	0.349	0.71
27.54	5.639	0.08519	1.029	0.457	0.64
27.52	0.5919	0.3154	0.152	0.047	0.72
27.64	0.7250	0.3140	0.184	0.055	0.73
27.76	0.8531	0.3127	0.259	0.058	0.90
27.45	1.936	0.3163	0.473	0.122	0.74
27.62	2.669	0.3143	0.702	0.169	0.82
27.63	3.321	0.3143	0.796	0.213	0.71
27.32	1.355	0.4863	0.455	0.158	0.87
27.44	1.839	0.4842	0.592	0.194	0.85

C_{SO_2} and C_{I^-}, the two corresponding mass balance equations and $[SO_2]$, the free SO_2 concentration deduced from P_{SO_2} and Henry's law constant H.

The usefulness of the vapour pressure method to study reaction 1 in AN proved to be limited for the following reasons. First, because the SO_2X^- complexes are relatively stable and because the presence of $(SO_2)_nX^-$ species cannot be ruled out, the range of C_{SO_2} and C_{X^-} concentrations studied was restricted to values of C_{SO_2}/C_{X^-} near 1. Second, owing to the high

TABLE 3. Comparison of thermodynamic parameters for reaction 1 in acetonitrile (K in $M\ell^{-1}$, ΔH^0 in kcal mol^{-1})

Cl^-		Br^-		I^-		
K	$-\Delta H^0$	K	$-\Delta H^0$	K	$-\Delta H^0$	Reference
361	2.32	99	3.08	27.4	2.52	3
372	3.603	161	5.360	38	4.179	4
	4.11 ± 0.18		3.42 ± 0.18	33 ± 10	3.05 ± 0.09	This work

solvent vapour pressure P_{AN}, C_{SO_2} and hence C_{X^-}, had to be relatively high to obtain meaningful values of $P_{SO_2} = P - P_{AN}$, but then the calculation of P_{AN} was approximate because the solutions were no longer dilute. The use of DMSO instead of AN, as solvent, was precluded because though this time P_{DMSO} is favourably low, P_{SO_2} values are also unfavourably low, the Henry's law constant H being now only 0.0076.

The calorimetric results are presented in Table 2. The measured heat effects, Q_{exp}, correspond to the reaction between 0.3–0.8 ml (0.2–3.0 M) SO_2 solutions with a known excess of halide solutions. The final SO_2 concentrations varied between 3×10^{-3} and 4×10^{-2} M whilst the halide concentrations ranged from 9×10^{-2} to 5×10^{-1} M. The lower limits for the SO_2 concentrations were dictated by the magnitude of the ΔH^0 and K values for the particular reaction investigated and the fact that the values of Q_{exp} once corrected had to be reasonably accurate. Since the heat changes observed are relatively small, corrections for dilution effects were applied. For this purpose, the molar heats of dilution of SO_2 were estimated from data obtained on separate calorimetric runs in which SO_2 solutions were mixed with the pure solvents. The minor heat effect on mixing of pure solvent with the halide solutions was also taken into account. The corrections Q_{dil} are entered in Table 2. The enthalpies ΔH^0(s) for reaction 1 were then obtained from corrected heat effects, the SO_2X^- concentrations calculated from mass balances, and the values of the equilibrium constant K listed in Table 3 (3).

Attempts to study the SO_2–F^- system in AN proved unsuccessful because of the very low solubility of dried $(CH_3)_4NF$ and KF.

Discussion

First we will discuss briefly our K values for SO_2I^- in AN, as determined from vapour pressure measurements. Considering the assumptions involved in the calculation of P_{SO_2} and $[SO_2]$, there is a fair agreement between our average value, 33, and the values of Norris *et al.*, 21.4, and of Wasif *et al.*, 38. These latter values were deduced from spectrophotometric data for very dilute solutions ($8 \times 10^{-4} - 5 \times 10^{-3}$ M). Our P_{SO_2} data for two solutions with a high ratio C_{SO_2}/C_{I^-} lead either to a high value for K or a value of $\bar{n}$, the average number of SO_2 moles bound per mole of I^-, which is above 1. These results are thought to be indicative of the presence in these SO_2-rich solutions of an additional species $(SO_2)_2I^-$. In this respect, it is worth noting that solid SO_2 solvates of halide salts containing up to $4SO_2$ per halide are known (1).

The formation of SO_2I^- and SO_2Br^- in aqueous solution has been reported, although the available supporting data are sketchy (4, 10). Taking into account the known decrease in stability of related complexes such as I_3^- and HCl_2^- when passing from a dipolar aprotic solvent, such as AN, to water (8, 11), the quoted stability of SO_2I^- in aqueous media was unexpected. We therefore attempted to estimate a value for $K_{SO_2I^-}$ in water from our $K_{SO_2I^-}$ value in AN. The procedure used followed that which led us to account for the known weak stability of HCl_2^- in water (8). Combining the AN values $K_{SO_2I^-} = 30$ and $P_{SO_2} = 0.104[SO_2]$, gives $[SO_2I^-]/[I^-] = 300 \times P_{SO_2}$. If we now assume that the free energies of transfer of the related anions SO_2I^- and I_2I^-, from water to AN, are about the same, then the calculated ratios $[I_3^-]/[I^-] = K_{I_3^-} \times S_{I_2} = 10^{7.3} \times 10^{-0.3}$ in AN (S_{I_2} is the I_2 solubility) and $[I_3^-]/[I^-] = K_{I_3^-} \times S_{I_2} = 10^{2.9} \times 10^{-2.9}$ in water (11), lead to $[SO_2I^-]/[I^-] \sim 300 \times P_{SO_2} \times 10^{-7.0}$. Since for aqueous solutions $P_{SO_2} = 0.80[SO_2]$ at 25°C (12), we finally get $K_{SO_2I^-} = [SO_2I^-]/[SO_2]\,[I^-] \sim 10^{-4.6}$. This very low value is to be contrasted with much higher values obtained from spectrophotometric data, respectively 0.35 (4) and 0.8

(10). We tend to attribute the large discrepancy to difficulties in the spectrophotometric measurements, possibly due to the susceptibility to oxidation of I^- (catalyzed by light) (13), and of SO_2. That the determinations on the system SO_2–I^- may be subject to errors, even in AN, has been pointed out (3) and it is also apparent when the spectrophotometric data of Wasif *et al.* (4) are compared with those of Norris *et al.* (3). It is difficult to predict from our results in AN what the SO_2X^- complexes stability order is in water. Considering the small differences in the K values in AN, the stability order in water might well be reversed, $SO_2I^- > SO_2Br^- > SO_2Cl^-$. We have shown that for the related series I_2X^-, the order is $I_3^- \sim I_2Br^- = I_2Cl^-$ in sulfolane (14) another dpa solvent but $I_3^- > I_2Br^- > I_2Cl^-$ in water (11). These changes in relative stabilities, when passing from dpa solvents to water, are mainly due to the increasingly stronger solvation by water of the halide ions in the order $I^- < Br^- < Cl^-$.

Turning now to our enthalpy data (Tables 2 and 3), the ΔH^0 values for reaction 1 in AN are, as expected, at variance with those derived indirectly from spectral data at 15, 25, and 35°C (3, 4). The exothermicity of [1] decreases slightly from X = Cl to Br and I just as the stability constants K do. The relationship between ΔH^0 and $\Delta G^0 = -RT \ln K$ is approximately linear as is often the case for donor–acceptor type reactions (15). The enthalpy-based halide basicity order $Cl^- > Br^- > I^-$ we observe here in AN, with SO_2 as the acid A, is the same as that obtained in sulfolane, another dpa solvent with A = HCl (8). From estimates of solvation enthalpies of gaseous ions X^- and AX^- (8), it is expected that the halide basicity order for A = SO_2 remains the same in the gas phase, with differences between the three individual ΔH^0 values larger in the gas phase than in AN.

The analysis of the solvent effect on reaction 1 (X = Cl) from our ΔH^0 values in AN and in DMSO, respectively -4.1 and -0.7 kcal mol^{-1}, is best carried out by taking into account the basicity-related solvent interaction with SO_2. We have therefore calculated ΔH^0(s,g) for

[2] $$SO_2(g) + Cl^-(s) \rightleftharpoons SO_2Cl^-(s)$$

by adding to ΔH^0(s) the heat of solution of gaseous SO_2 in AN and DMSO, respectively -6.8 and -11.5 kcal mol^{-1} (16). The obtained ΔH^0(s,g) values are -10.9 (AN) and -12.2 kcal mol^{-1} (DMSO). The difference, $\Delta\Delta H^0$(s,g), between these values, which is equal to 1.3 kcal mol^{-1}, represents the difference of the enthalpies of transfer between both solvents of the anions pair Cl^-–SO_2Cl^-. The value found for $\Delta\Delta H^0$ (s,g), 1.3 kcal mol^{-1} is in line with what we expected since we have recently established that the differences between the enthalpies of transfer of a number of pairs of anions X^-–AX^- are small and mainly governed by non-coulombic interactions when the transfers are between dpa solvents (6). These results make it possible to estimate, within 1–3 kcal mol^{-1}, the enthalpy change ΔH^0(s) of any X^-–A anion–molecule reaction such as [1] in a dpa solvent, from the value of ΔH^0(s,g) in a reference dpa solvent and the value of the enthalpy of solution of A in the dpa solvent of interest. We can now relate the acid strength of SO_2 to that of I_2, another Lewis acid, by comparing both ΔH(s,g) values for the reaction $A(g) + I^-(s) \rightleftharpoons AI^-(s)$ where s is AN. The corresponding ΔH^0(s,g), -9.8 kcal mol^{-1} (A = SO_2), and -20.0 kcal mol^{-1} (A = I_2) (6), indicate that in the gas phase SO_2 is a much weaker acid than I_2, with respect to the base I^-. The ΔH^0(s) values in AN for $A(s) + I^-(s) \rightleftharpoons AI^-(s)$, -3.0 kcal mol^{-1} (A = SO_2), -9.7 kcal mol^{-1} (A = I_2), give the same acidity order. Drago's compilation of data (17) also rank SO_2 as a weaker acid than I_2 with respect to any molecular base in inert media, since the enthalpy of adduct formation between a base B and an acid A is given by the four-parameter equation: $\Delta H = E_A E_B + C_A C_B$ with $E_A = C_A = 1$ for A = I_2 and $E_A = 0.92$, $C_A = 0.81$ for A = SO_2.

Finally, in view of the probable charge-transfer (CT) character of the SO_2X^- complexes, it is interesting to see to what extent these complexes follow some of the general correlations relating properties of such donor–acceptor complexes with those of the donors or acceptors. A linear relationship has been established (3) between the energies $h\nu_{max}$ corresponding to the frequencies of the uv–visible absorption maxima of the three SO_2X^- complexes and the ionization potentials (I_d) of the donors X^-. However, this linear correlation raises some unanswered questions. First, as pointed out by Norris *et al.* (3), the slope has not the expected unit value, and the calculated differences in binding energies between ground and excited states have a sign which is opposite to that found for CT complexes between

neutral species. Second, because of the abnormal value of the electron affinity of F in the halogen series which gives $I_d = 3.45$ eV for F^-, the linear correlation would predict for SO_2F^- an absorption band ($\lambda_{max} \sim 310$ nm) between those of SO_2Br^- and SO_2Cl^- whilst Norris *et al.* found no such band above 220 nm but a tail of an absorbance band at shorter wavelengths (3). Another type of general correlation sought for CT complexes involving a series of structurally related donors and a common acceptor is that between the stability of the complexes and the donor ionization potential I_d (15). The trend observed here for the SO_2X^- complexes is an increase in stability, as measured with ΔH^0 or K, in the order $SO_2I^- < SO_2Br^- < SO_2Cl^-$ which is the order of increasing I_d, $I^- < Br^- < Cl^-$. Surprisingly this trend is opposite to that usually observed for CT complexes with neutral donors in non-polar solvents (15). This reversal cannot be attributed to the polar nature of the solvent AN since we have seen that the stability order of the SO_2X^- complexes would be the same in the gas phase. The observed order is that of the proton affinity of the halides and is in line with predictions made from Drago's equation and the E_BC_B values calculated for gaseous X^- from gas phase ionic reactions (18). The sequence $Cl^- > Br^- > I^-$ is also that of nucleophilic reactivity of halides in dpa solvents but, interestingly enough, not in liquid SO_2 (19).

NOTE ADDED IN PROOF: The ΔH^0(g) value for $SO_2(g) + Cl^-(g) = SO_2Cl^-(g)$ has recently been found to be about -19.1 kcal mol^{-1} (21, 22). Thus the acidity order, with respect to the base Cl^-, is $HCl > SO_2 > H_2O$ both in the gas phase and in acetonitrile and sulfolane, two dpa solvents of similar basicity.

Acknowledgement

The financial assistance of the National Research Council of Canada is gratefully acknowledged.

1. D. F. BUROW. *In* The chemistry of non-aqueous solvents. Vol. 3. *Edited by* J. J. Lagowski. Academic Press, London. 1970.
2. T. C. WADDINGTON. *In* Non-aqueous solvent systems. *Edited by* T. C. Waddington. Academic Press, London. 1965.
3. E. J. WOODHOUSE and T. H. NORRIS. Inorg. Chem. **10**, 614 (1971).
4. (*a*) A. SALAMA, S. B. SALAMA, M. SOBEIR, and S. WASIF. J. Chem. Soc. A, 1112 (1971); (*b*) S. B. SALAMA and S. WASIF. J. Chem. Soc. Dalton, 151 (1975).
5. S. Y. LAM, C. LOUIS, and R. L. BENOIT. J. Am. Chem. Soc. **98**, 1156 (1976).
6. R. L. BENOIT, M. F. WILSON, and S. Y. LAM. Can. J. Chem. **55**, 792 (1977).
7. T. F. BOLLES and R. S. DRAGO. J. Am. Chem. Soc. **88**, 5015 (1965).
8. R. L. BENOIT, M. RINFRET, and R. DOMAIN. Inorg. Chem. **11**, 2603 (1972).
9. R. L. BENOIT and S. Y. LAM. Can. J. Chem. **52**, 718 (1974).
10. J. JANDER and B. TURK. Angew. Chem. **75**, 792 (1963).
11. (*a*) R. L. BENOIT and M. GUAY. Inorg. Nucl. Chem. Lett. **4**, 215 (1968); (*b*) R. L. BENOIT. Inorg. Nucl. Chem. Lett. **4**, 723 (1968).
12. H. F. JOHNSTONE and P. W. LEPPLA. J. Am. Chem. Soc. **56**, 2233 (1934).
13. T. NOVAK, E. J. POZLOMEK, V. A. MOSHER, and R. A. MACKAY. J. Phys. Chem. **80**, 2609 (1976).
14. M. DENEUX and R. L. BENOIT. Can. J. Chem. **48**, 674 (1970).
15. R. FOSTER. Organic charge-transfer complexes. Academic Press, London. 1969.
16. R. L. BENOIT, S. Y. LAM, and E. MILANOVA. To be published.
17. R. S. DRAGO. *In* Structure and bonding. Vol. 15. Springer-Verlag, New York. 1973.
18. A. P. MARKS and R. S. DRAGO. Inorg. Chem. **15**, 1800 (1976).
19. M. S. PUHAR. J. Chem. Educ. **47**, 473 (1970).
20. D. V. FENBY and L. G. HEPLER. Chem. Soc. Rev. **3**, 193 (1974).
21. P. KEBARLE. Ann. Rev. Phys. Chem. 1977. In press.
22. F. C. FEHSENFELD and E. E. FERGUSON. J. Chem. Phys. **61**, 3181 (1974).

The semiempirical derivation of ^{13}C nuclear magnetic resonance chemical shifts. Hydrocarbons, alcohols, amines, ketones, and olefins

HELMUT BEIERBECK AND JOHN K. SAUNDERS
Département de Chimie, Université de Sherbrooke, Sherbrooke (Qué.), Canada J1K 2R1
AND
JOHN W. APSIMON
Department of Chemistry, Carleton University, Ottawa, Ont., Canada K1S 5B6

Received February 21, 1977

HELMUT BEIERBECK, JOHN K. SAUNDERS, and JOHN W. APSIMON. Can. J. Chem. **55**, 2813 (1977).

Substituent parameters were derived for the semiempirical determination of ^{13}C chemical shifts in saturated hydrocarbons, alcohols, amines, ketones, and olefins. The olefin parameters are valid for six-membered rings and the remaining parameters for six-membered rings in chair conformations. The use of these parameters for the calculation of carbon resonances is illustrated with a number of examples.

HELMUT BEIERBECK, JOHN K. SAUNDERS et JOHN W. APSIMON. Can. J. Chem. **55**, 2813 (1977).

On a pu dériver des paramètres pour les substituants permettant la détermination semiempirique des déplacements chimiques du carbone 13 d'hydrocarbures saturés, d'alcools, d'amines, de cétones et d'oléfines. Les paramètres des oléfines sont valables pour les cycles à six chaînons et les autres paramètres pour des cycles à six chaînons dans des conformations chaises. On présente des exemples de l'utilisation de ces paramètres pour le calcul des résonances du carbone dans un certain nombre d'exemples.

[Traduit par le journal]

We have shown that β-carbon substituent effects on ^{13}C resonances are related to the number of hydrogen–carbon (HC) and carbon–carbon (CC) *gauche* interactions (1). Similarly, β-heterosubstituent effects depend on the number of hydrogen–heterosubstituent (HX) and carbon–heterosubstituent (CX) *gauche* interactions (2). If a *gauche* γ-substituent is added to an HC configuration, one observes a displacement which is equal in size, but opposite in sign, to the HC shift increment. An investigation of double bond substituent effects suggested that the γ-group has not introduced a new shielding mechanism which fortuitously cancels the HC shift increment, but rather that it has eliminated the HC shift contribution (3).[1] In other words, the observed *gauche* γ-effect is not associated with the γ-group but with the elimination of the

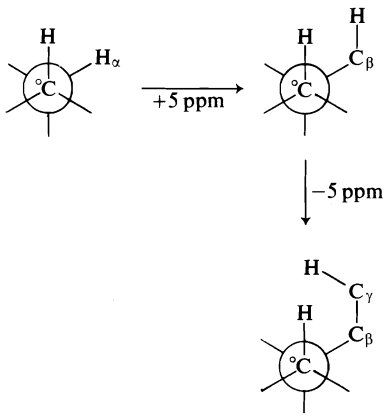

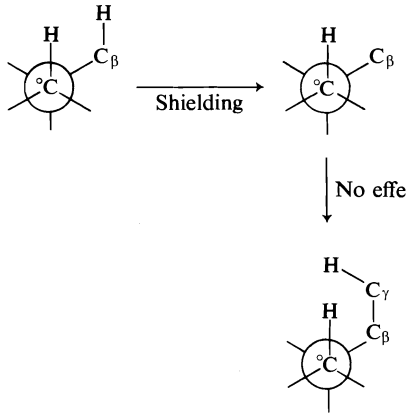

[1]After submission of our manuscript (ref. 3) we became aware of a publication by Boaz (4), in which the author shows that downfield shifts in ^{13}C and upfield shifts in proton spectra are related to the number of 1,3-diaxial hydrogen alignments.

β-hydrogen. This conclusion is based on the following observations (3).

(1) Elimination of γ-hydrogens by γ,δ-double bond formation has no noticeable effect on carbon resonances, i.e. nonbonded interactions with a γ-hydrogen cannot be responsible for the *gauche* γ-effect.

(2) The *gauche* γ-substituent effect is virtually independent of the nature of the γ-group X.

(3) The substituent effect of a β,γ-double bond depends on the number of displaced 1,3-diaxial hydrogen interactions.

(4) β-heterosubstituent shifts are found to depend on bond polarity, if 1,3-diaxial hydrogen alignments $H-^{0}C-C_{\alpha}-X_{\beta}-H_{\beta}$ are taken into account.

(5) Deviations from the cyclohexane chair conformation in heterocyclic systems lead to large *anti* γ-shifts only at carbons which are engaged in 1,3-diaxial hydrogen interactions, presumably because the HC shift contribution is sensitive to changes in hydrogen alignment.

(6) It seems more reasonable that the more severe *syn*-axial δ-interaction should give rise to larger shifts than the *gauche* γ-interaction. In the original interpretation of *gauche* γ-effects the γ-parameter was larger than the δ-parameter.

The general β-parameter HX therefore has to be redefined as the sum of contributions from 1,3-diaxial hydrogen interactions and from the C—X bond polarity. A *gauche* γ-parameter is now only required if the observed *gauche* γ-shift exceeds the magnitude of the eliminated HC contribution. With this revision the additivity parameters for saturated hydrocarbons, alcohols, and amines were redetermined, and new parameters were derived for ketones and olefins.

Results

The experimental data used in the derivation of the predictive parameters are found in Tables 1–5. The first two entries in Table 2 may serve to explain the symbols and abbreviations in the tables. Items 1/**32** and 2/**32** refer to carbons C(1) and C(2) in substrate **32**, 1β-hydroxy-*trans*-decalin. There are two parameter sets:

1/**32**—300 T 10000

2/**32** S 200—02000

The first sequence indicates hydrocarbon parameters and the second block functional group parameters, in this case hydroxyl parameters. The references for sp^2 and heterosubstituted sp^3 carbons are indicated by letters at the beginning of the second parameter sequence. For example C(1) in **32** is a tertiary carbinyl carbon and the hydroxyl parameter series therefore begins with the letter T. The remaining carbon references are indicated at the beginning of the hydrocarbon parameter series. Thus, C(2) in **32** is an unsubstituted secondary sp^3 carbon and the hydrocarbon parameter sequence therefore begins with the letter S. The reference shifts, like the structural parameters, were treated as variables. The number sequences indicate the number of occurrences of structural features. The hydrocarbon parameters are given in the sequence HC, CC, and δ, the hydroxyl parameters in the sequence OC, HO, CO, γ, and δ, etc. The definitions of the references and structural parameters, their numerical values, and standard errors are found in Table 6, in the same sequence as in Tables 1–5. The parameter sequences are also indicated in the footnotes of Tables 1–5. The symbols δ_{obs} and $\delta_{obs} - \delta_{calc}$ indicate observed resonances and deviations between observed and calculated shifts. The carbon and compound numbers, and the literature references for the experimental data are given in Chart 1. Experimental results which were obtained in this laboratory are collected in Table 7.

The hydrocarbon, hydroxyl, amine, and carbonyl parameters were derived from, and are only valid for, six-membered rings in chair conformations. The olefin parameters are valid only for six-membered rings. The eventual extension of this predictive scheme to the derivation of ^{13}C resonances in other conformations will require reference shifts, γ- and δ-parameters which are explicit functions of dihedral angles etc., similar to the generalized β-parameters $2 \times HX \times \cos\phi$ and $2 \times CX \times \cos\phi$ (2).

The use of these parameters for the derivation of ^{13}C resonances will now be demonstrated with a few examples.

Hydrocarbon Parameters

The hydrocarbon parameters in Table 6 are derived from the data in Table 1. P, S, T, and Q are the starting values for the derivation of primary, secondary, tertiary, and quaternary carbon resonances. The HC shift increment is associated with 1,3-diaxial hydrogen–hydrogen interactions, the CC parameter with exocyclic carbon–carbon *gauche* interactions, and the δ parameter with *syn*-axial δ-interactions.

TABLE 1. ^{13}C chemical shifts and structural parameters for some saturated hydrocarbons[a]

Carbon/ substrate	Parameters[b]	δ_{obs}	$\delta_{calc} - \delta_{obs}$	Carbon/ substrate	Parameters[b]	δ_{obs}	$\delta_{calc} - \delta_{obs}$
1/**3**	S 400	34.7	1.1	12/**11**	S 200	27.1	−0.4
2/**3**	S 200	27.2	−0.5	13/**11**	S 100	21.8	0.4
9/**3**	T 400	44.2	−1.8	14/**11**	S 310	33.1	0.0
1/**4**	T 310	38.4	1.3	1/**14**	S 410	39.7	−2.0
2/**4**	S 400	37.1	−1.3	2/**14**	S 000	19.4	−1.8
9/**4**	S 300	31.0	0.3	3/**14**	S 510	42.3	−0.3
10/**4**	T 510	50.6	−1.8	4/**14**	Q 040	33.5	0.4
Me/**4**	P 300	19.7	1.4	5/**14**	T 550	55.2	1.0
1/**5**	S 510	42.4	−0.2	19/**14**	P 301	22.5	1.1
2/**5**	S 100	22.2	0.0	1/**15**	S 410	38.8	−1.1
3/**5**	S 200	27.4	−0.7	7/**15**	S 300	32.6	−1.3
4/**5**	S 300	29.4	1.9	9/**15**	T 530	55.1	−2.6
5/**5**	T 420	46.2	−0.1	10/**15**	Q 060	36.4	1.2
9/**5**	Q 040	34.8	−0.9	11/**15**	S 100	20.9	1.3
Me/**5**	P 200	15.8	0.7	19/**15**	P 100	12.3	−0.3
1/**6**	T 420	44.3	1.8	9/**23**	T 430	48.8	−0.9
2/**6**	T 310	39.3	0.4	10/**23**	Q 060	37.2	0.4
3/**6**	S 400	35.8	0.0	11/**23**	S 100	20.1	2.1
9/**6**	S 300	31.0	0.3	19/**23**	P 101	13.9	0.6
10/**6**	T 510	49.4	−0.6	6/**28**	S 000	18.5	−0.9
Me-2/**6**	P 200	16.1	0.4	7/**28**	S 310	33.1	0.0
Me-3/**6**	P 300	20.9	0.2	10/**28**	Q 060	37.0	0.6
1/**7**	S 600	44.2	0.7	16/**28**	S 210	28.2	0.4
2/**7**	T 310	39.8	−0.1	20/**28**	T 310	39.7	0.0
Me-2/**7**	P 300	20.3	0.8	21/**28**	S 300	31.3	0.0
1/**8**	T 210	34.0	1.1	22/**28**	S 510	41.6	0.6
2/**8**	S 400	35.6	0.2	28/**28**	P 400	28.8	−3.2
5/**8**	T 300	36.8	1.0	29/**28**	P 200	17.5	−1.0
7/**8**	S 100	21.0	1.2	30/**28**	P 300	21.4	−0.3
8/**8**	S 310	34.6	−1.5	20/**29**	Q 020	31.0	−0.8
9/**8**	T 030	28.5	1.2	21/**29**	S 410	34.7	3.0
10/**8**	T 530	52.4	0.1	22/**29**	S 410	37.1	0.6
Me-1/**8**	P 300	19.2	1.9	25/**29**	P 102	15.6	1.5
Me-9/**8**	P 100	12.5	−0.5	26/**29**	P 101	16.7	−2.2
1/**9**	S 300	30.1	1.2	29/**29**	P 600	33.3	1.4
5/**9**	T 400	43.6	−1.2	30/**29**	P 400	23.6	2.0
7/**9**	S 400	35.0	0.8	6/**30**	S 000	18.2	−0.6
10/**9**	T 510	48.2	0.6	7/**30**	S 310	34.6	−1.5
1/**10**	S 300	30.4	0.9	8/**30**	Q 080	40.7	0.6
6/**10**	S 300	29.8	1.5	9/**30**	T 450	51.2	0.4
7/**10**	S 310	32.9	0.2	10/**30**	Q 060	37.3	0.3
8/**10**	T 220	38.0	−1.0	11/**30**	S 100	21.1	1.1
9/**10**	T 330	42.3	1.1	15/**30**	S 210	27.4	1.2
10/**10**	T 310	38.5	1.2	25/**30**	P 102	16.7	0.4
11/**10**	S 200	27.2	−0.5	26/**30**	P 101	16.1	−1.6
12/**10**	S 100	20.7	1.5	27/**30**	P 100	14.6	−2.6
14/**10**	S 200	27.0	−0.3	6/**31**	S 410	41.3	−3.6
1/**11**	S 300	31.0	0.3	7/**31**	S 000	18.3	−0.7
5/**11**	T 300	36.5	1.3	9/**31**	Q 060	37.5	0.1
7/**11**	S 200	26.1	0.6	11/**31**	S 310	35.6	−2.5
8/**11**	T 220	38.4	−1.4	12/**31**	S 210	30.5	−1.9
9/**11**	T 330	42.4	1.0	13/**31**	Q 060	39.7	−2.1
10/**11**	T 420	47.7	−1.6	24/**31**	P 101	14.7	−0.2
11/**11**	S 100	21.8	0.4	25/**31**	P 102	18.0	−0.9

[a]For substrate number, carbon numbering system, and literature references see Chart 1.
[b]Parameter definitions: Letters: P = primary, S = secondary, T = tertiary Q = quaternary. Numbers: n_{HC}, n_{CC}, n_{δ}. Root-mean-squares deviation between observed and calculated resonances is 1.28 ppm.

TABLE 2. ^{13}C chemical shifts and structural parameters for some alcohols[a]

Carbon/ substrate	Parameters[b]	δ_{obs}	$\delta_{calc} - \delta_{obs}$	Carbon/ substrate	Parameters[b]	δ_{obs}	$\delta_{calc} - \delta_{obs}$
1/**32**	—300 T 10000	74.6	2.0	5/**41**	T 420 —00200	48.5	2.1
2/**32**	S 200 —02000	35.8	−0.3	6/**41**	S 200 —00010	26.0	−0.6
3/**32**	S 200 —00010	24.1	1.3	Me/**41**	P 200 —00001	19.1	0.3
5/**32**	T 400 —00010	41.2	−0.1	1/**42**	—310 T 20000	78.8	1.6
9/**32**	S 300 —00010	29.1	0.9	9/**42**	T 530 —00000	55.4	−2.9
10/**32**	T 400 —01100	50.4	−1.3	10/**42**	Q 060 —00200	42.6	−0.4
1/**33**	—100 T 30000	70.4	1.0	11/**42**	S 100 —00001	24.7	0.3
2/**33**	S 200 —01100	34.3	−0.9	19/**42**	P 000 —00010	6.7	−0.5
3/**33**	S 100 —00010	20.0	0.9	1/**43**	—110 T 30000	71.5	1.8
5/**33**	T 300 —00010	35.6	0.9	9/**43**	T 430 —00010	47.5	−0.9
9/**33**	S 300 —00010	29.6	0.4	10/**43**	Q 060 —00200	40.2	2.0
10/**33**	T 400 —00200	47.4	−0.5	11/**43**	S 100 —00000	20.1	2.1
1/**34**	S 400 —02000	43.0	1.6	1/**44**	S 410 —01100	45.3	−0.9
2/**34**	—200 T 00000	70.2	−0.1	2/**44**	—000 T 20000	68.1	−3.2
3/**34**	S 200 —02000	35.6	−0.1	10/**44**	Q 060 —00010	36.1	0.3
4/**34**	S 400 —00010	32.0	2.5	19/**44**	P 100 —00001	14.8	0.1
10/**34**	T 400 —00010	41.2	−0.1	5/**45**	T 420 —00010	44.1	0.7
1/**35**	S 400 —01100	40.4	2.1	6/**45**	S 300 —02000	38.7	1.4
2/**35**	—000 T 20000	66.6	−1.7	7/**45**	—300 T 10000	75.2	1.4
3/**35**	S 200 —01100	33.9	−0.5	9/**45**	T 530 —00010	53.1	−1.9
4/**35**	S 300 —00010	27.6	2.4	5/**46**	T 320 —00010	39.2	1.0
10/**35**	T 300 —00010	36.4	0.1	6/**46**	S 300 —01100	36.8	1.2
1/**36**	—310 T 20000	79.6	0.8	7/**46**	—000 T 30000	68.2	−1.3
2/**36**	S 100 —02000	30.4	0.6	9/**46**	T 430 —00010	46.4	0.2
5/**36**	T 420 —00010	44.2	0.6	1/**47**	S 410 —00001	40.2	0.3
9/**36**	S 410 —00010	37.3	−0.9	9/**47**	T 530 —01100	61.2	−2.0
10/**36**	Q 040 —00200	39.2	−0.7	10/**47**	Q 060 —00010	38.4	−2.0
Me/**36**	P 100 —00010	9.8	0.9	11/**47**	—100 T 10000	69.2	−1.7
1/**37**	—210 T 30000	75.2	2.6	12/**47**	S 510 —02000	50.5	0.5
2/**37**	S 100 —01100	28.5	0.4	9/**48**	T 530 —00200	59.0	−2.0
5/**37**	T 320 —00010	37.5	2.7	10/**48**	Q 060 —00010	36.5	−0.1
9/**37**	S 310 —00010	34.8	−3.0	11/**48**	—000 T 30000	68.6	−1.7
10/**37**	Q 040 —00200	38.3	0.2	12/**48**	S 510 —01100	47.8	1.1
Me/**37**	P 200 —00000	16.1	0.4	18/**48**	P 200 —00001	20.0	−0.6
1/**38**	S 510 —02000	50.9	0.1	19/**48**	P 100 —00001	15.5	−0.6
2/**38**	—100 T 00000	66.9	−1.4	9/**49**	T 530 —00010	53.9	−2.7
3/**38**	S 200 —02000	36.4	−0.9	11/**49**	S 100 —02000	29.9	1.1
4/**38**	S 300 —00010	27.9	2.1	12/**49**	—310 T 20000	79.7	0.7
10/**38**	Q 040 —00010	34.7	−2.0	4/**21**	S 200 —02001	39.7	−1.3
1/**39**	S 510 —01100	47.8	1.1	5/**21**	T 330 —00020	42.1	−1.3
2/**39**	—000 T 20000	67.6	−2.7	6/**21**	S 210 —01100	35.4	−0.1
3/**39**	S 200 —01100	34.1	−0.7	7/**21**	—000 T 20000	67.8	−2.9
4/**39**	S 200 —00010	24.0	1.4	4/**22**	S 100 —02010	30.6	−0.9
Me/**39**	P 200 —00001	17.9	1.5	5/**22**	T 330 —01110	48.8	0.0
2/**40**	S 100 —00010	20.4	0.5	6/**22**	—110 T 10000	68.1	1.3
3/**40**	S 200 —02000	36.6	−1.1	7/**22**	S 200 —02000	35.3	0.2
4/**40**	—200 T 10000	70.0	2.1	10/**22**	Q 060 —00010	36.1	0.3
5/**40**	T 420 —01100	52.4	0.4	2/**29**	S 000 —02000	27.2	−0.8
6/**40**	S 200 —00010	23.0	2.4	3/**29**	—310 T 20000	78.9	1.5
10/**40**	Q 040 —00010	34.8	−2.1	4/**29**	Q 040 —00200	38.7	−0.2
2/**41**	S 000 —00010	16.9	−0.6	5/**29**	T 550 —00010	55.1	−0.2
3/**41**	S 200 —01100	34.1	−0.7	23/**29**	P 400 —00010	28.0	−3.6
4/**41**	—100 T 30000	71.8	−0.4	24/**29**	P 201 —00010	15.6	2.2

[a]For carbon numbering, substrate number, and literature references see Chart 1.
[b]Parameter definitions: first sequence gives hydrocarbon parameters (see footnote *b*, Table 1); second group gives hydroxyl parameters: T = tertiary carbinyl reference shift. Numbers: n_{OC}, n_{HO}, n_{CO}, n_{γ}, and n_{δ}. Root-mean-squares deviation between calculated and observed resonances is 1.49 ppm.

TABLE 3. ^{13}C chemical shifts and structural parameters for some saturated *N*-heterocycles[a]

Carbon/ substrate	Parameters[b]	δ_{obs}	$\delta_{calc} - \delta_{obs}$	Carbon/ substrate	Parameters[b]	δ_{obs}	$\delta_{calc} - \delta_{obs}$
1/**58**	S 300 —1000	33.6	1.7	8/**70**	S 400 —0001	34.9	−1.1
2/**58**	S 200 —0001	24.8	−0.1	9/**70**	T 200 —1100	37.5	1.0
3/**58**	S 100 —1000	26.0	0.2	10/**70**	—500 T 0000	68.0	−1.4
4/**58**	—400 S 0000	56.9	−0.4	Me/**70**	P 300 —0001	18.6	0.5
10/**58**	—400 T 0000	63.2	−1.1	5/**71**	T 200 —1000	35.6	1.7
1/**59**	T 210 —1000	36.6	2.5	9/**71**	T 020 —1100	33.2	−0.1
10/**59**	—510 T 0000	69.5	−1.0	Me/**71**	P 100 —0001	12.6	−2.6
Me/**59**	P 300 —0001	18.7	0.4	2/**72**	—400 S 0000	57.9	−1.4
1/**60**	T 120 —0100	33.0	0.6	3/**72**	S 100 —1000	25.8	0.4
2/**60**	S 310 —0001	32.4	−1.3	5/**72**	T 300 —1000	41.8	0.0
3/**60**	S 000 —1000	20.9	0.7	9/**72**	S 200 —1010	30.5	−0.6
10/**60**	—410 T 0000	65.9	−2.0	10/**72**	—510 T 0000	69.3	−0.8
Me/**60**	P 200 —0001	13.8	0.7	Me/**72**	—300 —0000	42.6	−0.1
2/**61**	S 310 —0000	30.1	3.0	2/**73**	—130 T 0000	56.0	−2.0
3/**61**	T 010 —0100	28.6	−1.4	10/**73**	—410 T 0000	60.0	3.9
4/**61**	—500 S 0000	62.1	−1.1	Me(N)/**73**	—200 P 0000	39.5	−1.6
Me/**61**	P 300 —0001	18.3	0.8	Me(2)/**73**	P 100 —0020	9.1	1.3
3/**62**	S 300 —0000	35.5	−0.2	2/**74**	—310 T 0000	59.7	−0.3
4/**62**	—310 T 0001	59.2	0.2	Me(N)/**74**	—200 P 0000	37.1	0.8
6/**62**	—300 S 0100	51.9	0.0	Me(2)/**74**	P 200 —1010	21.9	−2.1
Me/**62**	P 200 —0010	20.8	−1.0	2/**75**	—310 S 0000	56.1	−2.3
1/**63**	S 410 —1000	40.5	1.2	3/**75**	S 100 —0010	19.4	2.0
2/**63**	S 100 —0001	20.3	−0.2	9/**75**	T 200 —0110	34.5	−0.8
4/**63**	—300 S 0000	50.0	1.9	10/**75**	—520 T 0000	70.7	−0.4
10/**63**	—040 Q 0000	53.2	−0.1	Me(N)/**75**	—100 P 0000	33.2	0.2
Me/**63**	P 200 —0020	10.1	4.8	Me(9)/**75**	P 300 —0001	18.9	0.2
2/**64**	—200 S 0000	47.3	0.1	5/**76**	T 120 —1000	36.0	0.4
3/**64**	S 100 —1000	27.3	−1.1	9/**76**	S 100 —1010	27.7	−2.3
4/**64**	S 400 —0001	32.5	1.3	10/**76**	—220 T 0000	55.3	1.4
5/**64**	T 300 —1000	43.3	−1.5	Me/**76**	P 200 —2000	23.6	1.0
6/**64**	S 400 —0001	32.6	1.2	5/**77**	T 230 —1000	25.8	0.7
8/**64**	S 200 —0001	25.6	−0.9	6/**77**	S 210 —0001	38.3	4.4
9/**64**	S 200 —2000	34.0	0.7	9/**77**	S 210 —1010	41.1	−0.1
10/**64**	—400 T 0000	62.1	0.0	10/**77**	—040 Q 0000	50.5	−1.1
2/**65**	—020 T 0000	47.5	0.1	Me/**77**	P 200 —2000	26.0	−1.7
3/**65**	S 210 —1000	31.3	1.3	4/**78**	S 510 —0001	39.4	0.8
10/**65**	—300 T 0000	54.0	3.5	5/**78**	Q 030 —0100	32.0	1.3
Me/**65**	P 100 —1010	18.6	−3.4	9/**78**	S 100 —1100	28.2	−0.8
2/**66**	—200 T 0000	52.4	0.6	10/**78**	—310 T 0000	59.8	−0.4
3/**66**	S 300 —1000	35.0	0.3	Me/**78**	P 400 —0001	26.3	−0.7
Me/**66**	P 200 —2000	23.0	1.6	4/**79**	S 210 —0001	25.8	0.7
2/**67**	—400 S 0000	54.9	1.6	5/**79**	T 320 —0100	38.3	4.4
3/**67**	T 100 —1000	32.8	−0.1	9/**79**	S 400 —1100	41.1	−0.1
4/**67**	S 600 —0001	41.4	1.5	10/**79**	—020 Q 0000	50.5	−1.1
Me/**67**	P 400 —0001	19.6	4.0	Me/**79**	P 300 —1010	26.0	−1.7
2/**68**	—310 S 0000	52.3	1.5	9/**80**	T 400 —0110	44.6	−1.8
3/**68**	T 010 —0100	28.6	−1.4	11/**80**	S 300 —0001	29.4	−0.2
4/**68**	S 510 —0001	38.1	2.1	Me/**80**	—100 P 0000	33.2	0.2
5/**68**	T 200 —1000	37.5	−0.2	9/**81**	T 220 —0110	37.7	−0.3
Me/**68**	P 200 —0001	17.7	−3.2	11/**81**	S 210 —0001	26.9	−0.4
5/**69**	Q 030 —0100	33.9	−0.6	Me/**81**	—100 P 0000	33.0	0.4
10/**69**	—410 T 0000	64.3	−0.4	11/**82**	S 100 —0001	20.6	−0.5
Me/**69**	P 200 —0001	15.6	−1.1	Me/**82**	—300 P 0000	42.3	0.2

[a]For carbon numbering, substrate number, and literature references see Chart 1.
[b]Parameter definition: first sequence gives hydrocarbon parameters (see footnote *b*, Table 1), second group gives amine parameters: P, S, T, Q = references for primary, secondary, tertiary, and quaternary nitrogen-bearing carbons. Numbers: n_{HN}, n_{CN}, n_{HNC}, n_{γ}. Root-mean-squares deviation between calculated and observed resonances is 1.67 ppm.

TABLE 4. ^{13}C chemical shifts and structural parameters for some ketones[a]

Carbon/ substrate	Parameters[b]	δ_{obs}	$\delta_{calc} - \delta_{obs}$	Carbon/ substrate	Parameters[b]	δ_{obs}	$\delta_{calc} - \delta_{obs}$
1/**2**	—000 C 000	208.8	3.4	5/**54**	T 420 —100	58.8	2.0
2/**2**	S 200 —100	40.7	0.7	6/**54**	—000 C 000	211.8	0.4
3/**2**	S 100 —001	26.8	0.5	7/**54**	S 300 —100	47.1	−1.1
1/**50**	—010 C 000	215.8	−1.8	10/**54**	Q 060 —001	41.8	1.0
2/**50**	S 100 —100	38.3	−1.4	5/**55**	T 320 —001	49.1	−2.4
3/**50**	S 100 —001	28.0	−0.7	6/**55**	S 300 —100	46.6	−0.6
5/**50**	T 320 —001	49.8	−3.1	7/**55**	—000 C 000	211.3	0.9
9/**50**	T 430 —010	47.2	0.5	9/**55**	T 430 —001	55.1	−2.0
10/**50**	Q 060 —100	52.0	0.3	9/**56**	T 530 —100	64.9	2.3
19/**50**	P 000 —001	12.3	0.3	10/**56**	Q 060 —010	36.0	1.4
1/**51**	S 410 —100	54.1	−1.7	11/**56**	—000 C 000	210.7	1.5
2/**51**	—000 C 000	211.7	0.5	12/**56**	S 510 —100	56.9	0.0
3/**51**	S 200 —100	41.4	0.0	9/**57**	T 430 —001	56.5	−3.4
4/**51**	S 200 —001	28.3	3.6	11/**57**	S 100 —100	37.5	−0.6
10/**51**	Q 060 —001	40.6	2.2	12/**57**	—010 C 000	215.3	−1.3
1/**52**	S 310 —001	38.7	−0.4	18/**57**	P 100 —001	17.7	−0.6
2/**52**	S 100 —100	38.1	−1.2	2/**27**	S 000 —100	34.5	−2.2
3/**52**	—000 C 000	211.0	1.2	3/**27**	—010 C 000	217.6	−3.6
4/**52**	S 300 —100	44.6	1.4	4/**27**	Q 040 —100	47.2	1.4
5/**52**	T 320 —001	46.7	0.0	29/**27**	P 300 —010	21.2	−5.2
2/**53**	S 000 —001	22.7	0.1	30/**27**	P 201 —001	26.1	3.1
3/**53**	S 200 —100	41.2	0.2	1/**31**	S 000 —001	22.3	0.5
4/**53**	—000 C 000	212.6	−0.4	2/**31**	S 200 —100	42.2	−0.8
5/**53**	T 420 —100	59.3	1.5	3/**31**	—000 C 000	213.0	−0.8
6/**53**	S 100 —010	20.5	1.4	4/**31**	T 330 —100	58.2	−0.1
10/**53**	Q 060 —001	42.6	0.2	5/**31**	Q 060 —001	41.5	1.3
4/**54**	S 100 —010	20.4	1.5	23/**31**	P 000 —010	6.9	0.3

[a]For carbon numbering, substrate number, and literature references see Chart 1.
[b]Parameter definitions: first sequence gives hydrocarbon parameters (see footnote *b*, Table 1), second block gives carbonyl parameters: C = carbonyl reference. Numbers: n_β, $n_{\gamma s}$, $n_{\gamma a}$. Root-mean-squares deviation between calculated and observed resonances is 1.79 ppm.

A few examples may serve as illustration. The C(19) resonance in saturated steroids, e.g. item 19/**15** in Table 1, is calculated to be 7.44 + 4.55 = 12.0 ppm, since C(19) is a primary carbon and there is one HC contribution from the *gauche* interaction between a methyl C—H and the C—H(1e) bonds. In lanostanol the C(19) methyl group has a *syn*-axial δ-interaction with the C(30) methyl group, as well as the *gauche* HC interaction. The C(19) resonance in lanostanol, item 19/**23**, is therefore predicted to be 7.44 + 4.55 + 2.56 = 14.5 ppm. The steroidal C(9) resonance (item 9/**15**) is calculated to be 24.17 + 5 × 4.55 + 3 × 1.85 = 52.5 ppm, since C(9) is a tertiary carbon and there are five HC and three CC shift contributions. The five HC contributions arise from the alignment of the C(9)—H bond with the axial C—H bonds at positions 1, 5, 7, 12, and 14. The three exocyclic carbon–carbon *gauche* interactions are C(11)–C(9)–C(10)–C(1), C(11)–C(9)–C(10)–C(19), and C(8)–C(9)–C(10)–C(19).

Hydroxyl Parameters

The hydroxyl parameters in Table 6 are based on the data in Table 2. Only resonances for secondary alcohols are included in the table and therefore only a reference shift T for tertiary carbinyl carbons was derived. The OC, HO, and CO shift increments are associated with oxygen–carbon, hydrogen–oxygen, and carbon–oxygen *gauche* interactions. The γ parameter is used for *gauche* as well as for *anti* γ-interactions, provided the *anti* γ-hydroxyl group is equatorial. The δ parameter refers to *syn*-axial δ-interactions.

In monofunctional substrates the carbinyl carbon may only be engaged in HC, CC, or δ hydrocarbon interactions and in OC interactions. Of these structural features the HC interactions are the single most important factor determining the position of carbinyl carbon resonances, since the HC parameter has the largest value. For example, the axial C(2)—H bond in 2α-hydroxy,-10-methyl-*trans*-decalin is engaged in one HC interaction with the axial C(4)—H bond, and the C(2) signal is found at 66.9 ppm (item 2/**38**). The axial C(2)—H bond in 2α-hydroxy-*trans*-decalin is engaged in two HC interactions, with the axial C(4)—H and C(10)—H bonds, and the C(2) resonance is found at 70.2 ppm (item 2/**34**).

TABLE 5. ^{13}C chemical shifts and structural parameters for some olefins[a]

Carbon/ substrate	Parameters[b]	δ_{obs}	$\delta_{calc} - \delta_{obs}$	Carbon/ substrate	Parameters[b]	δ_{obs}	$\delta_{calc} - \delta_{obs}$
1/**1**	—000 T 0000	127.2	−1.2	4/**20**	—100 T 0000	129.9	0.6
3/**1**	S 100 —0100	25.5	0.5	5/**20**	—010 Q 0000	141.7	−2.1
4/**1**	S 100 —0010	23.1	0.5	6/**20**	—100 T 1000	123.2	−1.1
5/**12**	T 450 —0010	50.5	2.5	7/**20**	S 200 —0100	32.2	−1.6
6/**12**	S 000 —0100	23.5	−2.0	9/**20**	T 430 —0010	48.9	0.4
7/**12**	—100 T 1000	121.6	0.5	10/**20**	Q 050 —0000	35.5	0.3
8/**12**	—000 Q 0000	135.2	2.6	19/**20**	P 100 —0001	18.9	−1.7
9/**12**	T 430 —0100	52.2	−0.4	6/**24**	S 000 —0010	19.1	−0.1
10/**12**	Q 060 —0000	35.6	2.0	7/**24**	S 100 —0100	26.5	−0.5
1/**13**	S 310 —0001	36.7	1.7	8/**24**	—020 Q 1000	134.4	−1.4
5/**13**	T 450 —0010	52.0	1.0	9/**24**	—020 Q 1000	134.4	−1.4
6/**13**	S 000 —0010	21.3	−2.3	10/**24**	Q 050 —0000	37.0	−1.2
7/**13**	S 300 —0100	32.6	2.5	11/**24**	S 000 —0100	21.0	0.5
8/**13**	—000 Q 1000	124.4	4.9	12/**24**	S 210 —0010	31.0	−1.0
9/**13**	—020 Q 1000	134.4	−1.4	19/**24**	P 100 —0001	18.3	−1.1
10/**13**	Q 050 —0000	37.7	−1.9	7/**25**	S 100 —0001	28.1	−0.7
11/**13**	S 000 −0100	19.0	2.5	9/**25**	—030 Q 0000	148.2	−4.9
20/**13**	P 101 —0001	19.7	0.1	10/**25**	Q 060 —0000	39.5	−1.9
6/**14**	S 000 —0001	22.9	0.0	11/**25**	—000 T 1000	115.0	2.5
7/**14**	S 300 —0100	36.3	−1.2	19/**25**	P 101 —0001	21.5	−1.7
8/**14**	—000 Q 0000	138.8	−1.0	6/**26**	S 000 —0100	23.0	−1.5
9/**14**	T 430 —0100	51.8	0.0	7/**26**	—000 T 1000	120.1	−2.6
10/**14**	Q 060 —0000	38.8	−1.2	8/**26**	—030 Q 0000	142.7	0.6
11/**14**	S 000 —0010	19.1	−0.1	9/**26**	—030 Q 0000	145.9	−2.6
14/**14**	—200 T 1000	128.1	−1.5	10/**26**	Q 060 —0000	37.4	0.2
6/**16**	—100 T 1000	121.8	0.3	11/**26**	−000 T 1000	116.3	1.2
7/**16**	S 200 —0100	32.1	−1.5	19/**26**	P 101 —0001	22.8	−3.0
9/**16**	T 430 —0010	50.3	−1.0	18/**28**	T 540 —0100	59.2	−1.0
10/**16**	Q 050 —0000	36.6	−0.8	19/**28**	T 221 —0001	39.8	5.0
19/**16**	P 100 —0001	19.5	−2.3	8/**29**	Q 080 —0000	39.7	1.6
6/**17**	S 200 —0100	29.6	1.0	9/**29**	T 350 —0010	47.6	0.9
7/**17**	—000 T 1000	117.1	0.4	11/**29**	S 000 —0100	23.5	−2.0
8/**17**	—020 Q 0000	139.0	2.5	12/**29**	—100 T 1000	121.7	0.4
9/**17**	T 430 —0100	49.4	2.4	13/**29**	—020 Q 0000	145.1	−3.6
10/**17**	Q 060 —0000	34.1	3.5	14/**29**	Q 070 —0000	41.6	−2.1
6/**18**	—100 T 1000	119.2	2.9	15/**29**	S 110 —0001	26.1	3.2
7/**18**	—000 T 1000	116.5	1.0	17/**29**	Q 040 —0000	32.4	1.5
8/**18**	—020 Q 0000	140.4	1.1	18/**29**	T 330 —0100	47.1	0.1
9/**18**	T 330 —0110	46.3	2.3	19/**29**	S 411 —0001	46.8	−1.3
10/**18**	Q 050 —0000	37.0	−1.2	12/**30**	S 100 —0010	26.2	−2.6
11/**18**	S 000 —0001	21.0	1.9	13/**30**	T 240 —0100	38.4	6.1
19/**18**	P 100 —0001	15.8	1.4	14/**30**	Q 080 —0000	43.3	−2.0
6/**19**	S 200 —0100	29.8	0.8	16/**30**	S 310 —0001	37.7	0.7
7/**19**	—000 T 1000	118.0	−0.5	17/**30**	Q 030 —0000	34.3	−2.2
8/**19**	—020 Q 0000	135.7	5.8	18/**30**	—030 Q 0000	142.7	0.6
9/**19**	—030 Q 0000	143.4	−0.1	19/**30**	—200 T 1000	129.7	−3.1
10/**19**	Q 060 —0000	35.6	2.0	20/**30**	Q 010 —0000	32.3	−3.9
11/**19**	—000 T 1000	118.8	−1.3	21/**30**	S 310 —0010	33.3	1.2
12/**19**	S 310 —0100	42.1	−5.1	22/**30**	S 310 —0010	37.3	−2.8
19/**19**	P 100 —0001	19.3	−2.1	28/**30**	P 200 —0001	25.2	−3.4
1/**20**	S 210 —0011	34.3	0.9	29/**30**	P 400 —0001	31.3	−0.4
2/**20**	S 000 —0100	23.4	−1.9	30/**30**	P 500 —0001	32.3	3.1
3/**20**	—000 T 0000	124.6	1.4				

[a]For carbon numbering, substrate number, and literature references, see Chart 1.
[b]Parameter definitions: first group gives hydrocarbon parameters (see footnote *b*, Table 1), second block gives olefin parameters: T and Q = tertiary and quaternary sp^2 carbon references. Numbers: n_R, n_β, $n_{\gamma s}$, $n_{\gamma a}$. Root-mean-squares deviation between calculated and observed resonances is 2.19 ppm.

CHART 1. Definition of chemical structures and numbering systems for Tables 1–5 and 7. (Literature references)/structures: (7)/**1**; (8)/**2**; (9)/**3–8**; (10)/**9–11**; (11)/**12–14**; (12)/**15, 42–49**; (13)/**16**; (14)/**17–19**; (15)/**20**; (16)/**21, 22**; (17)/**23, 26, 28**; (18)/**32–41**; (19)/**50–57**; (20)/**58–63**; (21)/**64–75, 80–82**; (22)/**76–79**; (Table 7)/**24, 25, 27, 29, 30, 31**. *Note*, in Table 1 of ref. 13 the C(5) resonance of cholesterol should be 139.9 ppm and not 130.9 ppm.

1 Cyclohexene
2 Cyclohexanone

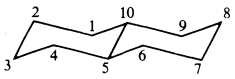

3 *trans*-Decalin
4 1β-Methyl-*trans*-decalin
5 10-Methyl-*trans*-decalin
6 1β,2α-Dimethyl-*trans*-decalin
7 2α,3β-Dimethyl-*trans*-decalin
8 1β,9α-Dimethyl-*trans*-decalin

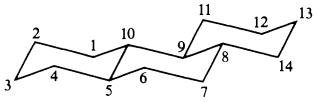

9 *trans-anti-trans*-Perhydrophenanthrene

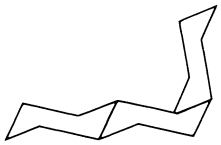

10 *trans-anti-cis*-Perhydrophenanthrene

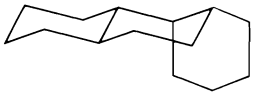

11 *trans-syn-cis*-Perhydrophenanthrene

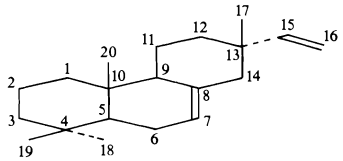

12 Pimara-7,15-diene
13 Pimara-8(9),15-diene

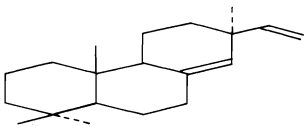

14 Pimara-8(14),15-diene

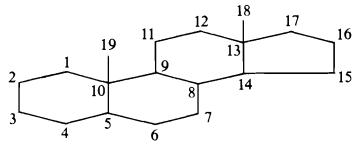

15 Androstane

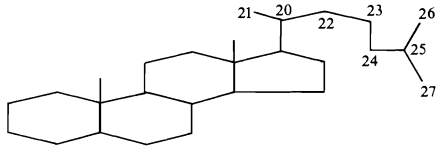

16 Cholest-5-en-3β-ol
17 Ergosta-7,22-dien-3β-ol
18 Ergosta-5,7,22-trien-3β-ol
19 Ergosta-7,9,22-trien-3β-ol
20 Cholesta-3,5-diene

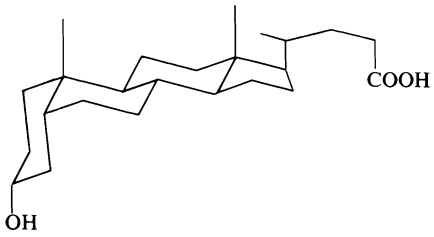

21 7α-Hydroxydesoxycholic acid
22 6α-Hydroxydesoxycholic acid

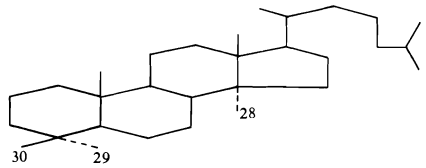

23 Lanostan-3β-ol
24 Lanost-8(9)-en-3β-ol
25 Lanost-9-en-3β-ol
26 Lanosta-7,9-dien-3β-ol
27 Lanost-8(9)-en-3-one

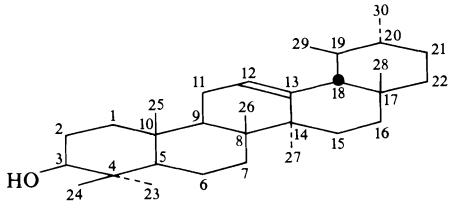

28 α-Amyrin

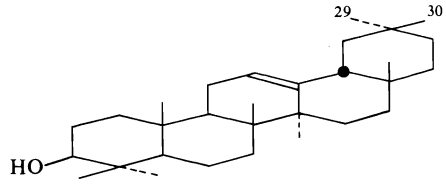

29 β-Amyrin

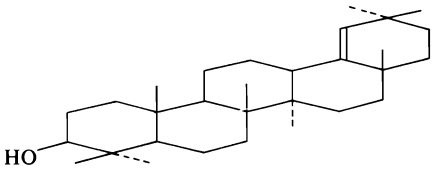

30 Germanicol

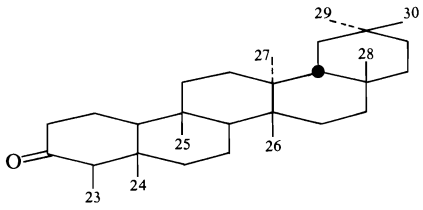

31 Friedelin
32 1β-Hydroxy-*trans*-decalin
33 1α-Hydroxy-*trans*-decalin
34 2α-Hydroxy-*trans*-decalin
35 2β-Hydroxy-*trans*-decalin
36 1β-Hydroxy,10-methyl-*trans*-decalin
37 1α-Hydroxy,10-methyl-*trans*-decalin
38 2α-Hydroxy,10-methyl-*trans*-decalin
39 2β-Hydroxy,10-methyl-*trans*-decalin
40 4α-Hydroxy,10-methyl-*trans*-decalin
41 4β-Hydroxy,10-methyl-*trans*-decalin
42 1β-Androstanol
43 1α-Androstanol
44 2β-Androstanol
45 7β-Cholestanol
46 7α-Cholestanol
47 11α-Androstanol
48 11β-Androstanol
49 12β-Androstanol
50 1-Androstanone
51 2-Cholestanone
52 3-Androstanone
53 4-Androstanone
54 6-Androstanone
55 7-Cholestanone
56 11-Androstanone
57 12-Androstanone

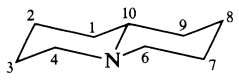

58 Quinolizidine
59 1β-Methylquinolizidine
60 1α-Methylquinolizidine
61 3α-Methylquinolizidine
62 4α-Methylquinolizidine
63 10-Methylquinolizidine

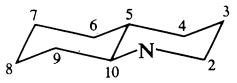

64 *trans*-Decahydroquinoline
65 2α-Methyl-*trans*-decahydroquinoline
66 2β-Methyl-*trans*-decahydroquinoline
67 3α-Methyl-*trans*-decahydroquinoline
68 3β-Methyl-*trans*-decahydroquinoline
69 5-Methyl-*trans*-decahydroquinoline
70 9α-Methyl-*trans*-decahydroquinoline
71 9β-Methyl-*trans*-decahydroquinoline
72 *N*α-Methyl-*trans*-decahydroquinoline
73 *N*α,2α-Dimethyl-*trans*-decahydroquinoline
74 *N*α,2β-Dimethyl-*trans*-decahydroquinoline
75 *N*β,9α-Dimethyl-*trans*-decahydroquinoline

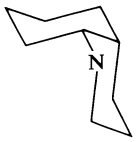

76 2β-Methyl-*cis*-decahydroquinoline
77 10-Methyl-*cis*-decahydroquinoline

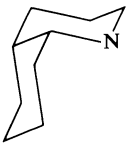

78 5-Methyl-*cis*-decahydroquinoline
79 10-Methyl-*cis*-decahydroquinoline

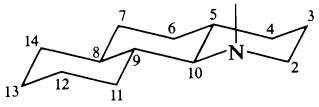

80 *N*β-Methyl-*trans-anti-trans*-perhydrobenzoquinoline

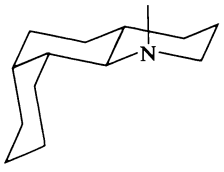

81 *N*β-Methyl-*trans-anti-cis*-perhydrobenzoquinoline

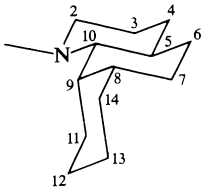

82 *N*α-Methyl-*trans-syn-cis*-perhydrobenzoquinoline

TABLE 6. Parameter definitions, numerical values, and standard errors

Hydrocarbons	Alcohols	Amines	Ketones	Olefins
P 7.44 0.42	T 60.99 0.72	P 28.82 0.63	C 212.19 0.54	T 125.99 0.93
		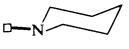	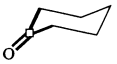	
S 17.62 0.32	OC 1.97 0.34	S 38.29 0.56	β 14.70 0.41	Q 137.80 0.59
				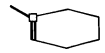
T 24.17 0.47	HO 4.41 0.18	T 43.89 0.40	γ_s −0.22 0.73	R −8.47 0.93
	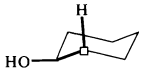			
Q 26.53 0.86	CO 2.28 0.22	Q 45.67 0.96	γ_a 5.16 0.42	β 3.86 0.47
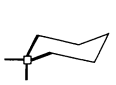	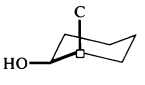	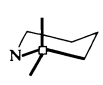	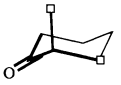	
HC 4.55 0.10	γ −1.28 0.23	HN 4.01 0.26		γ_s 1.41 0.57
		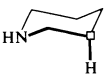		
CC 1.85 0.14	δ 2.86 0.53	CN 1.21 0.48		γ_a 5.23 0.49
		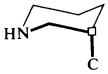		
δ 2.56 0.39		HNC −0.80 0.45		
		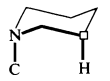		
		γ −2.04 0.34		
				

The axial C(1)—H bond in 1β-hydroxy-*trans*-decalin has three HC interactions, with the axial C(3)—H, C(5)—H, and C(9)—H bonds, plus the O(1)–C(1)–C(10)–C(9) OC *gauche* interaction, and the C(1) resonance occurs at 74.6 ppm (item 1/**32**).

The 2α- and 2β-hydroxy,10-methyl-*trans*-decalins may serve to illustrate the use of the β-, γ-, and δ-hydroxyl parameters. In the 2α isomer both C(1) and C(3) experience two HO *gauche* interactions, in addition to the hydrocarbon contributions (items 1/**38** and 3/**38**). C(4) and C(10) experience an *anti* γ-hydroxyl interaction (items 4/**38** and 10/**38**). In the 2β isomer both C(1) and C(3) are engaged in one HO and one CO interaction (items 1/**39** and 3/**39**), C(4) in

a *gauche* γ-interaction (item 4/**39**), and the methyl group in a *syn*-axial δ-interaction (item Me/**39**).

Amine Parameters

The amine parameters in Table 6 are based on the data in Table 3. The P, S, T, and Q parameters in the second block of parameters in Table 3 are the references for primary, secondary, tertiary, and quaternary nitrogen-bearing carbons. The HN parameter denotes a shift increment associated with a hydrogen–nitrogen *gauche* β-interaction, if a hydrogen or a lone pair electron at the nitrogen atom is aligned with a hydrogen on the carbon in question. However, if the 1,3-diaxial group is a carbon atom, the parameter HNC is used. The CN parameter denotes an increment associated with exocyclic carbon–nitrogen *gauche* β-interactions. The γ-parameter denotes the γ-nitrogen effect at both *gauche* and *anti* positions, exocyclic as well as endocyclic.

The derivations of the *N*-methyl, C(2) and C(10) resonances in *N*-methyldecahydroquinoline and of the C(10) resonance in 10-methylquinolizidine start from the P, S, T, and Q references, respectively (items Me/**72**, 2/**72**, 10/**72**, and 10/**63**). The remaining shift contributions arise from hydrocarbon interactions. For example, the alignment of the methyl C—H bonds with the two C(2)—H groups and with C(10)—H adds 3 × 4.55 ppm to the *N*-methyl reference of 28.82 ppm, for a total value of 42.5 ppm (item Me/**72**).

The C(3), C(5), and C(9) resonances in decahydroquinoline and its *N*-methyl and *N*,9α-dimethyl derivatives may illustrate the application of the HN and HNC parameters. It is assumed that the *N*-methyl group is exclusively equatorial in the monomethyl compound and exclusively axial in the dimethyl derivative. The HN interaction contributes 1 × 4.01, 1 × 4.01, and 2 × 4.01 ppm to the C(3), C(5), and C(9) resonances in decahydroquinoline, since the axial C—H bonds in positions 3 and 5 and both C—H bonds at position 9 are aligned either with a lone pair or a hydrogen on nitrogen (items 3/**64**, 5/**64**, and 10/**64**). In the *N*-methyl derivative the alignment of the axial C(9)—H bond with the lone pair on nitrogen again contributes one HN increment, but the equatorial C(9)—H bond is now aligned with an N—C bond, resulting in an HNC contribution (item 9/**72**). The calculation of the C(3) and C(5) resonances is unchanged by the introduction of the equatorial *N*-methyl group. In the 9α,*N*-dimethyl derivative the C(3), C(5), and C(9) resonances each receive an HNC contribution since all three axial C—H bonds are aligned with the axial N—C bond. In addition the exocyclic Me(9)–C(9)–C(10)–N carbon–nitrogen *gauche* interaction adds one CN increment to the C(9) resonance (items 3/**75**, 5/**75** and 9/**75**). The γ increment is added, for example, to the resonances of C(4) in decahydroquinoline (item 4/**64**, endocyclic *gauche* γ-interaction), to the methyl resonance in the 3β-methyl derivative (item Me/**68**, exocyclic *gauche* γ-interaction), to the C(6) resonance in decahydroquinoline, and to the methyl resonance in the 3α-methyl derivative (items 6/**64** and Me/**67**, *anti* γ-interactions).

Carbonyl Parameters

The carbonyl parameters in Table 6 are based on the data in Table 4. The parameter C is the reference for the carbonyl carbons. There is only one β parameter, but a *syn* and an *anti* γ parameter, γ_s and γ_a.

Since the carbonyl carbons do not bear any hydrogen, the only hydrocarbon interactions which may occur are the CC interactions. Thus, the parameter C itself is the predicted shift for the carbonyl carbons in the 2, 3, 4, 6, 7, and 11-ketosteroids. The carbonyl resonances in the 1- and 12-ketosteroids, on the other hand, receive additional downfield shift contributions of 1.85 ppm from the exocyclic C(2)–C(1)–C(10)–C(19) and C(11)–C(12)–C(13)–C(18) carbon–carbon *gauche* interactions, respectively (items 1/**50** and 12/**57**). The β increment of 14.70 ppm is added to the resonances of all carbons adjacent to the carbonyl group. The *syn* γ-interaction γ_s occurs, for example, at C(9) in 1-ketoandrostane (item 9/**50**) and at C(10) in 11-ketoandrostane (item 10/**56**). The *anti* γ_a interaction may occur at exocyclic or endocyclic carbons. C(19) in 1-ketoandrostane and C(18) in 12-ketoandrostane are examples for the exocyclic case (items 19/**50** and 18/**57**), and C(3) and C(5) in the 1-ketone for the endocyclic case. There are obviously two γ_a positions in every cyclohexanone ring.

Olefin Parameters

The olefin parameters in Table 6 are based on the data in Table 5. The parameters T and Q are the references for tertiary and quaternary sp^2 carbons. The increment R is added to the references T and Q if the second sp^2 carbon is

quaternary. There is only one β parameter, but there is a *syn* and an *anti* γ parameter. The β and γ parameters are not applied at quaternary sp^3 and sp^2 carbons. The hydrocarbon parameter HC is used for all 1,3-diaxial hydrogen interactions, whether the hydrogen is on an sp^2 or an sp^3 carbon. Exocyclic carbon–carbon *gauche* interactions at angles close to 0° are taken to make two CC contributions, in accordance with the cos φ dependence of the generalized β parameters 2 × HC × cos φ and 2 × CC × cos φ on the dihedral angle φ (2). Exocyclic carbon–carbon *gauche* interactions at angles $\phi \geq 90°$ are ignored (2).

A few examples may serve to demonstrate the derivation of sp^2 carbon resonances.

Item	Calculated resonances	Obsvd.
7/**17**	125.99−8.47+0×4.55=117.5	117.1
7/**12**	125.99−8.47+1×4.55=122.1	121.6
14/**14**	125.99−8.47+2×4.55=126.6	128.1
8/**12**	137.80 +0×1.85=137.8	135.2
5/**20**	137.80 +1×1.85=139.6	141.7
8/**18**	137.80 +2×1.85=141.5	140.4
9/**19**	137.80 +3×1.85=143.3	143.4

Carbons 7/**17**, 7/**12**, and 14/**14** are tertiary sp^2 carbons and therefore the reference shift of 125.99 ppm is used. The second sp^2 carbon, C(8) in all three cases, is quaternary and the R increment of −8.47 ppm is added. The sp^2 C—H bond at C(7) in cholest-7-en-3β-ol is not engaged in HC interactions (item 7/**17**). The sp^2 C—H bond in the Δ^7-pimaradiene has one HC interaction with the equatorial C(14)—H bond (item 7/**12**), and in the $\Delta^{8(14)}$-pimaradiene it has two HC interactions, with the equatorial C(7)—H and one C(17)—H bond (item 14/**14**). Items 8/**12**, 5/**20**, 8/**18**, and 9/**19** are examples of quaternary sp^2 carbons and the reference value of 137.80 ppm is used. In these four examples the second sp^2 carbon is tertiary and the R parameter is not required. The only hydrocarbon parameters which may contribute to quaternary sp^2 carbon resonances are the CC shift increments. C(8) in the Δ^7-pimaradiene is not engaged in exocyclic carbon–carbon *gauche* interactions along any of its three CC-bonds, and the predicted shift is simply equal to the reference value (item 8/**12**). The 60° C(6)–C(5)–C(10)–C(19) interaction in cholesta-3,5-diene makes one CC contribution to the C(5) resonance item (5/**20**). The segment C(7)–C(8)–C(14)–C(15) forms an angle of close to 0° and two CC contributions are added to the C(8) resonance in cholesta-5,7-dien-3β-ol (item 8/**18**). Segment C(11)–C(9)–C(10)–C(1) in cholesta-7,9-dien-3β-ol forms a dihedral angle of close to 0°, contributing two CC increments to the C(9) resonance, and the 60° C(8)–C(9)–C(10)–C(19) fragment accounts for the third CC parameter (item 9/**19**). In spite of obvious conformational problems in the olefin series the experimental values reflect this downfield shift with increasing number of HC and CC interactions.

The β parameter is added to the resonances of carbons adjacent to C=C double bonds, with the exception of quaternary or other sp^2 carbons. For example, the β parameter is included in the calculation of the C(2) and C(7), but not the C(4), C(5), or C(10) resonances in cholesta-3,5-diene (items 2/**20**–10/**20**). The γ_s and γ_a increments are also not used for quaternary and sp^2 carbons. For example, a γ_s contribution is added to the tertiary C(9), but not to the quaternary C(8) resonance in β-amyrin (items 8/**29** and 9/**29**). The two *anti* positions are treated as being equivalent. For example, the geometric relation of C(19) relative to the double bond in lanost-9-en-3β-ol is essentially equivalent to the orientation of C(5) or C(7) relative to the same bond. C(7) and C(19) are therefore taken to receive the same γ_a contributions (items 7/**25** and 19/**25**).

The data bases for the substituent parameters require some comments. The assignments in Table 7 are based on off-resonance decoupling, relaxation and shift reagent experiments, and on comparison with related compounds. Our assignments for lanost-8(9)-en-3β-ol and lanost-9-en-3β-ol differ from those in ref. 17 by the interchange C(7) → C(16), C(12) → C(7), and C(16) → C(12). Our β-amyrin assignments agree with ref. 17 and ref. 23 (according to our own results and those in ref. 24, the C(8) shift for β-amyrin in ref. 17 is in error by 1 ppm).

The C(3) and C(4) resonances of cholesta-3,5-diene in ref. 15 are interchanged (items 3/**20** and 4/**20** in Table 5). C(3) is neither engaged in HC or CC *gauche* interactions, nor is the parameter R required. Its predicted shift is therefore equal to the tertiary sp^2 carbon reference of 126.0 ppm, and the 124.6 ppm band, rather than the 129.9 ppm signal, is assigned to C(3).

The assignment of C(4) and C(7) of hydroxydesoxycholic acid in ref. 16 is also interchanged (items 4/**22** and 7/**22** in Table 2). Introduction of an equatorial hydroxyl group at position 6 in steroids with *cis* A/B ring junctions causes the

TABLE 7. ^{13}C chemical shifts for some tetra- and pentacyclic triterpenoids[a,b]

	Compounds[c]					
Carbon	**24**	**25**	**27**	**29**	**30**	**31**
1	35.6	36.2	36.0	38.6	38.9	22.3
2	27.7	28.3*	34.5	27.2	27.4	42.2
3	79.0	79.0	217.6	78.9	78.9	213.0
4	38.9	39.2	47.2	38.7	38.9	58.2
5	50.4	52.6	51.2	55.1	55.5	41.5
6	19.1	22.3	19.4	18.4	18.2	41.3
7	26.5	28.1*	26.3	32.6	34.6	18.3
8	134.4	41.9	133.1	39.7	40.7	53.1
9	134.4	148.2	135.3	47.6	51.2	37.5
10	37.0	39.5	36.8	36.9	37.3	59.5
11	21.0	115.0	21.0	23.5	21.1	35.6
12	31.0	37.3	30.8	121.7	26.2	30.5
13	44.5	44.4	44.4	145.1	38.4	39.7
14	49.8	47.1	49.8	41.6	43.3	38.3
15	30.8	34.0	30.8	26.1	27.4	32.5
16	28.2	28.2*	28.1	26.9	37.7	36.0
17	50.5	51.1	50.5	32.4	34.3	30.0
18	15.8	14.5	15.8	47.1	142.7	42.8
19	18.3	21.5	18.6	46.8	129.7	35.4
20	36.5	36.2	36.4	31.0	32.3	28.2
21	18.7	18.6	18.6	34.7	33.3	39.3
22	36.5	36.6	36.4	37.1	37.3	32.8
23	24.1	24.2	24.0	28.0	15.4	6.9
24	39.5	39.6	39.4	15.6	27.9	14.7
25	28.0	28.1*	27.9	15.6	16.7	18.0
26	22.5	22.6	22.5	16.7	16.1	18.7
27	22.8	22.9	22.7	26.1	14.6	20.3
28	24.3	18.6	24.2	28.4	25.2	32.1
29	27.9	27.9*	26.1	33.3	31.3	31.8
30	15.4	15.7	21.2	23.6	32.3	35.0

[a]The spectra were recorded on a Bruker HX 90 FT nmr spectrometer, with 0.1 *M* solutions in $CDCl_3$. The chemical shifts are given in ppm relative to internal TMS.
[b]Entries marked with * may be interchanged.
[c]For chemical structures, see Chart 1.

following changes at C(4) and C(7). At C(4) the HC interaction between C(4)—H(4β) and C(6)—H(6α) is eliminated and one *gauche* γ-hydroxyl interaction is introduced, for a substituent effect of $-4.55 + (-1.28) = -5.8$ ppm. At C(7) two HO interactions are introduced for

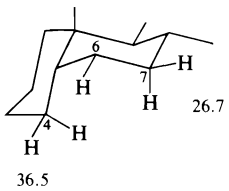

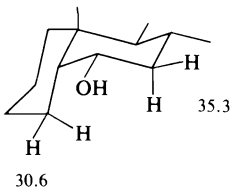

a substituent effect of $2 \times 4.41 = 8.8$ ppm. Therefore the signal at 30.6 ppm is assigned to C(4) and the 35.3 ppm band to C(7).

Finally, the assignment of C(9) and C(14) of 7-cholestanone in ref. 19 is interchanged (items 9/**55** and 14/**55** in Table 4). Introduction of the carbonyl group at C(7) eliminates the HC interaction between C(9)—H and C(7)—H(7α) and introduces an *anti* γ-carbonyl shift, for a substituent effect of $-4.55 + 5.16 = +1.6$ ppm. At C(14) the HC interaction between C(14)—H and C(7)—H(7α) disappears, but here a *gauche* γ-carbonyl interaction is added, for a substituent shift of $-4.55 + (-0.22) = -4.8$ ppm. There-

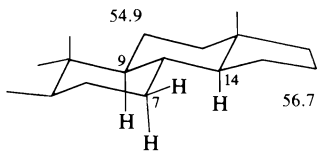

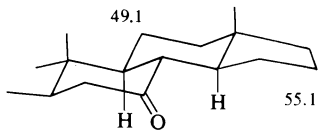

fore the 55.1 ppm band is due to C(9), and the 49.1 ppm signal is assigned to C(14).

Discussion

In the diamond lattice all α- and all β-positions, relative to any given lattice point, are equivalent. There are two nonequivalent γ- and four nonequivalent δ-positions, etc. The simplest possible parameter set for the derivation of ^{13}C resonances in saturated hydrocarbons would therefore consist of one reference value, one α-, one β-, two γ-, four δ-parameters, etc. Such a parameter set is insufficient for several reasons. Firstly, α-substituent effects are not additive. Thus, the shift increments caused by the successive replacement of the methane hydrogens by methyl groups are not constant. The simplest parameter modification to allow for this lack of additivity is the replacement of the one reference and one α-parameter by four separate reference values for primary, secondary, tertiary, and quaternary carbons. Secondly, the β-substituent effect depends on the α-substitution pattern at the carbon under observation. The simplest parameter modification to allow for this interdependence is the replacement of the one β-parameter by two parameters associated with hydrogen–carbon and carbon–carbon *gauche* interactions. Thirdly, the shifts observed upon replacement of a directly bonded hydrogen by an α-carbon, an α-hydrogen by a β-carbon, a β-hydrogen by a γ-carbon, a γ-hydrogen by a δ-carbon, etc., are in principle differences between shifts associated with the incoming group and increments associated with the eliminated hydrogen. The distinction between the two contributions is obviously important for an understanding of the relation between chemical structure and ^{13}C resonances. However, this question is particularly difficult to resolve since two steps, namely the removal of a hydrogen and the insertion of a methyl group, give rise to only one observation. An investigation of shielding in ketones and olefins led us to believe that the shift caused by the replacement of a β-hydrogen by a *gauche* γ-methyl group is essentially entirely due to the removal of the β-hydrogen (3). If the second step, the introduction of the *gauche* γ-methyl group, is of no consequence, it follows that the shift due to the replacement of a γ-hydrogen by a *syn*-axial δ-methyl group is associated with the δ-methyl group and not with the removal of the γ-hydrogen. The effect of removal of directly bonded and α-hydrogens on the observed α- and β-carbon shifts has not been investigated yet, but will undoubtedly become of considerable importance for an understanding of the conformational dependence of ^{13}C resonances.

In alcohols, amines, ketones, and olefins, polar and double bond effects create further complications. These contributions are equally difficult to resolve since they again increase the number of parameters without increasing the number of observations. Furthermore, polar and double bond substituents are more likely to cause substantial conformational changes, which in turn may lead to complex changes in chemical shifts. Thus, some of the parameters in Table 6 presumably represent combinations of (de)-shielding effects.

In the alcohol series the β-parameters HO and CO very likely contain polar shift contributions which are impossible to extract at this level of approximation. The *anti* γ-hydroxyl parameter is almost certainly a function of conformation. It seems that only equatorial hydroxyl groups cause upfield shifts at *anti* γ-carbons, whereas axial and bridgehead substituents give rise to downfield shifts (3). Since bridgehead substituents are least likely to cause conformational changes, for reasons of symmetry, the *anti* γ-shift in bicyclic compounds would be expected to correspond most closely to the genuine substituent effect, i.e. the *anti* γ-effect is probably positive. However, the antiperiplanar $^{0}C–C_{\alpha}–C_{\beta}–O_{\gamma}$ arrangement occurs most frequently in equatorially substituted rings, since there are always two ring carbons in an *anti* orientation. Therefore, a negative *anti* γ-hydroxyl parameter is required for most predictive purposes. All examples of *anti* γ-hydroxyl shifts in Table 2 occur in equatorially substituted rings. The γ_a parameter was found to be close to the γ_g value and the *gauche* and *anti* γ-hydroxyl parameters were combined to a general γ-hydroxyl parameter. It was noted (6) that the *anti* γ-hydroxyl shift is positive in tertiary hydroxides. However, axial hydroxyl groups in the secondary 1α- and 12α-hydroxysteroids also shift the methyl carbon resonances downfield (12).

The β-nitrogen parameters HN and CN, like the HO and CO parameters, presumably contain polar shift contributions. One would expect

different HN parameters for secondary and tertiary amines, since 1,3-diaxial hydrogen alignment is only possible in secondary amines. However separate analyses of chemical shifts for

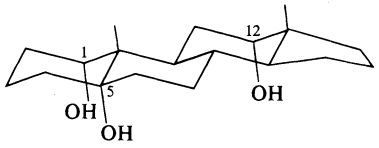

1α—OH	C(19)	+0.6 ppm
5α—OH	C(19)	+3.9 ppm
12α—OH	C(18)	+1.1 ppm

secondary and tertiary amines did not lead to significantly different HN parameters, and therefore no distinction between hydrogen–hydrogen and hydrogen–lone pair alignments is made in the present scheme. The expected parameter difference is possibly obscured by conformational effects. The HNC parameter has the following origin. If C(5) in 10-methyl-*trans*-decalin is replaced by nitrogen, the methyl carbon resonance is shifted upfield from 15.8 ppm (9) to 10.1 ppm (20). One might have

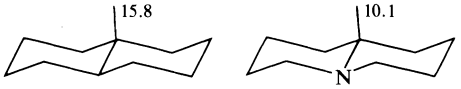

expected the insertion of the more electronegative nitrogen to deshield the angular methyl carbon. In other words, the magnitude of this shielding effect, whatever its origin, should exceed the observed upfield shift by the size of any dipolar nitrogen substituent effect. It is tentatively assumed that such a shielding effect arises whenever a ^{0}C—H bond is aligned with an N_β—C_γ bond.

The γ-carbonyl parameters are open to a number of interpretations. For example, it is possible that the carbonyl group only causes a downfield shift at the *anti*, but not at the *gauche* γ-position. It is equally possible that the keto group causes a general downfield shift at both *gauche* and *anti* γ-positions, of the order of magnitude of the γ_a parameter, and that an additional shielding mechanism in the *gauche* configuration cancels this general γ-effect. A distinction between these different interpretations is not possible at this moment.

The most striking observation in the olefin series is the apparent insensitivity of quaternary carbon resonances to the presence of β- or γ-double bonds. It is possible to find some dependence of quaternary carbon resonances on γ-double bond orientation, within a series of isomeric olefins (3). However, an examination of a larger number of olefins, and particularly the resonances of carbons adjacent to C=C bonds, suggests that, to a first approximation, quaternary carbon resonances may be assumed to be unaffected by the presence of olefinic double bonds. A plausible explanation for this observation might be that the double bond does not affect carbon nuclei directly, but rather C—H bonds. In other words, β-and γ-olefin substituent effects seem to depend on the presence and orientation of ^{0}C—H bonds relative to the C=C group.

Conformational effects have been invoked a number of times in the discussion, and there is little doubt that conformational changes influence chemical shifts. However, it is obviously difficult to demonstrate that a given substituent effect is conformational in origin. Nevertheless, there is an important difference between a (de)shielding substituent effect and a conformational substituent effect which in turn modifies other (de)shielding mechanisms. The analysis of conformational effects on carbon resonances requires the development of substituent parameters which are explicit functions of internal coordinates such as dihedral angles. Conformational effects will then be expressed by modifications of these (de)shielding parameters, and parameters which only represent conformational effects will disappear.

Acknowledgments

Generous financial support by the National Research Council of Canada is gratefully acknowledged.

1. H. Beierbeck and J. K. Saunders, Can. J. Chem. **53**, 1307 (1975).
2. H. Beierbeck and J. K. Saunders. Can. J. Chem. **54**, 632 (1976).
3. H. Beierbeck and J. K. Saunders. Can. J. Chem. **54**, 2985 (1976).
4. H. Boaz. Tetrahedron Lett. 55 (1973).
5. J. B. Stothers. Carbon-13 NMR spectroscopy. Academic Press, New York, NY. 1972.
6. W. A. Ayer, L. M. Browne, S. Fung, and J. B. Stothers. Can. J. Chem. **54**, 3272 (1976).
7. R. G. Parker and J. D. Roberts. J. Am. Chem. Soc. **92**, 743 (1970), quoted in ref. 5.

8. F. J. WEIGERT and J. D. ROBERTS. J. Am. Chem. Soc. **92**, 1347 (1970), quoted in ref. 5.
9. D. K. DALLING, D. M. GRANT, and E. G. PAUL. J. Am. Chem. Soc. **95**, 3718 (1973).
10. D. K. DALLING and D. M. GRANT. J. Am. Chem. Soc. **96**, 1827 (1974).
11. E. WENKERT and B. L. BUCKWALTER. J. Am. Chem. Soc. **94**, 4367 (1972).
12. H. EGGERT, C. L. VAN ANTWERP, N. S. BHACCA, and C. DJERASSI. J. Org. Chem. **41**, 71 (1976).
13. J. W. APSIMON, H. BEIERBECK, and J. K. SAUNDERS. Can. J. Chem. **51**, 3874 (1973).
14. R. J. ABRAHAM and J. R. MONASTERIOS. J. Chem. Soc. Perkin Trans. II, 662 (1974).
15. H. J. REICH, M. JAUTELAT, M. T. MESSE, F. J. WEIGERT, and J. D. ROBERTS. J. Am. Chem. Soc. **91**, 7445 (1969), quoted in ref. 5.
16. D. LEIBFRITZ and J. D. ROBERTS. J. Am. Chem. Soc. **95**, 4996 (1973).
17. S. A. KNIGHT. Org. Magn. Reson. **6**, 603 (1974).
18. S. H. GROVER and J. B. STOTHERS. Can. J. Chem. **52**, 870 (1974).
19. H. EGGERT and C. DJERASSI. J. Org. Chem. **38**, 3788 (1973).
20. R. T. LALONDE and T. N. DONVITO. Can. J. Chem. **52**, 3778 (1974).
21. E. L. ELIEL and F. W. VIERHAPPER. J. Org. Chem. **41**, 199 (1976).
22. H. BOOTH, D. V. GRIFFITHS, and M. L. JOSEFOWICZ. J. Chem. Soc. Perkin Trans. II, 751 (1976).
23. S. SEO, Y. TOMITA, and K. TORI. J. Chem. Soc. Chem. Commun. 954 (1975).
24. K. TORI, S. SEO, A. SHIMAOKA, and Y. TOMITA. Tetrahedron Lett. 4227 (1974).

Etude en résonance magnétique nucléaire du ^{13}C des paramètres de substitution de la fonction azide

A. PANCRAZI, I. KABORÉ, B. DELPECH, A. ASTIER, Q. KHUONG-HUU ET G. LUKACS

Institut de Chimie des Substances Naturelles du C.N.R.S., 91190 Gif/Yvette, France

Reçu le 16 février 1977

A. PANCRAZI, I. KABORÉ, B. DELPECH, A. ASTIER, Q. KHUONG-HUU et G. LUKACS. Can. J. Chem. **55**, 2829 (1977).

En rmn du ^{13}C, les différents effets-α, β, γ et δ de 16 azido-stéroïdes ont été mesurés. Les effets-α ont été évalués à 33.6 et 31.2 ppm pour des azides cyclohexaniques de configurations bloquées, équatoriale et axiale. Les effets-γ ainsi que les effets-δ ont des amplitudes voisines de ceux des groupes OH et NH_2. Par contre, l'effet-β des azides est sensiblement plus faible que celui des hydroxyles ou amines, son amplitude étant atténuée par un effet-γ du second atome d'azote de l'azide; cet effet-γ supplémentaire est fonction de la disposition spatiale de la liaison Cβ—H et du groupe azide.

A. PANCRAZI, I. KABORÉ, B. DELPECH, A. ASTIER, Q. KHUONG-HUU, and G. LUKACS. Can. J. Chem. **55**, 2829 (1977).

The various effects (α, β, γ and δ) on the ^{13}C nmr of azido steroids have been measured. For cyclohexane azides constrained to equatorial and axial configurations, the α-effects were determined to be 33.6 and 31.2 ppm. Both γ- and δ-effects have magnitudes near those for OH and NH_2 groups. On the other hand, the β-effect of the azides is slightly smaller than those of hydroxyls or amines as its magnitude is reduced by a γ-effect of the second nitrogen atom of the azide group. This additional γ-effect is a function of the spatial arrangement of the Cβ—H bond with respect to the azide group.

[Journal translation]

Les composés qui possèdent une fonction azide constituent des intermédiaires importants du point de vue de la synthèse de produits naturels complexes (amino-sucres, amino-stéroïdes et alcaloïdes). La rmn du ^{13}C est une technique de choix pour l'étude structurale de ces composés; cette méthode nécessitant une bonne connaissance des différents effets de type α, β, γ et δ de la fonction azide, nous avons entrepris une étude systématique d'un certain nombre d'azido-stéroïdes antérieurement synthétisés (1)[1].

Résultats et discussion

Azides saturés

Les déplacements chimiques en rmn du ^{13}C des azido-stéroïdes de **1** à **10** sont indiqués dans le tableau 1. L'attribution des signaux a été effectuée selon les règles générales de la rmn du ^{13}C (2), appuyée par des expériences de découplage partiel; l'interprétation des résultats est obtenue également par comparaison avec les spectres de modèles bien connus: androstane-5α (3*b*, 4), cholestane-5α (3*a*, 5), cholestane-5β (4, 6) et hydroxy-5α et -5β pregnane (7).

L'examen du tableau 1 permet de dégager les conclusions suivantes.

(*A*) L'effet-α d'un azide équatorial (**1** α = +33.5 ppm) est plus important que celui d'un azide axial (**2**, α = +31.1 ppm) (cf. tableau 1); la différence entre les deux effets $\Delta(\delta\alpha(\text{eq.}) - \delta\alpha(\text{ax})) = 2.4$ ppm semble être toutefois légèrement inférieure à celle observée dans le cas des alcools $\Delta(\delta\alpha(\text{eq.}) - \delta\alpha(\text{ax.})) = 4.6$ ppm (3, 5).

Il est à remarquer dans le cas de l'azido-6β pregnane-5α, **10**, un effet-α de 34.3 ppm relativement important pour un azide axial, ce qui est à rapprocher de l'effet-α d'un groupe hydroxyle en 6β (3*b*), également au dessus de la valeur attendue pour une fonction alcool axiale, ce qui doit être en rapport avec un changement de géométrie de la molécule.

En ce qui concerne les azides-17α et 17β, **5** et **6**, l'effet-α est pratiquement identique pour les deux épimères (31.2 et 30.9 ppm respectivement) alors que pour les deux hydroxy-17α et -17β la différence entre les deux effets-α est de 2 ppm environ (3b).

En position tertiaire les effets-α des azides

[1]Aussi, I. Kaboré, Q. Khuong-Huu et A. Pancrazi, résultats non publiés.

TABLEAU 1. Déplacements chimiques en rmn du ^{13}C d'azido-stéroïdes*

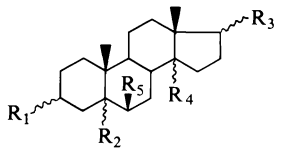

1 $R_1 = \blacktriangleleft N_3, R_2 = \cdots H, R_3 = \blacktriangleleft C_2H_5, R_4 = \cdots H, R_5 = H$
2 $R_1 = \cdots N_3, R_2 = \cdots H, R_3 = \blacktriangleleft C_2H_5, R_4 = \cdots H, R_5 = H$
3 $R_1 = H, R_2 = \blacktriangleleft N_3, R_3 = \blacktriangleleft C_2H_5, R_4 = \cdots H, R_5 = H$
4 $R_1 = H, R_2 = \cdots N_3, R_3 = \blacktriangleleft C_2H_5, R_4 = \cdots H, R_5 = H$
5 $R_1 = H, R_2 = \cdots H, R_3 = \blacktriangleleft N_3, R_4 = \cdots H, R_5 = H$
6 $R_1 = H, R_2 = \cdots H, R_3 = \cdots N_3, R_4 = \cdots H, R_5 = H$

7 $R_1 = H, R_2 = \cdots H, R_3 =$  $, R_4 = \cdots H, R_5 = H$
(20*R*)

8 $R_1 = H, R_2 = \cdots H, R_3 =$  $, R_4 = \cdots H, R_5 = H$
(20*S*)

9 $R_1 = H, R_2 = \cdots H, R_3 = H, R_4 = \blacktriangleleft N_3, R_5 = H$
10 $R_1 = H, R_2 = \cdots H, R_3 = \blacktriangleleft C_2H_5, R_4 = \cdots H, R_5 = N_3$

	1 N_3–3β	**2** N_3–3α	**3** N_3–5β	**4** N_3–5α	**5** N_3–17β	**6** N_3–17α	**7** N_3–20(*R*)	**8** N_3–20(*S*)	**9** N_3–14β	**10** N_3–6β
C-1	37.2	32.9	31.8	31.5	38.7	38.8	38.6	38.6[a]	38.9	40.4[a]
C-2	27.6	25.6	20.8	20.7	22.2	22.2	22.2	22.1	22.0	22.0
C-3	60.4	58.0	22.1	22.1	26.9	26.8	26.8[a]	26.7	26.8	26.9[b]
C-4	34.0	32.6	29.1	30.7[a]	29.1	29.1	29.0	28.9	28.9	26.7[b]
C-5	45.3	40.0	67.7	69.3	47.1	47.0	47.0	46.9	46.8	49.5
C-6	28.6	28.3	31.8	30.6[a]	29.1	29.1	29.0	28.9	28.9	63.5
C-7	32.0	32.0	28.3	26.8	31.8	32.4	32.2	32.0	28.9	36.5
C-8	35.4	35.4	34.9	34.7	35.7	35.9	35.4	35.2	39.4	30.9
C-9	54.6	54.5	43.2	46.5	54.9	54.4	54.7	54.6	49.9	54.8
C-10	35.4	35.9	39.8	38.7	36.4	36.4	36.2	36.1	36.7	36.5
C-11	21.0	20.5	20.2	20.7	20.4	20.3	20.6	20.6	20.3	20.4
C-12	38.0	38.0	38.0	37.9	37.4	32.8	38.6	39.2[a]	36.0	37.9[a]
C-13	42.1	42.0	42.0	42.1	44.5	45.9	42.5	42.0	46.6	42.2
C-14	55.8	55.8	55.9	55.5	52.4	49.7	55.9[b]	56.3[b]	79.4	55.5
C-15	24.5	24.5	24.5	24.3	23.5	24.6	24.3	24.0	28.7	24.5
C-16	28.1	28.1	28.2	28.0	26.9	28.6	26.5[a]	26.7	18.9	28.1
C-17	52.9	52.9	52.9	52.8	71.4	71.7	55.2[b]	56.0[b]	39.4	53.0
C-18	13.3[a]	13.3[a]	13.3[a]	13.3[b]	12.2	17.7	12.2	12.2	19.6	13.3[c]
C-19	12.6	11.6	18.0	15.4	12.2	12.2	12.2	12.2	12.2	15.0
C-20	23.0	23.0	23.1	23.0	—	—	58.9	60.8	—	23.0
C-21	12.2[a]	12.6[a]	12.4[a]	12.6[b]	—	—	18.8	19.5	—	12.6[c]

*[a], [b], [c], les attributions à l'intérieur d'une colonne verticale peuvent être inversées.

5α, **4** et 5β, **3** sur le carbone quaternaire C-5 sont respectivement de 22.6 et 24.4 ppm donc considérablement atténués par rapport aux azides secondaires ou primaires; dans le cas des hydroxy-5α et -5β prégnanes (7), ces effets sont également très atténués (26.0 et 29.9 ppm respectivement).

Pour les azides aliphatiques comme les azido-20(*R*), **7**, et -20(*S*) prégnane **8**, on observe des effets de 35.9 et 37.8 ppm; il semble donc que l'effet-α soit plus important en série aliphatique qu'en série alicyclique.

(*B*) L'effet-β dû à un groupe azide est en général nettement plus faible que celui dû à une fonction alcool ou amine de stéréochimie identique. Cette observation s'explique aisément en considérant que l'effet-β dû à l'azote fixé au site de substitution est atténué par un effet-γ dont l'origine est l'azote central de l'azide.

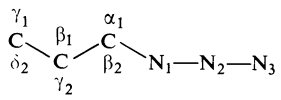

En série équatoriale, cet effet-β est de 4.9 à 5.4 ppm et d'environ 2.5 à 3.5 ppm en série axiale (cf. tableau 2).

La différence $\Delta(\delta\beta_{OH} - \delta\beta_{N_3})$ est de 3.9 à 4.2 ppm pour une substitution équatoriale et de 3.2 à 3.4 ppm en série axiale, ceci apparaissant comme constant dans tous les modèles étudiés.

Néanmoins, dans certains cas très particuliers, l'effet-γ supplémentaire de l'azote central est inexistant, l'effet-β observé se trouve alors voisin et même parfois supérieur à l'effet-β de l'hydroxyle de stéréochimie identique.

C'est ainsi que, pour l'azide-6β, **10**, l'effet sur le C-7 est de 4.3 ppm, soit un $\Delta(\delta\beta_{OH} - \delta\beta_{N_3}) = 3.1$ ppm, ce qui est attendu pour une substitution axiale, mais en C-5, l'effet-β de l'azide est de 2.5 ppm, ce qui correspond à un $\Delta(\delta\beta_{OH} - \delta\beta_{N_3})$ de 0.2 ppm.

De la même façon, pour les azido-17α et -17β androstane-5α, **5** et **6**, la différence $\Delta(\delta\beta_{OH} - \delta\beta_{N_3})$ au niveau du C-16 est de 3.7 et 3.9 ppm respectivement, donc en accord avec les valeurs attendues, mais pour le C-13 le $\Delta(\delta\beta_{OH} - \delta\beta_{N_3})$ est de −1.4 et −0.6 ppm respectivement, ce qui conduit à admettre un effet-β plus important pour l'azide que pour l'hydroxyle.

Au niveau des azides tertiaires-5α et -5β

TABLEAU 2. Effects de substitution des azides $\delta_{N_3} - \delta_H$ (ppm)

Composés	Effets α	β	γ	δ
Azides aliphatiques				
Hexylazide	+37.8	+3.7	−2.9	−0.3
N_3-20(*R*) **7**	+35.9	C-17 +2.3; C-21 +6.6	C-16 −1.6; C-13 +0.4	C-18 +1.1; C-14 +0.1; C-15 −0.2
N_3-20(*S*) **8**	+37.8	C-17 +3.1; C-21 +7.3	C-16 −1.4; C-13 −0.1	C-18 +1.1; C-14 +0.5; C-15 −0.5
Azides alicycliques				
N_3-17β **5**	+30.9	C-13 +3.7; C-16 +6.4	C-15 −2; C-14 −2.3; C-18 −5.4; C-12 −1.6	C-8 −0.3; C-11 −0.5
N_3-17α **6**	+31.2	C-13 +5.1; C-16 +8.1	C-15 −0.9 C-14 −5; C-18 +0.1; C-12 −5.2	C-8 −0.1; C-11 −0.6
N_3-3β **1**	+33.6	C-2 +5.4; C-4 +4.9	C-1 −1.4; C-5 −1.7	C-10 −0.8; C-6 −0.5
N_3-3α **2**	+31.2	C-2 +3.4; C-4 +3.5	C-1 −5.6; C-5 −7	C-10 −0.3; C-6 −0.7
N_3-6β **10**	+34.5	C-5 +2.5; C-7 +4.3	C-4 −2.3; C-10 +0.3; C-8 −4.5	C-3 +0.1; C-9 +0.1; C-19 +2.8; C-1 +1.8
N_3-5α **4**	+22.6	C-4 +1.7; C-6 +1.6; C-10 +2.6	C-1 −7.1; C-3 −4.7; C-7 −5.4 C-9 −8.2; C-19 +3.2	C-2 −0.5; C-8 −0.7
N_3-5β **3**	+24.4	C-4 +1.6; C-6 +4.6; C-10 +4.5	C-1 −5.7; C-3 −5; C-7 +1.8 C-9 +2.9; C-19 −6	C-2 −0.5; C-8 −0.9

TABLEAU 3. Effets de substitution des azides $\Delta(\delta\beta_{OH} - \delta\beta_{N_3})$

Composés	$\Delta(\delta\beta_{OH} - \delta\beta_{N_3})$ ppm		
N_3-3β **1**	(C-2)(*A*) +3.9	(C-4)(*A*) +4.2	
N_3-3α **2**	(C-2) (*A*) +3.4	(C-4)(*A*) +3.2	
N_3-5β **3**	(C-4)(*A*) +3.5	(C-6)(*A*) +3.7	(C-10)(*D*) +0.6
N_3-5α **4**	(C-4)(*A*) +3.5	(C-6)(*A*) +3.8	(C-10)(*D*) +0.4
N_3-17β **5**	(C-16)(*A*) +3.7	(C-13)(*D*) −1.4	
N_3-17α **6**	(C-16)(*A*) +3.9	(C-13)(*D*) −0.6	
N_3-14β **9**	(C-8)(*B*) +1.9	(C-15)(*A*) +4.2	(C-13)(*D*) −1.6
N_3-6β **10**	(C-5)(*C*) +0.2	(C-7)(*A*) +3.1	

prégnanes **4** et **3**, les effets observés en C-4 et C-6 ont des valeurs attendues (tableau 3) mais en C-10, les valeurs de $\Delta(\delta\beta_{OH} - \delta\beta_{N_3})$ sont respectivement de 0.4 et 0.6 ppm.

Compte-tenu que d'un point de vue purement stérique, l'enchaînement des atomes d'azote de l'azide doit être dirigé vers l'extérieur du reste stéroïdique, donc de façon "*exo*", (8), des conformations privilégiées de l'azide sont à envisager. A l'examen des modèles moléculaires et des projections de Newman, les faits suivants apparaissent le long des différents axes Cα–Cβ.

Lorsque le carbone-β possède un atome d'hydrogène tel que la liaison C-β—H se trouve parallèle à la liaison N_1—N_2, l'effet-γ supplémentaire de l'azote central est maximum (situation *A*); cet effet peut être apparenté à un effet-γ d'origine stérique; cette situation est déterminée par les conformations privilégiées du groupe azide, par rapport au stéroïde, qui imposent essentiellement un enchaînement des trois atomes d'azote dérivé vers l'extérieur du stéroïde, donc de façon '*exo*' (8).

C'est ainsi que dans le cas ou il existe un hydrogène sur le carbone-β, et que les conformations privilégiées du groupe azide ne permettent pas que les liaisons Cβ—H et N_1—N_2 soient parallèles (situation *B*: azido-14β **9** C-14 → C-8), l'effet-γ supplémentaire observé est d'amplitude plus faible que dans la situation A ($\Delta(\delta\beta_{OH} - \delta\beta_{N_3}) = 1.9$ en C-8).

Pour les autres situations dans lesquelles le carbone-β présente un atome d'hydrogène antipériplanaire à l'azide (situation *C*), ou que le carbone-β ne présente aucun atome d'hydrogène (situation *D*), l'effet-γ supplémentaire ne s'exerce plus; ceci est tout à fait comparable à l'interprétation des effets stériques de type δ, le remplacement d'une liaison Cγ—H par une liaison Cγ—Cδ ayant pour conséquence de supprimer l'effet de blindage sur le carbone-γ (9).

Dans les situations *A* et *D*, le nombre d'exemple présenté est suffisamment important pour l'interprétation du phénomène; par contre, pour les situations *C* et *B* notre explication ne repose que sur un seul cas et doit donc être confirmée par l'analyse spectrale d'autres composés.

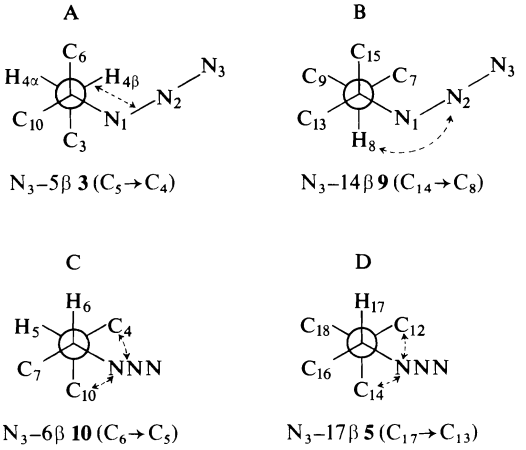

(*C*) L'effet-γ de type 1–3 diaxial de la fonction azide est tout à fait comparable à celui d'un groupe hydroxyle ou amine, les faibles variations observées devant être attribuées à des modifications mineures de la géométrie de la molécule; l'effet-γ antipériplanaire (10) (−1.5 à −2 ppm) est également observé dans nos exemples et possède la même amplitude que pour les alcools (3*b*).

Un nouvel effet-γ antipériplanaire provoqué par un groupement X en position tertiaire a été récemment observé par Stothers et ses collaborateurs (11); cet effet déblinde le C-19 de +3.2 ppm dans le cas de l'azide-5α, **4** et pour l'azide-5β, **3**, un déblindage des C-7

TABLEAU 4. Déplacements chimiques* en rmn du ^{13}C d'azides allyliques

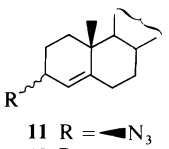

11 R = ◄N_3
12 R = ◄NH_2
13 R = ····N_3
14 R = ····NH_2

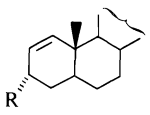

15 R = N_3
16 R = NH_2

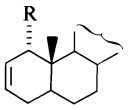

17 R = N_3
18 R = NH_2

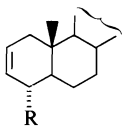

19 R = N_3
20 R = NH_2

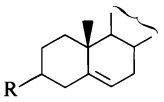

21 R = ◄N_3
22 R = ····N_3

	11	12	13	14	15	16	17	18	19	20	21	22
C-1	36.2	36.3	32.6	31.8	140.3	137.8	62.3	52.8	39.3	39.6	38.3	33.8
C-2	25.6	28.1	25.6	26.8	123.4	128.2	122.2	127.2	130.3	131.3	28.1	26.2
C-3	58.7	48.4	55.6	45.6	58.8	54.9	132.6	130.0	124.3	126.1	61.2	58.2
C-4	118.1	122.2	115.2	120.0	31.4	31.5	30.7	30.9	62.5	51.3	38.0	36.1
C-5	150.5	147.6	153.0	149.4	43.7	45.0	35.6	34.2	47.0	50.9	139.9	138.1
C-6	33.7	33.2	33.3	33.0	28.1	28.8	28.6	28.8	25.2	24.7	122.6	123.2
C-7	32.8	32.4	32.6	32.5	31.9	32.2	31.5	31.7	31.4	31.4	31.9	31.9
C-8	35.9	35.9	35.9	35.9	35.6	35.5	35.6	35.7	35.4	35.3	31.9	31.9
C-9	55.3	55.0	54.7	54.0	51.7	51.6	47.8	47.2	54.2	54.3	50.7	50.5
C-10	38.2	38.0	37.9	38.0	38.0	35.5	39.5	38.5	36.4	35.9	36.8	37.2
C-19	19.1	19.2	18.4	18.8	15.7	12.5	12.1	12.6	12.4	12.5	19.3	19.0

*Les déplacements chimiques des carbones de C-11 à C-18 et de C-20 et C-21 sont en accord avec des valeurs attendues pour un squelette non substitué.

et C-9 de 1.8 et 2.9 ppm[2] est observé; cet effet est général et son amplitude varie entre les groupes —CH_3, —OH, —NH_2 et —N_3.

Il a été vérifié sur d'autres exemples la validité de l'effet observé par Stothers.

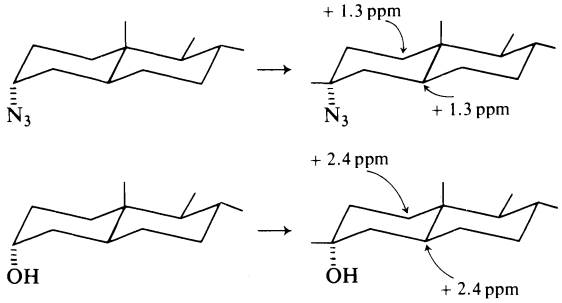

(*D*) Les effets de type-δ définis par Stothers (12) pour les hydroxyles se retrouvent également pour les azides; on notera par exemple un effet-δ_1 (effet stérique de type *syn*-diaxial) de +2.8 ppm sur le C-19 de l'azide-6β, **10** et un δ_2 de +1.8 ppm sur le C-1; pour l'azide 3β, les effets-δ_4 en C-6, δ_5 en C-10 sont de −0.5 ppm et −0.8 ppm; pour l'azide-3α, **2**, l'effet-δ_2 en C-6 est de −0.7 ppm et en C-10 l'effet-δ_3 est d'environ −0.2 ppm.

Azides allyliques et homoallyliques

Pour les azides homoallyliques, les déplacements chimiques sont comparables à ceux des alcools homoallyliques (13), compte-tenu des particularités de la fonction azide, précédemment définies.

Dans le cas d'azides allyliques (cf. tableau 4), on pourra observer pour le carbone-β, éthylénique, un déplacement vers les champs forts, par rapport à l'alcool allylique correspondant (effet-β des azides); par contre, le carbone-γ éthylénique subit un déblindage de 3 à 4 ppm.

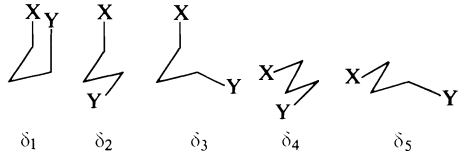

[2]Variation en ppm par rapport au dérivé non substitué X = H.

Cette propriété surprenante des azides stéroïdiques s'observe pour tous les composés étudiés sauf **19**; cette influence due à l'azote central de l'azide est un effet de type-δ de déblindage et pourrait être apparenté à l'effet de "l'acétylation allylique", de direction et de dimension tout à fait comparables (14).

Conclusion

L'effet-β des azides est inférieur à celui des groupes OH et NH_2 et présente une variation $\Delta(\delta\beta_{OH} - \delta\beta_{N_3})$ de 3.9 à 4.2 ppm en série équatoriale et 3.2 à 3.4 ppm en série axiale; ceci est expliqué par l'existence d'un effet-γ supplémentaire dû à l'atome d'azote central de l'azide. Il apparaît sans conteste à l'examen des modèles moléculaires que cet effet-γ supplémentaire n'existe que si le carbone-β considéré possède un hydrogène au voisinage du groupe azide.

1. (*a*) A. Pancrazi et Q. Khuong-Huu. Tetrahedron, **31**, 2041 (1975); (*b*) **30**, 2337 (1974).
2. J. B. Stothers. Carbon-13 NMR spectroscopy. Academic Press, New York, NY. 1972.
3. (*a*) H. Eggert et C. Djerassi. J. Org. Chem. **38**, 3788 (1973); (*b*) H. Eggert, C. L. Van Antwerp, N. S. Bhacca et C. Djerassi. J. Org. Chem. **41**, 71 (1976).
4. B. Balogh, D. M. Wilson et A. L. Burlingame. Nature, **233**, 261 (1971).
5. H. J. Reich, M. Jautelat, M. T. Messe, G. J. Weigert et J. D. Roberts. J. Am. Chem. Soc. **91**, 7445 (1969).
6. D. Leibfritz et J. D. Roberts. J. Am. Chem. Soc. **95**, 4996 (1973).
7. Q. Khuong-Huu, A. Pancrazi et I. Kaboré. Tetrahedron, **30**, 2579 (1974).
8. A. Pancrazi et Q. Khuong-Huu. Tetrahedron, **31**, 2041 (1975); **31**, 2049 (1975).
9. H. Beierbeck et J. K. Saunders. Can. J. Chem. **54**, 2985 (1976).
10. E. L. Eliel, W. F. Bailey, L. D. Kopp, R. L. Willer, D. M. Grant, R. Bertrand, K. A. Christensen, D. K. Dalling, M. W. Duch, E. Wenkert, F. M. Schell et D. W. Cochran. J. Am. Chem. Soc. **97**, 322 (1975).
11. W. A. Ayer, L. M. Browne, S. Fung et J. B. Stothers. Can. J. Chem. **54**; 3272 (1976).
12. (*a*) S. H. Grovers, J. P. Guthrie, J. B. Stothers et C. T. Tan. J. Magn. Reson. **10**, 227 (1973); (*b*) S. H. Grovers et J. B. Stothers. Can. J. Chem. **52**, 870 (1974).
13. E. Wenkert, D. W. Cochran, E. W. Hagaman, F. M. Schell, N. Neuss, A. S. Katner, P. Potier, C. Kan, M. Plat, M. Koch, M. Mehri, J. Poisson, N. Kunesh et Y. Rolland. J. Am. Chem. Soc. **95**, 4990 (1973).
14. E. Wenkert, M. Gasic, E. W. Hagaman et L. D. Kwart. Org. Magn. Reson. **7**, 51 (1975).

Long-range spin–spin coupling constants as an indicator of conformational preferences in ethyl and trifluoroethyl vinyl ethers

TED SCHAEFER AND WILLIAM J. E. PARR[1]

Department of Chemistry, University of Manitoba, Winnipeg, Man., Canada R3T 2N2

Received March 7, 1977

TED SCHAEFER and WILLIAM J. E. PARR. Can. J. Chem. **55**, 2835 (1977).

The observed and calculated, negative, long-range spin–spin coupling constants over five bonds between olefinic and methylene protons in ethyl vinyl ether and in 2,2,2-trifluoroethyl vinyl ether are consistent with predominant *s-cis* planar conformations. The five-bond couplings are sensitive to the proximity of the bonds containing the coupled nuclei and are unobservably small in 1-butene where the H,H distances are somewhat larger than in the ethers. The present results concur with the arguments based on other spectroscopic techniques.

TED SCHAEFER et WILLIAM J. E. PARR. Can. J. Chem. **55**, 2835 (1977).

Les constantes négatives observées et calculées pour les constantes de couplage spin–spin à longue distance à travers cinq liaisons entre les protons oléfiniques et méthyléniques de l'éthoxy-éthylène et du trifluoro-2,2,2 éthoxy-éthylène sont en accord avec des conformations prédominantes *s-cis*-planaires. Les couplages à travers cinq liaisons sont sensibles à la proximité des liens contenant le noyau couplé et sont trop faibles pour être observés dans le butène-1 où les distances H,H sont passablement plus grandes que dans les éthers. Les résultats obtenus dans le présent travail sont en accord avec les arguments basés sur d'autres techniques spectroscopiques.

[Traduit par le journal]

Introduction

The stable conformation of methyl vinyl ether is the *s-cis* form, **1**, defined by a dihedral angle,

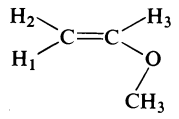

θ(C=C—O—C) = 0°

1

θ, of 0° (1–3). A second, skew, conformation is described by a θ of 90 ± 10°. In the liquid form **1** has a lower enthalpy than the skew form of about 1.5 kcal/mol (3). Consequently **1** is present to about 90% on the assumption that the entropies of the two conformers are equal.

Again, infrared (1, 3) and low resolution microwave (5) data are consistent with a stable form, **2**, for ethyl vinyl ether (EVE) and for

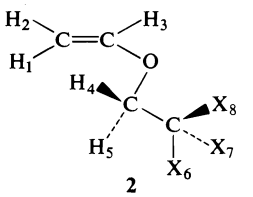

X = H or F
θ(C=C—O—C) = 0°
φ(C—O—C—CX_3) = 180°

2

2,2,2-trifluoroethyl vinyl ether (F_3-EVE). **2** has coplanar carbon and oxygen atoms and is defined by the two dihedral angles, θ and φ, *i.e.* by 0,180. Other plausible conformations would be described by 0,60; 180,180; and 180,0.

The vibrational spectra imply the additional presence of two other conformers for EVE in the liquid and gaseous states (3). Their enthalpies are again higher than that of **2** by about 1.5 kcal/mol (3). It was suggested on the basis of normal frequency calculations that the less stable forms both correspond to θ = 120° and that φ = 120° and 180° distinguishes these two isomers. In any event, the conformer **2** is predominant.

The microwave spectrum of F_3-EVE corresponds to 0,180, *i.e.* form **2**. No other species is observed and therefore the 180,180 conformation can be excluded. The dipole moment and the liquid phase spectra are consistent with this exclusion (4). Any other species in the vapor would be relatively nonpolar, having φ < 90° (5).

In summary, the most stable forms of all three ethers in the liquid and gaseous states are those in which the carbon and oxygen atoms are coplanar and θ = 0°, φ = 180°. In this conformation the C—H bonds of the methylene group in EVE and F_3-EVE are staggered about the O—C= bond. In the proton magnetic resonance spectrum of methyl vinyl ether the proximity of the C—H bonds and the C—H_1

[1]Postdoctoral fellow, 1974–1976.

TABLE 1. Proton chemical shifts[a] and coupling constants[b]

Parameter[c]	$H_2C=C(H_3)(H_1)$ (4)(5) CH_2CH_3			$H_2C=C(H_3)(H_1)$ (4)(5) OCH_2CF_3	
ν_3	631.861(2)			637.898(2)	
ν_2	384.868(3)			413.109(3)	
ν_1	402.650(2)			424.414(3)	
ν_4	363.817(3)			393.768(3)	
ν_5	123.200(3)			—	
^3J_c	6.865(3)			6.666(3)	
^3J_t	14.345(3)			14.157(3)	
^2J_g	−1.851(3)			−2.883(4)	
^3J_v	7.018(2)			8.205(2)	
$^4J^{H,CH_2}$	−0.527(2)	−0.56[d]	0.08[e]	−0.494(3)	−0.68[d]
$^5J_t^{H,CH_2}$	−0.172(4)	−0.14	−0.06	−0.194(4)	−0.14
$^5J_c^{H,CH_2}$	−0.304(3)	−0.28	0.02	−0.301(3)	−0.28
$^5J^{H,CH_3(F)_3}$	0.178(2)	0.67	−0.05	0.723(2)	1.87
$^6J_t^{H,CH_3(F)_3}$	0.165(4)	0.02	0.05	0.151(6)	0.06
$^6J_c^{H,CH_3(F)_3}$	0.149(4)	0.06	−0.03	0.162(4)	0.14
rms error	0.017			0.017	

[a]In Hz at 100 MHz and 305 K to low field of internal tetramethylsilane; 10 mol% solutions in CS_2.
[b]In Hz, numbers in parentheses representing the standard deviations in the last place.
[c]Subscripts *c*, *t*, *g*, and *v* represent *cis*, *trans*, geminal, and vicinal, respectively; subscripts 4 and 5 refer to CH_2 and $CH_3(CF_3)$ groups, respectively.
[d]These are the couplings from Table 2, averaged over the values calculated for protons or fluorine nuclei within the CH_2CH_3 or CH_2CF_3 group for conformation **2** of the text, $\theta = 0°$, $\phi = 180°$.
[e]For $\theta = 120°$, $\phi = 180°$.

bond is thought to account for the relatively large, negative, spin–spin coupling, $^5J_c^{H,CH_1}$, of −0.32 Hz (6). The INDO–MO–FPT calculations of the long-range couplings involving the methyl protons are in semiquantitative agreement (6) with the hypothesis that $^5J_c^{H,CH_1}$ contains a contribution from a direct coupling mechanism arising from interactions between electrons in the orbitals of the C—H bonds containing the coupled nuclei. For the *trans* conformation, $\theta = 180°$, $^5J_c^{H,CH_1}$ is calculated as positive.

It follows that $^5J_c^{H,CH_1}$ should be negative in EVE and in F_3-EVE if the conformer populations based on vibrational and microwave spectroscopy are correct. In this paper, full analyses of the proton magnetic resonance spectra of EVE and F_3-EVE in CS_2 solution are reported. The long-range couplings between the olefinic protons and the protons or fluorine nuclei in the saturated fragments are discussed in terms of the conformational preferences and are compared with the couplings calculated by INDO–MO–FPT.

Experimental

Solutions (10 mol%) of EVE and F_3-EVE in CS_2, containing a small amount of tetramethylsilane, were degassed by the freeze–pump–thaw technique. Proton magnetic resonance spectra were calibrated in the frequency sweep mode on an HA 100 spectrometer at 305K. Double resonance experiments (7, 8) established the relative signs of the coupling constants.

Results and Discussion

Spectral Analysis

The spectra were analyzed with the computer program LAME (9, 10), extended to cope with an 8 spin system. The spectral parameters are given in Table 1. The signs of the coupling constants assume that the vicinal couplings are positive. The standard deviations in the coupling constants imply an accuracy of 0.01 to 0.02 Hz in their magnitudes.

INDO–MO–FPT Calculations (11)

Because of the previous experimental data (3–5) and of the expense of these calculations, the latter were carried out for the $\theta = 0$, $\phi = 180$ conformations of EVE and F_3-EVE; and for one other form of EVE, that described by $\theta = 120$, $\phi = 180$. The calculated long-range coupling constants involving the olefinic protons are given in Table 2. The average values involving the protons of fluorine nuclei within a CH_2, CH_3, or CF_3 group correspond to the observed couplings in Table 1 and are tabulated there. The $\theta = 120$, $\phi = 180$ conformer of EVE is calculated as 0.67 kcal/mol less stable than **2**, in qualitative agreement with the vibrational data (3).

TABLE 2. INDO–MO–FPT coupling constants in ethyl vinyl ether and in 2,2,2-trifluoroethyl vinyl ether

	Value[b]				Value[b]		
	EVE				EVE		
Parameter[a]	θ = 0°	θ = 120°	F_3-EVE	Parameter[a]	θ = 0°	θ = 120°	F_3-EVE
$^5J_{1,4}$	−0.283	0.019	−0.284	$^6J_{2,6}$	0.068	0.190	0.220*
$^5J_{1,5}$	−0.283	0.027	−0.284	$^6J_{2,7}$	−0.003	−0.021	−0.019*
$^6J_{1,6}$	0.120	−0.064	0.318*	$^6J_{2,8}$	−0.003	−0.013	−0.020*
$^6J_{1,7}$	0.031	−0.018	0.065*	$^4J_{3,4}$	−0.555	−0.067	−0.677
$^6J_{1,8}$	0.031	−0.020	0.064*	$^4J_{3,5}$	−0.555	0.234	−0.677
$^5J_{2,4}$	−0.136	−0.003	−0.141	$^5J_{3,6}$	1.614	−0.125	5.354*
$^5J_{2,5}$	−0.136	−0.125	−0.141	$^5J_{3,7}$	0.199	−0.008	0.131*
—	—	—	—	$^5J_{3,8}$	0.200	−0.018	0.132*

[a]For the numbering see structure **2** in the text.
[b]These are proton–proton couplings in Hz, and, if starred, are proton–^{19}F couplings.

The Long-range Couplings to the Methylene Protons

The agreement between observed and calculated $^5J_c^{H,CH_2}$ and $^5J_t^{H,CH_2}$ is satisfactory for **2** (Table 1), the more negative value of $^5J_c^{H,CH_2}$ arising from the proximity of the coupled protons in **2**. In view of the calculated values for θ = 120, φ = 180 and of the previous calculations on methyl vinyl ether, in which negative values of these couplings were obtained only for θ values near 0 (6), it may be concluded that the coupling constant data and the INDO–MO–FPT calculations concur with the other spectroscopic conclusions that **2** is the predominant form for EVE and F_3-EVE in the liquid and gaseous states.

The observed and calculated values of $^4J^{H,CH_2}$ for **2** are in quantitative agreement for EVE but differ by 0.2 Hz for F_3-EVE. For θ = 120, φ = 180 in EVE, $^4J^{H,CH_2}$ is calculated as much larger than that observed.

The Long-range Couplings to Methyl Protons and Fluorine Nuclei

$^5J^{H,CH_3}$ and $^5J^{H,CF_3}$ are considerably smaller than their calculated magnitudes for **2**. The large predicted values can be attributed to the overestimate involving H_6 and F_6 (Table 2), INDO–MO–FPT being known to exaggerate couplings over five bonds in the all-*trans* arrangement (12, 13).

The calculations reproduce the positive signs of $^6J_{c,t}^{H,CH_3}$ and of $^6J_{c,t}^{H,CF_3}$ but underestimate the magnitudes by about 0.1 Hz, except for $^6J_c^{H,CF_3}$.

Comparison with Butene-1

$^5J_c^{H,CH_3}$ and $^5J_t^{H,CH_3}$ are both ±0.02 Hz or less in butene-1 (6), yet the microwave data (14) suggest that **3** is populated to a significant extent. It is interesting to note that INDO–MO–FPT calculations for the microwave geometry of **3** yield a $^5J_c^{H,CH_3}$ of −0.01 Hz. The contrast with

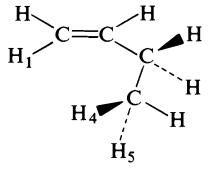

3

the corresponding couplings in **1** and **2** is attributable to the different H_1,H_4 distances. In **3**, the H_1,H_4 distance is 2.4 Å and is less than 2.0 Å in **1** and **2**. The direct interactions (6, 15–18) giving rise to a net negative $^5J_c^{H,CH_3}$ are very sensitive to these distances. The observation and calculation of $^5J_c^{H,CH_3}$ for 1-butene can be taken as a partial corroboration of the conformational deductions based on this coupling for the vinyl ethers.

Acknowledgments

We are grateful to the National Research Council of Canada for financial assistance.

1. N. L. OWEN and N. SHEPPARD. Trans. Faraday Soc. **60**, 634 (1964).
2. N. L. OWEN and H. M. SEIP. Chem. Phys. Lett. **5**, 162 (1970).
3. M. SASKAKIBARA, F. INAGAKI, I. HARADA, and T. SHIMANOUCHI. Bull. Chem. Soc. Jpn. **49**, 46 (1976).
4. S. W. CHARLES, F. C. CULLEN, and N. L. OWEN. J. Chem. Soc. Faraday Trans. II, **70**, 483 (1974).
5. N. S. TRUE and R. K. BOHN. J. Chem. Phys. **62**, 3951 (1975).
6. T. SCHAEFER, H. D. GESSER, and J. B. ROWBOTHAM. Can. J. Chem. **54**, 2235 (1976).

7. J. P. MAHER and D. F. EVANS. Proc. Chem. Soc. 208 (1961).
8. R. FREEMAN and W. A. ANDERSON. J. Chem. Phys. **37**, 2053 (1962).
9. S. CASTELLANO and A. A. BOTHNER-BY. LAOCOON 3. Mellon Institute Publications, Pittsburgh, PA. 1967.
10. C. W. HAIGH and J. M. WILLIAMS. J. Mol. Spectrosc. **32**, 398 (1969).
11. J. A. POPLE, J. W. MCIVER, JR., and N. S. OSTLUND. J. Chem. Phys. **49**, 2960 (1968); **49**, 2965 (1968).
12. R. WASYLISHEN and T. SCHAEFER. Can. J. Chem. **49**, 3216 (1971).
13. J. B. ROWBOTHAM, M. SMITH, and T. SCHAEFER. Can. J. Chem. **53**, 986 (1975).
14. S. KONDO, E. HIROTA, and Y. MORINO. J. Mol. Spectrosc. **28**, 471 (1968).
15. M. BARFIELD and M. KARPLUS. J. Am. Chem. Soc. **91**, 1 (1969).
16. R. E. WASYLISHEN and M. BARFIELD. J. Am. Chem. Soc. **97**, 4545 (1975).
17. T. SCHAEFER, K. CHUM, K. MARAT, and R. E. WASYLISHEN. Can. J. Chem. **54**, 800 (1976).
18. T. SCHAEFER and K. CHUM. Can. J. Chem. **54**, 2231 (1976).

Lichen substances. X. Physciosporin, a new chlorinated depsidone[1,2]

W. S. G. MAASS, A. G. MCINNES, D. G. SMITH, AND A. TAYLOR

Atlantic Regional Laboratory, National Research Council of Canada, Halifax, N.S., Canada B3H 3Z1

Received August 12, 1976[3]

W. S. G. MAASS, A. G. MCINNES, D. G. SMITH, and A. TAYLOR. Can. J. Chem. **55**, 2839 (1977).

Physciosporin, a new chlorinated depsidone, has been isolated from the lichen *Pseudocyphellaria physciospora* and identified as methyl 2-chloro-4-formyl-3,8-dihydroxy-1,6,9-trimethyl-11-oxo-11*H*-dibenzo[*b*,*e*][1,4]dioxepin-7-carboxylate (methyl 5-chlorovirensate), **1**.

W. S. G. MAASS, A. G. MCINNES, D. G. SMITH et A. TAYLOR. Can. J. Chem. **55**, 2839 (1977).

On a isolé la physciosporine, une nouvelle depsidone chlorée, à partir du lichen *Pseudocyphellaria physciospora* et on l'a identifiée comme étant le chloro-2 formyl-4 dihydroxy-3,8 triméthyl-1,6,9 oxo-11 11*H* dibenzo[*b*,*e*][1,4]dioxépincarboxylate-7 de méthyle (chloro-5 virensate de méthyle), **1**.

[Traduit par le journal]

Introduction

Our survey for unusual lichen constituents in the genus *Pseudocyphellaria* by means of two-directional thin layer chromatography (1, 2) revealed the presence of several unidentified constituents reacting with *p*-phenylenediamine (PD). One of these, tentatively named physciosporin, gave a deep orange color with this reagent and was found in two species of the Southern Hemisphere, *P. physciospora* (Nyl.) Malme and *P. granulata* (Bab.) Malme. Physciosporin was extracted and purified in amounts sufficient for chemical identification from thalli of *P. physciospora* collected on Campbell Island, N.Z., on the occasion of the Swedish-Antarctic Expedition 1929, by the late Professor G. Einar DuRietz of the University of Uppsala and Dr. Margareta DuRietz.

Results

Physciosporin, **1**, was isolated in a yield of 5.3% of the dry lichen via column chromatography in benzene. The compound was slightly soluble in 5% sodium bicarbonate solution and readily so in 5% sodium carbonate, although excessive saponification occurred, especially in the latter case. The two absorption maxima in the ultraviolet spectrum (in dioxane) at 248 and 323 nm are typical of depsidones. The presence of a non-bonded ester carbonyl in the ir spectrum (in CCl_4) at 1748 cm^{-1}, as well as ester bond cleavage via methanolysis or saponification to give the corresponding biphenylether derivatives **2** and **3**, respectively, confirmed this conclusion. The mass spectrum showed the presence of one chlorine atom and an apparent molecular formula of $C_{19}H_{15}ClO_8$ confirmed by elemental analysis. The ^{1}Hmr spectrum (in $CDCl_3$) revealed three aromatic methyls, one methoxyl, and three sharp one-proton singlets attributable to an aldehyde function and either two hydroxyls or one hydroxyl and one carboxyl. The assumption of the presence of at least one aldehyde group is consistent with the PD+ reaction as well as the presence, in the ir spectrum (in CCl_4), of an absorption at ν 1647 cm^{-1} (H-bonded aromatic aldehyde C=O). An *ortho* hydroxyaldehyde grouping would also account for the solubility in sodium bicarbonate solution which is normally indicative of carboxylic acids. Short methylation of physciosporin with diazomethane resulted in the formation of a product, **4**, which was completely insoluble in sodium bicarbonate solution and gave an extra methoxyl signal in the ^{1}Hmr spectrum at δ 3.95, replacing the OH singlet at δ 12.81 observed in the ^{1}Hmr spectrum of physciosporin. High resolution mass spectrometry showed that this derivative, $C_{20}H_{17}ClO_8$, no longer had the chlorinated fragments at *m/e* 211 (corresponding to $C_9H_4ClO_4$) and 213 (corresponding to $C_9H_6ClO_4$) obtained from physciosporin, but a fragment at *m/e* 227 corresponding to $C_{10}H_8ClO_4$. On the other hand, the non-chlorinated fragment at *m/e* 194 (corresponding to $C_{10}H_{10}O_4$) was the same as in the parent

[1]This study formed part of a symposium paper presented by one of us (Wolfgang Maass) at the XIIth International Botanical Conference in Leningrad, 1975.

[2]NRCC No. 15945.

[3]Revision received March 28, 1977.

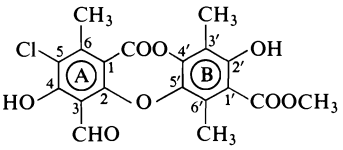

1

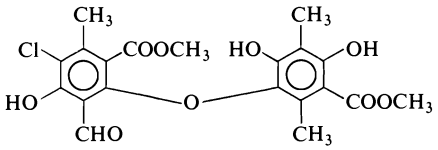

2

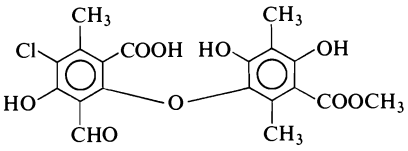

3

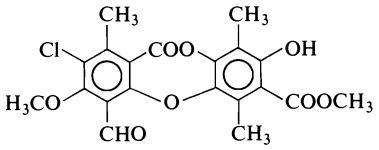

4

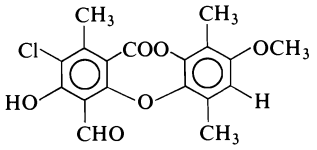

5

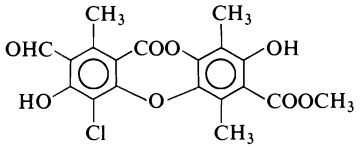

6

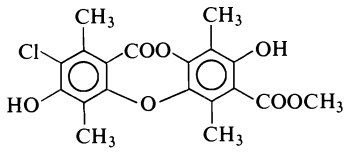

7

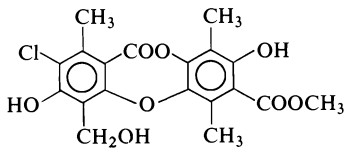

8

compound. Significantly, the biphenylether **3** obtained by cleavage of the depsidone bond gave molecular and daughter ions corresponding to $C_{19}H_{17}ClO_9$ and $C_{18}H_{17}ClO_7$ ($M - 44$), respectively, together with the chlorinated fragment ions found in the spectrum of physciosporin and a nonchlorinated fragment at *m/e* 212 (corresponding to $C_{10}H_{12}O_5$). The smaller ions may be interpreted as shown in Fig. 1*a–e* or as isomers thereof. The *m/e* 211 and 213 ions resemble those found in the mass spectrum of pannarin, **5** (3), a closely related monochlorodepsidone known from species of *Pannaria*, *Bombyliospora* and *Lecanora* (4, 5). Ions *a–c* would thus be derived from ring A and ion radicals *d* and *e* from ring B of a depsidone, clearly accounting for all functional groups implied by the spectral data and in particular ruling out the presence of a free carboxyl group in ring B. The observation of a loss of 32 mass units from the molecular ion of physciosporin supports a carboxymethyl substituent adjacent to a free hydroxyl and/or methyl group (6), and the relatively strong ion at *m/e* 44 (CO_2, 9% of the base peak) must then arise by fragmentation from the depside linkage. The biogenetically correct position of the phenolic hydroxyl in ring B of physciosporin follows from the positive calcium hypochlorite reaction of the saponified product in which the hydroxyl group must be located *meta* to that liberated from the ester bond (7). Typical absorption for an intramolecularly hydrogen-bonded ester function at 1665 cm^{-1} in the ir spectrum (in CCl_4) provides supporting evidence for the proposed locations of substituents on ring B.

On the basis of the above evidence, as well as on biogenetic grounds, physciosporin was likely to possess structure **1**. All presently known monochloro derivatives of naturally occurring depsides and depsidones (3, 5) have the chlorine in position 5 of ring A. However, alternative structures are possible, such as the 3-chloro, 5-formyl isomer, **6**.

Catalytic hydrogenation of physciosporin using platinum oxide as a catalyst and tetrahydrofuran as a solvent yielded hypophysciosporin, **7** or isomer, as the main product, as well as small amounts of the corresponding alcohol intermediate dihydrophysciosporin, **8** or isomer, and of deschlorohypophysciosporin, **9** or isomer. Hypophysciosporin was quantitatively converted to deschlorohypophysciosporin by hydrogenolysis using 10% palladized charcoal as a catalyst, triethylamine to neutralize the hydrochloric acid

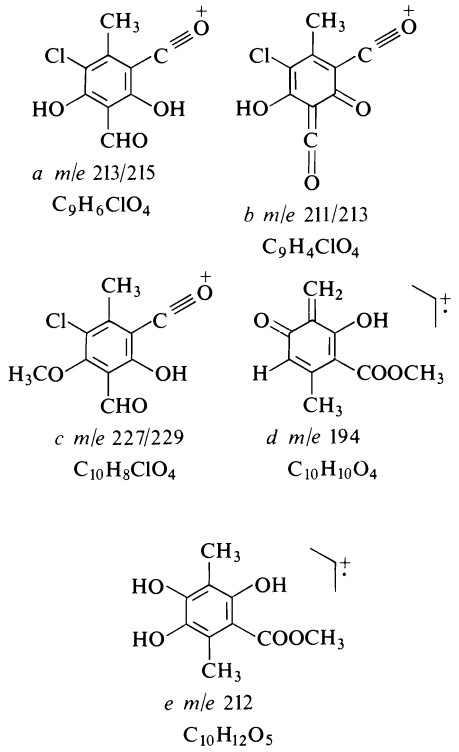

FIG. 1. Composition of important ions in the electron impact mass spectrum of physciosporin.

formed, and methanol as a solvent. The correct structure of deschlorohypophysciosporin was established by comparison with methyl hypoprotocetrarate, **9**, prepared by methylation of naturally occurring hypoprotocetraric acid, **10**, according to Culberson (8), by catalytic hydrogenation and subsequent methylation of fumarprotocetraric acid, **11**, isolated from *Cladonia rangiferina*, as well as by catalytic hydrogenation of the methylester of virensic acid, **12** (9). The physical data of all of these reduction products were in close agreement with each other and they all gave identical 4-*O*-methyl derivatives, **13**, and permethyl derivatives, **14**. The latter showed no depression of their melting points when mixed. Furthermore, the structure of naturally occurring 4-*O*-methylhypoprotocetraric acid, **15**, has recently been verified by synthesis (10) and shown to yield the methylester **13** (11). A comparison of 4-*O*-methyldeschlorohypophysciosporin with the methylester prepared from synthetic 4-*O*-methylhypoprotocetraric acid revealed their identity on the basis of an undepressed mixture mp and ^{1}Hmr spectroscopical data.

The conversion of physciosporin to the tetramethyl depsidone **9** confirmed a regular β-orcinol type of substitution pattern for rings A and B of physciosporin and fixed the chlorine and hydroxyl groups of ring A at the C-5 and C-4 positions, respectively. As a consequence, the intramolecularly hydrogen-bonded aldehyde group had to be placed on C-3 as usual. This assignment accounts for the loss of hydrogen bonding of the aldehyde C=O upon methylation of the C-4 hydroxyl group (ν_{max} for KBr 1700 cm^{-1} in **4** instead of 1648 cm^{-1} in **1**) and was substantiated by ^{1}Hmr studies as follows. Seven-bond spin–spin coupling between the two methyl groups (δ 2.28, 2.58) on ring B of **1** was visible in the ^{1}Hmr spectrum and confirmed by spin-decoupling experiments. Irradiation of the signal at δ 2.58 resulted in a nuclear Overhauser enhancement (25%) of the resonance for the hydrogen of the aldehyde group. This result requires that C-3 bears the aldehyde group, and permits the methyl groups at C-3′ (δ 2.28), C-6′ (δ 2.58), and C-6 (δ 2.60) to be assigned. Physciosporin is therefore firmly identified as methyl 5-chlorovirensate, **1**.

Experimental

Infrared (ir) spectra were recorded on a Perkin-Elmer model 521 spectrometer, ultraviolet (uv) spectra on a Unicam SP 8000 instrument, nmr spectra on a Varian HA-100D nmr spectrometer and mass spectra on a DuPont 21-491 or (for high resolution work) DuPont 21-110 B spectrometer. Chemical shifts are reported downfield from tetramethylsilane used as an internal standard. Precise mass measurements were obtained by the peak matching method using a suitable ion in the spectrum of perfluorokerosene as a standard. For chromatography, silicic acid (Mallinckrodt) and silica gel (Merck 60 F-254 plates) were used.

Methyl 2-Chloro-4-formyl-3,8-dihydroxy-1,6,9-trimethyl-11-oxo-11H-dibenzo[b,e][1,4]dioxepin-7-carboxylate (1, Physciosporin)

Thalli of *Pseudocyphellaria physciospora* were selected that contained a bright greenish yellow fluorescent, PD+ orange constituent. These (21 g, air dry) were extracted exhaustively with benzene. The benzene solution was chromatographed on silicic acid. The main crystalline fraction eluted with benzene (1.12 g or 5.3%) was recrystallized from chloroform–ether and acetone–ether to give fluffy colorless needles, mp 201–202°C; λ_{max}(dioxane) 248 (log ε 4.52), 323 (log ε 3.75), 351 (sh) nm, λ_{min} 229, 296 nm; ν_{max}(KBr) 2994w (br, OH), 2956w and 2929w (CH), 2850 sh(CHO?), 1739 (depsidone C=O), 1658 (H-bonded ester C=O), 1648 (H-bonded aldehyde C=O) cm^{-1}; ν_{max}($CHCl_3$) 1739, 1655 sh, 1643 cm^{-1}; ν_{max}(CCl_4) 1748, 1665 sh, 1647 cm^{-1}; δ ($CDCl_3$) 2.28, 2.58 and 2.60 (3 aromatic CH_3), 3.97 (1 $COOCH_3$), 10.73 (1 CHO), 11.41 and 12.81 (2 OH); *m/e* 408 (M^+, 34%), 406 (M^+, 100, found 406.0448, calcd. for $C_{19}H_{15}{}^{35}ClO_8$ 406.0456), 376(15), 374(40), 348(24), 346(73, found 346.0242, calcd. for $C_{17}H_{11}{}^{35}ClO_6$ 346.0245), 321(10), 319(29, found 319.0003, calcd. for $C_{15}H_8{}^{35}ClO_6$ 319.0010), 308(13),

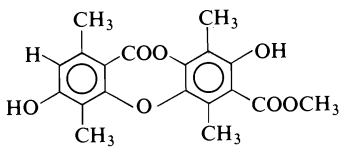

9

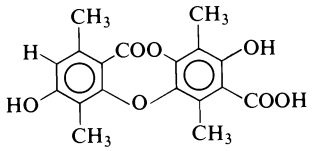

10

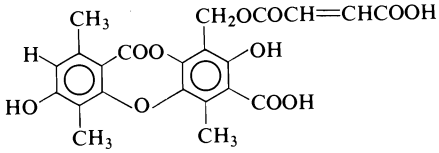

11

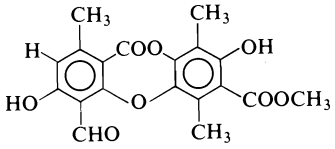

12

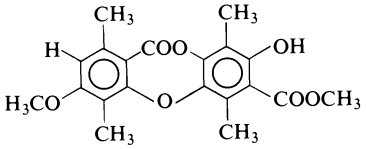

13

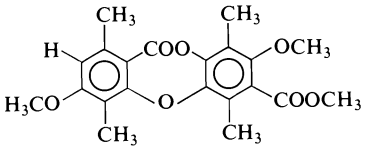

14

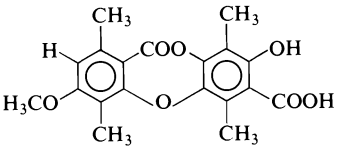

15

306(38, found 306.0288, calcd. for $C_{15}H_{11}{}^{35}ClO_5$ 306.0296), 294(17), 292(54, found 292.0138, calcd. for $C_{14}H_9{}^{35}ClO_5$ 292.0139), 281(5), 279(14, found 279.0062, calcd. for $C_{13}H_8{}^{35}ClO_5$ 279.0061), 215(4), 213(12, found 212.9952, calcd. for $C_9H_6{}^{35}ClO_4$ 212.9955), 211(7, found 210.9804, calcd. for $C_9H_4{}^{35}ClO_4$ 210.9799), 194(27, found 194.0578, calcd. for $C_{10}H_{10}O_4$ 194.0579), 164(6), 83(25), 44(9). *Anal.* calcd. for $C_{19}H_{15}ClO_8$ (mw 406.77): C 56.10, H 3.72, Cl 8.71, O 31.46; found: C 56.22, H 3.69, Cl 8.48, O 31.38.

*Methyl 2-Chloro-4-formyl-8-hydroxy-3-methoxy-1,6,9-trimethyl-11-oxo-11H-dibenzo[b,e][1,4]dioxepin-7-carboxylate (**4**, 4-O-Methylphysciosporin)*

Physciosporin (180 mg) was dissolved in acetone and treated with ethereal CH_2N_2 for 1 min. Excess reagent was destroyed by the addition of a few drops of acetic acid, and concentration of the solvent afforded a massive crystalline precipitate which was filtered off and washed with a minimum of ice-cold acetone to give **4** (100 mg), mp 242–243°C. Further purification via column chromatography raised the mp to 244°C (with slight decomposition); ν_{max}(KBr) 3010w, 2955m, 2880w and 2860w (CH), 1732 (depsidone C=O), 1700 (non-bonded aldehyde C=O), 1671 (H-bonded ester C=O) cm^{-1}; δ ($CDCl_3$) 2.25, 2.50 and 2.57 (3 aromatic CH_3), 3.95 and 3.97 (2 OCH_3), 10.64 (1 CHO, non-bonded), 11.45 (1 OH); *m/e* 422(M^+, 34%), 420(M^+, 100), 390(19), 388(43), 362(28), 361(20), 360(79), 335(11), 333(27), 322(14), 320(43), 308(16), 306(50), 229(5), 227(16, *anal.* calcd. for $C_{10}H_8{}^{35}ClO_4$: 227.0112; found 227.0111), 225(8), 194(33), 83(36), 67(22), 44(16), 28(24). *Anal.* calcd. for $C_{20}H_{17}ClO_8$ (mw 420.81): C 57.09, H 4.07, Cl 8.43, O 30.42; found C 56.84, H 4.11, Cl 8.69, O 29.85.

*3-Chloro-5-formyl-4-hydroxy-2-methyl-6-(3′-carbomethoxy-4′,6′-dihydroxy-2′,5′-dimethyl)phenoxybenzoic Acid (**3**, Saponified Physciosporin)*

When the ether extract from 5 g lichen was carefully fractionated into sodium bicarbonate, sodium carbonate, and neutral fractions as usual (2), physciosporin was isolated from the sodium bicarbonate fraction via column chromatography although only in poor yield (25 mg or 0.5% of the air-dry lichen). The sodium carbonate fraction consisted of 240 mg **3** which formed a very slow moving band on columns as compared to physciosporin. The same compound was obtained in quantitative yield by treatment of pure physciosporin with 5% aqueous solutions of either sodium carbonate or sodium hydroxide at room temperature for 10 min, followed by acidification. It was recrystallized from chloroform, mp 225°C dec. (with foaming); ν_{max}(KBr) 3471s (non-bonded OH), 3135 (br, COOH), 3075w, 3005w, and 2955m (CH), 2850sh (CHO?), 1724 (non-bonded carboxyl C=O), 1656sh (H-bonded ester C=O), 1643 (H-bonded aldehyde C=O) cm^{-1}; δ (THF-d_8) 2.03, 2.30 and 2.32 (3 aromatic CH_3), 3.87 (1 $COOCH_3$), 8.87 (br, 1 non-bonded OH), 10.43 (1 CHO), 11.83 and 12.63 (2 OH), COOH not found; *m/e* 426(M^+, 2%), 424(M^+, 6, found 424.0567, calcd. for $C_{19}H_{17}{}^{35}ClO_9$ 424.0561), 408(4), 406(11), 394(2), 392(4), 382(11), 380(30, found 380.0665, calcd. for $C_{18}H_{17}{}^{35}ClO_7$ 380.0662), 376(7), 374(20), 351(8), 350(26), 349(20), 348(64), 346(31), 321(9), 319(18), 308(5), 306(15), 294(9), 292(23), 215(4), 213(11, found 212.9954, calcd. for $C_9H_6{}^{35}ClO_4$ 212.9955), 212(12, found 212.0684, calcd. for $C_{10}H_{12}O_5$ 212.0685), 211(9), 194(9), 186(29), 185(39), 184(26), 180(26), 165(37), 164(36), 136(24), 85(51), 83(83), 77(34), 67(63), 51(36), 44(100), 43(29), 39(36), 32(16), 31(64), 29(26), 28(33).

*Methyl 3-Chloro-5-formyl-4-hydroxy-2-methyl-6-(3′-carbomethoxy-4′,6′-dihydroxy-2′,5′-dimethyl)phenoxybenzoate (**2**)*

Short treatment of saponified physciosporin, **3** (384 mg), with ethereal CH_2N_2 in acetone (1 min at room

temperature) gave a mixture of products which was separated over silicic acid. From the first fraction eluted with chloroform, **2** (115 mg) was obtained as colorless needles after two recrystallizations from ether, mp 226–227°C dec. (melt dark brown;[4] ν_{max}(KBr) 3280 (br, non-bonded OH), 2950w, 2846 sh, 1708 (non-bonded ester C=O), 1650 sh (H-bonded ester C=O), 1638 (H-bonded aldehyde C=O) cm^{-1}; δ ($CDCl_3$) 2.16, 2.28 and 2.31 (3 aromatic CH_3), 3.45 and 3.93 (2 $COOCH_3$), 6.44 (1 OH, non-bonded), 10.35 (1 CHO), 11.73 and 12.68 (2 OH, bonded); *m/e* 440(M^+, 7%), 438(M^+, 18), 408(15), 406(35), 348(41), 346(100). *Anal.* calcd. for $C_{20}H_{19}ClO_9$ (mw 438.82): C 54.74, H 4.36, Cl 8.08, O 32.81; found C 54.94, H 4.56, Cl 8.02, O 32.79.

The main fraction from this methylation (236 mg, mp 162.5–163°C) has not been fully characterized yet and will be reported elsewhere.

The methyl ester **2** was also formed upon methanolysis of physciosporin. The latter (100 mg) was suspended in 10% methanolic potassium hydroxide (50 ml) and stirred with heating for 30 min. The solution obtained was poured into ice-cold 10% hydrochloric acid (100 ml). The crude crystalline product was filtered off and dissolved in ether, which was shaken with a cold 5% sodium bicarbonate solution and then with dilute hydrochloric acid. Evaporation of the ether and purification by column chromatography gave creamy yellow needles (35 mg) from chloroform, mp 207°C (melt initially yellow, needles formed after cooling melted at 221–223°C with decomposition). Two recrystallizations from ether afforded a colorless product, mp 226–227°C dec. (melt dark brown).[4] Infrared, nmr, and mass spectral data were in good agreement with those of **2** prepared via saponified physciosporin (mixture mp undepressed).

Catalytic Hydrogenation of Physciosporin

Physciosporin (137 mg) was dissolved in tetrahydrofuran (300 ml) and the solution stirred for 5 h in a hydrogen atmosphere in the presence of platinum oxide (50 mg). After removal of the catalyst and evaporation of the solvent, the mixture of products was applied to a short (10 cm) silicic acid column packed in chloroform. Elution with chloroform gave the following fractions in the order mentioned: starting material, hypophysciosporin, **7** (incompletely separated from the former), and several constituents that moved slowly as a glossy band. The mixture of physciosporin and hypophysciosporin was fully resolved by rechromatography on a longer column (30 cm), yielding a total of 25 mg and 53 mg, respectively. The constituents from the glossy band were separated by preparative tlc in benzene – dioxane – acetic acid 90:25:1. Three bands were formed as detected by ultraviolet light (2200 Å). They were scraped off and eluted with acetone. After evaporation of the filtrates, the residues were redissolved in chloroform. The solutions thus obtained were washed with water, dried over anhydrous sodium sulphate, and passed through beds of silicic acid. The tlc eluate from the upper band thus purified gave 4 mg of an unidentified material, that from the middle band 9 mg deschlorohypophysciosporin, **9**, and that from the lower band 22 mg dihydrophysciosporin, **8**.

[4]One recrystallization of highly purified **2** from boiling chloroform gave the lower mp (207°C without decomposition) due to the formation of traces of a yellowish decomposition product not detectable in the nmr spectrum and preferentially soluble in ether. Mass spectrometry of the ether mother liquor gave ions at *m/e* 404 and 372 in addition to those obtained from highly purified **2**.

*Methyl 2-Chloro-3,8-dihydroxy-1,4,6,9-tetramethyl-11-oxo-11H-dibenzo[b,e][1,4]dioxepin-7-carboxylate (**7**, Hypophysciosporin)*

Colorless crystals were obtained from chloroform and washed with ether, mp 240–241°C dec.; ν_{max}(KBr) 3413s (OH), 2954w, and 2925w (CH), 1721 (depsidone C=O), 1656 (H-bonded ester C=O) cm^{-1}; δ (acetone-d_6, assignments on the basis of decoupling experiments) 2.20 (1 aromatic CH_3, ring B), 2.45 (2 aromatic CH_3, both on ring A), 2.68 (1 aromatic CH_3, ring B) 4.01 (1 $COOCH_3$), hydroxyl protons not found; *m/e* 394(M^+, 21%), 392(M^+, 56), 362(24), 360(59), 335(10), 334(40), 333(28), 332(98), 307(22), 306(24), 305(61), 304(43), 294(21), 292(65), 280(26), 279(23), 278(74), 277(30), 276(37), 267(11), 265(25), 199(17, ring A fragment), 198(11), 194(40, ring B fragment), 170(11), 166(35), 91(22), 89(20), 83(100), 77(31), 67(61), 65(24), 63(24), 55(25), 51(28), 44(18), 43(27), 39(41), 28(47). *Anal.* calcd. for $C_{19}H_{17}ClO_7$ (mw 392.80): C 58.10, H 4.36, Cl 9.03, O 28.51; found C 57.90, H 4.50, Cl 9.04, O 28.84.

Hydrogenolysis of Hypophysciosporin

Hypophysciosporin, **7** (39.2 mg or 0.1 mmol) was dissolved in methanol (150 ml). 10% Palladized charcoal (40 mg) was added and an excess of triethylamine (2 equiv. or 28 μl) for neutralization of the hydrochloric acid to be formed. The reaction mixture was stirred for 5 h in an atmosphere of hydrogen. The catalyst was filtered off and washed with methanol, and the combined filtrates were taken down to dryness. The residue was recrystallized from chloroform to give deschlorohypophysciosporin, **9** (30 mg).

*Methyl 3,8-Dihydroxy-1,4,6,9-tetramethyl-11-oxo-11H-dibenzo[b,e][1,4]dioxepin-7-carboxylate (**9**, Deschlorohypophysciosporin)*

The compound isolated from among the products of catalytic hydrogenation of physciosporin and the hydrogenolysis product from hypophysciosporin gave identical physical data; mp 264–265°C dec. (melt dark reddish brown); ν_{max}(KBr) 3346s (OH), 2958w and 2926w (CH), 1703 (depsidone C=O), 1663 (H-bonded ester C=O) cm^{-1}; δ (acetone-d_6, assignments by decoupling experiments) 2.19 (1 aromatic CH_3, ring B), 2.35 (2 aromatic CH_3, both on ring A), 2.67 (1 aromatic CH_3, ring B), 3.98 (1 $COOCH_3$), 6.70 (1 aromatic H), hydroxyl protons not found; δ (THF-d_8) 2.18, 2.31, 2.35 and 2.65 (4 aromatic CH_3), 3.92 (1 $COOCH_3$), 6.45 (1 aromatic H), hydroxyl protons not found; *m/e* 358(M^+, 57%), 326(53), 298(100), 271(53), 270(41), 258(56), 244(62), 243(37), 242(38), 231(33), 194(19), 149(34), 91(39), 83(63), 67(39), 44(9), 43(21), 39(38), 28(30).

*Methyl 2-Chloro-3,8-dihydroxy-4-hydroxymethyl-1,6,9-trimethyl-11-oxo-11H-dibenzo[b,e][1,4]dioxepin-7-carboxylate (**8**, Dihydrophysciosporin)*

Colorless crystals were obtained from chloroform and washed with *n*-hexane, mp 181–182°C; ν_{max}(KBr) 3200 (OH), 2958w and 2830 (CH), 1700 (depsidone C=O), 1664 (H-bonded ester C=O) cm^{-1}; δ ($CDCl_3$, assignments based on decoupling experiments and similar derivatives) 2.25 (C-3′ methyl), 2.50 (C-6 methyl), 2.64 (C-6′ methyl), 3.95 (1 $COOCH_3$), 4.48 (br, 1 OH, non-

bonded), 5.14 (2H, CH_2OH), 7.51 (1H, CH_2OH), 11.42 (1 OH, bonded); *m/e* 408(M − 2, 6%), 406(M − 2, 15), 394(M − 16, 6), 392(M − 16, 13), 348(8), 346(18), 334(12), 332(29), 308(6), 307(7), 306(15), 305(15), 294(9), 292(27), 280(7), 278(20), 194(16), 44(41), 38(57), 36(100), 32(19), 31(28), 28(37). *Anal.* calcd. for $C_{19}H_{17}ClO_8$ (mw 408.80): C 55.83, H 4.19; found C 55.34, H 4.36.

Methylation of Deschlorohypophysciosporin

Deschlorohypophysciosporin, **9** (30 mg), in acetone was treated with ethereal CH_2N_2 for 10 h. After evaporation of the solvent, the residue was taken up in chloroform and passed through a column of silicic acid. The 4-*O*-methyl derivative **13** (10 mg) was eluted first and then the fully methylated product **14** (21 mg).

*Methyl 8-Hydroxy-3-methoxy-1,4,6,9-tetramethyl-11-oxo-11H-dibenzo[b,e][1,4]dioxepin-7-carboxylate (**13**, 4-O-Methyldeschlorohypophysciosporin)*

The crystals obtained from chloroform were washed with a minimum of ether–*n*-hexane, mp 211–213°C, and recrystallized from benzene, mp 219°C, mixture mp with synthetic methyl 4-*O*-methylhypoprotocetrarate (mp 219°C) undepressed; ν_{max}(KBr) 2960 sh, 2927m and 2852w (CH), 1742 (depsidone C=O), 1656 (H-bonded ester C=O) cm^{-1}; δ ($CDCl_3$, assignments on the basis of decoupling experiments) 2.25 (C-3′ methyl), 2.32 (C-3 methyl), 2.49 (C-6 methyl), 2.65 (C-6′ methyl), 3.84 (1 OCH_3), 3.94 (1 $COOCH_3$), 6.56 (1 aromatic H), 11.42 (1 OH, bonded); *m/e* 372(M^+, 48%), 340(47), 312(100).

*Methyl 3,8-Dimethoxy-1,4,6,9-tetramethyl-11-oxo-11H-dibenzo[b,e][1,4]dioxepin-7-carboxylate (**14**, Fully Methylated Deschlorohypophysciosporin)*

The crystals obtained from chloroform were washed with a minimum of ether–*n*-hexane, mp 140–142°C (needle form, lit (8) mp 144–145°C), and recrystallized from methanol, mp 171–172°C (rhombic plate form, lit (8) mp 172–173°C), mixture mp with fully methylated hypoprotocetraric acid (mp 171–172°C) prepared from virensic acid as well as from fumarprotocetraric acid (9) undepressed; ν_{max}(KBr) 3000w, 2980w, 2960m, 2935m, and 2851w (CH), 1740s (depsidone C=O) and 1730s (non-bonded ester C=O), 1671w, 1612 cm^{-1}; δ ($CDCl_3$) 2.29, 2.31, 2.38, and 2.50 (4 aromatic CH_3), 3.74, 3.86, and 3.91 (3 OCH_3), 6.58 (1 aromatic H); *m/e* 386(M^+, 56%), 358(67), 180(100).

Acknowledgments

We are greatly indebted to Dr. Margareta DuRietz for the generous donation of the lichen, and to Dr. Chicita Culberson and Dr. John A. Elix for gifts of hypoprotocetraric acid, isolated from *Ramalina hypoprotocetrarica*, and synthetic 4-*O*-methylhypoprotocetraric acid, respectively. The spectral data were obtained through Messrs D. Embree, G. McCully, and J. Van Ingen.

1. W. S. G. Maass. Contributions to a chemotaxonomy of *Pseudocyphellaria*. XI. International Botanical Congress. Abstracts. 1969. p. 136.
2. W. S. G. Maass. Can. J. Bot. **53**, 1031 (1975).
3. J. A. Elix, D. A. Jackman, and M. V. Sargent. J. Chem. Soc. Chem. Commun. 892 (1974).
4. S. Huneck. Z. Naturforsch. Teil B, **21**, 80 (1966).
5. C. F. Culberson. Chemical and botanical guide to lichen products. The University of North Carolina Press, Chapel Hill, NC. 1969.
6. J. H. Beynon, R. A. Saunders, and A. E. Williams. The mass spectra of organic molecules. Elsevier Publishing Company, Amsterdam-London-New York. 1968.
7. J. Santesson. *In* The lichens. *Edited by* V. Ahmadjian and M. E. Hale. Academic Press, Inc., New York and London. 1973. p. 633.
8. C. F. Culberson. Phytochemistry, **4**, 951 (1965).
9. W. S. G. Maass, The Bryologist. In preparation.
10. P. Djura, J. A. Elix, U. Engkaninan, and M. V. Sargent. Aust. J. Chem. **25**, 2167 (1972).
11. T. M. Cresp, J. A. Elix, S. Kurokawa, and M. V. Sargent. Aust. J. Chem. **25**, 2167 (1972).

Photoisomerization of some bicyclooctanones in solution

SUSAN C. CRITCH[1] AND ALEX G. FALLIS

Department of Chemistry, Memorial University of Newfoundland, St. John's, Nfld., Canada A1C 5S7

Received November 24, 1976

SUSAN C. CRITCH and ALEX G. FALLIS. Can. J. Chem. **55**, 2845 (1977).

The ketene derived products and unsaturated aldehydes produced upon solution photolysis of a series of bicyclooctanones (bicyclo[2.2.2]octan-2-one (**1**), bicyclo[3.2.1]octan-2-one (**6**), 1,8,8-trimethylbicyclo[3.2.1]octan-2-one (**12**)) are reported. Estimated strain energies of the approximate transition states involved and conformational analysis are utilized as guides to rationalize the results. This approach should assist more accurate predictions of photolysis products from related systems in the same solvent(s). The product ratios are solvent sensitive and preliminary experiments indicate that a primary amine (cyclohexylamine) in the photolysis solution enhances the production of ketene derived product.

SUSAN C. CRITCH et ALEX G. FALLIS. Can. J. Chem. **55**, 2845 (1977).

On rapporte les produits dérivés de cétènes et les aldéhydes non-saturés qui sont formés par photolyse en solution d'une série de bicyclooctanones (bicyclo[2.2.2]octanone-2 (**1**), bicyclo-[3.2.1]octanone-2 (**6**) et triméthyl-1,8,8 bicyclo[3.2.1]octanone-2 (**12**)). On utilise les énergies de tension estimées des états de transition approximatifs impliqués et l'analyse conformationnelle comme guide pour rationaliser les résultats. Cette approche devrait permettre de meilleures prédictions concernant les produits de photolyse de systèmes qui sont reliés dans les mêmes solvants. Les rapports de produits sont très sensibles aux solvants et des expériences préliminaires indiquent qu'une amine primaire (cyclohexylamine) dans des photolyses en solution augmente la production de produit dérivé de cétène.

[Traduit par le journal]

Introduction

The photochemical reactions of saturated cyclic ketones in solution have been studied extensively (for pertinent reviews see ref. 1), nevertheless many facets are still imperfectly understood, and as Chapman and Weiss have pointed out "the factors determining the relative yields of aldehyde to ester are ... subtle (and) small changes in molecular structure ... cause drastic alterations in product ratios" (2). Thus, due in part to the difficulty of predicting product ratios accurately, the use of simple, photoinduced cleavage reactions of cycloalkanones in organic synthesis has been limited.

It is well established that photochemical α-cleavage (Norrish type I) of most cyclic ketones affords discrete acyl-alkyl diradicals (3) which partition themselves between three major pathways: (*i*) disproportionation to yield alkenal(s), (*ii*) disproportionation to yield ketene, and (*iii*) recoupling to yield ground state ketone. The relative importance of recombination (ring closure) *vs.* hydrogen abstraction is influenced by radical stability and the ease of formation of the transition states required for hydrogen transfer. Thus substituents and conformational preferences exert a significant influence on the product distribution. This product ratio is also sensitive to solvent and these effects may alter conformational factors. The study of relatively rigid bridged-ring ketones facilitates a better understanding of the conformational factors which influence aldehyde and ketene formation (4). We report herein a study of the product distributions upon photolysis of bicyclo[2.2.2]octan-2-one (**1**), bicyclo[3.2.1]octan-2-one (**6**), and 1,8,8-trimethylbicyclo[3.2.1]octan-2-one (**12**, homocamphor) in methanol and tetrahydrofuran–water solutions. Since completion of this study investigations of closely related systems have been published. Agosta and Wolff (5) have utilized a series of bicyclo[3.2.1]octan-6-ones and Hammond and Yeung (6) have examined a deuterated bicyclo[2.2.2]octan-2-one.

Results

Photolysis of *endo*-5,6-dideuteriobicyclo-[2.2.2]octane-2-one in benzene containing added methanol was recently reported (6) to afford the aldehyde as the only isolated product, while under similar conditions (benzene containing 3.5% methanol) others (5) detected both ester **2**

[1]Taken in part from the M.Sc. Thesis of S. C. Critch, Memorial University of Newfoundland, 1975.

TABLE 1. Relative product formation on the photolysis of **1**, **6**, and **12**

Ketone	Solvent	Relative yields		
		Aldehyde		Ketene
1 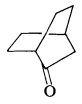	MeOH	4		1
	$THF-H_2O$	10		1
		syn-8	*endo-7*	
6 	MeOH	7	2	1
	$THF-H_2O$	8	2	1
12 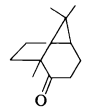	MeOH		4	1
	$THF-H_2O$		30	1

and aldehyde **4** upon photolysis of bicyclo[2.2.2]-octan-2-one (**1**). Under our conditions using either methanol or tetrahydrofuran–water, both the ketene derived product **2** (7) or **3** (8) and the unsaturated aldehyde **4** (9) were produced. Irradiation of **1** in methanol afforded the aldehyde **4** and ester **2** in a 4:1 ratio. The structure of the aldehyde was confirmed by silver oxide oxidation to 3-cyclohexenylacetic acid (**5**), a sample of which was prepared by homologation of 3-cyclo-

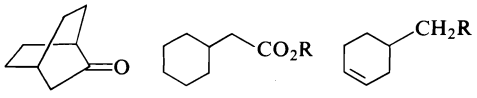

1 **2** R = CH_3, **3** R = H, **4** R = CHO, **5** R = CO_2H

hexenylcarboxylic acid (10).[2] It may be seen from Table 1 that photolysis of **1** in tetrahydrofuran–water (1:1) afforded an aldehyde–acid (**4**:**3**) ratio of 10:1.

Irradiation of a 0.1 *M* methanol solution of bicyclo[3.2.1]octan-2-one (**6**) gave a mixture, shown by glc analysis to contain three components in a ratio of 7:2:1 (8:2:1 in $THF-H_2O$) which were separated by preparative glc. The ^{1}Hmr spectrum of the major component (an aldehyde) possessed a triplet (J = 2 Hz) at δ 9.74 due to an aldehydic proton adjacent to a methylene group and a multiplet representing two protons at δ 5.63 indicating the presence of two vinyl hydrogens.

The second component displayed similar ^{1}Hmr characteristics, a triplet at δ 9.75 and a signal at δ 5.55 suggesting two equivalent vinyl protons in a symmetrical environment. Thus

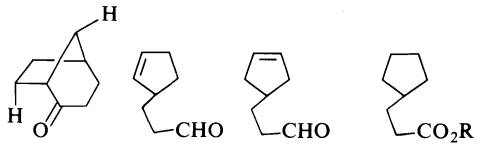

6 **7** **8** **9** R = H, **10** R = CH_3

tentatively the major aldehyde can be assigned structure **7** and the second component structure **8** (9). Silver oxide oxidation of **7** followed by hydrogenation (5% Pd/C) provided 3-cyclopentylpropionic acid (**9**) (11). This was repeated on a mixture of **7** and **8** and confirmed that these photoproducts were cyclopentene isomers arising from the same mode of α-cleavage. The minor component from the photolysis mixture was identified as the methyl ester **10** (12).

The exact position of the double bond in the aldehyde isomers, to prove which hydrogen was abstracted preferentially after α-cleavage, was established as follows. The benzene induced solvent shifts indicate that the vinyl hydrogens of **8** are in a symmetrical environment and also experience less shielding than those in **7** due to their greater separation from the carbonyl function. Additional support for the non-identity of the olefinic hydrogens in **7** was provided by the ^{1}Hmr spectrum recorded in the presence of a molar equivalent of $Eu(fod)_3$.

Ozonolysis of **7** followed by oxidative work-up

[2]We are grateful to E. R. Benson for preparing this sample.

(30% H_2O_2) and *in situ* methylation with diazomethane provided the ester **11** (13) which was identified by comparison with an authentic sample prepared from pentane-1,3,5-tricarboxylic acid (13), confirming the structural assignment.

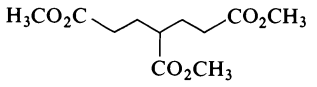

11

Prior to this work the only photochemical study of a bicyclo[3.2.1]octan-2-one was that of homocamphor (**12**) (14). Irradiation of homocamphor in diethyl ether containing cyclohexylamine had afforded only the ketene derived product (as the amide) and no aldehyde was detected. Based on the results above one would anticipate that the aldehyde **13** should be the major product upon photolysis of homocamphor in methanol. We have found this to be the case.

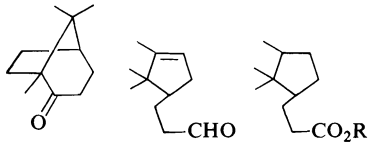

12 **13** **14** R = CH_3
15 R = H

The ^{1}Hmr spectrum of the total photolysis mixture contained a triplet at δ 9.67 ($J \sim 1.5$ Hz) due to the aldehydic proton and a singlet at δ 3.60 due to the methoxyl function. Integration of these signals indicated an aldehyde–ester ratio (**13**:**14**) of 4:1. As in the previous cases the THF–H_2O solvent system resulted in an enhancement of the aldehyde–ketene ratio (30:1). In view of these results it is surprising that in the earlier photolytic study of homocamphor in diethyl ether – cyclohexylamine no aldehyde was encountered (14). This solvent effect is very marked, for no aldehyde was detected when the photolysis was repeated under Quinkert's conditions nor was it present as the imine. In a preliminary study, with diethyl ether – cyclohexylamine, bicyclo[3.2.1]octan-2-one afforded an aldehyde–amide ratio of 1:1, and bicyclo[2.2.2]-octan-2-one, a ratio of 1:2. The aldehydes are partly converted to their imines as indicated by the ^{1}Hmr spectrum of the total crude photolysis mixture and could be freed by washing with aqueous acid. This solvent effect which enhances the production of ketene derived product (as the amides) should be of synthetic utility although further work is required and the exact role of amine is not clear at present.

Discussion

As expected, photolysis products arise from these ketones by cleavage of the bond between the carbonyl group and the bridgehead carbon to afford the most stable of the two possible acyl-alkyl diradicals. In these short lived 1,6-diradical systems the accurate prediction of their behaviour is difficult because of the multiple reaction pathways available. Their fate is also influenced by a variety of steric, conformational, and electronic factors. Nevertheless to rationalize the product distribution and to help improve the predictability and synthetic potential for photoinduced α-cleavage it is instructive to examine the conformational preferences of these intermediates. Chart 1 lists estimated 'strain energies' for the approximate transition states involved. Used in concert with steric considerations they provide a guide for predicting the major product from a given photolysis *in the same solvent system.*

For bicyclo[2.2.2]octan-2-one (**1**), as pointed out recently (5), neither product "can arise from the stable chair conformation of the biradical" since for hydrogen abstraction to be geometrically feasible the acyl side chain must be axial. The aldehyde **4** is the expected major product since α-cleavage releases the cyclohexane ring of **1** from its enforced boat conformation placing one of the geometrically equivalent *syn*-hydrogens in close proximity to the acyl radical for facile abstraction (**A**). The geometry of this system is clearly more easily achieved (less strained) than the competing transition state **B** for ketene formation which requires a boat cyclohexane incorporated into a bicyclo-octane-heptane type intermediate bearing an acyl substituent (Chart 1).

Similarly for bicyclo[3.2.1]octan-2-one it is apparent that the major aldehyde will arise from a hydrindanone type intermediate **C** which clearly involves less strain than either of the two competing pathways **D** and **E** (R = H). Cycloheptanones and bicyclo[3.3.1]nonan-3-one are known to be more stable than their parent hydrocarbons (1.5–3.4 kcal) (17). This feature increases the stability of **D** due to the presence of the carbonyl function while the axial acyl substituent in **E** introduces a destabilizing nonbonded interaction. In addition, the reduced freedom of the side chain increases the difficulty of approach to the

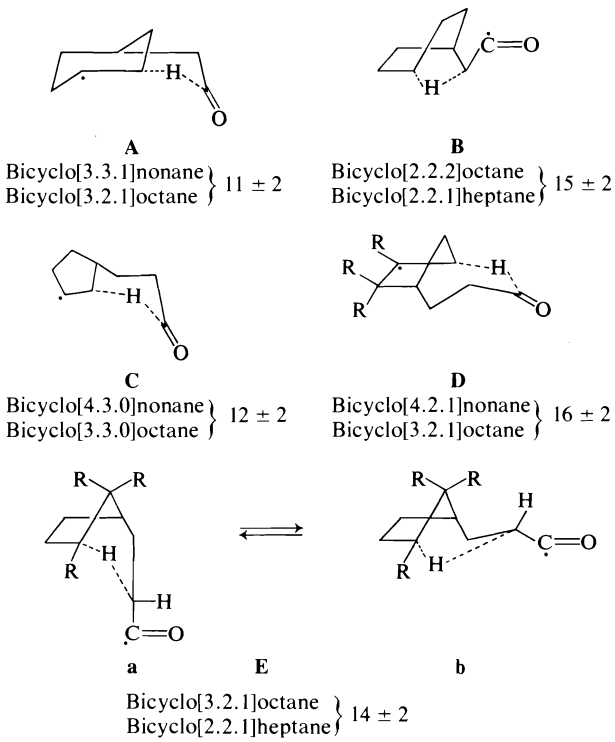

CHART 1. Estimated strain energies (kcal/mol); based on averages of hydrocarbon strain energies determined by Allinger (15), Schleyer (16), and their co-workers for the two bicyclic hydrocarbons being considered.

planar alkyl radical confined in the cyclopentane, and makes ketene formation more difficult. Indeed molecular models suggest that the required conformation is less easily achieved than diagram **E** implies. Thus in total these influences appear sufficient to tip the balance in favour of aldehyde formation via **D** over ketene formation via **E**.

Homocamphor (**12**) provides a measure of the direct competition between these aldehyde and ketene pathways. In this case also, product from **D** (R = CH_3) predominates, enhanced slightly by the *syn*-C_8 methyl function which introduces a further 1,3 interaction which appears more severe in **E** than **D**.

These considerations therefore account for the predominance of aldehydes over ketenes upon photolysis of these bicyclic ketones in methanol and THF–water solvents. The solvent plays a separate role from structure in radical disproportionations and generally the effects are poorly understood. It is possible that the amine solvates the acyl radical preferentially so that it is not able to abstract hydrogen as readily, permitting the ketene pathways to compete more efficiently. However as pointed out above, further work is required with simpler systems in order to fully understand this phenomenon. Bicyclo[5.2.1]decan-10-one may represent a previous example of this 'amine effect' (18).

A referee has recommended inclusion of a general conclusion to facilitate future predictions of major ketone photolysis products. There is at present insufficient data and understanding for predictions of this sort to be made with complete assurance. However based on this study and related examples in the literature (1–5) the following guidelines may be given for comparisons of photolyses of *bridged-ring ketones in the same solvent system*. The diradical intermediates will disproportionate preferentially by the lowest energy pathway consistent with the most geometrically feasible transition state for hydrogen abstraction. As a guide to determining the preferred conformation for the transition state it is useful to consider the approximate strain energy of the system, steric influences of substituents and their non-bonded interactions, the preferred orientation of the acyl radical side chain, and conformational equilibria. In addition the first

example of stereoelectronic control in a hydrogen transfer leading to aldehyde has recently been reported (19). This preference for abstraction of axial hydrogen adjacent to a radical centre may operate in other systems as well but its presence can only be ascertained at present by studying specifically deuterated ketones.

Experimental

Melting points were determined on a Fisher–Johns melting point apparatus or with a Thomas–Hoover Uni-Melt apparatus and are uncorrected. Elemental microanalyses were performed by Alfred Bernhardt, West Germany.

Infrared spectra were recorded on a Perkin-Elmer 237B grating spectrometer, and were calibrated against the 2850 and 1601 cm^{-1} bands of polystyrene film. Nuclear magnetic resonance spectra were determined with a Varian model A-60, Varian model EM-360, or Varian model HA-100 spectrometer; band positions are reported in parts per million downfield from tetramethylsilane as an internal standard. Mass spectra were recorded on a Hitachi–Perkin-Elmer model RMU-6E mass spectrometer at an ionization potential of 70 eV unless otherwise specified.

Gas–liquid chromatographic analyses were conducted on a Varian Aerograph model 1720 gas chromatograph using helium as the carrier gas. Column A refers to an 8 ft × ¼ in., 13% SE-30 column supported on Chromosorb W (AW-DMCS) (70–80 mesh); column B refers to a 8 ft × ¼ in., 20% Carbowax 20M column supported on Chromosorb W (AW-DMCS) (70–80 mesh).

Irradiations were carried out in stoppered Pyrex containers, using a water-cooled Hanovia 450-W medium pressure mercury arc lamp, on solutions (~0.01 *M*) which had been thoroughly flushed with nitrogen.

Solutions in organic solvents were dried over anhydrous magnesium sulphate and evaporated by means of a Büchi rotary evaporator under reduced pressure.

Bicyclo[2.2.2]octan-2-one (**1**) mp 177–178°C (lit. (20) mp 178.5–179°C) was prepared from bicyclo[2.2.2]oct-2-ene (Chem. Sample Co.) by hydroboration and oxidation with chromic acid (21).

*Photolysis of Bicyclo[2.2.2]octan-2-one (**1**)*

(i) In Methanol

A solution of bicyclo[2.2.2]octan-2-one (0.200 g, 0.0016 mol) in absolute methanol (20 ml), to which sodium bicarbonate (0.020 g) had been added, was irradiated for 4 h. After removal of the solvent and addition of petroleum ether, the solution was filtered and concentrated to afford a colourless oil (0.200 g, 100%). Gas–liquid chromatographic analysis indicated essentially complete reaction of the ketone. Comparison of aldehyde and methoxyl peaks of the nmr spectrum indicated an aldehyde–ester ratio of 4:1; ^{1}Hmr (CCl_4) δ 2.62 (s, 3H, OCH_3), 9.68 (t, $J \sim 2$ Hz, 1H, CHO) ppm.

A sample (0.167 g) from the methanol photolysis was added to a solution of silver nitrate (0.0170 g, 0.001 mol) and sodium hydroxide (0.080 g, 0.002 mol) in water (3 ml). After stirring at room temperature for 1.5 h, the solution was filtered, the residue washed several times with hot water, and the filtrate extracted with ether (twice). The combined organic extracts were washed with water, dried, filtered, and concentrated. The methyl ester **2** (7) was isolated as a colourless oil (0.045 g, 36%) which was purified by tlc on silica gel (5% ether – petroleum ether); ir (CCl_4): 1735 cm^{-1}; ^{1}Hmr (CCl_4): δ 3.60 (s, 3H, OCH_3) ppm.

The combined aqueous layers were acidified and extracted with ether to yield the unsaturated carboxylic acid **5** (0.075 g, 53.5%) which was purified by tlc on silica gel (30% ether – petroleum ether); ir (CCl_4): 3500–2400 (br OH), 1710 (C=O) cm^{-1}; ^{1}Hmr (CCl_4): δ 1.1–2.5 (complex), 5.57 (br s, 2H, CH=CH), 11.77 (br s, 1H, COOH) ppm. An authentic sample was prepared by Arndt–Eistert homologation of 3-cyclohexenyl carboxylic acid (10).

(ii) In Tetrahydrofuran–Water

A solution of bicyclo[2.2.2]octan-2-one (0.278 g, 0.0022 mol) in a 1:1 mixture of THF–water (22 ml) was irradiated for 7 h and extracted with ether (twice). The combined extracts were washed with aqueous 10% sodium bicarbonate solution (twice) and water, dried, filtered, and concentrated to provide the aldehyde **4** (0.243 g, 87.5%) (9) which was further purified by preparative glc (column B, 200°C); ir (CCl_4): 2700 (CHO), 1725 (C=O) cm^{-1}; ^{1}Hmr (CCl_4): 5.57 (br s, 2H, CH=CH), 9.63 (t, $J = 2$ Hz, 1H, CHO) ppm.

The combined aqueous layers were acidified and extracted with ether to yield 3-cyclohexylacetic acid (**3**) (0.013 g, 4.15%) (8) which was homogeneous by glc analysis (column A, 150°C); ir (CCl_4): 3500–2400 (br OH), 1705 (C=O) cm^{-1}; ^{1}Hmr (CCl_4): 5.60 (br s, 2H, CH=CH), 11.35 (br s, 1H, CO_2H) ppm. An authentic sample was prepared by the hydrogenation (5% Pd/C, EtOAc) of synthetic **5**. Treatment of **3** with ethereal diazomethane afforded the ester **2** (7).

*Photolysis of Bicyclo[3.2.1]octan-2-one (**6**)*

(i) In Methanol

A solution of bicyclo[3.2.1]octan-2-one (0.150 g, 0.0012 mol, Aldrich) in absolute methanol (13 ml), to which sodium bicarbonate (0.040 g) had been added, was irradiated for 6 h. After removal of the solvent, carbon tetrachloride was added and the solution filtered and concentrated to yield a colourless oil. Gas–liquid chromatographic analysis (column A, 140°C) revealed two major peaks in a ratio of 9:1. Analysis on column B allowed a resolution of the principal peak into two components in a ratio of 7:2 (**7**:**8**) which were separated by preparative glc (column B, 207°C). The major product **7** had the following spectral properties: ir (CCl_4): 2810 (CHO), 2705 (CHO), 1725 (C=O) cm^{-1}; ^{1}Hmr (CCl_4): δ 9.74 (t, $J = 2$ Hz, 1H CHO), 5.63 (m, 2H CH=CH); (benzene-d_6): 5.53 (m, 2H CH=CH), 9.25 (br s, 1H CHO); (CCl_4 + $Eu(fod)_3$ mol equiv.): δ 9.74 (t, $J = 6.5$ Hz, 2H), 6.68 (m, 1H), 6.43 (q, $J = 6.5$ Hz, 2H), 5.50 (m, 1H), 5.07 (br m, 1H), 4.10 (t, $J = 7$ Hz, 1H), 3.88 (d, $J = 6$ Hz) ppm. This material was further characterized as its semicarbazone derivative mp 126–126.5°C. *Anal.* calcd. for $C_9H_{15}ON_3$: C 59.63, H 8.35, N 23.19; found: C 59.65, H 8.16, N 23.37.

The minor aldehyde **8** (9), collected by preparative glc as a colourless oil, had the following spectral properties: ir (CCl_4): 1710 (CHO), 1725 (C=O) cm^{-1}; ^{1}Hmr (CCl_4): δ 9.75 (t, $J = 2$ Hz, 1H, CHO), 5.55 (s, 2H, CH=CH);

(benzene-d_6): 5.58 (br s, 2H, CH=CH), 9.70 (br s, 1H, CHO) ppm. The material was further characterized as its semicarbazone derivative mp 123–123.5°C. *Anal.* calcd. for $C_9H_{15}ON_3$: C 59.63, H 8.35, N 23.19; found: C 59.55, H 8.43, N 23.34.

Methyl 3-cyclopentylpropionate (**10**) (12) was also collected from the glc; ir (CCl_4): 1738 (C=O) cm^{-1}; ^{1}Hmr (CCl_4): δ 3.60 (s, 3H, OCH_3) ppm. An authentic sample was prepared from 3-cyclopentylpropionic acid (Aldrich) by esterification with ethereal diazomethane and purified by glc (column A, 140°C).

(ii) In Tetrahydrofuran–Water

A solution of bicyclo[3.2.1]octan-2-one (8.0 g, 0.064 mol) in a 1:1 mixture of THF–water (64 ml) was irradiated until glc analysis indicated the photolysis was 85% complete. The solution was extracted twice with diethyl ether and the combined organic layers washed with aqueous 10% sodium bicarbonate solution and water until the washings were neutral, dried, and concentrated to give a mixture of isomeric aldehydes, **7** and **8**, and starting ketone as a colourless oil (6.2 g, 78%). Gas–liquid chromatographic analysis indicated the aldehydes were present in a ratio of 8:2 (**7**:**8**).

The combined aqueous layers were acidified and extracted with ether to yield an acid (0.6 g, 7.5%) which was purified by preparative tlc on silica gel (30% ether – petroleum ether) and identified as 3-cyclopentylpropionic acid (11) by comparison with an authentic sample; ir (CCl_4): 3500–2400 (br OH), 1710 (C=O) cm^{-1}.

Silver Oxide Oxidation of Aldehyde 7

A cold (0°C) aqueous solution (5 ml) of silver nitrate (0.350 g, 0.002 mol) and sodium hydroxide (0.04 g, 0.01 mol) was added to a dioxane solution (5 ml) containing the aldehyde **7** (0.100 g, 8.1 mmol). The reaction was stirred for 24 h at room temperature, filtered, and the residue washed with hot water until these washings were neutral. The filtrate was extracted with ether, acidified with 6 *N* hydrochloric acid, and extracted with ether (twice). These latter extracts were combined, washed with water, dried, filtered, and concentrated. The oil so obtained was purified by tlc on silica gel (1% acetic acid – benzene) to give 2-cyclopenten-1-propionic acid, (0.091 g, 80%) (22); ir (CCl_4): 3400–2400 (br, OH), 1710 (C=O) cm^{-1}; ^{1}Hmr (CCl_4): 5.50 (m, 2H, CH=CH), 10.45 (br s, 1H, COOH) ppm.

Hydrogenation of this material (5% Pd/C, EtOAc) afforded 3-cyclopentylpropionic acid. The same result was obtained when the oxidation and reduction were conducted on a mixture of **7** and **8**.

*Ozonolysis and Methylation of 2-Cyclopenten-1-propionic Acid: Formation of Dimethyl 4-Carbomethoxyheptane-1,7-dioate (**11**)*

A methanol–dichloromethane solution (1:1) containing 2-cyclopenten-1-propionic acid (0.090 g, 6.5 mmol) was cooled to −78°C (solid CO_2 – acetone bath) and a stream of oxygen containing ozone (~6%) passed through the solution until it retained a blue colour. The reaction mixture was allowed to warm to room temperature, aqueous 30% hydrogen peroxide (0.5 ml) added, and the solution stirred for 12 h. An ethereal solution of diazomethane was then added at 0°C until the solution retained a yellow colour and the solvent was removed under reduced pressure. Water and ether were added and the ether extract washed with water, dried, filtered, and concentrated to give the triester (0.138 g, 86%) which was purified by preparative glc (column A, 150°C).

This material was identified as dimethyl 4-carbomethoxyheptane-1,7-dioate (**11**) (13) by comparison with an authentic sample prepared by treating 1,3,5-pentanetricarboxylic acid (Aldrich, recrystallized from CH_3CN, mp 112.5–113°C; lit. (13) mp 113–114°C) with ethereal diazomethane at 0°C; ir (CCl_4): 1740 cm^{-1}; ^{1}Hmr (CCl_4): δ 1.86 (br t, $J \sim 6.5$ Hz, 4H, CH_2-), 2.1–2.6 (m, 5H, α to C=O), 3.61 (s, 6H, CH_3O), 3.65 (s, 3H, CH_3O) ppm.

Similar ozonolysis of the mixture of cyclopentenylpropionic acids from **7** and **8** afforded a 7:1 mixture (glc, column A, 180°C) of two triesters and permitted identification of the minor component as dimethyl-3-(carbomethoxymethyl)pentane-1,5-dioate.

*Photolysis of 1,8,8-Trimethyl[3.2.1]octan-2-one (Homocamphor) (**12**)*

(i) In Methanol

A solution of homocamphor (0.055 g, 3.2 mmol) (**12**) in absolute methanol (3.5 ml) containing sodium bicarbonate (0.010 g) was irradiated for 7 h. After evaporation of the solvent and the addition of petroleum ether, the solution was filtered and concentrated to yield a colourless oil (0.054 g, 99%), shown by glc analysis (column A, 187°C) to be a mixture of two new components (ratio 4:1) in addition to **12** (~10%). The aldehyde–ester ratio of 4:1 was confirmed by the ^{1}Hmr spectrum (CCl_4): 3.60 (s, OCH_3), 9.67 (t, $J \sim 1.5$ Hz, CHO) ppm.

(ii) In Tetrahydrofuran–Water

A solution of homocamphor (0.035 g, 2 mmol) in 1:1 THF–water (2 ml) was irradiated for 4 h. Gas–liquid chromatographic analysis (column A, 185°C) indicated an aldehyde–acid ratio of 30:1. After extraction with diethyl ether (twice), the combined extracts were washed with aqueous 10% sodium bicarbonate solution (twice), then water until the washings were neutral. The extracts were then dried, filtered, and concentrated to afford a colourless oil (0.028 g, 80%), from which the aldehyde was separated by tlc on silica gel (10% ether–hexane); ir (CCl_4): 2710 (CHO), 1720 (C=O) cm^{-1}; ^{1}Hmr (CCl_4): δ 0.80 (s, 3H, CH_3), 1.00 (s, 3H, CH_3), 1.60 (br s, 3H, CH_3C=C), 5.16 (br s, 1H, CH=C), 9.67 (t, 1H, $J \sim 1.5$ Hz, CHO) ppm.

Acidification of the combined aqueous phases (6 *N* HCl) followed by extraction with ether, washing the combined extracts with water until the washings were neutral, drying, filtering, and concentrating provided the carboxylic acid **14** (0.008 g, 2.1%) (23) which was homogeneous by glc (column A, 150°C); ir (CCl_4): 3500–2400 (br, OH), 1712 (C=O) cm^{-1}.

*Isolation of (±)-Homocamphor (**12**)*

To a 1:1 mixture of (±)-homo- and (±)-homoepicamphor (1.01 g, 0.006 mol) obtained by ring expansion of (±)-camphorquinone (24) followed by reduction (24) was added aqueous semicarbazide hydrochloride solution (1.5 ml, 0.5 mol equiv.) and enough methanol (~3 ml) to produce a clear solution. After the addition of pyridine (0.38 ml, 0.005 mol), the mixture was heated gently on a steam bath for 10 min, cooled, and the semicarbazone filtered. The filtrate was acidified with 6 *N* hydrochloric acid, the layers separated, and the aqueous layer ex-

tracted with ether (twice). The combined organic extracts were washed with water until the washings were neutral, dried, filtered, and concentrated to afford a colourless oil which crystallized on the addition of a few drops of benzene. Purification of homocamphor was achieved by preparative glc (column A, 187°C) or by thin layer chromatography on silica gel (10% ether-hexane). The melting point of (±)-homocamphor was 178–179°C (sealed tube) (lit. (24) (−)-homocamphor mp 187–190°C);[3] ir (CCl_4): 1706 cm^{-1}; ^{1}Hmr (CCl_4): δ 0.79 (s, 3H, CH_3), 0.85 (s, 3H, CH_3), 0.88 (s, 3H, CH_3) ppm.

*Photolysis of Ketones **1** and **6** in Diethyl Ether – Cyclohexylamine*

Solutions (~0.3 *M*) of the individual ketones were prepared in diethyl ether – cyclohexylamine (20:1), flushed with nitrogen, and irradiated in Pyrex containers until glc analysis indicated 20–30% of the original ketone had reacted. (Prolonged irradiation altered the ratios, the aldehydes giving rise to a more volatile component, presumably oxetane(s), and the amide afforded nitrile.) The ether was removed under reduced pressure and the ^{1}Hmr spectra recorded, the imine hydrogens appearing as triplets $J \sim 5$ Hz at δ 7.50 and 7.49 for **1** and **6**, respectively. These samples were dissolved in chloroform, washed with dilute aqueous hydrochloric acid, dried, and the spectra rerecorded. The imine signals had disappeared and the characteristic triplets for the aldehydic protons were now present. Integration of these signals and the amide N-C-H signals indicated an aldehyde–amide ratio of 1:2 for **1** and 1:1 for **6**. The accuracy of this determination was compared with a synthetic mixture in the case of **6** prepared from the aldehydes **7** and **8** and authentic cyclohexylamide prepared below. The individual components from the photolyses were separated by tlc on silica gel (30% ether–hexane).

3-Cyclopentylpropionatecyclohexyl amide was prepared from 3-cyclopentylpropionic acid (Aldrich) via its acid chloride (thionyl chloride) and recrystallized from ethanol–water mp 99–101°C; ir ($CHCl_3$): 3425 (N—H), 3300 br (N—H), 1665 (C=O), 1515 (C=O) cm^{-1}; ^{1}Hmr ($CDCl_3$): δ 3.73 (br complex, 1H, H-C-N), 5.48 (br, 1H, N-H) ppm.

Acknowledgments

We are grateful to Memorial University of Newfoundland and the National Research Council of Canada for financial support of this research, the Newfoundland Provincial Government for a fellowship (to S.C.C.), and the referees for their comments.

1. G. Quinkert. Pure Appl. Chem. **9**, 607 (1964); Angew. Chem. Int. Ed. Engl. **4**, 211 (1965); N. J. Turro, J. C. Dalton, K. Dawes, G. Farrington, R. Hautala, D. Morton, M. Niemezyk, and N. Schore. Acc. Chem. Res. **5**, 92 (1972); O. L. Chapman and D. S. Weiss. Org. Photochem. **3**, 197 (1973).

[3]The lower mp is probably a result of racemic *vs.* optically active material, for example (−)-epicamphor mp 186–187°C, (±) mp 180°C.

2. O. L. Chapman and D. S. Weiss. Org. Photochem. **3**, 252 (1973).
3. C. C. Badcock, M. J. Perona, G. O. Pritchard, and B. Rickborn. J. Am. Chem. Soc. **91**, 543 (1969); G. L. Closs and C. E. Doubleday. J. Am. Chem. Soc. **94**, 9248 (1972); **95**, 2735 (1973); B. Blank, A. Henne, and H. Fischer. Helv. Chim. Acta, **57**, 920 (1974); W. B. Moniz and C. F. Poranski, Jr. J. Am. Chem. Soc. **97**, 3258 (1975).
4. P. J. Wagner and R. W. Spoerke. J. Am. Chem. Soc. **91**, 4437 (1969); W. C. Agosta and W. L. Schreiber. J. Am. Chem. Soc. **93**, 3947 (1971); J. C. Dalton, K. Dawes, N. J. Turro, D. S. Weiss, J. A. Barltrop, and J. D. Coyle. J. Am. Chem. Soc. **93**, 7213 (1971); N. C. Yang and R. H. K. Chen. J. Am. Chem. Soc. **93**, 530 (1971); J. D. Coyle. J. Chem. Soc. B, 1736 (1971); A. G. Fallis. Can. J. Chem. **53**, 1657 (1975); R. O. Duthaler, R. S. Stingelinschmidt, and C. Ganter. Helv. Chim. Acta. **59**, 307 (1976).
5. W. C. Agosta and S. Wolff. J. Am. Chem. Soc. **98**, 4182 (1976).
6. W. B. Hammond and T. S. Yeung. Tetrahedron Lett. 1173 (1975).
7. P. Sabatier and M. Murat. C. R. **156**, 424 (1913).
8. R. Adams and J. R. Marshall. J. Am. Chem. Soc. **50**, 1970 (1928); O. Wallach. Ann. Chem. **359**, 287 (1908).
9. M. Schwartz, A. Besold, and E. R. Nelson. J. Org. Chem. **30**, 2425 (1965).
10. W. R. Boehme. J. Org. Chem. **26**, 2107 (1961); J. Gillois-Doucet. Ann. Chim. (Paris), **10**, 497 (1955).
11. J. W. Barrett, A. H. Cook, and R. P. Linstead. J. Chem. Soc. 1065 (1935).
12. D. S. Deorha and P. Gupta. Chem. Ber. **98**, 1722 (1965).
13. H. T. Openshaw and R. Robinson. J. Chem. Soc., 912 (1946).
14. G. Quinkert, A. Moschel, and G. Buhr. Chem. Ber. **98**, 2742 (1965).
15. N. L. Allinger, M. T. Tribble, M. A. Miller, and D. W. Wertz. J. Am. Chem. Soc. **93**, 1637 (1971).
16. E. M. Engler, J. D. Andose, and P. von R. Schleyer. J. Am. Chem. Soc. **95**, 8005 (1973).
17. N. L. Allinger, M. T. Tribble, and M. A. Miller. Tetrahedron, **28**, 1173 (1972); N. L. Allinger. J. Am. Chem. Soc. **81**, 5727 (1959).
18. C. D. Gutsche and J. W. Baum. Tetrahedron Lett. 2301 (1965); J. Am. Chem. Soc. **90**, 5862 (1968).
19. W. C. Agosta and S. Wolff. J. Am. Chem. Soc. **98**, 4316 (1976).
20. O. Diels, K. Adler, E. Petersen, and F. Querberitz. Ann. Chem. **478**, 137 (1930); G. A. Abad, S. P. Jindal, and T. T. Tidwell. J. Am. Chem. Soc. **95**, 6326 (1973).
21. G. Zweifel and H. C. Brown. Org. React. **13**, 1 (1963).
22. M. Julia and F. Le Goffic. Bull. Soc. Chim. Fr. 1550 (1965).
23. A. G. Fallis. Ph.D. Thesis, University of Toronto, Toronto, Ont. 1967.
24. H. Favre, B. Marinier, and J. C. Richler. Can. J. Chem. **34**, 1329 (1956).

σ-Complexes as biophysical and biochemical probes. Part II.[1] Transformations of σ-complex intermediates from reaction of 4-nitrobenzofuroxan and methoxide ion

ERWIN BUNCEL, NOEMI CHUAQUI-OFFERMANNS, BRIAN K. HUNTER, AND ALBERT R. NORRIS

Department of Chemistry, Queen's University, Kingston, Ont., Canada K7L 3N6

Received November 15, 1976

ERWIN BUNCEL, NOEMI CHUAQUI-OFFERMANNS, BRIAN K. HUNTER, and ALBERT R. NORRIS. Can. J. Chem. **55**, 2852 (1977).

Reaction of 4-nitrobenzofuroxan with methoxide ion in methanolic dimethyl sulphoxide solution gives rise to 7-hydroxy-4-nitrobenzofurazan (as the anion) and 7-methoxy-4-nitrobenzofurazan (as the methoxide C-7 adduct); the proposed reaction mechanism invokes the formation of several transient intermediates. The results bear on the postulated mechanism for the antileukemic activity of 4-nitrobenzofuroxan.

ERWIN BUNCEL, NOEMI CHUAQUI-OFFERMANNS, BRIAN K. HUNTER et ALBERT R. NORRIS. Can. J. Chem. **55**, 2852 (1977).

La réaction du nitro-4 benzofuroxanne avec l'ion méthylate dans une solution de diméthylsulfoxyde méthanolique conduit à l'hydroxy-7 nitro-4 benzofurazanne (sous forme d'anion) et au méthoxy-7 nitro-4 benzofurazanne (sous forme d'adduit méthylate en C-7); le mécanisme proposé pour la réaction implique la formation de plusieurs intermédiaires de courte durée de vie. Ces résultats ont des implications sur le mécanisme postulé pour l'activité antileucémique du nitro-4 benzofuroxanne.

[Traduit par le journal]

Introduction

The discovery (2) that certain benzofuroxan and benzofurazan derivatives act as powerful inhibitors of nucleic acid and protein biosynthesis in many types of animal cells has heightened interest in these classes of compounds (3–11). Especially noteworthy was the observation that 4-nitrobenzofuroxan exhibits a toxic effect on the metabolism of leukocites *in vitro* (3), suggesting the possibility that such compounds may act as potential antileukemic and immunosuppressive drugs. Since 4-nitrobenzofuroxan readily formed Meisenheimer type σ-complexes with nucleophiles, and since drug action was abolished by preincubation with aliphatic thiols, it was concluded (2) that drug action was related to the interaction of 4-nitrobenzofuroxan with intracellular thiol groups, leading to σ-complex formation (10–12).

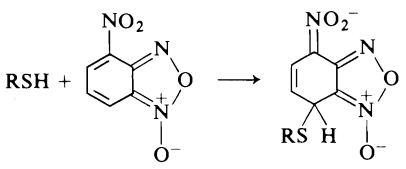

[1]For part I see ref. 1.

In our studies of the interaction of aromatic nitro compounds with bases, we have elucidated the structures of a variety of σ-complexes and have also derived kinetic and thermodynamic parameters relating to their formation and decomposition (13–19). Thus, we have extended these studies to the 4-nitrobenzofuroxan – methoxide ion system in dimethyl sulfoxide – methanol. Unexpectedly, we have discovered that the initially formed σ-complexes undergo some unusual transformations which lead, overall, to deoxygenation of the *N*-oxide function and to substitution of an aromatic hydrogen by the methoxy or hydroxy function.

Results

The interaction of 4-nitrobenzofuroxan (**1**) with potassium methoxide in methanolic dimethyl sulphoxide solution was investigated over a temperature range between −20 and +35°C. Five minutes after mixing, when the first spectrum could be taken, the solution of **1** (0.40 *M*) and CH_3OK (0.44 *M*) in DMSO-d_6–CH_3OD (70:30 v/v) at −20°C showed the absence of signals characteristic of **1**, and the appearance of a species which is identified as **2**. The identification was made on the basis of the following assignment for the ABC spin system (chemical

shifts, δ, quoted in ppm, relative to tetramethylsilane as internal standard, coupling constants in Hz): H-5 5.52, H-6 6.43, H-7 6.68; $J_{5,6}$ 4.7, $J_{5,7} < 1$, $J_{6,7}$ 9.8. On further monitoring of the reaction solution at −20°C new resonances developed which after 30 min were found to be sufficiently intense to allow for their identification as resonances due to complex **3**. The nmr spectrum presented an ABC pattern which was assigned as follows: H-5 7.19, H-6 5.23, H-7 5.32; $J_{5,6}$ 10.3, $J_{5,7} < 1$, $J_{6,7}$ 4.4. The computer simulated spectra (20) of **2** and **3** agreed well with the experimentally obtained nmr spectra.[2] Our data are also in agreement with the work of Simonnin and co-workers (10).

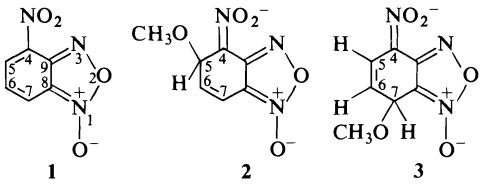

1 **2** **3**

Further changes in the nmr spectrum are observed on allowing the temperature of the solution to rise, first to −10°C (25 min) then to 0°C, corresponding to the formation of a new species, **X**; after 5 min at 0°C the species **2**, **3**, and **X** are present in about equal concentrations. A further rise in temperature causes the signals due to **2** to disappear entirely so that after 45 min at 10°C only **3** and **X** are present, in about equal concentration. When the temperature is then raised to 35°C for 10 min, **3** also disappears and **X** remains as the sole product. The species **X** is identified as the nitronate derivative **4**. The nmr spectrum consisted of a simple AX doublet, assignable as H-5 at 7.27 and H-6 at 5.70 ($J_{5,6}$ = 8), and in addition there was a signal at low field (δ 10.5) assignable to the NOH function. The CH_3O resonance is obscured by the methanol of the medium.

The reaction solution on standing 24 h at 30°C developed new sets of peaks in the nmr spectrum, this process becoming complete after 48 h at 30°C. The new resonance signals could be identified unambiguously as resulting from a mixture of the substances **7** and **9** (present in ratio of 3:1), both of which were prepared by authentic routes (7, 9) and were found to have concordant spectral characteristics under the reaction conditions. For **7**, H-5 occurs at 8.35 (d) and H-6 at 5.90 (d), $J_{5,6}$ = 10. For **9**, H-5 appears at 7.32 (d) and H-6 at 5.32 (d), $J_{5,6}$ = 11 (see Experimental section for complete characterization of **7** and **9**).

Discussion

The results which we have observed are interpreted as follows. Addition of methoxide ion to **1** leads to the initial formation of complex **2** as the product of a kinetically controlled reaction (21–26). In time **2** is replaced by complex **3** which is the thermodynamically controlled product.[3] The latter is unstable, as shown by further changes in the nmr spectra, and the products which are formed can be explained by the mechanisms given in Scheme 1. Initially there is a transfer of the sp^3 hydrogen in **3** to the *N*-oxide function yielding the nitronate derivative **4**. This intermediate is also unstable and becomes the precursor of the observed reaction products **7** and **9**. The former arises essentially via an intramolecular shift of the O^- function following deprotonation of **4**, *i.e.* **5** → **6**. This process is analogous to the Smiles rearrangement (for a review see ref. 28), though to our knowledge such has not been observed previously in the benzofuroxan system. The product **7** is obtained by loss of CH_3O^- from **6**. The second product, **9**, is obtained from **4** by expulsion of OH^- from the furoxan ring to yield **8**, followed by addition of CH_3O^-. Alternatively, attack of CH_3O^- on C-7 of **4** with concerted expulsion of OH^- would yield **9** directly.

In previous work on the interaction of **1** with methoxide ion, the complexes **2** (10) and **3** (2, 10) have been identified, but not their subsequent transformations. It is noteworthy that formation of complexes analogous to **3**, derived by attack of intracellular sulfhydryl and/or amino groups at C-7 of **1**, has been invoked in order to account for the observed antileukemic reactivity of 4-nitrobenzofuroxan (2, 3). This hypothesis must be reexamined in view of our findings that the complex **3** is unstable and decomposes through

[2]The species **3** could be obtained essentially free of **2** (and also of X) when the experiment was performed under the conditions [4-nitrobenzofuroxan] = [CH_3OK] = 0.2 *M*. However this solution on standing developed a green color, with concurrent loss of the proton resonances. Initial studies show that the course of the reaction is strongly influenced by the ratio of substrate to base and this aspect will be further investigated.

[3]Alternatively, it is possible that the transformation of **2** to **3** occurs by means of the Boulton–Katritzky rearrangement (27). This possibility is currently being investigated.

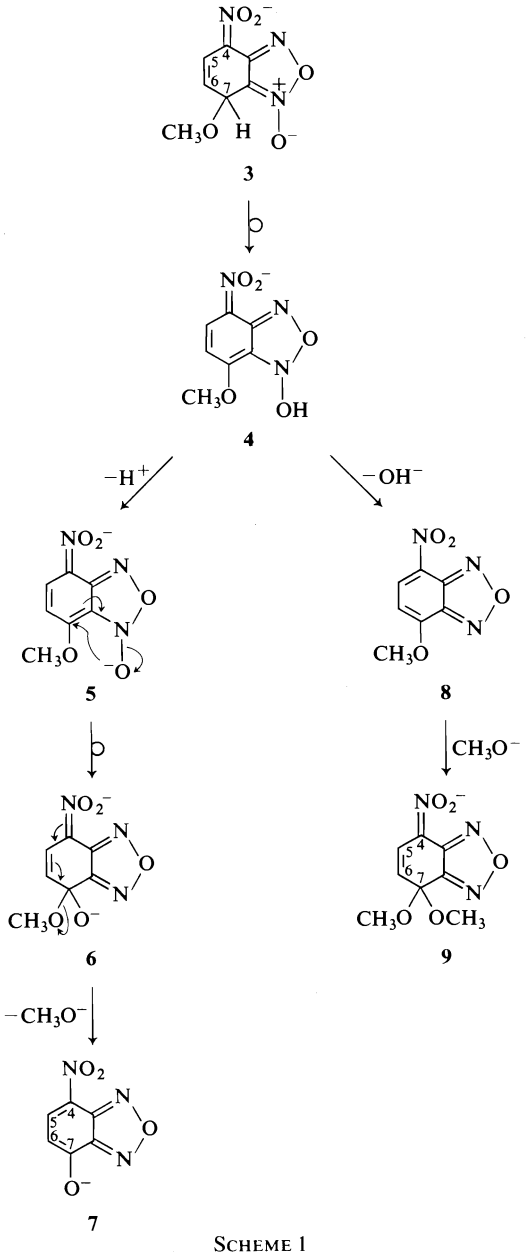

SCHEME 1

the involvement of several transient intermediates. An examination of the possible biological activity of all the species implicated in the present study is thus indicated, since it might be one or more of these intermediates or products and not 4-nitrobenzofuroxan itself which is responsible for the activity of this compound.

Experimental

Materials and Preparations

Dimethyl sulfoxide was distilled from barium oxide or calcium hydride under nitrogen. Methanol was distilled from magnesium metal. The deuterated solvents were dried over molecular sieves. A stock solution of CH_3OK/CH_3OD was prepared from freshly cut potassium metal and CH_3OD, stored under nitrogen, and standardized immediately before use.

4-Nitrobenzofuroxan was prepared according to ref. 4 (method *B*) mp 143°C. 7-Methoxy-4-nitrobenzofurazan was prepared from 7-chloro-4-nitrobenzofurazan and sodium methoxide, mp 115–116°C (29). Reaction of 7-methoxy-4-nitrobenzofurazan with hot aqueous NaOH yielded 7-hydroxy-4-nitrobenzofurazan, mp 200°C (29). The uv–visible spectrum of this compound was obtained in DMSO–methanol (70:30 v/v) containing trifluoroacetic acid (2.2 *M*): $\lambda_{max(1)}$ 395 nm, ε 9500; $\lambda_{max(2)}$ 285 nm, ε 5000 M^{-1} cm^{-1}. The spectrum of the anion (**7**) was obtained in this medium with added CH_3ONa: $\lambda_{max(1)}$ 466 nm, ε 20 000; $\lambda_{max(2)}$ 366 nm, ε 11 000 M^{-1} cm^{-1}. The nmr spectrum of 7-hydroxy-4-nitrobenzofurazan in DMSO-d_6: H-5 8.60, H-6 6.72 ($J_{5,6}$ 8 Hz), OH 11.6.

Complex **9** was obtained as a yellow-orange solid on treatment of 7-methoxy-4-nitrobenzofurazan in acetonitrile solution with sodium methoxide in methanol. Spectral data: nmr in DMSO-d_6: H-5 7.25, H-6 5.18 ($J_{5,6}$ 11 Hz), OCH_3 3.30; uv in DMSO–methanol (80:20 v/v): λ_{max} 354 nm, ε 22 000. Acidification of the solution (CF_3CO_2H) regenerated 7-methoxy-4-nitrobenzofuran: λ_{max} 380 nm, ε 11 500 M^{-1} cm^{-1}.

Methods

The reaction of 4-nitrobenzofuroxan (**1**) with methoxide ion was performed in DMSO-d_6–CH_3OD by the following procedure. A solution of **1** (72.4 mg) in 0.60 ml of DMSO-d_6–CH_3OD (70:30 v/v) was placed in a 5 ml round bottom flask sealed with a rubber septum, the flask immersed in a cryostat bath at −20°C, and the contents were stirred magnetically. To this cooled, stirred, solution 0.40 ml of a 1.1 *M* potassium methoxide solution in DMSO-d_6–CH_3OD (70:30 v/v) was added very slowly by means of a cooled syringe. A 0.5 ml portion of the resulting deep orange coloured solution was transferred under nitrogen to an nmr tube, which was then cooled to −80°C and stored until the nmr measurements could be made. A Bruker 60 MHz HFX-60 instrument was used, varying the temperature of the probe between −20 and +35°C.

Acknowledgments

We gratefully acknowledge financial support of this research by the National Research Council of Canada, the McLean Foundation (A.R.N.) and the Advisory Research Committee of Queen's University (A.R.N.).

1. E. BUNCEL, N. CHUAQUI-OFFERMANNS, and A. R. NORRIS. J. Chem. Soc. Perkin Trans. I, 415 (1977).
2. P. B. GHOSH and M. W. WHITEHOUSE. J. Med. Chem. **11**, 305 (1968).
3. M. W. WHITEHOUSE and P. B. GHOSH. Biochem. Pharmacol. **17**, 158 (1968).
4. P. B. GHOSH. J. Chem. Soc. B, 334 (1968).
5. P. B. GHOSH and M. W. WHITEHOUSE. J. Med. Chem. **11**, 158 (1969).
6. P. B. GHOSH, B. TERNAI, and M. W. WHITEHOUSE. J. Med. Chem. **15**, 255 (1972).

7. D. DALMONTE, E. SANDRI, and W. CERÉ. Ann. Chim. (Rome), **60**, 801 (1970).
8. D. DALMONTE, E. SANDRI, L. DINUNNO, S. FLORIO, and P. E. TODESCO. Chim. Ind. (Milan), **53**, 940 (1971).
9. L. DINUNNO, S. FLORIO, and P. E. TODESCO. J. Chem. Soc. Perkin Trans. II, 1469 (1975).
10. F. TERRIER, F. MILLOT, A. P. CHATROUSSE, M. J. POUET, and M. P. SIMONNIN. Org. Magn. Reson. **8**, 56 (1976).
11. F. TERRIER, F. MILLOT, and W. P. NORRIS. J. Am. Chem. Soc. **98**, 5883 (1976).
12. W. P. NORRIS and J. OSMUNDSEN. J. Org. Chem. **30**, 2407 (1965).
13. E. BUNCEL, A. R. NORRIS, and K. E. RUSSELL. Q. Rev. Chem. Soc. **22**, 123 (1968).
14. E. BUNCEL, A. R. NORRIS, and W. PROUDLOCK. Can. J. Chem. **46**, 2759 (1968).
15. E. BUNCEL, A. R. NORRIS, K. E. RUSSELL, P. J. SHERIDAN, and H. WILSON. Can. J. Chem. **52**, 1750 (1974).
16. A. R. NORRIS. Can. J. Chem. **47**, 2895 (1969).
17. L. H. GAN and A. R. NORRIS. Can. J. Chem. **52**, 1 (1974).
18. E. BUNCEL and J. G. K. WEBB. Can. J. Chem. **52**, 630 (1974).
19. E. BUNCEL, A. JONCZYK, and J. G. K. WEBB. Can. J. Chem. **53**, 3761 (1975).
20. DELOS F. DETAR. Computer programs for chemistry. Vol. 1. W. A. Benjamin, New York, N.Y. 1968, as modified for Fortran IV: NMRCAL, Nicolet Instrument Corp., NIC-05-40417, 1972.
21. K. L. SERVIS. J. Am. Chem. Soc. **89**, 1508 (1967).
22. M. R. CRAMPTON. Adv. Phys. Org. Chem. **7**, 211 (1969).
23. F. MILLOT and F. TERRIER. Bull. Soc. Chim. Fr. 2692 (1969).
24. M. J. STRAUSS. Chem. Rev. **70**, 667 (1970).
25. C. F. BERNASCONI. MTP Int. Rev. Sci. Org. Chem. Ser. One, **3**, 33 (1973).
26. J. H. FENDLER, W. L. HINZE, and L.-J. LIU. J. Chem. Soc. Perkin Trans. II, 1768 (1975).
27. A. J. BOULTON, P. B. GHOSH, and A. R. KATRITZKY. Angew. Chem. Int. Ed. Engl. **3**, 693 (1964).
28. J. F. BUNNETT and R. E. ZAHLER. Chem. Rev. **49**, 273 (1951); H. J. SHINE. Aromatic rearrangements. Elsevier, Amsterdam. 1967. p. 307.
29. D. DALMONTE, E. SANDRI, and P. MAZZARACCHIO. Boll. Sci. Fac. Chim. Ind. Bologna, **26**, 165 (1968).

Derivatives of 2-pyrazolin-5-one. V.[1] Preparation and properties of 1′,2′-dihydrospiro[[2]pyrazoline-4,3′(4′*H*)-quinoline]-5-one derivatives and related compounds

RONALD T. COUTTS AND ABDEL-MONAEM EL-HAWARI

Faculty of Pharmacy and Pharmaceutical Sciences, University of Alberta, Edmonton, Alta., Canada T6G 2N8

Received January 21, 1977

RONALD T. COUTTS and ABDEL-MONAEM EL-HAWARI. Can. J. Chem. **55**, 2856 (1977).

1′,2′-Dihydro-3-methyl-1-phenylspiro[[2]pyrazoline-4,3′(4′*H*)-quinoline]-5-one (**8***q*), the structurally related 1,3-diphenylspiro[pyrazolone–quinoline] **8***r* and numerous 2′-substituted derivatives of **8***q* and **8***r* are readily accessible from catalytic reduction of 3-methyl-1-phenyl- or 1,3-diphenyl-4-(2-nitrobenzyl)-2-pyrazolin-5-one (**1***a*, **1***b*, respectively) in alcohols (with the incorporation of the alkylidene moiety) or by interaction of the corresponding 2-aminobenzyl precursors (**3***a*, **3***b*) with appropriate aldehydes and ketones. All spiro compounds were characterized by mass, ir, and ^{1}Hmr spectra. The products obtained by reducing the spiro compounds with sodium borohydride and with lithium aluminum hydride are described. Reduction of **1***a* and **1***b* with zinc and acetic acid gave 3-methyl-1-phenyl- and 1,3-diphenyl-1*H*-pyrazolo-[3,4-*b*]quinoline (**2***a*, **2***b*, respectively).

RONALD T. COUTTS et ABDEL-MONAEM EL-HAWARI. Can. J. Chem. **55**, 2856 (1977).

La dihydro-1′,2′ méthyl-3 phényl-1 spiro[[2]pyrazoline-4,3′(4′*H*) quinoline] one-5 (**8***q*), la diphényl-1,3 spiro[pyrazolone–quinoline] qui lui est reliée d'une façon structurale (**8***r*) et plusieurs dérivés substitués en position 2′ de **8***q* et **8***r* sont facilement accessibles par la réduction catalytique des méthyl-3 phényl-1 ou diphényl-1,3 (nitro-2 benzyl)-4 pyrazolin-2 ones-5 (**1***a*, **1***b* respectivement) dans l'alcool (avec l'incorporation de la portion alkylidène) ou par interaction des précurseurs amino-2 benzyle correspondants (**3***a*, **3***b*) avec les aldéhydes ou cétones appropriés. On a caractérisé tous les composés spiro par spectrométrie de masse, ir ou rm^{1}H. Les produits obtenus en réduisant les composés spiro avec le borohydrure de sodium et l'hydrure double de lithium et d'aluminium sont décrits. La réduction de **1***a* et de **1***b* avec le zinc et l'acide acétique conduit aux méthyl-3 phényl-1 et au diphényl-1,3 1*H*-pyrazolo[3,4-*b*]-quinolines (**2***a* et **2***b* respectivement).

[Traduit par le journal]

Our previous studies (1, 2) have shown that the products of palladium–charcoal catalyzed sodium borohydride reductions of 3-methyl-4-(2-nitrobenzyl)-1-phenyl-2-pyrazolin-5-one (**1***a*), the 3-phenyl analog **1***b*, and structurally related 2-nitrobenzylidene compounds, vary according to the nature of the solvent employed. In further attempts to prepare cyclic hydroxylamines or related nitrones, we have continued our studies on the reduction of **1***a* and **1***b* using alternative reducing systems.

Initially, the 3-phenylpyrazolone **1***b* was reduced with zinc and acetic acid and yielded a yellow crystalline product, $C_{22}H_{15}N_3$, the ir spectrum of which lacked NH, OH, and CO absorption bands. The mass spectrum of the product had a strong molecular ion (*m/e* 321) and only three additional ions of appreciable intensity of *m/e* 320, 244, and 218, which resulted from the expulsion of a hydrogen atom, a phenyl radical, and a phenyl cyanide molecule, respectively, from the molecular ion. The product's ^{1}Hmr spectrum showed no signals other than those of aromatic protons. The compound, $C_{22}H_{15}N_3$, is identified, therefore, as the hitherto unknown 1,3-diphenyl-1*H*-pyrazolo[3,4-*b*]quinoline (**2***b*).

When the 3-methyl analog **1***a* was similarly reduced with zinc and acetic acid, the product obtained proved difficult to purify but possessed

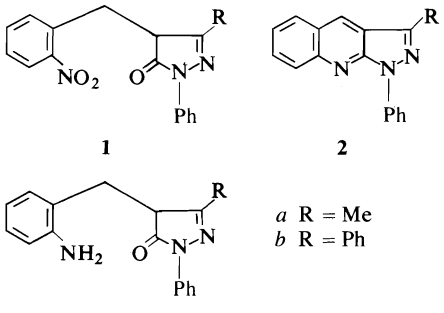

[1]For part IV, see ref. 3.

properties similar to those described for **2***b* and is identified as 3-methyl-1-phenyl-1*H*-pyrazolo-[3,4-*b*]quinoline (**2***a*) which was obtained previously (4) by heating together 5-chloro-4-formyl-3-methyl-1-phenylpyrazole and aniline. The mechanism of formation of **2***a* and **2***b* from **1***a* and **1***b* proceeds presumably via the amines **3***a*,*b* since prolonged heating of solutions of these amines in acetic acid produced **2***a* and **2***b*.

Catalytic hydrogenation of the *o*-nitrobenzylpyrazolone derivatives **1***a* and *b* was then attempted to determine whether *N*-hydroxy compounds could be obtained by this route. Reduction was initially carried out using platinum oxide or palladium–charcoal as a catalyst and absolute ethanol as solvent. When the 3-phenylpyrazolone **1***b* was reduced under these conditions, the product obtained, $C_{24}H_{21}N_3O$, designated compound A, was not the expected one. It was a weak base, but, unlike compound **3***b*, product A was insoluble in dilute sodium hydroxide solution. Its ir spectrum showed NH and C=O absorption bands, the latter at 1712 cm^{-1}. The presence of C=O absorption at this frequency in addition to the insolubility of product A in dilute alkali solution, indicated that the pyrazolone ring was no longer capable of enolization, i.e. the hydrogen atom α to the C=O group was no longer present. The ^{1}Hmr spectrum of compound A indicated the presence of a $CHCH_3$ group which undoubtedly originated from the ethanol employed as the solvent in the catalytic reduction of **1***b*. To verify this, the same reaction was repeated in dioxane, in methanol, in propanol, and in benzyl alcohol. With dioxane, 4-(2-aminobenzyl)-1,3-diphenyl-2-pyrazolin-5-one (**3***b*) was obtained in good yield, but when the other solvents were employed, the products obtained (B–D) in each case differed, and elemental analyses suggested that the alkyl or aryl group of the alcohol used had been incorporated into the molecule. The ir spectra of all products (A–D) were very similar. Their ^{1}Hmr and mass spectra confirmed that the alcohols used as solvents were involved in the formation of A–D.

From all these data, each of the compounds A–D was suspected to be a 2′-substituted-1′,2′-dihydro-1,3-diphenylspiro[[2]pyrazoline-4,3′(4′*H*)-quinoline]-5-one (**4**). A mechanism for the formation of spiro[pyrazolone–quinoline] (**4**) can be envisaged (Scheme 1). The nitro compound **1***b* is partially reduced to a hydroxylamine (**5**) which then interacts with the alcohol present; the former is reduced to the amine **3***b* while the latter is oxidized to the aldehyde. Both the amine and the aldehyde react to form a carbinolamine (**6**) which cyclizes to the spiro[pyrazolone-quinoline] derivatives (**4**). This suggested oxidation–reduction process, and subsequent interaction of the products, is another example of solvent/product interactions known to occur during catalytic hydrogenation (5).

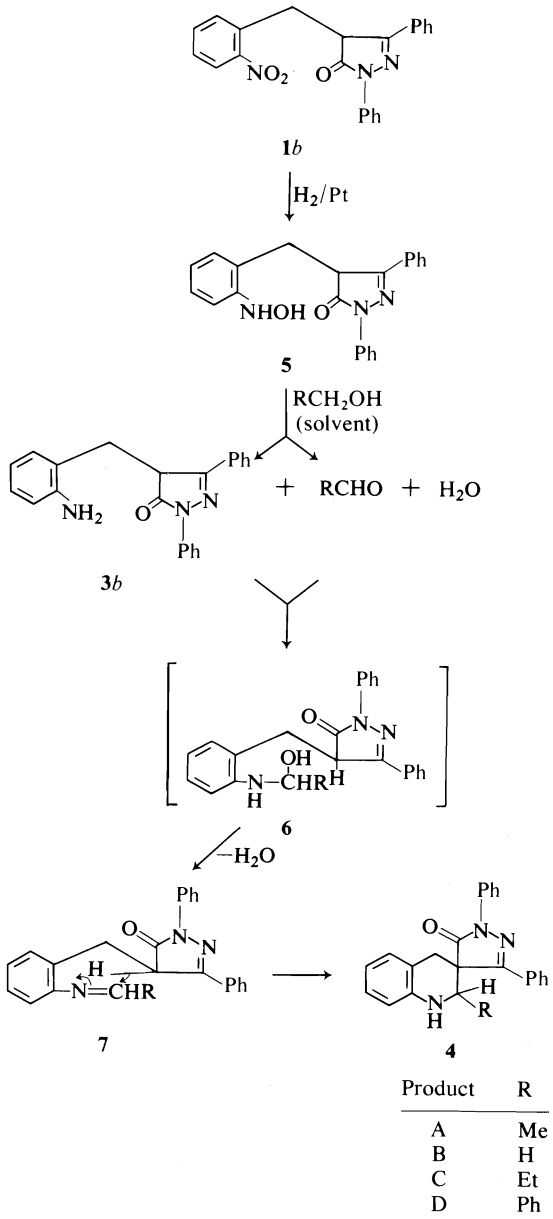

Product	R
A	Me
B	H
C	Et
D	Ph

SCHEME 1

The spiro[pyrazolone–quinoline] structure (**4**; Scheme 1) is isomeric with the imine (Schiff base) structure **7** but the ir and ^{1}Hmr data from compounds A–D are not compatible with these compounds being imines. Further evidence of the suitability of structure **4** was obtained from an analysis of the mass spectra of the four compounds A–D. None fragmented under electron impact in the manner that Schiff bases do. Mass spectral studies of some Schiff bases have recently been reported (6) and it has been shown that the molecular ion undergoes simple fission at the ring-nitrogen and ring-carbon bonds, the former fragmentation being more facile than the latter. No fragment ions due to ring-nitrogen fission were present in the mass spectra of any of the products isolated. On the other hand, the fragment pathways observed were reminiscent of the behaviour of tetrahydroquinoline derivatives under electron impact (7) (Scheme 2).

A final argument against the imine structure **7** was based on the fact that such a structure should not be isolated under these reduction conditions. Schiff bases are known to be reduced in virtually quantitative yields either by catalytic hydrogenation or by chemical reagents (8) and accordingly, the imine if it were formed would be reduced to the related secondary amine. The imine, however, may have a transitory existence in the formation of the spiro-compounds (**4**) (see Scheme 1). It is possible that the aldol **6** dehydrates directly to the spiro-compound, but literature evidence is available (9) in support of a Schiff base intermediate. The formation of the spiro-compounds (**4**) thus involves the addition of a C—H group to the C=N function of the Schiff base. Similar cyclizations of Schiff bases involving the addition of O—H across the C=N group to give 2*H*-1,3-benzoxazines, and the addition of S—H across the C=N group to yield thiazolidines have been reported (10, 11).

If the postulated mechanism depicted in Scheme 1 is factual, numerous compounds of general structures **8** and **9** could be prepared in the manner shown (Scheme 3) and this has proved possible. Eighteen spiro[pyrazolone–quinoline] derivatives (Table 1) were obtained from the interaction of the amines **3***a* and **3***b* and an appropriate aldehyde or ketone in refluxing ethanolic solution. The phenolic compounds **8***d*, *e*, *f*, *g* and *o* and the carboxylic acid derivatives **8***k* and *p* were prepared in particular because of their ability to dissolve in dilute

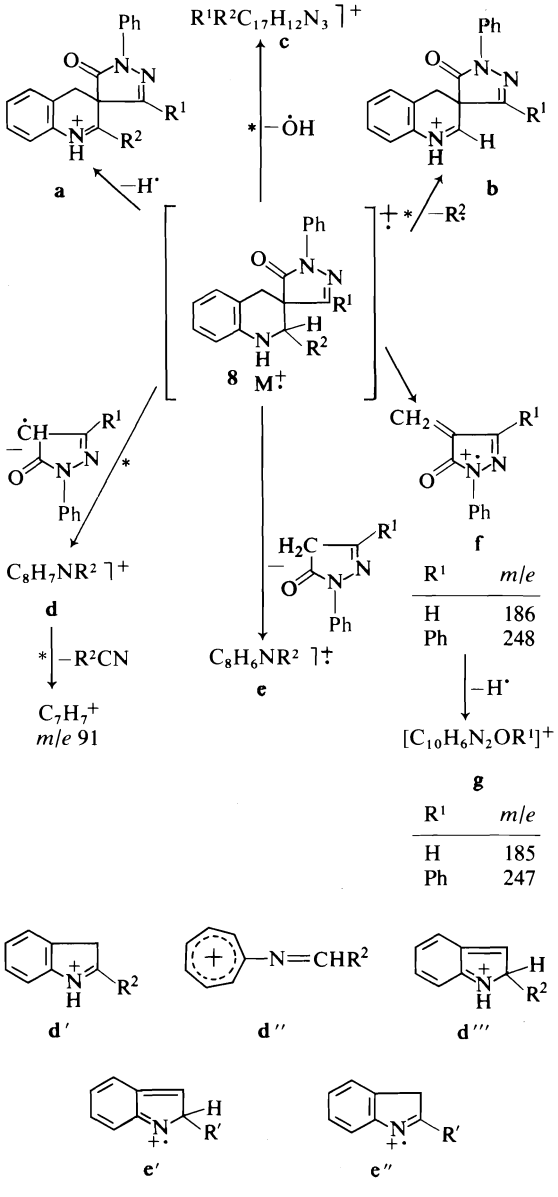

SCHEME 2. Percentage relative abundance of ions:

	M+·	a	b	c	d	e	f	g
8*a*	96	7	21	6	100	21	17	7
8*c*	100	7	4	4	76	54	8	9
8*l*	76	8	14	6	100	9	6	4
8*o*	100	9	5	4	62	33	—	—
9*b**	47	—	9	—	100	43	5	6
8*q*	85	16	—	11	87	35	16	25
8*r*	100	19	—	7	42	9	14	22

*For compound **9***b*, replace the —NHCHR²— group in general structure **8** with —NHCMe₂—; in fragment ions **b**, **d** and **e** derived from **9***b*, a methyl group, therefore, replaces the hydrogen atom indicated (—NHC*H*R²).

TABLE 1. 1′,2′-Dihydrospiro[[2]pyrazoline-4,3′(4′*H*)-quinoline]-5-one derivatives (**8**, R^3 = H; **9**, R^3 = Me)

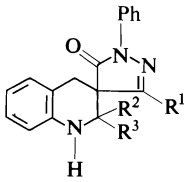

	R^1	R^2	mp(°C)		R^1	R^2	mp (°C)
8*a*	Me	Me	149–150	**8***j*	Me	2-NH_2-Ph	163–165
8*b*	Me	Et	143–144	**8***k*	Me	Ph-4-COOH	245–246
8*c*	Me	Ph	146–147	**8***l**	Ph	Me	174–175
8*d*	Me	4-OH-Ph	212–213	**8***m**	Ph	Et	160–162
8*e*	Me	2-OH-Ph	176–178	**8***n**	Ph	Ph	210–212
8*f*	Me	2,4-*di*OH-Ph	180–182	**8***o*	Ph	4-OH-Ph	237–239
8*g*	Me	3-OMe, 4-OH-Ph	181–182	**8***p*	Ph	Ph-4-COOH	253–254
8*h*	Me	3,4-*di*OMe-Ph	193–194	**9***a*	Me	Me	148–151
8*i*	Me	4-NH_2-Ph	193–195	**9***b*	Ph	Me	198–199

*These compounds are included for completeness and are identical with compounds A, C, and D respectively (see Scheme 1).

alkaline solution, a property which was required to facilitate a planned pharmacological evaluation.

Aliphatic ketones are known to react with amines more slowly than aldehydes to form imines. This was the case here; it necessitated the use of higher reaction temperature and longer reaction times to obtain the spiro-derivatives **9***a* and **9***b* in the absence of catalyst or dehydrating agent. Attempts to crystallize the isolated product **9***a* were unsuccessful, but the ir and ^{1}Hmr spectra of this product agreed with the proposed structure. The reaction between the phenyl analog **3***b* and acetone was more facile and the product **9***b* was easily characterized.

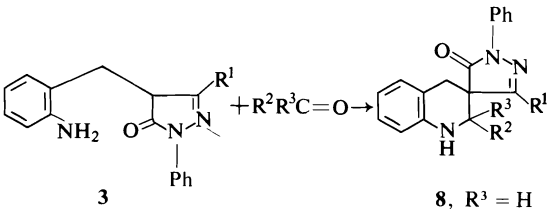

3 **8**, R^3 = H; **9**, R^3 = Me

SCHEME 3

When the amines **3***a* and **3***b* were reacted with formaldehyde, they failed to form spiro-compounds. The required spiro[pyrazolone–quinolines] (**8***q*, **8***r*) were readily obtained, however, when the nitro compounds **1***a*, *b* were catalytically hydrogenated over platinum using methanol as a solvent.

All the spiro-compounds (**8**, **9**) prepared in this study were identified by their correct elemental analysis and by the similarities between their ir and ^{1}Hmr spectra and those described earlier for compounds A—D. The mass spectra of some of these derivatives were recorded and possible fragmentation pathways are suggested in Scheme 2. Deuteration of compound **8***c* as well as an examination of the spectrum of 1′,2′-dihydro-2′,2′-dimethyl-1,3-diphenylspiro[[2]pyrazoline-4,3′(4′*H*)-quinoline]-5-one **9***b* were helpful in accounting for the origin of some of the fragment ions. Each compound gave a strong molecular ion which expelled a hydrogen atom as well as the radical (R^2) from C-2 of the tetrahydroquinoline ring giving rise to weak fragment ions (Scheme 2).

An interesting fragment found in all the spectra (except the dimethyl derivatives **9***a*, *b*) was due to the expulsion of an OH radical from the molecular ion. This expulsion was supported by metastable ions present at appropriate *m*/*e* values in most spectra. The origin of this ion is not known. Deuterium labelling ruled out any contribution from the amine proton since the ion at *m*/*e* 350 in **8***c* was located at *m*/*e* 351 in the deuterated compound.

A strong fragmentation ion (**d**) was present in the spectra of all compounds. This resulted from the expulsion of a pyrazolone radical from the molecular ions; appropriate metastable ions were present in the spectra in support of this assertion. Depending on which hydrogen is involved in the expulsion of the pyrazolone radical, three structures (**d**′–**d**‴) can be en-

visaged for the ion formed. It seems, however, that the amine hydrogen is more involved in the proposed migration than a C-2′ or a C-4′ hydrogen atom. That was indicated by examining the spectra of both the deuterated compound (**8***c*, N—D replaces N—H) and the 2′,2′-dimethyl derivative **9***b*. The former showed a major loss of 174 mass units from the molecular ion instead of 173 mass units lost in the non-deuterated compound **8***c*. The 2,2-dimethyl derivative **9***b* molecular ion also expelled a pyrazolone radical to give a fragment ion at *m/e* 146 (which retained both C-2′ methyl groups) thus implicating migration of the NH hydrogen atom, or alternatively, a hydrogen atom from the ring methylene group. Non-involvement of the protons at C-4′ was suggested, however, by the presence of similar strong ions resulting from the loss of a pyrazolone radical in the spectra of structurally related spiro-dihydrobenzothiazines (**10**)[2] in which the methylene group is replaced by a sulfur atom. Mechanisms for the formation of ions **d′**–**d‴** are readily suggested. The mechanism preferred, for the reasons just expounded, is given in Scheme 4.

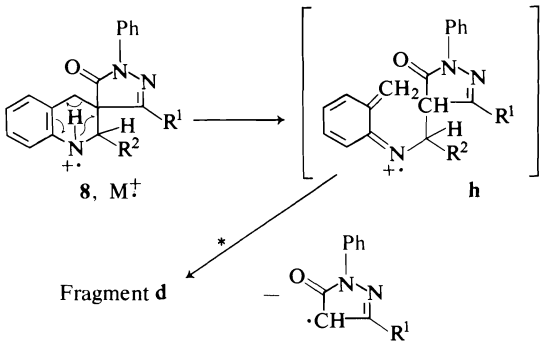

SCHEME 4

Another diagnostic fragmentation pathway is the decomposition of the molecular ion to give ions identified as **f** and **g** in Scheme 2. The intermediate ion **h** (Scheme 4) is also thought to be the origin of the fragment **e** which is present in relatively high abundance in the mass spectra of spiro[pyrazolone–quinolines] which possess aromatic substituents at the C-2′ position. A comparison of the spectrum of **8***c* with *N*-deuterated **8***c* confirmed that the amine hydrogen atom was expelled in the formation of this ion. Of the two possible structures for this ion (**e′** and **e″**), the latter is preferred since **e** is located at *m/e* 131 in the spectrum of **9***b*, indicating the loss of a methyl radical from C-2′ in its formation.

A difference between the *o*-aminobenzylpyrazolone **3***a* and its phenyl analog **3***b* was demonstrated in their reactions with salicylaldehyde. Whereas **3***a* was successfully converted to a spiro[pyrazolone-quinoline] (**8***e*), the phenyl analog reacted to give a yellow crystalline product $C_{29}H_{23}N_3O_2$, which had an ir spectrum that was devoid of both the lactam C=O and NH absorptions present in the spectra of all the spiro-compounds (**8**). The spectrum contained absorption bands comparable to those in the ir spectrum of the Schiff base, salicylideneaniline (**11**) which was prepared for comparison pur-

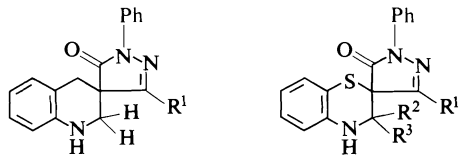

8 **10**

q R^1 = Me
r R^1 = Ph (product B)

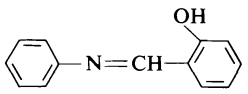

11

poses. Accordingly, the Schiff base structure **12** is suggested for the compound $C_{29}H_{23}N_3O_2$. Its mass spectrum was in agreement with the proposed structure. Although this spectrum displayed some similarities with the spectra of the spiro[pyrazolone–quinoline] (**8***e*), it also showed strong fragment ions resulting from cleavage at ring-nitrogen or ring-carbon bonds of the imine group (Scheme 5). Both these fissions are known

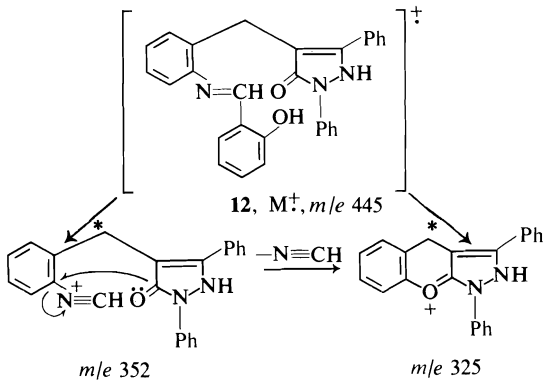

SCHEME 5

[2]R. T. Coutts and A.-m. El-hawari, work to be published.

(6, 12) to occur in the mass spectra of Schiff bases.

Reduction of **12** by means of sodium borohydride in aqueous dioxane did not yield a crystalline product. Methylation with dimethyl sulfate gave an alkali-insoluble product which was difficult to purify. The mass spectrum of the

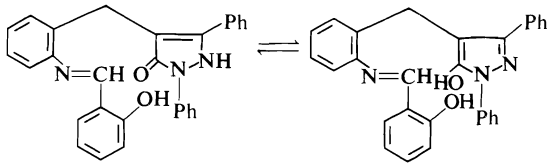

12

crude methylated product displayed a weak molecular ion at *m/e* 473 which indicated a dimethyl derivative in agreement with a Schiff base precursor (**12**) rather than a spiro-compound (**13**), since in **12**, methylation of the pyrazolone nucleus, could also occur. Interpretation of the ir and mass spectra of the isolated products showed that methylation occurred at the N-2 position of the pyrazolone ring. The ir spectrum displayed a C=O band at 1660 cm^{-1} which is expected only when the pyrazolone nucleus has an α,β-unsaturated carbonyl group (13). The mass spectrum displayed, in addition to the $M - 1$ and $M - 15$ ions, a fragment ion (the base peak) at *m/e* 118. A similar ion was identified earlier (1) in the mass spectrum of the N-2 methylated pyrazolone **15** as the fragment ($Ph—C\equiv\overset{+}{N}—CH_3 \leftrightarrow Ph—\overset{+}{C}=N—CH_3$). Accordingly, the structure **14** was assigned to the dimethyl derivative obtained from **12**.

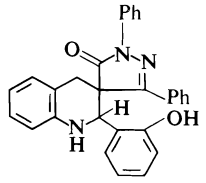

13

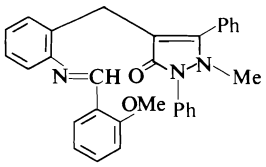

14

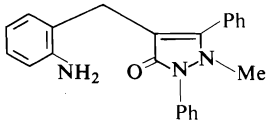

15

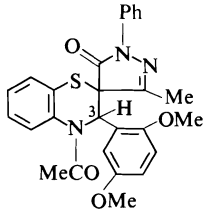

17

The Schiff base **12** is readily cyclized to the isomeric spiro-compound **13**. When the former was dissolved in DMSO-d_6 for a ^{1}Hmr study, a spectrum very similar to that of the spiro[pyrazolone–quinoline] **8***o* was obtained. In particular, the spectrum displayed a doublet of doublets for the methylene group. Such a signal was demonstrated, throughout the present study, solely in spiro-compounds (**8**). This case of conversion (**12** → **13**) supports the earlier suggestion that Schiff bases are intermediate products in the formation of spiro[pyrazolone–quinolines] in the manner illustrated in Scheme 1. Cyclization also occurred when the Schiff base **12** was acetylated. This is discussed further below.

In order to characterize further the spiro-compounds described in this study, some (**8***b*, *c*, *e*, *n*, and *o*) were acetylated with acetic anhydride. Compound **8***n* was converted to a monoacetyl derivative identified as **16***a*. This structure was confirmed by elemental analysis ($C_{31}H_{25}N_3O_2$), ir (carbonyl bands 1666 and 1720 cm^{-1}), and ^{1}Hmr spectra. When **8***e* was acetylated, it yielded a diacetylated product identified as **16***b*. It analyzed correctly for $C_{28}H_{25}N_3O_4$ and its ir spectrum showed three C=O absorption bands at 1766 (ester), 1700 (lactam), and 1670 cm^{-1} (cyclic amide). The nmr spectrum of this compound had three methyl signals at δ 0.78, 1.86, and 2.18. The first of these signals was surprisingly far upfield, a position not expected for any of the methyl groups in compound **16***b*. In order to assist in deciding its origin, the acetyl derivatives **16***c* and **17**[2] were prepared. The results of a ^{1}Hmr study on these compounds are summarized in Table 2 and indicate that it is the

TABLE 2. The ^{1}Hmr chemical shifts (relative to TMS) of the methyl and C_2-H signals in some acetyl derivatives of spiro[pyrazolone–quinolines]

	δ			
Compound	$NCOCH_3$	$OCOCH_3$	$N=\overset{\vert}{C}—CH_3$	C_2-H
16*a*	2.25	—	—	6.50
16*b*	2.18	1.86	0.78	6.25
16*c*	2.20	—	0.88	6.13
17	2.22	—	1.00	*
16*d*	2.23	2.10	—	*
16*e*	2.24	1.93	—	*
16*f*	2.23	—	1.74	5.16
8*b*†	—	—	1.88	

*Located within aromatic multiplet.
†Presented for comparison.

methyl group on the pyrazolone ring which produces the upfield methyl signal in compound **16***b*. A tentative explanation, based on an examination of Dreiding models, is that the N=C—CH_3 group is forced to align itself on top of the phenyl ring at C-2 of the tetrahydroquinoline ring (or C-3 of the dihydrobenzothiazine ring in **17**) and thus is greatly shielded. In addition, the hydrogen atom attached to the same carbon atom as the phenyl ring is forced into the plane of this phenyl ring, adopting 'aromatic-like' character and therefore a downfield position. This explanation is supported by a study of the spectrum of the acetyl derivative **16***f* which lacks an aromatic substituent at C-2 of the tetrahydroquinoline ring. In the ^{1}Hmr spectrum of this compound, the pyrazolone methyl signal came to resonance at δ 1.74. This signal was found to be at δ 1.88 in the non-acetylated tetrahydroquinoline **8***b*.

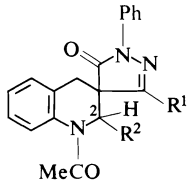

16

	R^1	R^2
a	Ph	Ph
b	Me	Ph-2-OCOMe
c	Me	Ph
d	Ph	Ph-4-OCOMe
e	Ph	Ph-2-OCOMe
f	Me	Et

Compound **16***e* (Table 2) was the product obtained when the Schiff base **12** was acetylated with acetic anhydride, again indicating the ease with which **12** is cyclized to **13**. Analysis ($C_{33}H_{27}N_3O_4$) confirmed the diacetate structure. Similarities in the ir and ^{1}Hmr spectra of the isolated product and the isomeric diacetate **16***d* obtained from **8***o* suggested two related structures. The ir spectrum of **16***d* had three carbonyl absorption bands at 1765 (ester), 1715 (lactam), and 1668 cm^{-1} (cyclic amide) which are closely related to those in the ir spectrum of acetylated **12**. The ^{1}Hmr spectrum of **16***d* displayed two methyl signals at δ 2.10 ($OCOCH_3$) and at 2.23 ($NCOCH_3$), a doublet of doublets centered at 3.37 (CH_2), and an aromatic multiplet which included the C-2 proton signal. The corresponding signals in acetylated **12** were located at δ 1.93, 2.24, and 3.26.

To complete this study on spiro[pyrazolone–quinolines] the effect of reducing these compounds was investigated. Whereas sodium borohydride reduction of the amine **12** in aqueous dioxane gave no crystalline products, similar reductions of the isomeric spiro-compounds (**8***a*, *b*, and *c*) yielded amphoteric products which analyzed correctly for $C_{18}H_{18}N_3OR$. The ease of solubility of these products in aqueous sodium hydroxide suggested the presence of an enolizable hydrogen at C-4 of the pyrazolone nucleus. Structure **18** is suggested for the reduction products; this suggestion is supported by the ir spectral characteristics. Their ir spectra displayed an N—H absorption band around 3300 cm^{-1}, lacked C=O absorption, and showed broad absorption between 2100 and 3300 cm^{-1} which could be attributed to a bonded OH stretching band. The ^{1}Hmr spectra of these products were very informative. In addition to the pyrazolone methyl signal and the aromatic signal, two deuterium-exchangeable protons and two methylene signals were also present in all spectra. One methylene signal was a singlet while the other was a singlet or multiplet depending on the adjacent substituent R. The mass spectra of the amphoteric products were also indicative of the suggested structure **18**. Important fragment ions in these spectra (i.e. molecular ion and three fragment ions of greatest mass) are identified in Scheme 6. The presence of ions **i** and **j** are of special interest since both contained an intact $NHCH_2R$ unit. Unlike compounds **18***a* and *b* which expelled the substituent R as a radical and gave fragment **k**, compound **18***c* lacked this ion, but instead expelled a C_7H_7 radical to give an ion of *m*/*e* 278.

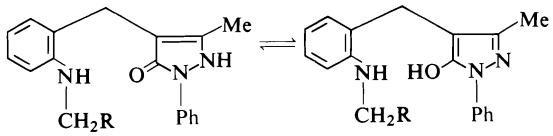

(NH-form) **18** (OH-form)

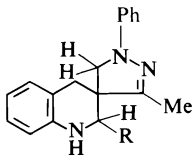

19

a R = Me
b R = Et
c R = Ph

Reductions of the spiro-compounds **8***a*, *b*, and *c* were also performed using lithium aluminum hydride in ether. Two products were isolated from each reduction mixture; the minor product

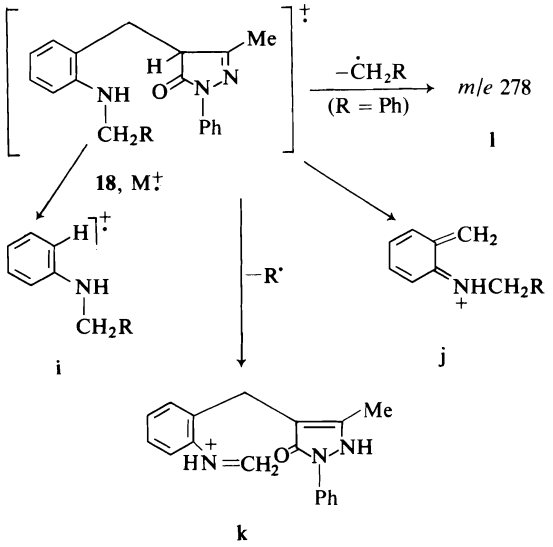

SCHEME 6. Percentage relative abundance of ions:

	R	$M^{+\cdot}$	i	j	k	l
18*a*	Me	21	46	100	3	—
18*b*	Et	34	50	100	12	—
18*c*	Ph	24	32	43	—	18

was basic while the major one was amphoteric. The proportion of these compounds was virtually reversed when the reduction of **8***a* was carried out in tetrahydrofuran. In contrast, only the amphoteric product was obtained, when **8***c* was reduced with lithium aluminum hydride/aluminum chloride in ether.

The amphoteric products were identical to the compounds obtained by sodium borohydride reduction of **8***a*, *b*, and *c*, respectively. The basic products analyzed for $C_{18}H_{18}N_3R$ (R = CH_3, C_2H_5, or Ph) and their mass spectra displayed molecular ions at appropriate *m/e* values for these formulae. This indicated that the lactam C=O groups in **8***a–c* had been reduced by the action of lithium aluminum hydride, a reagent which is known to reduce pyrazolones to pyrazoline and pyrazolidine derivatives (14–17). The basic properties, the elemental analyses, and the mass spectra of these products suggested that they were pyrazoline derivatives (**19**). Their ir spectra lacked carbonyl absorption bands but each had two absorption bands near 3400 (sharp band) and 3300 cm^{-1} (broad band) which is a puzzling observation since only one N—H stretching band was expected. The identity of the basic products, $C_{18}H_{18}N_3R$, as compounds **19***a–c* is therefore tentative until further studies of these compounds are made.

Experimental

Infrared spectra were recorded for Nujol mulls with a Beckman IR-10 spectrophotometer. Proton magnetic resonance spectra were recorded with a Varian A60 spectrometer, with tetramethylsilane as internal standard, and mass spectra were measured with an A.E.I. MS9 spectrometer at 70 eV (direct insertion technique). Melting points (capillary) are uncorrected. Deuterated compounds were prepared by repeated crystallization of the non-labelled precursor from dioxane–D_2O. Where elemental analyses are indicated, analytical results obtained for those elements were within ±0.45% of the theoretical values. Complete analyses are compiled in two tables (Table 3: elemental analyses of spiro[pyrazolone–quinolines] and related compounds; Table 4: elemental analyses and physical properties of spiro-[[2]pyrazoline-4,3′(4′*H*)-quinoline]-5-ones (**8**, **9**) prepared by a general method) which are available from the Depository of Unpublished Data.[3]

*Reduction of 1,3-Diphenyl-4-(2-nitrobenzyl)-2-pyrazolin-5-one (**1***b*)*

(*a*) Zinc dust (1.0 g) was added in small quantities to a stirred solution of the title compound (1) (2.0 g) in boiling glacial acetic acid (20 ml). The mixture was heated under reflux for 6 h then filtered. On cooling, a yellow solid (0.8 g), mp 158–160°C crystallized from the filtrate. An additional quantity (0.5 g) of product was obtained by diluting the filtrate with water. Crystallization from ethanol gave 1,3-diphenyl-1*H*-pyrazolo[3,4-*b*]quinoline (**2***b*), mp 162–163°C; ir ν_{max} 1618 (C=N) cm^{-1}, NH and OH bands absent; ^{1}Hmr ($CDCl_3$) δ 7.00–8.90 (aromatic protons); ms *m/e* (% relative abundance) 321(M^+, 100), 320(30), 244(11), 218(9). *Anal.* ($C_{22}H_{15}N_3$) C,H,N.

The same product (**2***b*) was obtained by heating a solution of 1,3-diphenyl-4-(2-aminobenzyl)-2-pyrazolin-5-one (1) (**3***b*, 0.5 g) in glacial acetic acid (10 ml) for 2 h. On cooling, 1,3-diphenyl-1*H*-pyrazolo[3,4-*b*]quinoline (0.35 g) separated as yellow crystals, mp 158–160°C, with properties identical to those described immediately above.

(*b*) The title compound (1.0 g) in methanol (200 ml) was hydrogenated over platinum oxide (30 mg) at room temperature and atmospheric pressure. When the calculated amount of hydrogen was taken up, the catalyst was filtered off and the solvent evaporated to give a yellow solid. Crystallization from methanol yielded pale-yellow crystals (0.35 g) of 1′,2′-dihydro-1,3-diphenylspiro[[2]pyrazoline-4,3′(4′*H*)-quinoline]-5-one (**8***r*, product B), mp 188–189°C; ir ν_{max} 1700 (C=O), 3365 (NH) cm^{-1}; ^{1}Hmr ($CDCl_3$) δ 3.34 (2H, s, CH_2), 3.57 (2H, br s, CH_2), 3.95 (1H, br s, NH), 6.50–8.30 (14H, m, aromatic protons); ms: see Scheme 2 caption; measured mass 118.0653 (calcd. for C_8H_8N, 118.0657). *Anal.* ($C_{23}H_{19}N_3O$) C,H,N.

(*c*) Reduction of **1***b* by method *b* was repeated except that ethanol (200 ml) was used as solvent. This gave 1′,2′-

[3]Copies of Tables 3 and 4 are available, at a nominal charge, from the Depository of Unpublished Data, CISTI, National Research Council of Canada, Ottawa, Canada K1A 0S2.

dihydro-1,3-diphenyl-2′-methylspiro[[2]pyrazoline-4,3′-(4′*H*)-quinoline]-5-one (**8***l*, product A) (0.75) g), as colorless crystals, mp 174–175°C; ir ν_{max} 1712 (C=O), 3405 (NH) cm^{-1}; ^{1}Hmr ($CDCl_3$) δ 1.15 (3H, d, J = 6.5 Hz, CH_3), 3.50 (2H, d of d, J = 17 Hz, CH_2), 3.60 (1H, q, J = 6.5 Hz, CH), 3.63 (1H, br s, D-exchangeable, NH), 6.40–8.30 (14H, m, aromatic protons); ms: see Scheme 2 caption; measured masses 367.1680 (calcd. for $C_{24}H_{21}N_3O$, 367.1685), 352.1450 (calcd. for $C_{23}H_{18}N_3O$, 352.1450), 132.0813 (calcd. for $C_{19}H_{10}N$, 132.0813). *Anal.* ($C_{24}H_{21}N_3O$) C,H,N.

(*d*) Reduction of **1***b* by method *b* was repeated except that propanol (200 ml) was the solvent. This gave 1′,2′-dihydro-1,3-diphenyl-2′-ethylspiro[[2]pyrazoline-4,3′(4′*H*)-quinoline]-5-one (**8***m*, product C) (0.59 g) as colorless crystals, mp 159–160°C; ir ν_{max} 1710 (C=O), 3415 (NH) cm^{-1}; ^{1}Hmr ($CDCl_3$) δ 0.90–1.50 (5H, m, J = 6.5 Hz, CH_2CH_3), 3.35 (2H, d of d, J = 17.5 Hz, CH_2), 3.64 (1H, br s, D-exchangeable, NH), 6.35–8.30 (14H, m, aromatic protons); ms *m/e* (% relative abundance) 381(M^+, 100), 364(2), 352(42), 146(78); measured masses 381.1837 (calcd. for $C_{25}H_{23}N_3O$, 381.1841), 146.0966 (calcd. for $C_{10}H_{12}N$, 146.0970). *Anal.* ($C_{25}H_{23}N_3O$) C,H,N.

(*e*) Reduction of **1***b* by method *b*, but using benzyl alcohol (200 ml) as solvent gave 1′,2′-dihydro-1,2′,3-triphenylspiro[[2]pyrazoline-4,3′(4′*H*)-quinoline]-5-one (**8***n*, product D) (0.28 g) as a pale yellow solid, mp 207–209°C; ir ν_{max} 1698 (C=O), 3380 (NH) cm^{-1}; ^{1}Hmr ($CDCl_3$) δ 3.45 (2H, d of d, J = 17 Hz, CH_2), 4.68 (1H, s, CH), 4.07 (1H, br s, D-exchangeable, NH), 7.00–7.80 (19H, m, aromatic protons); ms *m/e* (% relative abundance) 429(M^+, 100), 412(2), 352(3), 194(67), 193(25). *Anal.* ($C_{29}H_{23}N_3O$) C,H,N.

(*f*) Reduction of **1***b* by method *b* was repeated using dioxane (100 ml) as solvent and 4-(2-aminobenzyl)-1,3-diphenyl-2-pyrazolin-5-one (0.78 g, mp 151–152°C) was obtained as colorless crystals. The properties of this product were identical to those reported earlier (1).

*Reduction of 3-Methyl-4-(2-nitrobenzyl)-1-phenyl-2-pyrazolin-5-one (**1a**)*

(*a*) When the title compound (1) (2.0 g) was reduced with zinc dust in glacial acetic acid as described in the preparation of **1***b* by method *a*, a yellow solid (1.33 g), mp 166–168°C (from aqueous ethanol) was obtained and is identified as 3-methyl-1-phenyl-1*H*-pyrazolo[3,4-*b*]-quinoline (**2***a*) (lit. (4) mp 178°C); ir ν_{max} 1618 (C=N) cm^{-1}, NH and OH bands absent; ^{1}Hmr ($CDCl_3$) δ 2.78 (3H, s, CH_3), 7.30–9.05 (10H, m, aromatic protons); ms *m/e* (% relative abundance) 259(M^+, 100), 258(27), 244(33), 218(21). *Anal.* ($C_{17}H_{13}N_3$) N.

(*b*) The same product (**2***a*) was obtained in low yield (0.15 g) when 4-(2-aminobenzyl)-3-methyl-1-phenyl-2-pyrazolin-5-one (1) (**3***a*, 0.5 g) was heated under reflux in glacial acetic acid (10 ml) for 3 h.

(*c*) A solution of the title compound (1.0 g) in methanol (150 ml) was hydrogenated in the manner described in the reduction of compound **1***b*, method *b*. Crystallization of the product from methanol gave colorless crystals (0.28 g), mp 153–154°C, of 1′,2′-dihydro-3-methyl-1-phenylspiro[[2]pyrazoline-4,3′(4′*H*)-quinoline]-5-one (**8***q*); ir ν_{max} 1692 (C=O), 3425 (NH) cm^{-1}; ^{1}Hmr ($CDCl_3$) δ 2.01 (3H, s, CH_3), 3.00 (2H, d of d, J = 17.5 Hz, CH_2), 3.91 (1H, br s, D-exchangeable, NH), 6.60–8.30 (9H, m, aromatic protons); ms: see Scheme 2 caption. *Anal.* ($C_{18}H_{17}N_3O$) C,H,N.

*General Method of Preparing 1′2′-Dihydrospiro-[[2]pyrazoline-4,3′(4′H)-quinoline]-5-ones (**8**, **9**)-(See Tables 1 and 4)*

A hot solution of the 4-(2-aminobenzyl)-1-phenyl-2-pyrazolone **3***a* or **3***b* (1) (0.5 g) in either methanol or ethanol (15 ml) was mixed with a quantitative amount of the appropriate aldehyde. The reaction mixture was heated under reflux for 1 h. Upon cooling, many of the title compounds separated and were recrystallized from ethanol. In some cases, the reaction mixture was concentrated to about half its volume then diluted with water. The precipitate was washed with water, dried, and recrystallized from either methanol or ethanol as colorless crystals.

A similar reaction was carried out using acetone instead of an aldehyde. In this instance, the solvent used was either ethanol or butanol. Suitable reaction times were found to be 24 h when ethanol was the solvent, or 4–6 h when butanol was employed.

The compounds prepared by this method were obtained in 73–96% yields. Melting points are listed in Table 1. Individual yields and elemental analyses of all compounds are compiled in Table 4.[3] Their ir spectra displayed N—H absorption bands around 3400 and C=O bands around 1700 cm^{-1}. Each ^{1}Hmr spectrum showed, in addition to the signals ascribable to the aromatic protons and the different substituents at C-3 of the tetrahydroquinoline ring, a 2-proton doublet of doublets around δ 3.2 with J value ~ 17 Hz (CH_2), a one proton signal near δ 4.5 (-C*H*R) and a D-exchangeable N-H signal of variable chemical shift. The spectra of 3-methylpyrazolone derivatives also contained a methyl signal around δ 2.0. The mass spectra of some of these compounds were recorded and interpreted (see Scheme 2).

*Preparation and Reactions of 1,3-Diphenyl-4-[2-(2-hydroxybenzylidene)aminobenzyl]-2-pyrazolin-5-one (**12**)*

(*a*) *Preparation*

A solution of 4-(2-aminobenzyl)-1,3-diphenyl-2-pyrazolin-5-one (1) (**3***b*, 0.5 g) and salicylaldehyde (0.18 g) was heated under reflux for 1 h during which time the solution turned dark yellow. On cooling, a yellow solid separated from solution. Crystallization from ethanol gave the title compound (0.55 g), mp 199–200°C; mass spectrum *m/e* (% relative abundance) 445(M^+, 100), 444(44), 428(4), 352(18), 325(20), 248(7), 220(13), 210(41), 209(26); see also Scheme 5. *Anal.* ($C_{29}H_{23}N_3O_2$) C,H,N.

(*b*) *Isomerization*

A solution of **12** in DMSO-d_6 gave ^{1}Hmr δ 3.30 (2H, d of d, J = 16 Hz, CH_2), 5.31 (1H, s, CH), 6.20 (1H, br s, D-exchangeable, NH), 6.50–8.25 (18H, m, aromatic protons), 9.38 (1H, br s, D-exchangeable, OH), consistent with the formation of 1′,2′-dihydro-1,3-diphenyl-2′-(2-hydroxyphenyl)spiro[[2]-pyrazoline-4,3′(4′*H*)-quinoline]-5-one (**13**).

(*c*) *Methylation*

To an ice-cooled solution of the title compound (0.5 g) in dilute sodium hydroxide (15 ml), dimethyl sulfate (1.0 ml) was added dropwise with stirring and then the mixture was heated on a water bath for 1 h. The resulting oil which separated was extracted into chloroform. This

extract was washed with dilute sodium hydroxide then with water and dried. Evaporation of the organic solvent yielded an off-white solid (0.45 g), mp 128–132°C, which could not be purified by fractional crystallization from various solvents but which consisted mainly of 1,3-diphenyl-4-[2-(*o*-methoxybenzylidene)aminobenzyl]-2-methyl-3-pyrazolin-5-one (**14**); ir ν_{max} 1660 (C=O) cm^{-1}; ^{1}Hmr ($CDCl_3$) δ 2.98 (3H, s, NCH_3), 3.37 (2H, s, CH_2), 3.87 (3H, s, OCH_3), 6.40–7.90 (18H, m, aromatic protons); ms *m/e* (% relative abundance) 473(M^+, 4), 472(9), 458(8), 383(80), 118(100).

(*d*) *Acetylation*

A solution of the title compound (0.3 g) in acetic anhydride (5 ml) was heated under reflux for 15 min then poured into ice-water (30 ml). The resulting precipitate was crystallized from ethanol and yielded 1′-acetyl-2′-(2-acetoxyphenyl)-1′,2′-dihydro-1,3-diphenylspiro[[2]-pyrazoline-4,3′(4′*H*)-quinoline]-5-one (**16***e*) as colorless needles (0.22 g), mp 240–241°C; ir ν_{max} 1764 (ester C=O), 1720 (lactam C=O), 1666 (amide C=O) cm^{-1}; ^{1}Hmr (DMSO-d_6) δ 1.93 (3H, s, $OCOCH_3$), 2.24 (3H, s, $NCOCH_3$), 3.26 (2H, d of d, J = 15 Hz, CH_2), 6.30–8.30 (14H, m, C-2′ proton and aromatic protons). *Anal.* ($C_{33}H_{27}N_3O_4$) C,H,N.

*Reactions of 1′,2′-dihydrospiro[[2]pyrazoline-4,3′(4′H)-quinoline]-5-ones (**8**)*

(*a*) *Acetylation*

Each of the spiro[pyrazolone–quinolines] (**8***b*, *c*, *e*, *n*, and *o*) (0.3 g) was acetylated in the manner described above for the acetylation of compound **12**. Products were **16***f*, mp 220–221°C; **16***c*, mp 223–224°C; **16***b*, mp 205–206°C; **16***a*, mp 218–219°C; and **16***d*, mp 188–189°C, respectively. They were crystallized from ethanol as colorless compounds in 78–91% yields. Elemental analyses of the acetylated products are listed in Table 3.[3] The ir spectra of all five acetamides contained C=O absorption bands near 1665 (cyclic amide) and 1710 cm^{-1} (lactam) and were devoid of N—H bands. Compounds **16***b* and **16***d* contained an additional C=O band near 1765 cm^{-1} (ester). Important signals in the ^{1}Hmr spectra of these acetyl derivatives are listed in Table 2.

(*b*) *Reduction with Sodium Borohydride*

(*i*) A solution of 1′,2′-dihydro-2′,3-dimethyl-1-phenylspiro[[2]pyrazoline-4,3′(4′*H*)-quinoline]-5-one (**8***a*, 0.5 g) in dioxane (15 ml) was added dropwise to a stirred solution of sodium borohydride (0.5 g) in water (5 ml). After addition was completed, stirring was continued for 30 min then the reaction mixture was acidified with dilute acetic acid and diluted with water. Crystallization of the resulting precipitate from ethanol gave 4-(2-ethylaminobenzyl)-3-methyl-1-phenyl-2-pyrazolin-5-one (**18***a*) as a white crystalline powder (0.33 g), mp 181–182°C; ir ν_{max} 2100–3500 (OH) with maximum at 3380 (NH), 1620 (bonded C=O) cm^{-1}; ^{1}Hmr ($CDCl_3$) δ 1.02 (3H, t, CH_3), 1.91 (3H, s, CH_3), 3.40 (2H, s, CH_2), 3.62 (2H, q, CH_2), 6.40–7.40 (11H, m, aromatic protons overlapping NH and pyrazoline ring protons); ms, see Scheme 6. *Anal.* ($C_{19}H_{21}N_3O$) C,H,N.

(*ii*) 1′,2′-Dihydro-2′-ethyl-3-methyl-1-phenylspiro[[2]-pyrazoline-4,3′(4′*H*)-quinoline]-5-one (**8***b*, 0.5 g) was similarly reduced to give 3-methyl-1-phenyl-4-(2-*n*-propylaminobenzyl)-2-pyrazolin-5-one (**18***b*, 0.31 g) as white crystals, mp 149–150°C; ir ν_{max} 2040–3400 with maximum at 3380 (OH and NH), 1617 (C=O) cm^{-1}; ^{1}Hmr ($CDCl_3$) δ 0.70–1.75 (5H, m, CH_2CH_3), 2.05 (3H, s, CH_3), 3.30 (2H, s, CH_2), 3.45 (2H, t, NCH_2), 6.30–7.60 (10H, m, aromatic protons and pyrazoline ring proton), 9.02 (1H, br s, D-exchangeable, NH); ms, see Scheme 6. *Anal.* ($C_{20}H_{23}N_3O$) C,H,N.

(*iii*) 1′,2′-Dihydro-1,2′-diphenyl-3-methylspiro[[2] pyrazoline-4,3′(4′*H*)-quinoline]-5-one (**8***c*, 0.5 g) was similarly reduced and yielded 4-(2-benzylaminobenzyl)-3-methyl-1-phenyl-2-pyrazolin-5-one (**18***c*, 0.39 g) as white crystals, mp 155–156°C; ir ν_{max} 2000–3360 with maximum at 3305 cm^{-1} (OH and NH), 1612 (C=O) cm^{-1}; ^{1}Hmr ($CDCl_3$) δ 1.88 (3H, s, CH_3), 3.33 (2H, s, CH_2), 4.25 (2H, s, CH_2), 6.40–7.80 (16H, m, aromatic protons overlapping NH and pyrazoline ring protons); ms, see Scheme 6. *Anal.* ($C_{24}H_{23}N_3O$) C,H,N.

(*c*) *Reduction with Lithium Aluminum Hydride*

(*i*) A solution of 1′,2′-dihydro-2′,3-dimethyl-1-phenylspiro[[2]pyrazoline-4,3′(4′*H*)-quinoline]-5-one (**8***a*, 0.75 g) in ether (50 ml) was slowly added, with stirring, to a mixture of lithium aluminum hydride (0.15 g) and ether (20 ml). After heating under reflux for 10 h, water was added dropwise to the cooled reaction mixture until the evolution of hydrogen ceased. The solution was made alkaline by the addition of 30% aqueous sodium hydroxide (~20 ml) then the mixture was extracted with ether (2 × 50 ml). Evaporation of the dry (Na_2SO_4) combined ether extracts gave a white powder which crystallized from ethanol as a white solid (0.14 g), mp 178–179°C. This compound is tentatively identified as 1′,2′-dihydro-2′,3-dimethyl-1-phenylspiro[[2]pyrazoline-4,3′(4′*H*)-quinoline] (**19***a*); ir ν_{max} 3470, 3390 br, 1595 (NH) cm^{-1}, C=O absorption absent; ms *m/e* (% relative abundance) 291(M^+, 2), 263(97), 248(10), 171(100). *Anal.* ($C_{19}H_{21}N_3$) C,H,N.

The basic aqueous solution which remained was neutralized with dilute sulfuric acid then extracted with ether (3 × 50 ml). The combined ether extracts were dried (Na_2SO_4) and evaporated to give 4-(2-ethylaminobenzyl)-3-methyl-1-phenyl-2-pyrazolin-5-one (**18***a*, 0.29 g), identical (mp, ir, mass spectrum) to the product obtained by reducing **8***a* with sodium borohydride as described above.

(*ii*) 1′,2′-Dihydro-2′-ethyl-3-methyl-1-phenylspiro[[2]-pyrazoline-4,3′(4′*H*)-quinoline]-5-one (**8***b*, 0.8 g) was reduced with lithium aluminum hydride in a manner similar to reaction *i* above. The basic product was a white solid (0.12 g), mp 170–171°C and is tentatively identified as 1′,2′-dihydro-2′-ethyl-3-methyl-1-phenylspiro[[2] pyrazoline-4,3′(4′*H*)-quinoline] (**19***b*); ir ν_{max} 3405, 3290 br, 1600 (NH) cm^{-1}, C=O absorption absent; ms *m/e* (% relative abundance) 305(M^+, 25), 303(9), 276(13), 274 (34), 263(43), 171(65), 118(100). *Anal.* ($C_{20}H_{23}N_3$) C,H,N.

The product isolated from neutral solution was 3-methyl-1-phenyl-4-(2-*n*-propylaminobenzyl)-2-pyrazolin-5-one (**18***b*, 0.21 g), identical (mp, ir, mass spectrum) to the product formed by reducing **8***b* with sodium borohydride (see above).

(*iii*) Reduction of 1′,2′-dihydro-1,2′-diphenyl-3-methylspiro[[2]-pyrazoline-4,3′(4′*H*)-quinoline]-5-one (**8***c*, 1.0 g) with lithium aluminum hydride as described in reaction *i* gave basic material which was fractionally crystallized from ethanol and yielded starting material (**8***c*, 0.21 g) and another product (0.09 g), mp 205–206°C

which is tentatively identified as 1′,2′-dihydro-1,2′-diphenyl-3-methylspiro[[2]pyrazoline-4,3′(4′*H*)-quinoline] (**19***c*); ir ν_{max} 3380, 3290 br, 1597 (NH) cm^{-1}; ms *m/e* (% relative abundance) 353(M^+, 7), 351(100), 350(29), 336(8), 274(22), 193(36); accurate mass measurements: 353.1888 ($C_{24}H_{23}N_3$ requires 353.1892), 351.1730 ($C_{24}H_{21}N_3$ requires 351.1736). *Anal.* ($C_{24}H_{23}N_3$) C,H,N.

The product (0.32 g) isolated from the neutralized solution was identical (mp, ir) to the previously identified (see above) 4-(2-benzylaminobenzyl)-3-methyl-1-phenyl-2-pyrazolin-5-one (**18***c*).

Acknowledgments

The authors thank the Medical Research Council of Canada for operating grant MT-2993 (to R.T.C.) which financed this project and acknowledge the assistance of Mr. W. Dylke of our faculty and the Department of Chemistry, University of Alberta, for the elemental analyses.

1. R. T. Coutts and A.-M. El-hawari. Can. J. Chem. **53**, 3637 (1975).
2. R. T. Coutts, A.-M. El-hawari, and D. F. Biggs. Can. J. Chem. **53**, 3645 (1975).
3. R. T. Coutts, A.-M. El-hawari, N. J. Pound, and R. A. Abramovitch. Can. J. Chem. **54**, 993 (1976).
4. A. Brack. Belg. Patent No. 617180 (1962); Chem. Abstr. **59**, 636 (1963).
5. P. N. Rylander. Catalytic hydrogenation over platinum metal. Academic Press, New York, NY. 1967.
6. D. J. Elias and R. G. Gillis. Aust. J. Chem. **19**, 251 (1966).
7. P. M. Draper and D. B. MacLean. Can. J. Chem. **46**, 1499 (1968).
8. H. Adkins. Reaction of hydrogen with organic compounds over copper – chromium oxide and nickel catalysts. University of Wisconsin Press, Madison, WI. 1937.
9. M. Passerini and G. Ragni. Gazz. Chim. Ital. **66**, 684 (1936); Chem. Abstr. **31**, 3484 (1937).
10. A. F. McDonagh and H. E. Smith. J. Org. Chem. **33**, 1 (1968).
11. G. W. Stacey and P. L. Strong. J. Org. Chem. **32**, 1487 (1967).
12. J. H. Bowie, R. G. Cooks, J. W. Fisher, and T. M. Spotswood. Aust. J. Chem. **21**, 2021 (1968).
13. K. Nakanishi. Infrared absorption spectroscopy – Practical. Holden-Day, San Francisco and Nankodo Co., Tokyo. 1962. p. 42.
14. R. E. Bowman and C. S. Franklin. J. Chem Soc. 1583 (1957).
15. R. L. Hinman, R. D. Ellefson, and R. D. Campbell. J. Am. Chem. Soc. **82**, 3988 (1960).
16. P. Bouchet, J. Elguero, and R. Jacquier. Tetrahedron, **22**, 2461 (1966).
17. J. Elguero, R. Jacquier, and D. Tizané. Tetrahedron, **27**, 133 (1971).

Etude conformationnelle par spectroscopie photoélectronique de dihydro "épinnes"

P. MEUNIER
Laboratoire de Polarographie Organique, Faculté des Sciences, 21000 Dijon, France
ET
G. PFISTER-GUILLOUZO
Laboratoire de Chimie Organique Physique, I.U.R.S. B.P. 523, 64010 Pau-Université, France

Reçu le 25 novembre 1976

P. MEUNIER et G. PFISTER-GUILLOUZO. Can. J. Chem. **55**, 2867 (1977).

Les dithiéno[*c,e*] dihydro azépines, oxépinnes et thiépinnes ont fait l'objet d'une étude par spectroscopie photoélectronique. L'analyse de ces données expérimentales a permis de conclure pour ces composés, à l'existence en phase vapeur d'une conformation croisée.

P. MEUNIER and G. PFISTER-GUILLOUZO. Can. J. Chem. **55**, 2867 (1977).

Dithieno[*c,e*]dihydroazapines, oxepines, and thiepines have been studied by photoelectron spectroscopy. The results of this work are reasonably well interpreted in terms of a twisted conformation in the vapor phase.

Introduction

Les dithiéno[*c,e*] dihydro azépines, oxépinnes et thiépinnes peuvent être considérées soit comme des dérivés de substitution des dihydro-2,7 azépine, oxépinne et thiépinne, soit comme des bithiényls hétéropontés.

Selon la préférence conformationnelle de l'hétérocycle à sept chaînons (forme "semi-bateau" ou "croisée"), et l'encombrement stérique provoqué par la substitution, le squelette bithiénylique présentera une conformation *cis*, plane ou twistée.

A notre connaissance, les dihydro "épinnes" envisagées n'ont pas été isolées. Seules les données de diffraction électronique recueillies pour leur homologue carboné, le cycloheptadiène-1,3 (1, 2) avaient permis de conclure en la prépondérance en phase vapeur de la forme "semi-bateau" de ce composé. Par contre, le cycloheptadiène-1,3 et diverses dihydro "épinnes" benzo substituées ont fait l'objet d'une étude rmn (3, 4). Les auteurs proposent pour tous ces dérivés l'existence d'une forme "croisée" en solution, les barrières d'inversion étant d'environ 15 kcal/mol.

Des travaux récents ont mis en évidence l'apport de la spe à l'étude de nombreux problèmes conformationnels (5). Dans ce travail, nous avons appliqué cette technique à une série de dithiéno "épinnes" de type **1** et **2** afin d'en préciser la conformation privilégiée à l'état vapeur. Nos conclusions sont vérifiées par l'examen de certains de ces composés *gem* diméthylés en α et α′ de l'hétéroatome.

Dérivés de type **1** et **2**

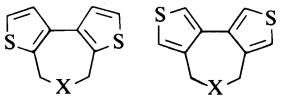

1 **2**

X = NR,O,S

Composés de type 1

Ces composés peuvent être considérés comme des dérivés du bithiényl-3,3′ hétéropontés en position 2 et 2′.

Pour le bithiényl-3,3′ lui-même (5*f*), nous avons attribué les potentiels d'ionisation à 8.2, 9.15 et 10.03 eV à l'ionisation des électrons π des quatre orbitales moléculaires schématisées sur la fig. 1. Celles-ci correspondent respectivement aux combinaisons antisymétrique et symétrique des deux orbitales A_2 et B_1 du thiophène. Les écarts observés (approximativement 1 eV et 0.9 eV) correspondent à une interaction moyenne entre les deux noyaux qui s'interprète bien compte tenu de l'angle de twist d'environ 30° déterminé par diffraction électronique (6).

Pour les composés de type **1**, on peut envisager des interactions similaires entre les deux noyaux thiophéniques liées directement à la conformation du cycle heptagonal. Ces interactions sont ainsi attendues nettement plus importantes pour

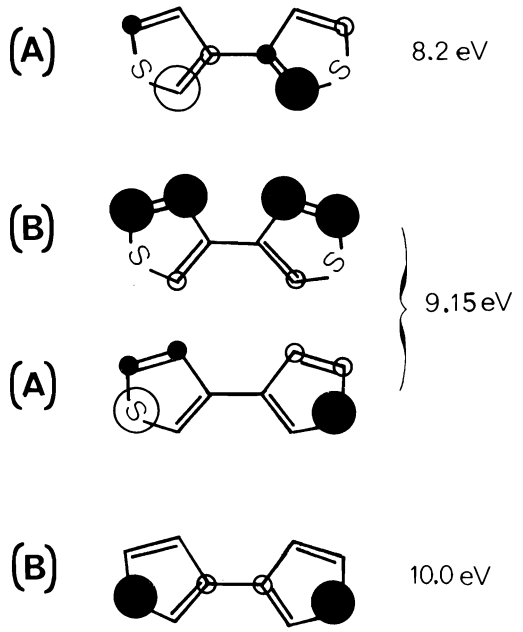

FIG. 1. Orbitales moléculaires du bithiényl-3,3′.

une conformation "enveloppe" que pour une conformation "croisée".

Par ailleurs, la présence de l'hétéroatome X entraine un léger effet de polarisation auquel doit s'ajouter compte tenu de la symétrie de la molécule, une interaction possible entre la paire π de cet hétéroatome et les combinaisons symétriques des orbitales A_2 et B_1 du thiophène (notamment cette dernière, compte tenu du recouvrement entre la paire π de l'hétéroatome et les paires π des atomes de soufre dans les cycles thiophéniques relativement plus important).

Spectres expérimentaux

Les spectres sont reportés dans les figs 2 à 5, et les valeurs des potentiels d'ionisation verticaux ont été rassemblées dans le tableau 1 avec celles observées pour le bithiényl-3,3′.

On note pour tous les composés étudiés des spectres dont l'allure est très voisine de celle du spectre du bithiényl-3,3′. La présence de l'hétéroatome se traduit par une bande supplémentaire dont nous précisons la position avant de discuter des bandes caractéristiques du système bithiényl.

Dithiéno[2′,3′-c;3″,2″-e] 4H, 5 éthyl, 6H azépine et dithiéno[2′,3′-c;3″,2″-e] 4H, 5 phényl, 6H azépine

Dans le cas du dérivé *N*-éthylé, on observe une bande à 8.3 eV qui peut être associée à l'ionisation de la paire libre de l'atome d'azote. Cette valeur peut être rapprochée de celle observée à 8.5 eV dans la triméthylamine (7).

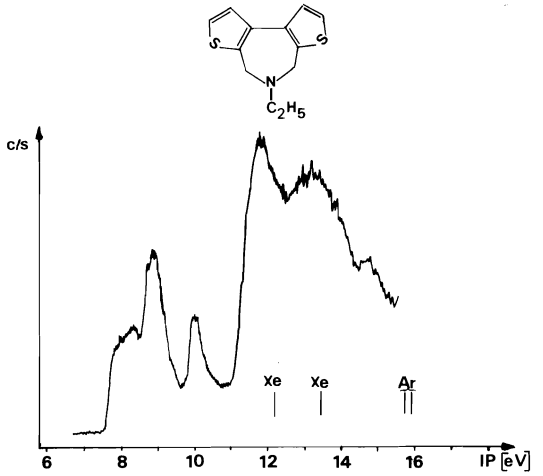

FIG. 2. Spectre photoélectronique du dithiéno[2′,3′-*c*; 3″,2″-*e*] 4*H*, 5 éthyl, 6*H* azépine.

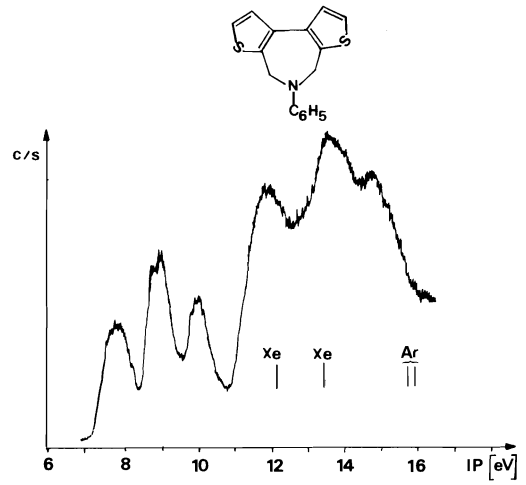

FIG. 3. Spectre photoélectronique du dithiéno[2′,3′-*c*; 3″,2″-*e*] 4*H*, 5 phényl, 6*H* azépine.

Pour le dérivé *N*-phénylé on observe comme pour les dérivés de l'aniline (8) une interaction entre la paire libre de l'azote et les orbitales dégénérées e_{1g} du benzène. Ces ionisations sont à l'origine (*i*) de l'élargissement de la première bande à 7.9 eV, (*ii*) d'une bande dans la région de 10 eV comme pour la *N*,*N*-diméthylaniline, (*iii*) de la bande à 9 eV (ionisation des électrons de l'orbitale e_{1g} antisymétrique).

Dithiéno[2′,3′-c;3″,2″-e] 4H, 6H oxépinne

Pour ce composé, l'ionisation d'un électron de

TABLEAU 1. Potentiels d'ionisation verticaux du bithiényl-3,3′ et des dérivés type **1**

Attribution	Symétrie	Bithiényl-3,3′	Composés type **1**			
			X = NC_2H_5	X = NC_6H_5	X = O	X = S
$\pi_{C=C}$	A	8.2	7.9	7.9	8.15	8.15
$\pi_{C=C}$	B	9.15	8.8	8.85	8.9	8.75
π_S	A	9.15	8.8	8.85	9.0	9.05
π_S	B	10.03	10.0	10.05	9.6	9.8
$\pi_{C_6H_5}$				9.0		
π_X	B		8.3	7.9	10.1	8.65
n_S	A					11.2

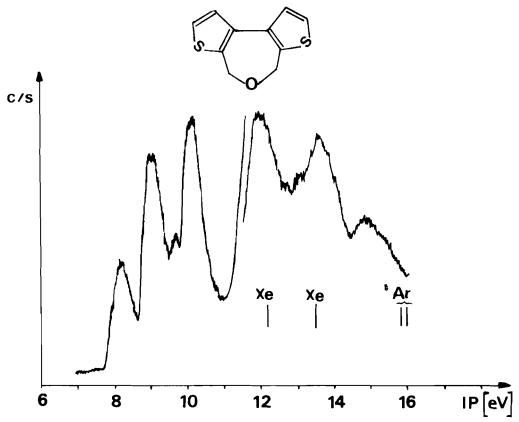

FIG. 4. Spectre photoélectronique du dithiéno[2′,3′-*c*; 3″,2″-*e*] 4*H* 6*H* oxépinne.

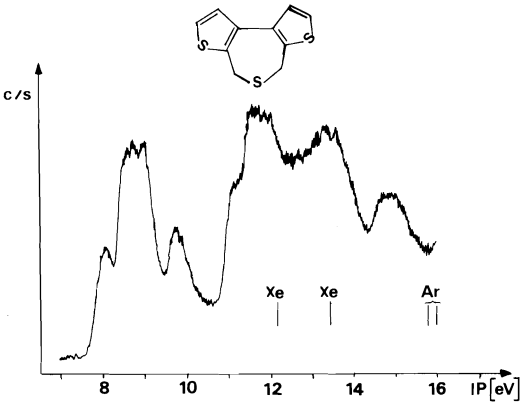

FIG. 5. Spectre photoélectronique du dithiéno[2′,3′-*c*; 3″,2″-*e*] 4*H* 6*H* thiépinne.

la paire π de l'oxygène correspond à la bande large et intense observée à 10.1 eV, valeur à rapprocher de celle observée à 10.04 eV dans le diméthyl éther (9).

Dithiéno[2′,3′-c;3″2,″-e] 4H, 6H thiépinne

L'ionisation de la paire π de l'atome de soufre intervient dans la même région que les deuxième et troisième bandes du système bithiényl. Le massif est large et l'on peut observer trois potentiels d'ionisation verticaux à 8.65, 8.75 et 9.05 eV.

L'ionisation de la paire π de l'atome de soufre intervenant à 8.7 eV dans le diméthyl sulfure (9) et 8.5 eV dans le pentaméthylène sulfure (10), il semble raisonnable de proposer pour les premières et deuxième bandes du bithiényl, celles à 8.15 et 8.75 eV. L'ionisation de la paire π du soufre interviendrait donc à 8.65 eV.

On observe de plus dans ce cas une bande de faible intensité apparaissant à 11.2 eV sous forme d'un épaulement d'une bande plus intense. On peut associer cette bande à l'ionisation des paires σ des atomes de soufre thiophéniques. Nous en apporterons d'ailleurs une confirmation ultérieurement.

Discussion des résultats

Les positions respectives des quatre potentiels d'ionisation associés au système bithiényl s'interprètent de façon qualitative par les interactions mises en jeu entre les paires libres de l'hétéroatome central et les combinaisons symétriques des orbitales des noyaux thiophéniques. Celles-ci sont schématisées sur la fig. 6.

L'effet de polarisation du pont CH_2—X—CH_2 tend à destabiliser les premières bandes du spectre de façon similaire.[1] Pour les trois composés, l'écart entre les premier et deuxième potentiels d'ionisation en première approximation permettra d'évaluer l'angle existant entre les deux noyaux thiophéniques.

Ces écarts sont de 0.9, 0.85 et 0.6 eV respectivement pour l'azépine, l'oxépinne et la thiépinne.

Si l'on rapproche ces données de celles recueillies pour le bithiényl-3,3′ (écart entre le premier

[1]Cet effet varie dans l'ordre NR > S > O, il peut être estimé pratiquement négligeable dans le cas de l'oxépinne.

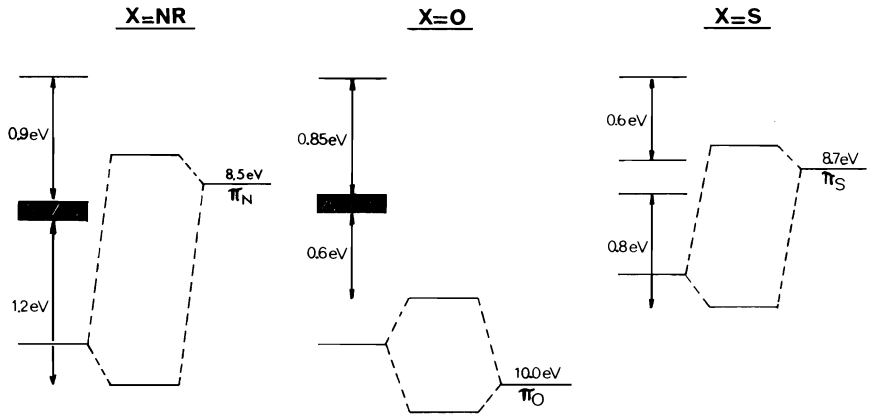

FIG. 6. Diagramme qualitatif des interactions orbitalaires mises en jeu entre le système bithiényl et l'hétéroatome X.

TABLEAU 2. Potentiels d'ionisation verticaux du bithiényl-3,3′ et des dérivés de type **2**

Attributions	Symétrie	Bithiényl-3,3′	Composés type **2**		
			X = NC_6H_5	X = O	X = S
$\pi_{C=C}$	A	8.2	8.15	8.3	8.4
$\pi_{C=C}$	B	9.15	8.9	8.9	8.9
π_S	A	9.15	8.9	8.9	8.9
π_S	B	10.0	10.0	9.5	9.75
π_X	B		7.5	10.0	8.4
n_S	A		8.9	11.2	11.1

et le deuxième potentiels d'ionisation: approximativement 1 eV) présentant en phase vapeur un angle twist d'environ 30° (6), on remarque que, dans le cas de l'azépine et de l'oxépinne, les éclatements observés sont sensiblement du même ordre, quoique un peu plus faibles, ce qui laisse présumer d'un angle de twist entre les deux noyaux de 30 à 40°. Pour la thiépinne, les faibles éclatements observés ne s'interprètent que par une rotation plus importante des cycles.

Dans tous les cas, l'existence privilégiée d'une forme "semi bateau" du cycle heptagonal où les deux cycles thiophéniques seraient coplanaires conduirait à une interaction plus forte entre les cycles thiophéniques que celle observée dans le bithiényl-3,3′, hypothèse incompatible avec les valeurs expérimentales observées.

Composés de type 2

Les spectres sont reportés dans les figs 7, 8 et 9 et les valeurs des potentiels d'ionisation verticaux sont rassemblés dans le tableau 2.

L'ionisation des électrons des paires libres des hétéroatomes du cycle heptagonal peut être associée aux bandes suivantes:

7.5 eV pour l'azépinne

10.0 eV pour l'oxépinne

Dans le cas de la thiépinne, la forte intensité de la première bande à 8.4 eV laisse présumer du recouvrement de deux ionisations. Compte tenu de la légère destabilisation observée pour les paires de l'oxygène et de l'azote comparativement aux dérivés de type **1**, il semble bien que l'on puisse attribuer à l'ionisation des électrons de la paire libre du soufre une valeur aux environs de 8.4 eV.

Dans le cas de l'azépine, la bande correspondant à l'ionisation des électrons du cycle benzénique (e_{1g} antisymétrique) peut être attribuée à celle observée à 8.9 eV, cette bande résultant du recouvrement de trois ionisations.

Discussion des résultats

Comme dans le cas des dérivés de type **1**, les éclatements observés entre les deux premiers potentiels d'ionisation associés aux orbitales A_2 du thiophène suivent le même classement: NR >

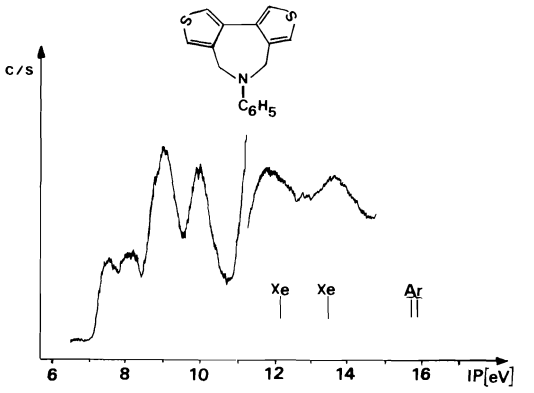

FIG. 7. Spectre photoélectronique du dithiéno[3′,4′-*c*; 3″,4″-*e*] 4*H*, 5 phényl, 6*H* azépine.

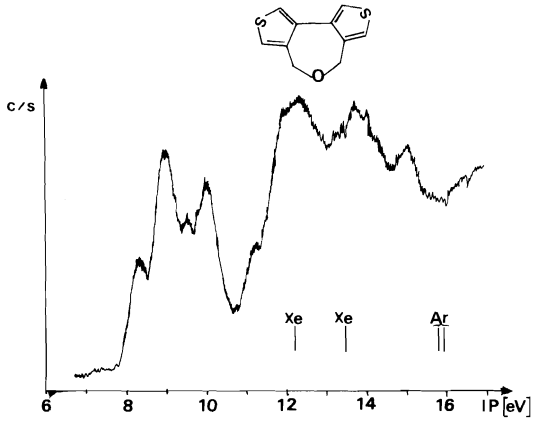

FIG. 8. Spectre photoélectronique du dithiéno[3′,4′-*c*; 3″,4″-*e*] 4*H*, 6*H* oxépinne.

O > S. Cet éclatement est nettement plus faible que pour les dérivés de type **1**: 0.75, 0.6 et 0.5 eV. Les interactions entre les orbitales semi-localisées du thiophène qui sont liées à la position différente des cycles thiophéniques ne permettent pas d'interpréter à elles seules ces données. Il semble logique de conclure pour les composés de type **2** à un angle de torsion légèrement plus important entre les deux cycles thiophéniques que pour les dérivés de type **1**. Comme précédemment l'azépinne et l'oxépinne auraient un angle de torsion voisin tandis que la thiépinne serait sensiblement plus twistée.

Composés tétraméthyles

Afin de compléter cette étude, nous avons examiné les spectres des composés dérivés des oxépinnes précédentes et substitués en α et α′ de l'oxygène par deux groupements méthyles.

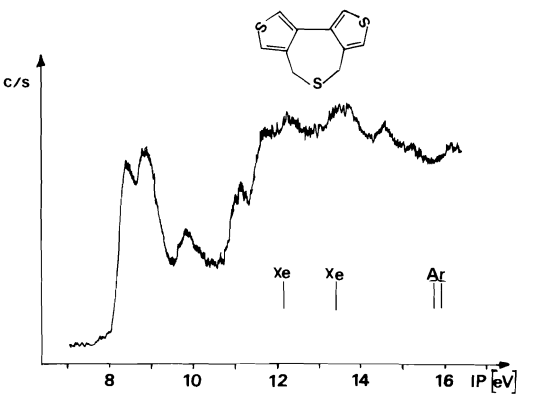

FIG. 9. Spectre photoélectronique du dithiéno[3′,4′-*c*; 3″,4″-*e*] 4*H*, 6*H* thiépinne.

Les spectres sont reproduits sur les figs 10 et 11 et les valeurs des potentiels d'ionisation sont rassemblées dans le tableau 3.

On constate pour les deux composés étudiés: (*i*) une destabilisation de toutes les premières bandes du spectre, (*ii*) une destabilisation plus importante (0.5 à 0.6 eV) de la dernière bande associée aux électrons σ des atomes de soufre thiophéniques. Dans ce cas, on n'observe plus un épaulement mais une bande bien définie.

Pour ces deux composés, l'allure des spectres et les éclatements observés conduisent à conclure à l'existence d'une conformation très voisine de celle existant pour les dérivés non méthylés. Le fait que ces composés fortement encombrés stériquement présentent le même type de conformation que ceux non substitués est cohérent avec les conclusions que nous avons

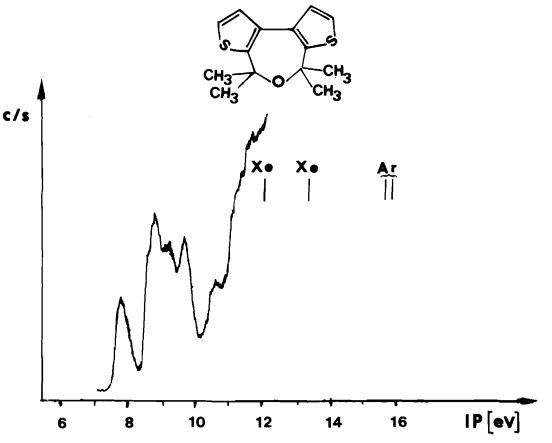

FIG. 10. Spectre photoélectronique du tétraméthyl-4,4,6,6 dithiéno[2′,3′-*c*;3″,2″-*e*] 4*H*, 6*H* oxépinne.

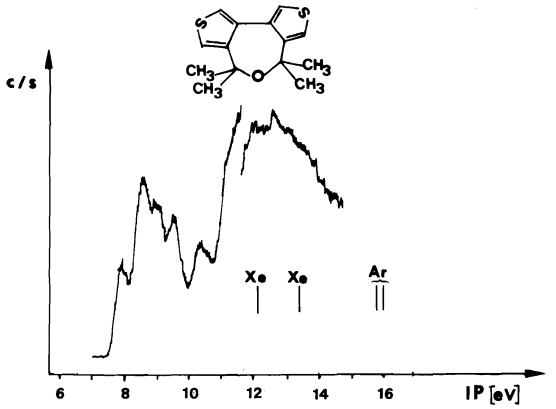

FIG. 11. Spectre photoélectronique du tétraméthyl-4,4,-6,6 dithiéno[3′,4′-*c*;3″,4″-*e*] 4*H*, 6*H* oxépinne.

TABLEAU 3. Potentiels d'ionisation verticaux des tétraméthyloxépinnes de type **1** et **2**

Attribution	Symétrie	Oxépinne de type **1**	Oxépinne de type **2**
$\pi_{C=C}$	A	7.8	8.0
$\pi_{C=C}$	B	8.8	8.8
π_S	A	8.8	8.8
π_S	B	9.2	9.2
π_O	B	9.75	9.7
n_S	A	10.8	10.45

formulées précédemment quant à l'existence d'une forme "croisée" en phase gazeuse.

Conclusion

L'analyse des spectres photoélectroniques des diverses dihydroépinnes étudiées met en évidence pour tous les composés une interaction entre les deux systèmes thiophéniques plus faible que celle observée dans le cas du bithiényl-3,3′. Ce composé présentant d'après les données de diffraction électronique un angle de twist d'environ 30°, il semble raisonnable de proposer pour tous les composés examinés une conformation privilégiée en phase gazeuse correspondant à une forme "croisée". Cette hypothèse est confirmée par l'examen des spectres d'oxépinnes substituées par des groupements méthyles en position αα′ pour lesquels une forme semi bateau n'est pas envisageable compte tenu de l'encombrement stérique.

De façon qualitative on peut estimer que pour les composés de type **1** l'angle de torsion entre les cycles est sensiblement identique (de l'ordre de 30 à 40°) pour les dérivés azotés et oxygénés et comparable à celui observé pour le bithiényl-3,3′ tandis que cet angle est nettement supérieur pour les dérivés sulfurés.

Par contre la conformation des dérivés pour lesquels les thiophènes sont reliés par leur chaînon (*c*) présente vraisemblablement un angle de torsion des cycles supérieur.

Conditions expérimentales

Les spectres ont été enregistrés sur un spectrophotomètre Perkin-Elmer PS 18 muni d'une source à hélium I (584 Å, 21.21 eV). L'étalonnage a été effectué avec les pics $^2P_{1/2}$ et $^2P_{3/2}$ du xénon (12.127 et 13.427 eV) et de l'argon (15.755 et 15.933 eV).

Les potentiels d'ionisation théoriques ont été calculés à l'aide de la méthode CNDO/S (11) dans le cadre du théorème de Koopmans (12).

Les orbitales *d* des atomes de soufre n'ont pas été prises en considération.

Les paramètres géométriques utilisés sont ceux déterminés théoriquement par optimisation énergétique à l'aide de la méthode PCILO (13).

1. J. F. CHIANG et S. H. BAUER. J. Am. Chem. Soc. **88**, 420 (1966).
2. K. HAGEN et M. TRAETTEBERG. Acta Chem. Scand. **26**, 3643 (1972).
3. K. MISLOW, M. A. W. GLASS, H. B. HOPPS, E. SIMON et G. H. WAHL, JR. J. Am. Chem. Soc. **86**, 1710 (1964).
4. I. O. SUTHERLAND et M. V. J. RAMSAY. Tetrahedron, **21**, 3401 (1965).
5. (*a*) J. P. MAIER et D. W. TURNER. J. Chem. Soc. Faraday Trans. II, 196 (1973); (*b*) J. P. MAIER et D. W. TURNER. Faraday Discuss. Chem. Soc. **54**, 149 (1972); (*c*) H. BOCK et G. WAGNER. Angew. Chem. **84**, 119 (1972); G. WAGNER et H. BOCK. Chem. Ber. **107**, 68 (1974); (*d*) S. F. NELSEN et J. M. BUSCHEK. J. Am. Chem. Soc. **95**, 2011 (1973); P. RADEMACHER. Angew. Chem. Int. Ed. Engl. **12**, 408 (1973); S. F. NELSEN et J. M. BUSCHEK. J. Am. Chem. Soc. **96**, 2392 (1974); (*e*) M. F. GUIMON, C. GUIMON, F. METRAS et G. PFISTER-GUILLOUZO. Can. J. Chem. **54**, 146 (1976); M. F. GUIMON, C. GUIMON, F. METRAS et G. PFISTER-GUILLOUZO. J. Am. Chem. Soc. **98**, 2078 (1976); (*f*) P. MEUNIER, M. COUSTALE, C. GUIMON et G. PFISTER-GUILLOUZO. J. Mol. Struct. **36**, 233 (1977).
6. A. SKANCKE. Acta Chem. Scand. **24**, 1389 (1970).
7. A. B. CORNFORD, D. C. FROST, F. G. HERRING et C. A. MCDOWELL. Can. J. Chem. **49**, 1135 (1971).
8. T. KOBAYASHI et S. NAGAKURA. Bull. Soc. Chem. Jpn. **47**, 2563 (1974).
9. H. BOCK, G. WAGNER et J. KRONER. Tetrahedron Lett. 3713 (1971).
10. D. A. SWEIGART et D. W. TURNER. J. Am. Chem. Soc. **94**, 5599 (1972).
11. C. GUIMON, D. GONBEAU et G. PFISTER-GUILLOUZO. Tetrahedron, **29**, 3399 (1973).
12. T. KOOPMANS. Physica, **1**, 104 (1934); W. RICHARDS. J. Mass. Spectrom. Ion Phys. **2**, 419 (1969).
13. (*a*) S. DINER, J. P. MALRIEU et P. CLAVERIE. Theor. Chim. Acta, **13**, 1 (1969); (*b*) J. P. MALRIEU, P. CLAVERIE et S. DINER. Theor. Chim. Acta, **13**, 18 (1969); (*c*) S. DINER, J. P. MALRIEU, F. JORDAN et M. GILBERT. Theor. Chim. Acta, **15**, 100 (1969).

Nuclear analogs of β-lactam antibiotics. VII. Synthesis of 2-isocephems[1]

TERRENCE WILLIAM DOYLE,[2,3] JAMES LESLIE DOUGLAS,[2] BERNARD BELLEAU, JACQUES MEUNIER, AND BING-YU LUH

Bristol Laboratories of Canada, 100 Industrial Boulevard, Candiac, P.Q., Canada J5R 1J1

Received March 17, 1977

TERRENCE WILLIAM DOYLE, JAMES LESLIE DOUGLAS, BERNARD BELLEAU, JACQUES MEUNIER, and BING-YU LUH. Can. J. Chem. **55**, 2873 (1977).

The synthesis of 7-β-phenoxyacetamido-3-methyl-Δ^3-2-isocephem-4-carboxylic acid **14***b* and its corresponding α-sulfoxide **15** and sulfone **17** is described. Treatment of the bismesylates **4***a*, **4***b*, and **10** with hydrogen sulfide triethylamine gave the corresponding 7-β-amino-Δ^3-2-isocephems **12***a–c* which were coupled with phenoxyacetic acid to yield the amides **13***a–c*. Hydrogenolysis of **13***b* and *c* gave the acids **14***a–b* which were active as antibiotics. Compound **14***b* was oxidized to its sulfoxide **15** with sodium metaperiodate and to its sulfone **17** with *m*-chloroperbenzoic acid. Conversion of **13***c* to its sulfoxide **16***b* followed by halogenation gave the 1α-chloro sulfoxide **18** which was converted to the acid **19**. The stereochemical assignments in the 2-isocephem series are discussed.

TERRENCE WILLIAM DOYLE, JAMES LESLIE DOUGLAS, BERNARD BELLEAU, JACQUES MEUNIER et BING-YU LUH. Can. J. Chem. **55**, 2873 (1977).

On décrit la synthèse de l'acide phénoxyacétamino-7β méthyl-3 Δ^3 isocéphem-2 carboxylique-4 (**14***b*) et de ses sulfoxyde α (**15**) et sulfone **17** correspondants. La réaction des bismésylates **4***a*, **4***b* et **10** avec le sulfure d'hydrogène dans la triéthylamine conduit aux amino-7β Δ^3 isocéphems-2 (**12***a–c*) correspondants qui peuvent réagir avec l'acide phénoxyacétique pour produire les amides **13***a–c*. L'hydrogénolyse de **13***b* et de **13***c* fournit les acides **14***a–b* qui sont actifs comme antibiotiques. On a oxydé le composé **14***b* en sulfoxyde **15** à l'aide du métapériodate de sodium et en sulfone **17** en faisant appel á l'acide métachloroperbenzoique. La transformation de **13***c* en sulfoxyde correspondant **16***b* suivie par une halogénation donne le chloro-1α sulfoxyde **18** qui peut être transformé en acide **19**. On discute des attributions stéréochimiques dans la série des isocéphems-2.

[Traduit par le journal]

In our earlier communications the synthesis of a number of *O*-2-isocephems and *N*-2-isocephems were described (1, 2). We now wish to describe the synthesis of the 2-isocephem system as well as its sulfoxide and sulfone (Fig. 1, X = S, SO, SO_2, Y = CH_2, R = ϕOCH_2, R_2 = H, R_3 = H, CH_3).[4]

To date there has been only one report of a synthesis of the 2-isocephem system by Brunwin and Lowe (4). They have described the synthesis of the 7-α-methyl-7-β-phenylacetamido-2-isocephem-4-carboxylic acid **1** (R_1 = ϕCH_2, R_2 = CH_3, R_3 = H, Y = CH_2, X = S). This material was reported to be devoid of antibiotic activity, which result was not surprising in view of the fact that substitution of the 6 position in penicillins or the 7 position in cephalosporins by a methyl group results in extensive loss of activity (5). In addition Woodward and co-workers have reported the syntheses of a number of cephalosporins containing disulfide linkages (**1**, X = Y = S) in which biological activity has been retained (6).

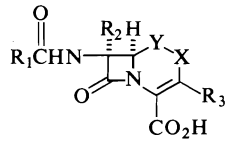

FIGURE 1

Our approach to these compounds is an extension of our synthesis of the *O*-2-isocephem system which we have reported earlier (2*b*). The key intermediates in our synthesis were the bismesylates **4***a*, **4***b*, and **10**. Compounds **4***b* and **10** were prepared in the same manner as **4***a* (1) (Scheme 1). Thus treatment of **2***a* (2*b*) with *p*-nitrobenzyl chloroformate followed by heating

[1]For part VI of this series see ref. 1.

[2]Authors to whom correspondence concerning this paper may be addressed.

[3]Present address: Bristol Laboratories, P.O. Box 657, Syracuse, NY 13201.

[4]For an explanation of the trivial nomenclature used in this series of papers see ref. 2. Alternatively the nomenclature suggested by Bose might be used. Under such nomenclature the Δ^3-2-isocephem system would be named as a 2-thia-3-octem (3).

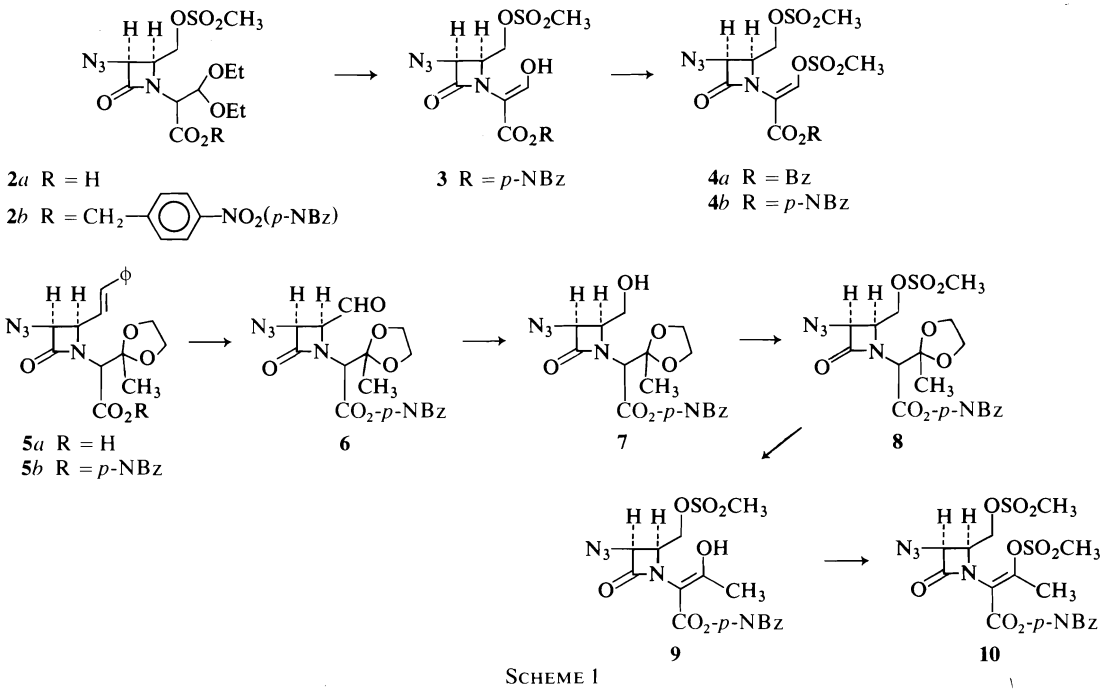

SCHEME 1

gave the ester **2***b* in 85% yield. Hydrolysis of the acetal function using 95% trifluoroacetic acid gave the enol **3** in 36% yield. Treatment of the enol **3** with methane sulfonyl chloride and base gave the desired bismesylate **4***b* in 93% yield.

The synthesis of **10** was carried out as follows. Treatment of the acid **5***a* (2*b*) with *p*-nitrobenzyl chloroformate followed by heating as in the preparation of **2***b* gave the ester **5***b* in quantitative yield. Ozonolysis of **5***b* followed by decomposition of the ozonide with dimethyl sulfide gave the aldehyde **6** in 41% yield when isolated. Generally the crude aldehyde was directly reduced with sodium borohydride in tetrahydrofuran at low temperature to give **7**. The crude alcohol was converted to its mesylate **8** which was isolated as a solid in 36% overall yield from **5***a*. Hydrolysis of **8** with trifluoroacetic acid (95%) gave the enol **9** in quantitative yield. Finally treatment of **9** with methane sulfonyl chloride – triethylamine gave the desired bismesylate **10** as an oil (85%).

Our initial experiment on the ring closure of bismesylate to 2-isocephem was carried out on **4***a*. Treatment of **4***a* with potassium acid sulfide in dimethyl sulfoxide gave **11***a* in 44% yield as a crystalline solid. The structure of **11***a* was indicated by its ir, nmr, and uv spectra as well as its correct elemental analysis. The nmr spectrum of **11***a* in $CDCl_3$ was deceptively simple (Table 1) showing a simple doublet of triplets for the C_6 proton and a doublet for the C_1 protons. When the spectrum was recorded in either deuterodimethyl sulfoxide or deuterobenzene the more complex ABX spectrum for these three protons was observed. An analysis of the coupling constants for the C_6, C_1, and C_3 protons of **11***a* permits one to assign each proton as well as to determine the conformation of **11***a* in solution. An examination of Dreiding models of the 2-isocephem system showed that **11***a* could exist in either of two possible conformations A or B (Fig. 2). The coupling constants of $H_{1\alpha}$–H_6 and $H_{1\beta}$–H_6 are 3.5 and 9.5 Hz, respectively, in (C_6D_6). Conformer A is the only conformer consistent with this observation. In addition the 1 Hz long range coupling constant between H_3 and $H_{1\alpha}$ confirms this assignment, these protons being properly aligned in the W configuration in this particular conformation (7). This assignment is in accord with that reached in the *O*-2-isocephem and *N*-2-isocephem systems (1, 2*b*). The uv spectrum of **11***a* showed a band at 303 nm with an extinction coefficient of 13 400. This is in contrast to the value of 296 nm with an extinction coefficient of 4300 reported by Lowe (3) for his 2-isocephem **1** (Fig. 1, X = S, Y = CH_2, R_1 = ϕCH_2, R_2 = Me, R_3 = H). It is apparent

TABLE 1. Nuclear magnetic resonance spectra[a]

Compd.	Aromatic and vinyl protons	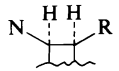		$ArCH_2^-$	CH_3	Other
2*b*[b]	8.14(d, 2H) 7.51(d, 2H) J = 7.5	4.92, 4.97 (d) J = 5.0		5.03(s)	3.04(s) 3.08(s) 1.14(t, J = 7.0) 1.20(t, J = 7.0)	3.60(m, 5H, C*H*CO_2R and CH_2Me) 4.5(m, 4H, C*H*CH_2Mes C*H*$(OEt)_2$)
3	8.10(d, 2H) J = 9.0 7.42(d, 2H) J = 9.0 7.53(s)	4.98(d) J = 5.0		5.23(m)	3.0(s)	4.40(m, C*H*—CH_2OMes, 3H)
4*b*	7.70(s, 1H) 8.10(d, 2H) 7.42(d, 2H) J = 9.0	4.98(d) J = 5.0		5.28(s)	2.97(s) 3.26(s)	4.40(m, 3H)
5*b*[b]	7.58(d) 8.22(d) J = 9 7.38(s, 5H) 6.76, 6.84(d) J = 16.0 6.20(m, 1H)	4.82(m, 2H)		5.20(s) 5.35(s)	1.52(s)	4.34, 4.66(s, C*H*CO_2R) 3.96, 3.98(s, 4H, ketal)
6	8.20(d) 7.54(d) J = 8.5	5.08(d) J = 5.0	4.65(m)	5.30(s)	1.47(s)	4.75(s, C*H*CO_2R) 3.88(m, 4H, ketal) 9.66(d, 1H, C*H*O) J = 4
7[b]	8.24(d) 7.67(d, $J \simeq$ 8)			5.32(s)	1.48	3.90(m, 4H, ketal) 4.4–5.0(m, 6H, CH_2*O*H, C*H*CO_2R, azetidinone protons)
8	8.16(d) 7.54(d) J = 8.5	5.07(d) $J \simeq$ 5	4.33(m)	5.28(s)	1.42(s) 3.0(s)	3.90(4H, m, ketal) 4.65(s, 1H, C*H*—CO_2R) 4.50(m, 3H, C*H*CH_2—OMes)
9	8.16(d) 7.50(d) J = 8.5	5.0(d) J = 4.5	3.88(dd) J_1 = 4.5 J_2 = 9	5.33(s)	3.03(s) 2.12(s)	4.40(m, 2H, CH_2—OMes)
10	8.10(d) 7.47(d) J = 8.5	4.94(d) J = 4.7		5.28(s)	3.25(s) 2.98(s) 2.53(s)	4.42(m, 3H, C*H*—CH_2—OMes)

TABLE 1 (*Continued*)

Compd.	Aromatic and vinyl protons	N–H H–R		$ArCH_2^-$	CH_3	Other
11*a*	7.41(s, 5H) 7.07(s, 1H)	5.18(d) $J = 5.0$	3.87(dt) $J_1 = 5.0$ $J_2 = 7.0$	5.28(s)		3.04(d, 2H, $J = 7.0$, —CH_2S)
11*a*[c]	7.63(s, 5H) 7.58(bs, 1H)	5.83(d) $J = 5.5$	4.12(ddd) $J_1 = 10.5$ $J_2 = 5.5$ $J_3 = 3.5$	5.39(s)		3.02(dd, 1H, $J_1 = 10.5$ $J_2 = 12.5$) 3.45(dd, 1H, $J_1 = 3.5$, $J_2 = 12.5$)
11*a*[d]	6.15(d, $J_1 = 1$)	3.61(d) $J = 5.0$	2.33(ddd) $J_1 = 9.5$ $J_2 = 5$ $J_3 = 3.5$	4.56(s)		1.79(dd, 1H, $J_1 = 12$, $J_2 = 9.5$ 1.37(ddd, 1H, $J_1 = 12$, $J_2 = 3.5$, $J_3 = 1$
11*b*[c]	8.10(d) 7.58(d) $J = 8.5$ 7.30(s, 1H)	5.59(d) $J = 5.0$	3.95(ddd) $J_1 = 10$ $J_2 = 5.0$ $J_3 = 3.5$	5.30(s)		2.88(dd, 1H, $J_1 = 10$, $J_2 = 13$) 3.34(dd, 1H, $J = 3.5$ $J_2 = 13$)
12*a*	7.32(s, 5H) 6.97(s, 1H)	4.68(d) $J = 5.0$	3.78(dt) $J_1 = 5.0$ $J_2 = 7.0$	5.24(s)		3.00(d, $J = 7.0$, 2H) 1.68(bs, 2H, NH_2)
12*c*	8.12(d) 7.55(d) $J = 8.5$	4.63(d) $J = 5.0$		5.13(d)[e] 5.38(d)[e] $J = 14.0$	2.25(s)	1.67(bs, 2H, NH_2) 3.17(dd, 1H, $J_1 = 9.0$, $J_2 = 12.0$) 2.90(dd, 1H, $J_1 = 4.5$, $J_2 = 12.0$)
13*a*[c]	7.32(s, 5H) 6.7–7.5(m, 5H) 7.0(s, 1H)	5.62(dd) $J_1 = 5.0$ $J_2 = 9.0$	3.87(m)	5.20(s)		4.55(s, 2H, ϕOCH_2—) 3.15(m, 2H) 8.77(d, 1H, NH, $J = 9.0$)
13*b*	8.10(d, 2H) $J = 8.5$ 6.7–7.7(m, 9H)	5.54(dd) $J_1 = 5.0$ $J_2 = 7.0$	3.95(m)	5.13(d)[e] 5.42(d)[e] $J = 13.5$		2.90(m, 2H, CH_2—S) 4.47(s, 2H, ϕOCH_2)
13*c*	8.0(d, 2H) 7.42(d, 2H) $J = 8.5$ 7.57(d, 1H, $J = 7.0$) 6.6–7.3(m, 5H)	5.43(dd) $J_1 = 5.0$ $J_2 = 7.0$	3.90(dt) $J_1 = 5.0$ $J_2 = 9.5$	5.14(bs)	2.23(s)	4.42(s, 2H, ϕOCH_2) 3.06(dd, 1H, $J_1 = 8.5$, $J_2 = 12$) 2.70(dd, 1H, $J_1 = 4.5$, $J_2 = 12$
14*a*[c]	6.7–7.5(6H, m)	5.56(dd) $J_1 = 5$ $J_2 = 9$	3.84(dt) $J_1 = 10$ $J_2 \simeq 5$			4.53(s, 2H, ϕOCH_2) 3.18(dd, $J_1 = 12$, $J_2 = 10$) 2.90(dd, $J_1 = 12$, $J_2 = 5$)

TABLE 1 (*Concluded*)

Compd.	Aromatic and vinyl protons	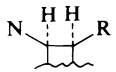		$ArCH_2^-$	CH_3	Other
14*b*[c]	8.66(d, J = 8, 1H, NH) 6.6–7.5(m, 5H)	5.45(dd) J = 5.0 J = 8.0	3.67(m)		2.12(s)	4.50(s, 2H, ϕOCH_2) 3.25(dd, 1H, J_1 = 9.5, J_2 = 12) 2.75(dd, 1H, J_1 = 4, J_2 = 12)
15[c]	8.80(d, NH, J = 9.0) 6.7–7.4(m, 5H)	5.70(dd) J = 5.0 J = 9.0	4.20(m)		2.18(s)	4.55(s, 2H, ϕOCH_2) 3.15(m, 2H, CH_2—SO)
16*a*[c]	7.38(m, 5H) 6.7–7.5(m, 5H) 7.05(s, 1H)	5.87(dd) J_1 = 5.5 J_2 = 9.0	4.30(m)	5.31(s)		4.58(s, 2H, ϕOCH_2) 3.06(m, 2H, CH_2—SO) 8.78(d, 1H, N*H*, J = 9.0)
16*b*[c]	8.13(d, 2H) 7.61(d, 2H) J = 8.5 6.7–7.4(m, 5H)	5.75(dd) J = 5.0 J = 8.0	4.22(m)	5.42(s)	2.22(s)	4.55(s, 2H, ϕOCH_2) 3.22(m, 2H, CH_2SO—) 8.70(d, 1H, N*H*, J = 8.0)
17[c]	8.70(d, NH, J = 9.5) 6.7–7.4(m, 5H)	5.67(dd) J = 5.0 J = 9.5	4.56(dt) J_1 = 5.0 J_2 = 11 Hz		2.0(s)	4.53(s, 2H, ϕOCH_2) 3.84(dd, 1H, J_1 = 13, J_2 = 11) 3.53(dd, 1H, J_1 = 13, J_2 = 5)
18[c]	8.20(d) 7.65(d) J = 8.5 6.7–7.4(m, 5H)	5.76(dd) J_1 = 6 J_2 = 9	4.85(dd) J = 6 J_2 = 1.5	5.44(s)	2.10(s)	4.68(s, 2H, ϕOCH_2) 6.0(d, 1H, J = 1.5, C*H*Cl) 8.67(d, 1H, N*H*, J = 9)
19[c,f]	6.8–7.5(m, 5H)	5.76(d) J = 6.0	4.86(dd) J_1 = 6.0 J_2 = 1.5		2.05(s)	5.95(d, 1H, J = 1.5, C*H*Cl) 4.75(s, 2H, ϕOCH_2)
20[c]	7.67(s, 5H) 7.50(d, 1H) J = 1.0	6.05(d) J = 5.5	4.47(ddd) J_1 = 3.5 J_2 = 5.5 J_3 = 13	5.50(s)		2.94(dd, 1H, J_1 = 14.5, J_2 = 13) 3.58(ddd, 1H, J_1 = 14.5, J_2 = 3.5, J_3 = 1)
21[c]	7.67(s, 5H) 7.28(d, 1H) J = 1.0	5.88(d) J = 5	4.47(dt) J_1 = 5 J_2 = 12	5.50(s)		3.84(2H, d, J = 12, CH_2—SO_2)

[a]Spectra were recorded at 60 MHz in $CDCl_3$ unless otherwise noted. Coupling constants are in Hz. [b]Mixture of diastereoisomers. [c]DMSO-d_6. [d]Recorded in C_6D_6. TMS external reference in $CDCl_3$. [e]Arms of AB quartet. [f]D_2O exchanged.

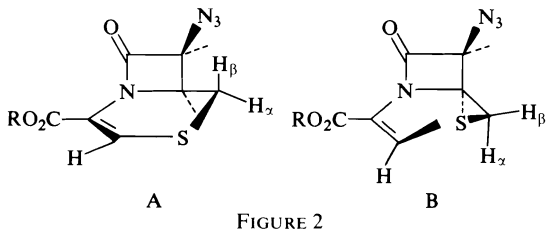

A B

FIGURE 2

that the material obtained by these workers cannot have been of much greater than 33% purity inasmuch as it is highly unlikely that substitution of the 7α-proton by methyl would produce such a difference in the extinction coefficient for the two compounds. The values for the extinction coefficients for all 2-isocephems prepared in this work ranged from 11 400 to 15 000.

Reduction of the azido function **11***a* was accomplished using hydrogen sulfide – triethylamine to give **12***a* in 77% yield. The amine was coupled to phenoxyacetic acid using *N*-ethoxycarbonyl-2-ethoxy-1,2-dihydroquinoline(EEDQ) (8) to give **13***a* (78%). Attempted conversion of the ester to the desired acid **14***a* by hydrogenolysis failed due to poisoning of the catalyst. Accordingly it was decided to prepare **14***a* via the *p*-nitrobenzyl ester.

Treatment of **4***b* with hydrogen sulfide and 2.2 equiv. of triethylamine followed by immediate work-up gave the desired 2-isocephem **11***b* in 55.5% yield. Reduction of **11***b* with triethylamine – hydrogen sulfide gave the amine **12***b* in quantitative yield. Coupling of **12***b* and phenoxyacetic acid with EEDQ proceeded in 64% yield to give **13***b*. The preparation of the 3-methyl substituted 2-isocephem was carried out similarly. Thus treatment of the bismesylate **10** with hydrogen sulfide – triethylamine for an extended period (45 min vs. 10 min) accomplished both the ring closure and azide reduction in one step giving the amine **12***c* in 77% yield from **10**. The conversion of the amine **12***c* to its phenoxyacetamide was carried out in the usual fashion to give **13***c* in 74% yield.

Hydrogenolysis of **13***b* over palladium-on-carbon gave the desired acid **14***a* in 40.5% yield. Similarly hydrogenolysis of **13***c* gave **14***b* in 70% yield. The structures of **14***a* and **14***b* were established by their mode of synthesis, elemental analyses, and spectral properties. Both **14***a* and **14***b* exhibited significant antibiotic activity.

Treatment of **14***b* with 1 equiv. of sodium metaperiodate gave the sulfoxide **15** in 77% yield as a single isomer. Alternatively **15** could be prepared by conversion of **13***c* to its sulfoxide **16***b* using *m*-chloroperbenzoic acid followed by reduction of **16***b* to **15** on 10% palladium-on-carbon. The overall yield of **15** from **13***c* was 84%. The material was identical in all respects with that obtained from **14***b*, thus indicating the stereochemistry of the sulfoxide to be the same in each case. Treatment of **14***b* with an excess of *m*-chloroperbenzoic acid gave the sulfone **17** in 25% yield.

Chlorination of the sulfoxide **16***b* using *tert*-butyl hypochlorite gave the monochloro derivative **18** as a single isomer in 67% yield. Compound **18** was converted to the acid by hydrogenolysis over 10% palladium-on-charcoal. Thus **19** was prepared in 56% yield.

Inasmuch as only a single sulfoxide isomer was produced in the oxidations of **14***b* to **15**, **13***a* to **16***a*, and **13***c* to **16***b* the assignment of configuration to these compounds (**15**, **16***a*, **16***b*) rests upon the assumption that oxidation of the sulfur should occur from the least hindered face of the molecule thus producing the α-sulfoxide in each instance. Unfortunately the nmr spectra of compounds **15**, **16***a*, **16***b* did little to resolve the question of their stereochemistry although the down field shift of the C_6 proton was suggestive of the formation of an α-sulfoxide with the pseudoaxial configuration (Fig. 3).

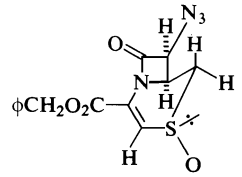

FIGURE 3

In order to help resolve this question the oxidation of **11***a* to its sulfoxide **20** was carried out. Treatment of **11***a* with 1 equiv. of *m*-chloroperbenzoic acid gave **20** in 74% yield as a single isomer. Prolonged treatment of **11***a* with an excess of *m*-chloroperbenzoic acid gave the sulfone **21** in 86% yield. Several attempts to convert **20** to **16***a* via the amine **22** failed.

A comparison of the nmr spectra of compounds **11***a*, **20**, and **21** permits the configurational assignment to **20** to be made and by inference to **15**, **16***a* and **16***b*. In the nmr spectrum of **20** a down field shift of 0.35 ppm for the C_6 proton was observed typical of the shift usually observed for a proton *syn*-axial to an axial sulfoxide group (9). Conversion of **20** to **21** results

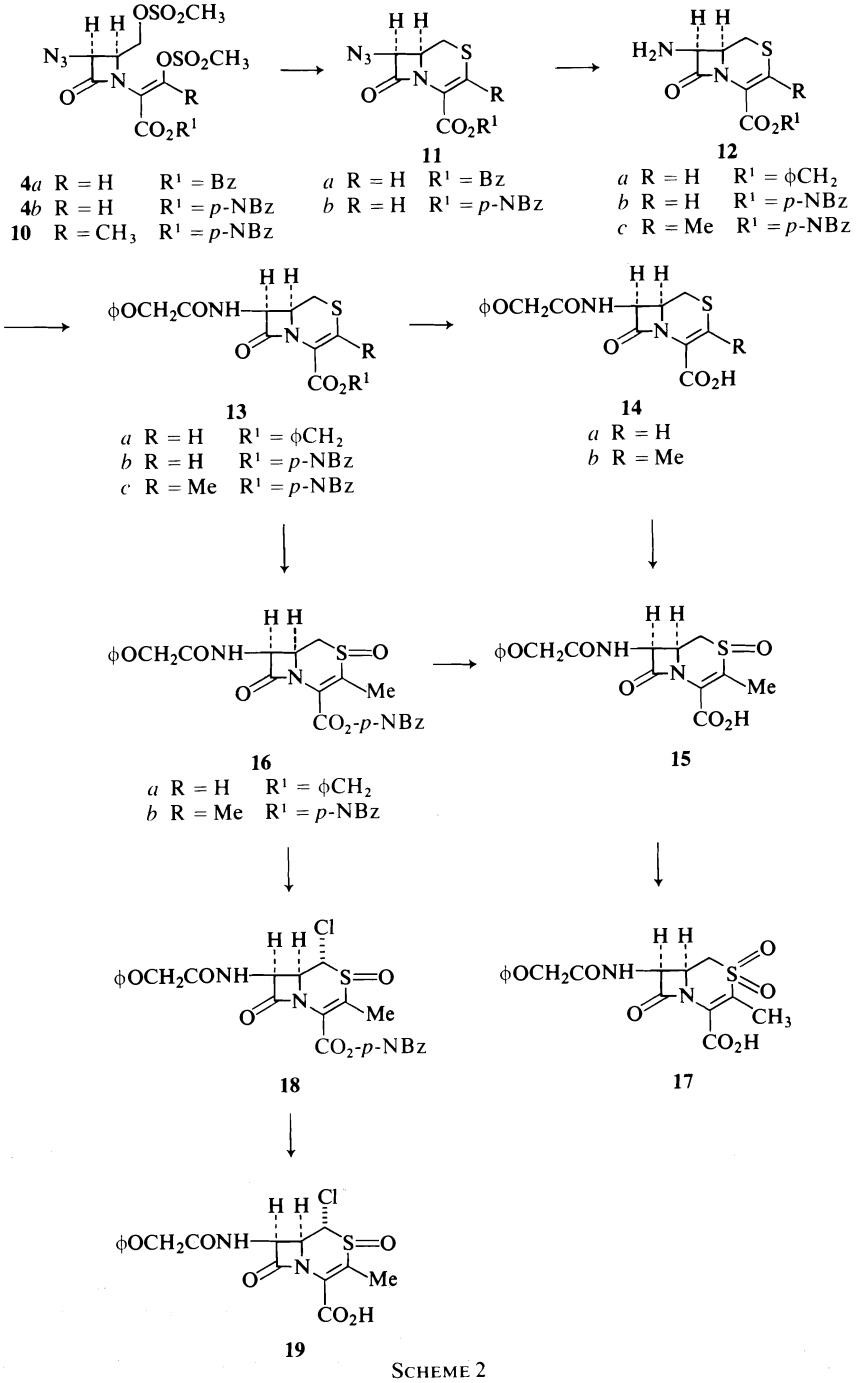

SCHEME 2

in no shift of the C_6 proton. From the coupling constants for the $C_{1\alpha}$ and $C_{1\beta}$ protons to the C_6 proton both **11***a* and **20** are in the same conformation as shown for **20** in Fig. 3. Thus based on the down field shift of the C_6 proton the α-sulfoxide configuration is assigned to **20**. This is also borne out by the size of the geminal coupling constant for $C_{1\alpha}$ and $C_{1\beta}$ protons in **20** vs. **11***a*. In compound **11***a* J_{gem} = 12.5 Hz while in **20** J_{gem} = 14.5 Hz. The increased J_{gem} is diagnostic

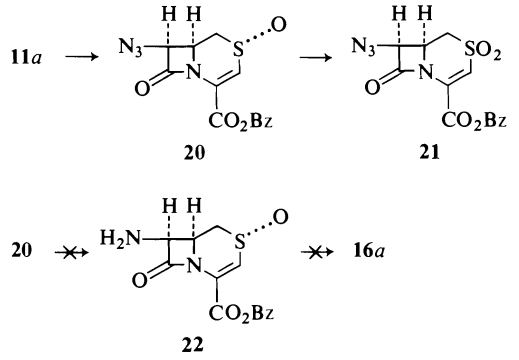

SCHEME 3

of an axial sulfoxide (10) although in the absence of the β-isomer this assignment must be viewed cautiously.

The stereochemical assignment to the α-chlorosulfoxide **18** is uncertain. Recent reports on the stereochemistry of α-halogenation of sulfoxides (11) and the mechanism of the reaction suggest that the chlorination of **17** probably proceeds via the intermediates **23** (Scheme 4) and **24**. A priori one would expect attack of the chloride ion on **24** to proceed from the less hindered α face to give the α-chloro sulfoxide. The nmr spectrum of **18** is in accord with this expectation, there being an ~1.5 Hz coupling constant between the proton α to chlorine and the C_6 proton. The only isomer in which such a small coupling is to be expected is the α-chloro isomer in the conformation shown.

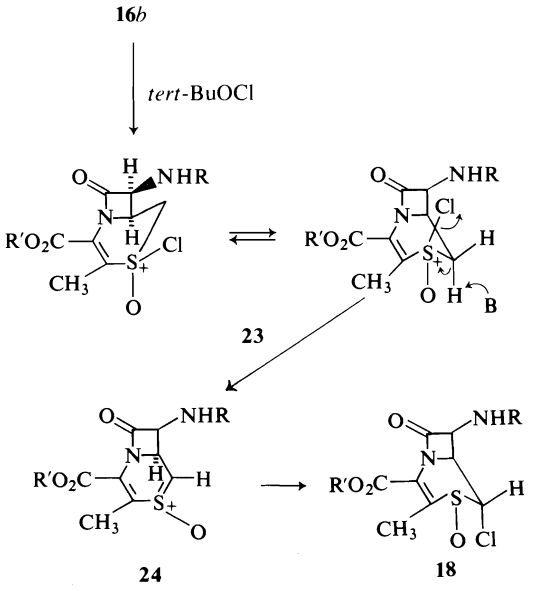

SCHEME 4

While the configuration of the α-chloro group may be thus assigned that of the sulfoxide is less certain. α-Halogenation has been shown to involve both retention and inversion of configuration at sulfur depending on the nature of the sulfoxide and the halogenating agent (11). Spry has reported that α-chlorination of the β-sulfoxide **25** proceeded with retention of configuration at sulfur although no details of the stereochemical assignment were given (12). Inasmuch as this chlorination of **25** probably proceeds via an intermediate **26** similar to **24**, by

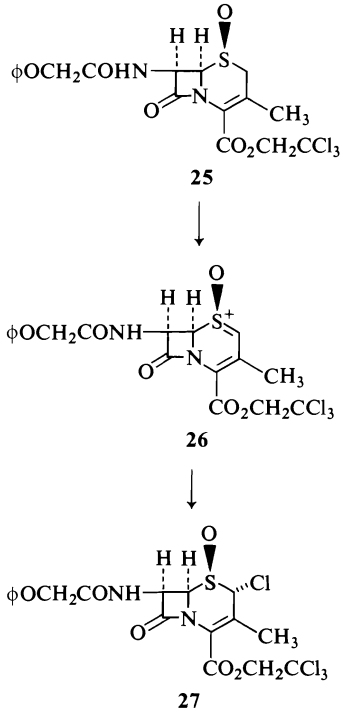

FIGURE 4

analogy the conversion of **16*b*** to **18** may well involve retention at sulfur (Fig. 4).

Experimental

The infrared spectra were recorded on a Unicam SP-200G grating, ir spectrometer. The nmr spectra were determined on a Varian A60-A spectrometer using tetramethylsilane as an internal standard. Melting points are uncorrected and were determined on a Gallenkamp melting point apparatus. The analyses were performed by Micro-Tech Laboratories, Skokie, IL.

Preparation of 4b

To a solution of 23.0 g crude acid **2*a*** in 150 ml CH_2Cl_2 at 0–5°C was added 15.4 g *p*-nitrobenzylchloroformate. A solution of 8.5 ml triethylamine in 50 ml CH_2Cl_2 was added dropwise. Vigorous gas evolution and darkening of the solution was observed. The solution was refluxed 15

min and diluted to 300 ml with ether. The solution was washed with 10% HCl (2 × 50 ml), 1% NaOH (1 × 50 ml), and brine (100 ml), dried over Na_2SO_4, and filtered through a pad of activity 3 alumina (~50 g). The filtrate was evaporated to give 26.6 g of crude *p*-nitrobenzyl ester **2***b*.

The crude *p*-nitrobenzyl ester **2***b* was taken up in 100 ml of 95% TFA and evaporated to dryness at 50°C under vacuum (rotary evaporator). This procedure was repeated once and the residual oil taken up in CH_2Cl_2. The solution was washed with brine (3 × 100 ml), dried over Na_2SO_4, filtered, and evaporated. The residual oil was taken up in ether and extracted with 1% NaOH. The aqueous fractions were acidified and extracted into ether – methylene chloride (3 × 100 ml). The extracts were dried over Na_2SO_4, filtered, and evaporated to give 8.0 g of enol **3**; uv (EtOH) λ_{max} 238 (ε 9900).

To a solution of 6.5 g (14.7 mmol) of **3** and 224 ml triethylamine in 75 ml CH_2Cl_2 was added 1.25 ml methanesulfonyl chloride in 10 ml CH_2Cl_2 at 0–5°C. The solution was stirred at 0–5°C for 30 min, washed with 10% HCl, saturated $NaHCO_3$, and brine, dried over Na_2SO_4, filtered, and evaporated to yield 7.08 g (93%) of **4***b*. The nmr and ir spectra of **4***b* were compatible with the assigned structure (as a mixture of geometrical isomers). The oil was used without further purification in the next step.

Preparation of ***10***

A solution of the acid **5***a* (89.5 g, 0.25 mol) and triethylamine (27.8 g, 0.275 mol) in 1.35 ℓ of CH_2Cl_2 was placed in a 2 ℓ flask equipped with magnetic stirrer, a nitrogen inlet, and a dropping funnel. A solution of *p*-nitrobenzylchloroformate (59.3 g, 0.275 mol) in 275 ml of CH_2Cl_2 was added slowly while the reaction mixture was maintained at 0–5°. After completion of the addition, the reaction mixture was maintained at 25°C for 30 min, then heated under reflux until gas evolution ceased (45 min). The resulting solution was washed with brine, 10% HCl (2 × 500 ml), and brine, then dried (Na_2SO_4) and evaporated *in vacuo* (35°C) to give ester **5***b* as an orange oil, 123 g (100%) which was used in subsequent reactions without purification.

A solution of compound **5***b* (123 g, 0.25 mol) in 1.7 ℓ of CH_2Cl_2 was cooled to −78°C and ozone passed through until a blue color persisted (3 h). The excess ozone was flushed out with nitrogen. Dimethyl sulfide (100 ml) was added over 30 min to the solution at −78°C, which was then allowed to come to 25°C over 1 h. The solution was evaporated *in vacuo* and the residue redissolved in 1.7 ℓ of CH_2Cl_2. This solution was washed with brine (2×), dried (Na_2SO_4), filtered through a pad of alumina (500 g, grade III), and evaporated *in vacuo*. The final evaporation was done at 40–45°C and 0.3 Torr for 24 h. The resulting oil, 93.3 g, was shown by nmr to be approximately 35% benzaldehyde and 65% aldehyde **6** (mol%). The oil was triturated with cold ether and the resulting solid was collected by filtration to give 42.5 g of **6** as a white solid, mp 143–146°C; ir (neat) 1785, 1735 cm^{-1}. *Anal.* calcd. for $C_{17}H_{17}N_5O_8$: C 48.69, H 4.09, N 16.70; found: C 48.71, H 4.16, N 16.52.

The crude aldehyde was generally used as such in subsequent reactions.

Sodium borohydride (4.2 g, 0.111 mol) was added in three portions to a stirred solution of crude aldehyde **6** (93.3 g, 0.222 mol) in 775 ml of THF at −5 to −10°C. The reaction was maintained at −5 to −10°C for 2 h, then acidified to p*H* 3 with 10% HCl, saturated with NaCl, and evaporated *in vacuo* (35°C). The resulting residue was mixed with 500 ml of brine and extracted (3 × 400 ml) with CH_2Cl_2. The extracts were dried (Na_2SO_4), filtered through a pad of alumina (500 g, grade III), and evaporated *in vacuo* to give a yellow oil, 80.0 g. The nmr and ir spectra of this oil were consistent with the major portion of the oil being the desired alcohol **7** plus some impurities, including benzyl alcohol.

A solution of 80.0 g (0.19 mol) of alcohol **7** and 30.7 g (0.304 ml) of triethylamine in 825 ml of CH_2Cl_2 was cooled to 0°C and a solution of methane – sulfonyl chloride (32.6 g, 0.285 mol) in 240 ml of CH_2Cl_2 was added over 45 min. The reaction mixture was stirred at 25°C for 5 h, then washed with brine (3 × 500 ml) and 10% HCl (3 × 500 ml). The resulting solution was dried (Na_2SO_4) and evaporated *in vacuo* to a red oil. The oil was crystallized from benzene–ether to give pure mesylate **8** as a colorless solid, 44.5 g, mp 133–136°C. The overall yield from **5***a* to **8** was 36%; ir (Nujol mull) 2110, 1775, 1742 cm^{-1}. *Anal.* calcd. for $C_{18}H_{21}N_5O_{10}S$: C 43.29, H 4.24, N 14.02, S 6.42; found: C 42.85, H 4.38, N 14.24, S 6.35.

A solution of ketal **8** (43.4 g, 87 mmol), trifluoroacetic acid (380 ml), and water (20 ml) was left at 25°C for 2.5 h, then evaporated *in vacuo* at 35°C. The residue was mixed with 400 ml of brine and extracted (3 × 200 ml) with CH_2Cl_2. The organic extract was washed (2 × 100 ml) with brine, dried (Na_2SO_4), and evaporated *in vacuo* to give the enol **9** as a yellow oil, 44.8 g; ir (neat) 2110, 1785, 1755, 1660, 1605 cm^{-1}.

A solution of enol **9** (32.0 g, 74 mmol) and methanesulfonyl chloride (9.32 g, 81.4 mmol) in 950 ml of CH_2Cl_2 was added over 1 h. The reaction mixture was stirred another 1 h at 0°C, then washed with brine (2 × 500 ml), 10% HCl (2 × 500 ml), and brine (500 ml). The solution was dried (Na_2SO_4), filtered through a pad of alumina (200 g, grade III), and evaporated *in vacuo* (35°C) to give the dimesylate **10** as an orange oil, 33.45 g; ir (neat) 2110, 1780, 1735, 1645, 1610 cm^{-1}.

Benzyl 7-β-Azido-Δ³-2-isocephem-4-carboxylate ***11a***

To a solution of 497.5 mg (1.05 mmol) of compound **4***a* in 9 ml dry DMSO at 25°C was added a solution of 160 mg (2.10 mmol) potassium acid sulfide in 5 ml DMSO in a dropwise fashion. As each drop was added a transient green color was observed. After approximately 50% of the KSH solution had been added, the green color faded to yellow (rather than colorless as previously observed). Addition was stopped and the solution was stirred 5 min. The solution was poured into 50 ml of brine to which 10 ml 10% HCl had been added. The solution was extracted with CH_2Cl_2–Et_2O, the extracts washed with water (3 × 50 ml) and brine (1 × 25 ml), dried over Na_2SO_4, filtered, and evaporated to yield 255 mg partially crystalline oil. The oil was passed through 2 g silica gel with CH_2Cl_2 and evaporated. Trituration with ether (5 ml) and filtration gave 145 mg of **11***a*, mp 97°C; ir ($CHCl_3$): 2110, 1782, 1715, 1580 cm^{-1}; uv (EtOH) λ_{max} 303 (ε 13 400). *Anal.* calcd. for $C_{14}H_{12}N_4O_3S$: C 53.15, H 3.82, N 17.71; found: C 53.19, H 3.75, N 17.94.

p-Nitrobenzyl 7-β-Azido-Δ³-2-isocephem-4-carboxylate ***11b***

Into a solution of 2.90 g (5.6 mmol) bismesylate **4***b* in 50 ml CH_2Cl_2 was bubbled H_2S gas for 3 min. To this

was added 1.35 g (13.3 mmol) triethylamine in 10 ml CH_2Cl_2 dropwise over 10 min. The solution was purged with a stream of N_2 and washed with 10% HCl, $NaHCO_3$, and brine. The solution was dried over Na_2SO_4 and concentrated. Trituration of the oil with CH_2Cl_2 induced crystallization. Filtration gave 1.12 g (55.5%) crystalline **11***b*, mp 187.5–188.5°C; uv (EtOH) λ_{max} 303 (ε 14 970); ir ($CHCl_3$): 2110, 1782, 1720, 1608, 1573, 1525 cm^{-1}. *Anal.* calcd. for $C_{14}H_{11}N_5O_5S$: C 46.53, H 3.07, N 19.38, S 8.87; found: C 46.69, H 3.07, N 19.65, S 9.18.

Benzyl 7-β-Amino-Δ³-2-isocephem-4-carboxylate ***12a***

To a solution of 316 mg (1 mmol) of **11***a* in 20 ml methylene chloride was added 101 mg (1 mmol) triethylamine. A stream of hydrogen sulfide was passed through the solution for 3 min and the solution was let stand 1 h at 25°C. The solvent was evaporated at reduced pressure and the residue was partitioned between 10% hydrochloric acid and ether. The aqueous layer was neutralized using sodium bicarbonate and extracted with methylene chloride. The extracts were dried over sodium sulfate and evaporated to yield 223 mg (77%) of **12***a*, mp 119–120°C, recrystallized from benzene; ir ($CHCl_3$): 3400, 1770, 1715, 1577 cm^{-1}; uv (EtOH) λ_{max} 305 (ε 14 060). *Anal.* calcd. for $C_{14}H_{14}N_2O_3S$: C 57.91, H 4.86, N 9.65, S 11.04; found: C 58.32, H 4.81, N 9.70, S 11.17.

p-Nitrobenzyl 7-β-Amino-Δ³-2-isocephem-4-carboxylate ***12b***

Reduction of 525 mg (1.45 mmol) of **11***b* in methylene chloride using triethylamine – hydrogen sulfide as in the above example gave 486 mg (100%) of **12***b*, mp 181.5–183°C recrystallized from acetonitrile–ether; ir ($CHCl_3$): 1775, 1720, 1610, 1580, 1530 cm^{-1}; uv (EtOH) λ_{max} 301 (ε 15 200). *Anal.* calcd. for $C_{14}H_{13}N_3O_5S$: C 50.14, H 3.91, N 12.53, S 9.56; found: C 49.85, H 3.85, N 12.67, S 9.59.

p-Nitrobenzyl 3-Methyl-7-β-amino-Δ³-2-isocephem-4-carboxylate ***12c***

Hydrogen sulfide was passed into a solution of dimesylate **10** (4.4 g, 8.24 mmol) in 90 ml of CH_2Cl_2 at 0–5°C for 15 min. With the temperature maintained at 0–5°C, a solution of triethylamine (2.5 g, 24.7 mmol) in 50 ml of CH_2Cl_2 was added over 10 min. The reaction mixture was stirred at 25°C for 45 min. The resulting solution was washed with brine (2 × 100 ml), dried (Na_2SO_4), treated with charcoal, and evaporated *in vacuo* to give a yellow oil. The oil was dissolved in a minimum volume of CH_2Cl_2 (an insoluble gum was removed by filtration) and saturated with HCl (gas). Ether was added to near opalescence and the solution was cooled to 0°C. The hydrochloride salt of **12***c* was obtained as a pale yellow solid, 2.5 g (77%), mp 194–195°C (dec.). The amine **12***c* was stored as its HCl salt; the free base was prepared as follows. The salt was suspended in water, $NaHCO_3$ added until basic, and the mixture extracted (3×) with CH_2Cl_2. The extracts were dried, treated with charcoal, and evaporated *in vacuo* to give the free base **12***c* as a pale yellow foam; ir (Nujol mull on HCl salt): 1782, 1695, 1610, 1580, 1530 cm^{-1}. *Anal.* calcd. for $C_{15}H_{15}N_3O_5S \cdot HCl$: C 46.70, H 4.18, N 10.89, Cl 9.19, S 8.31; found: C 46.50, H 4.20, N 10.85, Cl 9.08, S 8.18.

Benzyl 7-β-(Phenoxyacetamido)-Δ³-2-isocephem-4-carboxylate ***13a***

To a solution of 223 mg (0.77 mmol) of **12***a* in 25 ml methylene chloride was added 123 mg (0.81 mmol) phenoxyacetic acid followed by 200 mg (0.81 mmol) EEDQ. The solution was let stand 18 h at 25°C and washed with 10% hydrochloric acid, 5% sodium bicarbonate, water, and brine. After drying over sodium sulfate, the extracts were evaporated and the residual oil triturated with ether–chloroform. There was obtained 254.5 mg (78%) of **13***a*, mp 184–185°C with decomposition; ir ($CHCl_3$): 3430, 3350, 1770, 1712, 1690, 1601, 1590, 1575, 1530, 1500 cm^{-1}; uv (EtOH) λ_{max} 303 (ε 12 850). *Anal.* calcd. for $C_{22}H_{20}N_2O_5S$: C 62.26, H 4.75, N 6.60, S 7.55; found: C 62.32, H 4.98, N 6.63, S 7.50.

p-Nitrobenzyl 7-β-(Phenoxyacetamido)-Δ³-2-isocephem-4-carboxylate ***13b***

The coupling of 335 mg (1 mmol) of **12***b* with phenoxyacetic acid using EEDQ as in the above example gave 295.7 mg (64%) of **13***b*, mp 180°C after recrystallization from benzene; ir ($CHCl_3$): 3420, 1778, 1720, 1692, 1598, 1573, 1523, 1492 cm^{-1}; uv (EtOH) λ_{max} 302.5 (ε 15 060). *Anal.* calcd. for $C_{22}H_{19}N_3O_7S$: C 56.28, H 4.07, N 8.95, S 6.83; found: C 55.93, H 4.06, N 9.05, S 6.62.

p-Nitrobenzyl 3-Methyl-7-β-(phenoxyacetamido)-Δ³-2-isocephem-4-carboxylate ***13c***

Treatment of 4.0 g (11.4 mmol) of **12***c* with phenoxyacetic acid and EEDQ as in the above example gave after work-up **13***c* as a foam. The foam was recrystallized from benzene to yield 4.75 g (74%) of **13***c* as a beige solid; ir (Nujol mull): 3340, 3310, 1755, 1715, 1680, 1600, 1590, 1575 cm^{-1}. *Anal.* calcd. for $C_{23}H_{21}N_3O_7S$: C 57.14, H 4.38, N 8.69; found: C 57.46, H 4.44, N 8.20.

7-β-(Phenoxyacetamido)-Δ³-2-isocephem-4-carboxylic Acid ***14a***

Compound **13***b* (469 mg, 0.001 mol) in 2 ml DMF and 20 ml methanol (to which 5 drops 10% HCl had been added) were stirred with 700 mg of 10% Pd/C at atmospheric pressure and ambient temperature (20°C) under hydrogen. Rapid uptake of 3 equiv. of hydrogen was observed (35 min). The uptake of the fourth equivalent of hydrogen required an additional 2 h. The suspension was filtered through Celite (filter cake washed with CH_2Cl_2) and the filtrate evaporated. The residue was taken up in 50 ml CH_2Cl_2 and the filtrate evaporated. The solution was dried over Na_2SO_4 and filtered. The filtrate was evaporated to give a yellow solid. Trituration with 5 ml ether and filtration gave 135 mg (40.5%) of **14***a*, mp 209–210°C with decomposition (after recrystallization from acetone–ether); ir (KBr disc): 2400–3600, 3340, 1770, 1750, 1665, 1575 cm^{-1}; uv (EtOH) λ_{max} 298 (ε 12 750). *Anal.* calcd. for $C_{15}H_{14}N_2O_5S$: C 53.87, H 4.22, N 8.37, S 9.59; found: C 53.43, H 4.23, N 8.45, S 9.38.

3-Methyl-7-β-(Phenoxyacetamido)-Δ³-2-isocephem-4-carboxylic Acid ***14b***

A solution of **13***c* (2.0 g, 3.57 mmol) in dioxane (50 ml) and methanol (25 ml) containing 1.0 g of 10% palladium-on-charcoal was hydrogenated on a Parr shaker at 25°C and 50 psi for 3 h. The catalyst was filtered off and the solution evaporated to dryness *in vacuo*. The residue was dissolved in ethyl acetate (EtOAc) and washed with 10% HCl (3×), then with brine. The aqueous layers were extracted (2×) with EtOAc and each extract washed with brine. The combined organic layers were treated with charcoal and evaporated *in vacuo* to a solid. The solid was dissolved in very dilute $NaHCO_3$ containing slightly more

than 1 equiv. of base. This aqueous solution was washed with EtOAc, acidified to p*H* 2 with 10% HCl, and extracted 2× with EtOAc. The organic solution was dried (Na_2SO_4) and evaporated *in vacuo* to give the acid **14***b* as an off-white solid, 865 mg (70% yield). The product could be recrystallized from EtOAc, mp 219–220°C; ir (Nujol mull): 3340, 1755(s), 1745, 1705, 1660, 1590 cm^{-1}; uv (MeOH) λ_{max} 294 (ε 11 400). *Anal.* calcd. for $C_{16}H_{16}N_2O_5S$: C 55.16, H 4.63, N 8.04, S 9.20; found: C 55.03, H 4.62, N 7.98, S 9.07.

Benzyl 2-Oxido-7-β-(Phenoxyacetamido)-Δ³-2-isocephem-4-carboxylate ***16a***

To a solution of 215 mg (0.51 mmol) of **13***a* in 15 ml of methylene chloride was added 107 mg (~0.51 mmol) of *m*-chloroperbenzoic acid in 5 ml methylene chloride at 0–5°C over 15 min. The solution was stirred 15 min at 25°C and washed with 5% sodium bicarbonate solution. The solution was dried over sodium sulfate and concentrated to yield a semisolid which crystallized on trituration with ether to give 157.0 mg (70%) of **16***a*, mp 203–204°C; ir ($CHCl_3$): 3410, 1795, 1735, 1695, 1609, 1595, 1520, 1495 cm^{-1}. *Anal.* calcd. for $C_{22}H_{20}N_2O_6S$: C 59.98, H 4.58, N 6.36, S 7.27; found: C 59.91, H 4.40, N 6.44, S 7.05.

p-Nitrobenzyl 2-Oxido-3-methyl-7-β-(phenoxyacetamido)-Δ³-2-isocephem-4-carboxylate ***16b***

A solution of *m*-chloroperbenzoic acid (103 mg, containing 0.505 mmol) in 11 ml of CH_2Cl_2 was added over 75 min to a stirred solution of **13***b* (280 mg, 0.50 mmol) in 11 ml of CH_2Cl_2 at 0°C. After a further 15 min at 0°C, the solution was washed (3×) with 10% $NaHCO_3$ containing several drops of Na_2CO_3, dried, and evaporated *in vacuo* to give the sulfoxide **16***b* as a colorless foam, 281 mg.

2-Oxido-3-methyl-7-β-(phenoxyacetamido)-Δ³-2-isocephem-4-carboxylic Acid ***15***

From ***14b***

The isocephem **14***b* (454 mg, 1.30 mmol), 45 ml of water, $NaHCO_3$ (110 mg, 1.31 mmol), and sodium metaperiodate (280 mg, 1.30 mmol) were stirred together at 25°C for 24 h. The resulting solution was saturated with NaCl and 10% HCl added until p*H* 2 reached. This mixture was extracted (3×) with EtOAc containing some MeOH. The combined extracts were washed with brine, dried, and evaporated *in vacuo* to give the sulfoxide **15**, 363 mg (77% yield), as a beige solid. Recrystallization from EtOAc–MeOH gave a colorless solid, mp 229–232°C (dec.); ir (Nujol mull): 3360, 3310, 1775, 1720, 1635, 1600, 1595, 1545, 1495 cm^{-1}; uv (MeOH) λ_{max} 270, 275 (ε 9100). *Anal.* calcd. for $C_{16}H_{16}N_2O_6S$: C 52.75, H 4.43, N 7.69, S 8.80; found: C 52.65, H 4.45, N 7.64, S 8.60.

From ***16b***

A mixture containing the sulfoxide ester **16***b* (280 mg, 0.485 mmol), THF (28 ml), dioxane (14 ml), MeOH (2.8 ml), and 10% palladium-on-charcoal was hydrogenated on a Parr shaker at 25°C and 50 psi for 4 h. The catalyst was filtered off and the solution evaporated *in vacuo*. The residue was mixed with EtOAc and ½ ml of 10% HCl and enough MeOH added to make a nearly homogeneous solution. The filtered solution was extracted (2 × 20 ml) with 1% $NaHCO_3$. The aqueous layer was acidified with 10% HCl, saturated with NaCl, and extracted (2×) with EtOAc/MeOH. The organic layers were washed with brine, dried, and evaporated *in vacuo* to give 149 mg (84%) of **15**, the ir and nmr spectra of which were identical with the sample prepared from **14***b*.

2,2-Dioxo-3-methyl-7-β-(phenoxyacetamido)-Δ³-2-isocephem-4-carboxylic Acid ***17***

A solution of *m*-chloroperbenzoic acid (542 mg, containing 2.66 mmol) in 5 ml of EtOAc was added to a slurry of isocephem **14***b* (440 mg, 1.26 mmol) in 44 ml of EtOAc. The mixture was stirred at 25°C for 40 h, then evaporated to dryness under a nitrogen stream. The resulting solid was triturated with small volumes of EtOAc several times, then recrystallized from EtOAc–MeOH (3×) to give the sulfone **17** as a colorless solid, mp 203–204°C (dec.), 118 mg (25% yield); ir (Nujol mull): 3380, 2400–3600, 1795, 1735, 1665, 1620, 1600, 1590, 1520, 1495 cm^{-1}; uv (MeOH) λ_{max} 267 (ε 11 100). *Anal.* calcd. for $C_{16}H_{16}N_2O_7S$: C 50.53, H 4.24, N 7.37, S 8.43; found: C 50.38, H 4.25, N 7.38, S 8.60.

p-Nitrobenzyl 1-α-Chloro-2-oxido-3-methyl-7-β(phenoxyacetamido)-Δ³-2-isocephem-4-carboxylate ***18***

To a slurry of sulfoxide **16***b* (889 mg, 1.78 mmol) and potassium acetate (465 mg, 4.74 mmol) in 70 ml of CH_2Cl_2 at 0°C was added a solution of *tert*-butyl hypochlorite (0.213 ml, 1.92 mmol) in 4 ml of CH_2Cl_2. The mixture was stirred at 0°C for 3.5 h. Water (70 ml) was added and the mixture shaken and separated. The water was extracted with more CH_2Cl_2 and the combined organic layers were washed with brine, dried (Na_2SO_4), and evaporated *in vacuo* to give a yellow oil. A $CHCl_3$ solution of the oil deposited crystals on standing 24 h. The mother liquors were chromatographed on silica (15% water) with $CHCl_3$, the second fraction giving desired product and the third fraction, starting material. Total yield of chlorosulfoxide **18** was 635 mg (67%). The product could be recrystallized from $CHCl_3$ to give material with mp 182–184°C (dec.); ir (Nujol mull): 3330, 1780, 1733, 1675 cm^{-1}. *Anal.* calcd. for $C_{23}H_{20}ClN_3O_8S$: C 51.74, H 3.78, N 7.87, Cl 6.63, S 6.01; found: C 51.47, H 3.66, N 7.74, Cl 6.48, S 5.85.

1-α-Chloro-2-oxido-3-methyl-7-β-(phenoxyacetamido)-Δ³-2-isocephem-4-carboxylic Acid ***19***

A mixture of **18** (600 mg, 1.125 mmol), 10% palladium-on-charcoal (600 mg), dioxane (30 ml), and methanol (15 ml) was hydrogenated on a Parr shaker at 50 psi and 25°C for 3.5 h. The catalyst was filtered off and the filtrates evaporated *in vacuo*. The resulting oil was dissolved in ethyl acetate and this solution was washed with 10% HCl (2 × 50 ml) and brine (2 × 50 ml) and then extracted with 10% $NaHCO_3$ (3 × 50 ml). The basic extracts were washed with ether (2×), acidified to p*H* 3 with 10% HCl, and extracted with ethyl acetate (3 × 75 ml). The combined extracts were washed with brine, dried (Na_2SO_4), and evaporated *in vacuo*. The resulting oil was crystallized from ethyl acetate to give the acid **19**, 250 mg (56%), mp 204–205°C (dec.); ir (Nujol mull): 3400, 3600–2400, 1790, 1778, 1710, 1670, 1660 cm^{-1}; uv (MeOH) λ_{max} 275 (ε 9500) 286 (ε 9400). *Anal.* calcd. for $C_{16}H_{15}ClN_2O_6S$: C 48.19, H 3.79, N 7.02, Cl 8.89, S 8.04; found: C 48.11, H 3.77, N 6.95, Cl 8.77, S 7.94.

Benzyl 2-Oxido-7-β-azido-Δ³-2-isocephem-4-carboxylate ***20***

To a solution of 2.005 g (6.35 mmol) of compound **11***a*

in 45 ml $CHCl_3$ at 0–5°C was added 1.35 g (6.45 mmol) of *m*-chloroperoxybenzoic acid (85%) in 25 ml $CHCl_3$ over 15 min. Thin layer chromatography showed complete reaction after addition was complete. The solution was stirred 15 min, diluted to 400 ml with $CHCl_3$, extracted with Na_2CO_3 (2 × 50 ml of saturated aqueous solution), dried over Na_2SO_4, and concentrated to give compound **20** as a solid. Trituration with 25 ml Et_2O and filtration gave 1.5 g sulfoxide **20** (74%); mp 159–160°C (dec.) recrystallized from $CHCl_3$–Et_2O; ir ($CHCl_3$) 2110, 1800, 1738, 1580 cm^{-1}; uv (EtOH) λ_{max} 279 (ε 12 100). *Anal.* calcd. for $C_{14}H_{12}N_4O_4S$: C 50.59, H 3.64, N 16.86; found: C 50.28, H 3.34, N 16.81.

Benzyl 2,2-Dioxido-7-β-azido-Δ^3-2-isocephem-4-carboxylate ***21***

To a solution of 158 mg (0.5 mmol) of **11***a* in 20 ml methylene chloride was added 220 mg (1.10 mmol) of 85% *m*-chloroperbenzoic acid. The solution was stirred at 25°C for 18 h and then washed with 5% sodium bicarbonate solution. The organic phase was dried over sodium sulfate and evaporated to give an oil which crystallized on trituration with ether. Filtration gave 150 mg (86.5%) of **21**, mp 113.5–114.5°C after recrystallization from chloroform–ether; ir ($CHCl_3$) 2110, 1803, 1740 cm^{-1}; uv (EtOH) λ_{max} 274 (ε 10 100). *Anal.* calcd. for $C_{14}H_{12}N_4O_5S$: C 48.27, H 3.47, N 16.09, S 9.21; found: C 48.38, H 3.31, N 16.08, S 9.42.

Acknowledgements

Partial financial support of this work by the National Research Council of Canada through its Industrial Research Assistance Plan is gratefully acknowledged.

1. T. W. Doyle, B.-Y. Luh, D. T. Chu, and B. Belleau. Can. J. Chem. **55**, 2714 (1977).
2. (*a*) T. W. Doyle, B. Belleau, B.-Y. Luh, C. F. Ferrari, and M. P. Cunningham. Can. J. Chem. **55**, 468 (1977); (*b*) T. W. Doyle, B. Belleau, B.-Y. Luh, T. T. Conway, M. Menard, J. L. Douglas, D. T. Chu, G. Lim, L. R. Morris, P. Rivest, and M. Casey. Can. J. Chem. **55**, 484 (1977).
3. A. K. Bose. J. Heterocycl. Chem. **13**, 93 (1976).
4. D. M. Brunwin and G. Lowe. Chem. Commun. 589 (1972); J. Chem. Soc. Perkin Trans. I, 1321 (1973).
5. E. H. W. Bohme, H. E. Applegate, B. Toeplitz, J. E. Dolfini, and J. Z. Gougoutas. J. Am. Chem. Soc. **93**, 4324 (1971).
6. R. Scartazzini, H. Peter, H. Bickel, K. Heusler, and R. B. Woodward. Helv. Chim. Acta, **55**, 408 (1972); R. Scartazzini, J. Gosteli, H. Bickel, and R. B. Woodward. Helv. Chim. Acta, **55**, 2567 (1972).
7. F. A. Bovey (*Editor*). Nuclear magnetic resonance spectroscopy. Academic Press, New York and London. 1969.
8. B. Belleau and G. Malek. J. Am. Chem. Soc. **90**, 1651 (1968).
9. (*a*) R. Letl and A. Marquet. Tetrahedron, **30**, 3379 (1974); (*b*) R. Letl, S. Bory, B. Moreau, and A. Marquet. Bull. Soc. Chim. Fr. 2851 (1973).
10. J. B. Lambert and R. G. Keske. J. Org. Chem. **31**, 3429 (1966).
11. (*a*) P. Calzavara, M. Cinquini, S. Colonna, R. Fornasier, and F. Montanari. J. Am. Chem. Soc. **95**, 7431 (1973); (*b*) J. Klein and H. Stollar. J. Am. Chem. Soc. **95**, 7437 (1973).
12. D. O. Spry. Tetrahedron Lett. 3717 (1972).

Approaches toward the conformational analysis of carbocyclic hydroxyphosphono compounds: ^{13}C–^{31}P couplings and carbon shieldings[1]

GERALD W. BUCHANAN AND FREDERICK G. MORIN
Department of Chemistry, Carleton University, Ottawa, Ont., Canada K1S 5B6

Received February 18, 1977

GERALD W. BUCHANAN and FREDERICK G. MORIN. Can. J. Chem. **55**, 2885 (1977).

^{13}C nmr chemical shifts and ^{13}C–^{31}P couplings through one, two, and three bonds are reported for twelve carbocyclic hydroxyphosphonates and alkyl derivatives with all ring sizes from four to twelve, except the cyclodecyl system. On the basis of the vicinal couplings and carbon shieldings, inferences regarding preferred conformations are drawn. Evidence for ring flattening in some cyclohexyl compounds is presented. For a given ring size, it is demonstrated that $^1J_{CP}$ becomes less positive as the degree of steric congestion about the C—P bond increases.

GERALD W. BUCHANAN et FREDERICK G. MORIN. Can. J. Chem. **55**, 2885 (1977).

On rapporte les déplacements chimiques en rmn du ^{13}C et les constantes de couplage ^{13}C–^{31}P á travers un, deux et trois liens pour douze hydroxyphosphonates carbocycliques et pour leurs dérivés alkylés; les cycles de toutes les grandeurs allant de quatre á douze chaînons sont représentés á l'exception du système cyclodécyle. Sur la base des constantes de couplage vicinales et des blindages des carbones, on tire des conclusions concernant les conformations privilégiées. On présente des données concernant l'aplatissement du cycle dans quelques composés cyclohexaniques. Pour une grandeur de cycle donnée, on démontre que $^1J_{CP}$ devient plus positive à mesure que le degré de congestion stérique autour du lien C—P augmente.

[Traduit par le journal]

Introduction

Recent publications from these laboratories (1, 2) have dealt with the stereochemical dependence of ^{13}C–^{31}P couplings and ^{13}C chemical shifts for phosphonates of known geometry. For the direct ^{13}C–^{31}P interactions, some indications of a configurational dependence are evident (2), and there appears to be a Karplus-type relationship for the ^{13}C–C–C–^{31}P couplings, except when transmitted through a three-membered ring (1). Electronegative groups such as OH bonded to the carbon bearing the phosphorus have been shown to reduce the absolute value of J_{CCCP} substantially.

Presently we report the results of an investigation of twelve carbocyclic hydroxyphosphono compounds and some methylated derivatives with ring sizes ranging from four to twelve. Using ^{13}C–^{31}P couplings and ^{13}C chemical shifts as stereochemical probes, attempts to define preferred ring geometries are made. Where possible, comparisons with available X-ray data are presented.

[1]Presented in part at the International Symposium on Stereochemistry, Kingston, Ont., Canada. June 27 – July 2, 1976.

Results and Discussion

Spectral Assignments

Routinely the carbon spectra were obtained using complete ^1H noise decoupling. Subsequently the single frequency off-resonance decoupling technique was employed to identify CH_3, CH_2, CH, and quaternary carbons. Selective ^1H decoupling was used occasionally. Approximate signal intensities were an aid in cases where the molecules possessed obvious symmetry properties. Also the model compounds studied previously (1, 2) were valuable in many instances. The chemical shift data are collected in Table 1, while the one, two, and three bond ^{13}C–^{31}P J's are presented in Tables 2, 3, and 4 respectively.

Conformational Implications

In general the ^{13}C shifts and the vicinal couplings are the most useful for obtaining insight into conformational preferences. For the cyclobutyl system **1**, it is instructive to compare the C-3 shift (δ 13.4) with that of cyclobutane itself (δ 22.1) (3). In a puckered 1,1-disubstituted cyclobutane (4), one of the functions will be axial and one equatorial. The axial substituent experiences two *gauche*-butane type interactions

TABLE 1. ^{13}C chemical shifts for cyclic hydroxyphosphonates (δ from TMS ±0.1)*

	Position												
Compd.	C-1	C-2	C-3	C-4	C-5	C-6	C-7	C-8	C-9	C-10	C-11	C-12	OCH_3
1	71.9	33.0	13.4	33.0									53.7
2	79.0	36.7	24.1	24.1	36.7								53.5
3	80.8	41.6	30.9	30.9	41.6	13.8	13.8						53.8
4	71.6	31.7	20.1	25.4	20.1	31.7							53.5
5	74.6	36.2	29.9	25.8	20.0	33.4	17.2						53.4 53.0
6	72.0	39.8	26.0	34.3	20.0	31.0	22.5						53.3 53.1
7	71.9	30.6	28.7	28.1	28.7	30.6	19.4						53.5
8	74.7	35.9	21.8	29.8	29.8	21.8	35.9						53.5
9	74.9	31.4	21.1	28.9	24.8	28.9	21.1	31.4					53.4
10	75.7	28.8	18.1	27.2	21.5	21.5	27.2	18.1	28.8				53.5
11	75.6	32.0	20.3	(25.9)	(25.5)	27.3	27.3	(25.5)	(25.9)	20.3	32.0		53.4
12	75.2	30.6	18.8	(22.8)	(22.3)	26.6	26.1	26.6	(22.3)	(22.8)	18.8	30.6	53.3

*0.2–0.3 *M* solutions in $CDCl_3$.

with the C-3 ring carbon and should, therefore, induce substantial upfield shifts at this site (5). Our recent work (1, 2) indicates that an axial $P(O)(OCH_3)_2$ function induces a *gauche*-γ shielding effect of 2–3 ppm at C-3,5 of a cyclohexane, whereas an axial OH causes a shielding of 5–6 ppm at these sites (6). On this basis, it appears that the preferred conformer of **1** has an axial OH and an equatorial dimethylphosphono group. This is consistent with the observation in cyclohexyl systems that dialkylphosphono groups are sterically bulky ($-\Delta G^0 \geq 3$ kcal/mol) (2).

Electron diffraction of cyclobutane (7) gives a dihedral angle of 157° between C-3 and the equatorial H at C-1. In **1**, the ring may well be flattened more than in the hydrocarbon due to the axial OH, and the vicinal *J* of 6.5 Hz reflects this. The expected ^3J for θ = 180° is about 16 Hz (see discussion below). If the phosphorus were axial, the dihedral angle would be nearly 90° and minimal (<0.6 Hz) coupling is predicted (1).

For the cyclopentyl compound **2**, the chemical shifts at C-2,5 and C-3,4 are similar to those for cyclopentanol (36.0 and 24.1, respectively) (8) and C-3,4 of **2** are close to cyclopentane (25.3) (3). The large vicinal coupling of 13.0 Hz

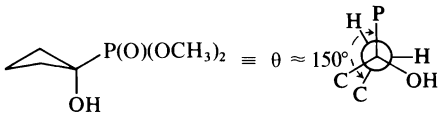

1

suggests that the conformer with equatorial phosphorus is highly favoured. In this form, the dihedral angle can be estimated from models at ca. 170°.

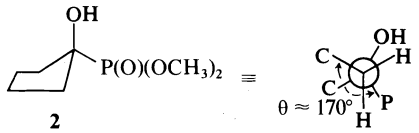

2

The fact that the axial OH of **2** does not perturb the γ-ring carbon shifts of cyclopentane has been noted earlier (8) and is attributed to the lesser amount of ring puckering in the five-membered case than in cyclohexane. Furthermore it is apparent that the influence of the equatorial dimethylphosphono moiety on C-2,5 is minor (presumably due to the offsetting effect of the β-phosphorus atom and the γ-oxygens bonded to it).

For the *cis*-dimethylcyclopentyl compound **3**, the large three-bond *J* from ^{31}P to C-3,4 (16.1 Hz) suggests additional ring puckering to permit the CH_3's to become staggered with respect to the OH and the dimethylphosphono group. We envisage the preferred form of **3** to be that

TABLE 2. One bond ^{13}C–^{31}P couplings (±0.2 Hz)*

Compd.	*J* (Hz)	Compd.	*J* (Hz)
1	164.3	**7**	161.2
2	169.0	**8**	159.6
3	164.1	**9**	161.2
4	165.5	**10**	156.8
5	158.8	**11**	157.1
6	165.2	**12**	157.9

*Sign assumed to be positive (24).

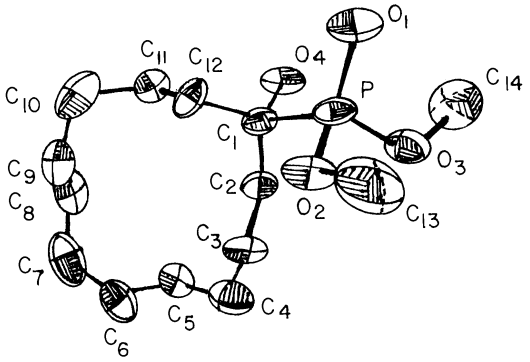

FIG. 1. Structures and numbering scheme for hydroxyphosphonates.

TABLE 3. Geminal ^{13}C–^{31}P couplings (±0.2 Hz)*

Compd.	Path	*J* (Hz)
1	$^{2,4}C$–^{1}C–P	N.R. (i.e. <0.6 Hz)
2	$^{2,5}C$–^{1}C–P	8.4
3	$^{2,5}C$–^{1}C–P	8.7
4	$^{2,6}C$–^{1}C–P	2.8
5	^{2}C–^{1}C–P	4.2
	^{6}C–^{1}C–P	N.R.
6	^{2}C–^{1}C–P	2.0
	^{6}C–^{1}C–P	N.R.
7	$^{2,6}C$–^{1}C–P	4.6
8	$^{2,7}C$–^{1}C–P	4.4
9	$^{2,8}C$–^{1}C–P	4.6
10	$^{2,9}C$–^{1}C–P	4.5
11	$^{2,10}C$–^{1}C–P	5.2
12	$^{2,11}C$–^{1}C–P	4.9

*$^{13}CH_3$–O–^{31}P *J*'s for **1**–**12** are all 7.2 ± 0.4 Hz, and are not listed individually.

depicted below. In such a conformation, the dihedral angle between phosphorus and C-3,4 is approximately 180° and accordingly the enhanced ^3J is noted. The population of the ring inverted form of **3** should be even lower than for **2** since 1,3-diaxial CH_3---CH_3 interactions would arise.

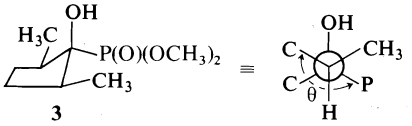

The non-resolvable coupling between phosphorus and the C-2,5 CH_3's of **3** ($\theta \approx 60°$) is reminiscent of the results for 4-*tert*-butylcyclohexylhydroxyphosphonates with axial phosphorus where no coupling to C-3,5 of the ring was found (1). It is notable that the CH_3's of **3** are shielded by 2 ppm relative to the CH_3 of *cis*-2-methylcyclopentanol (8, 9) as a consequence of the *gauche*-γ $P(O)(OCH_3)_2$ group in **3**.

TABLE 4. Vicinal ^{13}C–^{31}P couplings (±0.2 Hz)

Compd.	Path	*J* (Hz)
1	^{3}C–C–C–P	6.5
2	$^{3,4}C$–C–C–P	13.0
3	$^{3,4}C$–C–C–P	16.1
	CH_3–C–C–P	N.R. (i.e. <0.6 Hz)
4	$^{3,5}C$–C–C–P	11.1
5	^{3}C–C–C–P	11.2
	^{5}C–C–C–P	11.6
	CH_3–C–C–P	1.8
6	^{3}C–C–C–P	11.9
	^{5}C–C–C–P	12.7
7	$^{3,5}C$–C–C–P	15.6
8	$^{3,6}C$–C–C–P	10.9
9	$^{3,7}C$–C–C–P	8.8
10	$^{3,8}C$–C–C–P	6.7
11	$^{3,10}C$–C–C–P	6.7
12	$^{3,11}C$–C–C–P	5.7

For the series of cyclohexyl compounds **4**–**7** the magnitudes of the vicinal coupling between the C-3 and C-5 ring positions and ^{31}P indicate the predominance of conformers with equatorial phosphorus. The methyl stereochemistry in **5**, **6**, and **7**, however, remains to be elucidated. Our approach to this problem involves the use of the methylcyclohexanols (6) as models and consideration of the effect of introducing an equatorial $P(O)(OCH_3)_2$ moiety on the chemical shifts. Comparison of *cis*-4-*tert*-butylcyclohexanol and the corresponding dimethylphosphono compound yields a set of substituent parameters outlined below (1, 6).

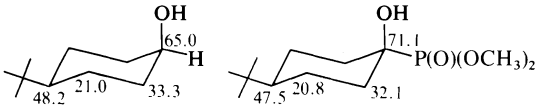

α = +6.1 ppm γ = −0.2 ppm
β = −1.2 ppm δ = −0.7 ppm

Model compounds selected were the *cis*-2-methyl, *trans*-3-methyl and *cis*-4-methylcyclohexanols. Equilibration data (10) indicate that the latter two exist at least 85% with axial OH and equatorial CH_3. Assuming approximate additivity of conformational energies (11), the 2-methyl case should be similar. With the alcohol data (6) and the α, β, γ, and δ effects of the equatorial dimethylphosphono group, predicted values for **5**, **6**, and **7** (assuming equatorial CH_3) are presented in Table 5. Observed shifts are in parentheses. Clearly, agreement is excellent for **6** and **7**, between predicted and observed

TABLE 5. Predicted and observed* ^{13}C shifts

	C-1	C-2	C-3	C-4	C-5	C-6
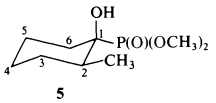 5	77.5 (74.6)	34.9 (36.2)	29.4 (29.9)	23.8 (25.8)	21.6 (20.5)	30.9 (33.4)
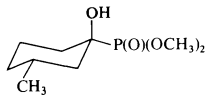 6	72.9 (72.0)	40.3 (39.8)	26.7 (26.0)	34.0 (34.3)	20.3 (20.0)	31.9 (31.0)
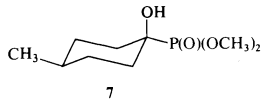 7	72.3 (71.9)	30.5 (30.6)	28.9 (28.7)	30.2 (28.1)	28.9 (28.7)	30.5 (30.6)

*In parentheses.

parameters, lending credence to our conformational assignments. Poorer agreement at all positions except C-3,5 is noted for **5**.[2] For the alcohol model, for which no equilibration data are available, there may be more axial CH_3 than predicted using additivity of $-\Delta G^0$ values. If this were the case, the axial 2-CH_3 which tends to shield C-4,6 (12) would lead to predicted shifts which are too high field (too low δ) for C-4,6 of **5** than would be the case if the CH_3 were exclusively equatorial in the alcohol.

The most interesting result in the series **4**–**7** is the vicinal coupling of 15.6 Hz in **7** which is 3 Hz larger than that found in the corresponding 4-*tert*-butylcyclohexyl compound (1) and 3–4.5 Hz larger than in **4**, **5**, or **6**. In view of the results for

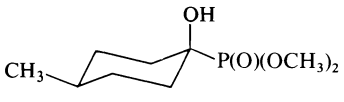

$^3J_{CCCP} = 15.6$

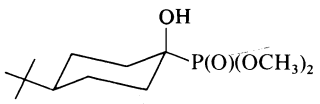

$^3J_{CCCP} = 12.6$

3, we interpret the findings for **7** as indicative of close to 180° dihedral angle between C-3,5 and the equatorial phosphorus. The attenuated coupling in the 4-*tert*-butyl compound can be attributed to ring flattening induced by the bulkier substituent at C-4, which may reduce the dihedral angle to near 170°.

Compound **4** which has been discussed previously (2) is no doubt a mixture of conformers, but the 11.1 Hz vicinal coupling of C-3,5 to phosphorus suggests a preponderance of the conformer with equatorial phosphorus. For **5** the vicinal couplings of 11.2 and 11.6 Hz to C-3 and C-5, combined with the 1.8 Hz vicinal coupling to the CH_3 indicate either ring flattening or measurable contributions from the ring inverted form. Low temperature experiments have been performed and we have not detected two conformers, thus we favor the former rationale. Similar arguments apply to the 3-methyl compound **6**, although it is interesting to observe that there appears to be more ring flattening in the vicinity of the substituent (^3J to C-3 is 11.9) than at the other vicinal carbon (^3J to C-5 is 12.7).

For the cycloheptyl compound **8**, variable temperature experiments (to −100°C) gave no spectral changes. It can be argued, however, that none would be expected until much lower temperatures since the substituent sites in seven-membered rings are known to equilibrate rapidly by pseudorotation and ring inversion even at very low temperatures (13). In fact, no nmr techniques have succeeded in freezing out conformers of cycloheptane to date (13). Several conformational energy calculations have been published for cycloheptane (13–15) and Hen-

[2]Comparing the predicted and observed shifts for **5**, **6**, and **7** at *all* sites indicates comparable differences. Carbons of **5** are, on the average, slightly less shielded than predicted, whereas carbons of **6** and **7** are slightly more shielded than predicted.

drickson (16) has carried out calculations for several methyl-substituted cycloalkanes. The latter results are most relevant for our purposes since the molecule of interest here is a *gem*-disubstituted cycloheptane. There seems to be general agreement (13–16) that the twist chair form represents an energy minimum. When methyl groups are considered in the calculations (16) the lowest energy form is the twist chair shown.

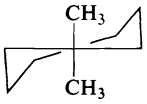

Recently[3] we have determined the X-ray crystal structure of **8**. The results indicate that the major form ($93 \pm 1\%$) is a twist chair, depicted below, in which the dihedral angles P–C_1–C_7-C_6 and P–C_1–C_2–C_3 are $-168.7°$ and $+90.0°$, respectively. In addition, a minor contribution ($7 \pm 1\%$) from a chair form of **8** is present, for which the angles P–C_1–C_2–C_3 and P–C_1–C_7–C_6 are $-168.7°$ and $-173.0°$. On the basis of the crystal structure and using models for coupling through angles of 90° (J ca. 0.5 Hz) and 170° (J ca. 13 Hz), the 'predicted' value for **8** is near 7 Hz. The observed value of 10.9 Hz suggests that in solution there may be an increase in the amount of chair cycloheptane leading to the enhanced vicinal ^{13}C–^{31}P coupling. It is notable that Hendrickson's calculations (14) give an energy difference of only 1.4 kcal/mol between twist chair and chair cycloheptane. Subtle factors of solvation in **8** may lead to a substantially larger amount of chair form in solution than in the solid phase.

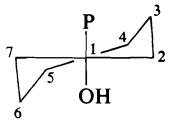

The situation for the cyclooctyl derivative **9** will also be complicated by ring inversion and pseudorotation. The latter process has a very low barrier, measured to be 4.9 kcal/mol in the 1,1-difluoro derivative of cyclooctane (17). Although several conformations will be populated appreciably at room temperature, it is most likely that the favored ring geometry is a boat–chair form (18). Hendrickson (16) calculated that the methyl strain energies are lowest in the 4a,4e(6a,6e) sites of the boat-chair form (each 0.5 kcal/mol). If one assumes that these sites will also be favored for the introduction of the OH and $P(O)(OCH_3)_2$ functions then a low energy form of **9** would be the boat–chair depicted.[4] In this form the dihedral angles

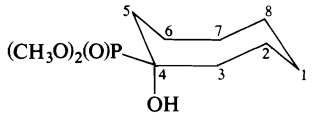

9

P–^{4}C–^{5}C–^{6}C and P–^{4}C–^{3}C–^{2}C are ca. 175° and 75°, respectively. Using models discussed earlier ^3J for $\theta = 175°$ can be estimated at ca. 14–15 Hz and that for 75° at ca. 0.5 Hz. On this basis the predicted ^3J is 7–8 Hz, in reasonable agreement with the observed value of 8.8 Hz. The possibility that the phosphorus and the OH have reversed stereochemistry cannot be disregarded since the calculations (16) indicate no difference in methyl strain energy between the 4a and 4e positions. In this conformer, the dihedral angles P–^{4}C–^{5}C–^{6}C and P–^{4}C–^{3}C–^{2}C are ca. 55° and 165°, respectively. For θ ca. 60°, J is less than 1 Hz (1, 2) while for 165° no reliable models exist, except perhaps a highly flattened cyclohexyl case ($J \approx 11$ Hz). Using these crude models, the ^3J for this conformer would be predicted to be somewhat smaller than for the first case, i.e. in poorer agreement with experiment. To date we have not been able to slow down ring inversion of **9** sufficiently at low temperature to obtain spectra of separate conformers, but efforts to do so are continuing. This should be feasible since ring inversion barriers are ca. 7–8 kcal/mol in cyclooctyl compounds (18).

For the cyclononanyl system **10** the X-ray crystal structure determination has been carried out (19) and the preferred form is the twist-boat–chair (TBC) shown which possesses D_3 symmetry. In this form, the dihedral angles P–^{1}C–

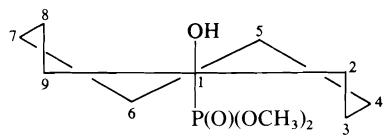

10

[3]Unpublished observations with G. I. Birnbaum.

[4]The numbering scheme used above denotes particular positions of Hendrickson's boat–chair form. Data in Tables 1–4 for **9** are based on the IUPAC numbering system.

^{9}C–^{8}C and P–^{1}C–^{2}C–^{3}C are 176° and 56°, respectively. Employing models for these angles, namely ca. 14–15 Hz and 0.5 Hz, again the predicted value for ^{3}J is 7–8 Hz in reasonable agreement with the experimental value of 6.7 Hz. Of course the usual problem of extrapolation of crystal structures to solution phase applies here.

The fact that only five ring carbon resonances are obtained in the ^{13}C spectrum of **10** is consistent with rapid ring inversion occurring at room temperature. From high frequency ^{1}H nmr (251 MHz) and ^{13}C (63 MHz) at low temperature, Anet and Wagner have measured a barrier of ca. 6 kcal/mol in the hydrocarbon (20). The high field position for the C-3,8 resonance of **10** (δ 18.1 ppm) reflects the averaged *gauche*-γ relationship of these positions to the OH and $P(O)(OCH_3)_2$ groups in the preferred conformer.

For the cycloundecanyl compound **11**, the observation of only six ring carbon resonances again indicates rapid conformational interconversions. In the hydrocarbon the ^{13}C spectrum is still one line at −135°C indicating rather low barriers (21). Dale (22) has calculated that there are four conformations of cycloundecane within 1 kcal/mol of each other. Accordingly for the hydroxyphosphonate **11** we feel that it is not meaningful to attempt to analyze the ^{3}J value of 6.5 Hz in terms of any preferred form.

The X-ray structure of the cyclododecyl compound **12** has been published (23). The molecule adopts a 'square' conformation in the crystal, with the substituents at a corner position. Observation of seven ring carbon signals again indicate rapid conformational interconversion. For the hydrocarbon (21), the 'square–square' interconversion barrier has been determined as 7.3 kcal/mol. The square form of **12** as found in the crystal (23) is depicted in Fig. 2. In the crystal, the dihedral angles P–^{1}C–^{2}C–^{3}C and P–^{1}C–^{12}C–^{11}C are 56° and 172°, respectively. Employing 0.5 Hz as a value for 56° and ca. 12–13 for the latter, the predicted vicinal coupling is 6–7 Hz, compared to the experimental value of 5.7.

To summarize, it is evident that vicinal ^{13}C–^{31}P couplings provide a useful, albeit somewhat local, probe for molecular conformations in these systems. The major drawback at present is the paucity of compounds with well defined geometries to serve as models.

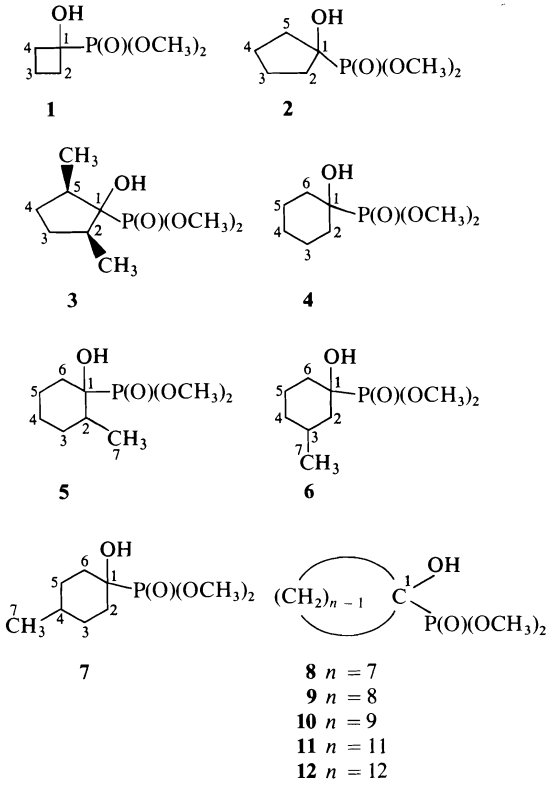

FIG. 2. The square form of **12** as found in the crystal.

Direct Couplings and Steric Congestion

From the data for compounds **2–7** in Table 2 and those published earlier (2), it is evident that for a given ring size, $^{1}J_{CP}$ is to some extent a measure of steric crowding about the C—P bond. It was noted earlier (2) for cyclohexylphosphonates and hydroxyphosphonates that $^{1}J_{CP}$ for compounds with axial phosphorus is 5–7 Hz less than when the dialkylphosphono function is equatorial. Comparing **4** and **5** it is clear that introduction of the 2-methyl group equatorially (i.e. *gauche* to the C—P bond) reduces $^{1}J_{CP}$ substantially. For **6** and **7** when the methyl is more remote, the $^{1}J_{CP}$ values increase, although the value for **7** seems anomalously low.

For the cyclopentyl systems **2** and **3**, $^{1}J_{CP}$ is reduced by 4.9 Hz in **3** where there are *gauche* interactions between phosphorus and the neighbouring methyl groups.

It is interesting that in P^{III} compounds steric hindrance about the phosphorus also reduces $^{1}J_{CP}$ (25). For example in trimethyl phosphine, $^{1}J_{CP}$ is −13.6 Hz, while in the tri-*tert*-butyl

phosphine, $^1J_{CP}$ is -33.9. For hydroxyphosphonates, $^1J_{CP}$ is positive (24), therefore the trends upon increase in steric congestion are consistent in P^{III} and P^{V} systems.

Recently Gorenstein (28) has noted the generality of such trends in directly bonded couplings as a function of stereochemistry. An interpretation involving the Fermi-contact mechanism and bond angle distortions was presented.

Experimental

Spectra

^{13}C spectra were obtained by techniques described previously (1), with the exception that sample tube size was 5 mm in the present study.

Materials

*1-Dimethylphosphono-1-hydroxycyclobutane (**1**)*

To cyclobutanone (0.5 g, 7.1 mmol) and dimethyl phosphite (0.9 g, 8.2 mmol) dissolved in benzene (2 ml) was added 2 drops of a saturated sodium methoxide solution. The reaction mixture was left at room temperature for 1 week and the solvent removed by rotary evaporator. The oily product was placed under vacuum before spectra were taken. The product remained an oil but showed no extraneous peaks in ^1H or ^{13}C nmr. Previously reported (26) as an oil, $\eta_D^{20} = 1.4630$.

*1-Dimethylphosphono-1-hydroxycyclopentane (**2**)*

Cyclopentanone (1.5 g, 17.8 mmol), dimethylphosphite (2.2 g, 20.0 mmol), and 15 drops of sodium methoxide solution were refluxed in benzene (10 ml) overnight and the solvent removed by rotary evaporator. The product was recrystallized (cyclohexane) mp 74.0–75.5°C (lit. mp 78°C) (27); yield 0.91 g (26%).

*1-Dimethylphosphono-1-hydroxy-cis-2,5-dimethylcyclopentane (**3**)*

2,5-Dimethylcyclopentanone (a mixture of *cis*- and *trans*-isomers, 5.0 g, 44.6 mmol), dimethyl phosphite (5.0 g, 45.4 mmol), and 10 drops of sodium methoxide solution were refluxed for 3 days. The reaction mixture was chromatographed on 100 g silica gel (Baker Analyzed Reagent 60–200 mesh) using benzene as eluent. The small amount of hydroxy phosphonate obtained was shown to be the one isomer by ^{13}C nmr. The product remained an oil and could not be crystallized, but was characterized by nmr and ir spectra; ^1H nmr ($CDCl_3$): δ 1.08 (d, $J = 6.5$ Hz, CH_3), 1.3–2.7 (bm, ring -CH_2-), 3.84 (d, $J = 10.3$ Hz, CH_3O-P).

*1-Dimethylphosphono-1-hydroxycyclohexane (**4**)*

The synthesis has been previously described (1).

*1-Dimethylphosphono-1-hydroxy-2-methylcyclohexane (**5**)*

2-Methylcyclohexane (2.0 g, 18.0 mmol), dimethyl phosphite (2.2 g, 20.0 mmol), and 10 drops of a saturated sodium methoxide solution were refluxed in benzene (5 ml) for ½ h. At this point five more drops of base were added and reflux continued for another ½ h. The solvent was removed and the flask placed in a freezer to induce crystallization of the resulting oil. The crystals obtained were recrystallized (ethyl acetate) mp 114–115°C. ^1H nmr ($CDCl_3$): δ 1.04 (d, $J = 6$ Hz, CH_3-), 1.3–2.3 (massive, ring -CH_2-), 3.1 (bs, -O*H*), 3.88 (d, $J = 11.1$ Hz, CH_3-O-P). *Anal.* calcd. for $C_9H_{19}O_4P$: C 48.64, H 8.62; found: C 48.63, H 8.54.

*1-Dimethylphosphono-1-hydroxy-3-methylcyclohexane (**6**)*

3-Methylcyclohexanone (6.0 g, 53 mmol), dimethyl phosphite (6.6 g, 60 mmol), and 25 drops of a saturated $NaOCH_3$ solution were refluxed in benzene (15 ml) for 1 h at which time 10 more drops of base were added. Reflux was continued overnight (ca. 18 h). The product obtained was recrystallized (ethyl acetate) mp 121.5–123°C; yield 10.1 g (86%); ^1H nmr ($CDCl_3$): δ 0.90 (d, $J = 6$ Hz, CH_3-), 1.4–2.3 (massive, ring -CH_2-), 3.3 (bs, -O*H*), 3.88 (d, $J = 10.6$ Hz, CH_3O-P). *Anal.* calcd. for $C_9H_{19}O_4P$: C 48.64, H 8.62; found: C 48.76, H 8.70.

*1-Dimethylphosphono-1-hydroxy-4-methylcyclohexane (**7**)*

The same procedure and amounts were used as for **6** to yield 3.6 g (31%) of the product, recrystallized (ethyl acetate) mp 120–122°C. ^1H nmr ($CDCl_3$): δ 1.0 (d $J = 6$ Hz, CH_3-), 1.3–2.4 (massive, ring -CH_2-), 4.02 (d, $J = 10.9$ Hz, CH_3O-P), 4.4 (bs, -O*H*). *Anal.* calcd. for $C_9H_{19}O_4P$: C 48.64, H 8.62; found: C 48.70, H 8.72.

*1-Dimethylphosphono-1-hydroxycycloheptane (**8**)*

Cycloheptanone (2.24 g 20.0 mmol), dimethyl phosphite (11.0 g, 100 mmol), and 20 drops of a saturated $NaOCH_3$ solution were refluxed in benzene (10 ml) overnight. The product was recrystallized (ethyl acetate) mp 106.0–107.5°C; yield 1.2 g (27%); ^1H nmr ($CDCl_3$): δ 1.4–2.5 (massive, ring -CH_2-), 4.00 (d, $J = 10.8$ Hz, CH_3O-P), 5.0 (bs, -O*H*). *Anal.* calcd. for $C_9H_{19}O_4P$: C 48.64, H 8.62; found: C 48.50, H 8.54.

*1-Dimethylphosphono-1-hydroxycyclooctane (**9**)*

Cyclooctanone (3.8 g, 30 mmol), dimethyl phosphite (3.6 g, 33 mmol), and 15 drops of a saturated $NaOCH_3$ solution were refluxed in benzene (10 ml) for 3 h. The solvent was removed to give a liquid residue. After 1 week in a freezer at −25°C, white crystals had formed. Recrystallized (cyclohexane) mp 92–93°C; yield 0.42 g (6%); ^1H nmr ($CDCl_3$): δ 1.5–2.1 (massive, ring -CH_2-), 3.95 (d, $J = 10.8$ Hz, CH_3O-P), 3.7 (bs, -O*H*). *Anal.* calcd. for $C_{10}H_{21}O_4P$: C 50.84, H 8.96; found: C 50.78, H 8.91.

*1-Dimethylphosphono-1-hydroxycyclononane (**10**)*

To cyclononanone (0.25 g, 1.78 mmol) dissolved in a minimum amount of benzene was added dimethyl phosphite (0.22 g, 2.00 mmol) and 1 drop of a saturated $NaOCH_3$ solution. The mixture turned pale yellow and then faded after 1 h, at which time another drop of base was added. This resulted in no colour change and the reaction mixture was placed in a freezer. The crystals that formed (66 mg, 15%) had mp 106.5–107.5°C (lit. (19) mp 105–106°C).

*1-Dimethylphosphono-1-hydroxycycloundecane (**11**)*

To cycloundecanone (1.14 g, 6.8 mmol) and dimethyl phosphite (1.77 g, 16 mmol) dissolved in benzene (3 ml) was added 10 drops of saturated $NaOCH_3$ solution. The mixture was placed in a freezer for 5 min until cool and the solvent removed by rotary evaporator to leave a liquid residue. After several days in a freezer crystals had formed. Recrystallized (cyclohexane) mp 79.0–80.5°C; yield 0.66 g (35%); ^1H nmr ($CDCl_3$): δ 1.4–2.1 (massive, ring -CH_2-), 4.02 (d, $J = 10.8$ Hz, CH_3O-P), 4.0 (bs,

-O*H*). *Anal.* calcd. for $C_{13}H_{27}O_4P$: C 56.09, H 9.78; found: C 56.13, H 9.85.

*1-Dimethylphosphono-1-hydroxycyclododecane (**12**)*

To cyclododecanone (3.1 g, 17 mmol) and dimethyl phosphite (2.2 g, 20 mmol) dissolved in benzene (5 ml) was added 15 drops of a saturated $NaOCH_3$ solution. This mixture was placed in a freezer until cool, and then removed. After 5 min at room temperature, **12** crystallized. Recrystallized (cyclohexane) mp 131–132.5°C (lit. (26) mp 127°C); yield 3.1 g (62%).

Acknowledgement

We thank the National Research Council of Canada for their financial support.

1. G. W. Buchanan and C. Benezra. Can. J. Chem. **54**, 231 (1976).
2. G. W. Buchanan and J. H. Bowen. Can. J. Chem. **55**, 604 (1977).
3. J. J. Burke and P. C. Lauterbur. J. Am. Chem. Soc. **86**, 1870 (1964).
4. R. M. Moriarty. Top. Stereochem. **8**, 273 (1974).
5. J. B. Stothers. Carbon-13 NMR spectroscopy. Academic Press, New York, NY. 1972.
6. J. D. Roberts, F. J. Weigert, J. I. Kroschwitz, and H. J. Reich. J. Am. Chem. Soc. **92**, 1338 (1970).
7. D. A. Dows and N. Rich. J. Chem. Phys. **47**, 333 (1967).
8. M. Christl, H. J. Reich, and J. D. Roberts. J. Am. Chem. Soc. **93**, 3463 (1971).
9. R. G. S. Ritchie, N. Cyr, B. Korsch, H. J. Koch, and A. S. Perlin. Can. J. Chem. **53**, 1424 (1975).
10. E. L. Eliel and T. J. Brett. J. Am. Chem. Soc. **87**, 5039 (1965).
11. J. A. Hirsch. Top. Stereochem. **1**, 199 (1967).
12. D. K. Dalling and D. M. Grant. J. Am. Chem. Soc. **89**, 6612 (1967).
13. D. F. Bocian, H. M. Pickett, T. C. Rounds, and H. L. Strauss. J. Am. Chem. Soc. **97**, 687 (1975).
14. J. B. Hendrickson. J. Am. Chem. Soc. **89**, 7036 (1967).
15. M. Bixon and S. Lifson. Tetrahedron, **23**, 769 (1967).
16. J. B. Hendrickson. J. Am. Chem. Soc. **89**, 7047 (1967).
17. J. E. Anderson, E. S. Glazer, D. L. Griffith, R. Knoir, and J. D. Roberts. J. Am. Chem. Soc. **91**, 1386 (1969).
18. F. A. L. Anet. *In* Conformational analysis. *Edited by* G. Chiurdoglu. Academic Press, New York, NY. 1971.
19. G. Samuel and R. Weiss. Tetrahedron Lett. 3529 (1969).
20. F. A. L. Anet and J. J. Wagner. J. Am. Chem. Soc. **93**, 5266 (1971).
21. F. A. L. Anet, A. K. Cheng, and J. J. Wagner. J. Am. Chem. Soc. **94**, 9250 (1972).
22. J. Dale. Acta Chem. Scand. **27**, 1115 (1973).
23. G. Samuel and R. Weiss. Tetrahedron, **26**, 3951 (1970).
24. W. McFarlane. Proc. R. Soc. London, Ser. A, **306**, 185 (1968).
25. B. E. Mann. J. Chem. Soc. Perkin Trans. II, 30 (1972).
26. C. Benezra and G. Ourisson. Bull. Soc. Chim. Fr. 1140 (1967).
27. C. Benezra and G. Ourisson. Bull. Soc. Chim. Fr. 2270 (1966).
28. D. G. Gorenstein. J. Am. Chem. Soc. **99**, 2254 (1977).

Electron mobilities in fluids through the liquid and critical regions: isomeric butenes[1]

JEAN-POL DODELET AND GORDON R. FREEMAN

Chemistry Department, University of Alberta, Edmonton, Alta., Canada T6G 2G2

Received March 2, 1977

JEAN-POL DODELET and GORDON R. FREEMAN. Can. J. Chem. **55**, 2893 (1977).

Electron mobilities are similar in all four isomeric butenes near the critical region, ~ 10 cm^2/V s at ~ 420 K, and again in the low temperature liquids, $\sim 10^{-3}$ cm^2/V s at ~ 150 K, but not at intermediate temperatures. The Arrhenius temperature coefficient of the mobility decreases with increasing temperature in *cis*-butene-2 and isobutene, and increases with temperature in butene-1 and *trans*-butene-2. This difference in behavior is reflected in the temperature dependence of the dispersion parameter σ in the assumed Gaussian distribution of transition energies between localized and extended states. The extreme cases are *trans*-butene-2, for which $d\sigma/dT = 0$, and *cis*-butene-2, for which $d\sigma/dT \approx (2kC_p)^{1/2}$. Mobilities in mixtures of *cis*- and *trans*-butene-2 do not display ideal solution behavior; the transition energies E_0 go through a maximum. The mobility in liquid *cis*-butene-2 under its vapor pressure goes through a maximum value of 17 cm^2/V s at 426 K, decreases to 14 cm^2/V s at $T_c = 433$ K, then increases with temperature in the constant density supercritical gas. Maxima are not observed in the other butenes. Electron migration in each of the supercritical gases is an activated process with an activation energy of ~ 0.3 eV. The present results emphasize the large role played by phase structure in electron migration.

JEAN-POL DODELET et GORDON R. FREEMAN. Can. J. Chem. **55**, 2893 (1977).

Les mobilités électroniques des quatre isomères du butène sont semblables près de la région critique: ~ 10 cm^2/V s à ~ 420 K, ainsi qu'en phase liquide à basse température: $\sim 10^{-3}$ cm^2/V s à ~ 150 K. Toutefois, ces mobilités diffèrent dans la région des températures intermédiaires. Pour ces mobilités, le coefficient de température d'Arrhénius décroît en augmentant la température du *cis*-butène-2 et de l'isobutène tandis qu'il augmente en élevant la température du butène-1 et du *trans*-butène-2. Cette différence de comportement se reflète dans la variation de σ avec la température. σ est le paramètre de dispersion dans la distribution, supposée gaussienne, des transitions entre les états localisés et étendus d'énergie. Les cas extrêmes sont le *trans*-butène-2 pour lequel $d\sigma/dT = 0$ et le *cis*-butène-2 pour lequel $d\sigma/dT \approx (2kC_p)^{1/2}$. Les mobilités dans les mélanges de *cis*- et *trans*-butène-2 ne présentent pas le comportement d'une solution idéale; les énergies de transition E_0 passent par un maximum. La mobilité dans le *cis*-butène-2 liquide, sous sa propre tension de vapeur, passe par un maximum de 17 cm^2/V s à 426 K pour ensuite décroître à 14 cm^2/V s à $T_c = 433$ K. Dans le gaz supercritique, à densité constante, cette mobilité augmente avec la température. Aucun maximum n'est observé pour les autres butènes. La migration électronique pour tous ces gaz au dessus de la température critique est un processus accompagné d'une énergie d'activation de ~ 0.3 eV. Ces résultats mettent l'accent sur le rôle joué par la structure de la phase dans la migration électronique.

Introduction

The Arrhenius temperature coefficient of electron migration in liquids is temperature dependent (1–6). The causes of the temperature dependence in different types of systems are not all the same (2, 5, 6), although none is understood in detail. To obtain more information about this phenomenon, electron mobilities have been measured in the isomeric butenes over a wide range of temperatures, from near the melting point to beyond the critical temperature. The butenes were chosen because of the extraordinary difference between the mobilities in *cis*- and *trans*-butene-2 at room temperature (7).

[1]Assisted by the National Research Council of Canada.

Experimental

Materials

The hydrocarbons were Phillips Research Grade, with initial purities 99.82% for butene-1, 99.57% for isobutene, 99.94% for *cis*-butene-2, and 99.92% for *trans*-butene-2. They were treated in a vacuum apparatus as follows: stirred several hours with lithium aluminum hydride powder and sodium hydroxide pellets, then degassed and distilled onto sodium–potassium alloy, stirred for several hours, then degassed and condensed into the conductance cell at 77 K. The cell was sealed after reducing the gas pressure in it to $< 5 \times 10^{-6}$ Torr.

Apparatus and Techniques

The conductance cell and temperature bath used for studies above room temperature were similar to those described in ref. 6. The cell could contain a pressure of 60 atm.

The cell used at low temperatures had larger electrodes

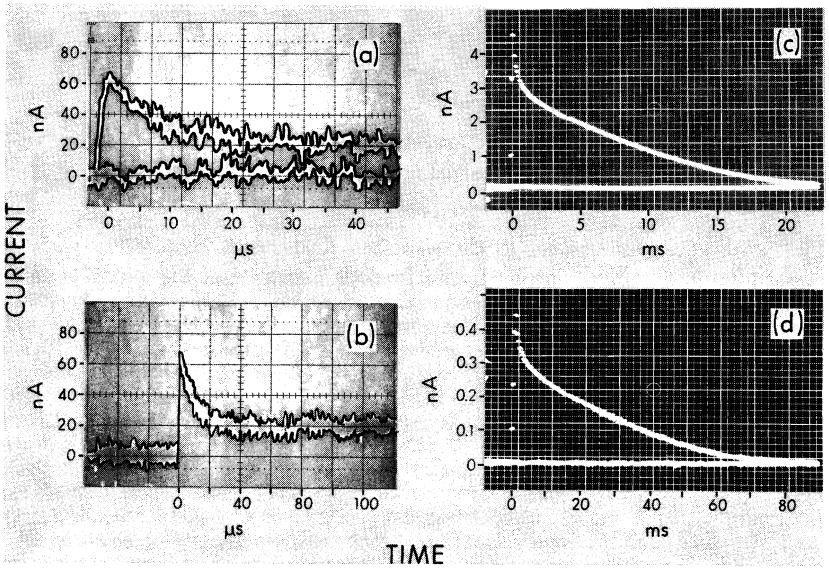

FIG. 1. Oscilloscope traces of transient electron and ion conductances in butene-1 after a 1 μs pulse of X rays. Dose/pulse $\approx 5 \times 10^{10}$ eV/g. (*a*) and (*b*) show the decay of the electron conductance on two time scales; applied field = 34 kV/cm, $T = 216$ K. (*c*) and (*d*) show the decay of the ionic conductance at 17 kV/cm averaged over 16 pulses; $T = 293$ and 192 K, respectively.

to compensate for the lower mobilities and lower ion yields. It was described earlier (8).

The low temperature bath was a Styrofoam box with walls 3 cm thick and a net inner volume $\sim$(10 cm)^3. Cold nitrogen gas from a 50 ℓ Dewar flask was piped into the center of the bottom of the box through a 13 mm diameter stainless steel tube that was insulated with a 5 cm layer of polystyrene. The cold gas was generated by putting controlled electric power into a 600 W heating element immersed in liquid nitrogen. The heater was fixed in a 20 cm long metal pipe attached to the bottom of a 5 cm diameter PVC tube. The pipe was near the bottom of the Dewar and the plastic tube conducted the cold gas up through the 10 cm wide neck.

Temperature gradients were reduced by having the cold nitrogen hit a 1 cm thick Styrofoam false bottom of the box with holes in the four corners, and by having the gas exit through a 15 mm inside diameter, 30 cm high chimney on the flanged lid of the box. The cell sat on the false bottom and was supported by Styrofoam projections from the sides of the box.

The Styrofoam box was placed inside an aluminum (0.5 mm thick) Faraday cage.

Two copper–constantan thermocouples were glued to the cell with silicone rubber. One thermocouple was connected to the temperature controller (LFE Corp. model 226-A21), and the other to a digital thermometer (Fluke 2100A). The best copper and constantan wire came from Thermoelectric Co., and it conformed to the 1974 ASTM standards.

The technique for measuring electron mobilities is described in refs. 7 and 9. The electron mobilities in the low temperature butenes are nearly as small as those of the heavy ions. The method of measurement gives the sum $(u_- + u_+)$, where u_- is the average mobility of the negative species and u_+ is that of the positive species. Immediately after the 1 μs radiation pulse u_- corresponds to the electron mobility u_e. The electron conductance transient decayed in microseconds (Fig. 1 *a,b*), probably due to reaction of the electrons with trace impurities. The remaining ion conductance transient decayed in milliseconds (Fig. 1 *c,d*).

Values of the sum $(u_- + u_+)$ for the heavy ions were obtained from the signal remaining at the right hand ends of pictures such as 1*a* and *b*. If the signals in 1*c* and *d* had decayed in two linear portions it would have been possible to obtain separate values of u_- and u_+ (5). The curvature in these traces indicates the presence of more than two types of ion. However, the total decay time t_d at high field strengths is the time required for the slowest ion to drift the distance $l = 0.30$ cm between the two electrodes. The value of u_{slowest} was obtained from [1].

$$[1] \qquad u_{\text{slowest}} = l^2/Vt_d$$

where V is the applied voltage. Comparing this to the value of $(u_- + u_+)$ just after the decay of the electron transient, the ratio $[(u_- + u_+)/u_{\text{slowest}}] \approx 3$ at 400–200 K, then appeared to increase to $\sim$5 at 140 K. The apparent increase may not have been real. There was considerable uncertainty in the ion mobility values at the lowest temperatures.

An Arrhenius plot of $(u_- + u_+)$ is not linear at the higher temperatures (Fig. 2). The upward curvature is probably associated with the decreasing liquid density and concomitant increasing fluidity (inverse viscosity) as the critical temperature is approached. The Arrhenius temperature coefficient of the ion mobilities is similar to that of the fluidity (10), 1.1 ± 0.2 kcal/mol, where the two types of measurement have been made over the same temperature range (Fig. 2).

The mobilities of the slowest ions may be roughly

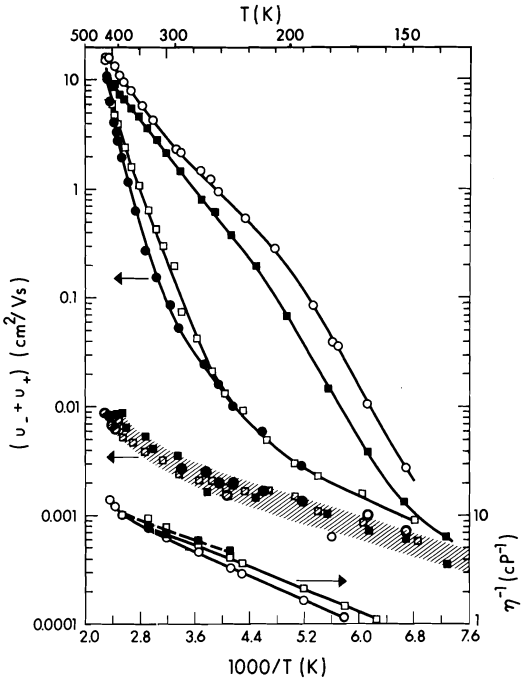

FIG. 2. Plots of $(u_- + u_+)$ and inverse viscosity against T^{-1}. Liquid phase only. For the upper curves the negative species is the electron, while in the hatched region it is a heavy negative ion. ○, *cis*-butene-2; ●, *trans*-butene-2; □, butene-1; ■, isobutene. The viscosities of *cis*- and *trans*-butene-2 are the same (10).

approximated by [2]

$$[2] \qquad u_{\text{slowest}} \approx 0.01 \exp(-700/T)$$

Physical Properties of the Liquids

The densities d were obtained from refs. 10 and 11.

The dielectric constants ε of the three polar butenes were calculated from Onsager's formula (12*a*):

$$[3] \qquad \frac{(\varepsilon - n^2)(2\varepsilon + n^2)}{\varepsilon(n^2 + 2)^2} = \frac{4\pi N d \mu^2}{9MkT}$$

where n is the refractive index, N is Avogadro's number, μ is the dipole moment (13), M is the molar weight, k is Boltzmann's constant, and T is the absolute temperature. The value of n at a given temperature was obtained from ref. 14 and the variation with temperature was calculated from the Lorenz–Lorentz equation (12*b*). The dielectric constant of *cis*-butene-2 was measured at temperatures between 197 and 296 K (15) and the values are 1% greater than those given by [3]. The latter were used in the present work for the sake of consistency over the entire liquid range and through the critical region.

The dielectric constant of *trans*-butene-2, which is nonpolar, was taken equal to n^2, with n determined in the manner described above.

The critical properties of the butenes are summarized in Table 1.

TABLE 1. Critical and other properties of the butenes*

Butene	T_c (K)	P_c (atm)	d_c (g/cm³)	ε_c†	n_c^2†	μ (D)‡
Isobutene	418	39.5	0.234	1.33	1.27	0.50
Butene-1	419	39.7	0.233	1.29	1.27	0.34
trans-Butene-2	428	41.5	0.238	1.28	1.28	0.0
cis-Butene-2	433	40.5	0.238	1.30	1.28	0.3

*References 10, 11, and 14.
†See text.
‡Gas phase dipole moment, ref. 10.

Results

The pressure on the liquids was the vapor pressure and the density of the supercritical gases was equal to the critical density.

Pure Compounds

Electron mobilities are similar in all four isomeric butenes near the critical region (~420 K) and again in the low temperature liquids (~150 K), but not at intermediate temperatures (Fig. 2). The behavior in isobutene is similar to that in *cis*-butene-2, while in butene-1 it is similar to that in *trans*-butene-2. The mobilities range from $\sim 10^{-3}$ cm²/V s at ~150 K to ~10 cm²/V s at ~420 K.

The relatively high melting point of *trans*-butene-2, 168 K, prevented measurements from being made at the lowest temperatures in that liquid.

The mobility in liquid *cis*-butene-2 goes through a maximum value of 17 cm²/V s at 426 K, decreases to 14 cm²/V s at the critical temperature 433 K, then increases with temperature in the supercritical gas (Fig. 3). Mobilities in the other butenes increase continuously with temperature, although there appears to be a change of slope when the system attains constant density in the supercritical gas (Fig. 3).

The mobilities were independent of field strength up to 30 kV/cm at $T < 300$ K and up to 10 kV/cm at the highest temperatures. Experimental difficulties prevented measurements at higher fields.

Mixtures of cis- and trans-Butene-2

To investigate the cause of the great difference between the behavior in *cis*- and *trans*-butene-2, mobilities were measured in mixtures of the two isomers. Addition of *trans*- to *cis*-butene-2 has a relatively greater effect on electron mobility at low than at high temperatures (Fig. 4).

As expected the ion mobilities in the solutions

were similar to those in the pure compounds (Fig. 4).

Discussion

To obtain values of the electron mobilities it was necessary to subtract u_+ from $(u_e + u_+)$. The value of u_+ was taken as one third of the sum of the heavy ion mobilities $(u_- + u_+)$. This is consistent with reports that $u_-/u_+ \approx 2$ for ions in many hydrocarbons (6, 16, 17). Although there is some doubt about the validity of this approximation in the butenes at $T < 200$ K (see earlier), shifting the fraction to reach $u_+ \approx 0.2(u_+ + u_-)$ at 140 K would have increased the estimated values of u_e only slightly.

The model of electron mobilities that was derived for ether solvents (18) has been applied to the present results. The model involves two types of transport, one important at low temperatures and another at higher temperatures. The low temperature type has been called ion-like, because the activation energy is similar to that for heavy ions and the magnitude of the mobility is a small factor greater than that of anions.[2] The transport mechanism at higher temperatures appears to involve electron transitions to a higher mobility state. The equations are as follows (18).

$$[4] \quad u_e = (1 - \chi)u_{i1}^0 \exp(-E_{i1}/kT) + \chi u_h^0$$

where χ is the fraction of electrons that are in the higher mobility state at a given instant, u_{i1}^0 and E_{i1} are respectively the pre-exponential factor and activation energy for ion-like mobility, k is Boltzmann's constant, T is the absolute temperature, and u_h^0 is the mobility in the higher state.

The fraction χ is given by [5].

$$[5] \quad \chi = \int_{-\infty}^{\infty} N(E)[1 + \exp(E/kT)]^{-1}\,dE$$

where $N(E)\,dE$ is the fraction of solvated electrons that require energies between E and $(E + dE)$ to be excited into the high mobility state, and $[1 + \exp(E/kT)]^{-1}$ is the fraction of electrons, for which the transition energy is E, that occupy the upper state. It has been assumed for simplicity that the entropy change of the transition is negligible.

The distribution function $N(E)$ is assumed to be a Gaussian with a most probable energy E_0 and a dispersion parameter σ.

$$[6] \quad N(E) = \pi^{-1/2}\sigma^{-1} \exp[-(E - E_0)^2/\sigma^2]$$

The present data permit evaluation of u_{i1}^0 and E_{i1} for butene-1 only. Similar values of these parameters were used in the four butenes, because the mobilities of heavy ions are similar in all the liquids (Fig. 2).

It was assumed that E_0 and σ vary linearly with temperature (6, 18).

$$[7] \quad E_0 = E(0) - \alpha T$$

$$[8] \quad \sigma = \sigma(0) + \beta T$$

where $E(0)$ and $\sigma(0)$ are the values extrapolated to zero Kelvin. Finally, u_h^0 was assumed to vary inversely as the temperature and the square of the fluid density (6).

$$[9] \quad u_h^0 = u_{ref}^0 \left(\frac{d_{ref}}{d_T}\right)^2 \frac{T_{ref}}{T}$$

where u_{ref}^0 is the value of u_h^0 at density d_{ref} and temperature T_{ref}.

Unique values of the parameters E_0, σ, and u_{ref}^0 cannot be obtained by fitting eq. 4 to the

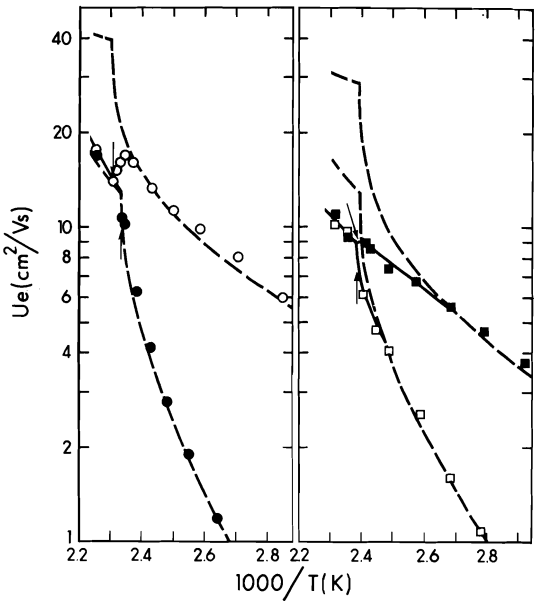

FIG. 3. Electron mobilities in the isomeric butenes near the critical region. The arrows mark T_c^{-1}. ○, *cis*-butene-2; ●, *trans*-butene-2; □, butene-1; ■, isobutene. The dashed lines were calculated from eqs. 4–9, using the parameter values in Table 2. Where the calculated curve deviates greatly from the experimental the latter is indicated by a full curve.

[2]The ion-like mechanism is conceptually similar to thermally assisted tunnelling to nearest neighbor centers (19) and small polaron hopping (20). It does not involve migration of the solvation shell of the electron.

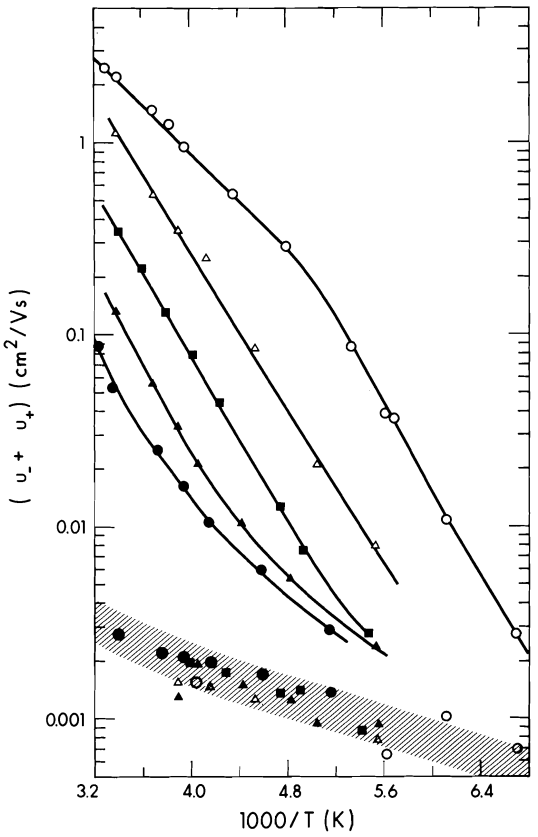

FIG. 4. Plots of $(u_- + u_+)$ against T^{-1} for mixtures of *cis*- and *trans*-butene-2. For the upper curves the negative species is the electron, while in the hatched region it is a heavy negative ion. ○, *cis*-butene-2; ●, *trans*-butene-2; △, 25 mol% *cis*; ■, 50 mol% *cis*; ▲, 75 mol% *cis*. The hatched portion marks the same region as that in Fig. 2.

observed mobilities, but lower limits can be estimated. Below certain values of the parameters, disagreement between the calculated and observed mobility curves becomes progressively greater. Thus for $T_{ref} = 295$ K we obtained $u_{ref}{}^0 \gtrsim 15$ cm^2/V s for isobutene, butene-1, and *trans*-butene 2, and $\gtrsim 30$ cm^2/V s for *cis*-butene 2. Lower limits of $E(0)$ and α were 0.5 eV and 0.001 eV/K in *trans*-butene-2 and butene-1, and about 0.3 eV and 0.0005 eV/K in isobutene and *cis*-butene-2. Corresponding values of σ were such that the ratio E_0/σ equalled 3–4 at 150 K and 0.5–1.3 at 400 K, depending on the liquid. As long as the minimum acceptable values of the parameters are equalled or exceeded, the electron mobility – temperature plot is governed mainly by the value of E_0/σ and its variation with temperature, and to a smaller extent by the absolute magnitude of E_0.

To facilitate comparison of the relative values of the parameters we chose for all the liquids $u_{ref}{}^0 = 30$ cm^2/V s at $T_{ref} = 295$ K, and $E(0) = 0.6$ eV. This makes the values of E_0 similar to the optical absorption energies of electrons in hydrocarbons at the lower temperatures (21, 22). The values of $E(0)/\alpha$ that were required to fit the mobilities in the butenes were similar to the ratio of the analogous parameters for the optical absorption energies of electrons in alkyl ethers (18), $E(0)/\alpha \approx 600$ K.

Within the framework of the present model, the change of shape of the mobility curves in Fig. 5 is embodied mainly in the temperature dependence of σ (Table 2). In *cis*-butene-2 σ has the form that would be expected if the width of the distribution of electron trap depths were governed by thermal energy fluctuations in the liquid (23, 24):

$$[10] \qquad \beta \approx (2kC_p)^{1/2}$$

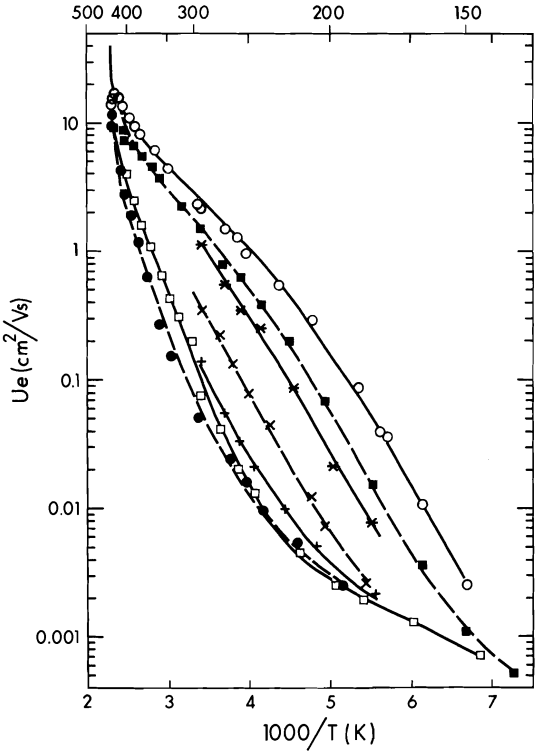

FIG. 5. Experimental (points) and calculated (curves) electron mobilities in *cis*-butene-2, ○; isobutene, ■; 75/25 *cis*/*trans*, *; 50/50 *cis*/*trans*, ×; 25/75 *cis*/*trans*, +; butene-1, □; *trans*-butene-2, ●. The curves for isobutene, 50/50 *cis*/*trans* and *trans*-butene-2 are dashed for clarity. The parameter values used to calculate the curves are given in Table 2.

TABLE 2. Parameter values for eqs. 4–9* and Fig. 5

Solvent	u_{11}^0 (cm^2/V s)	E_{11} (meV)	$E(0)$ (meV)‡	α (meV/K)	σ(0) (meV)	β (meV/K)
cis-Butene-2	0.115†	65†	600	0.98	0	1.08
Isobutene	0.115†	65†	600	0.86	8.1	0.97
Butene-1	0.115	64	600	0.96	49	0.35
trans-Butene-2	0.115†	64†	600	1.08	117	0
n-Pentane §	0.12	75	600	1.02	145	0
75*c* + 25*t* ‖	0.115†	65†	600	0.98	39	0.68
50*c* + 50*t*	0.115†	65†	600	0.84	43	0.58
25*c* + 75*t*	0.115†	65†	600	0.90	90	0.26

*u_{ref}^0 = 30 cm^2/V s at T_{ref} = 295 K was used for all liquids.
†Assumed, by comparison with butene-1.
‡These values are not unique, but have been placed at slightly larger than the minimum acceptable value for butene-1. To obtain larger values that fit the results $E(0)$, α, σ(0), and β are multiplied by approximately the same factor.
§The calculated curve is essentially the same as that in Fig. 5 of ref. 6.
‖75% *cis* + 25% *trans*-butene-2 mixture.

where C_p is the constant pressure heat capacity of the "cell" that contains the electron and exchanges energy with it. The magnitude of β for *cis*-butene-2, 1.08 meV/K, is equivalent to the thermal fluctuations in a cell that contains about four butene molecules.[3] At the other extreme, σ in *trans*-butene-2 appears to be independent of temperature. This implies that the localized state is more stable in *trans*- than in *cis*-butene-2, perhaps through anion formation in the former. However, the full implications are not known. The stability might be related more to entropy changes than to enthalpy changes.

Equation 9 for u_h^0 was devised to approximate the mobility in *n*-pentane (6), which increases rapidly as the critical temperature is approached. It is also adequate for the results in *trans*-butene-2 and butene-1 (Fig. 5). It does not however, reproduce the maximum and subsequent decrease of the mobility in high temperature *cis*-butene-2 (Fig. 3). The decrease is presumably due to the break up of the conduction band, caused by the rapidly decreasing fluid density in this region (4, 6). A similar process must occur also in isobutene, because the calculated mobilities are much too high in the critical region (Fig. 3). All of the approximations [7]–[9] might be expected to fail at the high temperatures where the liquid density changes rapidly. However, in *trans*-butene-2 the net effect of the approximations remains reasonable right through the critical region (Fig. 3). An alternative to [9] is required for *cis*-butene-2 and other liquids which display a maximum in the plot of electron mobility against temperature.

It should be stressed that electron migration in each of the supercritical gases is an activated process with an activation energy of ~0.3 eV. The similarity of behavior in the supercritical gases, and the great difference of that in the liquids at 300 K, emphasizes the large role played by phase structure.

Mixtures of cis- and trans-Butene-2

The experimental and calculated values of the

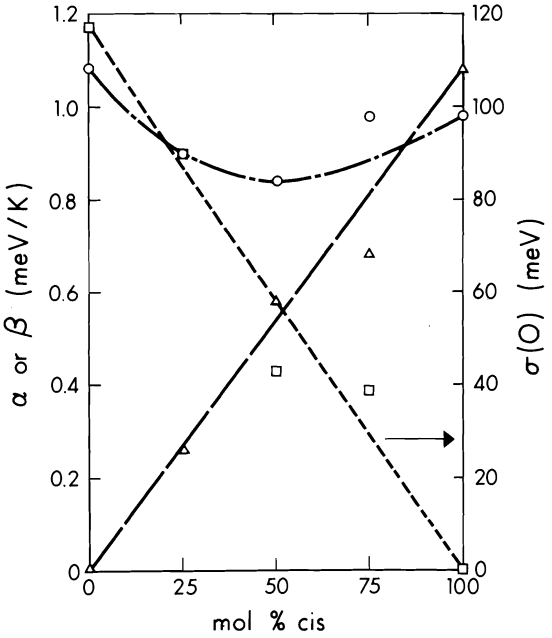

FIG. 6. Mobility parameter values in mixtures of *cis*- and *trans*-butene-2. ○, α; △, β; □, σ(0).

[3]The number of butene molecules that interact appreciably with an electron in the liquid is probably 10–20, so the solvated electron "cell" would be that large. The σ for the electronic state would be smaller than that for the total thermal energy fluctuation in the cell.

mobilities are compared in Fig. 5. The parameter values are listed in Table 2.

Although one cannot obtain the absolute values of E_0 and σ from mobility measurements alone, the relative values provide interesting information. The temperature coefficients of E_0 for the 100%, 75%, 50%, 25%, and 0% *cis* solutions are, respectively, α = 0.98, 0.98, 0.84, 0.90, and 1.08 meV/K. The lack of a linear variation between the two pure compounds indicates that the solutions are not ideal.

The parameters that change the most with solution composition are $\sigma(0)$, which ranges from 0 to 117 meV, and β, which ranges from 1.08 to 0.00 meV/K (Fig. 6).

The results from the mixtures confirm the unexpected behavior of σ. More work is needed to interpret it.

Acknowledgements

We are grateful to the staff of the Radiation Research Center for help with the electronics.

1. H. SCHNYDERS, S. A. RICE, and L. MEYER. Phys. Rev. **150**, 127 (1966).
2. J. A. JAHNKE, L. MEYER, and S. A. RICE. Phys. Rev. A**3**, 734 (1971).
3. M. G. ROBINSON and G. R. FREEMAN. Can. J. Chem. **52**, 440 (1974).
4. T. KIMURA and G. R. FREEMAN. Can. J. Phys. **52**, 2220 (1974).
5. J.-P. DODELET and G. R. FREEMAN. Can. J. Chem. **53**, 1263 (1975).
6. J.-P. DODELET and G. R. FREEMAN. Can. J. Chem. **55**, 2264 (1977).
7. J.-P. DODELET, K. SHINSAKA, and G. R. FREEMAN. J. Chem. Phys. **59**, 1293 (1973).
8. J.-P. DODELET, K. SHINSAKA, U. KORTSCH, and G. R. FREEMAN. J. Chem. Phys. **59**, 2376 (1973).
9. K. SHINSAKA and G. R. FREEMAN. Can. J. Chem. **52**, 3495 (1974).
10. R. W. GALLANT. Physical properties of hydrocarbons. Vol. 1. Gulf Publishing Co., Houston, TX. 1968.
11. (*a*) J. TIMMERMANS. Physico chemical constants of pure organic compounds. Elsevier Publishing Co., Amsterdam. Vol. 1, 1950; Vol. 2, 1965; (*b*) R. R. DRIESBACH. Adv. Chem. Ser. **22** (1959).
12. N. E. HILL, W. E. VAUGHAN, A. H. PRICE, and M. DAVIES. Dielectric properties and molecular behavior. Van Nostrand Reinhold Co., Toronto. 1969. (*a*) p. 23; (*b*) p. 191.
13. R. D. NELSON, JR., D. R. LIDE, JR., and A. A. MARYOTT. Selected values of electric dipole moments in the gas phase. NSRDS-NBS 10, U.S. Government Printing Office, Washington, DC. 1967.
14. R. C. WEST (*Editor*). Handbook of chemistry and physics. 50th ed. Chemical Rubber Co., Cleveland, OH. 1969.
15. J.-P. DODELET, K. SHINSAKA, and G. R. FREEMAN. To be published.
16. I. ADAMCZEWSKI. Acta Phys. Polon. **30**, 707 (1966).
17. P. H. TEWARI and G. R. FREEMAN. J. Chem. Phys. **49**, 4394 (1968).
18. J.-P. DODELET, F.-Y. JOU, and G. R. FREEMAN. J. Phys. Chem. **79**, 2876 (1975).
19. J. FRITZCHE. *In* Amorphous and liquid semiconductors. *Edited by* J. Tauc. Plenum Press, London. 1975. Chapts. 5 and 6.
20. W. E. SPEAR. Adv. Phys. **23**, 523 (1974).
21. H. A. GILLIS, N. V. KLASSEN, G. G. TEATHER, and K. H. LOGAN. Chem. Phys. Lett. **10**, 1481 (1971).
22. T. SHIDA, S. IWATA, and T. WATANABE. J. Phys. Chem. **76**, 383 (1972).
23. J.-P. DODELET, K. SHINSAKA, and G. R. FREEMAN. Can. J. Chem. **54**, 744 (1976).
24. R. SCHILLER, SZ. VASS, and J. MÁNDICS. Int. J. Radiat. Phys. Chem. **5**, 491 (1973).

Kinetics and mechanism of the oxidation of several ketones by tris(1,10-phenanthroline)Fe(III) in aqueous acid medium

FLORA T. T. NG AND PATRICK M. HENRY

Guelph–Waterloo Centre for Graduate Work in Chemistry, Guelph Campus, University of Guelph, Guelph, Ont., Canada N1G 2W1

Received August 16, 1976[1]

FLORA T. T. NG and PATRICK M. HENRY. Can. J. Chem. **55**, 2900 (1977).

The kinetics of the oxidation of acetone, 2-butanone, 2,4-dimethyl-3-pentanone, 3-methyl-2-butanone, and 3-pentanone by tris(1,10-phenanthroline)Fe(III) (ferriin) were determined in aqueous solutions containing either sulphuric or perchloric acid in the presence or absence of air. The kinetics are consistent only with a mechanism involving oxidation of the enol tautomer by ferriin. The rate constants of enolization calculated from this kinetic analysis agree well with the literature values. Relative reactivity of the four enols from symmetrical ketones were found to be in the order: 2,4-dimethyl-3-pentanone > 3-pentanone > cyclohexanone > acetone. The rate of oxidation of the enol form of 2,4-dimethyl-3-pentanone is approximately 1000 fold larger than that of the enol form of acetone, indicating that electron-donating methyl substituents enhance the rate of electron transfer from the enol tautomer to ferriin.

Kinetics of the oxidation carried out in air were generally the same as in its absence; the rates of oxidation were found to be slower by a factor of 2 in most cases. This suggests that the initially formed enol radical reacts with O_2 rather than a second ferriin to give the oxidized product. At high [ferriin] in air, pseudo zero-order kinetics were observed initially as in its absence. However, above about 50% reduction of ferriin, the reaction appears to involve autocatalysis and was not studied further.

FLORA T. T. NG et PATRICK M. HENRY. Can. J. Chem. **55**, 2900 (1977).

On a déterminé, en solutions aqueuses d'acide sulfurique ou d'acide perchlorique en présence ou en absence d'air, les cinétiques d'oxydation de l'acétone, de la butanone-2, de la diméthyl-2,4 pentanone-3, de la méthyl-3 butanone-2 et de la pentanone-3 par le tris(phenanthroline-1,10)-Fe(III) (ferriine). Les données cinétiques sont en accord uniquement avec un mécanisme impliquant l'oxydation du tautomère énolique par la ferriine. Les constantes de vitesse d'énolisation calculées à partir de cette analyse cinétique sont en bon accord avec les valeurs de la littérature. La réactivité relative des quatre énols provenant des cétones symétriques est dans l'ordre suivant: diméthyl-2,4 pentanone-3 > pentanone-3 > cyclohexanone > acétone. La vitesse d'oxydation de la forme énolique de la diméthyl-2,4 pentanone-3 est approximativement 1000 fois plus grande que celle de la forme énolique de l'acétone et ces résultats indiquent que les substituants méthyles électro-donneurs augmentent la vitesse du transfert d'électron du tautomère énolique vers la ferriine.

Les résultats cinétiques des oxydations effectués dans l'air sont généralement les mêmes que pour les réactions effectuées en son absence; on a trouvé que les vitesses d'oxydation sont plus lente par un facteur de 2 dans la plupart des cas. Ces résultats suggèrent que le radical énolique formé initialement réagit avec O_2 plutôt qu'avec une seconde molécule de ferriine pour donner le produit oxydé. A des taux élevés de ferriine dans l'air, on observe initialement un ordre cinétique pseudo zéro; et c'est aussi le cas en l'absence d'air. Toutefois une fois que 50% de la ferriine a été réduite, il semble que la réaction implique une autocatalyse et elle n'a pas été étudiée plus loin.

[Traduit par le journal]

Introduction

The oxidation of ketones by two electron oxidants such as Hg(II), Tl(III), Mn(VII), and Cr(VI) has been shown to proceed via the enol tautomer (1–3). However, there has been some discussion as to the mode of oxidation of ketones by one electron oxidants (4, 5). Although it has been suggested that one electron oxidants attack the keto form there is recent kinetic evidence that the oxidation of ketones by $Mn(OAc)_3$ in acetic acid occurs via the enol form (6), a route previously suggested for ketone oxidation by Ce(IV) (7) and Mn(III) pyrophosphates (8). Thus the rate of oxidation of ketone by $Mn(OAc)_3$ is independent of concentration of Mn(III) indicating the rate determining step is the formation of enol. Recently the authors reported similar kinetic evidence indicating that,

[1]Revision received March 25, 1977.

contrary to previous proposals (9), the oxidation of cyclohexanone in aqueous solution by tris-(1,10-phenanthroline)Fe(III) (Ferriin) occurs by way of the enol tautomer (10). The proposed mechanism is given in reactions 1–3.

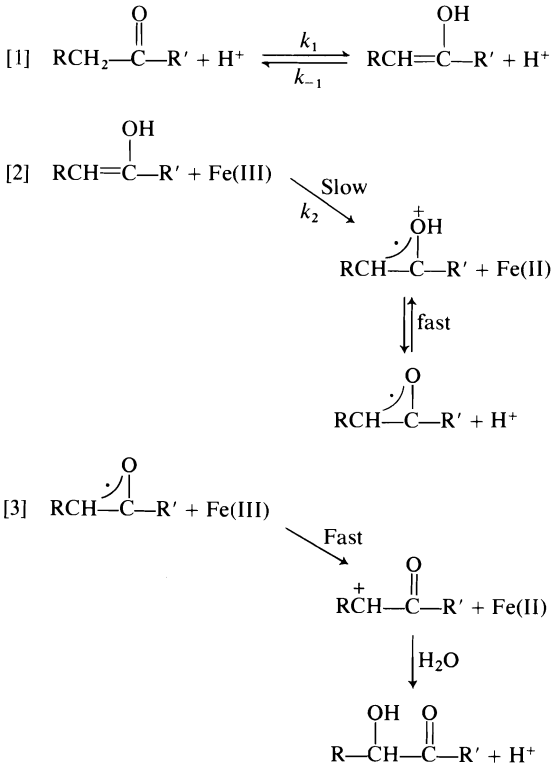

Thus the complete rate expression is given by [4],

$$[4]\qquad \text{Rate} = \frac{d[\text{Fe(II)}]}{dt} = \frac{2k_1k_2[\text{ketone}][H^+][\text{Fe(III)}]}{k_{-1}[H^+] + k_2[\text{Fe(III)}]}$$

[Fe(III)] = [Ferriin], where k_1 is the rate constant for enolization and k_2 the rate constant for oxidation of enol by Fe(III). This rate expression has two limiting forms. At low [Fe(III)] where $k_{-1}[H^+] \gg k_2[\text{Fe(III)}]$ the rate expression is given by [5] where $k_2' = k_1k_2/k_{-1} = Kk_2$, K being the keto–enol equilibrium constant.

$$[5]\qquad \frac{d[\text{Fe(II)}]}{dt} = \frac{2k_1k_2[\text{Fe(III)}][\text{ketone}]}{k_{-1}} = 2k_2'[\text{Fe(III)}][\text{ketone}]$$

This is the form of the rate expression reported earlier (10).

If high [Fe(III)] and low $[H^+]$ are used such that $k_2[\text{Fe(III)}] \gg k_{-1}[H^+]$ the expression becomes zero order in [Fe(III)] as shown by [6].

$$[6]\qquad \frac{d[\text{Fe(II)}]}{dt} = 2k_1[\text{ketone}][H^+]$$

At low [Fe(III)] and high $[H^+]$ [5] was obeyed while at high [Fe(III)] and low $[H^+]$ [6] was followed. Furthermore, the value of the enolization rate constant, k_1, calculated from these studies agreed with those previously reported. This result requires that the enol tautomer is the reactive species. We also found, by using substituted ferriins, that the rate of electron transfer from the enol to the Fe(III) depended on the reduction potential of the ferriin in the manner predicted by the Marcus relationship (10).

This paper describes a study of the oxidation of several additional ketones. Its main purpose was to see if the enol mechanism held for ketones other than cyclohexanone with different structures and rates of enolization. Also it was hoped to find how k_2 varied with enol structure. Finally we wished to test the effect of oxygen on the reaction mechanism. Earlier it was reported that O_2 increased the rate of cyclohexanone oxidation by ferriin (9), a result which was not duplicated in the later study (10).

Results

The kinetics of reduction of ferriin by acetone, 2-butanone, 2,4-dimethyl-3-pentanone, 3-methyl-2-butanone, and 3-pentanone were determined at 25°C in aqueous solution containing either $HClO_4$ or H_2SO_4. The kinetics were studied with either (*i*) solutions in which the oxygen had been removed by degassing and which were run under a nitrogen and argon atmosphere or (*ii*) with solutions containing air. The H_2SO_4 solutions were employed when high concentrations of ferriin were required, as ferriin is more soluble in aqueous H_2SO_4 than in aqueous $HClO_4$. Actually, it makes little difference which is used, as rates of enolization and oxidation are nearly the same in the two solvents (11).

Air Free System

Kinetic Dependence at Low [Fe(III)] and High [H+]

Kinetic studies were carried out under pseudo first-order conditions with excess ketone. A first-order dependence on [Fe(III)], first-order dependence on [ketone], and zero-order de-

TABLE 1. Oxidation of ketones by ferriin at 25°C under argon or nitrogen at high [H^+] and low [Fe(III)]

Ketone	[Ketone] $\times 10^2$ (M)	[Ferriin] $\times 10^4$ (M)	[$HClO_4$] (M)	[H_2SO_4] (M)	k_{obs} $\times 10^3$ (s^{-1})	$2k_2'$ $\times 10^2$ (M^{-1} s^{-1})
2-Butanone	3.73	1.0	1.0		2.46	6.60
	9.33	1.0	1.0		6.30	6.70
	9.33	2.0	1.0		6.30	6.70
	3.73	1.0	0.2		2.46	6.60*
3-Methyl-2-butanone	3.22	0.42		4.5	15.5	48
	1.67	0.42		4.5	8.4	50
	1.67	0.40		4.5	8.2	49†
3-Pentanone	3.20	1.0	1.0		3.0	9.5±1.0
2,4-Dimethyl-3-pentanone	2.35	≤0.4		4.5	8.0	34±2.0

*[$NaClO_4$] = 0.8 M.
†Peroxide free.

pendence on [H^+] was found. This corresponds to [5]. The values of $2k_2'$ for 2-butanone, 3-methyl-2-butanone, 3-pentanone, and 2,4-dimethyl-3-pentanone are shown in Table 1. 3-Methyl-2-butanone is known to form peroxides readily. However, the same value of k_2' was found for a peroxide free solution under N_2 (Table 1).

The rate of oxidation of acetone by ferriin at high acetone concentration is so slow that the rate of decomposition of ferriin was comparable to the observed rate of oxidation. Thus the rate could not be accurately measured. The value of k_2' was actually measured using 5-chloroferriin which is a more vigorous oxidant than ferriin. A value of 1.3×10^{-3} M^{-1} s^{-1} at 1.3 M H_2SO_4 for $2k_2'$ was found (Table 2). Assuming that the Marcus relationship holds as it does for cyclohexanone, a value of 1.3×10^{-4} M^{-1} s^{-1} can be calculated to be the value of $2k_2'$ for ferriin.

Kinetic Dependence at Low [H^+] and High [Fe(III)]

With excess ketone, pseudo zero-order kinetics were observed for more than 50% of the reaction followed by a gradual decrease in rate. Some reactions were carried out in H_2SO_4 because ferriin is more soluble in H_2SO_4 than in $HClO_4$. The rate expression in the linear region was found to be first-order in [ketone], first-order in [H^+], and zero-order in [Fe(III)]. This corresponds to [6]. Values of $2k_1$ for 2-butanone, 3-methyl-2-butanone, 3-pentanone, and 2,4-dimethyl-3-pentanone are shown in Table 3. No k_1 values for acetone were obtained since the rate expression corresponding to [6] could not be achieved under experimentally accessible conditions (see calculation in Discussion).

TABLE 2. Oxidation of acetone by 5-chloroferriin at 25°C in aqueous sulfuric acid*

[Acetone] (M)	[5-Chloroferriin] $\times 10^4$ (M)	k_{obs} $\times 10^3$ (s^{-1})
0.23	4.8	0.85
0.46	4.8	1.1
0.92	4.8	1.7
1.38	4.8	2.25
1.38†	4.8	2.35
1.82	4.8	3.0

*[H_2SO_4] = 1.3 M.
†Degassed with argon.

Since the products in the oxidation of ketones by ferriin are known to be 2-hydroxy ketones (initially) which are further oxidized, little product identification study was carried out. However, the oxidation of 2-butanone was shown by vapour phase chromatography to initially give 3-hydroxy-2-butanone. This was further oxidized to 2,3-butanedione.

Air Containing System

Kinetic Data at Low [Fe(III)] and High [H^+]

These runs were carried out essentially in the same way as the air free system except that no attempt was made to remove the air. Runs at low [Fe(III)] and high [acid] gave well behaved kinetics, first-order in [Fe(III)], first-order in [ketone], and zero-order in [H^+]. Values of $2k_2'$, given in Table 4, are usually about one half those in the absence of air (see Table 1). An exception is 3-methyl-2-butanone for which $2k_2'$ was found to be 1.2 M^{-1} s^{-1} or three times larger than in the absence of air.

Kinetic Data at High [Fe(III)] and Low [H^+]

The runs at high [Fe(III)] and low [acid] were

TABLE 3. Oxidation of ketones by ferriin at 25°C under argon or nitrogen at low [H^+] and high [Fe(III)]

Ketone	[Ketone] $\times 10^2$ (M)	[Fe(III)] $\times 10^4$ (M)	[H_2SO_4] (M)	[$HClO_4$] (M)	[H^+]* (M)	Initial rate $\times 10^7$ (M^{-1} s^{-1})	$2k_1 \times 10^5$ (M^{-1} s^{-1})
2-Butanone	3.73	19.3	0.24		0.25	11.8	12.7
	7.45	19.3	0.24		0.25	24.6	13.2
	3.73	38.0	0.24		0.25	10.9	11.7
	3.73	38.0	0.48		0.49	24.6	13.5
	3.73	72.0	0.48		0.49	22.8	12.5
	3.73	38.0	0.24		0.26	10.9	11.2†
	7.45	38.0	0.24		0.25	22.7	12.2
	14.9	38.0	0.24		0.25	45.5	12.2
3-Pentanone	3.16	19.2	0.24		0.25	10.9	13.8
	3.16	38.4	0.48		0.49	20.9	13.5
3-Methyl-2-butanone	3.22	2.0		0.2	0.2	1.9	3.0
	3.22	2.0		0.4	0.4	3.7	2.9
	3.22	2.0		0.6	0.6	6.1	3.2
	3.22	2.0		0.6	0.6	5.8	3.0
	3.22	2.0		1.0	1.0	11	3.4
	7.45	1.2		1.0	1.0	20	2.7
	3.22	2.0		0.4	0.4	3.4	2.6‡
2,4-Dimethyl-3-pentanone	2.35	1.0		0.6	0.6	0.46	0.33
	2.35	2.0		0.6	0.6	0.41	0.28
	2.35	2.0		0.6	0.6	0.61	0.43

*Dissociation constant of HSO_4^- is taken to be 0.012 M, ref. 12.
†[$NaHSO_4$] = 0.24 M.
‡Peroxide free.

TABLE 4. Oxidation of ketones by ferriin at 25°C in air at high [H^+] and low [Fe(III)]

Ketone	[Ketone] $\times 10^2$ (M)	[Ferriin] $\times 10^4$ (M)	[$HClO_4$] (M)	[H_2SO_4] (M)	k_{obs} $\times 10^3$ (s^{-1})	$2k_2' \times 10^2$ (M^{-1} s^{-1})
2-Butanone	4.50	1.0	1.0		1.64	3.65
	8.90	1.0	1.0		3.00	3.35
	13.4	1.0	1.0		4.51	3.34
	8.9	1.0	0.6		3.14	3.52
3-Pentanone	3.80	1.0	1.0		1.66	4.40
	6.60	1.0	1.0		3.09	4.70
	11.4	1.0	1.0		4.86	4.30
	6.60	0.6	0.6		3.14	4.78
3-Methyl-2-butanone	1.67	0.40		4.5		7,* 120†
	3.22	0.42		4.2	38.6	120
	3.22	0.17		4.2	38.6	120
2,4-Dimethyl-3-pentanone	2.35	0.40		4.5	3.46	15±0.15

*Initial rate data, peroxide free.
†Autocatalytic region, peroxide free.

also kinetically well-behaved initially. At a given acid and ketone concentration they gave pseudo zero-order plots for the reduction of [Fe(III)] to [Fe(II)]. However, at about 50% of the reaction the linear rate of [Fe(III)] reduction suddenly increased, giving a reduction plot for the remainder of the reaction which resembled that expected for a reaction first-order in [Fe(III)] (Fig. 1). The latter part of these plots indicate a complicated secondary reaction resulting from the build-up of some reactive species during the course of the ketone oxidation. Since the reaction scheme must be very complicated no kinetic analysis was attempted. Measurement of the initial rate yielded a rate expression corresponding to [6]; first-order in [ketone], first-order in [H^+], and zero-order in [Fe(III)]. Values of $2k_1'$ for all ketones but acetone are given in Table 5.

As the products from the oxidation in the

TABLE 5. Oxidation of ketones by ferriin at 25°C under air at low [H^+] and high [Fe(III)]

Ketone	[Ketone] $\times 10^2$ (M)	[Fe(III)] $\times 10^4$ (M)	[H_2SO_4] (M)	[$HClO_4$] (M)	[H^+] (M)	Initial rate $\times 10^7$ (M^{-1} s^{-1})	$2k_1 \times 10^5$ (M^{-1} s^{-1})
2-Butanone	3.73	38	0.24		0.25	4.55	4.88
	7.45	19	0.24		0.25	9.10	4.89
	7.45	38	0.24		0.25	9.00	4.83
	10.0	9.6	0.24		0.25	12.0	4.80
3-Pentanone	3.16	9.6	0.24		0.25	3.62	4.58
	6.32	9.6	0.24		0.25	7.27	4.60
	6.32	9.6	0.48		0.49	14.9	4.81
	6.32	19.2	0.48		0.49	15.5	5.00
3-Methyl-2-butanone	3.22	0.8		0.2	0.2	0.68	1.1*
	3.22	0.8		0.2	0.2	0.64	0.95
	3.22	0.4		1.0	1.0	3.2	0.97
	3.22	0.8		1.0	1.0	3.1	0.95
	3.22	1.7		1.0	1.0	3.4	1.0
	3.22	2.5		1.0	1.0	3.6	1.1
	3.22	3.3		1.0	1.0	3.6	1.1
	3.72	1.0		1.0	1.0	4.2	1.1
	7.46	1.0		1.0	1.0	8.7	1.2
	3.72	1.0		0.6	0.6	2.2	0.99
	1.24	1.0		1.0	1.0	1.3	1.1
	3.22	2.0		0.4	0.4	1.3	0.98†
2,4-Dimethyl-3-pentanone	4.70	1.0		1.0	1.0	0.85	0.18
	2.35	1.0		1.0	1.0	0.42	0.18
	2.35	1.0		0.6	0.6	0.25	0.18
	2.35	2.0		0.6	0.6	0.27	0.19

*(0.8 M) $NaClO_4$ added.
†Peroxide free.

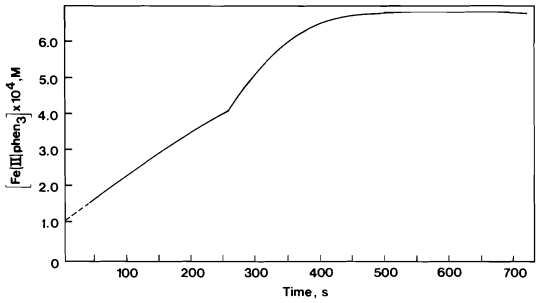

FIG. 1. Reaction profile for oxidation of 2-butanone by ferriin at 25°C, 0.24 M H_2SO_4 and in air. Rate of formation of ferroin vs. time at 510 nm. [Ferriin] = 9.6×10^{-4} M, [2-butanone] = 0.1 M.

presence of oxygen would result from formation and decomposition of peroxides in chain reactions they might be expected to be quite complicated. For that reason no product studies were carried out in this system.

Discussion

The air-free system is mechanistically the simplest and will be discussed first. The data are summarized in Table 6. The most important point is that four ketones in addition to cyclohexanone have now been shown to have a rate equation of the form of [4] clearly indicating they are oxidized via the enol mechanism. The five include ketones of quite different structure whose rates of enolization vary by a factor of 170. The agreement between calculated and literature values for the rates of enolization are quite good for cyclohexanone (13) and 2,4-dimethyl-3-pentanone (14) whose rates of enolization are well established (Table 6). The rest were obtained by determining relative rates of enolization as compared with acetone and are probably not as accurate. The values for 3-methyl-2-butanone agree well but those for 2-butanone and 3-pentanone are not as close. However, even with the worst case, 3-pentanone, the difference of a factor of ca. three in the two rates is not unreasonable, considering the difference in method of measurement. However, the value of k_1 for acetone could not be obtained because the limiting case of [4] when k_2[Fe(III)] $\gg k_{-1}$[H^+] is not experimentally accessible. This is readily verified by the following considerations. Values

TABLE 6. Values of k_1 and k_2 for several ketones in air-free aqueous solutions at 25°C*

Ketone	Enolization rate constant† Calcd. (k_1) (M^{-1} s^{-1})	Literature (M^{-1} s^{-1})	$2k_2' = 2Kk_2$ (M^{-1} s^{-1})	K	k_2 (M^{-1} s^{-1})
Acetone	—	2.7×10^{-5} (11)	1.3×10^{-4}	1.5×10^{-8} (15)	4.32×10^{3}
2-Butanone	6.2×10^{-5}	2.8×10^{-5} (7)	6.7×10^{-2}	—	—
Cyclohexanone‡	3.0×10^{-4}	3.1×10^{-4} (13)	1.1	4.1×10^{-6} (16)	1.34×10^{5}
2,4-Dimethyl-3-pentanone	1.5×10^{-6}	1.8×10^{-6} (14)	0.34	4.5×10^{-8} (15)	3.78×10^{6}
3-Methyl-2-butanone	1.5×10^{-5}	1.9×10^{-5} (7)	0.49	—	—
3-Pentanone	6.8×10^{-5}	2.0×10^{-5} (7)	9.5×10^{-2}	10×10^{-8} (15)	4.75×10^{5}

*All values of k_1 except that for 2,4-dimethyl-3-pentanone were determined in aqueous sulfuric acid. Value of k_1 for this ketone, as well as all values of k_2', were determined in aqueous $HClO_4$.
†Numbers in parentheses are literature references.
‡Data from ref. 10.

of k_2 and k_{-1} were calculated to be 4.3×10^3 M^{-1} s^{-1} and 1.8×10^3 M^{-1} s^{-1} from the literature values of K (1.5×10^{-8}) (15), k_1 (2.7×10^{-5} M^{-1} s^{-1}) (11), and the experimentally determined value of $2k_2'$ (1.3×10^{-4} M^{-1} s^{-1}) (Table 2). Using these values it can be shown that for k_2[Fe(III)] to be 10 times larger than k_{-1}[H$^+$], the ratio of [Fe(III)] to [H$^+$] must be about 4. The lowest [H$^+$] which can be used is 0.2 M since ferriin is readily hydrolyzed at lower [H$^+$] (17). This would require a [Fe(III)] of 0.8 M but it is not possible to make a ferriin solution more concentrated than 0.02 M when [H$^+$] is 0.2 M.

One objective of this work was to establish a correlation between enol structure and reactivity. Fortunately, for the symmetrical ketones, values of the equilibrium constant, K, for enolization have been determined (15). In making such a correlation we will assume that acetone reacts by way of the enol tautomer although this has not been proven kinetically. This is a reasonable assumption since all the other ketones studied are oxidized via the enol tautomer. However, it is possible that acetone is oxidized via the keto tautomer.

The values of the rate constants, k_2, for electron transfer from enol to ferriin are given in Table 6. The order of reactivity, 2,4-dimethyl-3-pentanone > 3-pentanone > cyclohexanone > acetone, indicates a methyl substituent increases the rate of electron transfer from enol. Correlations between enol structure and relative rates are shown in Table 7. This is reasonable if, as previously proposed for the oxidation of cyclohexanone (10), electron transfer occurs to give a radical cation (reaction 2). The electron donating substituents would stabilize such an intermediate. To our knowledge, this is the first quantitative correlation between enol structure and reactivity.

The oxidation rates of the unsymmetrical ketones 2-butanone and 3-methyl-2-butanone are also listed in Table 6. It is of interest to note that the values of $2k_2' = 2Kk_2$ for the two unsymmetrical ketones, 2-butanone and 3-methyl-2-butanone, are similar to the next more substituted symmetrical ketone, 3-pentanone and 2,4-dimethyl-3-pentanone (Table 6). Enols formed from unsymmetrical ketones exist in two tautomeric forms which differ in their degrees of substitution. The rates with symmetrical enols indicate the more highly substituted enol is the more reactive. Thus the rate of oxidation of the ketone will be determined by the rate of reaction of the more substituted enol if its equilibrium concentration is not much less than that of the less substituted enol. The values of K for 3-pentanone and 2,4-dimethyl-3-pentanone are within a factor of two indicating that the equilibrium concentration of enol is not strongly dependent on structure. Actually bromination studies with unsymmetrical ketones (7) suggest that the more substituted enol is the more abundant enol. On the basis of these considerations it would be predicted that the value of $2k' = 2Kk_2$ of unsymmetrical ketones would be close to that of the next more substituted ketone since the reactive enol for both is identical. This is the observed result.

The opposite order of reactivity was found for the oxidation of *para*-substituted benzyl phenyl ketones by $Mn(OAc)_3$ in acetic acid (6). Electron-withdrawing groups increased the rate of oxidation. Also unsymmetrical ketones gave products which indicated that CH_2=C(OH)— was more

TABLE 7. Relative rates of electron transfer from several enols to ferriin

Ketone	Enol structure	Relative rate
2,4-Dimethyl-3-pentanone	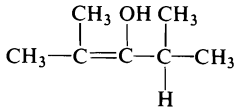	875
3-Pentanone	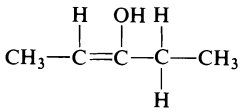	110
Cyclohexanone	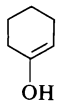	31
Acetone	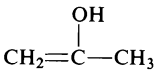	1

reactive than $(CH_3)_2C{=}C(OH)$—. This system is quite different from the aqueous system considered in this paper and the mechanisms could be quite different. Thus $Mn(OAc)_3$ could be an inner-sphere oxidant and the radical anion could be the more reactive species which would explain the order of reactivity. Also in the $Mn(OAc)_3$ system it is not clear if the rate determining step is the rate of electron transfer from the enol or the rate of enolization.

Earlier reports on the rates of oxidation of ketones by other oxidants deserve some comment. Petit found that in the oxidation of a series of methyl ketones by chromic acid, the rate of oxidation increased from acetone to 2-nonanone (18). Shorter found a linear correlation between the apparent rate of oxidation of ketones by ceric sulphate and the rate of enolization. He interpreted this result by suggesting that all enols have approximately the same reactivity since there is likely a Brønsted type of correlation between rate of enolization and the keto–enol equilibrium constant. Acetone was found to react much slower than would be expected on the basis of its rate of enolization. He attributed this lack of stabilization to hyperconjugation in the oxidation product of acetone. No correlation between rates of enolization and rates of oxidation of ketones by Mn(III) pyrophosphate was found; acetone was oxidized faster than 2,4-dimethyl-3-pentanone (8). Ceric sulphate, $Mn(OAc)_3$, chromic acid, as well as Mn(III) pyrophosphate are most likely inner-sphere oxidants and hence not comparable to ferriin. In addition, the rates of oxidation quoted by the above workers includes the keto–enol equilibrium constant and hence do not refer to the reactivity of the enol towards the oxidant.

Although detailed product distribution studies were not carried out, 3-hydroxy-2-butanone and 2,3-butanedione products were the expected ones, if the more substituted enol is reactive. Thus oxidation of 2-butanone by Fe^{3+} (19) and $[Fe(III)(X)(H_2O)phen_2]$ ($X = H_2O$, OH^-) (20) were reported to give 2,3-butanedione as the final product. Almost certainly, this product arose from further oxidation of the hydroxy ketone.

The most striking feature of the values k_1 and k_2 for the air containing system is that they are about the same or lower than those in the air-free system for all ketones but 3-methyl-2-butanone. In fact for three; 2-butanone, 2,4-dimethyl-3-pentanone, and 3-pentanone, the values of both k_1 and k_2 are roughly one-half of the corresponding values in the air-free system. This result can be explained by a change in stoichiometry of the reaction. Thus in the absence of O_2 the reaction would be given by [1] to [3].

In the presence of oxygen [3] could be re-

placed by reactions such as those shown in reactions 7 and 8.

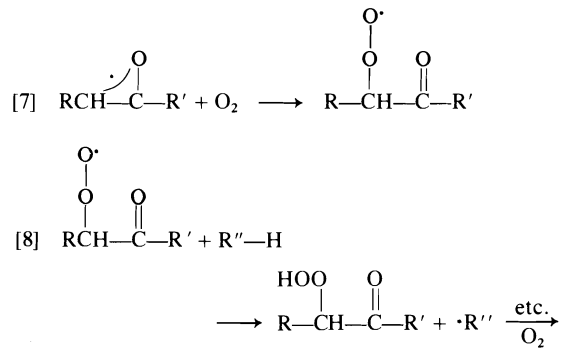

Thus, in the presence of O_2, only one Fe(III) is reduced per electron transfer from enol, i.e. the autoxidation chain reaction must be terminated without further reduction of Fe(III). This would have the effect of halving the rate of Fe(III) reduction. A similar argument has been put forward by Littler and co-workers on the effect of O_2 on rate in the oxidation of cyclohexanone by Ir(IV) (21).

The increase in $2k_2'$ in air for 3-methyl-2-butanone is apparently real. It could be that the rates of the steps in reactions 1–3, 7–8 are different, or alternatively that other reaction paths are operative for this ketone and some species which reduces Fe(III) is produced in high enough concentrations to become important. Thus in the oxidation of 2-butanone by Fe(III), oxygen is reported to increase the rate (19) while in the oxidation of cyclohexanone by Ir(IV), oxygen decreases the rate (21). Thus whether retardation or acceleration is observed will depend on the system and in fact may depend on reaction variables. As discussed next, apparently [Fe(III)] is an important variable.

Since Fe(III) reduction rather than oxygen uptake is measured, no information about the autocatalytic reaction sequence is obtained other than that Fe(III) takes part in the autocatalytic sequence by reacting with some of the products formed. This apparently happens in the runs at high [Fe(III)] and low $[H^+]$ used to measure k_1, since the rate of Fe(III) reduction suddenly departs from linearity at about 50% reduction of Fe(III). Since we were measuring the rate of formation of Fe(II) species the autocatalytic plot shows that in the autocatalytic region, there is a rapid build up of a certain species that is active in reducing Fe(III). The nature of this species is highly speculative; it could be a radical, or peroxide, or even $Fe^{2+}(aq)$[2] formed due to hydrolysis of ferroin (22). On the basis of present evidence further speculation does not seem warranted.

As reported previously, the values of k_1 and k_2 for cyclohexanone are altered little in the presence of air, suggesting Fe(III) reacts very fast with the enol radical (reaction 3) in this case. The value of k_2 for acetone is also little altered by oxygen but because of the uncertainty of mechanism little can be said about this case.

Since the product distribution would likely be very complicated in the air containing systems no product analysis was carried out.

Experimental

Materials

1,10-Phenanthroline, ferrous sulphate heptahydrate, and perchloric acid were purchased from G. Frederick Smith Chemical Company. Sulphuric acid was purchased from Matheson, Coleman and Bell Manufacturing Company.

2-Butanone, 3-pentanone, 3-methyl-2-butanone, and 2,4-dimethyl-3-pentanone were all reagent grade from J. T. Baker Chemical Company and were distilled before use. In some instances, peroxides were removed from the ketone by addition of Fe^{2+} to the ketone before distillation. This treatment did not alter the rates. Acetone was reagent grade from J. T. Baker Chemical Company and was used without purification.

Tris(1,10-phenanthroline)Fe(II) (ferroin) was prepared from a published procedure (23) which consisted of adding 1,10-phenanthroline to a solution of $FeSO_4 \cdot 7H_2O$ in a 3:1 molar ratio. Ferriin was obtained by oxidation of ferroin with PbO_2 in 1 M H_2SO_4. Ferriin was precipitated as a perchlorate salt. Stock solutions of ferriin were made up in concentrated H_2SO_4 or $HClO_4$ medium. Such solutions were diluted with water to appropriate acid strength immediately before each kinetic run.

Kinetic Studies

The rate of oxidation of ketones was monitored by following the increase in optical density at 510 nm with time. Ferroin has an extinction coefficient of 1.1×10^4 M^{-1} cm^{-1} at 510 nm while that of ferriin is 500 M^{-1} cm^{-1} (23). Kinetic studies were carried out on a Durrum stopped-flow spectrophotometer and a Cary 118 spectrophotometer. The reaction was carried out under pseudo first-order conditions with excess ketone. The pseudo first-order rate plots were analyzed by plotting log $(OD_\infty - OD_t)$ against time from which k_{obs} was found.

[2]Ferroin is known to hydrolyze with a rate constant $\sim 10^{-4}$ s^{-1} at 0.2 M $[H^+]$ to give $Fe^{2+}(aq)$. Since oxidations in air are slower than in its absence, we might expect a higher accumulation of $[Fe^{2+}(aq)]$ which subsequently undergoes a rapid outer-sphere electron transfer with ferriin to give ferroin (22) and thus produces autocatalytic behavior.

The k_{obs} values for pseudo zero-order kinetics were obtained by measurement of the slope of the linear region.

Reactions under argon or nitrogen were carried out by degassing solutions of Fe(III) in acid and ketone separately. Reaction was started by injecting the degassed solution of ketone into a solution of Fe(III) in a 1 cm optical cell fitted with a serum cap. Since degassing cannot be performed easily inside a 1 mm cell, such reactions were carried out by degassing solutions of Fe(III) and ketone separately. Mixing and transferring the reactants into the 1 mm cell were carried out under N_2 in a glove box.

The oxidation of acetone was studied at 2.4×10^{-3} *M* ferriin and 0.6 *M* H_2SO_4 and at 6×10^{-5} *M* ferriin and 6.3 *M* H_2SO_4. Even at acetone concentrations of 0.91 *M* and 1.82 *M* and at low [Fe(III)] no change in OD over a 2 h period was observed. At high [Fe(III)] and low [acid], pseudo first-order kinetics were observed with excess [acetone]; k_{obs} is ca. 2×10^{-4} s^{-1} which is about the same as the dissociation rate constant of ferriin in absence of acetone (22). Also, the rates changed little as the acetone concentration was doubled.

The rates of oxidation of acetone by 5-chloroferriin are given in Table 1. From the slope of the k_{obs} vs. acetone plot, k_2' was determined to be 1.3×10^{-3} M^{-1} s^{-1}. If the Marcus relationship is obeyed 5-chloroferriin would be 10 times more reactive than ferriin (10). This gives an oxidation rate of 1.3×10^{-4} M^{-1} s^{-1} for ferriin.

Product Analysis

2-Butanone (0.2 ml) was added to a suspension of 0.008 g of ferriin in 0.1 ml of 2 *M* H_2SO_4. The reaction was carried out under N_2. After stirring the solution for 5 min samples were taken at 1 min intervals for analysis on a Hewlett Packard 5750 research gas chromatograph on a $\frac{1}{4}$ in. diameter 12 ft Carbowax column. Products were identified by retention times. 3-Hydroxy-2-butanone was identified as the initial product. With time, butane-2,3-dione was formed.

Acknowledgements

The authors thank the National Research Council of Canada and Environment Canada for support of this research. Technical assistance by E. Makowsky is also gratefully acknowledged. We thank a referee for helpful suggestions and for drawing our attention to a pertinent reference.

1. J. S. Littler. J. Chem. Soc. 827 (1962).
2. J. Roček and Sr. A. Riehl. J. Am. Chem. Soc. **88**, 4749 (1966).
3. K. B. Wiberg and R. D. Geer. J. Am. Chem. Soc. **87**, 5202 (1965).
4. T. J. Kemp. Comprehensive chemical kinetics. Vol. 7. *Edited by* C. H. Bramford and C. F. H. Tipper. Elsevier Publishing Company, Amsterdam, London, New York. 1972. p. 380.
5. W. A. Waters. Mechanisms of oxidation of organic compounds. Methuen and Co. Ltd., London. 1964. p. 97.
6. E. I. Heiba and R. M. Dessau. J. Am. Chem. Soc. **93**, 525 (1971).
7. J. Shorter. J. Chem. Soc. 3425 (1950).
8. A. Y. Drummond and W. A. Waters. J. Chem. Soc. **93**, 525 (1971).
9. J. S. Littler and I. G. Sayce. J. Chem. Soc. 2454 (1964).
10. F. T. T. Ng and P. M. Henry. J. Am. Chem. Soc. **98**, 3606 (1976).
11. R. P. Bell and K. Yates. J. Chem. Soc. 1927 (1962); J. E. Dubois and J. Toullec. Chem. Commun. 478 (1969).
12. R. C. Weast (*Editor*). Handbook of chemistry and physics. 49th ed. The Chemical Rubber Co., Cleveland, OH. 1968. p. D-91.
13. A. J. Green, T. J. Kemp, J. S. Littler, and W. A. Waters. J. Chem. Soc. 2722 (1964).
14. R. P. Bell, G. R. Hillier, J. W. Mansfield, and D. G. Street. J. Chem. Soc. B, 827 (1967).
15. J. E. Dubois and J. Toullec. Tetrahedron, **29**, 2859 (1973).
16. R. P. Bell and P. W. Smith. J. Chem. Soc. B, 241 (1966).
17. T. S. Lee, I. M. Kolthoff, and D. L. Leussing. J. Am. Chem. Soc. **70**, 2348 (1948); **72**, 2173 (1950); F. Basolo, J. C. Hayes, and H. M. Neumann. J. Am. Chem. Soc. **76**, 3807 (1954); J. E. Dickens, F. Basolo, and H. M. Neumann. J. Am. Chem. Soc. **79**, 1286 (1957).
18. G. Petit. Bull. Soc. Chim. Fr. **12**, 568 (1945).
19. E. T. Denisov, V. D. Komissarov, and D. J. Metilitza. Discuss. Faraday Soc. **46**, 127 (1968).
20. V. D. Komissarov and E. T. Denisov. Russ. J. Phys. Chem. **43**, 426 (1969).
21. R. Cecil, J. S. Littler, and G. Easton. J. Chem. Soc. B, 626 (1970).
22. B. Z. Shakhashiri and G. Gordon. J. Am. Chem. Soc. **91**, 1103 (1969).
23. M. H. Ford-Smith and N. Sutin. J. Am. Chem. Soc. **83**, 1830 (1961).

Photoreactions of 1- and 2-naphthonitriles with tetramethylethylene in various solvents

JOHN J. MCCULLOUGH, RODERICK C. MILLER, AND WEI-SAI WU
Chemistry Department, McMaster University, Hamilton, Ont., Canada L8S 4M1

Received January 12, 1977

JOHN J. MCCULLOUGH, RODERICK C. MILLER, and WEI-SAI WU. Can. J. Chem. **55**, 2909 (1977).

The photoreactions of 1- and 2-naphthonitriles with tetramethylethylene have been studied in the solvents hexane, benzene, dimethoxyethane, methanol, and acetonitrile. In hexane, benzene, or dimethoxyethane, the exclusive products are the cyclobutanes 1-cyano-7,7,8,8-tetramethyl-2,3-benzobicyclo[4.2.0]octa-2,4-diene (from 1-naphthonitrile and tetramethylethylene), and 6-cyano-7,7,8,8-tetramethyl-2,3-benzobicyclo[4.2.0]octa-2,4-diene (from 2-naphthonitrile). In methanol, products of photoreduction are formed. From 2-naphthonitrile and tetramethylethylene in methanol are obtained 1-(2′-methoxy-1′,1′,2′,2′-tetramethyl)-3-cyano-1,4-dihydronaphthalene, 1-(2′-methoxy-1′,1′,2′,2′-tetramethyl)-2-cyano-2,4-dihydronaphthalene, and 1,2-dihydro-2-naphthonitrile. Deuterium incorporation is observed with CH_3OD as solvent, and the stereochemistry of solvent incorporation is discussed. Reaction in 2,2,2-trifluoroethanol proceeds similarly. In methanol, 1-naphthonitrile and tetramethylethylene give products of reductive dimerization, whose exact structures were not determined. In acetonitrile, both naphthonitriles give complex mixtures of products on reaction with tetramethylethylene. It is proposed that the cyclobutane formation in non-polar solvents involves exciplex intermediates, while in polar media electron transfer occurs and results in photoreduction.

JOHN J. MCCULLOUGH, RODERICK C. MILLER et WEI-SAI WU. Can. J. Chem. **55**, 2909 (1977).

On a étudié les photoréactions des naphtonitriles-1 et -2 avec le tétraméthyléthylène dans l'hexane, le benzène, le diméthoxyéthane, le méthanol et l'acétonitrile comme solvants. Dans l'hexane, le benzène ou le diméthoxyéthane, les produits exclusifs sont les cyclobutanes, cyano-1 tétraméthyl-7,7,8,8 benzo-2,3 bicyclo[4.2.0] octadiène-2,4 (à partir du naphtonitrile-1 et du tétraméthyléthylène) et le cyano-6 tétraméthyl-7,7,8,8 benzo-2,3 bicyclo[4.2.0] octadiène-2,4 (á partir du naphtonitrile-2). Dans le méthanol il y a formation de produits de photoréduction. A partir du naphtonitrile-2 et du tétraméthyléthylène dans le méthanol on obtient le (méthoxy-2′ tétraméthyl-1′,1′,2′,2′)-1 cyano-3 dihydro-1,4 naphtalène, le (méthoxy-2′ tétraméthyl-1′,1′,-2′,2′)-1 cyano-2 dihydro-2,4 naphtalène et le dihydro-1,2 naphtonitrile-2. On observe une incorporation de deutérium lorsque le CH_3OD est utilisé comme solvant et on discute de la stéréochimie de l'incorporation du solvant. La réaction dans le trifluoro-2,2,2 éthanol se produit d'une manière similaire. Dans le méthanol, le naphtonitrile-1 et le tétraméthyléthylène donnent des produits de dimérisation réductive dont on n'a pas déterminé les structures exactes. Dans l'acétonitrile, les deux naphtonitriles conduisent á des mélanges complexes de produits de réaction avec le tétraméthyléthylène. On propose que la formation de cyclobutane dans des solvants non-polaires implique des intermédiaires exciplexes alors que dans des milieux polaires, il se produit des transferts d'électrons et il en résulte une photoréduction.

[Traduit par le journal]

The formation, structure, and behaviour of exciplexes is an area of research attracting considerable current interest. Exciplexes and ion-pairs have been studied by a variety of physical (1–13) and chemical (14–21) approaches, and a great deal is now known about the factors affecting their formation and behaviour. The earlier work employed amino compounds (1–4, 6, 7, 14–16) as electron donors to study the physical and chemical effects of charge transfer. It was also shown, however, that simple alkyl substituted ethylene derivatives could act as electron donors, giving rise to exciplex and ion pair formation with various excited aromatic compounds (8–13, 18–21). We have given preliminary accounts of our physical and chemical investigations on exciplexes and ion pairs from the naphthonitriles and tetramethylethylene (18, 19). In the present paper, we describe the isolation and identification of products of these reactions, run in various solvents. In a later paper, the details of photokinetics and lifetime measurements on these systems will be described.

Results

Reactions in Non-polar Solvents

Products and Structural Assignments

Irradiation of 1-naphthonitrile and tetra-

methylethylene in benzene with 313 nm light results in the efficient formation of a 1:1 adduct, **1**. This was separated from residual 1-naphthonitrile by column chromatography and vpc. On sublimation at 1 Torr, crystals, mp 69–71°C were obtained. The nmr spectrum showed resonances as follows. Four singlets at 1.40, 1.32, 1.00, and 0.81 δ (each area 3) were assigned to the methyl groups. A doublet of doublets (area 1) with $J = 4.5$ and 2.0 Hz at 3.20 δ was assigned to the bridgehead methine proton. An AB system at 5.71 δ, $J = 10.0$ and 4.5 Hz and at 6.31 δ, $J = 10.0$ and 2.0 Hz was attributed to the vinylic protons. Protons of the benzene ring gave two multiplets, centered at 7.1 (area 3) and

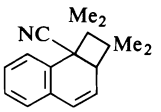

1

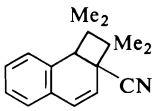

2

at 6.9 δ (area 1). The ultraviolet spectrum of **1** had λ_{max}(hexane) at 270 nm, log ε = 3.84. This is in good agreement with the spectrum of *endo*-7-cyano-2,3-benzobicyclo[4.2.0]octa-2,4-diene, whose structure is known from X-ray work, which had λ_{max}(hexane) at 268 nm, log ε = 3.86. In contrast, *o*-xylene has λ_{max}(EtOH) at 262 nm, log ε = 2.42. On the basis of this data, the adduct **1** is assigned the structure 1-cyano-7,7,8,8-tetramethyl-2,3-benzobicyclo[4.2.0]octa-2,4-diene. The same adduct was found to be by far the major product of this photoaddition in hexane or dimethoxyethane as solvents.

Irradiation of 2-naphthonitrile and tetramethylethylene in benzene also gave a single 1:1 adduct, **2**. The latter was difficult to separate from 2-naphthonitrile because it was thermally unstable to preparative vpc conditions, and moved at the same rate as 2-naphthonitrile on adsorption chromatography. Purification was achieved by high pressure liquid–liquid chromatography. This adduct is assigned the structure 6-cyano-7,7,8,8-tetramethyl-2,3-benzobicyclo[4.2.0]octa-2,4-diene (**2**). The nmr spectrum agrees with that reported by Cantrell (22). Singlet resonances were noted at 0.78, 1.07, 1.09, and 1.48 δ (each area 3) due to the methyl groups, and at 3.72 δ (area 1), assigned to the methine proton. The vinyl protons showed at 6.52 ($J = 10.0$ Hz) and at 5.72 δ ($J = 10.0$ Hz and 1.5 Hz). The smaller coupling constant is apparently due to coupling with a proton in the benzene ring. The protons of the benzene ring gave multiplets at 7.15 (area 3) and at 6.85 δ (area 1). Note that the product of 1,4-addition to the 2-naphthonitrile would have just one vinyl proton signal in the nmr spectrum. The same adduct was the only significant product of irradiation of 2-naphthonitrile and tetramethylethylene in dimethoxyethane.

Reactions in Polar Solvents

Irradiation of *2-naphthonitrile* and *tetramethylethylene in methanol* gave products assigned the structures **3**, **4**, and **5** shown in Scheme 1.

The products **3** and **4** (ratio 3:2) were isolated by silica gel chromatography. Compound **3** had mp 89.5–91.5°C. The nmr spectrum showed singlet resonances at 3.24 (area 3), due to the methoxy group, and at 0.56, 0.82, 1.10, and 1.26 δ (each area 3), due to the two pairs of diastereotopic methyl groups. The methylene and methine protons gave resonances between 3.30 and 3.80 δ, partly overlapping the singlet at 3.24 δ. A resonance at 7.05 δ was attributed to the vinyl proton, but detail was obscured by the resonance of the benzenoid protons at 7.08 δ (area 4). These resonances did have quite different chemical shifts on treatment with europium tris(dipivaloylmethide) (23). The resonance (area 1) of the vinyl proton showed a doublet, $J = 5.0$ Hz. As a final confirmation of structure, **3** was dehydrogenated with palladium-on-charcoal to give the naphthalene derivative **6**. The latter showed singlet resonances at 3.07 (area 3),

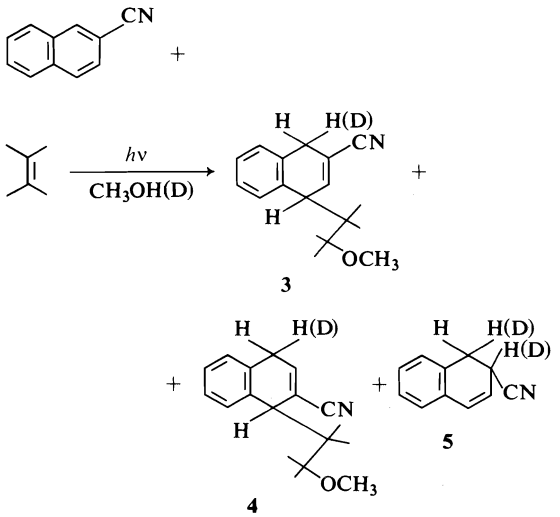

SCHEME 1

of the methoxy group, and at 1.12 and 1.66 δ (each area 6), due to the two pairs of side chain methyl groups. Most of the benzenoid protons resonated between 7.2 and 8.0 δ, except for a multiplet (area 1) at 8.9 δ. The latter is assigned to the proton at the *peri*-position, nearest to the side-chain, because of its low-field position (24). The structure 1-(2′-methoxy-1′,1′,2′,2′-tetramethylethyl)-3-cyano-1,4-dihydronaphthalene is thus assigned to compound **3**.[1]

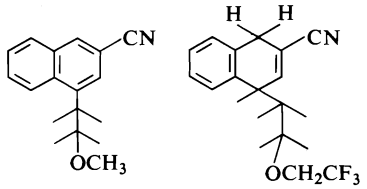

6 **7**

Compound **4**, mp 96.5–98°C, showed singlet resonances in the nmr spectrum at 7.08, for benzenoid protons (area 4), at 3.24 for the methoxy group (area 3), and at 0.71, 0.73, 1.12, and 1.35 δ (each area 3), for the side-chain methyl groups. A doublet at 3.75 δ, (area 1) with $J = 0.5$ Hz identified the methine proton, while the methylene group gave a multiplet from 3.24–3.50 δ, overlapping the methoxy-group singlet at 3.24 δ. The vinyl proton gave a doublet of doublets at 6.75 δ, (area 1) with $J =$ 7.0 and 3.0 Hz.

Attempted dehydrogenation as described for **3**, resulted in loss of the side-chain to give 2-naphthonitrile. The structure 1-(2′-methoxy-1′,1′,2′,2′-tetramethylethyl)-2-cyano-1,4-dihydronaphthalene is assigned to compound **4**. In the above reaction, there was also formed 1,2-dihydro-2-naphthonitrile **5**. This was isolated by distillation and characterized by its spectral properties.

Reaction of 2-Naphthonitrile and Tetramethylene in Methanol-O-d

Use of deuteroxylated methanol (CH_3OD) as solvent gave **3**, **4**, and **5** with deuterium incorporated in the methylene groups, as shown in Scheme 1. These labelled products will be referred to as **3**D, **4**D, and **5**D, respectively.

The presence of the deuterium label was evidenced by the weak M^+ ions of **3**D and **4**D with $m/e = 270$ ($C_{18}H_{22}DON$), and by the decrease in areas of the methylene group resonances in the nmr spectra.

By determining which proton–proton coupling constants were affected by the labelling, it was possible to deduce the stereochemistry of the deuterium label in **4**D. It was assumed that the reduced ring of the 1,4-dihydronaphthalene system adopts a shallow boat conformation (25) with the bulky substituent axial, as shown in Fig. 1.

The substituent apparently keeps the dihydronaphthalene system locked in one boat conformation, as shown by the proton spin–spin splitting pattern (25*c*). In **4** (unlabelled) the signal of the vinyl proton (H_v) shows as a doublet of doublets, with $J = 3.0$ and 7.0 Hz. Splitting of the H_v signal by H_a is assumed to have $J =$ 3.0 Hz (25*d*) and the splitting by H_e is assumed to have the larger ($J = 7.0$ Hz) coupling constant (25*c*).

In the spectrum of **4**D the signal of H_v appears as a *doublet* with $J = 7.0$ Hz. Thus, the deuterium in **4**D has apparently replaced H_a and not H_e and the deuterium label is *cis* to the side-chain substituent. Interestingly, the splitting of H_v in **3** has $J = 5.0$ Hz, which is consistent with H_e being equatorial with the bulky substituent axial. The above data are summarized in Fig. 1. Irradiation of *2-naphthonitrile* and *tetramethylethylene* in formic acid – methanol gave the same products as with pure methanol (Scheme 1), although the ratio of **3**:**4** did appear to change. Irradiation of *2-naphthonitrile* and *tetramethylethylene* in 2,2,2-trifluoroethanol gave a mixture of products from which compound **7** was isolated by preparative vpc. This compound had mp 150–152°C, and was identified by its nmr spectrum. This showed singlets at 0.73, 0.87, 1.19, and 1.36 (each area 3), due to the methyl groups, a quartet, $J = 9.0$ Hz (area 2), at 3.79 due to the methylene group of the trifluoroethyl substituent, and a partially resolved doublet at

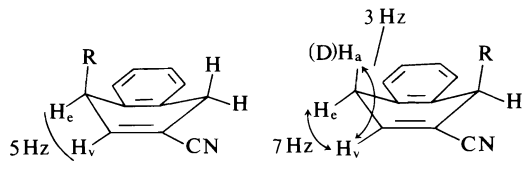

3 **4**

R = $CH_3OC(CH_3)_2C(CH_3)_2$—

FIG. 1. Conformations of the 1,4-dihydro-2-naphthonitrile derivatives **3** and **4**.

[1]The ultraviolet spectra of **3** and **4** also agreed with these assignments (see Experimental).

7.05 δ due to the vinylic proton. Multiplets at 3.53 (area 1), 3.73 (area 2), and 7.1–7.3 δ (area 4) corresponded to the methine, ring methylene, and aromatic ring protons respectively. The ^{19}F spectrum showed a triplet at 74.6 δ, (J = 9.0 Hz) from $CFCl_3$ confirming the presence of the trifluoroethyl group.

Irradiation of *1-naphthonitrile* and *tetramethylethylene* in methanol gave two crystalline adducts, which were separated by chromatography over silica gel. In spite of an intensive investigation of the structures of these products by chemical and spectroscopic techniques, their structures are still undetermined. They appear to be products of reductive dimerization of the naphthonitrile, and one of them contains the side chain which is present in **3** and **4**. This shows that solvent (methanol) has been incorporated.

Irradiation of 1- or 2-*naphthonitrile* and *tetramethylethylene* in acetonitrile gave an extremely complex mixture of products, shown by vpc analysis. No attempt was made to separate or characterize these compounds.

Discussion

It is clear from the above results that the photoreactions of the naphthonitriles and tetramethylethylene proceed by quite different mechanisms in the non-polar (hexane, benzene, dimethoxyethane) and polar (alcohols, acetonitrile) solvents. The non-polar media give highly specific reactions, the products being the cyclobutanes, **1** and **2**, formed by a formal $2\pi_S + 2\pi_S$ addition.[2] There is evidence, presented previously, that the cycloaddition involves exciplexes of the naphthonitrile and the olefin (19). The exciplex emission from 1-naphthonitrile and certain olefins is now well-known (10, 11).

Quenching of exciplex emission by polar solvents is also a widely recognized process. This quenching generally gives rise to ion-pairs, which are non-fluorescent. The photoreactions of many amino-compounds in polar solvents have been satisfactorily interpreted in terms of ion pairs, formed by electron transfer.

The products formed from the 2-naphthonitrile and tetramethylethylene in methanol are, by their nature, strongly suggestive of an electron transfer reaction pathway. In fact, all the products in Scheme 1 are dihydronaphthalenes, clearly formed by photoreduction of the naphthalene ring. The following mechanistic scheme (Scheme 2) is suggested to account for these

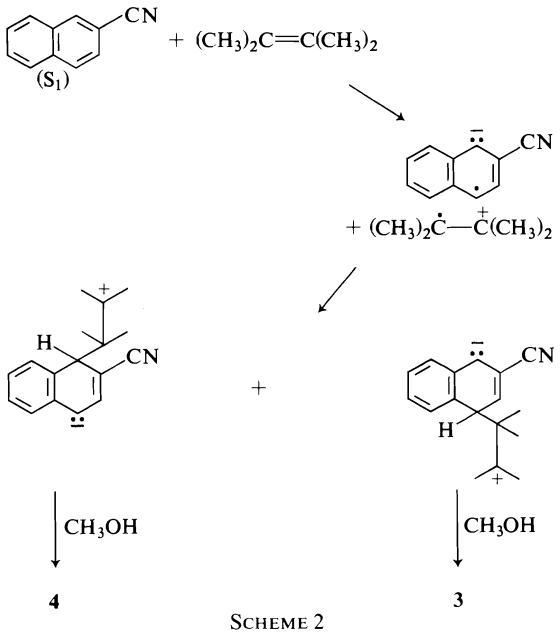

SCHEME 2

products. The stages are (*i*) electron transfer from olefin to the naphthonitrile ring, forming a pair of radical ions; (*ii*) collapse of the ion pair to a zwitterion; (*iii*) capture of solvent by the zwitterion to give products **3** and **4**. This is a rationale for the reaction, which accounts for the general features, e.g., it explains the formation of 1,2-dihydro-2-naphthonitrile which could be formed by escape of the radical anion from the ion-pair (26).[3]

We have one piece of evidence which gives insight into the timing of the above steps in the reaction. The *cis* arrangement in **4** of the proton (deuterium label) which comes from the solvent, and the side chain means that protonation cannot precede formation of the new carbon–carbon bond. If it did, a mixture of *cis* and *trans* deute-

[2]In a recent communication, Yang *et al.* (27) report the formation of 1-azetines on irradiation of the naphthonitriles or benzonitrile with olefins. We did not observe these products. However, as the authors point out (27), the cyclobutane ring system of **1** and **2** is photochemically labile (17), and under their reaction conditions (high conversion of reactant, Corex filter) the labile cyclobutanes are gradually replaced by the apparently stable 1-azetines. In contrast, our reactions giving **1** and **2** were always taken to low conversion, and Pyrex filters and 300 nm light were used. Under these conditions the initially formed cyclobutanes would be stable.

[3]Libman has observed reduction of 1-naphthonitrile on photoreaction with phenylacetic acid derivatives (26).

rium labelled **4** would result. Apparently, protonation *cis* to the bulky substituent (axial protonation) occurs preferentially.

The formation of **7** in trifluoroethanol may mean that this solvent, in spite of its much lower nucleophilicity, can be captured in the same way as methanol. This is consistent with the ion-pair mechanism, since the radical cation should be a powerful electrophile. Alternatively, protonation of the naphthonitrile ring may precede bonding of the side chain in this solvent (in contrast to methanol). We also note that the reduction product 1,2-dihydro-2-naphthonitrile **5** appears to be formed in trifluoroethanol. A final point can be made concerning product **5**. Since **5** is formed by reduction of the naphthonitrile, there must be an equivalent amount of products, from oxidation of the tetramethylethylene. We have not characterized these products, but note that Sakurai and co-workers (13) have reported a dimeric ether derivative in the photoreaction of 9-cyanophenanthrene with tetramethylethylene in methanol.

The reaction in acetonitrile is very complex, many products being formed, and a detailed analysis would involve an extensive investigation.

In conclusion, the results are consistent with the proposal (18, 19) that cycloaddition in nonpolar solvents proceeds via exciplexes, while electron-transfer in polar media leads to a totally different spectrum of photoreduction products. This scheme has been used to interpret the widely-studied photochemistry of amines and related compounds (14).

Experimental

Instruments

The nuclear magnetic resonance spectra were obtained with a Varian HA-100 or A-60 spectrometer. The chemical shifts are given as ppm (δ) and tetramethylsilane (δ = 0) was used as internal standard. Infrared and ultraviolet spectra were determined with a Perkin-Elmer 521 and Cary model 14 spectrophotometer respectively. Mass spectra were recorded on a Hitachi–Perkin-Elmer RMU 6A or a CEC 21-110B instrument. The vapor-phase chromatography (vpc) was performed, unless otherwise specified, with a Varian 204B dual column instrument with the flow rate of helium 30 ml/min. Two kinds of silica gel (Grace, 923, 100–200 mesh, and MN-silica gel G) were used as adsorbents in the adsorption column chromatography. For thin layer chromatography (tlc), Eastman plastic sheet precoated with silica gel was used. Melting points were measured on a Kofler hot stage and are uncorrected. Nitrogen was Canadian Liquid Air, certified grade. Preparative scale irradiations were generally performed either with a 450 W Hanovia type L mercury vapor lamp, using a Pyrex filter, or in sealed, deaerated Pyrex ampoules, irradiated with RPR-3000 Å lamps in a Rayonet reactor.

Microanalyses were determined by the Spang Microanalytical Laboratory, Ann Arbor, MI, by the Gygli Microanalysis Laboratory, Toronto, or by Galbraith Laboratories, Inc., Knoxville, TN.

Materials

All solvents for reactions were distilled before use.

1-Naphthonitrile from Eastman Organic Chemicals was recrystallized from light petroleum, mp 36.5–37°C. 2-Naphthonitrile was also from Eastman Organic Chemicals and was crystallized from 95% ethanol, mp 67–68°C. Tetramethylene was from Aldrich Chemicals ("Gold Label" grade) and was distilled at atmospheric pressure, bp 70.5°C. Deuterium oxide was from Columbia Organic Chemicals, and was specified at 99.7% D_2O. Dimethyl carbonate was from the British Drug Houses, Ltd., and was used to prepare methanol-*OD* by the method of Streitwieser *et al.* (28).

Photoaddition of 1-Naphthonitrile and Tetramethylethylene in Benzene

1-Naphthonitrile (3.0 g, 0.020 mol) and tetramethylethylene (8.0 g, 0.095 mol) in benzene (420 ml) were irradiated under argon with the Hanovia 450 W lamp for 50 h. The extent of reaction was determined from the nmr spectrum. The mixture was filtered through a 7 × 3 cm column of Grace 923 silica gel, using 1 ℓ of benzene to elute, and the solution was evaporated. The residue was chromatographed on a 3 × 35 cm column of silica gel (Machery–Nagel, type G) which was eluted with ether – benzene – light petroleum mixture in the ratio 15:15:70. The first 300 ml were discarded, and 25 ml fractions were collected. Fractions 1–10 contained mainly 1-naphthonitrile; fractions 11–70 contained a mixture of 1-naphthonitrile and cyclobutane **1**. The residue from fractions 11–70 was distilled at 0.1 Torr, at 110°C (oil bath). The distillate (0.621 g) when combined with fractions 1–10 gave 1.495 g of 1-naphthonitrile (50%). The residue from this distillation was chromatographed on 3 × 10 cm of silica gel, and 25 ml fractions were collected. Fractions 1–5 contained 1-naphthonitrile, while fractions 11–70 contained mixtures of 1-naphthonitrile and the cyclobutane **1**. The latter fractions were evaporated and a sample of **1** was isolated by preparative vpc on 10 ft × ¼ in. of 30% SE-30 on Chromosorb W at 210°C. The sample crystallized on cooling in ice, and the crystals were used to seed the residue from fractions 11–70. An analytical sample of **1** (0.420 g) mp 69–71°C from methanol, was obtained. *Anal.* calcd. for $C_{17}H_{19}N$: C 86.03, H 8.07, N 5.90; found: C 86.22, H 8.29, N 5.90.

Photoaddition of 2-Naphthonitrile and Tetramethylethylene

A solution of 2-naphthonitrile (0.536 g, 3.5 mmol) and tetramethylethylene (6.312 g, 0.075 mol) in benzene (50 ml) was degassed by three freeze–pump–thaw cycles and was sealed in a Pyrex tube. The sample was irradiated for 48 h using the Rayonet reactor and 11 RPR-3000 lamps. Analysis on 5 ft × ⅛ in. of 5% SE-30 on Chromosorb W at 175°C showed one major peak of retention time 5.1 min. In these runs, approximately half of the 2-naphthonitrile was unreacted. The adduct **2** was separated from 2-naphthonitrile by 'reverse phase' high pressure liquid chromatography. A Waters Associates

ALC-100 instrument was used with a 4 ft × $\frac{3}{8}$ in. column of Durapak *n*-octane/Porasil C. Elution was with 50:50 acetonitrile–water at 700 psi and elution rate of 2.0 ml/min. The 2-naphthonitrile was eluted first; the fractions containing the second component **2** were collected, extracted with methylene chloride, and dried over Na_2SO_4. Evaporation gave an oil (115 mg) which declined to crystallize. Analytical vpc showed one peak corresponding to photolysis product. This showed a parent ion of *m/e* 237.1515, corresponding to $C_{17}H_{19}N$. The structure was established from the nmr spectrum (22).

Irradiation of 2-Naphthonitrile and Tetramethylethylene in Methanol

A methanolic solution (400 ml) of 2-naphthonitrile (6.0 g, 0.039 mol) and tetramethylethylene (18.0 g, 0.214 mol) was irradiated under nitrogen with a Hanovia type L 450 W lamp (Pyrex filter) for 36 h. The progress of the addition was monitored by nmr spectroscopy and by vpc on 10 ft × $\frac{1}{8}$ in. of 5% QF-1 at 200°C. Two products were observed with retention times of 10 min and 8.3 min in a ratio of 60:40. The solvent was removed, and the crude mixture (8.14 g) was chromatographed on silica gel (Grace, 923), in a 27 × 3 cm column, slurry packed in and eluted with 30% ether – light petroleum, bp 30–60°C, and 400 ml fractions were collected. Fractions 1 and 2 contained 0.136 g of unidentified material; fractions 3 and 4 were 2-naphthonitrile (3.34 g), and fractions 5–10 contained products **3** and **4** (4.20 g), determined by vpc analysis. Fractions 5–10 were combined and chromatographed on a second column of silica gel (MN-silica gel G), (65 × 4.0 cm); elution was with a mixture of ether, benzene, and light petroleum in the ratio 10:10:80. The first litre of eluate was discarded, and thereafter 20 ml fractions were collected. Fractions 1–9 contained 0.355 g of unidentified material; fractions 13–23 contained a 50:50 mixture of **3** and **4** (2.128 g); fractions 24 and 25 were **4** contaminated with **3** (0.198 g), and fractions 26–37 contained **4** (1.184 g). The latter fractions were combined and crystallization from ethanol afforded **4**, 0.351 g, mp 96.5–98°C. *Anal.* calcd. for $C_{18}H_{23}NO$: C 80.25, H 8.61, N 5.20; found: C 80.38, H 8.62, N 5.22.

Fractions 13–23 from the above column were combined and chromatographed on a third column of MN-silica gel G (25 × 3.0 cm), and elution was with 3% ether – light petroleum, bp 30–60°C. Fractions of 25 ml were collected, and fractions 15–25 contained **3** and **5** (1.064 g) which gave **3**, 0.387 g, mp 89.5–91.5°C, from ethanol. *Anal.* calcd. for $C_{18}H_{23}NO$: C 80.25, H 8.61, N 5.20; found: C 80.31, H 8.55, N 5.31. The ultraviolet spectrum of **3** showed λ_{max}(EtOH) at 263 nm, log ε = 2.52, and that of **4** had λ_{max}(EtOH) 270 nm, log ε = 2.42 (compare *o*-xylene, above). The mother liquors from the crystallization of **3** were evaporated and distilled at 0.05 Torr (oil bath temperature 130°C) to afford **5**, (0.723 g) as an oil.

For the deuterium labelling experiment, the above reaction was repeated using methanol-*OD* as solvent. Deuterated **3**, **4**, and **5** were isolated as above and characterized by mass and nmr spectra.

Irradiation of 2-Naphthonitrile and Tetramethylethylene in 2,2,2-Trifluoroethanol

A solution of 2-naphthonitrile (77 mg, 0.5 mmol) and tetramethylethylene (2.1 g, 25 mmol) in freshly distilled trifluoroethanol (50 ml) was transferred to a Pyrex ampoule and degassed by purging with argon. The sample was irradiated at 300 nm for 25 h using 16 RPR-3000 Å lamps in the Rayonet reactor. Analysis by vpc on 5 ft × $\frac{1}{8}$ in. of SE-30 at 180°C showed peaks with retention times 1.6, 2.0, 7.6, 9.2, 11.5, and 17.5 min. The peak of longest retention time was isolated by preparative vpc on 8 ft × $\frac{1}{4}$ in. of 15% SE-30 on Chromosorb W at 197°C. This gave compound **7** as a yellow solid from which crystals, mp 150–152°C were obtained from ethanol. The mass spectrum showed *m/e* = 337.1663 corresponding to $C_{19}H_{22}NOF_3$. *Anal.* calcd. for $C_{19}H_{22}NOF_3$: C 67.64, H 6.57, N 4.15; found: C 67.43, H 6.63, N 4.30.

The two peaks at shortest retention time were collected together and the nmr spectrum showed that 1,2-dihydro-2-naphthonitrile and 2-naphthonitrile were present.

Irradiation of 2-Naphthonitrile and Tetramethylethylene in Acetonitrile

Irradiation of 2-naphthonitrile (2.0 g, 13 mmol) and TME (6.0 g, 71 mmol) in acetonitrile in the same way as for methanol, for 12 h resulted in the formation of many products, according to vpc analysis (10 ft × $\frac{1}{8}$ in. of 5% SE-30 at 185°C), and the mixture was not investigated further.

Dehydrogenation of Compound 3

A mixture of 0.2 g of compound **3** and 0.15 g 10% palladium–charcoal in 15 ml *p*-xylene was refluxed for 3 days. The catalyst was filtered and the solution distilled under aspirator pressure. The residue was crystallized from ethanol–water. The dehydrogenation product **6**, mp 124–126°C, was obtained (0.06 g, 30% yield). *Anal.* calcd. for $C_{18}H_{21}NO$: C 80.86, H 7.92, N 5.24; found: C 80.88, H 7.99, N 5.24.

Dehydrogenation of Deuterio-5

Deuterio-**5** and 10% palladium–charcoal (0.2 g) in 10 ml toluene were refluxed for 8 h. The solvent was removed and the residue chromatographed on a silica gel (MN-silica gel G) column (7 × 3 cm). First elution was with 0.5 ℓ light petroleum and this was discarded. Elution with 5% ether in light petroleum (1 ℓ) gave a residue which crystallized, giving 2-naphthonitrile, mp 65–68°C (lit. (29) 66°C) on removal of solvent. The product consisted of a 50:50 mixture of 2-naphthonitrile and 1-deuterio-2-naphthonitrile according to nmr and mass spectral analyses.

Acknowledgement

We thank the National Research Council of Canada for a postgraduate scholarship (to R.C.M.) and for financial support.

1. A. WELLER. Pure Appl. Chem. **16**, 115 (1968).
2. T. FORSTER. Angew. Chem. Int. Ed. Engl. **8**, 333 (1969).
3. M. OTTOLENGHI. Acc. Chem. Res. **6**, 153 (1973).
4. T. OKADA, H. OOHARI, and N. MATAGA. Bull. Chem. Soc. Jpn. **43**, 2750 (1970).
5. N. J. TURRO, J. C. DALTON, K. DAWES, G. FAR-

RINGTON, R. HAUTALA, D. MORTON, M. NIEMCZYK, and H. SCHORE. Acc. Chem. Res. **5**, 92 (1972), and references therein.
6. M. S. WALKER, T. W. BEDNAR, and R. LUMRY. J. Chem. Phys. **47**, 1020 (1967).
7. E. A. CHANDROSS and A. H. SCHIEBEL. J. Am. Chem. Soc. **95**, 611 (1973); **95**, 1677 (1973).
8. L. M. STEPHENSON and G. S. HAMMOND. Pure Appl. Chem. **16**, 125 (1968); Angew. Chem. Int. Ed. Engl. **8**, 261 (1969).
9. D. A. LABIANCA, G. N. TAYLOR, and G. S. HAMMOND. J. Am. Chem. Soc. **94**, 3679 (1972); G. N. TAYLOR and G. S. HAMMOND. J. Am. Chem. Soc. **94**, 3684; **94**, 3687 (1972).
10. G. N. TAYLOR. Chem. Phys. Lett. **10**, 355 (1971).
11. W. R. WARE, D. WATT, and J. D. HOLMES. J. Am. Chem. Soc. **96**, 7853 (1974).
12. (*a*) R. A. CALDWELL. J. Am. Chem. Soc. **95**, 1690 (1973); (*b*) R. A. CALDWELL and L. SMITH. J. Am. Chem. Soc. **96**, 2994 (1974); (*c*) D. CREED and R. A. CALDWELL. J. Am. Chem. Soc. **96**, 7369 (1974).
13. K. MIZUNO, C. PAC, and H. SAKURAI. J. Am. Chem. Soc. **96**, 2993 (1974).
14. S. G. COHEN, A. PAROLA, and G. H. PARSONS, JR. Chem. Rev. **73**, 141 (1973).
15. W. FEREE, JR., J. B. GRUTZNER, and H. MORRISON. J. Am. Chem. Soc. **93**, 5502 (1971); R. HOFFMAN, P. WELLS, and H. MORRISON. J. Org. Chem. **36**, 102 (1971).
16. R. S. DAVIDSON and S. P. ORTON. J. Chem. Soc. Chem. Commun. 209 (1974).
17. R. M. BOWMAN, T. R. CHAMBERLAIN, C. W. HUANG, and J. J. McCULLOUGH. J. Am. Chem. Soc. **96**, 692 (1974).
18. J. J. McCULLOUGH and W. S. WU. J. Chem. Soc. Chem. Commun. 1136 (1972).
19. J. J. McCULLOUGH, R. C. MILLER, D. FUNG, and W. S. WU. J. Am. Chem. Soc. **97**, 5942 (1975).
20. R. A. NEUNTEUFEL and D. R. ARNOLD. J. Am. Chem. Soc. **95**, 4080 (1973).
21. J. SALTIEL and D. E. TOWNSEND. J. Am. Chem. Soc. **95**, 6140 (1973).
22. T. S. CANTRELL. J. Am. Chem. Soc. **94**, 5929 (1972).
23. (*a*) C. C. HINCKLEY. J. Am. Chem. Soc. **91**, 5160 (1969); (*b*) B. C. MAYO.Chem. Soc. Rev. **2**, 49 (1973).
24. R. W. FRANCK and K. YANAGI. J. Org. Chem. **33**, 811 (1968); R. W. FRANCK and E. G. LESER. J. Am. Chem. Soc. **91**, 1577 (1969).
25. (*a*) A. H. BECKETT and B. A. MULLEY. J. Chem. Soc. 4159 (1955); (*b*) E. L. ELIEL, N. L. ALLINGER, S. J. ANGYAL, and G. A. MORRISON. Conformational analysis. Interscience, New York, NY. 1964. pp. 125, 242; (*c*) M. J. COOK, A. R. KATRITZKY, F. C. PENNINGTON, and B. M. SEMPLE. J. Chem. Soc. B, 523 (1969); (*d*) P. W. RABIDEAU, J. W. PASCHAL, and L. E. PATTERSON. J. Am. Chem. Soc. **97**, 5700 (1975).
26. J. LIBMAN. J. Am. Chem. Soc. **97**, 4139 (1975).
27. N. C. YANG, B. KIM, W. CHIANG, and T. HAMADA. J. Chem. Soc. Chem. Commun. 729 (1976).
28. A. STREITWIESER, JR., L. VERBIT, and P. STANG. J. Org. Chem. **29**, 3706 (1964).
29. R. C. WEAST (*Editor*). Handbook of chemistry and physics. 49th ed. The Chemical Rubber Company, Cleveland, OH. 1969–1970. p. C-386.

Pyrromethenes in the synthesis of polypyrranes[1]

AREND ROWOLD AND S. FERGUSON MACDONALD
Division of Biological Sciences, National Research Council of Canada, Ottawa, Ont., Canada K1A 0R6

Received April 18, 1977

AREND ROWOLD and S. FERGUSON MACDONALD. Can. J. Chem. **55**, 2916 (1977).

A new method makes appropriate 5-bromo-5′-methoxymethyl-pyrromethenes available for synthesizing polypyrranes related to uroporphinogens. In chloroform at 20°C, they react with α-free pyrroles (normally) and with 5-free pyrromethanes (losing the methoxymethyl-pyrrole ring) to give tripyrrenes which reduce to unblocked tripyrranes. Likewise, but in dioxane at 20°C and more cleanly, 5-bromo-5′-methylpyrromethenes convert pyrromethanes to tripyrrenes, and a tripyrrane to a tetrapyrrene (bilene).

AREND ROWOLD et S. FERGUSON MACDONALD. Can. J. Chem. **55**, 2916 (1977).

Une nouvelle méthode permet de préparer quelques bromo-5 méthoxyméthyl-5′ pyrrométhènes utilisés dans la synthèse de polypyrranes apparentés aux uroporphinogènes. Les pyrrométhènes réagissent (normalement) dans le chloroforme à 20°C avec des pyrroles de position α libre et avec des pyrrométhanes de position 5 libre (perdant le cycle méthoxyméthyl-pyrrole) conduisant à des tripyrrènes lesquels sont réduits en tripyrranes non empêchés. De la même façon, les bromo-5 méthyl-5′ pyrrométhènes, dans le dioxane à 20°C, transforment plus proprement les pyrrométhanes en tripyrrènes et un tripyrrane au tétrapyrrène (bilène).

[Traduit par le journal]

The unknown 5-bromo-5′-bromomethyl-pyrromethene (**2**) was promising for the synthesis of porphyrins via a,c-biladienes, and of aminomethyl-polypyrranes related to uroporphinogens. It was obtained from the pyrrole **1**[2] and bromine in ethanol-free chloroform at 0°C, a new method, and converted to the more stable methoxymethyl-pyrromethene **3** in methanol at 20°C. Three analogues of both, with alternating substituents (PAPA, MePMeP, and the known PMePMe (1)), were obtained likewise.

Pyrromethane-5-carboxylic acids with analogues of **3** in boiling benzene had given tetrapyrrenes (bilenes) and mixtures of porphyrins (2, cf. ref. 3). It was suggested that the latter were formed through an intermediate like **11** (R = CH_2OMe) which lost two pyrroles then self-condensed to the porphyrin.

In chloroform or methanol at 20°C, the bromomethyl- and methoxymethyl-pyrromethenes **2** and **3** both condensed rapidly with the α-free pyrrole **4**. The resulting tripyrrene was isolated as its free base **5** (≤40%),[3] which was reduced to the tripyrrane **6**. Unexpectedly, the methoxymethyl-pyrromethene **3** and the 5-free pyrromethane **7** in chloroform also gave **5**, but this retained some impurity (possibly the expected tetrapyrrene, cf. **10**). In boiling benzene, **3** and the 5-carboxylic acid of **7** again gave **5** (tlc), but still less cleanly.

On the face of it, the second electrophilic center in **3** reacted with **7**, resulting in **11** (R = CH_2OMe) and thence **5**. As suggested by this, the 5′-methylpyrromethene **8** (!) and **7** gave **5** exclusively. This reaction was slow in chloroform, and the tripyrrene was hard to separate from unreacted **7**. In dioxane, still at 20°C, the reaction was fast and pure **5** (≤30%) easily obtained. The methyl ester corresponding to **8** and the tripyrrane **6** gave the tetrapyrrene **10** (20%) analogously.

Thin layer chromatography of the products from **7** and **8** showed a pyrrole spot (cold Ehrlich's reaction: red) running as both **9** and its methyl ester. In the more complex and now devalued reaction between **7** and **3** the lost

[1]Issued as NRCC No. 16087.

[2]When it is not indicated that identification was by tlc or ^{1}Hmr, all compounds gave satisfactory analyses, etc.

[3]Such reactions were followed by tlc on alumina (MN, Brinkmann cat. 66130207) with $CHCl_3$–MeOH, ca. 95:5. Concentrated solutions of the products in $CHCl_3$ were filtered through alumina (Woelm, grade 1), washing with reagent $CHCl_3$, eluting with ca. 97:3 $CHCl_3$–MeOH. The dried residue usually crystallized when stirred with methanol.

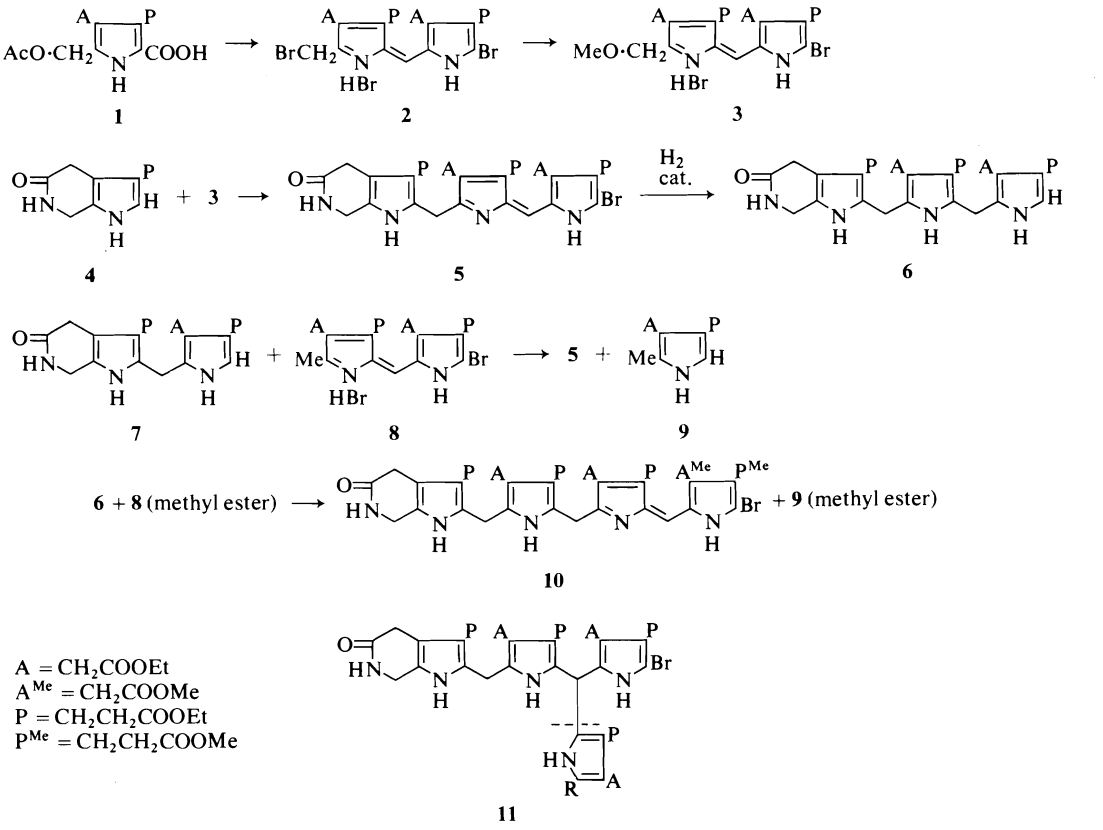

pyrrole was not accounted for. However, the ^{1}Hmr spectra of tripyrrenes from methoxymethyl-pyrromethene methyl esters and pyrromethane ethyl esters showed that it was the methoxymethyl-pyrrole ring in the former which was lost.

If isoporphobilinogen derivatives behave like those of porphobilinogen, the above reactions may represent general routes to the tripyrranes (from pyrroles or pyrromethanes via tripyrrenes) and the tetrapyrranes (from tripyrranes via tetrapyrrenes). Other routes to the relevant polypyrranes have all required acid-catalyzed condensations (4–7), and usually an element of symmetry (4) or the removal of carbobenzoxy groups (5, 6).

These reactions of **8** are typical pyrrole redistribution reactions. Although long indispensable in the rationalization of mishaps, such reactions have been useless in rational synthesis with one possible exception: the use of formylpyrroles as substitutes for formic acid (8).

Acknowledgement

The authors are grateful to the Deutsche Forschungsgemeinschaft for a stipendium supporting A.R.

1. A. H. Jackson, G. W. Kenner, and J. Wass. J. Chem. Soc. Perkin Trans. 1, 1475 (1972).
2. J. Ellis, A. H. Jackson, A. C. Jain, and G. W. Kenner. J. Chem. Soc. 1935 (1964).
3. H. Fischer and A. Kürzinger. Hoppe-Seyler's Z. Physiol. Chem. **196**, 213 (1931).
4. S. F. MacDonald, H. D. Mah, and M. F. Chen. Ann. N.Y. Acad. Sci. **244**, 396 (1975).
5. B. Frydman, R. B. Frydman, A. Valasenas, S. Levy, and G. Feinstein. Ann. N.Y. Acad. Sci. **244**, 371 (1975).
6. B. Franck and A. Rowold. Angew. Chem. Int. Ed. Engl. **14**, 423 (1975).
7. J. M. Osgerby, J. Pluscec, Y. C. Kim, F. Boyer, N. Stojanac, H. D. Mah, and S. F. MacDonald. Can. J. Chem. **50**, 2652 (1972).
8. J. S. Andrews, A. H. Corwin, and A. G. Sharp. J. Am. Chem. Soc. **72**, 491 (1950).

Canadian Journal of Chemistry

Published by
THE NATIONAL RESEARCH COUNCIL OF CANADA

Journal canadien de chimie

Publié par
LE CONSEIL NATIONAL DE RECHERCHES DU CANADA

Volume 55 Number 16 August 15, 1977

Volume 55 numéro 16 15 août 1977

N-Nitromethylphthalimide. A formyl anion equivalent[1]

FRANK G. COWHERD,[2] MARIE-CARMEN DORIA, EDVIGE GALEAZZI, AND JOSEPH M. MUCHOWSKI[3]

Research Laboratories, Syntex, S. A., Apartado Postal 10-820, Mexico 10, D.F.

Received July 27, 1976[4]

FRANK G. COWHERD, MARIE-CARMEN DORIA, EDVIGE GALEAZZI, and JOSEPH M. MUCHOWSKI. Can. J. Chem. **55**, 2919 (1977).

It is shown that the exclusive 1,4-addition of *N*-nitromethylphthalimide **4***a* to unhindered α,β-unsaturated ketones and esters can be effected by non-nucleophilic bases, such as sodium hydride or potassium fluoride, in dimethyl sulfoxide. The phthalimido moiety can be removed from the adducts with hydroxylamine or 1,2-dianilinoethane to give the oximes or diphenylimidazolidines of 1,4-ketoaldehydes. The ethylene ketal **5** of 3-formylcyclohexanone could easily be recovered from the imidazolidine **10**, but it was not possible to transform **11** into 3-formylcyclohexanone under similar conditions. It is further shown that reactions, such as the Knoevenagel condensation, or the Paal–Knorr synthesis of pyrroles, can be achieved directly on the adducts without the need for isolating the unstable 4-formyl carbonyl compounds. *N*-Nitromethylphthalimide thus serves as a new formyl anion equivalent.

FRANK G. COWHERD, MARIE-CARMEN DORIA, EDVIGE GALEAZZI et JOSEPH M. MUCHOWSKI. Can. J. Chem. **55**, 2919 (1977).

On démontre que l'addition-1,4 exclusive de la *N*-nitrométhylphtalimide **4***a* aux cétones et aux esters α,β-non-saturés non-empêchés peut être effectué par des bases non-nucléophiles telles que l'hydrure de sodium ou le fluorure de potassium dans le diméthylsylfoxyde. La portion phtalimido peut être enlevée des adduits avec l'hydroxylamine ou le dianilino-1,2 éthane pour conduire aux oximes ou aux diphénylimidazolidines de cétoaldéhydes-1,4. On peut récupérer facilement l'éthylène cétal **5** de la formyl-3 cyclohexanone à partir de l'imidazolidine **10** mais il n'est pas possible de transformer **11** en formyl-3 cyclohexanone dans de telles conditions. On montre de plus que des réactions, telles que la condensation de Knoevenagel ou la synthèse de Paal–Knorr des pyrroles, peuvent être réalisées sur les adduits sans qu'il soit nécessaire d'isoler les composés formyl-4 carbonylés instables. La *N*-nitrométhylphtalimide sert donc de nouvel équivalent de l'anion formyle.

[Traduit par le journal]

1,4-Diketones are compounds of immense synthetic importance and numerous useful procedures have been devised for the preparation of such substances (1–4, and refs. therein). A considerable number of 4-keto aldehyde syntheses (2, 3, 5–11, and refs. therein) have also been reported, but many of these are inconvenient and new practical syntheses of these useful intermediates are required. A conceptually very attractive route to the latter class of compounds is based on the conjugate addition of a formyl anion (4), or an equivalent thereof (2, 8–10), to an α,β-unsaturated carbonyl moiety. Nitromethane (9) and hydrogen cyanide (10), which historically are two of the oldest known formyl

[1]Contribution No. 473 from the Syntex Institute of Organic Chemistry.

[2]Syntex post-doctoral fellow, 1972–1973.

[3]Author to whom enquiries should be addressed.

[4]Revision received April 25, 1977.

anion equivalents, still remain the most versatile members of this group of reagents to be used for the synthesis of 4-keto aldehydes. An important characteristic of both of these reagents is that 1,4-addition to an α,β-unsaturated carbonyl system generally occurs in preference to 1,2-addition, even when the latter might be expected to be competitive (e.g., for nitromethane see ref. 12). To be useful, any new formyl anion equivalent should retain this desirable property, and in addition, the latent formyl group should be easily unmasked after the desired reaction has been effected. It was with these points in mind that a study of *N*-nitromethylphthalimide **1** as a formyl anion equivalent was undertaken.[5]

N-Nitromethylphthalimide has previously been prepared in 27% yield from the corresponding *N*-bromomethyl compound and silver nitrite in acetonitrile solution (13). The yield of this product was more than doubled when the reaction was effected with sodium nitrite in acetone solution (this work).

A convenient source of the nitro compound was thus at hand, and consequently a study was undertaken to determine the optimum conditions for the Michael addition of this substance (1 equiv.) to activated olefins (1 equiv.) such as cyclohexenone and methyl vinyl ketone. For these acceptors it was found that the 1,4-addition of **1** occurred most readily in dipolar aprotic solvents (preferably dimethyl sulfoxide) in the presence of weakly nucleophilic bases (1 equiv.) such as sodium hydride or potassium fluoride. These conditions (see Experimental section) were then applied to the preparative scale (5–100 mmol) reaction of **1** with various activated olefins **2**.

The data presented in Table 1 show that the addition of **1** to α,β-unsaturated ketones and esters occurred in satisfactory yields in those cases where the acceptor was unhindered. These yields are particularly notable in view of the fact that a 1:1 olefin–nitro compound ratio was utilized in all of the experiments. Non-cyclic β-substituted acceptors (e.g., benzalacetone and methyl crotonate) reacted rapidly with the anion of **1** to give an equilibrium mixture of the product and the reactants which was strongly in favour of the latter. The expected Michael adducts were isolable in low yields from the reaction mixtures, More highly substituted acceptors such as mesityl oxide, 1-acetylcyclohexene, neosterol, and neosterol acetate did not react at all with **1**, undoubtedly for steric reasons.

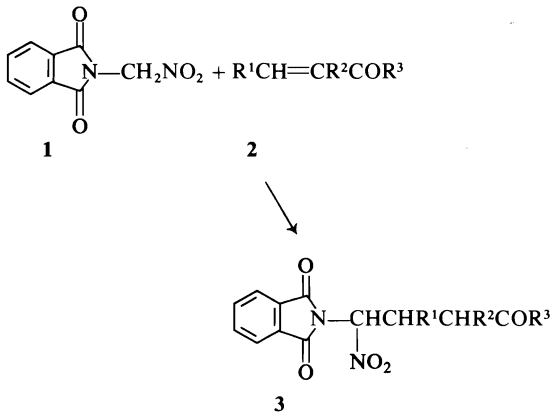

Whereas α,β-unsaturated ketones gave the best adduct yields when the anion of **1** was generated with sodium hydride, α,β-unsaturated esters and acrylonitrile, under the same conditions, gave complex mixtures which did not contain the desired products. The expected adducts were formed with α,β-unsaturated esters when the reaction was initiated with potassium fluoride, but no characterizable products were isolable when acrylonitrile was the acceptor, even though **1** was rapidly consumed. The addition of **1** to acrylonitrile was not examined further.

The adducts derived from the cyclic enones and the other β-substituted acceptors were obtained as mixtures of *threo* and *erythro* isomers. This was evident both from the broad melting points and the nmr spectra (see Table 3) of the crude products. For example, the nmr spectrum of the crude adduct from cyclohexenone showed a pair of doublets, of approximately equal intensity, centered at δ 6.24 and 6.25 (J = 10.6 and 8.4 Hz, respectively) for the proton α to the nitro group. In some cases (adducts from benzalacetone and methyl crotonate) one of the isomers could be obtained pure by fractional crystallization, and in one instance (ethylene ketal of adduct from cyclohexenone), both isomers were isolated in pure form by this technique. The resolution of these mixtures is, of course, unimportant because the centre of asymmetry which was created during the formation of the adducts is destined for destruction when the formyl group is unmasked.

[5]Presented in part at the 57th Canadian Chemical Conference of the Chemical Institute of Canada, Regina, Saskatchewan, June 1974.

TABLE 1. Addition of *N*-nitromethylphthalimide to activated olefins[a]

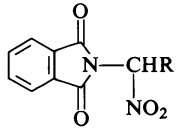

R	Base	Reaction time (h)	Yield (%)	mp (°C)	Cryst. solvent	Calcd.			Found		
						C	H	N	C	H	N
$CH_2CH_2COCH_3$	NaH	1	43–63	108–109[b]	Benzene–hexane	56.52	4.38	10.14	56.58	4.45	10.19
$(CH_2)_2CO(CH_2)_5CH_3$	NaH	1	15–28[c]	49–51	Hexane	62.41	6.40	8.09	62.50	6.22	8.14
$C_6H_5CHCH_2COCH_3$ |	NaH	48[d]	7–8	149–151[e]	Ether	64.76	4.57	7.95	64.42	4.64	7.90
	NaH	1	47–68	96.5–102.5	Hexane–ether	58.23	4.20	9.72	58.27	4.47	9.45
	NaH	1	50–67	138.5–168	Benzene–hexane	59.60	4.67	9.27	59.75	4.56	9.12
$CH_2CH_2CO_2CH_3$	KF	2.5	43–64	139.5–141.5	Hexane	53.43	4.14	9.59	53.34	4.25	9.60
$CH_3CHCH_2CO_2CH_3$ |	KF	72[d]	14	151–152[f]	Hexane	54.89	4.60	9.14	54.78	4.70	9.16

[a]All reactions were carried out at room temperature.
[b]The crude product had mp 100.5–103.5°C.
[c]The low yield is a reflection of the poor quality of the enone (purity ≤40%).
[d]The reaction rapidly reached a steady state and did not progress further during the time indicated.
[e]The mp of the isomer obtained by fractional crystallization of the crude (mp 132–151°C) product.
[f]The mp of the isomer obtained after purification by thin layer chromatography on silica gel and crystallization.

TABLE 2. Ethylene ketals of adducts from enones and **1**

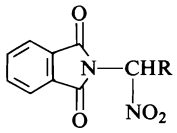

R	mp (°C)[a]	Cryst. solvent	Calcd. C	Calcd. H	Calcd. N	Found C	Found H	Found N
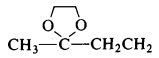	121–123	Acetone	56.24	5.03	8.74	56.11	5.00	8.73
	127–128.5	Hexane	58.95	5.24	8.09	58.87	5.32	8.16
	151–152	Ether	58.95	5.24	8.09	58.73	5.28	8.13
	151–153[b]	Ether	57.83	4.85	8.43	57.94	4.97	8.41

[a]The yields of the ketals were quantitative.
[b]The mp of the isomer obtained by fractional crystallization of the crude product.

Phthalimido protecting groups can be removed under basic or acidic conditions (14), but since the latter are generally very vigorous the use thereof was not considered feasible for the deprotection of the compounds described herein. In order to avoid the problems potentially associated with the use of basic reagents such as methylamine (pyrrole formation) or alkaline carbonates (internal aldolization), the enone adducts were converted into the corresponding ethylene ketals (Table 2) for the initial deprotection studies. The ketalized adduct **4***a* reacted rapidly with aqueous methanolic potassium carbonate at room temperature, boiling aqueous methanolic potassium bicarbonate, or aqueous methylamine (15) at room temperature, but in no case was the desired aldehyde **5** isolated after work-up, presumably because of the instability (e.g., aldolization) of this substance under the basic conditions of these reactions. Compound **4***a* was therefore subjected to the action of alkaline sodium borohydride with the expectation that the liberated aldehyde would be reduced before self condensation could occur. A mixture of products was then obtained, but the alcohol **6** was not present therein. The spectral properties and the elemental analysis of the major component of the mixture were fully consistent with the carbinolamide **7***a*. The yield of this compound was considerably improved when the reduction was effected in the absence of external alkali. This substance was considered to have been formed by the reduction of the very reactive acyl imine **9**, the intermediate occurrence of which is readily explicable by the loss of the elements of nitrous acid from the primary reduction product **8***a*. The above observations suggested that the removal of the phthalimido group might be achieved by the inclusion of a weakly basic,

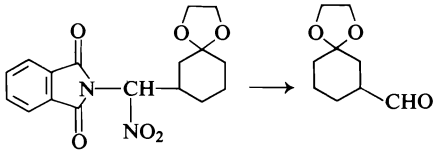

4*a* **5**

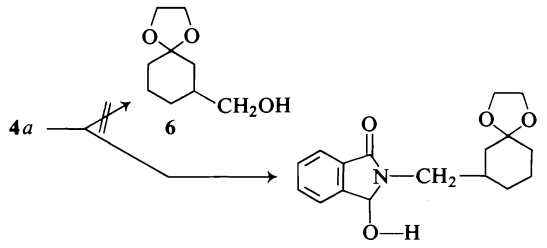

4*a* **6** **7***a*

TABLE 3. Spectral properties of the activated olefin–*N*-nitromethylphthalimide adducts and the corresponding ethylene ketals

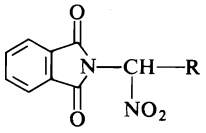

R	Infrared (cm^{-1})	Nuclear magnetic resonance δ (ppm)[a]
$CH_2CH_2COCH_3$	1794, 1742, 1727 sh, 1573	2.17 (s, 3H), 2.53–3.18 (m, 4H), 6.17 (q, 1H, J = 8.2, 8.6 Hz), 7.82 (m, 4H)
$(CH_2)_2CO(CH_2)_5CH_3$	1797, 1742, 1725 sh, 1572	0.83 (m, 3H), 1.22 (m, 8H), 2.17–3.15 (m, 6H), 6.17 (t, 3H, J = 8.2 Hz), 7.78 (m, 4H)
$CHC_6H_5CH_2COCH_3$	1793, 1740, 1570	2.07 (s, 3H), 3.12–3.29 (m, 2H), 4.97 (m, 1H), 6.52 (d, 1H, J = 10.4 Hz), 7.16 (m, 5H), 7.70 (m, 4H)
$CH_2CH_2CO_2CH_3$	1743, 1615, 1568	3.02–3.59 (m, 4H), 3.13 (s, 3H), 6.06 (t, 1H, J = 7.2 Hz), 7.55 (m, 4H)
$CHCH_3CH_2CO_2CH_3$	1742, 1568	1.30 (d, 3H, J = 7.2 Hz), 3.25 (s, 3H), 6.22 (d, 1H, J = 7.8 Hz), 7.57 (m, 4H)
	1793, 1740, 1572	1.67–2.87 (m, 6H), 3.84 (m, 1H), 6.02, 6.05 (d's, total 1H, J = 9.0, 9.6 Hz), 7.84 (m, 4H)
	1793, 1735, 1712, 1567	1.67–2.67 (m, 8H),[b] 3.50 (m, 1H), 6.24, 6.25 (d's, total 1H, J = 10.6, 8.4 Hz), 7.93 (s, 4H)
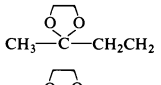	1793, 1738, 1571	1.48 (s, 3H), 1.77 (q, 2H, ΣJ = 6.4 Hz), 2.68–3.05 (m, 2H), 3.92 (s, 4H), 6.18 (t, 1H, J = 7.8 Hz), 7.82 (m, 4H)
	1790, 1738, 1568	1.35–2.47 (m, 6H), 3.70 (m, 1H), 3.80 (s, 4H), 5.95 (d, 1H, J = 10.6 Hz), 7.82 (m, 4H)
	1793, 1740, 1570[c]	1.15–2.20 (m, 8H), 3.45 (m, 1H), 3.87 (m, 4H), 6.05 (d, 1H, J = 11.6 Hz), 7.83 (m, 4H)
	1793, 1740, 1570[d]	1.07–2.27 (m, 8H), 3.45 (m, 1H), 3.92 (s, 4H), 6.02 (d, 1H, J = 9.6 Hz), 7.78 (m, 4H)

[a]Recorded in deuterochloroform unless specified otherwise.
[b]Measured in perdeuteroacetone.
[c]Isomer with mp 127–128.5°C.
[d]Isomer with mp 151–152°C.

nucleophilic, aldehyde trapping agent, such as the Wanzlick base (16; dianilinoethane), in the hydrolytic medium. This supposition was confirmed by the rapid formation of the imidazolidine derivative **10** when an aqueous methanolic solution of **4*a*** (1 mol), dianilinoethane (1.5 mol), and potassium carbonate (1.1 mol) was stirred at room temperature. The application of these conditions to the other adducts gave the corresponding imidazolidine derivatives (Table 4) in acceptable yields. Even sodium bicarbonate (at reflux temperature) could be used for the transformation, but dianilinoethane alone did not effect the cleavage of the phthalimido compounds.

The aldehyde **5** was easily recovered in good yield by treatment of **10** with 2 equiv. of *p*-toluenesulfonic acid monohydrate in dichloromethane–acetone (1:1) solution at 10°C. Decomposition of the imidazolidine **11** under the same conditions did not give a trace of the 4-ketoaldehyde **12**, even though the bis-toluenesulfonic acid salt of dianilinoethane was formed in high yield. The results were similar when the decomposition of **11** was effected at −30°C. The failure to isolate **12** under such mild conditions prob-

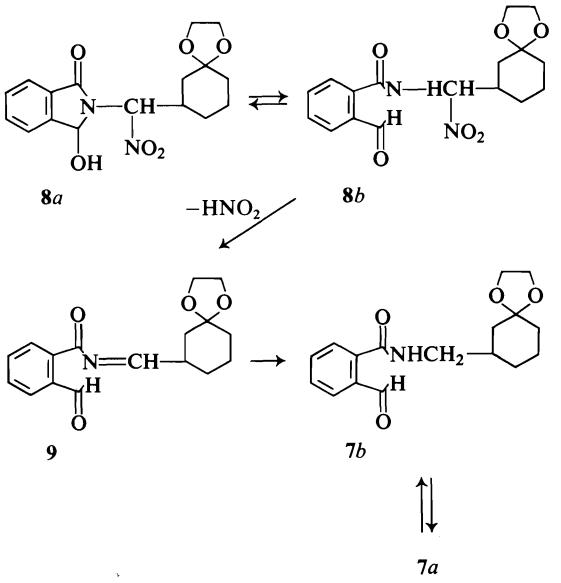

ably is a reflection of the known[6] instability of this type of 1,4-dicarbonyl compound.

Hydroxylamine could also be used to remove the phthalimido moiety from the adducts. For

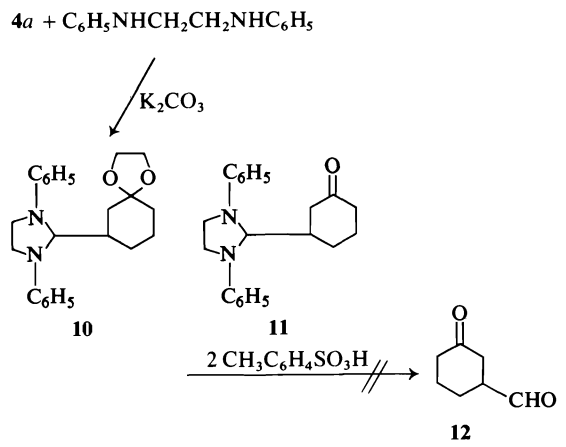

example, the oximes **13***a* and **13***b* were readily formed from **4***a* and **4***b*, and a method was devised whereby these oximes were transformed into the stable primary alcohols **14***a* and **14***b* without isolation of the intermediate aldehydes. This was accomplished by the addition of the oxime bisulfite adducts (17) to aqueous sodium carbonate containing sodium borohydride, the aldehydes thus being reduced immediately upon liberation from the bisulfite addition products.

[6]Professor B. Fraser-Reid (personal communication), University of Waterloo, also has observed that 1,4-keto-aldehydes are exceedingly unstable substances.

The alcohols (43–66% overall from the oximes) were characterized as the crystalline 4-nitrophenylazobenzoates **15** (18).

The intermediacy of the acyl imines implied

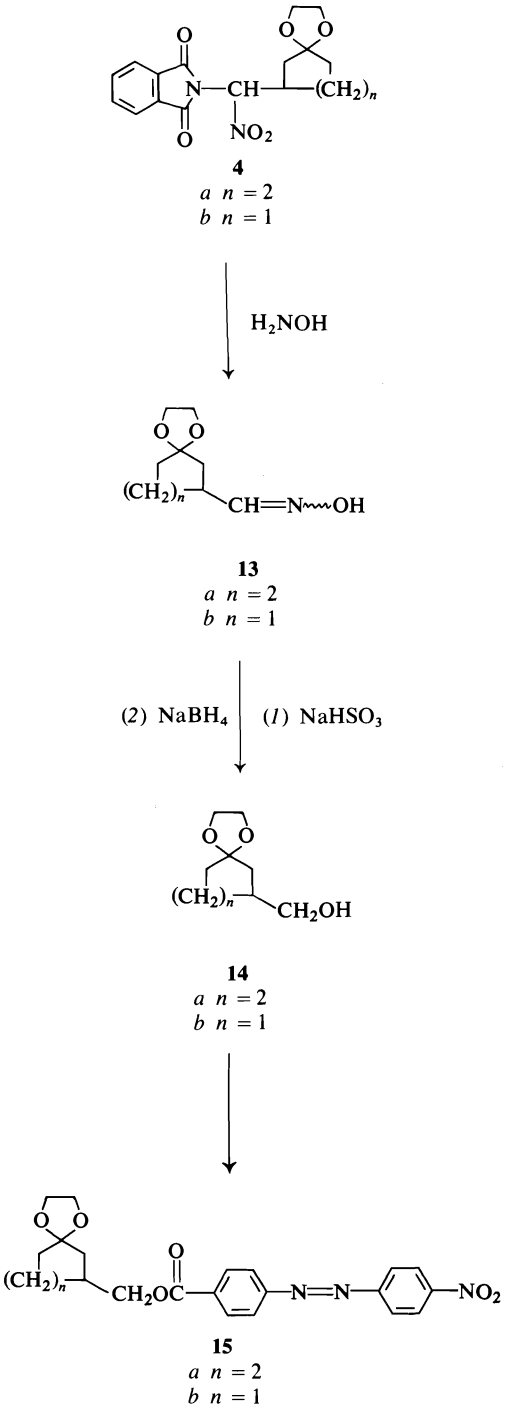

TABLE 4. 1,3-Diphenylimidazolidine derivatives of some 4-ketoaldehydes and derivatives thereof

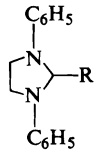

R	Base	Time (h)	Yield (%)	mp (°C)	Cryst. solvent	Calcd. C	Calcd. H	Calcd. N	Found C	Found H	Found N
$CH_2CH_2COCH_3$	K_2CO_3	5	79	137.5–138.5	Ether	77.52	7.53	9.52	77.39	7.62	9.56
	$NaHCO_3$	0.75	72								
	K_2CO_3	8	49	89.5–91.5	Ether	78.44	7.24	9.14	78.43	7.30	9.12
	$NaHCO_3$	0.75	58								
	K_2CO_3	5	60	123–124	Hexane	75.40	7.48	7.99	75.61	7.60	7.95
	$NaHCO_3$	0.75	60								
	K_2CO_3	18	49	119–121	Hexane–dichloromethane	78.71	7.55	8.74	78.69	7.65	8.74
	$NaHCO_3$	0.75	50								
	K_2CO_3	3.5	65	160–162	Ether	79.79	7.74	7.69	75.71	7.83	7.71
	$NaHCO_3$	0.75	41								

that for some reactions the isolation of the aldehyde would be unnecessary. This was confirmed by the direct formation of 1-phenyl-2-methylpyrrole **17** from the adduct **16** and aniline in the presence of sodium bicarbonate. Furthermore, it

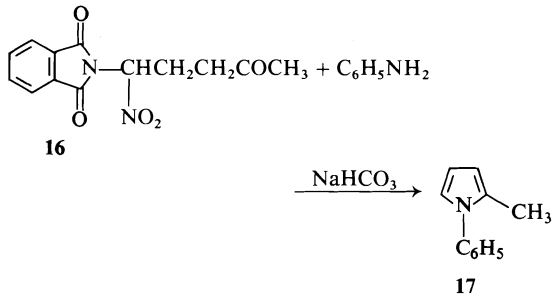

was possible to effect a Knoevenagel type condensation (19) of diethyl malonate with ***4a*** in the presence of sodium ethoxide. A mixture, which consisted of the expected unsaturated ester **18** and the Michael adduct **19** thereof with diethyl malonate, was obtained. The structures of the components of this mixture were assured by transformation into a single unsaturated ester **20** with sodium chloride in hot dimethyl sulfoxide (20). A Knoevenagel condensation of **21** with diethyl malonate gave a mixture of **22** and **23** analogous to that described above.

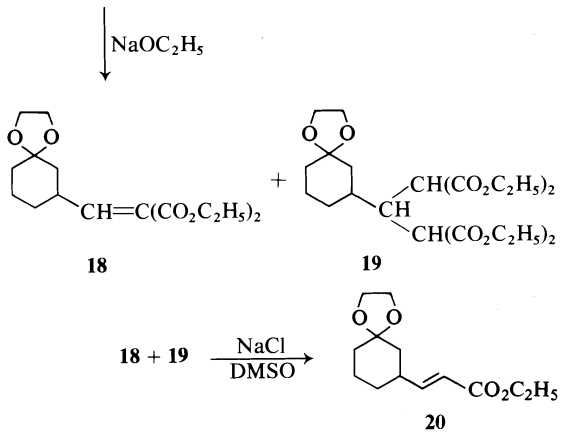

In summary, it has been shown that *N*-nitromethylphthalimide can be used as a formyl anion equivalent, but that the utility thereof is severely limited by the fact that 1,4-addition is successful only to those activated olefins which are unhindered. Nevertheless, the information described herein can be used as a basis upon

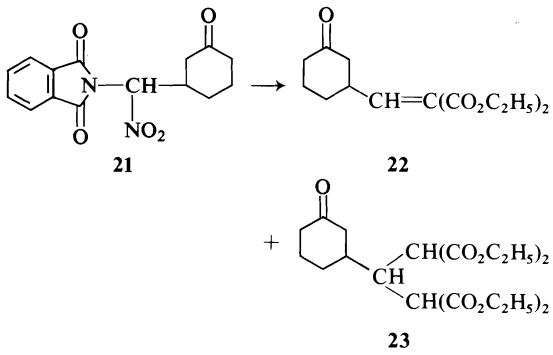

which the design of new formyl anion equivalents, devoid of the above limitation, can be commenced.

Experimental

The melting points were determined in a Mel-Temp melting point apparatus and are corrected. The ir spectra were measured with a Perkin-Elmer model 237 grating infrared spectrophotometer. The uv spectra were recorded with a Perkin-Elmer 402 uv spectrophotometer as solutions in methanol. The nmr spectra were measured with a Varian T-60 spectrometer. The mass spectrum was measured with an Atlas CH-4 spectrometer.

All of the activated olefins except *n*-hexyl vinyl ketone were purchased from commercial sources. The above mentioned unsaturated ketone was prepared from *n*-heptanoic acid and vinyl lithium (21) and was used without purification.

N-Nitromethylphthalimide ***2***

Sodium nitrite (12.5 g, 0.181 mol) was added at 0°C with stirring to a solution of *N*-bromomethylphthalimide (22) (25.0 g, 0.104 mol) in acetone (250 ml). After 0.5 h at this temperature, the reaction was left at room temperature for 1.5 h and then it was poured into water (500 ml). The product was extracted with ether (5 × 100 ml) and the extract was evaporated *in vacuo*. Benzene was added to the residue and the resultant was evaporated *in vacuo* (to remove water). The residue was purified by column chromatography on silica gel using 2.5% ether in benzene as the eluant. The product thus obtained (12.5 g, 58%) had mp 108–110°C (lit. (13) mp 110.5–111°C) after crystallization from benzene–hexane; λ_{max} 218, 237, 293.5 nm (ε 45 700, 9560, 2900); ν_{max} ($CHCl_3$) 1790, 1740, 1580, 1370 cm^{-1}; δ ($CDCl_3$) 6.10 (s, 2H), 8.07 (s, 4H). *Anal.* calcd. for $C_9H_6N_2O_4$: C 52.43, H 2.93, N 13.59; found: C 52.29, H 2.98, N 13.61.

Reaction of N-Nitromethylphthalimide with Activated Olefins

(a) Sodium Hydride as the Base

To a stirred mixture of sodium hydride (10 mmol; from a 50% suspension in mineral oil which had been washed with dry hexane) and anhydrous dimethyl sulfoxide (50 ml), maintained in an atmosphere of dry nitrogen, was added *N*-nitromethylphthalimide (9.7 mmol). After 1 h at room temperature gas evolution had ceased and the solution was cooled to 18°C. The α,β-unsaturated ketone (9.8 mmol) was added in one portion (exotherm

in some cases) and the solution was then left at room temperature until the reaction no longer advanced or the starting nitro compound was absent (see Table 1), as judged by thin layer chromatography (tlc) on silica gel. The solution was poured into a large excess of 10% hydrochloric acid and the product was extracted into ethyl acetate. The extract was washed with water until neutrality was achieved, it was dried over sodium sulfate, and then evaporated *in vacuo*. The adducts derived from cyclohexenone, cyclopentenone, and methyl vinyl ketone were purified by column chromatography on Fluorisil using benzene–ether (5:1) as the eluant. The adducts from benzal acetone and *n*-heptyl vinyl ketone were obtained pure by tlc on silica gel using hexane–ether (1:1) as the developing solvent. The yields and physical constants of these compounds are recorded in Tables 1 and 3.

(b) Potassium Fluoride as the Base

To a stirred solution of potassium fluoride (5.5 mmol, dried *in vacuo* at 60°C for 24 h) in dry dimethyl sulfoxide (30 ml), maintained in an atmosphere of nitrogen, was added the nitro compound (5.0 mmol) and then the α,β-unsaturated ester (5.5 mmol). The reactions were followed and worked-up as described for sodium hydride as the base. The methyl acrylate adduct was purified by column chromatography on Fluorisil using benzene as the eluant. The product from methyl crotonate was obtained pure by tlc on silica gel using benzene–ether (80:20) as the developing solvent. The yields and physical constants of the adducts are recorded in Tables 1 and 3.

Preparation of the Ketals

The adduct (5 g), ethylene glycol (10 ml), and *p*-toluenesulfonic acid (0.125 g) were heated in benzene solution at reflux temperature for 1–3 h. The water evolved was collected in a Dean–Stark apparatus. The solution was left to cool, pyridine (2.0 ml) was added, and the solution was washed successively with water, 10% hydrochloric acid solution, and water. The solution was dried over sodium sulfate and the solvent was removed *in vacuo*. The residue was crystallized from a suitable solvent. The ketal of the adduct from cyclohexenone **4***a* was separated into two isomers by crystallization first from ether. The substance which separated from solution was recrystallized from the same solvent to give an isomer with mp 151–152°C. The mother liquors from these crystallizations were evaporated *in vacuo* and the residue was crystallized from hexane to give the isomer with mp 127–128.5°C. The physical constants of these compounds are recorded in Tables 2 and 3.

*Reduction of **4***a* with Sodium Borohydride*

To a stirred solution of the ketal **4***a* (1.038 g, 3.0 mmol) in dry tetrahydrofuran (60 ml) was added sodium borohydride (0.150 g, 4 mmol). After 6 h at room temperature the mixture was poured into water and the products were extracted into ethyl acetate. The extract was washed with water, dried over sodium sulfate, and evaporated *in vacuo*. The residue (0.910 g) was separated by tlc (hexane – ethyl acetate; 1:1) into a less and a more polar fraction. The more polar fraction (**7***a*, 0.370 g) was crystallized from ether to give a solid mp 142–145°C. This material had λ_{max} 220, 228, 250 nm (ε 9120, 6620, 4370); ν_{max} 3585, 3340, 1690, 1622 cm^{-1}; δ ($CDCl_3$) 0.5–2.40 (m, 8H; H-2,4,5,6 of cyclohexane), 2.87–3.33 (m, 3H; H-3 of cyclohexane and N-CH_2), 3.80 (m, 4H; OCH_2CH_2O), 4.42 (d, 1H, J = 11.3 Hz, OH, exchanged with D_2O), 5.72 (d, 1H, J = 11.3 Hz, *CH*-OH, singlet with D_2O), 7.50 (m, 4H; aromatic H's). *Anal.* calcd. for $C_{17}H_{21}NO_4$: C 67.31, H 6.98, N 4.62; found: C 67.39, H 7.05, N 4.73.

Synthesis of the Diphenylimidazolidine Derivatives

(a) Potassium Carbonate as the Base

A solution of the nitro compound (1 mmol), dianilinoethane (1.5 mmol), and potassium carbonate (1.1 mmol) in methanol (25 ml) and water (5 ml) was stirred at room temperature for the time specified in Table 4. The imidazolidine derivative which had separated from solution was collected by filtration, washed with water, dried, and then crystallized from a suitable solvent. The yields and physical constants of these compounds are given in Table 4.

(b) Sodium Bicarbonate as the Base

A solution of the nitro compound (1 mmol), dianilinoethane (1.5 mmol), and sodium bicarbonate (1.1 mmol) in methanol (25 ml) and water (5 ml) was boiled under reflux for 45 min. The solution was cooled and the crystalline product was separated by filtration.

*Synthesis of the Aldehyde **5** by Decomposition of the Imidazolidine **10***[7]

To a solution of the imidazolidine **10** (1.00 g, 2.5 mmol) in 1:1 dichloromethane–acetone (100 ml), cooled to 10°C, was added *p*-toluenesulfonic acid monohydrate (1.06 g, 5.6 mmol). After 7 min the precipitated solid was removed by filtration, it was washed with dichloromethane (20 ml), and the combined filtrates were evaporated *in vacuo*. Ether was added to the residue, the resultant was washed with dilute sodium bicarbonate solution and then with water. The organic phase was dried over sodium sulfate, and evaporated *in vacuo*. The residual oil was purified by tlc on silica gel using ether–hexane (70:30) as the developing solvent. The oily aldehyde (0.32 g, 69%) was distilled *in vacuo* at 86–88°C/0.05 Torr; ν_{max} ($CHCl_3$) 2720, 1715 cm^{-1}; δ ($CDCl_3$) 1.20–2.12 (m, 8H; H-2,4,5,6), 2.48 (m, 1H; H-3), 3.80 (s, 4H; OCH_2CH_2O), 9.54 (s, 1H; CHO); ms (relative intensity) 170(1), 142(7), 141(33), 113(7), 99(29), 86(7), 73(100), 55(11), 45(19), 41(15). Even though this substance appeared to be pure by tlc and nmr a satisfactory microanalysis could not be obtained. *Anal.* calcd. for $C_9H_{14}O_3$: C 63.50, H 8.28; found: C 62.73, H 8.10. The identity of this substance nevertheless was assured by sodium borohydride reduction to the alcohol **14***a* (88%) which was converted into the crystalline 4-(4-nitro)phenylazo benzoate **15***a* (80%) described below.

*Conversion of **4***a* and **4***b* into the Alcohols **14***a* and **14***b*

*(a) Synthesis of the Oximes **13***a* and **13***b*

A solution of **4***a* (1.384 g, 4 mmol) in methanol (75 ml) and water (15 ml) containing hydroxylamine hydrochloride (0.562 g, 8.1 mmol) and potassium carbonate (1.133 g, 8.2 mmol) was boiled under reflux for 2 h. The solution was concentrated to a small volume *in vacuo*, ethyl acetate was added, and the resultant was washed with water. The organic phase was dried over sodium sulfate and evaporated *in vacuo*. The residue was purified by tlc on silica gel using benzene–ether (75:25) as the developing solvent. The oxime was obtained as an oily mixture of *syn* and *anti*

[7]We thank Dr. G. Jones for providing us with these experimental details.

isomers **13***a* in 70–100% yield; ν_{max} ($CHCl_3$) 3605, 3350, 1660 cm^{-1}; δ ($CDCl_3$) 1.12–2.00 (m, 8H; H-2,4,5,6), 2.50 (m, 1H; H-3), 3.90 (s, 4H; OCH_2CH_2O), 6.52, 7.31 (d's, total 1H, J = 6.8 and 5.4 Hz, respectively; CH=N), 8.31 (m, 1H, W_H = 24 Hz; N-OH). *Anal.* calcd. for $C_9H_{15}NO_3$: C 58.36, H 8.16, N 7.56; found: C 58.24, H 8.20, N 7.37.

Compound **4***b* was transformed into the oxime mixture **13***b* in 57% yield in the manner described for **4***a*. This material was used directly in the next step.

*(b) Synthesis of the Alcohols **14***a and **14***b*

A solution of the oxime (1.3 mmol) and sodium bisulfite (1.8 mmol) in 50% aqueous ethanol (20 ml) was boiled under reflux for 2 h. The solvent was evaporated *in vacuo* and the residue was dissolved in methanol (10 ml). This methanol solution was added slowly to a stirred solution of sodium borohydride (3 mmol) and sodium carbonate (1.2 mmol) in water (2 ml). After 1.5 h at room temperature, the solution was poured into a saturated sodium chloride solution and the product was extracted into ethyl acetate. The extract was washed with water, dried over sodium sulfate, and evaporated *in vacuo*.

The alcohol **14***a* was obtained in 43–65% yield; ν_{max} ($CHCl_3$) 3640, 3490 cm^{-1}; δ ($CDCl_3$) 0.68–2.00 (m, 10H, H-2,3,4,5,6, OH), 3.46 (d, 2H, J = 5.4 Hz; CH_2-OH), 3.89 (s, 4H; OCH_2CH_2O). This alcohol was converted into the crystalline 4-(4-nitro)phenylazo benzoate **15***a* for analysis in the manner described below.

The alcohol **14***b* was prepared in 57% yield; ν_{max} ($CHCl_3$) 3635, 3480 cm^{-1}; δ ($CDCl_3$) 1.08–2.92 (m, 7H; H-2,3,4,5), 2.17 (s, 1H; OH, exchanged with D_2O), 3.52 (d, 2H, J = 5.6 Hz; CH_2OH), 3.87 (s, 4H; OCH_2CH_2O). This alcohol was converted into the 4-(4-nitro)phenylazo benzoate **15***b* for analysis.

*(c) Synthesis of the 4-(4-Nitro)phenylazo Benzoates **15***a and **15***b*

To a stirred solution of the alcohol (1.0 mmol) in dry benzene (50 ml) containing pyridine (2.0 mmol) was added 4-(4-nitro)phenylazo benzoyl chloride (1.0 mmol). After 1.5 h at room temperature the solvent was removed *in vacuo*, the residue was taken up in benzene and passed through a short column of alumina (Fluka, neutral, Activity I). Evaporation of the solvent gave a red solid which was crystallized from a suitable solvent.

The ester **15***a* had mp 129–131°C after crystallization from hexane; λ_{max} 329.5 nm (ε 30 200); ν_{max} 1719, 1610, 1527, 1346 cm^{-1}; δ ($CDCl_3$) 0.75–2.52 (m, 9H; H-2,3,4,5,6), 3.93 (s, 4H; OCH_2CH_2O), 4.22 (d, 2H, J = 5.6 Hz; CH_2), 7.48–8.40 (m, 8H; aromatic H's). *Anal.* calcd. for $C_{22}H_{23}N_3O_6$: C 62.10, H 5.44, N 9.87; found: C 62.28, H 5.41, N 9.86.

The ester **15***b* had mp 130–133°C after crystallization from hexane; λ_{max} 329 nm (ε 30 200); ν_{max} ($CHCl_3$) 1720, 1610, 1528, 1346 cm^{-1}; δ ($CDCl_3$) 1.48–2.78 (m, 7H; H-2,3,4,5), 3.89 (s, 4H; OCH_2CH_2O), 4.27 (d, 2H, J = 6.4 Hz; CH_2), 7.84–8.40 (m, 8H; aromatic H's). *Anal.* calcd. for $C_{21}H_{21}N_3O_6$: C 61.30, H 5.14, N 10.21; found: C 60.99, H 5.26, N 10.67.

*1-Phenyl-2-methylpyrrole **17***

A solution of the adduct from methyl vinyl ketone **16** (4.45 g, 16.0 mmol) in methanol (400 ml) and water (80 ml) containing aniline (2.22 ml, 24.0 mmol) and sodium bicarbonate (1.47 g, 17.0 mmol) was boiled under reflux in an atmosphere of nitrogen for 30 min. The solution was concentrated to a small volume *in vacuo* and the residue was diluted with 10% hydrochloric acid. The product was extracted into ethyl acetate and the extract was washed with water and dried over sodium sulfate. The solvent was removed *in vacuo* and benzene was added to the residue. The mixture was filtered to remove phthalimide, silica gel was added to the residue, and the mixture was evaporated to dryness *in vacuo*. This solid was placed on top of a column of silica gel (250 g) and the column was developed with hexane (500 ml) and hexane–benzene (95:5, 750 ml). The product (0.500 g, 19.8%) was found in the hexane–benzene eluate; λ_{max} 241 nm (ε 9330); δ ($CDCl_3$) 2.17 (s, 3H; CH_3), 5.97 (m, 1H; H-3), 6.08 (t, 1H, ΣJ = 3.5 Hz; H-4), 6.64 (m, 1H; H-4), 7.24 (m, 5H; phenyl H's). This compound had previously been prepared by Yurev and Minkina (23).

*Reaction of **4***a with Diethyl Malonate*

To a stirred solution of sodium ethoxide (prepared from 50% sodium hydride in mineral oil (0.610 g, 12.7 mmol)) in absolute ethanol (50 ml) was added diethyl malonate (2.02 g, 12.7 mmol) and then the adduct **4***a* (2.2 g, 6.35 mmol). After 3 h at room temperature the solvent was removed *in vacuo*, water was added to the residue, and the mixture was extracted with ethyl acetate. The extract was washed with water, dried over sodium sulfate, and evaporated *in vacuo*. Benzene was added to the residue, the phthalimide was filtered off, and the solvent was evaporated *in vacuo*. The residual oil was chromatographed on a column of Fluorisil (200 g). The column was first eluted with benzene (200 ml) and then the product was removed with benzene–ether (1:1). The product (1.90 g) was then evaporatively distilled at 100°C/0.02 Torr. This oil was a 1:3 mixture of **18** and **19**. The separation of these esters was achieved by tlc on silica gel using hexane – ethyl acetate (85:15) as the developing solvent. In this way, samples of **18** and **19** of about 90% purity were obtained.

Compound **18** had the following spectral characteristics: λ_{max} 214 nm (ε 7220); ν_{max} ($CHCl_3$) 1733 cm^{-1}; δ ($CDCl_3$) 1.27 (m, 6H; ester CH_3's), 1.65 (m, 8H; ring CH_2's), 3.55 (m, 1H; allylic CH), 3.89 (s, 4H; OCH_2CH_2O), 4.22 (m, 4H; ester CH_2's), 6.68 (d, 1H, J = 10 Hz; olefinic CH). This material was not characterized further.

Compound **19** had the following spectral properties: ν_{max} ($CHCl_3$) 1757, 1734 cm^{-1}; δ ($CDCl_3$) 1.25 (m, 12H; ester CH_3's), 1.77 (m, 8H; ring CH_2's), 3.02 (m, 2H; —CH—CH—), 3.73 (m, 2H; CH-α-to ester), 3.85 (s, 4H; OCH_2CH_2-O), 4.14 (m, 8H; ester CH_2's). This ester was not characterized further.

*Preparation of the Unsaturated Ester **20***

A solution of the mixture of **18** and **19** (0.47 g) in dimethyl sulfoxide (10 ml) containing sodium chloride (0.064 g) and water (0.036 g) was heated at 150–170°C for 5 h. The solution was poured into water and the product was extracted into ethyl acetate. The extract was washed with saturated sodium chloride solution, dried over sodium sulfate, and evaporated *in vacuo*. The residue (0.280 g) was purified by tlc on silica gel using hexane – ethyl acetate (75:25) as the developing solvent. The oil (0.080 g) thus obtained was evaporatively distilled at

85°C/0.02 Torr to give an oil with λ_{max} 214 nm (ε 12 300); ν_{max} ($CHCl_3$) 1711, 1652, 972 cm^{-1}; δ ($CDCl_3$) 1.28 (t, 3H, J = 7.2 Hz; CH_3), 1.68 (m, 8H; ring CH_2's), 2.43 (m, 1H allylic CH), 3.92 (s, 4H; OCH_2CH_2O), 4.15 (q, 2H, J = 7.2 Hz; ester CH_2's), 5.72 (q, 1H, J = 1.3; O ‖ 16.0 Hz; =CH—C—), 6.84 (q, 1H, J = 16.0, 6.6 Hz; —CH—*CH*=). *Anal.* calcd. for $C_{13}H_{20}O_4$: C 64.98, H 8.39; found: C 65.11, H 8.49.

*Reaction of **4c** with Diethyl Malonate*

This reaction was carried out in the same manner as described for **4a**. The crude product was separated into its components by tlc on silica gel (benzene–ether; 4:1). The bis adduct **22** was purified (15–22% yield) further by tlc on silica gel (hexane – ethyl acetate; 3:1); ν_{max} ($CHCl_3$) 1731 cm^{-1}; δ ($CDCl_3$) 1.27 (t, 12H, J = 7.4 Hz; CH_3's), 2.12 (m, 9H; ring H's), 3.00 (m, 1H; CH), 3.73 O ‖ (d, 2H, J = 5.8 Hz); CH—C), 4.16 (q, 8H, J = 7.4 Hz; ester CH_2's). *Anal.* calcd. for $C_{21}H_{32}O_2$: C 58.86, H 7.52; found: C 58.85, H 7.69.

1. G. Rio and A. Lecas-Nawrocka. Bull. Soc. Chim. Fr. 317 (1976).
2. T. Mukaiyama, K. Narasaka, and M. Furusato. J. Am. Chem. Soc. **94**, 8641 (1972).
3. K. Oshima, H. Yamamoto, and H. Nozaki. J. Am. Chem. Soc. **95**, 4446 (1973).
4. H. Stetter and H. Kuhlmann. Tetrahedron Lett. 4505 (1974).
5. (*a*) J. L. Herrmann, G. R. Kieczykowski, R. F. Romanet, P. J. Wepplo, and R. H. Schlessinger. Tetrahedron Lett. 4711 (1973); (*b*) J. L. Herrmann, G. R. Kieczykowski, R. F. Romanet, and R. H. Schlessinger. Tetrahedron Lett. 4715 (1973).
6. B. M. Trost and M. Preckel. J. Am. Chem. Soc. **95**, 7862 (1973).
7. K. U. Acholonu and D. K. Wedegaertner. Tetrahedron Lett. 3253 (1974).
8. D. Seebach and R. Bürstinghaus. Angew. Chem. Int. Ed. Engl. **14**, 57 (1975).
9. H. Schecter and F. T. Williams. J. Org. Chem. **27**, 3699 (1962); F. S. Alvarez and D. Wren. Tetrahedron Lett. 569 (1973).
10. M. P. L. Caton, E. C. J. Coffee, and G. L. Watkins. Tetrahedron Lett. 773 (1972).
11. J. C. Stowell. J. Org. Chem. **41**, 560 (1976).
12. E. D. Bergmann, D. Ginsburg, and R. Pappo. Organic reactions. Vol. 10. John Wiley and Sons, Inc., New York, NY. 1959. p. 179.
13. L. W. Kissinger and H. E. Ungnade. J. Org. Chem. **23**, 815 (1958).
14. M. S. Gibson and R. W. Bradshaw. Angew. Chem. Int. Ed. Engl. **7**, 919 (1968).
15. S. Wolfe and S. K. Hasan. Can. J. Chem. **48**, 3572 (1970).
16. H. W. Wanzlick and W. Löchel. Chem. Ber. **86**, 1463 (1953).
17. S. H. Pines, J. M. Chemerda, and M. A. Kozlowski. J. Org. Chem. **31**, 3446 (1966).
18. W. H. Nutting, R. A. Jewell, and H. Rapoport. J. Org. Chem. **35**, 505 (1970).
19. G. Jones. Organic reactions. Vol. 15. John Wiley and Sons, Inc. New York, NY. 1967. p. 204.
20. A. P. Krapcho and A. J. Lovey. Tetrahedron Lett. 957 (1973).
21. J. C. Floyd. Tetrahedron Lett. 2877 (1974).
22. O. Mancera and O. Lemberger. J. Org. Chem. **15**, 1253 (1950).
23. Y. K. Yurev and G. A. Minkina. J. Gen. Chem. USSR, **8**, 116 (1937); Chem. Abstr. **32**, 5399 (1938).

Studies in the usnic acid series. VIII.[1] The biodegradation of (+)-usnic acid by *Mortierella isabellina*

JAMES P. KUTNEY, WILLIAM H. BAARSCHERS, OSCAR CHIN, YUTAKA EBIZUKA, LAURENCE HURLEY, JEFFREY D. LEMAN, PHILLIP J. SALISBURY, IGNACIO H. SANCHEZ, AND TREVOR YEE

Department of Chemistry, University of British Columbia, 2075 Wesbrook Place, Vancouver, B.C., Canada V6T 1W5

AND

ROBERT J. BANDONI

Department of Botany, University of British Columbia, 2075 Wesbrook Place, Vancouver, B.C., Canada V6T 1W5

Received March 15, 1977

JAMES P. KUTNEY, WILLIAM H. BAARSCHERS, OSCAR CHIN, YUTAKA EBIZUKA, LAURENCE HURLEY, JEFFREY D. LEMAN, PHILLIP J. SALISBURY, IGNACIO H. SANCHEZ, TREVOR YEE, and ROBERT J. BANDONI. Can. J. Chem. **55**, 2930 (1977).

A study involving the biodegradation of (+)-usnic acid (**1**) by the microorganism *Mortierella isabellina* is described. Three metabolic products, 6-acetyl-8,9bα-dimethyl-1,9b,2,3-tetrahydro-1α,7,9-trihydroxy-3-oxodibenzofuran (**2**, (+)-1α-hydroxy-2-desacetylusnic acid), (+)-2-desacetylusnic acid (**3**), and (+)-6-acetyl-8,9bα-dimethyl-1,9b-dihydro-2-acetoxy-3,7,9,trihydroxy-1-oxodibenzofuran (**4**, (+)-2-acetoxyusnic acid) are isolated and characterized. By means of radioactively labelled precursors, some information about the biodegradation sequence is derived.

JAMES P. KUTNEY, WILLIAM H. BAARSCHERS, OSCAR CHIN, YUTAKA EBIZUKA, LAURENCE HURLEY, JEFFREY D. LEMAN, PHILLIP J. SALISBURY, IGNACIO H. SANCHEZ, TREVOR YEE et ROBERT J. BANDONI. Can. J. Chem. **55**, 2930 (1977).

On décrit une étude impliquant la biodégradation de l'acide (+) usnique (**1**) par le microorganisme *Mortierella isabellina*. On a isolé et caractérisé trois produits métaboliques soit l'acétyl-6 diméthyl-8,9bα tétrahydro-1,9b,2,3 trihydroxy-1α,7,9 oxo-3 dibenzofuranne (**2**, l'acide (+) hydroxy-1α désacétyl-2 usnique), l'acide (+) désacétyl-2 usnique (**3**) et le (+) acétyl-6 diméthyl-8,9bα dihydro-1,9b acétoxy-2 trihydroxy-3,7,9 oxo-1 dibenzofuranne (**4**, l'acide (+) acétoxy-2 usnique). Faisant appel à des précurseurs marqués par des radioisotopes actifs, on a obtenu quelques informations sur les chemins de biodégradation.

[Traduit par le journal]

As part of our studies on the microbial degradation of the lichen antibiotic (+)-usnic acid (**1**) (1, 2) the fungal isolate *Mortierella isabellina* (Oudemans and Konig, 1902) (3, 4), a microorganism originally screened by Bandoni and Towers (5), was chosen as a promising candidate for a more comprehensive examination.

Thus a sample of the isolate identified as *Mortierella isabellina* (UBC culture collection #129) was used for the present study. The actual fermentation was carried out over a 10 day period at room temperature in shake culture flasks employing 3–4 day old cultures of the isolate. The representative extraction procedure indicated in Fig. 1 was developed in order to separate the complex product mixture into two main categories: (*i*) Neutral Fraction, and (*ii*) Acid Fraction. Moreover, this procedure allows for the facile recovery of any unreacted starting material by benzene extraction of the filtered solids.

Although the presence of several usnic acid-derived materials has been detected in both the Neutral and Acid Fractions, at the present time only those components which have been fully characterized will be discussed. Furthermore, approximately one-third (by weight) of the total biodegradation mixture resides in the Neutral Fraction, with the remaining two-thirds appearing in the Acid Fraction, as can be seen from Table 1.

In the initial phase of our program, experiments designed to evaluate the sequential production of metabolites according to varying time periods were performed in the hope that the results would allow a differentiation of the several possible biodegradation pathways which

[1]Part VII. See ref. 18.

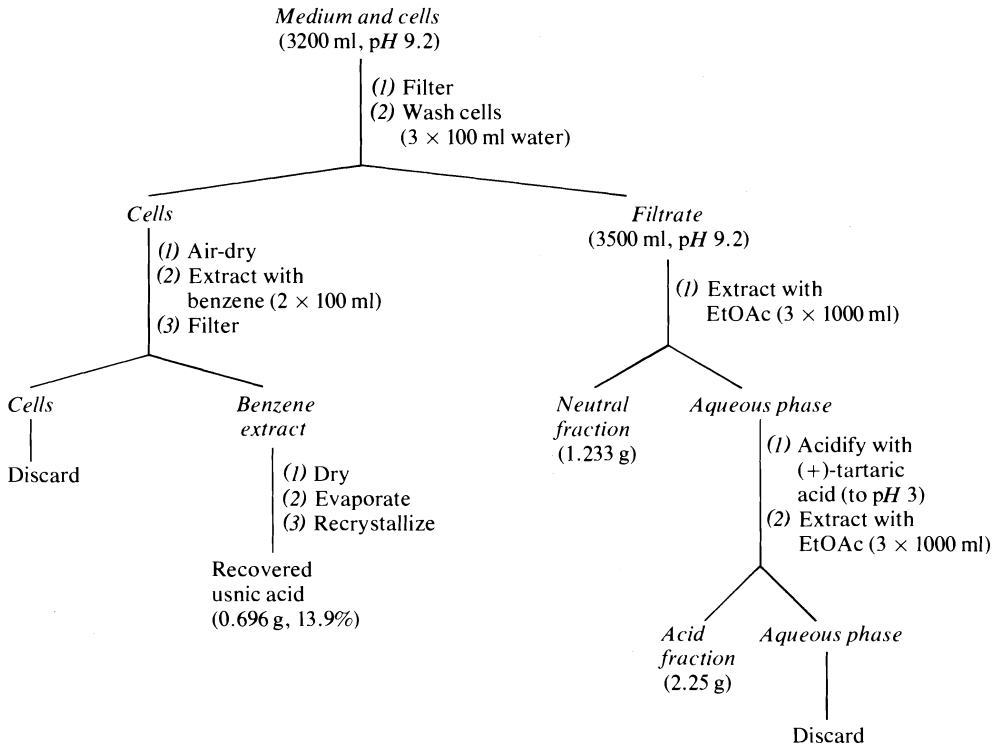

FIG. 1. A representative extraction procedure for the biodegradation of (+)-usnic acid (**1**) by *Mortierella isabellina*.

TABLE 1. Representative product distribution for the biodegradation of (+)-usnic acid (**1**) with *Mortierella isabellina**

Neutral fraction		Acid fraction	
Component	Weight (g)	Component	Weight (g)
FA(N)	0.940	FA(A)	1.250
A(N)	0.075	A(A)	0.060
B(N)	0.124	B(A)	0.700
C(N)	0.010	C(A)	0.150
	Total: 1.149		Total: 2.160

*Starting amount of (+)-usnic acid (**1**) = 5.0 g; FA = fatty acid ester residue; A, B, C = components (according to polarity).

may be involved. Our results indicate (Tables 2 and 3) that after a brief induction period of about 1–2 days, some biodegradation products begin to appear in the fermentation broth, which grows increasingly alkaline until days 9–10 when it reaches its final p*H* value of ~9.20. Whereas (+)-usnic acid (**1**) is being effectively incorporated throughout the time interval considered (20 days) (Fig. 2), the first product observed is the compound coded as B(A) (see Table 1) appearing initially on the second day (Table 3). After 5 days, detectable amounts of A(A) can be isolated from the growth medium (Table 3). It is interesting to note that the composite sequential production of these two materials approximately accounts for the overall behavior of the total Acid Fraction, as seen from Figs. 2 and 3. On the other hand, the Neutral Fraction, consisting mainly of two components, increases more slowly and seems to be at least partially dependent on the behavior of the Acid Fraction, with both reaching a maximum almost simultaneously about the 12–14 day period. Although it was not possible at this stage of the investigation to put forward a biodegradation pathway that would incorporate all the observations at hand, subsequent experiments with radioactively labelled precursors (see later) did shed some light on this aspect.

Purification of the Neutral Fraction afforded besides a fatty acid ester residue (see Table 1), which was not further studied at this time, two main components. The least polar of them, coded as A(N), has not been fully characterized due to its great instability although there appears little question of its derivation from usnic acid. The second component, designated as B(N), was

TABLE 2. Sequential study on the biodegradation of (+)-usnic acid (**1**) by *Mortierella isabellina*

Day	Recovered (+)-usnic acid (mg)	p*H* of medium	Total weight of acid fraction (mg)	Total weight of neutral fraction (mg)
0	500	5.20	—	—
1	272	7.22	18	0.5
2	265	7.48	19	1.5
3	234	7.35	26	5
4	250	7.65	30	10
5	210	8.15	52	21
6	197	8.05	56	19
7	151	8.45	111	40
8	142	8.82	86	27
9	129	9.25	95	40
10	140	9.10	137	51
11	113	9.20	164	48
12	71	9.18	245	59
13	30	9.40	277	85
14	30	9.20	289	62
15	15	9.22	324	51
16	10	9.20	221	38
17	7	9.20	247	—
18	5	9.20	—	—
19	3	9.20	—	—
20	2	9.20	—	—

TABLE 3. The biodegradation of (+)-usnic acid (**1**) by *Mortierella isabellina*. Product distribution in the acid fraction

Day*	Total weight (mg)	Compound A(A) (**3**) (mg)	Compound B(A) (**4**) (mg)
1	18	—	—
2	19	—	4
3	26	—	9
4	30	—	12
5	52	0.5	20
6	56	2	16
7	111	6	28
8	86	3	12
9	95	5	19
10	137	11	18
11	164	15	17
12	245	17	35
13	277	16	27
14	289	22	21
15	324	20	20
16	221	20	25

*After 16 days the fermentation mixture is too complex to allow proper isolation of the desired materials.

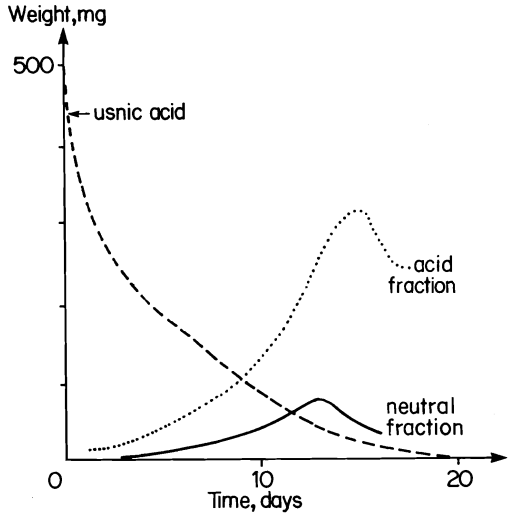

FIG. 2. Sequential study on the biodegradation of (+)-usnic acid (**1**) by *Mortierella isabellina*.

obtained crystalline, mp 236–238°C, $[\alpha]_D^{26}$ +187° (CH_3CN), and had the molecular formula $C_{16}H_{16}O_6$, the latter differing from that of usnic acid ($C_{18}H_{16}O_7$) by 40 mass units. While its ultraviolet spectrum ($\lambda_{max}(CH_3OH)$ 324, 282, 215 nm) suggested the presence of a methylphloroacetophenone system, its infrared spectrum indicated chelated hydroxyl groups (3300–3000 cm^{-1}) and a chelated *o*-hydroxyaryl-methyl ketone group (1625 cm^{-1}), in addition to a new band at 1658 cm^{-1} attributed to an α,β-unsaturated ketone system. At this point it became clear that the normal bands assigned to the ring C β-triketone system (1680 and 1540 cm^{-1}) of the usnic acid series were absent, thus

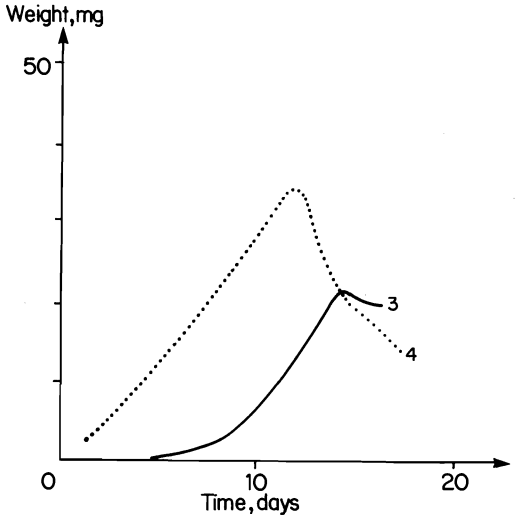

FIG. 3. Product distribution in the acid fraction of the biodegradation of (+)-usnic acid (**1**) by *Mortierella isabellina*.

providing the first firm indication that the microbial transformation involves ring C of the usnic acid molecule.

The ^{1}Hmr spectrum of B(N) showed, as expected, the characteristic signals corresponding to the angular and aromatic methyl groups and the aromatic methyl ketone at δ 1.48, 2.04, and 2.66 ppm, respectively, although that corresponding to the angular substituent had experienced a considerable upfield shift. The one-proton singlet at δ 5.75 ppm was in agreement with an olefinic proton at the α-position of an α,β-unsaturated ketone while the low field region of the spectrum indicated the presence of three hydroxyl groups, two of which appeared as a very broad band centered at δ 8.76 ppm and the other being typical of the chelated hydroxyl group at the 7-position (δ 13.32 ppm) in the usnic acid series.

The remaining proton signals in the ^{1}Hmr spectrum of B(N) were observed in the δ 2.50–4.30 ppm region and were clearly due to protons in ring C of an usnic acid derivative. The splitting patterns approximated an ABX system and the coupling constants obtained suggested the stereochemical assignment made to the C_2- and C_1-protons as shown in A. Thus the methylene protons H_A and H_B at C_2 (δ 2.82, J = 16.5 Hz) appear as a multiplet and are coupled to the methine proton at C_1 (δ 4.41, q, J = 16.5 Hz) with the magnitude of the coupling constant being consistent with a pseudoaxial orientation for the latter proton as shown.

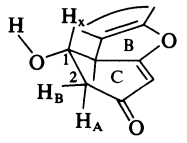

A

A previous detailed mass spectrometric investigation of a large number of usnic acid derivatives (6) was invaluable in applying this technique to the structural elucidation of B(N). The nature of the functionality in ring C of this metabolite, as suggested above, was fully substantiated by the fragmentation pattern observed and summarized in Fig. 4. The complete assignment of structure for B(N) or (+)-1α-hydroxy-2-desacetylusnic acid as shown in **2** was now possible.

Confirmation of this structural assignment was obtained when **2** was converted to a triacetate **5**, mp 92–93°C, $[\alpha]_D^{26}$ +152° (CH_3CN). This substance revealed the expected infrared absorptions for both phenolic (1770 cm^{-1}) and saturated acetate (1720 cm^{-1}) groups while in its ^{1}Hmr spectrum new signals at δ 2.23, 2.33, and 2.40 ppm were assigned to the $C_{1\alpha}$-, C_9-, and C_7-acetate groups, respectively. The proton at C_1 in **5** was observed at δ 5.50 ppm (J = 16.5 Hz, q) and as expected had shifted downfield in the conversion to the acetate derivative (δ 4.41 in **2** → δ 5.50 in **5**).

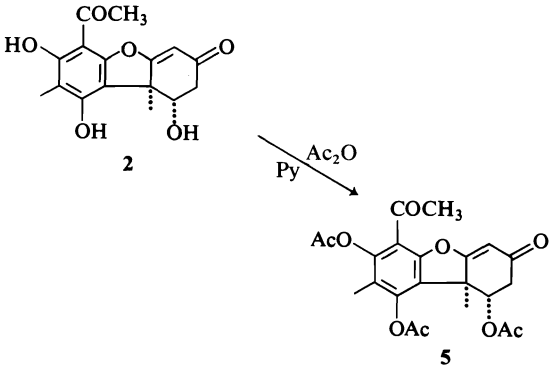

We then turned our attention to the structure elucidation of the metabolites present in the Acid Fraction. The least polar component designated as A(A) was crystalline mp 221–222°C, $[\alpha]_D^{26}$ +630° (CH_3CN), with molecular formula $C_{16}H_{14}O_6$. This compound proved to be identical with (+)-2-desacetylusnic acid (**3**) iso-

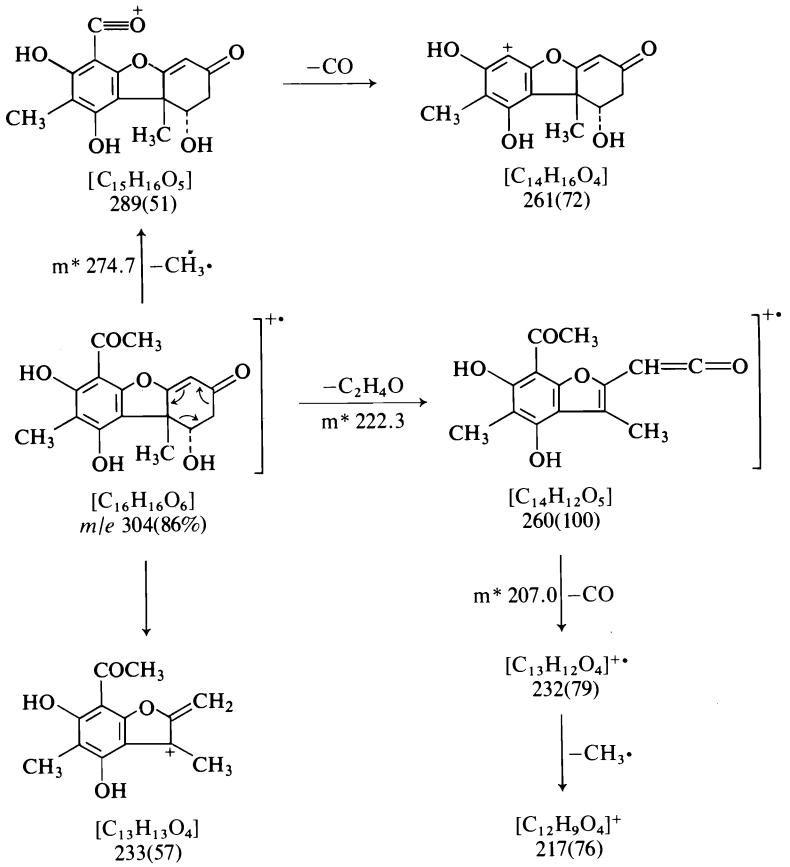

FIG. 4. Postulated fragmentation pattern for (+)-1α-hydroxy-2-desacetylusnic acid (**2**).

lated and characterized in a complementary series of investigations involving fermentations with *Mucor globosus* (7).

After successive purifications the second component, B(A), was isolated as an unstable bright yellow glassy material with molecular formula $C_{18}H_{16}O_7$, or 16 mass units higher than (+)-usnic acid (**1**). It was shown that the ultraviolet, infrared, and mass spectral data of B(A) were identical with those of synthetic (+)-2-acetoxyusnic acid (**4**), a compound which had already been prepared in our laboratory during studies relating to the synthesis of (+)-2-desacetylusnic acid (**3**) (7).

Further chemistry which substantiated the structural assignment **4** and which would be required for future experiments with radioactively labelled precursors was also developed. Acetylation of **4** and ozonolysis of the acetate provided the known (8, 9) α-coumaranone derivative **6**, thereby revealing that ring A of the usnic acid system had not been modified during the microbial transformation. Hydrogenation of **4** afforded the dihydro derivative **7** while chromous chloride reduction (11) allowed the conversion to the known (+)-2-desacetylusnic acid (**3**), thus providing a facile chemical interrelation between these two metabolites.

The conversion of usnic acid (**1**) to the metabolite **4** can be effectively carried out by reaction of **1** with hydrogen peroxide whereupon **4** is obtained in 83% yield. This latter experiment suggested a possible biological relationship between **1** and **4** (see later).

The above experiments have provided some evidence concerning the microbial degradation of usnic acid (**1**) with *Mortierella isabellina* (Fig. 5) and it was now desirable to substantiate these results and to define more accurately the sequential nature of the biodegradation pathway by the use of radioactively labelled precursors.

The preparation of appropriately labelled

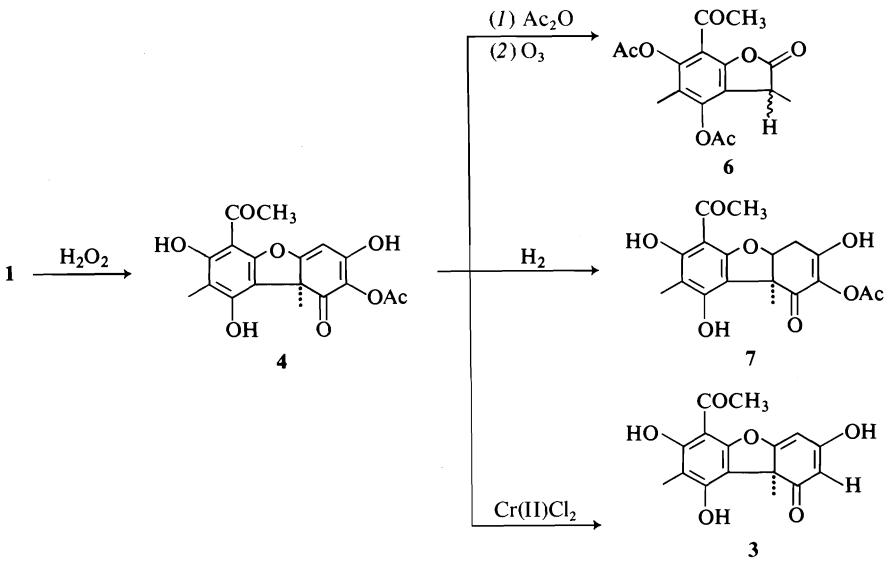

usnic acid and related derivatives, quite unexpectedly, became a difficult chemical problem. The most desired site of label in the usnic acid system was ring A since, as indicated above, the metabolic products retain this portion of the molecule. The most direct synthetic route was the introduction of the aromatic methyl ketone side chain via a Friedel–Crafts reaction or Fries rearrangement employing 6-desacetylusnic acid (**8**) as starting material, as shown in the sequence, **8** → **9**. Although the extensive chemistry of the usnic acid series was recorded in the literature, the earlier workers had not recognized the facile rearrangement of the 'normal' usnic acid series, as shown above, to the 'iso' or isousnic series. In the numerous experiments which followed, it became essential to reinvestigate and clarify the chemistry relating to the synthesis of **8** and the results thus obtained form the subject of a number of recent publications (12–18). Fortunately the desired synthesis of **8** was eventually achieved in an efficient manner *without* the complicating

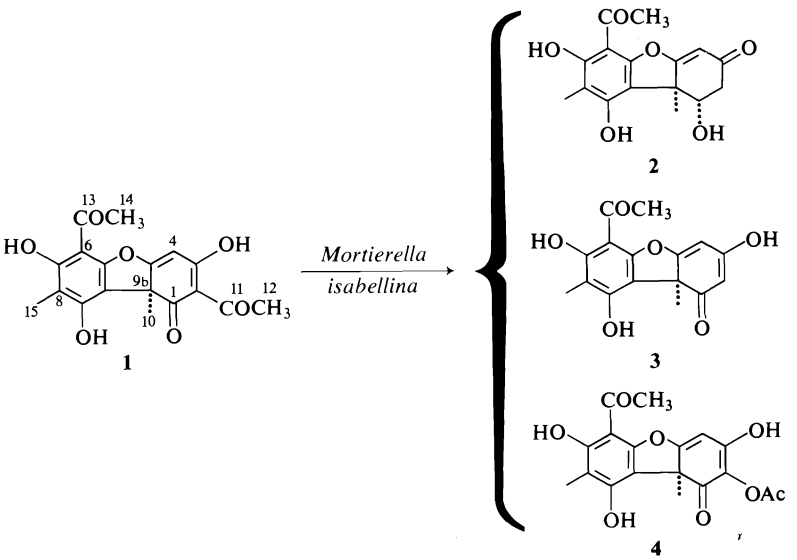

FIG. 5. A summary of metabolic products obtained from the biodegradation of usnic acid (**1**) with *Mortierella isabellina*.

rearrangement to the 'iso' series and the conversion of **8** to (+)-usnic acid (**1**) via the Fries method could be effectively employed (18). Repetition of this latter stage with acetyl chloride-*2*-^{14}C provided the desired usnic acid (**9**) with label in the methyl group of the aromatic ketone side chain (see Experimental). This material was then employed in the fermentation studies with *Mortierella isabellina*.

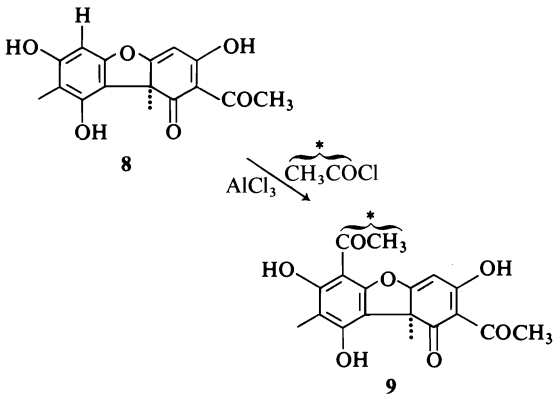

Various fermentations with [6-$^{14}CH_3CO$]-(+) usnic acid as the precursor were performed and, in each instance, the three metabolites (**2**, **3**, and **4**) were carefully purified and their radioactivity evaluated. These results left no doubt that these compounds were derived from (+)-usnic acid in the biodegradation process. The efficiency of utilization of this precursor by the microorganism varied depending upon the rate of shaking, volume of growth medium, and time period (usually 11–16 days). Under optimum conditions high levels of conversion (generally 70–90%) were obtained (see Experimental).

As mentioned earlier, the chemical conversion of (+)-usnic acid to (+)-2-acetoxyusnic acid (**4**) could be achieved in high yield by an oxidative process (hydrogen peroxide). Such a process could have significance in the biological transformation as well and therefore **4** could be an early stage metabolite serving as a precursor for **2** and/or **3**. For this purpose, radioactively labelled **4** obtained from a synthetic conversion of radioactive **1** and hydrogen peroxide, was added to the fermentation broth in the normal manner. Isolation and separation of the fermentation mixture provided unchanged **4** as a major component (about 60%) and an insignificant amount of the other metabolites.

In order to eliminate the possibility that the fungus requires usnic acid to induce the formation of enzymes responsible for the observed biodegradation, a fermentation experiment with radioactive **4** in the presence of non-radioactive usnic acid was carried out. Again no detectable amounts of the metabolites **2** and **3** were found. On this basis it is assumed that (+)-2-acetoxyusnic acid (**4**) does not serve as a precursor for **2** or **3**.

The relationship between **2** and **3** could be conclusively established from fermentation experiments with radioactive forms of these metabolites. When radioactive **3** was employed as the precursor it could be demonstrated that radioactive **2** is formed. On the other hand fermentation with radioactive **2** produces no evidence of active **3**. In summary these results provide definitive information about the biodegradation pathways involved. It appears that two independent pathways have been recognized, one involving the sequence, **1** → **4**, and the other, **1** → **3** → **2**. The intermediates involved in these conversions have not been established and further experiments will be required. The chemical instability associated with the anticipated intermediates may provide considerable difficulty since the instability of **4** has already prevented any more detailed studies with this metabolite.

Experimental

Melting points were determined on a Kofler block and are uncorrected.

Ultraviolet (uv) spectra were recorded on a Cary 15 spectrophotometer in methanol solution (unless otherwise noted). The wavelength of the absorption maxima are reported in nanometres (nm).

Infrared (ir) spectra were measured routinely on a Perkin-Elmer model 710 spectrophotometer. Analytical or comparison spectra were recorded on a Perkin-Elmer model 457 spectrophotometer using matched cells with a cell path of 0.2 mm in chloroform solution. Calibration was achieved using the 1601 cm^{-1} absorption band of polystyrene. The absorption maxima are quoted in wave numbers (cm^{-1}).

Proton magnetic resonance (^{1}Hmr) spectra were measured at 60 or 100 MHz in deuterochloroform ($CDCl_3$) solution (unless otherwise indicated) at room temperature. Line positions are given in the δ (ppm) scale using tetramethylsilane (TMS) as internal standard. The integrated peak areas, multiplicity, and proton assignments are indicated in parentheses.

Low resolution mass (ms) spectra were determined on either an AEI-902 or an Atlas CH-4B mass spectrometer, with high resolution mass spectra being recorded exclusively on an AEI-MS-902 mass spectrometer.

Optical rotations ($[\alpha]_D$) were measured on a Perkin-Elmer model 141 polarimeter at the sodium D line in

chloroform solution (unless otherwise noted) using cells with a 0.1 dm path.

Microanalyses were performed by Mr. P. Borda of the Microanalytical Laboratory, University of British Columbia.

Merck silica gel G (acc. to Stahl) impregnated with oxalic acid (2%) and with 2% fluorescent indicator added, was used as adsorbent for thin layer chromatography (tlc), unless otherwise noted. The tlc plates were activated in an oven at 90°C for 4 h before use. For qualitative chromatography, layers of 0.3 mm thickness were used and the spots were visualized by viewing under ultraviolet (uv) light or spraying with a 1% ethanolic ferric chloride solution. For preparative (plc) chromatography, large (20 × 20 and 20 × 60 cm) plates with a thicker layer (0.7 mm) were used. The developing systems were *A*, petroleum ether (30–60°C) – acetone (4:1), and *B*, chloroform – ethyl acetate (3:2), unless otherwise indicated.

Column chromatography was performed on either Mackerey–Nagel (0.2–0.5 mm grain size) or Merck 60 (0.063–0.2 mm grain size) silica gel.

(+)-Usnic acid was obtained from Koch-Light Laboratories, England.

In experiments involving radioactive precursors, the radioactivity was determined by the liquid scintillation counting method utilizing a Nuclear-Chicago Mark II Scintillation Counter. All specimens were counted in duplicate.

A sample of the isolate used and identified as *Mortierella isabellina* #129 was maintained on modified malt agar plates (18) by transfer every 2 weeks from a two-week old agar plate growth to a fresh sterile plate.

Maintenance, Growth, and Fermentation Conditions

A 'stock culture' of the purified fungal isolate was stored on modified malt agar in culture tubes placed in the refrigerator.

Aseptic techniques were used throughout in handling the cultures. To ensure proper aeration, the volume of the nutrient solution (18) should never exceed about two-fifths of the total volume of the flask.

Media and stock solutions utilized have been fully reported in ref. 18.

Fermentation Conditions and Extraction Procedure

Inoculation of *shake* culture flasks is carried out by transferring a small segment (about $\frac{1}{4}$ in. square) of active growth (not older than 2 weeks) and agar to a sterile Erlenmeyer flask containing an appropriate volume of nutrient medium.

Large scale production of biodegradation products is carried out in 6 ℓ Erlenmeyer flasks, each containing 3 ℓ of growth medium. Inoculation of these flasks is achieved by transferring the contents of a liquid culture of *Mortierella isabellina* (200 ml) which had been grown for 3–4 days in a shake culture flask (*vide supra*) and crystalline (+)-usnic acid (5 g, 14.534 mmol) into each fermentation flask. The flasks were then agitated on a rotary shaker at room temperature for 10 days. A typical extraction procedure routinely employed is summarized in Fig. 1.

Neutral Fraction

Purification by column chromatography on silica gel Woelm (activity II, 50 g) produced the following components.

Component FA(N)

Fatty acid ester(s) (940 mg). Not investigated.

Component A(N)

Usnic acid derived unstable compound (75 mg). Not investigated.

Component B(N): (+)-1α-Hydroxy-2-desacetylusnic Acid (2) (6-Acetyl-8,9bα-dimethyl-1,9b,2,3,-tetrahydro-1α,7,9-trihydroxy-3-oxodibenzofuran)

Colorless plates from acetone – petroleum ether (30–60°C) (124 mg, 0.408 mmol; 3%), mp 236–238°C; $[\alpha]_D^{26}$ (CH_3CN) +187° (*c* 0.123); uv: λ_{max} (log ε) 324 (3.74), 282 (4.13), 215 (4.19); ir: ν_{max} 3300–3000 (OH, chelated), 1658 (C=O, α,β-unsaturated), 1625 (C=O, chelated aromatic acetyl; C=C); ^{1}Hmr: δ 1.48 (3H, s, C_{9b}-CH_3), 2.04 (3H, s, C_8-CH_3), 2.60 (1H, ABX q, J_{AB} = 18 Hz, C_2-*H* (axial)), 2.66 (3H, s, C_6-$COCH_3$), 2.82 (1H, ABX q, J_{AB} = 18 Hz, C_2-*H* (equatorial)), 4.30 (1H, ABX q, $J_{AX} + J_{BX}$ = 16.5 Hz, C_1-*H* (axial)), 5.75 (1H, s, C_4-H), 8.76 (2H, b, C_1-O*H* and C_9-O*H*), 13.32 ppm (1H, s, C_7-O*H*); ^{1}Hmr (60 MHz, CD_3OD) δ 1.58 (3H, s, C_{9b}-CH_3), 2.13 (3H, s, C_8-CH_3), 2.76 (3H, s, C_6-$COCH_3$), 2.82 (2H, ABX multiplet, $J_{AX} + J_{BX}$ = 16.5 Hz, C_2-H_2), 4.41 (1H, ABX q, $J_{AX} + J_{BX}$ = 16.5 Hz, C_1-*H* (axial)), 5.98 ppm (1H, s, C_4-*H*); ms: *m/e* 304 (M^+), 289, 261, 260 (base peak), 247, 243, 233, 232, 217, 205, 115, 91, 83, 77, 69, 43. *Anal.* calcd. for $C_{16}H_{16}O_6$: C 63.15, H 5.30; found: C 63.05, H 5.28. High resolution molecular weight determination calcd.: 304.095; found: 304.096.

Component C(N)

Base line material (10 mg). Not investigated. Total weight of recovered materials from Neutral Fraction is 1.149 g.

Acid Fraction

Upon concentration of the ethyl acetate extract a yellow crystalline solid precipitated and was filtered. This material (40 mg) constitutes component A(A) and was combined with the one obtained during the purification of the mother liquors by preparative layer chromatography (silica gel – oxalic acid, 20 × 60 cm plates, solvent system *A*, developed three times). The following components were obtained.

Component FA(A)

Fatty-acid ester(s) (1.250 g). It showed an identical ^{1}Hmr spectrum with the one obtained for component FA(N) of the Neutral Fraction; ir: ν_{max} 1720, 1700, 1680, 1610, 1500, 1410. It was subsequently shown with radioactively labelled precursors that this component is *not* derived from usnic acid and it was not investigated further.

Component A(A): (+)-2-Desacetylusnic Acid (3)

Bright yellow plates from ethyl acetate (60 mg, 0.198 mmol; 1.5%), mp 221–222°C; mixture mp with an authentic sample of (+)-2-desacetylusnic acid (7), 220–222°C; $[\alpha]_D^{26}$ (CH_3CN) +630° (*c* 0.0755). This sample showed identical chromatographic and spectroscopic properties with those of the authentic product; uv: λ_{max} (log ε) 330 (3.53), 287 (4.02), 219 (4.33); ir (Nujol): ν_{max} 3300–2300 (OH, chelated), 1670 (C=O, enone system), 1630 (C=O, chelated aromatic acetyl; C=C), 1600 (C=C); ^{1}Hmr: δ 1.71 (3H, s, C_{9b}-CH_3), 2.02 (3H, s, C_8-CH_3), 2.65 (3H, s, C_6-$COCH_3$), 5.37 (1H, d, *J* = 2 Hz, C_2-*H*), 5.88 (1H, d, *J* = 2 Hz, C_4-*H*), 11.94

(1H, b, C_9-O*H*), 13.32 ppm (1H, s, C_7-O*H*); ms: *m/e* 302 (M^+), 287, 260 (base peak), 233, 232, 217. *Anal.* calcd. for $C_{16}H_{14}O_6$: C 63.57, H 4.67; found: C 63.51, H 4.72. High resolution molecular weight determination calcd.: 302.079; found: 302.077.

Component B(A): (+)-2-Acetoxyusnic Acid (4) (6-Acetyl-8,9bα-dimethyl-1,9b-dihydro-2-acetoxy-3,7,9-trihydroxy-1-oxodibenzofuran)

After three successive purifications by preparative chromatography (silica gel – oxalic acid plates, solvent *A*, developed twice) this material presented the following characteristics.

Unstable yellow glassy material that could not be induced to crystallize (700 mg, 1.944 mmol; 15.5%); $[\alpha]_D^{26}$ (CH_3OH) +392° (*c*, 0.025); uv: λ_{max} (log ε) 335 (3.35), 291 (3.83), 221 (4.15); ir: ν_{max} 3400–2500 (OH, chelated), 1765 (C=O, acetate), 1720, 1690 (C=O, β-diketone), 1625 (C=O, chelated aromatic acetyl; C=C); ^{1}Hmr: δ 1.80 (3H, s, C_{9b}-C*H*$_3$), 2.06 (3H, s, C_8-C*H*$_3$), 2.30 (3H, s, C_2-OCOC*H*$_3$), 2.65 (3H, s, C_6-COC*H*$_3$), 5.85 (1H, s, C_4-*H*), 9.00 (2H, b, C_3-O*H* and C_9-O*H*), 13.26 ppm (1H, s, C_7-O*H*); ms: *m/e* 360 (M^+), 318, 302, 290, 272, 262, 260 (base peak), 232, 217, 88, 73, 70, 60. High resolution molecular weight determination calcd. for $C_{18}H_{16}O_8$: 360.084; found: 360.083. This compound seems to be stable for 1–2 weeks if stored at 0°C in ethyl acetate solution.

Compound C(A)

Unstable usnic acid derived product (150 mg). Not investigated. Total weight of recovered materials from Acid Fraction is 2.160 g.

Formation of (+)-1α-Hydroxy-2-desacetylusnic Acid Triacetate (5) (6-Acetyl-8,9bα-dimethyl-1,9b,2,3-tetrahydro-1α,7,9-triacetoxy-3-oxodibenzofuran)

A solution of (+)-1α-hydroxy-2-desacetylusnic acid (**2**) (20 mg, 0.065 mmol) in a 1:1 mixture of pyridine – acetic anhydride (1 ml) was allowed to stand at room temperature for 5 h. The resulting pale brown reaction mixture was then poured onto crushed ice (10 g) and extracted with chloroform (3 × 5 ml). The combined extracts were washed with water, dried over anhydrous sodium sulfate, and evaporated under reduced pressure to yield a colorless semi-crystalline glass (22.8 mg). Purification by preparative layer chromatography (silica gel plates, (4:1) chloroform – ethyl acetate) produced pure (+)-1α-hydroxy-2-desacetylusnic acid triacetate (**5**) (16 mg, 0.0372 mmol; 57%). Although this material could not be induced to crystallize, upon sublimation (190°C, 0.03 Torr) colorless droplets (mp 93–95°C) were obtained; $[\alpha]_D^{26}$ (CH_3CN) +152° (*c* 0.052); uv: λ_{max} (log ε) 272 (3.87), 246 (3.78), 208 (4.29); ir: ν_{max} 1770 (C=O, aromatic acetates), 1720 (C=O, saturated acetate), 1690 (C=O, aromatic acetyl), 1660 (C=O, α,β-unsaturated ketone), 1605 (C=C), 1240 (C—O, saturated acetate), 1205 (C—O, aromatic acetates); ^{1}Hmr: δ 1.60 (3H, s, C_{9b}-C*H*$_3$), 1.94 (3H, s, C_8-C*H*$_3$), 2.23 (3H, s, C_1-α OCOC*H*$_3$), 2.33 (3H, s, C_9-OCOC*H*$_3$), 2.40 (3H, s, C_9-OCOC*H*$_3$), 2.51 (1H, ABX q, J_{AB} = 18 Hz, C_2-*H* (axial)). 2.63 (3H, s, C_6-COC*H*$_3$), 2.98 (1H, ABX q, J_{AB} = 18 Hz, C_2-*H* (equatorial)), 5.50 (1H, ABX q, $J_{AX} + J_{BX}$ = 16.5 Hz, J_{AX} = 10 Hz, J_{BX} = 6.5 Hz, C_1-*H* (axial)), 5.86 ppm (1H, s, C_4-*H*); ms: *m/e* 430 (M^+), 388, 346, 328, 317, 313, 302, 287, 286, 271, 260 (base peak), 232, 217, 83, 74, 59, 43. *Anal.* calcd. for $C_{22}H_{22}O_9$: C 61.39, H 5.15; found: C 61.14, H 5.33. High resolution molecular weight determination calcd.: 430.126; found: 430.128.

Ozonolysis of (+)-2-Acetoxyusnic Acid (4). Isolation of (±)-7-Acetyl-4,6-dihydroxy-3,5-dimethylcoumaran-2-one Diacetate (6)

Freshly isolated (+)-2-acetoxyusnic acid (**4**) (60 mg, 0.166 mmol) was dissolved in a 1:1 mixture of pyridine – acetic anhydride (2 ml) and allowed to stand at room temperature overnight. The resulting solution was poured onto ice (10 g), extracted with ethyl acetate (3 × 5 ml), and the combined extracts washed with water, dried over anhydrous sodium sulfate, and evaporated under reduced pressure to produce an orange glass (67 mg). The residue was dissolved in dry carbon tetrachloride (8 ml), cooled to 0°C (ice bath), and ozonized oxygen (26 mg O_3/min) bubbled through until a pale blue color was observed. The reaction mixture was diluted with distilled water (10 ml) and heated to reflux in a steam bath for 20 min. The organic layer was then separated, washed with 2.5% sodium bicarbonate solution and water, dried over anhydrous sodium sulfate, and evaporated under reduced pressure. The residue was recrystallized from ethyl alcohol – water to produce (±)-7-acetyl-4,6-dihydroxy-3,5-dimethylcoumaran-2-one diacetate (**6**) (20 mg, 0.0625 mmol; 37%), colorless crystals, mp 131–132°C (lit. (2) mp 130–132°C); mixture mp with authentic material, 131–132°C. The sample showed identical chromatographic and spectroscopic properties with those of the material obtained from (+)-usnic acid.

Preparation of (+)-Dihydro-2-acetoxyusnic Acid (7) (2-Acetoxy-6-acetyl-8,9bα-dimethyl-1,9b,4,4a-tetrahydro-3,7,9-trihydroxy-1-oxodibenzofuran)

(+)-2-Acetoxyusnic acid (**4**) (110 mg, 0.305 mmol) in absolute ethyl alcohol (10 ml) was hydrogenated at room temperature and atmospheric pressure over 5% platinum-on-carbon catalyst (50 mg). After the uptake of 1 mol equiv. of hydrogen (7.45 ml H_2 at 25°C) the reaction mixture was filtered through Celite, the Celite cake washed with absolute ethyl alcohol (2 × 5 ml), and the combined filtrates evaporated under reduced pressure to afford a colorless foam (83 mg). Purification by preparative layer chromatography (silica gel – oxalic acid plates, solvent *A*) yielded (+)-dihydro-2-acetoxyusnic acid (**7**) (41.3 mg, 0.114 mmol; 37%), colorless glassy material that could not be induced to crystallize $[\alpha]_D^{26}$ (CH_3OH) +45° (*c* 9.11); uv: λ_{max} (log ε) 322 (3.66), 286 (4.30), 222 (4.15); ir: ν_{max} 3500–3100 (OH, chelated), 1775 (C=O, acetate), 1730 (C=O, β-diketone), 1630 (C=O, chelated aromatic acetyl; C=C); ^{1}Hmr: δ 1.67 (3H, s, C_{9b}-C*H*$_3$), 2.03 (3H, s, C_8-C*H*$_3$), 2.20 (3H, s, C_2-OCOC*H*$_3$), 2.54 (3H, s, C_6-COC*H*$_3$), 3.06 (2H, d, J = 5 Hz, C_4-*H*$_2$), 4.84 (1H, t, J = 5 Hz, C_{4a}-α*H*), 7.13 (2H, b, C_3-O*H* and C_9-O*H*), 13.20 ppm (1H, s, C_7-O*H*); ms: *m/e* 362 (M^+), 334, 320, 305, 260, 233, 220, 219, 217, 215, 205, 201, 191, 149, 91, 83, 69, 57, 55, 43 (base peak). High resolution molecular weight determination calcd. for $C_{18}H_{18}O_8$: 362.100; found: 362.098.

The Chromium(II) Chloride Reduction of Natural (+)-2-Acetoxyusnic Acid (4). Isolation of (+)-2-Desacetylusnic Acid (3)

A solution of (+)-2-acetoxyusnic acid (**4**) (21 mg, 0.0583 mmol) in dry acetone (10 ml) was saturated at

0°C (ice bath) with carbon dioxide and treated under a stream of carbon dioxide with a freshly prepared chromium(II) chloride solution (10 ml). The reaction flask was properly sealed to exclude air (Parafilm) and allowed to stand at room temperature in the dark for 3 days. The resulting green reaction mixture was then concentrated under reduced pressure, diluted with distilled water (10 ml), and extracted with ethyl acetate (3 × 5 ml). The combined extracts were washed with water, dried over anhydrous sodium sulfate, and evaporated under reduced pressure. The yellow semicrystalline residue (18 mg) was purified by preparative layer chromatography (silica gel – oxalic acid plates, solvent *A*) to produce (+)-2-desacetylusnic acid (**3**) (13 mg, 0.043 mmol; 73%), bright yellow crystals from ethyl acetate, mp 220–222°C; mixture mp with authentic material, 221–222°C. The sample showed identity with the authentic material in all spectroscopic and chromatographic properties.

*Sequential Biodegradation of (+)-Usnic Acid (**1**) by Mortierella Isabellina*

A sequential study of the biodegradation of (+)-usnic acid (**1**) by *Mortierella isabellina* was set up by using 20-1000 ml Erlenmeyer flasks, each containing an adequate volume of growth medium (250 ml) and crystalline (+)-usnic acid (**1**) (500 mg, 1.453 mmol). Inoculation of these flasks was carried out by transferring aliquots (25 ml) from a 6-day old liquid culture of *M. isabellina* (500 ml).

Extraction of the fermentation mixture according to the scheme outlined in Fig. 1 was performed every day by processing the contents of one flask. The variations of p*H*, amount of recovered usnic acid, total weight of the Neutral and Acid Fraction, and individual weight of components present in each fraction were recorded. The results are presented in Tables 2 and 3.

Synthesis of [6-$^{14}CH_3CO$]-(+)-Usnic Acid

To a solution of aluminum chloride (63.1 mg) and [2-^{14}C]acetyl chloride (29.5 μl; total activity 1.0 mCi) in anhydrous nitrobenzene (1.2 ml) was added 6-desacetylusnic acid (30.3 mg) and the mixture was stirred for 1.5 h at 60°C under a nitrogen atmosphere. After cooling with ice, the mixture was diluted with chloroform (5 ml) and freshly prepared 1 *N* sodium hydroxide solution (5 ml) and stirred at room temperature for a further 0.5 h. The two layers were separated and the organic layer was extracted with 1 *N* sodium hydroxide (5 ml). The combined aqueous layers were carefully acidified with 1 *N* hydrochloric acid and thoroughly extracted with ethyl acetate (3 × 15 ml). These extracts were washed with brine, then with water, dried over anhydrous sodium sulfate, and evaporated *in vacuo* to provide the crude product (25.6 mg). Preparative layer chromatography (silica gel, 2% oxalic acid, petroleum ether – acetone 4:1) and crystallization from chloroform – ethyl alcohol afforded the radioactive usnic acid (11.0 mg). This material was diluted with inactive usnic acid to give a specimen (74.0 mg) with activity of 1.23 × 10^6 dpm/mg.

For the large scale fermentations this sample could be further diluted with inactive usnic acid to provide the required quantities and activities as noted below.

*Fermentation with [6-$^{14}CH_3CO$]-(+)-Usnic Acid (**1**)*

Radioactive usnic acid (4.55 g, activity 1.56 × 10^4 dpm/mg) was reacted in eight flasks innoculated with *Mortierella isabellina* and fermented in the manner already described earlier. Isolation according to the earlier described procedure provided a Neutral Fraction (654 mg) and an Acid Fraction (1.20 g).

Purification of the Neutral Fraction by preparative layer chromatography afforded radioactive **2** (30.2 mg, activity 1.78 × 10^4 dpm/mg) while the Acid Fraction afforded **3** (77.7 mg, activity 1.78 × 10^4 dpm/mg) and **4** (355 mg, activity 1.68 × 10^4 dpm/mg). In addition, 1.3 g of usnic acid was recovered.

This type of experiment was repeated on numerous occasions to provide similar results.

*Fermentation with [6-$^{14}CH_3CO$]-(+)-2-Desacetylusnic Acid (**3**)*

Radioactive (+)-2-desacetylusnic acid **3** (159.8 mg activity 0.57 × 10^3 dpm/mg) was exposed to fermentation in the normal manner over a 17 day period. Isolation of the resultant mixture provided a Neutral Fraction (63.4 mg) and an Acid Fraction (98.6 mg).

Purification of the Neutral Fraction provided an inactive oily material (19.6 mg) which was not characterized further and radioactive **2** (activity 0.60 × 10^3 dpm/mg). Blank experiments with inactive **2** gave values of 81 dpm/mg.

The Acid Fraction, upon purification, afforded unchanged **3** (27.5 mg, activity 0.50 × 10^3 dpm/mg) as the only radioactive components.

*Fermentation with [6-$^{14}CH_3CO$]-(+)-1α-Hydroxy-2-desacetylusnic Acid (**2**)*

Radioactive (+)-1α-hydroxy-2-desacetylusnic acid **2** (162 mg, activity 1.46 × 10^3 dpm/mg) was exposed to fermentation over a 2 week period. Isolation of the mixture afforded a Neutral Fraction (96.3 mg) which upon thin layer chromatographic purification gave unreacted **2** (74 mg) and an Acidic Fraction (31 mg) which on tlc revealed only very polar material. No detectable amounts of any of the other metabolites (**3** or **4**) were observed.

*Synthesis of [6-$^{14}CH_3CO$]-(+)-2-Acetoxyusnic Acid (**4**)*

[6-$^{14}CH_3CO$]-(+)-Usnic acid (500 mg, activity 1.35 × 10^4 dpm/mg) was dissolved in warm pyridine (8.5 ml) and treated at room temperature with 30% hydrogen peroxide (0.35 ml). After stirring for 1 h, the reaction mixture was cooled to 0°C, acidified with 0.1 *N* hydrochloric acid, and then extracted with ethyl acetate (3 × 35 ml). The extract was washed with water, dried over anhydrous sodium sulfate, and evaporated *in vacuo* to provide a brown oily residue. Thick layer chromatography (silica gel – oxalic acid, petroleum ether – acetone (3:1)) of the latter provided pure **4** (480 mg, activity 1.29 × 10^4 dpm/mg).

*Fermentation with [6-$^{14}CH_3CO$]-(+)-2-Acetoxyusnic Acid (**4**)*

Radioactive **4** (350 mg, activity 1.29 × 10^4 dpm/mg) was exposed to fermentation over a 2 week period. Isolation and purification of the Acid Fraction (315 mg) provided unreacted **4** (210 mg) while the Neutral Fraction (11.5 mg) did not reveal any of the expected metabolites **2** or **3**.

*Fermentation with [6-$^{14}CH_3CO$]-(+)-2-Acetoxyusnic Acid (**4**) in the Presence of Non-radioactive Usnic Acid*

Radioactive **4** (128 mg, activity 1.29 × 10^4 dpm/mg)

and non-radioactive usnic acid (150 mg) were exposed to fermentation over a 2 week period. Preparative layer chromatography of the Neutral Fraction (30 mg) provided only unchanged **4** (78 mg) and no evidence of the other metabolites. The normal unlabelled metabolites **2** and **3** formed from the non-radioactive usnic acid were noted in the medium.

Acknowledgement

Financial aid from the National Research Council of Canada is gratefully acknowledged. One of us (I.H.S.) wishes to thank NRCC for a scholarship during the period of this study. We would also like to acknowledge the efforts of Ms. I. B. Krizsan in preparing the illustrations.

1. C. F. CULBERSON. Chemical and botanical guide to lichen products. The University of North Carolina Press, Chapel Hill, NC. 1969. p. 171; The Bryologist, **73**, 201 (1970).
2. A. ASAHINA and S. SHIBATA. Chemistry of lichen substances. Japan Society for the Promotion of Science, Tokyo. 1954. p. 171.
3. N. A. NAUMOV. Clés des Mucorinées (Mucorales). Encyclopédie mycologique. Vol. IX. *Edité par* P. Lechevalier., Paris, France. 1939. p. 94.
4. H. ZYCHA. Mucorineae. Kryptogamenflora der Mark Brandenburg. Pilze II. Verlag von Gebriider Borntraeger, Leipzig. 1935. p. 197.
5. R. J. BANDONI and G. H. N. TOWERS. Can. J. Biochem. **45**, 1197 (1967).
6. J. P. KUTNEY, I. H. SANCHEZ, and T. YEE. Org. Mass Spectrom. **8**, 129 (1974).
7. J. P. KUTNEY, I. H. SANCHEZ, T. YEE, J. D. LEMAN, and L. HURLEY. In preparation.
8. Y. ASAHINA. Proc. Imp. Acad. (Tokyo), **15**, 311 (1939).
9. Y. ASAHINA and K. OKASAKI. J. Pharm. Soc. Jpn. **63**, 626 (1943).
10. F. M. DEAN and A. ROBERTSON. J. Chem. Soc. 2166 (1955).
11. J. R. HANSON. Synthesis, 1 (1974).
12. J. P. KUTNEY and I. H. SANCHEZ. Can. J. Chem. **54**, 2795 (1976).
13. J. P. KUTNEY, I. H. SANCHEZ, and T. YEE. Can. J. Chem. **54**, 3713 (1976).
14. J. P. KUTNEY, I. H. SANCHEZ, and T. YEE. Can. J. Chem. **54**, 3721 (1976).
15. J. P. KUTNEY, I. H. SANCHEZ, and T. YEE. Can. J. Chem. **55**, 1073 (1977).
16. J. P. KUTNEY and I. H. SANCHEZ. Can. J. Chem. **55**, 1079 (1977).
17. J. P. KUTNEY and I. H. SANCHEZ. Can. J. Chem. **55**, 1085 (1977).
18. J. P. KUTNEY, J. D. LEMAN, P. J. SALISBURY, I. H. SANCHEZ, T. YEE, and R. J. BANDONI. Can. J. Chem. **55**, 2336 (1977).

Transition state determination by the X-method

PAUL G. MEZEY, MICHAEL R. PETERSON, AND IMRE G. CSIZMADIA
Lash Miller Chemical Laboratories, University of Toronto, Toronto, Ont., Canada M5S 1A1

Received December 17, 1976

PAUL G. MEZEY, MICHAEL R. PETERSON, and IMRE G. CSIZMADIA. Can. J. Chem. **55**, 2941 (1977).

A simple direct procedure to locate saddle points (transition states) on energy surfaces is described. The advantage of the method is that it may utilize effective unconstrained optimization techniques while convergence may occur only to saddle points and not to minima. Thus no further tests are needed to decide the nature of the critical point located. Both the simplex and conjugate gradients optimization techniques were applied within the framework of the proposed method (the X-method) and numerical tests were carried out on both 'mathematical' and 'chemical' model surfaces.

PAUL G. MEZEY, MICHAEL R. PETERSON et IMRE G. CSIZMADIA. Can. J. Chem. **55**, 2941 (1977).

On décrit une méthode directe et simple pour localiser les points d'énergie maximale (états de transition) sur des surfaces d'énergie. L'avantage de la méthode est qu'elle peut utiliser des techniques d'optimisation non-contraintes et effectives alors que la convergence peut n'apparaître qu'au niveau maximum sans apparaître au niveau minimum. Il n'est donc pas nécessaire d'avoir d'autres vérifications pour décider de la nature du point critique localisé. On a appliqué les méthodes simplex et conjuguées d'optimisation des gradients dans le cadre de la méthode proposée (la méthode X) et on a effectué plusieurs vérifications numériques sur les surfaces modèles 'mathématiques' et 'chimiques'. [Traduit par le journal]

Introduction

The determination of saddle points is of considerable importance in chemistry as they represent transition states between the stable species, which occur at local minima on energy surfaces. The energy difference between the transition state and the minimum is the energy barrier of the reaction.

Transition states are extremely difficult to observe experimentally and hence only few transition state geometries are even approximately known. The theoretical determination of saddle points also presents great difficulties (1–6), as the calculation of the total energy of a chemical system using the Hartree–Fock method is itself a laborious procedure. In addition, traditional geometry optimization methods, that is, direct unconstrained minimization of the calculated total energy, can lead only to minima of energy hypersurfaces. While these minima are characterized by a positive definite Hessian matrix **H** with elements

$$[1] \qquad H_{ij} = \frac{\partial^2 E}{\partial x_i \partial x_j}$$

i.e., all eigenvalues of **H** are positive, for saddle points an indefinite Hessian is characteristic with one (or for higher order saddle points several negative eigenvalues). Consequently, at a saddle point **H** has at least one eigenvector along which the energy decreases, hence any unconstrained energy optimization should fall back into one of the minima (7).

Constrained optimization of the energy can be utilized if the reactant and product of the reaction or conformational change are of a symmetry different from the symmetry of the transition state, as for the planar (D_{3h}) transition state for the pyramidal inversion of ammonia (C_{3v}). The energy may be minimized within a given symmetry which may lead to a saddle point (or a minimum). However, this method is not generally applicable.

One previously proposed method (3, 6) is based on the fact that all saddle points are among the solutions of the equation

$$[2] \qquad S_g \equiv \sum_{i=1}^{3N-6} \left(\frac{\partial E}{\partial x_i}\right)^2 = 0$$

To find these solutions, a direct minimization method may be applied to S_g. The difficulty with this method, however, is that any critical point (i.e. any point where grad $E = 0$) is a solution of [2], and **H** must also be evaluated to decide whether the solution found is a minimum, saddle point of some order, or a maximum. The method requires many energy and (more costly) grad E evaluations.

Method

The method of the present paper was designed to utilize the effectiveness of direct optimization methods, assuring, however, that convergence may occur to saddle points only.

The basic idea of the method is intuitively transparent and simple. After suitable rotation and translation of the coordinate frame, the equation of the simplest saddle surface, the hyperbolic paraboloid, shown in Fig. 1, becomes

$$[3] \qquad f(x_1,x_2) = \frac{x_1^2}{a^2} - \frac{x_2^2}{b^2} = cx_3$$

At the saddle point $x_1 = x_2 = 0$ and $f(0,0) = 0$. For all points with $x_3 = 0$ eq. 3 becomes

$$[4] \qquad \frac{x_1^2}{a^2} - \frac{x_2^2}{b^2} = \left(\frac{x_1}{a} - \frac{x_2}{b}\right)\left(\frac{x_1}{a} + \frac{x_2}{b}\right) = 0$$

Consequently, there are two horizontal lines that lie completely on the surface:

$$[5] \qquad \frac{x_1}{a} = \frac{x_2}{b} \quad \text{or} \quad \frac{x_1}{a} = -\frac{x_2}{b}$$

The crossing point of these lines is the saddle point, $x_1 = x_2 = 0$. This result is general for any quadratic saddle surface. Taking coordinate x_3 as the calculated energy, the horizontal lines are of constant energy. Also there is only one pair of horizontal lines that lie wholly on the surface, necessarily the pair that cross at the saddle point. Consequently, the determination of the saddle point is equivalent to the determination of the best fitting horizontal line pair on the surface, which can be accomplished by simple least square fitting.

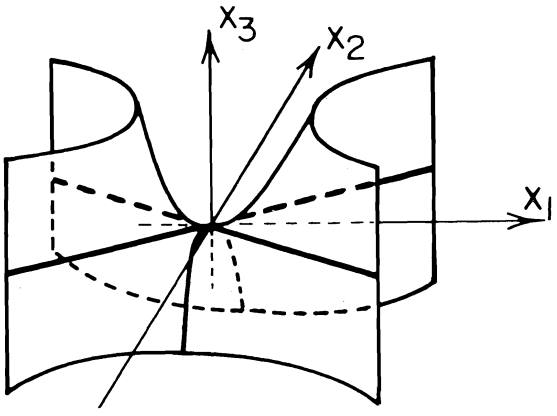

FIG. 1. Hyperbolic paraboloid: $x_1^2/a^2 - x_2^2/b^2 = cx_3$; horizontal lines: $x_1/a = \pm x_2/b$.

For saddle surfaces of chemical reactions only a neighbourhood of the saddle point can be regarded as quadratic, consequently the fit of line pairs is not perfect. As may be seen from Fig. 2, which is a contour plot of Fig. 1, two horizontal line segments that form an X (hence the name X-method) are needed to fit onto the surface. An attractive feature of the method is the fact that, after finding the two line segments, one of the two bisectors of the X gives a tangent to the reaction path. Consequently, a single determination of the saddle point also gives the direction of the reaction path at this point.

The concept of $n - 1$ linearly independent horizontal lines fitting to the saddle point is general for quadratic hypersurfaces in n dimensions (8), and may be utilized for the determination of saddle points. In this paper we present a simplified formulation of the general technique (8), that is suitable for the chemically most important $n = 3$ case, i.e. for saddle surfaces.

The actual formulation of the method for the determination of ordinary saddle points is outlined below. In the case of three dimensional saddle surfaces the energy may be written as

$$[6] \qquad \text{Energy} = E(\boldsymbol{x}) = E(x_1,x_2)$$

To define two line segments a reference vector $\boldsymbol{x}^0$ (the coordinates of the crossing point) and two direction vectors, $\boldsymbol{v}(\alpha)$ and $\boldsymbol{v}(\beta)$ are required. Let 'reference energy' E^0 be the energy of the crossing point. For any point of the 'horizontal X' the coordinate $x_3 = E^0$. The deviation of the line segment from the surface point $E(\boldsymbol{x})$ is

$$[7] \qquad d = E(\boldsymbol{x}) - E^0$$

The points $\boldsymbol{x}^{p_\alpha}$ and $\boldsymbol{x}^{p_\beta}$ along the arms of X are

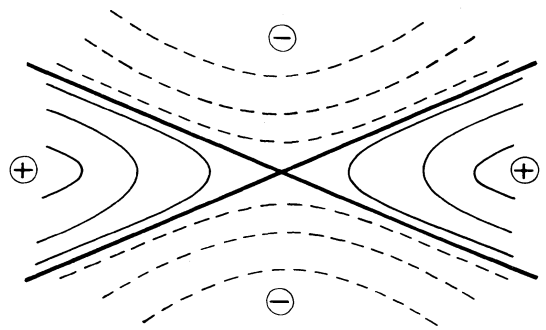

FIG. 2. Contour plot of a hyperbolic paraboloid showing the X of constant energy.

defined as

$$[8] \qquad \boldsymbol{x}^{p_\alpha} = \boldsymbol{x}^0 + p_\alpha z \boldsymbol{v}(\alpha)$$

$$[9] \qquad \boldsymbol{x}^{p_\beta} = \boldsymbol{x}^0 + p_\beta z \boldsymbol{v}(\beta)$$

Vectors $\boldsymbol{v}(\alpha)$ and $\boldsymbol{v}(\beta)$ are unit vectors, z is a suitably chosen positive scalar. The factors p_α and p_β give the multiples of $z\boldsymbol{v}(\alpha)$ and $z\boldsymbol{v}(\beta)$ to add to $\boldsymbol{x}^0$ in order to obtain a set of points on the lines defined by angles α and β with respect to the x_1 coordinate axis. The vectors $\boldsymbol{v}(\alpha)$ and $\boldsymbol{v}(\beta)$ may be generated by simple rotations,

$$[10] \qquad \boldsymbol{v}(\alpha) = \begin{pmatrix} \cos\alpha \\ \sin\alpha \\ 0 \end{pmatrix}$$

$$[11] \qquad \boldsymbol{v}(\beta) = \begin{pmatrix} \cos\beta \\ \sin\beta \\ 0 \end{pmatrix}$$

In order to fit an X to the saddle region of a surface the following function is to be minimized:

$$[12] \quad D = D(\boldsymbol{x}^0,\alpha,\beta) = \sum_{p=-k}^{k} \{[E(\boldsymbol{x}^{p_\alpha}) - E^0]^2 + [E(\boldsymbol{x}^{p_\beta}) - E^0]^2\}$$

where p_α and p_β take on values between $-k$ and k (k integer). The reference energy $E^0 = {x_3}^0$ may be restricted to $E^0 = E({x_1}^0,{x_2}^0)$, although faster convergence was achieved leaving ${x_3}^0 = E^0$, a free parameter just as the coordinates of points $\boldsymbol{x}^{p_\alpha}$ and $\boldsymbol{x}^{p_\beta}$. For quadratic surfaces, if $\boldsymbol{x}^0$ converges to the saddle point the reference energy E^0 becomes $E({x_1}^0,{x_2}^0)$, for intermediate $\boldsymbol{x}^0$ points, however, E^0 may deviate from $E({x_1}^0,{x_2}^0)$. For non-quadratic saddle surfaces, even if ${x_1}^0$ and ${x_2}^0$ are the coordinates of the saddle point, the E^0 value of the best fitting line segments is not necessarily equal to $E({x_1}^0,{x_2}^0)$. Since $\boldsymbol{x}^0$ involves three parameters, with α and β there are five parameters to be optimized.

In the course of the optimization the two angle parameters α and β must be different, since $\alpha = \beta$ would correspond to two coincident lines, that is, the X would collapse into one single line. If this single horizontal line fits onto the surface then the saddle point must fall on this line, nevertheless, the location of the saddle point along this line is still undetermined. Consequently, if the two angles approach each other beyond a preset limit, e.g. $|\alpha - \beta| < 1°$, then the optimization should be restarted with at least one of the angles altered. The choice of $\alpha_{new} = \alpha_{old}$, $\beta_{new} = \alpha_{old} + 90°$ appears to be appropriate, since then one well fitting line, $\boldsymbol{v}(\alpha)$, is preserved while the second line, $\boldsymbol{v}(\beta)$, fits rather poorly on the surface. The expected result of the new β in the next step is a translation along $\boldsymbol{v}(\alpha)$.

Two procedures to optimize these parameters were used: the simplex method (9) and the method of conjugate gradients (10–12). As the latter method requires the gradient of D, the following partial derivatives must be calculated:

$$[13] \qquad \frac{\partial D}{\partial {x_i}^0}, \frac{\partial D}{\partial \alpha}, \frac{\partial D}{\partial \beta}$$

Note that a similar application of the conjugate gradient method for the minimization of S_g (eq. 2) would require the evaluation of the *second derivatives* of the energy. For economy, during the testing of the X-method, the surfaces used were fitted by an analytic equation generated by a least-squares fitting procedure,[1] therefore, the explicit forms of [13] were available.

Results and Discussion

As would be expected, the conjugate gradients method generally converged to the minimum of D, i.e. to the saddle point in fewer function evaluations than the simplex method. However, in the simplex optimization procedure there is no need to evaluate the gradients and the actual optimization procedure follows a rather simple alogorithm. Consequently the conjugate gradient method appears to be more efficient in the most common cases of chemical applications, i.e., whenever the function evaluation is by far the most time consuming step. However, for functions that are readily calculable the simplex method is recommended. It appears that a rather crude approximation to the saddle point, based on chemical intuition, may yield a satisfactory starting point for the X-method.

As may be seen from Fig. 3, there are two additional 'parameters' in the X-method: (*1*) the number of points (NP) taken along each line segment, and (*2*) the distance (z) between those points. Both of these factors control the size of the X. A judicious choice of NP and z is necessary for, if the X is too small it may fit onto the surface reasonably well almost everywhere, while

[1]Programs SURFIT and SURFPLOT are available from the authors.

TABLE 1. A comparison of the simplex and conjugate gradients methods for the propanetriketone surface[a]

z	NP	ω_1 (rad)	ω_2 (rad)	Angle between the arms of the X (deg)	D evaluations: Simplex	D evaluations: Conjugate gradients[b]
0.02	3	1.5935	3.1951	64	131	99
	5	1.5927	3.1950	89	194	208
0.05	3	1.5926	3.1950	89	237	81
	5	1.5921	3.1950	89	236	87
0.10	3	1.5920	3.1950	89	221	124
	5	1.5901	3.1949	89	219	35
0.20	3	1.5896	3.1949	89	223	33
	5	1.5831	3.1946	89	165	23

[a]z, NP, ω_1, and ω_2 are defined in the text.
[b]One 'D evaluation' includes calculation of both D and grad D.

if it is too large, the approximation that the surface can be represented by a hyperbolic paraboloid is, in general, no longer valid.

As a chemical example, the calculated rotation–rotation surface of propanetrione (13), a surface of two coordinates, were taken. The conformational surface was calculated using the CNINDO program (14). An actual analytic approximation of this $E(\omega_1,\omega_2)$ surface by trigonometric functions is published elsewhere (13). The $\omega_1 = \omega_2 = 0$ conformation is defined by **1**. One saddle point occurs for ω_1 and ω_2 equal 1.5928 and 3.1950 rad (91° and 183°), respectively,[2] with a 90° angle between the arms of the X. The (91°,91°) and (89°,271°) conformations are minima.

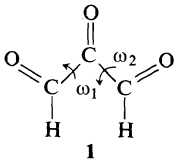

1

The results for this molecule are summarized in Table 1. They bear out the conclusions drawn above. It is also apparent from the table that the X-method performs almost equally well for NP = 3 or NP = 5, indicating that the number of function evaluations may be reduced to 3 per line. A proper choice for z seems to be important since for a z value of 0.02 the angle between the arms of the X is about 25° too small. For larger z, however, the correct angle was obtained consistently.

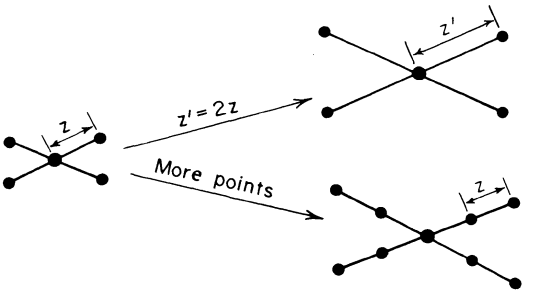

FIG. 3. Dependence of the size of the X on (*a*) the distance between the points and (*b*) the number of points per line segment.

Due to the large number of D evaluations, each involving 5 (for NP = 3) or 9 (for NP = 5) energy calculations, the computational costs appear too high to apply the method as an integral part of *ab initio* MO programs, such as the GAUSSIAN 70 program system (15). Instead, determination of saddle points on analytic surfaces fitted to the points calculated by such *ab initio* programs is recommended.

[2]The saddle point has been determined previously by the S_g method.

Acknowledgements

The authors express their thanks to the National Research Council of Canada for continuous financial support. One of us (M.R.P.) would like to thank the National Research Council of Canada for the award of a Postgraduate Scholarship.

1. J. W. McIver. Acc. Chem. Res. **7**, 72 (1974).
2. R. E. Shorter and J. W. McIver. J. Am. Chem. Soc. **97**, 3632 (1975).
3. J. W. McIver and A. Komornicki. J. Am. Chem. Soc. **94**, 2625 (1972).
4. F. Freeman. Chem. Rev. **75**, 439 (1975).
5. M. J. Dewar. Fortschr. Chem. Forsch. **23**, 1 (1971).
6. D. Poppinger. Chem. Phys. Lett. **35**, 550 (1975).
7. P. G. Mezey. Analysis of conformational energy hypersurfaces. *In* Progress in theoretical organic chemistry. Vol. 2. Elsevier. 1977. p. 127.
8. P. G. Mezey. To be published.
9. J. A. Nelder and R. Mead. Comput. J. **7**, 308 (1965).
10. R. Fletcher and M. J. D. Powell. Comput. J. **6**, 163 (1963).
11. W. C. Davidon. Variable metric method for minimization. A. E. C. Research and Development Report ANL-5990 (Rev.). 1959.
12. L. C. W. Dixon. Nonlinear optimization. Engl. Univ. Press, London. 1972.
13. S. Wolfe, J. E. Berry, and M. R. Peterson. Can. J. Chem. **54**, 210 (1976).
14. P. A. Dobosh. CNINDO, Program No. 141. Quantum Chemistry Program Exchange, Indiana University, Bloomington, Indiana.
15. W. J. Hehre, W. A. Lathan, R. Ditchfield, M. D. Newton, and J. A. Pople. GAUSSIAN 70, Quantum Chemistry Program No. 236, Indiana University, Bloomington, Indiana.

Polarographic studies of the interaction of boric acid with 1-hydroxy- and 1,2-dihydroxy-9,10-anthraquinones and -anthrahydroquinones

ARTHUR D. BROADBENT, W. DONALD HEWSON, HEATHER A. MCDONALD, AND RONALD J. MELANSON

Department of Chemistry, Mount Allison University, Sackville, N.B., Canada E0A 3C0

Received February 10, 1977

ARTHUR D. BROADBENT, W. DONALD HEWSON, HEATHER A. MCDONALD, and RONALD J. MELANSON. Can. J. Chem. **55**, 2946 (1977).

The interaction of 1-hydroxy-9,10-anthrahydroquinones (1-HOAHQ) with boric acid in aqueous borate buffer solutions at p*H* 9.5 causes a decrease in the anodic limiting current of the 1-HOAHQ and the simultaneous appearance of a new diffusion-controlled anodic wave at more positive potentials. This is attributed to the formation of a cyclic borate ester of the 1-HOAHQ involving the peri-hydroxyl groups. Ester formation is much slower but still complete when the boric acid – borate to 1-HOAHQ molar ratio exceeds 10–15. These esters are most stable at p*H* 7.5–9.5 and completely unstable above p*H* 12. 1,2-Dihydroxy-9,10-anthraquinones (1,2-diHOAQ) react with boric acid to give cyclic esters involving the 1- and 2-hydroxyl groups, but of lower stability than those from 1-HOAHQ. On reduction of a 1,2-diHOAQ in the presence of boric acid at p*H* 9.5, cyclic borate esters involving the peri-hydroxyl groups are rapidly produced in preference to those involving the ortho-hydroxyl groups.

ARTHUR D. BROADBENT, W. DONALD HEWSON, HEATHER A. MCDONALD et RONALD J. MELANSON. Can. J. Chem. **55**, 2946 (1977).

L'interaction d'hydroxy-1 anthraquinones-9,10 (1-HOAHQ) avez de l'acide borique en solutions aqueuses de borate tamponées à un p*H* de 9.5 produit une diminution du courant limitant anodique du 1-HOAHQ et l'apparition simultanée d'une nouvelle vague anodique contrôlée par la diffusion à des potentiels plus positifs. On attribue ces résultats à la formation d'un ester borate cyclique du 1-HOAHQ impliquant les groupes hydroxyles en péri. La formation d'ester est beaucoup plus lente mais elle demeure complète quand les rapports molaires acide borique – borate/1-HOAHQ dépassent 10–15. Ces esters sont les plus stables à des p*H* allant de 7.5–9.5 et complètement instables au dessus d'un p*H* 12. Les dihydroxy-1,2 anthraquinones-9,10 (1,2-diHOAQ) réagissent avec l'acide borique pour conduire à des esters cycliques impliquant les hydroxy-1 et -2 mais ces derniers ont une stabilité plus faible que ceux du 1-HOAHQ. Lors de la réduction d'un 1,2-diHOAQ en présence d'acide borique à un p*H* 9.5, des esters boriques cycliques impliquant les groupes hydroxyles en périe se forment rapidement de préférence à ceux impliquant les groupes hydroxyles en ortho.

[Traduit par le journal]

Introduction

The formation of chelated esters of boric acid and 1,2-diols is well-known (1–3). The rings in the cyclic esters are limited to five or six atoms, and the boron:diol ratio is usually 1:1 or 1:2.

1-Hydroxy-9,10-anthraquinones (1-HOAQ) form esters with boric acid in H_2SO_4 solution, but the esters readily hydrolyze in the presence of water, despite chelation between the boron and carbonyl oxygen atoms as in **1** (4). Russian workers have reported formation of chelated esters of boric acid and 1,2-dihydroxy-9,10-anthraquinones (1,2-diHOAQ) in aqueous solution, chelation occurring between the ortho-hydroxy groups as in **2** (5, 6).

Specific interaction between boric acid or borate ion and AQ derivatives was proposed by Furman and Stone (7) to account for anomalous polarographic results, but was subsequently repudiated by Gill and Stonehill (8), who observed normal polarographic behavior for such compounds in borate buffers. Polarographic studies of 1-HOAQ-4-SO_3H in ethanolamine and borate buffers of identical p*H*, and of the corresponding 9,10-anthrahydroquinone obtained by reduction (1-HOAHQ-4-SO_3H), indicated that

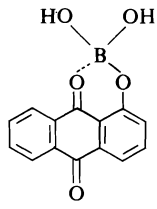

1

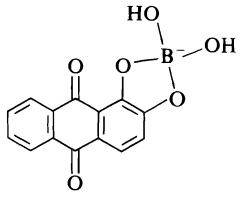

2

the AQ did not interact with boric acid while the AHQ gave an anodic wave at more positive potentials in the borate buffers attributed to oxidation of the ester **3** (9).

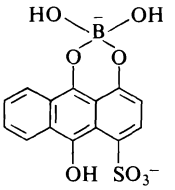

3

The purpose of the present study was to undertake a broader and more detailed study of the effect of boric acid on the polarography of hydroxyanthraquinone derivatives.

Results

The polarographic behavior of various 1-HOAQ, and the corresponding 1-HOAHQ generated by reduction with $Na_2S_2O_4$, was examined in borate and ethanolamine buffers of identical p*H*. After reduction of the AQ in borate buffer, or after addition of borate to an ethanolamine buffer solution of the AHQ, the anodic limiting current (i_d) for polarographic oxidation of the AHQ of half-wave potential ($E_{1/2}$) identical to that for polarographic reduction of the AQ, decreased with increasing time and simultaneously an anodic wave appeared at more positive potentials. The decrease in i_d for the 1-HOAHQ and the appearance of the new anodic wave were usually quite rapid in the borate buffer solution, total reaction taking only a few minutes or less with a 780-fold molar excess of boric acid – borate (except for 1-HOAHQ-4-SO_3H). The conversion was much slower but still complete when a 10–15-fold molar excess of boric acid – borate was added to the 1-HOAHQ. For ethanolamine buffer solutions of the 1-HOAHQ containing an equimolar quantity of boric acid – borate, the decrease in i_d for the 1-HOAHQ was very slow and when i_d became stable after several hours, both the anodic wave of the AHQ and the new anodic wave could be observed, the $E_{1/2}$ of the latter being about 10–20 mV more positive than in the presence of excess boric acid.

In the case of 1,5-diHOAHQ, no anodic wave was observed in the presence of excess borate buffer but the yellow solution had an intense green fluorescence. On adding a 10-fold molar excess of boric acid – borate to an ethanolamine buffer solution of 1,5-diHOAHQ (2.0×10^{-4} mol dm^{-3}), its anodic limiting current ($E_{1/2} = -581$ mV) decreased with simultaneous appearance of a new anodic wave with $E_{1/2} = -438$ mV. However, as i_d for the AHQ approached zero the limiting current of the new anodic wave ceased increasing and then gradually decreased to zero with development of the green fluorescence, indicating a stepwise reaction.

For every 1-HOAHQ, the decrease of i_d for the AHQ in the presence of borate buffer was accompanied by simultaneous changes in the visible absorption spectrum (Table 2). These changes were only slight and did not result in any observed colour changes. For 1,5-diHOAHQ, a stepwise reaction was again evident since addition of borate buffer to an ethanolamine buffer solution of the AHQ resulted in an initial increase in absorption at 399 nm followed by a decrease in absorption at this wavelength.

Addition of 2 mol $K_3Fe(CN)_6$ per mol of 1-HOAHQ in the borate buffer caused immediate oxidation and disappearance of the new anodic wave. The only observed oxidation product within 10 s was the corresponding 1-HOAQ, detected by its characteristic cathodic wave and absorption spectrum.

For the 1-HOAQ in borate buffer, and for both the 1-HOAQ and 1-HOAHQ in ethanolamine buffer, graphs of log $(i_d - i)/i$ vs. E were linear, but the slopes, although all constant for a given compound, were usually larger than the 29.7 mV expected for an electrode process involving transfer of 2 electrons per molecule, which was indicative of semiquinone formation (8, 9). For the ethanolamine buffer solutions, $E_{1/2}$ was identical with E_0' determined by redox potentiometry. Similar logarithmic analysis of the new anodic waves for the 1-HOAHQ in borate buffer gave linear graphs but the slopes were quite variable ranging from 29 mV for 1,8-diHOAHQ up to 45 mV for 1-HOAHQ-6-SO_3Na. In all cases, observed limiting currents were found to be directly proportional to the initial concentration of the 1-HOAQ and to the square root of the effective mercury height above the dropping mercury electrode.

Previous polarographic studies (10) indicated that 2-HOAQ and 2-HOAHQ and derivatives do not interact with boric acid as described above, and a similar result was found for

TABLE 1. Polarographic data for 1-HOAQ (2.0×10^{-4} mol dm^{-3}) and 1,2-diHOAQ (1.0×10^{-3} mol dm^{-3}) derivatives in ethanolamine and borate buffer solutions (p*H* 9.55, 25°C)

	AQ cathodic wave		AHQ anodic wave	
Compound (buffer)	$-E_{1/2}$ (mV)	i_d (μA)	$-E_{1/2}$ (mV)	i_d (μA)
1-HOAQ-4-SO_3H				
(Ethanolamine)	527	1.46	530	1.28
(Borate)	528	1.30	370	0.98
1-HOAQ-6-SO_3Na				
(Ethanolamine)	543	1.35	543	1.22
(Borate)	544	1.35	408	1.00
(Ethanolamine/$PhB(OH)_2$)	545	1.34	365	1.02
1-HOAQ				
(Ethanolamine/NaOH)	701	1.56	695	1.37
(Ethanolamine)	*		600	1.23
(Borate)	*		465	1.10
1,8-diHOAQ				
(Ethanolamine/NaOH)	720	1.53	712	1.35
(Ethanolamine)	*		610	1.30
(Borate)	*		497	1.11
1,5-diHOAQ				
(Ethanolamine/NaOH)	676	1.45	672	1.34
(Ethanolamine)	*		581	1.10
(Borate)	*		438†	
1,4-diHOAQ (35°)				
(Ethanolamine/NaOH)	727	1.41	724	1.32
(Ethanolamine)	*		‡	
1-NH_2AQ-6-SO_3Na				
(Ethanolamine)	691	1.33	688	0.96
(Borate)	689	1.32	683	1.03
1,2-diHOAQ				
(Ethanolamine)	747	7.37	748	6.99
(Borate)	673	4.41	670	7.01
	743	4.35		
1,2-diHOAQ-3-SO_3Na				
(Ethanolamine)	728	7.74	723	6.52
(Borate)	652	3.11	640	7.06
	731	4.62		

*Insoluble at p*H* 9.55.
†Disappears on standing.
‡Small irregular anodic currents unaffected by boric acid.

1-NH_2AHQ-6-SO_3Na (Table 1). It was observed that 1-NH_2AHQ-6-SO_3Na is not stable at p*H* 9.55 and its i_d decreases slightly with increasing time to a lower steady value with simultaneous appearance of two new cathodic waves with $E_{1/2}$ of -1124 and -1285 mV. This behavior is typical of tautomerism of the AHQ to the corresponding 10-hydroxy-9-anthrone derivative (10, 11) and no new anodic wave at potentials below 680 mV was observed in the presence of boric acid.

The variation of i_d for the new anodic wave with change in p*H* was examined for one compound (Fig. 1) and the optimum p*H* for its formation was established as 7.5–9.5. The $E_{1/2}$ data also provided information on acidic dissociation constants.

The rate of decrease of i_d for 1-HOAHQ-4-SO_3H, in the presence of a large molar excess of boric acid – borate, was sufficiently low that it could be conveniently measured. Graphs of log i_d vs. time were linear. The preliminary pseudo first order rate constant increased with increasing concentration of borate buffer at constant p*H*

TABLE 2. Visible absorption spectra of HOAQ derivatives at p*H* 9.55*

Compound	Borate buffer		Ethanolamine buffer	
	λ_{max} (nm)	$10^{-4}\ \varepsilon_{max}$	λ_{max} (nm)	$10^{-4}\ \varepsilon_{max}$
1-HOAQ-4-SO_3H	503	0.24	503	0.24
1-HOAHQ-4-SO_3H	389	1.17	394	1.68
	412(sh)	0.86		
1-HOAQ-6-SO_3Na	493	0.38	493	0.38
1-HOAHQ-6-SO_3Na	393	1.12	402	1.30
	418	1.04		
			395†	1.05
			417	0.97
1-HOAHQ	387	0.96	391	1.20
1,8-diHOAHQ	390	1.44	398	1.63
1,5-diHOAHQ	399	1.19	411	1.72
	425(sh)	0.69		
	452(sh)	0.47		
1,2-diHOAQ	465	0.67	522	0.86
1,2-diHOAHQ	384	0.74	393	1.17
	405	0.54	455	0.53
	450	0.49		
1,2-diHOAQ-3-SO_3Na	450	0.54	515	0.71
1,2-diHOAHQ-3-SO_3Na	387	0.66	396	0.82
	412	0.54	418(sh)	0.61
	462	0.41	468	0.39

*sh = shoulder.
†Ethanolamine buffer plus $PhB(OH)_2$.

and decreased on increasing the p*H* of the borate buffer in the range 8.9–10.3, with the tentative conclusion that the rate is first order with respect to boric acid.

The polarographic behavior of the 1,2-diHOAQ in the ethanolamine buffer appears quite normal. In the borate buffer, the 1,2-diHOAQ exhibits two overlapping cathodic waves, but only a single anodic wave was observed after reduction and this had $E_{1/2}$ corresponding to the first cathodic wave for the AQ. For the 1,2-diHOAQ in both buffer solutions, the total limiting current is diffusion controlled and corresponds to the transfer of two electrons per molecule. The first of the two cathodic waves observed in borate buffer, however, has a pronounced positive temperature coefficient, while the second cathodic wave decreases slightly with increasing temperature.

A more detailed examination of the polarography of 1,2-diHOAQ-3-SO_3Na in the borate buffer established that the first of the two cathodic waves ($E_{1/2} = -652$ mV) was only present in concentrated borate buffer solutions (Table 3). Such solutions of 1,2-diHOAQ-3-SO_3Na are yellow-range, while solutions in the ethanolamine buffer are violet (Table 2). In the solution composed of 60% of the ethanolamine buffer mixed with 20% of the borate buffer, 1,2-diHOAQ-3-SO_3Na did not give an observable cathodic wave at $E_{1/2} = -655$ mV, even though visible absorption spectra showed 50% conversion of the violet AQ to the yellow-orange chelated borate ester, e.g. **2**. Reduction of the AQ in this solution, however, gave a single anodic wave at $E_{1/2} = -650$ mV. With a 10-fold molar excess of boric acid – borate present, the visible absorption spectrum of 1,2-diHOAQ-3-SO_3Na was essentially identical with that of an ethanolamine buffer solution of the AQ with boric acid absent, but after reduction to the AHQ the spectrum of the latter rapidly changed to that typical of the AHQ in the presence of excess borate buffer. This coincided with a decrease in i_d of the AHQ anodic wave at $E_{1/2} = -735$ mV and the simultaneous growth of the new anodic current at $E_{1/2} = -655$ mV.

Discussion

The decrease of i_d of the AHQ, and the simultaneous appearance of a new anodic wave at more positive potentials, occurs only for 1-HOAHQ in the presence of boric acid. The

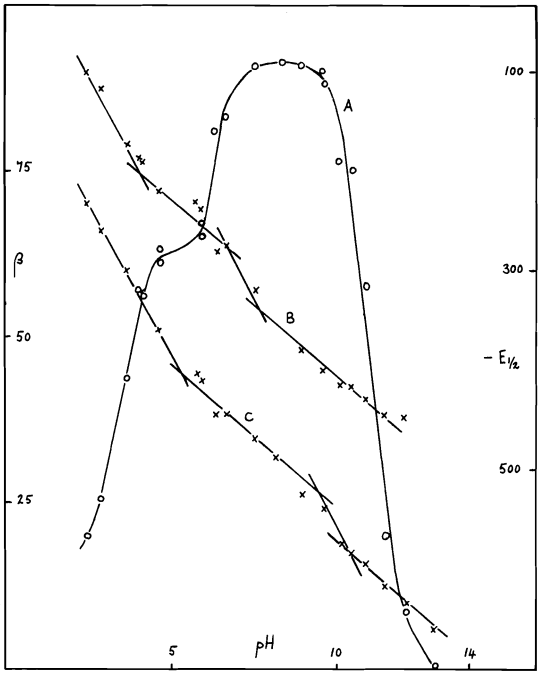

FIG. 1. Dependence of $E_{1/2}$ on pH for 1-HOAQ-6-SO_3Na (2.0×10^{-4} mol dm^{-3}) at 25°C (C) and the effects of pH on $E_{1/2}$ for the cyclic borate ester of 1-HOAHQ-6-SO_3Na (B) and upon the conversion (β) of 1-HOAHQ-6-SO_3Na to the ester (A) in the presence of boric acid – borate (2.0×10^{-3} mol dm^{-3}). $\beta = 100\ i_{ester}/i_{anodic}$.

new wave most probably arises because of anodic oxidation of a chelated borate ester (reaction 1).

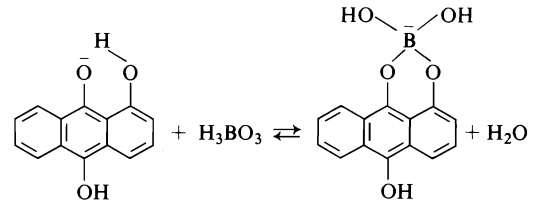

4 **5**

Chelated esters of *o*-diols are well-known but some involving peri-diols have been reported (12, 13). Polarographic and spectrophotometric examination of 1-HOAQ in the ethanolamine and borate buffers did not reveal any measureable interaction between the 1-HOAQ and boric acid. Borate esters of 1-HOAQ (e.g. **1**) are readily hydrolyzed in aqueous solution (4).

Reduction of a 1-HOAQ in the presence of excess borate buffer results in complete conversion of **4** into **5** and the observed changes in polarographic behavior of the 1-HOAHQ are quite specific for these compounds. The i_d of the new anodic wave is controlled by diffusion of **5** to the electrode surface but the electrode process is not polarographically reversible, possibly because the product of anodic oxidation of **5**, **1**, is rapidly hydrolyzed to the 1-HOAQ on the electrode surface.

Additional support for reaction 1 is provided by the observation of the analogous interaction of 1-HOAHQ-6-SO_3Na with benzene boronic acid, and by the obvious stepwise reaction of 1,5-diHOAHQ with boric acid, this being the only AHQ for which two rings involving boron could form. The observation of fluorescence towards completion of the reaction between boric acid and 1,5-diHOAHQ would be consistent with the rigid polycyclic structure of a dichelated ester.

In solutions containing equimolar boric acid, the formation of esters with a 1:2 boron: 1-HOAHQ ratio is possible, but no significant change in $E_{1/2}$ was observed.

The 1-NH_2AHQ-6-SO_3Na did not react with boric acid, in agreement with Böeseken's observations on *o*-aminophenols (14). There was also no indication of reaction of boric acid with reduced 1,4-diHOAQ. In strongly alkaline solution, the polarographic results for this compound seem quite normal, but at pH 9.5 1,4-diHOAHQ presumably exists as the tautomer 1,4-dioxo-1,2,3,4-tetrahydro-9,10-dihydroxyanthracene (15), which would account for the irregular behavior at this pH.

The variation of $E_{1/2}$ with changing pH for 1-HOAHQ-6-SO_3Na gave pK_a values of 5.2 and 10.2 for the AHQ and 9.4 for the AQ, these values being very similar to those found for 1-HOAHQ-4-SO_3H and 1-HOAQ-4-SO_3H (9). A pK_a of 5.33 for 1,8-dihydroxynaphthalene-3,6-disulfonate has been reported (16). Peri-diphenols exhibit enhanced acidity because of intramolecular hydrogen bonding, the non-hydrogen bonded proton at position 1 or 8 being most acidic.

Changes in slope in the plot of $E_{1/2}$ vs. pH for the chelated borate ester of 1-HOAHQ-6-SO_3Na (Fig. 1) must be considered with caution because of the polarographic irreversibility of the anodic oxidation process. These data did not give reliable pK_a values for the borate ester, which would have been valuable for interpretation of the dependence of the degree of chelate formation (β) on pH (Fig. 1). For 1-HOAHQ-6-

TABLE 3. Polarographic data for 1,2-diHOAQ-3-SO_3Na and 1,2-diHOAHQ-3-SO_3Na (4.0×10^{-4} mol dm^{-3}) at pH 9.55 and 25°C

Buffer composition*		1,2-diHOAQ-3-SO_3Na		1,2-diHOAHQ-3-SO_3Na	
Ethanolamine	Borate	$-E_{1/2}$ (mV)	i_d (μA)	$-E_{1/2}$ (mV)	i_d (μA)
80%	0	738	3.10	736	2.60
80%	0.4%	738	2.93	653	1.32
				743	1.07
80%	5.6%	736	2.84	654	2.50
				732	0
80%	14%	735	2.60	650	2.52
60%	20%	736	2.76	649	2.54
40%	40%	656	0.69	653	2.54
		735	2.19		
20%	60%	657	0.92		
		735	2.01		
0	80%	652	1.04		
		731	1.84		

*% by volume.

SO_3Na, optimum formation of **5** occurs at pH 7.0–8.5, where the maximum concentrations of **4** and boric acid exist. The decreased concentration of boric acid at pH > 9 must contribute to the decrease in β in alkaline solution. The stepwise decrease in β at pH < 7 must be a consequence of the acid–base equilibria of the reaction partners and products, or possibly of a noncyclic borate ester, which is a likely intermediate in the formation of **5**. Since β was determined using only a 10-fold molar excess of boric acid – borate, the values may be influenced by formation of chelate esters with a 2:1 AHQ:boron ratio.

Spectrophotometric measurements on the 1,2-diHOAQ showed that relatively high boric acid concentrations were required to give the chelated ester **2**. For 1-HOAHQ, total conversion to **5** was found at much lower boric acid concentrations. These results indicated that chelated esters such as **5** are formed more readily than **2**. An identical result was found for chelated esters of 1,8-dihydroxynaphthalene, when compared with those of 2,3-dihydroxynaphthalene (13, 16). The polarographic behavior of the 1,2-diHOAQ and 1,2-diHOAHQ can be interpreted in terms of the difference in stability of 1,2- (**6**) and 1,9-chelated borate esters (**7**) of 1,2-diHOAHQ. Reduction of **2** in the presence of boric acid results in preferential formation of **7** rather than **6** because in **7** the 1,9-oxygen atoms are closer together than the 1,2-oxygen atoms in **6**. The ester **7** is more stable as its formation involves less strain.

In the presence of a 10-fold molar excess of boric acid – borate, the 1,2-diHOAQ gave a single cathodic wave, with $E_{1/2}$ essentially identical to that in the ethanolamine buffer. On reduction, i_d for the 1,2-diHOAHQ rapidly decreased with simultaneous increase in the i_d for the anodic wave at more positive potentials, a process which proceeded to completion at boric acid concentrations insufficient to give detectable formation of **2**. The new anodic wave can be attributed to oxidation of **7** rather than **6**.

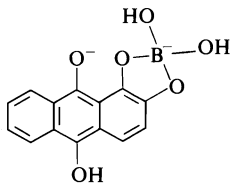

6

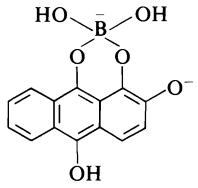

7

The occurrence of two cathodic waves on polarography of 1,2-diHOAQ at higher borate buffer concentrations can also be related to preferential formation of **7**. In such solutions, the 1,2-diHOAQ exist largely as **2**, but both species are polarographically active, being reduced to 1,2-diHOAHQ and **6**, respectively, with essentially identical $E_{1/2}$ values (−740 mV). At potentials corresponding to the foot of the first cathodic wave (−640 mV), the Nernst equilibrium concentration of 1,2-diHOAHQ at the electrode surface is very low, but, at high boric acid concentrations rapid conversion to **7** would disturb the redox equilibrium and result in further elec-

tron transfer to **2**. Thus, a significant current can arise at potentials more positive than anticipated. At lower boric acid concentrations, the rate of conversion of 1,2-diHOAHQ to **7** is insufficient to disturb the Nernst equilibrium. The pronounced positive temperature coefficient for the first cathodic wave indicates that its limiting current is controlled by a reaction rate. Although the exact pathway leading to **7** cannot be distinguished, the conversions **2** to 1,2-diHOAQ, **6** to 1,2-diHOAHQ or 1,2-diHOAHQ to **7** could be rate-controlling, assuming rapid electron transfer at the electrode surface. The $E_{1/2}$ of the first cathodic wave corresponds to that of the 1,2-diHOAHQ in borate buffer because of the redox equilibrium between **7** and its oxidation product. The situation is somewhat analogous to that where adsorption of the electrode product results in a polarographic wave at more positive potentials.

Experimental

The compounds examined were available from previous studies (18) or were commercial samples which were purified by chromatography on Al_2O_3 and recrystallization from ethanol and/or acetic acid. Solutions of the hygroscopic sulfonates were standardized by potentiometric titration of the AHQ with $K_3Fe(CN)_6$ solution.

Ethanolamine was dried by distillation of added benzene and purified by vacuum distillation. The buffer solutions were composed of 0.200 mol dm^{-3} ethanolamine/0.100 mol dm^{-3} HCl and of 0.078 mol dm^{-3} B_2O_3/0.100 mol dm^{-3} NaOH.

A known aliquot of the AQ solution was placed in the flat-bottomed, flanged reaction vessel, which was clamped to an aluminum plate fitted with sealed-in DME, salt bridge to the SCE, N_2 inlets and outlet for anaerobic operation, and burettes for N_2-saturated titrant solutions. The AQ were reduced by titration with freshly prepared, concentrated $Na_2S_2O_4$ solution in the appropriate buffer. HOAQ insoluble at p*H* 9.5 was dissolved in NaOH or NaOH–ethanolamine solution and, after reduction, the solutions were buffered to p*H* 9.5 by addition of B_2O_3 or HCl solution.

Polarograms were recorded on a Sargent Model XV1 polarograph at 25°C.

Acknowledgements

The authors wish to express their gratitude to the National Research Council of Canada for their support of this work and to Shell Canada Ltd. for the award of a Shell Canada Undergraduate Research Scholarship (to H.A.M.).

1. J. Böeseken. Adv. Carbohydr. Chem. **4**, 189 (1949).
2. H. Steinberg. Organoboron chemistry. Vol. 1. J. Wiley and Sons, Inc., New York. 1964.
3. R. P. Oertel. Inorg. Chem. **11**, 544 (1972).
4. E. H. Rodd (*Editor*). Chemistry of carbon compounds. Vol. IIIB. Elsevier Pub. Co. Inc., Amsterdam. 1956.
5. T. N. Nazarchuck. Ukr. Khim. Zh. **28**, 233 (1962).
6. L. S. Serdyuk and U. F. Silich. Ukr. Khim. Zh. **28**, 226 (1962).
7. N. H. Furman and K. G. Stone. J. Am. Chem. Soc. **70**, 3055 (1948).
8. R. Gill and H. I. Stonehill. J. Chem. Soc. 1845 (1952).
9. A. D. Broadbent and H. Zollinger. Helv. Chim. Acta, **49**, 1729 (1966).
10. A. D. Broadbent and E. F. Sommermann. J. Chem. Soc. B, 376 (1967); 519 (1968).
11. K. Brederek, F. Sommermann, and M. Diamantoglou. Chem. Ber. **102**, 1053 (1969); **103**, 1748 (1970).
12. M. Bartusek and L. Havelkova. Coll. Czech. Chem. Commun. **32**, 3853 (1967).
13. J. Böeseken, J. A. de Bruin, and W. E. van Rijswijk de Jong. Rec. Trav. Chim. **58**, 3 (1939).
14. J. Böeseken, W. Sturm, and G. Goettsch. Rec. Trav. Chim. **37**, 144 (1918).
15. S. M. Bloom and R. F. Hutton. Tetrahedron Lett. 1993 (1963).
16. L. Havelkova and M. Bartusek. Coll. Czech. Chem. Commun. **33**, 4188 (1968).
17. A. D. Broadbent and R. P. Newton. Can. J. Chem. **50**, 381 (1972).

Effect of the hexadecapole moment on the translational vibrational absorption by carbon-dioxide-type crystals[1]

E. WHALLEY
Division of Chemistry, National Research Council of Canada, Ottawa, Ont., Canada K1A 0R9

Received February 14, 1977

E. WHALLEY. Can. J. Chem. **55**, 2953 (1977).

The effect of a hexadecapole moment on the absorption by the translational vibrations of carbon-dioxide-type crystals has been calculated. If the qudrupole and hexadecapole moments have the same sign the absorption is relatively insensitive to the hexadecapole moment and the hexadecapole moment may reduce the integrated absorptivity to a minimum of about 0.85 of the value for the quadrupole moment alone. If the moments have opposite signs, the absorptivity can be increased significantly by a hexadecapole moment of the expected magnitude.

E. WHALLEY. Can. J. Chem. **55**, 2953 (1977).

On a calculé l'effet d'un moment hexadécapolaire sur l'absorption par des vibrations de translation de cristaux de type dioxyde de carbone. Si les moments quadrupolaires et hexadécapolaires ont le même signe l'absorption est relativement insensible au moment hexadécapolaire; le moment hexadécapole peut réduire l'absorptivité intégrée vers une valeur minimale d'environ 0.85 de la valeur du moment quadrupolaire seul. Si les moments ont des signes opposés, il peut y avoir une augmentation importante de l'absorptivité par un moment hexadécapolaire de grandeur attendue.

[Traduit par le journal]

A part of the interaction between molecules at relatively large distances is frequently described as being due to the permanent electrostatic moments acting according to classical laws. The electric field of dipole and successively higher moments decreases with increasing distance r from the molecule by the factors r^3, r^4, r^5, etc. Most observable effects are due either to the square of the field, when the observed effects should decrease by the factors r^6, r^8, r^{10}, etc., or to the square of the field gradient, when the effects should decrease by the factors r^8, r^{10}, r^{12}, etc. A particularly elegant way of studying this interaction is to measure the intensity of absorption of electromagnetic radiation by the translational vibrations of the molecules. For some crystals, such as those having the carbon-dioxide or halogen structures, symmetry requires that only the non-spherical part of the intermolecular interaction can contribute to the intensity, and so it can be studied in isolation.

Schnepp (1) has worked out the theory for the infrared intensity of crystals having the carbon-dioxide structure assuming that the quadrupole moment dominates, and it seems to agree reasonably well with experimental measurements on carbon dioxide (2, 3), although the experimental absorption intensity of solid nitrogen (4) is about one quarter of the calculated value, perhaps (4) because the large vibrational motion reduces the effective quadrupole moment. The theory is not adequate for all molecular crystals; for example, the absorption intensity of crystalline chlorine is (5) about 94 times that calculated by the theory adapted to the halogen structure.[2] This paper is concerned only with the crystals for which the multipole moment theory is an adequate approximation.

It is not clear that the multipole expansion converges rapidly at the intermolecular distances in the crystals, as the following arguments show. For approximate purposes, the charge distribution in a linear molecule like carbon dioxide can be represented by two equal and opposite point dipoles of moment μ, counted as positive if the positive end is on the inside, situated on the axis, and parallel to it a distance a from the center of the molecule. The nth moment of charge for such a distribution, when n is even, is characterized by the quantity $-2na^{n-1}\mu$. The integrated infrared intensity due to the nth even

[1]NRCC No. 16002.

[2]The calculations in this paper were made with the inaccurate published quadrupole moment of chlorine. A corrected value (6) results in the experimental integrated absorption intensity being 94 times greater instead of the published 35 times.

TABLE 1. Field derivatives (1) for carbon-dioxide-type crystals due to hexadecapole moments[a]

$$\frac{\partial E_x^i(p,q)}{\partial x(p,q)} = -\frac{H}{8r^7}(1365d_1^2d_3'^4 - 2520d_1d_3'^3l_1 - 315d_3'^4 - 90d_1^2d_3'^2 + 420d_3'^2l_1^2 + 840d_1d_3'l_1 - 75d_1^2 + 210d_3'^2 - 60l_1^2 - 15)_{p,q}$$

$$\frac{\partial E_y^i(p,q)}{\partial x(p,q)} = \frac{\partial E_z^i(p,q)}{\partial x(p,q)} = -\frac{H}{8r^7}(1365d_1d_2d_3'^4 - 1260d_1d_3'^3l_2 - 1260d_2d_3'^2l_1 - 90d_1d_2d_3'^2 + 420d_3'^2l_1l_2 + 420d_1d_3'l_2 + 420d_2d_3'l_1 - 75d_1d_2 - 60l_1l_2)_{p,q}$$

[a] r is the nearest-neighbor distance and the other symbols are defined by Schnepp (1).

moment is (1) $4n^2a^{2(n+1)}\mu^2/r^{2(n+2)}$ where r is the intermolecular distance, apart from an angular factor of the order unity and the product of some fundamental parameters. The ratio of the intensities due to, say, the quadrupole and hexadecapole moments, without the angular factor, is $4(a/r)^4$. An intermolecular distance is typically twice an intramolecular distance, and so this ratio is about $\frac{1}{4}$. The effects of quadrupole and hexadecapole moments may therefore be of the same magnitude. Furthermore, because the fields due to quadrupole and hexadecapole moments on the same molecule interfere destructively in some regions of space and constructively in others, it is not clear whether the effect of adding a hexadecapole moment is to increase or decrease the absorptivity from that of a quadrupole alone.

To determine if the hexadecapole moment of carbon dioxide and related molecules contributes significantly to the absorption intensity it is therefore necessary to work out the theory. This has been done following Schnepp's (1) procedure for the effect of the quadrupole moment. The derivatives of the field at the center of a molecule, due to the hexadecapole moment H of a linear neighboring molecule, with respect to the displacement of the molecule, are given in Table 1. The symmetry coordinates for the infrared-active vibrations of carbon-dioxide-type crystals are (7)

$$S_4(T_u) = \tfrac{1}{2}(x_1 - x_2 + x_3 - x_4)$$

$$S_7(T_u) = \tfrac{1}{2}(x_1 - x_2 - x_3 + x_4)$$

where x_q is the x cartesian displacement of molecule q, and molecules 1, 2, 3, and 4 are on the sites 000, $\frac{1}{2}\frac{1}{2}0$, $0\frac{1}{2}\frac{1}{2}$, and $\frac{1}{2}0\frac{1}{2}$. The derivatives of the fields at the centers of the molecules q are listed in Table 2, and the sums of the derivatives caused by the quadrupole (1) and hexadecapole moments are listed in Table 3.

If the moments have the same sign, the contributions of the quadrupole and hexadecapole moments to the field derivatives $\partial E_y/\partial S_4$ have opposite signs, and the contributions to $\partial E_z/\partial S_4$ and $\partial E_y/\partial S_7$ have the same sign. If the relatively small effect of the anisotropy of the polarizability is neglected, the integrated intensity A of the two bands is

$$[1]\quad A \propto 308160^2 + 286511H^2/r^4 - 733870H/r^2$$

where r is the nearest-neighbor distance. For a given θ, this expression has a minimum value as a function of H at

$$H/r^2 = 0.128070\theta$$

and the minimum value is $26\ 112\theta^2$ or 0.8475 of the absorption with zero hexadecapole moment. The experimental intensity for nitrogen is about one fourth of the calculated intensity (1, 4) and it appears that the effect of the hexadecapole moment cannot lower the absorption enough to account for more than a small fraction of the discrepancy. The integrated intensity is within 15% of the value for zero hexadecapole moment if $H/\theta r^2$ is between -0.27369 and $+0.78597$.

The intensity of absorption due to the quadrupole moment of a molecule with an insignificant hexadecapole, and that due to the hexadecapole moment of a molecule with an insignificant quadrupole, are equal, if the distance r is the same in both cases, when

$$H/\theta r^2 = 0.32795$$

A typical intermolecular distance in a crystal of small molecules is 4 Å, and then a pure hexadecapolar molecule having a moment of 5.25×10^{-42} esu cm^4 would have the same absorption intensity as a pure quadrupolar molecule having a moment of 10^{-26} esu cm^2. If the same molecule has a hexadecapole moment between -4.4 and 12.6×10^{-42} esu cm^4 its absorption intensity would be within 15% of that of the quadrupole acting alone.

The quadrupole moment of nitrogen is (8) -1.4×10^{-26} esu cm^2 and the hexadecapole

TABLE 2. The variation of the cartesian components of the electric field at the molecular centers with the symmetry coordinates S_4 and S_7 for carbon-dioxide-type crystals. The quantities listed are the coefficients of $H/r^7N^{1/2}$

Field derivative	Value for q = 1	2	3	4
$\frac{\partial E_x^q}{\partial S_4}$	$(1/3)700\sqrt{2}$	$-(1/3)700\sqrt{2}$	$(1/3)700\sqrt{2}$	$-(1/3)700\sqrt{2}$
$\frac{\partial E_y^q}{\partial S_4}$	$(1/3)800\sqrt{2}$	$(1/3)800\sqrt{2}$	$-(1/3)800\sqrt{2}$	$-(1/3)800\sqrt{2}$
$\frac{\partial E_z^q}{\partial S_4}$	$-80\sqrt{2}$	$-80\sqrt{2}$	$-80\sqrt{2}$	$-80\sqrt{2}$
$\frac{\partial E_x^q}{\partial S_7}$	$70\sqrt{2}$	$-70\sqrt{2}$	$-70\sqrt{2}$	$70\sqrt{2}$
$\frac{\partial E_y^q}{\partial S_7}$	$-80\sqrt{2}$	$-80\sqrt{2}$	$-80\sqrt{2}$	$-80\sqrt{2}$
$\frac{\partial E_z^q}{\partial S_7}$	0	0	0	0

TABLE 3. Sum of the contributions of the quadrupole and hexadecapole moments to the effect of the symmetry coordinates S_4 and S_7 on the electric field at the site of the qth atom. The factor $1/r^5N^{1/2}$ is omitted

Field derivative	Value for q = 1	2	3	4
$\frac{\partial E_x^q}{\partial S_4}$	$\frac{700}{3}\sqrt{2}\frac{H}{r^2}$	$-\frac{700}{3}\sqrt{2}\frac{H}{r^2}$	$\frac{700}{3}\sqrt{2}\frac{H}{r^2}$	$-\frac{700}{3}\sqrt{2}\frac{H}{r^2}$
$\frac{\partial E_y^q}{\partial S_4}$	$-100\sqrt{2}\left(\theta-\frac{8}{3}\frac{H}{r^2}\right)$	$-100\sqrt{2}\left(\theta-\frac{8}{3}\frac{H}{r^2}\right)$	$100\sqrt{2}\left(\theta-\frac{8}{3}\frac{H}{r^2}\right)$	$100\sqrt{2}\left(\theta-\frac{8}{3}\frac{H}{r^2}\right)$
$\frac{\partial E_z^q}{\partial S_4}$	$-4\sqrt{2}\left(13\theta+20\frac{H}{r^2}\right)$	$-4\sqrt{2}\left(13\theta+20\frac{H}{r^2}\right)$	$-4\sqrt{2}\left(13\theta+20\frac{H}{r^2}\right)$	$-4\sqrt{2}\left(13\theta+20\frac{H}{r^2}\right)$
$\frac{\partial E_x^q}{\partial S_7}$	$70\sqrt{2}\frac{H}{r^2}$	$-70\sqrt{2}\frac{H}{r^2}$	$-70\sqrt{2}\frac{H}{r^2}$	$70\sqrt{2}\frac{H}{r^2}$
$\frac{\partial E_y^q}{\partial S_7}$	$-4\sqrt{2}\left(13\theta+20\frac{H}{r^2}\right)$	$-4\sqrt{2}\left(13\theta+20\frac{H}{r^2}\right)$	$-4\sqrt{2}\left(13\theta+20\frac{H}{r^2}\right)$	$-4\sqrt{2}\left(13\theta+20\frac{H}{r^2}\right)$
$\frac{\partial E_z^q}{\partial S_7}$	0	0	0	0

moment is (9) about $\pm 3 \times 10^{-42}$ esu cm^2. If these acted independently, the hexadecapole would cause an absorption intensity of 0.1656 of the quadrupole, but if the two moments have the same sign the intensity due to the combined moments is 0.8454 of that of the quadrupole alone, which is nearly the smallest possible, and if they have the opposite sign, the absorptivity is 1.486 of the quadrupole acting alone. The quadrupole moment of carbon dioxide is -4.1×10^{-26} esu cm^2, and if the charge distribution is represented by two point dipoles located on the oxygen atoms the hexadecapole moment is $2a^2\theta$ where a is the C=O distance. The estimated hexadecapole moment is therefore -14×10^{-42} esu cm^4. The intensity of the combined quadrupole and hexadecapole moments is then 0.922 of that of the quadrupole alone. If the hexadecapole moment were 14×10^{-42} esu cm^4, the intensity would be about twice as high. An

accurate measurement of the intensity should therefore determine the sign of the hexadecapole moment if the effective quadrupole moment (4) were known.

The principal conclusions of this note are: (*1*) The hexadecapole moments of molecules like nitrogen and carbon dioxide contribute significantly to the fluctuation of the electric fields at the molecular centers in the crystal, but if the quadrupole and hexadecapole moments have the same sign, interference of the fields can reduce the absorption intensity of the translational vibrations to about 85% of that due to the quadrupole alone. The hexadecapole moment cannot therefore explain the difference between the experimental and theoretical absorption intensity of crystalline nitrogen. (*2*) Accurate infrared intensity measurements should allow the hexadecapole moment to be determined if $H/\theta r^2$ is significantly less than about -0.3 or greater than about 0.8.

1. O. SCHNEPP. J. Chem. Phys. **46**, 3983 (1967).
2. O. SCHNEPP and N. JACOBI. Adv. Chem. Phys. **22**, 205 (1972).
3. Y. A. SATATY and R. RON. J. Chem. Phys. **61**, 5471 (1974).
4. R. V. ST. LOUIS and O. SCHNEPP. J. Chem. Phys. **50**, 4177 (1969).
5. P. T. T. WONG and E. WHALLEY. Can. J. Phys. **50**, 1856 (1972).
6. P. T. T. WONG and E. WHALLEY. Can. J. Phys. **51**, 696 (1973).
7. S. H. WALMSLEY and J. A. POPLE. Mol. Phys. **8**, 345 (1964).
8. A. D. BUCKINGHAM, R. L. DISCH, and D. A. DUNMUR. J. Am. Chem. Soc. **90**, 3104 (1968).
9. G. BIRNBAUM and E. R. COHEN. Mol. Phys. **32**, 161 (1976).

ESCA investigations of Group IV derivatives. Part III. Binding energies for methyl substituted disilyl and digermyl chalcogenide series

JOHN E. DRAKE, CHRIS RIDDLE, H. ERNEST HENDERSON, AND BORIS GLAVINČEVSKI

Department of Chemistry, University of Windsor, Windsor, Ont., Canada N9B 3P4

Received February 3, 1977

JOHN E. DRAKE, CHRIS RIDDLE, H. ERNEST HENDERSON, and BORIS GLAVINČEVSKI. Can. J. Chem. **55**, 2957 (1977).

Core-level binding energies of all atoms are reported for the methyl substituted disilyl and digermyl chalcogenides, $(Me_nMH_{3-n})_2E$; where M = Si, Ge; E = O, S, Se, Te; n = 0, 1, 2, 3. Binding energies are also reported for the dimethyl series Me_2E; where E = O, S, Se, Te; for the hydrides H_2E; where E = O, S, Se; and for the methylhydrides MeEH; where E = O, S. Binding energy trends throughout these closely related series of compounds are discussed. The similarity of atomic charge patterns, deduced from the binding energies, for all molecules of a given silicon or germanium series are consistent with their ability to redistribute charge. The bonding mechanisms that make this possible are assessed.

JOHN E. DRAKE, CHRIS RIDDLE, H. ERNEST HENDERSON et BORIS GLAVINČEVSKI. Can. J. Chem. **55**, 2957 (1977).

On rapporte les énergies des liaisons au niveau du noyau de tous les atomes pour les chalcogénicides de disilyl et de digermyl substitués par des méthyles, $(Me_nMH_{3-n})_2E$; où M = Si, Ge; E = O, S, Se, Te; n = 0, 1, 2, 3. On rapporte aussi les énergies de liaisons pour les séries diméthyles Me_2E; où E = O, S, Se, Te; pour les hydrures H_2E où E = O, S, Se; et pour les méthylhydrures MeEH; où E = O, S. On discute des tendances des énergies des liaisons à travers toutes ces séries de composés extrêmement reliés. La similarité dans les répartitions des charges atomiques, déduite des énergies de liaison pour toutes ces molécules d'une série donnée de silicium ou de germanium, est en accord avec leur habilité à redistribuer les charges. On évalue les mécanismes de liaison qui rendent ces propriétés possible.

[Traduit par le journal]

Introduction

In earlier publications (1, 2) we reported core-level binding energies for various halogeno(methyl)-germanes and -silanes. Few ESCA studies of related Group VI B derivatives have appeared in the literature. Van Wazer *et al.* (3) reported silicon 2*p* level binding energies of several silicon–oxygen containing species and of the polymeric sulfide $(SiS_2)_\infty$; all recorded with solid or liquid samples. Their work was extended to similar derivatives of other Group IV B elements (4). Unfortunately, correlations between data collected from condensed phase samples are liable to be poor. Perry and Jolly have made extensive correlations between vapor-phase determined binding energies and calculated charge (5). In discussing the importance of *d*-orbital participation they concluded that "the data offer little support for the participation of *d*-orbitals in the bonding of silicon and germanium compounds" (6). Although they mainly reported binding energies for simple hydrides and halides, two Group VI derivatives, Me_2O and $(SiH_3)_2O$, were included (5, 6).

A communication by Pignataro *et al.* (7) reported sulfur $2p^{3/2}$ binding energies for a series of compounds C_6H_5—S—MMe_3 (M = C, Si, Ge, Sn, Pb). These were compared with the ^{13}C nmr chemical shifts of the ring carbon attached to sulfur. The authors concluded that the concept of ($p \rightarrow d$) π-bonding, from sulfur to the metal, M, is supported because the ionization energy of the sulfur $2p^{3/2}$ level increases along the series Si < Ge < Sn < Pb. However, the value of the binding energy of sulfur for C_6H_5—S—CMe_3 falls between those of the germanium and tin derivatives.

The hydrides $(MH_3)_2E$ (M = C, Si, Ge; E = O, S, Se, Te) have been the subject of a PES study (8) which assigned the observed bands to expected valence shell levels and concluded that the results were consistent with the existence of ($p \rightarrow d$) π-bonding for all compounds where M = Si or Ge. Glidewell (9) reconsidered these data, taking into account that the ionization energies for the lone-pairs of the Group VI B atoms increase in the order $(CH_3)_2E > (GeH_3)_2E > (SiH_3)_2E$. This leads him to conclude that the

SiH_3 and GeH_3 groups are not electron acceptors by means of ($p \rightarrow d$) π-interactions but are, in fact, net electron donors, relative to hydrogen. He suggested that a π-perturbation, caused by mixing of the $p\pi$ lone-pair orbital of M with another, more tightly bound, orbital of π-symmetry, is operative.

Bock *et al.* have published the results of extensive molecular orbital calculations assigning the PES of the two series $(CH_3)_n$—E—$(SiH_3)_{2-n}$; where n = 2, 1, 0 and E = O (10) and S (11). For the ether series they concluded that conformational changes are surprisingly important and that the bond-angle widening on substitution of silyl groups "may as much be a mechanism to relieve coulombic repulsions ... as it is partially a result of oxygen–silicon $p\pi$–$d\pi$ interaction" (10). For the sulfide series, they conclude that ($p \rightarrow d$) π-interactions from sulfur to silicon play a significant role in increasing the binding-energy of the sulfur "lone-pair" in the $2b_1$ molecular orbital; also the concentration of localized charge in the sulfides is far less critical than in the ethers (11).

With this limited background of ESCA and related studies, we decided to investigate a large number of silicon and germanium derivatives of Group VI B. As in our previous work (1, 2) we have measured core-level binding energies of *all* atoms in closely related series of compounds. In this way we can study the changes in binding energy and thence in charge throughout each molecule, as stepwise substitutions of atoms or groups occur. The series reported in this paper are the methyl substituted disilyl and digermyl chalcogenides, $(Me_nMH_{3-n})_2E$; where M = Si or Ge; E = O, S, Se, Te; n = 0, 1, 2, 3. Binding energies are also reported for the dimethyl series Me_2E; where E = O, S, Se, Te; for the hydrides H_2E; where E = O, S, Se; and for the methyl hydrides MeEH; where E = O, S.

Results and Discussion

Table 1 gives a complete listing of the binding energies observed in this work. The previously reported values for H_2O, MeOH, H_2S (12) and for Me_2O and $(SiH_3)_2O$ (5, 6) agree well with our values, allowing for minor calibration differences.

The quality of the peaks observed was dependent upon the stability of the samples under the instrumental operating conditions. All the tellurides had a tendency to decompose in the instrument and frequent cleaning of the system was necessary. Peak quality suffered slightly, due to the count rates being reduced. It is possible, however, that some of the minor anomalies in the data result from the effects of sample decomposition. Digermyl ether is known to be of low stability (13) and we were only able to obtain a weak spectrum, unsuitable for computer treatment, but of sufficient intensity to be able to fix the peak positions to ± 0.2 eV.

The most striking feature of the binding energy data is the *lack* of any substantial shifts. Intuitively, large differences might be expected between binding energies of oxygen compounds and those of the other Group VI B elements; or at least consistent trends along the series. Such is not generally the case.

Consider first the carbon 1*s* levels. Although it is true that in these levels the least change might be expected; along any series the value of the C 1*s* binding energy hardly varies, regardless of the nature of E. For example, in the series $(Me_3Ge)_2E$ the C 1*s* values are: 289.79 (E = O); 289.81 (S); 289.82 (Se); 289.84 eV (Te). A few individual values do vary within some series. For example, the sulfur compound has a value *ca.* 0.15 eV higher ($\Delta = +0.15$ eV) than the mean in the $(MeSiH_2)_2E$ series; the oxygen compound has $\Delta = -0.13$ for the $(Me_3Si)_2E$ series and $\Delta = +0.23$ for the $(Me_2GeH)_2E$ series. The few exceptions are random and could result from aberrations in the experimental determinations. Thus, the postulate that the R_3Ge— and R_3Si— groups (R = Me or H) behave as invariant moieties regardless of whether they are attached to oxygen, sulfur, selenium, or tellurium is generally upheld. Any changes in partial charges with a change in the central atom should therefore be most noticeable in the changing binding energies of the M and E atoms that are involved in mutual bonding. (The slight general increase in the value of the C 1*s* level as H atoms replace methyl groups in the R_3M moieties is possibly the result of changes in relaxation effects. In our studies on Me_3MX (X = Cl, Br, I) compounds (1) we noted a small but consistently higher value for corresponding C 1*s* levels when M = Ge compared with M = Si. In these Group VI B series, of the twelve possible corresponding pairs of compounds, the germanium compound has the higher C 1*s* value in all *four* $(Me_3M)_2E$ pairs of compounds, in three of the $(Me_2MH)_2E$ pairs, but only in *one* of the $(MeMH_2)_2E$ pairs.

TABLE 1. Observed binding energies of Group VI B derivatives

General formula	Core level*	E			
		O	S	Se	Te
H_2E	E	539.93†	170.51†	62.62	—
MeEH	C 1*s*	292.42†	291.41	—	—
	E	539.01	169.79		
Me_2E	C 1*s*	292.17‡	290.74	290.88	290.39
	E	538.50	169.28	61.52	47.02
$(SiH_3)_2E$	Si 2*p*	107.79‡	107.45	107.72	107.50
	E	538.17	168.60	61.91	46.93
$(MeSiH_2)_2E$	Si 2*p*	107.27	107.29	107.3	107.11
	C 1*s*	290.20	290.40	290.2	290.18
	E	537.80	168.29	61.6	46.60
$(Me_2SiH)_2E$	Si 2*p*	106.83	106.85	106.99	106.70
	C 1*s*	289.93	289.93	289.97	289.90
	E	537.32	168.00	60.89	46.94
$(Me_3Si)_2E$	Si 2*p*	106.57	106.57	106.58	106.67
	C 1*s*	289.64	289.79	289.79	289.85
	E	537.10	167.78	61.11	45.85
$(GeH_3)_2E$	Ge 3*d*	37.8	37.56	37.36	37.11
	E	537.2	168.66	61.05	46.86
$(MeGeH_2)_2E$	Ge 3*d*	36.82	36.92	36.93	36.78
	C 1*s*	290.25	290.10	290.14	290.10
	E	536.34	167.99	60.57	46.44
$(Me_2GeH)_2E$	Ge 3*d*	36.91	36.62	36.51	36.78
	C 1*s*	290.23	289.94	289.99	289.84
	E	536.45	167.85	60.28	46.11
$(Me_3Ge)_2E$	Ge 3*d*	36.53	36.50	36.40	36.39
	C 1*s*	289.79	289.81	289.82	289.84
	E	536.02	167.84	60.07	46.07

*The core levels observed and their average widths (eV) at half maximum height are: Si 2*p* (1.52), Ge 3*d* (1.53), C 1*s* (1.26), O 1*s* (1.21), S $2p^{3/2}$ (1.04), Se 3*d* (1.68), and Te 4*d* (1.35).
†These values compare with the following reported in Siegbahn *et al.* (10): H_2O, O 1*s* 539.7; MeOH, C 1*s* 292.3, O 1*s* 538.9; H_2S, S $2p^{3/2}$ 170.2.
‡These values compare with the following reported by Perry and Jolly (5, 6) and referenced to Ar $2p^{3/2}$ at 248.46 eV: Me_2O, C 1*s* 292.14, O 1*s* 538.86; $(SiH_3)_2O$, Si $2p^{3/2}$ 107.68, O 1*s* 538.46.

This could be related to the changes noted above on the introduction of H atoms into the R_3M moiety.)

In the Me_2E series the C *1s* binding energies are close for E = S, Se, Te but for E = O a considerably higher value results $\Delta = +1.5$ eV. A large shift, $\Delta = +1.0$ eV, occurs between MeOH and MeSH also. This is discussed later.

We next consider the silicon 2*p* and germanium 3*d* binding energies. Again, along a series, there is no dramatic change or general trend. All sixteen silicon values are contained within a 1.2 eV spread and all the germanium values are within a 1.4 eV spread. Thus for the $(Me_3Si)_2E$ series the experimental value for Si 2*p* is constant for E = O, S, and Se and rises for E = Te, whereas for the $(MeSiH_2)_2E$ series it is lowest for E = Te. The normal expectation, based on the relative Pauling electronegativities of O, S, Se, and Te would be for the silicon or germanium atoms to be relatively the most positive when attached to oxygen and therefore to have the highest binding energy for the $(R_3M)_2O$ species with a fairly regular decrease along the series $(R_3M)_2O \gg (R_3M)_2S > (R_3M)_2Se > (R_3M)_2Te$. Clearly the relative electron-withdrawing powers of the Group VI B elements are being equalized by some mechanism. Our studies on the halogeno(methyl)-silanes and -germanes also led to the conclusion that the halogens (Cl, Br, and I) all 'behave' as though they had similar electronegativities. On the basis of simple charge calculations, we rationalized that this comes about by the halogen *s*-orbitals being utilized to

varying degrees in the bonding between the halogen and the Group IV B element. Indeed, if the *s*-orbital participation is only *ca.* 5% greater for Cl than for Br and a further 3-5% greater for Br than for I, then the similarity of binding energies of the Me_nMX_{3-n} series can be explained (1, 2). It seems reasonable to assume a similar argument applies to the Group VI B elements. The increase in *s*-character would not be so large as to require a dramatic increase in the M—E—M angle, although it would require an angle greater than 90°. For example, the introduction of 10% *s*-character requires an increase in angle from 90 to 96°, which is approximately the angle at S or Se where known (12).

The same mechanism cannot be used for the $(R_3M)_2O$ compounds. It is well established (12) that the M—O—M bond angles are appreciably *larger* than the corresponding M—E—M angles (E = S, Se, Te). This wide angle requires an even larger involvement of the *s*-orbital of oxygen and hence a much higher binding energy is expected for the silicon and germanium atoms. However, bond angles of 120° and more are those required to maximize $(p \rightarrow d)$ π-bonding (10, 11, 14, 15). Where this is extensive, a significant redistribution of charge back from oxygen to silicon and germanium is expected, thus reducing the electropositive nature of the atoms and hence the value of their binding energies; exactly the situation that we have here. The fact that the binding energies are so close is possibly fortuitous because relaxation effects have been ignored. Nonetheless, a model that suggests that there are varying degrees of small *s*-orbital participation by S, Se, and Te to make the binding energies similar in $(R_3M)_2E$ compounds, without invoking *d*-orbital participation, is consistent with the observations. However, for $(R_3M)_2O$ species, where *s*-orbital participation must be large, the occurrence of $(p \rightarrow d)$ π-bonding appears to be the most logical rationalization. In the compounds MeOH and Me_2O, where $(p \rightarrow d)$ π-bonding cannot occur, there are indeed considerable binding energy shifts, the carbon atom being considerably more electropositive in the oxides than in the sulfides, selenides, or tellurides.

Finally, we examine the binding energies of the central atoms themselves. With three exceptions, $(MH_3)_2S$, $(Me_3M)_2S$, and $(Me_3M)_2Te$), all of the silicon compounds have higher binding energies for the core-level of the Group VI B elements than do the germanium analogues. In this respect the results parallel those found for the lone-pair orbitals in the two series $(SiH_3)_2E$ and $(GeH_3)_2E$ (E = O, S, Se) (5). Within the silicon and germanium compounds, as hydrogen atoms successively substitute for methyl groups, within the R_3M moieties, there is a corresponding general increase in the binding energies of all levels measured. Such changes could be the result of relaxation effects, however, the changes are as predicted if it is assumed that the hydrogen atom is 'behaving' as a weakly electronegative halogen atom. This is not unreasonable as the Si—H and Ge—H bonds are polarized with $H^{\delta-}$ (16). Thus the successive introduction of the more electronegative hydrogen atom increases all the binding energies within the molecule. For example, the binding energy increases in the $(R_3Si)_2O$ column as R = Me → H are: Δ O $1s = +1.07$; Δ Si $2p = +1.22$; and Δ C $1s = +0.70$ eV. With few exceptions, all columns show the same trend. This is exactly as we found for the Me_nGeX_{4-n} (X = Cl, Br, I) series (1, 2).

The collected data do not allow a definitive analysis of bonding mechanisms in the Group VI B compounds. Assuming that the changes in binding energy reflect the *overall* changes in charge distribution that result from a variety of competing 'mechanisms', such as $(p \rightarrow d)$ π-bonding, varying *s*-orbital participation, and inductive effects, then only the dominant mechanism, and not the relative importance of competing mechanisms, will be reflected in the data.

Experimental

Core-electron binding energies were determined on a McPherson ESCA-36 photoelectron spectrometer using magnesium K_α X-radiation (1253.6 eV) for photoelectron excitation. Samples were introduced in the vapor phase at pressures close to 5×10^{-5} Torr. Argon gas was bled in to form 20% of the total sample. Binding energies in excess of 120 eV were referenced to the argon $2p^{3/2}$ level at 248.63 eV (17). All other binding energies were referenced indirectly, via Ar $2p^{3/2}$, to the neon 2*s* level at 48.47 eV (17).

Details of the data accumulation procedures adopted and of the curve-fitting program used to compute the binding energies are given in Part I (1). The reproducibility from separate runs was such that binding energies are quoted to ± 0.05 eV for C 1*s*, Si 2*p*, O 1*s*, and S $2p^{3/2}$ and to ± 0.10 eV for Ge 3*d*, Se 3*d*, and Te 4*d*.

The observed binding energies are listed in Table 1.

Materials

Hexamethyldisiloxane and hexamethyldisilthiane were obtained commercially (Petrarch Systems) as were dimethyl ether (Matheson Gas Products), dimethyl sulfide,

methanol, methanethiol (Aldrich Chemical Co.), dimethyl selenide, and dimethyl telluride (Research Organic/Inorganic Chemical Corp.). Hydrogen sulfide, hydrogen selenide, and hydrogen telluride were prepared by hydrolysis of the corresponding aluminum compound, Al_2E_3 (E = S, Se, Te) (18, 19). The remaining methyl substituted disilyl and digermyl chalcogenides, $(Me_nMH_{3-n})_2E$ (M = Si, Ge; E = O, S, Si, Te; n = 0, 1, 2, 3) were prepared *either* by reaction of the corresponding silyl or germyl halide with a solution of the requisite lithium salt, Li_2E (20–23), *or* by cleavage of the corresponding bismethylgermanium carbodiimide with the appropriate Group VI hydride, H_2E (21, 24, 25).

All samples were distilled on the vacuum line and their purity checked by ir, Raman, and nmr spectroscopy. Where appropriate, vapor pressure determinations were also made.

Acknowledgment

We wish to thank the National Research Council of Canada for financial support.

1. J. E. Drake, C. Riddle, and L. Coatsworth. Can. J. Chem. **53**, 3602 (1975).
2. J. E. Drake, C. Riddle, H. E. Henderson, and B. Glavinčevski. Can. J. Chem. **54**, 3876 (1976).
3. R. Nordberg, H. Brecht, R. G. Albridge, A. Fahlman, and J. R. van Wazer. Inorg. Chem. **9**, 2469 (1970).
4. W. E. Morgan and J. R. van Wazer. J. Phys. Chem. **77**, 964 (1973).
5. W. B. Perry and W. L. Jolly. Inorg. Chem. **13**, 1211 (1974).
6. W. B. Perry and W. L. Jolly. Chem. Phys. Lett. **17**, 611 (1972).
7. S. Pignataro, L. Lunazzi, C. A. Boicelli, R. Di Marino, A. Ricci, A. Mangini, and R. Danieli. Tetrahedron Lett. **52**, 5341 (1972).
8. S. Cradock and R. A. Whiteford. J. Chem. Soc. Faraday II, 281 (1972).
9. C. Glidewell. Inorg. Chim. Acta, **13**, L 11 (1975).
10. H. Bock, P. Mollère, G. Becker, and G. Fritz. J. Organomet. Chem. **61**, 113 (1973).
11. P. Mollère, H. Bock, G. Becker, and G. Fritz. J. Organomet. Chem. **61**, 127 (1973).
12. K. Siegbahn, C. Nordling, G. Johansson, J. Hedman, K. Hamrin, U. Gelius, T. Bergmark, L. O. Werme, R. Manne, and Y. Baer. ESCA applied to free molecules. North-Holland, Amsterdam, and American Elsevier, New York, NY. 1969.
13. S. Cradock and E. A. V. Ebsworth. J. Chem. Soc. A, 1422 (1968).
14. J. E. Drake and C. Riddle. Q. Rev. **24**, 263 (1970) and references cited therein.
15. E. A. V. Ebsworth. *In* Organometallic compounds of the Group IV elements. Vol. 1, Part 1. Dekker, NY. 1968.
16. A. P. Altshuller and L. Rosenblum. J. Am. Chem. Soc. **77**, 272 (1955).
17. G. Johansson, J. Hedman, A. Berndtsson, M. Klasson, and R. Nilsson. J. Electron. Spectrosc. **2**, 295 (1973).
18. A. Tian and S. Aubanel. C. R. Trav. Fac. Sci. Marseille, **1**, 97 (1942).
19. G. R. Waitkins and R. Shutt. Inorg. Synth. **2**, 183 (1946).
20. D. W. H. Rankin. Inorg. Synth. **15**, 182 (1974).
21. S. Cradock, E. A. V. Ebsworth, and D. W. H. Rankin. J. Chem. Soc. A, 1628 (1969).
22. H. Bürger, V. Goetze, and W. Sawodny. Spectrochim. Acta, **24**A, 2003 (1968).
23. J. E. Drake, B. M. Glavinčevski, R. T. Hemmings, and H. E. Henderson. Can. J. Chem. To be published.
24. S. Cradock and E. A. V. Ebsworth. J. Chem. Soc. A, 1423 (1968).
25. J. E. Drake, R. T. Hemmings, and H. E. Henderson. J. Chem. Soc. Dalton, 366 (1976).

Liquid-junction potentials in ethylenediamine: Attempted calculations and evaluations using concentration cells

SURAJ P. MAKHIJA[1]

Department of Chemistry, Indiana University, Bloomington, IN, U.S.A. 47401

Received December 17, 1976

SURAJ P. MAKHIJA. Can. J. Chem. **55**, 2962 (1977).

Concentration cells of the type M(Hg)|MX(1)||MX(2)|M(Hg), where M(Hg) is potassium amalgam or sodium amalgam, were investigated with three electrolytes, potassium bromide, potassium iodide, and sodium iodide. An attempt was made to determine the necessity and magnitude of liquid-junction potential corrections. Only in the case of sodium iodide are the ionic mobilities of cation and anion quite different in ethylenediamine, and liquid-junction potential corrections are necessary to obtain agreement between observed and calculated data. The limiting equations of Nernst and of Lewis and Sargent were found to be appropriate for calculating liquid-junction potentials in ethylenediamine, provided that calculated activities were used in these equations.

SURAJ P. MAKHIJA. Can. J. Chem. **55**, 2962 (1977).

On a étudié, à l'aide des trois électrolytes, bromure de potassium, iodure de potassium et iodure de sodium, des cellules de concentration de types M(Hg)|MX(1)||MX(2)|M(Hg), où M(Hg) est un amalgame de potassium ou de sodium. On a effectué des essais pour déterminer la nécessité et l'amplitude des corrections pour les potentiels de jonction-liquide. Il n'y a que dans le cas de l'iodure de sodium où les mobilités ioniques du cation et de l'anion sont très différentes dans l'éthylènediamine et où des corrections de potentiel de jonction-liquide sont nécessaires pour obtenir une bonne concordance entre les valeurs observées et les valeurs calculées. On a trouvé que les équations limites de Nernst et de Lewis et Sargent sont appropriées pour calculer les potentiels de jonction-liquide dans l'éthylènediamine à condition que l'on utilise une activité calculée dans ces équations.

[Traduit par le journal]

Introduction

Whenever solutions containing various electrolytes are brought into contact a potential develops at the interface. This potential is known as liquid-junction potential, E_j, and develops due to mobilities of various ions across the interface. There are three types of liquid junctions. The simplest of all involves the same electrolyte at different activities, such as 0.1 *M* NaBr|0.01 *M* NaBr. Both sodium and bromide ions diffuse from more concentrated to less concentrated solution with a driving force proportional to the concentration gradient: the sign and magnitude of E_j are independent of which ion of the salt is involved in the electrode reaction.

This type of liquid-junction potential is approximated by an equation due to Nernst

$$[1] \qquad E_j = (1 - 2t^-)\frac{RT}{F}\frac{(M^+)_1}{(M^+)_2}$$

where t^- is the transference number of the anion, $(M^+)_1$ and $(M^+)_2$ are the activities of the cation in the two solutions, and the other terms have their usual meanings. It is obvious from the above equation that $E_j = 0$ if $t^- = 0.5$.

Various concentration cells of the type

M(Hg)|MX(I)||MX (2)|M(Hg)

were studied and an attempt was made to estimate the necessity and magnitude of corrections for liquid-junction potentials in non-aqueous solvents. Three electrolytes, KBr, KI, and NaI, were investigated.

The overall potential of a concentration cell is the difference between the potentials of the two electrodes, i.e.,

$$E_1 = E_{m+m(Hg)} + \frac{RT}{nF}\ln (M^+)_1$$

and

$$E_2 = E_{m+m(Hg)} + \frac{RT}{nF}\ln (M^+)_2$$

Therefore

$$[2] \quad E_{cell} = E_1 - E_2 = \frac{RT}{nF}\ln\frac{(M^+)_1}{(M^+)_2} - E_j$$

[1]Present address: Department of Chemistry, Alabama State University, Montgomery, AL, U.S.A. 36101.

The potential of the concentration cell is thus seen to be independent of the standard potentials of the electrodes, but to depend upon the ratio of the activities of metal ion in the two solutions and the liquid-junction potential.

In this study, an attempt was made to test out theories for the calculation of activities and liquid-junction potentials. If the exact expressions (1) for ionic activities are substituted into eq. 2, we get

$$[3]\quad E_{obs} = E_{cell} - E_j = E_1 - E_2 - E_j = \frac{RT}{nF} \times \ln \frac{(1 + 4\sum_{MX(1)} K_{mx} f_i^2)^{1/2} - 1}{(1 + 4\sum_{MX(2)} K_{mx} f_i^2)^{1/2} - 1} \times \frac{f_{i(2)}}{f_{i(1)}} - E_j$$

in which $\sum_{MX}$ is the stoichiometric concentration of 1:1 electrolyte, f_i is the activity coefficient, and K_{mx} is the ion-pair association constant. Conductance studies (2) have shown that the cations and anions of KBr and KI have approximately equal ionic mobilities in ethylenediamine, while NaI has a cation and anion with appreciably different mobilities. If the theories for liquid-junction potentials are correct, then only sodium iodide among the above three electrolytes should require liquid-junction potential corrections in order to obtain a reasonable fit of the experimental data to theoretically calculated curves.

As the system

$$M(Hg)|MX\ (1)||MX\ (2)|M(Hg)$$

involves only the simple type liquid-junction potential, the corrections were made using eq. 1. Since $t^+ \simeq t^-$ for K^+, Br^-, and I^- ions and t^+ and $t^- = 1$, eq. 1 shows that the E_j correction will approach zero for solutions containing KBr or KI. In case of Na^+ and I^-, however, $t^+ < t^-$ and the E_j corrections become significant.

Experimental

Material

Commercially available 98–100% ethylenediamine was doubly distilled from calcium hydride under reduced pressure in an atmosphere of purified nitrogen and was stored in a glass stoppered bottle. All alkali metal halides were of analytical reagent grade quality and were dried for 6 to 8 h in a vacuum at approximately 100°C. Sodium amalgam and potassium amalgam (both two-phase) were prepared by electrolyzing 5% solutions of NaOH or KOH in methanol with a mercury pool as cathode and a platinum wire as anode. Excess hydroxides were washed with methanol.

The dissolution of alkali metal halides was hastened by grinding the salts finely and using a rotatory disk for continuous shaking of the solution.

The reference electrodes were prepared by adding an ethylenediamine solution containing a fixed concentration of the alkali metal halide into compartments of the demountable H-shaped cell which also contained the two-phase alkali metal amalgam.

Instruments and Cells

An H-shaped cell of the following type was used for carrying out the experimental work.

M(Hg), MX(*i*)	MX	MX	MX(*ii*), M(Hg)
Reference	Salt bridge 1	Salt bridge 2	Indicating compartment

In the above cell, M refers to potassium or sodium and X to bromide or iodide. MX(*i*) denotes the potassium or sodium salt solution having a constant concentration while MX(*ii*) refers to the solution with varying con-

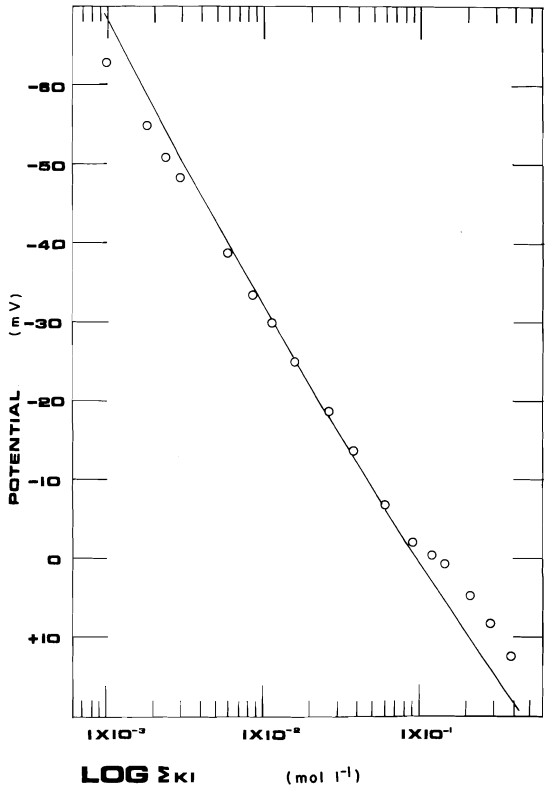

FIG. 1. Plot of potential (mV) of concentration cell K(Hg)|KI(1)||KI(2)|K(Hg) as a function of log Σ_{KI}. Open circles: experiment; solid line: potentials calculated with eq. 3.

centration of MX. Contact to the metal amalgam in the reference and indication electrode compartments were made by fusing a platinum wire through the glass at the bottom of each compartment

The indicating electrode and reference electrode were separated by two salt bridges, one of which (S.B.1) contained a standard solution of alkali metal halide in ethylenediamine and the other of which (S.B.2) contained the same stoichiometric concentration of alkali metal halide as the indicating electrode. The concentrations of the alkali metal halide in salt bridge 2 and in the indicating electrode compartment were changed simultaneously and equally by adding appropriate amounts of a concentrated solution of MX to both compartments with a buret. Two bridges containing MX were introduced in order to avoid any direct mixing of the solutions in the reference and indicating electrode compartments. Dry, prepurified nitrogen gas was bubbled through the indicating compartment to achieve good mixing and to remove any oxygen which might have been dissolved.

A null-type Rubicon potentiometer was used to measure all the potentials. A Honeywell high-gain electronic null-indicator, Model No. 104 WIG, was used with the potentiometer.

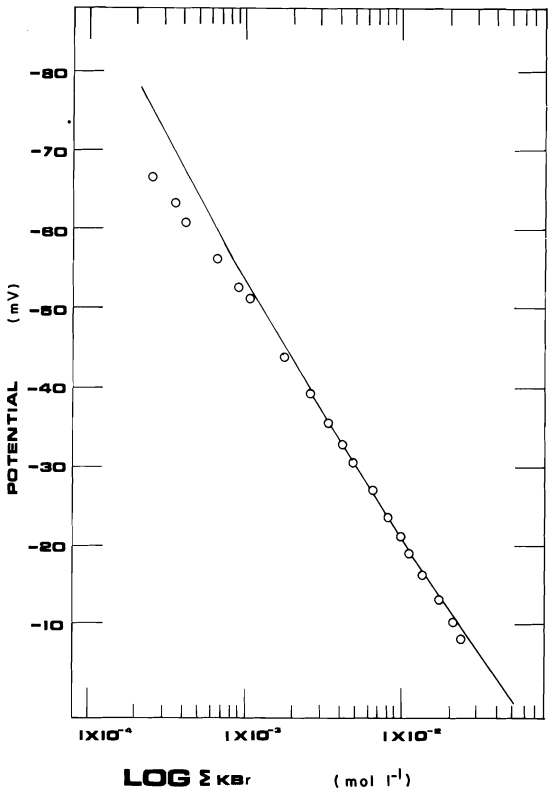

FIG. 2. Plot of potential (mV) of concentration cell K(Hg)|KBr(1)||KBr(2)|K(Hg) as a function of log Σ_{KBr}. Open circles: experiment; solid line: potential calculated with eq. 3.

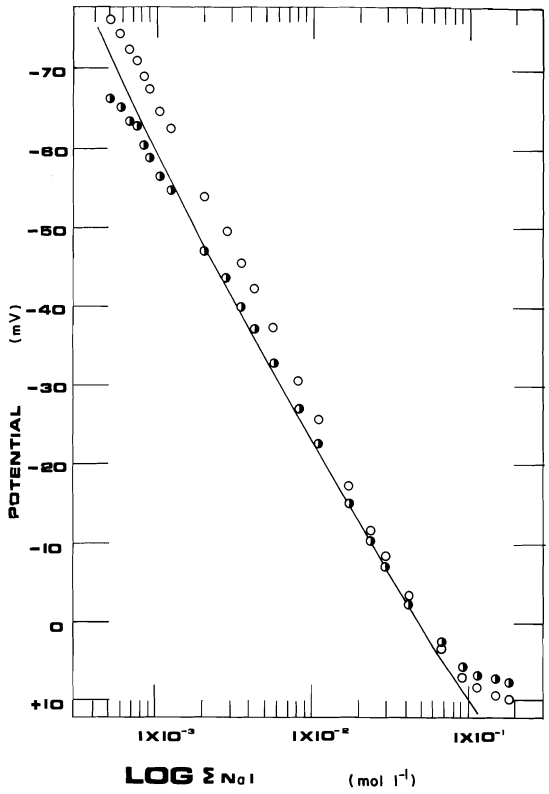

FIG. 3. Plot of potential (mV) of concentration cell Na(Hg)|NaI(1)||NaI(2)|Na(Hg) as a function of log Σ_{NaI}. Open circles: experimentally observed potentials; half-shaded circles: experiment corrected for liquid-junction potentials; solid line: potential calculated with eq. 3.

Results and Discussion

The potentials obtained with KI, KBr, and NaI were measured over a wide range of concentration.[2] Theoretical potentials, E_{calc}, are shown as solid lines in Figs. 1, 2, and 3 and were calculated as a function of electrolyte concentrations using eq. 3.

Experimental points as observed and after correction for liquid-junction potential, if any, are plotted for comparison with theoretical points. It is observed that liquid-junction potential corrections are necessary in the case of sodium iodide, i.e., for a concentration cell in which the cations and anions have different mobilities. In the cases of potassium bromide and iodide, where t^+ and t^- are very close

[2]Complete set of the actual experimental data is available, at a nominal charge, from the Depository of Unpublished Data, CISTI, National Research Council of Canada, Ottawa, Canada K1A 0S2.

to 0.50, the liquid-junction corrections are not necessary and good agreement between the theoretical lines and uncorrected experimental points is observed over a reasonably wide range of concentration.

A careful examination of Figs. 1, 2, and 3 shows that calculated curves fit the experimental data best at intermediate stoichiometric concentrations (between 1×10^{-3} to 1×10^{-1} M) of alkali metal halides. Deviations at higher concentrations (i.e., 1×10^{-1} M) are an indication of the probable formation of triple and perhaps quadruple ions (3).

Acknowledgement

The author wishes to acknowledge the support and suggestions given by Professor Ward B. Schaap of Indiana University.

1. W. B. SCHAAP, R. SEIFKER, R. BAYER, P. BREWSTER, J. KIM, and F. SCHMIDT. Rec. Chem. Prog. **22**, 197 (1961).
2. F. PUSPANADEN. Ph.D. dissertation, Indiana University, Bloomington, IN, U.S.A. 1966. p. 50.
3. H. LAITINEN and W. HARRIS. Chemical analysis. 2nd ed. McGraw-Hill, New York. 1975. pp. 68–69.

Oxygen-18 isotope effects in the liquid water–pyridine system as a probe of intermolecular forces

ROBERT H. BETTS, JAN BRON, WAYNE D. BUCHANNON, AND KWOK-YING D. WU

Department of Chemistry, University of Manitoba, Winnipeg, Man., Canada R3T 2N2

Received March 11, 1977

ROBERT H. BETTS, JAN BRON, WAYNE D. BUCHANNON, and KWOK-YING D. WU. Can. J. Chem. **55**, 2966 (1977).

Oxygen-18 exchange between gaseous carbon dioxide and water in liquid water–pyridine mixtures is used as a probe for changes in intermolecular forces when the composition of the system is changed from pure water to pure pyridine. In agreement with results obtained previously by other methods, it is found that the interaction energy of an 'average' water molecule with the medium decreases when the mole fraction of pyridine is varied from zero to unity. The experimental results are related to the vapour pressure isotope effect, $P(H_2{}^{18}O)/P(H_2{}^{16}O)$, of the binary mixtures. The utility of the Stern – Van Hook – Wolfsberg equation for vapour pressure isotope effects has been investigated. In addition, a plot of the equilibrium constant of the oxygen-18 exchange reaction vs. the mole fraction of pyridine presents no evidence of the formation of stoichiometric pyridine–water complexes.

ROBERT H. BETTS, JAN BRON, WAYNE D. BUCHANNON et KWOK-YING D. WU. Can. J. Chem. **55**, 2966 (1977).

On utilise l'échange d'oxygène-18 entre le dioxyde de carbone et l'eau dans des mélanges liquides eau–pyridine comme sonde pour des changements dans les forces intermoléculaires alors que la composition du système varie de l'eau pure jusqu'à la pyridine pure. En accord avec les résultats obtenus antérieurement par d'autres méthodes, on a trouvé que l'énergie d'interaction d'une molécule "moyenne" avec le milieu diminue quand la fraction molaire de pyridine varie de zéro jusqu'à unité. On relie les résultats expérimentaux à l'effet isotopique de pression de vapeur, $P(H_2{}^{18}O)/P(H_2{}^{16}O)$ des mélanges binaires. On a étudié l'utilité de l'équation de Stern – Van Hook – Wolfsberg pour les effets isotopiques de la tension de vapeur. De plus, une courbe de la constante d'équilibre de la réaction d'échange de l'oxygène-18 par rapport à la fraction molaire de la pyridine ne présente pas de données permettant de conclure à la formation de complexe stoechiométrique pyridine–eau.

[Traduit par le journal]

Introduction

The properties of liquid mixtures of water and pyridine have been the subject of numerous investigations. Amongst the properties examined have been the vapour pressures of binary mixtures (1) and the infrared (2, 3) and Raman (4) spectra. A recent very comprehensive paper by Chan and Van Hook (5) reports vapour pressure isotope effects for the C_5D_5N–H_2O and C_5H_5N–H_2O systems. An earlier related study by Rabinovich (6) involved measurements of enthalpy of mixing of water (both H_2O and D_2O) with pyridine, as well as a comparison of the relative vapour pressures of the H_2O–C_5H_5N and D_2O–C_5H_5N systems. In addition there have been many papers published of systems involving the H_2O–pyridine pair in which a third component is present as the solvent (7–9). Much of this latter work is summarized in a review by Christian *et al.* (10). While three-component systems are of intrinsic interest, they are not directly relevant to our investigations and we shall not enlarge on this aspect.

Broadly speaking, the following picture emerges from earlier work. The system is characterized by complete miscibility over the entire range of composition and over all temperatures examined above the melting points of the pure components. Positive deviations from Raoult's law are observed, i.e., the *excess* Gibbs free energy of mixing is positive, whilst ΔG(mixing) is of course negative. The latter quantity reaches a minimum value at 65 mol% of pyridine. Rabinovich (6) suggests that this minimum corresponds to the formation of molecular complexes involving hydrogen bonding of two pyridine molecules to a single water molecule. Similar conclusions are drawn by Chan and Van Hook from their vapour pressure isotope effect measurements. Spectral studies, usually involving a third component, also support the view that complexes containing two pyridine molecules per water mol-

ecule are present, especially for systems rich in pyridine relative to water (2, 8). The recent spectral work of Bonner and Choi (3) provides particularly strong evidence for the 1 : 1 complex as well. These authors interpret the absorption spectra in terms of a water molecule, singly hydrogen bonded to the π electrons of the aromatic ring. This conclusion is supported by experimental and theoretical studies by Hussein *et al.* (11) of the three component system water – pyridine – carbon tetrachloride.

Some years ago, O'Neil and Adami (12) measured the distribution of ^{18}O between gaseous CO_2 and liquid water in a search for evidence of discrete polymolecular species of water in the liquid phase. At that time, certain temperature dependent anomalies, or "kinks", in the physical properties of water were suspected and O'Neil and Adami indicated how ^{18}O distribution studies could be used to learn more about these anomalies and the molecular complexes responsible. We have adapted their method to the pyridine–water system in an attempt to learn more about the molecular interactions in this system.

The purpose of this paper is twofold: (*1*) To apply and test ^{18}O isotope effects as a probe of intermolecular forces and changes therein; abrupt changes, due to formation of complexes of definite composition, will lead to discontinuities in plots of physical properties vs. mole fraction. (*2*) To examine the general applicability of the SVHW (13) equation for vapour pressure isotope effects. For example, Chan and Van Hook found that a 15% decrease in the external frequencies for water on solution in pyridine could explain their results (5). Therefore, since the SVHW equation should be generally applicable and independent of the isotopes involved, measurements of the ^{18}O isotope effects in the water–pyridine system should give results which are consistent with the data in (5).

Experimental

Pyridine (0.04% water, Baker Analyzed Reagent) was distilled from *p*-toluene sulfonyl chloride to remove secondary and tertiary amines, and then redistilled from calcium hydride to remove final traces of water. It was stored over Linde Type 3A molecular sieve. A single supply of doubly-distilled water was used in all experiments.

Mixtures of pyridine and water of the desired composition were prepared by weight in a clean dry equilibration flask of approximately 110 ml volume. The flask was attached to a vacuum line, and the contents outgassed by repeated cycles of freezing, pumping, and thawing, using liquid nitrogen as a refrigerant.

A single batch of carbon dioxide was used for all experiments. It was first freed of permanent gases and water by distillation between traps using liquid nitrogen and dry ice – acetone as the refrigerants.

The same amount (0.00055 mol) CO_2 was added to each flask of pyridine–water, after which the flask was transferred to a water bath maintained at 298.1 K. The flasks were shaken mechanically for at least 9 h, a time found sufficient to reach isotopic equilibrium amongst the oxygens of CO_2 and H_2O.

After equilibration was complete, the CO_2 was removed quantitatively from the system by vacuum transfer, and freed from traces of pyridine and water by trap-to-trap distillation. We emphasize that all the CO_2 was collected, i.e., the CO_2 in the gas phase, as well as that dissolved in the pyridine–water liquid phase. This was done to avoid possible errors arising from fractionation of the isotopic carbon dioxides between the two phases; such effects are likely to be small, but have been observed in other liquid–vapour distributions involving CO_2 (14).

Both the H_2O and CO_2 used in this work were of normal isotopic composition.

A Varian-Mat GD-150 isotope ratio mass spectrometer was used for isotopic analysis of the recovered CO_2.[1] The relative abundance of ^{18}O in each sample was measured as the ratio of mass 46 ($^{12}C^{16}O^{18}O$) to the sum of masses (44 + 45 + 47 + 48). The relative ^{18}O content of each sample was compared repeatedly with that in the original purified but unequilibrated CO_2, which was taken as a reference. This is discussed further below.

Results

This isotope exchange equilibrium we are concerned with may be written as

$$H_2{}^{18}O(\ell) + \tfrac{1}{2}\,C^{16}O_2(g) \rightleftharpoons H_2{}^{16}O(\ell) + \tfrac{1}{2}\,C^{18}O_2(g)$$

and the equilibrium constant, K, has the form

$$[1] \qquad K = \frac{[C^{18}O_2]^{1/2}[H_2{}^{16}O]}{[C^{16}O_2]^{1/2}[H_2{}^{18}O]}$$

The square brackets denote the number of moles of the indicated species at equilibrium. Provided that the isotopes ^{16}O and ^{18}O are distributed statistically amongst $C^{16}O_2$, $C^{16}O^{18}O$, and $C^{18}O_2$, which may be confidently expected, the following relation applies:

$$[2] \quad \frac{[C^{18}O_2]^{1/2}}{[C^{16}O_2]^{1/2}} = \frac{2[C^{18}O_2] + [C^{16}O^{18}O]}{2[C^{16}O_2] + [C^{16}O^{18}O]}$$

[1]This spectrometer measures the ratio of the abundance of mass 46 ($^{12}C^{16}O^{18}O$) to the sum of the abundances of the masses ± 2 mass units on each side of mass 46, i.e., masses (44 + 45 + 47 + 48). The first two of these terms contribute >99.5% of the denominator, whilst the last term is negligibly small. In the text we refer to this ratio as R. Variations in R faithfully reflect variations in the $^{18}O/^{16}O$ ratio of the CO_2.

The expression on the right hand side of [2] is clearly a quantitative measure of the ratio $^{18}O/^{16}O$ in CO_2.

We now proceed to relate K, which is defined by [1], to measured quantities. The mass spectrometrically determined ratio R, where

$$R = \text{Mass}(46)/\text{Mass}(44 + 45 + 47 + 48)$$

is a good measure of the ratio shown in [2]. Let $R_{st} = {}^{18}O/{}^{16}O$ for reference CO_2 and $R_g = {}^{18}O/{}^{16}O$ for CO_2 after equilibrium with H_2O in pyridine. If δ_g is defined as

$$\delta_g = (R_g/R_{st} - 1)1000$$

it follows that

$$R_g = (1 + \delta_g/1000)R_{st}$$

Let R_l be equal to

$$R_l = [H_2{}^{18}O]/[H_2{}^{16}O]$$

and let δ_l be defined by

$$\delta_l = (R_l/R_{st} - 1)1000$$

it then follows that

$$R_l = (1 + \delta_l/1000)R_{st}$$

The equilibrium constant K can now be expressed in the following way

$$[3] \qquad \alpha = \frac{R_g}{R_l} = \frac{1 + (\delta_g/1000)}{1 + (\delta_l/1000)} \simeq K$$

the factor R_{st} cancelling out. An equation identical to [3] was used by O'Neil and Adami in the work already cited (12). In the following we shall use α as a measure of K.

In each experiment δ_g is a measured quantity from which α can be evaluated by means of [3], provided that we know δ_l. This latter quantity is obtained in the following way. For the H_2O–CO_2 system alone at 298 K, α is equal to 1.04073 (12) and measurement of δ_g for this system therefore gives directly δ_l for the equilibrated water (see entry 1 in Table 1). From this information, the value of $\delta_l{}^0$, where the superscript refers to the value of this quantity for our stock water *before* its equilibration with CO_2, is obtained from [4]

$$[4] \quad 2n_{CO_2}\delta_g{}^0 + n_{H_2O}\delta_l{}^0 = 2n_{CO_2}\delta_g + n_{H_2O}\delta_l$$

In [4], n refers to the number of moles; $\delta_g{}^0$ is of course equal to zero by definition.

In summary, to evaluate α for each CO_2–pyridine–H_2O system investigated, we measure δ_g, and from [4] evaluate δ_l, since $\delta_l{}^0$ is known. With these quantities, α is calculated by means of [3]. The relevant data are given in Table 1 and summarized in Fig. 1.

TABLE 1. Isotopic composition of equilibrated CO_2 and equilibrium constant for ^{18}O distribution between CO_2 and H_2O in H_2O–pyridine solutions at 298.1 K

Moles H_2O	Moles pyridine	δCO_2	α
0.111	0.000	14.77	(1.0407_3)*
0.111	0.0106	15.76	1.0417
0.111	0.0117	15.45	1.0414
0.111	0.0125	15.21	1.0412
0.111	0.0172	14.92	1.0409
0.111	0.0616	16.19	1.0422
0.0555	0.0539	16.62	1.0428
0.0555	0.0568	16.62	1.0428
0.0222	0.0389	17.16	1.0439
0.0222	0.0406	17.33	1.0441
0.0278	0.0684	17.87	1.0444
0.0278	0.0695	17.81	1.0449
0.0278	0.0819	17.99	1.0446
0.0278	0.0846	18.00	1.0446
0.0222	0.0818	18.66	1.0455
0.0222	0.0899	18.52	1.0454
0.0222	0.1039	18.69	1.0456
0.0222	0.1834	18.94	1.0459
0.0222	0.1984	19.02	1.0459
0.0222	0.2030	19.42	1.0463
0.0222	0.2049	19.02	1.0459

*Normalizing value (see text).

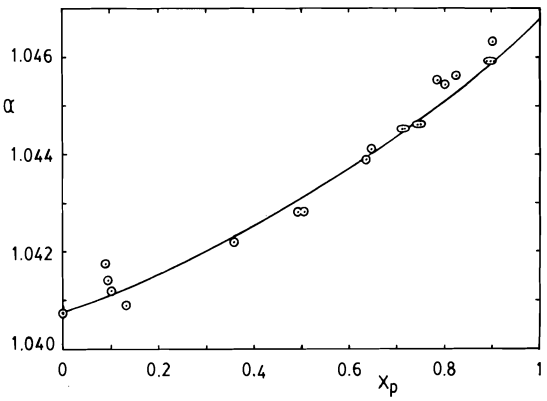

FIG. 1. A plot of α, defined by [1] in text, vs. the mole fraction of pyridine, X_p, at 298 K.

Discussion

Figure 1 displays the results of measurements of α as a function of the mole fraction, X_p, of pyridine. It may be observed that, within experimental error, no 'kinks' in the estimated line connecting the experimental points occur and that this line shows slight curvature. In order to

explain the variation of α with X_p a theoretical digression is required.

The equilibrium constant α can be written in terms of molecular partition functions

$$[5] \qquad \alpha = (q'/q)^{1/2}(\bar{q}/\bar{q}') = k^{1/2}r$$

In [5] the prime refers to the ^{18}O labelled species. The *molecular* canonical partition function for CO_2 in the ideal gas phase is q. The relationship between q and the *total* partition function, Q, is $q = (N!Q)^{N^{-1}}$. The partition function $\bar{q}$, which refers to the condensed phase of H_2O, is the *average* partition function as defined by Bigeleisen (15): $\bar{q} = Q^{N^{-1}}$. The constant k is equal to (q'/q) and r is equal to $(\bar{q}/\bar{q}')$. It is possible to calculate k, within the harmonic approximation, from the data for CO_2 given by Bottinga (16). At 298 K, k is equal to 1.783. Therefore, from a knowledge of α and k, r can be calculated by means of [5]. The value obtained for r will then be an 'experimentally observed' quantity; it quantifies the partition function ratio of the average isotopic water species in the *condensed* phase.

A relationship between r and α and the vapour pressure isotope effect can be obtained readily. Bigeleisen and Mayer (17) defined a reduced partition function as

$$[6] \qquad f = (q/q')\Pi_i(m_i'/m_i)^{3/2}$$

A similar definition has been given for $\bar{q}$. By using [6] and after making several simplifying assumptions SVHW (13) obtained an expression for the vapour pressure isotope effect:

$$[7] \qquad P'/P = f_l/f_g$$

In this case the subscripts l and g refer to the condensed and gas phase of water respectively. The vapour pressure ratio P'/P is then $P(H_2{}^{18}O)/P(H_2{}^{16}O)$. Note the following relationships

$$[8] \qquad f_l = r(18/16)^{3/2} \quad \text{and} \quad f_g = [(q/q')/(18/16)^{3/2}]_g^{(H_2O)}$$

The reduced partition function f_g may be calculated from literature data (18): at 298 K f_g is equal to 0.940. It follows, by means of [5], [6], [7], and numerical values for the quantities required, that

$$[9] \qquad P(H_2{}^{18}O)/P(H_2{}^{16}O) = 0.951\alpha$$

Hence, P'/P is directly proportional to α and, in this case, almost equal to α. By means of [9] and the experimental results for α, it can be concluded that the vapour pressure of $H_2{}^{18}O$ increases, relative to $P(H_2{}^{16}O)$, as X_p increases.

The variation of P'/P or α as a function of X_p can be explained as follows. Application of the SVHW expression and the assumption that the *ratios* of the internal partition functions of the $H_2{}^{16}O$ and $H_2{}^{18}O$ species in the condensed phase do not change considerably in going from pure water to pure pyridine, results in the following expression

$$[10] \qquad P'/P = \text{constant} \times \prod_{i=1}^{6} \frac{(\frac{1}{2}u_i)\sinh(\frac{1}{2}u_i')}{(\frac{1}{2}u_i')\sinh(\frac{1}{2}u_i)}$$

In [10] the number 6 represents the six external degrees of freedom: three hindered translations and three librations. The quantities u_i are equal to $hc\omega_i/kT$, in which all symbols have their usual meaning. Equation 10 states that the variation in P'/P at a particular temperature with X_p is caused only by a change in the six frequencies corresponding to the external degrees of freedom. Since the values of u_i are usually small at room temperature, [10] can be written as (19)

$$[11] \qquad P'/P \simeq A\sum_{i=1}^{6}\Delta u_i^2 + B$$

The constants A and B are positive. The difference Δu_i^2 is equal to $(u_i'^2 - u_i^2)$.

The change in the sum $\sum\Delta u_i^2$ accounts for variations in P'/P as the medium is changed from pure water to pure pyridine. As P'/P is linearly related to α and a plot of α vs. X_p is almost linear, the sum $\sum\Delta u_i^2$ should be an (almost) linear function of X_p. The sum $\sum\Delta u_i^2$ is always negative in the condensed phase, since Δu_i^2 is always negative or zero. It may be noted that Δu_i^2 can only be zero for some librational modes. The sign of Δu_i can be rationalized in the following way (13, 20). For translation

$$[12] \qquad \Delta u_t^2 = (h/kT)^2\sum_{i=1}^{3}(\nu_i'^2 - \nu_i^2) = (h/2\pi kT)^2 \times (M - M')(MM')^{-1}\nabla^2 V^{(t)}$$

The force constant of hindered translation is $\nabla^2 V^{(t)}$. It has been assumed that $\nabla^2 V^{(t)}$ is independent of isotopic substitution. Because by definition $M' > M$ and $\nabla^2 V^{(t)} > 0$, Δu_t^2 for the hindered translational modes is always negative. It can be shown by similar arguments that for the three librational modes the contributions to the sum in [11] must be negative or zero.

For the experimental results and [11] to be

consistent, $\sum\Delta u_i^2$ must increase with increasing X_p. Since the sum is always negative it should, therefore, become less negative (approach zero from the negative direction) when X_p is changed from zero to unity. The sum in [11] can only change via the (positive) force constants of hindered translation and libration and it may be concluded that these force constants for the average water molecule should decrease with increasing X_p. Also, a decrease in force constants of the external modes of vibration signifies a decreased interaction energy of the water molecule with the medium.

From [9], [11], and the experimental results it can be deduced that in our work we 'observed' a 15% increase in the sum $\sum\Delta u_i^2$, which is not the same result as the one by Chan and Van Hook (see above) but points in the same direction: a lowering of the force constants of the external degrees of freedom. It follows from [9] and the data in Table 1 that the vapour pressure ratio $P(H_2{}^{18}O)/P(H_2{}^{16}O)$, in solutions where X_p approaches unity, is 0.995 (0.951 × 1.046). This value is virtually the same as that reported by O'Neil and Adami (12) for concentrated dioxane–water mixtures. Hence, the external forces on the water molecule, when $X_p \simeq 1$, should be very similar in these two solutions.

Finally, by considering Fig. 1, the spread of experimental results does not allow us to draw any firm conclusions about the ambience of discrete molecular complexes of pyridine and water. Thus there are no plateaus or peaks in the values of α, corresponding to unique values of this quantity for particular molecular entities. This is perhaps not entirely unexpected, as there are undoubtedly a very large number of co-existing molecular environments for water and the nature and proportions of these will change as pyridine is added. Only some of these can be described as stoichiometric complexes. The ^{18}O equilibration method is evidently responding to the weighted chemical environment of all the water molecules in the system.

Acknowledgment

Financial support by the National Research Council of Canada is gratefully acknowledged.

1. R. J. L. Andon, J. Cox, and E. Herington. Trans. Faraday Soc. **53**, 410 (1957).
2. A. N. Sidorov. Opt. Spectrosc. **8**, 24 (1960).
3. O. D. Bonner and Y. S. Choi. J. Phys. Chem. **78**, 1723 (1974).
4. E. V. Sagitova, F. Kh. Tukhvallin, and A. K. Atakhodzhaev. Opt. Spectrosc. **28**, 250 (1970).
5. T. C. Chan and W. A. Van Hook. J. Chem. Soc. Faraday Trans. I, **72**, 583 (1976).
6. I. B. Rabinovich. Influence of isotopy on the physicochemical properties of liquids. Consultants Bureau, New York. 1970.
7. J. R. Johnson, P. J. Kilpatrick, S. D. Christian, and H. E. Affsprung. J. Phys. Chem. **72**, 3223 (1968).
8. S. C. Mohr, W. D. Wilk, and G. M. Barrow. J. Am. Chem. Soc. **87**, 3048 (1965).
9. A. Le Narvor, E. Gentric, J. Lauransan, and P. Saumagne. J. Chem. Soc. Faraday Trans. I, **72**, 1329 (1976).
10. S. D. Christian, A. A. Taha, and B. W. Gash. Q. Rev. **24**, 20 (1970).
11. M. A. Hussein, J. Almlof, and J. Lindgren. J. Mol. Struct. **27**, 391 (1975).
12. J. R. O'Neil and L. H. Adami. J. Phys. Chem. **73**, 1553 (1969).
13. M. J. Stern, W. A. Van Hook, and M. Wolfsberg. J. Chem. Phys. **39**, 3179 (1963).
14. J. C. Vogel, P. M. Grootes, and W. G. Mook. Z. Phys. **230**, 225 (1970).
15. J. Bigeleisen. J. Chem. Phys. **34**, 1485 (1961).
16. Y. Bottinga. J. Phys. Chem. **72**, 800 (1968).
17. J. Bigeleisen and M. G. Mayer. J. Chem. Phys. **15**, 261 (1947).
18. J. Bron, Chen Fee Chang, and M. Wolfsberg. Z. Naturforsch. **28**a, 129 (1973).
19. J. Bron. Can. J. Chem. **54**, 160 (1976).
20. K. F. Herzfeld and E. Teller. Phys. Rev. **54**, 912 (1938).

Acid-catalysed hydrolysis of bis(trifluoroethyl)sulfite in water and 60.7% *p*-dioxane in water

MARK SALOMON

Power Sources Technical Area, U.S. Army Electronics Technology and Devices Laboratory (ECOM), Fort Monmouth, NJ, U.S.A. 07703

Received January 5, 1977

MARK SALOMON. Can. J. Chem. **55**, 2971 (1977).

The rates of the catalysed hydrolysis of bis(trifluoroethyl)sulfite have been measured in concentrated acid solutions at 25 and 35°C in water and in an aqueous mixture containing 60.7% *p*-dioxane by weight. The results are analyzed in terms of a solvation model similar to that proposed by Bunnett, and the kinetic medium effect. The data indicate that the mechanism of the acid-catalysed hydrolysis is bimolecular and that catalysis by halide ions occurs only in acidified solutions.

MARK SALOMON. Can. J. Chem. **55**, 2971 (1977).

On a mesuré les vitesses d'hydrolyse catalysée des sulfites de bis(trifluoroéthyle) dans des solutions acides concentrées, à 25 et 35°C, dans l'eau et dans des mélanges aqueux contenant 60.7% de *p*-dioxanne par poids. On analyse les résultats en termes d'un modèle de solvatation similaire à celui proposé par Bunnett et d'un effet cinétique de solvant. Les données indiquent que le mécanisme de l'hydrolyse acido-catalysée est bimoléculaire et que la catalyse par des ions halogénures ne se produit que dans des solutions acidifiées.

[Traduit par le journal]

Introduction

The acid/base-catalysed hydrolysis of alkyl sulfites has been studied in detail by Bunton and co-workers (1), Tillett (1, 2), and Davis (3). The overall reaction has been shown to be

[1] $$(RO)_2SO + H_2O \rightarrow 2ROH + SO_2$$

which occurs by cleavage of the S—O bond in both acid and base. The mechanism of reaction 1 has been determined by these investigators to be bimolecular (Type A-2): i.e. in acid solution,

[2*a*] $(RO)_2 + H^+ \rightleftharpoons (RO)_2SOH^+$ rapid equilibrium

[2*b*] $(RO)_2SOH^+ + H_2O \rightarrow$ products slow

The unimolecular or A-1 mechanism, which has not been confirmed for any of the alkyl sulfites, can be written as

[3*a*] $(RO)_2SO + H^+ \rightleftharpoons (RO)_2SOH^+$ rapid equilibrium

[3*b*] $(RO)_2SOH^+ \rightarrow$ products slow

The present paper is concerned with the hydrolysis of bis(trifluoroethyl)sulfite, $(CF_3CH_2O)_2SO$, in water and in an aqueous–dioxane mixture containing 60.7% *p*-dioxane by weight. The objective of this study is to elucidate the mechanism of the hydrolysis of this fluorinated ester by investigating the dependence of the rate upon (*1*) the concentrations of various solutes, (*2*) the effect of temperature, and (*3*) the effect of solvent composition.

Experimental

(a) Materials

All salts and the ester $(CF_3CH_2O)_2SO$ were purified as described previously (4). The ester was stored in an argon-filled dry box and all salts were stored in a desiccator over P_2O_5. Reagent grade *p*-dioxane was distilled from activated alumina and type 4A molecular sieves. Reagent grade acids were used as received. Acid solutions for the water–dioxane mixture were prepared by mixing standard (aqueous) acid with the purified dioxane such that the wt% of dioxane was always 60.7 (this corresponds to the 60.0 vol% mixture used in related studies 2*b*, 5). The acid solutions were analyzed by titration with Fisher certified standard alkali. All titrations, both for standardization and product analysis (see below), were carried out at 25°C using water-jacketed burets.

(b) Rates of Hydrolysis

Since the acid hydrolysis of sulfite esters results in the production of SO_2 (cf. reaction 1), the rate of reaction is conveniently measured by iodometric titration (1–3). A hydrolysis cell with ~10 ml capacity is shown in Fig. 1. In each run, 3–5 cells were thermostated in series to within ±0.1°C. 5.0 ml of ester + acid solution were pipetted into each cell and, at specified times, the solutions were rapidly drained by N_2 pressure into small flasks containing excess 0.01 *N* I_2 (as I_3^-). The excess I_3^- was back-titrated with 0.01 *N* $Na_2S_2O_3$ and the first order rate constant was calculated from

[4] $$k^1 = \{\ln [a/(a - x)]\}/t$$

where *a* is the initial concentration of $(CF_3CH_2O)_2SO$

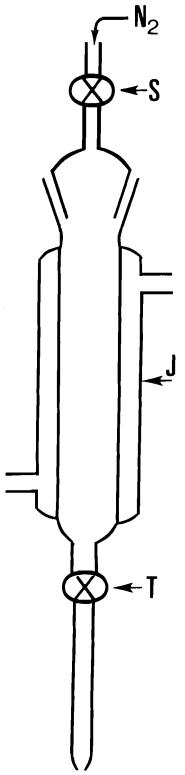

FIG. 1. Diagram of the hydrolysis cell. S = greased micro-stopcock, J = water jacket, T = Teflon micro-stopcock.

and x is the mol of SO_2 liberated after t min. The experimental k^1 values were reproducible to within $\pm 3\%$. Zero time for the kinetic runs was taken at the start of mixing the ester with the acid solutions. Typical initial concentrations of the sulfite ester in water were around 5×10^{-3} M and around 3×10^{-2} M in 60.7% dioxane. Several runs were carried out at 35°C and the majority of the runs were carried out at 25°C.

(c) Results

The results are summarized in Tables 1–5.[1] In Tables 2, 4, and 5, the rate constant k_x^1 is the observed rate constant for the acid–halide-catalysed reaction, and is obtained from the observed first order rate constant, k^1, by subtracting the value the rate constant would have in the absence of halide; i.e. as in $HClO_4$ solutions. Denoting this latter quantity as $k^1(HClO_4)$, we have

$$[5] \qquad k_x^1 = k^1 - k^1(HClO_4)$$

The values of $k^1(HClO_4)$ were obtained either graphically by interpolation or from a least squares fit to a suitable rate equation (see eqs. 11 and 14 below). Additional data given in these tables are the acidity functions, H_0, for $HClO_4$ in water (6) and 60.7% dioxane (5), and for HCl in water (6) and 60.7% dioxane (7). The molar activity coefficients, $y_\pm$, for HCl in water and 60.7% dioxane were obtained from Harned and Owens' compilations (8) (the latter values were interpolated from the data for 20, 45, 70, and 82% dioxane solutions). Values of $y_\pm$ for aqueous $HClO_4$ solutions and the activity of water in these solutions were obtained from the molal activity coefficients, $\gamma_\pm$, of Robinson and Baker (9). The density data of Markham (10) were used to make the conversions to the molar scale.

There are additional kinetic data in 60.7% dioxane which were not placed in the tables. In neutral solutions containing 0.274 and 0.512 M LiCl, the first order rate constant was too small to be determined by the present method ($k^1 < 10^{-5}$ min^{-1}); in 0.407 M KOH the second order rate constant was much too large to be accurately determined ($k^2 > 10$ ℓ mol^{-1} min^{-1}).

The enthalpies of activation, $\Delta H^\ddagger$, were estimated from the data at 25 and 35°C, and the entropies of activation were calculated from the data at 25°C using the relation

$$[6] \quad \Delta S^\ddagger = R \ln (k/T) + \Delta H^\ddagger/T - 47.216$$

where k is in units of s^{-1}. The results are given in Table 6 along with those for diethylsulfite (1*b*, 2*b*) which are presented for comparison.

Discussion

(a) Overall Kinetics

The observed rate constant may be written as

$$[7] \quad k^1 = k_N + k_H[H^+] + k_x[H^+][X^-] + k_{OH}[OH^-]$$

where k_N is the rate constant in neutral solution and k_{OH} is that for alkaline solution which, for the present experimental conditions, need not be considered. The data in Tables 1–5 indicate: (*1*) there is specific catalysis by H^+; (*2*) there is no catalysis by Li^+, Na^+, or ClO_4^-; and (*3*) there is catalysis by halide ions only in the presence of H^+. The existence of catalysis by halide ions appears to be unique as no such behaviour is observed for the hydrolysis of carboxylic esters (11). The reason for the existence the k_x term in eq. 7 is due to the fact that the sulfinyl sulfur is highly electrophilic (12, 13). It has also been suggested (14) that the sulfinyl sulfur can be classified as a hard Lewis acid in the Pearson sense (15), and on this basis, one would expect its reactivity towards anions would decrease according to $OH^- > Cl^- > Br^- > ClO_4^-$. The alkaline hydrolysis of alkyl sulfites and of $(CF_3CH_2O)_2SO$ is faster than the H^+—X^--catalysed hydrolysis, but the latter decreases according to $Br^- > Cl^-$ which suggests that the sulfinyl sulfur is a soft Lewis acid (4, 12). This acidic behaviour of the sulfinyl sulfur originates partly from an inductive effect (4) and partly from the possibility that the sulfinyl sulfur

[1]Tables 1–5 are available, at a nominal charge, from the Depository of Unpublished Data, CISTI, National Research Council of Canada, Ottawa, Canada K1A 0S2.

TABLE 6. Enthalpies and entropies of activation for the hydrolysis of $(CF_3CH_2O)_2SO$ and $(CH_3CH_2O)_2SO$ in water and in 60.7% dioxane*

Sulfite	Solvent	Acid	[Acid]	Salt	[Salt]	$\Delta H^{\ddagger}$	$\Delta S^{\ddagger}$
$(CF_3CH_2O)_2SO$	H_2O	$HClO_4$	0.961			15.74	−26.24
	H_2O	$HClO_4$	3.004			18.37	−14.73
	H_2O	HCl	0.500			12.21	−38.57
	H_2O	HCl	1.000			10.38	−41.63
	60.7% diox	$HClO_4$	0.872			14.49	−33.14
	60.7% diox	$HClO_4$	0.872	LiCl	0.128	14.56	−19.55
	60.7% diox	HCl	0.411			15.23	−24.33
$(CH_3CH_2O)_2SO$	H_2O	$HClO_4$	1.030			17.86	−14.45
	H_2O	$HClO_4$	3.090			20.06	−3.52
	H_2O	$HClO_4$	1.000	NaCl	0.250	18.33	−13.08
	H_2O	$HClO_4$	1.000	NaBr	0.100	18.30	−12.26
	60.7% diox	$HClO_4$	1.000			19.29	−11.10
	60.7% diox	$HClO_4$	1.500			18.91	−10.75

*$\Delta H^{\ddagger}$ units are kcal/mol; $\Delta S^{\ddagger}$ units are eu.

possesses *d* orbitals of low enough energy to undergo *d–p* π-bonding and *d–d* back-bonding with suitable anions (i.e. of appropriate symmetry) such as the halides, but not with ClO_4^- (12, 14). The two major terms involving k_H and k_x in eq. 7 are discussed below.

(b) The Acid-catalysed Reaction

For acid-catalysis, the first order rate constants for the A-1 and A-2 mechanisms are given by

$$[8]\quad \log k_{A\text{-}1}{}^{1} = \log k^0 + \log a_{H^+} + \log(y_s/y^{\ddagger})$$

and

$$[9]\quad \log k_{A\text{-}2}{}^{1} = \log k^0 + \log([H^+]a_w) + \log(y_{\pm}y_s/y^{\ddagger})$$

In these equations, *y* is the true (measurable) molar activity coefficient for the indicated species: s for the substrate $(RO)_2SO$, and ‡ for the activated complex. Explicit forms of eqs. 8 and 9 can be derived by using theoretical and/or empirical relations for the activity coefficients (16). One such relation is the extended Debye–Hückel equation

$$[10a]\quad \log y_i = -Az_i^2\mu^{1/2}/(1 + \mu^{1/2}) + b_i\mu$$

When the species *i* is a molecule ($z_i = 0$), eq. 10*a* reduces to

$$[10b]\quad \log y_i = b_i\mu$$

Substituting eqs. 10 into eq. 9 gives

$$[11a]\quad \log\{k^1/[H^+][H_2O]\} = \log k^0 + b'\mu$$

where $b' = b_{H^+} + b_{H_2O} + b_s - b^{\ddagger}$. For the range of concentrations over which eqs. 10 are valid, the variation in $[H_2O]$ is small and the log $[H_2O]$ term can be incorporated into the log k^0 term: i.e.

$$[11b]\quad \log(k^1/[H^+]) = \log k' + b'\mu$$

where

$$[12]\quad k' = k^0\chi_w$$

The thermodynamic reference state for ions and uncharged solutes is the hypothetical 1 *M* solution, whereas the reference state for the solvent is, by convention, that of the pure solvent: thus the terms in $[H_2O]$ in the above equations can be replaced by the mole fraction of water, χ_w.

A major problem associated with the use of eqs. 10 over a large range of concentrations is that the constant *b* is not constant. The variation in *b* for infinitely dilute aqueous solutions to 0.5 *M* solutions is ~25%, and from 1.0 to 3.0 *M*, *b* changes by ~9%. Bunnett (17) has shown that in concentrated solutions, satisfactory empirical relations for the activity coefficients should account for ionic/molecular hydration. In aqueous solutions for concentration ≤6 *M*, an accurate rate equation can be derived by use of the empirical equation (18)

$$[13]\quad \log y_i = -\frac{Az_i^2\mu^{1/2}}{1 + Ba_0\mu^{1/2}} - \bar{n}\log a_w - \log\left\{\frac{1}{d_0}[d - 0.001(36.03 - MW)c]\right\}$$

where $\bar{n}$ is the average solvation number, d_0 and *d* are, respectively, the densities of pure water and the solution, MW is the molecular weight of the solute whose concentration is *c* mol/ℓ, and all other terms have their usual significance. Combining eqs. 9 and 13 yields

TABLE 7. Least squares fit to the various rate equations for the hydrolysis of $(CF_3CH_2O)_2SO$ in water and 60.7% dioxane at 25°C

System	Equation	Slope	Intercept	σ
H_2O; $HClO_4$	18	0.579	−2.804	0.010
H_2O; $HClO_4$	19	3.50	−2.968	0.025
H_2O; $HClO_4$	11*a**	0.0631	−2.7212	0.001
H_2O; $HClO_4$	11*b**	0.0422	−2.7201	0.002
H_2O; $HClO_4$	14	−2.471	−2.746	0.017
H_2O; HCl	18	1.59	−2.477	0.010
H_2O; HCl	17	0.9585	−1.9956	0.008
60.7% diox; $HClO_4$	18	0.635	−2.782	0.021
60.7% diox; $HClO_4$	11*a*	0.324	−3.400	0.010
60.7% diox; $HClO_4$	11*b*	0.309	−3.521†	0.010
60.7% diox; HCl	18	1.772	1.368	0.034
60.7% diox; HCl	17	0.938	−0.102	0.024

*Based on data in solutions for which $[HClO_4] \leq 3\ M$.
†To obtain k^0 from this intercept, k' is divided by χ_w (0.760) for the pure solvent (cf. eq. 12) which yields $\log k^0 = -3.402$.

[14] $$\log (k^1/[H^+]) + \log \left\{\frac{1}{d_0}[d - 0.001(36.03 - MW)[H^+]]\right\} = w^* \log a_w + \log k^0$$

where w^* is the "Bunnett" slope defined by

[15] $$w^* = 1 + n^{\neq} - n_{H^+} - n_s$$

Taking $n_{H^+} = 4$ (19) and $n^{\neq} - n_s \simeq 0$, 1, the slope w^* is expected to have values around −2 to −3. The above treatment assumes that the average solvation number is constant over the entire concentration range studied. This is a reasonable assumption for solutions in which there are an excess of solvent molecules, but for concentrations greater than 2 to 3 *M*, this assumption is not valid (20).

(c) The Acid–Halide-catalysed Reaction

This reaction can be treated in a simple fashion since the mechanism appears to be (cf. also ref. 3*b*)

[16*a*] $(RO)_2SO + H^+ \rightleftharpoons (RO)_2SOH^+$ rapid equilibrium

[16*b*] $(RO)_2SOH^+ + X^- \rightarrow ROSOX + ROH$ slow

[16*c*] $ROSOX + H_2O \rightarrow ROH + H^+ + X^- + SO_2$ fast

Since both the substrate and activated complex are neutral species, it is assumed that $y_s/y^{\neq} = 1$ and the first order rate constant (i.e. the observed quantity) can be written as

[17] $$\log k_x^1 = \log k^0 + \log a_{\pm}^2$$

The data for hydrolysis in acidified Cl^- and Br^- solutions (Tables 2, 4, and 5) show that eq. 17 is obeyed within experimental error: i.e. $\log (k^1/a_{\pm}^2)$ is constant.

(d) Analysis of the Data

The data for hydrolysis in $HClO_4$ solutions can be analyzed in several ways as shown in Table 7. The data for 25°C in this table were treated by the least squares method and the σ's are the statistical standard deviations in $\log k^1$. In aqueous solution, the Bunnett slope w^* (eqs. 14, 15) is −2.5 which leads to the reasonable values of $n^{\neq} \simeq 1$ and $n_s \simeq 0$. An attempt was made to determine if the rates of these reactions could be fit to a first order mechanism. Use was made of the Zucker–Hammett (21) relation

[18] $$\log k^1 = \log k^0 - H_0$$

and the Bunnett (17) relation

[19] $$\log k^1 + H_0 = w \log a_w + \log k^0$$

and the results are also given in Table 7. The rate data for the fluorinated ester studied here are complementary to those for the non-fluorinated esters (1–3): i.e. the reaction mechanism appears to be bimolecular in both cases.

The energetics of the catalysed hydrolysis of $(RO)_2SO$ can offer additional insights as to the mechanism. Using the data in Table 7 for the k^0 terms,[2] the standard enthalpies and entropies of activation ($\Delta H_0^{\neq}$ and $\Delta S_0^{\neq}$) have been evaluated and are presented in Table 8 with corresponding data for $(CH_3CH_2O)_2SO$. These

[2]It is to be noted that $k^0 = k^2 K_e$, where k^2 is the true second order rate constant in units of $\ell\ mol^{-1}\ min^{-1}$ and K_e is the equilibrium constant for protonation of the substrate (eqs. 2*a* and 16*a*).

TABLE 8. Standard enthalpies and entropies of activation for the hydrolysis of $(CF_3CH_2O)_2SO$ and $(CH_3CH_2O)_2SO$

Sulfite	Solvent	Acid	Salt	$\Delta H_0^{\neq}$	$\Delta S_0^{\neq}$	k^0 (25°C)
$(CF_3CH_2O)_2SO$	H_2O	$HClO_4$		17.9	−19.3	1.79×10^{-3}
	H_2O	HCl		11.0	−39.0	0.0101
	60.7% diox	$HClO_4$		15.4	−30.5	3.98×10^{-4}
	60.7% diox	$HClO_4$	LiCl	14.6	−19.6	0.419
	60.7% diox	HCl		12.8	−23.6	1.036
$(CH_3CH_2O)_2SO$	H_2O	$HClO_4$		17.9	−14.7	0.0180
	H_2O	$HClO_4$	NaCl	18.9	−8.2	0.0857
	H_2O	$HClO_4$	NaBr	18.8	−5.5	0.377
	60.7% diox	$HClO_4$		19.2	−12.5	5.81×10^{-3}

data are not completely unambiguous, but several factors can be used to lend support to the A-2 mechanism. The fact that $\Delta S_0^{\neq}$ and $\Delta S^{\neq}$ are large and negative has been interpreted by Long and co-workers (22) as being due to the large loss in entropy on forming the activated complex which, by virtue of its mechanism, is more solvated than its A-1 counterpart. Considering the hydrolysis of $(CF_3CH_2O)_2SO$, Tables 6 and 8 indicate that in aqueous solution, $\Delta S^{\neq}$ is more negative for the H^+—Cl^--catalysed hydrolysis than it is for the acid-catalysed reaction; the reverse behaviour is noted in 60.7% dioxane. In aqueous HCl, the loss in entropy in forming the activated complex, $(RO)_2SOHCl$, may be augmented by a large net ordering effect of the solvent since in the initial state, Cl^- is a "structure-breaking" ion and the large activated complex may embody the "structure-making" properties typical of large non-polar solutes (23). In 60.7% dioxane, the increase in $\Delta S^{\neq}$ for the H^+—Cl^--catalysed reaction compared to the acid-catalysed reaction is almost certainly due to the more negative entropy of solvation of the Cl^- ion in the mixed solvent. This follows from the general observations of Criss and co-workers that entropies of ions are most positive in those solvents which have a greater degree of internal order in the pure state (24–26). For the aqueous $(CH_3CH_2O)_2SO$ system, $\Delta S_0^{\neq}$ is larger for the acid-catalysed reaction than for the H^+—Cl^--catalysed reaction. The reason for this is not clear, but may be attributed to a combination of effects such as a weaker S–Cl interaction compared to that involving $(CF_3CH_2O)_2SO$, and (2) the activated complex $(CH_3CH_2O)_2SOHCl$ may be a structure-breaker since it is expected to be more polar than its fluorinated analog. It is of course possible that this decrease in $\Delta S_0^{\neq}$ for $(CH_3CH_2O)_2SO$ hydrolysis in the presence of halide is an artifact of the extrapolations used to obtain k^0, but a large error seems unlikely since the differences cannot be attributed to experimental error.

Despite several uncertainties in the above treatments, there is no evidence supporting the A-1 mechanism. Another straightforward approach in mechanism confirmation involves the medium effect. In general, the ratio of standard rate constants for reactions in water (k_w^0) to that in solvent s (k_s^0) is given by (26*b*)

$$[20]\quad k_w^0/k_s^0 = \exp\{[\Delta G_t^0(\neq) - \textstyle\sum \Delta G_t^0(r)]/RT\}$$

where $\Delta G_t^0(\neq)$ and $\Delta G_t^0(r)$ are, respectively, the standard free energies of transfer of the activated complex and reactants from water to solvent s. For large neutral molecules or for large ions where the charge is diffusely distributed over the molecule, ΔG_t^0 approaches zero (27, 28) and eq. 20 can be greatly simplified. From eqs. 8 and 9 for the A-1 and A-2 mechanisms in the absence of halide, eq. 20 reduces to

$$[21]\quad (k_w^0/k_s^0)_{H(A\text{-}1)} = \exp\{-\Delta G_t^0(H^+)/RT\}$$

and

$$[22]\quad (k_w^0/k_s^0)_{H(A\text{-}2)} = \exp\{[-\Delta G_t^0(H^+) - \Delta G_t^0(H_2O)]/RT\}$$

For the H^+—Cl^--catalysed reaction, eq. 20 reduces to

$$[23]\quad (k_w^0/k_s^0)_{x(A\text{-}2)} = \exp\{-\Delta G_t^0(HCl)/RT\}$$

The terms in $\Delta G_t^0(HCl)$ and $\Delta G_t^0(H_2O)$ can be unambiguously evaluated from emf studies on cells of the type H_2/HX (in solvent s)/AgX,Ag (8, 29–31), and from equilibrium constants for the ionization of H_2O in water and mixtures with *p*-dioxane (32, 33) and the activities of water in these mixtures (34). For the transfer from water to 60.7% dioxane, the values of $\Delta G_t^0(HCl)$ and $\Delta G_t^0(H_2O)$ are, respectively, 2.45 and 3.96 kcal/mol. The evaluation of $\Delta G_t^0(H^+)$ requires

an extrathermodynamic assumption which is always subject to uncertainty (26–29). The method of Feakins and co-workers (29, 35) appears to be consistent with other techniques (26) and using the emf data (8, 29–31), it is found that $\Delta G_t^0(H^+) = -6.0$ kcal/mol. Substituting these values into the above equations yields

$$(k_w^0/k_s^0)_{H(A\text{-}1)} = 2.6 \times 10^4$$

$$(k_w^0/k_s^0)_{H(A\text{-}2)} = 33.0$$

$$(k_w^0/k_s^0)_{x(A\text{-}2)} = 0.016$$

Experimentally the specific rate ratios for $(CF_3CH_2O)_2SO$ hydrolysis are $(k_w^0/k_s^0) = 4.5$, and $(k_w^0/k_s^0)_x = 0.010$. Similarly, for the hydrolysis of $(CH_3CH_2O)_2SO$, it is found that $(k_w^0/k_s^0)_H = 3.1$.

Summary and Conclusions

The mechanism of the acid–halide catalytic hydrolysis of $(CF_3CH_2O)_2SO$ follows closely that of $(CH_3CH_2O)_2SO$: both are bimolecular, characterized by a large negative value for the entropy of activation, and exhibit analogous behaviour when the medium is changed from water to an aqueous–dioxane mixture. The observations that the acid–halide-catalysed reactions are faster for $(CH_3CH_2O)_2SO$ than for $(CF_3CH_2O)_2SO$ is attributed to a large inductive effect at the carboxylic oxygens which are the sites of the initial protonation (cf. eqs. 2*a*, 16*a*). A large inductive effect at the sulfinyl sulfur would lead to a stronger S–Cl interaction with the fluorinated ester which might conceivably lead to more rapid kinetics. There is some evidence that there is a stronger S–Cl interaction with the fluorinated ester: for the hydrolysis of $(CF_3CH_2O)_2SO$ in water, $\Delta S^{\neq}$ and $\Delta S_0^{\neq}$ are smaller for the acid–halide-catalysed reaction than it is for the acid-catalysed reaction. The reverse behaviour is observed for the hydrolysis of $(CH_3CH_2O)_2SO$ as seen in Tables 6 and 8. The effect of fluorination of diethyl sulfite thus appears to give rise to two major effects: the decrease in electron density at the carboxylic oxygens and the sulfinyl sulfur results in a decrease in K_e (the equilibrium constant for protonation of the substrate) which acts to decrease the rate of hydrolysis, while the increase in the S–Cl interaction acts in an opposing fashion.

1. C. A. Bunton, P. B. D. De La Mare, and J. G. Tillett. J. Chem. Soc. (*a*) 4754 (1958); (*b*) 1766 (1959).
2. J. G. Tillett. J. Chem. Soc. (*a*) 37 (1960); (*b*) 5138 (1960).
3. R. E. Davis. J. Am. Chem. Soc. **84**, 599 (1962).
4. M. Salomon. Can. J. Chem. **55**, 2499 (1977).
5. C. A. Bunton, J. B. Ley, A. J. Rhind-Tutt, and C. A. Vernon. J. Chem. Soc. 2327 (1957).
6. M. A. Paul and F. A. Long. Chem. Rev. **57**, 1 (1957).
7. C. A. Braude and E. S. Stern. J. Chem. Soc. 1976 (1948).
8. H. S. Harned and B. B. Owen. The physical chemistry of electrolytic solutions. Reinhold, NY. 1958.
9. R. A. Robinson and O. J. Baker. Trans. R. Soc. N.Z. **76**, 250 (1946).
10. A. E. Markham. J. Am. Chem. Soc. **63**, 874 (1941).
11. F. A. Long and M. A. Paul. Chem. Rev. **57**, 935 (1957).
12. M. Salomon. J. Phys. Chem. **79**, 2000 (1975).
13. M. C. Rykowski, K. J. Douglas, and E. T. Kaiser. J. Org. Chem. **41**, 141 (1976).
14. A. Salama, S. B. Salama, M. Sobeir, and S. Wasif. J. Chem. Soc. A, 1112 (1971).
15. R. G. Pearson. J. Am. Chem. Soc. **85**, 3533 (1963).
16. K. J. Laidler. Reaction kinetics. Vols. 1 and 2. Pergamon, London. 1963.
17. J. F. Bunnett. J. Am. Chem. Soc. **83**, 4956 (1961); **83**, 4968 (1961); **83**, 4973 (1961).
18. E. Hogfeldt. Chem. Scr. **8**, 23 (1975).
19. B. E. Conway. Modern aspects of electrochemistry. Vol. 3. *Edited by* J. O'M. Bockris and B. E. Conway. Butterworths, London. 1964. Chapt. 2.
20. R. A. Robinson and R. H. Stokes. Electrolyte solutions. Butterworths, London. 1959.
21. L. Zucker and L. P. Hammett. J. Am. Chem. Soc. **61**, 2791 (1939).
22. (*a*) F. A. Long, J. G. Pritchard, and F. E. Stafford. J. Am. Chem. Soc. **79**, 2362 (1957); (*b*) L. L. Schaleger and F. A. Long. Advances in physical organic chemistry. Vol. 1. *Edited by* V. Gold. Academic Press, NY. 1963. Chapt. 1.
23. (*a*) H. S. Frank and M. W. Evans. J. Chem. Phys. **13**, 507 (1945); (*b*) H. S. Frank and W.-Y. Wen. Discuss. Faraday Soc. **24**, 133 (1957).
24. C. M. Criss, R. P. Held, and E. Luksha. J. Phys. Chem. **72**, 2970 (1968).
25. C. M. Criss. J. Phys. Chem. **78**, 1000 (1974).
26. C. M. Criss and M. Salomon. (*a*) Physical chemistry of organic solvent systems. *Edited by* A. K. Covington and T. Dickinson. Plenum Press, London. 1973; (*b*) J. Chem. Educ. **53**, 763 (1976).
27. A. J. Parker. Chem. Rev. **69**, 1 (1969).
28. O. Popovych. Crit. Rev. Anal. Chem. **1**, 73 (1970).
29. D. Feakins and D. J. Turner. J. Chem. Soc. 4986 (1965).
30. T. Mussini, C. Massarani-Formaro, and P. Andrigo. J. Electroanal. Chem. **33**, 177 (1971); **33**, 189 (1971).
31. P. K. Das and U. C. Mishra. Electrochim. Acta, **22**, 59 (1976).
32. H. S. Harned and L. D. Fallon. J. Am. Chem. Soc. **61**, 2374 (1939).
33. E. M. Woolley, D. G. Hurkot, and L. G. Hepler. J. Phys. Chem. **74**, 3908 (1970).
34. J. R. Goates and R. J. Sullivan. J. Am. Chem. Soc. **62**, 188 (1958).
35. D. Feakins and P. Watson. J. Chem. Soc. 4734 (1963).

Molar excess enthalpies of acetonitrile + chloroform and of acetonitrile + chloroform-d_1 at 298 K

YASH PAUL HANDA[1] AND DAVID EDWARD JONES[2]
Department of Chemistry, University of Otago, Dunedin, New Zealand
Received February 10, 1977

YASH PAUL HANDA and DAVID EDWARD JONES. Can. J. Chem. **55**, 2977 (1977).

Molar excess enthalpies of acetonitrile + chloroform and of acetonitrile + chloroform-d_1 were measured at 298 K. The results for the former system were discussed in terms of an ideal associated solution model and the deuterium isotope effect was discussed.

YASH PAUL HANDA et DAVID EDWARD JONES. Can. J. Chem. **55**, 2977 (1977).

On a mesuré, à 298 K, les enthalpies molaires d'excès de l'acétonitrile + chloroforme et de l'acétonitrile + chloroforme-d_1. On discute des résultats obtenus dans le premier système en termes d'un modèle de solutions associées idéales et on discute de l'effet isotopique du deutérium.

[Traduit par le journal]

Introduction

There has been a revival of interest recently in the thermodynamic study of liquid mixtures of A and B in which association takes place. Often, the "physical" contribution, $X^E_{m,phys}$ and the "chemical" contribution, $X^E_{m,chem}$ to the molar excess function X^E_m are assumed independent (there is experimental evidence for this assumption (1)) i.e.

$$[1] \qquad X^E_m = X^E_{m,phys} + X^E_{m,chem}$$

If $X^E_{m,phys}$ is negligibly small compared with $X^E_{m,chem}$ or, alternatively, if $X^E_{m,phys}$ can be estimated (see, for example, ref. 2), the mixture can be treated as an ideal associated solution. The application of this model to calorimetric measurements on mixtures with AB association has been reviewed (3).

Triethylamine + chloroform and diethyl ether + chloroform have been exhaustively investigated by thermodynamic methods as a result of independent evidence for AB association in these systems. The earlier calorimetric studies in the former system at 298 K (4, 5) have been supplemented by vapour pressure measurements at 283 K (6) and 298 K (7) and by measurements of the molar excess volumes at 298 and 308 K (8). The ideal associated solution model has been extended and applied to these results. Similarly, the ideal associated solution model has been applied (3) to the results of calorimetric measurements at 298 K (9), to vapour pressure measurements at 298 K (7), and to the results (10) for the temperature dependence of the molar excess volumes of diethyl ether + chloroform (7).

For the system acetonitrile + chloroform vapour pressures at 313 K (11), constant pressure vapour liquid equilibria (12) and molar excess volumes at 293 and 313 K (13) have been measured. Spectroscopic measurements on this system (14, 15) have been interpreted in terms of AB association and the values of the equilibrium constants at 299 and 310.5 K have been calculated. However, it appears that the AB associated model is too simple and that a model which includes self-association (see accompanying paper) is required to interpret the thermodynamic results. We have measured the molar excess enthalpies of acetonitrile + chloroform at 298 K.

The deuterium isotope effect on thermodynamic measurements in liquid mixtures has been reviewed (16). The molar excess enthalpies of triethylamine + chloroform and of triethylamine + chloroform-d_1 at 298 K (17) have been interpreted in terms of a larger value of the equilibrium constant for the former system and a more exothermic enthalpy of AB association for the latter, assuming no difference in the physical contributions in the respective systems. No deuterium isotope effect was detected from comparison of the molar excess enthalpies of

[1]Present address: Department of Chemistry, Wright State University, Dayton, OH, U.S.A. 45431.
[2]To whom correspondence should be addressed. Present address: Environment Ontario, P.O. Box 487, Bracebridge, Ont., Canada P0B 1C0.

diethyl ether + chloroform and of diethyl ether + chloroform-d_1, and this may be attributed to a compensation of the respective differences in the equilibrium constants and the standard enthalpies of AB association (17). In order to assess the deuterium isotope effect in this study, we report the molar excess enthalpies of acetonitrile + chloroform-d_1 at 298 K.

Experimental

Materials

Chloroform (B.D.H. Analar) was purified as reported previously (7).

Chloroform-d_1 (Merck, for spectroscopy) was purified by a procedure similar to that for chloroform (7) except that the initial shaking with water (to remove ethanol) was omitted. A high amplification nmr study indicated a purity of 99.7 mol%, with chloroform being the only proton-containing impurity.

Acetonitrile (B.D.H. Analar) was refluxed over phosphorous pentoxide for 4 h, and subsequently fractionally distilled in a dry and oxygen-free nitrogen atmosphere using a column of 15 theoretical plates at a reflux ratio of 20. The distillation apparatus was wrapped in black cloth to exclude light. The middle fraction was degassed by vacuum sublimation (18) and the degassed sample was stored over freshly activated molecular sieve (Union Carbide, type 13X) in a sealed ampoule. A high amplification nmr study indicated that the sample was at least 99.5 mol% pure.

Calorimeter

The calorimeter was similar to that described by Larkin and McGlashan (19) and has been described elsewhere (20). Tests with the I.U.P.A.C. recommended system *n*-hexane + cyclohexane have previously been carried out and compared with literature values (22).

Results

The molar excess enthalpies, H_m^E of acetonitrile + chloroform and of acetonitrile + chloroform-d_1 at 298 K are given in Table 1. The results were fitted by a least-squares computer program to the expression

$$[2]\quad H_m^E/\text{J mol}^{-1} = x_A x_B \sum_{i=1}^{k} h_i(1 - 2x_B)^{i-1}$$

where x_B is the mole fraction of chloroform or of chloroform-d_1. For both systems the results in Table 1 were adequately fitted with $k = 3$ in eq. 2. The parameters h_i and their respective standard deviations are given for both systems in Table 2. Table 2 also gives the standard deviations $\sigma(H_m^E)$ defined by

$$[3]\quad \sigma(H_m^E) = \left\{\sum (H_m^E(\text{calcd}) - H_m^E(\text{expt}))^2/(N - k)\right\}^{1/2}$$

where H_m^E(calcd), H_m^E(expt) are respectively the calculated (from the parameters h_i given in Table 2) and experimental values of the molar excess enthalpies for N experimental values.

TABLE 1. Molar excess enthalpies H_m^E of $x_A CH_3CN + x_B CHCl_3$ and of $x_A CH_3CN + x_B CDCl_3$ at 298 K

$x_A CH_3CN + x_B CHCl_3$		$x_A CH_3CN + x_B CDCl_3$	
x_B	$-H_m^E$/J mol^{-1}	x_B	$-H_m^E$/J mol^{-1}
0.0731	119.5	0.1139	200.4
0.0996	162.6	0.2710	507.7
0.2051	369.1	0.3907	697.0
0.2761	500.6	0.4824	810.9
0.3884	689.8	0.5591	868.5
0.5007	808.5	0.6565	865.3
0.5943	855.0	0.7592	745.5
0.6923	809.0		
0.7444	735.6		
0.8198	606.4		

Discussion

Both the magnitude and asymmetry of the H_m^E results suggest the inadequacy of the AB association model used to interpret the nmr results. There is evidence (21) for self-association in acetonitrile for which Trouton's constant is 96.4 J mol^{-1} K^{-1}. In addition, the results for G_m^E are positive (11) which is not consistent with an AB association model. Hence, it appears that a more complex model is required to interpret the thermodynamic results for this system (see accompanying paper).

At 313 K $G_m^E(x_B = \frac{1}{2}) = 131$ J mol^{-1} and use of the Gibbs–Helmholtz equation gives $G_m^E(x_B = \frac{1}{2}) = 164$ J mol^{-1} and $TS_m^E = -974$ J mol^{-1} at 298 K.

From constant pressure liquid vapour equilibrium results (12) it appears that G_m^E is slightly more positive at higher temperatures and consequently that H_m^E changes sign. This is in accordance with the expectation that $C_{p,m}^E$ will be positive for mixtures in which AB association takes place. Consequently, measurements of $C_{p,m}^E$ would be of interest.

Both V_m^E and $(\partial V_m^E/\partial T)_p$ are negative (13), the former fact consistent with AB association and the latter as observed for triethylamine + chloroform (8).

Although there is no significant deuterium

TABLE 2. Coefficients in eq. 2, the standard deviations of these coefficients, and standard deviations $\sigma(H_m^E)$ defined by eq. 3

System	h_1	h_2	h_3	$\sigma(H_m^E)$/J mol^{-1}
Acetonitrile + chloroform	-3250 ± 11	1505 ± 21	319 ± 52	4.8
Acetonitrile + chloroform-d_1	-3317 ± 16	1611 ± 39	153 ± 97	6.8

isotope effect on V_m^E (13), the molar excess enthalpies of acetonitrile + chloroform-d_1 are more exothermic (by 16 J mol^{-1} at $x_B = \frac{1}{2}$) than those of acetonitrile + chloroform. The difference is beyond the experimental uncertainty (Table 2) and is therefore consistent with the idea that the strength of the hydrogen bond in the AB associated system is increased on substitution by deuterium. However, a different value of the physical contribution in the hydrogen and deuterium systems (23) may account for such a small difference in the values of H_m^E. It appears that there will be some interest in similar experimental results for acetonitrile-d_3 + chloroform and acetonitrile-d_3 + chloroform-d_1.

Further treatment of the thermodynamic results for the binary systems formed by carbon tetrachloride, chloroform, and acetonitrile will be found in the following paper.

Acknowledgement

Y.P.H. acknowledges the award of a Mellor Post-Graduate Scholarship.

1. D. L. ANDERSON, R. A. SMITH, D. B. MYERS, A. G. WILLIAMSON, and R. L. SCOTT. J. Phys. Chem. **66**, 621 (1962).
2. G. L. BERTRAND. J. Phys. Chem. **79**, 48 (1975).
3. D. V. FENBY and L. G. HELPER. Chem. Soc. Rev. **3**, 193 (1974).
4. L. G. HEPLER and D. V. FENBY. J. Chem. Thermodyn. **5**, 471 (1973).
5. T. MATSUI, L. G. HEPLER, and D. V. FENBY. J. Phys. Chem. **77**, 2397 (1973).
6. Y. P. HANDA, D. V. FENBY, and D. E. JONES. J. Chem. Thermodyn. **7**, 337 (1975).
7. Y. P. HANDA and D. E. JONES. Can. J. Chem. **53**, 3299 (1975).
8. A. CHAND, Y. P. HANDA, and D. V. FENBY. J. Chem. Thermodyn. **7**, 401 (1975).
9. L. A. BEATH and A. G. WILLIAMSON. J. Chem. Thermodyn. **1**, 51 (1969).
10. R. BATTINO. Chem. Rev. **71**, 5 (1971).
11. A. KREGLEWSKI. Bull. Acad. Polon. Sci. Ser. Sci. Chim. **13**, 723 (1965).
12. F. MATO and M. SANCHEZ. An. Real. Soc. Espan. Fis. Quim. Ser. B. **63**, 1 (1967).
13. Y. P. HANDA. J. Chem. Thermodyn. In press.
14. P. J. BERKELEY and M. W. HANNA. J. Phys. Chem. **67**, 846 (1963).
15. W. LIN and S. TSAY. J. Phys. Chem. **74**, 1037 (1970).
16. Y. P. HANDA and D. V. FENBY. J. Chim. Phys. Phys.-Chim. Biol. **72**, 1235 (1975).
17. Y. P. HANDA, B. I. MATTINGLEY, and D. V. FENBY. J. Chem. Soc. Faraday Trans. I, **72**, 1355 (1976).
18. T. N. BELL, E. L. CUSSLER, K. R. HARRIS, C. N. PEPELA, and P. J. DUNLOP. J. Phys. Chem. **72**, 4693 (1968).
19. J. A. LARKIN and M. L. MCGLASHAN. J. Chem. Soc. 3425 (1961).
20. D. V. FENBY, G. J. BILLING, and D. B. SMYTHE. J. Chem. Thermodyn. **5**, 49 (1973).
21. A. SAUM. J. Poly. Sci. **42**, 57 (1960).
22. B. I. MATTINGLEY, Y. P. HANDA, and D. V. FENBY. J. Chem. Thermodyn. **7**, 169 (1975).
23. B. I. MATTINGLEY and D. V. FENBY. Aust. J. Chem. **28**, 185 (1975).

Thermodynamics of complex formation in binary liquid mixtures: application to systems containing acetonitrile

JOHN W. LORIMER AND DAVID E. JONES[1]

Department of Chemistry, University of Western Ontario, London, Ont., Canada N6A 5B7

Received January 10, 1977

JOHN W. LORIMER and DAVID E. JONES. Can. J. Chem. **55**, 2980 (1977).

Equations for enthalpies and volumes of mixing are derived from thermodynamic association theory for complex binary liquid mixtures containing self-associating species and binary complexes. The various species can interact through general non-specific interactions of the simple mixture type.

The equations, along with equations for the excess Gibbs energy, are applied to experimental data on excess Gibbs energies, heats, and volumes of mixing for the three binary systems formed from acetonitrile, carbon tetrachloride, and chloroform. The data require a theoretical model that involves two types of self-association of acetonitrile, one type of self-association of chloroform and formation of a binary complex $CH_3CN{\cdot}2CHCl_3$. Thermodynamic parameters for the various types of association and interaction are derived by constrained least-squares methods, and provide a unified picture of the thermodynamic properties of these mixtures.

JOHN W. LORIMER et DAVID E. JONES. Can. J. Chem. **55**, 2980 (1977).

On a dérivé des équations pour les enthalpies et les volumes de mélange à partir de la théorie d'association thermodynamique pour des mélanges liquides binaires complexes contenant des espèces auto-associées et des complexes binaires. Les diverses espèces peuvent interagir par l'intermédiaire des interactions générales non spécifiques d'un type de mélange simple.

Les équations de même que les équations pour l'énergie d'excès de Gibbs peuvent être appliquées à des données expérimentales concernant les énergies d'excès de Gibbs, les chaleurs et les volumes de mélanges pour les trois systèmes binaires formés à partir de l'acétonitrile, du tétrachlorure de carbone et du chloroforme. Les données nécessitent un modèle théorique qui implique deux types d'auto-association de l'acétonitrile, un type d'auto-association du chloroforme et la formation d'un complexe binaire $CH_3CN{\cdot}2CHCl_3$. On a pu dériver les paramètres thermodynamiques pour les divers types d'association et d'interaction par la méthode des moindres carrés restreints et l'on obtient ainsi une image unifiée des propriétés thermodynamiques de ces mélanges.

[Traduit par le journal]

Introduction

Much recent interest in formation of complexes in binary liquid mixtures has emphasized the extraction of thermodynamic parameters from heats and volumes of mixing for systems in which simple complexes are assumed to form between non-associating components (1). In systems such as mixtures of alcohols and alkanes, self-association is extensive and it has proved difficult to construct a quantitative theory that correlates the experimental data (2). Recently, Lorimer *et al.* (3) combined thermodynamic association theory (4–6) with experimental Gibbs energies to find thermodynamic parameters for systems that involve self-association, formation of binary complexes, and non-specific interactions among the various species present. The theory, except in the case of simple complex formation between two non-associating components (4), has not been extended to include heats and volumes of mixing. This extension is described in the first part of this paper.

Extensive data are available for the three binary mixtures formed from acetonitrile, carbon tetrachloride, and chloroform. Handa and Jones (7) and Handa (8) have presented data on the heats and volumes of mixing for mixtures of acetonitrile and chloroform, and excess Gibbs energies have been obtained from measurements of total vapour pressures (9). Excess Gibbs energies (10, 11), heats of mixing (11, 12), and volumes of mixing (10, 11) have been measured for the systems acetonitrile – carbon tetrachloride and carbon tetrachloride – chloroform. Interpretation of the properties of liquid mixtures containing acetonitrile must take into account the high degree of association in pure

[1]Present address: Ministry of the Environment, P.O. Box 487, Bracebridge, Ont., Canada P0B 1C0.

acetonitrile, evidence for which has been summarized by Saum (13). It has also been considered that chloroform is an associated liquid (14) and that acetonitrile and chloroform form complexes (9, 15, 16). There is no evidence for formation of complexes between acetonitrile and carbon tetrachloride in the solid–liquid phase diagram (17); the phase diagram for acetonitrile–chloroform (18) will be discussed below. Association theory would appear, therefore, to be a reasonable approach to a comprehensive theory of the thermodynamic properties of these binary mixtures, an approach that is discussed in the second part of this paper.

Theory

(a) General Relations and Excess Gibbs Energies

Saum (13) has indicated that both antiparallel and head-to-tail association of acetonitrile dipoles is significant, with a larger energy of association for the antiparallel case. Thus, two association reactions for acetonitrile are assumed: a one-step association (corresponding to roughly antiparallel alignment of CN bond dipoles):

$$[1] \qquad 2A_1 = A_2' \qquad K_A' = x_{A_2}'/x_{A_1}^2$$

and chain association (corresponding to head-to-tail alignment of acetonitrile dipoles) with the same association constant for all steps (3, 6):

$$[2] \qquad A_1 + A_i = A_{i+1} \qquad K_A = x_{A_{i+1}}/x_{A_1}x_{A_i}, \quad i \geq 1$$

Chloroform molecules (B) are assumed to associate in chains, with the same equilibrium constant for each association step:

$$[3] \qquad B_1 + B_i = B_{i+1} \qquad K_B = x_{B_{i+1}}/x_{B_1}x_{B_i}$$

Acetonitrile and chloroform molecules are assumed to form simple complexes containing one or two $CHCl_3$ molecules:

$$[4] \qquad B_1 + AB_i = AB_{i+1} \qquad K_{i+1} = x_{AB_{i+1}}/x_{AB_i}x_{B_1}, \quad i = 0, 1$$

The symbols A_i and B_i represent i-mer molecules, x_{A_i}, x_{B_i} are the species mole fractions based on the total amount of all species in the mixture and x_{A_2}' refers to head-to-head dimers. These various species are assumed to form a mixture that is ideal except for a general non-specific interaction term involving all species (3–5). The quantities K_{i+1}, K_A', K_A, K_B are mole fraction equilibrium constants.

The stoichiometric mole fractional activity coefficients can be calculated by methods described elsewhere (3, 6), and are given by (cf. ref. 3):

$$[5] \qquad x_{A_1}{}^* f_A \exp(-wx_B^2) = x_{A_1}/x_A = Q(x_{A_1}, x_{B_1})/\{x_{B_1}K_1(1 + x_{B_1}K_2) + 2x_{A_1}K_A' + 1/(1 - x_{A_1}K_A)^2\}$$

$$[6] \qquad x_{B_1}{}^* f_B \exp(-wx_A^2) = x_{B_1}/x_B = Q(x_{A_1}, x_{B_1})/\{x_{A_1}K_1(1 + 2x_{B_1}K_2) + 1/(1 - x_{B_1}K_B)^2\}$$

where

$$[7] \qquad Q(x_{A_1},x_{B_1}) = 2x_{A_1}K_A' + x_{A_1}x_{B_1}K_1(2 + 3x_{B_1}K_2) + x_{A_1}/(1 - x_{A_1}K_A)^2 + x_{B_1}/(1 - x_{B_1}K_B)^2$$

Here, $x_{A_1}{}^*$, $x_{B_1}{}^*$ are the mole fractions of monomers in the pure liquids A, B respectively, and the exponential terms allow for non-specific interactions among all species. The species mole fractions are related by

$$[8] \qquad x_{A_1}^2K_A' + x_{A_1}/(1 - x_{A_1}K_A) + x_{B_1}/(1 - x_{B_1}K_B) + x_{A_1}x_{B_1}K_1(1 + x_{B_1}K_2) = 1$$

Equations 8 with either [5] or [6] constitute two simultaneous equations in x_{A_1} and x_{B_1} that may be solved by iteration if the interaction parameter w and the equilibrium constants are known. To estimate these parameters, it is convenient to use the limiting values of the activity coefficients (3):

[9] $$l_A^{(g)} \equiv \lim_{x_A \to 0} f_A = e^w / x_{A_1}^* x_{B_1}^* \{1 + x_{B_1}^* K_1 (1 + x_{B_1}^* K_2)\}$$

[10] $$l_B^{(g)} \equiv \lim_{x_B \to 0} f_B = e^w \{2 x_{A_1}^{*3} K_A' + (1 - x_{A_1}^{*2} K_A')^2\} / x_{A_1}^* x_{B_1}^* (1 + x_{A_1}^* K_1)$$

In deriving these limiting relations, the following relations derived from eq. 8 have been used (3):

[11] $$K_A = 1/x_{A_1}^* - 1/(1 - x_{A_1}^{*2} K_A')$$

[12] $$K_B = 1/x_{B_1}^* - 1$$

Note that, if $K_A = 0$, eq. 11 becomes

[13] $$K_A' = (1/x_{A_1}^* - 1)/x_{A_1}^*$$

If experimental data on excess Gibbs energies are fitted to the usual polynomial expansion

[14] $$G_m^E / RT = x_A x_B \sum_{r=1}^{n} g_r (x_A - x_B)^{r-1}$$

where R is the ideal gas constant and T the thermodynamic temperature, then it is found that (3)

[15] $$l_A^{(g)} = \exp \left\{ \sum_{r=1}^{n} (-1)^{r-1} g_r \right\}$$

[16] $$l_B^{(g)} = \exp \left\{ \sum_{r=1}^{n} g_r \right\}$$

It will be shown below how experimental values of $l_A^{(g)}$ and $l_B^{(g)}$ can be used to find values of the association parameters. Once these have been found, data on excess enthalpies and volumes can be analyzed.

(b) Excess Enthalpies

Well-known thermodynamic relations (19) give

[17] $$R \ln f_A = G_m^E / T - x_B \partial (G_m^E / T) / \partial x_B$$

and

[18] $$H_A - H_A^* = H_m^E - x_B \partial H_m^E / \partial x_B$$

where H_m^E is the molar excess enthalpy and H_A, H_A^* are the partial molar enthalpies of A in the mixture of composition x_B and in the pure liquid, respectively. Analogous equations for component B are found by interchanging the subscripts A and B. Differentiation of eq. 17 with respect to $1/T$ gives eq. 18. It follows that

[19] $$l_A^{(h)} = R \, \partial \ln l_A^{(g)} / \partial (1/T)$$

and that a similar relation holds for $l_B^{(h)}$, where $l_A^{(h)}$, $l_B^{(h)}$ are the limiting partial molar heats of mixing of components A and B. From eqs. 9, 10, and 19,

[20] $$l_A^{(h)} = u - \Delta H_A^* - \{1 + x_{B_1}^* K_1 (2 + 3 x_{B_1}^* K_2)\} \Delta H_B^* / \{1 + x_{B_1}^* K_1 (1 + x_{B_1}^* K_2)\} + x_{B_1}^* K_1 \{(1 + x_{B_1}^* K_2) \Delta H_1^{\ominus} + x_{B_1}^* K_2 \Delta H_2^{\ominus}\} / \{1 + x_{B_1}^* K_1 (1 + x_{B_1}^* K_2)\}$$

[21] $$l_B^{(h)} = u - \Delta H_B^* - \Delta H_A^* - x_{A_1}^* K_1 (\Delta H_A^* - \Delta H_1^{\ominus}) / (1 + x_{A_1}^* K_1) + 2 x_{A_1}^{*2} K_A' \{(1 - x_{A_1}^* K_A' - x_{A_1}^*) \Delta H_A'^{\ominus} + (3 x_{A_1}^* + 2 x_{A_1}^* K_A' - 2) \Delta H_A^*\} / Q'$$

where

[22] $$Q' = 2 x_{A_1}^{*3} K_A' + (1 - x_{A_1}^{*2} K_A')^2$$

In these equations, standard values of ΔH (indicated by superscript $\ominus$) are the usual derivatives $-R\partial/\partial(1/T)$ of the appropriate equilibrium constants. The starred quantities are (cf. (3))

[23] $$\Delta H_A^* = R\partial \ln x_{A_1}^*/\partial(1/T)$$

[24] $$\Delta H_B^* = R\partial \ln x_{B_1}^*/\partial(1/T) = (1 - x_{B_1}^*)\Delta H_B^{\ominus}$$

and

[25] $$u = R\partial w/\partial(1/T)$$

The enthalpy terms connected with self-association of acetonitrile are connected by the following relation derived from eq. 11:

[26] $$x_{A_1}^* K_A \Delta H_A^{\ominus} = \{1 + 2x_{A_1}^{*3} K_A'/(1 - x_{A_1}^{*2} K_A')^2\}\Delta H_A^* - x_{A_1}^{*3} K_A' \Delta H_A'^{\ominus}/(1 - x_{A_1}^{*2} K_A')^2$$

For the special case $K_A = 0$, eqs. 26 and 13 give:

[27] $$\Delta H_A^* = (1 - x_{A_1}^*)\Delta H_A'^{\ominus}/(2 - x_{A_1}^*)$$

From eq. 14, the experimental enthalpies can be represented as a series

[28] $$H_m^E = x_A x_B \sum_{r=1}^{n} h_r (x_A - x_B)^{r-1}$$

and from eq. 17,

[29] $$h_r = R\partial g_r/\partial(1/T)$$

From [28], [15], and [16],

[30] $$l_A^{(h)} = \sum_{r=1}^{n} (-1)^{r-1} h_r$$

[31] $$l_B^{(h)} = \sum_{r=1}^{n} h_r$$

The limiting partial molar heats of mixing can therefore be obtained from experimental data expressed in the form of eq. 28, and it will be shown below how these values can be used to evaluate the enthalpy parameters for association.

Once the enthalpy parameters have been determined, the excess enthalpy – composition curve can be calculated as follows. From eqs. 5, 6, 17, and 18,

[32] $$H_A - H_A^* = R\partial \ln x_{A_1}/\partial(1/T) - \Delta H_A^* + u x_B^2$$

and similarly for component B. The molar excess enthalpy is then

[33] $$H_m^E = x_A(H_A - H_A^*) + x_B(H_B - H_B^*)$$

Differentiation of eqs. 5 (or 6) and 8 gives two simultaneous linear equations in the temperature derivatives of x_{A_1} and x_{B_1}, with solutions

[34] $$\partial x_{A_1}/\partial(1/T) = (Q_2 Q_6 - Q_3 Q_5)/(Q_1 Q_5 - Q_2 Q_4)$$

[35] $$\partial x_{B_1}/\partial(1/T) = (Q_3 Q_4 - Q_1 Q_6)/(Q_1 Q_5 - Q_2 Q_4)$$

where

[36] $$Q_1 = x_B(1 + x_{A_1}K_A)/(1 - x_{A_1}K_A)^3 + 4x_B x_{A_1} K_A' + x_{B_1} K_1(2x_B - 1) + x_{B_1}^2 K_1 K_2(3x_B - 2)$$

[37] $$Q_2 = -x_A(1 + x_{B_1}K_B)/(1 - x_{B_1}K_B)^3 + x_{A_1} K_1(2x_B - 1) + 2x_{A_1} x_{B_1} K_1 K_2(3x_B - 2)$$

[38] $$\begin{aligned} RQ_3 = {} & -2x_B x_{A_1}^2 K_A \Delta H_A^{\ominus}/(1 - x_{A_1}K_A)^3 + 2x_A x_{B_1}^2 K_B \Delta H_B^{\ominus}/(1 - x_{B_1}K_B)^3 \\ & - 2x_B x_{A_1} K_A' \Delta H_A'^{\ominus} - (2x_B - 1)x_{A_1} x_{B_1} K_1 K_2 \Delta H_1^{\ominus} \\ & - (3x_B - 2)x_{A_1} x_{B_1}^2 K_1 K_2 (\Delta H_1^{\ominus} + \Delta H_2^{\ominus}) \end{aligned}$$

[39] $$Q_4 = 1/(1 - x_{A_1}K_A)^2 + 2x_{A_1} K_A' + x_{B_1} K_1(1 + x_{B_1} K_2)$$

[40] $$Q_5 = 1/(1 - x_{B_1}K_B)^2 + x_{A_1}K_1(1 + 2x_{B_1}K_2)$$

[41] $$RQ_6 = -x_{A_1}{}^2K_A\Delta H_A{}^{\ominus}/(1 - x_{A_1}K_A)^2 - x_{B_1}{}^2K_B\Delta H_B{}^{\ominus}/(1 - x_{B_1}K_B)^2 - x_{A_1}{}^2K_A{}'\Delta H_A{}'^{\ominus} - x_{A_1}x_{B_1}K_1\Delta H_1{}^{\ominus} - x_{A_1}x_{B_1}{}^2K_1K_2(\Delta H_1{}^{\ominus} + \Delta H_2{}^{\ominus})$$

For each pair of calculated values of x_{A_1} and x_{B_1}, the derivatives and the excess enthalpy can be calculated.

The significance of $x_{A_1}{}^*$, $x_{B_1}{}^*$, $\Delta H_A{}^*$, $\Delta H_B{}^*$ (and, as defined below, $\Delta V_A{}^*$ and $\Delta V_B{}^*$) should be recalled (3): $RT \ln x_{A_1}{}^*$ is the change in molar Gibbs energy for formation, in the pure liquid, of the equilibrium distribution of self-associated complexes from monomers, and $\Delta H_A{}^*$, $\Delta V_A{}^*$ are the accompanying changes in enthalpy and in volume. The standard quantities (superscript $\ominus$) specify as usual that all species are in their reference states, here the hypothetical pure liquid for each species in the mixture.

(c) Excess Volumes

Equations analogous to [17] to [19] may be derived by differentiating with respect to pressure instead of temperature. Thus,

[42] $$V_A - V_A{}^* = V_m{}^E - x_B\partial V_m{}^E/\partial x_B$$

where $V_m{}^E$ is the molar excess volume and V_A, $V_A{}^*$ are the partial molar volumes of A in the mixture of composition x_B and in the pure liquid, respectively. Differentiation of eq. 17 with respect to pressure p gives eq. 42. It follows that

[43] $$l_A{}^{(v)} = RT\partial \ln l_A{}^{(g)}/\partial p$$

and that a similar equation holds for $l_B{}^{(v)}$, where $l_A{}^{(v)}$, $l_B{}^{(v)}$ are the limiting partial molar volumes of mixing of components A and B. Analogues of eqs. 20 through 41 hold for the excess volumes, and are obtained from these equations by replacing H with V, h_r with v_r, u with v, and $R\partial/\partial(1/T)$ with $RT\partial/\partial p$.

Although the relations above have been developed for a specific model for association, analogous relations can be developed by the same method for other models.

(d) The Non-specific Interaction Parameters

Relations among the interaction parameters are useful for interpretation of available data on systems involving acetonitrile. If the interaction parameters w_{ij} refer to simple mixtures, the approximate relation of Malesinski (9, 20) connecting the values of w_{ij} for the three different binary systems that can be formed from components 1, 2, 3 is

[44] $$w_{23} = w_{13} - w_{12}$$

From this equation and eq. 25 it follows that (9)

[45] $$u_{23} = u_{13} - u_{12}$$

and that, analogously, $v = RT\partial w/\partial p$, giving

[46] $$v_{23} = v_{13} - v_{12}$$

For a series of systems that show formation of complexes between components 2 and 3, Kreglewski (9) assumed that w_{12} and w_{13} could be replaced by the appropriate experimental values of $4G_m{}^E/RT$ (i.e., at mole fraction $\frac{1}{2}$), and argued that self association effects for one component (3, say) would largely cancel. The value of w_{23} calculated in this way was taken to be the contribution of non-specific interactions to the total excess Gibbs energy of mixtures of components 2 and 3. However, it is clear from eqs. 5 and 6 that the effects of self-association and binary association are not additive, and here relations [44]–[46] are considered to apply only to the interaction parameters, and not to the excess Gibbs energies at mole fraction $\frac{1}{2}$.

McGlashan *et al.* (21) discussed formation of simple complexes from the point of view of lattice theory, pointing out that wRT is a Gibbs energy and that for many simple mixtures $w = A/T^2$ and $u = 2wRT$ hold approximately, where A is a constant. Bertrand (22) assumed that a non-specific interaction term existed for each species in a mixture containing simple complexes, and by a series of approximations reduced the problem to finding a single w that was estimated from solubility parameters. Bertrand's method is clearly a crude version of the correct lattice theory that ignores entropic contributions to w and that cannot be applied either to self-associating components or to polar molecules (23).

Applications and Discussion

(a) Excess Gibbs Energies

For analysis of complexes in mixtures of

TABLE 1. Coefficients for calculation of excess Gibbs energies (eq. 14)

System	T/K	g_1	$\sigma(g_1)$	g_2	$\sigma(g_2)$	g_3	$\sigma(g_3)$	g_4	$\sigma(g_4)$
CCl_4–$CHCl_3$*	318.15	0.148	0.010	—	—	—	—	—	—
CH_3CN–CCl_4	318.15	1.7842	0.0089	−0.180	0.030	0.322	0.020	−0.172	0.044
CH_3CN–$CHCl_3$	313.15	0.244	0.010	0.084	0.029	0.098	0.055	—	—
	318.15	0.264	0.010	0.084	0.029	0.096	0.055	—	—

*$G_m^E/RT = x_A x_B\{111.9(0.24)/T - 0.202(0.010)\}$; standard deviations in parentheses.

acetonitrile and chloroform, available data on binary mixtures of carbon tetrachloride, chloroform, and acetonitrile are used, where it is assumed that carbon tetrachloride takes no part in complex formation, but that both chloroform and acetonitrile are self-associated. The three possible systems are indicated by Roman numerals: CCl_4–$CHCl_3$(I), CH_3CN–CCl_4(II), CH_3CN–$CHCl_3$(III), and the first-named component is component A. For these three systems, eight parameters $w_{12}, w_{13}, w_{23}, x_{A_1}^*, x_{B_1}^*, K_1, K_2$, and K_A' appear in eqs. 9 and 10.

Excess Gibbs energies have been calculated from isothermal liquid–vapour equilibrium data for both CCl_4–$CHCl_3$ (11) and CH_3CN–CCl_4 (10). For CCl_4–$CHCl_3$, a one-constant equation of type [14] represents the data, with $g_1 = h_1/RT + g_0$. The value of h_1 is that recommended by McGlashan *et al.* (11), and its standard deviation was estimated from the summary of heats of mixing given by them. The constant g_0 and its standard deviation were found from least-squares evaluation of the G_m^E data at three temperatures; its value differs slightly from that of McGlashan *et al.* (11). For CH_3CN–CCl_4, the data (10) were fitted by least squares to an equation of type [14] in order to find estimated standard deviations. The coefficients differ slightly from those given by Brown and Smith (10).

Excess Gibbs energies for CH_3CN–$CHCl_3$ have been obtained at 40°C from measurements of total vapour pressures (9) by Barker's method (24), and by neglecting the second virial cross-coefficient for the vapour. It is known (3) that this coefficient is of considerable importance, and the data have been recalculated using virial coefficients estimated by the method[2] of Prausnitz *et al.* (25, 26). The necessary data (26) give the values $B_{AA} = -3256$, $B_{AB} = -698$, $B_{BB} = -1115$ cm^3 mol^{-1} at 40°C (A-acetonitrile) on calculation. The values for B_{AA} and B_{BB} are in good agreement with the average of tabulated values (27). The results of all recalculations of g_r are given in Table 1, along with estimated standard deviations σ. Correlation coefficients for the g_r values are necessary to find standard deviations for derived quantities such as activity coefficients, but are not listed here. The coefficients for CH_3CN–$CHCl_3$ at 45°C were estimated from the values at 40°C and the enthalpies of mixing (7), assuming that the enthalpies of mixing are independent of temperature over this range. For each system, the number of coefficients g_r tabulated is the number that gave the smallest standard deviation or that gave a variance ratio that indicated the minimum number of coefficients required.

Since the limiting activity coefficients for CCl_4–CH_3Cl are equal, there are only five limiting activity coefficients that can be used to find the eight association parameters. Estimation of the parameters proceeds as follows. For system II (CH_3CN–CCl_4), $K_1 = K_2 = K_B = 0$ and the ratio $l_B^{(g)}/l_A^{(g)}$ (eqs. 9, 10) gives a quadratic equation in K_A' for a given value of $x_{A_1}^*$. The value of $x_{A_1}^*$ is a maximum for $K_A = 0$, and, for this value of K_A, determines the values of K_A' and w_{13} through eqs. 9 and 13. These parameters are then used for an iterative solution of eqs. 5 and 8 by computer to find x_{A_1} and x_{B_1}, using initial values of these quantities found by setting the stoichiometric activity coefficients equal to unity. The activity coefficients and G_m^E are then calculated. The parameters found in this way reproduced the experimental G_m^E–x_B curve very well, the maximum deviation being only 4.2% at $x_B = 0.5$. Calculations of the enthalpy of mixing (see below) using these parameters were less successful, and, in fact, a better fit to the excess Gibbs energies was found by using a non-zero value of K_A. Values of K_A' were chosen, and the corresponding values of $x_{A_1}^*$,

[2]The sign of the association term in the equation for the virial coefficients is incorrect in refs. 25, 26, but correct in the computer program in ref. 26.

w_{13}, and K_A were found from eqs. 9, 10, and 11. The value of K_A' that gave the minimum χ^2 for nine values of G_m^E calculated from the experimental polynomial at equally-spaced mole fractions was taken as the final value (Table 4). The estimated standard deviation in K_A' was found by finding the values of K_A' that produced twice the minimum χ^2, while the standard deviations in K_A and in x_{A_1}* were calculated from this value and (through eqs. 9 to 11) the error matrix for the experimental polynomial. Agreement between the theoretical and experimental excess Gibbs energy curves (Fig. 1) is excellent, with an estimated standard deviation (28) of only 19 J mol^{-1}.

Non-specific interactions contribute 718 J mol^{-1} to G_m^E at mole fraction one-half. The remaining positive contribution to the almost symmetrical curve is due to self-association. Kreglewski's method (9) gives the much larger value 1082 J mol^{-1} for non-specific interactions at equal mole fractions.

Saum (13) has estimated x_{A_1}* = 0.04 at 30°C by consideration of heats of vapourization and viscosities of a homologous series of nitriles. His value of the enthalpy of association gives x_{A_1}* = 0.12 at 45°C from eqs. 23 and 27, in reasonable agreement with the value found here when the highly approximate nature of Saum's estimate is considered.

For mixtures of CH_3CN and $CHCl_3$, the relation of Malesinski (eq. 44), the ratio $l_A^{(g)}(III) \times l_A^{(g)}(I)/l_A^{(g)}(II)$ and the corresponding ratio for the $l_B^{(g)}$-values give an equation that relates x_{B_1}* to x_{A_1}*, if $K_2 = 0$. Numerous trials showed that $K_2 < K_1$ was a condition that was incompatible with the experimental data, that K_1 was at least 100 times smaller than K_2, and that x_{B_1}* was smaller than unity. The final values of the parameters and their standard deviations were found by the constrained least-squares procedure outlined above, this time setting $K_1 = 0$ and choosing a value of x_{B_1}* that gave a minimum χ^2. Agreement between the theoretical and experimental G_m^E-composition curves is again excellent, with a standard deviation of 3.9 J mol^{-1} (Fig. 1).

Non-specific interactions contribute −215 J mol^{-1} to G_m^E at equal mole fractions. This contribution and the negative contribution from complex formation are overbalanced by self-association of acetonitrile. The skewness of the curve results mainly from formation of a complex containing two molecules of $CHCl_3$. Use of volume fractions instead of mole fractions in the non-specific interaction term would also skew the curve in the same direction. However, the heat of mixing curve (Fig. 2) is skewed in the opposite direction.

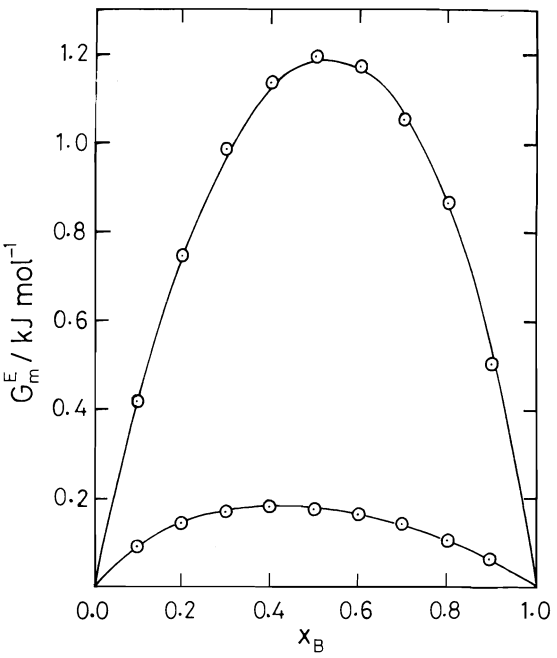

FIG. 1. Excess Gibbs energies at 318 K. Upper curve: CH_3CN–CCl_4; lower curve: CH_3CN–$CHCl_3$. Lines: experimental polynomials; open circles: values from association theory.

Values of K_1 for formation of AB-type complexes between acetonitrile and chloroform have been derived from nmr measurements (15, 16) by assuming that only these complexes are formed and that self-association of acetonitrile does not affect the calculations, or is included in a solvent shift. The nmr data, however, can be interpreted equally well by assuming that only an AB_2 complex is formed. The method of doing this is outlined in the Appendix, and gives $K_2 = 1.9$ at 297 K, which is the same value found for this temperature by extrapolation from 318 K using the enthalpy of complex formation (Table 4). From the constants in Tables 1 and 4 it is calculated that the fraction of CH_3CN molecules that is self-associated is 0.73 at $x_B = 0.336$ (the most concentrated solution of $CHCl_3$ used by Lin and Tsay (16)) and 0.86 at $x_B = 0$, while the fraction of CH_3CN molecules in AB_2 complexes varies from 0.063 to zero over the same range of

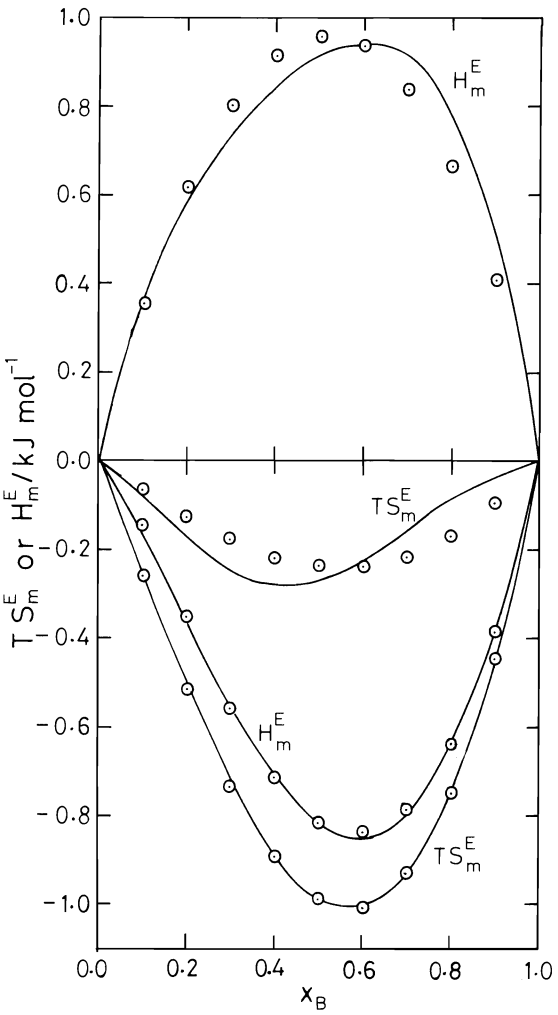

FIG. 2. Excess enthalpies and entropies (as TS_m^E). Upper curves: CH_3CN–CCl_4, 318 K; lower curves: CH_3CN–$CHCl_3$, 298 K for H_m^E, 318 K for TS_m^E. Lines: experimental polynomials; open circles: values from association theory.

composition. At $x_B = 0.0290$ (the lowest concentration of Lin and Tsay (16)), a fraction 0.85 of CH_3CN molecules are self-associated and a fraction 8.8×10^{-4} is in AB_2 complexes. Even at this low concentration it is estimated that the mole fraction of AB complexes is not more than one-quarter that of AB_2 complexes. The assumptions that self-association of acetonitrile is roughly constant and that AB complexes are negligible over the range of composition used in the nmr studies thus appears to be justified.

The solid–liquid phase diagram for $CHCl_3$–CH_3CN (18) shows no evidence for complex formation, while $CHCl_3$–propionitrile shows an AB complex and $CHCl_3$–butyronitrile shows both AB and AB_2 complexes. Murray and Schneider (18) proposed that self-association in acetonitrile was so extensive that formation of binary complexes was prevented. This question can be investigated by extrapolating the coefficients in Tables 1 and 4 to 183 K (where a solid compound might exist) and calculating the fraction of acetonitrile molecules that are self-associated. This fraction varies from 0.9 at $x_B = 0$ to 0.74 at $x_B = 0.5$ to 0.46 at $x_B = 0.67$ and is probably an overestimate; the enthalpy terms have been assumed independent of temperature, but there is probably a significant positive heat capacity of association. Thus, there should be sufficient opportunity for binary compounds to form at low temperatures, and a reinvestigation of the phase diagram is desirable.

The coefficient g_1 for CCl_4–$CHCl_3$, with the value of x_{B_1}*, yields the value of w_{12} in Table 2. This non-specific interaction term contributes 60 J mol^{-1} to G_m^E at equal mole fractions of $CHCl_3$ and CCl_4, or 61% of the total. Proton nmr measurements (14) give $K_B = 0.16$ for a one-step self-association of chloroform at 25°C, a value that corresponds to x_{B_1}* = 0.88. At 45°C, the value of x_{B_1}* should be closer to unity, and at the normal boiling point (61°C) the Trouton constant $\Delta S_1^v/R = 10.67$ has the "normal" value for an unassociated liquid (3). The value x_{B_1}* = 0.94 (Table 4) is in good agreement with these considerations. The fact that CCl_4–$CHCl_3$ mixtures have equal limiting activity coefficients in the range 298–328 K is incompatible with the assumption made in interpreting the nmr data that only $CHCl_3$ dimers are formed.

(b) Enthalpies of Mixing

In Table 2, the least-squares coefficient in the polynomial equation [28] is taken from values in the literature for CCl_4–$CHCl_3$ (11). For CH_3CN–$CHCl_3$ the tabulated coefficients (7) were recalculated to find the error matrix, and for CH_3CN–CCl_4 (12) the data were fitted to a least-squares polynomial. The same number of coefficients for polynomials [28] and [14] was found to give satisfactory fits in all cases and all coefficients are given in Table 2. It is assumed that, for CH_3CN–$CHCl_3$ mixtures, the enthalpies of mixing are independent of temperature between 25 and 45°C. This is a good assumption

TABLE 2. Coefficients for calculation of excess enthalpies (eq. 28) in J mol^{-1}

System	T/K	h_1	$\sigma(h_1)$	h_2	$\sigma(h_2)$	h_3	$\sigma(h_3)$	h_4	$\sigma(h_4)$
CCl_4–$CHCl_3$	289–328	930	2	—	—	—	—	—	—
CH_3CN–CCl_4	318.15	3636	40	−966	152	1657	154	−274	371
CH_3CN–$CHCl_3$	298.15	−3250	11	1505	21	319	52	—	—

for some associated mixtures (e.g., olefin–SO_2 (3)), but for others (e.g., aromatic hydrocarbons – CCl_4 (21)), the heat of mixing at $x_B = 0.5$ can vary as much as 30 J mol^{-1} over a range of 20 K.

Equations 20 and 21, when applied to CH_3CN–CCl_4 mixtures, give a single equation in $\Delta H_A'^{\ominus}$ and ΔH_A^*. A value of $\Delta H_A'^{\ominus}$ was chosen which, with the values of $x_{A_1}^*$, K_A', and K_A found previously, determines ΔH_A^*, $\Delta H_A^{\ominus}$, and u_{13}. These parameters were then used to find H_m^E from eqs. 32–41, along with values of x_{A_1} and x_{B_1} calculated from the experimental polynomial for G_m^E and eqs. 5 and 6. The value of $\Delta H_A'^{\ominus}$ was then varied until a minimum χ^2 was found, and the resulting parameters $\Delta H_A'^{\ominus}$, $\Delta H_A^{\ominus}$, ΔH_A^*, and u_{13} are given in Table 4. The theoretical curve is less skewed than the experimental curve (see Fig. 2), and deviations are considerably larger than the estimated random errors in the experimental polynomial. The standard deviation for the fit is 78 J mol^{-1}. However, only two experimental values of H_m^E are available for $x_B > 0.5$; more experimental values could alter the shape of the curve considerably. Use of volume fractions instead of mole fractions in the non-specific interaction term would skew the calculated curve in the wrong direction. Non-specific interactions amount to 653 J mol^{-1} at equal mole fractions.

Saum (13) estimated the energy of parallel dipole interaction in acetonitrile to be −28 kJ mol^{-1}, if the C—N distances between adjacent molecules are equal to the sum of the van der Waals' radii. This value is close to the value −23 kJ mol^{-1} estimated from the electrostatic reaction field (29) and to −22 kJ mol^{-1} estimated by Lambert *et al.* (30) from the virial coefficients of acetonitrile vapour. Meyer and coworkers (31, 32), on the other hand, estimated that induction forces contribute −11 kJ mol^{-1} to the cohesive energy of acetonitrile, and −4 kJ mol^{-1} to the orientation energy. Their calculation was based essentially on the curvature of heats of vaporization as a function of chain length in a homologous series of nitriles. The ΔH_A parameters presumably are measures of orientation energy, since they refer to formation of complexes from a hypothetical liquid consisting only of monomers. The "mean" enthalpy change, ΔH_A^*, has a value close to Meyer's value of orientation energy. Dipole–dipole attractions (13) at distances larger than the van der Waals' radii or at angles between adjacent dipoles of less than 180° (18) could account easily for the values of $\Delta H_A'^{\ominus}$ and $\Delta H_A^{\ominus}$.

For CH_3CN–$CHCl_3$ mixtures, values of the parameters for acetonitrile were used, and choosing ΔH_B^* then determines $\Delta H_2^{\ominus}$ and u_{23} through eqs. 20 and 21. The same constrained least-squares procedure then yielded the values in Table 4. The agreement between calculated and observed values is excellent with a standard deviation of 13 J mol^{-1}. The point of inflection at $x_B = 0.1875$ is reproduced well by the theory. As with the excess Gibbs energies, the main contribution to skewness is the formation of complexes containing two molecules of $CHCl_3$. The non-specific interaction term contributes −81 J mol^{-1} at equal mole fractions, a rather small value because of the large positive contribution from acetonitrile interactions. Use of volume fractions in the non-specific term would skew the curve in the wrong direction.

For CCl_4–$CHCl_3$ mixtures, the value of ΔH_B^* and eq. 20 determines the value of u_{12}. The calculated reaction field energy in chloroform is −0.75 kJ mol^{-1} (29), again larger than the value of ΔH_B^*, which presumably reflects orientation energy. Non-specific interactions contribute 200 J mol^{-1} or 22% of the heat of mixing at equal mole fractions.

(c) Excess Entropies

Excess entropies of mixing were calculated from both the experimental and theoretical values of G_m^E and H_m^E, and are shown in Fig. 2. As expected, the errors in the model or in the data for H_m^E are emphasized in taking differences between H_m^E and G_m^E, so that the agree-

TABLE 3. Coefficients for calculation of excess volumes (cf. eq. 28) in $cm^3\ mol^{-1}$

System	T/K	v_1	$\sigma(v_1)$	v_2	$\sigma(v_2)$	v_3	$\sigma(v_3)$	v_4	$\sigma(v_4)$
CCl_4–$CHCl_3$	297.15	0.695	0.036	—	—	—	—	—	—
CH_3CN–CCl_4	298.15	−0.533	0.025	0.016	0.078	0.391	0.054	−0.269	0.124
CH_3CN–$CHCl_3$	313.15	−1.265	0.002	0.838	0.005	−0.072	0.010	—	—
	318.15	−1.302	0.002	0.856	0.005	−0.076	0.010	—	—

ment between the experimental and theoretical curves for CH_3CN–CCl_4 is only qualitative. The most striking discrepancies are that the curves are skewed in opposite directions and that the two points of inflection in the experimental curve are not found by theory. Non-specific interactions account for -65 J mol^{-1} at equal mole fractions, so that there is a large negative contribution from self-association.

For CH_3CN–$CHCl_3$, the calculated and experimental curves agree closely. Non-specific interactions contribute -535 J mol^{-1} at equal mole fractions, and there is a negative contribution due to self-association and complex formation that is considerably larger than in CH_3CN–CCl_4. The excess entropy for CCl_4–$CHCl_3$ is always positive. At equal mole fractions, non-specific interactions contribute 140 J mol^{-1} to TS_m^E, or 104% of the total, leaving a contribution of -5 J mol^{-1} for self-association of chloroform.

Standard entropy changes can be calculated for each corresponding equilibrium constant and enthalpy of association, and are given in Table 4. It has been suggested (5, 6) that the decrease in entropy on association arises mainly from the loss of orientational degrees of freedom, i.e.,

$$[47] \qquad q = \exp(-\Delta S^{\ominus}/R)$$

where q is the number of nearest-neighbour contacts that are lost by a monomer on association. The values of q calculated from the data in Table 4 are 3 for reaction 1, 14 for reaction 2, 2 for reaction 3, and 27 for reaction 4, compared to the value of 6–10 expected for freely-rotating molecules in a liquid. Clearly, other contributions to the entropy of association are present, among them a change in entropy involving dipole orientation.

(d) Volumes of Mixing

Polynomial least-squares fits according to the volume analogue of eq. 28 were recalculated on the data for excess volumes of CCl_4–$CHCl_3$ (11) and CH_3CN–$CHCl_3$ (8) in order to estimate errors. For CH_3CN–CCl_4, excess volumes were calculated from density data (10) and fitted to a least-squares polynomial. The coefficients of all polynomials are given in Table 3.

Analysis of the experimental data by association theory proceeds exactly as for the analysis of the heats of mixing. For CCl_4–$CHCl_3$ and CH_3CN–CCl_4, the experimental data are for 298 K, and values of the required association parameters were calculated at this temperature using the enthalpy data in Table 4. For CH_3CN–$CHCl_3$, data are available at 293 and 313 K (8), permitting a linear extrapolation (33) to 318 K. The resulting parameters are given in Table 4. The volume changes for association are all negative, and are small compared to the molar volumes of the components (52.9, 97.1, and 80.7 $cm^3\ mol^{-1}$ at 298 K for CH_3CN, CCl_4, and $CHCl_3$, respectively). The theoretical excess volume–composition values (Fig. 3) agree well with the experimental values; the standard deviations are 0.011 $cm^3\ mol^{-1}$ for CH_3CN–CCl_4, and 0.015 $cm^3\ mol^{-1}$ for CH_3CN–$CHCl_3$. The predominantly negative excess volume for CH_3CN–CCl_4 becomes zero at $x_B = 0.962$, then reaches a positive maximum of 9.9×10^{-4} $cm^3\ mol^{-1}$ at $x_B = 0.982$, according to the polynomial equation (cf. 10, 33). One positive value has been measured (10): $V_m^E = 0.0015$ $cm^3\ mol^{-1}$ at $x_B = 0.9535$. The association theory curve also shows reversal of sign, which occurs at $x_B = 0.994$ and reaches a maximum of 1.6×10^{-4} $cm^3\ mol^{-1}$ at $x_B = 0.997$. While the quantitative agreement between these two sets of values is poor, they are both subject to large errors. The limiting partial molar volume of mixing is negative at $x_B = 0$ and positive at $x_B = 1$, so that the theoretical curve is constrained to undergo a change in sign. That this change in sign occurs at a mole fraction close to the experimental value is an indication of the high degree of consistency among the theoretical

TABLE 4. Association and interaction parameters for binary liquid mixtures containing carbon tetrachloride (1), chloroform (2,B), and acetonitrile (3,A)*

Parameter	Value	Parameter	Value	Parameter	Value	Parameter	Value
K_2	1.52(0.074)	$\Delta H_2^{\ominus}$	−9.81(0.57)	$\Delta S_2^{\ominus}$	−27.4(1.9)	$\Delta V_2^{\ominus}$	−3.92(0.32)
x_{A_1}*	0.245(0.036)	ΔH_A*	−3.9(1.6)	ΔS_A*	−0.63(4.9)	ΔV_A*	−0.89(0.76)
K_A'	8.35(0.12)	$\Delta H_A'^{\ominus}$	−8.9(1.4)	$\Delta S_A'^{\ominus}$	−10.2(4.3)	$\Delta V_A'^{\ominus}$	−1.90(0.16)
K_A	2.1(1.2)	$\Delta H_A^{\ominus}$	−6.7(2.1)	$\Delta S_A^{\ominus}$	−21.8(8.2)	$\Delta V_A^{\ominus}$	−1.64(0.60)
x_{B_1}*	0.943(0.023)	ΔH_B*	−0.129(0.020)	ΔS_B*	−0.41(0.21)	ΔV_B*	−0.029(0.025)
K_B	0.060(0.026)	$\Delta H_B^{\ominus}$	−2.14(0.099)	$\Delta S_B^{\ominus}$	−32.8(3.6)	$\Delta V_B^{\ominus}$	−0.48(0.11)
w_{12}	0.091(0.091)	u_{12}	0.801(0.020)	s_{12}	1.76(0.80)	v_{12}	0.667(0.044)
w_{13}	1.09(0.15)	u_{13}	2.6(1.6)	s_{13}	−0.82(1.2)	v_{13}	−0.73(0.77)
w_{23}	0.33(0.18)	u_{23}	−3.0(1.9)	s_{23}	−12.2(6.1)	v_{23}	−0.94(1.2)

*Parentheses show estimated standard deviations. Enthalpies in kJ mol^{-1}, entropies in J K^{-1} mol^{-1}, volumes in cm^3 mol^{-1}. T = 318 K except for volume parameters subscripted A, v_{12}, and v_{23}, which are for 298 K.

FIG. 3. Excess volumes. Upper curve: CH_3CN–CCl_4, 298 K; lower curve: CH_3CN–$CHCl_3$, 318 K. Lines: experimental polynomials; open circles: values from association theory.

parameters for the excess Gibbs energy and the excess volume. For this system, non-specific interactions contribute −0.183 cm^3 mol^{-1} at equal mole fractions, the contribution from self-association being positive.

The excess volume–composition curve for CH_3CN–$CHCl_3$ has a point of inflection at $x_B = 0.2367$ that is reproduced well by the theory. Non-specific interactions contribute −0.235 cm^3 mol^{-1} at equal mole fractions, the balance being the net result of self-association (positive contribution) and complex formation (negative contribution).

For CCl_4–$CHCl_3$, non-specific interactions contribute 0.167 cm^3 mol^{-1} or 96% of the excess volume at equal mole fractions. The remaining positive contribution is from self-association of chloroform. For all three systems, the product pV_m^E is negligible compared to G_m^E or H_m^E.

(e) Relations Among the Parameters

The data in Table 4 indicate clearly that eqs. 44–46 are poor approximations; the correct sign for the 2–3 interaction is obtained only for the volume interaction term v_{23}. The ratios u_{ij}/RTw_{ij} have the values 3.32, 0.91, and 3.49 for CCl_4–$CHCl_3$, CH_3CN–CCl_4, and CH_3CN–$CHCl_3$, respectively, all of which are close to the average value of 2 suggested by McGlashan *et al.* (21). The values of $\Delta S^{\ominus}$ for self-association decrease roughly linearly with $\Delta H^{\ominus}$; it follows that $\Delta G^{\ominus}$ increases roughly linearly with $\Delta H^{\ominus}$. The values found for chain self-association of SO_2 (3) fit these correlations as well, and are very close to the values for chain self-association of acetonitrile.

(f) General Remarks

The power series equations and association theory both represent the experimental data well (except for the heats of mixing of CH_3CN–CCl_4), and both representations satisfy the Gibbs–Duhem equation. The two representations are not, however, identical. The limiting curvatures of the excess Gibbs energy – composition curves can be calculated from association theory and from the series equations. Despite the exact agreement imposed on the limiting slopes, and the general good agreement between experiment and theory at intermediate compositions, the calculated and experimental curvatures differ markedly in magnitude but have the same sign. The association theory equations for heats and volumes of mixing involve derivatives of G_m^E, and thus resemble the equations for the curvature. Enthalpies and volumes of association and complexing are available as disposable parameters, however, so that the temperature and pressure derivatives of the limiting slopes are chosen to agree with experiment.

Hildebrand and Scott (34) have pointed out that in many cases both association theory and regular solution theory give equally satisfactory fits to experimental data. A similar equivalence between association theory and Barker's statistical mechanical theory of associated mixtures (35, 36) has been found by Smith and Brown (2) for alcohol–alkane mixtures. From a rigorous statistical mechanical point of view, it would be desirable to calculate thermodynamic properties from suitable molecular interaction parameters and then to look for statistical mechanical interpretation of the parameters found from thermodynamic association theory. In this paper, the separation of interactions into specific and non-specific types is to some extent arbitrary, and thus simple correspondences between molecular and thermodynamic parameters may not exist. This problem will be the subject of future work. We note, however, that association theory gives a self-consistent, if limited, picture of interactions in these complex systems.

Acknowledgement

The authors wish to thank Dr. Y. P. Handa for supplying data on molar volumes of acetonitrile–chloroform mixtures in advance of publication.

1. D. V. Fenby and L. G. H. Hepler. Chem. Soc. Rev. **3**, 193 (1974).
2. F. Smith and I. Brown. Aust. J. Chem. **26**, 691 (1973); **26**, 705 (1973).
3. J. W. Lorimer, B. C. Smith, and G. H. Smith. J. Chem. Soc. Faraday Trans. I, **71**, 2232 (1975).
4. I. Prigogine and R. Defay. Chemical thermodynamics. *Translated by* D. H. Everett. Longman Green, London, New York, Toronto. 1954. Chapt. XXVI.
5. I. Prigogine. The molecular theory of solutions. North-Holland, Amsterdam. 1957. Chapt. XV.
6. L. Saroléa-Mathot. Trans. Faraday Soc. **49**, 8 (1953).
7. Y. P. Handa and D. E. Jones. Can. J. Chem. This issue.
8. Y. P. Handa. J. Chem. Thermodyn. **9**, 117 (1977).
9. A. Kreglewski. Bull. Acad. Polon. Sci. Sér. Sci. Chim. **13**, 723 (1965).
10. I. Brown and F. Smith. Aust. J. Chem. **7**, 269 (1954).
11. M. L. McGlashan, J. E. Prue, and I. E. J. Sainsbury. Trans. Faraday Soc. **50**, 1284 (1954).
12. I. Brown and W. Fock. Aust. J. Chem. **9**, 180 (1956).
13. A. M. Saum. J. Polymer Sci. **42**, 57 (1960).
14. C. F. Jumper, M. T. Emerson, and B. B. Howard. J. Chem. Phys. **35**, 1911 (1961).
15. P. J. Berkeley and M. W. Hanna. J. Phys. Chem. **67**, 846 (1963).
16. W. Lin and S. Tsay. J. Phys. Chem. **74**, 1037 (1970).
17. J. Timmermans. The physico-chemical constants of binary systems in concentrated solutions. Vol. 1. Interscience Publishers, Inc., New York, NY. 1959. p. 766.
18. F. E. Murray and W. G. Schneider. Can. J. Chem. **33**, 797 (1955).
19. E. A. Guggenheim. Thermodynamics. 4th ed. North-Holland, Amsterdam. 1959. Sect. 5.44, 5.37.
20. W. Malesinski. Bull. Acad. Polon. Sci. Sér. Sci. Chim. **7**, 51 (1959).
21. M. L. McGlashan, D. Stubley, and H. Watts. J. Chem. Soc. (A), 673 (1969).
22. G. L. Bertrand. J. Phys. Chem. **79**, 48 (1975).

23. J. H. HILDEBRAND and R. L. SCOTT. Regular solutions. Prentice-Hall, Englewood Cliffs, NY. 1962. Chapt. 11.
24. J. A. BARKER. Aust. J. Chem. **6**, 207 (1953).
25. J. P. O'CONNELL and J. M. PRAUSNITZ. Ind. Eng. Chem. Process Design Dev. **6**, 245 (1967).
26. J. M. PRAUSNITZ, C. A. ECKERT, R. V. ORYE, and J. P. O'CONNELL. Computer calculations for multicomponent vapor–liquid equilibria. Prentice-Hall, Englewood Cliffs, NY. 1967.
27. J. H. DYMOND and E. B. SMITH. The virial coefficients of gases. Clarendon Press, Oxford. 1969.
28. P. R. BEVINGTON. Data reduction and error analysis for the physical sciences. McGraw-Hill Book Co., New York, NY. 1969. p. 187.
29. C. J. F. BÖTTCHER, O. C. VAN BELLE, P. BORDEWIJK, and A. RIP. Theory of electric polarization. Vol. 1. Elsevier, Amsterdam. 1973. p. 155.
30. J. D. LAMBERT, G. A. H. ROBERTS, J. S. ROWLINSON, and V. J. WILKINSON. Proc. R. Soc. London, A**196**, 113 (1949).
31. E. F. MEYER and R. E. WAGNER. J. Phys. Chem. **70**, 3162 (1966).
32. E. F. MEYER, T. A. RENNER, and K. S. STEC. J. Phys. Chem. **75**, 642 (1971).
33. J. BROWN and F. SMITH. Aust. J. Chem. **15**, 9 (1962).
34. J. H. HILDEBRAND and R. L. SCOTT. Solubility of non-electrolytes. 3rd ed. Reinhold Publishing Corp., New York, NY. 1950. Chapt. XI.
35. J. A. BARKER. J. Chem. Phys. **20**, 1526 (1952).
36. J. A. BARKER. J. Chem. Phys. **22**, 375 (1954).

Appendix

If only AB_2-type complexes form, the nmr data can be analyzed by standard methods (16). If Δ is the observed chemical shift of complexed chloroform relative to that of pure chloroform, δ_B, and $\Delta_{AB_2} = \delta_{AB_1} - 2\delta_B$ is the relative chemical shift of the complex, then it is found readily that

$$[48] \quad K_2 = \Delta(1 - 2x_B\Delta/\Delta_{AB_2})/(1 - 2\Delta/\Delta_{AB_2})^2 \times (x_A - x_B\Delta/\Delta_{AB_2})$$

This equation can be rearranged in the form of the equation for AB complexes (16):

$$[49] \quad (1 + 4K_2)\Delta/(1 - x_B) = K_2(\Delta_{AB_2} + 4\Delta_0^2/\Delta_{AB_2}) + 3K_2x_B\Delta/(1 - x_B) + 2x_B\Delta^2(1 - 2K_2\Delta/\Delta_{AB_2})/\Delta_{AB_2}(1 - x_B) + 4K_2\{\Delta^2/(1 - x_B) - \Delta_0^2\}/\Delta_{AB_2}$$

where Δ_0 is the value of Δ at $x_B = 0$. If $K_2 \sim 2$, $\Delta_{AB_2} \sim -0.6$, the third and fourth terms in eq. 49 have opposite signs, and at the highest x_B used by Lin and Tsay (16) total about 20% of the second term. Thus, approximately, $\Delta/(1 - x_B)$ is a linear function of $x_B\Delta/(1 - x_B)$. This is indeed the case for the results of Lin and Tsay (16), and the slope and intercept yield $K_2 = 1.87$, $\Delta_{AB_2} = -0.60$. The latter value is close to the value $\Delta_{AB} = -0.65$ (16). Inclusion of a solvent shift would alter these values slightly (16). The nmr data cannot, therefore, discriminate between the two cases $K_1 \ll K_2$ and $K_2 \ll K_1$ unless chemical shifts are measured over the whole range of compositions of the mixture.

C-Nucleosides and related compounds. XIII. Synthesis of D,L-2′-deoxyshowdomycin (1*d*)

GEORGE JUST AND MU-ILL LIM
Department of Chemistry, McGill University, Montreal, P.Q., Canada H3C 3G1

Received September 23, 1976[1]

GEORGE JUST and MU-ILL LIM. Can. J. Chem. **55**, 2993 (1977).

Starting from the Diels–Alder adduct of furan and methyl β-nitroacrylate, the synthesis of the title compound is described.

GEORGE JUST et MU-ILL LIM. Can. J. Chem. **55**, 2993 (1977).

Partant de l'adduit de Diels–Alder du furanne avec le β-nitroacrylate de méthyle, on décrit une synthèse du composé mentionné dans le titre.

[Traduit par le journal]

We have recently described the synthesis of the 2′-epimer **1***b* of D,L-showdomycin **1***a* (1), and of the carbocyclic analogues of D,L-showdomycin **1***c* (2) and D,L-2′-deoxypyrazofurin A (3), starting from the Diels–Alder adducts of methyl β-nitroacrylate and furan or β-bromoacrylic acid and cyclopentadiene, respectively.

We now should like to describe a similar sequence of reactions leading to D,L-2′-deoxyshowdomycin **1***d* (see Scheme 1).

Because of some variability in the ratio of adducts **2** and **3** obtained in the initial Diels–Alder reaction, the reaction was studied in some detail. At 45°C, the concentration of the *endo*-nitro adduct **2** reached a maximum after 8 h (**2**:**3** = 2). After 4 days, an equilibrium was reached in which the *exo*-nitro adduct **3** predominated (**2**:**3** = 0.5).

Konig and co-workers reported the similar result that the *endo*-nitro isomer predominated in early stages of the Diels–Alder reactions of furan or 2,5-dimethyl furan with nitroethylene (4).

Hydroboration of the *exo*-nitro adduct **3** and oxidation of the resulting organoborane with alkaline hydrogen peroxide (5) was unsatisfactory. However, reaction of **3** with diborane in tetrahydrofuran at 0°C, followed by oxidation with triethylamine *N*-oxide dihydrate as reported by Kabalka and Hedgecock (6), resulted in the formation of the isomeric mixture of the alcohols **4***a* in 42% yield after chromatography on silicic acid.

The resulting isomeric alcohols **4***a* could not be separated. Direct acetylation of the alcohol using acetic anhydride and *p*-toluenesulfonic acid monohydrate afforded the acetates **4***b* in good yield. All attempts to separate the isomeric acetates failed. It is interesting to note here that acetylation with acetic anhydride in pyridine led to decomposition products, as already noted for similar bicyclic systems (1).

The acetates **4***b* were treated with diazabicyclo[5.4.0]undec-5-ene (DBU) in methylene chloride under reflux for 1 h to give the olefin esters **5** (7). The products consisted of a 1:1 mixture of isomers according to the nmr spectral data and could not be separated.

The above synthetic route was repeated starting with the *endo*-nitro adduct **2**. Hydroboration of **2** and oxidation of the resulting borane with triethylamine *N*-oxide dihydrate, under conditions identical to those described above, gave the isomeric alcohols **6***a* and **7***a* which were obtained in 46% yield after column chromatography on silicic acid. Without separation of the isomers, the mixture was acetylated with acetic anhydride and *p*-toluenesulfonic acid monohydrate in 82% yield. Both isomers were formed in approximately equal amounts, based on the nmr spectral data of **6***b*, **7***b*.

It was possible to separate the two isomers by fractional crystallization from hexane – carbon tetrachloride. One isomer, mp 113–114°C, was later identified to be the desired acetate **6***b* and the other, mp 67–68°C, to be the undesired acetate **7***b*. At this stage, we were unable to confirm the structures by nmr spectroscopy.

Elimination of nitrous acid from the acetate **6***b* by means of DBU in refluxing methylene chloride gave the 2-acetate olefin ester **9** in 91% yield. Using the same conditions as above,

[1]Revision received April 21, 1977.

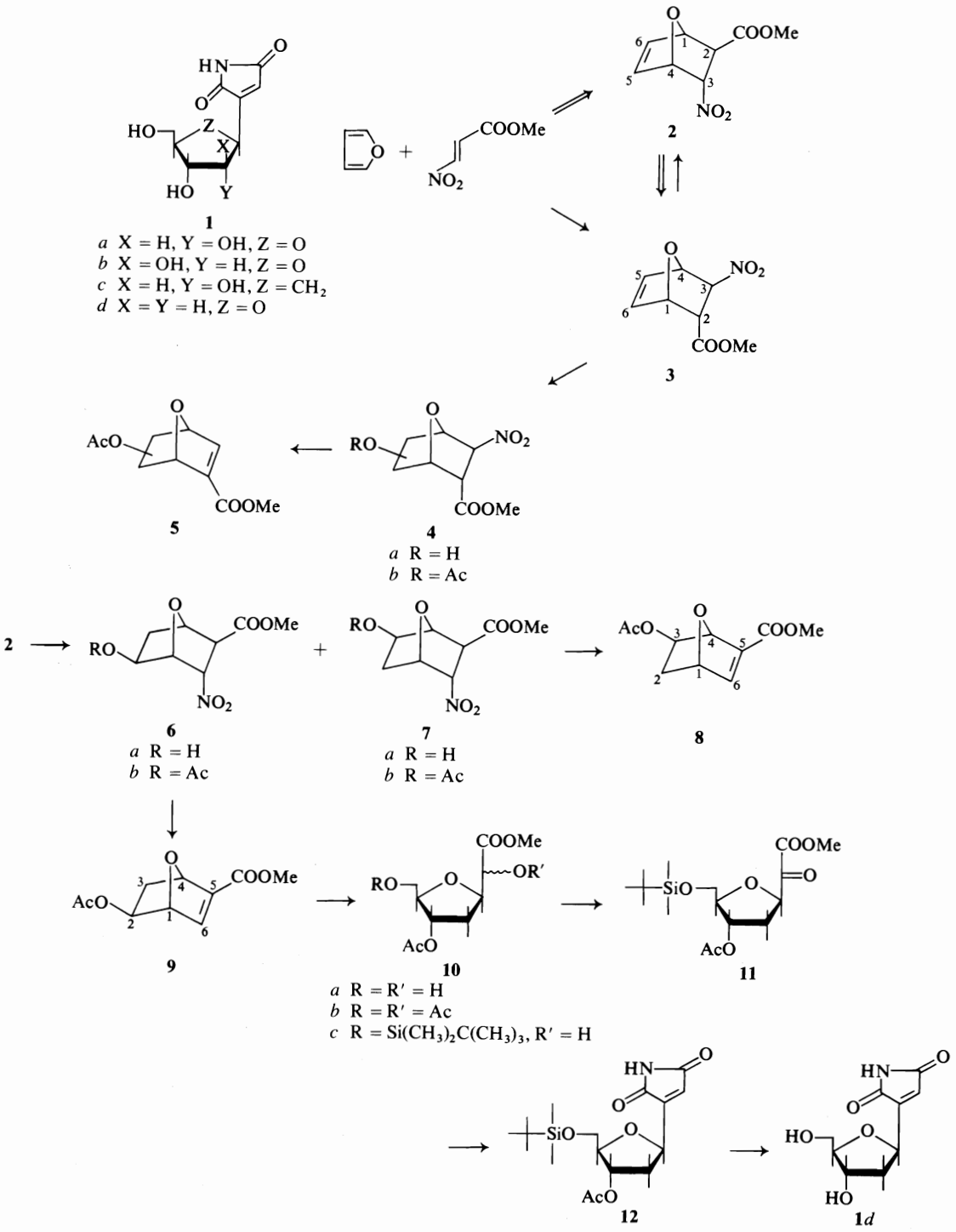

SCHEME 1

nitrous acid elimination from the acetate **7***b* afforded, after chromatography, a good yield of the 3-acetate olefin ester **8**. Both isomers had virtually identical ir and mass spectra but different nmr spectra.

In the nmr spectrum of the 2-acetate **9**, the C-4 proton gave a doublet at δ 5.16 (J = 4 Hz) due to coupling with the C-3 *exo* proton. A doublet for the C-6 proton at δ 6.92 resulted from $J_{6,1}$ = 2 Hz. Decoupling of the C-6 proton readily allowed identification of the C-1 proton at δ 5.00 (J = 2 Hz) because irradiation of the doublet for the C-6 proton collapsed the doublet for the C-1 proton to a singlet. The C-2 proton signal was split into a doublet of doublets with $J_{2,3endo}$ = 6 Hz and $J_{2,3exo}$ = 2 Hz (X part of AMX). The C-3 protons appeared as a complex multiplet at δ 1.73–2.20. The remaining two singlets for the carbomethoxy and acetyl protons were found at δ 3.70 and 2.03, respectively.

In the case of the acetate **8**, a singlet for the C-4 proton could be expected since there is no coupling between the C-4 proton and C-3 *endo* proton. In fact, a one-proton singlet overlapped with a one-proton multiplet at δ 4.90–5.10. Irradiation of the multiplet collapsed a doublet for the C-6 proton at δ 7.03 (J = 2 Hz) to a singlet. Therefore, it was obvious that a singlet arose from the C-4 proton and a multiplet from the C-1 proton which coupled with the C-6 and C-2 protons. Like the C-2 *endo* proton in the 2-acetate, the C-3 *endo* proton showed a doublet of doublets with $J_{3,2endo}$ = 6 Hz and $J_{3,2exo}$ = 2 Hz.

Ozonolysis of the olefin ester **9** in methylene chloride at low temperature, followed by mild reduction with dimethyl sulfide (7), afforded the crude aldehydo keto ester and its hydrated form in a ratio of 1:3, as established by nmr.

Since we knew from previous experience that the aldehyde could not be reduced selectively (1), the aldehydo keto ester was treated with 4 equiv. of lithium tri-*tert*-butoxyaluminum hydride in tetrahydrofuran at 0°C for 4 h to give the diol ester **10***a* in 62% yield after column chromatography on silicic acid. The structure of the diol ester was confirmed by acetylation to **10***b*.

Selective silylation of the diol ester **10***a* with 1 equiv. of *tert*-butyldimethylsilyl chloride and imidazole in dimethylformamide (9) at room temperature for 20 h provided the hydroxy ester **10***c* in 77% yield after purification by column chromatography on silicic acid.

Several different methods were examined for the oxidation of the hydroxy ester **10***c* to the keto ester **11**. By far the best results were obtained using dimethyl sulfoxide – acetic anhydride (10).

The keto ester **11** obtained by oxidation with dimethyl sulfoxide – acetic anhydride was treated with 1 equiv. of carbamoylmethylenetriphenylphosphorane (11) in chloroform at room temperature for 2 h. The reaction gave a single major product together with a considerable amount of polar products. By chromatography of the products on silica gel plates, the maleimide **12** was isolated in an overall yield of 38% from the hydroxy ester **10***c*. In agreement with the maleimide structure, this product showed a strong uv absorption characteristic for the maleimide chromophore at 222 nm in ethanol. The ir spectrum showed a broad absorption at 3420 cm^{-1} (NH) and the typical absorptions at 1780, 1740, 1725, and 1655 cm^{-1} (C=O, C=C). In the mass spectrum the major peak was found at m/e 312 ($M^+ - C(CH_3)_3$). The nmr spectrum displayed a single NH proton at δ 6.55. Similar reaction sequences in related systems indicate that no epimerization took place at the 'anomeric' center.[2]

The protected 2′-deoxyshowdomycin **12** was subjected to treatment with 0.1 *N* methanolic hydrochloric acid at room temperature for 26 h to remove the acetyl and silyl groups. Subsequent purification by a column of silicic acid using acetone – ethyl acetate (3:7) led to crystalline D,L-2′-deoxyshowdomycin **1***d*, mp 122–124°C, in 68% yield. Kalvoda (13) and Nakagawa *et al.* (14) used the same conditions to remove the acetyl groups of 2′,3′,5′-tri-*O*-acetylshowdomycin. The mass spectrum clearly indicated the complete removal of the protecting groups. A molecular ion was found at m/e 213 (M^+) and a major fragment corresponding to loss of water from the molecular ion at m/e 195 ($M^+ - H_2O$). The uv spectrum showed an absorption at 222 nm (log ε 4.18) like showdomycin and 2′-epishowdomycin and the molar extinction coefficient was also in accordance with that of known examples (1, 14), thus confirming the structure of the aglycon moiety of **1***d*. Furthermore, the elemental analysis confirmed the purity of the final product.

The synthetic route described seems to be

[2]From ref. 12 and unpublished results of T. J. Liak.

quite simple and straightforward, and should be applicable to other 2′-deoxy-analogues of *C*-nucleosides. No further work is at present being undertaken in this area.

Experimental

Melting points were determined on a Gallenkamp block and are uncorrected. Mass spectra were obtained on an AE1-MS-902 mass spectrometer at 70 eV using a direct-insertion probe. Nuclear magnetic resonance spectra were recorded on a Varian Associates T-60 spectrometer. Infrared spectra were obtained on a Unicam SP1000 and a Perkin-Elmer 257 ir spectrophotometer. Ultraviolet spectra were determined with a Unicam SP-800 spectrophotometer. Microanalyses were carried out by Dr. C. Daessle, Montreal.

*A Mixture of 2-exo-Carbomethoxy-5-exo-hydroxy-3-endo-nitro-7-oxabicyclo[2.2.1]heptane and 2-exo-Carbomethoxy-6-exo-hydroxy-3-endo-nitro-7-oxabicyclo[2.2.1]heptane (**6a**, **7a**)*

A solution of **2** (858 mg, 4.3 mol) in dry tetrahydrofuran (10 ml) was cooled to 0°C by means of an ice-water bath. To the reaction mixture was added 3 ml of 1 *M* diborane solution (3 mmol) in tetrahydrofuran and the mixture was stirred for 2.5 h under nitrogen. After evaporation to dryness *in vacuo* the residue and triethylamine *N*-oxide dihydrate (658 mg, 4.3 mmol) were dissolved in dry tetrahydrofuran (20 ml). The reaction mixture was heated under reflux for 2.5 h. The solvent was evaporated and the residue was dissolved in ethyl acetate, washed with 0.1 *N* hydrochloric acid, water, and with brine, dried, and evaporated. Chromatography of the residue on a column of silicic acid using chloroform afforded 416 mg (46%) of the isomeric mixture of **6***a* and **7***a* as an oil; ir ($CHCl_3$) 3650, 3500 (OH), 1735 (C=O), 1735 (C=O), 1578 cm^{-1} (NO_2); nmr ($CDCl_3$) δ 1.33–2.40 (m, 2H), 2.90 (m, 1H), 3.26 (m, 1H), 3.73 (s, 3H), 4.03 (m, 1H), 4.60–5.10 (m, 2H), 5.10–5.30 (m, 1H). *Anal.* calcd. for $C_8H_{11}NO_6$: C 44.24, H 5.11, N 6.45; found: C 44.35, H 5.10, N 6.78.

*5-exo-Acetoxy-2-exo-carbomethoxy-3-endo-nitro-7-oxabicyclo[2.2.1]heptane (**6b**) and 6-exo-Acetoxy-2-exo-carbomethoxy-3-endo-nitro-7-oxabicyclo[2.2.1]-heptane (**7b**)*

A mixture of the isomeric alcohols **6***a* and **7***a* (504 mg, 2.32 mmol) and acetic anhydride (4 ml) containing 1 equiv. of *p*-toluenesulfonic acid monohydrate was stirred overnight at room temperature. The reaction mixture was evaporated to dryness and the residue was dissolved in chloroform, washed with water, and dried over sodium sulfate. Following evaporation of the solvent chromatography of the residue on a column of silicic acid using chloroform afforded 495 mg (82%) of the isomeric mixture of **6***b* and **7***b* as an oil.

One isomer, the 5-acetoxy heptane **6***b*, was crystallized from hexane–carbon tetrachloride to give 220 mg, mp 113–114°C; ir (KBr) 1735 (C=O), 1550 cm^{-1} (NO_2); nmr ($CDCl_3$) δ 1.70–2.60 (m, 5H), 3.36 (d, 1H, J = 4 Hz), 3.70 (s, 3H), 4.70–5.03 (m, 3H), 5.30 (m, 1H); ms *m/e* 228 ($M^+ - OCH_3$), 213 ($M^+ - HNO_2$), 171, 153, 128, 43. *Anal.* calcd. for $C_{10}H_{13}NO_7$: C 46.33, H 5.06, N 5.40; found: C 46.53, H 5.26, N 5.43.

Upon evaporation the residue contaminated with **6***b* was chromatographed on a column of silicic acid using chloroform–hexane (1:1), giving 121 mg of the 6-acetoxy heptane **7***b* as an oil. The product solidified on standing, mp 67–68°C; ir (KBr) 1735 (C=O), 1550 cm^{-1} (NO_2); nmr ($CDCl_3$) δ 1.70–2.30 (m, 5H), 3.37 (d, 1H, J = 4 Hz), 3.70 (s, 3H), 4.70–5.06 (m, 3H), 5.20 (m, 1H); ms *m/e* 228 ($M^+ - OCH_3$), 213 ($M^+ - HNO_2$), 169, 127, 81. *Anal.* calcd. for $C_{10}H_{13}NO_7$: C 46.33, H 5.06, N 5.40; found: C 46.23, H 5.30, N 5.21.

*2-exo-Acetoxy-5-carbomethoxy-7-oxabicyclo[2.2.1]hept-5-ene (**9**)*

A solution of **6***b* (605 mg, 2.34 mmol) and DBU (444 mg, 281 mmol) in methylene chloride (20 ml) was refluxed for 1.5 h. The mixture was diluted with methylene chloride, washed with 0.1 *N* hydrochloric acid and water, dried, and evaporated. Chromatography of the residue on a column of silicic acid using chloroform–hexane (3:1) afforded 453 mg (91%) of **9** as an oil which solidified on standing, mp 62–63°C; ir (KBr) 1725, 1710 (C=O), 1610 cm^{-1} (C=C); nmr ($CDCl_3$) δ 1.73–2.20 (s + m, 5H), 3.70 (s, 3H), 4.76 (q, 1H, J = 3 Hz, H-2), 5.00 (d, 1H, $J_{1,6}$ = 2Hz, H-1), 5.16 (d, 1H, $J_{4,3exo}$ = 4 Ha, H-4), 6.92 (d, 1H, $J_{6,1}$ = 2 Hz, H-6); ms *m/e* 212 (M^+), 181 ($M^+ - OCH_3$), 169 ($M^+ - COCH_3$), 152 ($M^+ - CH_3COOH$), 137, 127, 109. *Anal.* calcd. for $C_{10}H_{12}O_5$: C 56.50, H 5.70; found: C 56.45, H 5.36.

*3-exo-Acetoxy-5-carbomethoxy-7-oxabicyclo[2.2.1]hept-5-ene (**8**)*

A mixture of **7***b* (189 mg, 0.73 mmol) and DBU (122 mg, 0.8 mmol) in methylene chloride was heated under reflux for 1.5 h. After the usual work-up chromatography of the residue on a column of silicic acid using chloroform–hexane (3:1) gave 108 mg (70%) of **8** as an oil which was crystallized from hexane–carbon tetrachloride, mp 119–120°C; ir (KBr) 1725, 1710 (C=O), 1610 cm^{-1} (C=C); nmr ($CDCl_3$) δ 1.70–2.10 (s + m), 3.70 (s, 3H), 4.75 (q, 1H, J = 3 Hz, H-3), 4.90–5.10 (s + m, 2H, H-4 and H-1), 7.03 (d, 1H, $J_{6,1}$ = 2 Hz, H-6); ms *m/e* 197 ($M^+ - CH_3$), 181 ($M^+ - OCH_3$), 169 ($M^+ - COCH_3$), 152 ($M^+ - CH_3COOH$), 127, 95, 43. *Anal.* calcd. for $C_{10}H_{12}O_5$: C 56.50, H 5.70; found: C 56.46, H 5.58.

*Methyl 2-(3-O-Acetyl-2-deoxy-β-D,L-ribofuranosyl)-glycolate (**10a**)*

To a solution of **9** (483 mg, 2.28 mmol) in dry methylene chloride at −78°C was bubbled ozone until a blue color persisted. Excess ozone was flushed with nitrogen and dimethyl sulfide (0.5 ml) was added. The reaction mixture was allowed to come to room temperature over a period of 5 h. The solution was then washed with brine three times, dried over magnesium sulfate, and evaporated. To a solution of the residue in dry tetrahydrofuran (20 ml) at 0°C was added lithium tri-*tert*-butoxyaluminum hydride (2.3 g, 9.1 mmol). The reaction mixture was stirred at 0°C for 4 h and a solution of ammonium sulfate (1.5 g) in water (2 ml) was added. After filtration over a layer of Celite and evaporation, the residue was dissolved in ethyl acetate, washed with water, dried, and evaporated. The residue was chromatographed on a column of silicic acid using chloroform–ethyl acetate (1:2), giving 349 mg (62%) of **10***a* as an oil; ir ($CHCl_3$) 3500 (OH), 1750 cm^{-1} (C=O); nmr ($CDCl_3$) δ 1.73–

2.56 (s + m, 5H), 3.43–4.16 (m, 7H), 4.16–4.80 (m, 3H), 5.10 (m, 1H). *Anal.* calcd. for $C_{10}H_{16}O_7$: C 48.38, H 6.50; found: C 48.49, H 6.28.

*Methyl 2-O-Acetyl-2-(3,5-di-O-acetyl-2-deoxy-β-D,L-ribofuranosyl)glycolate (**10***b*)*

The diol **10***a* (157 mg) was acetylated with acetic anhydride (1 ml) and pyridine (2 ml). After the usual work-up chromatography of the crude product on a column of silicic acid using chloroform–hexane (1:1) afforded 149 mg (70%) of **10***b* as an analytically pure oil; ir (neat) 1745 cm^{-1} (C=O), no hydroxyl group; nmr (CCl_4) δ 1.80–2.70 (m, 11H), 3.63 (m, 3H), 3.76–4.06 (m, 3H), 4.30 (m, 1H), 4.73–5.06 (m, 2H); ms *m/e* 332 (M^+), 301 ($M^+ - OCH_3$), 273 ($M^+ - CH_3COO$), 259, 201, 152, 81. *Anal.* calcd. for $C_{14}H_{20}O_9$: C 50.60, H 6.07; found: C 50.38, H 6.26.

*Methyl 2-(3-O-Acetyl-5-O-tert-butyldimethylsilyl-2-deoxy-β-D,L-ribofuranosyl)glycolate (**10***c*)*

To a solution of **10***a* (242 mg, 0.98 mmol) in dimethylformamide (5 ml) was added *tert*-butyldimethylsilyl chloride (148 mg, 0.98 mmol) and imidazole (166 mg, 2.45 mmol). The reaction mixture was stirred at room temperature for 20 h. The solvent was evaporated *in vacuo*. The residue was dissolved in chloroform, washed with water, dried over sodium sulfate, and evaporated. Chromatography of the residue on a column of silicic acid using chloroform gave 276 mg (77%) of **10***c* as an oil; ir (neat) 3450 (OH), 1740 cm^{-1} (C=O); nmr ($CDCl_3$) δ 0.13 (s, 6H), 0.93 (s, 9H), 1.76–2.53 (s + m, 5H), 3.23 (m, 1H), 3.53–3.97 (m, 6H), 4.10–4.46 (m, 2H), 5.03 (m, 1H). *Anal.* calcd. for $C_{16}H_{30}O_7Si$: C 53.04, H 8.29; found: C 53.27, H 8.05.

*2-(3-O-Acetyl-5-O-tert-butyldimethylsilyl-2-deoxy-β-D,L-ribofuranosyl)maleimide (**12**)*

A mixture of **10***c* (152 mg, 0.42 mmol) and acetic anhydride (1 ml) in dry dimethyl sulfoxide (4 ml) was stirred overnight at room temperature. The mixture was diluted with chloroform and washed with an aqueous sodium bicarbonate solution, water, and brine. The organic layer was dried over magnesium sulfate and evaporated to dryness, leaving the crude keto ester **11** as an oil which was contaminated with minor amounts of impurities. Without any further purification this material was directly used in the next step. A solution of the resulting keto ester and carbamoylmethylenetriphenylphosphorane (121 mg, 0.38 mmol) in dry chloroform was stirred at room temperature for 2 h. The solvent was then evaporated. The residue was chromatographed on a silica gel plate using ethyl ether – hexane (1:1), giving 58 mg (38% from **10***c*) of **12** as an oil; ir ($CHCl_3$) 3420 (NH), 1780, 1740, 1725 (C=O), 1645 cm^{-1} (C=C); uv λ_{max} (EtOH) 222 nm; nmr ($CDCl_3$) δ 0.06 (s, 6H), 0.86 (s, 9H), 1.70–2.76 (s + m, 5H), 3.70–3.90 (m, 2H), 4.10 (m, 1H), 4.83–5.23 (m, 1H), 5.33 (m, 1H), 6.55 (t, 1H, C=CH), 8.20 (m, 1H, NH); ms *m/e* 312 ($M^+ - C(CH_3)_3$), 253, 129, 117, 75, 73. *Anal.* calcd. for $C_{17}H_{27}NO_6Si$: C 55.28, H 7.32, N 3.79; found: C 55.12, H 7.35, N 3.68.

*2-(Z-Deoxy-β-D,L-ribofuranosyl)maleimide (**1***d*)*

A solution of **12** (102 mg, 0.28 mmol) in 0.1 *M* methanolic hydrochloric acid (15 ml) was stirred at room temperature for 26 h. After evaporation to dryness, chromatography of the residue on a column of silicic acid using acetone – ethyl acetate (3:7) afforded 40 mg (68%) of **1***d* as an oil which was crystallized from acetone–benzene; mp 122–124°C; ir (KBr) 3510, 3320, 3280, 3100 (OH, NH), 1770, 1700 (C=O), 1640 cm^{-1} (C=C); uv λ_{max} (EtOH) 222 nm (log ε 4.18); ms *m/e* 214 ($M^+ + 1$), 213 (M^+), 195 ($M^+ - H_2O$), 182, 165, 153, 136, 124, 81, 53, 44, 43, 39, 31, 29. *Anal.* calcd. for $C_9H_{11}NO_5$: C 50.70, H 5.20, N 6.57; found: C 50.85, H 5.40, N 6.64.

Acknowledgment

We wish to thank the National Research Council of Canada for financial assistance.

1. M. Lim. Ph.D. Thesis, McGill University, Montreal, P.Q. 1976.
2. G. Just and S. G. Kim. Tetrahedron Lett. 1063 (1976).
3. G. Just and S. G. Kim. Can. J. Chem. **55**, 427 (1977).
4. T. A. Eggelte, H. de Konig, and H. O. Huisman. Heterocycles, **4**, 19 (1976).
5. G. Zweifel and H. C. Brown. Org. React. **13**, 1 (1963).
6. G. N. Kabalka and H. C. Hedgecock. J. Org. Chem. **40**, 1776 (1975).
7. H. Oediger and Fr. Möller. Angew. Chem. Int. Ed. Engl. **6**, 76 (1967).
8. J. J. Pappas, W. P. Keaveney, E. Gancher, and M. Berger. Tetrahedron Lett. 4273 (1966).
9. E. J. Corey and A. Venkateswarlu. J. Am. Chem. Soc. **94**, 6190 (1972).
10. J. D. Albright and L. Goldman. J. Am. Chem. Soc. **89**, 2416 (1967).
11. (*a*) S. Trippett and D. M. Walker. J. Chem. Soc. 3874 (1959); (*b*) G. Trummlitz and J. G. Moffatt. J. Org. Chem. **38**, 1841 (1973).
12. G. Just and S. Kim. Tetrahedron Lett. 1063 (1976); G. P. Donnini. Ph.D. Thesis, McGill University, Montreal, P.Q. 1976.
13. L. Kalvoda, J. Farkas, and F. Sorm. Tetrahedron Lett. 2297 (1970).
14. Y. Nakagawa, H. Kano, Y. Tsukuda, and H. Koyama. Tetrahedron Lett. 4105 (1967).

C-Nucleosides and related compounds. XIV. The synthesis of a nitrogen analogue of showdomycin[1]

GEORGE JUST AND G. PAUL DONNINI[2]

Department of Chemistry, McGill University, Montreal, P.Q., Canada H3C 3G1

Received February 9, 1977

GEORGE JUST and G. PAUL DONNINI. Can. J. Chem. **55**, 2998 (1977).

Starting from teloidinone **5***a*, 2-(2′α,3′α-dihydroxy-4′β-hydroxymethyl-*N*-carbomethoxypyrrolidin-1β-yl)maleimide **1***b*, a showdomycin analogue in which the ribofuranosyl ring oxygen is replaced by an *N*-carbomethoxy group, has been synthesized in 7% overall yield.

GEORGE JUST et G. PAUL DONNINI. Can. J. Chem. **55**, 2998 (1977).

Utilisant la téloidinone **5***a*, on a synthétisé, avec un rendement global de 7%, la (dihydroxy-2′α,3′α hydroxyméthyl-4′β *N*-carbométhoxypyrrolidinyl-1β)-2 maléimide **1***b*, un analogue de la showdomycine dans lequel l'oxygène du cycle ribofurannosyle est remplacé par un groupe *N*-carbométhoxy.

[Traduit par le journal]

We wish to report the synthesis of an analogue of showdomycin (**1***a*), in which the ring oxygen is replaced by an *N*-carbomethoxy group. This ring oxygen seems to play an important role in the mechanism of action of showdomycin and pyrazofurin A, since its replacement by a methylene group leads to virtually complete disappearance of antiviral, antibacterial, and antifungal activity (1). The transformation of a ketoester of type **2** to showdomycin (**1***a*) (2) or its analogues (1, 3) being a relatively simple matter using Moffatt's procedure (2), we set out to synthesize the analogous ketoester **3** or **4**. However, the Diels–Alder approach that had been used successfully in the synthesis of the carbocyclic analogue of showdomycin (1) and other nucleoside analogues (4, 5) failed in this instance due to the unreactivity of N-substituted pyrroles towards the appropriate dienophiles.

Accordingly, we prepared the known teloidinone acetonide **5***b* (6) from teloidinone **5***a* (7).

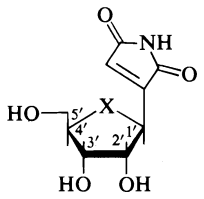

1*a* X = O
1*b* X = N—COOMe
1*c* X = N—H

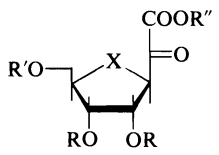

2 X = O
3 X = N—R‴
4 X = N—H

[1]Abstracted from the Ph.D. thesis of G. P. Donnini.
[2]Holder of an NRCC postgraduate scholarship, 1973–1976.

It was hoped that by selective oxidation, the two methylene groups adjacent to the carbonyl function could be differentiated. Thus, in order to protect the tertiary amine in **5***b* against oxidation, it was converted in high yield to the ethyl carbamate **6***a* by boiling with excess ethyl chloroformate (8) in toluene. An analogous reaction with methyl chloroformate in benzene gave, in addition to a 75% yield of the expected methyl carbamate **6***b*, a 15–20% yield of methochloride **7**. The structure of these products was supported by the usual spectroscopic and analytical data. Methochloride **7** could also be converted cleanly to the 8-thiatropan-3-one **8** by treatment with sodium sulphide in aqueous ethanol. The ^{1}Hmr spectrum of **8** clearly indicated a reversal of stereochemistry at C-6 and C-7. This arose from a double displacement of the nitrogen bridge of **7**, and attack by the sulfhydryl group from the least hindered side of the bicyclic system, as shown in Scheme 1. The methyl carbamate **6***b* was further characterized by hydrolysis with aqueous trifluoroacetic acid to diol **9***a*, which was converted to the diacetate **9***b*.

Oxidation of **9***b* with thallium trinitrate (9) gave the α-hydroxy ketone **10** in 40% yield. However, all attempts to oxidize **10** to an α-diketone by means of $Cu(OAc)_2 \cdot H_2O$ (10), DMSO – acetic anhydride (11), or RuO_2–KIO_4 (12) met with failure. Direct oxidation of the carbamate **6***b* with such reagents as selenium dioxide (13) was not attempted, because of the low yields of such transformations (13).

We next tried to form an α-monofurfurylidene

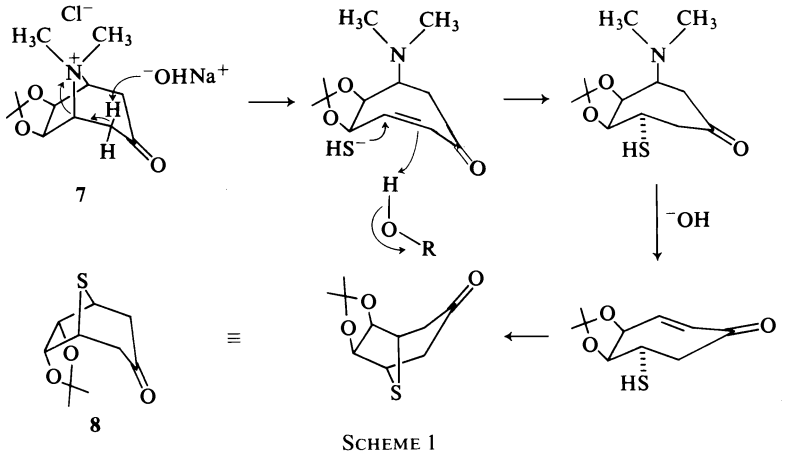

SCHEME 1

ketone derivative in order to ozonize it to an α-diketone. Unfortunately, all such attempts (14) afforded the di-substituted derivatives (**11** and **12**), even when only 1 equiv. of furfuraldehyde was utilized. We also prepared the morpholine enamines **13***a*, **13***b*, and **13***c* in the hope of converting them to α,β-unsaturated ketones of type **14** by the method of Birkofer *et al.* (15). The enamines were formed in high yield with a $TiCl_4$ catalyst (16), but once isolated they proved to be quite unstable, and they did not undergo clean reactions.

We next attempted to carry out a Baeyer–Villiger oxidation of ketone **6***a*. Prolonged treatment (36 h, 90°C) of ethyl carbamate **6***a* with *m*-chloroperbenzoic acid (MCPA) in refluxing 1,2-dichloroethane in the presence of a free radical inhibitor (17) gave impure lactone **15** in relatively good yield, as established by ^{1}Hmr, ir and mass spectra. However, it proved difficult to isolate in the pure state. On the other hand, the methyl carbamate **6***b* could be oxidized cleanly by treatment with MCPA at 60°C for 22 h. The crystalline D,L-lactone **16** was isolated in about 60% yield. It appears that the ethyl group in **6***a* possesses enough steric bulk to impede the approach of the oxidizing agent to the carbonyl group. This finding precluded the use of bulkier, more selectively removable N-protecting groups such as benzyl (18), phenyl (18, 19), and 2,2,2-trichloroethyl (20) carbamates.[3]

[3]We feel that this problem may be circumvented by the use of trifluoroperacetic acid (21). Unfortunately, 90–98% hydrogen peroxide used for its routine preparation is not commercially available anymore, thus precluding, for the time being, the synthesis of showdomycin analogue **1***c* by the scheme outlined.

Since conversions of lactones to their α-methylene derivatives with lithium diisopropylamide (22) have been reported to proceed in high yields, we hoped to convert lactone **16** to the α-methylene lactone **17***a*. The latter could be oxidized to the α-keto lactone **17***b*, which would be formally equivalent to the desired α-ketoester **3**. When the reaction of **16** with lithium diisopropylamide was carried out, substantial decomposition occurred, probably due to ring opening of the bicyclic structure. Thus, it was decided to open up the lactone and attempt to form an α-ketoester from the resulting ester.

Accordingly, lactone **16** was treated at room temperature with 1 equiv. of sodium methoxide in methanol, producing the hydroxy methyl ester **18***a*. The alcoholic function of **18***a* was protected with *tert*-butyldimethylsilyl chloride (23), affording the oily silyl ether **18***b* in greater than 85% yield, based on the lactone. This ether **18***b* was then treated with lithium diisopropylamide and carbon dioxide (22). The resulting malonic acid **19***a* could either be isolated as its methyl ester **19***b* (24) or directly decarboxylated in aqueous formaldehyde and diethylamine (22). In this way, an 80% yield of the α-methylene ester **20** was obtained, based on ether **18***b*. The ir spectrum of **20** exhibited a strong, broad carbonyl band between 1735 and 1720 cm^{-1}, plus a weaker olefinic absorption at 1650 cm^{-1}. Its ^{1}Hmr spectrum displayed two well-separated olefinic multiplets at δ 6.10 and 5.70 ppm, two carbomethoxy methyl singlets at 3.72 and 3.60, as well as *gem*-dimethyl singlets at 1.45 and 1.29 ppm.

Ozonolysis of the olefinic bond of **20** at −78°C, followed by reductive work-up with di-

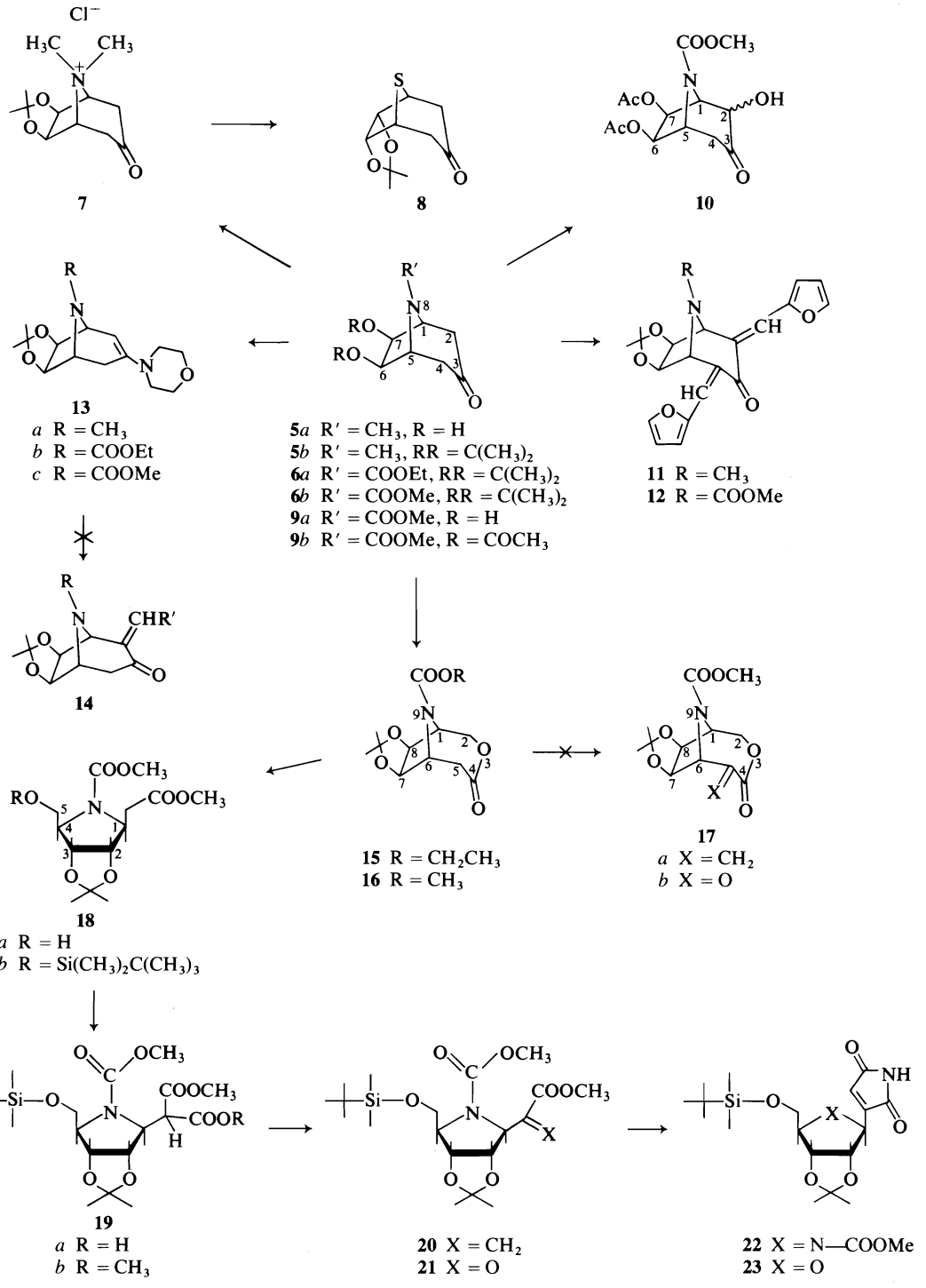

SCHEME 2

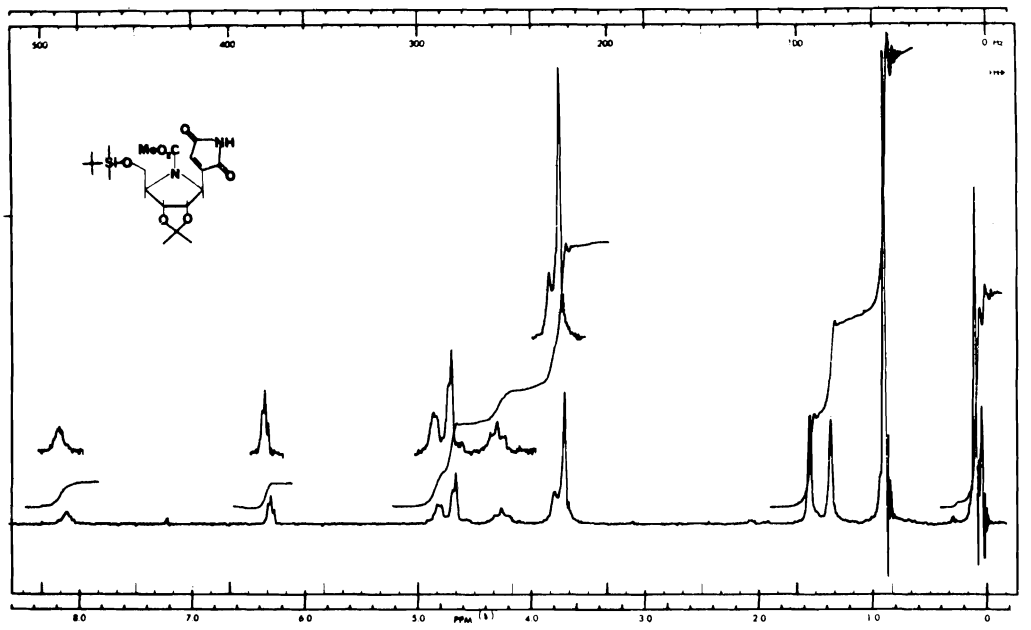

FIG. 1. ^{1}Hmr spectrum of the blocked azacyclic analogue **22** of showdomycin in deuterochloroform.

methyl sulphide (25), afforded the crude α-keto-ester **21**. This was reacted directly with carbamoylmethylenetriphenylphosphorane (2) in chloroform, yielding maleimide **22** in 40% yield based on the α-methylene ester **20**. The crystalline product (**22**) displayed ultraviolet and infrared absorptions extremely similar to those of showdomycin itself (26), and a ^{1}Hmr spectrum (Fig. 1) that was nearly superimposable on that of authentic, similarly blocked showdomycin **23**[4] (Fig. 2). The presence of an *N*-carbomethoxy methyl absorption at δ 3.66 ppm was the only major difference. Furthermore, the similarity of the separation between the *gem*-dimethyl singlets (0.18 ppm in Fig. 1 and 0.22 ppm in Fig. 2) supported the correct stereochemistry at C-1′ (27).

The protected maleimide **22** was deblocked with 50% aqueous trifluoroacetic acid, affording the triol **1***b* in 75% yield after purification by preparative thin layer chromatography. The product would not crystallize, but all spectral data supported the proposed structure. Biological testing of this compound has not yet been undertaken.

[4]Prepared by T. J. Liak. Removal of the protecting groups afforded showdomycin identical to that obtained in ref. 2.

Since malonic esters were known to undergo condensation with ethyl diazoacetate to produce 4-hydroxypyrazoles (28), we attempted to convert malonic ester **19***b* to an analogue of pyrazofurin A (**24**) by this scheme. However, no such conversion was observed. Substantial decomposition of the starting material always occurred. It should be noted, however, that Ohrui and Fox (29) successfully utilized a similar malonic ester of a *C*-glycoside to produce an analogue of pseudouridine.

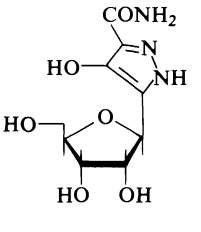

24

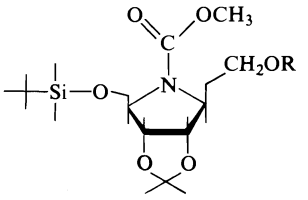

25*a* R = H
25*b* R = SO_2CH_3

Finally, we selectively reduced the ester function of ester **18***b* with borane–tetrahydrofuran, isolating the oily alcohol **25***a* in good yield. This was converted quantitatively to the mesylate **25***b*. But all attempts to eliminate methanesulphonic acid from this compound, in order to

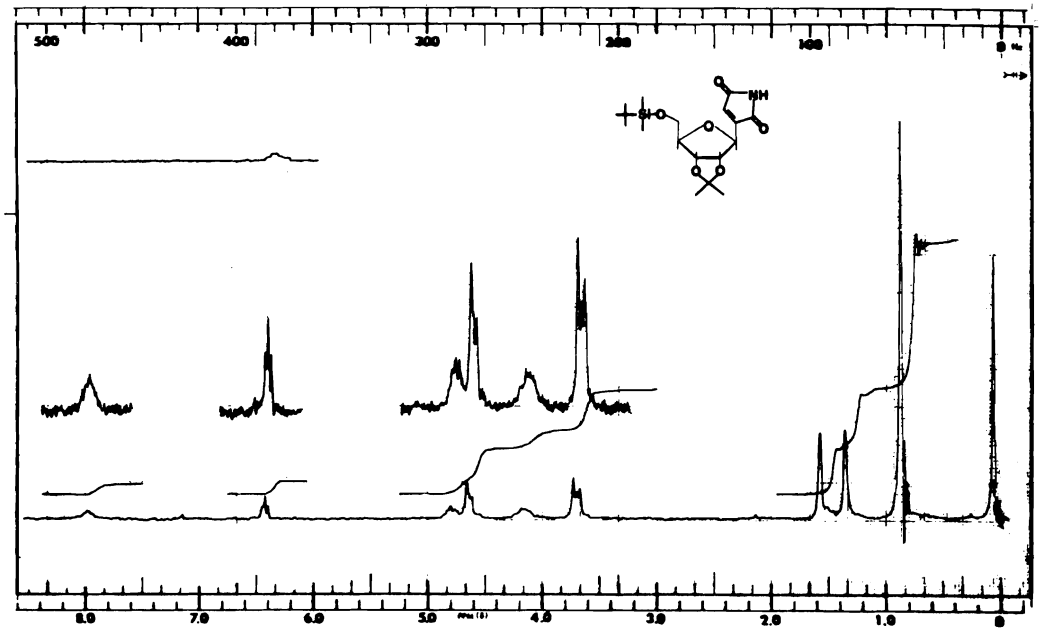

FIG. 2. ^{1}Hmr spectrum of blocked showdomycin **23** in deuterochloroform. Top scan is 100 Hz offset.

form a terminal olefin, failed. A terminal olefin would be an extremely useful dipolarophile for the production of many heterocyclic bases via 1,3-dipolar additions.

We have also been unable to remove efficiently the *N*-carbomethoxy group from any of our compounds, and as yet a reagent capable of cleaving simple *N*-carbalkoxy groups has not been reported in the literature.

Preliminary evaluation of the showdomycin analogue **1***b* failed to show any activity against 15 strains of bacteria and four strains of fungi up to levels as high at 256 μg/ml. Nine viral strains, including both DNA and RNA types, were not significantly affected by these drugs in tissue culture.

Experimental

Solvents were reagent grade unless otherwise specified. All evaporations were done under reduced pressure (water aspirator) with a bath temperature of 25–45° C unless otherwise noted.

Melting points were determined on a Gallenkamp block in open capillary tubes and are uncorrected. Mass spectra were obtained on an AEI-MS-902 mass spectrometer at 70 eV using a direct insertion probe. Infrared (ir) spectra were obtained on a Unicam SP1000 and a Perkin-Elmer 257 spectrophotometer. Ultraviolet (uv) spectra were obtained on a Unicam SP-800 and a Cary 17 spectrophotometer. Proton magnetic resonance (^{1}Hmr) spectra were recorded on a Varian T-60 instrument using tetramethylsilane (TMS) as an internal standard unless otherwise stated. Chemical shifts are given in the δ scale in parts per million (ppm). Doublets (d), triplets (t), quartets (q), and multiplets (m) were recorded at the centre of the peaks; other abbreviations used: singlet (s) and broad (b).

Analytical thin layer chromatography (tlc) was performed on silica gel-coated plates (Eastman Kodak or Machery-Nagel Polygram G) and on a preparative scale (plc) on silica gel (Merck $UV_{254,366}$) coated glass plates. Woelm alumina (neutral) and silica gel were used for column chromatography.

Elemental analyses were performed by C. Daessle, Montreal, and Heterocyclic Chemical Corporation, Missouri.

*6β,7β-Dihydroxy-O-isopropylidene-tropan-3-one (Teloidinone Acetonide) (**5b**)*

To a suspension of 4.71 g (27.5 mmol) teloidinone **5***a* (7) in 500 ml acetone was added 19.0 ml concentrated hydrochloric acid with vigorous stirring. This mixture was stirred at room temperature for 20 h, by which time it had become a clear, yellow solution. It was then neutralized by bubbling in anhydrous ammonia (to p*H* 8–9), and the resulting ammonium chloride filtered off. The precipitate was washed with another 100 ml acetone, and the filtrates were evaporated to dryness *in vacuo*. The yellow solid residue was recrystallized from petroleum ether (60–80° C); the product was obtained as white needles, mp 84–86°C (lit. (6) mp 87–90°C). The yield was 5.25 g (90%) in three crops; ^{1}Hmr ($CDCl_3$) δ 1.34 (s, 3H), 1.55 (s, 3H), 2.06 (bs, 0.67H), 2.34 (bs, 1.33H), 2.61 (d, 1.33H), 2.75 (s, 3H), 2.87 (d, 0.67H), 3.55 (m, 2H), 4.41 ppm (s, 2H); ir (KBr) 3025, 2980, 2945, 1720 (C=O), 1395 and 1390 (*gem*-dimethyl), 1220, 1080, 1055, 873 cm^{-1}; ms *m/e* 211 (M^+), 196 ($M^+ - CH_3$).

*6β,7β-Dihydroxy-O-isopropylidene-N-carbethoxy-tropan-3-one (**6a**)*

Freshly distilled ethyl chloroformate (6.2 ml, 76.3

mmol) was added to a solution of 805 mg (3.8 mmol) of teloidinone acetonide **5***b* in 15 ml dry toluene. This solution was heated to gentle reflux for 30 h, then evaporated to dryness under reduced pressure. The solid residue was recrystallized from petroleum ether (60–80°C) – ether, affording an 85% yield of white crystals, mp 77–78°C; ^{1}Hmr ($CDCl_3$) δ 1.23 (s, 3H), 1.27 (t, 3H), 1.40 (s, 3H), 2.48 (bm, 4H), 4.15 (q, 2H), 4.40 (s, 2H), 4.46 ppm (bm, 2H); ir (KBr) 1720 (ketone), 1705 (urethane), 1395 and 1385 cm^{-1} (*gem*-dimethyl); ms *m/e* 269 (M^+), 254 ($M^+ - CH_3$), 169, 168. *Anal.* calcd. for $C_{13}H_{19}NO_5$: C 57.98, H 7.11, N 5.20; found: C 57.82, H 7.09, N 5.22.

*6β,7β-Dihydroxy-O-isopropylidene-N-carbomethoxy-tropan-3-one (**6b**)*

Freshly distilled methyl chloroformate (29.6 ml, 0.384 mol) was added to a solution of 4.05 g (0.0192 mol) of teloidinone acetonide **5***b* in 50 ml dry benzene. This solution was warmed to 60°C and stirred for 20 h. Then the white precipitate (methochloride **7**) was filtered off, and the filtrate was evaporated to dryness. The white solid residue was recrystallized from anhydrous ether, mp 123–123.5°C. Further crops were obtained by adding petroleum ether (30–60°C) until the solvent was a 1:1 mixture. Total yield 3.6 g (75%) in four crops; ^{1}Hmr ($CDCl_3$) δ 1.30 (s, 3H), 1.46 (s, 3H), 2.56 (bm, 4H), 3.79 (s, 3H), 4.47 (s, 2H), 4.52 ppm (bm, 2H); ir (CCl_4) 2980, 2950, 2890, 1730 (C=O's), 1460, 1395 and 1385 cm^{-1} (*gem*-dimethyl); ms (150°C) *m/e* 255 (M^+), 240 ($M^+ - CH_3$), 155, 154. *Anal.* calcd. for $C_{12}H_{17}NO_5$: C 56.46, H 6.71, N 5.49; found: C 56.34, H 6.66, N 5.52. Evaporation of the last filtrate left 275 mg (6.3%) unreacted starting material.

6β,7β-Dihydroxy-O-isopropylidene-tropan-3-one Methochloride (7)

The side product isolated above was quite pure, and it was obtained in 17% yield (875 mg). An analytical sample was prepared by dissolving in methanol and adding anhydrous ether until partial reprecipitation had occurred, then cooling; mp 168–170°C with charring; ^{1}Hmr (D_2O) δ 1.53 (s, 3H), 1.79 (s, 3H), 2.80 (bs, 0.67H), 3.14 (bs, 1.33H), 3.43 (d, 1.33H), 3.60 (s, 3H), 3.70 (bm, 0.67H), 3.80 (s, 3H), 4.70 (d, 2H), 5.25 ppm (bs, 2H); ir (KBr) 3120, 3025, 3005, 2950, 1730 (C=O), 1395 (*gem*-dimethyl), 1215, 1160, 1065 cm^{-1}; ms (150°C) *m/e* 225 (M^+ – HCl, Hofmann elimination), 210 (M^+ – HCl – CH_3), 167. *Anal.* calcd. for $C_{12}H_{20}NO_3Cl$: C 55.06, H 7.70, N 5.35; found: C 55.01, H 7.52, N 5.07.

*6α,7α-Dihydroxy-O-isopropylidene-8-thiatropan-3-one (**8**)*

Sodium sulphide hydrate ($Na_2S \cdot 9H_2O$, 1.04 g, 4.3 mmol) was dissolved in 15 ml ethanol–water (2:1), and to this was added 378 mg (1.44 mmol) methochloride **7** in 15 ml ethanol–water (2:1). The solution was heated 30 min at 50°C, then stirred 1 h at room temperature. The ethanol was removed under reduced pressure, and the resulting aqueous mixture was extracted with methylene chloride (3 × 15 ml). Drying (Na_2SO_4) and evaporation afforded 200 mg of a yellow solid which consisted of a 6:1 mixture of 8-thiatropan-3-one **8** and teloidinone acetonide **5***b* by ^{1}Hmr. Purification by chromatography on 20 × 20 cm silica gel plates, using ether–hexanes (3:2) as the solvent system, afforded 145 mg (47%) of a white powder, mp 114–115.5°C. An analytical sample was obtained by recrystallization from petroleum ether (60–80°C), mp 115.5–116.5°C; ^{1}Hmr ($CDCl_3$) δ 1.35, 1.37 (s, s, 6H), 2.40 (d, 0.4H), 2.69 (d, 1.6H), 2.87 (d, 1.6H), 3.16 (d, 0.4H), 3.46 (bm, 2H), 4.88 ppm (q, 2H); ir (KBr) 3000, 2940, 1720 (C=O), 1390 and 1383 cm^{-1} (*gem*-dimethyl); ms (130°C) *m/e* 214 (M^+), 199 ($M^+ - CH_3$). *Anal.* calcd. for $C_{10}H_{14}O_3S$: C 56.07, H 6.59; found: C 56.10, H 6.53.

*6β,7β-Diacetoxy-N-carbomethoxy-tropan-3-one (**9b**)*

Urethane **6***b* (255 mg, 1 mmol) was dissolved in 10 ml 30% trifluoroacetic acid – water and heated to 55°C. After 4 h, its ^{1}Hmr spectrum showed the almost complete disappearance of the isopropylidene group, so the solution was evaporated to dryness, using benzene as chaser. Acetylation of the resulting diol **9***a* was carried out with 1 ml pyridine and 1 ml acetic anhydride for 4 h at room temperature. The solution was then evaporated to dryness and passed through a small silica gel column, eluting with methylene chloride. The eluate was evaporated to near dryness, and excess ethyl ether was added to precipitate the product **9***b*. Cooling the filtrate afforded a second crop; total yield 175 mg, 60%; mp 157–159°C; ^{1}Hmr ($CDCl_3$) δ 2.03 (s, 6H), 2.61 (bm, 4H), 3.73 (s, 3H), 4.47 (bm, 2H), 5.02 ppm (s, 2H); ir (KBr) 1755–1745 (acetates), 1720–1710 cm^{-1} (urethane and ketone); ms (150°C) *m/e* 299 (M^+), 239 ($M^+ - CH_3COO$), 197, 154. *Anal.* calcd. for $C_{13}H_{17}NO_7$: C 52.17, H 5.73, N 4.68; found: C 52.03, H 5.51, N 4.73.

*2-Hydroxy-6β,7β-diacetoxy-N-carbomethoxy-tropan-3-one (**10**)*

Diacetate **9***b* (205 mg, 0.685 mmol) was dissolved in 2 ml glacial acetic acid, and a solution of thallium trinitrate trihydrate (400 mg, 0.9 mmol) in 1.3 ml acetic acid was added. Five drops of concentrated nitric acid were then added, and the solution was stirred overnight at room temperature. The solid was filtered off, and the filtrate was neutralized with 10% sodium bicarbonate and with solid sodium bicarbonate. The resulting mixture (approximately 35 ml) was allowed to stand at room temperature overnight, then the precipitate was filtered off. The aqueous filtrate was extracted with 3 × 30 ml methylene chloride. Drying ($MgSO_4$) and evaporation afforded a white foam. This was dissolved in carbon tetrachloride and excess ethyl ether was added. On cooling, 80 mg (38% yield) of a white powder was recovered, mp 160–161.5°C; ^{1}Hmr ($CDCl_3$) δ 2.06 (s, 3H), 2.15 (s, 3H), 2.70 (m's, 2H), 3.88 (s, 3H), 4.60 (m, 1H), 4.82–5.63 ppm (m's, 5H; 1H at 5.4 moved downfield by CF_3COOH); ir (KBr) 1780 and 1760 (acetates), 1720 and 1705 (urethane), 1650 cm^{-1} (α-hydroxy ketone); ms (155°C) *m/e* 315 (M^+), 314 ($M^+ - H$), 272 ($M^+ - H - CH_2CO$), 235.7 (M*, 314 → 272), 212, 196, 184. *Anal.* calcd. for $C_{13}H_{17}NO_8$: C 49.52, H 5.44, N 4.44; found: C 49.38, H 5.21, N 4.49.

*2,4-Difurfurylidene-6β,7β-dihydroxy-O-isopropylidene-tropan-3-one (**11**)*

Teloidinone acetonide **5***b* (422 mg, 2 mmol) was dissolved in 4 ml of 95% ethanol and cooled in ice. A solution of 88 mg (2.2 mmol) sodium hydroxide in 1 ml water was added, followed by a solution of 200 mg (2.1 mmol) freshly distilled furfuraldehyde in 1 ml ethanol. A yellow precipitate was soon formed. The mixture was stirred 30 min, 5 ml water was added, and the precipitate was harvested. The bright yellow product was recrystallized from chloroform – absolute ethanol as yellow crystals in 50% yield, mp 218–221°C with charring; ^{1}Hmr ($CDCl_3$)

δ 1.34 (s, 3H), 1.66 (s, 3H), 2.50 (s, 3H), 4.60 (s, 2H), 4.86 (s, 2H), 6.58 (q, 2H), 6.80 (d, 2H), 7.66 ppm (bm, 4H); ir (KBr) 3160, 3120, 1675 (ketone), 1615, 1590, 1550, 1480 cm^{-1}; ms (200°C) *m/e* 367 (M^+), 352 ($M^+ - CH_3$), 267, 238.

*7β,8β-Dihydroxy-O-isopropylidene-N-carbomethoxy-3-oxa-9-azabicyclo[4.2.1^{1,6}]nonan-4-one (**16**)*

Ketone **6***b* (2.52 g, 9.9 mmol) was dissolved in 60 ml 1,2-dichloroethane, and to this was added 5.0 g (25 mmol) of 85% *m*-chloroperbenzoic acid and 20 mg 2,4,6-tri-(*tert*-butyl)phenol. This mixture was heated to 55°C and followed by gas chromatography (Hewlett-Packard 700 Laboratory Chromatograph, SE-30 Ultraphase (10% w/w) with Chromosorb W support in 6 ft × $\frac{1}{8}$ in. column). After 22 h the starting material had disappeared, and the solution was cooled to −15°C for 30 min to precipitate out most of the *m*-chlorobenzoic acid. The acid was filtered off, and the filtrate was washed successively with cold 10% sodium bisulphite (15 ml), cold 10% sodium bicarbonate (3 × 15 ml), and saturated salt solution (20 ml). The organic phase was dried ($MgSO_4$) and evaporated off, leaving a partially solidified oil. This was dissolved in anhydrous ether and allowed to crystallize out at −15°C, mp 117–118°C. More product was obtained by adding petroleum ether (30–60°C) and cooling, total yield 1.6 g (60%); ^{1}Hmr ($CDCl_3$) δ 1.26 (s, 3H), 1.40 (s, 3H), 2.93 (m, 2H), 3.73 (s, 3H), 4.33 (bm, 4H), 4.53 (d, 1H), 4.86 ppm (d, 1H); ir (CCl_4) 3000, 2960, 1755 (lactone), 1725 (urethane), 1455, 1392 and 1382 cm^{-1} (*gem*-dimethyl); ms (150°C) *m/e* 271 (M^+), 256 ($M^+ - CH_3$), 240 ($M^+ - CH_3O$), 214 ($M^+ - CH_3 - CH_2{=}C{=}O$), 179.0 (M*, 256 → 214), 142. *Anal.* calcd. for $C_{12}H_{17}NO_6$: C 53.13, H 6.32, N 5.16; found: C 53.29, H 6.41, N 5.11.

*Methyl-2-(2α,3α-dihydroxy-O-isopropylidene-4β-hydroxymethyl-N-carbomethoxypyrrolidin-1β-yl)-acetate (**18***a*)*

The lactone **16** (2.38 g, 8.8 mmol) was dissolved in 40 ml dry methanol under an atmosphere of dry nitrogen, and to this was added a solution of 223 mg (9.7 mmol) sodium in 20 ml dry methanol. The resulting yellow solution was allowed to stand at room temperature for 18 h, then cooled in ice and neutralized with 5 *N* hydrochloric acid. The resulting solution was evaporated to dryness, and the residue triturated with methylene chloride. The inorganic salt was filtered off and washed well, and the filtrate was dried ($MgSO_4$) and evaporated to dryness. The oily orange residue (2.4 g) was quite pure by ^{1}Hmr, and was used directly in the next step. ^{1}Hmr ($CDCl_3$) δ 1.30 (s, 3H), 1.47 (s, 3H), 2.71 (d, 2H, CH_2-COOMe), 3.50 (bm, 2H, exch. with D_2O), 3.70 (s, 6H, 2 × $COOCH_3$), 3.70 (bm, 2H), 3.92–4.85 ppm (m's, 4H); ir (film) 3480 (O—H), 1740–1710 (C=O's), 1460, 1390 cm^{-1}; ms (110°C) *m/e* 303 (M^+), 288 ($M^+ - CH_3$), 286 ($M^+ - OH$), 285 ($M^+ - H_2O$), 272 ($M^+ - CH_3O$), 256, 240, 230.

*Methyl-2-(2α,3α-dihydroxy-O-isopropylidene-4β-tert-butyldimethylsiloxymethyl-N-carbomethoxypyrrolidin-1β-yl)acetate (**18***b*)*

The crude alcohol **18***a* (2.4 g, 8 mmol) was dissolved in dry *N*,*N*-dimethylformamide (15 ml), and to this was added 1.6 g (10.5 mmol) *tert*-butyldimethylsilyl chloride (23) and 1.43 g (21 mmol) imidazole. This solution was stirred at room temperature overnight, then evaporated to dryness *in vacuo*. The residue was partitioned between methylene chloride (35 ml) and water (25 ml), and the organic layer was further washed with water (3 × 20 ml), dried ($MgSO_4$), and evaporated. The crude silyl ether was purified by passage through a short silica gel column, eluting with ethyl ether. The product was obtained as a slightly yellow oil, yield 3.0 g (85% based on lactone **16**); ^{1}Hmr (CCl_4, external TMS) δ 0.14 (s, 6H, dimethylsilyl), 0.96 (s, 9H, *tert*-butylsilyl), 1.30 (s, 3H), 1.46 (s, 3H), 2.55 (m, 2H, CH_2COOMe), 3.66 (s, 6H, 2 × $COOCH_3$), 3.68 (bm, 2H), 3.77–4.66 ppm (m's, 4H); ir (film) 2960, 1750 (ester), 1720 (urethane), 1460, 1390 cm^{-1}; ms (100°C) *m/e* 402 ($M^+ - CH_3$), 386 ($M^+ - CH_3O$), 360 ($M^+ - (CH_3)_3C$), 302, 272, 228. *Anal.* calcd. for $C_{19}H_{35}NO_7Si$: C 54.65, H 8.45, N 3.35; found: C 54.52, H 8.27, N 3.38.

*Methyl-2-(2α,3α-dihydroxy-O-isopropylidene-4β-tert-butyldimethylsiloxymethyl-N-carbomethoxypyrrolidin-1β-yl)acrylate (**20**)*

A three-necked 50 ml flask equipped with a septum, stopcocks, and a mercury bubbler was flushed with dry nitrogen and charged with 11.5 ml of a 0.26 *M* solution of lithium diisopropylamine in dry tetrahydrofuran. This was cooled to −78°C in an acetone – dry ice bath, and a solution of 1.015 g (2.45 mmol) of ester **18***b* in 15 ml tetrahydrofuran was added with a syringe over a 3 min period. The flask was allowed to slowly warm up to −25°C, and then dry carbon dioxide was bubbled into the solution for 10 min via a syringe needle. The resulting yellow solution was neutralized to p*H* 6 with 10% hydrochloric acid, and the precipitated diisopropylamine hydrochloride was filtered off. The filtrate was evaporated to dryness, and the residue **19***a* was used in the next reaction without further purification.

The crude malonic acid was heated to 50°C with 1.3 ml (12.25 mmol) diethylamine and 2.5 ml of 37% aqueous formaldehyde for 30 min, then 250 mg sodium acetate and 2.5 ml glacial acetic acid was added. The mixture was heated to 50°C for 20 min, then allowed to cool. Water (20 ml) was added, and the aqueous mixture was extracted with methylene chloride (3 × 25 ml). The organic extracts were dried ($MgSO_4$) and evaporated, and the crude product was chromatographed on silica gel. Elution with ether–hexane (2:1) afforded the product as a clear, colorless oil in 80% yield. An analytical sample was obtained by preparative tlc on a 20 × 20 cm silica gel plate using ether–hexane (1:1) as the solvent system; ^{1}Hmr (acetone-d_6) δ 0.12 (s, 6H), 0.92 (s, 9H), 1.29 (s, 3H), 1.45 (s, 3H), 3.60 (s, 3H), 3.72 (s, 3H), 3.75 (bm, 1H), 3.83–4.33 (m's, 2H), 4.40–4.85 (m's, 3H), 5.70 (m, 1H, C=C—*H*), 6.10 ppm (m, 1H, C=C—*H*); ir (film) 2975, 2950, 2875, 1735–1720 (C=O's), 1650 (C=C), 1460, 1390 cm^{-1}; ms (130°C) *m/e* 414 ($M^+ - CH_3$), 398 ($M^+ - CH_3O$), 372 ($M^+ - (CH_3)_3C$), 360. *Anal.* calcd. for $C_{20}H_{35}NO_7Si$: C 55.92, H 8.21, N 3.26; found: C 55.65, H 8.44, N 3.47.

*2-(2′α,3′α-Dihydroxy-O-isopropylidene-4′β-tert-butyldimethylsiloxymethyl-N-carbomethoxypyrrolidin-1′β-yl)maleimide (**22**)*

The olefin ester **20** (280 mg, 0.65 mmol) was dissolved in 45 ml dry ethyl acetate and treated with ozone at −78°C. Dry nitrogen was bubbled through the solution to remove excess ozone, and dimethyl sulphide (0.1 ml,

1.3 mmol) was added. The mixture was stirred for 30 min at −60°C, then allowed to warm up to room temperature and stand 5 h. It was washed with 3 × 25 ml of saturated salt solution, dried (Na_2SO_4), and evaporated to dryness. The residue (270 mg) displayed no olefinic absorption in the ir spectrum, but appeared impure by ^{1}Hmr.

The crude product was dissolved in 10 ml dry chloroform and 208 mg (0.65 mmol) of carbamoylmethylenetriphenylphosphorane (2) was added. The yellow solution was stirred for 3 h at room temperature, then evaporated to dryness. The oily residue was separated on 20 × 20 cm silica gel plates using ether–hexane (3:1) as the solvent system, and 150 mg of a clear, colorless oil was recovered. The product was crystallized from ether–hexane, mp 88–89°C in 40% overall yield based on olefin ester **20**; ^{1}Hmr ($CDCl_3$) δ 0.07 (s, 6H), 0.87 (s, 9H), 1.33 (s, 3H), 1.52 (s, 3H), 3.66 (s, 3H), 3.72 (bm, 2H), 4.22 (m, 1H), 4.50–4.90 (m's, 3H), 6.25 (t, 1H, C=C—*H*), 8.06 ppm (bm, N—*H*); ir (KBr) 3250 (maleimide N—H), 2970, 2950, 2870, 1787, 1738, 1695 (urethane), 1655 (maleimide C=C), 1460, 1390 cm^{-1}; uv (EtOH) λ_{max} 221.3 nm (ε 18 000), shoulder ~275 nm (ε 1000); ms (170°C) *m/e* 425 ($M^+ - CH_3$), 383 ($M^+ - (CH_3)_3C$), 325 ($M^+ - (CH_3)_3C(CH_3)_2Si$). *Anal.* calcd. for $C_{20}H_{32}N_2O_7Si$: C 54.52, H 7.32, N 6.36; found: C 54.54, H 7.52, N 6.50.

*2-(2′α,3′α-Dihydroxy-4′β-hydroxymethyl-N-carbomethoxypyrrolidin-1β-yl)maleimide (**1b**)*

Blocked showdomycin analogue **22** (130 mg, 0.30 mmol) was dissolved in 3 ml of 50% aqueous trifluoroacetic acid. After standing at room temperature for 5 min, the solution was evaporated to dryness. Separation on a 20 × 20 cm silica gel plate, eluting with ethyl acetate, afforded 70 mg (75%) of a clear colorless oil which would not crystallize; ^{1}Hmr (acetone-d_6, external TMS) δ 3.15 (bm, 2H), 3.60 (s, 3H), 3.65–4.80 (bm's, 7H), 6.60 (d, 1H), 9.5 ppm (bm, 1H); ir (film) 1780, 1730–1700, 1650 cm^{-1} (C=O, C=C), 3350 cm^{-1} (OH); ms (150°C) *m/e* 268 ($M^+ - H_2O$), 255 ($M^+ - CH_3O$), 237 ($M^+ - CH_3O - H_2O$), 220 (M*, 255 → 237), 205, 117, 59.

*Methyl-2-(2α,3α-dihydroxy-O-isopropylidene-4β-tert-butyldimethylsiloxymethyl-N-carbomethoxypyrrolidin-1β-yl)malonate (**19b**)*

The crude malonic acid **19***a* in 30 ml ethyl ether was esterified with etheral diazomethane generated from nitrosomethylurea (24). After reaction for 1 h at room temperature, the solution was evaporated to dryness, and the residue was purified by chromatography on a silica gel column, eluting with ether–hexane (1:1). The oily product was obtained in 60% yield based on methyl ester **18***b*. ^{1}Hmr spectrum ($CDCl_3$) δ 0.11 (s, 6H), 0.93 (s, 9H), 1.30 (s, 3H), 1.43 (s, 3H), 3.60–3.70 (3 × s, 9H), 3.7–4.3 (m's, 4H), 4.3–4.7 ppm (m's, 3H); ir (film) 2920, 2890, 2820, 1730 (malonic ester), 1700 (urethane), 1440, 1375 cm^{-1}; ms (160°C) *m/e* 460 ($M^+ - CH_3$), 444 ($M^+ - CH_3O$), 418 ($M^+ - Me_3C$), 386 ($M^+ - Me_3C$ – MeOH), 360 ($M^+ - Me_3C(Me_2)Si$), 356.5 (M*, 418 → 386), 228, 189. *Anal.* calcd. for $C_{21}H_{37}NO_9Si$: C 53.03, H 7.84, N 2.95; found: C 52.74, H 8.05, N 2.98.

*3,4-O-Isopropylidene 2β-(2′-Hydroxyethyl)-5β-tert-butyldimethylsiloxymethyl-N-carbomethoxypyrrolidine-3α,4α-diol (**25a**)*

Ester **18***b* (526 mg, 1.26 mmol) was dissolved in 10 ml dry tetrahydrofuran in a 50 ml 3-neck flask equipped with septum, stopcocks, and mercury bubbler. The apparatus was flushed with nitrogen, cooled to 0°C, and 4.2 ml of a 1 *M* borane–THF solution was added with a syringe. The ice was allowed to melt, and the solution was allowed to stand at room temperature for 2 days. Then 1 ml methanol was added, and the solution was evaporated to dryness. Coevaporation with methanol (2 × 15 ml) left an oily residue which was chromatographed on silica gel. Elution with ethyl acetate – methylene chloride (1:5) recovered unreacted ester, then elution with a 1:1 mixture of the same solvents afforded 350 mg (70% yield) of alcoholic product as a clear, colorless oil; ^{1}Hmr (CCl_4) δ 0.08 (s, 6H, dimethylsilyl), 0.91 (s, 9H, *tert*-butylsilyl), 1.27 (s, 3H), 1.42 (s, 3H), 1.60 (bm, 2H, CH—C*H*$_2$—CH$_2$), 3.24–4.17 (bm's, 7H, 1H exch. with D_2O at about 3.5), 3.60 (s, 3H), 4.24 (bd, 1H, C*H*—O), 4.51 ppm (bd, 1H, C*H*—O); ir (film) 3490 (O—H), 1710 and 1695 (urethane), 1460, 1390 cm^{-1}; ms (95°C) *m/e* 374 ($M^+ - CH_3$), 332 ($M^+ - Me_3C$), 300 ($M^+ - Me_3C - CH_3OH$), 274 ($M^+ - Me_3C$-$(CH_3)_2Si$), 271.0 (M*, 332 → 300).

*3,4-O-Isopropylidene 2β-(2′-Mesyloxymethyl)-5β-tert-butyldimethylsiloxymethyl-N-carbomethoxypyrrolidine-3α,4α-diol (**25b**)*

To a solution of 100 mg (0.257 mmol) of alcohol **25***a* in 6 ml dry methylene chloride was added 2.35 ml of a 0.167 *M* solution of triethylamine in dry dichloromethane. This solution was cooled to −50°C (dry ice – acetone), and 0.92 ml of a 0.32 *M* solution of methanesulphonyl chloride in methylene chloride was added to it dropwise. The solution was allowed to warm up to room temperature then stirred 1 h. It was then washed with 2 × 10 ml cold water. The organic layer was dried ($MgSO_4$) and evaporated, leaving the clear, colorless mesylate in nearly quantitative yield; ^{1}Hmr (CCl_4) δ 0.09 (s, 6H), 0.92 (s, 9H), 1.29 (s, 3H), 1.42 (s, 3H), 1.97 (bm, 2H), 2.93 (s, 3H, OSO_2CH_3), 3.60 (bm, 2H, C*H*$_2$OSi), 3.62 (s, 3H), 3.7–4.6 ppm (m's, 6H); ir (film) 1710 (urethane), 1460, 1365 and 1180 cm^{-1} (mesylate); ms (130°C) *m/e* 410 ($M^+ - Me_3C$), 322 ($M^+ - Me_3C(CH_3)_2SiOCH_2$). *Anal.* calcd. for $C_{19}H_{37}NSO_8Si$: C 48.80, H 7.97, N 3.00; found: C 48.52, H 7.81, N 2.83.

Acknowledgments

We wish to thank the National Research Council of Canada and E. Lilly Co., Indianapolis, for financial support, the NRCC for a fellowship (G.P.D.), and Dr. Donald C. DeLong of Lilly Research Laboratories for biological tests.

1. G. Just and S. Kim. Tetrahedron Lett. 1063 (1976).
2. G. Trummlitz and J. G. Moffatt. J. Org. Chem. **38**, 1841 (1973).
3. G. Trummlitz, D. B. Repke, and J. G. Moffatt. J. Org. Chem. **40**, 3352 (1975).
4. G. Just and G. Reader. Tetrahedron Lett. 1521 (1973); 1525 (1973).
5. G. Just and M. Ramjeesingh. Tetrahedron Lett. 985 (1975).
6. A. Heusner. Chem. Ber. **87**, 1032 (1954).
7. J. C. Sheehan and B. M. Bloom. J. Am. Chem. Soc. **74**, 3825 (1952).

8. (*a*) G. KRAISS and K. NADOR. Tetrahedron Lett. 57 (1971); (*b*) W. B. WRIGHT and H. J. BRABANDER. J. Org. Chem. **26**, 4057 (1961); (*c*) D. L. TREPANIER and S. SUNDER. J. Med. Chem. **16**, 342 (1973).
9. A. MCKILLOP, J. D. HUNT, and E. C. TAYLOR. J. Org. Chem. **37**, 3381 (1972).
10. A. T. BLOMQUIST and A. GOLDSTEIN. Org. Syn. Coll. Vol. IV, 838 (1963).
11. B. LINDBERG. *In* Methods in carbohydrate chemistry. Vol. VI. *Edited by* R. L. Whistler and J. N. BeMiller. Academic Press, New York and London. 1972. p. 323.
12. B. T. LAWTON, W. A. SZAREK, and J. K. N. JONES. Carbohydrate Res. **10**, 456 (1969).
13. C. C. HACH, C. V. BANKS, and H. DIEHL. Org. Syn. Coll. Vol. IV, 229 (1963).
14. W. S. JOHNSON, B. BANNISTER, and R. PAPPO. J. Am. Chem. Soc. **78**, 6331 (1956).
15. L. BIRKOFER, S. M. KIM, and H. D. ENGELS. Chem. Ber. **95**, 1495 (1962).
16. W. A. WHITE and H. WEINGARTEN. J. Org. Chem. **32**, 213 (1967).
17. Y. KISHI, M. ARATANI, H. TANINO, T. FUKUYAMA, T. GOTO, S. INOUE, S. SUGIURA, and H. KAKOI. Chem. Commun. 64 (1972); Y. KISHI, M. ARATANI, T. FUKUYAMA, F. NAKATSUBO, T. GOTO, S. INOUE, H. TANINO, S. SUGIURA, and H. KAKOI. J. Am. Chem. Soc. **94**, 9217 (1972).
18. J. D. HOBSON and J. C. MCCLUSKY. J. Chem. Soc. C, 2015 (1967).
19. M. M. ABDEL-MONEM and P. S. PORTOGHESE. J. Med. Chem. **15**, 208 (1972); J. FISCHER and G. MIKITE. Acta Chem. (Budapest), **68**, 253 (1971); **68**, 261 (1971).
20. K. C. RICE. J. Org. Chem. **40**, 1850 (1975).
21. L. F. FIESER and M. FIESER. Reagents for organic synthesis. Vol. I. John Wiley and Sons Inc., New York, London, Sydney. 1967. pp. 823–824.
22. P. A. GRIECO and K. HIROI. Chem. Commun. 500 (1973).
23. E. J. COREY and A. VENKATESWARLU. J. Am. Chem. Soc. **94**, 6190 (1972).
24. F. ARNDT. Org. Syn. Coll. Vol. II, 461 (1943).
25. J. J. PAPPAS, W. P. KEAVENEY, E. GANCHER, and M. BERGER. Tetrahedron Lett. 4273 (1966).
26. Y. NAKAGAWA, H. KANO, Y. TSUKUDA, and Y. KOYAMA. Tetrahedron Lett. 4105 (1967).
27. J.-L. IMBACH, J.-L. BARASCUT, B. L. KAM, and C. TAPIERO. Tetrahedron Lett. 129 (1974).
28. A. BERTHO and H. NÜSSEL. Ann. Chem. **457**, 278 (1927).
29. H. OHRUI and J. J. FOX. Tetrahedron Lett. 1951 (1973).

A critical evaluation of Lennard–Jones and Stockmayer potential parameters and of some correlation methods

FRANK M. MOURITS AND FRANS H. A. RUMMENS

Department of Chemistry, University of Regina, Regina, Sask., Canada S4S 0A2

Received November 10, 1976[1]

FRANK M. MOURITS and FRANS H. A. RUMMENS. Can. J. Chem. **55**, 3007 (1977).

Published values for the potential parameters σ and ε/k of the Lennard–Jones (12–6) and Stockmayer (12–6–3) potentials as based on viscosity measurements are reviewed, with particular reference to the problem of indeterminacy inherent to such calculations. A number of correlation techniques, calibrated on viscosity-based potential parameters, are critically reviewed; where possible, priority rules for the use of these correlations have been developed. In addition, several other criteria (i.e. not based on viscosity data) for the acceptance or rejection of σ and ε/k parameter values are also discussed. Upon application of the various criteria and priority rules it has been possible to give recommended σ and ε/k parameter values for 75 molecules.

FRANK M. MOURITS et FRANS H. A. RUMMENS. Can. J. Chem. **55**, 3007 (1977).

On passe en revue les valeurs publiées pour les paramètres σ et ε/k des potentiels de Lennard–Jones (12–6) et de Stockmayer (12–6–3); les potentiels sont basés sur des mesures de viscosité et on tient particulièrement compte des problèmes d'indéterminations inhérents aux tels calculs. On fait aussi une revue critique d'un certain nombre de techniques de corrélation, calibrées sur des paramètres de potentiel basés sur la viscosité; on a développé, dans les cas qui s'y prêtent, des règles de priorité pour l'utilisation de ces corrélations. De plus, on discute de plusieurs autres critères (qui ne sont pas basés, c'est-à-dire, sur la viscosité) pour l'acceptation ou le rejet de valeurs des paramètres σ et ε/k. Par l'application de divers critères et de règles de priorité, il est possible de présenter des valeurs recommandées pour les paramètres σ et ε/k pour 75 molécules.
[Traduit par le journal]

Introduction

The prediction of bulk properties of matter from molecular level models appears to be a well-developed science. Particularly in gases, properties like the second virial coefficient, viscosity, thermal conductivity *et cetera* can be molded into a unifying framework based on molecular pair interactions (see in particular Hirschfelder, Curtiss, and Bird's book (1*a*)). These models of pair interactions all start with the assumption that there exists a general potential function, different only for the various different molecules through one, two, or more parameters. Many such functions have been proposed (1*b*), but perhaps the one most commonly used is the Lennard–Jones (12–6) function of [1]:

$$[1] \qquad V(\text{pair}) = 4\varepsilon\left[\left(\frac{\sigma}{r}\right)^{12} - \left(\frac{\sigma}{r}\right)^{6}\right]$$

where r is the distance between the centres of mass of the two molecules, ε is the maximum depth of the potential well, and σ is the distance at which $V(\text{pair}) = 0$. Equation 1 can, strictly speaking, only be used for non-polar molecules, but in practice [1] is also used for polar molecules. However, for the latter the Stockmayer (12–6–3) potential of [2] should be preferred:

$$[2] \quad V(\text{pair}) = 4\varepsilon\left[\left(\frac{\sigma}{r}\right)^{12} - \left(\frac{\sigma}{r}\right)^{6} - \delta\left(\frac{\sigma}{r}\right)^{3}\right]$$

where $\delta = \zeta\,\mu^2/4\sigma^3\varepsilon$, $\zeta(\theta_1,\theta_2,\phi)$ being a function to describe the angular dependence of the dipole–dipole interaction energy. Used in their proper integrated forms, [1] or [2] can lead to expressions for transport properties (1*c*) and equation of state and thermodynamic properties (1*d*); data-fitting with accurate experimental data on these properties can be used to determine the parameters ε/k and σ. Mixing rules exist (1*e*) to predict macroscopic properties of binary mixtures. Particularly in engineering the possibility of calculating transport properties of gases has been explored and applied extensively. In our own attempts to construct a molecular model to account for the medium nmr shift of gases and liquids (see following paper (2)) we

[1]Revision received May 11, 1977.

have been confronted (as have many others before us) with several major drawbacks of the above outlined approach.

(*i*) Methods to extract the parameters ε/k and σ from different macroscopic properties often lead to substantially different values; this may happen even if the same property is employed.

(*ii*) All too often the ε/k and σ for the molecules of interest are not known, and even the required macroscopic properties may not have been measured. In these cases one has to resort to estimation methods, of which a bewildering collection is available in the literature, thus leaving one with the difficult task of deciding which approximation to believe most.

In this paper we will exclusively discuss ε/k and σ parameters either directly obtained from gas viscosities or estimated by correlation methods which have been calibrated on such viscosity-based parameters. This restriction is a pragmatic one; more parameters are known from viscosity than from all other sources combined. Second virial coefficients apply to a state of equilibrium and therefore potential parameters based on second virial coefficients should, in principle, be more relevant to nmr medium shift applications than those based on viscosity. Second virial coefficient data fits are, however, very sensitive to the choice of potential; in particular shape- and higher-order polarity terms are needed to obtain physically meaningful parameters (3). At present only Lennard–Jones parameters have been calculated from 2nd virial coefficients in any great number and these are notably poor for polar and large non-polar molecules (1*f*).

Directly viscosity-based parameters and their reliability are discussed first. Next some of the more prominent correlation methods will be discussed and several priority rules for the use of these will be proposed. A few extra tests will also be discussed; these are crude correlation guides for ε/k and σ which are nevertheless useful because even the best of the correlation techniques can on occasion produce extremely erroneous results. Finally, this critical analysis has enabled us to recommend best values for σ and ε/k. A list of such recommended parameters for 75 molecules concludes this paper.

Discussion

ε/k and σ Parameters Directly Obtained From Gas Viscosities

Before comparing in detailed fashion the various sets of parameters, it should be pointed out that for some molecules greatly varying parameter values have been reported. Reid and Sherwood (4*a*) have already discussed this in connection with the parameter values for *n*-butane as calculated by Flynn and Thodos and by Svehla, whose calculations were based on the *same* experimental viscosity data.

The explanation of these erratic results has recently been given by Kim and Ross (5). These authors noted that the Lennard–Jones collision integral $\Omega^{(2,2)*}$ in the reduced temperature range $0.4 < T^* < 1.4$ reduced to $1.604(T^*)^{-1/2}$ with an error of less than 0.7%. This has the effect (since $T^* = kT/\varepsilon$) that the Chapman–Enskog equation for the viscosity η is reduced to a simple proportionality with T, out of which only the *product* $\sigma^2\varepsilon^{1/2}$ can be deduced:

$$[3] \qquad \eta = \frac{266.95 \times 10^{-7}(MT)^{1/2}}{\sigma^2\Omega^{(2,2)*}} = \frac{166.43 \times 10^{-7}T(Mk)^{1/2}}{\sigma^2\varepsilon^{1/2}} \text{ (P)}$$

Reichenberg (6) has also studied this matter, reaching virtually the same conclusion, albeit with a slightly different indeterminacy range of $0.39 < T^* < 1.55$. Halkiadakis and Bowrey (7) have applied the same ideas to the Stockmayer potential and its parameters; they found that the range of indeterminacy increases slowly with polarity to become $0.2 < T^* < 1.8$ when δ_{max} reaches $\delta_{max} = 2.5$ ($\delta_{max} = \frac{1}{2}\mu^{*2}$, where $\mu^{*2} = \mu^2/\sigma^3\varepsilon$). Our own analysis confirmed the above, but it was found that in the indeterminate range $\Omega^{(2,2)*}$ for polar molecules reduces to $A(T^*)^{-n}$, where A and n depend strongly on the value of δ_{max}, with the result that η then becomes inversely proportional to the product $P(n) = \sigma^2(\varepsilon/k)^n$. Such indeterminacy is not really serious when viscosities are recalculated; any combination σ, ε/k such that the product $P(n)$ is equal to the experimental value will reproduce viscosities to good precision. Greater errors occur when viscosities of *mixtures* or other properties are calculated. Such errors take on catastrophic dimensions when a property like the nmr Van der Waals intermolecular shift σ_w is calculated, because σ_w is approximately proportional to $\sigma^{-3}\varepsilon$ (8); a σ which is too large combined with too small an ε now add up to give a much too small σ_w value.

Kim and Ross (5) also showed that the collision integral $\Omega^{(2,2)*}$ in the range $0.9 < T^*$

< 5 can be written, with an error of less than 0.1%, as:

$$[4] \qquad \Omega^{(2,2)*} = 0.7616\left(1 + \frac{1.09}{T^*}\right)$$

Equation 4 makes the Chapmann–Enskog equation (eq. 3) equivalent to the empirical Sutherland formula, which can be written as follows:

$$[5] \qquad \eta = \frac{266.95 \times 10^{-7}(MT)^{1/2}}{{\sigma_T}^2}$$

$$[5] \qquad {\sigma_T}^2 = {\sigma_\infty}^2\left(1 + \frac{C}{T}\right)$$

In the above stated T^* range the parameters in [3] and [5] are thus related as follows:

$$[6] \qquad \sigma = 1.146\sigma_\infty \quad \varepsilon/k = 0.917C$$

Through [6], therefore, the large compilation by Franck (9) of σ_∞ and C parameters can be converted to σ and ε/k parameters; the latter being just as much subject to indeterminacy, however, as when obtained directly through [3].

The indeterminacy problem thus obliges one to make a judgement on the quality of the experimental viscosity data. In Table 1 the viscosity-based parameters σ are listed as originating from Franck (abbrev. F) (9), Hirschfelder *et al.* (abbrev. HCB) (1*f*), Flynn and Thodos (abbrev. FT) (10), Svehla (abbrev. S) (11), Tee, Gotoh, and Stewart (abbrev. TGS) (12), Linakis and Bowrey (abbrev. LB) (13), and Halkiadakis and Bowrey (abbrev. HB) (7). In the column marked HB we have also indicated the total number of viscosity points (N_t) used by HB as well as the number (N_e) of viscosity points *outside* the indeterminate range. The parameters values of HCB and FT were obtained by a multiple two-point numerical fitting technique, whereas those given by S, TGS, LB, and HB were obtained by direct least-squares fitting on [3]. In Table A the corresponding ε/k values are listed.[2]

For polar molecules (Tables 2 and B)[2] a distinction must be made between parameters calculated following a Lennard–Jones potential [1], and those calculated according to a Stockmayer potential [2]. Only Monschick and Mason (referred to as MM), using a graphical curve-shifting procedure, have used [1] and [2] on the *same* set of viscosity data (14).

[2]Copies of Tables A, B, and C are available, at a nominal charge, from the Depository of Unpublished Data, CISTI, National Research Council of Canada, Ottawa, Canada K1A 0S2.

Because of the important role of the product $P(n) = \sigma^2(\varepsilon/k)^n$, the values of $P(n)$ for all parameter sets listed in Tables 1, 2, A, and B have been calculated; these are given in Tables 3 and 4. In Table 4 the calculated $P(n)$ values based on the Stockmayer potential are given both for the correct value of n (varying between 0.49 and 0.54) as well as for $n = 0.50$. The latter allows comparison with the Lennard–Jones based products $P(n)$, where $n = 0.50$. As will be shown, these products $P(n)$ can be used as a guide in analyzing and judging the various parameter sets. As expected, the $P(n)$ values for indeterminate parameter sets are fairly constant ($\pm 1\%$ or less), although the individual σ and ε/k parameters may vary strongly between the various authors. For determinate situations $P(n)$ is only constant, when the individual σ and ε/k parameters are the same. The $P(n)$ values based on the data of Franck (eq. 6 and ref. 9) were found to be systematically higher than all other $P(n)$ values; hence the corresponding σ and ε/k values were omitted from further consideration.

For the noble gases, N_2, O_2, CO_2, CH_4, C_2H_6, and H_2O the viscosities are known over a very large temperature range; therefore a high percentage of viscosity points falls outside the indeterminate range. Indeed the parameters from HCB, FT, S, TGS, and MM show a good mutual agreement for these molecules. The σ parameters of LB and HB seem to be systematically lower for the noble gases, N_2, O_2, and CO_2 in spite of a high percentage determinacy. We have traced this discrepancy back to their use of presmoothed viscosity data (15), even extrapolating outside the original experimental temperature range (O_2). In the HB study viscosity points outside the indeterminacy range were given a statistical weight 10 times larger than those inside the range, whereas in the LB study virtually the same data points were used but with *equal* statistical weight. The product $P(n)$ is a useful quantity to discuss the differences between the results of HB and LB. As the tables show, for highly determinate cases the products $P(n)$, as well as the individual σ and ε/k parameters are very similar in the HB and LB studies. The tables show also that the HB and LB products $P(n)$ are almost the same, but with widely different individual σ and ε/k values, for those molecules where the parameters are indeterminate. For molecules whose experimental points are partly inside, partly outside the indeterminate range, several sub-cases

TABLE 1. The Lennard–Jones parameters σ (in Å) for non-polar molecules, based on viscosity and calculated by empirical correlations, and recommended values for σ and ε/k (in K)

		σ_{visc}									σ_{calc}		σ (recommended)	ε/k (recommended)
#		F[a]	HCB[b]	FT[c]	S[d]	TGS[e]	LB[f]	HB[g]	N_t[h]	N_e[h]	ST Eq.7	TGS Eq.12		
1	Ne	2.578	*2.824*		*2.820*		2.664				2.745	2.796	2.822	32.0
2	Ar	3.426	*3.442*		*3.542*	*3.434*	3.320	3.302	13	13	3.460	3.432	3.465	113.5
3	Kr	3.690	*3.61*		*3.655*	*3.721*	3.563	3.539	13	10	3.741	3.677	3.662	178.0
4	Xe	4.068	*4.055*		*4.047*	*4.049*	3.909	3.890	13	9	4.111	4.019	4.050	230.2
5	N_2	3.690	*3.715*		*3.798*	*3.722*	3.606	3.584	13	13	3.687	3.668	3.738	82.0
6	O_2	3.460	*3.487*		*3.467*		3.374	3.354	13	13	3.480	3.431	3.480	102.6
7	CO_2	3.953	*3.964*		*3.941*	*3.881*	3.765	3.752	13	9	4.012	3.885	3.943	200.9
8	CS_2	4.526	4.438		4.483						4.748	*4.575*	4.575	414.6
9	SF_6		*5.24*		*5.128*						4.989	4.960	5.199	212.0
10	$(CN)_2$	4.538	4.38		4.361						5.137	*4.571*	4.571	275.7
11	F_2	3.644	3.653		3.357		3.534	*3.439*	5	3	3.362	3.325	3.439	152.1
12	Cl_2	4.217	*4.258*		*4.217*		*4.235*	*4.232*	21	10	4.380	4.176	4.240	307.2
13	Br_2	4.354	4.268		4.296						4.514	*4.266*	4.266	437.3
14	I_2	5.099	4.982		5.160		5.095	5.077	6	1	4.867	*4.630*	4.630	577.4
15	CH_4	3.816	*3.809*	*3.808*	*3.758*	*3.774*	3.863	*3.782*	67	51	3.845	3.787	3.790	142.1
16	CF_4				*4.662*		*4.407*	*4.390*	19	19	4.541	4.405	4.486	167.3
17	CCl_4	5.901	5.881		5.947		5.744	*5.611*	21	4	5.795	5.554	5.611	415.5
18	C_2H_6	4.446	*4.418*	*4.384*	*4.443*	*4.480*	*4.416*	*4.302*	70	30	4.452	4.395	4.407	227.9
19	C_3H_8	5.110	*5.061*	*5.240*	*5.118*	*5.136*	*5.147*	*4.982*	29	9	5.031	4.940	5.114	237.2
20	*n*-C_4H_{10}	5.248	4.997	5.869	4.687	5.339	5.179	5.176	11	0	5.595	*5.405*	5.405	305.0
21	*i*-C_4H_{10}	5.408	5.341	5.819	5.278		5.372	5.370	6	0	5.438	*5.392*	5.392	295.8
22	*n*-C_5H_{12}	5.798	*5.769*	*6.099*	*5.784*	*6.104*	*5.989*	*5.751*	44	9	6.260	5.851	5.916	308.3
23	*neo*-C_5H_{12}				6.464	6.520					6.058	*5.757*	5.757	312.2
24	*n*-C_6H_{14}	5.993	5.909	5.916	5.949		6.207	5.923	31	0	6.623	*6.269*	6.269	341.3
25	*n*-C_7H_{16}	6.405				7.144		6.543	8	0	7.006	*6.650*	6.650	351.4
26	*n*-C_8H_{18}	7.540	7.451	7.407			7.318	7.167	8	0	7.452	*7.024*	7.024	357.7
27	*n*-C_9H_{20}	8.433	8.448	8.302			8.467	8.286	4	1	7.883	*7.351*	7.351	360.3
28	*cyclo*-C_6H_{12}	6.130	6.093	6.143	6.182						5.984	*5.771*	5.771	394.8
29	C_2H_4	4.263	*4.232*	*4.066*	*4.163*	*4.257*	*4.240*	*3.971*	30	5	4.419	4.232	4.155	225.6
30	C_3H_6	4.732		4.670	4.678		4.730	4.424	36	1	4.969	*4.778*	4.778	271.2
31	butene-1	5.305		5.198							5.412	*5.274*	5.274	302.4
32	*i*-butene	5.191		4.776							5.451	*5.282*	5.282	299.6
33	C_2H_2	4.263	*4.221*	*4.114*	*4.033*		*4.060*	*3.964*	29	12	4.322	4.131	4.078	221.4
34	C_3H_4	4.790		4.742	4.761						4.787	*4.667*	4.667	284.7
35	C_6H_6	5.397	5.270	5.628	5.349	5.443	5.398	5.340	30	0	5.699	*5.455*	5.455	401.2
36	$C_6H_5CH_3$	6.210		5.932							6.284	*5.923*	5.923	407.8
37	mesitylene	8.525		7.706							6.995	*6.760*	6.760	400.5

[a]See ref. 9. [b]See ref. 1f. [c]See ref. 10. [d]See ref. 11. [e]See ref. 12. [f]See ref. 13. [g]See ref. 7. [h]N_t is the total number of viscosity points used by HB; N_e is the number of viscosity points outside the indeterminate range. See text for further details.

need to be considered. If the HB and LB procedures result in substantially different products $P(n)$, then the set of experimental points favored by the HB weighting method (normally the high-temperature points) is inconsistent with the complete set. In fact in such a case the HB parameters should be considered less reliable since even their product $P(n)$ does not optimally fit the

TABLE 2. The Lennard–Jones and Stockmayer potential parameters σ (in Å) for polar molecules, based on viscosity and calculated by empirical correlations, and recommended values for σ and ε/k (in K)

			$\sigma_{visc,L.J.}$				$\sigma_{visc,St.}$					σ_{calc}				σ	ε/k
																(recommended)	
#		μ^{*2}	F[a]	HCB[b]	S[c]	MM[d]	MM[e]	LB[f]	HB[g]	N_t[h]	N_e[h]	ST Eq.7	ST Eq.8	TGS Eq.12	MS Eq.15		
38	N_2O	0.02	3.724	*3.848*	*3.828*			*3.619*[i]	*3.740*	29	14	4.059	3.612	3.900	4.009	3.776	248.8
39	CO	0.02	3.701	3.648	3.690				3.633	28	0	3.660	3.558	*3.698*	3.598	3.698	104.5
40	COS	0.15	4.274	4.13	4.130							4.790	4.076	*4.424*	4.505	4.424	286.4
41	NO	0.03	3.541	*3.535*	*3.492*			*3.457*	*3.428*	34	20	3.794	3.039	3.553	3.236	3.489	117.2
42	HI	0.06	4.068	4.123	4.211		4.13	4.238				3.785	4.027	*4.080*	3.875	4.080	333.6
43	HBr	0.30	3.621		3.353		3.41					3.617	3.761	*3.852*	4.086	3.852	281.1
44	HCl	0.82	3.392	3.305	3.339		3.36	3.240	3.240	12	0	4.282	3.396	3.771	*3.168*	3.168	322.6
45	HF	2.33			*3.148*								3.220			3.148	330.
46	H_2S	0.43	3.644		3.623	3.591	3.49	3.628[i]	3.491	9	0	3.903	3.625	3.840	*3.733*	3.733	302.4
47	SO_2	0.85	4.251	4.290	4.112	4.026	*4.04*	*4.249*	*4.017*	44	17	4.494	3.893	4.283	4.054	4.102	328.5
48	HCN	2.36	3.254		*3.630*								4.066			3.630	569.1
49	NH_3	1.52	2.830		2.900		*3.15*	*3.288*[i]	*3.206*	40	15		3.273		3.121	3.215	309.9
50	H_2O	2.46	2.601		2.641		*2.71*	3.086	3.067	25	19		3.003		2.708	2.71	506.
51	$CHCl_3$	0.14	5.431	5.430	5.389		5.31	5.157	5.163	14	3	5.052	4.872	*5.179*	5.114	5.179	381.7
52	CH_2Cl_2	0.43	4.847	*4.759*	*4.898*	*4.748*	*4.62*	*4.759*	*4.830*	5	2	5.033	4.537	4.906	4.998	4.752	403.5
53	CH_3Br	0.71	4.423		4.118		4.25						*4.306*	4.278		4.306	416.2
54	CH_3Cl	0.97	4.091	3.375	4.182	4.151	3.94	4.047	4.057	21	2	4.693	4.067	4.419	*4.296*	4.296	328.1
55	C_2H_5Cl	0.83			4.898		4.45						4.583		*4.490*	4.490	402.9
56	n-C_3H_7OH	0.37	4.813		4.549		4.71	5.377	4.570	7	0	5.843	4.724	5.543	*4.867*	4.867	480.2
57	i-C_3H_7OH	0.41	4.961				4.64					6.003	*4.739*	5.623	4.491	4.739	456.0
58	C_2H_5OH	0.57	4.526	4.455	4.530	4.370	4.31	4.755[i]	4.756	15	9		4.323		*4.317*	4.317	450.2
59	CH_3OH	1.11	3.724	3.585	3.626	3.666	3.69	3.959	3.930	14	5		3.850		*3.657*	3.657	385.2
60	$(C_2H_5)_2O$	0.16	5.133		5.678	5.539	5.49	5.825	5.813	22	8	6.091	5.136	5.711	*5.553*	5.553	348.0
61	$(CH_3)_2O$	0.46	4.560		4.307	4.264	4.21	4.736[i]	4.359	14	0	4.425	4.513	4.718	*4.230*	4.230	352.3
62	$CH_3CO_2C_2H_5$	0.33	5.397		5.205	5.163	5.24					6.427	5.172	5.888	5.841	5.65	372.
63	$CH_3CO_2CH_3$	0.41	5.007		4.936	5.054	5.04					5.903	4.796	5.421	*5.141*	5.141	389.4
64	$(CH_3)_2CO$	1.35	4.778		4.600	4.669	4.50	4.601	4.601	9	0		4.659		*4.599*	4.599	458.0
65	CH_3CHO	1.56						3.972	3.972	4	0		*4.332*		3.883	4.332	413.5

[a] See ref. 9. [b] See ref. 1f. [c] See ref. 11. [d] Lennard-Jones parameters of ref. 14. [e] Stockmayer parameters of ref. 14. [f] See ref 13. [g] See ref. 7. [h] See footnote *h* of Table 1. [i] Total number of data points used less than N_t.

data points in the indeterminate range. On the other hand the LB *product* $P(n)$ is more reliable. It would have been better to employ the HB method, but with the LB product $P(n)$ kept as a fixed constant. Examples are C_3H_8, C_2H_4, N_2O, NH_3, and SO_2. If the HB and LB products $P(n)$ are essentially the same, when the individual σ and ε/k parameters are different, then one should prefer the HB parameters. Examples are F_2 and CCl_4. If the HB and LB products $P(n)$ and the σ and ε/k parameters are virtually the same, then apparently the case is already effectively determinate (noble gases, N_2, O_2, CO_2, NO). The fourth possibility relates to cases where N_e is very small. If these few points fall in a *narrow* T^* range (as they normally will do), then the extracted HB parameters may become effectively indeterminate (constant $P(n)$) again, as was pointed out already by Reichenberg (6). Examples are CH_3Cl, $CHCl_3$, C_2H_5OH, CH_3OH, and $(C_2H_5)_2O$. Although the degree of indeterminacy as indicated in Tables 1 and 2 refers, strictly speaking, only to the work of HB, it gives in general also a good indication of the indeterminacy of the parameters of the *other* authors for these same molecules, since the sources of viscosity data were largely the same. In addition, the latter data are for the most part

TABLE 3. The product $P(n)$ for the non-polar molecules of Table 1 with $n = 0.50$

#		P_{visc}[a]							P_{calc}		P_{ave}	P_{rec}	% dev.
		F	HCB	FT	S	TGS	LB	HB	ST Eq.7	TGS Eq.12			
1	Ne	72	*45*		*46*		55		46	43	48	45	
2	Ar	134	*130*		*121*	*130*	133	134	129	130	130	127	
3	Kr	179	*180*		*179*	*178*	177	178	174	176	178	179	
4	Xe	252	*249*		*249*	*249*	248	248	244	247	249	249	
5	N_2	134	*128*		*122*	*128*	134	134	133	134	129	126	
6	O_2	128	*122*		*124*		127	128	129	131	125	123	
7	CO_2	218	*221*		*217*	*221*	221	221	221	221	220	220	
8	CS_2	439	417		434				422	*426*	426	426	- 0.1
9	SF_6		*388*		*392*				365	365	389	389	
10	$(CN)_2$	358	353		355				418	*347*	354	347	+ 2.0
11	F_2	144	141		120		144	*146*	143	118	138	146	
12	Cl_2	319	*315*		*316*		*312*	*312*	310	313	314	314	
13	Br_2	419	415		416				377	*381*	415	381	+ 8.4
14	I_2	594	582		580		581	581	512	*515*	581	515	+11.3
15	CH_4	178	*172*	*172*	*172*	*171*	166	*169*	175	177	171	171	
16	CF_4				*252*		*262*	*263*	248	249	259	259	
17	CCl_4	637	635		635		640	*642*	614	618	638	642	
18	C_2H_6	301	*296*	*295*	*290*	*290*	*292*	*294*	292	295	293	293	
19	C_3H_8	417	*408*	*394*	*403*	*400*	*401*	*405*	400	403	402	402	
20	n-C_4H_{10}	512	506	497	506	502	507	506	507	*510*	504	510	- 1.3
21	i-C_4H_{10}	514	505	499	506		504	505	498	*500*	504	500	+ 0.7
22	n-C_5H_{12}	630	*618*	*610*	*618*	*602*	*610*	*614*	616	618	612	612	
23	*neo*-C_5H_{12}				581	575			581	*586*	578	586	- 1.3
24	n-C_6H_{14}	718	710	720	707		711	714	726	*726*	712	726	- 1.9
25	n-C_7H_{16}	829				818		829	832	*829*	823	829	- 0.7
26	n-C_8H_{18}	1000	993	1001			992	994	941	*933*	995	933	+ 6.2
27	n-C_9H_{20}	1132	1106	1124			1128	1121	1039	*1026*	1120	1026	+ 8.4
28	*cyclo*-C_6H_{12}	674	668	668	659				658	*662*	665	662	+ 0.5
29	C_2H_4	261	*256*	*251*	*256*	*257*	*261*	*264*	261	264	258	258	
30	C_3H_6	385		378	378		377	378	373	*376*	378	376	+ 0.6
31	butene-1	489		483					481	*484*	483	484	- 0.2
32	i-butene	475		470					481	*483*	470	483	- 2.7
33	C_2H_2	245	*242*	*246*	*248*		*248*	*250*	253	255	247	247	
34	C_3H_4	366		363	360				366	*368*	361	368	- 1.7
35	C_6H_6	591	583	580	581	583	584	583	593	*596*	582	596	- 2.4
36	$C_6H_5CH_3$	711		683					706	*708*	683	708	- 3.7
37	mesitylene	812		908					902	*915*	908	915	- 0.7

[a] For references see Table 1.

fairly old and are consequently not likely to be more accurate than 0.7%. It should be kept in mind, however, that recent viscosity data, particularly when measured with the rotating disc technique may be as precise as 0.1% (15), thereby narrowing or even eliminating the indeterminacy range. Except for the noble gases, N_2, O_2, and CO_2 no such accurate data appear to be available at this time.

As far as the fit on viscosity data of polar molecules is concerned, no significant improvement is obtained by replacing the Lennard–Jones

TABLE 4. The product $P(n)$ for the polar molecules of Table 2

#		$P_{visc,L.J.}$[a]				$P_{visc,St.}$[a]				P_{calc}				P_{ave}	P_{rec}	% dev.
		F	HCB	S	MM	MM	LB	HB	n	ST Eq.7	ST Eq.8	TGS Eq.12	MS Eq.15			
38	N_2O	235	*224*	*223*			*229*	*221*	0.50	228	217	230	237	224	224	
39	CO	132	132	130				135	0.50	139	138	*140*	136	132	140	- 5.6
40	COS	318	312	313					0.50	327	305	*331*	337	312	331	- 6.2
41	NO	136	*127*	*132*			*136*	*134*	0.50	130	117	125	129	131	131	
42	HI	313	306	301		302	299		0.50	303	316	*304*	288	302	304	- 0.6
43	HBr	243		238		224 237			0.49 0.50	248	255	*249*	262	238	249	- 4.6
44	HCl	210	207	207		193 204	193 204	193 204	0.49 0.50	219	197	222	*180*	204	180	-11.8
45	HF			*180*					0.50		211				180	
46	H_2S	231		228	227	213 226	217 230	218 231	0.49 0.50	247	240	249	*242*	228	242	- 6.2
47	SO_2	303	292	310	309	287 *304*	285 *301*	289 *306*	0.49 0.50	317	298	317	303	304	304	
48	HCN	304		*314*					0.50						314	
49	NH_3	192		199		*188*	*181*	*176*	0.50		204		190	181	181	
50	H_2O	201		198		212 *165*	198 158	196 156	0.54 0.50		217		184	160	165	
51	$CHCl_3$	546	533	536		531	541	542	0.50	524	521	*524*	522	537	524	+ 2.3
52	CH_2Cl_2	464	*456*	*453*	*450*	422 *449*	428 *454*	426 *452*	0.49 0.50	459	440	461	472	452	452	
53	CH_3Br	365		359		333 353			0.49 0.50		*378*			353	378	- 7.2
54	CH_3Cl	337	333	327	325	297 316	299 317	300 318	0.49 0.50	339	320	343	*334*	317	334	- 5.4
55	C_2H_5Cl			416		383 407			0.49 0.50		427		*405*	407	405	+ 0.6
56	n-C_3H_7OH	504		497		464 494	458 484	464 494	0.49 0.50	539	490	518	*519*	492	519	- 5.4
57	i-C_3H_7OH	506				460 490			0.49 0.50	534	*480*	508	462	490	480	+ 2.1
58	C_2H_5OH	396	392	391	389	363 386	356 377	356 377	0.49 0.50		402		*395*	380	395	- 4.2
59	CH_3OH	293	289	289	286	262 278	261 276	257 272	0.49 0.50		318		*282*	276	262	+ 4.7
60	$(C_2H_5)_2O$	507		571	575	573	568	565	0.50	581	540	582	*575*	570	575	- 0.8
61	$(CH_3)_2O$	370		369	369	347 368	353 374	347 368	0.49 0.50	378	386	377	*336*	370	336	+ 9.1
62	$CH_3CO_2C_2H_5$	626		619	614	576 613			0.49 0.50	639	579	637	653	615	615	
63	$CH_3CO_2CH_3$	538		528	522	489 519			0.49 0.50	538	490	539	*522*	523	522	+ 0.3
64	$(CH_3)_2CO$	509		501	497	474	475	474	0.50		463		*453*	475	453	+ 4.6
65	CH_3CHO						330	330	0.50		*382*		323	330	382	-15.8

[a]For references see Table 2.

(12–6) potential by a Stockmayer (12–6–3) potential (14). Indeed as MM stated (14), even more primitive potentials would have been equally successful. Klein and Hanley (16) analyzed this problem from a theoretical viewpoint and came to the important conclusion that within the range $2.0 < T^* < 5.0$ little can be learned about the precise nature of the potential function. One must have viscosity data of at least 0.5% accuracy and then either at $T^* < 2.0$ or $T^* > 5.0$ or both in order to distinguish between the various proposed potential func-

tions. The above does not imply, however, that the *parameter* sets for the Lennard–Jones and Stockmayer potentials would have to be the same. Inspection of the two MM columns of Tables 2 and B reveals in fact considerable, but non-systematic differences. Comparing each of the corresponding MM $P(n)$ values with the other $P(n)$ values for the same potential (Table 4), it is evident that all cases except SO_2 are effectively indeterminate. Although therefore no conclusion can be drawn regarding the relative merit of the two potentials with respect to their σ and ε/k parameters, it is evident from Table 4 that the Stockmayer $P(n)$ values are systematically smaller than the Lennard–Jones $P(n)$ values. Analysis of the collision integral $\Omega^{(2,2)*}$ as a function of δ_{max} has shown us that there are, to a good approximation, explicit relations between Stockmayer and Lennard–Jones parameters. Up to $\delta_{max} = 0.25$ the differences are negligible. Going from $\delta_{max} = 0.25$ to $\delta_{max} = 2.5$ the Stockmayer σ values decrease up to 5%, while the Stockmayer ε/k values decrease up to 51% relative to the Lennard–Jones ε/k; as a result Stockmayer $P(n)$ values are substantially smaller than Lennard–Jones $P(n)$ values for $\delta_{max} > 0.25$. This latter trend can be clearly observed in Table 4. The general conclusion therefore is, that, apart from indeterminacy problems, Stockmayer potential parameters are to be preferred for molecules with δ_{max} larger than 0.25.

ε/k and σ Parameters Obtained by Correlation Techniques

Stiel and Thodos (abbrev. ST) (17) have developed the following empirical relationship for non-polar molecules:

$$[7] \qquad \sigma = 0.1866 V_c^{1/3} Z_c^{-6/5}, \quad \varepsilon/k = 65.3 T_c Z_c^{18/5}$$

and similarly for polar, but non-hydrogen bonding molecules (18):

$$[8] \qquad \sigma = 0.785 V_c^{1/3}, \quad \varepsilon/k = 0.897 T_c$$

Here V_c is the critical volume (cm^3), T_c is the critical temperature (K) and Z_c is the critical compressibility. Selected values for Z_c, V_c, P_c, T_c, as well as for the dipole moment μ are given in Table C.[2] Equation 7 was calibrated on the viscosity-based Lennard–Jones (12–6) parameters of FT (10) and of HCB (1*f*). Equation 8 was calibrated on the viscosity-based Stockmayer parameters of MM (14). More recently, HB (7) have developed similar relations. For non-polar molecules only, they find:

$$[9] \qquad \sigma = 0.386 V_c^{1/3} Z_c^{-0.59}, \quad \varepsilon/k = 2.80 T_c Z_c^{0.97}$$

whereas for non-polar and polar molecules combined, they find:

$$[10] \qquad \sigma = 0.813 V_c^{1/3}, \quad \varepsilon/k = 0.404 T_c Z_c^{-0.53}$$

HB calibrated [9] and [10] on their own set of calculated viscosity-based Lennard–Jones (12–6) and Stockmayer (12–6–3) potential parameters.

For non-polar molecules an alternative was recently introduced by TGS (12). The method does not require knowledge of the often inaccurate V_c parameter, but utilizes P_c, T_c, and Pitzer's acentric factor ω, where ω is defined by

$$[11] \qquad \omega + 1 = -\log_{10} \frac{P}{P_c}\bigg|_{T_r = 0.7}$$

with P being the vapour pressure at the reduced temperature $T_r = 0.7$. Calibrating on their own set of viscosity-based Lennard–Jones (12–6) parameters, they found:

$$[12] \qquad \sigma = (2.3454 + 0.2972\omega)(T_c/P_c)^{1/3}$$
$$\varepsilon/k = (0.8082 - 0.4504\omega) T_c$$

The parameter ω can be calculated (eq. 11) from vapour pressure data or, if the latter are not available, be estimated within 5% from the following semi-empirical relation (19):

$$[13] \qquad \omega + 1 = \frac{3\theta}{7(1-\theta)} \log_{10} P_c, \quad \theta = T_b/T_c$$

where T_b (K) is the boiling point temperature.

Malek and Stiel (abbrev. MS) (20) have attempted to expand the TGS method to *polar* compounds, introducing a fourth parameter x to account for the polar interactions:

$$[14] \qquad x = \log_{10} \frac{P}{P_c}\bigg|_{T_r = 0.6} + 1.70\omega + 1.552$$

Calibrating on MM's set of Stockmayer parameters (14), they obtained the following relations:

$$[15] \qquad \sigma = (2.3454 + 0.2972\omega - 40.4271x + 61.7675\omega x - 15.8248x^2 - 0.9706\omega^2)(T_c/P_c)^{1/3}$$
$$\varepsilon/k = (0.8082 - 0.4504\omega + 27.3866x - 48.9402\omega x - 48.7293x^2 + 0.8784\omega^2) T_c$$

We have calculated ω and x values for all molecules concerned, directly from the best vapour pressure data available. These are given in Table 5. The right-hand side of Tables 1–4, A and B show calculated values of σ, ε/k and $P(n)$ as based on the critical values of Table C and our own set of ω and x parameters of Table 5.[2]

Critical Comparison of ε/k and σ Parameter Values

In Tables 1–4, A, and B we have italicized those values which we have used to arrive at the *recommended* values. For the values of σ(visc) and ε/k(visc) this judgement was arrived at by searching the original literature on the viscosity measurements as used by the various authors. Generally, when about 30% or more of the experimental points were outside the indeterminate range, the parameters were considered reliable, at least if and when the latter conformed with the criteria regarding $P(n)$ as discussed in the previous section. These preferred σ(visc) and ε/k(visc) values form a basis set against which the σ(calcd) and ε/k(calcd) can be compared.

Discussing first the non-polar molecules (Table 1), it may be seen that the σ(calcd) values according to [7] are not unreasonable but nevertheless slightly too large on the average. It is believed that this is due to the calibration of [7], which included many σ(visc) values now considered to be unreliable. Re-calibrating would be a possibility, but at this stage this would be rather unsatisfactory due to the lack of reliable σ(visc) data for *larger* molecules. Furthermore the strong dependence on the, usually inaccurately known, parameter V_c makes the ST method less attractive, particularly since the TGS method (see below) does not require V_c at all. The correlations given by HB (eqs. 9 and 10) show a lesser dependence on V_c. The σ(calcd) values obtained by [9] are reasonable, but in general somewhat too small. Equation 10 has in principle the great advantage of avoiding the discrimination between polar and non-polar molecules, but for non-polar molecules at least the results are often much too low.

The TGS results (eq. 12) show a very good agreement with our selected σ(visc) and ε/k(visc) parameters despite the fact that the original TGS calibration included some indeterminate parameters. Since the TGS method does not require knowledge of V_c but rather of the vapour pressure, which is usually accurately known, we prefer the TGS method over those of ST and HB. Based on this preference we have accepted as best values for those molecules, for which no sufficiently determinate σ(visc) and ε/k(visc) were available, the σ(calcd) and ε/k(calcd) calculated with [12]. The last two columns of Table 1 show the selected parameters σ and ε/k for all non-polar molecules; the ε/k values have, in all instances, been selected in conformity with the selection of σ values (see Table B).[2] Where more than one acceptable value was available, the *average* of these is given.

For slightly polar molecules (i.e. $\mu^* \leq 0.3$) [7] gives σ(calcd) values which are too high (as was already noticed for non-polar molecules), whereas the σ(calcd) values according to [8] are too low. Taking the *average* of the results of [7] and [8] gives good agreement for this μ^{*2} range. However, the HB method of [9] gives also good results, comparable with the above mentioned average. For polar molecules with $\mu^{*2} > 0.3$ reasonably good values are obtained with [8]. This is rather remarkable since the calibration of [8] included only one molecule (SO_2) with a large degree of determinacy in its parameters. Equation 10, being a correlation for non-polar and polar molecules combined shows systematic deviations; σ(calcd) is generally too low for slightly polar molecules and too high for polar molecules. It follows therefore that it is impossible to find a universal correlation based on critical constants, which gives good results for molecules of both low and high polarity. The claim of HB that [10] is superior to ST's [7] is irrelevant as far as polar molecules are concerned because the latter equation is designed to correlate non-polar molecules only!

The ω,x method of MS (eq. 15) is potentially the most powerful correlation, since it relates directly the potential parameters to the size and the degree of polarity of the molecule. However, because of the way in which ω and x are defined, these size and polarity factors are not separated, resulting in the need for a cross-term ωx and higher order terms such as ω^2. Ideally, such a method with well-separated parameters would correlate polar and non-polar molecules without discontinuity. However, because of the noted non-separation, one has to arbitrarily set ω^2 and x equal to zero for non-polar molecules (to reduce [15] to [12]), but also for slightly polar

TABLE 5. Values of ω and x for the molecules of Tables 1 and 2

#		ω[a]	#		ω	x	ω[f]	x[f]
1	Ne	0	38	N_2O	0.160[g]	−0.003[g]	0.160[l]	−0.003[l]
2	Ar	−0.002	39	CO			0.049[m]	0.002[m]
3	Kr	−0.002	40	COS			0.099[n]	−0.002[n]
4	Xe	0.002	41	NO	0.577[g]	−0.045[g]	0.581[o]	−0.025[o]
5	N_2	0.040	42	HI			0.047[p]	0.003[p]
6	O_2	0.021	43	HBr	0.083[g]	0.011[g]	0.076[p]	−0.004[p]
7	CO_2	0.225[b]	44	HCl	0.126[h]	0.008[h]	0.130[q]	0.011[q]
8	CS_2	0.127[c]	45	HF			0.377[r]	0.127[r]
9	SF_6	0.257	46	H_2S			0.096[s]	0.002[s]
10	$(CN)_2$	0.270[d]	47	SO_2	0.262[i]	0.005[i]	0.254[t]	0.003[t]
11	F_2	0.043[e]	48	HCN	0.409[g]	0.080[g]	0.372[u]	0.055[u]
12	Cl_2	0.074	49	NH_3	0.252[j]	0.013[j]	0.256[v]	0.013[v]
13	Br_2	0.132	50	H_2O	0.344[g]	0.023[g]	0.344[w]	0.023[w]
14	I_2	0.229	51	$CHCl_3$			0.215[x]	−0.001[x]
15	CH_4	0.011	52	CH_2Cl_2			0.197[y]	−0.003[y]
16	CF_4	0.191	53	CH_3Br			0.232[z]	
17	CCl_4	0.191[c]	54	CH_3Cl	0.152[g]	0.007[g]	0.152[aa]	0.001[aa]
18	C_2H_6	0.097	55	C_2H_5Cl	0.191[g]	0.005[g]	0.192[bb]	0.007[bb]
19	C_3H_8	0.154	56	n-C_3H_7OH	0.626[j]	−0.057[j]	0.621[cc]	−0.050[cc]
20	n-C_4H_{10}	0.201	57	i-C_3H_7OH	0.663[j]	−0.053[j]	0.665[cc]	−0.055[cc]
21	i-C_4H_{10}	0.185	58	C_2H_5OH	0.641[h]	0.003[h]	0.635[cc]	0.001[cc]
22	n-C_5H_{12}	0.252	59	CH_3OH	0.556[j]	0.037[j]	0.565[cc]	0.038[cc]
23	*neo*-C_5H_{12}	0.196	60	$(C_2H_5)_2O$	0.275[j]	−0.003[j]	0.280[dd]	−0.000[dd]
24	n-C_6H_{14}	0.301	61	$(CH_3)_2O$	0.206[j]	0.002[j]	0.202[ee]	0.007[ee]
25	n-C_7H_{16}	0.350	62	$CH_3CO_2C_2H_5$			0.360[ff]	−0.006[ff]
26	n-C_8H_{18}	0.398	63	$CH_3CO_2CH_3$	0.326[k]	0.005[k]	0.323[ff]	0.001[ff]
27	n-C_9H_{20}	0.449	64	$(CH_3)_2CO$	0.304[g]	0.013[g]	0.307[gg]	0.013[gg]
28	*cyclo*-C_6H_{12}	0.210	65	CH_3CHO	0.281[k]	0.019[k]		
29	C_2H_4	0.086						
30	C_3H_6	0.145						
31	butene-1	0.194						
32	i-butene	0.203						
33	C_2H_2	0.189						
34	C_3H_4	0.223						
35	C_6H_6	0.210						
36	$C_6H_5CH_3$	0.264						
37	mesitylene	0.399						

[a]The molecular parameters ω for the hydrocarbons were calculated from the API-44 vapour pressure data (28). The ω parameters for the inorganic gases, taken from Reid and Sherwood's tabulation (4b) are experimentally determined or calculated. Their value for CO_2 (ω = 0.420) is clearly in error. [b]K.S. Pitzer, *et al.* J. Am. Chem. Soc. *77*, 3433 (1955). [c]Calculated from vapour pressures given by Boublik and Aim (29). [d]Calculated from vapour pressures given by Edwards (26). [e]J.-H. Hu, D. White, and H.L. Johnston. J.Am. Chem. Soc. *75*, 5642 (1953). [f]Calculated (this paper) from vapour pressure data as referenced below. [g]R.L. Halm and L.I. Stiel. AIChE J. *13*, 351 (1967). [h]G.K. Stipp, S.D. Bai, and L.I. Stiel. AIChE J. *19*, 1227 (1973). [i]T.-F. Yuan and L.I. Stiel. Ind. Eng. Chem. Fundam. *8*, 393 (1970). [j]R.L. Halm and L.I. Stiel. AIChE. J. *16*, 3 (1970). [k]See ref. 20. [l]E.J. Couch, K.A. Kobe, and L.J. Hirth. J. Chem. Eng. Data *6*, 229 (1961); H.J. Hoge. J. Res. Natl. Bur. Standards *34*, 281 (1945). [m]A. Michels. T. Wassenaar, and Th. N. Zwietering. Physica *18*, 160 (1952); J.O. Clayton and W.F. Giauque. J. Am. Chem. Soc. *54*, 2610 (1932). [n]J.D. Kemp and W.F. Giauque. J. Am. Chem. Soc. *59*, 79 (1937). [o]H.L. Johnston and W.F. Giauque. J. Am. Chem. Soc. *51*, 3194 (1929). [p]See ref. 26. [q]W.F. Giauque and R. Wiebe. J. Am. Chem. Soc. *50*, 101 (1928); W. Thomas. Progr. Intern. Res. Thermod. Transp. Prop. ASME Second Symposium, 1962, 166–171; E. Cardoso and A.F.O. Germann. J. chim. phys. *11*, 632 (1913); O. Maass and D. McIntosh. Trans. Roy. Soc. Canada III, *VIII*, 65 (1914). [r]R.L. Jarry and W. Davis Jr. J. Phys. Chem. *57*, 600 (1953). [s]W.B. Kay and G.M. Rambosek, Ind. Eng. Chem. *45*, 221 (1953); W.F. Giauque and R.W. Blue. J. Am. Chem. Soc. *58*, 831 (1936). [t]W.F. Giauque and C.C. Stephenson. J. Am. Chem. Soc. *60*, 1389 (1938); K. Clusius, K. Schleich, and R.B. Bernstein. Helv. Chim Acta *45*, 258 (1962); T. Toriumi and R. Hara. J. Soc. Chem. Ind. Japan *47*, 502 (1944); E. Cardoso and U. Fiorentino. J. chim. phys. *23*, 841 (1926). [u]H. Sinosaki, R. Hara, and S. Mitsukuri. Tech. Repts. Tohoku Imp. Univ. *4*, 145 (1924). [v]International Critical Tables, Vol. III (1928). McGraw-Hill Book Company Inc., New York. [w]ASME Steam Tables 1967. The Am. Soc. of Mech. Eng. United Engineering Centre, New York. [x]M.A. Zmaczynski. J. chim. phys. *27*, 503 (1930). [y]See ref. 29; L.S. Dzung. The Brown Boveri Review *33*, 158 (1946). [z]C.J. Egan and J.D. Kemp. J. Am. Chem. Soc. *59*, 1265 (1937); *ibid.* *60*, 2097 (1938). [aa]G. Holst. Commun. Leiden, *144* b.c.d. (1913–1914). [bb]J. Gordon and W.F. Giauque. J. Am. Chem. Soc. *70*, 1506 (1948); A. Berthoud. J. chim. phys. *15*, 3 (1917). [cc]D. Ambrose, J.H. Ellender, and C.H.S. Sprake. J. Chem. Thermodynamics *6*, 909 (1974). [dd]D. Ambrose, C.H.S. Sprake, and R. Townsend. J. Chem. Thermodynamics *4*, 247 (1972). [ee]E. Cardoso and A. Bruno. J. chim. phys. *20*, 347 (1923); R.M. Kennedy, M.Sagenkahn and J.G. Aston. J. Am. Chem. Soc. *63*, 2267 (1941). [ff]J. Polak and I. Mertl. Coll. Czech. Chem. Comm. *30*, 3526 (1965). [gg]D. Ambrose, C.H.S. Sprake, and R. Townsend. J. Chem. Thermodynamics *6*, 693 (1974).

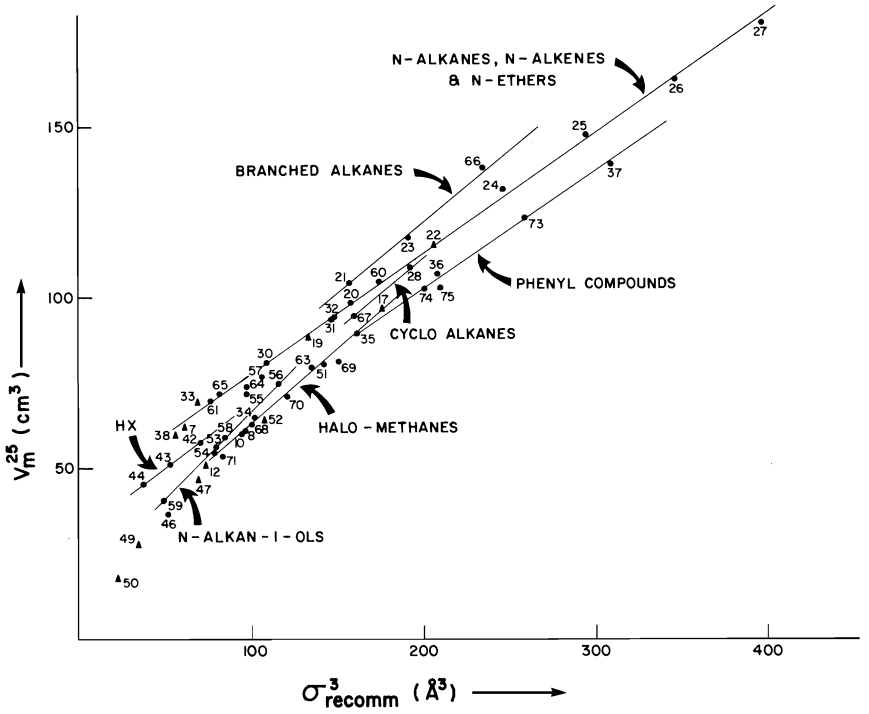

FIG. 1. Empirical correlation between the molar volume V_m^{25} and σ^3(rec) values of Tables 1, 2, and 6. σ(rec) values, based on determinate σ(visc) values are indicated by ▲; filled circles ● indicate σ(rec) values based on correlation techniques. Solid lines tie points within classes of compounds.

molecules (the limit appears to be at $\mu^{*2} = 0.3$). Another disadvantage of the MS method is that it requires extremely accurate vapour pressure data (*vide infra*). Finally it appears that for molecules with $|x| > 0.035$ grossly erroneous results may occur. Examples are HF, HCN, CH_3NO_2, and CH_3CN. In conclusion we prefer the MS method of [15] for polar molecules with $\mu^{*2} > 0.3$ whenever very accurate vapour pressure data are available. If with [15] physically unacceptable results are obtained according to supplementary tests (*vide infra*) (for example due to inaccurate vapour pressure data), it is recommended to use the ST method of [8]. For slightly polar molecules ($\mu^{*2} \leq 0.3$) it is recommended to use the TGS method of [12], to be consistent with the preference expressed with respect to non-polar molecules. Based upon the above recommendations, preferred σ and ε/k values (or their average) are given in the last columns of Table 2. Table B gives all the corresponding ε/k values for polar molecules.[2]

In Table 3 (non-polar molecules) P(av) is the average of all P(visc) values (except those of F), while P(rec) is the product based on σ(rec) and ε/k(rec). For the indeterminate cases (where η is only a function of $P(n)$), P(av) will give the best fit on all viscosity data combined. The deviation of P(rec) from P(av) is therefore a direct measure of the error if viscosities were recalculated on the basis of P(rec). These percentage deviations have been given in the last column of Table 3. In the determinate cases P(rec) is always taken from one or more P(visc) data and therefore will, of course, already constitute the best fit over the combined viscosity data.

For polar molecules (Table 4) with $\delta_{max} \leq 0.25$, P(av) is the average over the Lennard–Jones and Stockmayer P(visc) values; Stockmayer P(visc) values were used to calculate P(av) when $\delta_{max} > 0.25$. For reasons of consistent comparison all P(calcd), P(av), and P(rec) values have been calculated with $n = 0.50$. It should be noted that for indeterminate cases the determinate product $P(n)$ *may* have a value of n, different from 0.50; in these cases also P(visc) values for $n = 0.50$ were calculated to make comparison possible. As before, the % dev. column indicates the error

level in viscosities, recalculated on the basis of the recommended parameters.

Supplementary Test Methods for σ

In addition to already existing non-viscosity-based correlation techniques (1, 11) we have found three additional estimation methods. Figure 1 shows that there is a reasonable correlation between σ^3(rec) and V_m^{25}, the molar volume at 25°C. In fact, for chemically closely related molecules (such as the *n*-alkanes, the methyl benzenes and the *n*-alkan-1-ols) very good straight-line relationships exist. In principle a correlation between σ^3 and V_m^b (molar volume at boiling point) would be better; however, V_m^b is not available in many cases, whereas V_m^{25} is much more often available from literature sources. For low-boiling compounds the reverse is often true. An application of the above correlations is ethyl acetate which with the MS method appeared to give too high a value for σ. Using Fig. 1, an estimated σ(rec) = 5.65 was arrived at. Points which would fall clearly outside the indicated correlation band of Fig. 1 must be considered erroneous. In fact this criterion was used in the foregoing discussions; it did confirm that certain σ(visc) values (such as for mesitylene, *n*-hexane, neopentane, cyclohexane, CCl_4, and propanal) were not only indeterminate, but indeed erroneous.

A second test is based on the σ and ε/*k* parameters obtained by Wilhelm and Battino (abbrev. WB) (21) from the solubility of certain gases (He, Ne) in liquids. As Fig. 2 shows, there is an excellent straight-line relation between the WB σ values and our σ(rec) values. This relation formed an additional argument to accept the TGS method, particularly because of the excellent correlation for the higher *n*-alkanes. The only deviating point is that for acetone; since σ(rec) is based on highly accurate P_c, T_c, and vapour pressure data and since in Fig. 1 acetone falls well inside the correlation band, it is suspected that this deviation is caused by an error in the solubility measurements. The WB method in principle provides also ε/*k* values, but these seem to be rather inaccurate.

A third test is provided by the σ values, obtained by Goldman (22) by fitting a thermodynamic perturbation theory to experimental vapour pressure data. Figure 3 shows an excellent correlation between Goldman's σ and our σ(rec) values.

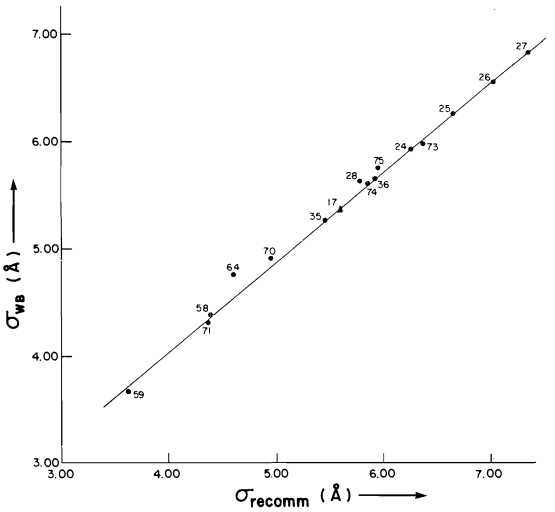

FIG. 2. Empirical correlation between the σ values based on noble gas solubility as given by Wilhelm and Battino (21) and the σ(rec) values of Tables 1, 2, and 6. σ(rec) values, based on determinate σ(visc) values are indicated by ▲; filled circles ● indicate σ(rec) values based on correlation techniques.

Whenever these test methods are used to *estimate* σ values, the problem of finding the corresponding ε/*k* value still remains. However, in these cases an accurate product $P(n)$ may be available, from which, in combination with the estimated σ value, the ε/*k* value can be abstracted (example: ethyl acetate).

Auxiliary Parameters

In all correlation techniques discussed above, critical constants are needed. Compilations of experimental critical constants are available (23–26). For molecules where such experimental data are not available, these can be calculated with good precision according to a method described by Curl and Pitzer (27). This method requires knowledge of the boiling temperature, the temperature at which the vapour pressure is 100 Torr and the density at some temperature below the boiling point, all of which data are usually easily accessible.

The TGS and MS methods require in addition knowledge of vapour pressures for the calculation of ω (and *x*). The potential parameters calculated according to TGS are not very sensitive to small (±5%) changes in ω. Therefore almost any source of vapour pressures (26, 28–32) at $T_r = 0.7$ is normally accurate enough as are values of ω estimated with the Edmister formula [13]. The situation is more complicated,

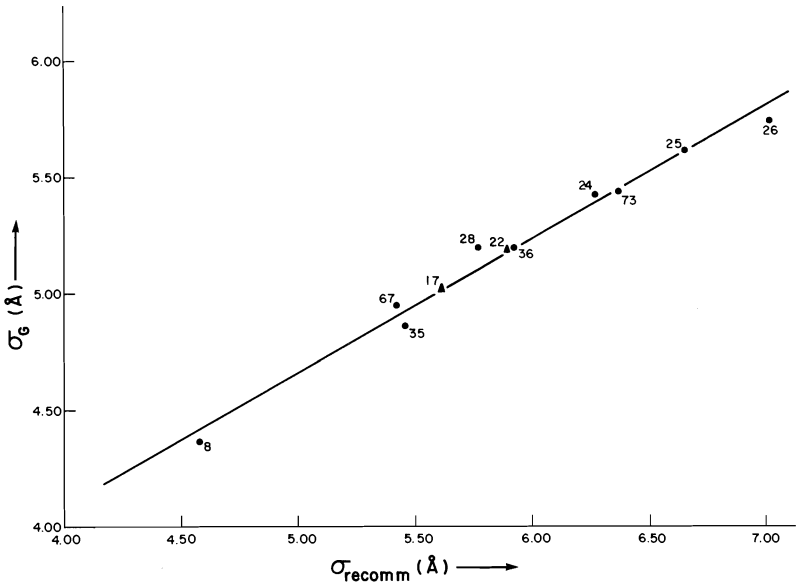

FIG. 3. Empirical correlation between the σ values of Goldman (22) and the σ(rec) values of Tables 1, 2, and 6. σ(rec) values based on determinate σ(visc) values are indicated by ▲; filled circles ● indicate σ(rec) values based on correlation techniques.

however, when the ω and x parameters of the MS method are to be determined. In their original paper, MS calculated Stockmayer parameters for 13 molecules for which, in their words, "reliable values of ω and x were available", without disclosing either their methods or their sources. In Table 5 we have listed the most recent values of ω and x used in other work of Stiel and co-workers. The fact that some of these values were revised several times reflects already the problems encountered when determining such parameters. With the above ω and x parameters we calculated σ and ε/k according to [15], but many of these were clearly unacceptable on the basis of the V_m^{25} or V_m^{b} test (example ethanal) or on the basis of a lacking consistency in homologous series (for example the σ(MS) for HBr and HCl). Partly because of the above we felt compelled to re-evaluate the ω,x method and to develop suitable criteria. Extensive trials have shown us that, in order to obtain reasonable σ and ε/k parameters through the MS method, one needs vapour pressures accurate to ±0.01 Torr (corresponding to a temperature accuracy of ±0.001°C), over an extended pressure range (normally between 0.1 and 2 atm) covering at least the $T_r = 0.6$ point but preferably also the $T_r = 0.7$ point. The requirement of highly accurate vapour pressure data is a direct result of the extreme sensitivity of σ and ε/k towards ω and x. In order to find the needed vapour pressures at reduced temperatures $T_r = 0.6$ and $T_r = 0.7$, it is necessary to fit experimental data into a vapour pressure equation. One of these is the Antoine equation [16]:

$$[16] \qquad \log_{10} P = A - \frac{B}{t + C}$$

Several compilations of Antoine parameters are available (28, 29, 31). The closeness of the data fit over the experimental range should be ±0.03% or less and the calculated critical pressure should be about 8% too low (33). If raw vapour pressure data were available, or if the Antoine equation was not adequate, we have successfully employed the following expression:

$$[17] \quad \log_{10} P = A - \frac{B}{T} + C \log T + DT$$

In our experience, [17] is at least equivalent in quality to the Antoine equation and in certain cases (such as alcohols) definitely superior; in addition, [17] is more easily adaptable to computerized least-squares fitting. Most of our own ω,x values (last two columns of Table 5) were obtained through the vapour pressure equation [17].

TABLE 6. Potential parameters σ and ε/k calculated by correlation techniques for some selected molecules

No.	Compound	μ*[2]	V_c[a] (cm^3)	T_c[a] (K)	P_c[a] (atm)	ω[c]	x[c]	σ (Å)	ε/k (K)
66	$Si(CH_3)_4$	0	372[b]	448.1[b]	26.9[b]	0.233[d]		6.167[m]	315.1[m]
67	c-C_5H_{10}	0	260	511.6	44.5	0.196[e]		5.423[m]	368.1[m]
68	CH_3I	0.48	173[b]	537.7[b]	71.7[b]	0.123[f]	0.005[f]	4.656[m]	405.5[m]
69	CH_2I_2	0.11	249[b]	756.1[b]	69.0[b]	0.185[g]	0.011[g]	5.327[m]	550.5[m]
70	$(CH_3)_2SO$	1.56	227[b]	754.1[b]	73.6[b]	0.263[h]	0.003[h]	4.940[o]	602.5[o]
71	CH_3NO_2	1.97	173	588	62.3	0.346[i]	0.038[i]	4.374[n]	527.4[n]
72	CH_3CN	2.70	173	548	47.7	0.320[j]	0.033[j]	4.374[n]	491.6[n]
73	p-Xylene	0	379	616.2	34.7	0.321[e]		6.371[m]	408.8[m]
74	C_6H_5Cl	0.25	308	632.4	44.6	0.249[k]	0.004[k]	5.856[m]	440.2[m]
75	$C_6H_5NO_2$	1.15	335[b]	758.3[b]	50.0[b]	0.270[l]	0.006[l]	5.95[p]	534[p]

[a]Taken from ref. 24, unless indicated otherwise. [b]Calculated by method of Curl and Pitzer (27). [c]Vapour pressures were fitted with [17] except where indicated otherwise. [d]$P(t)$ data from J. G. Aston *et al.* J. Am. Chem. Soc. 63, 2343 (1941). [e]From Antoine constants of ref. 28. [f]$P(t)$ data from ref. 29. [g]From Antoine constants of ref. 31. [h]From Antoine constants given by J. Heinrich and J. Surovy. Sb. Pr. Chem Fak. SVST. 207 (1966). [i]$P(t)$ data of McCullough; see ref. 30. [j]$P(t)$ data of Heim; see ref. 30. [k]$P(t)$ data of Zmackzymski; see ref. 30. [l]$P(t)$ data of Brown and of Maksimov; see ref. 30. [m]Calculated according to TGS method, eq. 12. [n]Calculated according to ST method, eq. 8; MS method rejected on the basis of V_m^{25} and WB tests. [o]Calculated according to MS method, eq. 15. [p]MS and ST methods rejected on the basis of V_m^{25} and WB tests; σ estimated from Figs. 1 and 2, ε/k calculated from product $\sigma^2\varepsilon^{1/2}$.

Some Further Applications

As mentioned above, for many molecules of interest no viscosity-based potential parameters are available at all. In such cases one has to rely exclusively on the correlation techniques as recommended in this paper. For some molecules, which were of particular interest to our nmr intermolecular interaction studies, we have thus calculated σ and ε/k values as given in Table 6.

Acknowledgement

The financial assistance of the National Research Council of Canada in the form of an operating grant (to F.R.) and an NRCC scholarship (to F.M.) is gratefully acknowledged.

1. (*a*) J. O. HIRSCHFELDER, C. F. CURTISS, and R. B. BIRD. Molecular theory of gases and liquids. 2nd ed. John Wiley and Sons Inc., New York, NY. 1964; (*b*) Chapt. 3; (*c*) Chapt. 8.4; (*d*) Chapt. 4.7; (*e*) pp. 222–223; (*f*) pp. 1110–1112 and pp. 1212–1214.
2. F. H. A. RUMMENS and F. M. MOURITS. Can. J. Chem. This issue.
3. J. R. JOHNSON and P. T. EUBANK. Ind. Eng. Chem. Fundam. **12**, 156 (1973).
4. (*a*) R. C. REID and T. K. SHERWOOD. The properties of gases and liquids. 2nd ed. McGraw-Hill Book Company, New York, NY. 1966. pp. 38–42; (*b*) Appendix A.
5. S. K. KIM and J. ROSS. J. Chem. Phys. **46**, 818 (1967).
6. D. REICHENBERG. AIChE J. **19**, 854 (1973).
7. E. A. HALKIADAKIS and R. G. BOWREY. Chem. Eng. Sci. **30**, 53 (1975).
8. F. H. A. RUMMENS, W. T. RAYNES, and H. J. BERNSTEIN. J. Phys. Chem. **72**, 2111 (1968).
9. E. U. FRANCK. Landolt-Börnstein. Physikalisch-Chemische Tabellen. Vol. 1, Part 1. 6th ed. Springer Verlag, Heidelberg. 1950.
10. L. W. FLYNN and G. THODOS. AIChE J. **8**, 362 (1962).
11. R. A. SVEHLA. NASA Technical Report R-132. 1962.
12. L. S. TEE, S. GOTOH, and W. E. STEWART. Ind. Eng. Chem. Fundamentals, **5**, 356 (1966).
13. K. N. LINAKIS and R. G. BOWREY. Aust. Chem. Eng. **14**, 3 (1973).
14. L. MONSCHICK and E. A. MASON. J. Chem. Phys. **35**, 1676 (1961).
15. G. C. MAITLAND and E. B. SMITH. J. Chem. Eng. Data, **17**, 150 (1972).
16. M. KLEIN and H. J. M. HANLEY. Trans. Faraday Soc. **64**, 2927 (1968).
17. L. I. STIEL and G. THODOS. J. Chem. Eng. Data, **7**, 234 (1962).
18. L. I. STIEL and G. THODOS. AIChE J. **10**, 266 (1964).
19. W. C. EDMISTER. Pet. Refiner, **37**, 173 (1958).
20. K. R. MALEK and L. I. STIEL. Can. J. Chem. Eng. **50**, 491 (1972).
21. E. WILHELM and R. BATTINO. J. Chem. Phys. **55**, 4012 (1971).
22. S. GOLDMAN. J. Phys. Chem. **80**, 1697 (1976).
23. J. F. MATHEWS. Chem. Rev. **72**, 71 (1972).
24. A. P. KUDCHADKER, G. H. ALANI, and B. J. ZWOLINSKI. Chem. Rev. **68**, 659 (1967).
25. K. A. KOBE and R. E. LYNN. Chem. Rev. **52**, 117 (1953).
26. D. G. EDWARDS. Vapour pressures of 30 inorganic liquids between one atmosphere and the critical point. University of California Radiation Laboratory (Livermore, California). Technical Report UCRL-7167 (Rev. 1). 1964.
27. R. F. CURL and K. S. PITZER. Ind. Eng. Chem. **50**, 265 (1958).
28. Selected values of properties of hydrocarbons and related compounds. American Petroleum Institute Research Project 44. Thermodynamics Research Centre, Department of Chemistry, Texas A & M University, College Station, TX.
29. T. BOUBLIK and K. AIM. Coll. Czech. Chem. Commun. **37**, 3513 (1972).
30. J. TIMMERMANS. Physico-chemical constants of pure organic compounds. Vol. 1 (1950) and Vol. 2 (1965). Elsevier Publ. Cie. New York, NY.
31. Advances in chemistry; physical properties of chemical compounds. Vol. 15 (1955), Vol. 22 (1959), and Vol. 29 (1962). The American Chemical Society, Washington, DC.
32. D. R. STULL. Ind. Eng. Chem. **39**, 517 (1947).
33. G. W. THOMSON. Chem. Eng. Progr. **45**, 153 (1949).

Intermolecular interactions in nuclear magnetic resonance. XI. The ^{13}C and proton medium shifts of CH_4 in the gas phase and in solution

FRANS H. A. RUMMENS AND FRANK M. MOURITS

Department of Chemistry, University of Regina, Regina, Sask., Canada S4S 0A2

Received September 23, 1976[1]

FRANS H. A. RUMMENS and FRANK M. MOURITS. Can. J. Chem. **55**, 3021 (1977).

The ^1H and ^{13}C resonances of methane have been measured at 298 K, both as pure CH_4 in the gas phase as function of the density as well as at low concentration in solution, using polar, non polar, isotropic, as well as magnetically anisotropic solvents. It is found that both the gas and the solution proton shift data can be readily understood in terms of the Van der Waals shielding σ_w and the mean-square field due to the dispersive interactions: $\sigma_w = -B\overline{F^2}$. Either a macroscopic reaction field model or a binary collision statistical mechanical model for $\overline{F^2}$ can be used with an approximately equal degree of success. Whereas the ^{13}C gas phase shifts of CH_4 are also proportional to the density, the ^{13}C gas-to-solution shifts indicate that, apart from σ_w, there exists even in non-polar isotropic solvents another effect which is not proportional to $\overline{F^2}$. The present study also includes a new proposal regarding $\overline{F^2}$, a discussion of anisotropy shielding σ_a in magnetically anisotropic solvents and a discussion of the effective B parameters (^1H and ^{13}C) of CH_4 in the gas and the solution state.

FRANS H. A. RUMMENS et FRANK M. MOURITS. Can. J. Chem. **55**, 3021 (1977).

On a mesuré les résonances de ^1H et ^{13}C du méthane à 298 K sous forme de CH_4 pur en phase gazeuse en fonction de la densité ainsi qu'à faible concentration en solution utilisant des solvants polaires, non-polaires, isotropes aussi bien que magnétiquement anisotropes. On a trouvé que les données de déplacement chimique des protons pour le gaz et les solutions peuvent être facilement expliquées en termes du blindage de Van der Waals σ_w et du moyen du carré du champ dû à des interactions dispersives: $\sigma_w = -B\overline{F^2}$. On peut utiliser soit un modèle de champ de réactions macroscopiques ou un modèle de méchanique statistique par collision binaire pour $\overline{F^2}$ et l'on a alors des chances approximativement égales de succès. Alors que les déplacements ^{13}C en phase gazeuse du CH_4 sont aussi proportionnels à la densité, les déplacements de ^{13}C qui se produisent lorsque l'on passe du gaz vers des solutions indiquent qu'il existe, en plus de σ_w, même dans des solvants isotropes non-polaires, un autre effet qui n'est pas proportionnel à $\overline{F^2}$. L'étude actuelle inclut aussi une nouvelle proposition concernant $\overline{F^2}$ soit une discussion du blindage anisotropique σ_a dans des solvants magnétiquement anisotropes et une discussion des paramètres B effectifs (^1H et ^{13}C) du CH_4 à l'état gazeux et en solution.

[Traduit par le journal]

Introduction

Solvent effect studies on nmr shifts have been studied hitherto mostly by proton spectroscopy. In view of the recent tremendous expansion of ^{13}C nmr it is surprising that very few ^{13}C solvent studies have appeared (for brief reviews see ref. 1 and the literature cited in ref. 2 therein). Apart from very recent work by Tiffon and Doucet (2) on ^{13}C gas-to-liquid shifts of *n*-pentane and by Cans *et al.* (3) on the ^{13}C solution shifts of a number of olefins, no other systematic study seems to have been undertaken. This situation appears precarious, because ^{13}C solvent shifts can now be estimated as being of very considerable magnitude; lack of knowledge of these effects can well precipitate errors of interpretation in general ^{13}C work. It was decided to study the medium shift effects of CH_4 to help fill in the aforementioned gap. Methane was chosen for several specific reasons. Firstly, it allows a study in the gas phase as function of density as well as in the liquid phase as gas-to-solution shifts. Secondly, the carbon being at the centre of mass, the site factor complications (ref. 4; see also pp. 46–50 of ref. 1 for a further discussion of this effect) are eliminated for the ^{13}C shifts. Finally, by measuring at the same time the proton shifts, a comparison between nuclear species would be feasible.

In general one can write for the shielding of a molecule in a medium:

$$[1] \quad \sigma = \sigma_0 + \sigma_b + \sigma_w + \sigma_a + \sigma_{E^2} + \sigma_{Ez} + \ldots$$

where the symbols have their usual meaning (5).

[1]Publication was delayed at the author's request.

The medium shift can be defined as $\sigma_m = \sigma - \sigma_0 - \sigma_b$; σ_m then contains exclusively the intermolecular effects. Since CH_4 is non polar, the reaction field term σ_{Ez} will be taken as zero. In addition the term σ_{E^2}, the direct field effect of polar solvents will also be taken as zero, since it has been estimated (6) that this effect, if it exists at all, is negligible in comparison to σ_w, at least for non polar solutes. For the Van der Waals term σ_w, most present theories start with Stephen's proposal (7) that σ_w is proportional to the mean-square electric field due to the spontaneous moments; $\sigma_w = -B\overline{F^2}$. Of these only the binary collision statistical mechanical model of Raynes, Buckingham, and Bernstein (abbreviated RBB) (5) and the macroscopic reaction field model of Rummens (6) have shown quantitative promise. In the latter model one has:

$$[2] \quad \sigma_w = -\frac{6KB\alpha_1 I_1}{a^6}\left(\frac{n_2^2 - 1}{2n_2^2 + 1}\right)^2 \frac{1}{(1 - q^2)^3}$$

The cavity radius a can be estimated from $a^3 = 3V_1/4\pi N_A$ but this has been shown (6) to be a poor approximation. Using proton shifts, Rummens has used the above model in reverse to determine the cavity radius; with a value of $KB(^1H) = 4.71 \times 10^{-18}$ esu he found $a^3(CH_4) = 13.9 \times 10^{-24}$ cm^3.[2] The site factor $(1 - q^2)^{-3}$ contains the parameter q which is defined as $q = d/r_{12}$, d being the distance from nuclear site to the centre of mass of the solute while $r_{12} = r_1 + r_2$, r_1 and r_2 being molecular radii. For ^{13}C of CH_4, $d = 0$ and therefore the site factor is unity. The parameter B is certainly much larger for ^{13}C than for ^1H; the parameter K contains only model approximations and can be expected to be independent of the nuclear species investigated. Following [2] one has therefore

$$[3] \quad \frac{\sigma_w(CH_4) \times (1 - q_H^2)^3}{\sigma_w(CH_4)} = \frac{B(^1H)}{B(^{13}C)}$$

In the virial model of RBB, and allowing only binary interactions, one has (5)

$$[4] \quad \sigma_w = \frac{\sigma_{1w}}{V} = \frac{1}{V}\int (\sigma_w)\text{pair} \exp(-u/kT)\, d\tau$$

where u is the intermolecular potential, for which the Lennard–Jones (6–12) potential is conveniently chosen:

$$[5] \quad u = 4\varepsilon\left\{\left(\frac{r_0}{r}\right)^{12} - \left(\frac{r_0}{r}\right)^6\right\}$$

The same authors (5) took as mean-square field on the solute the field of a (solvent) molecule at distance r

$$[6] \quad \overline{F}^2(\text{RBB}) = \frac{3\alpha_2 I_2}{r^6}$$

Rummens *et al.* (4, 8) introduced a site factor, which in the integrated form of [4] is given by

$$[7] \quad S_6^g = 1 + 5q_0^2\frac{\mathscr{H}_8(y)}{\mathscr{H}_6(y)} + 14q_0^4\frac{\mathscr{H}_{10}(y)}{\mathscr{H}_6(y)} + 30q_0^6\frac{\mathscr{H}_{12}(y)}{\mathscr{H}_6(y)} + 55q_0^8\frac{\mathscr{H}_{14}(y)}{\mathscr{H}_6(y)} \ldots$$

where $q_0 = d/r_0$. Using (σ_w) pair $= -B\overline{F^2}$, [4] combined with [5] and [6] becomes

$$[8] \quad \sigma_w = \frac{-\pi K_6^g B N_A \alpha_2 I_2}{r_0^3 V_2 y^4}\mathscr{H}_6(y) S_6^g$$

where $y = 2(\varepsilon/kT)^{1/2}$ and $\mathscr{H}_6(y)$ is an integral whose numerical values are known (9). For gas-phase work $K_6^g = 1$ by definition. A value of $K_6^g = 1.46 + 0.0064t$ has been proposed (8) for gas-to-liquid shifts. Apparently σ_w in liquids or in high pressure gases can be understood in terms of an *effective* binary collision, higher order collision contributions being apparently proportional to the binary effect. In this interpretation K_6^g represents this proportionality constant; its value should be independent of nuclear species. Analogous to [3], this model therefore predicts that

$$[9] \quad \frac{\sigma_w(CH_4)/S_6^g(H)}{\sigma_w(CH_4)} = \frac{B(^1H)}{B(^{13}C)}$$

Theory

A modification in the use of the binary collision model will be discussed here. It concerns the mean-square field $\overline{F^2}$, several criticisms having been made recently (ref. 1, pp 41–42) regarding the approach of [6]. At the rather short distances of interest (σ_w is nearly entirely determined by the nearest neighbors), it would seem that solute and solvent molecule would interact and that therefore a field in empty space would not be adequate For the dispersion energy ϕ^{disp} of two

[2]The value $a^3 = 34.3$ given in ref. 6 is in error; also the $(r_{01}/2)^3$ value quoted should read 6.80×10^{-24} cm.

molecules one may write;

$$[10] \qquad \phi^{disp} = -\frac{3\alpha_1\alpha_2 I_1 I_2}{2r^6(I_1 + I_2)}$$

This follows from the Drude model, but the same result can be obtained by London's perturbational method (10) or by variational methods (11, 12).

The energy of a polarizable particle in an electric field being $-\alpha E^2/2$, one has for a system of two particles in each other's mean-square field:

$$[11] \qquad \phi^{pol} = -\tfrac{1}{2}\alpha_1\overline{F^2}_{1(2)} - \tfrac{1}{2}\alpha_2\overline{F^2}_{2(1)}$$

where $F_{i(j)}$ is the field at i, caused by j. Equating [10] and [11], one has as a possible solution:

$$[12] \qquad \overline{F^2}_{1(2)} = \frac{3\alpha_2 I_1 I_2}{2r^6(I_1 + I_2)}$$

together with a similar expression for $\overline{F^2}_{2(1)}$.

For σ_w this results in:

$$[13] \qquad \sigma_w = \frac{-\pi N_A K_6{}^g B\alpha_2 I_1 I_2}{2r_0{}^3 V_2(I_1 + I_2)y^4}\mathscr{H}_6(y)S_6{}^g$$

Comparing [12] and [6] one notes that I_2 has been replaced by $I_1I_2/2(I_1 + I_2)$, so that even if the ionization potentials are equal, [12] gives a 4× smaller field and therefore a 4× smaller σ_w.

Many approximations were made in the derivation of the London dispersion energy, given by [10]. One may well wonder if its use is justified. Hirschfelder *et al.* (16) compared the sum of the first three terms in the dispersion energy with the r^{-6} coefficient in the Lennard–Jones potential as determined from viscosity and found that the latter coefficients were between 1.5 and 2.0 times larger. However, if one compares the r^{-6} coefficients of [10] with the results of other quantum-mechanical calculations, such as the variational methods of Slater and Kirkwood (11) and Buckingham (12), the uncoupled Hartree–Fock calculations of Karplus and Kolker (13) or the coupled version of Dalgarno and Victor (14), one can generally see a reasonable agreement. As Dalgarno and Davison have pointed out (15), one should not compare the r^{-6} coefficients based on viscosities, because the viscosity data are usually obtained at temperatures where the short-range repulsion forces play a significant role. One should extrapolate these viscosity data to absolute zero in order to get correct results. Atomic beam small-angle scattering at thermal energies is potentially the most valuable source of information about long-range forces. The few results obtained so far agree well with the above mentioned calculations (15). Bell (17) has calculated the r^{-6} coefficients for a number of gases, using a semi-empirical method which can be considered the best available. His results are somewhat larger than those of [10], but only about 5 to 20%. Thus, we have decided to adopt [10] because of its general applicability and its relatively good accuracy. As a corollary, [12] then must also be assumed correct, but this can be checked in an independent manner. If one takes the r^{-6} coefficient of $\sigma_w = -B\overline{F^2}$ with $\overline{F^2}$ as *per* [6] and equate this to the r^{-6} coefficient of σ_w for two interacting H atoms, as calculated by Marshall and Pople (18), one arrives at $B = 0.20 \times 10^{-18}$ esu for an H atom, in poor agreement with $B = 0.74 \times 10^{-18}$ esu for an H atom in an electric field, as calculated also by Marshall and Pople (19). However, if [12] is used rather than [6] then a value of $B = 0.80 \times 10^{-18}$ esu emerges, which shows a very good correspondence with the direct calculation of an H-atom in a field. In addition it has also been established empirically by Mohanty and Bernstein in their ^{19}F gas phase work (20) and by Rummens and De Meyer (ref. 1, p. 45) on gas-to-liquid shifts of $X(Me)_4$ that a form $I_1I_2/(I_1 + I_2)$ or, what is almost the same, $\sqrt{I_1I_2}$, gives much better coherence of σ_w data than does I_2 alone. Also a considerable improvement in constancy of B (though not enough) would be obtained if the data of Jameson *et al.* on ^{129}Xe in various solvent gases (21) would be treated according to [12] rather than [6].

The replacement of [6] by [12] has an effect that all B parameters obtained from gas phase studies would have to be recalculated; they will all become larger by a factor close to 4.

Experimental and Calculational Details

The ^1H and ^{13}C spectra were recorded on a Bruker HX-90 spectrometer by pulse Fourier transform techniques, using a ^{19}F field lock. Hexafluoroacetone – 1.6 D_2O (HFA) in a separate capillary was employed as the locking compound. The CH_4 proton resonance frequencies were derived directly from the offset frequency and from the spectral width employed. The ^{13}C resonance frequencies of $^{13}CH_4$ were measured relative to the ^{13}C resonance of HFA. The ^{13}C spectra were narrow-band proton decoupled. The probe temperature was maintained at 298 ± 0.5 K for all spectra. The CH_4 used for all gas phase measurements was supplied by Matheson of Canada, Ltd. (ultra high purity, CH_4 > 99.95%); for the

solution measurements, enriched $^{13}CH_4$ was used, supplied by Merck, Sharp and Dohme Canada, Ltd. (90 at.% ^{13}C). The various solvents were high purity chemical reagents, used without further purifications. A single nmr tube was used for all experiments. Its design followed closely that of Mohanty and Bernstein (20). A 5 mm od medium wall nmr tube (Wilmad Glass Co. Inc. #524-PP) was used, the open end of which was joined to the glass body of a Fischer and Porter Teflon valve, the side arm of the latter having been removed. The original Teflon valve was replaced by a modified valve which has an axial hole for the passage of the gas and a top designed to fit a 10/30 female glass joint on the vacuum system. A capillary (1.5 mm o.d.) containing the lock and reference compound HFA was placed in the nmr tube before the latter's assemblage; it was permanently centered by two Teflon washers. Tests have shown us that this kind of tube assembly can withstand pressures of over 100 atm. Alignment of the tube assembly on a precision lathe was found to be necessary in order that it will spin smoothly.

In order to enable the calculation of the CH_4 density in the nmr tube, a gas transfer system, which included a Toepler pump, was constructed. The design and operation of such systems have been described by Meinzer (22) and by Mohanty and Bernstein (20). Once all volumes concerned (nmr tube, Toepler pump, and manifold line) were calibrated, the amount of gas transferred could be calculated from its pV product.

The proton gas phase spectra of CH_4 were recorded on samples ranging in density from 1.5 mg cm^{-3} to 35 mg cm^{-3} (*i.e.* 2.4–53 atm). Below 2.4 atm the proton resonance line became too broad (because of spin–rotation relaxation) to be accurately measured. The corresponding ^{13}C spectra (of the natural abundancy CH_4) in the gas phase were recorded in the density range 5.9–35 mg cm^{-3}, the lower limit being determined by the low signal strength. The accuracy of the calculated gas densities was checked gravimetrically and found to be within 0.1%. The limits of error of the chemical shift measurements were ± 0.5 Hz for ^1H and ± 1.2 Hz for ^{13}C. For the gas-to-solution measurements the ^1H and ^{13}C shifts of $^{13}CH_4$ (90%) were determined in 18 solvents, which are listed in Table 1. The preparation of these samples was similar to the method described by Rummens and Louman (23); the solvent is brought into the nmr tube; it is then degassed by several freeze–pump–thaw cycles, followed by condensing an amount, equivalent to a pressure of 5 atm at 298 K, of $^{13}CH_4$ into the tube. The $^{12}CH_4$ proton resonance frequency was found by taking the center of the recorded doublet of the $^{13}CH_4$ and correcting this value for the isotope effect of 0.002 ppm. (This technique is more accurate than using the weak central line due to the 10% $^{12}CH_4$.)

The chemical shifts of CH_4 in the gas phase were found to be linear to the density, both for ^1H and ^{13}C. Extrapolation to $\rho = 0$ gave the values of $\sigma_0(^1H)$ and $\sigma_0(^{13}C)$, while the slopes provided the parameters $\sigma_1(^1H)/M$ and $\sigma_1(^{13}C)/M$, respectively.

Table 1 lists the physical properties used in the calculation of the medium shifts. All temperature dependent parameters were calculated at the temperature of the experiment. In the calculation of the site factors $d = 1.09$ Å was taken. Values of r_1 of CH_4 of $r_1 = 2.442$ Å for CH_4 (obtained by extrapolation on a plot of $V^{1/3}$ *vs.* r_0 for the halomethanes)[3] and r_2 (Å) = [0.293 V_2 (ml)]$^{1/3}$ (8) were used in the calculation of $q = d/r_1 + r_2$). The r_0 and ε/k parameters used have been given in the foregoing paper (31). Mixing rules (32) ($r_0^{(12)} = (r_0^{(1)} + r_0^{(2)})/2$ and $\varepsilon_{12} = \sqrt{\varepsilon_1\varepsilon_2}$ were used. A Hewlett Packard model 97 calculator was used for all calculations.

Results and Discussion

Gas Phase Measurements

Both for ^1H and ^{13}C the medium shift was found to be proportional to the density ρ. The results are given in Table 2. The experimental σ_1 value for $^1H(CH_4)$ compares well with earlier data (ref. 1, p. 34). The ratio $B(^{13}C)/B(^1H)$ is equal to 52 according to Table 2. This is reasonably close to similar ratios $B(Ne)/B(He)$ of 75 and 25 as calculated by Jameson *et al.* (21) and Kromhout and Linder (24), respectively. The large value for $B(^{13}C)$ indicates that σ_w is likely dominated by the paramagnetic shielding term.

Gas-to-solution Measurements

Table 3 gives the zero-pressure gas-to-solution shifts. The proton data can be compared with those at 30°C of Buckingham *et al.* (25). In general there is reasonable agreement, although there are sizeable differences. This is due in part to our extrapolation to zero gas pressure (in (25) a 10 atm CH_4 sample was used as the zero point) and to better χ_m data in the present study. Differences remain even after these corrections; our present results indicate σ_m values which are still 0.01 to 0.06 ppm larger. This systematic difference could be due to the lower probe temperature (25°C) of the present study.

A plot of $-\sigma_m(H)$ for 'isotropic' solvents vs. $(n^2 - 1)^2/(2n^2 + 1)^2(1 - q^2)^3$ for the proton data is given in Fig. 1. An unbiased least-squares straight line fit gave an intercept well below the standard deviation limit; a best straight line forced through the origin resulted in a slope of 8.05 ppm which is slightly different from a similar slope published earlier (6); this new slope value is henceforth adopted. A similar plot of $-\sigma_m(H)$ *vs.* $\sigma_w/K_6{}^gB$ of [13] gives also a reasonable straight line through the origin (see Fig. 2) although with somewhat larger scatter. However, if the binary collision model is subsequently used to extract σ_a values for the anisotropic solvents (by taking the difference of the experimental σ_m

[3]This value is different from the earlier used $r_1 = 2.068$ (6) because of re-calibration using better r_0 values (28).

TABLE 1. Physical properties of solvent and solute molecules

	No.	M	Density (g/cm^3)	n_D	$-\chi_m \times 10^6$ (esu)[j]	$\alpha \times 10^{24}$ (cm^3)[q]	$I \times 10^{12}$ (erg)[r]	μ (D)[x,y]
CH_4	1	16.04			17.4[k]	2.60[k]	20.58	0
TMS	2	88.23	$0.6687 - 1.12 \times 10^{-3}t$[e]	$1.3710 - 0.62 \times 10^{-3}t$[c,e]	74.85[l,m]	11.91	16.00[s,t]	0
c-C_5H_{10}	3	70.14	$0.76509 - 0.98 \times 10^{-3}t$[a,b,d]	$1.41753 - 0.56 \times 10^{-3}t$[a,b,d]	59.18	9.17	16.87	0
c-C_6H_{12}	4	84.16	$0.79686 - 0.92 \times 10^{-3}t$[a,b,d]	$1.43690 - 0.53 \times 10^{-3}t$[a,b,d]	66.09	10.99	15.83	0
CCl_4	5	153.82	$1.63258 - 1.93 \times 10^{-3}t$[a]	$1.47167 - 0.57 \times 10^{-3}t$[a]	66.60	10.49	18.38	0
$CHCl_3$	6	119.38	$1.52641 - 1.86 \times 10^{-3}t$[a,b]	$1.45652 - 0.54 \times 10^{-3}t$[a,b,c]	59.30	8.47	18.30	1.03
CH_3I	7	141.94	$2.33503 - 2.801 \times 10^{-3}t$[a,b]	$1.5464 - 0.76 \times 10^{-3}t$[a,b,c]	57.2[n]	7.64	15.29	1.65
CH_2I_2	8	267.84	$3.37279 - 2.59 \times 10^{-3}t$[a,b,h,i]	$1.7536 - 0.36 \times 10^{-3}t$[a,b,c,h]	93.10	12.91	14.96[w]	1.10[z]
CS_2	9	76.14	$1.29276 - 1.48 \times 10^{-3}t$[a]	$1.6443 - 0.82 \times 10^{-3}t$[a,b,c]	42.29[k]	8.48	16.15[u]	0
Ethyl ether	10	74.12	$0.73662 - 1.16 \times 10^{-3}t$[a,d]	$1.36459 - 0.60 \times 10^{-3}t$[a,d]	55.10	8.92	15.34	1.15
Ethyl acetate	11	88.11	$0.92485 - 1.21 \times 10^{-3}t$[a]	$1.3818 - 0.47 \times 10^{-3}t$[a,c]	54.10	8.83	16.20	1.78
DMSO	12	78.13	$1.1178 - 0.90 \times 10^{-3}t$[a,f,g]	$1.48858 - 0.48 \times 10^{-3}t$[f,g]	44.35[o,p]	7.98	14.74[v]	3.96
Acetone	13	58.08	$0.81251 - 1.10 \times 10^{-3}t$[a,d]	$1.36957 - 0.53 \times 10^{-3}t$[a,d]	33.80	6.41	15.52	2.91
CH_3NO_2	14	61.04	$1.16482 - 1.35 \times 10^{-3}t$[a,c]	$1.39099 - 0.455 \times 10^{-3}t$[a,c]	20.92[k]	4.95	17.83	3.46
CH_3CN	15	41.05	$0.80376 - 1.08 \times 10^{-3}t$[a]	$1.35275 - 0.45 \times 10^{-3}t$[a,b,c]	27.6[k]	4.41	19.55	3.92
C_6H_6	16	78.11	$0.90009 - 1.058 \times 10^{-3}t$[a,d]	$1.51393 - 0.64 \times 10^{-3}t$[a,b,d]	54.75	10.38	14.81	0
p-Xylene	17	106.17	$0.87840 - 0.868 \times 10^{-3}t$[a,b,d]	$1.50654 - 0.54 \times 10^{-3}t$[a,b,d]	76.78	14.27	13.53	0
C_6H_5Cl	18	112.56	$1.2753 - 1.06 \times 10^{-3}t$[a]	$1.53582 - 0.56 \times 10^{-3}t$[a]	69.60	12.35	14.53	1.69
$C_6H_5NO_2$	19	123.11	$1.22305 - 0.99 \times 10^{-3}t$[a,b]	$1.56138 - 0.45 \times 10^{-3}t$[a,b]	61.80	12.97	15.89	4.22

[a]J. Timmermans. Physico-chemical constants of pure organic compounds. Elsevier, New York, NY. Vol. 1. 1950 and Vol. 2. 1965. [b]Physical properties of chemical compounds. Advances in chemistry series. The American Chemical Society, Washington, DC. Vol. 29, 1961; Vol. 22, 1959; Vol. 15, 1955. [c]Beilstein, Handbuch der Chemie. Third and Fourth Supplement. [d]American Petroleum Institute Research Project 44. [e]Gmelin. Teil C, Silicium. 1958. [f]H. L. Schlaefer and W. Schaffernicht. Angew. Chem. 17, 618 (1960). [g]J. Heinrich and J. Surovy. Sb. Pr. Chem. Fak. SVST, 207 (1966). [h]R. Grzeskowiak, G. H. Jeffery, and A. I. Vogel. J. Chem. Soc. 4728 (1960). [i]V. Griffing, M.A. Cargyle, L. Corvese, and D. Eby J. Phys. Chem. **58**, 1054 (1954). [j]S. Broersma. J. Chem. Phys. **17**, 873 (1949). [k]Landolt- Börnstein. Zahlenwerte and Functionen. Vol. 2, 1967. [l]E. W. Abel, R. P. Bush, C. R. Jenkins, and T. Zobel. Trans. Faraday Soc. **60**, 1214 (1964). [m]M. W. Lister and R. Sarson. Can. J. Chem. **42**, 2104 (1964). [n]J. R. Lacker. J. Am. Chem. Soc. **69**, 2067 (1947). [o]G. Robinet, P. Dagnac-Amans, and J. F. Labarre. J. Chim. Phys. Physiochim. Biol. **66**, 63 (1969). [p]M. B. Kennedy, M. W. Lister, R. Marson, and R. B. Poyntz. Can. J. Chem. **51**, 674 (1973). [q]Calculated at 298 K from the Lorentz-Lorenz equation. [r]U.S. National Bureau of Standards. NSRDS-NBS 26 (1969). [s]G. G. Hess, F. W. Lampe, and L. H. Sommer. J. Am. Chem. Soc. **87**, 5327 (1965). [t]D. I. MacLean and R. E. Sacker. J. Organometal. Chem. **74**, 197 (1974). [u]Y. Tanaka, A. S. Jursa, and F. J. LeBlanc. J. Chem. Phys. **32**, 1199 (1960). [v]G. Distefano, A. Foffani, G. Innorta, and S. Pignataro. Int. J. Mass Spectrom. Ion Phys. **7**, 383 (1971). [w]K. Watanabe, T. Nakayama, and J. Mottl. U.S. Dept. Com. Office Tech. Serv. PB Rept. **158**, 317 (1963). [x]Landolt-Börnstein. New series. Group II, Vol. 4 (1967) and Vol. 6 (1974). [y]U.S. National Bureau of Standards. NSRDS-NBS 10 (1967). [z]A. L. McClellan. Tables experimental dipole moments. W. H. Freeman, London. 1963.

TABLE 2. Proton and ^{13}C medium shift of CH_4 in the gas phase at 25°C

Nucleus	σ_1 (exptl) (ppm cm^3 mol^{-1})	σ_{1w}	$B \times 10^{18}$ (esu) Eq. 13	$B \times 10^{18}$ (esu) Eq. 8
^1H	− 42.6 ± 1.6	− 6.1 ± 1.6	1.68 ± 0.44	0.42 ± 0.11
^{13}C	−276 ± 13	−239 ± 13	88.1 ± 4.9	22.0 ± 1.2

TABLE 3. Proton and ^{13}C gas-to-solution shifts of CH_4 at 24°C, corrected for susceptibility

Solvent	No.	$-\sigma_m$ (H)exptl (ppm)	$\frac{-\sigma_m + \sigma_a}{S_{con}}$	$\frac{-\sigma_m + \sigma_a}{S_6{}^g}$	$-\sigma_m$ (^{13}C)exptl (ppm)	$-\sigma_m + \sigma_a$
TMS	2	0.266	0.239	0.225	6.192	6.192
c-C_5H_{10}	3	0.276	0.244	0.227	5.860	5.860
c-C_6H_{12}	4	0.330	0.294	0.276	6.058	6.058
CCl_4	5	0.476	0.422	0.395	7.890	7.890
$CHCl_3$	6	0.435	0.383	0.355	7.625	7.625
CH_3I	7	0.543	0.471	0.431	8.979	8.979
CH_2I_2	8	0.781	0.686	0.636	12.096	12.096
CS_2	9	0.584	0.506	0.461	8.189	8.189
Et_2O	10	0.293	0.261	0.243	5.743	5.743
MeCOOEt	11	0.275	0.244	0.229	5.911	5.911
DMSO	12	0.474	0.414	0.381	8.887	8.887
Acetone	13	0.216	0.259	0.234	6.158	6.238
CH_3NO_2	14	0.240	0.284	0.257	5.386	5.476
CH_3CN	15	0.427	0.243	0.220	6.237	6.092
C_6H_6	16	−0.127	0.413	0.386	6.641	7.236
p-$C_6H_4(CH_3)_2$	17	−0.012	0.408	0.389	6.573	7.040
C_6H_5Cl	18	−0.015	0.439	0.414	6.929	7.438
$C_6H_5NO_2$	19	−0.225	0.470	0.444	6.340	7.093

values and σ_w contributions calculated on the basis of the straight line of Fig. 2), quite unacceptable values for σ_a result (see column 3 of Table 4). The σ_a values for acetone, acetonitrile, and nitromethane seem much too high, the one for acetonitrile even having the wrong sign, whereas those for the aromatics appear unrealistically low. The aberrations appear outside the limit of the errors due to uncertainties in r_0 and ε/k, but no alternate explanation can be offered. Because of this we have used the σ_a data based on [2] and the best straight line of Fig. 1; they are given in column 2 of Table 4.

The $\sigma_m(^{13}C)$ data were corrected, using this newly adopted set of σ_a values, (note that the site effect for σ_a is unity for spherical solutes (26, 27), independent of nuclear species) and subsequently tested against the expressions of [2] and [13]. As Figs. 3 and 4 indicate, neither of these plots goes through the origin while in addition the scatter is very large. The possibility of model or parameter errors can be eliminated by plotting $(\sigma_m - \sigma_a)$ for ^{13}C against $(\sigma_m - \sigma_a)$ or $(\sigma_m - \sigma_a)/S_{con}$ for ^1H. As [9] and [3] indicate this should result in perfect straight lines through the origin with a scatter no larger than that due to experimental error (note that $S_6{}^g$ and S_{con} are close to unity in this particular case). As Fig. 5 shows, however, this is not the case at all (using S_{con} rather than $S_g{}^6$ results in an almost identical plot). This can only mean that $\sigma_w = B\overline{F^2}$ is not a sufficient basis for the Van der Waals shifts of

TABLE 4. Neighbour anisotropy shifts σ_a, determined as the vertical deviation from the best straight line of Figs. 1 and 2

Solvent	σ_a (ppm) From Fig. 1	σ_a (ppm) From Fig. 2
C_6H_6	0.595	0.515
C_6H_5Cl	0.509	0.368
$C_6H_5NO_2$	0.753	0.619
p-Xylene	0.467	0.278
Acetone	0.080	0.212
CH_3NO_2	0.090	0.317
CH_3CN	−0.144	0.096

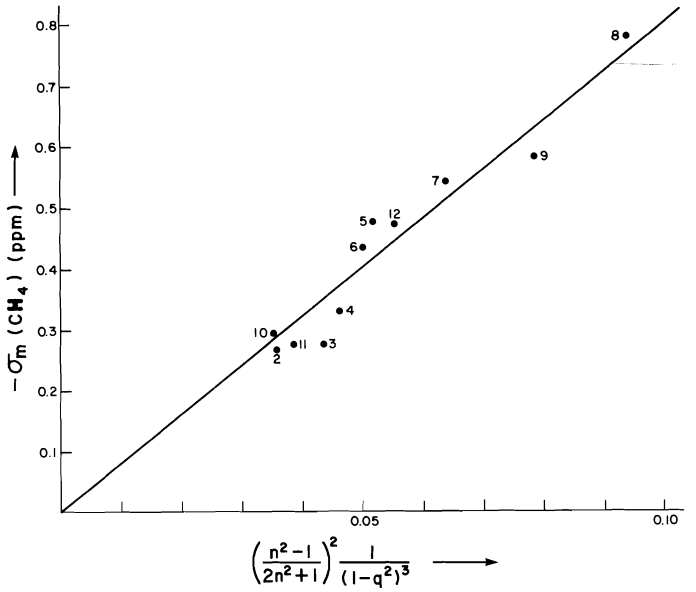

FIG. 1. Proton gas-to-solution shifts at 25°C of CH_4 corrected for σ_b, plotted against $f(n,q)$ of [2] for isotropic solvents. Slope of solid line is 8.05 ppm; standard deviation is ±0.045 ppm.

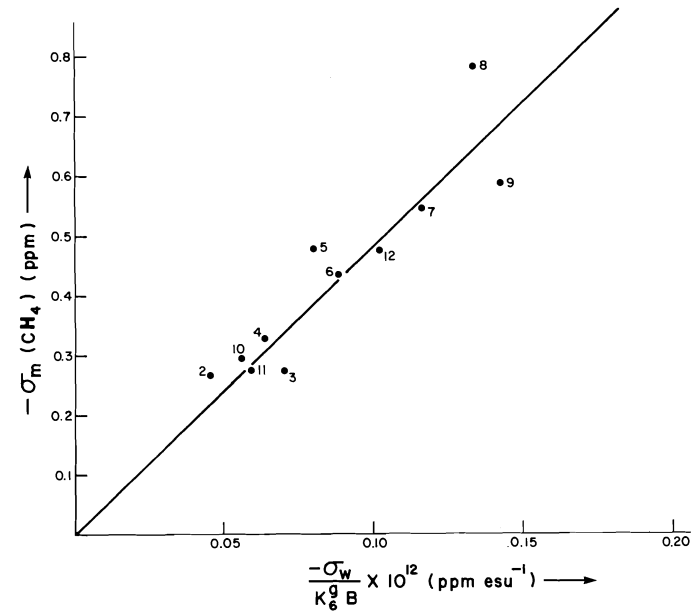

FIG. 2. Proton gas-to-solution shifts at 25°C of CH_4, corrected for σ_b, plotted against σ_w/BK_6^g, calculated according to [13]. Slope of solid line is $K_6^g B = 4.92 \times 10^{-18}$ (esu); standard deviation is ±0.07 ppm

^{13}C. Beyond dispersion forces there is clearly another effect at work, which is not proportional to $\overline{F^2}$. Apart from the suggestion that repulsive forces may be at the origin of this problem no definite explanation of this new effect can be offered at this stage.

The slope of Fig. 2 $K_6^g B = 4.92 \times 10^{-18}$ esu is in very satisfactory agreement with $KB =$

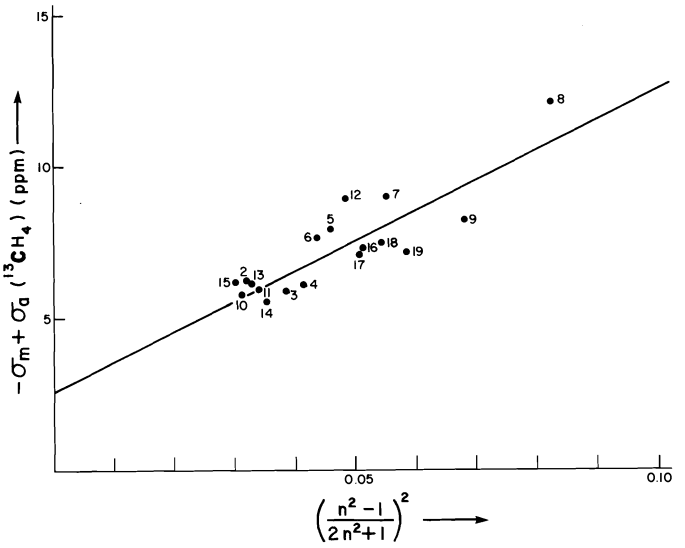

FIG. 3. ^{13}C gas-to-solution shifts at 25°C of $^{13}CH_4$, corrected for σ_b and σ_a, plotted against $f(n)$ of [2]. Best straight line is given by $y = 99.5x + 2.61$ ppm with a standard deviation of ± 0.84 ppm. Best line through the origin is $y = 151.4x$ with a standard deviation of ± 1.15 ppm.

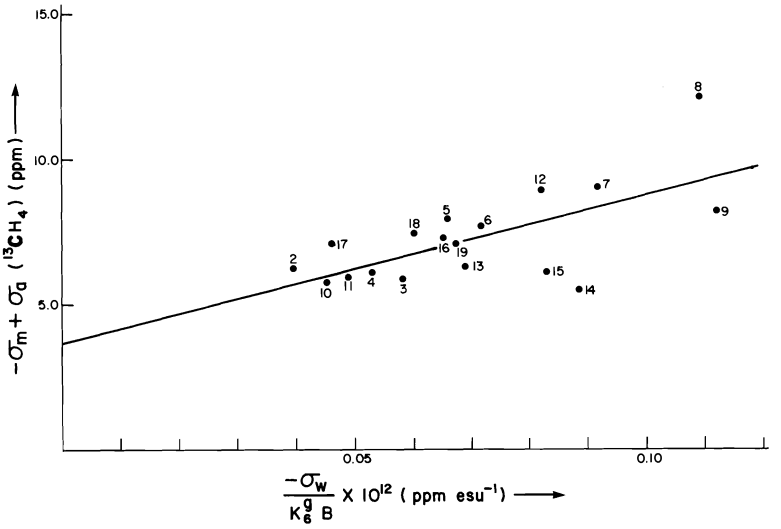

FIG. 4. ^{13}C gas-to-solution shifts at 25°C of $^{13}CH_4$, corrected for σ_b and σ_a, plotted against $\sigma_w/K_6^g B$ calculated according to [13]. Equation of solid line is $y = 50.0x + 3.74$ ppm; standard deviation is ± 1.28 ppm. Best line through the origin is $y = 99.4x$ with a standard deviation of ± 1.69 ppm.

4.71×10^{-18} esu determined previously (6). With a value of $B(CH_4) = 1.68 \times 10^{-18}$ esu (Table 2), this leads to $K = 2.80$ and $K_6^g = 2.93$. Although both these figures are somewhat larger than the $K_6^g(25°C) = 1.62$ (8), the close agreement shows again that both the continuous model and the binary collision model are essentially measuring the same property. Using the 'forced-through-the origin' lines of Figs. 3 and 4, combined with $B(CH_4) = 88.1 \times 10^{-18}$ esu (Table 2) one finds $K = 1.01$ and $K_6^g = 1.13$ respectively. Again the two K values are very similar but both are substantially lower than when determined from the proton shifts. If the slopes of the nonbiased best straight lines are used, the discrepancy becomes worse ($K = 0.66$

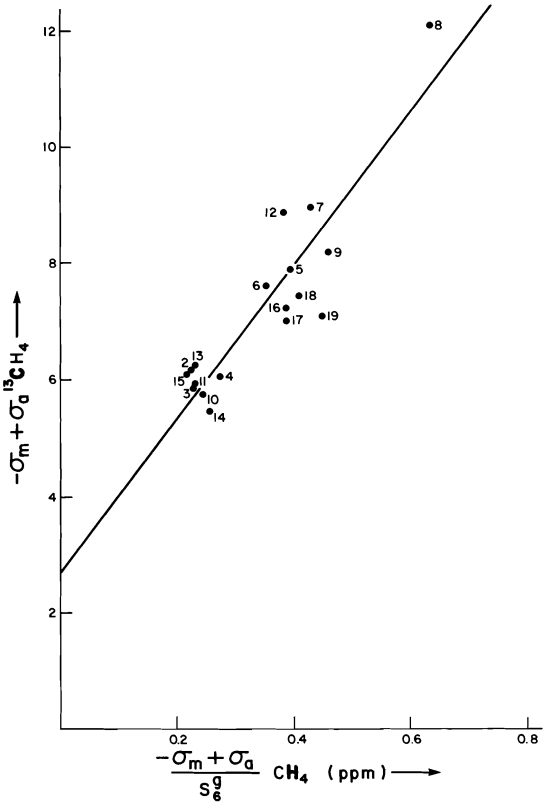

FIG. 5. ^{13}C Van der Waals shift $(-\sigma_m + \sigma_a)$ of $^{13}CH_4$ plotted against site-factor corrected proton Van der Waals shifts of $^{13}CH_4$. Best straight line is $y = 2.77 + 12.92x$; standard deviation is ± 0.71 ppm. Best line through the origin is $y = 20.2x$ with a standard deviation of ± 1.14 ppm.

and $K_6^g = 0.57$, respectively). This shows that the unidentified contribution to the ^{13}C Van der Waals shifts is not a constant term, but is definitely solvent dependent but with a dependency which is neither a smooth function of solvent refractive index, nor of the combined solvent factor of the binary collision model. Another way to look at the consistency between the models and the experimental facts is to calculate the $B(^{13}C)/B(^1H)$ ratios (eqs. 3 and 9). This ratio is 18.9 for the continuum model, 20.2 for the binary collision model, and 20.2 for the experimental ratio as given by Fig. 5.

In the ^{13}C work of Tiffon and Doucet on *n*-pentane (2) no nonzero intercepts, larger than the standard deviation, were observed in plotting σ_m *vs.* $(n^2 - 1)^2/(2n^2 + 1)^2$. This is probably due to the fact that these medium shifts are much smaller than for $^{13}CH_4$, but it also is possible that the particular choice of solvents has played a role in this. Calculating the site factors for pure *n*-pentane as S_{con} $(CH_3) = 1.67$, $S_{con}(CH_2) = 1.20$ and $S_{con} = 1.00$ for the central carbon respectively and dividing these into the observed slopes (see above), shows that the two types of CH_2 groups must have virtually the same KB values, whereas that for the CH_3 group must still be substantially larger. Using $\alpha_1 = 10.12 \times 10^{-24}$ cm^3, $I_1 = 16.9 \times 10^{-12}$ erg and $a^3 = 34.5 \times 10^{-24}$ cm^3 (this is actually the value for neopentane (6)) the *KB* parameters can be calculated using [2]. The σ_m *vs.* $(n^2 - 1)^2/(2n^2 + 1)^2$ slopes reported by Cans *et al.* (3) on the ^{13}C shifts of a number of olefinic hydrocarbons are not so easy to interpret because of the variety of solute molecular shapes. Taking the *average* observed slopes, assuming all $\alpha_1 I_1/a^6$ to be constant, assuming also a site factor for CH_3 groups, which is $1.2\times$ larger than for all other aliphatic groups, the ratios of *KB* factors $KB(CH_3R) : KB(CH_2R_2) : KB(CHR_3) : KB(CR_4)$ can be found, however. The first ratio, $KB(CH_3R) : KB(CH_2R_2)$, agreed very well with that same ratio found for *n*-pentane (see above). Anchoring on the *n*-pentane data, the *KB* values for the other aliphatic groups could thus be obtained. The final results are as follows

$$KB(CH_4) = 89 \times 10^{-18} \text{ esu}$$

$$KB(CH_3R) = 55 \times 10^{-18} \text{ esu}$$

$$KB(CH_2R_2) = 27 \times 10^{-18} \text{ esu}$$

$$KB(CHR_3) = 17 \times 10^{-18} \text{ esu}$$

$$KB(CR_4) = 38 \times 10^{-18} \text{ esu}$$

Although some of the above assumptions may seem drastic, the *qualitative* aspects of the above data are, in our opinion, nevertheless beyond reasonable doubt. The general trend of decreasing *KB* with increasing alkylation shows that this is not caused by a decrease in a presumed intermolecular repulsion effect (such an effect would have the opposite direction; see above), but that it is more likely a real bond effect. However, as the result for CR_4 shows, this cannot be the only effect. The three carbon types CH_3R, CH_2R_2, and CHR_3 are non-symmetrical, however, which makes these groups susceptible to electric field effects. Whereas the σ_{Ez} term cancels out to zero for CH_4 and CR_4, there could be a residual reaction field term σ_{Ez} in the other three substitution types.

Acknowledgement

The financial assistance of the National Research Council of Canada in the form of a research grant (to F.R.) and a scholarship (to F.M.) is gratefully acknowledged.

1. F. H. A. RUMMENS. Van der Waals forces in NMR intermolecular shielding effects. *In* NMR, basic principles and progress. Vol. 10. *Edited by* P. Diehl, E. Fluck, and R. Kosfeld. Springer Verlag, Heidelberg. 1975. pp. 94–95.
2. B. TIFFON and J-P. DOUCET. Can. J. Chem. **54**, 2045 (1976).
3. D. CANS, B. TIFFON, and J.-E. DUBOIS. Tetrahedron Lett. **24**, 2075 (1976).
4. F. H. A. RUMMENS and H. J. BERNSTEIN. J. Chem. Phys. **43**, 2971 (1965).
5. W. T. RAYNES, A. D. BUCKINGHAM, and H. J. BERNSTEIN. J. Chem. Phys. **36**, 3481 (1962).
6. F. H. A. RUMMENS. Can. J. Chem. **54**, 254 (1976).
7. M. J. STEPHEN. Mol. Phys. **1**, 223 (1958).
8. F. H. A. RUMMENS, W. T. RAYNES, and H. J. BERNSTEIN. J. Phys. Chem. **72**, 2111 (1968).
9. A. D. BUCKINGHAM and J. A. POPLE. Trans. Faraday Soc. **51**, 1173 (1955).
10. F. LONDON. Z. Phys. Chem. B, **11**, 222 (1930); Z. Phys. **63**, 245 (1930).
11. J. C. SLATER and J. G. KIRKWOOD. Phys. Rev. **37**, 682 (1931).
12. R. A. BUCKINGHAM. Proc. Roy. Soc. (London) Ser. A, **160**, 94 (1937); **160**, 113 (1937).
13. M. KARPLUS and H. J. KOLKER. J. Chem. Phys. **41**, 3955 (1964).
14. A. DALGARNO and G. A. VICTOR. Proc. Phys. Soc. (London), **90**, 605 (1967).
15. A. DALGARNO and W. D. DAVISON. Adv. Atom. Mol. Phys. **2**, 1 (1966).
16. J. O. HIRSCHFELDER, C. F. CURTISS, and R. B. BIRD. Molecular theory of gases and liquids. John Wiley, New York, NY. 1954.
17. R. J. BELL. Proc. Phys. Soc. **86**, 17 (1965).
18. T. W. MARSHALL and J. A. POPLE. Mol. Phys. **1**, 199 (1958).
19. T. W. MARSHALL and J. A. POPLE. Mol. Phys. **3**, 399 (1960).
20. S. MOHANTY and H. J. BERNSTEIN. J. Chem. Phys. **54**, 2254 (1971).
21. A. K. JAMESON, C. J. JAMESON, and H. S. GUTOWSKY. J. Chem. Phys. **53**, 2310 (1970).
22. R. A. MEINZER. Ph.D. Thesis, (No. 66-4238, University Microfilm Inc., Ann Arbor, MI) University of Illinois, IL. 1965.
23. F. H. A. RUMMENS and F. J. A. LOUMAN. J. Magn. Reson. **8**, 332 (1972).
24. R. A. KROMHOUT and B. LINDER. J. Magn. Reson. **1**, 450 (1969).
25. A. D. BUCKINGHAM, T. SCHAEFER, and W. G. SCHNEIDER. J. Chem. Phys. **32**, 1227 (1960).
26. J. K. BECCONSALL. Mol. Phys. **15**, 129 (1968).
27. F. H. A. RUMMENS. Mol. Phys. **19**, 423 (1970).
28. F. M. MOURITS and F. H. A. RUMMENS. Can. J. Chem. This issue.

Reaction of xenon difluoride. Part III. Oxidative-fluorination and α-fluorination of sulfur(II) compounds

RONALD KIRK MARAT AND ALEXANDER F. JANZEN
Department of Chemistry, University of Manitoba, Winnipeg, Man., Canada R3T 2N2

Received March 14, 1977

RONALD KIRK MARAT and ALEXANDER F. JANZEN. Can. J. Chem. **55**, 3031 (1977).

The reaction of XeF_2 with aryl and alkyl sulfides and thiols has been investigated. Oxidative-fluorination of diphenyl sulfide and *tert*-butylphenyl sulfide gives diphenylsulfur difluoride and *tert*-butylphenylsulfur difluoride, respectively. The presence of an α-hydrogen substituent leads to α-fluorination and, in some cases, to olefin formation while reaction of XeF_2 with thiols gives disulfides. HF catalyzed decomposition of products and intermolecular fluorine exchange is inhibited by the addition of $[(CH_3)_3Si]_2NH$.

RONALD KIRK MARAT et ALEXANDER F. JANZEN. Can. J. Chem. **55**, 3031 (1977).

On a étudié la réaction de XeF_2 avec des sulfures et des thiols d'aryles et d'alkyles. La fluoration oxydative du sulfure de diphényle et du sulfure de *tert*-butylphényle conduisent respectivement au difluorure de diphénylsulfure et au difluorure de *tert*-butylphénylsulfure. La présence d'un hydrogène comme substituant en α conduit à une α fluoration et dans quelques cas à la formation d'oléfine; la réaction de XeF_2 avec les thiols conduit aux disulfures. La décomposition catalysée par HF des produits et l'échange intermoléculaire du fluorure sont inhibés par l'addition de $[(CH_3)_3Si]_2NH$.

[Traduit par le journal]

Introduction

Xenon difluoride readily converts phosphorus(III) to phosphorus(V) (1, 2) and iodine(I) to iodine(III) (2–4) derivatives. We now report a similar oxidative-fluorination of sulfur(II) compounds. The presence of an α-hydrogen leads to α-fluorination and, in some cases, to olefin formation while reaction with thiols gives disulfides. Very recently, Zupan reported the XeF_2 fluorination of $C_6H_5SCH_3$ to $C_6H_5SCFH_2$ and $C_6H_5SCHF_2$ and the dehydrogenation of thiopyrone and thiochromanone (5). Previous methods of fluorination of sulfides include electrolytic fluorination in anhydrous HF and fluorination with F_2 or metal fluorides (6). α-Fluorination, accompanied by oxidative-fluorination, is often encountered in such reactions, as illustrated by the electrochemical conversion of CH_3SCH_3 to CF_3SF_5 and $CH_3SF_4CFH_2$ (7) and the formation of $CSHF_7$ (CHF_2SF_5?) (8) and $C_4H_8FSF_3$ ($C_3H_7CHFSF_3$?) (9) during fluorination of CH_3SH and $(n\text{-}C_4H_9S)_2$. Perfluoroalkyl-sulfides, -disulfides and -sulfenyl chlorides react with ClF to give sulfur(IV) and sulfur(VI) derivatives (10). Sulfides and CF_3OF give sulfur(IV) and sulfur(VI) derivatives, e.g. $(C_6H_5)_2SF_2$ and $(C_6H_5)_2SF_4$ (11).

Results and Discussion

XeF_2 and Diphenyl Sulfide and t-Butylphenyl Sulfide

Oxidative-fluorination of diphenyl sulfide occurred under mild conditions, eq. 1, to give diphenylsulfur difluoride which is stable indefinitely at room temperature if stored in a Teflon container. The product was characterized by elemental analysis, ^1H, ^{19}F, and ^{13}C nmr and by its hydrolysis to $(C_6H_5)_2SO$. The absence of

$$[1]\quad (C_6H_5)_2S + XeF_2 \xrightarrow[CH_3CN]{-5^\circ C} (C_6H_5)_2SF_2 + Xe$$

intermolecular fluorine exchange in $(C_6H_5)_2SF_2$ was confirmed by ^{13}C nmr since ring carbons C_1, C_2, and C_4 showed triplet fine structure due to carbon–fluorine coupling.

Under the mild conditions employed in this study, $(C_6H_5)_2SF_2$ was found to be stable towards further oxidative-fluorination by XeF_2.

Reaction of *t*-butylphenyl sulfide with XeF_2 gave $C_6H_5SF_2C(CH_3)_3$, identified by ^1H and ^{19}F nmr. The product was too unstable for elemental analysis.

XeF_2 and Alkyl Sulfides

The presence of methyl, ethyl, isopropyl, or

benzyl substituents prevented the isolation of dialkylsulfur difluorides; instead, the products were α-fluorinated sulfides, eq. 2, as listed in Tables 1 and 2.

[2] $RSCHR_2 + XeF_2 \rightarrow RSCFR_2 + HF + Xe$

Some reactions of $C_6H_5SCH(CH_3)_2$ produced only $C_6H_5SCF(CH_3)_2$ but others gave olefin, $C_6H_5SC(CH_3)=CH_2$, as well. The ratio of α-fluoride to olefin depended on reaction conditions; lower temperature (−10°C) favoured α-fluoride while higher temperature (0°C) favoured olefin. Once formed, the ratio of α-fluoride to olefin did not appear to vary, even at +40°C, suggesting that the olefin is not formed by simple loss of HF from $C_6H_5SCF(CH_3)_2$.

XeF_2 and Thiols

Reaction of XeF_2 with CH_3SH, $(CH_3)_2CHSH$, or C_6H_5SH (thiol:XeF_2 = 2:1) gave the corresponding disulfide, HF, and Xe as the only detectable products, eq. 3.

[3] $2RSH + XeF_2 \rightarrow RSSR + 2HF + Xe$

If the reaction is carried out with thiol:XeF_2 = 1:1 the same products are formed but only half of the XeF_2 is consumed. CH_3SSCH_3 is stable in the presence of excess XeF_2, however, after 3 days decomposition gives a very complex mixture of products.

Thiophene did not react with XeF_2 below +80°C; above that temperature decomposition occurred to give a black residue.

HF Catalyzed Decompositions and Exchange Reactions

The technique of removing HF by chemical reaction with silicon-nitrogen compounds, eq. 4, thereby slowing down HF catalyzed decom-

[4] $[(CH_3)_3Si]_2NH + 2HF \rightarrow 2(CH_3)_3SiF + NH_3$

positions and exchange reactions (12), proved useful in this work. For example, $(C_6H_5)_2SF_2$ gave a broad ^{19}F nmr signal on several occasions, however, the addition of a small amount of $[(CH_3)_3Si]_2NH$ produced a sharp peak; at the same time some of the $[(CH_3)_3Si]_2NH$ was converted to $(CH_3)_3SiF$ thereby strongly suggesting that HF catalyzed intermolecular fluorine exchange, perhaps involving intermediates $(C_6H_5)_2SF_3H$ or $(C_6H_5)_2SF^+FHF^-$, was the cause of line broadening.

Initial attempts to prepare $C_6H_5SF_2C(CH_3)_3$ were unsuccessful because of rapid decomposition, however, when the procedure was modified to include the addition of a small amount of $[(CH_3)_3Si]_2NH$ immediately after the reaction of XeF_2 with $C_6H_5SC(CH_3)_3$ then the product was stable for at least 3 h at +40°C.

The reaction of XeF_2 with sulfides produced equivalent amounts of HF, eq. 2, but the α-fluorinated sulfides $RSCFR_2$ decomposed in the presence of HF, for example, $CH_3CH_2SCFHCH_3$ decomposed within 15 min at +40°C while $C_6H_5CH_2SCFHC_6H_5$ decomposed after one week at −20°C. If a stoichiometric amount of $[(CH_3)_3Si]_2NH$ was added to remove HF, then the products appeared to be stable indefinitely.

Possible Intermediates in Fluorination Reactions

Our results are consistent with initial oxidative-fluorination of diaryl(alkyl) sulfides to give sulfur(IV) difluorides which are stable unless an α-hydrogen is present. Perhaps HF is lost via a 4-center step to give intermediate(i) i-**2** followed

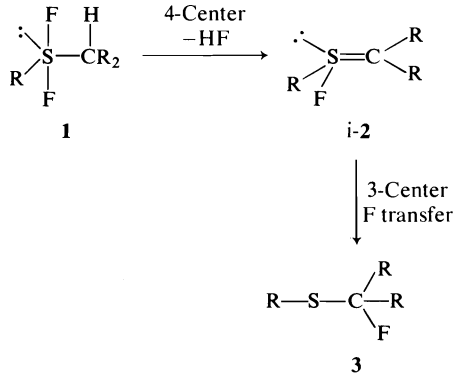

1 i-**2** **3**

by fluorine transfer via a 3-center step to give α-fluorinated sulfide **3**. Since the olefin $C_6H_5SC(CH_3)=CH_2$ is not formed by simple loss of HF from **3**, it is possible that **1** or i-**2** is the olefin precursor. Other intermediates could also be formed by reaction of HF with **1** or i-**2**, in that case, the mechanism of α-fluorination would be more complex than indicated here.

Attempts to identify intermediates in the reaction of XeF_2 with thiols were unsuccessful.

Experimental

Safety Note

Although no violent reactions were encountered in this work, the technique of destroying excess HF with $[(CH_3)_3Si]_2NH$ at the completion of the XeF_2 reactions is potentially hazardous because XeF_2 reacts explosively with some silicon-nitrogen compounds (2).

TABLE 1. Reaction of XeF_2 with sulfur(II) compounds

Sulfur(II) compound (mmol)		XeF_2 (mmol)	Reaction conditions	Products
$(C_6H_5)_2S$	1.09	1.09	−5°C, 10 min	$(C_6H_5)_2SF_2$, Xe
$C_6H_5SC(CH_3)_3$	0.42	0.42	0°C, 10 min	$C_6H_5SF_2C(CH_3)_3$, Xe
$(CH_3)_2S$	0.80	0.66	−20°C, 10 min	CH_3SCFH_2, Xe, HF
$(CH_3CH_2)_2S$	0.40	0.40	−5°C, 3 min	$CH_3CH_2SCFHCH_3$, Xe, HF
$(C_6H_5CH_2)_2S$	0.40	0.40	0°C, 5 min	$C_6H_5CH_2SCFHC_6H_5$, Xe, HF
$C_6H_5SCH(CH_3)_2$	0.40	0.40	−10°C, 30 min	$C_6H_5SCF(CH_3)_2$ (>90%), Xe, HF
	0.40	0.40	−5°C, 10 min	$C_6H_5SCF(CH_3)_2$ (60%), $C_6H_5SC(CH_3)=CH_2$ (40%)
	0.40	0.40	0°C, 2 min	$C_6H_5SC(CH_3)=CH_2$ (>90%)
Thiophene	0.45	0.45	+20 to +80°C	No reaction; dec. above +80°C
$(CH_3)_2CHSH$	0.55	0.27	−10°C, 20 min	$[(CH_3)_2CHS]_2$, Xe, HF
C_6H_5SH	0.59	0.55	0°C, 10 min	$[C_6H_5S]_2$, Xe, HF
CH_3SH	0.45	0.43	+20°C, 10 min	$[CH_3S]_2$, Xe, HF
$(CH_3)_3CSH$	0.80	0.80	−10°C, 30 min	$(CH_3)_3CF$, Xe, HF, S_8
CH_3SSCH_3	0.35	0.35	+20°C, 60 min	No reaction; very complex mixture after 3 days

TABLE 2. Proton, fluorine, and carbon nmr chemical shifts and coupling constants of some α-fluoroalkylsulfides and sulfur(IV) difluorides[a]

Compound	Chemical shift (ppm) F	Chemical shift (ppm) H(CF)	Coupling constant (J, Hz) HCF	HCCF	HCSCF	Additional nmr data
CH_3SCFH_2	+188.6	−5.63	54.0		2.6	δCH_3 −2.26
$CH_3CH_2SCFHCH_3$	+142.2	−6.05	59.0	21.2	1.8	$\delta CH_3(CFH)$ −1.59, $\delta CH_3(CH_2)$ −1.27, $\delta CH_2(CH_3)$ −2.77, $^3J(CH_3CH_2)$ = 7.6, $^3J(CH_3CH)$ = 6.4
$C_6H_5CH_2SCFHC_6H_5$	+149.7	−6.78	57.2		1.9	
$C_6H_5SCF(CH_3)_2$	+107.8			19.2		δCH_3 −1.69
$(C_6H_5)_2SF_2$[b]	−5.43					δC_1 −145.5, δC_2 −128.6, δC_3 −129.1, δC_4 −131.4, $^2J(C_1, F)$ = 4.55, $^3J(C_2, F)$ = 6.70, $^4J(C_3, F) \sim 0.5$, $^5J(C_4, F)$ = 1.78
$C_6H_5SF_2C(CH_3)_3$	+26.6					δCH_3 −1.45, $^4J(CH_3CSF_2)$ = 2.8

[a]Proton and carbon chemical shifts are relative to internal $(CH_3)_4Si$; fluorine chemical shifts are relative to internal $CFCl_3$. Positive values indicate shifts to high field.
[b]Sample for proton-decoupled ^{13}C nmr spectrum contained 1.0 mmol $(C_6H_5)_2SF_2$ and 10 μl $[(CH_3)_3Si]_2NH$ in CD_2Cl_2.

General

XeF_2 (PCR), CD_3CN (Aldrich), $[(CH_3)_3Si]_2NH$ (Aldrich), thiols, and dialkyl and diaryl sulfides were commercial samples and were used without further purification. Volatile compounds were handled in a conventional glass vacuum system. $C_6H_5SCH(CH_3)_2$ and $C_6H_5SC(CH_3)_3$ were prepared on a 0.1 mol scale (13). *tert*-Butanol, instead of isobutene, was used in the $C_6H_5SC(CH_3)_3$ synthesis.

Proton and fluorine nmr spectra were recorded on a Varian A-56/60A spectrometer and carbon nmr spectra were obtained on a Varian CFT-20 spectrometer (8 mm probe). Mass spectra were recorded on a Finnigan 1015 quadrupole mass spectrometer coupled to a Varian 1700 gas chromatograph. Thiols, sulfides, sulfoxides, S_8, HF, and Xe were identified by nmr and/or gc-ms by comparison with authentic samples. $C_6H_5SC(CH_3)=CH_2$ was identified by its known nmr and mass spectrum (14).

Elemental analyses were carried out by Alfred Bernhardt Laboratories, West Germany.

Diphenylsulfur Difluoride and tert-Butylphenylsulfur Difluoride

Diphenyl sulfide, in a microsyringe, was added to a solution of XeF_2 in CH_3CN (quantities given in Table 1) at −30°C in a 100 ml Teflon bottle. Reaction occurred on warming to about −5°C. After 10 min, all volatile components were removed under vacuum and the white residue (slightly purple coloured) was washed with three 10 ml portions of isopentane. The solid was again dried under vacuum to give $(C_6H_5)_2SF_2$, white needle-like crystals, mp 66–74°C, isolated yield 74%. Hydrolysis gave $(C_6H_5)_2SO$. *Anal.* calcd. for $C_{12}H_{10}SF_2$: C 64.27, H 4.49, F 16.94; found: C 64.20, H 4.62, F 16.71.

Using the procedure above, *t*-butylphenyl sulfide was added to XeF_2 in CH_3CN. Reaction occurred on warming to 0°C. After 10 min, 5 μl $[(CH_3)_3Si]_2NH$ was added and the solution transferred to a silylated and dried (210°C) quartz nmr tube. The nmr spectra were recorded at −20°C and the product was stable indefinitely at −20°C but decomposed within 18 h at +20°C to give

mainly $(CH_3)_3CF$, $C_6H_5SC_6H_5$, $(C_6H_5S)_2$, and $(C_6H_5)_2SO$.

Reaction of XeF_2 with Sulfides and Thiols

In a typical reaction, a solution of XeF_2 in CD_3CN was placed into a 2 ml vial, sealed with a Teflon lined septum cap and cooled to $-40°C$ with the aid of a Thermoelectrics Stir-Kool SK-31 apparatus. The sulfide or thiol was then added with a microsyringe and the temperature allowed to increase until reaction commenced. A 5 or 10 ml glass syringe was connected to the reaction vial and the reaction was conveniently monitored by observing the rise of the syringe plunger as Xe gas was liberated. Reaction with volatile CH_3SCH_3 and CH_3SH was carried out in a vacuum line by condensing reagents onto a XeF_2/CD_3CN solution. Reaction conditions and products are listed in Tables 1 and 2. The products were formed in essentially quantitative yield, as determined by nmr integration.

HF was observed in the proton nmr at about -7.8 ppm (half-height width ~ 4 Hz) and in the fluorine nmr at about $+170$ ppm (half-height width ~ 50 Hz).

Acknowledgements

The financial assistance of the National Research Council of Canada and the Research Board of the University of Manitoba is gratefully acknowledged. We thank Dr. R. E. Wasylishen, University of Winnipeg, for his assistance with the ^{13}C nmr measurements.

1. A. F. JANZEN and O. C. VAIDYA. Can. J. Chem. **51**, 1136 (1973).
2. J. A. GIBSON, R. K. MARAT, and A. F. JANZEN. Can. J. Chem. **53**, 3044 (1975).
3. J. A. GIBSON and A. F. JANZEN. J. Chem. Soc. Chem. Commun. 739 (1973).
4. M. ZUPAN and A. POLLAK. J. Fluorine Chem. **7**, 445 (1976).
5. M. ZUPAN. J. Fluorine Chem. **8**, 305 (1976).
6. W. A. SHEPPARD and C. M. SHARTS. Organic fluorine chemistry. W. A. Benjamin, New York, NY. 1969; S. P. VON HALASZ and O. GLEMSER. *In* Sulfur in organic and inorganic chemistry. Vol. 1. *Edited by* A. Sennig. Marcel Decker, New York, NY. 1971. Chapt. 7.
7. R. A. DRESDNER and J. A. YOUNG. J. Am. Chem. Soc. **81**, 574 (1959).
8. G. A. SILVERY and G. H. CADY. J. Am. Chem. Soc. **72**, 3624 (1950).
9. W. A. SHEPPARD. J. Am. Chem. Soc. **84**, 3058 (1962).
10. T. ABE and J. M. SHREEVE. J. Fluorine Chem. **3**, 17, (1973); **3**, 187 (1973).
11. D. B. DENNEY, D. Z. DENNEY, and Y. F. HSU. J. Am. Chem. Soc. **95**, 4064 (1973); **95**, 8191 (1973).
12. D. G. IBBOTT and A. F. JANZEN. Can. J. Chem. **50**, 2428 (1972); J. A. GIBSON, D. G. IBBOTT, and A. F. JANZEN. Can. J. Chem. **51**, 3203 (1973); R. K. MARAT and A. F. JANZEN. Can. J. Chem. **55**, 1167 (1977).
13. V. N. IPATIEFF, H. PINES, and B. S. FRIEDMAN. J. Am. Chem. Soc. **60**, 2731 (1938).
14. W. D. WERINGA. Tetrahedron Lett. 273 (1969); S. H. GROEN, R. M. KELLOGG, J. BUTER, and H. WYNBERG. J. Org. Chem. **33**, 2218 (1968).

The kinetics of the reaction of boric acid with salicylic acid

ALAN QUEEN

Parker Chemical Laboratory, University of Manitoba, Winnipeg, Man., Canada R3T 2N2

Received May 10, 1976[1]

ALAN QUEEN. Can. J. Chem. **55**, 3035 (1977).

Salicylic acid forms a 1:1 complex with boric acid, the reaction involving both the fully protonated ligand, and the salicylate ion. The kinetics of this reaction have been studied by the stopped-flow method. The stability constant for the reaction involving salicylate ion has been calculated from measurements of the absorbances of solutions at equilibrium and is the same as that obtained from the kinetic data. The kinetic results at p*H* values in the range 3.45–4.63 suggest that, when salicylic acid is the ligand, the complex is formed in two steps. A similar process may also occur with salicylate ions.

ALAN QUEEN. Can. J. Chem. **55**, 3035 (1977).

L'acide salicylique forme un complexe 1:1 avec l'acide borique; la réaction implique et le ligand complètement protoné et l'ion salicylate. On a étudié la cinétique de la réaction par la méthode des flux stoppés. On a calculé la constante de stabilité pour la réaction impliquant l'ion salicylate; ces calculs ont été effectués à partir de mesures d'absorption de solutions en équilibre et cette constante de stabilité est la même que celle obtenue à partir de données cinétiques. Les résultats cinétiques, à de valeurs de p*H* allant de 3.45 à 4.63, suggèrent que lorsque l'acide salicylique agit comme ligand, le complexe se forme en deux étapes. Un processus similaire peut aussi se produire avec les ions salicylates.

[Traduit par le journal]

Introduction

Boric acid forms 1:1 and 1:2 complexes with *cis* diols (1, 2), α-hydroxy acids (3), dicarboxylic acids (4) and nucleosides (5) as well as other compounds such as α-diketones (6). Most of the previous work has been concerned with equilibrium studies but recently Pizer and his coworkers have published the results of a series of kinetic studies of the reactions of boric acid with tartaric acid and phenylboronic acid with lactic, oxalic, and malonic acids (4, 7–10). The appearance of this work prompts the publication of results that have been obtained using boric and salicylic acids.

Pizer has interpreted his data in terms of several factors that influence the rate of complex formation. These are the acidity of the ligand and interactions that stabilize a four coordinate species. The first of these effects seems to be well established but the other effects are less easily identified. In particular, a proposal that in some cases there may be attractive interactions between the aromatic ring of phenylboronic acid and the carboxylate group of the ionized ligand is quite vague.

Salicylic acid was chosen for the present studies because complex formation could be followed spectroscopically in the absence of indicators and because the rates could be conveniently measured by the stopped-flow method.

Experimental

Salicyclic acid and boric acid were Fisher Certified Reagents and were used without further purification after drying *in vacuo* over phosphorus pentoxide.

Buffered solutions were made up by volume from standard solutions of acetic acid, sodium acetate, and sodium chloride, the final volume of the mixture being adjusted to give an ionic strength of 0.1 *M*. These solutions were used to prepare solutions of salicyclic acid and boric acid of known strength. p*H* measurements were carried out at 25°C on mixtures of equal volumes of the salicylic acid and boric acid solutions.

All kinetic experiments were carried out at 25°C, using a stopped-flow apparatus that has been described previously (11), except that it was fitted with a quartz cell having a bore of 2 mm square section and length of 20 mm. The flexible light pipes were discarded and light was passed from the monochromator to the cell by means of mirrors. By changing the position of a mechanical shutter, either transmitted light or fluorescence could be measured. In the fluorescence mode, light measurements were made at right angles to the exciting beam, which illuminated a 12 mm length of the reaction cell, starting 8 mm from the mixing chamber. Rate measurements were carried out by following the changes in fluorescence intensity using exciting light at a wavelength of 335 nm. Somewhat larger changes in fluorescence were observed when the exciting light was at 320 nm, but a better signal-to-noise ratio was obtained at the longer wavelength, where the output of the 200 W quartz–iodine lamp was

[1]Revision received March 1, 1977.

TABLE 1. Rates of reaction of boric acid and salicylic acid at 25°C. The effects of wavelength changes

pH	[Salicyclic acid] ($M \times 10^3$)	[H_3BO_3] (M)	λ (nm)	k_{obs} (s^{-1}) Absorbance method	k_{obs} (s^{-1}) Fluorescence method
5.29	1.5	0.03380	302		4.91
			322	4.99	5.07
			335	4.94	4.90
			343		4.80
		0.09387	335	7.15	7.18
4.63	0.4	0.02543	312	4.35	
			322	4.36	
			332	4.39	
3.45	1.5	0.05725	312	14.7	
			322	9.72	
			332	8.87	

TABLE 2. Stability constants for the complexation of boric acid and salicylate ions, 1.043×10^{-3} M, at pH 5.34 and 25°C

C_B^{0a} (M)	Absorbance at 322 nm	$K_{HA^-}^{b,c}$ (M^{-1})	Absorbance at 332 nm	$K_{HA^-}^{b,d}$ (M^{-1})
0.1989	1.451	10.36	0.351	10.60
0.1790	1.413	10.41	0.342	10.63
0.1591	1.368	10.43	0.331	10.59
0.1392	1.317	10.50	0.321	10.88
0.1194	1.257	10.60	0.304	10.64
0.09946	1.186	10.72	0.290	11.06
0.07957	1.085	10.54	0.267	10.96
0.05968	0.958	10.29	0.242	11.29
0.03978	0.803	10.17	0.202	10.83
0.01989	0.602	10.15	0.152	10.58
0	0.322		0.084	

[a] C_B^0 is the initial concentration of boric acid.
[b] $K_{HA^-} = 10.61 \pm 0.29$ M^{-1}.
[c] $\varepsilon_1 - \varepsilon_2 = 1610$, where ε_1 and ε_2 are the extinction coefficients of the complex **1** and salicylate ion, respectively.
[d] $\varepsilon_1 - \varepsilon_2 = 378$.

much greater. The apparatus used a Bausch and Lomb high intensity monochromator set at a bandwidth of 15 nm. It was shown that identical rate constants were obtained using either fluorescence or absorbance measurements. The fluorescence method was preferred because considerable loss of transmitted light occurs in our apparatus below 400 nm, resulting in a poor signal-to-noise ratio. The rate constants were calculated by an on-line method (12) and the results are summarized in Table 1. Each value is the mean of at least ten independent experiments. Good first-order rates were obtained over at least four half lives.

Results

Stability constants, K_{H_2A} and K_{HA^-}, for the formation of the complex **1** from salicylic acid and salicylate ion, respectively, are defined according to [1] and [2]. Values of K_{HA^-} have been obtained at 322 and 332 nm from the measurements of the absorbances of ten different solutions of boric acid and salicylic acid. The pH of the solutions was 5.34 and measurements were made at 25°C using a Gilford spectrophotometer, model 2400-2. For these conditions less than 0.5% of the ligand is in the protonated form. Calculations were based on the method of Rose and Drago (13) and the results are summarized in Table 2. The average value of $K_{HA^-} = 10.6$ can be compared to the approximate value of 17 ± 3, previously obtained at an ionic strength of 3 M and an unknown temperature using infrared data (14). Rose and Drago's method assumes that only two absorbing species are present in solution. Support for this assumption is gained from the convergence of the $K_{HA^-}^{-1}$ values in the Rose–Drago plots and from the

fact that excellent isosbestic points were observed at 258 and 299 nm when the pH of the solutions was 5.34.

[1] $$K_{H_2A} = \frac{[\text{complex}][H^+]}{[H_2A][\text{boric acid}]}$$

[2] $$K_{HA^-} = \frac{[\text{complex}]}{[HA^-][\text{boric acid}]}$$

Within the range of pH used, boric acid is virtually undissociated and only the first ionisation of salicyclic acid needs to be considered. The boric acid was always in large excess over salicyclic acid but at concentrations where the formation of dimers and larger aggregates could be neglected (15). For these conditions, the simplest reaction scheme is given by [3]. It can

[3]

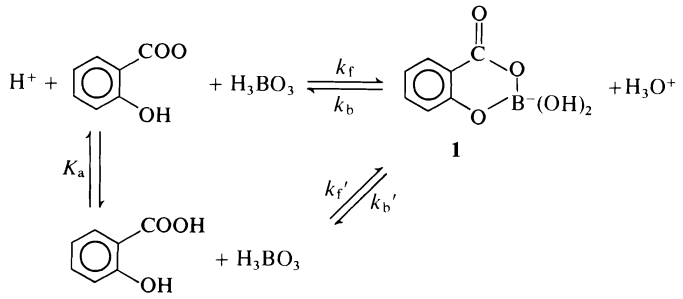

be readily shown that the observed rate constants are given by [4].

[4] $$k_{obs} = (k_b + k_b'[H^+]) + \left(\frac{k_f K + k_f'[H^+]}{K + [H^+]}\right)[H_3BO_3] = A + B[H_3BO_3]$$

In agreement with this scheme, plots of k_{obs} against boric acid concentration at constant pH were linear. The slopes and intercepts of these plots were obtained by a least-squares method and the values are given in Table 3. The values of the intercepts, A, varied linearly with hydrogen ion concentration, as required by [4]. The corresponding slopes, B, also increased linearly with hydrogen ion concentration, within the limits of the experimental errors, which is not inconsistent with [4], depending on the values of the constants and the range of hydrogen ion concentrations used. K_a, the acidity constant of salicylic acid, has been accurately measured in these laboratories by Dunn and Kung (16) at 25°C and an ionic strength of 0.1 M, the value being 1.02×10^{-3}. Values of k_b and k_b' were obtained from the variation of A with hydrogen ion concentration by a least squares method. k_f was similarly calculated from the hydrogen ion dependence of B. Values of k_b, k_b', and k_f obtained in these ways are shown at the bottom of Table 3. The results obtained at pH 5.29 were not included in these calculations, being used instead to check the validity of using [4] to obtain k_b and k_f. It can be seen that the values of these rate constants are in good agreement with those of A and B, respectively, obtained at low hydrogen ion concentration (pH = 5.29). Using these values of the rate constants, the ratio $k_f/k_b = 10.7 \pm 0.8\ M^{-1}$ is in good agreement with the value of K_{HA^-} given in Table 2. If k_f/k_b is calculated from the data obtained at pH 6.29, it equals $11.1 \pm 0.3\ M^{-1}$. The best value of k_f' leading to calculated values of B in agreement with those observed is $135\ s^{-1}\ M^{-1}$.

Discussion

The simple mechanism shown in [3] requires that $K_a = k_f'k_b/k_b'k_f = 1.02 \times 10^{-3}$. However, the rate constant quotient equals 2.8×10^{-3}, which suggests that the simple mechanism is either incorrect or incomplete. A logical expansion of this scheme allows for stepwise formation of the final complex **1** from both salicylate ion **2** and salicylic acid **4**, as shown in [6].

It might be argued that k_4 and k_{-4} should be associated with the quantities k_f' and k_b', so that K_a in [4] should be replaced by a composite-K_a', possibly equal to $k_{-3}K_a/k_3$. However, it is not possible to choose a value for K_a* which will simultaneously yield k_f' and a fit to the observed values of B. We have not attempted a full kinetic treatment of [6]. Instead we have preferred to argue from a consideration of a treatment in-

TABLE 3. Rates of reaction of boric acid and salicylic acid[a] at 25°C and an ionic strength of 0.1 *M*

p*H*	$[H_3BO_3]$ (*M*)	k_{obs} (s^{-1})	$A = (k_b + k_b'[H^+])$ (s^{-1})	$B = \frac{K_a k_f + [H^+]k_f'}{K_a + [H^+]}$ ($s^{-1}\,M^{-1}$)	B_{calcd}
5.290	0.03380	4.90	3.55±0.06	39.4±0.8	39.4
	0.05995	5.90			
	0.07453	6.48			
	0.09387	7.18			
	0.1143	8.01			
4.625	0.03333	4.98	3.71±0.10	40.4±1.2	41.1
	0.05615	6.07			
	0.07314	6.68			
	0.09284	7.50			
	0.1156	8.33			
3.969	0.03679	5.86	4.17±0.05	45.7±0.6	48.1
	0.05662	6.74			
	0.07636	7.63			
	0.09115	8.39			
	0.1170	9.50			
3.648	0.03623	6.71	4.53±0.04	59.6±0.5	56.3
	0.05472	7.79			
	0.07557	9.02			
	0.09570	10.2			
	0.1231	11.9			
3.450	0.03688	7.63	5.25±0.03	64.1±0.4	63.7
	0.05725	8.88			
	0.07352	9.96			
	0.09261	11.2			
	0.1148	12.6			

[a][Salicylic acid] = 1.5×10^{-3} *M*, $K_a = 1.02 \times 10^{-3}$, $k_b = 3.62 \pm 0.08\ s^{-1}$, $k_f = 38.9 \pm 2.6\ s^{-1}\,M^{-1}$, $k_b' = 4483 \pm 360\ s^{-1}\,M^{-1}$, $k_f' = 135\ s^{-1}\,M^{-1}$.

[6]

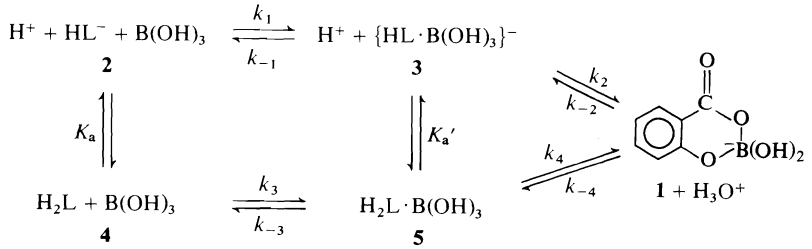

volving only the species **1**, **2**, and **3**; i.e. for the situation that would hold when the p*H* > 5.

If all three species change concentration simultaneously, then they will also contribute to the changes in fluorescence. It can then be shown that the value of k_{obs} is given by [7].

$$[7]\quad k_{obs} = \frac{1}{t}\ln\left\{\frac{(Y_e + Z_e)}{(Y_e + Z_e) - (Y + Z)}\right\} + \frac{1}{t}\ln\left\{\frac{P - (QY_e + RZ_e)/(Y_e + Z_e)}{P - \dfrac{Q(Y_e - Y) + R(Z_e - Z)}{(Y_e + Z_e) - (Y + Z)}}\right\}$$

In this equation, $Y_e = (C_2^e - C_2^0)$, $Y = (C_2^t - C_2^0)$, $Z_e = (C_1^e - C_1^0)$. The *C* values are concentrations at times 0, *t*, and equilibrium, as indicated by the superscripts 0, *t*, and e, respectively. The quantities *P*, *Q*, and *R* are the fluorescence coefficients of the species **2**, **3**, and **1**, respectively. These are likely to be different at a given wavelength and to change differently with wavelength. Hence, k_{obs} would be expected to vary with the wavelength of the incident light in a given experiment where the boric acid concentration and p*H* are fixed. If the reaction is followed by monitoring changes of absorbance,

the P, Q, and R values are extinction coefficients. It is likely that there will not be a 1:1 relation between these quantities for fluorescence and absorbance, so that k_{obs} might be expected to vary depending on the method used to measure it. The data in Table 1 show that neither of these differences are observed when the pH is 5.29. Indeed, the values of k_{obs} are independent of wavelength at pH 4.63, where the salicylic acid/salicylate ion ratio is 0.023. This suggests either that the complex **3** is not formed at all or that it reaches a low steady-state concentration early in the course of the reaction. The possibility that Q and R are equal is considered to be less likely. When the concentration of the complex **3** is small, Y and Y_e are small causing the second term of [7] to become zero. The steady state approximation may be applied to complex **3** and k_{obs} is then given by [8].

$$[8] \quad k_{obs} = \frac{k_{-1}k_2}{k_{-1} + k_2} + \frac{k_1k_2}{k_{-1} + k_2}[\text{boric acid}]$$

Hence,

$$k_b = \frac{k_{-1}k_2}{k_{-1} + k_2}, \quad k_f = \frac{k_1k_2}{k_{-1} + k_2}$$

$$K_{HL^-} = \frac{k_f}{k_b} = \frac{k_1k_2}{k_{-1}k_{-2}} = K_1K_2$$

This is consistent with the observation that the kinetic and equilibrium values of K_{HL^-} are the same.

The conclusion that complex **3** does not contribute significantly to changes in fluorescence suggests that the inequality of K_a and the quotient $k_f'k_b/k_b'k_f$ may require that complex **5** is not in low or steady state concentration during the course of the reaction. If this is so, the values of k_{obs} at low pH, when no salicylate ion is present, should be given by an equation similar to [7] and so should be wavelength dependent. No changes in light absorption or fluorescence could be detected at pH 1 and were too small to be useful at pH 2. A similar, but more complicated equation than [7] should apply to k_{obs} for intermediate pH values where both salicylic acid and salicylate ion react with boric acid. Table 1 shows that k_{obs} is indeed wavelength dependent at pH 3.45. It is therefore proposed that the results for the boric acid, salicylic acid system support a stepwise formation of the complex **1** from salicylic acid and probably from salicylate ion also. For this system, complex **3** is in low concentration during the reaction but complex **5** is not.

Pizer has previously assumed the formation of complexes corresponding to **3** and **5** in the reactions he has studied. However, he also assumes that these intermediates are formed at diffusion controlled rates, so that k_f and k_f' are considered to measure the rates of ring closure on loss of H_2O and H_3O^+, respectively. Although the present data have not been interpreted in the same way, mechanism [6] would appear to be capable of accommodating a variety of different possibilities since the various steps would be expected to be sensitive to the effects of substituent groups in the ligands. Indeed, it may be possible on this basis to explain the fact that k_f is larger than k_f' for the complexation of lactic and boric acids, this reaction being the only one so far reported where the fully protonated acid reacts more slowly than its conjugate base. It is worth noting that lactic acid is the only ligand having an electron donating group close to the reaction sites. Moreover, it is not certain that the same group acts as the nucleophile towards the boron atom in all cases. It may well be that the phenolic group acts in this way in the fully protonated ligands but that the carboxylate group is the reactive centre in the corresponding ionized ligands, at least in some cases.

1. J. Knoeck and J. P. Taylor. Anal. Chem. **41**, 1730 (1969) and literature cited therein.
2. L. B. Magnusson. J. Inorg. Nucl. Chem. **33**, 3602 (1970).
3. N. Veermaas. Recl. Trav. Chim. Pays-Bas, **51**, 955 (1932).
4. S. Friedman and R. Pizer. J. Am. Chem. Soc. **97**, 6059 (1975).
5. U. Weser. Z. Naturforsch. **22**, 457 (1967).
6. B. Pesetsky and N. R. Eldred. Tetrahedron, **25**, 4137 (1969).
7. K. Kustin and R. Pizer. J. Am. Chem. Soc. **91**, 317 (1969).
8. S. Friedman, B. Pace, and R. Pizer. J. Am. Chem. Soc. **96**, 5381 (1974).
9. S. Friedman and R. Pizer. J. Am. Chem. Soc. **97**, 6059 (1975).
10. G. Lorber and R. Pizer. Inorg. Chem. **15**, 978 (1976).
11. E. F. Caldin, J. E. Crooks, and A. Queen. J. Phys. E, **6**, 930 (1973).
12. A. Queen, J. L. Charlton, E. Dawson, and W. Buchannon. Chem. Instrum. **6**, 153 (1975).
13. N. J. Rose and R. S. Drago. J. Am. Chem. Soc. **81**, 6138 (1959).
14. R. Larsson and G. Nunziata. Acta Chem. Scand. **26**, 1503 (1972).
15. N. Ingri. Acta Chem. Scand. **16**, 439 (1962).
16. G. E. Dunn and Fei-Lin Kung. Can. J. Chem. **44**, 1261 (1966).

Definition of bond paths and bond directions in terms of the molecular charge distribution

G. R. RUNTZ, R. F. W. BADER,[1] AND R. R. MESSER

Department of Chemistry, McMaster University, Hamilton, Ont., Canada L8S 4M1

Received March 3, 1977

G. R. RUNTZ, R. F. W. BADER, and R. R. MESSER. Can. J. Chem. **55**, 3040 (1977).

The virial partitioning of a molecular electronic charge distribution, $\rho(\boldsymbol{r})$, divides a molecule into a collection of chemically identifiable atomic-like fragments. When two fragments interact strongly the distribution of charge in the region between their nuclei contains a saddle point ($\nabla\rho(\boldsymbol{r}) = 0$). The gradient paths (paths of steepest ascent through $\rho(\boldsymbol{r})$, as traced by the vectors $\nabla\rho(\boldsymbol{r})$) which *terminate* at this internuclear saddle point, define the virial partitioning surface which lies between the fragments. The two gradient paths which *originate* at the internuclear saddle point and terminate at each of the fragment nuclei define a *bond path*: the path which follows the ridge of maximum charge density between a pair of bonded nuclei. When the internuclear axis does not coincide with a symmetry axis, the internuclear stationary point will, in general, lie off the axis, and the bond path joining the nuclei will deviate or curve from this axis. The magnitude and direction of this 'bond curvature' as determined by the bond path agrees well with chemical expectations.

G. R. RUNTZ, R. F. W. BADER et R. R. MESSER. Can. J. Chem. **55**, 3040 (1977).

La départition virielle d'une distribution de charge électronique moléculaire, $\rho(\boldsymbol{r})$, divise une molécule en une collection de fragments du genre atomique qui sont identifiables d'une façon chimique. Lorsque deux fragments interagissent fortement la distribution de la charge dans la région entre les noyaux contient un point selle ($\nabla\rho(\boldsymbol{r}) = 0$). Les chemins gradients (les chemins qui ont la pente d'ascension la plus grande pour $\rho(\boldsymbol{r})$, lorsqu'on les trace en fonction des vecteurs $\nabla\rho(\boldsymbol{r})$) qui *aboutissent* à ce point maximal internucléaire, définissent la surface de départition virielle qui existe entre les fragments. Les deux chemins gradients *qui prennent origine* au point selle internucléaire et qui se terminent aux noyaux des fragments définissent un *chemin de liaison*: le chemin qui suit les hauteurs maximales de densité de charge entre une paire de noyaux liés. Quand l'axe internucléaire ne coïncide pas avec l'axe de symétrie, le point stationnaire internucléaire ne se situera généralement pas sur l'axe et le chemin de liaison joignant les noyaux déviera ou sera en courbe par rapport à cet axe. L'amplitude et la direction de cette 'courbature de liaison', telles que déterminées par le chemin de liaison, sont en bon accord avec les résultats attendus sur une base chimique.

[Traduit par le journal]

Introduction

In the virial partitioning of a molecular system and its properties the topographical features of the (observable) molecular charge distribution $\rho(\boldsymbol{r})$ define the partitioning surfaces (1–4). Specifically, $\rho(\boldsymbol{r})$ is partitioned by those *closed* surfaces through which the flux of $\nabla\rho(\boldsymbol{r})$ is *everywhere* zero,

$$[1] \qquad \nabla\rho(\boldsymbol{r})\cdot\boldsymbol{n}(\boldsymbol{r}) = 0 \quad \forall \boldsymbol{r} \in S(\boldsymbol{r})$$

where $\boldsymbol{n}(\boldsymbol{r})$ is the vector normal to the surface $S(\boldsymbol{r})$. Equation 1 is derived as a boundary condition through the application of the variational principle in the definition of a quantum subspace (5). The virial partitioning of a molecular system is obtained by constructing for the system all surfaces which satisfy eq. 1. This set of surfaces divides a molecule into a collection of chemically identifiable atomic-like fragments. Each fragment so defined possesses a unique set of quantum properties; the hypervirial and virial theorems are obeyed and all properties of the fragment, including its *total* energy are rigorously defined. Thus any property of the total system may be equated to a sum of contributions from spatially defined fragments. The properties of the fragments coincide with expectations based on experimental chemistry (2–4, 6).

In this attempt to find a quantum mechanical basis for the observations upon which descriptive chemistry is founded, the unit which emerges as the fundamental carrier of chemical information is atomic-like in nature and not bond-like. Thus the subspace variational principle demonstrates that the physical basis for additivity and near constancy of (functional) group properties has

[1]To whom correspondence should be addressed.

its origin in a constancy or near constancy, respectively, of the charge distribution and properties of the atomic-like (virial) fragments as defined in real space (5, 7). The only property of the observable charge distribution of a molecular system which is 'bond-like' in nature (that is, of bi-nuclear character) is the path defining the line of maximum charge density linking certain pairs of neighbouring nuclei. This paper is concerned with the definition of such a 'bond path' and with the delineation of its properties.

Topography of a Molecular Charge Distribution

The bond path linking two nuclei is defined in terms of the same topological property of the charge distribution used to define the virial partitioning surface which lies between the same two nuclei. For this reason we first discuss and illustrate the general topological features of a molecular electronic charge distribution.

Stationary Points

Stationary points in a charge distribution $\rho(\boldsymbol{r})$ are points at which $\nabla\rho(\boldsymbol{r}) = 0$. In an isolated molecule, these are generally *saddle points* (i.e., points at which $\rho(\boldsymbol{r})$ is a minimum with respect to certain directions, and a maximum with respect to others). There are two types: *internuclear* and *ring* saddle points. Internuclear saddle points normally occur on or near the internuclear axes joining pairs of so-called 'bonded' nuclei. Such stationary points are illustrated in Fig. 1 for the cyclopropane molecule, labelled as A, B, and C. When the internuclear axis is a rotational symmetry axis, the saddle point lies on the axis and is coincident with the density minimum on it. Otherwise it normally lies off the axis a short distance from this minimum. For example, the internuclear stationary point C lying between the out-of-plane carbons is displaced by 0.11 au from the point of intersection of the corresponding C—C internuclear axis with the σ_v plane (Fig. 1). Ring saddle points lie at or near the centres of ring compounds (e.g., point D in Fig. 1).

Stationary points at which $\rho(\boldsymbol{r})$ is a minimum or maximum with respect to all directions are less common. An example of true minima would be the intermolecular stationary points in $\rho(\boldsymbol{r})$ for a collection of molecules (i.e., in a liquid or a solid). Another example, as pointed out by Collard and Hall (8), is the density minimum near the centre of a cage compound. As far as we are aware[2] there are no examples of stationary points which are true maxima in $\rho(\boldsymbol{r})$. One must remember that the maxima which occur at nuclei are not stationary points, as $\rho(\boldsymbol{r})$ exhibits a cusp at a nuclear position and hence $\nabla\rho(\boldsymbol{r})$ is undefined (9).

Gradient Paths

A single gradient path (GP) passes through each point $\boldsymbol{r}_k$ in $\rho(\boldsymbol{r})$, providing $\nabla\rho(\boldsymbol{r}_k)$ is both defined and non-zero (i.e., providing $\boldsymbol{r}_k$ is not a nuclear cusp or a stationary point). The GP through $\boldsymbol{r}_k$ is the combination of the path of steepest *ascent* with the path of steepest *descent* from that point (as traced by the vectors $\nabla\rho(\boldsymbol{r})$ and $-\nabla\rho(\boldsymbol{r})$, respectively).

A number of GP's are illustrated in Figs. 1 and 2. Such two-dimensional representations of GP's are possible only in symmetry planes (as $\nabla\rho(\boldsymbol{r})$ has a zero component perpendicular to symmetry planes). In this case, GP's always intersect contour lines at right angles. The more general three-dimensional picture may be mentally constructed if one visualizes shells of constant density instead of contours. GP's can then be readily visualized as they must run *normal* to all density shells.

All GP's must *originate* and *terminate* at either a nuclear cusp (where $\nabla\rho(\boldsymbol{r})$ is undefined) or at a stationary point (where $\nabla\rho(\boldsymbol{r}) = 0$). (By *origin* and *terminus* of a GP we refer to the points of minimum and maximum $\rho(\boldsymbol{r})$, respectively, on that path.) In an isolated molecule most GP's originate at infinity (where both $\rho(\boldsymbol{r})$ and $\nabla\rho(\boldsymbol{r})$ tend to zero) and terminate at nuclei (e.g., all GP's represented by solid lines in Fig. 1). It is those which do not that are of particular interest.

Definition of Molecular Fragments and Bond Paths

In the virial partitioning of a molecular system, molecular fragments are objectively and unambiguously defined by those *closed* surfaces through which the flux of $\nabla\rho(\boldsymbol{r})$ is everywhere zero (7). The restriction that the flux of $\nabla\rho(\boldsymbol{r})$ be

[2]The only known possible exception is $Li_2(X^1\Sigma_g^+)$ for which the Hartree–Fock $\rho(\boldsymbol{r})$ exhibits a maximum at the bond midpoint (10). This molecule has an extremely long equilibrium bond length ($\sim$5.0 au) and apparently has a double minimum in $\rho(\boldsymbol{r})$ along the internuclear axis. Whether this is a true feature of the charge distribution, or simply a shortcoming of the approximate wavefunction, is not known.

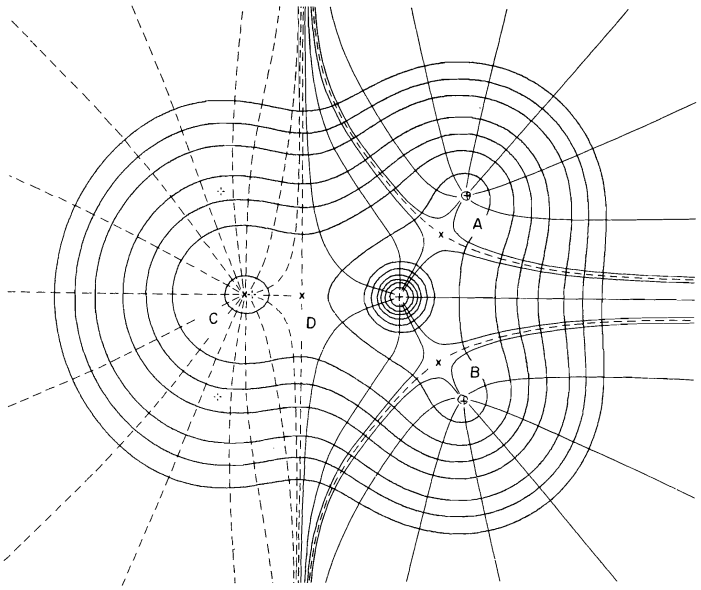

FIG. 1. Contour plot of the charge distribution in a σ_v symmetry plane of C_3H_6. Nuclei in the plane are denoted by plusses (+), and out-of-plane nuclei by broken plusses. The stationary points in $\rho(\boldsymbol{r})$ in this plane are denoted by × and labelled A through D. All gradient paths of $\rho(\boldsymbol{r})$ which lie in a partitioning surface are denoted by dashed lines; the two unique pairs of gradient paths which terminate at A and B denote the intersection with the σ_v plane of the partitioning surface between (C) and each (H); the gradient paths which terminate at stationary points C and D denote the partitioning surface between the out-of-plane carbons. All other gradient paths terminate at a nucleus. The contours increase inwards in the steps 2×10^n, 4×10^n, 8×10^n with n beginning at -3 and increasing in steps of unity.

everywhere zero is important in that it excludes surfaces which contain nuclei, since $\nabla\rho(\boldsymbol{r})$ is undefined there (9). The closure condition simply ensures a well-defined (not open-ended) fragment. Partitioning surfaces in an isolated molecule are generally closed by the zero-flux surface at infinity, where both $\rho(\boldsymbol{r})$ and $\nabla\rho(\boldsymbol{r})$ tend to zero.

The portions of the partitioning surfaces which occur at finite values of the coordinates are traversed by GP's which originate *and* terminate (both conditions are important) at stationary points in $\rho(\boldsymbol{r})$. Thus, a virial partitioning surface may be equivalently defined by *the collection of all gradient paths which both originate and terminate at stationary points in* $\rho(\boldsymbol{r})$. In Fig. 1, GP's which have this property are indicated by dashed lines. The GP's which terminate at stationary points A and B define the intersection with the σ_v symmetry plane of the partitioning surfaces which lie between the carbon and hydrogen fragments. There are actually six such surfaces. Only two of them intersect the plane illustrated. Those GP's which originate at infinity and terminate at stationary points C and D, together with the single gradient path which originates at D and terminates at C, define the partitioning surface which lies between the two out-of-plane carbon nuclei. There are actually three such surfaces. The two GP's which terminate at point D lie along the common intersection of these three surfaces (the C_3 rotational symmetry axis). The GP's denoted by dashed lines in Fig. 2 lie along the intersection of these surfaces with the σ_h symmetry plane.

Gradient paths may be used to define *bond paths* which link certain pairs of nuclei, as well as the partitioning surfaces which separate them. In a molecule, an internuclear saddle point may exist between a pair of neighbouring nuclei. The gradient paths which *terminate* at this saddle point define the partitioning surface which lies between them. The two gradient paths which *originate* at this same saddle point and terminate at each of the two nuclei define the *bond path*. Thus, whereas the paths of steepest descent from an internuclear saddle point define the partitioning surface, the two paths of steepest ascent from

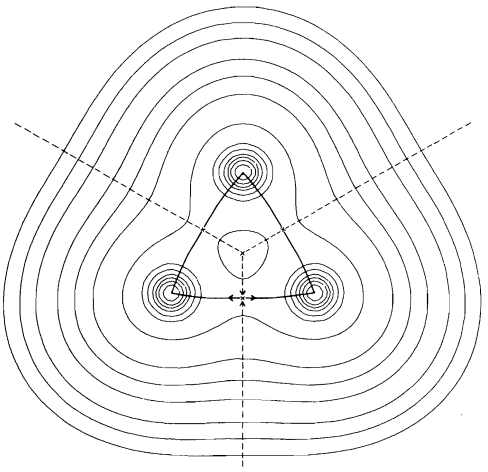

FIG. 2. Contour plot of $\rho(\boldsymbol{r})$ in the plane of the carbon nuclei in C_3H_6. Partitioning surfaces are denoted by dashed lines, the bond paths by solid lines joining the nuclei, and stationary points by ×. The directions of steepest ascent along the gradient paths in the partitioning surface and in the bond path are denoted by arrows for one pair of nuclei.

this same point to the nuclei define the *bond path*: *the path which follows the ridge of maximum charge density between a pair of bonded nuclei*. In those cases where an internuclear axis does not coincide with an axis of symmetry, the internuclear stationary point will not, in general, lie on the axis, and the bond path joining the two nuclei will deviate or curve from the internuclear axis. The magnitude and direction of this 'bond curvature' as reported below for a number of examples, agrees well with chemical expectations.[3]

Properties of the Bond Path

In cyclopropane (Fig. 2) the internuclear stationary points do not lie on the C—C internuclear axes. They are displaced outwards by 0.11 au. The line from a carbon nucleus to such a stationary point is called the *bond direction*, and the angle α formed by this line and the internuclear axis is 4.46°. The bond paths are curved out in this example. An experimental $\Delta\rho_{X-N}$ density difference map shows that the *bond density* (10*b*) in a three-membered ring compound peaks outside the nuclear triangle (13). Stevens *et al.* (14) have also noted that the ridge of maximum charge density obtained from an SCF wavefunction for cyclopropane is outwardly displaced from the internuclear axis.

The concept of 'ring strain', introduced to account for the increased reactivity of small ring compounds relative to that of their acyclic analogues, is given physical embodiment in the observed behaviour of the bond path in cyclopropane. The binding between a pair of nuclei is maximized when the bond path is coincident with the internuclear axis (10*b*, 15). In this case, the forces of attraction exerted on the nuclei by the charge density are maximized, as is the binding energy. In cyclopropane, not only does the ridge of maximum charge density lie off the internuclear axis, thereby resulting in a decrease in the binding energy, its displacement is such that it exerts a component of force on the nuclei tending to open the ring.

A ring structure may also exhibit an enhanced stability relative to its acyclic analogue. All nuclei comprising the ring are simultaneously attracted and bound by charge density lying within the geometrical boundary of the ring (16). If the bond path is displaced off each internuclear axis towards the interior of the ring, each nucleus will experience an increase in the force required to open the ring. An example of this behaviour is found for the benzene molecule, where the internuclear stationary points of the carbon ring are displaced off the axes towards the interior of the ring by 0.012 au with bond directions of 0.51°.

The recognition and definition of a bond path in an electronic charge distribution, together with the obvious electrostatic consequences its behaviour has on the forces which the electronic charge density exerts on the nuclei, provide a *common* explanation for the differing behaviour of cyclic compounds relative to their acyclic analogues: from 'ring strain energy' to 'resonance stabilization energy'.

In general, the bond direction (and its implied

[3]Martenson and Sperber (11) have previously suggested that one define "bond lines" as tracks of maximum charge density. However, no analytical definition of bond line was given and the authors expressed uncertainty as to which "density" function should be used to determine it. Qualitative bond lines were traced for cyclopropane using the density of a single bonded molecular orbital, and using the density difference distribution obtained from the valence electrons only. Neither distribution exhibits features common to the total charge distribution. Thus Martenson and Sperber found two maxima in these density functions lying off a C—C internuclear axis. These maxima determined the direction of the bond line. They concluded that any definition of bond line would be arbitrary. The definition of the bond path as given here in terms of a particular topological property of the *total* electronic charge distribution is nonarbitrary.

angle, α), as defined here in terms of a property of the charge density, is not expected to yield values as large as those obtained by models which both define and equate a 'bond' to some property of a localized or hybrid orbital. In their classic paper dealing with strain energy in cyclopropane, Coulson and Moffitt (17) obtained a value of 22° for the angle formed between the direction of the maximum in a hybrid orbital on carbon and the carbon–carbon internuclear axis.

There *are* preferred directions of bonding in a polyatomic system. The behaviour of the bond path offers a direct, quantitative measure of the importance, and with further study, of the energetic consequences of such geometrical restraints on the formation of a molecule.

The bond path, since it measures the real response of the electronic charge distribution to a particular nuclear arrangement, is not limited in its applicability or usefulness to systems where one postulates on *a priori* grounds the presence of strain or enhanced stability. Thus one finds the internuclear stationary points in the equilibrium geometries of H_2O and NH_3 to be displaced towards the interiors of these molecules, and their bond paths curved inwards. The bond direction, as measured in terms of the angle α with O or N at the apex, is 0.25° for H_2O and 0.24° for NH_3. In BH_3 with tetrahedral HBH angles, the bond paths are curved outwards and α, with B as apex, equals 6.26°.

The equilibrium geometry of BH_3 is planar and the charge distribution of pyramidal BH_3 is such that the ridge of maximum density is displaced off each B—H axis in a direction so as to exert an electrostatic force opening the bond angle. In H_2O (or NH_3), which is bent (or pyramidal) because of its ability to concentrate charge density in the binding region between the nuclei (16, 18), the ridge of maximum density is displaced so as to oppose an increase in the bond angles. Thus, information paralleling the relaxation of $\rho(\boldsymbol{r})$ caused by a change in bond angle, whether it facilitates or retards such a motion, is built into the static charge distribution as determined by the bond paths (19, 20).

If two fragments interact strongly within a molecular system, $\rho(\boldsymbol{r})$ in the region between their nuclei will exhibit a saddle point, and the nuclei will be linked by a bond path. This link will exist whether the strong interaction is a bonded one or a repulsive one, as in He_2 for example. Thus the existence of a bond path is a necessary (but not sufficient) condition for two atomic fragments to be bonded to one another.[4] In the charge distribution of H_2O for example, there are only two stationary points: internuclear saddle points between oxygen and each hydrogen. Thus, bond paths link the oxygen nucleus to each proton but no such link exists between the protons. The hydrogen fragments are not bonded to one another in the equilibrium water molecule. Alternatively, the two hydrogen fragments in H_2O do not share a common partitioning surface (12).

Bond path and bond direction are further examples of how chemically important concepts may be given rigorous definitions in terms of a property of the observable charge distribution.

Calculations

The electronic charge distributions used in the present study were calculated from the following wavefunctions: C_3H_6: a double-zeta function obtained by Snyder and Basch (21); C_6H_6: a minimal Slater function obtained by Stevens *et al.* (14); H_2O: a function of near Hartree–Fock quality obtained by Neumann and Moskowitz (22); NH_3: a function of near Hartree–Fock quality obtained by Rauk *et al.* (23); BH_3: a function of near Hartree–Fock quality obtained by Runtz and Bader (6).

1. R. F. W. BADER and P. M. BEDDALL. J. Chem. Phys. **56**, 3320 (1972).
2. R. F. W. BADER and P. M. BEDDALL. J. Am. Chem. Soc. **95**, 305 (1973).

[4]NOTE ADDED IN PROOF: It is possible that the sign of $\nabla^2\rho(\boldsymbol{r})$ at the saddle point $\boldsymbol{r}_s$ may be used to determine whether a given interaction is attractive or repulsive. It has been shown (24) that when $\nabla^2\rho(\boldsymbol{r}_s) < 0$, the potential energy density attains large negative values in the binding region while the kinetic energy density simultaneously is reduced in value. At an internuclear saddle point the curvature of $\rho(\boldsymbol{r}_s)$ parallel to the internuclear axis, $d^2\rho/dz^2 > 0$ while the perpendicular components, $d^2\rho/dx^2 = d^2\rho/dy^2 < 0$. When electronic charge is concentrated in the binding region as required for a bound state, the parallel curvature is decreased, the perpendicular values increased and hence $\nabla^2\rho(\boldsymbol{r}_s) < 0$. (In H_2 and N_2, $\nabla^2\rho(\boldsymbol{r}_s) = -1.27$ and -3.17 au at their respective R_e values.) In a repulsive state, charge density is removed from the binding region around $\boldsymbol{r}_s$, the parallel curvature of $\rho(\boldsymbol{r}_s)$ is greatly increased and $\nabla^2\rho(\boldsymbol{r}_s) > 0$. (In He_2 at $R = 2$ au, $\nabla^2\rho(\boldsymbol{r}_s) = +1.22$ au.) The stronger the binding, the more pronounced are the differing behaviours of the parallel and perpendicular curvatures of $\rho(\boldsymbol{r}_s)$. Thus the magnitude of $\nabla^2\rho(\boldsymbol{r}_s)$ is greater for N_2, than for C_2, than for Li_2.

3. R. F. W. BADER and R. R. MESSER. Can. J. Chem. **52**, 2268 (1974).
4. R. F. W. BADER. Acc. Chem. Res. **8**, 34 (1975).
5. S. SREBRENIK and R. F. W. BADER. J. Chem. Phys. **63**, 3945 (1975).
6. G. R. RUNTZ and R. F. W. BADER. Mol. Phys. **30**, 129 (1975).
7. R. F. W. BADER and G. R. RUNTZ. Mol. Phys. **30**, 117 (1975).
8. K. COLLARD and G. G. HALL. Int. J. Quantum Chem. To be published.
9. T. KATO. Commun. Pure Appl. Math. **10**, 151 (1975); E. STEINER. J. Chem. Phys. **39**, 2365 (1963); W. A. BINGEL. Z. Naturforsch. **18**a, 1249 (1963).
10. (*a*) S. BESNAINOU, M. ROUX, and R. DAUDEL. C. R. Acad. Bulg. Sci. **241**, 311 (1955); (*b*) R. F. W. BADER, W. H. HENNEKER, and P. E. CADE. J. Chem. Phys. 3341 (1967).
11. O. MARTENSON and G. SPERBER. Acta Chem. Scand. **24**, 1749 (1970).
12. R. F. W. BADER and R. A. GANGI. Specialist Periodical Reports, Theor. Chem. **2**, 1 (1975); Fig. 2.
13. D. A. MATTHEWS, G. D. STUCKY, and P. COPPENS. J. Am. Chem. Soc. **94**, 8001 (1972).
14. R. M. STEVENS, E. SWITKES, E. A. LAWS, and W. N. LIPSCOMB. J. Am. Chem. Soc. **93**, 2603 (1971).
15. R. F. W. BADER. The force concept in chemistry. *Edited by* D. B. Deb. In press.
16. R. F. W. BADER. J. Am. Chem. Soc. **86**, 5070 (1964).
17. C. A. COULSON and W. E. MOFFITT. Philos. Mag. **40**, 1 (1949).
18. R. F. W. BADER and H. J. T. PRESTON. Can. J. Chem. **44**, 1131 (1966).
19. R. F. W. BADER and A. D. BANDRAUK. J. Chem. Phys. **49**, 1666 (1968); R. F. W. BADER and J. L. GINSBURG. Can. J. Chem. **47**, 3061 (1969).
20. H. NAKATSUJI. J. Am. Chem. Soc. **96**, 24 (1973); **96**, 30 (1973).
21. L. C. SNYDER and H. BASCH. Molecular wave functions and properties. John Wiley and Sons, New York. 1972.
22. D. NEUMANN and J. W. MOSKOWITZ. J. Chem. Phys. **49**, 2056 (1968).
23. A. RAUK, L. C. ALLEN, and E. CLEMENTI. J. Chem. Phys. **52**, 4133 (1970).
24. R. F. W. BADER and H. J. T. PRESTON. Int. J. Quantum Chem. **3**, 327 (1969).

Vapour phase catalytic transformations of terpene hydrocarbons in the $C_{10}H_{16}$ series. IV. Effect of nitrogen, hydrogen, and pyridine on the dehydrogenation of Δ^3-carene over chromia and chromia–alumina catalysts

V. KRISHNASAMY[1] AND L. M. YEDDANAPALLI[2]

Department of Chemistry, Loyola College, Madras 600 034, India

Received January 25, 1977

V. KRISHNASAMY and L. M. YEDDANAPALLI. Can. J. Chem. **55**, 3046 (1977).

The influences of nitrogen, hydrogen, and pyridine on the conversion of 3-carene into various products over chromia catalyst at 450°C and over chromia–alumina at 400°C have been investigated. Nitrogen acts as a diluent over these catalysts; hydrogen at low partial pressures enhances the formation of cymenes over chromia, but suppresses its formation over chromia–alumina. Increase of the partial pressure of hydrogen increases the proportion of menthanes over chromia–alumina, but decreases it over chromia catalyst. Pyridine suppresses the over-all conversion of 3-carene and the formation of cymenes over chromia and chromia–alumina; however, it increases the formation of menthadienes over chromia–alumina. These observations are explained in terms of the acidity of chromia and chromia–alumina, the diluting effects of nitrogen, hydrogen, and pyridine, and their ability to adsorb and desorb over the catalyst surfaces.

V. KRISHNASAMY et L. M. YEDDANAPALLI. Can. J. Chem. **55**, 3046 (1977).

On a étudié l'influence de l'azote, de l'hydrogène et de la pyridine sur la conversion des carènes-3 en divers produits par passage sur un catalyseur de chrome à 450°C et sur un catalyseur de chrome–alumine à 400°C. L'azote agit comme un diluant sur ces catalyseurs; l'hydrogène, à des pressions partielles peu élevées, augmente la formation des cymènes sur le chrome mais supprime leur formation sur les complexes de chrome–alumine. Une augmentation de la pression partielle d'hydrogène augmente la proportion des menthanes sur le catalyseur de chrome–alumine mais la diminue sur le catalyseur de chrome. La pyridine supprime la conversion globale des carènes-3 et la formation des cymènes sur les catalyseurs de chrome et de chrome–alumine; toutefois elle augmente la formation des menthadiènes sur les catalyseurs de chrome–alumine. On explique ces observations en termes d'acidité des catalyseurs de chrome et de chrome–alumine, des effets diluant de l'azote, de l'hydrogène et de la pyridine et de leur habilité à s'adsorber et à se désorber sur les surfaces des catalyseurs.

[Traduit par le journal]

Introduction

Alumina, chromia, and chromia–alumina catalysts and their modified forms obtained by treating with hydrofluoric acid, potassium nitrate, sodium carbonate, etc. have been employed in this laboratory for the vapour-phase catalytic transformation of terpene hydrocarbons from Indian turpentine, with a view to convert them into stable useful intermediates. Isomerization and aromatization of β- and α-pinenes were already reported (1–4). Recently, the dehydrogenation of 3-carene over chromia and chromia–alumina catalysts, impregnated with potassium and fluoride ions, has been reported (5) with special reference to the ratio of *p*-cymene to *m*-cymene formed from 3-carene. The present study deals with the effect of nitrogen, hydrogen, and pyridine on the dehydrogenation of 3-carene. In the presence of these added substances the ratio between the cymenes does not show any appreciable change from that obtained in their absence; hence, this aspect is not reported here.

Experimental

Preparation of Materials

Alumina

Alumina was prepared by hydrolysing aluminium isopropoxide with distilled water (6). The precipitated aluminium hydroxide was filtered, washed thoroughly with water, and dried at 120°C for 24 h. It was activated at 500°C in dry air for 24 h, crushed into powder, and made into 4 × 4 mm cylindrical pellets.

Chromia Gel

The chromia gel catalyst was prepared and activated according to procedure described elsewhere (4, 7). The activated material was powdered and pelletized (4 × 4 mm cylindrical size). Prior to each run, the catalyst was reactivated by heating for 8 h in a current of dry air at 500°C until no oxides of carbon were detected in the exit

[1]Present address: Reader in Chemistry, A.C. College of Technology, University of Madras, Madras 600 025, India.

[2]Deceased.

gas, and then reduced by passing pure dry hydrogen for 6 h at the same temperature.

Chromia–Alumina

Chromia–alumina was prepared according to the methods of Selwood and Eischens (8) and Yeddanapalli *et al.* (9). The %Cr was estimated (9) to be 5.78.

3-Carene

First-quality Indian turpentine oil (Government Turpentine and Rosin Company, Bareilly, India) containing 50% 3-carene, 40% α-pinene, and 10% β-pinene was used. 3-Carene was obtained from this oil by fractionation at 10 mm, using a 152 cm glass column packed with stainless steel helices equivalent to 22 theoretical plates. The purity was found by gas chromatography to be better than 99%.

Pyridine

Analar pyridine (E. Merck) was refluxed over KOH pellets and fractionally distilled with careful exclusion of moisture, and the material distilling at 115.5°C/760 mm was collected. Its purity by gas chromatography was found to be better than 99%.

Nitrogen and Hydrogen

Nitrogen and hydrogen (Indian Oxygen Co.) were purified by passing successively through a silica gel drying tower, a tube containing freshly reduced copper turnings at 400°C, another silica gel tower, and finally through a trap cooled in liquid oxygen.

Apparatus and Procedure

The reactions were carried out at atmospheric pressure in a fixed-bed flow-type reactor. The catalyst (5 g) was placed in a Pyrex reaction tube, 25 cm long and 3 cm internal diameter. Above the catalyst bed, Pyrex glass beads (4 mm diameter) were placed to a height of 5 cm. The tube was inserted into the furnace, a cylindrical steel tube of internal diameter 4 cm, coated with a thin layer of asbestos and wound uniformly with nichrome wire, and heated electrically to the required temperature. 3-Carene was passed over the catalyst using a constant feed rate syringe pump that could be operated at different feed rates. The hydrogen and nitrogen supplies were controlled through precision 'Hoke' valves, and their flow rate was measured initially using a soap bubble flow meter, which was cut off during the experiment to avoid contamination of the catalyst with moisture. The flow rate was checked again at the end of the experiment. Various partial pressures of pyridine were achieved by mixing pyridine and 3-carene in different proportions.

The liquid products collected for the first 15 min of each run, which normally covers an hour, were discarded, and analysis was made only of the products collected after this time. This was done to ensure the attainment of a steady state for the reaction over the catalyst, and also to allow any temperature fluctuations due to the starting of the reaction to dissipate. After the reaction, the catalyst was regenerated as described earlier.

The liquid products of dehydrogenation were identified and estimated using a Perkin-Elmer Infracord Model-137 and a Perkin-Elmer Vapour Fractometer Model 154-D. Products other than cymenes were quantitatively estimated by a Perkin-Elmer Column K, consisting of a 2-m column of carbowax on chromosorb. The column temperature for the best resolution within a reasonable time was found to be 115°C with a hydrogen inlet pressure of 15 psi. *Para*- and *meta*-cymenes were separated and estimated in a specially prepared 2-m column filled with 40–60 mesh acid-washed kiesulguhr, coated with the stationary liquid, consisting by weight of 9% Bentone-34 and 4% Apiezon-L, heated at 108°C with hydrogen passed at a pressure of 28 psi.

For the identification of different peaks in a chromatogram, retention times for the different compounds were found by introducing pure substances kindly donated by Hercules Powder Company, U.S.A. For quantitative analysis, exactly reproducible quantities of synthetic mixtures containing the different compounds in varying proportions were introduced, and calibration curves relating the concentration with the peak heights were drawn. Since the peaks obtained were sharp and symmetrical, peak heights were used as a measure of concentration. Initial experiments, in which both peak heights and the total areas were compared using mixtures of known concentrations, gave identical results. The formation of the various products in this investigation can be accounted for by schemes presented earlier (5).

Results and Discussion

Results obtained over chromia and chromia–alumina in the presence of nitrogen, hydrogen, and pyridine are given in Figs. 1 to 3. To estimate the extent to which hydrogen and pyridine inhibit or enhance the over-all conversion of 3-carene, as well as the distribution of the products, the results were compared with those obtained using nitrogen as a diluent. The effects of partial pressures of nitrogen, hydrogen, and pyridine on the conversion of 3-carene over chromia and chromia–alumina are presented in Fig. 1. Figure 2 illustrates the influence of these substances on the formation of cymenes over chromia and chromia–alumina. The proportions of menthadienes and menthanes formed over these catalysts are shown in Fig. 3.

When 3-carene mixed with nitrogen at various partial pressures was passed over chromia gel catalyst, its conversion and product formation were reduced. The same effect of nitrogen was observed over chromia–alumina catalyst, but the formation of menthadienes increased directly with the partial pressure of nitrogen. The total acidities of chromia and chromia–alumina were 0.14 and 0.64 milliequivalent of *n*-butylamine, respectively (5). The higher acidity of chromia–alumina may be responsible for the increased formation of menthadienes.

Effect of Hydrogen

The increase in partial pressure of hydrogen, like that of nitrogen, decreased the total conversion of 3-carene. But, the decrease due to hydrogen was less pronounced at all partial

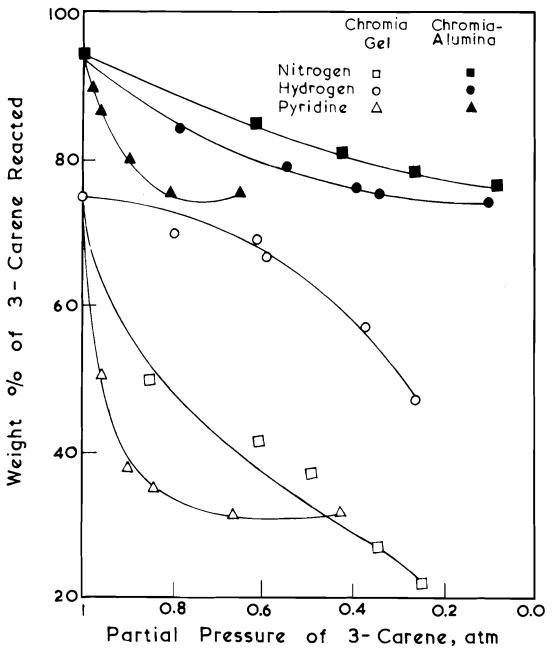

FIG. 1. Effect of partial pressure of nitrogen, hydrogen, and pyridine on the overall conversion of Δ^3-carene over chromia gel catalyst at 450°C and over chromia–alumina catalyst at 400°C. LHSV = 2.

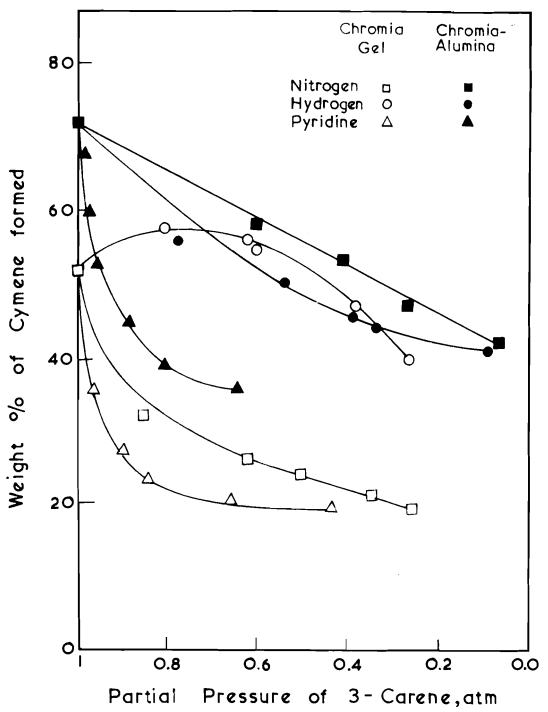

FIG. 2. Effect of partial pressure of nitrogen, hydrogen, and pyridine on the formation of cymenes from Δ^3-carene over chromia catalyst at 450°C and over chromia–alumina catalyst at 400°C. LHSV = 2.

pressures, as compared to nitrogen (Fig. 1). It may be noted that the formation of cymenes increases even though there is a decrease in the conversion of 3-carene.

The above observations may be explained as follows. Hydrogen over chromium oxide is easily desorbed (10) and therefore its presence on the surface of the catalyst does not seriously affect the conversion of 3-carene. It is presumed that hydrogen reduces the unsaturated compounds that precede the formation of polymers and of coke which would deposit on the active centers of the catalyst as in an earlier scheme (5). On suppressing the formation of polymers and coke, the formation of cymenes goes up. The fall in the activity of chromia at higher partial pressures of hydrogen may be due to further reduction of catalyst surface available for reaction.

Hydrogen has a different effect over chromia–alumina compared to chromia. Hydrogen decreases both 3-carene conversion and the formation of cymenes, but the level of reduction is much below that due to nitrogen (Figs. 1 and 2). Formation of menthadines does not vary significantly, but that of menthanes increases with the partial pressure of hydrogen. The decrease in the conversion of 3-carene and the formation of cymenes may be attributed to the preferential adsorption over chromia–alumina of hydrogen compared to 3-carene. The observed results are in agreement with the findings of Selwood (11) and Greensfelder (12). Presumably the adsorbed hydrogen is transferred to the adsorbed menthadines and hydrogenates them to menthanes, thus increasing the yield of menthanes.

Effect of Pyridine

Pyridine markedly reduces the conversion of 3-carene over chromia while only a small reduction is noted over chromia–alumina. In either case, the poisoning influence of pyridine is greater compared to nitrogen as diluent. These observations can be related to the acidity of these two catalysts. The alumina used as a support for chromia in this investigation was found (13) to contain strong, medium, and weak acid sites. Pyridine being a strong base can neutralise the strong and medium sites preferentially, without affecting the weak sites, which are still capable of isomerizing 3-carene to menthadienes. Parry (14) has also reported that pyridine does not affect the weak sites on alumina. The acid sites in chromia possibly may not be active in an

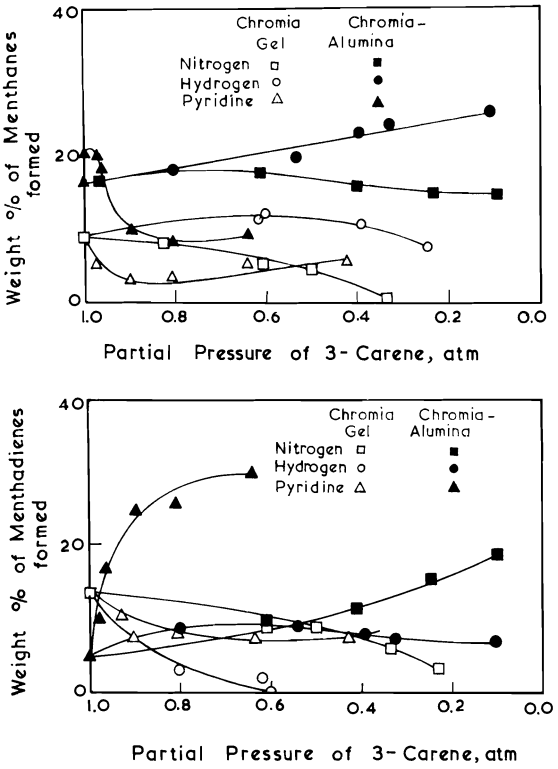

FIG. 3. Effect of partial pressure of nitrogen, hydrogen, and pyridine on the formation of menthadines and menthanes from Δ^3-carene over chromia catalyst at 450°C and chromia–alumina catalyst at 400°C. LHSV = 2.

atmosphere of pyridine, thus accounting for the observed reduction in the conversion of 3-carene.

Though there is a notable difference in the conversion of 3-carene over chromia and chromia–alumina, as discussed above, there is not much difference in the reduction of cymenes over these catalysts. For instance, cymenes formed over chromia and chromia–alumina in the absence of pyridine are 52 and 76% respectively; the amounts are reduced to 35 and 56% when the partial pressure of pyridine is 0.04 atm (Fig. 2). This effect may be attributed to the tendency of pyridine to interact with the chromium ions. This is supported by the findings of Stanislaus and Yeddanapalli (4) on the dehydrogenation of α-pinene over chromia–alumina. Quinoline is also found to reduce the dehydrogenation and the dehydration activity of chromia (15).

Over chromia pyridine suppresses the formation of both menthanes and menthadienes, but over chromia–alumina it favours the formation of menthadienes; menthanes, however, show only an initial increase. Heats of combustion (16) and of hydrobromination (17) show that cyclopropane ring has double bond character, and that the ring may undergo fission via addition. Hence, the cyclopropane ring in 3-carene can isomerize (5) to *p*- and *m*-menthadienes by the weak acid sites, which are left unaffected by pyridine. The menthadines formed may not possibly be dehydrogenated, since the dehydrogenation sites may have interacted with the pyridine molecules as mentioned above. Krishnasamy and Yeddanapalli (5) have observed a similar increase of menthadienes in the presence of potassium ions.

Pyridine at low concentrations may catalyse hydrogen transfer reactions among the menthadienes to form menthanes. Pines and Kolobielski (18) have also noted hydrogen transfer reactions among cyclic diolefins in the presence of base catalysts.

Acknowledgements

We thank the Ministry of Education, Government of India, and the Council of Scientific and Industrial Research, New Delhi for financial support.

1. V. KRISHNASAMY, P. RATNASAMY, and L. M. YEDDANAPALLI. Chem. Age India, **21**, 597 (1970).
2. V. KRISHNASAMY, P. RATNASAMY, and L. M. YEDDANAPALLI. Chem. Age India, **22**, 14 (1971).
3. A. STANISLAUS and L. M. YEDDANAPALLI. Can. J. Chem. **50**, 61 (1972).
4. A. STANISLAUS and L. M. YEDDANAPALLI. Can. J. Chem. **50**, 113 (1972).
5. V. KRISHNASAMY and L. M. YEDDANAPALLI. Can. J. Chem. **54**, 3458 (1976).
6. H. PINES and W. O. HAAG. J. Am. Chem. Soc. **83**, 2847 (1961).
7. J. TURKEVICH *et al.* J. Am. Chem. Soc. **63**, 1129 (1941).
8. P. W. SELWOOD and R. P. EISCHENS. J. Am. Chem. Soc. **69**, 1590 (1947).
9. L. M. YEDDANAPALLI *et al.* Symposium on contact catalysis. Calcutta. 1956.
10. H. PINES, C. T. GEOTSCHEL, and J. W. DEMBINSKI. J. Org. Chem. **30**, 3530 (1965).
11. P. W. SELWOOD. J. Am. Chem. Soc. **88**, 2676 (1966).
12. B. S. GREENSFELDER. Chem. Eng. Prog. **43**, 561 (1947).
13. V. KRISHNASAMY. Indian J. Chem. In press.
14. E. P. PARRY. J. Catal. **2**, 371 (1963).
15. J. C. KURIACOSE and M. V. C. SASTRI. Proceedings of the Third International Congress on Catalysis. Amsterdam. 1964. p. 507.
16. J. W. KNOWLTON and F. D. ROSSINI. J. Res. Nat. Bur. Stand. **19**, 249 (1937); **43**, 113 (1949).
17. J. R. LACHER, A. KINAPOUR, and J. D. PARK. J. Phys. Chem. **61**, 1124 (1957).
18. H. PINES and M. KOLOBIELSKI. J. Am. Chem. Soc. **79**, 1698 (1957).

Transition state activity coefficients in the acid-catalyzed hydrolysis of amides

TOMASZ A. MODRO, KEITH YATES, AND FRANÇOISE BEAUFAYS
Department of Chemistry, University of Toronto, Toronto, Ont., Canada M5S 1A1

Received March 8, 1977

TOMASZ A. MODRO, KEITH YATES, and FRANÇOISE BEAUFAYS. Can. J. Chem. **55**, 3050 (1977).

The transition-state activity coefficient ($f_{S\neq}$) approach has been applied to the acid-catalyzed hydrolysis of benzamide and its *N*-alkyl derivatives. For all systems (with the exception of the *N-tert*-butyl derivative which reacts via carbon–nitrogen bond cleavage) a uniform type of medium dependence of log $f^*_{S\neq}$ is observed. The reaction shows a pronounced destabilization of $S^{\neq}$ over the whole region of acidity studied, practically identical to that found for the A_{Ac}-2 type of ester hydrolysis. This is interpreted in terms of an A_OT2 mechanism of amide hydrolysis, that is the rate-determining formation of the oxonium-type tetrahedral intermediate from the O-protonated form of substrate conjugate acid.

TOMASZ A. MODRO, KEITH YATES et FRANÇOISE BEAUFAYS. Can. J. Chem. **55**, 3050 (1977).

On a appliqué le coefficient d'activité des états de transition ($f_{S\neq}$) à l'hydrolyse acido-catalysée de la benzamide et de ses dérivés *N*-alkylés. Pour tous les systèmes (à l'exception du dérivé *N-tert*-butylé qui réagit par l'intermédiaire d'une coupure du lien carbone–azote), on a observé un type uniforme de relation entre le milieu et le log $f^*_{S\neq}$. La réaction présente une déstabilisation prononcée de $S^{\neq}$ à toutes les valeurs d'acidité étudiées et cette déstabilisation est pratiquement identique à celle trouvée pour l'hydrolyse d'esters de type A_{Ac}-2. On interprète ces résultats en termes d'un mécanisme A_OT2 pour l'hydrolyse des amides qui implique la formation, dans l'étape déterminante, d'un intermédiaire tétraédrique de type oxonium à partir de la forme O-protonée de l'acide conjugué du substrat.

[Traduit par le journal]

The controversial question of the predominant protonation site in amides now seems to be definitely resolved in favour of oxygen-protonation;[1] this holds in both regions of moderate and low concentrations of aqueous acids (1). The O-protonated conjugate acid probably represents the major intermediate on the reaction path in the acid-catalyzed hydrolysis of amides, but this is not established. Recent results of Williams (2) on the acidic hydrolysis of *N,N*-dialkylacetamides indicate that the percentage of reaction proceeding via the N-protonated form of conjugate acid (existing in very low concentration but possibly highly reactive) is less than 0.02%. However, this conclusion involves necessary assumptions about the compounds used as models for N-protonated amides. The only reported example of amide hydrolysis via S_N2 displacement in the N-conjugate acid is a special case of acid-catalyzed collapse of *N*-nitrosoamides (3).

The present work concerns the hydrolysis of benzamide and a series of its *N*-alkyl and *N,N*-dialkyl derivatives in moderately concentrated aqueous sulfuric acid, and was undertaken to provide possible support for the mechanism involving O-protonated amide as the reactive intermediate. The approach used has been successfully applied previously in mechanistic studies of acid-catalyzed ester hydrolysis (4) and aromatic substitution (5). It is based on expected differences in solvation requirements of different types of transition state and involves examination of the behaviour of the activity coefficients of transition states as a function of the acidity (or water activity) of the reaction medium. For the acid-catalyzed hydrolysis of amides there are principally four distinct mechanistic schemes that have to be taken into account (6). Three of them involve bimolecular rate-determining nucleophilic attack of water on the substrate conjugate acid (A-2 mechanisms). The fourth scheme represents unimolecular rate-determining cleavage of the N-protonated amide (A-1 mechanism). The first of the A-2 reaction paths (designated as the A_OT2 mechanism (6)) involves rate-determining formation of the tetrahedral intermediate from the O-protonated substrate; in the second (designated as A_NT2) the tetrahedral intermediate is formed in a rate-determining step from the N-protonated substrate. The mechanism designated as A_ND2 involves a rate-

[1]See however the recent article of M. Liler in ref. 18.

determining, synchronous displacement of ammonia (or amine) by water from the N-protonated conjugate acid, and the last scheme (designated as A_N^D1) involves a unimolecular rate-determining cleavage of the N-protonated substrate to give the ammonia (or amine) molecule and an acylium ion. The possible transition states (and intermediates which directly follow them) for these four mechanistic schemes can be represented by the structures **i**–**iv**. Since the reactivity of the amides studied is

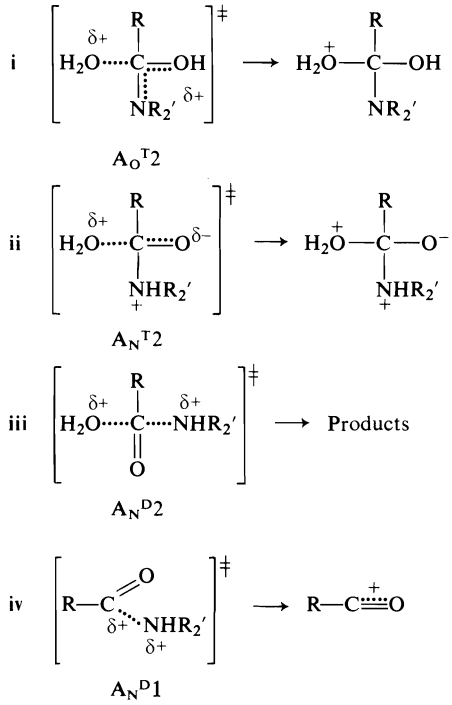

very low, on the basis of the Hammond postulate a 'late' transition state can be assumed for the hydrolysis pathway. The transition states **i**, **ii**, and **iv** would be therefore expected to resemble the intermediates which follow (tetrahedral structures or acylium ion); for **iii** a high degree of charge dispersion would be expected. The A_O^T2 scheme corresponds closely to the $A_{Ac}2$ mechanism of acid-catalyzed ester hydrolysis (4) and the transition state, due to advanced charge localization and a considerable degree of oxonium ion character, should be characterized by strong requirements for hydrogen-bonding type of solvation. By analogy with the $A_{Ac}2$ process (4), the transition state for A_O^T2 mechanism should exhibit a marked salting-out effect (or destabilization) when the availability of water in the reaction medium is decreased. By contrast, in the A_N^D2 and A_N^D1 mechanisms, the corresponding transition states are characterized by significant charge dispersion and at least partial ammonium ion character. This should result in much lower hydration requirements and therefore in lower sensitivity to changes in the composition of the reaction medium. Moreover, since the nitrogen in **iii** and **iv** has a partially ammonium ion character, it would be expected to show different hydration (hydrogen bonding) requirements depending on the number of hydrogen atoms present on nitrogen (R′ = H or alkyl). In consequence, a decrease in the salting-out effect should be observed in the series primary > secondary > tertiary amides (7).

It is difficult to predict the behaviour of the transition state corresponding to the polycharged intermediate **ii** in the A_N^T2 process. At any rate, it should be distinctly different from that for the A_O^T2 mechanism, for which a close resemblance to the transition state of the bimolecular ester hydrolysis is expected. In summary, essentially different behaviour is anticipated for the transition state activity coefficients for the alternative hydrolysis mechanisms as a response to the variation of the aqueous acid composition.

The transition state activity coefficient $f^*_{S\neq}$ (relative to a standard tetraethylammonium ion)[2] can be expressed as a sum of the following quantities (4):

$$[1]\quad \log f^*_{S\neq} = \log k_0 - \log k_\psi^{corr} + pK_{SH^+} + \log f_S + \log a^*_{H^+}$$

In [1] k_0 is the rate constant for the slow step and the log k_0 term can be separated as the intercept of a plot of log $(f^*_{S\neq}/k_0)$ vs. acid concentration. k_ψ^{corr} is the observed pseudo-first-order rate constant, corrected for partial protonation of the substrate; i.e. $k_\psi^{corr} = k_\psi^{obs}(1 + I)$, where I is the ionization ratio $[SH^+]/[S]$. pK_{SH^+} is the amide acidity constant and can be obtained from conventional ionization ratio measurements. f_S represents substrate activity coefficient and can be determined by means of solubility or distribution measurements. Finally, $a^*_{H^+}$ is the proton activity (expressed as relative

[2]Since the activity coefficients of single ionic species are not directly accessible, they are usually expressed as relative to the standard, tetraethylammonium ion (8): $f^*_{Z^+} \equiv f_{Z^+}/f_{TEA^+}$.

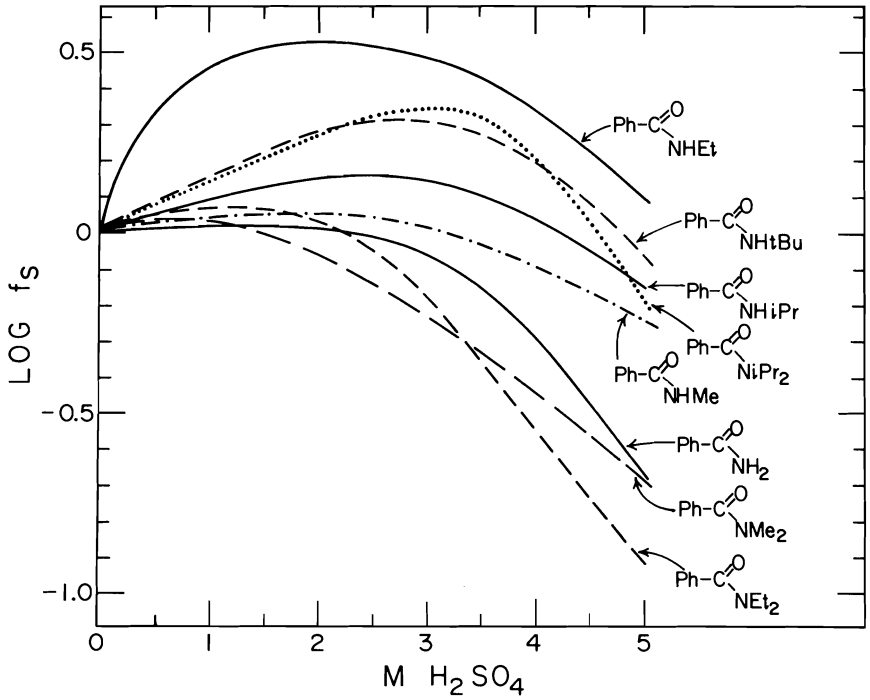

FIG. 1. Activity coefficient variation for benzamides.

to the TEA^+ ion) and its values are available (9) for various aqueous acid solutions.

We have determined the required quantities (eq. 1) for some amides of the structure PhC(O)-NRR′ (R,R′ = H, alkyl) in order to examine the log $f^*_{S\ddagger}$ dependence on the acidity of the reaction medium and to compare this behaviour with that of log $f^*_{S\ddagger}$ for related reactions and of log f_+* of some stable model cationic species.

Results and Discussion

Activity Coefficient Data

The distribution method (7) was employed in all cases, using chloroform as the inert organic solvent. The distribution coefficients were corrected for the partial ionization of amides in the aqueous phase. The activity coefficients determined for eight benzamides at different concentrations of sulfuric acid are represented graphically in Fig. 1.[3] For all compounds, similar behaviour was observed; an initial mild salting-out (destabilization) followed by a moderate salting-in (stabilization) effect. The variations in the individual values of f_S over the acidity range employed never exceed one logarithmic unit (usually ca. 0.5 log unit) and therefore the log f_S term in [1] does not contribute very significantly to the over-all calculation of the transition state activity coefficients.

Basicity of Amides

Ionization ratios ($I = [SH^+]/[S]$) for the five *N*-alkyl derivatives of benzamide were obtained spectrophotometrically by conventional methods (10). Plots of log I values against the amide acidity function H_A showed good linearity (correlation coefficients >0.99) over a wide range of acidity. The slopes m and intercepts of those plots for the series of benzamides discussed are presented in Table 1. The values of the slope m show significant deviations from 'ideal' behaviour (slope of unity) for some of the *N*-alkyl derivatives. For secondary amides these deviations are not large, although slightly greater than those (m = 1.03–0.93) reported by Barnett and O'Connor (12) for a series of ring-substituted *N*-alkylbenzamides. For the *N*,*N*-dialkyl substituted system, a systematic decrease in the d log I/d($-H_A$) value was observed with an increase of the size of the alkyl groups (0.90, 0.73,

[3]The values of activity coefficients (Table 4) are available, at a nominal charge, from the Depository of Unpublished Data, CISTI, National Research Council of Canada, Ottawa, Canada K1A 0S2.

TABLE 1. Protonation behaviour in aqueous H_2SO_4

Amide	m (slope of log I vs. $-H_A$) (corr. coef.)	pK_{SH^+} (intercept)
Ph—C(=O)—NH_2 [a]	0.99	−1.74
Ph—C(=O)—NHMe [a]	1.02	−1.7
Ph—C(=O)—NMe_2 [a]	0.90	−1.4
Ph—C(=O)—NHEt	0.88 (>0.999)	−1.60
Ph—C(=O)—NEt_2	0.73 (>0.995)	−1.28
Ph—C(=O)—NH-*i*-Pr	0.92 (>0.990)	−1.73
Ph—C(=O)—N-*i*-Pr_2	0.57 (>0.994)	−0.85
Ph—C(=O)—NH-*tert*-Bu	0.84 (>0.995)	−1.48

[a]Taken from ref. 11.

0.57, respectively). The reason for this steric effect on the acidity dependence of the ratio f_{SH^+}/f_S (which increases with diminishing water activity more rapidly for bulky tertiary than for primary and secondary amides) is not quite clear. In the conjugate acid Ph—$C(OH)NR_2^+$ the oxonium-like OH group is always syn to one of the alkyl groups R and its solvation is probably subject to significant steric hindrance. When water is removed from the medium, the (partly) compensating solvation by bisulfate ions may be less effective for steric reasons and the cation is more rapidly salted-out relative to the conjugate acids derived from primary and secondary amides.[4]

Rate Constants

Rates of hydrolysis were measured spectrophotometrically by a conventional method (13). For all compounds there is a sufficiently large difference in the uv spectrum of the substrate and product (benzoic acid) for the reaction to be followed by measuring the change of the absorbance of the reaction mixture in the range 210–240 nm. The hydrolysis is slow and all kinetic runs were carried out at elevated temperatures. In Table 2 are listed pseudo-first-order rate constants for the five amides as a function of acidity. In Fig. 2 some typical rate profiles, determined at 70.9°C, are displayed, together with data previously obtained (13) for benzamide and its *N,N*-dimethyl derivative, interpolated to the same temperature. All compounds show similar rate–acidity dependence, with a broad rate maximum at about 30% H_2SO_4, typical of amide hydrolysis in acidic solutions (cf. ref. 14). The only exception is *N-tert*-butylbenzamide, which will be discussed later. The overall hydrolysis rate is markedly suppressed by alkyl substitution at nitrogen particularly for the *N,N*-dialkyl derivatives. A systematic decrease in k_ψ values with an increase of the bulk of the alkyl groups is observed with the *N,N*-diisopropyl derivative being 3 to 4 × 10^3 times less reactive than the parent benzamide. This sensitivity of the rates to steric effects in itself argues against the mechanistic models of hydrolysis involving C—N bond cleavage in the rate-determining step (mechanisms A_N^D2 and A_N^D1). If these mechanisms were operating, some rate enhancement due to the relief of steric crowding would be expected with increasing substitution at nitrogen.

The behaviour of *N-tert*-butylbenzamide is quite different; spectrophotometrically measured rate constants increase with acidity more rapidly than those for other substrates, and at ca. 40% H_2SO_4 the rate profile merges into that of benzamide itself. Close similarity of rate profiles for acid-catalyzed hydrolysis of 4-chlorobenzamide and its *N-tert*-butyl derivative has also been observed by Hyland and O'Connor (15). It was demonstrated some time ago by Lacey (16) that the hydrolysis of various *N-tert*-alkyl substituted amides in strong mineral acids proceeds with an alkyl carbon – nitrogen bond fission, giving first the tertiary alcohol and unsubstituted amide. We have confirmed this observation for the *N-tert*-butylbenzamide; the nmr analysis of the reaction mixture showed the exclusive formation of *tert*-butyl alcohol, no *tert*-butylamine being detected in the products. In this case the hydrolysis can be therefore described by [2*a*] and [2*b*]. The uv spectro-

[4]Since the value of pK_{SH^+} is included in [1] as a constant, any possible error in its determination does not affect the behaviour of log f_+* as a function of acidity.

TABLE 2. Rates of hydrolysis in sulfuric acid

	$10^6 \times k_{obs}$ (s^{-1})								
	Ph—C(=O)—NHEt	Ph—C(=O)—NEt_2	Ph—C(=O)—NH-*i*-Pr			Ph—C(=O)—N-*i*-Pr_2	Ph—C(=O)—NH-*tert*-Bu		
H_2SO_4 (%)	70.9°C	70.9°C	70.9°C	85.2°C	98.8°C	70.9°C	59.8°C	70.9°C	85.4°C
8.06		0.625				0.00645		4.06	
11.00								5.41	
15.08	2.86	1.00	0.795	1.62	4.26	0.0132	2.89	10.70	46.00
20.61					7.85		5.32	16.90	
22.74	3.38	1.53	1.48	3.86	10.96				154.3
28.64	4.20	1.67		4.63	12.97	0.0262	11.05	40.75	230
34.49		1.15		3.76	10.78				
34.73			1.83				16.48	59.30	280
40.44	2.93	0.94	1.24	1.56		0.0269	21.80	64.60	276.3
44.96									204
45.52							17.04	53.40	

[2*a*] Ph—C(O)NH-*tert*-Bu $\xrightarrow{H^+, H_2O}$ Ph—C(O)NH_2 + *tert*-BuOH

[2*b*] Ph—C(O)NH_2 $\xrightarrow{H^+, H_2O}$ Ph—CO_2H + NH_3

photometric method enables one to follow only step [2*b*], since the spectroscopic changes accompanying the conversion secondary → primary benzamide are insignificant. It can be seen from the rate profiles in Fig. 2 that up to ca. 40% H_2SO_4 the step [2*a*] (de-*tert*-butylation) is slower than step [2*b*] (benzamide hydrolysis) whereas this order is reversed above that acidity. The alkyl–nitrogen cleavage step [2*a*] can be followed by nmr due to the different chemical shifts for the *tert*-butyl hydrogens of the substrate and the alcohol. We have determined the half-life of *N*-*tert*-butylbenzamide in 96% H_2SO_4 by the nmr method, and the corresponding value of k_ψ at 25°C is ca. 1.9×10^{-4} s^{-1}. This value can also be estimated indirectly from the uv measurements. From the rates determined at three different temperatures (Table 2), the corresponding rate profile for the hydrolysis of *N*-*tert*-butylbenzamide at 25°C could be obtained. The linear section of this log k_ψ – acidity plot (up to 30% H_2SO_4) has been extrapolated to higher acidities, giving approximate value of k_ψ (25°C) in 96% H_2SO_4 equal 2×10^{-4} s^{-1}. The good agreement with k_ψ value obtained by nmr indicates that the spectrophotometrically (uv) determined rate profile at acidities below 40% H_2SO_4 (Fig. 2) indeed corresponds to the acid-catalyzed de-*tert*-butylation step [2*a*]. Hydrolysis involving prior alkyl–nitrogen cleavage seems to operate only for tertiary alkyl derivatives. Nuclear magnetic resonance analysis of the reaction mixture for the hydrolysis of *N*,*N*-diisopropylbenzamide (the least reactive member of the series) showed the formation of diisopropylamine as the exclusive product, that is by the 'normal' acyl–nitrogen cleavage pathway.

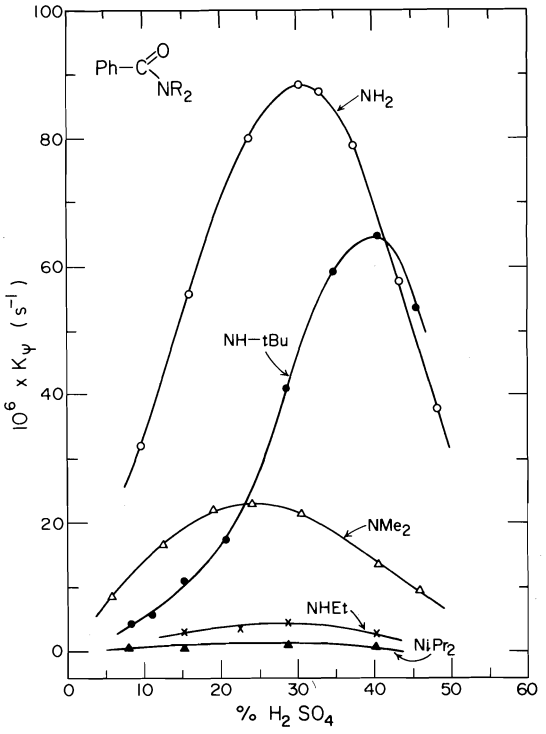

FIG. 2. Rate profiles for hydrolysis of benzamides.

The hydrolysis of the *N*-*tert*-butylbenzamide

TABLE 3. Transition state[a] activity coefficients for amide hydrolysis in sulfuric acid solutions at 25°C

	$\log f^*_{S\ddagger}$			
H_2SO_4 (M)	Benzamide[a]	*N*-Methylbenzamide[a]	*N*-Isopropylbenzamide	*N*,*N*-Dimethylbenzamide[a]
0.5	0.55	0.41	0.41	0.49
1.0	1.00	0.80	0.80	0.91
1.5	1.34	1.11	1.20	1.27
2.0	1.57	1.42	1.43	1.47
2.5	1.86	1.71	1.69	1.72
3.0	2.17	2.02	2.01	2.01
3.5	2.43	2.29	2.28	2.31
4.0	2.63	2.54	2.54	2.54
4.5	2.83	2.89	2.90	2.88
5.0	3.04	3.21	3.22	3.20

[a]Values of log $k\psi$ taken or extrapolated from data in ref. 13.

must be considered as a distinct type of acid-catalyzed cleavage of an amide system. This process by itself presents some interesting mechanistic problems, such as the role of water in the dealkylation step, and the structural requirements for the mechanistic change from the acyl–nitrogen to the alkyl–nitrogen bond fission pattern. These questions can only be answered by more comprehensive studies on the rate–acidity and rate–structure dependence for this type of hydrolysis and work on acid-catalyzed amide hydrolysis proceeding via alkyl–nitrogen cleavage is in progress in this laboratory. For the purpose of this work, however, the *N-tert*-butyl derivative has been excluded from the transition state activity coefficient treatment.[5]

Log $f^*_{S\ddagger}$ for Amide Hydrolysis

Values of log $f^*_{S\ddagger}$ as a function of sulfuric acid concentration have been calculated for benzamide and its *N*-methyl, *N*,*N*-dimethyl, and *N*-isopropyl derivatives. These models have been chosen in order to examine the behaviour of the log $f^*_{S\ddagger}$ values for primary, secondary, and tertiary systems, as well as for secondary amides substituted at nitrogen by alkyl groups of different size. The necessary rate data at 25°C were available for benzamide (13), and for remaining substrates were obtained by extrapolating the Arrhenius plots determined at higher temperatures. The values of log $f^*_{S\ddagger}$ (eq. 1) in the 0.5–5.0 M sulfuric acid region are listed in Table 3.

The data in Table 3 show the remarkable similarity in log $f^*_{S\ddagger}$ values for all four substrates over the whole range of acidity, despite the large variations in observed rate. This is evidence of the close structural parallel of the transition states involved, which in turn implies a uniformity of mechanism of hydrolysis for these derivatives. Since all systems are salted-out (destabilized) with an increase of acidity to approximately the same extent, it appears that the number of hydrogen atoms present at the nitrogen is not important in determining the overall solvation requirements of the transition state. Such a result indicates that only a minor fraction of the positive charge is localized on the nitrogen in the transition state. In Fig. 3, values of log $f^*_{S\ddagger}$ are plotted as a function of water activity in the aqueous solutions of sulfuric acid. The behaviour of log $f^*_{S\ddagger}$ for the amide hydrolysis is compared in Fig. 3 with the behaviour of the activity coefficients of some relevant systems, the transition state for the $A_{Ac}2$ type of ester hydrolysis (4) and two stable cationic species: the conjugate acids of alcohols (17) (oxonium ion with localized charge and high hydration requirements) and amides (7). The values of log $f^*_{S\ddagger}$ for benzamide and its *N*-alkyl derivatives parallel closely the plot characteristic for the $A_{Ac}2$ mechanism of ester hydrolysis. This is well illustrated by comparison of the behaviour of one of the amides studied with the log $f^*_{S\ddagger}$ – acidity plot for the hydrolysis of *p*-nitrobenzyl

[5]It is worth pointing out that the log $f^*_{S\ddagger}$ values for the *N-tert*-butylbenzamide calculated from the rate data up to 35% H_2SO_4 (Fig. 2) show that the transition state activity coefficient behaviour is indeed different from that of remaining amides. A weaker salting-out effect is observed, as might be expected for the essentially different mechanism not involving an oxonium ion-like transition state. However, this log $f^*_{S\ddagger}$ behaviour for the *N-tert*-butyl derivative is also different from that of *tert*-butyl acetate hydrolysis (4) indicating that the reaction does not represent the typical A-1 process in which the formation of the *tert*-butyl carbonium ion constitutes the rate-determining step.

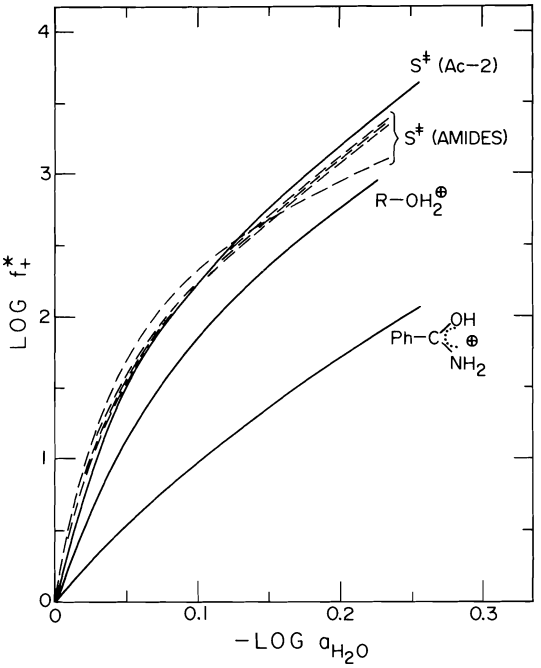

FIG. 3. Activity coefficients of cationic molecules and transition states (relative to TEA^+).

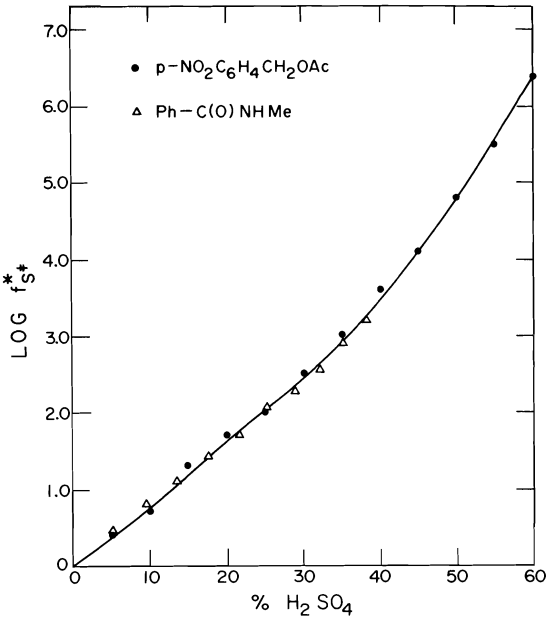

FIG. 4. Transition state activity coefficients for hydrolysis of *p*-nitrobenzyl acetate and *N*-methylbenzamide.

acetate, an ester which is believed to react according to the $A_{Ac}2$ mechanism over the whole range of sulfuric acid concentrations (4). Such a comparison, made for the *N*-methylbenzamide, is presented in Fig. 4. An examination of the log $f^*_{S^{\ddagger}}$ behaviour for hydrolysis of amides and esters leads to the obvious conclusion that for both systems the transition states must resemble each other very closely in solvation requirements, and in the degree of development of oxonium ion character. This can be interpreted in terms of highly advanced transition states, resembling in both cases the corresponding tetrahedral intermediate:

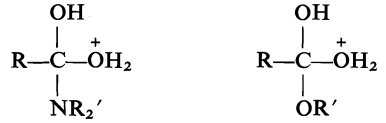

We believe therefore that the generally observed behaviour of the log $f^*_{S^{\ddagger}}$ for amide hydrolysis as a function of medium composition is only compatible with the $A_O{}^T2$ mechanistic pattern.

Experimental

Materials

N,N-Diethylbenzamide was prepared from benzoyl chloride and diethylamine in benzene; bp 99°C/0.6 Torr. *Anal.* calcd. for $C_{11}H_{15}NO$: C 74.54, H 8.53, N 7.90; found: C 74.64, H 8.55, N 7.93. Remaining amides were commercially available, and were purified by recrystallization.[6] Acid solutions were prepared by diluting the concentrated sulfuric acid with distilled water. The concentrations of these solutions were determined from their densities; densities were measured with a DMA 02C digital precision density meter at 25.0°C.

Activity Coefficient Measurements

All activity coefficients were determined by the distribution method (7): a 10^{-2}–10^{-3} *M* solution of the amide in chloroform (ACS Grade) was shaken mechanically with 5 ml of water or the aqueous sulfuric acid solution for 5 min in a thermostatically controlled (25 ± 0.5°C) box. The aqueous layer was transferred to the uv cell and the absorbance of the amide was measured at the wavelength maximum (Table 5), using a Cary 14 spectrophotometer. The concentration of the amide in acidic solution was corrected for partial ionization of the substrate. The values of the activity coefficients were calculated from the ratio of the distribution coefficient in pure water to that in an acid solution.

Measurements of Basicity Constants

A stock solution of the substrate in methanol (0.5 µl) was introduced into 3.0 ml of the aqueous acid in a uv cell by means of a Hamilton Precision Syringe, and the uv spectrum was measured immediately. The range of acid concentrations generally included at least ten

[6]The uv characteristics of the substrates and their conjugate acids (Table 5) are available, at a nominal charge, from the Depository of Unpublished Data, CISTI, National Research Council of Canada, Ottawa, Canada K1A 0S2.

samples in the region $-1.0 \leq \log I \leq 1.0$, as well as solutions in which the substrate is unprotonated and fully protonated.

Rate Determinations

A stock solution of amide was prepared in the appropriate sulfuric acid and 12–14 samples were prepared for each kinetic run by sealing 3 ml of the solution in glass ampoules. The ampoules were allowed to equilibrate in an oil bath thermostatted to ± 0.1°C, and were quenched in ice when withdrawn. Runs were followed to ca. 2 half-lives. Infinity points A_∞ were obtained in duplicate or triplicate and were reproducible to $\pm 1.0\%$. Rate constants were obtained in the usual way from plots of $\ln (A_t - A_\infty)$ vs. time.

Product Determination

The substrate was dissolved in aqueous sulfuric acid and the hydrolysis was followed by recording the nmr spectrum of the solution in the range of 0–3 δ. For the *N-tert*-butylbenzamide the initial signal of the *tert*-butyl group (δ ~ 1.8) disappeared gradually and was replaced by the signal corresponding to the *tert*-butyl group of *tert*-butyl alcohol (δ ~ 1.1); no signal corresponding to the *tert*-butylamine was detected. The cleavage product was identified by adding authentic samples of *tert*-butyl alcohol and *tert*-butylamine to the sample tube. Similar experiments for *N,N*-diisopropylbenzamide demonstrated exclusive formation of diisopropylamine; no traces of 2-propanol were observed.

The rate of the de-*tert*-butylation of *N-tert*-butylbenzamide was determined in a similar way. The progress of reaction was followed by measuring the ratio of the integrated peak areas for the *tert*-butyl group of the substrate and product as a function of time.

Acknowledgements

The continued financial assistance of the National Research Council of Canada is gratefully acknowledged.

1. R. A. McClelland and W. F. Reynolds. J. Chem. Soc. Chem. Commun. 824 (1974).
2. A. Williams. J. Am. Chem. Soc. **98**, 5645 (1976).
3. B. C. Challis and S. P. Jones. J. Chem. Soc. Perkin Trans. II, 153 (1975).
4. R. A. McClelland, T. A. Modro, M. F. Goldman, and K. Yates. J. Am. Chem. Soc. **97**, 5223 (1975).
5. T. A. Modro and K. Yates. J. Am. Chem. Soc. **98**, 4247 (1976).
6. C. R. Smith and K. Yates. J. Am. Chem. Soc. **94**, 8811 (1972).
7. K. Yates and R. A. McClelland. Prog. Phys. Org. Chem. **11**, 323 (1974).
8. R. H. Boyd. J. Am. Chem. Soc. **85**, 1555 (1963).
9. T. A. Modro, K. Yates, and J. Janata. J. Am. Chem. Soc. **97**, 1492 (1975).
10. K. Yates, J. B. Stevens, and A. R. Katritzky. Can. J. Chem. **42**, 1957 (1964).
11. K. Yates and J. B. Stevens. Can. J. Chem. **43**, 529 (1965).
12. J. W. Barnett and C. J. O'Connor. J. Chem. Soc. Perkin Trans. II, 1331 (1973).
13. C. R. Smith and K. Yates. J. Am. Chem. Soc. **93**, 6578 (1971).
14. J. T. Edward and S. C. R. Meacock. J. Chem. Soc. 2000 (1957); C. R. Smith and K. Yates. J. Am. Chem. Soc. **93**, 6578 (1971); C. J. Hayland and C. J. O'Connor. J. Chem. Soc. Perkin Trans. II, 1402 (1973); M. S. Shingare, D. B. Ingle, and D. D. Khandkar. J. Ind. Chem. Soc. 4, **L11**, 599 (1975).
15. C. J. Hyland and C. J. O'Connor. J. Chem. Soc. Perkin Trans. II, 1402 (1973).
16. R. N. Lacey. J. Chem. Soc. 1633 (1960).
17. D. C. Lee and R. Cameron. J. Am. Chem. Soc. **93**, 4724 (1971).
18. M. Liler. Adv. Phys. Org. Chem. **11**, 267 (1975).

Comment: Lifetimes of the solvated electron in liquid alcohols

J. H. BAXENDALE AND PETER WARDMAN[1]

Chemistry Department, University of Manchester, Manchester M13 9PL, England

Received February 22, 1977

J. H. BAXENDALE and PETER WARDMAN. Can. J. Chem. **55**, 3058 (1977).

The solvated electron, e_s^-, decays with first-order kinetics in pulse-irradiated aliphatic alcohols, attributed to reaction 1: $e_s^- + ROH \rightarrow$ products. It is suggested that a recent report of curved Arrhenius plots for the temperature dependence of the rate constants for reaction 1 can be ascribed to reaction of e_s^- with impurities.

J. H. BAXENDALE et PETER WARDMAN. Can. J. Chem. **55**, 3058 (1977).

Dans des alcools aliphatiques irradiés par pulsation, l'électron solvaté e_s^- se décroît avec une cinétique du premier ordre par une réaction attribuée á: $e_s^- + ROH \rightarrow$ des produits [1]. On attribue à la réaction de e_s^- avec des impuretés la nature recourbée des traces d'Arrhénius, décrivant la relation entre les constantes de vitesse et la temperature, pour la réaction 1 qui ont été rapportées dans un travail récent.

[Traduit par le journal]

Recently, Bolton, Jha, and Freeman (1) measured the lifetimes of the solvated electron produced by pulse radiolysis of liquid alcohols, and compared their values of the first-order rate constants, k_1

[1] $$e_s^- + ROH \rightarrow \text{products}$$

at various temperatures with the data previously reported by Baxendale and Wardman (2). Bolton *et al.* (1) observed an order of magnitude shorter lifetimes of e_s^- at low temperatures than Baxendale and Wardman, and also shorter lifetimes than are predicted from the Arrhenius extrapolation of their higher temperature values. In fact, their Arrhenius plots were curved, and they stated that "the earlier reported linearity (2) is questionable". No basis for this statement was given.

Our data were published (2) in the form of the equation

[2] $$k_1 = A_1 \exp(-E_1/RT)$$

with values of $\log_{10}(A/s^{-1})$ and E_1/kJ mol^{-1} together with the least-squares standard deviations from measurements at 12–15 temperatures between ca. 170 and 340 K. We present some details in Fig. 1, which shows that for changes in k_1 of three orders of magnitude, "Our direct measurements.....are closely described by the Arrhenius expression....." (2).

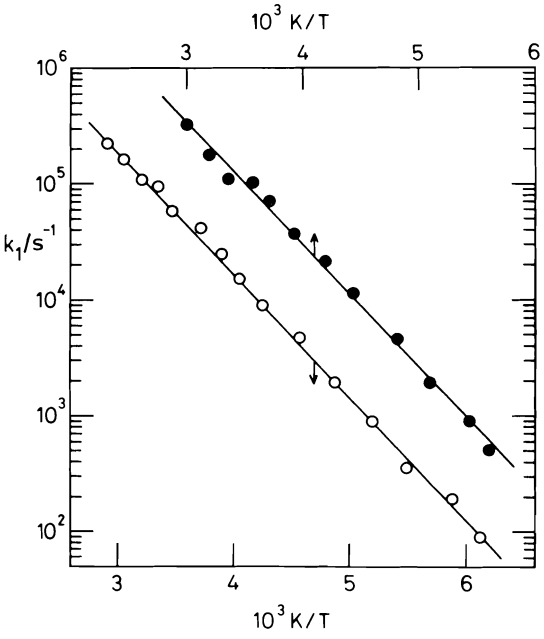

FIG. 1. Arrhenius plots for the exponential decay of e_s^- in alcohols containing 1 mmol dm^{-3} sodium alkoxide. ○, ethanol (lower abscissa). ●, methanol (upper abscissa).

Electron decay studies in 'pure' liquids have always been bedevilled by the question of liquid purity and hence we would hesitate to claim that our results are the last word on this matter. However, we found that impurities which shorten the lifetime of e_s^- had relatively more effect at lower temperatures, i.e. the apparent E_1 increased with purification. Clearly, curved

[1]Present address: Cancer Research Campaign Gray Laboratory, Mount Vernon Hospital, Northwood, Middlesex HA6 2RN, England.

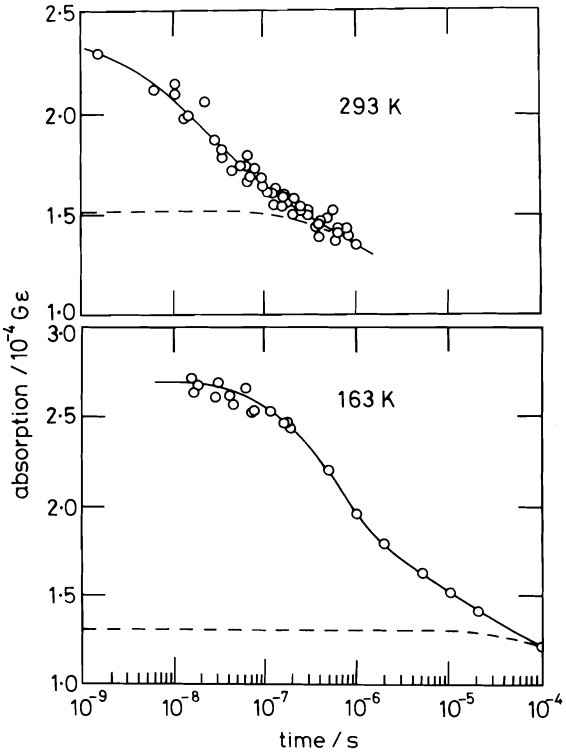

FIG. 2. Absorption of e_s^- after nanosecond pulse radiolysis of ethanol at 163 and 293 K. Dose ~600 rad.

Arrhenius plots may also arise in this way and the higher values of k_1 at low temperatures reported by Bolton *et al.* (1) suggest that impurities in the alcohols are the reason for their curves. We purified ethanol by the borohydride technique (3) and methanol by fractional distillation from basic solution under nitrogen.

Our values of k_1 were derived from analysis of the final, exponential portion of the decay of e_s^- after nanosecond pulse radiolysis of alcohols containing 1 mmol dm^{-3} base. Prior to this exponential 'free ion' decay, there is a more rapid decay process due to recombination with geminate ions or radicals in the spur. We showed (2) that in pure alcohols at low temperatures the whole of the 'free' and 'spur' e_s^- could be observed, and presented time–concentration data for methanol and 1-butanol at 187 K demonstrating the amounts of these two contributions. In Fig. 2 we give the corresponding data for ethanol at 163 and 293 K. The dotted line is the 'free ion' contribution to the total e_s^-, obtained by extrapolation of the exponential decay. The kinetic separation of 'free' and 'spur' ions can easily be made at both temperatures even in neutral alcohols, and is made easier by the addition of base. Values of k_1 and the ratio of geminate to free ions (2) were obtained from analyses of the final, exponential portion of the decay of e_s^-, over ca. 3 half-lives. The initial ~10% of the free-ion decay was ignored in this analysis (i.e. the whole of the data in Fig. 2 would be excluded) to eliminate possible contributions from a small amount of spur decay still occurring on this timescale.

1. G. L. BOLTON, K. N. JHA, and G. R. FREEMAN. Can. J. Chem. **54**, 1497 (1976).
2. J. H. BAXENDALE and P. WARDMAN. Chem. Commun. 429 (1971).
3. J. H. BAXENDALE and P. WARDMAN. J. Chem. Soc. Faraday Trans. I, **69**, 584 (1973).

Reply: Lifetimes of the solvated electron in liquid alcohols

GORDON R. FREEMAN
Chemistry Department, University of Alberta, Edmonton, Alta., Canada T6G 2G2

Received March 7, 1977

GORDON R. FREEMAN. Can. J. Chem. **55**, 3059 (1977).

A reply is given to the preceding Comment concerning the kinetics of the decay of e_s^- in alcohols.

GORDON R. FREEMAN. Can. J. Chem. **55**, 3059 (1977).

On fait une réponse au commentaire qui précède concernant la cinétique de la décroissance du e_s^- dans des alcools.

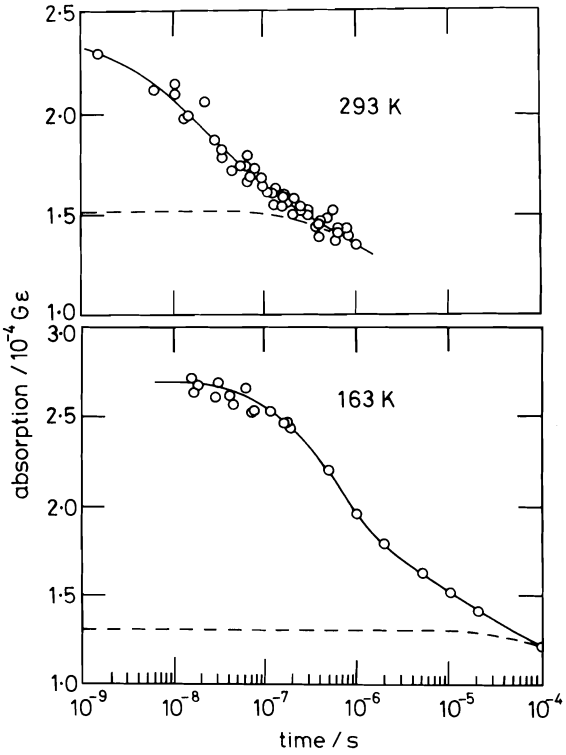

FIG. 2. Absorption of e_s^- after nanosecond pulse radiolysis of ethanol at 163 and 293 K. Dose ~600 rad.

Arrhenius plots may also arise in this way and the higher values of k_1 at low temperatures reported by Bolton *et al.* (1) suggest that impurities in the alcohols are the reason for their curves. We purified ethanol by the borohydride technique (3) and methanol by fractional distillation from basic solution under nitrogen.

Our values of k_1 were derived from analysis of the final, exponential portion of the decay of e_s^- after nanosecond pulse radiolysis of alcohols containing 1 mmol dm^{-3} base. Prior to this exponential 'free ion' decay, there is a more rapid decay process due to recombination with geminate ions or radicals in the spur. We showed (2) that in pure alcohols at low temperatures the whole of the 'free' and 'spur' e_s^- could be observed, and presented time–concentration data for methanol and 1-butanol at 187 K demonstrating the amounts of these two contributions. In Fig. 2 we give the corresponding data for ethanol at 163 and 293 K. The dotted line is the 'free ion' contribution to the total e_s^-, obtained by extrapolation of the exponential decay. The kinetic separation of 'free' and 'spur' ions can easily be made at both temperatures even in neutral alcohols, and is made easier by the addition of base. Values of k_1 and the ratio of geminate to free ions (2) were obtained from analyses of the final, exponential portion of the decay of e_s^-, over ca. 3 half-lives. The initial ~10% of the free-ion decay was ignored in this analysis (i.e. the whole of the data in Fig. 2 would be excluded) to eliminate possible contributions from a small amount of spur decay still occurring on this timescale.

1. G. L. BOLTON, K. N. JHA, and G. R. FREEMAN. Can. J. Chem. **54**, 1497 (1976).
2. J. H. BAXENDALE and P. WARDMAN. Chem. Commun. 429 (1971).
3. J. H. BAXENDALE and P. WARDMAN. J. Chem. Soc. Faraday Trans. I, **69**, 584 (1973).

Reply: Lifetimes of the solvated electron in liquid alcohols

GORDON R. FREEMAN
Chemistry Department, University of Alberta, Edmonton, Alta., Canada T6G 2G2

Received March 7, 1977

GORDON R. FREEMAN. Can. J. Chem. **55**, 3059 (1977).

A reply is given to the preceding Comment concerning the kinetics of the decay of e_s^- in alcohols.

GORDON R. FREEMAN. Can. J. Chem. **55**, 3059 (1977).

On fait une réponse au commentaire qui précède concernant la cinétique de la décroissance du e_s^- dans des alcools.

The preceding comment by Baxendale and Wardman (1) focusses attention on the important and difficult problem of interpreting data when the kinetics of the reaction are not simple. The decay of electrons in irradiated alcohols follows nonhomogeneous kinetics inside the spurs and homogeneous kinetics outside the spurs. The decay outside the spurs is generally accepted to occur by pseudo-first-order reactions which, in a purified alcohol, are much slower than the spur reactions. The rate of the former is obtained from the tail of the optical absorption signal at long times. However, it is not always clear at what point the contribution of spur electrons to the absorption signal becomes negligible (see Fig. 2 of ref. 1). The earlier (2) discussion of this problem may have been obscured by the mass of other data in that paper.

As a basis for questioning the linearity of the Arrhenius plots (1) we gave a full column of discussion (2). It is also difficult to assess data for which the pulse dose has not been given. Qualitatively, Wardman lowered the dose as the temperature was lowered, because the longer decay times permitted greater electronic smoothing.[1] The resulting smaller amount of secondary reaction at lower pulse doses might tend to straighten the Arrhenius plot of the electron decay rate. On the other hand, we have stated (2) and Wardman has emphasized (1) that artifacts might also have caused the curvature we observed.

Solution to the problem requires further work.

1. J. H. BAXENDALE and P. WARDMAN. Can. J. Chem. This issue.
2. G. L. BOLTON, K. N. JHA, and G. R. FREEMAN. Can. J. Chem. **54**, 1497 (1976).

[1]P. Wardman and J. H. Baxendale. Private communication. May 1977.

Erratum: Electronic excited states of small ring compounds. IV. Bicyclo[2.1.0]pentanes by the photocycloaddition of cyclopropenes to olefins

D. R. ARNOLD AND R. M. MORCHAT

The Photochemistry Unit, Department of Chemistry, University of Western Ontario, London, Ont., Canada N6A 5B7

Received May 19, 1977

(Ref.: Can. J. Chem. **55**, 393 (1977))

Our inconsistent use of units on page 398 may cause confusion. The rate constants listed in Table 1 are given in units of s^{-1} as indicated. In the Arrhenius plot (Fig. 5) and for the kinetic parameter given, the rate constants are in units of min^{-1} (not indicated). The preexponential term is $\log A = 12.9 \pm 0.4\ s^{-1}$.

A template synthesis of nickel 6,8,15,17-tetramethyldibenzo[*b*,*i*][1,4,8,11]-tetraazacyclotetradeca-2,4,7,9,12,14-hexaene

A. R. CUTLER AND D. DOLPHIN

Department of Chemistry, The University of British Columbia, Vancouver, B.C., Canada V6T 1W5

Received April 21, 1977

A. R. CUTLER and D. DOLPHIN. Can. J. Chem. **55**, 3062 (1977).

The title macrocyclic nickel complex has been conveniently prepared in moderate yield using 2,5-dimethyl-3*H*-1,5-benzodiazepine, or a mixture of *o*-phenylenediamine and pentane-2,4-dione in a template synthesis using nickel salts. The previous low yield synthesis of this macrocycle required condensation of nickel bisacetylacetonate in molten *o*-phenylenediamine.

A. R. CUTLER et D. DOLPHIN. Can. J. Chem. **55**, 3062 (1977).

Le complexe macrocyclique du nickel du titre est préparé avec un rendement moyen en utilisant la diméthyl-2,5 benzo[3*H*]diazépine-1,5 ou un mélange de *o*-phénylènediamine et de pentanedione-2,4 dans une synthèse modèle faisant intervenir des sels de nickel. La synthèse antérieure, à bas rendement de ce macrocycle, consiste en la condensation du bis-acétylacétonate de nickel dans la *o*-phénylènediamine fondue.

[Traduit par le journal]

Metal complexes of the fully conjugated macrocycle (**1**) are but one example of synthetic tetraaza macrocyclic complexes (1) that have gained importance as metalloporphyrin models (2). Synthetic entry into complexes of type **1** has

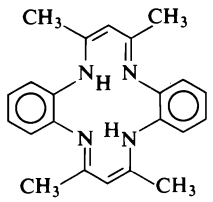

1

been limited by the availability of its nickel complex (**2**), which had previously been prepared in low yield from the reaction of nickel bisacetylacetonate in excess *molten* *o*-phenylenediamine (3). Removal of the nickel from **2** with acid, followed by remetallation, has then provided other metal complexes of **1** (4). We report here a convenient template synthesis of **2**.

The reaction of 2,4-dimethyl-3*H*-1,5-benzodiazepine (**3**) (5) and nickel(II) acetate (2:1) in refluxing aqueous ethanol gave a 31% yield of the emerald green nickel complex (**2**). Removal of solvent from this reaction mixture and washing with water left a green residue containing **2** and a magenta filtrate which contained nickel complexes of 2-methylbenzimidazole (6).[1] Similar work-up of a refluxing aqueous ethanol solution of *o*-phenylenediamine, pentane-2,4-dione, and nickel(II) acetate (2:2:1) provided a somewhat lower yield (15%) of **2**.

Similar reactions between the 2,4-dimethyl-1,5-benzodiazepinium salt (**5**) (R = CH_3) and nickel salts afforded only nickel complexes of 2-methylbenzimidazole. In contrast, the parent benzodiazepinium salt (**5**) (R = H) has been shown to undergo a stepwise template reaction, via the uncyclized nickel tetradentate complex of *N*,*N*′-di-(*o*-aminophenyl)-1-amino-3-iminopropene, to give the related nickel macrocyclic complex of 6,8,15,17-tetramethyldibenzo[*b*,*i*]-[1,4,8,11]tetraazacyclotetradeca-2,4,7,9,12,14-hexaene.

Formation of the nickel macrocyclic complex (**2**) under the above critical conditions involves two competing pathways via the monoanil intermediate (**4**). The monoanil (**4**) is the postulated intermediate for both the hydrolytic ring con-

[1]The yield of this reaction was evidently concentration dependent. Thus a decrease in the concentration of the reagents from that in the Experimental section greatly diminished the yield of **2**. In addition the choice of solvolytic conditions was critical and although this had not been optimized, substitution of either ethanol or water alone afforded only minor amounts of **2**.

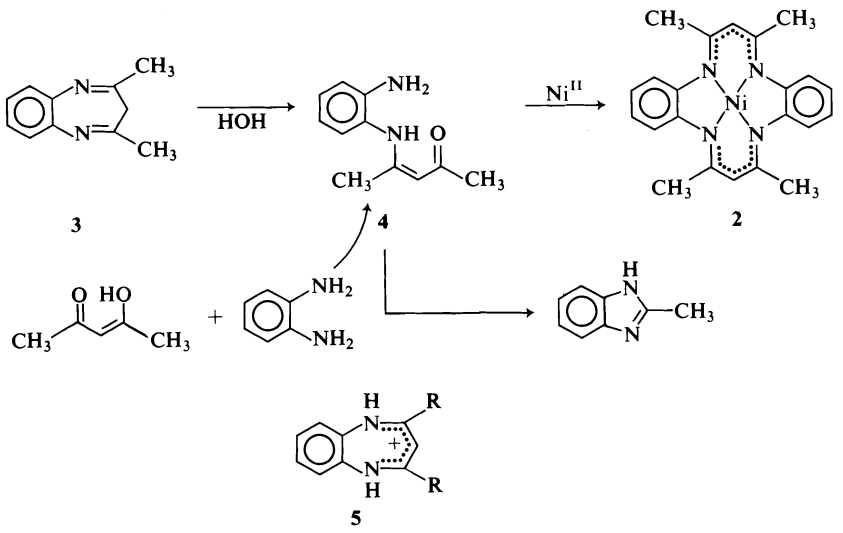

traction of **3** to 2-methylbenzimidazole as well as for the condensation of *o*-phenylenediamine and pentane-2,4-dione to **3** (5, 8). Thus the monoanil (**4**) generated in our reactions either degrades to 2-methylbenzimidazole or undergoes a metal template cyclization to **2**.

It is hoped that the straightforward template synthesis of **2** and analogous macrocyclic complexes (7, 9) will increase their availability.

Experimental

Nickel acetate (12.443 g, 0.050 *M*) was added as a hot aqueous solution (40 ml) to an ethanolic solution of 2,4-dimethyl-3*H*-1,5-benzodiazepine (17.223 g, 0.100 *M*). The resulting magenta solution changed to an emerald green suspension after refluxing 4 h. Removal of solvent under reduced pressure and washing the greenish brown residue with water (200 ml) afforded a green solid. After air drying, the green solid, in a minimum volume of methylene chloride (60 ml), was added to a column of dry alumina (18 × 6 cm; Camag neutral, activity I, 160 g). Elution of this column with methylene chloride cleanly removed a dark green band containing the desired nickel macrocycle (**2**) (6.323 g, 31.5%). The nmr spectrum of the highly soluble **2** was especially diagnostic, $CDCl_3$(TMS) δ 2.19 (s, 12H, CH_3), 4.73 (s, 2H, CH), 6.61 (multiplet, 8H, Ar-H).

Acknowledgments

This work is a contribution from the Bioinorganic Chemistry Group and was supported by operating and negotiated development grants from the National Research Council of Canada. In addition, the authors gratefully acknowledge the donors of the Petroleum Research Fund, administered by the American Chemical Society, for their generous support.

1. L. F. Lindoy and D. H. Busch. Prep. Inorg. React. **6**, 1 (1971); L. F. Lindoy. Chem. Soc. Rev. **4**, 421 (1975).
2. S. Koch, R. H. Holm, and R. B. Frankel. J. Am. Chem. Soc. **97**, 6714 (1975), and references cited therein.
3. E.-G. Jager. Z. Anorg. Allg. Chem. **364**, 177 (1969).
4. V. L. Goedkin, J. Molin-Case, and Y. Whang. J. Chem. Soc. Chem. Commun. 337 (1973); V. L. Goedkin, S. Peng, and Y. Park. J. Am. Chem. Soc. **96**, 284 (1974); V. L. Goedkin and Y. Park. J. Chem. Soc. Chem. Commun. 214 (1975); L. G. Bell and J. C. Dabrowiak. J. Chem. Soc. Chem. Commun. 512 (1975); D. R. Neves and J. C. Dabrowiak. Inorg. Chem. **15**, 129 (1976).
5. G. A. Archer and L. H. Sternbach. Chem. Rev. **68**, 747 (1968); D. Lloyd and H. P. Cleghorn. Adv. Heterocycl. Chem. **17**, 27 (1974).
6. R. J. Sundberg and R. B. Martin. Chem. Rev. **74**, 471 (1974).
7. A. R. Cutler and D. Dolphin. Submitted for publication.
8. J. A. Barltrop, C. G. Richards, D. M. Russel, and G. Ryback. J. Am. Chem. Soc. **81**, 1132 (1959); J. O. Halford and R. M. Fitch. J. Am. Chem. Soc. **85**, 3354 (1963); D. Lloyd, R. H. McDougall, and D. R. Marshall. J. Chem. Soc. 3785 (1965).
9. C. L. Honeybourne. Inorg. Nucl. Chem. Lett. **11**, 191 (1975).

Canadian Journal of Chemistry

Published by
THE NATIONAL RESEARCH COUNCIL OF CANADA

Journal canadien de chimie

Publié par
LE CONSEIL NATIONAL DE RECHERCHES DU CANADA

Volume 55 Number 17 September 1, 1977 Volume 55 numéro 17 1 septembre 1977

Crystal and molecular structure of 1,1′-bi(3,3,4,4-tetrafluoro-2-diphenylphosphinocyclobutene)

STEVEN J. RETTIG AND JAMES TROTTER

Department of Chemistry, University of British Columbia, 2075 Wesbrook Mall, Vancouver, B.C., Canada V6T 1W5

Received February 2, 1977

STEVEN J. RETTIG and JAMES TROTTER. Can. J. Chem. **55**, 3065 (1977).

Crystals of 1,1′-bi(3,3,4,4-tetrafluoro-2-diphenylphosphinocyclobutene) are monoclinic, a = 10.398(1), b = 18.484(1), c = 15.984(1) Å, β = 107.76(1)°, Z = 4, space group $P2_1/c$. The structure was solved by direct methods and was refined by full-matrix least-squares procedures to a final R of 0.042 and R_w of 0.057 for 4226 reflections with $I \geq 3\sigma(I)$. The molecule has a *cisoid* configuration about the central C—C bond, the angle between the two cyclobutene rings being 34.3°. The overall molecular symmetry is approximately C_2 with a P...P separation of 3.661(1) Å. Bond lengths and angles in the molecule are generally in good agreement with accepted values.

STEVEN J. RETTIG et JAMES TROTTER. Can. J. Chem. **55**, 3065 (1977).

Les cristaux du bis-(tétrafluoro-3,3,4,4 diphénylphosphino-2 cyclobutène)-1,1′ sont monocliniques, a = 10.398(1), b = 18.484(1), c = 15.984(1) Å, β = 107.76(1)°, Z = 4, groupe d'espace $P2_1/c$. On a résolu la structure par les méthodes directes et on l'a affinée par la méthode des moindres carrés (matrice complète) jusqu'à une valeur finale de R de 0.042 et de R_w 0.057 pour 4226 réflexions avec $I \geq 3\sigma(I)$. La molécule a une configuration *cisoide* autours du lien C—C central; l'angle entre les deux cyclobutènes est de 34.3°. La symétrie moléculaire globale est approximativement C_2 avec une séparation P...P de 3.661(1) Å. Les longueurs de liens et les angles dans la molécule sont généralement en bon accord avec les valeurs acceptées.

[Tradiut par le journal]

Introduction

The preparation and physical properties of a series of ditertiary phosphines and arsines with bialicyclic, 'butadiene', bridging groups, **1**, have recently been reported (1). This work was initiated by the discovery that a complex with this type of bridging group can be isolated when $[(CH_3)_2AsC{=}CAs(CH_3)_2CF_2CF_2]Co_2(CO)_6$ is warmed in solution (2, 3). Several metal carbonyl complexes were obtained from these new ligands and one of them, $(bif_{12}fars)Mo(CO)_4$, **2**, has been characterized by X-ray analysis (1).

Compound **1***b*, the ditertiary phosphine, has the unusual property of photochromism in the solid state. In the dark, the crystals are yellow, but turn bright orange-red when exposed to sunlight. The process is reversible (at a slower rate) provided the exposure has not been too great. A crystal structure analysis of **1***b* has been undertaken in the hope that the photochromic nature of the molecule might be explained by some feature of the structure.

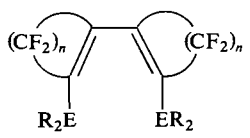

1

a $R_2E = (CH_3)_2As$, $n = 2$
b $R_2E = (C_6H_5)_2P$, $n = 2$
c $R_2E = (CH_3)_2As$, $n = 3$

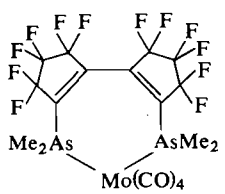

2

Experimental

The crystal chosen for study was mounted with (1 0 −6) normal to the goniostat axis and had dimensions of ca. 0.4 × 0.5 × 1.0 mm. Unit-cell and space group data were obtained from film and diffractometer measurements. The unit-cell parameters were refined by a least squares on 2 sin θ/λ values for 21 reflections measured on a diffractometer with CuKα radiation (λ = 1.5418 Å). Crystal data (at 22°C) are:

$C_{32}H_{20}F_8P_2$ fw = 618.5
Monoclinic, a = 10.398(1), b = 18.484(1), c = 15.984(1) Å, β = 107.76(1)°, V = 2925.4(4) Å^3, Z = 4, ρ_c = 1.4041(2) g cm^{-3}, $F(000)$ = 1256, μ(CuKα) = 20.1 cm^{-1}. Absent reflections: $h0l$, $l \neq 2n$ and $0k0$, $k \neq 2n$ define uniquely the space group $P2_1/c$ (C_{2h}^5, No. 14).

Intensities were measured with nickel-filtered CuKα radiation on a Datex-automated General Electric XRD-6 diffractometer. A θ–2θ scan at 4° min^{-1} over a range of (1.80 + 0.86 tan θ) degrees in 2θ was employed; 10 s background counts were measured at each end of the scan. Data were measured to 2θ = 146°. The intensities of the check reflections, measured every 50 reflections throughout the data collection, decreased uniformly to final values which were 80% of the initial values. Lorentz and polarization corrections and batch check reflection scaling were applied, and the structure amplitudes were derived. No absorption correction was made (maximum error in $|F_o|$ about 5%, apart from a few planes with extreme path lengths). Of the 5846 independent reflections measured, 4246 (73%) had intensities greater than 3σ(I) above background where $\sigma^2(I) = S + B + (dS)^2$ with S = scan count, B = time averaged background count, and d = 0.06 (the relatively high value of d was required to give a satisfactory weighting scheme in the final refinement).

The structure was solved by direct methods. Eight sets of signs for 500 reflections with $|E| \geq 1.69$ were determined by a computer program which uses Sayre relationships in an iterative procedure (4). One set of signs was outstanding in that it converged in six cycles to a set having the highest consistency index (0.93). Forty of the 42 non-hydrogen atoms were located on an E map calculated from this set of signs.

The 40 atoms located on the E map were refined by full-matrix least-squares procedures giving R = 0.179. An electron density difference map gave the positions of the two remaining carbon atoms. All 42 non-hydrogen atoms were refined isotropically for two cycles, and then anisotropically for two cycles reducing R to 0.065. A second difference map, calculated at this point, gave positions for all 20 hydrogen atoms which were included in all subsequent cycles of refinement with isotropic temperature factors. The entire structure (460 variables, full-matrix) was refined for four cycles giving a final R of 0.042 and R_w of 0.057 for 4226 reflections with $I \geq 3\sigma(I)$ (20 reflections which had $|F_o| - |F_c| > 3\sigma(F)$ were treated as unobserved in the final stages of refinement; instrumental error was suspected for these reflections, but it seemed unwise to bias the data by remeasuring them; none of the disagreements were exceptionally bad). For all 5846 reflections R = 0.060 and R_w = 0.066.

The least-squares refinement was based on the minimization of $\Sigma w[|F_o| - |F_c/(1 + gI)|]^2$ where g is the extinction parameter and I the uncorrected intensity. The final value of g was 6.3 × 10^{-8}. The scattering factors of ref. 5 were used for the non-hydrogen atoms and those of ref. 6 for the hydrogen atoms. Anomalous scattering factors from ref. 7 were used for the non-hydrogen atoms. The weighting scheme $w = 1/\sigma^2(F)$ where $\sigma^2(F)$ is derived from the previously defined $\sigma^2(I)$ gave uniform average values of $w(|F_o| - F_c|)^2$ over ranges of $|F_o|$ and was employed in the final stages of refinement.

On the final cycle of refinement some parameter shifts (particularly for hydrogen atoms associated with the C(27)—C(32) phenyl ring) were significant. The mean error in an observation of unit weight was 1.277. A final difference map showed maximum fluctuations of ±0.28 e Å^{-3} in the vicinity of the phosphorus atoms and ±0.16 e Å^{-3} elsewhere. The final positional and thermal parameters appear in Tables 1 and 2[1] respectively. Measured and calculated structure factors have been placed in the Depository of Unpublished Data.[1]

The ellipsoids of thermal motion for the non-hydrogen atoms are shown in Fig. 1. The thermal motion has been analysed in terms of the rigid-body modes of translation (**T**), libration (**L**), and screw (**S**) motion (8) using the computer program MGTLS. The rms standard error in the temperature factors σU_{ij} (derived from the least-squares analysis) is 0.0015 Å^2. Analyses were physically reasonable for the four phenyl groups C(9)—C(14) and P(1), C(15)—C(20) and P(1), C(21)—C(26) and P(2), and C(27)—C(32) and P(2) (rms ΔU_{ij} = 0.0017, 0.0023, 0.0020, and 0.0031 Å^2 respectively) and for the 10 atom group P(1), P(2), C(1)—C(8) (rms ΔU_{ij} = 0.0029 Å^2).

The appropriate bond distances have been corrected for libration (9, 10), using shape parameters q^2 of 0.08 for all atoms involved. Corrected bond lengths appear in Table 3[1] along with the uncorrected values.

Results and Discussion

Figure 1 shows a general view of the molecule with the crystallographic numbering scheme and Fig. 2 shows the packing arrangement viewed along a^*. Bond angles are given in Table 4[1] and deviations of atoms from weighted least squares mean planes in Table 5.[1] Selected inter- and intramolecular non-bonded distances are listed in Table 6.[1]

The 1,1′-bi(3,3,4,4-tetrafluoro-2-diphenylphosphinocyclobutene) molecule, **1***b*, has a *cisoid* configuration about the central C(2)—C(6) bond, the angle between normals to the two cyclobutene mean planes being 34.3°. The over-

[1]The structure factor table and Table 2 (thermal parameters), 3*b* (bond distances involving hydrogen), 4*b* (bond angles involving hydrogen), 5 (mean planes), and 6 (non-bonded distances) are available, at a nominal charge, from the Depository of Unpublished Data, CISTI, National Research Council of Canada, Ottawa, Canada K1A 0S2.

TABLE 1. Final positional parameters (fractional × 10^4, P × 10^5, H × 10^3) with estimated standard deviations in parentheses

Atom	x	y	z
P(1)	36201(5)	53805(3)	10573(3)
P(2)	62955(6)	44815(3)	27787(4)
F(1)	667(2)	5194(1)	2862(1)
F(2)	2237(2)	5909(1)	3609(1)
F(3)	2095(3)	6666(1)	2164(1)
F(4)	493(2)	5967(1)	1416(1)
F(5)	3021(2)	4149(1)	4360(1)
F(6)	2336(2)	3452(1)	3231(1)
F(7)	5553(2)	3677(1)	4634(1)
F(8)	4879(2)	2978(1)	3511(2)
C(1)	2747(2)	5458(1)	1867(1)
C(2)	2846(2)	5088(1)	2620(1)
C(3)	1814(3)	5529(2)	2851(2)
C(4)	1715(3)	5968(2)	2018(2)
C(5)	4940(2)	4266(1)	3210(1)
C(6)	3651(2)	4493(1)	3077(1)
C(7)	3322(3)	3924(2)	3639(2)
C(8)	4766(3)	3654(2)	3787(2)
C(9)	3178(2)	4462(1)	656(1)
C(10)	4124(3)	4087(1)	380(2)
C(11)	3822(3)	3407(2)	8(2)
C(12)	2599(3)	3096(1)	−72(2)
C(13)	1667(3)	3453(1)	219(2)
C(14)	1945(2)	4134(1)	577(2)
C(15)	2598(2)	5966(1)	180(1)
C(16)	1773(2)	5708(1)	−617(2)
C(17)	1129(3)	6192(2)	−1271(2)
C(18)	1297(3)	6923(2)	−1143(2)
C(19)	2119(3)	7179(2)	−358(2)
C(20)	2775(3)	6705(1)	295(2)
C(21)	7746(2)	4083(1)	3604(1)
C(22)	8293(3)	3458(1)	3371(2)
C(23)	9429(3)	3152(2)	3938(2)
C(24)	10039(3)	3461(1)	4742(2)
C(25)	9501(2)	4070(1)	4985(2)
C(26)	8359(2)	4385(1)	4423(2)
C(27)	6524(2)	5450(1)	2958(1)
C(28)	7290(4)	5800(2)	2514(2)
C(29)	7498(5)	6542(3)	2593(3)
C(30)	6922(5)	6934(2)	3103(3)
C(31)	6159(4)	6599(2)	3541(3)
C(32)	5954(3)	5862(1)	3480(2)
H(10)	502(3)	431(1)	46(2)
H(11)	447(3)	314(2)	−21(2)
H(12)	240(2)	258(1)	−29(2)
H(13)	88(3)	323(2)	19(2)
H(14)	128(2)	440(1)	77(1)
H(16)	170(3)	519(2)	−73(2)
H(17)	64(2)	603(1)	−168(1)
H(18)	84(3)	729(2)	−162(2)
H(19)	222(3)	763(2)	−24(2)
H(20)	339(3)	690(2)	86(2)
H(22)	782(3)	322(2)	279(2)
H(23)	976(3)	267(2)	377(2)
H(24)	1083(3)	320(2)	519(2)
H(25)	991(3)	429(2)	554(2)
H(26)	803(3)	483(2)	463(2)
H(28)	761(3)	554(2)	219(2)
H(29)	808(3)	672(2)	232(2)
H(30)	703(4)	744(3)	314(3)
H(31)	566(4)	690(2)	379(3)
H(32)	538(3)	566(2)	379(2)

all molecular symmetry is approximately C_2, the most obvious departure from C_2 symmetry being the orientation of the phenyl rings (torsion angles about the P—Ph bonds are: C(1)[P(1)—C(9)]C(14), 34.5(2), C(1)[P(1)—C(15)]C(20), 77.3(2), C(5)[P(2)—C(27)]C(32), 12.1(2), and C(5)[P(2)—C(21)]C(26), −75.8(2)°). The arsine ligand in **2** has exact C_2 symmetry and an As... As separation of 3.636 Å, close to the value of 3.661(1) Å for the P...P distance in the present structure.

Both cyclobutene rings are slightly, but significantly, nonplanar (see Table 5), with bond angles ranging from 85.9 to 94.8°. The mean[2] bond lengths (averaged assuming C_2 symmetry) in the cyclobutene rings (1.362(1), 1.490(4), 1.537(3), and 1.507(1) Å) may be compared to those in gaseous perfluorocyclobutene (1.342(6), 1.508(3), and 1.595(assumed) Å) (11). The C(sp^3)—C(sp^3) single bond (1.537 Å) is short compared to the values of 1.55–1.60 Å usually found in four-membered rings (see e.g. ref. 12 for numerous examples). The mean C—F bond distance of 1.350(5) Å is as expected. The geometry of the bi(cyclobutene) moiety indicates essentially localized double bonds. The shortening of the C(2)—C(6) (1.445(3) Å), C(1)—P(1) (1.804(2) Å), and C(5)—P(2) (1.798(2) Å) bonds relative to the distances of 1.485 and 1.828 Å (13) usually expected for C(sp^2)—C(sp^2) and C(sp^2)—P(tertiary) single bonds is believed to result primarily from σ-hybridization effects (14).

One of the four phenyl rings is rigorously planar within experimental error while the other three show small, but significant, deviations from planarity (see Table 5). Bond lengths and angles in the C_6H_5P groups are equal, within experimental error, to the mean values quoted for phenyl derivatives of trivalent phosphorus and their coordination compounds (13). The mean C(ar)—H distance of 0.95(8) Å is as expected for X-ray data.

The crystal structure of 1,1′-bi(3,3,4,4-tetrafluoro-2-diphenylphosphinocyclobutene) (see Fig. 2) consists of well-separated molecules. The shortest intermolecular distances (listed in Table 6) correspond to normal van der Waals interactions.

[2]Here and elsewhere in this paper, mean values refer to weighted means with rms deviations from the mean in parentheses.

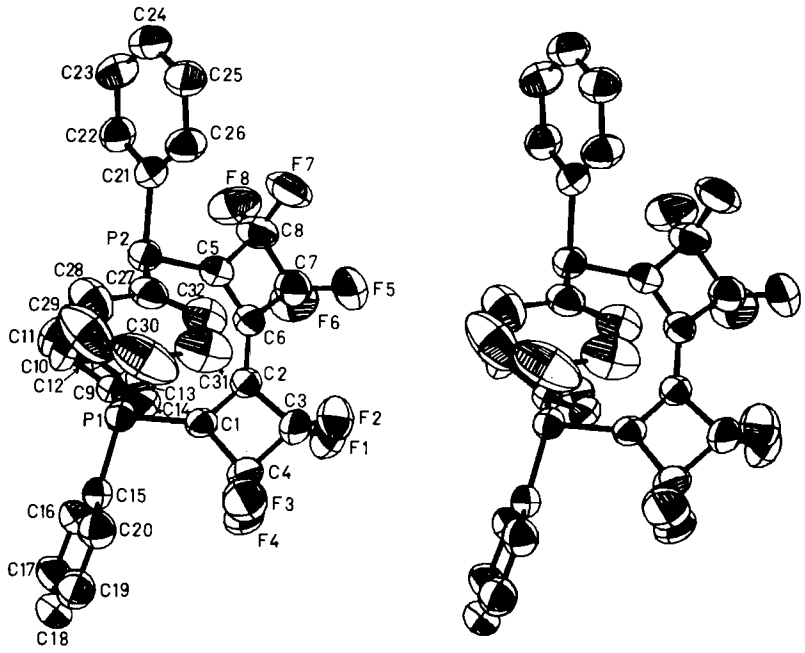

FIG. 1. A stereo view of the 1,1′-bi(3,3,4,4-tetrafluoro-2-diphenylphosphinocyclobutene) molecule; 50% ellipsoids are shown for the non-hydrogen atoms. Hydrogen atoms have been omitted for clarity.

TABLE 3. Bond lengths (Å) with estimated standard deviations in parentheses

(*a*) Non-hydrogen atoms

Bond	Uncorrected	Corrected	Bond	Uncorrected	Corrected
P(1) —C(1)	1.800(2)	1.804	P(2) —C(5)	1.793(2)	1.798
P(1) —C(9)	1.824(2)	1.829	P(12)—C(21)	1.817(3)	1.825
P(1) —C(15)	1.832(2)	1.838	P(2) —C(27)	1.829(2)	1.832
C(3) —F(1)	1.348(3)	1.351	C(7) —F(5)	1.349(3)	1.352
C(3) —F(2)	1.352(3)	1.354	C(7) —F(6)	1.353(3)	1.356
C(4) —F(3)	1.348(3)	1.349	C(8) —F(7)	1.353(3)	1.355
C(4) —F(4)	1.340(3)	1.342	C(8) —F(8)	1.342(3)	1.344
C(1) —C(2)	1.359(3)	1.363	C(5) —C(6)	1.358(3)	1.361
C(2) —C(3)	1.482(3)	1.486	C(6) —C(7)	1.490(3)	1.493
C(3) —C(4)	1.536(4)	1.540	C(7) —C(8)	1.531(4)	1.534
C(1) —C(4)	1.503(3)	1.507	C(5) —C(8)	1.504(3)	1.507
C(9) —C(10)	1.382(3)	1.395	C(21)—C(22)	1.388(3)	1.400
C(10)—C(11)	1.384(4)	1.389	C(22)—C(23)	1.373(4)	1.376
C(11)—C(12)	1.365(4)	1.374	C(23)—C(24)	1.372(4)	1.378
C(12)—C(13)	1.366(4)	1.379	C(24)—C(25)	1.365(4)	1.378
C(13)—C(14)	1.376(3)	1.380	C(25)—C(26)	1.381(3)	1.384
C(14)—C(9)	1.389(3)	1.397	C(26)—C(21)	1.387(3)	1.392
C(15)—C(16)	1.386(3)	1.397	C(27)—C(28)	1.379(4)	1.393
C(16)—C(17)	1.383(4)	1.388	C(28)—C(29)	1.387(6)	1.395
C(17 —C(18)	1.370(5)	1.377	C(29)—C(30)	1.360(7)	1.373
C(18)—C(19)	1.369(5)	1.380	C(30)—C(31)	1.356(6)	1.370
C(19)—C(20)	1.376(4)	1.381	C(31)—C(32)	1.377(4)	1.385
C(20)—C(15)	1.383(3)	1.390	C(32)—C(27)	1.389(4)	1.401
C(2) —C(6)	1.439(3)	1.445			

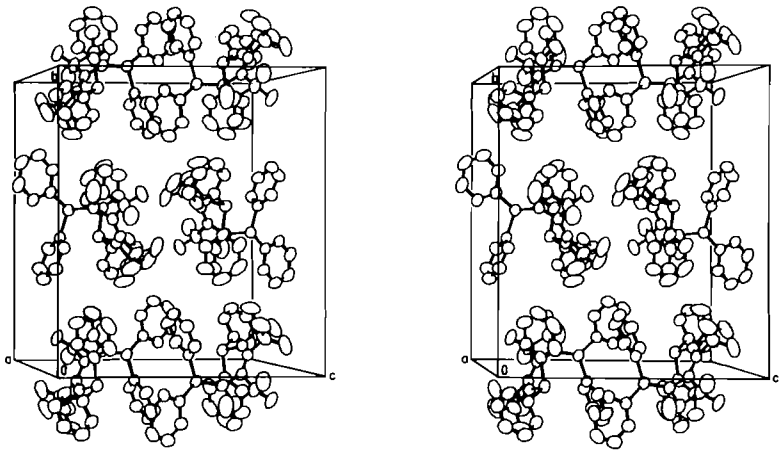

FIG. 2. The packing arrangement viewed along a^*.

TABLE 4. Bond angles (deg) with estimated standard deviations in parentheses

(*a*) Non-hydrogen atoms

Bonds	Angle (deg)	Bonds	Angle (deg)
C(1) —P(1) —C(9)	101.5(1)	C(5) —P(2) —C(21)	101.8(1)
C(1) —P(1) —C(15)	101.6(1)	C(5) —P(2) —C(27)	103.8(1)
C(9) —P(1) —C(15)	104.8(1)	C(21)—P(2) —C(27)	104.1(1)
P(1) —C(1) —C(2)	132.7(2)	P(2) —C(5) —C(6)	136.4(2)
P(1) —C(1) —C(4)	135.0(2)	P(2) —C(5) —C(8)	131.2(2)
C(2) —C(1) —C(4)	92.2(2)	C(6) —C(5) —C(8)	91.9(2)
C(1) —C(2) —C(3)	94.5(2)	C(5) —C(6) —C(7)	94.8(2)
C(1) —C(2) —C(6)	135.1(2)	C(5) —C(6) —C(2)	135.2(2)
C(3) —C(2) —C(6)	130.3(2)	C(7) —C(6) —C(2)	129.9(2)
C(2) —C(3) —C(4)	86.3(2)	C(6) —C(7) —C(8)	85.9(2)
C(2) —C(3) —F(1)	117.4(2)	C(6) —C(7) —F(5)	117.0(2)
C(2) —C(3) —F(2)	116.5(2)	C(6) —C(7) —F(6)	116.3(2)
C(4) —C(3) —F(1)	115.4(2)	C(8) —C(7) —F(5)	116.2(2)
C(4) —C(3) —F(2)	114.9(2)	C(8) —C(7) —F(6)	115.3(2)
F(1) —C(3) —F(2)	105.9(2)	F(5) —C(7) —F(6)	105.8(2)
C(1) —C(4) —C(3)	86.8(2)	C(5) —C(8) —C(7)	87.4(2)
C(1) —C(4) —F(3)	116.3(2)	C(5) —C(8) —F(7)	116.2(2)
C(1) —C(4) —F(4)	116.8(2)	C(5) —C(8) —F(8)	117.4(3)
C(3) —C(4) —F(3)	114.6(2)	C(7) —C(8) —F(7)	114.1(3)
C(3) —C(4) —F(4)	114.8(2)	C(7) —C(8) —F(8)	115.6(2)
F(3) —C(4) —F(4)	106.9(2)	F(7) —C(8) —F(8)	105.8(2)
P(1) —C(9) —C(10)	116.9(2)	P(2) —C(21)—C(22)	117.2(2)
P(1) —C(9) —C(14)	124.4(2)	P(2) —C(21)—C(26)	124.0(2)
C(10)—C(9) —C(14)	118.7(2)	C(22)—C(21)—C(26)	118.7(2)
C(9) —C(10)—C(11)	120.1(2)	C(21)—C(22)—C(23)	120.4(2)
C(10)—C(11)—C(12)	120.4(3)	C(22)—C(23)—C(24)	120.4(3)
C(11)—C(12)—C(13)	120.1(3)	C(23)—C(24)—C(25)	119.8(2)
C(12)—C(13)—C(14)	120.2(3)	C(24)—C(25)—C(26)	120.6(2)
C(13)—C(14)—C(9)	120.5(2)	C(25)—C(26)—C(21)	120.1(2)
P(1) —C(15)—C(16)	123.6(2)	P(2) —C(27)—C(28)	125.2(2)
P(1) —C(15)—C(20)	117.3(2)	P(2) —C(27)—C(32)	116.7(3)
C(16)—C(15)—C(20)	118.7(2)	C(28)—C(27)—C(32)	118.0(3)
C(15)—C(16)—C(17)	119.6(3)	C(27)—C(28)—C(29)	121.1(4)
C(16)—C(17)—C(18)	121.0(3)	C(28)—C(29)—C(30)	119.8(4)
C(17)—C(18)—C(19)	119.6(3)	C(29)—C(30)—C(31)	119.9(4)
C(18)—C(19)—C(20)	120.1(3)	C(30)—C(31)—C(32)	121.2(4)
C(19)—C(20)—C(15)	120.9(3)	C(31)—C(32)—C(27)	120.0(3)

The crystal structure reveals no unusual features which could definitely explain the photochromic behavior of the compound. Crystals of the orange-red material obtained by irradiation (with light or X rays) gave the same diffraction pattern as the original yellow crystals, so that any structural change must be small. One of the phenyl rings, C(27)—C(32), exhibits fairly large thermal vibration, which might suggest a possible rotation of the four-membered rings about the C(2)—C(6) bond, with consequent increase in electron delocalization, and hence color change. The lone-pair electrons of P(1) point towards the phenyl group, and the bis(phosphine oxide) of **1***b* is colorless, suggesting that the phosphorus lone pairs are involved. However, it is not yet understood why the compound should be colored at all (1).

Acknowledgments

We thank Prof. W. R. Cullen and Dr. A. W. Wu for suggesting the problem, providing the sample, and helpful discussion. We are indebted to the University of British Columbia Computing Centre for assistance and to the National Research Council of Canada for financial support.

1. W. R. CULLEN, A. W. WU, A. R. DAVIS, F. W. B. EINSTEIN, and J. D. HAZLETT. Can. J. Chem. **54**, 2871 (1976).
2. F. W. B. EINSTEIN and R. D. G. JONES. J. Chem. Soc. Dalton Trans. 2568 (1972).
3. W. R. CULLEN and A. J. T. JULL. Can. J. Chem. **51**, 1521 (1973).
4. R. E. LONG. Ph.D. Thesis, University of California at Los Angeles. 1965.
5. D. T. CROMER and J. B. MANN. Acta Crystallogr. Sect. A, **24**, 321 (1968).
6. R. F. STEWART, E. R. DAVIDSON, and W. T. SIMPSON. J. Chem. Phys. **42**, 3175 (1965).
7. D. T. CROMER and D. LIBERMAN. J. Chem. Phys. **53**, 1891 (1970).
8. V. SCHOMAKER and K. N. TRUEBLOOD. Acta Crystallogr. Sect. B, **24**, 63 (1969).
9. D. W. J. CRUICKSHANK. Acta Crystallogr. **9**, 747 (1956); **9**, 754 (1956).
10. D. W. J. CRUICKSHANK. Acta Crystallogr. **14**, 896 (1961).
11. C. H. CHANG, R. F. PORTER, and S. H. BAUER. J. Mol. Struct. **7**, 89 (1971).
12. BOHN, SCHELTEMA, and HOLKEMA. Structure reports. Utrecht. 1976.
13. A. DOMENICANO, A. VACIAGO, and C. A. COULSON. Acta Crystallogr. Sect. B, **31**, 231 (1975); **31**, 1630 (1975).
14. S. J. RETTIG. Ph.D. Thesis, University of British Columbia, Vancouver, British Columbia. 1974.

Crystal and molecular structure of phenylboronic acid, $C_6H_5B(OH)_2$

STEVEN J. RETTIG AND JAMES TROTTER

Department of Chemistry, University of British Columbia, 2075 Wesbrook Mall, Vancouver, B.C., Canada V6T 1W5

Received April 1, 1977

STEVEN J. RETTIG and JAMES TROTTER. Can. J. Chem. **55**, 3071 (1977).

Crystals of phenylboronic acid are orthorhombic, $a = 17.9049(7)$, $b = 15.3264(5)$, $c = 9.8113(2)$ Å, $Z = 16$, space group *Iba*2. The structure was solved by direct methods and was refined by full-matrix least-squares procedures to a final R of 0.031 and R_w of 0.041 for 1409 reflections with $I \geq 3\sigma(I)$. The asymmetric unit consists of two independent molecules linked by a pair of O—H...O hydrogen bonds. Each dimeric unit is also hydrogen bonded to four other such units (at $z \pm \frac{1}{2}$) to form an infinite array of layers which stack along the c axis. Mean bond lengths corrected for libration (rms deviations from the mean in parentheses) are: O—B, 1.371(7), B—C, 1.565(3), and C—C(phenyl), 1.394(11) Å.

STEVEN J. RETTIG et JAMES TROTTER. Can. J. Chem. **55**, 3071 (1977).

Les cristaux de l'acide phénylboronique sont orthorhombiques, $a = 17.9049(7)$, $b = 15.3264(5)$, $c = 9.8113(2)$ Å, $Z = 16$, groupe d'espace *Iba*2. On a résolu la structure par des méthodes directes et on l'a affinée par la méthode des moindres carrés (matrice complète) jusqu'à une valeur finale de R de 0.031 et R_w de 0.041 pour 1409 réflexions avec $I \geq 3\sigma(I)$. L'unité asymétrique comprend deux molécules indépendantes liées par une paire de ponts hydrogène O—H...O. Chaque unité dimère est aussi liée par des ponts hydrogène à quatre autres unités semblables (avec $z \pm \frac{1}{2}$) pour former un arrangement infini de couches qui sont superposées le long de l'axe c. Les longueurs moyennes de liaison corrigées pour la libration (les déviations rms à partir de la moyenne sont entre parenthèses) sont O—B, 1.371(7), B—C, 1.565(3) et C—C(phényle), 1.394(11) Å.

[Traduit par le journal]

Introduction

The structures of a number of esters and other derivatives of the organoboron acids R_2BOH and $RB(OH)_2$ have recently been reported (1–9). Two of these structures contain trigonally coordinated boron atoms (1, 2) while the other molecules feature tetrahedrally coordinated boron, occurring via intramolecular N → B (3, 4, 6, 8, 9) or O → B (5, 7) interactions. There is, however, little structural information available on the parent acids. Only one structure, that of $4\text{-}BrC_6H_4B(OH)_2$ (10), has been determined, but the presence of bromine obscures the structural details of the boron coordination group. In order to provide accurate geometrical parameters for a free organoboron acid the crystal structure of phenylboronic acid, $C_6H_5B(OH)_2$, has been determined.

Experimental

Crystals of phenylboronic acid (Alfa Inorganic) suitable for X-ray analysis were obtained by recrystallization from water. The crystal chosen for study was mounted with c parallel to the goniostat axis and had dimensions of ca. 0.36 × 0.40 × 0.93 mm. Unit-cell and space group data were obtained from film and diffractometer measurements. The unit-cell parameters were refined by a least squares on 2 sin θ/λ values for 17 reflections measured on a diffractometer with CuKα radiation (λ = 1.5418 Å). Crystal data (at 22°C) are:

$C_6H_7BO_2$ fw = 121.93

Orthorhombic, $a = 17.9049(7)$, $b = 15.3264(5)$, $c = 9.8113(2)$ Å, $V = 2692.4(1)$ Å^3, $\rho_m = 1.18$ (flotation in aqueous KI), $Z = 16$, $\rho_c = 1.203$ g cm^{-3}, $F(000) = 1024$, $\mu(CuK\alpha) = 7.18$ cm^{-1}. Absent reflections: hkl, $h + k + l \neq 2n$; $0kl$, $k \neq 2n$; and $h0l$, $h \neq 2n$. Space group *Iba*2 (C_{2v}^{21}, No. 45).

Intensities were measured with nickel-filtered CuKα radiation on a Datex-automated General Electric XRD-6 diffractometer. A θ–2θ scan at 4° min^{-1} over a range of (1.80 + 0.86 tan θ) degrees in 2θ was employed; 10 s background counts were measured at each end of the scan. Data were measured to 2θ = 160°. The intensities of two check reflections, measured every 50 reflections throughout the data collection, decreased slowly to a value which was 0.91 times the initial value. Lorentz and polarization corrections and batch check reflection scaling were applied, and the structure amplitudes were derived. An absorption correction was applied by a computer program using a Gaussian integration method (11, 12). Transmission factors ranged from 0.631 to 0.794. Of the 1563 independent reflections measured, 1419 (91%) had intensities greater than $3\sigma(I)$ above background where $\sigma^2(I) = S + B + (0.06S)^2$ with S = scan count and B = time averaged background count. These reflections were used in the solution and refinement of the structure.

The systematic absences allow space groups *Iba*2 or

Ibam, the former being indicated by the E statistics. The structure was solved by direct methods (13–15). The positions of the 18 non-hydrogen atoms were located among the 19 highest peaks on an E map calculated from the set of phases with the lowest value of R_k.

Two cycles of isotropic followed by three cycles of anisotropic full-matrix least-squares refinement of the non-hydrogen atoms gave $R = 0.064$. The z coordinate of O(1) was fixed to determine the origin. The positions of all 14 hydrogen atoms were located on a difference map at this point. The entire structure (including hydrogen atoms with isotropic thermal parameters) was refined for six cycles giving a final R of 0.031 and R_w of 0.041 for 1409 reflections with $I \geq 3\sigma(I)$ (10 reflections which had $|F_o| - |F_c| > 3\sigma(F)$ were treated as unobserved in the final stages of refinement; for all 1563 reflections $R = 0.036$ and $R_w = 0.044$).

The least-squares refinement was based on the minimization of $\Sigma w[|F_o| - |F_c/(1 + gI)|]^2$ where g is the extinction parameter and I the uncorrected intensity. The final value of g was $9.0(6) \times 10^{-8}$. The scattering factors of ref. 16 were used for the non-hydrogen atoms and those of ref. 17 for the hydrogen atoms. Anomalous scattering factors from ref. 18 were used for the non-hydrogen atoms. The weighting scheme: $w = 1.0$ if $|F_o| < 10.0$, $w = (10.0/|F_o|)^2$ if $|F_o| \geq 10.0$, and $w = 0.0625$ for the unobserved reflections gave uniform average values of $w(|F_o| - |F_c|)^2$ over ranges of $|F_o|$ and was employed in the final stages of refinement.

On the final cycle of refinement the mean parameter shift was 0.09σ, with no shift greater than 0.65σ. The mean error in an observation of unit weight was 0.3556. A final difference map showed maximum fluctuations of ± 0.3 e Å^{-3}. The final positional and thermal parameters appear in Tables 1 and 2[1] respectively. Measured and calculated structure factors have been placed in the Depository of Unpublished Data.[1]

The positive z direction (for the particular crystal used) has been determined through the anomalous scattering of the non-hydrogen atoms. Structure A is represented by the coordinates in Table 1 referred to a right-handed axial system and structure B, the mirror image of A, was generated by changing the z coordinates of A to $1 - z$. Both structures were refined and Hamilton's test (19) applied to the resulting R factor ratios. The ratios (B/A) and the percentage probabilities that A is the correct structure are: 1.0009 (90%) for R (all data), 1.0002 (50%) for R (3σ data), 1.0017 (95%) for R_w (all data), and 1.0017 (95%) for R_w (3σ data).

The ellipsoids of thermal motion for the non-hydrogen atoms are shown in Fig. 1. The thermal motion has been analysed in terms of the rigid-body modes of translation (**T**), libration (**L**), and screw (**S**) motion (20) using the computer program MGTLS. The rms standard error in the temperature factors σU_{ij} (derived from the least-squares analysis) is 0.0011 Å^2. Analyses were successful for each of the two independent molecules (rms $\Delta U_{ij} =$ 0.0024 and 0.0025 Å^2 for molecules 1 and 2 respectively).

[1]The structure factor table and Tables 2 (thermal parameters), 3*b* (individual bond lengths involving H), and 4*b* (individual angles involving H) are available, at a nominal charge, from the Depository of Unpublished Data, CISTI, National Research Council of Canada, Ottawa, Canada K1A 0S2.

TABLE 1. Final positional parameters (fractional $\times 10^5$, H $\times 10^3$) with estimated standard deviations in parentheses

Atom	x	y	z
O(1)	38888(9)	53251(10)	30217
O(2)	40098(8)	52140(9)	53622(16)
O(3)	49326(9)	66108(9)	34498(18)
O(4)	47315(9)	67834(10)	57598(17)
C(1)	30735(10)	41906(11)	41453(22)
C(2)	26929(12)	40146(15)	29366(28)
C(3)	21363(15)	33889(19)	28680(36)
C(4)	19446(16)	29351(18)	40162(41)
C(5)	23019(17)	30976(18)	52297(39)
C(6)	28632(13)	37186(14)	52946(28)
C(7)	55021(10)	79589(11)	46281(24)
C(8)	60263(13)	81636(15)	36328(30)
C(9)	64186(17)	89459(19)	36678(39)
C(10)	62920(15)	95310(16)	47035(41)
C(11)	57875(18)	93402(17)	57001(39)
C(12)	53955(14)	85577(15)	56830(32)
B(1)	36784(11)	49241(12)	42077(23)
B(2)	50508(11)	70900(12)	45955(24)
H(O1)	417(2)	571(2)	314(3)
H(O2)	385(2)	498(3)	599(5)
H(O3)	508(2)	685(2)	283(4)
H(O4)	453(2)	640(2)	562(3)
H(2)	283(2)	440(2)	211(4)
H(3)	187(3)	330(4)	204(7)
H(4)	156(2)	251(2)	394(4)
H(5)	217(2)	277(3)	601(5)
H(6)	308(2)	385(2)	615(3)
H(8)	610(2)	774(2)	282(4)
H(9)	682(2)	904(2)	289(4)
H(10)	656(2)	1013(2)	471(4)
H(11)	567(2)	975(2)	651(4)
H(12)	505(2)	843(2)	640(3)

The appropriate bond distances have been corrected for libration (21, 22), using shape parameters q^2 of 0.08 for all atoms involved. Corrected bond lengths appear in Table 3[1] along with the uncorrected values. Corrected bond angles differ by less than 1 standard deviation from the uncorrected values listed in Table 4.[1]

Results and Discussion

Figure 1 shows a view of the asymmetric unit with the crystallographic numbering scheme and Fig. 2 shows a view down b of the basic repeating structural unit. Details of the hydrogen bonding scheme are given in Table 5.

The asymmetric unit (Fig. 1) consists of two molecules of phenylboronic acid linked by a pair of O—H...O hydrogen bonds. Each of these dimeric units is hydrogen bonded to four other such units (at $z \pm \frac{1}{2}$) to form an infinite array of layers which stack along c. The basic repeating structural unit, including the interlayer hydrogen bonding, is shown in Fig. 2. The two dimeric units which make up each layer are related by the

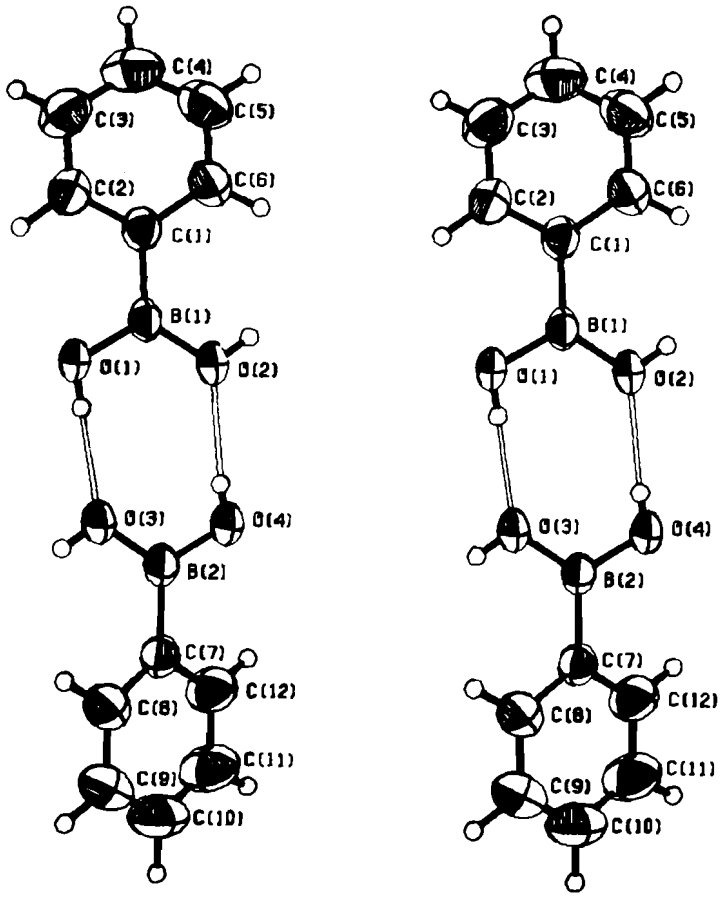

FIG. 1. A stereo view of the asymmetric unit of phenylboronic acid; 50% ellipsoids are shown for the non-hydrogen atoms. Hydrogen atoms have been assigned artificially small thermal parameters for the sake of clarity.

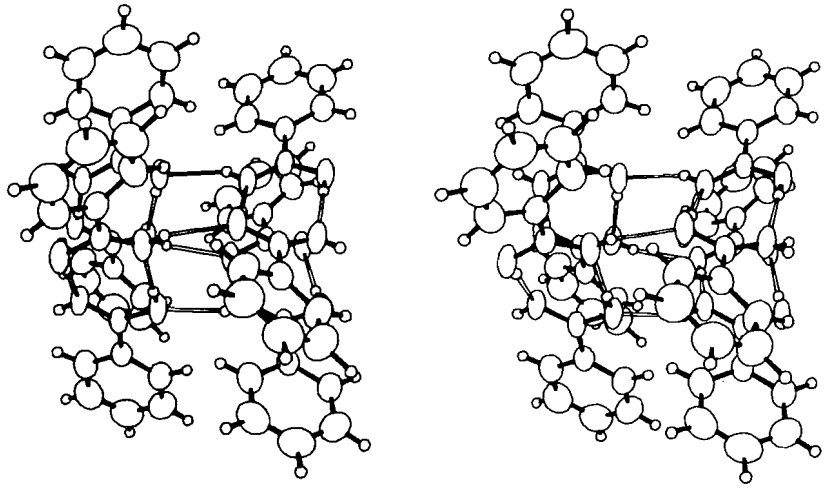

FIG. 2. The basic repeating structural unit of phenylboronic acid viewed down *b*. Unshaded bonds represent hydrogen bonds.

TABLE 3. Bond lengths (Å) with estimated standard deviations in parentheses

(*a*) Non-hydrogen atoms

Bond	Uncorrected	Corrected	Bond	Uncorrected	Corrected
O(1)—B(1)	1.369(2)	1.378	O(3) —B(2)	1.359(2)	1.371
O(2)—B(1)	1.354(2)	1.362	O(4) —B(2)	1.361(3)	1.373
C(1)—B(1)	1.562(3)	1.568	C(7) —B(2)	1.558(2)	1.563
C(1)—C(2)	1.394(3)	1.404	C(7) —C(8)	1.390(3)	1.403
C(1)—C(6)	1.392(3)	1.402	C(7) —C(12)	1.396(3)	1.410
C(2)—C(3)	1.385(3)	1.389	C(8) —C(9)	1.390(3)	1.394
C(3)—C(4)	1.368(5)	1.378	C(9) —C(10)	1.374(5)	1.388
C(4)—C(5)	1.374(5)	1.384	C(10)—C(11)	1.363(5)	1.374
C(5)—C(6)	1.386(4)	1.390	C(11)—C(12)	1.390(4)	1.394

(*b*) Bonds involving hydrogen atoms

Bonds	Bond lengths	Mean bond length
O—H	0.69–0.75(3–5)	0.75(5)
C—H	0.94–1.06(3–6)	1.00(5)

TABLE 4. Bond angles (deg) with estimated standard deviations in parentheses

(*a*) Non-hydrogen atoms

Bonds	Angle (deg)	Bonds	Angle (deg)
O(1)—B(1)—O(2)	116.3(2)	O(3) —B(2) —O(4)	116.2(2)
O(1)—B(1)—C(1)	118.7(2)	O(3) —B(2) —C(7)	124.0(2)
O(2)—B(1)—C(1)	125.0(2)	O(4) —B(2) —C(7)	119.7(2)
B(1)—C(1)—C(2)	120.8(2)	B(2) —C(7) —C(8)	121.9(2)
B(1)—C(1)—C(6)	122.0(2)	B(2) —C(7) —C(12)	120.4(2)
C(2)—C(1)—C(6)	117.2(2)	C(8) —C(7) —C(12)	117.7(2)
C(1)—C(2)—C(3)	121.8(2)	C(7) —C(8) —C(9)	121.2(2)
C(2)—C(3)—C(4)	119.5(3)	C(8) —C(9) —C(10)	119.9(3)
C(3)—C(4)—C(5)	120.3(2)	C(9) —C(10)—C(11)	120.0(2)
C(4)—C(5)—C(6)	120.1(3)	C(10)—C(11)—C(12)	120.7(3)
C(1)—C(6)—C(5)	121.1(2)	C(7) —C(12)—C(11)	120.5(2)

(*b*) Angles involving hydrogen atoms

Bonds	Bond angle	Mean bond angle
B—O—H	110–113(2–3)	111(1)
C—C—H	116–124(2–3)	120(2)

TABLE 5. Hydrogen-bond data* (distances in Å and angles in deg)

D—H...A	H...A	D...A	∠DHA	∠XAH
O(1)—H(O1)...O(3)	1.96(3)	2.748(2)	176(3)	128(1), 117(3)
O(2)—H(O2)...O(1)[1]	2.05(5)	2.746(2)	151(4)	136(1), 110(3)
O(3)—H(O3)...O(4)[2]	2.06(4)	2.720(2)	146(3)	138(1), 109(3)
O(4)—H(O4)...O(2)	2.07(3)	2.758(2)	174(3)	126(1), 119(4)

*Superscripts refer to atoms at positions: [1] $x, 1-y, \frac{1}{2}+z$; [2] $1-x, y, z-\frac{1}{2}$.

twofold axis ($\frac{1}{2}$, $\frac{1}{2}$, z) and are not directly hydrogen bonded to one another. Alternate layers are related by *c* glide planes and the dimers in each layer are bridged (via hydrogen bonds) by both dimers in the adjacent layers. There are two well-separated 'stacks' of molecules in the unit cell, related by the *I* centering.

The most obvious difference between the two molecules is in the orientation of the phenyl ring, twisted 6.6° with respect to the boron co-

ordination group in molecule 1 and 21.4° in molecule 2. The phenyl rings and boron coordination groups of both molecules are slightly, but significantly, nonplanar. B(1) and B(2) deviate by 0.009(2) and 0.012(2) Å from the respective OOC planes, and by 0.061(2) and 0.021(2) Å from the phenyl mean planes.

The bond angles at the trigonal planar boron atoms are distorted from ideal values in a manner which makes all of the hydrogen bonds more linear. The C(1)—B(1)—O(1) and C(7)—B(2)—O(4) angles (118.7(2) and 119.7(2)°) are significantly smaller than C(1)—B(1)—O(2) and C(7)—B(2)—O(3) (125.0(2) and 124.0 (2)°). The two independent O—B—O angles (116.3(2) and 116.2(2)°) are equal within experimental error. The two B—O distances in molecule 1 are significantly different while those in molecule 2 are not. The mean[2] B—O distance of 1.371(6) Å is somewhat shorter than the bond in 2-phenyl-1,3,2-benzodioxaborol (1.394(3) Å (1)), between the values of 1.337(2) and 1.404(2) Å in 8,8-dimethyl-3,5-diphenyl-2,4,6-trioxa-1-azonia-3-bora-5-boranatabicyclo[3.3.0]octane (2), and in good agreement with the mean value of 1.36 Å in $BrC_6H_4B(OH)_2$ (10). The B—C distances in the present structure (1.563 and 1.568 Å) lie between those in the above-mentioned molecules (1.537(6), 1.557(2), and 1.54 Å respectively) and those in Ph_3B (23) of 1.571(3) and 1.589(5) Å.

The corrected C—C distances in the phenyl rings range from 1.374(5) to 1.410(3) Å with a mean value of 1.394 Å. As in related molecules (e.g. ref. 2), the bond distances in the phenyl rings decrease as they are removed from the boron substituent (mean values are 1.405(4), 1.392(3), and 1.381(6) Å). This variation of bond lengths, as well as the pattern of bond angles in the phenyl rings, is consistent with that in related compounds (24). Distances and angles involving hydrogen atoms are as expected for X-ray data.

Acknowledgments

We thank the National Research Council of Canada for financial support and the University of British Columbia Computing Centre for assistance.

[2]Here and elsewhere in this report mean values refer to weighted means with rms deviations from the mean in parentheses.

1. F. Zettler, H. D. Hausen, and H. Hess. Acta Crystallogr. Sect. B, **30**, 1876 (1974).
2. S. J. Rettig, J. Trotter, W. Kliegel, and H. Becker. Can. J. Chem. **54**, 3142 (1976).
3. S. J. Rettig and J. Trotter. Can. J. Chem. **51**, 1288 (1973).
4. S. J. Rettig and J. Trotter. Acta Crystallogr. Sect. B, **30**, 2139 (1974).
5. S. J. Rettig, J. Trotter, and W. Kliegel. Can. J. Chem. **52**, 2531 (1974).
6. S. J. Rettig and J. Trotter. Can. J. Chem. **53**, 1393 (1975).
7. S. J. Rettig and J. Trotter. Can. J. Chem. **54**, 1168 (1976).
8. S. J. Rettig and J. Trotter. Can. J. Chem. **54**, 3130 (1976).
9. S. J. Rettig and J. Trotter. Can. J. Chem. **55**, 958 (1977).
10. Z. V. Zvonkova and V. P. Gluskova. Kristallografija, SSSR, **3**, 559 (1958).
11. P. Coppens, L. Leiserowitz, and D. Rabinovich. Acta Crystallogr. **18**, 1035 (1965).
12. W. R. Busing and H. A. Levy. Acta Crystallogr. **22**, 457 (1967).
13. J. Karle and I. L. Karle. Acta Crystallogr. **21**, 849 (1966).
14. J. Karle and H. Hauptman. Acta Crystallogr. **9**, 635 (1956).
15. M. G. B. Drew. Private communication. 1969. See, e.g., M. G. B. Drew, D. H. Templeton, and A. Zalkin. Acta Crystallogr. Sect. B, **25**, 261 (1969).
16. D. T. Cromer and J. B. Mann. Acta Crystallogr. Sect. A, **24**, 321 (1968).
17. R. F. Stewart, E. R. Davidson, and W. T. Simpson. J. Chem. Phys. **42**, 3175 (1965).
18. D. T. Cromer and D. Liberman. J. Chem. Phys. **53**, 1891 (1970).
19. W. C. Hamilton. Acta Crystallogr. **18**, 502 (1965).
20. V. Schomaker and K. N. Trueblood. Acta Crystallogr. Sect. B, **24**, 63 (1969).
21. D. W. J. Cruickshank. Acta Crystallogr. **9**, 747 (1956); **9**, 754 (1956).
22. D. W. J. Cruickshank. Acta Crystallogr. **14**, 896 (1961).
23. F. Zettler, H. D. Hausen, and H. Hess. J. Organomet. Chem. **72**, 157 (1974).
24. A. Domenicano, A. Vaciago, and C. A. Coulson. Acta Crystallogr. Sect. B, **31**, 221 (1975); **31**, 1630 (1975).

^{125}Te Mössbauer spectra of the polyatomic cations of tellurium

C. H. W. JONES

Department of Chemistry, Simon Fraser University, Burnaby, B.C., Canada V5A 1S6

Received March 14, 1977

C. H. W. JONES. Can. J. Chem. **55**, 3076 (1977).

^{125}Te Mössbauer data for frozen solutions of tellurium in HSO_3F and in oleum are reported together with data for solid samples which may have contained the Te_4^{2+}, Te_n^{n+}, and Te_6^{2+} cations. The data demonstrate that the quadrupole splitting reflects the sequential oxidation of the tellurium through the steps Te → Te_4^{2+} → Te_n^{n+} → Te(II) → Te(IV) → TeO_2. The quadrupole splittings for samples identified as containing Te_4^{2+} are consistent with a unit quadrupole splitting of 12 mm s^{-1} for ^{125}Te.

C. H. W. JONES. Can. J. Chem. **55**, 3076 (1977).

On rapporte des données de Mössbauer du ^{125}Te pour des solutions congelées de tellure dans HSO_3F et dans l'oléum de même que des données pour des échantillons solides qui pourraient contenir des cations Te_4^{2+}, Te_n^{n+} et Te_6^{2+}. Les données démontrent que les couplages quadrupolaires sont un reflet de l'oxydation en séquence du tellure par l'intermédiaire des étapes Te → Te_4^{2+} → Te_n^{n+} → Te(II) → Te(IV) → TeO_2. Les couplages quadrupolaires pour les échantillons qui sont identifiés comme contenant du Te_4^{2+} sont en accord avec un couplage quadrupolaire unitaire de 12 mm s^{-1} pour le ^{125}Te.

[Traduit par le journal]

Introduction

The formation and properties of the polycations of the Group VI elements have been reviewed by Gillespie and Passmore (1, 2). In particular, tellurium is known to form the red cation Te_4^{2+} in sulphuric and fluorosulphuric acid solutions (3, 4) and also on reaction with sulphur trioxide (5). Crystallographic studies of $Te_4(AlCl_4)_2$ and $Te_4(Al_2Cl_7)_2$ have established that the Te_4^{2+} ion is square-planar in geometry (6). On oxidation of the Te_4^{2+} ion in acid solution or in SO_3, a yellow diamagnetic ion Te_n^{n+}, which is possibly Te_4^{4+}, Te_6^{6+}, or Te_8^{8+}, is formed. Further oxidation produces a colorless Te(IV) species in solution and finally, in sulphuric acid solution, TeO_2 precipitates out (3). More recently the preparations and crystal structures of the compounds $Te_2Se_8(AsF_6)_2 \cdot SO_2$ and $Te_{3.7}Se_{6.3}(AsF_6)_2$ have been reported (7).

The reaction of tellurium with arsenic and antimony pentafluorides yields a number of solid derivatives of the Te_4^{2+} and Te_n^{n+} ions (3, 4) and the compound with the empirical formula Te_3AsF_6 has also been identified. The latter is diamagnetic and hence may be formulated as $Te_6^{2+}(AlF_6^-)_2$ (3). A single crystal X-ray diffraction study (8) of the compound $Te_6(AsF_6)_4 \cdot 2AsF_3$ has shown the presence of the cation Te_6^{4+}, which is a trigonal prismatic cluster cation.

The study of the phases formed in the system Te–$TeCl_4$–$AlCl_3$ has led to the identification (6) of the compounds $Te_4(AlCl_4)_2$ and $Te_4(Al_2Cl_7)_2$ referred to above and also to that of the compound $Te_6(AlCl_4)_2$ (9).

The present work was initiated to determine whether or not ^{125}Te Mössbauer spectroscopy could be used to distinguish between these different tellurium polycations and perhaps throw some light on the nature of the bonding in the Te_n^{n+} and Te_6^{2+} ions. The Mössbauer parameters for the Te_4^{2+} ion were also of some considerable interest because the structure of this ion is known and it was important to establish whether or not the data for this simple ion would support the previous models that we have used in interpreting quadrupole splittings in ^{125}Te Mössbauer spectra (10, 11).

Results and Discussion

Typical spectra are shown in Fig. 1 and the computed Mössbauer parameters are given in Table 1. Where more than one result is reported for any one compound or ion these represent independent measurements on separately prepared samples. For the solutions of tellurium in HSO_3F, the first sample prepared gave rather broad line-widths and the subsequent samples studied were prepared with less ^{125}Te present. This was also the case for the spectrum of the oxidation product of tellurium formed on warming in oleum.

It is clear from Table 1 that on dissolving tellurium in cold HSO_3F, the Mössbauer spec-

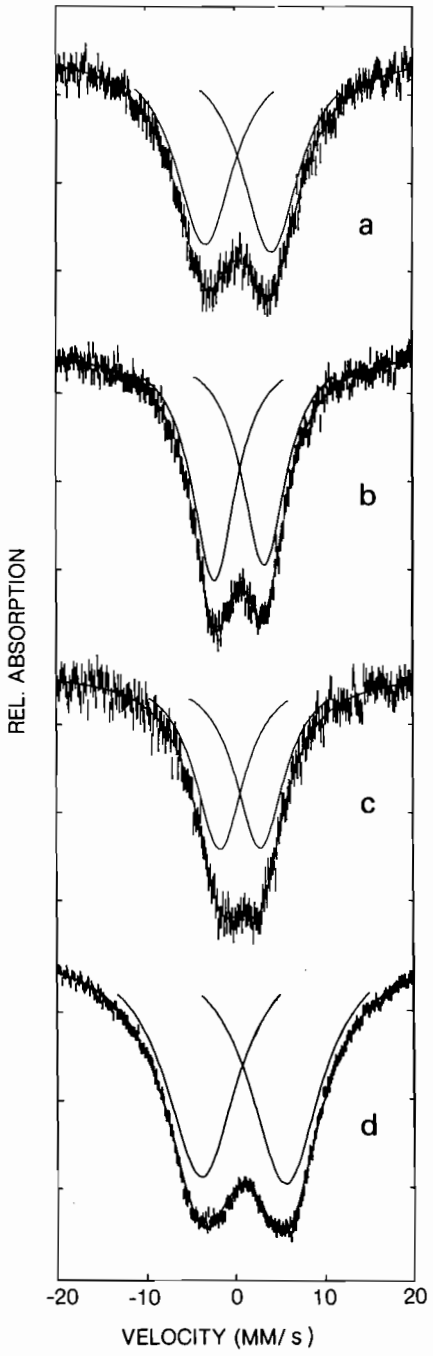

FIG. 1. ^{125}Te Mössbauer spectra for (*a*) Te, (*b*) Te in HSO_3F (Te_4^{2+}), (*c*) Te in 45% oleum (Te_n^{n+}), (*d*) Te in 45% oleum on warming (Te(II)).

trum of the frozen solution was significantly different from that of the elemental tellurium itself. Within the errors, the observed parameters for $Te_4(Sb_2F_{11})_2$, $Te_4(AlCl_4)_2$, and $Te_4(AsF_6)_2$ were in reasonable agreement with those of the HSO_3F frozen solutions.

Taking the average of the values for the HSO_3F solutions and the solids containing the Te_4^{2+} ion, the values $\delta = +0.44$ and $\Delta = 6.1$ mm s^{-1} for the Te_4^{2+} ion are arrived at. The Te_4^{2+} ion in $Te_4(AlCl_4)_2$ and $Te_4(Al_2Cl_7)_2$ is known (6) to be square-planar with bond-angles very close to 90° and bond-lengths of ca. 2.66 Å, which are shorter than those in elemental tellurium (2.864 Å). A simple description of the bonding would suggest that each tellurium contributes one 5*p* electron to each σ-bond in the (*xy*) plane, and that each tellurium possesses on average 1.5 electrons in the $5p_z$ orbital directed out of the plane, the p_z orbitals participating in π-bonding around the ring. This picture would suggest that V_{zz} the principal component of the efg tensor would be negative in sign and that in the Townes and Dailey theory the *p*-orbital imbalance, U_p, would be −0.5. Since Δ is 6.0 mm s^{-1} for Te_4^{2+} it follows that the quadrupole splitting for an imbalance of one 5*p* electron in ^{125}Te should be 12.0 mm s^{-1}. This value is in excellent agreement with our previous estimate of this parameter based on an analysis of the isomer shifts of the TeX_6^{2-} ions (X = Cl, Br, I) and the δ and Δ values of the Te(II) thiourea complexes (10, 11).

The isomer shift of Te_4^{2+} is a little more positive than that of elemental tellurium. Removal of 5*p*-electron density from tellurium results in deshielding of the 5*s*-electrons from the nucleus and increases the isomer shift by ca. +0.4 mm s^{-1} per 5*p* electron, while removal of 5*s*-electron density directly decreases δ (10). Assuming that the bonding in elemental tellurium is itself predominantly *p* in character, the removal of *p*-electron density on oxidation of Te^0 to $Te^{+1/2}$ would be expected to have only a small effect on the isomer shift, and, within the large errors, this appears to be the case.

A solution of tellurium in cold H_2SO_4 yielded a Mössbauer spectrum with a significantly smaller quadrupole splitting than Te_4^{2+}. The parameters for the H_2SO_4 solution were subsequently found to be very similar to those of solid derivatives thought to contain the yellow Te_n^{n+} cation. Solutions of tellurium in H_2SO_4 always contain both Te_4^{2+} and Te_n^{n+} and it would appear that, while the solutions were red in color, the yellow Te_n^{n+} ion predominated in the present case. There was no evidence in the spectrum for the presence of appreciable amounts of Te_4^{2+}. A solution of tellurium in

TABLE 1. ^{125}Te Mössbauer parameters

Compound	δ* (mm s^{-1})	Δ (mm s^{-1})	Γ (mm s^{-1})	χ^2/N§
Te	+0.35 (5)	7.8 (1)	7.2	246/240
Te in cold HSO_3F	+0.39 (7)	6.2 (1)	8.3	230/240
	+0.51 (6)	6.0 (1)	6.8	237/240
	+0.46 (3)	5.91 (5)	6.3	245/240
$Te_4(Sb_2F_{11})_2$	+0.59 (8)	5.9 (2)	7.3	247/240
$Te_4(AlCl_4)_2$	+0.37 (8)	5.9 (2)	7.7	232/240
$Te_4(AlCl_4)_2$†	+0.40 (5)	6.5 (1)	6.8	261/248
$Te_4(AsF_6)_2$†	+0.34 (10)	6.3 (3)	9.2	257/248
Te in cold H_2SO_4	+0.49 (6)	4.8 (1)	7.0	242/240
Te in 40% oleum	+0.67 (4)	4.5 (1)	6.0	265/240
Te SbF_6†	+0.74 (12)	4.4 (2)	5.6	243/248
$Te_x(AsF_6)_y$†	+0.50 (13)	4.6 (3)	6.7	217/248
$Te_m(AsF_6)_n$†	+0.52 (12)	4.9 (3)	6.7	250/248
Te in oleum on warming	+0.68 (4)	10.4 (1)	10.8	309/240
	+0.71 (3)	10.1 (1)	10.7	452/240
Te in oleum on further warming	+0.90 (3)	6.3 (1)	7.9	232/240
	+1.01 (4)	5.6 (1)	6.4	231/240
TeO_2	+0.67 (5)	6.2 (1)	7.5	211/240
$Te_6(AlCl_4)_2$	+0.30 (5)	8.7 (1)	8.6	244/240

*δ with respect to Pb^{125m}Te, source and absorbers at 4.2 K.
†For these samples the source was at 80 K and the absorbers at 4.2 K.
‡The line-widths were constrained as being equal in the computed fits of the doublets.
§χ^2 divided by the number of degrees of freedom, N.

oleum, which on prolonged standing turned orange, also gave a quadrupole splitting comparable with the H_2SO_4 solution and this is again tentatively identified as corresponding to the Te_n^{n+} ion. There is little question that the quadrupole splittings of these latter samples were all consistently smaller than those corresponding to the Te_4^{2+} ion, and that the isomer shift was consistently more positive, corresponding to an increase in oxidation state and a net removal of 5*p*-electron density from the tellurium.

A number of possible structures for the Te_n^{n+} ion are discussed in ref. 3. In the light of the known structure of the Te_6^{4+} ion, which is a trigonal prismatic cluster cation, it has been proposed that Te_n^{n+} is probably Te_6^{6+} and has the structure shown in Fig. 2*i*. The presence of a small quadrupole splitting in the Mössbauer spectrum is not inconsistent with that structure. The 60% bond angles within the triangular ring suggests the presence of bent bonds which lie off the interatomic axes. The bonding could be predominantly *p* in character and the small *p*-orbital imbalance would derive from the difference between the bonding within and between the triangular rings. The small increase in δ over that in tellurium and the Te_4^{2+} cation is consistent with the presence of predominantly *p*-character in the bonds.

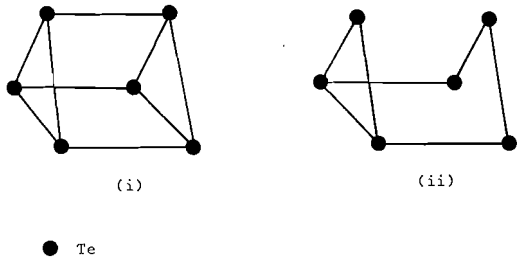

FIG. 2. Proposed structures (8) for Te_n^{n+} (i.e. Te_6^{6+}) and Te_6^{2+}. For the latter, 3 resonance forms may contribute to the structure.

On warming a solution of tellurium dissolved in oleum, a very marked increase in the quadrupole splitting was observed for the frozen solution, together with an increase in line-width. Attempts to fit the spectra to more than one pair of doublets yielded poorer fits to the data than that reported here. The broad line-widths and the poor χ^2 values suggest the presence of a spectrum of products with varying hyperfine parameters. The increase in Δ is consistent with oxidation of the tellurium to a Te(II) derivative, compounds which in general exhibit quadrupole splittings from 10 to 15 mm s^{-1}.

Following further heating, the spectrum of the frozen solution exhibited a significant decrease in Δ and an increase in δ, consistent with further oxidation of the tellurium to a Te(IV) species.

The decrease in Δ reflects the participation of all three 5*p* orbitals in bonding, in contrast with Te(II) compounds, and the increase in δ the increased withdrawal of *p*-electron density and a concomitant increase in the *s*-electron density at the nucleus.

Finally, TeO_2 precipitated out and the somewhat smaller isomer shift for this compound is consistent with that generally found for Te(IV) oxides and oxyanions in the solid state, reflecting some stereochemical activity of the 5*s* electrons (10).

From these experiments it appears that the Mössbauer quadrupole splitting reflects the step by step oxidation of the tellurium:

$$Te \rightarrow Te_4^{2+} \rightarrow Te_n^{n+} \rightarrow Te(II) \rightarrow Te(IV) \rightarrow TeO_2$$

	Value					
Parameter	Te	Te_4^{2+}	Te_n^{n+}	Te(II)	Te(IV)	TeO_2
Δ (mm s^{-1})	7.8	6.1	4.6	10.3	6.0	6.2
δ	+0.35	0.43	0.58	0.70	0.96	0.67

The isomer shifts for ^{125}Te are small because of the small value of $\Delta R/R$ for this transition. As a result the changes in δ are less useful in characterizing the change in chemical form of the tellurium. However, with the exception of TeO_2, the δ values show a trend to increasing (more positive) δ values with increasing oxidation state. This suggests that the 5*s* electrons are predominantly stereochemically inactive and that the electrons removed are primarily 5*p* in character.

Prince *et al.* (9) have prepared the compound $Te_6(AlCl_4)_2$ through the reaction

$$11Te + TeCl_4 + 4AlCl_3 \rightarrow 2Te_6(AlCl_4)_2$$

A ^{125}Te enriched sample prepared in this way yielded the parameters shown in Table 1. The quadrupole splitting is again significantly different from that of the other tellurium ions studied. While the line-width was rather broad, there is no conclusive evidence for the presence of more than one tellurium site in the sample. The broad line-width for this sample may have arisen from the presence of tellurium. A structure which has been suggested for this ion is shown in Fig. 2*ii*.

A crystal structure of Te_6^{2+} has not been reported but $Te_2Se_4^{2+}$ and $Te_3S_3^{2+}$ have been demonstrated (12) to have a six-membered boat-shaped ring structure with a Te—Te cross-ring bond, similar to that of Fig. 2(*ii*). The Te_6^{4+} ion may be viewed as a boat-shaped ring with two cross-ring bonds (8). In the Te_6^{2+} ion three resonance structures of the form shown in Fig. 2*ii* may contribute to the structure, in which case all six tellurium atoms would have similar environments. A similar situation has been found to hold for Te_6^{4+} (12).

The isomer shift of +0.3 mm s^{-1} (Table 1) is consistent with a small charge on the tellurium. The quadrupole splitting of 8.7 mm s^{-1} is greater than that proposed for tellurium in the Te_n^{n+} ion. Assuming the Te_n^{n+} and Te_6^{2+} ions to have the structures shown in Fig. 2(*i*) and (*ii*) respectively, a greater *p*-orbital imbalance would be expected for Te_6^{2+}.

With regard to the experiments where frozen solutions were studied, there is clearly some uncertainty as to whether the species being studied was present in a frozen glass or whether a compound had crystallized out of solution. However, since the Mössbauer parameters for ^{125}Te appear to be primarily determined by the valence orbital populations of the tellurium, and that lattice terms do not appear to be important, the similarity between the results for the frozen solutions and the solid compounds for the same tellurium cation was to be expected.

Experimental

The HSO_3F solutions were prepared by stirring 10 mg 70% enriched dry ^{125}Te with 2 ml of ice-cold HSO_3F (3). The solutions were transferred to Teflon holders with O-ring seals and frozen and stored in liquid nitrogen until such time as the Mössbauer spectra were run. The sample referred to as $Te_4(Sb_2F_{11})_2$ was prepared by reacting 20 mg of 70% enriched, dry ^{125}Te with an excess of SbF_5 (vacuum distilled) in liquid SO_2 at −23°C (3). The SO_2 solution was drawn off and on evaporation of the SO_2 the resulting red solid was sealed in a Teflon holder and stored in liquid nitrogen. The samples referred to as $Te_4(AlCl_4)_2$ and $Te_6(AlCl_4)_2$ were prepared (6, 9) by reacting 200 mg of unenriched tellurium, to which 50 mg of 70% enriched ^{125}Te was added, with the stoichiometric

quantities of vacuum sublimed $TeCl_4$ and $AlCl_3$ according to the equations:

$$7Te + TeCl_4 + 4AlCl_3 \rightarrow 2Te_4(AlCl_4)_2$$

$$11Te + TeCl_4 + 4AlCl_3 \rightarrow 2Te_6(AlCl_4)_2$$

The reactions were carried out in the molten phase under vacuum in sealed Pyrex tubes. On cooling, the purple-black solids were then mounted and stored as before. The solutions in oleum and the subsequent oxidation steps were studied using 10 mg portions of 70% enriched ^{125}Te. Preparations and sample-mounting were carried out in a dry-box.

None of the above samples were further purified or characterized. However the consistency of the Mössbauer data within any one set of experiments lends support to the identification of tellurium species present.

The compounds $Te_4(AsF_6)_2$, $TeSbF_6$, $Te_x(AsF_6)_y$, and $Te_m(AsF_6)_n$ were kindly provided by Dr. R. J. Gillespie. The latter samples were prepared by reaction of tellurium with excess AsF_5 in SO_2 and may have corresponded to $TeAsF_6$, although they were not analysed.

The bulk of the Mössbauer spectra were recorded with the source and absorbers at 4.2 K at the PCMU Harwell using a $Pb^{125m}Te$ source prepared by neutron irradiation of a $Pb^{124}Te$ sample prepared in our laboratory. The remaining spectra were recorded in our laboratory at Simon Fraser University, again using a $Pb^{125m}Te$ source but with the source at 80 K and the absorbers at 4.2 K (Table 1). The prepared absorbers had a thickness of 5–10 mg cm^{-2} of ^{125}Te. The general procedures used in recording the Mössbauer spectra have been reported elsewhere (10). The spectra were computer fitted to Lorentzians using a program described in ref. 13. The spectrometers were routinely calibrated using an iron foil and a $^{57}Co/Pd$ source and the standard parameters quoted in ref. 14 were used. A sample of $Te(thiourea)_4Cl_2 \cdot 2H_2O$ was used as an internal calibrant and gave parameters on both spectrometers in excellent agreement with previous measurements (10) ($\delta_{PbTe} = 0.78$ mm s^{-1}, $\Delta = 15.6$ mm s^{-1}).

Acknowledgements

The author wishes to thank Dr. A. G. Maddock for his period spent in Cambridge when these experiments were initiated, Dr. B. Dale and the staff at the PCMU Harwell for their help in recording Mössbauer spectra, and Dr. R. J. Gillespie, McMaster University, for kindly providing samples of four compounds. An operating grant from the National Research Council of Canada is gratefully acknowledged.

1. R. J. Gillespie and J. Passmore. Acc. Chem. Res. 413 (1971).
2. R. J. Gillespie and J. Passmore. Adv. Inorg. Chem. Radiochem. **17**, 49 (1975).
3. J. Barr, R. J. Gillespie, G. P. Pez, P. K. Ummat, and O. C. Vaidya. Inorg. Chem. **10**, 362 (1971).
4. J. Barr, R. J. Gillespie, P. K. Ummat, and O. C. Vaidya. J. Am. Chem. Soc. **92**, 1081 (1970).
5. R. C. Paul, C. L. Arora, J. K. Puri, R. N. Virmani, and K. C. Malhotra. J. Chem. Soc. A, 781 (1972).
6. T. W. Couch, D. A. Lokken, and J. D. Corbett. Inorg. Chem. **11**, 357 (1972).
7. P. Boldrini, I. D. Brown, R. J. Gillespie, P. R. Ireland, W. Luk, D. R. Slim, and J. E. Vekris. Inorg. Chem. **15**, 765 (1976).
8. R. J. Gillespie, W. Luk, and D. R. Slim. J. Chem. Soc. Chem. Commun. 791 (1976).
9. D. J. Prince, J. D. Corbett, and B. Garbisch. Inorg. Chem. **9**, 2731 (1970).
10. B. M. Cheyne, C. H. W. Jones, and P. Vasudev. Can. J. Chem. **50**, 3677 (1972).
11. B. M. Cheyne, J. J. Johnstone, and C. H. W. Jones. Chem. Phys. Lett. **14**, 545 (1972).
12. R. J. Gillespie, W. Luk, E. Maharajh, and D. R. Slim. Inorg. Chem. **16**, 892 (1977).
13. G. M. Bancroft, W. K. Ong, A. G. Maddock, R. H. Prince, and A. J. Stone. J. Chem. Soc. A, 1966 (1967).
14. A. M. Muir, K. J. Ando, and H. M. Coogan (*Editors*). Mössbauer Effect Data Index 1958–65. Interscience, New York. 1966. p. 26.

Crystal structure studies of Group V chalcogenide compounds. I. The structure of tricyclohexylphosphine sulphide

K. ANN KERR, P. M. BOORMAN, B. S. MISENER, AND J. G. H. VAN ROODE[1]

Chemistry Department, The University of Calgary, Calgary, Alta., Canada T2N 1N4

Received November 22, 1976

K. ANN KERR, P. M. BOORMAN, B. S. MISENER, and J. G. H. VAN ROODE. Can. J. Chem. **55**, 3081 (1977).

Crystals of tricyclohexylphosphine sulphide, $C_{18}H_{33}PS$, are orthorhombic, $a = 10.906(2)$, $b = 15.836(2)$, $c = 10.362(2)$ Å, $Z = 4$, space group $Pn2_1a$. The structure was solved by direct methods and refined by full-matrix least-squares procedures to a final R_ω of 0.058 for all 1209 reflexions with $\sin\theta/\lambda \leq 0.5377$.

Although second harmonic generation unambiguously established the correct space group as $Pn2_1a$, parameters reported here refer to the centrosymmetric space group *Pnma*. The geometry at phosphorus is approximately tetrahedral with an average P—C distance of 1.838(2) Å. Angles at phosphorus range from 105.4° to 113.2°. The P=S bond length of 1.966(2) Å is one of the longest bonds of this type so far reported. Rigid body analysis of thermal parameters suggests that the 'true' bond lengths are even longer.

K. ANN KERR, P. M. BOORMAN, B. S. MISENER et J. G. H. VAN ROODE. Can. J. Chem. **55**, 3081 (1977).

Les cristaux du sulfure de tricyclohexylphosphine, $C_{18}H_{33}PS$, sont orthorhombiques, $a = 10.906(2)$, $b = 15.836(2)$, $c = 10.362(2)$ Å, $Z = 4$, groupe d'espace $Pn2_1a$. On a résolu la structure par des méthodes directes et on l'a affinée par la méthode des moindres carrés (matrice complète) jusqu'à une valeur finale de R_ω de 0.058 pour les 1209 réflexions avec $\sin\theta/\lambda \leq 0.5377$.

Quoique la génération d'harmoniques secondes permet d'établir d'une façon non-ambigue le groupe d'espace correct $Pn2_1a$, les paramètres qui sont rapportés ici se réfèrent au groupe d'espace centrosymétrique *Pnma*. La géométrie au niveau du phosphore est approximativement tétraédrique avec une distance P—C moyenne de 1.838(2) Å. Les angles autour du phosphore varient de 105.4° à 113.2°. La longueur du lien P=S est de 1.966(2) Å et correspond à la plus longue liaison de ce type qui ait été rapportée jusqu'à maintenant. Une analyse selon les corps rigides des paramètres thermiques suggèrent que les "vraies" longueurs de liaison sont même plus longues.

[Traduit par le journal]

Introduction

Until recently the study of phosphine sulphide complexes was a neglected area of coordination chemistry. Although this situation has been rectified to some extent (1–3), discussions of P—S bonding in both free and complexed forms have been based mainly on studies of vibrational spectra. Since few crystallographic data are available and since there is wide variation in reported bond lengths among different structures and among 'chemically equivalent' bonds in the same structure, we are studying a group of ligands containing the P—S bond in both 'free' and 'bound' states. We are interested in the multiple bond character of the P—S bond and in the nature of the interaction that occurs when phosphine sulphides bond to different classes of metals. Our current structural studies complement our previous synthetic and spectroscopic work (4–6).

Experimental

The compound tricyclohexylphosphine sulphide was prepared by direct reaction between elemental sulphur and tricyclohexylphosphine in a sealed tube at 150°C, followed by extraction with ethanol (7). Recrystallization from ethanol gave clear, plate-like crystals. The sample chosen for analysis had dimensions ca. 0.30 × 0.14 × 0.40 mm (*b*-axis perpendicular to plate face) and was mounted about the *a*-axis. Preliminary unit cell and space group data were obtained by film methods. Unit cell parameters were refined by least-squares treatment of the $\sin^2\theta$ values of 12 high-angle reflexions measured on a 4-circle diffractometer with CuK_α radiation. Crystals data are:

$C_{18}H_{33}PS$ fw = 312.5
Orthorhombic, $a = 10.906(2)$, $b = 15.836(2)$, $c = 10.362(2)$ Å, $V = 1789.7(3)$ Å^3, $Z = 4$, $\rho_c = 1.160$ g cm^{-3}, $\lambda = 1.5418$ Å; $\mu = 22.75$ cm^{-1}, $F(000) = 172$. Absent reflexions: $0kl$, $k + l \neq 2n$ and $hk0$, $h \neq 2n$, space group

[1]Present address: Memorial University of Newfoundland Regional College at Cornerbrook, Cornerbrook, Nfld.

TABLE 1. Atomic parameters of heavy atoms*

Atom	X	Y	Z	U_{11}	U_{22}	U_{33}	U_{12}	U_{13}	U_{23}
S	6631(1)	2500	4416(1)	35(1)	62(1)	51(1)	—	1(1)	—
P	4845(1)	2500	4677(1)	35(1)	37(1)	29(1)	—	−0(0)	—
C1	4426(4)	2500	6398(4)	38(3)	36(3)	29(3)	—	2(2)	—
C2	4892(4)	3292(2)	7084(3)	62(3)	41(2)	35(2)	−2(2)	−2(2)	−1(2)
C3	4559(4)	3286(2)	8508(3)	83(3)	44(2)	36(2)	−2(2)	−0(2)	−8(2)
C4	5030(6)	2500	9163(5)	80(5)	64(4)	31(3)	—	−3(3)	—
C5	4170(3)	3469(2)	4008(3)	46(2)	38(2)	29(2)	−0(1)	1(1)	1(1)
C6	4375(4)	3581(2)	2557(3)	51(2)	39(2)	37(2)	0(2)	3(2)	3(2)
C7	4050(4)	4475(2)	2150(4)	76(3)	46(2)	38(2)	1(2)	5(2)	11(2)
C8	2756(4)	4703(3)	2504(4)	74(3)	46(2)	50(2)	10(2)	−7(2)	9(2)
C9	2500(5)	4552(3)	3930(4)	62(3)	60(3)	51(2)	18(2)	4(2)	2(2)
C10	2832(3)	3659(2)	4336(4)	49(2)	56(2)	41(2)	11(2)	7(2)	8(2)

*Coordinates ($\times 10^4$) and their standard deviations expressed as fractions of the cell edge. Anisotropic temperature factors ($\times 10^3$) have the form $T = \exp\{-2\pi^2(h^2a^{*2}U_{11} + \ldots + 2hka^*b^*U_{12} + \ldots)\}$. Those temperature factors that must have zero value in space group *Pnma* are indicated with a dash.

Pnma or $Pn2_1a$. Strong second harmonic generation (8*a*, *b*) unequivocally confirms that the correct space group is $Pn2_1a$.[2] Intensity data were measured at room temperature on a Picker four-circle diffractometer in the θ–2θ scan mode with a scintillation counter and Ni-filtered CuK_α radiation using a scan rate of 1° min^{-1}. The scan range was determined by the expression $\Delta 2\theta = 1.0° (0.93 + 0.285 \tan\theta)$ and background counts were measured for 40 s at either end of the scan. The three standard reflexions that were measured after every 75 reflexions throughout the data collection showed no systematic trend. Both *hkl* and *hkl̄* data were collected to a maximum 2θ value of 112°. These reflexions were averaged to give 1209 independent reflexions of which 271 had intensities less than $3\sigma(I)$. These were included in the structure factor calculation but given zero weight in the refinement if $F_c \leq F_o$.

Structure Analysis

The structure was solved in space group $Pn2_1a$ using the program MULTAN (9). The 300 reflexions with $E > 1.18$ were used in a symbolic addition procedure which generated 128 sets of phases of which 64 had identical figures of merit. One of these sets was used to calculate an E-map which revealed the positions of all heavy atoms in the molecule.

The structure was refined to convergence in the centrosymmetric space group *Pnma* using full-matrix least-squares with weights based on counting statistics. During the final cycles of refinement the 167 parameters refined included scale, extinction, positional parameters for all atoms, anisotropic temperature parameters for the heavy atoms and isotropic temperature parameters for hydrogen. The refinement converged with $R_\omega = \Sigma\omega||F_o| - |F_c||/\Sigma\omega|F_o| = 0.0581$ for the 966 reflexions of non-zero weight. The conventional *R*-value was 0.0472 for the 'observed' reflexions only and 0.0787 for the full data set.

Since the correct space group is $Pn2_1a$ we attempted refinement in this space group at two stages, once at the end of isotropic refinement and once after convergence of the anisotropic refinement. In both cases, the approach to convergence was slow, estimated standard deviations of parameters were high and agreement between chemically equivalent bonds became worse than in the preceding centrosymmetric refinement. For these reasons the results reported here refer to refinement in the centrosymmetric space group *Pnma*.

The quantity minimized was $\Sigma\omega(|F_o| - |F_c|)^2$ where $\sqrt{\omega} = \{\sigma^2(F) + 0.001F^2\}^{-1/2}$ and $\sigma(F)$ was derived from counting statistics. When the refinement was terminated the mean parameter shift was 0.076σ and no parameter shift was larger than 0.407σ. The standard deviation of an observation of unit weight was 1.56. Scattering factors and anomalous scattering corrections from ref. 10 were used for all atoms. A table of observed and calculated structure factors has been placed in the Depository of Unpublished Data.[3]

Results and Discussion

Positional and thermal parameters for the heavy atoms are given in Table 1 while those for hydrogen atoms are in Table 2. General features of the molecular structure are shown in Fig. 1. Molecular packing is illustrated in Fig. 2. In the centrosymmetric refinement, the mirror plane at $y = 0.25$ bisects the molecule so that atoms S, P, C(1), and C(4) lie on the mirror. The three cyclohexyl rings are in the chair form with bond angles close to the expected tetrahedral values.

The geometry at phosphorus is slightly but significantly distorted. The S—P—C angles and the C—P—C angle across the mirror plane are

[2]In this technique, laser light of wavelength 1.06 μm with peak pulse power in the kW range is used to irradiate the sample. The fundamental beam is eliminated with appropriate filters placed after the sample and any second harmonics of wavelength 0.53 μm are then detected with a photomultiplier. This provides a highly sensitive test for the absence of centres of inversion.

[3]Complete set of data is available at a nominal charge, upon request, from the Depository of Unpublished Data, CISTI, National Research Council of Canada, Ottawa, Canada K1A 0S2.

larger than the expected tetrahedral value, while the other C—P—C angles are significantly smaller than tetrahedral. This may well be a steric effect since the direction of the distortion is consistent with relief of very short intramolecular S---C(5) contact of 3.120(3) Å. The S---C(1) contact of 3.162(4) Å is not as severe. The only other short contacts of note are between the phosphorus atom and the hydrogens on the lead carbons of the cyclohexyl rings. The P---H(1) distance is 2.33(4) Å and the P---H(5) distances are 2.24(3) Å. There are no unusual inter-molecular contacts.

A comparison of bond lengths with other values in the literature demands that the values compared be measurements of the same quantity and be drawn from the same pool. The P=S and P—C values of 1.959(2) Å and 1.798(2) Å given for an X-ray determination of $(CH_3)_3PS$ (12) are too scantily reported to allow a reader to assess their reliability. The results for triorthotolyl phosphine sulphide (3) (P=S 1.953(6) Å, 1.942(5) Å with P—C ranging from 1.773(9) Å to 1.870(9) Å) are much less precise than the present determination. The electron diffraction results on $(CH_3)_3PS$ give a P=S of 1.940(2) Å with an average P—C distance of 1.812(2) Å. These results have the desired accuracy and precision but are not strictly comparable with the X-ray results since the two experiments measure different time-average distances. However, it can be noted that our value of 1.966(2) Å is the longest bond of this type so far reported. The two independent P—C bonds are identical within the precision of the experiment, and very close to the value of 1.84 Å calculated from Schomaker–Stevenson single-bond radii with electronegativity correction.

TABLE 2. Atomic parameters of hydrogen atoms, fractional coordinates, and isotropic temperature factors ($\times 10^3$)

Atom	x	y	z	U (Å²)
H1	348(4)	250	641(4)	33(10)
H2A	463(3)	377(2)	670(3)	45(10)
H2B	573(3)	330(2)	700(3)	49(10)
H3A	363(3)	332(2)	859(3)	59(11)
H3B	489(3)	383(2)	888(3)	55(9)
H4A	489(5)	250	1003(7)	82(18)
H4B	587(5)	250	907(5)	67(17)
H5	475(3)	390(2)	443(3)	47(9)
H6A	378(3)	321(2)	211(3)	51(9)
H6B	519(3)	346(2)	238(3)	43(9)
H7A	427(3)	454(2)	129(4)	61(11)
H7B	470(3)	486(2)	259(3)	63(11)
H8A	219(4)	436(2)	207(4)	68(12)
H8B	259(3)	529(3)	231(3)	67(11)
H9A	168(3)	462(2)	409(3)	55(11)
H9B	302(3)	496(2)	440(3)	52(10)
H10A	227(3)	330(2)	388(3)	56(11)
H10B	263(3)	360(2)	518(4)	52(10)

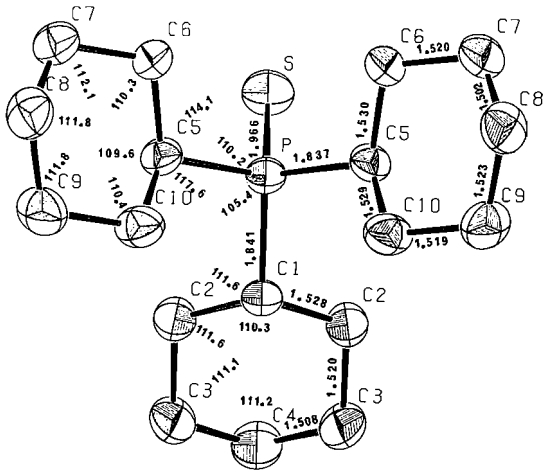

FIG. 1. A perspective view of tricyclohexylphosphine sulphide with hydrogen atoms omitted for clarity. The atoms S, P, C(1), and C(4) lie on the mirror plane. H—C bond lengths range from 0.90(4) to 1.04(4) Å with a mean value of 0.96(5) Å. Bond angles involving hydrogen range from 100(3)° to 117(2)° with a mean of 109(3)°. Bond angles not shown in the diagram: C(1)—P—S, 112.2(1); C(5)—P—C(5), 113.2(1).

TABLE 3. Bond distances corrected for rigid-body thermal motion

Bond	Distance
P —S	1.970
P —C1	1.844
P —C5	1.840
C1 —C2	1.530
C2 —C3	1.521
C3 —C4	1.510
C5 —C6	1.532
C6 —C7	1.522
C7 —C8	1.505
C8 —C9	1.525
C9 —C10	1.520
C10—C5	1.532

Orientation of the thermal ellipsoids in Fig. 1 suggests that the molecule may be librating as a rigid body (11). Thermal vibration analysis has been carried out using the method of Schomaker and Trueblood (13) with the rigid-body parameters constrained to have the same mirror symmetry as the individual U_{ij}'s. Although the analysis was successful in that the fit was reason-

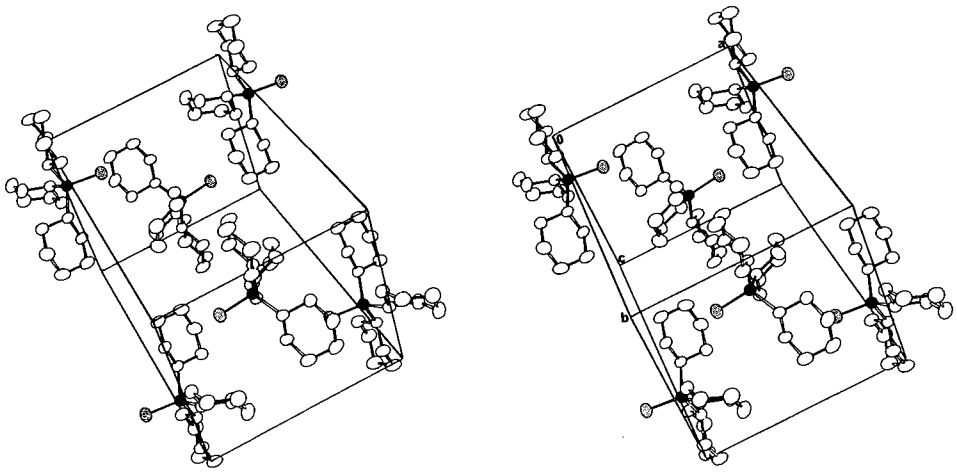

FIG. 2. A stereoscopic view of the crystal structure of tricyclohexylphosphine sulphide.

TABLE 4. Rigid-body parameters, tensor elements, and their esd's*

Tensor	11	22	33	12	13	23
T (Å²)	0.038(1)	0.041(1)	0.033(1)	—	0.003(1)	—
L (deg²)	2.0(4)	6.9(6)	7.9(7)	—	0.26(5)	—

	Rms amplitudes†		Principal axes‡		
	0.2020 (Å)	t_1	0.00	1.000	0.000
T	0.1988	t_2	0.906	0.000	0.423
	0.1776	t_3	0.423	0.000	0.906
	2.817 (deg)	l_1	0.044	0.000	0.999
L	2.626	l_2	0.000	−1.00	0.000
	1.420	l_3	0.999	0.000	−0.042

*Tensor elements have been calculated with respect to inertial tensors with origin at 0.4298, 0.2500, 0.4713, with l_1 and t_1 defined as vectors of the libration tensor **L** and the translation tensor, **T**.
†Rms discrepancy in U_{ij} = 0.0037 Å².
‡Referred to crystal coordinate system.

able, the corrections to the bond lengths are not significant. The systematic shortening in C—C bond length with distance from the centre of the molecule suggests that internal modes of vibration may be important in the cyclohexyl rings. Corrected bond distances are shown in Table 3. Rigid-body parameters and their esd's are shown in Table 4.

There are too few structure determinations on this class of compounds to allow a meaningful comparison with spectroscopic work. We are currently studying several related ligands in both free and bound states.

Acknowledgements

This work was supported by NRCC grants A4734 (P.M.B.) and A5881 (K.A.K.) and by a generous grant of computer time from the University of Calgary. Computer programs used include CUDLS (John Stevens), ORTEP (C. K. Johnson), MGTLS (P. K. Gantzel and K. N. Trueblood), and several programs from the Los Alamos Scientific Laboratory system of programs (A. C. Larson). All have been modified by the authors to include new features and/or to meet the constraints of the local computer. Tests for second harmonic generation were done by Philips Laboratories, Briarcliff Manor, New York.

1. D. E. C. CORBRIDGE. The structural chemistry of phosphorus. Elsevier Scientific Publishing Company, Amsterdam, London, New York. 1974.
2. C. J. WILKINS, K. HAGEN, L. HEDBERG, Q. SHEN, and K. HEDBERG. J. Am. Chem. Soc. **97**, 6352 (1975).
3. T. S. CAMERON and B. DAHLÈN. J. Chem. Soc. Perkin II, 1737 (1975).

4. P. M. BOORMAN and K. J. REIMER. Can. J. Chem. **49**, 2926 (1971).
5. P. M. BOORMAN and D. POTTS. Can. J. Chem. **52**, 2016 (1974).
6. P. M. BOORMAN, S. A. CLOW, D. POTTS, and H. WIESER. Inorg. Nucl. Chem. Lett. **9**, 941 (1973).
7. C. SCRETTAS and A. F. ISBELL. J. Org. Chem. 2753 (1962).
8. (*a*) S. K. KURTZ and T. T. PERRY. J. Appl. Phys. **39**, 3798 (1968); (*b*) J. D. DOUGHERTY and S. K. KURTZ. J. Appl. Crystallogr. **9**, 145 (1976).
9. G. GERMAIN, P. MAIN, and M. M. WOOLFSON. Acta Crystallogr. B**26**, 274 (1970).
10. International Tables for X-Ray Crystallography. Vol. IV. Kynoch Press, Birmingham, England. 1974.
11. D. W. J. CRUICKSHANK. Acta Crystallogr. **9**, 754 (1956).
12. P. G. ELLER and P. W. R. CORFIELD. Chem. Commun. 105 (1971).
13. V. SCHOMAKER and K. N. TRUEBLOOD. Acta Crystallogr. B**24**, 63 (1968).

Structural effects on reactivity in the oxymercuration reaction

I. C. AMBIDGE, STEPHEN K. DWIGHT, CAROLYN M. RYNARD, AND THOMAS T. TIDWELL

Department of Chemistry, University of Toronto, Scarborough College, West Hill, Ont., Canada M1C 1A4

Received March 10, 1977

I. C. AMBIDGE, STEPHEN K. DWIGHT, CAROLYN M. RYNARD, and THOMAS T. TIDWELL. Can. J. Chem. **55**, 3086 (1977).

The kinetics of the reaction of mercuric acetate with alkenes in methanol can be measured directly by observing the ultraviolet absorbance of the solution at 265 nm. For more reactive alkenes stopped flow techniques are required, but for less reactive substrates conventional spectrophotometers are adequate. The measured rates are in satisfactory agreement with values obtained by other methods. The rates of several cyclopropylalkenes were measured in this way, and relative reactivities of some of the same substrates were obtained by the competition method. Rates obtained by both methods are in qualitative agreement, and show very high reactivity for the cyclopropylalkenes. These rates are analyzed by comparison with model reactions involving open ions (acid-catalyzed hydration) and bridged ions (sulfenyl halide addition). The comparisons suggest that the oxymercuration of alkenes not substituted with strongly resonance electron-donating substituents, for example ethylene, proceeds through bridged rate-determining transition states that put very little positive charge on carbon, but that when strongly resonance electron-donating substituents such as cyclopropyls are present, the rate-determining transition state resembles an open carbonium ion.

I. C. AMBIDGE, STEPHEN K. DWIGHT, CAROLYN M. RYNARD et THOMAS T. TIDWELL. Can. J. Chem. **55**, 3086 (1977).

On peut mesuré la cinétique de la réaction de l'acétate mercurique avec les alcènes dans le méthanol d'une manière directe en observant l'absorption dans l'ultraviolet d'une solution à 265 nm. Pour les alcènes réactifs, on doit faire appel aux techniques de flux stoppés mais pour des substrats moins réactifs, des méthodes spectrophotométriques conventionnelles sont adéquates. Les vitesses mesurées sont en bon accord avec les valeurs obtenues par d'autres méthodes. De cette manière on a mesuré les vitesses de réaction de plusieurs cyclopropylalkènes et des réactivités relatives de quelques uns des mêmes substrats ont pu être obtenues par des méthodes compétitives. Les vitesses obtenues par les deux méthodes sont en bon accord qualitatif et indiquent une très grande réactivité pour les cyclopropylalkènes. On a analysé ces vitesses par comparaison avec des réactions modèles impliquant des ions ouverts (l'hydratation acido-catalysée) et des ions pontés (addition de l'halogénure de sulfényle). Ces comparaisons suggèrent que l'oxymercuration des alcènes non-substitués par des substituants agissant comme électro-donneurs puissants par résonance, par exemple l'éthylène, procède par des états de transition déterminant la vitesse de la réaction qui sont pontés et qui induisent très peu de charge positive au niveau du carbone; toutefois lorsque des substituants agissant fortement comme des électro-donneurs à cause de la résonance tel que le cyclopropyle, sont présents, l'état de transition déterminant la vitesse ressemble à un ion en forme ouverte.

[Traduit par le journal]

The oxymercuration reaction has been extensively studied and has been the subject of frequent reviews (1–11). Nevertheless it appears from the most recent surveys (9–11) that there is still dissension regarding the mechanism of this important reaction, although there is general agreement that its broad features can be described as in [1] and [2].

[1] $$R_1R_2C{=}CR_3R_4 + HgX_2 \underset{k_{-1}}{\overset{k_1}{\rightleftharpoons}} \text{Complex } \mathbf{1}$$

[2] $$\mathbf{1} + N \underset{k_{-2}}{\overset{k_2}{\rightleftharpoons}} R_1{-}\overset{R_2}{\overset{|}{C}}{-}\overset{R_3}{\overset{|}{C}}{-}R_4 \quad (HgX,\ N)$$

It has been established that the rate of oxymercuration is first order in both alkene and mercuric salt, but there are a number of other aspects of the reaction that are open to question. For example, the identity of the attacking mercury species is unknown in most cases. For reactions in 0.01 *M* $HClO_4$ the reaction involves the fully dissociated Hg^{2+} reagent (12), but for reactions utilizing mercuric acetate in methanol solution, the most common medium for kinetic studies (13–21), it has been proposed that a

number of possible electrophiles must be considered (14, 16). These include various acetatomercury(II) complexes (eq. 3) (16), as well as

[3] $Hg(OAc)_3^-$

$$\begin{array}{ccccc} & & \uparrow\downarrow OAc^- & & \\ Hg(OAc)_2 & \overset{OAc^-}{\rightleftharpoons} & Hg(OAc)^+ & \overset{OAc^-}{\rightleftharpoons} & Hg^{2+} \end{array}$$

protonated forms of these and complexes with other ligands (14). It has been suggested that attack by $HgOAc^+$ is of primary kinetic importance (16, 22), and in agreement with this hypothesis added acetate ions usually slow the reaction (13, 14, 16, 19, 20*b*,*c*), whereas added mineral acids (14, 16, 20) increase the rate. Added acetic acid has been reported to increase the rate in some cases (16, 20*b*,*c*), and decrease it in others (13, 19, 20*a*).

There is also some disagreement as to which step in [1] and [2] is rate-limiting, as both formation of the olefin–mercury complex (12, 16, 20), and attack of the nucleophile N (usually solvent) (7, 9, 17, 23) have been proposed as the slow step in the reaction. Finally, there is sharp disagreement about the structure of the alkene–mercury(II) complex **1**.

One proposal is that the complex is a rather symmetrical cyclic 'mercurinium' ion **2**. This view is endorsed in recent reviews (7–9) and

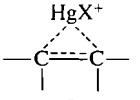

2

papers (14, 16, 17, 23). For example, the authors state "Such π-complexes were . . . called mercurinium ions. This intermediate is a commonly accepted tenet in the oxymercuration mechanism" (7); "It may well be that two polar mechanisms can operate; in one, a four-center transition state involving only the reagent and the olefin . . . while . . . a mercurinium ion or some kinetically equivalent species may be the more usual mode of reaction" (8); and "Studies of oxymercuration are generally consistent with the rapid and reversible formation of mercurinium ions" (9).

An opposing mechanistic interpretation is that oxymercuration occurs to give an unbridged open carbonium ion **3**. Recent examples of this view are "We discard the symmetrical

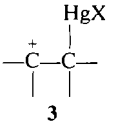

3

mercurinium ion in interpreting our results. We prefer the concept of electrophilic attack by the mercury species ^+HgX at the least substituted carbon atom of the double bond" (22*b*) and "oxymercuration . . . of olefins (is) considered to be electrophilic addition . . . passing through a classical carbenium ion" (24).

A viewpoint intermediate between the extremes of a symmetrical cyclic mercurinium ion (**2**) and an open β-mercuri carbonium ion (**3**) is an unsymmetrical ion (**4**) with partial charge on one carbon and on mercury (25). The positive charge in such an ion is partly delocalized onto mercury by hyperconjugation (25). It may be

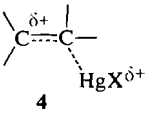

4

that the energy difference between transition states **2**–**4** are small and that structural differences in the alkenes determine which is involved in each case. Other more complex ions have been proposed for some special cases (26).

Most of the discussions in the literature have tacitly assumed that the olefins under consideration are symmetrically substituted and have neglected the role of unsymmetrical substitution on the double bond. It has been pointed out (27) that unsymmetrical substitution would of necessity require mercurinium ions to be unsymmetrical, and some of the kinetic data have been interpreted in terms of such intermediates (18).

The evidence for the different formulations of the oxymercuration intermediate has been thoroughly reviewed (1–11) and it is only briefly summarized here.

It would be anticipated that a reaction involving a bridged species would occur in an *anti* fashion, and oxymercuration usually (28–30), but not always, fulfils this expectation. The reverse reaction, deoxymercuration, also occurs in an *anti* fashion (28). Furthermore alkenes such as *tert*-butylethylene (18*b*) and 1-methylnorbornene (22*b*), which are prone to rearrangement during reactions involving carbonium ions, give unrearranged products in oxymercuration. Kinetic studies have been interpreted as

favoring a bridged intermediate (14, 16, 17, 20*a*,*b*), as have theoretical studies (25*a*,*b*, 31), and an nmr examination of stable ion complexes of Hg^{2+} and alkenes (27).

Evidence that oxymercuration involves open ions includes the fact that many strained species, such as norbornene (**6**) (32*a*), bicyclo[2.1.1]-hexene (**7**) (33), and cyclopropene (**8**) (34) add mercuric salts in a *cis* fashion. We discovered that even when there are *syn*-7 substituents in

6 **7** **8**

the norbornyl nucleus the addition still occurs *cis*,*exo*, [4] (22*b*, 32*b*), and a general correlation has been proposed that such behaviour is diagnostic of unbridged intermediates (22*b*).

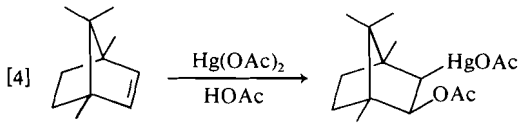

Further evidence that bridging is not a dominant factor in oxymercuration comes from the comparison of the oxymercuration and arylsulfenyl halide additions to the *cis*- and *trans*-1,2-di-*tert*-butylethylenes. The latter reaction is generally accepted to involve a strongly bridged intermediate, and occurs in an *anti* fashion to each of these compounds (35). Oxymercuration however, leads to the same product from each of these isomeric alkenes (17*b*). Although the results of the oxymercurations were interpreted in terms of a bridged intermediate the contrast with the arylsulfenyl halide results strongly suggests that bridging is less significant in the former reaction.

Some authors also conclude that the kinetic results do not provide compelling evidence for bridged ions (12, 22). Others believe that an asymmetrically bridged ion is implicated by the kinetics (18). Also the investigators of the long-lived ions stated "While these observations do lend credence to those reports in which mercurinium ions have been implicated as reaction intermediates, they do not prove that mercurinium ions are present under any other set of conditions" (27).

In view of the conflicting views and contradictory experimental findings regarding the oxymercuration reaction, as well as continuing interest in this reaction (36–38), it appeared that further studies were warranted.

Previous kinetic methods applied to this reaction have not been completely satisfactory. Because of the great rate of the reaction direct kinetic measurements have been confined to the less reactive alkenes (14–16, 19, 20, 39). More recently competition methods have been utilized (17, 18, 22*a*) but these are more subject to uncertainties in interpretation, and do not allow examination of the effects of variables such as concentration, solvent, and added ions. Direct measurement by ultraviolet absorption has been applied to rates in aqueous $HClO_4$, but the reactions in this medium are so fast that no alkene more reactive than isobutene could be measured, even using stopped flow techniques (12).

It appeared highly desirable therefore to develop an ultraviolet method for measuring rates in methanol solution. It was hoped that the use of both conventional and stopped flow spectrophotometers would allow the complete range of alkene reactivities to be observed, and furthermore the rates could be compared to all of the previous kinetic studies carried out in methanol solution (13–21).

In order to probe the possible structures of the methoxymercuration transition state it was of particular interest to test the influence of a strong resonance electron-donating substituent on the reaction. We have previously found the cyclopropyl substituent is a useful probe for the examination of the transition states of electrophilic additions to alkenes (40). Accordingly this investigation deals with the development and testing of the ultraviolet method for direct measurement of methoxymercuration and the use of this method to examine cyclopropyl-alkenes. To establish the validity of the method we began with a comparison with rates obtained by the competitive method and with rates measured by direct methods which have previously been reported.

Results

Relative rate constants for methoxymercuration of alkenes have been obtained by two different methods. Pritzkow and co-workers (18) reacted a mixture of alkenes with a smaller amount of mercuric acetate and analyzed the amounts of residual olefins by gas chromatography. Bach and Richter (17) carried out the

reaction in a similar fashion, but reduced the product organomercurial with $NaBH_4$ and analyzed the resultant ethers by gas chromatography [5].

[5] 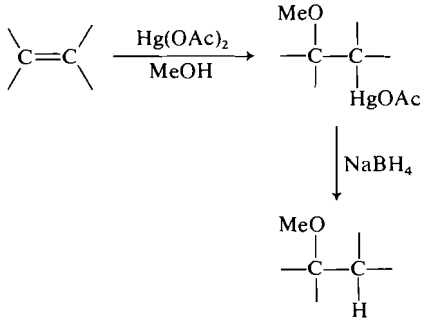

In our work competitive rates of vinylcyclopropane (**9**), 1-methyl-1-cyclopropylethylene (**10**), 1-phenyl-1-cyclopropylethylene (**11**), and 1,1-dicyclopropylethylene (**12**) were measured relative to cyclohexene by analysis of the yields of methyl ethers. The authentic methyl ethers corresponding to Markovnikoff addition were prepared by oxymercuration–demercuration or by reaction of the alkoxides with methyl iodide. Preparative scale oxymercuration–demercurations were also carried out and in every case the product expected from Markovnikoff addition without rearrangement was isolated and identified. Relative rates were calculated from the observed relative yields of methyl ethers when equimolar amounts of two different alkenes were allowed to react with a deficient amount of $Hg(OAc)_2$.

The relative rates obtained are compiled in Table 1. The cyclopropylalkenes **9**, **10**, and **12** were very reactive and no suitable standard more than one-tenth as reactive was available. Therefore, the rates of these compounds relative to cyclohexene are subject to error. The relative rates among these three compounds were measured independently and should be more precise.

The reactivities of several compounds in methanol which had previously been examined in other laboratories were also measured as a test of the reproducibility of the method. These data are also included in Table 1, along with data for some crowded alkenes. In general the agreement between methoxymercuration rates from different laboratories is quite satisfactory, although some discrepancies exist (cf, norbornene **6**).

In order to measure directly the rate of methoxymercuration it appeared that spectral measurements using fast-mixing techniques would be most suitable. The ultraviolet spectrum of mercuric acetate in methanol (Fig. 1) is characterized by a very strong absorption but no maximum above 200 nm (at 200 nm $\varepsilon = 7000$) which decreases smoothly and becomes imperceptible near 300 nm. Gowenlock and Trotman (41) in an aside reported a maximum for mercuric acetate in ethanol at 212 nm but we do not observe this feature in either methanol or ethanol, although we did confirm the maxima they report for mercuric halides in this region.

The ultraviolet spectra of 1-methyl-1-cyclopropylethylene (**10**) and the reaction product of **10** with equimolar $Hg(OAc)_2$ are also shown in Fig. 1. Above 210 nm it may be seen that the absorptivity of the alkene and the reaction product are lower than that of $Hg(OAc)_2$. We elected to follow the reactions by the decrease in absorbance at 265 nm.

Rates were monitored at 25°C using two different Durrum D110 stopped flow spectrophotometers, and Cary 14 and 118 spectrophotometers. Standard reaction conditions (0.035 *M* $Hg(OAc)_2$, alkene, and HOAc) were adopted for most runs. In some cases a 10-fold excess of alkene was present to give pseudo first-order conditions, and lower reagent concentrations were used in some of the stop-flow runs. Within the limits of reproducibility the second-order rate constants were independent of the concentrations of $Hg(OAc)_2$ and alkene, and were about 20% lower in the presence of 0.035 *M* HOAc. Equimolar NaOAc or NaOMe decreased the rates by factors of about 5.

The end-point absorptions of many of the reactions, especially for alkenes with allylic hydrogens, were unstable and drifted continually downward. For these cases the rate constants were calculated using estimated infinity points or by the Guggenheim method. Excellent linear rate plots for 1–2 half-lives were generally obtained by second-order or pseudo first-order calculations as appropriate. However the reproducibility of the rate constants was not good, despite extensive efforts at purification of reagents and solvents, and degassing of the solutions. The failure to reduce some of the average deviations below $\pm 20\%$ eliminated the possibility of a more detailed study of the effect of reaction variables. However relative reactivities

TABLE 1. Relative rates of methyoxymercuration of alkenes by $Hg(OAc)_2$ in MeOH at 25°C

Alkene	k_{rel}	k_{rel} (literature)
Cyclohexene	1.0	1.0
Norbornene	4.6	4.5[a], 10.6[b], 1.0[c]
1-Octene	7.4	9.5[a], 4.0[c]
c-PrCH=CH_2 (**9**)	700	1700[b]
c-PrCMe=CH_2 (**10**)	350	8600[b]
c-PrCPh=CH_2 (**11**)	15	
c-Pr_2C=CH_2 (**12**)	700	11000[b]
cis-4-Octene	0.22	0.10[c]
cis-3-Hexene	0.58	0.25[c]
tert-BuCH=CH_2	0.067	0.07[c]
tert-BuCMe=CH_2	0.50	
tert-Bu_2C=CH_2	<0.005[d]	

[a]Reference 17*a*.
[b]From direct measurement, this work.
[c]Reference 18.
[d]No reaction observed.

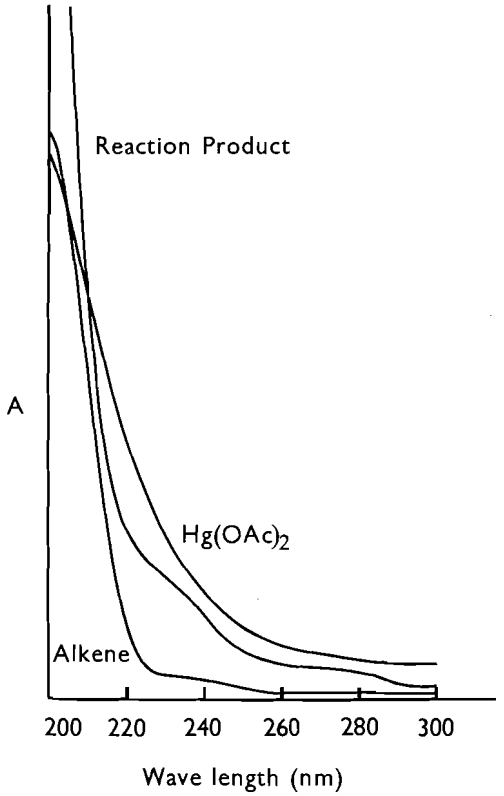

FIG. 1. Ultraviolet absorption of $Hg(OAc)_2$, *c*-PrCMe=CH_2, and *c*-PrMeCOMeCH_2HgOAc, each 1.0×10^{-3} *M* in MeOH, 1 mm cell.

of different substrates were consistently reproduced and the rate constants presented in Table 2 appear reliable for that purpose.

In the case of the isomeric 1,2-dicyclopropylethylenes an extremely rapid increase in uv absorbance was observed, so rates of addition for these substrates are not reported.

Discussion

The relative rate constants obtained for alkenes by the direct and competitive methods are compared in Table 1. These are in reasonable agreement but some deviations are apparent. One serious difficulty with the competitive rates is that the reactions do not proceed quantitatively to single products, and often several unidentified peaks are visible in the gas chromatograms.

[6] $$-CH_2CH{=}CH- \xrightarrow{Hg(OAc)_2} -CHOAcCH{=}CH-$$

Allylic oxidation (eq. 6), alkene exchange, and vinyl mercurial formation are well known examples of side reactions that occur in oxymercurations (42–44). The lack of agreement between some of the competitive rates from different laboratories is probably a consequence of these and other experimental problems.

The direct rate measurements suffer from the fact that their degree of reproducibility is only fair, and they may also be affected by side reactions. However, we believe the rate constants obtained by this method are reasonable indicators of the relative reactivities of the alkenes as the differences in reactivity were reproducible and were quite large in some cases. Qualitative agreement of rates obtained by competitive and direct methods lends considerable confidence that these reactivities can be reliably used for mechanistic interpretations.

In the introduction the possibility of reversi-

TABLE 2. Direct measurement of rates of methoxymercuration of alkenes by uv spectroscopy in MeOH at 25°C and comparative rates of hydration and sulfenyl halide addition

Alkene	Methoxymercuration			
	k_2 (M^{-1} s^{-1})	k_{rel}	H_3O^+ (k_{rel})[b]	ArSCl (k_{rel})[c]
CH_2=CH_2	1.04	0.50	3.4×10^{-7}	0.49
n-BuCH=CH_2	(2.06)[a]	1.0	1.0	1.0
tert-BuCH=CH_2	0.058	0.028	—	0.71
tert-BuCMe=CH_2	0.50	0.24	4.7×10^4	1.11
c-PrCH=CH_2	840	410	5.9×10^4	4.8
c-PrCMe=CH_2	4300	2100	4.6×10^7	14.1
c-Pr_2C=CH_2	5500	2700	2.5×10^9	23
c-PrCH=CHMe (*Z*)	1.37	0.67	1.4×10^4	6.4
c-PrCH=CHMe (*E*)	0.64	0.31	6.3×10^3	2.1
Cyclohexene	0.50[d]	0.24	10.3	2.2
Norbornene	5.3	2.6	7.9×10^3	20

[a]Derived by multiplying the cyclohexene rate by the cyclohexene–1-hexene competitive relative rate of 4.13.
[b]Reference 40.
[c]T. Cerksus, V. Csizmadia, G. H. Schmid, and T. T. Tidwell. Unpublished work, and ref. 45.
[d]A value of 0.29 M^{-1} s^{-1} has been found by a different method (13*b*).

bility of the different steps of the reaction was raised. The results available do not allow the assignment of the individual rate constants in [1] and [2]. In the discussion that follows it is assumed that the observed rates reflect the stability of the intermediate ion, so that k_{obs} is proportional to k_1 in [1]. A consistent interpretation does emerge on the basis of this assumption, but a detailed analysis of the kinetics, including the various mercury electrophiles (eq. 3), remains an unsolved problem.

Protonation is the best example of a reaction which proceeds with attack on one carbon of a double bond to form an open carbonium ion, and we have thoroughly examined the effects of structure upon reactivity in this case (40). The most clear-cut example of an electrophilic addition proceeding through rate-determining formation of a bridged three-center ion is sulfenyl halide addition to alkenes, and the structural effects on this reaction have also been well documented (45). Therefore the effect of structure on the rate of oxymercuration may be compared to these two reactions as a suitable guide to the mechanism of this reaction. The relevant data are compiled in Table 2.

It is apparent from Table 2 that there is not a direct correlation of the oxymercuration rates with the rates of hydration or of sulfenyl halide addition. However, inspection of the individual data does reveal some salient structural features that affect the rates. Most noticeably ethylene is extremely unreactive in hydration relative to 1-hexene or cyclohexene, but these three alkenes are of comparable reactivity in oxymercuration or sulfenyl halide addition. This rate comparison is what would be expected if protonation gave the very unstable open ethyl cation (eq. 7), but the other electrophiles led to bridged structures (eq. 8).

[7] $$CH_2{=}CH_2 \xrightarrow{H^+} CH_3\overset{+}{C}H_2$$

[8] $$CH_2{=}CH_2 \xrightarrow{E^+} CH_2{=}\overset{E^+}{CH_2}$$

(E^+ = HgX^+ or ArS^+)

On the other hand oxymercuration of the vinylcyclopropanes *c*-PrCR=CH_2 are accelerated relative to 1-hexene by factors of about 10^3, whereas the corresponding sulfenyl halide additions only increase by factors of 5 to 23. In these cases the behavior of the oxymercuration reactions resembles the hydrations much more than the sulfenyl halide additions and supports the formation of open ions for hydration and oxymercuration [9]. The more than 10^3 greater

[9] *c*-PrCH=CH_2 $\xrightarrow{Hg(OAc)^+}$ *c*-Pr$\overset{+}{C}$HCH_2HgOAc

reactivity of 2-cyclopropylpropene relative to the isomeric 1-cyclopropylpropenes strongly implicates an open ion in the former case.

In addition to these effects it is also apparent that steric factors are much more significant in the case of oxymercurations than in the other reactions. Thus the *tert*-butylethylenes show decreased reactivities in oxymercuration, as do the 1,2-disubstituted alkenes.

As pointed out in the introduction oxymercuration of the isomeric *cis*- and *trans*-1,2-di-*tert*-butylethylenes leads to the same product, a result which was interpreted in terms of bridged ions (17). However we believe the fact that sulfenyl halide additions to the same alkenes proceeds with *anti* attack in each case to give isomeric products indicates that bridged ions are involved in the latter case and a different mechanism in the former. The oxymercuration product was assigned *threo* stereochemistry by ^{1}H nmr but the *erythro* isomer was not available for comparison. The *threo* product could be formed by *syn* addition to a common open ion with *anti tert*-butyl groups formed directly by attack of the electrophilic mercury species on the *trans*-olefin and attack on the *cis*-olefin followed by rotation around the central C—C bond.

The overall picture that emerges is that the oxymercuration occurs by either open or bridged ions depending upon the particular substitution pattern. If strongly resonance electron-donating substituents are present then open ions are favored, and in the absence of electronic factors that would stabilize open carbonium ions bridging occurs. An alternative way of viewing the situation is in terms of hyperconjugatively stabilized ions such as **4** in which the degree of hyperconjugative electron donation depends on the electron demand placed on the C—Hg bond. This latter interaction in the intermediate would also give some bias towards *anti*-addition without rearrangement, as is frequently observed. We agree with the view (27) that a 'continuum' of ions is involved, and believe that the ion from ethylene resembles the bridged extreme and that the ion from **12** resembles the open ion structure.

The rapid increase in absorbance observed in the reaction of the 1,2-dicyclopropylethylenes indicates that some other reaction is occurring instead of addition to the double bond. The probable pathway is cleavage of the cyclopropane ring by electrophilic attack of mercury (eq. 10). This is a well documented reaction that

[10] 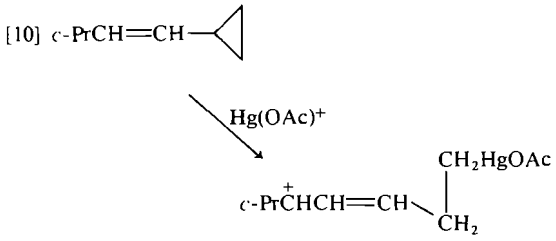

occurs under rather mild conditions (46) that should be particularly facile in this case because of the very stable carbonium ion intermediate that can be formed (eq. 10). An alternative route involving rate-determining attack of electrophilic $HgOAc^+$ on the double bond and then ring opening would be expected to be much slower, inasmuch as the 1,2-dicyclopropylethylenes are slower than the 1-cyclopropylpropenes in hydration and of about the same reactivity in arylsulfenyl halide addition.

We were successful in analyzing rates of hydration in terms of substituent parameters (40) so it was of interest to test this approach for oxymercuration.

There have been several attempts to define the rate-determining transition state by correlation of the rates with substituent parameters. Halpern and Tinker (12*a*) plotted log k vs. σ^* and reported an 'excellent' correlation for monosubstituted alkenes. They interpreted the plot as "implying a high degree of positive charge localization (approaching carbonium ion character), in the transition state, on the carbon adjacent to the substituent R, i.e."

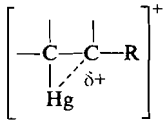

Kreshkov *et al.* (16), also correlated rates in terms of σ^* parameters but interpreted their results in terms of a cyclic mercurinium ion intermediate.

Charton and Charton (47) correlated part of the data of Halpern and Tinker with the equation $\log k/k_0 = \alpha\sigma_I + \beta\sigma_R$ and found an 'excellent' fit but stated "We conclude therefore that . . . the reaction . . . proceeds by way of the bridged intermediate."

Finally, Pritzkow and co-workers (18*b*) examined the correlation of the rates of methoxymercuration of 20 alkenes with σ^* and E_S parameters, and concluded that the transition state for the addition resembled an unsymmetrically bridged mercurinium ion.

We have examined the ability of each of these previously published correlations to accommodate the data for the cyclopropylalkenes, and in each case there is a very large deviation from the predicted rate. For example, the treatment of Halpern and Tinker (12*a*) predicts that vinylcyclopropane will have a reactivity of 0.4

relative to 1-butene in water, whereas the actual rate (in methanol) relative to 1-hexene is 400. The Charton correlation (47) derived from the same data also predicts the rate ratio as 0.4. The Pritzkow equation (log $k = a + \rho^*\sigma^* + \delta E_S$) (18*b*) predicts rates relative to cyclohexene of 2.2 and 4.9 for *c*-PrCH=CH_2 and *c*-PrCMe=CH_2, respectively, compared to the observed values of 10^3. Insufficient information was given in the work of Kreshkov and co-workers (16) to test for the quantitative agreement with the experimental results on vinylcyclopropanes, but qualitatively their treatment using σ^* is also unsatisfactory.

One reason for the inadequacy of these previous correlations is their failure to include the σ_p^+ parameter to account for the strong resonance electron donation by cyclopropyl. We were able to obtain a better correlation of the rates of 1,1-disubstituted alkenes with the equation log $k/k_0 = \rho\sum\sigma_p^+ + a\sum E_S$, but the correlation coefficient ($R = 0.64$) was not satisfactory.

The complexity of the steric interaction in oxymercuration contributes to the trouble in effecting a good correlation. Pritzkow, and co-workers used the multiparameter equation log $k/k_0 = \rho_1^*\sum\sigma_1^* + \rho_2^*\sum\sigma_2^* + \delta_2\sum E_{S1} + \delta_2\sum E_{S2}$ to account for the reactivities of tetrasubstituted alkenes (18*b*). This equation takes into account the unequal electronic and steric effects at the two alkene carbons due to the unsymmetrical structure of the transition state. The fact that the ratio k_Z/k_E for oxymercurations ranges between 2 and 8 (11, 18*c*, 22*a*) shows that even a more complicated equation would be required to account for this effect. However, this approach appears to us to have exceeded the limits of usefulness of the substituent parameter method and we have not pursued it further.

In summary the rates of the oxymercuration reaction show a dependence on structure that support a variable geometry for the rate-determining transition state and the intermediate as the substrate changes. At one extreme is the case of ethylene, whose rate determining transition state may best be represented as bridged, and at the other is 1,1-dicyclopropylethylene, which leads to a species closely resembling an open ion.

Experimental

Cyclopropylalkenes were obtained as in ref. 40*b*,*c*. Other alkenes were commercial samples, purified where necessary by gas chromatography before use. Mercuric acetate was crystallized twice from MeOH containing a little HOAc to give material completely soluble in MeOH under the kinetic conditions mp 175–177°C, lit (48) 178–180°C. Methanol was distilled from $Mg(OMe)_2$ (49). Nuclear magnetic resonance spectra were run on a Varian T60 instrument with tetramethylsilane as an internal standard. Gas chromatograph separations (glpc) were carried out using a Varian Aerograph 2440 flame ionization instrument, and 1420 and 920 thermal conductivity instruments.

Authentic methyl ethers for use as standards in the competition experiments were prepared by preparative oxymercuration–demercuration (50) of cyclohexene 3-hexene, 4-octene, norbornene, *tert*-butylethylene, and 1-cyclopropyl-1-phenylethylene. Methyl ethers of 2-octanol, cyclopropylmethylcarbinol, dicyclopropylmethylcarbinol, and cyclopropyldimethylcarbinol were prepared by treatment of the alcohols in dry THF with NaH followed by the addition of excess MeI and reflux. After work-up the ethers prepared by both methods were isolated by glpc and the structures confirmed by their nmr spectra.

Relative Rates by Competition

The conditions were designed to duplicate a published procedure (17*a*). Ten millilitres of a methanol solution, 0.33 *M* in each of two olefins, was stirred in a round bottom flask with a magnetic stirrer at room temperature and 10 ml of a 0.033 *M* solution in mercuric acetate was added in one portion. After 10 min 10 ml of a solution 3 *M* in NaOH and 0.5 *M* in $NaBH_4$ was added and the solution was stirred for 30 min. For the cyclopropylalkenes 2 ml of each solution was used. In all cases the solutions were freshly prepared to prevent loss of alkenes and deterioration of the mercuric acetate. The solution was suction filtered through Celite with the receiver in a dry ice bath. The filtrate was partitioned between water and ether and the ether layer was washed with saturated NaCl, dried over Drierite, concentrated to 2 ml by slow distillation through a Vigreaux column, and the relative amounts of the product ethers formed were determined by glpc. Relative rates were calculated from the peak areas using the measured glpc response factors from authentic samples.

Direct Rate Measurements

The slower rates were monitored by observing the decrease in absorbance at 265 nm using Cary 14 or 118 instruments. In a typical experiment 1.5 ml of a fresh MeOH solution 0.07 *M* in both alkene and acetic acid equilibrated at 25°C was injected into 1.5 ml of 0.07 *M* $Hg(OAc)_2$ in MeOH equilibrated at 25°C in a 1 cm cell in a thermostatted cell compartment and the absorbance change was monitored vs. time. When NaOMe or NaOAc were also present these were contained in the alkene solution. For pseudo first-order runs the alkene concentration was increased 10-fold.

More rapid reactions were followed using a Durrum D110 stopped flow spectrophotometer. The cyclopropyl alkenes were run at final concentrations between 0.005 and 0.035 *M*, and the others were measured at final concentrations of 0.035 *M*. The kinetic points were measured from the oscilloscope traces and used to calculate the second-order rate constants.

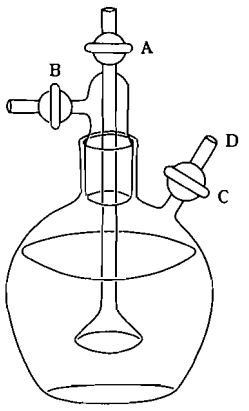

FIG. 2. Flask for dissolving ethylene in solvents. The flask is stirred magnetically and ethylene is passed through A and bubbled through the frit and vented at B. After 30 min A and B are closed, stirring is halted, and the flask left undisturbed for 15 min. Then the long needle of a syringe is inserted through a septum at D and through the bore of C into the solution. A pressure of gas is applied through B forcing the syringe to fill.

Rate constants obtained under pseudo first-order conditions (at least a 10-fold excess of alkene over mercuric acetate) were calculated graphically from plots of log $(A_0 - A)/(A_0 - A_\infty)$ vs. time. These were converted to second-order rate constants by division by the initial alkene concentration. Rate constants obtained under second-order conditions (equimolar mercuric acetate and alkene) were calculated from the formula $kt = (A_0 - A)/(A - A_\infty)c$ where c is the reactant concentration.

In the reactions of the 1,2-dicyclopropylethylenes the absorbance at 265 nm of solutions 0.035 M in each reagent on mixing immediately increased off the scale, whereas at 273 nm (with the *trans* olefin) the absorbance immediately increased from 0.5 to 1.3, then successively decreased for 90 min, increased again, and then began another decrease.

A solution of ethylene in MeOH was prepared by bubbling the gas into the stirred solution for about 30 min at 25°C. Samples were removed by applying a slight pressure of ethylene to the solution to fill the transfer syringe. These samples were either analyzed for ethylene content by injection into standard Br_2 solutions or were injected into the uv cell containing a $Hg(OAc)_2$–HOAc solution for kinetic determinations. Ethylene concentrations of about 0.09 M were obtained in this way. The apparatus for these transfers is shown in Fig. 2.

Usually excellent linearity in the rate plots was followed for 1–2 half-lives. However the reproducibility of the rate constants from day to day was sometimes erratic, and could not be improved despite strenuous attempts at degassing of the solutions and purification of the reagents. At least two and usually many more rate determinations were made on each alkene, with average deviations of as much as ±20%.

Acknowledgements

Financial support by the National Research Council of Canada and Undergraduate Research Fellowships from the Physical Sciences Division, Scarborough College, are gratefully acknowledged. We thank Professor T. G. Traylor, who first studied the kinetics of oxymercuration in methanol by uv, for providing details of his unpublished work.

1. G. F. WRIGHT. Chem. Can. **2**, 149 (1950).
2. J. CHATT. Chem. Rev. **48**, 7 (1951).
3. N. S. ZEFIROV. Usp. Khim. **34**, 1272 (1965).
4. W. KITCHING. Organomet. Chem. Rev. **3**, 61 (1968).
5. R. C. FAHEY. Top. Stereochem. **3**, 237 (1968).
6. T. G. TRAYLOR. Acc. Chem. Res. **2**, 152 (1969).
7. W. KITCHING. *In* Organometallic reactions. Vol. 3. *Edited by* E. I. Becker and M. Tsutsui. Wiley-Interscience, New York, NY. 1972. p. 319.
8. R. BOLTON. *In* Comprehensive chemical kinetics. Vol. 9. *Edited by* C. H. Bamford and C. F. H. Tipper. Elsevier, London. 1973.
9. D. S. MATTESON. Organometallic reaction mechanisms of the nontransition elements. Academic Press, New York, NY. 1974. pp. 202–218.
10. D. SEYFERTH. J. Organomet. Chem. **75**, 13 (1974); **98**, 133 (1975).
11. (*a*) G. H. SCHMID and D. G. GARRATT. *In* Chemistry of alkenes. Vol. 3. *Edited by* J. Zabicky. Wiley Interscience, New York, NY. 1977; (*b*) F. FREEMAN. Chem. Rev. **75**, 439 (1975).
12. (*a*) J. HALPERN and H. B. TINKER. J. Am. Chem. Soc. **89**, 6427 (1967); (*b*) P. ABLEY, J. E. BYRD, and J. HALPERN. J. Am. Chem. Soc. **95**, 2591 (1973).
13. (*a*) J. ROMEYN and G. F WRIGHT. J. Am. Chem. Soc. **69**, 697 (1947); (*b*) A. RODGMAN and G. F WRIGHT. J. Org. Chem. **28**, 1617 (1953).
14. (*a*) M. C. CABALEIRO, A. D. AYALA, and M. D. JOHNSON. J. Chem. Soc. Perkin. Trans. II, 1207 (1973); (*b*) D. DODD and M. D. JOHNSON. J. Chem. Soc. B, 662 (1971).
15. G. SPENGLER, H. FRÖMMEL, R. SCHAFF, P. FAUL, and P. LONSKY. Brennstoff-Chem. **37**, 47 (1956).
16. (*a*) A. P. KRESHKOV, L. N. BALYATINSKAYA, and S. M. CHESNOKOVA. Zh. Obshch. Khim. **43**, 166 (1973); (*b*) A. P. KHRESHKOV, L. N. BALYATINSKAYA, S. M. CHESNOKOVA, and T. V. KURCHENKO. Zh. Obshch. Khim. **41**, 2513 (1971); (*c*) A. P. KRESHKOV and L. N. BALYATINSKAYA. Zh. Obshch. Khim. **37**, 2211 (1967).
17. (*a*) R. D. BACH and R. F. RICHTER. Tetrahedron Lett. 4099 (1973); (*b*) R. D. BACH and R. F. RICHTER. J. Org. Chem. **38**, 3442 (1973).
18. (*a*) G. MÜLLER-HAGEN and W. PRITZKOW. J. Prakt. Chem. **311**, 874 (1969); (*b*) H. J. BERGMANN, G. COLLIN, G. JUST, G. MÜLLER-HAGEN, and W. PRITZKOW. J. Prakt. Chem. **314**, 285 (1972); (*c*) G. COLLIN, U. JAHNKE, G. JUST, G. LORENZ, W. PRITZKOW, M. RÖLLIG, L. WINGUTH, P. DIETRICH, C.-E. DÖRING, H. G. HAUTHAL, and A. WIEDENHÖFT. J. Prakt. Chem. **311**, 238 (1969).
19. (*a*) F. ASINGER, B. FELL, G. HADIK, and G. STEFFAN. Chem. Ber. **97**, 1568 (1964); (*b*) F. ASINGER. Hung. J. Ind. Chem. **2**, 33 (1974).
20. (*a*) A. K. CHAUDHURI and M. N. DAS. Tetrahedron. **21**, 457 (1965); (*b*) A. K. CHAUDHURI, K. L. MALLIK,

and M. N. DAS. Tetrahedron, **19**, 1981 (1963); (*c*) K. L. MALLIK and M. N. DAS. J. Am. Chem. Soc. **82**, 4269 (1960).
21. B. FLORIS and G. ILLUMINATI. Coord. Chem. Rev. **16**, 107 (1975).
22. (*a*) H. C. BROWN and P. J. GEOGHEGAN, JR. J. Org. Chem. **37**, 1937 (1972); (*b*) H. C. BROWN and J. H. KAWAKAMI. J. Am. Chem. Soc. **95**, 8665 (1973).
23. S. J. CRISTOL, J. S. PERRY, JR., and R. S. BECKLEY. J. Org. Chem. **41**, 1912 (1976).
24. G. A. OLAH, P. W. WESTERMAN, and J. NISHIMURA. J. Am. Chem. Soc. **96**, 3548 (1974).
25. (*a*) R. D. BACH, A. T. WEIBEL, J. PATANE, and L. KEVEN. J. Am. Chem. Soc. **98**, 6237 (1976); (*b*) R. D. BACH and H. F. HENNEIKE. J. Am. Chem. Soc. **92**, 5589 (1970); (*c*) J. M. JERKUNICA and T. G. TRAYLOR. J. Am. Chem. Soc. **93**, 6278 (1971); (*d*) W. HANSTEIN and T. G. TRAYLOR. Tetrahedron Lett. 4451 (1967).
26. (*a*) M. KOSAKI, S. SHINODA, and Y. SAITO. Bull. Chem. Soc. Jpn. **48**, 3745 (1975); (*b*) A. T. DO AMARAL, O. A. EL SEOUD, and L. DO AMARAL. J. Org. Chem. **40**, 2534 (1975); (*c*) N. TAKAISHI, Y. FUJIKURA, and Y. INAMOTO. J. Org. Chem. **40**, 3767 (1975); (*d*) A. J. BLOODWORTH, H. G. HUTCHINGS, and A. J. SOTOWICZ. J. Chem. Soc. Chem. Commun. 578 (1976).
27. G. A. OLAH and P. R. CLIFFORD. J. Am. Chem. Soc. **95**, 6067 (1973).
28. (*a*) M. M. KREEVOY and F. R. KOWITT. J. Am. Chem. Soc. **82**, 739 (1960); (*b*) M. M. KREEVOY, L. C. SCHALEGER, and J. C. WARE. Trans. Faraday Soc. **58**, 2433 (1962).
29. A. RODGMAN, D. A. SHEARER, and G. F WRIGHT. Can. J. Chem. **35**, 1377 (1957).
30. T. IBUSUKI and Y. SAITO. J. Organomet. Chem. **56**, 103 (1973).
31. S. SAKAKI, H. KATO, H. KANAI, and K. TARAMA. Bull. Chem. Soc. Jpn. **47**, 377 (1974).
32. (*a*) T. G. TRAYLOR and A. W. BAKER. J. Am. Chem. Soc. **85**, 2746 (1963); (*b*) T. T. TIDWELL and T. G. TRAYLOR. J. Org. Chem. **33**, 2614 (1968).
33. F. T. BOND. J. Am. Chem. Soc. **90**, 5326 (1968).
34. J. E. GALLE and A. HASSNER. J. Am. Chem. Soc. **94**, 3930 (1972).
35. C. L. DEAN, D. G. GARRATT, T. T. TIDWELL, and G. H. SCHMID. J. Am. Chem. Soc. **96**, 4958 (1974).
36. (*a*) T. SUGITA, Y. YAMASAKI, O. ITOH, and K. ICHIKAWA. Bull. Chem. Soc. Jpn. **47**, 1945 (1974); (*b*) R. D. BACH, J. PATANE, and L. KEVAN. J. Org. Chem. **40**, 257 (1975).
37. S. SHINODA and Y. SAITO. J. Organomet. Chem. **90**, 1 (1975).
38. (*a*) M. BARRELLE and M. APPARU. Tetrahedron Lett. 2611 (1976); (*b*) F. DELBECQ and J. GORÉ. Tetrahedron Lett. 3459 (1976); (*c*) W. HOLTMEIER and P. WELZEL. Tetrahedron Lett. 3423 (1976).
39. (*a*) E. R. ALLEN, J. CARTLIDGE, M. M. TAYLOR, and C. F. H. TIPPER. J. Phys. Chem. **63**, 1437, **63**, 1442 (1959); (*b*) M. H. THOMAS and F. E. W. WETMORE. J. Am. Chem. Soc. **63**, 136 (1941); (*c*) P. BRANDT and O. PLUM. Acta Chem. Scand. **7**, 97 (1953).
40. D. G. GARRATT, A. MODRO, K. OYAMA, G. H. SCHMID, T. T. TIDWELL, and K. YATES. J. Am. Chem. Soc. **96**, 5295 (1974); (*b*) K. OYAMA and T. T. TIDWELL. J. Am. Chem. Soc. **98**, 947 (1976); (*c*) P. KNITTEL and T. T. TIDWELL. J. Am. Chem. Soc. **99**, 3408 (1977); (*d*) W. K. CHWANG, V. J. NOWLAN, and T. T. TIDWELL. J. Am. Chem. Soc. **99**, 3395 (1977).
41. B. G. GOWENLOCK and J. TROTMAN. J. Chem. Soc. 1454 (1955).
42. (*a*) H. ARZOUMANIAN and J. METZGER. Synthesis, 527 (1971); (*b*) Z. RAPPOPORT, S. WINSTEIN, and W. G. YOUNG. J. Am. Chem. Soc. **94**, 2320 (1972).
43. (*a*) G. COLLIN, G. MULLER-HAGEN, and W. PRITZKOW. J. Prakt. Chem. **314**, 229 (1972); (*b*) R. D. BACH and R. N. BRUMMEL. J. Am. Chem. Soc. **97**, 453 (1975).
44. J. M. COXON, M. P. HARTSHORN, and A. J. LEWIS. Tetrahedron Lett. 3521 (1969).
45. G. H. SCHMID, C. L. DEAN, and D. G. GARRATT. Can. J. Chem. **54**, 1253 (1976).
46. R. G. SALOMON and R. D. GLEIM. J. Org. Chem. **41**, 1529 (1976) and references therein.
47. M. CHARTON and B. I. CHARTON. J. Org. Chem. **38**, 1631 (1973).
48. G. BRAUER. Handbook of preparative inorganic chemistry. Vol. 2. 2nd ed. Academic Press, New York, NY. 1965. p. 1121.
49. A. I. VOGEL. Practical organic chemistry. 3rd ed. John Wiley and Sons, New York, NY. 1956. p. 169.
50. H. C. BROWN and M.-H. REI. J. Am. Chem. Soc. **91**, 5646 (1969).

Etude par spectroscopie infrarouge de l'ion diacétylacétylium. Rôle de $AlCl_3$, $AlBr_3$ et $GaCl_3$ sur sa formation et sa structure. Mise en évidence d'une liaison hydrogène intramoléculaire dans le tétrachloroaluminate de diacétylacétylium

ALAIN GERMAIN

Laboratoire des Intermédiaires réactionnels et mécanismes de réactions, E.R.A. 555 C.N.R.S. U.S.T.L. 34060 Montpellier Cédex

ET

JEAN-LOUIS PASCAL ET JACQUELINE POTIER

Laboratoire des Acides Minéraux, L.A. 79 C.N.R.S. U.S.T.L. 34060 Montpellier Cédex

Reçu le 31 janvier 1977

ALAIN GERMAIN, JEAN-LOUIS PASCAL et JACQUELINE POTIER. Can. J. Chem. **55**, 3096 (1977).

L'étude des réactions de formation de l'ion diacétylacétylium à partir de CH_3COX (X = Cl ou Br) et des acides de Lewis $AlCl_3$, $AlBr_3$ et $GaCl_3$ montre que l'anion formé est un tétrahalogénométallate. Dans le cas du tétrachloroaluminate de diacétylacétylium le cation est un monomère avec une liaison hydrogène intramoléculaire à potentiel à double minimum: ν O—H—O = ν O—D—O = 1400 cm^{-1}; *d* O—O = 2.48 Å. Un comportement identique s'observe pour le tétrabromoaluminate mais est plus complexe dans le cas du tétrachlorogallate.

ALAIN GERMAIN, JEAN-LOUIS PASCAL, and JACQUELINE POTIER. Can. J. Chem. **55**, 3096 (1977).

The study of the reaction of formation of the diacetoacetylium ion from CH_3COX (X = Cl or Br) and the Lewis acids $AlCl_3$, $AlBr_3$, and $GaCl_3$ shows that the counterion is always the tetrahalogenometallate. In the solid tetrachloroaluminate the cation is a monomer with a double minimum type of intramolecular hydrogen bond: ν O—H—O = ν O—D—O = 1400 cm^{-1}; *d* O—O = 2.48 Å. An identical behaviour is observed with the tetrabromoaluminate, but the structure of the diacetoacetylium tetrachlorogallate is more complicated.

Introduction

Les intermédiaires d'acylation de Friedel et Crafts ont fait l'objet de nombreuses études, en particulier spectroscopiques (1, 2) (ir, rmn, esca, rayons X) et théoriques (3, 4). Ainsi, il est bien établi que le mélange d'un halogénure d'acide carboxylique avec un acide de Lewis conduit, suivant la nature des espèces en cause et les conditions expérimentales, à deux types de composés: soit un composé de coordination (I), soit un sel d'acylium (II).

Récemment, avec le chlorure d'aluminium comme acide de Lewis, en présence d'un excès de chlorure d'acétyle, Germain *et al.* (5) ont observé que l'ion acétylium (Ac), initialement formé, évolue lentement pour conduire au cation "trimère": l'ion diacétylacétylium (DAA) (6).

$$3CH_3CO^+ \rightarrow (CH_3CO)_2CHCO^+ + 2H^+$$
$$\text{(Ac)} \qquad\qquad \text{(DAA)}$$

Les deux cations (Ac) et (DAA) sont caractérisés par des fréquences ν CO bien distinctes: 2300 cm^{-1} pour (Ac), 2200 cm^{-1} pour (DAA).

Les auteurs ont proposé pour (DAA) la forme énolique chélatée (fig. 2), l'abaissement de la fréquence ν CO de 100 cm^{-1} est ainsi expliqué par la participation importante de la forme mésomère céténique.

L'hypothèse de la structure énolique se trouve

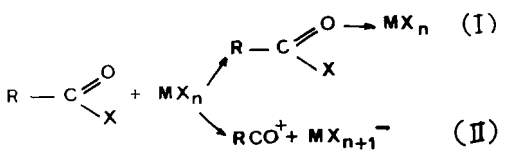

FIGURE 1

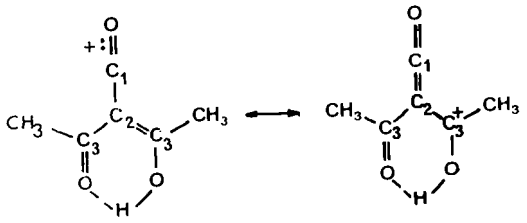

FIGURE 2

confirmée par la rmn du ^{13}C, qui montre l'absence d'hydrogène sur le carbone C_2 du carbonyle (6). Pulfer et Whitehead (7), à partir de calculs CNDO ont aussi adopté cette structure énolique plane.

Cependant, bien que la forme monomère chélatée représente la structure énolique la plus simple, aucun résultat ne permet d'éliminer la possibilité de formation de dimères ou polymères avec liaison hydrogène intermoléculaire selon les modèles de la fig. 3.

Une étude par spectroscopie de vibration doit permettre de résoudre cette ambiguité et de préciser la force et la nature de la liaison hydrogène (8–10). En plus de ce problème il paraît intéressant de rechercher le type de l'anion antagoniste en fonction de la nature de l'acide de Lewis (MX_3) et de l'halogénure d'acétyle utilisé. Ceci doit permettre également de généraliser la réaction de trimérisation et de préciser le rôle de l'acide de Lewis choisi dans le déroulement de cette réaction.

Nous analyserons d'abord les synthèses des différents sels et simultanément, nous caractériserons les différents anions présents à partir des données de la bibliographie (11, 13, 14) et ensuite nous étudierons le cation diacétylacétylium. Sur la fig. 4 nous reproduisons les spectres ir obtenus dans ce travail.[1]

Analyse des réactions et caractérisation des anions formés

(a) $CH_3COCl + AlCl_3$

Synthèse

Le produit solide est obtenu comme précédemment (5). Rappelons que l'addition de chlorure d'aluminium à un large excès de chlorure d'acétyle (rapport molaire > 3) conduit à la formation instantanée de l'ion acétylium (ν CO = 2300 cm^{-1}) suivie par l'apparition lente de l'ion diacétylacétylium (ν CO = 2180 cm^{-1}) (fig. 5*a*).

Après 6 h à température ambiante, l'ion acétylium est pratiquement totalement transformé. Le sel de diacétylacétylium est alors précipité par addition de dichloroéthane.

Caractérisation de l'anion

A priori deux anions sont possibles, $AlCl_4^-$ ou $Al_2Cl_7^-$. L'analyse des spectres infrarouge du sel cristallisé enregistrés à température ambiante est susceptible de caractériser ces anions. En effet, Manteghetti (11) a montré que la principale différence entre les spectres des ions $Al_2Cl_7^-$ et $AlCl_4^-$ est l'existence dans ceux du premier d'une bande à 300 cm^{-1}: ν_{as} AlClAl. Sur le spectre (fig. 4*a*) on note l'absence de cette bande ce qui permet de rejeter l'existence de $Al_2Cl_7^-$ dans ce sel. Par contre la présence des bandes intenses à 490 et 180 cm^{-1} sont compatibles avec la présence de $AlCl_4^-$, elles correspondent aux vibrations ν_3 et ν_4 (11). *Le sel obtenu est donc le tétrachloroaluminate de diacétylacétylium.*

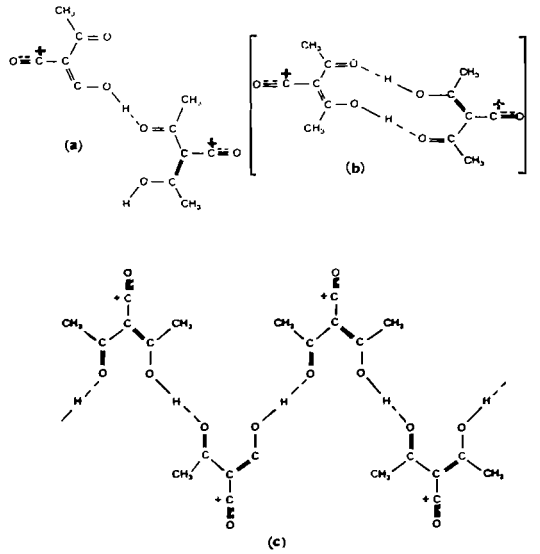

FIG. 3. (*a*) Dimère ouvert avec une seule liaison intramoléculaire. (*b*) Dimère fermé avec deux liaisons hydrogène intermoléculaire. (*c*) Polymère en chaînes.

(b) $CH_3COBr + AlBr_3$

Synthèse

Bien que réalisée dans des conditions expérimentales identiques à celles des chlorures, la réaction se déroule différemment. La première espèce qui apparaît sur le spectre infrarouge (fig. 4*c*) est le composé de coordination sur l'oxygène

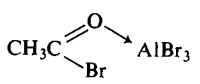

dont la vibration ν CO se situe à 1640 cm^{-1}.

Après 8 h à température ambiante la formation des ions acétylium et diacétylacétylium est très faible. Au bout de 5 jours, la formation de

[1]Malheureusement il n'a pas été possible d'enregistrer de spectres Raman par suite de diffusion parasite.

l'ion diacétylacétylium est nette mais loin d'être totale et même après 10 jours, il reste une grande proportion de composés de coordination. (fig. 4*c*, 4*d*). En ce qui concerne l'ion acétylium sa présence est toujours très faible. Pourtant ce cation doit être formé intermédiairement, il faut donc admettre que dans ce cas l'ion acétylium se forme lentement et se trimérise relativement rapidement (fig. 5*b*), comportement différent de celui observé précédemment. L'explication de ce phénomène peut être trouvée dans la différence de stabilité des composés de coordination du type $L \rightarrow AlX_3$. En effet, pour un même ligand L, le composé formé avec le bromure d'aluminium est généralement plus stable que celui formé avec le chlorure (12). Dans ce travail, cette différence est certainement accentuée du fait que la base est aussi un bromure. Il est, de plus, raisonable de penser que l'oxygène de l'halogénure d'acétyle est plus basique dans le cas du bromure que dans celui du chlorure.

Par évaporation sous vide de l'excès de bromure d'acétyle ou par addition de solvants, aucune cristallisation ne se produit.

Caractérisation de l'anion

Comme dans le cas du dérivé chloré deux anions peuvent être envisagés a priori: $AlBr_4^-$ et $Al_2Br_7^-$. Cependant, la bande observée à 400 cm^{-1} se situe à une fréquence trop faible pour correspondre à la vibration de valence des groupes $AlBr_3$ terminaux de $Al_2Br_7^-$ (11) et de plus, nous ne retrouvons pas dans les spectres de bandes entre 280 et 350 cm^{-1} (fig. 4*c*, 4*d*) caractéristiques des vibrations ν_s et ν_{as} AlBrAl. L'anion est donc, dans ce cas aussi, le plus simple c'est à dire $AlBr_4^-$. La bande large à 400 cm^{-1} correspond à ce qui est attendu pour la vibration triplement dégénérée ν_3 de cet anion. *Le sel obtenu est donc le tétrabromoaluminate de diacétylacétylium.*

(c) $CH_3COCl + GaCl_3$

Synthèse

Comme avec le chlorure d'aluminium, l'ion acétylium (ν CO = 2300 cm^{-1}) se forme rapidement, suivi immédiatement de l'ion diacétylacétylium (ν CO = 2180 cm^{-1}). Après 6 h à température ambiante la trimérisation est complète. Un liquide visqueux est alors obtenu après évaporation sous vide de l'excès de chlorure d'acétyle.

Caractérisation de l'anion

Dans le domaine de fréquence de l'anion, de profondes modifications du spectre se produisent selon que l'ion acétylium est présent ou non (fig. 6*a*, 6*b*).

Lorsque la réaction de trimérisation est totale (fig. 6*a*) nous relevons dans ce domaine la présence d'une bande à 380 cm^{-1}, mais constatons l'absence de bandes vers 270 cm^{-1} (ν_{as} GaClGa). Dans ce cas, comme pour les sels d'aluminium nous concluons à la formation de l'anion le plus simple $GaCl_4^-$ (13). *Le sel de diacétylacétylium obtenu est donc un tétrachlorogallate.*

Par contre, lorsque le monomère et le trimère coexistent (ν CO à 2300 et 2200 cm^{-1}), le spectre est différent (fig. 6*b*): la bande à 380 cm^{-1} (ν_3 $GaCl_4^-$) éclate en plusieurs composantes et deux nouvelles bandes moyennement fortes apparaissent à 280 et 255 cm^{-1}. Si l'éclatement ν_3 $GaCl_4^-$ peut être dû à la formation d'un composé de coordination

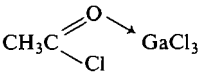

un tel complexe ne peut expliquer l'apparition des bandes à 280 et 255 cm^{-1} (14). Ces bandes sont analogues à celles observées pour $Ga_2Cl_7^-$ (15) (fig. 6*c*).

Rappelons qu'elles ont été attribuées respectivement aux vibrations ν_{as} et ν_s du pont GaClGa, l'abaissement de la fréquence ν_s de 20 cm^{-1} a déjà été observé pour KGa_2Cl_7 à l'état fondu (250 cm^{-1}) (15*b*). Ceci permet d'envisager que l'anion antagoniste du cation acétylium est $Ga_2Cl_7^-$. On est apparemment en contradiction avec l'observation par analyse thermique du composé solide du type 1–1 (F = 86°C) (16), ainsi qu'avec la détermination de la structure aux rayons X du composé $CH_3CO^+GaCl_4^-$ (17). Toutefois, en solution il n'est pas illogique d'observer $CH_3CO^+Ga_2Cl_7^-$

FIG. 4. Spectres ir. (*a*, *b*) Tétrachloraluminate de diacétylacétylium solide (poudre), normal (*a*) et totalement deutérié (*b*). (*c*, *d*) Solutions de bromure d'aluminium dans du bromure d'acétyle après 8 h (*c*) et 10 jours (*d*). (Les bandes hachurées appartiennent au bromure d'acétyle en excès.) (*e*, *f*) Mélanges de chlorure d'acétyle et chlorure de gallium après évaporation de l'excès de chlorure d'acétyle à 2 stades différents de l'avancement réactionnel (20 min (*e*) et 6 h (*f*)).

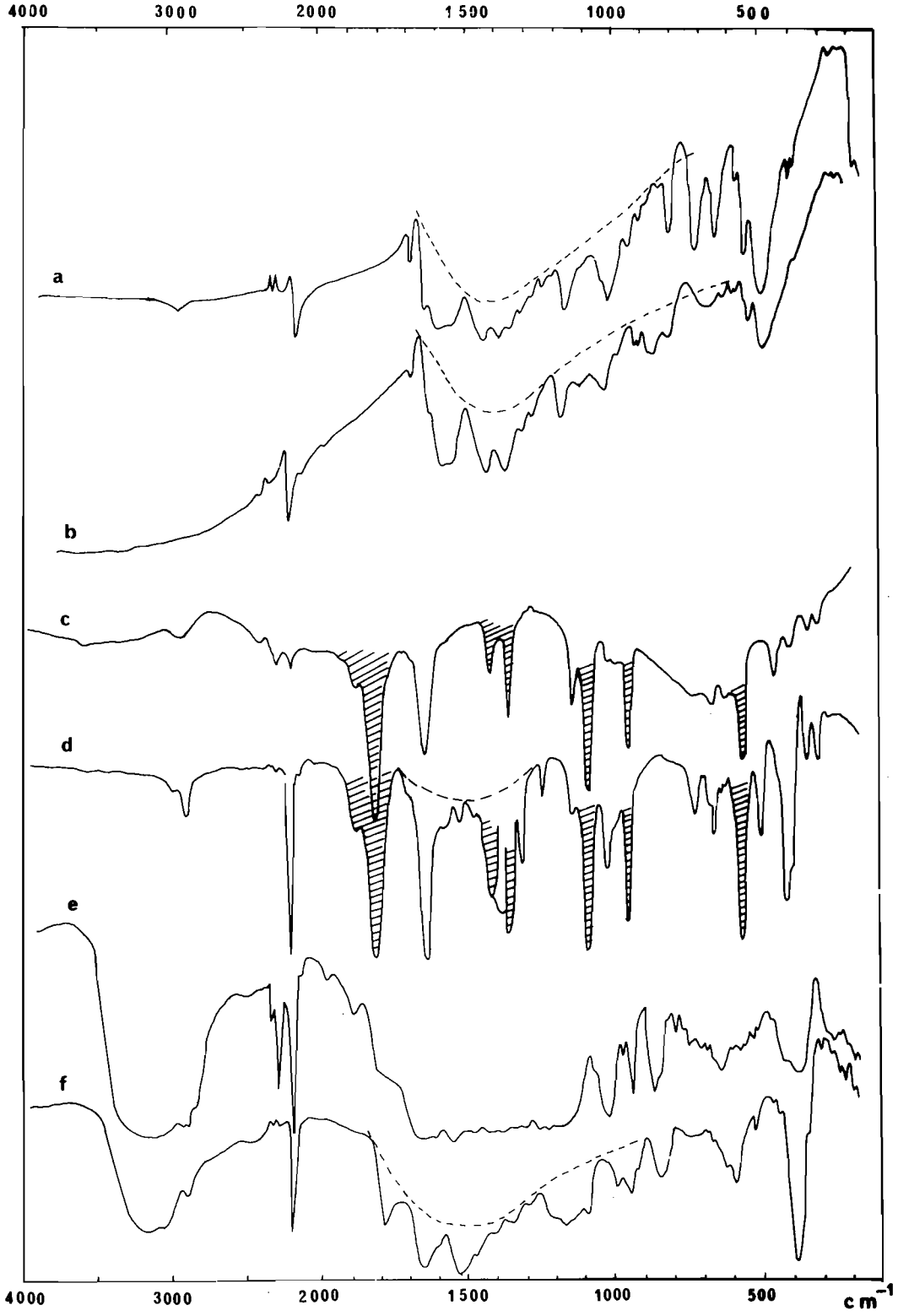

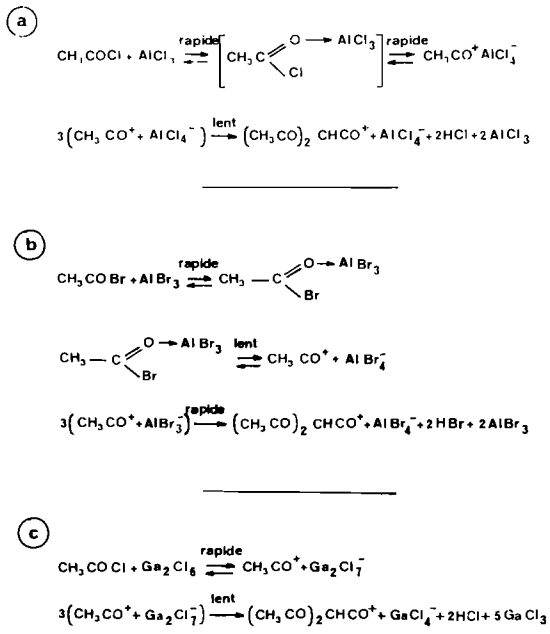

FIGURE 5

car Mascherpa-Corral (15*b*) a montré que l'existence d'ions condensés $Ga_2X_7^-$ en solution est beaucoup plus générale que dans l'état cristallin et Waddington et coll. (18) ont identifié par spectroscopie infrarouge l'existence du composé similaire $CH_3CO^+Al_2Cl_7^-$.

Le fait que l'anion associé à l'ion diacétylacétylium soit $GaCl_4^-$ est en accord avec la plus grande stabilité du cation trimère qui ne nécessite pas un anion de charge très délocalisée.

Structure de l'anion diacétylacétylium

Nous avons déjà écrit que la forme énolique de l'ion diacétylacétylium permettrait d'envisager plusieurs types de composés, suivant la nature de la liaison hydrogène.

Afin de préciser la structure de ce cation nous allons analyser plus en détails les spectres infrarouge des composés obtenus ainsi que ceux de composés énoliques voisins comme le diacétylacétate d'éthyle (DAAE) et l'acétylacétone (AA), en se référant, pour ce dernier, au travail de Nakamoto (19).

La nature de la liaison hydrogène sera analysée pour les trois sels synthétisés, mais ce n'est que pour le tétrachloroaluminate de diacétylacétylium, seul composé cristallin isolé, que nous proposerons une attribution plus complète du spectre.

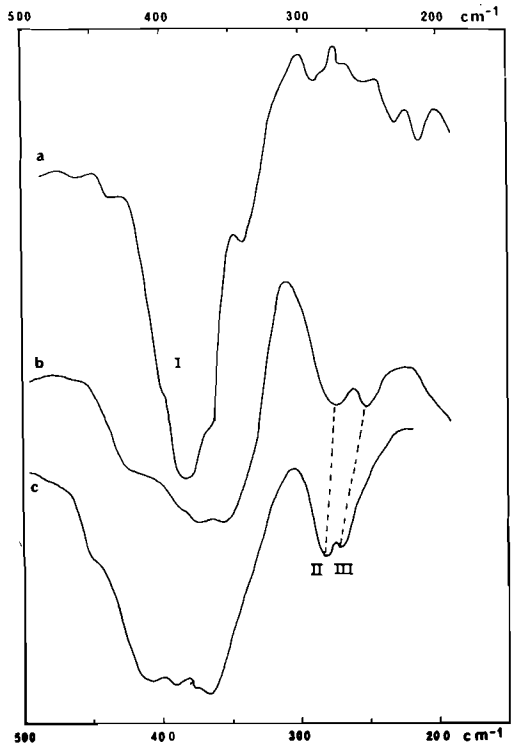

FIG. 6. Spectre ir dans la région des basses fréquences des dérivés du gallium. (*a*) Tétrachlorogallate de diacétylacétylium. (*b*) Mélange avant la formation complète de l'ion diacétylacétylium. (*c*) Heptachlorodigallate de potassium solide (avec la permission de Mme D. Mascherpa-Corral, Laboratoire des Acides Minéraux, Montpellier). I: ν_3 $GaCl_4^-$. II et III: ν_{as} et ν_s GaClGa.

Etude de la liaison hydrogène

Sur la fig. 7 sont représentés les spectres de DAAE liquide (*a*), en solution dilué dans CCl_4 (*b*) et deutérié sélectivement sur le proton énolique (*c*). Ces spectres sont semblables à ceux des différents tétrahalogénométallates de diacétylacétylium (fig. 4). Mis à part le spectre du sel de gallium (fig. 4*f*) on note en particulier, l'absence de forte absorption autour de 3000 cm^{-1}. Ce fait semble indiquer que la vibration de valence v OH dans les divers composés est perturbée par une liaison hydrogène. En 1966 Nakamoto (19) a étudié l'acétylacétone, composé voisin. Les spectres reproduits par cet auteur sont comparables à ceux observés dans ce travail, notamment absence d'absorption autour de 3000 cm^{-1}, Nakamoto positionne v OH à 2750 cm^{-1}. Cependant l'intensité de cette bande est très faible. Par contre on relève sur les différents spectres une absorption large autour de

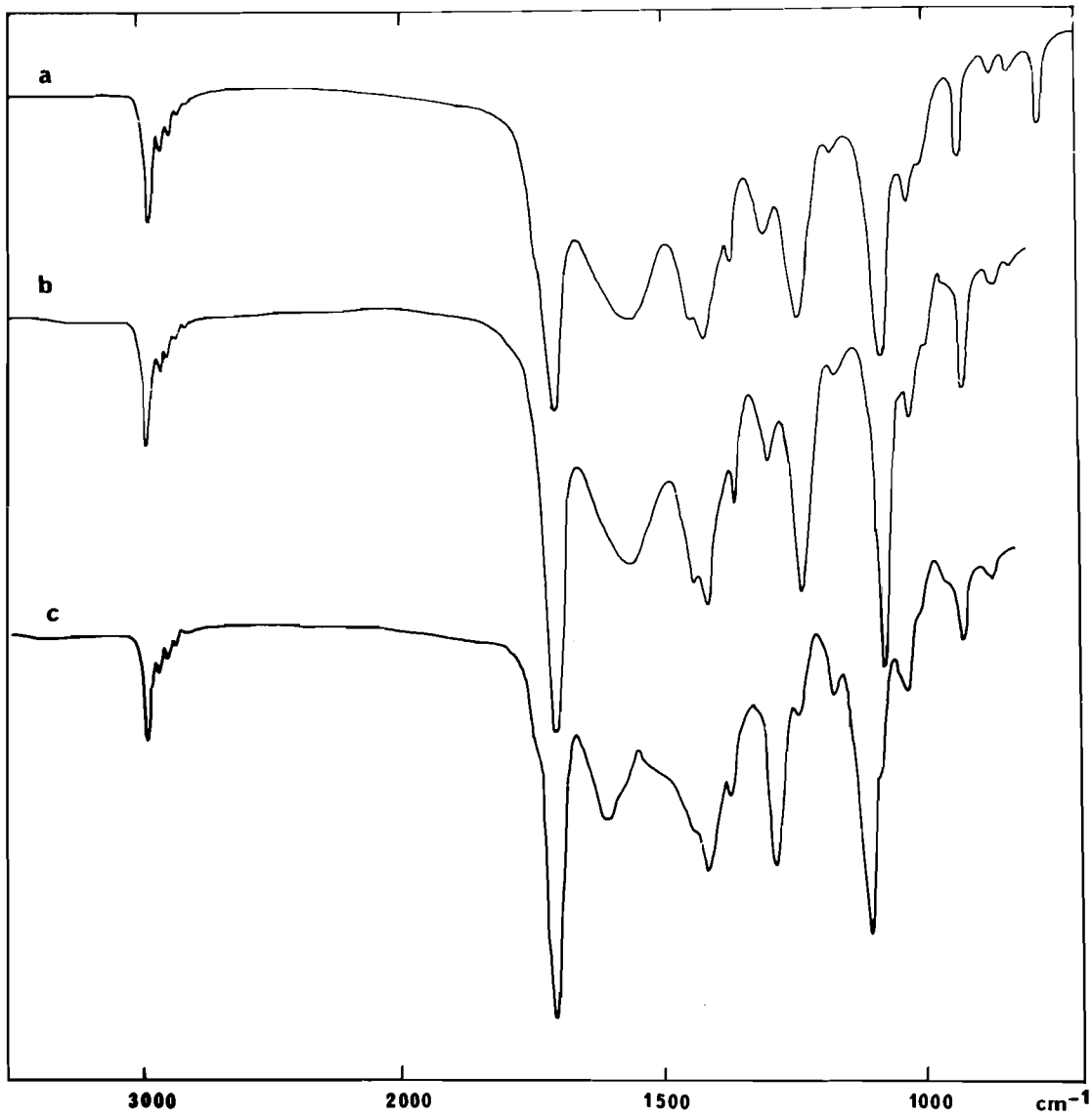

FIG. 7. Spectres ir de $(CH_3CO)_2CHCO_2C_2H_5$. (*a*) Liquide pur. (*b*) 0.2 *M* dans CCl_4. (*c*) $(CH_3CO)_2$-$CDCO_2C_2H_5$ 0.2 *M* dans CCl_4.

1500 cm^{-1} caractéristique d'une liaison hydrogène de forte (*d* O—O = 2.50 Å) liaison plus compatible avec la géométrie de cette molécule que celle déduite de l'attribution de Nakamoto (2.65 Å).

Pour notre part, quelque soit le composé étudié à l'exception du sel de gallium nous n'observons pas d'absorption sensible à la deutériation au-dessus de 2000 cm^{-1} qui puisse être attribué à la vibration ν OH. Par contre nous relevons une bande très large centrée vers 1400 cm^{-1} attribuable à la vibration ν OHO d'une liaison hydrogène forte. L'absence de déplacement par deutériation est en accord d'après Novak (10) avec l'existence d'une liaison hydrogène avec un potentiel à double minimum et une distance O—O de 2.48 Å. Cette valeur est parfaitement compatible avec la distance de 2.46 Å calculée pour un modèle d'ion diacétylacétylium plan possédant des

angles C_2—C_3—O de 120° et des longueurs de liaison C_1—C_2 comprises entre celles d'une simple et d'une double liaison (1.42 Å).

Cette constatation est donc tout à fait favorable à l'existence d'une liaison hydrogène intramoléculaire forte (9, 10, 20). Le seul argument défavorable est que, généralement la vibration ν OH d'une liaison hydrogène intramoléculaire est peu visible en infrarouge; toutefois, dans le cas des maléates acides, Hadzi[2] a très récemment montré la présence de la bande de vibration ν OH de faible intensité. De plus dans le cas de DAAE, on observe aussi bien sur le spectre du liquide pur que sur celui de la solution dans CCl_4 (0.2 *M*), une absorption large centrée à 1520 cm^{-1}. Puisque cette bande est insensible à la dilution on peut admettre *qu'elle prouve l'existence d'une liaison hydrogène intramoléculaire et non intermoléculaire.*

En ce qui concerne le spectre du tétrachlorogallate, le fait le plus marquant est la coexistence de deux bandes ν OH l'une centrée à 3200 cm^{-1} caractéristique d'un hydroxyle libre ou très faiblement lié, l'autre centrée vers 1500 cm^{-1} caractéristique d'une liaison hydrogène forte. Notons aussi la présence d'une bande à 1790 cm^{-1} attribuable à un carbonyle pratiquement libre.

Deux hypothèses peuvent expliquer ces faits; soit l'existence d'une forme dimère ouvert possédant ainsi un OH et un CO pratiquement libre[3] et un OH et un CO fortement liés; soit un équilibre conformationnel en phase liquide entre la forme liée intramoléculairement et la forme libre. Bien que la force de la liaison hydrogène soit un argument thermodynamique défavorable à l'existence d'un tel équilibre, rien ne permet de conclure définitivement.

Outre la vibration ν_{as} OHO qui traduit le mouvement du proton le long de l'axe O—O toute liaison hydrogène conduit à l'existence de deux vibrations de déformation et d'une autre vibration de valence: ν_s OHO. Cette dernière qui appartient au domaine des basses fréquences n'est généralement visible qu'en Raman. Les deux déformations δ OH et γ OH sont sensibles à la deutériation et à la force de la liaison hydrogène: plus la liaison est forte, plus leurs fréquences sont élevées. Dans le cas de l'ester, DAAE, la deutériation sélective du proton énolique entraîne une évolution au niveau de la bande à 1560 cm^{-1}, qui glisse de 60 cm^{-1} vers les hautes fréquences. Simultanément on relève dans le composé deutérié une nouvelle bande à 1280 cm^{-1}. Ces deux bandes sont attribuables à δ OH et δ OD. La faiblesse du rapport isotopique ($\rho = 1.22$) et le déplacement vers les hautes fréquences (1620 cm^{-1}) de la bande à 1560 cm^{-1} sont significatifs de l'existence d'un couplage.

La bande forte à 1240 cm^{-1} qui disparaît par deutériation sélective, est attribuée à γ OH. La vibration γ OD, attendue vers 925 cm^{-1} ($\rho = 1.34$) est peu discernable.

Pour ce qui est de l'ion diacétylacétylium nous observons un phénomène analogue bien que par deutériation l'évolution du domaine vers 1600 cm^{-1} soit peu spectaculaire. La bande centrée à 1580 cm^{-1} diminue d'intensité (participation de δ OH) tandis que δ OD est positionnée à 1260 cm^{-1} ($\rho = 1.25$). Pour γ OH et γ OD trois couples de bandes sont sensibles à la deutériation totale et sont dans un domaine de fréquence très convenable. Il s'agit de 1230–915 cm^{-1} ($\rho = 1.34$) 1205–865 cm^{-1} ($\rho = 1.39$) et 937–680 cm^{-1} ($\rho = 1.38$). Le premier couple est très proche de celui attribué à ce mouvement dans l'ester deutérié sélectivement, nous pensons que cette attribution est plus compatible avec la force de la liaison hydrogène que celle proposée par Nakamoto; 945 cm^{-1} est en effet une fréquence bien trop faible pour une liaison hydrogène de cette force.

Vibrations du squelette

Il n'est pas nécessaire de revenir sur la vibration ν C≡O de l'ion diacétylacétylium (2180 cm^{-1}). La vibration ν C=O du groupement ester du diacétylacétate d'éthyle se situe à 1710 cm^{-1}. En ce qui concerne la vibration ν C_1—C_2, nous devons nous attendre à une différence importante entre le cation et l'ester. En effet, pour le cation la participation notable de la forme céténique confère un caractère partiellement double à cette liaison, qui ne se retrouve pas dans l'ester. La bande intense à 1375 cm^{-1} (1353 dans le cas du composé totalement deutérié) est attribuée à ν C_1—C_2 dans l'ion diacétylacétylium. Pour l'ester nous la situons à 1080 cm^{-1}, bande intense que nous ne retrouvons pas dans le cation.

Pour les autres vibrations du squelette Nakamoto (19) distingue dans l'acétylacétone,

[2]Communication personnelle.

[3]Il est possible de considérer une association faible intermoléculaire entre l'hydroxyle "libre" d'un dimère et le carbonyle "libre" d'un dimère voisin, permettant ainsi la constitution d'un enchaînement polymérique.

TABLEAU 1. Fréquences comparées des vibrations de l'acétylacétone, de l'ion diacétylacétylium et du diacétylacétate d'éthyle*

AA (19)		$DAA^+AlCl_4^-$		DAAE		
d_0	d_8	d_0	d_7	d_0	d_1	Attributions
1623	1627	1580	1580	1560	1620	ν_{as} C···O
1432	1380	1430	1425	1450	1440	ν_s C···O
1623	1535	1540	1540	1570	1570	ν_{as} C_2—C_3
1250	1258	1260	1262	1280	1300	ν_s C_2—C_3
1432	1107	1390	1045	1470	1470	δ_{as} CH_3
1368	1042	1340	1018	1420	1415	δ_s CH_3
1170	795	1155	(784)	1170	1170	γ CH_3
—	—	1375	1353	1080	1080	ν C_1—C_2
908	902	937	900	925	920	ν_{as} C—CH_3
810	788	800	800	830	830	ν_s C—CH_3
2750	1960	1400	1400	1520	1520	ν O—H—O
1460	1076	1580	1160	1560	1280	δ OH
945	684	1230	915	1240	(925)	γ OH

*AA: acétylacétone; DAA: diacétylacétylium; DAAE: diacétylacétate d'éthyle; *d*: deutériation.

ν C=O et ν C—O et ν C=C et ν C—C. Pour notre part, nous pensons que la délocalisation des électrons le long du squelette conduit à raisonner en terme de vibrations symétriques et asymétriques. Pour DAAE l'attribution de la bande à 1560 cm^{-1} à la vibration ν_{as} C—O semble évidente. Rappelons que par deutériation partielle, cette bande glisse à 1620 cm^{-1}, valeur proche de celle trouvée par Nakamoto. Pour ν_{as} C—O le couplage signalé lors de l'étude de δ OH est donc celui de δ OH $\leftrightarrow$ ν_{as} C—O. Pour le cation DAA, par analogie, nous attribuons à la bande 1580 cm^{-1} à ce mouvement.

Dans certains spectres de DAA solide nous pouvons relever deux bandes faibles à des fréquences plus élevées (1630 et 1680 cm^{-1}) et dont les intensités varient suivant l'échantillon. Elles proviennent vraisemblablement d'impuretés comme par exemple l'acétylacétone (1630 cm^{-1}) due à une hydrolyse partielle:

$$(CH_3CO)_2CHCO^+ \xrightarrow{H_2O} [(CH_3CO)_2CHCO_2H] \rightarrow \underset{\text{instable}}{} (CH_3CO)_2CH_2 + CO_2\uparrow$$

Pour les trois autres mouvements du squelette de DAA: ν_s C—O, ν_{as} C_2—C_3 et ν_s C_2—C_3 nous avons retenu les attributions 1430, 1540 et 1260 cm^{-1}, valeurs proches de celles proposées pour AA (19).

Enfin, nous situons ν_{as} C—CH_3 et ν_s C—CH_3 à 937 et 800 cm^{-1}. Ces valeurs peuvent être comparées à celles trouvées pour AA (908 et 810 cm^{-1}). Les fréquences légèrement plus élevées pour le cation DAA s'expliquent par la présence d'une charge positive partielle sur le carbone C_3. Le tableau 1 représente l'ensemble des vibrations choisies.

Méthodes expérimentales

Produits utilisés

Le chlorure d'aluminium Schuchardt est purifié par sublimation sous vide. Le bromure d'aluminium et le chlorure de gallium sont synthétisés selon les méthodes déjà décrites (11, 13).

Les chlorure et bromure d'acétyle sont des produits Prolabo, ils ont été bidistillés. Le chlorure d'acétyle deutérié est obtenu à partir de l'acide acétique d_4 (CEA) et PCl_3, selon la méthode décrite par Vogel (21). Le diacétylacétate d'éthyle est préparé par acétylation de l'acétate d'éthyle selon la méthode de Spassow (22). La deutériation sélective sur l'hydrogène énolique du diacétylacétate d'éthyle en solution dans le tétrachlorure de carbone est obtenu par échange avec l'eau lourde.

Les tétrachloroaluminates de diacétylacétylium, non deutérié et deutérié, cristallisés sont obtenus selon (5). La même technique utilisée avec $AlBr_3$–CH_3COBr et $GaCl_3$–CH_3COCl n'a pas permis d'obtenir de produits cristallisés. Après évaporation sous vide du solvant et éventuellement de l'excès d'halogénure d'acétyle, des huiles jaunes ou rouges sont obtenues.

Etude spectroscopique

Les spectres infrarouges sont enregistrés sur un appareil Perkin-Elmer 180. Les produits solides pulvérulents sont placés entre faces en CsI et les liquides entre faces en silicium.

Conclusion

La réaction d'un halogénure métallique sur un grand excès d'halogénure d'acétyle conduit à un sel de diacétylacétylium dont l'anion est du type $M_nX_{3n+1}^-$. Dans le cas du tétrachloroaluminate obtenu cristallisé, le cation est un monomère à liaison hydrogène intramolé-

culaire forte à potentiel à double minimum. La distance O—O de 2.48 Å, estimée à partir des données de la littérature, est compatible avec la géométrie attendue pour un tel édifice.

1. G. A. OLAH, A. GERMAIN et A. WHITE. *In* Carbonium ions. Vol. V. *Edited by* G. A. Olah et P. V. R. Schleyer. Wiley-Interscience, New York, NY. 1976. Chapt. 35.
2. B. CHEVRIER et R. WEISS. Angew. Chem. Int. Ed. Engl. **13**, 1 (1974).
3. B. REES, A. VEILLARD et R. WEISS. Theor. Chim. Acta, **23**, 266 (1971).
4. D. R. YARKONG et H. F. SCHAEFER III. J. Chem. Phys. **63**, 4317 (1975).
5. A. GERMAIN, A. COMMEYRAS et A. CASADEVALL. Chem. Commun. 633 (1971); Bull. Soc. Chim. 3177 (1972).
6. G. A. OLAH, A. GERMAIN, H. C. LIN et K. DUNNE. J. Am. Chem. Soc. **97**, 5477 (1975).
7. J. D. PULFER et M. A. WHITEHEAD. Can. J. Chem. **51**, 2220 (1973).
8. K. NAKAMOTO, M. MARGOSHES et R. E. RUNDEL. J. Am. Chem. Soc. **77**, 6480 (1955).
9. D. HADZI. Pure Appl. Chem. **11**, 435 (1965).
10. A. NOVAK. Struct. Bonding, **18**, 177 (1974).
11. A. MANTEGHETTI. Thèse de 3ème Cycle, Montpellier. 1973.
12. G. A. OLAH. Friedel–Crafts and related reactions. Vol. I. John Wiley-Interscience, New York, NY. 1963.
13. E. CHEMOUNI. J. Inorg. Nucl. Chem. **33**, 2325 (1971).
14. J. ROZIERE, M. T. ROZIERE-BORIES, A. MANTEGHETTI et A. POTIER. Can. J. Chem. **52**, 3274 (1974).
15. (*a*) A. GRODZICKI et A. POTIER. J. Inorg. Nucl. Chem. **35**, 61 (1973); (*b*) D. MASCHERPA-CORRAL et J. POTIER. J. Chim. Phys. A paraître.
16. N. N. GREENWOOD et K. WADE. J. Chem. Soc. 1527 (1956).
17. J. M. LE CARPENTIER et R. WEISS. Acta Crystallogr. Sect. B, **28**, 1421 (1972).
18. M. E. PEACH, V. L. TRACY et T. C. WADDINGTON. J. Chem. Soc. A, **366** (1969).
19. H. OGOSHI et K. NAKAMOTO. J. Chem. Phys. **45**, 3113 (1969).
20. J. C. SPEAKMAN. Struct. Bonding, **12**, 141 (1972).
21. A. I. VOGEL. A text-book of practical organic chemistry. 3ème éd. Longman, London. 1970. p. 367.
22. A. SPASSOW. Org. Synth. **3**, 390 (1955).

Syntheses in the group of Nuphar alkaloids. III.[1] Total synthesis of (±)-nupharamine and (±)-3-epinupharamine[2]

JERZY SZYCHOWSKI, JERZY T. WRÓBEL, AND ANDRZEJ LENIEWSKI

Department of Chemistry, University of Warsaw, 02-093 Warsaw, Poland

Received August 12, 1976[3]

JERZY SZYCHOWSKI, JERZY T. WRÓBEL, and ANDRZEJ LENIEWSKI. Can. J. Chem. **55**, 3105 (1977).

The alkaloids (±)-nupharamine and (±)-3-epinupharamine were synthesized using 3-acetylfuran as the starting material. The conditions for stereoselective reduction of pyridine derivatives are described.

JERZY SZYCHOWSKI, JERZY T. WRÓBEL et ANDRZEJ LENIEWSKI. Can. J. Chem. **55**, 3105 (1977).

Utilisant l'acétyl-3 furanne comme produit de départ, on a synthétisé les alcaloïdes (±) nupharamine et (±) épi-3 nupharamine. On décrit les conditions permettant la réduction stéréosélective de dérivés de la pyridine.

[Traduit par le journal]

Deoxynupharidine **1** and castoramine **2** are the only alkaloids of the Nuphar type which have been totally synthesized (1). An attempted synthesis of a piperidine alkaloid, nupharamine **3**, resulted in deoxynupharamine **4** (2) since the synthetic procedure used excluded the possibility of introduction of the hydroxyl group, characteristic of this alkaloid. The common feature of the syntheses mentioned above was the construction of the A ring, or A and B rings in the first stages and the introduction of the furan nucleus in one of the last steps.

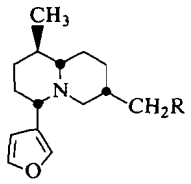

1 R = H
2 R = OH

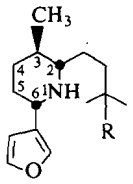

3 R = OH
4 R = H

The syntheses of the carbon skeletons of the piperidine Nuphar alkaloids reported here were carried out using a 3-furan derivative as a substrate. Construction of the nitrogen ring was followed by that of a side chain suitable for piperidine alkaloids or serving as a precursor of the B ring in the quinolizidine system. All chiral centers were formed in the reduction step in order to ensure a high stereoselectivity.

The main steps of the synthetic procedure are shown in Scheme 1. All the synthetic steps were checked to obtain first the model 2-furan and then the 3-furan derivatives.

The Claisen condensation of the initial material, acetylfuran **5** with ethyl formate results in a purple salt of furoylacetaldehydes **6**. Condensation of this salt **6***a* with ethyl 3-aminocrotonate in the presence of piperidine acetate (3) yields enamine **7** as the only basic product. The Hantzsch condensation of furoylacetaldehydes **8** with 3-aminocrotonate in benzene results in ethyl esters of 2-methyl-6-furylnicotinic acids **9**. In view of the instability of free β-ketoaldehydes **8** they were prepared from their sodium salts *in situ* in the reaction medium. In this way furyl derivatives **9** were obtained in satisfactory yields, namely 40% and 35% for compounds **9***a* and **9***b*, respectively.

The carboethoxy group was reduced to the hydroxymethyl group by the usual procedure with lithium aluminium hydride. Alcohols **10** were obtained in a quantitative yield. The removal of the hydroxyl group in **10***a* by treatment with thionyl chloride and subsequent reduction with zinc in 80% ethanol resulted in a very low yield of the expected dimethyl derivative **11***a*. The main product was a compound containing chlorine in position 4 of the furan ring **12**, as determined by ^{1}Hmr. 2,3-Dimethyl-6-furylpyridines **11***a* and **11***b* were obtained in 85% and 63% yield, respectively, by brief (few minutes) treatment of alcohols **10** with boiling 60% HBr and subsequent reduction with zinc in acetic acid. The above conditions ensure maximum yields.

The completion of the carbon skeleton of the

[1]For part II see ref. 10.

[2]Preliminary communications: Bull. Acad. Polon. Sci. Ser. Sci. Chim. **22**, 383 (1974); IUPAC, 9th International Symposium of Chemistry of Natural Products, Abstracts 4A, Ottawa, 1974.

[3]Revision received March 3, 1977.

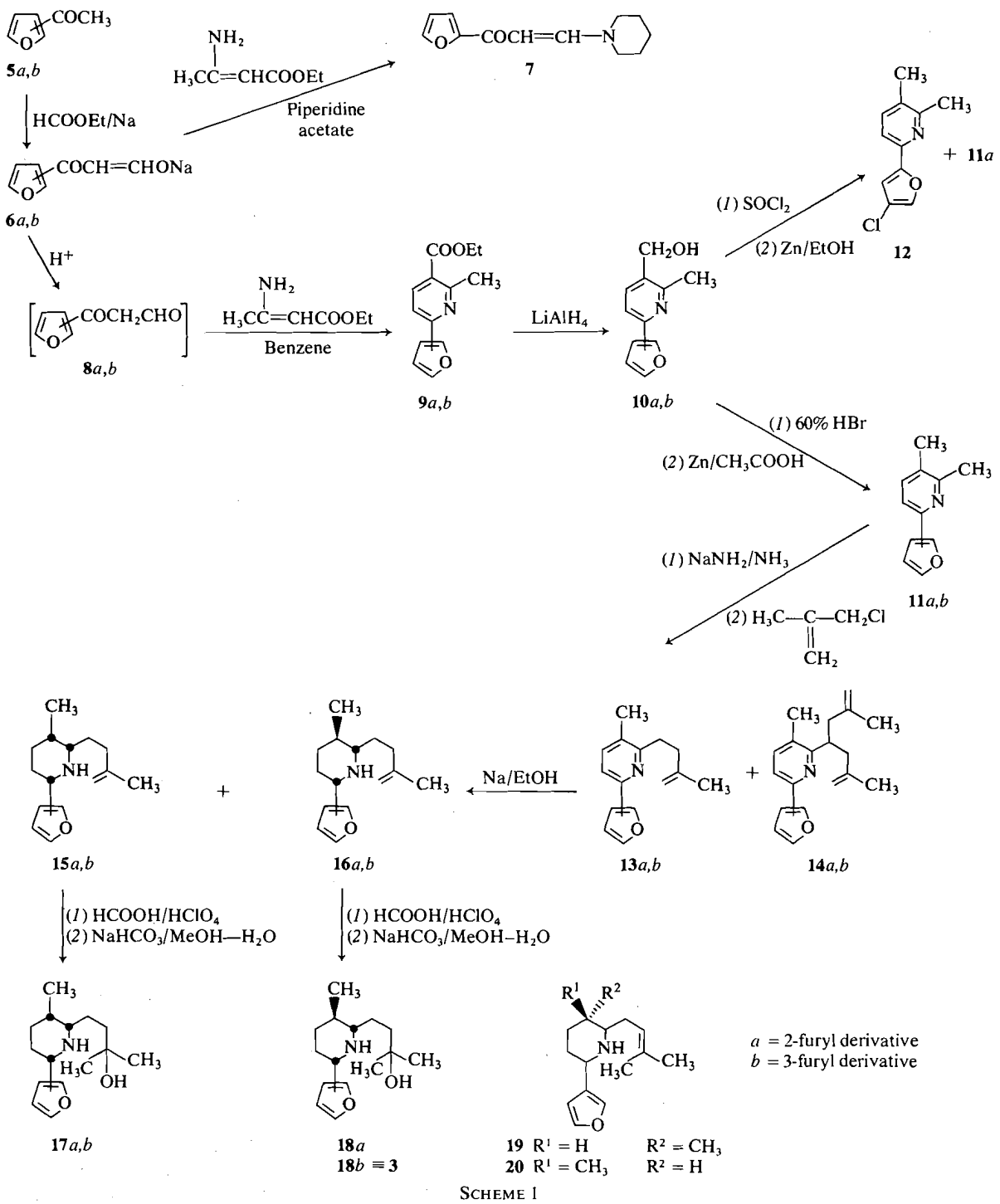

SCHEME I

piperidine Nuphar alkaloids requires the derivative **11***b* to be extended by an isobutene side chain. This was achieved by the reaction of **11** with β-methallyl chloride resulting in **13**. Methallyl chloride contains an active chlorine atom favouring the *C*-alkylation, moreover its structure prevents the formation of unwanted compounds as a result of a possible allylic rearrange-

ment. The presence and position of the ethylene bond makes possible the introduction of a hydroxyl group as well as ring closure to form the quinolizidine system. Compound **13** with the desired structure was obtained together with a dialkylated derivative **14**. The yield of the latter decreases with decreasing temperature and shorter rate of the methallyl chloride addition reaction.

The synthesis of **13***b* paved the way to the total synthesis of C_{15} piperidine Nuphar alkaloids. Compound **13***b* used as precursor required a chemically and stereochemically selective reduction of the pyridine ring and introduction of the tertiary hydroxyl group to the side chain. The latter reaction seemed to be relatively simple in view of the ethylene bond present in **13***b*. Conversely, a selective reduction of pyridine, which would retain unaffected both the furan ring and ethylene bond, presented serious difficulties.

Compounds **13***a,b* were reduced with sodium–ethanol in xylene. The resulting products consisted of a mixture of epimers at C3, **15** and **16**. Their R_f values were virtually identical in tlc on alumina but differed on silica gel. The ratio of **15** to **16** was determined by ^{1}Hmr spectroscopy. The 3-epi isomer **15** was usually the main product.

Epimers **15***a* and **16***a* were separated by chromatography on alumina (although their R_f values were virtually identical in tlc).

The stereochemistry of **15***a* was determined by ir and ^{1}Hmr spectroscopy by a method similar to that used in the case of piperidine Nuphar alkaloids (7).

Bohlmann bands in the ir spectrum show the presence of two axial hydrogen atoms in position 2 and 6 thus indicating the equatorial conformation of the furan ring and side chain. The chemical shift of the proton signal at C2 (δ = 2.78 ppm) and the value of the coupling constant with the proton at C3 (J = 2.5 Hz) indicated the presence of an equatorial hydrogen atom and an axial methyl group at C3.

The tertiary hydroxyl group was introduced by the addition of formic acid in the presence of $HClO_4$ and by subsequent gentle alkaline hydrolysis of the resulting ester. This method proved superior to the hydration in dilute HCl (8). The hydration was accompanied by a side reaction of isomerization of the ethylene bond to nuphenine **19**.

Anhydronupharamine **16***b* and 3-epianhydronupharamine **15***b* were hydrated as a mixture.

The mixture of (±)-nupharamine **18***b* and (±)-3-epinupharamine **17***b* thus obtained was separated by chromatography on alumina.

The identity of the synthetic and natural nupharamine was proven by direct comparison with a sample obtained from Professor Y. Arata. The identity of the synthetic (±)-3-epinupharamine with the natural alkaloid was demonstrated by comparison of spectroscopic data (8).

Experimental

All melting points and boiling points are uncorrected. Spectra were obtained as follows: uv in 95% ethanol on Jena-Specord UV-VIS spectrophotometer; ir on a UR-20 or UR-10 spectrophotometers (KBr pellets for solids or films for liquids); ^{1}Hmr at 100 MHz on a JOEL JNM-4H-100 spectrometer in $CDCl_3$ using TMS as internal standard, unless otherwise indicated (δ 0.0; symbols s, d, t, q, qu, br, m, stand for singlet, doublet, triplet, quartet, quintet, broad, multiplet, respectively); ms on an LKB-9000 low-resolution instrument with a direct inlet system operating at 70 eV. Fluka Al_2O_3 type H was used for tlc and BDH neutral alumina (activity III) for column chromatography.

Sodium Salts of the Enolic Forms of Furoylacetaldehydes 6

These compounds were obtained from the corresponding acetylfurans by condensation with ethyl formate in the presence of powdered sodium in ether, as in the case of the reaction with 2-acetylselenophene (5). 2-Acetylfuran (0.5 mol) and 3-acetylfuran (0.14 mol) gave in quantitative yields **6***a* and **6***b*, respectively, in the form of brown amorphous powders which were used for condensation with ethyl 3-aminocrotonate.

Condensation with Ethyl 3-Aminocrotonate in the Presence of Piperidine Acetate. Enamine 7

The procedure used in this reaction was similar to that employed in the condensation of acetone with ethyl formate and cyanoacetamide (3). 2-Acetylfuran **5***a* (0.2 mol) gave 8.5 g of **7** as the only basic reaction product; mp 86–87°C (from a mixture of ether and ethanol); picrate mp 134–136°C (ethanol). *Anal.* calcd. for $C_{12}H_{15}NO_2$ (mol. wt. 205.3): C 70.37, H 7.03, N 6.83; found (M^+ 205(100%)): C 70.32, H 7.23, N 6.48. Spectral data: uv λ_{max}(log ε): 208(3.37), 233(3.41), 277(3.86), 360(4.49) nm; ir ν_{max}: 3131, 3105, 1650, 1588, 873 cm^{-1}; ^{1}Hmr δ: 1.63 (6H, br t, β- and γ-piperidine protons), 3.32 (4H, br t, α-piperidine protons), 5.77 (1H, d, J = 13 Hz, CO—CH=), 6.42 (1H, m, H4-furan), 7.01 (1H, m, H3-furan), 7.45 (1H, m, H5-furan), 7.73 (1H, d, J = 13 Hz, N—CH=) ppm.

Ethyl Esters of 2-Methyl-6-furylnicotinic Acids 9

Ethyl 2-Methyl-6-(2-furyl)nicotinate 9a

The enol salt **6***a* (80 g) was added portionwise at room temperature to a vigorously stirred solution of ethyl 3-aminocrotonate (64.5 g) and glacial acetic acid (30 g) in 500 cm^3 of benzene. The mixture was stirred for 1 h. The resulting precipitate was filtered and washed twice with benzene. The filtrates were evaporated to about 300 cm^3 and were distilled azeotropically with a water–benzene separator for 10–15 h until the evolution of water ceased. The solvent and the excess ethyl 3-

aminocrotonate were distilled off and the residue was distilled collecting the fraction boiling at 111–112°C/0.04 Torr. Alternatively, the residue was dissolved in 200 cm^3 of acetone and the hydrobromide was precipitated by addition of 50 cm^3 of 40% HBr. The first method gave 40–46 g (35–40% yield) of a light yellow oil which crystallized on cooling. After recrystallization from *n*-hexane the product melted at 40–41°C. The second method gave 45.5 g (29% yield) of yellow hydrobromide **9***a* which crystallized from ethanol in the form of needles mp 182–184°C; picrate **9***a* mp 154–155°C (ethanol). *Anal.* calcd. for $C_{13}H_{13}NO_3$ (mol. wt. 231.2): C 67.52, H 5.67, N 6.06; found (M^+ 231(100%)): C 67.73, H 5.65, N 6.04. Spectral data: uv λ_{max}(log ε): 210(3.52), 229(3.73), 287(3.98), 319(4.39) nm; ir ν_{max}: 3160, 3129, 1730, 1604, 1594, 1500, 1277, 890 cm^{-1}; ^{1}Hmr δ: 1.43 (3H, t, J = 7 Hz, O-CH_2-CH_3), 2.88 (3H, s, C2-CH_3), 4.37 (2H, q, J = 7 Hz, O-CH_2-CH_3), 6.50 (1H, m, H4-furan), 7.15 (1H, m, H3-furan), 7.51 (1H, d, J = 8 Hz, C5-H), 7.55 (1H, m, H5-furan), 8.20 (1H, d, J = 8 Hz, C4-H) ppm.

Ethyl 2-Methyl-6-(3-furyl)nicotinate **9***b*

This compound was obtained by a method analogous to the preparation of **9***a*. From 0.14 mol of sodium salt of enol **6***b*, after removal of the excess of ethyl 3-aminocrotonate, the remaining dark oil was dissolved in benzene and the solution was filtered through alumina (50 g). The product **9***b* (11.5 g, 35% yield) was a light yellow oil which crystallized on cooling; mp 42–43°C (*n*-hexane); hydrobromide **9***b* mp 202–203.5°C (acetone–ethanol); picrate **9***b* mp 157–159.5°C (ethanol). *Anal.* calcd. for $C_{13}H_{13}NO_3$ (mol. wt. 231.2): C 67.52, H 5.67, N 6.06; found (M^+ 231(100%)): C 67.87, H 5.92, N 5.95. Spectral data: uv λ_{max}(log ε): 206(4.19), 248(3.91), 300(4.18) nm; ir ν_{max}: 3140, 1728, 1280, 881 cm^{-1}; ^{1}Hmr δ: 1.41 (3H, t, J = 7 Hz), O-CH_2-CH_3), 2.88 (3H, s, C2-CH_3), 4.35 (2H, q, J = 7 Hz, O-CH_2-CH_3), 6.91 (1H, m, H4-furan), 7.31 (1H, d, J = 8 Hz, C5-H), 7.51 (1H, m, H5-furan), 8.13 (1H, m, H2-furan), 8.21 (1H, d, J = 8 Hz, C4-H) ppm.

2-Methyl-3-hydroxymethyl-6-furylpyridines **10**

Aminoesters **9** were reduced with $LiAlH_4$ in the usual way adding it dropwise to a 1.5 molar excess of the hydride suspended in ether and then refluxing the mixture for 3 h.

2-Methyl-3-hydroxymethyl-6-(2-furyl)pyridine **10***a*

9*a* (49.7 g) gave 39.5 g (97% yield) of **10***a* in the form of a solid. An analytical sample was crystallized from ether and gave needles, mp 84–85°C; picrate **10***a* mp 191–193°C (ethanol). *Anal.* calcd. for $C_{11}H_{11}NO_2$ (mol. wt. 189.2): C 69.83, H 5.86, N 7.40; found (M^+ 189(100%)): C 69.54, H 5.83, N 7.26. Spectral data: uv λ_{max}(log ε): 206(3.62), 269(4.06), 276(4.05), 305(4.14) nm; ir ν_{max}: 3400 br, 3182, 1601, 1503, 1052, 893 cm^{-1}; ^{1}Hmr δ: 2.48 (3H, s, C2-CH_3), 6.44 (1H, m, H4-furan), 6.99 (1H, m, H3-furan), 7.42 (1H, d, J = 8 Hz, C5-H), 7.46 (1H, m, H2-furan), 7.60 (1H, d, J = 8 Hz, C4-H), and 2.7 (1H, br s, OH), 4.57 (2H, s, -CH_2-O) ppm.

2-Methyl-3-hydroxymethyl-6-(3-furyl)pyridine **10***b*

9*b* (9.3 g) gave 7.6 g (100% yield) of **10***b*; mp 78–79°C (benzene); picrate **10***b* mp 196–198°C (ethanol). *Anal.* calcd. for $C_{11}H_{11}NO_2$ (mol. wt. 189.2): C 69.83, H 5.86, N 7.40; found (M^+ 189(100%)): C 70.01, H 5.63, N 7.51. Spectral data: uv λ_{max} (log ε): 203(4.02), 213(3.98), 218(4.00), 247(3.95), 289(3.89) nm; ir ν_{max}: 3500–3000 br, 1610, 1595, 1514, 1053, 870 cm^{-1}; ^{1}Hmr δ: 2.45 (3H, s, C2-CH_3), 4.55 (2H, s, -CH_2-O), 6.81 (1H, m, H4-furan), 7.14 (1H, d, J = 8 Hz, C5-H), 7.43 (1H, m, H5-furan), 7.52 (1H, d, J = 8 Hz, C4-H), 8.00 (1H, m, H2-furan), and 3.75 (1H, br s, OH) ppm.

2,3-Dimethyl-6-furylpyridines **11**

2,3-Dimethyl-6-(2-furyl)pyridine **11***a*

Hydrobromic acid (60%, 110 cm^3) was added to amino alcohol **10***a* (30 g) and the mixture was refluxed for 5 min. After cooling the resulting dark red solution was added dropwise to a stirred hot suspension of zinc dust (50 g) in glacial acetic acid (600 cm^3).

The mixture was refluxed for 15 min and then it was stirred without heating for 30 min. The resulting, almost colourless solution was decanted from zinc, the precipitate was washed with glacial acetic acid (2 × 50 cm^3), the decanted liquid and the washings were combined, and after evaporation to a small volume under reduced pressure they were added slowly to 500 cm^3 of concentrated ammonia solution. An oil separated which was extracted with benzene (4 × 200 cm^3). The extract was washed with water and the solvent was evaporated. The remaining red oil (26 g) was distilled and the fraction boiling at 139–140°C/8 Torr was collected (23.4 g, 85% yield). On cooling the colourless product crystallized mp 60–61°C; hydrobromide **11***a* mp 206–207°C; picrate **11***a* mp 204–206°C (ethanol). *Anal.* calcd. for $C_{11}H_{11}NO$ (mol. wt. 173.2): C 76.28, H 6.40, N 8.09; found (M^+ 173(100%)): C 76.79, H 6.54, N 7.71. Spectral data: uv λ_{max}(log ε): 204(3.94), 268(4.15), 276(4.13), 306(4.20) nm; ir ν_{max}: 3152, 3122, 1605, 1562, 1501, 890 cm^{-1}; ^{1}Hmr δ: 2.23 (3H, s, C3-CH_3), 2.49 (3H, s, C2-CH_3), 6.45 (1H, m, H4-furan), 6.94 (1H, m, H3-furan), 7.38 (2H, s, C4-H and C5-H), 7.45 (1H, m, H5-furan) ppm.

2,3-Dimethyl-6-(3-furyl)pyridine **11***b*

Analogous to the preparation of **11***a*, 7.3 g of **10***b* gave 4.2 g (63% yield) of **11***b*; bp 133–136°C/8 Torr, mp 20–22°C; picrate **11***b* mp 212–215°C (ethanol). *Anal.* calcd. for $C_{11}H_{11}NO$ (mol. wt. 173.2): C 76.28, H 6.40, N 8.09; found (M^+ 173(100%)): C 76.38, H 6.65, N 7.96. Spectral data: uv λ_{max}(log ε): 203(3.96), 213(3.85), 218(3.87), 245(3.81), 252(3.81), 289(3.80) nm; ir ν_{max}: 3153, 3140, 3125, 1608, 1580, 1564, 880 cm^{-1}; ^{1}Hmr δ: 2.25 (3H, s, C3-CH_3), 2.52 (3H, s, C2-CH_3), 6.86 (1H, m, H4-furan), 7.16 (1H, d, J = 8 Hz, C5-H), 7.35 (1H, d, J = 8 Hz), 7.46 (1H, m, H5-furan), 8.01 (1H, m, H2-furan) ppm.

Reaction of Amino Alcohol **10***a with Thionyl Chloride and Reduction with Zinc and 80% Ethanol* **12**

A solution of **10***a* (19 g) in 30 cm^3 of benzene was added dropwise to $SOCl_2$ (47 g) at 0 to 5°C. The mixture was refluxed for 15 h, the excess $SOCl_2$ and benzene were evaporated, and the dark viscous residue was dissolved in 130 cm^3 of 80% ethanol. The solution was added dropwise during 30 min to a hot suspension of zinc dust (40 g) activated with $CuSO_4$ in 100 cm^3 of 80% ethanol, the mixture was refluxed for 3.5 h and was left to stand overnight. The excess of zinc was filtered off, the precipitate was washed with 80% ethanol and then ethanol and a part of water were evaporated from the acidic filtrate. One third of the residue was made alkaline with NaOH and was steam distilled. The remaining part of the residue

was made alkaline with concentrated ammonia solution and was extracted with ether. Both the semisolid distillation product and the ether extract were identical mixtures of two substances with similar R_f values in tlc, but their purity was different. The components of the mixture were separated by crystallization and distillation. The products were: 1.3 g of solid substance identical with **11***a* and 1.8 g of **12**. **12** had mp 98–100.5°C (*n*-hexane) and bp 147–165°C/11 Torr. *Anal.* calcd. for $C_{11}H_{10}ClNO$ (mol. wt. 207.7): C 63.70, H 4.87, N 6.75; found (M^+ 207(100%), 209(34%)): C 63.67, H 5.15, N 6.43. Spectral data: uv λ_{max}(log ε): 205(3.94), 267(4.12), 275(4.10), 303(4.21) nm; ir ν_{max}: 3153, 3112, 1595, 873 cm^{-1}; ^{1}Hmr δ: 2.24 (3H, s, C3-CH_3), 2.48 (3H, s, C2-CH_3), 6.93 (1H, m, H3-furan), 7.35 (2H, s, C4-H and C5-H), 7.41 (1H, m, H5-furan) ppm.

Alkylation of 2,3-Dimethyl-6-furylpyridines ***11*** *with β-Methallyl Chloride in the Presence of Sodium Amide in Liquid Ammonia*

Alkylation of 2,3-Dimethyl-6-(2-furyl)pyridine ***11a****. 13a and 14a*

A solution of **11***a* (6.06 g) in 25 cm^3 of ether was added at −33°C to a suspension of $NaNH_2$ in liquid ammonia prepared from 100 cm^3 of dry NH_3 and sodium (1.21 g). The dark red solution was stirred for 15 min, then it was cooled to −50°C and β-methallyl chloride (4.75 g) was added dropwise as rapidly as possible. The mixture became colourless. It was decomposed with 10 cm^3 of water, ammonia was evaporated, and the residue was extracted with ether. The product was 8.67 g of red oil which, after chromatography on alumina (700 g), gave 4.75 g (60% yield) of **13***a*, 0.14 g of **14***a*, and 2.1 g of unchanged **11***a*.

13*a* is an oil bp 101–106°C/0.085 Torr; picrate mp 143.4°C (ethanol – ethyl acetate). *Anal.* calcd. for $C_{15}H_{17}NO$ (mol. wt. 227.3): C 79.26, H 7.54, N 6.16; found (M^+ 227(45%)(213 = 100%)): C 79.58, H 7.54, N 5.86. Spectral data: uv λ_{max}(log ε): 205(4.06), 268(4.12), 276(4.06), 304(4.04) nm; ir ν_{max}: 3125, 3084, 1654, 891, 880 cm^{-1}; ^{1}Hmr δ: 1.84 (3H, s, CH_3—C═), 2.32 (3H, s, C3-CH_3), 2.5–3.1 (4H, m, -CH_2-CH_2-), 4.77 (2H, s, C═CH_2), 6.53 (1H, m, H4-furan), 7.07 (1H, m, H3-furan), 7.49 (2H, s, C4-H and C5-H), 7.54 (1H, m, H5-furan) ppm.

14*a* is an oil bp 116°C/0.1 Torr; picrate mp 156–158°C (ethanol). *Anal.* calcd. for $C_{19}H_{23}NO$ (mol. wt. 281.4): C 81.09, H 8.24, N 4.98; found (M^+ 281(18%)(226 = 100%)): C 81.38, H 8.90, N 4.48. Spectral data: uv λ_{max}(log ε): 205(4.06), 268(4.12), 276(4.06), 304(4.04) nm; ir ν_{max}: 3152, 3125, 3079, 1653, 893, 880 cm^{-1}; ^{1}Hmr δ: 1.70 (6H, s, 2CH_3—C═), 2.32 (3H, s, C3-CH_3), 2.4–2.6 (4H, m, 2—CH_2—C═), 3.39 (1H, qu, J = 7 Hz, C2-CH), 4.60 (2H, m, C═CH_2), 4.66 (2H, s, C═CH_2), 6.50 (1H, m, H4-furan), 7.08 (1H, m, H3-furan), 7.43 (2H, s, C4-H and C5-H), 7.49 (1H, m, H5-furan) ppm.

Alkylation of 2,3-Dimethyl-6-(3-furyl)pyridine ***11b****. 13b and 14b*

Analogous to the preparation of **11***a* 4.0 g of **11***b* gave 5.6 g of a mixture of products from which 2.36 g (45% yield) of **13***b* and 0.43 g of **14***b* were isolated by chromatography on alumina.

13*b* is an oil. *Anal.* calcd. for $C_{15}H_{17}NO$ (mol. wt. 227.3): C 79.26, H 7.54, N 6.16; found (M^+ 227(48%)(213 = 100%)): C 79.16, H 7.96, N 6.01. Spectral data: uv λ_{max}(log ε): 204(4.20), 219(3.96), 251(3.90), 291(3.84) nm; ir ν_{max}: 3155, 3140, 3081, 1643, 893, 880 cm^{-1}; ^{1}Hmr δ: 1.84 (3H, s, CH_3—C═), 2.50 (2H, d, d, J_1 = 10 Hz, J_2 = 5 Hz, —CH_2—C═), 2.92 (2H, d, d, J_1 = 10 Hz, J_2 = 5 Hz, C2-CH_2-), 2.31 (3H, s, C3-CH_3), 4.78 (2H, s, C═CH_2), 6.92 (1H, m, H4-furan), 7.17 (1H, d, J = 8 Hz, C5-H), 7.38 (1H, d, J = 8 Hz, C4-H), 7.50 (1H, m, H5-furan), 8.05 (1H, m, H2-furan) ppm.

14*b* is an oil. *Anal.* calcd. for $C_{19}H_{23}NO$ (mol. wt. 281.4): C 81.09, H 8.24, N 4.98; found (M^+ 281(79%) (226 = 100%)): C 81.16, H 8.50, N 5.11. Spectral data: uv λ_{max}(log ε): 205(4.27) 220(3.91), 253(3.83), 300(3.65) nm; ir ν_{max}: 3157, 3139, 3079, 1651, 896, 879 cm^{-1}; ^{1}Hmr δ: 1.70 (6H, s, 2CH_3—C═), 2.32 (3H, s, C3-CH_3), 2.4–2.6 (4H, m, 2—CH_2—C═), 3.40 (1H, qu, J = 7 Hz, C2-CH), 4.60 (2H, br s, C═CH_2), 4.66 (2H, s, C═CH_2), 6.93 (1H, m, H4-furan), 7.17 (1H, d, J = 8 Hz, C5-H), 7.38 (1H, d, J = 8 Hz, C4-H), 7.51 (1H, m, H5-furan), 8.07 (1H, m, H2-furan), ppm.

Reduction of Bases ***13*** *with Sodium and Ethanol*

Reduction of 13a

A solution of **13***a* (4.54 g, 0.02 mol) in 20 cm^3 of absolute ethanol was added dropwise during several minutes to a suspension of sodium (9.2 g, 0.4 mol) in 100 cm^3 of boiling xylene. During the reduction three further 2 cm^3 portions of ethanol were added. When the yellow-green colour of the solution disappeared, the metal was dissolved with water. The solution was diluted with water and extracted with benzene. The extract was washed with water and with dilute HCl in order to remove basic substances. The acid extract was washed with benzene and after making alkaline with concentrated NaOH it was reextracted with benzene. On evaporation the benzene extract gave 3.91 g of a light-red oil which was chromatographed on alumina column to isolate a mixture of epimers **15***a* and **16***a* (ratio about 1:1); yield 1.28 g (27%). Thin layer chromatography on silica gel showed the presence of two compounds of similar R_f values. The ^{1}Hmr spectrum of the mixture was compared with that of **15***a* and showed the presence of an additional signal at δ 2.3 corresponding to the C2-H proton of epimer **16***a*. The ratio of these two compounds was determined on the basis of integration of signals at δ 2.8 and 3.7 ppm. The crude products from several experiments (2.8 g) were chromatographed on alumina (330 g) and gave **15***a* (0.475 g) and **16***a* (0.425 g).

15a*: A Colourless Oil*—ir ν_{max}: 3330, 3120, 3075, 2790, 2728, 1653, 886 cm^{-1}; ^{1}Hmr δ: 0.98 (3H, d, J = 6 Hz, C3-CH_3), 1.73 (3H, s, ═C—CH_3), 1.4–2.2 (9H, m), 2.5 (1H, br s, NH), 2.78 (1H, d, t, J_1 = 2.5 Hz, J_2 = 7 Hz, C2-H), 3.72 (1H, m, C6-H), 4.68 (2H, s, ═CH_2), 6.12 (1H, m, H3-furan), 6.23 (1H, m, H4-furan), 7.27 (1H, m, H5-furan) ppm; ^{1}Hmr (C_6D_6) δ: 0.92 (3H, d, J = 6 Hz, C3-CH_3) ppm; ms: 233(11%)(M^+), 164(64%), 107(100%), 94(79%) *m/e*.

16a*: A Colourless Oil*—ir ν_{max}: 3330, 3130, 2810, 2740, 1659, 889 cm^{-1}; ^{1}Hmr δ: 0.92 (3H, d, J = 5.5 Hz, C3-CH_3), 1.74 (3H, s, ═C—CH_3), 1.2–2.1 (10H with NH, m), 2.26 (1H, m, C2-H), 3.73 (1H, m, C6-H), 4.70 (2H, s, ═CH_2), 6.12 (1H, m, H3-furan), 6.26 (1H, m, H4-furan), 7.32 (1H, m, H5-furan) ppm; ^{1}Hmr (C_6D_6) δ: 0.78 (C3-CH_3) ppm; ms: 233(17%)(M^+), 164(69%), 107-(100%), 94(75%) *m/e*.

Reduction of Base 13b

Analogous to the preparation of **13***a*, 0.73 g of **13***b*

gave 89 mg (yield 12%) of a mixture of **15***b* and **16***b* (ratio about 3:1). The product was used for hydration without previous separation of epimers.

Hydration of 15a, 16a and Mixture of 15b and 16b

General Procedure

A mixture of unsaturated compound **15***a*, **16***a*, or mixture of **15***b* and **16***b*, 99% formic acid, and 72% perchloric acid in the ratio 1:10:1 (wt./wt.) was allowed to stand at room temperature for about 40 h (optimal time) and then it was diluted with about 5 times its volume of 80% methanol. The mixture was gently boiled and solid sodium bicarbonate was added portionwise until the evolution of CO_2 ceased and the solution became alkaline. Then methanol was evaporated, water was added in order to dissolve the salts, and the mixture was extracted with ether. On drying with anhydrous $MgSO_4$ and evaporation the extract gave a viscous yellow oil. The amino alcohols can be readily separated from the substrates by column chromatography on alumina using first benzene and then ether as eluting solvents. The substrates (benzene fraction) always contain the isomerization products having the structure of natural compounds nuphenine **19** (7) and anhydronupharamine **20** (9) (^{1}Hmr of the mixture: br t, at δ = 5.1 and methyl groups singlets at 1.6 and 1.7 ppm). An unsatisfactory result was obtained by the HCl hydration method (8).

Hydration of 15a

15*a* (0.47 g) treated by the method described above gave 0.45 g of an oil which, on chromatography on alumina (40 g), gave 47 mg of substrate and 0.27 g (yield 54%) of **17***a* in the form of a colourless oil. Spectral data: ir ν_{max} (CCl_4): 3610, 3400, 3200, 2817, 2790, 2728, 888 cm^{-1}; ^{1}Hmr δ: 0.96 (3H, d, J = 7 Hz, C3-CH_3), 1.20 and 1.24 (6H, s, s, *gem*-dimethyl), 1.1–1.9 (9H, m), 2.76 (1H, d, t, J_1 = 2.5 Hz, J_2 = 7 Hz, C2-H), 2.95 (2H, br s, NH and OH), 3.70 (1H, m, C6-H), 6.12 (1H, m, H3-furan), 6.24 (1H, m, H4-furan), 7.32 (1H, m, H5-furan) ppm; ^{1}Hmr (C_6D_6) δ: 0.87 (C3-CH_3) ppm; ms: 251-(7%)(M^+), 236(12%), 164(100%), 107(48%), 94(60%) *m/e*.

Hydration of 16a

16*a* (0.42 g) gave 0.23 g (yield 51%) of **18***a* in the form of a colourless oil which crystallized on standing; mp 90–90.5°C (*n*-hexane). Spectral data: ir ν_{max} (KBr): 3270, 3142, 3120, 2800, 2740, 868, 2717 cm^{-1}; ^{1}Hmr δ: 0.92 (3H, d, J = 7 Hz, C3-CH_3), 1.21 (6H, s, *gem*-dimethyl), 1.0–2.0 (11H, with NH and OH, m), 2.39 (1H, m, C2-H), 3.72 (1H, d d, J_1 = 2.5 Hz, J_2 = 10 Hz, C6-H), 6.11 (1H, m, H3-furan), 6.24 (1H, m, H4-furan), 7.29 (1H, m, H5-furan) ppm; ^{1}Hmr (C_6D_6) δ: 0.76(C3-CH_3) ppm; ms: 251(6%)(M^+), 236(11%), 164(100%), 107(56%), 94(54%) *m/e*.

Hydration of Mixture of 15b and 16b

The mixture of epimeric anhydronupharamines obtained by reduction of **13***b* (142 mg) on hydration followed by preliminary chromatography gave 86 mg of mixture of synthetic alkaloids **17***b* and **18***b* (in tlc separate spots having similar R_f values). A quantity of 69 mg was rechromatographed on 15 g of alumina collecting 15 cm^3 portions of the eluate (4 benzene fractions, 4 fractions of the ether–benzene mixtures containing 2%, 5%, 10%, and 25% ether and 2 ether fractions, making the total of 22 fractions). Fraction 15 contained 6 mg of pure (±)-nupharamine **18***b*, which by ir, ms, and tlc were identical with those of natural (−)nupharamine isolated from picrolonate.

Combined fractions 17–21 gave 50 mg of pure (±)-3-epinupharamine **17***b*. Spectral data: ir ν_{max} (CCl_4): 3400, 3170, 2976, 2934, 2862, 2805, 2738, 1507, 1457, 1386, 1368, 1225, 1159, 1120, 1069, 1032, 984, 969, 930, 913, 877 cm^{-1}; ^{1}Hmr δ: 0.96 (3H, d, J = 7 Hz, C3-CH_3), 1.18 and 1.23 (6H, s, s, *gem*-dimethyl), 1.0–2.0 (9H, m), 2.42 (2H, br s, NH and OH), 2.78 (1H, d t, J_1 = 2.5 Hz, J_2 = 6 Hz, C2-H), 3.56 (1H, d d, J_1 = 3 Hz, J_2 = 9 Hz, C6-H), 6.39 (1H, m, H4-furan), 7.32 (2H, m, H2-furan and H5-furan) ppm; ^{1}Hmr (C_6D_6) δ: 0.79 (C3-CH_3) ppm ms: 251(1.5%)(M^+), 236(6%), 164(100%), 136(7%), 107(27%), 94(38%), 81(9%) *m/e*.

Hydrobromide of 17b

Hydrobromic acid (0.1 cm^3 of 40%) was added to 33 mg of synthetic 3-epinupharamine in 0.5 cm^3 of acetone and the mixture was allowed to stand in a refrigerator. After two crystallizations from acetone the product gave colourless needles mp 179–181°C.

1. J. T. Wróbel. Alkaloids, **9**, 441 (1967).
2. Y. Arata, T. Ohashi, Z. Okumura, Y. Wada, and M. Ishikawa. J. Pharm. Soc. Jpn. **83**, 79 (1963).
3. R. Mariella. Org. Synth. Coll. Vol. **4**, 210 (1963).
4. H. C. Brown and B. Kanner. J. Am. Chem. Soc. **75**, 3865 (1953).
5. Yu. K. Yur'ev, N. N. Mezentsova, and E. A. Kashutina. Zh. Obshch. Khim. **29**, 2597 (1959).
6. E. Profft. J. Prakt. Chem. **19**, 266 (1963).
7. R. Barchet and T. P. Forrest. Tetrahedron Lett. 4229 (1965).
8. T. P. Forrest and S. Ray. Can. J. Chem. **49**, 1774 (1971).
9. Y. Arata, T. Ohashi, M. Yonemitsu, and S. Yasuda. J. Pharm. Soc. Jpn. **87**, 1094 (1967).
10. Z. Dąbrowski, J. T. Wróbel, and J. Cybulski. Bull. Acad. Pol. Sci. Ser. Sci. Chim. **22**, 935 (1974).

Syntheses in the group of Nuphar alkaloids. IV.[1] Crystal structure and stereochemistry of synthetic (±)-3-epinupharamine

MICHAŁ SABAT AND TADEUSZ GŁOWIAK
Institute of Chemistry, University of Wrocław, 50-383 Wrocław, Poland[2]
AND
JERZY SZYCHOWSKI, JERZY T. WRÓBEL, AND ANDRZEJ LENIEWSKI
Department of Chemistry, University of Warsaw, 02-093 Warsaw, Poland
Received August 12, 1976[3]

MICHAŁ SABAT, TADEUSZ GŁOWIAK, JERZY SZYCHOWSKI, JERZY T. WRÓBEL, and ANDRZEJ LENIEWSKI. Can. J. Chem. **55**, 3111 (1977).

Racemic 3-epinupharamine hydrobromide ($C_{15}H_{26}BrNO_2$) crystals are monoclinic, space group $C2/c$, with $a = 18.163(3)$, $b = 13.346(2)$, $c = 13.847(2)$ Å, $\beta = 100.36(1)°$, $Z = 8$. The X-ray analysis proved the structural identity of the compound obtained by the total synthesis with the natural 3-epinupharamine. The empirical criterion indicating the axial or equatorial orientation of the *C*-methyl group on the basis of the direction of changes of the chemical shifts recorded in benzene solutions does not hold for the piperidine system investigated.

MICHAŁ SABAT, TADEUSZ GŁOWIAK, JERZY SZYCHOWSKI, JERZY T. WRÓBEL et ANDRZEJ LENIEWSKI. Can. J. Chem. **55**, 3111 (1977).

Les cristaux du bromhydrate d'épi-3 nupharamine racémique ($C_{15}H_{26}BrNO_2$) sont monocliniques, groupe d'espace $C2/c$ avec $a = 18.163(3)$, $b = 13.346(2)$, $c = 13.847(2)$ Å, $\beta = 100.36(1)°$, $Z = 8$. L'analyse par rayons-X a démontré l'identité structurale du composé obtenu par synthèse totale avec l'épi-3 nupharamine naturel. Les critères empiriques permettant de déterminer l'orientation axiale ou équatoriale des groupes *C*-méthyles en se basant sur la direction des changements dans les déplacements chimiques enregistrés en solutions benzéniques ne peuvent être utilisés dans le système pipéridine étudié.

[Traduit par le journal]

Introduction

The total synthesis of two stereoisomers: nupharamine and 3-epinupharamine was described previously (1). The identity of the synthetic and natural nupharamine was proved by a direct comparison of the respective samples. The comparison of the synthetic and natural 3-epinupharamine was carried out only on the basis of nmr, ir, and ms spectra obtained for the synthetic compounds with those reported in the literature for the natural alkaloid (2).

The structure of the natural 3-epinupharamine[1] was established (2) on the basis of the chemical correlation with another Nuphar alkaloid, nuphenine (3), and by a similar interpretation of the spectroscopic data for both compounds. The stereochemistry of the piperidine ring was established by analysis of nmr and ir spectra. The signal of the C2-H proton at $\delta = 2.78$ characteristic of all 3-epipiperidine Nuphar alkaloids has been found in the nmr spectra. Its structure indicates a coupling with two equivalent side chain protons as well as a coupling with the C3-H proton. In the latter case the value of the coupling constant $J = 2.5$ Hz, shows that the C2-H and C3-H protons can be in axial–equatorial or equatorial–equatorial positions with respect to each other. The presence of Bohlmann bands in the ir spectra lead to the conclusion that the side chain is in the equatorial and the methyl group in the axial position.

This conclusion was confirmed by the observed changes of the chemical shift of the C3-CH_3 group of 3-epinuphamine (4) in benzene solution. According to an empirical criterion found for the quinolizidine system (5) the signal of the axial methyl group is shifted downfield in benzene as compared to the chloroform solution.

The nmr spectra of the synthetic 3-epinupharamine show an opposite direction of the changes of the chemical shift of the C3-CH_3 group; in benzene the difference with respect to

[1]For part III see preceding paper.
[2]Address for X-ray analysis problems.
[3]Revision received May 9, 1977.

TABLE 1. Final atomic coordinates ($\times 10^4$, Br^- $\times 10^5$) and anisotropic thermal parameters ($\times 10$) for non-hydrogen atoms with e.s.d.'s in parentheses[a]

	x	y	z	B_{11}	B_{22}	B_{33}	B_{12}	B_{13}	B_{23}
Br^-	19887(5)	−4804(6)	−12755(4)	100.9(6)	59.8(4)	34.0(3)	14.9(5)	13.1(3)	5.9(4)
O(1)	3017(3)	205(3)	782(4)	46(3)	45(3)	50(3)	5(2)	11(2)	7(2)
O(2)	477(6)	2397(8)	1202(5)	123(7)	112(6)	63(4)	75(6)	−3(4)	−11(4)
N(1)	1793(3)	−498(5)	1491(4)	30(3)	43(3)	32(3)	4(3)	9(3)	0(3)
C(2)	1981(4)	−1594(5)	1396(5)	40(5)	39(4)	34(4)	−2(4)	7(3)	−2(3)
C(3)	1419(5)	−2235(7)	1803(6)	44(5)	55(5)	56(5)	−8(4)	12(4)	1(4)
C(4)	629(6)	−1968(9)	1304(7)	55(7)	94(8)	57(6)	−30(6)	19(5)	−2(5)
C(5)	465(6)	−842(9)	1376(7)	37(5)	112(9)	44(5)	6(5)	0(4)	6(5)
C(6)	1028(4)	−213(6)	947(5)	36(5)	73(7)	27(4)	6(4)	4(4)	1(4)
C(7)	930(6)	889(7)	970(6)	43(5)	65(6)	34(4)	27(5)	−1(3)	−4(4)
C(8)	391(7)	1396(11)	1325(7)	88(8)	88(8)	65(5)	46(7)	20(5)	12(6)
C(9)	1062(8)	2533(10)	766(8)	101(9)	56(8)	79(7)	26(7)	−16(6)	−10(6)
C(10)	1362(6)	1630(9)	608(7)	57(7)	67(7)	59(5)	12(7)	−3(5)	4(5)
C(11)	1510(7)	−2215(9)	2921(7)	68(7)	63(7)	51(5)	−4(6)	19(5)	17(5)
C(12)	2783(5)	−1796(7)	1856(6)	51(6)	40(5)	50(5)	7(4)	15(4)	6(4)
C(13)	3370(5)	−1535(6)	1234(6)	42(5)	47(5)	54(5)	20(4)	12(4)	6(4)
C(14)	3635(4)	−458(7)	1197(5)	36(4)	48(5)	64(4)	12(4)	15(3)	12(4)
C(15)	4225(6)	−346(9)	548(9)	51(6)	76(4)	97(8)	13(6)	34(5)	17(7)
C(16)	3912(6)	−15(9)	2226(8)	52(6)	66(6)	73(6)	−2(5)	−4(5)	3(5)

[a]Anisotropic thermal parameters are defined by $\exp[-\frac{1}{4}(B_{11}h^2a^{*2} + B_{22}k^2b^{*2} + B_{33}l^2c^{*2} + 2B_{12}hka^*b^* + 2B_{13}hla^*c^* + 2B_{23}klb^*c^*)]$.

the chloroform solution is 17 Hz upfield, thus indicating the equatorial methyl group. Similar effects were found for 3-epianhydronupharamine and analogous compounds of the α-furan series (1). Thus, either (*i*) the synthetic compound differs from the natural 3-epinupharamine, or (*ii*) the empirical criterion which establishes the orientation of the *C*-methyl group in quinolizidine systems on the basis of the changes of chemical shifts in benzene solution does not hold for the piperidine system.

In order to solve this problem the X-ray structural analysis of the hydrobromide of the synthetic racemic 3-epinupharamine was carried out.

Experimental

Crystals suitable for X-ray analysis were prepared using a method described elsewhere (1). Preliminary Weissenberg photographs established that the crystals were monoclinic. The persistent absence of *hkl* reflections for $h + k = 2n + 1$, and of *h*0*l* reflections for $l = 2n + 1$, showed that the space group is either *Cc* or *C*2/*c*. The centrosymmetric space group *C*2/*c* (No. 15) (6) was determined from the statistics of $|E|$ values and satisfactory structure refinement. The cell parameters were determined by a least-squares refinement of the setting angles of 15 reflections found by automatic centering routine of Syntex $P2_1$ diffractometer (MoKα radiation, $\lambda = 0.71069$ Å).

$C_{15}H_{26}BrNO_2$ mw 332.3
Monoclinic, *C*2/*c*, $a = 18.163(3)$ Å, $b = 13.346(2)$, $c = 13.847(2)$, $\beta = 100.36(1)°$, $V = 3301.8$ Å^3, $Z = 8$, $d_m = 1.34$ g cm^{-3}, $d_x = 1.35$, μ(MoKα) = 26.4 cm^{-1}.

The density of 1.34 g cm^{-3} as determined by flotation in $CHCl_3$–benzene mixture agrees well with that calculated for a unit cell containing eight molecules of the compound.

Intensity data for a crystal of approximate dimensions 0.15 × 0.15 × 0.20 mm were collected, using MoKα radiation, on a Syntex $P2_1$ computer-controlled four-circle diffractometer equipped with a scintillation counter and graphite monochromator. A total of 1658 independent reflections were measured up to $2\theta = 45°$ by the θ–2θ scan technique. The scan rate varied from 2.0 to 20.0°/min depending on the reflection intensity. The 1122 reflections, for which $F > 3.92\sigma(F)$ were used in the subsequent calculations. The intensity of the standard reflection (040) was monitored at 15 reflection intervals. No significant variation of this intensity was observed. The intensities of reflections were corrected for the Lorentz and polarization effects. No absorption or extinction corrections were made.

Structure Determination and Refinement

The structure was established using the heavy-atom method. The bromine atom position was determined from a three-dimensional Patterson map. The remaining non-hydrogen atoms were located using a three-dimensional Fourier synthesis, which was phased on the bromine atom ($R_1 = 0.45$). Full-matrix least-squares refinement of the obtained structure model with isotropic thermal parameters yields the value of $R_1 = 0.164$. Several cycles of refinement with anisotropic temperature factors result in the agreement factor

$$R_1 = \sum||F_o| - |F_c||/\sum|F_o| = 0.080$$

and

$$R_2 = (\sum w(|F_o| - |F_c|)^2/\sum w|F_o|^2)^{1/2} = 0.074$$

At this stage coordinates of the hydrogen atoms were derived from a difference synthesis. A further five cycles of full-matrix refinement with isotropic temperature factors for hydrogen atoms gave the final values R_1 of 0.040 and R_2 of 0.026. The subsequent difference synthesis showed no unexpected features. The function minimized during the refinement was defined as $\sum w(|F_o| - |F_c|)^2$, where the weight $w = 1/\sigma^2(F)$. The atomic scattering factors were those listed by Cromer and Waber (7). The anomalous dispersion correction for Br^- was made according to Temple-

TABLE 2. Atomic coordinates (× 10^3) and isotropic thermal parameters for the hydrogen atoms with e.s.d.'s in parentheses

	x	*y*	*z*	*B* (Å^2)
H(O1)	286(3)	2(4)	20(3)	3(2)
H(N1a)	219(3)	−14(4)	127(4)	1(2)
H(N1b)	186(3)	−23(4)	219(4)	6(2)
H(2)	192(2)	−171(3)	62(3)	3(1)
H(3)	155(3)	−293(5)	169(4)	6(2)
H(4a)	25(4)	−227(5)	165(5)	9(2)
H(4b)	59(4)	−206(5)	55(5)	9(2)
H(5a)	51(3)	−69(4)	206(4)	4(2)
H(5b)	0(3)	−68(5)	105(4)	6(2)
H(6)	102(3)	−46(4)	26(4)	5(2)
H(8)	−6(4)	107(5)	159(5)	9(2)
H(9)	131(3)	323(5)	48(4)	8(2)
H(10)	176(3)	159(5)	31(4)	4(2)
H(11a)	186(3)	−256(5)	320(4)	5(2)
H(11b)	106(3)	−254(4)	309(4)	5(2)
H(11c)	140(3)	−151(5)	312(4)	9(3)
H(12a)	282(3)	−252(5)	203(4)	6(2)
H(12b)	290(3)	−146(4)	254(4)	4(2)
H(13a)	384(4)	−197(5)	151(4)	7(2)
H(13b)	314(3)	−172(4)	53(4)	4(2)
H(15a)	442(3)	43(6)	57(5)	9(2)
H(15b)	405(3)	−67(5)	−12(4)	7(2)
H(15c)	460(3)	−77(4)	81(4)	4(2)
H(16a)	427(3)	−58(5)	249(4)	7(2)
H(16b)	348(3)	0(4)	258(4)	7(2)
H(16c)	415(4)	69(5)	222(5)	8(2)

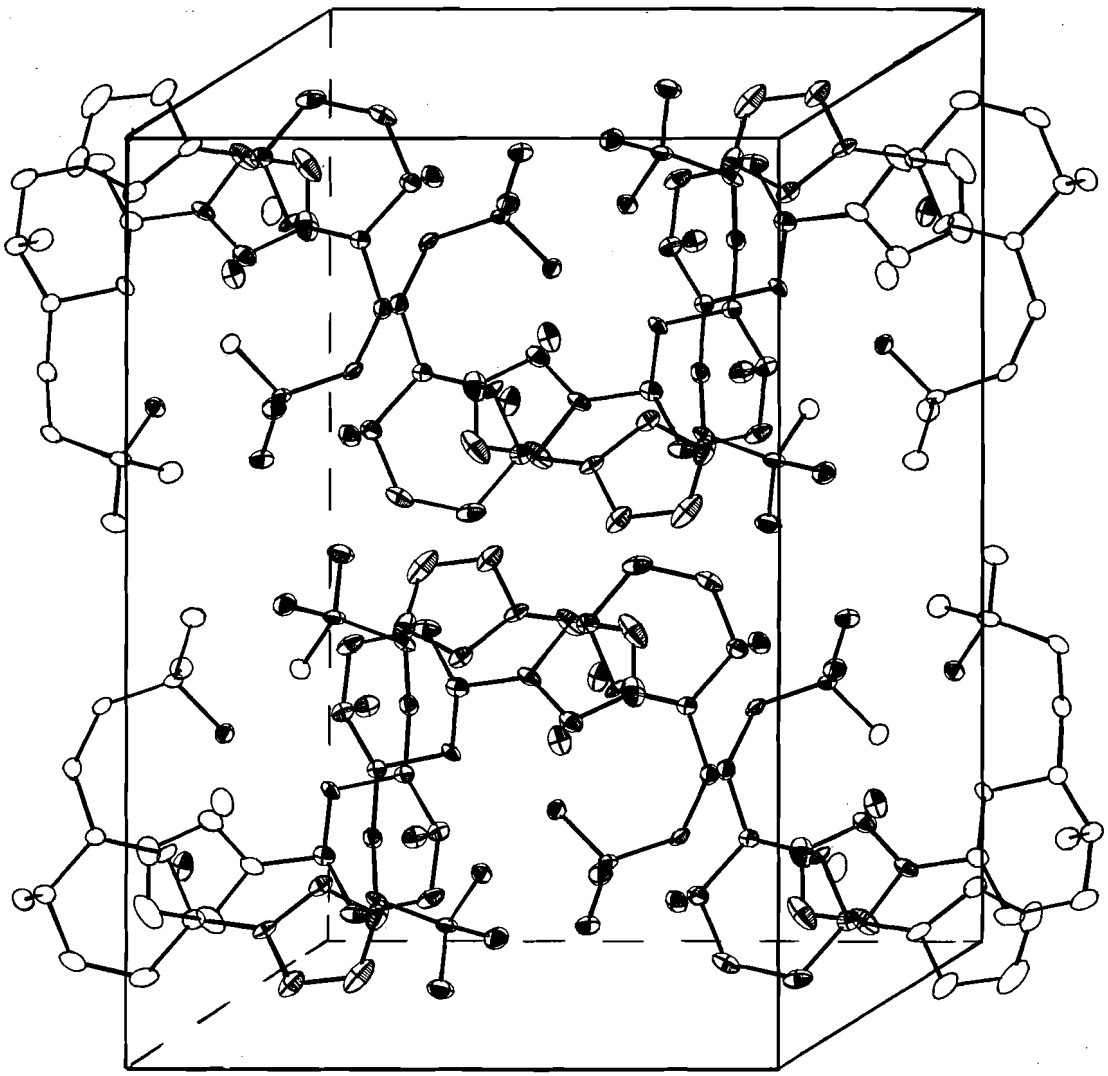

FIG. 1. ORTEP drawing illustrating the packing in the unit cell.

ton (8). The structure calculations were carried out using the Syntex XTL Structure Determination System (NOVA 1200 computer and additional external disk memory).[4] The figures were prepared with Johnson's ORTEP plotting program.

Table 1 contains the final atomic coordinates and anisotropic temperature factors with their standard deviations for non-hydrogen atoms. The final positional and isotropic thermal parameters for hydrogen atoms are listed in Table 2.

[4]The table of structure factors is available, at a nominal charge, from the Depository of Unpublished Data, CISTI, National Research Council of Canada, Ottawa, Canada K1A 0S2.

Description of the Structure and Discussion

The arrangement of molecules in the unit cell is shown in Fig. 1. The structural features of the molecule are illustrated in Fig. 2, while bond distances and angles are collected in Table 3. The furan ring and the side chain are equatorial, whereas the methyl group is axial (compare the distances of appropriate atoms from the plane 2, Table 4). Thus the stereochemistry of the synthetic alkaloid established by X-ray analysis re-

TABLE 3. (*a*) Bond lengths (Å) with e.s.d.'s in parentheses

Bond	Distance (Å)	Bond	Distance (Å)
O(1)–C(14)	1.464(9)	C(6)–C(7)	1.483(13)
O(2)–C(8)	1.359(19)	C(7)–C(8)	1.353(16)
O(2)–C(9)	1.327(17)	C(7)–C(10)	1.410(15)
N(1)–C(2)	1.513(9)	C(9)–C(10)	1.356(18)
N(1)–C(6)	1.504(10)	C(12)–C(13)	1.526(13)
C(2)–C(3)	1.516(12)	C(13)–C(14)	1.519(12)
C(2)–C(12)	1.506(11)	C(14)–C(15)	1.523(13)
C(3)–C(4)	1.519(14)	C(14)–C(16)	1.542(13)
C(3)–C(11)	1.528(12)	O(1)–H(O1)	0.84(5)
C(4)–C(5)	1.539(17)	N(1)–H(N1a)	0.96(6)
C(5)–C(6)	1.524(13)	N(1)–H(N1b)	1.01(5)

(*b*) Bond angles (deg) with e.s.d.'s in parentheses

Bonds	Angle (deg.)	Bonds	Angle (deg.)
N(1)–C(2)–C(3)	109.6(6)	C(8)–C(7)–C(10)	105.3(9)
N(1)–C(2)–C(12)	110.7(6)	C(7)–C(8)–O(2)	109.9(1.0)
C(3)–C(2)–C(12)	114.0(6)	C(8)–O(2)–C(9)	108.1(1.0)
C(2)–C(3)–C(4)	110.1(7)	O(2)–C(9)–C(10)	109.2(1.1)
C(2)–C(3)–C(11)	114.1(7)	C(9)–C(10)–C(7)	107.6(1.0)
C(4)–C(3)–C(11)	112.2(8)	C(2)–C(12)–C(13)	116.2(7)
C(3)–C(4)–C(5)	112.2(9)	C(12)–C(13)–C(14)	119.5(7)
C(4)–C(5)–C(6)	111.2(8)	C(13)–C(14)–C(15)	112.0(7)
C(5)–C(6)–N(1)	107.0(7)	C(13)–C(14)–C(16)	112.6(7)
C(5)–C(6)–C(7)	116.5(7)	C(13)–C(14)–O(1)	111.1(6)
N(1)–C(6)–C(7)	110.1(7)	C(15)–C(14)–C(16)	111.1(8)
C(6)–N(1)–C(2)	113.8(6)	C(15)–C(14)–O(1)	106.3(7)
C(6)–C(7)–C(8)	127.0(9)	C(16)–C(14)–O(1)	103.3(6)
C(6)–C(7)–C(10)	127.8(9)		

mains in good agreement with the results of spectroscopic measurements for natural 3-

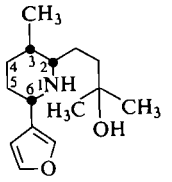

1

epinupharamine **1**. Therefore, it must be concluded that the empirical criterion correlating the changes of chemical shifts with the orientation (axial or equatorial) of the methyl group does not hold for the piperidine system.

The piperidine ring of 3-epinupharamine has a chair conformation with C(6)–N(1)–C(2)–C(3) and C(3)–C(4)–C(5)–C(6) torsion angles being of 55.8° and −56.5°, respectively. The furan ring is planar (within one standard deviation, Table 4) and the dihedral angle between the plane of furan ring and that through C(2), C(4), C(5), and N(1) atoms is 29.8°.

The bond lengths in 3-epinupharamine are similar to those reported in crystal structure determination of related quinolizidine systems (9, 10) and dimeric sulphur Nuphar alkaloids (11). The observed valence angles of the piperidine and furan rings do not differ significantly from those expected for such systems. On the other hand, the C(2)–C(12)–C(13) and C(12)–C(13)–C(14) angles from the side chain are considerably larger than the value characteristic for a tetrahedral arrangement. The distortion found seems to be caused by the strains in seven-membered system formed by N(1), C(2), C(12), C(13), C(14), O(1), and H(N1a) atoms.

The strain imposed by strong, almost linear hydrogen-bonding interaction N(1)–H(N1a)···O(1) results in the increase of bond angles inside this system with the C(2)–C(12)–C(13) and C(12)–C(13)–C(14) angles being the most affected. A similar effect was observed in the maleic acid molecule (12) where the analogical angles differ from the value expected for unstrained molecule by ca. 10°.

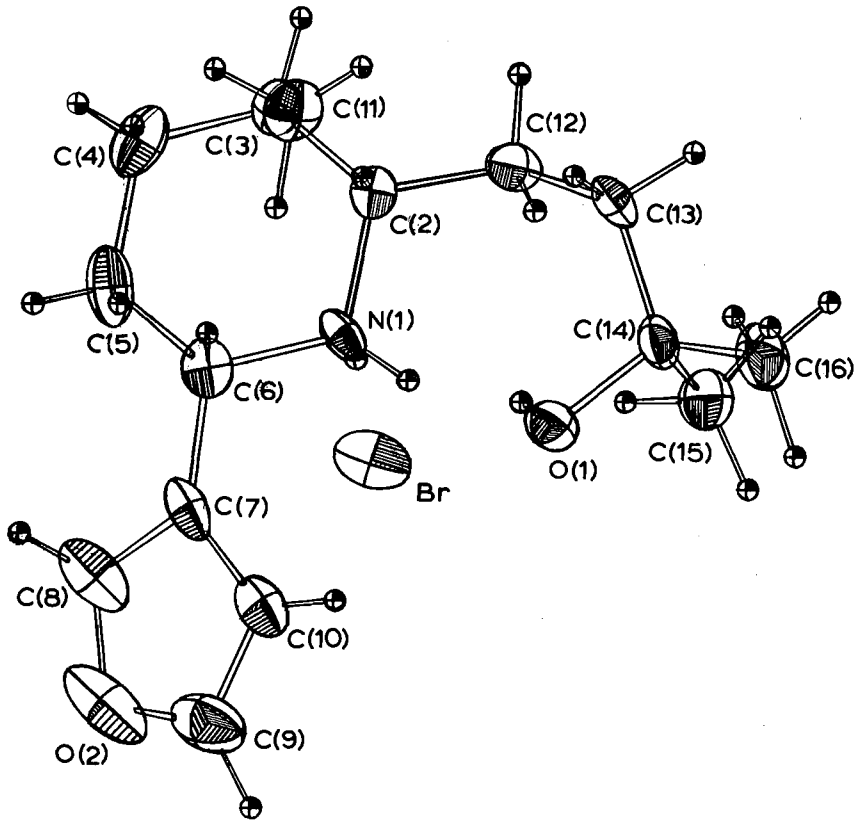

FIG. 2. A molecule of 3-epinupharamine hydrobromide with thermal ellipsoids scaled to include 50% probability. The hydrogen atoms are drawn with an arbitrary isotropic temperature factor.

TABLE 4. Equations of planes and deviations (in Å) of atoms from those planes[a]

Plane *1*: C(7), C(8), C(9), C(10), O(2)

Equation: $0.4427X + 0.0534Y + 0.8951Z = 1.8857$

Atom	Deviation	Atom	Deviation
C(7)*	0.001(9)	C(10)*	0.000(9)
C(8)*	−0.003(10)	O(2)*	0.002(8)
C(9)*	−0.002(12)	C(6)	−0.024(7)

Plane *2*: N(1), C(2), C(4), C(5)

Equation: $0.0406X + 0.0908Y - 0.9950Z = -1.9590$

Atom	Deviation	Atom	Deviation
N(1)*	−0.004(5)	C(11)	−2.187(9)
C(2)*	0.006(7)	C(12)	−0.588(8)
C(4)*	−0.014(10)	C(13)	0.337(8)
C(5)*	0.013(9)	C(14)	0.538(7)
C(3)	−0.669(8)	C(6)	0.716(7)

[a]The angle between plane *1* and plane *2*: 29.8°. Standard deviations are given in parentheses. Atoms used to define the planes are indicated by an asterisk.

There are three unique hydrogen bonds in the structure (Table 4). Each nitrogen atom is linked by an N—H···Br^- bond to the Br^- ion of the nearest neighbour molecule related by the glide plane *c*. The parameters characterizing the geometry of this bond are as follows: N–H 1.01(5) Å, N···Br^- 3.317(5) Å, N–H–Br^- 176(4)°. Another reasonably strong interaction consisting of the Br^- ion is O(1)–H(O1)···Br^-, where both donor and acceptor atom are from the same molecule. The hydroxyl bond length is 0.84(5) Å and the donor–acceptor distance is 3.244(5) Å with an O–H–Br^- angle of 159(4)°.

The O(1) atom is also involved in the intramolecular N(1)–H(N1a)···O(1) bond with the N(1)···O(1) contact being 2.751(8) Å and the N(1)–H(N1a)–O(1) angle (165°) not too much deviated from linearity.

1. J. SZYCHOWSKI, J. T. WRÓBEL, and A. LENIEWSKI. Can. J. Chem. This issue.

2. T. P. FORREST and S. RAY. Can. J. Chem. **49**, 1774 (1971).
3. R. BARCHET and T. P. FORREST. Tetrahedron Lett. 4229 (1965).
4. C. F. WONG and R. T. LALONDE. Phytochemistry, **9**, 1851 (1970).
5. R. T. LALONDE, C. F. WONG, and K. C. DAS. J. Am. Chem. Soc. **95**, 6342 (1973).
6. International tables for X-ray crystallography. Vol. I. Kynoch Press, Birmingham, England. 1965.
7. D. T. CROMER and J. T. WABER. International tables for X-ray crystallography. Vol. IV. Kynoch Press, Birmingham, England. 1974.
8. D. H. TEMPLETON. International tables for X-ray crystallography. Vol. III. Kynoch Press, Birmingham, England. 1962.
9. J. OHRT, R. PARTHASARATHY, R. T. LALONDE, and C. F. WONG. J. Cryst. Mol. Struct. **3**, 3 (1973).
10. K. ODA and H. KOYAMA. J. Chem. Soc. B, 1449 (1970).
11. G. I. BIRNBAUM. Acta Crystallogr. **23**, 526 (1967).
12. M. N. G. JAMES and G. J. B. WILLIAMS. Acta Crystallogr. Sect. B, **30**, 1249 (1974).

Crystal and molecular structure of dodecamethylcyclohexaphosphazene, $(NPMe_2)_6$

RICHARD T. OAKLEY, NORMAN L. PADDOCK, STEVEN J. RETTIG, AND JAMES TROTTER

Department of Chemistry, University of British Columbia, 2075 Wesbrook Mall, Vancouver, B.C., Canada V6T 1W5

Received March 9, 1977

RICHARD T. OAKLEY, NORMAN L. PADDOCK, STEVEN J. RETTIG, and JAMES TROTTER. Can. J. Chem. **55**, 3118 (1977).

Crystals of dodecamethylcyclohexaphosphazene are triclinic, $a = 13.898(1)$, $b = 8.690(1)$, $c = 10.790(1)$ Å, $\alpha = 109.84(1)$, $\beta = 92.01(1)$, $\gamma = 106.39(1)°$, $Z = 2$, space group $P\bar{1}$. The structure was solved by direct methods and was refined by full-matrix least-squares procedures to a final R of 0.034 and R_w of 0.042 for 4217 reflections with $I \geq 3\sigma(I)$. The unit cell contains two independent centrosymmetric molecules which are virtually identical. The 12-membered rings have the 'double tub' conformation. Bond lengths not involving hydrogen have been corrected for libration. Weighted mean bond lengths (rms deviations from the mean in parentheses) are: P—N, 1.593(6), C—P, 1.808(4), and C—H, 0.95(6) Å.

RICHARD T. OAKLEY, NORMAN L. PADDOCK, STEVEN J. RETTIG et JAMES TROTTER. Can. J. Chem. **55**, 3118 (1977).

Les cristaux du dodécaméthylcyclohexaphosphazène sont tricliniques, $a = 13.898(1)$, $b = 8.690(1)$, $c = 10.790(1)$ Å, $\alpha = 109.84(1)$, $\beta = 92.01(1)$, $\gamma = 106.39(1)°$, $Z = 2$, groupe d'espace $P\bar{1}$. On a résolu la structure par les méthodes directes et on l'a affinée par la méthode des moindres carrés (matrice complète) jusqu'à une valeur finale de R de 0.034 et de R_w de 0.042 pour 4217 réflexions avec $I \geq 3\sigma(I)$. La maille unitaire contient deux molécules centrosymétriques indépendantes qui sont pratiquement identiques. Les cycles à 12 chaînons ont la conformation "double bateau". On a corrigé les longueurs de liens n'impliquant pas les hydrogènes pour la libration. Les longueurs de liaison moyennes (la déviation rms de la moyenne est indiquée entre parenthèse) sont P—N, 1.593(6), C—P, 1.808(4) et C—H, 0.95(6) Å.

[Traduit par le journal]

Introduction

This report is the third in a series dealing with the crystal structures of large ring methylphosphazenes $(NPMe_2)_n$ $(n \geq 6)$. The two previous papers in this series dealt with the structures of the heptameric (1) and octameric (2) methylphosphazenes $(NPMe_2)_7$ and $(NPMe_2)_8$. The structure of the hexamer, $(NPMe_2)_6$, is the topic of the present report.

Experimental

Dodecamethylcyclohexaphosphazene was prepared as previously described (1). Crystals suitable for X-ray analysis were obtained by recrystallization from *p*-xylene. The crystal chosen for study was mounted with (1 1 1) perpendicular to the goniostat axis and had dimensions of ca. 0.30 × 0.44 × 0.56 mm. Unit-cell and space group data were obtained from film and diffractometer measurements. The unit-cell parameters were refined by a least squares on 2 sin θ/λ values for 50 reflections measured on a diffractometer with CuKα radiation (λ = 1.5418 Å). Crystal data (at 22°C) are:

$C_{12}H_{36}N_6P_6$ fw = 450.3

Triclinic, $a = 13.898(1)$, $b = 8.690(1)$, $c = 10.790(1)$ Å, $\alpha = 109.84(1)$, $\beta = 92.01(1)$, $\gamma = 106.39(1)°$, $V = 1164.4$ (2) Å^3, $\rho_m = 1.26$ (flotation in aqueous KI), $Z = 2$, $\rho_c = 1.284$ g cm^{-3}, $F(000) = 480$, μ(CuKα) = 43.0 cm^{-1}. Absent reflections: none. Space group $P\bar{1}$ (C_i^1, No. 2).

Intensities were measured with nickel-filtered CuKα radiation on a Datex-automated General Electric XRD-6 diffractometer. A θ–2θ scan at 4° min^{-1} over a range of (1.80 + 0.86 tan θ) degrees in 2θ was employed; 10 s background counts were measured at each end of the scan. Data were measured to 2θ = 160°. The intensities of the check reflections, measured every 50 reflections throughout the data collection, decreased slowly to a value which was 0.758 times the initial value. The structure amplitudes were derived and an absorption correction was applied by a computer program using a Gaussian integration method (3, 4). Transmission factors ranged from 0.190 to 0.410. Of the 5086 independent reflections measured, 4242 had intensities greater than $3\sigma(I)$ above background where $\sigma^2(I) = S + B + (0.06S)^2$ with S = scan count and B = time averaged background count. These reflections were used in the solution and refinement of the structure.

The centrosymmetric space group $P\bar{1}$ was indicated by the E statistics. The structure was solved by direct methods (5). All the P and N atoms and 4 of the 12 carbon atoms were located on an E map. The structure was found to consist of two independent molecules lying around inversion centres. These atoms were refined isotropically for two cycles giving $R = 0.248$. The remaining carbon atoms were found on a difference map at this point. The non-hydrogen atoms were refined isotropically for two cycles, and then anisotropically for

two cycles, reducing R to 0.079. The positions of all 36 hydrogen atoms were determined from a difference map. The entire structure (full-matrix, including hydrogen atoms with isotropic thermal parameters) was refined for eight cycles giving a final R of 0.034 and R_w of 0.042 for 4207 reflections with $I \geq 3\sigma(I)$ (35 observed reflections which had $|F_o| - |F_c| > 3\sigma(F)$ were treated as unobserved in the final stages of refinement; instrumental error was suspected for these reflections, but it seemed unwise to bias the data by remeasuring them; none of the disagreements were exceptionally bad). For all 5086 reflections $R = 0.044$ and $R_w = 0.045$.

The least-squares refinement was based on the minimization of $\Sigma w[|F_o| - |F_c/(1 + gI)|]^2$ where g is the extinction parameter and I the uncorrected intensity. The final value of g was $1.56(8) \times 10^{-7}$. The scattering factors of ref. 6 were used for the non-hydrogen atoms and those of ref. 7 for the hydrogen atoms. Anomalous scattering factors from ref. 8 were used for the non-hydrogen atoms. The weighting scheme $w = 1.00$ if $|F_o| < 16.0$, $w = (16.0/|F_o|)^2$ if $|F_o| \geq 16.0$, and $w = 0.0625$ for the unobserved reflections gave uniform average values of $w(|F_o| - |F_c|)^2$ over ranges of $|F_o|$ and was employed in the final stages of refinement.

On the final cycle of refinement the mean parameter shift was 0.04σ, with no shift greater than 0.4σ. The mean error in an observation of unit weight was 0.4819. The final positional and thermal parameters appear in Tables 1 and 2[1] respectively. Measured and calculated structure factors have been placed in the Depository of Unpublished Data.[1]

The ellipsoids of thermal motion for the non-hydrogen atoms are shown in Fig. 1. The thermal motion has been analysed in terms of the rigid-body modes of translation (**T**), libration (**L**), and screw (**S**) motion (9) using the computer program MGTLS. The rms standard error in the temperature factors σU_{ij} (derived from the least-squares analysis) is 0.0012 Å^2. Analyses of the entire molecules as rigid bodies were unsuccessful, but each of the independent phosphorus tetrahedra behaves as a rigid body (rms $\Delta U_{ij} = 10, 10, 10, 10, 9$, and 9×10^{-4} Å^2 for P(1) to P(6) respectively).

The appropriate bond distances have been corrected for libration (10, 11), using shape parameters q^2 of 0.08 for all atoms involved. Corrected bond lengths appear in Table 3 along with the uncorrected values. Corrected angles differ by no more than $\pm 0.1°$ from the uncorrected values given in Table 4.

Results and Discussion

Figure 1 shows general views of the two independent molecules with the crystallographic numbering scheme and Fig. 2 shows the packing arrangement viewed down the b^* axis. The unique intra-annular torsion angles in the 12-membered rings are given in Table 5 and the mean structural parameters for $(NPMe_2)_6$ are compared with those of the related molecules $(NPMe_2)_4$ (12), $(NPMe_2)_5$ (13), $(NPMe_2)_7$ (1), and $(NPMe_2)_8$ (2) in Table 6.

[1]The structure factor table and Table 2 (thermal parameters) are available, at a nominal charge, from the Depository of Unpublished Data, CISTI, National Research Council of Canada, Ottawa, Canada K1A 0S2.

TABLE 1. Final positional parameters (fractional, N, and C × 10^4, P × 10^5, H × 10^3) with estimated standard deviations in parentheses

Atom	x	y	z
P(1)	61811(4)	62400(7)	38181(5)
P(2)	44179(4)	35228(7)	20243(5)
P(3)	41869(4)	15030(6)	37076(5)
P(4)	3635(4)	80593(6)	9568(4)
P(5)	−14544(3)	29391(6)	13233(4)
P(6)	1651(4)	61331(6)	27044(4)
N(1)	5563(1)	4594(3)	2587(2)
N(2)	3818(1)	2164(3)	2632(2)
N(3)	4471(1)	2771(2)	5223(2)
N(4)	777(1)	8000(2)	−399(2)
N(5)	−970(1)	4884(2)	2308(2)
N(6)	685(1)	6900(2)	1662(2)
C(1)	7042(2)	5627(5)	4688(3)
C(2)	6999(3)	7661(5)	3139(4)
C(3)	4409(3)	2354(5)	286(3)
C(4)	3670(3)	4912(5)	2038(4)
C(5)	5267(3)	779(5)	3308(3)
C(6)	3188(3)	−444(4)	3528(3)
C(7)	−986(2)	7546(4)	639(3)
C(8)	801(3)	10287(3)	2043(2)
C(9)	−1888(2)	1675(3)	2333(3)
C(10)	−2592(2)	2813(4)	399(3)
C(11)	1030(2)	5181(4)	3203(3)
C(12)	132(2)	7827(3)	4226(2)
H(1*a*)	749(3)	520(4)	402(3)
H(1*b*)	743(3)	663(5)	543(4)
H(1*c*)	656(3)	466(5)	497(4)
H(2*a*)	726(3)	707(5)	261(4)
H(2*b*)	653(4)	790(6)	257(5)
H(2*c*)	745(3)	864(6)	386(4)
H(3*a*)	372(3)	185(5)	−11(4)
H(3*b*)	475(3)	319(5)	−9(4)
H(3*c*)	480(3)	159(6)	19(4)
H(4*a*)	302(3)	421(5)	160(4)
H(4*b*)	368(3)	560(5)	293(4)
H(4*c*)	391(3)	557(5)	154(4)
H(5*a*)	539(3)	25(5)	398(4)
H(5*b*)	514(3)	4(5)	236(4)
H(5*c*)	580(2)	172(4)	339(3)
H(6*a*)	335(3)	−91(5)	408(4)
H(6*b*)	258(5)	0(7)	389(6)
H(6*c*)	302(3)	−113(6)	272(5)
H(7*a*)	−108(3)	830(5)	31(3)
H(7*b*)	−129(2)	634(4)	3(3)
H(7*c*)	−126(2)	768(4)	146(3)
H(8*a*)	49(2)	1091(4)	167(3)
H(8*b*)	60(3)	1031(4)	280(4)
H(8*c*)	157(2)	1068(4)	206(3)
H(9*a*)	−231(2)	205(4)	287(3)
H(9*b*)	−222(2)	54(4)	181(3)
H(9*c*)	−130(3)	181(4)	286(3)
H(10*a*)	−293(2)	340(4)	101(3)
H(10*b*)	−240(2)	337(4)	−15(3)
H(10*c*)	−294(2)	161(4)	−21(3)
H(11*a*)	167(3)	602(4)	349(3)
H(11*b*)	74(2)	481(4)	395(3)
H(11*c*)	108(2)	437(4)	247(3)
H(12*a*)	84(2)	866(4)	454(3)
H(12*b*)	−32(2)	842(4)	397(3)
H(12*c*)	−14(2)	732(4)	487(3)

TABLE 3. Bond lengths (Å) with estimated standard deviations in parentheses

(*a*) Non-hydrogen atoms

Bond	Distance		Bond	Distance	
	Uncorrected	Corrected		Uncorrected	Corrected
P(1)—N(1)	1.577(2)	1.585	P(4)—N(4)	1.582(2)	1.588
P(1)—N(3)′	1.591(2)	1.598	P(4)—N(6)′	1.595(2)	1.600
P(2)—N(1)	1.575(2)	1.584	P(5)—N(4)	1.579(2)	1.586
P(2)—N(2)	1.590(2)	1.599	P(5)—N(5)	1.590(2)	1.597
P(3)—N(2)	1.587(2)	1.594	P(6)—N(5)	1.588(2)	1.594
P(3)—N(3)	1.592(2)	1.599	P(6)—N(6)	1.590(2)	1.596
P(1)—C(1)	1.794(3)	1.804	P(4)—C(7)	1.794(3)	1.801
P(1)—C(2)	1.799(3)	1.810	P(4)—C(8)	1.799(2)	1.807
P(2)—C(3)	1.803(3)	1.814	P(5)—C(9)	1.801(2)	1.809
P(2)—C(4)	1.798(3)	1.808	P(5)—C(10)	1.797(3)	1.805
P(3)—C(5)	1.797(3)	1.806	P(6)—C(11)	1.799(2)	1.806
P(3)—C(6)	1.806(3)	1.814	P(6)—C(12)	1.808(2)	1.815

(*b*) Bonds involving hydrogen atoms

Bond	Range	Weighted mean
Me—H	0.81–1.06(3–6)	0.95(6)

TABLE 4. Bond angles (deg) with estimated standard deviations in parentheses

(*a*) Non-hydrogen atoms

Bonds	Angle (deg)	Bonds	Angle (deg)
N(1) —P(1)—N(3)′	116.1(1)	N(4) —P(4)—N(6)′	116.3(1)
N(1) —P(1)—C(1)	107.7(1)	N(4) —P(4)—C(7)	106.9(1)
N(1) —P(1)—C(2)	105.9(1)	N(4) —P(4)—C(8)	106.0(1)
N(3)′—P(1)—C(1)	112.6(1)	N(6)′—P(4)—C(7)	112.0(1)
N(3)′—P(1)—C(2)	109.9(1)	N(6)′—P(4)—C(8)	110.2(1)
C(1) —P(1)—C(2)	103.7(2)	C(7) —P(4)—C(8)	104.7(2)
N(1) —P(2)—N(2)	120.2(1)	N(4) —P(5)—N(5)	119.7(1)
N(1) —P(2)—C(3)	105.1(1)	N(4) —P(5)—C(9)	104.9(1)
N(1) —P(2)—C(4)	111.2(2)	N(4) —P(5)—C(10)	112.2(1)
N(2) —P(2)—C(3)	107.2(1)	N(5) —P(5)—C(9)	107.0(1)
N(2) —P(2)—C(4)	107.3(1)	N(5) —P(5)—C(10)	107.2(1)
C(3) —P(2)—C(4)	104.8(2)	C(9) —P(5)—C(10)	104.6(1)
N(2) —P(3)—N(3)	118.7(1)	N(5) —P(6)—N(6)	119.2(1)
N(2) —P(3)—C(5)	112.1(1)	N(5) —P(6)—C(11)	112.7(1)
N(2) —P(3)—C(6)	105.0(1)	N(5) —P(6)—C(12)	103.6(1)
N(3) —P(3)—C(5)	105.7(1)	N(6) —P(6)—C(11)	105.2(1)
N(3) —P(3)—C(6)	110.7(1)	N(6) —P(6)—C(12)	111.3(1)
C(5) —P(3)—C(6)	103.6(2)	C(11)—P(6)—C(12)	103.8(1)
P(1) —N(1)—P(2)	137.5(1)	P(4) —N(4)—P(5)	137.3(1)
P(2) —N(2)—P(3)	131.2(1)	P(5) —N(5)—P(6)	131.9(1)
P(3) —N(3)—P(1)′	130.4(1)	P(6) —N(6)—P(4)′	130.4(1)

(*b*) Angles involving hydrogen atoms

Bonds	Range	Weighted mean
P—C—H	104—113(2–3)	107(2)
H—C—H	103—121(2–4)	111(4)

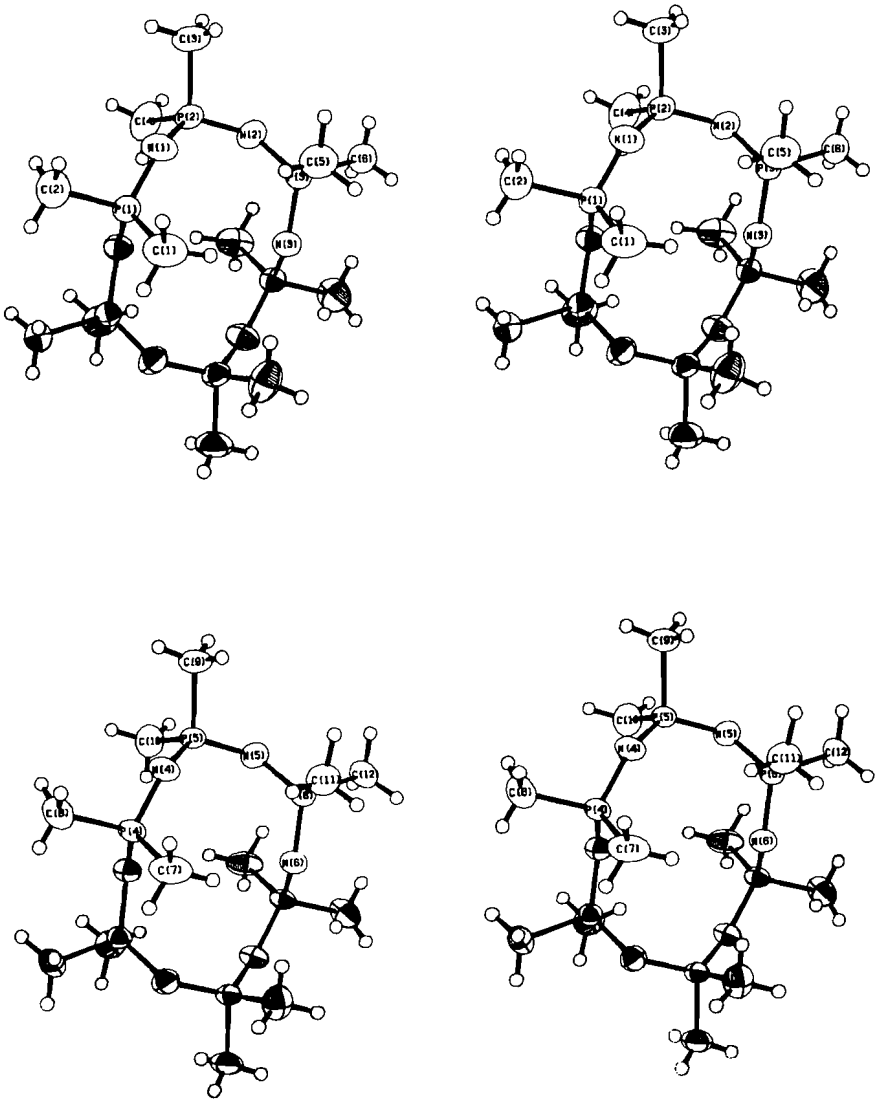

FIG. 1. Stereo views of the dodecamethylcyclohexaphosphazene molecules 1 (top) and 2 (bottom); 50% ellipsoids are shown for the non-hydrogen atoms. Hydrogen atoms have been assigned artificially small thermal parameters for the sake of clarity.

The crystal structure consists of well-separated molecules of dodecamethylcyclohexaphosphazene (see Fig. 2). The shortest non-bonded intermolecular distance (H(2*a*)...H(7*c*)[1 + *x*, *y*, *z*] = 2.46(5) Å) corresponds to a normal van der Waals interaction. The unit cell contains two independent centrosymmetric molecules. Molecule 1 is located at the crystallographic centre of symmetry ($\frac{1}{2}$, $\frac{1}{2}$, $\frac{1}{2}$) and molecule 2 at (0, $\frac{1}{2}$, 0). The two independent molecules are virtually identical; corresponding bond lengths are equal within experimental error while there are some small, but significant, differences between corresponding bond angles and torsion angles. The corresponding parameters are listed side by side in Tables 3–5 for comparison. Packing forces are believed to be responsible for the minor differences between the two molecules.

Both molecules have a 'double tub' conformation closely resembling that of the centro-

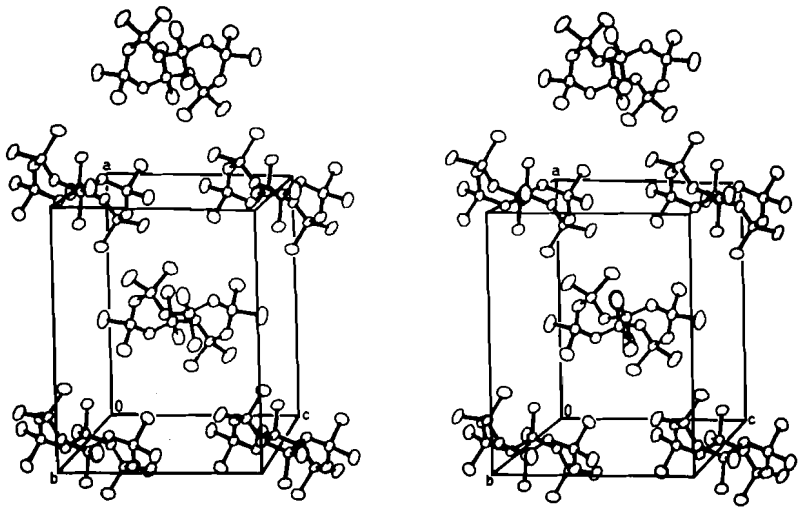

FIG. 2. The packing arrangement viewed down b^*.

TABLE 5. Intra-annular torsion angles (deg)

Bond	Observed	Bond	Observed
P(1)—N(1)	−3.8(1)	P(4)—N(4)	−0.5(1)
N(1)—P(2)	−80.0(1)	N(4)—P(5)	−79.6(1)
P(2)—N(2)	−5.8(1)	P(5)—N(5)	−7.8(1)
N(2)—P(3)	72.0(1)	N(5)—P(6)	73.2(1)
P(3)—N(3)	56.4(1)	P(6)—N(6)	59.0(1)
N(3)—P(1)′	−157.8(2)	N(6)—P(4)′	−157.1(1)

TABLE 6. Mean structural parameters for $(NPMe_2)_n$ (n = 4–8) (distances in Å and angles in deg)*

	$n = 4$	$n = 5$	$n = 6$	$n = 7$	$n = 8$
P—C	1.804(3)	1.801(4)	1.808(4)	1.804(11)	1.811(2)
P—N	1.596(5)	1.586(4)	1.593(6)	1.592(6)	1.590(13)
N—P—N	119.8(2)	118.7(18)	118.3(18)	117.1(16)	117.2(21)
P—N—P	132.0(2)	132.9(17)	133.1(34)	132.9(20)	139.9(84)
C—P—C	104.1(2)	104.3(8)	104.2(5)	103.9(5)	103.5(10)

*Root mean square deviations from the mean (in units of the last figure shown) in parentheses.

symmetric molecule $[NP(OMe)_2]_6$ (14). The mean intra-annular torsion angles in $(NPMe_2)_6$ differ from those in $[NP(OMe)_2]_6$ by no more than 17.2° (mean deviation = 7.3°). The conformation of the 12-membered rings is qualitatively similar to that found for $[NP(NMe_2)_2]_6$ (15) which has $\bar{3}$ symmetry and torsion angles which are alternately 17 and 97°. The local conformations (14, 16) at the phosphorus atoms are CT for P(1) and P(4), GG for P(2) and P(5), and GT for P(3) and P(6). The energetically less favorable CT conformation (14) does not occur in the larger, less-restricted rings of $(NPMe_2)_{7 \text{ and } 8}$ (1, 2).

The mean structural parameters of the methylphosphazenes in Table 6 show that the P—C and P—N bond lengths and the C—P—C angles are nearly the same in all five molecules. The N—P—N angles appear to be decreasing toward a limiting value with increasing n. The mean P—N—P angles span a range of about 8° for $(NPMe_2)_{4-8}$ and show large variations between the independent values found for each molecule (with the exception of the tetramer which has

crystallographic $\bar{4}$ symmetry). Ring strain resulting from steric and/or electronic forces in the phosphazenes is relieved primarily by distortions of the P—N—P angles. The σ-bonding orbitals at N have a high *s* component (confirmed by X_α calculations[2]), which would make them less directional. Large angles at nitrogen are therefore often associated with a large variability of the angle, as found in the structure of $[NP(NMe_2)_2]_8$ (17) where the P—N—P angles range from 145.9 (4) to 170.2(5)°.

The geometry involving hydrogen atoms is as expected for X-ray data. The weighted mean C—H distance is 0.95(6) Å and weighted mean P—C—H and H—C—H angles are 107(2) and 111(4)° respectively.

Acknowledgments

We thank the National Research Council of Canada for financial support and the University of British Columbia Computing Centre for assistance.

1. K. D. GALLICANO, R. T. OAKLEY, N. L. PADDOCK, S. J. RETTIG, and J. TROTTER. Can. J. Chem. **55**, 304 (1977).
2. R. T. OAKLEY, N. L. PADDOCK, S. J. RETTIG, and J. TROTTER. Can. J. Chem. **55**, 2530 (1977).
3. P. COPPENS, L. LEISEROWITZ, and D. RABINOVICH. Acta Crystallogr. **18**, 1035 (1965).
4. W. R. BUSING and H. A. LEVY. Acta Crystallogr. **22**, 457 (1967).
5. R. E. LONG. Ph.D. Thesis, University of California at Los Angeles. 1965.
6. D. T. CROMER and J. B. MANN. Acta Crystallogr. Sect. A, **24**, 321 (1968).
7. R. F. STEWART, E. R. DAVIDSON, and W. T. SIMPSON. J. Chem. Phys. **42**, 3175 (1965).
8. D. T. CROMER and D. LIBERMAN. J. Chem. Phys. **53**, 1891 (1970).
9. V. SCHOMAKER and K. N. TRUEBLOOD. Acta Crystallogr. Sect. B, **24**, 63 (1969).
10. D. W. J. CRUICKSHANK. Acta Crystallogr. **9**, 747 (1956); **9**, 754 (1956).
11. D. W. J. CRUICKSHANK. Acta Crystallogr. **14**, 896 (1961).
12. M. W. DOUGILL. J. Chem. Soc. 5471 (1961).
13. M. W. DOUGILL and B. SHELDRICK. Acta Crystallogr. Sect. B, **33**, 295 (1977).
14. M. W. DOUGILL and N. L. PADDOCK. J. Chem. Soc. Dalton Trans. 1022 (1974).
15. A. J. WAGNER and A. VOS. Acta Crystallogr. Sect. B, **24**, 1423 (1968).
16. S. MIZUSHIMA. Structure of molecules and internal rotation. Academic Press, NY. 1954.
17. H. P. CALHOUN, N. L. PADDOCK, and J. TROTTER. J. Chem. Soc. Dalton Trans. 38 (1976).

[2]L. Noodleman. Unpublished results.

Behavior of hydrogen atoms in the fragmentation of CH_3CD_3

ISAO H. SUZUKI AND KOGORO MAEDA
Electrotechnical Laboratory, Tanashi, Tokyo, Japan

Received February 17, 1977

ISAO H. SUZUKI and KOGORO MAEDA. Can. J. Chem. **55**, 3124 (1977).

The behavior of hydrogen atoms in the fragmentation of CH_3CD_3 has been studied by use of a monoenergetic electron beam. Ionization efficiency curves for ions (*m/e* 3, 4, 15 to 18, 26 to 33) from CH_3CD_3 have been measured over ranges of 12 to 30 eV near their appearance thresholds. Mass spectra over various ranges of *m/e* have been measured at several electron energies. It has been found that at least two processes participate in the formation of $C_2X_4^+$ and CH_3^+ (X = H or D) and the rates of these processes depend on the energy of electron beam. The formations of $C_2X_2^+$ and X_2^+ are independent of the electron energy.

ISAO H. SUZUKI et KOGORO MAEDA. Can. J. Chem. **55**, 3124 (1977).

On a étudié le comportement des atomes d'hydrogène dans la fragmentation de CH_3CD_3 en faisant appel à un faisceau d'électrons monoénergétiques. On a mesuré les courbes d'efficacité d'ionisation pour les ions (3, 4, 15 à 18, 26 à 33 *m/e*) pour CH_3CD_3 à des potentiels d'ionisation de 12 à 30 eV près de leur point d'apparition. On a mesuré les spectres de masse à diverses valeurs de *m/e* à plusieurs énergies des électrons. On a trouvé qu'au moins deux processus participent à la formation de $C_2X_4^+$ et CH_3^+ (X = H ou D) et les vitesses de ces processus dépendent de l'énergie du faisceau d'électrons. Les formations de $C_2X_2^+$ et X_2^+ sont indépendantes de l'énergie des électrons.

[Traduit par le journal]

Introduction

Many studies have been carried out on the ionization and fragmentation of ethane using mass spectra and appearance potentials (AP) of the fragment ions. Photoionization mass spectrometry provided reliable AP's for ions produced at relatively low energy (1) and a photoelectron–photoion coincidence method (2, 3) examined the quasi-equilibrium theory (4, 5) with respect to the fragmentation of the ethane ion. The theory was also compared with the breakdown curve obtained by an ion impact technique (6).

Amenomiya and Pottie measured mass spectra of normal and nine deuterated ethanes generated by 70 eV electrons and found that at least two processes contribute to the formation of $C_2X_4^+$ (X = H or D) and of CX_3^+ (7, 8). By observing metastable transitions Löhle and Ottinger reported that $C_2X_4^+$ is produced only through the detachment of two hydrogen atoms from different carbon atoms near the threshold and that CX_3^+ is produced from $C_2X_6^+$ via two processes: simple breaking of the C—C bond and hydrogen scrambling followed by bond breaking (9). The former finding is in agreement with the result by Lifshitz and Sternberg (10). Von Koch observed $C_2HD_3^+$ and $C_2H_3D^+$ from CH_3CD_3 by impact of Ar^+ but was unable to detect these ions with ground state Xe^+(6). Moreover, he found that the intensity ratios of CX_3^+ (*m/e* 15–18) by Ne^+ and He^+ impacts were different from each other (6).

The above results are summarized as follows. The mechanism of $C_2X_4^+$ formation depends upon the internal energy of $C_2X_6^+$; at least two processes participate and the thresholds of the two processes are different. The mechanism of CX_3^+ formation also depends on the internal energy.

In order to obtain more precise information on the formation of these ions, it is important to determine the thresholds more accurately and to clarify the energy dependence of the fragmentation mechanisms. In the present study ionization efficiency curves of $C_2X_4^+$ and CX_3^+ from CH_3CD_3 were measured over ranges of about 15 eV near their appearance thresholds by use of a monoenergetic electron beam. Mass spectra were measured at several electron energies and over several ranges of *m/e*. The formation of these ions was discussed on the basis of their energy dependences and isotope distributions. Similar studies were carried out on the formation of $C_2X_2^+$ and X_2^+. A total ionization efficiency curve of CH_3CD_3 was calculated from the intensity ratio and ionization efficiency curves for all ions.

Experimental

Measurements were made using the apparatus described in previous papers (11, 12). In observing the ionization efficiency curve each memory channel in the pulse height analyzer was assigned to each electron energy, while in observing the mass spectra the memory channels were used as a mass scale. The energy of the bombarding electron beam (f.w.h.m.: 0.15 eV) was scanned from 10 to 23 eV with 0.05 eV intervals for most ions measured (*m/e* 15, 18, 26 to 33). The energy was scanned from 12 to 30 eV with 0.1 eV intervals for ions of *m/e* 16 and 17, and scanned from 20 to 50 eV with 0.2 eV intervals for ions of *m/e* 3 and 4. Ion counts of about 40 cps were obtained for ions of *m/e* 30 at 23 eV and noise counts were less than 0.05 cps.

The electron energy was calibrated by using the 14.00 eV threshold of Kr. Ionization efficiency curves were processed by a computer to check reproducibility and to estimate a standard deviation at every energy (13). Error bars in the figures given in this paper were calculated from these standard deviations.

The ethane-1,1,1-d_3 (Merck Sharp & Dohme Co., Ltd., isotopic purity 98%) was introduced at about 1.7×10^{-5} Torr. No correction for isotopic purity was carried out in this study.

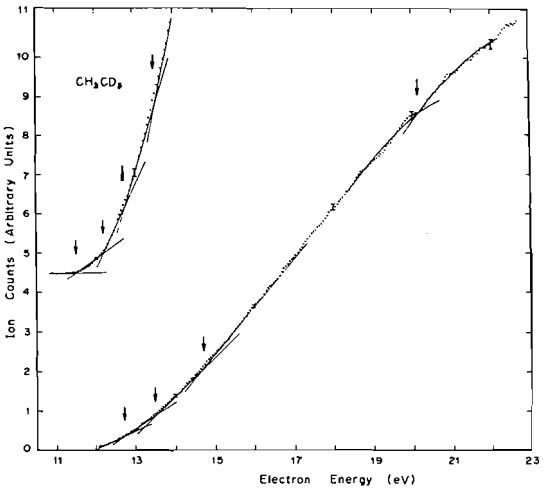

FIG. 1. Total ionization efficiency curve of CH_3CD_3. The curve near threshold is shown with an expanded scale in the upper part of the figure. Bars indicate statistical errors calculated from the standard deviations obtained in the data-processing of ionization efficiency curves.

Results

Total Ionization Efficiency Curve

A total ionization efficiency curve of CH_3CD_3 is shown over a range of bombarding electron energy from 11 to 22 eV in Fig. 1. This curve is a sum of the intensities of the ions *m/e* 15, 18, and 26 to 34. The mass discrimination effect in the present experimental system was not taken into account for the lack of established mass spectrum of CH_3CD_3 but the effect on the curve is expected to be quite small (13). The upper curve with an expanded scale indicates an onset at 11.5 eV followed by breaks at 12.2, 12.7, and 13.5 eV, slightly different from those of C_2H_6 (13). Breaks at 14.7 and 20.1 eV are supposed to correspond to third and fourth electronic states of ethane ion as seen in the case of C_2H_6 (13–16).

Ionization and Appearance Potentials

Table 1 shows IP's of CH_3CD_3 and AP's of the fragment ions including two carbon atoms from CH_3CD_3 as well as the corresponding values for C_2H_6 (13). There is no indication of an ion-pair process in the ionization efficiency curve for $C_2H_3D_2^+$ (*m/e* 31). This is probably due to the smearing out by the tailing of $C_2HD_3^+$ toward low energy and by the ethylene ion $^{13}CCH_2D_2^+$. The AP's of the ions of *m/e* 29 and 30 indicate those by $C_2X_4^+$ (X = H or D) because the vinyl ion $C_2H_3^+$ has a considerably higher AP (13). It is important to note that the $C_2H_3D^+$ produced through the detachment of two hydrogen atoms from the same carbon atom has a higher AP than the $C_2H_2D_2^+$ produced through the detachment of two hydrogen atoms from different carbon atoms. (The difference between these AP's was suggested to be 0.8 eV by Lorquet and Lorquet (22).) The AP of $C_2HD_3^+$ (*m/e* 31) is assumed to be equal to that of $C_2H_3D^+$ because both ions are produced through the same detachment process. Since $C_2H_3^+$ is responsible for the AP of 14.9 eV for *m/e* 27, the AP for C_2HD^+ is presumed to be close to that for $C_2H_2^+$, 15.5 eV.

Table 2 shows AP's of the fragment ions including one or no carbon atom from CH_3CD_3 and from C_2H_6 (13). Since CX_2^+ and CX_4^+ are lower in intensity and have higher AP's than CX_3^+, the CX_3^+ ion is responsible for AP's of ions of *m/e* 15 to 18. There is no indication of an ion-pair process in the ionization efficiency curve for CH_3^+ unlike that for CD_3^+. The two ions CH_3^+ and CD_3^+ produced through the simple breaking of C—C bond have lower AP's than CHD_2^+ and CH_2D^+ produced through the breaking of C—C bond after rearrangement of hydrogens. D'Or and co-workers measured the AP's of CX_3^+ from CH_3CD_3 by using the vanishing current method and found that the AP's of CX_3^+ from CH_3CD_3 and also from C_2H_6 were all equal to one another within their

TABLE 1. Ionization potentials of CH_3CD_3 and appearance potentials for the fragment ions with two carbon atoms from CH_3CD_3 (in units of eV). The table includes the corresponding values for C_2H_6 given in ref. 13

	CH_3CD_3				C_2H_6			
m/e	Species	IP or AP			Species	IP or AP		
33	$C_2H_3D_3^+$	11.5 ± 0.1	14.7 ± 0.1	20.1 ± 0.2	$C_2H_6^+$	11.5 ± 0.1	14.6 ± 0.1	20.0 ± 0.2
32	$C_2H_2D_3^+$	12.2 ± 0.1*	12.6 ± 0.1		$C_2H_5^+$	12.0 ± 0.1*	12.5 ± 0.1	
31	$C_2H_3D_2^+$, $C_2HD_3^+$	12.1 ± 0.1						
30	$C_2D_3^+$, $C_2H_2D_2^+$	12.1 ± 0.1			$C_2H_4^+$	12.1 ± 0.1		
29	$C_2HD_2^+$, $C_2H_3D^+$	12.5 ± 0.15						
28	$C_2H_2D^+$, $C_2D_2^+$	14.9 ± 0.15			$C_2H_3^+$	14.6 ± 0.1		
27	$C_2H_3^+$, C_2HD^+	14.9 ± 0.2			$C_2H_2^+$	14.7 ± 0.1		
26	C_2D^+, $C_2H_2^+$	15.5 ± 0.3						
25	C_2H^+				C_2H^+	25.6 ± 0.2		
24	C_2^+				C_2^+	31.5 ± 0.2		

*Denotes ion-pair process.

TABLE 2. Appearance potentials for the fragment ions with one or no carbon atom from CH_3CD_3 (in units of eV). The table includes the corresponding values for C_2H_6 given in ref. 13

	CH_3CD_3			C_2H_6		
m/e	Species	AP		Species	AP	
19	CHD_3^+			CH_4^+	20.4 ± 0.3	
18	$CH_2D_2^+$, CD_3^+	14.6 ± 0.3*	15.5 ± 0.3	CH_3^+	14.1 ± 0.1*	14.9 ± 0.1
17	CH_3D^+, CHD_2^+		16.9 ± 0.5			
16	CD_2^+, CH_2D^+		17.0 ± 0.5			
15	CHD^+, CH_3^+		15.4 ± 0.3			
14	CH_2^+, CD^+			CH_2^+	17.3 ± 0.15	
13	CH^+			CH^+	26.7 ± 0.5	
12	C^+			C^+	29.6 ± 0.2	
4	D_2^+	35.2 ± 0.8				
3	HD^+	35.2 ± 0.8		H_2^+	35.0 ± 0.5	
2	H_2^+, D^+					
1	H^+			H^+	23.5 ± 0.5	

*Denotes ion-pair process.

experimental accuracy (17). In the present study, all ions of CX_3^+ from CH_3CD_3 have slightly higher AP's than CH_3^+ from C_2H_6. Appearance potentials for X_2^+ from CH_3CD_3 agree with that for H_2^+ from C_2H_6 within experimental accuracy.

Intensity Ratio of Ions

Several measurements have been reported on the mass spectra of CH_3CD_3 at 50–75 eV, but the results are not always in agreement with one another (7, 9, 18–20). In the present study mass spectra of CH_3CD_3 were measured at several electron energies and over various ranges of *m/e*. Our results are the closest to those of Stief and Ausloos (20). The intensity ratio of ions obtained at 22.7 eV is shown in Table 3 as well as that of C_2H_6 at 22.6 eV without correction for mass discrimination. Most intense is the ion of *m/e* 30 which consists mostly of $C_2H_2D_2^+$. The intensity of *m/e* 26, mostly $C_2H_2^+$, is close to 25% of that of C_2HD^+ because $C_2H_3^+$ should be much lower than C_2HD^+ in intensity. The *m/e* 16 and 17 ions are due to CH_2D^+ and CHD_2^+, not due to CD_2^+ and CH_3D^+.

Behavior of Hydrogen Atoms in the Fragmentation Process

Formation of $C_2X_4^+$

Several investigators studied the formation of $C_2X_4^+$ (X = H or D) from $C_2X_6^+$ using deuterated ethanes and concluded that the ion is produced through detachment of two hydrogen atoms from different carbon atoms in the parent ion near the threshold (9, 10, 17).

[1] 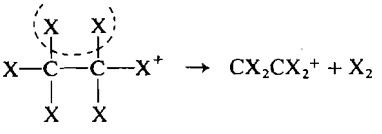 $\rightarrow CX_2CX_2^+ + X_2$

TABLE 3. Relative intensities of the ions produced from CH_3CD_3 at 22.7 eV and from C_2H_6 at 22.6 eV over ranges from *m/e* 14 to 34. Intensities of other ions are extremely low and neglected

	CH_3CD_3		C_2H_6	
m/e	Species	Intensity ratio	Species	Intensity ratio
34	$^{13}CCH_3D_3^+$	0.004		
33	$C_2H_3D_3^+$	0.202		
32	$C_2H_2D_3^+$	0.101		
31	$C_2H_3D_2^+$, $C_2HD_3^+$	0.190	$^{13}CCH_6^+$	0.004
30	$C_2D_3^+$, $C_2H_2D_2^+$	1.000	$C_2H_6^+$	0.205
29	$C_2HD_2^+$, $C_2H_3D^+$	0.209	$C_2H_5^+$	0.173
28	$C_2H_2D^+$, $C_2D_2^+$	0.084	$C_2H_4^+$	1.000
27	$C_2H_3^+$, C_2HD^+	0.042	$C_2H_3^+$	0.135
26	C_2D^+, $C_2H_2^+$	0.009	$C_2H_2^+$	0.056
25	C_2H^+	<0.001	C_2H^+	<0.001
19	CHD_3^+	<0.001		
18	$CH_2D_2^+$, CD_3^+	0.007		
17	CH_3D^+, CHD_2^+	0.002		
16	CD_2^+, CH_2D^+	0.002	CH_4^+	<0.001
15	CHD^+, CH_3^+	0.006	CH_3^+	0.020
14	CH_2^+	<0.001	CH_2^+	<0.001

In process 1 the X_2 is expected to form a hydrogen molecule, but the present method of analysis is not altered even if the X_2 is two atomic hydrogens. Von Koch measured $C_2H_3D^+$ and $C_2HD_3^+$ from $CH_3CD_3^+$ with excess internal energy by use of the charge exchange collision with ions which have higher recombination energies than the IP of CH_3CD_3 (6). Amenomiya *et al.* proposed the possibility of $C_2X_4^+$ formation through the detachment of two hydrogen atoms from the same carbon atom in the parent ion in order to reproduce mass spectra of nine deuterated ethanes at electron impact of 70 eV (7, 8).

[2] 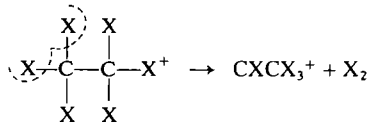 $\rightarrow CXCX_3^+ + X_2$

where the X_2 is similar to that of process 1.

Those results are consistent with the result shown in Table 1; the threshold for process 1 is lower than that for process 2. These suggest that the fragmentation of the ion proceeds through at least two processes and that the mechanism of the formation depends on the excess internal energy of the parent ion.

Apart from the two processes shown above, there is a possibility that a scrambling process participates in the formation of the ion (8, 12). In this process the exchange of hydrogen atoms is presumed to occur through an intermediate bridged structure

However this process is not considered in the present study, because it includes the ambiguous assumption of the intermediate; moreover the formation of the ion can be explained by adopting only two processes 1 and 2.

In the case that only process 1 participates in the formation of the ion, the intensity ratio of $C_2H_3D^+$, $C_2H_2D_2^+$, and $C_2HD_3^+$ (*m/e* 29 to 31) is 0:2:0, while in the case that only process 2 participates, the ratio is 1:0:1. Since the ratio estimated from the data observed at 22.7 eV is 0.14:1:0.12, two processes take part in the formation at this energy. When the intensity ratio is described as α:1:α at a bombarding electron energy, the rate at which process 1 participates is $1/(2\alpha + 1)$ at that energy. (In the present study the term 'rate' does not mean the velocity at which a reaction proceeds, but only the fraction of ion product formed by the process in question.) The participating rate of process 2 is $2\alpha/(2\alpha + 1)$.

In Fig. 2 are shown the energy dependence of the latter rate. The contribution of $C_2D_3^+$ to the intensity of *m/e* 30 is negligible because $C_2D_3^+$ is estimated to be less than 0.01 of $C_2H_2D_2^+$ (*m/e* 30) in intensity. In the calculation of the intensity of $C_2HD_3^+$ (*m/e* 31), the intensity of $C_2H_3D_2^+$ (*m/e* 31) was assumed to be 0.55 of that of $C_2H_2D_3^+$ (*m/e* 32) in all regions of

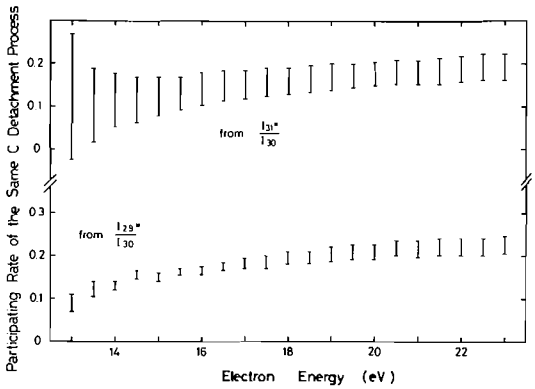

FIG. 2. Energy dependences of the participating rates of the same carbon atom-detachment process in $C_2X_4^+$ formation. The rates calculated from the intensity ratios of $C_2HD_3^+$ (*m/e* 31) to $C_2H_2D_2^+$ (*m/e* 30) and $C_2H_3D^+$ (*m/e* 29) to $C_2H_2D_2^+$ are shown in the upper and lower parts, respectively. The rates were calculated at 0.05 eV intervals and plotted at 0.5 eV intervals. Bars indicate statistical errors calculated from the standard deviations obtained in the data-processing of ionization efficiency curves. See the text with respect to I_{31}* and I_{29}*.

energy.[1] Although the factor was varied from 0.5 to 0.7, the rates calculated have similar trends. The intensity of $C_2H_2D_2^+$ including ^{13}C was considered in the calculation. In the calculation of the intensity of $C_2H_3D^+$ (*m/e* 29), $C_2HD_2^+$ (*m/e* 29) was assumed to have the same energy dependence as that of $C_2H_3^+$ from C_2H_6 and the intensity at 22.7 eV was assumed to be 0.069 of that of *m/e* 30.

The plots in Fig. 2 indicate that both rates are lower than 0.1 below 13 eV and gradually approach a plateau of about 0.2 around 20 eV. Amenomiya and Pottie estimated that the rate was 0.13 at 70 eV (8). Their rate is lower than that of the present study provided that the plateau continues towards higher energies. Most of $C_2X_4^+$ is produced from $C_2X_6^+$ through process 1 in all regions of energy with a slight contribution from process 2, at most 20%, above 12.5 eV.

On account of the AP for $C_2H_3D^+$ in Table 1, the state in which process 2 participates in $C_2X_4^+$ formation is assumed to be related to the upper state of the doublet which is caused by the Jahn–Teller effect in ^2E_g of $C_2X_6^+$ (14, 15). The lower state probably corresponds to process 1.

[1]Amenomiya and Pottie estimated the factor to be 0.57 in ref. 8.

Formation of $C_2X_2^+$

In the formation of $C_2X_2^+$ from $C_2X_6^+$, $C_2X_4^+$ has been proposed to be an intermediate by several authors (4, 9, 10, 21). The relevant ion is assumed to be produced from $C_2H_2D_2^+$ through the two following processes:

[3] 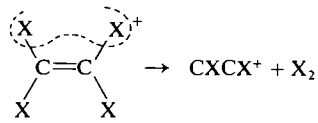

[4] 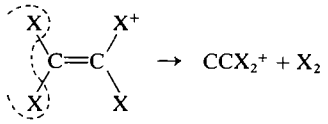

where X_2 is similar to that of the former section.

When the intensity ratio of C_2HD^+ to $C_2H_2^+$ is described as $1:\alpha$ at a given electron energy, the participating rate of process 4 is $2\alpha/(2\alpha + 1)$ at that energy. The energy dependence of the rate is shown at the lower part of Fig. 3. Since the intensities of $C_2H_3^+$ and C_2D^+ are expected to be extremely low over the range of the energy studied, contributions of the two ions were ignored in the calculation of the rate. The energy dependence of the intensity ratio of *m/e* 26 to 27 is shown at the upper part, with the scale indicated at the right side. Both are independent of the electron energy within the indicated accuracy.

The result suggests that processes 3 and 4 have the same threshold energy. This is, however, somewhat doubtful because the product ions differ considerably in stability (about 3 eV in a rough estimation).[2] If the present result is interpretable as a scrambling process (22), the scheme of $C_2X_2^+$ formation can be simplified to a single process.

[5] 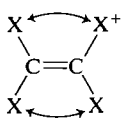

(scrambling state) → $CXCX^+ + X_2$

[2]The energy difference is roughly estimated from transfer of a hydrogen atom,

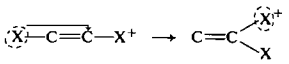

Thus the energy difference is calculated from an equation, $\Delta E = \{AP(C_2H^+ \text{ from } C_2H_2) - IP(C_2H_2)\} - \{AP(C_2H_3^+ \text{ from } C_2H_4) - IP(C_2H_4)\}$.

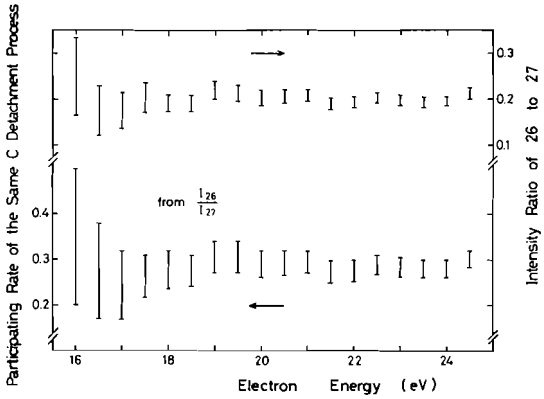

FIG. 3. Energy dependences of the participating rate of the same carbon atom-detachment process and of the intensity ratio of *m/e* 26 to 27 in $C_2X_2^+$ formation. The ratio and the rate were calculated at 0.05 eV intervals and plotted at 0.5 eV intervals in the upper and lower parts, respectively. Bars indicate statistical errors calculated from the standard deviations obtained in the data-processing of ionization efficiency curves.

As in the case of the fragmentation of ethylene ion, $C_2X_2^+$ is produced through process 5 over all ranges of energy, in which the intensity ratio of $C_2H_2^+$ to C_2HD^+ is 1:4 (12). Figure 3 is consistent with this interpretation; the indicated ratio of about 0.2 is a little smaller than the expected value 0.25 in all the energies observed. The difference of the ratios is due to the fact that the lighter neutral isotopic species departs faster than the heavier from the scrambling ion (9, 10, 12). If scrambling occurs in $C_2X_6^+$, the ratio is calculated to be 0.33. Therefore, the most probable interpretation for $C_2X_2^+$ formation from $C_2X_6^+$ is as follows: firstly $C_2X_6^+$ decomposes into $C_2X_4^+$ through process 1 and further $C_2X_4^+$ decomposes into $C_2X_2^+$ through process 5.

The state in which $C_2X_6^+$ decomposes at the first step described above is supposed to be related to the lower state of the doublet which is caused by the Jahn–Teller effect in ^2E_u (14, 15).

Formation of X_2^+

The present authors are unaware of any papers in which the mechanism of X_2^+ formation from $C_2X_6^+$ was studied. By analogy with former sections, it is assumed that X_2^+ formation proceeds through two processes.

[6] 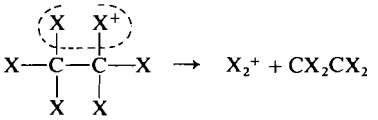 $\rightarrow X_2^+ + CX_2CX_2$

[7] 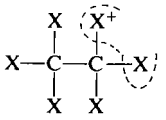 $\rightarrow X_2^+ + CX_3CX$

In the X_2^+ formation, there are possibilities that $C_2X_4^+$ and other ions are intermediate ions. Tentatively, however, these processes were not taken into account in the present analysis because no information on these intermediate ions exists. When the intensity ratio of HD^+ to D_2^+ is described as $1:\alpha$ at an energy, the participating rate of process 7 is $2\alpha/(2\alpha + 1)$ at that energy. The energy dependence of the rate is shown over a range of bombarding electron energy from 36 to 50 eV in Fig. 4. The rate is independent of energy within the indicated accuracy. The scrambling process, however, cannot be ruled out for the following reasons. The threshold energies for HD^+ and D_2^+ are the same, as seen in Table 2. The observed intensity ratio of these ions, 1:0.4, is close to the calculated one on the assumption of the scrambling in $C_2X_6^+$, 1:0.33. (The calculated ratio is 1:0.25 in the scrambling of $C_2X_4^+$.)

Formation of CX_3^+

Löhle *et al.* measured CX_3^+ (*m/e* 15 to 18) produced through metastable transition from CH_3CD_3 and concluded that the scrambling in $C_2X_6^+$ occurs incompletely before metastable C—C bond breaking (9). This finding is consistent

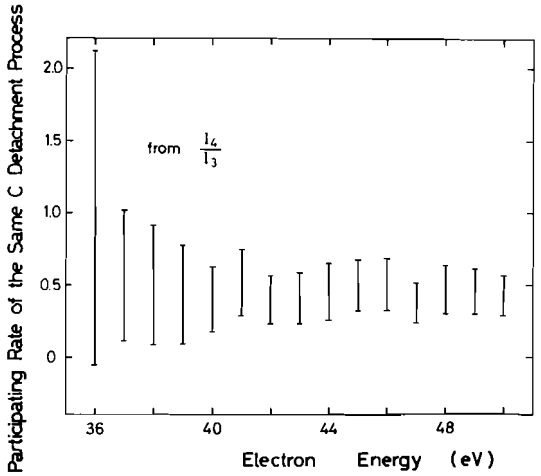

FIG. 4. Energy dependence of the participating rate of the same carbon atom-detachment process in X_2^+ formation. The rate was calculated at 0.2 eV intervals and plotted at 1 eV intervals. Bars indicate statistical errors calculated from the standard deviations obtained in the data-processing of ionization efficiency curves.

with mass spectra at 70 eV by Amenomiya and Pottie (7). By use of charge exchange collision von Koch found that the relative intensities of *m/e* 15 to 18 were dependent on the excess internal energy of $CH_3CD_3^+$ (6). Then, the CX_3^+ formation from CH_3CD_3 can be assumed to proceed through two following processes.

[8] $X_3C\text{-}CX_3^+ \rightarrow CX_3^+ + CX_3$

[9] $X_3C\text{—}CX_3^+ \rightarrow$ (scrambling state) $\rightarrow CX_3^+ + CX_3$

Table 2 suggests that the thresholds for processes 8 and 9 are about 15.5 and 17.0 eV. If only process 8 participates in CX_3^+ formation, the intensity ratio of CD_3^+, CHD_2^+, and CH_2D^+ (*m/e* 18 to 16) is 10:0:0. If only process 9 participates in the formation of CX_3^+, the ratio is 1:9:9. Since the ratio was estimated from the experimental result to be 1:0.22:0.25 at 22.7 eV, both processes took part in CX_3^+ formation at that energy. When the ratio is described as $1:\alpha:\alpha$ at an energy, the participating rate of process 9 is $10\alpha/9(\alpha + 1)$ at that energy.

The rates are shown over a range from 16 to 23.5 eV in Fig. 5. Since CX_2^+ and CX_4^+ are much lower than CX_3^+ in intensity, those ions were not taken into account in estimating the intensities of *m/e* 16 to 18. The rates are both zero at low energy and reach plateaus of about 0.2 around 18.5 eV. Decreases of the rates at 19 eV were caused by the decreases in slope in the ionization efficiency curves of *m/e* 16 and 17 at the energy, but the cause of the decreases cannot be clarified at present. The figure indicates that CX_3^+ is produced through the simple breaking of the C—C bond, process 8, at the rate of more than 80% in the region of the energy studied. The extent of reshuffling at 70 eV estimated by Amenomiya and Pottie 21% (8) corresponds to the rate of 0.23 in the present study. Therefore the plateaus in Fig. 5 are presumed to extend to 70 eV.

Löhle *et al.* detected metastable peaks of CX_3^+ produced from $C_2X_5^+$ which is produced from $C_2X_6^+$ and scrambles completely (9). Thus there

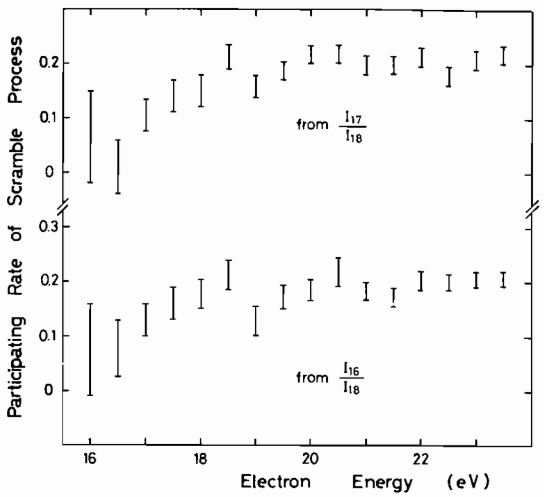

FIG. 5. Energy dependences of the participating rates of the scramble process in CX_3^+ formation. The rates calculated from the intensity ratios of CHD_2^+ (*m/e* 17) to CD_3^+ (*m/e* 18) and CH_2D^+ (*m/e* 16) to CD_3^+ are shown at the upper and lower parts, respectively. The rates were calculated at 0.1 eV intervals and plotted at 0.5 eV intervals. Bars indicate statistical errors calculated from the standard deviations obtained in the data-processing of ionization efficiency curves.

is a possibility in the present experiment that CX_3^+ is produced through the following process (23).

[10] $X_3C\text{—}CX_3^+ \rightarrow$ (scrambling state) $+ X \rightarrow CX_3^+ + CX_2 + X$

The threshold for this process is expected to be around 17 eV because AP of CH_2^+ from C_2H_6 is 17.3 eV (13) and the difference of IP's between CH_3 and CH_2 is 0.56 eV (24). The thresholds for CH_2D^+ and CHD_2^+ from CH_3CD_3 are nearly equal to the expected value. In the case that only process 10 participates in CX_3^+ formation from CH_3CD_3, the intensity ratio of *m/e* 18 to 16 is 1:9:9 on the assumption of equal probabilities in the detachment of H and D atoms before scrambling. This ratio is the same as that of process 9. Therefore the participating rate

calculated using process 10 instead of process 9 is the same as the one discussed above.

The rate of the scrambling process in Fig. 5 is interpreted to be the summed rate of processes 9 and 10. It is still uncertain which process is the main contributor to the scrambling process in CX_3^+ formation. Determination of the appearance threshold energy for each metastable peak should provide a clue to this question.

The state in which process 8 participates in CX_3^+ formation is supposed to be related to the lower state of the doublet which is caused by the Jahn–Teller effect in ^2E_u of $C_2X_6^+$. The upper state probably corresponds to the process 9 or 10 because the tail of the second band in the photoelectron spectrum extends to about 17 eV (14–16).

Acknowledgement

The authors wish to extend their sincere thanks to Professor J. L. Franklin of Rice University for helpful suggestions in the preparation of this manuscript.

1. W. A. Chupka and J. Berkowitz. J. Chem. Phys. **47**, 2921 (1967).
2. E. von Puttkamer. Z. Naturforsch. **25a**, 1062 (1970).
3. R. Stockbauer. J. Chem. Phys. **58**, 3800 (1973).
4. Z. Prášil and W. Forst. J. Phys. Chem. **71**, 3166 (1967).
5. L. K. Huy, W. Forst, and Z. Prášil. Chem. Phys. Lett. **9**, 476 (1971).
6. H. von Koch. Ark. Fys. **28**, 559 (1965).
7. Y. Amenomiya and R. F. Pottie. Can. J. Chem. **46**, 1735 (1968).
8. Y. Amenomiya and R. F. Pottie. Can. J. Chem. **46**, 1741 (1968).
9. U. Löhle and Ch. Ottinger. J. Chem. Phys. **51**, 3097 (1969).
10. C. Lifshitz and R. Sternberg. Int. J. Mass Spectrom. Ion Phys. **2**, 303 (1969).
11. K. Maeda, I. H. Suzuki, and Y. Koyama. Int. J. Mass Spectrom. Ion Phys. **14**, 273 (1974).
12. I. H. Suzuki and K. Maeda. Int. J. Mass Spectrom. Ion Phys. **15**, 281 (1974).
13. I. H. Suzuki and K. Maeda. Int. J. Mass Spectrom. Ion Phys. **24**, 147 (1977).
14. A. D. Baker, C. Baker, C. R. Brundle, and D. W. Turner. Int. J. Mass Spectrom. Ion Phys. **1**, 285 (1968).
15. J. W. Rabalais and A. Katrib. Mol. Phys. **27**, 923 (1974).
16. R. Stockbauer and M. G. Inghram. J. Chem. Phys. **54**, 2241 (1971).
17. L. D'Or, J. E. Collin, and J. Longree. Bull. Cl. Sci. Acad. R. Belg. **52**, 518 (1966).
18. D. O. Schissler, S. O. Thompson, and J. Turkevich. Discuss. Faraday Soc. Hydrocarbons, 46 (1951).
19. E. I. Quinn and F. L. Mohler. J. Res. Nat. Bur. Stand. **65A**, 93 (1961).
20. L. J. Stief and P. Ausloos. J. Chem. Phys. **36**, 2904 (1962).
21. M. Vestal and G. Lerner. Aerospace Res. Lab. Rep. 67-0114 (1967).
22. A. J. Lorquet and J. C. Lorquet. J. Chem. Phys. **49**, 4955 (1968).
23. A. Kropf, E. M. Eyring, A. L. Wahrhaftig, and H. Eyring. J. Chem. Phys. **32**, 149 (1960).
24. G. Herzberg. Molecular spectra and molecular structure. Vol. 3. D. van Nostrand Co., Inc., Princeton, NJ. 1967.

Photochemical decomposition of EDTA coordinated to cobalt(III): products, thermal reactions, and evidence for outer sphere alcohol oxidation by the excited state

COOPER H. LANGFORD AND GAY WIN QUANCE
Metal Ions Group, Chemistry, Carleton University, Ottawa, Ont., Canada K1S 5B6

Received March 7, 1977

COOPER H. LANGFORD and GAY WIN QUANCE. Can. J. Chem. **55**, 3132 (1977).

The photolysis of $Co(EDTA)^-$ in the ultraviolet is unlike analogous reactions of Fe(III) complexes. The ratio of products Co(II) to CO_2 is 1:1 but we find only $\frac{1}{2}$ as much CH_2O. For $Fe(EDTA)^-$, yields of photolysis products Fe(II):CO_2:CH_2O are 2:1:1. This is consistent only with a mechanism where primary photolysis yields Co(II), CO_2, and a radical which attacks EDTA in *preference* to reduction of the slowly reducible metal oxidation state, Co(III). Use of 2-propanol as a scavenger diagnostic of primary radicals is questioned because it is shown that LMCT excited states of Co(III) complexes exhibit the same outer sphere oxidations of alcohols earlier recognized in the photochemistry of a variety of Fe(III) complexes.

COOPER H. LANGFORD et GAY WIN QUANCE. Can. J. Chem. **55**, 3132 (1977).

La photolyse de $Co(EDTA)^-$ dans l'ultraviolet ne ressemble pas à la réaction analogue des complexes du Fe(III). Le rapport des produits Co(II) et CO_2 est de 1:1 mais on ne trouve que la moitié de la quantité équivalent de CH_2O. Dans le cas du $Fe(EDTA)^-$, les rendements de produits de photolyse Fe(II):CO_2:CH_2O sont de 2:1:1. Ceci est en accord uniquement avec un mécanisme dans lequel la photolyse primaire conduit à du Co(II) et du CO_2 et un radical qui attaque l'EDTA *de préférence* à une réduction lente de l'état d'oxydation III du Co. L'utilisation du propanol-2 comme piégeur pouvant servir de diagnostic pour les radicaux primaires est mise en question parce qu'il est connu que les états excités LMCT des complexes du Co(III) agissent dans l'oxydation des alcools aux sphères extérieures de la même façon que l'on a reconnu antérieurement dans la photochimie d'une variété de complexes Fe(III).

[Traduit par le journal]

Introduction

Photochemical decomposition of aminopolycarboxylates coordinated to metals in reducible oxidation states has attracted considerable interest both for the mechanistic photochemistry (1–3) and because photodecomposition may be environmentally important for aminopolycarboxylates in detergents and industrial wastes (4, 5). In the case of all the Fe(III) complexes examined (2–5), the oxidative decomposition of the aminopolycarboxylate yields CO_2 with a stoichiometry with respect to metal reductions of $\phi_{CO_2}:\phi_{Fe(II)} = 1:2$ (ϕ = quantum yield in mol einstein^{-1}). This is expected. Organic oxidations are two electron processes and that the primary radical formed reduces the second Fe(III) is not surprising. In fact, pathways are well documented (3, 4). A radical of the type

$$\geq N-CH_2^{\cdot}$$

appears to form following decarboxylation. This reduces a second Fe(III) to give

$$\geq \overset{\oplus}{N}=CH_2$$

which hydrolyses to the observed organic products, CH_2O, and a secondary amine.

The case of $Co(EDTA)^-$ (EDTA = *N*,*N*,*N*′,*N*′-1,2-ethanediaminetetraacetate) is anomalous (1). Explanation of this anomaly is the last outstanding question in this area to which our program has been addressed and we present in this article evidence showing the relation of this system to the environmentally important cases we have studied earlier. The yields of CO_2 and Co(II) are in the ratio $\phi_{CO_2}:\phi_{Co(II)} = 1:1$ and addition of 2-propanol increases the relative yield of Co(II). The organic products have not been well characterized and the significance of the 2-propanol effect is rendered ambiguous by the recent discovery that charge transfer excited states, including that of $Fe(EDTA)^-$, can oxidize primary and secondary alcohols in an outer sphere reaction (6). (Whereas it was assumed earlier (1) that 2-propanol only scavenges radicals from the primary photoprocess.)

The earlier work (1) has clearly established that photoreaction of $Co(EDTA)^-$ arises from the ligand to metal charge transfer (LMCT) excited state with an absorption maximum near

240 nm. It also clearly establishes the 1:1 ratio of Co(II) and CO_2 yields. The present article is addressed to two questions: improving understanding of the fate of EDTA especially quantifying CH_2O yield, and testing for outer sphere oxidation of 2-propanol which has previously been assumed to be simply a scavenger for free radicals.

Experimental

Crude KCoEDTA was generously supplied by Dr. J. H. Carey. It was recrystallized twice from distilled water. The spectrum agrees with earlier reports (1). $Co(NH_3)_6Cl_3$ was prepared by conventional procedures (7). It was converted to the perchlorate by precipitation with $HClO_4$. Alcohols were spectro grade materials used as supplied.

Stock solutions for photolysis were prepared in aqueous $HClO_4$ (0.15 *M* $HClO_4$). Co(III) concentrations were chosen to insure 100% absorption of incident light in a 1.8 cm diameter cylindrical quartz irradiation vessel which was inserted for irradiation at 254 nm in a Nuclear Supplies, Inc. photoreactor. The solutions irradiated were prepared by pipetting 1.0 ml of stock solution into the irradiation cell and diluting this to 5.0 ml with water or an alcohol–water mixture. The cell was then sealed with a rubber serum cap and deaerated by bubbling purified N_2 for 20 min with the aid of stainless steel needles. That this procedure did not alter Co(III) or alcohol concentrations significantly was confirmed.

The basic quantum yield determined was that for reduction to Co(II). The photolyte was analyzed by a modification of the procedure of Caspari *et al.* (8). A 4.0 ml aliquot of photolyte was mixed with 8.0 ml of 50% NH_4SCN in a 25.0 ml volumetric flask. Redistilled reagent grade acetone was added up to the mark. The absorbance of this solution was monitored at 625 nm (extinction coefficient 7.50×10^3 M^{-1} cm^{-1}). Thermal blanks were performed for each set of irradiations and thermal production of Co(II) was negligible in all systems. Irradiations were limited to 5% conversion or less to minimize product absorption and secondary photolysis. Light intensity was measured by ferrioxalate actinometry (9).

The other product assayed quantitatively in parts of this study was formaldehyde. The chromotropic acid method of Houle *et al.* (10) was employed. In this case, thermal blanks were of more significance because $Co(EDTA)^-$ has a distinct absorbance at the analytical wavelength of 570 nm.

Given a knowledge of yields of Co(II), CO_2, and CH_2O, the remaining products are dictated by stoichiometry and the need to remain within transformations having a precedent. However, the gas chromatographic procedure developed by Lockhart and Blakeley (4) can provide confirmation. This method used *N*-fluoroacetyl-*n*-butyl esters. Minor modifications of the procedure included use of 0.02 ml aliquots of solutions irradiated for 0, 2, and 30 min, immediate addition of the internal standard, 4-aminobutyric acid, and use of a 6 ft × $\frac{3}{16}$ in. column of 3% QF-1 on 100/120 mesh Chromosorb W mounted in an F and M Scientific 402 gas chromatograph with the oven temperature programmed from 110 to 250°C at 5°C/min. Thermal blanks and spiked samples containing $Co(EDTA)^-$ or Na_2H_2EDTA were also prepared. Authentic samples of *N,N,N'*-1,2-ethanediaminetriacetate (ED3A) and *N*-methyl-*N,N'N'*-1,1-ethanediaminetriacetate (MeED3A) were not available but they would be expected to be very similar and probably chromatographically unresolvable since ED3A and EDDA (*N,N'*-1,2-ethanediaminediacetate) are only minimally resolved (4). The difficulty of distinguishing these two compounds is a problem, but the *key stoichiometric question turns on CH_2O yield.*

Results and Discussion

1. The Outer Sphere Oxidation of 2-Propanol

The occurrence of outer sphere oxidation of primary and secondary alcohols by charge transfer excited states in contrast to the unreactivity of tertiary alcohols was established on the basis of the observation (6) of a limit to quantum yield as *tert*-butanol (2-methyl-2-propanol) concentration increases, whereas quantum yield in the presence of methanol, ethanol, or 2-propanol increases *linearly* with alcohol concentration in the high alcohol concentration region. This is to be understood in terms of the fact that *tert*-butanol scavenges *free* radicals (11) but reaches a limit when it captures all free radicals. The other alcohols also react with the charge transfer excited state itself and, therefore, do not approach a limiting reactivity at moderate concentrations because LMCT excited state lifetimes are shorter than radical lifetimes.

The outer sphere LMCT excited state reaction has been shown to be general over a range of oxidizable organic molecules including aldehydes, formic acid, and dicarboxylic acids as well as primary and secondary alcohols (12). It was shown to occur for the excited states of a diverse set of Fe(III) complexes including $Fe(OH_2)_6^{3+}$, $Fe(OH_2)_5Cl^{2+}$, $Fe_2(OH)_2(OH_2)_8^{4+}$, and $FeEDTA^-$. Whether the analogous LMCT states of Co(III) complexes are similarly reactive is an interesting question. Figures 1 and 2 show the dependence of Co(II) quantum yields on alcohol concentration for $Co(NH_3)_6^{3+}$ and $Co(EDTA)^-$ respectively. These figures confirm that the direct outer sphere reaction of the excited state is also occurring in Co(III) systems.

This result contains the subsidiary point that 2-propanol is an unreliable choice as a scavenger for study of the primary radical products of photolysis; for example, reduction to Co(II) could occur without leading to decarboxylation of EDTA (except perhaps in secondary reactions). Indeed, the curves in Fig. 2 where yields in the presence of *tert*-butanol are larger at low alcohol concentration than those in the presence

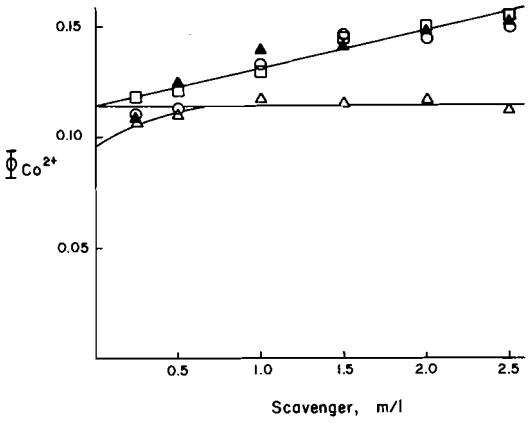

FIG. 1. The quantum yield for Co(II) production as a function of concentrations of various alcohols in the 254 nm irradiation of $Co(NH_3)_6^{3+}$: □, methanol, ▲, ethanol, ○, isopropanol, △, *tert*-butanol.

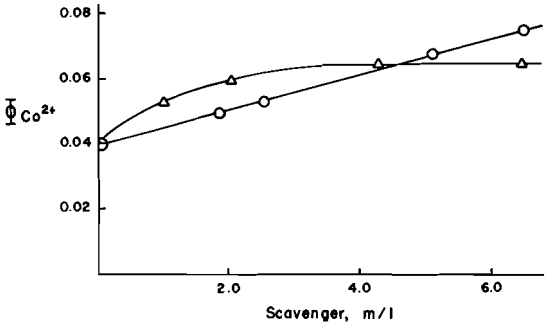

FIG. 2. The quantum yield for Co(II) production as a function of concentrations of two alcohols in the 254 nm irradiation of $Co(EDTA)^-$: ○, isopropanol, △, *tert*-butanol.

of 2-propanol suggest a plausible interpretation where the radical initially formed from photochemical decarboxylation of $Co(EDTA)^-$ reacts much more rapidly with *tert*-butanol than 2-propanol. The report (1) that ratios of Co(II) formation to CO_2 formation increase from 1.0–1.6 in 50% 2-propanol could be explained by decreases in EDTA decarboxylation associated with outer sphere reactions.

2. Stoichiometry of Photolysis of Co(EDTA)$^-$

The central result of our study is the CH_2O yield which has not previously been examined. Several runs in the absence of scavenging alcohols and using the chromotropic acid method for CH_2O determination gave $\phi_{Co(II)}:\phi_{CH_2O} = 2:1.01 \pm 0.03$. In conjunction with the results of Natarajan and Endicott (1), this establishes the stoichiometry $\phi_{Co(II)}:\phi_{CO_2}:_{CH_2O} = 2:2:1$. The implication of this is that each effective photon leads to the reduction of two $Co(EDTA)^-$ molecules and release of 2 mol CO_2. However, only one $-CH_2-$ group from an acetate of the aminopolycarboxylate is lost. In Fe(III) photochemistry the result is $\phi_{Fe(II)}:\phi_{CO_2}:\phi_{CH_2O} = 2:1:1$ (3, 4, 12). This is explained (3, 4) by the reaction sequences of eq. 1. (In the equation, partial decomposition of EDTA is indicated by writing a formula representing only the part of the molecules involved in the reaction.)

[1*a*] $Fe^{III}(EDTA)^- \xrightarrow{h\nu} {}^*Fe^{III}(EDTA)^-$

[1*b*] ${}^*Fe^{III}(EDTA)^- \longrightarrow Fe^{II}(\dot{C}H_2)N + CO_2$

[1*c*] $Fe^{II}(\dot{C}H_2)N + Fe^{III}(EDTA)^-$

$\searrow$

$Fe^{II}(\oplus CH_2{=}N) + Fe^{II}(EDTA)^{2-}$

[1*d*] $Fe^{II}(\oplus CH_2{=}N) + H_2O \longrightarrow Fe^{II}(H)N + CH_2O + H^+$

The step which differentiates Co(III) from Fe(III) is [1c]. The thermal reduction of low spin Co(III) complexes is known to be much slower than reductions of Fe(III). Thus, it is likely that the electron transfer step in Co(III) cases analogous to [1*c*] is to the EDTA ligand and initiates decomposition of a second molecule of EDTA which *yields the second* CO_2. We can write eqs. 2 to describe this mechanism.

[2*a*] $Co^{III}(EDTA)^- \longrightarrow {}^*Co^{III}(EDTA)^-$

[2*b*] ${}^*Co^{III}(EDTA)^- \longrightarrow Co^{II}(\dot{C}H_2)N + CO_2$

[2*c*] $Co^{II}(\dot{C}H_2)N + Co^{III}(EDTA)^-$

$\searrow H^+$

$Co^{II}(\oplus CH_2{=}N) + Co^{III}(N{-}O{-}CH_2{-}\dot{C}(OH))N$

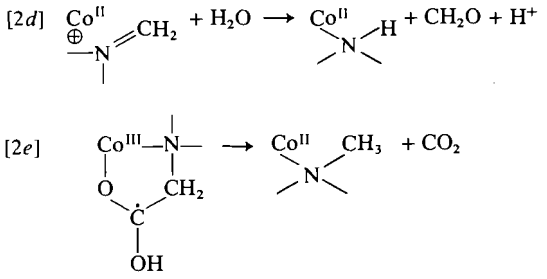

Mechanism [2] with electron transfer to EDTA preceding the reduction of the second Co(III) accounts for the anomalous stoichiometry of 1:1 CO_2:Co(II) and the clear accompanying requirement for only one CH_2O. (Inspection of as many alternative pathways as our research group could invent left no plausible alternative to the mechanism in [2] to account for the stoichiometry.) There is only one remaining requirement. The other organic products must be ED3A and MeED3A. In ref. 1 some nmr evidence for MeED3A was presented. (We have had some difficulty confirming these experiments and could not express confidence in this product, if the stoichiometry allowed us to ignore it.)

3. Gas Chromatography

The only acceptable mechanism (eq. 2) requires that ED3A and MeED3A be the only other products. Figure 3 shows the chromatogram of photolytes of $Co(EDTA)^-$ in the presence of the internal standard, 4-aminobutyric acid, and unreacted EDTA. The only product peak is a relatively broad one marked Q. EDTA and 4-aminobutyric acid appear at exactly the positions reported by Lockhart and Blakeley in their study of Fe(III) complexes (4). Q corresponds to the reported (4) ED3A position. But, in the context of evidence for MeED3A and the expected difficulty of resolutions of ED3A from MeED3A (*vide supra*) the chromatogram is *consistent with production of both* and the mechanism in eq. 2.

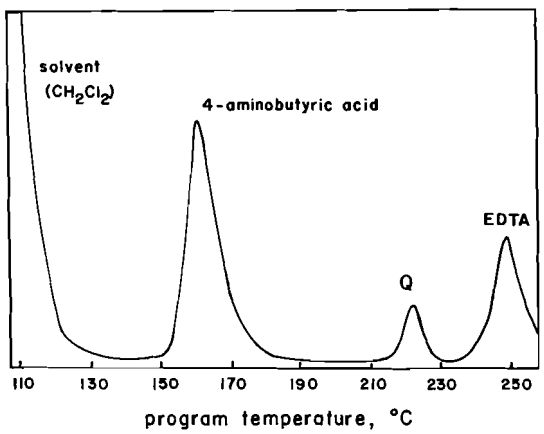

FIG. 3. Chromatogram of the photodegradation products of EDTA isolated as described in the text following 254 nm irradiation of $Co(EDTA)^-$.

Conclusion

Free radical scavenging is not the only role for alcohols. Thus, some earlier photochemical literature must be interpreted with caution. A mechanism consistent with the established aspects of reaction stoichiometry does provide a reasonable explanation of the anomalous reaction of $Co(EDTA)^-$ compared to Fe(III) complexes. It draws attention to the role of the well known *kinetic barrier to Co(III) reduction* in thermal radical pathways following photochemical initiation. Clearly, an attack on a second EDTA ligand is indicated and this is the critical point. The determination of aminopolycarboxylate products by nmr and gc remains somewhat ambiguous but is consistent with the proposed mechanism. Wide ranging exploration suggested no attractive alternatives to eqs. 2.

Acknowledgements

We thank Mr. Thomas Tennian for his work on the $Co(NH_3)_6^{3+}$ experiments. Dr. John H. Carey rendered both theoretical and experimental advice. The National Research Council of Canada supported this work financially.

1. P. NATARAJAN and J. F. ENDICOTT. J. Phys. Chem. **77**, 2049 (1973).
2. P. NATARAJAN and J. F. ENDICOTT. J. Am. Chem. **95**, 2470 (1973).
3. J. H. CAREY and C. H. LANGFORD. Can. J. Chem. **51**, 3665 (1973).
4. H. B. LOCKHART, JR. and R. V. BLAKELEY. Environ. Sci. Technol. **9**, 1035 (1975).
5. T. TROTT, R. W. HARWOOD, and C. H. LANGFORD. Environ. Sci. Technol. **6**, 367 (1971).
6. J. H. CAREY and C. H. LANGFORD. Can. J. Chem. **53**, 2436 (1975).
7. A. KING. Inorganic preparations. Allen & Unwin, London. 1950. p. 108.
8. G. CASPARI, R. G. HUGHES, J. F. ENDICOTT, and M. Z. HOFFMAN. J. Am. Chem. Soc. **92**, 6801 (1970).
9. C. G. HATCHARD and C. A. PARKER. Proc. R. Soc. London, Ser. A, **235**, 518 (1956).
10. M. J. HOULE, D. E. LONG, and D. SMETTE. Anal. Lett. **3**, 401 (1970).
11. C. WALLING and G. M. EL-TALIAWI. J. Am. Chem. Soc. **95**, 844 (1973).
12. J. H. CAREY. Ph.D. Thesis, Carleton University, Ottawa, Ont. 1974.

Reaction of the fluoroantimony(V) and fluoroarsenic(V) salts of the polyatomic cations of sulphur with tetrafluoroethylene and hexafluoropropylene. Reaction of tetraselenium bis(hexafluoroarsenate(V)) with tetrafluoroethylene

C. David Desjardins and Jack Passmore

Department of Chemistry, University of New Brunswick, Fredericton, N.B., Canada E3B 5A3

Received August 13, 1976[1]

C. David Desjardins and Jack Passmore. Can. J. Chem. **55**, 3136 (1977).

$S_8(AsF_6)_2$ reacts with C_2F_4 in SO_2 to form $(C_2F_5)_2S_x$ ($x = 2 \rightarrow 6$), $C_2F_5S_xCF_2C(O)F$ ($x = 2 \rightarrow 5$), $S_x(CF_2C(O)F)_2$ ($x = 2 \rightarrow 4$), $CF_3S_xCF_2C(O)F$ ($x = 3, 4$), $CF_3S_xC_2F_5$ ($x = 3 \rightarrow 5$), and $(CF_3)_2S_3$. Solid $S_8(AsF_6)_2$ reacts with C_3F_6 to form $(C_3F_7)_2S_x$ ($x = 2 \rightarrow 5$). In SO_2 solution, the same reactants yield the additional products

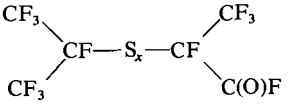

($x = 2 \rightarrow 5$)

and related species incorporating the C(O)F moiety. Solid $S_4(Sb_2F_{11})_2$ reacts with C_2F_4 to yield $(C_2F_5)_2S_x$ ($x = 1 \rightarrow 4$),

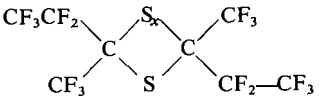

($x = 1, 2$)

and with C_3F_6 to give $(C_3F_7)_2S_x$ ($x = 1 \rightarrow 3$), and

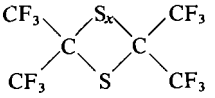

($x = 1, 2$)

Solid $Se_4(AsF_6)_2$ reacts with C_2F_4 to form $(C_2F_5)_2Se_x$ ($x = 1 \rightarrow 3$) and in SO_2 solution, the species $C_2F_5Se_2CF_2C(O)F$, $Se_2(CF_2C(O)F)_2$, $CF_3Se_2CF_2C(O)F$, $C_2F_5Se_2CF_3$, and $CF_3Se_2CF_3$ are also formed.

Products were identified by mass spectroscopy and the major species were isolated by vpc and further characterized by ^{19}F nmr. The mechanisms of these reactions are discussed.

C. David Desjardins et Jack Passmore. Can. J. Chem. **55**, 3136 (1977).

Le $S_8(AsF_6)_2$ réagit avec C_2F_4 dans le SO_2 pour former $(C_2F_5)_2S_x$ ($x = 2 \rightarrow 6$), $C_2F_5S_xCF_2$-$C(O)F$ ($x = 2 \rightarrow 5$), $S_x(CF_2C(O)F)_2$ ($x = 2 \rightarrow 4$), $CF_3S_xCF_2C(O)F$ ($x = 3, 4$), $CF_3S_xC_2F_5$ ($x = 3 \rightarrow 5$) et $(CF_3)_2S_3$. Le $S_8(AsF_6)_2$ à l'état solide réagit avec C_3F_6 pour former $(C_3F_7)_2S_x$ ($x = 2 \rightarrow 5$). En solution dans le SO_2, les mêmes réactifs conduisent aux produits additionnels

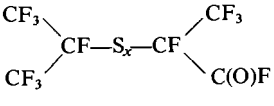

($x = 2 \rightarrow 5$)

et aux entités apparentées incorporant le groupement C(O)F. Le $S_4(Sb_2F_{11})_2$ à l'état solide réagit avec le C_2F_4 pour conduire au $(C_2F_5)_2S_x$ ($x = 1 \rightarrow 4$)

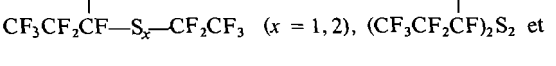

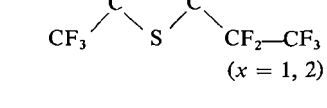

($x = 1, 2$)

---

[1]Revision received April 7, 1977.

et avec le C_3F_6 pour donner $(C_3F_7)_2S_x$ ($x = 1 \rightarrow 3$) et

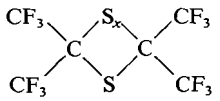

($x = 1, 2$)

Le $Se_4(AsF_6)_2$ à l'état solide réagit avec le C_2F_4 pour former $(C_2F_5)_2Se_x$ ($x = 1 \rightarrow 3$) et, en solution dans le SO_2, il y a aussi formation des entités $C_2F_5Se_2CF_2C(O)F$, $Se_2(CF_2C(O)F)_2$, $CF_3Se_2CF_2C(O)F$, $C_2F_5Se_2CF_3$ et $CF_3Se_2CF_3$.

On a identifié les produits par spectrométrie de masse et les produits majeurs ont été isolés par chromatographie en phase gazeuse et caractérisés par rmn du ^{19}F.

On discute des mécanismes de ces réactions.

[Traduit par le journal]

Introduction

Recently, various reactions of the Group VI polycations (1) with C_2F_4 have been studied. Tetrafluoroethylene reacts with $S_{16}(AsF_6)_2$ and $S_8(AsF_6)_2$ (2) to form $(C_2F_5)_2S_x$ ($x = 2 \rightarrow 6$), with $Se_8(AsF_6)_2$ (3) to give $(C_2F_5)_2Se_x$ ($x = 2$, 3), and with $Te_4(AsF_6)_2$ and $Te_6(AsF_6)_2$ (4) to give $(C_2F_5)_2Te_x$ ($x = 1$, 2). In SO_2 solution, C(O)F-containing species were also formed (*i.e.*, $Se_8(AsF_6)_2$ reacts with C_2F_4 in SO_2 solution (3) to yield $(C_2F_5)_2Se_2$ and $C_2F_5Se_2CF_2C(O)F$ as the major products). However, only preliminary evidence for the carbonyl fluoride species was obtained for the reaction of $S_8(AsF_6)_2$ with C_2F_4 in SO_2 solution (2). In this paper we have identified the C(O)F sulphur compounds and extended our work to reactions of $S_8(AsF_6)_2$ with $F_2C{=}CFCF_3$ and $CF_3FC{=}CFCF_3$, as well as to reactions of $S_4(Sb_2F_{11})_2$, $S_8(Sb_2F_{11})_2$, and $Se_4(AsF_6)_2$ with C_2F_4 and $S_4(Sb_2F_{11})_2$ with C_3F_6 in order to add to an understanding of the mechanism and reactivity of this system.

Experimental

A. Apparatus

Techniques used in this work have been described elsewhere (2–4). ^{19}F nmr were obtained using a Varian Associates HA-60 spectrometer operating at 56.4 MHz or with a Varian HA-100 at 94.1 MHz. Vapour phase chromatographic analysis and preparative separations were obtained as in ref. 4 but with a helium gas flow of 60 ml min^{-1}. Raman spectra were obtained using liquid samples in sealed melting point tubes and a Spex Ramalab RS2 spectrometer with a Spectra Physics 164 2W Ar–Kr ion laser as the exciting source (6471 Å). Spectra were calibrated (error ± 2 cm^{-1}) using appropriate lines from carbon tetrachloride and indene.

B. Reagents

Tetrafluoroethylene, hexafluoropropylene, octafluorobutene-2 (Columbia Organic Chemicals), selenium (Fisher Scientific Co., contains 0.1% sulphur determined by analysis), sulphur (McArthur Chemical Co.), triphenylphosphine (Eastman) were used without further purification. SO_2, HF, and AsF_5 were purified as in refs. 2 to 4. SbF_5 (Ozark–Mahoning) was purified by distillation *in vacuo*. $S_8(AsF_6)_2$ (5) and $Se_4(AsF_6)_2$ (1) were prepared by reported methods. $S_4(Sb_2F_{11})_2$ was prepared according to reaction 1 by a modification of the reported method (5).

[1] $S_8 + 12SbF_5 \rightarrow 2S_4(Sb_2F_{11})_2 + 2SbF_3{\cdot}SbF_5$

The products were mixtures of $S_4(Sb_2F_{11})_2$ and reduced species (*i.e.*, $SbF_3{\cdot}SbF_5$ and/or SbF_3).

Prep. *A*: S_8 (0.52 g, 2.03 mmol) was reacted with excess SbF_5 (7.19 g, 33.17 mmol) in AsF_3 solution for 3 days at 100°C under reflux. Volatiles were removed at room temperature under dynamic vacuum for 1 day. A Raman of the light blue solid (6.81 g) (681(s), 672(m), 646(s), 608(s), 582(vs), 540(s), 374(s), 286(m br)) contained peaks attributable to S_4^{2+}, Sb(V) fluoroanion and reduced products.

Prep. *B*: S_8 (2.0 g, 7.8 mmol) was reacted with SbF_5 (22.25 g, 102.65 mmol) at 140°C for several days under reflux, and treated as in *A* to give 18.77 g solid.

Prep. *C*: (S_8 (0.53 g, 2.07 mmol), SbF_5 (7.18 g, 33.12 mmol)) and Prep. *D*: (S_8 (2.4 g, 9.36 mmol), SbF_5 (24.75 g, 114.19 mmol)) were reacted as in Prep. *B*. We were, like earlier workers (5), unable to isolate pure $S_4(Sb_2F_{11})_2$.

$S_8(Sb_2F_{11})_2$ was prepared (5), according to reaction 2.

[2] $S_8 + 5SbF_5 \xrightarrow{SO_2} S_8(Sb_2F_{11})_2 + SbF_3$

Prep. *E*: S_8 (1.49 g, 5.6 mmol) and SbF_5 (6.3 g, 29.2 mmol) gave 6.41 g SO_2 soluble solid (6.55 g, expected for $S_8(Sb_2F_{11})_2$).

Prep. *F*: S_8 (0.37 g, 1.44 mmol) and SbF_5 (2.05 g, 9.46 mmol) in SO_2 yielded a blue solid. Half of the material obtained was filtered using SO_2 as in Prep. *E*.

Prep. *G*: In a typical reaction $Se_8(SbF_6)_2{\cdot}xSbF_5$ was made by reacting (6) selenium (3.50 g, 5.54 mmol 8Se) with excess SbF_5 (7.10 g, 32.76 mmol) in SO_2 solution for several days at room temperature. The soluble green solid (5.0 g) was filtered and dried. Insoluble products were antimony(III) containing species and a black solid.

C. Reactions

Volatile species obtained from reactions were isolated and characterized by previous methods (2–4). In SO_2 reactions, a small loss of AsF_3 and to a lesser extent perfluoroalkyl sulphides occur on removal of SO_2 solvent and therefore weights of products recovered are lower than the total produced in the reaction. Unless otherwise specified the reactions were carried out in 40 cm^3 Monel reaction vessels at room temperature. The dis-

TABLE 1. Vapour phase chromatographic retention times

Compound	Retention time (min)	Compound	Retention time (min)	Compound	Retention time (min)
AsF_3	0.1	$(C_2F_5)_2S_3$	2.2	$(C_4F_9)_2S_2$	6.9
$(C_2F_5)_2Se$	0.2	$CF_3Se_2CF_2C(O)F$	2.2	$CF_3S_4C_2F_5$	7.4
$(C_2F_5)_2S_2$	0.6	$C_2F_5Se_2CF_2C(O)F$	3.1	$C_3F_7S_3C_3F_5O$	7.8
$CF_3Se_2C_2F_5$	1.2	$C_2F_5S_3CF_2C(O)F$	4.1	$(C_2F_5)_2S_4$	9.2
$CF_3S_3C_2F_5$	1.4	$(C_3F_7)_2S_3$	5.3	$S_3(C_3F_5O)_2$	11.3
$(C_3F_7)_2S_2$	1.5	$C_8F_{16}S_2$	5.6	$C_2F_5S_4CF_2C(O)F$	17.2
$(C_2F_5)_2Se_2$	1.6	$(C_2F_5)_2Se_3$	6.4	$(C_3F_7)_2S_4$	21.5
$C_6F_{12}S_2$	1.6	$S_3(CF_2C(O)F)_2$	6.4	$C_8F_{16}S_3$	22.4
$C_2F_5S_2C_4F_9$	1.9	$C_6F_{12}S_3$	6.5	$C_3F_7S_4C_3F_5O$	34.1

tribution of the various sulphides and selenides was established by vpc analysis. A combination of vpc analysis and mass spectra data of different volatile fractions and various components isolated from preparative vpc confirmed the identity and retention times (Table 1) of the major species.

(1) Reaction of Solid $S_8(AsF_6)_2$ with C_2F_4

$S_8(AsF_6)_2$ (5.29 g, 8.34 mmol) was reacted with an excess of C_2F_4 (31.6 mmol) for 3 days. The volatile products at room temperature included C_2F_4 (26.40 mmol consumed), C_2F_6, AsF_3 (1.4 g, 62% of the available arsenic) and a clear liquid (4.32 g), consisting of 4% $(C_2F_5)_2S_2$, 68% $(C_2F_5)_2S_3$, 27% $(C_2F_5)_2S_4$, and traces of $(C_2F_5)_2S_x$, $x = 5$, 6 detected by mass spectroscopy. $(C_2F_5)_2S$ was not detected in the infrared or mass spectrum of the volatile products of this reaction. The clear liquid incorporates 82% of the available fluorine from AsF_6^- (*i.e.* 3 fluorines per AsF_6^-) and 61% of the available sulphur. An unidentified green solid (1.9 g) remained. Previously reported reactions (2) gave measurable amounts of $(C_2F_5)_2S_5$ (*ca.* 0.5%) under conditions of low pressure of C_2F_4. $S_8(AsF_6)_2$ was also reacted with C_2F_4 at −78°C for several weeks. A very low yield of similar products was obtained.

(2) Reaction of $S_8(AsF_6)_2$ with C_2F_4 in SO_2

$S_8(AsF_6)_2$ (6.36 g, 10.02 mmol) was dissolved in SO_2 (3.7 g) and treated with an excess of C_2F_4 (42.1 mmol) for 3 days.

The volatile products were C_2F_4 (27.30 mmol consumed), C_2F_6, SO_2, traces of CO, OSF_2, and a carbonyl-containing species, $CF_3C(O)F$, as identified by its infrared spectrum, AsF_3 (1.1 g, 41% of the available arsenic) and a clear liquid (3.95 g), a mixture of polysulphides containing 6% $CF_3S_3C_2F_5$, 19% $(C_2F_5)_2S_3$, 34% $C_2F_5S_3CF_2C(O)F$, 18% $(C_2F_5)_2S_4$, 14% $C_2F_5S_4CF_2C(O)F$, $CF_3S_3CF_2C(O)F$, $S_3(CF_2C(O)F)_2$, and $CF_3S_4C_2F_5$ (the latter three compounds constitute 9% of the liquid polysulphides). Molecular ions attributable to the above species were observed as well as less intense molecular ions and fragments attributable to $(C_2F_5)_2S_5$, $(C_2F_5)_2S_6$, $(C_2F_5)_2S_2$, $C_2F_5S_5CF_2C(O)F$, $S_4(CF_2C(O)F)_2$, $CF_3S_5C_2F_5$, $C_2F_5S_2CF_2C(O)F$, $(CF_3)_2S_3$, $S_2(CF_2C(O)F)_2$, and $CF_3S_4CF_2C(O)F$. 68% of the available fluorine and 51% of the available sulphur were incorporated into the liquid polysulphides. An unidentified purple solid (3.75 g) remained. In other reactions similar products were obtained with some change in the percentage distribution of products. $S_8(AsF_6)_2$ (5.60 g, 8.83 mmol) was also reacted with excess C_2F_4 (*ca.* 22.5 mmol) in SO_2 (7.45 g) at −78°C. The liquid polysulphides obtained (1.60 g, contains AsF_3) were predominantly $(CF_3)_2S_2$, $CF_3S_2C_2F_5$, and traces of $(C_2F_5)_2S_3$, $CF_3S_3C_2F_5$. A red solid mixture (4.52 g) remained that contained an unidentified reactive red volatile component.

(3) Reaction of Solid $S_8(AsF_6)_2$ with C_3F_6

The results of the reactions of solid $S_8(AsF_6)_2$ with C_3F_6 neat and in SO_2 solvent are summarised in Table 2.

(4) Reaction of Solid $S_8(AsF_6)_2$ with C_4F_8

Perfluorobutene-2 (28.8 mmol) was added in excess to solid $S_8(AsF_6)_2$ (5.03 g, 7.93 mmol) for 13 days. Volatiles contained C_4F_8 and a slightly coloured liquid (0.25 g). A vpc showed it to be essentially AsF_3. AsF_3 and traces of unidentified perfluoroalkyl sulphides were detected in the mass spectrum. A brownish blue solid mixture (4.94 g) remained.

(5) Reaction of $Se_4(AsF_6)_2$ with C_2F_4

The results of this reaction, neat, and in SO_2 solvent are summarised in Table 2. A reaction of $Se_8(SbF_6)_2 \cdot xSbF_5$ (5.21 g; see Prep. *G*) with C_2F_4 (2.61 g, 26.1 mmol) in SO_2 solution (2.93 g) for several weeks gave a mixture of polyselenides (3.49 g; $CF_3Se_2C_2F_5$ and $(C_2F_5)_2Se_2$ were major components, also contains traces of $(CF_3)_2Se_2$ and carbonyl containing species). An unidentified solid was obtained. 47% of selenium was incorporated into the liquid polyselenides.

(6) Reaction of Solid $S_4(Sb_2F_{11})_2$ with C_2F_4

Solid $S_4(Sb_2F_{11})_2$ (2.21 mmol; see Prep. *C*) (number of mmoles $S_4(Sb_2F_{11})_2$ was computed assuming 100% conversion of sulphur to $S_4(Sb_2F_{11})_2$ according to reaction 1) was placed in a Kel-F reaction vessel on a 50 cm^3 Monel vacuum line. An initial pressure of C_2F_4 (*ca.* 1.5 atm) was maintained. After one week, no further pressure drop was observed. Unreacted C_2F_4 (14.0 mmol consumed) was removed at −130°C leaving a light blue liquid (1.42 g) containing 4% $C_8F_{16}S_3$, 26% $(C_2F_5)_2S_2$ (contains shoulder due to $C_4F_9SC_2F_5$), 43% $C_4F_9S_2C_2F_5$, 16% $(C_4F_9)_2S_2$ (peak includes traces of $(C_2F_5)_2S_4$), 3% $C_8F_{16}S_2$, 4% $(C_2F_5)_2S$, and 4% unidentified component (possibly $C_6F_{12}S_2$). Less intense molecular ions and fragments were attributable to $C_4F_9S_3C_2F_5$, $C_4F_8S_2$, C_4F_8S, and $(C_2F_5)_2S_3$. Due to fragmentation patterns of higher molecular weight species in the mass spectra, unambiguous evidence could not be obtained for the

TABLE 2. Reactions of $S_8(AsF_6)_2$ with C_3F_6, and $Se_4(AsF_6)_2$ with C_2F_4

Reactants	Conditions[a]	Products	Yield[b]
(1) $S_8(AsF_6)_2$ (5.97 g, 9.42 mmol) C_3F_6 (34.53 mmol consumed, 34.73 mmol added)	3 days, neat	AsF_3 (1.73 g), 7.45 g polysulphides (85% $(C_3F_7)_2S_3$, 15% $(C_3F_7)_2S_4$ traces $(C_3F_7)_2S_x$ (x = 2, 5)) and a yellow solid (1.94 g)	70% As 95% F 71% S
(2) $S_8(AsF_6)_2$ (4.82 g, 7.60 mmol) C_3F_6 (22.0 mmol consumed, 51.0 mmol added)	3 days SO_2 solvent (6.3 g)	SOF_2, AsF_3 (0.9 g), 4.74 g polysulphides (22% $(C_3F_7)_2S_3$, 38% $C_3F_7S_3CF(CF_3)C(O)F$, 12% $S_3(CF(CF_3)(C(O)F))_2$, 7% $(C_3F_7)_2S_4$, 15% $C_3F_7S_4CF(CF_3)(C(O)F)$, 5% unidentified component (possibly $(C_3F_7)_2S_5$ or $S_4(CF(CF_3)(C(O)F))_2$, and traces of $C_3F_7S_5CF(CF_3)(C(O)F)$, $(C_3F_7)_2S_2$, $C_3F_7S_2CF(CF_3)(C(O)F)$, $S_2(CF(CF_3)(C(O)F)_2$, $(CF_3)(C(O)F)CFS_3CF(C(O)F)_2$, and $S_3(CFC(O)F)_2)_2$) and a yellow solid (2.47 g)	45% As 80% F 60% S
(3) $Se_4(AsF_6)_2$ (7.24 g, 10.42 mmol) (*i*) C_2F_4 (19.60 mmol consumed, 45.6 mmol added)	14 days, neat	C_2F_6, AsF_3 (1.25 g), 3.46 g polyselenides (9% $(C_2F_5)_2Se$, 87% $(C_2F_5)_2Se_2$, and 4% unidentified component (*m/e* 350, possibly $(C_2F_5)_2SSe$), traces of $(C_2F_5)_2Se_3$) and a yellow solid (3.9 g)	45% As 27% F 41% Se
(*ii*) Low pressure reaction (*ca.* 1 atm in a 50 cm^3 Monel line)		Gave a similar distribution of polyselenides to that in 3 (*i*).	
(4) $Se_4(AsF_6)_2$ (7.38 g, 10.63 mmol) C_2F_4 (22.20 mmol consumed, 45.5 mmol added)	14 days, SO_2 solvent (7.2 g)	Traces of SOF_2, CO, $CF_3C(O)F$, and AsF_3 (0.6 g), polyselenides (1.71 g; 1% $(C_2F_5)_2SSe$, 16% $CF_3Se_2C_2F_5$, 42% $(C_2F_5)_2Se_2$, 31% $C_2F_5Se_2CF_2C(O)F$, and 9% unidentified components (possibly $CF_3Se_2CF_2C(O)F$ and $Se_2(CF_2C(O)F)_2$), and traces of $(C_2F_5)_2Se_3$, $(C_2F_5)_2Se$, $(CF_3)_2Se_2$) and a yellow solid (6.1 g)	21% As 12% F 18% Se

[a]Room temperature throughout.
[b]For definition of yields see section 1.

TABLE 3. Reactions of $S_8(Sb_2F_{11})_2$ and $S_4(Sb_2F_{11})_2$ with C_2F_4

Reactants	Conditions[a]	Products	Yield[b]
(*a*) $S_4(Sb_2F_{11})_2$ (1.40 g, 1.36 mmol) (See Prep. *D*) C_2F_4 (4.76)[c]	14 days, pressure C_2F_4 < *ca.* 0.2 atm	0.44 g liquid[d] 1.98 g orange solid	44% S
(*b*) $S_4(Sb_2F_{11})_2$ (4.45 g, 4.31 mmol) (See Prep. *A*) C_2F_4 (16.10)[c]	7 days, pressure C_2F_4 *ca.* 17 atm	1.43 g liquid[d] 5.94 g yellow solid	49% S
(*c*) $S_8(Sb_2F_{11})_2$ (1.05 g, 0.90 mmol) (See Prep. *F*) C_2F_4 (3.06)[c]	7 days, pressure C_2F_4 *ca.* 1 atm	0.19 g liquid[d] 1.17 g green solid	17% S
(*d*) Unfiltered $S_8(Sb_2F_{11})_2 \cdot xSbF_3 \cdot ySbF_5$ (4.22 g) (See Prep. *F*) C_2F_4 (21.8)[c]	7 days, pressure C_2F_4 *ca.* 1 atm	1.90 g liquid[d] 6.12 g green solid	42% S

[a]Room temperature throughout.
[b]For definition of yield see section 1.
[c]C_2F_4 consumed in mmol.
[d]Light blue colour.

possible molecular ions $C_6F_{12}S_2$, $C_4F_8S_2$, and C_4F_8S. 83% of the available sulphur was incorporated into the liquid polysulphides. An amount of 3.14 g unidentified solid remained.

Reactions were also carried out at various pressures of C_2F_4. In one reaction (Table 3, part *a*) the polysulphides contained: 6% $C_8F_{16}S_3$, 35% $C_2F_5S_2C_4F_9$, 17% $(C_4F_9)_2S_2$, 3% unidentified component (possibly $C_6F_{12}S_2$), 25% $(C_2F_5)_2S_2$, 13% $C_4F_9SC_2F_5$, and 2% $(C_2F_5)_2S$. Traces of other species were not identified. Under the conditions of high pressure of C_2F_4, the reaction (Table 3, part *b*) gave polysulphides containing 58% (the sum of $(C_2F_5)_2S_2$ and $C_4F_9SC_2F_5$), 37% $C_4F_9S_2C_2F_5$, 2% $(C_4F_9)_2S_2$, 2% $C_8F_{16}S_2$, and 2% $(C_2F_5)_2S$. Less intense molecular ions and fragments were attributable to $(C_2F_5)_2S_4$, $(C_2F_5)_2S_3$, $C_8F_{16}S_3$, and probably $C_6F_{12}S_2$, $C_4F_8S_2$, and C_4F_8S.

(7) Reaction of Solid $S_8(Sb_2F_{11})_2$ with C_2F_4

$S_8(Sb_2F_{11})_2$ (4.37 g, 3.76 mmol; see Prep. *E*) was reacted with excess C_2F_4 (23.95 mmol) in a 30 cm^3 glass vessel and allowed to stand at room temperature for 4 days. Volatiles removed at −78°C contained C_2F_4 (13.54 mmol consumed) and traces of C_2F_6, SiF_4, OSF_2, and $(C_2F_5)_2S_3$. A volatile clear liquid (2.23 g) was removed at room temperature containing 22% $(C_2F_5)_2S_2$, 71% $(C_2F_5)_2S_3$, and 7% $(C_2F_5)_2S_4$. A grey-green solid (3.49 g) remained. 64% of the available sulphur was incorporated into the liquid polysulphides.

A reaction was carried out at low pressure of C_2F_4 (3.10 mmol consumed) (*i.e.*, pressure maintained at *ca.* 1 atm in a 50 cm^3 Monel vacuum line) (Table 3, part *c*). The light blue liquid (0.19 g) contained 80% $(C_2F_5)_2S_2$, 8% $C_4F_9S_2C_2F_5$, 5% $(C_2F_5)_2S_3$, 4% $C_8F_{16}S_2$, and 4% unidentified components. A reaction (Table 3, part *d*) was also undertaken using unpurified $S_8(Sb_2F_{11})_2$ with C_2F_4 (21.80 mmol consumed) at low pressure (*ca.* 1 atm). The sulphides contained 88% $(C_2F_5)_2S_2$, 4% $C_4F_9S_2C_2F_5$, 4% $C_8F_{16}S_2$, 2% $(C_2F_5)_2S_3$, 1% $(C_2F_5)_2S$ as well as traces of $C_8F_{16}S_3$, and unidentified components (possibly containing $C_6F_{12}S_2$, $C_4F_8S_2$, and C_4F_8S).

(8) Reaction of Solid $S_4(Sb_2F_{11})_2$ with C_3F_6

Solid $S_4(Sb_2F_{11})_2$ (3.86 g, 2.7 mmol) (Prep. *B*) was reacted with excess C_3F_6 (5.8 mmol) for 3 days. A yellow liquid (0.88 g) contained 60% $(C_3F_7)_2S_2$, 28% $C_6F_{12}S_3$, 5% unidentified component (probably $C_6F_{12}S_4$), and 7% of components possibly containing $(C_3F_7)_2S$ and $C_6F_{12}S_2$. 43% of the available sulphur was incorporated into the liquid polysulphides. An amount of 3.9 g unidentified solid was also obtained. The solid product (11.29 g) obtained from a similar reaction was further reacted with C_3F_6 (3.53 mmol) at 100°C for 3 days. The liquid polysulphides (1.98 g) obtained contained 91% $(C_3F_7)_2S$, 9% $C_6F_{12}S_2$, and small amounts of $(C_3F_7)_2S_2$. An unidentified solid (9.84 g) remained.

(9) Reaction of Solid Triphenyl Phosphine with $C_6F_{12}S_3$

$C_6F_{12}S_3$ (0.19 g, 0.48 mmol) obtained from the previous reaction and purified by preparative vpc (96% pure) was reacted with excess triphenylphosphine (0.26 g, 0.99 mmol) at room temperature in a 10 cm^3 glass reaction vessel. After 3 h, a clear liquid (0.16 g) was distilled from the reaction mixture. Vapour phase chromatography and mass spectrum analysis of the product showed 55% conversion to $C_6F_{12}S_2$.

Results and Discussion

The reactions of $S_8(AsF_6)_2$ and C_2F_4 in SO_2 solution at room temperature yield $(C_2F_5)_2S_4$, $C_2F_5S_4CF_2C(O)F$, $CF_3S_4C_2F_5$, $(C_2F_5)_2S_3$, $C_2F_5S_3CF_2C(O)F$, $CF_3S_3CF_2C(O)F$, $S_3(CF_2C(O)F)_2$, $CF_3S_3C_2F_5$, and traces of related species. This confirms our preliminary results (2). The major carbonyl species, $C_2F_5S_3CF_2C(O)F$,

TABLE 4. Schematic representation of the ^{19}F nmr spectra[a] of $(C_2F_5)_2S_x$ ($x = 2, 3, 4$), $C_2F_5S_3CF_2C(O)F$, $(C_3F_7)_2S_3$, and $C_3F_7S_3CF(CF_3)(C(O)F)$

Compound	Shift CF_3	Shift CF_2	$J_{CF_3-CF_2}$[b]
(*i*) $(C_2F_5)_2S_2$	83.2	95.0	1.2
$(C_2F_5)_2S_3$	83.2	96.0	2.7
$(C_2F_5)_2S_4$	83.1	94.3	2.8

(*ii*)

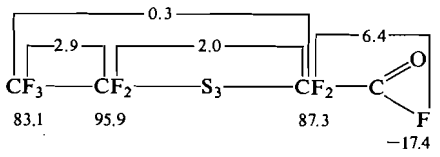

(*iii*)

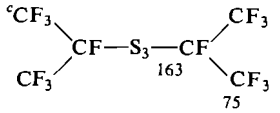

(*iv*)

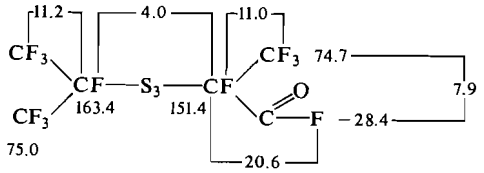

[a]$CFCl_3$ internal standard, all chemical shifts quoted are in ppm, coupling constants are in cps.
[b]Apparent coupling constants are given, although spectra are complex.
[c]Chemical shifts obtained under low resolution scan (accuracy ±1 ppm). Other chemical shifts accurate to ±0.1 ppm.

was isolated and characterized by ^{19}F nmr (Table 4) and mass spectroscopy (Table 5). The ^{19}F nmr of $S_2(CF_2C(O)F)_2$ (7) and the related sulphide $CF_3S_2C(O)F$ (8) have been reported. Similar products were observed in the reaction of $Se_8(AsF_6)_2$ and C_2F_4 in SO_2 solution. $S_8(AsF_6)_2$ reacts with C_2F_4 in SO_2 at −78°C to give $(CF_3)_2S_2$ and $CF_3S_2C_2F_5$. Compounds containing the carbonyl fluoride moiety were not observed. Low temperatures may favour increased formation of $(C_2F_5S_2CF_2C(O))^+$ $(AsF_6)^-$ involving participation of the solvent SO_2 in the reaction. Such salts may readily lose CO via routes outlined in ref. 3 yielding CF_3 derivatives (*i.e.*, $C_2F_5S_2CF_3$). Knunyants *et al.* (9) have reported a reaction of sulphur, the stronger acceptor SbF_5 and C_2F_4 in SO_2 to give $(C_2F_5)_2S_x$ and $CF_3S_xC_2F_5$ ($x = 2, 3$).

Solid $S_8(AsF_6)_2$ reacts with C_2F_4 at ambient temperature and at −78°C to yield AsF_3, $(C_2F_5)_2S_x$, $x = 2, 3, 4$. Reevaluation of the previous data (2) shows that the vpc distributions were in error due to misassignment of AsF_3 for $(C_2F_5)_2S_2$ and therefore $(C_2F_5)_2S_3$ was identified as $(C_2F_5)_2S_2$ (*i.e.*, 80% $(C_2F_5)_2S_2$ (2) should read 80% $(C_2F_5)_2S_3$). High resolution ^{19}F nmr spectra are given in Table 4. Coupling constants are quoted although the spectra are complex. Similar complexity was observed for bis(perfluoroethyl)selenides and tellurides (3, 4). The ^{19}F nmr spectra of perfluorobutane (10) has been analysed as a $(AA'X_3)_2$ system and the complexity of our spectra may, in part, be of similar origin. The ^{19}F nmr spectrum of $(C_2F_5)_2S_2$ has been previously reported (2, 9, 11). Previous results (2) were incorrect due to misassignment (see above).

Reaction of $S_8(AsF_6)_2$ and C_3F_6

Solid $S_8(AsF_6)_2$ reacts with perfluoropropylene to yield AsF_3, $S_x[CF(CF_3)_2]_2$ $x = 3, 4$, and traces $x = 2, 5$. A mass spectrum (Table 5) and ^{19}F nmr spectrum of isolated $(C_3F_7)_2S_3$ (Table 4) was consistent with the presence of

TABLE 5. Mass spectra of $C_8F_{16}S_3$, $(C_3F_7)_2S_3$, $(C_2F_5)_2S_3$, $C_2F_5S_3CF_2C(O)F$, $C_3F_7S_3CF(CF_3)(C(O)F)$, $C_6F_{12}S_3$, $C_4F_9S_2C_2F_5$, $(C_3F_7)_2S_2$, $C_8F_{16}S_2$, $(C_2F_5)_2S_2$, $(C_3F_7)_2S$ based on ^{32}S and ^{12}C[a]

Compound	Mass spectra
$C_8F_{16}S_3$	496 $C_8F_{16}S_3$ (47), 427 $C_7F_{13}S_3$ (20), 413 $C_8F_{15}S$ (34), 377 $C_6F_{11}S_3$ (84), 281 C_6F_{11} (24), 264 $C_4F_8S_2$ (33), 245 $C_4F_7S_2$ (50), 232 C_4F_8S (28), 231 C_5F_9 (54), 195 $C_3F_5S_2$ (100), 181 C_3F_7 (65), 163 C_3F_5S (98), 145 $C_2F_3S_2$ (100), 119 C_2F_5 (99), 113 C_2F_3S (100), 94 C_2F_2S (96), 76 CS_2 (51), 69 CF_3 (100)
$(C_3F_7)_2S_3$	434 $C_3F_7S_3C_3F_7$ (29), 265 $C_3F_7S_3$ (86), 233 $C_3F_7S_2$ (27), 96 S_3 (65), 69 CF_3 (100)
$(C_2F_5)_2S_3$	334 $C_2F_5S_3C_2F_5$ (64), 215 $C_2F_5S_3$ (64), 183 $C_2F_5S_2$ (40), 132 C_2F_4S (61), 119 C_2F_5 (23), 82 CF_2S (40), 69 CF_3 (100)
$C_2F_5S_3CF_2C(O)F$	312 $C_2F_5S_3CF_2C(O)F$ (38), 215 $C_2F_5S_3$ (89), 193 $S_3CF_2C(O)F$ (25), 183 $C_2F_5S_2$ (35), 161 $S_2CF_2C(O)F$ (19), 119 C_2F_5 (76), 96 S_3 (25), 83? (58), 82 CF_2S (100), 69 CF_3 (100)
$C_3F_7S_3CF(CF_3)(C(O)F)$	412 $C_3F_7S_3CF(CF_3)(C(O)F)$ (27), 265 $C_3F_7S_3$ (100), 243 $S_3CF(CF_3)(C(O)F)$ (25), 233 $C_3F_7S_2$ (10), 182 C_3F_6S (10), 132 C_2F_4S (28), 113 C_2F_3S (27), 96 S_3 (47), 69 CF_3 (100)
$C_6F_{12}S_3$	396 $C_6F_{12}S_3$ (54), 327 $C_5F_9S_3$ (60), 313 $C_6F_{11}S$ (36), 214 $C_3F_6S_2$ (53), 195 $C_3F_5S_2$ (25), 164 $C_2F_4S_2$ (26), 145 $C_2F_3S_2$ (58), 113 C_2F_3S (58), 94 C_2F_2S (20), 76 CS_2 (18), 69 CF_3 (100)
$C_4F_9S_2C_2F_5$	402 $C_4F_9S_2C_2F_5$ (26), 283 $C_4F_9S_2$ (15), 245 $C_4F_7S_2$ (11), 183 $C_2F_5S_2$ (92), 164 $C_2F_4S_2$ (16), 131 C_3F_5 (16), 119 C_2F_5 (100), 113 C_2F_3S (100), 100 C_2F_4 (19), 82 CF_2S (65), 69 CF_3 (93)
$(C_3F_7)_2S_2$	402 $C_3F_7S_2C_3F_7$ (34), 233 $C_3F_7S_2$ (100), 164 $C_2F_4S_2$ (10), 113 C_2F_3S (47), 100 C_2F_4 (13), 69 CF_3 (83)
$C_8F_{16}S_2$	464 $C_8F_{16}S_2$ (4), 445 $C_8F_{15}S_2$ (46), 395 $C_7F_{13}S_2$ (100), 345 $C_6F_{11}S_2$ (100), 232 C_4F_8S (66), 213 C_4F_7S (56), 163 C_3F_5S (100), 144 C_3F_4S (46), 131 C_3F_5 (33), 125 C_3F_3S (82), 119 C_2F_5 (100), 113 C_2F_3S (100), 94 C_2F_2S (100), 69 CF_3 (100)
$(C_2F_5)_2S_2$	302 $C_2F_5S_2C_2F_5$ (99), 283 $C_2F_4S_2C_2F_5$ (28), 183 $C_2F_5S_2$ (74), 164 $C_2F_4S_2$ (27), 119 C_2F_5 (99), 82 CF_2S (28), 69 CF_3 (100)
$(C_3F_7)_2S$	370 $C_3F_7SC_3F_7$ (23), 351 $C_3F_7SC_3F_6$ (43), 301 $C_3F_7SC_2F_4$ (78), 182 C_3F_6S (26), 169 C_3F_7 (100), 119 C_2F_5 (55), 100 C_2F_4 (26), 69 CF_3 (100)

[a]Obvious impurity peaks were deleted. Peaks of intensity < 10, and m/e < 69 were excluded.

the isopropyl isomer, and chemical shifts are very similar to those reported for bis(perfluoroisopropyl) monosulphide (12) (78 ppm (CF_3), 166 ppm (CF)) and bis(heptafluoroisopropyl) disulphide (75 ppm (CF_3), 164 ppm (CF)) (9).

The reactions carried out in SO_2 solution gave additional products incorporating the carbonyl fluoride moiety. The structure of the major carbonyl species isolated from the reaction products, $C_3F_7S_3CF(CF_3)(C(O)F)$, has been established from its mass spectrum (Table 5) and ^{19}F nmr (Table 4). Species involving elimination of CO were not detected. Carbonyl species obtained from reactions of $S_8(AsF_6)_2$ with C_2F_4 and C_3F_6 in SO_2 solution (*i.e.*, $C_2F_5S_xCF_2C(O)F$, $C_3F_7S_xCF(CF_3)(C(O)F)$, etc.) have not been previously reported with the exception of $S_2(CF_2C(O)F)_2$ (7).

Reaction of $Se_4(AsF_6)_2$ with C_2F_4

C_2F_4 reacts with solid $Se_4(AsF_6)_2$ to yield $(C_2F_5)_2Se_2$, small amounts of $(C_2F_5)_2Se$, and probably traces of $(C_2F_5)_2SSe$ and $(C_2F_5)_2Se_3$. (Sulphur is an impurity in the selenium used to make $Se_4(AsF_6)_2$.) The reaction carried out in liquid SO_2 gives additional products containing carbonyl fluoride groups as well as those involving elimination of CO (*i.e.*, $CF_3Se_2C_2F_5$). The carbonyl fluorides and related species are similar to those obtained in reactions of C_2F_4 and $Se_8(AsF_6)_2$ in SO_2 (3).

Reactions of $S_4(Sb_2F_{11})_2$ and C_2F_4

Solid $S_4(Sb_2F_{11})_2$ containing $SbF_3{\cdot}SbF_5$ and/or SbF_3 reacts vigorously with C_2F_4 at ambient pressure and temperature. A blue liquid is obtained containing $C_8F_{16}S_3$, $(C_2F_5)_2S_2$, $C_4F_9S_2C_2F_5$, $(C_4F_9)_2S_2$, $C_8F_{16}S_2$, $(C_2F_5)_2S$, and small amounts of $(C_2F_5)_2S_4$, $(C_2F_5)_2S_3$, $C_4F_9S_3C_2F_5$, $C_4F_9SC_2F_5$. $C_4F_9S_2C_2F_5$, $C_8F_{16}S_2$, and $C_8F_{16}S_3$ were isolated by preparative vpc and further characterized by their ^{19}F nmr and mass spectra. Structural identification of $C_4F_9S_2C_2F_5$ as perfluoro(3-methyl propyl, ethyl)disulphide **1** is based on its mass spectrum (Table 5) which gives a molecular ion and major fragments $C_4F_9S_2$, $C_2F_5S_2$, and its ^{19}F nmr spectrum (Table 6) which shows the presence of the $CF_3CF_2S_x$ and $CF_3CF_2CF(CF_3)S_x$ groups. The related species $(CF_3CF_2CF(CF_3)S)_2$ has been reported (13). Structural formulation of $C_8F_{16}S_2$ as perfluoro-(2,4-dimethyl, 2,4-diethyl)-1,3-dithietane **2** is based on its mass spectrum which gives a molecular ion and fragments (Table 5) and its ^{19}F nmr spectrum (Table 6) which is consistent with the related compound **3** (14).

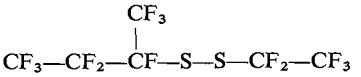

1

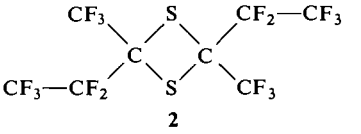

2

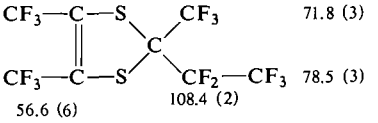

3

TABLE 6. ^{19}F nmr spectra of $C_2F_5CF(CF_3)S_2C_2F_5$, $C_8F_{16}S_2$, and $C_8F_{16}S_3$[a]

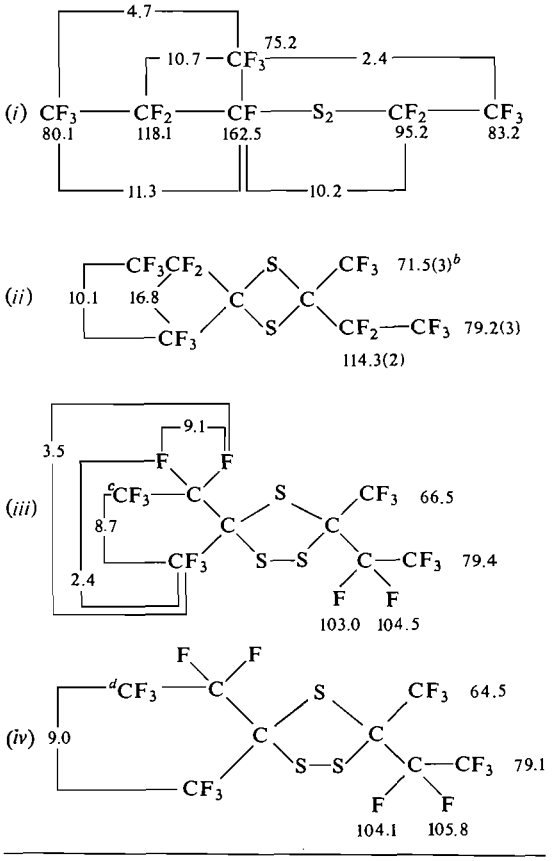

Chemical shift in ppm relative to CCl_3F (relative area in parentheses)

[a]CCl_3F internal standard, chemical shifts in ppm, coupling constants in cps.
[b]Relative area in parentheses.
[c]*cis* and *trans* isomers were both present, although we are unable to determine which data correspond to which isomer.
[d]High resolution spectra for one isomer was poor and only partial coupling constants were obtained.

High resolution ^{19}F nmr spectra of **2** reveal a complex, asymmetrical spectrum for the CF_2 group possibly due to restricted rotation about the CF_2 to ring carbon bond. Irradiation of the CF_3—C group (71.5 ppm) in a decoupling experiment resulted in collapse of the CF_2 group (114.3 ppm) to a singlet. Irradiation of the other CF_3 group (79.2 ppm) did not change

the complex structure of the CF_2 peak (114.3 ppm). **2** is designated as having the *trans* configuration although this has not been proved. Synthesis of **2** via dimerization of perfluorobutene-2-thione has been reported (13). ^{19}F nmr and mass spectra however were not given. $C_8F_{16}S_3$ assignment as perfluoro(3,5-dimethyl, 3,5-diethyl)-1,2,4-trithiolane, **4**, is consistent with its fragmentation pattern in the mass spectrum (Table 5).

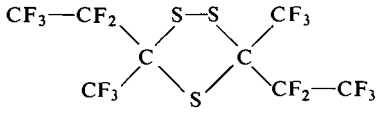

4

High resolution ^{19}F nmr of **4** (Table 6) combined with a series of irradiation experiments has established the presence of two sets of data consistent with the existence of two (probably *cis* and *trans*) isomers. Irradiation of the CF_3—C (66.5 ppm) group resulted in collapse of the CF_3—CF_2 (79.4 ppm) quartet and partial collapse of the CF_2 (104.5 ppm, 103.0 ppm) multiplet. Irradiation of the CF_3—CF_2 (79.4 ppm) group resulted in partial collapse of the CF_3—C (66.5 ppm) multiplet. Irradiation of the 103.0 ppm nuclei of the CF_2 group resulted in partial collapse of the CF_3—C (66.5 ppm) and 104.5 nuclei (CF_2 group) multiplet. Complementary experiments with the second isomer gave similar results and in both cases establish which nuclei are coupled. Related examples of non-equivalent methylene fluorines and hydrogens have been discussed by Mislow and Raban (15). The ^1H nmr of 3,5-dialkyl-1,2,4-trithiolanes (16) shows two isomers for each trithiolane as well as different conformers of each isomer at low temperatures.

Reaction of $S_8(Sb_2F_{11})_2$ and C_2F_4

In one reaction solid $S_8(Sb_2F_{11})_2$ reacts with C_2F_4 to yield $(C_2F_5)_2S_x$, $x = 2$, 3, 4. Other reactions gave mainly $(C_2F_5)_2S_2$ and small amounts of $C_4F_9S_2C_2F_5$, $(C_2F_5)_2S_3$, $(C_2F_5)_2S$, and $C_8F_{16}S_2$. Similar products were observed for reactions with $S_4(Sb_2F_{11})_2$ and C_2F_4 but in larger yields. In cases where $C_4F_9S_2C_2F_5$ and $C_8F_{16}S_2$ type products were found the amount of antimony pentafluoride consumed in preparing $S_8(Sb_2F_{11})_2$ was greater than that for the stoichiometric reaction. These products are therefore attributed to the presence of $S_4(Sb_2F_{11})_2$ in $S_8(Sb_2F_{11})_2$ reactant or more likely to some $S_8(Sb_3F_{16})_2$ which accounts for the formation of these species (see below).

Reaction of $S_4(Sb_2F_{11})_2$ with C_3F_6

Solid $S_4(Sb_2F_{11})_2$ reacts with perfluoropropylene at room temperature to yield predominantly $((CF_3)_2CF)_2S_2$ and $C_6F_{12}S_3$. At 100°C $S_4(Sb_2F_{11})_2$ and C_3F_6 react to yield largely $((CF_3)_2CF)_2S$ and smaller amounts of $(C_3F_7)_2S_2$ and $C_6F_{12}S_2$. $((CF_3)_2CF)_2S$ was characterized by its mass spectrum (Table 5). ^{19}F nmr spectra (Table 6) of perfluoro(3,3,5,5-tetramethyl)-1,2,4-trithiolane ($C_6F_{12}S_3$), **5**, gave a singlet at 66 (± 1) ppm suggesting rapid equilibrium between ring conformers thus rendering the CF_3 groups equivalent. The mass spectrum gave a fragmentation pattern (Table 5) quite similar to **4** suggesting their structures are similar.

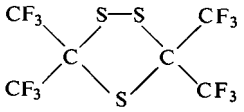

5

Raman spectra obtained for **2**, **4**, and **5** are also quite similar (Table 7). Based on C—S stretch assignments for $(CF_3)_2S_x$ ($x = 1$, 2) (17), $(C_2F_5)_2S_x$ ($x = 2 \rightarrow 4$) (18), and tetrafluoro-1,3-dithietane (19), it is probable that peaks observed at 420 ($C_8F_{16}S_3$, **4**), 424 ($C_6F_{12}S_3$, **5**), and 472 cm^{-1} ($C_8F_{16}S_2$, **2**) are of similar origin.

It is expected that $C_8F_{16}S_3$, **4**, should give a strong S—S stretch in the 500–550 cm^{-1} region (17, 18) and the medium, polarized band observed at 541 cm^{-1} is given this tentative assignment. The band at 538 cm^{-1} for $C_6F_{12}S_3$ may also be an S—S stretching vibration. Bands centered at about 750 cm^{-1} for **2**, **4**, and **5** are assigned as CF_3 deformation modes consistent with other CF_3-containing molecules (17). Complexity of this mode for the fluoroalkyl trithiolane **4** (754, 750, and 740 cm^{-1}) suggests the presence of different isomers confirmed by its ^{19}F nmr spectrum (Table 6). Raasch (20) has reported that similar compounds (*i.e.* trithiolanes) undergo reaction with triphenylphosphine resulting in sulphur abstraction and conversion to 1,3-dithietanes. A similar reaction with **5** gave perfluoro(2,2,4,4-tetramethyl)-1,3-dithietane, **6**, identified by a singlet (73.4 $\pm$ 1 ppm) in the ^{19}F nmr.

TABLE 7. Raman spectra in cm^{-1} of $C_8F_{16}S_3$, $C_6F_{12}S_3$, $C_8F_{16}S_2$

Compound	Raman spectra
$C_8F_{16}S_3$	1327(w), 1126(br), 1056(br), 754(s), 750(s), 740(vs), 718(w), 628(w), 620(w), 591(w), 560(w), 552(w), 541(s), 528(w), 450(m), 420(vs), 385(w), 370(m), 364(m), 350(w), 338(m), 308(s), 285(w), 271(m), 246(s), 230(m), 210(s), 192(w), 184(s), 170(w), 147(w), 130(w), 118(s), 92(m)
$C_6F_{12}S_3$	1291(vw), 1270(w), 1208(w), 1160(vw), 934(w), 907(vw), 847(w), 756(m), 744(vs), 704(w), 563(w), 555(m), 538(s), 424(vs), 395(m), 392(m), 362(w), 339(m), 325(m), 304(m), 276(m), 247(s), 216(m), 181(m), 171(w), 134(s), 78(w)
$C_8F_{16}S_2$	1332(w), 1252(br), 1218(br), 1184(vw), 1068(w), 911(w), 748(vs), 714(w), 634(w), 592(w), 564(w), 548(w), 532(m), 518(m), 472(s), 449(m), 436(w), 396(w), 387(w), 363(m), 348(w), 334(w), 328(w), 307(m), 298(w), 288(w), 240(s), 218(w), 188(w), 179(w), 154(w), 135(s), 82(s,br)

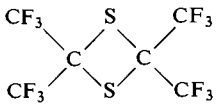

6

This is consistent with ^{19}F nmr data reported by Knunyants and co-workers (21) (singlet +70.4 ppm; CCl_3F external standard; recalculated) and Middleton *et al.* (13) (singlet +74.8 ppm; CCl_3F external standard). The perfluoroalkyl 1,2,4-trithiolanes **4** and **5** have not been previously reported.

Solids obtained from all the reactions were not identified. In most cases they are mixtures probably containing unreacted polycation and/or the respective element. They also may contain material related to the products of the reaction of bis(perfluoroethyl) diselenide and antimony pentafluoride (22).

The reactions previously described complete a series of reactions of S, Se, and Te polycations with C_2F_4. The mechanism postulated for these reactions (2–4) and those of Knunyants and co-workers for a related system (9), are applicable to the formation of the straight chain products of the type $(C_2F_5)_2S_x$. We note the intermediate $S_xC_2F_5^+$ is similar to the recently characterised S_7I^+ (23). The reactivity of the polyatomic cations towards C_2F_4 appears to increase as its size decreases (*e.g.* Se_4^{2+} is more reactive than Se_8^{2+} and Te_4^{2+}).

Reactions involving electrophilic addition of C_2F_4 which is typical for olefins are much less common for perfluoroolefins and have been recently reviewed (24, 25). It has been established by Knunyants and Polishchuk (26) that increased replacement of fluorine on C_2F_4 by fluorocarbon alkyl groups leads to decreasing ease of electrophilic attack. We observe a reaction scale consistent (see [3]) with these observations.

[3] $F_2CCF_2 \approx CF_3FC{=}CF_2 > (CF_3)FC{=}CF(CF_3)$

Products of type $C_4F_9S_xC_2F_5$, $(C_4F_9)_2S_x$ (x = 1, 2, 3), and $C_8F_{16}S_x$ (x = 2, 3) which account for 50% of the liquid polysulphides obtained from reaction of $S_4(Sb_2F_{11})_2$ and C_2F_4 cannot be accounted for by previous mechanisms. In the presence of antimony pentafluoride C_2F_4 may dimerize to give $CF_2{=}CF{-}CF_2{-}CF_3$ which may then react with the polyatomic cations leading to branched chain products.

Precedence for the electrophilic dimerization of a perfluorolefin in the presence of antimony pentafluoride has been established for hexafluoropropylene (27). Knunyants and co-workers have reported a reaction of Se, SbF_5, and C_2F_4, C_3F_6 in SO_2 solution (28) to give $(C_2F_5)_2Se_2$ (C_2F_4 reaction); $(C_3F_7)_2Se_x$ (x = 1, 2) and **7** (C_3F_6 reaction). However, products of type $C_4F_9S_xC_2F_5$, $(C_4F_9)_2S_x$, and dithietanes were not reported for the analogous sulphur system (9).

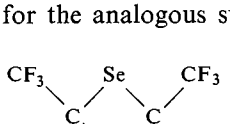

7

The mechanism for formation of 1,3-dithietanes may be similar to that outlined by Knunyants

and co-workers (28) and involve thioketones. One fraction of the volatile components from our reaction products was a deep blue liquid which decolourized on standing consistent with the presence of perfluorobutane-2-thione, C_4F_8S (13). 1,2,4-Trithiolanes may be formed by a related route. Reactions involving C_3F_6 and C_2F_4 presumably occur in a similar manner.

In reactions with four membered rings, $Se_4(AsF_6)_2$ and $S_4(Sb_2F_{11})_2$, some $(C_2F_5)_2Se$ and $(C_2F_5)_2S$ are formed. These species were not detected even in trace quantities by mass spectra for reactions of $S_8(AsF_6)_2$, $S_{16}(AsF_6)_2$, and $Se_8(AsF_6)_2$ with C_2F_4. This is probably a consequence of the greater oxidizing potential in the $S_4(Sb_2F_{11})_2$ and $Se_4(AsF_6)_2$ systems leading to more extensive S—S, Se—Se bond cleavage. Yakobson and co-workers (29, 30) have shown that bis(perfluorophenyl) polysulphides and -selenides react with SbF_5 in the presence of C_6F_5H to form bis(perfluorophenyl) monosulphide and -selenide. A similar reaction may be operative for our system involving intermediates of the type $(C_2F_5Se)_3^+$ or $(C_2F_5Se)_{2n}^{n+}$ identified in our recent work (22) and related sulphur compounds by Yakobson and co-workers (31). These intermediates may further react with perfluorolefin followed by fluoride ion abstraction to give bis(perfluoroalkyl) monosulphide and -selenide. Breakdown of long chain perfluoroalkyl polysulphides and -selenides may proceed by a similar mechanism to give shorter chain products rather than direct cleavage of S—S, Se—Se bonds by AsF_5 or SbF_5 as previously suggested (2–4).

Acknowledgements

We thank the National Research Council of Canada for financial support. We are also indebted to Grace S. H. Chen for preliminary studies on the $S_8(Sb_2F_{11})_2$ and C_2F_4 reaction, and to E. Keith Richardson and Dr. R. Kaiser for the ^{19}F nmr spectra, and Heather Schroeder for a fine ^{19}F nmr spectra of **4**.

1. R. J. GILLESPIE and J. PASSMORE. Advances in inorganic chemistry and radiochemistry. Vol. 17. *Edited by* H. J. Emeléus and A. G. Sharpe. Academic Press, London. 1975. p. 49 and references therein.
2. H. L. PAIGE and J. PASSMORE. Inorg. Chem. **12**, 593 (1973).
3. C. D. DESJARDINS and J. PASSMORE. J. Chem. Soc. Dalton, 2314 (1973).
4. (*a*) H. L. PAIGE and J. PASSMORE. Inorg. Nucl. Chem. Lett. **9**, 277 (1973); (*b*) C. D. DESJARDINS, H. L. PAIGE, J. PASSMORE, and P. TAYLOR. J. Chem. Soc. Dalton, 488 (1975).
5. R. J. GILLESPIE, J. PASSMORE, P. K. UMMAT, and O. C. VAIDYA. Inorg. Chem. **10**, 1327 (1971).
6. R. J. GILLESPIE and P. K. UMMAT. Can. J. Chem. **48**, 1239 (1970).
7. W. R. BRASEN, H. N. CRIPPS, C. G. BOTTOMLEY, M. W. FARLOW, and C. G. KRESPAN. J. Org. Chem. **30**, 4188 (1965).
8. A. HAAS, H. REINKE, and J. SOMMERHOFF. Angew. Chem. Intern. Ed. **9**, 466 (1970).
9. G. G. BELEN'KII, YU. L. KOPAEVICH, L. S. GERMAN, and I. L. KNUNYANTS. Dokl. Akad. Nauk SSSR, **201**, 603 (1971).
10. R. K. HARRIS and C. M. WOODMAN. J. Mol. Spectrosc. **26**, 432 (1968).
11. C. T. RATCLIFFE and J. M. SHREEVE. J. Am. Chem. Soc. **90**, 5403 (1968).
12. R. M. ROSENBERG and E. L. MUETTERTIES. Inorg. Chem. **1**, 756 (1962).
13. W. J. MIDDLETON, E. G. HOWARD, and W. H. SHARKEY. J. Org. Chem. **30**, 1375 (1965).
14. J. S. JOHAR and R. D. DRESDNER. Inorg. Chem. **7**, 683 (1968).
15. K. MISLOW and M. RABAN. Topics in stereochemistry. Vol. 1. *Edited by* N. L. Allinger and E. L. Eliel. Interscience, New York. 1967. p. 1.
16. S. B. TJAN, J. C. HAAKMAN, C. J. TEUNIS, and H. G. PEER. Tetrahedron, **28**, 3489 (1972).
17. H. A. CARTER, C. S.-C. WANG, and J. M. SHREEVE. Spectrochim. Acta, **29A**, 1479 (1973).
18. C. D. DESJARDINS and J. PASSMORE. J. Fluorine Chem. **9**, 53 (1977).
19. J. R. DURIG and R. C. LORD. Spectrochim. Acta, **19**, 769 (1963).
20. M. S. RAASCH. J. Org. Chem. **35**, 3470 (1970).
21. B. L. DYATKIN, S. R. STERLIN, L. G. ZHURAVKOVA, B. I. MARTYNOV, E. I. MYSOV, and I. L. KNUNYANTS. Tetrahedron, **29**, 2759 (1973).
22. J. PASSMORE, E. K. RICHARDSON, and P. TAYLOR. J. Chem. Soc. Dalton, 1006 (1976).
23. J. PASSMORE, P. TAYLOR, T. K. WHIDDEN, and P. WHITE. J. Chem. Soc. Chem. Commun. 689 (1976).
24. R. D. CHAMBERS and R. H. MOBBS. Advances in fluorine chemistry. Vol. 4. *Edited by* M. Stacey, J. C. Tatlow, and A. G. Sharpe. Butterworths, London. 1965. p. 50.
25. B. L. DYATKIN, E. P. MOCHALINA, and I. L. KNUNYANTS. Fluorine chemistry reviews. Vol. 3. *Edited by* Paul Tarrant. Marcel Dekker Inc., New York. 1969. p. 45.
26. I. L. KNUNYANTS and V. R. POLISHCHUK. Russ. Chem. Rev. **44**, 339 (1975).
27. YU. L. KOPAEVICH, G. G. BELEN'KII, E. I. MYSOV, L. S. GERMAN, and I. L. KNUNYANTS. Zhur. Vsesoyuz. Khim. obshch. im. D. I. Mendeleeva, **17**, 236 (1972).
28. YU. L. KOPAEVICH, G. G. BELEN'KII, L. S. GERMAN, E. I. MYSOV, and I. L. KNUNYANTS. Zhur. Vsesoyuz. Khim. obshch. im. D. I. Mendeleeva, **17**, 226 (1972).
29. G. G. YAKOBSON, G. G. FURIN, and T. V. TERENT'EVA. Zhur. Org. Khim. **10**, 799 (1974).
30. G. G. FURIN, T. V. TERENT'EVA, and G. G. YAKOBSON. Zhur. Org. Khim. **9**, 2206 (1973).
31. G. G. FURIN, L. N. SHCHEGOLEVA, and G. G. YAKOBSON. Zhur. Org. Khim. **11**, 1290 (1975).

Réaction oscillante de Belousov. 2. Etude d'un nouveau modèle cinétique[1]

GUY SCHMITZ
Faculté des Sciences Appliquées, Université Libre de Bruxelles, Bruxelles, Belgium
Reçu le 28 janvier 1976[2]

GUY SCHMITZ. Can. J. Chem. **55**, 3147 (1977).

Sur base de nos résultats concernant la réaction bromate–céreux nous proposons et discutons un nouveau modèle cinétique pour la réaction oscillante de Belousov–Zhabotinskii. L'existence d'un cycle limite est prouvée à l'aide d'un calculateur analogique pour un choix semi-empirique des paramètres cinétiques.

GUY SCHMITZ. Can. J. Chem. **55**, 3147 (1977).

On the basis of our results dealing with the bromate–cerous reaction we propose and discuss a new kinetic model for the Belousov–Zhabotinskii oscillating reaction. The existence of a limiting cycle is shown with an analog computer for a set of semi-empirically chosen kinetic parameters.

Introduction

Dans la première partie de ce travail (1) nous avons étudié la cinétique de l'une des composantes de la réaction oscillante de Belousov (2): l'oxydation du sulfate céreux par le bromate de potassium en solution sulfurique. Le modèle cinétique adopté nous a permis de rendre compte de nos résultats expérimentaux dans un très large domaine de concentrations initiales et est en accord avec les observations des autres auteurs (3, 4). Notre but est maintenant de montrer que ce modèle, complété par les réactions de réduction des ions cériques par les acides maloniques et bromomaloniques, peut expliquer les oscillations de concentrations observées pendant la réaction de Belousov.

Après une brève partie expérimentale nous détaillons le modèle proposé et discutons la cinétique des réactions qui le composent. Nous indiquons ensuite comment on peut comprendre intuitivement le comportement du système au cours d'une oscillation. Ce raisonnement intuitif ne suffisant pas à prouver que le modèle possède des caractéristiques impliquant de telles oscillations, nous avons tenu à étudier le système d'équations différentielles associé. Une étude très détaillée n'est cependant pas possible, trop de constantes cinétiques étant encore inconnues. Bien plus, malgré l'important travail de Jwo et Noyes (5), le mécanisme de réduction des ions cériques par les acides maloniques et bromomaloniques n'est pas entièrement élucidé. Il faut donc renoncer à retrouver par calcul le détail des courbes expérimentales. Notre but moins ambitieux a cependant été atteint: pour un choix semi-empirique des paramètres cinétiques en variables réduites nous avons vérifié, à l'aide d'un calculateur analogique, qu'un cas particulier de notre modèle conduit à des oscillations des concentrations des ions bromures et cériques.

Résultats expérimentaux

Plusieurs caractéristiques de la réaction de Belousov sont actuellement bien établies (3, 6–11). Les oscillations se produisent en phase homogène et ne résultent pas de phénomènes de transport. Les principaux produits de la réaction sont l'acide bromomalonique et le dioxyde de carbone. Les ions bromures jouent un rôle cinétique important et leur concentration oscille avec la même fréquence que le rapport Ce(III)/Ce(IV). On peut également obtenir des systèmes oscillants en remplaçant l'acide malonique par d'autres acides carboxyliques; de même le cerium peut être remplacé par le manganèse ou la ferroine.

En solution non agitée le couplage entre la cinétique de ce type de réaction et la diffusion peut conduire à l'apparition de bandes de concentration se propageant dans le système ou structures spatiales (12–15).

Les aspects théoriques et expérimentaux des oscillations chimiques ont été passés en revue par Nicolis et Portnow (16) et tout récemment par Gray (17).

[1]La publication de cet article a été retardée à la demande de la rédaction.

[2]Revision reçue le 26 août 1976.

En utilisant la technique expérimentale décrite antérieurement (1) nous avons enregistré quelques exemples d'oscillations en phase homogène. Dans l'ensemble les courbes obtenues sont analogues à celles obtenues par d'autres auteurs et, en particulier, à celles de Noyes et coll. (10). L'avantage de notre technique est de donner simultanément et avec une très bonne précision les concentrations en ions bromures et cériques. Un exemple à une échelle montrant les détails d'une oscillation est donné par la fig. 1. On remarque qu'il n'y a pas concordance exacte entre les positions des extrema des deux concentrations.

Le comportement des solutions en fin de réaction est tout à fait différent selon que l'on a initialement un excès de bromate ou d'acide malonique (figs 2 et 3). Avec un excès de bromate les oscillations s'amortissent et leur période s'allonge suite à la diminution de la concentration des réactifs. Par contre avec un excès d'acide malonique on a un comportement plus surprenant: l'amplitude et la fréquence des oscillations varient peu mais lorsque la concentration en bromate devient trop faible les ions céreux ne sont plus oxydés. Les oscillations s'arrêtent brusquement sans amortissement alors qu'il reste à la fois du bromate et de l'acide malonique dans le système. L'addition d'une petite quantité de bromate à ce moment les fait redémarrer immédiatement. Zhabotinskii (7) avait déjà signalé cet arrêt brutal des oscillations mais sans le relier à un niveau critique de la concentration en bromate.

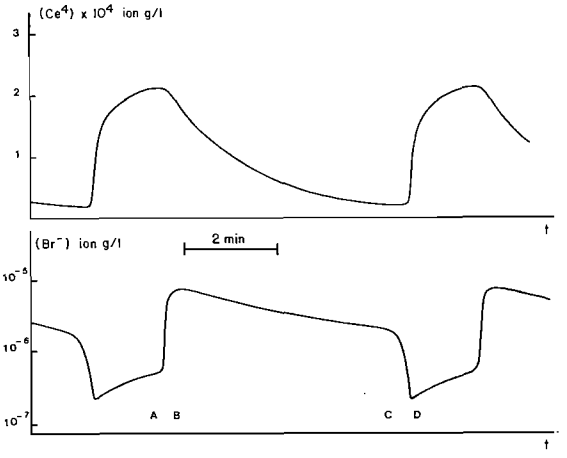

FIG. 1. Détails d'une oscillation: $-[KBrO_3] = 2 \times 10^{-2}$ *M*, $[CH_2(COOH)_2] = 3 \times 10^{-2}$ *M*, [Ce]total $= 10^{-3}$ *M*, $[H_2SO_4] = 1$ *M*, 23°C.

Modèle cinétique

Le cerium étant présent en petites quantités comme catalyseur, la réaction considérée correspond globalement à l'oxydation de l'acide malonique par le bromate. Elle résulte de trois réactions partielles que nous envisagerons successivement, l'oxydation du Ce(III) par le bromate, la formation de l'acide bromomalonique et la réduction du Ce(IV) par les acides malonique et bromomalonique. La stoechiométrie du système étudié ne résulte pas cependant d'une simple somme des stoechiométries de ces trois réactions partielles prises isolément. Par exemple l'acide formique qui semble être un produit final de la réduction du Ce(IV) par l'acide malonique ne se retrouve pas parmi les produits de la réaction oscillante (18). Jwo et Noyes ont étudié les réactions possibles du Ce(IV) et mis en évidence leur complexité (5). Ils sont cependant d'avis que cela a peu d'importance pour expliquer l'existence des oscillations (19). C'est ce que nous pensons également à condition de se limiter à l'aspect qualitatif du phénomène.

1. Oxydation du Ce(III) par le bromate

Le mécanisme de cette réaction a été établi dans la première partie de ce travail (1).

[1] $BrO_3^- + Br^- + 2H^+ \rightleftharpoons Br_2O_2 + H_2O$

[2] $Br_2O_2 + H_2O \rightleftharpoons HBrO_2 + HOBr$

[3] $HBrO_2 + Br^- + H^+ \rightarrow 2HOBr$

[4] $HBrO_2 + Br_2O_2 \rightleftharpoons 2BrO_2^{\cdot} + Br^- + H^+$

[5] $BrO_2^{\cdot} + Ce^{3+} + H^+ \rightleftharpoons HBrO_2 + Ce^{4+}$

L'acide hypobromeux formé peut être converti en brome suivant l'équilibre

$$HOBr + Br^- + H^+ \rightleftharpoons Br_2 + H_2O$$

Rappelons les caractéristiques principales de ce mécanisme. Lorsque la concentration du bromure dans le système est élevée elle maintient celles de $HBrO_2$ et de $BrO_2^{\cdot}$ très petites et le cerium n'est pas oxydé. La stoechiométrie est alors

[*A*] $BrO_3^- + 2Br^- + 3H^+ \rightarrow 3HOBr$

La concentration du bromure diminuant celle de $HBrO_2$ augmente. Lorsque l'on atteint une concentration critique la vitesse des pas [4] et [5] cesse d'être négligeable et la réaction d'oxydation des ions céreux prend une allure autocatalytique. La concentration en bromure

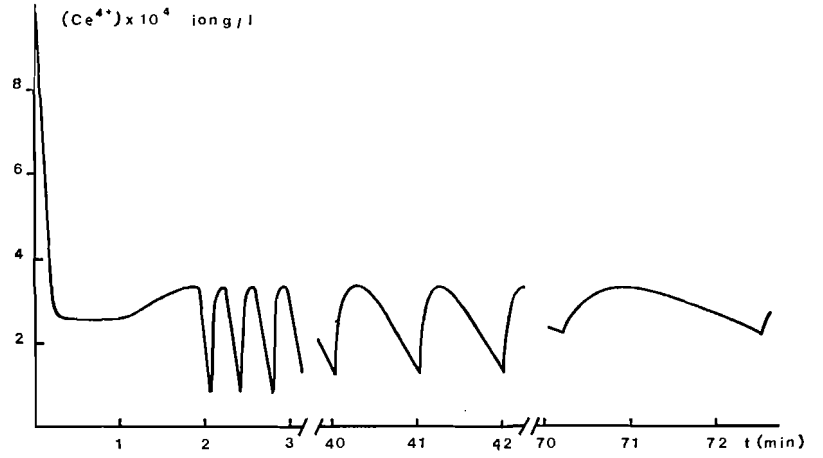

FIG. 2. Evolution de la fréquence et de l'amplitude des oscillations avec un excès de bromate: $-[KBrO_3] = 6.6 \times 10^{-2}$ *M*, $[CH_2(COOH)_2] = 3.3 \times 10^{-2}$ *M*, [Ce]total = 10^{-3} *M*, $[H_2SO_4] = 1$ *M*, 23°C.

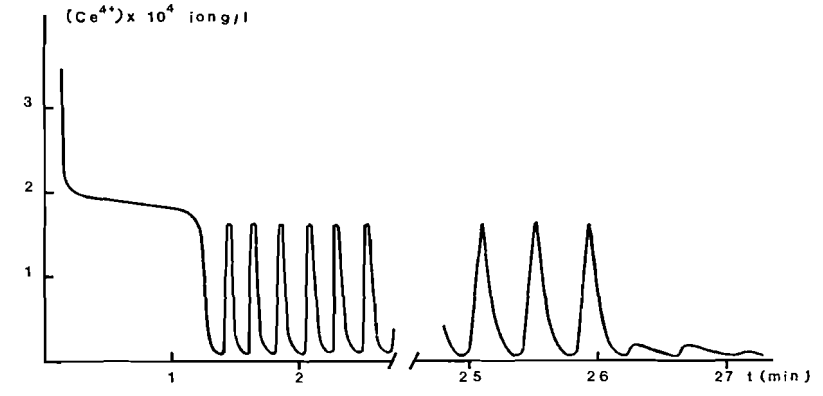

FIG. 3. Evolution de la fréquence et de l'amplitude des oscillations avec un excès d'acide malonique: $-[KBrO_3] = 5 \times 10^{-2}$ *M*, $[CH_2(COOH)_2] = 0.1$ *M*, [Ce]total = 10^{-3} *M*, $[H_2SO_4] = 1$ *M*, 23°C.

chute rapidement et la stoechiométrie principale devient

[*B*] $BrO_3^- + 4Ce^{3+} + 5H^+ \rightarrow HOBr + 4Ce^{4+} + 2H_2O$

2. Formation de l'acide bromomalonique

En milieu acide le brome et l'acide hypobromeux réagissent avec l'acide malonique pour donner de l'acide bromomalonique. On peut également obtenir de l'acide dibromomalonique mais suivant les résultats de Field et coll. (10) cette formation est négligeable dans les conditions de la réaction oscillante. Par contre il est possible que l'on forme un peu d'acide mono ou dibromoacétique (19).

La réaction de l'acide malonique avec le brome obéit à la loi cinétique (20, 21)

$$\frac{d}{dt}[BrCH(COOH)_2] = k[H^+][CH_2(COOH)_2]$$

Son étape déterminante est l'énolisation de l'acide catalysée par les ions H^+. Par analogie avec les autres réactions de ce type (22) nous admettons que l'énol réagit ensuite avec le cation Br^+ ce qui implique que les réactions avec le brome ou avec l'acide hypobromeux obéissent à la même loi cinétique.

Zhabotinskii (7) a recherché mais n'a pas trouvé de brome dans la solution oscillante. D'autre part les mesures d'absorbance à 400 et 500 nm de Franck et Geiseler (23) laissent présumer, mais ne prouvent pas, sa présence dans ce milieu complexe. Quoi qu'il en soit, il résulte de ce qui a été dit ci-dessus qu'au point

de vue cinétique on peut se borner à ne considérer que la réaction [6] pour la formation de l'acide bromomalonique.

[6] $HOBr + CH_2(COOH)_2 \rightarrow BrCH(COOH)_2 + H_2O$

3. Réduction du Ce(IV) par les acides maloniques et bromomaloniques

Les stoechiométries de ces deux réactions sont vraisemblablement (10, 24)

[7] $CH_2(COOH)_2 + 6Ce^{4+} + 2H_2O \rightarrow 6Ce^{3+} + HCOOH + 2CO_2 + 6H^+$

[8] $BrCH(COOH)_2 + 4Ce^{4+} + 2H_2O \rightarrow 4Ce^{3+} + HCOOH + 2CO_2 + Br^- + 5H^+$

Il est possible que le rapport $CO_2/HCOOH$ soit un peu supérieur à 2 (25) ou même, la concentration en Ce^{4+} restant très faible au cours de la réaction oscillante, un peu inférieur à 2. Cela n'aurait cependant aucune incidence notable sur la suite de notre raisonnement. On sait également qu'en présence d'ions bromures l'acide formique peut être oxydé par le Ce(IV) (5) mais cette réaction est lente et probablement négligeable à l'échelle de temps d'une oscillation.

La cinétique de la réaction [7] a été étudiée par Sengupta et Aditya (24) qui, avec un excès d'acide malonique, trouvent un ordre 1 par rapport au Ce(IV). Kasperek et Bruice (3) ont étudié les deux réactions. Ils concluent que le Ce(IV) est en partie complexé par l'acide et obtiennent dans les deux cas une loi cinétique de la forme

$$r = k \frac{[A]\, Ce(IV)_T}{K_m + [A]}$$

A désignant l'acide malonique ou bromomalonique et $Ce(IV)_T$ la concentration totale du Ce(IV). Jwo et Noyes (5) trouvent un ordre 1 dans des conditions ou $K_m \gg [A]$ mais observent une cassure dans leurs courbes cinétiques pour la réaction [8].

Lorsque les deux acides sont présents simultanément la situation est certainement beaucoup plus complexe (5), la présence d'acide malonique modifiant fortement la vitesse de production du bromure par la réaction [8]. Il subsiste donc une incertitude quant aux lois à adopter au cours de la réaction oscillante. Cela ne modifie certainement pas notre description qualitative du phénomène mais bien sa description quantitative.

Explication intuitive de l'évolution du système

Lorsque l'on introduit le cerium initialement sous la forme Ce(IV) on observe dès l'instant initial sa réduction rapide (figs 2 et 3), ce qui correspond évidemment à la réaction [7]. Simultanément si l'on a des traces de bromure elles sont oxydées par le bromate. Lorsque la concentration en bromure est devenue suffisamment faible le Ce(III) produit par la réaction [7] commence à être oxydé par le bromate suivant la stoechiométrie [*B*]. La compétition entre ces deux réactions donne une période où le rapport Ce(III)/Ce(IV) varie lentement. Que cette variation lente soit due à une compétition et non pas à la petitesse des vitesses de réactions est démontré par la production importante de CO_2 observée par Degn (8) au cours de cette période. L'acide hypobromeux produit par la réaction [*B*] brome l'acide malonique suivant [6]. La concentration de l'acide bromomalonique augmentant, la réduction du Ce(IV) ne résulte plus seulement de [7] mais également de [8]. C'est à ce moment qu'apparait le phénomène fondamental permettant de comprendre l'apparition des oscillations: si dans un système siège à la fois des réactions [*B*] et [8] la vitesse de cette dernière est assez grande, la concentration du bromure augmentera et finira par inhiber la réaction [*B*]. Degn (8) a montré que la période d'induction est raccourcie par l'introduction dans le système d'acide bromomalonique ou d'autres dérivés bromés, ce qui confirme que la fin de cette période soit liée à la production de bromure par la réaction [8] ou par une réaction analogue.

A la fin de la période d'induction la situation est identique à celle existant au point A de la fig. 1. La réaction bromate–céreux [*B*] se déroule avec une vitesse importante et tend à maintenir des concentrations quasi-stationnaires, très petite pour Br^- et relativement grande pour $HBrO_2$. Cependant la réaction [8] produit du bromure ce qui perturbe de plus en plus vite ces concentrations: l'augmentation de $[Br^-]$ provoque la diminution de $[HBrO_2]$ et de la vitesse de la réaction [*B*] qui s'oppose donc de moins en moins à l'augmentation de $[Br^-]$. On voit que l'allure autocatalytique prise par la courbe donnant la concentration du bromure ne provient pas de l'augmentation de sa vitesse de production (la vitesse de [8] varie peu) mais bien de la chute de sa vitesse de consommation par le pas [3].

Au point B de la fig. 1 le bromure a atteint une concentration telle que la réaction [*B*] est inhibée et remplacée par la réaction [*A*]. Le cerium n'est plus oxydé et la concentration $[Ce^{4+}]$ diminue du fait des réactions [7] et [8]. Entre les points B et C la vitesse de ces réactions diminue et la production de CO_2 tend vers son minimum (8).

Lorsque la formation de Br^- par la réaction [8] est devenue suffisamment petite l'état du système est comparable à celui existant à la fin de la période d'induction de la réaction bromate–céreux. La seule réaction importante est la réaction [*A*] qui fait diminuer $[Br^-]$ jusqu'à une valeur critique permettant le démarrage de la réaction [*B*]. $[HBrO_2]$ augmente de façon autocatalytique du fait des pas [4] et [5], $[Br^-]$ chute rapidement et les ions Ce^{3+} sont à nouveau oxydés par le bromate. L'acide hypobromeux formé brome l'acide malonique suivant [6].

Au point D de la fig. 1 le cerium est oxydé rapidement par le bromate et est réduit par les acides maloniques et bromomaloniques. La réaction [8] provoque l'augmentation de $[Br^-]$ et l'on se retrouve dans la même situation qu'au point A.

Système différentiel associé au modèle cinétique

Pour démontrer que le modèle proposé implique des oscillations du type de celles que nous venons d'expliquer intuitivement il faut étudier le système différentiel qui lui est associé. Sa complexité est cependant telle que dans le cas général et avec les moyens de calcul dont nous disposons cette étude est irréalisable. Face à ce problème on peut chercher à construire un modèle chimique moins réaliste mais plus simple dont la forme est suggérée par le modèle initial. On en trouve de nombreux exemples dans la littérature aussi bien pour la réaction de Belousov que pour d'autres réactions oscillantes.[3] Cette approche, utile sur le plan de la théorie des systèmes oscillants, ne constitue cependant pas un test sûr du modèle initial. En effet en groupant certains pas, en réduisant le nombre d'intermédiaires etc. . . . on introduit et l'on supprime certaines caractéristiques cinétiques pouvant être importantes. Nous avons donc préféré conserver le modèle général mais en limitant les développements mathématiques à des cas particuliers du système différentiel associé, choisis en fonction de leur sens physique. Si l'on peut démontrer qu'un cas particulier ainsi obtenu admet des solutions périodiques non amorties il est évident que le cas général en admet également.

Un autre résultat important de notre étude mathématique sera l'explication de la différence de comportement du système à la fin des oscillations suivant que l'on a initialement un excès de bromate ou d'acide malonique.

En désignant par r_i la vitesse globale vers la droite du pas i, le système différentiel associé à notre modèle cinétique s'écrit:

$$\frac{d[Br^-]}{dt} = -r_1 - r_3 + r_4 + r_8$$

$$\frac{d[HOBr]}{dt} = r_2 + 2r_3 - r_6$$

$$\frac{d[HBrO_2]}{dt} = r_2 - r_3 - r_4 + r_5$$

$$\frac{d[BrO_2^{\bullet}]}{dt} = 2r_4 - r_5$$

$$\frac{d[Br_2O_2]}{dt} = r_1 - r_2 - r_4$$

$$\frac{d[Ce^{4+}]}{dt} = -\frac{d[Ce^{3+}]}{dt} = r_5 - gr_8$$

Le nombre d'oscillations observées étant toujours grand les concentrations du bromate et de l'acide malonique varient très peu au cours de chaque oscillation. Mis à part les premiers temps de la réaction, il en est de même de la concentration de l'acide bromomalonique Enfin on constate expérimentalement que la concentration $[H^+]$ est quasi-constante. Nous n'écrivons donc pas d'équation différentielle pour ces concentrations et les incluons dans les constantes cinétiques.

La vitesse des pas [1] à [4] est donnée par

$$r_1 = k_1[Br^-] - k_{-1}[Br_2O_2]$$

$$r_2 = k_2[Br_2O_2] - k_{-2}[HBrO_2][HOBr]$$

$$r_3 = k_3[HBrO_2][Br^-]$$

$$r_4 = k_4[HBrO_2][Br_2O_2] - k_{-4}[BrO_2^{\bullet}]^2[Br^-]$$

Pour que la réversibilité du pas [5] apparaisse on sait (1) qu'il faut non seulement que $[Ce^{4+}]$

[3]Des modèles dans des domaines très divers ont été passés en revue récemment par Gray (17). Pour la réaction de Belousov voir les réfs 26–28.

soit grand mais également que $[Br^-]$ soit très petit. Bien que manquant d'indications quantitatives précises, nous pensons que cette réversibilité n'influence pas le déroulement de la réaction oscillante.

$$r_5 = k_5[BrO_2^{\cdot}][Ce^{3+}]$$

Si l'on tient compte de la réversibilité de ce pas on fait apparaître un nouveau point singulier instable tandis que la stabilité de celui qui nous intéressera est peu influencée.

Le pas [6] étant d'ordre zéro par rapport à HOBr sa vitesse s'écrit simplement:

$$r_6 = k_6$$

Les lois cinétiques et même la stoéchiométrie des réactions [7] et [8] prises simultanément sont, comme nous l'avons vu, mal connues. Pour des concentrations en acides malonique et bromomalonique quasi-constantes nous admettons:

$$r_8 = k_8[Ce^{4+}]$$

Le coefficient g dans l'expression de $d[Ce^{4+}]/dt$ correspond au nombre d'ions Ce^{4+} consommés par les réactions [7] et [8] lorsque la réaction [8] produit un ion bromure. Sa valeur peut être comprise entre 1 et 6 (5). Nous adopterons $g = 4$.

1. Explication de l'arrêt des oscillations à la fig. 3

On sait que des oscillations ne peuvent se produire qu'autour de points singuliers du système différentiel. Les concentrations en ces points, que nous désignerons par des valeurs surlignées, sont obtenues en annulant toutes les dérivées par rapport au temps. En posant

$$a = 3k_1k_4/4k_{-1}k_3$$

$$b = (5k_8/2k_6)c_t - 1$$

c_t = Concentration totale en cérium

$$c = 12k_{-4}k_8^2/k_1k_5^2b^2$$

on obtient notamment

$$\overline{[Br^-]} = \frac{3k_6}{5k_1}\alpha$$

$$\overline{[HOBr]} = \frac{k_3k_6}{5k_1k_{-2}}\alpha\left[1 + 3\frac{k_2}{k_{-1}}(\alpha - 1)\right]$$

$$\overline{[HBrO_2]} = k_1/\alpha k_3$$

$$\overline{[Ce^{4+}]} = 2k_6/5k_8$$

Le paramètre α étant donné par l'équation [9] on obtient deux points singuliers[4] que nous désignerons par $\alpha(+)$ et $\alpha(-)$.

$$[9] \qquad c\alpha^2 - (a - 1)\alpha + a = 0$$

Pour qu'ils aient un sens physique il faut que les trois conditions suivantes soient satisfaites.

$$[10] \qquad b > 0$$

$$[11] \qquad a > 1$$

$$[12] \qquad (a - 1)^2 > 4ac$$

La condition [10] impose une valeur minimum du rapport [acide bromomalonique]/[acide malonique] pour une concentration totale en cérium donnée. Si elle est satisfaite à un moment de l'évolution du système, elle le restera ensuite. La condition [11] impose une valeur minimale de la concentration en bromate. Dans les systèmes étudiés il est probable qu'elle est toujours satisfaite et que, comme lors de l'étude de la réaction bromate–céreux (1), on a même $a \gg 1$. La condition [12] est beaucoup plus critique car elle cessera d'être satisfaite si le rapport [bromate]/[acide malonique] devient trop petit. A ce moment les deux racines de l'équation donnant α deviennent complexes, les points singuliers du système différentiel perdent leur sens physique et dans le cas où il existait un cycle limite, il disparait. Ceci explique la différence de comportement du système en fin de réaction montrée par les figs 2 et 3. Si l'on a initialement un excès de bromate, le rapport [bromate]/[acide malonique] augmente au cours de la réaction et si la condition [12] est satisfaite, elle le reste. Si l'on a initialement un excès d'acide malonique ce rapport diminue ce qui finit par provoquer la disparition brutale du cycle limite. Une explication aussi simple d'un fait expérimental à priori assez étonnant nous parait être un argument solide en faveur de notre modèle.

2. Stabilité des points singuliers

Nous avons étudié cette stabilité par la première méthode de Liapounov (17): on linéarise le système différentiel au voisinage

[4]Bien qu'ayant toujours un sens physique le point singulier correspondant à des concentrations nulles n'apparait pas ici à cause de la loi de vitesse admise pour le pas [6]. Si la concentration en acide hypobromeux tend vers zéro cette loi ne reste évidemment pas valable et l'on doit avoir $r_6 \to 0$.

d'un point singulier et l'on étudie le signe de la partie réelle des racines de son équation caractéristique en utilisant les critères de Routh–Hurwitz (29). Les calculs, très laborieux, montrent que le point singulier correspondant à $\alpha(-)$ est toujours instable et que celui correspondant à $\alpha(+)$ peut l'être dans un domaine de valeurs des constantes cinétiques. Dans ce domaine il est possible que les solutions du système différentiel admettent un cycle limite et donc que son intégration fasse apparaître des oscillations des concentrations.

3. *Intégration du système différentiel dans un cas particulier*

L'intégration de systèmes différentiels correspondant à des modèles cinétiques tels que celui étudié ici est rendue particulièrement difficile par la présence de constantes cinétiques d'ordres de grandeur très différents. Pour ces systèmes mal conditionnés, (stiff équations) il existe des méthodes numériques (30, 31) mais les calculs sont longs et couteux. Comme de plus notre système comporte de nombreuses constantes inconnues, ce qui rend illusoire une tentative de reproduire les courbes expérimentales, nous nous sommes borné à prouver l'existence de solutions oscillantes en utilisant un calculateur analogique avec des variables réduites et l'approximation de l'état quasi-stationnaire pour les intermédiaires très réactifs $BrO_2^{\bullet}$ et Br_2O_2.

Lors de notre étude de la réaction bromate–céreux (1) nous avons considéré que l'équilibre du pas [4] n'était quasi pas perturbé. Nous admettons qu'il en est de même au cours des oscillations. En outre, ne connaissant les valeurs ni de k_1 ni de k_{-1}, nous admettons également l'équilibre du pas [1]. Cette hypothèse simplificatrice implique, outre la condition $a \gg 1$ déjà connue, que l'on oscille autour du point singulier $\alpha(+) \simeq a/c \gg 1$. Elle devrait être abandonnée pour un calcul plus élaboré car nous savons que l'équilibre du pas [1] peut être perturbé pendant la période AB de la fig. 1.

On pose:

$$[Br^-] = 10x\overline{[Br^-]} \qquad [HOBr] = 4y\overline{[HOBr]}$$

$$[HBrO_2] = 4u\overline{[HBrO_2]} \qquad [Ce^{4+}] = 2z\overline{[Ce^{4+}]}$$

$$t = \tau\overline{[Ce^{4+}]}/2k_6 \qquad a_2 = 3k_2\alpha(+)/k_{-1}$$

$$A = 10\overline{[Br^-]}/\overline{[Ce^{4+}]} \qquad B = 4\overline{[HOBr]}/\overline{[Ce^{4+}]}$$

$$C = 5\overline{[HBrO_2]}/\overline{[Ce^{4+}]}$$

Les valeurs surlignées se rapportent au point singulier $\alpha(+)$. On obtient ainsi le système différentiel que nous avons étudié.

$$A\frac{dx}{d\tau} = -a_2x + 1.6(1 + a_2)uy - 12ux + 0.4z$$

$$B\frac{dy}{d\tau} = a_2x - 1.6(1 + a_2)uy + 24ux - 0.5y/(y + \varepsilon)$$

$$C\frac{du}{d\tau} = a_2x - 1.6(1 + a_2)uy - 12ux + \frac{0.8}{b}(b + 1 - 2z)\sqrt{u}$$

$$\frac{dz}{d\tau} = \frac{0.8}{b}(b + 1 - 2z)\sqrt{u} - 0.8z$$

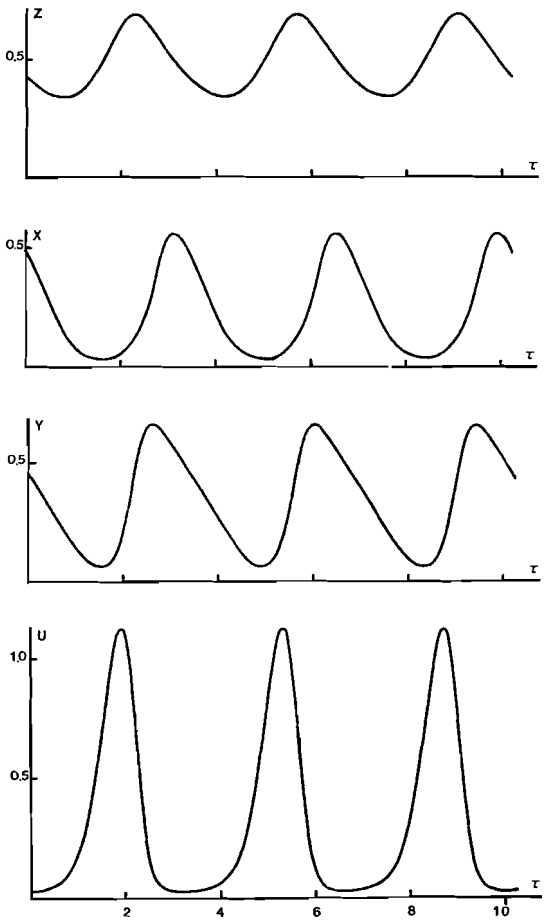

FIG. 4. Exemple d'oscillations obtenues par le calcul analogique: $a_2 = 0.1$; $b = 8$; $A = 5 \times 10^{-2}$; $B = 0.5$; $C = 0.25$; $\varepsilon = 0.01$.

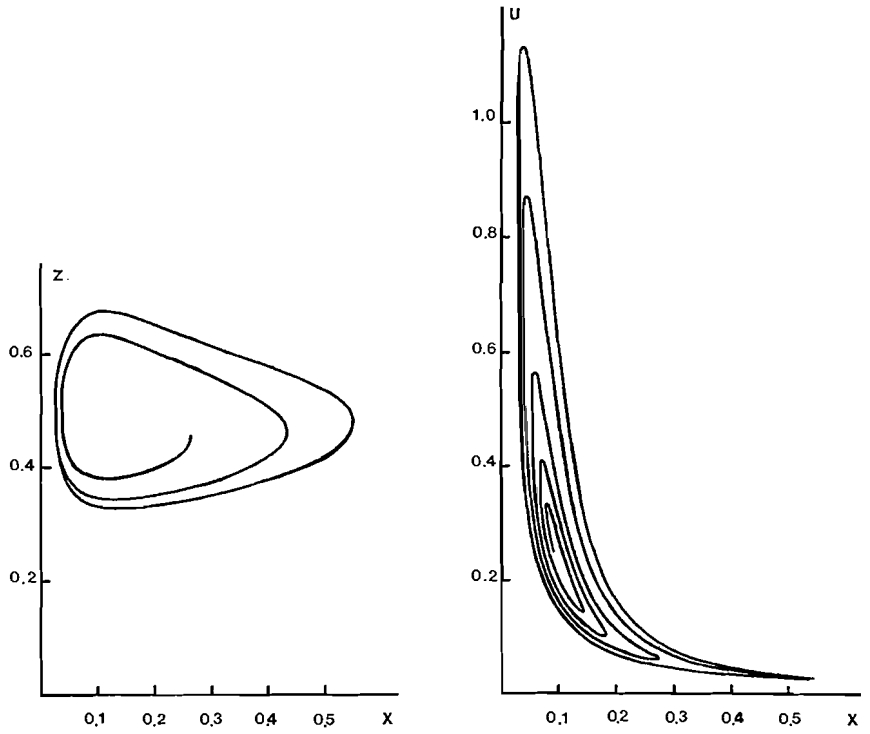

FIG. 5. Plans des phases correspondants à la fig. 4.

Nous avons du introduire le facteur $y/(y + \varepsilon)$ car sinon y tendait à devenir négatif. Cela résulte de l'ordre zéro admis pour le pas [6], ordre qui ne se maintient évidemment pas si y tend vers zéro. ε influence la position et la stabilité du point singulier mais cette influence peut être rendue négligeable en prenant ε suffisamment petit. Nous avons vérifié par le calcul analogique que pour $\varepsilon = 0.01$ la stabilité du point singulier correspond correctement aux résultats des calculs évoqués au paragraphe *2*. Lorsque ce point est instable on obtient, comme prévu, des oscillations entretenues dont un exemple est donné par les figs 4 et 5. Les valeurs de A et b correspondent à des ordres de grandeurs expérimentaux, celle de a_2 à l'idée que le pas [2] est réversible mais pas à l'équilibre, celles de B et c ne sont pas connues expérimentalement et ont été prises sans autre considération que l'instabilité du point singulier.

Le cas particulier étudié pouvant donner des oscillations il en est de même du cas général mais son étude qui devrait permettre de mieux reproduire les courbes expérimentales nécéssiterait la connaissance à priori de plusieurs constantes cinétiques ainsi que des moyens de calcul beaucoup plus puissants.

Conclusions

Sur base de nos résultats cinétiques antérieurs relatifs à la réaction bromate–céreux, nous proposons un nouveau modèle pour la réaction oscillante de Belousov. Après avoir montré intuitivement l'origine des oscillations nous avons étudié le système différentiel associé à notre modèle. Nous avons montré d'une part qu'il rend compte de la différence de comportement des solutions oscillantes en fin de réaction selon le rapport initial des concentrations du bromate et de l'acide malonique, d'autre part qu'il peut admettre des points singuliers instables. Face à la difficulté que présente l'étude de systèmes aussi complexes nous n'avons pas cherché à construire un modèle cinétique simplifié mais nous avons préféré étudier un cas particulier du système différentiel correspondant au modèle dans son intégralité. Le calcul analogique a montré que ce cas particulier peut admettre un cycle limite.

Les courbes cinétiques obtenues par le calcul

ne correspondent que qualitativement aux courbes expérimentales. Des essais d'ajustement quantitatifs nous sembleraient prématurés tant que l'on ne connait pas certaines constantes cinétiques ainsi que les lois de réduction du Ce(IV) par les acides maloniques et bromomaloniques simultanément.

Remerciements

Je remercie très vivement Monsieur le Professeur C. Herbo pour l'intérêt qu'il a porté à ce travail. Les nombreuses discussions que j'ai eues avec lui ont toujours été très fructueuses.

1. C. HERBO, G. SCHMITZ et M. VAN GLABBEKE. Can. J. Chem. **54**, 2628 (1976).
2. B. P. BELOUSOV. Sb. Ref. Radiat. Med. (1958) Medzig, Moscow. 1959.
3. G. J. KASPEREK et T. C. BRUICE. Inorg. Chem. **10**, 382 (1971).
4. R. C. THOMPSON. J. Am. Chem. Soc. **93**, 7315 (1971).
5. J. J. JWO et R. M. NOYES. J. Am. Chem. Soc. **97**, 5422 (1975).
6. R. M. ZHABOTINSKII. Dokl. Akad. Nauk SSSR, **157**, 392 (1964).
7. A. M. ZHABOTINSKII. Biofizika, **9**, 306 (1964).
8. H. DEGN. Nature (London), **213**, 589 (1967).
9. R. M. NOYES, R. J. FIELD et E. KOROS. J. Am. Chem. Soc. **94**, 1934 (1972).
10. R. J. FIELD, E. KOROS et R. M. NOYES. J. Am. Chem. Soc. **94**, 8649 (1972).
11. E. KOROS et M. BURGER. Ion selective electrodes. Symposium de Matrafüred, 1972. *Edité par* E. Pungor. Akadémian Kiado, Budapest. 1973.
12. H. BUSSE. J. Phys. Chem. **73**, 750 (1969).
13. A. N. ZAIKIN et A. M. ZHABOTINSKII. Nature (London), **225**, 535 (1970).
14. A. T. WINFREE. Science, **181**, 937 (1973).
15. R. J. FIELD et R. M. NOYES. J. Am. Chem. Soc. **96**, 2001 (1974).
16. G. NICOLIS et J. PORTNOW. Chem. Rev. **73**, 365 (1973).
17. B. F. GRAY. *Dans* Reaction kinetics. Vol. 1. The Chemical Society, London. 1975.
18. L. BORNMANN, H. BUSSE et B. HESS. Z. Naturforsch. Teil C, **28**, 514 (1973).
19. R. M. NOYES et J. J. JWO. J. Am. Chem. Soc. **97**, 5431 (1975).
20. R. W. WEST. J. Chem. Soc. **125**, 1277 (1924).
21. S. L. BAFNA, V. M. BHALE et W. V. BHAGWAT. Agra Univ. J. Res. Sci. **4**, 341 (1955).
22. M. JULIA. Mécanismes électroniques en chimie organique. Gauthier Villars, Paris. 1963. p. 54.
23. V. FRANCK et W. GEISELER. Naturwiss, **58**, 52 (1971).
24. K. K. SENGUPTA et S. ADITYA. Z. Phys. Chem. (Frankfurt am Main), **38**, 25 (1963).
25. H. U. WILLARD et P. YOUNG. J. Am. Chem. Soc. **52**, 136 (1930).
26. B. L. CLARKE. J. Chem. Phys. **58**, 5605 (1973).
27. R. J. FIELD et R. M. NOYES. J. Chem. Phys. **60**, 1877 (1974).
28. G. WEISBUCH, J. SALOMON et M. ATLAN. J. Chim. Phys. **72**, 71 (1975).
29. F. PORTER. Stability criteria for linear dynamical systems. Oliver and Boyd, Mech. Eng. Monograph. 1968.
30. C. W. GEAR. Numerical initial value problems in ordinary differential equations. Prentice-Hall, New Jersey. 1971.
31. G. M. COME, C. BOURLIER et C. GUILLERM. J. Chim. Phys. **72**, 123 (1975).

A comparison of mechanisms for the oxidation of cerium(III) by acidic bromate[1]

RICHARD M. NOYES
Department of Chemistry, University of Oregon, Eugene, OR, U.S.A. 97403
AND
K. BAR-ELI
Department of Chemistry, University of Tel-Aviv, Tel-Aviv, Israel and Department of Chemistry, University of Oregon, Eugene, OR, U.S.A. 97403

Received January 14, 1977

RICHARD M. NOYES and K. BAR-ELI. Can. J. Chem. **55**, 3156 (1977).

The preceding paper by Schmitz suggests a mechanism of the oscillating Belousov–Zhabotinsky reaction that differs significantly from the mechanism previously proposed by Field, Körös, and Noyes. The most important differences are associated with the mechanism assumed for the oxidation of cerium(III) by bromate. The alternative mechanisms for this oxidation are examined and compared with relevant experimental information on similar systems. We conclude the mechanism developed by Schmitz and associates is inconsistent with several observations and that it is doubtful it can be the correct interpretation of this reaction.

RICHARD M. NOYES et K. BAR-ELI. Can. J. Chem. **55**, 3156 (1977).

La communication précédente par Schmitz suggère un mécanisme pour la réaction oscillante de Belousov–Zhabotinsky qui diffère d'une façon importante du mécanisme proposé antérieurement par Field, Körös et Noyes. Les différences les plus importantes sont reliées au mécanisme présumé pour l'oxydation du cérium(III) par le bromate. On fait un examen des mécanismes alternatifs pour cette oxydation et on les compare avec les informations expérimentales disponibles pour des systèmes similaires. On conclut que le mécanisme développé par Schmitz et ses associés n'est pas en accord avec plusieurs observations et qu'il est peu probable qu'il puisse expliquer correctement cette réaction.

[Traduit par le journal]

Introduction

The Belousov–Zhabotinsky (2, 3) reaction is of interest because it is one of very few known oscillating chemical reactions taking place in homogeneous solution. Schmitz (4) has proposed a mechanism for this reaction that differs significantly from that previously proposed by Field *et al.* (5). Both mechanisms generate unstable steady states for certain combinations of rate constants, but they differ primarily in their explanation of the oxidation of cerium(III) by bromate ion. The purpose of this paper is to compare the two mechanistic proposals for this critical component of the oscillating system.

General Characteristics of Reaction

There have been several recent experimental studies of this reaction (6–10). It starts with an induction period of difficultly reproducible length during which initial traces of bromide ion are consumed and no cerium(III) is oxidized. If the initial bromide ion concentration is no more than about 1% that of bromate, the appropriate stoichiometry is that of equation [T1]. If more bromide is present initially, Br_2 will be produced in amount comparable to or greater than that of HOBr.

$$[T1] \qquad BrO_3^- + 2Br^- + 3H^+ \rightarrow 3HOBr$$

After the induction period is over, reaction with the stoichiometry of equation [T2] is suddenly initiated. Thermodynamic calculations confirm that this is the principal stoichiometry to be expected in systems containing a considerable excess of bromate ion. However, the final product should be mostly Br_2 when cerium(III) is in considerable stoichiometric excess. Nevertheless, Thompson (8) reports the final product is HOBr even under these conditions; the reasons the system does not react further must be kinetic rather than thermodynamic.

$$[T2] \qquad BrO_3^- + 4Ce^{3+} + 5H^+ \rightarrow HOBr + 4Ce^{4+} + 2H_2O$$

[1]This is paper No. 20 in the series "Oscillations in Chemical Systems"; for part 19 see ref. 1.

Assignment of Elementary Processes

Reactions [T1] and [T2] certainly do not take place in single steps. There have been two detailed efforts to devise a set of elementary processes generating the observed experimental facts (9, 11). They agree in ascribing significance to the three steps with [C] designations.

[C1] $HBrO_2 + Br^- + H^+ \rightleftarrows 2HOBr$

[C2] $HOBr + Br^- + H^+ \rightleftarrows Br_2 + H_2O$

[C3] $BrO_2\cdot + Ce^{3+} + H^+ \rightleftarrows HBrO_2 + Ce^{4+}$

The mechanism of Noyes *et al.* (11), hereafter designated NFT, includes the four other steps with [A] designations.

[A1] $BrO_3^- + Br^- + 2H^+ \rightleftarrows HBrO_2 + HOBr$

[A2] $BrO_3^- + HBrO_2 + H^+ \rightleftarrows 2BrO_2\cdot + H_2O$

[A3] $BrO_2\cdot + Ce^{4+} + H_2O \rightleftarrows BrO_3^- + Ce^{3+} + 2H^+$

[A4] $2HBrO_2 \rightleftarrows BrO_3^- + HOBr + H^+$

These seven elementary processes include only one species for each oxidation state of bromine and assume proton transfers to and from oxygen and bromine are so rapid that acid–base equilibria are maintained at all times. Four species contain one bromine atom in each odd oxidation number from -1 to $+5$, and steps [C1], [A1], and [A4] represent the only ways they could be interchanged by oxygen atom transfers. Steps [C2] and [A2] represent the ways even oxidation numbers 0 and $+4$ could be formed reversibly from the species with adjacent odd oxidation numbers. Cerium ions can only undergo one-equivalent changes, and steps [C3] and [A3] represent the only ways they could react with $BrO_2\cdot$ radicals. Step [A3] was originally (11) proposed to explain the dramatic slowing of the reaction long before the equilibrium of process [T2] is approached. It involves formation of a Br—O bond, while step [C3] is a simple electron transfer. The modeling calculations of Barkin *et al.* (10) subsequently demonstrated that step [A3] could be omitted entirely and that the slowing of reaction rate arose because the equilibrium constant for step [C3] is not much over 0.01 M^{-1}.

The alternative mechanism of Herbo *et al.* (9), hereafter designated HSV, omits the [A] steps and proposes three others with [B] designations.

[B1] $BrO_3^- + Br^- + 2H^+ \rightleftarrows Br_2O_2 + H_2O$

[B2] $Br_2O_2 + H_2O \rightleftarrows HBrO_2 + HOBr$

[B3] $HBrO_2 + Br_2O_2 \rightleftarrows 2BrO_2\cdot + Br^- + H^+$

All three steps involve the intermediate Br_2O_2, which is inferred from kinetic data without direct spectroscopic or other evidence. Two hydrolysis reactions are included for this species, and it is postulated that step [$-$B1] is much faster than [B2]. Step [B3], which produces $BrO_2\cdot$ radicals, is chemically unprecedented and contains three bromine atoms in the transition state. This high order in intermediate bromine oxidation states appears to be necessary if the HSV mechanism is to generate an unstable steady state in the Belousov–Zhabotinsky reaction (4).

General Comparison of Mechanisms

Both mechanisms can easily account for the stoichiometry of process [T1]. The NFT mechanism uses [A1] + [C1] with $HBrO_2$ the only intermediate species. The HSV mechanism replaces [A1] with [B1] + [B2] and considers Br_2O_2 another intermediate. The predictions of the two mechanisms are not significantly different during the induction period.

When the principal reaction commences, the NFT mechanism can generate the stoichiometry of process [T2] by combining three steps that treat $HBrO_2$ and $BrO_2\cdot$ as the only intermediates.

[A2] $\times$ 2 $2BrO_3^- + 2HBrO_2 + 2H^+ \rightarrow 4BrO_2\cdot + 2H_2O$

[C3] $\times$ 4 $4BrO_2\cdot + 4Ce^{3+} + 4H^+ \rightarrow 4HBrO_2 + 4Ce^{4+}$

[A4] $2HBrO_2 \rightarrow BrO_3^- + HOBr + H^+$

The HSV mechanism requires a combination of five steps to generate the same stoichiometry, and Br_2O_2, Br^-, and HOBr are also species that are both created and destroyed during the reaction.

[B1] $BrO_3^- + Br^- + 2H^+ \rightarrow Br_2O_2 + H_2O$

[B3] $\times$ 2 $2Br_2O_2 + 2HBrO_2 \rightarrow 4BrO_2\cdot + 2Br^- + 2H^+$

[C3] $\times$ 4 $4BrO_2\cdot + 4Ce^{3+} + 4H^+ \rightarrow 4HBrO_2 + 4Ce^{4+}$

[C1] $HBrO_2 + Br^- + H^+ \rightarrow 2HOBr$

[$-$B2] $HBrO_2 + HOBr \rightarrow Br_2O_2 + H_2O$

We can identify at least three ways in which the two mechanisms lead to different predictions that can be tested by means of experimental data presently available.

(*a*) The NFT mechanism regards HOBr as a product formed almost irreversibly in step [A4], while the HSV mechanism both forms this species in step [C1] and consumes it in step [−B2]. Therefore, the NFT mechanism predicts deliberate manipulation of [HOBr] should have no effect on the rate of oxidation of cerium(III), while the HSV mechanism predicts an effect.

(*b*) The NFT mechanism assumes that any Br^- initially present is destroyed by process [T1] during the induction period, and this species is at negligibly small concentration during all of the principal reaction. The HSV mechanism requires that Br^- is both created and destroyed at significant rates during most of the reaction. This requirement leads to predictions that can be tested.

(*c*) The NFT mechanism produces $BrO_2\cdot$ radicals by potentially reversible step [A2], and the HSV mechanism produces them by step [B3]. Information available on analogous systems permits definite conclusions about the relative plausibilities of these two mechanisms.

Detailed Comparison of Mechanisms

Effect of HOBr

We are not aware of any deliberate manipulations of [HOBr] during the oxidation of cerium(III), but Knight and Thompson (12) did examine effects on the analogous oxidation of neptunium(V) by bromate. They found that added HOBr shortened the induction period as would be predicted by both mechanisms. However, they found the rate of the principal reaction was not affected by addition of allyl alcohol, which is an effective scavenger for HOBr. This result is consistent with the predictions of the NFT mechanism but is inconsistent with the HSV predictions.

Effect of Br^-

Reaction [C2] has been studied kinetically by Eigen and Kustin (13). It is so rapid that equilibrium is established in much less than 1 s. If we accept the equilibrium constant used by Herbo *et al.* (9), then at all times we may assume

$$[Br^-] = 5.8 \times 10^{-9} \frac{[Br_2]}{[HOBr][H^+]}$$

As indicated above, the data of Thompson (8) in 1 *M* acid indicate that $[HOBr] \gg [Br_2]$ at least near the end of a reaction with cerium(III) in stoichiometric excess, and thermodynamic considerations suggest the inequality would be even more severe during the intermediate stages when BrO_3^- is still present in significant amount.

These restrictions create no difficulty for the NFT mechanism which considers $[Br^-]$ to be negligibly small during all of the principal reaction. However, the HSV mechanism predicts that Br^- is being produced at a rate equal to $\frac{1}{2}d[Ce^{4+}]/dt$. It is difficult to see how the inequality $[Br^-] \ll 6 \times 10^{-9}$ *M* can be maintained toward the end of the reaction unless steps [B1] and [C1] are much more rapid than is permissible even for diffusion control (14).

Mechanism of $BrO_2\cdot$ Formation

One of the greatest differences between the two mechanisms relates to the alternative steps [A2] and [B3] by which oxybromine radicals are proposed to be formed. We are not aware of any other chemical system for which a reaction like [B3] has been proposed. However, step [A2] is an exact analogue of a reaction that Taube and Dodgen (15) studied directly in the oxychlorine system. The thermodynamic estimates of Field *et al.* (5) indicate the equilibrium constant of step [A2] is not greatly different from that for the oxychlorine reaction (16), although Taube and Dodgen (15) do find the chlorine reaction is much slower than the analogous bromine one is predicted to be. An attempt to devise a mechanism for the oscillating iodate catalyzed decomposition of hydrogen peroxide (17) indicated the oxyiodine analogue of step [A2] had very similar rate and equilibrium parameters to [A2].

Further support for our rate estimates for [A2] is provided by the radiation chemical observations of Buxton and Dainton (18) on the reverse reaction. Their experiments were conducted in alkaline solution. However, if their interpretations may be extrapolated to the strongly acidic solutions employed for the oxidation of cerium(III), step [−B3] must have been much slower than step [−A2] at the very low bromide concentrations prevailing. The HSV mechanism regards step [B3] as reversible, and it then appears difficult to justify their ignoring of step [A2]. It also seems significant that Buxton and Dainton (18) found no effect of bromide ion on the rate of $BrO_2\cdot$ disproportionation even though step [B3] suggests that a large effect should have been observed.

The isotopic exchange studies of Betts and MacKenzie (19) provide still stronger evidence

for step [A2] of the NFT mechanism for radical formation. A small amount of tracer Br^- was added to an acidic solution prepared from Br_2 and BrO_3^-, and the rate of appearance of tracer in BrO_3^- was followed. The bromine species were not initially in equilibrium, and the ratio $[HOBr]/[Br^-]$ increased greatly over a period of days. During the same period, the rate at which BrO_3^- was gaining radioactivity changed by less than a factor of two. These observations seem to require that the rate-determining step for exchange of BrO_3^- and Br_2 does not involve either HOBr or Br^-; $HBrO_2$ is the only non-radical species left for consideration. It is the contention of Field *et al.* (5) that step [A2] of the NFT mechanism is also rate-determining for the isotopic exchange.

Further support for this interpretation is provided by the kinetic data of Betts and MacKenzie (19). They made a number of runs in which tracer was not added until the BrO_3^- and Br_2 had been in contact for 100 h. Although these systems had not yet attained equilibrium concentrations of HOBr, they had moved a considerable distance in that direction. Rates of exchange in those systems were proportional to $[BrO_3^-]^{1.7}[Br_2]^{0.3}$. If a single step were rate-determining for the exchange, and if all bromine species were in equilibrium, the rate of exchange would be proportional to $[BrO_3^-]^{\alpha}[Br_2]^{\beta}$ where $\alpha + 2\beta$ would equal the number of bromine atoms in the transition state and $5\alpha/(\alpha + 2\beta)$ would equal the average oxidation number of those bromines. The experimental data suggest a transition state with 2.3 bromine atoms having an average oxidation number of +3.7. Step [A2] has a transition state with 2 bromine atoms having an average oxidation number of +4 and predicts kinetics $[BrO_3^-]^{1.6}[Br_2]^{0.2}$. Step [B3] has 3 bromine atoms in a transition state having an average oxidation number of +2.33 and predicts kinetics $[BrO_3^-]^{1.4}[Br_2]^{0.8}$. The NFT prediction certainly comes much closer to fitting the experimental observations. No other step in the HSV mechanism has an average oxidation number greater than +2 for the average oxidation number of bromines in the transition state.

Summary

Overall stoichiometries like [T1] and [T2] can be established precisely if the necessary free energies are known. We can never determine with certainty the precise elementary processes by which a complicated chemical change is accomplished. It is difficult even to prove with absolute certainty that a particular mechanistic proposal is invalid. However, the accumulation of evidence can often generate a strong preference for one of two alternative mechanistic proposals. We believe such a situation applies to the present case.

The NFT (11) mechanism includes all of the possible oxygen atom transfer processes between bromine species with odd oxidation number. It includes the possible hydrolysis reactions of Br(0) and Br(IV); we have argued elsewhere (ref. 5, p. 8655) why reversible hydrolysis of Br(II) is also fast even though this process does not need to be included in the NFT mechanism. The possible reactions of cerium species with bromine dioxide free radicals are both considered, although we show (10) that only one contributes significantly. The proposed steps and rate constants for bromine reactions are also consistent with what is known about the chemistry of chlorine (15, 16) and of iodine (17), with independent studies of radiation chemistry in alkaline solution (18), and with the kinetics of isotopic exchange reactions between bromine and bromate (19). The resulting mechanism has been subjected to computer simulation (10) and found to be consistent with experimental information. We are not aware of any serious discrepancies with any known experimental facts. We therefore believe this mechanism can appropriately be applied with confidence to the still more complicated Belousov–Zhabotinsky reaction (5).

The HSV (9) mechanism omits oxygen transfer and hydrolysis steps like [A1], [A2], and [A4] for which there is considerable precedent, and it includes a peculiar [B3] step that differs from any we have seen proposed for an oxyhalogen system. This mechanism has not been subjected to computer simulation, but it predicts effects of [HOBr] manipulation different from those observed in an analogous system (12) and seems to require some bromide ion reactions to proceed at rates greater than would be permitted even for diffusion control (14). It also seems to us to be inconsistent with the results from radiation chemical (18) and isotopic exchange (19) studies. Unless these apparent inconsistencies can be explained, and unless the NFT mechanism can be proved inconsistent with some experimental fact, we believe a definite choice between the two

mechanistic proposals should strongly favor the NFT mechanism or some minor modification of it.

Acknowledgement

This work was supported in part by the Energy Research and Development Administration.

1. R. M. NOYES and R. J. FIELD. Acc. Chem. Res. In press.
2. B. P. BELOUSOV. Ref. Radiat. Med. (1958) Medgiz, Moscow. 1959. p. 145.
3. A. M. ZHABOTINSKY. Dokl. Akad. Nauk SSSR, **157**, 392 (1964); Biofizika, **9**, 306 (1964)
4. G. SCHMITZ. Can. J. Chem. This issue.
5. R. J. FIELD, E. KÖRÖS, and R. M. NOYES. J. Am. Chem. Soc. **94**, 8649 (1972).
6. V. A. VAVILIN and A. M. ZHABOTINSKY. Kinet. Katal. **10**, 83 (1969).
7. G. J. KASPEREK and T. C. BRUICE. Inorg. Chem. **10**, 382 (1971).
8. R. C. THOMPSON. J. Am. Chem. Soc. **93**, 7315 (1971).
9. C. HERBO, G. SCHMITZ, and M. VAN GLABBEKE. Can. J. Chem. **54**, 2628 (1976).
10. S. BARKIN, M. BIXON, R. M. NOYES, and K. BAR-ELI. Int. J. Chem. Kinet. In press.
11. R. M. NOYES, R. J. FIELD, and R. C. THOMPSON. J. Am. Chem. Soc. **93**, 7315 (1971).
12. G. C. KNIGHT and R. C. THOMPSON. Inorg. Chem. **12**, 63 (1973).
13. M. EIGEN and K. KUSTIN. J. Am. Chem. Soc. **84**, 1355 (1962).
14. R. M. NOYES. Prog. React. Kinet. **1**, 129 (1961).
15. H. TAUBE and H. DODGEN. J. Am. Chem. Soc. **71**, 3330 (1949).
16. W. M. LATIMER. Oxidation potentials. 2nd ed. Prentice-Hall, New York, NY. 1952.
17. K. R. SHARMA and R. M. NOYES. J. Am. Chem. Soc. **98**, 4345 (1976).
18. G. V. BUXTON and F. S. DAINTON. Proc. R. Soc. Ser. A, **304**, 427 (1968).
19. R. H. BETTS and A. N. MACKENZIE. Can. J. Chem. **29**, 655 (1951).

Substituent effects on the ^{13}C chemical shifts of monosubstituted twistanes

HELMUT BEIERBECK AND JOHN K. SAUNDERS
Département de chimie, Université de Sherbrooke, Sherbrooke (Qué.), Canada J1K 2R1

Received December 2, 1976

HELMUT BEIERBECK and JOHN K. SAUNDERS. Can. J. Chem. **55**, 3161 (1977).

The ^{13}C chemical shift data for some hydroxy, chloro, bromo, and oxo twistane derivatives are presented and compared to the shifts observed in corresponding adamantanes. The substituent effect at the α and β carbons is more pronounced in twistanes than in adamantanes. The substituent shift induced at an antiperiplanar γ carbon is shown to depend on the presence or absence of 1,3-diaxial hydrogen–hydrogen interactions between the substituted and γ carbons. If such an interaction is present the effect is of shielding whereas if it is absent, the effect is of deshielding. The deshielding effect appears to occur via a through bond interaction.

HELMUT BEIERBECK et JOHN K. SAUNDERS. Can. J. Chem. **55**, 3161 (1977).

Les déplacements chimiques du ^{13}C pour quelques hydroxy, chloro, bromo et oxo twistanes sont donnés et sont comparés aux déplacements chimiques observés dans les dérivés d'adamantane correspondants. L'effet d'un substituant sur les carbones α et β est plus grand dans les twistanes que dans les adamantanes. On démontre que le déplacement induit sur le carbone γ antiperiplanar, par un substituant, dépend de la présence ou de l'absence d'interactions hydrogène–hydrogène 1,3 diaxiales entre les hydrogènes sur le carbone substitué et le carbone γ. Si une telle interaction est présente, on observe un effet de blindage tandis que si elle est absente, le carbone γ est déblindé. Il semble que l'effet de déblindage soit dû à une interaction à travers les liaisons.

Substituent effects on ^{13}C chemical shifts have received a lot of attention since the earliest ^{13}C nmr studies (1). These studies have led to the development of empirical correlations between the substituent induced shift and the stereochemistry of the compound. Also such correlations can give insight into the fundamental interpretation of ^{13}C chemical shifts with respect to molecular and electronic structural characteristics. Molecular systems of well defined and rigid geometry provide good models for a study of the electronic effects on carbon shieldings. Adamantane is such a system, and thus the effect of substitution at either carbon 1 or 2 has been studied (2–4).

The difference in substituent induced shift at the α and β carbons between 1- and 2-substituted adamantanes is readily explained in terms of differences in *gauche* interactions (5). However, the effect at the γ carbon appears anomalous in that, for example, substitution of an OH at carbon 1 deshields the γ carbon by 2.4 ppm whereas substitution of an OH at carbon-2 results in shielding of both carbons by 6.7 and 1.2 ppm for the γ carbon *syn* and *anti* to the OH, respectively. For the carbon *syn*, the C_α—OH, C_β—C_γ bonds are in a *gauche* orientation, an orientation well known to give rise to shielding at the γ carbon, whereas for the carbon *anti*, the C_β—C_γ bond is antiperiplanar to the C—O bond, a relative orientation found for the γ carbon in 1-adamantanol.

Another class of compounds which have well defined geometry and which are relatively rigid are the twistane derivatives. However, the six membered rings in these compounds exist in a twist boat conformation in comparison with the chair conformation of adamantanes, hence the relative bond orientations are quite different in the two series of compounds. In this paper, we report the ^{13}Cmr data of a number of twistane derivatives and compare this data with that obtained in the corresponding adamantane derivatives.

Results and Discussion

The ^{13}C chemical shifts for twistane (**1**), 1-substituted twistanes (**2–4**), and 4-substituted twistanes (**5–7**) are given in Table 1 as are the data for the disubstituted adamantanes **8** and **9**. The resonances for **1** were readily assigned from the single-frequency, off-resonance decoupled (SFORD) spectrum and the relative intensities. For **2**, carbons 1, 2, 6, and 10 were assigned from the SFORD spectrum. The remaining resonances could be assigned as corresponding to either CH or CH_2 carbons but could not be assigned to a particular carbon. Consequently,

TABLE 1. Chemical shift data for twistane and adamantane derivatives[a]

	1	**2**			**3**	**4**	**5**			**6**			**7**			**8**			**9**
			Δδ[b]					Δδ[b]			Δδ[b]			Δδ[b]			Δδ[b]		
Carbon	δ	δ	Calcd.	Exp.	δ	δ	δ	Calcd.	Exp.	δ	Calcd.	Exp.	δ	Calcd.	Exp.	δ	Calcd.	Exp.	δ
1	28.4	72.4	20.4[c]	25.7	70.2	67.7	26.0	4.4	4.4	26.7	5.6	5.5	25.8	3.5	3.5	39.0	12.0	11.7	42.1
2	28.8	37.9	12.9	12.8	40.7	41.8	27.1	5.3	5.1	22.0	9.1	9.5	25.8	5.6	5.6	73.7	24.2	—[e]	69.7
3	28.4	30.2	6.0	5.9	31.3	31.6	35.0	14.0[c]	11.3	37.4	14.2	14.2	46.7	10.0[c]	7.7	39.0	11.9	11.7	42.1
4	24.4	24.0	5.1	4.8	24.4	24.7	71.2	24.7[c]	28.1	68.8	33.2[c]	31.0	212.1	13.3[c]	12.0	32.9	8.3	9.0	34.6
5	24.4	21.9	7.2	7.6	22.7	22.5	36.2	10.1	11.3	35.4	13.3	13.1	43.0	8.1	8.2	27.5	4.6	4.8	27.5
6	28.4	37.5	10.1[c]	12.1	39.7	40.6	28.8	6.6	6.7	29.1	6.3	6.3	30.1	4.7	4.5	38.3	4.3	4.8	39.5
7	28.8	29.8	5.9	5.6	30.8	31.0	29.0	8.0	7.8	28.4	5.0	5.2	31.8	4.4	4.2	27.1	6.5	6.2	27.4
8	28.4	28.6	5.2	5.4	28.0	27.1	24.6	9.1	9.2	28.2	5.9	5.9	27.2	5.1	5.3	34.4	5.6	5.5	36.0
9	24.4	26.6	5.5	5.4	27.7	28.0	24.2	3.8	3.9	24.2[d]	3.8	3.9	22.9	2.5	2.4	34.4	5.6	5.5	36.0
10	24.4	33.7	14.0	14.1	35.7	36.8	25.3	3.1	3.2	24.6[d]	3.4	3.4	24.5	2.0	2.2	32.9	8.6	9.0	34.6
CH_3																34.4	5.6	5.5	32.8

[a]In ppm relative to TMS; approximately 1 *M* in $CDCl_3$.
[b]Chemical shift changes resulting from the addition of 0.5 *M* equivalent of Pr(fod)$_3$. Calculated values obtained using expanded pseudo contact equation (6).
[c]Deleted from calculations due to the presence of contact shifts (6).
[d]Can be interchanged vertically.
[e]Not observed.

the effect of the addition of Pr(fod)$_3$ was used in order to complete the assignments. The Pr(fod)$_3$ induced shifts were treated using the McConnell equation as described previously (6). The calculated and observed induced shifts are given in Table 1. The observed resonances for **3** and **4** were assigned using the respective SFORD spectra and the recorded data for **2**. The spectra

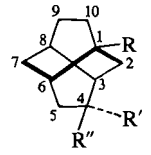

1 R = R′ = R″ = H
2 R = OH R′ = R″ = H
3 R = Cl R′ = R″ = H
4 R = Br R′ = R″ = H
5 R = R″ = H R′ = OH
6 R = R′ = H R″ = OH
7 R = H R′ + R″ = O

for the 4-substituted twistanes were assigned using the corresponding SFORD spectrum and the Pr(fod)$_3$ induced shift data given in Table 1.

The spectrum for **8**, was assigned on the basis of relative intensities, the SFORD spectrum, and the Pr(fod)$_3$ induced shift data included in Table 1. The spectrum of **9** was assigned using

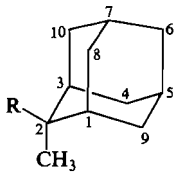

8 R = OH
9 R = Br

the relative intensities, the SFORD spectrum, and by comparison with the spectrum of **8**. Inspection of Table 1 indicates that the combination of SFORD spectra and Pr(fod)$_3$ induced shifts leads to relatively unambiguous assignments of all carbons with the possible exception of carbons 9 and 10 for compound **6**.

In Table 2 the chemical shift difference, Δδ, due to the introduction of each substituent for the twistane derivatives is compared to that observed in the corresponding adamantanes. The relative shift at the β carbon resulting from the introduction of the substituent depends on the dihedral angle between the C—X and C—H and/or C—C bonds (5). The γ carbons of the 1-twistane derivatives are deshielded, with the exception of C-5, by the introduction of a sub-

stituent, as are the γ carbons of 1-adamantanes although the magnitude is somewhat smaller in the case of the twistanes. In the adamantane compounds an approximative correlation between substituent induced shift at the γ carbon and σ* was observed (2) and thus it was concluded that the dominant factor causing the deshielding at this carbon was the through-bond interaction. If the transmission of this effect occurs by a hyperconjugative interaction (7) between the electrons of the C_β—C_γ bonds and the back lobe of the carbon sp^3 orbital of the C—X bond then this interaction will be a maximum when the C_β—C_γ and C_α—X bonds are *trans* antiperiplanar as is the case in adamantanes. The smaller shifts in twistanes are a consequence of the angle between the C_β—C_γ and C_α—X bonds differing from 180°. Although only a limited number of substituents have been studied, the same trend is apparent for both series of compounds i.e. bromine > chlorine > OH > H. Carbon 5 has a C—H bond in a pseudo 1,3-diaxial interaction with the C—X bond and will thus be shielded. For each substituent, the α shift is larger for twistanes than for adamantanes. This could also be a consequence, at least in part, of the lack of coplanarity between the C_β—C_γ and C_α—X bonds. Since the hyperconjugative effect which deshields the γ carbon will tend to shield the α carbon and, as mentioned above, this interaction will be a maximum when the C_β—C_γ and C_α—X bonds are coplanar.

The twistanols **5** and **6** exhibit both shielding and deshielding at the γ carbons whereas in 2-adamantanol both γ carbons are shielded. Recently, it has been suggested (8) that the ~5 ppm shielding of the γ carbon for C—X and C_β—C_γ in a *gauche* orientation is not a consequence of a steric interaction between the group X and a proton on the γ carbon but rather is due to the replacement of the hydrogen of the α carbon i.e.

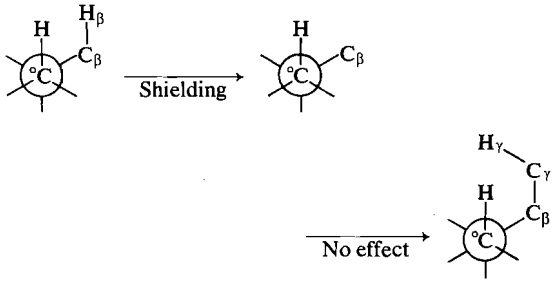

TABLE 2. Substituent effects[a] on substituted twistane and adamantane derivatives[b]: Δδ values

	1-OH		1-Cl		1-Br		Twistan-4-ols			Ketones	
Carbon	Twist.	Adam.	Twist.	Adam.	Twist.	Adam.	5	6	Adamantan-2-ol	Twistan-4-one	Adamantan-2-one
α	44.0	39.1	41.8	38.5	39.3	35.7	46.8	44.4	36.5	187.7	175.1
β	9.1(2)	7.8	11.9(2)	10.0	13.0(2)	11.5	6.6(3)	9.0(3)	6.4	18.3(3)	18.5
	9.1(6)		11.3(6)		12.2(6)		11.8(5)	11.0(5)		18.6(5)	
	8.7(10)		11.3(10)		12.4(10)						
γ	1.8(3)	2.4	2.9(3)	3.3	3.2(3)	4.1	−1.7(2)	−6.8(2)	−6.7(*syn*)	−3.0(2)	1.1(*syn*)
	−2.5(5)		−1.7(5)		−1.9(5)		0.6(6)	0.7(6)	−1.2(*anti*)	1.3(6)	
	1.0(7)		2.0(7)		2.2(7)		−3.8(8)	−0.6(8)		−1.2(8)	
	2.2(9)		3.1(9)		3.6(9)						
δ	−0.4(4)	−1.4	0 (4)	−2.0	0.3(4)	−2.1	−2.4(1)	−1.7(1)	−1.2(*syn*)	−2.6(1)	−0.9(*syn*)
	−0.2(8)		−0.4(8)		−1.3(8)		0.2(7)	−0.4(7)	−0.7(*anti*)	3.0(7)	
							−0.2(9)	−0.2(9)		−1.5(9)	
ε							0.9(10)	0.2(10)	0	0.1(10)	−1.4

[a]Negative values imply shielding.
[b]Adamantane values taken from ref. 3 with the exception of adamantan-2-one (2).

Thus the chemical shift will depend on the relative orientation of the C_α—H and C_γ—H bonds. Introduction of an electronegative substituent causes changes in valency angles of the substituted carbon and it is quite possible that the distance between the hydrogen on the α carbon and that on the γ carbon *anti* is increased upon substitution of X at the α carbon which would lead to a relative shielding of the γ carbon. The observed shift will then be a function of the through bond effect plus the effect due to a decrease in the 1,3-diaxial hydrogen–hydrogen interaction. In twistane, the two hydrogens of C-4 have pseudo 1,3-diaxial interactions with the hydrogens of carbons 2 and 8. Introduction of an OH at C-4 causes shielding of both of these carbons for both orientations of the OH group with the effect being more pronounced when the C—OH and C_β—C_γ bonds are in the pseudo *gauche* orientation. The third γ carbon, C-6, is in an orientation such that the angles between its C—H bond and the carbon–hydrogen bonds of C-4 are 90° or greater and thus introduction of an OH at C-4 results in deshielding.

The effect of introduction of an OH or Br on the chemical shift of the γ carbons in adamantane derivatives is given in Table 3. The γ carbon *syn* to the OH in **8** is shielded by 6.9 ppm relative to 2-methyladamantane (3) whereas the γ carbon *anti* is deshielded by 2.6 ppm. Thus the OH has a similar effect on the carbon *syn* to that observed in adamantan-2-ol. However, the effect on the carbon *anti* does not correlate with that observed in adamantan-2-ol, but rather to that found in adamantan-1-ol. The effect of the Br is similar in that the γ carbon *anti* is deshielded by 4.2 ppm which resembles the induced shift in 1-bromoadamantane. Thus, it appears that in order to observe an upfield shift of the γ carbon *anti*, the substituted carbon must bear a hydrogen. Eliel *et al.* (7) found that electronegative substituents on secondary or tertiary carbons shielded the γ carbon *anti* whereas Ayer *et al.* (9) observed deshielding at this carbon when the substituted carbon was quaternary.

The effect at the γ carbon (C-3) on substitution of a keto group in cyclohexane is a combination of two effects, namely a polar effect (either a through bond or a through space effect) which deshields, and the removal of one 1,3-diaxial hydrogen–hydrogen interaction which shields. This can be seen from the comparison

TABLE 3. Substituent induced shifts for adamantane[a] derivatives

Compound	γ Carbon	
	syn	*anti*
Adamantan-1-ol		2.4
Adamantan-2-ol	−6.7	−1.2
8	−6.9	2.6
1-Bromoadamantane		4.1
2-Bromoadamantane	−6.3	0.7
9	−5.8	4.2

[a]Shifts of mono substituted adamantanes taken from ref. 3.

of the chemical shifts recorded for 3,3,5-trimethylcyclohexanone (10) and 1,1,3-trimethylcyclohexane (11). For the former the quaternary carbon resonance appears at 35.1 ppm and the tertiary carbon at 29.5 ppm, whereas in the latter these carbons absorb at 31.4 and 28.9 ppm respectively. Thus the quaternary carbon is deshielded by 3.7 ppm whereas the tertiary carbon is only deshielded by 0.6 ppm. In **7**, the γ carbons (C-2 and 8) whose hydrogens had 1,3-diaxial interactions with the C-4 hydrogens in twistane, are shielded whereas the γ carbon (C-6), which did not have such an interaction, is deshielded. The results parallel those observed for OH substitution. The polar effect is probably, at least in part, a through bond effect and consequently will depend on the relative orientation of C—C and C=O bonds. Thus the magnitude of the observed shift caused by the introduction of the carbonyl group will depend on the severity of the replaced 1,3-diaxial interaction as well as the angle between the C—C and C=O bonds.

The effect of the OH group on the chemical shift of the δ carbon is of shielding, with the exception of C-7 in **5**. This is in the same direction as that observed in adamantane derivatives although, for the twistane, the numerical value is less due to lack of coplanarity between the C—X and C_β—C_γ bonds. The steric interaction between a substituent and the hydrogen of the δ carbon has been shown to deshield the δ carbon (12) which explains the downfield shift observed for C-7 in **5**. The substituent shifts for the δ carbons in **7** are somewhat larger and can in part be attributed to polar effects. Also, inclusion of an sp^2 carbon at C-4 changes the relative orientations of a number of C—H bonds and this will also influence the observed shift.

Conclusion

The shifts recorded at the γ carbons of the 1-substituted twistane derivatives agree in direction though not in magnitude to the corresponding 1-substituted adamantanes. This is interpreted as evidence for a through bond type mechanism since the substituent effect is a maximum where the C_α—X and C_β—C_γ bonds are *trans* antiperiplanar. The relatively larger α substituent effects in twistane are in agreement with this statement. The substituent shifts on γ carbons observed in 4-twistanols, 4-twistanone, and 2-adamantanols are shown to be a combination of field effects and conformational changes.

Experimental

All spectra were recorded on a Bruker HX-90 spectrometer equipped with a Nicolet 1083 computer operating in the Fourier transform mode. The compounds were analyzed as approximately 1 *M* $CDCl_3$ solutions with TMS used as internal reference. The experimental procedure for determining the effect of $Pr(fod)_3$ as well as the data analysis has been reported elsewhere (6). The calculated Pr—O internuclear distances varied between

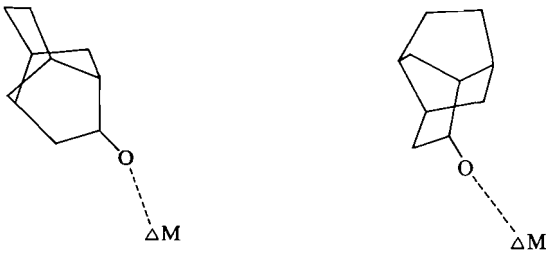

2.8 and 3.5 Å. A typical position for the Pr is shown. The syntheses and structure proof of all twistane derivatives have been given elsewhere (13). Compound **8**, 2-methyladamantan-2-ol, was prepared by the reaction of CH_3Li on adamantanone (14). Compound **9** was prepared by reacting **8** with PBr_3/HBr (15).

Acknowledgement

We are very grateful to Professor Deslongchamps for the generous donation of all twistane derivatives and to Mr. Normand Pothier for the preparation of the adamantane derivatives. Financial support from the National Research Council of Canada is also gratefully acknowledged.

1. (*a*) J. B. Stothers. Carbon-13 NMR spectroscopy. Academic Press, New York, NY. 1972; (*b*) G. C. Levy and G. L. Nelson. Carbon-13 nuclear magnetic resonance for organic chemists. Wiley-Interscience, New York, NY. 1972.
2. T. Pehk, E. Lippmaa, V. V. Sevostjanova, M. M. Krayuschkin, and A. I. Tarasova. Org. Magn. Reson. **3**, 783 (1971).
3. G. E. Maciel, H. C. Dorn, R. L. Greene, W. A. Kleschick, M. R. Peterson, and G. H. Wahl. Org. Magn. Reson. **6**, 178 (1974).
4. H. Duddeck. Org. Magn. Reson. **7**, 151 (1975).
5. H. Beierbeck and J. K. Saunders. Can. J. Chem. **54**, 632 (1976).
6. J. W. ApSimon, H. Beierbeck, and J. K. Saunders. Can. J. Chem. **51**, 3874 (1973).
7. E. E. Eliel, W. F. Bailey, L. D. Kopp, R. L. Willer, D. M. Grant, R. Bertrand, K. A. Christensen, D. K. Dalling, M. W. Duch, E. Wenkert, F. M. Schell, and D. W. Cochran. J. Am. Chem. Soc. **97**, 322 (1975).
8. H. Beierbeck and J. K. Saunders. Can. J. Chem. **54**, 2985 (1976).
9. W. A. Ayer, L. M. Brown, S. Fung, and J. B. Stothers. Can. J. Chem. **54**, 3272 (1976).
10. J. B. Stothers and C. T. Tan. Can. J. Chem. **52**, 308 (1974).
11. D. K. Dalling and D. M. Grant. J. Am. Chem. Soc. **89**, 6612 (1967).
12. S. H. Grover, J. P. Guthrie, J. B. Stothers, and C. T. Tan. J. Magn. Reson. **10**, 227 (1973).
13. A. Bélanger, Y. Lambert, and P. Deslongchamps. Can. J. Chem. **47**, 795 (1969); R. C. Bingham, P. von R. Schleyer, Y. Lambert, and P. Deslongchamps. Can. J. Chem. **48**, 3739 (1970).
14. W. J. Hickinbottom, A. A. Wyatt, and M. B. Sparke. J. Chem. Soc. 2533 (1954).
15. J. C. H. Hwa and H. Sims. Org. Synth. **41**, 49 (1961).

The comparative chemistry of ammine and methylamine complexes of rhodium(III) and cobalt(III)

THOMAS WILSON SWADDLE

Department of Chemistry, The University of Calgary, Calgary, Alta., Canada T2N 1N4

Received April 12, 1977

THOMAS WILSON SWADDLE. Can. J. Chem. **55**, 3166 (1977).

For the aquation of $(CH_3NH_2)_5RhCl^{2+}$, the first order rate coefficients are represented by $\Delta H_{aq}^* = 101.9$ kJ mol^{-1} and $\Delta S_{aq}^* = -50.2$ J K^{-1} mol^{-1} in 0.1 *M* $HClO_4$, while for base hydrolysis the rate is first order in $[(CH_3NH_2)_5RhCl^{2+}]$ and $[OH^-]$ at ionic strength 0.10 *M* and the rate coefficients (in M^{-1} s^{-1}) are represented by $\Delta H_{OH}^* = 108.6$ kJ mol^{-1} and $\Delta S_{OH}^* = 74.1$ J K^{-1} mol^{-1}. Acid dissociation constants are reported for $(RNH_2)_5MOH_2^{3+}$ (R = H or CH_3; M = Rh or Co), and these, combined with spectral data, show CH_3NH_2 to be a poorer electron donor than NH_3 in complexes of this type, contrary to expectations. The comparative kinetics of reactions of $(RNH_2)_5MCl^{2+}$ support the assignment of an I_a mechanism to aquation when M = Rh or Cr, I_d to aquation when M = Co, and D_{cb} for base hydrolysis in all these cases.

THOMAS WILSON SWADDLE. Can. J. Chem. **55**, 3166 (1977).

Pour l'aquation de $(CH_3NH_2)_5RhCl^{2+}$, dans $HClO_4$ 0.1 *M*, les coefficients de vitesse du premier ordre sont représentés par $\Delta H_{aq}^* = 101.9$ kJ mol^{-1} et $\Delta S_{aq}^* = -50.2$ J K^{-1} mol^{-1}, et pour l'hydrolyse basique à force ionique de 0.10 *M* la vitesse est du premier ordre en $[(CH_3NH_2)_5RhCl^{2+}]$ et en $[OH^-]$ et les coefficients de vitesse (en M^{-1} s^{-1}) sont représentés par $\Delta H_{OH}^* = 108.6$ kJ mol^{-1} et $\Delta S_{OH}^* = 74.1$ J K^{-1} mol^{-1}. On rapporte les constantes de dissociation acide pour $(RNH_2)_5MOH_2^{3+}$ (R = H ou CH_3; M = Rh ou Co) et ces valeurs, combinées avec des données spectrales, montrent que le CH_3NH_2 est un plus mauvais donneur d'électron que le NH_3 dans des complexes de ce type et ceci contrairement aux anticipations. Les cinétiques comparées des réactions de $(RNH_2)_5MCl^{2+}$ sont en accord avec l'attribution d'un mécanisme I_a pour l'aquation quand M = Rh ou Cr, d'un mécanisme I_d pour l'aquation quand M = Co, et D_{cb} pour l'hydrolyse basique dans tous ces cas.

[Traduit par le journal]

Introduction

The hypothesis has been advanced (1, 2) that simple ligand substitution reactions of cationic octahedral complexes in solution occur by an associative interchange (I_a) mechanism for trivalent transition metals in general, with the important exception of cobalt(III), for which a dissociative interchange (I_d) mechanism evidently operates. The term 'simple' implies exclusion of special cases, notably conjugate-base solvolysis pathways in which a dissociative (D_{cb}) mechanism is considered to be generally applicable.

If this hypothesis is valid, then the effects of replacing R = H by R = CH_3 in $(RNH_2)_5MCl^{2+}$ (hereinafter called '*N*-methylation') on the rates of chloride aquation

[1] $(RNH_2)_5MCl^{2+} + H_2O \rightarrow (RNH_2)_5MOH_2^{3+} + Cl^-$

should be qualitatively different for M = Co relative to M = Cr, Rh, etc. Indeed the methylamine complex aquates 22 times more *rapidly* than the ammine for M = Co, but 33 times more *slowly* when M = Cr, at 298 K (3–5). In the simplest view, this can be attributed to the different roles of steric effects in the mechanistic dichotomy (1, 6–8), since it is known (9) that marked steric compression exists in both of these methylamine complexes, although there are fewer nonbonded contacts in the chromium one (as expected, since the ionic radius of Cr^{3+} is 61.5 pm as opposed to 52.5 pm for Co^{3+} (10)). We may therefore naively predict that $(CH_3NH_2)_5RhCl^{2+}$ should aquate more slowly than $(NH_3)_5RhCl^{2+}$, if the mechanism is indeed I_a, but that the rates should be more nearly equal than in the chromium(III) analogues, since the relatively large radius of Rh^{3+} (67 pm) (10) should reduce the number of nonbonded contacts in $(CH_3NH_2)_5MCl^{2+}$ still further.

On the basis of a common conjugate-base mechanism for the alkaline hydrolysis of $(RNH_2)_5MCl^{2+}$

[2] $(RNH_2)_5MCl^{2+} + OH^- \rightleftharpoons (RNH_2)_4M(NHR)Cl^+ + H_2O$

[3] $(RNH_2)_4M(NHR)Cl^+ + H_2O \rightarrow (RNH_2)_5MOH^{2+} + Cl^-$

one can similarly predict a marked steric acceleration of reaction 3 in all cases on *N*-methylation (6), but the decline in the number of nonbonded interactions in $(CH_3NH_2)_5MCl^{2+}$ on going from M = Co to Cr to Rh should reduce this effect rather sharply. Thus, if it can be shown that the effect of *N*-methylation on reaction 2 is not very much different for the various M, it can be predicted that the acceleration of base hydrolysis on *N*-methylation will fall in the sequence M = Co ≫ Cr > Rh.

The purpose of this study was to test these predictions experimentally, especially since Buchacek and Harris (11) have recently pointed out anomalies in the assignments of mechanism in octahedral rhodium(III) complexes. The predictions are based on the more obvious steric consequences of *N*-methylation, such as have been considered by many authors both recently (12, 13) and in the formative years of inorganic mechanistic studies (14). Consideration must be given, however, to possible indirect influences of *N*-methylation on reactivity such as through solvational and electronic effects, especially since the latter are of an unexpected kind in the complexes considered here.

Experimental

Materials

Chloropentaamminerhodium(III), aquopentaamminerhodium(III), and aquopentaamminecobalt(III) perchlorates were made as described previously (15, 16). Chloropentakis(methylamine)cobalt(III) chloride was made from dichlorotetrapyridinecobalt(III) chloride (17) by the method of Mitzner *et al.* (18), with minor variations in reagent quantities and reaction conditions between successive preparations.

Preparation of Chloropentakis(methylamine)rhodium(III) Perchlorate

Liquid methylamine (30 cm³) was obtained by adding the 40% aqueous solution dropwise to NaOH pellets with warming, drying the liberated gas over sodalime, and condensing it under reduced pressure at −78°C. To this liquid, 0.5 g $RhCl_3 \cdot 3H_2O$ (freshly prepared from Rh residues) was added, a little at a time, allowing the solid to dissolve after each addition. The red solution was allowed to evaporate, the yellow residue was dissolved in the minimum amount of hot dilute HCl, and the solution was filtered. On cooling, yellow crystals of $[Rh(NH_2CH_3)_5Cl]Cl_2$ (0.4 g) separated, and were converted to the perchlorate salt by dissolving them in 10 cm³ water at 65°C, adding about 8 cm³ 60% $HClO_4$, and cooling the solution to 0°C. The resulting pale yellow needles were filtered, washed with 2–3 cm³ ice-cold water, and dried in a vacuum desiccator over silica gel. *Anal.* calcd. for $[Rh(NH_2CH_3)_5Cl](ClO_4)_2$: C 12.2, H 5.1, N 14.2, Cl 21.6, Rh 20.9; found: C 12.3, H 5.2, N 14.1, Cl 21.5, Rh 20.9.

Preparation of Aquopentakis(methylamine)rhodium(III) Perchlorate

$[Rh(NH_2CH_3)_5Cl](ClO_4)_2$ (0.702 g) in 150 cm³ $HClO_4$ (0.01 *M*; *M* = mol dm^{-3}) was heated with $AgClO_4$ (0.305 g, a 3% excess) for 24 h at 95°C. The pale yellow solution was filtered, evaporated on the steam bath to about 15 cm³, and again filtered. The solution was treated with 5 cm³ 60% $HClO_4$, evaporated to 10 cm³, filtered, and kept overnight at 0°C. The resulting pale yellow crystals were filtered, washed quickly three times with ice-cold water, and dried under vacuum over fresh NaOH pellets. Yield, 0.36 g. *Anal.* calcd. for $[Rh(NH_2CH_3)_5OH_2](ClO_4)_3$: C 10.5, H 4.7, N 12.2, Cl 18.5 (formula weight 575); found: C 10.6, H 4.5, N 12.3, Cl 18.7 (formula weight by p*H* titration (see below) 580 ± 6).

Spectra

All spectrophotometric measurements were made using a freshly serviced Cary 15 spectrophotometer. The spectra of the pure compounds in acidic aqueous solution are listed in Table 1.

Kinetics

The kinetics of the aquation reactions were followed by thermostatting (±0.01°C) 10 cm³ aliquots of a solution of the rhodium(III) complex in $HClO_4$ in Pyrex ampoules in a darkened oil bath, quenching these to room temperature at appropriate times *t*, and measuring the optical density A_t of the solution at 200 nm. At this wavelength, the molar absorptivities ε of $Rh(NH_2CH_3)_5Cl^{2+}$, $Rh(NH_2CH_3)_5OH_2^{3+}$, $Rh(NH_3)_5Cl^{2+}$, and $Rh(NH_3)_5OH_2^{3+}$ in aqueous $HClO_4$ are 35 400, 18 000, 11 200, and 300 M^{-1} cm^{-1} respectively, while ε for Cl^- is negligible, and the final absorbance values A_∞ of the reaction mixtures after 10 half-lives were compared to these to show that the reactions being followed were indeed chloride aquations (reaction 1) and went to completion under the experimental conditions.

For the base hydrolysis reactions (reactions 2 and 3), accurately measured aliquots were pipetted from the thermostatted bulk reaction mixtures at appropriate intervals and quenched in a measured excess of 0.5 *M* $HClO_4$ at room temperature. The absorbances of the resulting solutions were measured at 200 nm, and again the final values A_∞ verified that the products were indeed $(RNH_2)_5RhOH^{2+}$ (identified in acid as the aquo complex).

All temperature measurements were made with calibrations traceable to NBS.

Acid Dissociation Constants of Aquo Complexes

For $Rh(NH_2CH_3)_5OH_2^{3+}$, $Rh(NH_3)_5OH_2^{3+}$, and $Co(NH_3)_5OH_2^{3+}$, aliquots of 0.0100 *M* solutions made from the solid perchlorates were thermostatted in a jacketted beaker and titrated with standardized 0.1 *M* NaOH solution from a microburette, while monitoring the p*H* with a Beckman 39502 combination electrode in conjunction with an Orion 801A potentiometer. This procedure gave both the acid equivalent weights of the complexes (which agreed with the theoretical values within the experimental uncertainty in all cases) and the pK_a

TABLE 1. Spectra of $(RNH_2)_5MX^{(3-n)+}$ in dilute perchloric acid[a]

M	X^{n-}	R	λ_1	λ_2	λ_3	Reference
Rh	Cl^-	H	347(101)	276(106)	<195	This work
		CH_3	357(122)	284(144)	195(38 800)	This work
	H_2O	H	314(107)	262(92.7)	<195	This work
		CH_3	321(164)	269(150)	<195	This work
Co	Cl^-	H	536(53)	367(50)	229(17 400)	19
		CH_3	555(63)	383(69)	240(28 200)	19
	H_2O	H	490(47.1)	344(44.5)	192(25 700)	16, 20
		CH_3	515(66.2)	362(68.3)	229(30 200)	This work, 20
Cr	Cl^-	H	513(36.5)	376(38.2)		21
		CH_3	524(49.1)	386(55.1)		21

[a]Wavelengths λ of maxima in nm are followed by molar absorptivities ε in M^{-1} cm^{-1}.

values at the ionic strength I of the midpoint of the titration curve.

This procedure was inapplicable to $Co(NH_2CH_3)_5OH_2^{3+}$, which was not obtained as a solid salt and which decomposed slowly with methylamine release in the course of a pH titration. Instead, solutions of $[Co(NH_2CH_3)_5Cl]Cl_2$ in dilute standard $HClO_4$ with the stoichiometric amount of $AgClO_4$ were kept at 22°C in the dark for 44 to 68 h, i.e., for times corresponding to over 99% chloride aquation even in the absence of the anticipated Ag^+ catalysis (3, 5). The solutions were then chilled to 0°C to ensure maximum precipitation of AgCl, filtered, and made to 100 cm^3 at 22°C such that $[HClO_4] = [(Co(NH_2CH_3)_5OH_2)(ClO_4)_3] = 0.0100\ M$. These freshly prepared solutions were used to obtain the spectrum of $Co(NH_2CH_3)_5OH_2^{3+}$, given in Table 1, which agrees well with that reported by Mitzner and Blankenburg (20). Aliquots of these solutions were placed in the darkened, thermostatted beaker as above but at a low temperature (2°C), and enough 0.1 M NaOH was added under thorough stirring to neutralize all the $HClO_4$ and precisely one-half of the aquo complex. The pH of the mixtures ($\equiv pK_a$ of the aquo complex) was then measured as above, arranging for the momentary pH meter reading immediately before immersion into the test solution to be within 1 pH unit of the anticipated pK_a value so as to expedite the attainment of a stable final reading without decomposition of the complex.

Results

Aquation of $Rh(NH_2R)_5Cl^{2+}$

Plots of ln $(A_t - A_\infty)$ vs. t were linear over at least 87% reaction (correlation coefficients $r^2 > 0.9994$), and the corresponding pseudo-first-order rate coefficients k_{aq} are collected in Table 2. For R = CH_3, standard errors in k_{aq} were typically $\pm 0.8\%$, and reproducibility was $\pm 1.8\%$. Precision was better than this for R = H because the final absorbances A_∞ were much smaller than for R = CH_3. The rate coefficients were the same in 0.01 M as in 0.10 M $HClO_4$, and over a twofold range of initial complex concentrations, within these limits of uncertainty.

The Eyring plot for R = CH_3 is linear ($r^2 = 0.9998$) and leads to $\Delta H_{aq}^* = 101.9 \pm 0.9$ kJ mol^{-1}, with $\Delta S_{aq}^* = -50.2 \pm 2.3$ J K^{-1} mol^{-1}. The data for R = H indicate $\Delta H_{aq}^* \sim 102$ kJ mol^{-1} and $\Delta S_{aq}^* \sim -44$ J K^{-1} mol^{-1}; the k_{aq} values agree well with those interpolated from the work of Poë *et al.* (22) and Lalor and Bushnell (23), and all these data taken together give $\Delta H_{aq}^* = 101.5 \pm 1.2$ kJ mol^{-1} and $\Delta S_{aq}^* = -45.6 \pm 3.4$ J K^{-1} mol^{-1} with $r^2 = 0.9992$ (the activation parameters calculated by Lalor and Bushnell are in error).

TABLE 2. Pseudo-first-order rate coefficients k_{aq} for the aquation of $Rh(NH_2R)_5Cl^{2+}$ in 0.1 M $HClO_4$

Complex	T (°C)	$10^5 k_{aq}$ (s^{-1})
$Rh(NH_2CH_3)_5Cl^{2+}$[a]	113.59	32.6
	108.00	20.5
	100.25	10.5
	92.36	4.90
	84.90	2.40
$Rh(NH_3)_5Cl^{2+}$[b]	100.21	20.5
	84.90	4.80

[a][Rh] = (1.66 to 3.31) × 10^{-5} M.
[b][Rh] = 6.34 × 10^{-5} M.

Base Hydrolysis of $Rh(NH_2R)_5Cl^{2+}$

Plots of ln $(A_t - A_\infty)$ vs. t were linear to at least 86% reaction, with r^2 always exceeding 0.995 for R = CH_3 and 0.999 for R = H. The corresponding pseudo-first-order rate coefficients k_{obs} were seen to be directly proportional to $[OH^-]$ at constant I, and accordingly Table 3 lists $k_{OH} = k_{obs}/[OH^-]$, together with the standard errors. The temperature dependence of k_{OH} gives $\Delta H_{OH}^* = 108.6 \pm 1.8$ kJ mol^{-1} and $\Delta S_{OH}^* = 74.1 \pm 6.1$ J K^{-1} mol^{-1} with $r^2 = 0.9995$ for $Rh(NH_2CH_3)_5Cl^{2+}$, and $\Delta H_{OH}^* = 114.8 \pm 0.7$ kJ mol^{-1} and $\Delta S_{OH}^* = 66.4 \pm 2.1$ J K^{-1} mol^{-1} with $r^2 = 0.99997$ for $Rh(NH_3)_5$-

TABLE 3. Specific rate coefficients k_{OH} for the base hydrolyses of $(RNH_2)_5RhCl^{2+}$ at ionic strength 0.100 M ($NaOH/NaClO_4$)

Complex	T (°C)	$[OH^-]$ (M)	$10^3 k_{OH}$ (M^{-1} s^{-1})
$Rh(NH_2CH_3)_5Cl^{2+}$ [a]	35.00	0.0251	18.6 ±0.4
	30.00	0.0251	9.0 ±0.1
		0.0497	9.0 ±0.1
		0.0989	9.3 ±0.3
	20.01	0.0989	2.14±0.05
	13.43	0.0989	0.69±0.01
$Rh(NH_3)_5Cl^{2+}$ [b]	50.42	0.0497	5.77±0.02
	44.98	0.0497	2.66±0.01
	45.00	0.0989	2.87±0.03
	34.99	0.0989	0.65±0.01
	34.99	0.0873 [c]	0.65±0.01

[a] $[Rh] = 3.2 \times 10^{-5}$ M.
[b] $[Rh] = 1.2 \times 10^{-4}$ M.
[c] Ionic strength 0.088 M.

TABLE 4. Acid dissociation constants for the ions $(RNH_2)_5MOH_2^{3+}$ in aqueous solution [a]

Complex	T (°C)	pK_a [b]	ΔH^0 (kJ mol^{-1})	ΔS^0 (J K^{-1} mol^{-1})
$Rh(NH_2CH_3)_5OH_2^{3+}$	43.0	5.82	24±2	−36±6
	22.0	6.10±0.01		
	10.4	6.27		
$Rh(NH_3)_5OH_2^{3+}$	35.0	6.24 [c]	25±4 [c]	−38±12 [c]
	22.0	6.53±0.02		
	9.4	6.63 [c]		
$Co(NH_2CH_3)_5OH_2^{3+}$	1.9	5.73±0.01		
		5.68 [d]		
$Co(NH_3)_5OH_2^{3+}$	30.0	5.97 [e]	33±2	−5±6
	22.0	6.08		
	1.9	6.53±0.02		

[a] Counterions Na^+, ClO_4^-; ionic strength 0.047 M except where indicated.
[b] Triplicate measurements where error ranges cited; otherwise, single determinations.
[c] Reference 22; ionic strength 0.2 M.
[d] Using solution kept 24 h at 22°C after filtration.
[e] Extrapolated from higher ionic strengths (ref. 25).

Cl^{2+}, at $I = 0.100$ M. The latter parameters give $k_{OH} = 1.39 \times 10^{-3}$ M^{-1} s^{-1} for $Rh(NH_3)_5Cl^{2+}$ at 40.16°C, in excellent agreement with the value reported by Bushnell *et al.* (24) for this temperature and similar ionic strength.

Acid Dissociation Constants K_a of the Aquo Complexes

Values of pK_a (Table 4) obtained by the pH titration and the direct half-neutralization methods were equally reliable, according to experiments using $Co(NH_3)_5OH_2^{3+}$, were independent of variations in the mode of preparation of the complexes, and agreed well with literature values (22, 25, 26), allowing for ionic strength differences. The pH values of solutions of the pure solid salts were in good agreement with those calculated from the measured pK_a data.

Discussion

The *retardation* (×0.50 at 85°C) of the aquation of $(RNH_2)_5RhCl^{2+}$ on *N*-methylation, though modest, originates in ΔS_{aq}^* rather than ΔH_{aq}^* and so persists over the entire temperature range of interest. It is *opposite in direction* to the *acceleration* (×22 at 25°C) observed for the cobalt(III) analogues (3, 5, 6), and the simplest explanation is that the mechanism is I_a for M = Rh and I_d for M = Co, as previously contended (1, 2, 15). Steric effects can account for the consequences of the presumed mechanistic difference, and indeed the retardation is less striking for Rh than for Cr (3, 5), as expected on steric grounds. Steric factors in aliphatic substitution produce much larger effects than these, but organic S_N2 reactions involve attack remote from the replaced ligand with stereochemical inversion of the entire molecule, whereas octahedral sub-

stitution by an I_a process evidently involves flanking ('*cis*') attack with little disturbance of the ligands other than the one being replaced (1). Similarly, the large kinetic effects of steric decompression associated with organic S_N1 reactions, in which the geometry goes from tetrahedral to trigonal planar, may be matched in octahedral substitutions of the D type, in which the five-coordinate intermediate survives long enough to undergo major rearrangement (27), but will be less striking in I_d processes in which the configuration of the intermediate is less likely to change prior to resumption of six-coordination.

In the base hydrolysis of $Rh(NH_2R)_5Cl^{2+}$, we observe an *acceleration* (×29 at 35°C) on *N*-methylation. If a conjugate base mechanism (reactions 2 and 3) is operating, part of this acceleration could be due to an increased acidity of the N protons (reaction 2), but $Rh(NH_2CH_3)_5OH_2^{3+}$ is only 2.7 times more acidic than $Rh(NH_3)_5OH_2^{3+}$ (Table 4), so that an acceleration of about 10-fold still needs to be accounted for, if N-proton and O-proton acidity trends are at all similar. This acceleration contrasts with the retardation displayed in the aquation reactions of the same compounds, but is in accordance with the asssignment of a D_{cb} mechanism to base hydrolysis reactions in general, on the basis of steric acceleration of reaction 3. This argument applies much more forcefully when M = Co (6); $Co(NH_2CH_3)_5OH_2^{3+}$ is 6.3 times more acidic then $Co(NH_3)_5OH_2^{3+}$ (Table 4) but this still leaves an acceleration factor of about 2×10^3 to be attributed to *N*-methylation in reaction 3. The overall acceleration factors associated with *N*-methylation in base hydrolysis of $M(NH_2R)_5Cl^{2+}$ are 1.5×10^4, 225, and 29 for M = Co, Cr, and Rh respectively, as expected for a common D_{cb} mechanism, for which the steric acceleration of reaction 3 will decline with the decrease in the number and severity of the nonbonded interactions as the ionic radii of M^{3+} increase (9, 10).

While the above analysis explains the phenomena on the basis of steric effects alone, consideration must be given to the contributions of the rather unusual electronic effects revealed by Tables 1 and 4, and to solvational factors, even though these contributions will be similar for all the three M considered and hence do not seriously affect the foregoing conclusions. Table 1 shows that *N*-methylation in $(RNH_2)_5MCl^{2+}$ *decreases* the energy of the lowest spin-allowed ligand field band in every case, i.e., it decreases the ligand field strength of the nonreacting ligands, which in $(RNH_2)_5MCl^{2+}$ is a measure of σ electron release from N to M. This is surprising, since the methyl group is invariably electron releasing in organic molecules, yet Table 4 shows that the $(CH_3NH_2)_5MOH_2^{3+}$ are more *acidic* than the corresponding $(NH_3)_5MOH_2^{3+}$ even though CH_3NH_2 itself is 25 times more *basic* than NH_3 (28). Parris and Feiner (29) noted a similar spectroscopic effect in $M(NH_2R)_6^{3+}$, and attributed the anomaly to steric constraints on six-coordination when R = CH_3. The work of Foxman (9) suggests that the distortion of metal-to-ligand bond angles from 90° may account for the reduced effectiveness of N → M σ-electron donation in the methylamine complexes.

It is difficult to gauge the effect of reduced electron release from RNH_2 on the aquation rates of $(RNH_2)_5MCl^{2+}$. A lowered rate would be expected for an I_d process, on the basis of the lowered electron density at M, yet marked acceleration is observed when M = Co, where the I_d mechanism is almost certainly operative (1, 14); the steric effects discussed above are evidently much more important than these electronic factors. Furthermore, the replacement of NH_3 by H_2O in $(NH_3)_5CrCl^{2+}$ results in a decrease of over 3000 cm^{-1} in the wavenumber $\bar{\nu}_1$ of the first ligand field band and a 31-fold decrease in the chloride aquation rate (30), whereas replacement of NH_3 by CH_3NH_2 decreases $\bar{\nu}_1$ by only 410 cm^{-1} yet k_{aq} is reduced 33-fold. These observations also run counter to the expectation that increasing the ligand field should decrease the reaction rate of d^6 (spin-paired) or d^3 complexes (ref. 14, pp. 145–158). For M = Rh and Co, $\bar{\nu}_1$ decreases on *N*-methylation of $(NH_3)_5MCl^{2+}$ by amounts that are sufficiently small and similar (810 and 640 cm^{-1}, or 2.8 and 3.4%, respectively) to indicate that electronic effects cannot account for the differences in the kinetic consequences of *N*-methylation between M = Co, Rh, and Cr (compare ref. 14, p. 161).

Qualitatively, however, the spectroscopic data can be taken as evidence for a general electronic destabilization of $(RNH_2)_5MCl^{2+}$ through geometrical strain, leading to an expectation of labilization of the complexes in the order Co ≫ Cr > Rh, on *N*-methylation. Viewed in this way, the deactivation of the Cr and Rh complexes towards aquation becomes all the more significant.

Finally, solvational factors cannot account satisfactorily for the different kinetic consequences of *N*-methylation for M = Co, Cr, and Rh, since they will be rather similar in each case. Progress from R = CH_3 to R = C_2H_5, *n*-C_3H_7, etc. (the chief consequence of which will be desolvation) leads to modest stepwise *accelerations* of the aquations of $(RNH_2)_5MCl^{2+}$ for both Co and Cr (4–6), indicating that the *retardations* of aquation observed in *N*-methylation of $(NH_3)_5RhCl^{2+}$ and $(NH_3)_5CrCl^{2+}$ would be more striking if solvational factors could be allowed for. Again, this effect can be viewed as one of general labilization through destabilization of the complexes.

In summary, then, the kinetic phenomena observed in reactions 1–3 can be rationalized in terms of steric effects if aquation proceeds by an I_a mechanism for M = Rh or Cr but I_a for M = Co, and base hydrolysis by a D_{cb} process in all these cases.

Acknowledgements

I thank Dr. S. J. Cartwright for preparing chloropentakis(methylamine)rhodium(III) chloride, Dr. B. M. Foxman for permission to refer to his results prior to publication, and the National Research Council of Canada for financial assistance.

1. T. W. Swaddle. Coord. Chem. Rev. **14**, 217 (1974).
2. S. B. Tong and T. W. Swaddle. Inorg. Chem. **13**, 1538 (1974).
3. M. Parris. J. Chem. Soc. A, 583 (1967).
4. M. Parris and W. J. Wallace. Can. J. Chem. **47**, 2257 (1969).
5. R. Mitzner, P. Blankenburg, and W. Depkat. Z. Phys. Chem. (Leipzig), **245**, 260 (1970).
6. D. A. Buckingham, B. M. Foxman, and A. M. Sargeson. Inorg. Chem. **9**, 1790 (1970).
7. G. Guastalla and T. W. Swaddle. Can. J. Chem. **51**, 821 (1973).
8. T. W. Swaddle. Inorg. Chem. Submitted.
9. B. M. Foxman. J. Chem. Soc. Chem. Commun. 515 (1972); private correspondence.
10. R. D. Shannon and C. T. Prewitt. Acta Crystallogr. Sect. B, **25**, 925 (1969); **26**, 1046 (1970).
11. R. J. Buchacek and G. M. Harris. Inorg. Chem. **15**, 926 (1976).
12. R. Romeo, D. Minnitti, and M. Trozzi. Inorg. Chem. **15**, 1134 (1976).
13. P. W. Mak and C. K. Poon. Inorg. Chem. **15**, 1949 (1976).
14. F. Basolo and R. G. Pearson. Mechanisms of inorganic reactions. 2nd ed. J. Wiley and Sons, Inc., New York, NY. 1967. pp. 158–170.
15. T. W. Swaddle and D. R. Stranks. J. Am. Chem. Soc. **94**, 8347 (1972).
16. W. E. Jones and T. W. Swaddle. Can. J. Chem. **45**, 2647 (1967).
17. P. Spacu, A. Ianu, and E. Nicolau. An. Univ. C. I. Parhon Bucuresti Ser. Stiint. Nat. **15**, 73 (1957).
18. R. Mitzner, P. Blankenburg, and W. Depkat. Z. Chem. **9**, 68 (1969).
19. R. Mitzner, W. Depkat, and P. Blankenburg. Z. Chem. **10**, 34 (1970).
20. R. Mitzner and P. Blankenburg. Z. Chem. **11**, 25 (1971).
21. C. F. C. Wong and A. D. Kirk. Can. J. Chem. **53**, 419 (1975).
22. A. J. Poë, K. Shaw, and M. J. Wendt. Inorg. Chim. Acta, **1**, 371 (1967).
23. G. C. Lalor and G. W. Bushnell. J. Chem. Soc. A, 2520 (1968).
24. G. W. Bushnell, G. C. Lalor, and E. A. Moelwyn-Hughes. J. Chem. Soc. A, 719 (1966).
25. J. Bjerrum. Metal ammine formation in aqueous solution. P. Haase and Son, Copenhagen. 1957. p. 280.
26. S. C. Chan and K. Y. Hui. Aust. J. Chem. **21**, 3061 (1968).
27. S. B. Tong, H. R. Krouse, and T. W. Swaddle. Inorg. Chem. **15**, 2643 (1976).
28. R. C. Weast (*Editor*). Handbook of chemistry and physics. 47th ed. Chemical Rubber Co., Cleveland, OH. 1966. p. D85.
29. M. Parris and N. F. Feiner. Inorg. Nucl. Chem. Lett. **3**, 337 (1967).
30. T. W. Swaddle and E. L. King. Inorg. Chem. **4**, 532 (1965).

Single crystal electronic spectra of a series of *trans* nickel(II) complexes with *N,N'*-diethyl- and *N,N'*-dimethylethylenediamine

A. B. P. LEVER AND G. LONDON

Department of Chemistry, York University, Downsview, Ont., Canada M3J 1P3

AND

P. J. MCCARTHY

Department of Chemistry, Canisius College, Buffalo, NY 14208, U.S.A.

Received February 3, 1977

A. B. P. LEVER, G. LONDON, and P. J. MCCARTHY. Can. J. Chem. **55**, 3172 (1977).

We have measured the polarized crystal spectra at 10 K of Ni(*s*-Et_2en)$_2X_2$, where X = Cl, Br, NCS, and H_2O (with Cl, Br, and I counterions) and *s*-Et_2en is *N,N'*-diethylethylenediamine, and of Ni(*s*-Me_2en)$_2X_2$, where X = NCS and NO_3, and *s*-Me_2en is *N,N'*-dimethylethylenediamine. Transition energies were calculated for D_{4h} symmetry using symmetry adapted functions and a normalized spherical harmonic Hamiltonian. When the differences between calculated and observed band positions are minimized, the ligand-field and angular overlap parameters listed in Table 2 are obtained. The criteria for the band assignments are discussed. The principal conclusions are: (*1*) The π interactions between Ni(II) and the axial ligands are small in contrast to tetragonal Cr(III) complexes. (*2*) Equatorial and axial parameters are relatively independent, in contrast to tetragonal Cu(II) complexes. (*3*) The more basic *s*-Et_2en exerts a stronger ligand field than *s*-Me_2en. (*4*) The σ-bonding strength of the axial ligands follows the spectrochemical series. (*5*) DQ for the axial ligands in the ethyl complexes is lower than anticipated, probably due to steric hindrance of the bulky ethyl groups. (*6*) B values are all near 850 cm^{-1}, except for an anomalously low value for Ni(*s*-Et_2en)$_2$(NCS)$_2$.

A. B. P. LEVER, G. LONDON et P. J. MCCARTHY. Can. J. Chem. **55**, 3172 (1977).

On a mesuré les spectres polarisés de cristaux à 10 K de Ni(*s*-Et_2en)$_2X_2$ où X = Cl, Br, NCS et H_2O (alors que Cl, Br et I agissent comme contrions) et *s*-Et_2en = *N,N'*-diéthyléthylènediamine et de Ni(*s*-Me_2en)$_2X_2$ où X = NCS et NO_3 et *s*-Me_2en = *N,N'*-diméthyléthylènediamine. On a calculé les énergies de transition pour la symétrie D_{4h} utilisant des fonctions adaptées pour la symétrie et un hamiltonian harmonique sphérique normalisé. Lorsque l'on minimise les différences entre les positions calculées et observées des bandes, on obtient les paramètres de champ de ligand et de recouvrement angulaire qui sont rapportés dans la tableau 2. On discute des critères pour l'attribution des bandes. Les principales conclusions sont: (*1*) Les interactions π entre le Ni(II) et des ligands axiaux sont plus petites que celles observées dans les complexes tétragonaux du Cr(III). (*2*) Les paramètres équatoriaux et axiaux sont relativement indépendants, ce qui est en opposition avec les observations effectuées avec les complexes tétragonaux du Cu(II). (*3*) Le groupe *s*-Et_2en qui est plus basique exerce un champ de ligand plus fort que celui exercé par le groupe *s*-Me_2en. (*4*) La force de liaison σ des ligands axiaux est en accord avec la série spectrochimique. (*5*) Les valeurs de DQ pour les ligands axiaux dans les complexes d'éthyle sont plus basses que celles anticipées et l'on attribue ce résultat à un empêchement stérique qui est probablement plus grand dans les groupes éthyles volumineux. (*6*) Les valeurs de B sont toutes près de 850 cm^{-1} excepté pour la valeur qui est basse d'une façon anormale pour Ni(*s*-Et_2en)$_2$(NCS)$_2$.

[Traduit par le journal]

The study of electronic spectra has played a dramatic role in our understanding of the nature of the metal–ligand bonds in coordination complexes. Much effort has been concentrated in studying complexes of high symmetry, generally containing only one kind of ligand. Numerous models exist to convert these data into chemical information. They range from simple crystal-field models through more sophisticated ligand-field approaches and various molecular orbital methods ranging from *ab initio* to semi-empirical (1). Most of these methods can adequately describe the behaviour of molecules of high symmetry, but generally are of less utility with molecules of lower symmetry, a direct consequence of the increase in the number of parameters required to describe such systems. However, since the number of observables also increases, generally, to a greater degree, this is not a serious drawback. Indeed, by using the extra

information contained within the spectrum of a low-symmetry complex much can be learned about how one metal–ligand bond interacts with another in the molecule. Such information is not generally available, at least from electronic spectra, because of some skepticism about the chemical significance of individual parameters in any given model, and because there has been little concentrated effort to obtain a large body of data particularly from closely related series of complexes. Moreover, the lack of any standardized approach to a study of low-symmetry systems makes it difficult to compare the results of one study with those of another (2).

We have recently introduced the normalized spherical harmonic (nsh) Hamiltonian approach as a means of standardizing spectroscopic analysis of low-symmetry systems (2–4). This method provides numerical values of *DQ*, *DS*, *DT*, *DM*, *DN*, etc., which have precise group theoretical significance and whose numerical values are independent of the choice of coordinate axes. Such a procedure standardizes the collection of data, but does not necessarily preclude its further analysis by means of other models, in particular the orbital angular overlap model (5 and references cited therein).

Useful information can only be derived satisfactorily from highly resolved electronic spectra, obtained preferably from polarized-light, single-crystal studies at cryogenic temperatures. While such studies are now routine, they are usually carried out on complexes of known structure (X ray), and thus tend to involve isolated individual complexes rather than closely related series.

We report here the polarized single-crystal spectra of the closely related series Ni(*s*-$Et_2en)_2X_2$ where X is Cl, Br, NCS, and H_2O (with Cl, Br, and I counterions) and *s*-Et_2en is *N*,*N*′-diethylethylenediamine. We also report the spectra of Ni(*s*-$Me_2en)_2X_2$ (X = NCS, NO_3) which contain *N*,*N*′-dimethylethylenediamine. In due course we will report data for complexes containing chloroacetate, NO_2, and NO_3 ligands, as well as those for several analogous cobalt(II) complexes. X-ray structures are not generally available for this series. If the spectral data are interpreted with care, however, useful chemical information can be derived. Publication of such spectra without X-ray data is not common (see, however, refs. 6, 7), but can nevertheless be exceedingly useful, and is certainly preferable to conventional solution or diffuse reflectance or transmittance spectra of solids.

Spectra are obtained by lining up extinction axes of the crystal parallel to the electric vector of the polarized light. Where the crystal morphology permits, spectra can be obtained along each of three orthogonal extinction axes. In general, for this series of compounds one expects that all or most of the spin-allowed bands will appear in every polarization, but not necessarily with the same intensity. The reasons for this are several: (*1*) The selection rules for D_{4h} symmetry do not strictly apply to the chromophores in this study, since the latter possess no true C_4. The rather small distortions from this symmetry could be a cause of finite intensity in bands which would be symmetry forbidden in D_{4h}. It is quite clear, however, from the observed spectra, that the designation of the split states with D_{4h} labels remains a rather good approximation. (*2*) Since the bands in the spectra studied here almost uniformly decrease in size upon cooling, vibronic mechanisms must contribute significantly to the intensity. When this situation obtains even bands which are symmetry forbidden could be vibronically allowed and appear in the spectra with significant intensity. (*3*) Since we have no information about the orientation of the chromophores, we cannot assume that their axes are collinear with the extinction axes. In this situation each of the observed polarizations will be a mixture of the spectra expected with light polarized along the three molecular axes. When one or more bands in the spectra are strongly polarized, the extinction axes may be assumed to be more nearly coincident with the molecular axes. In this case the selection rules may be used by induction (see Discussion).

In summary, we demonstrate below that unambiguous assignments can be made and useful chemical information obtained from spectra without the benefit of X-ray structural information.

Experimental

Preparation of the Compounds

The anhydrous complexes described here have been previously reported (8, 9). In growing the halo complexes from ethanol open to the atmosphere for a prolonged period, the hydrated versions were obtained. No problem of dehydration was experienced in obtaining electronic spectra at cryogenic temperatures even though the samples were evacuated in the Dewar assembly.

Analysis of the halo aquo complexes gave the following results: Ni(*s*-$Et_2en)_2(H_2O)_2 \cdot 2Cl \cdot 2H_2O$ requires Cl 16.3;

found Cl 16.1%. Ni(*s*-$Et_2en)_2(H_2O)_2 \cdot 2Br$ requires Br 32.8; found Br 32.5%. Ni(*s*-$Et_2en)_2(H_2O)_2 \cdot 2I$ requires I 43.7; found I 44.5%.

Spectral Measurements

The polarized absorption spectra of single crystals of all the compounds in this study were measured at room temperature (~295 K) and at approximately 10 K using an Air Products Displex cryogenic refrigerator. A Cary 14 spectrophotometer was employed, and the full range available (2500–185 nm) was scanned until complete absorption of light by the crystal occurred. The light was polarized by means of a pair of Glan-Thompson prisms, and spectra were recorded with the electric vector of the light parallel and perpendicular to an extinction axis of the crystal. The extinction axes are generally not coincident with any of the prominent crystal edges. Although we interpret the spectra in terms of D_{4h} symmetry, the chromophores have only an approximate C_4 axis, and so in principle three distinct spectra should be observable. In some cases we have obtained three distinct spectra, while in other cases the shape and size of the crystals permitted only two spectra. In all cases we are confident that we have observed all major features of the spectra. Tomlinson *et al.* (10) have measured the spectra of (Zn, Co)$(P\phi_3)_2I_2$ and of the corresponding bromide, the first along the *a*, *b*, *c* axes of the crystal, the second along the extinction axes. All the features appeared in each set, but in the former, the polarization of the bands is more complete, as expected. Similar measurements were made on $Ni(en)_2(NCS)_2$ by Bertini *et al.* (11). Again all major features could be seen both in the spectra taken along two of the crystal axes and in those taken along two extinction axes.

In calculating the band positions for the complexes, we have employed the symmetry adapted functions and a normalized spherical harmonic Hamiltonian for D_{4h} (2). A fitting program was used to minimize the differences between the calculated and observed positions for the spin-allowed bands.

Experimental Results

Structure of the Chromophores

In a previous study infrared spectra were used to demonstrate that the complexes under discussion here have a *trans* configuration (8). This conclusion was based on the close similarity of the finger-print region of the infrared spectra of each complex of a given amine, with each other, and with analogous copper complexes for which X-ray structural data had indicated a *trans* structure. Emphasis was also placed on the N—H stretching region and on the lack of splitting of the ν(C–N) mode of the thiocyanate complexes even at low temperature. A preliminary X-ray study of Ni(*s*-$Me_2en)_2(NO_3)_2$ (9) revealed that the molecule possesses a centre of symmetry and must therefore be *trans*. In this fashion we can conclude with confidence that the compounds in this study are all *trans*. As shown below, the electronic spectra of these complexes also confirm this assignment.

Criteria of Assignment

The splitting of the F and P terms of the nickel ion in a tetragonal field are shown in Fig. 1. Six spin-allowed transitions may be anticipated and in practice at least five are observed. The $^3A_{2g}$ component of the $^3T_{1g}$(P) term is rarely seen as a discrete band but may be observed as a shoulder. In addition, some spin-forbidden bands will appear and may be fitted.

In the absence of crystal structures and therefore the absence of an unambiguous use of selection rules, we have developed some criteria to aid in the assignment of these spectra. These are:

(*a*) Similarity to previous assignments. The spectra of tetragonal nickel complexes have been treated many times in the past (1, 2, 6, 12–14). Comparison of these new data with those previously reported often leads to a direct, essentially unequivocal assignment of the spectra. The transitions to the doubly degenerate ^3E_g levels are usually the most intense features. The highest energy *d–d* band near 28 kK may safely be assigned to the highest ^3E_g transition (from $^3T_{1g}$(P)), and the most intense feature near 17 kK to the second highest ^3E_g transition (from $^3T_{1g}$(F)). The $^3A_{2g}$ (from $^3T_{1g}$(F)) seems in these complexes usually to lie as a well-defined feature to lower energy of the latter *E* band. The $^3T_{2g}$ level generally splits to a greater degree than the other orbital triplets, and one of its components may lie at a sufficiently high energy to lead to some doubt as to the identity of the lowest energy $^3A_{2g}$. Spin–singlet transitions in this region often steal enough intensity from nearby spin-allowed bands (1) that these also cause some ambiguity in the assignment. In particular the $^1B_{1g}$ transition may lie very close to, and appear very similar to, the $^3B_{2g}$ transition, which may be a weak feature. The main peak near 9–11 kK is likely to be the lowest energy ^3E_g level (from $^3T_{2g}$).

The sense of the $^3T_{2g}$ splitting also provides information, in that tetragonal complexes with axial field weaker than equatorial field split $^3E_g < {}^3B_{2g}$, whereas the reverse is true for complexes whose axial field is stronger (12).

(*b*) In comparing data from two orthogonal polarizations, we observe that the energies of the ^3E_g transitions usually differ slightly, whereas transitions to orbital singlet states have essen-

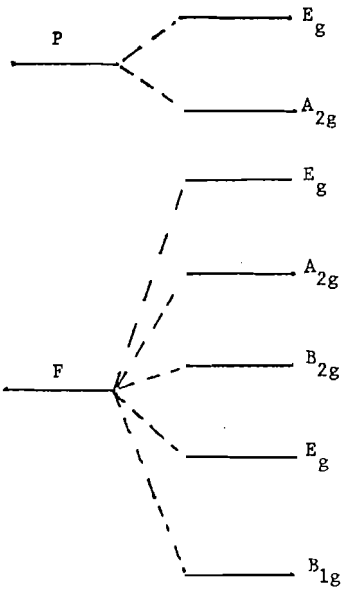

FIG. 1. Energy diagram for Ni^{2+} (d^8) in a tetragonal field.

tially the same energy in both polarizations. This may be due to some splitting of the E mode by lower symmetry and/or spin–orbit coupling. Whatever the mechanism, this observation provides a means of identifying transitions to E levels.

(*c*) Generally speaking, transitions dependent upon DQ increase significantly in energy upon cooling, whereas those independent of DQ are less temperature sensitive. This provides a mechanism for distinguishing spin-allowed transitions (always dependent upon DQ) from certain spin–singlet transitions.

(*d*) While selection rules cannot be used directly, we must require consistency in our assignments. In general *d–d* bands increase in intensity as their energy increases because they are closer to higher energy (uv) charge-transfer bands to which they are coupled. It would, therefore, be unreasonable to assign identical symmetry labels to two bands in the same polarization if the higher energy band were the weaker. Likewise, if a given band appears only in one polarization while another appears in two polarizations, it is unlikely that the two bands have the same symmetry label.

(*e*) There must be an acceptable fit between the observed energy levels and those calculated from the energy matrices (3). We are dealing basically with a four-parameter theory (DQ, DS, DT, and B). These four parameters should predict the six (or often only five) observed bands with a deviation in any given band of less than about 300 cm^{-1}. Often fits much better than this can be achieved. A good fit is not in itself an indicator of a correct assignment. However, the theory is now sufficiently well developed that even though vibrational and spin–orbit contributions are omitted, a really poor fit *is* an indicator of an incorrect assignment.

(*f*) The resulting parameters must make chemical sense. Thus, for example, it is well established that the crystal-field strength of the chloride ion is less than the crystal-field strength of the diamine. An assignment which failed to reproduce this would have to be rejected. However, one of the main purposes of this work is to gain further chemical insight into the nature of the metal–ligand bond. It is therefore to be hoped that some of the results will extend our chemical thinking and will not be rejected because they have not hitherto been observed.

Results for the Individual Compounds

The room temperature and 10 K spectra for the compounds used in this study are shown in Figs. 2–9. The band energies at 10 K, their probable assignments, and the parameters used in obtaining the best fits between observed and calculated energies are listed in Table 1. The root mean square deviations of the calculated from the observed energies are listed to give an indication of goodness of fit. Measurements of band areas for five compounds which show that the 18 and 28 kK bands are only 68 ± 10% and 50 ± 3% as intense at 10 K as they are at room temperature are indicative of vibronic coupling. The values for the 18 kK band vary between 57 and 88%, and so may involve different enabling vibrations in the different compounds. The value for the 28 kK band is quite constant, and seems to indicate a single enabling vibration, which on the basis of the coth law (1*b*) is calculated to be 225 ± 17 cm^{-1}. Many $Ni(diamine)_2X_2$ complexes have a fundamental vibration in this range (8). A band in the spectrum of $Cu(en)_2(SCN)_2$ at 230 cm^{-1} has been assigned to an N—Cu—N deformation mode (18). It is probably the N—Ni—N deformation which is the activating vibration for the 28 kK band in the nickel complexes.

(*a*) *$Ni(s\text{-}Et_2en)_2(NCS)_2$*

The reflectance spectrum of this complex has

TABLE 1. Assigned absorption energies, normalized spherical harmonic parameters, Racah parameters, and rms values[a]

	Complex[b]									
	Et NCS	Et Cl	Et Br	Et H_2O(Cl)	Et H_2O(Br)	Et H_2O(I)	Me NCS	H NCS[c]	Me NO_3[d]	$Ni(NH_3)_4(NCS)_2$[e]
^3E	11 310	8 600	8 215	9 795	9 195	9 245	11 135	9 600	9 130	10 750
$^3B_2$	13 050	11 915	11 770	12 525	12 505	12 620	11 990	12 000	12 590	10 750
$^1B_1$		12 630	12 660	13 190	13 300	13 485	13 200	13 200	13 400	13 000
$^3A_2$	16 650	14 670	13 810	16 000	15 440	15 405	18 410	16 000	14 365	17 500
^3E	18 115	17 285	17 380	18 240	17 815	18 375	18 525	17 900	18 570	17 350
^1E	21 340	20 940	20 245		21 550	21 385	23 635	22 000		
$^1A_2$	24 110									
$^1B_2$			23 585				24 935			
$^3A_2$	(28 285)	(25 480sh)	(24 875sh)	(27 030sh)			29 110	27 700		28 000
^3E	28 460	27 365	27 030	29 000	28 415	28 700	29 250	28 300	28 985	27 900
Singlets?	34 150	~32 720		33 950(?)	37 850	36 185				
	34 560									
DQ	32 655	27 561	27 171	29 868	28 858	29 437	31 741	29 104	29 394	29 775
DS	−2 545	−5 072	−6 777	−4 419	−4 672	−5 682	514	−3 063	−8 116	742
DT[g]	−2 727	−4 394	−4 383	−3 863	−4 670	−4 447	−1 043	−3 288	−4 414	184
B	690	864	845	895	890	882	862	895	887	851
C	2 600	3 100	3 000	3 220	3 225	3 100	3 335	3 100	3 350	3 300
$\gamma(=C/B)$	3.77	3.59	3.55	3.60	3.62	3.52	3.87	3.46	3.78	3.88
rms[f]	247(7)	88(7)	173(8)	20(6)	125(7)	274(7)	237(9)	174(8)	12(6)	81(7)

[a]All data are in cm^{-1}; they represent the band peaks at 10 K. Bands in parentheses were not used in obtaining the best fit. The ground state of all compounds is $^3B_1$. Weak bands which are found in some spectra (see Figs. 2–9) above 30 kK are probably triplet–singlet transitions.
[b]$Ni(s\text{-}R_2en)_2X_2$; the aquo complexes are $[Ni(s\text{-}Et_2en)_2(H_2O)_2X_2]$. Et = ethyl; Me = methyl.
[c]Data are from ref. 11.
[d]A shoulder at 26.64 kK is probably due to triplet–singlet transitions; no reasonable parameters allow its assignment to the $^3B_1 \rightarrow {}^3A_2$ transition.
[e]Data are for room temperature; from ref. 23.
[f]The number of bands used in calculating the rms deviation is given in parentheses.
[g]The sign of DT follows the convention used in ref. 4; it is the opposite of that given earlier in refs. 2 and 3.

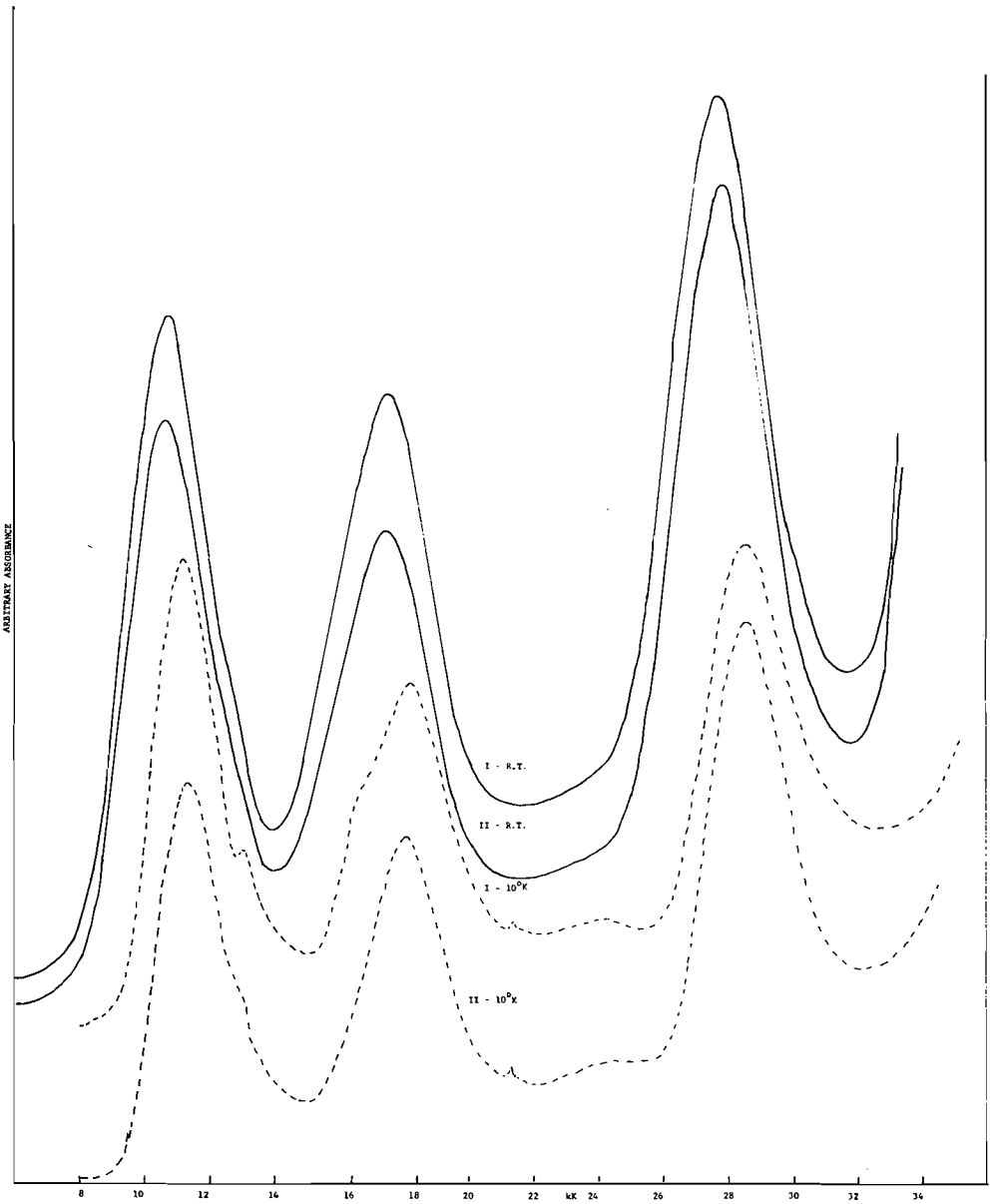

FIG. 2. Polarized crystal spectra of Ni(*s*-$Et_2en)_2(NCS)_2$. Polarization III is not shown; it is very similar to II, but also shows a weak band at 13 245 cm^{-1} and very weak absorptions at 34 150 and 34 560 cm^{-1}. The band positions in Table 1 are the averages of the three polarizations except that the value listed for $^3A_2$ (28 285 cm^{-1}) is the band maximum in III. The weak absorption at 21 340 cm^{-1} is a multiplet that contains up to six irregularly spaced bands. The Appendix contains a complete listing of the energies of all peaks and shoulders shown in Figs. 2–9.

been reported by Goodgame and Hitchman (15). The polarized spectra (Fig. 2) show little dichroism, and the spectroscopic details are very much like those of $Ni(en)_2(NCS)_2$ (11). The latter molecule has a *trans* configuration, and the NiN_6 departs from effective D_{4h} symmetry principally by the unequal N—Ni—N angles (82° and 98°) in the $Nien_2$ group. A similar structure may be assumed for the present compound.

The polarized spectra of three different crystals were recorded, and three distinct spectra were obtained, as was ascertained by the very different intensities of two sharp vibrational bands at 6464 and 6330 cm^{-1}. These have relative heights of 0.42 to 1, 1.56 to 1, and 37.5 to 1 in the three polarizations. The assignments of the triplet states agree completely with those made by Bertini *et al.* (11) for $Ni(en)_2(NCS)_2$. In addition, several spin-forbidden bands are observed. Of special interest is a group of weak bands starting at about 21 340 cm^{-1}. Similar bands with varying degrees of sharpness and complexity appear in the spectra of several of the compounds studied in this series. The bands are best ascribed to the $^3B_1 \rightarrow {}^1A_1$ spin-forbidden transition plus various associated vibronic bands.

(b) $Ni(s\text{-}Et_2en)_2Cl_2$

Because of the habit of the crystals of this complex, spectra along only two of the extinction axes were recorded (Fig. 3). The spectra in the two polarizations are very similar, the principal difference being in the intensities of the lower energy bands. At low temperature the band at ~17 kK shows a real difference of ~300 cm^{-1} between the two polarizations. The band at 8.6 kK also shows a difference of about 120 cm^{-1}, which may be beyond the limits of experimental error. As noted above, these splittings suggest the assignment of these bands to *E* states.

The spectra of this compound (as well as the others studied) show some features below 10 kK which from their intensity, position, and sharpness are readily assigned to overtones of the N—H and C—H stretching modes. In some cases the assignment is confirmed by the appearance of the band at an identical place in the spectra of the Co(II) analog (unpublished data).

(c) $Ni(s\text{-}Et_2en)_2Br_2$

The polarized spectra (Fig. 4) of this complex are quite similar to those of the analogous chloro compound, and again only two polarizations were recorded on the two crystals studied. The rapidly rising base line appears to be caused by light scattering due to the rather small crystals used in the study. Similar spectra on a third crystal at 77 K showed a more normal base line.

(d) The Halo–Aquo Complexes

Recrystallization of the halo complexes from aqueous ethanol or water yields crystals whose ir spectra and chemical analysis indicate the presence of water. The electronic spectra (Figs. 5–7) are similar to those of the anhydrous complexes with the bands in general shifted to higher energy, as expected if H_2O replaces a halogen in the coordination sphere. It is most probable that we have the *trans* diaquo complexes rather than complexes containing water and halogen bonded to the nickel. For example, substitution of bromine for chlorine in the anhydrous compounds causes *DS* to change significantly (−5072(Cl) to −6777(Br)). The change in *DS* for the analogous hydrated compounds is very much smaller. The iodo complex shows no low-lying charge-transfer absorption associated with coordinated iodine; so it cannot have iodide ions as ligands. It appears therefore that in all three compounds both halogens are replaced by H_2O in the coordination sphere. The different appearance of the three halo–aquo spectra and the rather significant differences in some band positions may then be attributed to variations in hydrogen bonding, and possibly to lattice effects due to the different sizes of the halo ions.

Both the bromo–aquo and iodo–aquo complexes show an absorption of moderate intensity ~36–38 kK. Attempts to assign this to one of the components of the third *d–d* band result in quite unacceptable parameters and fits of observed and calculated data. It may be a spin-forbidden band which shows rather large intensity because of its position as a shoulder on the charge-transfer rise. The chloro–aquo complex shows a similar band but it is poorly reproducible.

Two crystals of the chloro–aquo complex and two of the bromo–aquo complex were studied, and only two distinct spectra were observed in each case. A single robust crystal of the iodo–aquo complex was used to obtain three distinct spectra.

(e) $Ni(s\text{-}Me_2en)_2(NCS)_2$

The polarized spectra of three crystals were recorded and three distinct polarizations were obtained (Fig. 8). The band positions in the polarizations are quite similar except for the lowest *d–d* band where a difference of 860 cm^{-1} between two polarizations is seen.

(f) $Ni(s\text{-}Me_2en)_2(NO_3)_2$

The spectra of two crystals were recorded (Fig. 9). A unique feature of the spectra is the appearance at room temperature of a clear band

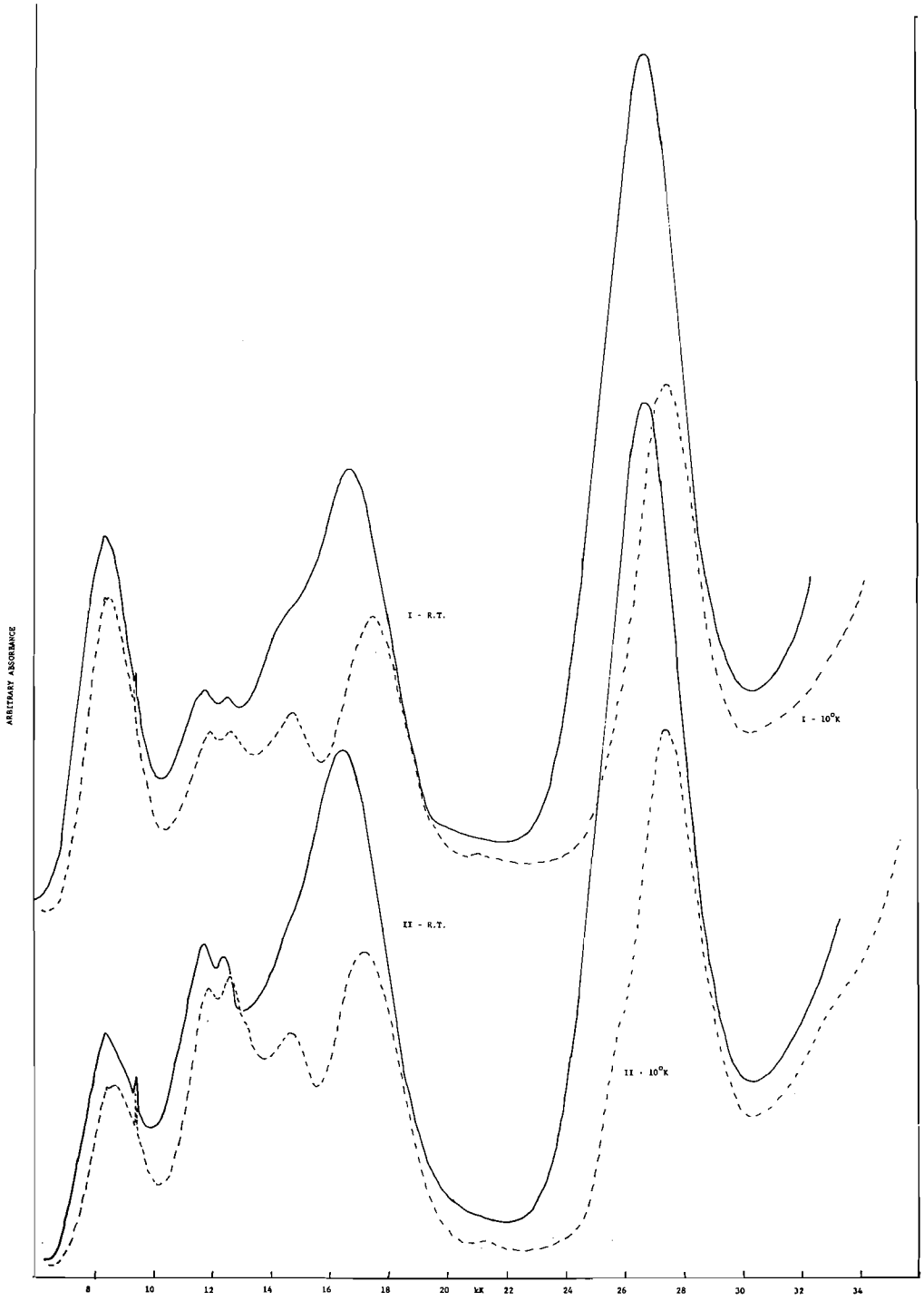

FIG. 3. Polarized crystal spectra of Ni(*s*-Et_2en)$_2Cl_2$. The bands at 8400 and 9470 cm^{-1} appear in the spectra of the analogous Co(II) complex, and so are probably ligand vibration second overtones. Stronger bands corresponding to the first overtones are found in the expected regions.

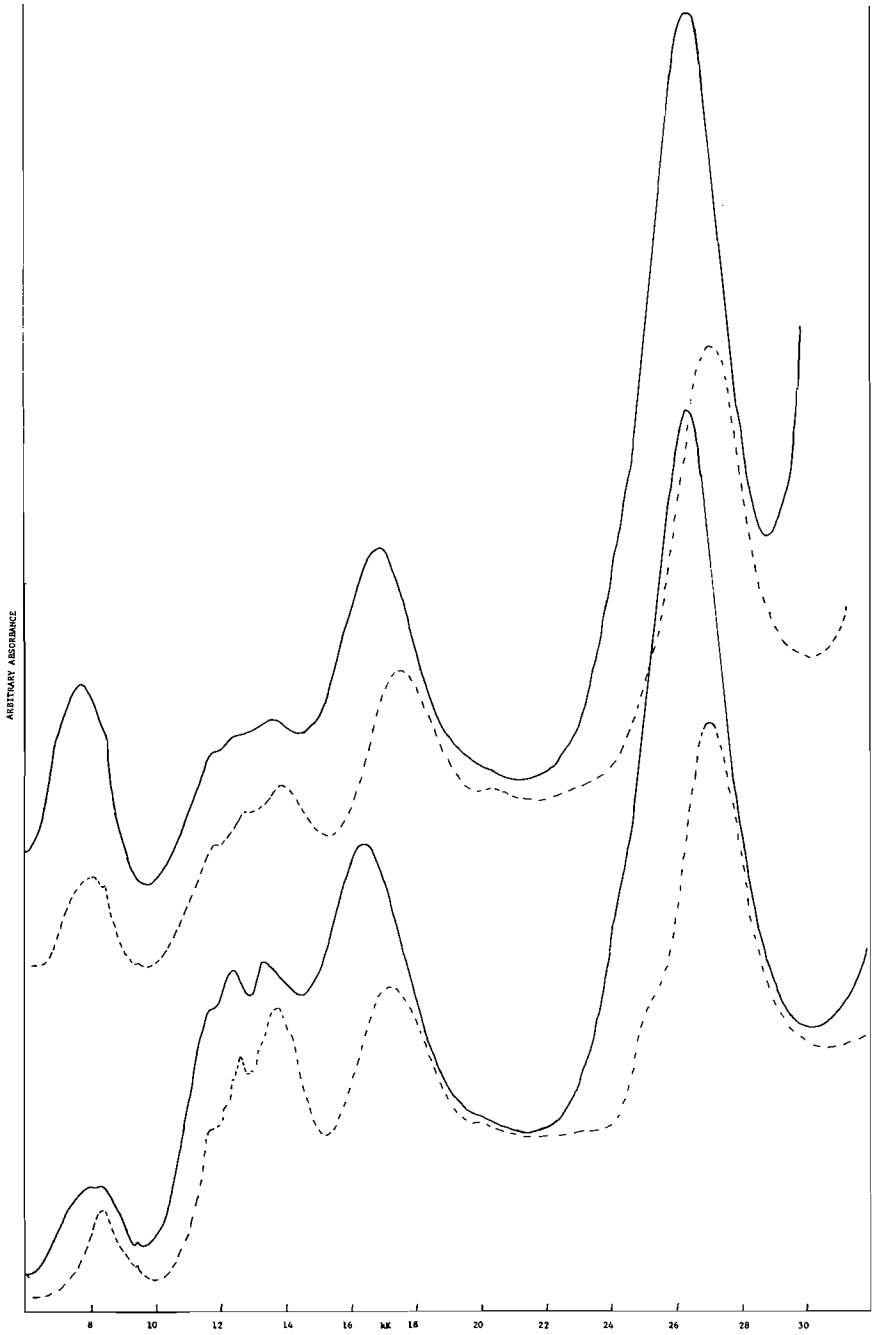

FIG. 4. Polarized crystal spectra of $Ni(s\text{-}Et_2en)_2Br_2$. The weak features at ca. 8.4 kK and 9.4 kK appear on other spectra also and are probably due to ligand vibrations.

in polarization I at 28.3 kK, which is reduced to a shoulder at 10 K. So the position of the third spin-allowed transition at 10 K is less certain for this compound.

Discussion

A complete listing of the experimental results (two or more sets of polarized data at room temperature and at 10 K) is given in the Ap-

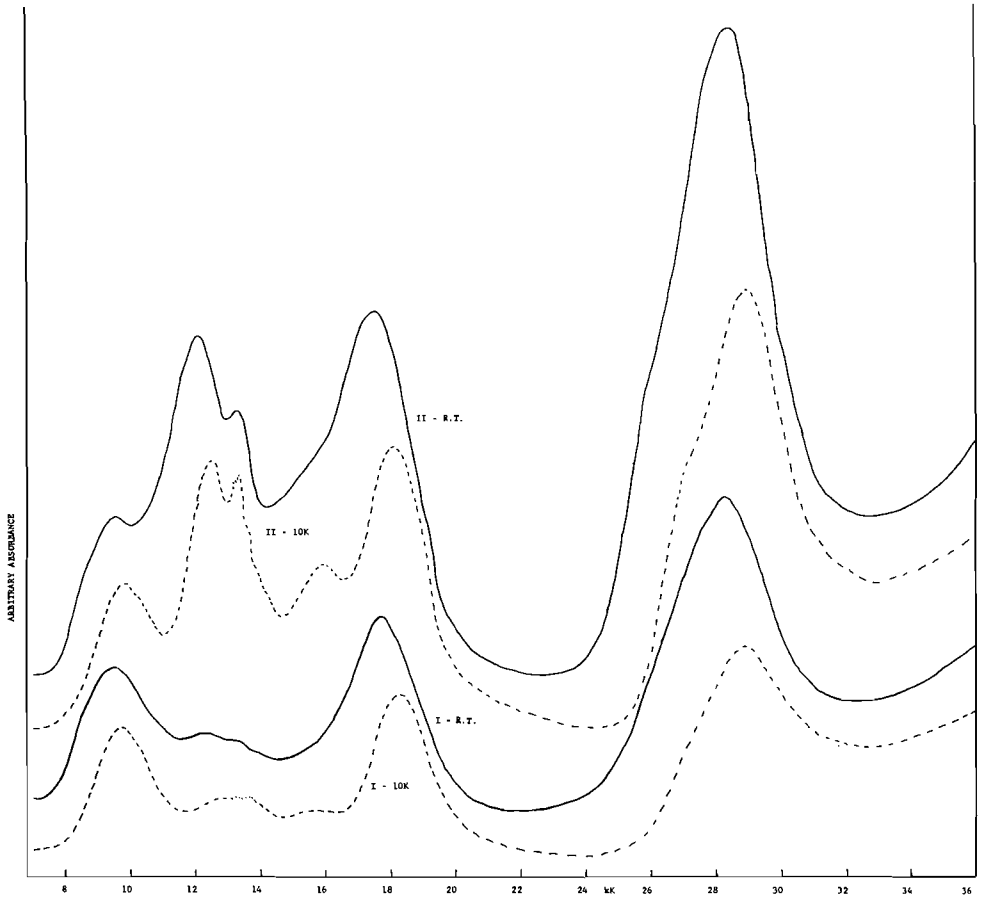

FIG. 5. Polarized crystal spectra of $Ni(s\text{-}Et_2en)_2(H_2O)_2^{2+} \cdot 2Cl^- \cdot 2H_2O$. The weak features at 10.4 kK (10 K) and 8.4 kK (room temperature and 10 K) are not shown in the spectra; they are probably ligand vibrations.

pendix. The energies cited in Table 1, used to derive the parameters shown in Table 2, are the average of the energies seen in each polarization at 10 K. In some cases several sets of data were obtained from different crystals. These data are included in the average; however, the Appendix cites data relating to the specific measurement shown in the appropriate figure.

In some cases there is doubt concerning the distinction between the transitions to $^1B_{1g}$ and $^3B_{2g}$, the alternate assignments both giving good fits. This need not be a serious cause of concern in that these two states are mixed together (1), and therefore the true parameter set is an average. The same general trends are observed using either set. Furthermore, since we are more interested in well-defined trends in parameters, the absolute values, in view of the approximations involved, are of less import. Since the upper band, in several spectra, has associated vibronic structure, and since the lower band often shows a greater shift to higher energy on cooling, we are assuming $^3B_{1g} < {}^1B_{1g}$ for all the complexes. Accordingly we list in Tables 1 and 2 only the energies and parameters based on this assignment.

As previously noted, we have neglected spin–orbit coupling and vibrational contributions to the energies. This is likely to introduce an error of up to $\pm 200\ cm^{-1}$ into the energies of the observed electronic transitions used to calculate the parameters. Since most of the orbital degeneracy has been removed in the energy levels of concern, first-order spin–orbit coupling should have little effect on the calculated energies. Second-order spin–orbit coupling will cause

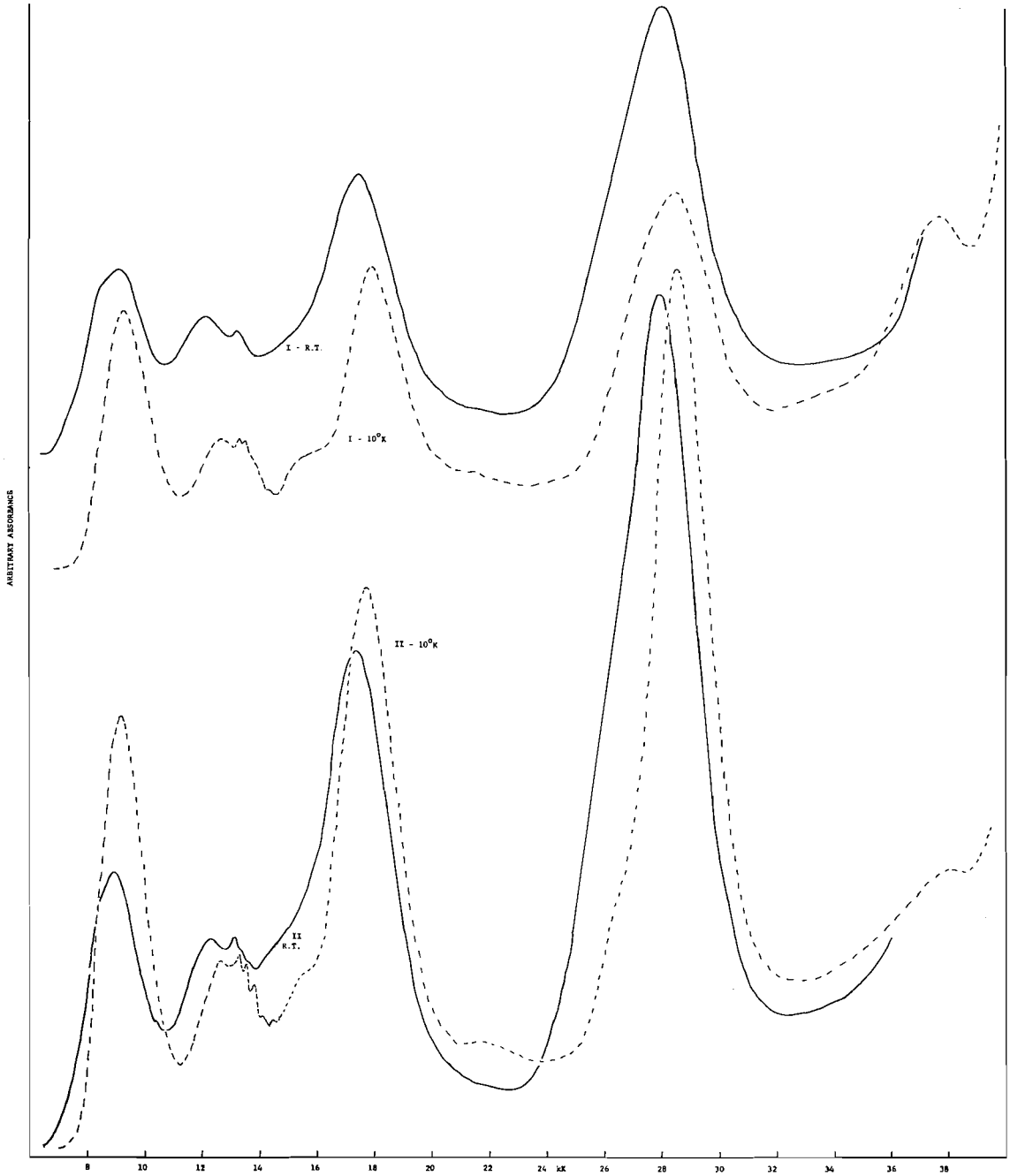

FIG. 6. Polarized crystal spectra of $Ni(s\text{-}Et_2en)_2(H_2O)_2^{2+}\cdot 2Br^-$. The 17.9 kK band (10 K) in polarization I shows some very weak structure beginning at ca. 16.9 kK which may be a progression in about 260 cm^{-1}. The bands at 8.4 kK (polarization I) and 10.4 kK (polarization II) appear to be ligand vibrations.

mixing, in particular, of the $^3B_{2g}$ and $^1B_{1g}$ levels alluded to previously, resulting in a small uncertainty in the value of DS (16).

Most bands can be measured with an accuracy of better than ± 100 cm^{-1} but larger errors may result for the broader bands and particularly the shoulders. Gaussian analysis of the 18 kK band for $Ni(s\text{-}Et_2en)_2(NCS)_2$ yields, however, band

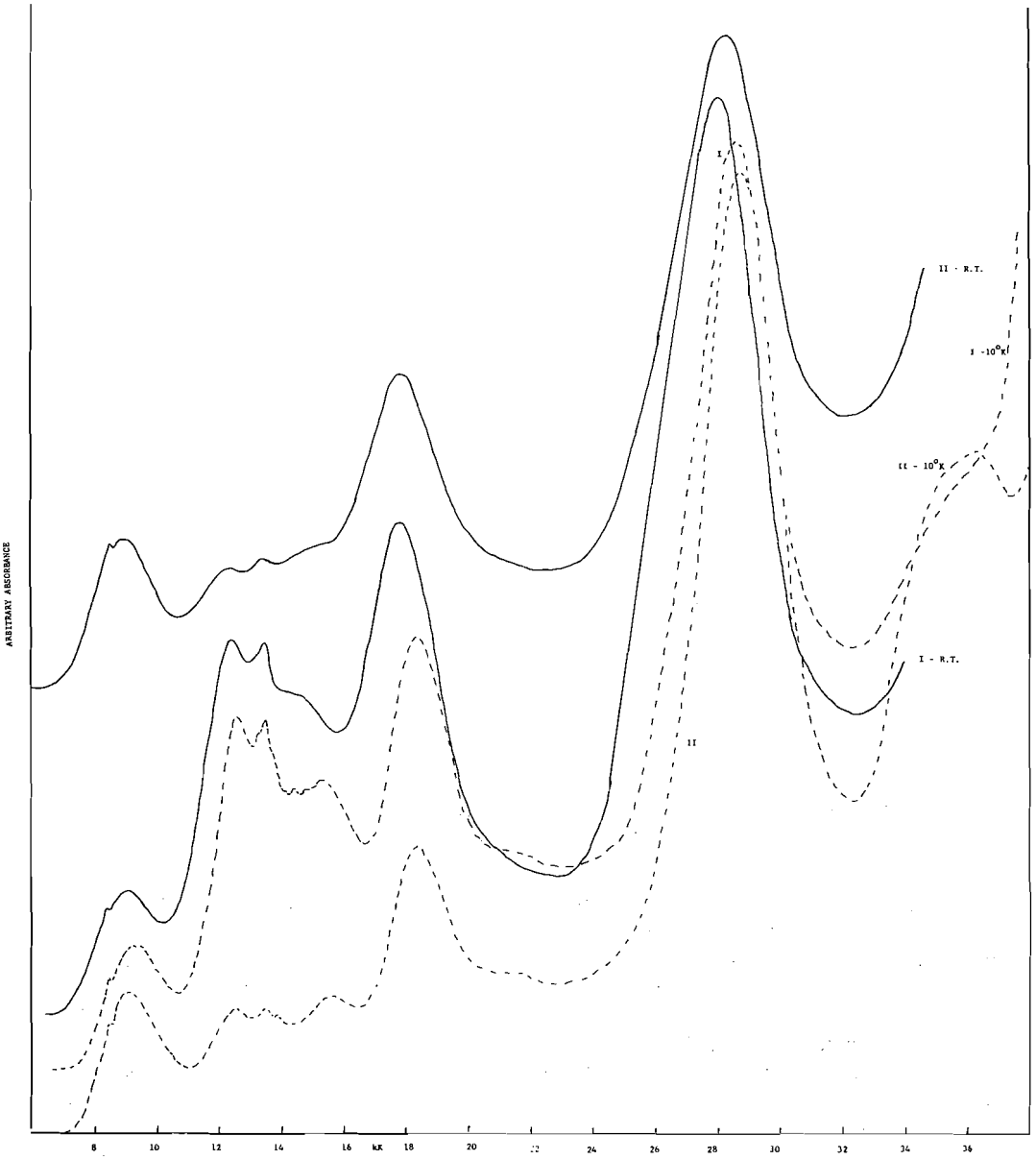

FIG. 7. Polarized crystal spectra of $Ni(s\text{-}Et_2en)_2(H_2O)_2^{2+} \cdot 2I^-$. Polarization III is not shown, since it is very similar to II. The positions listed in Table 1 are the averages of the three polarizations. The weak band at 8.4 kK (10 K, polarization I) consists of four closely spaced components, all probably ligand vibrations.

maxima not substantially different from those measured directly from the spectra. Trial calculations reveal that DS is most sensitive to these possible errors, the variations in DT and DQ being rather smaller. Thus, discussion of any trends in DS would be futile at this stage and must await a more complete analysis of the data.

For these reasons no attempt has been made to obtain a perfect fit to the observed energies, though with enough computer time this may be possible. Instead, a root mean square deviation of about 200 cm^{-1} or less is considered a thoroughly acceptable result. Once the spin-allowed transitions have been fitted, the positions of the

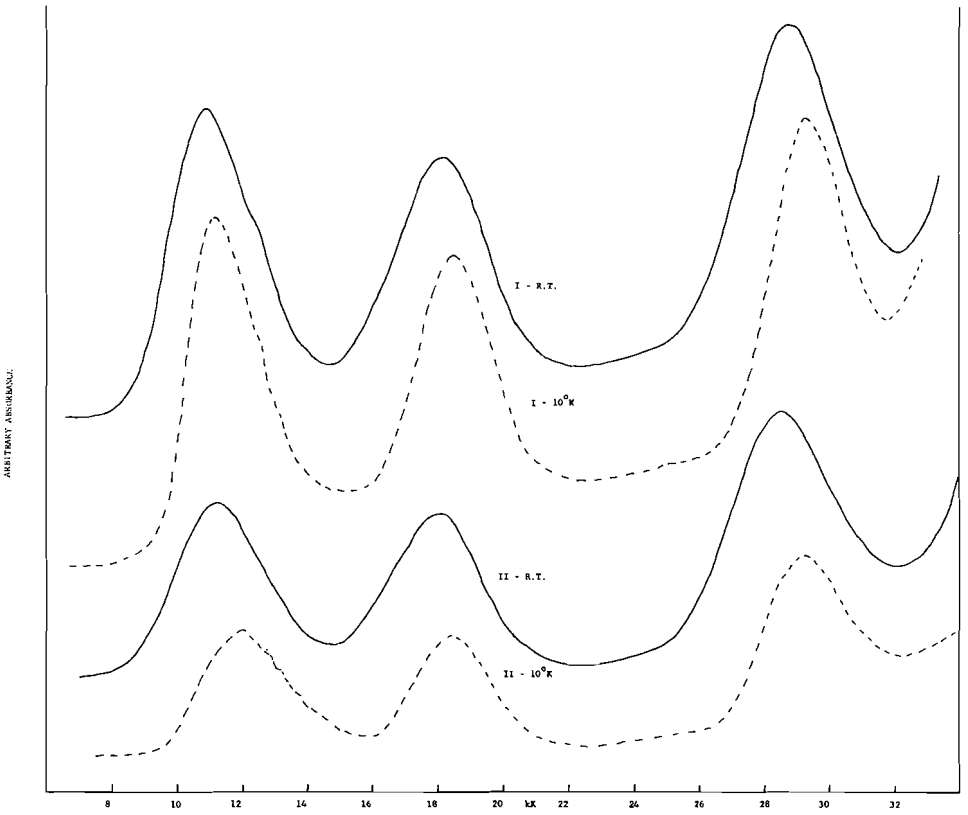

FIG. 8. Polarized crystal spectra of Ni(*s*-Me_2en)$_2$($NCS)_2$. Polarization III is not shown; it is very similar to II except that the 13.2 kK band is more clearly resolved in III. This band probably represents the transition to the $^1B_1$ state.

spin-forbidden transitions are computed and a value of C determined which will reproduce the dominant spin–singlet transitions observed in the spectra. These data are also shown in Table 1.

The orbital angular overlap parameters[1] e_{σ_N}' and e_{σ_Z}', which convey potentially the most chemical insight, are much less sensitive to the possible errors indicated above. Trends in these parameters are well defined and seem to make chemical sense. It has been pointed out that the angular overlap parameters refer only to the nonspherical part of the ligand field, and furthermore only to that part of it which is associated with bonding to the metal d orbitals (5). Thus they may possess chemical significance, yet not be very important with regard to total metal–ligand bond energy. For the complexes in this study, e_{π_N}' is assumed equal to zero. Values for the parameter e_{π_Z}' are for the most part close to zero. So it appears that π interactions between nickel(II) and the axial ligands are of relatively little importance, in contrast to tetragonal chromium(III) complexes, where this parameter can be quite large (17). This is explicable if the π interactions are largely ligand to metal π donation, since Cr(III) has a half-filled $t_{2g}(O_h)$ shell, whereas that of Ni(II) is full. Moreover, the higher positive charge of Cr(III) will cause greater ionic polarization of the ligand π pairs effectively increasing the magnitude of the e_{π_Z}' parameter.

The directional covalent contribution to the σ bond between the *s*-Et_2en ligand and the metal, as demonstrated by the magnitude of e_{σ_N}' (or

[1] e_σ' and e_π' represent respectively the nonspherical σ-antibonding and π-antibonding (or bonding) effects exerted on the metal d orbitals by interactions with the ligand orbitals (5). The additional subscript N refers to the four ammine nitrogens in the equatorial plane, while Z refers to the two axial ligands.

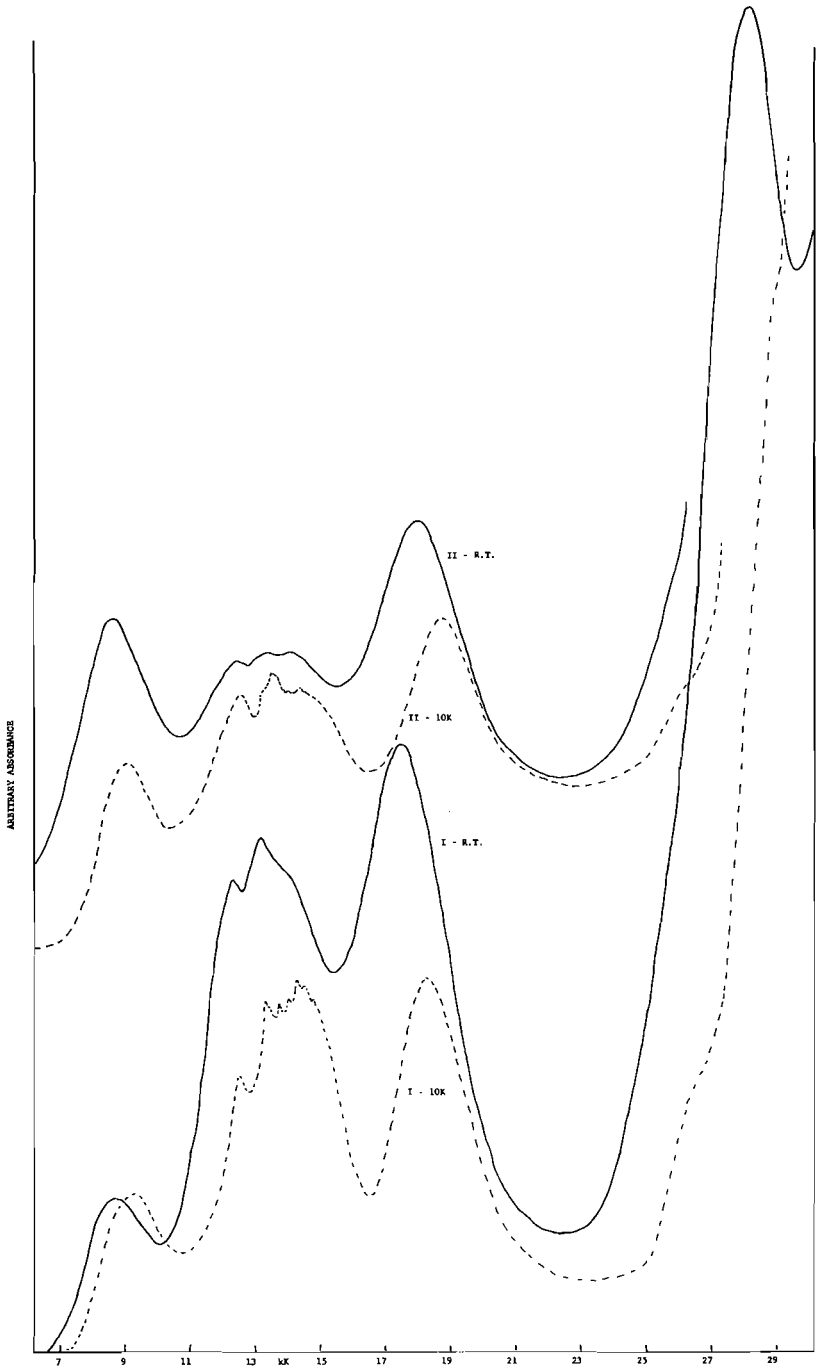

FIG. 9. Polarized crystal spectra of $Ni(s\text{-}Me_2en)_2(NO_3)_2$. A weak feature at ca. 8.4 kK in both polarizations and one at ca. 9.3 kK in II have been omitted. They probably represent ligand vibrations.

TABLE 2. Empirical parameter sets

	$R^a = H^c$ $X^a = NCS$	$R^a = Me$ $X^a = NCS$	$R^a = {}^d$ $X^a = NCS$	$R^a = Et$ $X^a = NCS$	$R^a = Et$ $X^a = Cl$	$R^a = Et$ $X^a = Br$	$R^a = Et$ $X^a = H_2O(Cl)$	$R^a = Et$ $X^a = H_2O(Br)$	$R^a = Et$ $X^a = H_2O(I)$	$R^a = Me$ $X^a = NO_3$
$d\sigma$	−1 111	−34	184	−923	−1 695	−2 058	−1 481	−1 647	−1 833	−2 350
$d\pi = (e_{\pi_Z}'(\text{axial}))^b$	−50	303	125	−42	−276	−644	−234	−140	−397	−925
DQ (axial)	21 323	29 273	30 210	26 202	17 163	16 799	20 726	17 807	18 913	18 949
DQ (equatorial)	32 994	32 975	29 557	35 882	32 760	32 357	34 439	34 384	34 699	34 617
e_{σ_Z}' (axial)	2 518	3 952	3 829	3 120	1 712	1 178	2 200	1 972	1 763	1 064
e_{σ_N}'(equatorial)	4 000	3 998	3 583	4 350	3 972	3 923	4 175	4 168	4 207	4 197

[a]Ni(*s*-R_2en)$_2X_2$; the aquo complexes are [Ni(*s*-Et_2en)$_2$(H_2O)$_2$]X_2. Et = ethyl; Me = methyl. For the first three compounds all six triplet states were used to calculate the parameters; for the others the position of the upper $^3A_2$ was varied until a best fit was obtained. All values in cm^{-1}.
[b]e_{π_N}' (equatorial) is assumed equal to zero.
[c]Based on data of Bertini *et al.* (11).
[d]This compound is Ni(NH_3)$_4$(NCS)$_2$; based on room temperature data of Hare and Ballhausen (23).

DQ_{eq}), has an average value of 4132 cm^{-1} (or 34 087 for DQ_{eq}) in this series with rather small variation from one complex to another. This provides further support for the validity of the assignment made, and reflects the relative independence of the equatorial and axial parameters for these nickel complexes. This is in contrast to similar copper(II) complexes, in which the two parameters are quite dependent on one another (19). Gazo and Bersuker (20) describe this as the plasticity of the copper coordination sphere (see also ref. 24).

An infrared study of several Ni(diamine)$_2X_2$ compounds indicates that for a given X the ν(Ni–N) mode is higher for the *s*-Et_2en complex than for the *s*-Me_2en complex (9). This should be reflected by a larger DQ_{eq} for the former. We find DQ_{eq} to be about 9% greater for Ni(*s*-Et_2en)$_2$(NCS)$_2$ than for the corresponding Me complex. For the trichloroacetate complexes it is about 2% greater in the Et complex (unpublished data). While more data are needed in order to verify this as a general trend, the values correspond to what one would expect from the greater basicity of the *s*-Et_2en ligand. An earlier study (21) using data of much poorer quality led to the reverse conclusion. An apparent decrease in Dq for the *s*-Et_2en complexes was ascribed to increased steric hindrance. The importance of obtaining high quality data cannot be overemphasized.

The σ bonding strength of the axial ligand naturally depends upon the nature of this ligand. The parameter e_{σ_Z}' varies in the sequence:

[1] $$\begin{array}{lccccc} NCS \gg H_2O & > & Cl & > & Br & > NO_3 \\ 3536^2 & & 1979 & & 1712\ 1178 & 1064\ cm^{-1} \end{array}$$

certainly the anticipated order on the basis of the spectrochemical series. Recall that the crystal-field strength is related to the orbital angular overlap parameters by the relationship (3):

[2] $$(5/3)\sqrt{21}\,DQ = 10Dq = (3e_\sigma' - 4e_\pi')$$

The spectrochemical series reflects a relative order of DQ. Since in the case of nickel, the e_π' parameter is usually small, the spectrochemical series will also reflect the value of e_σ'.

In general, the axial field strengths are rather low. The conventional DQ values for an unhindered Ni(II)L_6 hypothetical complex would

[2]Average for the methyl and ethyl complexes.

be: 24.47 kK for L = H_2O, 19.58 for L = Cl, and 18.60 for L = Br (22). The calculated DQ values for these axial ligands (L) in the *s*-Et_2en complexes are: 17.81 to 20.73 kK for H_2O, 17.16 for Cl, and 16.80 for Br. The reduced values observed in these complexes may reliably be attributed to a weakened axial interaction as a consequence of steric hindrance by the *N*-ethyl groups. In the case of the thiocyanates shown in Table 2, the field strength of NCS in the less sterically hindered *s*-Me_2en complex is markedly greater than in the *s*-Et_2en complex. Curiously, however, the field strength of the NCS group in *trans*-Ni(en)$_2$(NCS)$_2$ is much smaller (Table 2). This is attributed by Bertini *et al.* (11) to a somewhat longer than normal Ni—NCS bond length. It is certainly not clear why *en* should behave so differently from its *N*-substituted derivatives in this respect. In this last complex the Ni—NCS bond is bent (140°) and this may be the reason for the low DQ value through decreased overlap. The equatorial field strength of this ethylenediamine complex is the same as that of the *s*-Me_2en complex.

In the sterically unhindered *trans*-Ni$(NH_3)_4$(NCS)$_2$ complex (23) the σ-bonding strength of ammonia is seen to be below that of the diamines whereas the thiocyanate has e_σ' and DQ values comparable to that of the *s*-Me_2en complex, where presumably steric hindrance is small, at least towards the sterically undemanding linear NCS group. It should be noted that these are room temperature spectral data, and so not directly comparable to the other data gathered at ~10 K.

The Racah B values do not vary a great deal, clustering with one important exception near 850 cm^{-1}. The exception is Ni(*s*-Et_2en)$_2$(NCS)$_2$ for which the low value of 690 cm^{-1} is observed. There can be no doubt that the value is correct in that the two highest energy bands in the spectrum (arising from the F and P terms) are closer together than in the other complexes considered. It is this fact which results in a decreased B value. The reason for the lower B value is by no means clear. The possibility of S bonding by the thiocyanate is absolutely ruled out both by the electronic and vibrational spectra.

This is the initial report of a series of papers describing the analysis of the spectra of both cobalt(II) and nickel(II) complexes of this general class. The cobalt data are, as expected, much more complicated. They can be fitted with parameters very similar to those reported here, but further supporting evidence, in particular magnetic circular dichroism data, are necessary to confirm the assignments. These cobalt data and those for other nickel(II) complexes will be reported in due course. At that time a more detailed analysis of the variation of the parameters as a function of both metal and stereochemistry will be attempted.

Acknowledgements

ABPL and GL are indebted to the National Research Council of Canada for financial support. PJM acknowledges a grant from the Research Corporation for the purchase of the Displex Cryogenic refrigerator.

1. (*a*) A. B. P. Lever. Inorganic electronic spectroscopy. *Edited by* M. F. Lappert. Elsevier, Amsterdam. 1968. (*b*) C. J. Ballhausen. Introduction to ligand field theory. McGraw-Hill, New York, NY. 1962.
2. J. C. Hempel, J. C. Donini, B. R. Hollebone, and A. B. P. Lever. J. Am. Chem. Soc. **96**, 1693 (1974); **97**, 4151 (1975).
3. J. C. Donini, B. R. Hollebone, G. London, A. B. P. Lever, and J. C. Hempel. Inorg. Chem. **14**, 455 (1974).
4. J. C. Donini, B. R. Hollebone, and A. B. P. Lever. Prog. Inorg. Chem. **22**, 225 (1977).
5. J. Glerup, O. Mønsted, and C. E. Schäffer. Inorg. Chem. **15**, 1399 (1976).
6. J. S. Merriam and J. R. Perumareddi. J. Phys. Chem. **79**, 142 (1975).
7. L. Dubicki, M. A. Hitchman, and P. Day. Inorg. Chem. **9**, 188 (1970); L. Dubicki and P. Day. Inorg. Chem. **10**, 2043 (1971).
8. A. B. P. Lever and E. Mantovani. Can. J. Chem. **51**, 1567 (1973).
9. R. Nasanen, L. Lemmetti, U. Lamminsivu, and H. Abdalla. Suom. Kemistil. B, **41**, 1 (1968).
10. A. A. G. Tomlinson, C. Bellitto, O. Piovesana, and C. Furlani. J. Chem. Soc. Dalton Trans. 350 (1972).
11. I. Bertini, D. Gatteschi, and A. Scozzafava. Inorg. Chem. **15**, 203 (1976).
12. A. B. P. Lever. Coord. Chem. Rev. **3**, 119 (1968).
13. D. A. Rowley and R. S. Drago. Inorg. Chem. **7**, 795 (1968).
14. A. F. Schreiner and D. J. Hamm. Inorg. Chem. **12**, 2037 (1973).
15. D. M. L. Goodgame and M. A. Hitchman. Inorg. Chem. **3**, 1389 (1964).
16. R. Grinter, M. J. Harding, and S. F. Mason. J. Chem. Soc. A, 667 (1970).
17. M. Keeton, B. F-C. Chou, and A. B. P. Lever. Can J. Chem. **49**, 192 (1971).
18. Y. Omura, I. Nakagawa, and T. Shimanouchi. Spectrochim. Acta Part A, **27**, 2227 (1971).
19. A. B. P. Lever and E. Mantovani. Inorg. Chem. **17**, 817 (1971).

20. J. GAZO and I. B. BERSUKER. Coord. Chem. Rev. **19**, 253 (1976).
21. A. B. P. LEVER. Adv. Chem. Ser. **62**, 430 (1966).
22. C. K. JØRGENSEN. Absorption spectra and chemical bonding in complexes. Addison-Wesley, Reading, MA. 1962. p. 113.
23. C. R. HARE and C. J. BALLHAUSEN. J. Chem. Phys. **40**, 792 (1964).
24. L. Y. MARTIN, C. R. SPERATI, and D. H. BUSCH. J. Am. Chem. Soc. **99**, 2968 (1977).

Appendix

Parameters

The various parameters are calculated from the following equations (4). Note change in sign of DT effective in our publications dating from 1976.

$$[3] \quad d\sigma = (6DS + \sqrt{15}\,DT)/28$$

$$[4] \quad d\pi = (3DS - 2\sqrt{5/3}\,DT)/14$$

$$[5] \quad DQ_{ax} = DQ + 2\sqrt{7/5}\,DT$$

$$[6] \quad DQ_{eq} = DQ - \sqrt{7/5}\,DT$$

$$[7] \quad e_{\sigma N}' = 5DQ_{eq}/9\sqrt{21} = 5/9(DQ/\sqrt{21} - DT/\sqrt{15})$$

$$[8] \quad e_{\sigma z}' = 4/3d\sigma + e_{\sigma N}' = \frac{1}{189} \times (5\sqrt{21}\,DQ + 54DS + 2\sqrt{15}\,DT)$$

$e_{\pi N}'$ is assumed to be zero; therefore $e_{\pi z}' = d\pi$.

The relationships with the conventional parameters are (2):

$$[9] \quad DQ = 6\sqrt{21}\,Dq - 3.5\sqrt{21}\,Dt$$

$$[10] \quad DT = -3.5\sqrt{15}\,Dt$$

$$[11] \quad DS = -7Ds$$

Experimental Energies

Listed here are the energies observed for all shoulders (sh) and peaks illustrated in Figs. 2–9. R.T.-I and R.T.-II are the two room temperature orthogonal polarizations, 10 K-I and 10 K-II, the corresponding data at 10 K. Sharp spikes are indicated by sp.

In Fig. 2.

R.T.-I. 10 810, 17 525, 27 645 cm^{-1}.

10 K-I. 11 240, 13 050, 16 650sh, 18 155, 21 340sp, 24 110, 28 460 cm^{-1}.

R.T.-II. 10 835, 17 445, 27 745 cm^{-1}.

10 K-II. 9 480sp, 11 405, 13 050sh, 13 730sh, 18 050, 21 340sp, 24 110, 28 460 cm^{-1}.

In Fig. 3.

R.T.-I. 8 405, 9 470sp, 11 785, 12 545, 14 350sh, 16 690, 26 710 cm^{-1}.

10 K-I. 8 545, 9 476sp, 11 905, 12 640, 14 685, 17 435, 20 940, 27 350, 32 595sh cm^{-1}.

R.T.-II. 8 490, 9 470sp, 11 730, 12 420, 16 450, 26 775 cm^{-1}.

10 K-II. 8 382sp, 8 660, 9 473sp, 11 920, 12 615, 13 100sh, 14 660, 17 130, 20 940, 25 480sh, 27 375, 32 850sh cm^{-1}.

In Fig. 4.

R.T.-I. 7 660, 8 415sh, 11 800, 12 360, 13 650, 16 830, 26 320 cm^{-1}.

10 K-I. 8 065, 8 415sp, 9 435, 11 840, 12 725, 13 825, 17 550, 20 245, 23 585sh, 27 030 cm^{-1}.

R.T.-II. 8 115, 8 375, 11 680, 12 370, 13 195, 13 495sh, 16 350, 26 300 cm^{-1}.

10 K-II. 8 370, 9 425sp, 11 695, 12 175sh, 12 415sh, 12 590, 13 000sp, 13 310sh, 13 800, 14 165sh, 17 210, 20 000, 24 965sh, 27 025 cm^{-1}.

In Fig. 5.

R.T.-I. 9 560, 12 080, 13 100, 15 150sh, 17 495, 26 315sh, 28 280 cm^{-1}.

10 K-I. 9 830, 12 525, 13 210sp, 13 395, 13 705sh, 14 005sh, 14 320sh, 14 560sh, 16 000, 18 165, 27 030sh, 29 000 cm^{-1}.

R.T.-II. 9 390, 12 300, 13 330, 17 720, 28 275 cm^{-1}.

10 K-II. 9 760, 12 675, 13 430, 13 740, 15 750, 18 310, 28 965 cm^{-1}.

In Fig. 6.

R.T.-I. 8 400sh, 8 990, 12 060, 13 140, 17 405, 27 950 cm^{-1}.

10 K-I. 9 240, 12 505, 13 300sp, 13 472sp, 13 830sh, 14 105sh, 14 465sh, 14 715sh, 15 440sh, 17 950, 21 550, 28 415, 37 700 cm^{-1}.

R.T.-II. 8 925, 10 410sp, 12 150, 13 080, 13 420sh, 13 710sh, 17 350, 27 915 cm^{-1}.

10 K-II. 9 150, 12 505, 13 300sp, 13 554sp, 13 836sp, 14 142sp, 14 390, 14 450, 14 735sh, 15 440sh, 17 680, 21 550sh, 26 200sh, 28 415, 38 000 cm^{-1}.

In Fig. 7.

R.T.-I. 8 420sp, 8 840, 12 335, 13 280, 14 710, 17 820, 28 210 cm^{-1}.

10 K-I. 8 420sp, 9 360, 12 650, 13 255sh, 13 485, 13 780sh, 14 095sh, 14 400, 14 665sh, 15 295, 18 375, 21 385, 28 610, 35 400sh cm^{-1}.

R.T.-II. 8 405sp, 9 020, 12 480, 13 320, 14 570sh, 17 765, 27 815 cm^{-1}.

10 K-II. 8 410sp, 9 155, 10 440sh, 12 570, 13 485, 13 780, 15 520, 18 375, 21 385sh, 28 810, 35 200sh, 36 185 cm^{-1}.

In Fig. 8.

R.T.-I. 10 945, 12 560sh, 13 090sh, 18 185, 28 715 cm^{-1}.

10 K-I. 11 135, 12 750sh, 13 200sh, 18 525, 24 935sh, 29 250 cm^{-1}.

R.T.-II. 11 190, 17 970, 28 475 cm^{-1}.

10 K-II. 11 990, 12 895sh, 13 200sh, 18 410, 29 110 cm^{-1}.

In Fig. 9.

R.T.-I. 8 590, 12 500, 13 380, 14 255, 18 020 cm^{-1}.

10 K-I. 9 055, 12 590, 13 200sh, 13 475, 13 655sh, 13 980sh, 14 350, 14 835sh, 18 765, 26 165sh cm^{-1}.

R.T.-II. 8 620, 12 360, 13 120, 14 270sh, 17 560, 28 310 cm^{-1}.

10 K-II. 9 210, 12 585, 13 330, 13 800sp, 14 050sp, 14 385sp, 14 565, 14 870, 18 375, 26 315sh, 28 985sh cm^{-1}.

All data, except spikes, are rounded to the nearest 5 cm^{-1}.

Canadian Journal of Chemistry

Published by
THE NATIONAL RESEARCH COUNCIL OF CANADA

Journal canadien de chimie

Publié par
LE CONSEIL NATIONAL DE RECHERCHES DU CANADA

Volume 55 Number 18 September 15, 1977

Volume 55 numéro 18 15 septembre 1977

Studies on metal–acetylene complexes. VII. The molecular structure of bis(tricyclohexylphosphine)(hexafluorobut-2-yne)platinum(0)

JOHN F. RICHARDSON AND NICHOLAS C. PAYNE

Department of Chemistry, University of Western Ontario, London, Ont., Canada N6A 5B7

Received February 21, 1977

JOHN F. RICHARDSON and NICHOLAS C. PAYNE. Can J. Chem. **55**, 3203 (1977).

The acetylene complex $Pt(P(cyclo\text{-}C_6H_{11})_3)_2(F_3CC{\equiv}CCF_3)$ crystallizes in the monoclinic space group $P2_1/c$ with four formula units in a cell of dimensions $a = 10.902(2)$, $b = 21.766(3)$, $c = 19.808(3)$ Å, and $\beta = 116.52(1)°$. Three-dimensional X-ray data were collected on a four circle automatic diffractometer using Cu radiation. The structure was solved by the heavy atom method, and refined by full-matrix least-squares methods on F. A conventional agreement factor of 0.062 was achieved, employing 6678 observations for which $I > 0$. The coordination geometry at the platinum atom is essentially planar, for the acetylene triple bond makes an angle of 6.5(5)° with the plane formed by the Pt and the two P atoms. The triple bond length is 1.260(10) Å. The acetylene adopts a *cis*-bent geometry, with a mean bend-back angle of 45.5(8)°. The ligand is considerably perturbed upon coordination to the Pt atom, as is evident from the $\Delta\nu(C{\equiv}C)$ value of 578 cm^{-1}.

JOHN F. RICHARDSON et NICHOLAS C. PAYNE. Can. J. Chem. **55**, 3203 (1977).

Le complexe acétylène $Pt(P(cyclo\text{-}C_6H_{11})_3)_2(F_3CC{\equiv}CCF_3)$ cristallise dans le groupe d'espace monoclinique $P2_1/c$ avec quatre unités dans la maille de dimensions $a = 10.902(2)$, $b = 21.766(3)$, $c = 19.808(3)$ Å et $\beta = 116.52(1)°$. On a recueilli les données de rayons-X en trois dimensions à l'aide d'un diffractomètre automatique à quatre cycles utilisant la radiation Cu. On a résolu la structure par la méthode des atomes lourds et on l'a affinée par la méthode des moindres carrés (matrice complète) autour de F. On a pu obtenir un facteur de R de 0.062 utilisant 6678 réflexions pour lesquelles $I > 0$. La géométrie de la coordination au niveau de l'atome de platine est essentiellement planaire puisque le lien triple de l'acétylène fait un angle de 6.5(5)° avec le plan formé par le platine et les deux atomes de phosphore. La longueur de la liaison triple est de 1.260(10) Å. L'acétylène adopte une géométrie *cis*-déformée avec un angle de déformation de 45.5(8)°. Le ligand est très perturbé par la coordination avec l'atome de platine et ceci est mis en évidence à l'aide d'une valeur de $\Delta\nu(C{\equiv}C)$ de 578 cm^{-1}.

[Traduit par le journal]

Introduction

The interaction between a metal atom and an acetylene molecule results in a π-bonded complex in which the acetylene ligand adopts a *cis*-bent geometry. The magnitude of the deviation from linearity may be determined from the bend-back angle. Such effects have been successfully explained by a modification of the Chatt–Dewar–Duncanson synergic bonding scheme (1, 2). The crystallographic studies completed to date suggest that, except in cases where the acetylene is cyclic, for example cyclohexyne or cycloheptyne (3), the maximum bend-back angle observed is around 40° (2). For example, a value of 39.9(5)° was found in the complex bis(triphenylphosphine)(hexafluorobut-2-yne)platinum(0) (2).

Thus the preparation and characterization (4) of the complex bis(tricyclohexylphosphine)-(hexafluorobut-2-yne)platinum(0) provided an opportunity to examine the geometry of the same acetylene ligand in the presence of phosphine ligands of greater basicity than triphenyl-

phosphine, and hence presumably greater electron-donating abilities (5, 6).

Further interest in the title compound is provided by the increased steric bulkiness of the tertiary phosphine ligand. In 1969 Tolman introduced the concept of a cone angle as a measure of the steric properties of a phosphine ligand (5). The value of 179(10)° given for tricyclohexylphosphine, later revised to 170(10)°, suggests that the acetylene complex should not exist. It was thus of interest to examine the interligand steric interactions with a view to determining the relative importance of the electronic and steric effects. The results of the study are presented herein.

Experimental

Colourless crystals of $Pt(P(C_6H_{11})_3)_2(F_3CC{\equiv}CCF_3)$ were kindly supplied by Attig and Clark (4). A preliminary photographic study using Weissenberg and precession techniques showed the crystals belonged to the monoclinic system. The systematic absences observed, l odd for $h0l$ and k odd for $0k0$, uniquely define the space group as $P2_1/c$, C_{2h}^5, No. 14 (7).

The crystal chosen for data collection was carefully measured with a microscope fitted with a filar eyepiece to permit an absorption correction. Approximate dimensions of 0.41 mm × 0.23 mm × 0.17 mm were observed. The crystal possessed nine faces, namely {010}, $(\bar{1}10)$, $(1\bar{1}0)$, $(\bar{1}\bar{1}0)$, (100), (001), and (011) as determined by optical goniometry. A fractured face was best approximated as $(10\bar{6})$. The crystal was mounted on a Picker FACS-1 diffractometer with the long dimension [100] offset from coincidence with the spindle axis by approximately 5°.

Unit cell dimensions were determined from a least-squares refinement[1] of the angular settings for 20 reflections centered using $CuK\alpha_1$ radiation. The crystal density, determined by the flotation method using carbon tetrachloride and n-hexane, was 1.46(1) g cm^{-3}. This is in good agreement with the density of 1.450 g cm^{-3} calculated assuming four molecules per unit cell. There are no crystallographic symmetry constraints imposed upon the molecule.

Crystal data and the conditions for data collection are summarized in Table 1. Intensity data were recorded over a period of 8 days giving a total of 7301 reflections. Of these 186 were standards, which were recorded every 150 reflections for the range $2.5° \leq 2\theta \leq 60°$, and then every 250 reflections up to the maximum 2θ of 125° as a check on the crystal quality and electronic stability. These were found to increase with time, the increase being relatively constant for each standard. This increase was attributed to an increase in crystal mosaicity, and a correction was therefore applied to the data. The intensity of the nth reflection, observed at I_0 was adjusted to I_n, where

$$I_n = I_0/(1.0 + n(3.789 \times 10^{-5}))$$

The raw data were then corrected for background and Lorentz-polarization effects, and standard deviations were assigned according to the expression

$$\sigma(I) = [T_C + \tfrac{1}{4}(t_c/t_b)^2(B_h + B_l) + (pI)^2]^{1/2}$$

where T_C is the integrated count over the scan range, measured in time t_c, B_h and B_l are background counts, each measured in times t_b. I, the corrected intensity, is given by $T_C - \frac{1}{2}(t_c/t_b)(B_h + B_l)$. A series of absorption correction trials using $\mu = 70.72$ cm^{-1} for $CuK\alpha$ radiation showed transmission factors varying from 0.185 to 0.321, so an absorption correction was applied. The analytical method of de Meulenaer and Tompa was used.[1] There were 5672 reflections regarded as observed ($I > 3\sigma(I)$) and used in the structure solution and preliminary refinement.

Structure Solution and Refinement

The positions of the Pt atom and the two P atoms were readily located from a three-dimensional Patterson synthesis. One cycle of full-matrix least-squares refinement on F, varying positional parameters and isotropic temperature factors, and minimizing the function $\sum w(|F_o| - |F_c|)^2$, led to the agreement factors

$$R_1 = \sum||F_o| - |F_c||/\sum|F_o| = 0.222$$

$$R_2 = (\sum(|F_o| - |F_c|)^2/\sum wF_o^2)^{1/2} = 0.308$$

The weight w is defined as $4F_o^2/\sigma^2(F_o^2)$.

The atomic scattering factors for neutral Pt, P, F, and C atoms were those of Cromer and Waber (8), while that of H was taken from Stewart *et al.* (9). Anomalous dispersion contributions to the scattering factor were included for Pt, P, and F atoms, and were taken from Cromer and Liberman (10).

The remaining 46 non-hydrogen atoms were located by means of a difference Fourier synthesis. Subsequent least-squares refinements were carried out with the Pt, P, and F atoms assigned anisotropic thermal parameters and the acetylene C atoms isotropic Debye factors. The cyclohexyl rings were treated as rigid groups, having the chair conformation with C—C bond lengths of 1.54 Å and C—C—C angles of 109.47° (11). Ten cycles of refinement gave agreement factors $R_1 = 0.048$ and $R_2 = 0.052$ (5672 observations, 190 variables).

[1]Computing was performed on the CDC Cyber 73-14 at the University of Western Ontario. Programs used include local modifications of: orientation matrix and cell refinement, a version of Hamilton's MODE1; absorption correction, AGNOST, as modified by Cahen and Ibers; Fourier syntheses, FORDAP, by Zalkin; least-squares refinements and structure factor calculations, a version of NUCLS, by Ibers; error calculations, ORFFE, by Busing, Martin, and Levy; and molecular illustrations, ORTEP, by Johnson.

TABLE 1. Summary of crystal data and conditions for data collection

$PtP_2F_6C_{40}H_{66}$	fw = 918.0
Crystal description	Colourless prisms
Cell constants	a = 10.902(2) Å, b = 21.766(3) Å, c = 19.808(3) Å, β = 116.52(1)°
Cell volume	4205.7 Å^3
Radiation	CuKα, Ni foil (0.018 mm thick) prefilter
Temperature	21°C
Mean ω scan width at half height	0.09°
Scan speed	2° min^{-1}
Stationary background count time	10 s at scan limits
Standard reflections	$\bar{1}00$, 020, 002, 100, $0\bar{2}0$
Take-off angle	1.4°
Crystal–counter distance	34 cm
Aperture size	5 × 5 mm

An analysis of the structure at this point revealed a probable disorder of one of the CF_3 groups, as indicated by C—F bond distances ranging from 1.203 to 1.362 Å and F—C—F bond angles from 87.1 to 116.8°. An examination of a difference Fourier synthesis indicated six F-atom sites. This disorder apparently occurs as a result of a 60° rotation of the group around the C—CF_3 bond. To account for this disorder a rigid group having D_{6h} symmetry and F—F nonbonded distances of 1.215 Å was refined with each F having a multiplicity of 0.5. Least-squares refinement of the group parameters proved successful, resulting in an acceptable model geometry and a slight increase in the agreement factors to $R_1 = 0.055$ and $R_2 = 0.057$ (5672 observations, 247 variables).

The positions of the 66 H atoms were calculated assuming a C—H distance of 1.00 Å, and sp^3 hybridization at the C atoms. All were found to correspond to regions of positive electron density (0.4–0.8 e Å^{-3}) in a difference Fourier synthesis. The H-atom contributions were henceforth included in structure factor calculations.

In the final stages of refinement the group constraints were lifted from the cyclohexyl substituents, and each C atom was allotted an isotropic thermal parameter. Idealized H-atom positions were recalculated. For the final cycle only the disordered hexagonal F entity was refined as a group with an overall group thermal parameter. The 36 cyclohexyl C atoms were allotted isotropic thermal parameters. Only unique data with $I > 0$ were used, and with 6678 observations and 247 variables, the refinement converged at $R_1 = 0.0624$ and $R_2 = 0.0631$. No parameter shifts other than those associated with the F6 group exceeded 0.14 of an estimated standard deviation, and a statistical analysis of R_2 in terms of $|F_o|$, indices, $\lambda^{-1} \sin\theta$, and the diffractometer setting angles χ and ϕ showed no unusual trends. The standard deviation on an observation of unit weight was 2.73 electrons. A final difference Fourier synthesis was calculated and showed no areas of significant positive electron density. The largest residual peak (1.85(18) e Å^{-3}) occurred at (−0.1279, 0.1212, 0.1662) and was associated with the F6 rigid group. No evidence was observed for secondary extinction.

The final positional and thermal parameters of the nongroup atoms are given in Table 2. The group parameters and the derived atom positional and isotropic thermal parameters for the F atoms in the F6 group are given in Table 3. Cyclohexyl H-atom parameters are given in Table 4 and final values of $10|F_o|$ and $10|F_c|$ in electrons are given in Table 5.[2]

Description of the Structure

The structure consists of discrete molecular units with the closest intermolecular distance of approach being 2.30 Å between cyclohexyl H atoms bonded to 4C5 and 5C6. Selected bond lengths and bond angles are given in Table 6. The inner coordination sphere of the Pt atom, showing the atom-labelling scheme and significant bond lengths and angles, is given in Fig. 1. A stereoview of the molecule is found in Fig. 2.

The coordination geometry around the Pt atom is essentially planar. A weighted least-squares plane was calculated using the Hamilton method[1] and results are shown in Table 7. The

[2]Tables 4 and 5 are available, at a nominal charge, from the Depository of Unpublished Data, CISTI, National Research Council of Canada, Ottawa, Canada K1A 0S2.

TABLE 2. Atomic positional and thermal parameters*,†,‡

Atom	x	y	z	$U(1,1)$	$U(2,2)$	$U(3,3)$	$U(1,2)$	$U(1,3)$	$U(2,3)$
Pt	995.5(3)	2188.41(13)	−2467.4(2)	410(2)	392(2)	514(2)	5(1)	216(1)	−34(1)
P(1)	1152(2)	1158.5(8)	−2698.0(10)	443(9)	396(9)	475(10)	0(7)	188(8)	−27(8)
P(2)	3131(2)	2636.3(8)	−1971.9(11)	453(9)	431(10)	467(10)	−25(7)	208(8)	−47(8)
F(1)	−2814(5)	1750(3)	−3745(5)	498(31)	1588(65)	2151(84)	0(36)	116(40)	−995(63)
F(2)	−3098(6)	2126(4)	−2898(4)	763(41)	3018(117)	1088(53)	−283(52)	540(40)	88(61)
F(3)	−3226(6)	2667(3)	−3764(5)	858(42)	1271(57)	1643(71)	85(39)	32(44)	509(52)
C(1)	−2527(9)	2232(4)	−3316(6)	509(47)	709(58)	996(73)	156(45)	329(50)	−47(56)
C(2)	−1053(8)	2377(3)	−2885(5)	553(45)	440(42)	804(57)	51(34)	365(42)	7(39)
C(3)	−399(8)	2860(4)	−2586(5)	520(45)	672(56)	846(64)	85(42)	301(44)	−8(48)
C(4)	−772(10)	3500(5)	−2489(6)	799(72)	980(80)	1028(84)	195(59)	298(63)	−82(68)

Atom	x	y	z	U (Å²)	Atom	x	y	z	U (Å²)
1C1	551(7)	680(3)	−2134(4)	54(2)	4C1	3340(7)	3067(3)	−2721(4)	49(2)
1C2	−876(8)	839(4)	−2240(5)	65(2)	4C2	2132(8)	3505(4)	−3146(5)	67(2)
1C3	−1303(9)	411(4)	−1760(5)	73(2)	4C3	2242(9)	3848(4)	−3787(5)	73(2)
1C4	−289(9)	451(4)	−931(5)	80(3)	4C4	2436(10)	3395(5)	−4327(6)	86(3)
1C5	1146(9)	294(4)	−818(5)	75(2)	4C5	3686(9)	2988(4)	−3894(5)	71(2)
1C6	1580(8)	714(3)	−1296(4)	58(2)	4C6	3502(7)	2634(3)	−3285(4)	55(2)
2C1	−128(7)	1036(3)	−3691(4)	49(2)	5C1	3224(7)	3252(3)	−1308(4)	53(2)
2C2	−323(8)	390(4)	−4017(5)	61(2)	5C2	4493(10)	3660(4)	−986(5)	81(3)
2C3	−1567(9)	375(4)	−4799(5)	72(2)	5C3	4264(11)	4222(5)	−577(6)	99(3)
2C4	−1432(9)	832(4)	−5331(5)	79(3)	5C4	3957(11)	4006(5)	44(6)	100(3)
2C5	−1215(8)	1472(4)	−5011(5)	67(2)	5C5	2724(11)	3590(5)	−223(6)	94(3)
2C6	23(8)	1497(4)	−4234(4)	59(2)	5C6	2868(10)	3042(5)	−688(6)	83(3)
3C1	2775(7)	758(3)	−2542(4)	49(2)	6C1	4697(7)	2153(3)	−1526(4)	51(2)
3C2	3298(7)	951(3)	−3109(4)	51(2)	6C2	4824(9)	1841(4)	−809(5)	69(2)
3C3	4747(8)	705(4)	−2882(5)	64(2)	6C3	5982(10)	1360(4)	−526(6)	84(3)
3C4	4772(9)	12(4)	−2823(5)	73(2)	6C4	7330(10)	1661(5)	−409(6)	89(3)
3C5	4229(9)	−194(4)	−2279(5)	73(2)	6C5	7225(9)	1980(4)	−1086(5)	76(2)
3C6	2796(8)	54(4)	−2481(5)	62(2)	6C6	6052(8)	2452(4)	−1385(5)	66(2)

*Estimated standard deviations in this and other tables are given in parentheses and correspond to the least significant digits.
†Positional parameters are multiplied by 10^4.
‡$U_{ij} = \beta_{ij}/(2\pi^2 a_i^* a_j^*)$ Å². Values have been multiplied by 10^4. The thermal ellipsoid is given by $\exp[-(\beta_{11}h^2 + \beta_{22}k^2 + \beta_{33}l^2 + 2\beta_{12}hk + 2\beta_{13}hl + 2\beta_{23}kl)]$. Isotropic thermal parameters are multiplied by 10^3.

TABLE 3. Group parameters and derived atom positional and thermal parameters*

x_g	y_g	z_g	δ	ε	η
−920(5)	3723(2)	−2442(3)	−1.217(5)	2.936(6)	1.313(8)

Atom	x	y	z	B (Å² × 10)
F1	−2064(6)	3533(3)	−2598(6)	57(2)
F2	−1197(10)	3546(4)	−1944(5)	130(5)
F3	−53(8)	3735(4)	−1788(4)	120(5)
F4	224(6)	3912(3)	−2286(5)	52(2)
F5	−643(10)	3900(4)	−2939(4)	125(5)
F6	−1787(8)	3710(4)	−3095(4)	117(4)

*x_g, y_g, and z_g are the fractional coordinates of the group centre; δ, ε, and η (in radians) are the group orientation angles.

TABLE 6. Selected bond distances and bond angles

Bond	Distances (Å)
Pt—P(1)	2.309(2)
Pt—P(2)	2.301(2)
Pt—C(2)	2.047(7)
Pt—C(3)	2.045(8)
P(1)—1C1	1.848(8)
P(1)—2C1	1.854(7)
P(1)—3C1	1.871(7)
P(2)—4C1	1.854(7)
P(2)—5C1	1.849(8)
P(2)—6C1	1.859(7)
C(1)—C(2)	1.478(11)
C(2)—C(3)	1.260(10)
C(3)—C(4)	1.487(13)

Atoms	Angle (deg)	Atoms	Angle (deg)
P(1)—Pt—P(2)	110.23(6)	C(1)—C(2)—C(3)	133.7(8)
P(1)—Pt—C(2)	106.1(2)	C(4)—C(3)—C(2)	135.4(8)
P(2)—Pt—C(3)	107.7(2)	C(2)—Pt—C(3)	35.87(29)
Pt—P(1)—1C1	110.5(2)	Pt—P(2)—4C1	109.6(2)
Pt—P(1)—2C1	105.2(2)	Pt—P(2)—5C1	109.5(2)
Pt—P(1)—3C1	124.6(2)	Pt—P(2)—6C1	120.2(2)
1C1—P(1)—2C1	105.0(3)	4C1—P(2)—5C1	102.5(3)
1C1—P(1)—3C1	101.6(3)	4C1—P(2)—6C1	104.6(3)
2C1—P(1)—3C1	108.5(3)	5C1—P(2)—6C1	109.0(3)

dihedral angle between planes defined by the Pt, P(1), P(2) and Pt, C(1), C(2) indicates only a small deviation from planarity of 6.5(5)°.

The Pt—P distances of 2.301(2) and 2.309(2) Å may be considered statistically equivalent. The Pt—C distances to C(2) and C(3) of 2.047(7) and 2.045(8) Å respectively are also equivalent, and comparable to the values of 2.024(5) and 2.047(7) Å found in the triphenylphosphine complex (2). The two P atoms of the tricyclohexylphosphine ligands subtend an angle of 110.23(6)° at the Pt atom and the acetylene C atoms C(2) and C(3) form an angle of 35.9(3)° with the Pt atom. The angle of 36.1(2)° subtended in the triphenylphosphine complex by the acetylene ligand is comparable, but the P—Pt—P angle of 100.17(4)° is much less than that in the complex containing the bulkier tricyclohexylphosphine ligand.

The disorder of the CF_3 group bonded to C(3) renders comparisons of the CF_3 groups doubtful, but it should be noted that the ordered CF_3 group has dimensions comparable to those in the triphenylphosphine complex. Thus the mean

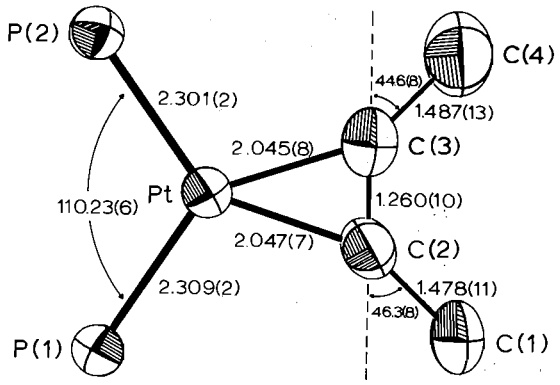

FIG. 1. Inner coordination sphere, showing the atom-labelling scheme and selected bond distances and angles.

C—F distance is 1.282(10) Å, and the mean F—C—F angle is 104.6(9)°. Mean values of 1.327(10) Å and 105.0(8)° respectively resulted from the refinement of the hexagonal F group. The mean P—C distance in the tricyclohexylphosphine ligands is 1.856(6) Å and the mean angle subtended by the cyclohexyl C1 atoms at the P atoms is 114.1(5)°. Within the C_6H_{11} rings a mean C—C bond length of 1.524(10) Å was observed, with an average C—C—C angle of 110.9(7)°.

Upon coordination to the Pt atom the $\nu(C{\equiv}C)$ is reduced by 578 cm^{-1}, an extent significantly greater than the value of 525 cm^{-1} observed for the triphenylphosphine complex (2). That the acetylene has been greatly perturbed upon coordination is shown by a mean bend-back angle of 45.5(8)°, also significantly larger than that found in the triphenylphosphine case (39.9(5)°). The acetylenic triple bond length

TABLE 7. Weighted least-squares plane

Atom	Distance from plane (Å)
Pt	0.0007(3)
P(1)	−0.0065(19)
P(2)	−0.0076(19)
C(2)	−0.1748(91)
C(3)	−0.0580(96)

Equation of plane

$-3.491x - 4.750y + 19.17z + 6.118 = 0$

Atoms	Dihedral angle between planes (deg)
Pt P(1) P(2) Pt C(2) C(3)	−173.5(5)

of 1.260(10) Å is indistinguishable from the triphenylphosphine complex value of 1.255(9) Å, but significantly larger than the average value of 1.202(5) Å found in free acetylenes (12).

Discussion

Differences between the title compound and the triphenylphosphine complex are summarized in Table 8. As indicated, the relative basicities of the phosphine ligands were determined by two independent means. Thus Tolman (5) showed that in the complexes $Ni(CO)_3L$ the value of $\nu(C{\equiv}O)$ was a sensitive indicator of the ligand basicities. The infrared stretching frequency of the C≡O was found to decrease with increasing basicity of the ligand L, and thus tricyclohexyl-

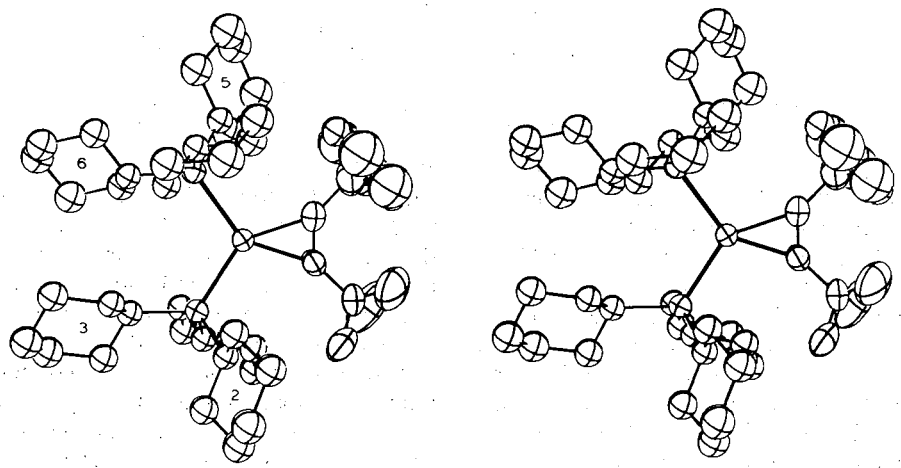

FIG. 2. A stereoview of the molecule. Thermal ellipsoids are drawn at the 50% probability level.

TABLE 8. A comparison of bis(tricyclohexylphosphine)-(hexafluorobut-2-yne)platinum(0) and bis(triphenylphosphine)(hexafluorobut-2-yne)platinum(0)

	$P(C_6H_{11})_3$	$P(C_6H_5)_3$
Basicity ν(C≡O) in	2056	2069
$Ni(CO)_3L$ (cm^{-1})	1973	1990
pK_a	9.70	2.73
C≡C bond length (Å)	1.260(10)	1.255(9)
Bend-back angles (deg)	45.5(8)	39.9(5)
Δν(C≡C) (cm^{-1})	578	525
Tolman cone angles (deg)	170(10)	145(2)
Cone angles		
Minimum	128	92
Maximum	168	160

phosphine was considered a stronger electron donor than triphenylphosphine. Similarly, pK_a values determined by Trogler and Marzilli (6) show tricyclohexylphosphine to be the stronger base.

A greater basicity in the phosphine ligands is expected to cause a greater distortion in the acetylene due to increased back donation from the metal atom (1). An increase is indeed found, as the bend-back angle of the title compound is 5.6(8)° larger than that found in the triphenylphosphine analogue. The triple bond lengths do not indicate this as clearly, for the increase is 0.005(13) Å, a difference of only 0.4σ. However, a greater distortion of the bond is indicated by the larger reduction in the infrared stretching frequency ν(C≡C) which occurs for the acetylene in the title compound compared to that observed for the triphenylphosphine complex (4).

The greater distortion from linearity of the acetylene ligand might therefore be explained solely on the basis of electronic effects. However, it is apparent that steric considerations play a major role in this complex. That a symmetric cone angle is not applicable to the tricyclohexylphosphine ligand is evident from the disposition of the cyclohexyl groups in this complex. Thus cyclohexyl groups 'bracket' the CF_3 substituents on the acetylene ligand. The distances of approach noted are 2.325 Å (F(1)—2C1H1), 2.434 Å (F3—5C5H2), and 2.34 Å (F4—5C1H1) and steric constraints could be causing the large bend-back angle observed. In an analogous way the presence of the acetylenic triple bond within a small cyclic organic molecule (3) introduced steric constraints which resulted in bend-back angles of 52.7° and 41.3° respectively for the cyclohexyne and the cycloheptyne complexes. At present we cannot unambiguously attribute the magnitude of the bend-back angle observed in this complex to an electronic rather than a steric effect.

Modified cone angle calculations have also been performed, based upon the geometry of this complex.[3] In these calculations the conical symmetry has been removed, and maximum and minimum cone angle values determined for the phosphine ligand. The maximum value agrees well with Tolman's values, as is to be expected from the original hypothesis. The minimum values are more applicable to complexes of this type. It is apparent that the tricyclohexylphosphine ligand is significantly larger than triphenylphosphine, and thus sterically more demanding.

However, the phosphine interactions do not dictate the conformation of the complex. If the plane containing the Pt and the two P atoms is taken as a reference in each complex, then different ligand orientations are observed. In the triphenylphosphine complex, one phenyl ring on P(2) lies closest to the plane, while two rings on P(1) lie above and below the plane, 'bracketing' the ring on P(2). Such a conformation results in a relatively close approach between one CF_3 group and the third phenyl ring on P(1). By contrast, in the tricyclohexylphosphine complex, a cyclohexyl group on each phosphorus atom lies close to the reference plane, with a resulting unfavourable interligand interaction. The greater P—Pt—P angle (110.23(6)° for this study, compared to 100.17(4)° for the triphenylphosphine complex) could result from this interaction. Also the mean Pt—P distance is longer, being 5.4σ greater in the title complex. As a result of this close approach of the cyclohexyl groups to the reference plane, each CF_3 group is 'bracketed' by the two remaining cyclohexyl groups on each phosphorus atom. These observations would seem to indicate that the interactions between the CF_3 groups on the acetylene ligand and the phosphorus substituents are of major importance in the tricyclohexylphosphine complex. These interactions will of course affect the bend-back angles observed, and at present we are unable to distinguish conclusively between electronic and steric effects. Further studies are underway on complexes of hexafluorobut-2-yne with phos-

[3]N. C. Payne and R. F. Stepaniak. Unpublished results.

phines of varying steric properties with a view to identifying the relative importance of these effects.

Acknowledgement

We thank the National Research Council of Canada for financial support of this work.

1. E. O. Greaves, C. J. L. Lock, and P. M. Maitlis. Can. J. Chem. **46**, 387 (1968).
2. B. W. Davies and N. C. Payne. Inorg. Chem. **13**, 1848 (1974).
3. G. B. Robertson and P. O. Whimp. J. Am. Chem. Soc. **97**, 1051 (1975).
4. T. G. Attig, H. C. Clark, and C. S. Wong. Can. J. Chem. **55**, 189 (1977).
5. C. A. Tolman. J. Am. Chem. Soc. **92**, 2953 (1970); **92**, 2956 (1970).
6. W. C. Trogler and L. G. Marzilli. Inorg. Chem. **14**, 2942 (1975).
7. International Tables for X-ray Crystallography. Kynoch Press, Birmingham, England. 1962.
8. D. T. Cromer and J. T. Waber. Acta Crystallogr. **18**, 104 (1965).
9. R. F. Stewart, E. R. Davidson, and W. T. Simpson. J. Chem. Phys. **42**, 3175 (1965).
10. D. T. Cromer and D. Liberman. J. Chem. Phys. **53**, 1891 (1970).
11. O. Hassel and H. Viervoll. Acta Chem. Scand. **1**, 149 (1947).
12. Special Publication No. 18. The Chemical Society, London. 1965. p. S16s.

'Breaking' and formation of hydrogen bonds by proton donor anesthetics

RACHEL MASSUDA AND C. SANDORFY
Département de chimie, Université de Montréal, Montréal (Qué.), Canada H3C 2V1

Received March 21, 1977

RACHEL MASSUDA and C. SANDORFY. Can. J. Chem. **55**, 3211 (1977).

It has been shown previously that halofluorocarbons having anesthetic potency hinder the formation of hydrogen bonds (HB) of the N—H - - - N, O—H - - - O, N—H - - - O=C types and it has been suggested that this is linked to a competitive mechanism involving another type of association. Since some of the most potent and widely used fluorocarbon anesthetics contain a mobile hydrogen atom the question arises if in such molecules the competitive mechanism involves the formation of HB's with the anesthetic as the proton donor instead of, or in addition to, association due to the electron acceptor properties of the higher halogens as seems to be the case for those fluorocarbon anesthetics which contain no hydrogen. Chloroform, halothane, methoxyflurane, enflurane, and 4,5-dichloro-2,2-difluoro-1,3-dioxolane have been studied from this point of view with the result that both mechanisms appear to operate.

RACHEL MASSUDA et C. SANDORFY. Can. J. Chem. **55**, 3211 (1977).

Nous avons montré antérieurement que les fluorocarbures contenant des halogènes supérieurs et ayant un pouvoir anesthésique entravent la formation des liaisons hydrogène (LH) de types N—H - - - N, O—H - - - O et N—H - - - O=C. Nous avons suggéré, en outre, que cela est dû à une association de type différent qui entre en compétition avec l'association par LH. Comme quelques uns des anesthésiques les plus puissants et les plus utilisés contiennent un hydrogène mobile, on peut se demander si cette association compétitive implique la formation d'une autre LH avec l'anesthésique comme donneur de proton, ou en plus des associations qui font intervenir les propriétés électron-accepteur des halogènes supérieurs, comme cela semble être le cas des fluorocarbures anesthésiques ne possédant pas d'atome d'hydrogène, ou les deux à la fois. Nous avons examiné le cas du chloroforme, de l'halothane, du méthoxyflurane, de l'enflurane et du dichloro-4,5 difluoro-2,2 dioxolanne-1,3 et nous concluons que les deux mécanismes contribuent à la dissociation des LH de types N—H - - - N, O—H - - - O et N—H - - - O=C par ces molécules anesthésiques.

Introduction

It has been observed in our laboratory through infrared spectroscopic measurements that fluorocarbon anesthetics containing higher halogens hinder the formation of ('break') hydrogen bonds of the N—H - - - N, O—H - - - O, and N—H - - - O=C type (1–3). Such hydrogen bonds (HB) are typical of the most frequently occurring HB's in the living organism. This effect can become very pronounced at low temperatures. While low temperatures normally favor association, in the presence of such halofluorocarbons the opposite is observed: a large relative decrease in the infrared intensities of the 'associated' NH or OH bands and an increase in the intensity of the 'free' band or bands due to less associated species. A qualitative correlation has been found between anesthetic potency and this HB 'breaking' property by Di Paolo and Sandorfy (2) who have shown by infrared spectroscopic measurements that, in general, halofluorocarbons known to have anesthetic potency are efficient HB breakers. The large changes observed at low temperatures made it easier to observe the smaller effects occurring at room temperature. Similar low temperature measurements have been carried out in the course of the work reported in the present paper.

In order to explain the hindering of HB formation by halofluorocarbon anesthetics it is natural to stipulate that there exists in these solutions a competitive mechanism of association which, under given circumstances, might be energetically favored over HB formation. This mechanism might be the formation of *another* hydrogen bond, charge transfer complex formation, Van der Waals interactions, or a combination of these. Many of the most potent anesthetics contain a mobile hydrogen atom as well as chlorine or bromine. In our previous work, the emphasis was laid on the role of the halogens. In this paper, we concentrate on the role of the mobile hydrogen atom. The following anesthetic compounds have been studied: chloroform $CHCl_3$, halothane $CF_3CHClBr$, enflurane

CF_2HOCF_2CHFCl, methoxyflurane CH_3OCF_2-$CHCl_2$, and 4,5-dichloro-2,2-difluoro-1,3-dioxolane henceforth abbreviated as DDD:

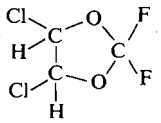

This latter compound has been recently prepared and proposed as an anesthetic by Denson *et al.* (4). Our aim has been to ascertain if a competitive formation of HB's of the C—H - - - N or C—H - - - O type takes place when these molecules are added to solutions of amines, amides, or alcohols which are engaged in HB's of the N—H - - - N, N—H - - - O=C, or O—H - - - O type.

Experimental

The solvents used were 1:1 mixtures of Freon-11 ($CFCl_3$) and methylcyclohexane (FM), or methylcyclohexane-d_{14}; the latter was needed for the investigation of the CH stretching bands. These solvents set to a glass at about −150°C; they are still glasses at liquid nitrogen temperature. The nondeuterated solvents were dried over P_2O_5 and distilled. Chloroform was washed several times with water, dried, and distilled. The other anesthetic compounds were high purity commercial products (Ayerst Laboratories for halothane, Abbott Laboratories for enflurane, and Pitman-Moore for methoxyflurane). The absence of any major impurity was verified by gas chromatography. The sample of 4,5-dichloro-2,2-difluoro-1,3-dioxolane (DDD) was supplied to us by D. D. Denson. All samples were stored over molecular sieves. The samples of amines, amides, and alcohols were all purified by distillation. The deuterated ones were obtained from Merck, Sharp and Dohme of Canada Ltd. and were used without purification. Halothane-*d* and methoxyflurane-d_1 were prepared by the method of Hine *et al.* (6). The disappearance of the CH bands was observed by infrared and nmr spectroscopy. The estimated yield was 97 and 89%, respectively. All preparations of solutions and the filling of cells were carried out in a dry box under nitrogen atmosphere.

The spectra were measured with a Perkin-Elmer model 621 infrared spectrophotometer at temperatures ranging from room to liquid nitrogen temperature. The low temperature cells were described previously (5).

The limits of error affecting the intensity measurements in these low temperature spectra are hard to estimate. Although every effort has been made to standardize the conditions of the cooling down procedure as much as possible the variations between repeated measurements remained nonnegligible. For this reason, we refrain from presenting quantitative results. However, we indicate the observed trends where they are clearly beyond possible experimental error. By 'intensity' we mean roughly estimated integrated intensities obtained by planimetering out the area under the bands taking approximate account of mutual overlapping between bands. A new series of works is underway in our laboratory using a nearly free-standing combination band with all spectra measured at room temperature.

Results

Our results indicate that HB formation takes place between our five anesthetic compounds and the amines, alcohols, and amides with the anesthetics as proton donors. The evidence is as follows.

Association with Amines

Figure 1*a* shows the NH stretching band for a 0.6 *M* solution of diethylamine in FM. The associated band which appears at 3268 cm^{-1} at 22°C increases in intensity on lowering the temperature and shifts to lower frequencies. At −180°C, a weak free NH band is still present at 3310 cm^{-1} and the much stronger associated band moves to 3224 cm^{-1}. Figure 1*b* shows the NH stretching band for a similar amine solution with 1.4 *M* chloroform added. It is observed that the growth of the associated band on lowering the temperature is much slower. At −150°C, for example, the free band is still more intense than the associated band indicating the much lesser extent of N—H - - - N association. Thus the HB 'breaking' property of chloroform appears clearly.

Similar observations have been made on chloroform-*d*, halothane, halothane-*d*, methoxyflurane, methoxyflurane-d_1, enflurane, and DDD. To illustrate these conditions in Fig. 2 the apparent molar extinction coefficient (computed with the initial room temperature concentration but corrected for changes in volume on lowering the temperature) has been plotted against temperature for the NH stretching band of diethylamine, first with no anesthetic present (curve *A*, concentration 0.61 *M*) and then for an equimolar (0.48 *M*) mixture of diethylamine and enflurane. At moderately low temperatures the difference is slight but from about −50°C it becomes rather sizeable. Similar plots have been obtained for the other four anesthetics.

The next step naturally consists of looking at the CH stretching band of chloroform and the other anesthetics. In order to avoid interference from the CH vibrations of diethylamine and from the methylcyclohexane component of the solvent (FM) we had to use $(CD_3)_2NH$ in a 1:1 mixture of $CFCl_3$ and methylcyclohexane-d_{14}. The associated CH stretching band appeared clearly in all cases between 2950 and 2900 cm^{-1}

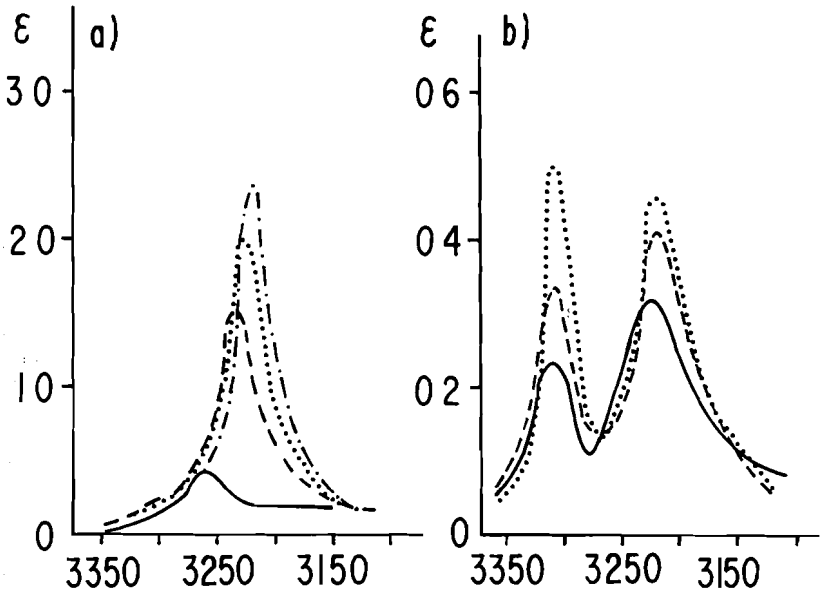

FIG. 1. (*a*) The infrared NH stretching band of a 0.6 *M* solution of diethylamine in a 1:1 mixture of $CFCl_3$ and methylcyclohexane (FM) at different temperatures. (*b*) The same with a 1.4 *M* $CHCl_3$ added to the solution. (Note the change of scale.) Apparent molar extinction coefficients (ℓ mol^{-1} cm^{-1}) against wave numbers in cm^{-1}. — −50°C; - - - −120°C; ··· −150°C; -·-·- −180°C.

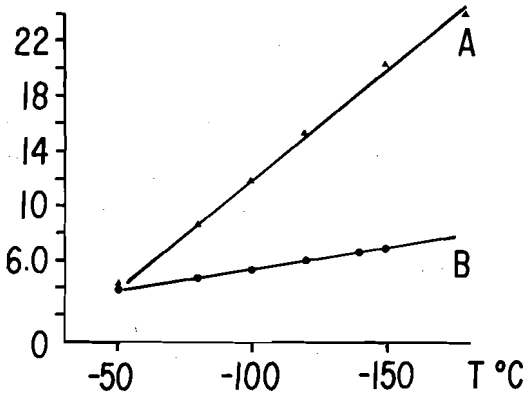

FIG. 2. Plot of the apparent molar extinction coefficient of the associated NH stretching band of diethylamine against temperature, from −50 to −180°C. Curve *A*: 0.61 *M* in FM, no anesthetic present. Curve *B*: equimolar mixture (0.48 *M*) of diethylamine and enflurane in FM.

(Table 1). The intensity of this band increases gradually for all our anesthetics with decreasing temperature and the band shifts to lower frequencies. For chloroform the intensity increased by a factor of six on lowering the temperature to −100°C and the band shifted to 2909 cm^{-1}. Enflurane which has two CH groups has also two free CH stretching bands, at 3023 and 2998 cm^{-1}. The latter is believed to correspond to the associated band at 2932 cm^{-1}. For methoxyflurane the presence of the methyl group gives rise to additional CH bands and we see four of these at 2960, 2910, and 2860 cm^{-1} while the band related to the tertiary CH group is at 3006 cm^{-1}. The increases in the intensity on lowering the temperature were in the order chloroform > halothane > methoxyflurane > enflurane > DDD. At the same time the intensity of the NH stretching band increased but much less than for diethylamine in solutions containing no anesthetics. This slowing down of the rate of increase was greatest for chloroform, > halothane > enflurane.

The first overtone of the CH bending mode is observed at 2398 and 2500 cm^{-1} for the free and associated species, respectively. The associated band increases in intensity, lowering the temperature as does the associated CH stretching band.

The free CD stretching band of $CDCl_3$ appears at 2250 cm^{-1}. In the presence of diethylamine an associated CD band appears at 2187 cm^{-1} at room temperature ($\Delta\nu$ = 63 cm^{-1}). The intensity of this band increases on lowering the temperature and it broadens on its low frequency side. Figure 3 shows the associated CD stretching band at different temperatures.

TABLE 1. CH stretching frequencies of anesthetic molecules

Anesthetic	Association with: Diethylamine or dimethylamine-d_6 $\nu_{CH(free)}$	$\nu_{CH(assoc)}$	$\Delta\nu$	*tert*-Butanol $\nu_{CH(assoc)}$	$\Delta\nu$	*N,N*-Dimethylacetamide $\nu_{CH(assoc)}$*	$\Delta\nu$
$CHCl_3$	3018	2925	93	2990	28	2982	36
Halothane	3003	2925	78	2963	40	2975	28
Methoxyflurane	3006	2928	78			2965	41
Enflurane	3023						
	2998	2932	66	2972	26	2992	6
DDD	3040	2982	58	3015	25	3018	22
$CDCl_3$	2250	2187	63	2230	20	2245[a]	5
Halothane-*d*	2260	2203	57	2210	50	2215[b]	45
	2218	2150	68	2182	36	2185[c]	33
Methoxyflurane	2245	2175	70	2223	22	2225[d]	20

*N-methylacetamide: [a]2238 cm^{-1}; [b]2220 cm^{-1}; [c]2182 cm^{-1}; [d]2230 cm^{-1}.

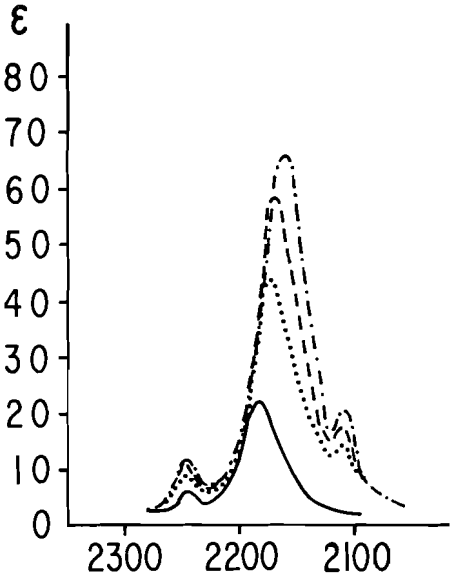

FIG. 3. The associated CD stretching band of $CDCl_3$ (0.88 *M*) at different temperatures in a solution of FM containing 0.50 *M* of diethylamine. Only the free band is seen in the absence of diethylamine. Apparent molar extinction coefficients against wave numbers. — −20°C; ··· −80°C; - - - −120°C; -·-·- −150°C.

The apparent increase in the intensity of the free band is largely due to overlap with the strong associated band. The weak band at the low frequency side of the associated band belongs probably to a more highly associated species (possibly a trimer) but we made no attempt to ascertain this.

Halothane-*d* exhibits two free CD stretching bands, at 2260 and 2218 cm^{-1}, respectively. The splitting is probably due to Fermi resonance. In the presence of diethylamine two additional bands appear, one at 2203, the other at 2150 cm^{-1} ($\Delta\nu$ = 57 and 68 cm^{-1}).

For methoxyflurane-d_1 the free CD band appears at 2245 cm^{-1}, the associated band at 2175 cm^{-1} ($\Delta\nu$ = 70 cm^{-1}). For both halothane-*d* and methoxyflurane-d_1 the associated band increases in intensity on lowering the temperature.

In all cases the increase in the intensity of the CH (or CD) bands was accompanied by the decrease of the NH bands showing that C—H - - - N and N—H - - - N HB formation compete with each other in these systems.

Association with Alcohols

In these studies we chose *tert*-butanol. In an FM solution its well known (composite) associated OH stretching band, centered at 3380 cm^{-1}, increases in intensity regularly with decreasing temperature. This increase is strongly reduced in the presence of chloroform or our other anesthetics (Fig. 4). At the same time the associated CH or CD band of the anesthetics appears and its intensity increases with decreasing temperature. In the presence of the anesthetics the *free* OH band is still seen at −20°C while it has disappeared in their absence.

The wave numbers of the free and associated CH bands are given in Table 1. The associated CD stretching band of $CDCl_3$ also increases in intensity on lowering the temperature, with a slight shift to lower frequencies (2230 cm^{-1} at −50°C and 2218 cm^{-1} at −180°C; its intensity

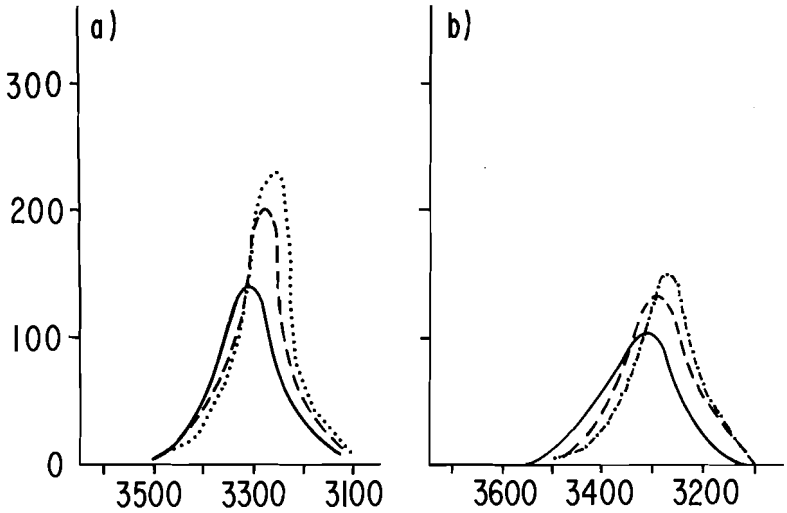

FIG. 4. (*a*) The infrared OH stretching band of *tert*-butanol in a 0.2 *M* solution in FM at different temperatures. (*b*) The same with 0.80 *M* $CDCl_3$ added to the solution. Apparent molar extinction coefficients against wave numbers. — −50°C; - - - −100°C; ··· −120°C; -·-·- −150°C.

increases about seven-fold). Deuterated halothane and methoxyflurane gave similar results. For deuterated halothane the associated CD stretching band is again split into two (2210 and 2182 cm^{-1}).

Association with Amides

The chosen amide, *N*-methylacetamide, presented us with some problems due to its insolubility in FM although the solubility increased in the presence of the anesthetics. This makes the determination of the concentrations more uncertain than in the previous case. We studied its association with chloroform-*d*, halothane-*d*, and methoxyflurane-d_1.

With $CDCl_3$ the free CD stretching band is at 2248 cm^{-1} (room temperature) (Table 1). On lowering the temperature, a slightly shifted associated band appears, first as a shoulder at 2238 cm^{-1}, then it increases in intensity and eventually becomes predominant. At room temperature the frequencies of free and associated NH stretching bands were measured as 3475 and 3312 cm^{-1} respectively. The latter shifted to 3268 cm^{-1} at −150°C. The first overtone of the bending band was measured as 3110 cm^{-1} at −20°C and shifted gradually to higher wave numbers on lowering the temperature. In general the CD bands were broader and less well defined for amides than for association with amines and alcohols.

With halothane-*d* again two free and two associated CD stretching bands are found but the lower free and the higher associated band coalesce into one broad band near 2220 cm^{-1}. The higher free band is at 2260 cm^{-1} and the lower associated band at 2182 cm^{-1}. The associated bands increase in intensity on lowering the temperature. With methoxyflurane the free CD stretching band is at 2248 and the associated one is at 2230 cm^{-1} and behaves similarly, but at −80°C precipitation occurred.

As in the case of amines and alcohols the increase in CH association is accompanied by a decrease in NH association. The intensity of the CD bands followed the order chloroform > halothane > methoxyflurane while the slowdown in the temperature increase of the N—H - - - O=C band followed the order chloroform > methoxyflurane > halothane.

We also studied a tertiary amide, *N*,*N*-dimethylacetamide and its deuterated analog against our five anesthetics. The wave numbers of the CH and CD stretching bands are included in Table 1. On lowering the temperature, the associated bands increase in intensity and shift to lower frequencies (Fig. 5) in a way similar to that observed for *N*-methylacetamide. The free and associated CD bands of $CDCl_3$ were mutually overlapped with an apparent maximum at 2245 cm^{-1}.

In all the cases discussed above, we checked our spectra for the self-association of our anesthetic molecules. Even at the lowest tempera-

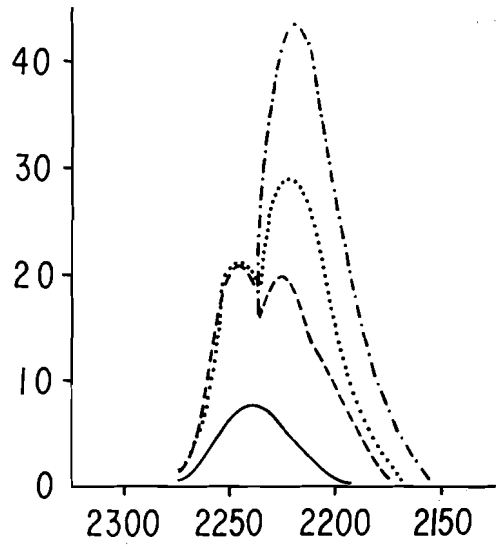

FIG. 5. The CD stretching band of methoxyflurane (0.28 *M*) associated with *N*,*N*-dimethylacetamide (0.25 *M*) at different temperatures in FM. Apparent molar extinction coefficients against wave numbers. — 25°C; - - - −10°C; ··· −80°C; -·-·- −120°C.

tures it caused only a slight broadening and intensification and a very slight shift of the free bands and no new bands due to self-association were ever found. In no case could it have interfered with the associations discussed above.

Discussion and Conclusions

It has been known for many years that the frequencies, intensities, and shapes of infrared absorption bands due to species associated by HB's are affected by solvent effects in addition to being affected by the formation of the HB itself (see, for example, refs. 7–11). The nature of these solvent effects has been investigated in the case of halogenated solvents by a number of different methods and various types of interactions, contact pair formation, charge transfer, 'electrostatic' interactions have been invoked (12–15).

The formation of HB's involving chloroform and similar molecules as proton donors was also established a long time ago (16–20), including, among many others, HB formation between chloroform and trimethylamine (21–25).

The investigation reported in this paper concerned five compounds widely used as anesthetics. Like the many fluorocarbons containing higher halogens which were studied previously in our laboratory, these compounds have been found to be potent hydrogen bond breakers. It has been shown that the remaining hydrogen atoms in these anesthetics do enter HB's. Brown and Chaloner (26) reported nmr evidence to the same effect.

The main point emerging from these observations is the following. Many of the fluorocarbon molecules which were studied by Di Paolo and Sandorfy (2, 3) do not contain hydrogen at all yet they are efficient HB breakers (CF_3Br, C_3F_7Br, $CF_2Br—CF_2Br$, and several fluoroiodides). Actually, when the work reported here was undertaken, we were wondering if chloroform's action is through proton donation or through interactions involving its chlorines or both. Combining the previous results of Di Paolo and Sandorfy and those presented in this paper leads to the conclusion that both mechanisms must be operating in halofluorocarbon anesthetics which contain a mobile hydrogen. The relative importance of the two is likely to vary from one anesthetic to the other. At the present stage, this cannot be assessed quantitatively because of the difficulties involved with the experimental techniques, but it seems that the mechanism by proton donation is the preponderant mechanism for chloroform while both mechanisms are important for halothane, methoxyflurane, enflurane, and DDD.

In a recent work, Martire *et al.* (14) applied nmr and gas chromatographic methods to investigate the thermodynamics of the association between chloroform and an ether, a thioether, and an amine. They found evidence to the effect that chloroform enters associations with these molecules both by forming HB's as a proton donor and by interacting with the chlorine atoms, although the latter interaction is probably not of the charge transfer type. This is entirely in line with the above interpretation of our results.

Although our work was done on model compounds the HB's they form are similar in type and energy to those which the living organism uses most. For this reason, we continue to believe that our observations do have relevance to the problem of the mechanism of anesthetic action.

Inhalation anesthetics are known to exert their action without undergoing chemical reactions (although they might be metabolized later) and recent theories of anesthesia (27, 28) concentrate on the perturbation of the permeability of the nerve cell membrane by the anesthetics. Since the permeability depends on the

conformation of the proteins and lipids which constitute the membrane and the right conformation is insured by intermolecular associations both within these macromolecules themselves and with the molecules forming their environment, the study of the possible perturbations of these intermolecular associations by anesthetics appears to be necessary and important for the elucidation of the mechanism of anesthesia.

We plan to present in subsequent publications the results of our efforts to obtain more quantitative relationships, our work done on systems representing in vivo conditions more closely as well as studies on anesthetics other than those of the fluorocarbon type.

Acknowledgements

Our thanks are due to Dr. K. C. Cole for helping us with his experience at the beginning of this work.

We are indebted to Dr. D. D. Denson for a highly stimulating conversation and for supplying us with samples of anesthetics including that of 4,5-dichloro-2,2-difluoro-1,3-dioxolane which he synthesized and to Dr. R. Denis from Hôpital Notre-Dame of Montreal for other anesthetics samples.

We thank the National Research Council of Canada and the Ministère de l'éducation du Québec for financial support.

1. M. C. BERNARD-HOUPLAIN and C. SANDORFY. J. Chem. Phys. **56**, 3412 (1972).
2. T. DI PAOLO and C. SANDORFY. Can. J. Chem. **52**, 3612 (1974).
3. T. DI PAOLO and C. SANDORFY. J. Med. Chem. **17**, 809 (1974).
4. D. D. DENSON, E. T. UYENO, R. L. SIMON, and H. M. PETERS. ACS Symp. Ser. 28 (1976).
5. M. ASSELIN and C. SANDORFY. J. Mol. Struct. **8**, 145 (1971).
6. J. HINE, R. WIESBOECK, and R. G. GHIRARDELLI. J. Am. Chem. Soc. **83**, 1219 (1961).
7. G. C. PIMENTEL and A. L. MCCLELLAN. The hydrogen bond. W. H. Freeman and Company, San Francisco and London. 1960.
8. L. J. BELLAMY and R. J. PACE. Spectrochim. Acta, **22**, 535 (1966).
9. A. ALLERHAND and P. VON R. SCHLEYER. J. Am. Chem. Soc. **85**, 1233 (1963).
10. A. ALLERHAND and P. VON R. SCHLEYER. J. Am. Chem. Soc. **85**, 371 (1963).
11. K. B. WHETSEL. Spectrochim. Acta, **17**, 614 (1961).
12. D. P. STEVENSON and G. M. COPPINGER. J. Am. Chem. Soc. **84**, 149 (1962).
13. M. GOMEL. Ann. Chim. **3**, 415 (1968).
14. D. E. MARTIRE, J. P. SHERIDAN, J. W. KING, and S. E. O'DONNELL. J. Am. Chem. Soc. **98**, 3101 (1976).
15. C. J. BIASELLE and J. G. MILLER. J. Am. Chem. Soc. **96**, 3813 (1974).
16. A. ALLERHAND and P. VON R. SCHLEYER. J. Am. Chem. Soc. **85**, 1715 (1963).
17. R. C. LORD, B. NOLIN, and H. D. STIDHAM. J. Am. Chem. Soc. **77**, 1365 (1955).
18. C. M. HUGGINS and G. C. PIMENTEL. J. Phys. Chem. **23**, 896 (1955); **23**, 1244 (1955).
19. R. D. GREEN. Hydrogen bonding by CH groups. John Wiley and Sons, New York, NY. 1974.
20. K. B. WHETSEL and J. H. LADY. J. Phys. Chem. **68**, 1010 (1964).
21. R. E. GLICK. Chem. Ind. (London), 413 (1956).
22. L. J. SEGAL. J. Phys. Chem. **65**, 697 (1961).
23. B. N. KHARE, S. S. MITRA, and G. LENGYEL. J. Chem. Phys. **47**, 5173 (1967).
24. W. E. THOMPSON and G. C. PIMENTEL. Z. Electrochem. **64**, 748 (1960).
25. Y. P. HANDA and D. E. JONES. Can. J. Chem. **53**, 3299 (1975).
26. J. M. BROWN and P. A. CHALONER. Can. J. Chem. **55**, 3380 (1977).
27. H. EYRING, J. W. WOODBURY, and J. S. D'ARRIGO. Anesthesiology, **38**, 415 (1973).
28. J. P. CHANGEUX, R. BLUMENTHAL, M. KASAI, and T. PODLESKI. *In* Molecular properties of drug receptors. *Edited by* R. Porter and M. O'Connor. J. A. Churchill, London, England. 1970.

Raman and infrared spectral studies of polycrystalline thallium(I) halates, $TlXO_3$

ARLEN VISTE
Department of Chemistry, Augustana College, Sioux Falls, SD 57102, U.S.A.
AND
DONALD E. IRISH
Department of Chemistry, University of Waterloo, Waterloo, Ont., Canada N2L 3G1

Received March 8, 1977

ARLEN VISTE and DONALD E. IRISH. Can. J. Chem. **55**, 3218 (1977).

Raman and infrared spectra have been recorded for polycrystalline samples of $TlClO_3$, $TlBrO_3$, and $TlIO_3$ at room temperature. The vibrational spectra of these rhombohedral ($R3m$, C_{3v}^5) crystals are closely related to each other, and to single crystal Raman spectra of isomorphous $RbClO_3$ and $KBrO_3$ reported by others. Spectral assignments are made. The unimolecular unit cell yields no correlation field splitting, but lack of a center of inversion leads to TO/LO splitting of each active mode in these uniaxial piezoelectric crystals. Relationships between the thallium(I) halates and the NaN_3 and MXY_3 perovskite structures are considered.

ARLEN VISTE et DONALD E. IRISH. Can. J. Chem. **55**, 3218 (1977).

On a enregistré les spectres Raman et infrarouges d'échantillons polycristallins de $TlClO_3$, de $TlBrO_3$ et de $TlIO_3$ à température de la pièce. Les spectres vibrationnels de ces cristaux rhomboédriques ($R3m$, C_{3v}^5) se ressemblent beaucoup entre eux et ressemblent aussi aux spectres Raman de cristaux uniques de $RbClO_3$ et $KBrO_3$ isomorphes rapportés par d'autres. On effectue des attributions spectrales. La maille unitaire unimoléculaire ne fournit aucun couplage de corrélation de champ mais le fait qu'il lui manque un centre d'inversion conduit à une division TO/LO de chaque mode actif dans ces cristaux uniaxiaux piézoélectriques. On considère les relations entre les halates de thallium(I) et les structures perovskite de NaN_3 et de MXY_3.

[Traduit par le journal]

Introduction

Thallium halates, $TlXO_3$, with X = Cl, Br, or I, are isomorphous, each having the $KBrO_3$ structure, the space group $R3m$ (C_{3v}^5), and one formula unit per unit cell (1). Both $KBrO_3$ (2) and the isomorphous $RbClO_3$ (3–5) have been studied by single crystal Raman techniques. The present investigation concerns the observation and interpretation of the Raman and infrared spectra of polycrystalline thallium halates. These are structurally related, to various degrees, with NaN_3, space group $R\bar{3}m$ (D_{3d}^5), with linear azide ions rather than pyramidal halate (6) and with cubic perovskite, for which comparison is made by Wyckoff (1). Existing interpretations of the vibrational spectra of $KBrO_3$ (2), $RbClO_3$ (3–5), NaN_3 (7–9), and perovskite MXY_3 (10), have aided us in the present study.

Experimental

The thallium halates were prepared by simple precipitation from aqueous solution, as follows: $TlIO_3$ from $TlNO_3$ and KIO_3 solutions (11), $TlBrO_3$ from $TlNO_3$ and $KBrO_3$ (12), and $TlClO_3$ from $TlNO_3$ and $NaClO_3$ by an adaptation of the $TlBrO_3$ preparation (12) and solubility data (13). $TlClO_3$, the most soluble of the three (14), was recrystallized from water. The chemicals used in the preparations were $TlNO_3$, Laboratory BDH Reagent; KIO_3, Baker Analyzed Reagent 99.7%; $KBrO_3$, Fisher Certified Reagent; $NaClO_3$, Baker Analyzed Reagent.

Raman spectra, excited by the 514.5 nm or 488.0 nm line of a Coherent Radiation Model 52G argon ion laser, were recorded with a Jarrell-Ash 25–100 1.0-m double Czerny-Turner monochromator equipped with an SSR model 1105/1120 photon-counting system. Spectral slit widths of 2.4 or 1.2 cm^{-1} were used. Polycrystalline samples were generally in glass melting point capillaries. Low laser power was necessary with $TlIO_3$ and $TlBrO_3$ because of a tendency toward decomposition in the beam when at full power. $TlClO_3$ appeared to be more stable in this regard. A trace of NO_3^- impurity in the first $TlClO_3$ product, prior to recrystallization, was suggested by the appearance of a Raman line at about 1039 cm^{-1}; the strongest line of NO_3^- (ν_1) appears at 1042 cm^{-1} in pure $TlNO_3$ (15). This trace impurity was largely removed by recrystallization. Infrared spectra were also recorded, principally as Nujol mulls between AgCl or polyethylene windows, with the Perkin-Elmer 180 spectrophotometer. Except for shoulders and perhaps broad bands, the frequencies reported should be reliable to about ± 2 cm^{-1} for Raman and about ± 5 cm^{-1} for infrared spectra. All measurements were carried out at room temperature, $\simeq 22°C$.

Results and Discussion

Infrared and Raman data for $TlClO_3$, $TlBrO_3$, and $TlIO_3$ are presented in Tables 1 and 2. The

TABLE 1. Raman and infrared frequencies (cm^{-1}) of the internal modes of $TlXO_3$*

Mode†	$TlClO_3$		$RbClO_3$ (5)	$TlBrO_3$		$KBrO_3$ (2)		$TlIO_3$	
	Raman	Infrared	Raman	Raman	Infrared	Raman	Infrared	Raman	Infrared
ν_2 $2A_1$(TO)	601	598 (sp)	612	406	415	419	421	(326)§	340
$2A_1$(LO)	609	—	621	426	—	450	—	§	—
ν_1 $3A_1$(TO)	911	‡	928	777	≃767 (br)	793	≃788	740	≃748‡
$3A_1$(LO)	‡	—	935	784	—	803	—	760	—
ν_4 $3E$(TO)	473	472 (sp)	486	343	348 (sp)	358	358	287	290 (sp)
$3E$(LO)	480	—	492	356	—	370	—	304	—
ν_3 $4E$(TO)	(894)‡	900 (br)	943	749	≃740 (br)‡	779	777	711	≃694 (br)‡
$4E$(LO)	983	—	1013	808	—	840	—	785	—

*sp = sharp; br = broad.
†The modes are numbered in a manner consistent with ref. 5.
‡Overlapping bands make placement difficult.
§Too weak to determine with confidence.

TABLE 2. Raman frequencies (cm^{-1}) of the lattice modes of $TlXO_3$

Mode	$TlClO_3$	$TlBrO_3$	$TlIO_3$	$RbClO_3$ (5)	$KBrO_3$ (2)
$1A_1$(TO)	62	56	≃53*	81	90
$1A_1$(LO)	†	†	†	119	128
$1E$(TO)	68	61	≃53*	104	113
$1E$(LO)	114	93	82	130	143
$2E$(TO)	135	142	145	141	158
$2E$(LO)	148	158	163	150	171

*Near coincidence of two bands (see text).
†Apparently too weak to identify.

bands are identified by numbers which increase with increasing cm^{-1} for a given species; this scheme is identical to that used by Hwang and Solin (5) and thus facilitates comparison. Data for $RbClO_3$ (5) and $KBrO_3$ (2) are also tabulated. Photographs of Raman spectra of $TlXO_3$ (X = Cl, Br, I) are shown in Figs. 1–4; photographs of infrared spectra of these thallium halates, as Nujol mulls, are presented in Fig. 5. It is clear that the infrared spectra exhibit the distortion characteristic of strongly absorbing crystals and thus the frequencies of minimum transmission could differ from the frequencies of the TO modes. In fact, however, they agree closely with the Raman frequencies.

The free halate ion XO_3^-, of C_{3v} symmetry, has stretching modes ν_1 (A_1) and ν_3 (E), and bending modes ν_2 (A_1) and ν_4 (E). In solution, the Raman frequencies for ClO_3^-, BrO_3^-, and IO_3^- respectively are as follows (16): ν_2 (A_1), 610, 421, 390 cm^{-1}; ν_1 (A_1), 930, 806, 779 cm^{-1}; ν_4 (E), 479, 356, 330 cm^{-1}; ν_3 (E), 982, 836, 826 cm^{-1}. The irreducible representations of the point group, site group, and factor group are correlated in Table 3. There is one molecule of $TlXO_3$ per unit cell, and for the XO_3^- halate ion the point group of the free ion as well as the site group and the factor group are all C_{3v}. Similarly for the Tl^+ cation, C_{3v} is both the site group and the factor group. Thus, treatment by standard methods (10, 15, 17–20) indicates that correlation field splitting should not occur in this system.

Vibrational modes of a crystal which are infrared active are split into transverse and longitudinal components: TO/LO splitting (21). For a thallium halate $TlXO_3$, A_1 and E modes are active in both the infrared and the Raman spectra, prior to TO/LO splitting, whereas the A_2 mode is inactive. As a result, the number of bands in the Raman spectrum should be doubled by this TO/LO splitting (Table 3). However, for the thallium halates, as for $KBrO_3$ and $RbClO_3$ (5), even though infrared-active modes are subject to TO/LO splitting, in first approximation only the TO modes appear in the infrared spectrum (2, 5, 21). Table 3 indicates this. For directions of phonon propagation other than parallel or perpendicular to the C_3 or optic axis ($0° < \theta < 90°$), the phonon frequencies vary smoothly between their 0° and 90° limiting values (5, 20, 22). For such intermediate directions of phonon propagation, if short-range anisotropy forces

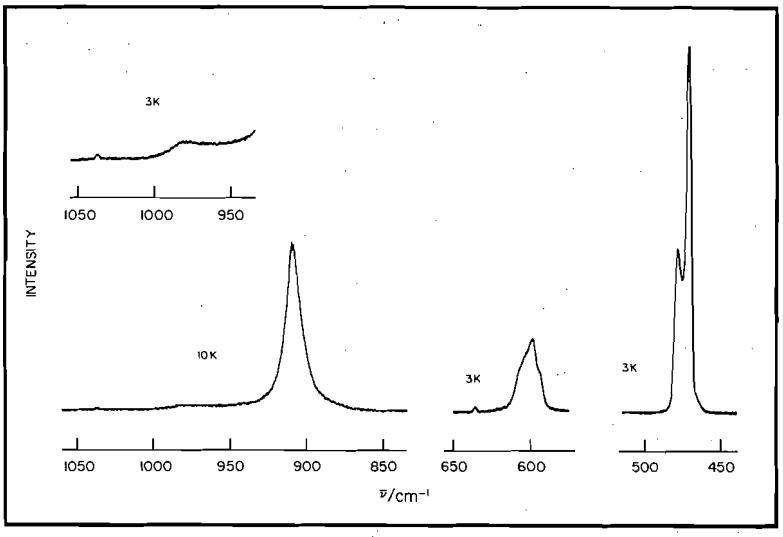

FIG. 1. Portions of the Raman spectrum of polycrystalline $TlClO_3$, for the internal mode region. Counting rates are designated. The relative sensitivity of the lower left spectrum is 0.3 that of the other three.

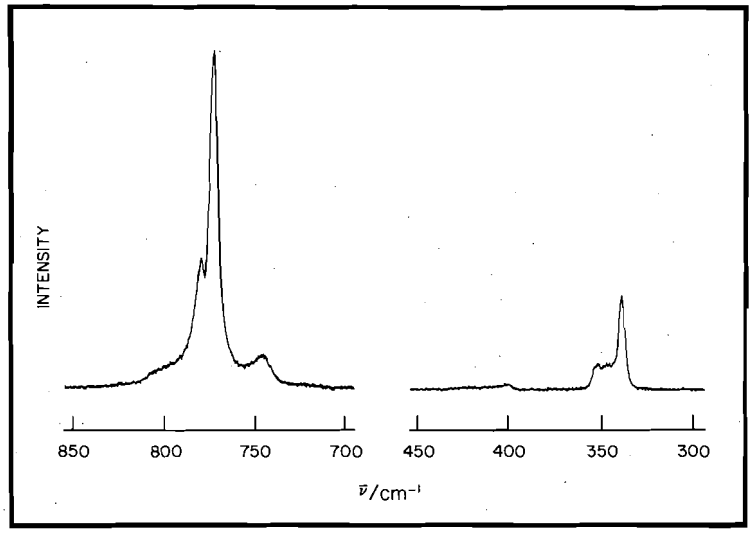

FIG. 2. Portions of Raman spectra of polycrystalline $TlBrO_3$, for the internal mode region.

(SRAF) predominate then the phonon may be idealized as having definite symmetry (A_1 or E) but mixed polarization (TO, LO), whereas if instead long-range electrostatic forces (LREF) predominate then the phonon may be idealized as of definite polarization (TO or LO) but mixed symmetry (A_1, E) (5, 23). The corresponding phonon dispersion curves of frequency vs. θ have been determined through single crystal Raman measurements for $RbClO_3$ by Hwang and Solin (5) and for $KBrO_3$ by Unger and Haussühl (2). As a further cautionary note, Hwang and Solin (5) have pointed out that in the general (real) case, strictly speaking "at oblique angles, each polar phonon mixes with every other polar phonon in the crystal".

In the present study, polycrystalline samples of the thallium halates have been observed because single crystals of suitable size and quality could not be grown. The relation of Raman spectra of

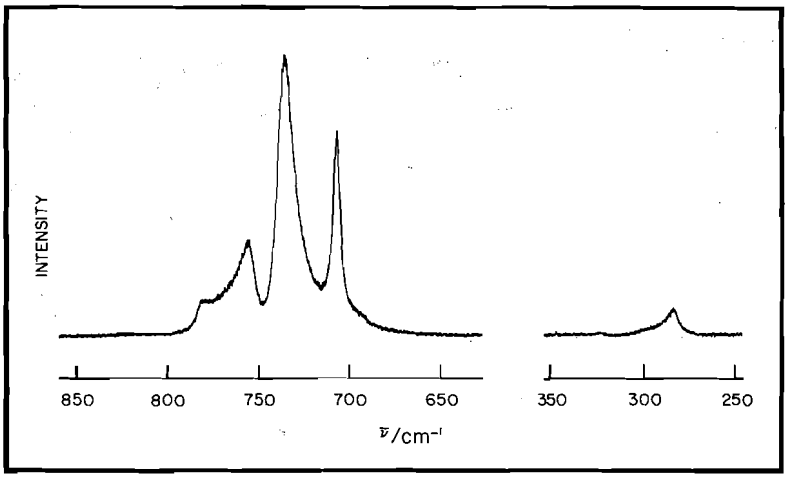

FIG. 3. Portions of Raman spectra of polycrystalline $TlIO_3$, for the internal mode region.

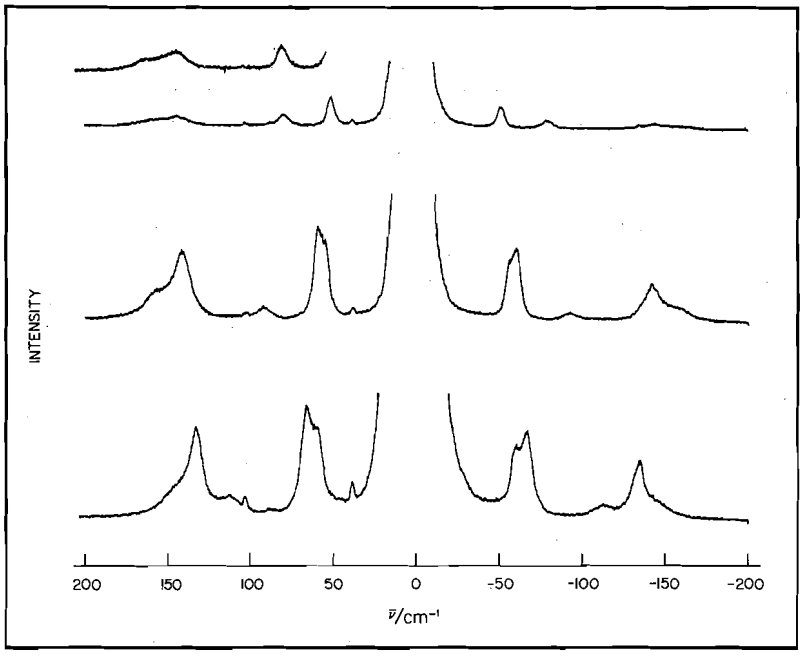

FIG. 4. Stokes and anti-Stokes Raman spectra of polycrystalline $TlXO_3$ (X = Cl, Br, I), for the lattice mode region. From the top, spectra are $TlIO_3$ (two), $TlBrO_3$, and $TlClO_3$.

such polycrystalline substances to dispersion curves of single crystals has been discussed by Burns and Scott (22). The availability of single crystal phonon dispersion curves for $RbClO_3$ (5) and $KBrO_3$ (2) is valuable because they have provided model systems for comparison. For these two systems, the ordering of levels agrees except for the order and composition of the states associated with the $3A_1$ and $4E$ TO and LO modes (2, 5). Beyond the ordering of levels, one notes that only the $1E$(TO), $2E$(TO), $3E$(TO), and $4E$(TO) frequencies are independent of direction of phonon propagation (5). For the other phonon dispersion curves, one anticipates a tendency for the directions with large θ (approaching 90°) to appear more prominently in the spectrum than those with small θ, due in part to simple statistics since the random distri-

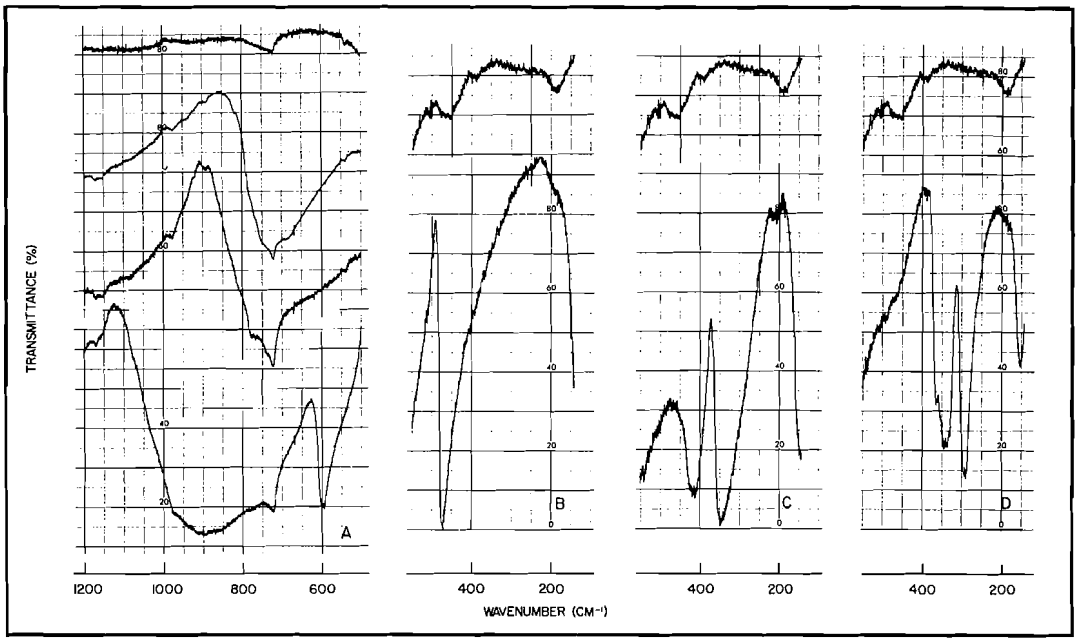

FIG. 5. Portions of infrared spectra of polycrystalline $TlXO_3$ (X = Cl, Br, I). The upper spectrum in each panel is that of Nujol. *A*, From the bottom: $TlClO_3$, $TlBrO_3$, $TlIO_3$. *B*, $TlClO_3$. *C*, $TlBrO_3$. *D*, $TlIO_3$.

TABLE 3. Correlation table for $TlXO_3$ (X = Cl, Br, I); space group $R3m$ (C_{3v}^5), 1 molecule per unit cell

Mode	Point group C_{3v}	Site group C_{3v}	Factor group C_{3v}	TO/LO splitting
ν_1, ν_2, T_z	A_1(R,I)	A_1(R,I)	A_1(R,I)	A_1(TO) (R,I)
				A_1(LO) (R)
R_z	A_2(ia)	A_2(ia)	A_2(ia)	A_2 (ia)
ν_3, ν_4, (R_x, R_y) (T_x, T_y)	E(R,I)	E(R,I)	E(R,I)	E(TO) (R,I)
				E(LO) (R)

bution of orientation population varies as sin θ (22).

Using these considerations as helpful guides, the observed bands for the Raman and infrared spectra of $TlXO_3$ (X = Cl, Br, I) have been assigned, as summarized in Tables 1 and 2. The assignments are quite compatible with the ordering of levels in the isomorphous model compounds $RbClO_3$ (5) and $KBrO_3$ (2). The latter two systems differ in the order of the upper four levels. In $RbClO_3$, the order is given by $3A_1$(TO) < $3A_1$(LO) < $4E$(TO) < $4E$(LO), whereas in $KBrO_3$ $4E$(TO) < $3A_1$(TO) < $3A_1$(LO) < $4E$(LO). Unger and Haussühl (2) note that in the phonon dispersion curves, a symmetry selection rule prevents a quasi E [$4E$(TO) → $4E$(LO)] curve from crossing a quasi A_1 [$3A_1$(LO) → $3A_1$(TO)] curve. In consequence of this and the level ordering, in this region in $KBrO_3$ the curves may be described as quasi TO [$4E$(TO) → $3A_1$(TO)] and quasi LO [$3A_1$(LO) → $4E$(LO)], whereas in $RbClO_3$ the corresponding phonon dispersion curves are instead quasi $3A_1$[$3A_1$(LO) → $3A_1$(TO)] and quasi $4E$ [$4E$(TO) → $4E$(LO)] as the phonon direction θ varies from 0° to 90° (2, 5). Thus, for these four modes, it appears that there is dominance by LREF in $KBrO_3$ but by SRAF in $RbClO_3$ (2, 5).

In the case of the thallium halates, the $KBrO_3$ order of these upper four levels appears to hold at least for $TlIO_3$ and $TlBrO_3$, and probably for $TlClO_3$ as well. This conclusion is based on the following considerations. First, on the basis of the two alternative patterns of phonon dispersion curves (2, 5) and their relationship to the polycrystalline Raman spectrum (22), it is anticipated that the band intensities will be related as $3A_1(LO) < 3A_1(TO)$ and $4E(LO) < 4E(TO)$. Second, as noted earlier, to a first approximation the infrared spectrum is expected to display the TO rather than the LO component of each mode (2, 5, 21). Third, for ClO_3^- in $RbClO_3$ (5) as for the planar NO_3^- (15) the symmetric stretch ν_1 appears more intense in the Raman than the antisymmetric stretch ν_3, and similarily $3A_1(TO)$ will be more intense than $4E(TO)$ in $TlXO_3$ thallium halates.

To illustrate the application of these interpretive principles, consider the case of $TlIO_3$. For the lower two bands in the ν_1, ν_3 region, the intensity of the 711 cm^{-1} Raman band is substantially less than that of the 740 cm^{-1} Raman band. This is compatible with the $KBrO_3$ order but not with the $RbClO_3$ order, since for the latter it would imply a greater intensity for $3A_1$-(LO) (as $\theta \rightarrow 0°$) than for $3A_1(TO)$ (as $\theta \rightarrow 90°$), which is unlikely. Similar arguments apply to $TlBrO_3$. The resulting $KBrO_3$ order of levels for $TlIO_3$ and $TlBrO_3$ also leads to a greater Raman intensity for $3A_1(TO)$ (ν_1) than for $4E(TO)$ (ν_3), a reasonable result. In going from $TlIO_3$ to $TlBrO_3$, the intensity of $4E(TO)$ and $4E(LO)$ fall off in comparison with that of $3A_1(TO)$ and $3A_1(LO)$. In addition the separation between $3A_1(TO)$ and $3A_1(LO)$ decreases from about 20 cm^{-1} to about 7 cm^{-1}. Apparently these trends continue, in going further to $TlClO_3$. The resulting spectrum (Fig. 1) is less clearcut in this region than that of $TlBrO_3$ (Fig. 2) or $TlIO_3$ (Fig. 3). However, it appears that $TlClO_3$, like $TlBrO_3$ and $TlIO_3$, conforms to the $KBrO_3$ level ordering in this ν_1, ν_3 region. The magnitude of the LO/TO splitting has been related to the square of the dipole derivative, $(\partial\mu/\partial Q)^2$, and thus a large separation of the components implies an intense infrared absorption (24–27). Although infrared band overlap is severe, the infrared intensities suggest that the splitting $4E(LO) - 4E(TO)$ should be greater than $3A_1(LO) - 3A_1(TO)$, as assigned.

The assignment of the levels arising from the other internal modes of XO_3^- (ν_2 and ν_4) is straightforward, since these occur reasonably well separated from other modes. However, the falling off in Raman intensity of these bending modes in $TlBrO_3$ and $TlIO_3$ in comparison with $TlClO_3$ is worth noting. The Raman intensities of $2A_1(TO)$ and $2A_1(LO)$ in particular drop to almost vanishingly small magnitudes.

The lattice modes of the $TlXO_3$ thallium halates are assigned in Table 2. The close relationships and smooth frequency trends for the lattice modes are clearly exhibited in the Raman spectra for the lattice mode region, displayed in Fig. 4. The order of levels utilized in the band assignments is as in $RbClO_3$ (5) and $KBrO_3$ (2). The approximate accidental degeneracy of $1A_1(TO)$ and $1E(TO)$ in $TlIO_3$ cited in Table 2 is inferred from the trend toward coalescence of these two bands observed in $TlClO_3$ and $TlBrO_3$. The missing $1A_1(LO)$ is expected to be of low intensity and probably a shoulder on the low frequency side of the $1E(LO)$ band, on the basis of the phonon dispersion curves of $RbClO_3$ (5) and $KBrO_3$ (2). However, the intensity of this missing $1A_1(LO)$ is apparently too low to confirm this expectation in the present case.

Comparison of frequencies within Table 2 indicates that the expected inverse dependence of frequencies of translatory modes on ionic mass is borne out. (Formula weights of the various ions are: Tl^+ 204.4, Rb^+ 85.5, K^+ 39.1, ClO_3^- 83.5, BrO_3^- 127.9, IO_3^- 174.9.) From Table 3 it follows that $1A_1(TO)$, $1A_1(LO)$, $1E(TO)$, and $1E(LO)$ are essentially translatory modes, and $2E(TO)$ and $2E(LO)$ are rotatory modes. There is a trend toward decreasing frequency for each of the translatory modes with increasing anion mass in the sequence $TlClO_3$, $TlBrO_3$, $TlIO_3$, and with increasing cation mass in the pairs $RbClO_3$, $TlClO_3$ and $KBrO_3$, $TlBrO_3$. The dependence on cation mass is considerably stronger for the translatory modes than for the rotatory modes, as seems reasonable. In connection with such mass comparisons, it is helpful that the cation radii are rather similar. For coordination numbers 12 and 8 respectively these are: Tl^+ 1.76, 1.60; Rb^+ 1.73, 1.60; K^+ 1.60, 1.51 Å (28). Moreover, in contrast to the translatory modes, the proposed rotatory modes $2E(TO)$ and $2E$-(LO) actually increase slightly in frequency in the series $TlClO_3$, $TlBrO_3$, $TlIO_3$ (Table 2). Such an increase would be quite out of character for a translatory mode. At first sight it also seems surprising for a rotatory mode, in view of the expected inverse dependence of rotatory

TABLE 4. Correlation diagrams*

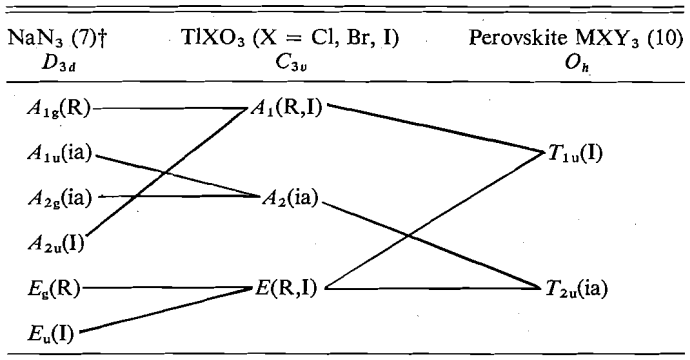

*R = Raman active; I = infrared active; ia = inactive.
†NaN_3 has no modes of A_{1u} or A_{2g} symmetry.

mode frequency on XO_3^- anion moment of inertia, and in turn the involvement in this of the atomic weight of X for (R_x, R_y). However, it is pertinent to note that the Yatsimirskii thermochemical radii of the anions are ClO_3^- 2.00, BrO_3^- 1.91, IO_3^- 1.82 Å (29, 30), with the counterintuitive decrease in size due in part perhaps to differences in bond angles (31). Since the trends in atomic weight of X and Yatsimirskii thermochemical radii of XO_3^- tend to result in opposing influences on the rotatory mode frequencies, the slight increase in frequency from $TlClO_3$ to $TlIO_3$ does not appear to be unreasonable for the rotatory modes.

Bhagavantam and Venkatarayadu argue that among lattice modes, rotatory modes should normally tend to be more intense than translatory modes in the Raman spectrum (32). This appears to be the case in $RbClO_3$ for the $2E$(TO) mode in particular (5), and similarly for the Raman-active rotatory mode (E_g) of the planar NO_3^- ion in $LiNO_3$ and $NaNO_3$ (15). For $TlXO_3$ thallium halates, however, the rotatory mode Raman intensities do not seem to be as prominently enhanced. For example in $TlClO_3$ and $TlBrO_3$ the $2E$(TO) mode is considerably more intense than the translatory $1E$(LO), but roughly comparable to the translatory $1E$(TO) (Fig. 4). The significance of this more moderate Raman intensity of the rotatory modes in the $TlXO_3$ thallium halates is not clear. It may for example simply serve as a reminder that a conceptual distinction between translatory and rotatory lattice modes, while very useful, is not without its limitations (33). Since in our assignments the $1E$(TO) translatory mode and the $2E$(TO) rotatory mode in particular are of the same symmetry, some mixing of translatory and rotatory character is allowed by symmetry. It is conceivable that the admixture of a limited amount of rotatory character in the nominally translatory $1E$(TO) might appreciably enhance its intensity, along the lines of the observations.

Isotope splitting of vibrational bands by ^{35}Cl and ^{37}Cl has been observed in $RbClO_3$, with $2A_1$(TO) split by 4 cm^{-1} and $3A_1$(TO) split by 7 cm^{-1} (5). In $TlClO_3$, isotope splitting of $2A_1$-(TO) is indicated by the appearance of a shoulder on the low-frequency side of the band; the magnitude of the splitting is about 5 cm^{-1} (Fig. 1). Splitting of the $3A_1$(TO) band is not apparent, due perhaps to band overlap by $4E$(TO) and the quasi TO phonon dispersion curve connecting $4E$(TO) and $3A_1$(TO).

The $TlXO_3$ thallium halates are related to some extent to two other crystal types: NaN_3 (6, 8, 9) and perovskite MXY_3 (10).

NaN_3 (6, 7) belongs to space group $R\bar{3}m$ (D_{3d}^5). Placement of the Na^+ and N_3^- ions is similar to that of Tl^+ and XO_3^- in $TlXO_3$, with the C_∞ axis of N_3^- and the C_3 axis of XO_3^- aligned along the C_3 axis of the unit cell. However, NaN_3 has a center of inversion which is not present in $TlXO_3$. A correlation diagram relating the D_{3d} factor group of NaN_3 and the C_{3v} factor group of $TlXO_3$ is shown in Table 4. Since C_{3v} is a subgroup of D_{3d} and since both NaN_3 and $TlXO_3$ have one molecule per unit cell, the relationship between them is rather close. A thorough study of the lattice dynamics of NaN_3 has been carried out by Rafizadeh and coworkers (7), involving both theoretical calculation of dispersion curves within the Brillouin zone, and experimental neutron scattering with polycrystalline NaN_3. At $\boldsymbol{k} = 0$, in NaN_3 the rotatory E_g mode occurs at 122 cm^{-1}, below the translatory modes E_u(TO) and A_{3u}(TO) at about 175 cm^{-1} and E_u(LO) and A_{2u}(LO) at about 250

cm^{-1} (7). The formula weights of the ions are quite low (Na^+ 23.0, N_3^- 42.0) in comparison with Tl^+ and XO_3^-, and so the position of the translatory modes above the rotatory E_g in NaN_3 is not surprising. The A_{2u}(TO) and E_u(TO) translatory modes in NaN_3 are nearly accidentally degenerate (7), similar to the behavior of the corresponding $1A_1$(TO) and $1E$(TO) translatory modes in the $TlXO_3$ thallium halates (Table 2). The frequency of the rotatory E_g mode in NaN_3 is actually not greatly different from the $2E$(TO) rotatory component in $TlXO_3$ (Table 2); it is slightly lower, due perhaps to a somewhat larger moment of inertia for linear N_3^- than the corresponding moment of inertia of pyramidal XO_3^-.

Finally, consider the MXY_3 perovskite structure with space group $Pm3m$ (O_h^1) (10). Both perovskite MXY_3 and $TlXO_3$ have one molecule per unit cell. The C_{3v} factor group of $TlXO_3$ is a subgroup of the factor group O_h of the perovskite MXY_3, and the corresponding correlation diagram appears in Table 4. From one perspective the thallium halates $TlXO_3$ may be regarded as distorted perovskite structures (1, 32, 34), particularly in the case of the iodate. The relationship involves a trigonal distortion of the perovskite unit cell, together with a transition from an octahedral XO_6 unit to pyramidal XO_3 by the shortening of three X—O bonds and lengthening the other three. (An alternative C_{4v} distortion of the perovskite structure is also known in other systems (22).) The perovskite structure has only lattice modes, which (apart from acoustic modes) consist only of translatory modes: three T_{1u} and one T_{2u}, of which the T_{1u} are infrared active and the T_{2u} inactive; there are no Raman active modes. Trends in the $TlXO_3$ spectra from $TlClO_3$ to $TlIO_3$ appear to be compatible in part with a trend in the direction of the perovskite structure. Thus in the sequence $TlClO_3$, $TlBrO_3$, $TlIO_3$ the ν_2 and ν_4 bending modes [$2A_1$(TO), $2A_1$(LO), $3E$(TO), $3E$(LO)] are approaching one another and becoming markedly less intense, as if collapsing into the perovskite T_{1u} band. Similar movement of the TO and LO frequency components of $1A_1$ and $1E$ can be seen. The $2E$(TO) and $2E$(LO) modes would presumably coalesce with the inactive rotatory mode A_2, into the perovskite T_{2u} mode.

Conclusions

The Raman and infrared spectra of polycrystalline thallium halates $TlClO_3$, $TlBrO_3$, and $TlIO_3$ have been investigated, and the bands assigned. Although there is no correlation field coupling in these crystals, since there is only one molecule per unit cell, the existence of TO/LO splitting is important to the analysis of the spectrum. The band assignments are in accord with the Unger and Haussühl order of levels for $KBrO_3$ (2), though agreeing also in the majority of cases with the $RbClO_3$ order of levels found by Hwang and Solin (5). ^{35}Cl, ^{37}Cl isotope splitting was observed for the $2A_1$(TO) band of $TlClO_3$. Relationships between the results for the $TlXO_3$ thallium halates and the related systems NaN_3 and MXY_3 perovskite have been discussed.

Acknowledgments

This work was supported by the National Research Council of Canada. One of us (A.V.) also thanks the Augustana Research-Artist Fund for summer support. Helpful discussions with A. Anderson and B. H. Torrie are gratefully acknowledged.

1. R. W. G. Wyckoff. Crystal structures. 2nd ed. Vol. 2. Interscience, New York, NY. 1964. p. 381 ff.
2. B. Unger and S. Haussühl. Phys. Status Solidi B, **54**, 183 (1972).
3. D. Hwang, R. Kobliska, and S. A. Solin. Proceedings of the Second International Conference on Light Scattering in Solids, Paris, July 19–23, 1971. *Edited by* M. Balkanski. Flammarion Sciences, Paris, France. 1971. p. 260.
4. D. M. Hwang and S. A. Solin. Appl. Phys. Lett. **20**, 181 (1972).
5. D. M. Hwang and S. A. Solin, Phys. Rev. B, **7**, 843 (1973).
6. R. W. G. Wyckoff. Crystal structures. 2nd ed. Vol. 2. Interscience, New York, NY. 1964. p. 294.
7. H. Rafizadeh, S. Yip, and H. Prask. J. Chem. Phys. **56**, 5377 (1972).
8. T. A. Richter, M. L. Malhotra, and K. D. Möller. Mater. Res. Bull. **5**, 203 (1970).
9. J. I. Bryant. J. Chem. Phys. **40**, 3195 (1964).
10. W. G. Fateley, F. R. Dollish, N. T. McDevitt, and F. F. Bentley. Infrared and Raman selection rules for molecular and lattice vibrations: the correlation method. Wiley-Interscience, New York, NY. 1972.
11. E. A. Gyunner and I. G. Poltavtseva. Izv. Vyssh. Uchebn. Zaved. Khim. Khim. Tekhnol. **13**, 452 (1970); Chem. Abstr. **73**, 81303*h* (1970).
12. J. Simpson, D. Taylor, R. S. Fanshawe, J. M. Norbury, and W. J. Watson. J. Chem. Soc. 3323 (1958).
13. A. Seidell and W. F. Linke. Solubilities of inorganic and metal-organic compounds. 4th ed. Vol. 2. American Chemical Society, Washington, DC. 1965. pp. 1015, 1069, 1578, 1588.
14. A. Seidell and W. F. Linke. Solubilities of inorganic and metal-organic compounds. 4th ed. Vol. 2. Ameri-

can Chemical Society, Washington, DC. 1965. pp. 1557, 1578, 1582.
15. M. H. BROOKER and D. E. IRISH. Can. J. Chem. **48**, 1183 (1970).
16. K. NAKAMOTO. Infrared spectra of inorganic and coordination compounds. Wiley, New York, NY. 1963. p. 87.
17. W. G. FATELEY. Appl. Spectrosc. **27**, 395 (1973).
18. D. E. IRISH and M. H. BROOKER. Appl. Spectrosc. **27**, 395 (1973).
19. S. BHAGAVANTAM and T. VENKATARAYADU. Theory of groups and its application to physical problems. Academic Press, New York, NY. 1969.
20. G. TURRELL. Infrared and Raman spectra of crystals. Academic Press, London. 1972.
21. G. TURRELL. Infrared and Raman spectra of crystals. Academic Press, London. 1972. p. 176.
22. G. BURNS and B. A. SCOTT. Phys. Rev. Lett. **25**, 1191 (1970).
23. C. A. ARGUELLO, D. L. ROUSSEAU, and S. P. S. PORTO. Phys. Rev. **181**, 1351 (1969).
24. C. HAAS and D. F. HORNIG. J. Chem. Phys. **26**, 707 (1957).
25. R. SAVOIE and M. PÉZOLET. J. Chem. Phys. **50**, 2781 (1969).
26. J. B. BATES and M. H. BROOKER. Chem. Phys. Lett. **21**, 349 (1973).
27. R. SAVOIE. *In* The Raman effect. Vol. 2. *Edited by* A. Anderson. Marcel Dekker, Inc., New York, NY. 1973. pp. 800–802.
28. R. D. SHANNON and C. T. PREWITT. Acta Crystallogr. B, **25**, 925 (1969).
29. T. C. WADDINGTON. Adv. Inorg. Chem. Radiochem. **1**, 180 (1959).
30. J. E. HUHEEY. Inorganic chemistry. Harper and Row, New York, NY. 1972. p. 77.
31. A. F. WELLS. Structural inorganic chemistry. 3rd ed. Oxford University Press, London. 1962. p. 332.
32. S. BHAGAVANTAM and T. VENKATARAYADU. Theory of groups and its application to physical problems. Academic Press, New York, NY. 1969. p. 148 ff.
33. B. J. BERENBLUT, P. DAWSON, P. MORSE, and G. R. WILKINSON. J. Raman Spectrosc. **1**, 523 (1973).
34. A. J. SMITH and A. J. E. WELCH. Acta Crystallogr. **13**, 653 (1960).

Total synthesis of indole and dihydroindole alkaloids. X.[1,2] The preparation of novel oxygenated catharanthine derivatives

JAMES P. KUTNEY, GORDON H. BOKELMAN, MASAHIRO ICHIKAWA, EDWIN JAHNGEN, ALUMMOOTTIL V. JOSHUA, PING-HUANG LIAO, AND BRIAN R. WORTH

Department of Chemistry, University of British Columbia, 2075 Wesbrook Place, Vancouver, B.C., Canada V6T 1W5

Received March 31, 1977

JAMES P. KUTNEY, GORDON H. BOKELMAN, MASAHIRO ICHIKAWA, EDWIN JAHNGEN, ALUMMOOTTIL V. JOSHUA, PING-HUANG LIAO, and BRIAN R. WORTH. Can. J. Chem. **55**, 3227 (1977).

Detailed investigations involving the electrophilic attack of various reagents on the 3,4-double bond of catharanthine derivatives (e.g. **3**, R = O) furnished a series of novel derivatives of potential use in the syntheses of naturally occurring bisindole alkaloids. These studies include such reagents as peracid, osmium tetroxide, and positive iodine.

JAMES P. KUTNEY, GORDON H. BOKELMAN, MASAHIRO ICHIKAWA, EDWIN JAHNGEN, ALUMMOOTTIL V. JOSHUA, PING-HUANG LIAO et BRIAN R. WORTH. Can. J. Chem. **55**, 3227 (1977).

Des études détaillées impliquant l'attaque électrophile de divers réactifs sur la double liaison-3,4 de dérivés de la catharanthine (e.g. **3**, R = O), permettent d'obtenir une série de nouveaux dérivés susceptibles d'être utilisés pour la synthèse d'alcaloïdes bisindoles trouvés dans la nature. Ces études comportent des réactifs tels que les peracides, le tétroxyde d'osmium et de l'iode positif.

[Traduit par le journal]

The bisindole or 'dimeric' alkaloids of which vinblastine (VLB, **1**) may be cited as one of the best known members, are an important class of natural products (for a recent review see ref. 1). Vinblastine and vincristine (**1**, N—CH_3 replaced by N—CHO) are already well known as clinically important anti-tumor agents (2), while other members within this family exhibit considerable potential in this regard. A number of these alkaloids for example, leurosine (3–5), leurosidine (5), and vincadioline (6) differ in the nature of their oxygen functionality at the $C_{3'}$ and $C_{4'}$ positions of the indole unit (see **1**). Thus any research program directed at the synthesis of such bisindole alkaloids via coupling of appropriate indole and dihydroindole units (7–11) must consider, as one of its important phases, the preparation of requisite 3,4-oxygenated indole units. The results of such investigations form the subject of this publication.

Catharanthine (**2**), a major alkaloid in *Catharanthus roseus* G. Don (*Vinca rosea* L.) for which several total syntheses are now available (12, 13), was selected as the starting material in our experiments.

The high reactivity of the indole system and the basic nitrogen atom in **2** toward a variety of electrophilic reagents necessary for addition to the olefinic linkage dictated appropriate protection of these sites in **2**. An electron-withdrawing group present in the indole ring would be expected to reduce its reactivity while removal of the basic nitrogen, perhaps via lactam formation, seemed desirable to remove any undesirable interference at this site of the molecule.

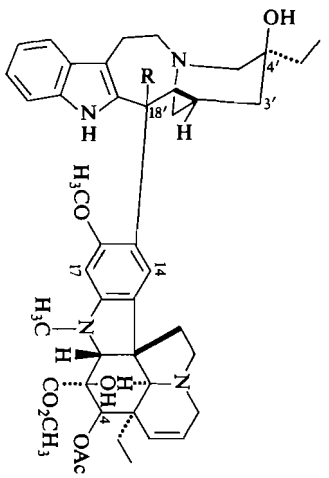

1, R = $COOCH_3$

Reaction of catharanthine (**2**) with potassium hydride in anhydrous tetrahydrofuran at 0°C to form the indole anion and subsequent reaction of the latter with methyl chloroformate provided

[1]For part IX, see ref. 9.

[2]For a preliminary report on a portion of this work, see ref. 17.

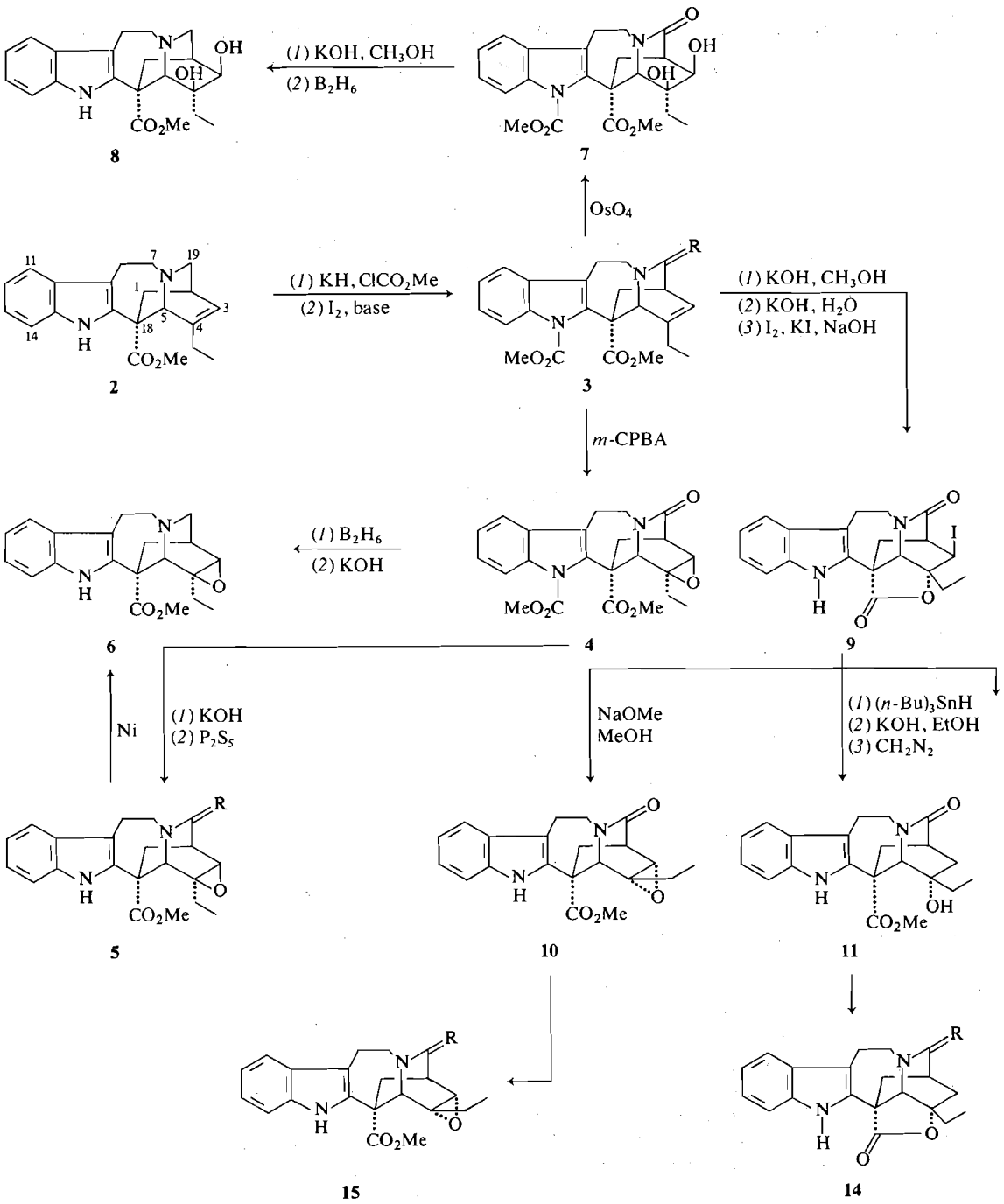

FIG. 1. The synthesis of a series of novel oxygenated catharanthine derivatives.

N_a-carbomethoxycatharanthine (**3**, R = H_2) in 91% yield. This intermediate, upon reaction with iodine in a basic medium (14) undergoes a facile conversion to the lactam **3** (R = O, 70% yield), (ir: 1735, 1670, 1650 cm^{-1}; nmr: δ 6.24 (m, 1H, olefinic), 3.95, 3.62 (2s, 2 × CO_2CH_3); ms: *m/e* 408 (M^+, $C_{23}H_{24}N_2O_5$)). As expected, this compound possessed the required properties for

further studies toward the synthesis of various novel oxygenated catharanthine derivatives. A summary of the various synthetic pathways is provided in Fig. 1.

The alkaloid leurosine, already noted above, possesses an epoxy group at the 3′,4′ positions of the fundamental bisindole skeleton and it was essential to develop synthetic routes to the 3,4-epoxy catharanthine series so as to utilize such derivatives in the eventual synthesis of this bisindole alkaloid. Direct epoxidation of lactam **3** (R = O) with *m*-chloroperbenzoic acid (*m*-CPBA) in refluxing dichloromethane provided the crystalline epoxide **4** in 80% yield. Its characteristic spectral data (ir: 1720, 1665 cm^{-1}; nmr: δ 3.7 (s, 3H, C_{18}-CO_2CH_3), 3.98 (s, 3H, N-CO_2CH_3); ms: *m/e* 424 (M^+, $C_{23}H_{24}N_2O_6$), 285 (base peak)) left little doubt about the gross structure although the β-orientation assigned to the epoxide ring was established with certainty only after a comparison of this compound with the isomeric epoxide **10** prepared in an unambiguous manner (see later).

Removal of the lactam carbonyl in **4** (R = O) could be accomplished in two ways. Initial investigations involved reduction with diborane in tetrahydrofuran but the yields of the desired amine **6** were generally low (approximately 30%). Reductive opening of the epoxide ring became a serious side reaction in these studies. A preferable route involved the conversion of **4** to 3β,4β-epoxy-19-oxodihydrocatharanthine (**5**, R = O) by alkaline hydrolysis and reaction of the latter with phosphorus pentasulfide in refluxing benzene to provide the crystalline thiolactam **5** (R = S) in 73% yield (ir: 1730, 1480, 1455, 1440 cm^{-1}; nmr: δ 7.98 (bs, 1H, NH), 3.72 (s, 3H, C_{18}-CO_2CH_3); ms: *m/e* 382 (M^+, $C_{21}H_{22}N_2O_3S$), 227, 195). Raney Nickel desulfurization of **5** (R = S) provides 3β,4β-epoxydihydrocatharanthine (**6**).

Vincadioline has been recently shown (6) to contain a vicinal diol system in the indole unit and consequently studies directed at the synthesis of 3,4-dihydroxy catharanthine derivatives were undertaken. For this purpose the intermediate **3** (R = O) was treated with osmium tetroxide in tetrahydrofuran at low temperature (−78°C) and the resultant product characterized as N_a-carbomethoxy-3β,4β-dihydroxy-19-oxodihydrocatharanthine **7** (ir: 3700–3150, 1735, and 1660 cm^{-1}; nmr: δ 4.87 and 4.28 (2bs, 2H, 2 × OH), 3.92 and 3.62 (2s, 6H, 2 × CO_2CH_3); ms: *m/e* 442 (M^+, $C_{23}H_{26}N_2O_7$, base peak), 410, 384, and 285). These spectral data do not allow unambiguous stereochemical assignment of the hydroxyl groups but since, as will be shown later, electrophilic attack at the double bond in **3** (R = O) by iodine (see iodolactone **9**) and peracid (see **4**) have occurred from the β face of the molecule, a similar assumption appears reasonable here. Molecular models of catharanthine or any of its derivatives carrying the double bond clearly reveal less hindrance, to attack at the β face.

A considerable amount of research was performed in developing conditions for removal of the indole protecting group and the lactam carbonyl in **7**. Alkaline hydrolysis of the indole ester group could be achieved in high yield (97%) but diborane removal of the lactam carbonyl group provided a relatively low yield (39%) of the desired 3β,4β-dihydroxydihydrocatharanthine **8** (ir: 3560–3400, 1720 cm^{-1}; nmr: δ 7.79 (bs, 1H, NH), 3.73 (m, 2H, C_3H and C_5H), 3.67 (s, 3H, CO_2CH_3); ms: *m/e* 370 (M^+, $C_{21}H_{26}N_2O_4$, base peak)).

An improved procedure for the preparation of the catharanthine glycol derivatives was obtained when catharanthine hydrochloride (**12**) was reacted at low temperature (0°C) with osmium tetroxide in tetrahydrofuran. Two products, the lactam diol **13** (R = O) and the diol **8** were obtained as the major and minor components, respectively.

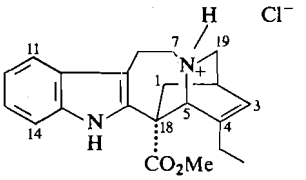

12

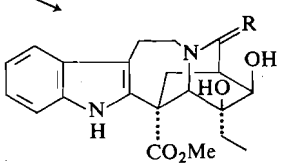

13

It is clear from structure **1**, that vinblastine and vincristine both possess a tertiary hydroxyl group in the indole unit and the preparation of C_4-hydroxy derivatives of catharanthine would be required for eventual coupling with vindoline to provide these bisindole alkaloids. Experi-

ments directed to the synthesis of such intermediates were not only successful for this purpose but were important in terms of allowing stereochemical assignments to all of the novel oxygenated catharanthine derivatives shown in Fig. 1.

The above investigations have already demonstrated the facile electrophilic addition of peracids, for example, to the olefinic linkage in **3** (R = O). Consequently it was felt that the addition of 'positive' iodine should proceed equally well and the intermediate iodonium ion could undergo reaction with the C_{18} carboxyl function to provide an iodolactone (see **9**). The highly rigid bicyclic quinuclidine system present in **3** clearly demands a particular stereochemistry in the resultant lactone as shown in **9**. Further elaboration of such a system would impart definite stereochemistry to any functional groups at C_3 and C_4. Indeed this synthetic strategy has resulted in the successful syntheses of various catharanthine derivatives and an opportunity to interrelate their stereochemical differences.

Basic hydrolysis of the *N*-carbomethoxy group in **3** (R = O) provided 19-oxocatharanthine (**3**, R = O, N-CO_2CH_3 replaced by NH) in 74% yield (ir: 1740, 1668 cm^{-1}; nmr: δ 3.68 (s, 3H, C_{18}-CO_2CH_3); ms: *m/e* 350 (M^+, $C_{21}H_{22}N_2O_3$)). Further hydrolysis of the C_{18} ester group in the latter provides 19-oxocatharanthinic acid which, without purification, is subjected to reaction with potassium iodide and iodine in a basic medium. The product obtained, in overall 75% yield, is the desired iodolactone **9** (ir: 3435, 1770, 1690 cm^{-1}; nmr: δ 9.45 (bs, 1H, NH), 4.6 (dd, 1H, J = 3.5 and 1.5 Hz, CHI); ms: *m/e* 462 (M^+, $C_{20}H_{19}N_2O_3I$)). Clearly the successful formation of the iodolactone demands initial attack of iodine from the β face of the molecule and, in turn, the stereochemical assignments portrayed in **9**.

Deiodination of **9** with tri-*n*-butyltin hydride in tetrahydrofuran furnished the desired 4α-hydroxy-19-oxodihydrocatharanthinic acid lactone (**9**, I replaced by H) in 89% yield (ir: 1765, 1680 cm^{-1}; ms: *m/e* 366 (M^+ $C_{20}H_{20}N_2O_3$)). This intermediate provides a direct route to the required C_4-hydroxy dihydrocatharanthine series which, as noted above, could be employed in the eventual synthesis of vinblastine or vincristine.

Hydrolysis of 4α-hydroxy-19-oxodihydrocatharanthinic acid lactone under alkaline conditions and subsequent esterification of the resulting acid provided 4α-hydroxy-19-oxodihydrocatharanthine (**11**) in 54% yield (ir: 1725, 1635 cm^{-1}; nmr: δ 3.6 (s, 3H, CO_2CH_3), 1.85 (q, 2H, J = 7.5 Hz, CH_2CH_3), 1.15 (t, 3H, J = 7.5 Hz, CH_2CH_3). Thus the overall sequence, **3** → **9** → **11**, provides an effective method for the stereospecific introduction of an hydroxyl function at C_4 starting with the alkaloid, catharanthine.

The reductive removal of the lactam carbonyl in **11** appeared, in view of our previous success, to be a routine reaction. However contrary to expectation, reaction of **11** with diborane in the above-mentioned procedures provided instead, 4α-hydroxydihydrocatharanthinic acid lactone (**14**, R = H_2) as a crystalline product, mp 142–143°C (78% yield) (ir: 1750 cm^{-1}; ms: *m/e* 322 (M^+, $C_{20}H_{22}N_2O$)). Clearly the close proximity of the ester and hydroxyl groups in **11** have allowed a facile lactonization reaction to occur.

The lactone **14** was remarkably stable and showed no reaction even under rather drastic hydrolytic conditions (sodium methoxide in methanol or potassium hydroxide in refluxing aqueous ethanol).

It was hoped that lactone formation could be suppressed by converting **11** into its thiolactam derivative and then performing the desulfurization in the manner described earlier for the epoxide series. Unfortunately reaction of **11** with phosphorus pentasulfide under mild conditions (benzene, room temperature) provided the thiolactam lactone derivative **14** (R = S) again indicating the rapid lactonization reaction in this series. The structure of **14** (R = S) (ir: 1775, 1460 cm^{-1}; ms: *m/e* 352 (M^+, $C_{20}H_{20}N_2O_2S$)) was confirmed by reacting the lactone **9** (I replaced by H) under similar conditions with phosphorus pentasulfide whereupon the product isolated was shown to be identical with that obtained earlier.

The final series of reactions which were performed involved the synthesis of the 3α,4α-epoxy derivatives, which would be isomeric to the compounds derived from *m*-CPBA addition. The iodolactone **9** was an important starting material in these investigations. Reaction of **9** with sodium methoxide in methanol, at room temperature, provided 3α,4α-epoxy-19-oxodihydrocatharanthine **10** (79% yield) (ir: 1725, 1665 cm^{-1}; nmr: δ 8.17 (s, 1H, NH), 3.8 (s, 3H, $COOCH_3$); ms: *m/e* 366 (M^+, $C_{21}H_{22}N_2O_4$)). It is obvious that this conversion involves a methoxide-cata-

lyzed ring opening of the lactone with subsequent displacement of iodide ion by internal attack of the resultant alkoxide ion. Such a process demands α-orientation of the resulting epoxide and serves to substantiate the earlier statements concerning β attack of electrophilic reagents onto the olefinic linkage of catharanthine derivatives.

Removal of the lactam carbonyl group in **10** was accomplished via the thiolactam procedure already described. The final product, 3α,4α-epoxydihydrocatharanthine (**15**, R = H_2) was crystalline and revealed chromatographic as well as spectral characteristics which were clearly different from those of the isomeric epoxide **6**.

In conclusion, these investigations have provided a series of novel 3,4-oxygenated catharanthine derivatives which we hope will prove useful in the syntheses of various bisindole alkaloids. Some results in this direction are described in the accompanying publication (15).

After our studies in this area were completed and published in preliminary fashion, (17) an independent investigation by Ban and coworkers was published (16).

Experimental

Melting points were determined on a Kofler block and are uncorrected. Ultraviolet (uv) spectra were recorded on a Cary 15 spectrophotometer in ethanol solution. The wavelengths of absorption maxima are reported in nanometres (nm) with log ε values in parentheses. Infrared (ir) spectra were measured on a Perkin-Elmer model 710 or 457 spectrophotometer in chloroform solution. The absorption maxima are reported in wavenumbers (cm^{-1}), calibrated with respect to the absorption band of polystyrene at 1601 cm^{-1}. Proton magnetic resonance (^{1}Hmr) spectra were measured in deuterochloroform ($CDCl_3$) solution at ambient temperature on either a Varian HA-100 or XL-100 spectrometer. Chemical shift values are given in the δ (ppm) scale relative to tetramethylsilane (TMS) used as internal standard. The integrated peak areas, signal multiplicities, and proton assignments are given in parentheses. Low resolution mass spectra (ms) were determined on either an AEI-MS-902 or an Atlas CH-4B spectrometer. High resolution mass spectra were measured on an AEI-MS-902 intrument. Microanalyses were carried out by Mr. P. Borda of the Microanalytical Laboratory, University of British Columbia.

Thin layer chromatography (tlc) utilized Merck silica gel G (acc. to Stahl) containing 2% fluorescent indicator. For preparative layer chromatography (plc), plates (20 × 20 or 20 × 60 cm) of 1 mm thickness were used. Visualization was effected by viewing under ultraviolet light and/or by colour reaction with ceric sulphate spray reagent. Column chromatography utilized Merck silica gel 60 (70–230 mesh) or Merck aluminum oxide 90 (neutral).

As a matter of routine, all reagents and solvents were recrystallized or distilled prior to use.

N_a-Carbomethoxycatharanthine (3, R = H_2)

A suspension of potassium hydride (KH), oil dispersion (0.6 ml, 24%, 2.0 mmol) in dry tetrahydrofuran (THF), (20 ml) was cooled to ca. −5°C under an atmosphere of nitrogen. Catharanthine **2** (500 mg, 1.35 mmol) in dry THF (2 ml) was added and the mixture stirred at −5°C for 1 h. Methyl chloroformate (190 mg, 2 mmol) was added and after 30 min, alumina (ca. 1 g of grade III) to quench excess KH. The mixture was filtered and the filtrate evaporated *in vacuo*. The oily product was triturated with hexane (3 × 15 ml) to remove the oil and yield *N_a-carbomethoxycatharanthine* (487 mg, 92%) as a white foam, homogeneous by tlc (silica gel; hexane–acetone, 3:2); uv: λ_{max} 293 (3.67), 281 (3.80), 263 (4.13), 226 (4.32); ir: ν_{max} 2950, 2850, 1730; ^{1}Hmr: δ 7.45 (1H, m, C_{14}-*H*), 7.35–7.2 (3H, m, aromatic protons), 5.70 (1H, m, C_3-*H*), 3.93 (3H, s, N-CO_2CH_3), 3.70 (3H, s, CO_2CH_3), 1.13 (3H, t, J = 7 Hz, —CH_2CH_3); ms: *m/e* 394 (M^+, base peak), 305, 188, 155, 121. High resolution molecular weight determination calcd. for $C_{23}H_{26}N_2O_4$: 394.463; found: 394.457. *Anal.* calcd. for $C_{23}H_{26}N_2O_4$: C 70.03, H 6.64, N 7.10; found: C 70.23, H 6.80, N 7.00.

N_a-Carbomethoxy-19-oxodihydrocatharanthine (3, R = O)

(*i*) Mercuric acetate (108 mg, 0.34 mmol) and EDTA disodium salt (125 mg, 0.34 mmol) were dissolved in 1% aqueous acetic acid (3 ml). A solution of **3** (R = H_2) (50 mg, 0.127 mmol) in dioxane (3 ml) was added and the mixture stirred for 24 h, diluted with water (20 ml), and extracted with ethyl acetate (2 × 20 ml). The organic phase was washed with 5% HCl solution (2 × 10 ml) then with saturated NaCl solution (2 × 10 ml), dried (Na_2SO_4), and evaporated *in vacuo*. The residue was chromatographed on silica gel (ca. 10 g) to yield the *lactam* **3** (R = O) as a white foam (39.5 mg, 76%), mp 166–167°C; uv: λ_{max} 294 (3.90), 282 (3.95), 260 (4.33), 227 (4.51); ir: ν_{max} 2940, 2890, 1735, 1670, 1650; ^{1}Hmr: δ 6.24 (1H, m, C_3-*H*), 4.88 (1H, d, J = 1 Hz, C_5-*H*), 4.0 (1H, m, C_2-*H*), 1.92 (2H, m, —CH_2CH_3), 1.00 (3H, t, J = 7 Hz, —CH_2CH_3); ms: *m/e* 408 (M^+), 285 (base peak), 286, 226, 168, 167. High resolution molecular weight determination calcd. for $C_{23}H_{24}N_2O_5$: 408.168; found: 408.171. *Anal.* calcd. for $C_{23}H_{24}N_2O_5$: C 67.63, H 5.92, N 6.86; found: C 67.56, H 5.93, N 6.73.

(*ii*) Sodium bicarbonate (680 mg, 8 mmol), water (40 ml), **3** (R = H_2) (110 mg, 0.28 mmol), and benzene (5 ml) were stirred vigorously at ambient temperature. A solution of iodine (354 mg, 1.4 mmol) in benzene (20 ml) was added and stirring continued for 1 h. Sodium bicarbonate (1 g) and sodium thiosulphate (500 mg) were added, the organic layer was separated and the aqueous phase washed with dichloromethane (3 × 20 ml). The extracts were combined, dried (Na_2SO_4), and evaporated *in vacuo*. Chromatography on silica gel afforded the *lactam* **3** (R = O) (81 mg, 71%), identical with that obtained above.

N_a-Carbomethoxy-3β,4β-epoxy-19-oxodihydrocatharanthine (4)

The *lactam* **3** (R = O) (816 mg, 2 mmol), purified *m*-CPBA (850 mg, 5 mmol), and 3-*tert*-butyl-4-hydroxy-5-methylphenylsulphide (ca. 10 mg) were stirred in refluxing 1,2-dichloroethane (50 ml) under an atmosphere of dry nitrogen for 5 h. The cooled solution was washed successively with saturated Na_2SO_3 solution and saturated $NaHCO_3$ solution, dried (Na_2SO_4), and filtered

through a small plug of Celite. Evaporation of the filtrate gave the *epoxide* **4** (677 mg, 80%); mp 234–236°C (acetone – petroleum ether (40–60°C)); uv: λ_{max} 294 (3.71), 285 (3.74), 282 (3.76), 267 (4.17), 259 (4.18), 232 (4.31), 227 (4.33); ir: ν_{max} 1720, 1665; ^{1}Hmr: δ 4.59 (1H, d, J = 1 Hz, C_5-*H*), 4.15 (1H, m, C_2-*H*), 3.98 (3H, s, N_a-CO_2CH_3), 3.72 (3H, s, CO_2CH_3), 1.4–2.2 (2H, m, —CH_2CH_3), 0.94 (3H, t, J = 7 Hz, —CH_2CH_3); ms: *m/e* 424 (M^+), 285 (base peak), 192 (metastable peak). *Anal.* calcd. for $C_{23}H_{24}N_2O_6$: C 65.08, H 5.70, N 6.60; found: C 65.14, H 5.80, N 6.56.

3β,4β-Epoxydihydrocatharanthine (6)

The *epoxide* **4** (42 mg, 0.1 mmol) in dry THF (2 ml) was treated with a solution of borane in THF (0.2 ml, 1 *M*, 0.2 mmol) in dry THF (2 ml). The solution was stirred at 0°C under an atmosphere of dry argon for 30 min, then at ambient temperature for 1 h. Acetone (0.5 ml) and triethylamine (2 ml) were added, followed by 1% methanolic KOH solution (1 ml). After 30 min the mixture was poured into dichloromethane (50 ml), washed with water, dried (Na_2SO_4), and evaporated *in vacuo*. Chromatography on silica gel afforded the *lactam* **5** (R = O) (11.4 mg, 31%) plus the *epoxide* **6** (5.3 mg, 15%); uv: λ_{max} 292 (3.91), 284 (3.96), 277 (3.93), 225 (4.66); ir: ν_{max} 3450, 1725; ^{1}Hmr: δ 7.60 (1H, bs, D_2O exchangeable, N-*H*), 4.18 (1H, s, C_5-*H*), 3.79 (3H, s, CO_2CH_3), 1.00 (3H, t, J = 7 Hz, —CH_2CH_3); ms: *m/e* 352 (M^+, base peak), 323, 138. High resolution molecular weight determination calcd. for $C_{21}H_{24}N_2O_3$: 352.1787; found: 352.1790. *Anal.* calcd. for $C_{21}H_{24}N_2O_3$: C 71.57, H 6.86, N 7.95; found: C 71.52, H 6.77, N 7.75.

3β,4β-Epoxy-19-oxodihydrocatharanthine (5, R = O)

A solution of **4** (340 mg, 0.8 mmol) in 1% methanolic KOH (20 ml) was stirred at ambient temperature for 20 min, diluted with dichloromethane (30 ml), and filtered through a short plug of silica gel. Evaporation of the filtrate gave **5** (R = O), (300 mg, quantitative), mp 276–278°C dec. (acetone – petroleum ether (40–60°C)); uv: λ_{max} 292 (3.91), 283 (3.96), 275 (3.91), 222 (4.56); ir: ν_{max} 3460, 1725, 1665; ^{1}Hmr: δ 8.3 (1H, bs, D_2O exchangeable, N-*H*), 4.76 (1H, d, J = 1 Hz, C_5-*H*), 4.3 (1H, bm, C_2-*H*), 3.64 (3H, s, CO_2CH_3), 2.22 (6H, s, acetone), 1.4–2.2 (2H, bm, —CH_2CH_3), 0.97 (3H, t, J = 7 Hz, —CH_2CH_3); ms: *m/e* 366 (M^+, base peak), 228, 227, 214, 195, 168, 167, 154. *Anal.* calcd. for $C_{21}H_{22}N_2O_4 \cdot C_3H_6O$: C 67.91, H 6.65, N 6.60; found: C 67.63, H 6.46, N 6.77.

3β,4β-Epoxy-19-thionodihydrocatharanthine (5, R = S)

The *lactam* **5** (R = O) (366 mg, 1 mmol) and excess phosphorous pentasulphide (366 mg) were stirred in refluxing benzene (40 ml) under an atmosphere of dry nitrogen for 30 min. Water (5 ml) was added to the cooled mixture and stirring continued for 5 min. The mixture was diluted with dichloromethane (60 ml), washed with $NaHCO_3$ solution, dried (Na_2SO_4), and evaporated *in vacuo*. Recrystallization from methanol gave the *thiolactam* **5** (R = S) (278 mg, 73%), mp 259–260°C; uv: λ_{max} 291 (4.13), 279 (4.38), 272 (4.45), 222 (4.66); ir: ν_{max} 3450, 1730, 1480, 1455, 1440; ^{1}Hmr: δ 7.98 (1H, bs, D_2O exchangeable, N-*H*), 5.2 (1H, bm, C_2-*H*), 5.10 (1H, s, C_5-*H*), 3.72 (3H, s, CO_2CH_3), 1.4–2.2 (2H, bm, —CH_2CH_3), 1.00 (3H, t, J = 7 Hz, —CH_2CH_3); ms: *m/e* 382 (M^+, base peak), 227, 195. *Anal.* calcd. for $C_{21}H_{22}N_2O_3S$: C 65.95, H 5.80, N 7.32, S 8.38; found: C 65.89, H 5.90, N 7.20, S 8.22.

3β,4β-Epoxydihydrocatharanthine (6)

The *thiolactam* **5** (R = S), (76 mg, 0.2 mmol) and a large excess of Raney Nickel (pre-washed with distilled water and ethanol) were stirred in ethanol (10 ml) at ambient temperature for 8 min. The mixture was diluted with dichloromethane (10 ml), filtered, and evaporated *in vacuo*. Chromatography on silica gel gave the *epoxide* **6** (37 mg, 53%), identical with that obtained above. A sample recrystallized from ether had mp 214–215°C.

N_a-Carbomethoxy-3β,4β-dihydroxy-19-oxodihydrocatharanthine (7)

The *lactam* **3** (R = O) (325 mg, 0.796 mmol) in dry THF (1.7 ml) and pyridine (3.25 ml) was treated at −78°C with osmium tetroxide (210 mg, 0.826 mmol) in dry THF (1.7 ml). After 2 h at −78°C, the mixture was diluted with ether (130 ml) and the resultant precipitate collected by filtration. This product was dissolved in dichloromethane, saturated with hydrogen sulphide, filtered, and evaporated *in vacuo*. Chromatography on silica gel afforded the *diol* **7** (201 mg, 57%) as an amorphous solid; uv: λ_{max} 294 (3.73), 285 (3.79), 282 (3.83), 261 (4.21), 228 (4.34); ir: ν_{max} 3700–3150, 3620, 1735, 1660; ^{1}Hmr: δ 4.87 (1H, bs, D_2O exchangeable, —O*H*), 4.50 (1H, s, C_5-*H*), 4.28 (1H, bs, D_2O exchangeable, —O*H*), 3.92 (3H, s, N_a-CO_2CH_3), 3.87 (1H, d, J = 2 Hz, C_3-*H*), 3.62 (3H, s, CO_2CH_3), 0.91 (3H, t, J = 7 Hz, —CH_2CH_3); ms: *m/e* 442 (M^+, base peak), 410, 384, 285, 100. High resolution molecular weight determination; calcd. for $C_{23}H_{26}N_2O_7$: 442.1739; found: 442.1693. *Anal.* calcd. for $C_{23}H_{26}N_2O_7$: C 62.43, H 5.92, N 6.33; found: C 62.19, H 6.00, N 6.47.

3β,4β-Dihydroxy-19-oxodihydrocatharanthine

The *diol* **7** (60 mg, 0.136 mmol) was stirred in 3 *N* methanolic KOH solution (3 ml) for 1 h. The mixture was diluted with water (15 ml) and extracted with dichloromethane (3 × 10 ml). The organic phase was dried (Na_2SO_4) and evaporated *in vacuo* to yield *3β,4β-dihydroxy-19-oxodihydrocatharanthine* (50.5 mg, 97%), mp 207–209°C dec. (acetone); uv: λ_{max} 292 (3.90), 284 (3.95), 278 (3.89), 222 (4.51); ir: ν_{max} 3540–3400, 3460, 1725, 1665; ^{1}Hmr: δ 8.02 (1H, bs, D_2O exchangeable, N-*H*), 4.62 (1H, s, C_5-*H*), 4.42 (1H, bs, D_2O exchangeable, —O*H*), 4.08 (1H, bs, D_2O exchangeable, —O*H*), 3.78 (1H, d, J = 3 Hz, C_3-*H*), 3.65 (3H, s, CO_2CH_3), 0.96 (3H, t, J = 6 Hz, —CH_2CH_3); ms: *m/e* 384 (M^+, base peak), 298, 228, 227, 215, 214, 195, 168, 167, 154, 143. High resolution molecular weight determination calcd. for $C_{21}H_{24}N_2O_5$: 384.1685; found: 384.1685. This compound decomposes during attempted removal of solvent. *Anal.* calcd. for $C_{21}H_{24}N_2O_5 \cdot \frac{1}{2}H_2O$: C 64.11, H 6.40, N 7.12; found: C 64.00, H 6.41, N 7.20.

3β,4β-Dihydroxydihydrocatharanthine (8)

3β,4β-Dihydroxy-19-oxodihydrocatharanthine (21.9 mg, 0.057 mmol) in dry THF (3.5 ml) was treated with a solution of borane in THF (0.29 ml, 1 *M*, 0.29 mmol) at ambient temperature under an atmosphere of dry argon for 2 h. The solution was diluted with dry acetone (1.5 ml), refluxed for 5 min, and evaporated *in vacuo*. The residue was stirred in 3 *N* HCl (10 ml) at ambient temperature for 30 min, the solution basified with NH_4OH to p*H* 9–10 and extracted with dichloromethane. The extract was dried (Na_2SO_4) and evaporated. Chromatography on silica gel gave **8** (8.2 mg, 39%) as a colourless oil; uv: λ_{max} 293 (3.77), 284 (3.81), 276 (3.77), 224 (4.44); ir: ν_{max} 3560–3400, 3460, 1720; ^{1}Hmr: δ 7.79 (1H, bs,

D_2O exchangeable, N-*H*), 3.73 (2H, m, C_3-*H* and C_5-*H*), 3.67 (3H, s, CO_2CH_3), 0.99 (3H, t, J = 7 Hz, $—CH_2CH_3$); ms: *m/e* 370 (M^+, base peak), 353, 313, 282, 228, 168, 165, 156, 100. High resolution molecular weight determination calcd. for $C_{21}H_{26}N_2O_4$: 370.1892; found: 370.1896.

3β,4β-Dihydroxy-19-oxodihydrocatharanthine

Osmium tetroxide (179 mg, 0.704 mmol) in dry THF (2 ml) was added to a slurry of catharanthine hydrochloride (150 mg, 0.403 mmol) in dry THF (5 ml) at −10°C under an atmosphere of argon. Dry pyridine (118 mg, 0.12 ml, 1.49 mmol) was added and the mixture stirred at ca. −10 to −5°C for 2 h. Hydrogen sulphide was bubbled through the cool mixture for 5 min. The mixture was diluted with ethyl acetate and washed with dilute NH_4OH solution. The aqueous phase was extracted with ethyl acetate, the extracts combined, dried (Na_2SO_4), and evaporated *in vacuo*. Chromatography on silica gel afforded: **8** (5.4 mg, 4%), catharanthine **2** (40 mg), and *3β,4β-dihydroxy-19-oxodihydrocatharanthine* (52 mg, 48%) identical with that obtained above.

19-Oxocatharanthine

Potassium hydroxide (3 *N*, 1 ml) was added to a solution of **3** (R = O) (300 mg, 0.735 mmol) in methanol (3 ml). The mixture was stirred at ambient temperature for 1 h, carefully neutralized with Amberlite IR-120 at ca. 0°C, filtered, and evaporated *in vacuo*. Trituration of the oily residue gave *19-oxocatharanthine* (234 mg, 91%), mp 231°C (methanol).

19-Oxocatharanthinic Acid

19-Oxocatharanthine (870 mg, 2.49 mmol) and 6 *N* KOH solution (5 ml) were heated in refluxing ethanol (15 ml) under an atmosphere of dry nitrogen for 6 h. The solution was cooled to 0°C, carefully neutralized with Amberlite IR-120, filtered, and evaporated *in vacuo* to give crude *19-oxocatharanthinic acid* (835 mg, quantitative), which was used, without further purification, in the next reaction.

4α-Hydroxy-3β-iodo-19-oxodihydrocatharanthinic Acid Lactone (9)

19-Oxocatharanthinic acid (101 mg, 0.3 mmol) was dissolved in the minimum required amount of 3 *N* NaOH solution and water (30 ml) added. Powdered iodine (305 mg, 1.2 mmol) and potassium iodide (75 mg, 0.45 mmol) were added and the mixture stirred in the dark, under an atmosphere of nitrogen for 24 h. Sodium thiosulphate (1 g) was added and the mixture extracted with dichloromethane (5 × 20 ml). The organic extract was dried (Na_2SO_4) and evaporated *in vacuo* to yield crude *iodolactone* **9** (135 mg, 97.5%). Purification by chromatography on silica gel gave **9** (75.5%) as an amorphous solid; uv: λ_{max} 288 (3.84), 280 (3.89), 272 (3.88), 222 (4.54); ir: ν_{max} 3435, 1770, 1690; ^{1}Hmr: δ 9.45 (1H, bs, D_2O exchangeable, N-*H*), 4.66 (1H, dd, J = 3.5, 1.5 Hz, C_3-α*H*), 4.45–4.70 (1H, m, C_2-*H*), 4.34 (1H, s, C_5-*H*), 2.22 (2H, m, $—CH_2CH_3$), 1.06 (3H, t, J = 7 Hz, $—CH_2CH_3$); ms: *m/e* 462 (M^+, base peak), 169, 168, 167, 128. High resolution molecular weight determination calcd. for $C_{20}H_{19}N_2O_3I$: 462.0440; found: 462.0462.

4α-Hydroxy-19-oxodihydrocatharanthinic Acid Lactone

The *iodolactone* **9** (615 mg, 1.33 mmol) and tri-*n*-butyltin hydride (744 mg, 2.66 mmol) were stirred in anhydrous THF (5 ml) under a nitrogen atmosphere for 72 h. Evaporation *in vacuo* and chromatography on silica gel gave *4α-hydroxy-19-oxodihydrocatharanthinic acid lactone* (400 mg, 90%) mp 196–196.5°C (dichloromethane–pentane); uv: λ_{max} 288 (3.86), 280 (3.91), 272 (3.89), 221 (4.65); ir: ν_{max} 3440, 1765, 1680; ^{1}Hmr: δ 9.56 (1H, bs, D_2O exchangeable, N-*H*), 4.40–4.65 (1H, bm, C_2-*H*), 4.20 (1H, s, C_5-*H*), 1.06 (3H, t, J = 7 Hz, $—CH_2CH_3$); ms: *m/e* 336 (M^+, base peak), 195, 168, 167. High resolution molecular weight determination calcd. for $C_{20}H_{20}N_2O_3$: 336.1474; found: 336.1471. *Anal.* calcd. for $C_{20}H_{20}N_2O_3$: C 71.40, H 6.00, N 8.33; found: C 71.23, H 6.25, N 8.03.

4α-Hydroxy-19-oxodihydrocatharanthine (11)

4α-Hydroxy-19-oxodihydrocatharanthinic acid lactone (33.6 mg, 0.1 mmol) and 6 *N* KOH solution (1 ml) were heated in refluxing ethanol (2 ml) under an atmosphere of nitrogen for 6 h. The solvents were removed *in vacuo* and the residue dissolved in water (2 ml). The solution was carefully neutralized at 0°C with oxalic acid, and extracted with dichloromethane (5 × 10 ml). The extract was dried (Na_2SO_4) and evaporated *in vacuo*. The residue was dissolved in anhydrous THF (2 ml) and treated with an excess of diazomethane in ether at 0°C for 30 min. Evaporation and trituration with chloroform–hexane (1:1) afforded **11** (20 mg, 55%), decomposes without melting above 200°C; uv: λ_{max} 291 (3.82), 282 (3.88), 275 (3.84), 221 (4.48); ir: ν_{max} 3400, 1725, 1635; ^{1}Hmr: δ (pyridine-d_5) 4.98 (1H, s, C_5-*H*), 4.6–4.9 (1H, m, C_2-*H*), 3.60 (3H, s, CO_2CH_3), 1.85 (2H, q, J = 7 Hz, $—CH_2CH_3$), 1.15 (3H, t, J = 7 Hz, $—CH_2CH_3$); ms: *m/e* 336 ($(M - CH_3OH)^+$, base peak), 195, 168, 167. High resolution molecular weight determination calcd. for $C_{20}H_{20}N_2O_3$: 336.1474; found: 336.1471. *Anal.* calcd. for $C_{21}H_{24}N_2O_4 \cdot 2H_2O$: C 62.38, H 6.93, N 6.93; found: C 62.74, H 6.65, N 6.86.

4α-Hydroxydihydrocatharanthinic Acid Lactone (14, R = H_2)

A solution of **11** (340 mg, 1.01 mmol) in anhydrous THF (25 ml) was treated with borane/THF solution (10 ml, excess). The solution was stirred at ambient temperature under an atmosphere of dry nitrogen for 4 h. Acetone (5 ml) was added and the solution refluxed for 5 min, triethylamine (5 ml) was added, and reflux continued for 1½ h. The solvents were removed *in vacuo* and the residue partitioned between dichloromethane (20 ml) and water (10 ml). The p*H* was adjusted to ca. 10 with 6 *N* NaOH and saturated NaCl solution (10 ml) added. The organic layer was separated and the aqueous layer extracted with dichloromethane (4 × 20 ml). The extract was dried (Na_2SO_4) and evaporated *in vacuo*. Chromatography on silica gel afforded the *lactone* **14** (R = H_2) (255 mg, 78%), mp 142–143°C (pentane); uv: λ_{max} 288 (3.77), 280 (3.80), 273 (3.77), 222 (4.47); ir: ν_{max} 3420, 1750; ^{1}Hmr: δ 9.60 (1H, bs, D_2O exchangeable, N-*H*), 3.54 (1H, s, C_5-*H*) 1.04 (3H, t, J = 7 Hz, $—CH_2CH_3$); ms: *m/e* 322 (M^+, base peak), 263, 130. High resolution molecular weight determination calcd. for $C_{20}H_{22}N_2O_2$: 322.1681; found: 322.1678. *Anal.* calcd. for $C_{20}H_{22}N_2O_2$: C 74.50, H 6.88, N 8.69; found: C 74.43, H 6.70, N 8.86.

4α-Hydroxy-19-thionodihydrocatharanthinic Acid Lactone (14, R = S)

(*i*) Phosphorous pentasulphide (10 mg, 0.045 mmol) was added to a suspension of **11** (5 mg, 0.0135 mmol) in dry benzene (1 ml). After 24 h at ambient temperature,

the mixture was filtered and the filtrate evaporated *in vacuo*. Chromatography on silica gel gave the *thiolactam* **14** (R = S), (3.9 mg, 82%) as an amorphous solid; uv: λ_{max} 288 (4.04), 278 (4.13), 272 (4.14), 219 (4.42); ir: ν_{max} 3420, 1775, 1460; ^{1}Hmr: δ 9.54 (1H, bs, D_2O exchangeable, N-*H*), 5.2–5.4 (1H, m, C_2-*H*), 4.43 (1H, s, C_5-*H*), 1.15 (3H, t, J = 7 Hz, —CH_2CH_3); ms: *m/e* 352 (M^+), 248, 195, 168, 167, 140. High resolution molecular weight determination calcd. for $C_{20}H_{20}N_2O_2S$: 352.1246; found: 352.1253.

(*ii*) Phosphorous pentasulphide (50 mg, 0.23 mmol) and *4α-hydroxy-19-oxodihydrocatharanthinic acid lactone* (26 mg, 0.077 mmol) were stirred in dry benzene (2 ml) for 24 h. Filtration, evaporation, and chromatography on silica gel gave **14** (R = S), (23 mg, 85%) identical with that obtained above.

3α,4α-Epoxy-19-oxodihydrocatharanthine (10)

The *iodolactone* **9** (35 mg, 0.075 mmol) was added to a solution of sodium methoxide in methanol (sodium metal ca. 2 mg in 3 ml of dry methanol). The solution was stirred at ambient temperature for 3 h, evaporated *in vacuo*, and the residue chromatographed on silica gel. Recrystallization from methanol gave the *epoxide* **10** (21 mg, 79%), mp 278–280°C; uv: λ_{max} 292 (3.92), 282 (4.02), 272 (3.99), 219 (4.60); ir: ν_{max} 3425, 1725, 1665; ^{1}Hmr: δ 8.17 (1H, bs, D_2O exchangeable, N-*H*), 4.82 (1H, s, C_5-*H*), 4.21–4.53 (1H, m, C_2-*H*), 3.80 (3H, s, CO_2CH_3), 1.02 (3H, t, J = 7 Hz, —CH_2CH_3); ms: *m/e* 366 (M^+, base peak), 308, 195, 164, 137. High resolution molecular weight determination calcd. for $C_{21}H_{22}N_2O_4$: 366.1579; found: 366.1586. *Anal.* calcd. for $C_{21}H_{22}N_2O_4 \cdot CH_3OH$: C 66.33, H 6.53, N 7.03; found: C 66.27, H 6.21, N 7.35.

3α,4α-Epoxy-19-thionodihydrocatharanthine (15, R = S)

The *epoxide* **10** (38 mg, 0.1 mmol) and phosphorous pentasulphide (44 mg, 0.2 mmol) were stirred in dry benzene (3 ml) for 4 h at ambient temperature. The mixture was filtered and the filtrate evaporated *in vacuo*. The residue was chromatographed on silica gel to yield starting material (8 mg) and the *thiolactam* **15** (R = S), (17 mg, 55%), mp 118–121°C (ethyl acetate – hexane); uv: λ_{max} 292 (4.13), 278 (4.36), 272 (4.38), 220 (4.59); ir: ν_{max} 3425, 1725, 1450, 1430; ^{1}Hmr: δ 8.17 (1H, bs, D_2O exchangeable, N-*H*), 5.09–5.40 (1H, m, C_2-*H*), 5.01 (1H, s, C_5-*H*), 3.82, (3H, s, CO_2CH_3), 1.02 (3H, t, J = 7 Hz, —CH_2CH_3); ms: *m/e* 382 (M^+ base peak), 227, 195, 178, 166, 149. High resolution molecular weight determination calcd. for $C_{21}H_{22}N_2O_3S$: 382.1331; found: 382.1341.

3α,4α-Epoxydihydrocatharanthine (15, R = H_2)

The thiolactam **15** (R = S) (40 mg) and excess Raney Nickel (pre-washed with distilled water and ethanol) were stirred in ethanol (5 ml) for 1.5 h. After filtration and evaporation *in vacuo*, the residue was chromatographed on silica gel to yield the *epoxide* **15** (R = H_2), (26 mg, 74%), mp 67–70°C (acetone–hexane); uv: λ_{max} 292 (4.02), 282 (4.19), 273 (4.08), 222 (4.61), ir: ν_{max} 3425, 1725; ^{1}Hmr: δ 8.04 (1H, bs, D_2O exchangeable, N-*H*), 3.91 (1H, s, C_5-*H*), 3.80 (3H, s, CO_2CH_3), 0.99 (3H, t, J = 7 Hz, —CH_2CH_3); ms: *m/e* 352 (M^+), 293 (base peak), 167, 166, 149, 138. High resolution molecular weight determination calcd. for $C_{21}H_{24}N_2O_3$: 352.1787; found: 352.1793. *Anal.* calcd. for $C_{21}H_{24}N_2O_3 \cdot \frac{1}{2}H_2O$: C 69.81, H 6.91, N 7.76; found: C 69.75, H 7.18, N 7.69.

Acknowledgement

Financial aid from the National Research Council of Canada and from Contract NO1-CM-23223, National Cancer Institute, National Institutes of Health, Bethesda, Maryland, is gratefully acknowledged. We are grateful to the Lilly Research Laboratories for supplies of catharanthine and vindoline.

1. G. H. Svoboda and D. A. Blake. *In* The catharanthus alkaloids. *Edited by* W. I. Taylor and N. R. Farnsworth. Marcel Dekker, New York, NY. 1975. p. 45.
2. R. C. De Conti and W. A. Creasy. *In* The catharanthus alkaloids. *Edited by* W. I. Taylor and N. R. Farnsworth. Marcel Dekker, New York, NY. 1975. p. 237.
3. N. Neuss, M. Gorman, N. J. Cone, and L. L. Huckstep. Tetrahedron Lett. 783 (1968).
4. D. J. Abraham and N. R. Farnsworth. J. Pharm. Sci. **58**, 694 (1969).
5. E. Wenkert, E. W. Hagsman, B. Lal, G. E. Gutowski, A. S. Katner, J. C. Miller, and N. Neuss. Helv. Chim. Acta, **58**, 1560 (1975).
6. W. E. Jones and G. J. Cullivan. U.S. Patent No. 3,887,565 June, 1975; Chem. Abstr. **83**, 97687d (1975).
7. J. P. Kutney, J. Beck, F. Bylsma, J. Cook, J. W. Cretney, K. Fuji, R. Imhof, and A. M. Treasurywala. Helv. Chim. Acta, **58**, 1690 (1975).
8. J. P. Kutney, A. H. Ratcliffe, A. M. Treasurywala, and S. Wunderly. Heterocycles, **3**, 639 (1975).
9. J. P. Kutney, T. Hibino, E. Jahngen, T. Okutani, A. H. Ratcliffe, A. M. Treasurywala, and S. Wunderly. Helv. Chim. Acta, **59**, 2856 (1976).
10. P. Potier, N. Langlois, Y. Langlois, and F. Gueritte. Chem. Commun. 670 (1975).
11. N. Langlois, F. Gueritte, Y. Langlois, and P. Potier. J. Am. Chem. Soc. **98**, 7017 (1976).
12. G. Buchi, P. Kulsa, K. Ogasawara, and R. L. Rosati. J. Am. Chem. Soc. **92**, 999 (1970).
13. J. P. Kutney and F. Bylsma. J. Am. Chem. Soc. **92**, 6090 (1970); Helv. Chim. Acta, **58**, 1672 (1975).
14. V. C. Agwada, Y. Morita, Y. Renner, M. Hesse, and H. Schmid. Helv. Chim. Acta, **58**, 1001 (1975).
15. J. P. Kutney, G. H. Bokelman, A. V. Joshua, P. Liao, and B. R. Worth. Can. J. Chem. This issue.
16. Y. Honma and Y. Ban. Heterocycles, **6**, 285 (1977).
17. J. P. Kutney, G. H. Bokelman, M. Ichikawa, E. Jahngen, A. V. Joshua, P. Liao, and B. R. Worth. Heterocycles, **4**, 1267 (1976).

Total synthesis of indole and dihydroindole alkaloids. XI.[1,2] The synthesis of leurosine and the coupling of 3α,4α-substituted catharanthine derivatives with vindoline

JAMES P. KUTNEY, ALUMMOOTTIL V. JOSHUA, PING-HUANG LIAO, AND BRIAN R. WORTH
Department of Chemistry, University of British Columbia, 2075 Wesbrook Place, Vancouver, B.C., Canada V6T 1W5

Received March 31, 1977

JAMES P. KUTNEY, ALUMMOOTTIL V. JOSHUA, PING-HUANG LIAO, and BRIAN R. WORTH. Can. J. Chem. 55, 3235 (1977).

A detailed study involving the Polonovski-type coupling of vindoline (**2**) with several novel catharanthine derivatives is described. Coupling of vindoline (**2**) with the *N*-oxide intermediate of 3β,4β-epoxydihydrocatharanthine (**1**) provides a laboratory synthesis of the bisindole alkaloid leurosine (**3**, R = CO_2CH_3) and an unambiguous proof of the stereochemistry of the epoxide function in that alkaloid. The coupling of **2** with the *N*-oxides of 3α,4α-epoxydihydrocatharanthine (**4**) and 4α-hydroxydihydrocatharanthinic acid lactone (**6**) provide the rearranged bisindole products **5**, **7**, and **8**.

JAMES P. KUTNEY, ALUMMOOTTIL V. JOSHUA, PING-HUANG LIAO et BRIAN R. WORTH. Can. J. Chem. 55, 3235 (1977).

On décrit en détail l'étude impliquant un couplage du type Polonovski de la vindoline (**2**) avec quelques dérivés de la catharanthine. Le couplage de la vindoline (**2**) avec l'intermédiaire *N*-oxyde de l'époxy-3β,4β dihydrocatharanthine (**1**) permet de poursuivre la synthèse de la bis-indole leurosine (**3**, R = CO_2CH_3) et apporte une preuve très nette de la stéréochimie du pont époxyde dans l'alkaloïde. Le couplage de **2** avec les *N*-oxydes de l'époxy-3α,4α dihydrocatharanthine (**4**) et d'hydroxy-4α dihydrocatharanthinolactone (**6**) conduit aux bis-indoles réarrangées **5**, **7** et **8**.

[Traduit par le journal]

In the previous publication in this series (14) we presented a discussion of the experiments which provided a variety of novel oxygenated catharanthine derivatives. It was noted that such intermediates could prove valuable in the synthesis of various bisindole alkaloids and their derivatives. The present discussion exemplifies some of our studies in this direction.

The bisindole alkaloid leurosine (**3**, R = CO_2CH_3) was isolated some years ago and its structure has been investigated by several groups (1–3). These studies provided a structural assignment but the stereochemical assignment of the epoxide function remained unsettled. Analysis of proton magnetic resonance data provided a tentative assignment of a β orientation to this function (2) while more recent studies involving ^{13}C magnetic resonance and an acid-catalyzed rearrangement of leurosine assumed an α orientation (3). Since *N*-formyl leurosine (**3**, R = CO_2CH_3, N-CH_3 replaced by N-CHO) is presently in clinical studies in Hungary, it appeared particularly important to provide an unambiguous proof for the stereochemical orientation of the epoxide ring since this feature of the bisindole system may be important in terms of its antitumor activity. Consequently our initial studies with the oxygenated catharanthine derivatives (4, 14) were directed toward this objective. The two possible 3,4-epoxydihydrocatharanthine derivatives available from the previous studies (4, 14) were utilized in coupling experiments with vindoline (**2**) according to procedures developed independently in our laboratories (5, 6) and elsewhere (7, 8).

The *N*-oxide derivative of 3β,4β-epoxydihydrocatharanthine (**1**), prepared from the epoxide and *m*-chloroperbenzoic acid, was coupled with vindoline (**2**) in the presence of trifluoroacetic anhydride at −50°C (5, 6) to provide the alkaloid leurosine (**3**, R = CO_2CH_3) in 20% yield. This study not only provided a laboratory synthesis of this bisindole alkaloid but, most importantly, settled unambiguously the stereochemistry of the epoxide function at $C_{3'}$–$C_{4'}$ as shown in **3**. It is also of interest to note that, unlike the earlier studies involving the coupling of catharanthine derivatives lacking

[1]Part X, see ref. 14.

[2]For preliminary reports on a portion of this work, see refs. 15 and 16.

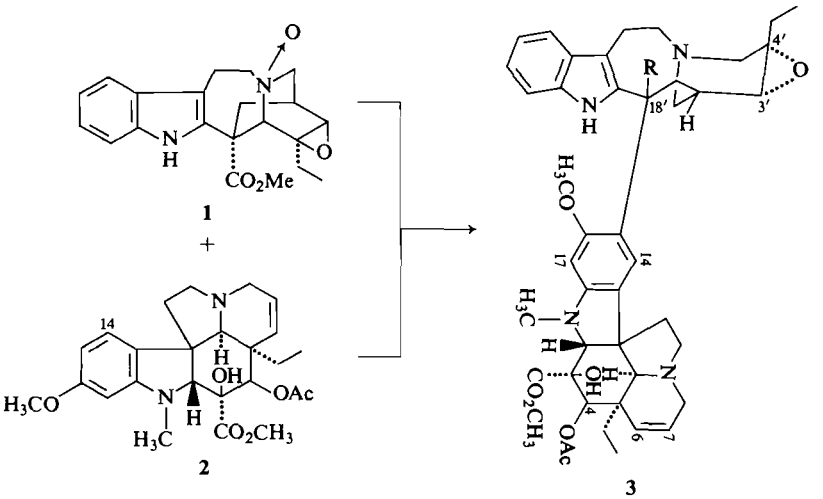

oxygen functionality at the C_3–C_4 positions (5, 6), other bisindole products, particularly those bearing unnatural configuration at $C_{18'}$, are not isolated. The other byproducts obtained are monomeric in nature clearly arising from transformations of the catharanthine and indole systems.

It was now of particular interest to compare the results obtained when the isomeric 3α,4α-epoxide **4** was employed in the coupling studies. Indeed an unexpected result was obtained in that the only isolated bisindole product (51% yield) possessed spectral data which were not consistent with the 3′,4′-epileurosine structure which would be formed if normal fission of the C_{18}—C_5 bond in **4** had occurred. Careful analysis of the spectral data allowed the assignment of structure **5** to this product. The 'dimeric' nature of this compound was evident from the high resolution mass spectrum (*m/e* calcd. for $C_{46}H_{54}N_4O_9$: 806.409; found: 806.402) while the uv spectrum (λ_{max} 222, 255, 285, 292 nm) clearly revealed the presence of indole and dihydroindole units. The point of attachment of the indole unit at C_{15} of the vindoline ring system was readily ascertained from the ^{1}Hmr spectrum (singlets at δ 6.48 and 6.12 for the C_{14} and C_{17} protons, respectively). As in the previous studies (6, 9), this spectrum was highly informative, being essentially a summation of the appropriate signals for the indole and dihydroindole portions, and virtually on its own established the postulated structure **5**. Although the normal proton signals attributed to the vindoline unit were clearly evident in the ^{1}Hmr spectrum of **5**, several important differences in

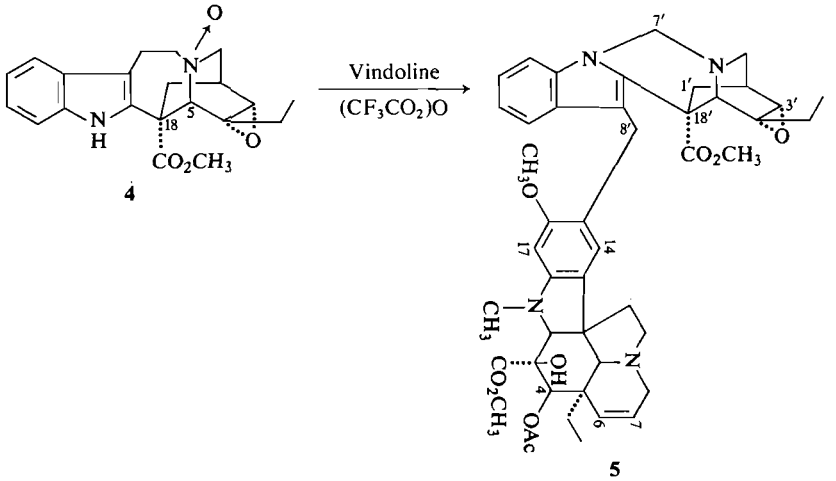

the signal patterns for the indole unit were noted. The absence of the indole NH signal, so characteristic in all the previous bisindole products isolated previously (5, 6, 9) and in leurosine prepared above, was immediately noted and a new two-proton AB quartet centered at δ 5.02 (J = 11 Hz) never observed in any of the ^{1}Hmr spectra of the previously studied bisindole products, was noted. This quartet was attributed to the methylene group at C_7' in **5**, a product arising from a rearrangement of the *N*-oxide **4** prior to coupling with vindoline (see later).

In a complementary series of investigations involving the coupling of the *N*-oxide intermediate of 4α-hydroxydihydrocatharanthinic acid lactone (**6**) (4, 14) with vindoline, a similar series of rearrangement products were isolated and characterized. Thus when **6** was coupled with vindoline in the presence of trifluoroacetic anhydride (methylene chloride, −50°C), three products resulting from the coupling of these units could be isolated. On the basis of careful spectroscopic analyses two of these products were assigned the bisindole structures **7** and **8** (R = $COCH_3$) while the third was a trimer resulting from the reaction of two vindoline units with an indole system.

The major component (62% yield) was assigned the bisindole structure **7** on the basis of the following spectral data. The molecular formula, $C_{45}H_{52}N_4O_8$ as determined by high resolution mass spectrometry (calcd: 776.388; found: 776.376), was consistent with the presence of an indole and dihydroindole unit and this was supported by the uv (λ_{max} 223, 250, 285, 292 nm) and ^{1}Hmr data. With respect to the latter, all the normal vindoline proton signals were evident in the spectrum but again the indole NH was absent and an AB quartet centered at δ 4.95 (2H, J = 12 Hz) could be assigned to the $C_{7'}$-methylene group. In this instance the ^{1}Hmr spectrum also revealed clearly a second new two-proton AB quartet (δ 4.43, J = 16 Hz) attributed to the methylene group ($C_{8'}$) linking the indole and dihydroindole units. The presence of the γ-lactone in **7** was clear from its ir spectrum (1775 cm^{-1}). Chemical experiments to substantiate the structural assignment are discussed later.

The second component (10% yield) differed from **7** in several respects. Its mass spectrum established a molecular formula, $C_{45}H_{54}N_4O_8$, (calcd.: 778.394; found: 778.394) which was two mass units higher than that of **7** while its ir spectrum indicated that the γ-lactone system was absent. The remaining spectral features were consistent with the structural assignment **8** (R = $COCH_3$) for this product. It was tempting to speculate that **8** (R = $COCH_3$) could arise via sodium borohydride reduction of the lactone carbonyl group since this reagent is employed prior to isolation of the coupling products from the reaction mixture. Indeed when **7** was exposed to such reduction (methanol, 0°C) lactol **8** (R = $COCH_3$) is obtained in 75% yield. The stereochemical assignment to the chiral center $C_{20'}$ in **8** remains an open question.

The third product (6% yield) obtained from the coupling of **6** with vindoline is a trimer corresponding to a structure derived from one indole unit and two vindoline units. The thermal lability of this compound in the mass spectrometer made it difficult to obtain the true molecular ion, but under carefully controlled conditions peaks in the desired mass range (*m/e* 1232 and 1234) corresponding to the molecular formulae $C_{70}H_{84}N_6O_{14}$ and $C_{70}H_{86}N_6O_{14}$, respectively, were observed. The ir spectrum of trimer **9** does not show the γ-lactone absorption at 1775 cm^{-1} observed in the spectrum of **7** but possesses a strong carbonyl absorption at 1740 cm^{-1}. In the uv spectrum, the absorption bands due to the dihydroindole chromophore (for example, 313 nm) were of significantly higher intensity than normally observed in spectra of the bisindole alkaloids. The ^{1}Hmr spectrum clearly revealed two vindoline units as evidenced by two sets of aromatic singlets (δ 6.82, 6.38, 6.08, 6.02), two N-CH_3 signals (δ 2.66, 2.64) and two methyl triplets (δ 0.28 and 0.0, J = 7 Hz) in addition to the proton signals for the indole unit. In summary the above data are insufficient to allow a definitive assignment of structure for trimer **9**.

The bisindole products **7** and **8** (R = $COCH_3$) were of more direct interest to this study so further experiments were conducted to substantiate the assignments made. For this purpose the lactone **7** was reacted with sodium methoxide (methanol, room temperature) and the product obtained in 77% yield was the hydroxyester **10** (R = CO_2CH_3) [ir: no γ-lactone absorption; ^{1}Hmr: δ 3.87, 3.84 (2s, 6H, OCH_3 and C_3-$COOCH_3$), 3.54 (s, 3H, $C_{18'}$-$COOCH_3$), no acetyl; ms: *m/e* calcd. for $C_{44}H_{54}N_4O_8$:

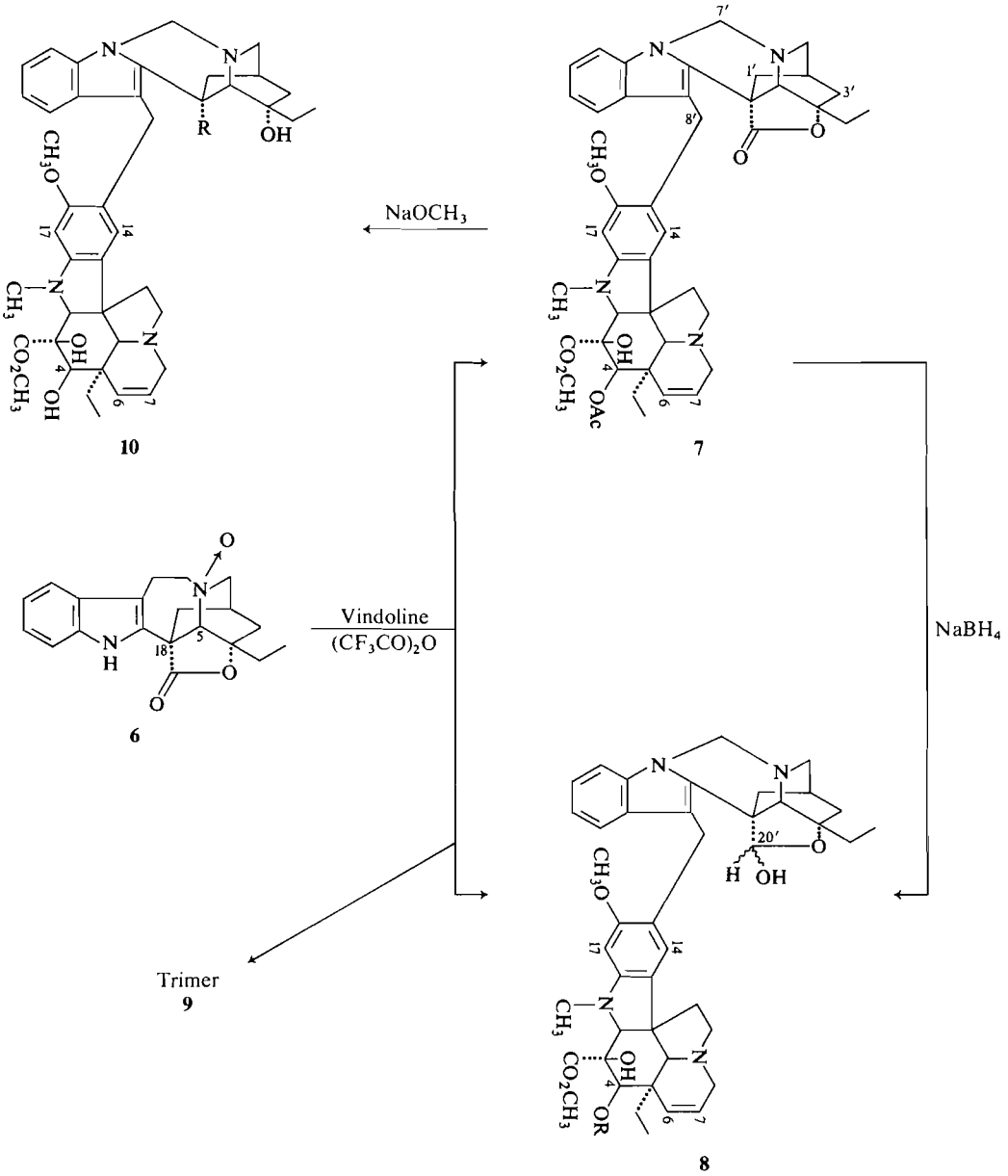

766.394; found: 766.399]. Under identical conditions, catharanthine lactone (4α-hydroxydihydrocatharanthinic acid lactone, **12**) is *not* converted to the corresponding hydroxyester thereby revealing a significant difference in reactivity of the lactone system when the rigid Iboga alkaloid skeleton is intact. Similarly lactol **8** (R = $COCH_3$) is stable to these conditions, the only reaction being hydrolysis of the acetate group to provide **8** (R = H).

The close relationship between **7** and **8** was confirmed when lithium aluminum hydride reduction of each compound provided the identical product. Thus when **7** or **8** (R = $COCH_3$) were reacted with $LiAlH_4$ in tetrahydrofuran at room temperature, the expected product **11** [ir: 3540, 3390 cm^{-1}, no carbonyl absorption; ^{1}Hmr δ 3.86 (s, 3H, OCH_3), 2.98 (s, 3H, NCH_3), no acetyl or carbomethoxy methyl signals; ms: *m/e* calcd. for $C_{42}H_{54}N_4O_6$: 710.404; found:

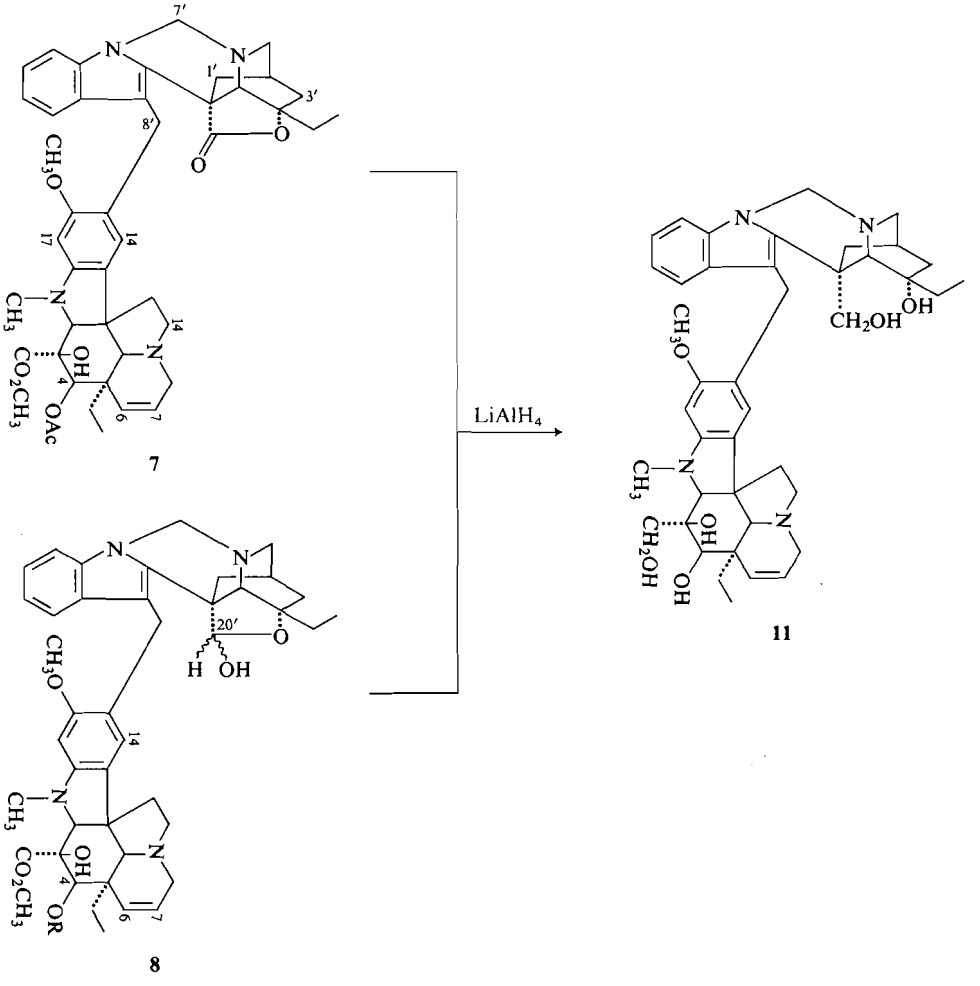

710.401) was isolated in 94% yield from the lactone **7** and 60% yield from the lactol **8** (R = $COCH_3$).

It was again of interest to compare the reactivity of catharanthine lactone (**12**) toward hydride reducing agents in order to evaluate the relative differences in reaction of this carbonyl system in the normal Iboga series with that of the rearranged system shown in **7**. For this purpose **12** was reacted under mild conditions with sodium borohydride and more severe conditions with lithium aluminum hydride. With the former reagent in methanol at room temperature, **12** was converted to the lactol **13** in 86% yield [ir: no carbonyl absorption; ms: *m/e* calcd. for $C_{20}H_{24}N_2O_2$: 324.184; found: 324.1844]. This product was a 1:1 mixture of the isomeric lactols as evidenced by the appropriate signals in the ^{1}Hmr spectrum. Thus two indole NH signals (δ 8.32, 7.99), two singlets (δ 5.29, 5.24) attributed to C_{20}-H, and two methyl triplets (δ 0.97, 0.94, $J = 7$ Hz) of essentially equal intensity were observed. This mixture was not separated into its pure components.

Somewhat surprisingly, the lactone **12** proceeded to the lactol **13** (77% yield) with lithium aluminum hydride even under rather severe conditions (refluxing tetrahydrofuran). These results portray, on the one hand, a similarity in reaction of the bisindole lactone **7** and **12** with borohydride (**7** → **8** and **12** → **13**) but a distinct difference with $LiAlH_4$ (compare **7** and **8** → **11** vs. **12** → **13**).

The isolation of the rearranged bisindole products **5**, **7**, and **8** was of considerable interest

since it portrayed the first instance in our extensive studies of the Polonovski-type coupling process (5, 6) where such substances had been observed as the predominant, if not exclusive, products. All previous coupling products were shown to arise from initial fragmentation of the C_{18}—C_5 bond in the *N*-oxide intermediate and subsequent reaction of this intermediate with the dihydroindole unit. The bisindole products **5**, **7**, and **8** clearly arise from fragmentation of the C_7—C_8 bond and subsequent reaction of the intermediate thus formed with vindoline as shown in the sequence **14** → **15** → **7**.

A comparison of the results in the isomeric epoxide series is particularly striking with the normal C_{18}—C_5 bond fragmentation process being predominant in the 3β,4β-epoxide (**1** → **3**) while with the 3α,4α-isomer only the alternative C_7—C_8 bond fragmentation is observed (**4** → **5**) under *identical* conditions of coupling. This latter fragmentation process has been recently observed in other laboratories (8, 10)[3] although there are differences in their experimental procedures when compared to ours.

It is interesting to note that in all of our studies thus far which are internally consistent in terms of the reaction conditions employed, the two examples which have led to the rearranged products are catharanthine derivatives containing C_3 and/or C_4 oxygen functionality in the α orientation as shown in **4** and **6**. Whether this pattern will continue in our future studies is of considerable importance since one of the obvious extensions of the Polonovski-type coupling to the synthesis of the clinical drugs vinblastine and vincristine would involve a

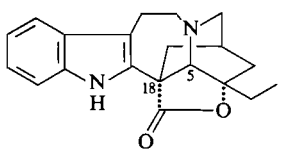

12

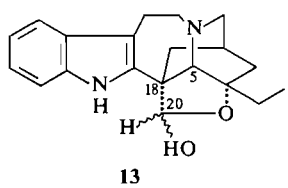

13

[3]We are grateful to Professor Ban for communicating his results to us prior to publication.

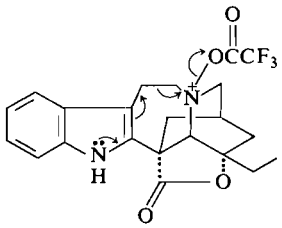

14

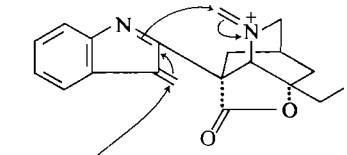

15

→ **7**

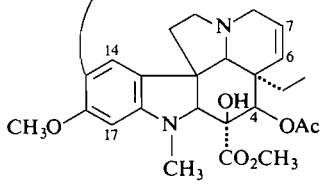

2

C_4α-oxygenated catharanthine derivative (11). Studies in this direction are presently underway.

It should be noted that the synthesis of leurosine, as reported herein, is less efficient than the first synthesis of this alkaloid reported earlier from these laboratories (12). Another low yielding synthesis of this alkaloid has been reported from another laboratory (13).

Experimental

All details concerning spectral measurements, chromatographic separations, etc. are provided in the accompanying publication (14).

Coupling of 3β,4β-Epoxydihydrocatharanthine-N-oxide (1) with Vindoline (2): Leurosine 3 (R = CO_2CH_3)

3β,4β-Epoxydihydrocatharanthine (34 mg, 0.1 mmol) and *m*-CPBA (19 mg, 0.11 mmol) were stirred in dichloromethane (1 ml) at −20°C for 20 min under an atmosphere of dry argon to form the *oxide* **1**. The solution was cooled to −50°C and vindoline **2** (50 mg, 0.11 mmol) followed by redistilled trifluoroacetic anhydride (60 µl, 0.5 mmol) were added. The mixture was stirred at −45 to −55°C for 4 h, quenched with excess $NaBH_4$ slurry in ethanol, and extracted with dichloromethane. The extracts were dried (Na_2SO_4) and evaporated *in vacuo*. Chromatography on silica gel afforded the previously described (6) isomers of 15-(2,2,2-trifluoro-1-hydroxyethyl)-vindoline, together with leurosine **3** (R = CO_2CH_3) (16 mg, 20%), identical with an authentic sample.

Coupling of 3α,4α-Epoxydihydrocatharanthine-N-oxide (4) with Vindoline (2): the Bisindole Product 5

3α,4α-Epoxydihydrocatharanthine (62 mg, 0.176 mmol) and *m*-CPBA (33 mg, 0.193 mmol) were stirred in dichloromethane (2 ml) at −20°C for 2 h under an atmosphere of dry argon to form the *oxide* **4**. The solution was cooled to −50°C and vindoline **2** (56 mg, 0.123 mmol) followed by redistilled trifluoroacetic anhydride (120 μl) were added. The mixture was stirred at ca. −50°C for 5 h, quenched with excess $NaBH_4$ slurry in ethanol, and extracted with dichloromethane. The extracts were dried (Na_2SO_4) and evaporated *in vacuo*. Chromatography on silica gel afforded an unidentified catharanthine derivative (14 mg), vindoline (14 mg), and the *bisindole* **5** (41 mg, 51%) as an amorphous solid; uv: λ_{max} 292 (4.61), 285 (4.52), 255 (4.05), 222 (3.91); ir: ν_{max} 1740; ^{1}Hmr: δ 6.80–7.41 (4H, m, aromatic protons), 6.48 (1H, s, C_{14}-*H*), 6.12 (1H, s, C_{17}-*H*), 5.78 (1H, dd, J = 10, 4 Hz, C_7-*H*), 5.39 (1H, s, C_4-*H*), 5.18 (1H, d, J = 10 Hz, C_6-*H*), 5.02 (2H, 2d, J = 11 Hz, $C_{7'}$-H_2), 3.95 (3H, s, -OCH_3), 3.81 (3H, s, -OCH_3), 3.62 (3H, s, -OCH_3), 2.02 (3H, s, -OCOCH_3), 0.98 (3H, t, J = 7 Hz, -CH_2CH_3), 0.09 (3H, t, J = 7 Hz, -CH_2CH_3); ms: *m/e* 806(M^+), 790, 737, 736, 731, 730, 718, 714, 684, 680, 658, 648, 647, 646, 645, 630, 624, 538, 351, 338, 282, 200, 188, 169, 149, and 135 (base peak). High resolution molecular weight determination calcd. for $C_{46}H_{54}N_4O_9$: 806.4090; found: 806.4022. *Anal.* calcd. for $C_{46}H_{54}N_4O_9$: C 68.48, H 6.69, N 6.94; found: C 68.28, H 6.35, N 6.76.

Coupling of 4α-Hydroxydihydrocatharanthinic Acid Lactone-N-oxide (6) with Vindoline (2): the Bisindole Products 7 and 8 and the Trimer 9

4α-Hydroxydihydrocatharanthinic acid lactone (100 mg, 0.31 mmol) and *m*-CPBA (56 mg, 0.325 mmol) were stirred in dichloromethane (3 ml) at −25°C under an atmosphere of dry nitrogen for 45 min. The solution was cooled to −50°C and vindoline **2** (100 mg, 0.219 mmol) followed by redistilled trifluoroacetic anhydride (216 μl) were added. The mixture was stirred at −50 to −60°C for 5 h, poured into a slurry of $NaBH_4$ (500 mg) in methanol (10 ml), shaken for 5 min, and extracted with dichloromethane. The combined extracts were dried (Na_2SO_4) and evaporated *in vacuo*. Chromatography on silica gel and crystallization from ethyl acetate – pentane afforded the following.

(*i*) *The bisindole lactone* **7**, mp 182–187°C (105 mg, 62%); uv: λ_{max} 292 (3.92), 285 (3.92), 250 (4.05), 223 (4.52), 211 (4.61); ir: ν_{max} 1775, 1740; ^{1}Hmr: δ 9.44 (1H, s, D_2O-exchangeable, -O*H*), 6.90–7.45 (4H, m, aromatic protons), 6.60 (1H, s, C_{14}-*H*), 6.09 (1H, s, C_{17}-*H*), 5.73 (1H, dd, J = 10, 4 Hz, C_7-*H*), 5.38 (1H, s, C_4-*H*), 5.13 (1H, d, J = 10 Hz, C_6-*H*), 4.95 (2H, 2d, J = 12 Hz, $C_{7'}$-H_2), 4.43 (2H, 2d, J = 16 Hz, $C_{8'}$-*H*), 3.83 (3H, s, -OCH_3), 3.73 (3H, s, CO_2CH_3), 2.62 (3H, s, N-CH_3), 2.00 (3H, s, -OCOCH_3), 1.03 (3H, t, J = 7 Hz, $C_{4'}$-CH_2CH_3), 0.10 (3H, t, J = 7 Hz, C_5-CH_2CH_3); ms: *m/e* 776(M^+), 717, 716, 702, 701, 700, 630, 629, 617, 616, 615, 509, 508, 494, 321, 323, 322, 309, 308, 296, 282, 269, 267, 263, 236, 235, 234, 222, 209, 202, 200, 188, 139, 135 (base peak), 122, 121. High resolution molecular weight determination calcd. for $C_{45}H_{52}N_4O_8$: 776.388: found: 776.376. *Anal.* calcd. for $C_{45}H_{52}N_4O_8$: C 69.59, H 6.70, N 7.22; found: C 69.71, H 6.87, N 6.99.

(*ii*) *The bisindole lactol* **8** (R = $COCH_3$), mp 176–182°C (18 mg, 11%); uv: λ_{max} 292 (3.97), 285 (3.96), 250 (4.08), 223 (4.55), 210 (4.64); ir: ν_{max} 3575, 3450, 1740; ^{1}Hmr: δ 6.9–7.4 (4H, m, aromatic protons), 6.69 (1H, s, C_{14}-*H*), 6.09 (1H, s, C_{17}-*H*), 5.88 (1H, dd, J = 10, 4 Hz, C_7-*H*), 5.39 (2H, s, $C_{19'}$-*H*, C_4-*H*), 5.18 (1H, d, J = 10 Hz, C_6-*H*), 4.97 (2H, 2d, J = 12 Hz, $C_{7'}$-*H*), 3.81 (3H, s, -OCH_3), 3.75 (3H, s, CO_2CH_3), 2.65 (3H, s, -NCH_3), 2.03 (3H, s, -OCOCH_3), 1.01 (3H, t, J = 7 Hz, $C_{4'}$-CH_2CH_3), 0.25 (3H, t, J = 7 Hz, C_5-CH_2CH_3); ms: *m/e* 778(M^+), 776, 762, 719, 718, 702, 701, 700, 698, 660, 659, 658, 657, 644, 619, 618, 617, 512, 511, 510, 509, 497, 496, 495, 494, 481, 470, 469, 338, 324, 323, 322, 321, 310, 309, 307, 283, 234, 222, 202, 200, 188, 188, 174, 171, 154, 149, 136, 135 (base peak), 122, 121, 107. High resolution molecular weight determination calcd. for $C_{45}H_{54}N_4O_8$: 778.394; found: 778.395. *Anal.* calcd. for $C_{45}H_{54}N_4O_8$: C 69.41, H 6.94, N 7.20; found: C 69.73, H 6.68, N 7.21.

(*iii*) *The trimer* **9**, mp 205–211°C (9 mg, 7%); uv: λ_{max} 313 (4.34), 293 (4.30), 286 (4.26), 250 (4.49), 226 (5.01), 211 (5.07); ir: ν_{max} 1740; ^{1}Hmr: δ 6.82, 6.38, 6.08, 6.02 (4H, 4 s, vindoline aromatic protons), 3.80 (6H, s, 2× -OCH_3), 3.75 (6H, s, 2× -OCH_3), 2.66 (3H, s, -NCH_3), 2.64 (3H, s, -NCH_3), 2.01 (6H, s, 2× -OCOCH_3, 0.76 (3H, t, J = 7 Hz, $C_{4'}$-CH_2CH_3), 0.29 (3H, t, J = 7 Hz, -CH_2CH_3), 0.00 (3H, t, J = 7 Hz, -CH_2CH_3); ms: *m/e* 1235, 1234, 1233, 1232, 1231, 1151, 1150, 1149, 1148, 1066, 802, 516, 475, 441, 440, 360, 359, 327, 287, 283, 239, 169, 149. *Anal.* calcd. for $C_{70}H_{84}N_6O_{14}$: C 68.18, H 6.82, N 6.82; found: C 68.30, H 6.71, N 6.84.

$NaBH_4$ Reduction of (7): the Lactol 8 (R = $COCH_3$)

A solution of **7** (20 mg) and trifluoroacetic anhydride (100 μl) in dichloromethane (2 ml) was added dropwise to $NaBH_4$ (50 mg) in methanol (2 ml) at 0°C. Excess $NaBH_4$ (50 mg) was added in two portions at 15 min intervals. The mixture was stirred at 0°C for 30 min, diluted with water (1 ml), saturated NaCl solution (5 ml), and extracted with dichloromethane. The combined extracts were dried (Na_2SO_4), and evaporated *in vacuo*. Chromatography on silica gel gave **7** (9.8 mg, 49%) and **8** (R = $COCH_3$) (7.7 mg, 38%) identical with that obtained above.

Reaction of (7) with NaOMe: the Hydroxyester 10

A solution of **7** (10 mg, 0.013 mmol) in anhydrous methanol (1 ml) was added to sodium methoxide in methanol (10 mg of sodium metal in 1 ml of anhydrous methanol) and the mixture stirred under an atmosphere of dry nitrogen for 20 h. The reaction mixture was cooled to 0°C, carefully neutralized with Amberlite IR-120, and filtered. The filtrate was evaporated *in vacuo*. Chromatography on silica gel and crystallization from ethyl acetate – methanol pentane afforded the *hydroxyester* **10** mp 170–177°C (7.6 mg, 77%); uv: λ_{max} 293 (4.03), 288 (4.00), 250 (4.13), 224 (4.59), 212 (4.68); ir: ν_{max} 3550, 1720; ^{1}Hmr: δ 6.8–7.25 (4H, m, aromatic protons), 6.47 (1H, s, C_{14}-*H*), 6.14 (1H, s, C_{17}-*H*), 5.62-5.86 (2H, m, C_7-*H*, C_6-*H*), 5.06 (2H, 2d, J = 12 Hz, $C_{7'}$-*H*), 3.87 (3H, s, -OCH_3), 3.84 (3H, s, -CO_2CH_3), 3.54 (3H, s, -CO_2CH_3), 2.73 (3H, s, -NCH_3), 0.96 (3H, t, J = 7 Hz, $C_{4'}$-CH_2CH_3), 0.42 (3H, t, J = 7 Hz, C_5-CH_2CH_3); ms: *m/e* 766(M^+), 735, 734, 702, 701, 700, 675, 674, 619, 618, 617, 615, 536, 509, 508, 495, 494, 481, 354, 321, 308, 297, 263, 248, 246, 240, 234, 202, 200, 188, 174, 172, 170, 154, 149, 135 (base peak), 122, 121, 108, 107. High resolution molecular weight determination calcd. for $C_{44}H_{54}N_4O_8$: 766.394; found: 766.399. *Anal.* calcd. for

$C_{44}H_{54}N_4O_8 \cdot CH_3OH$: C 67.66, H 7.27, N 7.01; found: C 67.80, H 7.30, N 6.66.

NaOMe Opening of the Lactol **8** *(R = $COCH_3$): the Lactol* **8** *(R = H)*

A solution of **8** (R = $COCH_3$) (8 mg) in anhydrous methanol (1 ml) was added to sodium methoxide (from 10 mg of sodium metal) in anhydrous methanol (1 ml) and the mixture stirred at ambient temperature under a nitrogen atmosphere for 17 h. Work-up, as described for the preparation of **10**, gave the *lactol* **8** (R = H), (5.8 mg, 77%); uv: λ_{max} 292 (3.89), 287 (3.88), 250 (4.014), 222 (4.40), 212 (4.45); ir: ν_{max} 3550, 3450, 1725; ^{1}Hmr: δ 6.9–7.4 (4H, m, aromatic protons), 6.72 (1H, s, C_{14}-*H*), 6.12 (1H, s, C_{17}-*H*), 5.76 (2H, m, C_7-*H*, C_6-*H*), 5.45 and 5.42 (1H, 2s, $C_{19'}$-*H*), 5.08 (1H, d, *J* = 12 Hz, $C_{7'}$-*H*), 4.99 (1H, d, *J* = 12 Hz, $C_{7'}$-*H*), 3.86 (3H, s, OCH_3), 3.84 (3H, s, OCH_3), 2.74 (3H, s, $-NCH_3$), 1.04 (3H, t, *J* = 7 Hz, $C_{4'}$-CH_2CH_3), 0.46 (3H, t, *J* = 7 Hz, C_5-CH_2CH_3); ms: *m/e* 736(M^+), 734, 703, 702, 701, 700, 677, 676, 674, 660, 620, 619, 618, 617, 538, 511, 510, 509, 508, 497, 495, 494, 393, 354, 337, 336, 321, 308, 277, 265, 263, 248, 240, 234, 202, 200, 195, 188, 168, 154, 149, 135 (base peak), 122, 121, 107. High resolution molecular weight determination calcd. for $C_{43}H_{52}N_4O_7$: 736.384; found: 736.388.

LAH Reduction of Lactone 7: the Pentahydroxy Bisindole **11**

Lithium aluminum hydride (30 mg) was added to a solution of the *lactone* 7 (20 mg) in anhydrous THF (1.5 ml). The mixture was stirred at ambient temperature for 18 h, treated with a few drops of water, and filtered. The filtrate was concentrated *in vacuo*, chromatographed on silica gel, and crystallized from ethyl acetate – pentane to afford **11**, mp 188–197°C (dec) (17 mg, 94%); uv: λ_{max} 294 (3.96), 288 (3.91), 250 (4.05), 226 (4.43), 213 (4.46); ir: ν_{max} 3540, 3390; ^{1}Hmr: δ 8.62 (1H, s, -O*H*), 6.8–7.4 (4H, m, aromatic protons), 6.48 (1H, s, C_{14}-*H*), 6.15 (1H, s, C_{17}-*H*), 5.75 (1H, dd, *J* = 10, 4 Hz, C_7-*H*), 5.56 (1H, d, *J* = 10 Hz, C_6-*H*), 5.04 (1H, d, *J* = 12 Hz, $C_{7'}$-*H*), 4.86 (1H, d, *J* = 12 Hz, $C_{7'}$-*H*), 3.86 (3H, s, $-OCH_3$), 2.98 (3H, s, $-NCH_3$), 0.96 (3H, t, *J* = 7 Hz, $C_{4'}$-CH_2CH_3), 0.38 (3H, t, *J* = 7 Hz, C_5-CH_2CH_3); ms: *m/e* 710(M^+), 709, 708, 692, 679, 677, 676, 675, 674, 662, 660, 658, 622, 621, 542, 541, 513, 512, 511, 498, 494, 429, 399, 398, 381, 380, 366, 365, 364, 363, 355, 354, 352, 325, 324, 312, 311, 297, 295, 294, 281, 278, 233, 229, 226, 223, 221, 210, 202, 200, 188, 169, 168, 167, 149 (base peak), 135, 124, 122, 115, 107. High resolution molecular weight determination calcd. for $C_{42}H_{54}N_4O_6$: 710.404; found: 710.401.

LAH Reduction of Lactol **8** *(R = $COCH_3$): the Pentahydroxy Bisindole* **11**

Reaction of **8** (R = $COCH_3$) (7 mg) with LAH (10 mg) as described above, gave **11** (3.8 mg, 60%) identical with that prepared earlier.

Reduction of 4α-Hydroxydihydrocatharanthinic Acid Lactone **12**: *the Lactol* **13**

(*a*) The *lactone* **12** (10 mg) was added to a solution of $NaBH_4$ (50 mg) in methanol (2 ml) at 0°C. Excess $NaBH_4$ (50 mg) was added in two portions at ca. 15 min intervals. The mixture was stirred at ambient temperature for 2 h. Work-up, as described above for the reduction of **7**, gave the *lactol* **13** (8.7 mg, 87%) as a mixture of diastereomers; uv: λ_{max} 283 (3.80), 280 (3.84), 274 (3.83), 222 (4.273); ir: ν_{max} 3550, 3425, 3340; ^{1}Hmr: δ 8.32 and 7.99 (1H, 2 bs, -N*H*), 6.9–7.6 (4H, m, aromatic protons), 5.29 and 5.24 (1H, 2s, C_{19}-*H*), 0.97 and 0.94 (3H, 2t, *J* = 7 Hz, $-CH_2CH_3$); ms: *m/e* 324 (M^+,base peak), 322, 307, 306, 278, 277, 263, 249, 236, 235, 234, 221, 209, 205, 204, 193, 184, 168, 167, 159, 154, 144, 141, 135, 130, 128, 122, 121, 115, 108, 105. High resolution molecular weight determination calcd. for $C_{20}H_{24}N_2O_2$: 324.184; found: 324.184.

(*b*) Lithium aluminum hydride (10 mg) was added to a solution of **12** (10 mg) in anhydrous THF (1.5 ml) and the mixture stirred at ambient temperature for 18 h. Work-up, as described above for the preparation of **11**, gave the *lactol* **13** (7.8 mg, 78%) identical with that described above.

Acknowledgements

Financial aid from the National Research Council of Canada and from Contract N01-CM-23223, National Cancer Institute, National Institutes of Health, Bethesda, Maryland, is gratefully acknowledged. We are grateful to the Lilly Research Laboratories for supplies of catharanthine and vindoline and a sample of leurosine.

1. N. Neuss, M. Gorman, N. J. Cone, and L. L. Huckstep. Tetrahedron Lett. 783 (1968).
2. D. J. Abraham and N. R. Farnsworth. J. Pharm. Sci. **58**, 694 (1969).
3. E. Wenkert, E. W. Hagsman, B. Lal, G. E. Gutowski, A. S. Katner, J. C. Miller, and N. Neuss. Helv. Chim. Acta, **58**, 1560 (1975).
4. J. P. Kutney, G. H. Bokelman, M. Ichikawa, E. Jahngen, A. V. Joshua, P. Liao, and B. R. Worth. Heterocycles, **4**, 1267 (1976).
5. J. P. Kutney, A. H. Ratcliffe, A. M. Treasurywala, and S. Wunderly. Heterocycles, **3**, 639 (1975).
6. J. P. Kutney, T. Hibino, E. Jahngen, T. Okutani, A. H. Ratcliffe, A. M. Treasurywala, and S. Wunderly. Helv. Chim. Acta, **59**, 2858 (1976).
7. P. Potier, N. Langlois, Y. Langlois, and F. Gueritte. Chem. Commun. 670 (1975).
8. N. Langlois, F. Gueritte, Y. Langlois, and P. Potier. J. Am. Chem. Soc. **98**, 7017 (1976).
9. J. P. Kutney, J. Beck, F. Bylsma, J. Cook, W. J. Cretney, K. Fuji, R. Imhof, and A. M. Treasurywala. Helv. Chim. Acta, **58**, 1690 (1975).
10. Y. Honma and Y. Ban. Heterocycles, **6**, 291 (1977).
11. A. Atta-ur-Rahman, A. Basha, and M. Ghazala. Tetrahedron Lett. 2351 (1976).
12. J. P. Kutney, J. Balsevich, G. H. Bokelman, T. Hibino, I. Itoh, and A. H. Ratcliffe. Heterocycles, **4**, 997 (1976).
13. Y. Langlois, N. Langlois, P. Mangeney, and P. Potier. Tetrahedron Lett. 3945 (1976).
14. J. P. Kutney, G. H. Bokelman, M. Ichikawa, E. Jahngen, A. V. Joshua, P. Liao, and B. R. Worth. Can. J. Chem. This issue.
15. J. P. Kutney and B. R. Worth. Heterocycles, **4**, 1777 (1976).
16. J. P. Kutney, A. V. Joshua, and P. Liao. Heterocycles, **6**, 297 (1977).

Long-range proton–^{19}F spin–spin coupling interactions in phenyltrifluorosilane

WILLIAM J. E. PARR,[1] T. SCHAEFER, AND K. MARAT
Department of Chemistry, University of Manitoba, Winnipeg, Man., Canada R3T 2N2

Received March 14, 1977

WILLIAM J. E. PARR, T. SCHAEFER, and K. MARAT. Can. J. Chem. **55**, 3243 (1977).

Analysis of the proton magnetic resonance spectrum of phenyltrifluorosilane yields the spin–spin coupling constants between the fluorine nuclei and the protons. These are compared with the analogous long-range coupling constants in benzotrifluoride, toluene, and phenylsilane and are rationalized in terms of coupling mechanisms. The coupling over six bonds is assessed as a base point for the estimation of hindered rotation about the carbon–silicon bond.

WILLIAM J. E. PARR, T. SCHAEFER et K. MARAT. Can. J. Chem. **55**, 3243 (1977).

L'analyse du spectre de résonance magnétique du proton du phényltrifluorosilane nous fournit les constantes de couplage spin–spin entre le noyau fluor et les protons. Celles-ci sont comparées à des constantes de couplage analogues à longue distance pour le trifluorobenzyle, le toluène et le phénylsilane et sont rationalisées en termes de mécanismes de couplage. Le couplage au delà de six liaisons est assigné comme référence pour l'estimation de la rotation empêchée autour du lien carbone–silicium.

[Traduit par le journal]

Introduction

The long-range spin–spin coupling constants between ring protons and protons or fluorine nuclei in the sidechain of benzene derivatives have been investigated in some detail (1–17). In addition to providing tests of theories of the transmission of spin state information, the couplings are often sensitive to the conformation of the molecule and have been employed in the empirical determination of free energy differences between conformational isomers (17, 18). It has also proved possible to extend their application to the derivation of twofold rotational barriers of magnitudes between about 0.2 and 2.2 kcal/mol (19, 20), such values being inaccessible to lineshape methods. For example, a careful comparison of the long-range coupling over six bonds, $^6J_p^{H,CH}$, in toluene and in phenylethane, combined with a hindered rotor treatment, yields a twofold barrier of 1.2 ± 0.1 kcal/mol to rotation about the C—CH_2 bond in the latter molecule in solution. In addition it is clear that **1** is the low-energy conformation (19).

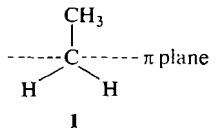

1

It has also been seriously suggested (20, 21) that analogous couplings to fluorine nuclei on the sidechain, $^6J_p^{H,CF}$, are useful in finding small twofold internal barriers in $C_6H_5CHF_2$ and $C_6H_5CH_2F$.

An attempt to extend the approach to phenyl derivatives of the third row of the periodic table was partially successful when the barriers to rotation about the C_6H_5—Si bond were found for $C_6H_5SiH(CH_3)_2$ and $C_6H_5SiHCl_2$ and were estimated for $C_6H_5SiH_2Cl$ and $C_6H_5SiH_2CH_3$ (22).

All this work depends on having reliable values for couplings over six bonds to protons in the *para* position. These are now known for $C_6H_5CH_3$, $C_6H_5CF_3$, and $C_6H_5SiH_3$.

This paper reports the analysis of the proton magnetic resonance spectrum of $C_6H_5SiF_3$ and the determination of the long-range couplings from the ring protons to ^{19}F nuclei. The latter are compared with the analogous couplings in the three molecules above and are assessed for their possible use in the measurement of barriers to internal rotation. The magnitudes of the coupling constants are rationalized in terms of σ, σ–π, and direct (through-space) mechanisms.

Experimental

Antimony trifluoride (50 g, 0.28 mol) and tetramethylenesulphone (50 ml) were placed in a 250 ml flask equipped with a reflux condenser, dropping funnel, and thermometer. Phenyltrichlorosilane (14.1 g, 0.067 mol) was added from the dropping funnel at a rate such that the reaction temperature never exceeded 100°C. The phenyltrifluorosilane was distilled through a 15 cm

[1]Postdoctoral fellow, 1974–1976.

TABLE 1. Proton chemical shifts* and spin–spin coupling constants† for a 20 v/v % solution of $C_6H_5SiF_3$ in C_6D_6. Includes data for $C_6H_5CF_3$, $C_6H_5CH_3$, $C_6H_5SiF_3$

Parameter	Value		Parameter	Value
ν_F	1216.85‡	—	$^4J_o^{H,SiF_3}$	+0.090(5)
$\nu_{2,6}$	738.70	744.85§	$^5J_m^{H,SiF_3}$	0.829(4)
$\nu_{3,5}$	703.21	718.92	$^6J_p^{H,SiF_3}$	−0.278(4)
ν_4	717.36	725.71	$^4J_o^{H,CF_3}$	−0.74
$^3J_{2,3}$	7.541(5)	7.91	$^5J_m^{H,CF_3}$	0.82
$^3J_{3,4}$	7.648(4)	7.59	$^6J_p^{H,CF_3}$	−0.64
$^4J_{2,4}$	1.358(5)	1.24	$^4J_o^{H,CH_3}$	−0.75
$^4J_{2,6}$	1.345(6)	1.99	$^5J_m^{H,CH_3}$	0.36
$^4J_{3,5}$	1.200(5)	1.30	$^6J_p^{H,CH_3}$	−0.62
$^5J_{2,5}$	0.760(5)	0.62	$^4J_o^{H,SiH_3}$	−0.14
$^1J(^{29}Si, F)$	267.0‖	—	$^5J_m^{H,SiH_3}$	0.20
rms error	0.026 Hz	—	$^6J_p^{H,SiH_3}$	−0.34

*In Hz at 100 MHz at 305 K to low field of internal tetramethylsilane.
†In Hz, numbers in parentheses giving the standard deviation in the last place.
‡In Hz to low field of internal C_6F_6 at 301 K and 56.443 MHz.
§This column refers to $C_6H_5CF_3$, ref. 8.
‖The sign is taken as positive. See ref. 36.

column, collecting the portion that boiled at 95–98°C. The yield was 10.7 g (98%).

Due to the air sensitivity of the phenyltrifluorosilane, it was necessary to prepare the sample under anhydrous conditions. C_6D_6, C_6F_6, and TMS were all dried for 24 h over a molecular sieve. Sufficient phenyltrifluorosilane for a 20 vol.% solution was condensed into a dried nmr tube from a bulb on the vacuum system. C_6D_6 and small quantities of C_6F_6 and TMS were condensed into the tube which was then flame sealed under dynamic vacuum.

The proton magnetic resonance spectrum was calibrated on a HA 100 spectrometer at 305 K. Calibration lines were placed at approximately 5 Hz intervals and the sweep and manual oscillator frequencies were recorded for each such line. The spectral dispersion was 1 Hz/cm, the sweep rate was 0.02 Hz/s, and the other instrumental parameters were adjusted to minimize distortion from saturation or filtering phenomena. The ^{19}F resonance spectrum was recorded in a similar way on a DA60I spectrometer at 301 K, employing C_6F_6 as an internal lock. The peak positions determined in this manner had rms deviations near 0.02 Hz.

Ab initio calculations at the STO-3G level of molecular orbital theory (23) employed a standard geometry (24) for the phenyl group, tetrahedral angles at silicon, and C—Si, Si—F bond lengths of 1.843 and 1.561 Å, respectively.

Results and Discussion

Spectral Analysis

The proton magnetic resonance spectrum was analyzed with the computer program LAME (25, 26). The spectral asymmetry was sufficient to establish the sign sequence given in Table 1. Figure 1 illustrates the sensitivity of the calculated spectrum to the sign of the small coupling, $^4J_o^{H,SiF_3}$. The *meta* and *para* proton peaks could only be fitted if $^5J_m^{H,SiF_3}$ and $^6J_p^{H,SiF_3}$ had opposite signs. The ^{19}F spectrum was consistent with a positive sign for $^5J_m^{H,SiF_3}$ and a negative sign for $^6J_p^{H,SiF_3}$. The sign sequence in Table 1 is firmly established. The standard deviations of 0.004 to 0.005 Hz (Table 1) in the long-range couplings suggest an accuracy of 0.02 Hz.

The Spectral Parameters within the Phenyl Group

The chemical shifts are no doubt influenced by the anisotropy of the benzene solvent molecules, but a comparison with the shifts for neat benzotrifluoride (8) is partially valid. It suggests that the CF_3 group withdraws slightly more charge from the ring than does the SiF_3 group. A similar conclusion follows from the ^{13}C chemical shifts (27).

In benzene, $^3J_o^{H,H}$, $^4J_m^{H,H}$, and $^5J_p^{H,H}$ are 7.54, 1.37, and 0.69 Hz, respectively (28). Comparison with the data in Table 1 indicates a very small perturbation of these values by the SiF_3 group. In fact, the sum of the six coupling constants in Table 1 is 19.86 Hz as compared to the 19.88 Hz for the corresponding sum in benzene. This sum is 20.65 Hz for $C_6H_5CF_3$.

Long-range Coupling Constants $^6J_p^{H,XH}$ and $^6J_p^{H,XF}$ (X = C or Si)

The sixfold barrier to internal rotation is 0.014 kcal/mol in toluene (29) and 0.010 kcal/mol in benzotrifluoride (30). Consequently their coupling constants in Table 1 represent averages over the essentially free rotation about the C—CH_3 and C—CF_3 bonds. The barrier to rotation about the C—SiH_3 bond in phenylsilane is 0.018 kcal/mol (31) and, on the assumption that it is no higher in phenyltrifluorosilane, the coupling constants for these two compounds in

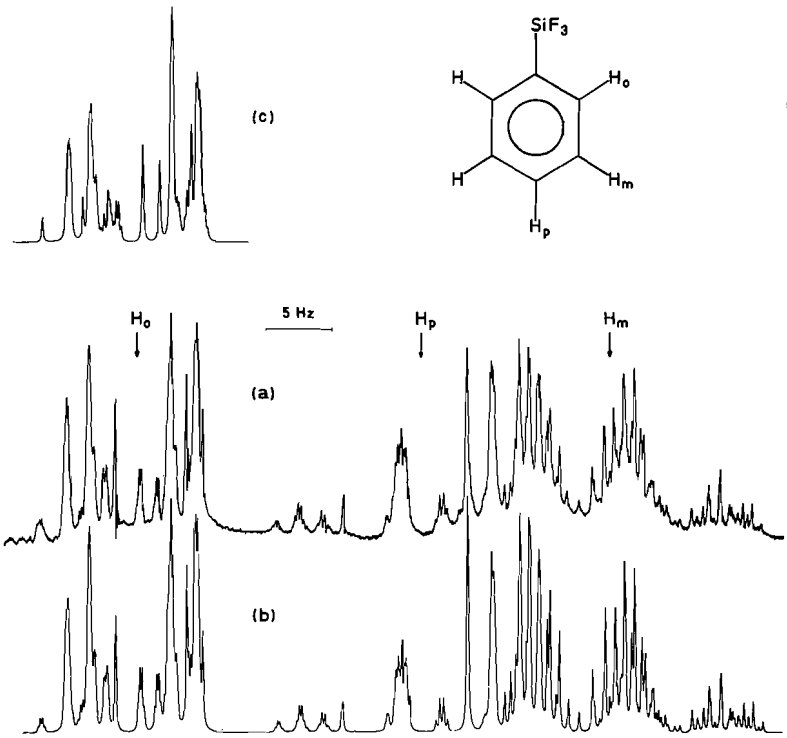

FIG. 1. The ring proton magnetic resonance spectrum at 100 MHz of a 20 vol.% solution of phenyltrifluorosilane in benzene-d_6 is shown in *a*. In *b* the spectrum calculated with the parameters in Table 1 is presented. The appearance of the calculated spectrum of the *ortho* protons, under conditions where $^4J_o^{H,SiF_3}$ is negative, is illustrated in *c*.

Table 1 may also be taken as averages over free rotation.

On the basis of INDO-MO-FPT calculations (7) and of measurements of $^6J_p^{CH_3,CH_3}$ (3, 4) it is apparent that $^6J_p^{H,CH_3}$ is proportional to $\sin^2\theta$, where θ is the angle by which a C—H bond of the methyl group twists out of the plane of the aromatic ring. The calculations agree quantitatively with the observed value of -0.62 Hz. This number is a base point in the derivation of barriers to internal rotation in α- and α,α-substituted toluene derivatives (19).

Similar calculations on $^6J_p^{H,CF_3}$ (32) also suggest a $\sin^2\theta$ dependence but predict a magnitude almost twice as large as the observed one of 0.64 Hz.

When the sidechain carbon atom is replaced by a silicon atom a σ–π hyperconjugative model suggests that the increased bond lengths may well reduce the overlap between the orbitals in the sidechain and the $p\pi$ orbitals in the phenyl group, thereby reducing the magnitude of the σ–π parameters. Indeed (see Table 1), $^6J_p^{H,SiH}$ is just over half as large in magnitude as $^6J_p^{H,CH}$. Similarly, $^6J_p^{H,SiF}$ is just under half as large in magnitude as $^6J_p^{H,CF}$.

$^6J_p^{H,SiF}$ is -0.28 Hz in $C_6H_5SiF_3$, so small a modulus that use of it as a base in determining barriers to rotation about the C—Si bond becomes relatively difficult for the following reasons. $^6J_{90}^{H,SiF}$ is -0.56 Hz. Now, for example, in $C_6H_5SiF(CH_3)_2$ it seems reasonable that the low-energy conformation is **2** and that the high-energy conformation is **3**. In **2**, $\sin^2\theta$ is zero. For free rotation, $\langle\sin^2\theta\rangle$ is 0.5 so that the observed $^6J_p^{H,SiF}$ would be -0.28 Hz. For a barrier lying between 0 and about 3 kcal/mol, $\langle\sin^2\theta\rangle$ would vary between 0.5 and 0.05. An error of 0.02 Hz in the measurements of $^6J_p^{H,SiF}$

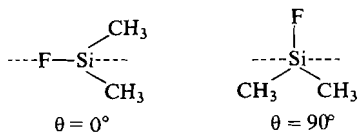

in $C_6H_5SiF_3$ and of $C_6H_5SiF(CH_3)_2$ would introduce an error of about 20% into the determination of the barrier (33). Furthermore, small perturbations of ^6J by the substituents attached to silicon may introduce a further uncertainty into the barrier. It appears that the value of $^6J_p^{H,SiF}$ is near the limit at which significant deductions about conformational preferences and rotational barriers are still possible in compounds of formula $C_6H_5SiFX_2$.

$^5J_m^{H,XH}$ and $^5J_m^{H,XF}$ (X = C or Si)

The π electron contribution to $^5J_m^{H,CH_3}$ is 0.21 Hz (3, 4), leaving 0.15 Hz to the σ electron mechanism. The 0.20 Hz observed for $^5J_m^{H,SiH}$ can be attributed to reduced magnitudes of both coupling mechanisms. Clearly, both $^5J_m^{H,CF}$ and $^5J_m^{H,SiF}$ have a large σ component and, in view of their equality and of the relative magnitudes of the corresponding six-bond couplings, this component is larger in the silicon compound. INDO-MO-FPT calculations overestimate $^5J_m^{H,CH}$ and $^5J_m^{H,CF}$ (7, 32).

$^4J_o^{H,XH}$ and $^4J_o^{H,XF}$ (X = C or Si)

The magnitudes of $^4J_o^{H,CF_3}$ and $^4J_o^{H,CH_3}$ are equal (Table 1). According to INDO-MO-FPT calculations, the equality is coincidental. In addition to the σ–π and σ electron mechanisms common to both $^4J_o^{H,CH_3}$ and $^4J_o^{H,CF_3}$, the latter contains in addition a contribution from a direct interaction dependent on the proximity of the bonds carrying the coupled nuclei (7, 32).

The relatively small magnitude of $^4J_o^{H,SiH_3}$ can plausibly be attributed to a decrease in the magnitude of the σ–π mechanism (see $^6J_p^{H,CH_3}$) combined with a small positive σ electron contribution. The decrease in the former and the change in sign of the latter contributions relative to their role in determining $^4J_o^{H,CH_3}$ (7) could well be a consequence of the C—Si and Si—H bond lengths.

The positive sign of $^4J_o^{H,SiF_3}$ can be rationalized by assigning a lesser importance to the direct (through-space) mechanism which depends critically on the ^{19}F, ^1H internuclear distance (34), combined with a positive σ electron contribution which outweighs the expected negative σ–π mechanism (compare $^6J_p^{H,SiF_3}$).

STO-3G Calculations

These gave a barrier of 0.005 kcal/mol to rotation about the C—Si bond. Although such a small value is below the level of significance of these *ab initio* MO calculations (35), it is consistent with the very small barriers measured for the other three compounds.

Acknowledgment

We are grateful to the National Research Council of Canada for financial assistance.

1. G. Kotowycz and T. Schaefer. Can. J. Chem. **44**, 2743 (1966).
2. M. P. Williamson, R. Kostelnik, and S. M. Castellano. J. Chem. Phys. **49**, 2218 (1968).
3. C. J. Macdonald and W. F. Reynolds. Can. J. Chem. **48**, 1002 (1970).
4. J. B. Rowbotham and T. Schaefer. Can. J. Chem. **52**, 489 (1974).
5. R. Wasylishen and T. Schaefer. Can. J. Chem. **49**, 94 (1971).
6. D. J. Blears, S. S. Danyluk, and T. Schaefer. J. Chem. Phys. **47**, 5037 (1967).
7. R. Wasylishen and T. Schaefer. Can. J. Chem. **50**, 1852 (1972).
8. R. J. Kostelnik, M. P. Williamson, D. E. Wisnosky, and S. M. Castellano. Can. J. Chem. **47**, 3313 (1969).
9. T. Schaefer, R. Schwenk, C. J. Macdonald, and W. F. Reynolds. Can. J. Chem. **46**, 2187 (1968).
10. A. F. Janzen and T. Schaefer. Can. J. Chem. **49**, 1818 (1971).
11. H. M. Hutton, J. B. Rowbotham, B. H. Barber, and T. Schaefer. Can. J. Chem. **49**, 2033 (1971).
12. J. A. Weil, A. Blum, A. H. Heiss, and J. K. Kinnaird. J. Chem. Phys. **46**, 3132 (1967).
13. R. Wasylishen and T. Schaefer. Can. J. Chem. **48**, 1263 (1970); **48**, 1343 (1970); **49**, 3216 (1971).
14. S. Forsén and R. A. Hoffman. J. Mol. Spectrosc. **20**, 168 (1968).
15. J. B. Rowbotham, M. Smith, and T. Schaefer. Can. J. Chem. **53**, 986 (1975).
16. T. Schaefer and J. B. Rowbotham. Chem. Phys. Lett. **29**, 633 (1974).
17. W. Danchura, T. Schaefer, J. B. Rowbotham, and D. J. Wood. Can. J. Chem. **52**, 3986 (1974).
18. J. B. Rowbotham and T. Schaefer. Can. J. Chem. **52**, 3037 (1974).
19. T. Schaefer, W. Niemczura, and L. Kruczynski. Chem. Phys. Lett. **38**, 498 (1976).
20. T. Schaefer, J. B. Rowbotham, W. J. E. Parr, K. Marat, and A. F. Janzen. Can. J. Chem. **54**, 1322 (1976).
21. J. B. Rowbotham, A. F. Janzen, J. Peeling, and T. Schaefer. Can. J. Chem. **52**, 481 (1974).
22. W. J. E. Parr and T. Schaefer. Can. J. Chem. **55**, 557 (1977).
23. W. J. Hehre, R. F. Stewart, and J. A. Pople. J. Chem. Phys. **51**, 2657 (1969); Program 236, Quantum Chemistry Program Exchange, University of Indiana, Bloomington, Indiana.
24. J. A. Pople and M. Gordon. J. Am. Chem. Soc. **89**, 4254 (1967).

25. S. CASTELLANO and A. A. BOTHNER-BY. Laocoon 3, Mellon Institute Publication, Pittsburgh, PA. 1967.
26. C. W. HAIGH and J. M. WILLIAMS. J. Mol. Spectrosc. **32**, 398 (1969).
27. NGUYEN-DUC-CHUY, V. CHVALOVSKY, J. SCHRAML, M. MÄGI, and E. LIPPMA. Coll. Czech. Chem. Commun. **40**, 875 (1975).
28. J. M. READ, R. E. MAYO, and J. H. GOLDSTEIN. J. Mol. Spectrosc. **22**, 419 (1967).
29. H. D. RUDOLPH, H. DREIZLER, J. JAESCHKE, and P. WENDLING. Z. Naturforsch. Teil A, **22**, 940 (1967).
30. T. OGATA and A. P. COX. J. Mol. Spectrosc. **61**, 265 (1976).
31. W. CAMINATI, G. CAZZOLI, and A. M. MIRRI. Chem. Phys. Lett. **35**, 475 (1975).
32. R. E. WASYLISHEN and M. BARFIELD. J. Am. Chem. Soc. **97**, 4545 (1975).
33. P. B. AYSCOUGH, M. C. PRICE, and R. E. D. MCCLUNG. Mol. Phys. **20**, 41 (1971).
34. T. SCHAEFER, K. CHUM, K. MARAT, and R. E. WASYLISHEN. Can. J. Chem. **54**, 800 (1976).
35. W. J. HEHRE, L. RADOM, and J. A. POPLE. J. Am. Chem. Soc. **94**, 1496 (1972).
36. S. S. DANYLUK. J. Am. Chem. Soc. **86**, 4505 (1964).

Cupric ion binding by coal humic acids at p*H*'s 1–3

JOHN B. GREEN AND STANLEY E. MANAHAN[1]
Chemistry Department, University of Missouri-Columbia, Columbia, MO 65201, U.S.A.

Received October 25, 1976[2]

JOHN B. GREEN and STANLEY E. MANAHAN. Can. J. Chem. **55**, 3248 (1977).

The extent and mechanism of cupric ion binding by humic acid (HA) at low p*H*'s where the material was insoluble in aqueous media was investigated. It was shown that significant amounts of Cu(II) were bound by HA even at p*H*'s as low as 1.35. Two major types of HA–Cu^{2+} binding were observed. Binding which was accompanied by exchange of H^+ was more prevalent at high p*H*'s and $[Cu^{2+}]$. Nonexchange bonding occurred at all p*H*'s, but assumed greater importance at low p*H*'s. Since the pattern of Cu(II) uptake could not be interpreted in terms of basic ion exchange or surface adsorption theory, a new model was proposed which qualitatively explained the dependence of Cu(II) on p*H* and $[Cu^{2+}]$. The model assumed that the intermolecular bonding in flocculated HA was determined by the relative amounts of H^+ and Cu^{2+} available for forming bridging bonds between the HA molecules. The model suggested that at high concentrations of Cu(II) and/or high p*H*'s, the floc structure was such that the formation of copper bridge bonds was maximized.

JOHN B. GREEN et STANLEY E. MANAHAN. Can. J. Chem. **55**, 3248 (1977).

On a étudié l'étendue et le mécanisme de liaisons de l'ion cuprique par l'acide humique (AH) à de bas p*H* où les matériaux sont insolubles dans un milieu aqueux. On a pu montrer que des quantités importantes de Cu(II) sont liées en AH même à des p*H* aussi bas que 1.35. On a observé deux types majeurs de liaisons AH et Cu^{2+}. La liaison qui est accompagnée par un échange de H^+ est plus importante à des p*H* élevés et des concentrations de $[Cu^{2+}]$ élevées. La liaison sans échange se produit à tous les p*H*, mais elle est plus importante à des p*H* plus bas. Puisque l'on ne pouvait pas interpréter l'évolution de l'absorption de $[Cu^{2+}]$ en termes d'échange d'ions basiques ou de la théorie de l'adsorption par la surface, on propose un nouveau modèle qui explique qualitativement la relation entre le Cu(II) et le p*H* et la concentration en $[Cu^{2+}]$. Dans ce modèle, on fait l'hypothèse que la liaison intermoléculaire dans du AH floculé est déterminée par les quantités relatives de H^+ et de Cu^{2+} disponibles pour la formation de liens effectuant des ponts entre les molécules de AH. Le modèle suggère qu'à des concentrations élevées de Cu(II) et/ou des p*H* élevés, la structure flocculée est telle que la formation des liens pontés de cuivre est maximale.

[Traduit par le journal]

Introduction

A large portion of the recent literature on humic acids (HA) extracted from soil, peat, and coal has been devoted to study of their metal ion binding properties (1, 2). However, practically all work has been at p*H* values where appreciable ionization of acidic functional groups on HA occurs. One mechanism of binding at the commonly studied p*H* range is thought to involve chelation by *ortho* phenolate and carboxylate groups on aromatic rings (1–5). This type of binding at acidic p*H*'s is unlikely, however, due to intense competition by hydrogen ion for very weakly acidic phenolate groups.

Two plausible mechanisms for interaction of HA and Cu(II) under acidic conditions are adsorption and ion exchange. A cation exchange reaction is usually symbolized in the following way for synthetic cation resins in hydrogen form:

$$[1] \qquad n\mathrm{HR} + \mathrm{M}^{n+}{}_{(aq)} = \mathrm{MR} + n\mathrm{H}^{+}{}_{(aq)}$$

HR and MR are resin-bound H^+ and M^{n+}.

The corresponding equilibrium quotient for [1] is, of course:

$$[2] \qquad K = \frac{[\mathrm{M}]_r[\mathrm{H}^+]_s{}^n}{[\mathrm{H}]_r{}^n[\mathrm{M}^{n+}]_s}$$

Davies *et al.* (5) referred to equations analogous to [1] and [2] in their work on retention of low levels of Cu(II) on HA. They found, however, that the quotient (K) varied with the extent of cupric ion saturation of HA. Also, Szalay (6) explained $UO_2{}^{2+}$ uptake by HA in terms of ion exchange.

Adsorption isotherms have also been used in conjunction with metal binding by HA precipitates. For example, sorption of Cu(II) (7) and

[1]Author to whom correspondence should be addressed.
[2]Revision received May 5, 1977.

Cd(II) (8) reportedly follows the well-known Langmuir equation. Log–log plots corresponding to the Freundlich isotherm were used to describe Ga^{3+} sorption on peat and HA (9). Titanium's interactions with peat have been interpreted in terms of an adsorption model (10). Adsorption isotherms have also been used to describe binding of organic molecules to HA. For example, adsorption to linuron (a herbicide) is best represented by a Freundlich isotherm (11). Hayword and Trapnell (12) describe adsorption isotherms in detail, hence they need not be discussed here.

Both ion exchange and adsorption equations were tested by the authors using Cu(II)–HA equilibration data taken in acidic media. Neither was found to be satisfactory.

Experimental

The HA's used in these experiments were prepared from Illinois No. 6 coal by oxidation with nitric acid followed by extraction with NaOH (13). The different batches were designated by their date of preparation and were stored in plastic bottles under slightly alkaline conditions. The HA's were characterized with regard to their gravimetric concentration (mg dry weight/ml) using a straightforward technique (14). Also, the hydrogen exchange capacity was determined by potentiometric titration; and the Cu(II) exchange capacity was determined by adding excess $CuSO_4$ at p*H* 5.0, filtering off the copper humate, and titrating an aliquot of the filtrate with EDTA (14). Prior to equilibration with Cu^{2+} at low p*H*, the p*H*-dependent solubility behavior of each HA was determined to ensure that the equilibration experiments would be performed at p*H*'s where the HA was insoluble.

I. Procedure for the Determination of the Precipitation pH

A series of tared 15 cm^3 centrifuge tubes was filled with 8.00 ml of sodium humate (NaHA) from a single batch. The p*H*'s of the humate solutions were adjusted to p*H* values between 8 and 2 at 0.3–0.5 p*H* intervals with HCl and NaOH allowing 15 min equilibration time. The adjusted solutions were centrifuged for 0.5 h and the liquid decanted. The entire collection of tubes was vacuum dried and weighed. A plot of mg dry solid vs. p*H* described the solubility behavior of the given batch of HA.

II. Procedures for Cu(II) Binding at Low pH's

A. Equilibration of HA and Cu(II) at Low pH's

The equilibration experiments were carried out in the following manner. Two millilitres of NaHA was pipetted into each of several vials. Various amounts of standard copper solutions were measured into the vials in order to obtain the desired concentrations of Cu(II). Deionized water was added to make the total volume of 10 ml. Then, the entire series of solutions was adjusted to within 0.02 units of the desired p*H* with small additions of HCl or NaOH. The samples were analyzed for soluble Cu after standing overnight by centrifuging, removing an aliquot of the clear liquid, diluting if necessary, followed by atomic absorption analysis. In a few samples (especially at low concentrations of Cu^{2+} and at p*H* 3), incomplete HA precipitation after centrifugation was observed. In those cases, approximately 0.05 g of NaCl solid was added, the solution stirred, and recentrifuged. Usually, the sample would precipitate out quantitatively after this treatment. If incomplete precipitation was still obtained, the sample was discarded.

B. Measurement of the pH Drop Upon Addition of $CuSO_4$

In order to determine if H^+ was released upon the uptake of Cu^{2+} by insoluble HA, the following procedure was followed. Five millilitres of NaHA stock was pipetted into a centrifuge tube and acidified. The solution was centrifuged and washed once. HCl and/or NaOH plus deionized water was added for p*H* adjustment and dilution, and the HA solid in the centrifuge tube was shaken vigorously until it was in suspension. The suspension was diluted to 10 ml, transferred to a beaker, and the p*H* was measured precisely. Twenty-five millilitres of standard $CuSO_4$ was added, and the new p*H* measured. Attainment of a steady p*H* was achieved in a few seconds, although this did not necessarily imply that equilibrium was reached in such a short time. After at least 1 h of equilibration, the contents of the beaker were then gravity filtered through medium porosity paper. An aliquot of the filtrate was titrated for Cu(II) using EDTA and Murexide indicator after a procedure by Flaschka (15). At the end of each series of experiments, the p*H* of the $CuSO_4$ standard solution was measured precisely. The p*H* expected on the basis of dilution of the HA with 25.00 ml of $CuSO_4$ of known p*H* assuming no interaction between Cu^{2+} and HA was calculated and compared with the observed p*H*. The hydrogen ion released (Δmmol H^+) through Cu^{2+} uptake was calculated from that p*H* difference. The cupric ion bound by the HA (Δmmol Cu^{2+}) was calculated from the initial concentration of $CuSO_4$ and the EDTA titration results. A comparison of Δmmol H^+ and Δmmol Cu^{2+} enabled determination of the extent of H^+ exchanged for Cu^{2+} bound by HA.

Results

I. pH-dependent Solubility Behavior

Figure 1 shows a typical solubility curve for coal HA's. The exact range of precipitation for a given preparation was observed to vary with the concentration of HA and the concentrations of cations present. The very narrow p*H* range between onset and completion of precipitation shown in Fig. 1 is typical of coal HA's.

II. Analytical Data

The analytical data for two different batches of HA appear in Table 1. The near equivalence of the mmol titratable H^+ and mmol Cu(II) bound at p*H* 5 for both HA's tends to support the *ortho* carboxylate–phenolate binding model mentioned in the Introduction. It should be noted, however, that Cu(II) uptake at p*H* 5 was considerably higher than at p*H*'s 1–3, and that considerable ionization of carboxylate groups on HA occurred at p*H* 5. Hence, caution is warranted in drawing analogies between Cu(II)

TABLE 1. Analytical data for two HA preparations*

Preparation date	Gravimetric concentration	Hydrogen ion exchange capacity (mmol/ml)	Hydrogen ion exchange capacity (mmol/g)	Cupric ion exchange capacity (mmol/ml)	Cupric ion exchange capacity (mmol/g)	Precipitation p*H* Onset	Precipitation p*H* Completion
9/21/73	22.2 ±0.1	0.0462 ±0.0002	2.08 ±0.02	0.0481 ±0.0002	2.16 ±0.02	4.6	3.0
5/24/74	6.55 ±0.07	0.0113 ±0.0011	1.7 ±0.1	0.0112 ±0.0004	1.71 ±0.05	4.2	3.2

*Uncertainties given are average deviations for 3–5 determinations.

TABLE 2. Ratio of HA bound and aqueous Cu(II) at three p*H*'s

Initial $[Cu^{2+}]$ (ppm)	At p*H* (±0.02): 1.37 Final $[Cu^{2+}]$ (ppm)	1.37 *X**	2.00 Final $[Cu^{2+}]$ (ppm)	2.00 *X*	3.00 Final $[Cu^{2+}]$ (ppm)	3.00 *X*
1.00	0.20	610	0.05	2900	0.20	610
2.00	0.55	400	0.14	1980	0.30	870
3.00	0.84	400	0.27	1530	0.51	750
4.00	1.35	310	0.53	990	0.40	1370
5.00	1.77	270	—	—	0.51	1340
6.00	2.37	230	0.97	760	0.80	990
7.00	2.93	210	1.32	660	0.71	1360
8.00	3.37	210	1.51	660	0.98	1100
9.00	3.65	230	1.38	840	1.11	1080
10.0	4.38	200	1.64	780	1.37	960

*$X = [Cu^{2+}]_{HA}/[Cu^{2+}]_{aq}$ (mmol/g HA *M*). A 2.00 ml HA suspension containing 65.5 mg HA was added to each sample. Total volume = 10.0 ml.

binding under the acidic conditions studied here, and at p*H*'s where HA is soluble.

III. Results of Equilibration Experiments

The insoluble HA was observed to bind significant amounts of Cu(II). This binding depended on the initial concentration of Cu(II) to a large extent and on p*H* to a smaller extent. In general, linear least-squares regression of log (mg Cu^{2+} absorbed) vs. log ($[Cu^{2+}]_0$) ($[Cu^{2+}]_0 = [Cu^{2+}]$ before absorption of Cu^{2+} by HA) yielded significantly smaller slope standard deviations than any other method of plotting the data. For example, Fig. 2 is linear within 2.02% over four orders of magnitude of $[Cu^{2+}]_0$ (0.1–700 ppm). Figures 3 and 4 show the same data plotted on linear axes. Other methods of plotting the data included attempts at fitting the Freundlich and Langmuir equations to the data, and fitting equations analogous to [1] and [2] in the Introduction. Langmuir plots were nonlinear even over small concentration ranges. Ion exchange equilibrium quotients (see [2]) were also not constant over small Cu(II) concentration ranges. The failure of ion exchange quotients is especially obvious in the relatively small p*H* dependence of Cu^{2+} uptake, as seen in Table 2. For example, eq. 2 predicts that the ratio of bound to free Cu(II) should increase 100-fold as the p*H* is raised 1 unit. However, inspection of Table 2 reveals that the ratio changes only about a factor of 4 as the p*H* increases from 1.37 to 3.00. It should be noted that the term $[H^+]_r''$ in [2] did not change significantly under conditions employed in taking data for Table 2. In other words, the H^+ exchanged from HA by 1–10 ppm Cu(II) solutions was small compared to the total H^+ capacity. Table 3 summarizes slopes and intercepts of log (mg Cu^{2+} adsorbed) vs. log $[Cu^{2+}]_0$ plots and Freundlich isotherm plots. The relative standard deviations in Table 3 show the superiority of the empirical log–log relation over the Freundlich relation for all data sets.

IV. Results Comparing Δmmol H^+ to Δmmol Cu^{2+}

Table 4 shows sample data and calculated quantities obtained from procedure II(B) in the Experimental. Surprisingly little variation in the

TABLE 3. Comparison of empirical and Freundlich linear regression analysis for HA–Cu(II) equilibration data

Empirical

Humic* acid	p*H*	Concentration range of Cu(II) (ppm)	Log (mg Cu(II) absorbed) vs. log ([Cu(II)]$_0$‡) (ppm)		
			Slope	rsd (%)	*y* intercept ± sd†
a	1.35	1–8	1.2	15.0	−2.6 ±0.1
a	2.00	0.1–700	0.83	2.02	−2.38±0.03
b	1.37	1–10	0.84	1.47	−2.09±0.01
b	2.00	1–10	0.93	1.17	−2.02±0.01
b	3.00	1–10	1.04	1.23	−2.09±0.01

Freundlich

Humic* acid	p*H*	Concentration range of Cu(II) (ppm)	Log (mol Cu(II) adsorbed/equiv. HA vs. log ([Cu(II)]$_{eq}$§) (*M*)		
			Slope	rsd (%)	*y* intercept ± sd
a	1.35	1–8	0.8	27.7	2 ±1
a	2.00	0.1–700	0.76	2.78	2.3±0.1
b	1.37	1–10	0.63	2.87	1.5±0.1
b	2.00	1–10	0.58	5.19	1.6±0.2
b	3.00	1–10	1.2	11.9	4.7±0.7

*(*a*) 1:5 diluted HA prepared 5/24/74, 2.00 ml = 13.1 mg. (*b*) Stock HA prepared 5/24/74, 2.00 ml = 65.5 mg.
†sd = standard deviation, rsd = relative standard deviation. All p*H*'s ± 0.02 units.
‡[Cu(II)]$_0$ was the initial [Cu(II)].
§[Cu(II)]$_{eq}$ was the equilibrium soluble [Cu(II)].

TABLE 4. Comparison of mmol Cu^{2+} bound and mmol H^+ released at different initial p*H*'s*

Initial p*H*	Predicted final p*H*	Observed final p*H*	Δmmol H^+ released by HA	Δmmol Cu^{2+} bound by HA
1.84 ±0.01	2.35 ±0.01	2.30 ±0.01	0.018	0.0450 ±2%
2.07	2.55	2.43	0.032	0.0454
2.41	2.83	2.57	0.042	0.0496
2.74	3.05	2.65	0.047	0.0573
3.06	3.21	2.75	0.041	0.0558

*p*H* $CuSO_4$ = 3.29, [$CuSO_4$] = 0.03468 *F*, 5.00 ml (111 ± 1 mg) of HA prepared 9/21/73 used per run.

amount of Cu^{2+} bound occurred throughout the p*H* range studied. (Variation was larger for some other HA's studied, but was never greater than a factor of 3 over three orders of magnitude of hydrogen ion concentration.) However, the considerable increase in the mmol H^+ exchanged as the initial p*H* increased shows that the Cu(II) binding mechanism approached an ion exchange type at p*H* 3 and above.

Discussion

The results clearly indicate that two major types of Cu(II) binding occur under acidic conditions: (*1*) binding where at least one proton is exchanged and (*2*) binding where no protons are exchanged. The relative importance of each type appears to be p*H* dependent. For example, Table 4 shows fairly consistent amounts of Cu(II) bound between p*H* 1.84 and 3.06, but shows considerable increase in hydrogen ion exchange with increasing p*H*. In addition, the overall increase in amount of Cu(II) bound with increasing p*H* (Table 2) tends to substantiate the idea of greater hydrogen ion exchange with increasing p*H*.

On the other hand, considerable evidence exists for Cu(II) binding without exchange throughout the p*H* range studied. For example, Table 4 shows the amount of Cu(II) bound to be always in

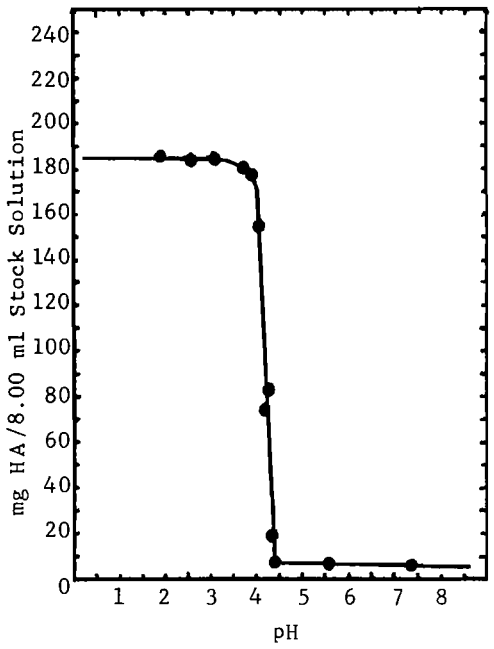

FIG. 1. Solubility vs. pH curve for HA prepared 5/30/74.

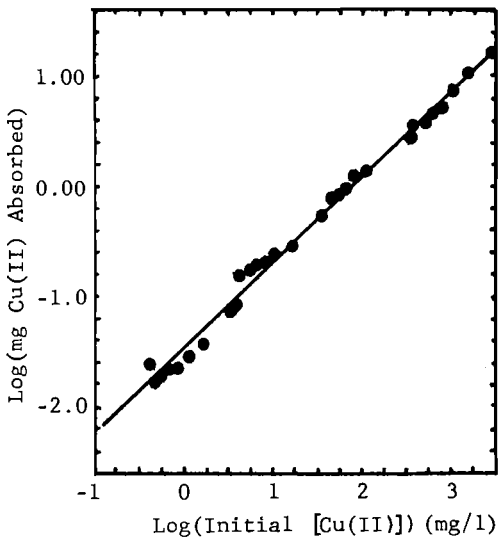

FIG. 2. Log–log plot of mg Cu(II) bound by HA vs. initial concentration of Cu(II) (HA prepared 5/24/74, pH = 2.00 ± 0.02).

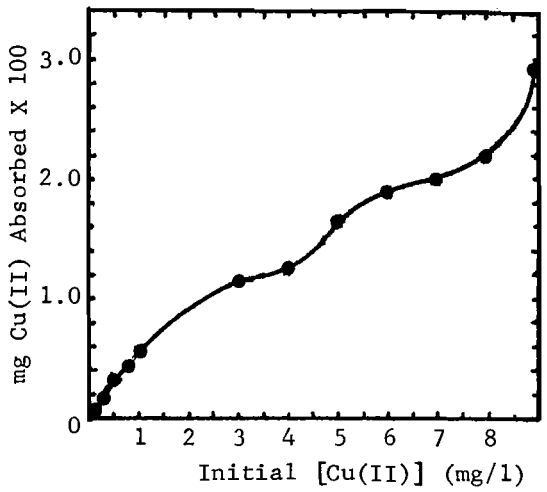

FIG. 3. Linear plot of data in Fig. 2 ($[Cu^{2+}]_0$ = 0–9 ppm).

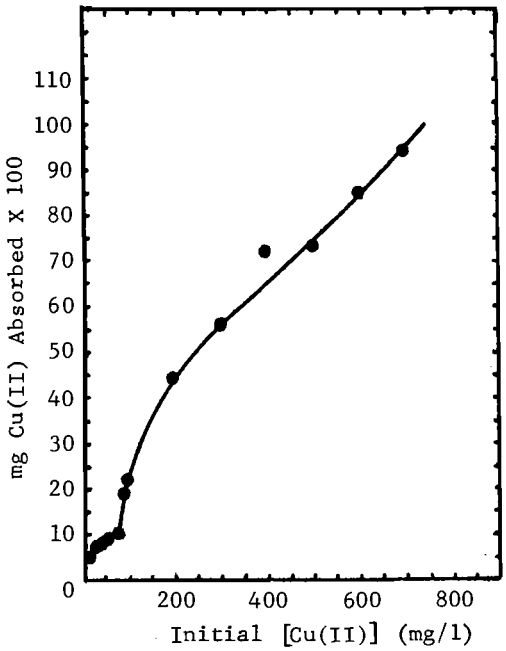

FIG. 4. Linear plot of data in Fig. 2 ($[Cu^{2+}]_0$ = 10–700 ppm).

excess of H^+ exchanged, especially at lower pH values. Also, the consistency of y intercepts obtained from the empirical least-squares fits (Table 3) indicates that nearly the same amount of Cu(II) would be bound at any pH value from 1–3 from a 1 ppm Cu(II) solution. (This conclusion follows from the fact that y intercept = log (mg Cu^{2+} absorbed) when $[Cu(II)]_0$ = 1 ppm.) Such a pH-independent uptake of Cu(II) would, of course, indicate a nonexchange mode of binding.

Since both exchange and nonexchange binding occur simultaneously, it is not surprising that neither ion exchange nor surface adsorption theory alone adequately account for the pattern

of Cu(II) uptake by HA. And, although the empirical equation described in the Results section fits the data within 2% except in one case (see Table 3), it unfortunately yields no direct clues to the mechanism(s) of the HA–Cu(II) interaction. However, the fact that the Cu(II) bound by HA can be related to the initial concentration of Cu(II) present does suggest at least one model which is consistent with that fact plus the observations mentioned above.

I. Proposed Binding Model

The fact that HA can be precipitated by adding hydrogen ion or other cations indicates that they are important links in the intermolecular bonding resulting in HA flocculation. The importance of hydrogen bonding in HA structure has been widely recognized (1, 16, 17), but the similar influence of metal cations has only recently become apparent in the literature. For example, substantial molecular size increases with increasing hydrogen ion (18, 19) and/or other cation (20) concentrations indicate their intermolecular bridging function. Formation of metal ion linked molecules is also consistent with recent complexation studies (21, 22). Thus, it appears that if aggregation occurs beyond a given point for HA, flocculation is induced and a solid HA results. Intuitively, the concentration and chemical properties of a given cation should determine the extent to which it participates in intermolecular bonding between flocculated HA molecules. For example, calcium ion is much more effective than magnesium or sodium ions in flocculating HA (23). The concentration dependence for intermolecular bonding by a given ion is suggested by the following example. Addition of excess cupric ion to NaHA at p*H* 5 causes precipitation of Cu(II)–humate; and evidence such as Table 1 indicates that most hydrogen ions are displaced from HA by Cu(II). However, addition of excess Cu(II) to NaHA at p*H* 4.5 (assuming that the HA is soluble at that p*H*) also causes precipitation of HA; yet the Cu(II) bound is less than that at p*H* 5.0.[3] Assuming that approximately the same number of bridge bonds are formed in each case, the obvious conclusion is that the p*H* 4.5 precipitate is a mixed hydrogen–copper linked floc.

Given the above points, one can postulate that the same process is operable in the p*H* range 1–3. Hence, the pattern of Cu(II) binding observed can be explained in terms of Cu(II) and H^+ competition for intra- and for intermolecular bonding in the HA solid. At low p*H*'s and low [Cu(II)], hydrogen bonding is the dominant form of bonding. Cu(II) incorporated in HA under these conditions is largely without ion exchange and thus is most likely to be at sites where hydrogen bonding does not occur. At higher p*H*'s and [Cu(II)], it appears that Cu(II) replaces hydrogen bonding at many sites as evidenced by the observed increase in H^+ exchange and Cu(II) uptake under those conditions. Incorporation of Cu(II) may involve changes in floc structure, which is suggested by the stair-step pattern evident in Figs. 3 and 4. That is, Cu(II) uptake levels off until sufficient amounts are present to cause a shift in floc structure, which allows for increased Cu(II) absorption. Thus, the empirical relation between the Cu(II) bound by HA and the initial concentration (amount) of Cu(II) present can be explained in terms of HA forming a solid structure which best utilizes available H^+ and Cu^{2+} for bonding.

The observed deviation of Cu(II) uptake from that predicted by ion exchange theory is consistent with the above model. For example, if the hydrogen on a carboxylate group is bonded to another polar group on the same or another HA molecule, two bonds must be broken in order for the Cu(II) ion exchange to occur. Because of its increased size and charge, the incorporation of Cu(II) in place of H^+ may also necessitate a shift in HA structure. Finally, a multiple intra- or intermolecular Cu(II) bond may form in place of the hydrogen bond, along with the added possibility of HA bonding with Cu(II)'s waters of hydration or other coordinated ligands. Thus, such a complicated exchange would not be expected to follow a simple ion exchange quotient (eq. 2). In light of the model, deviation from surface adsorption theory is not surprising since incorporation of Cu(II) is not a surface type of phenomenon. Surface chemistry concepts such as 'adsorbed monolayer,' etc. do not apply.

The last feature of the model is the question of anion incorporation into the HA floc to maintain the electrical neutrality of the precipitate. Since all evidence indicates that on the average at most one proton is exchanged for each Cu^{2+} incorporated into HA, anions must accompany the bound copper. Chloride ion was present in all samples, and thus was probably incorporated

[3]Typical values are 0.0426 (p*H* 4.93) and 0.0353 (p*H* 4.34) mmol Cu(II) bound/ml HA.

into the floc. Bergseth *et al.* (24) have shown that $SrCl^+$ instead of Sr^{2+} was bound by humus, hence it seems reasonable that $CuCl^+$ was also bound.

II. Comparison of Findings with Previous Work

The 'binding model' presented here incorporates the concepts of ion exchange and adsorption, but goes beyond both in that cupric ion is assumed to be an integral part of the HA structure. The findings presented here are consistent with some previous work, yet contradict other papers. For example, Davies *et al.* (5) also found that ion exchange quotients were not constant in their work with Cu(II) and HA, but explained the variation in terms of different functional groups on HA having different affinities for Cu(II). From this work, it appears that variation of Cu^{2+} binding by HA would be more p*H* dependent than actually observed if variation was simply due to interaction with carboxylate groups with different acidities, for example. Guy *et al.* (7) observed no Cu^{2+} binding in the p*H* range studied here; this may be due to differences in HA's used in the two works. Porphyrin rings in HA have also been implicated in the binding of small amounts of Cu(II) (25). The importance (or existence) of such in our HA preparations is unknown; however, infrared spectra of the coal HA's indicate that most of the N is in the form of nitro groups. Participation of nitro groups in hydrogen and metal ion bonding is likely, but as yet unconfirmed.

Acknowledgement

The financial support of the U.S. Department of the Interior Office of Water Research and Technology matching grant B-115-MO is acknowledged.

1. M. Schnitzer and S. U. Khan. Humic substances in the environment. M. Dekker, NY. 1972.
2. S. E. Manahan. Environmental chemistry. 2nd ed. Willard Grant, Boston, MA. 1975.
3. H. Van Dijk. Geoderma, **5**, 53 (1971).
4. M. Schnitzer and S. Skinner. Soil Sci. **99**, 278 (1965).
5. R. I. Davies, B. R. Singh, and A. Stuanes. J. Soil Sci. **20**, 65 (1969).
6. A. Szalay. Geochim. Cosmochim. Acta, **28**, 1605 (1964).
7. R. D. Guy, C. L. Chakrabarti, and L. L. Schramm. Can. J. Chem. **53**, 661 (1975).
8. R. Riffaldi and R. Levi-Minzi. Water Air Soil Pollut. **5**, 179 (1975).
9. Gr. Eskenazy. Fuel, **46**, 187 (1967).
10. Gr. Eskenazy. Fuel, **51**, 221 (1972).
11. S. U. Khan and R. Mazurkewich. Soil Sci. **118**, 339 (1974).
12. D. O. Hayword and B. M. W. Trapnell. Chemisorption. Butterworths, London. 1964.
13. J. B. Green and S. E. Manahan. J. Inorg. Nucl. Chem. In press.
14. J. B. Green. M.A. Thesis, University of Missouri-Columbia, Columbia, MO. 1975.
15. H. Flaschka. Mikrochem. Ver. Mikrochim. Acta, **39**, 38 (1952); **40**, 42 (1952).
16. D. S. Orlov, Yd. M. Ammosova, and G. I. Glebova. Geoderma, **13**, 211 (1975).
17. M. Schnitzer and S. M. Griffith. Can. J. Soil Sci. **55**, 491 (1975).
18. R. L. Wershaw and D. J. Pinckney. U.S. Geol. Surv. Prof. Pap. 750-D, pp. D216–8 (1971).
19. W. A. J. Flaig and H. Beutelspacher. Proc. Symp. Use Isot. Radiat. Soil Org. Mat. Studies. International Atomic Energy Agency, Vienna. 1968. pp. 23–30.
20. A. Ramunni and F. Palmieri. Agrochimica, **19**, 224 (1975).
21. F. J. Stevenson. Environ. Biogeochem., Proc. Int. Symp., 2nd ed., 1975. Vol. 2. *Edited by* J. O. Nriagu. Ann. Arbor Sci., Ann Arbor, MI. 1976. pp. 519–540.
22. F. J. Stevenson. Soil Sci. **123**, 10 (1977).
23. J. M. Eckert and E. R. Sholkovitz. Geochim. Cosmochim. Acta, **40**, 847 (1976).
24. H. Bergseth. Colloid Polym. Sci. **252**, 555 (1974).
25. B. A. Goodman and M. V. Cheshire. Nature (London) New Biol. **244**, 158 (1973).

Nuclear magnetic resonance studies of the solution chemistry of metal complexes. XIV. The aqueous chemistry of trimethyllead(IV) and its carboxylic acid complexes

T. L. SAYER, S. BACKS, C. A. EVANS, E. K. MILLAR, AND D. L. RABENSTEIN

Department of Chemistry, University of Alberta, Edmonton, Alta., Canada T6G 2G2

Received March 14, 1977

T. L. SAYER, S. BACKS, C. A. EVANS, E. K. MILLAR, and D. L. RABENSTEIN. Can. J. Chem. **55**, 3255 (1977).

The aqueous solution chemistry of the trimethyllead(IV) species and the trimethyllead(IV) complexes of six carboxylic acids of pK_a values ranging from 2.75 to 4.95 has been investigated by proton magnetic resonance spectroscopy. Equilibrium constants for the reaction of $(CH_3)_3Pb^+$ with hydroxide ion to form $(CH_3)_3PbOH$ and $((CH_3)_3Pb)_2OH^+$, and the formation constants of the carboxylic acid complexes were determined from the pH dependence of the chemical shift of the methyl protons of trimethyllead. The formation constants of the complexes increase as the pK_a of the ligand increases. The lead-207–proton coupling constant was found to be insensitive to complexation.

T. L. SAYER, S. BACKS, C. A. EVANS, E. K. MILLAR et D. L. RABENSTEIN. Can. J. Chem. **55**, 3255 (1977).

On a étudié par résonance magnétique du proton la chimie aqueuse des solutions d'espèces triméthylplomb(IV) et de complexes triméthylplomb(IV) de six acides carboxyliques de pK_a se situant de 2.75 à 4.95. Les constantes d'équilibre pour la réaction de l'espèce $(CH_3)_3Pb^+$ avec l'ion hydroxyde pour former $(CH_3)_3PbOH$ et $((CH_3)_3Pb)_2OH^+$ ainsi que les constantes de formation des complexes d'acid carboxylique ont été déterminées à partir de la dépendance du pH du déplacement chimique des protons méthyliques du triméthylplomb. Les constantes de formation des complexes augmentent à mesure que croit la valeur des pK_a. Il apparaît que la constante de couplage proton–plomb-207 soit insensible à la complexation.

[Traduit par le journal]

Introduction

Inhalation or absorption of tetraalkyllead compounds results in the presence of lead in the fluids and tissues of the body, primarily as dissolved trialkyllead salts (1). Also, recent research by Wong, Chau, and Luxon (2) has revealed the methylation of certain organic and inorganic lead compounds by microorganisms in lake sediments. Although the organometallic chemistry of the trialkyllead compounds has been the subject of much study (3–6), their aqueous solution chemistry and coordination chemistry have not been characterized. In response to the need for such information, we have initiated a program directed towards characterizing the aqueous solution chemistry of trimethyllead and its complexes. For example, chelation therapy, a common form of treatment for inorganic lead poisoning (7), has thus far proven to be rather ineffective in the treatment of organic lead poisoning because of the lack of an effective chelating agent for organic lead salts (1).

In this paper, results are presented which provide the first characterization of the aqueous solution species and equilibria of $(CH_3)_3Pb^+$ and of the coordination chemistry of $(CH_3)_3Pb^+$ with carboxylic acid ligands.[1] The equilibrium constants for the acid–base equilibria of $(CH_3)_3Pb^+$ and the formation constants of the carboxylic acid complexes were determined by proton magnetic resonance spectroscopy. ^1H nmr is a direct method for studying the solution chemistry of $(CH_3)_3Pb^+$ and its complexes; the chemical shift of the methyl protons of $(CH_3)_3Pb^+$, the coupling constant for spin–spin coupling between ^{207}Pb ($I = \frac{1}{2}$, natural abundance = 21.1%) and the protons of the methyl group, and the chemical shift of the ligand protons all provide information about the complexes at the molecular level. The type of detailed information ^1H nmr can provide about the binding of organometallic ions by polydentate biological ligands is illustrated by the study of the binding of methylmercury by glutathione (8).

[1]For simplicity, waters of hydration are omitted from the formula throughout this paper. Hydrated $(CH_3)_3Pb^+$ is assumed to be trigonal bipyramidal with water molecules in the axial positions.

Experimental

Chemicals

The carboxylic acids were of the highest grade commercially available and were used without further purification. Sodium formate was used as the source of formate ligand. The trimethyllead – acetic acid studies were carried out using trimethyllead acetate (Alfa Inorganics) as the source of both $(CH_3)_3Pb^+$ and acetate.

Trimethyllead acetate was the only water soluble form of trimethyllead commercially available and was converted to a stock solution of trimethyllead perchlorate prior to use in the acid–base and complexation studies. An initial attempt to extract $(CH_3)_3PbOH$ from benzene, using a method developed for triethyllead chloride (9), yielded only an insoluble, gelatinous mass of unknown composition. Ion exchange has been used to remove acetate from methylmercuric hydroxide solutions (10), and a similar method was developed for the conversion of $(CH_3)_3PbO_2CCH_3$ to trimethyllead perchlorate.

A solution of trimethyllead acetate ($\sim 0.25\ M$) was passed two or three times through a column containing anion exchange resin (Dowex 2 × 8) in the hydroxide form. The column was regenerated between passes with 1 *M* NaOH. The ^1H nmr spectrum, at high amplitude, of an aliquot was then checked to ensure the absence of acetate (in basic solution the resonance of the methyl protons of acetate is located approximately 0.67 ppm downfield from the *tert*-butyl resonance of tertiary butanol and is detectable at concentration levels of $\gtrsim 0.001\ M$). The solution was filtered twice through Nalgene filter units, 0.2 μm pore, and then neutralized with concentrated perchloric acid (to p*H* ~ 5) and stored in the dark. Before use, this solution was standardized as described below.

pH Measurements

All p*H* measurements were made at 25 ± 1°C using an Orion Model 701 digital p*H* meter equipped with a standard glass electrode – porous ceramic junction electrode pair. Initially a saturated calomel reference electrode was used; to avoid precipitation of $KClO_4$ in the liquid junction, electrical contact between the solution and the reference electrode was made in a salt bridge containing 4.0 *M* NaCl solution. In later experiments, Na_2SO_4 was used as the reference solution in a Ag/AgCl electrode. The p*H* meter was calibrated using Fisher certified standard solutions of p*H* 4.01, 7.00, and 10.00.

^1H Nuclear Magnetic Resonance Measurements

^1H nmr spectra were obtained on a Varian A-60-D high resolution spectrometer at a probe temperature of 25 ± 1°C. Spectra were recorded at sweep rates of 0.1 Hz s^{-1}. Reported results are the average of 2–3 scans. Chemical shifts were measured relative to the *tert*-butyl resonance of *tert*-butanol (TBA) or the central resonance of the tetramethylammonium (TMA) cation, but are reported relative to the methyl resonance of sodium 2,2-dimethyl-2-silapentane-5-sulphonic acid (DSS). Positive shifts correspond to resonances of protons less shielded than the methyl protons of DSS. The *tert*-butyl resonance of TBA is 1.243 ppm downfield from the methyl resonance of DSS; the central triplet of the methyl resonance of TMA is 3.175 ppm downfield from DSS.

Solution Preparation

(i) ^1H Nuclear Magnetic Resonance Studies

Solutions for the ^1H nmr studies were prepared from an aliquot of stock $(CH_3)_3PbClO_4$ solution and the appropriate amount of sodium perchlorate and/or carboxylic acid. All solutions were prepared using doubly distilled water.

For the studies of the acid–base chemistry of trimethyllead, the initial sample was taken at a p*H* no higher than 5. Samples were taken approximately every 0.3 p*H* unit to a maximum p*H* between 11 and 12. The ionic strength was kept constant at 0.3 *M* with $NaClO_4$.

The initial p*H* of the $(CH_3)_3Pb^+$ – carboxylic acid solutions was reduced to a value about 3.0 p*H* units below the pK_a of the acid in order to obtain the chemical shift of the fully protonated acid and of the free $(CH_3)_3Pb^+$ ion. For acids with a pK_a below 3.75, a minimum p*H* of 0.75 was used. Samples were taken every 0.3 of a p*H* unit to a p*H* value 3.0 p*H* units above the pK_a of the acid and then every p*H* unit to a maximum p*H* of 11.00.

All p*H* adjustments were made with concentrated $HClO_4$ or carbonate-free NaOH solution. The temperature was maintained at 25 ± 1°C using a water bath.

(ii) Standardization of Trimethyllead Stock Solutions

The ion exchanged $(CH_3)_3Pb^+$ stock solutions were standardized by potentiometric titration using a glass electrode. The titrations were carried out using carbonate-free NaOH and the ionic strength was controlled using $NaClO_4$. To ensure complete neutralization of all the $(CH_3)_3PbOH$ present in solution, the initial p*H* was reduced to a value between 2 and 3 using concentrated $HClO_4$. The solution is thus a mixture of a strong acid ($HClO_4$) and a weak acid ($(CH_3)_3Pb^+$) and the titration yields two inflection points. Titration of the added perchloric acid yields a sharp inflection point at p*H* 5 and the $(CH_3)_3Pb^+$ an inflection point at p*H* 10.5. The exact position of the $(CH_3)_3Pb^+$ endpoint was determined using a second derivative plot of the titration curve (11). The titration with base converts the trimethyllead from $(CH_3)_3Pb^+$ to $(CH_3)_3PbOH$, so that the amount of NaOH added between the first and second endpoints provides the concentration of trimethyllead in the stock solution.

The potentiometric method was verified by determining the trimethyllead concentration of several stock solutions using both atomic absorption spectroscopy, and EDTA titration of aliquots following conversion to Pb^{2+}.

The atomic absorption measurements were made at the 282.3 nm line using a Perkin-Elmer 290-B atomic absorption spectrophotometer. A working curve was prepared using $Pb(NO_3)_2$ and a 0.1 *M* solution of the disodium salt of ethylenediaminetetraacetic acid was used as a common matrix. Standard solutions were prepared containing 10–40 μg/ml of lead and an aliquot of the trimethyllead stock solution was diluted to yield a solution of approximately 20–30 μg/ml of lead. Although the atomic absorption results tended to be slightly higher than the trimethyllead concentrations obtained by potentiometry, the agreement is sufficient to support the potentiometric standardization.

Further confirmation of the validity of potentiometric titrations as a convenient and rapid method of standardiz-

ing the $(CH_3)_3PbClO_4$ stock solutions was obtained from EDTA titrations of the $Pb(NO_3)_2$ solutions resulting from digestion of portions of the stock solution with aqua regia. Aliquots (typically 5.00 ml) of the stock solution were digested with aqua regia (15 ml) and then with nitric acid to remove chloride which causes separation of $PbCl_2$. The solution was adjusted to about neutral with solid sodium hydroxide, and the aliquots titrated with standard EDTA, using hexamine and xylenol orange indicator (12).

Results and Discussion

The Stability of Trimethyllead in Aqueous Solution

The stability of the carbon–lead bonds towards hydrolysis has been considered to establish that the trimethyllead moiety is stable on the time scale of these experiments. Acidic, neutral, and alkaline solutions of trimethyllead were tested periodically for the presence of Pb(II) using chemical spot tests. Sodium rhodizonate was used as detailed by Feigl and Anger (13), and is sensitive to inorganic lead at concentrations greater than approximately 10^{-4} *M*. The results, after 7 months of monitoring, indicate that the concentration of inorganic lead is not greater than 10^{-4} *M* in solutions at neutral or alkaline p*H* and is approximately 10^{-3} *M* in solutions at p*H* 1.0 and 2.0.

The Acid–Base Chemistry of Trimethyllead

The acid–base chemistry of trimethyllead has been characterized by fitting of proton magnetic resonance data to various acid–base models. The chemical shift of the methyl protons is given by the position of the central resonance and the lead–proton coupling constant by the separation of the satellite lines. A typical spectrum is shown in Fig. 1. Both of these quantities are p*H* dependent; the variation of the chemical shift as a function of p*H* is shown by the bottom curve in Fig. 2, and the variation of the coupling constant in Fig. 3. This p*H* dependence is caused by formation of hydroxyl complexes as the p*H* of an acidic solution is increased above ca. p*H* 6. There is no evidence for the addition of more than one hydroxide ion per trimethyllead cation up to p*H* 12, at which point essentially all of the trimethyllead has been converted to $(CH_3)_3PbOH$.

Of various models tested, the best fit was obtained with the model described by eqs. 1–4,

[1] $$(CH_3)_3Pb^+ + OH^- \rightleftarrows (CH_3)_3PbOH$$

[2] $$K_1 = \frac{[(CH_3)_3PbOH]}{[(CH_3)_3Pb^+]a_{OH^-}}$$

[3] $$(CH_3)_3Pb^+ + (CH_3)_3PbOH \rightleftarrows ((CH_3)_3Pb)_2OH^+$$

[4] $$K_2 = \frac{[((CH_3)_3Pb)_2OH^+]}{[(CH_3)_3Pb^+][(CH_3)_3PbOH]}$$

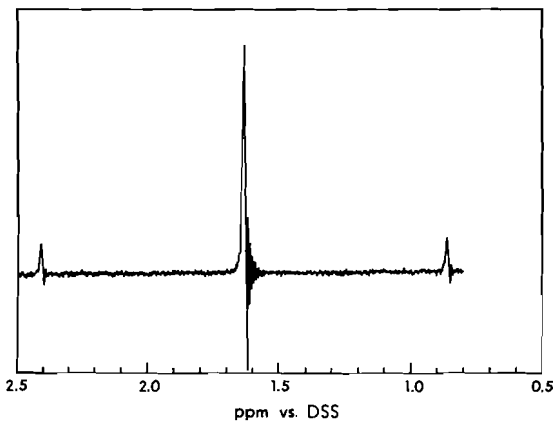

FIG. 1. ^1H nmr spectrum of the methyl groups of trimethyllead in 0.140 *M* solution at approximately neutral p*H*.

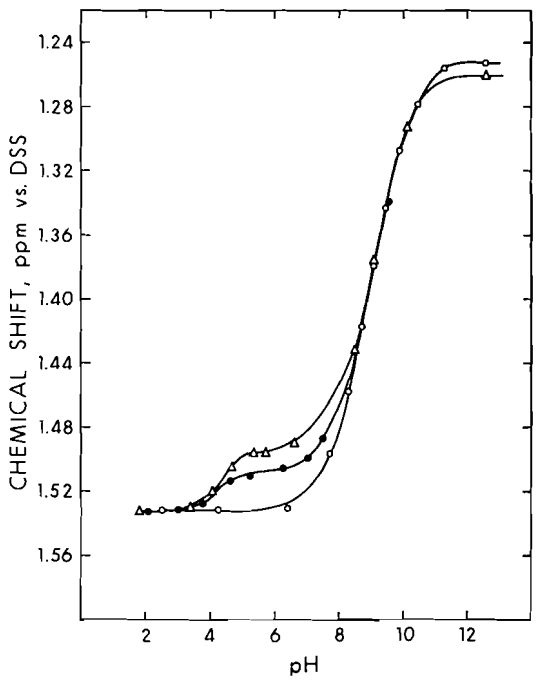

FIG. 2. p*H* dependence of the methyl protons of trimethyllead in a 0.140 *M* aqueous solution (open circles), in an aqueous solution containing 0.153 *M* trimethyllead and 0.071 *M* pivalic acid (closed circles), and in an aqueous solution containing 0.102 *M* trimethyllead and 0.093 *M* pivalic acid (triangles).

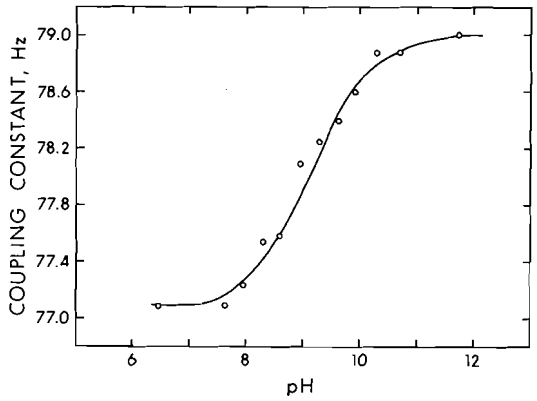

FIG. 3. pH dependence of the lead-207 – proton coupling constant in a 0.140 M aqueous solution.

where K_1 and K_2 are the formation constants for the mononuclear and dinuclear hydroxyl complexes, respectively, and a_{OH^-} represents the activity of hydroxide ion.

K_1 and K_2 were evaluated from chemical shift data of the type shown in Fig. 2. Since the exchange of the trimethyllead moiety between its various solution forms is fast on the nmr scale, the observed chemical shift (or coupling constant), δ_{obs}, is an average of the chemical shifts of the various molecular forms present in solution, weighted proportionally to their individual populations. For the system described by eqs. 1–4

$$[5] \qquad \delta_{obs} = P_a\delta_a + P_b\delta_b + P_c\delta_c$$

where a, b, and c refer to the species $(CH_3)_3Pb^+$, $(CH_3)_3PbOH$, and $((CH_3)_3Pb)_2OH^+$ respectively, P refers to the fraction of the total trimethyllead present in each of the forms, and δ is the chemical shift of that form. The fractions are defined as

$$[6] \qquad P_a = [(CH_3)_3Pb^+]/TMLT$$

$$[7] \qquad P_b = [(CH_3)_3PbOH]/TMLT$$

$$[8] \qquad P_c = 2[((CH_3)_3Pb)_2OH^+]/TMLT$$

where TMLT represents the total concentration of trimethyllead. Manipulation of these equations leads to an expression for δ_{obs}, viz.

$$[9] \qquad \delta_{obs} = P_a\delta_a + K_1a_{OH}P_a\delta_b + 2K_1K_2a_{OH}P_a^2\delta_c$$

where

$$[10] \qquad P_a = \frac{(-(1 + K_1a_{OH}) + [(1 + K_1a_{OH})^2 + 8K_1K_2a_{OH}(TMLT)]^{1/2})}{4K_1K_2a_{OH}(TMLT)}$$

K_1, K_2, and δ_c were evaluated from chemical shift data, over the pH range 0.5–13.0 and trimethyllead concentrations in the range 5×10^{-3} M to 2×10^{-1} M, using the nonlinear least-squares fitting program described by Dye and Nicely (14). δ_a and δ_b were measured directly on solutions sufficiently acidic and alkaline, respectively. The values obtained are $K_1 = 7.34\ (\pm 0.1) \times 10^4\ M^{-1}$ and $K_2 = 3.12\ (\pm 0.1) \times 10^1\ M^{-1}$, where the uncertainties are linear estimates of the standard deviation. The ionic strength was 0.3 M. The chemical shifts of the species are 1.535 ($(CH_3)_3Pb^+$), 1.253 ($(CH_3)_3PbOH$), and 1.327 ppm ($((CH_3)_3Pb)_2OH^+$), quoted from DSS.

Attempts to fit the observed chemical shift data to models involving either the species $((CH_3)_3Pb)_2O$ or $((CH_3)_3PbOH)_2$ in addition to $(CH_3)_3Pb^+$ and $(CH_3)_3PbOH$ gave poor fits. The model giving the best fit is analogous to that for methylmercury (10, 15, 16) and in view of the low value estimated for the formation constant of the oxonium species, $(CH_3Hg)_3O^+$ (16), such a species is not considered in the present system.

Because of the unsymmetrical nature of eq. 3, the importance of $((CH_3)_3Pb)_2OH^+$ is dependent on the total concentration of trimethyllead. The species distribution, calculated using the above values of K_1 and K_2 and a trimethyllead concentration of 0.100 M is shown in Fig. 4. At 0.005 M the maximum fractional concentration of trimethyllead as $((CH_3)_3Pb)_2OH^+$ is 0.07.

Carboxylic Acid Complexes of Trimethyllead

The formation constants have been derived for binding of trimethyllead by the carboxylate group of carboxylic acids with a range of acid dissociation constants. The results are listed in Table 1. Representative chemical shift data for the trimethyllead protons in the presence of a carboxylic acid are shown in Fig. 2, in this case for the trimethyllead – pivalic acid system. Qualitatively the effect of complexation can be observed as the upfield displacement of the trimethyllead resonance in the pH region below

TABLE 1. Acid ionization constants and formation constants of the trimethyllead and the methylmercury complexes of selected carboxylic acids, and the trimethyllead chemical shifts of their trimethyllead complexes

Carboxylic acid	pK_a[a]	$\delta_{Complex}$[c]	Log K_f[a,b,e] $(CH_3)_3Pb^+$	Log K_f[a,b,d] CH_3Hg^+
Pivalic	4.95	1.436	1.22	3.53
Propionic	4.80	1.449	1.08	3.37
Acetic	4.65	1.450	0.97	3.16
Formic	3.55	1.492	0.86	2.65
Acetylglycine	3.40	1.479	0.82	2.61
Chloroacetic	2.75	1.493	0.52	2.19

[a]25°C.
[b]Mixed activity-concentration constant.
[c]Chemical shift of the methyl protons of trimethyllead, ppm vs. DSS, ±0.005.
[d]From Libich and Rabenstein (10).
[e]Standard deviation 0.05, except for formic acid, 0.1.

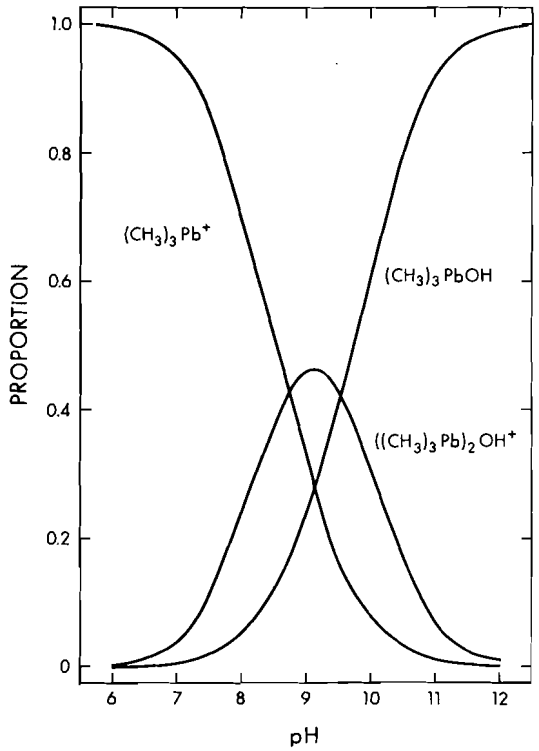

FIG. 4. pH dependence of the trimethyllead species distribution in a 0.100 M aqueous solution calculated using K_1 and K_2 as in the text.

pH 7 when the solution contains a carboxylic acid. Above pH 7 the hydroxide ion competes effectively with the carboxylate ligand for trimethyllead and by a pH of 11 the great majority of the trimethyllead is present as a hydroxide complex. The small plateau in the 1:1 plot at approximately pH 6 indicates that complexation by the pivalic acid has reached its greatest extent (43% of the trimethyllead is as the pivalate complex) in this pH region.

The formation constant of the trimethyllead–carboxylate complex is defined by eqs. 11 and 12:

[11] $$(CH_3)_3Pb^+ + RCO_2^- \rightleftarrows (CH_3)_3PbO_2CR$$

[12] $$K_f = \frac{[(CH_3)_3PbO_2CR]}{[(CH_3)_3Pb^+][RCO_2^-]}$$

Exchange of the trimethyllead moiety among the various species in solution is fast on the nmr time scale and thus the formation constant and chemical shift of the complex were determined by procedures similar to those outlined previously for the trimethyllead hydroxide equilibria.

The upper curves in Fig. 2 are described by the equation

[13] $$\delta_{obs} = P_a\delta_a + P_b\delta_b + P_c\delta_c + P_d\delta_d$$

where P_d and δ_d represent respectively the fractional concentration of trimethyllead complexed by carboxylate and the chemical shift of the trimethyllead protons of this complex, and other symbols are as defined in connection with eq. 5. In this case, the polynomial in P_a is a cubic in which the coefficients are expressions in K_1, K_2, K_a, and K_f; this was solved by an iterative method (SSP Library Subroutines, DRTMI). Values for P_b, P_c, and P_d were then calculated using modified versions of eqs. 2, 4, and 12, yielding the values for K_f and $\delta_{complex}$ listed in Table 1. The distribution of trimethyllead among the various species is shown as a function of pH in Fig. 5 for the trimethyllead – pivalic acid system.

There are no formation constants for trimethyllead complexes available for comparison

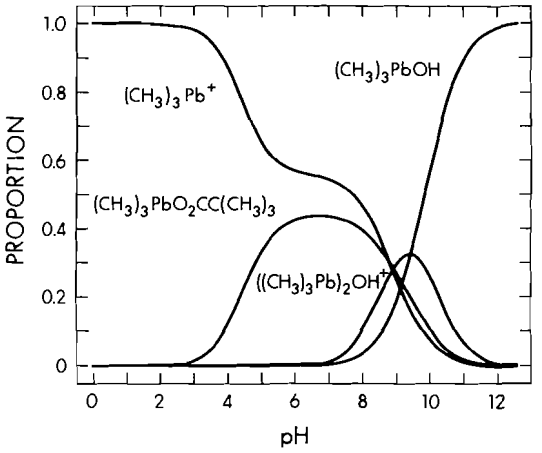

FIG. 5. pH dependence of the trimethyllead species distribution in an aqueous solution containing 0.102 M trimethyllead and 0.093 M pivalic acid.

with the results in Table 1. Comparison is made in the table with the previously reported formation constants for the methylmercury complexes of the same carboxylic acids, which are consistently larger than those for trimethyllead by a factor of approximately 10^2 (10). The logarithms of the formation constants of Pb^{2+} with formate and acetate, respectively, are reported as being 0.85 and 2.33 (17); that for formate is close to the value reported here for the trimethyllead complex.

By analogy to methylmercury (8, 10), it was expected that the ^{207}Pb–^1H coupling constant would be sensitive to complex formation. However, the coupling-constant data presented in Fig. 3 for hydroxyl complexes and the even smaller changes in $J_{^{207}Pb-^1H}$ observed for the carboxylic acid complexes indicates that the lead-207 proton coupling constant is not sensitive to the complexation of trimethyllead by the ligands studied. Any changes in the hybridization of lead, due to complexation, which involve the bond angles at the lead atom should be reflected in changes in $J_{^{207}Pb-^1H}$ (18). Shier and Drago (18) have shown, however, that $J_{^{207}Pb-^1H}$ changes from 77.5 Hz for $(CH_3)_3PbBF_4$ in water to 85.0 for $(CH_3)_3PbClO_4$ in hexamethylphosphoramide and that the change is not solely dependent upon any apparent geometrical change in the planar $(CH_3)_3Pb^+$ ion. Raman spectroscopy studies (19) have indicated that $(CH_3)_3Pb^+$ is planar in aqueous solutions of perchlorate salt. It is possible, then, that complex formation with the carboxylic acids studied does not bring about any significant change in the geometrical configuration or in the hybridization of the lead ion in trimethyllead.

Acknowledgements

This research was supported in part by a Water Resources Research Support Program Grant from the Inland Waters Directorate, Environment Canada, and by the University of Alberta.

1. H. SHAPIRO and F. W. FREY. The organic compounds of lead. Interscience Publishers, New York, NY. 1968. pp. 17–21.
2. P. T. S. WONG, Y. K. CHAU, and P. L. LUXON. Nature, **253**, 263 (1975.
3. H. SHAPIRO and F. W. FREY. The organic compounds of lead. Interscience Publishers, New York, NY. 1968. p. 248.
4. G. J. M. VAN DER KERK. Third International Conference on Lead. Vol. 3. Pergamon Press, London. 1969. p. 409.
5. M. GIELERN and M. SPRECHER. Organomet. Chem. Rev. **54**, 101 (1954).
6. I. P. BELETSKAYA, K. BUTIN, A. N. RYABTSEV, and O. H. REUTOV. J. Organomet. Chem. **59**, 1 (1973).
7. N. I. SAX. Dangerous properties of industrial materials. Reinhold Publishing Corporation, New York, NY. 1968. p. 886.
8. D. L. RABENSTEIN and M. T. FAIRHURST. J. Am. Chem. Soc. **97**, 2086 (1975).
9. G. CALINGAERT, F. J. DYKSTRA, and H. SHAPIRO. J. Am. Chem. Soc. **67**, 190 (1945).
10. S. LIBICH and D. L. RABENSTEIN. Anal. Chem. **45**, 118 (1973).
11. A. I. VOGEL. Quantitative inorganic analysis. 3rd ed. John Wiley and Sons Inc., New York, NY. 1961. p. 931.
12. A. I. VOGEL. Quantitative inorganic analysis. 3rd ed. John Wiley and Sons Inc., New York, NY. 1961. p. 443.
13. F. FEIGL and V. ANGER. Spot tests in inorganic analysis. Elsevier Publishing Co., Amsterdam, Netherlands. 1972. p. 284.
14. J. L. DYE and V. A. NICELY. J. Chem. Educ. **48**, 443 (1971).
15. G. SCHWARZENBACH and M. SCHELLENBERG. Helv. Chim. Acta, **48**, 28 (1965).
16. D. L. RABENSTEIN, C. A. EVANS, M. C. TOURANGEAU, and M. T. FAIRHURST. Anal. Chem. **47**, 338 (1975).
17. Stability constants. Chemical Society Special Publications No. 17 (1964) and No. 25 (1971). The Chemical Society, London.
18. G. D. SHIER and R. S. DRAGO. J. Organomet. Chem. **6**, 359 (1966).
19. I. R. BEATTIE. Q. Rev. Chem. Soc. **17**, 382 (1963).

^{13}C chemical shifts in medium ring and macrocyclic ketolactones

JASWANT R. MAHAJAN AND HUGO C. ARAÚJO
Universidade de Brasília, Dept. de Química, 70.000 Brasília, DF. Brasil

Received March 28, 1977

JASWANT R. MAHAJAN and HUGO C. ARAÚJO. Can. J. Chem. **55**, 3261 (1977).

Natural abundance ^{13}C Ft nmr spectra of four different series of title compounds have been examined. Unambiguous chemical shift assignments could be made for all the carbons of the 11-membered *cis*-3,3-dimethyl-5-keto-6-alkyl-8-decenolides. In the rest of the 9- to 16-membered ketolactones, unique as well as logical assignments have been made using the standard ^{13}C chemical shift rules. In the case of two benzo- and naphthoketolactone series examined, the available shielding parameters for the substituted benzenes were employed with success to the naphthalene series for the assignment of aromatic carbons.

JASWANT R. MAHAJAN et HUGO C. ARAÚJO. Can. J. Chem. **55**, 3261 (1977).

On a examiné les spectres rmn en tf du ^{13}C en abondance naturelle de quatre séries différentes de composés mentionnés dans le titre. On a pu faire l'attribution non-ambigue des déplacements chimiques de tous les carbones des diméthyl-3,3 céto-5 alkyl-6 décen-8 olides-*cis* à onze chaînons. Dans le cas des cétolactones possédant de 9 à 16 chaînons, on a pu faire des attributions aussi précises que logiques en faisant appel aux règlements standards de déplacements chimiques du ^{13}C. Dans le cas de deux séries de benzo- et naphtocétolactones qui ont été examinées, on a utilisé avec un certain succès les paramètres de blindage disponibles pour les benzènes substitués afin de faire l'attribution des carbones aromatiques en série naphthalénique.
[Traduit par le journal]

We have recently reported the synthesis of several medium ring and macrocyclic ketolactones **2**, **4**, **6**, **9** by the intramolecular reverse Dieckmann reaction of 2,2-dialkyl-1,3-cyclohexanediones (1) as well as by the oxidative procedures (2, 3), as shown in Scheme 1. These ketolactones are related to some of the macrolide antibiotics (4, 5). Recently, ^{13}C nmr spectral studies have been reported for some of the 14- and 16-membered macrolides (6, 7). It seemed likely that ^{13}C spectral examination of our synthetic polyfunctional large ring lactones would be valuable in the spectral interpretation of the more complex natural products. We now report the results of this study.

The proton noise decoupled as well as the single-frequency off-resonance decoupled (SFORD) natural abundance ^{13}C Ft nmr spectra of 0.3–1.0 *M* solutions of the ketolactone in $CDCl_3$, containing 10% TMS (v/v), were recorded on a Varian CFT-20 (20 MHz) spectrometer using standard parameters, with pulse width of 30–37.5° (8–10 μs) and aquisition time of 0.75–0.91 s, without any pulse delay. The line positions and intensities were obtained relative to internal TMS. The reported values (δ ppm) have been rounded to the nearest first decimal place for simplicity.

Results and Discussion

cis-3,3-Dimethyl-5-keto-6-alkyl-8-decenolides (2; R = CH_3, CH_2—CH=CH_2, $CH_2C_6H_5$)

The ^{13}C chemical shifts of the carbon atoms of three ketolactones examined in this series, including those of the substituent at C-6, could be unambiguously assigned on the basis of chemical shift rules (8), aided by the lower relative intensity of the quaternary carbon atom and further confirmed by the observed multiplicity in the SFORD spectra. These assignments, along with the SFORD results, are recorded in Table 1.

A close examination of Table 1 reveals that all the functionalities in these 11-membered ketolactones, except for the diversely substituted C-6, show constant chemical shifts and appear around the expected values. For instance, the observed chemical shifts for the carbonyl and lactonic carbons in these compounds, ~210.5 and 171.5 ppm, respectively, compare very favorably with the corresponding chemical shifts of 2-methylcyclohexanone (210.3) (8*a*), cycloundecanone (211.1) (8*b*) and medium to large ring lactones (172.2 ppm) (8*c*). Similarly, the C-6 substituent is expected to occupy a quasi equatorial position in the more stable conformation, e.g. **2***a*. Accordingly, the C-6 methyl group appearing at 16.8 ppm compares favorably with that of 2-methyl-

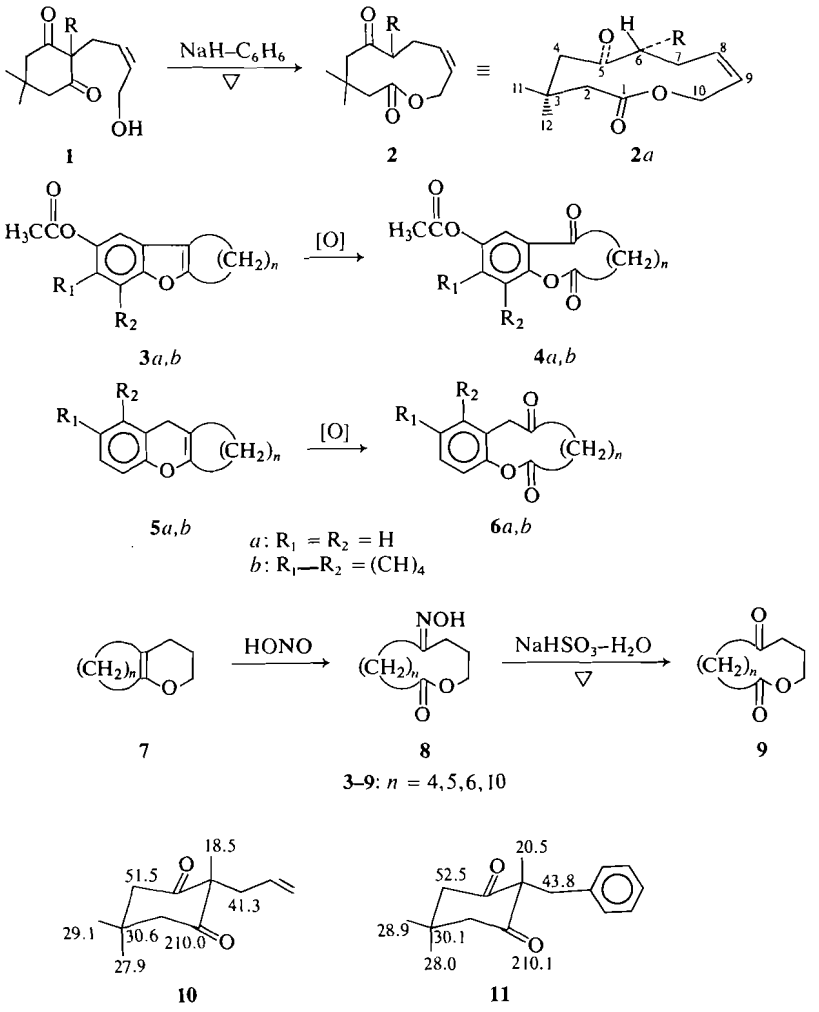

SCHEME 1

cyclohexanone at 13.8 ppm, (8*d*), bearing in mind that the 11-membered ring is more flexible than the 6-membered one. It indicates that the C-6 substituent is occupying a quasi equatorial position, partially eclipsed by the carbonyl group (9), as depicted in the chair-boat-boat conformation **2***a*. Moreover, this chemical shift of 16.8 ppm compares very favorably with that of the similarly situated methyl group at C-8 of the 14-membered (6) as well as the 16-membered (7) macrolides: erythromycin A 16.2, erythromycin B 15.6, magnamycin A 17.1, magnamycin B 17.3, tylosin 17.4, and cirramycin A 17.5 ppm, despite the greater functional complexity of these molecules.

In the case of 14-membered macrolides (erythromycins A, B) ^{1}H and ^{13}C nmr studies have suggested the presence of a single conformation in the solution of these compounds, with the ring atoms occupying cyclohexane-like positions (6). In the case at hand, a stable conformation could be represented by **2***a* and would lead to non-equivalent axial and equatorial methyl groups at C-3. The observed chemical shifts for these two methyl groups, in the three lactones, are very close to one another and are separated by only 1.1–1.5 ppm. Usually, the geminal axial and equatorial methyl groups in a frozen conformation are expected to appear about 8 ppm apart. For example, the axial and equatorial methyl groups of 1,1,3-trimethylcyclohexane appear at 25.5 and 34.3 ppm, respectively (8*e*). Similarly, the corresponding values in the case of 3,3,5-trimethylcyclohexanol are 25.7 and 33.1 ppm

TABLE 1. ^{13}C chemical shifts of *cis*-3,3-dimethyl-5-keto-6-alkyl-8-decenolides **2***a*

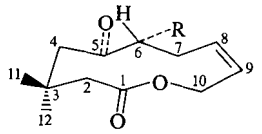

2*a*

		R[a]		
		CH_3	CH_2—CH=CH_2	CH_2—
		16.8q	35.6t, 116.9t, 135.9d	37.6t, 129.0d*, 128.4d*, 126.2d†, 139.8s
Carbon	Multiplicity[b]			
C-1	s	171.5	171.4	171.6
C-2	t	43.4	43.4	43.4
C-3	s	34.7	34.7	34.6
C-4	t	51.7	52.8	52.2
C-5	s	210.9	210.0	210.2
C-6	d	44.7	50.1	53.4
C-7	t	34.9	32.5	32.5
C-8	d	136.0	135.9	135.9
C-9	d	125.9	126.1	126.0†
C-10	t	57.3	57.3	57.4
C-11	q	30.2	30.2	30.2
C-12	q	29.1	28.9	28.7

[a]*, †: indicate interchangeable values.
[b]s = singlet; d = doublet; t = triplet; q = quartet, as observed in SFORD spectra.

(10). The small difference (1.1–1.5 ppm) between the two methyl groups in the present case could probably arise due to two factors: (*a*) the absence of hydrogen atoms at the γ-positions, which has thus eliminated the major cause of lowering the chemical shift of the axial methyl group (8*f*); and (*b*) the presence of chirality at C-6, in a conformationally equilibrating system. This reasoning is supported by examining the ^{13}C spectra of several conformationally mobile 2,2-dialkyl-5,5-dimethyl-1,3-cyclohexanediones.[1] It has been found that while the 5,5-dimethyl groups become equivalent (~28.5 ppm) in compounds bearing two identical substituents at C-2, they are separated by a small difference (~1 ppm) in the compounds bearing a chiral carbon atom. For example, the chemical shifts for the C-5′ methyls in 2-methyl-2-allyldimedone **10** and 2-methyl-2-benzyldimedone **11** are 27.9, 29.1 ppm and 28.0, 28.9 ppm, respectively. A few more chemical shifts relevant to the present case are shown along with the structures **10** and **11**.

*4-Acetoxybenzo- and 4-Acetoxynaphthoketolactones **4a,b** (Table 2)*

The ketonic, lactonic, and the acetate carbonyls as well as the methylenes adjacent to the ketone (C-α) and lactone (C-α′) carbonyls could be easily assigned due to their unambiguous and well-separated chemical shifts. The acetate methyl was distinguished from the other upfield signals as a quartet in the SFORD spectra, which also confirmed all the quaternary carbons which had been assigned on the basis of their lower relative intensities in the noise-decoupled spectra. Although there is as yet no unequivocal way of assigning all the carbons in a large cycloalkanone (9, 11) or a large-ring lactone, we have attempted to assign the remaining methylenes in the present investigation guided by the following two main arguments. Firstly, the known β-effect of a ketone (1 ppm) is smaller than that of the ester carbonyl (3 ppm), while their γ-effects are equal (−2 ppm) (12*a*); the shielding effect of the carbonyl at the γ-position (−2 ppm) cannot override the increased substitution effect at that position. Secondly, the chemical shift should increase from the β- to the γ-position, from each functional group, while the δ- and ε-carbons are expected to show a slight successive decrease and increase, in their respective values. Although relevant bifunctional model compounds have not yet been examined, the observed trends in the

[1]Our unpublished results.

TABLE 2. ^{13}C chemical shifts of 4-acetoxybenzo- and 4-acetoxynaphthoketolactones **4***a*,*b*

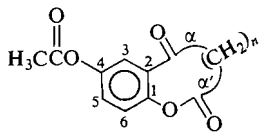

4*a*

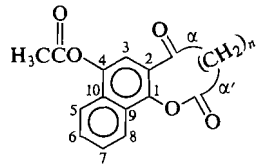

4*b*

Carbon[a]	*n* = 4	5	6	10	4	5	6	10
Ar—*C*O—	201.9	198.0	202.3	199.7	—	198.5	202.5	200.0
Ar—O*C*O—	171.7	171.6	172.0	172.2	—	172.1	172.6	172.2
CH_3CO_2—	168.9	169.0	168.9	168.9	—	169.1	169.1	169.0
C-α	41.5	39.5	40.9	41.0	—	39.1	41.1	41.2
C-α′	33.7	34.5	34.8	33.0	—	34.5	35.0	32.7
C-β	23.6	20.3	23.3	21.6	—	20.7	23.6	21.5
C-β′	24.9	22.4	23.3	22.9	—	22.0	23.6	22.8
C-γ	—	26.7	25.6	27.0	—	26.7	26.2	26.9; 25.4
C-γ′	—	—	26.1	27.1	—	—	26.4	27.2; 25.4
C-δ	—	—	—	25.5	—	—	—	25.4; 25.6
C-δ′	—	—	—	25.5	—	—	—	25.4; 26.2
C-ε	—	—	—	25.8	—	—	—	25.6; 26.9
C-ε′	—	—	—	26.1	—	—	—	26.2; 27.2
CH_3CO_2—	20.9	20.9	20.9	20.9	—	20.8	20.8	20.9
C-1* (147.9)	147.0	146.9	145.8	146.0	(147.5)	144.9	143.9	143.4
C-2* (131.2)	134.6	131.0	134.6	133.4	(128.6)	128.6	129.4	128.4
C-3 (122.1)	121.9	123.6	122.3	122.2	(119.5)	117.8	117.5	117.0
C-4* (147.9)	148.5	148.6	148.3	148.0	(147.5)	145.8	144.8	144.4
C-5 (126.0)	125.7	126.8	125.5	125.5	(125.8)	123.7	122.9	123.2
C-6 (122.1)	124.4	125.7	124.7	124.5	(127.5)	127.5	127.7	127.7
C-7	—	—	—	—	(123.6)	121.8	121.8	121.7
C-8	—	—	—	—	(129.7)	129.1	128.6	128.6
C-9*	—	—	—	—	(127.3)	126.8	128.0	128.3
C-10*	—	—	—	—	(131.2)	130.0	129.8	129.3

[a]*Indicates quaternary carbon. Calculated values in parenthesis; for explanation see text.

dibasic acids are consistent with this reasoning (8*g*). This leads to the prediction of slightly lower chemical shifts for the methylenes on the ketonic side (C-β to C-ε) than those on the lactonic side (C-β′ to C-ε′). The observed chemical shifts can thus be assigned in a self consistent way for all the polymethylenic ketolactones reported in Tables 2–4.

It is interesting to note that the highest observed chemical shifts for the aliphatic methylenes in these compounds (Tables 2–4) are very close to those in the 10- to 16-membered cycloalkanes. This could lead to an alternative way of assigning the γ–ε methylenes, assuming a decreasing shielding effect of each functional group along the chain. Thus the highest chemical shift, among the γ to ε methylenes, would be assigned to the farthest position from the functional group (C-ε and C-ε′) and the decreasing trend followed to the γ-position. These alternative assignments are illustrated only for the ketolactone **4***b* ($n = 10$), in Table 2.

The aromatic carbons of both the benzene and naphthalene series could be assigned on the basis of proton noise-decoupled and SFORD spectra, aided by the calculated values. As the required shielding parameters for substituted naphthalenes are not available (13),[2] the values reported for OAc and COC_2H_5 for the substituted benzenes (8*h*) were also used for the naphthoketolactones. The base values used for α, β, and junction carbons in the naphthalene series were 128.3, 126.1, and 133.9 ppm, respectively. The substituent was counted as *para* or *meta* to a

[2]For the ^{13}C spectra of some substituted naphthalenes (OH, OCH_3, CH_3, F, CN, and NO_2) see ref. 13 and references cited therein. We thank the referees for bringing this report to our notice.

TABLE 3. ^{13}C chemical shifts of benzo- and naphthoketolactones *6a,b*

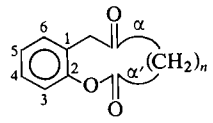

6a

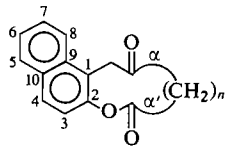

6b

Carbon[a]	*n* = 4	5	6	6 (5-NO_2)	10	*n* = 4	5	6	10	
C=O	208.4	208.8	207.5	206.4	207.1	207.8	208.7	207.7	207.8	
ArO*C*O—	170.9	170.5	171.4	170.3	171.7	171.6	171.0	171.6	172.1	
Ar—*CH_2*CO—	44.5	43.5	46.1	45.5	44.5	42.0	43.0	41.9	41.4	
C-α	42.9	42.8	41.4	41.8	41.1	41.6	37.8	39.8	40.5	
C-α′	35.1	33.7	34.7	34.8	33.6	34.8	33.4	34.9	33.7	
C-β	22.1	22.1	22.8	22.6	22.8	21.8	22.4	23.5	22.4	
C-β′	23.3	22.8	23.3	23.3	23.7	22.8	23.1	23.5	24.0	
C-γ	—	25.2	26.5	26.6	26.9	—	25.0	26.4	26.7	
C-γ′	—	—	27.0	27.3	27.0	—	—	27.0	27.0	
C-δ	—	—	—	—	25.7	—	—	—	25.9	
C-δ′	—	—	—	—	25.7	—	—	—	25.9	
C-ε	—	—	—	—	25.8	—	—	—	25.7	
C-ε′	—	—	—	—	26.0	—	—	—	26.0	
C-1* (131.8)	128.7	127.5	126.7	128.6	126.5	122.5	122.2	121.2	121.3	(131.6)
C-2* (152.3)	148.0	148.4	149.4	153.3	149.2	145.2	146.2	147.0	147.0	(149.9)
C-3 (122.5)	122.9	122.0	122.5	123.3	122.5	122.2	121.3	121.5	121.6	(120.1)
C-4 (126.6)	127.9	127.9	128.4	123.8	128.2	128.3	128.1	128.5	128.7	(126.4)
C-5 (126.5)	126.1	125.5	125.9	145.1	125.9	128.7	128.5	128.6	128.8	(126.4)
C-6 (130.3)	131.6	132.5	132.0	127.3	131.4	123.2	124.2	123.8	124.0	(124.1)
C-7	—	—	—	—	—	125.6	125.4	125.3	125.6	(124.2)
C-8	—	—	—	—	—	126.9	126.8	126.7	127.0	(126.3)
C-9*	—	—	—	—	—	132.9	133.7	133.4	133.2	(135.7)
C-10*	—	—	—	—	—	131.8	131.7	131.8	131.8	(131.9)

[a]*Indicates quaternary carbon. Calculated values in parenthesis; for explanation see text.

position in the unsubstituted part of the naphthalene molecule (C-5 to C-8), depending on whether it was conjugated or not to that position. It is gratifying to note a close correspondence between the calculated and observed chemical shifts for both the series (Table 2).

*Benzo- and Naphthoketolactones **6a,b** (Table 3)*

All the assignments in these compounds were also made on the basis established in the preceding series. The chemical shifts of benzenic and naphthalenic carbons were calculated using the available data for the closely resembling substituents, OAc and CH_3, as compiled by Wehrli and Wirthlin (12*b*). In this case, the recommended value of 128.5 ppm was used for benzene, instead of 128.7 ppm employed by Stothers (8*h*). The base values used for C-1, C-2, and C-9 of the naphthalene system were the same as in the previous case: 128.3, 126.1, and 133.9 ppm, respectively. An examination of the aromatic carbons in Table 3 reveals that, but for C-1 and C-2, there is a remarkable agreement between the calculated and observed chemical shifts. The lower observed values for C-1 and C-2 are undoubtedly, in part, due to the shielding influence of the ketonic carbonyl, which has not been taken into account, while 1,8-*peri* interactions may also contribute to the excessive shielding of the C-1 in the naphthalene series. Moreover, it is well known that the additive relationship does not work very well when the substituents are *ortho* to each other.

*Ketolactones **9** and their Corresponding Oximes **8** (Table 4)*

In these compounds, apart from the unique assignments for the carbonyl functions and the two methylenes adjacent to the lactonic carbonyl and the oxygen atom, the β-carbon in the three

TABLE 4. ^{13}C chemical shifts of ketolactones **9** and their oximes **8**

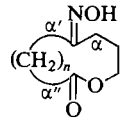

8

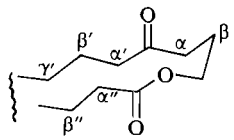

9

	$n = 4$		$n = 5$			$n = 6$		$n = 10$	
Carbon[b]	Ketone	Oxime	Ketone	Oxime[a]		Ketone	Oxime	Ketone	Oxime
CO/C=NOH	210.3	159.3	211.4	160.3	159.9	209.7	159.7	210.1	160.8
$-CO_2-$	173.0	173.7	173.3	174.4	174.1	173.4	174.1	173.3	173.8
$-CH_2-O-$	64.2	65.1	64.1	64.6	63.3	64.6	64.7	63.0	63.6
C-α	41.7	28.8	41.3	26.9	33.7	40.7	26.1	41.9	27.7
Δ	(12.9)			(14.4)	(7.6)	(14.6)		(14.2)	
C-α′	39.0	31.9	40.2	29.9	26.6	40.4	31.7	38.6	31.1
Δ	(7.1)			(10.3)	(13.6)	(8.7)		(7.5)	
C-α″	34.5	34.9	34.9	34.0	33.9	33.6	33.8	34.0	34.4
C-β	20.9	20.1	22.1	22.9	22.5	21.3	22.8	22.8	23.9
C-β′	22.8	24.5	22.3	23.1	23.0	22.8	23.2	23.6	24.9
C-β″	26.7	25.3	24.4	24.8	24.2	23.4	24.0	24.7	25.9
C-γ′	—	—	26.2	26.5	25.7	25.0	25.2	27.0	27.2
C-γ″	—	—	—	—	—	25.1	25.2	27.6	27.2
C-δ′	—	—	—	—	—	—	—	26.4	26.2
C-δ″	—	—	—	—	—	—	—	26.6	26.7
C-ε′	—	—	—	—	—	—	—	26.8	27.0
C-ε″	—	—	—	—	—	—	—	26.8	27.0

[a]Two oximes were observed only in this case and could not be separated by repeated fractional crystallization.
[b]Δ = (Chemical shift of ketone — chemical shift of oxime).

carbon chain was unambiguously assigned the highest field value, because it carries the least number of substituents among the methylenes β to the functional groups. The most difficult choice was between the two methylenes adjacent to the ketone carbonyl. However, as the three carbon chain remains constant while successive methylenes are added to the other side of the ring, one would expect comparatively constant chemical shift for the α-methylene in this chain. Thus the higher chemical shifts varying over 1.2 ppm only (40.7–41.9 ppm) were allotted to this carbon (C-α), while the upfield values (38.6–40.4 ppm) ranging over 1.8 ppm were assigned to the other methylene (C-α′). Although these assignments are arbitrary, the chemical shift comparison with the corresponding oximes (described below) seems to support them. The rest of the methylenes (γ,γ′ to ε,ε′) were assigned on arguments already elaborated in the previous two series.

In the ketoximes the α-methylenes *syn* to the oxime OH are known to be upfield by about 14–16 ppm, while the α-methylene *anti* to this hydroxyl should be shielded by only 8–10 ppm, as compared with the corresponding ketone (11). So the observed chemical shifts for the α-methylenes of the oximinolactones **8** (n = 4, 5, 6, 10) were allotted to fit the expected trend. An examination of Table 4 shows that the observed shieldings in these oximes indeed correspond very nicely to the expected values.

The shielding parameters at the β-carbons in oximes are not well defined and can be either positive or negative (11). So the rest of the methylenes were assigned to afford the closest fit to that of the corresponding ketolactone.

In conclusion, we may point out that molecular models reveal that the 9- to 16-membered ketolactones examined in the present study are conformationally very flexible molecules. It is

noteworthy that although subtle conformational changes causing slight variations in the chemical shift of certain carbons are evident in Tables 1–4, for the most part these compounds show remarkably constant values for the respective series.

Acknowledgments

This work was carried out at the Biological Sciences Division of the National Research Council, Ottawa, Canada. J. R. Mahajan thanks Dr. O. E. Edwards for the kind hospitality, research facilities, and helpful discussion and Dr. I. C. P. Smith for technical guidance and fruitful comments. Special thanks are due to both the National Research Council of Canada and Brazil (CNPq) for granting a visiting fellowship to J. R. Mahajan.

1. J. R. MAHAJAN. Synthesis, 110 (1976).
2. J. R. MAHAJAN and H. C. ARAÚJO. Synthesis, 54 (1975); 111 (1976).
3. J. R. MAHAJAN, G. A. L. FERREIRA, and H. C. ARAÚJO. J. Chem. Soc. Chem. Commun. 1078 (1972).
4. W. KELLER-SCHIERLEIN. Fortschr. Chem. Org. Naturst. **30**, 313 (1973).
5. M. BINDER and C. TAMM. Angew. Chem. **85**, 369 (1973); Angew. Chem. Int. Ed. Engl. **12**, 370 (1973).
6. S. OMURA, A. NESZMÉLYI, M. SANGARÉ, and G. LUKACS. Tetrahedron Lett. 2939 (1975).
7. S. OMURA, A. NAKAGAWA, A. NESZMÉLYI, S. D. GERO, A. M. SEPULCHRE, F. PIRIOU, and G. LUKACS. J. Am. Chem. Soc. **97**, 4001 (1975).
8. J. B. STOTHERS. Carbon-13 NMR spectroscopy. Academic Press, New York, NY. 1972. (*a*) p. 290; (*b*) p. 289; (*c*) p. 300; (*d*) p. 173; (*e*) p. 64; (*f*) p. 66; (*g*) p. 148; (*h*) p. 197.
9. F. J. WEIGERT and J. D. ROBERTS. J. Am. Chem. Soc. **92**, 1347 (1970).
10. L. F. JOHNSON and W. C. JANKOWSKI. Carbon-13 NMR spectra. Wiley-Interscience, New York, NY. 1972.
11. G. E. HAWKES, K. HERWIG, and J. D. ROBERTS. J. Org. Chem. **39**, 1017 (1974).
12. F. W. WEHRLI and T. WIRTHLIN. Interpretation of carbon-13 NMR spectra. Heyden and Sons, Ltd., London. 1976. (*a*) Table 2.5; (*b*) Table 2.13.
13. L. ERNST. Chem. Ber. **108**, 2030 (1975).

Tricyclic aromatic hydrocarbons. III. Isomerically pure *meta*-bis-annelated benzenes: a simple synthesis

M. ELAINE ISABELLE, DARRYL H. LAKE,[1] AND ROBERT H. WIGHTMAN[2]

Department of Chemistry, Carleton University, Ottawa, Canada K1S 5B6

Received March 21, 1977

M. ELAINE ISABELLE, DARRYL H. LAKE, and ROBERT H. WIGHTMAN. Can. J. Chem. **55**, 3268 (1977).

A short, general synthetic sequence has been developed, involving cycloaddition and a new decarboxylation/aromatization step, to prepare isomerically pure *meta*-bis-annelated benzenes. Some new bis annelated benzoic acids were isolated as by-products. Examples of a new decarboxylation of (annelated) benzoic acids catalyzed by Pd/C are reported.

M. ELAINE ISABELLE, DARRYL H. LAKE et ROBERT H. WIGHTMAN. Can J. Chem. **55**, 3268 (1977).

On a développé une séquence synthétique générale et courte impliquant une cycloaddition et une nouvelle étape de décarboxylation/aromatisation afin de préparer des benzènes *méta*-bis accolés isomériquement purs. Des nouveaux acides benzoïques bis accolés sont isolés comme sous-produits. On rapporte aussi des exemples d'une nouvelle décarboxylation d'acides benzoïques (accolés) qui est catalysée par le Pd/C.

[Traduit par le journal]

Introduction

Tricyclic hydrocarbons in which a central benzene ring has been fused to two saturated carbocyclic rings have been prepared for their contribution to bonding studies (1–3), as rearrangement products of macrocyclic annulenes (4) or as intermediates in the synthesis of analogues with extended unsaturation (5, 6). The two most commonly encountered configurations involving two annelations on the benzene ring are the so-called *para-* or 'linear' (**1**) and *meta-* or 'angular' (**2**) isomers, neither of which has a generally applicable synthetic approach.

Previous synthetic attempts to obtain compounds of type **2** have been rather cumbersome (7, 8), specific for one type of saturated ring (9, 10) or complicated by the presence of the corresponding linear isomer (**1**) (11, 12). One recently published approach seems best suited to *meta* annelations of small (4- or 5-membered) rings (13).

In this paper we wish to outline a four step synthetic sequence (Scheme 1) which can produce isomerically pure 'angular' hydrocarbons (**2**) with various combinations of ring sizes. We have tested ring sizes from 5–8 carbons and believe the method to be quite general. It also nicely complements the aforementioned approach for small ring compounds (13).

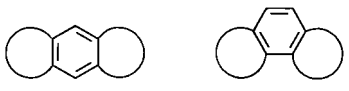

1 **2**

Results and Discussion

The General Sequence

As outlined in Scheme 1 the most direct approach to the carbocyclic skeleton corresponding to 'angular' compounds of type **2** would appear to proceed via some Diels–Alder cycloadduct, e.g. **5** or **6**, derivable from bicyclic dienes (**4**). The dienes can be obtained directly by dehydration of the corresponding diols (**3**) using phosphorus oxychloride/pyridine to avoid rearrangements (14, 15). The diols **3** are now available from the cyclanones in excellent yield by employing the titanium tetrachloride modification of the pinacol reduction as recently reported by Corey *et al.* (16). Bicyclic dienes **4** are known to react readily with a variety of dieneophiles (15, 17, 18) but it is the efficient conversion of these cycloadducts to hydrocarbons such as **2** that has presented the synthetic problem.

We have been unable to obtain practically useful conversions of the anhydrides **6** or the corresponding diacids to unsaturated hydro-

[1]Present address: Department of Chemistry, Cambrian College of Applied Arts and Technology, Sudbury, Ont.

[2]Author to whom correspondence should be addressed.

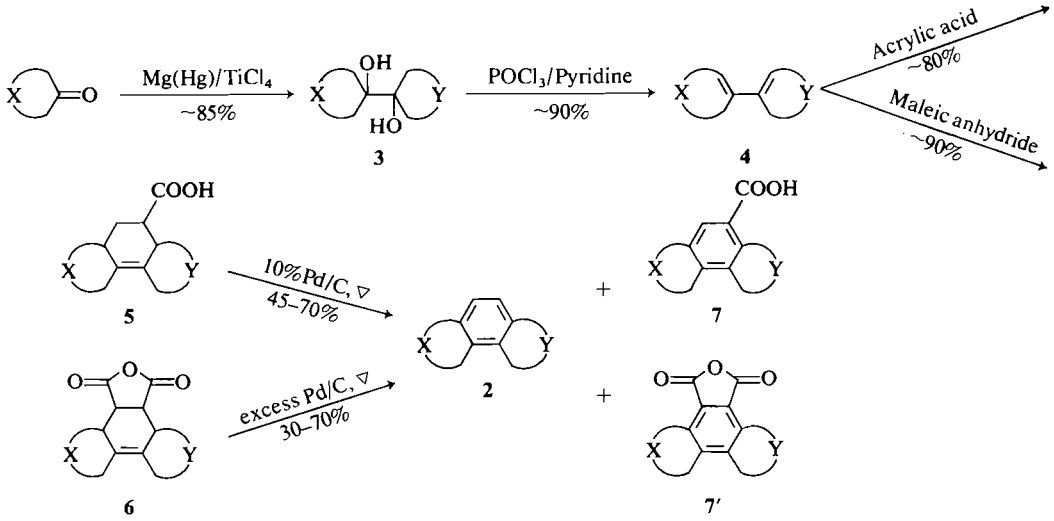

a X = Y = $(CH_2)_2$; *b* X = Y = $(CH_2)_3$; *c* X = $(CH_2)_2$, Y = $(CH_2)_4$; *d* X = Y = $(CH_2)_4$; *e* X = Y = $(CH_2)_5$

SCHEME 1

carbon products employing traditional decarboxylation reagents such as lead tetraacetate (19), electrolysis (20), or bis(triphenylphosphine)-nickel dicarbonyl (21). Similarly neither halodecarboxylation of the acids **5** with lead tetraacetate/lithium chloride (22) plus base-promoted elimination nor Diels–Alder reactions of the dienes **4** with ethylene (22) followed by dehydrogenation produced **2** in acceptable yields.

In an earlier publication we had observed that the Diels–Alder anhydride **6** could be directly converted into the corresponding 'angular' hydrocarbon **2** by pyrolytic (~350°C) decarboxylation/dehydrogenation in the presence of an excess of 10% palladium-on-carbon (11). At the time the large amounts of Pd/C seemed to preclude this method as practical for the preparative synthesis of these hydrocarbons. We now find that the monocarboxylic acids **5**, obtained from Diels–Alder addition of the dienes **4** with acrylic acid (**5***a* (18*a*), **5***b* (18*b*), **5***d* (18*c*), **5***a* and **5***b* (18*d*)), on pyrolytic decomposition with small amounts of 10% Pd/C lead directly to the isomerically pure *meta*-bis-annelated benzenes **2**. Absence of any 'linear' isomers (**1**) can be readily verified by ^{13}Cmr (23). Furthermore either of these catalytic aromatizations, i.e. of **5** or **6**, can be effected with catalyst which has been 'recovered' by simply filtering and drying in an oven at 110°C. This now makes the method economically feasible for preparative scale runs.

Reaction Parameters

A representative list of specific reaction conditions are included in Tables 1 and 2 to indicate the variations in yield of **2** (and **7**) which can be encountered by altering such parameters as substrate structure, activity (source) of catalyst, ratio of reactants, and time or temperature of reaction. However, several points should be noted.

(*a*) We have found the activity of the catalyst drops significantly during storage on the laboratory shelf interspersed with frequent usage. A brief period of heating, e.g. 110°C for 24–48 h or 300°C for 30 min, appears to rejuvenate the catalyst or suffice for recycling.

(*b*) All cyclohexane rings were completely dehydrogenated in the process, i.e. **5***b* or **6***b* produced only phenanthrene.

(*c*) An interesting variation on the method is the formation of the tetracyclic hydrocarbon **10** from diacid **9** in 25% yield via the sequence outlined in Scheme 2. In contrast the corresponding dianhydride produced no **10** on pyrolysis with 10% Pd/C and only 6% of **10** on heating with phosphorus pentoxide (24).

The above example emphasizes the conclusion that the acids **5** generally afford better conversions to **2** than the corresponding anhydrides **6**. Such 'aromatizations' have been noted before on similar types of anhydrides (ref. 17, p. 455) but we believe this to be the first report of

TABLE 1. Typical 'aromatizations' of Diels–Alder acids **5**

Substrate/weight (mg)	Weight of 10% Pd/C (mg)	Temp. (°C)/Time (min)	Yield of **2** (%) (Yield of **7** (%))
5*a*/500	100	200/30	(83)
5*a*/200	100	390/15	33
5*a*/200	40	350/30	26 (41)
5*b*/200	40	350/15	86 of phenanthrene
5*c*/200	40	390/15	44
5*d*/200	40	350/15	55–68
5*d*/200	40 (recycled)	350/15	61
5*d*/200	20	350/30	55 (10)
5*d*/200	67	300/30	55 (10)
5*d*/200	67	200/30	6 (83)
5*d*/1000	200	360/15	45 (31)
5*e*/200	40	350/30	24 (67)
5*e*/200	40	390/15	60
5*e*/500	100	200/30	(90)
7*d*/200	0	360/30	<1
7*d*/130	30	390/15	47
7*a*/200	40	390/15	13
7*e*/200	40	390/15	60
9/500	200	350/15	25 of **10**

such a process occurring directly from the cyclohexene carboxylic acids **5** with Pd/C. Additionally we report the first examples of the Pd/C catalyzed decarboxylation of aromatic acids (e.g. **7***a*,*d*,*e*). The method could be considered a viable alternate to traditional methods for aromatic decarboxylations (25) and somewhat resembles the reported Pd/C catalyzed decarboxylations of aromatic aldehydes (26). Thus the formation of **2** from **5** may well involve initial dehydrogenation to **7** followed by decarboxylation.

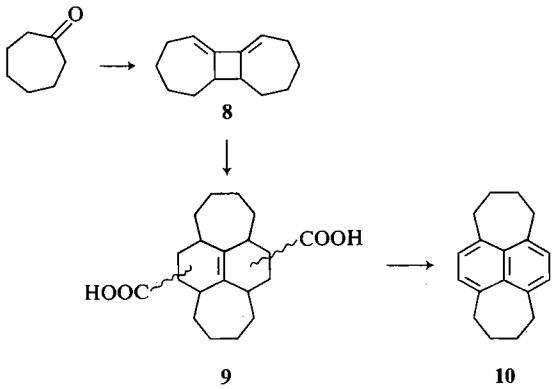

8 **9** **10**

SCHEME 2

Experimental

Melting points were obtained on a Buchi SMP-20 melting range apparatus. Infrared spectra (ν_{max} in cm^{-1}) were recorded on a Perkin-Elmer 237B spectrophotometer. Ultraviolet spectra (λ_{max} in nm (ε)) were obtained in 95% EtOH on a Perkin-Elmer–Coleman-124 spectrophotometer. ^{13}Cmr data were obtained on a Varian XL-100 (100 MHz) instrument and proton nmr spectra were recorded on a Varian T-60 (60 MHz) instrument; all values are recorded in ppm (δ) with reference to TMS. All nmr spectra were taken in $CDCl_3$ with 1% TMS. Band shape is indicated by s(singlet), d(doublet), t(triplet), m(multiplet), b(broad). Thin layer chromatography was performed using silica gel G (0.25 mm layers) on glass plates (Merck). Petroleum ether with boiling range 30–60°C was used exclusively. Microanalyses were obtained from Organic Microanalyses, Montreal, Canada, and Spang Microanalytical Laboratory, Ann Arbor, USA.

Preparation of Diols 3a–e

A typical procedure modified from the method of Corey *et al.* (16) is as follows. Magnesium turnings (24.3 g, 1.0 mol) were amalgamated and treated with $TiCl_4$ (42.7 g, 24.8 ml, 0.225 mol) at 0°C in dry THF under a nitrogen atmosphere. To this mixture at −10°C was slowly added a solution of cyclopentanone (21.0 g, 0.25 mol) and cycloheptanone (28.0 g, 0.25 mol) in THF then the cooling bath was removed and the temperature rose to 42°C over a period of 30 min, then dropped. The usual work-up produced a viscous oil (47.5 g) which contained only the diols (**3***a*, **3***c*, and **3***d*) as indicated by tlc. Such mixtures cannot be separated by conventional column chromatography (11, 14); however, the short, wide column (35 cm × 10 cm diameter) technique (27) using silica gel H (1000 g, Merck, particle size 10–40 × 10^{-6} m) and ethyl acetate – benzene (3:7 v/v) produced **3***a* (1.8 g, mp 107–109°C), **3***c* (6.3 g, mp 62–63°C), and **3***d* (4.0 g, mp 76–77°C) from 15.0 g of the crude mixed diols. Similarly **3***a*, **3***b*, **3***d*, and **3***e* could be prepared in yields ≥85% from the corresponding ketones and the crude product used directly for preparation of the dienes.

TABLE 2. Typical 'aromatizations' of Diels–Alder anhydrides **6**

Substrate/weight (mg)	Weight of 10% Pd/C (mg)	Temp. (°C)/Time (min)	Yield of **2** (%)
6*a*/200	400	350/30	30
6*a*/200	400	400/15	22
6*a*/200	67	350/30	7
6*b*/200	400	390/30	74 (phenanthrene)
6*c*/500	900	350/20	52
6*d*/200	400 (recycled)	350/30	68
6*d*/200	400	315/30	47
6*d*/200	100	350/30	54
6*e*/200	400	350/30	26
6*e*/200	400	400/15	20
6*e*/200	67	350/30	13

Preparation of Bicyclic Dienes 4a–e

Essentially the method of Greidinger and Ginsberg (15) was followed involving heating the diols with freshly distilled phosphorus oxychloride and dry pyridine. Reaction times of 2–4 h and a temperature of 90°C were found to be sufficient. Yields of the dienes (**4**) were 80–95% and as before (11, 15) the crude dienes were found to be of sufficient purity for direct use in the ensuing Diels–Alder reactions.

Preparation of Tricyclic Acids 5a–e

Following the procedure of Christol *et al.* (18) diene **4***e* (5.7 g, 0.026 mol) and acrylic acid (1.87 g, 0.026 mol) in refluxing benzene for 9 h produced unreacted diene **4***e* (1.63 g), mp 41°C, and **5***e* (4.89 g, 90% when corrected for recovered diene), mp 125°C; ir 3300–2600, 1700 (-COOH); ^{1}Hmr 11.31 (1H, bs, COOH) 2.90–1.90 (7H, bm, allylic H's), 1.90–1.00 (22H, m, all other H's). *Anal.* calcd. for $C_{19}H_{30}O_2$: C 78.57, H 10.41; found: C 78.72, H 10.30.

We have found that extended reflux times (up to 30 h) or temperatures (e.g. refluxing toluene) may be required depending on the reactivity of the dienes. Thus the following acids were prepared (mp, corrected yield, (lit.) mp): **5***a* (118–122°C, 87%, (18*a*) 128°C), **5***b* (172–176°C, 90%, (18*b*) 185°C), **5***d* (80–92°C, 92%, (18*c*), 75–90°C), and **5***c* (72%, presumably as a mixture of the two regioisomers which were not separated). The acids **5** were crystallized from petroleum ether.

Preparation of Tricyclic Anhydrides 6a–e

Again the method of Greidinger and Ginsberg (15) was employed, namely heating the dienes **4** with maleic anhydride for 2–5 h depending on the reactivity of each individual diene. Yields of anhydrides (**6**) were ≥ 85% and all compounds agreed by mp with previously reported values (11, 15).

Preparation of Hydrocarbons 2a–e and Benzoic Acids 7a–e

For specific conditions of time, temperature, and amounts, see Tables 1 and 2.

The acid **5** or anhydride **6** was intimately mixed with a certain amount of 10% Pd/C and this mixture placed in a glass tube (~50 cm × 0.10 cm diameter) open at one end. This tube was placed vertically in a preheated (usually 350–400°C) furnace (25 cm × 8 cm diameter) for a short period of time. The tube was removed, allowed to cool, and the contents rinsed out with CH_2Cl_2. The catalyst was filtered (to be oven dried at 110°C and reused), the filtrate stripped of solvent, and the crude product either separated into acidic and neutral fractions or adsorbed directly onto a short column of silica gel. The hydrocarbon **2** was eluted with petroleum ether and easily identified by ^{1}Hmr and ^{13}Cmr (23). The major by-product from **5** at lower temperatures proved to be the benzoic acid **7** which could be eluted from the column with benzene–ether (19:1 v/v). These acids were crystallized from petroleum ether and characterized as follows.

7*a*: mp 203–204°C; lit. mp 202–204°C (28); ir: 3300–2700, 1680 (aryl COOH); uv: 244 (14 833), 290 (3 300); ^{1}Hmr, 11.00 (1H, bs, COOH), 7.64 (1H, s, ArH), 2.95 (8H, m, benzylic H), 1.53 (4H, m, other H). *Anal.* calcd. for $C_{13}H_{14}O_2$: C 77.19, H 6.98; found: C 77.20, H 6.94.

7*d*: mp 141°C; ir: 330–2700, 1680 (aryl COOH); uv: 245 (2466), 288 (304); ^{1}Hmr: 11.50 (1H, bs, COOH), 7.63 (1H, s, ArH), 3.00 (8H, m, benzylic H), 1.70 (12H, m, other H). *Anal.* calcd. for $C_{17}H_{22}O_2$: C 79.02, H 8.59; found: C 79.30, H 8.58.

7*e*: mp 151°C; ir: 3300–2800, 1680 (aryl COOH); uv: 244 (8375), 298 (1175); ^{1}Hmr: 11.13 (1H, bs, COOH), 7.64 (1H, s, ArH), 2.95 (8H, m, benzylic H), 1.53 (16H, m, other H). *Anal.* calcd. for $C_{19}H_{26}O_2$: C 79.67, H 9.16; found: C 79.86, H 9.30.

Preparation of Tetracyclic Hydrocarbon 10

Tricyclic diene **8** (8.0 g, 0.022 mol) (24), acrylic acid (3.4 g, 0.061 mol), and hydroquinone (0.1 g) in dry benzene (50 ml) were heated at reflux under a nitrogen atmosphere for 54 h. After the benzene was removed and the residue triturated with petroleum ether to remove any unreacted diene, there remained an amorphous glass (10.0 g) which could not be induced to crystallize but appeared to be diacid **9** (perhaps a mixture of regioisomers) on the basis of the following spectral data; ir: 3300–2600, 1720 (COOH); nmr: 10.65 (2H, bs, COOH), 3.10–2.40 (6H, m, H α to C=C and C=O), 2.4–1.0 (16H, m, other H). When this crude diacid **9** was subjected to the usual decomposition in the presence of 10% Pd/C, the hydrocarbon **10** mp 140–142°C, lit. mp 143°C (24), could be isolated in 25% yield after chromatography on alumina (Woelm, neutral, activity I). In preparation for the reaction a concentrated solution of **9**

in CH_2Cl_2 was added to the catalyst in the reaction tube and the solvent then carefully evaporated. Specific conditions are outlined in Table 1.

Acknowledgments

We acknowledge with thanks the National Research Council of Canada which provided the operating grants to finance much of this work. Mr. David Laycock prepared the diene **8** and diacid **9**. The continued assistance of Mr. G. K. Diedrich is much appreciated. ^{13}Cmr were obtained through Dr. G. W. Buchanan, Carleton University.

1. R. T. Arnold and E. Rondestvedt. J. Am. Chem. Soc. **67**, 1267 (1945).
2. R. D. Bushick. J. Org. Chem. **33**, 4085 (1968).
3. (*a*) D. Davalian and P. J. Garrat. J. Am. Chem. Soc. **97**, 6883 (1975); (*b*) C. J. Saward and K. P. C. Vollhardt. Tetrahedron Lett. 4539 (1975).
4. J. Mayer and F. Sondheimer. J. Am. Chem. Soc. **88**, 602 (1966).
5. J. Beeby and P. J. Garrat. J. Org. Chem. **38**, 3051 (1973).
6. A. D. Campbell and S. N. Slater. J. Chem. Soc. 4353 (1952).
7. W. J. Rosenfelder and D. Ginsberg. J. Chem. Soc. 1301 (1957).
8. T. J. Katz, V. Balogh, and J. Shulman. J. Am. Chem. Soc. **90**, 734 (1968).
9. H. Rapoport and G. Smolinsky. J. Am. Chem. Soc. **82**, 1171 (1960).
10. W. F. Erman and H. C. Kretschman. Tetrahedron Lett. 1717 (1965).
11. R. H. Wightman, R. J. Wain, and D. H. Lake. Can. J. Chem. **49**, 1360 (1971).
12. R. T. Arnold and R. A. Barnes. J. Am. Chem. Soc. **65**, 2393 (1943).
13. R. P. Thummel. J. Am. Chem. Soc. **98**, 628 (1976).
14. H. Christol, A. P. Krapcho, and F. Pietrasanta. Bull. Chim. Soc. Fr. 4059 (1969).
15. D. S. Greidinger and D. Ginsberg. J. Org. Chem. **22**, 1406 (1957).
16. E. J. Corey, R. Danheiser, and S. Chandrasekaran. J. Org. Chem. **41**, 260 (1976).
17. A. S. Onishchenko. Diene synthesis. Printed by S. Monson, Jerusalem, 1964 for Israel Program for Scientific Translations Ltd. p. 446–456.
18. (*a*) H. Christol, F. Pietrasanta, and Y. Pietrasanta. Bull. Soc. Chim. Fr. 4068 (1969); (*b*) H. Christol, D. Moers, and Y. Pietrasanta. Bull. Soc. Chim. Fr. 962 (1969); (*c*) H. Christol, H. Combe, and Y. Pietrasanta. Bull. Soc. Chim. Fr. 4493 (1969); (*d*) H. Christol and M. Levy. Bull. Soc. Chim. Fr. 3056 (1964).
19. C. M. Cimarusti and J. Wolinsky. J. Am. Chem. Soc. **90**, 113 (1968).
20. (*a*) P. Radlick, R. Klem, S. Spurlock, J. Sims, E. van Tamelen, and T. Whitesides. Tetrahedron Lett. 5117 (1968); (*b*) H. H. Westberg and H. J. Dauben, Jr. Tetrahedron Lett. 5123 (1968).
21. B. M. Trost and F. Chen. Tetrahedron Lett. 2603 (1971).
22. H. Christol, H. Coombe, F. Pietrasanta, and Y. Pietrasanta. Bull. Soc. Chim. Fr. 4501 (1969).
23. G. W. Buchanan and R. H. Wightman. Can. J. Chem. **51**, 2357 (1973).
24. D. E. Laycock, R. J. Wain, and R. H. Wightman. Can. J. Chem. **55**, 21 (1977).
25. C. A. Buehler and D. E. Pearson. Survey of organic synthesis. Wiley-Interscience, NY. 1970. p. 52.
26. J. O. Hawthorne and M. H. Wilt. J. Org. Chem. **25**, 2215 (1960).
27. B. J. Hunt and W. Rigby. Chem. Ind. 1868 (1967).
28. R. T. Arnold and E. Rondestvedt. J. Am. Chem. Soc. **68**, 2176 (1946).

Sterically hindered aromatic compounds. VII. Deoxygenation of 2,5-di-*tert*-butyl- and 2,4,6-tri-*tert*-butylnitrosobenzene

L. Ross C. Barclay, Prabhaker G. Khazanie, Kenneth A. H. Adams, and Elaine Reid

Department of Chemistry, Mount Allison University, Sackville, N.B., Canada E0A 3C0

Received February 2, 1977

L. Ross C. Barclay, Prabhaker G. Khazanie, Kenneth A. H. Adams, and Elaine Reid. Can. J. Chem. **55**, 3273 (1977).

Deoxygenation of 2,5-di-*tert*-butylnitrosobenzene (**1**) by triethylphosphite gave a complex mixture containing 2,5-di-*tert*-butylaniline, 2,5,2′,5′-tetra-*tert*-butylazobenzene, *N*-(2,5-di-*tert*-butylphenyl)-α-*tert*-butyl-α-2-(5-*tert*-butylpyridyl)nitrone, and diethyl *N*-(2,5-di-*tert*-butylphenyl)phosphoramidate. In contrast deoxygenation of 2,4,6-tri-*tert*-butylnitrosobenzene (**2**) yielded mainly 3,3-dimethyl-5,7-di-*tert*-butyl-2,3-dihydroindole (80%), together with small amounts of 2,4,6-tri-*tert*-butylaniline and a product of side chain rearrangement, 2-(2-methyl-3-propenyl)-4,6-di-*tert*-butylaniline. Reaction pathways involving nitrenoid intermediates account for the various products. The different types of products from **1** and **2** are explained in terms of differential steric and conformational effects.

L. Ross C. Barclay, Prabhaker G. Khazanie, Kenneth A. H. Adams et Elaine Reid. Can. J. Chem. **55**, 3273 (1977).

La déoxygénation du di-*tert*-butyl-2,5 nitrosobenzène (**1**) par la triéthylphosphite donne un mélange complexe de di-*tert*-butyl-2,5 aniline, tétra-*tert*-butyl-2,5,2′,5′ azobenzène, *N*-(di-*tert*-butyl-2,5 phényl)-α *tert*-butyl-α (*tert*-butyl-5 pyridyl)-2 nitrone et *N*-(di-*tert*-butyl-2,5 phényl) phosphoramidate de diéthyle. Par contre, la déoxygénation du tri-*tert*-butyl-2,4,6 nitrosobenzène (**2**) conduit principalement au diméthyl-3,3 di-*tert*-butyl-5,7 dihydro-2,3 indole (80%), avec un faible pourcentage de tri-*tert*-butyl-2,4,6 aniline contenant un produit de réarrangement de la chaîne latérale, le (méthyl-2 propényl-3)-2 di-*tert*-butyl-4,6 aniline. Les sentiers réactionnels impliquant des intermédiaires nitrénoïde sont responsables des composés divers. Les différents type de produit obtenus à partir de **1** et **2** sont expliqués en terme d'environnement stérique et d'effets conformationnels.

[Traduit par le journal]

Introduction

Deoxygenation of aromatic nitro and nitroso compounds by tervalent phosphorus reagents results in reactions indicative of the presence of nitrenes as discrete intermediates. The generation and reactions of aryl nitrenes have been reviewed (1–5). They are of continuing interest in the synthesis of heterocyclic compounds (3, 6–8), and the detailed nature of the intermediates involved in reactions, such as cyclizations of 2-azidobiphenyl to carbazole, is still an interesting question (9).

Ortho tert-butyl groups are known to affect the lifetimes of various types of radicals (10, 11) in aromatic compounds. As part of our continuing study of steric influences on reactions and reactive intermediates, we have examined the steric effect of one and of two *ortho tert*-butyls on the reactions of aryl nitrenes derived from 2,5-di-*tert*-butylnitrosobenzene (**1**) and 2,4,6-tri-*tert*-butylnitrosobenzene (**2**) by triethyl phosphite deoxygenation. These conveniently exist as the monomers and preferentially with the nitroso group in the coplanar *anti* (**1**) and out-of-plane (**2**) conformations shown (12).

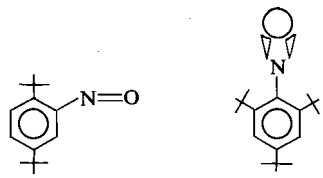

Results and Discussion

(a) Deoxygenations of 1 and 2. Analysis of Products

Deoxygenation of **1** yielded four identifiable products as illustrated in Scheme 1 and Table 1.

The major product, diethyl *N*-(2,5-di-*tert*-butylphenyl)phosphoramidate (**3**) (35%) was identified from its spectroscopic properties and hydrolysis to the known amine (**5**). The structure of the rearrangement product, the pyridine derivative or nitrone (**4**) (29%) was determined from its analytical and spectroscopic proper-

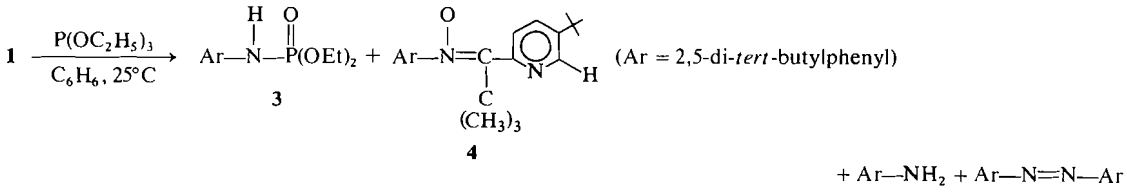

SCHEME 1

ties.[1] The elemental and mass spectroscopic data agreed with the formula $C_{28}H_{42}N_2O$. A peak at *m/e* 407 is assigned to $M - CH_3$, one at *m/e* 406 to $M -$ oxygen, and the base peak at *m/e* 365 to $M -$ *tert*-C_4H_9. The structure assigned to **4** is based mainly on its nmr spectrum, especially the low field portion of the aromatic absorption. In addition to a multiplet at 7.64 δ (5-hydrogens), a weakly coupled peak at 8.70 δ (doublet, $J \simeq 1$ Hz) is attributed to the α-H of a 2,5-disubstituted pyridine ring.

Deoxygenation of **2** with triethyl phosphite required elevated temperature and longer reaction times. However, the product mixture was not so complex as in the reduction of **1** (compare Scheme 2 and Table 2), in that reduction of **2** gave a high yield of 3,3-dimethyl-5,7-di-*tert*-butyl-2,3-dihydroindole (**7**). The cyclic amine **7** was identified by its spectroscopic properties and by preparing it through hydride reduction of 5,7-di-*tert*-butyl-3,3-dimethyloxindole (**10**), a known photolysis product from 2,4,6-tri-*tert*-butylnitrobenzene (13).

The rearranged unsaturated amine **8** is an unexpected product from the reduction of **7**. Its infrared spectrum indicated a primary amine. The structure assigned is based mainly on the nmr spectrum, especially the bands for the rearranged side chain, $Ar—CH_2—\overset{CH_2}{\overset{\|}{C}}—CH_3$ (see Experimental). The broad nature of these bands is presumably due to weak allylic coupling.

TABLE 1. Deoxygenation products of 2,5-di-*tert*-butylnitrosobenzene (**1**) by triethyl phosphite

Compound	Isolated yields[a]
3	31–35
4	31–29[b]
5	11–13
6	3

[a]The percent yields actually isolated from two separate runs by column and tlc.
[b]The yield of 4 was increased to 70% from a run using direct nmr observations.

(b) Proposed Reaction Pathways

A pathway (Scheme 3) for deoxygenation of 2,5-di-*tert*-butylnitrosobenzene through the dipolar intermediate **11** (14) should account both for products arising directly from an aryl nitrene (e.g., **3**, **5**, and **6**) and also for products of molecular rearrangement and recombination (e.g., the nitrone **4**). The amine **5** and the azo compound **6** would form from the aryl nitrene **13** by hydrogen abstraction and dimerization respectively. There is also precedent for the reaction of aryl nitrenes with triethyl phosphite to form a phosphoramidate via an *N*-aryl phosphorimidate intermediate (15); in our case for the sequence **13** → **14** → **3**.

Several suggestions have been made for the reaction pathway to account for intermolecular reactions and rearrangements of aryl nitrenes leading to pyridine derivatives (16–19). Phenylnitrene and 2-pyridylcarbene are known to interconvert, at least in the gas phase (19), and one could formulate nitrone formation as simply a combination of a 2-pyridylcarbene with a nitroso compound (i.e., in this case **18** and **1**). The exclusive formation of isomer **4** is an interesting example of the directional specificity of the rearrangement. This presumably occurs by preferential ring expansion involving migration of the *unsubstituted* carbon *ortho* to the electron deficient nitrogen. This kind of specificity has been observed before in the triethyl phosphite deoxygenation of *o*-methylnitrosobenzene (16), in the photochemical deoxygenation of aromatic nitro-compounds in triethyl

[1]Unlike a similar aryl nitrone containing an α-methyl substituent (16), nitrone **4** failed to undergo acid-catalyzed hydrolysis. The α-*tert*-butyl group of **4** evidently results in steric hindrance to nucleophilic attack at the

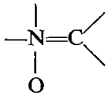

group.

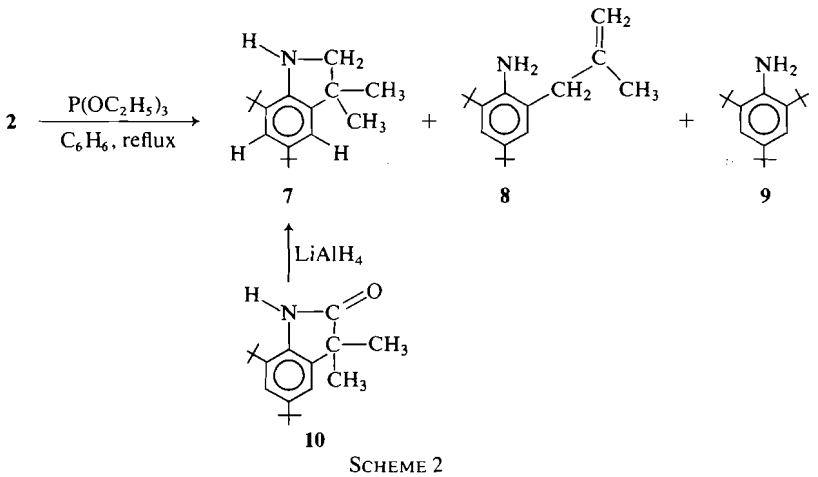

SCHEME 2

TABLE 2. Deoxygenation products of 2,4,6-tri-*tert*-butylnitrosobenzene (**2**) by triethyl phosphite

Compound	Relative yield[a]	Isolated yield[b]
7	81.3	79
8	11.4	9
9	7.3	7

[a]Determined by glc methods.
[b]Actually isolated by tlc methods.

phosphite (17), and in the photolysis of *ortho*-substituted aryl azides in diethylamine (20).

The specificity in the present deoxygenation–rearrangement of **1** may be explained on the basis of conformational or steric control. The preferred *anti* conformation for **1** is presumably retained in the more bulky dipolar intermediate (**11**). We speculate that the preferential bonding at the *ortho* site on the same side of the benzene ring as the leaving group ($(EtO)_3P{=}O$) may be a result of polarization of the *ortho* position by the electrophilic phosphorus in **11**. This could be formulated in terms of a cyclic intermediate such as **12** which could preferentially form the azirine (**15**). Alternatively **15** could be the preferred azirine simply due to steric inhibition of attack of the nitrene centre at the *tert*-butylated site-2. The rearrangement can be formulated as proceeding via ring expansion of **15** in the direction indicated leading to **16** then **17** (or **18**). Reaction of the aryl nitroso compound with the latter would yield the nitrone **4**. This pathway has the advantage of accommodating both the directional specificity and the required C-1 to C-3 shift (17).

The major product (**7**) from deoxygenation of 2,4,6-tri-*tert*-butylnitrosobenzene (**2**) resulted from reductive cyclization into an *o-tert*-butyl group. The marked difference in behaviour of **1** and **2** can be attributed to differential conformational or steric effects. The dipolar intermediate from **2** is expected to retain the out-of-plane conformation (Scheme 4, **19**). This would inhibit the coplanar conformation of the charged leaving group which may be preferred for the rearrangement of the aromatic ring, as suggested above for the deoxygenation–rearrangement of **1**. Alternatively, and more simply, the different products from **2** could be a result of steric inhibition of attack of the nitrene (**20**) at *both tert*-butylated *ortho* positions coupled with steric hindrance to intermolecular reactions, such as dimerization and reaction with triethyl phosphite. As a result, cyclization into a methyl group of an *o-tert*-butyl leading to **7** in high yield is the predominant reaction. Such cyclizations can be formulated via insertion involving an initial singlet nitrene or through hydrogen abstraction by triplet nitrene followed by radical coupling (2, 4). The latter is the suggested route to account for the cyclization yielding **7** because a radical intermediate[2] can also account for the interesting side product (**8**), where an *o-tert*-butyl group has undergone skeletal rearrangement (**21** → **22** → **8**) *leading to a nonconjugated*

[2]NOTE ADDED IN PROOF: The esr spectrum measured directly on the deoxygenation reaction of **2** showed a very persistent 1:1:1 triplet ($a_N \simeq 10.0$ G) with unresolved fine structure. This is probably due to an anilino radical of the type Ar—N̈—OR (Ar = 2,4,6-tri-*tert*-butylphenyl) formed by spin trapping of radical intermediates by unreacted **2** (see Terabe and Konaka (22)).

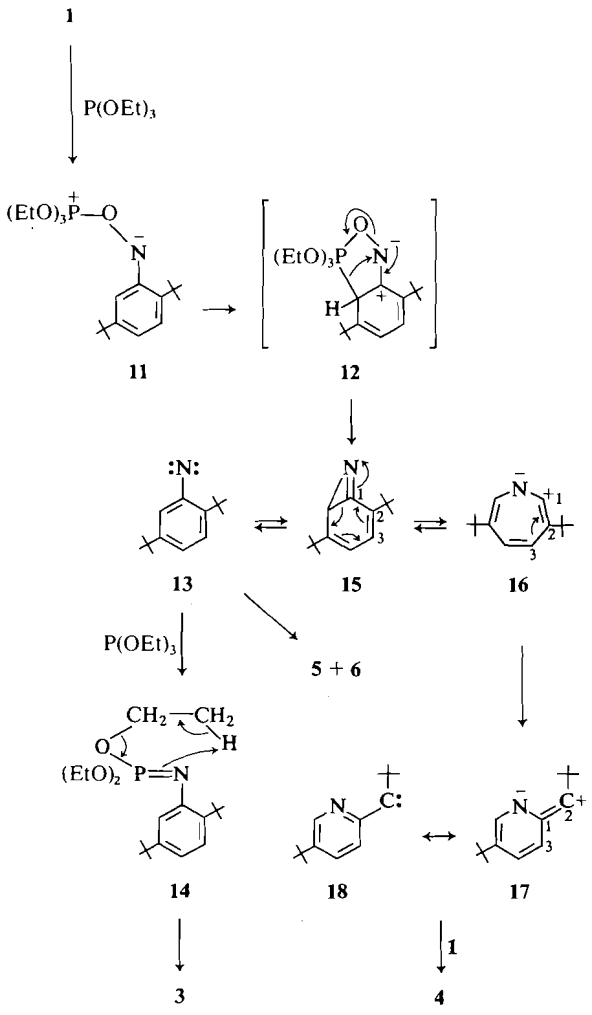

SCHEME 3

double bond in the side chain. This result provides an interesting contrast to results of Sundberg (16) who found a selectivity in H-abstracting for *ortho* alkyl aryl nitrenes derived from *o*-azidopropylbenzene pyrolysis and from triethyl phosphite reduction of *ortho* propyl or butylnitrobenzene. The formation of only the nonconjugated alkene in those cases was an argument against any mechanism involving a radical or carbonium ion at the β and γ carbon. That particular concerted pathway is not open for the intermediate **20** since it lacks a γ carbon. The formation of the nonconjugated double bond in **8** may be a result of kinetic control in elimination of hydrogen in the rearrangement **21** → **22**. Alternatively the second hydrogen atom might be abstracted from the γ position as illustrated in **23**, although the latter involves a relative unfavourable seven-membered cyclic transition state.

It is of interest to note that the nitro compounds, 2,5-di-*tert*-butylnitrobenzene and 2,4,6-tri-*tert*-butylnitrobenzene, failed to undergo triethylphosphite deoxygenations, even on prolonged treatment at elevated temperatures.

Experimental

The nmr spectra were recorded on a Varian A-60 nmr spectrometer using carbon tetrachloride solvent containing tetramethylsilane as an internal reference. The ir spectra were recorded on a Perkin-Elmer model 467 grating infrared spectrophotometer using potassium bromide pellets for solids and films for liquids. Mass spectra were determined on a Varian MAT-111 GC/MS system using a direct probe. Gas–liquid chromatography (glc) analysis were determined on a F & M model 500 gas chromatograph equipped with a dual column attachment, using 8 ft × 14 in. columns packed with 20% Carbowax on Chromosorb P and helium flow rate of 60 ml/min at 175°C. Thin layer chromatographic (tlc) preparative separations were carried out on plates (20 × 20 cm × 0.5 mm thick) prepared from Woelm Silica Gel F with 10% calcium sulfate binder added. Melting points were determined on a hot stage equipped with a microscope and are uncorrected. Elemental analyses were determined by Alfred Bernhardt, West Germany.

(a) Deoxygenation Procedure

The deoxygenations were carried out in dry benzene under a nitrogen atmosphere. The solutions were prepared from 2–3 mmol of the nitroso compound (**1** or **2**) (21) and excess (20–30 mmol) triethyl phosphite (Aldrich Chemical Co.) in 15–25 ml of benzene. It was convenient to follow the progress of the reductions by measuring the decrease in the visible absorbance readings at 790 nm for **1** and 750 nm for **2**. The reduction of **1** was complete in approximately 11 h at room temperature. The reduction of **2** did not appear to take place at room temperature but was complete after 20 h at the reflux temperature of benzene.

The relative ease of reduction of **1** and **2** was also followed by direct nmr observations of the aromatic proton region using equimolar solutions of the nitroso compound and triethyl phosphite in carbon tetrachloride. Under these conditions, the reduction of **1** was complete in 6 h. In contrast, the reduction of **2** was only ⅓ complete after 1 week.

The reaction mixtures were worked up by first evaporating the solvent and excess triethyl phosphite under reduced pressure. The residues were dissolved in ethyl ether, washed with water, the ether extract dried over anhydrous calcium chloride, and the ether evaporated. The crudes obtained were analyzed by chromatographic methods as described below.

(b) Product Analysis

(1) Deoxygenation Products from 2,5-Di-tert-butylnitrosobenzene (1)

The crude product from reduction of **1** (0.657 g) was

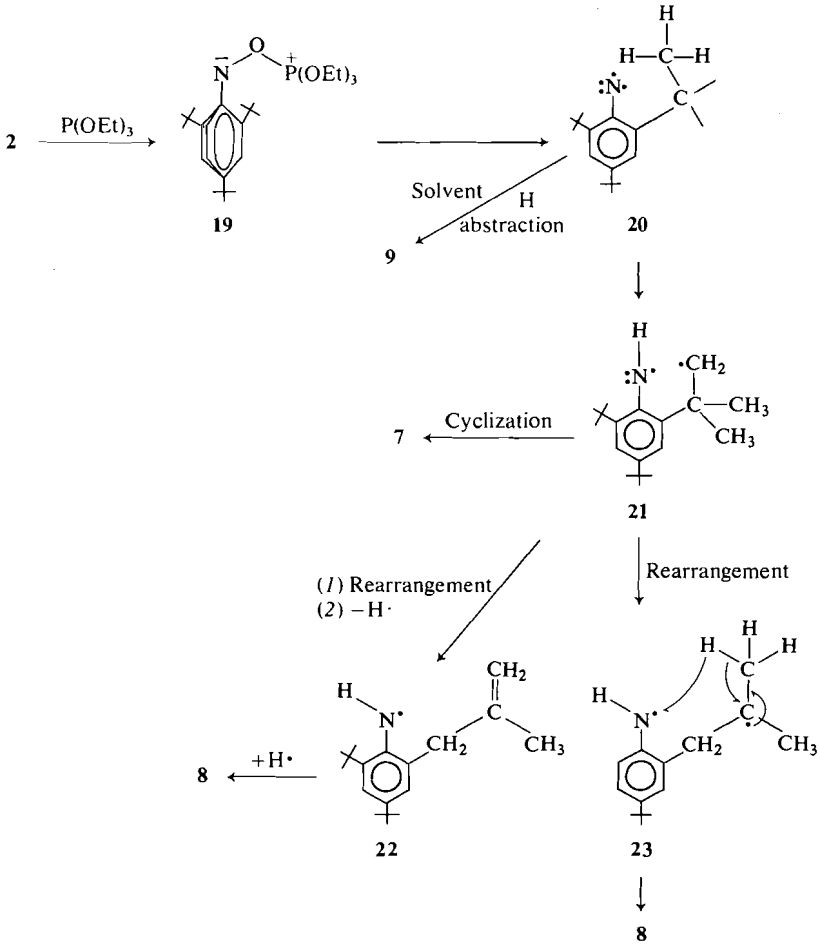

SCHEME 4

found to be a complex mixture by tlc analysis. It was dissolved in petroleum ether (bp 30–60°C) and separated into various fractions by column chromatography on a 2.5 × 28 cm column of neutral alumina as outlined in Table 3. Pure compounds were isolated by further separation of the column chromatograph fractions by means of preparative tlc.

2,5,2',5'-Tetra-tert-butylazobenzene (6)—The azo compound (**6**) was purified by preparative tlc using cyclohexane solvent. The compound separated as a narrow orange-red band by rapid elution near the solvent front. Sublimation *in vacuo* gave orange crystals, mp 227°C. The nmr spectrum showed a singlet at 1.38 (18H, 2 *tert*-butyls) and 1.64 (18H, 2 *tert*-butyls) and multiplets at 7.61 (4H, aryl) and 7.94 δ (2H, aryl). The mass spectrum showed a molecular ion peak at *m/e* 406 expected. *Anal.* calcd. for $C_{28}H_{42}N_2$: C 82.70, H 10.41, N 6.89; found: C 82.59, H 10.30, N 6.95.

N-(2,5-Di-tert-butylphenyl)-α-tert-butyl-α-2-(5-tert-butylpyridyl)nitrone (4)—Fractions 4–6 from the column chromatography (Table 3) yielded 305 mg of crystalline material. This material was chromatographed on five preparative tlc plates using benzene as the developer. There resulted two well-separated bands. The first band (near the solvent front) yielded, on extraction with ethyl ether, 197 mg (31%) of near colorless crystalline material identified as the nitrone (**4**). The analytical sample was obtained by sublimation *in vacuo* and gave a mp 189°C. The nmr spectrum showed four singlets of equal intensity at 1.39, 1.41, 1.47, and 1.53 δ (36H, three aryl *tert*-butyls and *tert*-butyl in $(CH_3)_3C-\overset{|}{\underset{|}{C}}=N-O$), a multiplet at 7.53–7.78 (5H, three hydrogens on benzenoid ring plus hydrogens 3,4 of pyridine ring), and a doublet at 8.70 ($J \simeq 1$ Hz, 1H, α-pyridyl hydrogen).

The mass spectrum showed a molecular ion peak at *m/e* 422 and an accurate mass measurement indicated the formula $C_{28}H_{42}N_2O$ (calcd. mass 422.3297; found 422.3288). *Anal.* calcd.: C 79.59, H 10.02, N 6.63; found: C 79.62, 79.47, H 9.96, 9.86, N 6.63, 6.56.

The nitrone (**4**) was recovered unreacted from an attempted hydrolysis by treatment in boiling ethanol–hydrochloric acid for 2 days.

The second band from the above tlc separation yielded 66 mg (11%) of 2,5-di-*tert*-butylaniline identified by a mixture melting point and comparison of its nmr spectrum with an authentic sample.

Diethyl N-(2,5-Di-tert-butylphenyl)phosphoramidate

TABLE 3. Column chromatography of deoxygenation products from 2,5-di-*tert*-butylnitrosobenzene (**1**)

Fraction	Solvent (ml)[a]	Yield (mg)	Identity of products[b]
1	PE (20)	44	Di-*tert*-butylazobenzene (**6**)
2, 3	PE (20)	19	Unidentified mixture
4–6	PE–bnz (80)	305	Di-*tert*-butylaniline (**5**), nitrone (**4**)
7–8	bnz (80)	7	Unidentified polymeric
9–14	bnz (300)	311	Phosphoramidate (**3**), traces of TEP

[a]PE = petroleum ether (bp 30–60°C), bnz = benzene.
[b]Products were further separated and purified by preparative tlc.

(3)—Fractions 9–14 from the column chromatography (Table 3) contained 311 mg (31%) of the crude phosphoramidate (**3**). It was separated from traces of a colored (violet) impurity by preparative tlc on four plates using 20% ethyl ether in benzene as developer. The ester **3** developed very slowly and was readily separated in this way. It was isolated as a colorless, thick, oily material. The nmr spectrum showed a singlet at 1.32 superimposed on a triplet between 1.47–1.22 (J in Hz) (15H, a *tert*-butyl and two CH_3-[s] of the CH_3CH_2O- groups), a singlet at 1.50 (9H, a *tert*-butyl), a multiplet at 3.9–4.5 (4H, $J = 7$ Hz, two -CH_2-[s] of CH_3CH_2O- groups), a doublet, exchangeable with D_2O at 5.28 (1H, —N—H), and an abc type of multiplet at 7.2–7.7 δ (3H, $J_{ab} = 9$ Hz, $J_{bc} = 2$ Hz, aryl). The ir spectrum showed a band at 3480 cm^{-1} attributed to N—H. A strong band at 1250 cm^{-1} is assigned to P=O and very strong absorption at 970–1060 to P—O—ethyl. The mass spectrum showed a molecular ion peak at *m/e* 341 as expected. *Anal.* calcd. for $C_{18}H_{32}NPO_3$: C 63.32, H 9.45, N 4.10, P 9.07; found: C 63.13, H 9.44, N 4.15, P. 8.99.

A sample (39 mg) of the phosphoramidate (**3**) was hydrolyzed by refluxing in a mixture of ethanol (10 ml) and concentrated hydrochloric acid (5 ml) for 2 days. The alcohol was distilled, the solution neutralized with sodium carbonate and the product extracted with ether. There was obtained 19 mg (81%) of 2,5-di-*tert*-butylaniline, identified by its nmr spectrum and melting point.

The deoxygenation of **1** with triethylphosphite was repeated in order to test the reproducibility of the rather complex reaction. The work-up and separation of products by a combination of column chromatography and tlc was carried out in a similar manner to the first run. The yields of the main products from this second run were azo compound **6** 3%, nitrone **4** 29%, amine **5** 13%, and the phosphoramidate **3** 35%. These results are in reasonably good agreement with those described above. When an equimolar mixture of **1** and triethylphosphite was used as described in the direct nmr observation, the yield of **4** (tlc) was increased to 70%.

(2) Deoxygenation Products from 2,4,6-Tri-tert-butylnitrosobenzene (2)

The crude product from reduction of **2** (0.550 g) was separated into three main bands by preparative tlc using benzene as developer. The first band gave 37 mg (6.9%) of 2,4,6-tri-*tert*-butylaniline (**9**) identified by its ir and nmr spectra. The second band yielded the major product, a colorless solid material (482 mg, 90%) which was shown by the nmr spectrum to be a mixture of the two amines **7** (*mainly*) and **8** described below. This mixture was separated on preparative tlc plates prepared from acid-treated silica gel. For this purpose, the plates were prepared from a slurry of the silica gel and binder in 1:1 ethanol–acetone containing 5% concentrated hydrochloric acid. The minor component (**8**) (48 mg, 9%) of this mixture eluted first with benzene followed by the major reaction product (**7**, 424 mg, 79%).

This deoxygenation of nitroso compound **2** was repeated in order to determine more precisely the percent composition of the products by glc. The compounds eluted from the column in the order **7**, **9**, and **8** and in the relative yields of 81.3%, 7.3%, and 11.4% respectively.

3,3-Dimethyl-5,7-di-tert-butyl-2,3-dihydroindole (7)—The major product **7** from the deoxygenation of **2** was sublimed *in vacuo* for analysis. It was a colorless crystalline compound, mp 105–106°C. The nmr and ir spectra established this compound to be identical to **7** obtained earlier (13) from hydride reduction of 5,7-di-*tert*-butyl-3,3-dimethyloxindole. It gave a parent mass at *m/e* 259 as expected. *Anal.* calcd. for $C_{18}H_{29}N$: C 83.33, H 11.26, N 5.40; found: C 83.52, 83.48, H 11.27, 11.25, N 5.20, 5.16.

2-(2-Methyl-3-propyl)-4,6-di-tert-butylaniline (8)—The amine **8** from the deoxygenation was isolated as an oil and distilled *in vacuo* for analysis. The nmr spectrum showed sharp singlets at 1.32 and 1.47 (9H each, *tert*-butyls), a broad singlet at 1.78 (3H, methyl of $CH_2{=}C(CH_3)$—), a broad singlet at 3.37 (2H, benzylic methylene of $Ar{-}CH_2{-}C(CH_2){-}CH_3$), two broad singlets at 4.92–5.00 (2H, nonequivalent olefinic H[s] of $>C{=}CH_2$), a singlet at 3.80 (2H exchangeable, -NH_2), and doublets at 7.11 and 7.37 δ ($J \simeq 3$ Hz) (1H each, *meta* aryl hydrogens). The ir spectrum showed bands at 3520 and 3420 cm^{-1} attributed to N—H stretching absorption of a primary amine and a band at 3090 cm^{-1} to the C—H stretching absorption of the $>C{=}CH_2$ group. The mass spectrum showed a parent mass at *m/e* 259 as expected. *Anal.* calcd. for $C_{18}H_{29}N$: C 83.01, H 11.22, N 5.38; found: C 83.21, H 11.09, N 5.53.

Acknowledgments

The authors are grateful to the National Research Council of Canada for financial support of this research. We thank Donald Embree of the National Research Council, Atlantic Regional Laboratory, for the accurate mass determination.

1. J. I. G. CADOGAN and R. K. MACKIE. Chem. Soc. Rev. **3**, 86 (1974).
2. R. A. ABRAMOVITCH. Organic reactive intermediates.

Edited by S. P. McManus. Academic Press. 1973. Chapt. 3.
3. J. I. G. CADOGAN. Acc. Chem. Res. **5**, 303 (1972).
4. W. LWOWSKI. Nitrenes. J. Wiley and Sons, New York. 1970.
5. R. A. ABRAMOVITCH and B. A. DAVIS. Chem. Rev. **64**, 149 (1964).
6. J. I. G. CADOGAN, D. S. B. GRACE, P. K. K. LIM, and B. S. TAIT. J. Chem. Soc. Perkin Trans. I, 2376 (1975).
7. A. H. JACKSON, D. N. JOHNSTON, and P. V. R. SHANNON. J. Chem. Soc. Chem. Commun. 911 (1975).
8. R. N. CARDE and G. JONES. J. Chem. Soc. Perkin Trans. I, 510 (1975).
9. R. J. SUNDBERG, D. W. GILLESPIE, and B. A. DEFRAFF. J. Am. Chem. Soc. **97**, 6193 (1975).
10. L. R. C. BARCLAY, D. GRILLER, and K. U. INGOLD. J. Am. Chem. Soc. **96**, 3011 (1974).
11. D. GRILLER, L. R. C. BARCLAY, and K. U. INGOLD. J. Am. Chem. Soc. **97**, 6151 (1975).
12. R. OKAZAKI and N. INAMOTO. J. Chem. Soc. B, 1583 (1970).
13. L. R. C. BARCLAY and I. T. MCMASTER. Can. J. Chem. **49**, 676 (1971).
14. R. J. SUNDBERG and R. H. SMITH. J. Org. Chem. **36**, 295 (1971).
15. J. I. G. CADOGAN, D. J. SEARS, D. M. SMITH, and M. J. TODD. J. Chem. Soc. C, 2813 (1969).
16. R. J. SUNDBERG. J. Am. Chem. Soc. **88**, 3781 (1966).
17. R. J. SUNDBERG, B. P. DAS, and R. H. SMITH. J. Am. Chem. Soc. **91**, 658 (1969).
18. J. I. G. CADOGAN. Q. Rev. **22**, 222 (1968).
19. C. WENTRUP. Tetrahedron, **30**, 1301 (1974); C. THÉTAZ and C. WENTRUP. J. Am. Chem. Soc. **98**, 1258 (1976).
20. R. J. SUNDBERG, S. R. SUTER, and M. BRENNER. J. Am. Chem. Soc. **94**, 513 (1972).
21. R. OKAZAKI *et al.* Bull. Chem. Soc. Jpn. **42**, 3559 (1969); **42**, 3611 (1969).
22. S. TERABE and R. KONAKA. J. Chem. Soc. Perkin Trans. II, 369 (1973).

Synthesis of enantiomers of sulcatol

HERMANN R. SCHULER[1] AND KEITH N. SLESSOR

Department of Chemistry, Simon Fraser University, Burnaby, B.C., Canada V5A 1S6

Received February 22, 1977

HERMANN R. SCHULER and KEITH N. SLESSOR. Can. J. Chem. **55**, 3280 (1977).

The synthesis of *R*-(−)- and *S*-(+)-6-methylhept-5-en-2-ol (sulcatol) is reported from commercially available carbohydrate precursors. The synthesis of the *R*-(−) enantiomer utilizes the four hydroxy function of 2-deoxy-D-ribose as a preformed precursor of the chiral secondary alcohol centre. The five hydroxy group of L-fucose provides the basis for a similar synthesis of the *S*(+) enantiomer. These isomers are to be used to test the aggregation response of *Gnathotricus sulcatus*, a northwestern American timber pest.

HERMANN R. SCHULER et KEITH N. SLESSOR. Can. J. Chem. **55**, 3280 (1977).

On rapporte la synthèse des *R*-(−)- et *S*-(+)-méthyl-6 heptène-5 ols-2 (sulcatol) à partir de précurseurs carbohydrates disponibles commercialement. La synthèse de l'énantiomère *R*-(−) utilise la fonction hydroxyle quatre du déoxy-2 D-ribose comme des précurseurs préformés du centre alcoolique secondaire chiral. Le groupe hydroxyle cinq du L-fucose fournissent la base pour une synthèse similaire de l'énantiomère *S*(+). Ces isomères seront utilisés pour déterminer une réponse d'agrégation de *Gnathotricus sulcatus*, un insecte des bois du nord ouest de l'Amérique.

[Traduit par le journal]

The ambrosia beetle, *Gnathotricus sulcatus*, a widely occurring timber pest in western North America, has been found to possess an aggregation pheromone (1), identified as 6-methylhept-5-en-2-ol (sulcatol). Furthermore, it was shown to consist of a 65:35 mixture of the (*S*)-(+) and the (*R*)-(−) enantiomers (2). This finding was rather unexpected as racemic sulcatol, which can be readily obtained by borohydride reduction of 6-methylhept-5-en-2-one, produced a beetle response comparable to the 65:35 mixture. Thus the question arose whether one or both enantiomers are needed to trigger an aggregation response by the beetle.

To investigate this question, pure enantiomers of sulcatol were required. Initially attempts were made to resolve racemic sulcatol by counter current distribution of diastereoisomeric sulcatol esters of 2,3:4,6-di-*O*-isopropylidene-L-*xylo*-hexulofuranosonic acid (3, 4). Although resolution was possible using this method, its quantitative aspects were unfavorable and led us to look for an alternative approach. We decided to design synthetic routes which utilize as starting materials compounds already containing the stereochemical requirements of the desired isomeric products. Sugars seemed well suited for this approach as their absolute configuration and optical purity are well established.

In the course of our synthetic work we learned of another preparation of the isomers of sulcatol by Mori (5), whose approach was similar as it uses optically active precursors, namely the two enantiomers of glutamic acid. Both of these enantiomers were subjected to the same reaction sequence leading to the two enantiomers of sulcatol. Initial studies, using Mori's enantiomers, gave evidence that *G. sulcatus* would not respond to either pure enantiomer, only to a mixture of the isomers. To our knowledge this is the first report (6) of a synergistic response to optical isomers. To further study this response, more pheromone was necessary, preferably from a different route to establish the weak, but possibly real response of the *S*(+) isomer.

In this paper we wish to describe the synthesis of the two pure enantiomers of sulcatol by two different routes starting from two different sugar precursors, namely L-fucose **1** and 2-deoxy-D-ribose **13** which are both commercially available. In **1**, the centre C-5 with its (*S*)-configuration was intended to become the chiral centre C-2 in (*S*)-sulcatol **12**. Great care was taken to maintain this configuration throughout the reaction sequence by keeping the C-5 oxygen of **1** fixed in a pyranose ring and by working under basic or very weakly acidic reaction conditions.

[1]Present address: Halifax Laboratory, Fisheries and Marine Service, Department of the Environment, P.O. Box 429, Halifax, N.S. B3J 2R3.

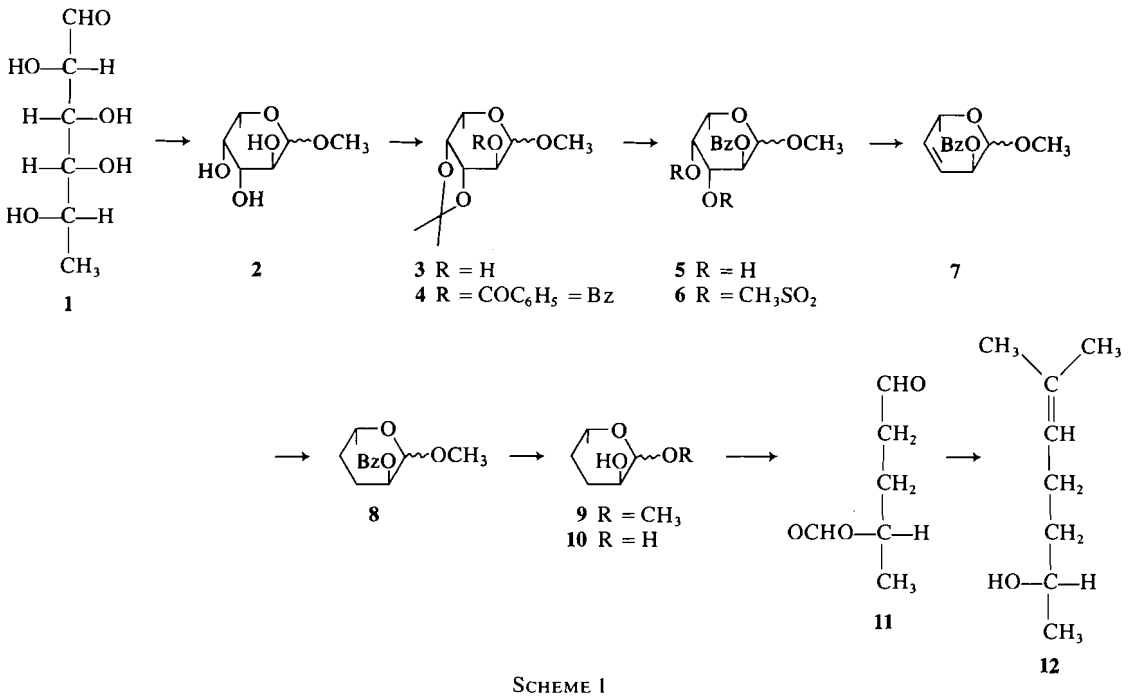

SCHEME I

The obvious transformations to be carried out on the sugar moiety were the removal of the hydroxy functions and the introduction of a double bond and a methyl branch. The latter two changes appeared to be most easily effected by a Wittig reaction. This gave the framework for the conversion of **1** to **12** as shown in reaction Scheme 1.

L-Fucose was converted to the methyl α,β-pyranoside **2** (7). As for the products of the subsequent reactions no attempts were made to isolate pure anomers. Treatment of **2** with acetone and zinc chloride led to the 3,4-*O*-isopropylidene derivative **3** which was then benzoylated to **4**. Hydrolysis with 50% aqueous acetic acid removed the isopropylidene group to give methyl 2-*O*-benzoyl-α,β-L-fucopyranoside **5**. Mesylation yielded the 3,4-di-*O*-mesyl derivative **6** which was used to introduce 3,4-unsaturation by the Tipson–Cohen method (8). Refluxing a mixture of **6**, sodium iodide, and zinc dust in dimethylformamide for 1 h thus gave the unsaturated derivative **7** in a yield of 52%. Catalytic reduction furnished the saturated compound **8**. The benzoyl group was then removed by reaction with methanolic potassium hydroxide to produce **9**. This was followed by hydrolysis to the pyranose **10**, which was carried out with a cation exchange resin, Dowex 50[H^+], as catalyst. Subsequent oxidation with sodium periodate afforded 2,3,5-trideoxy-4-*O*-formyl-L-*glycero*-pentose **11**. In the final step, **11** was treated with isopropylidenetriphenylphosphorane in THF. The product of this Wittig reaction was purified by column chromatography and distillation. Dextrorotatory (*S*)-sulcatol **12** was thereby obtained in a yield of 57%. The overall yield from **1** amounted to 13%.

The same sequence of reactions can be followed in order to synthesize (*R*)-sulcatol starting from D-fucose. However, the fact that D-fucose is not as readily available as its L-enantiomer led us to search for another starting material and an alternative synthetic route. Our choice of 2-deoxy-D-ribose **13** as such a precursor rested upon its availability and its synthetic potential. The centre C-4 in **13** with its (*R*)-configuration, its oxy and methyl functions appeared appropriate for becoming the chiral C-2 centre in (*R*)-sulcatol **19**. Furthermore, the aldehyde function of **13** seemed to allow the necessary elongation and modification to the sulcatol skeleton via a Wittig reaction. Another change to be brought about on the route from 2-deoxy-D-ribose to (*R*)-sulcatol was the removal of the two hydroxy groups attached to C-3 and C-5 of the sugar precursor. Primary hydroxy groups such as the one attached to C-5 can be readily removed by the

following method which has been widely used in carbohydrate chemistry for the preparation of deoxy sugars (9, 10):

$$R—OH \rightarrow R—OSO_2R' \rightarrow R—X \rightarrow R—H$$

$$R' = CH_3 \text{ or } p\text{-}CH_3C_6H_4$$

The hydroxy function to be removed is converted into a sulfonyloxy group which serves as leaving group in the subsequent substitution by halogen. Reductive dehalogenation then furnishes the deoxy compound. The displacement of a secondary sulfonyloxy group has in most cases proved to be rather difficult, if not impossible. However, there are reports describing the successful removal of the secondary hydroxy group bound to C-3 of 2-deoxy-D-ribose forming the glycone part in thymidine and other nucleosides (11, 12). This gave encouragement for our synthetic approach outlined in Scheme 2.

As in the synthesis of (*S*)-sulcatol, it was of utmost importance to retain the configuration at the carbon which was to become the chiral centre in (*R*)-sulcatol. This was again achieved by forming and maintaining a glycoside ring throughout the synthesis. 2-Deoxy-D-ribose **13** was first refluxed in 0.01% methanolic hydrogen chloride to furnish the methyl α,β-furanoside **14** (13). In view of the intermediacy of product **18**, it did not appear necessary to separate the anomeric mixture obtained. Similarly no attempts were made in the following steps to obtain pure anomers and therefore optical rotations were not determined. Reaction of **14** with an excess of methylsulfonyl chloride yielded syrupy dimesylate **15***a*. Treatment of **15***a* with sodium iodide in DMF at 70°C resulted in the effective displacement of the primary methylsulfonyloxy group at C-5 within 5 h. In contrast, the substitution of the secondary sulfonyloxy function at C-3 proceeded much more slowly and was still incomplete after 5 days at this temperature. Higher temperatures did not so much accelerate the formation of the diiodide **16** but promoted discoloration and gradual decomposition of the reaction mixture. So, even at 70°C, undesirable side reactions became noticeable from the 5th day onwards, and it was necessary at this point to isolate the diiodide from the reaction mixture and subject the unreacted 5-deoxy-5-iodo-3-mesylate to further reaction with sodium iodide. A 51% yield of diiodide was thus obtained after two recycling steps. Earlier attempts to prepare the diiodide via the ditosyl analogue of **15***a* were

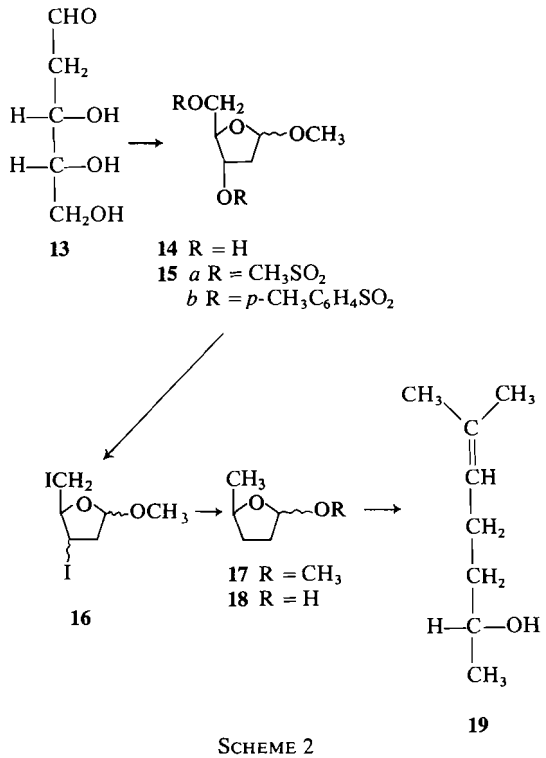

13 **14** R = H
15 *a* R = CH_3SO_2
b R = *p*-$CH_3C_6H_4SO_2$
16 **17** R = CH_3
18 R = H
19

SCHEME 2

even less successful. This was mainly due to the thermal instability of the ditosylate **15***b*. After twofold recrystallization from petroleum and chloroform, **15***b* could be obtained as a white crystalline solid with a melting point of 88°C. In pure form it decomposed shortly after melting. Likewise, heating of **15***b* with sodium iodide and dimethylformamide at 60°C resulted in extensive charring before any sizeable amount of diiodide **16** could be detected.

Hydrogenolysis of **16** using a Raney nickel (W-7) catalyst in methanolic potassium hydroxide furnished the volatile methyl 2,3,5-trideoxy-α,β-D-*glycero*-pentofuranoside **17**. This was hydrolyzed in the presence of a cation exchange resin catalyst, Dowex 50[H^+]. Serious difficulties were encountered in the isolation of the hydrolysis product **18** as this hemiacetal was found to be soluble not only in various organic solvents but also in water and, moreover, appeared to be rather unstable. These solubility characteristics as well as the instability had already been pointed out in the case of the optically inactive 4-hydroxypentanal (14). The crude hemiacetal **18**, which was recovered in a 52% yield, was therefore used in the following step without further

purification. Treatment with isopropylidenephosphorane in THF produced the (*R*)-sulcatol **19** which was purified by column chromatography and distillation. The yield of laevorotatory (*R*)-sulcatol was 30% in this Wittig reaction and 5% overall from 2-deoxy-D-ribose.

The purity of our sulcatol products was examined by glc and found to be greater than 99% for both the (*R*)- and the (*S*)-isomers. The spectroscopic characteristics were in good agreement with the data reported for natural sulcatol (2). The optical rotations $[\alpha]_D^{20}$ for ethanolic solutions of our (*R*)- and (*S*)-sulcatol were $-13.9°$ and $+14.0°$, respectively. They differ somewhat from Mori's determinations of $-14.5°$ and $+14.4°$ (5). It should be pointed out that the absolute rotation values do not differ significantly for our stereoisomers which, in contrast to the ones prepared by Mori, have been synthesized from chemically different precursors and by different routes.

In order to assess the optical purity we reacted both sulcatol isomers with (*R*)-(+)-α-methoxy-α-trifluoromethylphenylacetyl chloride (15). The nmr spectra (60 MHz) of the two diastereomeric esters (**20***a* and **20***b*) exhibited significant differences which are in line with the correlation of configuration and nmr shifts for diastereomeric MTPA esters derived by Dale and Mosher (16). The methyl group attached to the chiral centre of the sulcatol appeared as doublets at δ 1.35 and 1.25 for the (*S*,*R*)- and the (*R*,*R*)-MTPA esters, respectively.

Both MTPA esters appeared free of any cross contamination by the alternate diastereoisomer, thus proving the optical purity of our two sulcatol enantiomers. Since the (*R*,*R*)- and (*S*,*S*)- like the (*R*,*S*)- and (*S*,*R*)-MTPA esters are enantiomers having identical nmr spectra, a comparison is possible between the above-mentioned methyl absorptions and the corresponding shifts in (*S*)-MTPA esters of (*S*)- and (*R*)-sulcatol prepared by Mori (5). This shows good agreement between our results and Mori's values of δ 1.34 and 1.23 for his (*R*,*S*)- and (*S*,*S*)-MTPA esters. Our shift values are also in accord with the recently published results of the nmr study (100 MHz) which established the enantiomeric composition of natural sulcatol (17). In the (*R*)-MTPA ester of (*S*)-sulcatol, the C-1 methyl signal appeared at δ 1.33 whereas the corresponding absorption for the diastereomeric ester of (*R*)-sulcatol was found at δ 1.26.

Preliminary results of the biological testing of our sulcatol isomers in the laboratory as well as in the field seem to corroborate our purity assessment. The biological work will be published elsewhere.

Experimental

All solvents were dried and distilled before use. Silica gel G, E. Merck, type 60, was used for tlc. The following solvent systems were employed: A: ethyl acetate – ethanol, 10:1; B: toluene – diethyl ether, 1:2; C: petroleum (boiling ranges 30–60°C) – diethyl ether, 2:3; D: petroleum – diethyl ether, 7:3; E: butanone–water, 9:1. Spots were visualized by spraying with aqueous sulfuric acid (10%). Column chromatography was performed using Silica gel powder, 60–200 mesh. Symbols like PE10 stand for a 90:10 (vol) mixture of petroleum (boiling range 30–60°C) and diethyl ether.

All nmr spectra, unless stated otherwise, were recorded at 60 MHz on a Varian A-56/60A. All shift values are given in ppm downfield from TMS (δ = 0). Coupling constants (*J*) are given in Hz. Mass spectra were recorded on a Hitachi–Perkin-Elmer RMU-6E spectrometer using an ionization potential of 80 eV. Optical rotations were determined on a Perkin-Elmer P22 spectropolarimeter.

L-Fucose and 2-deoxy-D-ribose were commercially obtained from Sigma Chemical Company.

Methyl α,β-L-Fucopyranoside **2**

L-Fucose (**1**, 7.60 g, 46.3 mmol) was dissolved in methanolic hydrochloric acid (0.5 *M*, 150 ml) and stirred under reflux. The course of the reaction was followed by tlc (solvent A) which showed the disappearance of **1** (R_f 0.14) and the appearance of the product (R_f 0.21) and traces with R_f values of 0.27 and 0.40. After 1.5 h, the acid was neutralized with methanolic sodium methoxide (2.4 *M*, 30 ml). The precipitate was filtered and the filtrate was evaporated. The solid residue was triturated with dry acetone. Filtration and removal of acetone gave a white solid (8.82 g) which was used in the following step without further purification.

Methyl 3,4-O-Isopropylidene-α,β-L-fucopyranoside **3**

A solution of zinc chloride (8.82 g) and concentrated phosphoric acid (0.05 ml) in dry acetone (80 ml) was added with stirring to a suspension of crude product **2** (8.82 g) in dry acetone (80 ml). After a few minutes an only slightly turbid solution was obtained. Stirring at room temperature was continued for 1.5 h. Then tlc (A) indicated complete conversion to a product of R_f 0.56 with two minor components corresponding with R_f values of 0.27 and 0.40. The reaction solution was neutralized by stirring in sodium methoxide (7.0 g) and was filtered. The filtrate was evaporated. The residue was taken up in aqueous ammonia (1 *M*, 100 ml) and extracted with chloroform (5 × 50 ml). The chloroform layers were washed with water (3 × 40 ml), combined, and dried over anhydrous magnesium sulphate. Filtration and evaporation yielded a viscous liquid (10.0 g) which was pure by tlc giving a single spot (R_f 0.56). Spectral data: nmr: δ 1.26–1.54 (m, 9H), 3.2 (bs, 1H), 3.46 and 3.55 (two s, total of 3H), 3.7–4.2 (m, 4H), 4.73 (d, J = 3.5, 1H), ms: *m/e* 203($M - CH_3$, 21), 187($M - OCH_3$, 5), 143(5), 129(16), 101(69), 100(74), 99(71), 87(53), 85(50), 83(35), 71(74), 59(90), 42($C(CH_3)_2$, 100).

Methyl 2-O-Benzoyl-3,4-O-isopropylidene-α,β-L-fucopyranoside **4**

Benzoyl chloride (8.39 g, 59.7 mmol) was run into a stirred and ice cooled solution of **3** (10.0 g, 45.9 mmol) in dry pyridine (130 ml) over a period of 1 h. After stirring at room temperature for 1 h, the reaction mixture was concentrated *in vacuo* and partitioned between aqueous sodium hydroxide (1 *M*, 70 ml) and chloroform (3 × 100 ml). The chloroform extracts, after washing with brine and drying over anhydrous magnesium sulphate, yielded a viscous liquid (14.2 g, 95% from **1**). It had no ir absorption for O—H and ran on tlc (B) as two spots with R_f values of 0.76 and 0.79. Spectral data: nmr: δ 1.36–1.63 (m, 9H), 3.37 and 3.48 (two s, total of 3H), 3.9–4.6 (m, 3H), 4.92–5.4 (m, 2H), 7.2–7.7 (m, 3H), 7.95–8.25 (m, 2H); ms: *m/e* 307($M - CH_3$, 11), 291($M - OCH_3$, 2), 205(10), 200($M - C_6H_5COOH$, 17), 185(200 − CH_3, 7), 156(8), 147(17), 122(22), 105(C_6H_5CO, 100), 100(44), 99(61), 86(35), 85(63), 84(48), 83(72), 77(C_6H_5, 49).

The two compounds (**4***a* and **4***b*) corresponding with the two tlc spots (R_f 0.79 and 0.76) could be separated by chromatography through silica gel column eluting with PE 15. In contrast to their mass spectra, their nmr spectra exhibited significant differences indicating that **4***a* and **4***b* were anomers: **4***a* (R_f 0.79): δ 1.37 (s, 3H), 1.42 (d, J = 7, 3H), 1.57 (s, 3H), 3.37 (s, 3H), 4.92–5.28 (m, J_1 = 7, J_2 = 3.5, 2H); **4***b* (R_f 0.76): δ 1.36 (s, 3H), 1.47 (d, J = 7, 3H), 1.63 (s, 3H), 3.47 (s, 3H), 5.16 (d, J = 7, 1H), 5.29 (d, J = 7, 1H).

Methyl 2-O-Benzoyl-α,β-L-fucopyranoside **5**

A solution of **4** (14.2 g) in aqueous acetic acid (50%, 150 ml) was stirred for 1 h at 70°C. Evaporation and repeated coevaporation with toluene left a white solid residue (11.91 g). The product gave two major spots (R_f 0.14 and 0.23) on tlc (C) along with traces of **4** (R_f 0.71 and 0.82). The nmr spectrum indicated the anomeric nature of product **5**: δ 1.32 and 1.37 (two d, J = 6.5, total of 3H), 3.36 and 3.47 (two s, total of 3H), 3.63–4.52 (m, 3H), 5.05, 5.28, and 5.45 (three d, J = 4, 2H), 7.18–7.68 (m, 3H), and 8.00–8.18 (m, 2H).

Methyl 2-O-Benzoyl-3,4-di-O-(methylsulfonyl)-α,β-L-fucopyranoside **6**

A solution of crude product **5** (11.91 g) in dry pyridine (125 ml) was cooled in ice and methanesulphonyl chloride (11.91 g) was slowly added. The reaction mixture was stirred at room temperature overnight. After evaporation aqueous sodium hydroxide (1 *M*, 50 ml) was added to the residue. Extraction with petroleum (bp 30–60°C, 2 × 70 ml) removed the small amount of **4** carried over by the preceding reaction as well as traces of other by-products. Chloroform (4 × 70 ml) extracted a viscous brown liquid which was decolorized by treatment with charcoal. The product (19.2 g) had the same mobility on tlc (C) as the starting material **5** but showed no O—H absorption in the ir. The nmr spectrum indicated a mixture of two anomers in equal amounts. This was confirmed by comparison of the spectra obtained for compounds **6***a* and **6***b* which had been derived separately from **4***a* and **4***b*: **6***a*: δ 1.38 (d, J = 6.5, 3H), 3.02 (s, 3H), 3.21 (s, 3H), 3.40 (s, 3H), 4.18 (m, J = 6.5, 1H), 5.12 (m, 2H), 5.37 (m, 2H), 7.40–7.65 and 8.00–8.26 (two m, total of 5H); **6***b*: δ 1.43 (d, J = 6.5, 3H), 2.98 (s, 3H), 3.23 (s, 3H), 3.50 (s, 3H), 4.62 (d, J = 7, 1H), 5.13 and 5.35 (two m, total of 4H), 7.40–7.65 and 8.00–8.26 (two m, total of 5H); ms: *m/e* 315 ($M - C_6H_5CO$, H_2O; 3), 299($M - C_6H_5COO$, H_2O, 1), 283(1), 238(1), 226(6), 199(15), 122(C_6H_5COOH, 32), 105(C_6H_5CO, 100), 77(C_6H_5, 69).

Methyl 2-O-Benzoyl-3,4,6-trideoxy-α,β-L-erythro-hex-3-enopyranoside **7**

Product **6** (19.0 g, 43.4 mmol) in DMF (150 ml) was added to a hot solution of sodium iodide (90 g) in DMF (450 ml). Zinc powder (35 g) was added and the mixture was refluxed for 1 h. Removal of the solvent was followed by addition of water (200 ml) and extraction with chloroform (4 × 200 ml). The chloroform layers were washed with aqueous sodium thiosulphate (ca. 2 *M*, 200 ml) and brine (200 ml) and evaporated to yield a brown liquid (11.0 g). It was shown by tlc (D) to consist of several components corresponding with R_f values of 0.63, 0.52, 0.23, 0.12, and 0.02. The main component with R_f 0.63 (5.58 g, 22.5 mmol, 52%) was eluted from a silica gel column with PE 10. Its anomeric nature was again evident from its nmr spectrum: δ 1.28 and 1.33 (two d, J = 7, total of 3H), 3.47 and 3.52 (two s, total of 3H), 4.38 (m, J = 7, 1H), 4.72 (d, J = 5) and 5.18 (d, J = 3.5) (both 4.72 and 5.18 corresponding with 1H in total), 5.50 (m, 1H), 5.82 (m, 2H), 7.32–7.62 and 7.98–8.22 (two m, total of 5H); ms: *m/e* 248(M, 1), 217($M - OCH_3$, 7), 188($M - CHOOCH_3$, 47), 143(8), 127(7), 105(C_6H_5CO, 100), 77(C_6H_5, 71).

Methyl 2-O-Benzoyl-3,4,6-trideoxy-α,β-L-erythrohexopyranoside **8**

A Parr hydrogenator was used to hydrogenate **7** (5.51 g, 22.2 mmol) dissolved in methanol (75 ml) with Pd (10% on charcoal, 0.30 g) as a catalyst. An atmosphere of hydrogen (ca. 70 psi) was maintained at room temperature for 12 h. Filtration and evaporation left the product (5.39 g, 21.6 mmol, 97%) which on tlc (D) gave two spots with R_f values of 0.62 and 0.71 apparently being an anomeric mixture. Spectral data: nmr: δ 1.18 and 1.28 (two d, J = 7, total of 3H), 1.43–2.32 (4H), 3.43 and 3.50 (two s, total of 3H), 3.58–4.10 (m, 1H), 4.45 and 5.12 (two m, total of 1H), 7.17–7.55 and 7.60–8.30 (two m, total of 5H); ms: *m/e* 249(M − H, 1), 219($M - OCH_3$, 18), 190($M - CHOOCH_3$, 20), 165(20), 162(22), 148(10), 134(14), 128($M - C_6H_5COOH$, 48), 105(C_6H_5CO, 100), 77(C_6H_5, 68).

Methyl 3,4,6-Trideoxy-α,β-L-erythrohexopyranoside **9**

A solution of **8** (5.33 g, 21.3 mmol) in methanolic potassium hydroxide (0.5 *M*, 150 ml) was refluxed for 1 h. The solution was cooled and neutralized with methanolic hydrogen chloride (ca. 1 *M*). Filtration and evaporation left a residue which was taken up in water (100 ml). Extraction with chloroform (5 × 100 ml) yielded a crude product (3.78 g) which contained some methyl benzoate as indicated by its smell. Methyl benzoate was eluted from a silica gel column by PE 2, whereas PE 10 was used to elute product **9** (2.14 g, 14.7 mmol, 69%). The product **9**, an anomeric mixture, appeared on tlc (D) as a double spot with R_f values of 0.09 and 0.16. The ir spectrum had a strong O—H peak but no carbonyl absorption as had the ester **8**. Spectral data: nmr: δ 1.13 and 1.21 (two d, J = 6, total of 3H), 1.35–1.92 (m, 4H), 2.69 (bs, 1H), 3.42 and 3.51 (two s, total of 3H), 3.60–3.99 (m, 1H),

4.07 (d, J = 7) and 4.61 (d, J = 3.5) (both 4.07 and 4.61 corresponding with a total of 1H); ms: *m/e* 146(M, 2), 144(3), 115(M − OCH_3, 27), 104(M − C_3H_6, 80), 97(6), 75(41), 61($CHOHOCH_3$, 100), 57(41), 44(CH_3CHO, 78).

2,3,5-Trideoxy-4-O-formyl-L-glyceropentose ***11***

A mixture of **9** (2.10 g, 14.4 mmol), distilled water (50 ml), and Dowex 50[H^+] (prepared from 10 g of resin) was stirred and heated to 60°C. After 3 h, tlc (C) showed the conversion of **9** (R_f 0.34) to product **10** (R_f 0.10) to be complete. The resin was filtered off and washed with distilled water (50 ml). This washing solution was used to dissolve sodium periodate (3.39 g, 15.8 mmol) for the subsequent oxidation. The solution containing the hydrolysis product **10** was cooled to 0°C and mixed with the ice cooled solution of sodium periodate. The oxidation appeared to be complete after 10 min as indicated by a single spot (R_f 0.44) on tlc (C). In order to remove the excess sodium periodate, the reaction mixture was run through an anion exchange column (25 ml) of Dowex 1 X-4[Cl^-] which was then washed with distilled water (50 ml). The aqueous solution was extracted with chloroform (5 × 70 ml). The combined chloroform extracts were dried over anhydrous magnesium sulphate, filtered, and evaporated at atmospheric pressure. The liquid product (1.46 g) had a smell reminiscent of an aldehyde. As indicated by its nmr spectrum it consisted of compound **11** (1.32 g, 10.2 mmol, 71%) and a small amount of chloroform (0.14 g). For the use in the subsequent Wittig reaction, the contaminating chloroform was removed by repeated coevaporation with THF. Spectral data: nmr: δ 1.30 (d, J = 6.5, 3H), 1.72–2.15 (m, 2H), 2.38–2.73 (m, J_1 = 6, J_2 = 1.5, 2H), 5.09 (sextet, J = 6, 1H), 8.05 (s, 1H), 9.80 (t, J = 1.5, 1H); ms: *m/e* 129(M − H, 1), 101(M − CHO, 7), 84(M − CHOOH, 56), 72(37), 71(36), 69(36), 67(13), 56(C_4H_8, 100), 45(CHO_2, 78), 29(CHO, 69); ir: 1720 cm^{-1} (s) and 1185 cm^{-1} (vs).

(S)-(+)-6-Methylhept-5-en-2-ol [(S)-(+)-Sulcatol, ***12****]*

Care was taken to exclude moisture and to maintain an atmosphere of dry nitrogen throughout the following Wittig reaction. To a suspension of isopropyltriphenylphosphonium iodide ((18) 15.1 g, 35 mmol) in dry THF (60 ml) was slowly added a solution of *n*-butyllithium in hexane (2.1 M, 16.7 ml, 35 mmol). The resulting red-brown solution of the ylide was stirred at room temperature for 0.5 h and then cooled in an ice bath. A solution of **11** (1.30 g, 10 mmol) in dry THF (7.5 ml) was slowly added with stirring. After 1 h, the excess ylide was quenched by addition of ice (60 g). The product was extracted with petroleum (bp 30–60°C, 3 × 100 ml). The extracts were washed with water (50 ml), combined and dried over anhydrous sodium sulphate. Filtration and evaporation gave a crude product (5.5 g) which tlc (D) showed to consist of several components with R_f values of 0.04, 0.23, 0.34, 0.39, 0.69, 0.76, and 0.82. The tlc spot of racemic sulcatol coincided with the component with R_f 0.34. The product was purified by eluting from a silica gel column. PE 2.5 and PE 5 were used to elute the components with R_f values larger than 0.34. (*S*)-Sulcatol (1.09 g), eluted with PE 10, was subjected to vacuum distillation (29 Torr, bath temperature 120–130°C) to give a clear, colorless liquid (0.73 g, 5.7 mmol, 57%); $[\alpha]_D^{32}$ +13.20°, $[\alpha]_D^{20}$ +13.96° (*c* 4.56, EtOH); nmr; δ 1.19 (d, J = 6.5, 3H), 1.35–1.75 (m, J = 7, 2H), 1.65 (s, 3H), 1.72 (d, J = 1.3, 3H), 2.09 (q, J = 7, 2H), 2.53 (bs, 1H), 3.80 (sextet, J = 6.5, 1H), 5.17 (m, J_1 = 7, J_2 = 1.3, 1H); ms: *m/e* 128(M, 14), 113(M − CH_3, 4), 110(M − H_2O, 29), 95(110 − CH_3, 100), 85(27), 83(M − CH_3CHOH, 10), 81(12), 71(26), 69(CH_2CH=$C(CH_3)_2$, 58), 67(30), 55(CH=$C(CH_3)_2$, 36), 43(33), 42($C(CH_3)_2$, 36). Gas–liquid chromatography (column: 5% Carbowax 20 M on Chromosorb G70/80, 12 ft × ⅛ in; 150°C; carrier gas, He 40 ml/min): *Rt* 5.7 min, 99%; impurity *Rt* 2.3 min, 1%. *Anal.* calcd. for $C_8H_{16}O$: C 74.94, H 12.58; found: C 74.78, H 12.63.

Methyl 2-Deoxy-α,β-D-ribofuranoside ***14***

A solution of 2-deoxy-D-ribose (**13**, 11.6 g, 87.6 mmol) in methanolic hydrogen chloride (0.01 M, 250 ml) was stirred at room temperature. Monitoring by tlc (E) showed the conversion of **13** (R_f 0.26) to a single product with R_f 0.40 to be complete after 0.5 h. This solution was neutralized by addition of methanolic sodium methoxide (0.5 M). Evaporation gave a syrup which was taken up in dry acetone. A white precipitate formed and was filtered off. The filtrate was evaporated and coevaporated (2×) with dry pyridine to give **14** (12.5 g).

Methyl 2-Deoxy-3,5-di-O-(methylsulfonyl)-α,β-D-ribofuranoside ***15a***

Product **14** (12.5 g) was dissolved in dry pyridine (150 ml) and cooled in an ice bath. A solution of methanesulfonyl chloride (24.0 g, 210 mmol, ca. 25% excess) in dry pyridine (50 ml) was slowly added. The reaction mixture was stirred at room temperature for 15 h. The salt formed was filtered off and washed with pyridine (50 ml). The filtrate and washing solution were combined and evaporated. After addition of aqueous sodium hydroxide (1 M, 100 ml), the product was extracted with chloroform (4 × 100 ml). The chloroform layers were washed with water (2 × 50 ml), combined, and decolorized with charcoal. Removal of chloroform gave product **15***a* (24.6 g, 80.9 mmol, 92% from **13**) which on tlc (B) ran as a double spot with R_f values of 0.17 and 0.19. There was no O—H absorption in the ir spectrum but two strong peaks at 1350 and 1180 cm^{-1}. Spectral data: nmr: δ 2.23–2.55 (m, 2H), 3.10 (s, 6H), 3.37 and 3.39 (two s, total of 3H), 4.33–4.48 (m, 3H), 5.07–5.28 (m, 2H); ms: *m/e* 304(M, 1), 273(M − OCH_3, 2), 209(M − OSO_2CH_3, 7), 195(M − $CH_2OSO_2CH_3$, 34), 149(15), 117(13), 113(11), 111(13), 109(11), 99(100), 87(70), 81(83), 79(98), 71(43), 59(57), 52(55).

Methyl 2,3,5-Trideoxy-3,5-diiodo-α,β-D-glyceropentofuranoside ***16***

Compound **15***a* (24.3 g, 80 mmol) in DMF (40 ml) was added to a solution of sodium iodide (75 g) in DMF (300 ml). The reaction mixture was kept stirred and heated to 70°C. Higher temperatures caused the gradual decomposition of the starting material and of the products formed. Frequent checking by tlc revealed that all starting material had reacted within the first 5 h. The product appeared on tlc (B) as a double spot with R_f values of 0.48 and 0.53. It was accompanied by a component (R_f 0.80) whose concentration increased up to the fifth day when the reaction mixture started to turn dark brown. At this point the solvent was removed and water (300 ml) was added. The product was extracted with petroleum (bp 30–60°C) followed by chloroform (3 ×

200 ml). The organic layers were washed with aqueous sodium thiosulphate (5%, 2 × 100 ml) and brine (50 ml). The combined chloroform extracts yielded a crude product (14.0 g) which consisted mainly of the component B with R_f values 0.48 and 0.53 and of small amounts of more polar by-products. The petroleum extracts (13.1 g) contained the component A (R_f 0.80) as well as component B. These were separated by percolation through a column of silica gel (200 g). PE 15 eluted the component A (6.0 g) being the pure diiodide **16**. Component B (6.4 g, methyl 5-deoxy-5-iodo-3-*O*-(methylsulfonyl)-α,β-D-ribofuranoside) was eluted with PE 50. It was combined with the chloroform extract for further reaction with sodium iodide which was carried out and worked-up as described above giving another 5.8 g of diiodide. A second repetition of the reaction and extraction cycle made a further contribution (3.4 g) to the total of 15.2 g of **16** (41.0 mmol, 51%). Attempts to improve this yield by further recycling failed as charring occurred.

Component A, i.e. **16**, had the following spectral features: nmr: δ 2.23–2.68 (m, 2H), 3.23–3.57 (m, 2H), 3.40 (s, 3H), 3.75–3.95 (m, 1H), 4.03–4.38 (m, 1H), 4.95–5.18 (m, 1H); ms: *m/e* 368(*M*, 15), 337(*M* − OCH_3, 6), 241(*M* − I, 7), 227(*M* − CH_2I, 89), 209(241 − CH_3OH, 13), 181(100), 128(15), 127(13), 114(11), 113(9), 100(94), 71(51), 59(66).

Component B, nmr: δ 2.21–2.60 (m, 2H), 3.10 (s, 3H), 3.27–3.48 (m, 2H), 3.40 (s, 3H), 4.00–4.60 (m, 1H), 5.05–5.17 (m, 2H); ms: *m/e* 336(*M*, 5), 305(*M* − OCH_3, 2), 240(*M* − $HOSO_2CH_3$, 18), 227(6), 209(*M* − I, 72), 195(*M* − CH_2I, 16), 181(15), 179(31), 166(84), 149(39), 139(8), 128(3), 127(5), 113(62), 99(71), 87(100), 82(50), 81(34), 79(56), 71(57), 59(82).

Methyl 2,3,5-Trideoxy-α,β-D-glyceropentofuranoside ***17***

The catalytic hydrogenation of **16** to **17** was carried out in a Parr hydrogenator. A mixture of **16** (14.9 g, 40.5 mmol) and Raney Nickel (W-7) (freshly prepared from 10 g NiAl alloy) in methanolic potassium hydroxide (1.0 *M*, 85 ml) was vigorously shaken at room temperature in a hydrogen atmosphere of 70 psi. After 14 h, the mixture was filtered. Most of the solvent was removed by slow distillation through a Vigreaux column (12 cm) at atmospheric pressure. The residue was then partitioned between water (25 ml) and petroleum (bp 30–60°C, 4 × 50 ml). Evaporation of the petroleum left product **17** (3.16 g, 27.2 mmol, 67%) which ran on tlc (D) as a single spot R_f 0.52). Spectral data: nmr: δ 1.23 and 1.31 (two d, *J* = 6, total of 3H), 1.67–2.20 (m, 4H), 3.33 (s, 3H), 2.52 (sextet, *J* = 6, 1H), 2.93–3.09 (m, 1H).

2,3,5-Trideoxy-α,β-D-glyceropentofuranose ***18***

A mixture of product **17** (3.10 g, 26.7 mmol), water (40 ml), and Dowex 50[H^+] (from 15 g resin) was stirred at 50°C. The hydrolysis was monitored by tlc (D) which after 1 h showed complete conversion of **17** to a product consisting of a major component with R_f 0.11 and small amounts of by-products (R_f 0.15 and 0.18). The resin was then filtered off and the filtrate extracted with ether (6 × 75 ml). The ether extracts yielded the crude product **18** (1.40 g). Earlier attempts to purify product **18** by column chromatography had proved unsuccessful due to its instability. The crude product **18** was therefore employed in the subsequent Wittig reaction.

(R)-(−)-6-Methylhept-5-en-2-ol, (R)-(−)-Sulcatol, ***19***

Isopropyltriphenylphosphonium iodide (17.8 g, 41.1 mmol) was suspended in dry THF (80 ml) and reacted with *n*-butyllithium in hexane (2.1 *M*, 19.6 ml, 41.1 mmol). After stirring for 0.5 h, the red-brown ylide solution was cooled in an ice bath. Crude compound **18** (1.4 g) in THF (5 ml) was slowly added. After 1.5 h, the excess ylide was destroyed by addition of ice (100 g). Extraction with petroleum (bp 30–60°C, 6 × 100 ml) yielded a crude product consisting of several components (R_f 0.10, 0.34, 0.43, 0.53, 0.68, 0.75, and 0.81) as indicated by tlc (D). The product was purified by column chromatography (silica gel). The components with R_f values larger than 0.34 were eluted with PE 1, 2.5, and 4.0, whereas PE 7.5 was used to elute (*R*)-sulcatol (0.71 g, R_f 0.34). Vacuum distillation (29 Torr, bath temperature 130°C) gave colorless clear (*R*)-sulcatol (0.524 g, 4.1 mmol, 15.4%) from **17**. $[\alpha]_D^{20}$ −13.89°, $[\alpha]_D^{32}$ −13.24° (*c* 4.76, EtOH). Gas–liquid chromatography (for operating conditions see preparation of (*S*)-sulcatol **12**) *Rt* 5.7 min, impurity less than 1%, *Rt* 9.2 min. The nmr, ms, and ir data were essentially the same as for (*S*)-sulcatol. *Anal.* calcd. for $C_8H_{16}O$: C 74.94, H 12.58; found: C 74.97, H 12.48.

(R)-(+)-α-Methoxy-α-trifluoromethylphenylacetates of Sulcatol (S)-Sulcatol-(R)-MTPA Ester ***20a***

(*S*)-Sulcatol **12**, (32 mg, 0.25 mmol) dissolved in carbon tetrachloride (0.7 ml) was added to a solution of (*R*)-MTPA chloride (15) (65.6 mg, 0.26 mmol) in dry pyridine (0.7 ml). The mixture was stirred for 12 h, added to dilute aqueous hydrochloric acid (0.5 *M*, 10 ml) and extracted with chloroform (3 × 10 ml). The chloroform extracts were washed with saturated aqueous sodium bicarbonate followed by water. The product obtained after drying and removal of the solvent was purified by preparative tlc (PE 40) to give **20***a* (81.7 mg, 0.24 mmol, 96%). Spectral data: nmr: δ 1.35 (d, *J* = 6, 3H), 1.54 (s, 3H), 1.68 (s, 3H), 1.54–2.21 (m, 4H), 3.58 (t, *J* = 1, 3H), 4.86–5.37 (m, 2H), 7.21–7.73 (m, 5H); ms: *m/e* 262(*M* − C_6H_{10}, 11), 232(*M* − C_8H_{16}, 18), 189($C_9H_8F_3O$, 100), 139(22), 127($C_8H_{15}O$, 23), 119(32), 110(C_8H_{14}, 49), 105(41), 95(C_7H_{11}, 37), 69(C_5H_9, 39).

(R)-Sulcatol-(R)-MTPA Ester ***20b***

The conversion of (*R*)-sulcatol **19** to the (*R*, *R*)-MTPA ester **20***b* was carried out in the same way. The mass spectrum of **20***b* did not differ significantly from that of **20***a*. However, distinction of the two diastereomeric esters was possible on the basis of their nmr spectra. The nmr spectrum of **20***b* contains the following features: δ 1.25 (d, *J* = 6.5, 3H), 1.58 (s, 3H), 1.69 (s, 3H), 1.58–2.33 (m, 4H), 3.57 (t, *J* = 1, 3H), 4.85–5.37 (m, 2H), 7.22–7.75 (m, 5H).

No sign of cross contamination could be detected in the nmr spectrum of either diastereoisomer.

Acknowledgements

We thank K. Wiltshire for technical assistance, the Canadian Forestry Service Science Subvention Program, and the National Research Council of Canada (operating A 3785 and Co-op A 0243 grants) for financial support.

1. J. H. BORDEN and E. STOKKINK. Can. J. Zool. **51**, 469 (1973).
2. K. J. BYRNE, A. A. SWIGAR, R. M. SILVERSTEIN, J. H. BORDEN, and E. STOKKINK. J. Insect Physiol. **20**, 1895 (1974).
3. T. REICHSTEIN and A. GRÜSSNER. Helv. Chim. Acta, **17**, 311 (1934).
4. A. BROSSI and S. TEITEL. J. Org. Chem. **35**, 3559 (1970).
5. K. MORI. Tetrahedron, **31**, 3011 (1975).
6. J. H. BORDEN, L. CHONG, J. A. MCLEAN, K. N. SLESSOR, and K. MORI. Science, **192**, 894 (1976).
7. O. T. SCHMIDT, W. MAYER, and A. DISTELMAIER. Ann. **555**, 26 (1943).
8. R. S. TIPSON and A. COHEN. Carbohydr. Res. **1**, 338 (1965).
9. W. A. SZEREK. Adv. Carbohydr. Chem. **28**, 225 (1973).
10. S. HANESSIAN. Adv. Carbohydr. Chem. **21**, 143 (1966).
11. P. A. LEVENE and R. S. TIPSON. J. Biol. Chem. **109**, 623 (1935).
12. A. M. MICHELSON and A. R. TODD. J. Chem. Soc. 816 (1955).
13. R. E. DERIAZ, W. G. OVEREND, M. STACEY, and L. F. WIGGINS. J. Chem. Soc. 2836 (1949).
14. B. HELFERICH. Ber. Dtsch. Chem. Ges. **52**, 1123 (1919); **52**, 1800 (1919).
15. J. A. DALE, D. L. DULL, and H. S. MOSHER. J. Org. Chem. **34**, 2543 (1969).
16. J. A. DALE and H. S. MOSHER. J. Am. Chem. Soc. **95**, 512 (1973).
17. E. L. PLUMMER, T. E. STEWART, K. BYRNE, G. T. PEARCE, and R. M. SILVERSTEIN. J. Chem. Ecol. **2**, 307 (1976).
18. G. WITTIG and D. WITTENBERG. Ann. **606**, 1 (1957).

Radiation chemistry of acetylene at high intensity: the initial product distributions[1]

C. WILLIS, R. A. BACK, AND R. H. MORRIS[2]

Division of Chemistry, National Research Council of Canada, Ottawa, Canada K1A 0R6

Received May 18, 1977

C. WILLIS, R. A. BACK, and R. H. MORRIS. Can. J. Chem. **55**, 3288 (1977).

The distribution of products observed in the radiation chemistry of acetylene at high dose rate is dramatically different from that observed at low dose rate. The dominant products observed at high dose rate are vinyl acetylene and diacetylene with C_3 to C_9 compounds having smaller but significant yields. At low dose rate benzene and cuprene are the exclusive products. The difference in product distribution is attributed to the suppression of secondary attack on products at high dose rate so that the observed distribution approximates more closely the 'zero dose' or 'initial' distribution.

C. WILLIS, R. A. BACK et R. H. MORRIS. Can. J. Chem. **55**, 3288 (1977).

La répartition des produits observés dans la chimie du rayonnement de l'acétylène à grande intensité est très différente de celle observée à faible intensité. Les principaux produits observés à grande intensité sont le butène-3 yne-1 et le butadiyne-1,3, des composés en C_3 jusqu'à C_9 ayant des rendements plus faibles mais importants. A faible intensité, les seuls produits formés sont le benzène et le cuprène. La différence dans la répartition des produits est attribuée à l'absence, à grande intensité, d'une attaque secondaire sur les produits formés. Il en résulte que la répartition observée est plus proche de la répartition de "l'intensité zéro" ou "initiale".

[Traduit par le journal]

Introduction

The radiation-induced polymerization of acetylene has been a subject of study almost since it was first recognized that ionizing radiation could induce chemical change (1). Several groups have shown that at conventional low dose rate, about 10^{16} eV g^{-1} s^{-1}, two major products are formed, benzene and an acetylenic polymer loosely called cuprene, with a yield of disappearance of acetylene, $G(-C_2H_2)$, of between 50 and 100 molecules per 100 eV of energy absorbed (2). Trace amounts of vinyl acetylene, diacetylene, and butadiene, have been observed but with very small yields (3, 4).

It has been difficult to suggest a reasonable mechanism for the radiation chemistry of acetylene and indeed it is uncertain whether the predominant processes are ionic, involve free radicals, or are more comparable to those occurring in the thermal pyrolysis where it is thought that polymerization takes place via a triplet biradical species (5).

We decided to investigate the radiation chemistry of acetylene at very high dose rates in an attempt to map out the general features of the system. The high dose rate should reduce the length of both ionic and free radical chains, which have bimolecular termination steps, but should have a lesser effect on biradical chains, which have predominantly unimolecular termination steps. Furthermore, the short lifetime of ions and free radicals at high dose rates should also tend to reduce consumption of primary products by secondary attack by these species.

Experimental

The source of radiation was a Febetron 706. This gives short (~3 ns) pulses of approximately 600 keV electrons at high currents (~10 000 A) which correspond to a dose rate of the order of 10^{28} eV g^{-1} s^{-1}. Samples were irradiated in a cylindrical aluminum cell, 5 cm long and 4 cm in diameter. The front face of the cell had a 2.5 cm diameter electron window which had been machined down to a thickness of approximately 0.025 cm. The dose per pulse averaged over the cell volume was about 0.1 Mrad which was determined by irradiating CO_2 in the cell and assuming $G(CO) = 7.8$ (6). The cell was also fitted with a thermal syphon so that the gas could be circulated through a U-trap. In some experiments this trap was held at dry-ice temperature to maintain a low partial pressure of the higher molecular weight products. No differences were noted in the product distribution between experiments with the low temperature trap and experiments where the trap was at room temperature.

Products were analyzed by gas chromatography with flame ionization detection. The irradiated sample was condensed in the U-trap in the thermal syphon which was then used as part of the injection system of the gas

[1]NRCC No. 16115.

[2]NRCC Summer Student 1975. Present address: Chemistry Department, University of British Columbia, Vancouver, B.C.

chromatograph. Because of the large number of peaks observed a mass spectrometer was interfaced with the chromatograph so that part of the exit flow was injected directly into the mass spectrometer. Peaks were identified from standard tables of mass spectra. Two different column packings were used. Poropak Q, programmed between 80 and 160°C, was used for C_3–C_6 species and Durapak OPN/Poracil C, programmed between 30 and 120°C, was used to separate C_4–C_9 species. Stainless steel column tubing was used to avoid the possibility that copper tubing might distort the observations by acetylenic reactions.

Acetylene (Matheson, C.P. Grade) was passed through a trap at dry-ice temperature followed by a U-tube, packed with activated charcoal and also held at dry-ice temperature. These remove all traces of acetone contamination. The final purification stage involved several bulb-to-bulb distillations using alternately liquid nitrogen and dry-ice temperatures (3).

Results

Yield of Disappearance of Acetylene, $G(-C_2H_2)$

We attempted to measure the yield for disappearance of acetylene by the change in pressure. The aluminum cell was connected directly to a high precision quartz spiral gauge (Texas Instruments) and the average temperature of the cell was monitored by an array of 10 iron–constantin thermocouples taped to the cell body. This should have allowed measurement of pressure differences of about 20 μm. Unfortunately pressure changes were dominated by small geometry changes associated with flexing of the thin electron window of the cell and this allowed only measurement of an upper limit of $G(-C_2H_2) \leq 50$ for the disappearance of acetylene.

Products Observed

Table 1 gives a summary of the gas chromatograph peaks and their probable assignments as determined by mass spectrometry. Although compounds having up to six carbon atoms were assigned with reasonable certainty, above this it became increasingly difficult to determine more than a carbon count. The yields given in Table 1 are taken relative to benzene on the basis of peak areas assuming that relative sensitivities depend only on the number of carbon atoms in the species.

Effect of Pressure and Dose

The yields of benzene obtained for different acetylene pressures and for different numbers of irradiation pulses are given in Table 2. There is no apparent dependence on either pressure or dose within the rather large experimental scatter. A similar behaviour was observed for all C_6 products where again the yields appear to be independent of irradiation dose over the range 10–90 pulses.

Yield of Polymer

Only qualitative observations on polymer formation were made. In a series of experiments acetylene was irradiated in glass cells of a similar size and shape to the aluminum cell and a He–Ne laser beam was shone through the cell. About 2 s after a single irradiation pulse scintillations were observed, and the beam became clearly visible. Despite this evidence for light-scattering particles, we did not observe settling out of a cuprene-like polymer even after more than a hundred pulses. In fact, only a slight blooming of the glass thermal syphon trap on the aluminum cell was noted after more than a thousand pulses had been used to irradiate different samples of acetylene at atmospheric pressure. This is in direct contrast to the low dose rate behaviour where cuprene is seen to settle out after a dose of a few megarads.

Discussion

In an earlier paper (7) a four stage mechanism for the low dose rate radiation chemistry of acetylene was presented. This was: (*i*) *A primary polymerization* of acetylene to form polyunsaturated hydrocarbons with molecular weights in the C_4 to C_{20} range. (*ii*) *A secondary polymerization* of the polyenes initially formed. (*iii*) *A physical condensation* of the polyenes formed by primary and secondary polymerization. (*iv*) *Rapid and extensive polymerization and cross-linking in the liquid polyene droplets*, induced by radiation and leading to the final intractable cuprene product.

The present results lend some support to this mechanism. The observation that the yield per pulse was independent of the number of pulses for all of the products examined implies that no secondary reactions of these products were occurring. Thus the second stage of the mechanism is suppressed and we are seeing the products from the first stage alone, the primary polymerization. This is to be expected at high dose rate since the lifetimes of ions, atoms, and radicals will be greatly reduced because of their high concentrations and consequent fast second order combination reactions. The average ion lifetime in the present experiments is estimated to be of the order of 3×10^{-8} s which will limit even the

TABLE 1. Yields of observed products in acetylene radiolysis

Carbon number	Formula	Probable structure	Relative yield	Yield (*G*-units)	Yield as acetylene loss	Total for group
2	C_2H_2	$HC{\equiv}CH$	—	—	—	—
3	C_3H_4	$H_2C{=}C{=}CH_2$	0.16	0.05	0.08	0.11
	C_3H_6	$CH_3{-}CH{=}CH_2$	0.06	0.02	0.03	
4	C_4H_2	$HC{\equiv}C{-}C{\equiv}CH$	5.63	1.75	3.50	5.24
	C_4H_4	$H_2C{=}CH{-}C{\equiv}CH$	2.81	0.87	1.74	
	C_4H_6	$H_2C{=}CH{-}CH{=}CH_2$	trace	—	—	
5	C_5H_4	$HC{\equiv}C{-}CH{=}C{=}CH_2$	0.01	0.003	0.01	0.41
	C_5H_6	$HC{\equiv}C{-}CH{=}CH{-}CH_3$	0.50	0.16	0.40	
6	C_6H_2	$HC{\equiv}C{-}C{\equiv}C{-}C{\equiv}CH$	1.25	0.39	1.17	3.18
	C_6H_4	$HC{\equiv}C{-}CH{=}CH{-}C{\equiv}CH$	0.37	0.11	0.33	
	C_6H_6	$HC{\equiv}C{-}CH_2{-}CH_2{-}C{\equiv}CH$	0.64	0.20	0.60	
	C_6H_6		1.00	0.31	0.93	
	C_6H_8		trace	—	—	
	C_6H_{10}		0.16	0.05	0.15	
7	C_7H_x	—	0.30	0.09	0.32	1.28
	C_7H_6	—	0.11	0.03	0.11	
	C_7H_8		0.11	0.03	0.11	
	C_7H_x	—	0.22	0.07	0.25	
	C_7H_x	—	0.14	0.04	0.14	
	C_7H_x	—	0.08	0.02	0.07	
	C_7H_x	—	0.20	0.06	0.21	
	C_7H_x	—	0.05	0.02	0.07	
8	C_8H_6	—	0.04	0.01	0.04	0.56
	C_8H_8		0.14	0.04	0.16	
	C_8H_8	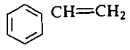	0.22	0.07	0.28	
	C_8H_{10}	—	0.05	0.02	0.08	
9	C_9H_8	—	0.04	0.01	0.05	0.10
	C_9H_8	—	0.03	0.01	0.05	
			Total	4.43	—	10.88

primary polymerization of the acetylene substrate to only a few steps. Product concentrations were always much less than 1% of that of acetylene so that secondary ionic polymerization of products, stage 2 in the low intensity mechanism, was quite negligible. At typical gamma ray dose rates, on the other hand, ion lifetimes would be 10–100 ms and the kinetic chain length in both primary and secondary polymerization would be much longer.

Very similar arguments apply to free-radical polymerization reactions which are also probably operative in acetylene radiolysis. A polymerization propagated by biradicals, however, might still be efficient at high dose rate if termination were first order (e.g. by ring closure, isomerization to a stable molecule, or by internal conversion of a triplet state) rather than second order. Biradical polymerization reactions initiated by the triplet state have been postulated in

TABLE 2. Yield of benzene as a function of pressure and dose

Acetylene pressure (Torr)	Number of pulses	G(benzene)
72	15	0.15
80	30	0.48
260	15	0.44
502	25	0.31
545	5	0.28
632	1	0.27
760	10	0.25
760	30	0.27
760	100	0.34
Average yield = 0.31 ± 0.10		

the pyrolysis of acetylene (5) and are not unlikely in the radiolysis, but the independence of the product yields on dose indicates again that reaction with products was negligible. It is possible that triplet–triplet annihilation becomes an important loss process which reduces the biradical lifetime at high intensity.

In low intensity radiolysis of acetylene benzene was the only volatile product of any importance. This was confirmed in the present work by a few experiments in which acetylene was irradiated with gamma rays, which showed that even at the lowest conversions, only negligible traces of other products were detectable with the same analytical techniques used in the Febetron experiments. It was suggested previously that benzene was the only volatile product not because it was the only one formed but because it is relatively unreactive towards secondary polymerization. The present results support this suggestion as it seems probable that many of the volatile polyunsaturated products observed in the present study were also transient intermediates in the low intensity radiolysis. It should be noted, however, that the distribution of the primary products was probably quite different in the two systems, as the primary polymerization may have been much attenuated at high intensity as noted earlier.

The average yield of benzene, G(benzene) = 0.31 ± 0.10, is very much smaller than the value of 5 ± 1 observed at low dose rate, perhaps reflecting the reduced extent of primary polymerization. Many reaction sequences were apparently limited to a single step, yielding C_4 products, which at low dose rate might have proceeded further to yield benzene or higher products. Both the product distribution and the G-value of about 4.4 for the total of all the volatile products observed demonstrate the absence of long chain reactions.

It is difficult to account quantitatively for the products observed although some generalizations can be offered. Table 3 shows the main ion–molecule sequences which will occur following the initial generation of primary species. The yields are derived from the W-value of 24 eV per ion pair (8) and mass spectral abundances (9). The various reaction sequences were identified by Derwish *et al.* (9) using high pressure mass spectrometry. Although the rates of the first stage reactions are reasonably well known, with values of the order of 3×10^{-10} cm^3 molecule^{-1} s^{-1}, the rates of subsequent stages are much less certain although it is apparent that the reaction rates decrease as polymerization proceeds. For ion lifetimes with respect to charge neutralization of approximately 3×10^{-8} s it seems very doubtful that any primary ions or those produced in the first stage took part in neutralization which probably involved ions of C_6 and higher carbon numbers. What is clear from the suggested reaction sequence is that the ions all tend to be less hydrogenated than the substrate, an effect which will be enhanced since neutralization will tend to decrease rather than increase the hydrogen content. The yields of species predicted from the data given in Table 3 are very much larger than were observed and either our yield measurements are very wrong or the majority of products formed by ion–molecule sequences are not being detected.

Similar problems are encountered with a quantitative accounting for products from neutral processes. The ion–molecule sequence given in Table 3 will generate a yield of H-atoms in excess of 6 G-units and presumably more are formed by dissociative excitation processes,

$$C_2H_2 \rightsquigarrow C_2H + H$$

A series of workers have investigated the reactions of H-atoms with acetylene and suggest that the main ultimate products are benzene and polymer (see, for example, ref. 10). Quantitative rate data are not available, but simple arguments suggest that yields of these products are much lower than expected from the estimated yield of H-atoms. Again, if chain reactions are involved, they may be minimized at the high dose rates employed, accounting for the low yields.

TABLE 3. Main ion–molecule sequences in acetylene radiolysis

Yield	Primary event	First stage reaction*	Second stage	Third stage
2.96	$C_2H_2^+ + e$	$(1.97)C_4H_3^+ + H \rightarrow$	$C_6H_5^+ \rightarrow$	$C_8H_7^+$
		$(0.99)C_4H_2^+ + 2H \rightarrow$	$C_6H_4^+ \rightarrow$	$C_8H_6^+$
0.48	$C_2H^+ + H + e$	$(0.23)C_4H_2^+ + H \rightarrow$	$C_6H_4^+ \rightarrow$	$C_8H_6^+$
		$(0.16)C_2H_3^+ + C_2 \rightarrow$	$C_3H_3^+ + CH_2 \rightarrow$	$C_5H_3^+ + H_2$
		$(0.09)C_4H^+ + H_2 \rightarrow$	$C_6H_2^+ + H \rightarrow$	$C_8H_4^+$
0.16	$C_2^+ + 2H + e$	$(0.07)C_4H^+ + H \rightarrow$	$C_6H_2^+ + H \rightarrow$	$C_8H_4^+$
		$(0.09)C_3H_2^+ + C \rightarrow$	$C_5H_3^+ + H \rightarrow$	$C_7H_5^+$
0.16	$C^+ + CH_2 + e$	$(0.40)C_3H^+ + H(+H) \rightarrow$	$C_5H_2^+ + H \rightarrow$	$C_7H_4^+$
0.24	$CH^+ + CH + e$			

*Yields are given in parentheses.

The production of vinyl acetylene and diacetylene can most easily be attributed to reactions of excited states,

$$C_2H_2^* + C_2H_2 \rightarrow C_4H_4 \text{ and } C_4H_2 + H_2$$

but it is difficult to assess the possible contribution from other sources. Reaction of triplet $C_2H_2^*$ formed by cadmium photosensitization (11) yielded only benzene and vinyl acetylene. The mercury-photosensitized decomposition, which can form both free radicals and the triplet state (12) gave benzene, vinyl acetylene, H_2, C_2H_4, diacetylene, cyclooctatetrene, and polymer (13). Direct photolysis (14, 15) which would proceed through the singlet $C_2H_2^*$ and probably free radicals gave relatively large amounts of diacetylene. It is clear that a variety of concurrent processes could be and probably are operating in the high-intensity radiolysis and there is no difficulty in writing plausible sequences of addition, combination, and abstraction reactions of free radicals and excited molecules leading to the products observed.

There is about a 20% deficit of hydrogen in the observed products which probably lies beyond the errors in analysis. Low limits can be put on the yields of H_2 and CH_4 as the irradiated samples were totally condensible in liquid nitrogen and ethane and ethylene were not detected by gas chromatography. One possible explanation of the hydrogen deficit is the dehydrogenation of some unstable polyunsaturated compounds in the heated inlet of the gas chromatograph, a process previously observed with vinyl acetylene, and it must be recognized that some of the highly unsaturated compounds reported (e.g. C_6H_2, C_4H_2) may not be entirely true primary products of the radiolysis. However, it is also possible that hydrogen-rich higher hydrocarbons, undetected by our analysis, could account for the deficit.

Finally, despite our conclusions that at high dose rate secondary polymerization is virtually eliminated and primary polymerization much attenuated, physical condensation, probably of liquid droplets, was observed within a couple of seconds after a single pulse of radiation. These droplets persisted for several hours, suspended in the gas, only detectable by their scattering of a laser beam. We have not been successful in further characterizing this high molecular weight fraction. It probably accounts for the product deficit noted in conjunction with the ion–molecule chemistry and with the H-atom chemistry. It can be shown on the basis of simple vapor pressure arguments that the molecular weight of these condensing species must be above C_{12}, and they were not observed by our analytical procedure.

1. (*a*) S. C. LIND and D. C. BARDWELL. Science, **62**, 422 (1925); (*b*) W. D. COOLIDGE. Science, **62**, 441 (1925); (*c*) S. C. LIND, D. C. BARDWELL, and J. H. PERRY. J. Am. Chem. Soc. **48**, 1556 (1926).
2. F. H. FIELD. J. Phys. Chem. **68**, 1039 (1964).
3. J. H. FUTRELL and L. W. SIECK. J. Phys. Chem. **69**, 892 (1965).
4. D. YASHIRO and T. NAITO. Reports of the Government Chemical Industrial Research Institute, Tokyo, Japan. Vol. 62. 1967. p. 91.
5. C. F. CULLIS and N. H. FRANKLIN. Proc. R. Soc. London, Ser. A, **280**, 139 (1964).

6. C. WILLIS, A. W. BOYD, and O. A. MILLER. Radiat. Res. **46**, 428 (1971).
7. J. P. BRIGGS and R. A. BACK. Can. J. Chem. **49**, 3789 (1971).
8. L. G. CHRISTOPHOROU. Atomic & molecular radiation physics. Wiley-Interscience, New York, NY. 1971. p. 37.
9. G. A. W. DERWISH, A. GALLI, A. GIARDINI-GUIDONI, and G. G. VOLPI. J. Am. Chem. Soc. **87**, 1159 (1965).
10. J. K. CASHION and D. J. LEROY. Can. J. Chem. **32**, 906 (1954); D. J. LEROY. J. Chem. Phys. **45**, 3482 (1966).
11. S. TSUNASHIMA and S. SATO. Bull. Chem. Soc. Jpn. **41**, 2281 (1968).
12. C. S. BURTON and H. E. HUNZIKER. J. Chem. Phys. **57**, 339 (1972).
13. S. SHIDA and M. TSUKADA. Bull. Chem. Soc. Jpn. **43**, 2740 (1970).
14. M. TSUKADA and S. SHIDA. Bull. Chem. Soc. Jpn. **43**, 3621 (1970).
15. S. TAKITA, Y. MORI, and I. TANAKA. J. Phys. Chem. **73**, 2929 (1969).

The crystal structure of bis(diethylamino)dithiaboretane, a compound with a four-membered alternating boron–sulfur ring

G. W. BUSHNELL AND G. A. RIVETT

Chemistry Department, University of Victoria, Victoria, B.C., Canada V8W 2Y2

Received January 19, 1977

G. W. BUSHNELL and G. A. RIVETT. Can. J. Chem. **55**, 3294 (1977).

The crystal structure of bis(diethylamino)dithiaboretane, $C_8H_{20}B_2N_2S_2$, is determined by single crystal X-ray diffraction and refined to $R = 0.120$, $R_w = 0.091$ for 373 independent reflections. The tetragonal cell dimensions are $a = 10.396(3)$, $c = 25.589(7)$. The space group is $P_{4_12_12}$ (No. 92) or its enantiomorph (No. 96); $D_m = 1.08(8)$, $D_c = 1.10$ g cm^{-3}; $n = 8$. The asymmetric unit is one half of a pair of molecules. Both molecules have approximate symmetry 222 with one of these symmetry elements being a crystallographic axis. The latter passes through all the B and N atoms of molecule 1, and is perpendicular to the B,S ring of molecule 2. The four-membered B,S rings are planar. The nitrogen coordination is trigonal, planar, and set at $<10°$ to the ring planes within each molecule. The mean bond lengths are: B—S = 1.84(4), B—N = 1.38(5) Å, and the mean bond angles: S—B—S = 105(3)°, B—S—B = 76(2)°. The results suggest single B—S and double exocyclic BN bonds.

G. W. BUSHNELL et G. A. RIVETT. Can. J. Chem. **55**, 3294 (1977).

La structure cristalline du bis(diéthylamino)dithiaborétane, $C_8H_{20}B_2N_2S_2$, est déterminée à l'aide d'un seul cristal par diffraction aux rayons X et affinée à $R = 0.120$, $R_w = 0.091$ pour 373 réflections indépendantes. Les dimensions de la cellule tétragonale sont $a = 10.396(3)$, $c = 25.589(7)$. Le groupe spatial est $P_{4_12_12}$ (No. 92) ou son énantiomorphe (No. 96); $D_m = 1.08(8)$, $D_c = 1.10$ g cm^{-3}; $n = 8$. L'unité asymétrique est la moitié de la paire de molécules. Les deux molécules ont une symétrie approximative de 222 dont l'un des éléments de symétrie est un axe cristallographique. Cet axe passe par tous les atomes B et N de la molécule 1 et est perpendiculaire au cycle B,S de la molécule 2. Les cycles B,S à quatre chaînons sont planaires. La coordination de l'atome d'azote est trigonale, planaire et fait un angle de 10° avec les plans des cycles à l'intérieur de chaque molécule. La longueur moyenne des liaisons principales ainsi que les angles formés entre ces liaisons sont: B—S = 1.84(4), B—N = 1.38(5) Å, S—B—S = 105(3)°, B—S—B = 76(2)°. Les résultats suggèrent une simple liaison B—S et une double liaison BN exocyclique.

[Traduit par le journal]

Introduction

The dithiaboretane ring system has been known for many years, but no X-ray structure determination has been done. In 1966, Forstner and Muetterties (1) reported a synthesis of bis-(diethylamino)dithiaboretane, **1**, by the reaction of H_2S with triethylamine borane. The crystal structure of **1** was undertaken to confirm the structure and investigate the geometry and bonding of the four-membered ring system.

Preparation

The literature method (1) yielded $(Et_2NBS)_3$, $(m/e)_{max} = 347$ in the mass spectrum. To obtain **1**, conditions were modified as follows: molar ratio H_2S: $Et_3NBH_3 = 4.3$, reaction time = 24 h at 175°C, sublimation temperature = 75°C, yield 50%. Identification was by mass, infrared, and proton magnetic resonance spectra. Crystals were obtained by cooling a solution in *n*-pentane. A dry box was used for all manipulations, as the compound is unstable in air.

Experimental Crystallography

The crystal data are shown in Table 1. Compound **1** formed tetragonal tablets showing the faces {110},{001}.

A large single crystal was measured and weighed to obtain the density. Smaller crystals were wedged into Lindemann tubes and sealed in with black wax. Over 40 crystals were mounted, of which 4 were single crystals. Three of these were used for photography, while the best crystal with dimensions 0.4 × 0.4 × 0.1 mm (shortest dimension along C) was used on the diffractometer. The crystals were mounted with the 1,1,0 planes approximately parallel to the axes of the Lindemann tube and the goniometer head. The space group $P_{4_12_12}$ (No. 92) is enantiomorphous with $P_{4_32_12}$ (No. 96) and no attempt to distinguish between these alternatives was made. The unit cell was refined by least-squares using diffractometer measurements at $\pm 2\theta$ for 28 reflections. A C-centred tetragonal cell was used for the intensity measurements only, which were done on a manual Picker 4-circle diffractometer using Zr-filtered Mo radiation ($\lambda = 0.71069$ Å). All reflections in one octant up to $2\theta = 30°$

TABLE 1. Crystal data for bis(diethylamino)dithiaboretane

System	Tetragonal
Space group	$P_{4_12_12}$, No. 92 (or $P_{4_32_12}$, No. 96)
Molecular weight	230.01 g mol^{-1}
Cell dimensions	$a = 10.396 \pm 0.003$ Å $b = 10.396 \pm 0.003$ Å $c = 25.589 \pm 0.007$ Å $\alpha = \beta = \gamma = 90.00°$
Cell volume	2765 × 10^{-24} cm^3
Density (measured)	1.08 ± 0.08 g cm^{-3}
Density (calculated)	1.10 g cm^{-3}
Molecules per cell	8
Absorption coefficient (MoK$_\alpha$)	3.43 cm^{-1}

were measured. Scans were in the $\theta/2\theta$ mode for 1 min, at 2° in 2θ min^{-1}. Background measurements were for 30 s at each extremity of the scan. Reflection 8,0,0 which was measured hourly as the standard reflection, had an intensity of 45 200 counts initially, falling to 9600 counts at the end of the data collection 59 h later. In the X-ray beam the material lost crystallinity in 2–5 days by a process which seemed to start where the crystal touched the glass. The crystal orientation was checked frequently and adjustments were necessary. Lorentz and polarization factors were applied and the intensities were corrected for crystal deterioration using the current intensity of the standard reflection. The indices were transformed to correspond to the primitive unit cell. As the Laue symmetry was 4/*mmm*, pairs of equivalent reflections were averaged. Four pairs of reflections showed differences in $|F_o|$ greater than 5% and were rejected. The final data set contained 373 reflections.

Structure Determination

The structure was solved by conventional Patterson and Fourier methods. All atomic scattering curves were from the *International Tables for X-Ray Crystallography* (2) with the atoms assumed to be uncharged. The programs used were supplied by Penfold (3). The refinement minimized $w(|F_o| - |F_c|)^2$ by full matrix least squares initially with unit weights. In the final stages of refinement, through analysis of $w\Delta^2$, a weighting scheme $w = (25/|F_o|)^2$ was employed. No significant shifts in positional or thermal parameters were observed. The final agreement factors were $R = 0.120$, $R_w = 0.091$ for all reflections and $R = 0.109$, $R_w = 0.088$ when those reflections for which $I < \sigma(I)$ were omitted. The final difference synthesis, with a maximum of 0.38 e Å^{-3} and $\sigma(\rho) = 0.18$ e Å^{-3}, gave no evidence of misplaced atoms. The structure factor table has been deposited.[1] The fractional atomic coordinates and isotropic temperature factors are given in Table 2.

[1]Copies may be obtained, at a nominal charge, from the Depository of Unpublished Data, CISTI, National Research Council of Canada, Ottawa, Canada K1A 0S2.

Results

One unit cell and its contents are shown in Fig. 1 with the atoms of the asymmetric unit labelled. For descriptive purposes, consider the twofold rotation axes in space group $P_{4_12_12}$ lying diagonally in the planes $Z = 0$, $Z = \frac{1}{4}$, $Z = \frac{1}{2}$, and $Z = \frac{3}{4}$. A pair of molecules occurs at each Z level, and the asymmetric unit is one-half of such a pair. In one molecule the twofold axis passes through the atoms NBBN and in the other molecule this same axis is perpendicular to the plane of the four-membered ring and passes through its centre. The symmetry of both molecules is approximately 222. All intramolecular S–S vectors are at a small angle (< 10°) to the c axis. The bond lengths and angles are given in Table 3 and the mean planes in Table 4. Assuming the covalent radii for B, N, and S to be 0.85, 0.70, and 1.04 Å, respectively, the single bond length for B—N is 1.55 Å, and B—S 1.89 Å.

A suitable reference compound for the single B—S bond is $(BrBS)_3$ (4) B—S = 1.74–1.88 (3). A double bond length of 1.5994(4) for B=S has been measured by microwave spectroscopy on thioborine H—B=S (5). The mean bond length of 1.84(4) in compound **1** indicates single bonding.

Single B—N bonds have been observed in many compounds, a good example being cyclotriborazane (6) B—N = 1.576(2) Å corrected for thermal motion. In borazine (7), where multiple bonding is expected, BN = 1.4355(21) Å. The microwave spectrum (8) of aminodifluoroborane $F_2B{=}NH_2$, shows that the molecule is planar and gives 1.402(24) Å for B=N. The BN lengths for compound **1** indicate double bonding.

Table 4 shows the planarity of the four-membered rings and of the nitrogen atom coordination. Where $\chi^2 = 0$, crystallographic symmetry ensures perfect planarity. The nitrogen planes are rotated by ±9.4° from the ring plane in the case of the molecule containing S1. In the molecule containing S2, the ring plane is only 2.9° from the nitrogen plane. Near-coplanarity of the ring plane and the nitrogen coordination plane is necessary for N—B π-bonding. The B octet is thus completed by $p\pi$–$p\pi$-bonding between first row elements, rather than by B—S π-bonding.

The mean angles are 76(2)° for BSB and 105(3)°

TABLE 2. Fractional atomic coordinates and isotropic thermal parameters for bis(diethylamino)dithiaboretane*

Atom	X	Y	Z	U_{iso} (Å^2)
S1	0.3793(8)	−0.3845(9)	0.3072(4)	0.067(4)
S2	−0.1112(8)	0.1214(8)	0.3059(3)	0.060(3)
C1	0.140(3)	−0.174(3)	0.301(1)	0.06(1)
C2	0.013(3)	−0.237(4)	0.310(1)	0.10(1)
C3	−0.380(3)	0.404(3)	0.300(1)	0.08(1)
C4	−0.256(3)	0.473(3)	0.313(1)	0.09(1)
C5	0.106(3)	0.351(3)	0.295(1)	0.06(1)
C6	0.233(3)	0.271(4)	0.306(1)	0.11(1)
C7	0.086(3)	0.343(3)	0.193(1)	0.09(1)
C8	0.022(3)	0.474(3)	0.180(1)	0.09(1)
B1	0.31(1)	−0.31(1)	0.2500	0.12(2)
B2	0.454(8)	−0.454(8)	0.2500	0.11(2)
B3	−0.039(3)	0.201(3)	0.247(1)	0.06(1)
N1	0.212(5)	−0.212(5)	0.2500	0.06(1)
N2	−0.448(5)	0.448(5)	0.2500	0.08(1)
N3	0.049(2)	0.291(2)	0.245(1)	0.072(8)

*Temperature factor = exp $(-8\pi^2 U_{iso} \sin^2\theta/\lambda^2)$. Standard deviations are given in the units of the last decimal place.

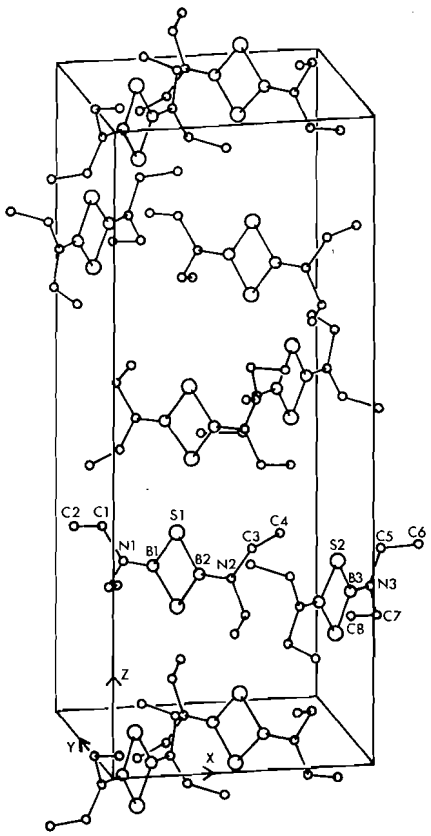

FIG. 1. The unit cell of bis(diethylamino)dithiaboretane.

TABLE 3. Bond lengths and angles

Bond	Length (Å)	Bonds	Angle (deg)
S1—B1	1.83(4)	S1—B1—S1′	106(4)
S1—B2	1.81(4)	S1—B2—S1′	108(3)
S2—B3	1.85(4)	S2—B3—S2′	101(2)
S2—B3′	1.87(4)	B1—S1—B2	73(2)
B1—N1	1.39(6)	B3—S2—B3′	79(2)
B2—N2	1.44(5)	S1—B1—N1	127(2)
B3—N3	1.32(3)	S1—B2—N2	126(2)
N1—C1	1.55(3)	S2—B3—N3	130(3)
		S2′—B3—N3	130(3)
N2—C3	1.54(3)	B1—N1—C1	122(2)
N3—C5	1.48(3)	B2—N2—C3	122(2)
N3—C7	1.54(3)	B3—N3—C5	119(3)
C1—C2	1.52(4)	B3—N3—C7	119(3)
C3—C4	1.49(4)	N1—C1—C2	116(3)
C5—C6	1.59(4)	N2—C3—C4	116(3)
C7—C8	1.55(4)	N3—C5—C6	105(2)
		N3—C7—C8	114(3)

TABLE 4. Mean planes in bis(diethylamino)-dithiaboretane*

Plane	Defining atoms	χ^2
1	N1, B1, S1, N2, B2, S1′	0
2	C1, C1′, N1, B1	0
3	C3, C3′, N2, B2	0
4	S2, B3, S2′, B3′	5.9
5	C5, C7, N3, B3	1.8

*Angles between planes 1,2 = 9.4°; 1,3 = −9.4°; 4,5 = −2.9°. $\chi^2 = \sum_i (p_i^2/[\sigma_i(p)^2])$, where p_i = the perpendicular distance of the atom (i) from the mean plane.

for SBS and seem to be strained equally and by approximately 15° from 90° and 120°. The bond angles at the nitrogen atoms are very close to 120°.

Conclusion

The structure proposed by Forstner and Muetterties (1) is confirmed. The accuracy of the structure is limited by experimental difficulties but the molecular geometry and the bond lengths taken in conjunction suggest double bonding in the exocyclic BN bonds and single bonding in the ring.

Acknowledgments

The authors are grateful to Dr. S. G. Gibbins, who helped initiate this work, and provided vacuum line facilities. Operating grants were obtained from the National Research Council of Canada and the University of Victoria Faculty Research Funds.

1. J. A. FORSTNER and E. L. MUETTERTIES. Inorg. Chem. **5**, 164 (1966).
2. J. A. IBERS (*Editor*). International tables for X-ray crystallography. Vol. III. Kynoch Press, Birmingham. 1962. p. 201, Table 3.3.1.A.
3. B. R. PENFOLD. University of Canterbury Crystallographic Programs, Christchurch, New Zealand.
4. W. SCHWARZ, H.-D. HAUSEN, and H. HEINZ. Z. Naturforsch. Teil B, **29**, 596 (1974).
5. E. F. PEARSON and R. V. MCCORMICK. J. Chem. Phys. **58**, 1619 (1973).
6. P. W. R. CORFIELD and S. G. SHORE. J. Am. Chem. Soc. **95**, 1480 (1973).
7. W. HARSHBARGER, G. LEE, R. F. PORTER, and S. H. BAUER. Inorg. Chem. **8**, 1683 (1969).
8. F. J. LOVAS and D. R. JOHNSON. J. Chem. Phys. **59**, 2347 (1973).

Structures of toxic constituents in kraft mill caustic extraction effluents from ^{13}C and ^{1}H nuclear magnetic resonance

A. N. THAKORE
B.C. Research, 3650 Wesbrook Mall, Vancouver, B.C., Canada V6S 2L2
AND
A. C. OEHLSCHLAGER
Department of Chemistry, Simon Fraser University, Burnaby, B.C., Canada V5A 1S6

Received May 6, 1977

A. N. THAKORE and A. C. OEHLSCHLAGER. Can. J. Chem. **55**, 3298 (1977).

Arguments based on ^{13}C and ^{1}H nmr spectroscopy are presented to elucidate the structures of 3,4,5- and 4,5,6-trichloroguaiacol, 12- and 14-monochlorodehydroabietic acid, and 12,14-dichlorodehydroabietic acid. These compounds were recently isolated and tentatively identified as major components toxic to fish in kraft mill caustic extraction effluents.

A. N. THAKORE et A. C. OEHLSCHLAGER. Can. J. Chem. **55**, 3298 (1977).

On présente une discussion basée sur la spectroscopie rmn du carbone ^{13}C et du proton ^{1}H afin d'éclaircir la structure des composés suivants: les trichloro-3,4,5 et -4,5,6 guaiacols, les acides monochloro-12 et -14 déhydroabiétiques et l'acide dichloro-12,14 déhydrobiétique. Ces composés ont été récemment isolés des eaux s'écoulant d'une usine de pâte et papier et identifiés comme étant les produits toxiques majeures responsables de l'empoisonnement des poissons.
[Traduit par le journal]

Introduction

In a typical pulping process, the unbleached pulp becomes fully bleached in five or six sequential stages designated CEHDED, where C is chlorination, E is caustic extraction, H is hypochlorite, and D is chlorine dioxide. Effluents produced by washing the pulp after each stage are combined into acid and caustic streams before being sewered. In the present work the elucidation of the structures of chlorinated compounds previously isolated from the caustic stream and found to be responsible for a major part of the effluent toxicity to fish (1) are presented. The compounds discussed were isolated from the caustic effluent by the fractionation procedure outlined in Fig. 1 and explained in detail in previous reports (1). Toxicity of the effluent was traced during the fractionation by 96 h bioassays with juvenile rainbow trout as previously described (1). Since exact structures of several of the compounds isolated have not been reported in the literature we wish to present arguments based on ^{13}C and ^{1}H nmr spectral data which lead to structural assignments.

Results and Discussion

Column and thin layer chromatographic fractionation of the acidic portion of the effluent (Fig. 1) yielded two apparently fish-toxic compounds (**1** and **2**, never isolated from the same sample of effluent) mass spectral analysis of which showed each had a molecular ion peak *m/e* 226, together with $(M^+ + 2)$ and $(M^+ + 4)$ peaks, in the ratio of 3:3:1. Methylation of these effluent derived toxicants (**1** and **2**) with diazomethane gave the same dimethoxy derivative (**3**, $M^+ = 240$), which had methoxyl resonances at δ 3.93 and a downfield signal due to an aromatic proton at δ 6.88. The proton magnetic resonance spectrum of the least polar isomer (**1**) contained signals due to one methoxyl group (δ 3.92), one exchangeable hydrogen (δ 5.90), and one aromatic hydrogen (δ 6.88), whereas the more polar isomer (**2**) gave resonances at δ 5.08 (D_2O exchangeable), and δ 7.05 (aromatic), and a methoxyl signal at δ 3.92. On this evidence effluent derived **1** and **2** were believed to be trichloroguaiacol isomers.

Controlled chlorination of guaiacol gave only one crystalline trichloroguaiacol which was identical by mass and nmr spectroscopy to **1** isolated from caustic effluent. Methylation of the synthesized trichloroguaiacol gave a veratrol derivative that was identical to **3**. Attempts to synthesize **2** by chlorination of guaiacol failed.

An additional toxic constituent isolated from

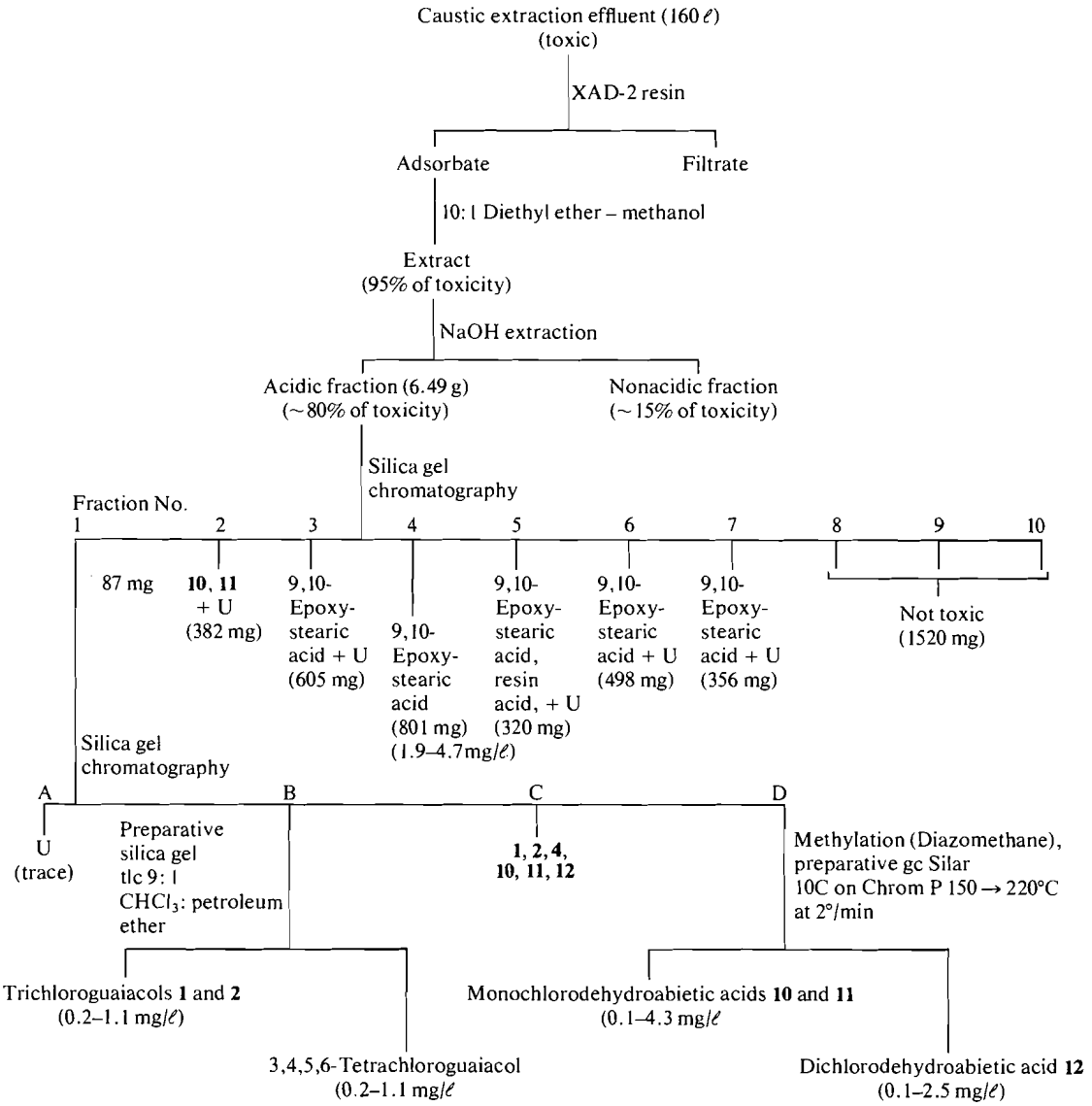

FIG. 1. Fractionation scheme for caustic extraction effluent and calculated concentrations of toxicants (1). U = unidentified constituents.

the same fraction of effluent as **1** and **2** was found by mass spectroscopic analysis to have a molecular weight of 260 with a M^+:(M^+ + 2):(M^+ + 4):(M^+ + 6) peak ratio of 1:1.3:0.6:0.1 indicating the presence of four chlorines. The proton magnetic resonance spectrum of this compound (**4**) contained signals due to one exchangeable hydrogen (δ 6.00) and one methoxyl group (δ 3.97). On the basis of the above data it was considered likely that **4** was tetrachloroguaiacol. Chlorination of guaiacol under vigorous conditions according to the method of Sarkanen and Dence (3) yielded a tetrachloroguaiacol, which was identical to **4** on the basis of nmr and mass spectroscopic analysis and by mixture melting point. Methylation of both the synthetic and isolated tetrachloroguaiacol **4** gave the same veratrole derivative **5** (M^+ = 274).

Structure determination of trichloroguaiacols **1** and **2** involved comparison of the ^1H and ^{13}C magnetic resonance spectra of **1**–**5**, guaiacol **6**, and veratrole **7**. A priori four trichloroguaiacol

TABLE 1. ^1H and ^{13}C chemical shifts*† of guaiacol derivatives

Compound No.	OCH_3	C_1OCH_3	C_2OCH_3	C_1	C_2	C_3	C_4	C_5	C_6
1	3.92	56.7	—	147.4	143.8	120.8	124.8	124.8	109.7
2	3.92	61.3	—	148.6	145.8	115.5	126.4	128.4	125.5
3	3.93	56.9	66.1	152.0	145.3	125.1	128.1	128.6	109.2
4	3.97	61.5	—	147.0	144.2	115.4	120.9	124.4	109.4
5	3.95	61.5	61.5	149.8	149.8	127.5	128.2	128.2	127.5
6	3.63	56.3	—	147.2	146.2	115.3	120.8	121.8	111.9
7	3.77	55.5	55.5	148.4	148.4	109.4	120.6	120.6	109.4

*Shifts pertain to nuclei underlined at the top of each column.
†Shifts reported in ppm relative to tetramethylsilane.

isomers **1**, **2**, **8**, **9** are possible. Although it is known (4) that substitution patterns influence the ^1H chemical shift of aromatic bound methoxyls, no significant differences were observed in the chemical shifts of the methoxyls of **1**, **3**, and **4** which would allow us to deduce the substitution patterns in **1** and **3**. However, examination of the ^{13}C magnetic resonance spectra of **1**–**7** revealed correlations in the chemical shifts of the methoxyl carbons as reported in Table 1.

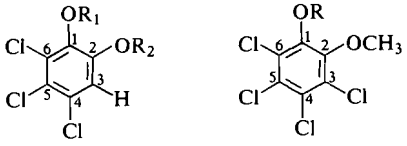

1 $R_1 = H, R_2 = CH_3$
2 $R_1 = CH_3, R_2 = H$
3 $R_1 = R_2 = CH_3$

4 R = H
5 R = CH_3

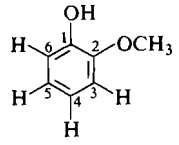

6

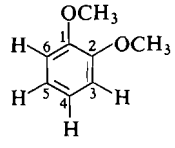

7

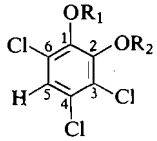

8 $R_1 = H; R_2 = CH_3$
9 $R_1 = CH_3; R_2 = H$

The data show that in tetrachloroguaiacol **4** and tetrachloroveratrole **5** the methoxyl carbons are deshielded relative to their nonchlorinated analogs (**6** and **7** respectively). This observation is analogous to that of Stothers *et al.* (5) who observed a downfield chemical shift of aromatic alkoxyl carbon resonances upon di-*ortho* substitution. The methoxyl carbon resonance of **1** does not indicate this deshielding effect whereas one of the methoxyl resonances in its methylated derivative **3** is deshielded. From these observations one can deduce that **1** possesses an aromatic hydrogen adjacent to its methoxyl and a chlorine adjacent to its hydroxyl. This uniquely defines the structure of **1**.

The carbon resonance attributable to the methoxyl of **2** is deshielded compared to **1**, guaiacol **6**, or veratrole **7**. This suggests that a chlorine is situated adjacent to the methoxyl of **2**. Since treatment of **2** with diazomethane yields a chlorinated veratrole identical with **3** (derived from **1**) compound **2** is uniquely defined.

The assignment of the aromatic ^{13}C resonances for **1**–**7** given in Table 1 are based on internal comparisons within the series and not on calculation, which for *ortho* substituted aromatics gives approximate results at best (6).

Since several unsuccessful attempts were made to synthesize **2** by chlorination of guaiacol it is considered unlikely that **2** is produced by direct chlorination of guaiacol during pulp bleaching. A more likely route for formation of **2** is considered to be dealkylation of chlorinated alkyl guaiacols present in the pulp slurry during the bleaching stage. The present experimental results indicate that a likely route for formation of **1** is chlorination of guaiacol during the first bleaching stage.

As shown in Fig. 1 silica gel chromatography of the acidic fraction of caustic extraction effluent yielded fractions containing both mono- (**10** and **11**) and dichlorodehydroabietic (**12**) acids. Methylation (diazomethane) of the fraction containing the chlorinated resin acids followed by preparative glpc facilitated separation of the mono- from dichloro derivatives. Gas–liquid partition chromatography also revealed that the methyl monochlorodehydroabietate was a separable 2:1 mixture of two isomers.

Controlled chlorination of dehydroabietic acid gave a 2:1 mixture of two crystalline monochlorodehydroabietic acids. Methylation of this mixture with diazomethane gave a mixture of methyl monochlorodehydroabietates which by nmr and gc/ms was identical to the mixture of **10** and **11** isolated from caustic extraction effluent.

Chlorination of dehydroabietic acid with excess chlorine gave only one dichlorodehydroabietic acid which was identical to **12** by mixture melting point, nmr, and mass spectroscopic analysis. Methylation of both synthetic and effluent derived **12** gave methyl esters that were identical when examined by gc/ms. The structures of **10** and **11** as well as that of the methyl dichlorodehydroabietate **12** were determined by comparison of their ^{1}H nmr spectra with those of dehydroabietic acid **13** and trichlorodehydroabietic acid **14**. The latter derivative was prepared by halogenation of **13** with an excess of chlorine. Integration of the aromatic region in the ^{1}H nmr spectra of **10–14** indicated that chlorination of **13** (to produce **10**, **11**, **12**, and **14**) occurred exclusively in the aromatic ring.

Examination of data in Table 2 indicates significant deshielding (δ 1.22 → δ 1.52) of the C-10 methyl in **14** (compared to the C-10 methyl of dehydroabietic acid, **13**) due to the chlorine atom at C-11. The observation that this deshielding does not occur in the dichloro derivative, **12**, uniquely defines the position of chlorine atoms to be C-12 and C-14. Structures can be assigned to the monochlorodehydroabietic acid isomers on the basis of the above deductions and the observation that the aromatic resonances of the methyl ester of one monochloro isomer appear as a two hydrogen singlet (δ 7.14) and the corresponding resonances in the other occur as two single hydrogen singlets (δ 7.03, 6.89). These latter signals cannot be due to two *ortho* hydrogens (no coupling observed) hence they must be due to two *para* hydrogens. The isomer yielding the methyl ester with aromatic resonances at δ 7.03 and δ 6.89 must therefore be **11**. The sequence of chlorination of dehydroabietic acid in the kraft mill bleach plant and in the laboratory synthesis can therefore be deduced as shown in Scheme 1.

TABLE 2. ^{1}H nmr chemical shifts* of methyl groups in dehydroabietic acid and its chlorinated derivatives

Compound No.	C_4-CH_3	C_{10}-CH_3	$C_{15}(CH_3)_2$†
10	1.28	1.22	1.24
11	1.28	1.22	1.26
12	1.28	1.22	1.41
13	1.28	1.22	1.23
14	1.32	1.52	1.41

*Shifts reported in ppm relative to tetramethylsilane internal standard.
†Doublet, J = 7 Hz.

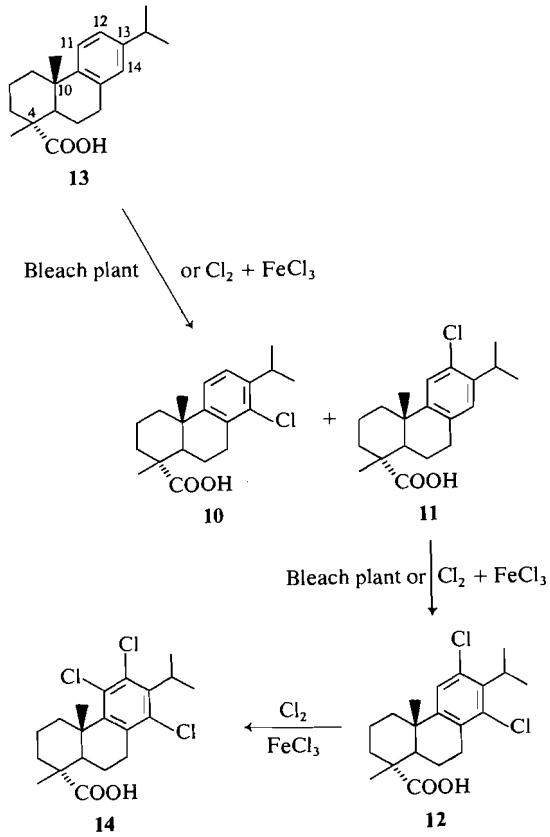

SCHEME 1

Experimental

General

Gas–liquid partition chromatography (glpc) was carried out on a Perkin-Elmer Model 881 instrument fitted with dual flame ionization detectors. Stainless steel (ss) columns (6 ft × ⅛ in.) were used containing 10% (w/w) Silar-10C on 100–120 mesh Gas Chrom P.

Gas chromatography – mass spectrometry was carried out using a 10% Silar-10C column in a Varian Associates Model 1400 Aerograph GC connected via a glass interface to a Hitachi Perkin-Elmer RMU-GE mass spectrometer.

Proton nuclear magnetic resonance (^{1}H nmr) spectra were obtained on a Varian A 56/60 spectrometer in deuteriochloroform solution using tetramethylsilane (TMS) as an internal standard. ^{13}C magnetic resonance spectra (^{13}C nmr) were taken at 25.2 MHz on a Varian XL-100

Fourier transform spectrometer. Chemical shifts for ^{13}C nmr spectra are in ppm downfield from TMS. In deuteriochloroform solution $\delta(TMS) = \delta(CDCl_3) + 77.6$ ppm.

Melting points (mp) were measured on a Kofler hot stage apparatus.

Synthesis of Toxicants

Guaiacol **6** was purchased from MCB Chemicals. Pure dehydroabietic acid **11** was isolated from a commercial preparation of dehydrogenated wood resin according to the method described by Halbrook and Lawrence (2). Methylations were carried out on guaiacol and dehydroabietic acid derivatives with diazomethane (in ether) which was generated by base treatment of *N*-nitroso-*N*-methyl urea.

4,5,6-Trichloroguaiacol 1

Trichloroguaiacol **1** isolated from caustic extraction effluent (1) had mp 105–107°C. A melting point of 107–108°C is given (7) for one trichloroguaiacol isomer generated on methylation of 3,4,5-trichlorocatechol.

An authentic sample was obtained by treating guaiacol (0.1 mol) with chlorine (0.3 mol) in acetic acid (500 ml) at room temperature for 1 h. The product was isolated by concentration of the reaction mixture *in vacuo* and crystallization three times from petroleum ether to give 4,5,6-trichloroguaiacol (**1**, yield 30%); mp 105–107°C; ^1H nmr δ 6.88 (1H, s, aromatic), 5.90 (1H, s, D_2O exchangeable hydrogen), and 3.92 (3H, s, OCH_3); ms *m/e* 226 (M^+), 228 ($M^+ + 2$), 230 ($M^+ + 4$), ratio 3:3:1 for M^+, ($M^+ + 2$), ($M^+ + 4$) peaks. Mixture melting point of **1** from both sources was undepressed.

3,4,5-Trichloroguaiacol 2

Trichloroguaiacol **2** isolated from caustic extraction effluent had mp 127–128°C. A melting point of 127–128°C is reported (7) for one trichloroguaiacol isomer generated on methylation of 3,4,5-trichlorocatechol; ^1H nmr δ 7.05 (1H, s, aromatic), 5.08 (1H, s, D_2O exchangeable), and 3.92 (3H, s, OCH_3); ms *m/e* 226 (M^+), 228 ($M^+ + 2$), 230 ($M^+ + 4$) (ratio 3:3:1), 211, 183, 147, 113.

4,5,6-Trichloroveratrole 3

Synthesization by methylation with diazomethane (75% yield) of **1** and **2** isolated from caustic extraction effluent gave **3**; mp 68–69°C (lit. (7) mp 68–69°C); ^1H nmr δ 6.88 (1H, s, aromatic) and 3.93 (3H, s, OCH_3); ms *m/e* 240 (M^+, base peak), 242 ($M^+ + 2$), 244 ($M^+ + 4$), 225, 162, 197, 147.

Methylation of **1** synthesized from guaiacol gave a crystalline veratrol, mp 68–69°C; nmr and ms identical to the veratrol derived above from **1** and **2**.

3,4,5,6-Tetrachloroguaiacol 4

Guaiacol (0.01 mol) was reacted with chlorine (0.04 mol) in 50 ml of acetic acid. After 1 h the solvent was removed *in vacuo* and the crude product was crystallized once from $MeOH–H_2O$ and twice from petroleum ether to yield 32% of **4**. Mixture melting point of this sample and that of material isolated from caustic extraction effluent was undepressed; mp 119–120°C (lit. (3) mp 119–121°C); ^1H nmr δ 6.00 (1H, s, D_2O exchangeable), 3.97 (3H, s, OCH_3); ms *m/e* 260 (M^+), 262 ($M^+ + 2$), 264 ($M^+ + 4$), 266 ($M^+ + 6$) (ratio 1:1.3; 0.6:0.1), 246 (base peak), 244, 219, 183.

Tetrachloroguaiacol **4**, isolated from the effluent had the same spectroscopic characteristics as synthetic **4**.

3,4,5,6-Tetrachloroveratrole 5

Methylation of **4** with diazomethane gave **5** (yield 70%); nmr δ 3.97 (3H, s, OCH_3); ms *m/e* 274 (M^+, base peak), 276 ($M^+ + 2$), 278 ($M^+ + 4$), 206, 261, 218.

Monochlorodehydroabietic Acids

The monochlorodehydroabietic acids were obtained from effluent as a 2:1 mixture of **10** and **11** (1). The same 2:1 mixture was generated upon chlorination (0.24 g) of dehydroabietic acid (1.00 g) and a crystal (~5 mg) of $FeCl_3$ in carbon tetrachloride for 1 h at room temperature with the exclusion of light. The solvent was removed *in vacuo* and the crude product was treated with 2-amino-2-methyl-1-propanol. The resulting salt was crystallized three times from acetone. Acid hydrolysis of the salt gave monochlorohydroabietic acids (0.4 g) as a 2:1 mixture of **10** and **11** (yield 36%) revealed by gas chromatography–mass spectrometry of the methyl esters. The methyl esters of the isolated compounds were separated by preparative glpc.

The methyl ester of the major isomer **10** (shorter retention time) had the following spectral characteristics: ^1H nmr near Cl δ 7.14 (2H, s, aromatic), 3.70 (3H, s, CO_2CH_3), 1.28 (3H, s, C_4CH_3), 1.23 (6H, d, $J = 7$ Hz, $C(CH_3)_2$), 1.20 (3H, s, $C_{10}CH_3$); ms *m/e* 273 (base peak), 275, 348 (M^+), 333, 207, 181, 350 ($M^+ + 2$); mass measurement, M^+ calcd. for $C_{21}H_{29}O_2Cl$: 348.193; found: 348.184.

The spectroscopic characteristics of the methyl ester of **11** were ^1H nmr δ 7.03 (1H, s, aromatic), 6.89 (1H, s, aromatic), 3.70 (3H, s, CO_2CH_3), 1.28 (3H, s, C_4CH_3), 1.23 (6H, d, $J = 7$ Hz, $C(CH_3)_2$), 1.20 (3H, s, $C_{10}CH_3$); ms *m/e* 273 (base peak), 275, 219, 348 (M^+), 221, 207, 181, 165, 333. M^+ calcd. for $C_{21}H_{29}O_2Cl$: 348.193; found: 348.184.

12,14-Dichlorodehydroabietic Acid 12

This compound was isolated from caustic extraction effluent (1) and also synthesized by addition of chlorine (0.7 g), dissolved in CCl_4, to a solution of dehydroabietic acid (1.5 g) and $FeCl_3$ (~5 mg) in CCl_4 at 20°C for 1 h in the dark. The mixture was worked up according to the procedure described for monochlorodehydroabietic acid to give 0.6 g of dichlorodehydroabietic acid (yield 33%); both isolated and synthesized samples had identical spectroscopic properties; nmr δ 7.14 (1H, s, aromatic), 1.41 (6H, d, $J = 7$ Hz, $C_{15}(CH_3)_2$), 1.27 (3H, s, C_4-CH_3), 1.20 (3H, s, C_{10}-CH_3); spectral details of the methyl ester were ^1H nmr δ 7.18 (1H, s, aromatic), 3.68 (3H, s, CO_2CH_3), 1.41 (6H, d, $J = 7$ Hz, $C(CH_3)_2$), 1.27 (3H, s, C_4, CH_3), 1.20 (3H, s, $C_{10}CH_3$); ms *m/e* 307 (base peak), 309, 382 (M^+), 241, 308; mass measurement, M^+ calcd. for $C_{21}H_{28}O_2Cl_2$: 382.146; found: 382.144.

11,12,14-Trichlorodehydroabietic Acid 14

This compound was obtained by addition of chlorine (0.8 g) and ~5 mg of $FeCl_3$ to a solution of dehydroabietic acid (1 g) in CCl_4 at 20°C for 1 h in the dark. After the usual work-up procedure, trichlorodehydroabietic acid (0.66 g) was obtained; nmr δ 1.52 (1H, s, C_{10}-CH_3), 1.41 (6H, d, $J = 7$ Hz, $C_{15}(CH_3)_2$, 1.32 (1H, s, C_4-CH_3). Spectral details for the methyl ester were ^1H nmr δ 3.70 (3H, s, $COOCH_3$), 1.52 (3H, s, $C_{10}CH_3$), 1.41 (6H, d, $J = 7$ Hz, $C(CH_3)_2$), 1.32 (3H, s, C_4CH_3); ms *m/e* 341 (base peak) 343, 345, 416 (M^+), 418 ($M^+ + 2$), 420 ($M^+ + 4$).

Acknowledgements

We wish to thank CPAR for financial support in the isolation of toxic constituents from bleach plant effluents and Dr. J. M. Leach for invaluable discussion and scientific goodwill.

1. J. M. LEACH and A. N. THAKORE. J. Fish. Res. Bd. Canada, **32**, 1249 (1975); CPAR Rep. No. 245. Canadian Forestry Service, Ottawa, Ont.
2. N. J. HALBROOK and R. V. LAWRENCE. J. Org. Chem. **31**, 4246 (1966).
3. K. V. SARKANEN and C. W. DENCE. J. Org. Chem. **25**, 715 (1960).
4. C. HEATHCOCK. Can. J. Chem. **40**, 1865 (1962).
5. K. S. DHAMI and J. B. STOTHERS. Can. J. Chem. **44**, 2855 (1966).
6. J. B. STOTHERS. Carbon-13 NMR spectroscopy. Academic Press, New York, NY. 1973.
7. I. HEILBRON and H. M. BUNBURY. Dictionary of organic compounds. Vol. 4. Eyre and Spottiswoode, London. 1953. p. 560.

^{13}C nuclear magnetic resonance spectra of the spirobenzylisoquinoline alkaloids and related model compounds

DONALD W. HUGHES, BALA C. NALLIAH, HERBERT L. HOLLAND,[1] AND DAVID B. MACLEAN

McMaster University, Department of Chemistry, Hamilton, Ont., Canada L8S 4M1

Received March 2, 1977

DONALD W. HUGHES, BALA C. NALLIAH, HERBERT L. HOLLAND, and DAVID B. MACLEAN. Can. J. Chem. **55**, 3304 (1977).

The natural abundance ^{13}C nuclear magnetic resonance spectra of a number of spirobenzylisoquinoline alkaloids and related model compounds have been recorded. The carbon resonances of the alkaloids were assigned by comparison with the spectra of other isoquinoline alkaloids and with those of the model compounds. It has been shown that ^{13}C nmr spectroscopy may be used to differentiate between diastereomers in this series.

DONALD W. HUGHES, BALA C. NALLIAH, HERBERT L. HOLLAND et DAVID B. MACLEAN. Can. J. Chem. **55**, 3304 (1977).

On a enregistré par résonance magnétique nucléaire ^{13}C les spectres de plusieurs alkaloïdes spirobenzylisoquinoléiques ainsi que d'autres composés de structure analogue. Par comparaison avec d'autres spectres d'alkaloïdes isoquinoléiques et de composés analogues, on assigne les valeurs trouvées à chaque carbone des alkaloïdes. On a montré que la spectroscopie rmn ^{13}C peut être utilisée pour différencier entre diastéréoisomères dans ces séries.

[Traduit par le journal]

Several classes of isoquinoline alkaloids have been examined recently by ^{13}C nuclear magnetic resonance spectroscopy. In a recent review (1) Wenkert has reported spectra of a simple benzylisoquinoline, several tetrahydroprotoberberines, several aporphines, the pavine alkaloid argemonine, and cularine. Other reports have appeared on the protoberberines (2, 3), the phthalideisoquinolines (2), and the protopines (4). We report here on our investigation of the spirobenzylisoquinoline system in which we have examined several model systems, some synthetic analogues, and alkaloids of this family.

We have made use of what are now standard techniques in ^{13}C magnetic resonance spectroscopy. The spectra of all compounds were recorded using broad band decoupling, and where applicable the off-resonance technique was used to determine the substitution at carbon. In some cases the alternately pulsed or gated decoupling method (5–7) was employed. Deuterium labelling and selective proton decoupling have also been used to make unequivocal assignments of several carbon resonances. Reference is made to model systems in which the assignments are already secure and in other appropriate cases calculated chemical shifts of model systems have been used.

The spirobenzylisoquinoline alkaloids are a relatively small group of alkaloids within the isoquinoline family. Their structure and chemistry are the subject of several recent reviews (8, 9). Ochotensimine **1***a* was the first member of this family to be investigated and it and ochotensine (8, 9) are the only alkaloids that carry an exocyclic methylene on the spiro ring. More common are the alkaloids that are oxygenated in the five-membered ring and carry the oxygens in the form of carbonyl, hydroxy, or acetoxy groups on one or both of carbons 8 and 13. The structures of alkaloids of this group and synthetic analogues used in this study are shown as the formulas **1***a*–**1***j* in Fig. 3.

The appropriately substituted 1,2,3,4-tetrahydroisoquinolines and indanes serve as models for rings A and B, and rings C and D, respectively, of the spiro alkaloids. A discussion of the ^{13}C spectra of the former has already appeared (2) and the information is used here in making assignments in rings A and B in this series. Several indane derivatives have been prepared in this study and their spectra have been recorded and interpreted to aid in the assignment of the ^{13}C resonances in rings C and D of the spiro compounds.

[1]Present address: Department of Chemistry, Brock University, St. Catharines, Ontario.

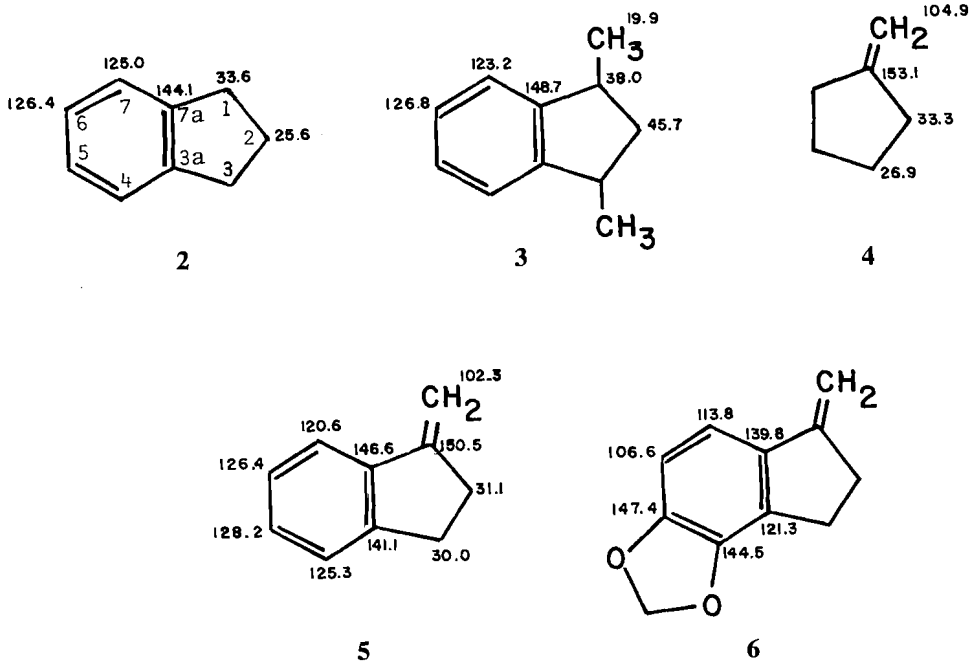

FIG. 1. ^{13}C resonances of indanes **2**–**6**.

The spectra of indane **2** and of 1,3-dimethylindane **3** have been published (10, 11), and the indane assignments recently verified (12). By using the indane spectra and the already reported spectrum of methylenecyclopentane **4** (13) as models, we assigned the spectrum of 1-methyleneindane **5** as shown in Fig. 1. Of the two substituted aromatic carbons, C-7*a* has been assigned at lower field because of β substitution at C-1. Of the four signals associated with unsubstituted aromatic carbons that at 120.6 was assigned to C-7 because of the γ-steric effect of the C-1 substituent. While the signal at 125.3 could not be unambiguously differentiated from that at 126.4, it was assigned to C-4 since this carbon is in an environment analogous to that in indane. Of the two remaining signals, that at lower field is tentatively assigned to C-5 because it is *para* to the double bond system. The aromatic spectrum of 4,5-methylenedioxy-1-methyleneindane **6** was then calculated using the substituent parameters already derived for a methylenedioxy group (2) and it served as model for rings C and D of ochotensimine.

The spectrum of 1-indanone **7***a* and several derivatives were examined to serve as models for the alkaloids bearing a carbonyl group in ring C (Table 1). In the case of indanone itself assignments were made initially by comparison with the spectrum of phthalide (2) and verified by examination of the spectrum of 6-deuterio-1-indanone **7***b*. In the latter the signal at 127.1 had virtually disappeared so that the assignment at C-6 was secure. Carbon 5 follows from consideration of the substituent effect for a carbonyl group on a *para* carbon. The remaining positions C-4 and C-7 were determined from the gated decoupled spectrum since deuterium substitution at C-6 removes the 7.0 Hz *meta* coupling between C-4 and the C-6 hydrogen. With the spectrum of 1-indanone established it was a simple matter to assign the resonances in the substituted 1-indanones **8** and **9** by making use of the substituent parameters for *o*-dimethoxy and methylenedioxy groups (2). The calculated chemical shifts show a resonable agreement with observed values except for the expected deviation at C-3*a* in the dimethoxy compound (2). The assignments of the protonated aromatic carbons were verified in all cases by selective proton decoupling.

Another series of models, the 1,3-indandiones, was also studied. No 1,3-diones have yet been found in nature among the spiro alkaloids but since the diols and the hydroxyketones are well known they may be present but undetected. The diones have been prepared, however, as

TABLE 1. ^{13}C chemical shifts of indanones and indandiones **7-12**

Compound	Carbon															
	1	2	3	3*a*	4	5	6	7	7*a*	4-OCH_3	5-OCH_3	OCH_2O	1′	2′, 6′	3′, 5′	4′	N—CH_3
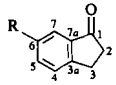 *7a*, R = H *7b*, R = D	206.5	36.0	25.5	155.0	126.6	134.4	127.1	123.4	137.0								
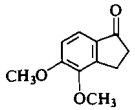 **8**	205.2	36.4	22.5	145.6	147.9	157.6	112.5	120.0	131.2	60.3	56.3						
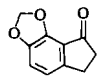 **9**	204.1	37.3	25.8	148.3	118.9	114.3	147.4	143.6	120.4			103.0					
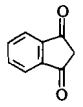 **10**	197.3	45.0	197.3	141.5	123.8	136.4	136.4	123.8	141.5								
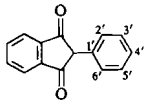 **11**	198.2	59.8	198.2	142.8	123.8	136.0	136.0	123.8	142.8				133.2	125.5	128.4	127.9	
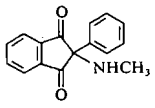 **12**	200.8	73.5	200.8	141.5	123.8	136.4	136.4	123.8	141.5				136.3	127.5	129.0	128.8	31.6

intermediates in several synthetic approaches to the spiro alkaloids (8, 9) and their spectra are also reported here. The compounds examined are also shown in Tables 1 and 2. In two of them the complete skeleton of the spiro alkaloids is present.

The spectra of the 1,3-indandiones **10**, **11**, and **12** were used in the interpretation of the spectra of the spiro compounds **13** and **14**. Assignment of the resonances of **10** was made without difficulty because of the molecular symmetry of the system and by taking into account the substituent effects of the two carbonyl groups. As C-2 becomes more substituted in going from **10** to **12**, its chemical shift moves downfield as expected. Substitution at C-2 also deshields the carbonyl carbons but has very little influence on the aromatic carbons of the indandione system.

In the spiro compounds, **13** and **14**, the indandione part of the molecule retains its symmetry and chemical shifts are observed which are similar to the models **10**, **11**, and **12**. The resonances of the ring A carbons are very similar to those found in other tetrahydroisoquinolines (2). The assignments made for C-4*a* and C-14*a* are based on the argument that C-14*a* has a greater number of β substituents. In the proton spectrum of **14** the hydrogen at C-1 is shielded relative to that at C-4 (14) and it was through selective proton decoupling that the resonances of these carbon atoms were established. The major difference between **13** and **14** lies in the chemical shifts of C-6 and C-14, both of which are deshielded as expected in the *N*-methyl relative to the N–H compound. Calculations, using the β equatorial methyl parameter derived from methylcyclohexane (11, 15), work well for C-6 but because of the highly substituted nature of C-14 there was a deviation between the observed and calculated chemical shift.

We turn now to (+)-ochotensimine **1***a* (Fig. 3) which is distinguished from the other alkaloids of the series examined here by the presence of an exocyclic methylene at C-13. The assignments (Table 3) in rings A and B were made by comparison with the spectrum of **15** (2) (Fig. 2). Carbons 1, 2, 3, 4, and 4*a* are not greatly different from the model and the assignments of C-1 and C-4 were differentiated from C-11 and C-12 by selective proton decoupling. Since carbons 2 and 3 are separated by only 0.2 ppm unambiguous assignments could not be made. C-14*a* and C-12*a* cannot be differentiated but it is noteworthy that relative to the model C-14*a* has shifted considerably downfield. This shift is attributed to greater substitution at C-14 in **1***a* relative to **15**.

TABLE 2. ^{13}C chemical shifts of the spiro diones **13** and **14**

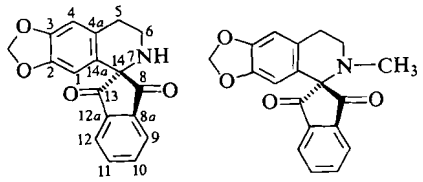

Carbon	**13**	**14**
1	105.3	105.2
2	146.4	146.3
3	147.3	147.2
4	110.1	109.5
4*a*	131.0	129.9
5	29.4	29.1
6	40.1	48.1
8,13	200.0	202.8
8*a*,12*a*	142.0	142.4
9,12	124.5	123.8
10,11	136.3	136.6
14	66.2	71.7
14*a*	136.1	137.7
OCH_2O	101.6	101.1
$N—CH_3$		40.5

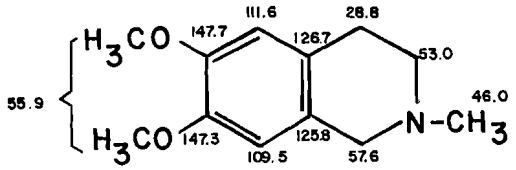

15

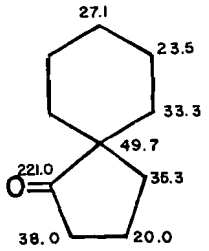

16

FIG. 2. ^{13}C chemical shifts of model compounds **15** and **16**.

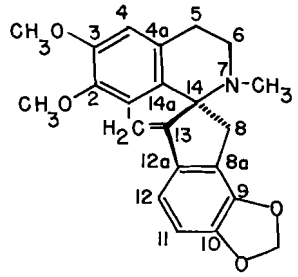

1*a*

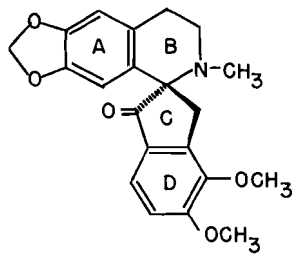

1*b*

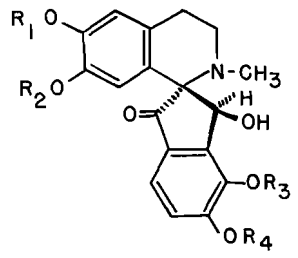

1*c* $R_1 + R_2 = CH_2$; $R_3 = R_4 = CH_3$
1*e* $R_1 + R_2 = R_3 + R_4 = CH_2$
1*g* $R_1 = R_2 = CH_3$; $R_3 + R_4 = CH_2$

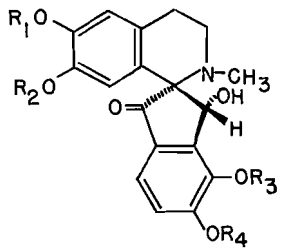

1*d* $R_1 + R_2 = CH_2$; $R_3 = R_4 = CH_3$
1*f* $R_1 + R_2 = R_3 + R_4 = CH_2$
1*h* $R_1 = R_2 = CH_3$; $R_3 + R_4 = CH_2$

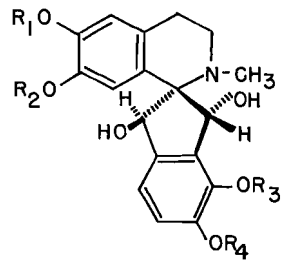

1*i* $R_1 + R_2 = R_3 + R_4 = CH_2$
1*j* $R_1 = R_2 = CH_3$; $R_3 + R_4 = CH_2$

FIG. 3. Structures of the spirobenzylisoquinoline alkaloids **1***a*–**1***j*. (The absolute stereochemistry is not implied in this figure.)

In ring B the changes between **15** and **1***a* are as follows: C-14, +14.3; C-6, −4.9; C-5, +0.3; N—CH_3, −7.0. The shielding of both C-6 and the *N*-methyl group may be attributed to the combined γ-gauche effect of both C-8 and C-13. Creation of the spiro ring junction at C-14 causes a significant deshielding in a manner analogous to that observed for the spiro carbon in spiro[4.5]decan-1-one **16** (16) relative to cyclohexane.

Chemical shift assignments for rings C and D were determined with the aid of the model compounds **5** and **6**, already discussed. The chemical shifts assigned to **6** served as a guide in assigning the substituted aromatic carbons of ring D. Selective proton decoupling was used to differentiate between C-11 and C-12. The exocyclic methylene of ring C was identified in a gated decoupling experiment. This resonance appears at 106.7 with $^1J\,^{13}C\,^1H = 160.6$ Hz.

The synthetic spiro ketone **1***b* was examined as a model for the sibiricine type alkaloids where we have examined three diastereomeric pairs, the compounds **1***c* and **1***d*, sibiricine **1***e* (17) and corydaine **1***f* (18), and raddeanone **1***g* (19) and yenhusomidine **1***h* (20), all of established stereochemistry (Fig. 3 and Table 3). The resonances of the carbon atoms of rings A and B of **1***b* were assigned through comparison with other benzylisoquinoline alkaloids that carry methylenedioxy substitution in ring A, e.g. hydrastine and berberine (2). The resonances of C-1 and C-4 were confirmed through selective proton decoupling. The fact that C-1 and C-4 are not equivalent as they are in ochotensimine may be a reflection of the difference in anisotropic shielding between the exocyclic methylene in **1***a* and the carbonyl in **1***b*. C-4*a* and C-14*a* follow the same trend observed in **1***a* but C-14*a* is less deshielded.

The chemical shifts of the aliphatic carbons of **1***b* are virtually identical with those of **1***a*. The indanone **8** serves as an excellent model for the carbons of rings C and D of **1***b*; however, one cannot differentiate between C-8*a* and C-9 because of their similar resonances.

Alkaloids of the sibiricine group differ from **1***b* by the presence of a hydroxy function at C-8

TABLE 3. ^{13}C chemical shifts of the spirobenzylisoquinoline alkaloids

	Compound									
Carbon	**1***a*	**1***b*	**1***c*	**1***d*	**1***e*	**1***f*	**1***g*	**1***h*	**1***i*	**1***j*
1	110.5	104.8	107.2	105.7	106.9	105.8	110.7	110.7	109.7	110.1
2	147.5	146.5	146.9	146.8	147.4	146.9	147.2	148.5	146.2	147.3
3	147.7	146.5	146.9	146.8	147.4	146.9	148.9	148.6	146.8	148.3
4	110.5	108.5	109.1	108.2	109.6	108.2	112.5	111.4	110.0	113.0
4*a*	126.1	128.3	125.9	129.3	125.0	129.3	124.0	128.7	126.0	124.9
5	29.1	29.4	28.9	29.4	29.2	29.5	28.5	29.3	22.8	22.0
6	48.1	48.4	48.7	50.3	48.9	50.2	48.9	50.3	47.6	47.8
8	37.0	37.3	70.5	75.9	70.3	75.0	70.1	75.1	73.4	73.4
8*a*	123.8	145.4	145.4	146.7	132.7	134.3	132.9	134.6	121.5	121.5
9	143.0	145.6	145.5	147.0	146.1	144.4	145.0	144.4	144.7	144.9
10	148.2	158.5	159.2	159.3	154.8	154.5	154.5	154.6	148.6	148.4
11	108.0	113.8	114.5	114.3	110.9	110.6	110.4	109.5	107.1	109.7
12	113.6	121.1	120.6	120.4	119.9	119.6	119.5	119.6	116.1	115.7
12*a*	136.1	131.0	130.0	130.1	132.5	131.2	132.5	131.3	140.0	140.9
13	155.5	206.4	202.4	202.7	201.5	202.2	201.7	202.7	79.5	79.0
14	71.9	71.2	76.8	72.0	77.2	72.0	76.9	72.0	75.2	75.2
14*a*	137.2	131.8	130.9	130.1	130.6	129.8	129.7	128.7	129.5	128.3
NCH_3	39.0	39.2	39.4	41.8	39.7	41.7	39.6	41.9	37.7	37.9
2,3 OCH_2O		100.9	100.9	101.0	101.3	101.1			101.0	
9,10 OCH_2O	101.3				103.2	103.1	103.1	103.2	101.9	101.8
2* OCH_3	56.1						56.1	56.1		56.0
3* OCH_3	55.8						56.0	56.5		55.5
9 OCH_3		60.4	61.3	61.2						
10 OCH_3		56.3	56.4	56.5						
13 $=CH_2$	106.7									

*These assignments may be reversed.

and may exist in diastereomeric forms. The chemical shift assignments for the synthetic compounds **1***c* and **1***d* follow directly from the model **1***b*. The ring D assignments for the pairs **1***e* and **1***f* and **1***g* and **1***h* were made by selective proton decoupling and by comparison with chemical shifts calculated for 4,5-methylenedioxy-1-indanone: C-3*a*, 135.2; C-4, 145.8; C-5, 153.6; C-6, 107.3; C-7, 116.6; C-7*a*, 130.2.

In **1***c*, C-8 and C-14 show the expected downfield shifts relative to **1***b* because of the α- and β-OH substituent effects, respectively. The carbonyl group is shielded by −4.0 ppm. In **1***d* there are a number of significant changes relative to its diastereomer. Hydrogen bonding between the hydroxy group and the nitrogen (18) causes slight conformational and electronic changes in the system resulting in a deshielding of C-8, C-6, and the *N*-methyl. At the same time C-14 is appreciably shielded. Differences of similar sign and magnitude are also observed between sibiricine (**1***e*) and corydaine (**1***f*) and raddeanone (**1***g*) and yenhusomidine (**1***h*). It is apparent then that ^{13}C nmr may be used to differentiate between diastereomers in this series of compounds.

Ochrobirine **1***i* and yenhusomine **1***j* (20) carry hydroxy groups in each of C-8 and C-13 and they represent another structural variation. We wished to determine if ^{13}C nmr could differentiate between C-8 and C-13 in these compounds and be used to assign the configuration of the hydroxy groups.

The data presented in Table 3 show that a number of significant chemical shift changes occur when corydaine **1***f* is transformed to ochrobirine **1***i*. Upon replacement of the carbonyl function by hydroxy, the aromatic carbon C-1 is deshielded by 3.9 ppm relative to corydaine while C-12 is shielded by −3.5 ppm. Examination of the aliphatic carbons of **1***i* indicates a distinct difference between C-8 and C-13. Selective proton decoupling was used to resolve these assignments since in the ^1H nmr spectrum of **1***i*, C-8 and C-13 hydrogens appear at 4.88 and 5.42 ppm, respectively (8). Although C-8 is shielded relative to that in corydaine **1***f*, C-8 is still downfield from the corresponding carbon in sibiricine (**1***e*) which indicates a retention of the corydaine relative configuration.

Of the ring B carbons of ochrobirine **1***i*, only C-14 has undergone a downfield shift whereas

C-5, C-6, and the *N*-methyl are shielded by −6.7, −2.6, and −4.0 ppm respectively, relative to corydaine **1***f*. The γ steric effect of the sp^3 centre at C-13 accounts for the shielding of C-6 and the *N*-methyl. Examination of molecular models demonstrates that the C-13 hydrogen and both the *N*-methyl and pseudo-axial C-6 hydrogen are quite sterically crowded when ring B adopts a half-chair conformation. Distortion of the B ring half-chair to a slightly more flattened conformation partially relieves these steric interactions while maintaining the internal hydrogen bond. This conformational change may contribute to the upfield shift of C-5.

Yenhusomine **1***j* is a *trans* diol like ochrobirine with the hydroxy at C-8 hydrogen bonded to nitrogen. The changes that occur in going from yenhusomidine **1***h* to yenhusomine exactly parallel those that take place in the corydaine to ochrobirine transformation. Unfortunately the *cis* diols were not available for examination. It is apparent that ^{13}C nmr is of value in the assignment of both gross structure and relative stereochemistry of the spirobenzylisoquinoline alkaloids.

Experimental

Apparatus, Methods, and Materials

Natural abundance ^{13}C nuclear magnetic resonance spectra were recorded on a Bruker WH-90 Fourier transform spectrometer at 22.62 MHz and a temperature of +35.0°C. Samples were 0.16 *M* to 0.41 *M* in $CDCl_3$; TMS was used as an internal reference. Field/frequency locking was provided by the deuterium signal of $CDCl_3$.

^1H nuclear magnetic resonance spectra were obtained on either a Varian HA-100 or a Varian EM-390 spectrometer in the frequency sweep mode. $CDCl_3$ and TMS were again used as solvent and internal reference, respectively.

Mass spectra were determined on a C.E.C. 21-110B mass spectrometer at an ionizing voltage of 80 eV and a source temperature of 200–250°C. Melting points were determined on a Kofler hot stage and are uncorrected. Infrared spectra were recorded on a Perkin-Elmer 337 spectrometer. Thin layer chromatography was performed either on silica gel ($F\text{-}60_{254}$) or alumina. 1-Indanone and 1,3-indandione were obtained commercially. All other compounds were synthesized in this laboratory by standard procedures or isolated from natural sources: 1-methyleneindane **5** (21), 4,5-dimethoxy-1-indanone **8** (22), 6,7-methylenedioxy-1-indanone **9** (23), 2-phenyl-1,3-indandione **11** (24), 2-methylamino-2-phenyl-1,3-indandione **12** (25), spiro diones **13** and **14** (14), spiro ketone **1***b* (26), (±)-sibiricine **1***e* (27), (±)-corydaine **1***f* (27), (±)-raddeanone **1***g* (27), (±)-yenhusomidine **1***h* (27), (±)-ochrobirine **1***i* (27), (±)-yenhusomine **1***j* (27), (+)-ochotensimine **1***a* (28).

6-Deuterio-1-indanone

6-Amino-1-indanone (29) was diazotized and converted to its diazonium fluoborate (30). The solid fluoborate (210 mg) was added with vigorous stirring in portions to 4 ml of hypophosphorous acid-d_3 (4 ml) at −5 to 0°C. Stirring of the mixture was continued for 15 min after addition was complete and the mixture was allowed to stand in a refrigerator for 48 h before work-up. D_2O (10 ml) was added to the reaction mixture and the mixture was extracted with chloroform, the extract dried and evaporated, and the residue purified by tlc on alumina using $CHCl_3$ as eluent. The 6-deuterio-1-indanone (40 mg, 35%) so obtained gave the following analysis by mass spectrometry: d_0 31%; d_1 69%; ^1H nmr δ 2.75 (2H, m, CH_2CO), 3.21 (2H, m, benzylic CH_2), 7.62 (3H, m, aromatic H's).

Acknowledgments

We thank Mr. B. Sayer for his assistance in recording the ^{13}C spectra and the National Research Council of Canada for financial support.

1. E. Wenkert, B. L. Buckwalter, I. R. Burfitt, M. J. Gasic, H. E. Gottlieb, E. W. Hagaman, F. M. Schell, and P. M. Wovkulick. Topics in carbon-13 NMR spectroscopy. Vol. 2. *Edited by* G. C. Levy. Wiley-Interscience, New York, NY. 1976.
2. D. W. Hughes, H. L. Holland, and D. B. MacLean. Can. J. Chem. **54**, 2252 (1976).
3. T. Kametani, K. Fukumoto, M. Ihara, A. Ujiie, and H. Koizumi. J. Org. Chem. **40**, 3280 (1975).
4. T. T. Nakashima and G. E. Maciel. Org. Magn. Reson. **5**, 9 (1973).
5. O. A. Gansow and W. Schittenhelm. J. Am. Chem. Soc. **93**, 4294 (1971).
6. R. Freeman and H. D. W. Hill. J. Magn. Reson. **5**, 278 (1971).
7. J. Feeney, D. Shaw, and P. J. S. Pauwels. Chem. Commun. 554 (1970).
8. M. Shamma. The isoquinoline alkaloids: chemistry and pharmacology. Academic Press, New York, NY. 1972.
9. S. McLean and J. Whelan. MTP International review of science. Vol. 9. Alkaloids. *Edited by* K. F. Wiesner. *Consultant editor* D. H. Hey. University Park Press, Baltimore, MD. 1973.
10. H. L. Retcofsky and R. A. Friedel. Spectrometry of fuels. *Edited by* R. A. Friedel. Plenum Press, New York, NY. 1970.
11. J. B. Stothers. Carbon-13 NMR spectroscopy. Academic Press, New York, NY. 1972.
12. W. Adcock, B. D. Gupta, T. C. Khor, D. Doddrell, and W. Kitching. J. Org. Chem. **41**, 751 (1976).
13. S. H. Grover and J. B. Stothers. Can. J. Chem. **53**, 589 (1975).
14. R. H. F. Manske and Q. A. Ahmed. Can. J. Chem. **48**, 1280 (1970).
15. D. K. Dalling and D. M. Grant. J. Am. Chem. Soc. **89**, 6612 (1967).
16. D. Zimmermann, R. Ottinger, J. Reisse, H. Christol, and J. Brugidou. Org. Magn. Reson. **6**, 346 (1974).
17. R. H. F. Manske, R. Rodrigo, D. B. MacLean, D.

E. F. GRACEY, and J. K. SAUNDERS. Can. J. Chem. **47**, 3585 (1969).
18. KH. SH. BAISHEVA, D. A. FESENKO, B. K. ROSTOTSKII, and M. E. PEREL'SON. Khim. Prir. Soedin. **6**, 456 (1970).
19. T. KAMETANI, M. TAKEMURA, M. IHARA, and K. FUKUMOTO. Heterocycles, **4**, 723 (1976).
20. S.-T. LU, T.-L. SU, T. KAMETANI, and M. IHARA. Heterocycles, **3**, 301 (1975).
21. I. H. SADLER. J. Chem. Soc. B, 1024 (1969).
22. W. H. PERKIN and R. ROBINSON. J. Chem. Soc. **105**, 2388 (1914).
23. B. NALLIAH, Q. A. AHMED, R. H. F. MANSKE, and R. RODRIGO. Can. J. Chem. **50**, 1819 (1972).
24. F. NATHANSON. Chem. Ber. **26**, 2576 (1893).
25. E. YA. OZOLA, YA. YA. OZOL, A. K. AREN, and G. YA. VANAG. Zh. Org. Khim. **4**, 88 (1968).
26. B. NALLIAH, R. H. F. MANSKE, R. RODRIGO, and D. B. MACLEAN. Tetrahedron Lett. 2795 (1973).
27. B. C. NALLIAH, D. B. MACLEAN, R. G. A. RODRIGO, and R. H. F. MANSKE. Can. J. Chem. **55**, 922 (1977).
28. R. H. F. MANSKE. Can. J. Res. Sect. B, **18**, 75 (1940).
29. C. K. INGOLD and H. A. PIGGOT. J. Chem. Soc. **123**, 1469 (1923).
30. D. T. FLOOD. Org. Synth. **2**, 295 (1943).

Competitive adsorption of urea and Et_4NBr at the electrode/electrolyte interface

FRANK M. KIMMERLE AND HUGUES MÉNARD

Département de chimie, Université de Sherbrooke, Sherbrooke (Qué.), Canada J1K 2R1

Received September 9, 1976[1]

FRANK M. KIMMERLE and HUGUES MÉNARD. Can. J. Chem. **55**, 3312 (1977).

The simultaneous adsorption of urea and tetraethylammonium bromide has been investigated in ternary solutions varying in composition from 10^{-3} to 1 mol ℓ^{-1}. The adsorption of urea at the electrode/electrolyte interface can be described at low surface coverage by a Langmuir isotherm taking into account the surface unoccupied by the ionic components of the Et_4NBr salt. At high surface coverage, perturbation of Γ_{urea} by the simultaneous adsorption of the electrolyte is explained in terms of the lateral attractive forces previously observed in concentrated bulk solutions.

FRANK M. KIMMERLE et HUGUES MÉNARD. Can. J. Chem. **55**, 3312 (1977).

Nous avons étudié l'adsorption simultanée de l'urée et du bromure de tétraéthylammonium à l'interface électrode/électrolyte dans des solutions ternaires de composition variant de 10^{-3} à 1 mol ℓ^{-1}. L'adsorption de l'urée à l'interface électrode/électrolyte suit, à faible recouvrement de surface, l'isotherme de Langmuir en tenant compte de la surface non occupée par les composants ioniques du sel Et_4NBr. A recouvrement élevé, la perturbation du terme $\Gamma_{urée}$ par l'adsorption simultanée de l'électrolyte, est expliquée par des forces d'attraction latérales antérieurement observées en solutions concentrées.

[Traduit par le journal]

Introduction

The interfacial region separates two regions: one which can be described by the bulk electrolyte properties, the other by the bulk electrode properties. While the anisotropic distribution of cations and anions in this 'electrical double layer region' may depend to a large degree on the electron charge density on the metal surface, the distribution of solvent molecules and neutral solutes can be expected to strongly reflect the bulk electrolyte properties. Knowledge of the bulk thermodynamic properties is thus essential for the study of the structure of the interfacial region; not only in order to calculate correctly the thermodynamic parameters of the interfacial region, but also in order to postulate models of the anisotropic structure in agreement with this experimentally accessible thermodynamic data.

The thermodynamics of aqueous urea solutions have been reviewed by Stokes (1), the thermodynamics of aqueous tetraalkylammonium solutions by Wen and Hung (2), and recently the ternary aqueous – urea – tetraalkylammonium bromide solutions have been examined by a number of workers (3–5). Schrier *et al.* (5) have succinctly summarized the Friedman cosphere model (6) as it applies to these results. Within slightly different frameworks, e.g. that of Desnoyers and Jolicoeur (7), or that of Parker (8), it is also taken for granted that urea salt solutions have less structure than pure water. Furthermore, it is admitted that entropy considerations are largely responsible for the negative free energy of transfer of R_4NBr to a more highly concentrated urea solution as well as the spontaneous transfer of urea to a R_4NBr solution.

The adsorption of Et_4NBr at the mercury/aqueous electrolyte interface has been studied by Verdier *et al.* (9), Piro *et al.* (10), and Ménard and Kimmerle (11). Piro *et al.* interpreted the adsorption over a range of 0.04 C m^{-2} at high negative potentials in terms of specific cation adsorption and postulated monolayer coverage by the cations ($r + \sim 4$ Å) in contact with each other. Just as Sarma and Ahluwalia (12) contend that the quaternary ammonium salts behave as soluble hydrocarbons with respect to the free energy of transfer, we have contended that Et_4NBr behaves in the interfacial region quite unlike the ionic alkali salts whose anionic and cationic attributes can be readily identified. Therefore, we have insisted (11) that Br^- and R_4N^+ ions are not adsorbed as separated entities and that one might treat instead the adsorption of an entity 'R_4NBr'.

[1]Revision received May 25, 1977.

The adsorption of urea had received little attention until Parsons *et al.* (13) recently undertook an experimental and theoretical study of the adsorption of urea from aqueous 1.0 *M* KNO_3 solutions. Although they neglected the activity coefficients of urea and employed instead the concentration terms in their data analysis, some very useful information was obtained. Weak lateral interactions of the adsorbed urea molecules and a Langmuir fit corresponding to a molecular area at saturation coverage of 24 $Å^2$ were reported. It was suggested that adsorbed urea molecules displace about three water molecules and that the urea is most strongly adsorbed at an electrode charge $q_M = +0.08$ C m^{-2} in a configuration with its dipole at a small angle to the surface. They also suggested that the nitrate ion modifies substantially the neighbouring water structure but in their numerical calculations did not explicitly consider interactions between the solvent shell of urea and the nitrate ion at the interface or in solution. The interpretation of the simultaneous adsorption of urea and Et_4NBr presents two challenges. (*i*) It is necessary to take into account the variation of activity coefficients of urea with varying salt concentration and vice versa. (*ii*) It is necessary to use a simple model of the interfacial region which will allow for the competitive adsorption. The first condition has only recently been examined for a ternary solution by Nakadomari *et al.* (14) who arranged to keep the activity of a Na_2SO_4 base electrolyte constant while varying the concentration of the 2-butanol solute. We chose to vary the concentrations of both the salt and neutral solute and to calculate both Γ_{urea} and Γ_{Et_4NBr} by use of the appropriate relationship (viz. eq. 4 *b* and *c* below). In order to meet condition (*ii*) the results presented here will emphasize the solution compositions where Γ_{urea} predominates, i.e., high urea and low Et_4NBr concentrations. We will extrapolate these results to Et_4NBr concentrations where the ionic population of the interfacial region is given by electrostatic considerations only. We will thus distinguish between three different types of phenomena in the interfacial region: (1) The adsorption of urea molecules on the electrode surface. (2) The attraction of Et_4NBr into the interfacial region. (3) The interaction between adsorbed urea molecules and adsorbed ionic components of the electrolyte.

Theory

A general electrocapillary equation for an ideally polarized electrode at constant pressure and temperature, where the indicator electrode is reversible with respect to the anion of a uni-univalent electrolyte can be written as:

$$[1]\quad d\gamma = -q_M\,dE^- - \Gamma_{1,h}\,d\mu_1 - \Gamma_{2,h}{}^+\,d\mu_2$$

where the subscripts 1 and 2 refer to the neutral and the ionic solute, respectively. The relative surface excess parameters can be given in terms of the mole fractions X_{urea}, X_{Et_4NBr}, X_{H_2O} and the experimentally inaccessible absolute surface excess, e.g.

$$[2]\quad \Gamma_{1,h} = \Gamma_{urea} - \frac{X_{urea}}{X_{H_2O}}\Gamma_{H_2O}$$

and

$$[3]\quad \Gamma_{2,h}{}^+ = \Gamma_{Et_4N^+} - \frac{X_{Et_4NBr}}{X_{H_2O}}\Gamma_{H_2O}$$

Differentiating [1] with respect to the activity of one solute at constant activity of the second solute will immediately yield the relative surface excess values: e.g.

$$[4a]\quad -(\partial\gamma/\partial\mu_1)_{E^-,\mu_2} = \Gamma_{1,h}$$

and

$$[5a]\quad -(\partial\gamma/\partial\mu_2)_{E^-,\mu_1} = \Gamma_{2,h}{}^+$$

This approach used by Nakadomari *et al.* (14) is very inconvenient to realize experimentally if both $\Gamma_{1,h}$ and $\Gamma_{2,h}{}^+$ are sought but it could be used with surface tension values interpolated from data obtained at fixed concentrations. Differentiating [1] with respect to the activity of one solute at constant molarity or molality of the second solute will yield two terms:

$$[4b]\quad -\left(\frac{\partial\gamma}{\partial\mu_1}\right)_{E^-,c_2\text{ or }m_2} = \Gamma_1' = \Gamma_{1,h} + \Gamma_{2,h}{}^+\left(\frac{\partial\mu_2}{\partial\mu_1}\right)_{c_2\text{ or }m_2}$$

and

$$[5b]\quad -\left(\frac{\partial\gamma}{\partial\mu_2}\right)_{E^-,c_1\text{ or }m_1} = \Gamma_2' = \Gamma_{2,h}{}^+ + \Gamma_{1,h}\left(\frac{\partial\mu_1}{\partial\mu_2}\right)_{c_1\text{ or }m_1}$$

where Γ_1' and Γ_2' are apparent surface excess values. Differentiating [1] with respect to the logarithm of the concentration will yield terms involving the activity coefficients f_1 and $f_{\pm,2}$.

$$[4c] \quad -\left(\frac{\partial\gamma}{RT\,\partial \ln c_1}\right)_{E^-,c_2} = \Gamma_{1,h} \times \left(1 + \frac{\partial \ln f_1}{\partial \ln c_1}\right)_{c_2} + 2\Gamma_{2,h}{}^{+}\left(\frac{\partial \ln f_{\pm,2}}{\partial \ln c_1}\right)_{c_2}$$

and

$$[5c] \quad -\left(\frac{\partial\gamma}{2RT\,\partial \ln c_2}\right)_{E^-,c_1} = \Gamma_{2,h}{}^{+} \times \left(1 + \frac{\partial \ln f_{\pm,2}}{\partial \ln c_2}\right)_{c_1} + \Gamma_{1,h}\left(\frac{\partial \ln f_1}{2\,\partial \ln c_2}\right)_{c_1}$$

The latter approach has frequently been used in the past but all terms involving the activity coefficients have generally been neglected.

Activity coefficients can be calculated from potentiometric results, although isopiestic results lead to unequivocal interpretations and are to be preferred (5), particularly if solute 1 may be thought to influence one ion of the solute 2 differently than its counterion. Such data were not available for aqueous urea Et_4NBr solutions, although Wen and Chen (3) have calculated the activity coefficients of the ternary solutions of urea, Me_4NBr, or Bu_4NBr. Interpolation from these systems is necessary in order to estimate μ_{Et_4NBr} at varying urea concentrations and μ_{urea} at varying Et_4NBr concentrations. Furthermore, it is necessary to estimate the derivative of the activity coefficients of one solute at fixed concentration with respect to concentration of the second solute.

As can be expected, the activity corrections given by the second terms on the right-hand side of [4*b*] and [5*b*] become important at high solute concentrations. Increasing the urea concentration depresses the activity of Et_4NBr and vice versa. $(\partial\mu_2/\partial\mu_1)_{c_2 \text{ or } m_2}$ and $(\partial\mu_1/\partial\mu_2)_{c_1 \text{ or } m_1}$ are therefore both negative quantities. For ternary solutions involving strong salting out (e.g. the butanol solutions (14)) the opposite trends are observed. Neglecting these changes in bulk solution activity and retaining only the first term of [4*c*] or [5*c*] would lead to erroneous high Γ values for solutions having less structure than bulk water and to erroneous low Γ values for ternary solutions having greater structure.

Experimental

The surface tension values were calculated from drop-time measurements using the computational techniques and instrumentation described previously (11).

Solutions were used within 24 h of preparation from water twice distilled from alkaline permanganate, Et_4NBr (Eastman Kodak Co.) recrystallized twice from ethanol, and urea (Baker Chem. Co.). We recorded drop-time for eight concentrations of urea varying from 0.005 to 2 *M* and for nine concentrations of Et_4NBr varying from 0.0025 to 1 *M* over 1.4 V intervals. Eighty-one different solution compositions were thus investigated in order to determine simultaneously the surface excess of the ionic species $\Gamma_{Et_4N^+}$ and Γ_{Br^-} and the surface excess of the neutral molecule, Γ_{urea}. Electrode potentials, E^-, were calculated with respect to a reversible Br^- electrode and verified by measuring the potential difference between a saturated calomel and a specific Br^- electrode (Orion 94-35A) in the urea–Et_4NBr solutions. All experiments were carried out at 25.0 ± 0.05°C.

Results and Discussion

Interpolation of Activity Coefficients

Wen and Chen (3) have shown that the molal activity coefficient of the nonelectrolyte γ_1 and the mean molal activity coefficient of the electrolyte $\gamma_{\pm,2}$ in a ternary system urea – tetraalkylammonium bromide – water may be expressed as a function of the concentration of the nonelectrolyte m_1 and the electrolyte m_2. Schrier *et al.* (5) used a somewhat simpler expression:

$$[6] \quad \log \gamma_1/\gamma_1{}^0 = -m_2\{g_{12}{}^{(0)} + \tfrac{2}{3}g_{12}{}^{(1)}\, m_2{}^{1/2} + g_{12}{}^{(2)}\, m_1\}$$

to express γ_1 in terms of the activity coefficient in the binary solution, $\gamma_1{}^0$, and a correction term, the right-hand side of [6]. Although $\log \gamma_1/\gamma_1{}^0$ and also $\log \gamma_{\pm,2}/\gamma_{\pm,2}{}^0$ differ somewhat with the nature of the electrolyte, as illustrated in Fig. 1,

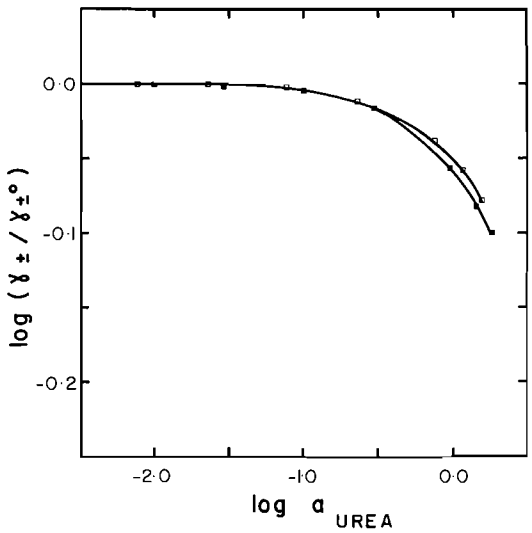

FIG. 1. Mean molal activity coefficient of Et_4NBr vs. activity of urea in a ternary Et_4NBr–urea–H_2O solution: ■ 0.01 *M* Et_4NBr, □ 1.0 *M* Et_4NBr.

for $(\log \gamma_{\pm,2}/\gamma_{\pm,2}{}^0)$ in Me_4NBr and Bu_4NBr solutions, this variation is surprisingly small. The correction terms become appreciably large for $m_1 > 0.1$ *m* and vary slightly more as a function of urea concentration at low electrolyte concentrations. The difference in the behaviour of the two salts becomes more apparent at high urea concentrations. Similarly, the differences in the behaviour of the urea molecule in Me_4NBr or Bu_4NBr solutions become somewhat more appreciable at high electrolyte concentrations. Since these correction terms reflect the effects of the interactions between the nonelectrolyte and electrolyte solutes it is to be expected that the chemical nature of the species would manifest itself when three or more solute particules are likely to interact.

Nevertheless, even at the highest concentrations employed, 2 *m* urea and 1 *m* R_4NBr, the differences in the correction terms for Me_4NBr and Bu_4NBr, Fig. 1, are less than 0.08 units. We therefore suggest that

$$[7]\quad (\ln \gamma_{\pm,2}/\gamma_{\pm,2}{}^0)_{Et_4NBr} = \tfrac{1}{2}\{(\ln \gamma_{\pm,2}/\gamma_{\pm,2}{}^0)_{Me_4NBr} + (\ln \gamma_{\pm,2}/\gamma_{\pm,2}{}^0)_{Bu_4NBr}\}$$

and

$$[8]\quad (\ln \gamma_1/\gamma_1{}^0)_{Et_4NBr} = \tfrac{1}{2}\{(\ln \gamma_1/\gamma_1{}^0)_{Me_4NBr} + (\ln \gamma_1/\gamma_1{}^0)_{Bu_4NBr}\}$$

constitute approximations for the activity coefficients in the ternary system Et_4NBr–urea–water to within 0.04 units. When $\gamma_{urea}{}^0$ and the right-hand sides of [7] and [8] are calculated from the data of Wen and Chen (3), and $\gamma^0{}_{\pm,Et_4NBr}$ taken from the work of Lindenbaum and Boyd (15), γ_{urea} and $\gamma_{\pm,Et_4NBr}$ are likely to be correct to within 1% for all but the most concentrated solutions examined.

Calculation of Relative Surface Excess Values

In order to verify that adsorption equilibrium had been attained within less than 5 s, we re-examined by the droptime technique the urea – 1 *M* KNO_3 solutions recently studied by Parsons *et al.* (13). The surface pressure curves as calculated from droptime data are in agreement with those calculated from differential capacitance data as are the surface excess results up to a concentration of 2 *M* in urea.

Typical electrocapillary results in Et_4NBr solutions containing up to 2 *M* urea are not remarkably different from those containing no urea. The influence of electrolyte concentration on the electrocapillary curves at varying urea concentrations is much more remarkable. At the lower Et_4NBr concentrations, 0.01 *M* Et_4NBr, the series of curves resemble that found for 1.0 *M* KNO_3. At higher concentrations, 0.1 *M* Et_4NBr, the family of curves has shrunk and at 1.0 *M* Et_4NBr the curves at different urea concentrations become practically indistinguishable. The surface pressure curves for the adsorption of urea are congruent with respect to charge in 1 *M* KNO_3 and in Et_4NBr at the concentrations below 0.01 *M*. Above these concentrations, charge congruency is not observed and the surface pressure values have considerably diminished.

This behaviour is even more clearly illustrated in Fig. 2 by the variation of Γ_{urea,H_2O} with surface charge. Whereas in Fig. 2*a* at 0.01 *M* Et_4NBr, the adsorption of urea tends toward a maximum at $q_M = +0.08\ C\ m^{-2}$ and resembles that found for 1.0 *M* KNO_3 solutions, no maximum is attained in Fig. 2*b* at 0.1 *M* Et_4NBr. At intermediate and high Et_4NBr concentrations, Γ_{urea,H_2O} is depressed considerably showing little charge dependency, Fig. 2*c*. Both the incongruency of the surface pressure curves, and the variation of charge dependence illustrated in Fig. 2*b* indicate strong lateral interactions involving adsorbed urea molecules. These interactions evidently also involve the adsorbed ionic species. It is generally accepted that adsorbed solute molecules replace adsorbed water molecules and that adsorbed ions replace adsorbed water molecules or at least influence their orientation. The free surface area open for this competition thus diminishes if the fractional surface coverage, θ_{urea}, or the surface excess of ionic components increase.

As indicated, apparent and relative surface excess values differ by the term $\Gamma_{2,h}{}^+ (\partial\mu_2/\partial\mu_1)$. In Fig. 3, Γ' at 0.1 *M* Et_4NBr is given to illustrate this point. The apparent values are consistently lower and in error by as much as 50% at negative charges with respect to the true values, Fig. 2*b*. At yet higher Et_4NBr concentrations this difference is even more important. In the past, calculations of apparent surface excess values have been made using the solute concentration instead of the solute activity in [2]. Since a_{solute} is normally less than [solute] even smaller values of apparent surface excess values would be obtained if such an erroneous data treatment were adopted here.

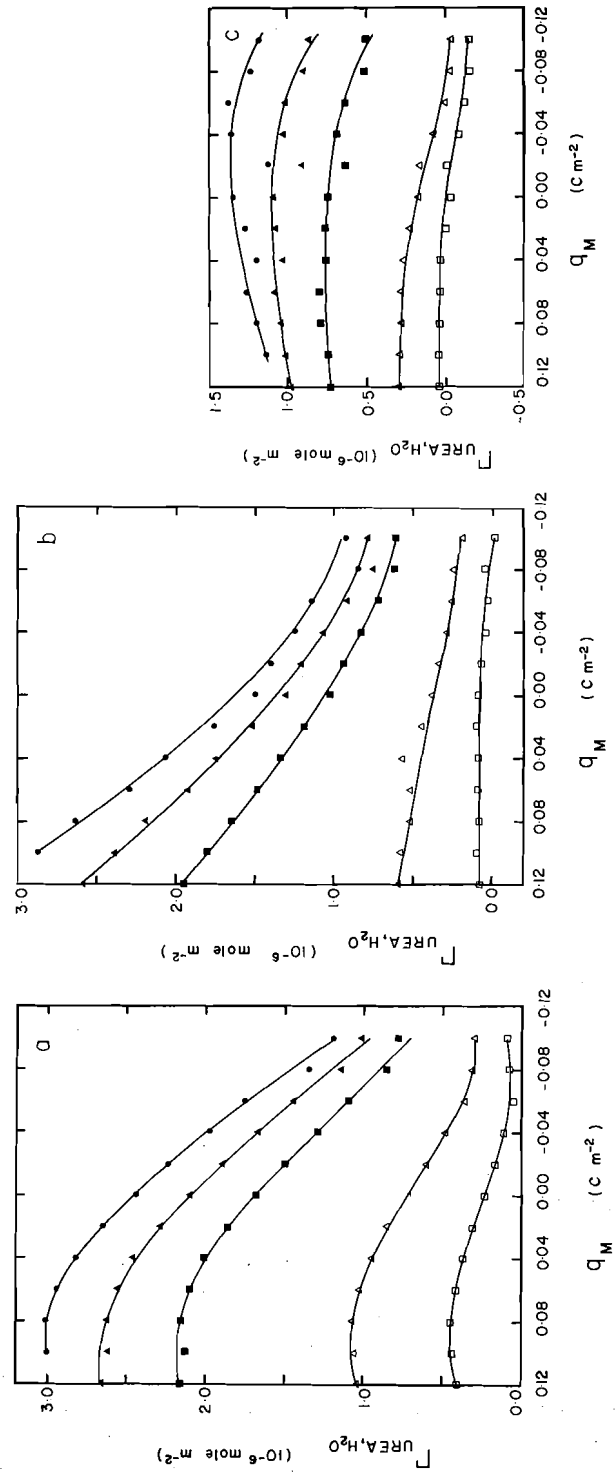

FIG. 2. (*a*) Surface excess Γ_{urea,H_2O} vs. surface charge at 0.01 *M* Et_4NBr: □ 0.1 *M*, △ 0.3 *M*, ■ 1.0 *M*, ▲ 1.5 *M*, ● 2.0 *M* urea. (*b*) Surface excess Γ_{urea,H_2O} vs. surface charge at 0.1 *M* Et_4NBr. Scale and symbols as in Fig. 2*a*. (*c*) Surface excess Γ_{urea,H_2O} vs. surface charge at 1.0 *M* Et_4NBr. Scale and symbols as in Fig. 2*a*.

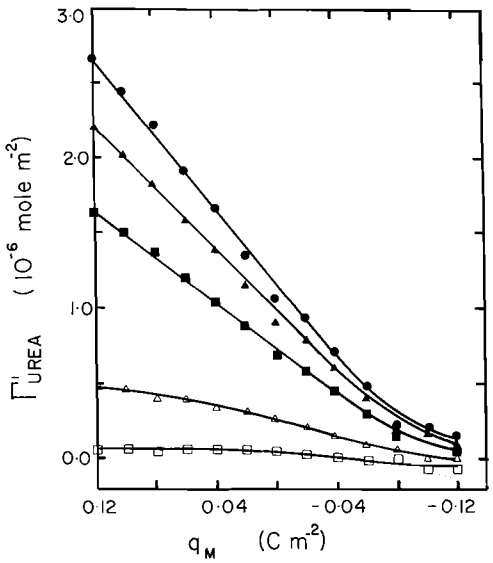

FIG. 3. Apparent surface excess Γ_{urea}' vs. surface charge at 0.1 *M* Et_4NBr. Scale and symbols as in Fig. 2*a*.

It cannot be denied that the injudicious treatment of thermodynamic data can lead to erroneous results difficult to interpret in terms of simple microscopic models. We should therefore view with caution any explanation of double layer phenomena in ternary systems unless it is established that the activity corrections have been applied or that they are indeed of negligible magnitude.

The ternary system urea–R_4NX–water reflects the behaviour of two binary systems: urea–water and R_4NX–water. Whereas the adsorption of R_4NX at different electrode charges can be studied, the system urea–water cannot be investigated directly without an electrolyte. However, extrapolating the surface excess value Γ_{urea,H_2O} to low electrolyte concentrations should yield results corresponding to the binary urea–water system. Thus

$$[9] \qquad \lim_{a_2 \to 0} \{\Gamma_{1,h}\} = \Gamma_{1,h} \quad (a_2 = 0)$$

However, plotting $\Gamma_{1,h}$ as a function of a_2 does not permit a linear extrapolation and involves highly curved regions at low Et_4NBr concentrations. Indeed, it would be surprising if the surface activity of urea varied linearly with the bulk Et_4NBr electrolyte activity. It is more useful to carry out the extrapolation with respect to the Et_4NBr population of the interfacial region itself.

It is possible (11) to divide the ionic surface excess $\Gamma_{2,h}^{+}$ into electrostatic and nonelectrostatic contributions:

$$[10] \qquad \Gamma_{2,h}^{+} = \Gamma_2^{+}\ \text{Electrostatic} + \Gamma_2^{\Delta}$$

where

$$\Gamma_2^{+}\ \text{Electrostatic} = A\ [\exp -(\sinh^{-1}(q_M/2A)) - 1]$$

and

$$A = (RT\varepsilon c/2\pi)^{1/2}$$

Extrapolating the surface excess Γ_{urea,H_2O} to a double layer composition where anions and cations are found only in the Outer Helmholtz region, i.e., where $\Gamma^{\Delta}_{Et_4NBr} = 0$, was carried out as in Fig. 4. The extrapolation is fairly linear, and the intercepts

$$[11] \qquad \lim_{\Gamma_2^{\Delta} \to 0} \{\Gamma_{1,h}\} = \Gamma_{1,h}^{0} \quad (\Gamma_2^{\Delta} = 0)$$

It now becomes possible to plot the isotherms for the adsorption of urea at different electrode charges without needing to consider the nature of the electrolyte. Such a plot is given in Fig. 5.

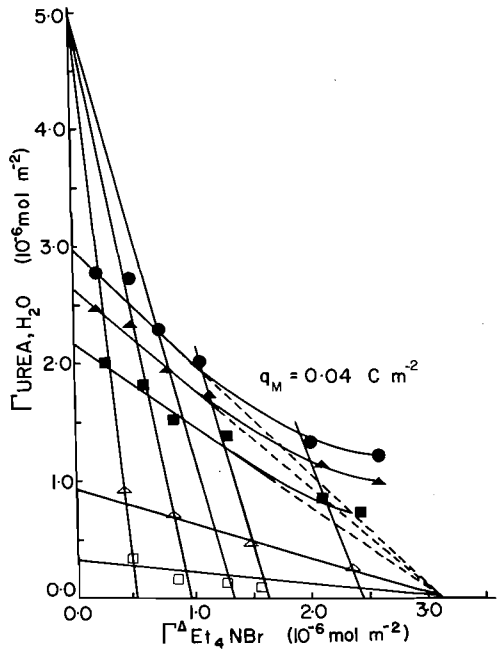

FIG. 4. Surface excess Γ_{urea,H_2O} vs. surface excess $\Gamma^{\Delta}_{Et_4NBr}$ at $q_M = 0.04$ C m^{-2} at fixed urea concentrations: □ 0.1 *M*, △ 0.3 *M*, ■ 1.0 *M*, ▲ 1.5 *M*, ● 2.0 *M* urea and at fixed Et_4NBr concentrations (left to right) 0.005, 0.01, 0.025, 0.05, 0.1, 0.5, 1.0 *M* Et_4NBr (10^{-6} mol m^{-2}) vs. (10^{-6} mol m^{-2}).

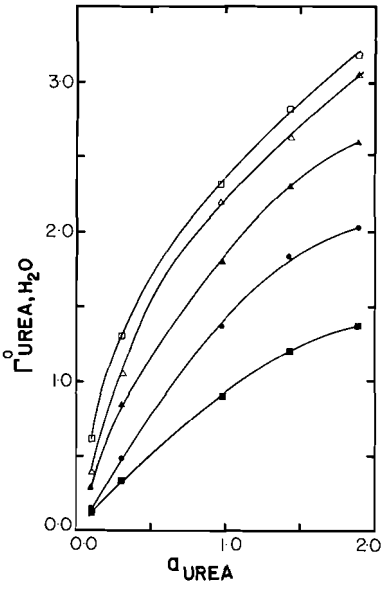

FIG. 5. Surface excess Γ^{o}_{urea,H_2O} extrapolated to $a_{Et_4NBr} = 0$ vs. activity of urea: $q_M = 0.08$, 0.04, 0.0, −0.04, −0.08 C m^{-2}.

Although different adsorption isotherms have been used (16) the Langmuir isotherm and variations thereof describe adequately the adsorption of simple molecules at the electrode/electrolyte interface. For the adsorption of a neutral solute (1) we may write:

$$[12] \quad \beta_1 a_1 = \theta_1/1 - \theta_1, \quad \theta_1 = \Gamma_1/\Gamma_{1\,max}$$

where $\beta_1 = \exp -(\Delta\bar{G}_1^{o}/RT) \exp -(g_1/RT)$ and where $\Delta\bar{G}_1^{o}$ is the free energy of adsorption of solute 1 and g_1 is a function of electrode charge, and where $\Gamma_{1\,max}$ is the surface excess corresponding to monolayer coverage.

Although we recognize that the Langmuir isotherm is unlikely to describe adequately the adsorption of the ionic components of an electrolyte, it is useful to employ this mathematical framework in order to describe the competitive adsorption of two solutes. For the simultaneous adsorption of two solutes (1) and (2) we may suppose that:

$$[13] \quad \beta_1' a_1 = \frac{\theta_1}{1 - \theta_1 - \theta_2}$$

where

$$\beta_2' = \beta_1 \exp -(\Delta\bar{G}_{1,2}/RT)$$

and where $\Delta\bar{G}_{1,2}$ refers to the lateral interaction energy between two adsorbed solutes (1) and (2).

The surface coverage θ_1 will diminish when θ_2 or $\beta_2' a_2$ becomes appreciably large, even in the absence of intersolute interactions. Since the surface activity of urea is considerably less than that of the tetraalkylammonium salt, θ_{urea} is expected to diminish by the simultaneous adsorption of the electrolyte.

The free energy terms β_1 and β_2 are normally charge dependent variables. The variation with charge of θ_1 will therefore be influenced by the variation of θ_2. If $\Delta\bar{G}_{1,2} = 0$, θ_1 should decrease most appreciably at those values of q_M where θ_2 becomes most significant because of increased competition for the space occupied by adsorbed water molecules. If $\Delta\bar{G}_{1,2} < 0$, the adsorption of the more weakly adsorbed species, here species (1), will be somewhat enhanced, particularly so at charges where solute (2) is strongly adsorbed.

We hesitate to identify θ_2 in the case of electrolytes although we recognize that the accepted mathematical treatment separates the ions into 'specifically' or 'contact' adsorbed and electrostatically adsorbed species. Different assumptions concerning the relative strength of the specific adsorption of the cation and anion will lead to different anion and cation profiles as a function of the distance from the electrode (17). At $q_M = 0$, the use of $\Gamma^{\Delta}_{Et_4NBr}$, the quantity of Et_4NBr adsorbed beyond that predicted from electrostatic behaviour, does not in itself presume any particular concentration profile. The use of $\theta_2 = \Gamma_2^{\Delta}/\Gamma_{2\,max}^{\Delta}$ in a Langmuir type isotherm does however presume adsorption of anion–cation pairs on the electrode surface. We shall examine the results for the ternary urea–Et_4NBr–water system to see to what degree this simplification is justified. A Langmuir type isotherm, [12], was imposed on the data given in Fig. 6 by a least-squares fit, varying $\Gamma_{1\,max}$ from 4×10^{-6} to 6×10^{-6} mol m^{-2} to obtain a concentration independent value of β_1. The results plotted in Fig. 6 indicate clearly, in agreement with Parson's conclusions (13), that little interaction exists between adsorbed urea molecules. We find $\Gamma_{max}^{urea} = 4.96 \times 10^{-6}$ mol m^{-2}, significantly less than that calculated by Parsons by neglecting activity coefficients in 1 M KNO_3. Our value in infinitely dilute electrolyte would allow full rotational freedom for the adsorbed molecule. In the absence of nonelectrostatic adsorption of Et_4NBr, the adsorption of urea follows a relatively simple pattern with a free energy of adsorption symmetrical about $q_M^{max} = +0.08$ C m^{-2}. A parabolic charge dependence was ob-

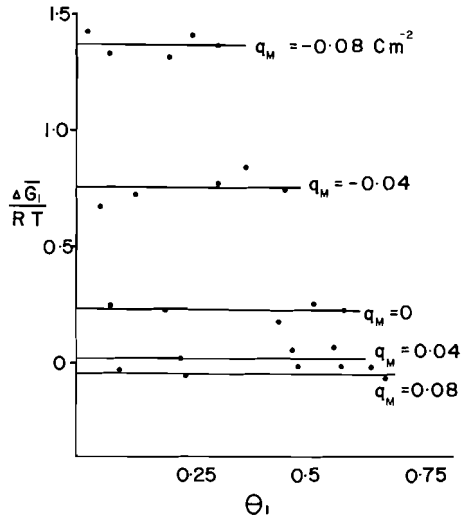

FIG. 6. Free energy of adsorption of urea vs. θ_{urea}. Calculated for $\Gamma_{max}^{urea} = 4.96 \times 10^{-6}$ mol m^{-2}: q_M = 0.08, 0.04, 0.0, −0.04, −0.08 C m^{-2}.

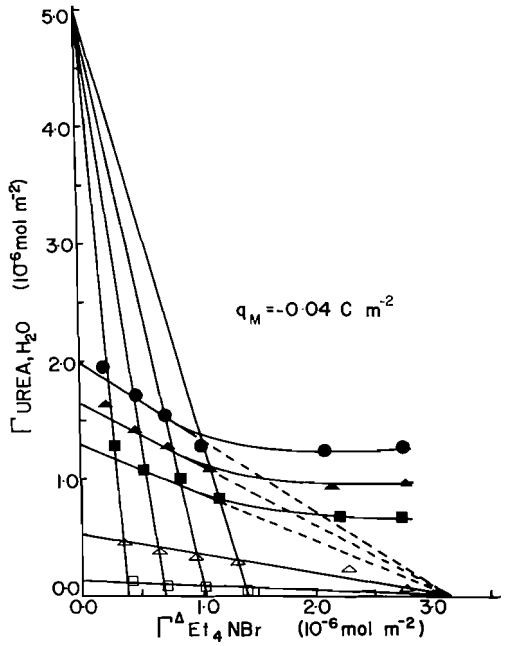

FIG. 7. Surface excess Γ_{urea,H_2O} vs. surface excess $\Gamma^{\Delta}_{Et_4NBr}$ at $q_M = -0.04$ C m^{-2}. Symbols as in Fig. 4.

served with $g_1/RT \propto -(q - q_{max})^2$, as expected if urea replaces absorbed water molecules.

Equation 12 constitutes a satisfactory description of the binary system. We can now examine Figs. 4 and 7 to see to what extent [13] describes the ternary system.

At any given urea activity a linear relationship exists between Γ_{urea,H_2O} and $\Gamma^{\Delta}_{Et_4NBr}$ at low Et_4NBr concentrations. Similarly, at any given salt activity a quasi-linear relationship is found, although the variations of $\Gamma^{\Delta}_{Et_4NBr}$ are slight and of the same magnitude as the experimental uncertainty. Extrapolation of $\Gamma^{\Delta}_{Et_4NBr}$ to $\Gamma_{urea} = 0$ yields values unaffected by the presence of adsorbed urea molecules and identical to those observed in binary solutions. Extrapolation of Γ_{urea,H_2O} to $\Gamma^{\Delta}_{Et_4NBr} = 0$ yields Γ^{0}_{urea,H_2O} whose numerical value is thought to be relatively little influenced by the chemial nature of the quaternary ammonium salts.

The intercepts Γ^{0}_{urea,H_2O} ($\Gamma^{\Delta} = 0$) at values of q_M from $q_M = +0.08$ to -0.08 C m^{-2} were used to establish an unique value of Γ_{max}^{urea} as indicated above. An attempt to evaluate Γ_{max}^{Δ} from a Langmuir isotherm at different values of q_M was not successful. Obviously the Langmuir model which supposes monolayer coverage and absence of lateral interactions is inadequate to describe the adsorption of an electrolyte. The value $\Gamma^{\Delta}_{max} = 3.15 \times 10^{-6}$ mol m^{-2} obtained by linear extrapolation of data such as in Figs. 4 and 7 is nevertheless in good agreement with that calculated from the theoretical model of the surface occupied by the voluminous cation (18).

From these two values, Γ_{max}^{urea} and Γ_{max}^{Δ}, obtained in 'binary' solutions, we can calculate θ_1 and θ_2 and evaluate [13] in the ternary solutions. Competition for the number of sites available is probably the underlying cause for the linear portions in Figs. 4 and 7. At low surface coverage $\Delta\bar{G}_{1,2} \simeq 0$ and little lateral interaction between adsorbed urea and adsorbed Et_4NBr is evident. Thus $(\theta_1 + \theta_2)$ remain relatively constant provided that a_1 or a_2 is held fixed. At high surface coverage θ_2, and fixed activity a_1, the lateral interaction term $\exp -(\Delta\bar{G}_{1,2}/RT)$ (eq. 13) is responsible for attracting increased amounts of species (1). Similarly, at high surface coverage θ_1, and fixed activity a_2, more species (2) are attracted than would be predicted if no lateral interactions existed. Again, the overwhelming surface activity of Et_4NBr vs. urea is such that the lateral urea–Et_4NBr interactions have a more prominent effect (at all surface charges) on the adsorption of urea than on the adsorption of Et_4NBr.

Interactions between adsorbed urea molecules are minimal, perhaps because appreciably large surface coverages were not attained, $\theta_{urea} < 0.6$. The perturbation due to adsorbed ionic components of Et_4NBr can be rationalized in a

manner analogous to the free energy of transfer of urea from a binary aqueous solution to a ternary Et_4NBr–urea–water solution. The overlap of a structure breaking type II_{sb} cosphere (5) of the Br^- ion with that of urea will lead to a relaxation of unstructures water to bulk water and a concomitant loss of enthalpy and entropy. In homogeneous solution this overlap leads to negative values of the free energy. In homogeneous solution a similar contribution due to the Et_4N^+ is thought to be minor. At the interface the analogous overlap of the hydration shells could also be responsible for the negative value of $\Delta\bar{G}_{1,2}$. For any given $\Gamma^{\Delta}_{Et_4NBr}$, this effect is relatively charge independent (viz. Figs. 4 and 7) and is consistent with the underlying assumption for the adsorption of Et_4NBr, namely that both anion and cation are found in the Inner Helmholtz Layer.

Conclusions

For ternary systems, surface excess values, Γ_{1,H_2O}, obtained at fixed concentration of species (2) should be calculated according to [4] and [5]. Neglect of the activity corrections would lead to erroneous results for urea–Et_4NBr–H_2O solutions. Since Et_4NBr is much more readily adsorbed than urea at the mercury/electrolyte interface, it competes most successfully for vacant sites and displaces adsorbed urea molecules at all but the highest concentrations and for $q_M \gg 0$. At high surface coverage, lateral attractive forces between adsorbed urea and Br^- species are probably due to overlap of hydration cospheres similar to that found in concentrated ternary solutions.

Acknowledgements

Our thanks are due to F. Comtois for technical assistance and the National Research Council of Canada for financial support of this work.

1. R. H. Stokes. Aust. J. Chem. **20**, 2087 (1967).
2. W.-Y. Wen and J. H. Hung. J. Phys. Chem. **74**, 170 (1970).
3. W.-Y. Wen and C. M. Y. Chen. J. Phys. Chem. **73**, 2895 (1969).
4. N. Desrosiers, G. Perron, J. G. Mathieson, B. E. Conway, and J. E. Desnoyers. J. Solution Chem. **3**, 789 (1974).
5. M. Y. Schrier, P. J. Turner, and E. E. Schrier. J. Phys. Chem. **79**, 1391 (1975).
6. H. Friedman. *In* Water, a comprehensive treatise. Vol. 3. *Edited by* F. Franks. Plenum Press, New York, NY. 1973. p. 50.
7. J. E. Desnoyers and C. Jolicoeur. *In* Modern aspects of electrochemistry. Vol. 5. *Edited by* J. O'M. Bockris and B. E. Conway. Plenum Press, New York, NY. 1969.
8. A. J. Parker. Electrochim. Acta, **21**, 671 (1976).
9. E. Verdier, G. H. Nancy, and P. Vanel. J. Chem. Phys. **1**, 368 (1973).
10. J. Piro, R. Bennes, and E. Ban Karam. J. Electroanal. Chem. **57**, 399 (1974).
11. H. Ménard and F. M. Kimmerle. Can. J. Chem. **54**, 2488 (1976).
12. T. S. Sarma and J. C. Ahluwalia. J. Phys. Chem. **76**, 1366 (1972).
13. R. Parsons, R. Peat, and R. M. Reeves. J. Electroanal. Chem. **62**, 151 (1975).
14. H. Nakadomari, D. V. Mohilner, and P. R. Mohilner. J. Phys. Chem. **80**, 1761 (1976).
15. S. Lindenbaum and G. G. Boyd. J. Phys. Chem. **68**, 911 (1964).
16. R. Parsons. J. Electroanal. Chem. **7**, 136 (1964).
17. F. M. Kimmerle and H. Ménard. Electroanal. Chem. **54**, 101 (1974).
18. F. M. Kimmerle and H. Ménard. *In* Chemistry and physics of aqueous gas solutions. *Edited by* W. A. Adams. The Electrochemical Society, Princeton, NJ. 1975. p. 337.

Arrhenius parameters for the reactions of $O(^3P)$ atoms with several aldehydes and the trend in aldehydic C—H bond dissociation energies[1]

D. L. SINGLETON, R. S. IRWIN, AND R. J. CVETANOVIĆ

Division of Chemistry, National Research Council of Canada, Ottawa, Ont., Canada K1A 0R9

Received March 23, 1977

D. L. SINGLETON, R. S. IRWIN, and R. J. CVETANOVIĆ. Can. J. Chem, **55**, 3321 (1977).

The phase-shift technique has been used to determine the temperature dependence of the reaction of ground state oxygen atoms with several aldehydes. Oxygen atoms were generated by modulated photosensitized decomposition of nitrous oxide and were monitored by the chemiluminescence from their reaction with nitric oxide. The Arrhenius expressions determined over the temperature interval 298–472 K are: k_1(acetaldehyde) = $(7.21 \pm 1.49) \times 10^9 \exp(-1960 \pm 153/RT)$; k_1(propionaldehyde) = $(7.78 \pm 0.75) \times 10^9 \exp(-1727 \pm 66/RT)$; k_1(butyraldehyde) = $(9.99 \pm 0.56) \times 10^9 \exp(-1702 \pm 40/RT)$; k_1(isobutyraldehyde) = $(7.92 \pm 1.02) \times 10^9 \exp(-1445 \pm 91/RT)$, where the units are ℓ mol^{-1} s^{-1} and cal mol^{-1}. The indicated uncertainties are one standard deviation. After small corrections were made for the potential abstraction of alkyl hydrogens, the activation energies of aldehydic hydrogen abstraction were used to estimate the aldehydic C—H bond dissociation energies, D(RCO—H). The trend of slightly decreasing values of D(RCO—H) thus obtained for the sequence H_2CO, CH_3CHO, C_2H_5CHO, n-C_3H_7CHO, i-C_3H_7CHO was also indicated by the aldehydic C—H stretching frequencies.

D. L. SINGLETON, R. S. IRWIN et R. J. CVETANOVIĆ. Can. J. Chem. **55**, 3321 (1977).

La technique de déphasage est utilisée afin de déterminer l'effet de la température sur la réaction de l'oxygène atomique à l'état fondamental avec plusieurs aldéhydes. Les atomes d'oxygène sont formés par décomposition photosensibilisée de l'oxyde nitreux. Ces atomes sont ensuite mesurés par chemiluminescence résultant de leur réaction avec l'oxyde nitrique. Les expressions d'Arrhénius déterminées pour l'écart de température 298–472 K sont: k_1(acétaldéhyde) = $(7.21 \pm 1.49) \times 10^9 \exp(-1960 \pm 153/RT)$; k_1(propionaldéhyde) = $(7.78 \pm 0.75) \times 10^9 \exp(-1727 \pm 66/RT)$; k_1(butyraldéhyde) = $(9.99 \pm 0.56) \times 10^9 \exp(-1702 \pm 40/RT)$; k_1(isobutyraldéhyde) = $(7.92 \pm 1.02) \times 10^9 \exp(-1445 \pm 91/RT)$, avec les unités exprimées en ℓ mol^{-1} s^{-1} et cal mol^{-1}. Les incertitudes indiquées correspondent à l'écart type. Après avoir fait les corrections pour l'abstraction possible des hydrogènes d'un groupe alkyle, les énergies d'activation de l'abstraction d'un hydrogène aldéhydique sont utilisée afin d'évaluer les énergies de dissociation du lien carbone hydrogène D(RCO—H). La tendance qu'ont les valeurs à décroître légèrement dans la série H_2CO, CH_3CHO, C_2H_5CHO, n-C_3H_7CHO, i-C_3H_7CHO est indiquée aussi par les fréquences d'élongation du lien C—H.

[Traduit par le journal]

Introduction

The reactions of ground state oxygen atoms with aldehydes occur in the initiating stages of photochemical smog and in the combustion of aldehydes. In the primary step for the reaction of $O(^3P)$ with acetaldehyde at 298 K, reactive acetyl and hydroxyl radicals are formed by abstraction of hydrogen from the aldehydic group (1, 2). An analogous mechanism should occur for the other aldehydes, and has indeed been shown to occur for the simplest member of the series, formaldehyde (3–5).

Kinetically obtained thermochemical data for various aldehydes indicate that the bond dissociation energies of the aldehydic hydrogen are about the same, within 1 or 2 kcal mol^{-1} (6). However, the reported rate constants and Arrhenius parameters for the $O(^3P)$ + aldehyde reactions are significantly different for the simpler aldehydes and do not appear to follow a consistent trend. The preferred room temperature rate constant for formaldehyde has recently been given as 0.9×10^8, and for acetaldehyde, 3.1×10^8 ℓ mol^{-1} s^{-1} (7). Nearly identical values of 1.4 and 1.5×10^8 have been reported for propionaldehyde (8) and butyraldehyde (9). Activation energies of 2.6, 2.3, and 3.8 kcal mol^{-1} have been reported for formaldehyde (10), acetaldehyde (11), and propionaldehyde (8).

[1]NRCC No. 16096.

Almost all the available values of the rate constants for the reactions of $O(^3P)$ with aldehydes have been determined by the discharge-flow technique. It is desirable to verify the values of these rate constants by an independent technique in order to establish the actual sequence of reactivity and the trends in the values of the Arrhenius parameters.

The modulated chemiluminescence ('phase-shift') technique has been used previously in this laboratory to determine rate constants and Arrhenius parameters for the addition of $O(^3P)$ atoms to several olefins (12). The rate constants determined with this technique were precise, and the agreement with the flash photolysis–resonance fluorescence results and the competitive (product analysis) results was generally very good. In the present work we use the modulated chemiluminescence technique to determine the temperature dependence of the rate constants for the abstraction reactions of $O(^3P)$ with acetaldehyde, propionaldehyde, butyraldehyde, and isobutyraldehyde. Estimates of the aldehydic C—H bond dissociation energies are made, based on correlations with (*1*) the activation energies for abstraction by $O(^3P)$ and (*2*) the aldehydic C—H stretching frequencies.

Experimental

Details of the experimental technique have been given previously (13–15). Ground state oxygen atoms are generated by modulated mercury photosensitized decomposition of nitrous oxide in a flowing mixture of Hg, N_2O, NO, and aldehyde. The $O(^3P)$ atoms react with both nitric oxide and aldehyde.

[1] $$O(^3P) + RCHO \rightarrow OH + RCO$$

[2] $$O(^3P) + NO + M \rightarrow NO_2 + M$$

The reaction with NO produces the well known NO_2 chemiluminescence, the intensity of which is also modulated. The phase difference between the 254 nm light, which initiates the reaction sequence, and the chemiluminescence is the primary measurement and is related to the rate constants k_1 and k_2 for reactions 1 and 2,

$$\frac{2\pi\nu}{\tan\phi} = k_1[RCHO] + k_2[NO][M]$$

where ϕ is the phase shift and ν is the modulation frequency. The phase shift is measured with photomultipliers and a lock-in amplifier.

The flow rate of N_2O was determined by a frequently calibrated rotameter. The flow rates of NO and the aldehydes were determined by calibrated capillaries. The pressure drops across the capillaries were measured with a DC-704 silicone oil manometer in the case of nitric oxide, and with an electronic pressure transducer (Dynisco DPT 85-2 or Decker 306) in the case of the aldehydes. Flows of the aldehydes were controlled by stainless steel bellows sealed needle valves. Teflon stopcocks with which the aldehydes came in contact were provided with ethylene propylene rubber O-rings.

At each of the experimental temperatures between 298–472 K, the following conditions were used. The modulation frequency was usually varied by a factor of two within the range 1500–8000 Hz. Experiments were done at both 30 and 60 Torr, except for butyraldehyde and isobutyraldehyde for which experiments were done only at 30 Torr because of difficulties associated with their lower volatilities. The NO concentration was 5 to 10% of the N_2O concentration, and the aldehyde concentration was varied from about 1–10% of the N_2O concentration.

The rate of absorption of 254 nm radiation, less than 1×10^{12} quanta cm^{-3} s^{-1}, was determined by gas chromatographic analysis of the products of the reaction: $O(^3P)$ + 1-butene.

All the aldehydes were obtained from Eastman Organic Chemicals, except isobutyraldehyde which was obtained from Anachemia. The aldehydes were distilled into a storage reservoir with care being taken always to maintain the aldehydes above their melting points to reduce polymerization. Gas chromatographic analysis on β,β′-thiodipropionitrile and β,β′-thiodipropionitrile + squalane capillary columns gave the following detectable impurity levels: acetaldehyde, <0.01%; propionaldehyde, 0.09% (0.05% as butyraldehyde); butyraldehyde, 0.01% (as isobutyraldehyde); isobutyraldehyde, 0.01%. Nitrous oxide and nitric oxide were obtained from Matheson. The nitric oxide was passed through Linde 13X molecular sieve to remove traces of NO_2.

Results

In the present experiments, an emission signal could be detected when only Hg, N_2O, and aldehyde were irradiated with the modulated low pressure mercury lamp. The intensity of the emission signal was proportional to the aldehyde concentration. A Corning 2-61 filter effectively blocked the extraneous emission, and transmitted the longer wavelength portion of the NO_2 chemiluminescence. The measured chemiluminescence intensity was decreased by about a factor of 2.5, relative to the intensity detected with the previously used 3-70 filter. This caused a corresponding decrease in the signal to noise ratio. It was estimated that the extraneous emission signal contributed less than 5% error to the measurement of tan ϕ. The error approached this value for only three points; usually it was much less.

The extraneous emission proved to be fluorescence from the aldehydes excited by absorption of the 313 nm line from the modulated low pressure mercury lamp. The spectrum of the

TABLE 1. Rate constants for the reactions of ground state oxygen atoms with aldehydes (k_1), and with nitric oxide (k_2)[a]

T (K)	Rate constant	Acetaldehyde	Propionaldehyde	Butyraldehyde	Isobutyraldehyde	Nitric oxide[b]
298	k_1	2.59±0.08	4.21±0.11	5.71±0.15	7.15±0.17	
	k_2	4.69±0.18	4.72±0.13	4.97±0.17	5.00±0.20	4.84
339	k_1	4.11±0.08	6.04±0.10	7.90±0.21	9.00±0.19	
	k_2	2.92±0.12	3.57±0.11	3.89±0.20	4.27±0.18	3.80
396	k_1	5.83±0.08	8.32±0.26	11.3 ±0.35	12.3 ±0.4	
	k_2	2.67±0.21	3.07±0.23	2.96±0.31	3.27±0.24	2.92
472	k_1	9.54±0.28	12.6 ±0.4	16.5 ±0.5	17.4 ±0.4	
	k_2	2.31±0.20	2.52±0.19	2.75±0.31	2.63±0.21	2.27

[a]Units are: $k_1 \times 10^{-8}$ ℓ mol^{-1} s^{-1}; $k_2 \times 10^{-10}$ ℓ^2 mol^{-2} s^{-1}. The uncertainties are one standard deviation.
[b]Values were calculated from the Arrhenius expression, determined for k_2 in mixtures of Hg, N_2O, and NO, reported in ref. 15.

emission from irradiated isobutyraldehyde + mercury, determined with a Bausch and Lomb monochromator and EMI 9558 photomultiplier, extended from 364 nm to beyond 500 nm with a maximum at about 418 nm. Also, the extraneous emission was eliminated when the 313 nm line was removed by placing an interference filter (center wavelength ~254 nm) between the Hg lamp and the reaction cell. The emission spectrum is similar to the reported fluorescence spectrum of acetaldehyde excited at 313 nm (16). However, in the present work, emission is detected at even longer wavelengths, (using Corning filters in place of the monochromator) up to about 600 nm, for all four aldehydes. This probably reflects somewhat greater sensitivity in the present experiments.

Rate constants of reactions 1 and 2 were obtained from plots of $2\pi\nu$/[aldehyde]tan ϕ vs. [NO][M]/[aldehyde]. The intercepts of linear least-squares lines through the points gave the values of k_1, and the slopes gave the values of k_2. The plots for the four aldehydes are given in Fig. 1 for $T = 298$ K. The slopes of the plots are the same, as they should be, and are within 4% of the value of k_2 determined previously in the absence of aldehyde. Also, the precision of the points indicates that the rate constants, k_1, of the four aldehydes are significantly different.

Several points were obtained for isobutyraldehyde at 298 K with a 254 nm interference filter placed in front of the reaction cell to block the 313 nm light in order to eliminate fluorescence of the aldehyde. In these additional experiments, the Corning 2-61 filter in front of the photomultiplier monitoring the chemiluminescence was replaced by a 3-70 filter. As shown in Fig. 1, elimination of the 313 nm line had no significant effect on the results.

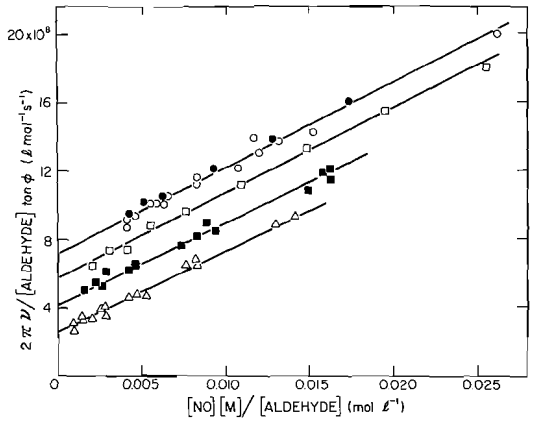

FIG. 1. Plots of $2\pi\nu$/[aldehyde] tan ϕ vs. [NO][M]/[aldehyde] for the reactions of $O(^3P)$ atoms with aldehydes at 298 K. △ Acetaldehyde; ■ propionaldehyde; □ butyraldehyde; ○ isobutyraldehyde; ● isobutyraldehyde with a 253.7 nm interference filter between the lamp and the reaction cell.

The rate constants, k_1, determined for the aldehydes at four temperatures are listed in Table 1. Also listed are values of k_2 determined from the slopes of plots similar to those in Fig. 1. With one exception (acetaldehyde at 339 K) the values of k_2 are in good agreement with the values of k_2 determined previously in the absence of aldehyde. (The Arrhenius parameters for acetaldehyde would be altered only slightly if the value of k_1 at 339 K were excluded.)

The rate constants, k_1, are plotted in Arrhenius form in Fig. 2. The points can be adequately represented by the Arrhenius equation. The least-squares Arrhenius parameters are given in Table 2.

TABLE 2. Comparison of the present room temperature rate constants and Arrhenius parameters with previously reported values for $O(^3P)$ + aldehyde reactions[a]

Reference	Method	$k_{298} \times 10^{-8}$ (ℓ mol^{-1} s^{-1})	$A \times 10^{-9}$ (ℓ mol^{-1} s^{-1})	E (kcal mol^{-1})
		Acetaldehyde		
This work	Hg sensitization – Chemiluminescence	2.59	7.21±1.49	1.960±0.153
Mack and Thrush (17)	Discharge flow – Chemiluminescence and esr	2.88		
Cadle and Powers (11)	Discharge flow – Chemiluminescence	2.7	14[b]	2.36[b]
Cvetanović (1)	Hg sensitization – Product analysis	3.0[c]		
		Propionaldehyde		
This work	Hg sensitization – Chemiluminescence	4.21	7.78±0.75	1.727±0.066
Cadle and Allen (8)	Discharge flow – Chemiluminescence	1.4	85	3.8
		Butyraldehyde		
This work	Hg sensitization – Chemiluminescence	5.71	9.99±0.56	1.702±0.040
Jaffe and Wan (9)	NO_2 photo-oxidation – Quantum loss of NO_2	1.5		
		Isobutyraldehyde		
This work	Hg sensitization – Chemiluminescence	7.15	7.92±1.02	1.445±0.091

[a]The uncertainties indicated in the present work are 1σ.
[b]Calculated by least-squares treatment of the rate constants reported in ref. 11.
[c]The reported relative rate was converted to an absolute rate using the $O(^3P) + C_2H_4$ rate constant of ref. 12.

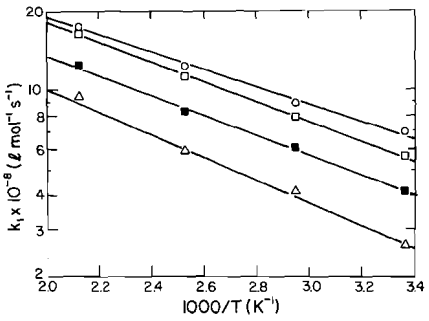

FIG. 2. Arrhenius plots of the reactions of $O(^3P)$ atoms with aldehydes. △ Acetaldehyde; ■ propionaldehyde; □ butyraldehyde; ○ isobutyraldehyde.

On the basis of a previously suggested generalized reaction scheme (14), it is estimated that less than 0.5% of the oxygen atom consumption in the presence of the aldehydes was by secondary reactions with primary reaction products. Less than 0.1% of the aldehydes were consumed by oxygen atoms, as estimated from the rate of oxygen atom production and the residence time of the aldehydes in the reaction cell.

Discussion

Comparison of the Rate Constants with Literature Values

A comparison of the present results with other reported values of k_1 is made in Table 2. The agreement among all the reported values for acetaldehyde is good. The value of Cadle and Powers (11) at 476 K is about 25% larger than the present value at 472 K, and their room temperature value is within 5%. The value determined by Cvetanović (1) for acetaldehyde, measured relative to ethylene, is also in good agreement, as is the value by Mack and Thrush (17).

The present Arrhenius expression for propionaldehyde differs considerably from that reported by Cadle and Allen (8), who used the same technique as was used by Cadle and Powers (11) with acetaldehyde. They determined the

rate constants from the initial $O(^3P)$ decay rate in a discharge flow system, using the chemiluminescence from reaction 2 to monitor the $O(^3P)$ concentration. At higher temperatures their values are in reasonable agreement with the present values (the Arrhenius lines intersect at 433 K), but at room temperature their value is only $\frac{1}{3}$ of the present value. It is not clear why such a discrepancy occurs, but it may not be significant when the scatter in the experimental values is taken into account.

There is apparently only one previously reported value of k_1 for butyraldehyde. Jaffe and Wan (9) reported a value, which is $\frac{1}{4}$ the present value, in a study of the photochemical reaction of NO_2 with butyraldehyde. The value of k_1 was obtained from the quantum yield for NO_2 loss as a function of [aldehyde]/[NO_2]. Within the experimental error, the results of Jaffe and Wan for acetaldehyde and butyraldehyde suggested that both aldehydes react with similar rates in the photochemical reactions with NO_2, implying similar values of k_1. However, these are indirect determinations of k_1, and various complicating factors may be involved.

Allowances for Abstraction of H Atoms from the Alkyl Groups

At room temperature the mechanism of the $O(^3P)$ + acetaldehyde reaction involves abstraction of the aldehydic hydrogen atom. There is no evidence of other reactive paths, such as abstraction of hydrogen from the methyl group (1, 2). However, abstraction of hydrogen from the alkyl group of the aldehydes will become more significant (*1*) as the C—H bonds become weaker on going from primary to secondary to tertiary, (*2*) as the temperature increases, and (*3*) as the number of alkyl C—H bonds increases.

It is possible to estimate the contributions to the observed rate constants made by alkyl hydrogen abstraction by assuming that the rate constants for abstraction (per C—H bond) from primary, secondary, and tertiary C—H bonds in the compounds C_2H_6, n-C_4H_{10}, and $(CH_3)_2CHCH(CH_3)_2$, respectively, as reported in ref. 18, are transferable to the alkyl groups in the aldehydes. The percentages estimated in this way for abstraction from the alkyl group relative to the total observed rate at 298 and 472 K are: acetaldehyde 0.1, 1.4; propionaldehyde 1.8, 12; butyraldehyde 2.6, 18; isobutyraldehyde 0.9, 4.2. These estimates show that abstraction from the alkyl groups probably becomes significant at the higher temperatures used in the present work as the number of alkyl $\rangle CH_2$ groups increases.

TABLE 3. Estimated[a] Arrhenius parameters for the reaction $O(^3P)$ + RCHO → OH + RCO[b]

Aldehyde	$A \times 10^{-9}$ (ℓ mol^{-1} s^{-1})	E (cal mol^{-1})
CH_3CHO	7.00±1.40	1941±148
CH_3CH_2CHO	5.67±0.51	1543± 62
$CH_3(CH_2)_2CHO$	6.23±0.13	1428± 15
$(CH_3)_2CHCHO$	7.18±0.87	1390± 86

[a]The estimated rate of H abstraction from the alkyl group is subtracted from the total measured rate.
[b]The indicated uncertainties are one standard deviation.

Rate constants corresponding to abstraction of the aldehydic hydrogen by $O(^3P)$ are estimated by substracting from the observed rates the calculated rates of abstraction of hydrogen atoms from the alkyl groups. The Arrhenius parameters for abstraction of the aldehydic hydrogen were evaluated from these 'corrected' rate constants. The least-squares values of the Arrhenius parameters, obtained using the statistical weights of the observed rate constants, are given in Table 3. The pre-exponential factors are the same, within about one standard deviation, for the four aldehydes, and are comparable to values, per C—H bond, for the $O(^3P)$ + alkane reactions (18). The Arrhenius activation energies are significantly lower (by 1 to 8 kcal mol^{-1}) than the activation energies for the $O(^3P)$ + alkane reactions, consistent with the weaker aldehydic C—H bond. There is a trend of decreasing activation energies in the series acetaldehyde–propionaldehyde–butyraldehyde–isobutyraldehyde. A question of considerable interest is whether this trend signifies that there is a corresponding trend in the bond dissociation energies of the aldehydic hydrogen, D(RCO—H),[2] for the four aldehydes.

Thermochemical Values of D(RCO—H)

The aldehydic C—H bond dissociation energies reported for formaldehyde, acetaldehyde, and propionaldehyde are very similar. Some recent values, in kcal mol^{-1}, are: CH_2O 88.5 (19), 87 (20), 76 (21); CH_3CHO 87.7 (22), 87 (20), 87.3 (21); CH_3CH_2CHO 87.4 (23). To our knowledge there are no values reported for the

[2]The bond dissociation energies in this paper refer to D^o_{298} values.

butyraldehydes. All of the values except Fletcher and Pilcher's value (19) for formaldehyde are based on kinetic data (i.e., differences in activation energies for various forward and reverse reactions). Within the experimental errors of about 1 or 2 kcal mol^{-1}, the bond dissociation energies are the same. The thermochemical data are not sufficiently precise to ascribe the small variation in activation energies in Table 3 to changes in D(RCO—H). Thus it is necessary to examine other physical properties of the aldehydes that might provide a more precise relative ordering of D(RCO—H).

Estimates of D(RCO—H) from the Trend in the Arrhenius Activation Energies

In a review of reactions of $O(^3P)$ atoms with hydrocarbons, Huie and Herron (18) correlated C—H bond dissociation energies with the activation energies for $O(^3P)$ abstraction reactions. Although the correlation is not necessarily linear, as they discussed, we have used their plot to estimate D(RCO—H) for the aldehydes in the present study and also for formaldehyde, for which the temperature dependence of the rate constant of reaction with $O(^3P)$ has been reported (10) as $3.7 \times 10^9 \exp(-2.4 \text{ kcal mol}^{-1}/RT)$ ℓ mol^{-1} s^{-1}. Values of D(RCO—H) were calculated from the line in Huie and Herron's plot of D vs. E using the values of E in Table 3 and Cadle's activation energy for H_2CO. The values D(RCO—H) thus obtained are given in Table 4 under the 'E vs. D' heading. The most significant decreases in D(RCO—H) occur going from formaldehyde to acetaldehyde (1.5 kcal mol^{-1}) to propionaldehyde (1.3 kcal mol^{-1}), but there is little further change on going to the butyraldehydes.

Because the correlation of bond energy with activation energy is not necessarily linear, and because the 'corrections' for abstraction from the alkyl portion of the aldehydes are estimates, the above correlation must be made advisedly. However, in support of this correlation, C—H stretching frequencies also indicate a similar trend in D(RCO—H).

Estimates of D(RCO—H) from the Trend in the Aldehydic C—H Stretching Frequencies

The stretching frequencies of C—H bonds have been correlated recently with the bond dissociation energies for a variety of molecules (24). We arbitrarily use the line drawn by McKean *et al.* (24) connecting the data for HCN and CH, and estimate D(RCO—H) for each aldehyde using the C—H stretching frequencies in Table 4. The trend in the D(RCO—H) values obtained from the stretching frequencies is similar to the trend obtained from the activation energy correlation, and in fact, the absolute values are in fairly good agreement, as shown in Table 4. However, only the relative values are sought, and the values are therefore normalized to $D(CH_3CO—H) = 87.3$ kcal mol^{-1}, the mean of the values in refs. 20–22. The trend in D(RCO—H) is perhaps shown more convincingly by comparing these normalized values, which are enclosed in parentheses in Table 4. It is interesting to note that Bernstein (27), in an earlier correlation of C—H stretching frequencies, predicted values of 88 and 85 kcal mol^{-1} for D(RCO—H) for formaldehyde and acetaldehyde, respectively.

Discussion of the Trend in D(RCO—H)

It should be emphasized that the trend in D(RCO—H) values suggested by the present work and by the C—H stretching frequencies is relatively small, and is within the uncertainties in the thermochemical results based on kinetic techniques such as iodine atom reactions. The near constancy of the aldehydic hydrogen bond dissociation energies has been discussed by Solly and Benson (28). Within the precision of the thermochemical data available, they concluded that there was no effect of alkyl group substitution of the magnitude exhibited by CH_3—H (104 kcal mol^{-1}) and C_2H_5—H (98 kcal mol^{-1}). It would be interesting to compare the aldehydes with the isoelectronic series $RC(=CH_2)$—H, but unfortunately there does not appear to be much thermochemical data on vinylic hydrogen dissociation energies.

The difference of $\sim$20 kcal mol^{-1} in the dissociation energies of the vinylic ($\sim$108 kcal mol^{-1} in C_2H_4) and the analogous aldehydic C—H bonds is very striking. The potential electronic interactions which may affect the strength of the aldehydic C—H bonds and the stability of the radicals formed after removal of H have been discussed (28–30). The fact that the C—H stretching frequencies are low, and that they predict fairly well the observed values of D(RCO—H), would seem to indicate that the bond weakening factors are operative in the

TABLE 4. Estimates of the aldehydic C—H bond dissociation energies, D(RCO—H), from the correlations E vs. D and ν vs. D, i.e., of activation energies, E, and of vibrational frequencies, ν, with the C—H bond dissociation energies, D

Aldehyde	E[b] (kcal/mol)	ν (cm^{-1})	D(RCO—H) from correlations[a]: E vs. D (kcal/mol)	ν vs. D (kcal/mol)
Formaldehyde	2.4[c]	2812[d]	87.6 (88.8)	87.7 (91.0)
Acetaldehyde	1.94	2770[e]	86.1 (87.3)	84.1 (87.3)
Propionaldehyde	1.54	2758[e]	84.8 (86.0)	83.1 (86.3)
Butyraldehyde	1.43	2757[e]	84.5 (85.7)	83.0 (86.2)
Isobutyraldehyde	1.39	2750[e]	84.3 (85.5)	82.4 (85.5)

[a]The values in the parentheses are normalized taking $D(CH_3CO—H) = 87.3$ kcal mol^{-1}, i.e., the mean of the values quoted in refs. 20–22.
[b]The activation energies have been corrected for the potential contribution of alkyl hydrogen abstraction.
[c]Reference 10.
[d]Average of the symmetric and asymmetric stretches (25).
[e]Average of the Fermi doublets (26).

aldehyde, and not solely through stabilization (28) of the radical, because the stretching frequencies are expected to be sensitive to properties of the aldehyde rather than to the separated radical and H atom. This is exemplified by comparing benzaldehyde and toluene. For the former, the aldehydic C—H stretch (average) is the same as that in acetaldehyde, 2770 cm^{-1} (24), as is the bond dissociation energy, 86.9 kcal mol^{-1} (28). Benzyl radical, on the other hand, exhibits about 15 kcal mol^{-1} stabilization. The value of $D(C_6H_5CH_2—H)$ that would be predicted by the C—H stretching frequency is 99.9 kcal mol^{-1} (24), whereas the observed value is only 85 kcal mol^{-1} (20).

1. R. J. CVETANOVIĆ. Can. J. Chem. **34**, 775 (1956).
2. H. E. AVERY and R. J. CVETANOVIĆ. J. Chem. Phys. **43**, 3727 (1965).
3. H. NIKI. J. Chem. Phys. **45**, 2330 (1966).
4. J. T. HERRON and R. D. PENZHORN. J. Phys. Chem. **73**, 191 (1969).
5. G. P. R. MACK and B. A. THRUSH. J. Chem. Soc. Faraday Trans. I, **69**, 208 (1973).
6. Z. B. ALFASSI and D. M. GOLDEN. J. Am. Chem. Soc. **95**, 319 (1973).
7. J. T. HERRON and R. E. HUIE. J. Phys. Chem. Ref. Data, **2**, 467 (1974).
8. R. D. CADLE and E. R. ALLEN. *In* Chemical reactions in urban atmospheres. *Edited by* C. S. Tuesday. American Elsevier, New York, NY. 1971. p. 63.
9. S. JAFFE and E. WAN. Environ. Sci. Technol. **8**, 1024 (1974).
10. R. D. CADLE, H. H. WICKMAN, C. B. HALL, and K. M. EBERLE. Chemosphere, **3**, 115 (1974).
11. R. D. CADLE and J. W. POWERS. J. Phys. Chem. **71**, 1702 (1967).
12. D. L. SINGLETON and R. J. CVETANOVIĆ. J. Am. Chem. Soc. **98**, 6812 (1976).
13. R. ATKINSON and R. J. CVETANOVIĆ. J. Chem. Phys. **55**, 659 (1971).
14. S. FURUYAMA, R. ATKINSON, A. J. COLUSSI, and R. J. CVETANOVIĆ. Int. J. Chem. Kinet. **6**, 741 (1974).
15. D. L. SINGLETON, S. FURUYAMA, R. J. CVETANOVIĆ, and R. S. IRWIN. J. Chem. Phys. **63**, 1003 (1975).
16. C. S. PARMENTER and W. A. NOYES, JR. J. Am. Chem. Soc. **85**, 416 (1963).
17. G. P. R. MACK and B. A. THRUSH. J. Chem. Soc. Faraday Trans. I, **70**, 178 (1974).
18. R. E. HUIE and J. T. HERRON. Prog. React. Kinet. **8**, 1 (1975).
19. R. A. FLETCHER and G. PILCHER. Trans. Faraday Soc. **66**, 794 (1970).
20. D. M. GOLDEN and S. W. BENSON. Chem. Rev. **69**, 125 (1969).
21. J. L. FRANKLIN, J. G. DILLARD, H. M. ROSENSTOCK, J. T. HERRON, K. DRAXL, and F. H. FIELD. Natl. Stand. Ref. Data Ser. Natl. Bur. Stand. **26** (1969).
22. K. W. WATKINS and W. W. WORD. Int. J. Chem. Kinet. **6**, 855 (1974).
23. K. W. WATKINS and W. W. THOMPSON. Int. J. Chem. Kinet. **5**, 791 (1973).
24. D. C. MCKEAN, J. L. DUNCAN, and L. BATT. Spectrochim. Acta, Part A, **29**, 1037 (1973).
25. K. YAMADA, T. NAKAGAWA, K. KUCHITSU, and Y. MORINO. J. Mol. Spectrosc. **38**, 70 (1971).
26. J. S. BYRNE, P. F. JACKSON, and K. J. MORGAN. J. Chem. Soc. Perkin Trans. II, 1291 (1972).
27. H. J. BERNSTEIN. Spectrochim. Acta, **18**, 161 (1962).
28. R. K. SOLLY and S. W. BENSON. J. Am. Chem. Soc. **93**, 1592 (1971).
29. L. J. BELLAMY and D. W. MAYO. J. Phys. Chem. **80**, 1217 (1976).
30. J. S. SHIRK and G. C. PIMENTEL. J. Am. Chem. Soc. **90**, 3349 (1968).

Metal-ion oxidations in solution. Part XVIII.[1] Characterization, rates, and mechanism of formation of the intermediates in the oxidation of thiols by chromium(VI)

ALEXANDER McAULEY[2] AND M. ADEGBOYEGA OLATUNJI[3]

Department of Chemistry, University of Glasgow, Glasgow G12 8QQ, Scotland, and Department of Chemistry, University of Victoria, Victoria, B.C., Canada V8W 2Y2

Received March 7, 1977

ALEXANDER McAULEY and M. ADEGBOYEGA OLATUNJI. Can. J. Chem. **55**, 3328 (1977).

The stopped-flow technique has been used to study the reactions of $[HCrO_4^-]$ and penicillamine, glutathione and β-mercaptoethylamine (RSH) in perchlorate media, $[H^+] = 0.02$–0.100 M, $I = 1.00$ M over the temperature range 10–30°C. The transient orange species formed as intermediates are 1:1 chromate esters,

$$RSH + [(HO)CrO_3]^- \overset{K_1}{\rightleftharpoons} [(RS)CrO_3]^- + H_2O$$

with $\lambda_{max} \sim 420$–430 nm and $K_1 \sim 700$ (DL-penicillamine) to 1440 M^{-1} (glutathione) at $T = 25$°C. Thermodynamic parameters for complex formation have been derived from initial absorbance data and the evidence for sulphur bonding is discussed. Kinetics of the reactions conform to the rate law

$$d[Complex]/dt = (k_f + k_f^{H^+}[H^+])[HCrO_4^-][RSH]$$

Activation enthalpies lie in the range 6–10 kcal/mol but ΔS^* values vary considerably possibly reflecting solvation effects. The rate constants $k_f^{H^+}$ are several orders of magnitude lower than those found for this parameter in other reactions of this type. The complex formation mechanisms are discussed and the possibility of some associative character in the present reactions is considered.

ALEXANDER McAULEY et M. ADEGBOYEGA OLATUNJI. Can. J. Chem. **55**, 3328 (1977).

On a employé la technique du "flux stoppé" pour étudier les réactions de $[HCrO_4^-]$ avec la penicillamine, le glutathion et la β-mercaptoethylamine en milieu perchlorique, $[H^+] = 0.02$–0.100 M, $I = 1.00$ M, entre 10–30°C. Les espèces transitoires de couleur orange ont été identifiées comme étant des esters chromiques 1:1 ($\lambda_{max} \sim 420$–430 nm),

$$RSH + [(HO)CrO_3]^- \overset{K_1}{\rightleftharpoons} [(RS)CrO_3]^- + H_2O$$

avec $K_1 = 700$ M^{-1} (DL-penicillamine) jusqu'à 1440 M^{-1} (glutathion) à 25°C. Les paramètres thermodynamiques pour la formation de ces complexes ont été obtenus à partir des mesures d'absorption initiale. On suggère un liaison soufre–metal pour ces espèces. Les vitesses de ces reactions obéissent à l'expression

$$d[complexe]/dt = (k_f + k_f^{H^+}[H^+])[HCrO_4^-][RSH]$$

Les enthalpies d'activation se situent entre 6–10 kcal mol^{-1}, mais les valeurs de ΔS^* présentent une grande variation reflètant probablement des effets de solvatation.

Les constantes de vitesse $k_f^{H^+}$ sont plus petites, par plusieurs ordres de magnitude, que celles mesurées pour d'autres réactions comparables. Les mécanismes de formation d'un complexe intermédiaire sont discutés, ainsi que la possibilité d'un caractère associatif pour les réactions présentées.

Whilst oxygen-bonded chromate esters are well characterized (2–4), having been identified as intermediates in the oxidation of organic substrates by chromium(VI), much less is known of the corresponding sulphur-bonded complexes. Recent kinetic studies using rapid reaction techniques (5–9) have demonstrated the existence of these transient species, but they are very much more susceptible to oxidation than the O-bonded analogues. Also, the formation constants and spectra of the oxygen- and thioesters show marked differences, e.g. in the reaction with acid thiosulphate (7, 8), a complex is formed with $HCrO_4^-$ with an equilibrium constant of $\sim 10^4$

[1]For part XVII see ref. 1.

[2]Author to whom correspondence should be addressed. Present address: Department of Chemistry, University of Victoria, Victoria, B.C., Canada V8W 2Y2.

[3]Present address: Department of Chemistry, Ahmadu Bello University, Zaria, Nigeria.

M^{-1} compared with $\sim 4\ M^{-1}$ for the bisulphate system (10). The red shift of about 30 nm of the charge-transfer band in the near uv ($\lambda = 350$ nm) has been interpreted as evidence for an S-bonded intermediate. Changes in the absorption maxima of this magnitude have also been observed with thiocyanate (11) and thioureas (12) whilst the displacement is even greater (to 420 nm) for cysteine (6). In all cases, however, the extinction coefficients are ~ 1.2–$1.4 \times 10^3\ M^{-1}\ cm^{-1}$, substantially in excess of that for the hydrogen chromate ion or the O-bonded esters. In view of the need for more information on these systems and of the importance of the sulphydryl group in electron-transport processes an extension of these studies into more biologically important substrates was undertaken.

Experimental

DL-Penicillamine (puriss), glutathione, and β-mercaptoethylamine hydrochloride (Koch Light) were used without further purification. Potassium dichromate (Analar grade) was used for kinetic runs, the sodium salt (BDH Reagent) being used where concentrations were such as to have caused precipitation of potassium perchlorate. Perchloric acid (A.R.) and sodium perchlorate (Fluka, puriss) were used to maintain a constant ionic strength of 1.00 M at varying hydrogen ion concentrations. Stock solutions of perchloric acid were analysed by titration against weighed quantities of sodium tetraborate.

Kinetic Studies

The complex formation reactions of glutathione and β-mercaptoethylamine were investigated using the stopped-flow apparatus described previously (13). Oscilloscope displays of transmission curves were photographed using a Polaroid camera and by comparison with a known reference voltage, the optical density of any point on the trace could be calculated using a Nova 1200 computer. The slower reaction with penicillamine was monitored using a hand driven (two jet glass mixer) stopped-flow system which utilized a Unicam SP800 spectrophotometer both as monochromatic light source and detection system (6). Experiments were carried out using a 1 cm flow-through cell, the dead time being 0.30 ± 0.05 s. For the formation reactions conditions were carefully chosen such that a state of equilibrium was reached prior to the subsequent redox reactions.

Results and Discussion

Interpretation of the kinetic data is strongly dependent on a detailed knowledge of the reactant species. The concentration of chromium(VI) was such that the predominant species was $HCrO_4^-$ throughout the acidity range used (4, 5). For the thiols, the pK_a values corresponding to the loss of a proton from —SH and $\overset{+}{N}H_3$ are >8 (14, 15). The carboxyl group pK values, on the other hand, are much lower, 2.44 for penicillamine and 2.1 and 3.5 for glutathione (14, 16). Under the conditions used in these investigations ($[H^+] = 0.04$–$0.10\ M$), the carboxylic acid is the predominant species although a small proportion of zwitterion is also present. Attempts were made to determine the effects of these proton equilibria on the actual concentration of hydrogen ions present. This was achieved by measuring the pH's of various solutions of the ligand prepared under conditions identical to those used for kinetic runs. Using a calibration curve derived from measurements of accurate dilutions of perchloric acid (0.01–0.10 M) at $I = 1.0\ M$, the pH's of mixed solutions at the start and completion of reaction were compared with those of the ligand alone. Representative data are presented in Table 1 where it is seen that no differences were observed. Interestingly, no trend was observed between the lowest and highest ligand concentrations at constant $[H^+]$. Hence, although a small proportion of deprotonated carboxylate may be formed the effective concentration of hydrogen ion is the initial value $[H^+]_0$.

In all the kinetic measurements carried out for the determination of the formation rate constants, the initial absorbance ($t = 0$) was found to be identical with that of chromium(VI) containing no ligand. By measuring the optical

TABLE 1. The pH's of solutions of penicillamine and glutathione (RSH) at differing $[H^+]_0$ as used in kinetic experiments, $I = 1.0\ M$ ($NaClO_4$)

		pH		
$[H^+]_0/M$	$10^3[RSH]/M$	Ligand	Mixture	End of reaction
		Glutathione		
0.02	2.0	1.10	1.09	1.10
0.06	2.0	0.91	0.91	0.90
0.08	2.0	0.79	0.80	0.80
0.10	2.0	0.70	0.71	0.71
0.06	8.0	0.92	0.92	0.92
0.10	8.0	0.69	0.70	0.70
		Penicillamine		
0.04	2.0	1.08	1.08	1.08
0.04	8.0	1.10	1.10	1.10
0.06	2.0	0.90	0.92	0.92
0.08	2.0	0.78	0.80	0.80
0.08	5.0	0.80	—	—
0.08	8.0	0.80	0.80	0.80
0.10	2.0	0.70	0.70	0.69
0.10	8.0	0.72	0.70	0.69

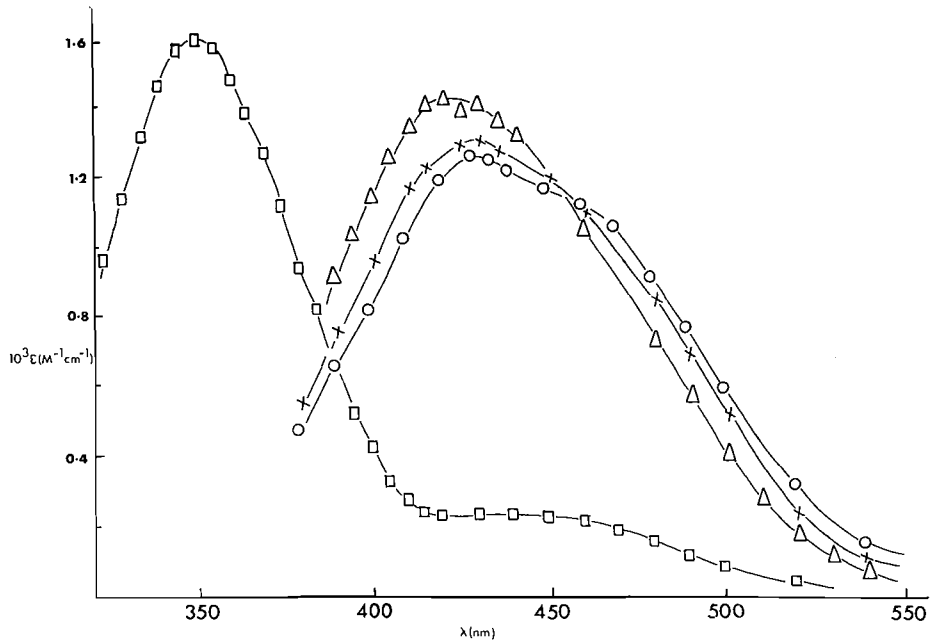

FIG. 1. Spectra of intermediate complexes. □, $HOCrO_3^-$; ○, Cr(VI)–glutathione ester; △, Cr(VI)–β-mercaptoethylamine ester; ×, Cr(VI)–penicillamine ester.

density changes, ΔOD, at various wavelengths under normal reaction conditions it was possible to compile the spectra of these complexes. In all cases λ_{max} was found to be 420–430 nm as is shown in Fig. 1. Kinetic and equilibrium measurements were carried out at this wavelength. Repeated spectroscopic scans of the relatively slowly reacting mixtures of Cr(VI) and penicillamine show an absorbance decrease at $\lambda = 350$, an increase at $\lambda \sim 420$, and an initial isobestic point at 390 nm.

In the acid concentration range 0.02–0.10 *M* the formation of the intermediate was sufficiently rapid compared with the subsequent decay that an equilibrium condition was achieved. Since $HCrO_4^-$ is generally considered to form only 1:1 complexes under the conditions employed in this study, eq. 1 may be derived where [RSH] is the

$$[1] \quad \frac{[Cr(VI)]_0[RSH]}{\Delta OD} = \frac{[RSH]}{\Delta\varepsilon \cdot l} + \frac{1}{K\Delta \cdot l}$$

ligand concentration and *K* the equilibrium constant. Plots of $[Cr(VI)]_0[RSH]/\Delta OD$ against [RSH] showed good linearity at all temperatures studied (Fig. 2). The absence of any variation of intercept with $[H^+]_0$ is an indication of little or no net uptake of protons on complex formation. In addition the linearity supports the assumption of only a monoester being formed.

Equilibrium data are presented in Table 2 where the associated thermodynamic parameters for complex formation are also reported. The magnitude of the formation constants when compared with the oxygen-bonded esters provides evidence for the Cr–S linkage in these systems (8). Also, the similarity of the spectroscopic and thermodynamic parameters of the α-aminocarboxylic acids and mercaptoethylamine suggests that there is little influence of oxygen as a donor atom in a possible chelate. In these systems where the amino group is protonated, any chelation via the nitrogen atom would require a preliminary deprotonation. In the oxidation of the hydrazinium ion, $\overset{+}{N}H_3NH_2$, there is evidence (17) for a very weakly bonded Cr(VI)–N complex ($K_f = 3 \pm 0.3\ M^{-1}$). Again the significant difference between this value and that of $\sim 10^3\ M^{-1}$ observed in the present case would argue in favour of the Cr–S linkage as contributing to the heat and entropy effects. If, in fact, the site of attack by the metal is the sulphydryl group it would appear that the equilibrium constants for the (carboxylate) protonated and anionic forms of the ligand with Cr(VI) are iden-

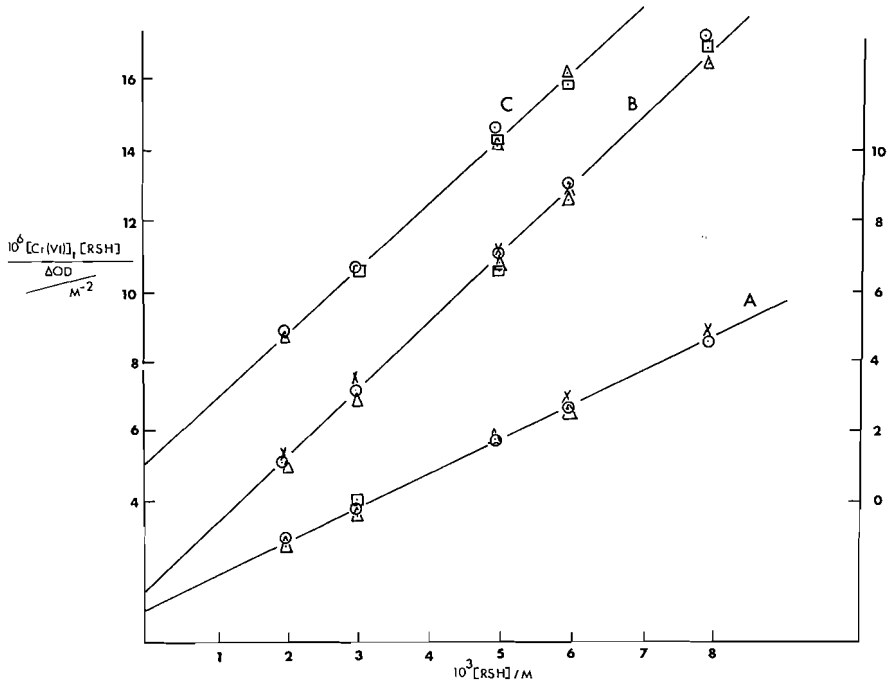

FIG. 2. Plots of $[Cr(VI)]_{tot}[RSH]/\Delta OD$ against [RSH] (eq. 1). (*A*) Penicillamine, $T = 12.0°C$; (*B*) glutathione, $T = 25.0°C$; (*C*) β-mercaptoethylamine, $T = 20.0°C$. $[H^+] = 0.04\ M$ ⊙; $0.06\ M$ △; $0.08\ M$ ⊡; $0.10\ M$ ×.

TABLE 2. Thermodynamic parameters for complex formation

T/°C	K/M^{-1}	$\varepsilon/(M^{-1}\ cm^{-1})$
	DL-Penicillamine[a]	
12.0	1150 ± 50	1248
17.0	889 ± 40	1248
25.0	700 ± 40	1228
30.0	510 ± 30	1268
	Glutathione[b]	
15.0	1643 ± 100	1338
20.0	1550 ± 100	1288
25.0	1436 ± 50	1290
30.0	1180 ± 80	1367
	β-Mercaptoethylamine[c]	
20.0	1470 ± 100	1328
25.0	1300 ± 100	1328
30.0	1170 ± 100	1308

[a] $\Delta H_f = -6.8 \pm 0.6$ kcal mol^{-1}; $\Delta S_f = -9.9 \pm 5$ cal deg^{-1} mol^{-1}.
[b] $\Delta H_f = -4.5 \pm 1.2$ kcal mol^{-1}; $\Delta S_f = -1 \pm 2$ cal deg^{-1} mol^{-1}.
[c] $\Delta H_f = -3.7 \pm 1.5$ kcal mol^{-1}; $\Delta S_f = 2 \pm 2$ cal deg^{-1} mol^{-1}.

tical to within the limits of experimental error in this study.

The formation kinetics were measured in conditions of excess of the ligands. Plots of log $(OD_{max} - OD_t)$ against time showed good linearity to greater than 80% of reaction. Pseudo-first-order rate constants, k_{obs}, were derived from the slopes of such plots and representative data at 25°C are presented for each ligand in Table 3. Plots of k_{obs} as a function of $[ligand]_0$ at constant $[H^+]_0$ were linear with positive intercepts. If the total ligand concentration is $[RSH]_0$ the various reactions contributing to the complex formation may be formulated as in eqs. 2 and 3.

$$[2]\qquad HCrO_4^- + RSH \underset{k_b}{\overset{k_f}{\rightleftharpoons}} RSCrO_3^- + H_2O$$

$$[3]\qquad HCrO_4^- + RSH + H^+ \underset{k_b^{H^+}}{\overset{k_f^{H^+}}{\rightleftharpoons}} RSCrO_3^- + H_2O + H^+$$

On the basis of this scheme, [4] may readily be derived

$$[4]\qquad k_{obs} = \{k_f^{H^+}[RSH]_0 + k_b^{H^+}\}[H^+]_0 + k_f[RSH]_0 + k_b$$

Rearrangement of [4] leads to an expression of the form

$$[5]\qquad k_{obs} = \alpha[RSH]_0 + \beta$$

TABLE 3. Rate constants[a] for the formation of Cr(VI)–thiol complexes. $T = 25.0°C$, $[Cr(VI)]_{tot} = 2.0 \times 10^{-4}$ M, $I = 1.00$ M, $\lambda = 420$ nm[b]

	k_{obs}/s^{-1} for $[H^+]/M$ of			
10^3[Pen]/M	0.02	0.04	0.06	0.08
2.00	0.79	1.26	1.76	2.21
3.00	1.02	1.59	2.13	2.63
5.00	1.53	2.21	2.69	3.64
6.00	1.79	2.56	3.42	3.90
8.00	2.22	3.42	4.46	4.88

	k_{obs}/s^{-1} for $[H^+]/M$ of			
10^3[Glut]/M	0.02	0.04	0.06	0.08
2.00	0.0472	0.093	0.14	0.192
3.00	0.062	0.123	0.18	0.254
5.00	0.089	0.184	0.256	0.366
6.00	0.101	0.208	0.310	0.424
8.00	0.127	0.264	0.392	0.550

	k_{obs}/s^{-1} for $[H^+]/M$ of				
10^3[Merc]/M	0.02	0.04	0.06	0.08	0.10
2.00	0.025	0.051	0.070	0.094	0.124
3.00	0.033	0.068	0.097	0.126	0.164
5.00	0.053	0.105	0.150	0.192	0.246
6.00	0.062	0.120	0.170	0.224	0.282
8.00	0.076	0.152	0.220	0.288	0.360

[a]Individual rate constants reproducible to ±3%.
[b]DL-Penicillamine, Pen; glutathione, Glut; β-mercaptoethylamine, Merc.

where

$$\alpha = (k_f + k_f^{H^+}[H^+]_0) \text{ and } \beta = (k_b + k_b^{H^+}[H^+]_0)$$

On plotting the slope (α) and intercepts (β) derived from [5] against $[H^+]_0$ good straight lines were obtained (Figs. 3, 4) from which the rate constants $k_f^{H^+}$, k_f, and $k_b^{H^+}$ were derived. In all cases the constant k_b was too small to be determined with any certainty and was taken to be negligible. Overall rate constants are shown in Table 4 where thermodynamic parameters for the principal (hydrogen-ion dependent) pathway are also presented.

Several interesting conclusions derive from the data and from the observed hydrogen-ion dependence which differs from many other reactions of this type (e.g. for the reaction with $(H_3N)_5$-$CoOH_2^{3+}$ the expression corresponding to the α above is of the form (18, 19) $k_f + k_f^1[H]_0^{-1}$ and may be interpreted in terms of the prior dissociation of a proton before the attack on the $HOCrO_3^-$ unit). In previous studies one reaction pathway has been observed (9) involving the rate law

$$[6] \qquad R = k_f^{H^+}[H^+][L^-][HOCrO_3^-]$$

and the constancy of the $k_f^{H^+}$ ($\sim 5 \times 10^5$ M^{-2} s^{-1}) has led to the suggestion that a weak L–$Cr(OH)O_3$ species is formed which reacts with H^+ to liberate water. An alternative postulate has been advanced by Haim (20) who reasoned that since the pathway is proton dependent the H^+ must be incorporated prior to the rate-determining step and so protonation of the $HCrO_4^-$ would be the first step with rate of loss of water as rate determining.

In the present study the $k_f^{H^+}$ values for substitution on $HCrO_4^-$ are all $\sim 10^3$–10^4 lower than the values obtained previously. The similarity of the rate for mercaptoethylamine with those of the aminocarboxylic acids is significant. In these systems either formation of the Cr—S bond or dissociation of the S—H bond is rate determining. Protonation occurs prior to the slow step and coordination of the sulphur is either rate determining or occurs before it. Following the mechanism preferred by Haim (20), water loss, which is not rate determining in this reaction, takes place with a specific rate of $\sim 5 \times 10^5$ s^{-1} as the equilibrium constant for $[(H_2O)CrO_3]$ is almost certainly less than unity. If protonation at sulphur is diffusion controlled (21) and the strength of the S—H bond is unaffected by a weak Cr---S linkage, then the rate of dissociation may be estimated from the dissociation constant of the thiol group.

$$RSH \underset{k_{-d}}{\overset{k_d}{\rightleftharpoons}} RS^- + H^+$$

$$K_a' = k_d/k_{-d} \quad k_d \sim 10^{10}K_a'$$

Since $K_a' \sim 10^{-7}$–10^{-8} (14, 22), values of k_d obtained in this way are of the order of 10^2–10^3 s^{-1}. The mechanism of reaction may then be written as

$$HOCrO_3^- + H^+ \rightleftharpoons (H_2O)CrO_3$$

$$RSH + (H_2O)CrO_3 \rightleftharpoons R\text{—}\underset{\vdots\atop H}{\overset{OH_2\atop\vdots}{S}}\cdots CrO_3$$

where the water loss is more rapid than proton dissociation which is the final step. The activation energies for the systems studied so far all fall within the range 6–10 kcal/mol. The entro-

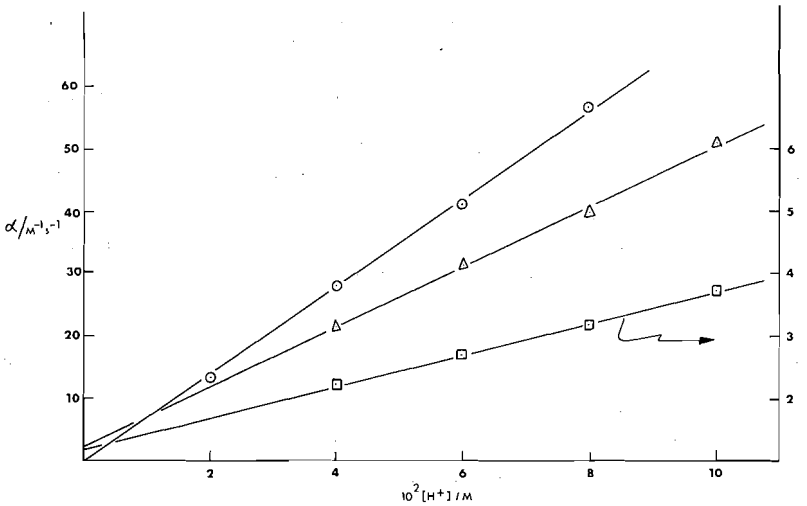

FIG. 3. Dependence of slope (α) (eq. 5) on $[H^+]$. ⊙, Glutathione, $T = 25.0°C$; △, β-mercaptoethylamine, $T = 30.0°C$; ⊡, penicillamine, $T = 17.0°C$ (right-hand ordinates).

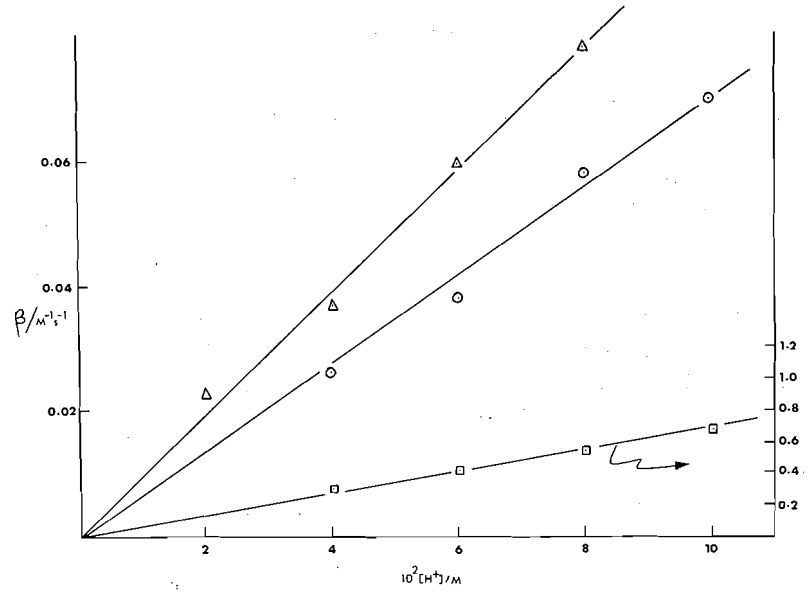

FIG. 4. Plots of β (eq. 5) as a function of $[H^+]$. △, Glutathione, $T = 25.0°C$; ⊙, β-mercaptoethylamine, $T = 30.0°C$; ⊡, penicillamine, $T = 12.0°C$ (right-hand ordinates).

pies of activation differ markedly, however, and may reflect differing degrees of solvation, a result not altogether surprising considering the differences in the nature of the substrates.

Desolvation of the transition state may be approximated to a melting process. This process with the attendant change in geometry has a marked influence on $\Delta S^{\neq}$ and $\Delta H^{\neq}$ and the effects work in opposition to one another (23). The free energy of solvation is considered to contribute only a fraction of the rate. Differences in $T\Delta S^{\neq}$ which roughly parallel differences in $\Delta H^{\neq}$ thus confirm the solvational effects in this study.

The hydrogen-ion independent pathway, k_f, is detectable only in the reactions of penicillamine and mercaptoethylamine, the values being of the same order of magnitude (~ 1–$2\ M^{-1}\ s^{-1}$) as that of cysteine (6). Values of k_f tend to vary with the acidity of the H—L bond and an inter-

TABLE 4. Rate constants[a] for the formation of the intermediate complexes at differing temperatures ($I = 1.00\ M$)

T/°C	$10^{-2}k_f^{H^+}/(M^2\ s^{-1})$	$k_f/(M^{-1}\ s^{-1})$	$k_b^{H^+}/(M^{-1}\ s^{-1})$
	DL-Penicillamine		
12.0	0.188±0.005	0.75±0.4	0.037±0.02
17.0	0.25 ±0.01	1.20±0.7	0.066±0.03
25.0	0.338±0.02	1.82±2.0	0.160±0.10
30.0	0.463±0.06	2.1 ±1.0	0.219±0.15
	ΔH^* 5.9±2 kcal mol^{-1}; ΔS^* −31.9±12 cal deg^{-1} mol^{-1}		
	Glutathione		
15.0	4.40 ±0.10	—	0.36 ±0.15
20.0	5.33 ±0.20	—	0.68 ±0.40
25.0	7.06 ±0.50	—	0.98 ±0.60
30.0	9.60 ±0.50	—	1.29 ±0.80
	ΔH^* 10.2±4 kcal mol^{-1}; ΔS^* −11.3±6 cal deg^{-1} mol^{-1}		
	β-Mercaptoethylamine		
20.0	3.22 ±0.10	0.50±0.30	0.32 ±0.10
25.0	3.79 ±0.15	1.70±0.60	0.44 ±0.20
30.0	4.88 ±0.20	2.0 ±1.0	0.68 ±0.35
	ΔH^* 7.2±3 kcal mol^{-1}; ΔS^* −25±10 cal deg^{-1} mol^{-1}		
	L-Cysteine[b]		
25.0	1.30 ±0.20	2±1	
	ΔH^* 7±3 kcal mol^{-1}; ΔS^* −24±11 cal deg^{-1} mol^{-1}		

[a]Derived from an unweighted least-squares analysis. Errors quoted represent twice the standard mean.
[b]Reference 6.

nal proton transfer governs the rate of water elimination. More data are required, however, before too much credence can be attributed to these values.

Acknowledgements

We wish to thank the Federal Government of Nigeria and Ahmadu Bello University for the award of a grant (to M.A.O.) and the Science Research Council and the National Research Council of Canada for financial support. Valuable discussion with Dr. J. P. McCann is also acknowledged.

1. Z. AMJAD and A. MCAULEY. J. Chem. Soc. Dalton Trans. 304 (1977).
2. F. H. WESTHEIMER. Chem. Rev. **45**, 419 (1949).
3. K. B. WIBERG. Oxidation in organic chemistry. Part A. Academic Press, New York, NY. 1965. p. 69.
4. J. H. ESPENSON. Acc. Chem. Res. **3**, 347 (1970).
5. J. K. BEATTIE and G. P. HAIGHT. Prog. Inorg. Chem. **17**, 93 (1972).
6. J. P. MCCANN and A. MCAULEY. J. Chem. Soc. Dalton Trans. 783 (1975).
7. I. BALDEA and G. NIAC. Inorg. Chem. **7**, 1232 (1968).
8. K. A. MUIRHEAD, G. P. HAIGHT, and J. K. BEATTIE. J. Am. Chem. Soc. **94**, 3006 (1972).
9. C. T. LIN and J. K. BEATTIE. J. Am. Chem. Soc. **94**, 3011 (1972).
10. G. P. HAIGHT, D. C. RICHARDSON, and N. H. COBURN. Inorg. Chem. **3**, 1777 (1964).
11. K. A. MUIRHEAD and G. P. HAIGHT. Inorg. Chem. **12**, 1116 (1973).
12. M. A. OLATUNJI and A. MCAULEY. J. Chem. Soc. Dalton Trans. 682 (1975).
13. K. J. ELLIS and A. MCAULEY. J. Chem. Soc. Dalton Trans. 1533 (1973).
14. E. M. CROOK (*Editor*). Glutathione. Biochem. Soc. (London) Symposium. No. 17. Cambridge University Press. 1959.
15. E. W. WILSON and R. B. MARTIN. Arch. Biochem. Biophys. **142**, 445 (1971).
16. G. SCHWARZENBACH, A. E. MARTELL, and L. G. SILLEN (*Editors*). Stability constants. Chemical Society (London) Special Publication No. 25. 1971.
17. G. P. HAIGHT, T. J. HUANG, and H. PLATT. J. Am. Chem. Soc. **96**, 3137 (1974).
18. M. WOODS and J. C. SULLIVAN. Inorg. Chem. **12**, 1459 (1973).
19. G. P. HAIGHT. Inorg. Chem. **12**, 1461 (1973).
20. A. HAIM. Inorg. Chem. **11**, 3147 (1972).
21. M. EIGEN. Discuss. Faraday Soc. **39**, 7 (1965).
22. L. E. ASHER and E. DEUTSCH. Inorg. Chem. **12**, 1774 (1973).
23. M. E. BALDWIN, S. C. CHAN, and M. L. TOBE. J. Chem. Soc. 4367 (1961).

Metal-ion oxidations in solution. Part XIX.[1] Redox pathways in the oxidation of penicillamine and glutathione by chromium(VI)

ALEXANDER McAULEY[2] AND M. ADEGBOYEGA OLATUNJI[3]

Department of Chemistry, The University of Glasgow, Glasgow G12 8QQ, Scotland, and Department of Chemistry, University of Victoria, Victoria, B.C., Canada V8W 2Y2

Received March 7, 1977

ALEXANDER McAULEY and M. ADEGBOYEGA OLATUNJI. Can. J. Chem. **55**, 3335 (1977).

Three moles of penicillamine or glutathione are required to reduce chromium(VI) to chromium(III). The kinetics and mechanism of the redox reaction have been studied using the stopped-flow method. The reaction proceeds via the formation of a transient intermediate (K_1) which decomposes either in a proton-catalyzed pathway or by reaction with a second mole of thiol. The rate law

$$-\mathrm{d[Cr(VI)]}/\mathrm{d}t = \frac{K_1[\mathrm{RSH}](k_a[\mathrm{H}^+]^n + k_2[\mathrm{RSH}])[\mathrm{Cr(VI)}]}{1 + K_1[\mathrm{RSH}]}$$

where $n = 1$ for penicillamine and 2 for glutathione has been shown to hold over a range of thiol and hydrogen-ion concentrations. At 25°C $k_2 = 14.3 \pm 1.0\ M^{-1}\ s^{-1}$ for penicillamine ($\Delta H^{\ddagger} = 9 \pm 2$ kcal mol^{-1}, $\Delta S^{\ddagger} = -33 \pm 6$ cal K^{-1} mol^{-1}) and $12.1 \pm 0.4\ M^{-1}\ s^{-1}$ for glutathione ($\Delta H^{\ddagger} = 7 \pm 2$ kcal mol^{-1}, $\Delta S^{\ddagger} = -40 \pm 5$ cal K^{-1} mol^{-1}). Several chromium(III) products have been identified by ion-exchange methods. The significance of the second-order pathways in these reactions is discussed.

ALEXANDER McAULEY et M. ADEGBOYEGA OLATUNJI. Can. J. Chem. **55**, 3335 (1977).

La penicillamine ou le glutathion présent dans un rapport 3:1 réduit le chrome(VI) en chrome(III). La cinétique et le mécanisme de ces réactions d'oxydo-réduction ont été étudiés au moyen d'un appareil de "flux-stoppé". Le mécanisme de ces réactions implique la formation d'un complexe intermédiaire (K_1) qui peut, soit se décomposer selon une voie catalysée par les protons, soit réagir avec une deuxième mole de thiol. La vitesse de la réaction obéit à l'expression

$$-\mathrm{d[Cr(VI)]}/\mathrm{d}t = \frac{K_1[\mathrm{RSH}](k_a[\mathrm{H}^+]^n + k_2[\mathrm{RSH}])[\mathrm{Cr(VI)}]}{1 + K_1[\mathrm{RSH}]}$$

dans laquelle $n = 1$ pour la penicillamine et $n = 2$ pour le glutathion. Cette expression est valable pour une variété de concentrations de thiol et de [H$^+$]. A 25°C, $k_2 = 14.3 \pm 1.0\ M^{-1}\ s^{-1}$ pour penicillamine ($\Delta H^{\ddagger} = 9 \pm 2$ kcal mol^{-1}, $\Delta S^{\ddagger} = -33 \pm 6$ cal K^{-1} mol^{-1}) et $12.1 \pm 0.4\ M^{-1}\ s^{-1}$ pour le glutathion ($\Delta H^{\ddagger} = 7 \pm 2$ kcal mol^{-1}, $\Delta S^{\ddagger} = -40 \pm 5$ cal K^{-1} mol^{-1}). Plusieurs complexes du chrome(III) ont été identifiés au moyen de colonnes échangeuses d'ions. On discute de l'implication d'un terme du second ordre en thiol pour ces réactions.

The oxidation of nonmetallic substrates by both metal ions and oxy-anions is often accomplished by way of inner-sphere complexes (2–5), presumably since they provide a low energy pathway for electron transfer. The ability of $HCrO_4^-$ to form esters with electron pair donors, particularly those with —OH groups, is already well established (6) and an increasing amount of data is now being provided on the corresponding thiol complexes. For these transient sulphur-bonded esters the formation constants are significantly higher than the oxygen-bonded species (7–10). Most metal-ion oxidants require only a one-electron transfer to attain a lower stable oxidation state; chromium(VI), however, requires three electrons for this purpose and only in a relatively small number of instances has a simultaneous three-electron transfer been reported (11). In other cases both one- and two-electron redox reaction pathways are important. Identification of the final products which usually include various inert Cr(III) complexes yields information on the elementary steps which take place after the transition state (12).

The oxidation of thiols to disulphides is an

[1]For Part XVIII see ref. 1.

[2]Author to whom correspondence should be addressed. Present address: Department of Chemistry, University of Victoria, Victoria, B.C., Canada V8W 2Y2.

[3]Present address: Chemistry Department, Ahmadu Bello University, Zaria, Nigeria.

important biological process and the role of metal ions in the reactions of penicillamine, glutathione, and β-mercaptoethylamine (RSH) is of significance in view of the nature of electron-transport enzymes which often incorporate sulphydryl groups of this type. The reactions of penicillamine with heavy metal ions have been extensively studied and characteristic reductive chelate formation with Cu(II), Fe(III), etc. has been observed (13). Few data are available for the Cr(VI) reactions. One reference (14) to the reaction at pH 7 has described the characterization of a 1:3 Cr(III)–penicillamine complex. The significance of this study was related to the effectiveness of various chelating agents for the removal of chromium bound to haemoglobin. The present investigation deals with the kinetics and mechanism of the redox processes involving these systems in the context of the reaction of intermediate S-bonded esters characterized previously (1).

Experimental

Details of the preparation and purification of reagents are available elsewhere (1). Kinetic studies were carried out using stopped-flow spectrometers described previously (10, 15) over a temperature range 12–30°C with the thiol ligand in excess. The redox reactions were in all cases at least a factor of 10 slower than the formation of the intermediate complexes and pseudo-first-order rate constants were derived from plots showing linearity to greater than 90%. Data were reproducible to ±2%.

Stoichiometry

Attempts to determine the stoichiometries of the overall redox reactions by spectrophotometric titration were unsuccessful as has been observed in the corresponding reaction with thiosulphate (16). For this reason and because it was considered desirable to measure the stoichiometry under conditions related directly to the kinetic data, acidimetric titration of the sulphydryl group was used (17). In this analysis, 50 ml of 0.2 M thiol was mixed with 25 ml of 4×10^{-2} M chromium(VI) and the requisite volumes of $NaClO_4$ and $HClO_4$ to give $[H^+] = 0.10$ M and $I = 1.0$ M on dilution of the mixture to 100 ml. After completion of the reaction a 50 ml sample of this mixture was used to charge a Dowex 50W × 8, 100–200 mesh cation-exchange column. Rinsing first with water, then with 0.10 M $HClO_4$, and finally a solution containing 0.10 M $HClO_4$ and 1.0 M $NaClO_4$ until the first coloured complex had reached the lower part of the resin ensured the removal of all excess free ligand. The fraction collected was analyzed as outlined (17).

Products

After the excess ligand had been removed, continued elution with various $HClO_4$–$NaClO_4$ mixtures resulted in a separation of the Cr(III) complexes. In order to minimize aquation, the ion-exchange column was maintained at 0°C during the separation procedure. The chromium content was determined by bromine oxidation in basic media with spectrophotometric measurement of the resulting $[CrO_4]^{2-}$ ($\varepsilon = 4814\ M^{-1}\ cm^{-1}$ at $\lambda = 372$ nm) (18).

Results and Discussion

The electron-transfer reactions of the penicillamine and glutathione systems were studied. Under the experimental conditions used, the redox reactions involving β-mercaptoethylamine were found to be very slow. In order to simplify the kinetics, a sufficient excess of the thiol was present so that no $[HCrO_4^-]$ was present in the redox step. Representative rate data at various $[H^+]$ and [RSH] at 25°C are presented in Table 1. Degassing the reactant solutions had no effect on the reaction rates. Also, no difference was observed in experiments where 0.0416 M Mn(II) was present.

Plots of k_{obs} as a function of $[RSH]_0$ yielded straight lines with positive intercepts. The gradients of these lines were acid independent although in each case the thiol-independent pathway showed a dependence on $[H^+]$.

For the reaction of penicillamine, the data are consistent with the rate scheme

$$[1]\quad RSH + [HOCrO_3^-] \overset{K_1}{\rightleftharpoons} [RSCrO_3^-] + H_2O$$

$$[2]\quad [RSCrO_3^-] + H^+ \overset{k_1}{\rightarrow} Cr(V)$$

$$[3]\quad [RSCrO_3^-] + RSH \overset{k_2}{\rightarrow} Cr(IV)$$

The rate law [4] may thus be derived.

$$[4]\quad \frac{-d[Cr(VI)]_{tot}}{dt} = \frac{K_1[RSH](k_1[H^+] + k_2[RSH])[Cr(VI)]_{tot}}{1 + K_1[RSH]}$$

Rearrangement of the observed rate constant (k_{obs}) in [4] yields the expression

$$[5]\quad \alpha = k_{obs}(1 + K_1[RSH])/K_1[RSH] = k_1[H^+] + k_2[RSH]$$

From a knowledge of the equilibrium constants at the various temperatures (1), plots of α against [RSH] were made (Fig. 1) from which the rate constant k_2 was derived directly from the gradients. The thiol-independent rate constant was derived from a plot of intercepts (I) of such plots against $[H^+]$ (Fig. 2). In the reaction of penicillamine only one proton is required in the one-electron reduction to Cr(V) (eq. 2).

TABLE 1. Rate constants for the redox reactions $[HCrO_4^-]_{tot} = 2 \times 10^{-4}$ M, $I = 1.0$ M

$[H^+]/M$	$10^2[RSH]/M$	$10^3k_{obs}/s^{-1}$	$[H^+]/M$	$10^2[RSH]/M$	$10^3k_{obs}/s^{-1}$
		DL-Penicillamine (T = 25.0°C)			
0.020	2.00	0.85	0.040	2.00	1.55
	3.00	1.01		3.00	1.90
	5.00	1.42		5.00	2.47
	6.00	1.60		6.00	2.62
	8.00	2.04		8.00	3.01
0.060	2.00	2.20	0.080	2.00	2.67
	3.00	2.75		3.00	3.37
	5.00	3.50		5.00	4.36
	6.00	3.628		6.00	4.73
	8.00	3.84		8.00	5.02
		Glutathione (T = 15.0°C)			
0.040	5.0	0.51	0.060	5.0	0.74
	8.0	0.82		8.0	1.06
	10.0	1.00		10.0	1.20
	12.0	1.21		12.0	1.36
	14.0	1.40		14.0	1.60
0.080	5.0	1.19	0.10	5.0	1.48
	8.0	1.50		8.0	1.80
	10.0	1.80		10.0	1.95
	12.0	2.01		12.0	2.20
	14.0	2.15		14.0	2.40

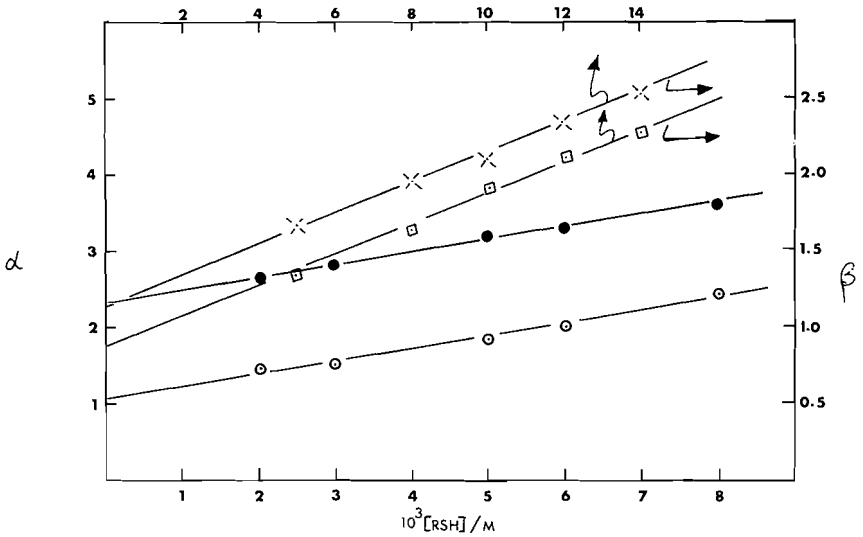

FIG. 1. Plots of α against [RSH] (eq. 5) for penicillamine reaction. T = 25.0°C. ⊙, $[H^+] = 0.02$ M; ●, $[H^+] = 0.04$ M. Plots of β against [RSH] (eq. 7) for glutathione oxidation. T = 15.0°C. ⊡, $[H^+] = 0.080$ M; ×, $[H^+] = 0.10$ M (upper and right-hand ordinates).

Using a similar treatment for glutathione, it was found that no single proton pathway was present. The thiol-independent rate derived from the reaction

$$[6] \qquad [RSCrO_3^-] + 2H^+ \xrightarrow{k_3} Cr(V)$$

and incorporation of this pathway into the rate scheme leads to [7]. Plots of β against [RSH]

$$[7] \qquad \beta = k_{obs}(1 + K_1[RSH])/K_1[RSH] = k_3[H^+]^2 + k_2[RSH]$$

again showed good linearity (Fig. 1) and the rate constant k_3 was derived from plots of the intercept (I') of such curves against $[H^+]^2$ (Fig. 3).

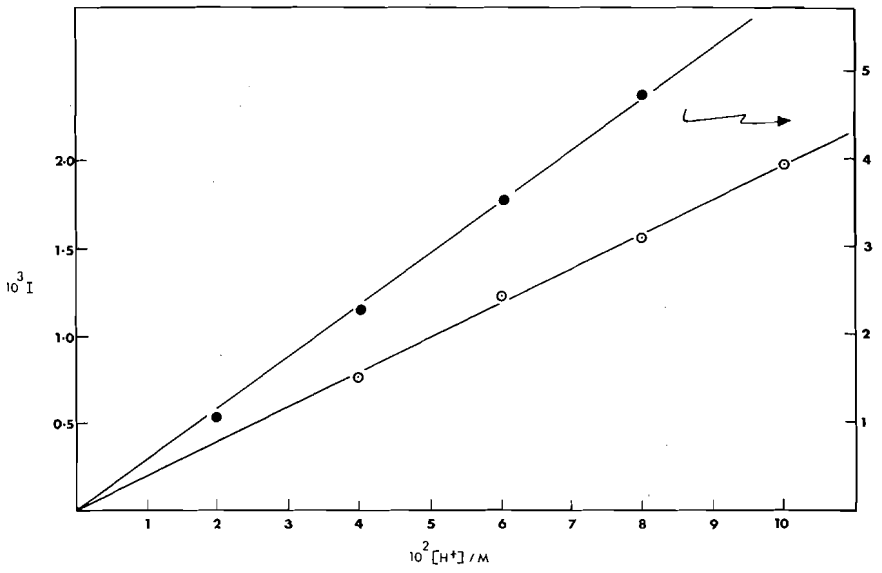

FIG. 2. Plot of intercepts (I) derived from graphical evaluation of eq. 5 against $[H^+]$. Slopes yield rate constant k_1: ⊙, T = 12.0°C; ●, T = 25.0°C (right-hand ordinates).

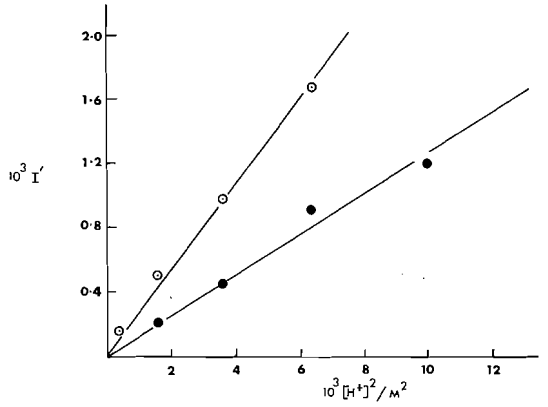

FIG. 3. Plots of intercepts (I') derived from eq. 7 against $[H^+]^2$. ●, T = 15.0°C; ⊙, T = 25.0°C.

TABLE 2. Dependence of k_1 and k_2 on temperature

T/°C	$10^2k_1/(M^{-1}\,s^{-1})$	$10^2k_2/(M^{-1}\,s^{-1})$
	DL-Penicillamine	
12.0	1.95±0.2	8.0±0.5
17.0	2.90±0.5	11.8±0.5
25.0	5.7±1.0	14.3±1.0
$\Delta H^{\ddagger}$/(kcal mol^{-1})	14.1±3	9±2
$\Delta S^{\ddagger}$/(cal K^{-1} mol^{-1})	17±5	−33±6
	Glutathione	
15.0	11.2 ±2[a]	9.7±0.2
25.0	25.0 ±4[a]	12.1±0.4
30.0	26.6 ±5[a]	21.2±0.6
$\Delta H^{\ddagger}$/(kcal mol^{-1})	11±3	7±2
$\Delta S^{\ddagger}$/(cal K^{-1} mol^{-1})	−24±7	−40±5

[a]Third-order rate constant, units $M^{-2}\,s^{-1}$.

Individual rate constants and thermodynamic parameters are presented in Table 2. It is known that the reduction from Cr(VI) to Cr(V) is often accompanied by proton dependences (6) (usually two are required) and it is probable that the penicillamine itself provides one of the protons required for reduction. Why the same process does not take place with the glutathione is not certain at present but it may be that conformational changes in the tripeptide require an external rather than an internal proton transfer for reduction to take place.

The reaction mechanisms for [2], [3], and [6] may be discussed in terms of single and multiple electron-transfer reactions. In steps 2 and 6 the rate-determining step is envisaged as the first of three consecutive one-electron transfers which have been well documented previously (6). Second-order ligand dependences (k_2 pathway) have been encountered in a number of systems, some of which involve sulphur centres. In Table 3 are listed the activation parameters for such reactions involving essentially similar processes with negligible dissociative character. In these systems the expansion of the chromium coordination sphere from four to six may be important. For sulphur-containing one-electron substrates, such as those under consideration,

TABLE 3. Activation data for chromium(VI) oxidation paths involving second-order ligand dependences

Reductant	$\Delta H^{\ddagger}$/ (kcal mol^{-1})	$\Delta S^{\ddagger}$/ (cal K^{-1} mol^{-1})	Ref.
Penicillamine	9 ± 2	-33 ± 6	[a]
Glutathione	7 ± 2	-40 ± 5	[a]
Thiourea	11[b]	−19	21
L-Cysteine	10.8	−27	10
Thiosulphate	8.2	−21	8
Sulphite	4.5	−13	7
Iodide	9.7	−16	22
Oxalic Acid	12.8	−19	23

[a]This work.
[b]First-order acid pathway.

cysteine, thiourea, and thiocyanate (19), routes corresponding to such terms may also provide a low energy pathway for the formation of a disulphide via a 'template' reaction with a transition state of the form

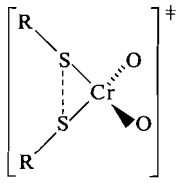

Such a system would be formally similar to chromyl chloride CrO_2Cl_2 but the differences in electronegativities of the halide and sulphur atoms are probably responsible for the differing stabilities. A similar incipient RS—SR bond formation has been observed (20) in the redox reactions of iron(III)–thiolate complexes in which a rate-determining dimerization involving the formation of a Fe_2S_2 four-centre electron-transfer transition state is observed rather than the unimolecular decomposition of the complex to yield Fe(II) and the RS$^{\bullet}$ radical. The fact that a two-electron transfer to Cr(IV) is possible thus facilitates disulphide formation.

The lack of an effect of Mn(II) on the reaction rate is similar to that observed in reactions with other thiols (10, 21) and with iodide (21). This transition metal ion has been used successfully as a trapping agent for Cr(IV) thus rendering impossible reaction of a second Cr(VI) species with either chromium(IV) or the radical produced if the latter reacts with another substrate molecule. Thus participation of a second mole of complex [$RSCrO_3^-$] in the reduction of Cr(IV) to Cr(III) complexes is eliminated and support is lent to the view that it is the ligand which is involved in this (rapid) step.

The results obtained by the acidimetric titration method are consistent with a ligand–chromium(VI) ratio of $(3.0 \pm 0.1):1$ in the reactions involving penicillamine and glutathione, consistent with the overall reaction

$$n\mathrm{H}^+ + 2[\mathrm{HCrO_4}]^- + 6\mathrm{RSH} \rightarrow 2\mathrm{Cr(III)} + 3\mathrm{RS{-}SR}$$

The thiol acts as a one-equivalent reductant under conditions of excess ligand. In spectrophotometric titrations solutions having Cr(VI) in excess were found to undergo further reaction, presumably overoxidation of the thiol to sulphoxide or sulphone.

Using the conditions referred to in the Experimental section, ion-exchange procedures indicated several complexes as products in the reaction of each thiol. With penicillamine, the first complex to be eluted was purple in colour. Comparison of elution rates with those of known complex ions showed the species to be doubly charged and containing about 60% of the total chromium. The second species had a more intense purple colour and could not be eluted even under extreme conditions of eluant concentration (2 *M* $HClO_4$ – 4 *M* $NaClO_4$). The complex did appear to aquate on prolonged elution to yield $[Cr(H_2O)_6]^{3+}$. This latter species is presumably a dimeric 4+ charged ion which could have resulted from the parallel reaction of $Cr_2O_7^{2-}$ which was present in the original solution. The results are similar to those obtained for cysteine where it was concluded (10) that the monomeric complex ion has cysteine coordinated to the chromium(III) centre via an α-aminocarboxyl binding site. Product mixtures from the glutathione reactions yielded three species, $Cr(H_2O)_6^{3+}$ ~ 50%, a green second complex (containing about 40% of the total chromium) also +3 in charge, and approximately 10% of the dimeric complex which was difficult to isolate. Although the presence of sulphur in the green species was confirmed by $BaSO_4$ precipitation after oxidation of the complex the low concentrations involved prevented an accurate determination of the Cr–S ratio. It is of interest to note that similar products were identified in the reaction of β-mercaptoethylamine with 78% of the aquo complex, ~20% of the green monomeric ion with little trace of the dimer. The fact that green chromium(III) complexes are observed as products in the oxidation of thioureas (21) is consistent with a postulate of nitrogen coordination in these species. It may be that (1)

in the case of the glutathione only the amine groups are accessible for binding to the metal centre.

Oxidations of thiols by chromium(VI) appear to be a route to chromium(III) species with coordinated disulphides. Before the mechanism of such reactions can be established with certainty more work is required on the nature of the radical intermediates and of the concentrations of chromium(V) generated. Flow esr will be of use in this regard and such studies are in progress.

Acknowledgements

We thank the Federal Government of Nigeria and Ahmadu Bello University for a grant (to M.A.O.). Thanks are also due to Drs. J. P. McCann and A. G. Lappin for helpful discussions. Support from the Science Research Council and the National Research Council of Canada are acknowledged.

1. A. McAuley and M. A. Olatunji. Can. J. Chem. This issue.
2. D. Benson. Mechanisms of oxidation by metal ions. Elsevier, Amsterdam. 1976.
3. A. McAuley. Coord. Chem. Rev. **5**, 245 (1970).
4. R. G. Wilkins. The study of kinetics and mechanism of reactions of transition metal complexes. Allyn and Bacon, Boston. 1974. Chapt. 5.
5. G. Davies and B. Warnqvist. Coord. Chem. Rev. **5**, 349 (1970).
6. J. K. Beattie and G. P. Haight. Prog. Inorg. Chem. **17**, 93 (1972).
7. G. P. Haight, E. Perchonock, F. Emmeneger, and G. Gordon, J. Am. Chem. Soc. **87**, 3835 (1965).
8. I. Baldea and G. Niac. Inorg. Chem. **7**, 1232 (1968); **9**, 110 (1970).
9. K. A. Muirhead, G. P. Haight, and J. K. Beattie. J. Am. Chem. Soc. **94**, 3006 (1972).
10. J. P. McCann and A. McAuley. J. Chem. Soc. Dalton Trans. 783 (1975).
11. F. Hasan and J. Rocek. J. Am. Chem. Soc. **96**, 534 (1974); **97**, 1444 (1975).
12. J. N. Cooper, G. E. Standt, M. L. Senalser, L. M. Setto, and G. P. Haight. Inorg. Chem. **12**, 2075 (1973).
13. E. W. Wilson and R. B. Martin. Arch. Biochem. Biosphy. **142**, 445 (1971).
14. Y. Sugiura, Y. Hojo, and H. Tanaka. Chem. Pharm. Bull. Tokyo, **20**, 1362 (1972).
15. K. J. Ellis and A. McAuley. J. Chem. Soc. Dalton Trans. 1533 (1973).
16. M. I. Edwards, K. E. Howlett, and B. L. Wedzicha. J. Chem. Soc. A, 2866 (1970).
17. G. W. Haupt. J. Res. Natl. Bur. Stand. **48**, 414 (1952).
18. C.-T. Lin and J. K. Beattie. J. Am. Chem. Soc. **94**, 3011 (1972).
19. K. A. Muirhead and G. P. Haight. Inorg. Chem. **12**, 1116 (1973).
20. K. J. Ellis, A. G. Lappin, and A. McAuley. J. Chem. Soc. Dalton Trans. 1930 (1975).
21. M. A. Olatunji and A. McAuley. J. Chem. Soc. Dalton Trans. 682 (1975).
22. D. C. Gaswick and J. H. Krueger. J. Am. Chem. Soc. **91**, 2240 (1969).
23. G. V. Bakore and C. L. Jain. J. Inorg. Nucl. Chem. **31**, 805 (1969).

Chemistry of chelocardin II[1]: chemical modifications at $C_{2''}$ and C_{12a}

DANIEL T. W. CHU, STUART N. HUCKIN, AND EDITH BERNSTEIN
Abbott Laboratories, Limited, P.O. Box 6150, Montreal, P.Q., Canada H3C 3K6

Received February 24, 1977

DANIEL T. W. CHU, STUART N. HUCKIN, and EDITH BERNSTEIN. Can. J. Chem. **55**, 3341 (1977).

A selective reduction of chelocardin has been developed leading to 12a-deoxychelocardin which retains much of the antibacterial potency of the parent antibiotic, unlike the analogous reduction of tetracycline. Reaction of an *N*-protected chelocardin with amide acetals leads exclusively to products in which the condensation has occurred at the methyl group of the acyl side chain.

DANIEL T. W. CHU, STUART N. HUCKIN et EDITH BERNSTEIN. Can. J. Chem. **55**, 3341 (1977).

On a réalisé une réduction sélective de la chelocardine qui a donné la 12a-deoxychelocardine. Ce dernier retient en grande partie l'activité antibiotique de la chelocardine, contrairement à la réduction similaire de la tetracycline. La réaction des chelocardines *N*-bloquées avec certains amidoacétals a donné des composés dont la condensation s'est produite uniquement sur le groupe méthylique de l'acétyle.

Chelocardin, a broad spectrum antibiotic that was first described in 1962 (1) and subsequently shown to be **1** (2), bears a marked structural resemblance to the tetracycline (**2**) and specifically to the anhydrotetracycline (**3**).

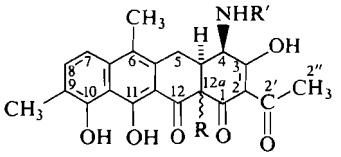

1 R = α-OH, R′ = H
5 R = α-OH, R′ = $CO_2CH_2C_6H_5$
6 R = H, R′ = $CO_2CH_2C_6H_5$
7 R = H, R′ = H·HBr

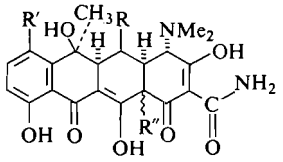

2 R′ = R = H, R″ = α-OH tetracycline
2 R′ = H, R = OH, R″ = α-OH oxytetracycline
2 R′ = Cl, R = H, R″ = α-OH chlorotetracycline
4 R′ = R = H, R″ = H

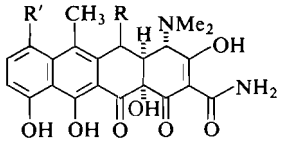

3 R′ = R = H anhydrotetracycline
3 R′ = H, R = OH anhydrooxytetracycline
3 R′ = Cl, R = H anhydrochlorotetracycline

[1]For Part I of this series, see ref. 12.

Since the discovery of the tetracycline class of antibiotics in 1948 (3) much effort has been expended to elucidate the structure–activity relationship of this class of compounds and considerable progress toward this end has been made (for a review of the structure–activity relationship see ref. 4*a*; for a more recent but less comprehensive review, see ref. 4*b*). However, during the course of our studies in the chemical modification of chelocardin, it became increasingly apparent that this body of literature concerning the tetracycline structure–activity relationship did not apply to chelocardin despite their structural similarities.

This divergence was first noted when the structure of chelocardin was elucidated (3) in that all of the modifications of the tetracycline ring system toward chelocardin are individually correlated with a decrease in antibiotic activity. For example, 2-acetyl-2-decarboxamidotetracycline possesses (depending upon the species of bacteria) between 6 and 15% of the activity of tetracycline (5), anhydrotetracycline has only slight antibacterial activity (6), 4-epitetracycline has only slight antibacterial activity in vitro (6), whereas the introduction of a methyl group at C_9 in deoxycycline gives an analogue with less than 10% of the parent antibiotic's antibacterial activity (7).

We now wish to report our chemical investigation on the modifications of chelocardin at C_{12a} and $C_{2''}$. It appears that there is a further difference between chelocardin and tetracyclines, namely the retention of antibacterial activity

upon removal of the 12a-hydroxyl function of chelocardin.

Modification at C_{12a}

12a-Deoxytetracycline (**4**) has been prepared by hydrogenolysis of O^{12a}-formyltetracycline (8) and by direct reduction of tetracycline with zinc and aqueous ammonia (9). Chelocardin, without protection of the amine functionality, would not withstand prolonged basic treatment. Even with the amine converted to the benzyl urethane, strong base causes epimerization at C_4 of chelocardin derivatives. However, it was found that treatment of *N*-carbobenzoxychelocardin (**5**) with zinc under acidic conditions gave a mixture of products, the major of which was characterized as the desired *N*-carbobenzoxy-12a-deoxychelocardin (**6**).

The removal of the hydroxyl functionality from the 12a position in both chelocardin and tetracycline permits the two, normally isolated, π-systems to interact, and this is reflected in the appearance of a new absorption band in the uv spectrum of **6** at 382 nm (cf. the additional band at 378 nm in the uv spectrum of anhydro-12a-deoxytetracycline (8) compared to anhydrotetracycline (10)). Further evidence for the assignment of the reduction products as **6** is the presence in its Hmr spectrum of two additional resonances; one at δ 4.0 ppm, assignable to the C_{12a}-hydrogen, and one in the enol region (δ 15–17 ppm) which together account for one proton (indicating that **6** in chloroform solution exists as a mixture of keto and enol forms). The ^{13}C nmr of the product is also compatible with reduction at the 12a position showing substantial shifts in the resonances previously assigned to C_{12}, C_{12a}, C_{4a}, and C_1.[2]

The carbobenzoxy group could be easily removed from **6** by treatment with hydrobromic acid in acetic acid to give 12a-deoxychelocardin as its hydrobromide salt (**7**) which could be purified more readily than **6**. Whereas reduction of the 12a-hydroxyl group of tetracycline reduces the antibacterial properties substantially (**4** is reported to possess only 2% of the activity of tetracycline toward *Staphylococcus aureus* (8)), 12a-deoxychelocardin possesses comparable efficacy toward Gram-positive bacteria as chelocardin and shows about one quarter of the latter's activity toward Gram-negative bacteria.

[2]R. S. Egan, R. S. Stanaszek, E. Bernstein, D. T. W. Chu, and S. N. Huckin, manuscript in preparation.

Modification at $C_{2''}$

Modification of the acyl side chain was initially achieved by substitution at the carbonyl group of the acyl side chain to give hydrazones (11*a*,*b*) and anils (11*c*), but subsequent indirect attempts at this modification via reacylation of 2-deacetylchelocardin (**8**) (12) have not been promising (19, 12).

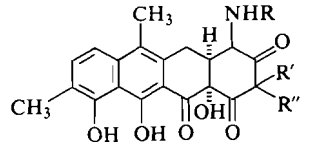

8 R = H, R′ = R″ = H

9 R = $CO_2CH_2C_6H_5$, R′, R″ = 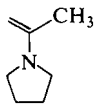

Direct reaction at the 2″ methyl group appeared to be chemically infeasible, as the enolization of the tricarbonyl system occurs initially with loss of the proton at C_2.[3] Subsequent enolization occurs by loss of the C_4 proton as evidenced by the epimerization of the amino groups in a wide variety of chelocardin derivatives under moderately basic conditions (for example see preparation of **9**). Modification of the tricarbonyl system by formation of the enamine at $C_{2'}$, to give **9**, also failed to allow reaction at $C_{2''}$, either directly or formally via acylation–deacylation at C_2. Compound **9** being a vinylogous imide was inert to the usual enamine alkylation and acylation conditions[4] and the presence of the other acidic groups in chelocardin precluded the preparation of the carbanion at $C_{2''}$ (14).

It is well known that *N*,*N*-disubstituted amide acetals (e.g. 1,1-dimethoxy-*N*,*N*-dimethylmethylamine **10**) undergo condensation with acid groups, such as a methyl ketone giving in this instance enamino-ketone (15). Although chelocardin contains several acidic groups with which a highly reactive compound such as **10** might react,[5] it was hoped that conditions which favored reaction at the 2″ methyl group could be

[3]However, no indication of reaction at C_2 was observed in a variety of acylations of chelocardin and derivatives even under forcing conditions (12).

[4]Vinylogous amides are somewhat deactivated (13) toward alkylation and acylation compared to enamines, **9** having two carbonyl groups in conjugation with the enamine can be expected to be even less reactive.

[5]For example, *trans* ketalization could occur involving the phenolic groups or the 12*a* hydroxyl and C_1 enol of chelocardin. For a review of amide acetals see ref. 20.

found. Accordingly, *N*-carbobenzoxychelocardin (**5**) was treated with an excess of **10** in refluxing benzene and tlcs taken after only 5 min reaction time indicated the complete conversion to a more polar product, subsequently shown to be the desired compound **11***a*.

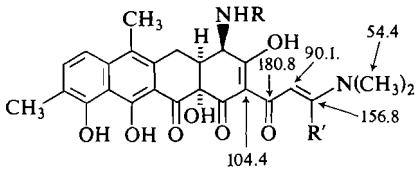

11*a* R = $CO_2CH_2C_6H_5$ and R′ = H
11*b* R = $CO_2CH_2C_6H_5$ and R′ = CH_3
11*c* R = H·HBr and R′ = H
11*d* R = H·HBr and R′ = CH_3
(^{13}C nmr data refer to **11***a* only)

Reaction at $C_{2''}$ was indicated by the presence in the Hmr spectrum of the product of a pair of doublets at δ 6.67 and δ 8.02 (J = 11 Hz) characteristic of *trans* vicinal vinylic protons and by the absence of the signals analogous to those assigned to the 2″ methyl group of *N*-carbobenzoxychelocardin. Compounds **11** possess a new band in their uv spectra at ca. 377 nm, and the model compounds **12**, derived from 2-acetyldimedone and the corresponding amide acetal, exhibit similar uv spectra.

The structure of **11***a* is further confirmed by its ^{13}C nmr spectrum which shows a striking parallel to that of **12***a* in that the corresponding carbon resonances for the side chain in both compounds are almost coincident. The relevant ^{13}C nmr data in ppm downfield, from internal TMS for **11***a* and **12***a*, are shown in their structures.

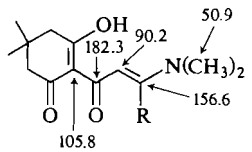

12*a* R = H
12*b* R = CH_3
(^{13}C nmr data refer to compound **12***a* only)

All attempts to hydrolyze the enamine moiety of the side chain in the formamide condensation products **11***a*, **11***c*, and **12***a* to produce the corresponding β-aldehydoketones failed. However, the corresponding ketamine compounds **11***b* and **12***b* derived from the dimethyl acetal of dimethylacetamide could be hydrolyzed to the corresponding carbonyl compounds **13** and **14**, by aqueous sodium carbonate.

Hydrolysis of compound **12***b* was very facile, even occurring during attempted purification by column chromatography on silica. If acidic hydrolysis conditions were employed, cyclization to the pyrone **15** occurred. Attempts to obtain the corresponding cyclization of **13** under similar conditions were not successful.

Unfortunately, the extension of conjugation of the 2′ carbonyl group away from the 1 and 3 carbonyls alters the electronic environment of the tricarbonyl system sufficiently that most of the antibacterial activity of chelocardin is lost and the nitrogen deprotected compounds **11***c* and **11***d* have only weak inhibitory effects on Gram-positive bacteria and are ineffective against Gram-negative bacteria at concentrations up to 100 μg/ml.

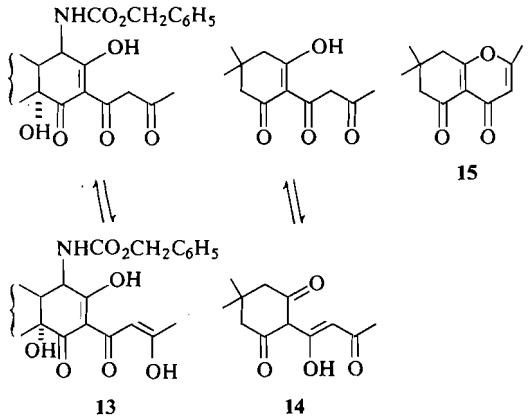

Experimental

The Hmr spectra were recorded on a Varian Associates EM-360 spectrometer in $CDCl_3$ solutions, resonance positions were reported using the δ scale relative to internal tetramethylsilane. The abbreviations used in reporting the signals are: s, singlet; d, doublet; m, multiplet, and b, broad. The mass spectra were recorded on an AEI MS-902 double focussing mass spectrometer. The uv spectra were recorded on a Unicam SP800A spectrometer in 0.1 *N* methanolic HCl solutions. Melting points were determined on a Thomas Hoover capillary melting point apparatus and are uncorrected. The ^{13}C nmr spectra were recorded on a Varian Associates XL-100-15/TT-100 spectrometer system in DMSO; resonance positions are given in ppm relative to internal tetramethylsilane.

Preparation of N-Carbobenzoxychelocardin (5)

Chelocardin hydrochloride (10 g, 0.022 mol) and benzyl chloroformate (20 ml) were dissolved in a mixture of tetrahydrofuran (300 ml) and water (60 ml), and a solution of sodium bicarbonate (15 g) in water (250 ml) was added, with vigorous stirring, over 15 min. The mixture was acidified with concentrated hydrochloric acid to p*H* 2.0 and the organic layer was separated and concentrated

to approximately 50 ml, before being dissolved in chloroform (250 ml). The chloroform solution was washed with saturated brine (2 × 30 ml) and dried over anhydrous sodium sulfate. Evaporation at reduced pressure gave 10.7 g (88%) of yellow amorphous solid which was essentially pure *N*-carbobenzoxychelocardin. Recrystallization from glacial acetic acid (6 ml/g) gave crystalline material, mp 206–211°C; Hmr δ 2.22 (s, 3H, C_9—CH_3), 2.30 (s, 3H, C_6—CH_3), 2.56 (s, 1.4H, $C_{2'}$—CH_3), 2.62 (s, 1.6H, $C_{2'}$—CH_3), 3.0–3.6 (m, 3H, C_5—H_2 and C_{4a}—*H*), 5.03 (m, 1H, —N*H*), 5.17 (m, 2H, —O—CH_2—C_6H_5), 6.05 (m, 1H, —C_4—*H*), 7.0–7.6 (m, 7H, C_7—*H*, C_8—*H*, and C_6H_5), 9.85 (s, 1H, C_{10}—O*H*), 15.1 (bs, 1H, C_{11}—O*H*), 18.1 (vbs, 1H, ring A enol —O*H*); uv λ_{max} 226, 275, and 435 nm; ms *m/e* 545 $M^{+}\cdot$. *Anal.* calcd. for $C_{30}H_{27}NO_9$: C 66.06, H 4.99, N 2.57; found: C 65.78, H 5.29, N 2.55.

*N-Carbobenzoxy-12a-deoxychelocardin (**6**)*

Zinc dust was activated by vigorous agitation with 1 *N* hydrochloric acid (10 ml/g), rapidly filtered, washed with water (3 × 25 ml/g) and acetone (2 × 10 ml/g), and dried under high vacuum.

N-Carbobenzoxychelocardin **5** (10 g, 18.2 mmol) was dissolved in glacial acetic acid (500 ml) and freshly activated zinc dust (30 g, 0.46 g-atom) added. The mixture was stirred at ambient temperature for 18 h and filtered. The filtrate was diluted with water (250 ml) and the resulting precipitate collected by filtration. The precipitate was dissolved in chloroform (500 ml) and the solution was washed with saturated brine (3 × 100 ml), dried over anhydrous sodium sulfate, and evaporated at reduced pressure to give 7.3 g (74%) of crude **6** as a red solid. Purification of **6** was achieved by chromatography on Sephadex LH20 using chloroform as eluent to give an amorphous solid having a melting point of 175–183°C; uv λ_{max} 226, 275, 382, and 445 nm; Hmr ($CDCl_3$) δ 2.27 (s, 6H, C_6—CH_3 and C_9—CH_3), 2.60 (s, 3H, $C_{2'}$—CH_3), 2.9–3.4 (m, 3H, C_5—H_2 and C_{4a}—*H*), 4.0 (d, 0.5H, C_{12a}—*H*), 4.6 (m, 1H, N—*H*), 5.17 (s, 2H, —O—CH_2—C_6H_5), 6.1 (m, 1H, C_4—*H*), 7.0–7.6 (m, 7H, C_7—*H*, C_8—*H* and C_6H_5), 10.1 (s, 0.5H, C_{10}—O*H*), 10.2 (s, 0.5H, C_{10}—O*H*), 15.1 (s, 0.5H, C_{11}—O*H*), 16.1 (s, 0.5H, C_{11}—O*H* or C_{12}—O*H*), 16.3 (s, 0.5H, C_{11}—O*H* or C_{12}—O*H*), 17.7 (bs, 0.5H, ring A enol O*H*) and 18.1 (bs, 0.5H, ring A enol O*H*); ^{13}C nmr (DMSO-d_6) δ 197.2 (s, C_3), 193.6 (s, C_2—*C*=O), 185.7 (s, C_{12}), 174.5 (s, C_1), 160.4 (s, C_{11}), 156.6 (s, N—CO_2), 154.5 (s, C_{10}), 137.0 (s, C_{6a}), 136.4 (s, C_1 of C_6H_5), 133.5 (d, C_8), 129.6 (s, C_{11a}), 128.2 (d, C_2 and C_6 of C_6H_5), 127.7 (d, C_4 of C_6H_5), 127.5 (d, C_3 and C_5 of C_6H_5), 119.8 (s, C_{5a}), 118.4 (s, C_9), 114.3 (d, C_7), 112.0 (s, C_2), 108.1 (s, C_6), 105.8 (s, C_{10a}), 99.6 (s, C_{12a}), 65.6 (t, OCH_2), 58.6 (d, C_4), 31.9 (d, C_{4a}), 29.0 (t, C_5), 25.6 (q, CO—CH_3), 15.1 (q, C_6—CH_3), 13.7 (q, C_9—CH_3); ms: *m/e* 529 $M^{+}\cdot$. *Anal.* calcd. for $C_{30}H_{27}NO_8$: C 68.04, H 5.14, N 2.64; found: C 68.75, H 5.43, N 2.63.

*12a-Deoxychelocardin Hydrobromide (**7**)*

Crude *N*-carbobenzoxy-12a-deoxychelocardin (5 g) was dissolved in hydrobromic acid (30% solution in glacial acetic acid, 75 ml) and the solution stirred for 5 min. The solution was poured into ether (500 ml) and the resulting precipitate collected by filtration and dried under high vacuum. The solid was dissolved in methanol (27 ml) and after 0.5 h, filtered. The filtrate was diluted to 50 ml with methanol and charcoal (2 g) added. The resulting suspension was stirred for 1 h, filtered, and concentrated to approximately 20 ml. Addition of ethanol (30 ml) and evaporation under reduced pressure gave 2.2 g (45%) of semicrystalline 7, mp 232–236°C (dec.); uv λ_{max} 225, 275, and 440 nm; Hmr (DMSO-d_6) δ 2.17 (s, 6H, C_6—CH_3 and C_9—CH_3), 2.67 (s, 3H, CO—CH_3), 3.0–3.5 (m, 3H, C_5—2*H* and C_{4a}—*H*), 5.0 (m, 1H, C_4—*H*), 7.0–7.5 (q, 2H, C_7—*H* and C_8—*H*), 9.0 (bs, 3H, —NH_3), 10.0 (bs, 1H, C_{10}—O*H*), 16.3 (bs, 1H, C_{11}—O*H*); ms *m/e* 395 $M^{+}\cdot$. *Anal.* calcd. for $C_{22}H_{22}NO_6Br$: C 55.47, H 4.65, N 2.94, Br 16.78; found: C 55.85, H 4.88, N 3.02, Br 16.45.

*2'-Pyrrolidine Enamine of N-Carbobenzoxychelocardin (**9**)*

Pyrrolidine (35 µl, 0.42 mmol) was added to a solution of *N*-carbobenzoxychelocardin (200 mg, 0.37 mmol) in benzene (10 ml) and the mixture was refluxed for 10 min. After cooling to room temperature, the mixture was poured into a large excess of hexane (~75 ml) and the resulting precipitate was filtered off, washed with a little hexane, and dried under high vacuum to give 210 mg (96%) of **9** as a mixture of epimers at C_4. Hmr δ 2.0 (m, 4H, pyrrolidine β-H), 2.26 (s, 3H, $C_{2'}$—CH_3), 2.40 (s, 3H, C_9—CH_3), 2.47 (s, 3H, C_6—CH_3), 3.0–3.9 (m, 7H, C_{4a}—*H* and C_5—H_2 and pyrrolidine α-*H*), 4.2 (m, 0.6H, N—*H*), 4.6 (m, 0.4H, N—*H*), 5.1 (d, 2H, —O$CH_2C_6H_5$), 5.5 (d, 0.4H, β-C_4—*H*), 6.05 (d, 0.6H, α-C_4—*H*) and 7.0–7.7 (m, 7H, C_7—*H*, C_8—*H*, and C_6H_5); high resolution mass spectrum calcd. for $C_{34}H_{34}N_2O_8$: *m/e* 598.2315; found: *m/e* 598.2357.

*N-Carbobenzoxy-2''-dimethylaminomethylene-chelocardin (**11a**)*

Dimethylformamide dimethyl acetal (70 µl, 0.65 mmol) was added to a refluxing solution of carbobenzoxychelocardin (100 mg, 0.18 mmol) in benzene (5 ml) and reflux was continued for 5 min. The mixture was cooled, washed with water (2 × 2 ml), dried by percolation through a small amount of anhydrous sodium sulfate, and poured into a large excess of hexane (40 ml). The resulting precipitate was collected by filtration, washed with a small quantity of ice-cold hexane, and dried under high vacuum to give 104 mg (95%) of pure **11***a*; Hmr δ 2.20 (s, 3H, C_9—CH_3), 2.30 (s, 3H, C_8—CH_3), 2.93 (s, 3H, N—CH_3), 3.13 (s, 3H, N—CH_3), 3.2–3.5 (m, 3H, C_{4a}—*H*, C_5—H_2), 4.2 (m, 1H, N—*H*), 5.20 (s, 2H, —O—CH_2—C_6H_5), 6.0 (d, 1H, C_4—*H*), 6.67 (d, J = 11 Hz, 1H, *H*C=CH—N—$(CH_3)_2$), 7.37 (m, 7H, C_7—*H*, C_8—*H*, and C_6H_5), 8.02 (d, J = 11 Hz, 1H, CO—CH=C*H*), 10 (bs, 1H, C_{10}—O*H*); uv λ_{max} 223, 271, 377, and 430 nm; high resolution mass spectrum calcd. for $C_{33}H_{30}N_2O_8$(**11***a*–H_2O): *m/e* 582.2002; found: *m/e* 582.2004. The relevant ^{13}C nmr data are given in the text.

*N-Carbobenzoxy-2''-(1-dimethylaminoethylidene)-chelocardin (**11b**)*

Dimethyl acetamide dimethyl acetal (100 µl, 0.65 mmol) was added to a refluxing solution of carbobenzoxychelocardin (100 mg, 0.18 mmol) in benzene (5 ml) and reflux was continued for 8 min. The mixture was cooled and poured into a large excess of hexane (40 ml). The resulting precipitate was collected by filtration, washed with a small quantity of ice-cold hexane, and dried under high vacuum to give 100 mg (98%) of pure **11***b*; Hmr δ 2.17 (s, 3H, C_9—CH_3), 2.23 (s, 3H, C_6—CH_3), 2.43 (s, 3H, C=C—CH_3), 2.83 (s, 3H,

N—CH_3), 2.90 (s, 3H, N—CH_3), 3.2 (m, 3H, C_5—H_2 and C_{4a}—H), 4.9 (m, 1H, N—H), 5.2 (s, 2H, —O—CH_2—C_6H_5), 6.03 (m, 1H, C_4—H), 6.87 (s, 1H, CH=C), 7.33 (m, 7H, C_7—H, C_8—H and C_6H_5); uv λ_{max} 225, 271, 377, and 420 nm; high resolution mass spectrum calcd. for $C_{33}H_{32}NO_9$(**11***b*–CH_2NO): *m/e* 570.2128; found: *m/e* 570.2139.

*2''-Acetyl-N-carbobenzoxychelocardin (**13**)*

A solution of sodium carbonate (40 mg) in water (4 ml) was added to **11***b* (100 mg, 0.16 mmol) dissolved in THF (20 ml) and the resulting mixture was stirred at room temperature for 2 h. The mixture was acidified to p*H* 2.0 with 1 *N* hydrochloric acid and the THF removed by evaporation under reduced pressure. The aqueous suspension was extracted with chloroform (2 × 15 ml) and the extract dried over sodium sulfate and concentrated to about 5 ml before being poured into hexane (30 ml). The resulting precipitate was collected by filtration and dried under high vacuum to give 76 mg (81%) of **13**; Hmr δ 2.05 (s, 1.5H, CH_3—C(OH)=C), 2.12 (s, 1.5H, CH_3—C=O), 2.30 (s, 3H, C_9—CH_3), 2.35 (s, 3H, C_6—CH_3), 3.1 (m, 3H, C_5—H_2 and C_{4a}—OH), 4.05 (s, 1.5H, CO—CH_2—CO), 5.2 (s, 2H, —OCH_2—C_6H_5), 5.4 (m, 1H, N—H), 5.9 (d, 1H, C_4—H), 6.8 (s, 0.5H, CO—CH=COH), 7.3 (m, 7H, C_7—H, C_8—H, and C_6H_5), 9.9 (bs, 0.5H, C_{10}—OH), 10.3 (bs, 0.5H, C_{10}—OH), 14.8 (bs, 0.5H, C_{11}—OH) and 15.4 (bs, 0.5H, C_{11}—OH); uv λ_{max} 228, 272, and 425 nm; high resolution mass spectrum calcd. for $C_{32}H_{29}NO_{10}$: *m/e* 587.1791; found: *m/e* 587.1820.

*5,5-Dimethyl-2-(3-dimethylaminopropenoyl)-1,3-cyclohexanedione (**12***a*)*

Dimethylformamide dimethyl acetal (0.24 ml, 1.75 mmol) was added to a solution of 2-acetyl dimedone (16) (100 mg, 0.55 mmol) in benzene (10 ml) and the solution was quickly heated to reflux which was maintained for 2 min. The solution was concentrated to ca. 2 ml under reduced pressure and chromatographed on a silica gel (25 g) column using chloroform – ethyl acetate (9:1) as eluent. The first component eluted from the column was **12***a* 98 mg (75%), mp 121–122°C; Hmr δ 1.03 (s, 6H, C_5—$(CH_3)_2$), 2.32 (s, 2H, C=C(OH)—CH_2), 2.40 (s, 2H, —CO—CH_2), 2.97 (s, 3H, N—CH_3), 3.17 (s, 3H, N—CH_3), 6.77 (d, J = 12 Hz, 1H, CO—CH=CH), 7.93 (d, J = 12 Hz, CO—CH=CH), 18.7 (s, 1H, C=C—OH); uv λ_{max} 270 and 370 nm; ms *m/e* 237 M^+·; *Anal.* calcd. for $C_{13}H_{19}NO_3$: C 65.80, H 8.07, N 5.90; found: C 66.05, H 8.34, N 5.72.

*5,5-Dimethyl-2-(3-dimethylamino-2-butenoyl)-1,3-cyclohexanedione (**12***b*)*

Dimethylacetamide dimethyl acetal (0.25 ml, 1.6 mmol) was added to a refluxing solution of 2-acetyldimedone (16) (100 mg, 0.55 mmol) in benzene (10 ml) and reflux was maintained for 10 min. The solution was cooled and concentrated, under reduced pressure to ca. 1 ml. The mixture was purified by preparative thin layer chromatography on a 20 × 20 cm silica gel plate (Quantagram PQIF 1000) using chloroform – ethyl acetate (9:1) as eluent. The band, visualized under uv light, at R_f 0.35 was removed and extracted with ethyl acetate. Upon concentration of this ethyl acetate solution, the product **12***b* crystallized yielding 94 mg (68%) of pure product, mp 132–134°C; Hmr δ 1.05 (s, 6H, C_5—$(CH_3)_2$), 2.39 (s, 2H, CH_2—C—(OH)=C), 2.57 (s, 2H, CH_2—C=O), 3.17 (s, 6H, N—$(CH_3)_2$), 7.05 (s, 1H, C=CH), 13.4 (bs, 1H, C=C—OH); uv λ_{max} 265 and 371 nm; high resolution mass spectrum calcd. for $C_{14}H_{21}NO_3$: *m/e* 251.1521; found: *m/e* 251.1530.

*Hydrolysis of (**12***b*)*

(*a*) *Basic Hydrolysis*

A solution of sodium carbonate (50 mg) in water (2 ml) was added to a solution of **12***b* (60 mg, 0.24 mmol) in THF (10 ml) and the mixture was stirred at room temperature for 2 h. The THF was removed by evaporation under reduced pressure and the aqueous residue extracted with chloroform (2 × 30 ml). Concentration of the dried (sodium sulfate) extract gave 42 mg (85%) of pale yellow crystals of 5,5-dimethyl-2-(1,3-dioxobutyl)-1,3-cyclohexanedione (**14**), mp 59–60°C (lit. (17) mp 60–61°C). The Hmr of **14** was essentially the same as the previously reported (17) differing only in the proportion of enol form present.

(*b*) *Acidic Hydrolysis*

Aqueous hydrochloric acid (5 ml, 1 *N*) was added to a solution of **12***b* (160 mg, 0.63 mmol) in THF (25 ml) and the mixture stirred at room temperature overnight. The THF was evaporated under reduced pressure and the aqueous residue extracted with chloroform (2 × 30 ml). Concentration of the dried (Na_2SO_4) extract gave 110 mg (84%) of colourless crystals identified as 7,8-dihydro-2,7,7-trimethyl-4H-1-benzopyran-4,5-(6H)-dione (**15**); mp 118–120°C (lit. (17) 121–122°C; lit. (18) 207–208°C) which exhibited an identical Hmr to that previously reported (17).

Acknowledgments

We thank G. Nettleship and Ms. S. Mueller of Abbott Laboratories for Hmr and mass spectra, respectively, and R. S. Egan and Ms. R. S. Stanaszek for the ^{13}C nmr spectra, and the staff of the microanalytical department of Abbott Laboratories for elemental analyses. We also thank D. L. Garmaise for his interest and encouragement throughout the course of this work.

1. T. J. Oliver, J. F. Prokop, R. R. Bower, and R. H. Otto. Antimicrob. Agents Chemother. 583 (1962); A. C. Sinclair, J. R. Schenck, G. C. Post, E. V. Cardinal, S. Burkas, and H. H. Fricke. Antimicrob. Agents Chemother. 592 (1962).
2. L. A. Mitscher, W. Rosenbrook, Jr., W. W. Andres, R. S. Egan, J. Schenck, and J. V. Juvarkar. Antimicrob. Agents Chemother. 38 (1970); L. A. Mitscher, J. V. Juvarkar, W. Rosenbrook, Jr., W. W. Andres, J. Schenck, and R. S. Egan. J. Am. Chem. Soc. **92**, 6070 (1970).
3. B. M. Duggar. Ann. N.Y. Acad. Sci. **51**, 177 (1948).
4. (*a*) G. C. Barrett. J. Pharm. Sci. **52**, 309 (1963); (*b*) W. Durckheimer. Angew. Chem. Int. Ed. Engl. **14**, 721 (1975).
5. M. W. Miller and F. A. Hochstein. J. Org. Chem. **27**, 2525 (1962).
6. J. R. McCormick, E. R. Jensen, P. A. Miller, and A. P. Doerschuk. J. Am. Chem. Soc. **81**, 4748 (1959).

7. L. BERNARDI, R. DECASTIGLIONE, P. MASI, R. MAZZOLENI, and U. SCARPONI. Il Farmaco Educ. Sci. **30**, 1025 (1975).
8. R. K. BLACKWOOD, H. H. RENNHARD, and C. R. STEPHENS. J. Am. Chem. Soc. **82**, 5194 (1960).
9. A. GREEN and I. H. BOOTHE. J. Am. Chem. Soc. **82**, 3950 (1960).
10. C. W. WALLER, B. L. HUTCHINGS, R. W. BROSCHARD, A. A. GOLDMAN, W. J. STEIN, C. F. WOLF, and J. H. WILLIAMS. J. Am. Chem. Soc. **74**, 4981 (1952).
11. (*a*) M. INABA, E. BERNSTEIN, and D. L. GARMAISE. U.S. Patent No. 3,907,889 (1975); (*b*) E. BERNSTEIN, M. INABA, and D. L. GARMAISE. U.S. Patent No. 3,910,906 (1975); (*c*) D. CHU and D. L. GARMAISE. U.S. Patent No. 3,894,061 (1975).
12. D. T. W. CHU, D. L. GARMAISE, and E. BERNSTEIN. Can. J. Chem. **53**, 1434 (1975).
13. M. E. KUELNE. *In* Enamines: synthesis, structures and reactions. *Edited by* A. G. Cook. Marcel Dekker, New York, NY. 1969. Chapt. 8, p. 355 (alkylation); p. 392 (acylation).
14. M. YOSHIMOTO, N. ISHIDA, and T. HIRAOKA. Tetrahedron Lett. 39 (1973).
15. H. BREDERECK, F. EFFENBERGER, and H. BOTSCH. Chem. Ber. **97**, 3397 (1964).
16. W. DIECKMANN and R. STEIN. Ber. **37**, 3370 (1904).
17. T. KATO, Y. YAMAMOTO, and T. HOZUMI. Chem. Pharm. Bull. **21**, 1840 (1973).
18. L. L. WOODS. J. Org. Chem. **34**, 2796 (1969).
19. D. CHU, E. BERNSTEIN, and S. N. HUCKIN. To be published.
20. R. H. DEWOLFE. Carboxylic ortho acid derivatives. Academic Press, New York, NY. 1970. Chapt. 7.

Benzannelated annulenes. II.[1] The synthesis of *trans*-12*b*,12*c*-dimethyl-12*b*,12*c*-dihydrobenzo(e)pyrene. An indication of the exceptional aromaticity of the 15,16-dimethyldihydropyrene[2] system

REGINALD H. MITCHELL[3] AND JOSEPH SHUE-HEN YAN

Department of Chemistry, University of Victoria, Victoria, B.C., Canada V8W 2Y2

Received June 22, 1977

REGINALD H. MITCHELL and JOSEPH SHUE-HEN YAN. Can. J. Chem. **55**, 3347 (1977).

The synthesis of *trans*-12*b*,12*c*-dimethyl-12*b*,12*c*-dihydrobenzo(e)pyrene **4**, in 10 steps from *o*-dibromobenzene and 2,6-dichlorotoluene utilizing a Wittig rearrangement – Hofmann elimination sequence on the benzothiacyclophane **6** is described. The diatropicity of **4** is compared to the parent *trans*-10*b*,10*c*-dimethyl-10*b*,10*c*-dihydropyrene **1**, and to other benzannelated annulenes.

REGINALD H. MITCHELL et JOSEPH SHUE-HEN YAN. Can. J. Chem. **55**, 3347 (1977).

On décrit la synthèse comportant 10 étapes du diméthyl-12*b*,12*c* dihydro-12*b*,12*c* benzo(e)pyrène *trans* **4** à partir du *o*-dibromobenzène et dichloro-2,6 toluène en utilisant une séquence comportant un réarrangement de Wittig et une élimination d'Hofmann sur le benzothiacyclophane **6**. La diatropicité de **4** est comparée à une molécule analogue le diméthyl-10*b*,10*c* dihydro-10*b*,10*c* pyrène *trans* **1** et à d'autres annulènes benzannelés.

[Traduit par le journal]

Like benzene, *trans*-15,16-dimethyl-15,16-dihydropyrene **1** has both a $(4n + 2)$–π electron periphery and two identical Kekulé structures and, moreover, since models indicate the macro-ring of **1** to be nearly planar, it could reasonably be expected to be aromatic. The synthesis of **1** by Boekelheide and Phillips (2) confirmed this point, and in its ^{1}H nmr spectrum, **1** showed its internal methyl protons to be exceptionally shielded at τ 14.25 by the strong diamagnetic ring current. A more recent (3) synthesis of **1**, utilizes the ready conversion of [2,2]metacyclophane-1,9-diene **2** into the thermodynamically (4) more stable photoisomer **1**. In this conversion, the delocalization of the electrons in both the benzene rings has to be interrupted in order to achieve conjugation in the macro-ring of **1**. In light of the fact that many tri and higher benzannelated annulenes have been known for a considerable number of years (see, for example, ref. 5) and none of them show any detectable delocalization in the macro-ring at the expense of the benzene rings, we thought it worthwhile to prepare the tribenzo compound **3** to determine whether it is possible to partially disrupt three benzene rings to form the macrocyclic system **4** which can be considered to be a benzannelated derivative of **1**.

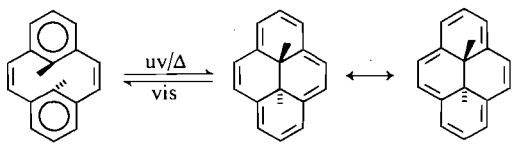

2 **1**

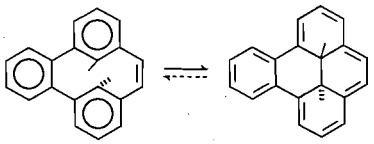

3 **4**

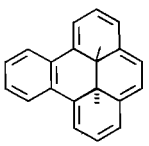

[1]For part I, see ref. 1.

[2]Chemical Abstract name is now *trans*-10*b*,10*c*-dimethyl-10*b*,10*c*-dihydropyrene.

[3]To whom correspondence should be addressed.

The synthesis of **3** required the dibromide **5**, which we prepared (mp 129–130°C)[4] in six steps[5] from *o*-dibromobenzene and 2,6-dichlorotoluene. Treatment of **5** under high dilution conditions (3) with sodium sulphide gave ca. 40% of the *anti*-thiacyclophane **6**, mp 201–202°C (along with a nearly equal amount of *syn*-isomer, mp 251–253°C). Separation was readily accomplished by chromatography on silica gel, the *anti*-cyclophane **6** being eluted first. *Anti*-**6** was readily distinguishable from *syn*-**6** by its ^{1}H nmr spectrum in which the shielded internal methyl protons appear at τ 9.1, whereas in *syn*-**6** they are in the normal toluene region (τ 7.9). Application of our Wittig rearrangement – Hofmann elimination sequence (6) to **6** then gave an 80% overall yield (from **6**) of the deep purple hydrocarbon **4**, mp 137–138°C, no detectable amount of the photoisomer **3** being present. The presence of a strong diamagnetic ring current in **4** was clearly evident from its ^{1}H nmr spectrum in which the internal methyl protons were strongly shielded at τ 11.85 and the external protons strongly deshielded at τ 1.0–3.6. The position of the internal methyl protons of **4** indicates[6] that

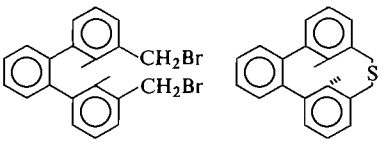

5 **6**

[4]The structure of all new compounds was fully supported by mass and nmr spectral data, and elemental analyses.

[5]Reaction of Mg with 2,6-dichlorotoluene in dry THF yielded the mono-Grignard reagent which on addition of *o*-dibromobenzene and 0.1 mol% $Ni(acac)_2$ gave 60% of 3,3″-dichloro-2,2″-dimethyl-*o*-terphenyl which was then converted through the dinitrile, dialdehyde, dialcohol to the dibromide **5** in 59% yield using the same reagent sequence (3) as for 2,6-bis(bromomethyl)toluene.

[6]This assumes that shielding is proportional to ring current. Calculated by comparison to a nonaromatic cyclic model, where methyl protons in a similar environment are at τ 9.0 (2).

4 sustains about 55% of the ring current of **1**. This is much greater than for benzo[14]annulene itself (7) or benzodidehydro[14]annulene (8), and must reflect on the considerably greater aromaticity of the rigid dihydropyrene nucleus of **1** than that of [14]annulene. Indeed **4** must be a contender for sustaining the largest ring current of any monobenzoannulene yet reported.[7]

This together with the fact that to disrupt the delocalization of each benzene ring of **3** may cost up to 36 kcal/mol (9) must point to the exceptional aromatic stability of the dihydropyrene system. We have not yet succeeded in converting *syn*-**6** into the corresponding *syn*-isomer of **4**.

Acknowledgments

We thank the University of Victoria and the National Research Council of Canada for support of this work.

1. R. H. MITCHELL and R. J. CARRUTHERS. Tetrahedron Lett. 4331 (1975).
2. V. BOEKELHEIDE and J. B. PHILLIPS. J. Am. Chem. Soc. **89**, 1695 (1967).
3. R. H. MITCHELL and V. BOEKELHEIDE. J. Am. Chem. Soc. **96**, 1547 (1974).
4. H. R. BLATTMANN and W. SCHMIDT. Tetrahedron, **26**, 5885 (1970).
5. G. WITTIG, G. KOENIG, and K. CLAUSS. Annalen, **593**, 127 (1955); C. E. GRIFFEN, K. R. MARTIN, and B. E. DOUGLAS. J. Org. Chem. **27**, 1627 (1962); H. A. STAAB, F. GRAF, and B. JUNGE. Tetrahedron Lett. 743 (1966); K. GROHMANN and F. SONDHEIMER. J. Am. Chem. Soc. **89**, 7119 (1967); R. H. MITCHELL and F. SONDHEIMER. J. Am. Chem. Soc. **90**, 530 (1968); Tetrahedron Lett. 2873 (1968).
6. R. H. MITCHELL, T. OTSUBO, and V. BOEKELHEIDE. Tetrahedron Lett. 219 (1975).
7. U. E. MEISSNER, A. GENSLER, and H. A. STAAB. Angew. Chem. Int. Ed. Engl. **15**, 365 (1976).
8. R. T. WEAVERS and F. SONDHEIMER. Angew. Chem. Int. Ed. Engl. **13**, 141 (1974).
9. A. YASUHARA, T. SATAKE, M. IYODA, and M. NAKAGAWA. Tetrahedron Lett. 895 (1975).

[7]Nakagawa and co-workers (9) have reported a strongly diatropic monobenzodidehydro[14]annulene.

Photochemistry of oxalate esters as a route to free radicals. Decay routes of crowded free radicals[1]

SIDDIK IÇLI,[2] VINCENT J. NOWLAN, PARVIZ M. RAHIMI, CHACKO THANKACHAN, AND THOMAS T. TIDWELL

Department of Chemistry, University of Toronto, Toronto, Ont., Canada M5S 1A1

Received June 14, 1977

SIDDIK IÇLI, VINCENT J. NOWLAN, PARVIZ M. RAHIMI, CHACKO THANKACHAN, and THOMAS T. TIDWELL. Can. J. Chem. **55**, 3349 (1977).

Photolysis of suitable oxalate esters leads to alkyl radicals which in the case of di- and tri-*tert*-butylmethyl abstract hydrogen and for triisopropylmethyl-d_{18} gives an esr spectrum consistent with the 'cogwheel' conformation for this species.

SIDDIK IÇLI, VINCENT J. NOWLAN, PARVIZ M. RAHIMI, CHACKO THANKACHAN et THOMAS T. TIDWELL. Can. J. Chem. **55**, 3349 (1977).

La photolyse d'oxalates appropriés conduit à des radicaux alkyles qui, dans le cas des di-, et tri-*tert*-butylméthyles, enlevent un hydrogène, et du tri-isopropylméthyle-d_{18}, présentent un spectre rpe compatible avec une conformation "roue dentée".

[Traduit par le journal]

Oxalate esters have been used to prepare free radicals by pyrolysis (1) and reduction (2), but although the photochemistry of esters has been a topic of intense recent interest (3), only scattered reports of oxalate photolysis have appeared (4). Oxalate esters have an attractive potential stoichiometry for photolysis to give only radicals and carbon dioxide, and absorb light at lower energies than ordinary esters (λ_{max} ethyl oxalate = 244 nm).

We now have found that photolysis of the oxalates **1–3** in cyclohexane with a medium pressure Hg lamp through quartz gave the products shown in eqs. 1–3 which implicate the radicals **4–6** as intermediates.[3] The esr spectrum of **6** was also observed during the photolysis (5). Oxalates with reactive β-hydrogens such as *tert*-butyl and cumyl gave mostly photoelimination (3*a*) to alkenes.

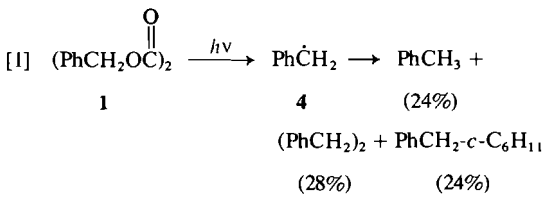

[1] $(PhCH_2OC(=O))_2 \xrightarrow{h\nu} PhC\dot{H}_2 \longrightarrow PhCH_3 + (PhCH_2)_2 + PhCH_2\text{-}c\text{-}C_6H_{11}$

1 4 (24%) (28%) (24%)

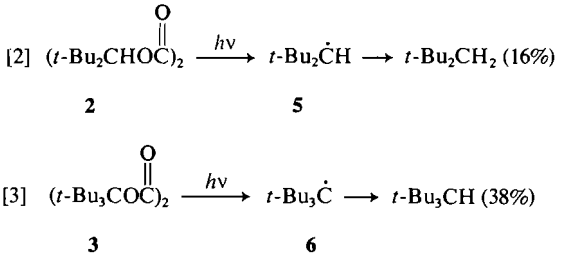

[2] $(t\text{-}Bu_2CHOC(=O))_2 \xrightarrow{h\nu} t\text{-}Bu_2\dot{C}H \longrightarrow t\text{-}Bu_2CH_2$ (16%)

2 5

[3] $(t\text{-}Bu_3COC(=O))_2 \xrightarrow{h\nu} t\text{-}Bu_3\dot{C} \longrightarrow t\text{-}Bu_3CH$ (38%)

3 6

The isolation of t-Bu_2CH_2 and t-Bu_3CH from the corresponding radicals establishes hydrogen abstraction as an important decay route for these long lived radicals (6[4]). This point has been unsettled (5), and the current results suggest these radicals may be very much longer lived in the absence of abstractable hydrogens.

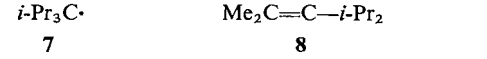

i-$Pr_3C\cdot$ $Me_2C{=}C{-}i$-Pr_2

7 8

A well resolved esr spectrum of **7** (7) was observed on photolysis of the oxalate, but interestingly the only volatile product observed was **8** (91% by vpc). This product may arise partly from photoelimination but studies of **7** from the perester (7) show that it can also arise from disproportionation reactions of **7** with cyclohexyl radicals. A sample of **7** fully deuterated in the methyl groups was prepared (eq. 4). Irradiation gave **7**-d_{18} whose esr spectrum in cyclopropane

[1]Presented in part at the 59th Congress of the Chemical Institute of Canada, London, Ontario, June, 1976.

[2]Present address: Department of Chemistry, Middle East Technical University, Ankara, Turkey.

[3]The new oxalates **3** (mp 114–115°C) and triisopropylcarbinyl oxalate (mp 51–52°C) were identified by spectral and elemental analysis.

[4]Also H. H. Lee and M. Stiles. University of Michigan. Unpublished data.

$$(CD_3)_2C{=}O \longrightarrow (CD_3)_2CHOH \longrightarrow (CD_3)_2CHCl \longrightarrow (CD_3)_2CHLi$$

[4]

$$(CD_3)_2CHLi \xrightarrow{CO_2} ((CD_3)_2CH)_3COH \xrightarrow[(2)\,C_2Cl_2O_2]{(1)\,n\text{-BuLi}} (((CD_3)_2CH)_3COC)_2 \xrightarrow{h\nu} \mathbf{7}$$

was a simple quartet (Fig. 1). The a_H^β values were found to vary with temperature as previously suggested in our interpretation of the spectrum of the undeuterated material (7). This is consistent with a planar geometry for the radical (Fig. 2), with small a_H^β values arising from the methine C—H bonds being orthogonal to the p orbital carrying the unpaired spin. The increase in a_H^β with temperature would arise from an increased amplitude of the torsional vibrations of the C—C bonds from the sp^2 carbon. The esr spectrum of undeuterated **7** is not fully resolved due to the γ splittings.

Thus this procedure provides improved routes to radicals such as **5**–**7** and the theoretically interesting tri-*tert*-butylmethane (6), and also resolves the questions as to the decay routes of **5** and **6** and the structure of **7**.

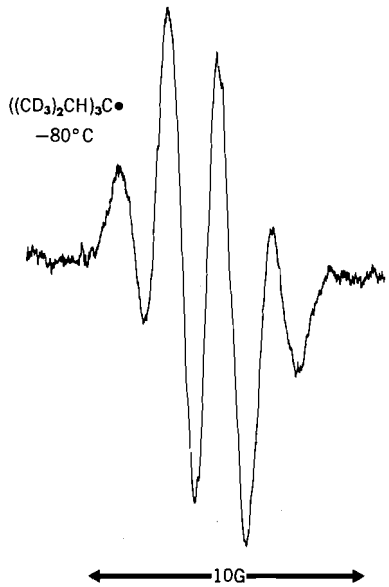

FIG. 1. Electron spin resonance spectrum of triisopropylmethyl-d_{18}.

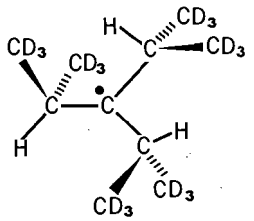

T(°C)	a_H^β (Gauss)
−80	1.85
−50	1.99
−25	2.12
10	2.38
25	2.49

FIG. 2. Temperature dependence of hyperfine splittings of **7**-d_{18}.

Acknowledgements

We thank the National Research Council of Canada for financial support and Professor Stiles for unpublished details regarding the synthesis of tri-*tert*-butylmethane. This work was partially supported by NATO Research Grant No. 1243.

1. (*a*) W. S. TRAHANOVSKY and P. W. MULLEN. J. Chem. Soc. Chem. Commun. 102 (1971); (*b*) R. E. LEHR and J. M. WILSON. J. Chem. Soc. Chem. Commun. 666 (1971); (*c*) J. WARKENTIN and D. M. SINGLETON. Can. J. Chem. **45**, 3035 (1967).
2. (*a*) H. REGENSTEIN, W. AHRENS, and A. BERNDT. Tetrahedron, **31**, 2837 (1975); (*b*) K. SCHREINER and A. BERNDT. Angew. Chem. Int. Ed. Engl. **14**, 366 (1975).
3. (*a*) J. D. COYLE and D. H. KINGSTON. J. Chem. Soc. Perkin Trans. II, 1475 (1976); (*b*) R. S. GIVENS, B. MATUSZEWSKI, N. LEVI, and D. LEUNG. J. Am. Chem. Soc. **99**, 1896 (1977); (*c*) N. A. MARRON and J. E. GANO. J. Am. Chem. Soc. **98**, 4653 (1976).
4. (*a*) Y. ODAIRA, T. TOMINAGA, T. SUGIHARA, and S. TSUTSUMI. Tetrahedron Lett. 2527 (1964); (*b*) W. M. HORSPOOL AND P. L. PAUSON. J. Chem. Soc. 5162 (1965).
5. G. D. MENDENHALL, D. GRILLER, D. LINDSAY, T. T. TIDWELL, and K. U. INGOLD. J. Am. Chem. Soc. **96**, 2441 (1974).
6. H. H. LEE. Ph.D. Thesis. University of Michigan. 1970.
7. D. GRILLER, S. IÇLI, C. THANKACHAN, and T. T. TIDWELL. J. Chem. Soc. Chem. Commun. 913 (1974).

Solvated electrons and the effect of coordination on the optical spectra of alkali metal cation – electron pairs in ethers[1]

WILLIAM ARTHUR SEDDON, JOHN WALLACE FLETCHER, FRED CHARLES SOPCHYSHYN, AND RON CATTERALL[2]

Physical Chemistry Branch, Atomic Energy of Canada Limited, Chalk River Nuclear Laboratories, Chalk River, Ont., Canada K0J 1J0

Received April 28, 1977

WILLIAM ARTHUR SEDDON, JOHN WALLACE FLETCHER, FRED CHARLES SOPCHYSHYN, and RON CATTERALL. Can. J. Chem. **55**, 3356 (1977).

Pulse radiolysis of tetrahydrofuran (THF), dimethoxyethane (DME), diglyme (DG), and triglyme (TG), results in the formation of solvated electrons, e_s^-, with optical band maxima $\lambda_{max} \geq 1840$ nm. In the presence of alkali metal salts transient optical bands are observed with λ_{max} at ~ 900 and ≥ 1600 nm. The latter bands are assigned to the formation of 'monomeric' species of stoichiometry M considered to be 'tight' and 'loose' ion-pairs, respectively. The proportion of 'loose' ion-pairs increases with decreasing temperature and increasing coordination of the solvent in the order THF $\ll$ DME $<$ DG $<$ TG. These results demonstrate a good correlation with established electron spin resonance data in alkali metal solutions and substantiate the coexistence of at least two 'monomeric' species in DME and the glymes.

WILLIAM ARTHUR SEDDON, JOHN WALLACE FLETCHER, FRED CHARLES SOPCHYSHYN et RON CATTERALL. Can. J. Chem. **55**, 3356 (1977).

La radiolyse par impulsion du tétrahydrofuranne (THF), diméthoxyéthane (DME), diglyme (DG) et triglyme (TG) conduit à la formation d'électrons solvatés e_s^- ayant des bandes optiques de maxima $\lambda_{max} \geq 1840$ nm. En présence de sels de métaux alkalins on observe des bandes optiques transitoires ayant des λ_{max} à ~ 900 et ≥ 1600 nm. Ces dernières bandes sont attribuées à la formation d'espèces "monomères" de stoechiométrie M que l'on considère comme étant respectivement des ions-pairés "près" et "loin". La proportion d'ions-pairés "loin" croît avec la diminution de la température et l'augmentation des sites de coordination du solvant: THF $\ll$ DME $<$ DG $<$ TG. Ces résultats démontrent une bonne corrélation avec les données établies par résonance de spin électronique en solutions de métaux alkalins et justifient la coexistence d'au moins deux espèces "monomères" dans le DME et les glymes.

[Traduit par le journal]

Introduction

The nature of the blue solutions of alkali metals in ethers has aroused considerable interest since their original discovery in 1957 (1, 2). Optical (3), electron spin resonance (esr) (4, 5), conductivity (6), flash photolysis (7–9), and pulse radiolysis (10–12) techniques have now clearly established the contribution of solvated electrons, e_s^-, cation–electron aggregates (M^+, e_s^-), and alkali metal anions M^- to the chemistry of such solutions.

Nevertheless, considerable controversy revolves around the precise identity of the (M^+, e_s^-) species. Pulse radiolysis of alkali metal salts in several amines and tetrahydrofuran (THF) (13) has established the formation of transient optical bands of stoichiometry M, resulting from the reaction of the cation M^+, with e_s^-.

[1] $$e_s^- + M^+ \rightarrow (M^+, e_s^-) \text{ or } M$$

Such bands exhibit a distinct blue shift from that of e_s^- observed in the same solvent. The magnitude of this shift shows a clear correlation with the percent atomic character, deduced from the esr hyperfine splitting constants, A_{iso}, for the corresponding 'monomeric' M species produced in alkali metal solutions (14–16). The value of A_{iso} is markedly temperature dependent and two different models have been proposed to explain this behaviour. In a static or continuum model, a single species is proposed whose structure is temperature dependent while a dynamic or multistate model envisages a temperature-

[1]AECL No. 5886.

[2]Visiting scientist, May–September 1976. Permanent address: Chemistry Department, University of Salford, Salford M54WT, England.

dependent equilibrium between two (or more) species of the same stoichiometry whose structures are relatively insensitive to temperature (17–23).

The observation of a single optical absorption band, and its correlation with esr (16), would appear to contradict the multistate theory. However, in progressing along the series THF, dimethoxyethane (DME), and the polyglycoldimethyl ethers (glymes), evidence was obtained for the existence of two distinct optical bands resulting from the reaction of e_s^- with Na^+ (24). Glymes have the general formula $CH_3O[CH_2CH_2O]_nCH_3$ and for $n = 1$, 2, and 3 correspond to DME, diglyme (DG), and triglyme (TG), respectively. In this series the chelating or cation solvating ability is well established (25) and increases markedly in the order THF < DME < DG < TG. This paper expands our preliminary account (24), compares our results with esr, and presents our conclusions with respect to the influence of solvent structure on the nature of (M^+, e_s^-).

Experimental

Details of the pulse radiolysis equipment, flow systems, and general techniques have been discussed elsewhere (26, 27). In this work all experiments were conducted using a 1.0 cm cell and 0.3 μs pulses of 2.25 MeV electrons. Solution preparation and purification of THF were as described previously (12). DME (Eastman) and the glymes (Matheson, Coleman and Bell, and Aldrich Chemicals) were purified by refluxing over calcium hydride in an inert atmosphere followed by fractional distillation. The middle fractions were degassed and allowed to stand over Na/K alloy until a stable blue color was obtained. This solution was then cooled and decanted, under vacuum, from the alloy and the ethers subsequently redistilled into the appropriate flow system. Sodium and potassium tetraphenylboron salts were used to give solutions of the alkali metal cations (12).

Results and Discussion

Solvated Electrons

Figure 1 shows the optical absorption spectra of e_s^- observed at 21°C immediately after the pulse in pure DME, DG, and TG. In each case there is good agreement with the normalized spectra (solid lines) observed previously having band maxima of 2050, 1915, and 1840 nm, respectively (10). As in other work (11, 28, 29) both the yield, $G_{e_s^-}$ molecules per 100 eV, and extinction coefficient ε_{max} at the band maximum, were determined by comparison with $G\varepsilon$ (anion) in the presence of $\leq 5 \times 10^{-4}$ M biphenyl (B) as an electron scavenger. Assuming $\varepsilon_{B^-} = 4 \times 10^4\ M^{-1}\ cm^{-1}$ at 410 nm (29) yields were calculated from linear plots of optical density against the energy absorbed per pulse for doses $\leq 1 \times 10^{20}$ eV ℓ^{-1}. On this basis we obtain $G_{e_s^-} = 0.40 \pm 0.03$ and $\varepsilon_{max} = 3.8 \pm 0.3 \times 10^4\ M^{-1}\ cm^{-1}$ for each ether. Again this is in good agreement with previous work in DME and THF where $\varepsilon_{max} = 3.4 \pm 0.7$ (10) and 4.0 ± 0.8 or $5.0 \pm 0.5 \times 10^4\ M^{-1}\ cm^{-1}$, respectively (10, 12).

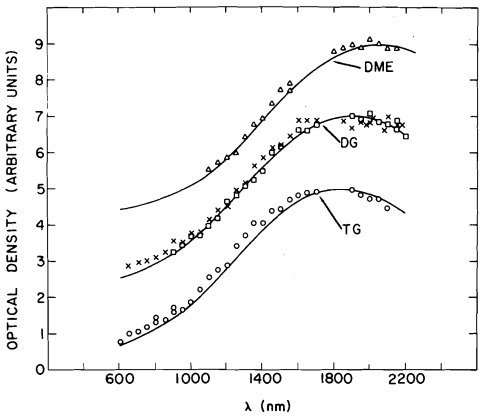

FIG. 1. Optical absorption spectra of e_s^- in ethers at 21°C. The solid lines represent the normalized spectra obtained previously (10). The DG and DME spectra are successively displaced vertically by two units for clarity in presentation.

With increasing temperature the absorption maxima shift toward lower energies with temperature coefficients of -17 ± 2, -19 ± 3, and $-20 \pm 3\ cm^{-1}\ deg^{-1}$ from −50, −64, and −40°C to 21°C for DME (mp −58°C), DG (mp −64°C), and TG (mp −45°C), respectively. At temperatures close to the melting point (mp) where the band maxima are more clearly resolved the corresponding widths at half height, $\Delta\nu_{1/2}$, are found to be ~5200, 5500, and 5900 cm^{-1}. Using the approximation $f \sim 4.32 \times 10^{-9}\ \varepsilon_{max} \times \Delta\nu_{1/2}$ (30), and substituting the appropriate values from above the oscillator strengths, f, of the e_s^- absorption bands are estimated as 0.85, 0.90, and 0.97, respectively.

Solvated Electron – Cation Aggregates

Optical Spectra

Figure 2 shows the optical spectra observed at the end of the pulse in DG solutions containing 7.2×10^{-4} and 9×10^{-3} M sodium tetraphenylboron ($NaB\phi_4$). The dotted line shows

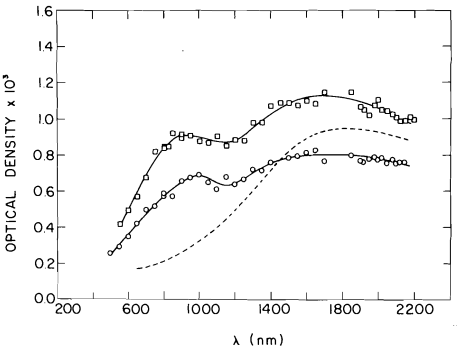

FIG. 2. Transient optical spectra observed immediately after the pulse in DG at 21°C. Dotted line, e_s^-; ○ and □ solutions containing 7.2×10^{-4} *M* and 9×10^{-3} *M* $NaB\phi_4$, respectively. Doses/pulse were $\sim 1 \times 10^{20}$ eV ℓ^{-1} with the optical densities normalized to a dose of 4.1×10^{18} eV ℓ^{-1}.

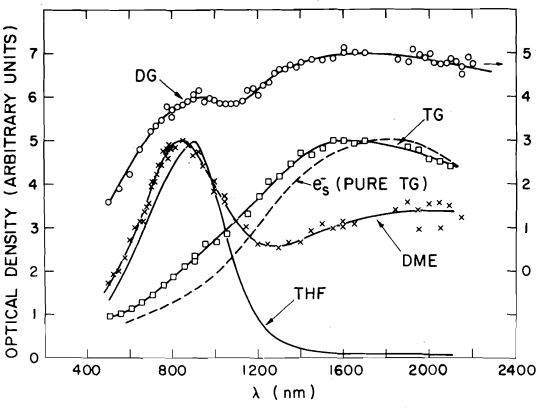

FIG. 3. Transient optical spectra observed immediately after the pulse in $\sim 10^{-2}$ *M* $NaB\phi_4$ solutions in THF, DME, DG, and TG. For THF and DME the spectra are normalized to a peak height of five units for the 900 and 850 nm band maxima, respectively. In DG and TG the spectra are normalized with respect to the 1600 nm band with the ordinate for the DG spectrum displaced two units (right hand scale). The dotted line shows the spectrum of e_s^- in TG.

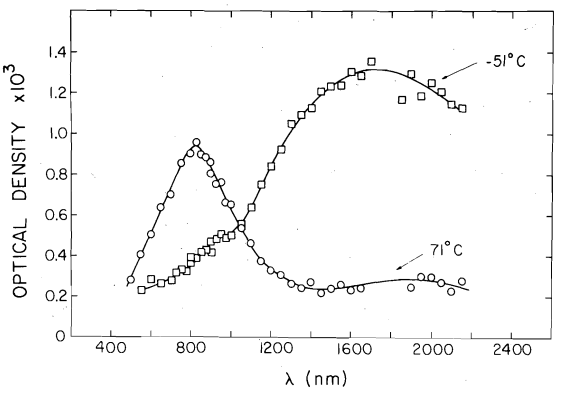

FIG. 4. Transient optical spectra observed immediately after the pulse as a function of temperature in $\sim 10^{-2}$ *M* $NaB\phi_4$ solutions in DME. Optical densities correspond to a dose of 2.66×10^{18} eV ℓ^{-1} at 71°C and 2.96×10^{18} eV ℓ^{-1} at −51°C. Typical doses/pulse were $\sim 6 \times 10^{19}$ eV ℓ^{-1}.

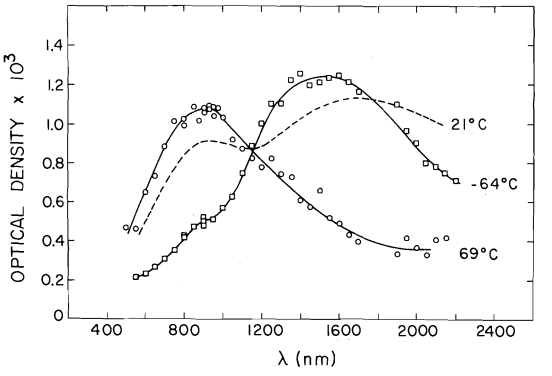

FIG. 5. Transient optical spectra observed immediately after the pulse as a function of temperature in $\sim 10^{-2}$ *M* $NaB\phi_4$ in DG. Optical densities correspond to doses of 2.3, 4.1, and 3.61×10^{18} eV ℓ^{-1} at −64, 21, and 69°C, respectively. Doses/pulse ranged from 0.7 to 1.0×10^{20} eV ℓ^{-1}.

the spectrum of e_s^- in DG from Fig. 1. Figure 3 shows the corresponding normalized spectra obtained in $\sim 10^{-2}$ *M* $NaB\phi_4$ solutions in DME and TG together with those observed in DG and THF for comparison. Similar spectra are obtained in solutions containing $NaAlH_4$. Figures 4, 5, and 6 show the effect of temperature on the DME, DG, and TG spectra presented in Fig. 3. Corresponding temperature studies from 21 to −17°C in THF gave no change in the spectrum. Figure 7 shows the optical spectrum observed at the end of the pulse in $\sim 10^{-2}$ *M* $KB\phi_4$ solutions in THF, DG, and DME along with the spectrum of e_s^- in DG for comparison.

The spectra, extinction coefficients, and oscillator strengths for e_s^- are in good agreement with previous work (10) and require no further comment. The blue shifts in band maxima with decreasing temperature are also typical of e_s^- in other systems (31).

With the addition of $NaB\phi_4$ the optical bands show a progression from a single peak at 900 nm in THF, through a composite spectrum in DME and DG with peaks at ~900 and ≥1600

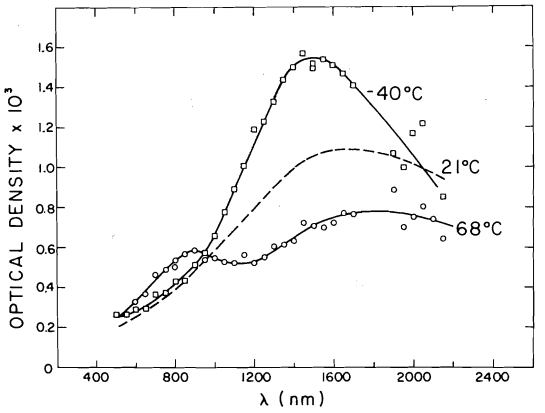

FIG. 6. Transient optical spectra observed immediately after the pulse as a function of temperature in $\sim 10^{-2}$ *M* $NaB\phi_4$ in TG. Optical densities correspond to doses of 3.24, 4.20, and 2.95 $\times$ 10^{18} eV ℓ^{-1} at -40, 21, and 68°C, respectively. Doses/pulse ranged from 0.6 to 1.0 $\times$ 10^{20} eV ℓ^{-1}.

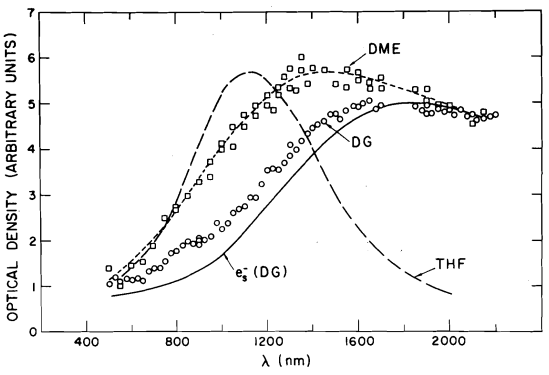

FIG. 7. Transient optical spectra observed immediately after the pulse in $\sim 10^{-2}$ *M* $KB\phi_4$ solutions in THF, DME, and DG. The dashed line shown for DME represents a calculated composite spectrum containing 25% of the THF species and 75% of the DG species (see text).

nm, until finally only the latter band is observed in TG. It can be seen in Figs. 2, 3, and 7 that although small, there is in the presence of $NaB\phi_4$ or $KB\phi_4$, a distinct blue shift in the long wavelength maximum from that of the corresponding e_s^- band in the same solvent.

In THF it is well established that [2] produces the 900 nm band with a second order rate constant $k_2 = 7.9 \times 10^{11}\ M^{-1}\ s^{-1}$ (10, 12)

[2] $$e_s^- + Na^+ \rightarrow (Na^+, e_s^-)$$

Because of spectral overlap it is not possible to measure the corresponding rate constants in DG, DME, or TG. However, changes in spectra such as depicted in Figs. 2 and 3 are observed immediately after the pulse at concentrations of $\sim 10^{-4}$ *M* $NaB\phi_4$. Since, as in THF (32, 33), it is likely that $NaB\phi_4$ is only weakly dissociated this indicates that the corresponding values of k_2 are $\geq 5 \times 10^{10}\ M^{-1}\ s^{-1}$.

On the basis of the optical–esr correlation (15, 16) we propose that in these ethers the 900 nm (r band) corresponds to the formation of a 'tight' ion-pair structure, whereas the 1600 nm (ir band) relates to a 'loose' ion-pair aggregate. By 'tight' we envisage a structure which allows a significant degree of interaction between e_s^- and the outer *s*-orbital of M^+ resulting in an appreciable atomic character of $\geq 30\%$ as found in THF (4). By 'loose' we imply a greater degree of solvent separation between M^+ and e_s^- resulting in less hyperfine interaction and an atomic character ≤ 2–5%. In both DME and DG (and THF) we suggest that the 'tight' aggregates represent coordination of M^+ with a single oxygen lone-pair whereas the ir bands reflect cation solvation by coordination with more than one site. In the latter case the glyme effectively shields the outer *s*-orbital of the cation from overlap with the e_s^-. These two types of aggregates we designate as $(M^+, e_s^-)_{tight}$ and $(M^+, e_s^-)_{loose}$, analogous to the well established ion-pair concepts in organic anion systems (34).[3]

From spectra such as shown in Fig. 2 it is apparent that the relative intensities of the r and ir bands remain the same over a 25-fold range of $NaB\phi_4$ concentration. This indicates that any contribution from e_s^- to the overall optical spectrum must be very small and a rapid equilibrium, predominantly in favour of 'loose' and 'tight' ion pairs, is established during the pulse.

[3] $$M^+ + e_s^- \rightleftarrows (M^+, e_s^-)_{loose} \rightleftharpoons (M^+, e_s^-)_{tight}$$

Such an interpretation is in accord with esr multistate models which require the existence of two or more distinct cation–electron aggregates in equilibrium (19).

In $KB\phi_4$ in THF, DG, and DME solutions (Fig. 7) only a single broad absorption band is observed. This again is consistent with the esr–optical correlation (16) in that the corresponding

[3]After submission of our original manuscript essentially the same description for the M species in alkali metal solutions appeared elsewhere (35).

potassium 'tight' ion-pair is expected to be red shifted by ~200 nm from that observed in $NaB\phi_4$ solutions. The lack of any obvious shoulder at ~1100 nm suggests that the equilibria in [3] lie more in favour of the 'loose' structure potassium solutions than for sodium. For example in DME the dashed line in Fig. 7 corresponds to a composite spectrum containing 25% of the 'tight' structure, as observed in THF, and 75% of the 'loose' structure observed in DG. For the corresponding sodium species at 21°C we estimate the fraction of 'tight' ion-pairs to be ~50% (see below).

In general the percent atomic character observed in alkali metal solutions for a given solvent increases in the order Na < K < Rb < Cs (16). The above observation is therefore not necessarily inconsistent with this trend since the expected increase in atomic character for K may compensate for the relative difference in equilibria from Na to K.

Another well established feature of the esr spectra is the marked temperature dependence of the metal hyperfine splitting constants, A_{iso} (3, 4). Increasing the temperature increases A_{iso} (and hence the percent atomic character) and vice versa. For organic anions and ethereal solvents the formation of loose ion-pairs is usually exothermic and is determined by the coulombic interaction between anion and cation in the tight and loose configurations and by the solvation energy of the two ion-pairs (25). In general the exothermicity and degree of solvent separation increases in the more polar solvents. Therefore, as suggested previously (36), a decrease in temperature is not inconsistent with a shift of [3] to the left. It can be seen from Figs. 4–6 that a clear shift in the optical spectrum corresponding to the formation of $(M^+, e_s^-)_{loose}$ is observed at low temperatures and vice versa at high temperatures. It is difficult to make precise quantitative comparisons with esr because of the corrections for spectral overlap and the uncertainty in relating esr data for potassium solutions with optical spectra for the corresponding sodium species. However, relative contributions of the 'tight' and 'loose' species can be estimated provided the extinction coefficients are known. The latter were estimated by comparison of the appropriate $G\varepsilon$ values obtained in $\sim 10^{-2}$ M $NaB\phi_4$ solutions with the corresponding values for B^- produced via [4] (12).

TABLE 1. Molar extinction coefficients for the tight and loose ion-pair species in ethers

		ε_{max} (M^{-1} cm^{-1}) ($\times 10^{-4}$)	
Solvent	Cation	Tight	Loose
THF*	Na^+	2.4 ± 0.2	
	K^+	2.9 ± 0.2	
	Cs^+	2.5 ± 0.2	
DME	Na^+	2.7 ± 0.4	2.9 ± 0.4
	K^+		2.8 ± 0.4
DG	Na^+	2.4 ± 0.4	2.4 ± 0.4
	K^+		2.4 ± 0.4
TG	Na^+	2.2 ± 0.4	2.4 ± 0.4

*See refs. 10 and 12.

[4] $$(Na^+, e_s^-) + B \rightarrow (Na^+, B^-)$$

For DME, DG, and TG at 21°C we find $G(B^-) = G(Na^+, e_s^-)_{tight} + G(Na^+, e_s^-)_{loose} = 0.9 \pm 0.1$. For DME this value was independent of temperature from −50 to 70°C. At −50°C only the ir band is observed from which we deduce $\varepsilon_{loose} = 2.9 \pm 0.3 \times 10^4$ M^{-1} cm^{-1}. However, at 71°C the r band predominates. Assuming the contribution of the r band to the ir band maximum to be negligible, and taking the above ε_{loose} to calculate the fraction of 'loose' ion-pairs, we then estimate $\varepsilon_{tight} = 2.7 \pm 0.3 \times 10^4$ M^{-1} cm^{-1}. This value is corrected for the overlap due to the ir band. At intermediate temperatures corrections for spectral overlap are more significant but adopting the same technique we obtain values in good agreement with the above. A similar procedure was utilized for DG and TG. However, at temperatures close to the mp the yield is approximately twice that observed at 21°C, presumably due to the enhanced escape probability of e_s^- from the spur (37). The appropriate extinction coefficients in each of the ethers are summarized in Table 1.

Utilizing the fraction tight/(tight + loose) and taking $A_{iso}(r) = 30$ G (by comparison with THF) and $A_{iso}(ir) = 0.3$ G as representative of splitting constants for the 'tight' and 'loose' ion-pairs in this series of ethers we can, since [3] is established in ≤0.3 μs, estimate the observed esr parameters from the weighted average of each form (38). These values are summarized in Table 2. Although the comparison is not exact the trend, particularly in DME, is remarkably good. We believe this adds further weight to the esr models in which the observed A_{iso} is thought to

TABLE 2. Optical ratio of tight and loose ion-pairs as a function of temperature for sodium species in ethers

Solvent	Temperature (°C)	Tight (Tight + Loose)	A_{iso} (G)* Calc.	Expt.
DME	−51	0.04	1.5	
	−20	0.11	3.6	0.0
	21	0.54	16.3	12.5
	71	0.75	22.5	28.5
DG	−64	≤0.05	≤1.8	
	−44	~0.05	~1.8	
	−21	0.10	3.3	0.0
	21	0.21	6.6	3.0
	69	0.74	22.2	10.6
TG	−40	0.0	≤0.3	
	21	0.0	≤0.3	3.0†
	68	0.22	6.8	

*Calculated values based on optical ratios for sodium species as described in text. Experimental values are for potassium solutions interpolated from a linear extrapolation of data in refs. 41 and 5 for DME and DG, respectively.
†Reference 42.

arise from a rapidly fluctuating hyperfine interaction between two discretely different solvated cation – electron aggregates.

In contrast it is interesting to note that in THF no shift or change in the (Na^+, e_s^-) spectrum was observed from 21 to −17°C. However, esr studies in potassium solutions show a decrease in A_{iso} over this temperature range of ~5 G (4), indicative of a looser structure. Since both the e_s^- and Na^- shift to the blue with decreasing temperature the relative position of the (Na^+, e_s^-) band is therefore closer to that of e_s^- and consequently we would predict a lower A_{iso} and a somewhat looser structure. This observation would imply a somewhat enhanced degree of cation-solvation with decreasing temperature compatible with the static model. For the multistate model to apply one might also consider an equilibrium between two slightly different 'tight' species (21) rather than a distinct contribution from a 'loose' species characteristic of the glymes.

This situation would also seem to apply in the glymes as a lower order effect in that there appears to be no shift in the position of the corresponding r band maxima with change in temperature. Furthermore, for the ir band, blue shifts of ~4, 7, and 9 cm^{-1} deg^{-1} observed in Figs. 4–6 for DME, DG, and TG, respectively, are significantly less than observed for e_s^- (this work) or M^- in the same solvents (31). Again this can be interpreted in favour of a slightly looser structure for the ir species. We suggest therefore that a combination of both the static and dynamic models are applicable in these systems either one of which can predominate according to the nature of the solvent. Such a conclusion is analogous to that suggested previously in the interpretation of esr spectra for organic radical anions (38).

Reaction Kinetics

No detailed kinetic studies of the subsequent ion-pair decay processes were investigated since the bulk of the decay probably occurs by reaction with other radiolytically produced radicals (12). However, in each case for solutions containing ~10^{-2} *M* $NaB\phi_4$ or $KB\phi_4$ and doses per pulse of ~1×10^{20} eV ℓ^{-1}, the decay at wavelengths ≥1150 nm is complete with ~10 μs. At lower wavelengths the absorption initially decays at the same rate but is then followed by a slow build up which reaches its maximum intensity some 30 μs after the pulse. The spectrum observed on this time scale peaks at 900 nm, reaches a maximum intensity ~30% of that observed initially at 2000 nm, and decays completely after ~500 μs. This additional absorption is not produced in $NaAlH_4$ solutions. A weak absorption observed ~7 μs after the pulse in $NaB\phi_4$ solutions peaks at ~700 nm and is undoubtedly due to Na^- (13).

We have been unable to identify the intermediate long-lived absorption at 900 nm but the available evidence indicates that this results from a reaction involving the tetraphenylboron anion.

Comparisons with Flash Photolysis

In an earlier study on the flash photolysis of Na^- in DG at −60°C (8, 39) the immediate formation of an ir band, with a maximum at 1600 nm, was followed by the slow (t_{max} = 0.1 s) formation of an intense absorption peaking at 830 nm and the subsequent regeneration of Na^-. Similar results were observed in DME containing NaCl dissolved in potassium solutions. These observations were attributed to the formation of e_s^- (ir band) and (Na^+, e_s^-) as precursors of Na^-.

Comparing this work with our pulse radiolysis results it is clear that at low temperatures the ir band observed by flash photolysis is consistent with the formation of $(Na^+, e_s^-)_{loose}$ or e_s^-. However, the 830 nm band cannot be identified with $(Na^+, e_s^-)_{tight}$ since the latter is absent, or is seen only as a minor component, at low tem-

peratures. Furthermore the pulse radiolysis results (see earlier) show that the formation of the ion-pair in [2] is diffusion controlled whereas the flash photolysis interpretation indicates the contrary (8, 39). Further experiments are in progress in an attempt to rationalize these puzzling discrepancies.

Non-chelating Solvents

In the non-chelating amine solvents such as methylamine MA (40), ethylamine EA (25), and isopropylamine IPA (14) only a single optical band attributed to ion-pair formation is observed. In MA we would consider such ion-pairs to be of a 'loose' type which, with decreasing solvent polarity, become progressively tighter in the order MA < EA < IPA (16, 35). In this respect one cannot refer to distinct 'tight' and 'loose' entities but must instead consider a continuous range of ion-pair species. Likewise in THF/EA mixtures the species varies between the 'tight' and the 'loose' as a function of solvent composition suggesting again a successive replacement of solvent molecules and the formation of an intermediate type of ion-pair consistent with the static model (15). For a dynamic equilibrium to be applicable it would seem that any two species would have to be structurally very similar but necessarily intermediate in character to our conception of 'tight' and 'loose' pairs in the pure solvents. Practically, this situation is impossible to distinguish from the static model.

In contrast mixtures containing a chelating solvent such as in THF/DG solutions[4] clearly show a change in the proportion of 'tight' and 'loose' species with increasing DG and are qualitatively, at least, consistent with the dynamic model.

1. J. L. Down, J. Lewis, B. Moore, and G. Wilkinson. Proc. Chem. Soc. 209 (1957).
2. J. L. Down, J. Lewis, B. Moore, and G. Wilkinson. J. Chem. Soc. 3767 (1959).
3. J. L. Dye. Electrons in fluids. *Edited by* J. Jortner and N. R. Kestner. Springer-Verlag, Berlin. 1973. p. 77.
4. R. Catterall, J. Slater, and M. C. R. Symons. Metal ammonia solutions. Colloque Weyl II. *Edited by* J. J. Lagowski and M. J. Sienko. Butterworths and Co., London, England. 1970. p. 329.
5. R. Catterall, J. Slater, and M. C. R. Symons. Can. J. Chem. **55**, 1979 (1977).
6. F. Cefasso and B. R. Sundheim. J. Chem. Phys. **31**, 809 (1959).
7. L. J. Giling, J. G. Kloosterboer, R. P. H. Rettschnick, and J. D. W. Van Voorst. Chem. Phys. Lett. **8**, 457 (1971).
8. J. G. Kloosterboer, L. J. Giling, R. P. H. Rettschnick, and J. D. W. Van Voorst. Chem. Phys. Lett. **8**, 462 (1971).
9. M. Fisher, G. Rämme, S. Claesson, and M. Szwarc. Proc. R. Soc. London, Ser. A, **327**, 481 (1972).
10. F. Y. Jou and L. M. Dorfman. J. Chem. Phys. **58**, 4715 (1973).
11. B. Bockrath and L. M. Dorfman. J. Phys. Chem. **77**, 1002 (1973).
12. G. A. Salmon, W. A. Seddon, and J. W. Fletcher. Can. J. Chem. **52**, 3259 (1974).
13. J. W. Fletcher and W. A. Seddon. J. Phys. Chem. **79**, 3055 (1975).
14. W. A. Seddon, J. W. Fletcher, and F. C. Sopchyshyn. Chem. Phys. **15**, 377 (1976).
15. R. Catterall, J. Slater, W. A. Seddon, and J. W. Fletcher. Can. J. Chem. **54**, 3110 (1976).
16. W. A. Seddon, J. W. Fletcher, and R. Catterall. Can. J. Chem. **55**, 2017 (1977).
17. K. Hofelmann, J. Jagur-Grodzinski, and M. Szwarc. J. Am. Chem. Soc. **91**, 4645 (1969).
18. K. Bar-Eli and T. R. Tuttle, Jr. J. Chem. Phys. **40**, 2508 (1964).
19. R. Catterall and P. P. Edwards. J. Phys. Chem. **79**, 3010 (1975).
20. J. H. Sharp and M. C. R. Symons. Ions and ion-pairs in organic reactions. Vol. 1. *Edited by* M. Szwarc. Wiley-Interscience, New York, NY. 1972. p. 177.
21. N. Hirota. J. Am. Chem. Soc. **90**, 3603 (1968).
22. N. Hirota, R. Carraway, and W. Schook. J. Am. Chem. Soc. **90**, 3611 (1968).
23. L. R. Dalton, J. D. Rynbrandt, E. M. Hansen, and J. L. Dye. J. Chem. Phys. **44**, 3969 (1966).
24. W. A. Seddon, J. W. Fletcher, R. Catterall, and F. C. Sopchyshyn. Chem. Phys. Lett. **48**, 584 (1977).
25. J. Smid. Ions and ion-pairs in organic reactions. Vol. 1. *Edited by* M. Szwarc. Wiley-Interscience, New York, NY. 1972. p. 85.
26. J. W. Fletcher, W. A. Seddon, and F. C. Sopchyshyn. Can. J. Chem. **51**, 2975 (1973).
27. W. A. Seddon, J. W. Fletcher, J. Jevcak, and F. C. Sopchyshyn. Can. J. Chem. **51**, 3653 (1973).
28. W. A. Seddon, J. W. Fletcher, F. C. Sopchyshyn, and J. Jevcak. Can. J. Chem. **52**, 3269 (1974).
29. W. A. Seddon, J. W. Fletcher, and F. C. Sopchyshyn. Can. J. Chem. **54**, 2807 (1976).
30. J. G. Calvert and J. N. Pitts, Jr. Photochemistry. J. Wiley and Sons, Inc., New York, NY. 1966. p. 172.
31. M. T. Lok, F. J. Tehan, and J. L. Dye. J. Phys. Chem. **76**, 2975 (1972).
32. D. N. Bhattacharyya, C. L. Lee, J. Smid, and M. Szwarc. J. Phys. Chem. **69**, 608 (1965).
33. D. Nicholls, C. Sutphen, and M. Szwarc. J. Phys. Chem. **72**, 1021 (1968).
34. M. Szwarc. Ions and ion-pairs in organic reactions. Vol. 1. *Edited by* M. Szwarc. Wiley-Interscience, New York, NY. 1972. p. 1.
35. J. L. Dye. Pure Appl. Chem. **49**, 3 (1977).
36. M. Szwarc and J. J. Grodzinski. Ions and ion-pairs in organic reactions. Vol. 2. *Edited by* M. Szwarc. J. Wiley and Sons, Inc., New York, NY. p. 1.

[4]R. Catterall, W. A. Seddon, and J. W. Fletcher. Unpublished results.

37. J. W. FLETCHER and W. A. SEDDON. Disc. Faraday Soc. In press.
38. K. S. CHEN, S. W. MAO, K. NAKAMURA, and N. HIROTA. J. Am. Chem. Soc. **93**, 6004 (1971).
39. J. G. KLOOSTERBOER. Thesis. University of Amsterdam, Amsterdam, The Netherlands. 1971.
40. J. W. FLETCHER, W. A. SEDDON, J. J. JEVCAK, and F. C. SOPCHYSHYN. Can. J. Chem. **53**, 3571 (1975).
41. S. H. GLARUM and J. H. MARSHALL. J. Chem. Phys. **52**, 5555 (1970).
42. J. SLATER. Thesis. University of Leicester, Leicester, England. 1970.

Volumes and heat capacities of some amino acids in water at 25°C

JAGDISH C. AHLUWALIA,[1] CLAUDE OSTIGUY, GERALD PERRON, AND JACQUES E. DESNOYERS[2]

Department of Chemistry, Université de Sherbrooke, Sherbrooke, P.Q., Canada J1K 2R1

Received April 13, 1977

JAGDISH C. AHLUWALIA, CLAUDE OSTIGUY, GERALD PERRON, and JACQUES E. DESNOYERS. Can. J. Chem. **55**, 3364 (1977).

The apparent molal volumes and heat capacities of nine amino acids were measured in water at 25°C with a flow densimeter and a flow microcalorimeter. It is shown that the poor additivity of the standard partial molal quantities of amino acids in water are attributable to the ionization of the two groups NH_2 and COOH. The hydration of these ionic groups interfere with each other when they are separated by less than three carbon atoms.

JAGDISH C. AHLUWALIA, CLAUDE OSTIGUY, GERALD PERRON et JACQUES E. DESNOYERS. Can. J. Chem. **55**, 3364 (1977).

Les volumes et capacités calorifiques molaires apparents de neuf acides aminés ont été mesurés dans l'eau à 25°C avec un densimètre et un microcalorimètre dynamiques. On peut démontrer que la pauvre additivité de groupe que l'on observe avec les acides aminés peut être attribuée à l'ionisation des deux groups NH_2 et COOH. L'hydratation de ces groupes se gêne lorsqu'ils sont séparés par moins de trois atomes de carbone.

Introduction

In recent years there has been a large effort to accumulate thermodynamic data on model organic molecules in water with the aim of devising simple additivity schemes for the prediction of the properties of biochemical systems. Volumes and heat capacities have drawn particular attention, since their standard partial molal quantities readily lead themselves to such an analysis.

Nichols *et al.* (1) have proposed a very simple group additivity scheme which predicts surprisingly well the standard partial molal heat capacities $\bar{C}_p^0$ of aliphatic nonionic solutes in water. However, parallel work by Spink and Wadsö (2) and by Prasad and Ahluwalia (3) shows that the additivity is far from being as good with amino acids. As a check of the reliability of the data by the integral heat method used by Prasad and Ahluwalia, concurrent measurements were made on nine amino acids with the flow microcalorimetric technique. The purpose of this paper is to report these heat capacities and the accompanying standard partial molal volumes $\bar{V}^0$. As it will be shown, the present data on $\bar{C}_p^0$ and $\bar{V}^0$ support the interpretation of Cabani *et al.* (4) that the poor additivity with amino acids is related to the ionization of the NH_2 and COOH groups.

Experimental

The flow microcalorimeter (5, 6) and flow densimeter (7) used in this study have been described elsewhere. Essentially heat capacities per unit volume and densities of the solution were measured relative to pure water and from these differences the apparent molal quantities ϕ_C and ϕ_V were calculated.

The amino acids studied were the following: DL-α-alanine (Fisher Scientific), DL-β-alanine (BDH chemicals, 99%), DL-α-aminobutyric acid (Sigma Chemical Co.), L-leucine (Anachemia Chemicals Company), DL-norleucine (Sigma Chemical Co), DL-β-amino-*n*-butyric acid (Sigma Chemical Co.), DL-γ-amino-*n*-butyric acid (Sigma Chemical Co., 99%), DL-5-amino-*n*-valeric acid (Aldrich Chemical), and DL-6-amino-*n*-caproic acid (Sigma Chemical Co.). The amino acids were not purified but dried under vacuum for 48 h. The solutions were prepared by weight with distilled deionized water (Continental Deionizer).

Results

For each amino acids about 8 to 15 data points were taken for m above 0.02 mol kg^{-1}, the highest concentration depending on the solu-

[1]Permanent address: Department of Chemistry, Indian Institute of Technology, Delhi, New Delhi, 110029, India.

[2]Author to whom correspondence should be addressed.

TABLE 1. Volumes and heat capacities of some amino acids in water at 25°C

Compound	$\bar{V}^0$ ($cm^3\ mol^{-1}$)	A_V ($cm^3\ mol^{-2}\ kg$)	$\bar{C}_p^0$ ($J\ K^{-1}\ mol^{-1}$)	A_C ($J\ K^{-1}\ mol^{-2}\ kg$)
α-Alanine $CH_3—CH(NH_2)COOH$	60.47	0.63	142.5	6.4
β-Alanine $NH_2—CH_2—CH_2COOH$	58.28	0.94	73.2	12.7
DL-α-Amino-*n*-butyric acid $CH_3CH_2—CH(NH_2)—COOH$	75.54	0.53	227.2	5.8_5
DL-β-Amino-*n*-butyric acid $CH_3—CH—(NH_2)—CH_2—COOH$	76.33	0.56	177.6	5.3
DL-γ-Amino-*n*-butyric acid $NH_2—CH_2—CH_2—CH_2—COOH$	73.02	1.08	136.2	5.6_5
5-Amino valeric acid $NH_2—CH_2—CH_2—CH_2—CH_2—COOH$	87.58	1.53	198.5	12.7
2-Amino caproic acid (DL-Norleucine) $CH_3—CH_2—CH_2—CH_2—CH_2(NH_2)COOH$	107.72	0.70	400.0	0.0
L-Leucine $(CH_3)_2—CH—CH_2—CH(NH_2)COOH$	107.75	0.00	399.0	0.0
6-Amino caproic acid $H_2N—CH_2—CH_2—CH_2—CH_2—CH_2COOH$	104.02	0.00	278.0	0.0

TABLE 2. Standard partial molal heat capacities of DL-α-alanine at 25°C

Reference*	$\bar{C}_p^0$ ($J\ K^{-1}\ mol^{-1}$)	Method
Present results	142.5±1	Flow microcalorimetry
Prasad and Ahluwalia (3)	150 ±25	At 30°C, integral heat method
Spink and Wadsö (2)	146 ±5	Drop heat capacity calorimetry
	141 ±4	Integral heat method
Cabani *et al.* (4)	147.7±2	Mean value, adiabatic calorimetry
Zittle and Schmidt (8)	167	
Gucker and Allen (9)	140	

*Numbers in parentheses are the corresponding reference numbers from which data are quoted.

bility.[3] In general the amino acids show little concentration dependence. The standard partial molal quantities, $\bar{C}_p^0$ and $\bar{V}^0$, and slopes, A_C and A_V, derived by least-squares analysis of the equations

$$[1] \qquad \phi_C = \bar{C}_p^0 + A_C m$$

$$[2] \qquad \phi_V = \bar{V}^0 - A_V m$$

are summarized in Table 1.

The heat capacities for DL-α-alanine are compared with other data in Table 2. Most results agree inside the experimental uncertainty of each technique. The agreement with the other amino acids is also good in most cases where literature values were available (see refs. 2–4 for a survey of $\bar{C}_p^0$ values). In addition to the uncertainties attached to a different technique, some errors probably result from the impurities of the amino acids. Impurities of 1% can probably cause uncertainties of 5 to 10 $J\ K^{-1}\ mol^{-1}$. Most of the amino acids used were guaranteed to 99% and attempts to determine by chromatography the extent of residual impurities failed.

The volumes of α-alanine, β-alanine, and 6-amino caproic acid are also compared with those of other authors in Table 3. The agreement is quite good with α-alanine and β-alanine but less so with β-alanine. Here again the disagreement

[3]Complete set of the actual experimental data is available, at a nominal charge, from the Depository of Unpublished Data, CISTI, National Research Council of Canada, Ottawa, Canada K1A 0S2.

TABLE 3. Standard partial molal volumes of some amino acids at 25°C

Reference[a]	$\bar{V}^0$ (cm^3 mol^{-1})		
	α-Alanine	β-Alanine	6-Amino caproic acid
Present results	60.47±0.1	58.28±0.1	104.02±0.1
Jolicoeur[b]	60.45		
Papela and Dunlop (10)		59.65	
Devine and Lowe (11)		57.9	103.9
Daniel and Cohn (12)		58.6	104.35

[a]Numbers in parentheses are the corresponding reference numbers from which data are quoted.
[b]C. Jolicoeur, unpublished data.

might be reflecting more the purity of the samples than the precision of the techniques.

Discussion

A comparison of the present $\bar{C}_p^0$ with those of the literature (2–4) shows that the CH_2 contribution of the α-amino acids are similar to those of other homologous *n*-alkyl solutes but are significantly different with ω-amino acids. To find the origin of this difference, $\bar{C}_p^0$ of the amino acids were calculated from the additivity scheme of Nichols *et al.* (1). The difference between the experimental and predicted values are about -40 to -50 J K^{-1} mol^{-1} for the α-amino acids, -90 to -100 for the β-amino acids and -140 to -170 for the γ and higher amino acids. Cabani *et al.* (4) have recently shown that the change in heat capacity for the reaction

[3] $\quad RCOOH + RNH_2 \rightarrow RCOO^- + RNH_3^+$

is between -160 to -170 J K^{-1} mol^{-1}. Therefore, the present observations suggest that the amino acids when the amino group is separated from the carboxylate group by more than two carbons, act as two independent ions. When the groups are closer together the hydration of the groups interfere with each other and the experimental $\bar{C}_p^0$ are intermediate to those for fully ionized and unionized amino acids. This interpretation is essentially the same as that offered by Cabani *et al.* (4).

The same reasoning can be applied to volumes. From the work of Jolicoeur and Lacroix (13), Høiland and Vikingstad (14), and Cabani *et al.* (15), the group contribution to $\bar{V}^0$ in cm^3 mol^{-1} for neutral molecules in water at 25°C are: CH_3, 26.4; COOH, 25.8; CH_2, 16.0; NH_2, 15.3; CH, 6.5; OH, 12.2. Here the mean differences between measured and predicted $\bar{V}^0$ for α, β, and higher amino acids are -13, -14, and -17 cm^3 mol^{-1}. The change in volume for reaction 3 can be estimated from the data of King (16), Cabani *et al.* (16), Palma and Morel (17), and Desnoyers and Arel (18) to be about -18 cm^3 mol^{-1}. This ΔV for different alkyl groups is not as constant as ΔC_p since the values for CH_2 near ionic groups are usually different from 16.0 cm^3 mol^{-1} (19). Still, the difference between the measured and predicted $\bar{V}^0$ can be largely attributed to the ionization of the amino acids: the effect is complete if the groups are far apart and partial if they are close together. This effect is less spectacular with $\bar{V}^0$ than with $\bar{C}_p^0$ since the hydration contribution to $\bar{V}^0$ is mostly electrostatic while that to $\bar{C}_p^0$ is mostly structural in origin. The interference between the hydration cospheres of the two ionic groups will thus be more important with $\bar{C}_p^0$ since the structural hydration effects are of longer range than the electrostatic ones. This higher sensitivity for $\bar{C}_p^0$ results from the fact that it is a second derivative with respect to free energies while $\bar{V}^0$ is a first derivative.

Acknowledgement

The authors are grateful to the National Research Council of Canada for financial support.

1. N. NICHOLS, R. SKÖLD, C. SPINK, J. SUURKUUSK, and I. WADSÖ. J. Chem. Thermodyn. **8**, 1081 (1976).
2. C. SPINK and I. WADSÖ. J. Chem. Thermodyn. **7**, 561 (1975).
3. K. P. PRASAD and J. C. AHLUWALIA. J. Solution Chem. **5**, 491 (1976).
4. S. CABANI, G. CONTI, E. MATTEOLI, and A. TANI. J. Chem. Soc. Faraday Trans. I, **73**, 476 (1977).
5. P. PICKER, P.-A. LEDUC, P. R. PHILIP, and J. E. DESNOYERS. J. Chem. Thermodyn. **3**, 631 (1971).
6. J. E. DESNOYERS, C. DE VISSER, G. PERRON, and P. PICKER. J. Solution Chem. **5**, 605 (1976).

7. P. PICKER, E. TREMBLAY, and C. JOLICOEUR. J. Solution Chem. **3**, 377 (1974).
8. C. A. ZITTLE and C. L. A. SCHMIDT. J. Biol. Chem. **108**, 161 (1935).
9. F. T. GUCKER and T. W. ALLEN. J. Am. Chem. Soc. **64**, 191 (1942).
10. C. N. PEPELA and P. J. DUNLOP. J. Chem. Eng. Data, **17**, 207 (1972).
11. W. DEVINE and B. M. LOWE. J. Chem. Soc. A, 2113 (1971).
12. J. DANIEL and E. J. COHN. J. Am. Chem. Soc. **58**, 415 (1936).
13. C. JOLICOEUR and G. LACROIX. Can. J. Chem. **54**, 624 (1976).
14. H. HØILAND and E. VIKINGSTAD. Acta Chem. Scand. Ser. A, **30**, 182 (1976).
15. S. CABANI, G. CONTI, and L. LEPORI. J. Phys. Chem. **78**, 1030 (1974).
16. E. J. KING. J. Phys. Chem. **73**, 1220 (1969).
17. M. PALMA and J. P. MOREL. J. Chim. Phys. **73**, 645 (1976).
18. J. E. DESNOYERS and M. AREL. Can. J. Chem. **45**, 359 (1967).
19. M. SAKURAI, T. KOMATSU, and T. NAKAGAWA. Bull. Chem. Soc. Jpn. **48**, 3491 (1975).

Heat capacities, volumes, and expansibilities of sodium phenyl carboxylates in water

CLAUDE OSTIGUY, JAGDISH C. AHLUWALIA,[1] GERALD PERRON, AND JACQUES E. DESNOYERS[2]

Department of Chemistry, Université de Sherbrooke, Sherbrooke, P.Q., Canada J1K 2R1

Received April 13, 1977

CLAUDE OSTIGUY, JAGDISH AHLUWALIA, GERALD PERRON, and JACQUES E. DESNOYERS. Can. J. Chem. **55**, 3368 (1977).

The heat capacities per unit volume at 25°C and densities from 10 to 55°C of sodium phenyl carboxylates were measured with a flow microcalorimeter and a flow densimeter. The apparent molal heat capacities and volumes were used to derive standard partial molal heat capacities $\bar{C}_p^0$, volumes $\bar{V}^0$, and expansibilities $\bar{E}^0$. The CH_2 contribution to $\bar{V}^0$ is the same as that usually observed for aliphatic solutes but the contribution to $\bar{C}_p^0$ and $\bar{E}^0$ is not constant and significantly different. No simple explanation can be offered for this anomaly.

CLAUDE OSTIGUY, JAGDISH C. AHLUWALIA, GERALD PERRON et JACQUES E. DESNOYERS. Can. J. Chem. **55**, 3368 (1977).

Les capacités calorifiques par unité de volume à 25°C et les masses volumiques de 10 à 55°C des phenyl carboxylates de sodium ont été mesurées avec un microcalorimètre dynamique et un densimètre dynamique. Les capacités calorifiques et volumes molaires apparents ont été utilisés pour calculer les valeurs molaires partielles standard pour les capacités calorifiques $\bar{C}_p^0$, les volumes $\bar{V}^0$ et les expansibilités $\bar{E}^0$. La contribution de chaque CH_2 à $\bar{V}^0$ est essentiellement la même que celle des solutés aliphatiques mais la contribution à $\bar{C}_p^0$ et $\bar{E}^0$ n'est pas constante et est très différente. Aucune explication simple n'a pu être proposée pour expliquer ces anomalies.

Introduction

There is much interest in the group additivity of organic molecules in water. In particular Nichols *et al.* (1) have shown that a very simple group additivity scheme can predict the standard partial molal heat capacities, $\bar{C}_p^0$, of many aliphatic nonionic molecules in water with a precision which is often comparable with the experimental uncertainty. Similarly, the work of Yalkowsky and Zografi (2), Jolicoeur and Lacroix (3), Høiland and Vikingstad (4), and Cabani *et al.* (5) indicates that reasonably good additivity schemes can be devised for standard partial molal volumes, $\bar{V}^0$, although the presence of charged groups can have a significant contribution on the adjacent groups (6). Cabani *et al.* (7) have also been accumulating data on standard partial molal expansibilities, $\bar{E}^0$, from which it will eventually be possible to obtain group additivity contributions.

Recent work in our laboratory (8) has shown that it is also possible to get an excellent additivity scheme of $\bar{C}_p^0$ and $\bar{V}^0$ of aromatic molecules in water. These group contributions are fairly similar to those of aliphatic molecules for $\bar{V}^0$ but significantly different with $\bar{C}_p^0$. Also, Nichols and Wadsö (9) found that the methylene contribution to $\bar{C}_p^0$ of homologous aromatic alcohols and amines are different from the normal aliphatic compounds. Similar differences, although less important, were also observed with diol (1).

In an attempt to find the origin of this lack of additivity of homologous aromatic solutes in water we determined $\bar{C}_p^0$, $\bar{V}^0$, and $\bar{E}^0$ of a series of aromatic carboxylate salts.

Experimental

The flow microcalorimeter (10, 11) and flow densimeter (12) used in this study have been described elsewhere. The expansibilities were obtained from the temperature dependence of the volumes, $\bar{E}^0 = d\bar{V}^0/dT$. All acids except phenyl pentanoic acid (Ash Stevens) were purchased from J. T. Baker Chemicals. The salts were prepared by neutralization of the acids in water followed by dry evaporation. The salts were then recrystallized in ethanol adding acetone to initiate the crystallization.

All solutions were prepared by weight with deionized distilled water (Continental Deionizer). The temperature was measured to 0.01°C with a Hewlett-Packard Quartz Thermometer, calibrated at the factory.

[1]On leave of absence from the Indian Institute of Technology, Delhi, New Delhi, 110029, India.

[2]Author to whom correspondence should be addressed.

TABLE 1. Volumes and heat capacities of sodium phenyl carboxylates in water; parameters of eq. 1

T (°C)	Solute	$\bar{V}^\theta$ (cm^3 mol^{-1})	B_V (cm^3 mol^{-2} kg)	$\bar{C}_p^\theta$ (J K^{-1} mol^{-1})	B_C (J K^{-1} mol^{-2} kg)
10	ϕCOONa	82.97	+0.89		
	ϕCH_2COONa	97.49	+1.06		
	$\phi(CH_2)_2COONa$	114.82	−0.08		
	$\phi(CH_2)_3COONa$	128.84	−0.12		
25	ϕCOONa[a]	85.92	+0.13	250.9	+5.5
	ϕCH_2COONa	100.61	+0.70	305.3	−0.0
	$\phi(CH_2)_2COONa$	118.36[b]	−1.21[b]		
		116.82	+1.17	361.7	−20.1
	$\phi(CH_2)_3COONa$	132.40	+0.11	422.7	−50.9
	$\phi(CH_2)_4COONa$	148.54	+0.92	504.0	−67.4
40	ϕCOONa	88.06	−0.26		
	ϕCH_2COONa	102.89	+0.53		
	$\phi(CH_2)_2COONa$	121.37	+0.06		
	$\phi(CH_2)_3COONa$	135.12	+0.18		
55	ϕCOONa	89.56	−0.26		
	ϕCH_2COONa	104.47	+0.44		
	$\phi(CH_2)_2COONa$	123.76	−2.11		
	$\phi(CH_2)_3COONa$	137.28	+0.47		

[a]Desnoyers *et al.* (14): $\bar{C}_p^\theta$ corrected as indicated in ref. 11.
[b]Old data: probably impure salt.

Results

The apparent molal volumes ϕ_V and heat capacities ϕ_C are obtained from the relative change in heat capacities per unit volume (11) and from the change in densities (12) in the usual way. The standard values, $\phi_Y^\theta = \bar{Y}^\theta$, are then obtained from a least-squares analysis with the general equation

$$[1] \qquad \phi_Y = \bar{Y}^\theta + A_Y m^{1/2} + B_Y m$$

where A_Y is the limiting slope of the Debye–Hückel law and has been given elsewhere (13) for ϕ_V and ϕ_C. About 8 to 12 data points were measured for each system.[3] The parameters $\bar{V}^\theta$, $\bar{C}_p^\theta$, B_V, and B_C are given in Table 1. The expansibilities obtained from the differences $\Delta\bar{V}^\theta/\Delta T$ are given in Table 2. It became apparent that the data for sodium phenyl propanoate were definitely out of line. A new sample was therefore purified and $\bar{V}^\theta$ was remeasured at 25°C. The anomalies with $\bar{V}^\theta$ and $\bar{C}_p^\theta$ then disappeared. The temperature dependence of $\bar{V}^\theta$ was not repeated however, and it will be apparent later on that the derived $\bar{E}^\theta$ are too large for this salt.

[3]Complete set of the actual experimental data is available, at a nominal charge, from the Depository of Unpublished Data, CISTI, National Research Council of Canada, Ottawa, Canada K1A 0S2.

TABLE 2. Standard partial molal expansibilities $\bar{E}^\theta$ (cm^3 K^{-1} mol^{-1}) of sodium phenyl carboxylates in water at 25 and 40°C

Solute	At 25°C	At 40°C
ϕCOONa	0.170	0.122
ϕCH_2COONa	0.180	0.129
$\phi(CH_2)_2COONa$	0.219	0.180
$\phi(CH_3)_3COONa$	0.209	0.163

Discussion

The values of $\bar{C}_p^\theta$, $\bar{V}^\theta$, and $\bar{E}^\theta$ at 25°C are plotted against the number of methylene groups of the homologous sodium phenyl carboxylates in Fig. 1. The $\bar{C}_p^\theta$ of phenylamines and alcohols (9) are also given for comparison. The expected slope from the CH_2 contribution of aliphatic solutes in water, 90 J K^{-1} mol^{-1} (1), 16.0 cm^3 mol^{-1} (4), and 0.023 cm^3 K^{-1} mol^{-1} (7) are also given in Fig. 1. With $\bar{V}^\theta$ the predicted and experimental slopes coincide. Only sodium benzoate falls slightly out of line as with aliphatic carboxylates (6). On the other hand the CH_2 contribution to $\bar{C}_p^\theta$ is not constant and is approaching the expected value only when there are more than 4 carbon atoms in the chain. The alcohols and amines also show a smaller contribution per CH_2 but here the deviation from the expected slope is much smaller. In the case

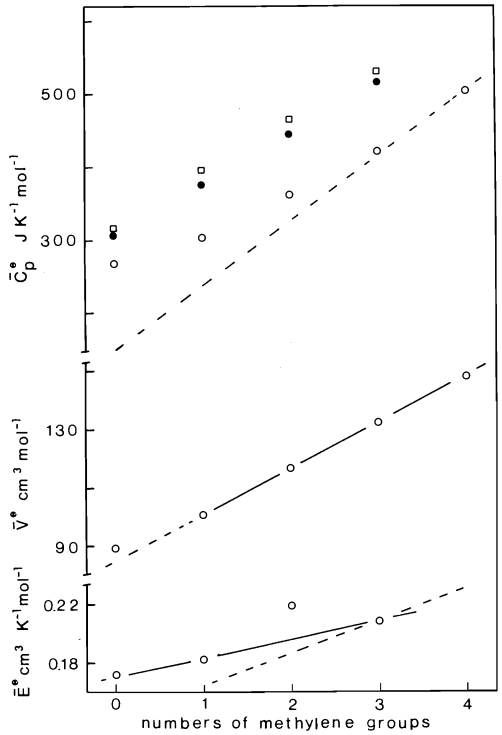

FIG. 1. Dependence of standard partial molal functions of aromatic solutes in water at 25°C on the number of methylene groups: ○, $\phi(CH_2)_nCOONa$; □, $\phi(CH_2)OH$; ●, $\phi(CH_2)_nNH_2$.

of $\bar{E}^\theta$ the carboxylates seem to fall on a straight line if we assume that the value of sodium phenyl propanoate is erroneous (see Results), and this experimental slope is, as with $\bar{C}_p{}^\theta$, significantly lower than the expected one for aliphatic solutes.

The interaction between the two groups increases significantly as the number of CH_2 groups between $NH_2{}^+$ and COO^- decreases. These interactions have a large effect on $\bar{C}_p{}^\theta$ but a smaller one on $\bar{V}^\theta$. By analogy with the amino acids it would seem that there are some interactions between the phenyl group and the ionic or polar end groups. These relatively weak interactions mostly affect second derivative functions, such as $\bar{C}_p{}^\theta$ and $\bar{E}^\theta$, implying that they are very temperature dependent or related to some shift in equilibrium with temperature. The exact nature of these interactions is still unknown.

Acknowledgement

The authors are grateful to the National Research Council of Canada for financial support.

1. N. NICHOLS, R. SKÖLD, C. SPINK, J. SUURKUUSK, and I. WADSÖ. J. Chem. Thermodyn. **8**, 1081 (1976).
2. S. H. YALKOWSKY and G. ZOGRAFI. J. Pharm. Sci. **61**, 793 (1972).
3. C. JOLICOEUR and G. LACROIX. Can. J. Chem. **54**, 624 (1976).
4. H. HØILAND and E. VIKINGSTAD. Acta Chem. Scand. Ser. A, **30**, 182 (1976).
5. S. CABANI, G. CONTI, and L. LEPORI. J. Phys. Chem. **78**, 1030 (1974).
6. M. SAKURAI, T. KOMATSU, and T. NAKAGAWA. Bull. Chem. Soc. Jpn. **48**, 3491 (1975).
7. S. CABANI, G. CONTI, and E. MATTEOLI. J. Solution Chem. **5**, 751 (1976).
8. G. PERRON, J. E. DESNOYERS, and W. A. ADAMS. Scientific report, Environment Canada. In preparation.
9. N. NICHOLS and I. WADSÖ. J. Chem. Thermodyn. **7**, 329 (1975).
10. P. PICKER, P.-A. LEDUC, P. R. PHILIP, and J. E. DESNOYERS. J. Chem. Thermodyn. **3**, 631 (1971).
11. J. E. DESNOYERS, C. DE VISSER, G. PERRON, and P. PICKER. J. Solution Chem. **5**, 605 (1976).
12. P. PICKER, E. TREMBLAY, and C. JOLICOEUR. J. Solution Chem. **3**, 377 (1974).
13. P.-A. LEDUC. J.-L. FORTIER, and J. E. DESNOYERS. J. Phys. Chem. **78**, 1217 (1974).
14. J. E. DESNOYERS, R. PAGE, G. PERRON, J.-L. FORTIER, P.-A. LEDUC, and R. F. PLATFORD. Can. J. Chem. **51**, 2129 (1973).
15. J. C. AHLUWALIA, C. OSTIGUY, G. PERRON, and J. E. DESNOYERS. Can. J. Chem. This issue.

^{13}C and $^{33,34}S$ isotope effects on the vapor pressure of liquid carbon disulfide

GÁBOR JANCSÓ[1] AND W. ALEXANDER VAN HOOK
Chemistry Department, University of Tennessee, Knoxville, TN 37916, U.S.A.
Received February 25, 1977

GÁBOR JANCSÓ and W. ALEXANDER VAN HOOK. Can. J. Chem. **55**, 3371 (1977).

Prompted by the experimental investigation of Betts and Buchannon a thorough analysis of CS_2 vapor pressure isotope effects has been made in the context of the theory of isotope effects in condensed phases and the available spectroscopic information. The agreement between the calculated and experimental results is satisfactory. The calculated results may be empirically described by the equations

$$\ln (P_{^{12}C^{32}S_2}/P_{^{13}C^{32}S_2}) = \frac{-0.529}{T} + 0.00035$$

and

$$\ln (P_{^{12}C^{32}S^{32}S}/P_{^{12}C^{32}S^{34}S}) = \frac{0.185}{T} - 0.00040$$

The analysis indicates that the principal contribution to the ^{13}C isotope effect is due to the shift on condensation of the asymmetric stretching frequency $\Delta\nu_3$, and quantitatively corroborates the theoretical conclusion reached earlier by Akopyan, Girin, and Bakshiev and others of the magnitude of the dielectric correction for this band. The ^{34}S effects are principally determined by the hindered rotation and translation in the liquid and the shift in the symmetric stretching motion $\Delta\nu_1$.

GÁBOR JANCSÓ et W. ALEXANDER VAN HOOK. Can. J. Chem. **55**, 3371 (1977).

A la lumière des résultats expérimentaux obtenus par Betts et Buchannon, on a fait une analyse complète des effets isotopiques de la pression de vapeur du CS_2 en tenant compte de la théorie des effets isotopiques en phase condensées et des informations spectroscopiques disponibles. Les valeurs calculées sont en bon accord avec les résultats expérimentaux. Les résultats calculés peuvent être empiriquement décrits par les équations;

$$\ln (P_{^{12}C^{32}S_2}/P_{^{13}C^{32}S_2}) = \frac{-0.529}{T} + 0.00035$$

et

$$\ln (P_{^{12}C^{32}S^{32}S}/P_{^{12}C^{32}S^{34}S}) = \frac{0.185}{T} - 0.00040$$

L'analyse indique que la contribution principale à l'effet isotopique ^{13}C est due au déplacement sur la condensation de la fréquence assymétrique d'élongation $\Delta\nu_3$ et confirme entièrement la conclusion théorique postulée antérieurement par Akopyan, Girin et Bakshiev puis d'autres, sur l'ampleur de la correction diélectrique de cette bande. Les effets du ^{34}S sont déterminés principalement par la rotation et la translation empêchée dans le liquide et par le déplacement dans le mouvement d'élongation symétrique $\Delta\nu_1$.

[Traduit par le journal]

Introduction

The theory of isotope effects on the properties of condensed phases as formulated in 1961 by Bigeleisen (1) has been successfully applied in the quantitative interpretation of the vapor pressure isotope effect (vpies) of a large number of different molecules. The literature in this field has been critically analyzed by Jancsó and Van Hook (2) who conclude (in agreement with previous authors (1, 3–6)) that the measurement of the vpie is a useful tool for determining the effects of molecular structure and the influence of intermolecular forces on the motions of molecules in condensed phases. The appearance of new data on a simple molecular system is therefore of considerable interest, because in such a case the spectroscopic parameters are often defined to relatively high precision, and the data can be used in a straightforward test of the theory. The recently reported measurements of Betts and Buchannon (7) therefore attracted our interest

[1]Permanent address: Central Research Institute for Physics, Hungarian Academy of Sciences, Budapest.

for this reason, and also because of their claim that the measured $^{13}C/^{12}C$ and $^{34}S/^{32}S$ effects were independent of the temperature over the range -20 to $+60°C$. This was puzzling for theoretical reasons. Earlier workers have also noted the inverse carbon isotope effect in this system but there is no other mention in the literature of sulfur isotope studies or of the temperature dependencies of the effects (2).

Background

The vapor pressure ratio between two isotopic isomers of a given molecule has been related to the reduced partition function ratio of the molecules by Bigeleisen (1). Following Jancsó and Van Hook (2) we write

$$[1]\quad \ln\frac{P'}{P} = \ln\left(\frac{f_c}{f_g}\right) + (RT)^{-1}(P'V' - PV) - (B_0P + \tfrac{1}{2}C_0P^2)' + (B_0P + \tfrac{1}{2}C_0P^2) - (RT)^{-1}\int_V^{V'} P'\,dV$$

The logarithmic vapor pressure ratio, $\ln(P'/P)$ (the prime denotes the lighter isotope), is given by the difference in quantum effects for the condensed and gaseous states (the first term) and correction terms which account for the difference between the Helmholtz and Gibbs free energies for the condensed phase (second term), gas imperfection (term 3), and the difference in the condensed phase molar volumes of the isotopic isomers. We have estimated the correction terms from available data on the virial coefficient (8) and molar volume (9) (neglecting the isotope effects on these parameters) and find them negligible in comparison with the experimental error (7). The reduced partition function ratio is then well approximated by the vapor pressure ratio. Following Stern *et al.* (3) we have elected to make a calculation in the harmonic approximation obtaining for a working equation,

$$[2]\quad \frac{f_c}{f_g} = \prod_{\text{int}}^{3n-5}\left[\frac{(u_i/u_i')_c \exp((u_i' - u_i)_c/2)}{(u_i/u_i')_g \exp((u_i' - u_i)_g/2)}\right] \times \left[\frac{(1-\exp(-u_i')_c)/(1-\exp(-u_i)_c)}{(1-\exp(-u_i')_g)/(1-\exp(-u_i)_g)}\right] \times \prod_{\text{ext}}^{5}\frac{u}{u'}\left[\exp\left(\frac{u'-u}{2}\right)\right]\left[\frac{1-\exp(-u')}{1-\exp(-u)}\right]$$

where $u_i = h\nu_i/kT$. In the derivation of eq. 2 a harmonic cell model has been assumed where the average condensed phase n-atom molecule is assigned $3n$ degrees of freedom. Of these, the $3n-5$ internal modes are treated in a fashion analogous to that used in the gas phase and the remaining hindered translations and rotations are assumed to be subject to harmonic restoring forces. In the calculation of the condensed phase frequencies due account is to be taken of terms which couple the internal and external motions of the molecules. These are often isotope dependent and give rise to interesting effects. In the presentation of eq. 2 we have not written the small correction which accounts for the effect of nonclassical rotation in the gas phase. We have, however, calculated this correction and found it to be negligible within the experimental precision of the results discussed in this paper.

In the next section of the paper, which describes the results of the calculation, our approach will be to present isotope independent force constant matrices which reproduce the spectroscopically observed frequencies in the gas and liquid phases. These will then be employed to calculate frequencies and isotopic frequency shifts in both phases which are then substituted into eq. 2 to obtain the calculated vapor pressure ratios.

It is clear for such a simple molecule as CS_2 the approach outlined above can be refined so that a calculation which takes account of anharmonic corrections in both phases can be made. However, the additional complexity and the marked increase in the number of parameters (as well as the additional labor) is not warranted, either by the precision of the presently available spectroscopic data, or by the precision of the vapor pressure results.

Analysis

A selection of spectroscopic data for the condensed and vapor phases of CS_2 is presented in Table 1. We note that the data are unusually complete and can be used to define effective harmonic gas and liquid force fields in a relatively unequivocal fashion. In the gas phase the recently reported high precision measurements of Smith and Overend (10) are in excellent agreement with the best of the earlier work. They have been used to define the gas phase force field reported in Table 2. In the liquid phase we have selected

TABLE 1. Spectroscopic properties of $^{12}C^{32}S_2$

(*A*) Recent observed and calculated gas phase frequencies (cm^{-1})

	ν_1	Ref.	ν_2	Ref.	ν_3	Ref.
Observed	658.01	10	396.09	10	1535.35	10
	657.98	33	396	35	1535.35	36
	658	34			1535.5	37
					1535	38
Calculated	658.003		396.090		1535.350	

(*B*) Recent observed liquid phase frequencies (cm^{-1})

	ν_1	Ref.	ν_2	Ref.	ν_3	Ref.
Observed	652.8 ir	11	390.6 ir	11	1508.3 ir	11
	655 ir	41	392 ir	35	1510 ir	35
	654 ir	39	390 R	39	1508.5 ir	27
	656 R	40	393 ir	39	1515 R	39
	656.5 R	12			1510 ir	41
	655.7 R	13				
	656 R	14				

(*C*) Observed condensed phase lattice frequencies

Solid	
Translation (ir)	66 (18, 79 K) (ref. 22); 66 (130 K) (ref. 15)
Libration (R)	73, 83 (79 K) (ref. 21); 75, 79, 85 (18 K) (ref. 21); 73, 83, 145 (74 K) (ref. 19); 85–90 (293 K) (ref. 17); 74, 83.8 (74 K) (ref. 20)
Liquid	70 (ref. 15); 70 (ref. 16); 52, 55 (ref. 21); 70 (ref. 17); 71 (ref. 18)

(*D*) Calculated and observed frequency shifts

Frequency	Degeneracy	$(\nu_g - \nu_l)_{obs}$	$(\nu_g - \nu_l)_{calc}$
ν_1	1	5.2	5.2
ν_2	2	5.5	5.5
ν_3	1	27.05[a](10–15)[b]	13.1
ν_{tr}	3	−52	−52
ν_{llbr}	2	−70	−70

[a]Observed.
[b]Corrected for dielectric effect; see text.

the results of Ribnikar and Puzić (11) thereby obtaining the set of experimental internal frequency shifts on condensation reported in the second part of Table 1. The observed shifts in the asymmetric stretching frequency, ν_3, and the bending mode, ν_2, are in general agreement among the different laboratories (Table 1) but Ribnikar's value for ν_1 lies 2 ± 1 cm^{-1} below values reported by other workers. We are inclined, however, to accept his value as it is based on a thorough study of the entire ir spectrum of the liquid, including the assignment of many overtone and combination bands, and a complete anharmonic analysis. In the Raman spectrum the band around 650–660 consists of an overlapped doublet including the fundamental and a satellite assigned to the (11′0), (030) ← (01′0) transition which has tended to complicate the assignment. Some authors (12–14) have reported the shifts on condensation in ν_1 for $^{34}S^{12}C^{32}S$ variously at 2.3, 3.5, and 7.2 cm^{-1} and this also indicates the difficulty of the assignment problem. (For CS_2 the phase frequency shift of this internal mode is much larger than is its isotope dependence, so to first order $\Delta\nu \cong \Delta\nu'$.) We note that the shift calculated from

TABLE 2. Gas and liquid force fields (mdyn/Å) and molecular parameters of CS_2

Gas and liquid force fields for CS_2

Force fields		Gas	Liquid
f_{11}, f_{22}	C–S stretch	7.585717	7.461838
f_{12}	Stretch–stretch	0.569683	0.564927
f_{33}, f_{44}	S–C–S bend	0.233472	0.227045
f_{55}, f_{66}, f_{77}	Translation	0	0.120978
f_{88}, f_{99}	Libration[a]	0	0.445149

The molecular parameters of CS_2

Parameters	Value	Ref.
$r_{C=S}$	1.5529 Å	33
m_{12_C}	12.00000 amu	
m_{13_C}	13.00335 amu	
m_{32_S}	31.97207 amu	42
m_{33_S}	32.97146 amu	
m_{34_S}	33.96786 amu	

[a]mdyn Å.

Ribnikar's assignment, $\Delta\nu = 5.2$ cm^{-1}, is certainly good to ± 2 cm^{-1} (i.e. even if the alternative assignment is accepted), and most probably is good to better than ± 1 cm^{-1}. The other two phase frequency shifts $\Delta\nu_2 = 5.5$ and $\Delta\nu_3 = 27.1$ cm^{-1} we also estimate as good to better than ± 1 cm^{-1}. All shifts are to the red on condensation.

We now turn attention to the hindered external translational and rotational modes. The 70 cm^{-1} frequency observed in the liquid (15–18) has been assigned to the doubly degenerate libration. The 70 cm^{-1} frequency has been observed in the solid phase at liquid nitrogen temperature blue shifted to the region between 73 and 85 cm^{-1} where the librational assignment is much more certain (19–21). The magnitude of the red shift observed on melting and lattice expansion is reasonable. The assignment is further substantiated by the ir high pressure studies of Bradley *et al.* (17) who found that by applying pressure to the liquid at room temperature the 70 cm^{-1} peak shifted to a value of 85–90 cm^{-1} in the solid at 12–13 kbar.

The liquid frequency observed at 52 cm^{-1} (21) near the melting point has been assigned to the triply degenerate hindered translation. Although the authors (21) did not discuss the origin of this band we note that in the solid at 77 K these frequencies are observed at 66 cm^{-1} (15, 22) and have been assigned to the translational modes. By employing the known volume expansion on melting (23) together with a reasonable estimate of the Grüneisen constant using the method of Slater (24) and Mizushima (25) we calculate a liquid frequency of about 45 cm^{-1} (300 K) which is in fair agreement with the observed band at 52 cm^{-1}. We conclude that the assignment is reasonable. In any event the details of the results are not very sensitive to the choice of the translational frequency.

The gas phase frequencies and phase frequency shifts as assigned above have allowed the definition of gas and liquid force fields which are presented in Table 2. The phase frequency shifts as calculated for $^{12}C^{32}S_2$ from these force fields have already been presented at the bottom of Table 1. For the asymmetric stretching motion, ν_3, an important correction must be applied to the spectroscopic data. This is discussed in detail in the material on $^{13}C/^{12}C$ which follows.

The $^{13}C/^{12}C$ Effect

The interpretation of the carbon isotope vpie is considerably simplified by virtue of the symmetry of the molecule. Since the carbon is located at the center of mass there is no isotope shift on the symmetric stretch, ν_1, nor is there any isotope effect on the moments of inertia and the librational frequencies. The observed effect is therefore due to a combination of the triply degenerate translations and the isotope dependencies of the phase frequency shifts in the doubly degenerate bending motion and the single asymmetric stretch. The isotope dependence of the translational and bending modes is small and cannot begin to explain the magnitude of the unusually large inverse vpie for this isomer. The value of the phase frequency shift, $\Delta\nu_3$, required to fit the experimental data at -14.8°C (where the experimental scatter is at its minimum) is 13.09 cm^{-1}. This compares to the experimentally observed shift of 27 cm^{-1} which is independent of temperature (26). However, it is now well established that the observed shift must be corrected for dielectric effects which take account of the difference between the mean field and the effective field of the light wave acting on the molecule in the condensed phase. This point has been discussed in considerable detail by Akopyan *et al.* (27), Lefranc *et al.* (28), and Clifford and Crawford (29). The correction is only important for very intense bands such as the

one under discussion. The value of the corrected shift (i.e. that portion due to the effect of intermolecular forces on the motion) has been variously estimated as 10–15 cm^{-1} (27), 8 cm^{-1} (Onsager correction following ref. 30), and 15 cm^{-1} (Lorentz correction following ref. 30). The value of 13 cm^{-1} obtained from the vpie measurements via the present interpretation is comfortably in the middle of these theoretical estimates. The result is one of useful precision (± 2 cm^{-1} if the error in the vpie at -14°C can be taken as $\pm 1 \times 10^{-4}$ (7) and the uncertainties in the frequency phase shifts are those discussed above). It can be usefully employed to test theories of the spectroscopic corrections to the contours of very intense bands (43).

The $^{34}S/^{32}S$ Effect

The vpie, $R_{34} = P_{^{12}C^{32}S_2}/P_{^{12}C^{32}S^{34}S}$, is now defined in terms of the parameters developed above. The rotational and translational contributions predominate for this isomer and determine the sign of the positive (normal) effect.

Results

The results of the calculation are plotted in Fig. 1 where they are compared with the data points reported by Betts and Buchannon (7). The temperature dependence of the calculated effects is evident and in our opinion the calculations are in satisfactory agreement with the experimental data. The calculated results can be satisfactorily described by the relations $\ln(P_{12}/P_{13}) = -0.529/T + 0.00035$ and $\ln R_{34} = 0.185/T - 0.00040$. These equations are purely empirical and should not be used to extrapolate the results outside the temperature limits of the calculation. We have not reported fits to the more commonly employed approximation, $\ln R = A/T^2 + B/T$ because the frequency distribution of the CS_2 molecule is such that this relation is not a good approximation to the complete eq. 2 in the liquid temperature range. We have also calculated the vpies for other isotopic isomers of CS_2 and find (as expected) that the results are reasonably well described by the law of the geometric mean (certainly well within the precision of the data under discussion). Thus, for example, $(\ln R_{34}/\ln R_{33}) - 2.0 \cong 0.06$.

Discussion

The vpies of the isotopic isomers of CS_2 are

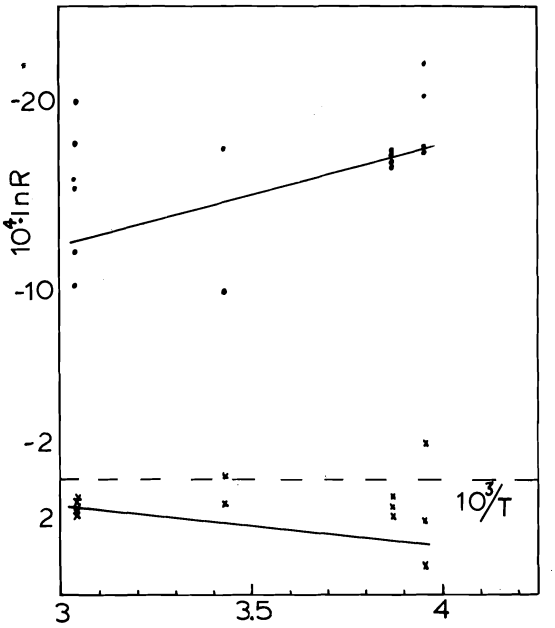

FIG. 1. Vapor pressure isotope effects of CS_2. Upper line $R = (P_{^{12}C^{32}S_2}/P_{^{13}C^{32}S_2})$ (calculated). Lower line $R = (P_{^{12}C^{32}S_2}/P_{^{34}S^{12}C^{32}S})$ (calculated). The data points are from ref. 7.

amenable to interpretation with the theory of isotope effects in condensed phases as applied in the harmonic approximation. Both carbon and sulfur effects show decided temperature dependences in accord with experiment. The large inverse carbon isotope effect is due principally to the red shift in the very intense asymmetric stretching frequency near 1535 cm^{-1}. Its magnitude offers confirmation of the theoretical conclusion that only about half of the observed spectroscopic shift is due to the influence of intermolecular forces on this motion. Our calculated value of the carbon vpie is in good agreement with the earlier estimate of Baertschi and Kuhn (31) of the inverse contribution to this effect, -1.6×10^{-3}, made from other (but related) considerations.

Earlier in a qualitative interpretation Betts and Buchannon (7) leaned heavily on comparisons between the CO_2 and CS_2 systems. Isotope effects in CO_2 have been recently reinterpreted by Bikladi *et al.* (32) using the same kind of approach as that employed here. Most of their attention was focused on vpies in the solid, but the liquid phase effects were also considered. Certainly comparisons between the two mole-

cules are pertinent and interesting but it must be emphasized that important differences between the molecules exist. These markedly influence the choice of parameters and the nature of the results. First, and most importantly, the spectroscopic information on the liquid phase is much more nearly complete for CS_2 than for CO_2. The phase frequency shift of the CO_2, and additionally the intensity change, is also smaller, so dielectric effect corrections are not as important. The ^{13}C vpie is therefore much larger for CS_2 than CO_2. The difference in intensity changes in the ν_3 band has been correlated with the difference in the crystal structure of the two solids (39) and it has been further indicated that the intermolecular forces in the liquid and the 'liquid structure' of the materials are different in kind (38), due to the same effect. The sulfur or oxygen effects are relatively independent of the asymmetric stretching motion and are predominantly determined by the hindered rotation and translational modes. Comparisons between the two materials for these effects are therefore more useful.

Acknowledgements

Partial supports from the U.S. National Science Foundation and the Hungarian Institute of Cultural Relations as part of the cooperative research program between the Central Research Institute for Physics and the University of Tennessee, the NSF Chemical Thermodynamics Program, and the National Institutes of Health are gratefully acknowledged.

1. J. Bigeleisen. J. Chem. Phys. **34**, 1485 (1961).
2. G. Jancsó and W. A. Van Hook. Chem. Rev. **74**, 689 (1974).
3. M. J. Stern, W. A. Van Hook, and M. Wolfsberg. J. Chem. Phys. **39**, 3179 (1963).
4. J. Bigeleisen. J. Chim. Phys. Phys. Chim. Biol. **61**, 87 (1964).
5. J. Bigeleisen, M. J. Stern, and W. A. Van Hook. J. Chem. Phys. **38**, 497 (1963).
6. W. A. Van Hook. J. Chem. Phys. **44**, 234 (1966).
7. R. H. Betts and W. D. Buchannon. Can. J. Chem. **54**, 3007 (1976).
8. J. H. Dymond and E. B. Smith. Virial coefficients of gases. Clarendon Press, Oxford. 1969.
9. Landolt-Bornstein. Tabellen II/1. Springer Verlag, Berlin, Heidelberg, New York. 1971. p. 473.
10. D. F. Smith and J. Overend. J. Chem. Phys. **54**, 3632 (1971).
11. S. V. Ribnikar and O. S. Puzić. Spectrochim. Acta Part A, **29**, 307 (1973).
12. J. A. Creighton and T. J. Sinclair. Spectrochim. Acta Part A, **29**, 817 (1973).
13. H. W. Schrötter. Ber. Bunsenges. Phys. Chem. **64**, 853 (1960).
14. R. Mierzecki and N. I. Rezaev. Bull. Acad. Pol. Sci. Cl. 3, **5**, 643 (1957).
15. G. W. Chantry, H. A. Gebbie, B. Lassier, and G. Wyllie. Nature, **214**, 163 (1967).
16. G. W. F. Pardoe. Trans. Faraday Soc. **66**, 2699 (1970).
17. C. C. Bradley, H. A. Gebbie, A. C. Gilby, V. V. Kechin, and J. H. King. Nature, **211**, 839 (1966).
18. V. S. Starunov. Sov. Phys. Dokl. **8**, 1206 (1964).
19. M. Ito. J. Chem. Phys. **42**, 815 (1965).
20. I. I. Kondilenko, P. A. Korotkov, and G. S. Litvinov. Opt. Spectrosc. **34**, 466 (1973).
21. S. L. Shapiro and H. P. Broida. Phys. Rev. **154**, 129 (1967).
22. A. Anderson, P. J. Grout, J. W. Leech, and T. S. Sun. Chem. Phys. Lett. **21**, 9 (1973).
23. Landolt-Bornstein. Tabellen II/1. Springer Verlag, Berlin, Heidelberg, New York. 1971. p. 723.
24. J. C. Slater. Introduction to chemical physics. McGraw-Hill, New York. 1939.
25. S. Mizushima. J. Phys. Soc. Jpn. **15**, 70 (1960).
26. Yu E. Zabiyakin and N. G. Bakshiev. Opt. Spectrosc. **26**, 38 (1969).
27. S. Kh. Akopyan, O. P. Girin, and N. G. Bakshiev. Opt. Spectrosc. **36**, 185 (1974) and references therein.
28. B. Lefranc, J. Jacob, and J. Vincent-Geisse. Spectrochim. Acta, **22**, 1057 (1966).
29. A. A. Clifford and B. Crawford, Jr. J. Phys. Chem. **70**, 1536 (1966).
30. J. Jacob and J. P. Benaich. J. Chim. Phys. Phys. Chim. Biol. **64**, 1282 (1967).
31. P. Baertschi and W. Kuhn. Proceedings of the international symposium on isotope separation. *Edited by* J. Kistemaker, J. Bigeleisen, and A. O. C. Nier. North Holland Publ. Co., Amsterdam. 1958. p. 65.
32. Z. Bilkadi, N. W. Lee, and J. Bigeleisen. J. Chem. Phys. **68**, 2087 (1975).
33. B. P. Stoicheff. Can. J. Phys. **36**, 218 (1958).
34. I. I. Kondilenko, G. A. Vorobyova, and I. F. Klassen. Opt. Spectrosc. **27**, 225 (1969).
35. W. B. Person and L. C. Hall. Spectrochim. Acta, **20**, 771 (1964).
36. I. David and M. Hallam. Spectrochim. Acta, **23**, 593 (1967).
37. D. Agar, E. K. Plyler, and E. D. Tidwell. J. Res. Natl. Bur. Stand. Sect. A, **66**, 259 (1962).
38. D. B. Cunliffe-Jones. Spectrochim. Acta, Part A, **25**, 779 (1969).
39. J. C. Evans and H. J. Bernstein. Can. J. Chem. **34**, 1127 (1956).
40. A. M. Amorim da Costa, M. A. Norman, and J. H. R. Clarke. Mol. Phys. **29**, 191 (1975).
41. E. K. Plyler and C. J. Humphreys. J. Res. Natl. Bur. Stand. **39**, 59 (1947).
42. R. C. Weast (*Editor*). Handbook of chemistry and physics. 56th ed. The Chemical Rubber Company, Cleveland, OH. 1975.
43. G. Jancsó and W. A. Van Hook. Chem. Phys. Lett. **48**, 481 (1977).

Studies on metal hydroxy compounds. XV. Electrical conductivity measurements on Cd(OH)Cl, Cu(OH)Cl, and PbOHCl

MAHADEVA NATARAJAN AND ETALO A. SECCO[1]

Chemistry Department, St. Francis Xavier University, Antigonish, N.S., Canada B2G 1C0

Received April 28, 1977

MAHADEVA NATARAJAN and ETALO A. SECCO. Can. J. Chem. **55**, 3377 (1977).

The electrical conductivity dependence on temperature measurements for three metal basic chlorides are reported. The conductivity results yield energy values which are interpreted in terms of active solid state processes leading up to, and including, the decomposition step.

MAHADEVA NATARAJAN et ETALO A. SECCO. Can. J. Chem. **55**, 3377 (1977).

On étudie la dépendance de la conductivité électrique sur les mesures de la température pour trois chlorures de métaux basiques. Les résultats obtenus pour la conductivité, nous amène à des valeurs d'énergie qui sont interprétées en termes de processus actifs de l'état solide se rapprochant et incluant l'étape de décomposition.

[Traduit par le journal]

Introduction

Thermal decomposition of a metal hydroxyhalide usually occurs via dehydroxylation (1, 2). The dehydroxylation step was speculated to be effected by (*i*) OH abstraction by a mobile H or (*ii*) H abstraction by a mobile OH (3). Since these species are expected to be electrically charged it was thought that electrical conductivity data on hydroxyhalide compounds might lead to a better understanding of the decomposition reaction.

Electrical conductivity, by its nature, can be more sensitive, than gravimetry, to the elementary or microscopic solid state effects. Therefore, conductivity has the added potential of providing a more detailed preview of the solid state processes leading up to the decomposition step. On the other hand, in the region of active decomposition conductivity data can be less reliable in view of the measurement's susceptibility to composite or masking effects arising from product presence.

This report contains electrical conductivity measurements done on three hydroxychlorides, viz. CuOHCl, CdOHCl, PbOHCl, selected as representative members of hydroxyhalide compounds which undergo first-order, second-order, and diffusion rate decomposition kinetics, respectively. The chloride derivatives were chosen on the probable basis of a constant overall anion conductivity.

[1]To whom correspondence should be addressed.

Experimental

All hydroxyhalides were prepared by the procedures already described (1–3); each compound was identified by its characteristic thermal analysis trace and X-ray diffraction pattern.

Electrical conductivity measurements were done on compressed polycrystalline discs held between Pt plates in a stainless steel conductivity cell (4) using Gr-1608A Impedance bridge; disc measurements were recorded both in ambient air and flowing N_2 (2SCFH). The normal heating rate was 20°C h^{-1} but lower heating rates were maintained as the cell temperature approached the region of active decomposition.

Results and Discussion

Plots of the logarithm of conductivity σ vs. $1/T$ K for CuOHCl, CdOHCl, and PbOHCl are presented in Figs. 1, 2, and 3, respectively. The activation energy values determined from the regional slopes on each plot are tabulated in Table 1; the activation energy E_a for each decomposition reaction obtained from gravimetric kinetic data is also included for comparison. Although the conductivity results obtained in air atmosphere are assumed to be valid, our discussion will be restricted to N_2 atmosphere conductivity results in view of their consistent nature and in the expectation that meaningful comparisons or correlations can be made with the gravimetric kinetic results.

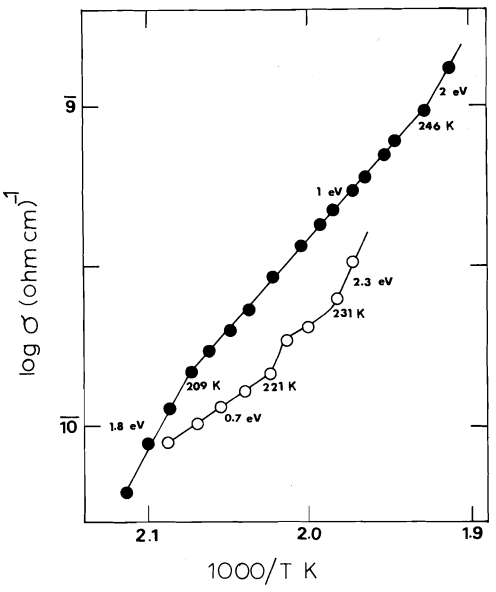

FIG. 1. Logarithm of conductivity, σ, vs. $10^3/T$ K for Cu(OH)Cl in air ○, and in N_2 ●.

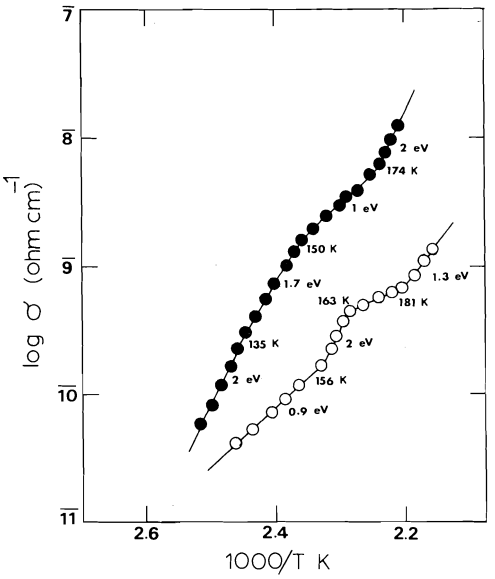

FIG. 3. Logarithm of conductivity, σ, vs. $10^3/T$ K for Pb(OH)Cl in air ○, and in N_2 ●.

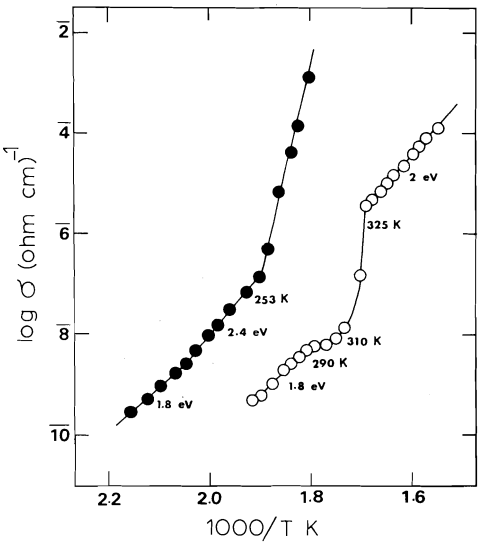

FIG. 2. Logarithm of conductivity, σ, vs. $10^3/T$ K for Cd(OH)Cl in air ○, and in N_2 ●.

The conductivity plots of Table 1 reveal (*i*) $\sigma_{N_2} > \sigma_{air}$; (*ii*) $\sigma_{(CuOHCl)} \approx \sigma_{(CdOHCl)} < \sigma_{(PbOHCl)}$ at ~200°C; (*iii*) common low temperature $E_1 = 43 \pm 2$ kcal; (*iv*) CuOHCl energies pass through minimum to attain E_3 in agreement with its E_a, PbOHCl energies drop to E_3 consistent with its E_a, and E values for CdOHCl jump to E_3 much higher than its E_a.

The common E_1 value is attributed to the migration energy of OH^- species in some form of complexes (5, 6). These complexes are expected to break up at higher temperatures accompanied in the absence of secondary effects, by lower energies as in CuOHCl and PbOHCl. The E_3 values consistent with their E_a values, viz. PbOHCl and CuOHCl, suggest active decomposition whereas E_2 represents the stage prior to the onset of decomposition. The agreement between E_2 for CdOHCl and its E_a suggests decomposition to be active under these conditions and the high E_3 value results from the high conductivity contribution by the product CdO.

The suggested condition of H^+ mobility governing first-order rate kinetics in the decomposition of hydroxyhalides requires σ(CuOHCl) to be much greater than σ(PbOHCl). The conductivity data do not support this condition. The initial fundamental step in a solid state decomposition reaction is most likely a nucleation process. The observed overall rate kinetics and activation energy is eventually determined by the specific boundary condition, if any, imposed on the reaction relative to the nucleation process. The first-order rate can be interpreted in terms of

TABLE 1. Regional energies (kcal) from conductivity vs. temperature data (°C)

Compound	Medium	E_1	E_2	E_3	E_a	Rate
CuOHCl	N_2	42(190–210)	23(210–245)	46(>246)	41.0(230–280)	First order
	Air	16(200–220)	—	53(>231)		
PbOHCl	N_2	46(120–135)	39(135–150)	23(150–175)	20.0(150–200)	Diffusion
	Air	21(125–155)	46(155–165)	30(>180)		
CdOHCl	N_2	42(175–220)	55(215–255)	~110(>255)	54.3(300–350)	Second order
	Air	42(250–310)	~110(310–325)	46(>325)		

a limiting case of the A–E type equation, $-\ln(1-\alpha) = (kt)^n$, with the boundary condition $n = 1$. This condition implies a collapse of the interface between the product and reactant phases leaving isolated blocks of solid with each molecule possessing equal probability for reaction.

In summary, the conductivity measurements provided more details regarding the solid state processes leading up to the decomposition stage and a basis for the interpretation of first-order rate in hydroxyhalide compounds.

Acknowledgment

The authors are indebted to the National Research Council of Canada for financial support of this study.

1. O. K. SRIVASTAVA and E. A. SECCO. Can. J. Chem. **45**, 1375 (1967).
2. P. RAMAMURTHY and E. A. SECCO. Can. J. Chem. **47**, 2185 (1969); **47**, 3915 (1969).
3. P. RAMAMURTHY, E. A. SECCO, and M. BADRI. Can. J. Chem. **48**, 2617 (1970).
4. M. NATARAJAN and E. A. SECCO. Can. J. Chem. **52**, 712 (1974).
5. R. NASANEN. Suom. Kemistil. B, **39**, 105 (1966).
6. T. G. STOEBE. J. Phys. Chem. Solids, **28**, 1375 (1967).

Strong amide–halothane hydrogen-bonding observed by nuclear magnetic resonance

JOHN M. BROWN AND PENNY A. CHALONER
Dyson Perrins Laboratory, South Parks Road, Oxford, England OX1 3QY

Received May 10, 1977

JOHN M. BROWN and PENNY A. CHALONER. Can. J. Chem. **55**, 3380 (1977).

The widely-used halothane anaesthetic $CF_3CHBrCl$ exhibits a proton magnetic resonance signal in CCl_4 solution which is strongly deshielded by addition of *N*-methylpyrrolidone. This is interpreted as a hydrogen-bonding interaction with halothane C—H as donor and carbonyl as acceptor. From the temperature dependence of the halothane C—H proton chemical shift in the presence of varying concentrations of *N*-methylpyrrolidone, thermodynamic parameters $\Delta H_0 = -4.7$ kcal mol^{-1} and $\Delta S_0 = -14$ cal mol^{-1} deg^{-1} were obtained. The carbon magnetic resonance spectrum of the two components in CCl_4 shows deshielding of the carbonyl carbon at higher concentrations of $CF_3CHBrCl$. The halocarbons (1-*H*)undecafluorobicycloheptane and (1-*H*,4-*H*)decafluorobicycloheptane show similar H-bonding behaviour which is comparable with that exhibited by $CHCl_3$.

These results are discussed in relation to their possible relevance to the mechanism of action of halocarbon anaesthetics.

JOHN M. BROWN et PENNY A. CHALONER. Can. J. Chem. **55**, 3380 (1977).

L'halothane anesthésique grandement utilisé $CF_3CHBrCl$ présente un signal dans son spectre rmn, enregistré dans le CCl_4, qui est fortement déblindé par addition de *N*-méthylpyrrolidone. Ceci est expliqué par une interaction hydrogène-lié avec le C—H de l'halothane comme donneur et le carbonyle comme accepteur. A partir de l'effet de la température sur le déplacement chimique du proton C—H en présence de différentes concentrations de *N*-méthylpyrrolidone on obtient les paramètres thermodynamiques suivants: $\Delta H_0 = -4.7$ kcal mol^{-1} et $\Delta S_0 = -14$ cal mol^{-1} deg^{-1}. Le spectre de résonance magnétique nucléaire du carbone des deux composés en solution dans le CCl_4 montre un déblindage du carbone du groupe carbonyle à fortes concentrations en $CF_3CHBrCl$. Les hydrocarbures halogénés (1-*H*) undécafluorobicycloheptane et (1-*H*,4-*H*) décafluorobicycloheptane présentent un comportement similaire H-lié, ce qui est comparable avec celui observé pour le $CHCl_3$.

Ces résultats sont discutés en fonction d'un rapprochement possible avec le mécanisme d'action des hydrocarbures halogénés anesthésiques.

[Traduit par le journal]

Introduction

The mechanism and site of action of inhalant anaesthetics have been the subject of much discussion (1), without evidence of any general agreement. Anaesthetic potency correlates more satisfactorily with lipid solubility than with other physicochemical properties (2) although there is some suggestion that a "polar factor" may also be important (3). Anaesthesia can be reversed by high pressures of inert gases (4) which corroborates the idea that dissolution of the anaesthetic in a lipid membrane, or its interaction with the hydrophobic region of a nerve protein causes a local volume expansion and neurotransmitter inhibition. Attempts to simulate these effects in simple systems have proved equivocal. One group of workers suggest that halothanes at a concentration of 0.16 m*M* or 0.32 m*M* increase the order parameter *S* determined by esr, in palmitoyllauryllecithin vesicles containing ketostearate-derived spin-labels, but cause a decrease at 9.3 m*M* (5). The effect on membrane fluidity in these and related experiments is slight, leading to criticism of the membrane-expansion model. A more specific role may be inferred from the effect of anaesthetic fluoroethers on the crab neuromuscular junction (6) which preferentially block the action of glutamate receptor sites, whereas convulsants of related structure act at γ-aminobutyrate receptors.

In view of the long-standing emphasis on the solubility characteristics of inhalant anaesthetics, and a chemically non-specific mechanism of

interaction, some recent findings are of particular interest. The effect of $CF_3CHBrCl$ on the nmr spectrum of haemoglobin has been studied in detail, and the major perturbation involves a small number of histidine H-2 resonances on residues remote from the site of oxygenation, together with (unassigned) hydrophobic resonances (7). Sandorfy (8) has shown that a variety of halocarbons, both fluorocarbon anaesthetics and others, perturb intermolecular hydrogen-bonding in amides, phenols, and amines. The dominant role is assigned to donor-acceptor complex formation between the halocarbon and addend, there being a correlation between hydrogen-bond breaking potency as observed by infrared spectroscopy and the lowest lone-pair ionisation potential of the halocarbon. Whilst this must be important in several cases (e.g., CF_3I, CF_2BrCF_2I) it seemed to us that many others might be better explained by competitive hydrogen-bonding by the C—H bond of the halocarbon. More recent infrared studies by Sandorfy (9) support this idea, and in the present paper we demonstrate the existence of strong hydrogen-bonds between $CF_3CHBrCl$ and *N*-methylpyrrolidone by nmr spectroscopy.

Experimental

Chloroform was purified before use by passage through a short column of Laporte type 'H' chromatographic alumina, and carbon tetrachloride was freshly distilled. Trifluorochlorobromomethane was a gift from the Department of Pharmacology, Oxford University and fluorobicycloheptanes were donated by Dr. R. Stephens of Birmingham University. The purity of all samples was checked by nmr.

^1H nmr spectra were obtained on a Perkin-Elmer R32 spectrometer equipped with variable temperature accessory which was calibrated with a standard methanol sample. Solutions were prepared by addition of aliquots of neat acceptor to standard solutions of donor in carbon tetrachloride. Frequencies are recorded in ppm downfield from an internal tetramethylsilane lock. The shift parameter (Δ) and binding constants K for a given system were calculated by the iterative procedure of Higuchi (10) using a Hewlett-Packard 91 desk calculator. Carbon magnetic resonance spectra were recorded on a Bruker WH-90 instrument with a D_2O external lock. Frequencies are recorded in ppm downfield from tetramethylsilane.

Results and Discussion

1,1,1-Trifluorobromochloroethane/N-methylpyrrolidone

The ^1H nmr spectrum of **1** in carbon tetrachloride shows a quartet, $J_{H-F} = 5.2$ Hz, at 5.75 ppm. The position is slightly temperature dependent, there being a shift to lower field of 0.03 ppm between 35 and −20°C. Addition of portions of **2** to standard solutions of **1** produces a substantial downfield shift, and Fig. 1 shows a series of runs at different concentrations of **2** and various temperatures between 35 and −20°C. Under these conditions complex formation is incomplete, and an iterative procedure was employed to derive Δ, defined as the chemical shift difference between **1** and the 1:1 association complex, and the complexation equilibrium constant K. The thermodynamics of complexation were derived from a standard Arrhenius plot incorporating data from runs at five different temperatures (Fig. 2).

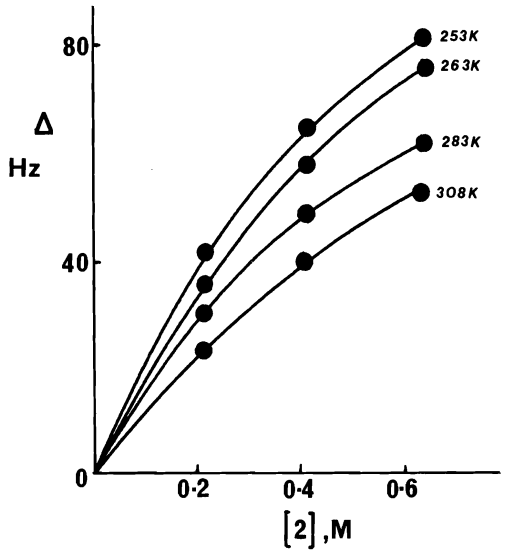

FIG. 1. Chemical shift changes induced by addition of **2** to solutions of **1** (0.38 *M* in CCl_4).

The ^{13}C nmr spectrum of **2** (1.1 *M* in CCl_4) has absorbances at 178.9 (*C*=O), 54.9 (CH_2—N), 36.1 (CH_2—CO), 35.3 (CH_3—N), and 23.9 (CH_2—CH_2—CH_2) ppm. Addition of portions of **1** to the solution causes downfield shifts of the carbonyl carbon resonance of up to 1 ppm at 2 *M* addend, without affecting other resonances by more than 0.15 ppm (Fig. 3). The C-1 carbon of **1** (127.0 ppm, $J_{C-F} = 278$ Hz) is slightly deshielded in mixed solutions but the C-2 carbon (55.8 ppm, $J_{C-F} = 41$ Hz) is more substantially affected.

Taken together, this evidence strongly suggests that hydrogen-bonding is the major interaction leading to complexation. The data may

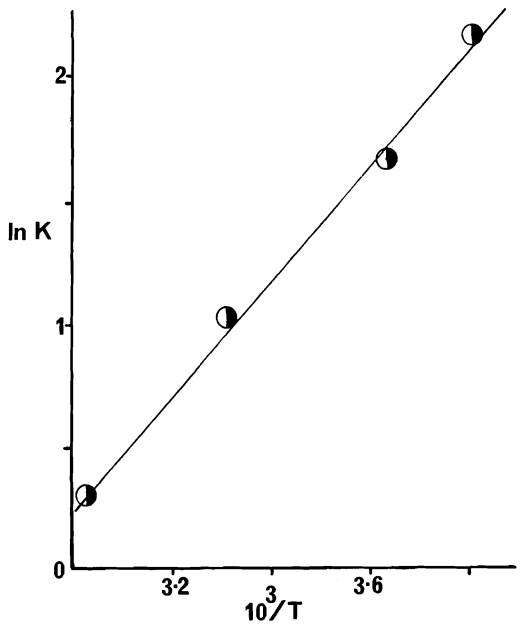

FIG. 2. Arrhenius plot and least-squares line correlating complexation data for mixtures of **1** and **2** in CCl_4.

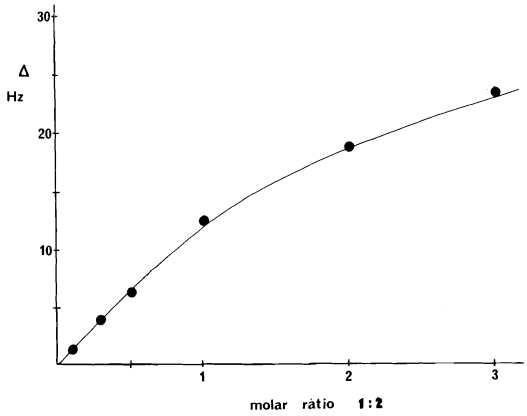

FIG. 3. Concentration dependence of the ^{13}C nmr carbonyl chemical shift of **2** in mixtures of **1** and **2** in CCl_4.

be compared with more extensive studies on hydrogen-bonding by chloroform to a variety of carbonyl compounds (11). For example, recent work on mixtures of chloroform and **2** (12), studied by ^1H nmr in cyclohexane, gave $\Delta H_0 = -3.99$ kcal mol^{-1} and $\Delta S_0 = -10.9$ cal mol^{-1} deg^{-1}, which may be compared with our values for **1** and **2** of $\Delta H_0 = -4.7$ kcal mol^{-1} and $\Delta S_0 = -14$ cal mol^{-1} deg^{-1}. Miller found the limiting chemical shift for complexation of chloroform and **2**, Δ, to be 84 Hz at 28°C as compared with our value of Δ = 132 Hz for **1** and **2** in CCl_4 at 35°C. Insofar as this parameter reflects changes in charge-density at the hydrogen-bonding proton, it provides a measure of the tightness of the hydrogen-bond.

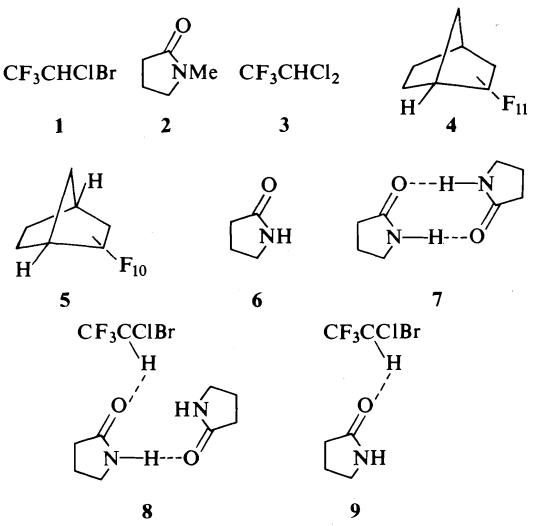

These results demonstrate that halothane **1** hydrogen-bonds strongly to a typical model tertiary amide. It would clearly be useful to correlate the hydrogen-bonding ability of this and other halothane anaesthetics with some readily measurable molecular property. Allen (13*a*), in a recent theoretical study of hydrogen-bonding, found that donor reactivity correlated well with the C—H bond dipole moment μ_{A-H}.[1] This is, however, difficult to evaluate in unsymmetrical organic molecules. Nevertheless, the electrostatic properties it represents may be reflected in the acidity of that C—H bond provided that the carbanion is charge-localized and of similar geometry to the hydrocarbon. It is particularly interesting that the pK_a's of **1**, **3**, and chloroform in cyclohexylamine (14) are 24.0, 24.4, and 24.4, respectively, that pentafluorobenzene, which has significant anaesthetic properties (15), has a pK_a of 24.2, and that **4** and **5** are extremely powerful anaesthetics (16), and have pK_a's of 20.5 and 22.3. Less acidic fluorocarbons (CF_3H, pK_a, 30.5; CF_3CF_2H, pK_a 28.2) are much less potent anaesthetics than **1** (1).

[1]Compare more recent theoretical studies of hydrogen-bonding (13*b*,*c*).

1,1,1-Trifluorobromochloromethane/pyrrolidone

It was of interest to determine whether hydrogen-bonding of **1** to a secondary amide might compete with inter-amide association (17) in CCl_4 solution. ^1H nmr measurements were carried out with mixtures of **1** and **6** as before, and the data treated to give $\Delta H_0 = -2.2$ kcal mol^{-1} and $\Delta S_0 = -6.5$ cal deg^{-1} mol^{-1} for hydrogen-bonding association. This may be compared with literature values (17) of $\Delta H_0 = -6.73$ kcal mol^{-1} and $\Delta S_0 = -13.1$ cal mol^{-1} deg^{-1} for self-association of **6**.

Amide dimers in solution may have a doubly hydrogen-bonding structure **7** (17), and our data do not distinguish between structures **8** and **9** for the halothane complex. They do, however, demonstrate that the hydrogen-bond between **1** and **6** is qualitatively similar in strength to a single inter-amide hydrogen-bond, one of the strongest known between organic molecules.

Fluorobicycloheptanes/N-Methylpyrrolidone

The polyfluorinated bicyclic compounds **4** and **5** are both highly acidic (14) and potent anaesthetics (16) and it was of interest to determine their C—H donor properties. Unlike **1** the chemical shift of the C—H in **4** is strongly temperature dependent, implying considerable self-association. Quantitative temperature dependence studies were therefore not attempted, but we have established that considerable deshielding of the C—H resonance in **4**, which is a complex multiplet centred at 3.50 ppm (0.26 *M*, CCl_4) occurs on addition of portions of **2**. The complexation chemical shift, Δ, is 122 Hz and $K = 1.9\ M^{-1}$ at 35°C. Similar results were obtained with **5**, showing that both of these fluorocarbons are capable of forming strong hydrogen bonds to amides.

Overall, these results suggest that halothane anaesthetics such as **1** may operate in vivo by a mechanism involving hydrogen-bonding, which may augment the more generally accepted role of lipid solubility (1).

Acknowledgments

We thank I.B.M. for a Fellowship (to P.A.C.), Dr. R. Stephens for samples of **4** and **5**, and Professor C. Sandorfy for communicating his later results to us, and for an exchange of manuscripts.

1. B. R. Fink (*Editor*). Cellular biology and toxicity of anaesthetics. Williams and Wilkins, Baltimore. 1972; J. C. Miller and K. W. Miller. MTP international review of biochemistry, **12** Ser. **1**, 33 (1975); E. R. Larsen. Fluorine Chem. Rev. **3**, 1 (1969); A. Spinks. Chem. Ind. (London), 475 (1977) and references therein.
2. T. Di Paolo, L. B. Kier, and L. H. Hall. Mol. Pharmacol. **13**, 131 (1977).
3. C. Hansch, A. Vittoria, C. Silipo, and P. Y. C. Jow. J. Med. Chem. **18**, 546 (1975).
4. K. W. Miller, W. D. M. Paton, R. A. Smith, and E. B. Smith. Mol. Pharmacol. **9**, 131 (1973).
5. P. H. Rosenberg, H. Eibl, and A. Stier. Mol. Pharmacol. **11**, 879 (1975); J. M. Boggs, T. Yoong, and J. C. Hsia. Mol. Pharmacol. **12**, 127 (1976).
6. J. Richter, E. M. Landau, and S. Cohen. Nature, **266**, 70 (1977).
7. F. F. Brown, M. J. Halsey, and R. E. Richards. Proc. R. Soc. London, Ser. B, **193**, 387 (1976).
8. T. Di Paolo and C. Sandorfy. J. Med. Chem. **17**, 807 (1974).
9. R. Massuda and C. Sandorfy. Can. J. Chem. **55**, 3211 (1977).
10. M. Nakano, N. I. Nakano, and J. Higuchi. J. Phys. Chem. **71**, 3954 (1967).
11. R. D. Green. Hydrogen-bonding by C—H groups. Macmillan, London. 1974.
12. G. R. Wiley and S. I. Miller. J. Am. Chem. Soc. **94**, 3287 (1972).
13. (*a*) L. C. Allen. J. Am. Chem. Soc. **97**, 6921 (1975); (*b*) H. Umeyama and K. Morukama. J. Am. Chem. Soc. **99**, 1316 (1977); (*c*) H. Umeyama, K. Morukama, and S. Yamabe. J. Am. Chem. Soc. **99**, 330 (1977).
14. A. Streitwieser, D. Holtz, G. R. Ziegler, J. O. Stoffer, M. L. Brokow, and F. Guibe. J. Am. Chem. Soc. **98**, 5229 (1976).
15. T. H. S. Burns, J. M. Hall, A. Bracken, and G. Gouldstone. Anaesthesia, **19**, 167 (1964).
16. P. J. N. Brown, R. Stephens, J. C. Tatlow, and J. R. Taylor. J. Chem. Soc. Perkin Trans I, 937 (1972) and references therein.
17. K. Wagner, G. Rudakoff, and P. Frolich. Z. Chem. **15**, 272 (1975); R. F. W. Hopmann. J. Phys. Chem. **78**, 2341 (1974); G. Montando, S. Caccamese, and A. Recca. J. Phys. Chem. **79**, 1554 (1975) and reference therein.

An electron impact study of the two isomeric tricarbonylchromium complexes of *N*-benzylideneaniline

EBERHARD W. NEUSE

Abteilung für Organische Chemie der Universität Ulm, D-7900 Ulm, Federal Republic of Germany[1]

Received January 4, 1977

EBERHARD W. NEUSE. Can. J. Chem. **55**, 3384 (1977).

Under electron impact, the two isomers resulting from tricarbonylchromium complexation of *N*-benzylideneaniline decarbonylate completely before the chromium-ring bond is broken and the azomethine ligand undergoes further fragmentation. The loss of two CO molecules is favored over the competitive process involving elimination of a single CO molecule, especially at high ionizing voltage. In both cases the highly stable benzylideneanilinechromium cations decompose primarily through fission of the metal-ring bond, although additional fragmentation pathways of minor importance are also observed. The decay patterns of the benzylideneaniline ligand cation are identical in the spectra of both complexes and very nearly coincide with that shown by benzylideneaniline itself under the same conditions of electron impact.

EBERHARD W. NEUSE. Can. J. Chem. **55**, 3384 (1977).

Sous impact électronique, les deux isomères provenant de la complexation du tricarbonylchrome avec le *N*-benzylidèneaniline se décarbonylent complètement avant que le lien chrome-cycle soit brisé et le ligand azométhine subisse des fragmentations subséquentes. La perte de deux molécules de CO est favorisée par rapport au processus compétitif impliquant l'élimination d'une seule molécule de CO spécialement à des hauts voltages d'ionisation. Dans chaque cas, les cations benzylidèneanilinechromes très stables se décomposent en premier lieu par la fission du lien métal-cycle, quoique des chemins additionnels de fragmentation d'importances mineures ont aussi pu être observés. Les patrons de décomposition du cation ligand-benzylidèneaniline sont identiques dans chacun des spectres des deux complexes et coincident presque complètement avec celui présenté par le benzylidèneaniline lui-même dans les mêmes conditions d'impact électronique.

[Traduit par le journal]

Introduction

The synthesis of mono- and bis(π-tricarbonylchromium) complexes of *N*-benzylideneaniline was first reported by Mostardini *et al.* (1), and their spectroscopic behavior was investigated more recently (2). In the following, we examine the fragmentation under electron impact of the two isomeric mono-complexes, (1,2,3,4,5,6-hexahapto-benzylideneaniline)tricarbonylchromium, **1**, and (1′,2′,3′,4′,5′,6′-hexahapto-benzylideneaniline)tricarbonylchromium, **2**.

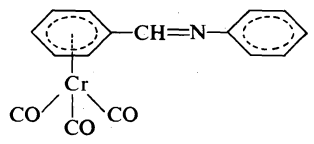

1

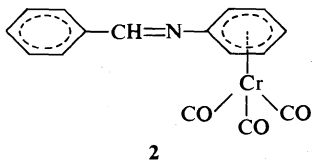

2

Results and Discussion

(1,2,3,4,5,6-η⁶-Benzylideneaniline)tricarbonylchromium (1)

The mass spectral fragmentation characteristics of arenetricarbonylchromium complexes (3) depend primarily on the relative strength of the bonds between the chromium atom and the various ligands, as well as on the type and inherent stability of the arene ligand involved. Two factors deserve attention here: (*i*) fission of the Cr—CO bonds entails the elimination of carbon monoxide molecules as uncharged, stable entities, and (*ii*) the metal-to-

[1]Permanent address: Department of Chemistry, University of the Witwatersrand, Johannesburg, Republic of South Africa.

carbonyl backdonation as a contributor to Cr—CO bonding, brought about by the pronounced π^* acceptor properties of carbon monoxide, is appreciably reduced on ionization, because the electron removed, stemming from a high-energy chromium *d* orbital with predominant metal character (4), leaves a cation characterized by an effectively lowered metal *d* electron population involved in the backbonding.[2] Both factors combine to cause Cr—CO dissociation energies in the various metal carbonyl ions to be lower than the Cr–arene dissociation energy and thus generally render carbon monoxide elimination a facile and preferred process. We find this trend confirmed in the 70 eV mass spectrum of complex **1**: initial degradation proceeds through carbon monoxide loss, and no other parent ion fragmentation steps, such as C_{ring}—C, C_{ring}—N, or C═N fission, are indicated in the spectrum. As a result, both the parent ion, $P^{+\cdot}$ (*m/e* 317), and the carbonyl-containing fragment ions are less abundant than the carbonyl-free *m/e* 233, the benzylideneanilinechromium cation.

The successive removal of CO ligands from metalpolycarbonyl ions entails a concomitant increase in the dissociation energies of the remaining M—CO bonds in the product ions (3, 8). In the fragmentation of **1**, simple stability arguments should, therefore, predict an increase in peak intensity as one follows the cascade sequence $P^{+\cdot}$(*m/e* 317) → $[P - CO]^{+\cdot}$(*m/e* 289) → $[P - 2CO]^{+\cdot}$(*m/e* 261) → $[P - 3CO]^{+\cdot}$(*m/e* 233). At low ionizing voltages this is seemingly the case, relative intensities at 15 eV increasing in the order 18 (*m/e* 317), 20 (*m/e* 289), 58 (*m/e* 261), 100 (*m/e* 233). At 70 eV, however, a different pattern obtains; while the order of increasing yields still holds for the ions *m/e* 317, 261, and 233 (and, similarly so, for their doubly charged counterparts), the peak at *m/e* 289 is drastically attenuated (*m/e* 289 to *m/e* 261 abundance ratio, 0.14). This suggests that, at the higher ionizing voltage, the parent ion prefers to convert directly to *m/e* 261 through the expulsion of two CO molecules, either concertedly or in a fast consecutive two-step process, and indeed we find the process *m/e* 317 → *m/e* 261 + 2CO unambiguously confirmed as a metastable transition. Although this process requires a higher activation energy than does the reaction *m/e* 317 → *m/e* 289 + CO (otherwise, the *m/e* 289 to *m/e* 261 ratio should decrease, rather than increase as the ionizing voltage is lowered to the more selective 15 eV level), it must proceed with a higher frequency factor in order to account for its absolute predominance at both voltage limits. Within the framework of quasi-equilibrium theory (9–11), the relationship between the unimolecular rate constant of decomposition, $k(E)$, and the total internal energy, E, imparted to the ion by the applied ionizing voltage can be expressed in simplified form by eq. 1, in which ν represents a frequency factor, E_0 is

$$k(E) = \nu((E - E_0)/E)^{s-1} \qquad [1]$$

the energy of activation of the decay process, and *s* indicates the effective number of weakly coupled harmonic oscillators (i.e. vibrational modes) operating in the molecule.[3] The relationship has been used extensively, notably by Williams (11, 15) and Shapiro (16, 17) with their collaborators, in the analysis of concurrent decomposition mechanisms under electron impact. With the aid of eq. 1, the trend of rate constants in two competitive parent ion decompositions can be depicted schematically (ref. 14, Chapt. 8, 18–20) by diagrams of the type shown in Fig. 1, in which log $k(E)$ is plotted against E

[2]While it is recognized (5, 6) that ionization will generally lead to immediate electronic reorganization, which is unaffected by the site of the original electron removal, the resultant charge distribution in the product cation must be consistent with the tendency for the lower-lying electronic states to be more highly populated at a given internal energy (in comparison with higher-lying states) because of the greater number of vibrational quanta present and concomitantly greater vibrational degeneracy (7). The increased population and enhanced vibrational energy of the lower-lying electronic states both combine to render further fragmentation more probable from these lower states than from the higher-lying ones. The lower-lying states, however, are precisely those characterized by reduced occupancy of the high-energy antibonding π^* orbitals of the Cr—CO bond system. Abandoning the concept (now somewhat outdated (6)) of charge localization and concomitant selective bond fission does, therefore, not invalidate the argument presented.

[3]For large molecules, the number of oscillators is given by $3n - 6$ (n = number of atoms). The effective number of modes is usually taken as one-half to one-third (one-fifth near threshold) of that value (11, 12). The more rigorous Rice–Ramsperger–Kassel–Marcus formulation (13) employs an exact enumeration of states and is, therefore, sometimes preferred (ref. 14, Chapt. 8) over the simple quasi-equilibrium theory formulation of eq. 1 and modified forms. Qualitatively, however, both theories lead to the same conclusions presented in the text.

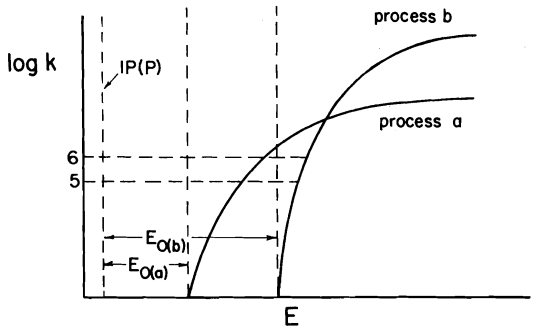

FIG. 1. Log k vs. E curves (schematic) for two competitive, unimolecular parent-ion degradation reactions.

for both reactions. In such systems of competing decay steps, in which ΔE_0, the difference in activation energy between the two reactions, determines their relative rates at low E, while $\Delta\nu$ becomes the controlling factor at high E (16), process b (high ν, E_0) passes through a relatively loose activated complex (ref. 14, Chapt. 8, 18) and so generally represents a direct bond cleavage. Process a (low ν, E_0), on the other hand, passing through a tighter (and perhaps anchimerically assisted) transition state, tends to involve a rearrangement (ref. 14, Chapt. 8, 16–19). The observed energy dependence of the reactions m/e 317 → m/e 289 and m/e 317 → m/e 261 suggests these two processes to be congruent with the depicted model, the former reaction being represented by a, and the latter by b. (Appearance potential measurements for the two daughter ions, not feasible with our present spectrometer set-up, will be necessary to confirm the implicit assumptions.) It appears, therefore, that the loss of two carbon monoxide molecules proceeds by direct breaking of Cr—CO bonds, whereas the competing expulsion of a single monoxide molecule proceeds through a transition state with a reduced number of active rotational modes as exemplified in a structure comprising pentacovalent chromium through coordinate bonding interaction with the C=N system. This question requires further study.

The benzylideneanilinechromium cation, m/e 233, is the most stable intermediate in the overall decay pattern of **1** and so, if one excepts $Cr^{+\cdot}$ as the highly abundant terminal fragmentation product ion, represents the base peak in the m/e 50–317 range, reflecting the higher arene–chromium bond dissociation energy (2.4 eV in benzenechromium cation (21)) relative to the various M—CO dissociation energies associated with the preceding CO expulsion steps (1.2–2.0 eV in benzenetricarbonylchromium decarbonylation (21)). The subsequent decay processes are straightforward. Arene–chromium bond fission, as the principal path, leads to chromium cation and probably also (albeit not associated with a detectable m^*) to benzylideneaniline cation.[4] Loss of chromium hydride, supported by the increased intensity ratio of m/e 180 to m/e 181 (1.03) in the spectrum of **1** relative to that of benzylideneaniline (0.88), and elimination of benzene (subsequent to a hydrogen migration) with generation of m/e 155 both represent low-abundance steps. The benzene elimination path is paralleled by the even less significant transition m/e 233 → m/e 78 involving loss of benzonitrile-chromium,[5] the benzene ion peak intensity being only moderately enhanced relative to the corresponding peak in the benzylideneaniline spectrum (measured against m/e 181 in both cases). Further fragmentations of m/e 155 give rise to $Cr^{+\cdot}$ and to $CrCN^+$, in the latter case through rearrangement and ejection of phenyl free radical (allowed by the even-electron rule). The transition m/e 155 → m/e 77, the species eliminated being neutral CrCN,[6] is suggested by the observation of a metastable peak, whose abundance, however, is too low to permit an unambiguous assignment. Should this latter reaction indeed occur, it would represent the only observed

[4]We are grateful to one of the referees for suggesting the possibility of benzylideneaniline cation formation through loss of neutral $Cr(CO)_n$ from $RCr(CO)_n^{+\cdot}$ (R = benzylideneaniline). In view of the prominence of m/e 181, this proposal appears quite valid, although we were unable to find corroboration by metastable peaks.

[5]Although the m^* associated with m/e 233 → m/e 78 also holds for m/e 317 → m/e 91 (C=N fission), we neglect this latter transition on energetic grounds; indeed, we were unable to detect metastable peaks for the corresponding C=N fission steps in m/e 289, 261, or 233, all of which should be energetically more amenable to such fission than the parent ion, and even in the uncomplexed benzylideneaniline the incidence of azomethine double bond fission is remarkably low (22).

[6]There is precedence in the literature for the generation of ions of the type CrX^+ by the reaction: $CrC_6H_5X^{+\cdot} \rightarrow CrX^+ + C_6H_5\cdot$, provided only that X represents a substituent of higher electronegativity (21). The analogous process in which the positive charge remains with the ring ligand, whereas a neutral species CrX departs, is feasible in cases where the resultant organic cation exhibits high stability (23).

metastable transition originating from Cr-containing fragment ions that would contribute directly to the phenyl cation[7] peak; the latter, only moderately intensified relative to its *m/e* 77 counterpart in the benzylideneaniline spectrum, appears to derive most of its intensity from fragmentations of the azomethine cation, although a minor additional contribution from *m/e* 233 decomposition by a rapid (and therefore not necessarily metastable) direct bond cleavage cannot be discounted.

The phenylchromium cation, manifested by a peak of low abundance at *m/e* 129, is probably (no *m**) formed in part by C_{ring}—C bond cleavage in *m/e* 233. Yet the principal mode of formation, substantiated by a relative ion yield increase with rising source pressure, involves phenyl radical capture by $Cr^{+}\cdot$. The phenylchromium ion decays through fission of the C—Cr bond and so contributes to the ion yield of *m/e* 52. The spectrum shows a peak of low intensity at *m/e* 80, identified as $[CrCO]^{+}\cdot$ by an accurate mass number determination. The peak's observed intensity increase at higher source pressure or inlet temperature suggests $[CrCO]^{+}\cdot$ formation to be due to an ion–molecule reaction involving CO capture by $Cr^{+}\cdot$.

In addition to the fragment ion peaks discussed in the foregoing, which are derived from chromium-containing species, the spectrum in the lower mass-number range extending up to *m/e* 181 shows the typical fragmentation pattern of benzylideneaniline (22, 25) as verified by comparison with the mass spectrum of this compound recorded separately under identical conditions. Additionally, the characteristic $[C_4H_3]^{+}$ peak at *m/e* 51 (through expulsion of acetylene from phenyl cation) should be mentioned, as should the low-intensity peaks at *m/e* 63, 64, 78, and 89. The ion of *m/e* 63 most probably is a fragment of *m/e* 77 (expulsion of methylene); a contribution may reasonably be ascribed to $[C_7H_5]^{+} \rightarrow [C_5H_3]^{+} + HC{\equiv}CH$. Loss of HCN from the ion of *m/e* 91 (identified as $[C_6H_5N]^{+}\cdot$ by accurate mass number determination) accounts for *m/e* 64. The benzene cation peak, *m/e* 78, derives most of its intensity from the fragmentation *m/e* 181 → *m/e* 78 + 103. (The minor transition *m/e* 233 → *m/e* 78 was mentioned above.)

[7]Both $[C_6H_5]^{+}$ and $[C_6H_6]^{+}\cdot$, although for convenience designated here as phenyl and benzene cations, respectively, may well possess non-cyclic isomer structures (24).

We expected a contribution from the reaction *m/e* 77 + H· → *m/e* 78; however, the injection of D_2O into the ionization chamber failed to produce a significant peak at *m/e* 79, suggesting hydrogen capture by the phenyl cation to be a negligible process. The benzene cation undergoes further breakdown in a straightforward manner through elimination of acetylene. No reasonable mode of formation of the ion of *m/e* 89 is apparent from the spectrum. Although the ion could result from *m/e* 181 by a hydrogen migration, followed by azomethine bond cleavage, the involved rearrangement should provide kinetic conditions conducive to the appearance of a metastable peak; this, however, was not observed.

In the previous papers (22, 25) the generation of *m/e* 77 in the fragmentation of benzylideneaniline was accounted for in terms of loss of $C_7H_6N\cdot$ from *m/e* 181 (*m** reported at *m/e* 32.8). However, we find the metastable peak more accurately at *m/e* 32.9, reflecting the transition *m/e* 180 → *m/e* 77, and this step in fact appears more plausible than *m/e* 181 → *m/e* 77 on energetic grounds. The species expelled from *m/e* 180 represents a stable molecular entity (benzonitrile), which on account of its high IP shows little tendency to accept the positive charge. In contrast, the species $C_7H_6N\cdot$ that would be ejected in the corresponding fragmentation of *m/e* 181 represents a free radical of low stability; hence, the preferred path originating from *m/e* 181 clearly comprises the formation of the highly stabilized even-electron cation $[C_7H_6N]^{+}$ (*m/e* 104) as indeed observed, and the elimination of the $C_7H_6N\cdot$ free radical is likely to constitute at best a competitive process of very low abundance.

(1′,2′,3′,4′,5′,6′-η⁶-Benzylideneaniline)tricarbonylchromium (2)

The mass spectrum of **2**, as would be expected, closely resembles that of isomer **1**, showing the *m/e* 317 parent ion and fragmentation peaks at all the positions cited in the foregoing section. The peaks and their relative abundances are juxtaposed in Table 1 to their counterparts derived from **1**, and the overall fragmentation patterns proposed for both compounds are depicted in Fig. 2. Table 2 lists the metastable transitions observed; it is seen that, with few exceptions, the respective *m** signals appear at virtually identical positions. On comparison of

TABLE 1. Significant peaks in the mass spectra of complexes **1** and **2**[a]

m/e	Ion	Relative intensity[b] Complex **1**	Complex **2**
317	$P^{+\cdot}$	9.6	16.6
289	$[P - CO]^{+\cdot}$	2.8	—
261	$[P - 2CO]^{+\cdot}$	19.8	15.7
233	$[P - 3CO]^{+\cdot}$	100.0	100.0
181	$[C_6H_5—CH=N—C_6H_5]^{+\cdot}$	26.8	32.6
180	$C_6H_5—C\equiv\overset{+}{N}—C_6H_5$	27.7	34.2
155	$[C_7H_5NCr]^{+\cdot}$	3.3	3.0
152	$[C_6H_4C_6H_4]^{+\cdot}$	2.3	4.1
145[d]	$[C_6H_7NCr]^{+\cdot}$	—	<1–2[e]
129	$[C_6H_5Cr]^{+}$	3.3[c]	3.4
104	$[C_7H_6N]^{+}$	6.3	6.8
93[d]	$[C_6H_7N]^{+\cdot}$	<1–3[e]	<1–2[e]
91	$[C_6H_5N]^{+\cdot}$	5.6	4.2
90	$[C_7H_6]^{+\cdot}$	2.1	2.5
89	$[C_7H_5]^{+}$	3.5	3.5
80	$[CrCO]^{+\cdot}$	5.4[f]	4.0
78	$[C_6H_6]^{+\cdot}$[g]	8.1	8.9
77	$[C_6H_5]^{+}$	39.7	41.8
64	$[C_5H_4]^{+\cdot}$	2.0	2.1
63	$[C_5H_3]^{+}$	2.9	3.5
52	$Cr^{+\cdot}$[h]	125	112
51	$[C_4H_3]^{+}$	16.3	17.2

[a]Within range *m/e* 50–317.
[b]Average of 24 scans, normalized for *m/e* 233 = 100.0. Peaks with abundances <2.0% neglected.
[c]Increases to 4.8 at 5×10^{-5} Torr.
[d]Suspected contamination.
[e]Maximum range.
[f]Increases to 7.9 at 5×10^{-5} Torr.
[g]Contains contribution by $CrCN^{+}$.
[h]Contains contribution by $[C_4H_4]^{+\cdot}$.

the spectra of **1** and **2**, several features deserve comment as detailed.

(*1*) The breakdown pattern from *m/e* 181 down to *m/e* 50 is about the same, which is, of course, in accord with the common ion intermediate role of the benzylideneaniline cation and needs no further discussion.

(*2*) Resulting from differences in both stability and ionization potential, the abundance of the parent ion in relation to the carbonyl-free complex ion (*m/e* 233) is distinctly lower in **1** than in **2**. The stability of **1**, in terms of resistance to the primary steps involving Cr—CO bond fission, is probably lower than that of **2** because of increased backbonding from Cr to ring ligand (and accordingly reduced Cr—CO backdonation), brought about by the lower charge density on the complexed ring of **1** (mildly electron-withdrawing —CH=N—Ph substituent (2)) as compared to the situation in **2** (weakly electron-donating —N=CH—Ph substituent (2)). In contrast, **1** can be expected to possess the higher IP[8] for the very same reason of electron withdrawal by the substituent on the complexed ring in this compound. Lower stability and higher ionization potential both will combine to render $P^{+\cdot}$ of **1** the less abundant one (ref. 14, pp. 35, 36) of the two parent ions.

(*3*) The decarbonylation pattern of **2** differs from that of **1** insofar as the $[P - 2CO]^{+\cdot}$ species is of noticeably lower relative intensity than the isomer ion derived from **1**, and the $[P - CO]^{+\cdot}$ daughter ion peak is effectively absent (<0.5%) in the spectrum at 70 eV, becoming significant only as the electron beam energy is lowered (2.9% at 20 eV, 6.0% at 15 eV). This indicates

[8]Accordingly, by plotting IP (by electron impact (26)) against k_{CO}, the carbonyl stretching force constant (from ν_{CO} (27)), for 12 representative arenetricarbonylchromium complexes as previously done by Müller (26), we obtain a least-squares fit, from which for **1** ($k = 15.000 \times 10^5$ dyn cm^{-1} (2, 27)) and **2** ($k = 14.867$ dyn cm^{-1} (2, 27)), respectively, IP values of 7.38 and 7.26 eV can be derived.

TABLE 2. Metastable transitions[a] in the fragmentation patterns of complexes **1** and **2**

Transition $m/e \rightarrow m/e$	m^* calcd.	m^* observed	
		Complex **1**	Complex **2**
317 → 289	263.5	263–264 vs, br	263.5 w
317 → 261	214.9	~215 w–m	~215 w–m
289 → 261	235.7	235.7 w–m	—
261 → 233	208.0	~208 vs	~208 s
233 → 180	139.1	139.2 w	—
233 → 155	103.1	103–104 w, br	103–104 w, br
233 → 78	26.1	26.1 w	26.1 w
233 → 52	11.6	11.6 vs	11.6 vs
181 → 180	179.0	179–180 s, br	179–180 vs, br
181 → 104	59.8	~59.5 w, br	59.6 w
181 → 78	33.6	~33.7 vs	~33.7 vs
180 → 153	130.0_5	~130 w–m, br	~130 w–m, br
180 → 77	32.9	32.9 vs	32.9 vs
155 → 78[b]	39.2_5	39.2 vw	39.2 vw
155 → 77[c]	38.2_5	38.3 vw	38.3 vw
155 → 52	17.4_5	17.4 s	17.4 s
153 → 152	151.0	~151 m	151 m
129 → 52	20.9_5	20.9 m–s	20.8 m–s
91 → 64	45.0	44.6–45 w, br[f]	44.6–44.9 w, br[f]
89 → 63[c]	44.6		
80 → 52[d]	33.8	~33.7 vs	~33.7 vs
78 → 52[e]	34.7	34.8 w	34.7 w
77 → 63[c]	51.5_5	51.8 m–s	51.7 m
77 → 51	33.8	~33.7 vs	~33.7 vs

[a]See Experimental for recording conditions. vw = very weak; w = weak; m = medium; s = strong; vs = very strong; br = broad.
[b][CrCN]$^+$, ascertained by accurate mass number determined.
[c]Tentative.
[d]Not unambiguous because of coincidence with transitions *m/e* 181 → *m/e* 78 and *m/e* 77 → *m/e* 51; see text.
[e][C_4H_4]$^{+\cdot}$.
[f]Tail at *m/e* 44.6–44.7 vw.

that the velocity curve for the transition *m/e* 317 → *m/e* 289 (Fig. 1) is even shallower, and approaches a lower limiting value of $k(E)$, in the decarbonylation of **2** than holds for the analogous step in the decarbonylation of **1**. For **2**, hence, the monodecarbonylation step is associated with a lower frequency factor, and thus passes through a tighter transition state, than in the case of **1**. Anchimeric assistance by the proximate N donor atom in a suitably adapted transition-state geometry, resulting in further rotational restrictions, may be responsible for this trend.

(*4*) The *m/e* 181 to *m/e* 233 ion yield ratio is higher, and so indicates a more favored Cr–ring bond cleavage, in *m/e* 233 (**2**) than in *m/e* 233 (**1**). This is not what one would expect on the basis of stability considerations: in the former ion, the more powerful π donating effect exerted by the complexed ring, brought about by the electron-releasing —N=CH—Ph substituent, should result in a stronger Cr–ring bond and, thus, in a correspondingly reduced relative *m/e* 181 ion yield. Possibly, competitive degradation reactions, at the expense of Cr–ring bond fission, are faster in the *m/e* 233 ion stemming from **1** than in the isomer derived from **2**. It can be argued, for example, that the higher stability of the benzonitrilechromium ion (possibly further stabilized by rearrangement to the *N*-substituted tropylium isomer) arising from *m/e* 233(**1**) decomposition, as compared to the isonitrile-type isomer resulting from degradation of *m/e* 233(**2**), should render benzene expulsion from *m/e* 233 a relatively more favorable process in the fragmentation sequence of **1**, and indeed the slightly enhanced abundance of *m/e* 155(**1**) relative to 155(**2**) corroborates this proposition. However, in view of the possibility of isomerizations at the more advanced stages of fragmentation, the difference in abundances is not significant enough to permit any rationalizations, which

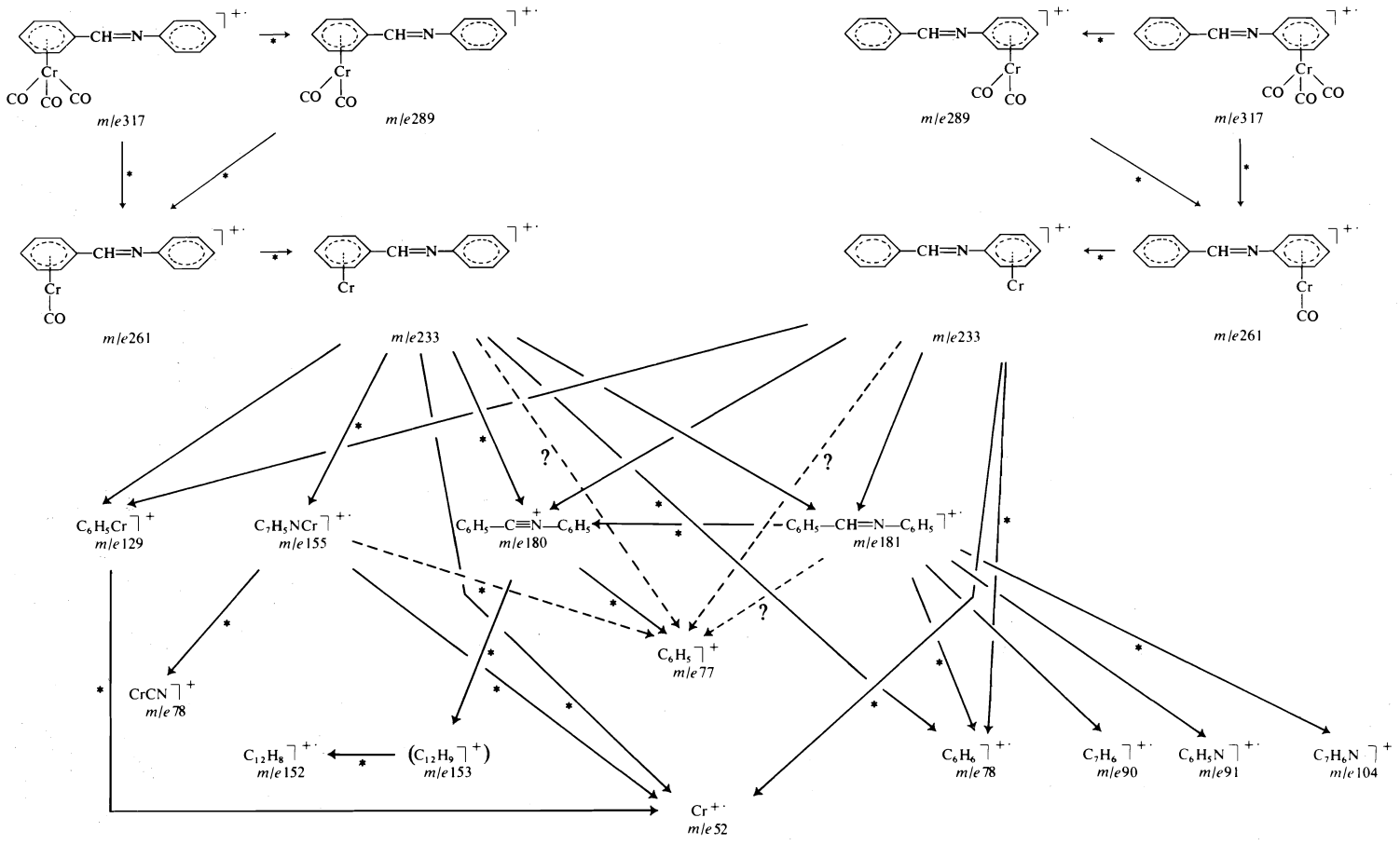

FIG. 2. Fragmentation patterns of complexes **1** ($P^{+\cdot}$ in upper left) and **2** ($P^{+\cdot}$ in upper right). Solid arrows marked with asterisk: metastable transitions; dotted arrows: questionable transitions. Only one species *m/e* 155 shown for simplicity. Ultimate fragmentations of daughter ions from *m/e* 180, 181 not indicated.

must await the availability of appearance potential data on all fragment ions involved.

Experimental

Compounds

Complexes **1** and **2**, obtained from precomplexed starting materials (1), were further purified by repeated recrystallization from dry, deoxygenated heptane under rigorously controlled anhydrous conditions in the dark; **1**, mp 106.5–107.5°C; **2**, mp 109–110°C (sealed). Failure to observe these precautions resulted in samples giving noticeably variant mass spectra. *N*-Benzylideneaniline (28) was recrystallized from dry methanol (moisture protection); mp 50.5–52°C.

Instrumental Conditions

Mass spectra of **1**, **2**, and *N*-benzylideneaniline were obtained on a Varian Mat CH5 single-focusing mass spectrometer operating at 15–70 eV ionizing voltage, 3 kV (nominal) accelerating voltage, 6×10^{-6} Torr source ion gauge pressure, and 150°C source temperature. Unless specifically stated otherwise, information was retrieved from the 70 eV spectra. Samples were admitted through a direct inlet system. Within the probe temperature range of 60–80°C no temperature sensitivity of relative peak intensities was observed; probe temperatures were therefore maintained at 71 ± 1°C. At this level, satisfactory intensities were obtained without the risk of thermal decomposition. Peaks and relative intensities are recorded in Table 1 for both **1** and **2**; for each compound, the abundance values represent averages of 24 scans taken on 12 samples individually prepared and admitted (i.e. two scans per sample), with normal bake-out procedures interposed between successive sample applications. Metastable peaks were recorded at the Inorganic Chemistry Laboratory, Technical University, Munich, with the aid of an Atlas-CH4 mass spectrometer equipped with a TO 4 ion source; ionizing voltage, 50 eV; probe temperature, 75 ± 2°C. The peaks are listed in Table 2.

Acknowledgments

This work was supported by the South African Atomic Energy Board, and a stimulating discussion with Dr. S. Gordon of that organization is gratefully acknowledged. Thanks are due to Mrs. M. Stein for her patient experimental assistance, and to Professor J. Müller, now at the Technical University of Berlin, for his invaluable help in obtaining spectra on the Atlas instrument under conditions conducive to the observation of metastable transitions. The kind hospitality extended by Professor H. A. Brune during the author's stay in Ulm, where the final preparation of the manuscript was done, is deeply appreciated.

1. E. Mostardini, F. Calderazzo, and R. Ercoli. Chim. Ind. (Milan), **42**, 1231 (1960).
2. E. W. Neuse. J. S. Afr. Chem. Inst. **28**, 365 (1975).
3. J. Müller. Angew. Chem. Int. Ed. Engl. **11**, 653 (1972).
4. J. Müller, K. Fenderl, and B. Mertschenk. Chem. Ber. **104**, 700 (1971).
5. C. Krier, J. C. Lorquet, and A. Berlingin. Org. Mass Spectrom. **8**, 387 (1974).
6. T. W. Bentley. *In* Mass spectrometry. Vol. 3. *Edited by* R. A. W. Johnstone. The Chemical Society, London. 1975. p. 78.
7. I. Howe. *In* Mass spectrometry. Vol. 1. *Edited by* D. H. Williams. The Chemical Society, London. 1971. p. 82; I. Howe and D. H. Williams. J. Am. Chem. Soc. **90**, 5461 (1968).
8. J. R. Gilbert, W. P. Leach, and J. R. Miller. J. Organomet. Chem. **49**, 219 (1973).
9. H. M. Rosenstock, M. B. Wallenstein, A. L. Wahrhaftig, and H. Eyring. Proc. Natl. Acad. Sci. USA. **38**, 667 (1952).
10. H. M. Rosenstock. *In* Advances in mass spectrometry. Vol. 4. *Edited by* E. Kendrik. The Institute of Petroleum, London. 1968. p. 523.
11. D. H. Williams and I. Howe. Principles of organic mass spectrometry. McGraw-Hill, London. 1972. Chapt. 4.
12. A. N. H. Yeo and D. H. Williams. J. Am. Chem. Soc. **92**, 3984 (1970).
13. R. A. Marcus and O. K. Rice. J. Phys. Colloid Chem. **55**, 894 (1951); R. A. Marcus. J. Chem. Phys. **20**, 359 (1952).
14. F. W. McLafferty. Interpretation of mass spectra. 2nd ed. Benjamin, London. 1973.
15. D. H. Williams and R. G. Cooks. Chem. Commun. 663 (1968).
16. R. H. Shapiro and T. F. Jenkins. Org. Mass Spectrom. **2**, 771 (1969).
17. R. H. Shapiro and K. B. Tomer. Org. Mass Spectrom. **3**, 333 (1970).
18. J. C. Tou. J. Phys. Chem. **75**, 1903 (1971); J. C. Tou and R. M. Rodia. Org. Mass Spectrom. **6**, 493 (1972).
19. R. D. Smith and J. H. Futrell. Org. Mass Spectrom. **11**, 445 (1976).
20. I. Howe. *In* Mass spectrometry. Vol. 2. *Edited by* D. H. Williams. The Chemical Society, London. 1973. p. 36.
21. J. Müller and P. Göser. Chem. Ber. **102**, 3314 (1969).
22. D. J. Elias and R. G. Gillis. Aust. J. Chem. **19**, 251 (1966).
23. J. Müller and K. Fenderl. Chem. Ber. **103**, 3128 (1970).
24. R. G. Cooks, J. H. Beynon, and J. F. Litton. Org. Mass Spectrom. **10**, 503 (1975).
25. J. H. Bowie, R. G. Cooks, J. W. Fisher, and T. McL. Spotswood. Aust. J. Chem. **21**, 2021 (1968).
26. J. Müller. J. Organomet. Chem. **18**, 321 (1969).
27. E. W. Neuse. J. Organomet. Chem. **99**, 287 (1975).
28. W. F. Smith. Tetrahedron, **19**, 445 (1963).

Organic electrode processes: generalized reduction mechanisms[1]

PHILIP J. ELVING

The University of Michigan, Ann Arbor, MI 48109, U.S.A.

Received February 28, 1977

PHILIP J. ELVING. Can. J. Chem. **55**, 3392 (1977).

Prototype formulations are considered for the reaction pathways commonly encountered for the electrolytic reduction of organic compounds in aqueous and nonaqueous media on the basis that the essential feature is severance of a chemical bond which requires transfer into the reaction site of one or two electrons; multiple electron processes result from instability at the applied potential of initially produced species or their chemically altered products. To obtain electrical neutrality, uptake of electrons may have to be accompanied by that of a cation, generally a proton. Pertinent factors in the path followed in the overall electrode process may include a sequence of free radical or radical anion going to dimeric or carbanion species (depending on the relative rates of chemical and charge-transfer steps), possible interaction of intermediate products with their progenitors, proton donor activities, medium properties (e.g in respect to rates of chemical reactions accompanying charge-transfer and control of the chemical states of reactants and intermediates), stereochemical factors inherent in reactant and intermediate species, and chemical interaction with the electrode material. Application of the general mechanistic considerations are illustrated by various types of electrolytic reductions: aromatic hydrocarbon, nitrogen heterocycle, carbon–halogen bond, ketone carbonyl group, and beta halogenated and/or unsaturated acids.

PHILIP J. ELVING. Can. J. Chem. **55**, 3392 (1977).

Des formules modèles sont considérées pour des chemins réactionnels souvent rencontrés dans la réduction électrolytique de composés organiques en milieu aqueux et non aqueux. On se base sur le fait que la rupture du lien chimique exige le transfert d'un ou deux électrons au site réactionnel. Les processus multi-électroniques résultent de l'instabilité au potentiel appliqué des espèces initialement produites ou de leurs produits transformés. Afin d'obtenir une neutralité électrique, le transfert d'un électron doit être accompagné par celui d'un cation, généralement un proton. Les facteurs appropriés dans ce chemin réactionnel suivi, tout au long du processus prenant place aux électrodes, peut impliquer: (*a*) la séquence d'un radical libre ou d'un radical anionique donnant des dimères ou carbanions (dépendant des vitesses relatives des étapes chimiques et celles de transfert de charge); (*b*) l'interaction possible des intermédiaires avec les produits initiaux, (*c*) des activités proton-donneur; (*d*) des propriétés de milieu (i.e. par rapport aux réactions chimiques accompagnant le transfert de charge ainsi que du contrôle des états chimiques des réactifs et intermédiaires); (*e*) des facteurs stéréochimiques propres aux réactifs et intermédiaires; (*f*) l'interaction chimique avec l'électrode. L'application des considérations mécanistiques générales est illustrée par différents types de réduction électrolytique, un hydrocarbure aromatique, un hétérocycle contenant un atome d'azote, un lien carbone–halogène, le groupe carbonyle d'une cétone et des acides bêta-halogénés ou insaturés.

[Traduit par le journal]

Introduction

The prototype formulation for the half-cell reaction mechanism for the electrolytic reduction of an organic compound, can be expressed in its simplest form as

$$[1] \qquad Ox + ne^- = Red$$

Although the stoichiometric form of eq. 1 is usually quite simple, involving small integral ratios of oxidized and reduced forms with perhaps the addition for reactions in aqueous media of hydrogen ions and/or water, and in nonaqueous media of proton donors and/or acceptors, the actual course of the reaction is often quite complex since it is heterogeneous in nature, involving electron transfer between a solution species (or its adsorbed or otherwise altered form) and the electrode, and occurring in the interfacial region between bulk solution and bulk electrode.

In 1961, Elving and Pullman (1) discussed three general approaches to the description of organic electrode reaction pathways: (*a*) the *chemical* reaction mechanism as stated in terms

[1]Presented at the International Conference on Modern Electrochemical Techniques for Investigating Chemical Systems, Carleton University, Ottawa, Canada, July 13–16, 1976.

of the species involved, following the format usually used in describing organic reaction mechanisms in homogeneous solution; (*b*) the *electrochemical* reaction mechanism, which involves a more detailed analysis of the physical situation at the solution–electrode interface; (*c*) the *energetic* reaction mechanism, in which a more precise (if possible) mathematical statement is attempted. This sequence was considered to be a logical development in the elucidation of a mechanism and its interrelations with the factors involved.

Since 1961, much work has been done on the elucidation of organic electrode reaction paths with extensive examination of the behavior of free radical and other intermediate species as well as of the roles of adsorption and kinetics in guiding the overall reaction in one direction in preference to another. The magnitude of the available literature and the complexity of effects involved can be seen from the compendia by Baizer (2), Tomilov *et al.* (3), and Mann and Barnes (4), two Faraday Society Discussions (5, 6), and the discussions on basic concepts in organic electrochemical reaction paths by Cauquis (ref. 7, pp. 13–91) and methods for such reaction elucidation by Cauquis (ref. 7, pp. 93–154) and by Fleischmann and Pletcher (8).

The present discussion, consequently, attempts to bring prototype formulations for the general reductive mechanism up to date by explicating possible alternate paths, particularly as these may cast light on reactive configurations at the solution–electrode interface and on the interplay of thermodynamic and kinetic effects. Stress is placed on the 'chemical reaction mechanism'. To conserve space, correlations of proposed mechanistic schemes with theoretical calculations, e.g. of the HMO type (cf. refs. 9 or 10), will not be explored. Similarly, correlation of reaction schemes with heterogeneous rate constants for electron-transfer (charge-transfer) steps will be largely omitted due, in this instance, to the paucity of $k_{s,h}$ data for organic compounds.

The discussion is largely focussed on data obtained by polarography, derived technics (e.g. cyclic voltammetry and ac polarography), and related approaches (e.g. controlled electrode potential electrolysis). Frequently, solutions of products prepared by the latter approach have been examined and products identified by diverse electrochemical, spectrophotometric, chemical, and enzymatic means; often, periodic examination of the test solution during electrolysis provides helpful information.

Basic Mechanistic Considerations

Because an electrochemical reaction is a heterogeneous process, a completely satisfactory mechanistic description must await a detailed understanding of phenomena in the electrical double layer and the immediately surrounding solvent region, e.g. ref. 11. Meanwhile, elucidation of a mechanism for an organic electrode reaction optimumly includes specification of (*a*) state of the compound in solution and on approaching the interface, (*b*) redox reaction sites in the molecule, (*c*) adsorption sites (and evaluation of adsorption in relation to electron-transfer), (*d*) the sequence of charge-transfer and coupled chemical steps, and (*e*) kinetic and energetic parameters for these steps. Where possible, the effects should be specified of variation in experimental conditions which may alter, for example, nature of the electroactive and intermediate species and extent of participation of other solution species, and attempts should be made to describe possible structures for the transition states involved, including orientation of the compound relative to the electrode when electron transfer occurs.

These goals are often approached with many descriptions stating in more or less detail the sequence of steps including the presence of accompanying chemical reactions, the reversibility of electron-transfer processes, the roles of free radical and other short- and long-lived intermediate species, the product ratio if more than one product is formed, the extent and manner of adsorption and orientation of reactant and products at the interface, and any changes produced at the electrode surface, e.g. film formation.

A limiting factor is the ability of the experimental technics used to discriminate between the various steps in the electrode process, and to follow these steps adequately, i.e., the relative time scales of reaction sequence and experimental approach. An obvious example is the increasing amount of information available from cyclic voltammetry as the potential scan rate (dE/dt) is increased; variation in initial and reversal potentials, and nonsymmetrical and repeated scanning may further amplify the information obtainable.

Bond Rupture

Electrolytic reduction of both organic and inorganic species involves the net transfer of electrons from electrode to electroactive species; an essential difference is that in inorganic reductions 'normal' largely covalent chemical bonds are only apt to be broken in cases where the electroactive element is present as an oxygenated species or has a lesser coordination number in the reduced than in the oxidized state. In contrast, the fundamental process in an electrolytic organic reduction is a change in the structure of a functional group due to bond rupture, which requires only one electron to produce a free radical species; addition of a second electron completes rupture of the bond. Accordingly, from the mechanistic viewpoint, only one-electron (1e) or two-electron (2e) processes need to be considered; apparent multiple electron processes result from the instability at the potential of its formation of the initially produced species, perhaps following an intermediate chemical reaction, and, consequently, its immediate further reduction, i.e., multiple electron processes are due to combinations (simultaneous and/or successive) of 1e and/or 2e processes. Polarographic waves, for example, may also overlap due to a succession of electrode processes at only small potential separation from each other, e.g. behavior of nicotinamide in alkaline solution (12).

It is reasonable to assume on the basis of the evidence accumulated on the mechanisms of homogeneous and heterogeneous (including electrode) reactions, both inorganic and organic, that the occurrence of an electrode reaction involving the actual simultaneous transfer of more than two electrons is likely to be small. Indeed, a question might be raised as to whether observed simultaneous 2e transfer processes are not actually two 1e processes which follow each other, for example, within less than either the lifetime of an intermediate species or the time of a single molecular vibration (cf. suggestion by Jacq, Cavalier, and Bloch (13)). Since the previous argument often is a nonoperational one and since dimers indicating the presence of 1e processes are found, we may safely assume that a simultaneous 2e process is the rapid succession of the 1e reactions represented in Fig. 1 with the proviso that electrons may follow each other so rapidly that the transition state

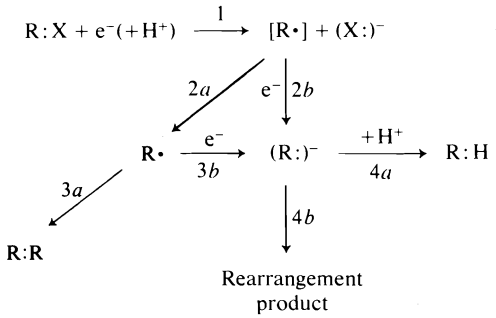

FIG. 1. Generalized chemical reaction mechanism (discussed in the text). If R and X were connected by multiple bonds, the initial reaction product may be [Ṙ—X—Z] (from ref. 1).

effectively represents a combination of the electroactive species and two electrons.

General Mechanism

Based on the previous discussion, a general mechanistic pattern for organic reductions (Fig. 1) can be proposed, which permits rationalization of the course of such processes and of variation in mechanism with experimental conditions or between members of a homologous series (cf. ref. 1). The pattern assumes a reaction site, R—X, where R may be a reactive carbon center (or another atom, e.g. nitrogen, oxygen, or sulfur), X another carbon, oxygen, nitrogen, halogen, or other atom, and the bond an electron pair; there may be more than one bond between R and X, e.g. C=N in a heterocyclic ring. (In the subsequent discussion and equations, H^+ or (H^+) represents a proton source, e.g. HA; hydrogen, hydroxide ions, and water are not usually shown except where necessary to indicate final establishment of an electrically balanced species.)

In the primary charge-transfer reaction, which is generally potential-determining, a single electron enters the reaction site to form presumably an activated complex, which can dissociate to a free radical precursor and an anionic species (step 1); if a multiple bond was originally present between R and X, a radical anion could be formed. The exact nature of species will be modified by the extent of participation of protons, solvent molecules, other solution constituents, and the electrode surface (participation of these species in subsequent steps is not explicitly indicated but may be involved), e.g. H^+ can participate by chemical polarization of the R—X bond through formation of an H—X

bond; H^+ is the most common third participant in the initial step, although another Lewis acid may act similarly.

The free radical precursor can either immediately (or after rapid chemical rearrangement) accept a second electron to form a carbanion (step 2*b*) or can exist as a discrete free radical (step 2*a*), which eventually either dimerizes (step 3*a*) or is reduced at more negative potential to the equivalent of a carbanion (step 3*b*). The charge on the carbanion, formed by either path, is usually neutralized either by acceptance of a Lewis acid, e.g. H^+ derived from a solution species (step 4*a*), or by electronic rearrangement (step 4*b*) with the charge being transferred to another part of the molecule where it can be suitably handled, e.g. elimination of an atom or group from an atom adjacent to the original reactive site with consequent formation of a double bond between this atom and that of the reactive site.

Completion of the initial electron addition (and perhaps displacement of the X moiety) by step 2*a* or 2*b*, depends on which route requires the less activation energy, i.e., on the difference in free energies of the transition states. Chemical reactions such as protonation, dimerization, rearrangement and elimination, which precede, accompany and/or follow charge-transfer, often play significant roles in the overall process, as has been noted and will be subsequently discussed.

Effect of the Medium

The effects of solution composition and experimental conditions on electrochemical behavior have been abundantly discussed, e.g. refs. 2–4 and 14–19, typically in respect to interaction of solvent and background electrolyte components with participants in the electrode process.

The principal effect of the medium is generally related to the sensitivity of the mechanistic pathways to proton availability. Thus, pyrimidine and nicotinamide are each initially reduced in a 1e process to the neutral free radical in acidic aqueous solution and to the radical anion in aprotic media; however, their behavior in aqueous solution differs markedly as the p*H* is increased, e.g. pyrimidine undergoes an initial 2e reduction by p*H* 6 and a 4e reduction by p*H* 9, whereas nicotinamide undergoes an initial 1e reduction up to p*H* 12. Furthermore, many initial 1e reactions in aprotic media may (in the presence of sufficient proton activity) become overall multiple electron reactions, e.g. reduction of aromatic hydrocarbons (2e reactions), nitro groups (4e or 6e reactions), and purines (2e, 4e, or 6e reactions).

Hydrogen ion can affect the reduction mechanism by (*a*) direct interaction with the chemical system and electrons at the reaction site, e.g. via polarization of the bond to be ruptured, (*b*) control of the nature of chemical participants in various steps via, for instance, acid–base equilibria, (*c*) effect on species behavior at the electrode in terms of adsorption and/or steric phenomena, and (*d*) alteration of relative reaction rates for electrochemical and chemical reactions.

Among the specific effects seen are the fusing of consecutive electron-transfer steps, the splitting of multiple electron-transfer steps, and the removal or formation of reduction sites such as double bonds as a result of tautomeric shifts and intramolecular chemical reactions, e.g. deamination and dehydration.

As previously noted, in many subsequent equations, H^+ can represent hydrogen ion furnished by dissociation of a sufficiently strong acid (e.g. $HClO_4$) or a slightly dissociated proton donor, e.g. H_2O. The latter is frequently the case in nonaqueous media, where reaction, for example, of an anion or radical anion, R^-, with a proton donor, HA, is likely to follow the course,

$$[2] \qquad R^- + HA \rightleftharpoons [R\text{---}H\text{---}A]^- \rightleftharpoons RH + A^-$$

Multiple bond reductions frequently involve an additional reactant, e.g., a solution component, Z, such as hydrogen ion,

$$[3] \qquad R{=}X + e + Z = [\dot{R}{-}X{-}Z]$$

Succeeding reactions of the intermediate species can still be depicted by the equations of Fig. 1.

Referring, then, to Fig. 1, the p*H*-dependence of organic electrolytic reductions is commonly associated with step 1; there are few well-defined examples of steps 2 and 3 being p*H*-dependent. For example, in the reduction of nitrogen heterocycles or ketones, where two polarographic waves are observed with wave I being due to formation of a free radical and II to its reduction, wave I may be p*H*-dependent but wave II rarely is. The p*H*-dependence of wave I may then be associated with hydrogen ion being involved in

formation of the energy-determining activated complex or transition state, regardless of whether hydrogen ion is involved in the final stoichiometry of the first step (eq. 3) or not. This does not necessarily mean that every first reaction step representable by eq. 3 is p*H*-dependent. The importance of H^+ in determining the state of the electroactive species and, consequently, the energy of the reaction is considerable in many situations, e.g. those involving acid–anion and keto–enol systems. For example, $E_{1/2}$ for the 2-bromoalkanoic acids is p*H*-dependent in the p*H* region where the shift from anion to more readily reduced acid form is appreciable; the fundamental carbon–bromine bond fission process is p*H*-independent throughout the p*H* range involved.

The argument is general, since other solution components may also affect the reactive species, e.g. the effect of ammonia and amines on carbonyl group reductions. An analogous argument concerns the effect of ion pair formation between, for example, a carbanion or other anion and a metallic cation.

An important reason for examining compounds in nonaqueous media has to do with their nonreducibility in aqueous media (20). If nonavailability of potential range is the cause, the use of solvents such as *N*,*N*-dimethylformamide (DMF), acetonitrile (AN), and dimethylsulfoxide (DMSO) provides at least a limited answer as the available potential range is a volt or more greater than in aqueous alkaline medium.

Reversibility and Characteristic Potentials

The energy level at which an electrode process occurs is indicated by a potential characteristic of the faradaic reaction, e.g. the half-wave potential, $E_{1/2}$, which (for a thermodynamically reversible redox half-reaction system) corresponds to the formal potential, E_c^0, for the specified experimental conditions, corrected for diffusion coefficient differences. For an irreversible system, $E_{1/2}$ corresponds to the formal potential plus terms involving the diffusion coefficient ratio, the activation energy for the electron-transfer, certain experimental conditions, and, at times, rate constants for chemical steps in the overall electrode process (cf. refs. 16, 18, 19, 21, and 22) for a summary of the nature of $E_{1/2}$ and related potentials, and the factors which enter into their measured values.

It is important to characterize the kinetics of both heterogeneous electron-transfer and homogeneous chemical reaction steps in the overall electrode process, since irreversible redox behavior may be shown, for example, by electrode processes involving either slow electron-transfer or rapid electron-transfer coupled to a subsequent (follow-up) rapid but irreversible chemical reaction; such a distinction is crucial for proper mechanistic evaluation. In the case of the compounds to be discussed, irreversibility is often associated with follow-up chemical reactions. In order to apply various approaches for calculating the rates of chemical reactions coupled to an electron-transfer reaction, it is essential to know that the latter is reversible, e.g. that the standard formal heterogeneous rate constant, $k_{s,h}$, is 0.1 cm s^{-1} or greater.

Signs of the potentials for the half-reactions discussed are determined by their being formulated as reductions with the usual thermodynamic conventions. Numerical potential values for aqueous media are based on comparison with the saturated calomel electrode (sce). Where possible, potentials for processes in nonaqueous media are also given vs. aqueous sce and, consequently, include liquid junction potentials of unknown magnitude.

Kinetics as a Factor in Electrode Reaction Mechanisms

If a compound can be transformed by different reactions into different products, the relative amounts of the products formed will be proportional to the relative rate constants (k). Thus, a free radical (or radical anion) can undergo a variety of reactions with the products formed being dependent on the relative rates, which are affected by medium composition and applied potential:

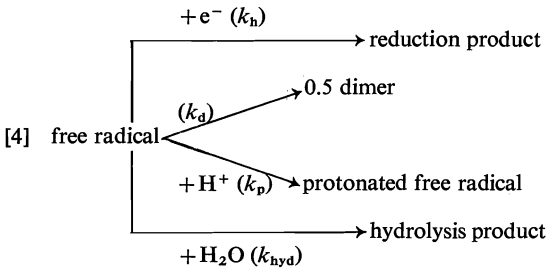

Enough studies have been made, for example, on electrode processes involving nitrogen hetero-

cyclic compounds of the pyridine, pyrimidine, and purine types to allow reasonable estimates to be made of rate constants and reaction sequences (22–24), e.g. $k_{s,h}$ for the initial 1e and 2e reductions seems to exceed 0.1 cm s^{-1}; the free radical reduction rate seems to be comparable. In any event, reduction of a free radical is rapid if the potential is sufficiently negative; as would be expected, it is more difficult to reduce an anionic free radical, $\dot{R}^-$, than the corresponding neutral radical, $\dot{R}H$. Dimerization rate constants (k_d) for anion radicals in nonaqueous media are about 10^4 or 10^5 M^{-1} s^{-1} and for neutral free radicals in aqueous or nonaqueous media are about 10^6 or 10^7.

Protonation rates of anionic species are quite rapid (25); those of neutral species are often slower but still rapid. The effective rate depends on the proton donor activity, e.g. whether it is water, a slightly ion-paired Brønsted acid, or a slightly dissociated acid. The protonation rate constant for pyrimidine anion radical by residual water (k_{hyd}) in AN is about 7 M^{-1} s^{-1}. Pseudo first order protonation rate constants at pH 3–5 for pyrimidine, cytosine, and purine carbanions are about 10^4 s^{-1}; those for adenine species are about an order of magnitude more rapid.

Thus, if a free radical can dimerize or hydrolyze, dimerization will predominate unless solution conditions increase the hydrolysis rate by several orders of magnitude. The dimer, once formed, may itself hydrolyze but the rate would, again, be much less than that of dimerization.

Chemical reactions, other than dimerization and protonation, are generally relatively slower. Pseudo first order rate constants for the acid-catalyzed hydrolytic decomposition of the dihydropyridine nucleotides in aqueous solution are about 10^{-3} s^{-1} at pH 4 and 10^{-5} s^{-1} at pH 7 (26). The deamination rate constant of reduced cytosine is about 10 s^{-1}; that of reduced adenine is much less (27, 28). Consequently, deamination to produce a species reducible at the potential of its formation is a factor in the reduction of cytosine at the dme but not in that of adenine.

The multitude of theoretically possible reaction paths is well exemplified for the case of the reaction,

$$[5] \qquad R + 2H^+ + 2e^- = RH_2$$

by Fig. 2, which scheme was originally proposed by Jacq (29) and has been discussed by Kastening

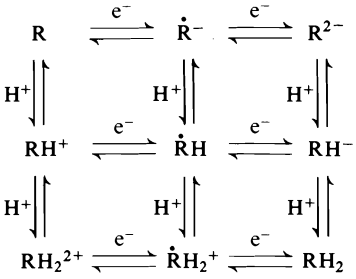

FIG. 2. Generalized scheme of theoretically possible reaction paths for a two-electron, two-proton reduction, i.e., $R + 2e + 2H^+ = RH_2$. Based on Jacq's formulation (29) (cf. ref. 7, pp. 13–91, and ref. 30).

(30) and Cauquis (ref. 7, pp. 13–91). In Fig. 2, horizontal reactions involve electron transfer; vertical reactions hydrogen ion transfer. The left column represents the original electroactive species in various states of protonation; the center column similarly represents the free radical species; the right column represents the fully reduced (2e process) product. It is apparent that the course of the reaction in an actual situation (for example, double bond reduction) will be critically dependent on the electron activity (i.e., the potential), the pK_a magnitudes for the various acid–base equilibria, the H^+ activity, and the relative rates of the various charge-transfer and chemical reactions involved. (Some subsequently discussed reaction paths, e.g. that for aromatic hydrocarbons (Fig. 4), involve a portion of the general scheme of Fig. 2.)

Such rates must be taken into account when considering possible alternate reaction paths. The variety of factors, which can effect rate and rate constants, have been amply considered in the literature. For example, due to the easier reducibility of the protonated member (conjugate acid) of a conjugate acid–base pair, the conversion of base to acid by a fairly rapid protonation will affect the observed polarographic pattern (25):

$$[6] \qquad RH^+ \rightleftharpoons R + H^+$$

An example of the effect of rates on the products obtained is provided by Mairanovsky's comparison (31) of two studies (32, 33) on the electrolytic reduction of carbon–oxygen bonds in unsaturated alcohols and related compounds. One paper (32) cited the mechanism as being

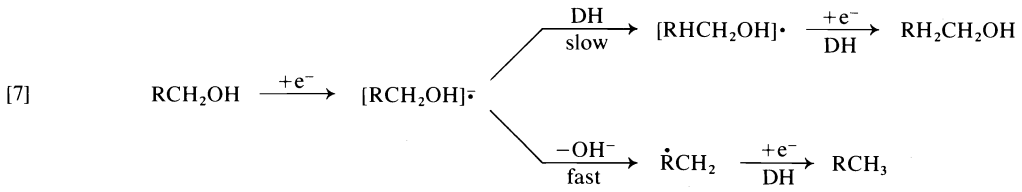

where DH represents a proton donor. The mechanism described in the other paper (33) was considered to be identical:

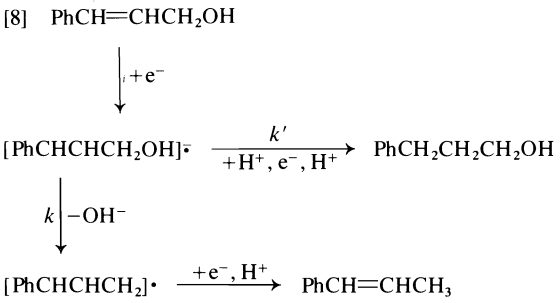

where $k \gg k'$. Mairanovsky *et al.* (32) pointed out that change in direction of the overall process to favor alcohol (ether) or hydrocarbon formation by variation in proton donor content (and the resulting effect on kinetics) has been used for selective syntheses.

Electrode Oriented Reaction Mechanisms

Since the electrode reaction locus is the solution–electrode interface, the structure of the electrical double layer is important in electrochemical kinetics and, therefore, in the potentials of many organic electrode reactions because of its influence, *inter alia*, on the effective potential difference which favors the electrochemical reaction and on the effective concentration of the electroactive species (34).

Furthermore, in many instances, adsorption of reactant, intermediate, and/or product is an important factor. A preferred orientation of the organic species in the interphase may often be necessary before electron transfer occurs; the energy for such a process woud be apt to vary similarly to that for an adsorption process. Many investigators have considered the energy of adsorption, if involved, to be negligible compared to the other energies acting, although adsorption energy has been suggested as the possibly significant factor in the variation of $E_{1/2}$ for an aliphatic homologous series (35).

Attempts to define the physical path for the overall electrode reaction usually lead to a more detailed geometric description, as is subsequently illustrated by considering those for two fundamentally different types of electrochemical bond rupture: (*a*) sigma bond breaking in single bond systems as in carbon–halogen bond fission and (*b*) pi bond rupture in multiple bond systems as in ketone carbonyl reduction. The geometrical treatment outlined is essentially descriptive but does help to define kinetic and energetic factors which must be considered.

Reduction of aromatic hydrocarbons, carbon–carbon double bonds in C_4 dibasic acids, and carbon–nitrogen double bonds will also be used to illustrate mechanistic generalities.

Digital Simulation of Reaction Mechanisms

In recent years, there has been increasing activity in the use of computer digital simulation studies, using ranges of reaction rate constants for the various reactions which may be involved if experimental rate constant data are not available, to generate the experimental results that would be expected for a particular investigative technic for postulated electrode reaction mechanisms. The general approaches involved have been described by Feldberg (36) and others, e.g. Bard and collaborators in papers in the *Journal of the Electrochemical Society* from 1970 to the present. In Feldberg's words,

"The simulation approach to problem solving no doubt tends to abort the search for an analytical solution. It can, however, greatly facilitate this search by providing the correct quantitative relationships and by indicating valid approximations (e.g., steady-state approximations)."

"Accessibility to the quantitative aspects of any system would seem to be greatly advantageous to the experimentalist. Paradoxically, he may actually find his task more difficult because of the variety of theoretical mechanisms that may seemingly describe a given experimental system. The mechanistic subtleties will take on added importance; a significant decrease

in the radius of Frost's "ring" will require utmost effort in development, selection, and application of *experimental* techniques."

Father–Son Reactions

Since mother–daughter reaction is a well established designation for a sequence in which the product of an initial reaction becomes a reactant in a second reaction, the term, father–son reaction, will be used to describe the situation where the principal product of a reaction reacts with the original reactant, e.g.

[9] $$R + \text{reagent} = R'$$

[10] $$R' + R = \text{products}$$

where the reagent may be an electron. (The term, father–son reaction, is obviously based on the frequently discussed conflict which arises from competition between father and son with the offspring (here, for example, a radical anion) attacking its immediate progenitor (here, the parent compound). An alternative term would obviously be the "Oedipus reaction".)

Reactions of this general type are not infrequently encountered (or, at the least, postulated) in connection with the electrochemistry of inorganic and organic species, e.g. the reverse disproportionation sequence such as the following:

[11] $$R + 2e^- = R^{2-}$$

[12] $$R^{2-} + R = 2R^-$$

For example, the following reaction sequence has been invoked to explain the presence of coupled products (dimers) on electrolysis of halides, R—X, where SH represents the solvent or a solution species:

[13] $$R\text{—}X + e^- = \begin{bmatrix} \delta^+ & \delta^- \\ R & \text{---} X \end{bmatrix}^-$$

[14] $$\begin{bmatrix} \delta^+ & \delta^- \\ R & \text{---} X \end{bmatrix}^- + e^- \xrightarrow{\text{rapid}} R^- + X^-$$

[15] $$R^- + SH = R\text{—}H + S^-$$

[16] $$R^- + R\text{—}X = \dot{R} + \dot{R} + X^-$$

[17] $$2\dot{R} = R\text{—}R$$

[18] $$\dot{R} + SH = RH + \dot{S}$$

In electrochemical studies of heterocyclic nitrogen bases in nonaqueous media, we have encountered a number of cases where a compound, RH, can serve as a proton source for neutralization of the radical anion, which it forms on 1e reduction, i.e.

[19] $$RH + e^- = \dot{R}H^-$$

[20] $$\dot{R}H^- + RH = \dot{R}H_2 + R^-$$

Since such father–son reactions may account for many situations, where, for example, polarographic wave heights and coulometric faradaic *n* values are less than expected for a 1e process, the mechanistic paths possibly involved will be considered. The patterns seen with some pyrimidines, e.g. 2-hydroxypyrimidine, in nonaqueous medium are illustrated in Fig. 3; dme polarographic waves and hmde cyclic voltammetric peaks are designated by a Roman number with addendum c indicating a cathodic faradaic reaction and a an anodic reaction.[2]

2-Hydroxypyrimidine (2-HP) is reversibly reduced (1e process; Ic) to a radical anion, whose dimerization is slower than its attack (it is a strong base) on unreduced pyrimidine to abstract a proton, producing the neutral free radical, which dimerizes much more rapidly than the radical anion, and the anion of 2-HP. (The radical anion of pyrimidine itself dimerizes in AN at about 0.1 of the rate of the neutral free radical produced in water (37, 38).) The 2-HP anion is involved in a Hg(I)–Hg(0) couple (IVa–IVc).

On addition of strong base (hydroxide ion) to a 2-HP solution, all of the 2-HP is converted to the anion and the only electrochemical activity seen is that due to the mercury couple (IVa–IVc).

On strong acid addition, the protonated pyrimidine formed is more easily reduced (IIc) than the neutral pyrimidine (Ic); the current (IIc) considerably exceeds that for the neutral pyrimidine; the couple ascribed to the pyrimidine anion – mercury reaction (IVa–IVc) is not seen. The neutral free radical can dimerize or, when the proton/pyrimidine ratio exceeds 1, can be protonated and reduced in an ECE reaction.

Addition of a weak acid apparently causes formation of an adduct as a result of hydrogen bridging between acid anion and pyrimidine reduction site, since reduction is facilitated (IIIc); the free radical produced can dimerize or can hydrogen-bond another molecule of acid to form an adduct reducible to a dihydropyrimidine within the available potential range. The

[2]T. Wasa and P. J. Elving, unpublished results.

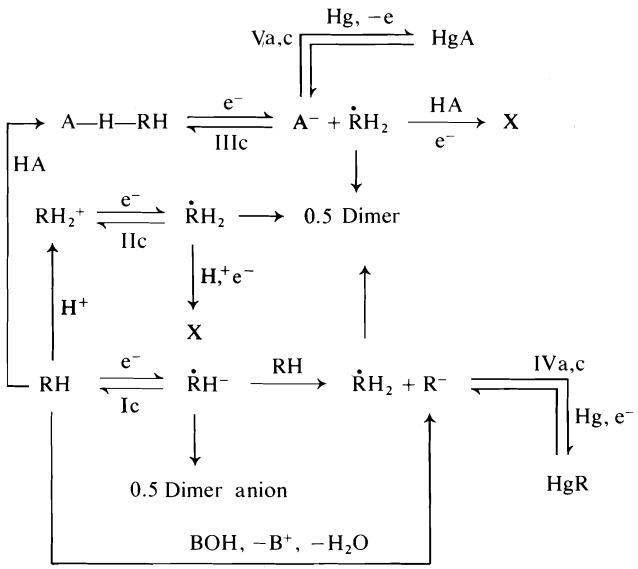

FIG. 3. Pattern for a 'father–son' reaction sequence and accompanying reactions in nonaqueous media in absence of added acid or base and on addition of a strong base (BOH), of a strong acid (H^+), and of a weak acid (HA). In the case of 2-hydroxypyrimidine in DMSO (0.1 *M* TEAP), the approximate potentials (dme polarography and hmde cyclic voltammetry) are as follows (vs. aqueous sce): Ic, −1.7 V; IIc, −0.8 V (HCl; $HClO_4$); IIIc, −1.2 to −1.3 V (benzoic and chloroacetic acids); IVa–IVc, −0.2 V; Va–Vc, 0.2 to −0.1 V.

acid anion can be involved in a Hg(I)–Hg(0) couple (Va–Vc) at a potential characteristic for the acid used; the mercury–pyrimidine anion couple (IVa–IVc) occurs at a potential characteristic of the pyrimidine.

Reduction of Aromatic Hydrocarbons

Much of our mechanistic conception of how the electrochemical reduction of hydrocarbons (largely, aromatic) occurs (39–42) is due to Hoytink. The relationships between redox potentials, ionization potentials, electron affinities, and solvation energies of alternant aromatic hydrocarbons for the initial 1e reduction or oxidation in aprotic media have recently been well reviewed by Parker (43) on the basis of the pioneering approach of Hoytink and van Schooten (44).

In nonaqueous media (commonly necessary to obtain the desired potential range), reduction generally proceeds through two successive 1e additions, producing two waves:

[21] $$R + e^- = \dot{R}^-$$

[22] $$\dot{R}^- + e^- = \ddot{R}^{2-}$$

Proton donor addition increases the wave I height with a corresponding decrease in wave II; in presence of excess donor, most aromatic hydrocarbons show a single 2e wave. The mechanism is usually considered to be

[23] $$R + e^- = \dot{R}^-$$

[24] $$\dot{R}^- + H^+ = \acute{R}H$$

[25] $$\dot{R}H + e^- = \ddot{R}H^-$$

Since protonated $\dot{R}H$ has a higher electron affinity than R itself, it is reduced at the same potential as R, resulting in a typical ECE process. Anion $\ddot{R}H^-$ can be protonated by an available proton source. A possible reaction is reduction of the free radical $\dot{R}H$ by the radical anion $\dot{R}^-$, which is the homogeneous equivalent of heterogeneous reaction [25] (45–47):

[26] $$\dot{R}H + \dot{R}^- = \ddot{R}H^- + R$$

The radical anion may disproportionate,

[27] $$2\dot{R}^- = R + \ddot{R}^{2-}$$

followed by protonation of the dianion (48, 49).

Based on extensive studies of electrochemical aromatic hydrocarbon reduction (due, at least in part, to the ready application of HMO theory to these compounds and the resulting feasibility of comparing experimentally measured and theoretically calculated ease of reduction for

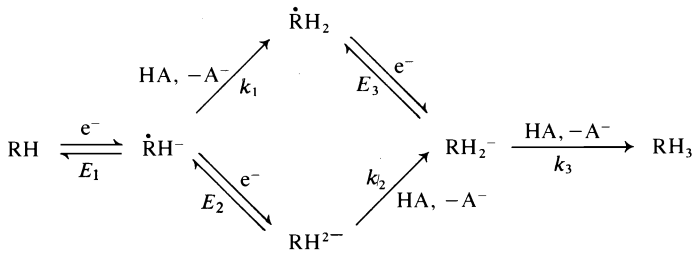

FIG. 4. Alternative patterns for reduction of aromatic hydrocarbons and other organic compounds containing unsaturated double bonds. Modelled after reaction sequences given in refs. 50 and 51. RH represents the parent compound; HA represents a potential proton donor.

compound sequences), the interrelated equilibria and reactions involved in aromatic hydrocarbon reduction (as well as for other highly conjugated compounds such as aromatic ketones and amines) have been frequently summarized in general schemes; Fig. 4 is a composite of those by Janata *et al.* (50) and Fry and Reed (51) (the parent hydrocarbon is represented as RH to indicate its availability as a proton donor).

As Janata *et al.* (50) and Fry and Reed (51) point out, Fig. 4 illustrates the major influence of proton availability on the courses of reaction. In media of high proton donor concentration (EtOH; aqueous organic solvent; added donor such as phenol), initially formed $\dot{R}H^-$ radicals will be rapidly protonated. Since E_3 for reduction of $\dot{R}H_2$ is generally less negative than E_1 for reduction of the parent RH, $\dot{R}H_2$ will be reduced as formed (ECE process). In media of low proton availability (aprotic solvent; alkaline aqueous solution), the lifetime of radical anion $\dot{R}H^-$ is sufficiently long that 1e reduction to a dianion is observed at more negative potential E_2 on dme polarography as well as on hmde cyclic voltammetry; the dianion can abstract protons from the medium. The importance of the relative magnitudes of the rate constants, k_i, for the various protonation steps is discussed in the references cited (50, 51) (cf. Jacq's general formulation (29), (Fig. 2), and the provocative study by Wightman *et al.* (52) of the protonation kinetics and mechanism of the 2e quinone reduction, which parallels that for aromatic hydrocarbons in aprotic media).

Dietz (39) has reviewed possible mechanistic paths (chemical and electrochemical) for the electrogenerated anions and dianions.

Carbon–Halogen Bond Fission

The voluminous data on reduction of organic halogen-containing compounds in aqueous and nonaqueous media have been interpreted from a variety of viewpoints, e.g. refs. 53–55; ref. 4, pp. 201–244. Any attempt to force all of the data into a strict ionic or free-radical mechanism leads to a formulation of limited utility because of the essentially dual nature of the process (cf. subsequent discussion of the dibromosuccinic acids).

In electrochemical carbon–halogen (C—X) bond fission, the carbon to which the halogen is attached can be considered as an electrophilic reaction center, on which nucleophilic displacement occurs with electrons from the electrode acting as displacing agent. As the compound diffuses towards the electrode, the C—X bond or dipole is increasingly oriented, finally approaching in a direction normal to the electrode plane with the halogen as the more negative portion of the C—X bond oriented away from the electrode. In immediate vicinity of the electrode, electrostatic repulsion causes elongation of the C—X bond; a state is finally reached where the attractive forces between carbon and electrode, and between carbon and halogen are in balance; this may be considered as the transition state since movement of carbon towards the halogen tends to reform the C—X bond, whereas movement towards the electrode results in the forces between carbon and halogen being insufficient to retain the halogen, which separates as the negative halide ion since the electron pair constituting the C—X bond has been driven even closer to it during the process described. Departure of the halogen with the electron pair makes the carbon even more electropositive and an electron (or two) will flow to it from the electrode to form a free radical (or carbanion); the free radical normally rapidly adds a second electron to form a carbanion, which then neutralizes its charge by abstracting a proton from a solution or interfacial region

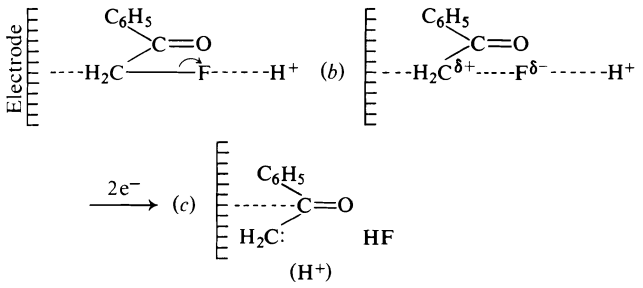

FIG. 5. Reaction path for the fission of the carbon–fluorine bond in phenacyl fluoride at a mercury electrode. The approach of the phenacyl fluoride to, and its orientation at, the electrode is represented by (*a*); polarization and subsequent reduction of the bond are represented by (*b*) and (*c*), respectively (from ref. 56).

species, or by electronic rearrangement and expulsion of an anion (cf. subsequent discussion of vicinal dihalides).

Final products of the 2e C—X fission are normally halide ion and an organic compound in which hydrogen has replaced halogen. In the case of compounds with halogens on adjacent carbons, $R_1R_2CX—R_3R_4CX$, the products of the initial 2e reaction are the halide ions and a more unsaturated species, $R_1R_2C{=}CR_3R_4$.

Since proton acquisition is not part of the rate-determining step in the C—X bond fission, it is clear why the process per se is normally p*H*-independent. The effect of p*H* on carbon–fluorine bond fission in aqueous solution further illuminates the process (56). $E_{1/2}$ for C—F fission is p*H*-independent above p*H* 6, but shows a sigmoidal dependence below p*H* 6. This is due to H^+ being able to assist the electrode in polarization of the C—F bond by H—F bonding in the transition state (Fig. 5). With decreasing H^+ concentration, the effect decreases and the fission becomes p*H*-independent. The marked tendency for ion pairing between fluoride and hydrogen ions is evident from the aqueous pK_a for hydrofluoric acid ($HF = H^+ + F^-$) of 3.17.

Sease (57) and Lambert and co-workers (58, 59) discuss whether electrochemical reduction of bridgehead bromides proceeds through back-side attack on carbon, as described, or through front-side attack on bromine. Alternate mechanisms involving, for example, attack by an electron from the electrode surface in a direction perpendicular to the C—X bond (9), have also been proposed (cf. pp. 885–891 of ref. 60 for a succinct summary).

Ketone Reduction

In aqueous acidic solution, aromatic ketones exhibit a p*H*-dependent 1e wave I and a p*H*-independent 1e wave II; these merge at about p*H* 6 to form a single p*H*-dependent wave III; the latter reaches 2e magnitude at about p*H* 9 and then decreases with increasing p*H* to near 1e magnitude; a more negative wave IV appears above p*H* 9 (61, 62). (In the case of some aromatic alkyl ketones, waves II and/or IV are obscured by background discharge.)

The proposed mechanism postulates (*a*) formation of a free radical as the fundamental process, (*b*) modification of this process with change in p*H*, i.e., anion radical formation in the alkaline region, and (*c*) possible reduction of the radical before dimerization occurs.

The process producing wave I can be explained as follows (Fig. 6) (61): (*a*) As the ketone diffuses into the field of the electrode, the latter initiates polarization of the carbonyl group. (*b*) Simultaneously, the carbonyl oxygen attracts neighboring protons, favoring increased polarization (the negligible effect of ionic strength indicates that little, if any, of the diffusing material is charged before it enters the electrode field). (*c*) The ketone, under influence of both proton and field completes diffusion (now supplemented by electromigration) into the interphase and acquires an electron. These steps are continuous and involve a transition state in which, as an electron is transferred to the carbonyl carbon, a proton is simultaneously bonded to the carbonyl oxygen.

The free radical produced dimerizes until a potential is reached at which it is reducible; it can then dimerize or be reduced; the latter reduction (wave II) is p*H*-independent.

The p*H*-dependency seen in the alkaline region, even though lessened, indicates continued proton participation in the potential-determining step. Since the decreased H^+ concentration

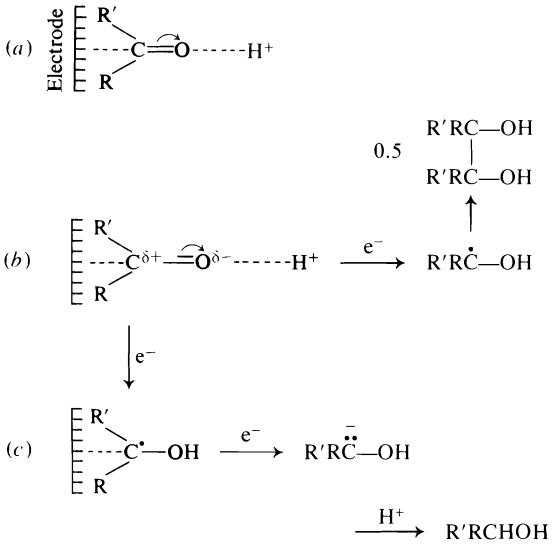

FIG. 6. Electrochemical reduction of a ketone in acidic, neutral, and slightly alkaline media: (*a*) initial diffusion–polarization process; (*b*) formation of the carbinol free radical (wave I); (*c*) reduction of the carbinol free radical (wave II) and subsequent acquisition of a proton. In neutral and slightly alkaline media, the combined sequence of electron-transfer steps represented by (*b*) and (*c*) produces the combined wave (from ref. 61).

greatly diminishes the probability of forming an O—H bond simultaneously with electron transfer, increasing amounts of carbinolate radical anion are formed (Fig. 7*b*). The latter, which is more difficultly reducible than the neutral radical, dimerizes until its reduction potential is reached. The needed additional energy for its reduction arises from the coulombic repulsion between it and the electrode, and from the electron having to enter an area of increased electron density. If the carbinolate radical anion is at the electrode when it acquires a proton, the resulting radical will be reduced to carbinol, thereby contributing to the wave III magnitude. Conversely, if the radical anion has diffused away from the electrode, the carbinol free radical subsequently formed will not be reduced but will dimerize.

Formation of the radical anion decreases the magnitude of wave III above p*H* 9, while its reduction produces wave IV. Since reduction of the carbinol free radical is unaffected by p*H*, the wave III height increases to a maximum at about p*H* 9 even though free radical formation becomes more difficult with increasing p*H*.

Electrochemical reduction of benzophenone in aprotic medium (63) supports the mechanism outlined. The benzophenone is reduced in successive 1e steps, first to the radical anion and then to the benzhydrol dianion. Proton addition causes the second 1e step to merge with the first since the neutral free radical is reduced at the potential of initial benzophenone reduction.

Further formulations of reduction paths for the carbonyl group are given by Zuman *et al.* (64) and Feoktistov and Lund (65).

Significance of pH-Dependence of $E_{1/2}$

Based on the foregoing discussion, a p*H*-dependent potential for an electrochemical bond fission may be due to H^+ aiding the electrode in polarization of the bond to be broken, i.e., a concerted push–pull attack on that bond by both electrode and H^+ (or proton donor). Thus, as shown in Figs. 6 and 7, the p*H*-dependence of carbonyl group reduction is ascribable to a transition species analogous for that described for C—F bond fission (Fig. 5):

[28] 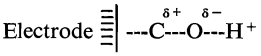

All multiple bond reductions in neutral organic compounds in aqueous or partially aqueous solutions are likely to be p*H*-dependent in the region of appreciable H^+ activity. Unfortunately, reduction of some types of multiple bonds (such as those of the phenyl-substituted olefins) occur at such negative potentials that, in solutions of appreciable H^+ activity, H^+ would be reduced at less negative potential than the multiple bond. However, $E_{1/2}$ for some such compounds in nonaqueous media is shifted to more positive potential on addition of a proton source with often an increased current flow due to the change from a 1e to a multielectron process. Thus, on proton donor addition, the 1e wave shown by purine, adenine, and other 6-substituted purines in nonaqueous media generally shifts positively and grows in magnitude to that expected for a 4e process (two 2e waves for purine itself and 6-methylpurine) (20).

Effect of Substitution: Reduction of Nitrogen Heterocycles

The alteration of reaction path by substitution can be illustrated by the electrochemical reduction of azabenzene ring systems, e.g., the three classes of nitrogen heterocycles: pyridines in the form of nicotinamides; pyrimidines; purines

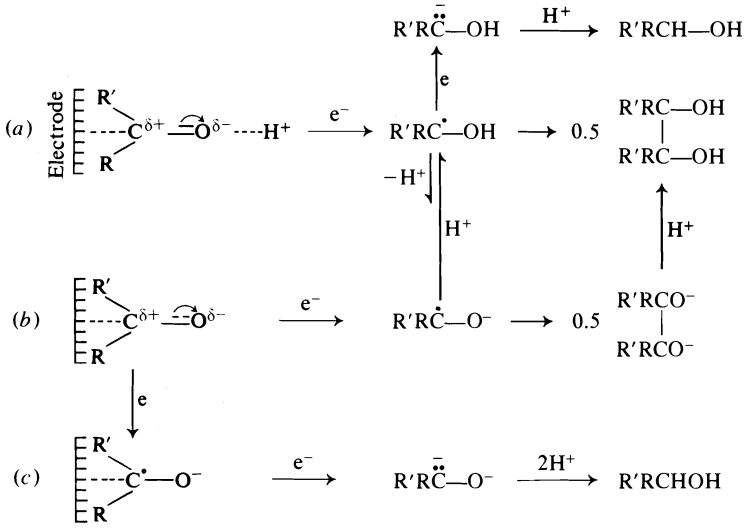

FIG. 7. Electrochemical reduction of a ketone in alkaline media (above p*H* 9): (*a*) and (*b*) processes producing the combined wave; (*c*) reduction of carbinolate radical anion (wave III); the steps shown should be considered as continuous. The position of the equilibrium between carbinol free radical (*a*) and its anion (*b*) is dependent on p*H* (from ref. 61).

(cf. refs. 24 and 66 for a review of the electrochemistry of these compounds). A general reduction path can be schematically formulated as follows, where RN represents an electroactive nitrogen heterocycle:

$$[29] \quad RN + e^- = \dot{R}N^- = \text{product(s)}$$

$$[30] \quad RN + ne^- + mH^+ = \text{product(s)}$$

$$[31] \quad pRN = (RN)_p$$

$$[32] \quad RN + R'N = RNR'N$$

$$[33] \quad RN + \text{electrode} = RN_{ads}$$

$$[34] \quad qRN_{ads} = (RN_{ads})_q$$

$$[35] \quad RN_{ads} + ne^- + mH^+ = \text{product(s)}$$

$$[36] \quad \text{product} + \text{electrode} = \text{product}_{ads}$$

Equations 29 and 30 refer to the initial and overall electron-transfer processes; eq. 35 refers to reduction of an adsorbed reactant (eq. 33), which may associate in the adsorbed state (eq. 34). Adsorption of product is indicated by eq. 36. Possible association of reactant, e.g. formation of a complementary purine–pyrimidine pair, is accounted for by eqs. 31 and 32; the associated species may then be the reactant of eqs. 29, 30, and 33. In proton-containing media, the electroactive reactant may be protonated RN or corresponding species. Complications may be introduced in nonaqueous media by father–son reactions (cf. supra).

The polarographic and allied chemical behavior of the 1-substituted nicotinamides and the equivalent protonated nicotinamides in aqueous media is exemplified by that of NAD^+ (nicotinamide adenine dinucleotide), which can be summarized as follows (approximate potentials are shown) (67):

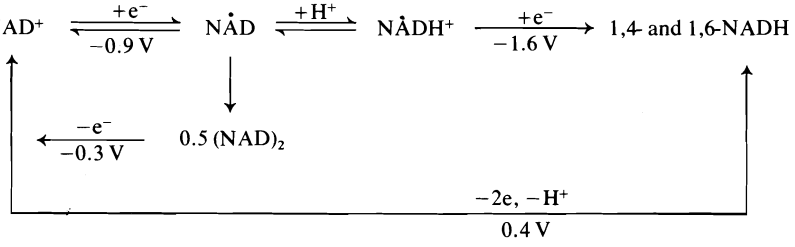

Reduction occurs in the cationic pyridinium ring. The first 1e reduction is p*H*-independent. The free radical rapidly dimerizes, largely to the 4,4′ isomer, reflecting the transition from the 6,6′ isomer in the case of nicotinamide itself to the 4,4′ form as the substituent on the pyridinium nitrogen increases in size. At more negative potential, NAD^+ is reduced to a dihydropyridine via 1e reduction of the free radical; the dimer is not reduced at this potential. The free radical reduction must be preceded by a protonation, e.g. in nonaqueous media in absence of a suitable proton donor, a second charge transfer is not seen. The dimer can be oxidized to NAD^+ at a potential considerably more positive than that for the initial reduction; NADH is oxidized to NAD^+ at still more positive potential in a nearly p*H*-independent process.

Reduction of Pyrimidine

Electrochemical reduction of the pyrimidine (1,3-diazine) ring differs markedly from that of the nicotinamide (3-carbamoylpyridine or 3-carbamoyl-1-azine) ring, which, within the available potential range, shows at most two separate 1e steps, which fuse only in rather alkaline aqueous medium. Pyrimidine, however, can be reduced in a series of 1e, 2e, and 4e steps depending on proton availability.

In aqueous media, pyrimidine exhibits five cathodic waves over the p*H* range (38, 68, 69) (Fig. 8). In acid solution, only p*H*-dependent 1e wave I is seen. At about p*H* 3, nearly p*H*-independent 1e wave emerges from background discharge. Because of the difference in p*H*-dependence, waves I and II merge at about p*H* 5 to form p*H*-dependent 2e wave III. Near p*H* 7, p*H*-independent 2e wave IV emerges from background and, due to the differing p*H*-dependencies, merges at about p*H* 9 with wave III to form p*H*-dependent 4e wave V. This wave pattern can be readily explained on the basis of the general electrode reaction mechanism (Fig. 1), as indicated in Fig. 9, which also shows the relation between reaction paths in protic and aprotic media.

Wave I results from 1e reduction of the 3,4 N=C bond with simultaneous (or prior) acquisition of a proton at N(3) to form a free radical, which may dimerize to 4,4′-bipyrimidine or be reduced (1e process) at more negative

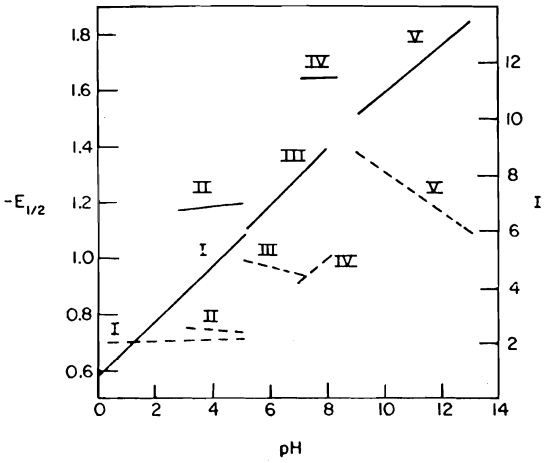

FIG. 8. Variation with p*H* of half-wave potentials ($E_{1/2}$; solid lines) and diffusion current constants (*I*; dashed lines) for pyrimidine. Roman numerals refer to the waves (cf. text).

potential (wave II) to a carbanion, which then acquires a proton to form 3,4-dihydropyrimidine. Wave III results when the potential necessary to transfer the first electron into the 3,4 N=C bond becomes, as a result of decreasing proton activity, more negative than that required to reduce the free radical. Wave IV results from a probably stepwise 2e reduction at still more negative potential of the 1,2 N=C bond in the dihydropyrimidine to form a tetrahydropyrimidine. When the energy necessary to transfer the first electron into the 3,4 N=C bond exceeds that necessary for a similar addition to the 1,2 N=C bond, wave V (4e process) results as an example of the cascading effect mentioned in connection with the general mechanism, i.e., separate faradaic processes may merge into a single wave due to the instability of the various products at the potential required to introduce the first electron.

Reduction of Substituted Pyrimidines

Substitution may alter the prototype pyrimidine reduction path, e.g. the initially produced free radical or a chemically altered form of it may be unstable at the potential of its formation and, consequently, would be immediately reduced to produce a 2e wave.

Tautomeric shifts due to substituents having divalent oxygen singly bonded to carbon, e.g. C—O—H, may result in migration of double bonds out of the ring to form less readily re-

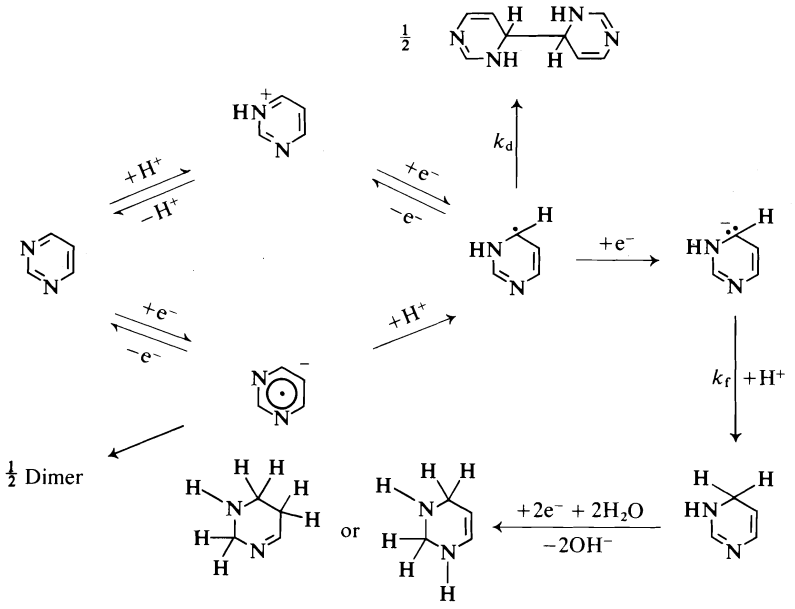

FIG. 9. Interpretation of the electrochemical behavior observed for pyrimidine in aqueous media. The lower reaction sequence involving electron addition to unprotonated pyrimidine is that in aprotic media. The reactions involved in the reduction of the 1,2 N=C bond are analogous to those indicated for the 3,4 N=C bond reduction (from ref. 38).

ducible external double bonds, thus limiting the extent of reduction or making it more difficult. Two commonly occurring nucleic acid pyrimidines, uracil (2,4-dihydroxypyrimidine) and thymine (2,4-dihydroxy-5-methylpyrimidine), are not reducible in aqueous media but are reduced in nonaqueous media at very negative potential.[3]

Chemical reactions such as deamination or hydrolysis, which follow electron-transfer, may generate electroactive species, e.g. reduction of 4-aminopyrimidines hydrogenates the 3,4 N=C bond to produce a *gem* diamine on C(4); resulting deamination regenerates the 3,4 N=C bond, which is reduced as formed since presence of the C(4) amino group made reduction of the original 3,4 N=C bond more difficult.

Effects may be compounded. Presence of a hydroxyl group on C(2) removes the 1,2 N=C bond, facilitates 3,4 N=C bond reduction, and increases markedly the dimerization rate of the initially produced free radical; its presence also seems to accelerate deamination of a C(4) diamine. Thus, 2-hydroxypyrimidine undergoes only a 1e reduction over the entire p*H* range to produce a bipyrimidine.

The result of such substitution effects is evident in the reduction path observed for cytosine, which is the most important pyrimidine occurring in nucleic acids.

Reduction Path: Cytosine

At p*H* 3.7–5.7, cytosine (4-amino-2-hydroxypyrimidine) gives a well defined dme reduction wave (27, 28, 68). Cyclic voltammetric and ac polarographic data support at the least a CECCEC process.

The proposed mechanism (Fig. 10) for the overall 3e process involves reduction of the protonated 3,4 N=C bond in cytosine (Cy) to a carbanion, protonation of the latter, deamination of the resulting *gem* diamine to 2-hydroxypyrimidine (2-HP), protonation of the latter followed immediately by a 1e reduction, and dimerization of the resulting free radical:

$$[38] \quad Cy + H^+ \underset{}{\overset{{}_1k_p}{\rightleftharpoons}} CyH^+$$

$$[39] \quad CyH^+ + 2e^- \overset{{}_1k_{s,h}}{\rightleftharpoons} CyH^-$$

$$[40] \quad CyH^- + H^+ \xrightarrow{{}_2k_p} CyH_2$$

$$[41] \quad CyH_2 \xrightarrow{k_{da}} 2\text{-HP} + NH_3$$

[3]T. E. Cummings and P. J. Elving, unpublished results.

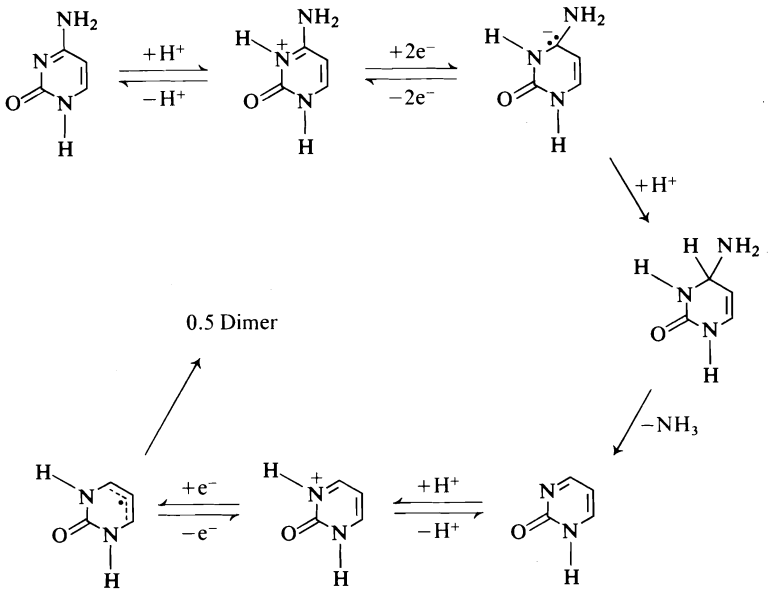

FIG. 10. Proposed reaction pathway for the reduction of cytosine in aqueous media (from ref. 27).

[42] $$2\text{-HP} + H^+ \underset{}{\overset{{}_3k_p}{\rightleftharpoons}} 2\text{-HPH}^+$$

[43] $$2\text{-HPH}^+ + e^- \underset{}{\overset{{}_2k_{s,h}}{\rightleftharpoons}} 2\text{-H}\dot{\text{P}}\text{H}$$

[44] $$2\ 2\text{-H}\dot{\text{P}}\text{H} \xrightarrow{k_d} (2\text{-HPH})_2$$

where k_p, k_{da}, and k_d are rate constants for homogeneous chemical reactions involving protonation, deamination, and dimerization, respectively. Protonation reactions 38 and 42 are very rapid and do not affect the equilibria of the other reactions. Deamination is somewhat slow on the time scale involved in dme polarography but occurs completely on prolonged electrolysis.

Structural Effects on Mechanistic Paths

The influence of structure on electrode mechanisms can be illustrated by phenomena observed on reduction of carbon–halogen (C—X) bonds and C_4 dibasic acids. The stereochemistry of organic electrode processes has been reviewed by Eberson and Horner (62).

Steric Effects and Steric Hindrance

Little or no steric hindrance is evident to electron transfer from electrode to carbon center in C—X fission, e.g. contrary to behavior of such groups to OH^- attack, a C—Br bond is more readily broken electrochemically in a tribromomethyl group than in a dibromomethyl and more readily in the latter than in monobromomethyl. However, steric effects may be manifest through adsorption or orientation of the molecule at the interface relative to the distance between electrode and reactive center (35), and possible interference with electrode-compound overlap by the bulk of the compound, e.g. due to side chains on the reactive center.

In reduction of the 2-bromoalkanoic acids, the shift of $E_{1/2}$ in the alkaline region to more negative values than expected for acids having ethyl or larger groups on the same carbon as the halogen was ascribed to the tendency towards stable ring formation in compounds having chains of at least six members with terminal atoms differing in electronegativity (35, 70, 71).

Steric Control of Products

Control of product structure by external conditions is indicated by the effect of p*H* on reduction of *meso-* and *racemic*-α,α′-dibromosuccinic acids (72).

Although some maleic acid production might be expected in the p*H* range where each acid exists as the monoanion, as a result of the *cis* configuration being maintained during reduction due to chelation between undissociated carboxyl group hydrogen and carboxylate group oxygen, polarographic and macroscale re-

ductions of the *meso* acid and the diethyl esters do not yield any detectable maleate species; the sole product formed in the single 2e wave is fumerate. However, the *racemic* acid yields a varying amount of maleic acid in the p*H* range of 1–7 with a maximum yield (70%) at p*H* 4; the remainder of the product is fumaric acid. These results can be explained in terms of a hydrogen bonding whose strength is influenced by p*H* and steric factors irrespective of the mechanistic route proposed.

Examination of molecular models of the *meso* and *racemic* acids (both carboxyl groups undissociated; one group ionized; both groups ionized) and consideration of other pertinent factors indicate that, of the six species, in only one (singly ionized *racemic* acid) do the charge and steric factors combine energetically to favor cyclic hydrogen bond formation. The stability of this cyclic form is supported by the fact that steric factors alone tend to keep both *meso*- and *rac*-2,3-dibromobutane (73) in the *trans* position. This, coupled with the added energy of interaction between hydroxyl hydrogen and carboxylate ion, should lead to a relatively stable configuration.

In reduction of the *meso* acid over the whole p*H* range and of the *racemic* acid in the intermediate p*H* range, step 2*b* (Fig. 1) is followed by step 4*b* since the conformation of the molecules is such that the two Br atoms are essentially *trans* and coplanar so that, as an electron pair is added to one C atom as its Br departs as a bromide ion, rearward displacement of the second Br atom as a bromide ion and formation of the C=C double bond can occur simultaneously due to electronic rearrangement, i.e., the electron pair on the original reactive center shifts towards the adjacent more positive C which still has a halogen attached to it. Such an action would have a relatively low activation energy.

The preferred configuration for the *racemic* acid at high p*H* and probably also at low p*H*, however, has the Br atoms constrained in a *cis* position and single step rearward elimination is not possible. In such a situation, a reaction involving step 2*a* is postulated; a planar free radical is formed and the second electron is so added that the remaining Br can be displaced at the same time (rotation of the sigma bond joining the two carbon centers in the anion produced on the second electron addition would help give the thermodynamically favored fumerate product).

Stereospecific Reduction

Dibromomaleic and dibromofumaric acids are quantitatively reduced (2e process) to acetylenedicarboxylic acid (ADCA) (Fig. 11); their diesters behave similarly (74). Between p*H* 0.4 and 3, ADCA is reduced in a 3e process to *rac*-α,α′-dimethylsuccinic acid; its monoester yields diethyl *rac*-α,α′-dimethylsuccinate in a 3e process; however, its diethyl ester is reduced to diethyl fumarate (2e process). The stereospecificity of these reductions is due to structural factors inherent in the compounds involved and not to interaction between them and the electrode.

The ADCA reduction mechanism is moderately complex (Fig. 11). Addition of two H^+ (one is formally the lost carboxyl group hydrogen) and one electron converts ADCA to fulgenic acid (enclosed in square in the figure) with loss of CO_2. The nature of the activated state is uncertain; however, comparison of acid, monoester and diester behavior shows that the second carboxyl group plays no direct role in the decarboxylation. A possible path would be addition of one e and one H^+ to form the free radical, HOOC—Ċ=CH—COOH, which could then decarboxylate as such structures often do to yield HOOC—Ċ—CH_2, whose dimerization would produce fulgenic acid. Reduction of the latter produces dimethylmaleic acid which, in turn, is specifically reduced to *rac*-α-α′-dimethylsuccinic acid. This mechanism indicates why the monoester with one unprotected carboxyl group also forms the *rac*-succinate, whereas the diester, both of whose carboxyl groups are esterified, goes to the fumarate.

The reduction of dimethylmaleic and dimethylfumaric acids by single 2e waves to *rac*- and *meso*-α,α′-dimethylsuccinic acids, respectively (Fig. 11), is direct evidence that reduction of the double bonds at the electrode proceeds through *trans* hydrogen addition. Evidence excluding certain intermediates, as indicated in Fig. 11, is discussed in the original paper (74).

The effects of structure and rates on electrode reaction stereochemistry are further indicated by polarographic and macroscale electrolysis of the monobromo C_4 dibasic acids and their esters (75), although in this case interaction with the electrode may be a significant factor. Be-

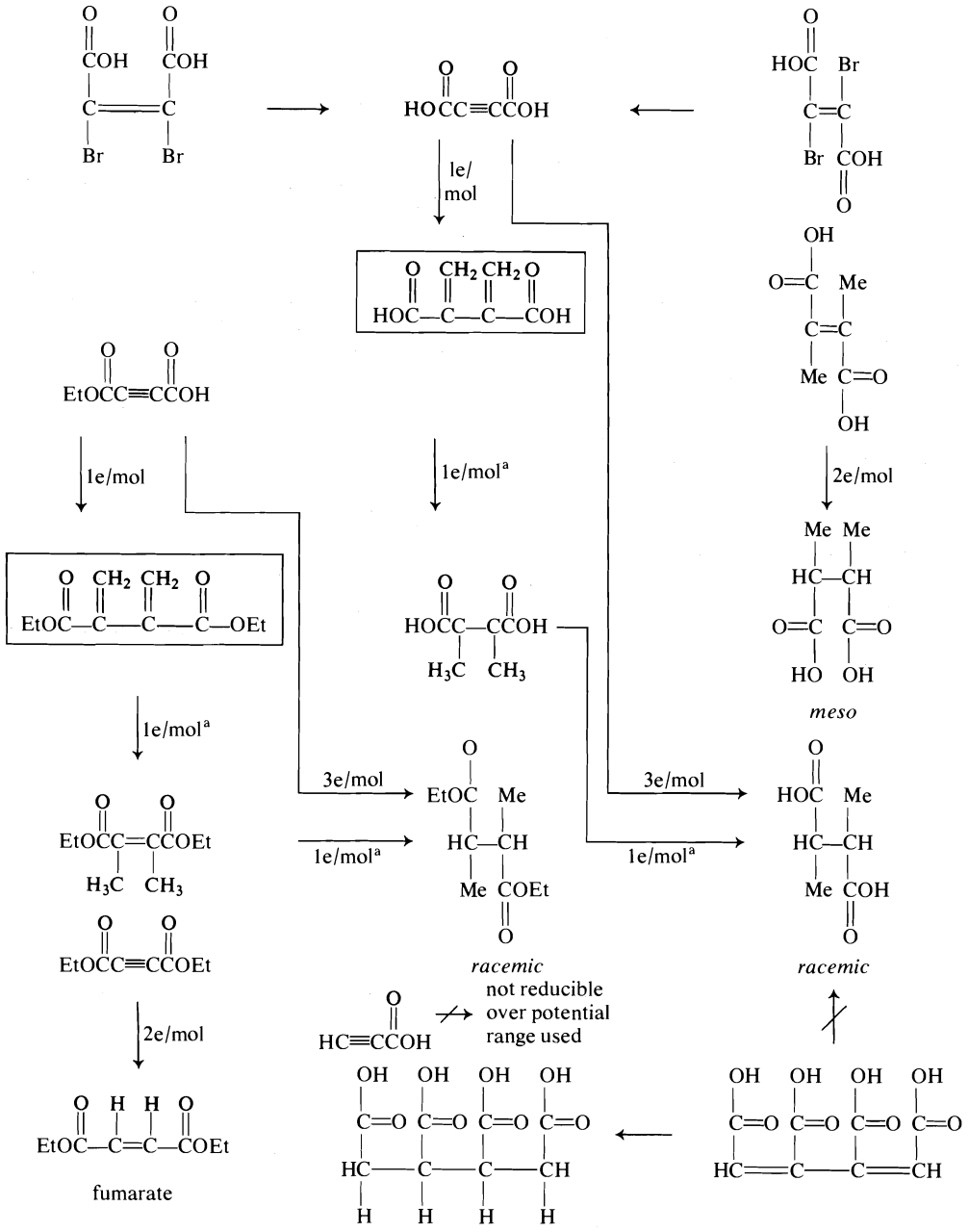

FIG. 11. Interrelation and proposed mechanisms for the electrochemical reduction of acetylenedicarboxylic acid (ADCA) and related compounds. Compounds enclosed in rectangles are postulated intermediates. The superscript a indicates that the electron transfer shown is calculated on the basis of the constituent (ADCA) acid or ester. A crossed arrow indicates that the reaction does not proceed under normal polarographic conditions (from ref. 74).

tween p*H* 0.5 and 10.5, the diethyl esters of monobromomaleic acid (MBMA) and monobromofumaric acid (MBFA) are quantitatively reduced (2e process) to diethyl fumerate (C—Br bond fission occurs before C=C bond reduction); MBFA is reduced (2e process) to fumaric acid. MBMA, however, is reduced to maleic and fumaric acids, and a dimer, butadiene-

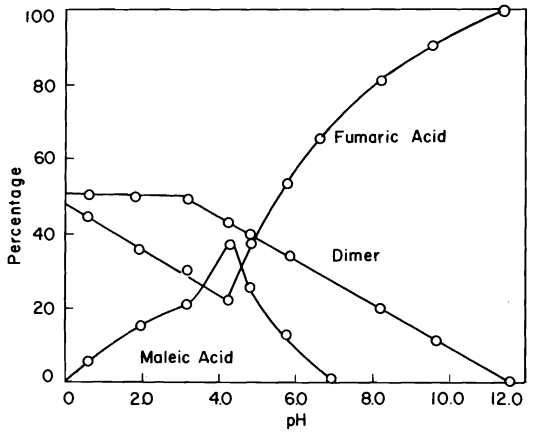

FIG. 12. Variation with p*H* of relative amounts of reduction products of monobromomaleic acid produced on coulometric (macro scale) electrolysis (from ref. 75).

1,2,3,4-tetracarboxylic acid; the relative amounts of these products are dependent on p*H* (Fig. 12), but the maleic–fumaric ratio at any p*H* is the same as that found on reduction of *rac*-α,α′-dibromosuccinic acid (cf. supra).

The mechanism outlined in Fig. 13 was proposed to explain the product observed (the structures drawn are meant not to define rigidly the structures but to aid the discussion). Electron addition to MBMA (I) liberates a bromide ion and forms a radical (II). The latter can dimerize to IV or add a second electron to form III, which is the intermediate common to the dibromosuccinic acid reduction. During the formation and/or existence of II or III, rotation can occur to form the *trans* product as obtained from the unionized, doubly ionized and ester species. With the singly ionized form, an intramolecular hydrogen bond between the carboxyl groups hinders rotation.

The same general mechanism can be applied to MBFA reduction, whose intermediate structures, however, are stable to rotation. Single-bonded intermediates II and III exist for an extremely short time and, if the species has no great need to rotate, the reaction will proceed and refreeze to the original structure without rotation. The energy diagrams for species II and

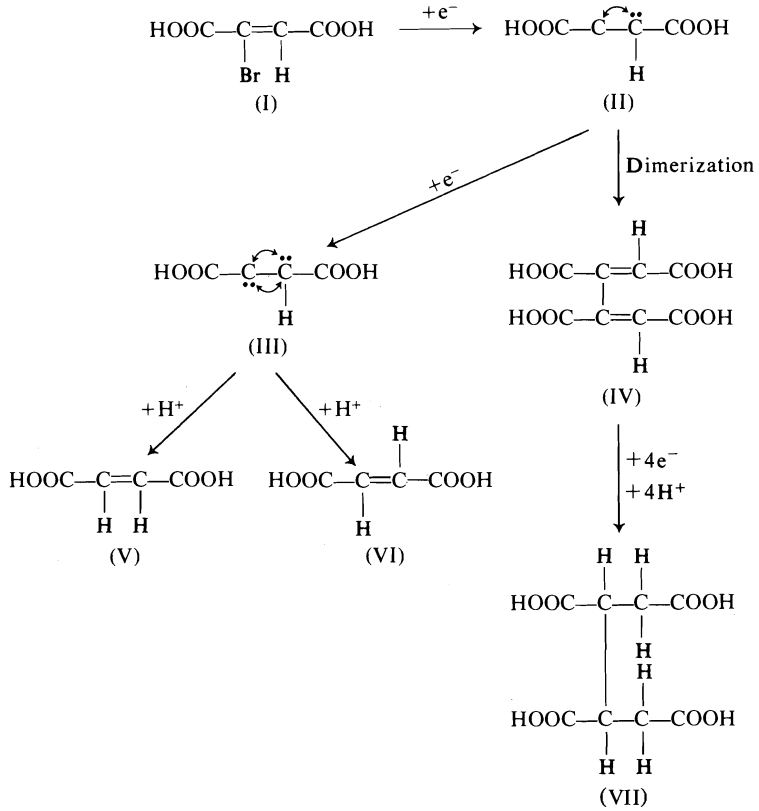

FIG. 13. Reaction mechanism proposed for electrochemical reduction of monobromomaleic and monobromofumaric acids (from ref. 75).

III with regard to orientation show one energy minimum for the ionized, double ionized, and ester species of both acids, corresponding to a *trans* conformation, and two minima for the singly ionized species, corresponding to *trans* and *cis* (hydrogen bound species) configurations. An energy barrier exists between the latter forms, so that, interconversion to the *cis* structure requires time and energy, which the reaction makes unavailable.

As to why only MBMA reduction yields a dimer, intermediate structure II can undergo two opposing reactions, whose rates, in the case of the *cis* form, are nearly equal up to p*H* 3 (Fig. 12). The double bond in maleic acid reacts with mercury while that in fumaric acid does not (76); the effect of this reaction and that of a free radical with mercury (77) will be to stabilize the *cis* form of intermediate II, thus slowing its reaction to III and resulting in a large free radical concentration at the interface. These effects enhance dimerization with the *cis* form.

Since dimer production is strong, if not conclusive, evidence for the existence in the course of a reaction of a free radical intermediate, formation of a dimeric product on MBMA reduction offers the strongest experimental support for electrochemical carbon–halogen bond fission in aqueous media proceeding, at least in part, through a free radical intermediate.

A potentially important approach is that of asymmetric reduction as a result of addition of suitable chemical reagents to the solutions being electrolyzed (78) or covalent attachment of such reagents to the electrode surface (79). Thus, addition of alkaloids has been found to induce optical activity in some electrolytic reductions, e.g. of acetyl pyridines at a mercury electrode. Recent studies are listed in ref. 78.

Acknowledgment

The author thanks the National Science Foundation for helping to support the present study.

1. P. J. ELVING and B. PULLMAN. *In* Advances in chemical physics. Vol. III. *Edited by* I. Prigogine. Interscience Publishers, New York, NY. 1961. pp. 1–31.
2. M. M. BAIZER (*Editor*). Organic electrochemistry. Marcel Dekker, New York, NY. 1973.
3. A. P. TOMILOV, S. G. MAIRANOVSKII, M. YA. FIOSHIN, and V. A. SMIRNOV. Electrochemistry of organic compounds. Halsted Press, New York, NY. 1972.
4. C. K. MANN and K. K. BARNES. Electrochemical reactions in nonaqueous systems. Marcel Dekker, New York, NY. 1970.
5. Electrode reactions of organic compounds. Discussions of the Faraday Society. No. 45. 1968.
6. Intermediates in electrochemical reactions. Discussions of the Faraday Society. No. 56. 1973.
7. G. CAUQUIS. *In* Organic Electrochemistry. *Edited by* M. Baizer. Marcel Dekker, New York, NY. 1973.
8. M. FLEISCHMANN and D. PLETCHER. *In* Reactions of molecules at electrodes. *Edited by* N. S. Hush. Wiley-Interscience, New York, NY. 1971. pp. 347–402.
9. A. STREITWIESER, JR. and C. PERRIN. J. Am. Chem. Soc. **86**, 4938 (1964).
10. B. J. TABNER and J. R. YANDLE. *In* Reactions of molecules at electrodes. *Edited by* N. S. Hush. Wiley-Interscience, New York, NY. 1971. pp. 283–303.
11. A. A. VLČEK. *In* Progress in inorganic chemistry. Vol. 5. *Edited by* F. A. Cotton. Interscience Publishers, New York, NY. 1963. p. 216.
12. C. O. SCHMAKEL, K. S. V. SANTHANAM, and P. J. ELVING. J. Electrochem. Soc. **121**, 345 (1974).
13. J. JACQ, B. CAVALIER, and O. BLOCH. Electrochim. Acta, **13**, 1119 (1968).
14. W. J. BLAEDEL and R. A. JENKINS. Anal. Chem. **47**, 1337 (1975).
15. W. M. CLARK. Oxidation–reduction potentials of organic systems. Williams and Wilkins, Baltimore. 1960.
16. P. J. ELVING. Pure Appl. Chem. **7**, 324 (1963).
17. J. HEYROVSKY and J. KUTA. Polarography. Academic Press, New York, NY. 1966.
18. L. MEITES. Polarographic techniques. 2nd ed. Interscience Publishers, New York, NY. 1965.
19. P. ZUMAN. *In* Progress in polarography. Vol. III. *Edited by* P. Zuman and L. Meites. Wiley-Interscience, New York, NY. 1972. pp. 73–156.
20. K. S. V. SANTHANAM and P. J. ELVING. J. Am. Chem. Soc. **96**, 1653 (1974).
21. P. J. ELVING and S. J. PACE. Experentia Suppl. **18**, 35 (1971).
22. E. R. BROWN and R. F. LARGE. *In* Physical methods of chemistry. Part IIA. *Edited by* A. Weissberger and B. W. Rossiter. Wiley-Interscience, New York, NY. 1971. pp. 423–530.
23. P. J. ELVING, C. O. SCHMAKEL, and K. S. V. SANTHANAM. Crit. Rev. Anal. Chem. **6**, 1 (1976).
24. P. J. ELVING. *In* Topics in bioelectrochemistry and bioenergetics. Vol. 1. *Edited by* G. Milazzo. John Wiley and Sons, London, England. 1976. pp. 180–286.
25. R. BRDIČKA, V. HANUS, and J. KOUTECKY. *In* Progress in polarography. Vol. 1. *Edited by* P. Zuman. Interscience Publishers, New York, NY. 1962. pp. 145–199.
26. R. D. BRAUN, K. S. V. SANTHANAM, and P. J. ELVING. J. Am. Chem. Soc. **97**, 2591 (1975).
27. J. W. WEBB, B. JANIK, and P. J. ELVING. J. Am. Chem. Soc. **95**, 991 (1973).
28. J. W. WEBB, B. JANIK, and P. J. ELVING. J. Am. Chem. Soc. **95**, 8495 (1973).
29. J. JACQ. J. Electroanal. Chem. **29**, 149 (1971).
30. B. KASTENING. Chem. Ing. Tech. **44**, 199 (1972).
31. V. G. MAIRANOVSKY. Electrochim. Acta, **20**, 807 (1975).
32. V. G. MAIRANOVSKY, L. A. VAKULOVA, and G. I. SAMOKHVALOV. Elektrokhimiya, **3**, 23 (1967).

33. H. LUND, H. DOUPEUX, M. A. MICHEL, G. MOUSSET, and G. SIMONET. Electrochim. Acta, **19**, 629 (1974).
34. M. BREITER, M. KLEINERMAN, and P. DELAHAY. J. Am. Chem. Soc. **80**, 5111 (1958).
35. P. J. ELVING, C. H. ALBRIGHT, and I. ROSENTHAL. J. Electrochem. Soc. **99**, 227 (1952).
36. S. W. FELDBERG. *In* Electroanalytical chemistry. Vol. 3. *Edited by* A. J. Bard. Marcel Dekker, New York, NY. 1969. pp. 199–296.
37. J. E. O'REILLY and P. J. ELVING. J. Am. Chem. Soc. **93**, 1871 (1971).
38. P. J. ELVING, S. J. PACE, and J. E. O'REILLY. J. Am. Chem. Soc. **95**, 647 (1973).
39. R. DIETZ. *In* Organic electrochemistry. *Edited by* M. Baizer. Marcel Dekker, New York, NY. 1973. pp. 253–277.
40. G. J. HOYTINK. *In* Advances in electrochemistry and electrochemical engineering. Vol. 7. *Edited by* P. Delahay. Interscience Publishers, New York, NY. 1970. pp. 221–281.
41. M. E. PEOVER. *In* Electroanalytical chemistry. Vol. 2. *Edited by* A. J. Bard. Marcel Dekker, New York, NY. 1967. pp. 1–51.
42. M. E. PEOVER. *In* Reactions of molecules at electrodes. *Edited by* N. S. Hush. Wiley-Interscience, New York, NY. 1971. pp. 259–281.
43. V. D. PARKER. J. Am. Chem. Soc. **98**, 98 (1976).
44. G. J. HOIJTINK and J. VAN SCHOOTEN. Recl. Trav. Chim. Pays-Bas, **71**, 1089 (1952).
45. M. D. HAWLEY and S. W. FELDBERG. J. Phys. Chem. **70**, 3459 (1966).
46. S. W. FELDBERG. J. Phys. Chem. **75**, 2377 (1971).
47. L. NADJO and J. M. SAVEANT. J. Electroanal. Chem. **33**, 419 (1971).
48. S. W. FELDBERG. J. Phys. Chem. **73**, 1238 (1969).
49. M. MASTRAGOSTINO, L. NADJO, and J. M. SAVEANT. Electrochim. Acta, **13**, 721 (1968).
50. J. JANATA, J. GENDELL, R. G. LAWTON, and H. B. MARK. J. Am. Chem. Soc. **90**, 5226 (1968).
51. A. J. FRY and R. G. REED. J. Am. Chem. Soc. **91**, 6448 (1969).
52. R. M. WIGHTMAN, J. R. COCKRELL, R. W. MURRAY, J. N. BURNETT, and S. B. JONES. J. Am. Chem. Soc. **98**, 2562 (1976).
53. N. S. HUSH and G. A. SIEGAL. Discuss. Faraday Soc. **45**, 23 (1968).
54. M. R. RIFI. *In* Organic electrochemistry. *Edited by* M. Baizer. Marcel Dekker, New York, NY. 1973. pp. 279–314.
55. M. R. RIFI and F. H. COVITZ. Introduction to organic electrochemistry. Marcel Dekker, New York, NY. 1974. pp. 194–219.
56. P. J. ELVING and J. T. LEONE. J. Am. Chem. Soc. **79**, 1546 (1957).
57. J. W. SEASE, P. CHANG, and J. L. GROTH. J. Am. Chem. Soc. **86**, 3154 (1964).
58. F. L. LAMBERT and K. KOBAYAS. J. Am. Chem. Soc. **82**, 5324 (1960).
59. F. L. LAMBERT, A. H. ALBERT, and J. P. HARDY. J. Am. Chem. Soc. **86**, 3155 (1964).
60. L. EBERSON and L. HORNER. *In* Organic electrochemistry. *Edited by* M. Baizer. Marcel Dekker, New York, NY. 1973. pp. 869–903.
61. P. J. ELVING and J. T. LEONE. J. Am. Chem. Soc. **80**, 1021 (1958).
62. M. SUZUKI and P. J. ELVING. J. Phys. Chem. **65**, 391 (1961).
63. R. F. MICHIELLI and P. J. ELVING. J. Am. Chem. Soc. **90**, 1989 (1968).
64. P. ZUMAN, D. BARNES, and A. RYVOLOVA-KEJHAROVA. Discuss. Faraday Soc. **45**, 202 (1968).
65. L. G. FEOKTISTOV and H. LUND. *In* Organic electrochemistry. *Edited by* M. Baizer. Marcel Dekker, New York, NY. 1973. pp. 372–375.
66. P. J. ELVING, J. E. O'REILLY, and C. O. SCHMAKEL. *In* Methods of biochemical analysis. Vol. 21. *Edited by* D. Glick. Interscience Publishers, New York, NY. 1973. pp. 287–465.
67. C. O. SCHMAKEL, K. S. V. SANTHANAM, and P. J. ELVING. J. Am. Chem. Soc. **97**, 5083 (1975).
68. D. L. SMITH and P. J. ELVING. J. Am. Chem. Soc. **84**, 2741 (1962).
69. J. E. O'REILLY and P. J. ELVING. J. Electroanal. Chem. **21**, 169 (1969).
70. P. J. ELVING, J. M. MARKOWITZ, and I. ROSENTHAL. J. Electrochem. Soc. **101**, 195 (1954).
71. P. J. ELVING, J. M. MARKOWITZ, and I. ROSENTHAL. Chem. Ind. (London), 1192 (1959).
72. P. J. ELVING, I. ROSENTHAL, and A. J. MARTIN. J. Am. Chem. Soc. **77**, 5218 (1955).
73. D. P. STEVENSON and V. SCHOMAKER. J. Am. Chem. Soc. **62**, 3173 (1939).
74. I. ROSENTHAL, J. R. HAYES, A. J. MARTIN, and P. J. ELVING. J. Am. Chem. Soc. **80**, 3050 (1958).
75. P. J. ELVING, I. ROSENTHAL, J. R. HAYES, and A. J. MARTIN. Anal. Chem. **33**, 330 (1961).
76. F. C. WHITMORE. Organic compounds of mercury. Chemical Catalog Co., New York, NY. 1929. p. 150.
77. H. GILMAN (*Editor*). Organic chemistry. Vol. I. 2nd ed. John Wiley and Sons, New York, NY. 1943. p. 549.
78. J. KOPILOV, S. SHATZMILLER, and E. KARIV. Electrochim. Acta, **21**, 535 (1976).
79. B. F. WATKINS, J. R. BEHLING, E. KARIV, and L. L. MILLER. J. Am. Chem. Soc. **97**, 3549 (1975).

Vibrational analysis of alkyl bromides. II. Secondary bromides

G. A. CROWDER AND MAURICE IWUNZE

Department of Chemistry, West Texas State University, Canyon, TX 79016, U.S.A.

Received March 30, 1977

G. A. CROWDER and MAURICE IWUNZE. Can. J. Chem. **55**, 3413 (1977).

Infrared and Raman spectra were obtained for 2-bromopentane, 3-bromopentane, 2-bromohexane, and 3-bromohexane. Vibrational assignments were made for several conformers of each compound with the aid of normal coordinate calculations. A 48 parameter modified valence force field was obtained that fit 221 frequencies of three conformers of 2-bromopentane, 4 conformers of 3-bromopentane, and 1 conformer of 2-bromobutane with an average error of 4.1 cm^{-1}. This force field was transferred to the bromohexanes, with good results.

G. A. CROWDER et MAURICE IWUNZE. Can. J. Chem. **55**, 3413 (1977).

On a obtenu les spectres infrarouge et Raman des composés suivants: bromo-2 pentane, bromo-3 pentane, bromo-2 hexane et bromo-3 hexane. L'attribution des vibrations est déterminée pour plusieurs conformères de ces composés grâce à des calculs de coordonnées normales. Un champ modifié de force de valence est obtenu et celui-ci comporte 48 paramètres, lequel s'adapte à 221 fréquences pour trois conformères du bromo-2 pentane, quatre conformères du bromo-3 pentane et un conformère du bromo-2 butane avec une erreur moyenne de 4.1 cm^{-1}. Ce champ de force appliqué aux bromohexanes donne de bons résultats.

[Traduit par le journal]

Introduction

Infrared spectra have been reported for 2-bromopentane and 3-bromopentane only in the 400–800 cm^{-1} region by Gates, Mooney, and Willis (1). Carbon–bromine stretching bands were assigned to four conformers of 2-bromopentane and five conformers of 3-bromopentane. These authors made analogous assignments for 2-chloro- and 2-iodopentane and 3-chloro- and 3-iodopentane, which included assignment of bands to the C—X stretch of a '*cis* X—H' conformer of 2-halopentane and the S_{CC} conformer of 3-halopentane. These bands have been interpreted by other authors as being due to the other conformers present for the chloro- (2) and iodo- (3) pentanes, rather than to the *cis* X—H and S_{CC} conformers.

Since the previous study (1) included only the 400–800 cm^{-1} region of the infrared spectra and did not include any Raman data, infrared and Raman spectra have been obtained in this laboratory in order to make vibrational assignments and to learn more about the conformational behavior of these compounds. Normal coordinate calculations were made for three conformers of 2-bromopentane and for four conformers of 3-bromopentane to aid in making vibrational assignments and identifying conformations and to develop a force field that will be useful for interpretations of the spectra of other secondary bromides.

No spectra have been published for 2-bromohexane or 3-bromohexane, so infrared and Raman spectra have been obtained for these two compounds and vibrational assignments were made with the aid of normal coordinate calculations that utilized the force constants obtained from the bromopentanes. The first paper of this series presented results for a series of primary bromides (4).

Experimental

Infrared spectra were obtained with a Beckman IR12 spectrophotometer, and Raman spectra were obtained with a Beckman Model 700 spectrometer equipped with a Coherent Radiation Model 54 argon laser. The 488.0 nm line was used. The samples were obtained from K & K Laboratories or Aldrich Chemicals, and were used without further purification. Gas chromatographic analysis showed no appreciable amounts of impurity.

Calculations

Normal coordinate calculations were made with a PDP-10 computer and utilized programs written by Schachtschneider (5, 6) for calculation of the **G**-matrix (GMAT), solution of the vibrational secular equation (VSEC), and for the least-squares refinement of designated force constants to fit the calculated to the observed frequencies (FPERT). These references should be consulted for details of the calculations, treatment of the redundancy problem, etc. The molecular parameters used were C—C = 1.54

Å, C—H = 1.09 Å, C—Br = 1.94 Å, and all angles were assumed to be tetrahedral.

Results and Discussion

Normal Coordinate Calculations for 2-Bromobutane

In order to obtain force constants to use initially for the bromopentanes, calculations were first made for the three conformers of 2-bromobutane, i.e., S_{HH}, $S_{HH'}$, and S_{CH}. A 48 parameter modified valence force field was used, with initial values being taken from the secondary iodides (3), except for the C—Br stretch force constant, which was taken from the force field of 2-bromobutane developed by Benedetti and Cecchi (7).

The band assignments made by Benedetti and Cecchi were used in our initial calculations. Seventeen force constants were refined by the least-squares program, and 69 frequencies of the three conformers were fitted with an average error of 5.4 cm^{-1}, as compared with an average error of 6.75 cm^{-1} obtained by Benedetti and Cecchi (7). The present calculations resulted in a change of only two of the band assignments given by those authors, both for the S_{CH} conformer. We have assigned the 1360 and 1120 cm^{-1} bands to this conformer, rather than those observed at 1346 and 1145 cm^{-1}. Our calculated values are 1363 and 1118 cm^{-1}, whereas the calculated values of Benedetti and Cecchi are 1345 and 1143 cm^{-1}. The difference between the present results for this compound and those of Benedetti and Cecchi are not significant enough to warrant listing our results here.

2-Bromopentane and 3-Bromopentane

Liquid-state ir and Raman spectra of 2-bromopentane were obtained with salt plates. Solid-state spectra were obtained by cooling a liquid film held between salt plates, in hopes that some simplification from the liquid-state spectrum would be observed, as a result of the disappearance of some of the conformers upon crystallization. However, crystallization did not take place, even with annealing for 1 h. Gates *et al.* (1) also reported only the amorphous solid. The solid-state spectrum is essentially identical to that for the liquid. There were, however, two bands observed in the solid-state spectrum that were not present in the spectra of the liquid.

As an aid in assigning the observed bands to the appropriate conformers, normal coordinate calculations were made for the S_{HH}, $S_{HH'}$, and S_{CH} conformers of 2-bromopentane (carbons 2, 3, 4, and 5 are coplanar in all three conformers) and for the S_{HH}, $S_{HH'}$, S_{CH}, and $S_{CH'}$ conformers of 3-bromopentane. Initially, zero-order calculations were made for the three conformers of 2-bromopentane and for the S_{HH}, $S_{HH'}$, S_{CH}, and $S_{CH'}$ conformers of 3-bromopentane. Initial calculations were made for the three conformers of 2-bromopentane, using the values of the force constants that had been obtained for 2-bromobutane. Band assignments were made by comparison of the observed and calculated wave numbers, and then a least-squares refinement was made to simultaneously fit the frequencies of the three conformers of 2-bromobutane and the three conformers of 2-bromopentane. Fifteen force constants were adjusted and 144 wave numbers of the six conformers were fit with an average error of 5.5 cm^{-1}.

The next step in the development of the force field was to make preliminary calculations for the four conformers of 3-bromopentane, using the force constants that were determined as described in the preceding paragraph. Again, band assignments were made by comparison of observed and calculated wave numbers. Our computer facility was limited to inclusion of eight molecules in the FPERT program, and several combinations of eight of the ten conformers of the butane and two pentanes were used, with essentially the same results for the conformers common to all the calculations. In the final computer run reported here, 16 force constants were refined to provide the best fit for 221 wave numbers below 1500 cm^{-1} of the 3 conformers of 2-bromopentane, the 4 conformers of 3-bromopentane, and the S_{HH} conformer of 2-bromobutane. The average difference between observed and calculated wave numbers for the 221 values was 4.1 cm^{-1}. The calculated wave numbers are available on request from the authors, and the force constants are given in Table 2. Comparison of the values of the force constants listed in Table 2 with those obtained for secondary iodides (3) shows 30 values used for both bromides and iodides and several others that are quite close. Of course, quite a few of those iodide values were transferred from a hydrocarbon force field.

The calculated wave numbers strongly support the presence of the three conformers of 2-bromo-

TABLE 1. Observed wave numbers (cm^{-1}) of 2-bromopentane and 3-bromopentane

Infrared		Raman	Infrared		Raman
Liquid	Solid	Liquid	Liquid	Solid	Liquid
		2-Bromopentane			
1462s	1467s		916mw	917m	919mw
ca. 1450s	ca. 1450s	1449m	873m	871m	871w
ca. 1430m	1426m		864m	861mw	
1382s	1379s	1379vw	843mw	843w	845mw
1340vw	1344vw		814mw	812m	813vw
ca. 1330vw	1333vw	1331vw	805mw	801w	802vw
1303m	1305m	1305w	753ms	ca. 755sh	753vw
1288mw	1287w	ca. 1285sh	743ms	745ms	745w
1269m	1269m	1268vw	616m	613m	617m
1254s	1254s	1254w	578w		580mw
1203s	1204s	1200m	536ms		537vs
1150s	1153s		512mw		517w
	1144w	1145w	490w		491w
ca. 1135sh	1133vw	ca. 1133vw	430w		431m
	1121w	1120w			ca. 420sh
ca. 1080sh	ca. 1079vvw	ca. 1080sh	361w		359mw
1071mw	1072mw	1073w			314w
1051w	1051mw	1053vw	293m		294vs
1027m	1027m	1028w			ca. 275sh
1000w	1000w	1002vvw			225vw
981m	980m	981w			181vw
928m	927m	ca. 930sh			144vw
		3-Bromopentane			
	1462ms				
1459m	1455ms	1457m			1009w
1439m	1436m	1438m	ca. 980sh		
1382ms	1376ms	1380vw	969w		
		1360vw	955w	958w	
1341w	1342mw		923mw	928mw	
		1327vw	914mw	915w	913w
1303s	1301s	1301w	870ms	870s	872w
1285w			863ms	862w	863w
1273w	1270w	1275w	843s	844m	
1254w	1255w		814s	811vs	814mw
		1240vvw	801s	800m	801mw
1201vs	1205s	1199m	786vw		
	1151mw		774w		773vw
1144s	1143m	1143w	753vw		
1123w	1125vw	1123w	744vw	745vw	
1105w	1106w	1104vw	616w		ca. 616sh
1082vw	1080vw		604ms		607m
	1068vw		ca. 596sh		ca. 595sh
1055w	1052vw	1060vw	532ms		534m
1036w	1034mw	1028m			ca. 520sh
ca. 1030sh			491m		491m
1020vw	1019vw				450vw
415w		420m			278mw
		374vw			ca. 265sh
		359vw			ca. 208sh
		317s			190mw
		294vw			ca. 110vw

pentane for which calculations were made. There are seven observed bands assigned solely to the S_{HH} conformer (1340, 1150, 1071, 928, 536, 420, and 181 cm^{-1}), four bands assigned to the $S_{HH'}$ (1135, 578, 512, and 314 cm^{-1}), and two bands assigned to the S_{CH} (743 and 616 cm^{-1}). Several other bands were assigned to different pairs of conformers, i.e., S_{HH} and $S_{HH'}$; S_{HH} and S_{CH};

TABLE 2. Force constants for secondary bromides

Force constant	Group	Coordinate(s) involved	Common atom(s)	Value[a]	Standard error[b]
Stretch					
K_r	CH_3	C—H	—	4.699	—
K_d	CH_2	C—H	—	4.554	—
K_s	CHI	C—H	—	4.588	—
K_R	CH_2—CH_3	C—C	—	4.387	—
$K_R(X)$	C—CHBr—C	C—C	—	4.586	—
K_X	CHBr	C—Br	—	2.320	—
Bend					
H_α	CH_3	H—C—H	—	0.539	—
H_β	CH_2—CH_3	C—C—H	—	0.593	0.007
$H_\beta(X)$	CHBr—CH_3	C—C—H	—	0.618	0.003
H_δ	CH_2	H—C—H	—	0.532	0.002
H_γ	C—CH_2—C	C—C—H	—	0.656	—
H_ξ	C—CHBr—C	C—C—H	—	0.656	—
H_ε	CHBr	Br—C—H	—	0.649	0.031
H_ω	C—C—C	C—C—C	—	1.160	—
H_Ξ	C—CHBr—C	C—C—Br	—	0.975	—
Torsion					
H_Υ	CH_2—CH_2—(HorC)	C—C	—	0.0095	—
H_τ	CHBr—CH_2—(HorC)	C—C	—	0.0087	—
Stretch–stretch					
F_r	CH_3	CH, CH	C	0.043	—
F_d	CH_2	CH, CH	C	0.006	—
F_R	C—CH_2—C	CC, CC	C	0.064	—
$F_R(X)$	C—CHBr—C	CC, CC	C	0.101	—
F_{RX}	C—CHBr—C	CC, CBr	C	0.121	—
Stretch–bend					
$F_{R\gamma} = F_{R\xi}$	C—CH—C	C—C, CCH	C—C	0.301	—
$F_{R\gamma}' = F_{R\xi}'$	C—CH—C	C—C, CCH	C	0.079	—
$F_{R\omega}$	C—C—C	C—C, CCC	C—C	0.405	0.012
$F_{R\Xi}$	C—C—Br	C—C, CCBr	C—C	0.292	0.035
$F_{X\varepsilon}$	C—CHBr—C	C—Br, CCH	C—Br	0.226	—
$F_{X\Xi}$	C—C—Br	C—Br, CCBr	C—Br	0.276	0.019
$F_{X\omega}$	C—CBr—C	C—Br, CCC	C	−0.058	0.034
Bend–bend					
F_β	C—CH_3	CCH, CCH	C—C	0.003	0.003
$F_\beta(X)$	CBr—CH_3	CCH, CCH	C—C	0.004	0.002
F_γ	C—CH_2—C	CCH, CCH	C—C	−0.021	—
$F_\gamma' = F_\xi'$	C—CH—C	CCH, CCH	C—H	0.012	—
$F_{\xi\varepsilon}$	CH_3—CHBr—CH_2	CCH, BrCH	C—H	0.026	0.014
$F_{\xi\varepsilon}'$	CH_2—CHBr—CH_2	CCH, BrCH	C—H	0.039	0.014
$F_{\gamma\omega} = F_{\xi\omega}$	C—CH_2—C	CCH, CCC	C—C	−0.031	—
$F_{\omega\Xi}$	C—CHBr—C	CCC, CCBr	C—C	−0.133	—
F_Ξ	C—CHBr—C	CCBr, CCBr	C—Br	−0.007	0.040
f_γ^g	—CH—CH—	HCC, CCH *gauche*	C—C	—0.009	0.002
f_γ^t	—CH—CH—	HCC, CCH *trans*	C—C	0.080	—
f_ω^g	C*—C—C—C^+	C*CC, CCC^+ *gauche*	C—C	0.011	—
f_ω^t	C*—C—C—C^+	C*CC, CCC^+ *trans*	C—C	−0.011	—
$f_{\gamma\omega}^g$	CH—C—C	HCC, CCC *gauche*	C—C	−0.088	0.006
$f_{\gamma\omega}^t$	CH—C—C	HCC, CCC *trans*	C—C	0.049	—

TABLE 2 (*Concluded*)

Force constant	Group	Coordinate(s) involved	Common atom(s)	Value[a]	Standard error[b]
$f_{\gamma\Xi}{}^{g}$	CH—C—Br	HCC, CCBr *gauche*	C—C	−0.037	—
$f_{\gamma\Xi}{}^{t}$	CH—C—Br	HCC, CCBr *trans*	C—C	0.054	0.020
$f_{\omega\Xi}{}^{g}$	C—C—C—Br	CCC, CCBr *gauche*	C—C	−0.024	—
$f_{\omega\Xi}{}^{t}$	C—C—C—Br	CCC, CCBr *trans*	C—C	−0.174	—

[a]Stretching constants are in units of mdyn/Å; stretch–bend constants are in units of mdyn/rad; bending constants are in units of mdyn Å/(rad)^2.
[b]Force constants for which no standard error is given were constrained to the transferred values.

$S_{HH'}$ and S_{CH}. The assignment of the C—Br stretch bands by Gates *et al.* (1) to these three conformers was confirmed. However, these authors assigned the band they observed at 515 cm^{-1} to the C—Br stretch of a '*cis* X—H' conformer, whereas our calculations indicate assignment of this band to the $S_{HH'}$ conformer. The potential energy distribution shows this band to be due to a mixture of skeletal bending and C—Br stretching modes. This interpretation is identical to that for 2-iodopentane (3).

Table 1 lists several observed bands that were unassigned to the three conformers for which calculations were made. This probably indicates the presence of one or more additional conformers.

The S_{HH}, $S_{HH'}$, and S_{CH} conformers of 2-bromopentane are interconverted by internal rotation about the C_2—C_3 bond. Rotation about the C_3—C_4 bond leads to additional conformers, two of which are shown in Fig. 1. These seem to be the conformers most likely to be present, in addition to the three already discussed. In an effort to determine if these two conformers are present, normal coordinate calculations were made for them, using the force constants given in Table 2. These calculated wave numbers are available from the authors. Comparison of the calculated values with the observed values given in Table 1 shows that the conformer shown in Fig. 1*a* can account for the band observed at 490 cm^{-1}, and the other calculated values are in good agreement with observed values. None of the bands previously unassigned can be unambiguously assigned to the conformer shown in Fig. 1*b*, and there is therefore no evidence to indicate the presence of this conformer, although this conformer seems as probable as that of Fig. 1*a*. There are still four unassigned bands listed in Table 1, and at least two of these can be explained as summation bands. No further attempt was made to try to determine the source of these bands.

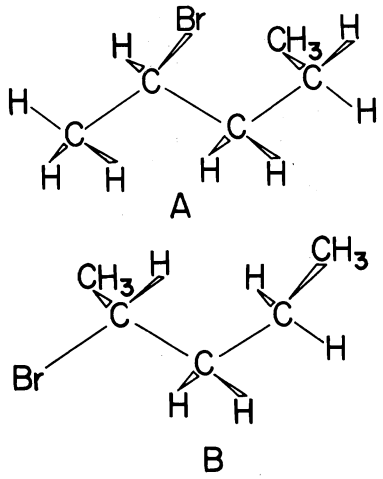

FIG. 1. Additional conformers of 2-bromopentane for which calculations were made.

Gates *et al.* (1) show the liquid-state infrared spectrum and list the observed bands of 3-bromopentane only for the 425–700 cm^{-1} region. The liquid-state infrared and Raman spectra of this compound were obtained in this laboratory. Solid-state infrared spectra were also obtained for this compound, but crystallization did not take place. The solid obtained by Gates was also amorphous.

Evidence has been given for the presence of four conformers of 3-chloropentane (8) and 3-iodopentane (3), and the present results indicate the same behavior for 3-bromopentane. There are seven bands assigned solely to the S_{HH} conformer (1254, 1151, 1082, 1068, 532, and 415 cm^{-1}), three bands to the $S_{HH'}$ (597, 374, and 265 cm^{-1}), six bands to the S_{CH} (1123, 870, 604, 450, 359, and 294 cm^{-1}), and three to the $S_{CH'}$ (616, 520, and 278 cm^{-1}).

Gates *et al.* assigned the band they observed

TABLE 3. Observed wave numbers (cm^{-1}) for 2-bromohexane and 3-bromohexane

Infrared		Raman	Infrared		Raman
Liquid	Solid	Liquid	Liquid	Solid	Liquid
		2-Bromohexane			
1466m	1467m		981m	980s	986vw
1461m		1457m	915mw	913m	
1454m	1456m		905m	904m	907mw
1428w	1427w		900mw	892m	
1380s	1378s	1386vvw	886mw		881mw
	1355w			874w	
1346w			829w	830w	837w
1326w	1327w		810w	810w	818w
	1310m	1312w	791m	790m	
1301w	1305w		748m		
1291m	1290m		731s	733s	744w
1260w	1261m		614s	611m	619m
1253w			579w		586w
1239s	1240s	1245w	540s		543vs
1195s	1197s	1201w	508w		
1149s	1151s	1155w	475vw		
1131w	1133w	1136w	455vw		
	1123m				437w
1090w	1091w	1096vvw	415vw		421w
1066w	1067m	1075w			402vw
1045m	1045ms		359vw		363w
		1029vvw	347vw		347m
1019w	1019w				325w
	1011w	1007vvw	295w		295s
1000m	998mw				222mw
		3-Bromohexane			
1461s	1464m			911w	
1455sh	1454m	1454ms	903m	902ms	898m
1437mw	1435m	1441ms	889m	890ms	
1381s	1380s	1382vw	873ms	872s	872m
1358w	1356mw		829mw	830m	832w
1346w	1346w		791s	788vs	792m
1325w	1328w		747ms	742s	750w
1310mw	1310s	1308m	612s	608m	612s
1300w			ca. 590sh		
1282s	1280s			ca. 535s	538s
1259m	1260ms	1260w	ca. 520sh		
1240m	1239s				508w
1232w	1233w	1235w	495w		496m
1196vs	1200vs	1197m	430w		432mw
	1148m		398mw		403m
1143s	1142s	1142w	352w		
1117w	1116m	1120w			343mw
1081w	1082m	1084w			316m
	1066w		285w		283s
1055w	1057m				245[a]
1047w	1047ms	1048mw			227[a]
1028w	1025w	1029m			212[a]
1001w	1007m				158[a]
980mw	980ms	980w			

[a]The existence of these bands is uncertain.

at 491 cm^{-1} to the S_{CC} conformer. Moore and Krimm (8) found no evidence for the presence of S_{CC} 3-chloropentane, nor was any evidence found for the presence of S_{CC} 3-iodopentane (3), as would be expected from steric considerations. Therefore, calculations were not made for the S_{CC} conformer of 3-bromopentane. Calculation shows that the 491 cm^{-1} band is due to both S_{HH} and $S_{HH'}$ conformers.

In order to conserve space, the potential

energy distributions will not be given here, but they are available from the authors.

2-Bromohexane and 3-Bromohexane

Liquid and solid-state infrared spectra and liquid-state Raman spectra for these compounds were obtained, and the observed wave numbers are listed in Table 3. The solid-state spectra for these compounds were due to all conformers and aided in the analysis only by the presence of some bands that were not resolved in the liquid-state spectra.

In order to make vibrational assignments, preliminary normal coordinate calculations were made for both compounds, using the force constant values given in Table 2. For 2-bromohexane, calculations were made only for the three conformers that differ by rotation about the C_2—C_3 bond, so the C_2 through C_6 carbons are all coplanar. The calculated wave numbers indicate five bands due solely to the S_{HH} conformer (1312, 1066, 900, 540, and 475 cm^{-1}), five bands to the $S_{HH'}$ (981, 579, 508, 402, and 347 cm^{-1}), and five bands to the S_{CH} (1260, 915, 791, 614, and 455 cm^{-1}). Not all of these band assignments are unambiguous, however. For example, the band observed at 540 cm^{-1} can be confidently assigned to the S_{HH} conformer and not to the other two, but the calculated value of 1316 cm^{-1} for the S_{HH} could be due to either the 1310 or 1326 cm^{-1} observed band. Nevertheless, we believe these results justify the conclusion that all three of these conformers are present. There are several unassigned bands listed in Table 3, which probably indicates the presence of additional conformers. However, the number of conformers possible from internal rotation about the other C—C bonds is relatively large and no attempt was made to identify additional conformers.

There are nine possible conformers of 3-bromohexane that differ in the *trans–trans* environment of the bromine atom as a result of rotation about the C_2—C_3 and C_3—C_4 bonds, and calculations were made for all but the S_{CC} and $S_{H'H'}$. The calculated wave numbers for this compound are available from the authors. There are only two observed bands assigned solely to one conformer (1310 and 483 cm^{-1}); but this is not surprising because major overlapping of bands is expected when seven conformers are involved. However, there are several bands assigned to only two or three conformers (1346, 1325, 1240, 1232, 1148, 1066, 1047, 1001, 911, 903, 889, 590, 508, 430, 398, 352, and 245 cm^{-1}).

Torsional Modes

Only the CH_3—CHI torsion was included in the calculations of the secondary iodides (3) because observed torsional frequencies were available only for 2-iodopropane and it was thought that neglect of the other torsions would not affect the calculations appreciably. Therefore, all torsions except CH_3—CHBr were neglected in the initial calculations of the secondary bromides. During the time this work was in progress, calculations were completed for a series of *n*-alkyl bromides that showed the necessity of including the torsional coordinates in order to fit certain low frequencies (4). Therefore, calculations were repeated for the secondary bromides, including all torsional coordinates.

Comparison of the calculations that included the torsional coordinates with those that excluded them shows only minor differences. However, the overall average error was lowered by 0.5 cm^{-1}. The major effect involves the lowest-frequency CH_2 rocking frequency of 2-bromopentane and 2-bromohexane. The calculated wave number was 20–30 cm^{-1} too low for all conformers of these two compounds, and could not be increased by the least-squares program. Inclusion of the other torsions increased the calculated wave numbers of this mode in all conformers. Examination of the Jacobian matrix showed that force constant H_τ has a very large effect on this frequency.

Acknowledgements

The authors are grateful to The Robert A. Welch Foundation, Houston, Texas, and the Killgore Research Center for financial support of this work.

1. P. N. Gates, E. F. Mooney, and H. A. Willis. Spectrochim. Acta, Part A, **23**, 2043 (1967).
2. C. G. Opaskar and S. Krimm. Spectrochim. Acta, Part A, **23**, 2261 (1967).
3. G. Crowder and Z. Najafi. Can. J. Chem. **55**, 310 (1977).
4. G. A. Crowder and M. R. Jalilian. Can. J. Spectros. **22**, 1 (1977).
5. J. H. Schachtschneider. Shell Development Co. Tech. Rept. Nos. 231-64 (1964); 57-65 (1965).
6. J. H. Schachtschneider and R. G. Snyder. Spectrochim. Acta, **19**, 117 (1963).
7. E. Benedetti and P. Cecchi. Spectrochim. Acta, Part A, **28**, 1007 (1972).
8. W. H. Moore and S. Krimm. Spectrochim. Acta, Part A, **29**, 2025 (1973).

Semi-empirical non-adiabatic potential energy curves for hydrogen, deuterium, and their molecule-ions

MARY KURIYAN AND HUW O. PRITCHARD

Centre for Research in Experimental Space Science, York University, Downsview, Ont., Canada M3J 1P3

Received February 17, 1977

MARY KURIYAN and HUW O. PRITCHARD. Can. J. Chem. **55**, 3420 (1977).

Effective non-adiabatic potential curves were constructed for the ground states of the deuterium molecule and of the hydrogen and deuterium molecule-ions by scaling our empirical non-adiabatic coupling correction for hydrogen according to the approximate rules given by Bunker. These effective potentials were refined by the techniques we have described previously, and were then used to generate the rotation–vibration energy-level spectra for H_2^+ and D_2^+; tables of these energy levels, which we consider to be the best available at the present time, are presented.

MARY KURIYAN et HUW O. PRITCHARD. Can. J. Chem. **55**, 3420 (1977).

Des courbes effectives de potentiel non-adiabatique sont construites pour les états fondamentaux de la molécule de deutérium et des ions-moléculaires d'hydrogène et de deutérium en calibrant notre correction du couplage empirique non-adiabatique pour l'hydrogène selon les règles approximatives rapportées par Bunker. Les potentiels effectifs sont affinés par les techniques décrites précédemment. Pour chacun de ces ions-moléculaires H_2^+ et D_2^+, ces calculs engendrent une série de niveaux d'énergie de rotation–vibration. On présente plusieurs tables des niveaux d'énergie que l'on considère les mieux réalisées jusqu'à maintenant.

[Traduit par le journal]

We have recently used an RKR-like procedure to invert the rotation–vibration energy-level spectrum of H_2 to an accuracy approaching ± 0.1 cm^{-1} (1). This procedure made use of the best available theoretical adiabatic potential $V(R)$ tabulated by Bishop and Shih (2) as the starting approximation, and an effective correction function $\Delta V(R)$ was deduced which would

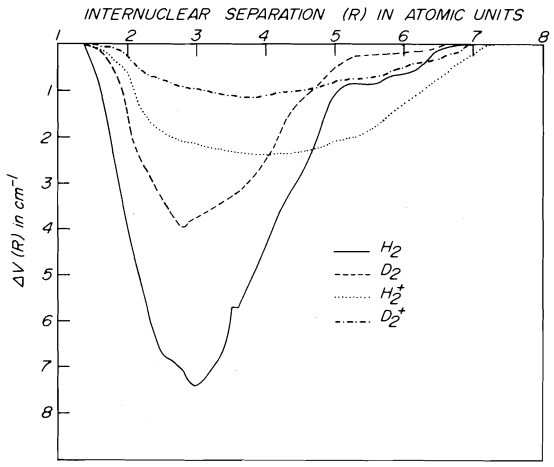

FIG. 1. Effective corrections required for H_2^+, D_2^+, H_2, and D_2 in order to make the best available adiabatic potential curves for these molecules yield the known energy-level spectra. For use in future computations, the corrections are also listed in Table 1.

TABLE 1. Effective non-adiabatic correction terms for H_2^+, D_2^+, H_2, and D_2 used to construct Fig. 1

R (au)	$-\Delta V(R)$ (cm^{-1})			
	H_2^+	D_2^+	H_2	D_2
1.6	0.11	0.04	0.88	0.18
1.8	0.33	0.13	2.41	0.53
2.0	0.69	0.26	3.95	1.54
2.2	1.43	0.57	5.16	2.52
2.4	1.76	0.70	6.36	3.11
2.6	1.98	0.79	6.80	3.60
2.8	2.11	0.92	7.13	3.95
3.0	2.20	0.99	7.42	3.80
3.2	2.28	1.05	7.13	3.62
3.4	2.35	1.10	6.58	3.40
3.6	2.37	1.14	5.71	3.29
3.8	2.39	1.19	5.05	2.96
4.0	2.41	1.12	4.39	2.50
4.2	2.39	1.08	3.62	1.95
4.4	2.37	1.03	3.07	1.40
4.6	2.33	0.99	2.63	1.10
4.8	2.26	0.94	1.76	0.80
5.0	2.17	0.90	1.10	0.50
5.2	2.09	0.83	0.88	0.30
5.4	2.00	0.79	0.88	0.25
5.6	1.82	0.70	0.88	0.20
5.8	1.54	0.61	0.75	0.18
6.0	1.32	0.53	0.66	0.15
6.2	1.10	0.44	0.55	0.13
6.4	0.88	0.35	0.22	0.11
6.6	0.66	0.26	0.09	0.10
6.8	0.44	0.18	0	0
7.0	0.22	0.09	0	0
7.1	0.11	0.04	0	0

TABLE 2. Rotation–vibration energy levels for H_2^+ in cm^{-1}

V / J	<0>	<1>	<2>	<3>	<4>	<5>	<6>	<7>	<8>
0	-21360.2	-19185.1	-17125.2	-15184.2	-13362.7	-11657.7	-10066.9	-8588.6	-7221.9
1	-21321.9	-19133.9	-17073.0	-15134.9	-13316.2	-11613.9	-10025.8	-8550.2	-7186.1
2	-21265.9	-19024.1	-16969.0	-15036.6	-13223.5	-11526.7	-9943.9	-8473.7	-7114.9
3	-21033.1	-18860.3	-16814.1	-14890.3	-13085.4	-11396.8	-9822.1	-8359.7	-7008.9
4	-20804.8	-18644.0	-16609.5	-14697.0	-12903.2	-11225.3	-9661.2	-8209.4	-6869.1
5	-20522.7	-18376.9	-16356.7	-14458.3	-12678.1	-11013.6	-9462.8	-8024.0	-6696.8
6	-20188.9	-18060.8	-16057.8	-14176.0	-12412.1	-10763.5	-9228.3	-7805.2	-6493.4
7	-19805.9	-17696.2	-15715.0	-13852.3	-12107.1	-10476.9	-8955.8	-7554.7	-6260.9
8	-19376.2	-17291.5	-15330.5	-13489.5	-11765.4	-10156.0	-8659.4	-7274.5	-6001.1
9	-18902.8	-16843.6	-14907.2	-13090.1	-11389.5	-9803.0	-8329.1	-6966.9	-5716.2
10	-18388.7	-16357.2	-14447.7	-12656.8	-10981.8	-9420.5	-7971.5	-6634.1	-5408.3
11	-17837.0	-15835.4	-13964.9	-12192.3	-10544.9	-9010.9	-7589.0	-6278.6	-5079.9
12	-17250.9	-15281.2	-13431.8	-11699.4	-10081.7	-8577.0	-7184.1	-5902.7	-4733.3
13	-16633.5	-14697.7	-12881.2	-11181.0	-9594.8	-8121.2	-6759.4	-5509.0	-4371.0
14	-15988.1	-14087.9	-12306.1	-10639.8	-9087.0	-7646.4	-6317.3	-5100.0	-3995.5
15	-15317.7	-13454.9	-11709.3	-10078.6	-8560.8	-7155.0	-5860.6	-4678.3	-3609.2
16	-14625.5	-12801.5	-11093.8	-9500.2	-8019.0	-6649.6	-5391.7	-4246.2	-3214.8
17	-13914.4	-12130.6	-10462.2	-8907.2	-7464.2	-6132.8	-4913.1	-3806.3	-2814.7
18	-13187.3	-11445.0	-9817.2	-8302.1	-6898.8	-5607.0	-4427.3	-3361.2	-2411.5
19	-12446.5	-10747.3	-9161.4	-7687.6	-6325.4	-5074.8	-3936.7	-2913.3	-2007.9
20	-11695.8	-10040.1	-8497.2	-7066.1	-5746.3	-4538.4	-3443.7	-2465.0	-1606.5
21	-10936.6	-9325.7	-7827.0	-6439.7	-5163.6	-4000.2	-2950.8	-2019.1	-1210.1
22	-10171.6	-8606.6	-7153.1	-5810.9	-4580.2	-3462.5	-2460.4	-1578.0	-821.9
23	-9403.1	-7884.8	-6477.7	-5181.7	-3997.7	-2927.7	-1974.9	-1144.7	-445.3
24	-8633.2	-7162.5	-5802.8	-4554.3	-3418.5	-2397.9	-1496.9	-722.1	-84.4
25	-7864.0	-6441.8	-5130.4	-3930.8	-2844.7	-1875.7	-1029.2	-313.8	255.5
26	-7097.3	-5724.5	-4462.6	-3313.1	-2278.6	-1363.5	-574.7	76.1	566.0
27	-6334.9	-5012.4	-3801.2	-2703.4	-1722.3	-863.9	-137.1	441.7	
28	-5578.7	-4307.4	-3148.1	-2103.6	-1178.4	-379.9	279.4	773.4	
29	-4830.2	-3611.2	-2505.2	-1515.9	-649.3	84.8	668.3		
30	-4091.1	-2925.5	-1874.4	-942.6	-138.0	525.7	1018.5		
31	-3362.9	-2252.0	-1257.7	-386.2	351.7	938.8			
32	-2647.2	-1592.5	-657.2	150.4	815.2				
33	-1945.5	-948.9	-75.3	663.5	1244.5				
34	-1259.4	-323.0	485.0	1148.0					
35	-590.6	282.7	1020.2	1595.2					
36	59.2	865.7	1524.9						
37	687.8	1422.4	1989.6						
38	1292.9	1947.4							
39	1871.3	2431.4							
40	2418.2								
41	2883.7								

V / J	<9>	<10>	<11>	<12>	<13>	<14>	<15>	<16>	<17>	<18>
0	-5966.5	-4822.6	-3791.4	-2875.0	-2076.2	-1399.0	-848.7	-431.7	-155.5	-24.0
1	-5933.3	-4792.1	-3763.7	-2850.1	-2054.3	-1380.2	-833.1	-419.8	-147.6	-20.6
2	-5867.4	-4731.6	-3708.7	-2800.7	-2010.7	-1342.8	-802.4	-396.3	-132.2	-14.2
3	-5769.3	-4641.5	-3626.8	-2727.3	-1946.1	-1287.5	-757.0	-361.9	-110.0	-5.9
4	-5640.1	-4523.0	-3519.1	-2630.8	-1861.3	-1215.1	-696.0	-317.6	-82.4	
5	-5480.8	-4377.0	-3386.8	-2512.5	-1757.7	-1127.0	-626.7	-264.8	-51.1	
6	-5293.2	-4205.2	-3231.2	-2373.7	-1636.4	-1024.5	-544.5	-205.3	-18.5	
7	-5078.7	-4009.1	-3054.0	-2216.0	-1499.3	-909.3	-453.4	-141.4		
8	-4839.5	-3790.8	-2857.1	-2041.4	-1348.3	-783.6	-355.5	-75.8		
9	-4577.4	-3552.1	-2642.4	-1851.9	-1185.4	-649.4	-253.6	-12.3		
10	-4294.8	-3295.2	-2412.2	-1649.6	-1012.9	-509.5	-150.6			
11	-3993.9	-3022.6	-2168.8	-1437.0	-833.4	-366.6	-50.5			
12	-3677.1	-2736.4	-1914.6	-1216.6	-649.6	-224.1				
13	-3346.8	-2439.2	-1652.1	-991.1	-464.7	-86.1				
14	-3005.6	-2133.6	-1383.9	-763.4	-282.2	41.8				
15	-2655.9	-1822.0	-1113.0	-536.8	-106.4					
16	-2300.4	-1507.4	-842.3	-314.9	57.1					
17	-1941.7	-1192.5	-575.1	-102.2						
18	-1582.5	-880.4	-315.3	95.3						
19	-1225.7	-574.6	-67.4							
20	-874.3	-278.8	162.2							
21	-531.9	2.2								
22	-202.3	261.4								
23	109.3									
24	395.6									

regenerate the experimental energy-level spectrum for all J. It is widely believed (see ref. 1) that the inability of the function $V(R)$ to generate the known energy-level spectrum of H_2 arises from the neglect of non-adiabatic effects, and if this is so, our effective correction term $\Delta V(R)$ represents an approximate way of incorporating the non-adiabatic coupling. However, as Bunker has shown (3), the non-adiabatic effects at small internuclear separation should be about four times as large for H_2 as they are for H_2^+, and consequently the addition of $0.25\Delta V(R)_{H_2}$ to the exact adiabatic potential curve for H_2^+ (4) should give a good representation of the energy-level spectrum for the hydrogen molecule-ion. The known spectrum consists principally[1] of some experimental observations by Herzberg and Jungen (5) for most members of the group

[1]Six quasibound levels for H_2^+ and five for D_2^+ have also been observed (14), but their accuracy is not such that they are suitable as calibration points in our energy-level inversion scheme.

TABLE 3. Rotation–vibration energy levels for D_2^+ in cm^{-1}

v / J	<0>	<1>	<2>	<3>	<4>	<5>	<6>	<7>	<8>
0	-21711.9	-20134.8	-18622.4	-17173.1	-15785.3	-14457.9	-13189.6	-11979.4	-10826.7
1	-21682.5	-20106.5	-18595.2	-17146.9	-15760.2	-14433.7	-13166.4	-11957.2	-10805.4
2	-21623.8	-20050.0	-18540.9	-17094.7	-15710.0	-14385.5	-13120.2	-11912.9	-10763.0
3	-21536.1	-19965.6	-18459.6	-17016.5	-15634.9	-14313.5	-13051.0	-11846.7	-10699.7
4	-21419.7	-19853.6	-18351.8	-16912.9	-15535.3	-14217.8	-12959.3	-11758.9	-10615.6
5	-21275.1	-19714.4	-18217.9	-16784.1	-15411.6	-14099.1	-12845.4	-11649.8	-10511.3
6	-21102.8	-19548.5	-18058.4	-16630.7	-15264.2	-13957.6	-12709.8	-11519.8	-10387.0
7	-20903.4	-19356.7	-17873.8	-16453.3	-15093.8	-13794.0	-12552.9	-11369.6	-10243.4
8	-20677.8	-19139.5	-17665.0	-16252.6	-14901.0	-13609.0	-12375.5	-11199.8	-10081.0
9	-20426.7	-18897.9	-17432.6	-16029.2	-14686.4	-13403.1	-12178.2	-11010.9	-9900.4
10	-20151.1	-18632.7	-17177.5	-15784.1	-14451.0	-13177.3	-11961.8	-10803.8	-9702.5
11	-19851.8	-18344.7	-16900.6	-15518.0	-14195.6	-12932.3	-11727.0	-10579.1	-9487.9
12	-19529.9	-18035.1	-16602.9	-15232.0	-13921.0	-12668.9	-11474.8	-10337.8	-9257.4
13	-19186.4	-17704.7	-16285.3	-14926.9	-13628.2	-12388.2	-11205.9	-10080.7	-9011.9
14	-18822.5	-17354.7	-15948.9	-14603.8	-13318.1	-12090.9	-10921.3	-9808.6	-8752.2
15	-18439.2	-16986.1	-15594.7	-14263.6	-12991.8	-11778.1	-10621.9	-9522.4	-8479.2
16	-18037.6	-16600.0	-15223.7	-13907.4	-12650.1	-11450.8	-10308.7	-9223.2	-8193.6
17	-17619.0	-16197.5	-14837.1	-13536.3	-12294.2	-11109.9	-9982.6	-8911.8	-7897.0
18	-17184.4	-15779.8	-14435.8	-13151.2	-11925.0	-10756.4	-9644.6	-8589.1	-7589.6
19	-16734.9	-15347.9	-14021.0	-12753.3	-11543.6	-10391.3	-9295.6	-8256.1	-7272.6
20	-16271.8	-14902.8	-13593.8	-12343.4	-11150.9	-10015.5	-8936.6	-7913.8	-6946.8
21	-15796.1	-14445.8	-13155.1	-11922.7	-10748.0	-9630.1	-8568.5	-7563.0	-6613.2
22	-15308.6	-13977.9	-12706.0	-11492.2	-10335.8	-9236.0	-8192.4	-7204.6	-6272.7
23	-14811.2	-13500.0	-12247.5	-11052.9	-9915.2	-8834.1	-7809.0	-6839.7	-5926.2
24	-14304.2	-13013.3	-11780.7	-10605.6	-9487.3	-8425.4	-7419.3	-6469.0	-5574.6
25	-13788.8	-12518.6	-11306.4	-10151.4	-9053.0	-8010.7	-7024.2	-6093.5	-5218.7
26	-13266.1	-12017.1	-10825.7	-9691.2	-8613.1	-7591.0	-6624.6	-5714.0	-4859.5
27	-12737.0	-11509.5	-10339.4	-9225.9	-8168.5	-7167.1	-6221.3	-5331.4	-4497.7
28	-12202.4	-10996.9	-9848.4	-8756.3	-7720.2	-6739.8	-5815.2	-4946.5	-4134.2
29	-11663.2	-10480.1	-9353.6	-8283.3	-7268.8	-6310.1	-5407.1	-4560.2	-3769.9
30	-11120.4	-9959.9	-8855.8	-7807.7	-6815.3	-5878.6	-4997.8	-4173.2	-3405.6
31	-10574.7	-9437.2	-8355.9	-7330.3	-6360.6	-5446.3	-4588.1	-3786.4	-3042.1
32	-10026.9	-8912.7	-7854.5	-6851.9	-5905.0	-5013.8	-4178.7	-3400.5	-2680.2
33	-9477.8	-8387.3	-7352.5	-6373.3	-5449.7	-4581.9	-3770.6	-3016.5	-2320.9
34	-8928.2	-7861.6	-6850.6	-5895.1	-4995.2	-4151.4	-3364.4	-2635.1	-1964.9
35	-8378.7	-7336.3	-6349.4	-5418.1	-4542.4	-3723.1	-2960.9	-2257.0	-1613.3
36	-7830.1	-6812.2	-5849.8	-4942.9	-4091.9	-3297.6	-2560.9	-1883.3	-1266.8
37	-7283.0	-6290.0	-5352.3	-4470.3	-3644.4	-2875.6	-2165.1	-1514.6	-926.6
38	-6738.0	-5770.1	-4857.6	-4000.9	-3200.7	-2458.1	-1774.5	-1152.0	-593.6
39	-6195.9	-5253.4	-4366.4	-3535.4	-2761.4	-2045.6	-1389.8	-796.5	-269.2
40	-5657.1	-4740.3	-3879.2	-3074.5	-2327.2	-1639.0	-1011.9	-449.1	45.2
41	-5122.2	-4231.5	-3396.7	-2618.7	-1898.9	-1239.1	-641.9	-111.0	348.0
42	-4591.8	-3727.6	-2919.5	-2168.9	-1477.2	-846.8	-280.7	216.3	636.8
43	-4066.5	-3229.1	-2448.3	-1725.6	-1063.0	-463.0	70.3	530.9	908.4
44	-3546.8	-2736.6	-1983.7	-1289.7	-657.0	-88.9	409.7	830.6	1156.8
45	-3033.3	-2250.8	-1526.3	-861.8	-260.2	274.4	735.5	1111.4	
46	-2526.4	-1772.1	-1076.8	-442.8	126.4	625.3	1045.3		
47	-2026.7	-1301.3	-635.9	-33.6	501.4	961.9	1334.9		
48	-1534.8	-838.9	-204.5	364.8	863.4	1281.4			
49	-1051.2	-385.7	216.7	751.2	1210.3	1579.0			
50	-576.5	57.7	626.5	1123.9	1539.1				
51	-111.4	490.4	1023.8	1480.9	1844.5				
52	343.6	911.4	1407.1	1819.1					
53	787.5	1319.6	1774.3	2132.5					
54	1219.6	1713.6	2122.1						
55	1638.9	2091.3							
56	2043.9	2449.6							
57	2433.0								
58	2803.4								
59	3151.1								

of states $0 \leq v \leq 3$, $0 \leq J \leq 4$, and the non-adiabatic calculations by Bishop (6) for $0 \leq v \leq 11$, $J = 0$.

It should be noted at the outset that no single potential can reproduce exactly all the rotation–vibration levels reported by Herzberg and Jungen (5), and irregularities somewhat larger than the estimated uncertainties ($\pm 0.2\ cm^{-1}$) are apparent. However, there is no guarantee that a single potential curve will be able to regenerate all the known levels, since it may be necessary to construct one effective potential curve for each vibrational state: this would represent an inherent limit in our effective potential method, but although the associated errors are not known at this time, they are certainly small (2, 7).

Figure 1 shows the effective correction to the known adiabatic potential (4) required to produce the best fit to the experimental data (5) and an exact fit to the theoretical data (6) for H_2^+. In the region of $2 \leq R \leq 3a_0$, the required correction is roughly one quarter of that required for H_2, as predicted by Bunker (3), but it becomes progressively larger relative to the H_2 correction term as the internuclear separation increases: this manifests itself in the calculation in that the first guess of $0.25\Delta V(R)_{H_2}$ for the correction term reproduces quite well the low-lying states of H_2^+, but not the higher ones; however, having established the magnitude of the correction term at small R, it is a simple matter to generate the whole correction function by the method we described previously (1).

TABLE 3 (*Concluded*)

v / J	<9>	<10>	<11>	<12>	<13>	<14>	<15>	<16>	<17>
0	-9730.6	-8690.6	-7706.5	-6778.1	-5905.4	-5088.5	-4327.9	-3624.1	-2978.0
1	-9710.3	-8671.3	-7688.1	-6760.7	-5888.9	-5073.0	-4313.3	-3610.5	-2965.3
2	-9669.8	-8632.7	-7651.4	-6725.8	-5855.9	-5041.9	-4284.2	-3583.3	-2940.1
3	-9609.3	-8575.0	-7596.5	-6673.7	-5806.7	-4995.5	-4240.6	-3542.7	-2902.5
4	-9529.0	-8498.4	-7523.7	-6604.7	-5741.4	-4934.0	-4183.0	-3489.0	-2852.8
5	-9429.3	-8403.4	-7433.4	-6519.0	-5660.4	-4857.7	-4111.5	-3422.3	-2791.1
6	-9310.7	-8290.4	-7325.9	-6417.1	-5564.1	-4767.1	-4026.6	-3343.2	-2718.0
7	-9173.6	-8159.8	-7201.7	-6299.4	-5452.5	-4662.5	-3928.6	-3252.1	-2633.8
8	-9018.6	-8012.1	-7061.5	-6166.5	-5327.4	-4544.4	-3818.2	-3149.4	-2539.1
9	-8846.3	-7848.1	-6905.7	-6018.9	-5188.1	-4413.6	-3695.8	-3035.7	-2434.3
10	-8657.5	-7668.3	-6735.0	-5857.4	-5035.7	-4270.5	-3562.2	-2911.7	-2320.2
11	-8452.8	-7473.6	-6550.2	-5682.5	-4870.9	-4115.6	-3417.8	-2777.9	-2197.3
12	-8233.1	-7264.6	-6351.9	-5495.1	-4694.4	-3950.3	-3263.5	-2635.2	-2066.4
13	-7999.1	-7042.2	-6141.1	-5295.6	-4506.8	-3774.7	-3100.1	-2484.1	-1928.2
14	-7751.8	-6807.2	-5918.4	-5085.6	-4309.1	-3589.7	-2928.1	-2325.6	-1783.5
15	-7491.9	-6560.4	-5684.7	-4865.1	-4102.1	-3396.2	-2748.6	-2160.4	-1633.2
16	-7220.4	-6302.7	-5440.9	-4635.3	-3886.5	-3195.1	-2562.3	-1989.3	-1478.1
17	-6938.1	-6035.0	-5187.8	-4397.0	-3663.2	-2987.1	-2370.0	-1813.4	-1319.1
18	-6645.9	-5758.1	-4926.3	-4151.1	-3433.0	-2773.1	-2172.7	-1633.3	-1157.2
19	-6344.8	-5473.0	-4657.3	-3898.4	-3196.9	-2554.1	-1971.2	-1450.2	-993.3
20	-6035.6	-5180.5	-4381.6	-3639.8	-2955.8	-2330.9	-1766.6	-1264.9	-828.6
21	-5719.3	-4881.5	-4100.2	-3376.2	-2710.5	-2104.4	-1559.6	-1078.6	-664.2
22	-5396.7	-4576.9	-3814.0	-3108.6	-2462.0	-1875.6	-1351.5	-892.2	-501.2
23	-5068.8	-4267.7	-3523.7	-2837.8	-2211.1	-1645.5	-1143.1	-706.9	-341.1
24	-4736.3	-3954.7	-3230.4	-2564.7	-1958.9	-1416.0	-935.6	-524.1	-185.5
25	-4400.2	-3638.7	-2934.9	-2290.2	-1706.2	-1185.2	-730.1	-345.0	-36.1
26	-4061.4	-3320.6	-2638.1	-2015.3	-1454.2	-957.3	-528.0	-171.4	104.4
27	-3720.7	-3001.4	-2341.0	-1741.0	-1203.8	-732.3	-330.6	-5.1	232.5
28	-3379.0	-2681.9	-2044.4	-1468.3	-956.2	-511.6	-139.7		
29	-3037.1	-2363.1	-1749.3	-1198.2	-712.5	-296.7	42.9		
30	-2695.9	-2045.7	-1456.8	-931.7	-474.1	-89.2	214.2		
31	-2356.3	-1730.6	-1167.7	-670.2	-242.5	108.7	370.2		
32	-2019.2	-1415.3	-883.3	-414.8	-19.3	294.1			
33	-1685.4	-1112.3	-604.8	-167.3	193.1	462.4			
34	-1356.0	-810.5	-333.4	70.7	391.7				
35	-1031.9	-516.2	-70.8	296.8	571.0				
36	-714.3	-229.6	181.2	507.4					
37	-404.3	47.2	419.9						
38	-103.4	312.2	641.6						
39	186.8	562.8							
40	464.1	794.5							
41	725.6								
42	966.2								

v / J	<18>	<19>	<20>	<21>	<22>	<23>	<24>	<25>	<26>	<27>
0	-2390.5	-1862.9	-1397.0	-994.5	-657.8	-385.3	-191.7	-67.0	-12.1	-1.0
1	-2378.9	-1852.4	-1387.6	-986.3	-650.7	-383.5	-187.4	-64.2	-10.9	-0.7
2	-2355.7	-1831.4	-1368.8	-969.8	-636.7	-372.1	-178.8	-58.7	-8.6	
3	-2321.2	-1800.1	-1340.7	-945.2	-615.8	-355.2	-166.2	-50.8	-5.4	
4	-2275.5	-1758.6	-1303.8	-912.9	-588.4	-333.1	-149.8	-40.8	-1.9	
5	-2219.0	-1707.4	-1258.1	-873.0	-554.8	-306.1	-130.1	-29.2		
6	-2152.1	-1646.8	-1204.1	-826.1	-515.3	-274.7	-107.5	-16.6		
7	-2075.0	-1577.3	-1142.3	-772.5	-470.5	-240.8	-82.7	-4.0		
8	-1988.5	-1499.2	-1073.2	-712.8	-420.9	-200.8	-56.5			
9	-1892.9	-1413.2	-997.3	-647.6	-367.1	-159.7	-29.8			
10	-1789.0	-1320.0	-915.3	-577.5	-310.1	-116.9	-4.0			
11	-1677.4	-1220.2	-827.9	-503.5	-250.4	-73.6				
12	-1556.8	-1114.5	-735.9	-426.1	-189.3	-31.1				
13	-1434.0	-1003.8	-640.1	-346.6	-127.7	9.0				
14	-1303.8	-888.8	-541.5	-265.8	-67.1					
15	-1169.1	-770.6	-441.0	-184.9	-9.1					
16	-1030.7	-650.0	-339.8	-105.4						
17	-889.6	-528.2	-239.1	-29.0						
18	-746.9	-406.3	-140.4							
19	-603.7	-285.6	-45.4							
20	-461.1	-167.6	43.7							
21	-320.6	-54.1								
22	-183.5	52.7								
23	-51.8									
24	72.1									

Again, following from the earlier work of Bunker (8), we may argue that to a first order of approximation the effective corrections for D_2 and D_2^+ will be respectively about one half of those appropriate to H_2 and H_2^+ (cf. also the results of Bishop and Shih (2)). These correction functions are also shown in Fig. 1, and it can be seen that for both pairs a factor of two is remarkably close to the truth. The data fitted in these two cases are as follows: for D_2, the experimental values of Bredohl and Herzberg (9) for $0 \leq v \leq 21$, $0 \leq J \leq 9$; for D_2^+, the non-adiabatic theoretical results of Bishop (6) for $0 \leq v \leq 11$, $J = 0$, and of Hunter and Pritchard (10) for $0 \leq v \leq 3$, $0 \leq J \leq 2$. It is worth remembering here that for HD^+, a more complicated theoretical problem than either H_2^+ or D_2^+, non-adiabatic calculations (10, 11) are in virtually exact agreement with experiment (12).

In general, the correction functions shown in

Fig. 1, when applied to the existing adiabatic potentials, will reproduce the known bound-state energy levels to within about $\pm 0.2\ cm^{-1}$. We may draw two conclusions from this observation. (*i*) That the correspondence of the effective correction terms shown in Fig. 1 with the relative magnitudes expected from Bunker's analyses (3, 8) identifies these correction terms more positively than ever with non-adiabatic coupling effects. (*ii*) That in the absence of costly and time-consuming non-adiabatic calculations for about 1400 individual states of H_2^+ and D_2^+, the best energy-level spectra available at the present time are those derived using these effective correction potentials. Hence, the complete energy-level spectra for these two species are reproduced in Tables 2 and 3. Comparison with an earlier tabulation of these energy levels (13) based on *adiabatic* internuclear potentials shows that the inclusion of non-adiabatic effects lowers most states of H_2^+ by some $1–3\ cm^{-1}$, with the lowerings for D_2^+ being somewhat less.[2] It should also be noted that we have not included resonance widths for the quasi-bound states in the present tables, for two reasons. (*i*) It is not clear to us that our effective potential method, although yielding good answers for the energies of the levels, need represent the tunnelling properties at all well. (*ii*) The tunnelling lifetimes are *very sensitive indeed* to small changes in the assumed potential, and the level widths quoted previously (13) change by as much as a factor of four when the effective potential is used instead of the adiabatic one; hence, numerical values of resonance widths can only have qualitative significance at the present time.

[2]Throughout these calculations 1 au = 219 474.72 cm^{-1}, but the present tables use a slightly different value for the mass of the deuteron viz. $M_D = 3673.17 m_e$ (15) from that used previously (13). Missing from the table for H_2^+ is an entry corresponding to $v=19$, $J=0$, which has been reported by other workers (16, 17); we searched extensively for an eigenvalue corresponding to such a state, both in this work and previously (13), but our potential does not support such a state. Also, we have omitted from the present tables a few of the topmost quasi-bound levels whose positions are rather difficult to locate and consequently cannot be quoted with the accuracy claimed.

Acknowledgment

This work was supported by the National Research Council of Canada.

1. M. KURIYAN and H. O. PRITCHARD. Can. J. Chem. **54**, 1865 (1976).
2. D. M. BISHOP and S.-K. SHIH. J. Chem. Phys. **64**, 162 (1976).
3. P. R. BUNKER. J. Mol. Spectrosc. **46**, 504 (1973).
4. G. HUNTER, B. F. GRAY, and H. O. PRITCHARD. J. Chem. Phys. **45**, 3806 (1966); P. R. BUNKER and E. A. COLBOURNE. J. Mol. Spectrosc. **63**, 155 (1976).
5. G. HERZBERG and CH. JUNGEN. J. Mol. Spectrosc. **41**, 425 (1972).
6. D. M. BISHOP. J. Mol. Spectrosc. **61**, 474 (1976).
7. D. M. BISHOP and G. HUNTER. Mol. Phys. **30**, 1433 (1975).
8. P. R. BUNKER. J. Mol. Spectrosc. **42**, 478 (1972).
9. H. BREDOHL and G. HERZBERG. Can. J. Phys. **51**, 867 (1973).
10. G. HUNTER and H. O. PRITCHARD. J. Chem. Phys. **46**, 2153 (1967).
11. D. M. BISHOP. Phys. Rev. Lett. **37**, 484 (1976).
12. W. H. WING, G. A. RUFF, W. E. LAMB, JR., and J. J. SPEZESKI. Phys. Rev. Lett. **36**, 1488 (1976).
13. G. HUNTER, A. W. YAU, and H. O. PRITCHARD. At. Data Nucl. Data Tables, **14**, 11 (1974).
14. J. G. MAAS, N. P. F. B. VAN ASSELT, and J. LOS. Chem. Phys. **8**, 37 (1975).
15. E. R. COHEN and B. N. TAYLOR. J. Phys. Chem. Ref. Data, **2**, 663 (1973).
16. C. L. BECKEL, B. D. HANSEN, and J. M. PEEK. J. Chem. Phys. **53**, 3681 (1970).
17. R. J. LEROY and R. B. BERNSTEIN. J. Mol. Spectrosc. **37**, 109 (1971).

Mécanisme d'apparition de la coloration jaunâtre dans les poudres de sulfate stanneux[1]

G. VERVILLE

Division Sources d'énergie électrique, Centre de recherches pour la Défense, Ottawa, Ont., Canada K1A 0Z4

Reçu le 13 janvier 1977

G. VERVILLE. Can. J. Chem. **55**, 3425 (1977).

Une étude spectrophotométrique des poudres de sulfate stanneux nous a permis de définir le mécanisme d'apparition de la coloration jaunâtre dans ces poudres. La formation des complexes de transfert de charge 1Sn(II)–4Sn(IV) dans le film d'eau adsorbée et acidifiée entourant certains grains de sulfate stanneux est à la base du mécanisme proposé. Ces complexes sont formés par fixation d'ions $Sn^{2+}\cdot xH_2O$ ou $SnHSO_4^+$ à la surface des colloïdes $Sn(OH)_4\cdot xH_2O$ obtenus par oxydation et hydrolyse du sulfate stanneux.

G. VERVILLE. Can. J. Chem. **55**, 3425 (1977).

A spectrophotometric study of stannous sulphate powders has enabled the mechanism of the yellow coloration of these powders to be defined. It is shown that the yellow coloration results from the formation of charge transfer complexes of the type 1Sn(II)–4Sn(IV) in a film of adsorbed and acidified water which surrounds some stannous sulphate particles. The charge transfer complexes are formed by the adsorption of $Sn^{2+}\cdot xH_2O$ or $SnHSO_4^+$ ions onto the surface of colloidal $Sn(OH)_4\cdot xH_2O$ that is formed by the oxidation and hydrolysis of the stannous sulphate.

Introduction

Les poudres de sulfate stanneux se présentent sous forme de cristaux aciculaires incolores qui laissés au repos en présence d'air se colorent en jaune avec le temps. Donaldson et Moser (1) attribuent cette coloration à l'apparition progressive de composés stanniques dans les poudres de sulfate stanneux. D'après ces auteurs, lorsque les premiers signes de coloration apparaissent, les échantillons contiennent plus de 2% de composés stanniques.

Mis à part le sulfure stannique, à notre connaissance il n'existe pas de composés stanniques purs ayant une coloration jaune en soi et à première vue, la présence de composés stanniques ne semble pas constituer une condition suffisante pour donner aux poudres leur aspect jaunâtre. Nous avons donc entrepris une étude spectrophotométrique des poudres et celle-ci nous a permis de préciser les résultats antérieurs et de définir le mécanisme d'apparition de la coloration jaunâtre dans les poudres de sulfate stanneux.

Mode opératoire

Les poudres de sulfate stanneux sont obtenues de diverses sources dans le commerce. Après réception, les poudres sont mélangées et broyées dans un mortier pendant 5 min. Les poudres sont ensuite analysées par spectrométrie de masse (spectre d'étincelles) afin de déceler les impuretés métalliques et la concentration en étain (stanneux, stannique, totale) est déterminée.

A la suite de ces analyses, les spectres de réflectance uv–visible des poudres sont enregistrés sur un spectrophotomètre SAFAS 1700 à l'aide d'un accessoire de réflectance diffuse $_{45}R^\circ$ où les poudres sont placées en vrac dans le compartiment échantillon et de l'oxyde de magnésium en poudre dans le compartiment référence. Les études dans le domaine infra-rouge sont effectuées sur un appareil Perkin-Elmer 137, par pastillage dans le bromure de potassium.

Résultats

Les analyses par spectrométrie de masse n'ont pas permis de déceler de différence fondamentale au niveau des impuretés métalliques, par conséquent la coloration jaunâtre n'apparait pas liée à la présence d'impuretés métalliques dans les poudres.

Par contre, nous avons enregistré des écarts importants, entre les poudres, dans la concentration en composés stanniques et stanneux. Dans la majorité des cas, les poudres ayant une concentration supérieure à 2% en composés stanniques présentaient déjà un aspect jaunâtre lors de la réception. Les analyses des poudres par réflectance diffuse nous ont permis d'établir la raison de ce critère de 2%. La fig. 1 montre les spectres de réflectance diffuse uv–visible d'une poudre blanche, courbe *a*, et d'une poudre

[1]Travail effectué à l'Ecole Nationale Supérieure d'Electrochimie et d'Electrométallurgie de Grenoble lors du travail de thèse de l'auteur.

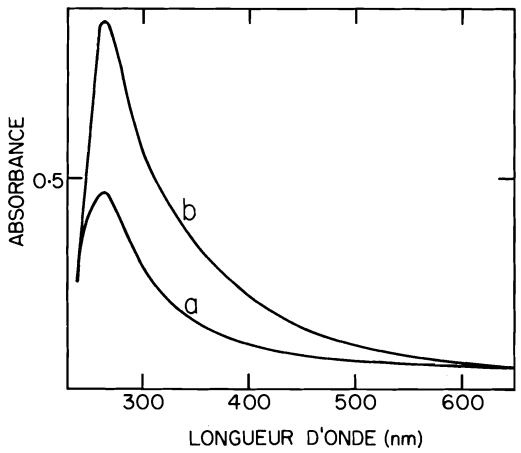

FIG. 1. Spectres de réflectance diffuse de poudres $SnSO_4$. *a*, Poudre blanche, 1.8% d'étain stannique; *b*, poudre jaunâtre, 2.8% d'étain stannique.

jaunâtre, courbe *b*. Ces poudres contiennent respectivement 1.8 et 2.8% d'étain stannique. Les spectres présentent la même allure générale et sont caractérisés par une bande d'absorption dans l'ultra-violet qui se prolonge vers le visible. Bien que très ressemblant, le spectre de la poudre jaunâtre se distingue du spectre de la poudre blanche par une absorption beaucoup plus intense dans l'uv et le proche uv. Il apparait que la coloration jaunâtre est due à un seuil continu d'absorption entre 400 et 600 nm et que la différence d'absorbance entre 400 et 600 nm détermine l'absence ou la présence de la coloration jaunâtre dans les poudres. Par exemple, sur le spectre *a*, la différence d'absorbance entre 400 et 600 nm est trop faible pour être perçu par un oeil de sensibilité moyenne, et par conséquent la poudre apparait blanche (un oeil d'une sensibilité supérieure pourrait éventuellement détecter des signes de coloration sur cette poudre). Aux concentrations supérieures à 2% en étain stannique, la différence d'absorbance entre 400 et 600 nm devient suffisamment importante pour permettre à l'oeil de percevoir la coloration jaunâtre qui devient de plus en plus intense à mesure que la concentration en étain stannique augmente dans les poudres. Cette observation a pu être reliée à une augmentation de la différence d'absorbance entre 400 et 600 nm et au déplacement progressif du seuil d'absorption vers les grandes longueurs d'onde.

Les résultats antérieurs sont donc bien confirmés et la coloration apparait bien liée à la présence d'étain stannique dans les poudres. Cependant, comme Donaldson et Moser (1), nous avons constaté que l'apparition de la coloration jaunâtre au cours du temps, sur les poudres initialement blanches, n'était pas uniforme. Les premiers signes visibles de coloration apparaissent souvent sur les parois des contenants. Nous avons recueilli et analysé les grains provenant de ces zones jaunâtres. Certains échantillons ont présenté des concentrations de l'ordre de 30–40% en étain stannique. A la suite de ces constatations nous avons été amené à considérer l'humidité atmosphérique comme un élément essentiel dans le processus d'obtention de la coloration jaunâtre.

Influence de l'humidité atmosphérique

Les échantillons jaunâtres contenant 30–40% d'étain stannique sont placés dans un four à 200°C pendant 24 h. Les échantillons perdent leur coloration et sont ensuite remis à la température ambiante sous l'atmosphère du laboratoire. Les poudres redeviennent progressivement jaunâtres en adsorbant de l'eau qui est mise en évidence par spectrophotométrie infra-rouge (ir). Les spectres ir ont également révélé la présence de groupements hydroxyles liés à l'étain stannique (doublet entre 3500 et 3600 cm^{-1}) (2, 3) et la présence du groupement HSO_4^- (bande située à 2900 cm^{-1}) dans ces échantillons.

Après un séjour prolongé à l'air libre les échantillons se transforment en boue dont le p*H* est inférieur à zéro. Ceci est révélateur d'une hydrolyse d'ions qui conduit à la formation d'ions H_3O^+. Quel que soit le degré de transformation de ces poudres, la diffraction des rayons X ne révèle que la présence de sulfate stanneux. Les composés stanniques résultant de l'oxydation se trouvent donc à l'état colloïdal.

Mécanisme d'apparition de la coloration

L'ensemble de ces constatations nous amène à proposer, pour l'apparition de la coloration, trois étapes principales:

1. Oxydation de Sn^{2+} en Sn^{4+} à la surface de certains grains de poudre

Cette étape est nécessaire mais non suffisante.

2. Formation d'un film d'eau adsorbée sur ces grains

Les Sn^{4+} à la surface des grains jouent le rôle d'acide de Lewis et l'adsorption de la vapeur d'eau se fait préférentiellement sur ces sites. Les $Sn^{4+}\cdot xH_2O$ isolés sur la surface servent ensuite de germes à la formation d'un film d'eau qui

entoure finalement les grains qui commencent alors à s'agglomérer entre eux. Le film formé est le siège de la prochaine étape conduisant à la coloration jaunâtre.

3. Formation des colloïdes $Sn(OH)_4 \cdot xH_2O$ et des ions $Sn^{2+} \cdot xH_2O$ et $SnHSO_4^+$ dans le film: apparition de la coloration

Le film d'eau étant formé, les ions $Sn^{4+} \cdot xH_2O$ et Sn^{2+} à la surface des grains se dissolvent dans le film. La poursuite de l'hydrolyse des ions stanniques conduit principalement à la formation des colloïdes $Sn(OH)_4 \cdot xH_2O$ (4) qui ont été mis en évidence par spectrophotométrie infra-rouge alors que l'hydrolyse des ions stanneux conduit à la formation des ions $SnOH^+$, $Sn_2(OH)_2^{2+}$, $Sn_3(OH)_4^{2+}$ (5). Cette hydrolyse augmente l'acidité du film d'eau adsorbée. Lorsque l'acidité devient suffisante les ions $Sn^{2+} \cdot xH_2O$ et $SnHSO_4^+$ prédominent sur les autres ions stanneux (6). La présence simultanée de composés stanneux et des colloïdes stanniques dans le film d'eau acidifiée conduit à la formation des complexes de transfert de charge 1Sn(II)–4Sn(IV) déjà étudiés dans les mélanges de solutions stanneuses et stanniques par Paul *et al.* (7) et Feldstein *et al.* (8). Ces complexes sont caractérisés, comme l'illustre les spectres de la fig. 2 par une absorption intense dans l'uv qui s'étend parfois jusqu'au visible pour conférer aux mélanges une coloration jaunâtre. Durant nos travaux (9) nous avons confirmé les résultats de ces auteurs et nous avons montré que les complexes 1Sn(II)–4Sn(IV) sont observés chaque fois que l'on met en présence des colloïdes stanniques et des complexes stanneux du type $Sn^{2+} \cdot xH_2O$ ou SnX^+ où X représente les anions usuels à l'exception de F^-.

Une vérification du mécanisme proposé nous est fournie par la mise en solution des poudres de sulfate stanneux contaminées; la fig. 3 présente les spectres d'absorption uv–visible de trois solutions $SnSO_4$ 30 g/ℓ, en milieu H_2SO_4 10% V. Ces spectres ont été réalisés immédiatement après la dissolution des poudres qui contenaient respectivement 0.8, 1.5 et 2.6% d'impuretés stanniques. On constate que l'absorption se présente sous la forme d'un seuil qui

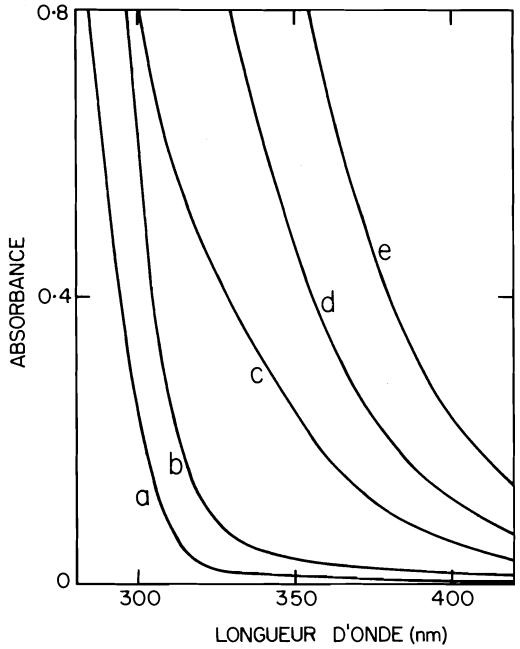

FIG. 2. Spectres d'absorption uv–visible d'une solution stanneuse, d'une solution stannique et de leurs mélanges en milieu HCl, pH = 0.6. *a*, Solution stanneuse fraichement préparée ($SnCl_2 \cdot 2H_2O$, 5×10^{-3} *M*); *b*, solution stannique vieillie pendant 24 h ($SnCl_4 \cdot 5H_2O$, 5×10^{-3} *M*); *c*, mélange équimolaire, 2.5×10^{-3} *M* Sn total; *d*, mélange équimolaire, 5.0×10^{-3} *M* Sn total; *e*, mélange équimolaire, 1.0×10^{-2} *M* Sn total.

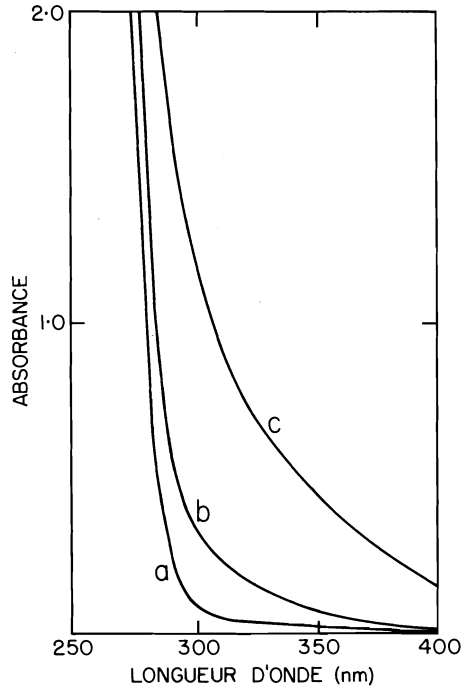

FIG. 3. Spectres d'absorption uv–visible de solutions $SnSO_4$ 30 g/ℓ, H_2SO_4 10%. *a*, Poudre contenant 0.8% d'étain stannique; *b*, poudre contenant 1.5% d'étain stannique; *c*, poudre contenant 2.6% d'étain stannique.

se déplace vers le visible lorsque la concentration en impuretés stanniques augmente. L'allure de ces spectres dans le proche uv est à comparer avec l'allure des spectres des solutions jaunâtres résultant des mélanges des solutions stanneuses et des solutions contenant des colloïdes stanniques de la fig. 2 et avec l'allure des spectres des poudres de la fig. 1. La dissolution du sulfate contenant 2.6% d'impuretés stanniques a entraîné l'apparition immédiate de la coloration jaunâtre de la solution (spectre *c*).

Conclusion

La coloration qui apparait progressivement sur les poudres blanches de sulfate stanneux est attribuable à la formation de complexes de transfert de charge 1Sn(II)–4Sn(IV) dans le film d'eau adsorbée et acidifiée entourant certains grains. Ces complexes sont formés par la fixation d'ions $Sn^{2+}\cdot xH_2O$ ou $SnHSO_4^+$ à la surface des colloïdes $Sn(OH)_4\cdot xH_2O$ obtenus par oxydation et hydrolyse du sulfate stanneux. Le mécanisme proposé rend compte des résultats observés et met bien en évidence le rôle de l'oxydation et de l'humidité dans l'obtention de la coloration; pour qu'apparaisse cette coloration les conditions d'obtention des constituants du complexe de transfert de charge doivent être respectées, c'est-à-dire que $Sn(OH)_4\cdot xH_2O$ d'une part et $Sn^{2+}\cdot xH_2O$ ou $SnHSO_4^+$ d'autre part puissent exister. Ainsi en chauffant à 200°C une poudre jaunâtre, celle-ci contient toujours les colloïdes stanniques mais la disparition du film d'eau adsorbée entraine la disparition des complexes stanneux et cause la disparition de la coloration. La dissolution en milieu acide de cette poudre, entraine l'apparition immédiate de la coloration jaunâtre de la solution.

Dans un cadre plus général, nous pensons que la coloration jaunâtre rapportée dans les poudres des composés stanneux et stanniques autres que les sulfures pourrait être due à une seule et même cause, c'est-à-dire à la présence des complexes de transfert de charge dans ces poudres.

1. J. D. Donaldson et W. Moser. J. Chem. Soc. 4000 (1960).
2. M. Maltese et W. J. Orville-Thomas. J. Inorg. Nucl. Chem. **29**, 2533 (1967).
3. R. A. Nyquist et R. O. Kagel. Infrared spectra of inorganic compounds (3800–45 cm^{-1}). Academic Press, New York, NY. 1971. p. 111, spectre 124.
4. J. Gueron. Ann. Chim. **11**, 225 (1935).
5. R. S. Tobias. Acta Chem. Scand. **12**, 198 (1958).
6. I. Takuji et A. Mitsuo. Kogyo Kagaku Zasshi, **63**, 1699 (1960).
7. A. D. Paul, K. I. Robbins et C. V. Overfield. Proc. W. V. Acad. Sci. **38**, 237 (1966).
8. N. Feldstein, J. A. Weiner et G. L. Schnable. J. Electrochem. Soc. **119**, 1486 (1972).
9. G. Verville. Thèse Docteur-Ingénieur, Université Scientifique et Médicale de Grenoble, Grenoble, France. 1975. N° d'ordre: A.O. 11 738.

A detailed assignment of the O–H stretching bands of ice I[1]

E. WHALLEY

Division of Chemistry, National Research Council of Canada, Ottawa, Ont., Canada K1A 0R9

Received March 15, 1977

E. WHALLEY. Can. J. Chem. **55**, 3429 (1977).

A detailed assignment of the infrared and Raman O–H stretching bands of disordered ice Ih and Ic is proposed. It is based on the assumptions that the spectra of disordered ice Ic are closely related to those of ordered ice Ic, and that the spectra of the as yet unrealized ordered ice Ic can be predicted from the spectra of ice VIII. The supposed similarity between the spectra of ordered and disordered ice Ic is justified by the observed similarity of the spectra of ice VIII and VII, which are respectively ordered and disordered forms of the same structure and are closely related to ordered and disordered ice Ic. The assignment takes into account the intermolecular coupling, which is particularly strong for the ν_1 vibrations but weak for the ν_3, and the TO–LO splitting, particularly of the ν_3 vibrations, which is shown to be required by the high infrared intensity. The infrared and Raman bands of amorphous ice have been assigned by analogy with the assignments of ice I.

E. WHALLEY. Can. J. Chem. **55**, 3429 (1977).

On propose une attribution détaillée des bandes d'élongation O–H en ir et en Raman des glaces désordonnées Ih et Ic. Cette attribution est basée sur l'hypothèse que le spectre de la glace désordonnée Ic ressemble beaucoup à celle de la glace ordonnée Ic et que le spectre qui n'a pas encore été obtenu pour la glace ordonnée Ic peut être prédit à partir du spectre de la glace VIII. Les similarités supposées entre les spectres des glaces Ic ordonnée et désordonnée sont justifiées par la similarité observée dans les spectres des glaces VIII et VII qui sont respectivement les formes ordonnées et désordonnées de la même structure et sont très reliées aux glaces Ic ordonnée et désordonnée. L'attribution rend compte du couplage intermoléculaire, qui est particulièrement fort pour les vibrations ν_1 mais faible pour ν_3, et le dédoublement TO–LO, en particulier des vibrations ν_3, qu'on démontre être nécessaire par conséquence de la grande intensité du spectre infrarouge. On a attribué les bandes infrarouges et Raman de la glace amorphe par analogie avec les attributions de la glace I.

[Traduit par le journal]

1. Introduction

The detailed origin of vibrational bands in crystalline solids can usually be determined by using techniques such as the infrared or Raman intensities and polarizations, transferability of force constants, normal coordinate calculations, etc. These techniques can be applied because there is always a high symmetry (even if it is only the translational symmetry) which restricts the number of spectroscopically active bands to a countable number. The vibrational bands of solids with a high degree of disorder cannot be so easily assigned in detail because 10^{24} or more vibrations per mole are actually observed, and because polarization does not provide much information.

The spectra in the 3-μm region in ice are undoubtedly due to the O–H stretching vibrations, but in spite of many discussions, little real progress has been made in assigning them in detail, as is described in Section 2. Many of the assignments are based on *ad hoc* assumptions that cannot be justified by appeal to other evidence. One reason for this lack of progress is that nearly all discussions have concentrated on the vibrations of a single water molecule, and have ignored the strong intermolecular coupling. To understand the spectrum of ice in detail, it must be approached from the point of view of solid-state spectroscopy, not isolated-molecule spectroscopy. A start has already been made in this program (1), and the strong O–H stretching Raman band at 3083 cm^{-1} at 100 K has been firmly assigned to intermolecularly coupled ν_1 vibrations moving in phase with one another, and it has been shown (2) that at least 25 molecules take part in each vibration.

The purpose of this paper is to propose a detailed assignment based on the following assumptions.

1. The spectra of ice Ic are closely related to the spectra of orientationally ordered ice Ic.

[1]NRCC No. 16037.

2. The spectra of ordered ice Ic can be predicted by analogy with the spectra (3–5) of ice VIII (6–8), whose crystal is made (9, 10) of two interpenetrating ice Ic structures oriented antiparallel to one another.

3. The spectra of ice Ih can be assigned by direct analogy with the spectra of ice Ic, with which they are identical within experimental uncertainty.

2. Previous Assignments

The vibrational spectrum of ice has probably been studied more than the spectrum of any other crystal, but its interpretation is still in a primitive state and the purpose of this section is to review the progress that has been made so far as an introduction to the proposals of this paper. A number of papers that report experimental measurements without an interpretation have been omitted; the earlier ones are reviewed by Ockman (11).

The absorption of ice in the 3-μm region has been known for many years (12, 13) but it was not until 1940 that films thin enough to show the structure were examined (14), and the peak at 3256 cm^{-1} at −9°C was identified. Typical spectra are reproduced in Fig. 1 in the 5th and 7th frame from the top.

Ice was studied (15, 16) in the very early days of Raman spectroscopy, and three bands were observed near 3200 cm^{-1}. They have been assigned in many ways. Rao (15, 17, 18) thought they were due to the water monomer, dimer, and trimer, which had been supposed to occur by W. Sutherland (19). G.B.B.M. Sutherland (20) dismissed the trimer but assigned the strong low-frequency peak to the dimer, and the two higher frequency peaks to Fermi resonance between the stretching and the overtone of the bending vibrations. Sutherland was influenced by Dennison's (21) (correct) finding of a hexagonal unit cell and proposal that it was a hexagonal close packed arrangement of dimers. Although the proposal is not entirely incorrect, Bragg (22) soon showed that the correct configuration allowed no unique choice of dimers, and this was later fully confirmed by Barnes (23). Rao (17) and Cross *et al.* (24) introduced a distinction between the symmetric ν_1 and asymmetric ν_3 stretching vibrations in discussing the spectrum of ice, and Ellis (25) had discussed the spectrum of the liquid in these terms several years earlier, before in fact the symmetric stretching had been identified in the vapor (26). However, Rao (17) interpreted the spectrum in terms of polymers and Cross *et al.* (24) made their interpretation in terms of differently hydrogen-bonded water molecules although it had been known (22, 23, 27) for some years that the water molecules are crystallographically equivalent. This interpretation has been revived (28) recently, but with no greater cogency. Venkatesh *et al.* (29)[2] have made a related suggestion that the 3370-cm^{-1} Raman band of amorphous ice is due to ν_1 of molecules with bent hydrogen bonds. There appear to be no arguments that strongly support this assignment, but there are two strong arguments against it. The first is that ice Ih and Ic (30) have a similar band which probably has the same origin, but have only one kind of hydrogen bond. The second is that the resolution proposed by the authors assigns about 30% of the Raman intensity to the bent hydrogen bonds, whereas the supposed contribution of the bent hydrogen bonds to the uncoupled O–H stretching band is only 12% of the band.

Fox and Martin (14) assigned the strongest Raman band to ν_1 and the strongest infrared band to ν_3. The only significant improvements on this assignment are the recognition (31) of the fact that intermolecular coupling is responsible for a large part of the breadth of the band and that disorder would result in broadened bands, and specifically (32) that all 10^{24} or so normal vibrations are infrared and Raman active, and a more precise assignment (1) of the low-frequency Raman band to the ν_1 vibrations that are intermolecularly coupled in phase with one another.

Hornig *et al.* (31) dismissed assignments based on different coordinations, and suggested that the three principal infrared bands were, in order of increasing frequency, $2\nu_2$, ν_3, and ν_1. The strongest Raman band was identified as $2\nu_2$, an impossible assignment as the stronger component of a Fermi doublet is principally the fundamental, and they were apparently unaware of Sutherland's (20) different assignment of $2\nu_2$. Ockman (11) reversed this assignment of ν_1 and $2\nu_2$ to the Raman bands, and this reversal was accepted by Haas and Hornig (33), and by many later workers (34, 35).

Val'kov and Maslenkova (36) assigned the

[2]Since this paper was submitted Dr. Rice has told me that this suggestion is withdrawn in a paper accepted by Chem. Phys. Lett.

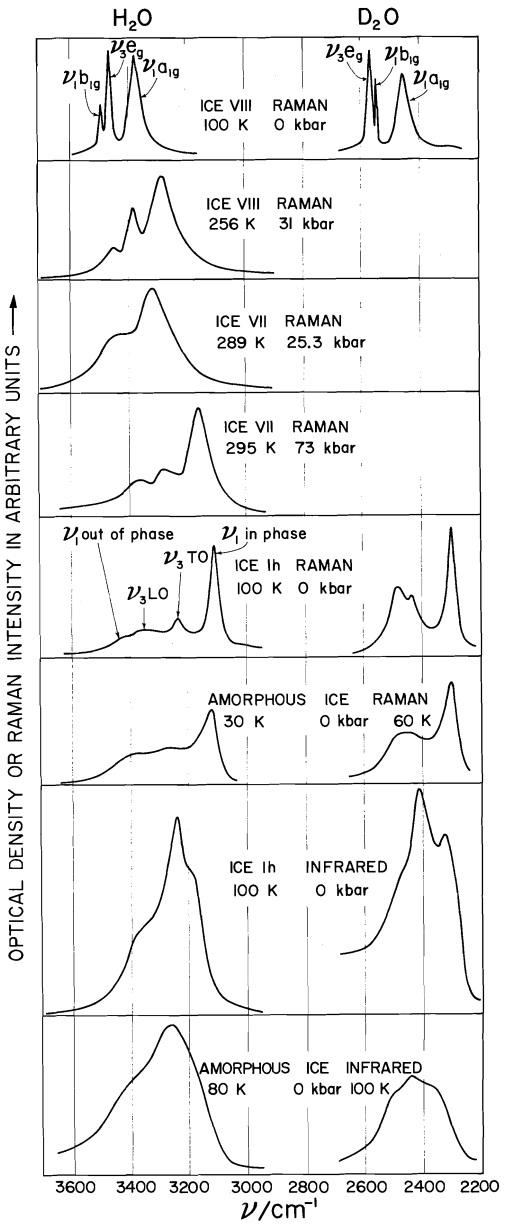

FIG. 1. Infrared and Raman spectra in the O–H stretching region of ice VIII (Raman only), VII (Raman only), Ih, and amorphous ice under various conditions as indicated.

3323- and 3400-cm^{-1} Raman bands to combinations of 3083-cm^{-1} and the 230- and 310-cm^{-1} lattice vibrations respectively. Ockman (11) suggested other combinations, and Hardin and Harvey (37) accepted that the 3340-cm^{-1} infrared band is a combination. But the bands seem too strong for this, and the corresponding difference bands are not observed in the Raman even at 0°C (11). White (38), Miller (39), Maisch (40), and Ockman (41) were the first to take account of coupling between water molecules, although the work was never fully published, and although the work was important in contributing to our general understanding, it did not lead to any significant advance in the assignment of the spectra. Maisch (40), Ockman (41), and Ockman and Sutherland (42) took specific account for the first time of the orientational disorder which had been known for nearly 20 years (43, 44*a*)[3] and calculated the Raman (40) and infrared (41, 42) polarizations. Bertie and Whalley (32) argued that because of the strong intermolecular coupling and the lack of selection rules caused by the disorder, the number of peaks and shoulders could not be predicted from the vibrations of an uncoupled water molecule, and that there was no strong evidence that $2\nu_2$ contributed significantly. These points were made again later (45), and it was emphasized that the observed absorption or scattering intensity is the density of vibrational states multiplied by an absorption or a scattering intensity function. Venkatesh *et al.* (29) found no evidence for $2\nu_2$ in the Raman spectrum of amorphous ice. Little further progress was made until Wong and Whalley (1) assigned the 3083-cm^{-1} Raman band to the particular group of ν_1 in-phase vibrations in which the molecules move in phase with one another.

A theoretical investigation by Shawyer and Dean (46) showed that the orientational disorder ensured that the vibrations were much more localized than in a perfect crystal, but used too little intermolecular coupling and so obtained too narrow ν_1 and ν_3 bands. The calculated degree of localization is therefore unreliable. Recently (2), a lower limit of about 25 molecules to the extent of the coupling has been obtained from the width of the strong Raman band.

Gurikov (47) assigned the 3210-cm^{-1} infrared band to the vibrations of O—H bonds parallel to the *c* axis and the 3450-cm^{-1} band to the vibrations of bonds inclined to the *c* axis. Mikhailov and Zolotarev (48) described a more elaborate assignment based on the same distinction between the bonds. There are two strong reasons for not accepting this assignment. The first is that the infrared spectrum of dilute

[3]See ref. 44*b* for a summary.

solutions of HDO (32, 33, 37) are not consistent with two significantly different kinds of O—H bond, and the ratio (49, 50) of the unit cell edges is only 0.3% from the ideal value for perfect tetrahedral coordination. The second is that all the bonds in ice Ic are crystallographically identical, but nevertheless its infrared (32, 37)[4] and Raman spectra (30) are identical with the spectra of ice Ih within experimental error.

The present state of knowledge can be summarized by saying that the strong Raman band is due to ν_1 vibrations (14) in which the molecules are vibrating largely in phase with one another (1), and the strong infrared band is due to ν_3 vibrations (14) in which the molecules are vibrating largely in a phase correlated with their orientation (1).

3. Spectra of Ice VIII and VII

3.1. Ice VIII

Ice VIII forms a tetragonal crystal consisting of two interpenetrating ice Ic structures, one with the axes of its water molecules parallel to the *c* axis, and the other with the axes antiparallel to the *c* axis (9, 10). The primitive cell contains four translationally inequivalent molecules, which are illustrated in Fig. 2. The crystal space group is $I4_1/amd$, D_{4h}^{19} and the water molecules are on sites of symmetry C_{2v}. Consequently the ν_1 (symmetric stretching) and ν_3 (antisymmetric stretching) motions do not couple with each other at the center of the Brillouin zone. The ν_1 vibrations of the individual molecules couple to form Raman-active A_{1g} and B_{1g} vibrations, an infrared-active A_{2u} vibration, and an inactive B_{2u} vibration. The ν_3 vibrations form a Raman-active E_g and an infrared-active E_u vibration (3).

The Raman spectra of H_2O and D_2O ice VIII (3) at 100 K and zero pressure are shown in Fig. 1, and the bands are labelled by their form and species. The spectrum agrees well with an earlier spectrum (51) using mercury excitation. The infrared spectrum has not been reported; there should be two bands in this region, $\nu_1 a_{2u}$ and $\nu_3 e_u$. $\nu_3 e_g$ should be close in frequency to $\nu_3 e_u$ for the following reason. If the coupling between molecules in the same substructure of ice Ic can be described by a coupling constant between two O—H bonds that are hydrogen bonded together, as in O—H---O—H, the contribution to the potential energy of the interaction

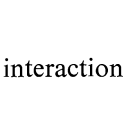

is zero because in the ν_3 vibration one O—H expands and the other contracts. For a similar reason the coupling between the near-neighbor nonbonded molecules

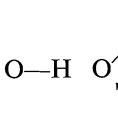

is zero. Consequently, $\nu_3 e_g$ and $\nu_3 e_u$ have approximately the same frequency, and that frequency is approximately the same as that of a water molecule uncoupled from the rest of the crystal (3).

This conclusion can be stated more formally in terms of group theory. Each ice Ic substructure belongs to the space group $I4_1md$, C_{4v}^{11}, and molecules 1 and 2 are related by the operation $\pm C_4$ and a *z*-axis translation. The character of $\pm C_4$ for the *E* species is zero, and consequently if coupling of the ν_3 vibrations with translational and rotational motions is neglected, the two

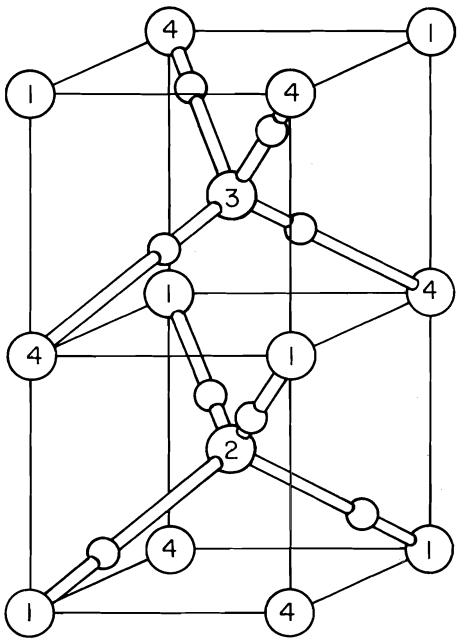

FIG. 2. The relationship between the four molecules in the primitive unit cell of ice VIII. Molecules 1 and 2 form an ice Ic structure with its dipole moment upwards, and molecules 3 and 4 form one with its dipole moment downwards.

[4]Hardin and Harvey (37) relied on making cubic ice by warming amorphous ice, and did not verify independently that ice Ic was formed.

components of the $\nu_3 e$ normal coordinate can be considered as the ν_3 vibration of molecule 1 and the ν_3 vibration of molecule 2. The ν_3 vibrations are therefore coupled only between molecules having their planes parallel to one another, i.e. only between second, fourth, etc. neighbors.

In D_2O ice VIII, the weak $\nu_1 b_{1g}$ band is at a lower frequency than the medium $\nu_3 e_g$, whereas in H_2O ice VIII it is at a higher frequency. The separation between them in H_2O ice VIII is 29.8 cm^{-1} at ~100 K and zero pressure. The hydrogen–deuterium isotope ratios for the ν_1 and ν_3 vibrations are respectively 1.365 and 1.342 (3), which are close to the values in the vapor (52), and arise from the different reduced masses. The effect of these ratios is to change $\nu_1 b_{1g}$–$\nu_3 e_g$ from 29.8 cm^{-1} in H_2O to -20.7 cm^{-1} in D_2O. At 103 kbar and 118 K the intermolecular coupling has increased so much that the $\nu_1 a_{1g}$ band of H_2O has decreased to ~3030 cm^{-1} (as read from Fig. 1 of ref. 4) or about 53 cm^{-1} below the corresponding ice Ih band at zero pressure, and the distance between the $\nu_1 a_{1g}$ and $\nu_1 b_{1g}$ bands is ~400 cm^{-1}, which is comparable to the breadth of the ice Ih band. At the same time, the separation of $\nu_1 b_{1g}$ and $\nu_3 e_g$ has increased to 185 cm^{-1}, and it is very unlikely that the isotope effect can reverse the order. In fact, if the isotope ratios that occur at 100 K and zero pressure (3) occur at 103 kbar, which seems likely as at zero pressure they are only 0.4% below the value in the vapor, the frequencies are ~2454 and ~2358 cm^{-1}, a separation of 95 cm^{-1}. In Section 4, the Raman spectrum of ice VIII will be used to assign the Raman spectrum of ice Ic. A reversal of order is unlikely to occur in ice Ic, where the intermolecular coupling is of comparable magnitude to that in ice VIII at 103 kbar and 118 K, but the two bands may be much closer together in D_2O than in H_2O.

Away from the zone center, the $\nu_1 a_{2u}$ and $\nu_3 e_u$ vibrations should be split by the long-range electric field arising from the transition moments of the molecules. The $\nu_1 a_{2u}$ vibrations propagating along the z direction, which are longitudinal optic (LO) vibrations, should be raised in frequency by the long-range field, while the $\nu_1 a_{2u}$ vibrations propagating along the x,y directions, which are transverse optic (TO) vibrations, would not be affected. The degeneracy of the $\nu_3 e_u$ vibrations is split by a similar process. The ratio of the two frequencies is given by the generalized Lyddane–Sachs–Teller relation (53)

$$\frac{\nu_1 a_{2u}\mathrm{LO}}{\nu_1 a_{2u}\mathrm{TO}} = \frac{n_{0z}}{n_{\infty z}}$$

$$\frac{\nu_3 e_g\mathrm{LO}}{\nu_3 e_g\mathrm{TO}} = \frac{n_{0x}}{n_{\infty x}}$$

where n_0 and n_∞ are the limiting low-frequency and high-frequency refractive indices of the infrared band, and subscripts x and z indicate the x and z principal values.

The change of refractive index across the O–H stretching bands of ice VIII is not known, but the contribution of all the infrared bands is. The mean permittivity at 10 kHz extrapolated to 100 K and 22 kbar, which is $\frac{1}{3}(2n_{0x}^2 + n_{0y}^2)$, is 4.32 (8). The effect of pressure is not known; increasing the pressure will increase the permittivity by increasing the density and probably the infrared absorption intensity, and decreasing some frequencies, and will decrease it by increasing some frequencies. It will be neglected. The mean permittivity at visible frequencies is 2.59, calculated assuming that the electronic polarizability of the water molecule is the same in ice I and ice VIII (8). The change of the mean refractive index across the infrared bands is (8) therefore 0.47 which is the same as the corresponding value for ice I (54). Because nothing further is known, it seems not too unreasonable to assume that the O–H stretching region contributes the same proportion of the infrared contribution to the refractive index in ice I and ice VIII. Then the change of the mean refractive index across the O–H stretching bands in ice VIII is (54) about 0.0308.

The ν_1 band contributes to the z component of the refractive index and the ν_3 band to the x and y components, which are equal. We have then

$$[1] \quad 2(n_{0x} - n_{\infty x}) + (n_{0z} - n_{\infty z}) = 0.0924$$

The contribution of a band to the change of refractive index across it is proportional to the Kramers–Kronig integral $\int K\nu^{-2}\,d\nu$ across it. If the changes of dipole moment when the two O—H bonds stretch independently are at the tetrahedral angle to one another, the integrated intensity of the ν_1 band is a half that of the ν_3 band. If the difference of the frequencies is ignored, as they must be at present because they are not known, then because of the Kramers–

Kronig integral,

$$[2] \qquad n_{0x} - n_{\infty x} = 2(n_{0z} - n_{\infty z})$$

From eqs. 1 and 2

$$[3] \qquad \begin{aligned} n_{0x} - n_{\infty x} &= 0.037 \\ n_{0z} - n_{\infty z} &= 0.019 \end{aligned}$$

As the optical birefringence of ice VIII is not known, it will be neglected. We then find

$$[4] \qquad \begin{aligned} \frac{\nu_1 a_{2u}\mathrm{LO}}{\nu_1 a_{2u}\mathrm{TO}} &= 1.012 \\ \frac{\nu_3 e_u\mathrm{LO}}{\nu_3 e_u\mathrm{TO}} &= 1.023 \end{aligned}$$

There is in the Raman spectrum of ice VIII (3) an unreported weak band at $\sim 3524\ \mathrm{cm}^{-1}$ in H_2O and $\sim 2625\ \mathrm{cm}^{-1}$ in D_2O. If these are the $\nu_3 e_u$LO vibrations, the corresponding TO vibrations are at 3445 and 2566 cm^{-1} respectively. These frequencies are 2 and 3 cm^{-1} respectively below the $\nu_3 e_g$ vibrations. The e_u vibrations should be similar in frequency to the e_g because the first-neighbor intermolecular coupling of the ν_3 vibrations should be small (3), as was shown earlier. The e_u vibrations should of course be Raman inactive, and if this assignment is correct they must be activated by some as yet unrecognized disorder. In any case, it seems likely that they are close to the $\nu_3 e_u$LO frequencies because $\nu_3 e_u$ and $\nu_3 e_g$ are close and eq. 4 holds. The assignments are summarized in Table 1.

3.2. Ice VII

The Raman spectra of ice VIII at 31 kbar and −17.4°C and of ice VII at 25 kbar and 16.1°C according to Hawke *et al.* (5)[5] are also shown in Fig. 1. The spectrum of ice VIII is broadened from that at ~100 K, no doubt because of thermal excitations, and $\nu_1 a_{1g}$ is displaced downwards in frequency from 3358.8 cm^{-1} to ~3277 cm^{-1}, $\nu_1 b_{1g}$ from 3477.4 cm^{-1} to ~3436 cm^{-1}, and $\nu_3 e_g$ from 3447.6 to ~3368 cm^{-1}. No doubt the decrease of frequency due to increased pressure dominates the increase due to increased temperature. Bands corresponding to $\nu_3 e_u$LO cannot be clearly identified because of overlap, but there is a high-frequency tail at ~3460 cm^{-1} that might be caused partly by LO vibrations.

When ice VII is formed, the spectrum, which is shown in Fig. 1 at 25 kbar and ~292 K retains[6] its character except that the bands broaden enough to cause the two higher frequency peaks to merge, and the frequencies of all the peaks increase by about 30 cm^{-1}. At 73 kbar (4), all the bands shift to lower frequency and the lower the frequency the more the shift, no doubt for reasons similar to those causing a related temperature effect in ice I (1). Because of this, the two higher frequency peaks again separate.

The orientational disorder that is produced (6–8) when ice VIII is converted to ice VII destroys all the selection rules that limit the spectrum of the crystal, and all vibrations become active. The normal vibrations can no longer be characterized by wave vectors, and they presumably become more localized. They do not shift much in frequency so they do not become localized enough to seriously reduce the effect of the intermolecular coupling on the frequency. It has been concluded (2) that in ice Ih more than about 25 molecules take part in the ν_1 in-phase stretching vibrations, and perhaps the increase in frequency and band width from ice VIII to VII is partly due to a reduced extent of intermolecular correlation.

The similarity of the spectra of ice VII and VIII indicates that the vibrations of ice VII retain a good deal of the ν_1 or ν_3 character that they had in ice VIII. The 3130-cm^{-1} band (at 73 kbar) is therefore due largely to coupled ν_1 oscillations with the molecules moving nearly in phase; the 3350-cm^{-1} band is due largely to ν_1 oscillations in which neighboring molecules move out of phase; and the 3260-cm^{-1} band is due largely to ν_3 oscillations whose frequencies are expected to be little influenced by intermolecular coupling, as was argued above. This assignment is summarized in Table 2.

The similarity of the Raman spectra of ice VIII and VII suggests that the Raman spectra of orientationally ordered and disordered ice Ic should also be similar to one another. Therefore, a detailed assignment of disordered ice Ic can be based on an assignment of ordered ice Ic. By an extension of this argument, it seems likely that the spectra of orientationally ordered and disordered ice Ih are also closely related to one another. This argument will be pursued in Section 4.

[5]The frequencies were read from a photocopy of the original of ref. 5, Fig. 6.

[6]Similar spectra are reported at this pressure and 295 K in ref. 4 and 289 K in ref. 5.

TABLE 1. Summary of assignments of the O–H stretching Raman bands of ice VIII

Vibrational form and species	ν/cm^{-1}			
	H_2O			D_2O
	0 kbar, 100 K	31 kbar, 256 K	103 kbar, 118 K	0 kbar, 100 K
$\nu_1 a_{1g}$	3358.8[a]	3277[d]	3030[e]	2462.7[a]
$\nu_1 b_{1g}$	3477.4[a]	3436[d]	3350[e]	2548.0[a]
$\nu_3 e_g$	3447.6[a]	3368[d]	3165[e]	2568.7[a]
$\nu_3 e_u$TO	3445[b]	3382[b]	—	2566[b]
$\nu_3 e_u$LO	~3524[c]	~3460[d]	—	~2624[c]

[a]Wong and Whalley (3).
[b]Calculated in this paper.
[c]From the spectra of Wong and Whalley (3).
[d]From Fig. 6 of Hawke *et al.* (5).
[e]From Fig. 4 of Holzapfel *et al.* (4).

4. Ice Ic and Ih

The Raman spectrum of ice VII is very similar to that of ice Ih and Ic. This is shown in Fig. 1 for ice VII and Ih, and the Raman spectra of ice Ih and Ic are identical to one another within present accuracy in both the Raman (30) and the infrared (32, 37).[4] However, the mercury-excited Raman (30) spectrum did not contain the bands at 3420 (1) and 2515 cm^{-1} (1) in H_2O and D_2O respectively, so it can only be inferred that they are present in ice Ic. The similarity of the structures of ice VII and Ic suggests that the bands of ice Ic can be assigned by analogy with the bands of ice VII. The assignment of ice Ih can then be made by analogy with ice Ic.

4.1. Ordered Ice Ic

Before discussing the actual disordered ice Ic it is worth discussing the hypothetical ordered structure in which the molecular dipoles are parallel to one another. The unit cell is represented by molecules 1 and 2 (or alternatively 3 and 4) in Fig. 2. It is tetragonal and belongs to space group $I4_1md$, C_{4v}^{11} with two molecules in the primitive cell and four in the conventional body-centered cell. It forms one of the interpenetrating substructures of ice VIII, the other being the same structure with its polarity reversed. The molecular site symmetry is C_{2v}, so that the ν_1 and ν_3 vibrations do not couple at the center of the Brillouin zone.

TABLE 2. Assignment of O–H stretching bands of ice VII

ν/cm^{-1}[a]		
25 kbar, 16°C	73 kbar, 22°C	Assignment
~3305	3130 s	ν_1 in-phase
~3400[b]	3260 m	ν_3
~3450[b]	3350 w	ν_1 out-of-phase

[a]From Fig. 6 of Holzapfel *et al.* (4).
[b]These bands are not resolved.

The ν_1 vibrations are split by intermolecular correlation into a $\nu_1 a_1$ and a $\nu_1 b_1$ vibration, and ν_3 forms a degenerate $\nu_3 e$ vibration. Each of these is of course split into a gerade and an ungerade vibration when two such structures are combined to form ice VIII (3) and the corresponding gerade vibrations are active in the Raman spectrum. All the vibrations of ordered ice Ic are active in the Raman, and $\nu_1 a_1$ and $\nu_3 e$ but not $\nu_1 b_1$ are active in the infrared.

The effective charge for the stretching of an O—H bond is (54, 58) 4.0 D $Å^{-1}$ or about 0.8 of an electronic charge, and the direction is uncertain. The zone-center vibrations of ordered ice Ic then split, as one moves from the zone center, into a TO branch whose frequency is little changed from the zone center, and an LO branch, whose frequency is increased by the long-range electric field generated by the vibration. Both the a_1 and the e vibrations have a finite infrared activity and so generate a TO–LO splitting.

The change of refractive index across the O–H stretching vibrations of disordered ice Ih is 0.0308 (54). It will be assumed that the same change of refractive index occurs in disordered ice Ic, whose infrared (32, 37) and Raman (30) spectra are identical within present experimental error with that of ice Ih, and in ordered ice Ih and Ic, which have not yet been prepared.

If the dipole-moment changes caused by stretching the two O—H bonds in ice I are at the

tetrahedral angle to one another, the integrated infrared intensities of the ν_1 and ν_3 bands are the ratio 1 to 2. This implies that the change of refractive index across the $\nu_1 a_1$ band is 0.019 and across the $\nu_3 e$ band is 0.037, where the difference in frequencies has been neglected. The optical refractive index of ice Ih is nearly isotropic, and hence that of ordered ice Ic will be assumed to be so. Then

$$\frac{\nu_1 a_1\text{LO}}{\nu_1 a_1\text{TO}} = 1.015 \qquad \frac{\nu_3 e\text{LO}}{\nu_3 e\text{TO}} = 1.028 \qquad [5]$$

The $\nu_1 a_1$ vibration of ordered ice Ic will surely have a frequency similar to that of the strong Raman band of disordered ice Ih, which is due to ν_1 in-phase vibrations (1). It is therefore at 3083 cm^{-1}. The $\nu_3 e$ is surely the second peak, at 3209 cm^{-1}. It almost coincides with the infrared maximum at 3220 cm^{-1}, as it should because ν_3 is much stronger than ν_1 in the infrared. The $\nu_1 b_1$ frequency can be estimated as follows. Holzapfel *et al.* (4) have plotted the $\nu_1 a_{1g}$, $\nu_1 b_{1g}$, and $\nu_3 e_g$ frequencies of ice VIII against the O--O bond length. When $\nu_1 a_{1g}$ is at 3083 cm^{-1}, $\nu_1 b_{1g}$ is at 3390 cm^{-1} and $\nu_3 e_g$ is at 3210 cm^{-1}. In ordered ice Ic, it is expected therefore that when $\nu_1 a_1$TO is at 3083 cm^{-1} and $\nu_3 e$TO at 3209 cm^{-1}, then $\nu_1 b_1$ would be about 3390 cm^{-1}. From eq. 5 $\nu_1 a_1$LO is predicted to be at 3129 cm^{-1} and $\nu_3 e$LO at 3299 cm^{-1}. These bands and the corresponding bands for D_2O and the methods of obtaining them are listed in Table 3.

TABLE 3. Predicted infrared and Raman bands of ordered ice Ic in space group $I4_1md$, C_{4v}^{11}

Form and species	Optical activity	ν/cm^{-1} H_2O	ν/cm^{-1} D_2O	Isotope ratio
$\nu_1 a_1$TO	R, ir	3083[a]	2295[a]	1.343[a]
$\nu_1 a_1$LO	R, ir	3129[b]	2329[b]	1.343
$\nu_1 b_1$	R	3390[c]	2524[d]	(1.343)[e]
$\nu_3 e$TO	R, ir	3209[a]	2429[a]	1.321
$\nu_3 e$LO	R, ir	3299[b]	2497[b]	1.321

[a]By analogy with ice Ih (1) and ice VIII (3, 4).
[b]Calculated from eq. 5.
[c]By analogy with ice VIII (3, 4).
[d]Calculated from the frequency for H_2O and the quoted isotope ratio.
[e]Assumed the same as for $\nu_1 a_1$TO.

4.2. *Disordered Ice Ic*

The similarity between the spectra of ice VII and VIII suggests that the spectra of disordered and ordered ice Ic will be similar and that the bands of disordered ice Ic can be assigned by analogy with those of ordered ice Ic.

It is important to be clear about what is meant by an assignment of the bands of a highly disordered material; it is not quite the same as the assignment of a perfect crystal. Of course, all the 1.2×10^{24} O–H stretching vibrations per mole of ice are optically active, and so the bands are usually broader than the bands of the crystal. The spectrum is the density of states at each frequency multiplied by a mean intensity function at that frequency. The identification attempted in this paper is a description of the kinds of vibration that dominate the absorption or scattering at a particular frequency and that give rise to recognizable features. No doubt other vibrations overlap in frequency with the recognized features and also contribute to the spectrum and no doubt there is some coupling between ν_1 and ν_3 vibrations, at least in some regions. To identify these more precisely is both an experimental and theoretical problem for the future.

The observed infrared and Raman frequencies of ice Ih and Ic are summarized in Table 4 along with their assignments. The basis of the assignments is as follows.

There seems little doubt that the 3083-cm^{-1} band is due to coupled ν_1 vibrations moving in phase, and corresponds to the $\nu_1 a_1$TO vibration of ordered ice Ic. The corresponding band in ice Ih has already been assigned to these motions (1). The TO–LO splitting is predicted to be only 46 cm^{-1}, and the LO band may be hidden in the high-frequency end of the 3083-cm^{-1} band. The ν_1 in-phase infrared band has its maximum at 3150 cm^{-1}, which is 67 cm^{-1} higher than the Raman maximum. In ordered ice Ic they would coincide. The difference of frequency is no doubt due to the different rules for adding the polarizability-derivative scalars, which determine the Raman intensity, and the dipole-moment-derivative vectors, which determine the infrared intensity. In the vibrations having the maximum infrared intensity, the molecules vibrate in phases that are as much as possible correlated with their orientations, whereas the maximum Raman intensity occurs when the molecules are all in phase (1). The intermolecular coupling constant is negative (33), so the maximum infrared intensity should be somewhat higher than the maximum Raman intensity.

TABLE 4. Assignment of the O–H stretching infrared and Raman bands of ice I

	ν/cm^{-1}[a]					
	H_2O		D_2O		Isotope ratio	
Vibration	Raman[b]	Infrared[c]	Raman[b]	Infrared[c]	Raman	Infrared
ν_1 in-phase[d]	3083	3150	2295	2332	1.343	1.349
ν_3TO	3209	3220	2427	2425	1.322	1.328
ν_3LO	3323	3380	2502[e]	2485	1.343[f]	1.360
ν_1 out-of-phase[d]	3420[g]		2547[g]		1.322[f]	

[a]Frequencies are at 100 K.
[b]From Wong and Whalley (1). References to earlier work are given in that paper.
[c]Many authors have observed these bands. The frequencies quoted are from Bertie and Whalley (32). The 3150-, 3380-, and 2485-cm^{-1} bands are shoulders and the characteristic frequency is to some extent arbitrary.
[d]The adjectives 'in-phase' and 'out-of-phase' mean that the molecules are moving, by and large, in phase and out of phase respectively with their immediate neighbors.
[e]Calculated frequencies using the quoted isotope ratios. They are not experimentally resolved and the Raman maximum is at 2482 cm^{-1}.
[f]Assumed isotope ratios.
[g]Not observed in ice Ic, probably because it is too weak for the technique used, as is the corresponding band of ice Ih.

The strongest infrared band is at 3220 cm^{-1} and undoubtedly corresponds to the $\nu_3 e$ band of ice Ic. The ν_3 vibrations probably occupy a much narrower band than the ν_1 except for the TO–LO splitting, as was shown in Section 3. Accordingly, the 3209-cm^{-1} Raman band is assigned to the same vibration. The difference between the infrared and Raman bands is 11 cm^{-1}, about $\frac{1}{6}$ of the difference between the infrared and Raman ν_1 in-phase bands. This is as expected if the ν_3 vibrational band is much narrower than the ν_1. Because the Raman peak corresponds to vibrations that are nearly in phase it will be taken as the ν_3TO band. The corresponding LO band is therefore predicted to be at 3299 cm^{-1}. There is a weak Raman peak at 3323 cm^{-1} which is therefore identified with ν_3LO. The ν_1 out-of-phase band, corresponding to $\nu_1 b_1$ of ordered ice Ic, should be weak in the Raman spectrum and is assigned to the 3420-cm^{-1} Raman band. A frequency of 3390 cm^{-1} was predicted earlier in this section for ordered ice Ic by analogy with the spectrum of ice VIII. In the infrared spectrum, only a single high-frequency shoulder at 3380 cm^{-1} can be identified with overlapping ν_3LO and ν_1 out-of-phase bands. These assignments are summarized in Table 4.

For a model of ordered ice Ic which includes only nearest-neighbor coupling, the mean of the $\nu_1 a_1$ and $\nu_1 b_1$ frequencies would be the frequency of an uncoupled ν_1 vibration. If this is also true for disordered ice I, as it should be, at least approximately, the uncoupled ν_1 frequency would be 3252 cm^{-1}. The uncoupled O–H stretching frequency is 3273 cm^{-1} (32, 37, 59), which is 22 cm^{-1} higher. In the vapor the corresponding bands differ by 50 cm^{-1}. This difference may be due to a smaller ν_1–ν_3 splitting in the crystal than in the vapor or to the vibrations that contribute to the ν_1 in-phase and out-of-phase bands not having near neighbors moving precisely in phase or out of phase respectively, or to a combination of both. Fifer and Schiffer (60) have shown that the ν_1–ν_3 splitting of water molecules in several metal chloride hydrates is significantly smaller than in the vapor. While the hydrogen bonding in these salts may not be exactly comparable to that in ice I, the observation is consistent with the proposed assignment of ice I.

Longitudinal optic vibrations have occasionally been identified in the past in disordered materials. Fournier *et al.* (61) have identified what appears to be an LO band in the Raman spectrum of liquid carbon tetrafluoride, Devlin *et al.* (62, 63) have identified LO bands in the Raman and attenuated total reflection spectra of orientationally disordered and molten nitrate salts, and Galeener and Lucovsky (64) have identified LO bands in the Raman spectra of vitreous silica and germania. A TO–LO splitting also appears to occur in the translational infrared and Raman spectra of ice I (65). The occurrence of TO–LO splitting in disordered materials appears to be now well established. It presumably means that at least some of the normal vibrations are coupled over significant distances.

The assignment of D_2O follows similar arguments except that the ν_3LO and ν_1 out-of-phase bands appear to overlap, and so their frequencies were calculated from the H_2O

frequencies using the isotope ratios obtained for the ν_3TO and ν_1 in-phase bands respectively. The frequencies are summarized in Table 4.

4.3. Ice Ih

Ice Ih has four molecules in a hexagonal cell. It can be considered as being made from two hexagonal puckered sheets stacked one on top of the other, and two molecules from each sheet make a unit cell. Each sheet has only one ordered arrangement of the protons having two molecules in the repeating unit, and it is shown by either the upper or lower pairs of either Fig. 3*a* or 3*b*. Two equivalent arrangements can be made by rotating the sheet $\pm 2\pi/3$ about a vertical axis through any oxygen atom. Two ordered arrangements of ice Ih in the four-molecule unit can be made by stacking equivalent sheets on top of one another, puckered in the right way, or by alternately stacking rotationally equivalent but not identical sheets. The first gives a C_{2v} structure in space group $Pmc2_1$, C_{2v}^2 shown in Fig. 3*a*, and the second a C_1 structure in space group Pl, C_1 shown in Fig. 3*b*.

In the C_{2v} structure, the molecules are all on sites of C_s symmetry. Two have the plane perpendicular to the molecular plane, so that ν_1 and ν_3 do not couple for these molecules at the zone center. The other two have the plane in the molecular plane, and so symmetry does not forbid the coupling of ν_1 and ν_3.

Both structures have eight Raman-active vibrations, four ν_1 and four ν_3, which may of course couple. The ν_1 in-phase vibration will be particularly strong, and no doubt corresponds to the 3083-cm^{-1} band of ice Ih and Ic. The ν_3 vibrations will be only slightly coupled intermolecularly, and all are active in the Raman. They no doubt correspond to the 3209-cm^{-1} band. Only three ν_3 infrared bands of the C_{2v} structure are allowed, that belonging to the A_2 species being infrared inactive. Hence, a small difference in the infrared and Raman ν_3 frequencies, which is experimentally about 11 cm^{-1}, can be understood. The TO–LO splitting will occur, much as in ice Ic, and the 3323-cm^{-1} Raman band is assigned to ν_3LO. The ν_1 out-of-phase Raman band, which would belong to the A_1 species in C_{2v} ice, no doubt corresponds to the 3420-cm^{-1} band.

It seems likely therefore that this discussion provides an approximation to the assignment of the infrared and Raman bands of ice Ih, and that the assignment in Table 4 applies to disordered ice Ih as well as to Ic. The caveat incorporated into Section 4.2 should of course be kept in mind.

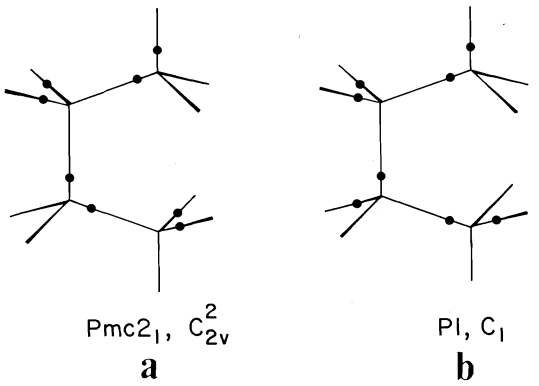

FIG. 3. The two ordered arrangements of the water molecules in the four-molecule unit cell of ice Ih and their symmetry species.

Although ice Ih (43, 44) and Ic appear[7] to be fully disordered within the restrictions of the ice rules, there is still a good deal of order. If there were no correlation of the orientations of neighboring molecules, the mean value of the reduced scalar product $(\boldsymbol{\mu}_1 \cdot \boldsymbol{\mu}_2)/\mu^2$ of the dipole moments of near-neighbor molecules 1 and 2 would be zero, and if it were fully ordered it would be 1. As the orientations are fully disordered within experimental uncertainty and within the limits of the ice rules, the product is $\frac{1}{3}$. Perhaps this large amount of local order is partly responsible for the visibility of particularly the Raman bands of ice I.

5. Amorphous Ice

The infrared (31, 32, 37, 68, 69) and Raman (29, 35, 70) spectra of amorphous ice have been investigated several times, and typical spectra are reproduced in Fig. 1. The infrared H_2O and D_2O spectra are from Buontempo (68) and Bertie and Whalley (32) respectively, and the Raman spectra are from Venkatesh *et al.* (29). The spectra of others are in substantial agreement. They are all similar to the spectra of ice Ih, the main differences being an increase in frequency, due no doubt to the distortion of the hydrogen bonds and an increased band width. The increase in band width is partly due to the variable distortion of the bonds, which causes a variation of the frequencies of the O–H oscilla-

[7]The similarity of the low-frequency permittivities of ice Ih and Ic (67) shows this.

TABLE 5. Assignment of the infrared and Raman bands of amorphous ice

	ν/cm^{-1}[a]					
	H_2O		D_2O		Isotope effect	
Vibration	Raman[b]	Infrared[c]	Raman[b]	Infrared	Raman	Infrared
ν_1 in-phase	3116	3191	2318		1.344	1.377
ν_3TO	3220	3253	3281	2436	1.352	1.366
ν_3LO	3372	3367	2483	2499	1.358	1.347
ν_1 out-of-phase	3483		2530		1.377	

[a]Frequencies are at ~100 K.
[b]As resolved using Gaussian line shapes by Venkatesh *et al.* (29). The frequencies are somewhat arbitrary because the band is a product of a density of states and an intensity, and there is no reason to assume it is a sum of a limited number of Gaussian bands.
[c]Frequencies taken from Hardin and Harvey (37). The spectra of D_2O (32) and H_2O (68) agree.

tors (32), and perhaps to a decrease in the extent of the intermolecular coupling, so that small variations of the extent from vibration to vibration will cause a variation of frequency. It appears (2) that the frequency of the in-phase ν_1 vibrations that dominate the low-frequency Raman peak at 3108 cm^{-1} at 30 K is not significantly broadened from its width in ice Ih by a decrease of coupling, but it is not known whether the other bands behave similarly.

The similarity of the crystalline and amorphous bands strongly suggests that they have similar causes. Consequently they can be assigned by analogy with the assignments of ice I, as given in Table 5.

6. Ice VI

The Raman spectrum of ice VI (5) at 14 kbar and 292 K resembles the spectrum of ice I, but the bands are broader, and are more like the bands of amorphous ice. Their centers are at ~3180, 3310, and 3400 cm^{-1}, and there may be a significant band at ~3500 cm^{-1}. At atmospheric pressure and 77 K the strong Raman band is (51) at 3204 cm^{-1} in H_2O and 2370 cm^{-1} in D_2O. By analogy with ice I, the bands can be assigned to ν_1 in-phase, ν_3(TO), and ν_1 out-of-phase mixed with ν_3(LO), in order of increasing frequency.

7. Discussion

It appears that a fairly detailed justifiable assignment of a quite complicated spectrum of a highly disordered material has been achieved, perhaps for the first time. The most likely avenue for further progress on ice is lattice dynamical calculations on ordered and eventually, but with much more difficulty, on disordered ice. Two calculations have been published, one (71) on the C_{2v} ordered ice in the four-molecule cell and one (46) on disordered ice. Both, however, used too little intermolecular O–H coupling, and so result in two too narrow and nonoverlapping bands of ν_1 and ν_3 vibrations.

One of the conclusions from this work is that the spectra of disordered phases are frequently closely related to the spectra of the corresponding crystalline phases, and in the O–H stretching region in ice I there appears to be almost a one-to-one correspondence. The correspondence extends even to the longitudinal vibrations, whose frequencies in the crystal are raised above the frequencies of the corresponding transverse vibrations by the long-range electric field in a well understood way (55). Their existence in disordered phases is less well understood.[8] When a crystal is disordered, the integrated infrared intensity of its strong bands is not markedly changed. The transition-moment coupling that causes the TO–LO splitting in the crystal is therefore still present with about the same magnitude. It will cause a long-range coupling of the atomic motions, and so also of course will the short-range forces which will also cause a finite range of coupling of the motions (46, 57, 66). The vibrational spectra of models of disordered solids resemble in general features the spectra of models of the corresponding crystals (46, 57, 66) and it appears that for most of the vibrations "the localization, although somewhat higher than for a crystalline solid, is by no means intense" (57). If this is so, it seems likely that many of the vibrations will have a significant plane-wave component of finite extent and can be approximately characterized by a local wave

[8]See the comments of E. Galeener appended to the paper by Galeener and Lucovsky (56).

vector. There will be vibrations in which the polarization is mainly parallel or respectively perpendicular to the wave vector, and so there will be local LO and TO vibrations having approximately the same separation as in the crystal.

It appears therefore that the appearance of LO vibrations in highly disordered solids can be understood, at least on a qualitative and somewhat intuitive level.

8. Summary

The arguments and conclusions of this paper can be summarized as follows.

1. The O–H stretching bands of ice are strongly coupled and can only be understood in detail from the point of view of solid-state spectroscopy, not from single-molecule spectroscopy.

2. Ice VIII is composed of two interpenetrating ordered ice Ic structures. Its experimental Raman and predicted infrared spectra have been used to predict the Raman and infrared spectra of ordered ice Ic.

3. Ice VII is an orientationally disordered ice VIII whose Raman spectrum has similar features to that of ice VIII. An assignment of the ice VII bands follows from the assignment of the ice VIII bands.

4. The similarity of the spectra and assignments of ice VIII and VII suggests that there will be a corresponding similarity in the spectra and assignments of ordered and disordered ice Ic. This allows the bands of disordered ice Ic to be assigned in some detail.

5. The infrared and Raman spectra of ice Ih and Ic are indistinguishable at present accuracy, and so the ice Ih bands can be assigned by analogy with the ice Ic bands.

6. The high infrared intensity of the O–H stretching bands of ice requires that there shall be strong TO–LO splitting of the bands of ordered ice Ic, particularly of the $\nu_3 e$ band. The bands in ordered ice Ih should be split in a similar way. A band that can be considered to be derived from the $\nu_3 e$(LO) band of ordered ice has been identified in the Raman and infrared spectra. The ν_1 bands should also show LO–TO splitting, perhaps by a smaller amount, but their effects have not been observed. The assignments are summarized in Table 4.

7. The corresponding bands in amorphous ice and ice VI have been assigned by analogy with the assignment for ice Ih and Ic.

1. P. T. T. Wong and E. Whalley. J. Chem. Phys. **62**, 2418 (1975).
2. E. Whalley. Intermolecular coupling of ν_1 vibrations in ice. To be published.
3. P. T. T. Wong and E. Whalley. J. Chem. Phys. **64**, 2359 (1976).
4. W. B. Holzapfel, R. S. Hawke, and K. Syassen. Proc. 4th Intl. Conf. High Pressure Research, Kyoto. Physico-Chemical Society of Japan, Kyoto. 1975. pp. 344–347.
5. R. S. Hawke, K. Syassen, and W. B. Holzapfel. Rev. Sci. Instrum. **45**, 1598 (1974).
6. E. Whalley, D. W. Davidson, and J. B. R. Heath. J. Chem. Phys. **45**, 3976 (1966).
7. A. J. Brown and E. Whalley. J. Chem. Phys. **45**, 4360 (1966).
8. G. P. Johari, A. Lavergne, and E. Whalley. J. Chem. Phys. **61**, 4292 (1974).
9. B. Kamb. Acta Crystallogr. Sect. A, **25**, S117 (1969).
10. B. Kamb. Trans. Am. Crystallogr. Assoc. **5**, 61 (1969).
11. N. Ockman. Adv. Phys. **7**, 199 (1958).
12. F. A. Saunders. Johns Hopkins Univ. Circ. No. 18, 58–59 (1899).
13. G. Bode. Ann. Phys. Leipzig, **30**, 326 (1909).
14. J. J. Fox and A. E. Martin. Proc. R. Soc. A, **174**, 234 (1940).
15. I. K. Rao. Indian J. Phys. **3**, 123 (1928).
16. A. S. Ganesan and S. Vankateswaran. Indian J. Phys. **4**, 195 (1929).
17. I. K. Rao. Proc. R. Soc. A, **130**, 489 (1931).
18. I. K. Rao. Philos. Mag. **17**, 1113 (1934).
19. W. Sutherland. Philos. Mag. **50**, 460 (1900).
20. G. B. B. M. Sutherland. Proc. R. Soc. A, **141**, 535 (1933).
21. D. M. Dennison. Phys. Rev. **17**, 20 (1921).
22. W. H. Bragg. Proc. Phys. Soc. **34**, 98 (1921).
23. W. H. Barnes. Proc. R. Soc. A, **125**, 670 (1929).
24. P. C. Cross, J. Burnham, and P. A. Leighton. J. Am. Chem. Soc. **59**, 1134 (1937).
25. J. W. Ellis. Phys. Rev. **38**, 693 (1931).
26. R. Mecke. Phys. Z. **30**, 907 (1929).
27. J. D. Bernal and R. H. Fowler. J. Chem. Phys. **1**, 515 (1933).
28. Z. A. Gabrichidze. Opt. Spektrosk. **19**, 575 (1965); Engl. Transl., Opt. Spectrosc. USSR, **19**, 319 (1965).
29. C. G. Venkatesh, S. A. Rice, and J. B. Bates. J. Chem. Phys. **63**, 1065 (1975).
30. M. J. Taylor and E. Whalley. J. Chem. Phys. **40**, 1660 (1964).
31. D. F. Hornig, H. F. White, and F. P. Reding. Spectrochim. Acta, **12**, 338 (1958).
32. J. E. Bertie and E. Whalley. J. Chem. Phys. **40**, 1637 (1964).
33. C. Haas and D. F. Hornig. J. Chem. Phys. **32**, 1763 (1960).
34. C. Wu and M. Nicol. Chem. Phys. Lett. **18**, 83 (1973).
35. P. C. Li and J. P. Devlin. J. Chem. Phys. **59**, 547 (1973).
36. V. I. Val'kov and G. L. Maslenkova. Opt. Specktrosk. **1**, 881 (1956).
37. A. H. Hardin and K. B. Harvey. Spectrochim. Acta Part A, **29**, 1139 (1973).
38. H. F. White. Thesis, Brown University. 1952. *Quoted by* Ockman in ref. 11.

39. R. L. MILLER. Thesis, Brown University, 1954. *Quoted by* Ockman in ref. 11.
40. W. MAISCH. Thesis, Brown University, 1956. *Quoted by* Ockman in ref. 11.
41. N. OCKMAN. Thesis, University of Michigan, 1957. *Quoted by* Ockman in ref. 11.
42. N. OCKMAN and G. B. B. M. SUTHERLAND. Proc. R. Soc. A, **247**, 434 (1958).
43. W. F. GIAUQUE and J. W. STOUT. J. Am. Chem. Soc. **58**, 1144 (1936).
44. (*a*) L. PAULING. J. Am. Chem. Soc. **57**, 2680 (1935); (*b*) L. PAULING. The nature of the chemical bond. 3rd ed. Cornell University Press, Ithaca, NY. 1960. p. 466.
45. E. WHALLEY. Dev. Appl. Spectrosc. **6**, 277 (1968).
46. R. E. SHAWYER and P. DEAN. J. Phys. C, **5**, 1028 (1972).
47. YU. V. GURIKOV. *In* Water in biological systems. *Edited by* L. P. Kayushin. *Translated by* Consultant's Bureau, New York. 1969. pp. 1–8 (1968).
48. B. A. MIKHAILOV and V. M. ZOLATAREV. *In* Water in biological systems. Vol. 2. *Edited by* M. F. Vuks and A. I. Sidorova. *Translated by* Consultant's Bureau, New York, 1971. pp. 83–88.
49. S. J. LAPLACA and B. POST. Acta Crystallogr. **13**, 503 (1960).
50. R. BRILL and A. TIPPE. Acta Crystallogr. **23**, 343 (1967).
51. J. P. MARCKMANN and E. WHALLEY. J. Chem. Phys. **41**, 1450 (1964).
52. W. S. BENEDICT, N. GAILAR, and E. K. PLYLER. J. Chem. Phys. **24**, 1139 (1956).
53. W. COCHRAN and R. A. COWLEY. J. Phys. Chem. Solids, **23**, 447 (1962).
54. J. E. BERTIE, H. J. LABBÉ, and E. WHALLEY. J. Chem. Phys. **50**, 4501 (1969).
55. G. VANKATARAMAN, L. A. FELDKAMP, and V. C. SAHNI. Dynamics of perfect crystals. MIT Press, Cambridge, MA. 1975. Chapt. 4.
56. F. E. GALEENER and G. LUCOVSKY. Longitudinal optical vibrations in vitreous SiO_2. *In* Structure and excitations of amorphous solids. *Edited by* G. Lucovsky and F. L. Galeener. Am. Inst. Phys., New York. 1976. pp. 223–227.
57. P. DEAN. Rev. Mod. Phys. **44**, 127 (1972).
58. S. IKAWA and S. MAEDA. Spectrochim. Acta Part A, **24**, 655 (1968).
59. T. A. FORD and M. FALK. Can. J. Chem. **46**, 3579 (1968).
60. R. A. FIFER and J. SCHIFFER. J. Chem. Phys. **52**, 2664 (1970).
61. R. P. FOURNIER, R. SAVOIE, F. BERSETTE, and A. CABANA. J. Chem. Phys. **49**, 1159 (1968).
62. J. P. DEVLIN, D. W. JAMES, and R. FRECH. J. Chem. Phys. **53**, 4394 (1970).
63. J. P. DEVLIN, G. RITZHAUPT, and T. HUDSON. J. Chem. Phys. **58**, 817 (1973).
64. F. L. GALEENER and G. LUCOVSKY. Phys. Rev. Lett. **37**, 1474 (1976).
65. D. D. KLUG and E. WHALLEY. Origin of the 300-cm^{-1} infrared and Raman band of ice I. To be published.
66. R. J. BELL. Rep. Prog. Phys. **35**, 1315 (1972).
67. S. R. GOUGH and D. W. DAVIDSON. J. Chem. Phys. **52**, 5442 (1970).
68. U. BUONTEMPO. Phys. Lett. A, **42**, 17 (1973).
69. G. RITZHAUPT, N. SMYRI, and J. P. DEVLIN. J. Chem. Phys. **64**, 435 (1976).
70. V. MAZZACURATI and M. NARDONE. Chem. Phys. Lett. **32**, 99 (1975).
71. P. BOSI, R. TUBINO, and G. ZERBI. J. Chem. Phys. **59**, 4578 (1973).

Etude par résonance paramagnétique électronique de la radiolyse de la pyridine *N*-oxyde en matrice vitreuse de methanol

J. P. QUAEGEBEUR ET B. PERLY

Service de Chimie Physique, C.E.N. de Saclay, B.P. N° 2-91190 Gif-Sur-Yvette, France

ET

G. SURPATEANU ET A. LABLACHE-COMBIER

Laboratoire de Chimie Organique Physique, Université des Sciences et Techniques de Lille, B.P. N° 36-59650 Villeneuve d'Ascq, France

Reçu le 21 janvier 1977

J. P. QUAEGEBEUR, B. PERLY, G. SURPATEANU et A. LABLACHE-COMBIER. Can. J. Chem. **55**, 3442 (1977).

L'analyse des spectres de rpe de la pyridine *N*-oxyde soumise au rayonnement γ, en matrice vitreuse méthanolique à 77 K montre la présence d'un mélange de radicaux 2 et 4-azacyclohexadienyles *N*-oxydes (respectivement **1** et **2**), formés par addition de l'espèce primaire hydroxyméthyle sur le cycle pyridinique. La détermination de la structure des différents radicaux a été facilitée par l'utilisation de pyridines *N*-oxydes substituées.

J. P. QUAEGEBEUR, B. PERLY, G. SURPATEANU, and A. LABLACHE-COMBIER. Can. J. Chem. **55**, 3442 (1977).

The analysis of esr spectra derived from γ irradiated pyridine *N*-oxide in a methanolic vitreous matrix at 77 K shows the presence of a mixture of 2- and 4-azacyclohexadienyl *N*-oxide radicals (respectively **1** and **2**) formed by the addition of the hydroxymethyl primary species to the pyridine ring. The structure of the different radicals was determined by comparison with spectra derived from several substituted pyridine *N*-oxides.

Introduction

Les radicaux libres dérivés des composés hétérocycliques azotés, générés aussi bien sous rayonnement γ que par photolyse ont fait l'objet de nombreux travaux (par ex. réf. 1). Dans le cadre de l'étude des effets des radiations sur la pyridine et ses dérivés, nous nous proposons d'examiner les espèces radicalaires formées à partir de la pyridine *N*-oxyde (py *N*-O), dans le but de mettre en évidence l'influence du groupement *N*-oxyde sur la réactivité du cycle pyridinique. La radiolyse à 77 K de ce composé en matrice méthanolique vitreuse donne naissance aux espèces primaires $\cdot CH_2OH$ lesquelles, par addition sur les molécules de soluté engendrent un nouveau radical dont le spectre de rpe semble différent de ceux obtenus à partir de la pyridine.

Afin d'identifier ce nouveau radical et d'élucider le mécanisme de sa formation, des études complémentaires effectuées sur différentes py *N*-O deutérées sélectivement ou méthylées ont été effectuées et ont permis de mettre en évidence la non sélectivité de l'addition du groupement hydroxyméthyle sur le cycle pyridinique.

Mode expérimental

Les expériences de rpe ont été effectuées à l'aide d'un spectromètre Varian V 4502, en bande **X**, avec une fréquence de modulation de 100 kHz. Les échantillons dégazés et scellés sous vide ont été irradiés à 77 K à l'aide d'une source ^{60}Co de 10 kCi (doses de 1 à 2 Mrad). Les spectres ont été enregistrés à 90 K après réchauffement des échantillons vers 115 K, afin de faire disparaître les radicaux provenant de la matrice.

La dideutéro-3,5 pyridine *N*-oxyde ($^2H_2$-3,5 py *N*-O) a été préparée par oxydation de la $^2H_2$-3,5 pyridine (dont la synthèse a été décrite dans la référence 1*c*) par l'acide peracétique suivant la méthode mentionnée dans la réf. 2. La lutidine-3,5 *N*-oxyde a été préparée à partir de la 3,5 lutidine de la même façon. La 2,6 dideutero pyridine *N*-oxyde ($^2H_2$-2,6 py *N*-O) a été synthétisée suivant la méthode décrite par Hershenson et Bauer (3). La pureté isotopique de ces composés a été vérifiée par spectroscopie rmn à 60 MHz (Jeol C 60 HL) ou 250 MHz (Cameca TSN 250). Les autres dérivés méthylés de la pyridine *N*-oxyde, provenant de chez Aldrich, ont été utilisés sans purification préalable.

Identification des spectres de résonance paramagnétique électronique

A 77 K, les signaux de rpe obtenus sous irradiation γ de la py *N*-O en concentration 0.3 *M* en matrice vitreuse CH_3OH (ou CD_3OD) sont attribués exclusivement aux radicaux issus du solvant, c'est à dire $\cdot CH_2OH$ et $\cdot CD_2OD$

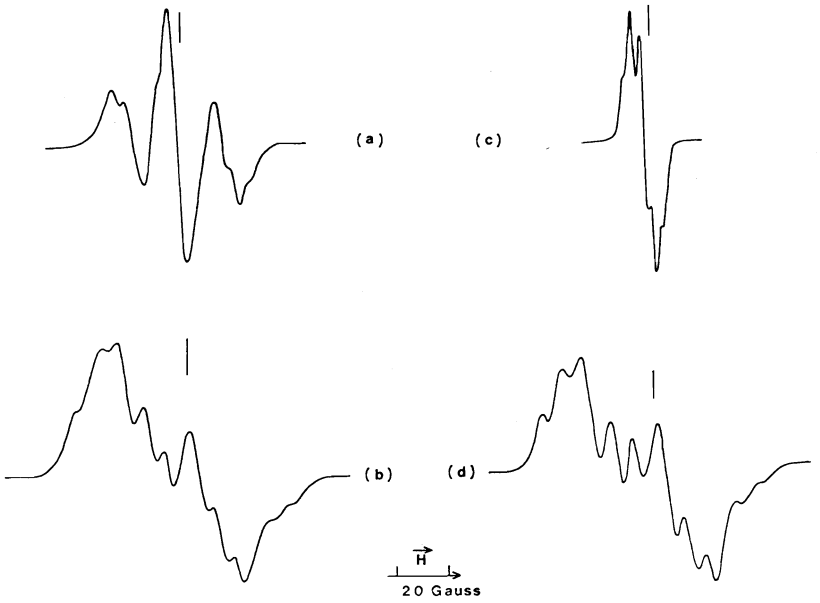

FIG. 1. Spectres rpe après irradiation à 77 K de la py *N*-O en matrice CH_3OH (spectres de gauche) et CD_3OD (spectres de droite). (*a*) et (*c*): respectivement des radicaux $\cdot CH_2OH$ et $\cdot CD_2OD$ (enregistrés à 90 K avant réchauffement de l'échantillon). (*b*) et (*d*): enregistrés à 90 K après réchauffement vers 115 K. Trait vertical: $g = 2.0028$.

respectivement. Lors du réchauffement de l'échantillon de 90 à 115 K, nous assistons à une décroissance progressive de ce signal puis ensuite à l'apparition d'un nouveau signal (fig. 1) avec conservation du paramagnétisme. Cette dernière constatation, ainsi que l'allure générale du spectre dont la structure hyperfine principale se compose d'un doublet partiellement structuré nous permettent d'envisager une espèce radicalaire différente de celles obtenues à partir de la pyridine dans diverses conditions (1*b*, *c* et *d*).

Par ailleurs, la deutération de la matrice ne se manifeste que par une diminution légère de la largeur de raie, sans modification notable du spectre de rpe (fig. 1), ce qui nous permet de supposer que le radical obtenu dans ces conditions provient d'une addition du groupement $\cdot CH_2OH$ (ou $\cdot CD_2OD$) sur le cycle pyridinique et peut être assimilé à un radical du type aza-cyclohexadiényle substitué.[1] Trois espèces radicalaires peuvent être envisagées, selon que l'addition de $\cdot CD_2OD$ se fait en position 2, 4 ou 3 par rapport à l'azote (numérotation cf. tableau 2).

[1]Le groupement hydroxyméthyle ne contribuant pas au spectre, CD_3OD a été utilisé comme solvant dans les expériences suivantes.

L'attribution du spectre provenant de la py *N*-O a été effectuée par comparaison avec ceux issus de différents dérivés deutérés ou

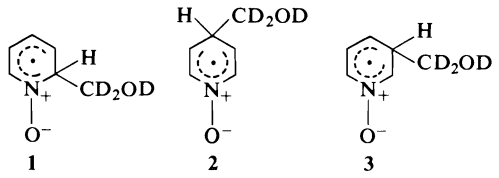

méthylés. Les différentes constantes de couplage ont été déduites des largeurs totales et des seconds moments des spectres de rpe (4), dont l'analyse a été décrite précédemment (5). La validité des attributions a été vérifiée par calcul INDO des densités de spin. La simulation des spectres a été effectuée d'après le programme de Lefebvre et Maruani (6), en tenant compte de l'anisotropie du couplage des protons σ et du tenseur **g**. Les différents paramètres ont été légèrement modifiés jusqu'à obtenir un accord satisfaisant entre les spectres calculés et expérimentaux.

Compte tenu de la délocalisation partielle de la densité de spin sur l'atome d'oxygène, conduisant à un paramètre de couplage spin–orbite important, nous avons déterminé les composantes principales $g_{\parallel}$ et $g_{\perp}$ du tenseur **g**.

En supposant que ce dernier est à symétrie axiale, $g_{\|}$ est donné par la position moyenne des deux raies extrêmes du spectre et sera pris comme la composante la plus petite, perpendiculaire au plan du cycle ($g_{\|} = g_{xx}$) (7). Les composantes $g_{\perp}$ ne pouvant être déterminées directement à partir du spectre, nous avons calculé la valeur isotrope g_{iso} de **g** à partir du premier moment mesuré par rapport à H_0:

$$[1] \qquad M_1 = -H_0(g_{iso}/g_0 - 1)$$

où $H_0 = 3320$ G et g_0 la valeur correspondante de **g** étant égale à 2.0028.

La valeur moyenne de M_1 étant (-4.41 ± 0.20) G, il s'en suit $g_{iso} = 2.0055 \pm 0.0004$; par suite comme $g_{\|} = 2.0028$, $g_{\perp} = \frac{1}{2}(3g_{iso} - g_{\|}) = 2.0068 \pm 0.0004$. La contribution au second moment de l'anisotropie du tenseur **g** est alors égale à (6):

$$[2] \quad \langle \Delta H^2 \rangle_g = (H_0{}^2/5)\{\varepsilon_{xx}{}^2 + \varepsilon_{yy}{}^2 + \varepsilon_{zz}{}^2 + \tfrac{2}{3}(\varepsilon_{xx}\varepsilon_{yy} + \varepsilon_{yy}\varepsilon_{zz} + \varepsilon_{zz}\varepsilon_{xx})\}$$

avec $\varepsilon_{uu} = g_{uu}/g_0 - 1$ ($u = x$, y ou z) et g_{uu} étant la composante principale de **g** suivant l'axe u soit

$$\langle \Delta H^2 \rangle_g \simeq (20 \pm 4)\ \mathrm{G}^2$$

Ces valeurs principales du tenseur **g** sont voisines de celles des radicaux nitroxydes pour lesquels $g_{\|} = g_{xx} \simeq 2.0030$ et $g_{iso} \simeq 2.0060$. Différents calculs INDO effectués sur les formes **1**, **2** et **3** (tableau 2) font apparaitre tout d'abord que l'addition de $\cdot CD_2OD$ en position 3 par rapport à l'azote conduirait à un spectre de rpe dont la largeur totale serait voisine de 95 G et le second moment M_2 supérieur à 440 G^2, valeurs incompatibles avec les résultats expérimentaux.

Le choix entre les espèces **1** et **2** semble plus difficile: en particulier les densités de spin voisines dans les deux cas (cf. tableau 2) fourniraient des spectres de rpe identiques, hypothèse vérifiée ultérieurement lors de la simulation des spectres. Nous envisagerons dans un premier temps, l'existence d'une espèce radicalaire du type **1**.

Les constantes de couplage $a^H{}_3$ et $a^H{}_5$ sont déterminées par la comparaison des largeurs totales et seconds moments de la py *N*-O et de son dérivé deutéré en 3 et 5 ($^2H_2$-3,5 py *N*-O) (tableau 1). En supposant que les densités de spin portées par les carbones C_3 et C_5 sont pratiquement égales,

$$\Delta(\Delta H) = (86 - 75)\ \mathrm{G} = 2(a^H{}_3 - 2 \times a^D{}_3)$$

soit, comme $a^D \sim 0.154a^H$,

$$|a_3| \sim |a_5| \sim (8 \pm 0.5)\ \mathrm{G}$$

Des valeurs du même ordre sont retrouvées en comparant les résultats expérimentaux de la py *N*-O et de la diméthyl-3,5 py *N*-O. Dans ce cas la largeur totale est augmentée de:

$$[3] \qquad \Delta(\Delta H) = 2(3 \times a^H{}_{CH_3} - a^H{}_3)$$

En supposant d'autre part que la substitution des protons par les groupements méthyles ne modifie pas de manière appréciable la répartition des densités de spin, le second moment est accru de:

$$[4] \quad \Delta(M_2) = 2\left\{-\frac{3.5}{12}(a^H{}_3)^2 + \tfrac{3}{4}(a^H{}_{CH_3})^2\right\}$$

si

$$\rho_3 = a^H{}_3/Q^H{}_{\alpha 3} = a^H{}_{CH_3}/Q^H{}_{CH_3}$$

avec $Q^H{}_{\alpha} = -23$ G et $Q^H{}_{CH_3} = 28$ G, nous en déduisons

$$|a_3| \sim |a_5| \sim (7.0 \pm 0.5)\ \mathrm{G}$$

$$|\rho^{\pi}{}_3| \sim |\rho^{\pi}{}_5| \sim (0.30 \pm 0.02)$$

Les spectres expérimentaux provenant des 2 et 4 picolines *N*-oxydes étant sensiblement identiques (fig. 3) et leurs caractéristiques voisines de celles de la py *N*-O, les constantes de couplages $a^H{}_4$ et $a^H{}_2$ (ou $a^H{}_6$), dans l'hypothèse des espèces du type **1** ou **2**, sont du même ordre de grandeur et inférieures à la largeur de raie σ: $|a_2| \sim |a_4| < 2$ G.

Il est alors possible, dans le cas du radical

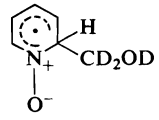

1

d'estimer approximativement la densité de spin $\rho_N{}^{\pi}$ ainsi que la constante de couplage isotrope $a^H{}_2$, à partir de ΔH et M_2. En incluant $a^H{}_4$ et

TABLEAU 1. Largeurs totales (ΔH) et seconds moments (M_2) des spectres de rpe des radicaux azacyclohexadienyles *N*-oxydes (matrice CD_3OD)

Composé	ΔH/G	M_2/G²*
py *N*-O	86	(347 ± 15)
$^2H_2$-2,6 py *N*-O	86	(217 ± 15)
$^2H_2$-3,5 py *N*-O	75	(304 ± 15)
Méthyl-2 py *N*-O	87	(343 ± 20)
Méthyl-4 py *N*-O	87	(343 ± 20)
Diméthyl-3,5 py *N*-O	119	(405 ± 20)

*Mesurés par rapport à $g = 2.0028$ à $T = 90$ K après réchauffement de l'échantillon à 115 K.

TABLEAU 2. Densités de spin et constantes de couplage données par calcul INDO des radicaux azacyclohexadienyles *N*-oxydes

Radical	Position	Densités de spin Π	Constantes de couplage (G) INDO*	Valeurs expérimentales	Valeurs optimisées pour la simulation des spectres
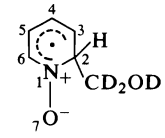 **1**	1	0.340	$a_N = 9.23$	$\begin{cases} A_{N\parallel} = 18.7 \\ A_{N\perp} = 3.3 \end{cases}$	$\begin{cases} A_{N\parallel} = 20 \\ A_{N\perp} = 3.5 \end{cases}$
	2	—	$a^H_{iso} = 24.8$	$a^H_{iso} = 27.4$	$a^H_{iso} = 27.5$
	3	0.240	$a^H = -6.94$	$\lvert a^H\rvert = 8.0 \pm 0.5$	$a^H = -8$
	4	−0.164	$a^H = 4.35$	$a^H < 2$	$a^H = 1.2$
	5	0.236	$a^H = -6.35$	$\lvert a^H\rvert = 8.0 \pm 0.5$	$a^H = -7.2$
	6	−0.252	$a^H = 5.96$	$a^H < 2$	$a^H = 1.5$
	7	0.468			$\begin{cases} g_\parallel = 2.0028 \\ g_\perp = 2.0064 \end{cases}$
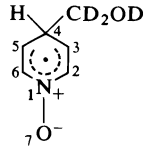 **2**	1	0.285	$a_N = 6.47$		$\begin{cases} A_{N\parallel} = 20 \\ A_{N\perp} = 3.5 \end{cases}$
	2,6	−0.178	$a^H = 4.32$		$a^H = 1.5$
	3,5	0.214	$a^H = -6.27$		$a^H = -7.5$
	4	—	$a^H_{iso} = 21.7$		$a^H_{iso} = 27.5$
	7	0.520			$\begin{cases} g_\parallel = 2.0028 \\ g_\perp = 2.0064 \end{cases}$
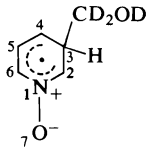 **3**	1	−0.204	$a_N = -6$		
	2	0.573	$a^H = -14.7$		
	3	—	$a^H_{iso} = 44.8$		
	4	0.428	$a^H = -11.7$		
	5	−0.201	$a^H = 6.09$		
	6	0.44	$a^H = -11.1$		
	7	−0.31			

*Les valeurs des distances interatomiques et des angles de liaison utilisées dans ces calculs sont données dans la réf. 8, en supposant la liaison N—O située dans le plan du cycle et l'angle θ (cf. texte) égal à 50°.

a^H_6 dans la largeur de raie σ,

[5] $$\Delta H - \sigma - a^H_3 - a^H_5 = 2A_{N\parallel} + a^H_2$$

soit

$$2A_{N\parallel} + a^H_2 \sim 65 \text{ G}$$

De même, la contribution des couplages hyperfins au second moment étant (4):

$$M_2 - \langle \Delta H^2 \rangle_g - \sigma^2/4 = \langle \Delta H^2 \rangle_{hf} = \tfrac{1}{3} \sum_i \sum_u n_i S_i A_{ui}^2$$

il s'en suit:

[6] $$(2/9)(A_{N\parallel}^2 + 2A_{N\perp}^2) + (1/4)(a^H_2)^2 \sim 278 \text{ G}^2$$

Les valeurs principales du tenseur de couplage de l'azote sont reliées à ρ_N^Π par:

[7] $$A_{N\parallel} = a_N + 2B \sim 62\rho_N^\Pi$$

[8] $$A_{N\perp} = a_N - B \sim 11\rho_N^\Pi$$

Dans ces expressions, dans la limite des incertitudes expérimentales, nous avons négligé la contribution $S^N\rho_N^\Pi$ de l'orbitale 1*s* de l'azote ainsi que l'interaction entre les noyaux N et O, si bien que

$$a_N \sim Q_N^N \rho_N^\Pi$$

Le couplage isotrope a^H_2 est relié aux densités de spin ρ_3^Π et ρ_N^Π portées par les atomes adjacents, par la relation (9):

[9] $$a^H_2 = Q(\rho_3^{1/2} + \rho_N^{1/2}) \cos^2 \theta$$

où $Q = (58 + 55)/2 = 56.5$ G et θ est l'angle que fait le plan $(C_3C_2H_2)$ ou (NC_2H_2) avec l'axe de l'orbitale de l'e^- non apparié, en admettant que la liaison N—O se trouve dans le plan du cycle.[2]

La substitution de [7], [8] et [9] dans [5] et [6] nous fournit ainsi $|\rho_N| \sim 0.303$ et $\theta \sim 50°$.

Dans l'hypothèse du radical **2** et en supposant que ρ_N reste du même ordre (cf. calcul INDO du tableau 2), nous obtenons $\theta = 51°$.

La validité de nos résultats est confirmée par simulation des spectres de rpe des radicaux

[2]Nous avons démontré, par calcul INDO que la distribution de densités de spin et l'énergie électronique totale n'étaient que faiblement affectées par l'inclinaison $\alpha (0 < \alpha < 20°)$ du groupement N—O par rapport au plan du cycle.

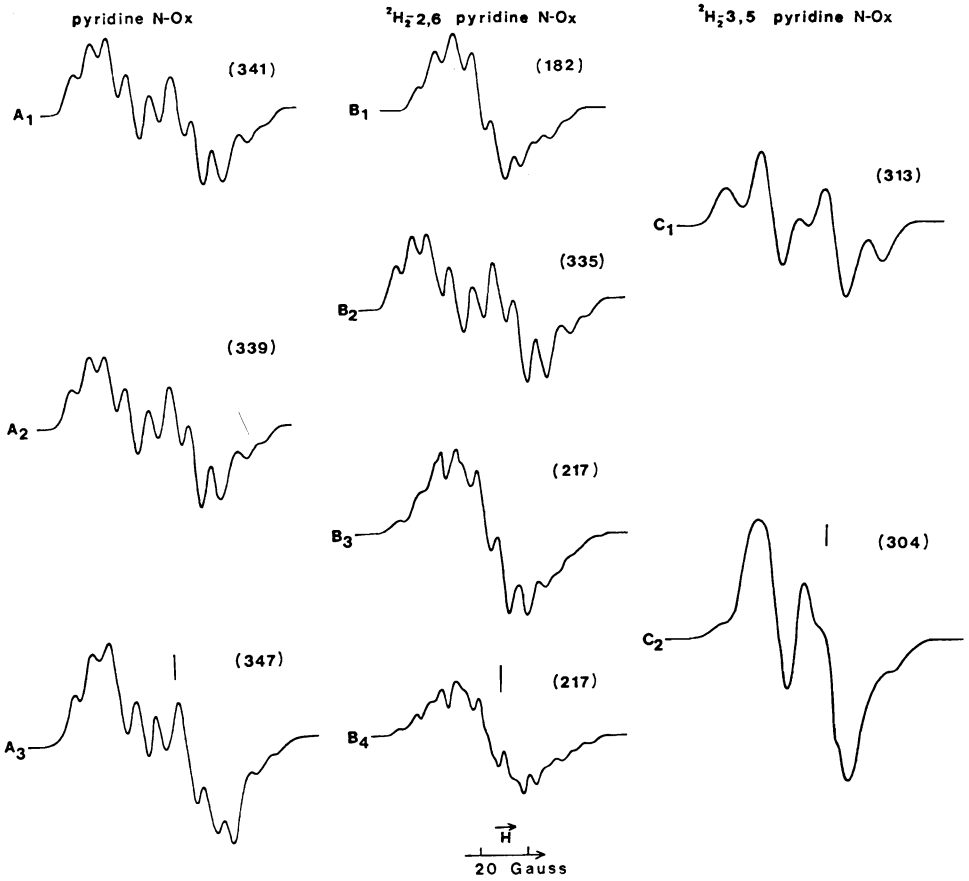

FIG. 2. Spectres rpe expérimentaux et calculés des radicaux azacyclohexadiényles *N*-oxydes (matrice: CD_3OD). A_3, B_4 et C_2: spectres expérimentaux. A_1 et A_2: spectres calculés correspondant aux espèces **1** et **2** respectivement (cf. tableau 2). B_1 et B_2: spectres calculés correspondant aux radicaux **4** et **5**. B_3 résulte de la superposition de B_1 et B_2 dans les proportions respectives 2:1. C_1: spectre calculé correspondant au radical **1**. Entre parenthèses figurent les seconds moments. Trait vertical: $g = 2.0028$.

1 et **2** (figs 2 et 3), pour lesquels les paramètres optimisés figurent dans le tableau 2. Il apparait ainsi que les spectres calculés des radicaux **1** et **2** sont pratiquement semblables de sorte que nous ne pouvons conclure à la présence préférentielle de l'une ou de l'autre espèce. Le cas de la $^2H_2$-2,6 py *N*-O permet de lever cette ambiguité. En admettant l'existence de la seule espèce **4** formée dans ces conditions,

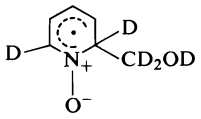

4

la largeur et le second moment théoriques, calculés à partir des caractéristiques $\langle \Delta H \rangle_{\text{py } N\text{-O}}$ et $\langle M_2 \rangle_{\text{py } N\text{-O}}$ du spectre de py *N*-O sont respectivement égales à:

$$\langle \Delta H \rangle = \langle \Delta H \rangle_{\text{py } N\text{-O}} - a^{\text{H}}{}_2 + 2a^{\text{D}}{}_2 = 66 \text{ G}$$

et

$$\langle M_2 \rangle = \langle M_2 \rangle_{\text{py } N\text{-O}} - \tfrac{1}{4}(a^{\text{H}}{}_2)^2 + \tfrac{2}{3}(a^{\text{D}}{}_2)^2 = 163 \text{ G}^2$$

De la même façon, les caractéristiques du spectre de rpe d'un radical du type **5**

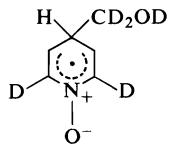

5

seraient voisines de 84 G et 335 G^2 respectivement. Ces valeurs théoriques des seconds moments ne sont pas compatibles avec M_2 expérimental = 217 G^2. De plus les spectres

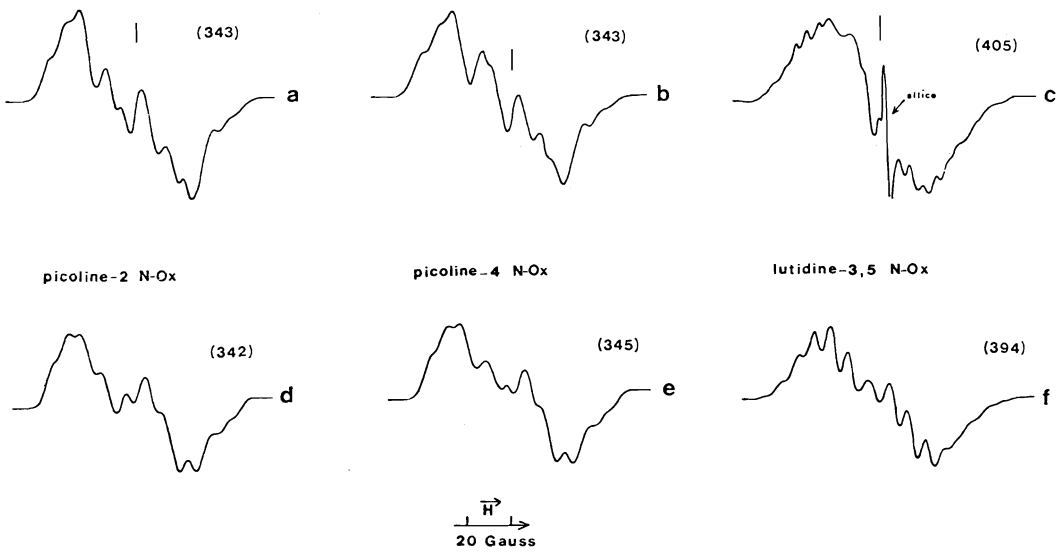

FIG. 3. Spectres rpe expérimentaux (ligne du haut) et calculés (ligne du bas) des radicaux dérivés des méthyl pyridines *N*-oxydes, avec leurs seconds moments correspondants. (*a*): Radicaux **1** et **2**; (*b*): radical **1**; (*c*): radicaux **1** et **2**. Trait vertical: $g = 2.0028$.

calculés pour les formes **4** et **5** ne correspondent pas précisément au spectre expérimental obtenu à partir de la $^2H_2$-2,6 py *N*-O (fig. 2). En supposant alors que l'addition du groupe hydroxyméthyle se fasse sur les positions 2 (ou 6) et 4, nous aurons un mélange des radicaux **4** et **5** dans les proportions respectives 2:1.

Ce rapport est effectivement celui obtenu en appliquant la règle d'additivité des seconds moments:

$$M_{2\text{exp}} = x(M_2)_{(5)} + (1 - x)(M_2)_{(4)}$$

soit

$$x \sim 0.31$$

Une vérification supplémentaire de notre hypothèse est apportée par la comparaison entre le spectre expérimental provenant de la $^2H_2$-2,6 py *N*-O et celui obtenu par addition des spectres calculés des radicaux **4** et **5** dans ces proportions relatives (fig. 2).

Il devient alors possible, compte tenu des données rassemblées pour les différents radicaux étudiés, d'attribuer avec plus de certitude les spectres de rpe obtenus. En particulier dans le cas de la py *N*-O et de ses dérivés 3–5 disubstitués, et 2–6 dideutéré nous obtenons les deux espèces correspondantes **1** et **2** dans les proportions 2:1, alors que l'addition de $^{\cdot}CD_2OD$ se fait préférentiellement en position 2 (ou 6) dans la methyl-4 py *N*-O, et en position 4 dans le cas de la methyl-2 py *N*-O (fig. 3). Ce résultat est différent de ceux obtenus par Symons et coll. (1*a*) lors de la radiolyse de l'ion pyridinium. Dans ce dernier cas l'addition de H sur le cycle se faisait exclusivement en position 4 pour donner naissance au radical 4-azacyclohexadienyle **6.**

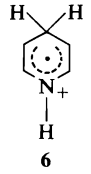

6

Dans le cas de la py *N*-O, la non sélectivité de la réaction serait induite par le groupe *N*-oxyde lequel favoriserait l'attaque sur les positions 2 et 4 de densités électroniques faibles. Ceci suggère que le groupement hydroxyméthyle piégé dans la matrice possède un caractère nucléophile faible:

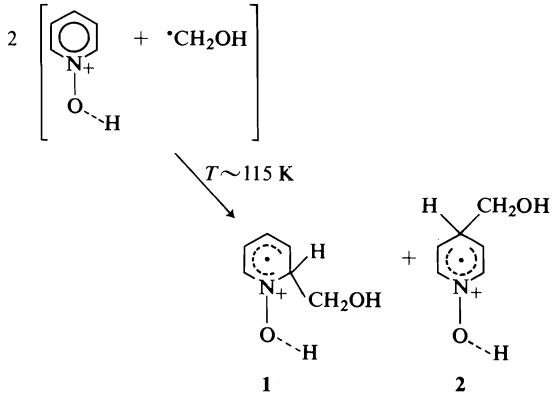

1 **2**

Conclusion

Bien qu'un accord satisfaisant entre les spectres expérimentaux et ceux calculés ait nécessité l'introduction d'une anisotropie du tenseur **g** dont la détermination des composantes principales reste assez approximative, les résultats obtenus par simulation des spectres de rpe et par la méthode des moments confirment notre hypothèse concernant l'existence d'un mélange de deux radicaux. Cependant nous n'avons pu détecter ces radicaux lors de l'irradiation uv en phase liquide et à température ambiante d'une solution 10^{-3} *M* de py *N*-O dans CH_3OH + 1% H_2O_2, selon la méthode de Livingston et Zeldes (10) à cause de la durée de vie trop courte de l'espèce primaire $\cdot CH_2OH$ ou parce que la transformation des espèces **1** et **2** en une molécule stable diamagnétique est beaucoup plus rapide que celle de la formation des radicaux.

Remerciements

Les auteurs tiennent à remercier le Dr. Chachaty du CEN/SACLAY pour ses suggestions et ses remarques qui nous ont été très utiles.

1. (*a*) H. J. Bower, J. A. McRae et M. C. R. Symons. J. Chem. Soc. A, 1918 (1968); (*b*) C. Chachaty et A. Forchioni. C. R. Acad. Sci. Ser. C, **264**, 1421 (1964); (*c*) J. P. Quaegebeur, H. Ofenberg, A. Lablache-Combier, J. C. Ronfard Haret et C. Chachaty. J. Chem. Soc. Faraday Trans. I, **72**, 143 (1976); (*d*) C. Chachaty. J. Chim. Phys. **64**, 608 (1967).
2. H. S. Mosher, L. Turner et A. Carlsmith. *Dans* Organic synthesis collective. Vol. 4. 2nd ed. *Edité par* N. Rabjohn. John Wiley and Sons Inc., New York, NY. 1967. p. 828.
3. F. M. Hershenson et L. Bauer. J. Org. Chem. **34**, 660 (1969).
4. G. Vincow et P. Johnson. J. Chem. Phys. **39**, 1143 (1963).
5. J. C. Ronfard Haret, A. Lablache-Combier et C. Chachaty. J. Phys. Chem. **78**, 899 (1974).
6. R. Lefebvre et J. Maruani. J. Chem. Phys. **42**, 1480 (1965).
7. H. M. McConnell et R. E. Robertson. J. Phys. Chem. **61**, 1018 (1957).
8. J. F. Chiang. J. Chem. Phys. **61**, 1280 (1974).
9. D. H. Whiffen. Mol. Phys. **6**, 223 (1963).
10. R. Livingston et H. Zeldes. J. Chem. Phys. **44**, 1245 (1966).

Ligand substitution kinetics of nickel(II) ion in *N,N*-dimethylformamide

PRAPHULLA KUMAR CHATTOPADHYAY AND BYRON KRATOCHVIL

Department of Chemistry, University of Alberta, Edmonton, Alta., Canada T6G 2G2

Received April 20, 1977

PRAPHULLA KUMAR CHATTOPADHYAY and BYRON KRATOCHVIL. Can. J. Chem. **55**, 3449 (1977).

Rate constants and activation parameters for formation of the monocomplexes of Ni(II) ion with several mono-, bi-, and terdentate ligands in *N,N*-dimethylformamide were obtained by stopped-flow spectrophotometry. The gross features of substitution for all the ligands studied could be accommodated within the structure of an I_d-type mechanism. 4-Phenylpyridine behaves most 'normally', and 1,10-phenanthroline stabilized most strongly outer-sphere complex formation with Ni(II). Comparison of these data with previously reported work by other authors for substitution at Ni(II) in acetonitrile with the same ligands indicates that in dimethylformamide pyridine-type ligands generally affect the stability of metal–ligand outer-sphere complexes less dramatically than in acetonitrile. Hammett correlation is observed for 1,10-phenanthroline and its 5- and 5,6-substituted derivatives. The slope of the Hammett correlation plot in dimethylformamide is in the order of -0.2, about half the value of -0.4 reported previously in acetonitrile by other authors. This indicates that the stability of the metal–ligand outer-sphere complex is affected more greatly by small differences in the electronic nature of the coordinating substituted 1,10-phenanthrolines in acetonitrile than it is in dimethylformamide.

PRAPHULLA KUMAR CHATTOPADHYAY et BYRON KRATOCHVIL. Can. J. Chem. **55**, 3449 (1977).

On obtient, par spectrophotométrie à flux stoppé, les constantes de vitesse et les paramètres d'activation pour la formation de monocomplexes d'ion Ni(II) avec plusieurs ligands mono-, bi- et terdentate dans la *N,N*-diméthylformamide. Les traits caractéristiques de la substitution pour tous les ligands étudiés peuvent être assimilés à l'intérieur d'un mécanisme de type I_d. La phényl-4 pyridine se comporte le plus souvent 'normalement' et la phénanthroline-1,10 stabilise plus fortement la formation d'un complexe à sphère extérieure avec le Ni(II). La comparaison de ces valeurs avec celles rapportées antérieurement par d'autres auteurs pour la substitution au site Ni(II) dans l'acétonitrile avec les mêmes ligands indique que pour les ligands de types pyridine dans la diméthylformamide, la stabilité des complexes métal–ligand aux sphères extérieures est moins affectée que dans l'acétonitrile. On observe une corrélation d'Hammett pour la phénanthroline-1,10 et ses dérivés 5- et 5,6-substitués. La pente de la courbe pour la corrélation d'Hammett dans la diméthylformamide est de l'ordre de -0.2 correspondant à environ la moitié de la valeur -0.4 rapportée antérieurement par d'autres auteurs pour l'acétonitrile. Ces résultats indiquent que la stabilité des complexes métal–ligand aux sphères extérieures est affectée plus grandement par de petites différences dans la nature électronique des phénanthrolines substituées si la coordination se produit dans l'acétonitrile que si elle se produit dans la diméthylformamide.

[Traduit par le journal]

Introduction

N,N-Dimethylformamide is an important dipolar aprotic solvent frequently used as a reaction medium for inorganic and organic reactions because of its ability to solvate both metal ions and nonpolar organic compounds. In recent years considerable data have been collected on metal–ligand equilibria and reaction rates in a variety of solvents, especially between nickel(II) and amines, and it has been found that a dissociative-interchange (I_d) type mechanism (1) fits the rate data for the reaction of nickel(II) with simple mono-dentate ligands in water (2), methanol (3), ethanol (4), acetonitrile (5), and propylene carbonate (6). Little data are available in dimethylformamide, however, and the mechanism of substitution at nickel(II) in this solvent has not yet been determined. Bennetto and Caldin have investigated the nickel(II)–bipyridine system (7*a*), and Hoffman and co-workers have made preliminary measurements on rates of reaction between nickel(II) and thiocyanate, chloride, trifluoroacetate, and *p*-toluenesulfonate ions (7*b*). The nickel(II)–isoquinoline reaction has also been investigated (7*c*).

For an I_d mechanism the pathways for

reaction between nickel(II) and a monodentate ligand L can be represented by

$$[1] \qquad NiS_6 + L \underset{\longleftarrow}{\overset{K_{12}}{\rightleftharpoons}} \underset{I}{NiS_6, L} \underset{k_{32}}{\overset{k_{23}}{\rightleftharpoons}} \underset{II}{NiS_5L, S}$$

in which the rate-determining step for the formation of the inner-sphere complex (process II, forward rate constant k_{23}) is preceded by rapid formation of an outer-sphere complex (process I, equilibrium formation constant K_{12}). In eq. 1 S stands for a solvent molecule and charges on the metal ion and ligand have been omitted for convenience.

For a 'normal' type of substitution (5*b*), when $K_{12}[L] \ll 1$, the second order rate constant k_f for formation of the inner-sphere complex is given by

$$[2] \qquad k_f = K_{12}k_{23}$$

As discussed before, for a 'normal' reaction the quantity R, given by

$$[3] \qquad R = (4/3)k_{23}/k_{ex} = (4/3)k_f/(k_{ex}K_{12})$$

should be close to unity (7*c*). Here k_{ex} and K_{12} have their usual significance (8). For normal substitution with a neutral monodentate ligand the enthalpy of activation for formation ($\Delta H_f^{\ddagger}$) of the complex is expected to be close to the corresponding quantity for solvent exchange ($\Delta H_{ex}^{\ddagger}$) for a given metal–ligand system in the same solvent.

Investigations of ligand substitution reactions at nickel(II) in solution have led to the identification of several specific rate-determining effects. These include (*a*) a solvent-dependent steric requirement exhibited by multidentate ligands during chelation, (*b*) a solvent-dependent rotational barrier to the proper orientation in space of coordinating ligand atoms during chelation, and (*c*) stabilization of metal–ligand outer-sphere complexes by π orbital or electrostatic interactions between the incoming ligand and polarized solvent molecules in the first coordinating sphere of the metal ion. All these effects influence the rate of substitution at nickel(II), especially in dipolar aprotic solvents such as acetonitrile and dimethylsulfoxide (5).

Of the solvents studied thus far, acetonitrile is the one in which nickel–ligand outer-sphere complexes are most influenced by variations in electronic character of the entering ligands (5*a*). Similar outer-sphere stabilization is absent in water, and has not been reported in any other dipolar aprotic solvent, although with phenanthroline there may be some stabilization in poor donor solvents such as propylene carbonate or sulfolane (9).[1] The specific property of acetonitrile that causes the stability of the metal–ligand outer-sphere complex to be so sensitive to the electronic character of the ligand has not been identified. Dimethylformamide and acetonitrile have similar dipole moments but differ considerably in size and in donor properties towards metal ions, acetonitrile being a weaker Lewis base toward nickel(II) than dimethylformamide. Hence a study of substitution at nickel(II) in dimethylformamide with ligands of varying electronic and steric properties could aid in improving understanding of the specific properties of the solvent that contribute to the stability of metal–ligand outer-sphere complexes, and will help establish the gross features of the mechanism of substitution at nickel(II) in dimethylformamide.

Experimental

Solvent

N,N-dimethylformamide (Fisher, Certified ACS) was purified as described before (7*c*). Purified solvent was used within 24 h after the final purification step.

Reagents

4-Phenylpyridine (Aldrich, mp 69–73°C) was recrystallized from ethanol. 2,2′-Bipyridine (G. F. Smith, mp 70°C), 2,2′,2″-terpyridine (G. F. Smith, Reagent Quality, mp 68–69°C), 1,10-phenanthroline monohydrate (B.D.H., mp 98°C), 5x-1,10-phenanthroline monohydrate (x = chloro, nitro, methyl) (G. F. Smith, Reagent Quality), and 5,6-dimethyl-1,10-phenanthroline (J. T. Baker, Baker Grade) were used as received. Nickel was used as $Ni(ClO_4)_2 \cdot H_2O$; the method of preparation of the salt was described previously (5*b*). Concentrations of nickel(II) solutions were determined by EDTA titration with murexide indicator after dilution with water and buffering at p*H* 10 with ammonia–ammonium chloride.

Procedure

Kinetic measurements were made with a stopped-flow spectrophotometer (Durrum Instrument Co., Model D-110). Descriptions of the instrument, along with modifications for better temperature control, were given previously (7*c*, 10). All other instruments and techniques used were as described before (7*c*).

Kinetic measurements for formation rate constants were made under pseudo-first-order conditions, the ratio of nickel(II) to ligand being held in the range of 10 to 100 throughout. All ligand and metal ion solutions were used within 4 to 6 h of preparation. Measurements were made

[1]Confer both ref. 9 and J. F. Coetzee, private communication.

TABLE 1. Rate constants for formation of the monocomplexes of pyridine-type ligands with nickel(II) in dimethylformamide at various temperatures

Ligand	Rate constant (k_f) × 10^{-3} (ℓ mol^{-1} s^{-1})			
	15°C	25°C	35°C	45°C
4-Phenylpyridine	0.968	2.00	[a]	
Bipyridine	0.227	0.564	1.09_0	2.25
Terpyridine	0.135	0.300	0.578	1.13_2
Phenanthroline	1.62_5	3.28	6.46	1.23
5-Chlorophenanthroline	1.06_7	2.39	4.61	9.33
5-Nitrophenanthroline	0.677	1.59	3.11	5.95
5-Methylphenanthroline	1.81_0	3.51	6.60	1.34
5,6-Dimethylphenanthroline	1.82_8	4.00	7.83	1.44

[a]Additional values: 0.409 at 4.75°C, 1.46_9 at 20°C, and 3.27 at 30°C.

at wavelengths where the complex absorbed more strongly than the reactants: 277 nm for 4-phenylpyridine, 335 nm for 2,2′,2″-terpyridine, 308 nm for 2,2′-bipyridine, and 272 nm for 1,10-phenanthroline and the substituted 1,10-phenanthrolines. Reaction rates were calculated from the rate of change of absorbance of the reaction solutions with time. All other experimental procedures were as described before (*7c*).

Results

The rate constants for substitution of the ligands studied at nickel(II) are presented in Table 1. Under the experimental conditions used, only 1:1 complexes are expected. A pseudo-first-order rate plot with terpyridine as the ligand is shown in Fig. 1. Except for 4-phenylpyridine and bipyridine, plots for all the ligands studied pass near the origin. This indicates that the equilibrium constants for formation of the nickel(II) monocomplexes are all relatively large; on the basis of the experimental uncertainty in the pseudo-first-order rate constants we estimate formation constants greater than 3×10^4 at 25°C for all the systems studied. In Table 2 rate constants and associated activation parameters for substitution of the above ligands at nickel(II) are compared with those for solvent exchange (11).

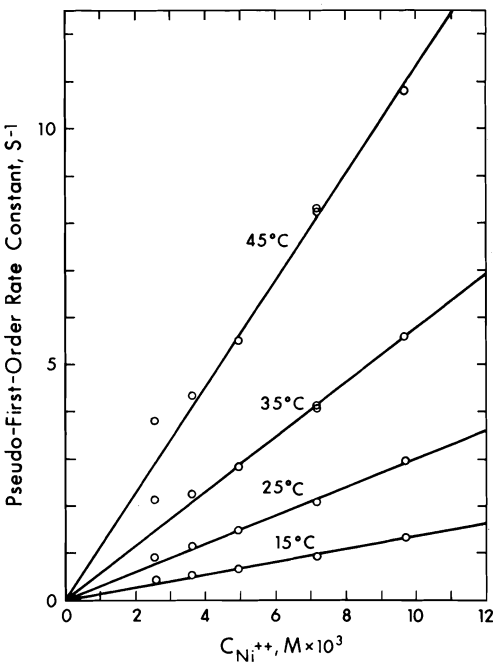

FIG. 1. Pseudo-first-order rate constants for formation of the monocomplex of nickel(II) with terpyridine as a function of nickel(II) concentration in dimethylformamide. $C_L = 2.52 \times 10^{-5}$ *M*.

Discussion

Pseudo-first-order Rate Constants

In a simple pseudo-first-order kinetic plot, the intercept is equal, in theory, to the dissociation rate constant for the reaction. This was found previously to hold for the nickel(II)–isoquinoline complex in dimethylsulfoxide (8). Intercepts that do not correspond to k_d have been observed in some solvents, however (*7a*). This may result from the presence of substances that affect the rate of reaction. Thus, traces of amine-type impurities in the solvent that can form stable complexes with nickel(II) can increase the magnitude of the real intercept owing to simultaneous formation of ternary complexes. This was observed in earlier work on the nickel(II)–isoquinoline system in dimethylformamide, where the value of 19.5 for k_b obtained from the intercept of pseudo-first-order plots agreed only approximately with the value of 26.5 obtained from K_{eq} and k_f measurements (8). A parallel but better-behaved system exists in dimethylsulfoxide, where intercepts of pseudo-first-order

TABLE 2. Rate constants at 25°C and associated activation parameters for formation of the monocomplexes of pyridine-type ligands with nickel(II) in dimethylformamide

Ligand	$k_f \times 10^{-3}$ (ℓ mol^{-1} s^{-1})	R	$\Delta H_f^{\ddagger}$ (kcal mol^{-1})	$\Delta S_f^{\ddagger}$ (eu)
Dimethylformamide[a]	3.8	—	15.0	+8
Isoquinoline[b]	2.42	0.98	12.4±0.4	−2±1
4-Phenylpyridine	2.00	0.81	13.6±0.6	−2.0±2.0
Bipyridine	0.564	0.23	13.2±0.5	−1.8±1.7
Phenanthroline	3.28	1.33	11.7±0.1	−3.2±0.4
5-Chlorophenanthroline	2.39	0.97	12.5±0.2$_6$	+1.3±0.9
5-Nitrophenanthroline	1.59	0.64	12.5±0.4	−1.9±1.4
5-Methylphenanthroline	3.51	1.42	11.5±0.4	−3.7±1.4
5,6-Dimethylphenanthroline	4.00	1.62	12.0±0.2	−2.0±0.8
Terpyridine	0.300	0.12	12.2±0.2	−6.1±0.7

[a]Data from ref. 11.
[b]Data from ref. 7c.

plots for formation of the 4-phenylpyridine and isoquinoline complexes of nickel(II) both agree with directly measured k_b values (8, 12). Since both complexes are of comparable stability in dimethylsulfoxide (K_{eq} = 35.8 and 31.3) it seems likely that the reaction of 4-phenylpyridine with nickel(II) in dimethylformamide has an equilibrium constant of about the same size as that of isoquinoline, and that an intercept value for k_b at 25°C on the order of 15 may be reasonable.

In general, however, dissociation rate constants should be determined either directly or calculated from directly measured overall equilibrium constants and formation rate constants rather than being obtained from the intercepts of pseudo-first-order kinetic plots for formation of the complex. Thus the intercepts observed with 2,2′-bipyridine in this work cannot be assumed to give correct values for k_d, especially since Bennetto and Caldin did not observe a positive intercept for this system in dimethylformamide (*7a*). Our values for the formation rate constant of this complex as measured from the slopes of the pseudo-first-order plots, and for the activation enthalpy for the formation of the complex, agree with their results within 1%. The discrepancy in intercept may be due to the presence in our solvent of a constant trace amount of a complexing impurity such as dimethylamine, a hydrolysis product of dimethylformamide. The concentration of bipyridine being on the order of 10^{-5} *M*, a concentration of dimethylamine in the solvent as low as 10^{-4} *M* would be likely to increase the pseudo-first-order rate constant with different concentrations of nickel(II) by a constant amount, and thereby cause a shift in the pseudo-first-order plots (13). Of the systems studied in this work, the one involving nickel(II) and terpyridine is most effected by the addition of low concentrations of dimethylamine. For example, the pseudo-first-order rate constant for the reaction between nickel(II) at 2.5 × 10^{-3} *M* and terpyridine at 2.5 × 10^{-5} *M* was doubled by the addition of about 5 × 10^{-4} *M* dimethylamine. The presence of traces of a complexing impurity is further indicated by the deviation from linearity of the points in Fig. 1 at nickel(II) concentrations below about 3 × 10^{-3} *M*. Therefore, we suspect the presence of a contaminant, probably dimethylamine, in the range of 10^{-5} to 10^{-6} *M* in our solvent; however, values for formation rate constants obtained from the slopes of pseudo-first-order plots using data measured at higher concentrations of nickel(II) are considered to be accurate within ±2 to ±3%.

Formation Rate Constants

From the k_f and R values listed in Table 2 it appears that the reaction with nickel(II) of 4-phenylpyridine, like isoquinoline, is 'normal' in dimethylformamide, and that an I_d type of reaction mechanism is involved. Recently Coetzee and co-workers reported that the reaction of 4-phenylpyridine with nickel(II) is normal in propylene carbonate, 2-propanol, and isobutyronitrile (6). Analysis of the values of R listed in Table 2 shows that the same conclusion can be applied to all the ligands studied in this work.

Terpyridine reacts more slowly with nickel(II) in dimethylformamide than does bipyridine, while 1,10-phenanthroline reacts more rapidly. This order is the same as that observed in all the nonaqueous solvents studied. Chattopadhyay and Coetzee (5) explained this order in acetonitrile by considering the thermodynamic parameters associated with the reactions. As in

acetonitrile, in dimethylformamide also the rings of bipyridine and terpyridine may experience some solvent-hindrance to attainment of the *cis* position during formation of the outer-sphere complex, while the rigid phenanthroline ligand is not affected.[1]

Enthalpy of Activation ($\Delta H_f^{\ddagger}$)

The variation in $\Delta H_f^{\ddagger}$ found for the ligands studied in this work is relatively small. Despite this, some significance can be attached to the differences because the formation rate constants vary by over an order of magnitude for the same set of ligands, and because the experimental uncertainty in $\Delta H_f^{\ddagger}$ values is smaller relative to the spread of results for the ligands studied. The observed $\Delta H_f^{\ddagger}$ values can be related to $\Delta H_{ex}^{\ddagger}$ for solvent exchange at nickel(II) in dimethylformamide by considering (*a*) the effect of the ligand on the stability of the metal–ligand outer-sphere complex, and (*b*) the steric effect exhibited by the ligand molecule. In this discussion it is assumed that the stability of the metal–ligand outer-sphere complex increases with an increase in the number of pyridine nitrogens and benzene rings in the ligand, and that benzene rings fused to pyridine rings have a greater stabilizing effect on the metal–ligand outer-sphere complex than do those connected by a carbon–carbon bond. On this basis the value of $\Delta H_f^{\ddagger}$ for 4-phenylpyridine is expected to be closest to $\Delta H_{ex}^{\ddagger}$; this is indeed observed (Table 2). The values of $\Delta H_f^{\ddagger}$ for bipyridine, isoquinoline, and phenanthroline would be expected to be lower than for 4-phenylpyridine in the order given; this is in agreement with experimental results for all but bipyridine. As mentioned above, bipyridine may be hindered by solvent interaction from ready attainment of the *cis* configuration necessary for chelation with nickel(II). The energy required to overcome this rotational barrier is compensated for by the extra stabilization of the metal–ligand outer-sphere complex provided by the additional pyridine nitrogen. The difference between the $\Delta H_f^{\ddagger}$ values for bipyridine and 4-phenylpyridine depends on the magnitude of the two opposing effects; since that for bipyridine is only 0.4 kcal lower than the corresponding quantity for 4-phenylpyridine, and about at the level of experimental uncertainty, we conclude that the two opposing effects for bipyridine are either about equal in magnitude or the stabilizing effect is slightly stronger than the steric effect.

In the solid state the rings of bipyridine are coplanar, with the nitrogen atoms in the *trans* position (14); this conformation is likely in solution also. For chelation with nickel(II) the two nitrogens must rotate from the *trans* to the *cis* position. The energy required for this rotation being small, it can be concluded that the decrease in $\Delta H_f^{\ddagger}$ due to extra stabilization of the metal–ligand outer-sphere complex by the additional pyridine nitrogen atom in bipyridine, as compared to 4-phenylpyridine, is also small. This may explain why $\Delta H_f^{\ddagger}$ for the reaction of nickel(II) with 4-phenylpyridine is only 1.4 kcal lower than $\Delta H_{ex}^{\ddagger}$ for solvent exchange and why 4-phenylpyridine follows a 'normal' I_d-type mechanism. Similarly, comparison of $\Delta H_f^{\ddagger}$ for the reaction of terpyridine with that of 4-phenylpyridine can be rationalized by assuming that in dimethylformamide the extra stabilizing effect on the metal–ligand outer-sphere complex of the additional two pyridine nitrogen atoms is greater than the energy required to put all the terpyridine nitrogen atoms in the *cis* position for chelation with nickel(II). We conclude that of the ligands studied in this work 5-methylphenanthroline has the strongest influence on the stability of the metal–ligand outer-sphere complex. 1,10-Phenanthroline and its 5-methyl derivative behave similarly; the difference in $\Delta H_f^{\ddagger}$ values is within experimental uncertainty.

Hammett Correlation

In dimethylformamide pyridine-type ligands generally affect the stability of metal–ligand outer-sphere complexes less dramatically than in acetonitrile. This is demonstrated in Fig. 2, in which the slope of Hammett plots for reactions of nickel(II) with substituted 1,10-phenanthro-

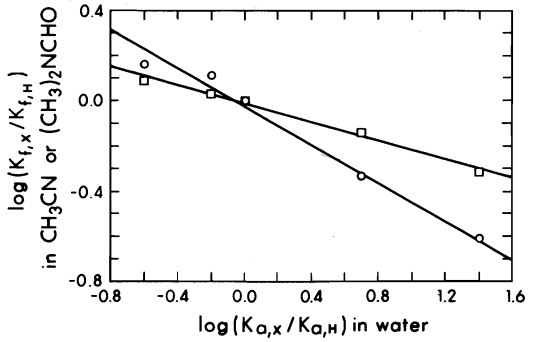

FIG. 2. Hammett correlation plots for reaction of substituted phenanthrolines with nickel(II) in acetonitrile (circles, slope = −0.40) and in dimethylformamide (squares, slope = −0.20).

lines in dimethylformamide are compared with previous results in acetonitrile by Chattopadhyay and Coetzee (5*a*).

The Hammett correlation shown is based on relative pK_a values of the ligands in water (15). The correlation in any solvent preferably should be based on relative pK_a values of the ligand in that solvent. It has been reported that a virtually constant difference exists between pK_a values in acetonitrile and water for a series of closely-related bases (16). Therefore the use of relative pK_a values in water for Hammett correlation in dimethylformamide should be feasible.

The different reaction rates observed in dimethylformamide for substitution at nickel(II) with 5- and 5,6-substituted 1,10-phenanthrolines may be the result of different electronic effects of the substituent groups on the stabilities of the metal–ligand outer-sphere complexes. A similar trend in rates was observed in acetonitrile (5*a*). The nature of the reaction mechanism in both cases is I_d rather than I_a. Slopes of Hammett correlations in the order of -0.4 ± 0.03 in acetonitrile and -0.2 ± 0.01 in dimethylformamide indicate that the metal–ligand outer-sphere complexes are more susceptible to the electronic nature of substituent groups on the parent phenanthroline in acetonitrile than in dimethylformamide.

Acetonitrile coordinates to nickel(II) through the nitrogen atom in the cyanide group, while dimethylformamide coordinates through the oxygen atom in the amide group, but the dipole moments of 3.92 and 3.86 D at 25°C are similar (17). Dimethylformamide is more bulky and exerts more steric hindrance to the approach of an incoming ligand to a dimethylformamide-solvated metal cation than does acetonitrile. Also, Gutmann donor numbers of 26.8 for dimethylformamide and 14.1 for acetonitrile (18) indicate that dimethylformamide is a much stronger Lewis base toward nickel(II) than acetonitrile. If the stability of the metal–ligand outer-sphere complex is mainly dependent on the intensity of π orbital or simple electrostatic interaction between the incoming ligand and a polarized solvent molecule in the inner sphere of the central cation, then from consideration of the molecular size and dipole moments of dimethylformamide and acetonitrile it is predicted that the outer-sphere complex with the phenanthrolines will be stabilized more in acetonitrile than in dimethylformamide. Comparisons of $\Delta H_f^{\ddagger}$ and $\Delta H_{ex}^{\ddagger}$ values in Table 2 with earlier results in acetonitrile (5*a*) show this to be the case. Similarly, the solvent donicity values suggest that stability of the outer-sphere phenanthroline complex is influenced by variation of 5- and 5,6-substitution more in acetonitrile than it is in dimethylformamide. This also is substantiated by the greater slope of the Hammet correlation plot for acetonitrile in Fig. 2.

In summary, we conclude that pathways for ligand substitution reactions between nickel(II) and the mono-, bi- and terdentate ligands studied so far in dimethylformamide can be accommodated within the framework of an I_d-type mechanism if effects of possible fine interactions between solvent and solute are considered. Of the ligands studied 4-phenylpyridine shows least interaction with dimethylformamide, whether the dimethylformamide is considered as bulk solvent or as polarized individual solvent molecules in the inner sphere of nickel(II). Consequently its reaction with nickel(II) in this solvent appears to be guided most 'normally' by an I_d-type mechanism. As was previously observed in acetonitrile, in dimethylformamide also 1,10-phenanthroline among all the ligands studied stabilizes most strongly the outer-sphere complex in reaction with nickel(II), but this influence on stabilization of the outer-sphere complex is less significant in dimethylformamide than in acetonitrile. Also, the stability of the metal–ligand outer-sphere complex is affected more greatly by small differences in the electronic nature of the coordinating substituted 1,10-phenanthrolines in acetonitrile than it is in dimethylformamide.

1. C. H. Langford and H. B. Gray. Ligand substitution processes. W. A. Benjamin, New York, NY. 1965.
2. (*a*) M. Eigen and R. G. Wilkins. Adv. Chem. Ser. No. 49, 55 (1965); (*b*) R. G. Wilkins. Acc. Chem. Res. **3**, 408 (1970).
3. (*a*) R. G. Pearson and P. Ellegen. Inorg. Chem. **6**, 1379 (1967); (*b*) F. Dickert, H. Hoffman, and W. Jaenicke. Ber. Bunsenges. Phys. Chem. **74**, 500 (1970).
4. M. L. Sanduja and W. M. Smith. Can. J. Chem. **50**, 3861 (1972).
5. P. K. Chattopadhyay and J. F. Coetzee. (*a*) Anal. Chem. **46**, 2014 (1974); (*b*) Inorg. Chem. **12**, 113 (1973).
6. (*a*) J. F. Coetzee and K. Umemoto. Inorg. Chem. **15**, 3109 (1976); (*b*) J. F. Coetzee and C. G. Karakatsanis. Inorg. Chem. **15**, 3112 (1976).
7. (*a*) H. P. Bennetto and E. F. Caldin. J. Chem. Soc. A, 2191 (1971); 2198 (1971); (*b*) H. Hoffmann. Pure

Appl. Chem. **41**, 327 (1975); (*c*) P. K. CHATTOPADHYAY and B. KRATOCHVIL. Can. J. Chem. **54**, 2540 (1976).
8. P. K. CHATTOPADHYAY and B. KRATOCHVIL. Inorg. Chem. **15**, 3104 (1976).
9. J. F. COETZEE. Pure Appl. Chem. **49**, 27 (1977).
10. P. K. CHATTOPADHYAY and J. F. COETZEE. Anal. Chem. **44**, 2117 (1972).
11. N. A. MATWIYOFF. Inorg. Chem. **5**, 788 (1966).
12. P. MOORE and D. M. W. BUCK. J. Chem. Soc. Dalton Trans. 1602 (1973).
13. P. K. CHATTOPADHYAY and J. F. COETZEE. Inorg. Chem. **15**, 400 (1976).
14. W. W. BRANDT, F. P. DWYER, and E. C. GYARFAS. Chem. Rev. **54**, 959 (1954).
15. R. K. STEINHAUS and D. W. MARGERUM. J. Am. Chem. Soc. **88**, 441 (1966).
16. J. F. COETZEE and G. R. PADMANABHAN. J. Am. Chem. Soc. **87**, 5005 (1965).
17. A. K. COVINGTON and T. DICKINSON. *In* Physical chemistry of organic solvent systems. *Edited by* A. K. Covington and T. Dickinson. Plenum Press, London. 1973.
18. V. GUTMANN. Top. Curr. Chem. **27**, 59 (1972).

Conformational study of a series of 6-substituted 5,6,7,12-tetrahydrodibenzo[*a*,*d*]-cyclooctenes by nuclear magnetic resonance spectroscopy[1]

ROGER N. RENAUD AND JOHN W. BOVENKAMP[2]

Division of Chemistry, National Research Council of Canada, Ottawa, Ont., Canada K1A 0R6

AND

ROBERT R. FRASER AND JEAN-LOUIS A. ROUSTAN

Department of Chemistry, University of Ottawa, Ottawa, Ont., Canada K1N 6N5

Received May 4, 1977

ROGER N. RENAUD, JOHN W. BOVENKAMP, ROBERT R. FRASER, and JEAN-LOUIS A. ROUSTAN. Can. J. Chem. **55**, 3456 (1977).

The conformational properties of seven 5,6,7,12-tetrahydrodibenzo[*a*,*d*]cyclooctenes bearing substituents at C-6 have been studied using variable temperature proton nmr spectroscopy. The position of the equilibrium between boat-chair (BC) and twist-boat (TB) conformers has been measured in several solvents. In contrast to the unsubstituted dibenzocyclooctene, appreciable amounts of TB conformer are present when C-6 is substituted by alkyl, hydroxy, or cyano substituents. Measurements at different temperatures showed the TB form to possess the greater entropy. Barriers to the BC → TB interconversion were determined by coalescence studies, using both approximate and complete line shape methods. Barriers ranged from 10.1 kcal/mol for the 6-keto derivative to 16.7 kcal/mol for the 6-hydroxy-6-methyl derivative.

ROGER N. RENAUD, JOHN W. BOVENKAMP, ROBERT R. FRASER et JEAN-LOUIS A. ROUSTAN. Can. J. Chem. **55**, 3456 (1977).

On étudie, par résonance magnétique du proton (rmn) et variant la température, les propriétés conformationnelles de sept tétrahydro-5,6,7,12 dibenzo[*a*,*d*]cyclooctènes ayant des substituants en C-6. La position de l'équilibre entre les conformères chaise-bateau (CB) et bateau-croisé (BC) est mesurée dans plusieurs solvants. Contrairement au dibenzocyclooctène non substitué, une quantité appréciable de conformères (BC) est présente lorsque le C-6 est substitué par un groupe alkyle, hydroxy ou cyano. Les mesures à différentes températures montrent que la forme BC possède une plus grande entropie. Les barrières d'interconversion CB → BC sont déterminées par des études de coalescence en utilisant les méthodes approximatives et complètes basées sur la forme des courbes. Les barrières s'étalent de 10.1 kcal/mol pour le dérivé céto-6 à 16.7 kcal/mol pour le dérivé hydroxy-6 méthyl-6.

[Traduit par le journal]

In the past few years the dibenzocycloocta-1,4-diene[3] ring system **1***a* has attracted considerable interest regarding its conformational properties. The first evidence on this topic came from a ^{1}H nmr study of compounds related to **1***a*, specifically the azocines **2***a–f* (1, 2). Subsequently studies on a variety of other heterocyclic analogs **3***a–l* were reported (3) and, most recently, the conformational properties of the hydrocarbon **1***a* itself have been described (4). The parent compound, 1,4-cyclooctadiene, has been the subject of analysis by ^{13}C and ^{1}H techniques (5) as well as by strain energy or force field calculations (5, 6). In this paper we wish to describe the elucidation of the conformational properties of a series of dibenzocyclooctadiene derivatives **1***b–h* (7) by the use of ^{1}H nmr techniques.

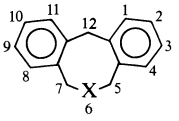

1

a X = CH_2
b X = C=O
c X = C=CH_2
d X = $CHCH_3$
e X = $CHCOOCH_3$
f X = $C(OH)CH_3$
g X = $C(CH_3)CH_2OH$
h X = $C(CN)_2$

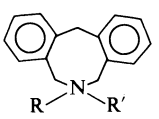

2

a R = CH_3, R′ = lone pair
b R = H, R′ = lone pair
c R = $CD_2C_6H_5$, R′ = lone pair
d R = $CH(CH_3)_2$, R′ = lone pair
e R = $C(CH_3)_3$, R′ = lone pair
f R = R′ = CH_3, I^-

[1]NRCC No. 16120.

[2]Present address: Defence Research Establishment Ottawa, Ottawa, Ont., Canada K1A 0Z4.

[3]The eight-membered ring **1***a*, whose correct name is 5,6,7,12-tetrahydrodibenzo[*a*,*d*]cyclooctene, has the numbering shown in formula **1**. This numbering is employed throughout the paper.

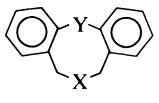

3

a X = CH_2; Y = S
b X = CH_2; Y = SO_2
c X = CH_2; Y = $NCH_2C_6H_5$
d X = O; Y = S
e X = O; Y = SO_2
f X = O; Y = $NCH_2C_6H_5$
g X = S; Y = S
h X = S; Y = $NCH_2C_6H_5$
i X = SO_2; Y = S
j X = SO_2; Y = SO_2
k X = SO_2; Y = $NCH_2C_6H_5$
l X = CO; Y = $NCH_2C_6H_5$

Initial proton studies of the azocine series, **2**, established the presence of two conformational isomers having comparable energies (1, 2). Depending upon the substituent at nitrogen either the boat-chair (BC) or the twist-boat (TB) conformer predominated in the equilibrating mixture. Barriers to this interconversion were found to be of the order of 15–17.5 kcal/mol. In a recent paper by Gellatly *et al.* (3) the relative energies of the various conformers of **2***a* as well as the possible pathways to their interconversion were computed using force-field calculations. The values they obtained for the enthalpy difference between BC and TB conformers was 1.2 kcal/mol (BC more stable) in fair agreement with the experimental value for ΔH of 3.2 kcal/mol (1). Two additional results of the calculations are pertinent in relation to the general properties of the ring system **2**. Calculations for a number of boat-like geometries indicated that of three possible conformers, a boat (BB) having C_s symmetry, a twist-boat (TB) having C_2 symmetry, and an asymmetric distorted twist-boat (DTB), the boat (BB) was of higher energy than either of the others.[4,5] The geometries of these conformers are depicted in Fig. 1. Calculations were also performed on three possible transition states for the BC → TB interconversion. One of these, involving rotation about the C-4 to C-5 and C-5 to C-6 bonds of the BC form, was of much lower energy than the other two. The activation energy of 18.3 kcal/mol calculated for the BC → TB process is in remarkably good agreement with the experimentally derived value of 17.0 kcal/mol.[6] On the basis of these calculations we need consider only one transition state, with the result that the interconversion pathways available to **1***a–h* can be represented as shown in Scheme 1.

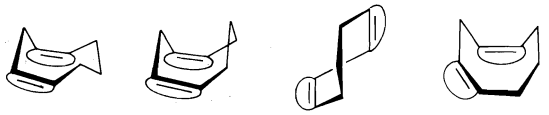

BC(C_s) BB(C_s) TB(C_2) DTB(C_1)

FIG. 1. Possible low energy conformations of 5,6,7,12-tetrahydrodibenzo[*a*,*d*]cyclooctene with their symmetry classification.

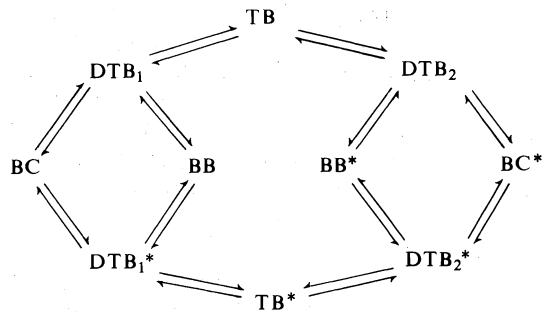

SCHEME 1. Allowed conformational interconversions for 5,6,7,12-tetrahydrodibenzo[*a*,*d*]cyclooctene. The species designated by an asterisk are mirror images of those lacking an asterisk. Subscripts are used to differentiate DTB_1 from DTB_2 since, although the two forms represent the same enantiomer, they can in principle be differentiated by the proton shifts at C-5 and C-7.

A. Criteria for Assignment of Conformation

Several parameters diagnostic of either the TB or BC conformation have been employed in our earlier studies of the azocines (1, 2). The same criteria to be applied to compounds **1***b–h* are summarized as follows.

i. The flexibility of the TB conformer gives it a greater entropy than the rigid BC conformer (e.g. ΔS = 7 eu for **2***a* (1)).

ii. The geminal coupling constant between the

[4]This nomenclature has been adopted to coincide with that employed by Anet (5) for 1,4-cyclooctadiene. It differs from that of Gellatly *et al.* (3) which uses C rather than BC and Boat rather than DTB.

[5]The small energy differences between the DTB and TB forms suggest that the more stable conformer may well differ for various members of series **1** and **2**. In the absence of definitive evidence on relative stabilities we will arbitrarily refer to any twist-boat conformer as TB.

[6]Previously $\Delta G^{\ddagger}_{211}$ (TB → BC) has been measured as 15.3 kcal/mol, ΔS_{eq} as −7 eu, and ΔH^0 as 3.2 kcal/mol. If we make the assumption that $S^{\ddagger}$ = 0, then $\Delta S^{\ddagger}$ = −7 eu, and thus $\Delta H^{\ddagger}$(TB → BC) = 13.8 kcal/mol. To obtain the BC → TB barrier one must then add ΔH^0 = 3.2 kcal/mol giving $\Delta H^{\ddagger}$(BC → TB) = 17.0 kcal/mol.

protons at C-12 is much more positive for the BC (−12 to −14 Hz) than for the TB (−19 Hz) conformation, as was anticipated on the basis of the previous known effect of a benzene ring (8).

iii. Two of the vicinal coupling constants between protons at C-5 and C-6 will be close to zero in the BC conformer only. This results from the fact that in the BC conformer the dihedral angles for two pairs of vicinal protons are approximately 90°.

iv. The BC conformer will normally give rise to two sets of nonequivalent methylene proton absorptions whereas the TB conformer, whenever the equilibration process (TB $\rightleftharpoons$ TB*) is rapid, will give rise to two singlets (except when C-6 bears two different substituents).

B. Criteria for Assignment of Configuration at C-6

In the derivatives **1***d–h* two BC conformers are possible, one in which the bond to the substituent at C-6 is essentially in the plane of either benzene ring (which will be referred to as the pseudoequatorial position), the other having the substituent oriented downwards from this plane (a pseudoaxial orientation). Distinction between these conformers can be made in two ways.

i. As was observed in the azocines, there should be a marked difference in chemical shift between a pseudoaxial and pseudoequatorial substituent. The shift of the pseudoaxial substituent to higher field by 0.6–0.8 ppm is attributable to the ring currents of the two benzene rings (9).

ii. Examination of a Dreiding model of the rigid BC conformer indicates the dihedral angles to be 90° and 150° between the protons at C-5 and the pseudoaxial proton at C-6. When the C-6 proton is pseudoequatorial the angles are 90° and 30°. From the extensive studies on the Karplus relation it is clear that the protons oriented at 150° to one another will exhibit a larger vicinal splitting than those oriented 30° to one another.[7] Thus of two BC conformers, that with pseudoequatorial substituent (pseudoaxial proton) will exhibit the larger vicinal splitting.

Determination of Barrier Heights from Variable Temperature Nuclear Magnetic Resonance Data

The measurement of free energies of activation for the interconversion of conformers has been accomplished for compounds **1***b*, *c*, *e*, *f*, *g*, and *h*. In each case the free energy has been calculated from the standard expression (10, 11) for coalescence of an AB system. For compounds **1***b* and *c* the coalescence of an AB pattern to a singlet was complicated by the presence of about 10% of the TB conformer whose singlet coalesced at the same time. However, it has been demonstrated by a comparison of a complete line shape (cls) analysis with the simple AB coalescence that the only effect of the second conformer is to cause unequal line widths of the A and B signals. Its presence in minor amounts does not affect the accuracy of determination of the coalescence temperature (3).

For compounds **1***e*, *f*, and *g* the coalescence being monitored involved two singlets of not quite equal intensities (the most unequal ratio was 2:1 (CH_{3a} vs. CH_{3e}). It has been shown previously by Raban and Carlson (12) that in such cases, treatment of the system by the simple two-site equation for equal populations still gives the same resultant $\Delta G^{\ddagger}$ as that obtained by cls analysis. For compound **1***h* measurement of the TB $\rightleftarrows$ TB* interconversion involved straightforward analysis of the AB coalescence of two protons at C-5 and C-7. To obtain the BC $\rightleftarrows$ BC* barrier the coalescence of two approximately equal intensity singlets[8] for the BC and TB absorptions at C-5 and C-7 was observed. To convert the derived barrier TB $\rightleftarrows$ BC into BC $\rightleftarrows$ BC* one simply adds $RT \ln 2$ to correct for the fact that for the equilibrium involved, BC $\rightleftarrows$ TB $\rightleftarrows$ BC*, the BC $\rightleftarrows$ BC* process is half as fast (probable) as the BC $\rightleftarrows$ TB process.

For compound **1***h*, a complete line shape analysis was carried out for comparison with the results obtained by use of the two-site approximation.

One additional method of measuring the TB $\rightleftarrows$ BC process was used with **1***d*. This method, previously used by us (1) to study **2***a* measured the rate of equilibration of a sample of **1***d* containing excess TB conformer (at −72°C) produced by plunging a heated sample into liquid N_2 before transferring to the nmr probe for monitoring. Similar 'T-jump' techniques have recently been elegantly exploited (13) to obtain observable concentrations of the boat conformation of cyclohexane.

The basic nmr spectral parameters, equilib-

[7]While application of the Karplus relation to stereochemical problems must be made with caution, as was discussed extensively by Jackman and Sternhell (9, p. 280), there is general agreement that the right hand side ($90° < \theta \leq 180°$) gives rise to larger coupling constants.

[8]The BC absorption of the C-5,7 protons appeared as a singlet in toluene but as an AB pattern in $CDCl_3$.

TABLE 1. Equilibrium constants for BC ⇄ TB equilibria

Compound	T (K)	K_{eq}	Solvent*
1*a*		0.02†	
1*b*	166	0.1	B
	166	1.0	C
1*c*	208	0.05	A
1*d*	243	0.14 (BC_a)‡ 0.17 (BC_e)	A
	243	0.17 (BC_e)	B
	200	0.06 (BC_e)	B
1*e*	253	0.08 (BC_e)	A
1*f*	233	0.45 (BC_a) 0.33 (BC_e)	A
1*g*	255	0.10 (BC_a) 0.18 (BC_e)	A
1*h*	213	0.62	A
	300	1.0	A
	300	1.0	E
	300	0.2	F

*The solvents used to obtain the data in Tables 1–4 are as follows: (A) $CDCl_3$; (B) acetone-d_6–$CDCl_3$–CS_2(1:1:1); (C) toluene-d_8–CS_2(1:1); (D) toluene-d_8–CS_2(4:1); (E) toluene-d_8; (F) acetone-d_6.
†Reference 3.
‡The subscript a or e designates the orientation of the methyl substituent at C-6.

rium concentrations of conformers and barriers to interconversion, are presented in Tables 1–4. Distinctive aspects of these spectral studies will be best considered individually.

5,6,7,12-Tetrahydrodibenzo[a,d]cyclooctene-6,6-d_2, 1a-d_2

The analysis of the ^{1}H nmr spectrum of **1***a* at several temperatures has been described by Elhadi *et al.* (4). They conclude that the molecule exists in the BC conformation in equilibrium with 2% of a TB conformer. Our results of examination of the spectra of **1***a*-6,6-d_2 in several solvents lead us to essentially the same conclusion.

The dideuteroderivative of **1***a* was used to study the coalescence of both methylene quartets by variable temperature. The barrier to interconversion BC ⇄ BC* was found to be 15.1 kcal/mol at 36.5°C, in good agreement with both the recent experimental (15.2) and calculated (15.2) values reported by Elhadi *et al.* (4). Since the presence of 2% of a TB conformer was indicated by their studies of line shapes, we attempted to observe weak peaks ascribable to the TB form in the simplified spectrum of **1***a*-d_2. No peaks due to a second conformer could be detected.

5,6,7,12-Tetrahydrodibenzo[a,d]cycloocten-6-one, 1b

The presence of two singlet methylene absorptions in the nmr spectrum of **1***b* indicates either a TB conformer or a mobile equilibrium between BC and TB conformers. As the temperature is lowered the two singlets broaden and diverge to several overlapping multiplets (in a 1:1:1 mixture of acetone-d_6, CS_2, and $CDCl_3$). From a study of 5,5,7,7-tetradeutero **1***b* in this solvent mixture over the temperature range −107 to −50°C the barrier to interconversion of BC conformers was found to be 10.1 kcal/mol. At −107°C the BC to TB ratio was 10:1. The absorption of the C-12 protons of the BC conformer appeared as an AB quartet while the TB absorption was a singlet. When the spectrum of **1***b*-d_4 was measured in toluene-d_8–CS_2(1:1) at the same temperature the ratio of conformers changed to 1:1 again appearing as a quartet and a singlet. Comparison of this latter spectrum with that of **1***b* (undeuterated) allowed the identification of an AB quartet and a singlet due to the protons at C-5,7. All shifts and coupling constants thereby obtained are given in Table 2. An interesting value was found for the geminal coupling constant between the methylenes adjacent to the carbonyl group of the BC conformer. This coupling constant is 3 Hz more positive than the value for ^2J at C-5 in the hydrocarbon **1***a*. This increment to ^2J, caused by replacing a CH_2 group with a C=O oriented orthogonal to the antisymmetric MO of the CH_2 group (14), is in perfect agreement with the value predicted from the empirical relation of Montecalvo and St-Jacques (15).

6-Methylene-5,6,7,12-tetrahydrodibenzo[a,d]cyclooctene, 1c

The spectrum of **1***c* at room temperature showed three sharp singlets for the three types of methylene groups at δ 3.65 (C-5,7), 4.06 (C-12), and 5.0 (vinyl). At −65°C the protons at C-12 and those at C-5,7 appeared as AB quartets while the olefinic protons remained as a singlet. The nonequivalence of the C-12 protons indicates a BC conformer. A small amount of TB conformer (5%) is also present as indicated by a second singlet peak in the *exo* methylene region (δ 5.11). The barrier to the BC ⇄ BC* interconversion was found to be 13.1 kcal/mol.

It is interesting to note that the difference in the BC ⇄ BC* barrier for the ketone versus the *exo* methylene derivative is 3.0 kcal/mol, reminiscent of the difference between cyclohexanone (ΔG^+ = 4.0 kcal/mol (16)) and methylene cyclohexane (ΔG^+ = 8.4 kcal/mol (17)).

6-Methyl-5,6,7,12-tetrahydrodibenzo[a,d]cyclooctene, 1d

The spectrum of this compound shows a

TABLE 2. Nuclear magnetic resonance parameters* for BC conformers

Compound	Solvent (T (K))	C-12	C-5,7	C-6
1*b*	A (300)	4.01	3.86	
1*b*-d_4	B (253)	4.06		
1*b*-d_4	B (166)	4.47, 3.99 (J = 13.0)		
1*b*	C (183)	3.61, 3.28 (J = 12.0)	3.67, 2.96 (J = 11.2)	
1*c*	A (300)	4.06	3.65	4.95
1*c*	A (208)	4.36, 3.82 (J = 12.7)	3.88, 3.55 (J = 13.0)	4.98
1*d*(CH_{3ax})	A (253)	4.28, 3.65 (J = 12.3)	3.44, 2.88 (J = 14.0)	0.47
			J_{5_a6} = 0, J_{5_e6} = 6.7	2.5 (C—H)
1*d*(CH_{3eq})	A (253)	4.20, 3.65 (J = 12.4)	3.15, 2.69 (J = 14.0)	1.27
			J_{5_a6} = 10.0, J_{5_e6} = 0.0	1.8 (C—H)
1*e*	A (228)	4.25, 3.71 (J = 12.4)	3.42, 3.08 (J = 14.3)	3.81
			J_{5_a6} = 10.0, J_{5_e6} = 0.0	2.48 (C—H)
1*f*(CH_{3ax})	A (233)	4.27, 3.73 (J = 12.7)	3.59, 2.87 (J = 13.5)	0.85
1*f*(CH_{3eq})	A (233)	4.27, 3.76 (J = 12.7)	3.49, 2.97 (J = 14.4)	1.65
1*g*(CH_{3ax})	A (238)	4.27, 3.69 (J = 12.7)	3.29, 2.66 (J = 13.6)	0.41, 3.57 (CH_2)
1*g*(CH_{3eq})	A (238)	4.27, 3.69 (J = 12.7)	3.24, 2.78 (J = 14.0)	1.35, 2.89 (CH_2)
1*h*	A (233)	4.13, 3.83 (J = 13.0)	3.90, 3.57 (J = 14.6)	
1*h*	E (255)	3.16, 3.00 (J = 12.5)	2.67	
1*h*	F (300)	4.40, 3.84 (J = 12.8)	4.22, 3.67 (J = 14.4)	

*Chemical shifts are in δ units, coupling constants in Hz. Coupling constants without subscripts represent geminal interactions which are negative in sign (ref. 9, p. 270).

similarity to its nitrogen analog, **2***a*, in the methyl region, having three distinct methyl absorptions representing TB, BC_e and BC_a conformers in a ratio of 8:42:50. The identification of the methyl signal of weakest intensity as a TB absorption follows from the observation of its increase in intensity from 3% of total methyl absorption at −73°C to 8% at −30°C, indicative of its greater entropy (+4 eu) than either of the more intense signals whose ratio stays constant. Furthermore the coupling constants for the methylene protons at C-12 of the two most abundant conformers confirm their identity as BC conformers. The assignment of an equatorial configuration to the methyl group of the weaker BC doublet rests on both the chemical shift and vicinal coupling constant criteria mentioned earlier.

All temperature dependent spectra were run using the 6,12,12-trideutero derivative. The barrier to interconversion, $BC_e \rightarrow BC_a$ was determined to be 15.9 kcal/mol at 55°C, the coalescence temperature of the two methyl singlets. Using the quenching technique the TB → BC barrier was found to be 14.2 kcal/mol from the rate of equilibration of the TB signal. The rate constant for this process represents the TB → BC_e and TB → BC_a transformations. Thus the TB → BC_a rate constant will be half as large giving $\Delta G^{\ddagger}$ (TB → BC_a) = 14.5 kcal/mol at −72°C. A comparison with $\Delta G^{\ddagger}$ (BC_a → TB) = 15.5 kcal/mol at 55°C reveals a good agreement between the two methods. If one assumes $\Delta S^{\ddagger} = 0$, and $\Delta S_{eq} = 4$ eu then $\Delta G^{\ddagger}$ (TB → BC_a) can be calculated to be 15.0 kcal/mol at 55°C. These two barriers, having a common transition state, should differ by ΔG_{eq} for TB ⇄ BC_a which is 0.5 kcal/mol at 55°C, consistent with the experimental values.

Methyl 5,6,7,12-tetrahydrodibenzo[a,d]cyclooctene-6-carboxylate, 1e

The methyl ester **1***e* gives rise to a simple ^1H spectrum at −20°C which shows a dominant conformer to be present accompanied by 7% of a second isomer. The major component can be identified as the BC conformer from both the chemical shift and the coupling constant data. The pseudoequatorial orientation of the carbomethoxy group of the BC form is indicated by the 10 Hz vicinal coupling constant involving the methine proton at C-6. The second isomer can be assigned to the TB conformation. A sample of 6,12,12-trideuterated ester clearly showed a small singlet for the protons at C-5 and 7 (δ 2.86) whose intensity diminished as the temperature was lowered (i.e. it has greater entropy than the BC form).

6-Hydroxy-6-methyl-5,6,7,12-tetrahydrodibenzo[a,d]cyclooctene, 1f

The tertiary alcohol, **1***f*, gives rise to a ^1H spectrum which is considerably broadened by

TABLE 3. Nuclear magnetic resonance parameters for TB conformers*

Compound	Solvent (T(K))	C-12	C-5,7	C-6
1*b*-d_4	B (166)	3.79	†	
1*b*	C (178)	3.32	3.10	
1*c*	A (208)	†	†	5.11 (CH_2)
1*d*	A (253)	†	†	0.93 (J_{CH_3-H} = 6.5)
1*f*	A (233)	†	†	1.28 (CH_3)
1*g*	A (273)	†	†	0.95 (CH_3)
1*h*	A (231)	4.45	3.28, 3.12 (J = 14.1)	
1*h*	F (300)	4.50	3.26	

*Chemical shifts are given in δ units, coupling constants in Hz.
†Peaks not identifiable.

TABLE 4. Barrier to ring inversion (kcal/mol)

Compound	Solvent	$\Delta G^{\ddagger}$ (T_c (K))	Process	Coalescence type
1*a* 6,6-d_2	A	15.1 (309)	BC → BC*	AB → A_2 at C-12
1*b* 5,5,7,7-d_4	B	10.1 (207)	BC → BC*	AB → A_2 at C-12
	C	10.2 (205)	BC → BC*	AB → A_2 at C-12
1*c*	A	13.0 (264)	BC → BC*	AB → A_2 at C-5,7
		13.1 (270)	BC → BC*	AB → A_2 at C-12
1*d*	A	15.9 (328)	BC_e → BC_a	*
	D	14.2 (200)	TB → BC	T-jump
1*f*	E	16.7 (341)	BC_e → BC_a	*
1*g*	E	16.5 (340)	BC_e → BC_a	*
1*h*	E	16.4 (332)	BC → TB	AB + S → S by cls
	E	16.5 (332)	BC → TB	†
	A	16.3 (333)	BC → TB	AB + S → S at C-12
	A	13.4 (270)	TB → TB*	AB → A_2 at C-5,7

*Unequal singlets coalescence.
†Equal singlets coalescence.

interconversions between the various conformers at 0°C or above. At −40°C the spectrum shows three sharp methyl singlets indicating the presence of three conformers comprising 50, 16, and 34% of the total and representing the BC_e, TB, and BC_a conformers, respectively, whose assignments followed from the customary applications of criteria *A*, *i* and *ii*, and *B*, *i*. A measurement of the coalescence of the two more intense singlets at 68°C indicates the barrier to interconversion of boat chairs to be 16.7 kcal/mol. The increase in this barrier over that of the parent (15.2) is quite consistent with the additional eclipsing of both the CH_3 and OH substituents with their vicinal protons in the transition state.

6-Hydroxymethyl-6-methyl-5,6,7,12-tetrahydrodibenzo[a,d]cyclooctene, 1g

From the nmr spectrum, the primary alcohol **1***g* at −18°C was found to exist in the three conformations BC_e (methyl equatorial), BC_a, and TB in the ratio 34:6:60, assignable on the basis of criteria *A*, *i* and *ii*. The barrier to interconversion of the two BC conformers was found to be the same as for **1***f*, as one would expect for two compounds, each having two substituents of similar size at C-6.

6,6-Dicyano-5,6,7,12-tetrahydrodibenzo[a,d]cyclooctene, 1h

The conformational properties of **1***h* differ significantly in several ways from the other members of the series. In $CDCl_3$ at −30°C, the proton spectrum of **1***h* shows the presence of a BC conformer (59%) represented by two AB quartets in the methylene region and a TB conformer (41%) whose methylene absorptions are a singlet (C-12 protons) and an AB quartet (protons at C-5 and C-7). As the temperature is raised to −3°C the quartet for the C-5,7 protons of the TB conformers broadens and coalesces, indicating the conformational process which averages the proton environments to have $\Delta G^{\ddagger}$ = 13.4 kcal/mol. This process, already observed by us in the structurally similar quaternary methiodide of the azocine **2***a*, was termed a

racemization process, i.e. TB ⇄ TB*. One distinctive property of **1***h*, as indicated by the data in Table 1, is that its conformational equilibrium is less influenced by temperature than was **1***d*. That the entropy difference between BC and TB conformers is smaller in **1***h* by 2 eu is consistent with the presence of two cyano groups restricting the mobility of the twist-boat. Interestingly this BC ⇄ TB equilibrium is surprisingly sensitive to solvent. At 27°C, the ratio [TB]/[BC] is unity in both $CDCl_3$ and toluene-d_8, whereas in acetone it is 0.2.

The barrier to the TB ⇄ BC interconversion for **1***h* was determined in several solvents. In toluene-d_8, a $\Delta G^{\ddagger}$ of 16.5 kcal/mol was obtained by observing the coalescence T_c = 59°C of the singlet for C-5,7 for the TB conformer with the equally intense absorption of the C-5,7 protons of the BC form which in this solvent appears as a singlet. At the same time the singlet (TB) and the AB quartet (BC) representing the C-12 protons also coalesced (T_c = 59°C). This latter coalescence was subjected to a complete line shape analysis (18) which yielded a value for $\Delta G^{\ddagger}$ of 16.4 kcal/mol.

In $CDCl_3$, observation of coalescence of the AB quartet (BC) and the singlet (TB) due to the protons at C-5 and C-7 indicates a $\Delta G^{\ddagger}$ of 16.3 kcal/mol. Thus for **1***h*, the effect of solvent on the BC → TB barrier is negligible.

The similarity in the geminal coupling constants for the methylene protons at C-5 and C-7 in the BC (−14.6 Hz) and TB (−14.1 Hz) conformers gives some indication of the geometry of the TB conformer of **1***h*. Recently we have shown that the hyperconjugative effect of a phenyl substituent on the geminal coupling constant of an attached methylene group varies from 0–5.5 Hz (19). Specifically the coupling constant is 5.5 Hz more negative when the π orbitals of the ring and a line drawn through the two protons are parallel (projected angle ϕ = 0°) rather than perpendicular (ϕ = 90°). Since MO theory predicts the effect to be proportional to $\cos^2\phi$, the hyperconjugative shift can be expressed as $\Delta J = 5.5\cos^2\phi$. Dreiding models show that the projected angle ϕ for **1***h* is 75° in the BC, 85° in the dissymmetric TB form and 0° in the symmetric BB. Models indicate that the DTB conformer produced from the symmetrical TB form by a 30° rotation about the C-5 to C-6 bond has the projected angle changed to 75°. Any further rotation would lead to a projected angle sufficiently smaller to cause a difference of greater than 0.5 Hz in the geminal coupling constants of the TB and BC conformers. Thus for **1***h* at least, the conformation of the twist-boat is either the symmetric TB or a DTB in which the change from the TB form is not great.

Experimental

All nmr spectra were recorded on a Varian HA-100 spectrometer, using simultaneous deuterium spin-decoupling by means of an SD-100 decoupler for those measurements involving deuterated derivatives. All coupling constants were determined with an accuracy of ±0.2 Hz. At temperatures other than ambient, the probe temperature was measured before and after recording the spectra by means of a copper–constantan thermocouple inserted into a nonspinning sample tube containing solvent. Such measurements are thought to be accurate to better than ±1°C. Spectra near the coalescence temperature were recorded at sweep widths of 250 Hz using a sweep time of 0.25 Hz/s. Care was taken to avoid saturation. The $\Delta\nu$'s used in calculating $\Delta G^{\ddagger}$ were determined over the range 213–263 K. No significant temperature dependences were encountered. Spectral calculations using the complete line shape program of Kleier and Binsch (18) were carried out on an IBM 360/65 computer.

The preparation of all the compounds except **1***b*-d_4 and **1***f* used in this study has been published elsewhere (7).

5,6,7,12-Tetrahydrodibenzo[a,d]cycloocten-6-one-5,5,7,7-d_4

The 5,5,7,7-tetradeuterio ketone **1***b* was obtained by the exchange of **1***b* with a DCl – D_3PO_3 – D_2O–dioxane solution according to the method of Seible and Gäumannl (20). No peaks for the C-5 and C-7 protons were seen in the ^{1}H nmr.

6-Hydroxy-6-methyl-5,6,7,12-tetrahydrodibenzo[a,d]cyclooctene ***1f***

Using the procedure of Cope and Fenton (21), the ketone **1***b* was reacted with methylmagnesium iodide in dry ether to give a quantitative yield of the alcohol **1***f*. An analytical sample was obtained by passing the crude oil through silica gel and distilling it at an air bath temperature of 100°C (0.01 Torr) using a Späth bulb apparatus to give a colorless viscous oil. *Anal.* calcd. for $C_{17}H_{18}O$: C 85.67, H 7.61; found: C 85.46, H 7.43.

Acknowledgments

We are grateful to Mr. R. Capoor of the University of Ottawa for technical assistance. Two of the authors (R.R.F. and J.-L.A.R.) acknowledge the financial support of the National Research Council of Canada.

1. R. N. Renaud, R. B. Layton, and R. R. Fraser. Can. J. Chem. **51**, 3380 (1973).
2. R. R. Fraser, M. A. Raza, R. N. Renaud, and R. B. Layton. Can. J. Chem. **53**, 167 (1975).
3. R. P. Gellatly, W. D. Ollis, and J. O. Sutherland. J. Chem. Soc. Perkin Trans. I, 913 (1976).
4. F. E. Elhadi, W. D. Ollis, and J. F. Stoddart. Angew. Chem. Int. Ed. Engl. **15**, 224 (1976).

5. F. A. L. ANET. Lecture presented at the International Stereochemistry Symposium, Kingston, Ont., Canada. June, 1976.
6. G. FAVINI, F. ZUCCARELLO, and G. BUERNI. J. Mol. Struct. **3**, 385 (1969).
7. R. N. RENAUD and J. W. BOVENKAMP. Can. J. Chem. **55**, 650 (1977).
8. R. C. COOKSON, T. H. CRABB, J. J. FRANKEL, and J. HUDEC. Tetrahedron, Supp. No. 7, 355 (1966).
9. L. M. JACKMAN and S. STERNHELL. Applications of nuclear magnetic resonance spectroscopy in organic chemistry. 2nd ed. Pergamon Press, London. 1969. p. 94.
10. G. BINSCH. Top. Stereochem. **3**, 97 (1968).
11. D. KOST, E. H. CARLSON, and M. RABAN. Chem. Commun. 656 (1971).
12. M. RABAN and E. CARLSON. J. Am. Chem. Soc. **93**, 685 (1971).
13. M. SQUILLACOTE, R. S. SHERIDAN, O. L. CHAPMAN, and F. A. L. ANET. J. Am. Chem. Soc. **97**, 3244 (1975).
14. J. A. POPLE and A. A. BOTHNER-BY. J. Chem. Phys. **42**, 1339 (1965).
15. D. MONTECALVO and M. ST-JACQUES. J. Org. Chem. **40**, 940 (1975).
16. F. A. L. ANET, G. N. CHMURNY, and J. KRAME. J. Am. Chem. Soc. **95**, 4423 (1973).
17. J. T. GERIG and R. A. RIMERMAN. J. Am. Chem. Soc. **92**, 1219 (1970).
18. D. A. KLEIER and G. BINSCH. J. Magn. Reson. **3**, 146 (1970).
19. R. N. RENAUD, J. W. BOVENKAMP, R. R. FRASER, and R. CAPOOR. Can. J. Chem. **55**, 2642 (1977).
20. J. SEIBLE and T. GÄUMANNL. Helv. Chim. Acta, **46**, 2857 (1963).
21. A. C. COPE and S. W. FENTON. J. Am. Chem. Soc. **73**, 1673 (1951).

Studies of a model of hydrogen recombination

NEIL S. SNIDER

Department of Chemistry, Queen's University, Kingston, Ont., Canada K7L 3N6

Received March 24, 1977

NEIL S. SNIDER. Can. J. Chem. **55**, 3464 (1977).

A Morse oscillator model for recombination of hydrogen and its isotopes was investigated computationally. The model is very similar to one recently studied by Pritchard and co-workers. The aims of the study were the test of certain approximations and the determination of the range of validity of the model. It was found that at low temperatures the steady state approximation is an increasingly accurate and increasingly convenient approximation. A way of estimating the error arising from this approximation was proposed. Other approximations which were tested gave unsatisfactory results. The rate constant vs. temperature curve for the model does not agree well with the experimental curve for hydrogen in argon except insofar as it reproduces the observed levelling-off at high temperatures. For the model this result may be ascribed to increasing relative rates for multiquantum transitions among the levels of the diatom. The model does give the experimentally observed ratios of the rate constants for H- and D-atom recombination. This result indicates that the important factor in determining the isotope ratio is the effect of mass change on the density of states rather than its effect on the collision dynamics.

NEIL S. SNIDER. Can. J. Chem. **55**, 3464 (1977).

On a étudié, à l'aide d'un calculateur, la recombinaison de l'hydrogène et de ses isotopes en prenant comme modèle l'oscillateur de Morse. Le modèle est très proche de celui récemment étudié par Pritchard et ses collaborateurs. Le but de cette étude est de vérifier certaines approximations et de déterminer la zone où le modèle est valable. Il apparaît qu'à basse température l'approximation de l'état stationnaire est de plus en plus exacte et convenable. On propose une méthode d'évaluation de l'erreur sur cette approximation. Plusieurs autres approximations n'ont pas donné de bons résultats. La courbe de la constante de vitesse vs. la température pour ce modèle ne correspondent pas bien à la courbe expérimentale pour l'hydrogène dans l'argon. On peut utiliser cette courbe en autant qu'elle reproduit le palier observé à haute température. Le résultat obtenu pour ce modèle peut être attribué à l'accroissement des vitesses relatives de transitions multiquantiques parmi les niveaux du diatome. D'ailleurs, le modèle reproduit les rapports qui sont observés expérimentalement pour les constantes de vitesse pour la combinaison des atomes H et D. Ce résultat suggère que le phénomène majeur dans la détermination du rapport isotopique est l'effet de la variation de masse sur la densité des états plutôt que son effet sur la dynamique des collisions.

[Traduit par le journal]

Introduction

It has been understood for some time (1) that a theoretical description of thermal dissociation of diatomic molecules A_2 in the presence of a diluent gas M,

$$A_2 \underset{}{\overset{M}{\rightleftharpoons}} 2A$$

entails the solution of a set of N coupled linear differential equations,

$$[1] \qquad \frac{dn_i}{dt} = \sum_{\substack{j=1 \\ \neq i}}^{N} k_{ij}n_j - \sum_{\substack{j=1 \\ \neq i}}^{N+1} k_{ji}n_i$$

where n_i is the concentration of A_2 in level i, N is the number of levels of A_2, level $N + 1$ corresponds to atoms, and k_{ji} is the frequency of transitions to j from i. The k_{ji}'s are directly proportional to n_M, the concentration of the diluent. The solution of [1] is characterized by the eigenvalues of κ, the matrix of coefficients of the n_i's. The dissociation rate constant k_d is related to λ_1, the smallest (in magnitude) of these eigenvalues,

$$k_d = -\lambda_1/n_M$$

The rate constant for recombination k_r is k_d divided by K, the equilibrium constant for dissociation.

Computation of the eigenvalues of κ is a straightforward task, but it is a lengthy one if N is large. Hence, approximation methods are normally employed to find λ_1. It has been known for some time (2) that the steady state approximation is useful here. A further simplification can be effected by approximate conversion of [1] to an equivalent diffusion (Fokker–Planck) equation (3). Recently still another approxima-

tion has been proposed (4) wherein the distribution of level populations is assumed to have a plausible functional form which is characterized by two parameters. The best values of the parameters for a given case are found by the variational method. The accuracy of the steady state approximation for k_d and k_r has been discussed at some length (4–6). Less attention has been paid to the accuracies of the second (3, 4) and the third (4) of the just mentioned approximations.

In this article are presented computational tests of these approximations for a model similar to one which has been assumed for H_2 dissociation in helium (7). The k_{ij}'s are given by

$$[2]\quad k_{ij}(\tilde{T}, \Delta_{ij}) = \tau^{-1}[1 - \exp(-49.6\Delta_{i,i-1})] \exp[-49.6\Delta_{ij} + (617 + 223 \ln \tilde{T})\Delta_{ij}^2] \quad \text{for } 0 < \Delta_{ij} < 0.157,\ 1 \le i \le N$$

$$= \tau^{-1} \exp[-49.6\Delta_{ij} + (617 + 223 \ln \tilde{T})\Delta_{ij}^2] \quad \text{for } 0 < \Delta_{ij} < 0.157,\ i = N + 1$$

$$= k_{ij}(\tilde{T}, 0.157) \exp[-67.2(\Delta_{ij} - 0.157)] \quad \text{for } \Delta_{ij} > 0.157$$

$$= k_{ji}(\tilde{T}, \Delta_{ji}) \exp(\Delta_{ij}/\tilde{T}) \quad \text{for } \Delta_{ij} < 0$$

where $\tilde{T}$ is kT/D_e, D_e is the depth of the potential well for the ground electronic state of H_2, $\Delta_{ij}D_e$ is the difference between the energies ε_i and ε_j of the levels i and j, and τ is the average time between collisions. The model, as characterized by [2], applies just to transitions between vibrational levels of the molecule. A simple generalization which takes account of rotation is introduced later in this article. This model differs from the one treated in ref. 7 in two ways: the Morse oscillator formula[1] is used for the ε_i's,

$$[3]\quad \varepsilon_i = -D_e[1 - s(i - \tfrac{1}{2})]^2$$

and a factor

$$1 - \exp(-49.6\Delta_{i,i-1})$$

is included (admittedly arbitrarily) to prevent the total rate of transitions out of closely spaced levels from becoming anomalously large.

None of the aforementioned approximations has yet been tested on a model of the type just described. Such a study is warranted since the model, hereafter referred to as the Morse oscillator model, has some realistic features.

The present article has as its other goal the test of the model itself as a predictor of isotope effect and temperature dependence for H- and D-atom recombination rate constants. The effect on rate constants of a change in level density has been examined for the Morse oscillator model (8) and for the so-called separable exponential model (4). In both studies the preexponential factor of k_d was found to increase with increasing level density, but it is not evident that the cause of the increase is the same in both cases. The present article attempts to clarify this point and to answer the related question of whether or not changes in level density alone can account for experimentally observed isotope effects.

Finally, it has been argued (9) that much of the temperature dependence of k_r is due to a simple factor which accounts for the rotation of A_2. It is therefore of interest to treat a simple generalization of the Morse oscillator model which includes rotation. In the present article such a treatment is carried out, and comparison is made between the temperature dependence of k_r for the model and the observed temperature dependence of k_r for H_2 in argon.

Tests of Approximations

The equations which underlie the various approximations to be tested have been presented in ref. 4. They are briefly summarized here to provide an immediate frame of reference. In the steady state approximation the time derivatives in [1] are set equal to 0 for all i greater than 1. The resulting equations can be cast in the form of $N - 1$ linear algebraic equations for N unknown δ_i's given by

$$\delta_i = (x_i/x_{i,e}) - 1$$

[1]Equation 3 differs slightly from the standard Morse oscillator energy level expression because the levels are numbered from 1 to N rather than from 0 to $N - 1$ as is usually the case. The parameter s in terms of the potential parameters a and D_e and the reduced mass μ is equal to $a\hbar/(2\mu D_e)^{1/2}$.

where x_i is the fraction of molecules in level i, and $x_{i,e}$ is the fraction of molecules which level i would contain if a Boltzmann distribution were maintained. For the Morse oscillator model $x_{i,e}$ is given by

$$[4a] \quad x_{i,e} = q_v^{-1} \exp[-s(2 - si)(i - 1)/\tilde{T}]$$

$$[4b] \quad q_v = \sum_{i=1}^{N} \exp[-s(2 - si)(i - 1)/\tilde{T}]$$

The aforementioned equations for the δ_i's are as follows:

$$[5] \quad \sum_{i=1}^{N} R_{ji}(\delta_{j,s} - \delta_{i,s}) - R_{N+1,i}(1 + \delta_{i,s}) = 0 \qquad \text{for } 2 \le i \le N$$

where R_{ji} is given by

$$R_{ji} = k_{ji}x_{i,e} = k_{ij}x_{j,e} = R_{ij}$$

The additional subscript s is appended to the δ_i's in [5] to indicate that they are the steady state approximations to these quantities. The dissociation rate constant is given by

$$k_{d,s} = \sum_{i=1}^{N} R_{N+1,i}(1 + \delta_{i,s})$$

In the computations reported here $\delta_{i,s}$ was set equal to zero for all i less than m where m is an appropriate integer greater than 1. Equations 5 for i equal to and greater than m were then solved for the remaining δ_i's. A subroutine based on the square root method (10) was employed in the solution of the equations.

For the approximately equivalent stepladder model the R_{ij}'s, call them R^*_{ij}, are given by

$$R^*_{ij} = R^*_{ji} = \sum_{k=1}^{N} \frac{(k - i + 1)(k - i)}{2} R_{ki} \qquad \text{for } j = i + 1$$

$$= 0 \qquad \text{for } j > i + 1$$

The dissociation rate constant, call it $k_{d,1}$, is given by

$$k_{d,1} = \left(\sum_{i=1}^{N} R_{N+1,i} \sum_{j=i}^{N} \frac{1}{R^*_{i+1,i}}\right)\left(\sum_{j=1}^{N} \frac{1}{R^*_{i+1,i}}\right)^{-1}$$

This approximation is the simplest of the three to carry through computationally.

In the final approximation considered, δ_i is taken to have the form

$$[6] \quad \delta_i = -\sigma(\rho - 1 + \sigma)^{-1} \rho^{-(N-i)}$$

where ρ and σ are variational parameters. The best values of ρ and σ, denoted below by subscript zeros, are given by

$$[7a] \quad a'(\rho_0)b(\rho_0) = a(\rho_0)b'(\rho_0)$$

$$[7b] \quad \sigma_0 = (\rho_0 - 1)a(\rho_0)/[a(\rho_0) - b(\rho_0)]$$

provided that ρ_0 differs sufficiently from 1. The primes in [7a] denote differentiation with respect to ρ, and the functions a and b are given by

$$[7c] \quad a(\rho) = \sum_{i=1}^{N} \left[\sum_{j=i+1}^{N} R_{ij}(\rho^{j-i} - 1)^2 + R_{N+1,i}\right]\rho^{-2(N-i)}$$

$$[7d] \quad b(\rho) = \sum_{i=1}^{N} R_{N+1,i}\rho^{-(N-i)}$$

The dissociation rate constant in this approximation is denoted $k_{d,v}$ and is given by

$$k_{d,v}n_M = k_{d,e}n_M - b^2(\rho_0)/a(\rho_0)$$

where $k_{d,e}$ is the rate constant which applies if the level populations maintain a Boltzmann distribution,

$$k_{d,e}n_M = \sum_{i=1}^{N} R_{N+1,i}$$

The basic approximation here is [6]. This equation is suggested by results for the separable exponential model (4), a model which reproduces the important features (although perhaps not the details) of many models of dissociation and recombination of diatomic molecules.

Calculations were carried out on a Burroughs B-6700. In finding the eigenvalues of κ, the matrix was first symmetrized by a standard similarity transformation (1). The symmetrized matrix was then tridiagonalized using the library subroutine TRED1, and the eigenvalues of the tridiagonalized matrix were found using the library subroutine RATQR. Because of technical difficulties, eigenvalues were only obtained for temperatures 3000 K and above. However, as will be shown, there is good reason to take the steady state approximation to be essentially exact below 3000 K.

For H_2 a value of s equal to 0.0575 was chosen. This gives the best fit to the known spacings of the low-lying vibrational levels of this molecule. There is probably no really suitable criterion for choosing a most appropriate value of s. The results of this study indicate that the Morse oscillator expression for the energy levels is

probably inadequate in any case. For T greater than 7000 K [2] gives a range of Δ_{ij} for which k_{ij} increases with increasing Δ_{ij}. It was considered best to terminate this study at a temperature well short of that at which the model develops this unphysical feature. The temperature 5000 K was chosen.

In Table 1 exact and approximate results are compared. Said results are expressed in terms of the dimensionless preexponential factor p given by

$$p = \tau k_d n_M \exp(D/kT)$$

where D is the dissociation energy. As before, subscripts s, l, v refer to steady state, equivalent stepladder, and variational approximations, respectively. The steady state approximation is clearly the most reliable of the three approximations. As mentioned above, $\delta_{i,s}$ was set equal to zero for all i less than some m. Results accurate to three or more significant figures were obtained provided ε_m was $-8kT$ or less relative to the dissociation energy. The variational method, although it gives somewhat better values of p at the highest temperatures, gives values of δ_N at 3000 and 5000 K which are less than -1. This result has the physically absurd implication that level N has a negative population. The variational approximation is also unsatisfactory in that eqs. 7 are difficult to solve computationally because of spurious roots.

It has been shown (4–6) that the fractional error f in the steady state approximation is of the same order as λ_1/λ_2, the ratio of the first two eigenvalues of κ,

$$f \equiv |k_d - k_{d,s}|/k_d \approx \lambda_1/\lambda_2$$

The present calculations confirm this assertion, as is shown by Table 2. At 5000 K, f is about a factor of four larger than λ_1/λ_2. It has been argued (1) that $-\lambda_2$ is τ_v^{-1}, the reciprocal of the vibrational relaxation time. For the harmonic oscillator model τ_v is given by (11)

$$\tau_v = q_v/k_{12}$$

Values of $-\lambda_2\tau$ and $k_{12}\tau/q_v$ for the Morse oscillator model are given in Table 2. As found previously (7), the latter quantity is larger, but by less than a factor of two. Since $k_{d,s}n_M$ is very close to $-\lambda_1$, a rough estimate of the error in the steady state approximation is given by

$$f \approx k_{d,s}n_M q_v/k_{12}$$

Since k_d increases much more rapidly with T than does k_{12}, the steady state approximation is sufficiently accurate below a certain temperature. As is seen from Table 1, that temperature is about 3000 K for the model under investigation.

TABLE 1. Comparison of approximate and exact preexponential factors for the Morse oscillator model of H_2 dissociation

T (K)	p	p_s	p_l	p_v
300	[a]	0.8169	1.1544	[a]
1500	[a]	0.2778	0.5533	0.6146
3000	0.1354	0.1354	0.2965	0.2979
5000	0.0834	0.0832	0.1845	0.1255

[a]Technical difficulties precluded the computation of these values.

TABLE 2. Exact and estimated eigenvalues of κ and error in the steady state approximation for the Morse oscillator model of H_2 dissociation

T (K)	λ_1/λ_2	f	$-\lambda_2\tau$	$k_{12}\tau/q_v$
3000	1.86×10^{-6}	$<10^{-3}$	0.0022	0.0027
5000	5.25×10^{-4}	2×10^{-3}	0.0049	0.0082

Rate Constants and Distribution Functions

Vibrational Levels Only

In Table 3 are shown values of p for the various values of s considered.[2] In descending order, these values of s are meant to correspond to H_2, D_2, T_2, and a hypothetical isotope of H_2 with a molecular weight of 10. Decreasing s implies increasing N as indicated in the table. An increase in N always produces an increase in p. This result is in agreement with earlier findings (8).

In order to better understand this result, the variation of r with s was considered where r is the factor by which the rate constant is reduced due to deviations from a Boltzmann distribution,

$$[8] \qquad r \equiv k_d/k_{d,e} = p/p_e$$

Figure 1 shows logarithmic plots of r vs. T for H_2, T_2, and the hypothetical isotope. In all three cases the curves level off at the temperature extremes. As s decreases, the rate of change of r with T decreases so that r increases with increasing s at low temperatures but decreases with increasing s at high temperatures. From [8] and Table 3 it is seen that p_e must decrease with increasing s at low temperatures. It was found

[2]In what follows, p is taken to be equal to p_s.

TABLE 3. Preexponential factors at two temperatures for Morse oscillator models with different level spacings

T (K)	s	N	p
77	0.0575	17	1.229
77	0.0406	25	1.831
77	0.0332	30	2.187
77	0.0257	39	2.818
5000	0.0575	17	0.083
5000	0.0406	25	0.122
5000	0.0332	30	0.143
5000	0.0257	39	0.167

that p_e decreases with increasing s at all temperatures.[3]

Figure 2 shows curves of ln $(-\delta_i)$ vs. ε_i/kT at 3000 K for the three cases discussed above.[4] The curves coincide near the dissociation limit, but for the underlying levels the population at given ε_i is closer to being in a Boltzmann distribution at smaller s. Nevertheless, even for the case with the smallest s, deviations from a Boltzmann distribution are already as high as 50% for a few of the levels which are more than kT below the dissociation limit. Similar results were found at the other temperatures investigated.

In Fig. 3 are shown plots of contributions to the rate from the individual levels as a function of level energy. Curves are shown only for T_2 because they are very similar for the other isotopes. The contributions are expressed in terms of p_i which is given by

$$[9] \qquad p_i = \tau R_{N+1,i}(1 + \delta_i) \exp(D/kT)$$

As can be seen from [2], $k_{N+1,i}$ increases monotonically with ε_i at the temperatures in question. However, because of the drastic depletion of the uppermost levels, p_i goes through a maximum. Also of note is that the maximum is broader at the higher temperature.

These results enable one to account for the variation of r with temperature for the various values of s. At low temperatures most of the dissociation comes from levels in the energy range for which δ_i at given ε_i is the same for all the isotopes. The pattern of levels and the variation of $k_{N+1,i}$ with ε_i are such that a decrease in s produces a decrease in r. At high temperatures this effect is offset by the relatively greater contribution to the rate from levels for which the populations come closer to maintaining a Boltzmann distribution at the smaller values of s. Since this contribution is decisive at the higher temperatures, r increases with decreasing s.

[3]The values of p_e and r for D_2 are out of step with these trends. However, D_2 can be regarded as the exception which proves the rule because the Nth level in this case is exceedingly close to the dissociation limit.

[4]As will be seen later, this representation of the δ's was chosen in order to facilitate comparison with predictions of the separable exponential model.

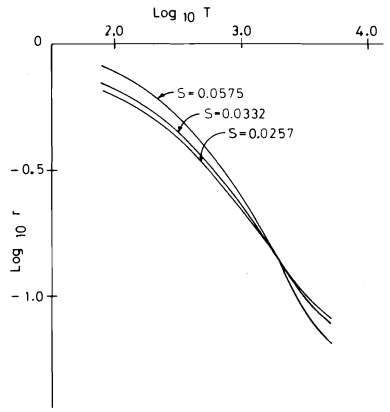

FIG. 1. Rate reduction due to non-Boltzmann distribution as a function of temperature for Morse oscillator models with different level spacings.

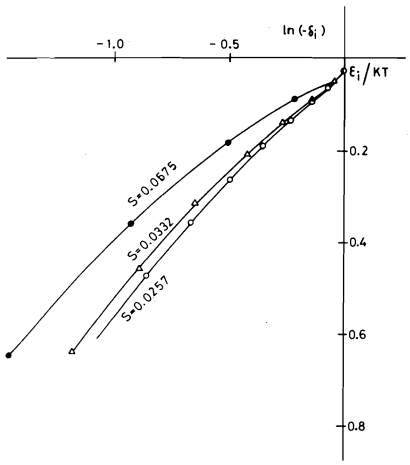

FIG. 2. Semilog plot of fractional deviation of level populations from a Boltzmann distribution as a function of level energy at 3000 K for Morse oscillator models with different level spacings.

A Rotational–Vibrational Model

In order to make meaningful comparisons with experiment, one must generalize the Morse oscillator model to account for rotation. It is also necessary to assume an explicit expression for τ^{-1}. The simplest assumption in the latter case is based on hard sphere collision theory,

$$[10] \qquad \tau^{-1} = \sigma(8kT/\pi\mu)^{1/2} n_M$$

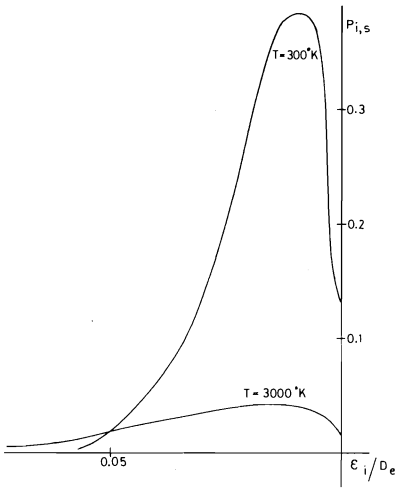

FIG. 3. Contributions to the rate from individual levels as a function of level energy for the Morse oscillator model of T_2 at 300 K and at 3000 K.

where σ is the hard sphere collision cross section (not to be confused with the σ of [6] and [7]) and μ is the reduced mass of the A_2–M pair.

Let L be the angular momentum of A_2 and let $P_{N+1,i}(L)$ be given by

$$P_{N+1,i}(L) = \tau k_{N+1,i}(L)$$

where $k_{N+1,i}(L)$ is the rate constant for dissociation of A_2 with angular momentum L and vibrational quantum number i. The dissociation rate constant $k_{d,e}$ is a thermal average of $k_{N+1,i}(L)$,

$$[11] \quad k_{d,e} = (\tau q_{INT})^{-1} \exp(-D/kT) \times \int_0^{L_m} \sum_{i=1}^{N(L)} P_{N+1,i}(L) \exp\{-[\epsilon_i(L) + \epsilon_b(L)]/kT\} \frac{L\,dL}{\hbar^2}$$

where q_{INT} is the partition function for the rotational–vibrational degrees of freedom of A_2, L_m is the maximum angular momentum which a bound A_2 may possess, $\epsilon_i(L)$ is the energy of level iL relative to the top of the centrifugal barrier, $N(L)$ is the number of vibrational levels for given L, and $\epsilon_b(L)$ is the height of the centrifugal barrier relative to the dissociation energy at $L = 0$. Strictly speaking, the integral over L in [11] should be a sum over the allowed values of the angular momentum quantum number. However, for the model assumed, the discrepancy between sum and integral is small even at the lowest temperature considered.

The recombination rate constant $k_{r,e}$ is related to $k_{d,e}$ by a factor K^{-1}. With K^{-1} written in terms of molecular parameters, this relation takes the form

$$k_{r,e} = k_{d,e} R_g q_{INT} \left(\frac{h^2}{\pi m_A kT}\right)^{3/2} \exp(D/kT)$$

where m_A is the mass of A and R_g is the ratio of the electronic degeneracy of the ground state of A_2 to the square of the electronic degeneracy of the ground state of A. Substitution of [10] and [11] for τ and $k_{d,e}$ and multiplication by r gives the following equation for k_r:

$$[12] \quad k_r = R_g \frac{2\sigma h^3}{\pi^2 m_A{}^2 D_e \tilde{T}} \left(\frac{m_M + 2m_A}{m_M}\right)^{1/2} r \times \int_0^{L_m} \sum_{i=1}^{N(L)} P_{N+1,i}(L) \exp\{-[\epsilon_i(L) + \epsilon_b(L)]/kT\} \frac{L\,dL}{\hbar^2}$$

The right-hand side of [12] really only contains a factor of Planck's constant to the first power since only the vibrational degree of freedom of A_2 is being regarded as quantum mechanical. For most diatomic molecules one likely can, to a good approximation, treat this degree of freedom classically as well.

Equation 12 is based on a reasonably realistic model for atom recombination, but further approximations are necessary in order to obtain numerical results. First, $\epsilon_i(L)$ and $P_{N+1,i}$ are taken to be independent of L so that the sum and the integral in [12] become separable. Next, ϵ_b is taken to have the form

$$[13] \quad \epsilon_b = D_e(X/X^*)^n$$

where X^* and n are constants. The variable X is related to L by

$$X = L^2/2\mu_{A-A} r_e{}^2 D_e$$

where μ_{A-A} is the reduced mass of A_2 and r_e is its equilibrium internuclear separation. This approximation for ϵ_b may be fairly good since [13] has been found (5) to provide an accurate representation of the angular momentum dependence of ϵ_b for the potential of the rotating Morse oscillator,

$$D_e[\exp[-2a(r - r_e)] - 2\exp[-a(r - r_e)] + Xr_e{}^2/r^2]$$

With the two just mentioned approximations, [11] becomes

$$[14]\quad k_r = \frac{R_g \sigma h^3 X^*}{n\pi^2 m_A{}^2 k\Theta_r}\left(\frac{m_M + 2m_A}{m_M}\right)^{1/2} \times \tilde{T}^{(1/n)-1}\gamma\left(n^{-1}, \frac{\varepsilon_c}{kT}\right) r \times \sum_i P_{N+1,i} \exp(-\varepsilon_i/kT)$$

where Θ_r is the rotational temperature of A_2, $\gamma(n^{-1}, \varepsilon_c/kT)$ is the incomplete gamma function, and ε_c is $\varepsilon_b(L_m)$. The factor

$$\frac{h^2 X^*}{n\pi m_A k\Theta_r}\tilde{T}^{(1/n)-1}\gamma\left(n^{-1}, \frac{\varepsilon_c}{kT}\right)$$

can be regarded as a rotational equilibrium constant. It corresponds to the formation of metastable A_2 at the top of the rotational barrier. The decrease with temperature can be ascribed to the slow increase of the thermally averaged ε_b relative to that of the average energy associated with orbital motion of the unbound atoms. The contribution of this effect to the temperature fall-off of k_r has recently been emphasized (9).

For the Morse potential used in the previous section one obtains values of 9.21 and 1.46 for X^* and n, respectively. The potential has a minimum only for X less than 2.26, which in conjunction with [13] implies that ε_c equals $0.136D_e$. Equation 13 with these specific values of the parameters gives for H_2

$$[15]\quad \int_0^{L_m} \exp[-\varepsilon_b(L)/kT]\frac{L\,dL}{\hbar^2} = 1837\tilde{T}^{0.685}\gamma(0.685, 0.136/\tilde{T})$$

For D_2 the result is exactly twice as large. At a temperature of 77 K the right-hand side of [15] is smaller by about 4% than the corresponding quantum mechanical sum. Furthermore, the ratio of ortho and para contributions to the sum is almost exactly 3:1. Therefore, this model predicts no significant para enrichment of H_2 due to recombination at 77 K, a result which agrees with experiment (12).

For r times the sum of the $P_{N+1,i}$'s, one may take pq_v where p is given by the computations reported in the previous sections, and q_v is readily computed from [4*b*]. As shown by Fig. 1, r decreases with T, albeit more slowly at the highest temperatures considered. The factor $p_c q_v$ increases with temperature, which may be the most unrealistic feature of the model. The hard sphere collision cross section σ in [14] is treated here as an adjustable parameter. Assuming for it a not unreasonable value of 10 Å^2, one obtains for hydrogen

$$[16]\quad k_{r,H} = (5.4 \times 10^8)\,\tilde{T}^{-0.315}\gamma(0.685, 0.136/\tilde{T}) \times q_v p\ \ell^2\ \text{mol}^{-2}\ \text{s}^{-1}$$

For deuterium the factor $m_A{}^2\,\Theta_r$ in the denominator of [14] is twice as large as it is for hydrogen. Thus the isotopic ratio is given by

$$[17]\quad k_{r,H}/k_{r,D} = 2(q_v p)_H/(q_v p)_D$$

The factor of two more than outweighs the larger $q_v p$ values for deuterium.

Figure 4 shows a logarithmic plot of [16] along with the most recent experimental values (13–15) of k_r for H_2 in argon. The graph of [16] is seen to level off at the extremes of temperature, a reflection of the levelling-off of r. Agreement with experiment is not very good. The experi-

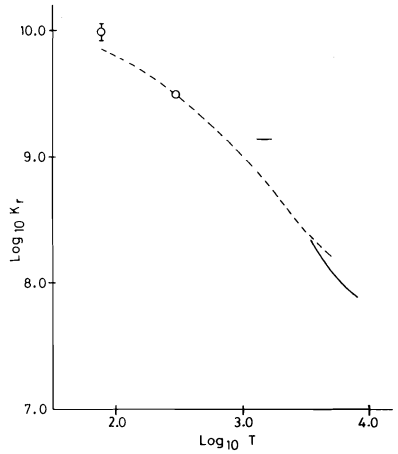

FIG. 4. Recombination rate constant as a function of temperature for H_2 in Ar. Dashed line was calculated from [16], circles represent data of ref. 13, and solid lines represent data of refs. 14 and 15.

TABLE 4. Calculated and experimental ratios of rate constants for H- and D-atom recombination in argon

	$k_{r,H}/k_{r,D}$	
T (K)	Calculated[a]	Experimental
300	1.3	1.55±0.43[b]
4000	1.1	1.1[c,d]

[a]Equation 17.
[b]Reference 20.
[c]Reference 15.
[d]Reference 21.

mental curve does level off at the highest temperatures. However, it does not level off at low temperatures, and there appears to be a shoulder between 1000 and 2000 K. It is of some significance that the modified phase space theory (16) does predict these latter two features of the experimental curve.

In Table 4 values of the isotope ratio calculated from [17] are compared with values obtained from experiment. Here the agreement is good.

Discussion

Comparison with the Separable Exponential Model

The separable exponential model (4) is defined by the equations

$$[18]\quad R_{ij} = \tau^{-1}(1 - e^{-\theta})^2 \exp[\beta(N - i)\theta - \alpha(N - j)\theta - N\theta] \quad \text{for } j < i < N + 1$$
$$= \tau^{-1}(1 - e^{-\theta})^2(e^{\beta\theta} - 1)^{-1} \exp[\beta(N - i)\theta - \alpha(N - j)\theta - N\theta] \quad \text{for } i = N + 1$$
$$= R_{ji} \quad \text{for } j > i$$

The model is characterized by parameters α, β, and θ. The parameter θ is a measure of the level spacing and is of greatest interest in the present discussion. In ref. 4 it was shown that the steady state approximation gives for this model

$$[19]\quad \delta_i = -(e^{\alpha\theta} - 1)(e^{\beta\theta} - 1)^{-1} e^{(\beta-\alpha)\varepsilon_i}$$

$$[20]\quad p = (1 - e^{-\theta})^2(e^{\beta\theta} - 1)^{-3}(1 - e^{-\alpha\theta})^{-1}(e^{\beta\theta} - e^{\alpha\theta})(e^{\beta\theta} - e^{-\alpha\theta})$$

$$[21]\quad r = 1 - \sinh^2(\tfrac{1}{2}\alpha\theta)\sinh^{-2}(\tfrac{1}{2}\beta\theta)$$

where ε_i is $-(N - i)\theta$.

The monotonic increase of p with decreasing s for the Morse oscillator model has been ascribed to network effects (17). The monotonic increase of p with decreasing θ for the separable exponential model cannot be explained in this way (4). The present study goes beyond ref. 17 by showing which independent paths are important for bringing about the increase, namely those which lead directly to the dissociated state. Increase of the number of these paths increases p_e, and p is thereby increased even at low temperatures where r decreases markedly with increasing s.[5]

As mentioned above, the increase of r with decreasing s for the Morse oscillator model at high temperatures is apparently due to differences in the variation of δ_i with ε_i for the different values of s. From Fig. 2 one would surmise that the curves of $\ln(-\delta_i)$ vs. ε_i converge to a continuum ($s \to 0$) limit and that this limit is approached more rapidly for ε_i's near the dissociation energy. From [19] one sees that the continuum limit of the $\ln(-\delta_i)$ vs. ε_i curves for the separable exponential model is approached at the same rate for all ε_i. Furthermore, the curves approach this limit from below whereas the corresponding curves for the Morse oscillator model appear to approach their continuum limit from above. These differences between the $\ln(-\delta_i)$ vs. ε_i curves for the Morse oscillator model and those for the separable exponential model can be explained on the basis of the variable level spacings for the former model. Simply because the levels for the Morse oscillator approach a continuum most rapidly near the dissociation limit, it would seem reasonable that δ_i should approach its continuum value most rapidly here as well. The downward concavity of the $\ln(-\delta_i)$ vs. ε_i curves for the Morse oscillator model can also be ascribed to the variation in level spacing since a greater number of levels per energy interval of given size is almost certain to imply less tendency for any one of them to be replenished. Thus the populations of the lower, less densely packed levels come closer to being in a Boltzmann distribution than would be expected on the basis of a linear extrapolation from the higher levels. Finally, since the relatively high depletions of the uppermost levels account for the maxima in the p_i vs. ε_i curves for the Morse oscillator model, this effect can be ultimately traced back to the variation of level spacing with ε_i.

[5]For the separable exponential model as well it is the increase of p_e with decreasing θ that is decisive, but here the increase can be ascribed only in part to network effects.

Comparisons with Experiment and with other Theories

As already mentioned, the modified phase space theory (16) gives a k_r vs. T curve more nearly in agreement with the experimental curve for H_2 in Ar than does the cruder theory discussed here. However, it has been pointed out (7) that the Morse oscillator model is really intended to describe H-atom recombination in He at high temperatures. No experimental data are available for this case, but the differences between He and Ar as third bodies are probably not large. Mass effects appear not to be important (18), and the effects of attractive forces are important only at low temperatures. One sees from Fig. 4 that the Morse oscillator model does come closest to representing the experimental variation of k_r with T at high temperatures. What is notable about this variation is the levelling-off of the curves as T increases. In the case of the model this levelling-off is a consequence of the levelling-off of r. The levelling-off of r is probably due to the increase with T of the probabilities of multiquantum transitions. Such an increase would slow the decrease of r in two ways: by evening out the reactivities of the various levels and by causing the reactive levels to be more easily replenished.

The failure of the Morse oscillator model to reproduce the low temperature portion of the k_r vs. T curve is most likely a consequence of the neglect of atom – third body attraction. As can be seen from the results of ref. 16, the prediction of the modified phase space theory as to the rapidity of the fall-off of k_r with T at low temperatures is quite sensitive to the assumed depth of the H–M potential well. The absence of a shoulder on the curve for the model in the intermediate temperature range may be due to a decline of r with T which is too gradual. Calculations, the results of which were not presented here, show that a relative widening of the level spacings near the dissociation limit results in a more abrupt fall-off of r with T. It is known (19) that [3] gives energy levels near the dissociation limit which are more closely spaced than those actually observed for H_2. It may be that the k_r vs. T curve for a model with level spacings somewhere between those of a harmonic oscillator and those of a Morse oscillator would exhibit the observed shoulder. Such an explanation of the shoulder would be, nevertheless, ambiguous. The modified phase space theory of ref. 16 is also based on a Morse oscillator model, and it does predict the shoulder.

Conclusions

The present study of the Morse oscillator model of hydrogen dissociation and recombination has two parts: a test of approximations to the smallest eigenvalue λ_1 of the matrix κ for the model and an analysis of rate constants and level populations for the model in the light of experimental and of other theoretical results. It was found that the steady state approximation gives a highly accurate result for λ_1 provided that T is sufficiently low. A rough estimate of the error due to the steady state approximation is given by

$$k_{d,s}n_M q_v/k_{12}$$

This ratio increases rapidly with temperature, but it does not become appreciable compared to one until temperatures such as are only occasionally investigated experimentally. The steady state approximation reduces the problem of calculating the rate constant and the level populations to one of solving a system of simultaneous linear algebraic equations. The number of equations which must be solved to get an accurate result decreases as T decreases. No satisfactory further simplification of the calculations was found. Conversion to an approximately equivalent stepladder model led to inaccurate results.

Transformation to an equivalent separable exponential model by means of the variational principle was also found to lead to inaccurate results. The failure of this approximation is elucidated by comparing curves of $\ln(-\delta_i)$ vs. ε_i for the two models. For the Morse oscillator model the curves are concave downward over most of the range of ε_i whereas they are linear for the separable exponential model. This difference can be ultimately related to the decrease in level spacing with increase in ε_i for the Morse oscillator model.

The recombination rate constant for the Morse oscillator model decreases as T increases. The decrease is due in part to the decrease of the rotational equilibrium constant for the formation of metastable A_2. The rest of the decrease is due to the fall-off of r. The temperature variation of k_r with T for the model does not agree well with that observed for H-atom recombination in argon. It seems fairly certain that neglect of atom – third body attraction is partly to blame for this discrepancy. The use of a rather unrealistic energy level expression may also be partly to blame.

The model best reproduces the observed variation of k_r with T at high temperatures where a levelling-off of both curves is found. For the model this levelling-off is due to increase with T of the relative rates of multiquantum transitions. The model also reproduces the experimentally observed ratios of the rate constants for H-atom and D-atom recombination. Phase space factors for degrees of freedom other than vibration of A_2 give a ratio of $k_{r,H}$ to $k_{r,D}$ equal to 2. The effect of increasing the vibrational level density is to reduce this ratio to values not much greater than one, which agrees with experiment. Apparently the effect which requires special consideration in predictions of $k_{r,H}/k_{r,D}$ is the effect of the change in the spacing of vibrational levels.

Acknowledgments

Financial support by the National Research Council of Canada is gratefully acknowledged. A word of thanks is due to Mr. Derek Leaist for assistance with the computations.

1. E. E. NIKITIN. Dokl. Akad. Nauk SSSR, **116**, 584 (1957) (*Engl. transl.*: Sov. Phys.-Dokl. **2**, 453 (1957)); E. W. MONTROLL and K. E. SHULER. Adv. Chem. Phys. **1**, 361 (1958).
2. E. V. STUPOCHENKO and A. I. OSIPOV. Zh. Fiz. Khim. **33**, 1526 (1959) (*Engl. transl.*: Russ. J. Phys. Chem. **33**, 36 (1959)).
3. J. C. KECK and G. CARRIER. J. Chem. Phys. **43**, 2284 (1965).
4. N. S. SNIDER. J. Chem. Phys. **65**, 1800 (1976).
5. N. S. SNIDER. Ph.D. Thesis, Princeton University, Princeton, NJ. 1963.
6. N. S. SNIDER. J. Chem. Phys. **45**, 3299 (1966).
7. D. L. S. MCELWAIN and H. O. PRITCHARD. Symp. (Int.) Combust. (Proc.), **13**, 37 (1971).
8. D. L. S. MCELWAIN and H. O. PRITCHARD. Can. J. Chem. **49**, 3915 (1971).
9. H. O. PRITCHARD. Can. J. Chem. **51**, 3152 (1973); Acc. Chem. Res. **9**, 99 (1976).
10. R. L. KETTER and S. P. PRAWEL. Modern methods of engineering computation. McGraw-Hill Book Co., New York, NY. 1969. p. 81.
11. E. W. MONTROLL and K. E. SHULER. J. Chem. Phys. **26**, 454 (1957).
12. L. P. WALKAUSKAS and F. KAUFMAN. J. Chem. Phys. **64**, 3885 (1976).
13. D. W. TRAINOR, D. O. HAM, and F. KAUFMAN. J. Chem. Phys. **58**, 4599 (1973).
14. W. G. MALLARD and J. H. OWEN. Int. J. Chem. Kinet. **6**, 753 (1974).
15. W. D. BRESHEARS and P. F. BIRD. Symp. (Int.) Combust. (Proc.), **14**, 211 (1972).
16. V. H. SHUI and J. P. APPLETON. J. Chem. Phys. **55**, 3126 (1971).
17. H. O. PRITCHARD. Spec. Per. Rep.: React. Kinet. **1**, 243 (1975).
18. W. H. WONG and G. BURNS. J. Chem. Phys. **62**, 1712 (1975).
19. G. HERZBERG and L. L. HOWE. Can. J. Phys. **37**, 636 (1959).
20. V. V. AZATYAN, R. R. BORODULIN, and E. I. INTEZAROVA. Dokl. Akad. Nauk SSSR, **213**, 856 (1973) (*Engl. transl.*: Dokl. Phys. Chem. **213**, 1053 (1973)).
21. D. APPEL and J. P. APPLETON. Symp. (Int.) Combust. (Proc.), **15**, 701 (1975).

Intrinsic acidities of carbon acids: the nitroalkanes. Solvation effects in water and DMSO

J. B. CUMMING, T. F. MAGNERA, AND P. KEBARLE

Department of Chemistry, University of Alberta, Edmonton, Alta., Canada T6G 2G2

Received May 3, 1977

J. B. CUMMING, T. F. MAGNERA, and P. KEBARLE. Can. J. Chem. **55**, 3474 (1977).

The ion equilibria $R_1H + R_2^- = R_1^- + R_2H$ involving nitroalkanes and compounds with known gas phase acidity were measured at 500 K with a pulsed high pressure mass spectrometer. The resulting $\Delta G^0 = -RT \ln K$ combined with calculated ΔS^0 values lead to the corresponding ΔH changes. The enthalpy changes are used for the evaluation of the difference between the bond dissociation energy and the electron affinity D(R—H) − EA(R). The values obtained are: CH_3NO_2 44.0, $CH_3CH_2NO_2$ 43.7, $(CH_3)_2CHNO_2$ 43.0 kcal/mol. D(R—H) − EA(R) is a measure of the gas phase acidity. The nearly equal gas phase acidities of the nitroalkanes above are due to a decrease of D(R—H) and to a decrease of EA(R) with methyl substitution. In aqueous solution the acidities are known to increase substantially for the above nitroalkane order. Decrease of EA with methyl substitution indicates that there will be more charge localization on the O atoms in R^- with methyl substitution. This leads to better H bonding and solvation of R^- in protic solvents. This explains the higher acidity of the methyl substituted nitroalkanes in aqueous solution. The acidities in DMSO are closer to those in the gas phase since DMSO is not so sensitive to the charge distribution in R^-.

J. B. CUMMING, T. F. MAGNERA et P. KEBARLE. Can. J. Chem. **55**, 3474 (1977).

L'équilibre ionique $R_1H + R_2^- = R_1^- + R_2H$ impliquant des nitroalkanes et des composés d'acidité connue en phase gazeuse sont mesurés à 500 K avec un spectromètre de masse à haute pression impulsive. L'expression $\Delta G^0 = -RT \ln K$ résultante, combinée avec les valeurs calculées du ΔS^0 conduisent aux valeurs ΔH correspondantes. Les changements d'enthalpie sont utilisés pour évaluer la différence entre l'énergie de dissociation d'une liaison et l'affinité électronique D(R—H) − EA(R). Les valeurs obtenues sont: CH_3NO_2 44.0, $CH_3CH_2NO_2$ 43.7, $(CH_3)_2CHNO_2$ 43.0 kcal/mol. La différence D(R—H) − EA(R) est une mesure de l'acidité des composés en phase gazeuse. Cette similarité des valeurs de l'acidité, en phase gazeuse des nitroalkanes ci-dessus, est due à une diminution des termes D(R—H) et EA(R) avec la substitution par un groupe méthyle. Par contre, pour la même séquence que ci-dessus, on note une augmentation de l'acidité de ces nitroalkanes en solution aqueuse. La diminution du terme EA avec la substitution par un groupe méthyle indique qu'il y a une localisation de charge plus grande sur les atomes d'oxygène O dans R^- avec la substitution par un groupe méthyle. Ceci nous amène à un meilleur établissement de la liaison H et une meilleure solvatation du radical R^- dans les solvants protiques. Ceci explique l'acidité plus grande des nitroalkanes méthyl-substitués en solution aqueuse. Les acidités dans le DMSO sont proches de celles obtenues en phase gazeuse puisque le DMSO n'est pas aussi sensible à la distribution de charge dans R^-.

[Traduit par le journal]

Introduction

Recently we reported gas phase acidities of a large variety of carbon acids RH obtained from measurements of the gas phase proton transfer equilibria 1 and 2 (1).

$$[1] \qquad R_1H + R_2^- = R_1^- + R_2H$$

$$[2] \qquad RH + Cl^- = R^- + HCl$$

The proton transfer process 2 relates the acidities to that of a common standard HCl. The previous measurements included only one nitro compound, p-NO_2 toluene. The anion of p-NO_2 toluene is highly delocalized and therefore not essentially different from the other highly delocalized anions reported in that work. The nitroalkanes, whose acidities are reported in the present work, are of special interest for several reasons. They are similar to the carbonyl carbon acids for which recently gas phase acidities (1, 2) and electron affinities (3) have become available. Therefore comparisons between the alkyl substituent effects prove to be quite fruitful even in the absence of electron affinities and bond dissociation energies for the nitro compounds. The nitroalkanes undergo measurable acid dissociation in aqueous solution so that acidity constants for that medium are available (4).

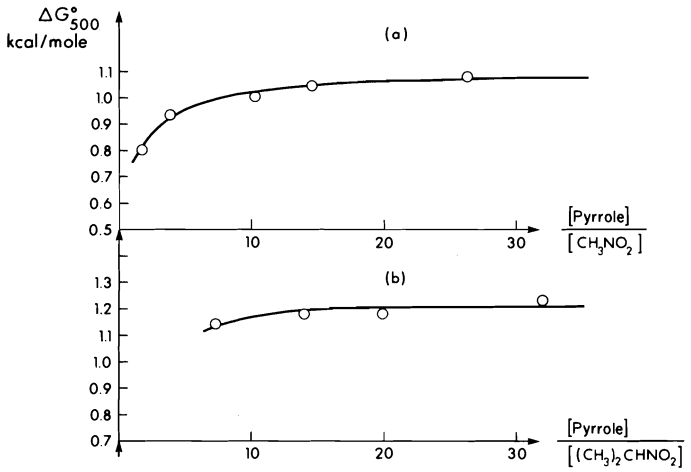

FIG. 1. Dependence of $\Delta G_1^0 = RT \ln K_1$ for proton transfer reaction involving nitroalkane and reference acid pyrrole. (*a*) $CH_2NO_2^- + PyH = CH_3NO_2 + Py^-$. (*b*) $(CH_3)_2CNO_2^- + PyH = (CH_3)_2CHNO_2 + Py^-$. Because of reaction producing NO_2^- (see text) consistent equilibrium constants could be obtained only for large [pyrrole]/[nitroalkane] ratios.

Acidity measurements in the important aprotic solvent DMSO have also been determined (5). Therefore comparisons between the acidities in the dilute gas phase, water, and DMSO are possible and, as will be seen, prove very informative.

Experimental

The measurements of the proton transfer equilibria 1 were made in a high pressure mass spectrometer (6) using procedures very similar to those described earlier (1). A gas mixture containing the buffer gas methane at 1–4 Torr, R_1H and R_2H generally in the 1–100 mTorr range, and NF_3 at ~20 mTorr was passed in slow flow through the ion source. Fluoride ions are formed by the dissociative electron capture: $e^- + NF_3 = F^- + NF_2$. The ions R^- result from the proton transfer: $F^- + RH = HF + R^-$. This reaction removes all the fluoride ions, since HF is a much weaker acid than RH. Pulsing of the electron beam permits one to follow the temporal change of R_1^- and R_2^-. In normal measurements, after a kinetic stage of some 50 μs, the concentration ratio R_1^-/R_2^- becomes constant, which indicates the achievement of equilibrium 1.

Some difficulties were encountered with the nitro compounds. For all nitroalkanes RH, the major ion observed was not R^- but NO_2^-. This ion was present directly after the electron pulse and continued to grow slowly in intensity at the expense of the R^- ions. Low pressure mass spectrometric studies (7) have shown that NO_2^- is produced directly by dissociative electron capture $e^- + C_nH_{2n+1}NO_2 = NO_2^- + C_nH_{2n+1}$. While this reaction might be responsible for the NO_2^- observed at the beginning of the pulse, the growth of NO_2^- with time after the pulse must be due to some ion molecule reaction. One possibility is the occurrence of nucleophilic displacement reactions of the type: $CH_2NO_2^- + CH_3NO_2 = CH_3CH_2NO_2 + NO_2^-$. Another possibility is proton transfer from HNO_2 i.e. $CH_2NO_2^- + HNO_2 = CH_3NO_2 + NO_2^-$, where the HNO_2 is either a minor impurity present in the nitroalkanes or a product of some reaction occurring in the ion source. Since HNO_2 is a much stronger acid, HNO_2 present at 10^{-4} Torr i.e. less than 0.1% of RH will still be able to convert half of the R^- to RH in ~1 ms.

It was found that equilibrium 'constants' K_1 obtained at longer reaction times where the anion ratio had become constant were not always independent of the neutral acid ratio used. Constant values of K_1 could be obtained only if the concentration of the nitroalkane RH was much lower than the concentration of the reference acid (pyrrole). This situation is illustrated by the results shown in Fig. 1. $\Delta G_1^0 = RT \ln K_1$ is seen initially to increase with the [pyrrole]/[nitroalkane] ratio but the value becomes constant for a ratio larger than ~10. This behaviour may be a result of the side reactions producing NO_2^-, which were mentioned above. The following scheme written for nitromethane AH and pyrrole PyH may be considered:

$$[3] \qquad PyH + A^- \underset{k_r}{\overset{k_f}{\rightleftarrows}} Py^- + AH$$

$$[4] \qquad Py^- + AH \xrightarrow{k_{s1}} NO_2^- + \text{neutrals}$$

$$[5] \qquad A^- + AH \xrightarrow{k_{s2}} NO_2^- + \text{neutrals}$$

The possible neutrals being $PyCH_3$ and $C_2H_5NO_2$ respectively if the side reactions are nucleophilic substitution processes. The results shown in Fig. 1*a* were measured for long reaction times where $[A^-]/[Py^-] =$ constant. For this condition to hold: $d[A^-]/dt = d[Py^-]/dt$. Expressing the rates in terms of the concentrations and the rate constants one obtains, after rearranging

[6] $$Q = \frac{2k_f}{2k_r + k_{s1}} + \frac{k_{s2}}{2k_r + k_{s1}} \frac{[AH]}{[PyH]}$$

where,

$$Q = \frac{[AH][Py^-]}{[PyH][A^-]}$$

Q is the equilibrium quotient for the proton transfer reaction 3.

A replot of the data used in Fig. 1*a* is shown in Fig. 2, where Q is plotted vs. the concentration ratio [AH]/[PyH]. An (approximately) straight line is obtained, which shows that the experimental results are consistent with the mechanism [3]–[5]. The slope of the straight line obtained is 0.2 while the intercept with the Q axis is ~0.325. This leads to the expressions:

$$Q = 2k_f/(2k_r + k_{s1}) = 0.325$$

and,

$$k_{s2}/(2k_r + k_{s1}) = 0.2$$

Evidently Q will be close to the equilibrium constant K for [3], only if $2k_r > k_{s1}$. Unfortunately quantitative measurements of the rate constants were not made; however qualitative examinations of the concentration changes of the ions before the ion ratio $[A^-]/[Py^-]$ becomes constant did indicate that k_r, which corresponds to the exothermic direction of equilibrium 3, is considerably larger than $k_{s1} + k_{s2}$. The equilibrium constant therefore should be equal to 0.325 the same value as that obtained by the extrapolation in Fig. 1*a*. An additional reason for confidence in the results is the thermodynamic consistency of the data presented in Fig. 3. The results of Fig. 3 are considered in the next section.

It should be pointed out that an equation of the same form as [6] will be obtained if the side reactions 4 and 5 involved not AH directly but some impurity like HNO_2 whose concentration is proportional to that of AH.

Results and Discussion

The free energy changes for reaction 1, $\Delta G_1^0(500) = RT \ln K$ for $T = 500$ K, are shown in Fig. 3. The determinations include, for the ion equilibria,

$$R_1H + R_2^- = R_1^- + R_2H$$

$$RH + Cl^- = R^- + HCl$$

some multiple thermodynamic cycles which are

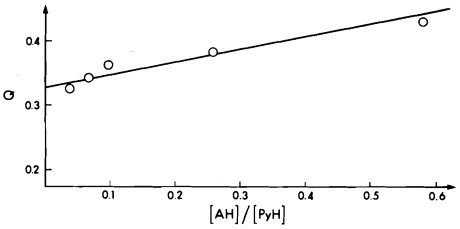

FIG. 2. Replot of data from Fig. 1*a* as a test of eq. 6. $Q = [AH][Py^-]/[PyH][A^-]$ is the equilibrium coefficient of reaction: $PyH + A^- = Py^- + AH$, slope of line equals 0.2 and intercept of Q axis equals 0.325.

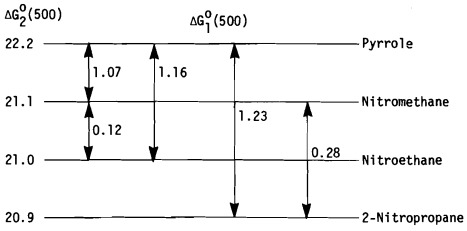

FIG. 3. Summary of gas acidity measurements. Numbers beside double arrows represent directly measured $\Delta G_1^0(500) = -RT \ln K_1$ for reaction 1: $R_1H + R_2^- + R_2H$ measured at 500 K. R_1H is the compound on the upper end of the double arrow. $\Delta G_2^0(500)$, given in column on the left are values for reaction 2: $RH + Cl^- = R^- + HCl$, relating present acidities to the primary standard HCl.

consistent to 0.1 kcal/mol. The $\Delta G_2^0(500)$, also shown in Fig. 3, relate the acidities to the primary standard HCl. They were obtained from ΔG_1^0 and the ΔG_2^0 for pyrrole which was determined in separate measurements (1, 9).

From ΔG_2^0, ΔH_2^0 can be evaluated by using calculated ΔS_2^0 values. Since $\Delta H_2^0 = D(R—H) - EA(R) - D(H—Cl) + EA(Cl)$, it is possible to evaluate $D(R—H) - EA(R)$ by using the known $D(H—Cl) - EA(Cl) = 20$ kcal mol (8). The entropy change in reaction 2 was evaluated (9) by considering the appearance of two rotational degrees of freedom in the change $Cl^- \rightarrow HCl$ and the conversion of an internal rotation to a restricted rotation in the change $C_nH_{2n+1}NO_2 \rightarrow C_nH_{2n}NO_2^-$. Symmetry number changes were considered also. The barrier to internal rotation around the C—N bond arises because of the formation of a partial double bond in the anion. The corresponding structures for the nitromethane anion are shown in **1**.

1 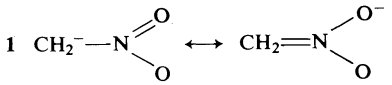

A full account of entropy calculations for reactions 2 involving all measurements done in our laboratory is given elsewhere (9). The calculated (9) $T\Delta S_2^0$ are approximately 2.2 kcal/mol (at 500 K) for the nitroalkanes. Since they don't change much for the three nitroalkanes studied, they do not have a significant effect on the relative acidities. However, this correction improves the accuracy of the absolute $D - EA$ results. The $D - EA$ values for the nitroalkanes are shown in Table 1.

A key to the changes of gas phase acidities of the nitroalkanes can be obtained by comparison

TABLE 1. Thermochemical information for carbon acids RH[a]

RH	D(R—H) − EA(R)[b]	EA(R)	D(R—H)
$HCOCH_2$—H	53.4[c]	41.7±1.4[e]	95.1[f]
$HCOCH(CH_3)$—H	52.8[c]	38.9±1.2[e]	91.7[f]
CH_3COCH_2—H	56.4[c]	40.6±1.3[e]	97.0[f] 98.0[g]
$CH_3COCH(CH_3)$—H	54.6[c]	38.6±1.2[e]	93.2[f] 92.3[g]
NO_2CH_2—H	44.0[d]	(~53)[h]	(~97)[h]
$NO_2CH(CH_3)$—H	43.7[d]	(~49.3)[h]	(~93)[h]
$NO_2C(CH_3)_2$—H	43.0[d]	(~48.5)[g]	(~91.5)[h]
$CNCH_2$—H	58.7[k]	34.8[l]	93.5[f] 93[m]

[a]All values in kcal/mol.
[b]From gas phase equilibria measurements of reaction $R_1^- + R_2H = R_1H + R_2^-$ and evaluations of entropy change.
[c]Cumming and Kebarle (2).
[d]Present work. Absolute D − EA values believed to be accurate to ±2 kcal/mol, relative values to ±0.2 kcal/mol.
[e]Zimmerman, Reed, and Brauman (3).
[f]From D(R—H) − EA(R) and EA(R).
[g]Direct (kinetic) determinations of bond dissociation energy, Solly, Golden, and Benson (13).
[h]Estimated electron affinities on the basis of assumed D(R—H) and determinations of D(R—H) − EA(R), see text.
[k]Gas phase acidity determinations and entropy change evaluation (1, 9).
[l]Richardson, Stephenson, and Brauman (14).
[m]Direct (kinetic) determination by King and Goddard (15).

with the acidities of the carbonyl compounds also shown in Table 1.

Recent determinations of the photodetachment thresholds of the enolate ions R^- by Zimmerman, Reed, and Brauman (3) have provided electron affinities for the enolate radicals R. With these data the D(R—H) − EA(R) obtained from gas phase acidity measurements (2) can be separated into substituent effects on EA(R) and on D(R—H) for the carbonyl compounds. Examining the pairs $HCOCH_2$—H, $HCOCH(CH_3)$—H and CH_3COCH_2—H, $CH_3COCH(CH_3)$—H (Table 1), we notice that methyl substitution on the carbon carrying the acidic hydrogen lowers the electron affinity of R by 2.8 and 2 kcal/mol and the bond energies D(R—H) are lowered by 3.4 and 3.8 kcal/mol, respectively. Since electron affinity and bond energy have opposite effects on the acid dissociation energy, the net result is a very small increase of acidity with methyl substitution. The bond energy change with methyl substitution is the familiar decrease which occurs from a primary to a secondary C—H bond. Since for the nitroalkanes CH_3NO_2, $C_2H_5NO_2$, and i-$C_3H_7NO_2$ we have again a change from primary to secondary and to tertiary C—H bonds one may certainly expect that decreases of D(R—H) of some 3–4 kcal/mol will be occurring with each methyl that is introduced. Since the measured D − EA values change (decrease) by much smaller amounts the electron affinities must be decreasing with methyl substitution. It is interesting to note that $D(CH_3CH_2$—H) = 98 and $D(CH_3CH(CH_3)$—H) = 94.5 kcal/mol (10) are very close to $D(CH_3COCH_2$—H) ≈ 97 and $D(CH_3COCH(CH_3)$—H ≈ 93 kcal/mol (Table 1). The lack of change when CH_3 is replaced by the electron withdrawing group CH_3CO makes it plausible to assume that the R—H bond energies in the nitromethanes might also be approximately equal to the bond energies of the primary, secondary, and tertiary C—H in the alkanes. Using $D((CH_3)_3C$—H) = 91.5 kcal/mol (10) and the values 97 and 93 kcal/mol for primary and secondary C—H given above one obtains the approximate values for EA(R) of the nitroalkanes given in Table 1.

It is interesting to compare the three substituted 'methanes' $(CN)CH_3$, $(CH_3CO)CH_3$, and $(NO_2)CH_3$ (Table 1). The D − EA values are 58.7, 56.4, and 44 kcal/mol, an acidity order observed previously in the more qualitative measurements by Bohme (11). The lack of a reliable $D(NO_2CH_2$—H) is unfortunate, but the available data indicate that the observed acidity change is determined by increases in the electron affinities: 34.8, 40.6, and ~53 kcal/mol. The bond energies also increase in this order but the changes are much smaller.

A comparison between the nitroalkane acidities in the dilute gas phase, in aqueous solution, and in DMSO can be made on the basis of the data shown in Table 2. This is best done by considering the experimental ΔG data for proton transfer in the gas phase, water, and DMSO since these do not involve corrections for symmetry number as do the D − EA data. While the acidity in the gas

TABLE 2. Acidities in the dilute gas phase, in water, and in DMSO

RH	D − EA[a]	pK(H_2O)[b]	pK(DMSO)[c]	ΔG^0(500)[d]	ΔG^0(H_2O)[d]	ΔG^0(DMSO)[d]
CH_3NO_2	44.0	10.2	17.2	0.0	0.0	0.0
$CH_3CH_2NO_2$	43.7	8.5	16.7	0.1	2.3	0.7
$(CH_3)_2CHNO_2$	43.0	7.7	16.9	0.2	3.4	0.5

[a] D(R—H) − EA(R) from Table 1.
[b] Pearson and Dillon (4).
[c] Bordwell (5).
[d] Free energy change for proton transfer reaction $CH_3NO_2 + R^- = CH_2NO_2^- + RH$ in kcal/mol. Water and DMSO measurements at 300 K.

phase experiences practically no increase with methyl substitution to the carbon carrying the acidic hydrogen, in water a substantial increase of acidity is observed. Generally alkyl substitution decreases the aqueous acidity relative to that in the gas phase so that, at a first glance, the results for the nitroalkanes appear surprising. However there is a good explanation for these observations. As noted earlier methyl substitution decreases the electron affinity EA(R). Therefore it may be assumed that methyl relative to H has a charge localization effect in the anion, i.e. the partial negative charge on the oxygen atoms increases in the order $CH_2NO_2^-$ < $CH_3CHNO_2^-$ < $(CH_3)_2CNO_2^-$. This means that the first and the few subsequent strong hydrogen bonds with HOH molecules, which will occur to the oxygen atoms as in structure **2**, will be stronger for the more highly methyl substituted anions.

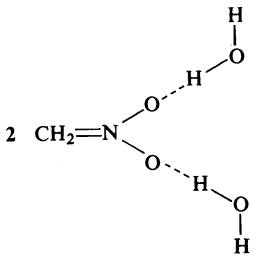

Therefore the solvation of the methyl substituted anions will be more favorable. The favorable solvation effect will partially offset the unfavorable decrease of electron affinity and a substantial increase of acidity will result from the decreasing bond energies R—H.

In DMSO the situation is quite different. As pointed out earlier (12), the behavior of aprotic solvents like acetonitrile and DMSO toward anions can be explained on the basis of the electric dipole charge distribution in the solvent molecules. Since the positive charge in aprotic dipolar molecules is distributed diffusely over bulky hydrocarbon groups, the centre of the positive pole of the dipole is relatively inaccessible to the negative ion. The strength of the interaction of the first few solvent molecules with the negative ion is therefore less sensitive to increase of ionic radius or delocalization of negative charge from a small functional group. Therefore, the solvation of the nitro anions in DMSO will not increase appreciably with charge localization on the O atoms upon methyl substitution and consequently the relative DMSO acidities will follow approximately the gas phase acidities.

Acknowledgments

Financial support by the National Research Council of Canada is gratefully acknowledged. Encouragement for us to undertake the above measurements came from Prof. F. G. Bordwell who also provided us with a pure sample of $2NO_2$–propane.

1. T. B. McMahon and P. Kebarle. J. Am. Chem. Soc. **98**, 3399 (1976).
2. J. B. Cumming and P. Kebarle. J. Am. Chem. Soc. Submitted for publication.
3. A. H. Zimmerman, K. J. Reed, and J. I. Brauman. J. Am. Chem. Soc. In press.
4. R. G. Pearson and R. L. Dillon. J. Am. Chem. Soc. **75**, 2439 (1953); J. Hine. Structural effects on equilibria in organic chemistry. John Wiley & Sons, Inc., N.Y., NY. 1975.
5. W. S. Matthews, J. E. Bares, J. E. Bartmess, F. G. Bordwell, F. J. Conforth, G. E. Drucker, Z. Margolin, R. J. McCallum, G. J. McCollum, and N. R. Vanier. J. Am. Chem. Soc. **97**, 7006 (1975); F. G. Bordwell, N. R. Vanier, W. S. Matthews, J. B. Hendrickson, and P. L. Skipper. J. Am. Chem. Soc. **97**, 7160 (1975).
6. A. J. Cunningham, J. D. Payzant, and P. Kebarle. J. Am. Chem. Soc. **94**, 7628 (1972).
7. R. Large and H. Knof. Org. Mass. Spectrom. **11**, 582 (1976).

8. R. S. BERRY and C. W. REIMANN. J. Chem. Phys. **38**, 1540 (1963); Selected values of chemical thermodynamic properties NBS Technical Note 270-3. U.S. Department of Commerce (1968).
9. J. B. CUMMING and P. KEBARLE. J. Am. Chem. Soc. To be published.
10. J. O. KERR. Chem. Rev. **148**, 11 (1966).
11. D. K. BOHME, E. LEE-RUFF, and L. B. YOUNG. J. Am. Chem. Soc. **94**, 5153 (1972).
12. T. B. MCMAHON and P. KEBARLE. J. Am. Chem. Soc. **99**, 2222 (1977); W. R. DAVIDSON and P. KEBARLE. J. Am. Chem. Soc. **98**, 6125 (1976); J. B. CUMMING, M. FRENCH, and P. KEBARLE. J. Am. Chem. Soc. In press.
13. R. K. SOLLY, D. M. GOLDEN, and S. W. BENSON. Int. J. Chem. Kinet. **2**, 11 (1970); **2**, 381 (1970).
14. J. H. RICHARDSON, L. M. STEPHENSON, and J. I. BRAUMAN. J. Chem. Phys. **59**, 5068 (1973).
15. K. D. KING and R. D. GODDARD. Int. J. Chem. Kinet. **7**, 837 (1975).

Microwave spectrum of *trans*-1-methoxy-1,3-butadiene

R. KEWLEY AND S. C. DASS[1]

Department of Chemistry, Queen's University, Kingston, Ont., Canada K7L 3N6

Received May 4, 1977

R. KEWLEY and S. C. DASS. Can. J. Chem. **55**, 3480 (1977).

The microwave spectra of two conformers of 1-methoxy-1,3-butadiene have been studied in the 18 to 40 GHz region. One conformer is the s-*trans* conformer of *trans*-1-methoxy-1,3-butadiene. The other is most likely the corresponding s-*cis* conformer. The rotational constants for the ground vibrational state are (in MHz) s-*trans*: $A = 24\,524(16)$; $B = 1336.51(1)$; $C = 1277.76(1)$; s-*cis*: $A = 12\,642.73(23)$; $B = 1607.61(1)$; and $C = 1439.64(1)$. The centrifugal distortion parameters D_{JK} and D_J have also been determined for each conformer.

For the s-*trans* conformer two series of torsional satellites have been found which are assigned as O—CH torsion with frequency 60(20) cm^{-1} and =C—C= torsion, frequency 80(30) cm^{-1}. For the s-*cis* conformer one series of satellites has been observed, which has been assigned to =C—C= torsion, of frequency 103(30) cm^{-1}.

R. KEWLEY et S. C. DASS. Can. J. Chem. **55**, 3480 (1977).

On a enregistré les spectres microondes de deux conformères du méthoxy-1 butadiène-1,3 dans la région de 18 à 40 GHz. L'un d'eux est le conformère s-*trans* du méthoxy-1 butadiène-1,3 *trans*. L'autre est vraisemblablement le conformère s-*cis* correspondant. Les constantes de rotation pour l'état vibratoire fondamental sont (en MHz) pour le s-*trans*: $A = 24\,524(16)$; $B = 1336.51(1)$; $C = 1277.76(1)$; et pour le s-*cis*: $A = 12\,642.73(23)$; $B = 1607.61(1)$; $C = 1439.64(1)$. Les paramètres de distorsion centrifuge D_{JK} et D_J sont aussi déterminés pour chaque conformère.

On a trouvé pour le conformère s-*trans* deux séries de satellites de torsion auxquelles sont assignées la torsion O—CH de fréquence 60(20) cm^{-1} et la torsion =C—C= de fréquence 80 (30) cm^{-1}. Pour le conformère s-*cis*, on observe une série de satellites à laquelle on attribut la torsion =C—C= de fréquence 103(30) cm^{-1}.

[Traduit par le journal]

Introduction

Recently a number of straight chain methoxy compounds have been studied by microwave spectroscopy. These include methyl ethyl ether (1), chloromethyl ether (2, 3), bromomethyl ether (3), methyl propargyl ether (4), methoxyacetonitrile (5), and 3-methoxypropionitrile (6).

Less work has been done on fairly small molecules of the type in which a methoxy oxygen is attached directly to an unsaturated carbon atom. The only conformer of methoxyethyne, $CH_3OC{\equiv}CH$, is planar except for two of the methyl hydrogens (7) and in methyl formate, $HCOOCH_3$, the O—CH_3 and C=O bonds are *cis* to one another (8). Of all the molecules investigated previously the one which has the greatest structural similarity to 1-methoxy-1,3-butadiene is methyl vinyl ether, $CH_3OCH{=}CH_2$. The conformer observed in the microwave study of this molecule (9) is the one which is structurally analogous to methyl formate, having the CH_3—O bond *cis* to C=C. The gas phase infrared spectrum of methyl vinyl ether (10) also showed the *cis* conformer to be predominant with about 12% *trans* conformer also present. In an infrared study of the molecules $CH_3OCH{=}CHCH_3$ and $CH_3OCH{=}CHC_2H_5$ Owen and co-workers (11) concluded that in the geometric isomer in which the CH_3O and CH_3 (or C_2H_5) are *trans* to one another the situation is like that in methyl vinyl ether, i.e. the conformer with an s-*cis* CH_3O predominates and there is also a less abundant s-*trans* CH_3O conformer. The other isomer, which has CH_3O and CH_3 (or C_2H_5) *cis*, is considered to have a slightly nonplanar s-*trans* structure (11).

The *cis* and *trans* isomers of 1-methoxy-1,3-butadiene have been the subjects of an nmr solution investigation by Diez and Rico (12).

In their study the *trans* and *cis* isomers were synthesized separately, the *cis* by hydrogenation of *cis*-$CH_3OCH{=}CH{-}C{\equiv}CH$ and the *trans* by treatment of crotonaldehyde, $CH_3CH{=}CH{-}CHO$, with methanol. The analysis of the nmr coupling constants data led to the conclusions

[1]Present address: Microwave Technology, 7512 Bath Road, Mississauga, Ont., Canada L4T 1L2.

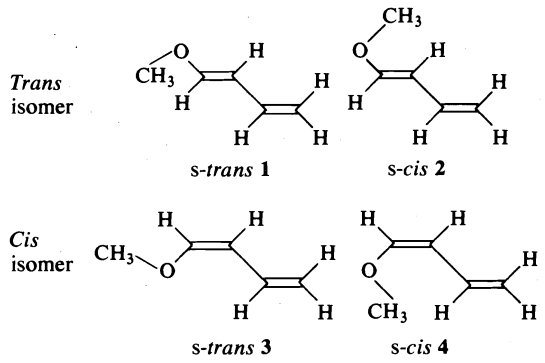

that the preferred conformation of the *trans* isomer is planar s-*cis* (conformer **2**) and that the *cis* isomer has the s-*trans* conformer **3** as its preferred configuration. The corresponding conclusion was reached, by dipole moment studies, for the related molecule 1-methoxy-but-1-ene-3-yne (13).

Because of the relative lack of microwave data on unsaturated methoxy compounds and because of the possibility of comparing the results with those found in a liquid medium by nmr it was considered to be of interest to use the microwave rotational spectrum of 1-methoxy-1,3-butadiene as a means of studying the conformational situation in the vapor state.

Experimental

Three samples of 1-methoxy-1,3-butadiene (technical grade), consisting of 88–95 of the *trans* isomer[2], were purchased on separate occasions from the Aldrich Chemical Company. Even a sample from a freshly opened vial gave strong microwave absorption lines due to *trans*-crotonaldehyde, for which the *a*-type $J = 5 \leftarrow 4$, $6 \leftarrow 5$, $7 \leftarrow 6$, $8 \leftarrow 7$, and $9 \leftarrow 8$ transitions fall within the frequency region studied (14). Although the presence of this strong spectrum caused some initial confusion its overlap with that of the molecule under study was not a serious difficulty, so that it was possible to use the commercial samples throughout without further purification. A few weak lines of methanol were also noticed in the 15–30 GHz region.

The initial work in the 18–26.5 GHz region was carried out at Queen's University using a Hughes-Wilson 100 kHz Stark-modulated spectrometer (15) at both room and dry ice temperatures. Samples pressures between 100 and 200 mTorr and Stark voltages in the range 100 to 2000 V cm^{-1} were used. Later work, in the 26.5 to 40 GHz region, was done using a Hewlett-Packard model 8460A MMR spectrometer in the laboratory of Professor R. F. Curl at Rice University, Houston, TX. All the measurements on this instrument were made at room temperature with pressures of 20–60 mTorr and Stark voltages of 800–2000 V cm^{-1}. The accuracy of the frequency measurements is 0.1 MHz or better. All computations were carried out in double precision arithmetic on the Queen's University Burroughs 6700 computer.

[2]This information was kindly provided by Technical Services, Aldrich Chemical Company, Milwaukee, WI, U.S.A.

Rotational Spectrum

Prediction and Assignments, Ground Vibrational State

As an aid to the initial assignment the rotational constants and spectra were predicted for conformers **1–4**, see Introduction, using structural parameters taken from refs. 5 and 16. The resulting values of $B + C$ and the asymmetry parameter κ are given in Table 1.

It was considered unnecessary to include in these predictions isomers in which the carbon–carbon double bonds are s-*cis* since Carreira[3], in a Raman study, found the s-*cis* configuration of 1,3-butadiene to be 873 cm^{-1} higher in energy than the s-*trans* form.

For conformers **1–4** estimates were also made of the μ_a and μ_b dipole moment components and were based on the observed magnitude and direction of the dipole moment of methyl vinyl ether (9). The estimated values of (μ_a, μ_b) were (in D): **1** (0.07, 0.96); **2** (0.65, 0.72); **3** (0.51, 0.83); **4** (0.95, 0.16).

The *a*-type $J = 9 \leftarrow 8$ and $10 \leftarrow 9$ transitions of conformer **1** were identified on a scan of the 22–26.5 GHz region. The $J = 12 \leftarrow 11$ and $14 \leftarrow 13$ transitions were then examined in detail using the Hewlett-Packard instrument. Only in these transitions was it found possible to make a detailed assignment of the high K_{-1} components. This is because the value of the centrifugal distortion parameter D_{JK} is such as to largely nullify the asymmetry shifts for lines with smaller K_{-1} values. This results in considerable overlapping of lines that would be well resolved for a rigid rotor. Once a satisfactory high K_{-1} assignment had been achieved the $K_{-1} = 1$ lines were identified by using the $(B + C)$, $(A - \frac{1}{2}(B + C))b_p^2$, D_J, and D_{JK} values from the high K_{-1} fit together with the condition that the out-of-plane hydrogen coordinate, c_H, is expected to be close to 0.89 Å. The value in methyl vinyl ether is 0.889 Å (9) and similar values are found in other methoxy compounds (5, 6). In addition a further check on the $K_{-1} = 1$ assignment was made by comparing the resulting A, B, and C values with those obtained from the assumed structure; see also below. The $K_{-1} = 1$ lines

[3]L. A. Carreira, private communication.

TABLE 1. Predicted $B + C$ values (MHz) and Ray's asymmetry parameters for four conformers of 1-methoxy-1,3-butadiene

Conformer[a]	$B + C$	κ
1	2578	−0.995
2	3131	−0.963
3	2998	−0.979
4	4563	−0.761

[a]For the numbering of the conformers, see Introduction.

TABLE 2. Some observed *a*-type transition frequencies (MHz) of *trans*-1-methoxy-1,3-butadiene, s-*trans* conformer (**1**), ground vibrational state

Transition	Observed	Obs. − Calcd.
7(3, 4) ← 6(3, 3)	18 300.30	−0.55
8(4, 4) ← 7(4, 3)	20 915.16	0.06
9(4, 5) ← 8(4, 4)	23 529.76	0.16
10(4, 6) ← 9(4, 5)	26 144.16	0.02
11(0, 11) ← 10(0, 10)	28 732.60	0.87
11(1, 10) ← 10(1, 9)	29 073.33	−0.33
11(1, 11) ← 10(1, 10)	28 427.40	0.11
11(2, 9) ← 10(2, 8)	28 776.60	−0.52
11(2, 10) ← 10(2, 9)	28 753.40	0.81
12(0, 12) ← 11(0, 11)	31 339.60	1.15
12(1, 11) ← 11(1, 10)	31 714.60	−0.29
12(1, 12) ← 11(1, 11)	31 010.50	0.30
12(2, 10) ← 11(2, 9)	31 397.96	0.63
12(2, 11) ← 11(2, 10)	31 365.60	0.14
12(3, 9) ← 11(3, 8)	31 375.48	0.41
12(3, 10) ← 11(3, 9)	31 374.62	−0.18
12(4, 8) ← 11(4, 7)	31 373.45	0.11
12(5, 7) ← 11(5, 6)	31 372.74	−0.16
12(6, 6) ← 11(6, 5)	31 372.90	−0.03
12(7, 5) ← 11(7, 4)	31 373.21	0.00
12(8, 4) ← 11(8, 3)	31 373.66	0.00
12(9, 3) ← 11(9, 2)	31 374.30	0.06
12(10, 2) ← 11(10, 1)	31 375.04	0.10
12(11, 1) ← 11(11, 0)	31 375.87	0.13
14(0, 14) ← 13(0, 13)	36 547.10	−0.60
14(1, 13) ← 13(1, 12)	36 997.00	0.20
14(1, 14) ← 13(1, 13)	36 174.30	−0.64
14(2, 12) ← 13(2, 11)	36 641.61	0.58
14(4, 10) ← 13(4, 9)	36 602.30	−0.45
14(5, 9) ← 13(5, 8)	36 601.58	−0.32
14(9, 5) ← 13(9, 4)	36 603.04	−0.04
14(10, 4) ← 13(10, 3)	36 603.92	0.06
14(11, 3) ← 13(11, 2)	36 604.72	−0.04

however were weak and difficult to assign as Stark lobes were not observed. The assigned transitions of conformer **1** are given in Table 2 and the derived constants in Table 4. The constants given were obtained using the program DLSQF which fits the observed transition frequencies to the asymmetric rotor constants $(A + C)/2$, $(A - C)/2$, and κ and the centrifugal distortion constants D_{JK} and D_J of a slightly asymmetric rotor. Since this program does not yield directly the standard errors in the rotational constants A, B, and C a second fit was carried out as a check and to obtain consistent standard errors. In this fit multiple linear regression was carried out using the known derivatives of the line frequencies with respect to D_{JK} and D_J and the derivatives with respect to A, B, and C, calculated using the rigid rotor frequency prediction program ROTSPE with the values from the DLSQF fit as the initial ones. The second fit gave essentially the same constants as the first. In both fits the centrifugal distortion constant D_K was set equal to zero. Some use was also made of the program CDANAL (written by Dr. W. H. Kirchoff and modified by Dr. R. S. Lowe) for predicting unobserved lines. However, this program was not used in the final fit as for this type of molecule, with very slight asymmetry, a constrained value of τ''_{aaaa} has to be used giving rather dubious values for the other τ coefficients. The absence of observed *b*-type lines for conformer **1**, in spite of the relatively large μ_b component, is due to the large uncertainties (over 100 MHz) attached to the prediction of such lines from the CDANAL program. Also only a few widely spaced *b*-type transitions would be expected to lie in the region studied.

The initial scan also revealed a group of lines near 24.4 GHz which was assignable as the *a*-type $J = 8 \leftarrow 7$ transition of a second conformer. Vibrational satellites are much less in evidence for this conformer. This may be seen on the trace shown in Fig. 1. Work at higher frequencies led to detailed assignments for the $J = 9 \leftarrow 8$,

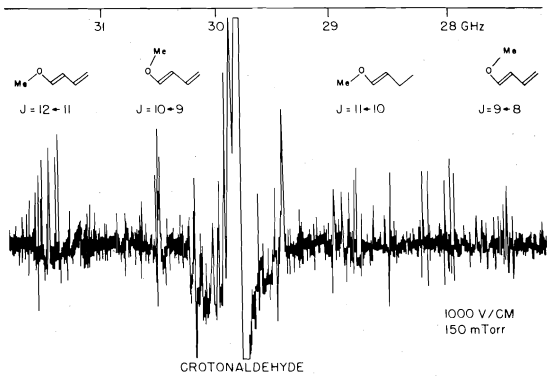

FIG. 1. A trace of the spectrum of *trans*-1-methoxy-1,3-butadiene in the 27 to 32 GHz region, showing the vibrational satellite patterns of the s-*trans* and s-*cis* conformers and the strong absorption due to the presence of crotonaldehyde impurity.

TABLE 3. Some observed *a*-type and *b*-type transition frequencies (MHz) of *trans*-1-methoxy-1,3-butadiene, s-*cis* conformer (**2**), ground vibrational state

Transition	Observed	Obs. − Calcd.	Transition	Observed	Obs. − Calcd.
6(2, 4) ← 5(2, 3)	18 341.10	−0.11	11(5, 6) ← 10(5, 5)	33 541.05	0.06
6(3, 4) ← 5(3, 3)	18 293.63	−0.01	11(6, 5) ← 10(6, 4)	33 535.97	0.09
6(4, 2) ← 5(4, 1)	18 290.16	−0.01	11(7, 4) ← 10(7, 3)	33 533.16	0.05
6(5, 1) ← 5(5, 0)	18 288.85	0.21	11(8, 3) ← 10(8, 2)	33 531.59	−0.01
7(2, 6) ← 6(2, 5)	21 315.75	−0.08	11(9, 2) ← 10(9, 1)	33 530.92	0.09
8(2, 7) ← 7(2, 6)	24 354.72	0.17	11(10, 1) ← 10(10, 0)	33 530.62	0.07
8(2, 6) ← 7(2, 5)	24 511.76	−0.58	12(0, 12) ← 11(0, 11)	36 053.80	−0.02
8(3, 6) ← 7(3, 5)	24 399.42	0.33	12(1, 12) ← 11(1, 11)	35 437.89	−0.11
8(3, 5) ← 7(3, 4)	24 402.29	−0.19	12(1, 11) ← 11(1, 10)	37 426.88	0.03
8(4, 4) ← 7(4, 3)	24 391.08	−0.43	12(2, 11) ← 11(2, 10)	36 480.62	−0.09
8(5, 3) ← 7(5, 2)	24 387.37	−0.31	12(2, 10) ← 11(2, 9)	36 992.16	−0.17
8(7, 1) ← 7(7, 0)	24 384.94	−0.03	12(3, 9) ← 11(3, 8)	36 652.46	0.10
9(0, 9) ← 8(0, 8)	27 200.89	−0.12	12(4, 8) ← 11(4, 7)	36 607.27	0.01
9(1, 9) ← 8(1, 8)	26 616.94	−0.16	12(5, 7) ← 11(5, 6)	36 593.68	0.02
9(1, 8) ← 8(1, 7)	28 122.53	−0.04	12(6, 6) ← 11(6, 5)	36 587.07	0.14
10(0, 10) ← 9(0, 9)	30 167.18	−0.12	12(7, 5) ← 11(7, 4)	36 583.17	−0.07
10(1, 10) ← 9(1, 9)	29 561.19	0.00	12(8, 4) ← 11(8, 3)	36 581.08	−0.07
10(1, 9) ← 9(1, 8)	31 230.23	0.02	12(9, 3) ← 11(9, 2)	36 579.85	−0.17
11(0, 11) ← 10(0, 10)	33 118.21	−0.02	12(10, 2) ← 11(10, 1)	36 579.38	−0.12
11(1, 11) ← 10(1, 10)	32 501.63	0.09	5(1, 5) ← 4(0, 4)	25 110.76	−0.22
11(1, 10) ← 10(1, 9)	34 331.86	−0.07	8(1, 8) ← 7(0, 7)	32 623.70	0.04
11(2, 10) ← 10(2, 9)	33 453.97	−0.12	9(1, 9) ← 8(0, 8)	35 020.90	0.00
11(2, 9) ← 10(2, 8)	33 854.47	−0.06	10(1, 10) ← 9(0, 9)	37 380.90	−0.18
11(3, 9) ← 10(3, 8)	33 567.26	0.13	14(0, 14) ← 13(1, 13)	36 504.20	−0.49
11(4, 7) ← 10(4, 6)	33 551.38	0.04			

10 ← 9, 11 ← 10, and 12 ← 11 transitions. In the case of this conformer the $K_{-1} = 1$ lines were quite easy to assign from an accurate prediction based on the frequencies of the remaining K_{-1} components, no assumptions concerning the value of c_H being needed. The CDANAL program was used to predict a few *b*-type transition frequencies. This allowed an improvement in the accuracy of the *A* rotational constant to be brought about. The observed frequencies and derived constants for this conformer are given in Tables 3 and 4. In the DLSQF fit for this conformer D_K was again set equal to zero because of the small number of *b*-type lines measured and their weak dependence of their frequencies upon D_K.

On the basis of the $B + C$ of 3047.25 MHz and κ value of −0.970 it would not be possible to assign this second conformer unequivocally as conformer **2** or conformer **3**. However it would be surprising to find no observable spectrum from the s-*cis* form of the *trans* isomer when the s-*trans* form has already been detected, since the similar molecule methyl vinyl ether is mainly in the s-*cis* form (9). An additional point is that the two s-*trans* isomers (**1** and **3**), in which the methoxy group is situated rather similarly in each case, might be expected to have rather similar vibrational satellite patterns, mainly as regards intensity, but this is not what is observed; see Fig. 1.

Abundance of Conformers

Because of the rather large *J* values involved in the observed transitions of both conformers and because the spectra are not very intense it has not proved possible to obtain any Stark shift measurements. This makes it difficult to make meaningful estimates of the relative abundances of the conformers **1** and **2**. The small estimated μ_a (0.07 D) for the s-*trans* form is particularly susceptible to large uncertainty. By comparing the intensity of the s-*trans* peak at 36 602.30 MHz, which is assigned as a superposition of the $K_{-1} = 4$, 7, and 8 components of the $J = 14 \leftarrow 13$ transition, with that of the s-*cis* peak at 36 607.27 MHz, assigned as $J = 12 \leftarrow 11$, $K_{-1} = 4$, the intensity ratio was determined as

$$[1] \quad \frac{\text{s-}trans\ (J = 14 \leftarrow 13\ (K_{-1} = 4, 7, 8))}{\text{s-}cis\ (J = 12 \leftarrow 11\ (K_{-1} = 4))} = 1.6$$

The deduction of the relative proportion of the

TABLE 4. Rotational and centrifugal distortion constants of *trans*-1-methoxy-1,3-butadiene, ground vibrational state

Constant[b]	s-*trans* Conformer (**1**)	s-*cis* Conformer (**2**)
A (MHz)	24 524 (16)	12 642.73 (23)
B (MHz)	1 336.51 (1)	1 607.61 (1)
C (MHz)	1 277.76 (1)	1 439.64 (1)
κ	−0.994946 (4)	−0.970015 (1)
D_{JK} (kHz)	−1.70 (5)	−1.75 (4)
D_J (kHz)	0.131 (20)	0.147 (22)
Number of transitions	T 74	100
Standard deviation of fit	0.345	0.178
$I_a + I_b - I_c$ (amu Å^2)	3.221 (20)[a]	3.296 (3)[a]
A'' (MHz)		12 646.07 (100)
B'' (MHz)		1 607.60 (1)
C'' (MHz)		1 439.64 (1)
τ_1 (MHz)		0.00574 (36)
τ_2 (MHz)		0.00106 (34)
τ_3 (MHz), assumed		0.315 (103)
τ''_{aaaa} (MHz)		−14.3 (40)
τ''_{bbbb} (MHz)		−0.000541 (272)
τ''_{cccc} (MHz)		−0.000767 (236)

[a]Conversion factor 505 379.2 MHz amu Å^2 from the constants in ref. 17.
[b]The figure given in parentheses after the value of the constant represents one standard error of the quantity.

two conformers from this ratio is, unfortunately, so highly dependent on the assumptions made in estimating μ_a (s-*trans*) that it is not considered meaningful to quote a precise figure. About all that can be said is that the s-*trans* form is probably between about 50 and 98% in abundance (corresponding to an energy difference E(s-*cis*) − E(s-*trans*) in the range 0 to 8 kJ mol^{-1}). Comparing this result with that of the nmr study (12) indicates that, for the *trans* isomer, the proportion of the s-*trans* conformer increases on going from the liquid solution phase (in TMS) to the vapor phase.

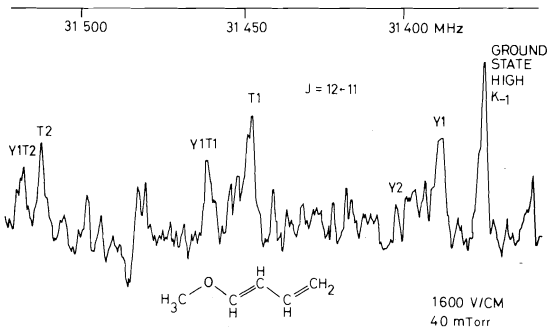

FIG. 2. A trace of a portion of the $J = 12 \leftarrow 11$ transition of the s-*trans* conformer showing some of the torsional satellites.

Vibrational Satellites

In addition to the ground vibrational state spectrum the s-*trans* conformer exhibits two series of vibrational satellites to higher frequency; see Fig. 2. For one series four successive excited states are easily observable. These are designated $T1$–$T4$. Relative intensity measurements on the high K_{-1} bunches in the $J = 11 \leftarrow 10$, $12 \leftarrow 11$, and $14 \leftarrow 13$ transitions yielded a vibrational frequency of 60 ± 20 cm^{-1} for the T series. Two excited states of the second (Y) vibrational motion were assigned and a vibrational frequency of 80 ± 30 cm^{-1} obtained from intensities. The B^* values for these states are given in Table 5 together with the values for two states in which both vibrations are excited. The B^* values for the T series fit the equation (for $T = 1$–4)

$$[2] \quad B_T^* = 2611.01 + (6.865)(T + \tfrac{1}{2}) - (0.350)(T + \tfrac{1}{2})^2$$

indicating a fairly harmonic potential. The T and Y vibrational satellites clearly must be those due to progressive excitation of the torsional motions about the O—CH and =C—C= bonds. The lower frequency (60 cm^{-1}) may be assigned to the O—CH torsion. This is comparable with the O—CH_2 torsional frequencies in methoxyacetonitrile, CH_3OCH_2CN and 3-methoxypropionitrile, $CH_3OCH_2CH_2CN$, which are, re-

TABLE 5. Effective rotational constants B^* (MHz) for the ground and excited vibrational state peaks of s-*trans trans*-1-methoxy-1,3-butadiene

State	B^* [a]
Ground	2614.42
$T1$	2620.56
$T2$	2626.04
$T3$	2630.77
$T4$	2634.86
$Y1$	2615.63
$Y2$	2616.71
$Y1T1$	2621.75
$Y1T2$	2627.08

[a]Obtained by dividing the frequency of the peak of the high K_{-1} group by $J + 1$. $B^* \simeq B + C$.

spectively, 74 ± 32 and 90 ± 17 cm^{-1} (5, 6). These molecules are not exactly analogous to the present one. In methyl vinyl ether the lowest vibration frequency of the molecule, at 219 ± 20 cm^{-1}, was assigned to the O—CH torsional mode (9). However for a molecule of this type in the s-*cis* conformation interaction between the methyl hydrogens and the nearby CH hydrogen should restrict the torsional motion, giving it a relatively high frequency. In s-*trans trans*-1-methoxy-1,3-butadiene the methyl group is situated further away from the closest CH hydrogen and the O—CH torsion is evidently less restricted.

The other frequency (80 cm^{-1}) is assigned to torsion about the =C—C= bond. The frequency is surprisingly low compared to the corresponding one in unsubstituted 1,3-butadiene, of 162 cm^{-1},[3] even though a lower frequency would be expected because of increased mass in the present case.

The only vibrational satellites observed for the s-*cis* conformer were the first and second excited states of a vibration for which the satellites are to the low frequency side of the ground state transition; see Table 6. The intensities yield a frequency of 102 ± 30 cm^{-1}. These excited states ($Y1$ and $Y2$) are assigned as due to =C—C= torsion on account of the proximity in frequency to the value of 80 cm^{-1} for the s-*trans* conformer and also because of the absence of any such low frequency modes in methyl vinyl ether.

For neither of the two observed conformers has an assignment been made of a satellite due to methyl torsion. Possibly this is due to the fact that in a relatively long-chain molecule the

TABLE 6. Observed frequencies (MHz) and relative intensities[a] for vibrational satellites in the $J = 11 \leftarrow 10$ transition of s-*cis trans*-1-methoxy-1,3-butadiene

Transition	Vibrational state: Ground	$Y1$	$Y2$
11(4, 8) ← 10(4, 7)	33 551.38	33 525.7	33 503.1
11(4, 7) ← 10(4, 6)	(1.00)	(0.72)	(0.36)
11(6, 6) ← 10(6, 5)	33 535.97	33 511.4	33 489.9
11(6, 5) ← 10(6, 4)	(1.00)	(0.46)	(0.31)
11(7, 5) ← 10(7, 4)	33 533.06	33 500.4	
11(7, 4) ← 10(7, 3)	(1.00)	(0.55)	
11(8, 4) ← 10(8, 3)	33 531.59	33 506.1	33 485.7
11(8, 3) ← 10(8, 2)	(1.00)	(0.68)	(0.45)
11(9, 3) ← 10(9, 2)	33 530.92	33 505.5	33 485.2
10(9, 2) ← 10(9, 1)	(1.00)	(0.63)	(0.41)

[a]The relative intensity of a vibrational satellite is in each case given with respect to the corresponding ground state peak.

excitation of methyl torsion does not cause enough change in the rotational constants to shift the satellite clear of the corresponding ground state transition. This is more likely to be a cause in the s-*trans* conformer, with its bunched high K_{-1} lines, than in the s-*cis*. If the barrier to internal rotation were 3820 cal mol^{-1} in the s-*cis* conformer, as it is in the structurally similar s-*cis* methyl vinyl ether, then using the equation

$$[3] \qquad V_3 = (8/9)\,\pi^2\,\nu^2\,I_r$$

together with an assumed methyl top moment of inertia $I_\alpha = 3.123$ amu Å^2 and a resulting I_r of 3.088 amu Å^2, calculated from the assumed structure, a value of ν of 256 cm^{-1} is estimated for the frequency of the methyl torsion mode. A similar calculation for the s-*trans* conformer predicts a frequency of 268 cm^{-1}. With a lower assumed barrier of 3000 cal mol^{-1} a value of 237 cm^{-1} is obtained. The barrier is likely to be less in the s-*trans* conformer due to a smaller interaction between the CH_3 group and the nearest CH hydrogen. These considerations serve to confirm that the vibrational satellites already assigned (T and Y for s-*trans*, Y for s-*cis*) are not due to methyl torsion.

Structure Calculations

On the basis of the observed rotational constants of the two conformers estimates have been made of the CCO and COC bond angles in each.

Since the constants are more accurate for the s-*cis* conformer an assumed structure for it was

first set up using data from the molecule methyl formate (8) to established the C—O—CH_3 parameters and from *trans*-1,3-pentadiene for the remainder of the structure (16). This initial structure was

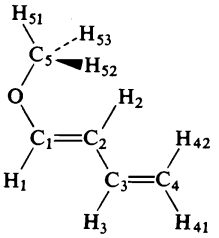

All C—H distances = 1.09 Å, HC_5H angles all 110.67°, $C_1C_2 = C_3C_4 = 1.337$ Å, all HC_5O angles equal, $C_2C_3 = 1.476$ Å, $C_1O = 1.334$ Å, $OC_5 = 1.437$ Å, $\angle H_{41}C_4C_3 = 121.5°$, $\angle H_{42}C_4C_3 = \angle H_1C_1C_2 = 120.5°$, $\angle C_4C_3H_3 = 119°$, $\angle C_2C_3C_4 = 122.9°$, $\angle H_2C_2C_3 = 118.1°$, $\angle H_2C_2C_1 = 119°$, $\angle C_2C_1O = 124.5°$, $\angle C_1OC_5 = 114.8°$.

When the C_2C_1O and C_1OC_5 angles were varied, holding the other parameters constant, a fit to the observed P_a and P_b planar moments of the s-*cis* conformer was achieved at $\angle C_2C_1O = 131.0°$ and $\angle C_1OC_5 = 114.3°$. The increased value of the first angle possibly indicates the effect of the repulsion between H_2 and the methyl group. When 131.0° and 114.3° were used as starting angles for the s-*trans* conformer and these angles were then varied, with other parameters fixed, the P_a and P_b planar moments of the s-*trans* conformer were reproduced when $\angle C_2C_1O = 123.5°$ and $\angle C_1OC_5 = 114.1°$. This appears to be a reasonable result and can be taken as additional confirmation of the correctness of the observed rotational constant of the s-*trans* conformer.

The P_c planar moments for the two conformers, which were kept fixed in the above calculations, are related to the observed moments of inertia and out-of-plane hydrogen coordinates by

$$[4] \quad P_c = (1/2)(I_a + I_b - I_c) = 2m_H c_H^2$$

The values of $I_a + I_b - I_c$ from Table 4 give a c_H coordinate of 0.894 ± 0.003 Å for the s-*trans* conformer and one of 0.904 ± 0.001 Å for the s-*cis* conformer. These values may be compared with that for the c_H coordinate in methyl vinyl ether (9), which is 0.889 Å, and with the values in *trans*- and *cis*-1,3-pentadiene (16) which are respectively 0.900 and 0.905 Å.

Acknowledgements

The authors are greatly indebted to Professor R. F. Curl of Rice University for the use of his Hewlett-Packard spectrometer and for helpful suggestions. Support for the study was provided by grant number A-2046 from the National Research Council of Canada. Dr. R. S. Lowe gave valuable help with the computer programs.

1. M. Hayashi and K. Kuwada. J. Mol. Struct. **28**, 147 (1975).
2. T. Ikeda, R. F. Curl, Jr., and H. Karlsson. J. Mol. Spectrosc. **53**, 101 (1974).
3. M. Hayashi, K. Kuwada, and H. Imaishi. Chem. Lett. 913 (1974).
4. K.-M. Marstokk and H. Møllendal. J. Mol. Struct. **32**, 191 (1976).
5. R. Kewley. Can. J. Chem. **52**, 509 (1974).
6. R. S. Lowe and R. Kewley. J. Mol. Spectrosc. **63**, 216 (1976).
7. D. Den Engelsen, H. A. Dijkerman, and J. Kerssen. Recl. Trav. Chim. **84**, 1357 (1965).
8. R. F. Curl, Jr. J. Chem. Phys. **30**, 1529 (1959).
9. P. Cahill, L. P. Gold, and N. L. Owen. J. Chem. Phys. **48**, 1620 (1968).
10. N. L. Owen and N. Sheppard. Trans. Faraday Soc. **60**, 634 (1964).
11. S. W. Charles, F. C. Cullen, and N. L. Owen. J. Mol. Struct. **18**, 183 (1973).
12. E. Diez and M. Rico. J. Mol. Spectrosc. **37**, 131 (1971).
13. R. M. LeQuan and M. P. Simonnin. C. R. Acad. Sci., Ser. C, **265**, 125 (1967); **266**, 825 (1967).
14. M. Suzuki and K. Kozima. Bull. Chem. Soc. Jpn. **42**, 2183 (1969).
15. R. Kewley. Can. J. Chem. **50**, 1690 (1972).
16. S. L. Hsu and W. H. Flygare. J. Chem. Phys. **52**, 1053 (1970).
17. E. R. Cohen and B. N. Taylor. J. Phys. Chem. Ref. Data, **2**, 663 (1973).

Preparation and Mössbauer spectra of organotin(IV) compounds containing the $CH_3(C_6H_5)Sn(IV)$ moiety

T. K. SHAM, J. S. TSE, V. WELLINGTON, AND G. M. BANCROFT

Department of Chemistry, The University of Western Ontario, London, Ont., Canada N6A 5B7

Received May 3, 1977

T. K. SHAM, J. S. TSE, V. WELLINGTON, and G. M. BANCROFT. Can. J. Chem. **55**, 3487 (1977).

The synthesis and Mössbauer spectra of 16 organotin compounds of the type $MePhSnX_2$ (X = F, Cl), $[Et_4N]MePhSnCl_3$, $MePhSnCl_2L_2$ (L = oxygen and nitrogen neutral donor ligands), and $MePhSnL_2'$ (L' = acetylacetonates and 8-hydroxyquinolate) are reported. The Mössbauer quadrupole splittings (qs) are used to assign the structures of the complexes. The $MePhSnX_2$ (X = F, Cl) compounds have similar structures to their Me_2Sn analogues, while the six-coordinate complexes show a greater structural similarity to their Ph_2Sn analogues. Thus $MePhSnF_2$ is a highly associated structure like Me_2SnF_2 with a six-coordinate Sn atom; while the $MePhSnL_2'$ complexes have the *cis* structure like their Ph_2Sn analogues. The structures of the six-coordinate organotin complexes are rationalized using steric calculations and the known bonding properties of the ligands. The quadrupole splittings and centre shifts (cs) are also used to suggest variations in ligand bonding properties, and to discuss variations in C—Sn—C angles from the MePhSn complexes to their Ph_2Sn analogues.

T. K. SHAM, J. S. TSE, V. WELLINGTON et G. M. BANCROFT. Can. J. Chem. **55**, 3487 (1977).

On présente la synthèse et les spectres Mössbauer de 16 composés organostanniques de types $MePhSnX_2$ (X = F, Cl), $[Et_4N]MePhSnCl_3$, $MePhSnCl_2L_2$ (L = ligand neutre ayant un oxygène ou azote donneur), et $MePhSnL_2'$ (L' = acétylacétonate et hydroxy-8 quinolate). Les dédoublements quadrupolaires (dq) tirés des spectres Mössbauer sont utilisés pour déterminer la structure des complexes. Les composés $MePhSnX_2$ (X = F, Cl) ont une structure similaire à leurs analogues Me_2Sn alors que les complexes hexacoordonnés montrent une plus grande similarité structurale à leurs analogues Ph_2Sn. Le composé $MePhSnF_2$ a une structure très associée comme Me_2SnF_2 et possède un atome Sn hexacoordonné; tandis que les complexes $MePhSnL_2'$ possèdent une structure *cis* comme leurs analogues Ph_2Sn. Les structures des complexes organostanniques hexacoordonnés sont rationalisées en faisant appel à des calculations stériques et des propriétés liantes déjà connues pour ces ligands. Les dédoublements quadrupolaires ainsi que le centre des déplacements (cd) sont aussi utilisés pour expliquer les variations des propriétés liantes du ligand et de discuter les variations des angles C—Sn—C lorsqu'on passe des complexes MePhSn à leurs analogues Ph_2Sn.

[Traduit par le journal]

Introduction

The stereochemistry of diorganotin compounds has been a subject of recent interest (1–3). The variable C—Sn—C angle in Me_2Sn compounds has been rationalized using ligand–ligand repulsion calculations (2), and the Mössbauer quadrupole splittings (qs) are useful for estimating this angle (1, 3). However, the stereochemical preference of *trans* and *cis* configurations in six-coordinate dimethyl and diphenyl compounds is not clearly understood. Accumulated X-ray structures (1, 3, 4) of dimethyl tin compounds indicate that with the exception of $Me_2Sn(oxin)_2$ (5) [oxin = anion of 8-hydroxyquinoline] and $Me_2Sn(ONHCOMe_2)$ (6), all the six-coordinate dimethyl tin compounds have the *trans* or distorted *trans* configurations. By contrast, Mössbauer data (7, 8) strongly suggest that all the diphenyl compounds with chelating ligands have the *cis* configuration. This *trans–cis* difference is manifested in the study of diorganotin acetylacetonates (8). All the dimethyl tin acetylacetonates are *trans*, whereas all the corresponding diphenyl compounds are *cis*. It is also interesting that while Me_2SnF_2 (9) is six coordinate with a linear Me—Sn—Me group and Me_2SnCl_2 (10) forms an associated compound, Ph_2SnCl_2 (11) is a monomer in the solid state.

The above differences in Me_2Sn and Ph_2Sn compounds make structural studies of MePhSn-(IV) compounds very desirable, but only a few MePhSn compounds have been previously prepared (12, 13), and the ^{119}Sn Mössbauer spectra of only two compounds have been recorded (13). The previous preparations of

TABLE 1. Melting points and analytical data

Compound[a]	Melting point (°C)	Found (calculated) (%) C	H
$MePhSnF_2$	>300	32.5(33.8)	3.1(3.2)
$MePhSnCl_2$	45.5	29.7(29.8)	2.8(2.9)
$[Et_4N]$ $[MePhSnCl_3]$	>200 decomp.	40.5(40.3)	6.6(6.3)
$MePhSnCl_2py_2$	>200	45.4(46.4)	4.1(4.1)
$MePhSnCl_2$bipy	189–192	46.8(46.6)	3.7(3.7)
$MePhSnCl_2$phen	246–248	50.6(49.2)	3.9(3.9)
$MePhSnCl_2(Ph_3PO)_2$	120–121	61.8(61.6)	4.7(4.6)
$MePhSnCl_2(dmso)_2$	105–106	30.4(30.2)	4.5(4.6)
$MePhSnCl_2(HMPA)_2$	79–82	35.4(35.7)	6.6(6.9)
$MePhSnCl_2$(bipyo)	173	43.7(43.2)	3.5(3.8)
$MePhSnCl_2$(opo)	228–229	54.9(55.1)	4.3(4.3)
$MePhSnCl_2$(diphoso)	219–220	55.7(55.5)	4.5(4.5)
$MePhSn(BzBz)_2$	157	41.1(40.0)	6.7(6.0)
$MePhSn(oxin)_2$	210–213	60.1(59.9)	4.1(4.4)

[a]The $MePhSn(AcAc)_2$ and $MePhSn(BzAc)_2$ compounds could not be prepared analytically pure (see text). Abbreviations used stand for: py = pyridine; bypy = 1,1′-bipyridine; phen = 1,10-phenanthroline; dmso = Me_2SO; HMPA = $(Me_2N)_3PO$; bipyo = 2,2′bipyridine *N*′,*N*-dioxide; opo = methylenebis (diphenylphosphine oxide); diphoso = ethylenebis (diphenylphosphine oxide); BzBz = anion of dibenzoylmethane; oxin = anion of 8-hydroxyquinoline; AcAc = anion of acetylacetone; BzAc = anion of benzoylmethane.

MePhSn compounds, and the very similar bonding properties of Me and Ph from Mössbauer partial quadrupole splittings (pqs) (8, 14–18), strongly suggested that a large number of MePhSn compounds could be prepared. In this study, we report the preparation and Mössbauer parameters of 16 compounds of the type $MePhSnX_2$ (X = F, Cl), $[Et_4N]$ $MePhSnCl_3$, $MePhSnCl_2L_2$ (L = nitrogen or oxygen donor), and $MePhSnL_2'$ (L′ = anion of acetylacetonates and 8-hydroxyquinoline). The structures of these compounds are assigned using the ^{119}Sn Mössbauer quadrupole splittings. Our results show that the stereochemical behaviour of MePhSn(IV) and Ph_2Sn(IV) units are similar in six-coordinate Sn(IV) compounds, and that the relatively bulky phenyl group plays an important stereochemical role in both types of complexes.

Experimental

All the reagents are commercially available or prepared with well established techniques (16). The starting material, $MePhSnCl_2$, was prepared by reacting Me_4Sn with $PhSnCl_3$ as described by Kuivila *et al.* (12). Reactions (13, 16) described previously in preparing analogous Me_2Sn(IV) and Ph_2Sn(IV) compounds were used with slight modification. All the compounds appear to be air stable although most of them were prepared under a dry N_2 atmosphere. Yields are always excellent (>90%) except in the cases of $MePhSnL_2'$ compounds (L_2' = acetylacetonates) where oily products make the separation of the pure product difficult (L_2' = AcAc, BzAc). We were, however, able to crystallize $MePhSn(BzBz)_2$ as light yellow needles.

The new compounds were characterized by spectroscopic techniques (ir, nmr, and Mössbauer), melting points, and elemental analyses (Table 1). Typical preparative procedures are as follows:

(*i*) $[Et_4N]$ $[MePhSnCl_3]$: $MePhSnCl_2$ (0.27 g) was dissolved in a minimum amount of ethyl alcohol. Dried tetraethylammonium chloride (0.17 g) was added to the solution. Crystallization of the product was obtained after the solvent was evaporated under reduced pressure. Recrystallization was from alcohol. The yield was quantitative.

(*ii*) $MePhSn(oxin)_2$: $MePhSnCl_2$ (0.56 g) was dissolved in a minimum amount of alcohol. 8-Hydroxylquinoline (0.58 g) was added, and the solution was neutralized with aqueous ammonia. The yellow precipitate was collected through suction filtration. Yield ~90%.

(*iii*) $MePhSn(BzBz)_2$: TlBzBz (0.64 g) was dissolved in 20 ml of benzene. $PhMeSnCl_2$ (0.21 g) was added, and the solution was stirred under nitrogen for an hour. The TlCl was filtered off, and the excess solvent was evaporated under vacuum. The oily residue was dissolved in hexane, and the yellow crystals of $MePhSn(BzBz)_2$ were collected.

Mössbauer spectra were recorded at 110 K for all the compounds. A 10 mCi $BaSnO_3$ source was used for ^{119}Sn spectra. The spectrometer was calibrated using a 99.99% Fe foil. All the spectra were fitted to Lorentzian line shapes using methods described previously (8, 19). The magnetic spectrum of $MePhSn(BzBz)_2$ (Fig. 1) was obtained at the PCMU Harwell.

Nuclear magnetic resonance spectra of MePhSn(IV) compounds, with sufficient solubility in organic solvents, were obtained using T60 and HA 100 spectrometers. The chemical shifts and coupling constants are given in Table 2. Infrared spectra were obtained using a Perkin-Elmer 621 spectrometer.

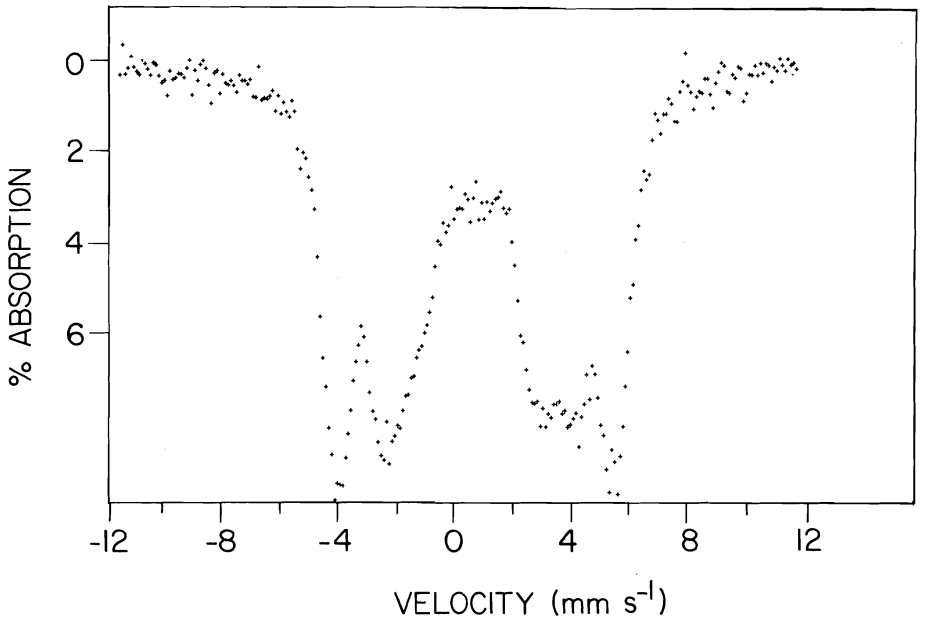

FIG. 1. ^{119}Sn Mössbauer spectrum of *cis*-MePhSn(BzBz)$_2$ taken at 4 K in a magnetic field of 6 T.

Results and Discussion

(*1*) *Chemistry*

The compounds reported in this study were prepared using the following well documented reactions (16):

[1] $MePhSnCl_2 + L_2 \rightarrow MePhSnCl_2L_2$

where L = neutral nitrogen or oxygen ligands.

[2] $MePhSnCl_2 + 2TlL' \rightarrow MePhSnL_2 + 2TlCl$

where L′ = AcAc, BzAc, BzBz.

[3] $MePhSnCl_2 + 2H\ oxin \rightarrow MePhSn(oxin)_2 + 2HCl$

[4] $MePhSnCl_2 + Et_4NCl \rightarrow [Et_4N]\,[MePhSnCl_3]$

These reactions yield the desired products readily except in eq. 2 where reactions between $MePhSnCl_2$ and the thallium salts seem to be less smooth than those reported previously for Me_2SnCl_2 and Ph_2SnCl_2 (8, 17). Oily products always result from reaction 2. We had difficulty in isolating the $MePhSn(AcAc)_2$ and $MePhSn(BzAc)_2$ from the oily substance. The Mössbauer spectra of these two compounds are however very good, and indicate no visible Sn impurity.

(*2*) *Structure and Bonding from Mössbauer Spectra*

(*a*) *Structure from Quadrupole Splittings*

The Mössbauer parameters for the MePhSn compounds are given in Tables 3 and 4 along with those for the corresponding Me_2Sn and Ph_2Sn compounds. It is immediately apparent that all the $MePhSnCl_2L_2$ adducts have qs values in the 4 mm s^{-1} range, while the $MePhSnL_2'$ compounds (L′ = AcAc, BzAc, BzBz, and oxin) have qs values in the 2 mm s^{-1} range. As discussed previously (18, 19), these results strongly indicate that all the $MePhSnCl_2L_2$ compounds have *trans*-C—Sn—C structures whereas the $MePhSnL_2'$ compounds have *cis* structures.

The *cis* structure occurring in the $MePhSnL_2'$ compounds is particularly interesting, since the analogous compounds Me_2SnL_2' and Ph_2SnL_2' have the *trans* and *cis* configurations respectively. These configurations are consistent with the

TABLE 2. Nuclear magnetic resonance data of $RR'SnCl_2$ and $RR'SnL_2'$ (R = Me, R′ = Ph, L′ = BzBz and oxin)

Compound	τ	$^2J_{CH_3-^{119}Sn}$ (Hz)
$MePhSnCl_2$[a]	8.62	70.5
cis-$MePhSn(BzBz)_2$[a]	9.03	83.0
cis-$MePhSn(oxin)_2$[a]	9.28	82.0
Me_2SnCl_2[b]	8.76–8.85	69.0–70.0
trans-$Me_2Sn(BzBz)_2$[c]	9.50	97.2
cis-$Me_2Sn(oxin)_2$[b]	9.56	71.2

[a]This work; solvent $CDCl_3$ with TMS as reference.
[b]Reference 16.
[c]Reference 8.

TABLE 3 Mössbauer parameters of $RR'Sn(IV)Cl_2L_2$ complexes (mm s^{-1}, ± 0.03 mm s^{-1})[a]

Compound	Me_2Sn[a]		MePhSn[b]		Ph_2Sn[a]	
	cs	qs	cs	qs	cs	qs
$RR'SnF_2$	1.33	4.38	1.32	4.44	1.28	3.43
$RR'SnCl_2$	1.56	3.55	1.44	3.11	1.38	2.82
$RR'SnCl_3^-$	1.40	3.30	1.28	2.95	1.25	2.62
$RR'SnCl_2py_2$	1.37	3.92	1.30	3.66	1.32	3.39
$RR'SnCl_2$bipy	1.46	4.09	1.26	3.75	1.26	3.45
$RR'SnCl_2$phen	1.32	4.03	1.34	3.74	1.21	3.37
$RR'SnCl_2(Ph_3PO)_2$	1.37	4.30	1.36	3.99	—	—
$RR'SnCl_2(dmso)_2$	1.40	4.13	1.33	3.86	1.23	3.54
$RR'SnCl_2(HMPA)_2$	1.32	4.28	1.31	3.97	—	—
$RR'SnCl_2$(bipyo)	1.39	4.08	1.30	3.69	1.28	3.49
$RR'SnCl_2$(opo)	1.44	4.32	1.30	3.67	1.27	3.78
$RR'SnCl_2$(diphoso)	1.27	4.19	1.38	4.24	1.26	3.65

[a]From refs. 7, 8, 14, and 15.
[b]This work. All measurements at 110 K. Centre shifts are quoted relative to $BaSnO_3$.

TABLE 4. Mössbauer parameters of $RR'Sn(IV)L_2'$ (R,R′ = Me,Ph) (mm s^{-1})

Compound	Centre shift	Quadrupole splitting	Reference
trans-$Me_2Sn(AcAc)_2$	1.16	+4.02	8
trans-$Me_2Sn(BzAc)_2$	1.06	+3.87	8
trans-$Me_2Sn(BzBz)_2$	1.18	+4.08	8
cis-$Me_2Sn(oxin)_2$	0.88	+2.02	27
cis-$MePhSn(AcAc)_2$	0.62	1.81	This work[a]
cis-$MePhSn(BzAc)_2$	0.59	1.75	This work[a]
cis-$MePhSn(BzBz)_2$	0.63	+1.89	This work[a]
cis-$MePhSn(oxin)_2$	0.82	1.76	This work[a]
cis-$Ph_2Sn(AcAc)_2$	0.71	2.07	8
cis-$Ph_2Sn(BzAc)_2$	0.73	2.23	8
cis-$Ph_2Sn(BzBz)_2$	0.73	2.15	8
cis-$Ph_2Sn(oxin)_2$	0.68	+1.69	27

[a]Uncertainty (± 0.03 mm s^{-1}). Measurement at 110 K. Centre shifts are all quoted relative to $BaSnO_3$.

donor properties of Me and Ph, and our steric calculations (20) based on the ligand–ligand repulsion arguments introduced by Kepert (2) and steric angle calculations introduced by Zahrobsky (21). For any $RR'SnL_2'$ structure (R,R′ = Me or Ph), the *cis* structure is always favoured sterically (2, 20), with the *cis* preference increasing in the order $Me_2SnL_2' < MePhSnL_2' < Ph_2SnL_2'$. The *trans* configurations in Me_2SnL_2' (L′ = AcAc, BzAc, BzBz) can be attributed to the small differences in the *cis–trans* repulsive energies (20), and the electronic effect of the two methyl groups. Since the methyl group is a very good donor, and tends to acquire most of the tin 5*s* character (Bent's rule (22)), a linear C—Sn—C structure results. If the methyl group(s) is (are) replaced by a poorer σ donor (e.g. chloride or phenyl), the *cis*-structure becomes more favourable for both steric and electronic reasons. The *cis*-Ph_2Sn (8, 18) and Cl_2Sn (23, 24) structures are consistent with this argument. Our calculations (20) indicate that the C—Sn—C angle in MePhSn compounds should be smaller than those in the analogous Ph_2Sn compounds. Consistent with these steric calculations, the qs and cs for the MePhSn acetylacetonates are smaller than those for the analogous Ph_2Sn compounds (Table 4, and see next section for discussion).

The qs values for $MePhSnF_2$ and $MePhSnCl_2$ show that the former compound has an associated six-coordinate Me_2SnF_2 structure (9); while the latter compound has a very weakly associated structure intermediate between the

TABLE 5. Observed and calculated quadrupole splittings (mm s^{-1})

Type	L (or L′)	Quadrupole splitting	
		Observed	Calculated[a]
$MePhSnL_2$'[b]	AcAc	1.81	−1.92
	BzAc	1.75	−1.86
	BzBz	+1.89	−1.96
	oxin	1.76	−1.88
$MePhSnCl_2L_2$[c]	py	3.66	+3.76
	bipy/2	3.75	+3.88
	phen/2	3.74	+3.80
	Ph_3PO	3.99	+4.14
	dmso	3.86	+4.18
	HMPA	3.97	+4.12
	bipyo/2	3.69	+3.90
	opo/2	3.67	+4.16
	diphoso/2	4.24	+4.10

[a]Using the pqs values in refs. 8, 14, and 15, and the electric field gradient expressions in ref. 7.
[b]*cis* structures.
[c]*trans*-Me-Sn-Ph and *cis*-Cl-Sn-Cl moieties.

weakly associated Me_2SnCl_2 (10) structure and the unassociated Ph_2SnCl_2 (11) structure.

(*b*) *Application of Partial Quadrupole Splitting Values in the MePhSn(IV) System*

The quadrupole splittings for the MePhSn complexes can be used once again to test the validity of the additive model (7, 19, 25). It is immediately apparent from additive model expressions (7, 19, 25) that the qs for a *trans*-MePhSn compound (C—Sn—C angle = 180°) should be midway between the qs values for the analogous *trans*-MeSn and *trans*-Ph_2Sn analogues. The results in Table 3 show that most of the MePhSn compounds have qs midway between the two analogues. The exceptions (e.g. $RR'SnCl_2$(opo) and $RR'SnCl_2$(diphoso) in Table 3) may be due to the different degrees of distortion of the C—Sn—C moiety between the three types of organotin complexes.

Using the pqs values in refs. 8, 14, and 15, the calculated qs for the *trans* compounds are compared with the observed values in Table 5. The agreement is generally good, although the calculated qs values are larger (with one exception) than the observed qs. This trend has already been observed in the corresponding $Me_2SnCl_2L_2$ and $Ph_2SnCl_2L_2$ systems studied previously (15). This trend is due either to a distortion of the C—Sn—C bond angle, or to a slight change of bonding properties of the ligands from $R_2SnL_4^{2+}$ compounds to the $R_2SnCl_2L_2$ compounds.

It is also interesting to compare the qs values of the *trans*-$RPhSnCl_2$ phen compounds (R = Me, Ph, and $Mn(CO)_5$, with qs = 3.74, 3.37, and 3.25 mm s^{-1}, respectively (26)). This trend is entirely consistent with the pqs values derived for these ligands (26), and confirms the σ donor series, Me > Ph > $Mn(CO)_5$.

Considering the *cis* compounds (Tables 4 and 5), it is apparent that the MePhSn compounds have smaller qs values than their Ph_2Sn analogues. Also, the calculated *cis*-MePhSn |qs| are in good agreement with the observed Ph_2Sn qs values (8). Because $(pqs)_{Me} > (pqs)_{Ph}$, the smaller MePhSn qs are perhaps surprising. However, the trend is consistent with the repulsion calculations described above: the C—Sn—C bond angle in the MePhSn compounds is closer to 90° than in the Ph_2Sn analogues, and a smaller qs results (1).

We had hoped that the proposed smaller C—Sn—C angle in the MePhSn compounds would lead to the first negative *cis*-^{119}Sn qs (27), but the observed sign for *cis*-$MePhSn(BzBz)_2$ is still positive ($\eta \simeq 0.5$). This result, combined with recent ^{121}Sb Mössbauer results[1] and our steric calculations (20), shows that the chelates are important in determining the C—Sn—C angle and/or contribute substantially to the electric field gradient themselves. X-ray determinations of *cis*-Ph_2Sn and *cis*-MePhSn compounds are now needed.

[1]A negative ^{121}Sb qs has been observed in *cis*-Ph_2SbCl_2(oxin) (28) which has only one chelating ligand. The C—Sb—C angle is thus probably less than 109.5° (27).

(*c*) *Centre Shifts and Bonding*

Centre shift (cs) values (Table 3) show that all the *trans*-MePhSn compounds have similar cs values ($\sim$1.3 mm s^{-1}) to the Me_2Sn and Ph_2Sn compounds. The general order of cs (Me_2Sn > MePhSn > Ph_2Sn) is consistent with the pqs values for Me and Ph, which show that Me is a better donor than Ph and/or that the Me C—Sn bond has a higher *s* character than the Ph C—Sn bond. These similar cs values also indicate that the bonding properties of Me and Ph (and thus the C—Sn—C angle) do not vary substantially from the *trans*-MePhSn compounds to their Me_2Sn and Ph_2Sn analogues.

The *cis*-$MePhSnL_2'$ complexes (like other *cis*-R_2Sn compounds) have considerably lower cs values than their *trans*-Me_2Sn analogues, due to the lower Sn 5*s* character in the Sn—C bonds in the *cis* position (7, 8, 25). The nmr coupling constant $^2J_{CH_3-^{119}Sn}$ of *cis*-$MePhSn(BzBz)_2$ (83 Hz) compared with the *trans*-$Me_2Sn(BzBz)_2$ value (97.2 Hz) is entirely consistent with these differences in cs and *s* character arguments (16).

From the above *trans*-R_2Sn cs values and the known donor properties of Me and Ph, it is perhaps surprising that the cs values for *cis*-$MePhSnL_2'$ (L' = AcAc, BzAc, BzBz) are consistently *smaller* than those for the corresponding Ph_2Sn compounds (Table 4). This trend can be readily rationalized if the C—Sn—C bond angle in the MePhSn compounds is smaller than that in their Ph_2Sn analogues, as previously suggested by the steric calculations and the qs values. The Sn 5*s* character in the Sn—C bonds in the MePhSn compounds would be smaller than in the Ph_2Sn compounds, and a lower cs for the MePhSn compounds would result. If our conclusions are correct, the MePhSn compounds violate Bent's rule. Thus, the Me—Sn bond in MePhSn compounds does not have a higher Sn 5*s* character than the Ph—Sn bond in Ph_2Sn compounds. Ligand–ligand repulsion effectively forces this situation (20).

The relative cs (and qs) values for the *cis*-$R_2Sn(oxin)_2$ (R = Me, Ph) are consistent with the above argument. The chelate ligand oxin has a substantially smaller bite than the AcAc ligands, and ligand–ligand repulsion will not be as important for the oxin compounds. Due to the normal electronic effect of the Me group to maximize Sn 5*s* density in its C—Sn bond, the C—Sn—C bond angle probably increases in the order Ph_2Sn < MePhSn < Me_2Sn in the oxin compounds. The normal trend in cs (and qs) for the oxin compounds is thus not surprising.

Finally, it is interesting (and puzzling) that the cs of the four-coordinate Sn(IV) compounds (such as $MePhSnCl_2$) have substantially larger cs values than the six-coordinate complexes. Similar trends have been observed previously (7, 25). This trend is not expected on *s* character arguments, which are supported by proton and ^{13}C nmr results (16, 29). Thus, the *s* character in R—Sn bonds in tetrahedral structures (sp^3 hybridized Sn) should be less than in R—Sn bonds in *trans*-R_2SnL_2' structures (*sp* hybridized Sn for the C—Sn bonds). Also, the bond lengths in four coordinate Me—Sn compounds are, if anything, larger than those in six coordinate Me—Sn compounds. Thus, there is no evidence that the R groups in tetrahedral compounds are better donors than in octahedral compounds. On both hybridization and bond length criteria, we would expect the tetrahedral compounds to have a *smaller* cs than the octahedral compounds.

Acknowledgement

We are grateful to the National Research Council of Canada for financial support.

1. T. K. Sham and G. M. Bancroft. Inorg. Chem. **14**, 2281 (1975) and references cited therein.
2. D. L. Kepert. J. Organomet. Chem. **107**, 49 (1976); Private communication.
3. P. G. Harrison. In Organotin compounds: new chemistry and applications. *Edited by* J. J. Zuckerman. ACS Advances in Chemistry, No. 157. 1977.
4. B. K. Y. Ho and J. J. Zuckerman. J. Organomet. Chem. **49**, 1 (1973).
5. E. O. Schlemper. Inorg. Chem. **6**, 2012 (1967).
6. P. G. Harrison, T. J. King, and R. C. Phillips. J. Chem. Soc. Dalton Trans. 2317 (1976).
7. G. M. Bancroft and R. H. Platt. Adv. Inorg. Chem. Radiochem. **15**, 59 (1972).
8. G. M. Bancroft and T. K. Sham. Can. J. Chem. **52**, 1361 (1974).
9. E. O. Schlemper and W. C. Hamilton. Inorg. Chem. **5**, 995 (1966).
10. A. G. Davies, H. J. Milledge, D. C. Puxley, and P. J. Smith. J. Chem. Soc. A, 2862 (1970).
11. P. T. Greene and R. F. Bryan. J. Chem. Soc. A, 2549 (1971).
12. H. G. Kuivila, R. Sommer, and D. C. Green. J. Org. Chem. **33**, 1119 (1968).
13. M. Gielen and J. Topart. Bull. Soc. Chim. Belg. **84**, 13 (1975).
14. M. G. Clark, A. G. Maddock, and R. H. Platt. J. Chem. Soc. Dalton Trans. 281 (1972).
15. G. M. Bancroft, V. G. Kumar Das, and K. D. Butler. J. Chem. Soc. Dalton Trans. 2355 (1974).
16. R. C. Poller. Chemistry of organotin compounds.

Academic Press, New York, NY. 1970; and references cited therein.
17. W. H. NELSON and D. F. MARTIN. J. Inorg. Nucl. Chem. **27**, 89 (1965); A. L. ALLRED and D. W. THOMPSON. Inorg. Chem. **7**, 196 (1968).
18. B. W. FITZSIMMONS, N. T. SEELEY, and A. W. J. SMITH. Chem. Commun. 390 (1965); J. Chem. Soc. A, 143 (1969).
19. G. M. BANCROFT. Mössbauer spectroscopy: an introduction for inorganic chemists and geochemists. McGraw-Hill, Maidenhead, England. 1973.
20. T. K. SHAM, J. TSE, and G. M. BANCROFT. To be published.
21. R. F. ZAHROBSKY. J. Am. Chem. Soc. **93**, 3313 (1971).
22. H. A. BENT. J. Inorg. Nucl. Chem. **19**, 43 (1961).
23. E. O. SCHLEMPER. Private communication. *Cited in* G. A. Miller and E. O. Schlemper. Inorg. Chem. **12**, 677 (1973).
24. P. G. HARRISON, T. J. KING, and J. A. RICHARDS. J. Chem. Soc. Dalton Trans. 1414 (1976).
25. R. V. PARISH. Prog. Inorg. Chem. **15**, 101 (1972).
26. G. M. BANCROFT and T. K. SHAM. J. Chem. Soc. Dalton Trans. 467 (1976).
27. R. V. PARISH and C. E. JOHNSON. J. Chem. Soc. A, 1906 (1971).
28. J. N. R. RUDDICK and J. R. SAMS. Inorg. Nucl. Chem. Lett. **11**, 229 (1975).
29. T. N. MITCHELL. J. Organomet. Chem. **59**, 189 (1973).

Canadian Journal of Chemistry

Published by
THE NATIONAL RESEARCH COUNCIL OF CANADA

Volume 55 Number 20 October 15, 1977

Journal canadien de chimie

Publié par
LE CONSEIL NATIONAL DE RECHERCHES DU CANADA

Volume 55 numéro 20 15 octobre 1977

Comparison of the charge distributions and barriers to ring inversion of protonated eucarvone and its boron trihalide adducts[1]

RONALD F. CHILDS[2] AND YEE-CHEE HOR
Department of Chemistry, McMaster University, Hamilton, Ont., Canada L8S 4M1

Received April 6, 1977

RONALD F. CHILDS and YEE-CHEE HOR. Can. J. Chem. **55**, 3495 (1977).

The protonation and formation of the boron trifluoride, trichloride, and tribromide adducts of eucarvone, **1**, are described. Examination of the nmr and uv spectra of these systems showed that in each case the proton or Lewis acid was bonded to the carbonyl oxygen of **1**. From the various ^{13}C chemical shifts of the Lewis acid adducts of **1**, it is concluded that there is significantly less positive charge induced on the dienylic part of these molecules than is found with protonated **1**. All of these cationic systems undergo a ring inversion process, the barriers of which are about 1 kcal/mol greater than that reported for the comparable inversion of **1**.

RONALD F. CHILDS et YEE-CHEE HOR. Can. J. Chem. **55**, 3495 (1977).

On décrit la protonation ainsi que l'addition du trifluorure, trichlorure et tribromure de bore sur l'eucarvone **1**. L'examen des spectres rmn et uv de ces systèmes montre que, dans chaque cas, le proton ou acide de Lewis est lié à l'oxygène du groupe carbonyle de l'eucarvone **1**. En se basant sur les différents déplacements chimiques du ^{13}C obtenus pour les adduits des acides de Lewis sur **1**, il apparaît que la charge positive induite sur la partie diénylique de ces molécules est plus petite que celle observée pour la forme protonée de **1**. Tous ces systèmes cationiques subissent une inversion de cycle, les barrières d'énergie étant environ 1 kcal/mol plus grande que celles rapportées pour une inversion comparable de **1**.

[Traduit par le journal]

In the following paper we present the results of our investigation into the effect on the photochemistry of eucarvone on its complexation with various boron trihalides (1). There are numerous reports of the protonation of aldehydes and ketones and the spectroscopic characterization of the resulting hydroxy substituted carbocations (2). Well defined complexes of carbonyl compounds and boron trifluoride have also been known for a long time (3, 4) and recently there has been a spate of publications defining their spectral properties (5–7). In contrast, comparatively few complexes of ketones and boron trichloride or tribromide have been described (4, 7–9). Before the excited state behaviour of the complexed or protonated cycloheptadienones can be examined, it is necessary to establish their ground state properties and this question is addressed in this paper. In particular, the different effects of complexation and protonation on the charge distribution and conformational mobility of eucarvone are examined.

Results and Discussion

Dissolution of eucarvone, **1**, in FSO_3H at $-78°C$ gave a clear yellow solution which exhibited nmr spectra (Tables 1 and 2) which

[1]The chemistry of cycloheptadienones, Part IX.
[2]Author to whom correspondence should be addressed.

TABLE 1. Proton chemical shifts of eucarvone, protonated eucarvone, and the boron trihalide complexes of eucarvone*

Compound	Solvent	T (°C)	Chemical shifts (ppm)						Coupling constant (Hz)	
			H_3	H_4	H_5	H_7	C_2Me	C_6Me	$J_{3,4}$	$J_{4,5}$
1	$CDCl_3$	37	6.36	5.68	5.90	2.53	1.84	1.03	8.0	11.3
2	FSO_3H	−50	7.86	6.50	6.87	3.33	2.22	1.28	8.2	11.5
3	$CDCl_3$	−50	7.50	6.34	6.68	3.64	2.10	1.20	8.0	11.5
4	$CDCl_3$	−50	7.53	6.27	6.62	3.62	2.11	1.21	8.0	11.5
5	$CDCl_3$	−50	7.62	6.24	6.60	3.72	2.14	1.27	8.0	11.5

*HA 100 spectra using tetramethylsilane (δ = 0.00) as internal standard for **1** and CH_2Cl_2 (δ = 5.30) as internal standard for **2**, **3**, **4**, and **5**.

TABLE 2. Carbon chemical shifts of eucarvone, protonated eucarvone, and boron trihalide complexes of eucarvone*

Compound	Solvent	T (°C)	Chemical shifts (ppm)								
			C_1	C_2	C_3	C_4	C_5	C_6	C_7	C_2Me	C_6Me
1	$CDCl_3$	30	200.1	138.5	133.8	122.2	148.8	33.1	54.1	19.9	26.9
2	FSO_3H	30	210.2	134.1	164.6	125.6	167.4	34.1	48.8	17.2	23.3
3	$CDCl_3$	−40	210.6	138.0	157.0	124.7	159.7	33.4	47.2	20.2	24.5
4	$CDCl_3$	−40	210.9	138.3	156.8	124.7	159.6	33.5	47.6	20.1	24.8
5	$CDCl_3$	−40	209.8	138.2	159.9	125.3	161.0	33.3	47.1	20.3	24.3
6	$CDCl_3$	30	201.3	131.2	137.9	126.5	140.5	22.2	41.4	—	—
7	FSO_3H	30	214.4	124.3	169.6	130.8	158.0	21.8	35.7	—	—

*22.63 MHz spectra using tetramethylsilane (δ 0.00) as internal standard for **1** and **6**, $CDCl_3$ (δ 77.2) for **3**, **4**, and **5**, and CD_2Cl_2 (δ 53.6) for **7**. External dimethylsulfoxide-d_6 (δ 39.6) was used as a standard for **2**. Carbon resonances were assigned on the basis of gated and selective proton decoupling.

were completely consistent with the formation of the hydroxydienyl cation **2**. For example, the downfield shifts of the various proton resonances of **1** on protonation are very comparable to those found in protonation of 6,6-disubstituted-cyclohexa-2,4-dienones (10). At temperatures above −60°C, no signal attributable to an OH resonance could be detected in FSO_3H solutions of **2**; however on cooling the samples to −90°C a singlet at δ 12.02 was observed. This signal, which is in a typical position for an OH resonance of a protonated enone (11), broadened and appeared to average with the solvent peak when the acid solution was warmed to −60°C. No change in the ^{1}Hmr spectrum of **2** occurred when FSO_3H solutions of this cation were kept at room temperature for several hours. Neutralization of the acid solution of **2** led to the recovery of **1** in 90–95% yield.

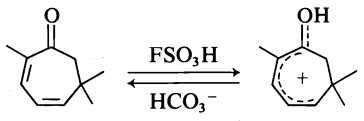

1 **2**

Eucarvone was reacted with the boron trihalides, BX_3 (X = F, Cl, and Br), by condensing the appropriate Lewis acid into a $CDCl_3$ or CH_2Cl_2 solution of **1**. The spectroscopic properties of the resulting yellow solutions indicated that the various boron trihalides had in each case formed a complex with **1**.

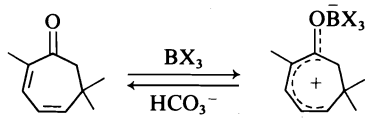

1 **3** X = F
4 X = Cl
5 X = Br

As is shown in Tables 1 and 2, the nmr spectral changes associated with the protonation of **1** or its reaction with the three boron trihalides are very similar. There are some differences in the magnitude of the shifts involved but the overall pattern of changes is the same in each case, indicating that the Lewis acids have coordinated with the carbonyl oxygen of **1** to give **3**, **4** and **5**.

The similarity of the structures of **2**, **3**, **4**, and **5** is also demonstrated in their uv spectra. The

TABLE 3. Ultraviolet spectra of eucarvone, protonated eucarvone, and boron trifluoride complexes of eucarvone*

Compound	Solvent	λ_{max}(nm)	log ε
1†	C_2H_5OH	303	3.83
2‡	96% H_2SO_4	400	3.63
3	CH_2Cl_2	389	3.85
4	CH_2Cl_2	389	3.89
5	CH_2Cl_2	400	3.93

*At 20°C.
†Reference 24.
‡Reference 25.

absorption maximum of **1** is red shifted by about the same amount on either the protonation or complexation of eucarvone (Table 3). Shifts of this magnitude of what would appear to be a π,π* band, are consistent with either coordination (12) or protonation (13) of the carbonyl oxygen.

Dilute solutions of **2**, **3**, and **4** were stable at temperatures below 0°C for long periods of time and could be reacted with bicarbonate to regenerate **1** in high yield. The complexes slowly decomposed on standing at room temperature for a few hours (14). This decomposition was more rapid when BBr_3 was used as the Lewis acid or when the concentrations of the complexes were increased beyond 0.1 *M*.

Charge Distribution

There has been considerable discussion over the question of the charge distribution in protonated aldehydes and ketones (2, 11, 15). In this present case, however, the issue is not only one of how the positive charge is distributed but how this distribution is affected by change of the group attached to the oxygen from a proton to a Lewis acid.

Examination of the chemical shift data presented in Tables 1 and 2 indicates that it is the C_1, C_3, C_5, and C_7 carbon resonances and the C_3, C_4, C_5, and C_7 proton resonances which are most affected by protonation or complexation of eucarvone. Apart from the C_1 and C_7 carbon and C_7 proton resonances, the changes in chemical shifts observed on complexation of **1** are smaller than those found on its protonation (Table 4). As the carbon–oxygen bond in these cationic systems will still have some double bond character, formally a proton or Lewis acid bonded to the oxygen of **1** could take a position which is either *cis* or *trans* with respect to C_7. It is known that a proton (11) or Lewis acid (6) normally adopts the sterically least hindered position which in this case is *cis* to C_7. The large deshielding effects observed with the C_7 proton and carbon resonances of **3**, **4**, and **5** as compared to **2** most probably result from the anisotropy of the adjacent boron trihalide group.

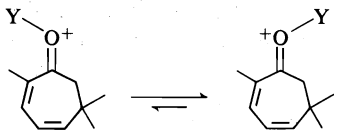

Y = H or $\bar{B}X_3$

Carbons C_3, C_4, and C_5 are well removed from any anisotropic effects of the Lewis acid groupings and the change in chemical shifts of these carbon resonances should reflect the fraction of positive charge induced on the dienylic part of the system by reaction with a proton or a Lewis acid. The downfield shifts observed for these carbons on complexation of **1** (Table 4) are in general only some 70% as large as those found on its protonation. Thus significantly less charge is induced at these carbons when a boron

TABLE 4. Change in chemical shifts on protonation or complexation of eucarvone and cyclohepta-2,4-dienone*

Transformation	Downfield shift (ppm)											
	H_2	H_3	H_4	H_5	H_7	C_1	C_2	C_3	C_4	C_5	C_6	C_7
1 → 2	—	1.50	0.82	0.97	0.80	10.1	−4.4	30.8	3.4	18.6	1.0	−5.3
1 → 3	—	1.14	0.66	0.78	1.11	10.5	−0.5	23.2	2.5	10.9	0.3	−6.9
1 → 4	—	1.17	0.59	0.72	1.09	10.8	−0.2	23.0	2.5	10.8	0.4	−6.5
1 → 5	—	1.26	0.56	0.70	1.19	9.7	−0.3	26.1	3.1	12.2	0.2	−7.0
6 → 7†	0.92	1.46	0.78	0.81	0.80	13.1	−6.9	31.7	4.3	17.5	−0.4	−5.7

*Positive number indicates a downfield shift.
†Proton data taken from ref. 18.

TABLE 5. Barriers to ring inversion of eucarvone, protonated eucarvone, and boron trihalide complexes of eucarvone

Compound	Solvent	Coalescence temp. T_c (°C)*	Limiting separation of C_6Me resonances (Hz)	Rate constant at T_c (s^{-1})	$\Delta G‡$ (kcal/mol)
1†	CD_2Cl_2–$CHClF_2$	−105.0	22.0	48.9	8.3
1‡§	CF_2Cl_2	−105.0	24.1	—	8.3
2‡	FSO_3H–SO_2ClF	−89.0	25.0	55.5	9.1
3†	CD_2Cl_2–$CHClF_2$	−90.0	19.0	42.2	9.1
4‖	CD_2Cl_2–$CHClF_2$	−86.9	13.0	28.9	9.4
5‖	CD_2Cl_2–$CHClF_2$	−91.0	8.5	18.9	9.4

*For C_6-Me resonances.
†At 90 MHz.
‡At 100 MHz.
‖At 60 MHz.
§Result of Cuthbertson and MacNicol (17).

trihalide rather than a proton is coordinated to the carbonyl oxygen of eucarvone.

The charge distribution in these Lewis acid adducts should also vary as a function of the boron trihalide used. It is anticipated that positive charge should be increasingly located on the dienylic portion of the molecule as the halogens bonded to the boron are changed from fluorine to chlorine to bromine (7, 9, 16). Examining the chemical shifts of the C_3, C_4, and C_5 carbon resonances of **3**, **4**, and **5** (Table 2), it can be seen that this is indeed the case for **5** as compared to **3** or **4**. The resonances of the C_3, C_4, and C_5 carbons of **5** occur at significantly lower field than those of the comparable carbons of **3** and **4**. There would appear, however, to be little difference in the charge distributions of **3** and **4**. It is not clear at this stage whether this is a general feature of boron trichloride and fluoride complexes of enones, or specific to the eucarvone complexes.

While the fraction of the positive charge residing on the dienylic portion of **2**, **3**, **4**, and **5** varies, the distribution of the charge between the various sp^2 hybridized carbons of these systems would appear to be much the same. Cornelis and Laszlo (17) have pointed out that the changes in the nmr spectrum of **1** as it is protonated closely parallel those observed on the protonation of cyclohexa-2,4-dienones. As the cyclohexadienones and protonated cyclohexadienones are planar species this would strongly suggest that the dienylic portions of **2**, **3**, **4**, and **5** are also close to being planar.

Included in Table 2 are details of the ^{13}C nmr spectra of cyclohepta-2,4-dienone, **6**, and protonated cyclohepta-2,4-dienone, **7** (18). As is shown in Table 4, the magnitude of the shifts observed of both the ^1H and ^{13}C resonances of **6** on its protonation are very similar to those observed on the protonation of **1**, indicating that the charge distribution in these systems is not affected to any great degree by the methyl substituents on eucarvone.

Ring Inversion

Despite the apparent simplicity of the room temperature nmr spectra of eucarvone, the seven-membered ring of this molecule is not planar. Cuthbertson and MacNicol (19) have shown that by cooling a sample of eucarvone to −130°C, it is possible to sufficiently slow a ring inversion process for the C_6 methyl proton resonances to appear as two singlets and C_7 methylene proton signals to occur as an AB quartet in its ^1Hmr spectrum. The barrier to this ring inversion was found to be 8.3 kcal/mol.

The ^1Hmr spectra of **2**, **3**, **4**, and **5** each exhibited a similar temperature dependence to that described by Cuthbertson and MacNicol for **1**. For example at −106°C the C_6 methyl signals of **3** appeared as two singlets at 1.13 and 1.34 δ and the C_7 protons as an AB quartet at 3.31 and 4.02 δ (J = 16.8 Hz). Apart from some general line broadening, the rest of the resonances of **3** were unchanged on cooling the sample to −106°C. On warming the solution, the *gem* dimethyl and methylene proton resonances reverted to singlets. The resolution of the ^1Hmr spectra of **2**, **3**, **4**, and **5** at temperatures below −100°C were not sufficient to warrant a full line shape analysis of these systems. The coalescence temperatures and low temperature limiting separation of the *gem* dimethyl group resonances of compounds **2** to **5** were obtained and are given in Table 5.

In view of the similarity in the temperature dependence of the ^{1}Hmr spectra of **1** and **2** to **5**, it would appear that a ring inversion process is occurring with these latter systems similar to that suggested for **1** itself. To confirm this and completely eliminate the possibility of involvement of any exchange or isomerization reactions involving the groups coordinated to the oxygen, the variable temperature ^{13}C nmr spectrum of **3** was examined. It was found that the resonance attributed to the C_6 methyl carbons of **3**, a sharp singlet at temperatures above -40°C, broadened at low temperatures and below -80°C, two singlets at 33.1 and 20.1 ppm were observed for these methyl carbons. No changes in any of the other carbon resonances were detected as the temperature was varied. The temperature dependencies described above of both the ^{13}C and ^{1}H nmr spectra of these cationic systems are thus fully consistent with a ring inversion process which interconverts the two C_6 methyl groups and also the C_7 methylene protons on the seven-membered ring.

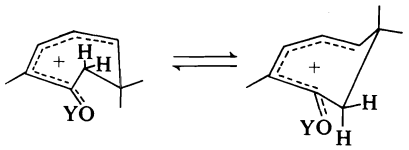

Y = H or $\bar{B}X_3$

It is interesting to compare the barriers to this ring inversion of the seven-membered ring of eucarvone and its complexed and protonated forms. The barrier to inversion of **1** ($\Delta G^{\ddagger}$ = 8.3 kcal/mol) is somewhat less than that found for **2** ($\Delta G^{\ddagger}$ = 9.1 kcal/mol). An examination of models suggests that ring inversion is helped if the five sp^2 hybridized carbons of these systems are allowed to be twisted somewhat away from a planar configuration. The higher energy barrier found for **2**, compared to **1**, is consistent with this view as conjugation, which would be more important with **2**, would be diminished as the dienylic portion of the molecule is twisted. However, the magnitude of the difference in the barrier to inversion of **1** and **2** and the similarity of the barriers of **2**, **3**, **4**, and **5** would indicate that conjugation is by no means completely lost in the transition state of this inversion process.

In conclusion, it is instructive to note that the conversion of cyclic unsaturated ketones to their corresponding cationic forms can, in some cases, have very large effects on the conformational mobility of the ring. Thus the barriers to ring inversion of cyclooctatrienone, 8, (E_a = 11.9 kcal/mol) (20) and the corresponding methoxy cation, **9**, ($\Delta G^{\ddagger}$ = 19.6 kcal/mol) (21) are considerably different. In this case, however, the conversion of the trienone to the cationic system involves the formation of a cyclically delocalized system, for **9** has been shown to be homoaromatic. The difference in the barriers to inversion of **8** and **9** in this case reflects the importance of homoaromaticity in a charged versus a neutral system.

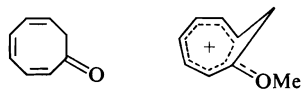

8 **9**

Experimental

Materials

Eucarvone was prepared from carvone by the procedure of Corey and Burke (22). FSO_3H was doubly distilled through a 12 in. glass column and stored in glass ampoules. CH_2Cl_2 was purified by the procedure of Jones and Wood (23). The boron trihalides, $CHCl_2F$, and SO_2ClF were all distilled on a vacuum line before use.

Protonation of Eucarvone

Protonations were carried out by slowly adding precooled FSO_3H (0.5 ml) to a dry nmr tube which contained **1** (ca. 20 mg) and which was kept in a dry-ice – acetone bath. Solution was achieved by agitating the sample with a quartz rod.

Formation of Complexes

Eucarvone (10–15 mg) was weighed into a dry nmr tube which was attached to a high vacuum line. The tube was cooled with liquid N_2 and the appropriate solvent distilled in. The sample was warmed to room temperature to allow **1** to dissolve, cooled again, and a known amount of the appropriate boron trihalide distilled over. The sample tube was sealed under vacuum and allowed to warm to -78°C.

For the uv measurements, a similar procedure was adopted except that a 200 ml reaction flask fitted with a side arm leading to a 2 mm quartz cuvette was used. The complexes were prepared in the 200 ml flask and after completion of the reaction some of the solution was transferred into the cuvette which was then sealed under vacuum. All these operations were carried out at low temperatures.

Quenching Procedure

The solution of protonated or complexed **1** was added dropwise to a stirred suspension of $NaHCO_3$ (5 g for **2**; 0.5 g for **3**, **4**, or **5**) in ether (25 ml) at -78°C. Upon warming to 0°C ice water (5 ml) was added, and the mixture stirred and filtered under suction. The organic layer was washed with saturated brine solution and dried

($MgSO_4$). The products were recovered by careful evaporation of the solvent at atmospheric pressure through a 6 in. Vigreux column and analyzed by glpc. (Varian Aerograph 204 using a 10 ft × $\frac{1}{8}$ in. column packed with 20% Carbowax 2000 M on Chromosorb W) and ^{1}Hmr. In each case only **1** was detected and recoveries were in the 90–95% range.

Spectroscopic Procedures

^{1}Hmr spectra were obtained on Varian HA-100 and A-60 spectrometers and both ^{1}H and ^{13}C nmr spectra on a Bruker WH 90 instrument. All three instruments were fitted with variable temperature probes, the probe temperature being measured with a copper–constantan thermocouple mounted at the appropriate depth in a nonspinning nmr tube. The rate constants for ring inversion at the coalescence temperature were obtained by using the equation $k = \pi\nu_{AB}/\sqrt{2}$. Ultraviolet spectra were obtained with a Cary 14 spectrometer.

Acknowledgment

This work was supported by a grant from the National Research Council of Canada.

1. R. F. Childs and Y. C. Hor. Can. J. Chem. This issue.
2. G. A. Olah, A. M. White, and D. H. O'Brien. Chem. Rev. **70**, 561 (1970).
3. F. Landolph. Compt. Rend. **86**, 1463 (1878).
4. D. R. Martin and J. M. Cannon. *In* Friedel-Crafts and related reactions. Vol. 1. *Edited by* G. A. Olah. Interscience Publishers, Inc., New York. 1963. p. 399.
5. G. Torri, J. P. Rosset, and M. Azzaro. Bull. Soc. Chim. Fr. 2167 (1970); A. Fratiello and C. S. Stover. J. Org. Chem. **40**, 1244 (1975); M. Rabinovitz and A. Grinvald. J. Chem. Soc. Perkin Trans. II, 514 (1973); R. J. Gillespie and J. S. Hartman. Can. J. Chem. **46**, 2147 (1968); P. N. Gates and E. F. Mooney. J. Chem. Soc. 4648 (1964); R. F. Childs and M. Zeya. J. Am. Chem. Soc. **96**, 6418 (1974).
6. J. S. Hartman, P. Stilbs, and S. Forsén. Tetrahedron Lett. 3497 (1975); P. Stilbs and S. Forsén. Tetrahedron Lett. 3185 (1974); U. Henricksson and S. Forsén. Chem. Commun. 1229 (1970).
7. R. G. Pews, Y. Tsuno, and R. W. Taft. J. Am. Chem. Soc. **89**, 2391 (1967); C. S. Giam and R. W. Taft. J. Am. Chem. Soc. **89**, 2397 (1967).
8. P. N. Gates, E. J. McLauchlan, and E. F. Mooney. Spectrochim. Acta, **21**, 1415 (1965); A. Fratiello, T. P. Onak, and R. E. Schuster. J. Am. Chem. Soc. **90**, 1194 (1968); R. C. Paul, R. Parkash, and S. S. Sandhu. J. Inorg. Nucl. Chem. **29**, 1915 (1967); H. Hirai. J. Polym. Sci. Macromol. Rev. **11**, 47 (1976).
9. M. Zeya. Ph.D. Thesis. McMaster University, Hamilton, Ontario. 1973.
10. E. C. Friedrich. J. Org. Chem. **33**, 413 (1968); R. F. Childs and B. D. Parrington. Can. J. Chem. **52**, 3303 (1974); N. Filipescu and J. W. Pavlik. J. Am. Chem. Soc. **92**, 6062 (1970).
11. T. Birchall and R. J. Gillespie. Can. J. Chem. **43**, 1045 (1965); M. Brookhart, G. C. Levy, and S. Winstein. J. Am. Chem. Soc. **89**, 1735 (1967); G. A. Olah, Y. Halpern, Y. K. Mo, and G. Liang. J. Am. Chem. Soc. **94**, 3554 (1972); D. M. Brouwer. Tetrahedron Lett. 453 (1968).
12. M. Rabinovitz and A. Grinvald. J. Am. Chem. Soc. **94**, 2724 (1972).
13. G. A. Olah, C. U. Pittman, Jr., and M. C. R. Symons. *In* Carbonium ions. Vol. 1. *Edited by* G. A. Olah and P. von R. Schleyer. Interscience, New York, NY. 1968. p. 153.
14. R. J. Gillespie and J. S. Hartman. Can. J. Chem. **46**, 3799 (1968).
15. H. Hogeveen. Recl. Trav. Chim. Pays Bas, **86**, 696 (1967); D. M. Brouwer. Recl. Trav. Chim. Pays Bas, **86**, 879 (1967).
16. D. G. Brown, R. S. Drago, and T. F. Bolles. J. Am. Chem. Soc. **90**, 5706 (1968); R. W. Taft and J. W. Carten. J. Am. Chem. Soc. **86**, 4199 (1964); D. P. N. Satchell and R. S. Satchell. Q. Rev. Chem. Soc. **25**, 171 (1971).
17. A. Cornelis and P. Laszlo. Org. Magn. Reson. **5**, 99 (1973).
18. K. E. Hine and R. F. Childs. J. Am. Chem. Soc. **95**, 3289 (1973).
19. E. Cuthbertson and D. D. MacNicol. Tetrahedron Lett. 2689 (1974).
20. C. Ganter, S. M. Pokras, and J. D. Roberts. J. Am. Chem. Soc. **88**, 4235 (1966).
21. M. S. Brookhart and M. A. M. Atwater. Tetrahedron Lett. 4399 (1972).
22. E. J. Corey and H. J. Burke. J. Am. Chem. Soc. **78**, 174 (1956).
23. D. E. H. Jones and J. L. Wood. J. Chem. Soc. A, 1448 (1966).
24. H. Hart and T. Takino. J. Am. Chem. Soc. **93**, 720 (1971).
25. K. E. Hine and R. F. Childs. J. Am. Chem. Soc. **93**, 2323 (1971).

Photoisomerization of the boron trihalide complexes of eucarvone[1]

RONALD F. CHILDS[2] AND YEE-CHEE HOR
Department of Chemistry, McMaster University, Hamilton, Ont., Canada L8S 4M1

Received April 6, 1977

RONALD F. CHILDS and YEE-CHEE HOR. Can. J. Chem. **55**, 3501 (1977).

The photoisomerization of the BF_3, BCl_3 and BBr_3 complexes of eucarvone (2,6,6-trimethylcyclohepta-2,4-dienone), **1**, have been examined. Irradiation of these zwitterions at low temperature gave, after subsequent recovery of decomplexed materials, 3,7,7-trimethylbicyclo-[4.1.0]hept-2-en-4-one, **2**, 2-methyl-5-isopropylphenol, **3**, 2-methyl-6-isopropylphenol, **4**, dehydrocamphor, **5**, and carvone, **6**. In the case of **1**·BF_3 and **1**·BCl_3 the initial photoproducts were shown to be the complexes of **2**, **3**, **4**, and **5**. The complexes of **6** were shown to arise from a secondary photoisomerization of **2**·BX_3. It was not possible to establish the primary product distribution, obtained from **1**·BBr_3 as further photoisomerization of **2**·BBr_3 occurred even at very low degrees of conversion. The mechanisms and synthetic utility of these reactions is discussed.

RONALD F. CHILDS et YEE-CHEE HOR. Can. J. Chem. **55**, 3501 (1977).

On examine la photoisomérisation des complexes BF_3, BCl_3 et BBr_3 de l'eucarvone (triméthyl-2,6,6 cycloheptadiène-2,4 one), **1**. L'irradiation de ces ions hermaphrodites à basse température conduit, après récupération des substances décomplexées, au triméthyl-3,7,7 bicyclo [4.1.0]heptène-2 one-4, **2**, méthyl-2 isopropyl-5 phénol, **3**, méthyl-2 isopropyl-6 phénol, **4**, déshydrocamphre, **5**, et à la carvone, **6**. Dans le cas des espèces **1**·BF_3 et **1**·BCl_3 on a montré que les produits initiaux de photolyse sont les complexes de **2**, **3**, **4** et **5**. Les complexes de **6** proviennent d'une seconde photoisomérisation de **2**·BX_3. Il n'a pas été possible de déterminer la distribution des produits primaires obtenu à partir de **1**·BBr_3 étant donné qu'une photoisomérisation plus poussée de **2**·BBr_3 a lieu même à très bas degré de conversion. On discute des mécanismes et des avantages synthétiques de ces réactions.

[Traduit par le journal]

In preceding papers we have examined the interrelationship of the photochemistry of neutral and protonated ketones (1–3). It is apparent from these and related studies (4–6) that protonation represents a method of exerting considerable control over the excited states reached and products obtained in the photoisomerization of a carbonyl compound. However, several problems stand in the way of the effective utilization of protonation as a general technique for the regulation of a photoreaction.

One of the major difficulties rests in the use of a strong acid such as FSO_3H to effect the complete protonation of a carbonyl compound. While the transfer of a ketone into such an acid is usually straightforward and the photochemical transformations are remarkably clean and free from intermolecular side reactions, the subsequent recovery of the products from the acid solution can be troublesome. On a small scale, substrates may readily be recovered in high yield on quenching the acid solutions with an appropriate base. However, in our experience the yields of recovered materials drop significantly as the scale of the reaction is increased.

Coordination of the carbonyl oxygen of a ketone with a Lewis acid induces changes in its ground state properties similar to those encountered on protonation (7). As the regeneration of a ketone from a Lewis acid complex is generally facile, the question arises whether a Lewis acid might not be used in a similar manner to a proton to modify the photochemistry of a ketone. Photochemically induced reactions of certain complexes of carbonyl compounds have been previously reported (8, 9). However, it would appear that no systematic study of their behaviour has been made. To this end we have examined the photoisomerizations of the boron trihalide adducts of eucarvone, **1**, a ketone for which the effects of protonation have been previously investigated (1). The boron halide complexes were selected for this study on the basis of their ready availability, ease of manipulation, and solubility characteristics as well as

[1]The chemistry of cycloheptadienones, Part X.
[2]Author to whom correspondence should be addressed.

the possibility that the nature of the photoisomerizations could change as an increasingly heavy atom is introduced into the system on going from BF_3 to BBr_3.

Results

Product Characterization

Irradiation of a CH_2Cl_2 solution of **1**·BCl_3 (λ_{max} = 389 nm (7)) at −90°C with light of wavelength greater than 370 nm caused it to isomerize to give a series of products. The low temperature ^{1}Hmr spectrum of the resulting solution was too complex to be readily interpretable and accordingly the products were recovered by quenching the solution with an ether–bicarbonate slurry. Five major components were found to be present by glpc and these were collected and shown to be **2**, **3**, **4**, **5** and **6**.[3] Samples of **2** and **5** were available from the photoisomerizations of protonated (1) and neutral eucarvone (6, 10), while **3** and **6** were both obtained commercially. In each case the glpc retention time and spectroscopic properties of the authentic material were identical to those of the corresponding compound isolated from the photoisomerization.

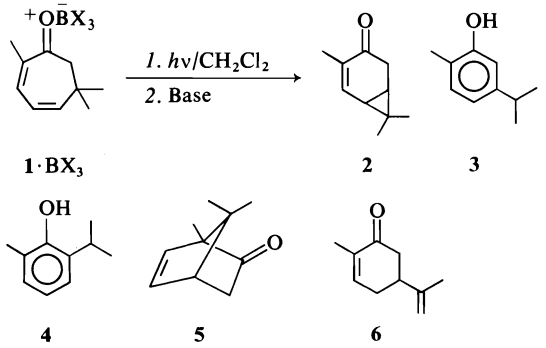

The ir, mass, and nmr spectra of the remaining compound were entirely consistent with the structure shown as **4**. A sample of **4** was prepared by the procedure of Sowa *et al.* (11) and found to be identical in every respect to the material obtained in the photoreaction. 2-Methyl-4-isopropylphenol, **7**, prepared by the method of Carpenter and Easter (12), had different spectral and glpc properties from any of the above products. The phenol **7** could have been detected as a photoproduct if it had been formed in greater than 1% yield.

The photoisomerizations of **1**·BF_3 and **1**·BBr_3 were examined in a similar manner to that outlined above for **1**·BCl_3. In each case the same five products were formed.

Quantitative product analyses were carried out on each of these systems and the results are given in Table 1. The yields of the recovered material were generally high (>94%) and the compositions were reproducible.

These photoisomerizations were also examined in a nonchlorinated solvent medium. Difluoroethane was eventually found to be a suitable solvent for the three complexes at low temperatures. The same products were formed in CH_3CHF_2 as were found in CH_2Cl_2 and details of the product compositions are given in Table 1.[4]

Product Stability

The composition of the photoproducts obtained on irradiation of **1**·BF_3 and **1**·BCl_3 was found to be a function of the degree of conversion of the initial complex. This was particularly noticeable with **1**·BCl_3, entries 4 and 5, Table 1, where **6**, a major product in the latter stages of the photoisomerization, could not be detected when the reaction was only taken to 4% completion. It would seem that **6** is arising from a secondary photochemical or thermal reaction of one of the photoproducts, most likely, in fact, **2**·BX_3. Accordingly, the individual photoproducts and several related potential products were reacted with BX_3 and the stability of the resulting complexes examined.

The bicyclic compound **2** was reacted with BCl_3 in CH_2Cl_2 at −90°C to give **2**·BCl_3. The ^{1}Hmr spectrum of this complex was very similar to that of protonated **2** (1) (Table 2) and **2** was recovered in high yield on treatment of the solution with base. While **2**·BCl_3 was stable at −90°C, it underwent a slow decomposition when kept at −78°C. No products could be recovered on quenching the CH_2Cl_2 solution after this decomposition had occurred. The reaction of **2** with BF_3 and BBr_3 proceeded in a comparable manner to give **2**·BF_3 and **2**·BBr_3. Both of these complexes were stable at −90°C and gave back the starting ketone when treated with base.

[3]Other minor products (each much less than 1%) were detected by glpc. These were not characterized.

[4]There appeared to be a slow thermal reaction of BBr_3 with CH_3CHF_2 which resulted in the formation of a yellow solid. This reaction was not investigated further.

TABLE 1. Products arising from the photoisomerization of $1 \cdot BX_3$ and related species*

Entry No.	Compound	Solvent	Conversion (%)	Products (%)† 2	3	4	5	6	9	11
1	$1 \cdot BF_3$	CH_2Cl_2	74	68	18	10	1	3	nd	nd
2		CH_2Cl_2	5	69	20	10	1	nd	nd	nd
3		CH_3CHF_2	5	74	16	9	1	nd	nd	nd
4	$1 \cdot BCl_3$	CH_2Cl_2	83	29	38	10	1	22	nd	nd
5		CH_2Cl_2	4	69	20	10	1	nd	nd	nd
6		CH_3CHF_2	5	72	19	8	1	nd	nd	nd
7	$1 \cdot BBr_3$	CH_2Cl_2	61	7	60	8	0.5	25	nd	nd
8		CH_2Cl_2	4	7	60	8	0.5	25	nd	nd
9		CH_3CHF_2	5	48	28	7	3	14	nd	nd
10	$2 \cdot BF_3$	CH_2Cl_2	—	nd	56	nd	nd	44	nd	nd
11	$2 \cdot BCl_3$	CH_2Cl_2	—	nd	57	nd	nd	43	nd	nd
12	$2 \cdot BBr_3$	CH_2Cl_2	—	nd	40	nd	nd	60	nd	nd
13	**1**‡	CH_2Cl_2	5	6	nd	nd	nd	nd	nd	94
14	**1**H§	FSO_3H/SO_2	70	73	17	nd	nd	nd	10‖	nd

*At −90°C, unless otherwise specified; recovery of material in each case in excess of 94%; nd, not detected, < 0.5%.
†Expressed as relative percentage of total products after quenching the reactions; error ±2%.
‡Reference 21.
§At −75°C. Products both thermally and photochemically stable under the reaction conditions.
‖9H undergoes a subsequent thermal rearrangement (1).

TABLE 2. ^{1}Hmr spectra of various BCl_3 complexes in CH_2Cl_2*

Compound	Chemical shifts (ppm) H_1	H_2	H_3	H_4	H_5	H_6	H_7	Other
$2 \cdot BCl_3$	1.30	8.07	—	—	3.52	2.00	—	0.88, 1.47, 1.88 (Me)
$6 \cdot BCl_3$	—	—	7.81	2.78	2.78	2.78	—	1.69, 1.88 (Me), 4.81 (=CH_2)
$9 \cdot BCl_3$	—	6.67	6.67	3.68	—	1.67 1.60	—	0.92, 1.10, 1.24 (Me)
$10 \cdot BCl_3$	—	—	7.63	8.60	3.34	—	2.25 1.76	0.90, 1.40, 1.42 (Me)
$8 \cdot BCl_3$	—	—	7.3	—	7.3	7.3	—	2.31, 4.52 (Me), 1.17 (Me_2C), 2.89 ($CHMe_2$)

*All spectra recorded at −50°C apart from that of $2 \cdot BCl_3$ which was obtained at −90°C.

The complexes of **2** were found to be photolabile under the conditions used in the irradiations of $1 \cdot BX_3$. Two products were formed in each case and these were identified after quenching the solutions as **3** and **6** (Table 1, entries 10–12). Qualitatively it was found that the relative efficiencies of the photoisomerization of the three complexes of **2** were quite different. Thus while $2 \cdot BF_3$ and $2 \cdot BCl_3$ each reacted about a factor of two more slowly than $1 \cdot BF_3$ or $1 \cdot BCl_3$, respectively, when irradiated under comparable conditions, $2 \cdot BBr_3$ photoisomerized some four times more rapidly than $1 \cdot BBr_3$. A mixture of $1 \cdot BBr_3$ and $2 \cdot BBr_3$ in a ratio 2.5:1 in CH_2Cl_2 was irradiated at −90°C for the time normally taken to achieve a 5–10% photoconversion of $1 \cdot BBr_3$. After quenching the solution the ratio of **1**:**2** was found to be 20:1, indicating that competitive photoisomerization of $2 \cdot BBr_3$ is significant even in the early stages of the rearrangement of $1 \cdot BBr_3$. It is clear that for $1 \cdot BF_3$ and $1 \cdot BCl_3$ and quite possibly also for $1 \cdot BBr_3$, that the complexes of **6** are not initial photoproducts but are produced in secondary photoreactions of $2 \cdot BX_3$. While complexes of **3** are also produced in this subsequent photoisomerization, it would seem that they are also produced directly from $1 \cdot BX_3$.

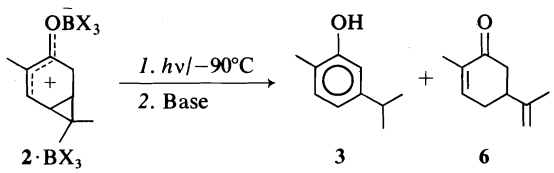

$2 \cdot BX_3$ **3** **6**

TABLE 3. ^{1}Hmr spectra of protonated phenols*

Phenol	Site of protonation	Chemical shifts (ppm) C_2Me	C_3H	C_4H	C_5H	C_6H	$CHMe_2$
3	C_4	2.25	8.10	4.13	—	7.15	1.35d
4	C_4	2.15	8.22	4.18	8.22	—	1.30d
7	C_4	2.33	8.4	3.92m	8.50d	7.23d	1.13d
7	C_6	2.33	8.4	—	7.21	4.32d	1.30d
7	O	2.37	7.2	—	7.2	7.2	1.30d

*In FSO_3H at $-50°C$; d = doublet, m = multiplet.

Reaction of **6** with BCl_3 in CH_2Cl_2 at $-78°C$ resulted in the formation of the corresponding complex **6**·BCl_3. The ^{1}Hmr spectrum of **6**·BCl_3 was entirely consistent with its assigned structure (Table 2) and **6** was recovered in good yield on reacting the solution with ether–HCO_3^- slurry. The complex was found to be stable at $-20°C$ for long periods of time and to be photochemically stable under the conditions used in the photoisomerization of **1**·BCl_3.

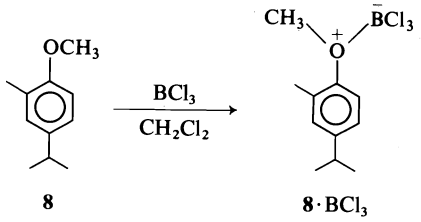

8 **8**·BCl_3

The phenols **3**, **4**, and **7** gave solutions with rather ill-defined ^{1}Hmr spectra when reacted with BCl_3 in CH_2Cl_2. This is in contrast, for example, with the reaction of the anisole **8** with BCl_3 which results in the formation of **8**·BCl_3 (Table 2).

The presence of a resonance at ca. δ 1.3 in the ^{1}Hmr spectra of solutions of these phenols and BCl_3 which was absent when the O-deuterated phenols were used, suggested that HCl was being formed in these reactions. Solutions of anhydrous HCl and BCl_3 in CH_2Cl_2 at low temperatures exhibited a signal in a comparable position. Phenols are known to react with BCl_3 to give mixtures of phenoxyboron halides and triaryl borates together with HCl (13) and it would appear that similar reactions take place between **3**, **4** and **7** and BCl_3. The phenols were recovered unchanged on reaction of these solutions with base.

It would seem likely from a mechanistic consideration, *vide infra*, that complexes of the keto tautomers of phenols **3** and **4** are obtained in the photoisomerization of **1**·BCl_3. As it was not possible to form this type of complex directly, the protonation of **3**, **4**, and **7** was examined in order to see if migration of the isopropyl groups would occur in these systems.

The cation **3H**, formed on protonation of **3** in FSO_3H, is known to be stable below 0°C (1). Dissolution of **4** in FSO_3H gave a cation with a ^{1}Hmr spectrum (Table 3) completely consistent with protonation in the *para* position, while **7** gave, as would be expected on the basis of the protonation of 2,4-dimethylphenol (14), a mixture of carbocations. No isopropyl group migrations could be detected in any of these systems at temperatures up to $-20°C$.

Unlike the photoisomerizations of **1H**, none of the 7-norbornenone **9** could be detected as a product of **1**·BX_3. To ensure that complexes of **9** would be stable under the reaction conditions,

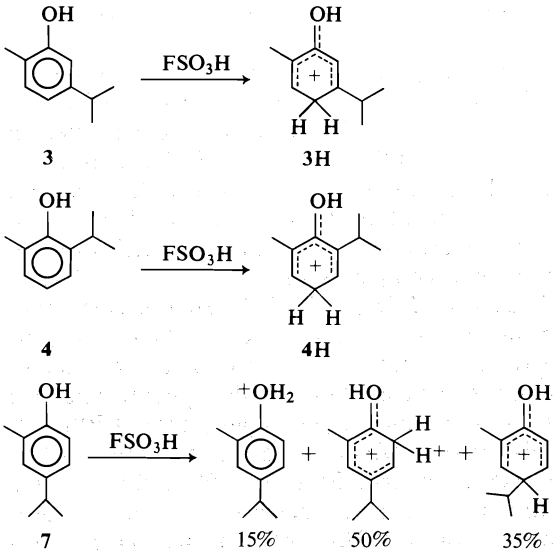

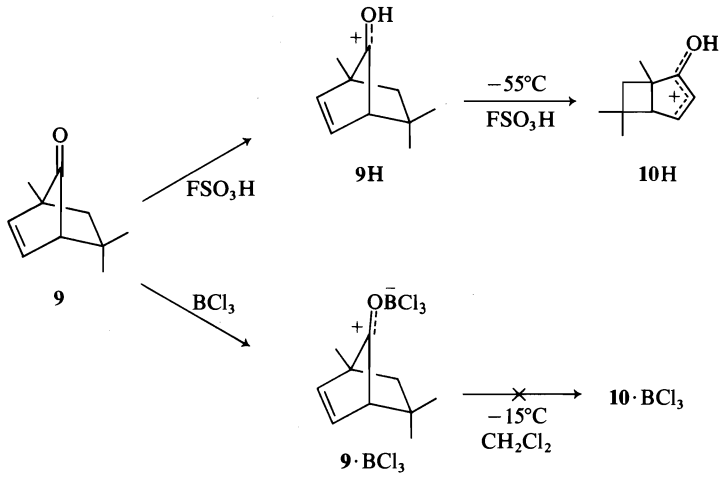

$9 \cdot BCl_3$ was prepared. This complex (^{1}Hmr spectral data in Table 2) was found to be thermally stable up to at least −15°C and unchanged when irradiated under the same conditions as used with $1 \cdot BCl_3$ The thermal stability of $9 \cdot BCl_3$ is in marked contrast with that of the corresponding protonated material which isomerized to give **10**H in FSO_3H −55°C (1).

Discussion

It is clear from the results presented above that the boron trihalide complexes of **1** predominantly undergo isomerization reactions on irradiation. In each case, apart from small manipulative losses, the yields of recovered materials are essentially quantitive and can be accounted for, after quenching, entirely in terms of isomers of **1**. It should be noted, however, that the wavelength of the incident light was such that only the complexed dienone chromophore and not any free boron halide could be excited (15). BCl_3 and BBr_3 are known to undergo dissociation on direct irradiation and this can lead to the occurrence of substitution reactions with hydrocarbon solvents (16). No such substitution reactions would appear to be occurring during the photoisomerizations of $1 \cdot BX_3$ nor were they observed by Griffith and Hart (8) on irradiation of the BF_3 complex of 2,4,6,6-tetramethylcyclohexa-2, 4-dienone, a system with a similar chromophore.

The profound effect of protonation on the photoisomerizations of eucarvone has largely been attributed to the reversal in the relative energies of the n,π^* and π,π^* states attendant upon protonation (1, 6). The uv spectra of $1 \cdot BX_3$ and **1**H are very similar (7) and it is again likely that the lowest energy transition in $1 \cdot BX_3$ is of π,π^* character.

It is interesting to compare the photoproducts obtained on irradiation of protonated eucarvone, **1**H, with those formed from $1 \cdot BX_3$. In each case **2** and **3** are the major products obtained on neutralization of the acid solutions and no materials corresponding to 1,4,4-trimethylbicyclo-[3.2.0]hept-6-en-2-one, **11**, are formed. The bicyclic ketone **11** is the predominant material obtained on irradiation of eucarvone itself in a wide variety of solvents, including CH_2Cl_2, Table 1, entry 13 (17). While the major products obtained on irradiation of $1 \cdot BX_3$ and **1**H are the same, they differ in that **4** ($4 \cdot BX_3$) and a trace of **5** ($5 \cdot BX_3$) are produced in the Lewis acid cases whereas **9**H is obtained from **1**H.

At first sight it is attractive to consider that the production of **4** or **9** in the complexed or protonated eucarvone photoisomerization respectively are somehow linked, especially as they are both formed in about the same yield. However, such a possibility is very unlikely. The control experiments described earlier showed that the products **4** and **9** do not interconvert when either protonated or complexed with BCl_3. It has also been shown by trapping experiments (1) that the precursor to **9**H is the bicyclic cation **12** and it is

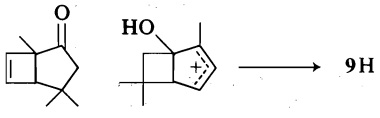

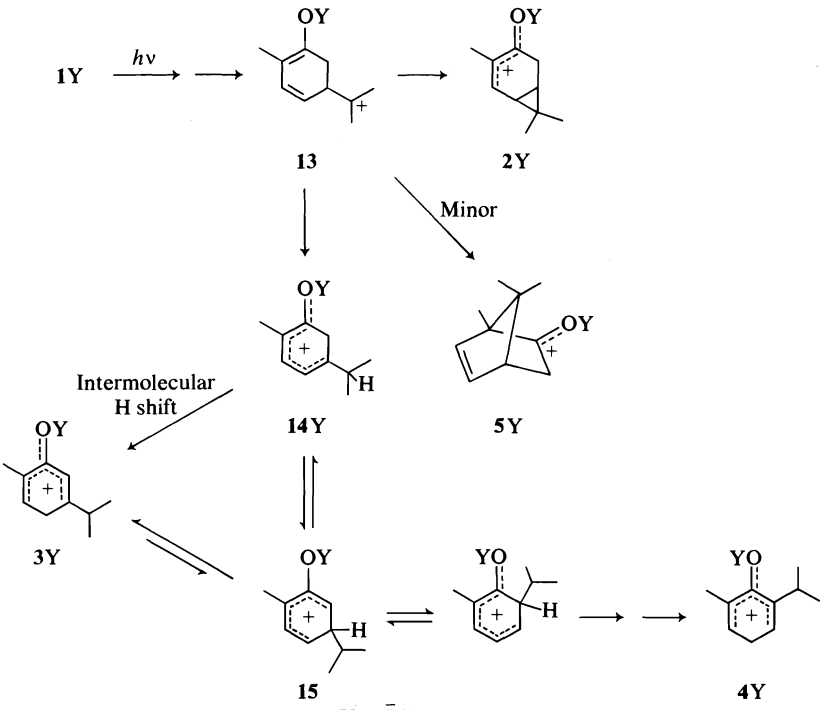

Y = $\bar{B}X_3$ or H

SCHEME 1

very difficult to conceive how an analogous species, differing only in the replacement of the OH group by an $O\bar{B}Cl_3$ group, could rearrange to give **4**·BCl_3.

The formation of the major photoproducts in both the complexed and protonated cases can be understood in terms of the intermediacy of the same type of carbocation. As is shown in Scheme 1, an intermediate such as **13** could, by bonding the positive centre to either C_4 or C_2, yield derivatives of **2** and **5** respectively, the latter process only occurring to a minor extent with **13**·BX_3 and not being detectable with **13**H. Alternatively, a 1,2 hydride shift would in each case convert **13** to **14**. While **14** would yield **3** on reaction with base, it is known that **14** rearranges in FSO_3H to give the more stable, isomeric cation **3**H (1). This thermodynamic preference for the formation of the cross conjugated dienone derivative should still be maintained in the corresponding Lewis acid complexes.[5]

[5]While the same relative order of stability is expected between the protonated and BX_3 complexed forms of **3**, **14**, and **15**, the exact positions of the various equilibria will be dependent on the nature of the group coordinated to the oxygen atom (18).

One possible difference between these protonated and complexed systems which might account for the formation of **4**·BX_3 in the latter case involves the mechanism of this hydride shift. In FSO_3H, the rearrangement of **14**H to **3**H most probably occurs via an intermolecular hydride shift (14, 19). On the other hand, if the isomerization of **14**·BX_3 were to proceed by successive intramolecular hydride shifts, **15** would be involved as an intermediate. This zwitterion could undergo subsequent hydride or isopropyl group migrations, the latter possibility eventually leading to **4**·BX_3. It is somewhat surprising that if **4**·BX_3 is indeed formed by such a route, there is no concurrent migration of the isopropyl group to the C_4 position (3, 5).

It has been suggested that the formation of **9**H from protonated eucarvone involves a triplet, π,π^* state, whereas the other photoproducts, **2**H and **3**H are derived from a singlet π,π^* state (1). With these complexes, an increasingly heavy atom is introduced into the zwitterions as the Lewis acid is changed from BF_3 to BCl_3 to BBr_3. It might well have been expected that the rates of intersystem crossing between the singlet and triplet states of **1**·BX_3 would be dependent on the halogen atom present. If such an effect is

operative, it is not apparent in terms of the photoproducts obtained from these complexes. Even in CH_3CHF_2, a solvent comprised solely of light atoms, there are no different photoproducts obtained from **1**·BBr_3 as are formed from **1**·BF_3 and no evidence for the formation of **9**·BX_3.

Overall it is apparent that a Lewis acid and a proton exert a comparable modifying effect on the direction of photoisomerization of a carbonyl compound. In view of the very large differences in the polarity of the halocarbon solvents used with the Lewis acid complexes and the FSO_3H employed in the photoisomerizations of **1**H, it is remarkable how similar the initial product distributions are in these two systems. In the case of eucarvone, the thermal and photochemical lability of the complexes of **2** strictly limits the synthetic utility of using a Lewis acid to direct the course of the photoisomerization. This extreme lability of **2**·BX_3 is unexpected in view of the known properties of **2**H and the stability of the boron halide complexes of the other related ketones. It is likely that the difficulties encountered are specific to the eucarvone system and that they do not detract from the general usage of a Lewis acid to direct the course of the photoisomerization of a carbonyl compound.

Experimental

General

^{1}H nmr spectra were recorded on Varian HA-100 and A-60 spectrometers equipped with variable temperature probes. The probe temperature was measured with a copper–constantan thermocouple mounted at the appropriate depth in a nonspinning sample tube. Chemical shifts of neutral materials are referred to internal tetramethylsilane and those of the complexes and protonated compounds are referred to internal CH_2Cl_2 taken as 5.30 δ. Infrared spectra were obtained with a Perkin-Elmer Model 337 grating spectrometer. A Nicolet 1080 Mini-Computer using the Nuclear Resonance Spectrum Calculation Programme (NMRCAL NIC-80/S-7117-D) was used to simulate the ^{1}Hmr spectrum of **4** and obtain the coupling constants of the ring protons. Varian Aerograph 204 (analytical) and Aerograph A-90-P3 (preparative) gas chromatographs were used with He as a carrier gas. The columns employed were: A, 10 ft × $\frac{1}{8}$ in., 20% Carbowax 2000 M on Chromosorb W; B, 10 ft × $\frac{1}{4}$ in., 15% SE 30 on Chromosorb W; C, 13 ft × $\frac{1}{4}$ in., 20% Carbowax 2000 M on Chromosorb W.

Materials

The purification of solvents, formation of the various complexes and protonation of the phenols were carried out as outlined in the previous paper (7).

2-Methyl-6-isopropylphenol, 4

2-Methyl-6-isopropylphenol was prepared by the method of Sowa *et al.* (11) and purified by preparative glpc, column C; ^{1}H nmr (CCl_4) δ 6.92 (1, H-3), 6.67 (1, H-4), 6.82 (1, H-5), $J_{3,4}$ = 7.74 Hz, $J_{4,5}$ = 7.54 Hz, $J_{3,5}$ = 1.66 Hz, 4.24 (s, 1, OH), 3.14 (h, 1, $CH(CH_3)_2$), 2.20 (s, 3, 2-CH_3), 1.15 (d, J = 7 Hz, 6, $C(CH_3)_2$).

2-Methyl-4-isopropylphenol, 7

This phenol was prepared by standard procedures (12); ^{1}H nmr (CCl_4) δ 6.82 (d, $J_{3,5}$ = 2.1 Hz, 1, H_3), 6.80 (q, $J_{3,5}$ = 2.1 Hz, $J_{5,6}$ = 7.8 Hz, 1, H-5), 6.52 (d, $J_{5,6}$ = 7.8 Hz, 1, H-6), 4.46 (s, 1, OH), 2.75 (h, 1, $CH(CH_3)_2$), 2.17 (s, 3, 2-CH_3), 1.16 (d, J = 7 Hz, 6, $C(CH_3)_2$).

Photochemical Procedures

A Phillips SP 500 W lamp was used in conjunction with the apparatus previously described (20). A Corning Glass filter #3850 was used in all irradiations and this cut off light with wavelength less than 370 nm. The temperature of the sample was maintained at −90°C during the course of the photoisomerizations, the temperature being monitored by a glass encased copper–constantan thermocouple inserted into the solution.

Following completion of the photoreaction the products were recovered by the addition directly to the sample tube of 2 ml of a cold (−90°C) slurry of $NaHCO_3$ (0.5 g) in ether (25 ml). The sample tube was agitated with a glass rod during this addition. The quenched solution was quickly transferred into the remaining ether–$NaHCO_3$ mixture and allowed to warm to 0°C. Ice water (5 ml) was added to the ether slurry, the mixture swirled and filtered under suction. The organic layer was washed with brine until neutral (litmus) and dried ($MgSO_4$). The solution was concentrated by careful evaporation of the solvent at atmospheric pressure through a 6 in Vigreux column and subjected to glpc analysis.

Large scale photoisomerizations of **1**·BCl_3 (prepared from 200 mg of **1**) in CH_2Cl_2 (2 ml) required some 4–5 h of irradiation and after quenching the solution, the products were collected by preparative glpc using column B. The products obtained were identified as **2**, **3**, **4**, **5** and **6** on the basis of the comparison of their ir and ^{1}Hmr spectra with those of authentic samples.

The product distributions (Table 1) were obtained with samples containing the appropriate complex (formed from ca. 15 mg of **1**) in CH_2Cl_2 or CH_3CHF_2 (0.5 ml). Following recovery of the products, a weighed amount of cycloheptanone was added and the percent recovery and product compositions determined by analytical glpc, column A. The areas of the peaks were found by triangulation or by cutting and weighing. Detector response curves were established in the usual manner.

Acknowledgment

This work was supported by a grant from the National Research Council of Canada.

1. K. E. Hine and R. F. Childs. J. Am. Chem. Soc. **95**, 6116 (1973); **93**, 2323 (1971).
2. K. E. Hine and R. F. Childs. J. Chem. Soc. Chem. Commun. 145 (1972); R. F. Childs and V. Taguchi. J. Chem. Soc. Chem. Commun. 695 (1970).

3. B. PARRINGTON and R. F. CHILDS. J. Chem. Soc. Chem. Commun. 1581 (1970).
4. R. NOYORI, Y. OHNISHI, and M. KATÔ. J. Am. Chem. Soc. **94**, 5105 (1972); **97**, 928 (1975); J. W. PAVLIK and J. KWONG. J. Am. Chem. Soc. **95**, 7914 (1973); J. W. PAVLIK and R. J. PASTERIS. J. Am. Chem. Soc. **96**, 6107 (1974).
5. N. FILIPESCU and J. W. PAVLIK. J. Am. Chem. Soc. **92**, 6062 (1970).
6. H. HART and T. TAKINO. J. Am. Chem. Soc. **93**, 720 (1971); H. HART. Pure Appl. Chem. **33**, 247 (1973).
7. R. F. CHILDS and Y-C. HOR. Can. J. Chem. This issue.
8. J. GRIFFITH and H. HART. J. Am. Chem. Soc. **90**, 5297 (1968).
9. T. SATO, G. IZUMI, and T. IMAMURA. J. Chem. Soc. Perkin Trans. 1, 788 (1976); T. SATO, K. TAMURA, K. MARUYAMA, O. OGAWA, and T. IMAMURA. Chem. Lett. 295 (1976); H. HIRAI. J. Polym. Sci. Macromol. Rev. **11**, 47 (1976).
10. D. I. SCHUSTER, M. J. NASH, and M. L. KANTOR. Tetrahedron Lett. 1375 (1964).
11. F. J. SOWA, G. F. HENNION, and J. A. NIEUWLAND. J. Am. Chem. Soc. **57**, 709 (1935).
12. M. S. CARPENTER and W. M. EASTER. J. Org. Chem. **20**, 401 (1955).
13. T. COLCLOUGH, W. GERRARD, and M. F. LAPPERT. J. Chem. Soc. 907 (1955); W. GERRARD. *In* The organic chemistry of boron. Academic Press, London. 1961. p. 34.
14. R. F. CHILDS and B. D. PARRINGTON. Can. J. Chem. **52**, 3303 (1974); S. M. BLACKSTOCK, K. E. RICHARDS, and G. J. WRIGHT. Can. J. Chem. **52**, 3313 (1974); G. A. OLAH and Y. K. MO. J. Org. Chem. **38**, 353 (1973).
15. H. J. MARIA, J. R. MACDONALD, and S. P. MCGLYNN. J. Am. Chem. Soc. **95**, 1050 (1973).
16. R. A. BOWIE and O. C. MUSGRAVE. J. Chem. Soc. C, 485 (1970); Y. OGATA, Y. IZAWA, H. TOMIOKA, and I. UKIGAI. Tetrahedron, 1817 (1969).
17. G. BÜCHI and E. M. BURGESS. J. Am. Chem. Soc. **82**, 4333 (1960); D. I. SCHUSTER and D. H. SUSSMAN. Tetrahedron Lett. 1657 (1970).
18. R. F. CHILDS. Chem. Commun. 946 (1969).
19. D. M. BROUWER, E. L. MACKOR, and C. MACLEAN. *In* Carbonium ions. Vol. 2. *Edited by* G. A. Olah and P. von R. Schleyer. Wiley-Interscience, New York. 1970. p. 837.
20. R. F. CHILDS, M. SAKAI, B. D. PARRINGTON, and S. WINSTEIN. J. Am. Chem. Soc. **96**, 6403 (1974).
21. K. E. HINE. Ph.D. Thesis. McMaster University, Hamilton, Ont. 1973.

Tricarbonylferrole iron tricarbonyl derivatives: formation from thiophenes and iron atoms in a CO atmosphere and fluxional behaviour

TRISTRAM CHIVERS[1] AND PETER L. TIMMS[2]

Department of Chemistry, The University of Calgary, Calgary, Alta., Canada T2N 1N4

Received May 13, 1977

TRISTRAM CHIVERS and PETER L. TIMMS. Can. J. Chem. **55**, 3509 (1977).

Co-condensation of metal atoms (Cr, Fe) with thiophenes 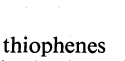 (R = R′ = H, Me; R = H, R′ = Me) at −196°C leads to desulphurization of the thiophene. Warm-up of the iron–thiophene co-condensate in a CO atmosphere produces derivatives of tricarbonylferrole iron tricarbonyl, $C_4H_2RR'Fe_2(CO)_6$. ^{13}C nmr studies of these complexes show that the tricarbonyl ferrole unit is static from −95°C to +60°C, while the π-$Fe(CO)_3$ group exhibits fluxional behaviour. Addition of dienes or Me_3P in hexane to the iron–thiophene co-condensate at −196°C yields thermally unstable red solutions on melting.

TRISTRAM CHIVERS et PETER L. TIMMS. Can. J. Chem. **55**, 3509 (1977).

La co-condensation d'atomes de métaux (Cr, Fe) avec les thiophènes 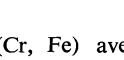 (R = R′ = H, Me; R = H, R′ = Me) à −196°C, conduit à la désulfuration de ces derniers. Le réchauffement du composé co-condensé thiophène–fer dans un atmosphère de CO, conduit aux dérivés du tricarbonyle tricarbonylferrole–fer $C_4H_2RR'Fe_2(CO)_6$. Les études par rmn du ^{13}C de ces complexes montre que la partie tricarbonylferrole est statique de −95°C à +60°C, alors que le groupe π-$Fe(CO)_3$ présente un comportement variable. L'addition de dienes ou du Me_3P dans l'hexane au composé co-condensé thiophène–fer à −196°C, conduit par fusion à des solutions rouges, thermiquement instables.

[Traduit par le journal]

Introduction

Since the first report of a π-complex of thiophene with a transition metal, viz. $(C_4H_8S)Fe(CO)_3$ (1, 2), numerous studies of related complexes have appeared (3–5) and corresponding cationic manganese complexes have been prepared(6). Bis(tetramethylthiophene)$Fe^{2+}(PF_6^-)_2$ has recently been isolated (7), but no neutral bis(thiophene)metal complexes are known although electrochemical reduction of this salt suggested the possibility of isolating bis(tetramethylthiophene)iron(0).

The direct synthesis of bis(arene)metal complexes from arenes and metal vapours at −196°C (8) is a versatile route to such complexes (9), and this approach has recently been extended to the synthesis of bis(2,6-dimethylpyridine)chromium (10). We describe here parallel investigations of the reactions of thiophenes with iron or chromium vapours at −196°C (for a preliminary communication see ref. 11), carried out as a possible source of bis(thiophene)metal(0) complexes.

[1]Author to whom correspondence should be addressed.
[2]Department of Chemistry, University of Bristol, Bristol, England.

Experimental

Apparatus and Techniques

Evaporation and low temperature co-condensation reactions of Fe and Cr were carried out in a glass apparatus previously described (12) and in a prototype of the commercially available Kontes metal atom reactor. Metals were evaporated from alumina-coated molybdenum wire crucibles at 25–30 A and 5–6 V. Solvents were dried, freshly distilled, and de-aerated before use.

The following instruments were used to obtain spectroscopic data: Perkin-Elmer 457 (ir spectra), Atlas CH5 (mass spectra), Varian HA100 (^1H nmr spectra), Bruker WH90 (^{13}C nmr spectra) operating in the pulsed Fourier transform mode at 22.63 MHz. The latter instrument is equipped with a Nicolet B-NC 12 data system. The ^{13}C chemical shifts were measured relative to tetramethylsilane as internal standard. Tris(acetylacetonato)chromium(III) (ca. 0.05 *M*) was added to each nmr sample to reduce T_1 relaxation times, and the spectra were recorded at various temperatures in the range −95°C to +60°C. The thiophenes were commercially available samples (Aldrich) and were used without further purification.

Iron, Thiophenes, and Carbon Monoxide

The typical reaction procedure is described here for 2,5-dimethylthiophene. Analogous products were ob-

tained from thiophene and 2-methylthiophene (see Discussion).

Iron (1.0 g, 18 mmol) was vaporized and condensed at −196°C with 2,5-dimethylthiophene vapour (20 g, 179 mmol) in 2 h. After addition of the thiophene, the reaction flask was allowed to slowly warm up under nitrogen. A deep purple-plum solution was observed when the co-condensate melted. The solution retained this colour up to ca. −20°C, whereupon it gradually became colourless with deposition of Fe metal. When the co-condensate was allowed to warm up under CO (½ atm), the solution remained purple up to ca. −30°C when CO uptake occurred and the solution became red-brown. Excess of thiophene was removed by vacuum transfer, and the residue was extracted with benzene (150 ml). The solution was filtered by forcing it under a pressure of N_2 through a stainless steel tube (1 mm diameter) with filter paper attached to one end. Benzene was removed from the clear red-brown filtrate by vacuum transfer to give a brown oil which was purified by chromatography on alumina using *n*-hexane. Orange crystals of tricarbonyl-2,5-dimethylferrole – iron tricarbonyl (mp 45°C) were obtained after solvent removal under vacuum. The yield was 91 mg or ca. 5% (allowing for 40% loss of the metal evaporated). *Anal.* calcd. for $C_{12}H_8Fe_2O_6$: C 40.0, H 2.24; found: C 39.9, H 2.35. The mass spectrum showed a molecular ion (M^+) at *m/e* 360 (59) together with major peaks at 332 (22), 304 (34), 276 (29), 248 (100), 220 (54), 192 (47) corresponding to the stepwise loss of six CO's from M^+. The infrared spectrum of the product was identical to that of an authentic sample prepared from $Fe_3(CO)_{12}$ and 2,5-dimethylthiophene by the literature procedure (13, 14).

The benzene-insoluble residue was washed several times with benzene, dried under vacuum, and ground up in a mortar before analyzing for sulphur. Values in the range 11–17% S were obtained for several residues resulting from the reactions with different thiophenes.

Vapour and liquid phase ir spectra and ^1H nmr spectra of the recovered volatiles provided no evidence for volatile products other than the recovered thiophene, with the exception of ir bands at 2970 (m) (aliphatic C—H) and 911 (m) cm^{-1} in the vapour phase ir spectrum of the volatiles from the reaction with thiophene.

Chromium, Thiophene, and Carbon Monoxide

Chromium (1.5 g, 29 mmol) was vaporized and condensed at −196°C with thiophene (12 g, 143 mmol) during 1.5 h. The co-condensates were allowed to melt under a nitrogen atmosphere to give a yellow-brown solution which became colourless at room temperature (15).[3] Excess of thiophene was removed in vacuo and the dark-green solid residue was washed with hexane and benzene, dried under vacuum (25°C; 10^{-2} Torr), and analyzed for sulphur. Found S = 13.5%. The ir spectrum (Nujol) showed no bands (other than Nujol) in the 2000–600 cm^{-1} region.

In a separate experiment the chromium-2,5-dimethylthiophene co-condensate was allowed to warm up under a CO atmosphere (0.5 atm). The solution was orange-brown on melting but colourless at room temperature. Excess of thiophene was removed under vacuum to give a pale-yellow solid (on the sides of the reaction flask), insoluble in benzene and involatile at 50°C/10^{-2} Torr. This solid became green in air and showed no bands in the 2000–600 cm^{-1} region of the ir spectrum. After drying under vacuum, the sulphur content of this solid was 11.4%. Infrared spectra of the volatile products (vapour phase and liquid film) showed no peaks other than those attributable to 2,5-dimethylthiophene.

Synthesis of Tricarbonylferrole Iron Tricarbonyl Derivatives from Iron Carbonyls

For comparison with the products from the iron atom – thiophene–CO reactions and for spectral measurements, tricarbonylferrole iron tricarbonyl and the 2-methyl, 3-methyl, and 2,5-dimethyl derivatives were prepared from the appropriate thiophene and $Fe(CO)_5$ or $Fe_3(CO)_{12}$ according to the literature procedures (13, 14). The 2-methyl and 3-methyl compounds were obtained as orange oils, after chromatography on alumina, and their ir and mass spectra were entirely consistent with the spectra expected for tricarbonylferrole iron tricarbonyl derivatives.

Results and Discussion

Co-condensation Reactions

The co-condensation of Cr atoms with thiophenes at −196°C produces yellow-brown solutions on melting which become colourless at room temperature. Analysis of the solid residues for sulphur, after removal of excess of thiophene, gave values in the range 10–13.5%, demonstrating that desulphurization of the thiophene had occurred. There was no evidence for the formation of a thermally stable organometallic product.

Similarly the co-condensation of Fe atoms with thiophene, 2-methyl- or 3-methyl-, or 2,5-dimethylthiophene at −196°C gives a plum-coloured matrix which retains its colour on melting up to ca. −20°C but becomes colourless at room temperature. After removal of excess ligand, the solid residues gave values in the range 11–17% for sulphur. When the iron–thiophene co-condensate was allowed to warm up in an atmosphere of CO, orange-brown crystals of **1** or **4** were isolated in low yield. The compounds **2** and **3** were obtained as orange oils.

Nature of the Iron–Thiophene Co-condensate

The isolation of the organometallic complexes **1**–**4** confirms that thiophenes are desulphurized after co-condensation with iron vapour at −196°C. It has previously been observed that tricarbonylferrole derivatives are formed via desulphurization of thiophenes by iron car-

[3]The reaction of thiophene with chromium atoms has been reported to give a dark, involatile product insoluble in the common organic solvents, but no details were given.

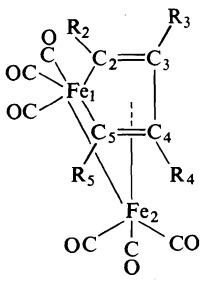

1 $R_2 = R_3 = R_4 = R_5 = H$
2 $R_2 = CH_3$; $R_3 = R_4 = R_5 = H$
3 $R_3 = CH_3$; $R_2 = R_4 = R_5 = H$
4 $R_2 = R_5 = CH_3$; $R_3 = R_4 = H$
5 $R_2 = R_5 = t$-Bu; $R_3 = R_4 = H$

bonyls (13). In the metal atom reactions, it is necessary to decide whether desulphurization occurs immediately on co-condensation or on warm-up of an unstable (thiophene)$_2$metal complex, which may involve σ- or π-coordination of thiophene to iron (16[4], 17[5]) or a combination of both.

The following observations and experiments indicate that the former pathway predominates. (*a*) Whereas the thermal stability of (arene)$_2$Fe complexes increases markedly with alkyl substitution on the arene ligand, the thermal stability of the plum-coloured Fe–thiophene co-condensates appears to be independent of alkyl substitution on the thiophene. (*b*) Addition of cyclopentadiene to an Fe–benzene co-condensate at −196°C produces ferrocene in 40% yield (8), but no ferrocene is obtained when an Fe–thiophene co-condensate is treated in a similar manner. (*c*) No (thiophene)Cr(CO)$_3$ was obtained from warm-up of the Cr–thiophene co-condensate in a CO atmosphere.

We therefore pursued the possibility that the Fe–thiophene co-condensate contained ferroles e.g. 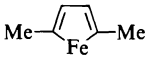 which might be trapped by the addition of suitable ligands, e.g. dienes, Me_3P (18).[6] When trimethylphosphine (20% solution in *n*-hexane) was added to an Fe–2,5-dimethylthiophene co-condensate at −196°C, a bright-red solution was observed on melting. At 0°C the red colour was much less evident, and the solution became orange-yellow with deposition of some black solid at 20°C. No derivatives of the type described by Rathke and Muetterties (18) could be isolated. Similarly, the addition of dienes, e.g. butadiene, 1,5-cyclooctadiene to Fe–thiophene co-condensates at −196°C gave, on melting, red solutions which were unstable above ca. −20°C. Thus the exact nature of the species responsible for the plum colour of the Fe–thiophene co-condensate remains uncertain.

Tricarbonylferrole Derivatives: ^1H Nuclear Magnetic Resonance Spectra

The ^1H nmr spectra and crystal structure of $C_4H_4Fe_2(CO)_6$ have been reported recently (14). The spectrum was analyzed as an AA′XX′ system and chemical shifts of 6.2 and 6.8 ppm, respectively, were assigned to the pairs of protons $H_{2,5}$ and $H_{3,4}$ (the subscripts refer to the carbon atoms to which the hydrogens are attached in **1**). The coupling constants are indicated in Table 1 together with our data for the tricarbonylferrole derivatives **2**–**4** which suggest that the chemical shift assignments reported for **1** (14) should be reversed. For the 2,5-dimethyl derivative, **4**, two singlets are observed at 5.82 ppm and 2.30 ppm and these can readily be assigned to ferrole protons and methyl substituents respectively. The ^1H nmr spectrum of the ferrole protons of the 2-methyl derivative, **2**, is that of an AMX system. In addition to the signal for the methyl group, three equally intense signals are observed at 6.66, 6.18, and 5.94 ppm, which appear as two doublet of doublets and a triplet, respectively. The triplet clearly arises accidentally as a result of two approximately equal couplings to non-equivalent protons as expected for H_3 on the basis of coupling constants reported for **1**. The assignment of the other two signals to H_4 or H_5 is, at this stage, ambiguous. The ^1H nmr spectrum of the 3-methyl derivative, **3**, showed two doublets at 6.84 and 6.37 ppm, respectively, and a doublet of doublets at 6.14 ppm, in addition to the signal for the methyl substituent. From the data for compound **1** in Table 1, the larger doublet (6.84 ppm) is assigned to H_5 and the smaller doublet (6.37 ppm) to H_2. Thus the signal at 6.14 ppm must be due to H_4, which

[4]The detection of CrS^+ in the mass spectrum of $(C_4H_8S)Cr(CO)_3$ suggests that σ-bonding of sulphur to chromium is important in the $C_4H_8SCr^+$ ion.

[5]The σ-bonded thiophene complex, (2-methyl,5-diethylborylthiophene)chromium pentacarbonyl has recently been described.

[6]The novel iron heterocycle 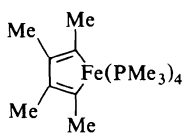 has recently been isolated and is described as a blue, highly volatile solid of high thermal reactivity. It was purified by vacuum sublimation at 40°C.

TABLE 1. ^{1}H nmr data for tricarbonylferrole iron tricarbonyl derivatives

Compound	δ (ppm)[a]					J (Hz)			
	H_2	H_3	H_4	H_5	CH_3	$H_{23}(=H_{45})$	H_{34}	$H_{24}(=H_{35})$	H_{25}
1[b]	6.2	6.8	6.8	6.2	—	5.3	2.4	2.3	0
2	—	5.94(dd)	6.18(t)	6.66(dd)	2.41(s)	5.26	2.34	2.34	—
3	6.37(d)	—	6.14(dd)	6.84(d)	2.25(s)	5.18	—	2.73	—
4	—	5.82(s)	5.82(s)	—	2.30(s)	—	—	—	—

[a]s, singlet, dd, doublet of doublets, t, triplet. Recorded in $CDCl_3$ solution with tetramethylsilane (0 ppm) as internal reference.
[b]Data from ref. 14.

shows two couplings of ca. 5.2 and 2.7 Hz, as expected. The high field signal therefore corresponds to the ferrole proton remote from the iron atom, and this assignment together with the chemical shift (5.82 ppm) of the ferrole protons in **4** suggests that the signals at 6.66 and 6.18 ppm in **2** can be assigned to H_5 and H_4, respectively. We, therefore, propose that the reported assignments for the ferrole protons in **1** should be reversed, i.e. $\delta_{H_2} = \delta_{H_5} = 6.8$ ppm and $\delta_{H_3} = \delta_{H_4} = 6.2$ ppm. Thus the chemical shifts of the protons (H_2, H_5) nearest to iron in tricarbonylferrole derivatives are consistently to high field of the chemical shift for the remote protons (H_3, H_4).

^{13}C *Nuclear Magnetic Resonance Spectra and Fluxional Behaviour*

The crystal structure of **1** shows that one of the CO groups of the π-bonded $Fe(CO)_3$ unit forms a highly unsymmetrical bridge to the other iron atom (Fe_1) (14). This structural feature has been observed in a number of other (19–21), but not all (22), tricarbonylferrole iron tricarbonyl derivatives. The static structure suggests, therefore, that such molecules should exhibit four carbonyl resonances with relative areas of 2:2:1:1. A number of recent ^{13}C nmr studies have shown, however, that in solution the π-$Fe(CO)_3$ group is stereochemically nonrigid. For example, the 3 carbonyl resonances of this group in the tricarbonylferrole derivative ($R_2 = R_4 = CH_3$; $R_3 = R_5 = C{\equiv}CCH_3$) remain magnetically equivalent down to −78°C (23). Similarly, the derivative in which $R_2 = R_5 = Ph$; $R_3 = R_4 = H$ shows an unchanged ^{13}C nmr spectrum over the temperature range −125°C to +95°C (21), although other authors (24)[7] report significant broadening at −75°C. It was suggested that the area 3 resonance was due either to a coincidental overlap of two signals or to a very low energy fluxional process (21). Resolution of the ^{13}C signals of the π-$Fe(CO)_3$ group has been reported for compound **5** ($R_2 = R_5 = t$-Bu) (24). At −100°C two signals (intensities 2:1) were observed at 214.1 and 222.2 ppm. This result suggests that a fluxional process is indeed responsible for the apparent equivalence of carbonyl groups on Fe_2 at higher temperatures, and that the steric bulk of the *tert*-butyl group results in a higher activation energy for rotation of the π-$Fe(CO)_3$ group in **5** compared to other tricarbonylferrole derivatives.

Our ^{13}C nmr data for compounds **2–4** are compared with the literature data for **1** (21) and **5** (25) in Table 2. Methyl substitution results in a deshielding of the ferrole ring carbon signals by 20–25 ppm. A similar deshielding is observed for phenyl (21) and *tert*-butyl substituents (25). Compounds **2–4** show three sharp resonances at room temperature with relative intensities 3:1:2. The area 3 resonance was not significantly broadened down to −95°C suggesting that the exchange of the CO groups on Fe_2 via rotation of the $Fe(CO)_3$ unit has a lower activation energy for compounds **2–4** compared with **5**. There was no evidence for exchange between carbonyls on Fe_1 and Fe_2 at higher temperatures (+60°C, see also ref. 21) and, thus, in solution the two $Fe(CO)_3$ groups in these complexes behave independently despite the observation of a *semi-bridging* CO in the solid state structure (*vide supra*). The loss of the plane of symmetry which bisects C_3–C_4 results in distinct signals for C_3 and C_4 in **2** and for C_2 and C_5 in **3**. For the same reason the equatorial CO's on Fe_1 are no longer equivalent in **2** and **3**, although separate signals could only be resolved for **2**.

It is instructive to compare these results with the extensive studies of the fluxional behaviour

[7]This paper also reports some ^{13}C nmr data for various methylsubstituted tricarbonylferrole iron tricarbonyls, including **4**, but they were not obtained as pure samples, and thus the carbonyl carbon signals were not resolved.

TABLE 2. ^{13}C nmr data for tricarbonylferrole iron tricarbonyl derivatives

	δ (ppm)[a]							
Compound	CH_3	C_2	C_3	C_4	C_5	Unique CO on Fe_1	Equivalent CO's on Fe_1	CO's on Fe_2
1[b]	—	154.9	110.6	110.6	154.9	209.0	206.9	211.1
2	32.1	180.8	110.6	110.3	152.9	209.8	207.2 206.9	212.3
3	19.4	154.7	131.1	112.3	151.8	209.8	207.1	211.7
4	32.2	178.3	110.4	110.4	178.3	210.4	206.8	213.7
5[c]	—	197.0	109.7	109.7	197.0	211.6 (211.8)	208.9 (209.1)	216.7 222.2 214.7

[a]For conditions of measurement see Experimental section.
[b]Data from ref. 21. The pattern of the CO signals does not change in the temperature range −125°C to +95°C.
[c]Data from ref. 24; values in parenthesis are for −100°C. The *tert*-butyl group shows signals at 33.7 (CH_3) and 43.1 (*C*) ppm.

of (η-diene)$Fe(CO)_3$ derivatives carried out by Kruczynski and Takats (25) who found a marked dependence of the rate of carbonyl scrambling on the nature of the diene. For nonconjugated dienes, e.g. cycloocta-1,5-diene, no evidence for line broadening was observed even at the lowest accessible temperatures (−130°C), whereas for conjugated 1,3-dienes, e.g. butadiene, the activation barrier was sufficiently large to be observable by nmr. This difference was attributed to significant contributions from six-coordinate structures (B) in the case of conjugated dienes and the relative unimportance of such contributions in complexes with nonconjugated dienes.

Our results suggest that, in contrast to the general accepted bonding description for butadiene iron tricarbonyl (25, 26) back-bonding between filled metal *d* orbitals and the LUMO (π_3*) of the diene is an unimportant component of the ligand–metal bonding in tricarbonylferrole iron tricarbonyl derivatives. For the tricarbonylferrole ligand there is good evidence from X-ray structural data for multiple bonding in the Fe—C bonds of the ferrole ring (14).Thus these bonds are 1.94–1.95 Å compared to 2.08–2.12 Å expected for the sum of the covalent radii of iron and carbon. Such multiple bonding can arise via interaction of d_{xz} and d_{yz} on Fe_1 with π_3* of butadiene. This electron donation would greatly diminish contributions to π_3* from the π-bonded $Fe(CO)_3$ group and hence six-coordinate structures would be less important in the bonding of tricarbonylferrole $Fe(CO)_3$ complexes compared to $C_4H_6Fe(CO)_3$. This conclusion is in accord with the observed low activation energies for carbonyl exchange in ferrole complexes and provides further support for the arguments used by Kruczynski and Takats to explain the dynamic behaviour of (diene)$Fe(CO)_3$ compounds (25).

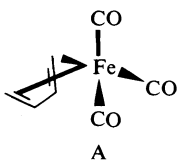

A

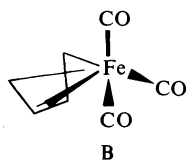

B

Acknowledgements

Most of this research was carried out at the University of Bristol and supported by the Science Research Council. One of the authors (T.C.) is grateful to the National Research Council of Canada and to the Royal Society and Nuffield Foundation for financial support which enabled this work to be carried out while on leave from the University of Calgary. Thanks are also due to Mrs. Eileen Gilmour for experimental assistance and to Dr. R. Yamdagni for recording the ^{13}C nmr spectra at the University of Calgary.

1. E. O. FISCHER and K. OFELE. Z. Naturforsch. **133**, 458 (1958); Chem. Ber. **91**, 2395 (1958).
2. M. F. BAILEY and L. F. DAHL. Inorg. Chem. **4**, 1306 (1965).
3. R. GUILARD, J. TIROUFLET, and P. FOURNARI. J. Organomet. Chem. **33**, 195 (1971), and references cited therein.
4. (*a*) H. LUMBROSO, C. SEGARD, and B. ROQUES. J. Organomet. Chem. **61**, 249 (1973); (*b*) C. SEGARD, C. POMMIER, B. ROQUES, and G. GUIOCHON. J. Organomet. Chem. **77**, 49 (1974).
5. M. NOVI, G. GUANTI, and C. DELL'ERBA. J. Heterocycl. Chem. **12**, 1055 (1975).
6. H. SINGER. J. Organomet. Chem. **9**, 135 (1967).
7. D. M. BRAITSCH and R. KUMARAPPAN. J. Organomet. Chem. **84**, C37 (1975).

8. P. L. TIMMS. Chem. Commun. 1033 (1969).
9. (*a*) V. GRAVES and J. J. LAGOWSKI. Inorg. Chem. **15**, 577 (1976); (*b*) P. S. SKELL, D. L. WILLIAMS-SMITH, and M. J. MCGLINCHEY. J. Am. Chem. Soc. **95**, 3337 (1973); (*c*) F. W. S. BENFIELD, M. L. H. GREEN, S. J. OGDEN, and D. YOUNG. J. Chem. Soc. Chem. Commun. 866 (1973); M. T. ANTHONY, M. L. H. GREEN, and D. YOUNG. J. Chem. Soc. Dalton Trans. 1419 (1975); (*d*) K. J. KLABUNDE and H. F. EFNER. Inorg. Chem. **14**, 789 (1975).
10. L. H. SIMONS, P. E. RILEY, R. E. DAVIS, and J. J. LAGOWSKI. J. Am. Chem. Soc. **98**, 1044 (1976).
11. T. CHIVERS and P. L. TIMMS. J. Organomet. Chem. **118**, C37 (1976).
12. R. MIDDLETON, J. R. HULL, S. R. SIMPSON, C. H. TOMLINSON, and P. L. TIMMS. J. Chem. Soc. Dalton Trans. 120 (1973).
13. H. D. KAESZ, R. B. KING, T. A. MANUEL, L. D. NICHOLS, and F. G. A. STONE. J. Am. Chem. Soc. **82**, 4749 (1960).
14. G. DETTLAF and E. WEISS. J. Organomet. Chem. **108**, 213 (1976).
15. V. GRAVES and J. J. LAGOWSKI. Inorg. Chem. **15**, 577 (1976).
16. YU. S. NEKRASOV and N. I. VASYUKOVA. J. Organomet. Chem. **122**, 227 (1976).
17. H. NOTH and U. SCHUCHARDT. J. Organomet. Chem. **125**, 155 (1977).
18. J. W. RATHKE and E. L. MUETTERTIES. J. Am. Chem. Soc. **97**, 3272 (1975).
19. (*a*) A. A. HOCK and O. S. MILLS. Acta Crystallogr. **14**, 139 (1961); (*b*) P. Y. DEGRÈRE, J. MEUNIER-PIRET, M. VAN MEERSSCHE, and P. PIRET. Acta Crystallogr. **23**, 119 (1967).
20. H. B. CHIN and R. BAU. J. Am. Chem. Soc. **95**, (1973) 5068.
21. L. J. TODD. J. P. HICKEY, J. R. WILKINSON, J. C. HUFFMAN, and K. FOLTING. J. Organomet. Chem. **112**, 167 (1976).
22. J. A. D. JEFFREYS and C. M. WILLIS. J. Chem. Soc. Dalton Trans. 2169 (1972).
23. F. R. YOUNG, D. H. O'BRIEN, R. G. PETTERSEN, R. A. LEVENSON, and D. L. VON MINDEN. J. Organomet. Chem. **114**, 157 (1976).
24. S. AUNE, L. MILONE, and E. SAPPA. J. Chem. Soc. Dalton Trans. 839 (1976).
25. L. KRUCZYNSKI and J. TAKATS. Inorg. Chem. **15**, 3140 (1976), and references cited therein.
26. M. ELIAN and R. HOFFMANN. Inorg. Chem. **14**, 1058 (1975).

Homogeneous catalysis of deuterium transfer by potassium hydroxide and potassium methoxide D_2–H_2O and D_2–CH_3OH exchange[1]

GRAEME G. STRATHDEE, DAVID M. GARNER, AND RUSSELL M. GIVEN

Atomic Energy of Canada Limited, Whiteshell Nuclear Research Establishment, Pinawa, Man., Canada R0E 1L0

Received February 25, 1977

GRAEME G. STRATHDEE, DAVID M. GARNER, and RUSSELL M. GIVEN. Can. J. Chem. **55**, 3515 (1977).

The kinetics and mechanism of exchange of deuterium between D_2 and water and between D_2 and methanol, catalyzed respectively by concentrated potassium hydroxide and potassium methoxide, has been studied between 348 and 398 K. In the D_2–KOH–H_2O case, the transfer of deuterium was found to be controlled by the rate of activation of the D_2 molecule by OH^-. Rapid exchange of D^+ with the aqueous solution followed. From the D_2–$KOCH_3$–CH_3OH studies, it was concluded that deuterium exchange depended upon the rates of both D_2 activation by methoxide and interaction of the solvent with the transition, or encounter, complex. The dependence of second-order rate constants on solvent activity for both systems was determined by normalization of the exchange reaction rates to unit reagent activity. Analysis of the kinetic isotope effects for each system suggested that their increase with base concentration or temperature was due to solvation effects.

GRAEME G. STRATHDEE, DAVID M. GARNER et RUSSELL M. GIVEN. Can. J. Chem. **55**, 3515 (1977).

On étudie entre 348 K et 398 K les cinétiques et le mécanisme d'échange du deutérium entre D_2 et l'eau puis entre D_2 et le méthanol, catalysé respectivement par des solutions concentrées d'hydroxyde de potassium et de méthylate de potassium. Dans le cas D_2–KOH–H_2O, le transfert du deutérium semble être contrôlé par la vitesse d'activation de la molécule D_2 par l'ion OH^-. Un échange rapide de l'ion D^+ avec la solution aqueuse s'en suit. A partir des études faites sur D_2–$KOCH_3$–CH_3OH, on en déduit que l'échange du deutérium dépend de la vitesse d'activation de D_2 par le méthylate et de la vitesse d'interaction du solvant avec le complexe de transition ou rencontre. La dépendance des constantes de vitesse du second ordre sur l'activité du solvant pour les deux systèmes est déterminée par normalisation des vitesses d'échange par unité d'activité du réactif. L'analyse des effets isotopiques cinétiques pour chaque système suggère que leur augmentation avec la concentration en base ou la température est due à des effets de solvatation.

[Traduit par le journal]

Introduction

Strong bases such as alkali metal hydroxides (1–6), alkoxides (4), amides (7, 8), and alkylamides (9–11) are effective homogeneous catalysts for the exchange of deuterium between D_2 and their corresponding protic solvents. The general pattern of reactivity of these catalyst systems is well known: the nitrogen bases are substantially better for the D_2-exchange application than are the oxygen bases and alkyl substitution of the amide anion, NH_2^-, yields higher specific rate constants for this proton transfer process. The present research has dealt mainly with the relative activity of aqueous KOH with respect to methanolic $KOCH_3$ and has allowed us to make a better comparison of the performance of these oxygen bases with that of KNH_2 in ammonia or $KNHCH_3$ in methylamine.

We have also investigated in detail the mechanism of deuterium transfer from D_2 to the protic solvent. The solution properties were nonideal because of the high electrolyte concentrations. To enable us to analyze the data at unit activity of the reagents we have evaluated the activities of the solutes and solvent in both the D_2–KOH–H_2O and D_2–$KOCH_3$–CH_3OH systems. Our kinetic studies have shown that in these solutions where the proportion of 'free' solvent is small, the manner in which the solvent participates in the proton transfer process may be defined. The mechanism which we propose to explain our results requires that D—D bond-breaking and solvation steps are of comparable importance in determining the overall rate of the exchange reaction. In this respect our con-

[1]Issued as AECL No. 5871.

clusions differ from that of Ritchie and King (12) who have argued that solvation is of greater importance.

It was also our intent to investigate why the oxygen bases promote D_2 exchange at rates which are unattractive from the chemical processing standpoint. Solutions of these catalysts are thermally stable and easily handled and are therefore of interest because of potential application for heavy water production, for example, in a bithermal hydrogen–water system. By describing the mechanism of proton transfer we hoped to assess if chemical modification of the system would lead to enhancement of rates of exchange.

Experiment

Purifications

Deuterium gas was C.P. grade (Matheson) and was used as received or was evolved from uranium deuteride (UD_3) at 723 K. The UD_3 was formed by reaction of commercial D_2 with uranium metal turnings at 600 K. No difference between exchange rates was found using D_2 from these sources. Water was distilled and deionized. Methanol was percolated through a bed of Linde 4A molecular sieves and distilled under dry nitrogen.

Preparations

Hydroxide solutions were made gravimetrically with reagent grade KOH. Alkoxide solutions were prepared by dissolution of the alkali metal in freshly distilled methanol. The metal was handled in a nitrogen filled glove box. The solution concentrations were determined by acid titration.

Procedures

The transfer of deuterium from D_2 gas to the protic solvents was followed by sampling the gas phase of a stirred two-phase reactor and by analyzing the gas for D_2, HD, and H_2 mass spectrometrically. The exchange reactions were run in either a 116 cm^3 Pyrex glass cell or in a glass-lined 248 cm^3 stainless steel autoclave, depending upon the total pressure at the operating temperature. The gas space – solution volume ratio was 7.7 in each case. Stirring speeds were always above 25 Hz to maintain satisfactory dispersion of the gas in the solution. Reaction rates were independent of agitation speed under those conditions. Constant temperatures were obtained by circulating a hydrocarbon oil from a thermoregulated bath through fluid-jackets around the reaction cells.

In other experiments, solubilities of H_2 in methanol and in alkali metal methoxide solutions in methanol were measured by gas chromatography using our dissolved gas stripping technique (13). The solutions were saturated with H_2 at known pressure and temperature. Liquid samples were withdrawn into a 1 cm^3 sampling valve loop, and were injected into a 10 cm^3 stripping cell held at room temperature. Sampling valves and all lines were heated to avoid precipitation of methoxides from the concentrated solutions. The partial pressure of H_2 in the autoclave was readjusted after each sampling step.

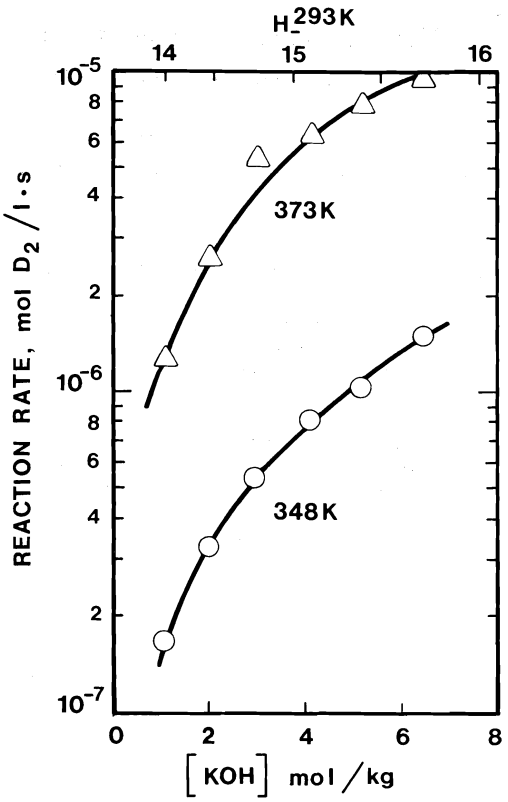

FIG. 1. Rate of D_2–H_2O exchange catalyzed by KOH.

Results

In this section, D_2 exchange rate, physical property, and kinetic isotope effect data are presented for both the D_2–KOH–H_2O and D_2–$KOCH_3$–CH_3OH cases. Our method of calculation of rate constants is considered in the section on Treatment of Data. The two systems are compared in the Discussion.

Deuterium Exchange Rates

D_2–KOH–H_2O

The rates of exchange of D_2 with water catalyzed by KOH at 348 and 373 K are shown in Fig. 1 as a function of KOH molality. The rates were calculated as described later in the section on Treatment of Data. These rates are essentially the same as those quoted by Flournoy and Wilmarth (3) and by Schindewolf (4). A plot of log exchange against log base concentration showed that the apparent reaction orders in hydroxide were greater than unity, although in dilute solution Wilmarth and co-workers have

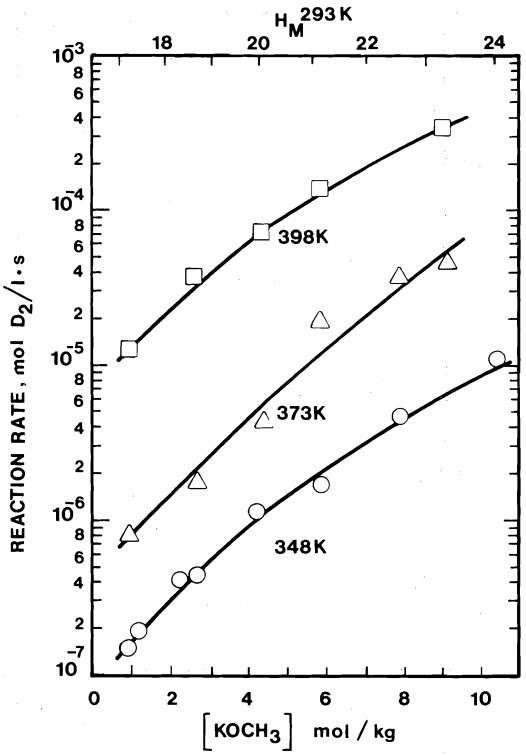

FIG. 2. Rate of D_2–CH_3OH exchange catalyzed by $KOCH_3$.

shown that the rate law for deuterium transfer contains first-order terms in hydroxide and D_2 (2). The remainder of this paper deals with the factors which contribute to the form of these results.

For reference purposes, the H_- basicity scale at 293 K for these aqueous KOH solutions (14) has been included on the upper abscissa of Fig. 1. It is noteworthy that for a unit increase in H_- (factor of 10 in basicity) there is approximately a 5-fold increase in D_2 reaction rate. This topic is also considered later in the Discussion.

D_2–$KOCH_3$–CH_3OH

In Fig. 2, the D_2 exchange rate data for the D_2–$KOCH_3$–CH_3OH system are presented for 348, 373, and 398 K as a function of base concentration. The absolute rates are very similar to those reported for the D_2–KOH–H_2O case, although there is somewhat less curvature on this logarithmic plot at high concentrations. The apparent order of the exchange reaction in $KOCH_3$ at 373 K, obtained from a plot of log (rate) against log [$KOCH_3$], increased from 1 at low concentration to about 3 above 4 mol/kg. The H_M basicity scale for these solutions determined at 20°C (15*a*) is shown as the upper scale of Fig. 2. As was the case with the D_2–KOH–H_2O system, the exchange rates increased by approximately a factor of 5 per unit of H_M.

Activities and Activity Coefficients

Our results for each system will be discussed in this order: activity coefficients for dissolved H_2, activity of the solvent, activity coefficient of the solute base. For the D_2–KOH–H_2O ternary mixture, data were available in the literature. For the D_2–$KOCH_3$–CH_3OH solutions, our new data were employed to derive the appropriate functions. In each case the mean activity coefficient for the catalyst was calculated from solvent vapour pressure data by integration of the Gibbs-Duhem equation as discussed below. All activity coefficients for D_2 and KOH were unsymmetrically normalized (16) and refer to the standard state of infinitely dilute base. The subscripts 1, 2, and 3 refer to the solvent, D_2, and base respectively.

D_2–KOH–H_2O

Shoor, Walker, and Gubbins (17) have reported activity coefficients for H_2 in water at temperatures up to 373 K, and their results have been used to calculate the activity of D_2 in our aqueous solutions. It is probable that D_2 is slightly more soluble than H_2 in aqueous KOH (5, 18) but in the absence of specific data we have employed results for H_2. The activity coefficient for H_2 does not vary with temperature between 298 and 373 K (17) and for a given KOH molality c, it is given by $\gamma_2^* = 10^{0.129c}$ as shown in Fig. 3.

The activity of water was calculated from the ratio of the vapour pressure of the aqueous KOH solution to that of pure water at the temperature of interest using the data of Anisimov (19). The activity of water for a given KOH mole fraction x_3 was essentially independent of temperature. The activity coefficients were calculated using the usual relation $\gamma_1 = a_1/x_1$ and are summarized in Fig. 3 for 373 K.

To calculate the activity coefficients for KOH from the activity of the solvent we employed the integral form of the Gibbs-Duhem equation:

$$[1] \quad \log \gamma_3^* = -\int_{\gamma_1=1}^{\gamma_1=\gamma_1} (x_1/x_3)\, d \log \gamma_1$$

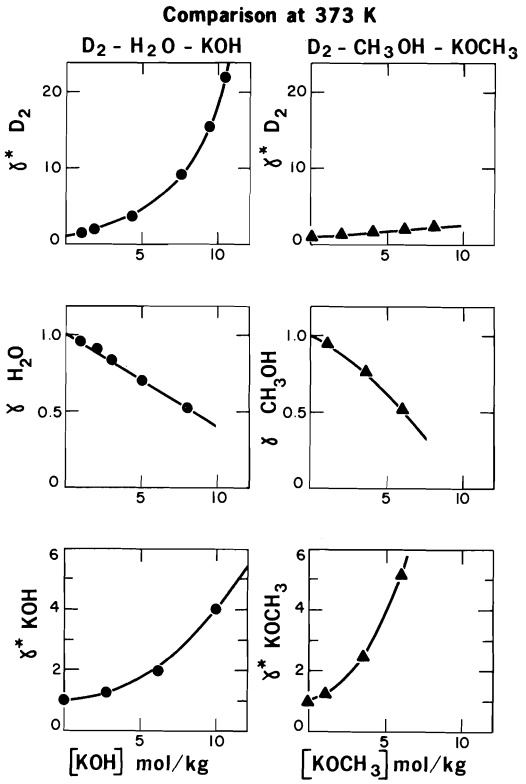

FIG. 3. Comparison of activity coefficients for D_2, the solvent, and the base for each exchange reaction mixture at 373 K. In the text, the subscripts 1–3 refer to solvent, D_2, and base respectively.

It was assumed that the resultant binary solution activity coefficients could be used for our three-component system calculations because the mole fraction of D_2 was exceedingly low. The right-hand side of eq. 1 was made explicit in x_1 by differentiation of $\log \gamma_1 = \log a_1 - \log x_1$:

$$[2] \qquad d \log \gamma_1 = [f'(x_1) - x_1^{-1}]\, dx_1$$

in which $f'(x_1)$ was the first derivative of the computer-fit polynomial $\log a_1 = f(x_1)$. Also, we made the approximation $x_3^{-1} = (1 - x_1)^{-1}$ and expanded that as a binomial series in x_1. Since $f(x_1)$ for the KOH–H_2O system using Anisimov's data for 373 K was:

$$[3] \quad \log a_1 = -10.6216 + 20.6578x_1 - 10.0365x_1^2$$

eq. 1 became:

$$[4] \quad \log \gamma_3^* = 4.0144x_1^5 - 0.1463x_1^4 + 0.0500x_1^3 - 10.1115x_1^2 + 0.434x_1 + 13.791$$

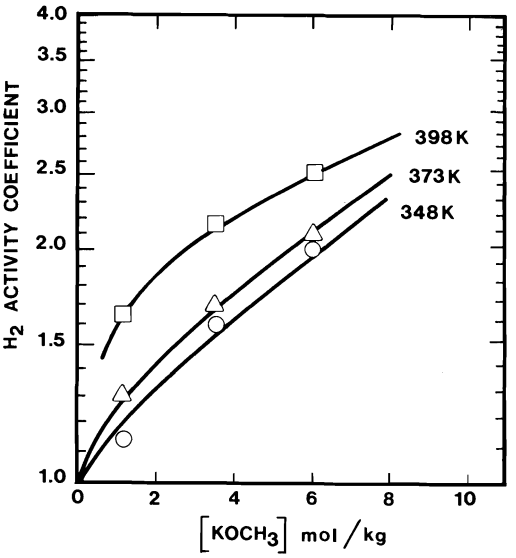

FIG. 4. Dependence of activity coefficients for H_2 in methanol on $KOCH_3$ concentration.

between the integration limits of $x_1 = 1$ to $x_1 = x_1$. These equations are valid up to a KOH molality of 8 mol/kg. The values for γ_3^* plotted in Fig. 3 apply to both 348 and 373 K since [4] holds at each temperature. Activity coefficients calculated in this way are similar to those tabulated by Robinson and Stokes for aqueous KOH up to 6 kmol/m^3 (6.55 mol/kg) at 298 K (20).

D_2–$KOCH_3$–CH_3OH

Solubilities of H_2 in methanolic $KOCH_3$ were measured by the solution purging method described in the Experiment section. The resultant data were treated in the same way as those of Shoor *et al.* (17) for the aqueous KOH system. The effect of $KOCH_3$ concentration c_3 on H_2 solubility was slight, and our results are summarized in Fig. 4 as a plot of activity coefficient γ_2^* values for H_2 in each catalyst solution at each temperature. Presumably, dissolution of H_2 is less affected by $KOCH_3$ concentration in methanol than by KOH in water because the free energy of cavity formation for the small H_2 molecule is much less in the methanolic system. The greater molar volume of methanol compared with water is consistent with the lesser dependence of γ_2^* on c_3 in the methanolic case.

The vapour pressures of methanolic $KOCH_3$ solutions were measured and used to calculate solvent activities and activity coefficients.

Activities, $a_1 = P/P_0$ where P and P_0 are the solution and pure solvent vapour pressures respectively, were found to be independent of temperature and the correlation given by [8] held between 348 and 398 K.

Potassium methoxide activity coefficients were calculated from those of the solvent by using [1] and [2] in which:

$$[5] \quad \log a_1 = f(x_1) = -7.6312 + 14.0291x_1 - 6.3919x_1^2$$

This gave

$$[6] \quad \log \gamma_3^* = 2.5568x_1^5 - 0.3113x_1^4 - 0.2704x_1^3 - 6.7975x_1^2 + 0.4340x_1 + 4.3884$$

which holds up to 10 mol/kg $KOCH_3$ in methanol. The results for 373 K are shown in Fig. 3 together with those for aqueous KOH.

The greater dependence of γ_3^* for $KOCH_3$ in methanol compared to KOH in water was due mainly to the higher molecular weight of $KOCH_3$. For a given molal concentration, the former solution contained fewer moles of solvent than did the latter. This relative reduction of available solvent in the $KOCH_3$ solutions resulted in the greater sensitivity of γ_3^* to $KOCH_3$ concentration.

Kinetic Isotope Effects

We have defined the kinetic isotope effect (kie) to be the ratio of the best first-order rate constants, $2k_{HD}/k_{D_2}$, calculated by the procedure discussed later in the section on Treatment of Data. The factor of 2 is a statistical correction for the fact that although either end of the HD molecule can react, only removal of the D by base can be observed. The standard deviation on the calculated kie was usually much less than 10% of the value, particularly at large overall conversion of D_2 to yield the products HD and H_2.

D_2–KOH–H_2O

At both 348 and 373 K the kie was found to be greater than 1, as expected for a normal HD:D_2 kie. As illustrated in Fig. 5, at 348 K the kie was independent of KOH concentration, but at 373 K a significant increase of kie was found. Our kie data are similar to those of Schindewolf (4), who reported a kie of 1.42 ± 0.06 for D_2–H_2O exchange catalyzed by NaOH at 388 K, although the kie was independent of base concentration.

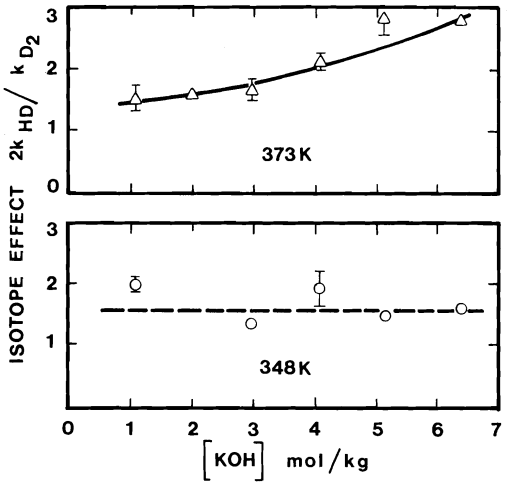

Fig. 5. Variation in the kinetic isotope effect for D_2–H_2O exchange with KOH concentration at 348 and 373 K.

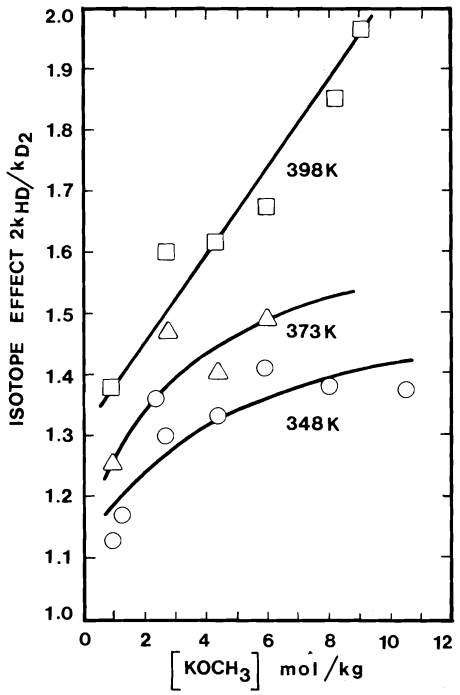

FIG. 6. Variation in the kinetic isotope effect for D_2–CH_3OH exchange with $KOCH_3$ concentration between 348 and 393 K.

D_2–$KOCH_3$–CH_3OH

The kie's for this system increased with base concentration at each temperature we selected. The scatter in the results at 348 and 373 K was primarily due to the low total conversion of D_2 for cases where the D_2 exchange rates were

slow. The trend of each set of data in Fig. 6 is clear. We believe these observations are due to a transition in the mode of solvent participation in the component steps of the deuterium transfer mechanism. This topic is dealt with in the Discussion.

Treatment of Data

Calculation of Exchange Rates

In-solution rates of exchange of D_2 to yield HD were calculated from the change of D_2 in the gas phase with the equation:

$$[7] \quad -\mathrm{d}[D_2]/\mathrm{d}t = \ln [(n_0 - n_e)/(n_t - n_e)]\, A/t$$

where n_0, n_t, and n_e represent the mol% D_2 at time $t = 0$, t, and at equilibrium, respectively. A is the total gas-to-liquid mole/volume ratio in moles D_2 per litre of solution at 293 K. The reaction rates which we quote at elevated temperature T_2 are high by an amount equal to the ratio of specific volumes of the electrolyte solutions at T_2 compared to 293 K. Densities of the methanolic solutions at high temperatures were unavailable. We were, thus, unable to correct solution volumes to T_2. It was necessary to treat our data in this manner because H_2 solubilities were measured on a volumetric basis. The resultant error in the D_2 exchange rates given below was small and less than the experimental error.

In each D_2 experiment, the sequential conversion of both D_2 to HD (k_{D_2}) and of HD to H_2 (k_{HD}) by reaction with the protic solvent were accurately first-order.

$$[8] \quad D_2 + ROH \xrightarrow{k_{D_2}} HD + ROD$$

$$[9] \quad HD + ROH \xrightarrow{k_{D_2}} H_2 + ROD$$

Back reactions were ignored because ROD was always less than 1 mol% of the ROH. To calculate apparent kinetic isotope effects, kie = $2k_{HD}/k_{D_2}$, an iterative curve-fitting technique was employed in which the computer program minimized the standard deviation between the observed and calculated HD yield and gave the best values for k_{HD} and k_{D_2}. Provision was made for the possibility that initial concentrations of HD and H_2 (in the feed D_2) might be significant. This procedure was necessary when overall D_2 conversions were low, e.g., 10–35% (21).

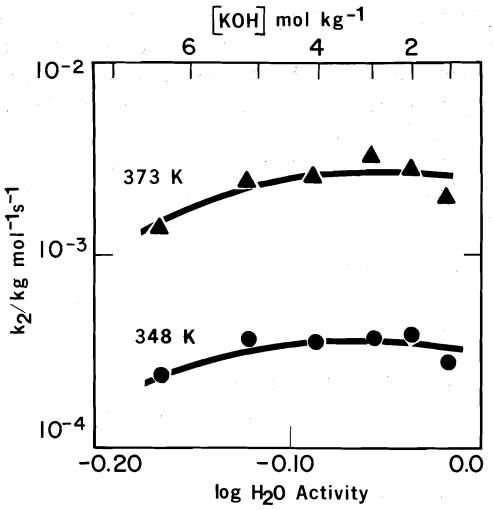

FIG. 7. Second-order rate constants for D_2–H_2O exchange catalyzed by KOH.

Rate Constants for D_2 Exchange

Wilmarth and co-workers (2) and Lin (22) have demonstrated the rate law for deuterium exchange with dilute aqueous KOH (less than 1 kmol/m^3) to be:

$$[10] \quad -\mathrm{d}[D_2]/\mathrm{d}t = k_2[D_2][KOH]$$

We have assumed that the deuterium transfer mechanism was the same as in dilute solution, that is the reaction order in D_2 and base remained unity in concentrated alkali. A corresponding equation was considered to hold for $KOCH_3$ in methanol. Accordingly, we have calculated second-order rate constants (identified by the subscript 2) for both systems in this way:

$$[11] \quad k_2 = \mathrm{Rate}/(a_2 a_3) = \mathrm{Rate}/(\gamma_2{}^*\gamma_3{}^*[D_2][K\beta])$$

where K refers to the potassium cation, and β to the anion OH^- or $OCH_3{}^-$ of the corresponding solvent.

The results are presented in Fig. 7 for D_2–KOH–H_2O and in Fig. 8 for D_2–$KOCH_3$–CH_3OH. All numerical values have also been summarized in Tables 1 and 2.[2] In each figure the logarithm of the rate constant k_2 is plotted against the logarithm of the solvent activity. The

[2]Copies are available, at a nominal charge, from the Depository of Unpublished Data, CISTI, National Research Council of Canada, Ottawa, Canada K1A 0S2.

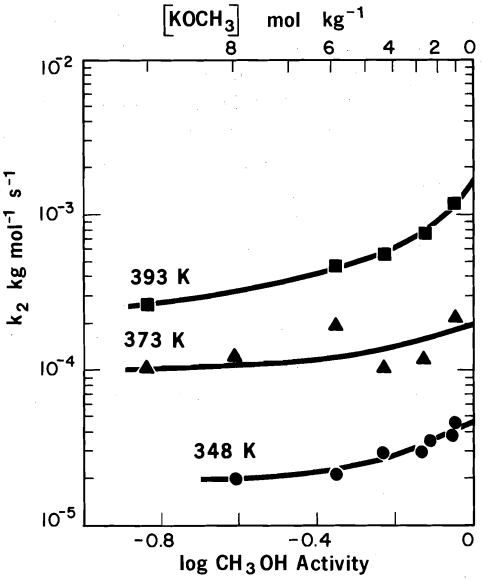

FIG. 8. Second-order rate constants for D_2–CH_3OH exchange catalyzed by $KOCH_3$.

corresponding base concentration is indicated on the upper abscissa in each figure.

In the aqueous system, k_2 appears to exhibit a slight maximum at about 3 mol/kg of KOH at both 348 and 373 K, although additional data below 2 mol/kg would be required to confirm that trend. The cumulative error associated with the evaluation of k_2 was approximately 10%; therefore assignment of significance to that trend requires caution. The reaction mechanism which we propose in the Discussion considers k_2 to be essentially independent of KOH concentration below about 5 mol/kg. At that point, the molar ratio of solvent:solute is 6.25, which is somewhat less than the sum of solvation numbers of 3 for hydroxide plus 4 for K^+ (23, 24).

In Fig. 8, k_2 initially decreases with decreasing methanol activity, that is, with increasing $KOCH_3$ concentration at each temperature. Above about 6 mol/kg $KOCH_3$, k_2 is only slightly dependent upon solvent activity. This unexpected result suggested that the solvent plays an important part in determining the overall rate of the D_2 exchange reaction and also that there was no increase in the intrinsic reactivity of $KOCH_3$ upon reduction of solvent molecules available for stabilization of $KOCH_3$. In the following section we present a mechanism which explains the dependence of k_2 on methanol activity in the D_2–$KOCH_3$–CH_3OH system and the independence of k_2 from water activity in the D_2–KOH–H_2O case.

Activation Energy

An apparent activation energy at infinite dilution of the base may be calculated from the limiting values

$$\lim_{a_3 \to 0} k_2$$

taken from Figs. 7 and 8. Our results for the D_2–KOH–H_2O system do not extend to sufficiently low concentrations of base to permit satisfactory extrapolation. That uncertainty, plus the limited data and cumulative error in evaluation of the two k_2 values at 75 and 100°C as described above, suggests that the activation energy for the D_2–KOH–H_2O case falls within the range 88 $\pm$ 20 kJ/mol. The studies of Wilmarth and coworkers (2) of the temperature dependence of para-hydrogen conversion or of Schindewolf (4) of HD exchange yielded comparable activation energies of about 100 kJ/mol.

The values of k_2 taken from Fig. 8 for the D_2–$KOCH_3$–CH_3OH system are more reliable, and an activation energy of 81 $\pm$ 5 kJ/mol was obtained.

Discussion

Review of Base-catalyzed Activation of D_2

This discussion of the mechanism of base-catalyzed D_2 exchange is essentially a consideration of the nature of an unidentified unstable intermediate. A brief review of this topic is necessary.

In the early work of Wilmarth and his colleagues (2), attack of OH^- on D_2 to yield an intermediate deuteride anion was thought to be the most probable rate-determining process (reaction 12):

[12] $$D_2 + OH^- \rightarrow D^- + HDO$$

which was followed by the rapid abstraction of a proton from water and regeneration of the base:

[13] $$D^- + H_2O \rightarrow HD + OH^-$$

It was also recognized that the exchange rate data could not be employed to distinguish between this reaction sequence and the concerted proton transfer process (reaction 14):

[14] $$D_2 + OH^- \rightarrow HD + OD^-$$

whereby D^+ transfer occurred smoothly via a multicentered intermediate. One argument against the former scheme rests on the inability of these aqueous KOH solutions containing H_2 to catalyze reductions of unsaturated organics or hydride-transfer reactions (4).[3] However, the former mechanism, which requires rate-controlling cleavage of the D—D bond, can account for the relatively high activation energy of the exchange reaction of about 100 kJ/mol. Note also that [13] specifically requires discharge of the D^- anion by water.

The calculations of Ritchie and King (12) on the gas phase reaction:

[15] $$H^- + H_2O \rightarrow HOHH^-$$

which showed the $HOHH^-$ species to be slightly stabilized with respect to the reactants, caused Ritchie to speculate that the rate-determining step in the D_2 exchange sequence was the loss of one molecule of solvation from the primary solvation shell of the OH^- anion prior to rapid attack of D_2. In that scheme, the high energy of activation was attributed to the enthalpy of solvation of OH^- by 1 mol of water. The structure of the intermediate encounter complex in that mechanism was considered to be similar to that of the product in [15].

Catalytically Active Species in Concentrated Solution

In eqs. 16 and 17 which follow, the anionic species OH^- and CH_3O^- have been considered to be catalytically active. Ion-pair formation is probably an important process in each base system. However, the limited data available in the literature do not allow us to treat that topic quantitatively. Under our experimental conditions, KOH was likely highly dissociated in water (26, 27) and the dominant catalyst species was $OH^-(H_2O)_3$ (23). Evidence from other proton-transfer reactions at carbon centers has suggested that the ion pair K^+OH^- does not promote rapid deuterium exchange (26).

Information on $KOCH_3$ in methanol (27) also favours ion-pair formation, although Barthel, Wachter, and Knerr (28) reported an association constant of zero based on conductometric studies on dilute $KOCH_3$ at 298 K. Jones has concluded from a review of the kinetic studies of proton transfer that ion-pairing of alkoxides is significant in concentrated solution (26). Our own unpublished data on D_2–methanol exchange have shown that $NaOCH_3$ and $KOCH_3$ possess identical reactivities which are about an order of magnitude greater than that of $LiOCH_3$ at a given base concentration and temperature. That suggests that ion-pairing of $KOCH_3$ is incomplete. The anion CH_3O^- is probably the species which activates D_2, firstly, because of its close relationship to OH^- and, secondly, because k_2 falls off at high $KOCH_3$ concentration where ion-pairing is greater (cf. Fig. 8). If $KOCH_3$ were a superior catalyst to CH_3O^-, k_2 would be expected to increase in that region.

Exchange Reaction Mechanism

In the mechanism which we present below, two points are noteworthy, (*i*) the exact structure of the intermediate need not be specified, but (*ii*) the stage at which solvent participation is essential must be identified to account particularly for the form of the D_2–$KOCH_3$–CH_3OH data presented in Fig. 8. The simple reaction sequence which we favour is as follows:

[16] $$D_2 + \beta^- \underset{k_{-16}}{\overset{k_{16}}{\rightleftharpoons}} D_2\beta^-$$

[17] $$D_2\beta^- + n\mathrm{S} \xrightarrow{k_{17}} \mathrm{HD} + \beta^- + (n-1)\mathrm{S} + \mathrm{S}\text{-}d_1$$

We consider that the initial equilibrium of D_2 with the solvated base β^- occurs with no net change in solvation and that is followed by decay of the intermediate $D_2\beta^-$ to yield products by reaction with n mol of solvent. The symbols β^- and S refer to the solvated base anion and solvent respectively, and S-d_1 denotes monodeuterated solvent.

If we consider the species $D_2\beta^-$ to be present in a low, steady-state concentration, the rate of exchange of D_2 may be written as:

[18] $$-\mathrm{d}[D_2]/\mathrm{d}t = \left(\frac{k_{16}k_{17}a_1{}^n}{k_{-16} + k_{17}a_1{}^n}\right)\gamma_2{}^*\gamma_3{}^*[D_2]\,[\beta^-]$$

where the subscripts 2 and 3 refer to D_2 and β^- as previously defined. For the case in which the terms in the denominator $k_{-16} + k_{17}a_1{}^n$ are of similar magnitude, this expression can be used to explain the decrease in k_2 of eq. 11 with decrease in solvent activity in the D_2–$KOCH_3$–

[3]The hydride-transfer mechanism is a plausible one for the D_2–$KOCH_3$–CH_3OH system (25).

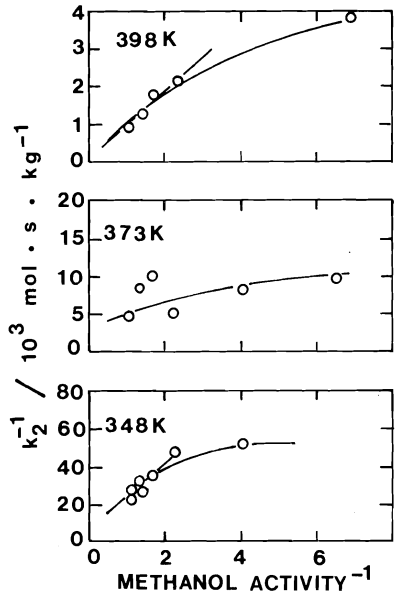

FIG. 9. Variation of k_2^{-1} with a_1^{-1} for D_2–$KOCH_3$–CH_3OH system.

CH_3OH system (cf. Fig. 8).[4] Equation 18 can also account for the independence of k_2 from water activity in the D_2–KOH–H_2O case (cf. Fig. 7) if $k_{17}a_1^n \gg k_{-16}$ since k_{16} alone would account for the observed D_2 exchange rate.

We may test the validity of this mechanism by transforming eq. 18 to give:

$$[19] \quad \frac{a_2a_3}{\text{Rate}} = \frac{1}{k_2} = \left(\frac{k_{-16}}{k_{16}k_{17}}\right)\frac{1}{a_1^n} + \frac{1}{k_{16}}$$

For the D_2–methanol exchange, k_2^{-1} and a_1^{-n} can be linearly correlated reasonably well up to 7 mol/kg $KOCH_3$ for $n = 1$ as shown in Fig. 9 at 348, 373, and 398 K. Above that concentration the solvent:solute molar ratio is less than 4.5 and our mechanism appears to become unsatisfactory with respect to the constraint that $n = 1$. Note that our results plotted in Fig. 8 as log k_2 against log a_1 also suggest that n (=d log k_2/d log a_1) decreases from 1 at $a_1 = 1$ to apparent fractional values at high $KOCH_3$ concentrations. That behaviour was expected as the amount of 'free' solvent became negligible.

The two-step mechanism which we have presented (eqs. 16 and 17) accounts for the fall-off in k_2 with decrease of the solvent activity. Alternative models such as that in which D_2 activation by β^- is rate-controlling, or that described by Ritchie (12, 29) in which loss of one molecule of solvent from β^- precedes attack upon D_2, cannot explain the form of our D_2–$KOCH_3$–CH_3OH data of Fig. 8. Those two mechanisms cannot, however, be rejected for the D_2–KOH–H_2O case because the slight dependence of k_2 on water activity up to 5 mol/kg KOH does not allow identification of the best option. Experiments at higher KOH concentrations may show the hydroxide and methoxide behaviour to be similar.

To review, we conclude that in both strongly basic media, the activation of D_2 by β^- is generally the rate-determining process but in concentrated solutions reaction of an unstable complex involving transfer of D^+ to the solvent may be of comparable magnitude.

Kinetic Isotope Effects

Three topics will be considered: (*i*) the magnitude of the kie's, and the effect of (*ii*) base concentration, and (*iii*) temperature on the experimental values (cf. Figs. 5 and 6). Two points must be clarified: firstly, because we quote the kie as a ratio of two pseudo-first-order rate constants, each of which is affected equally by reagent activities to a first approximation, then that ratio should be independent of those variables; secondly, we consider that dual exchange of D_2 to yield H_2 without transfer of the intermediate product HD to the gas phase is improbable for the reasons cited in the following text. The effect of such an event would be to yield an abnormally high kie compared to that calculated assuming the sequential first-order conversion $D_2 \rightarrow HD \rightarrow H_2$.

The kie's for both systems were always above 1 and are normal in that HD, with the higher zero-point energy, reacted more rapidly than D_2. This is consistent with our assignment of the rate-controlling process in the D_2–KOH–H_2O system to be D_2 bond cleavage (reaction 16 forward) and in the D_2–$KOCH_3$–CH_3OH case to be that plus solvation of the encounter-complex intermediate (reaction 17).

The effect of base concentration and temperature on the kie requires a more tentative interpretation. Recall that in the aqueous system, rate constant k_2 was independent of, but the kie increased with, KOH activity (i.e., reduction of solvent activity). Alteration of the relative

[4]Note that k_2 is equal to the bracketed rate constant in eq. 18.

solvation of ground and encounter-complex species during the overall proton-transfer process must therefore favour HD over D_2 exchange. We suggest that an increase in the entropy of activation of DH compared to D_2 occurs with KOH concentration. Furthermore, to account for the increase in kie with temperature at a given KOH molality it is necessary that the activation energy for HD must exceed that for D_2, which is contrary to the usual sequence (30). Since the difference in the zero point energies between HD and D_2 is approximately given by the difference between their fundamental stretching modes of 3632 and 2993 cm^{-1}, respectively (31), it is necessary that the ground-state difference of 639 cm^{-1} be exceeded by 450 $\pm$ 110 cm^{-1} for the corresponding encounter complexes to account for our observed dependence of kie on temperature. An explanation of the constraints thus placed on the activation entropy and enthalpy may lie in the marked reduction of 'free' solvent with increased electrolyte concentration.

Our data do not justify more detailed speculation upon the chemical bonding interactions which control the observed kie's. However, in principle it may be argued that reorientation of the H-bonded solvent structure surrounding an intermediate of the type proposed by Ritchie and King (12) could result in appropriate changes in the relative energetics of the different isotopically substituted species.

The comments above have been restricted to the D_2–KOH–H_2O system but are also applicable to the D_2–$KOCH_3$–CH_3OH case. In the latter, however, the interpretation of kie results must include the fact that the experimental constant k_2 is a function of k_{16}, k_{17}, and methanol activity. If the kie for k_{17} is less than that for k_{16}, the above discussion is directly applicable.

Reactivity of KOH and $KOCH_3$ and Basicity Scales

The acidity function approach has been applied to the investigation of the participation of the solvent in proton-transfer reactions by several workers. Rochester (15*b*) and Boyd (32) have each reviewed this subject. It is the purpose of this section to consider the manner in which D_2 exchange rates for each system vary with the corresponding basicity scales.

First-order rate constants for D_2–H_2O exchange, $k_1 = -(1/[D_2])(d[D_2]/dt)$ plotted against H_- values for aqueous KOH at 298 K (15) are shown in Fig. 10. Since temperature will mainly affect the K_w term in this definition of H_- (15*c*),

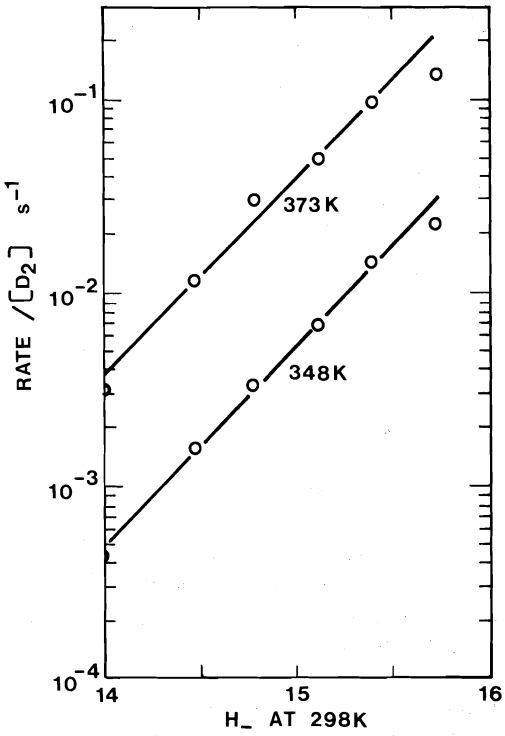

FIG. 10. Dependence of the first-order rate constant for D_2–H_2O exchange on H_-.

[20] $$H_- = pK_w + \log [OH^-] - \log a_w + \log (\gamma_{SH}{}^*\gamma_{OH^-}/\gamma_S)$$

where the subscript w refers to water, SH to the indicator acid, and S to its anion. It is reasonable to correlate our rate data at 348 and 373 K with H_- (298 K).

The slopes of the two straight lines for the D_2–KOH–H_2O system were 0.97 and 0.98 at 348 and 373 K, respectively. This direct dependence of k_1 on H_- supports our conclusion that activation of D_2 is the rate-controlling process in aqueous solution (15*b*). Our attempts to evaluate the difference between solvation of species in the ground and transition states by the methods of Yagil and Anbar and co-workers (23, 33), Rochester (34), and others (15) (i.e., from plots of our log k_2 data against logarithm of water

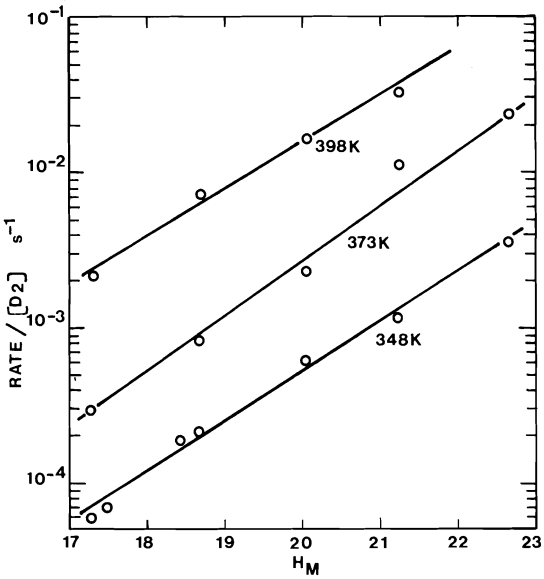

FIG. 11. Dependence of the first-order rate constant for D_2–CH_3OH exchange on H_M.

concentration or activity) yielded spuriously high results. We attributed that to the invalidity of the usual approximation, that the activity coefficient ratio term (in our case $\gamma_2^*\gamma_3^*/\gamma_{DDOH^-}$) was unity, mainly because of the extensive salting-out of D_2 (17).

The slopes of the three straight lines given in Fig. 11 for the D_2–$KOCH_3$–CH_3OH case were as follows: 348 K, 0.32; 373 K, 0.35; 398 K, 0.30. These values are smaller than those found for other correlations between rate constants for proton-transfer reactions at carbon acids and H_M (15). Perhaps our slopes are low because our D_2 exchange mechanism has shown the first-order rate constant employed here to be complex:

$$[21] \quad \text{Rate}/[D_2] = \frac{k_{14}k_{15}a_1\gamma_2^*\gamma_3^*[K\beta]}{k_{-14} + k_{15}a_1}$$

All parameters in [21] are functions of H_M except for $[\beta^-]$, therefore unequivocal identification of the origin of the slight dependence of Rate/$[D_2]$ on H_M cannot be made. The basicity scale approach is therefore of limited utility for detailed analysis of the deuterium exchange mechanism in this system.

Acknowledgements

The authors wish to thank their colleagues, particularly Dr. N. H. Sagert, Dr. E. A. Symons, Dr. J. H. Rolston, and Prof. E. Buncel, for their continued interest in, and helpful comments about, this research. We also thank D. Bell and the Staff of the Analytical Science Branch for deuterium analyses.

1. K. WIRTZ and K. F. BONHOEFFER. Z. Phys. Chem. **177**A, 1 (1936).
2. W. K. WILMARTH, J. C. DAYTON, and J. M. FLOURNOY. J. Am. Chem. Soc. **75**, 4549 (1953).
3. J. M. FLOURNOY and W. K. WILMARTH. J. Am. Chem. Soc. **83**, 2257 (1961).
4. U. SCHINDEWOLF. Ber. Bunsenges. Phys. Chem. **67**, 219 (1963).
5. E. A. SYMONS and E. BUNCEL. Can. J. Chem. **51**, 1673 (1973).
6. E. BUNCEL and E. A. SYMONS. J. Am. Chem. Soc. **98**, 656 (1976).
7. W. K. WILMARTH and J. C. DAYTON. J. Am. Chem. Soc. **75**, 4553 (1953).
8. K. BAR-ELI and F. S. KLEIN. J. Chem. Soc. 1378 (1962).
9. K. BAR-ELI and F. S. KLEIN. J. Chem. Soc. 3083 (1962).
10. E. ROCHARD and J. RAVOIRE. J. Chim. Phys. Phys.-Chim. Biol. **68**, 1183 (1971).
11. H. KALRA and F. D. OTTO. Can. J. Chem. Eng. **52**, 258 (1974).
12. C. D. RITCHIE and H. F. KING. J. Am. Chem. Soc. **90**, 825 (1968).
13. G. G. STRATHDEE and R. M. GIVEN. J. Catal. **30**, 30 (1973).
14. G. YAGIL. J. Phys. Chem. **71**, 1034 (1967).
15. C. H. ROCHESTER. Acidity functions. Academic Press, New York, NY. 1970. (*a*) p. 247; (*b*) p. 241; (*c*) p. 238.
16. J. M. PRAUSNITZ. Molecular thermodynamics of fluid-phase equilibria. Prentice-Hall, Inc., Englewood Cliffs, NJ. 1969. p. 190.
17. S. K. SHOOR, R. D. WALKER, JR, and K. E. GUBBINS. J. Phys. Chem. **73**, 312 (1969).
18. M. W. COOK, D. N. HANSON, and B. J. ALDER. J. Chem. Phys. **26**, 748 (1957).
19. V. M. ANISIMOV. Russ. J. Phys. Chem. **47**, 601 (1973).
20. R. A. ROBINSON and R. H. STOKES. Electrolyte solutions. 2nd ed. Butterworths, London. 1959. p. 494.
21. G. G. STRATHDEE and R. M. GIVEN. Can. J. Chem. **52**, 2216 (1974).
22. C.-F. LIN. J. Res. Inst. Catal. Hokkaido Univ. **15**, 218 (1967).
23. G. YAGIL and M. ANBAR. J. Am. Chem. Soc. **85**, 2376 (1963).
24. R. W. CREEKMORE and C. N. REILLEY. J. Phys. Chem. **73**, 1563 (1969).
25. C. WALLING and L. BOLLYKY. J. Am. Chem. Soc. **86**, 3750 (1964).
26. C. B. MONK. Electrolytic dissociation. Academic Press, New York, NY. 1961. p. 277.
27. J. R. JONES. Prog. Phys. Org. Chem. **9**, 255 (1972).
28. J. BARTHEL, R. WACHTER, and M. KNERR. Electrochim. Acta, **16**, 723 (1971).

29. C. D. RITCHIE. *In* Solute–solvent interactions. *Edited by* J. F. Coetzee and C. D. Ritchie. Marcel Dekker, New York, NY. 1969. p. 261.
30. L. MELANDER. Isotope effects on reaction rates. Ronald Press, New York, NY. 1960. p. 43.
31. K. NAKAMOTO. Infrared spectra of inorganic and coordination compounds. Wiley, New York, NY. 1963. p. 72.
32. R. H. BOYD. *In* Solute–solvent interactions. *Edited by* J. F. Coetzee and C. D. Ritchie. Marcel Dekker, New York, NY. 1969. p. 98.
33. M. ANBAR, M. BOBTELSKY, D. SAMUEL, B. SILVER, and G. YAGIL. J. Am. Chem. Soc. **85**, 2380 (1963).
34. C. H. ROCHESTER. J. Chem. Soc. B, 1076 (1967).

The crystal structure of bis(ethyldiazoacetate) mercury(II) $Hg(CN_2CO_2C_2H_5)_2$

R. A. SMITH, M. TORRES, AND O. P. STRAUSZ

Department of Chemistry, University of Alberta, Edmonton, Alta., Canada T6G 2G2

Received April 19, 1977

R. A. SMITH, M. TORRES, and O. P. STRAUSZ. Can. J. Chem. **55**, 3527 (1977).

Bis(ethyldiazoacetate) mercury(II) is orthorhombic with the following unit cell data at 20°C: *Fdd*2, $a = 19.810(8)$, $b = 14.387(5)$, $c = 9.015(2)$ Å, $V = 2569.3$ Å^3, $\rho_o = 2.17(2)$, $\rho_c = 2.21$, $Z = 8$ (MoK_{α_1}, $\lambda = 0.70930$ Å). The structure was solved by heavy atom methods and refined to $R = 2.2\%$ for 706 reflections. The molecule has a 2-fold axis of symmetry and all thermal parameters are large in the direction of this axis; diffuse scattering was observed in the rotation photograph taken about this axis. As expected the diazoacetate portion is planar.

R. A. SMITH, M. TORRES et O. P. STRAUSZ. Can. J. Chem. **55**, 3527 (1977).

Le bis-éthyldiazoacétate de mercure(II) cristallise dans le système orthorhombique avec des valeurs de maille suivantes à 20°C: *Fdd*2, $a = 19.810(8)$, $b = 14.387(5)$, $c = 9.015(2)$ Å, $V = 2569.3$ Å^3, $\rho_o = 2.17(2)$, $\rho_c = 2.21$, $Z = 8$ (MoK_{α_1}, $\lambda = 0.70930$ Å). La structure est résolue par la méthode des atomes lourds et affinée à $R = 2.2\%$ pour 706 réflections. La molécule possède un axe de symétrie d'ordre 2 et tous les paramètres thermiques sont élevés en direction de cet axe; une diffraction est observée sur un cliché lorsqu'on fait une rotation autour de cet axe. Conformément aux prévisions, la partie diazoacétate est planaire.

[Traduit par le journal]

Introduction

Bis(ethyldiazoacetate) mercury(II), $Hg(CN_2CO_2C_2H_5)_2$, (I), was synthesized by Buchner in the past century (1). Together with its analog bis(methyldiazoacetate) mercury(II) it remained the only known representative of a metal α-diazo structure until the last decade. Since then a large number of molecules with the same generic structure has been synthesized (2). The crystal structure of these molecules, with the exception of *tert*-butyl ethyldiazoacetate mercury(II) (3), has not been determined and for this reason we have currently undertaken a systematic X-ray diffraction study to elucidate the crystal structure and molecular geometry of the known diazomercurial compounds.

Some of these diazomercurials, in particular (I), have been employed as a photolytic source of carbynes (4) in the liquid phase and a knowledge of the molecular geometry may be helpful in the elucidation of the primary photochemical step.

Experimental

$C_8H_{10}HgN_4O_4$ fw = 426.70

*Fdd*2, $a = 19.810(8)$, $b = 14.387(5)$, $c = 9.015(2)$ Å, $V = 2569.3$ Å^3, $\rho_o = 2.17(2)$, $\rho_c = 2.21$, $Z = 8$ (MoK_{α_1}, $\lambda = 0.70930$ Å; 20°C).

The crystals were yellow prisms with all faces of the form {1,1,1}. Rotation photographs were taken about each axis and that about c showed very weak diffuse scattering corresponding to $hk\frac{1}{2}$ only. Mercury exhibits large anomalous dispersion with MoK_α radiation and unless these effects are correctly allowed for, large errors in bond distances are possible in polar space groups (5). Therefore, intensities of both hkl and $hk\bar{l}$ were collected and used in refinement. A very regular crystal with all faces 0.0067 cm from the center was selected, mounted about a, and placed on a Picker FACS-1 diffractometer. Twelve highangle reflections were carefully centered and accurate cell constants were derived. (MoK_{α_1} radiation, no monochromator.)

Data sets hkl and $hk\bar{l}$ with $0 \leq 2\theta \leq 45°$ were collected (MoK_α radiation, graphite (002) monochromator) by the coupled $\theta/2\theta$ scan method. A scan width of 2° was employed, the scan rate was 2° min^{-1} and background counts were accumulated for 20 s either side of the scan. Decomposition was monitored by measurement of standards every 100 reflections. A total of 844 reflections were measured and corrected for Lorentz-polarisation, decomposition, and absorption (μ, $MoK_\alpha = 122$ cm^{-1}) (6). The data were reduced to $|F|$, $\sigma(F)$, and $\sigma(I)$ using a p value of 0.06 (7). Using an acceptance criterion $I \geq 3\sigma(I)$ 706 reflections had significant intensity and of these only 40 had no net contribution from the Hg atom.

The Hg is required to occupy a position 0,0,z and in view of the polar nature of the space group it was assigned coordinates 0,0,0. The mercury was allowed anisotropic thermal parameters and anomalous dispersion corrections were applied to a refinement of this atom to the 666 reflections of the data sets $h, k, l, = 2n + 1$ and $h + k + l = 4n$ only. This model refined to $R = 8.0\%$ and a difference Fourier map was then calculated. The procedure outlined above led to false site symmetry, 222, that expected for the centrosymmetric case. The inclusion of anomalous dispersion had greatly favoured one

TABLE 1. Atomic parameters and std. dev. ($\times 10^3$; Hg $\times 10^4$) for bis(diethyldiazoacetate) mercury(II)
Temperature factors, exp $(-2\pi^2\{a^{*2}h^2U_{11} + \cdots + 2a^*b^*hkU_{12} + \cdots\})$
$(0,0,0;\ 0,\frac{1}{2},\frac{1}{2};\ \frac{1}{2},0,\frac{1}{2};\ \frac{1}{2},\frac{1}{2},0) + (x,y,z;\ x,y,z;\ \frac{1}{4}-x,\frac{1}{4}+y,\frac{1}{4}+z;\ \frac{1}{4}+x,\frac{1}{4}-y,\frac{1}{4}+z)$

Atom	x	y	z	U_{11}	U_{22}	U_{33}	U_{12}	U_{13}	U_{23}
Hg	0	0	0	298(3)	671(3)	851(4)	−4(6)	0	0
O(1)	136(1)	−40(1)	156(2)	61(7)	118(8)	258(16)	−24(7)	−51(9)	82(10)
O(2)	202(1)	83(7)	97(2)	34(5)	80(5)	190(10)	−4(4)	−27(5)	−15(6)
N(1)	97(1)	151(8)	−51(1)	36(5)	74(7)	132(9)	−15(5)	−13(5)	20(6)
N(2)	102(1)	221(1)	−96(3)	90(11)	126(12)	198(17)	−18(10)	−48(12)	35(12)
C(1)	88(1)	71(7)	12(2)	54(7)	67(6)	98(8)	12(5)	−11(7)	−9(7)
C(2)	148(1)	40(1)	88(2)	24(6)	87(8)	156(13)	3(6)	−16(7)	15(9)
C(3)	194(1)	−74(2)	281(3)	114(16)	126(14)	166(21)	−23(12)	−3(14)	−12(13)
C(4)	220(1)	−127(2)	170(4)	143(18)	142(19)	215(29)	−26(17)	−37(20)	−36(17)

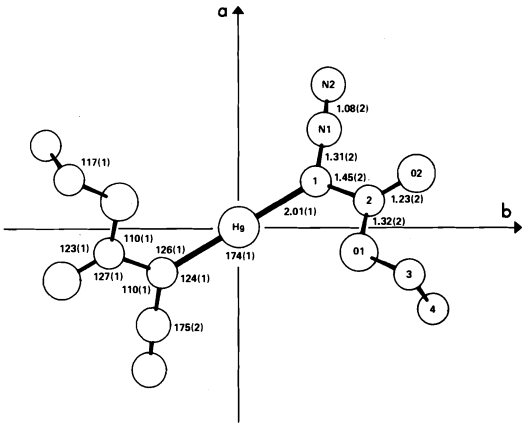

FIG. 1. A schematic representation of $Hg(CN_2CO_2C_2H_5)_2$ showing the atom numbering scheme and important bond angles, distances, and associated standard deviations.

logical set of 8 atoms and with anisotropic vibration allowed for all atoms R was reduced to 2.3% for all 706 reflections of the general data set. Structure factors were taken from Cromer and Mann (8). A weight of $4F^2/\sigma^2(F^2)$ was applied to every reflection. The model with $z = -z$ would not refine below 7% and the thermal parameters of several atoms reached absurd proportions at R of 7.4%. The first model can thus be taken as the correct one (9). The secondary extinction parameter was refined after examination of the data indicated such a problem (10), the refined value was $4.1(6) \times 10^{-7}$ and the final R value was 2.2%. The R value for all 844 measured reflections was 3.2%. A final difference Fourier map contained peaks of the order 1.25 e Å^{-3} and consequently no attempt was made to determine the H atom coordinates.

Results and Discussion

The atomic numbering scheme and important bond angles and distances are given in the schematic representation in Fig. 1. Final atom parameters are given in Table 1 and the Table of Structure Factors has been placed in the Depository of Unpublished Data.[1]

The thermal parameter U_{33} is large for all atoms and is expected in a polar space group in view of the weak diffuse scattering from a doubled polar axis. A slight disorder in the z coordinate of the mercury atom is possible, the fixing of the z value at 0 for all Hg atoms would give a ghost molecule slightly displaced in z from the chosen molecule and lead to large U_{33} values for all atoms during refinement compensating for the unexplained electron density. All 7 atoms of the $HgCN_2CO_2$ portion of the molecule lie within 0.03 Å of the mean plane, and the shape and dimensions of the diazo moiety are similar to those found in (II). The standard deviations in (II) were large because of problems associated with severe decomposition; however the Hg—C distance in this case, 2.01(1) Å, is significantly shorter than that observed in (II), 2.12(2) Å. The strength of the Hg—C bond to the carbon atom of the diazoacetate moiety and that of the C—N bond in compounds of the form R—Hg—$CN_2CO_2C_2H_5$ are of great interest, in view of the changes in photolysis products as a function of R and the proven formation of carbethoxymethyne during these reactions (4).

A detailed discussion of the structural implications of various bond strengths in these systems would require further data on diazomercurials and on the compound ethyldiazoacetate, the latter requiring a low temperature

[1]The Structure Factor Table is available, at a nominal charge, from the Depository of Unpublished Data, CISTI, National Research Council of Canada, Ottawa, Ont., Canada K1A 0S2.

study. Other members of the diazomercurial series are currently under investigation.

Acknowledgements

We thank the National Research Council of Canada for financial support and Dr. E. M. Lown for assistance.

1. E. BUCHNER. Chem. Ber. **28**, 215 (1895).
2. P. YATES and F. X. GARNEAU. Tetrahedron Lett. 71 (1968); T. DO MINH, O. P. STRAUSZ, and H. E. GUNNING. Tetrahedron Lett. 5237 (1968); M. EDGITZ, A. LIEDHEGENER, V. ECKSTEIN, M. MARTIN, and W. AUSCHUTZ. Justus Liebigs Ann. Chem. **748**, 207 (1971); S. T. VALENTY and P. S. SKELL. J. Org. Chem. **38**, 3937 (1973); P. YATES, F. X. GARNEAU, and J. P. LOKENSGARD. Tetrahedron, **31**, 1979 (1975).
3. R. A. SMITH, M. TORRES, and O. P. STRAUSZ. Can. J. Chem. **55**, 2752 (1977).
4. T. DO MINH, H. E. GUNNING, and O. P. STRAUSZ. J. Am. Chem. Soc. **89**, 6785 (1967); O. P. STRAUSZ, T. DO MINH, and J. FONT. J. Am. Chem. Soc. **90**, 1930 (1968); G. KENNEPOHL. Ph.D. thesis, University of Alberta. 1973; O. P. STRAUSZ, G. KENNEPOHL, F. X. GARNEAU, T. DO MINH, B. KIM, S. VALENTY, and P. S. SKELL. J. Am. Chem. Soc. **96**, 5723 (1974); T. B. PATRICK and G. H. KOVITCH. J. Org. Chem. **40**, 1527 (1975).
5. T. UEKI, A. ZALKIN, and D. H. TEMPLETON. Acta Crystallogr. **20**, 836 (1966).
6. P. COPPENS, L. LEISEROWITZ, and D. RABINOVITCH. Acta Crystallogr. **18**, 1035 (1965).
7. R. J. DOEDENS and J. A. IBERS. Inorg. Chem. **6**, 204 (1967).
8. D. T. CROMER and J. B. MANN. Acta Crystallogr. Sect. A, **24**, 321 (1968).
9. W. C. HAMILTON. Acta Crystallogr. **18**, 502 (1965).
10. W. H. ZACHARIASEN. Acta Crystallogr. **16**, 1139 (1963).

Thermochemical measurement of the ligand field splitting energies for hexaammine complexes of Mn(II), Fe(II), and Zn(II)[1]

M. BADRI AND J. W. S. JAMIESON[2]

Department of Chemistry, Universiti Pertanian Malaysia, Serdang, Selangor, Malaysia

Received September 8, 1976

M. BADRI and J. W. S. JAMIESON. Can. J. Chem. **55**, 3530 (1977).

Various lower ammines and high-energy modifications of lower ammines of the sulphates of Mn(II), Fe(II), and Zn(II) have been prepared and their heats of solution have been measured. For each of these ammine systems, the maximum difference in heat of solution, expressed in kcal/mol of heptaammine, has been found to be of the right order of magnitude to be regarded as the ligand field splitting energy for the hexaammine complex of the metal ion.

M. BADRI et J. W. S. JAMIESON. Can. J. Chem. **55**, 3530 (1977).

On a préparé et mesuré les chaleurs de solutions de diverses ammines de bas poids moléculaires et de diverses modifications riches en énergie d'ammines de bas poids moléculaires de sulphates de Mn(II), Fe(II) et Zn(II). Pour chacun de ces systèmes ammines, on a trouvé que la différence maximum dans la chaleur de solution exprimée en kcal/mol d'heptaammine est du bon ordre de grandeur pour l'énergie de dissociation du champ de ligand pour le complexe hexaammine de l'ion métallique.

[Traduit par le journal]

Introduction

The maximum differences in heat of solution between the normal crystalline lower hydrates and the high-energy modifications of the lower hydrates of manganese(II) sulphate, iron(II) sulphate, cobalt(II) sulphate, and nickel(II) sulphate, when expressed in kcal/mol of each heptahydrate, have been observed (1) to be equivalent to the ligand field splitting energies of the corresponding hexaaquo metal(II) ions. Further experimental verification of the validity of this thermochemical method for the measurement of ligand field splitting energies, which had previously been obtainable only from rather complex interpretation of observed spectra, has recently been provided (2) by the results of studies with the ammine complexes of cobalt(II) sulphate and nickel(II) sulphate. Thus it has been shown that the maximum differences in heat of solution between the normal crystalline lower ammines and the high-energy modifications of the lower ammines of these salts, when expressed as kcal/mol of each heptaamine, are equivalent to the ligand field splitting energies of the hexaamine metal(II) ions.

Experimental

The anhydrous manganese(II) sulphate, iron(II) sulphate, and zinc(II) sulphate were prepared by heating their respective hydrates at suitable temperatures which were experimentally determined using thermogravimetric analysis (TGA) and differential thermal analysis (DTA). Thus $MnSO_4 \cdot H_2O$ (Merck and Co. Ltd.) and $ZnSO_4 \cdot 7H_2O$ (J. T. Baker 'analyzed' reagent) were heated gradually to 265°C in an oven and kept at that temperature for a period of two days. Anhydrous $FeSO_4$, from the Fisher Scientific Company, was found to contain some water which was removed by heating the salt *in vacuo* at 170°C.

The anhydrous salts were finely powdered and samples of about 3 g were taken for reaction with anhydrous ammonia (supplied by Matheson of Canada, Ltd.) in the manner previously described for the preparation of the ammine complexes of nickel(II) sulphate and cobalt(II) sulphate (2–7). Since the hexaammines are unstable at room temperature, each sample prepared was analyzed for ammonia content. These samples were stored in an atmosphere of ammonia in sealed tubes.

The lower ammines were prepared by heating the hexaammines of the metal(II) sulphates in an oven or *in vacuo* at various temperatures. They were kept in sealed glass tubes to ensure that no reactions with water vapour from the air would take place. Such reactions may produce mixed ligand complexes and these would have different heats of solution depending on the amount of water absorbed.

Integral heats of solution were measured as previously described (1). To ensure complete solubility, the ammines of zinc(II) sulphate were dissolved in 0.75 *M* NH_4OH solution and the ammines of manganese(II) sulphate and iron(II) sulphate were dissolved in 1 *M* HCl solution.

[1]The experimental work was done while the authors were at Dalhousie University, Halifax, N.S., Canada.

[2]Present address: Kars, Ont., Canada.

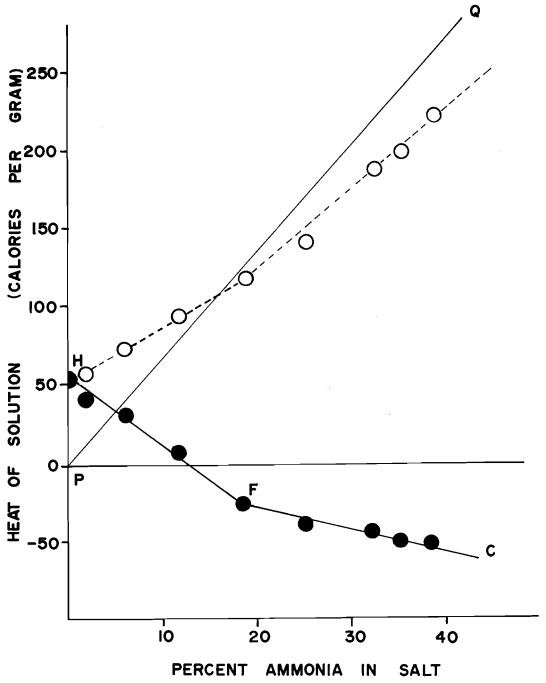

FIG. 1. Heats of solution for various ammines of $MnSO_4$ in 1 *M* aqueous HCl. ○, uncorrected; ●, corrected.

Results

For the ammine complexes of manganese(II) sulphate and iron(II) sulphate the heats of solution were found to increase with increasing ammonia content. Such results for some of the ammine complexes of manganese(II) sulphate are shown by the open circles in Fig. 1. This increase seems to disagree with the previous observations of the heats of solution for the ammine complexes of cobalt(II) sulphate and nickel(II) sulphate as well as the aquo complexes. In the case of the latter, the heat of solution decreases as the percent ligand increases. Thus it appears that all the ammonia in the ammine complexes of manganese(II) sulphate and iron(II) sulphate has been neutralized by hydrochloric acid. The heat of neutralization has been represented in Fig. 1 by the straight line *PQ* passing through the origin having a slope of 7.10 cal/1% ammonia. The lines *HF* and *FC* in Fig. 1 denote the differences between the heats of solution measured and the heats of neutralization of the ammonia, thus giving normal linear relations as have been observed for other systems. Values corrected in this way (Tables 1 and 2) have been plotted in Fig. 2 for the ammine complexes of manganese(II) sulphate and in Fig. 3 for the ammine complexes of iron(II) sulphate.

TABLE 1. Heats of solution for various ammines of manganese(II) sulphate

% Ammonia in sample	Heat of solution (cal/g)	Method of preparation
18.17	−24.1	Heated at 75°C
19.20	−26.1	Heated at 75°C
24.92	−38.2	Heated at 75°C
25.28	−38.5	Heated at 75°C
31.08	−44.9	Heated at 75°C
32.36	−42.4	Direct preparation
35.15	−50.0	Direct preparation
38.31	−50.8	Direct preparation
0.0	54.1	Heated at 300°C
1.90	42.6	Heated at 300°C
2.16	45.2	Heated at 300°C
6.02	29.6	Heated at 300°C
8.07	20.0	Heated at 300°C
9.68	8.91	Heated at 141°C
11.68	2.87	Heated at 141°C
11.83	9.22	Heated at 141°C
12.17	6.91	Heated at 141°C
12.54	−1.71	Heated at 141°C
13.83	−5.09	Heated at 141°C
0.0	93.1	Vacuum at 112°C
2.53	78.0	Vacuum at 112°C
8.40	56.4	Vacuum at 112°C
9.05	49.4	Vacuum at 112°C
10.75	46.0	Vacuum at 112°C
11.91	41.2	Vacuum at 22°C
12.36	36.3	Vacuum at 22°C
13.34	37.3	Vacuum at 22°C
13.44	36.5	Vacuum at 22°C
18.26	19.0	Vacuum at 22°C
25.58	−14.9	Vacuum at 22°C
26.24	−21.0	Vacuum at 22°C

Manganese(II) Sulphate

Using the method of least squares, the heat of solution data of Fig. 2 for the ammine complexes of manganese(II) sulphate can be expressed as

$$y_{BC} = -1.32x - 2.36$$

$$y_{FH} = -4.17x + 52.4$$

and

$$y_{IK} = -4.15x + 90.6$$

Extrapolation of the line *BC* gives the heat of solution of $[Mn(NH_3)_6]^{2+}SO_4^{2-}\cdot NH_3$ (with 44.11% ammonia) as −60.5 cal/g and that of $MnSO_4\cdot NH_3$ (with 10.13% ammonia) as −15.7 cal/g. The line *CE* has been drawn through the

TABLE 2. Heats of solution for various ammines of iron(II) sulphate

% Ammonia in sample	Heat of solution (cal/g)	Method of preparation
15.05	−42.2	Sealed at 123°C
18.31	−45.0	Over H_2SO_4 at 22°C
20.46	−48.2	Heated at 79°C
23.06	−54.4	Heated at 79°C
25.80	−53.9	Heated at 79°C
25.90	−57.3	Heated at 79°C
34.08	−65.6	Direct preparation
37.24	−68.5	Direct preparation
39.66	−72.1	Direct preparation
3.78	68.4	Vacuum at 79°C
4.76	60.7	Vacuum at 79°C
8.63	41.8	Vacuum at 79°C
14.62	14.9	Vacuum at 22°C
15.82	7.74	Vacuum at 22°C
7.65	6.76	Sealed at 123°C
9.13	−6.30	Heated at 79°C
9.20	−3.81	Sealed at 123°C
11.25	−16.6	Heated at 79°C
12.97	−20.3	Sealed at 123°C
15.95	−34.7	Sealed at 123°C
16.77	−38.0	Over H_2SO_4 at 22°C
4.01	−6.67	Sealed at 123°C

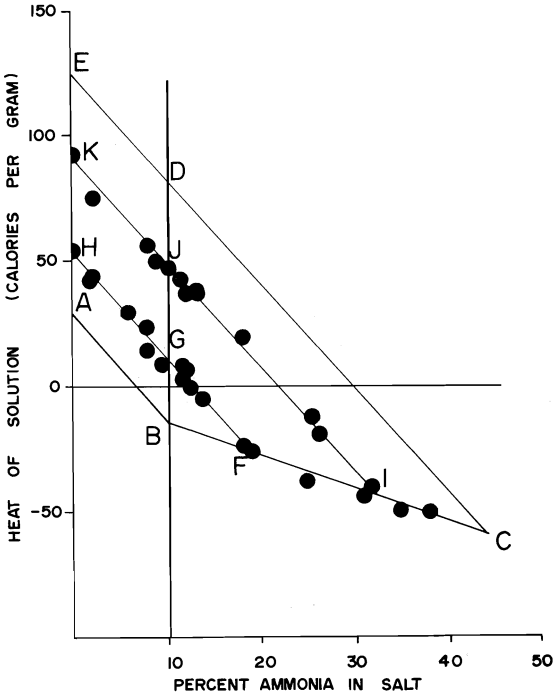

FIG. 2. Heats of solution for various ammines of $MnSO_4$.

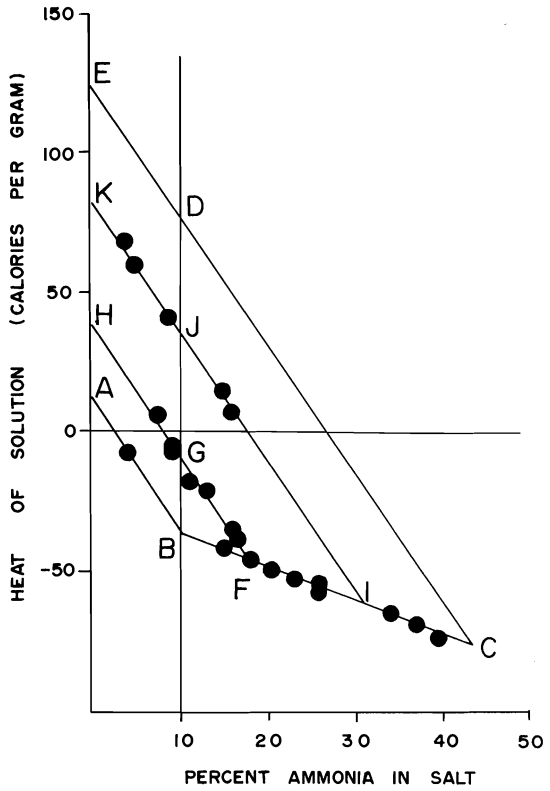

FIG. 3. Heats of solution for various ammines of $FeSO_4$.

point *C* for $MnSO_4 \cdot 7NH_3$, the species which would probably contain the hexaammine-manganese(II) ion, with a slope equal to that of the line *IK*. Thus it is possible to estimate the heat of solution for the high-energy modification of $MnSO_4 \cdot NH_3$ at the point *D* as 80.5 cal/g. The maximum energy of transition *DB* is therefore 96.2 cal/g of monoammine, or 26.0 kcal/mol of heptaamine, which is equivalent to 9.10×10^3 cm^{-1}.

Iron(II) Sulphate

To prevent oxidation of iron(II) the normal lower ammines of iron(II) sulphate were prepared by heating higher ammines in a nitrogen atmosphere.

Using the method of least squares, the heat of solution data of Fig. 3 for various ammine complexes of iron(II) sulphate can be expressed by the linear relations

$$y_{BC} = -1.22x - 24.0$$

$$y_{FH} = -4.57x + 38.1$$

TABLE 3. Heats of solution for various ammines of zinc(II) sulphate

% Ammonia in sample	Heat of solution (cal/g)	Method of preparation
0.0	124	Heated at 350°C
1.05	118	Heated at 240°C
2.06	113	Heated at 350°C
6.56	75.1	Heated at 300°C
9.60	52.7	Heated at 300°C
5.27	89.9	Heated at 300°C
5.88	89.4	Heated at 335°C
9.60	52.7	Heated at 300°C
19.43	15.4	Heated at 50°C
24.03	−2.08	Heated at 36°C
27.32	−14.4	Direct preparation
29.67	−22.9	Direct preparation
34.15	−38.8	Direct preparation
0.0	198	Vacuum at 298°C
9.63	131	Vacuum at 210°C
10.86	125	Vacuum at 203°C
13.47	101	Vacuum at 100°C
16.43	81.8	Vacuum at 87°C
24.61	16.4	Vacuum at 22°C
25.21	17.4	Vacuum at 22°C

and

$$y_{IK} = -4.59x + 82.5$$

Extrapolation of the line *BC* gives the heat of solution of $[Fe(NH_3)_6]^{2+}SO_4^{2-}\cdot NH_3$ (with 43.96% ammonia) as −77.4 cal/g and that of $FeSO_4\cdot NH_3$ (with 10.08% ammonia) as −36.2 cal/g. The line *CE* has been drawn through the point *C* for $FeSO_4\cdot 7NH_3$, the species which would probably contain the hexaammineiron(II) ion, with a slope equal to that of the line *IK*. Thus the heat of solution of the high-energy modification of the monoammine at point *D* is estimated as 78.3 cal/g, and the maximum energy of transition *DB* is therefore 114.5 cal/g of monoammine, or 31.0 kcal/mol of hepta-ammine, which is equivalent to 1.09×10^4 cm^{-1}.

Zinc(II) Sulphate

The heat of solution data for the ammine complexes of zinc(II) sulphate (Table 3, Fig. 4) have been similarly treated. The relations are:

$$y_{AB} = -7.32x + 127$$

$$y_{BC} = -3.74x + 88.2$$

and

$$y_{FH} = -7.32x + 201$$

The heat of solution for $Zn(NH_3)_6SO_4\cdot NH_3$ (with 42.76% ammonia) was estimated as

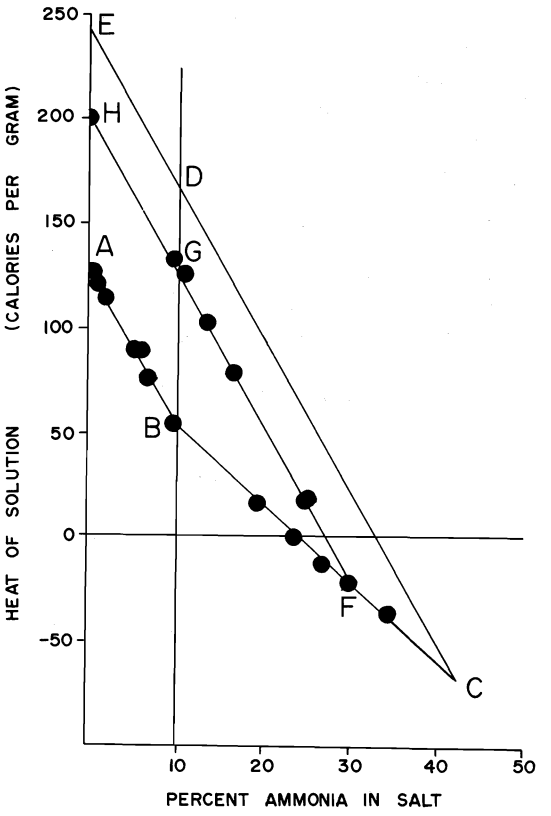

FIG. 4. Heats of solution for various ammines of $ZnSO_4$.

−71.6 cal/g and that for $ZnSO_4\cdot NH_3$ as 52.5 cal/g. Using the slope of the line *FH*, the line *CE* has been drawn having the equation

$$y_{CE} = -7.32x + 240$$

which gave the heat of solution for the mono-ammine at *D* as 170 cal/g. The maximum heat of transition is 117.5 cal/g or 32.9 kcal/mol of heptaammine which is equivalent to 11.5×10^3 cm^{-1}.

Discussion

Unfortunately no spectroscopic values have been given for the ligand field splitting energies of the hexaammines of manganese(II), iron(II), and zinc(II). Therefore the values now obtained for these complexes cannot be compared with the spectroscopic values as has been done for the hydrates and the hexaammines of cobalt(II) and nickel(II) (1, 2).

In aqueous ammonia the ammines of manganese(II) and iron(II) are hydrolyzed to their

hydroxides which precipitate as black solids. These salts dissolve readily in 1 *M* aqueous hydrochloric acid. This could be due to marked lability of ammonia ligands which allow reactions such as

[1] $[M(NH_3)_6]^{2+} + 6L \rightarrow [ML_6]^{2+} + 6NH_3$

where L could be either H_2O or Cl^- in solution. The ammonia released could then undergo hydrolysis to produce the hydroxide ions which in turn could react with the complex $[ML_6]^{2+}$ to form the black hydroxide observed.

In the presence of excess hydrogen ions, the net reaction can be written as

[2] $[M(NH_3)_6]^{2+} + 6H^+ + 6L \rightarrow [ML_6]^{2+} + 6NH_4^+$

From the heat of solution data, *e.g.*, Fig. 1 for the ammines of manganese(II) sulphate, it is apparent that all the ammonia ligands in the heat of solution samples have been replaced by water molecules or chloride ions, and therefore it is necessary to subtract the heat of neutralization of ammonia from the heat of solution of every sample except the anhydrous salt. The quantity to be subtracted, 7.10 cal/1% ammonia content, is obtained from thermochemical data (8) for the equation

$$NH_{3(aq)} + HCl_{(aq)} \rightarrow NH_4Cl_{(aq)}$$

[3] $$\Delta H^0 = 12.09 \text{ kcal/mol}$$

It is probably due to this that no attempt has been made to measure ligand field splitting energies spectroscopically for the hexaammines of maganese(II) and iron(II), since the hexaammines (or any lower ammine) do not exist in aqueous solution. It is, of course, impossible to measure the ligand field splitting energies for zinc(II) complexes spectroscopically since all the 3*d*-orbitals are filled so that no absorption spectra due to the *d–d* transitions could be observed.

However, the values obtained both by the present calorimetric technique and the spectroscopic method for other complexes of the metal ions may be used for the purpose of comparison. From the spectrochemical series it is known that the ligand field splitting energies due to H_2O, NH_3, and ethylenediamine (en) are in the order

$$H_2O < NH_3 < en$$

The values (9–15) for those ligands and various cations under consideration are reproduced in Table 4 and Fig. 5 together with the values found for the hexaammines of mangenese(II), iron(II), and zinc(II). It seems that they all are of the same order of magnitude; thus giving confidence in the present method. For the reason discussed above, it is unfortunate that no ligand field splitting energy for the tris(ethylenediamine) zinc(II) has yet been given. However, the ligand field splitting energy obtained for hexaaquozinc(II) (10) appears to suggest that the present assignment of $10Dq$ for hexaamminezinc(II) is correct.

TABLE 4. Ligand field splitting energies for some complexes of metal(II) ions

		$10Dq$ in 10^3 cm^{-1}		
Cation	Ligand	H_2O	NH_3	en
Mn^{2+}		7.80	9.10	10.1
Fe^{2+}		10.4	10.9	11.4
Co^{2+}		9.30	10.1	11.0
Ni^{2+}		8.50	10.8	11.6
Cu^{2+}		12.6*	15.1*	16.4*
		11.2†	11.0‡	
Zn^{2+}		8.30	11.5	—

*From ref. 9.
†From ref. 15.
‡From ref. 14.

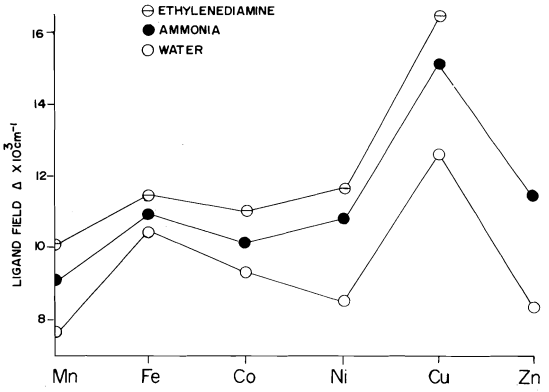

FIG. 5. Ligand field splitting energies for some complexes of metal(II) ions.

1. J. W. S. JAMIESON, G. R. BROWN, D. W. GRUENER, R. V. PEILUCK, and R. A. LAMONTAGNE. Can. J. Chem. **43**, 2148 (1965).
2. B. MUHAMMAD and J. W. S. JAMIESON. Can. J. Chem. **48**, 2177 (1970).
3. Gmelins Handbuch der Anorg. Chem. Vol. 8, Part B. No. 59. 1929. p. 58.
4. P. PASCAL. Noveau traite de chimie minerale. Vol. 5. Masson et Cie. 1962. p. 256.
5. F. EPHRAIM. Ber. **52**, 957 (1919).
6. J. W. MELLOR. A comprehensive treatise on inor-

ganic and theoretical chemistry. Longmans, Green and Co., Inc., London. 1936. Vol. III, p. 251; Vol. XII, p. 411; Vol. XIV, pp. 63, 273, 770; Vol. XV, p. 463.
7. W. W. WENDLANDT and J. P. SMITH. Nature, **201**, 73 (1964).
8. F. D. ROSSINI, D. D. WAGMAN, W. H. EVANS, S. LEVINE, and I. JAFFE. Nat. Bur. Stand. (U.S.) Circ. No. 500, 1952.
9. L. E. ORGEL. An introduction to transition metal chemistry, ligand field theory. Methuen, London. 1960. p. 46.
10. J. W. S. JAMIESON, R. A. LAMONTAGNE, B. A. PATTERN, and G. R. BROWN. Can. J. Chem. **43**, 3129 (1965).
11. C. J. BALLHAUSEN and C. K. JØRGENSEN. Acta Chem. Scand. **9**, 397 (1955).
12. C. K. JØRGENSEN. Absorption spectra and chemical bonding in complexes. Pergamon, Oxford. 1962. p. 110.
13. M. GIANPOEINI, P. PAOLETTI, and L. SACCONE. J. Chem. Soc. 4553 (1960).
14. H. ELIOTT and B. J. HATHAWAY. Inorg. Chem. **5**, 885 (1965).
15. R. PAPPALARDO. J. Mol. Spectrosc. **6**, 554 (1961).

Polar radicals. XI. Kinetic studies on the mechanism of the liquid phase bromination of 1-chlorobutane[1,2]

DENNIS D. TANNER, TAMEICHI OCHIAI,[3] JEFF ROWE,[4]
TONY PAĊE, HIDEKI TAKIGUCHI,[5] AND PETER W. SAMAL[6]
Department of Chemistry, University of Alberta, Edmonton, Alta., Canada T6G 2G2

Received November 18, 1976[7]

DENNIS D. TANNER, TAMEICHI OCHIAI, JEFF ROWE, TONY PAĊE, HIDEKI TAKIGUCHI, and PETER W. SAMAL. Can. J. Chem. **55**, 3536 (1977).

A general method for the evaluation of the kinetics of the solution phase bromination of alkanes and substituted alkanes is presented. The model used considers reversible transfer reactions of the radicals formed with both hydrogen bromide and hydrogen tribromide. Cage reversal of the geminate radical – hydrogen bromide pair and reversal with hydrogen tribromide are used to rationalize the differences observed between the vapor and solution phase kinetics. The method is applied to the bromination of 1-chlorobutane.

DENNIS D. TANNER, TAMEICHI OCHIAI, JEFF ROWE, TONY PAĊE, HIDEKI TAKIGUCHI et PETER W. SAMAL. Can. J. Chem. **55**, 3536 (1977).

On présente une méthode générale d'évaluation de la cinétique pour la bromation en solution d'alkanes substitués et non substitués. Le modèle utilisé tient compte des réactions réversibles de transfert des radicaux formés avec le bromure et le tribromure d'hydrogène. L'inversion en cage de l'ensemble, radical géminé et bromure d'hydrogène, et l'inversion avec le tribromure d'hydrogène sont utilisées pour rationaliser les différences observées entre la cinétique en solution et en phase vapeur. La méthode est appliquée à la bromation du chloro-1 butane.
[Traduit par le journal]

Introduction

The detailed mechanism of the liquid phase photobromination of alkanes and substituted alkanes has been a topic of both theoretical and synthetic concern. Recently several new details of the mechanism have been reported which make possible a clearer understanding of the reaction (2, 3). The more detailed pathway suggested for the reaction is presented in Scheme 1.

Cage reversal (the reverse of A), the reaction of the caged geminate radical – hydrogen bromide pair, was found to be a reaction which is competitive with diffusion of the radical from the solvent cage, reaction B. The cage reversal reaction was deemed to be competitive with diffusion since k_{-a} is a rate constant whose magnitude is near the diffusion controlled limit and the concentration of the species in the individual cage can be approximated as their bulk concentrations.[8] It was suggested that in the bromination of a substrate which can yield

$$\text{[A]}\quad RH + Br^{\bullet} \underset{k_{-a}}{\overset{k_a}{\rightleftharpoons}} (R^{\bullet} + HBr)^{cage}$$

$$\text{[B]}\quad (R^{\bullet} + HBr)^{cage} \xrightarrow{k_d} R^{\bullet}$$

$$\text{[C]}\quad R^{\bullet} + HBr \xrightarrow{k_{-a}} RH + Br$$

$$\text{[D]}\quad R^{\bullet} + HBr_3 \xrightarrow{k'_{-a}} RH + Br_3^{\bullet}$$

$$\text{[E]}\quad R^{\bullet} + Br_2 \xrightarrow{k_t} RBr + Br.$$

SCHEME 1

[1]For Part X, see ref. 9.

[2]Presented in part at 1st International Symposium on Organic Free Radicals, Sirmione, Italy (10) and in part at 57th Canadian Chemical Conference, C.I.C., Regina, Sask. (11).

[3]Postdoctoral Fellow, University of Alberta, Edmonton, Alta. 1974–1975.

[4]Taken in part from the Doctoral Dissertation of Jeff Rowe, University of Alberta, Edmonton, Alta. 1974.

[5]Postdoctoral Fellow, University of Alberta, Edmonton, Alta. 1975.

[6]Postdoctoral Fellow, University of Alberta, Edmonton, Alta. 1976.

[7]Revision received May 16, 1977.

[8]For a discussion of this assumption for reactions involving cage recombination reactions see ref. 8.

isomeric products, the variation of the rates of reversal of the isomeric radicals, when competing with diffusion, could lead to a differentiation in the proportion of each radical that escaped from the cage and ultimately formed products (3). In solution the relative rates of transfer, with bromine and with hydrogen bromide, of the radicals free of the solvent cage were found to be dependent upon the concentration of bromine and hydrogen bromide. The rate of transfer with hydrogen relative to bromine was found to be increased at higher concentration of transfer agents since a new species HBr_3, was found to react with an organic radical at a faster rate (k'_{-a}) than hydrogen bromide itself.

$$HBr + Br_2 \rightleftharpoons HBr_3$$

$$R^{\cdot} + HBr_3 \xrightarrow[k'_{-a}]{} RH + {}^{\cdot}Br_3$$

No information was available concerning the possibility that the species hydrogen tribromide could, likewise, act as a bromine atom donor. If this were so, however, the measured value, k'_{-a}/k_{-a}, would be even larger than reported. The possibility also existed that hydrogen abstraction in solution could take place by, the presumably more selective and less reactive species, $Br_3^{\cdot}$. Although this process would complicate the kinetic expression used to evaluate the relative rates of product formation for reactions carried out in solution, the values of the relative rates of abstraction used to evaluate the kinetics were obtained from vapor phase studies where this complication is not important. Both of these processes are not further considered in the development of this model although they can conceivably occur.

The liquid phase bromination of 1-chlorobutane has been previously studied and the product distribution obtained from the reaction has been rationalized on the basis of both the polar effects of the electronegative substituent and the strength of each carbon hydrogen bond that is broken in the abstraction process.[9]

A study of the kinetics of the bromination of perdeuterio-1-chlorobutane in the vapor phase allowed the determinations of the relative rates of abstraction of hydrogen in each position of 1-chlorobutane and the relative rates of transfer with bromine and hydrogen bromide of the isomeric set of radicals formed from the abstraction reaction (1). When the bromination was carried out in the vapor phase, to low conversion, and at high concentrations of molecular bromine, neither the cage reactions nor the transfer reactions with HBr_3 were present as competing processes.

In this publication we would like to report a study of the kinetics of the liquid phase photobromination of 1-chlorobutane which takes into account all of the details established previously, reactions A–E. The report details a general method which can be applied to evaluate the solution phase kinetics of bromination of substrates which yield isomeric mixtures of bromination products.

Discussion and Results

The simplest mechanism for the solution phase bromination of a molecule which yields isomeric radicals on hydrogen abstraction can be exemplified by the bromination of 1-chlorobutane (see Scheme 2). The relative rates of the appearance of any two products can be derived, using this mechanism (i.e. $(d[R^{\alpha}Br]/dt)/(d[R^{\gamma}Br]/dt)$, [1]; $(d[R^{\beta}Br]/dt)/(d[R^{\gamma}Br]/dt$, [2]).

$$[1]\quad \frac{d[R^{\alpha}Br]/dt}{d[R^{\gamma}Br]/dt} = \left(\frac{k_2}{k_{-1}}\right)\left(\frac{k_{-5}}{k_6}\right)\left(\frac{k_1}{k_5}\right)\left(\frac{k_{-5}[HBr]^c + k_d}{k_{-1}[HBr]^c + k_d}\right) \times \left(\frac{(k_6/k_{-5})[Br_2] + [HBr] + (k'_{-5}/k_{-5})[HBr_3]}{(k_2/k_{-1})[Br_2] + [HBr] + (k'_{-1}/k_{-1})[HBr_3]}\right)$$

$$[2]\quad \frac{d[R^{\beta}Br]/dt}{d[R^{\gamma}Br]/dt} = \left(\frac{k_4}{k_{-3}}\right)\left(\frac{k_{-5}}{k_6}\right)\left(\frac{k_3}{k_5}\right)\left(\frac{k_{-5}[HBr]^c + k_d}{k_{-3}[HBr]^c + k_d}\right) \times \left(\frac{(k_6/k_{-5})[Br_2] + [HBr] + (k'_{-5}/k_{-5})[HBr_3]}{(k_4/k_{-3})[Br_2] + [HBr] + (k'_{-3}/k_{-3})[HBr_3]}\right)$$

[9]For reference on the bromination of 1-chlorobutane see ref. 1 and the references quoted therein.

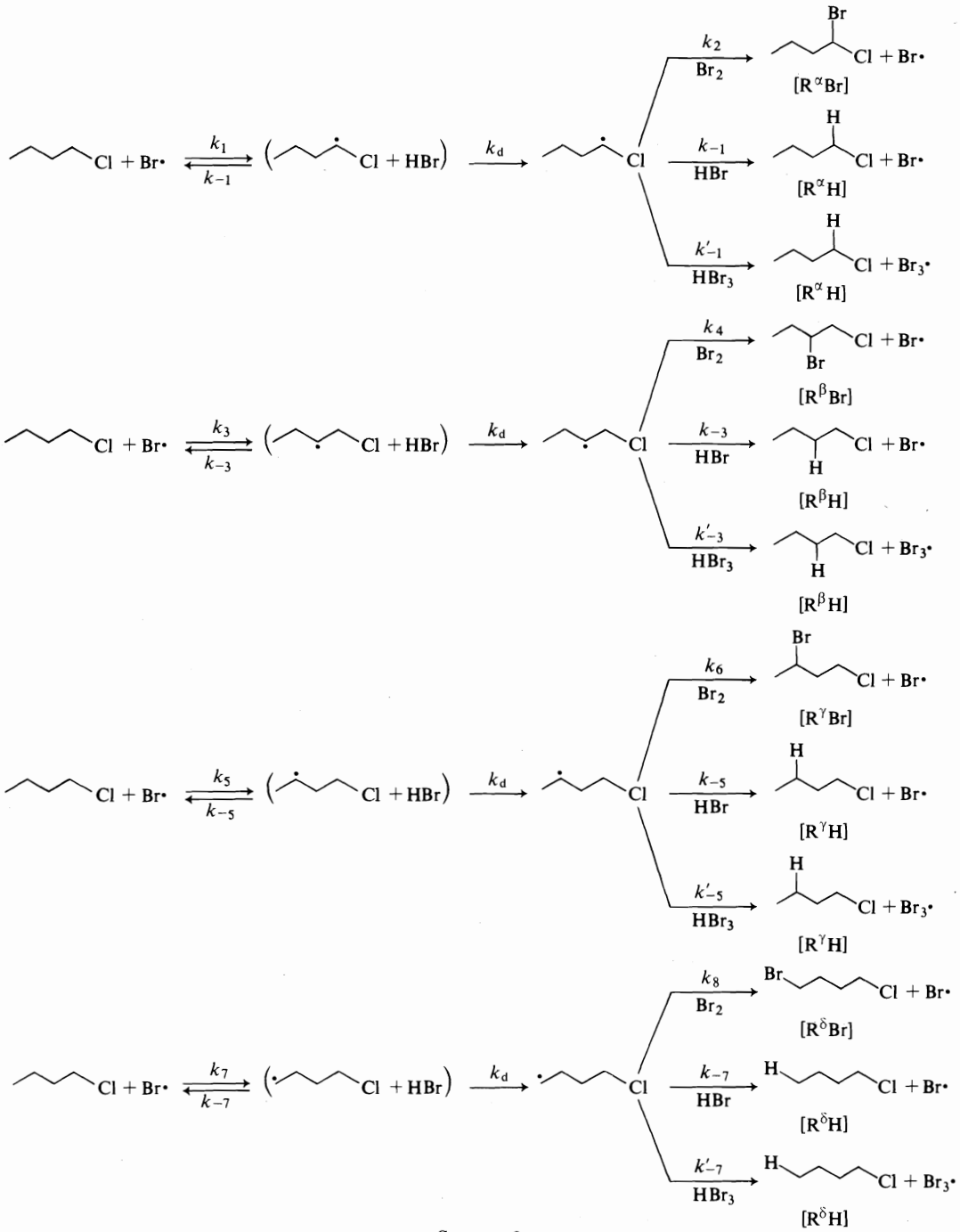

SCHEME 2

Equations 1 and 2 were derived using a steady state approximation for the concentrations of both 'free' and caged radicals and by assuming that k_d, the specific rate constant for diffusion, was the same for all of the 1-chlorobutyl radicals involved. If the reaction is carried out with high concentrations of bromine and hydrogen bromide, to low conversion, where the concentra-

tions of bromine and hydrogen bromide are relatively constant, then [1] and [2] can be integrated.

The relative rates of transfer, other than cage transfer, can be evaluated at each position in the molecule by a study of the relative rate of product formation (R^iH and R^iBr) for each position of perdeuterio-1-chlorobutane. The expression takes the form of [3] (α-position), [4] (β-position), and [5] (γ-position), and each expression may in turn be integrated when the reaction is carried out to low conversion using high concentrations of bromine and hydrogen bromide.

$$[3]\quad \frac{d[R^\alpha H]/dt}{d[R^\alpha Br]/dt} = \frac{[HBr] + k'_{-1}/k_{-1}[HBr_3]}{k_2/k_{-1}[Br_2]}$$

$$[4]\quad \frac{d[R^\beta H]/dt}{d[R^\beta Br]/dt} = \frac{[HBr] + k'_{-3}/k_{-3}[HBr_3]}{k_4/k_{-3}[Br_2]}$$

$$[5]\quad \frac{d[R^\gamma H]/dt}{d[R^\gamma Br]/dt} = \frac{[HBr] + k'_{-5}/k_{-5}[HBr_3]}{k_6/k_{-5}[Br_2]}$$

By a combination of the integrated forms of [3], [5], and [1] or [4], [5], and [2], two expressions ([6] and [7]) can be obtained that will allow an experimental evaluation of the effect of cage reversal on the ratio of products formed.

$$[6]\quad C_\gamma^{\ \alpha} = \left(\frac{k^D_{-1}(DBr)^c + k_d}{k^D_{-5}(DBr)^c + k_d}\right) = (k_1/k_5)\left(\frac{\Delta[R^\gamma H] + [R^\gamma Br]}{\Delta[R^\alpha H] + [R^\alpha Br]}\right)$$

$$[7]\quad C_\gamma^{\ \beta} = \left(\frac{k^D_{-3}[DBr]^c + k_d}{k^D_{-5}[DBr]^c + k_d}\right) = (k_3/k_5)\left(\frac{\Delta[R^\gamma H] + [R^\gamma Br]}{\Delta[R^\beta H] + [R^\beta Br]}\right)$$

The effect of cage reversal, $C_j^{\ i}$, may be evaluated from the results of the bromination of perdeuterio-1-chlorobutane if one invokes the assumption proposed by Mayo (4) that there will be negligible solvent effects on the relative rates of competitive free radical reactions of the same kinetic order. If one makes the substitution $(k_1/k_5)^{vapor} \simeq (k_1/k_5)^{solution}$ then [6] and [7] may be evaluated using the vapor phase values previously reported (ΔR^iH is the change from the initial to the final concentration of protium at each position i and $[DBr]^c$ is the cage concentration of deuterium bromide).

TABLE 1. Photobromination of perdeuterio-1-chlorobutane in Freon 113 (23.0°C)

	Concentration (mol/ℓ × 10^3)		
	Run 1	Run 2	Run 3
Reactants[a]			
$[RD(H)]^0$	20.2	13.3	21.9
$[Br_2]^0$	39.1	50.4	37.7
$[HBr]^0$	41.8	44.6	108.1
$[R^\alpha H]^0$	0.677	0.436	0.380
$[R^\beta H]^0$	0.279	0.180	0.425
$[R^\gamma H]^0$	0.796	0.513	0.550
$[R^\delta H]^0$	1.223	0.789	1.143
Products[b]			
[RD(H)]	18.6	11.9	21.0
$[R^\alpha H]$	0.727	0.474	0.457
$[R^\beta H]$	0.356	0.236	0.556
$[R^\gamma H]$	1.163	0.778	0.953
$[R^\delta H]$	1.292	0.853	1.199
$[R^\alpha Br]$	0.440	0.355	0.259
$[R^\beta Br]$	0.482	0.392	0.288
$[R^\gamma Br]$	0.699	0.573	0.318
$[R^\delta Br]^c$	0.000	0.000	0.000

[a][RD(H)] refers to the concentration of perdeuterio-1-chlorobutane, and $[R^iH]$ is the average concentration of the residual protium at position i.

[b]The values for $[R^iH]$ at the end of the reaction were calculated as: $[R^iH]^f + 1/2([R^iH]^0 + [R^iH]^f)([RDH]^0 - [RDH]^f/[RDH]^0)$, in order to correct for the small amount of protiated material that has undergone reaction.

[c]Not detected by glpc.

The photobrominations of perdeuterio-1-chlorobutane were carried out at 23°C in Freon 113 solution. The reactions were carried out to low conversion where multiple exchange reactions (H for H or D for D) will be negligible and where the concentration of bromine or the initially added hydrogen bromide were not appreciably changed during the reaction. The reaction mixture after photolysis was freed from excess bromine and hydrogen bromide and the yields of the bromination products were determined by glpc analysis. The analysis showed the presence of only the perdeuterated analogs of 1-bromo-1-chlorobutane, 2-bromo-1-chlorobutane, 3-bromo-1-chlorobutane, and the unbrominated substrate. A material balance of >97% for each of the brominated materials was obtained (in control experiments) using this analytical procedure (1). The unbrominated substrate was collected by preparative glpc and the change in the relative amount of incorporated protium at each position (see Table 1) was determined from a comparison of the ^1H 100 MHz nmr spectrum of the residual protium in the (Merck, Sharp and Dohme, 98.3 at.% D) starting perdeuterio-1-chlorobutane and the

TABLE 2. Relative kinetic values calculated for 1-chlorobutyl radicals[a]

I. Relative rates of transfer of 1-chlorobutyl radicals with Br_2 and HBr (vapor phase, 23°C)[b]
(α-position) $k_2/k_{-1} = 65.5 \pm 7.9$
(β-position) $k_4/k_{-3} = 15.6 \pm 3.0$
(γ-position) $k_6/k_{-5} = 8.1 \pm 0.5$

II. Relative rates of transfer of 1-chlorobutyl radicals with HBr_3 and HBr (Freon 113, 23.0°C)
(α-position) $k'_{-1}/k_{-1} = 57.6 \pm 1.2$
(β-position) $k'_{-3}/k_{-3} = 13.0 \pm 0.4$
(γ-position) $k'_{-5}/k_{-5} = 26.8 \pm 1.8$

III. Cage reversal effect, C_γ^i for the 1-chlorobutyl radicals (Freon 113, 23.0°C)
$C_\gamma^\alpha = 0.73 \pm 0.01$
$C_\gamma^\beta = 0.89 \pm 0.04$
$C_\gamma^\gamma = (1.00)$

[a]Errors quoted are based on the reproducibility between kinetic determinations.
[b]Data taken from ref. 1.

spectrum of the recovered unbrominated substrate. The total amount of protium in the starting material and the recovered substrate was determined by mass spectrometry. The concentrations, conditions, and values obtained for the kinetic analysis are listed in Table 1.

The ratio of rate constants for the abstraction of a deuterium atom from perdeuterio-1-chlorobutane in the α-, β-, and γ-positions can be equated to the same ratio of rate constants in the undeuterated substrate if the assumption is made that analogous ratios of rate constants for the two substrates are the same, eq. 8.

$$[8] \qquad k^H{}_i/k^H{}_j = k^D{}_i/k^D{}_j$$

From the data in Table 1, using the integrated forms of [3], [4], and [5], and the vapor phase relative rate data for transfer of each radical with bromine and hydrogen bromide (see Table 2) the ratio of transfer rates with HBr_3 vs. HBr could be calculated for each position in the molecule. The value of $[HBr_3]$ could be obtained from the equilibrium constant, $K = 2.8 \pm 0.3$ (23°C), determined by the nmr method previously described (2). Although the experimental error is large the value of k'_{-5}/k_{-5} listed in Table 2 is quite similar to the analogous value reported for perdeuteriocyclohexyl radicals, $k'_{-i}/k_{-i} = 22 \pm 7$ (32°C) (2). The similarity of these values was expected for structurally and energetically similar secondary radicals.

The effect of cage reversal, C_γ^i, as was expected, follows the same trend as that observed for the relative rate of transfer with bromine compared with hydrogen bromide (1). As the radical center involved was further removed from the electron withdrawing chlorine substituent the ratio of transfer rates for the three secondary radicals decreased in the order, $k_2/k_{-1} > k_4/k_{-3} > k_6/k_{-5}$. This change in relative rates was rationalized on the basis of a polar deactivation to transfer with hydrogen bromide which falls off as the distance from the electronegative substituent was increased, while the transfer with molecular bromine was little affected. The cage reversal effect is the result of a competition between diffusion and the reversal of the isomeric radicals formed with deuterium bromide, and since from the above reasoning $k^D{}_{-1} < k^D{}_{-3} < k^D{}_{-5}$, then it follows that cage reversal, C_γ^i, should increase as observed from C_γ^α to C_γ^γ (see Table 2).[10]

In the absence of external reversal [1] (or [2]) reduces to an expression [9] (or [10]) which can be integrated to obtain the predicted ratios of products obtained for the bromination of the natural protiated material.

$$[9] \qquad \frac{d(R^\alpha Br)/dt}{d(R^\gamma Br)/dt} = \left(\frac{k_1}{k_5}\right)\left(\frac{k_{-5}[HBr]^c + k_d}{k_{-1}[HBr]^c + k_d}\right)$$

$$[10] \qquad \frac{d[R^\beta Br]/dt}{d[R^\gamma Br]/dt} = \left(\frac{k_3}{k_5}\right)\left(\frac{k_{-5}[HBr]^c + k_d}{k_{-3}[HBr]^c + k_d}\right)$$

When the bromination of 1-chlorobutane was carried out to low conversion (see Table 3, reactions 1–8) under conditions where the reversal reaction was negligible the ratio of products found agreed reasonably well with the values predicted using [9] and [10] (Table 4, entries 1 and 2). The agreement between the observed and calculated values of the product ratios lends support to the assumption made, that the vapor phase values of the relative rate constants may be substituted into the kinetic expression for the solution phase reactions, and the cage reversal expression C_γ^i, evaluated using the data obtained from the bromination of the perdeuterated substrate, can equally well be used to predict the products obtained from the natural protiated substrate.

[10]Using [6] the cage reversal effect at the δ-position, C_γ^δ, was found to have a value of 0.56, rather than one closer to unity, as expected. This result may be due to the large error in the calculated value, since $[R^\delta Br]$ and $[R^\delta H]$ are both rather small.

TABLE 3. Photobromination of 1-chlorobutane in the liquid phase[a]

Reaction number	Concentration (M) $[C_4H_9Cl]^0$	Concentration (M) $[Br_2]^0$	Temperature (°C)	% conversion[b]	$\frac{[R^\alpha Br]}{[R^\gamma Br]}$	$\frac{[R^\beta Br]}{[R^\gamma Br]}$	$\frac{[R^\gamma Br]}{[R^\gamma Br]}$
1	0.219	0.556	21.0	2	0.55	0.55	(1.00)
2	0.219	0.556	21.0	3	0.49	0.54	(1.00)
3	0.219	0.556	21.0	4	0.54	0.55	(1.00)
4	0.217	0.567	23.0	1	0.51	0.51	(1.00)
5	0.217	0.567	23.0	1	0.53	0.56	(1.00)
6	0.217	0.567	23.0	3	0.49	0.53	(1.00)
7	0.217	0.567	23.0	4	0.50	0.53	(1.00)
8	0.217	0.567	23.0	10	0.52	0.53	(1.00)
9	2.60	10.3	21.0	2	0.31	0.47	(1.00)
10	2.60	10.3	21.0	3	0.35	0.47	(1.00)
11	0.199	11.6	21.0	1	0.31	0.48	(1.00)
12	0.199	11.6	21.0	1	0.33	0.47	(1.00)

[a]Reactions 1–8 were run in Freon 113 solvent; reactions 9–12 were run in liquid bromine solvent.
[b]Based on 1-chlorobutane.

TABLE 4. Comparison of the vapor and liquid phase product distribution in the photobromination of 1-chlorobutane and perdeuterio-1-chlorobutane

Conditions	$\frac{[R^\alpha Br]^a}{[R^\gamma Br]}$	$\frac{[R^\beta Br]^a}{[R^\gamma Br]}$	$\frac{[R^\gamma Br]^a}{[R^\gamma Br]}$
1. Freon 113, 23°C, 1–10% reaction of 1-chlorobutane[b]	0.52±0.02	0.54±0.01	1.0
2. Calculated (eqs. 8, 9) for the liquid phase bromination of 1-chlorobutane, 23°C	0.47±0.04	0.55±0.07	1.0
3. Liquid bromine, 1–3% reaction of 1-chlorobutane, 21°C[c]	0.33±0.02	0.47±0.00	1.0
4. Vapor phase, 4.5% reaction of 1-chlorobutane, 24°C[d]	0.36±0.02	0.47±0.02	1.0
5. Calculated from the vapor phase rates of bromination of perdeuterio-1-chlorobutane[d]	0.35±0.02	0.48±0.04	1.0

[a]Ratio of 1-bromo-, $[R^\alpha Br]$, and 2-bromo-1-chlorobutane, $[R^\beta Br]$, to 3-bromo-1-chlorobutane, $[R^\gamma Br]$.
[b]Taken from Table 3, reactions 1–8.
[c]Taken from Table 3, reactions 9–12.
[d]Taken from ref. 1.

We have previously suggested that the values obtained for the relative rates of bromination of several pairs of substrates in solvent liquid bromine (10–18 M) could be rationalized on the basis of competitive abstraction reactions which proceeded to products without internal (cage) or external return (5). In support of this suggestion that cage return can be interfered with by carrying out the brominations in very high concentrations of bromine it has been recently demonstrated that the deuterium isotope effect for the bromination of cyclohexane and perdeuteriocyclohexane, in the absence of external reversal, gave the same value, k_{RH}/k_{RD}, in the vapor phase and in solution (10–18 M liquid bromine) (3). The brominations of 1-chlorobutane in liquid bromine (reactions 9–12, Table 3), likewise, show the same product distribution as the vapor phase reactions of perdeuterio-1-chlorobutane and of 1-chlorobutane carried out under irreversible conditions, low conversion in the presence of excess bromine (see Table 4, compare entries 3 and 4 or 5). The coincidence of the product distributions obtained from these experiments in the vapor phase and in solution further substantiates the concept of cage scavenging of an alkyl radical by liquid bromine, and serves as a further example of the importance of considering differential cage reversal of isomeric radicals in solution phase brominations. The conclusions reached in the vapor phase study (1), that hydrogen abstraction and its reversal are both deactivated by the polar influence of the substituent, and that the effect

TABLE 5. The nmr determination of $HBr + Br_2 \rightleftharpoons HBr_3$ equilibrium constant (23.0°C)

Spectrum	HBr (M)	Br_2 (M)	δ (Hz)[a]	K
1	0.0509		357.3	
2	0.0681		354.5	
3	0.0764		355.4	
4	0.0814		354.7	
5	0.0925		355.1	
6	0.0675	0.0311	353.6	2.4
7	0.0655	0.1899	344.1	3.7
8	0.0630	0.3098	341.4	3.1
9	0.0594	0.5091	338.8	2.6
10	0.0651	1.040	333.8	2.6
11	0.0638	2.123	329.8	2.7
			Average	2.8 ± 0.3, $\Delta = 29.9$ Hz[b]

[a]Average δ (Hz) for HBr in Freon 113 was 355.4 ± 0.8 upfield from TMS.
[b]Computed shift of HBr_3 signal relative to that of HBr.

falls off as the distance of the substituent from the C—H bond involved increases, are consistent with the results of this study. The conclusion previously reached (1) that there is no evidence for anchimeric assistance by a neighboring chlorine atom during hydrogen abstraction is further enforced.

Experimental

Materials

1-Chlorobutane was washed with concentrated sulfuric acid, water, 10% aqueous sodium carbonate solution, and water, dried over calcium chloride, and distilled twice through a 1 ft Vigreaux column. The middle fraction was collected, bp 72.5–73.5°C (708 mm). Commercial perdeuterio-1-chlorobutane (Merck, Sharp and Dohme of Canada Ltd.) was used without further purification: glpc analysis showed it to be 99.5% pure. Analysis by mass spectroscopy showed it to contain 98.3 at.% D, while nmr analysis, using 1,1-diphenylethene as internal standard, showed it to be 98.0 at.% D.

Molecular bromine (Raylo Chemicals Ltd.) was washed with concentrated sulfuric acid and distilled, bp 56.7°C (700 mm). Hydrogen bromide (Matheson) was distilled prior to use.

Freon 113 (Matheson) and Freon 112 (PCR) were distilled from phosphorus pentoxide through a 1 ft Vigreaux column, bp 45.5°C and 88.0°C (700 mm), respectively.

1,1-Diphenylethene (Eastman Organic Chemicals) was distilled under reduced pressure, bp 133.5–133.8°C (7.6 mm), n_D^{20} 1.6088 (lit. (6) bp 139°C (11 mm), n_D^{20} 1.6085); nmr spectroscopy and glpc analysis showed it to have no detectable impurities.

Photobromination of Perdeuterio-1-chlorobutane with Excess Bromine and Excess Hydrogen Bromide

A Freon 113 solution of hydrogen bromide was allowed to equilibrate in a water bath maintained at 23.0 ± 0.1°C. The solution was protected from the atmosphere by a mercury bubbler. Perdeuterio-1-chlorobutane, bromine, and Freon 112 (internal standard) were added in the absence of light, and the concentrations of bromine and hydrogen bromide were determined by iodometric titration (7). The solution was irradiated (2 × 200 W incandescent lamps) until 4–10% of the perdeuterio-1-chlorobutane had reacted. The reaction mixture was washed with ice-cold, 5% aqueous sodium bisulfite solution and with water. It was dried over anhydrous sodium sulfate, and then analyzed by glpc (10 ft × ¼ in. 10% UCON 50 LB 550X on Chromosorb P AW, glass column) for the remaining perdeuterio-1-chlorobutane and products (1). The solution was concentrated by distillation on a 24 in. Teflon spinning band column and the unbrominated perdeuterio-1-chlorobutane was collected by preparative glpc. The protium content was then determined (using nmr and mass spectroscopy) as previously described (1).

Equilibrium Constant Measurements

Solutions of hydrogen bromide and bromine in Freon 113 (1% in TMS) were prepared in 4 mm id nmr tubes as previously reported (1). The tubes were allowed to equilibrate to the probe temperature, 23.0 ± 0.2°C, and the nmr spectrum was obtained. All line positions were measured in Hertz relative to TMS by counting the difference between the lock and sweep oscillator frequencies using a Varian HA 100 spectrometer. Reproducibility of the measurement was better than 0.2 Hz. The equilibrium constant was determined as described in our previous paper (1). The results are given in Table 5.

Photobromination of 1-Chlorobutane

Aliquots of Freon 113 solutions of 1-chlorobutane, bromine, and Freon 112 (internal standard) were placed in Pyrex tubes. The tubes were degassed three times by the freeze–thaw method and sealed. They were placed in a water bath, equilibrated in the absence of light for 10 min, and then irradiated until 1–10% of the 1-chlorobutane had been brominated. The tubes were opened, the excess bromine destroyed with aqueous sodium bisulfite solution, and the organic layer washed with water and dried (Na_2SO_4). It was then analyzed by glpc (10 ft × ¼ in. 10% UCON 50 LB 500X on Chromosorb P AW, glass column).

Acknowledgment

The authors wish to thank the National Research Council of Canada and the University of Alberta for their generous support of this work.

1. D. D. TANNER, T. PAĊE, and T. OCHIAI. Can. J. Chem. **53**, 2202 (1975).
2. D. D. TANNER, T. PAĊE, and T. OCHIAI. J. Am. Chem. Soc. **97**, 4303 (1975).
3. D. D. TANNER, T. OCHIAI, and T. PAĊE. J. Am. Chem. Soc. **97**, 6162 (1975).
4. F. R. MAYO. J. Am. Chem. Soc. **89**, 2654 (1967).
5. D. D. TANNER, J. E. ROWE, T. PAĊE, and Y. KOSUGI. J. Am. Chem. Soc. **95**, 4705 (1973).
6. C. F. H. ALLEN and S. CONVERSE. Organic Synthesis, Collected Vol. 1, 226 (1951).
7. G. H. CADY. Inorg. Synth. **5**, 156 (1957).
8. C. WALLING. Free radicals in solution. Wiley and Sons, Inc., New York, NY. 1957. pp. 76–77.
9. D. D. TANNER, T. PAĊE, Y. KOSUGI, E. V. BLACKBURN, and T. RUO. Tetrahedron Lett. 2413 (1976).
10. D. D. TANNER, J. ROWE, and T. OCHIAI. Abstracts, 1st International Symposium on Organic Free Radicals, Sirmione, Italy. 1974.
11. D. D. TANNER, J. ROWE, and T. OCHIAI. Abstracts, 57th Canadian Chemical Conference, C.I.C., Regina, Sask. June 3–5, 1974.

Ultrasonic velocities for deuterium oxide – water mixtures at 298.15 K[1,2]

OSAMU KIYOHARA,[3] CARL J. HALPIN, AND GEORGE C. BENSON
Division of Chemistry, National Research Council of Canada, Ottawa, Ont., Canada K1A 0R6

Received May 12, 1977

OSAMU KIYOHARA, CARL J. HALPIN, and GEORGE C. BENSON. Can. J. Chem. **55**, 3544 (1977).

Ultrasonic velocities in deuterium oxide – water mixtures were measured at 298.15 K and 1 atm pressure using the pulse-echo-overlap method in a successive dilution mixing cell. On a mole fraction basis, the velocities show negative deviations from linearity. Excess adiabatic compressibilities derived from the results are almost zero or slightly negative.

OSAMU KIYOHARA, CARL J. HALPIN et GEORGE C. BENSON. Can. J. Chem. **55**, 3544 (1977).

On mesure les vitesses ultrasonores dans des mélanges oxide de deutérium – eau à 298.15 K sous 1 atm de pression en utilisant le recouvrement impulsion-écho dans une cellule à mélange par dilution successive. En se basant sur la fraction molaire, les vitesses montrent des écarts negatifs à la linéarité. Les compressibilités adiabatiques d'excès dérivées à partir des résultats sont presque nuls ou légèrement négatifs.

[Traduit par le journal]

Introduction

In spite of the physical similarity between water and deuterium oxide, the difference of the velocities of ultrasound in these liquids is relatively large, ~ 98 m s^{-1} at 298 K. There have been several previous ultrasonic studies of deuterium oxide – water mixtures (1–4). Mathieson and Conway (3) found that a plot of ultrasonic velocity against mole fraction showed a small but significant curvature away from the composition axis. Gupta *et al.* (4) reported that the speed of sound varies linearly with volume fraction.

Our ultrasonic velocity measurements were undertaken as part of an on-going study of the thermodynamic properties of deuterium oxide – water mixtures. To avoid the exchange of deuterium oxide with atmospheric water vapor, a new mixing cell was designed in which the mixing could be carried out in the absence of any vapor space.

Experimental

Component Liquids

The deuterium oxide was Merck, Sharp and Dohme reagent with a specified minimum isotopic purity of 99.7 at.% D. An Anton Paar densimeter (5) was used to determine its density (1.10420 g cm^{-3} at 298.15 K) just before making the ultrasonic measurements. Assuming the only impurity to be H_2O, the mole fraction of D_2O in our sample was estimated to be 0.9976, based on a value of 1.104449 g cm^{-3} (6) for the density of pure D_2O at 298.15 K.

The water was distilled and deionized. Both component liquids were partially degassed prior to their use in the ultrasonic measurements.

Measurements of Ultrasonic Velocity

Ultrasonic velocities were determined by the pulse-echo-overlap method (7, 8) in which the time interval is measured between a pair of echoes of an ultrasonic wave travelling between a transducer and reflector. For the present work the rf generator was operated at 3 MHz. Details of our equipment have been described previously (9); only the mixing cell was new.

Ultrasonic Cell

A schematic drawing of the cell is shown in Fig. 1, and structural details are given in the legend. The whole unit is securely mounted on a brass frame which can be immersed in a thermostated water bath. The cell was designed to allow successive additions of one component to a known mass of the other component in the absence of any vapor space. The body of the cell is a Pyrex cylinder with a small U-shaped side chamber. The bottom is closed by a transducer–reflector assembly, the top by a movable plunger. The total inner volume when the plunger is withdrawn to its highest position is about 120 cm^3.

The transducer (Panametrics Type 5070 VIP) is mounted in a brass holder. In our previous cell (9), the face of the transducer was gold plated to protect it from the action of the liquid in the cell. It was found that this coating deteriorated with exposure to a variety of solvents. In the new cell direct contact between the transducer and the cell liquid is avoided by coupling through a double transition layer resonator (10). The latter consists of a thin layer of epoxy resin mixed with tungsten powder which couples the transducer to a piece of brass shim

[1]NRCC No. 16175.

[2]This work was presented in part at the 32nd Annual Calorimetry Conference, Université de Sherbrooke, Sherbrooke, Québec, Canada, July 6–9, 1977.

[3]National Research Council of Canada Research Associate.

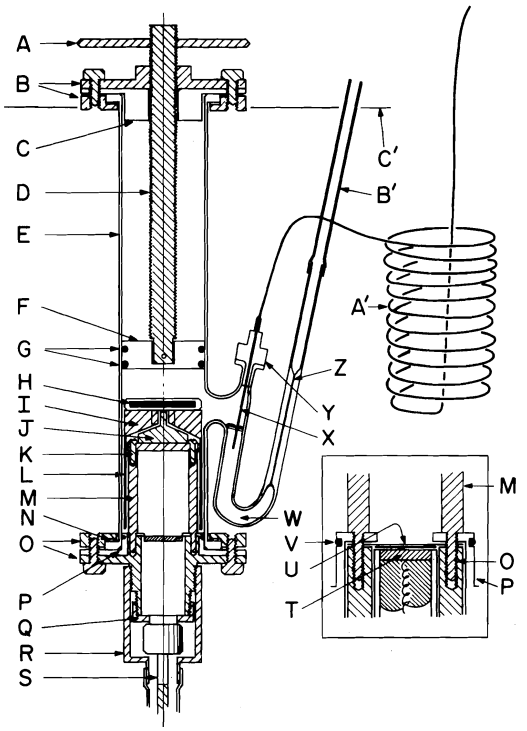

FIG. 1. Schematic drawing of the ultrasonic cell. A, control handle for plunger; B, brass collar and plunger support; C, Teflon insert; D, threaded brass rod; E, cylindrical Pyrex glass tube; F, Teflon plunger; G, O-ring seals; H, magnetic stirrer; I, stirrer blades; J, reflector; K, adjusting screws; L, stirring arm; M, brass support rods for reflector; N, rubber gasket; O, brass collar and transducer holder; P, Teflon insert; Q, cap for transducer holder; R, protective cap for connector and cable; S, coaxial cable; T, transducer and backing material (Panametrics Type 5070 VIP); U, brass shim stock (0.025 mm) coupled to transducer by a layer of epoxy resin containing tungsten powder; V, O-ring seal; W, U-shaped side chamber containing mercury; X, stainless steel and Teflon feed tube (id 1 mm); Y, filling port closed by Teflon stopper; Z, pyrex capillary (id 1 mm); A′, coil of Teflon tubing connected to piston burette; B′, nylon extension; C′, water level in thermostat.

stock (thickness 0.025 mm) (see Fig. 1 insert). The transducer and reflector are connected by a rigid framework which also supports the pivot of the magnetic stirrer. Four screws are provided for adjusting the parallelism between the transducer and reflector faces.

The plunger sealing the upper end of the cell is moved by a threaded rod. Thus the volume of the cell can be increased during the addition of the feed component, and the level of mercury in the capillary part of the side chamber can be altered to maintain a constant pressure within the cell.

The mercury also keeps the two components separate before mixing. The feed component is delivered by a calibrated piston displacement burette (11). The liquid flows through Teflon and stainless steel tubing and is injected into the mercury. The magnetic stirrer is activated by a rotating magnet outside the cell. It has four blades with long narrow brass arms attached and provides quick mixing of the liquid above and below the reflector.

Loading and Operating Procedure

After the cell is cleaned, the plunger is set just above the connection to the side chamber. Mercury (~ 3 cm^3) is placed in the U-tube and one of the component liquids (~ 40 cm^3) is introduced through the filling port from a weighing burette. All weighings are corrected to *vacuo*. The filling port Y is temporarily closed with an auxiliary stopper to prevent evaporation while the piston burette is loaded with the other component. The burette is operated to expel all air bubbles from it and the attached feed tubes (X and A′). The end of tube X is dipped into a dish containing mercury and the burette motor is reversed briefly, sucking a small amount of mercury into X before the motor is stopped. The filling port is then opened and the level of liquid in the cell is raised to the top of the side chamber by readjusting the plunger. The feed tube, still sealed by mercury, is inserted and the cell is closed without any vapor space by the Teflon stopper.

The loaded cell is immersed in a water bath operated at 298.15 $\pm$ 0.01 K and controlled to better than $\pm$0.003 K during a run. The temperature is monitored by a quartz crystal thermometer. After thermal equilibrium is reached, the mercury level in the feed tube is set close to a reference mark on the tube X by operating the piston burette, and the mercury levels in the two arms of the U-tube are set at the same height by readjusting the plunger.

After measuring the ultrasonic velocity of the liquid in the cell, the feed component is slowly added by the piston burette. At the same time the plunger is gradually raised to increase the inner volume of the cell. A balance is achieved by keeping the level of the mercury in the capillary nearly constant. The amount of the component added is obtained from the difference of the readings of the counter coupled to the piston burette. A small correction is subtracted from the first addition to allow for the mercury initially present in the feed tube. The imprecision of the composition of the mixture is estimated to be less than 0.02%.

Calibration of the distance between the transducer and reflector was based on the value of the ultrasonic velocity for pure water (1496.687 m s^{-1} at 298.15 K) reported by Del Grosso and Mader (12). The relative error of velocities measured with our equipment is estimated to be less than 0.2 m s^{-1}.

Measurements on Aqueous NaCl Solutions

Results of very accurate ultrasonic velocity measurements are avilable for aqueous NaCl solutions (13–15). Although the mercury and brass in the present cell make it rather unsuitable for measurements of this type, a few test runs were carried out. An aqueous NaCl solution of known concentration (~ 3 *m*) was prepared by mass from Anachemia reagent which had been dried in an oven at 338 K. This solution was successively added to the cell which was originally filled with water. Velocity measurements were made as rapidly as possible but changes in the appearance of the mercury indicated that some reaction

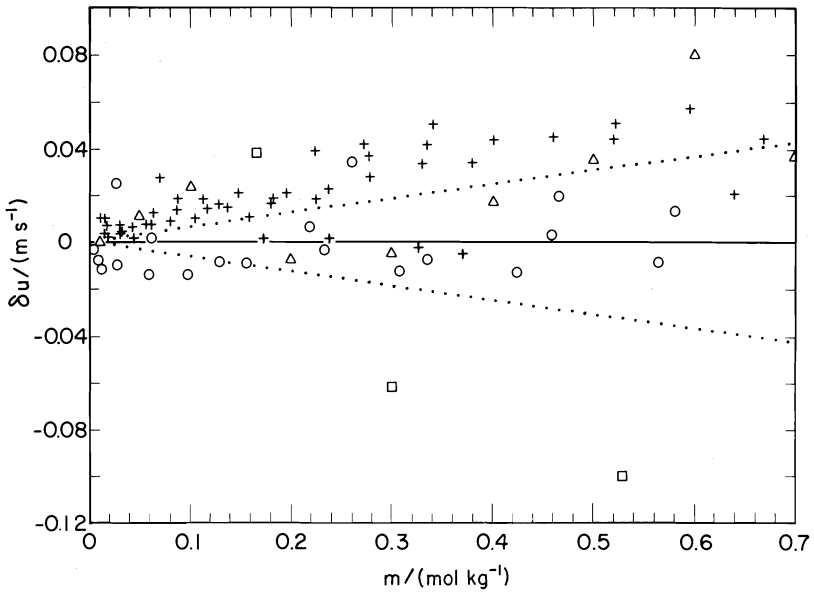

FIG. 2. Deviation plot for ultrasonic velocities, u, at 298.15 K in aqueous NaCl solutions with molality m. Plot shows deviations from eq. 1. $\delta u = u - u_0 - m(64.804 - 4.679m^{1/2})$. Experimental results: ○, present work; +, Sakurai *et al.* (13); □, Gucker *et al.* (14); Δ, Millero *et al.* (15). Dotted lines represent deviations of ±0.1%.

was occurring within the cell. The results obtained for $m < 0.7$ are represented by

$$[1] \quad (u - u_0)/(\text{m s}^{-1}) = m(64.804 - 4.679m^{1/2})$$

where u and u_0 (1496.687 m s^{-1}) are the velocities for a solution of molality m and for water respectively. The standard deviation of the representation is 0.014 m s^{-1}.

Our results, compared in Fig. 2 with values from the literature (13–15), are in close agreement with those of Sakurai *et al.* (13) and of Millero *et al.* (15). The apparent molal adiabatic compressibility $\phi_{K_S}{}^0$ of NaCl in water at infinite dilution, calculated from our velocity results using the limiting value of the apparent molal volume of NaCl (16) is −50.2 cm^3 mol^{-1} GPa^{-1} at 298.15 K. This agrees reasonably well with values reported by other workers: −50.45 (13), −52.88 (14), −50.5 (15, 17), −49.8 (18), and −50.8 (19).

Results and Discussion

Ultrasonic velocities, u, measured at 298.15 K in $D_2O(1) + H_2O(2)$ mixtures with various mole fractions x_1 of D_2O are listed in Table 1. These results were obtained in two independent dilution runs starting with H_2O, and with D_2O, in the cell. The smooth overlap of the results in the central part of the mole fraction range provides a good check on the consistency of the dilution technique. Extrapolation of the results for D_2O-rich mixtures leads to a value of u = 1398.74 m s^{-1} at $x_1 = 1$. This agrees well with the value 1398.6 m s^{-1} obtained by Yosioka (1) using the optical method. Other published values for u/(m s^{-1}) in pure D_2O at 298.15 K are: 1403.31 (4) and 1401 (20), interferometer method; 1402 (21) and 1399.24 (22), pulse method; ~1396 (3), sing-around method.

The deviation of the ultrasonic velocity in a mixture from additivity on a mole fraction basis is

$$[2] \quad \Delta u = u - \sum x_i u_i{}^0$$

where $u_i{}^0$ is the velocity in pure component i. Our results for the present system are represented by the polynomial expression

$$[3] \quad \Delta u/(\text{m s}^{-1}) = x_1x_2[-8.047 - 0.137(x_2 - x_1) + 0.171(x_2 - x_1)^2]$$

with a standard deviation σ = 0.007 m s^{-1}. A comparison of our results with values taken from the literature (1, 4) is given in Fig. 3. Our results are in close agreement with those of Yosioka (1). We find that Δu is negative over the whole mole fraction range, and this behavioral pattern is qualitatively unchanged if volume fractions are used in place of mole fractions in eq. 2. This is in contrast to the findings of Gupta

TABLE 1. Ultrasonic velocities and adiabatic compressibilities for $D_2O(1) + H_2O(2)$ mixtures at 298.15 K

x_1	u (m s^{-1})	κ_s (TPa^{-1})	κ_s^E (TPa^{-1})
0.0034	1496.33	447.79	0.00
0.0092	1495.72	447.88	0.00
0.0209	1494.48	448.05	0.00
0.0319	1493.32	448.22	−0.01
0.0455	1491.89	448.42	−0.02
0.0592	1490.42	448.64	−0.01
0.0786	1488.42	448.91	−0.03
0.0978	1486.41	449.21	−0.02
0.1218	1483.90	449.57	−0.02
0.1467	1481.30	449.96	−0.02
0.1741	1478.47	450.37	−0.03
0.2041	1475.39	450.82	−0.03
0.2366	1472.06	451.31	−0.03
0.2700	1468.65	451.82	−0.04
0.3015	1465.47	452.30	−0.04
0.3336	1462.21	452.79	−0.03
0.3619	1459.38	453.22	−0.03
0.3882	1456.75	453.62	−0.03
0.4090	1454.66	453.94	−0.01
0.4152	1454.06	454.03	−0.02
0.4445	1451.16	454.47	−0.02
0.4454	1451.07	454.49	−0.02
0.5157	1444.17	455.55	−0.02
0.5507	1440.77	456.07	−0.01
0.5873	1437.23	456.62	−0.01
0.6247	1433.62	457.20	0.00
0.6666	1429.62	457.82	−0.01
0.7130	1425.23	458.51	−0.01
0.7541	1421.36	459.12	−0.01
0.8010	1416.98	459.83	−0.01
0.8417	1413.20	460.44	0.00
0.8878	1408.96	461.12	−0.01
0.9188	1406.10	461.59	0.00
0.9467	1403.55	462.01	0.01
0.9682	1401.61	462.32	0.01
0.9831	1400.28	462.53	−0.01
0.9892	1399.71	462.63	0.00
0.9946	1399.23	462.71	0.00
0.9976	1398.96	462.75	0.00
1.0000	1398.74*	462.79	0.00

*Extrapolated value.

et al. (4) who reported that the speed of sound varied linearly with volume fraction.

Adiabatic compressibilities, κ_s, were calculated from the ultrasonic velocities using the relation

$$[4] \quad \kappa_s = [u^2 \sum M_i x_i/(V^E + \sum x_i V_i^0)]^{-1}$$

where M_i and V_i^0 are the molecular mass and molar volume of component i, and V^E is the molar excess volume of the mixture. Estimates of V^E for $D_2O + H_2O$ mixtures were based on the work of Bottomley and Scott (23). Results for κ_s are given in Table 1. Also included in Table 1 are values of the excess adiabatic compressibility defined by

$$[5] \quad \kappa_s^E = \kappa_s - \kappa_s^{id}$$

where κ_s^{id} is the adiabatic compressibility of an ideal mixture of the components at the same temperature and pressure. Previously we approximated κ_s^{id} by a volume fraction average of the adiabatic compressibilities $\kappa^0_{s,i}$ for the pure components (9). However in the present work we used the exact expression (24)

$$[6] \quad \kappa_s^{id} = \sum \phi_i^0 \gamma_i^0 \kappa^0_{s,i} \times (\sum x_i (C^0_{p,i}/\gamma_i^0)/\sum x_i C^0_{p,i})$$

where

$$[7] \quad \phi_i^0 = x_i V_i^0 / \sum x_i V_i^0$$

and

$$[8] \quad \gamma_i^0 = 1 + T V_i^0 (\alpha^0_{p,i})^2/(\kappa^0_{s,i} C^0_{p,i})$$

In eq. 8, T is the temperature, and $C^0_{p,i}$ and $\alpha^0_{p,i}$ are the isobaric molar heat capacity and thermal expansibility for pure component i. Numerical values of C_p/(J K^{-1} mol^{-1}) equal to 84.68 (25) and 75.297 (26), and of $10^3\alpha_p$/K^{-1} equal to 0.1918 (27) and 0.2572 (26) were adopted for D_2O and H_2O respectively.

Although our results for κ_s^E are only slightly larger than the estimated imprecision of κ_s ($\sim$0.02 TPa^{-1}), it appears that the adiabatic compressibilities of $D_2O + H_2O$ mixtures display small negative deviations from ideal behavior, and that the variation of these with mole fraction is somewhat asymmetric. Our value of $\kappa^0_{s,1}$ for pure D_2O corresponds to an isothermal compressibility $\kappa^0_{T,1}(=\gamma_1^0 \kappa^0_{s,1})$ of 465.13 TPa^{-1}, in excellent agreement with 465.3 TPa^{-1} (27) and 465.2 TPa^{-1} (28) obtained from direct PVT measurements by Millero and co-workers.

NOTE ADDED IN PROOF: Since the submission or our manuscript, correspondence with Dr. J. G. Mathieson has revealed that the ultrasonic velocities in ref. 3 should be increased by about 0.24% to allow for a change in calibration constant. The corrected value for D_2O, 1399.2 m s^{-1}, is thus much closer to our result than indicated in our text. We are indebted to Dr. Mathieson for sending us a copy of the primary data. It also appears from this that there is excellent agreement between our values of Δu for $D_2O + H_2O$ mixtures and the results of Mathieson and Conway.

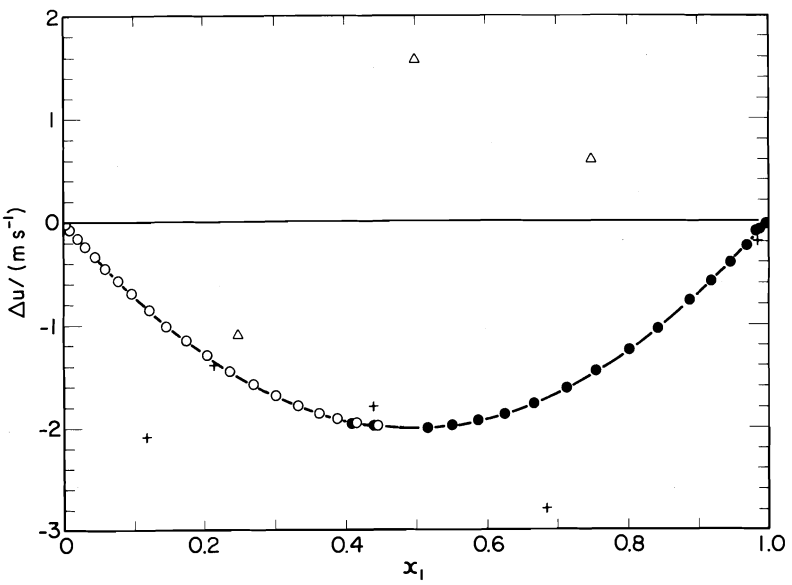

FIG. 3. Plot of Δu for $D_2O(1) + H_2O(2)$ mixtures at 298.15 K against mole fraction of D_2O. Experimental results: ○ and ●, present work (two separate dilution runs); +, Yosioka (1); △, Gupta *et al.* (4). Curve calculated from eq. 3.

1. K. YOSIOKA. Sci. Papers Inst. Phys. Chem. Res. **34**, 843 (1938).
2. S. K. KOR, B. K. SINGH, and S. C. DEORANI. Nuovo Cimento B, **8**, 367 (1972).
3. J. G. MATHIESON and B. E. CONWAY. Anal. Chem. **44**, 1517 (1972).
4. R. N. GUPTA, P. C. JAIN, and V. S. NANDA. J. Chem. Thermodyn. **8**, 627 (1976).
5. O. KIYOHARA and G. C. BENSON. Can. J. Chem. **51**, 2489 (1973).
6. G. S. KELL. J. Chem. Eng. Data, **12**, 66 (1967).
7. E. P. PAPADAKIS. J. Acoust. Soc. Am. **42**, 1045 (1967).
8. E. P. PAPADAKIS. Rev. Sci. Instrum. **47**, 806 (1976).
9. O. KIYOHARA, J.-P. E. GROLIER, and G. C. BENSON. Can. J. Chem. **52**, 2287 (1974).
10. P. J. HIGHMORE. Ultrasonics international 1973 conference proc. p. 112.
11. S. MARTIN, R. E. ROBERTSON, and G. C. BENSON. J. Sci. Instrum. **41**, 237 (1964).
12. V. A. DEL GROSSO and C. W. MADER. J. Acoust. Soc. Am. **52**, 1442 (1972).
13. M. SAKURAI, T. NAKAJIMA, T. KOMATSU, and T. NAKAGAWA. Chem. Lett. 971 (1975).
14. F. T. GUCKER, D. STUBLEY, and D. J. HILL. J. Chem. Thermodyn. **7**, 865 (1975).
15. F. J. MILLERO, G. K. WARD, and P. V. CHETIRKIN. J. Acoust. Soc. Am. **61**, 1492 (1977).
16. F. VASLOW. J. Phys. Chem. **70**, 2286 (1966).
17. J. G. MATHIESON and B. E. CONWAY. J. Solution Chem. **3**, 455 (1974).
18. M. V. KAULGUD. Z. Phys. Chem. **47**, 24 (1965).
19. R. GARNSEY, R. J. BOE, R. MAHONEY, and T. A. LITOVITZ. J. Chem. Phys. **50**, 5222 (1969).
20. D. R. MCMILLAN, JR. and R. T. LAGEMANN. J. Acoust. Soc. Am. **19**, 956 (1947).
21. M. PANCHOLY. J. Acoust. Soc. Am. **25**, 1003 (1953).
22. W. D. WILSON. J. Acoust. Soc. Am. **33**, 314 (1961).
23. G. A. BOTTOMLEY and R. L. SCOTT. Aust. J. Chem. **29**, 427 (1976).
24. W. VAN DAEL. *In* Experimental thermodynamics. Vol. 2. *Edited by* B. LeNeindre and B. Vodar. Butterworths, London. 1974. Chapt. 11.
25. G. C. BENSON. Unpublished data.
26. G. S. KELL. J. Chem. Eng. Data, **20**, 97 (1975).
27. R. T. EMMET and F. J. MILLERO. J. Chem. Eng. Data, **20**, 351 (1975).
28. F. J. MILLERO and F. K. LEPPLE. J. Chem. Phys. **54**, 946 (1971).

Mixed valence properties of a pyrazine bridged ruthenium–iron complex

HENRIQUE E. TOMA AND PAULO S. SANTOS

Instituto de Química, Universidade de São Paulo, Caixa Postal 20780, São Paulo, Brazil

Received March 14, 1977

HENRIQUE E. TOMA and PAULO S. SANTOS. Can. J. Chem. **55**, 3549 (1977).

A study is presented on the chemistry of the binuclear complex $[(CN)_5FepzRu(NH_3)_5]^n$ ($n = 0$ for the II–III complex and $n = -1$ for the II–II complex, pz = pyrazine) in solid state and in aqueous solution. Evidence for a mixed valence transition for the II–III complex was observed in the near infrared region. Based on infrared and resonance Raman spectra, a trapped-valence or class II formulation was proposed for the complex. Cyclic voltammetry indicated the occurrence of two reversible waves at 0.48 V and 0.72 V vs. NHE, which were assigned to the oxidation of the ruthenium(II) and iron(II) centers, respectively.

HENRIQUE E. TOMA et PAULO S. SANTOS. Can. J. Chem. **55**, 3549 (1977).

On présente l'étude de la chimie du complexe binucléaire $[(CN)_5FepzRu(NH_3)_5]^n$ ($n = 0$ pour le complexe II–III et $n = -1$ pour le complexe II–II, pz = pyrazine) dans l'état solide et en solution aqueuse. On a observé dans la région proche-infrarouge, l'existence d'une transition de valence mixte pour le complexe II–III. En se basant sur les spectres infrarouge et Raman, on propose pour le complexe, une valence piégée ou une formulation de classe II. Des mesures polarographiques cycliques nous indiquent la présence de deux ondes réversibles à 0.48 V et 0.72 V vs. NHE, lesquelles sont attribuées respectivement à l'oxydation des sites ruthénium(II) et fer(II).

[Traduit par le journal]

Introduction

Binuclear complexes of ruthenium ammines have been much studied over the last 6 years (1–5) since the mixed valence complex $[(NH_3)_5RupzRu(NH_3)_5]^{5+}$ was first described by Creutz and Taube (1, 2). Similar studies involving cyanoferrate complexes have also appeared in the literature (6–8). In the present work we report some properties of the binuclear complex $[(CN)_5FepzRu(NH_3)_5]^n$ ($n = 0, -1$, pz = pyrazine) in solid state and in aqueous solution.

Experimental

Materials

$[Ru(NH_3)_5pz](ClO_4)_2$ was prepared as described by Anson and co-workers (9). The *p*-toluenesulfonate salt was also prepared as described (9) but using silver *p*-toluenesulfonate instead of silver trifluoroacetate to remove the chloride ions from the starting materials. $Na_3[Fe(CN)_5NH_3]\cdot 3H_2O$ was prepared from sodium nitroprusside according to the conventional procedure (10). The purity of these complexes was checked spectrophotometrically and by microanalysis.

The dark red II–II ($n = -1$) complex can be easily prepared in aqueous solution by mixing equimolar solutions of the pentaammine(pyrazine)ruthenium(II) complex and of the aquopentacyanoferrate(II) ion (10–14) under argon atmosphere. The 1:1 composition of the complex in solution was demonstrated using Job's method. The II–II complex was isolated as the sodium salt $Na[Fe(CN)_5pzRu(NH_3)_5]\cdot 3H_2O$ according to the following procedure: 0.12 g (0.2 mmol) of $[Ru(NH_3)_5pz](C_7H_7SO_3)_2\cdot 3H_2O$ was dissolved in ca. 50 ml of water, and mixed with 10 ml of aqueous solution containing 0.065 g (0.2 mmol) of $Na_3[Fe(CN)_5NH_3]\cdot 3H_2O$ under argon atmosphere. After 20 min, the dark-violet solution was treated with argon saturated ethanol to precipitate the binuclear complex. *Anal.* calcd. for $Na[Fe(CN)_5pzRu(NH_3)_5]\cdot 3H_2O$: C 20.42, N 31.75, H 4.7; found: C 20.2, N 31.5, H 5.5.

The II–III complex was prepared in a similar way of the II–II analog, except that aqueous bromine (10^{-2} *M*) was added in nearly stoichiometric amounts to the final solution to oxidize the binuclear complex. The II–III complex is neutral and practically insoluble in water, precipitating immediately after the addition of aqueous bromine. *Anal.* calcd. for $[Fe(CN)_5pzRu(NH_3)_5]\cdot 5H_2O$: C 19.93, N 31.00, H 5.3; found: C 20.0, N 31.3, H 4.9.

Spectra

Near infrared and visible spectra were measured on a Cary 14 spectrophotometer in aqueous solution or in KBr pellets. Infrared spectra were recorded on either a Perkin-Elmer 337 or 180 spectrophotometer. A Jarrel-Ash, Model 25-300 spectrometer was used for the Raman measurements with argon ion laser excitation at 5145 Å, and a spinning cell to prevent or minimize the decomposition of the sample.

Studies in Solution

The kinetics of formation and dissociation of the II–II binuclear complex were investigated with a Durrum D-110 stopped-flow spectrophotometer equipped with a Kel-F flow system, or with a Cary 14 spectrophotometer in the conventional way. Pseudo-first-order behavior was observed during at least three half lives. For the cyclic voltammetry measurements, a PAR system consisting of a Model 173 Potentiostat and a Model 175 Universal

Programmer was employed. Platinum wires were used as auxiliary and working electrodes, with saturated calomel as the reference electrode.

Results and Discussion

The II–II binuclear complex is rapidly formed when solutions containing the aquopentacyanoferrate(II) ion and the pentaammine(pyrazine)-ruthenium(II) complex are mixed.

$$Fe(CN)_5H_2O^{3-} + pzRu(NH_3)_5^{2+} = (CN)_5FepzRu(NH_3)_5^{-}$$

The reaction can be monitored at 520 nm, the maximum wavelength for the visible absorption band of the product, with the stopped-flow apparatus. Using always freshly prepared solutions of the aquopentacyanoferrate(II) ion (3×10^{-5} *M* to 2×10^{-4} *M*) the specific rate of the formation reaction was $3.1 \pm 0.1 \times 10^3$ M^{-1} s^{-1}, at 25°C, $\mu = 0.10$ *M* (lithium perchlorate), and p*H* 4.5 (acetate buffer, 10^{-2} *M*), under argon atmosphere. The rates decrease with the ionic strength (e.g., for $\mu = 0.015$ *M* and 0.20 *M*, $k_2 = 1.60 \times 10^4$ and 1.58×10^3 M^{-1} s^{-1}, respectively), suggesting a S_N1, dissociative ion-pair mechanism (15).

The complex dissociates very slowly in aqueous solution, in the presence of ligands such as dimethyl sulfoxide. This ligand reacts with the aquopentacyanoferrate(II) ion to form the stable and inert pentacyano(dimethylsulfoxide)-ferrate(II) complex (16), driving to completion the dissociation of the binuclear complex. As expected for a limiting S_N1 dissociative mechanism (11–14), the rates were independent of the concentration of dimethyl sulfoxide (0.05 *M* – 0.5 *M*). For $\mu = 0.20$, 0.10, and 0.015 *M* (lithium perchlorate), at 25°C, the specific rates were 6.5×10^{-4}, 6.9×10^{-4}, and 8.1×10^{-4} s^{-1}, respectively. From the rates of formation and dissociation of the binuclear complex, the equilibrium constants were calculated to be 2.4×10^7, 4.5×10^6, and 1.9×10^6 M^{-1}, at 25°C and $\mu = 0.015$, 0.10, and 0.20 *M*, respectively.

The electronic spectra of KBr pellets of the II–II and II–III complexes, in the visible and near infrared region are shown in Fig. 1. As in the system described by Creutz and Taube (1, 2), combination of the filled Ru and Fe d_π orbitals with the vacant pyrazine π^* orbital of appropriate symmetry would result in a set of three π–MO orbitals, ψ_b, ψ_n, ψ_a, having respectively a bonding, nonbonding, and antibonding character. The band centered at 19.1 kK for the II–II and II–III complexes can be assigned to the transition from the occupied, nonbonding (metal) orbitals to the antibonding (ligand) orbitals. For the II–III complex, the new band appearing at 7.5 kK could be assigned to the ψ_b–ψ_n transition, or using a valence trapped description, to a metal(II)-to-metal(III) transition. A comparison of the absorption spectra of the binuclear Ru–pz–Ru, Fe–pz–Fe, and Ru–pz–Fe complexes can be seen in Table 1.

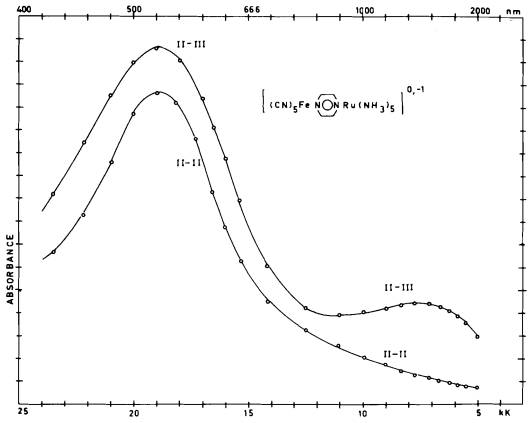

FIG. 1. Absorption spectra of the II–II and II–III binuclear complexes, in KBr pellets.

The absorption bands of the mononuclear and binuclear cyanoferrates occur systematically at higher energies than those of the corresponding ammine complexes. The hypsochromic shift of the visible band of the cyanoferrates from 19.8 to 21.8 kK contrast with the bathochromic shift from 18.3 to 17.7 kK, for the binuclear ruthenium ammines, when the II–II complexes are oxidized to the II–III mixed valence species. It is therefore remarkable that the visible absorption band of the Ru–pz–Fe complex is not shifted in the oxidation process, but remains at an intermediate position with respect to those for the Fe–pz–Ru and Ru–pz–Ru complexes. A similar behavior is shown by the intervalence transitions in the near infrared region.

In an attempt to identify the nature of the donor and acceptor centers in the asymmetric mixed valence complex, $(NH_3)_5RupzFe(CN)_5$, the infrared and Raman spectra were recorded and compared to those for the original II–II complex. This can be seen in Table 2.

The wavelength of the exciting radiation from

TABLE 1. Charge transfer and intervalence transitions in binuclear ruthenium–pyrazine–iron and similar complexes

Complexes	Charge transfer (kK (nm))	Intervalence transition (kK (nm))	Ref.
$(CN)_5Fepz^{3-}$	22.2 (452)		11
$(NH_3)_5Rupz^{2+}$	21.2 (472)		30
$(CN)_5FepzFe(CN)_5^{6-}$	19.8 (505)		8
$(CN)_5FepzFe(CN)_5^{5-}$	21.8 (458)	8.5 (1170)	8
$(CN)_5FepzRu(NH_3)_5^{1-}$	19.1 (523)		This work
$(CN)_5FepzRu(NH_3)_5$	19.1 (523)	7.5 (1330)	This work
$(NH_3)_5RupzRu(NH_3)_5^{4+}$	18.3 (547)		1, 2
$(NH_3)_5RupzRu(NH_3)_5^{5+}$	17.7 (565)	6.4 (1570)	1, 2

TABLE 2. Infrared (ir) and resonance Raman (rr) frequencies (cm^{-1}) for $[(NH_3)_5RupzFe(CN)_5]^n$ complexes

$n = -1$ (II–II)		$n = 0$ (III–II)		
ir[b]	rr[b]	ir[b]	rr[b]	Tentative assignment[a]
3400 br,s		3440 br,s		ν_{H_2O}
3300 br,s		3250 br,s		ν_{NH_3}
2080 m 2040 s		2085 m 2045 s		ν_{CN}
1630 s		1700 s 1640 m		δ_{deg,NH_3}, δ_{H_2O}
1590 m	1594 s	1595 m	1595 s	pz, ring stretch
1485 m 1465 m 1430 m		1485 sh 1430 m		pz, ring stretch
1340 sh		1335 sh		pz, ring stretch (δ_{sym,NH_3})
1280 s		1310 s		δ_{sym,NH_3}
1225 m 1190 w	1228 s	1225 m 1185 w	1228 s	pz, δ_{CH} in plane
1095 w 1075 m	1100 w 1075 m	1100 vw 1075 m	1103 w 1074 s	pz, δ_{CH} in plane
1040 w 1015 m	 1018 m	1030 m 1015 s	 1018 m	pz, ring stretch
825 m		Masked		pz, τ_{CH} out of plane
770 m		800 s		ρ_{NH_3}
675 m	675 m	675 m	675 m	pz, ring def. in plane
575 m 525 w		570 m 515 w		ν_{MC}, δ_{MCN}
420 w		420 w		pz, ring def. out of plane
300 w[c]	310 s 270 w	300 w[c]	313 s 270 w	ν_{MN}, pz, ring def. out of plane

[a]See ref. 20 for the vibrational modes of pyrazine.
[b]Infrared of KBr pellets, Raman of pure solid; br = broad, s = strong, m = medium, w = weak, vw = very weak, sh = shoulder.
[c]In Nujol.

the argon laser (5145 Å) practically coincides with the maximum of the visible absorption band of the complexes. This is especially convenient for the purposes of investigating the occurrence of resonance Raman phenomena (17–19) which can be very useful in the assignment of the vibrational spectra. Analogously to a recent work (5) with the binuclear Ru–pz–Ru complex, we have observed that the enhancement of the Raman bands is associated exclusively with the pyrazine ligand, the MNH_3 and MCN groups being practically undetectable in the presence of the enhanced bands.

Since the resonance effect is related to the excited electronic state of the molecule (17–19), the enhancement of the pyrazine bands can be taken as evidence for its involvement in the electronic excitation responsible for the absorption in the visible region. The enhancement has been observed essentially with the totally symmetric vibrations of pyrazine. According to Albrecht and Hutley (18) this may be the case of a typical vibrational interaction with a single excited electronic state. When two or more electronic states are involved in the excitation process, vibronic mixing should enhance any symmetry mode which is contained in the direct product of the representations of the two electronic states.

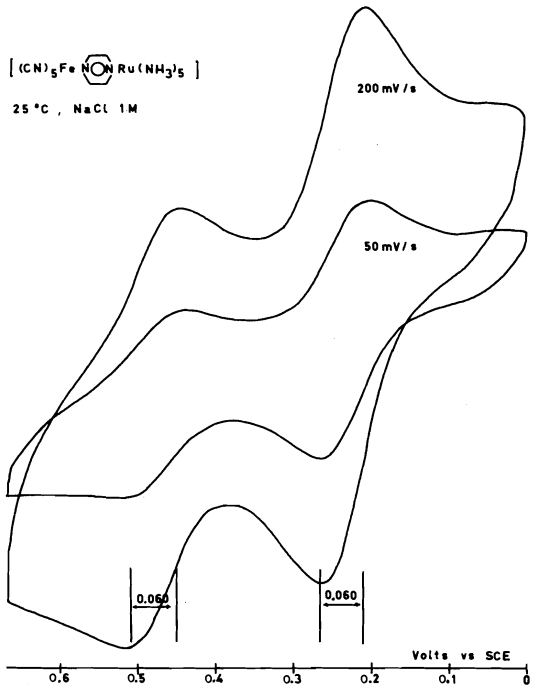

FIG. 2. Cyclic voltammograms of the binuclear complex $[(CN)_5FepzRu(NH_3)_5]^n$ in aqueous solution.

Comparison of the data collected in Table 2 shows that except for the NH_3 bands, the spectra of the II–II and II–III complexes are very nearly the same. This is an important observation if we are interested in the problem of valence delocalization in the system.

It is currently known (21) that the frequencies associated to the vibrations of the CN and NH_3 groups depend on the nature and charge of the metal ions to which they are coordinated. The symmetric deformation and rocking vibrational modes of the coordinated NH_3 group occur at frequencies which usually increase with the oxidation state and electronegativity of the central ion in the complex (22). For ruthenium hexaammines in the oxidation states II and III, they occur at 1220 and 769 cm^{-1} (23) and 1316–1362 and 788 cm^{-1} (24), respectively. Therefore, the observed shifts from 1280 and 770 cm^{-1} in the II–II complex to 1310 and 800 cm^{-1} in the II–III complex are consistent with the oxidation of the ruthenium(II) center.

The similar cyanide stretching frequencies, in the range of 2080–2040 cm^{-1}, for the II–II and II–III species, are characteristic of cyanoferrate(II) complexes (21, 25). In the case of cyanoferrate(III) complexes they are usually observed in the 2100–2150 cm^{-1} region. We therefore conclude that the complex II–III belongs to a valence trapped, or a class II type of system (26, 27) in which the oxidized center is mainly localized on the ruthenium ammine moiety.

Cyclic voltammetry waves for the binuclear complex, recorded at 25°C, $\mu = 1.0\ M$ in NaCl, at several sweep rates, are shown in Fig. 2.

The two reversible waves with $E_{1/2}$ of 0.48 and 0.72 V vs. NHE were ascribed to the oxidation of the ruthenium(II) and iron(II) centers, respectively. They can be compared to 0.37 and 0.76 V for the analogous binuclear ruthenium ammine complex (2).

Without additional information, the choice of the oxidized center could represent a real challenge in the present system. The oxidation potentials of the mononuclear $Ru(NH_3)_5L^{n+}$ and $Fe(CN)_5L^{m-}$ complexes (28, 29) do not necessarily constitute a criterium, since they are very sensitive to substituent effects on the ligand L, as well as to the nature of the metal–ligand bond. For example, the oxidation potentials for

the ruthenium ammine complexes of pyridine, pyrazine, *N*-methyl pyrazinium, and dimethyl sulfoxide are −0.35, −0.49, −0.89, and −1.0 V, in comparison to −0.47, −0.55, −0.78, and −0.89 V, respectively, for the analogous pentacyanoferrate(II) complexes.

These ligands were ordered according to their π-acceptor affinities (29) to show that the oxidation potentials of the ruthenium ammines decrease more rapidly in comparison to those for the cyanoferrates, becoming nearly the same at the proximity of ligands such as pyrazine. Therefore, in the case of the binuclear complexes here reported, the prediction of the oxidized center will depend on the knowledge of the relative stabilities of the Ru(III)–pz–Fe(II) and Ru(II)–pz–Fe(III) species, which can not be estimated from the properties of each moiety, isolately.

NOTE ADDED IN PROOF: The spectra of the mixed valence complex have been measured only for the solid, since it is not stable in aqueous solution. We would like to acknowledge Dr. Albert Haim for calling our attention to the possibility of decomposition even in the solid, which we neglected in the tentative assignment of the electronic and vibrational spectra.

Acknowledgement

A grant from the CNPq is gratefully acknowledged.

1. C. CREUTZ and H. TAUBE. J. Am. Chem. Soc. **91**, 3988 (1969).
2. C. CREUTZ and H. TAUBE. J. Am. Chem. Soc. **95**, 1086 (1973).
3. G. M. TOM, C. CREUTZ, and H. TAUBE. J. Am. Chem. Soc. **96**, 7827 (1974); G. M. TOM and H. TAUBE. J. Am. Chem. Soc. **97**, 5310 (1975); H. KRENTZIEN and H. TAUBE. J. Am. Chem. Soc. **98**, 6380 (1976).
4. R. W. CALLAHAN, G. M. BROWN, and T. J. MEYER. J. Am. Chem. Soc. **96**, 7830 (1974); M. J. POWERS, D. J. SALMON, R. W. CALLAHAN, and T. J. MEYER. J. Am. Chem. Soc. **98**, 6731 (1976).
5. T. C. STREKAS and T. G. SPIRO. Inorg. Chem. **15**, 974 (1976), and references therein.
6. G. EMSCHWILLER and C. K. JORGENSEN. Chem. Phys. Lett. **5**, 561 (1970).
7. A. LUDI, R. GLAUSER, H. SIEGENTHALER, U. HAUSER, F. HERREN, P. RODER, E. SCHMIDT, and F. WENK. J. Am. Chem. Soc. **95**, 8457 (1973).
8. F. FELIX, U. HAUSER, H. SIEGENTHALER, F. WENK, and A. LUDI. Inorg. Chim. Acta, **15**, 17 (1975).
9. H. S. LIM, D. J. BARCLAY, and F. C. ANSON. Inorg. Chem. **11**, 1460 (1972).
10. G. BRAUER. Handbook of preparative inorganic chemistry. Vol. 2. 2nd ed. Academic Press, NY. 1965. p. 1511.
11. H. E. TOMA and J. M. MALIN. Inorg. Chem. **12**, 1039 (1973).
12. H. E. TOMA and J. M. MALIN. Inorg. Chem. **12**, 2080 (1973).
13. H. E. TOMA and J. M. MALIN. Inorg. Chem. **13**, 1772 (1974).
14. H. E. TOMA. J. Inorg. Nucl. Chem. **37**, 785 (1975).
15. K. KUSTIN and J. SWINEHART. Prog. Inorg. Chem. **13**, 107 (1970); H. E. TOMA. J. Coord. Chem. In press.
16. H. E. TOMA, J. M. MALIN, and E. GIESBRECHT. Inorg. Chem. **12**, 2084 (1973).
17. J. BEHRINGER. *In* Raman spectroscopy. Vol. 1. *Edited by* H. A. Szymanski. Plenum Press, NY. 1967; R. E. HESTER. *In* Raman spectroscopy. Vol. 1. *Edited by* H. A. Szymanski. Plenum Press, NY. 1967.
18. J. TANG and A. C. ALBRECHT. *In* Raman spectroscopy. Vol. 2. *Edited by* H. A. Szymanski. Plenum Press, NY. 1970; A. C. ALBRECHT and M. C. HUTLEY. J. Chem. Phys. **55**, 4438 (1971).
19. R. J. H. CLARK. *In* Advances in infrared and Raman spectroscopy. Vol. 1. *Edited by* R. J. H. Clark and R. E. Hester. Heyden, London, NY, Rheine. 1975.
20. F. R. DOLLISH, W. G. FATELEY, and F. F. BENTLEY. *In* Characteristic Raman frequencies of organic compounds. Wiley-Interscience, NY. 1974. p. 274.
21. K. NAKAMOTO. Infrared spectra of inorganic and coordination compounds. 2nd ed. Wiley-Interscience, NY. 1970.
22. J. K. WILMSHURST. Can. J. Chem. **38**, 467 (1960); L. SACCONI, A. SABATINI, and P. GANS. Inorg. Chem. **3**, 1772 (1964).
23. M. B. FAIREY and R. J. IRVING. Spectrochim. Acta, **22**, 359 (1966).
24. A. D. ALLEN and C. V. SENOFF. Can. J. Chem. **45**, 1337 (1967).
25. E. F. HERINGTON and W. KYNASTON. J. Chem. Soc. 3555 (1955).
26. M. B. ROBIN and P. DAY. Adv. Inorg. Chem. Radiochem. **10**, 247 (1967).
27. N. S. HUSH. Prog. Inorg. Chem. **8**, 391 (1967).
28. C. G. KUEHN and H. TAUBE. J. Am. Chem. Soc. **98**, 689 (1976).
29. H. E. TOMA and C. CREUTZ. Inorg. Chem. **16**, 545 (1977).
30. P. C. FORD, D. F. P. RUDD, R. GAUNDER, and H. TAUBE. J. Am. Chem. Soc. **90**, 1187 (1968).

Matrix dependence of the electron spin resonance spectra of the $(CH_3)_3N^{\ddagger}$ radical trapped in different single crystals

J. P. MICHAUT AND J. RONCIN

Laboratoire de Résonance Electronique et Ionique (associé au CNRS), Université de Paris-Sud, Centre d'Orsay, 91405 Orsay, Cedex, France

Received April 18, 1977

J. P. MICHAUT and J. RONCIN. Can. J. Chem. **55**, 3554 (1977).

Nitrogen and proton coupling tensors have been measured for the $(CH_3)_3N^{\ddagger}$ radical trapped in five different single crystal matrices. As all isotropic coupling constants are the same within experimental error (a_N = 21.2 G, a_H = 28.4 G), no measurable crystal field effect is found. In these solids the motions of the radical depend on the dimension of the trapping cage and the motions of the surrounding molecules.

J. P. MICHAUT et J. RONCIN. Can. J. Chem. **55**, 3554 (1977).

Les tenseurs de couplage de l'azote et des protons ont été mesurés pour le radical $(CH_3)_3N^{\ddagger}$ piégé dans cinq matrices monocristallines. Pour ces cinq matrices les constantes de couplage isotrope sont semblables aux erreurs expérimentales près (a_N = 21.2 G, a_H = 28.4 G). Ceci indique que le champ cristallin a un effet négligeable sur la structure du radical. Les mouvements qui animent ce radical dépendent de la matrice de piègeage premièrement par la dimension de la cage de piègeage, deuxièmement par les mouvements des molécules voisines.

Introduction

Several studies (1, 2) have pointed out the influence of the polarity of the trapping matrix on the structure of some Si, Sn, Ge, or P centered free radicals: variations from 10–25% of the central atom spin densities are observed when replacing a nonpolar matrix by a polar one. It is known also that the matrix strongly influences the motion of the trapped radicals. It is for these two reasons that we have studied the temperature dependence of the coupling tensors of the radical $N^{\ddagger}(CH_3)_3$ trapped in five different matrices. We have chosen this radical firstly because the isotropic nitrogen coupling constants quoted in the literature seem to be very matrix sensitive (from 18.0 G (3) up to 22.6 G (4)) and secondly, because from its high degree of symmetry it is expected that it may have various kinds of reorientational motions in these solids.

Experimental

All the single crystals, except betaine hydrochloride, were grown from saturated alcoholic solutions by slow cooling. The betaine hydrochloride single crystals come from saturated aqueous solutions. Due to their highly hygroscopic character all the methylammonium salts were manipulated in a dry box. The crystal habits are hexagonal plates for betaine hydrochloride, rectangular plates for betaine, and square plates for betaine monohydrate. The methylammonium salts also give plates but with a tendency to twinning.[1] All crystals have been irradiated in a ^{60}Co source (doses of about 10^{20} eV/g). The esr spectra were recorded on a JEOL ME 1X spectrometer.

Results

1. Betaine Hydrochloride

Two magnetically unequivalent trapping sites are present in this matrix. The principal values of N and H coupling tensors are given in Table 1. They are quite different from the values reported in a previous study on this compound (4). However, the isotropic couplings agree quite well within experimental error with the value determined in the liquid phase (5) (a_N = 20.55 G, a_H = 28.56 G). We found no temperature dependence of the couplings between 77 and 293 K. As expected from the symmetry of the radical the nitrogen coupling tensor is cylindrical within the limits of experimental error. The direction cosines of the largest principal value of this tensor give the direction of the free electron π orbital axis of the radical. The angle between these directions for the two radical sites is about 30°, a value which corresponds approximately to that of the angle between the N—CH_2 bonds of the undamaged molecules in the crystals (35°)

[1]We are greatly indebted to Mister Jean Godard, Laboratoire de Physique cristalline Orsay, for the growth of a tetramethylammonium chloride single crystal.

TABLE 1. Coupling of nitrogen and proton in the five different matrices

Sample	Nitrogen			Proton		
	Total coupling tensor	Isotropic coupling	Dipolar coupling tensor	Total coupling tensor	Isotropic coupling	Dipolar coupling tensor
Betaine hydrochloride	49.40		28.20	27.00		−0.90
	6.80	21.20	−14.40	28.40	27.90	0.50
	7.30		−13.90	28.40		0.50
Betaine monohydrate	47.60		26.50	27.50		−1.10
	8.90	21.10	−12.20	29.30	28.60	0.70
	6.80		−14.30	29.10		0.50
Betaine (168 K)	50.80		29.50	27.10		−1.10
	7.90	21.30	−13.40	28.70	28.20	0.50
	5.30		−16.00	28.70		0.50
Trimethylammonium chloride (100 K)	53.80		28.90	22.40		−1.30
	11.40	24.90	−13.50	24.30	23.70	0.60
	9.40		−15.50	24.30		0.60
Trimethylammonium chloride (293 K)	48.10		26.40	23.80		−1.20
	7.00	21.70	−14.70	25.50	25.00	0.50
	10.00		−11.70	25.70		0.70
Tetramethylammonium chloride	13.60		−7.50	29.30		0.40
	25.00	21.10	3.90	28.70	28.90	−0.20
	24.60		3.50	28.70		−0.20

(6). The H coupling tensor is also cylindrical and the direction of its smallest principal value is parallel to that of the largest principal value of the nitrogen coupling tensor. This fact, together with the equivalence of the coupling tensors of all the nine protons and the very low values of the dipolar part of the H tensors, indicates that the $N^{\pm}\dot{}(CH_3)_3$ radical undergoes two types of motion in this matrix: a reorientation of the CH_3 groups around the N—C bonds and another reorientation of the whole radical around its C_{3v} symmetry axis. The frequencies of these motions are certainly higher than 10^8–10^9 even at 77 K.

2. Betaine Monohydrate

In that matrix too, two magnetically unequivalent sites for the radical in the crystal are present. The measured N and H coupling tensors are given in Table 1. The angle between the orbital directions in the two sites is about 20°. Here also no temperature dependence of the coupling was found between 77 K and room temperature.

The behaviour of $N^{\pm}\dot{}(CH_3)_3$ in matrices I and II is very similar, However, in betaine monohydrate the values of the nitrogen dipolar coupling tensors are smaller. This difference may arise from a small librational oscillation of the C_{3v} symmetry axis of the radical around its mean direction in the crystal.

3. Betaine

Figure 1 shows a spectrum of the $N^{\pm}\dot{}(CH_3)_3$ radical trapped in a room temperature γ-irradiated single crystal of betaine. In this matrix there is only one trapping site. The nitrogen and proton coupling tensors principal values measured at 168 K are given in Table 1. These couplings are not temperature dependent between 77 and 168 K. Above 168 K all the couplings continuously and reversibly decrease and at 345 K the $N^{\pm}\dot{}(CH_3)_3$ radical disappears. Since all the couplings decrease by the same amount (about 9% between 168 K and 345 K as seen in Table 2), these variations are certainly due to a reduction of the π spin density in the $2p$ orbital of this planar radical. The origin of this decrease of spin density is not yet understood.

Figure 1 shows that a second radical is produced during the irradiation of betaine. Its spectrum consists of two broad lines arising from a very anisotropic interaction of the free electron with an α proton and some other nuclei which

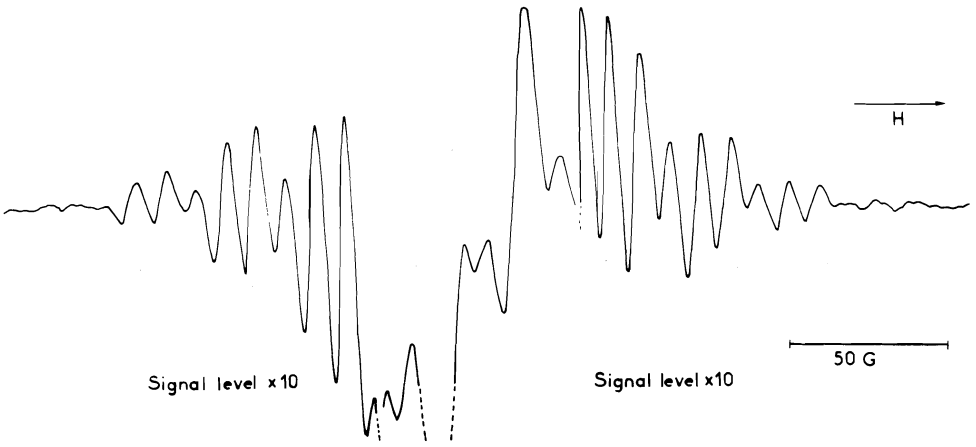

FIG. 1. Electron spin resonance spectrum of $(CH_3)_3N^{\ddagger}$ radical trapped in betaine single crystal. Spectra obtained for matrices 1–2 and 4 are quite similar to this one.

TABLE 2. Temperature variation of the coupling in the betaine matrix

	Nitrogen			Proton		
T (K)	Total coupling tensor	Isotropic coupling	Dipolar coupling tensor	Total coupling tensor	Isotropic coupling	Dipolar coupling tensor
168	50.80		29.50	27.10		−1.10
	7.90	21.30	−13.40	28.65	28.20	0.45
	5.30		−16.00	28.75		0.55
232	50.20		29.20	26.95		−1.05
	7.70	21.00	−13.30	28.50	28.00	0.50
	5.10		−15.90	28.60		0.60
293	48.90		28.30	26.30		−1.00
	5.40	20.60	−15.20	27.80	27.30	0.50
	7.60		−13.00	27.70		0.40
330	47.60		27.60	25.70		−0.20
	6.60	20.00	13.40	26.90	26.50	0.40
	5.80		14.20	26.90		0.40
345	45.40		26.90	25.10		−0.60
	5.50	19.50	−14.00	26.10	25.70	0.40
	6.60		−12.90	25.90		0.20

gives unresolved couplings. On the basis of the great similarity (Table 3) of the coupling tensor of this proton to that found by Ghosh and Whiffen (7) for the proton of the radical $N^+H_3\dot{C}HCOO^-$ trapped in irradiated glycine we tentatively attribute this spectrum to the $N^+(CH_3)_3\dot{C}HCOO^-$ radical.

4. Trimethylammonium Chloride

In this matrix $N^{\ddagger}(CH_3)_3$ has only one trapping site. The couplings are temperature dependent. The values of N and H coupling tensors measured at 100 K and 393 K are given in Table 1. The low temperature values are quite different from those obtained in other crystals. The isotropic nitrogen coupling is larger and the isotropic proton coupling is smaller than those found in the betaines while the dipolar tensors are the same. All these observations may be accounted for in the following way. When the $N^{\ddagger}(CH_3)_3$ radical is formed by γ irradiation of trimethylammonium chloride crystal it is not in its equilibrium planar configuration. A slightly pyramidal structure of the radical in the crystal may account for the 3.5 G increase of the isotropic nitrogen coupling constant which corresponds to a variation of the CNC angle from 120° to around 119.5° at 100 K. This deviation

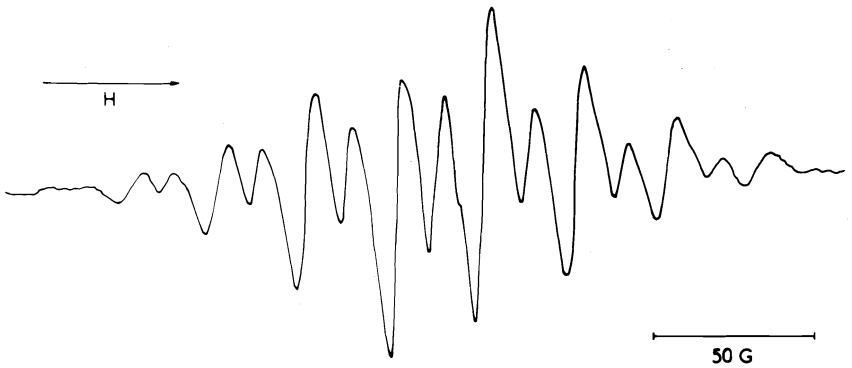

FIG. 2. Electron spin resonance spectrum of $(CH_3)_3N\dot{+}$ radical trapped in tetramethylammonium chloride single crystal.

TABLE 3. Comparison of the couplings of the alleged additional radical $N^+(CH_3)_3\dot{C}HCOO^-$ in betaine and the couplings of the $N^+H_3\dot{C}HCOO^-$ radical in glycine

Radical	Total coupling tensor	Isotropic coupling	Dipolar coupling tensor
$N^+(CH_3)_3\dot{C}HCOO^-$	−34.80		−10.60
in betaine	−22.10	−24.20	+2.10
	−15.60		+8.60
$N^+H_3\dot{C}HCOO^-$	−35.20		−11.50
in glycine	−22.00	−23.70	+1.70
	−13.90		+9.80

from the equilibrium configuration may result from a balance between the intramolecular electronic interactions which tend to give to the radical a planar configuration and the intermolecular repulsion interactions which tend to keep the pyramidal structure of the parent molecule. Then the variations of isotropic couplings (decrease for nitrogen, increase for proton) as temperature increases is due to a thermal expansion of the matrix. However, one difficulty still remains. The hypothesis of steric hindrance seems to be in contradiction with the existence of fast reorientational motions of the radical in the crystal as shown by the values of the dipolar coupling tensors. In fact this contradiction is only apparent because, even at low temperature, the trimethylammonium chloride molecules undergo fast intra- and intermolecular motions in the crystal so that the radical may be carried as if in a set of gear wheels. This explanation also supposes that the deformation energy of the radical is small.

5. Tetramethylammonium Chloride

Figure 2 shows a spectrum of the $N\dot{+}(CH_3)_3$ radical trapped in a room temperature γ-irradiated tetramethylammonium chloride single crystal. No site splitting is observed above the transition temperature of the matrix (185 K) and the couplings are not temperature dependent between 185 K and room temperature. From Table 1, it can be seen that the values of the nitrogen and proton isotropic couplings are in good agreement with those found in the other matrices but they are different from those reported in a previous study on the same compound (a_N = 18 G, a_H = 26.7 G) (3).

The dipolar parts of the couplings in this matrix are very different both in magnitude and in sign from those obtained in the betaines and in trimethylammonium chloride. This indicates a difference in the motion of $N\dot{+}(CH_3)_3$ in this matrix which is probably an additional motion of the radical reducing the parallel values of the tensor from the mean values of these couplings in the betaines ($b_N\| = 27.7$ G, $b_H\| = -1.1$ G) to $b_N\| = -7.5$ G and $b_H\| = 0.38$ G. This motion may be either free rotation or jumping reorientation between at least three equivalent positions in the crystal. In both cases the motion has to occur around an axis making an angle of about 23° with the C_{3v} symmetry axis of the radical. Then the parallel coupling becomes

$$2B \sin^2 (23) - B \cos^2 (23) = -7.5$$

where $2B$ is the mean parallel value of the nitrogen dipolar coupling for the $N^+(CH_3)_3$ radical in the matrices studied in this paper (28.3 G).

Conclusion

The measured N and H isotropic coupling constants of the $N\dot{+}(CH_3)_3$ radical are the same within experimental error in all the matrices studied. The only exception is the trimethylam-

monium chloride crystal but it seems that, in this case, steric hindrances may explain the observed distorted structure. Furthermore, the mean values of these couplings in the solid matrices studied (a_N = 21.2 G and a_H = 28.4 G) are in very good agreement with isotropic couplings found in the liquid phase (a_N = 20.55 G and a_H = 28.56 G) (5). This shows that the crystal field has a negligible effect on the structure of the radical, its only effect being to allow or inhibit some kinds of motion of the trapped radical. These motions depend on the dimensions of the trapping cage and also on the motions of the surrounding molecules. A good example is given by the tetramethylammonium chloride matrix. In this crystal the spectrum of $N^{\dagger}\bullet(CH_3)_3$ is well resolved only above 185 K, the transition temperature of the matrix, when the reorientations of the $N^{+}(CH_3)_3$ ions are allowed (4). From the crystal structure (8) it may be shown that even at these temperatures the cage is not large enough to allow the motion seen by esr so that a cooperative motion of the radical with the surrounding molecules has to be invoked to explain the nitrogen and proton couplings.

1. C. HESSE, N. LERAY, and J. RONCIN. J. Chem. Phys. **57**, 749 (1972).
2. L. BONAZZOLA, N. LERAY, and J. RONCIN. Can. J. Chem. **55**, 1617 (1977).
3. A. J. TENCH. J. Chem. Phys. **38**, 593 (1963).
4. D. J. WHELAN. Aust. J. Chem. **26**, 681 (1973).
5. R. W. FESSENDEN and P. NETA. J. Phys. Chem. **76**, 2857 (1976).
6. M. S. FISCHER, D. H. TEMPLETON, and A. ZALKIN. Acta Crystallogr. Sect. B, **26**, 1392 (1970).
7. D. K. GHOSH and D. W. WHIFFEN. Mol. Phys. **2**, 285 (1959).
8. R. W. G. WYCKOFF. Z. Kristallogr. **67**, 91 (1928).

Kinetics of ligand exchange between a uranium(IV) β-diketonate and free β-diketone

G. FOLCHER, N. KELLER, C. KIENER, AND J. PARIS

CEN-Saclay, Division de Chimie, S.E.P.C.P., B.P. nº 2–91190 Gif-sur-Yvette

Received March 1, 1977

G. FOLCHER, N. KELLER, C. KIENER, and J. PARIS. Can. J. Chem. **55**, 3559 (1977).

The intermolecular ligand exchange kinetics between a uranium(IV) β-diketonate and free β-diketone were studied by ^{1}H nmr as a function of temperature and concentration. The reaction was found to be of first order in both chelate and free ligand. The results suggest that the exchange mechanism involves a ninth coordination site in the uranium(IV) chelate.

G. FOLCHER, N. KELLER, C. KIENER et J. PARIS. Can. J. Chem. **55**, 3559 (1977).

La cinétique d'échange intermoléculaire du ligand entre une β-dicétonate d'uranium(IV) et la β-dicétone libre a été étudiée par rmn du proton en fonction de la température et de la concentration. On montre que la cinétique est du premier ordre par rapport aux deux espèces en échange. Les résultats suggèrent que le mécanisme d'échange implique un neuvième site de coordination dans la chélation de l'uranium(IV).

The kinetics of intermolecular ligand exchange in coordination compounds of uranium(IV) is little known. Johnson and Larsen (1) have measured oxalate exchange lifetimes by using C^{14}-labeled oxalate in tetraoxalatometallates of zirconium(IV), hafnium(IV), and uranium(IV). In the case where uranium(IV) β-diketonates form adducts with a variety of Lewis bases, we have noticed (2) that the base exchange rate is rapid on an nmr time scale. The same holds for the ligand exchange rate between free amino acids and the corresponding uranium(IV) complexes in aqueous solutions (3). By contrast the coordinated proton lifetime in the aquo-ion of uranium(IV) lies between 10 ms and 1 s (4).

Intermolecular ligand exchanges in metal β-diketonate complexes have been followed by nmr spectroscopy: quadrivalent (5, 6), trivalent (6, 7), and divalent (8) compounds have been studied.

The present paper describes the kinetics of intermolecular ligand exchange between a uranium(IV) paramagnetic complex and free ligand in solution. The exchange rates have been followed by high-resolution nmr techniques and have been studied as a function of temperature and concentration (9, 10).

Experimental Section

The $U(fod)_4$ (1,1,1,2,2,3,3-heptafluoro-7,7-dimethyl octane-4,6 dione) is prepared as follows: an aqueous solution of UCl_4 (0.5 *M*) and HCl (1 *N*) is mixed with one Hfod (Pierce Chemicals) equivalent and stirred. Within a few minutes, a solid compound forms. It is filtered, washed with a little petroleum ether, dried, and sublimated at 250°C in a water cooled apparatus under 10^{-2} Torr. The product is reasonably pure (*Anal.* calcd.: U 16.8, C 33.8; found: U 16.8, C 33.6; mp 165°C). The nmr spectra are obtained with a 60 MHz Varian NV-14 spectrometer fitted with a variable temperature probe.

Results

The ^{1}H nmr spectrum of $U(fod)_4$ in solution displays two resonance signals. The first one is assigned to the 36 protons of the four *tert*-butyl groups shifted 5.5 ppm upfield from the corresponding Hfod signal. The second signal is assigned to the four methylene protons. We have chosen to investigate ligand exchange between $U(fod)_4$ and Hfod, by following the variations of the strong *tert*-butyl signals.

Figure 1*A* displays the experimental ^{1}H nmr spectra between 30 and 100°C in deuterated toluene and for concentrations of $[U(fod)_4] = 0.046\ M$ and $[Hfod]_{enol} = 0.238\ M$. In the low temperature range ($T \lesssim 40$°C), the *tert*-butyl proton resonances are separated and remain approximately Lorentzian. As temperature is increased, the two signals collapse at about 100°C.

This behaviour can be explained in terms of ligand exchange between the acid form and the bound form by the following reaction:

$$[1] \qquad U(fod)_4 + Hfod^* \underset{k_{-1}}{\overset{k_1}{\rightleftharpoons}} U(fod)_3(fod^*) + Hfod$$

In the slow exchange limit, the bound ligand

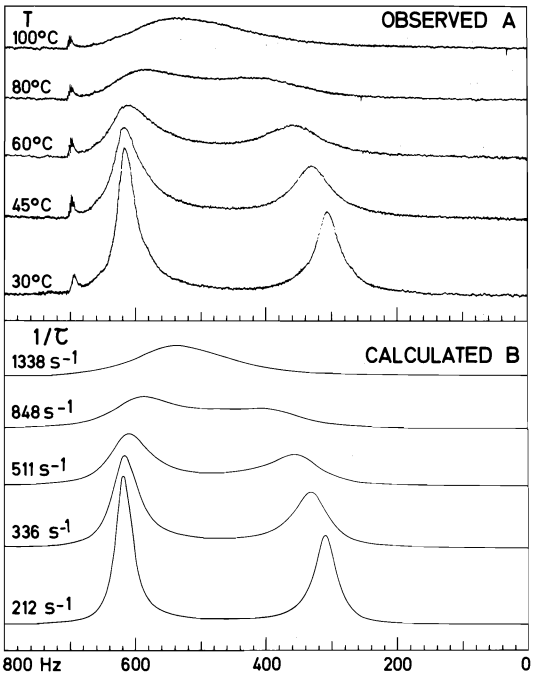

FIG. 1. Proton resonance signals of the (*tert*-butyl) groups in a toluene-d_8 solution of U(fod)$_4$ and Hfod, as a function of temperature, [U(fod)$_4$] = 0.046 *M*, [Hfod] = 0.238 *M*. *A*, experimental spectra; *B*, calculated spectra.

lifetime τ_{UL_4} is given by:

$$[2] \quad \frac{1}{\tau_{UL_4}} = \frac{1}{[UL_4]}\frac{d[UL_4]}{dt} = \frac{1}{T'_{2UL_4}} - \frac{1}{T_{2UL_4}}$$

Transverse relaxation times are obtained from the linewidths observed in the high resolution nmr spectra. T_{2UL_4} stands for the transverse relaxation time of the complex in absence of exchange. The corresponding linewidth $(\Pi T_{2UL_4})^{-1}$ does not vary significantly with temperature and is roughly equal to 1 Hz. The free ligand lifetime τ_{HL} is obtained from an equation analogous to [2].

The exchange reaction rate can be described by the following equation:

$$[3] \quad \frac{4d[UL_4]}{dt} = \frac{d[HL]_{enol}}{dt} = k[UL_4]^m[HL]_{enol}{}^n$$

The kinetic law is first order in UL_4 and HL (Fig. 2).

Temperature Dependence

In the higher temperature range ($T > 40°C$) the condition $1 \lesssim 2\Pi\tau\Delta\nu$ is realized. $\Delta\nu$ is the chemical shift difference between the protons in the free and coordinated sites and $\tau^{-1} =$

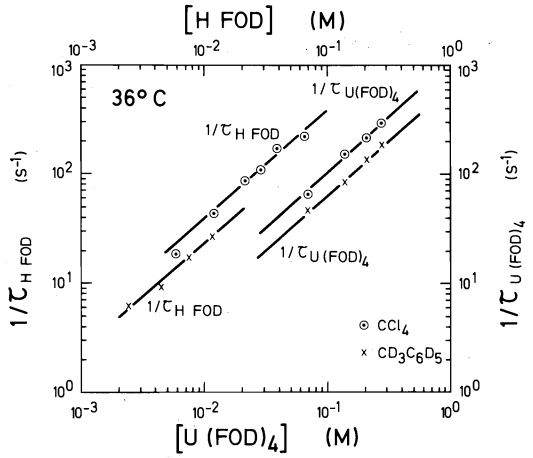

FIG. 2. Log $(\tau_{U(fod)_4}{}^{-1})$ vs. log [Hfod]$_{enol}$ and log $(\tau_{Hfod}{}^{-1})$ vs. log [U(fod)$_4$] at 36°C, ⊙ CCl_4 and × toluene-d_8.

$\tau^{-1}{}_{HL_4} + \tau^{-1}{}_{HL}$ is the ligand exchange rate. The absorption band shapes are calculated under the assumption that the exchange model between two unequally populated sites (11) is applicable. These are fitted to the experimental band shapes. The parameters involved in the fit are temperature dependent: i.e. the exchange time τ and the chemical shift of the bond ligand which is mainly paramagnetic. This paramagnetic contribution varies similarly to the magnetic susceptibility and follows a Curie Law in this temperature range. The best fit for the lineshapes is obtained using the following equation yielding the exchange time:

$$[4] \quad \tau\,(s) = \frac{2365 \times 10^{-7}}{T\,(K)} \exp\left(\frac{5238}{RT\,(K)}\right)$$

There is good agreement between the calculated lineshapes and the experimental spectra (Fig. 1 *A*, *B*). The free energy of activation can be calculated from the value of the rate constant k according to Eyring's equation:

$$[5] \quad k = \frac{\kappa k_B T}{h} \exp -\left(\frac{\Delta G^{\ddagger}}{RT}\right)$$

where the symbols have their usual meanings and by making the assumption that the transmission coefficient κ is equal to 1 (12). The exchange rate is given by:

$$[6] \quad \frac{1}{\tau} = \frac{1}{\tau_{UL_4}} + \frac{1}{\tau_{HL}} = k\left(\frac{[HL]_{enol}}{4} + [UL_4]\right)$$

Hence, the enthalpy and the entropy of activation can both be calculated: $\Delta H^{\ddagger} = 5.2$ kcal/mol and $\Delta S^{\ddagger} = 26$ eu.

Base Dependence

As one equivalent of DMSO is added to a CCl_4 or toluene-d_8 solution of $U(fod)_4$ containing also free Hfod, the bound and free ligand resonances become much narrower. Their linewidths are again of the same order of magnitude (1 Hz) as in the absence of exchange. Simultaneously, we observe an important upfield shift of the DMSO proton signals resulting from the DMSO molecule bounding onto the $U(fod)_4$ chelate (2). The same results have been obtained with strong bases like HMPA, DMF. Therefore the strong bases hinder ligand exchange by forming adducts with the chelates.

Discussion

The crystal structures of several uranium(IV) β-diketonates have been determined by X-ray crystallography (13, 14). The uranium(IV) atom is coordinated to eight oxygen atoms according to a square antiprismatic or dodecahedral arrangement. Besides, a recent study (2) shows that uranium(IV) β-diketonates form adducts with Lewis bases with a possible nine-coordination configuration. The absence of ligand exchange in the presence of a Lewis base suggests that the base occupies the ninth coordination site which is then no longer available. We propose here an exchange mechanism where a free β-diketone (in an enolic form) binds with an UL_4 chelate. From this adduct, the enolic proton escapes along with another ligand L (Fig. 3). Our mechanism differs from that proposed by Adams and Larsen (5) and assumed by Glass and Tobias (6) and also by Tanner, Tuck, and Wells (7). Their mechanism, which appears to apply to the transition metals and tin(II) (8), includes a first step involving the breaking of one metal–oxygen bond which consequently lowers the coordination number. In our case, the breaking of one bond leads to a 7 coordinated uranium which is not likely, while the 9 coordinance is more favorable. Adams and Larsen (5) have reported a faster ligand exchange for thorium(IV) than for zirconium(IV) and hafnium(IV) chelates. The exchange rate for a uranium(IV) chelate is found to be similar to that of the corresponding thorium(IV) chelate. A possible explanation of this behaviour is the existence of an accessible ninth coordination site which confers to the actinide complexes a greater lability as compared to transition metal complexes.

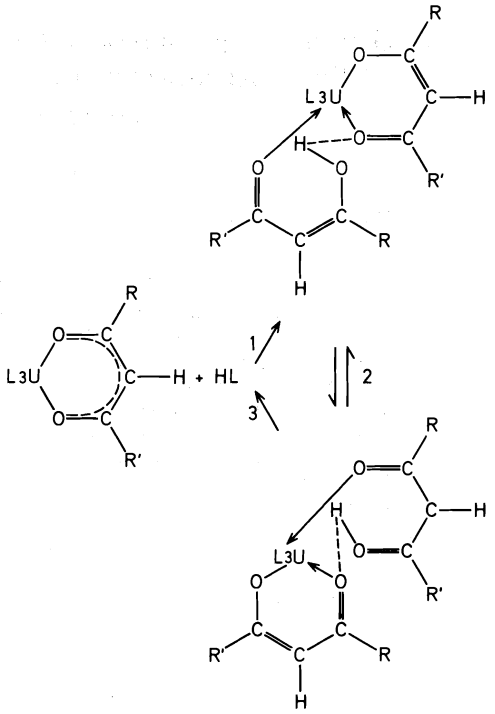

FIG. 3. Exchange mechanism where L represents a β-diketone ligand.

Acknowledgment

The authors wish to thank Dr. Rigny for the helpful discussions, the advice, and the interest that he has shown throughout this work.

1. F. A. JOHNSON and E. M. LARSEN. Inorg. Chem. **1**, 159 (1962).
2. G. FOLCHER, J. PARIS, P. PLURIEN, P. RIGNY, and E. SOULIE. Chem. Commun. 3 (1974).
3. C. NEVEU, G. FOLCHER, and A. M. LAURENT. J. Inorg. Nucl. Chem. **38**, 1223 (1976).
4. C. KIENER, G. FOLCHER, P. RIGNY, and J. VIRLET. Can. J. Chem. **54**, 303 (1976).
5. A. C. ADAMS and E. M. LARSEN. Inorg. Chem. **5**, 814 (1966).
6. G. E. GLASS and R. S. TOBIAS. J. Organomet. Chem. **15**, 481 (1968).
7. G. M. TANNER, D. G. TUCK, and E. J. WELLS. Can. J. Chem. **50**, 3950 (1972).
8. N. SERPONE and R. ISHAYEK. Inorg. Chem. **13**, 52 (1974).
9. G. N. LA MAR, W. DE W. HORROCKS, JR., and R. H. HOLM. Nmr of paramagnetic molecules. Academic Press. 1973. Chapt. 2.
10. L. M. JACKMAN and F. A. COTTON. Dynamic nuclear magnetic resonance spectroscopy. Academic Press. 1975. Chapts. 3 and 8.
11. J. M. EMSLEY, J. FEENEY, and L. H. SUTCLIFFE. High resolution nuclear magnetic resonance spectroscopy. Pergamon Press, 1965. Chapt. 9.
12. A. A. FROST and R. G. PEARSON. Kinetics and mechanism. Wiley and Sons, Inc., New York, NY. 1961. Chapt. 5.
13. V. L. WOLF and H. BÄRNIGHAUSEN. Acta Crystallogr. **13**, 778 (1960).
14. H. TITZE. Acta Chem. Scand. **24**, 405 (1970).

Cyclization of glycol monoesters to give hemiorthoesters: a test of the thermochemical method for determining free energies of tetrahedral intermediates

J. Peter Guthrie[1]

Department of Chemistry, University of Western Ontario, London, Ont., Canada N6A 5B7

Received November 9, 1976[2]

J. Peter Guthrie. Can. J. Chem. **55**, 3562 (1977).

From calorimetric heat of formation data, free energies of cyclization (to the hemiorthoester) for the following glycol monoesters have been calculated: ethylene glycol monoformate, +7.54; ethylene glycol monoacetate, +10.72; pinacol monoformate, +3.21; ethylene glycol monotrifluoroacetate, +2.83; pinacol monotrifluoroacetate, −3.38. The latter two results are shown to be in satisfactory agreement with experimental results. This investigation represents a further test of the thermochemical method for calculating free energies of tetrahedral intermediates in acyl transfer reactions which was reported earlier.

In the course of this work, various thermochemical quantities were determined. Heats of reaction for the process:

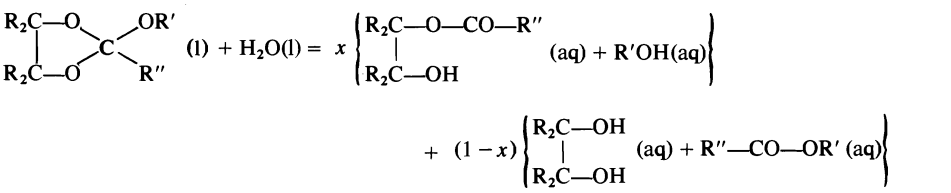

have been measured for three compounds: **1**, R = H, R′ = CH_3, R″ = H; $x = 0.92$, $\Delta H_{obs} = -7.13 \pm 0.60$ kcal/mol; **2**, R = H, R′ = CH_3, R″ = CH_3; $x = 0.98$, $\Delta H_{obs} = -10.11 \pm 0.40$ kcal/mol; **9**, R = CH_3, R′ = C_2H_5, R″ = H; $x = 0.98$, $\Delta H_{obs} = -4.76 \pm 0.19$ kcal/mol. From these may be obtained heats of formation of the liquids: **1**, −126.01 ± 0.94; **2**, −137.25 ± 0.87; **9**, −173.87 ± 2.09 kcal/mol. For some related esters, heats of hydrolysis were measured, leading to the following heats of formation of the liquids: *tert*-butyl formate, −117.85 ± 0.80; *tert*-butyl trifluoroacetate, −271.28 ± 1.14; pinacol monoformate, −175.02 ± 2.12 kcal/mol. Heats of hydrolysis were measured for methoxyethyl formate and acetate, but in the absence of a reliable value for the heat of formation of methoxyethanol, do not lead to calorimetric heats of formation. Equilibrium constants for formation of the monoesters of ethylene glycol with formic, acetic, and trifluoroacetic acids were measured (nmr analysis of equilibrated solutions) and lead to free energies of hydrolysis of −2.34, −1.65, and −2.75 kcal/mol respectively.

J. Peter Guthrie. Can. J. Chem. **55**, 3562 (1977).

On calcule, à partir des enthalpies de formation, obtenues par calorimétrie, les énergies libres de cyclisation (pour former l'hémiorthoester) des monoesters de glycol suivants: le monoformiate d'éthylène glycol, +7.54; le monoacétate d'éthylène glycol, +10.72; le monoformiate de pinacol, +3.21; le monotrifluoroacétate d'éthylène glycol, +2.83; le monotrifluoroacétate de pinacol, −3.38. Ces deux derniers résultats sont en bon accord avec les résultats expérimentaux. Cette étude représente un autre essai de la méthode thermochimique pour le calcul des énergies libres des intermédiaires tétrahédriques dans les réactions de transfert de groupes acyle rapportée antérieurement.

Dans ce travail, plusieurs entités thermochimiques sont déterminées. Les chaleurs de réaction pour le processus suivant:

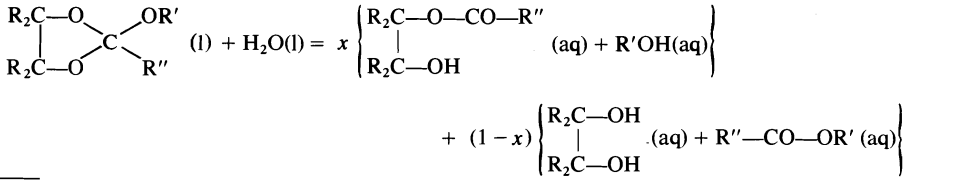

---

[1]Alfred P. Sloan Fellow, 1975–1977.

[2]Revision received May 5, 1977.

sont mesurées pour trois composés: **1**, R = H, R′ = CH_3, R″ = H; $x = 0.92$, $\Delta H_{obs} = -7.13 \pm 0.60$ kcal/mol; **2**, R = H, R′ = CH_3, R″ = CH_3; $x = 0.98$, $\Delta H_{obs} = -10.11 \pm 0.40$ kcal/mol; **9**, R = CH_3, R′ = C_2H_5, R″ = H; $x = 0.98$, $\Delta H_{obs} = -4.76 \pm 0.19$ kcal/mol. De ces données, on peut obtenir les chaleurs de formation des liquides; **1**, -126.01 ± 0.94; **2**, -137.25 ± 0.87; **9**, -173.87 ± 2.09 kcal/mol. A partir des mesures des chaleurs d'hydrolyse de quelques esters analogues, on obtient les chaleurs de formation suivantes des liquides: formiate de *tert*-butyle, -117.85 ± 0.80; trifluoroacétate de *tert*-butyle, -271.28 ± 1.14; monoformiate de pinacol, -175.02 ± 2.12 kcal/mol. Les chaleurs d'hydrolyse sont obtenues pour le formiate et l'acétate de méthoxyéthyle; n'ayant pas une bonne valeur de chaleur de formation du méthoxyéthanol, il n'est pas possible de calculer les chaleurs de formation calorimétriques. Les constantes d'équilibre de formation des monoesters d'éthylène glycol par les acides formique, acétique et trifluoroacétique sont mesurées (analyse rmn des solutions équilibrées), puis on en déduit les énergies libres d'hydrolyse qui sont respectivement de -2.34, -1.65 et -2.75 kcal/mol.

[Traduit par le journal]

Introduction

The vast majority of acyl transfer reactions proceed by way of tetrahedral intermediates (1), although other mechanisms intervene for some special situations (2). These intermediates are normally much too unstable to be detected, although stable analogs are known in the form of orthoesters and related compounds (3). In some cyclic or polycyclic compounds species analogous to the tetrahedral intermediates in ester hydrolyses, i.e. orthoacid diesters or hemiorthoesters, are thermodynamically favored relative to the ordinary ester plus alcohol (4, 5). There have been to date only two cases where the equilibrium constant for formation of a neutral tetrahedral species has been directly measured (4, 5), and one for formation of an anionic species (6, 7).

Recently, a method has been developed for evaluating the free energies of formation of tetrahedral intermediates (7–10), starting with the free energies of formation of the orthoester analogs. The basis of this method is that the dependence of the (symmetry corrected) free energy change for process [1] upon steric and electronic factors can be evaluated for alcohols,

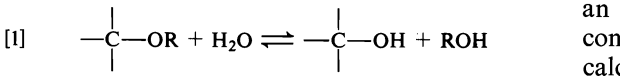

[1]

carbonyl hydrates, and hemiacetals from experimental data, and then (with a small extrapolation) applied to orthoesters. All available data for free energies of formation of ethers and alcohols and for equilibrium constants for hemiacetal and acetal formation involving methanol or ethanol and carbonyl compounds could be fitted to a straight line relating ΔG^0 to $\Sigma\sigma^*$, once steric and symmetry factors were allowed for (10).

This procedure has been applied to esters (7, 8), and amides (9), and gave results which were intuitively reasonable. Having a method for evaluating the equilibrium constant for addition to acyl groups should prove very useful in mechanistic analysis since it permits calculation of all the microscopic rate constants in favorable cases, whereas the best that can be done without the equilibrium constant for formation of the tetrahedral intermediate is to evaluate the rate constant for addition and the partitioning ratio. Indeed, the method has already been employed in this way (11). Although the basis of the method appears sound, it does involve an extrapolation, so that it seems desirable to test it as thoroughly as possible.

The first such test involved the addition of methanol to methyl trifluoroacetate (7). The equilibrium constant for addition of methoxide ion, in methanol, to methyl trifluoroacetate to give the anionic addition compound is readily measurable. Unfortunately, a direct test of the thermochemical approach was not possible, since the hydrolysis of trimethyl orthotrifluoroacetate was too slow to permit measurement of the heat of hydrolysis (7). In the absence of a heat of combustion for this orthoester, only an indirect test was possible. The equilibrium constants for addition of water to the acids, calculated using equilibrium constants for [1], and starting from the free energies of formation of trimethyl orthoacetate and trimethyl orthoformate, and the equilibrium constant for addition of methanol to methyl trifluoroacetate, showed a linear dependence upon σ^* with a slope similar to, but somewhat larger than, the slope which was observed for addition of water to the analogous carbonyl compounds (8).

This paper reports another test of the method, employing it to calculate the equilibrium constants for cyclization of glycol monoesters to

hemiorthoesters. Hine *et al.* (5) found that pinacol monotrifluoroacetate (and monotrichloroacetate) was partially or predominantly (depending upon the solvent) present as the hemiorthoester. For the monoesters of ethylene glycol the presence of the hemiorthoester could be demonstrated by trapping experiments, although it could not be detected spectroscopically (5). A direct application of the thermochemical method is not practical, since the heats of hydrolysis of the appropriate orthoesters are not measurable for technical reasons (7). Accordingly, an indirect test has been carried out, by determining the heats of formation, and hence the free energies of formation of analogous orthoformates and acetates, and then calculating the desired free energies of formation of the orthotrifluoroacetates by methods based upon the assumption of group additivity. From these values, equilibrium constants for the cyclization reactions could be deduced; these will be seen to be in satisfactory agreement with the experimental values.

Results

Calorimetric heats of reaction and solution determined in this work are found in Table 1. For the cyclic orthoesters, it was necessary to determine the stoichiometry of the reaction, expressed as x, the fraction of hydrolysis leading to the glycol monoester. Nuclear magnetic resonance analysis of product solutions permitted the determination of the product ratio; the final heat of formation of the orthoester is relatively insensitive to experimental errors in the stoichiometry. In order to calculate the heat of formation of the orthoester from the heat of reaction [2], it is also necessary to have heats of

[2]

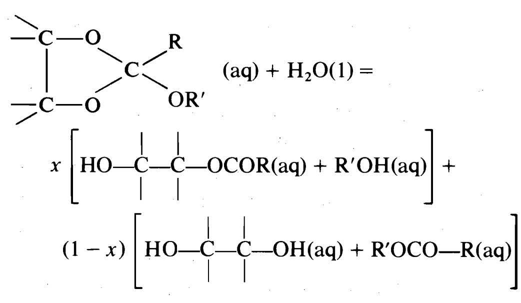

formation for the products. Literature values are available for methanol, ethanol, methyl formate, ethyl formate, methyl acetate, ethylene glycol, methoxyethanol, and pinacol (see Table 2; for the latter two, see also the Discussion section). The heat of formation in aqueous solution of pinacol monoformate could be calculated from the heats of hydrolysis and solution measured in this work. Although the monoformate and monoacetate of ethylene glycol are known compounds (12), it seemed likely that they would be difficult to obtain free of the diester and glycol (13). Accordingly, the heats of formation have been calculated on the assumption that the heat of hydrolysis for reaction [3] is independent of

$$[3]\quad R{-}O{-}CH_2{-}CH_2{-}O{-}\overset{\overset{\displaystyle O}{\|}}{C}{-}R'(aq) + H_2O(l) = ROCH_2CH_2OH(aq) + HO\overset{\overset{\displaystyle O}{\|}}{C}{-}R'(aq)$$

whether R is H or CH_3, using heats of reaction and solution for methoxyethyl formate and acetate determined in this work. The heats of formation of the orthoesters are found in Table 2. Entropy values were calculated by standard estimation procedures. Where possible, free energies of transfer from gas to aqueous solution were calculated from solubility and vapor pressure data. For those compounds which were excessively water soluble (methoxyethyl acetate, methoxyethyl formate, 2-methoxydioxolane, 2-methoxy-2-methyldioxolane), free energies of transfer were calculated by the group equivalent method of Hine and Mookerjee (14).

Equilibrium constants for the formation of the ethylene glycol monoesters of acetic, formic, and trifluoroacetic acids were determined by nmr analyses of solutions containing the acid, the glycol, and (except in the case of trifluoroacetic acid) 0.1 N HCl as a catalyst. The ester signal was integrated relative to the signal from the acid, or, when very little ester was present, the ^{13}C satellite of the signal from the acid. In some cases it was necessary to shift the pH to 7 after equilibrium had been established in order to get adequate separation of the ester and acid signals, since the acid and not the ester undergoes titration and consequently the resonance position shifts. The results of these experiments are found in Table 3. Free energies of formation of the esters were calculated from these results and the free energies of formation of the other reactants, and are found in Table 2. The free energy of formation (in aqueous solution) of pinacol monoformate is more difficult to obtain, since the equilibrium is quite far on the side of hydrolysis. For neither pinacol nor pinacol monoformate could the free energy of transfer

TABLE 1. Heats of reaction and solution[a]

Reaction	ΔH_{obs}[b] (kcal mol^{-1})	Stoichiometry
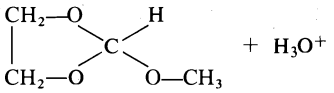	−7.13(0.60)	0.92(0.10)
	−1.56(0.17)	
	−16.20(0.65)	
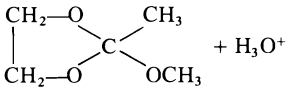	−10.11(0.40)	0.98(0.10)
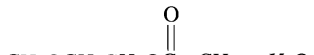	−3.14(0.12)	
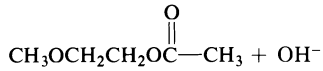	−16.87(0.67)	
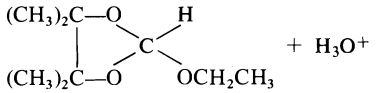	−4.76(0.19)	0.98(0.07)
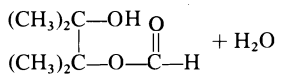	−3.07(0.12)	
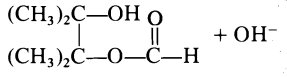	−17.26(0.69)	
	−9.72(0.39)	
HCOOH + OH$^-$ [c]	−8.44(0.67)	
H_2O + OH$^-$ [c]	−0.29(0.03)	
$(CH_3)_3C$—OH + OH$^-$ [c]	−0.27(0.11)	
$(CH_3)_3C$—O—$COCF_3$ + OH$^-$ [c]	−12.88(0.57)	
CF_3COOH + OH$^-$ [c]	−13.63(0.55)	

[a]For aqueous solutions unless otherwise specified.
[b]Average values (normally for three trials) with standard deviations in parentheses.
[c]75% (v/v) methanol used as solvent.

be determined by the simple method involving solubilities and vapor pressures, since pinacol forms a hexahydrate on contact with water and solubility and vapor pressure do not therefore refer to the same species, and pinacol monoformate is miscible with water. Two methods were used to calculate the free energy of pinacol monoformate. In the first, free energies of transfer were calculated by methods based upon the assumption of group additivity. From the known free energy of transfer of ethylene glycol, and the group contributions for $CH_2(C)(O)$, $CH_3(C)$, and $C(C)_3(O)$ a free energy of transfer for pinacol could be calculated. For pinacol monoformate, a

TABLE 2. Thermodynamic quantities for compounds used in this paper[a]

Compound	ΔH_f°(g)[b]	S°(g)[c]	ΔG_f°(g)[b]	ΔH_v[b,d]	ΔH_f°(l)[b]	ΔH_{soln}[b,e]	ΔH_f°(aq)[b]	ΔG_t[b,f]	ΔG_f°(aq)[b,g]
H_2O	−57.80[h]	45.11[h]	−54.68[h]		−68.32[h]				−56.69[h,i]
HCOOH	−90.49[j]	59.45[j]	−83.89[j]		−101.60[k]	−0.16[l]	−101.76[m]	−4.94[n]	−88.83[n]
CH_3OH	−48.08[h]	56.8[h]	−38.09[h]		−57.02[h]	−1.74[o]	−58.76[m]	−3.19[n]	−41.88[n]
CF_3COOH	−243.2(1.1)[x]	79.6(1.5)[x]	−225.2(1.1)[x]		−253.0(0.8)[k]			−4.75[x]	−230.0(1.2)[x]
$HCOOCH_3$	−84.97[p]	72.0[j]	−72.40[m]		−92.28[p]	−0.85[q]	93.13[m]	−0.98[n]	−73.38[m]
CH_3COOH	−103.26[k]	67.52[j]	−89.36[m]		−115.75[k]	−0.34[h]	−116.09[m]	−4.85[n]	−94.21[n]
CH_3CH_2OH	−56.24[h]	67.4[n]	−40.30[n]		−66.42[k]	−2.43[o]	−68.85[m]	−3.01[n]	−43.31[n]
$CH_2(OH)CH_2(OH)$	−93.9(1.5)[k]	77.3[r]	−73.6(1.6)[m]	13.6(1.4)[k]	−108.73(0.18)[k]	−1.65(0.09)[o]	−110.38(0.20)[m]	−5.78[s]	−79.3(1.6)[m]
	[−92.0]*	[77.36]	[−71.73]*					[−7.75]*	[−79.47]
$HCOOCH_2CH_3$	−94.90(1.03)[m]	82.0(1.5)[t]	−75.61(1.12)[m]	7.69(1.0)[u]	−102.59(0.23)[u]	−1.64(0.34)[v]	−104.23(0.41)[m]	−0.76[w]	−76.36(1.12)[m]
CH_3COOCH_3	−98.00[p]	76.45[n]	−77.05[m]		−106.57[p]	−1.89[q]	108.46[m]	−1.38[n]	−78.43[m]
CF_3COOCH_3	−237.3(1.3)[x]	96.0(1.5)[x]	−214.4(1.2)[x]		−243.9(1.4)[x]			+0.80[x]	−213.6(1.2)[x]
$CH_3OCH_2CH_2OH$	−104.0(?)[m]		−76.76(?)[m]	10.80[z]	−114.8(?)[j,y]	−3.65[cc]		−2.86[aa]	−79.6(?)[m]
	−90.07(1.93)[bb]		−62.83(1.88)[bb]		−100.87(1.82)[bb]		−104.52(1.82)[bb]		−65.69(1.94)[bb]
	[−87.40]*	[86.57]	[−60.17]*					[−4.82]*	[−64.99]
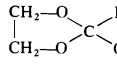	−115.10(1.27)[m]	86.64(1.0)[ff]	−80.17(1.31)[m]	9.95(1.00)[ee]	−125.05(0.79)[dd]				−84.03(1.40)[m]
	[−118.40]		[−83.47]					[−3.86]	[−87.33]
$(CH_3)_3COH$	−77.87[j]	77.98[j]	−45.66[j]		−85.87[j]	−4.29[o]	−90.16[m]	−2.63[s]	−46.81[m]
H—COO—CH_2—CH_2—OCH_3				10.40(1.00)[ee]	−135.10(1.83)[m]	−1.56(0.17)[dd]	−136.66(1.81)[m]		
	[−124.70]	[100.79]	[−93.99]					[−2.43]	[−96.43]
$H—C(OCH_3)_3$	−126.58[gg]	94.57[n]	−84.70[m]		−135.71[gg]			−2.52[n]	−87.22[m]
	−126.86(1.16)[m]		−83.81(1.25)[m]	10.04(1.00)[ee]	−136.90(0.59)[dd]				−87.63(1.34)[m]
	[−127.96]	[91.97]	[−84.91]					[−3.82]	[−88.72]
$H—COOC(CH_3)_3$	−109.18(1.28)[m]		−73.52(1.36)[m]	8.67(1.00)	−117.85(0.80)[dd]			−0.64(0.10)[dd]	−74.16(1.36)[m]
	[−108.60]	[92.24]	[−72.93]					[−0.31]	[−73.25]
$CH_3COOCH_2CH_2$—OCH_3	−136.85(2.05)[m]		−98.85(2.10)[m]	12.01(0.01)[hh]	−148.86(2.05)[dd]	−3.14(1.2)[dd]	−152.00(2.05)[m]		−101.62(2.15)[m]
	[−137.80]	[108.90]	[−99.80]					[−2.77]	[−102.56]
$CH_3C(OCH_3)_3$	−136.63[gg]	99.70[n]	−86.57[m]		−146.00[gg]			−2.48[n]	−89.05[m]
$HOC(CH_3)_2C$—$(CH_3)_2OH$	−129.15(2.24)[m]		−77.54(2.28)[m]	15.75(1.00)	−144.90(2.00)	−0.60[dd]	−145.50(2.00)[m]		−82.43(2.34)[m]
								[−4.89]	
	[−126.52]*	[102.54]	[−74.91]*					[−6.84]*	−[81.76]*
$CF_3—COOC(CH_3)_3$	−262.50(1.51)[m]	112.37(5.0)[ii]	−215.35(2.12)[m]	8.78(1.00)	−271.28(1.14)[dd]			2.26(0.50)[bb]	−231.09(2.18)[m]
$HCOOC(CH_3)_2C$—$(CH_3)_2OH$	−161.65(2.34)[m]		−106.97(2.39)[m]	13.37(1.0)[bb]	−175.02(2.12)[dd]	−3.07(0.12)[dd]	−178.09(2.12)[m]		−109.46(2.59)[m]
								[−2.49]	
	[−160.38]	[118.14]	[−105.71]					[−4.45]*	[−110.17]
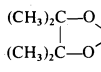	−162.43(2.32)[m]		−88.84(2.36)[m]	11.44(1.00)[bb]	−173.87(2.09)[dd]			−2.15(0.50)[dd]	−90.99(2.42)[m]
		[119.81]						−2.77]	
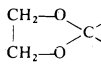									−100.72(1.42)[bb]
$HOCH_2CH_2OCHO$									

TABLE 2 (*Concluded*)

Compound	ΔH_f^0(g)[b]	S^0(g)[c]	ΔG_f^0(g)[b]	ΔH_v[b,d]	ΔH_f^0(l)[b]	ΔH_{soln}[b,e]	ΔH_f^0(aq)[b]	ΔG_t[b,f]	ΔG_f^0(aq)[b,g]
	[−129.30]*	[92.96]	[−105.97]*					[−5.35]*	−109.22(1.58)[jj] [−111.32] −104.23(1.36)[bb]
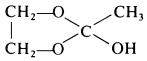 $HOCH_2CH_2OCOCH_3$	[−142.40]*	[101.06]	[−111.78]*					−5.68]*	−115.29(1.59)[jj] [−117.46] −106.24(2.43)[bb]
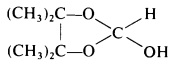									
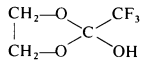									−245.73(1.66)[bb]
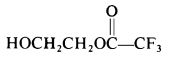									−249.24(1.99)[jj]
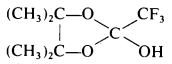									−252.09(2.77)[bb]
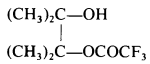									−249.04(4.28)[bb]
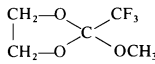									−228.70(1.63)[bb]
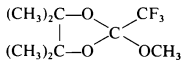									−233.34(2.75)[bb]
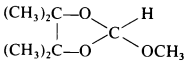									−89.56(2.42)[b]

[a]At 25°C; standard states are ideal gas at 1 atm, pure liquid, and 1 *M* aqueous solution with an infinitely dilute reference state, unless otherwise noted. Quantities in parentheses are estimated standard deviations. Quantities in brackets were estimated by group additivity; an asterisk indicates an ideal quantity, calculated assuming no hydrogen bond is present. [b]kcal mol^{-1}. [c]cal deg^{-1} mol^{-1}. [d]Heat of vaporization. [e]Heat of solution, liquid to infinitely dilute aqueous solution, unless otherwise noted. [f]Free energy of transfer, gas at 1 atm to 1 *M* aqueous solution with an infinitely dilute reference state. [g]Standard state is infinitely dilute aqueous solution. [h]Reference 34*a*. [i]Standard state is the pure liquid. [j]Reference 15. [k]Reference 34*b*. [l]Reference 35. [m]Calculated from other values in this table. [n]Reference 8. [o]Reference 36. [p]Reference 37. [q]Reference 9. [r]Reference 38. [s]Reference 14. [t]Reference 39. [u]Reference 40. [v]J. P. Guthrie. Unpublished results. [w]Reference 14. [x]Reference 7. [y]An old value of uncertain reliability (see ref. 15). [z]Reference 41. [aa]Calculated by group additivity, after ref. 14, using the distant polar interaction correction for ethylene glycol. [bb]Calculated as described in the text. [cc]Reference 42. [dd]This work. [ee]Estimated from the boiling point (see text). [ff]Estimated from the entropy of a model compound (see text). [gg]Calculated from the heats of hydrolysis and vaporization given in ref. 40. [hh]Reference 43. [ii]Estimated by the method of atomic additivity; ref. 17. [jj]Calculated from equilibrium constants as described in the text.

TABLE 3. Equilibrium constants for ester formation from ethylene glycol[a]

Acid	Final concentrations: Acid	Alcohol	Ester	K(eq.)[b]	K(av.)	ΔG^0
CH_3COOH	0.90	0.98	0.057	0.064(0.02)	0.062(0.01)	1.65(0.07)
	0.94	1.85	0.105	0.060(0.01)		
HCOOH	1.02	0.99	0.018	0.018(0.002)	0.019(0.002)	2.34(0.08)
	0.97	2.00	0.040	0.021(0.002)		
CF_3COOH	0.55[c]	1.13	0.0060	0.0097(0.002)		2.75(0.12)

[a]In aqueous solution at 25 ± 2°C.
[b]Error limits based upon the standard deviations for the integrations.
[c]Total trifluoroacetic acid concentration was 1.93 M; corrected for partial ionization and medium effects as described in ref. 7.

TABLE 4. Free energies of hydrolysis of tertiary esters[a]

Reaction	ΔG^{0b} (kcal mol^{-1})
$(CH_3)_3C{-}O{-}C(=O){-}H + H_2O = (CH_3)_3C{-}OH + HCOOH$	−4.79(1.37)
$(CH_3)_2C(C(CH_3)_2{-}OH){-}O{-}C(=O){-}H + H_2O = (CH_3)_2C(C(CH_3)_2{-}OH){-}OH + HCOOH$	−5.12(1.40)
$(CH_3)_3C{-}O{-}C(=O){-}CF_3 + H_2O = (CH_3)_3C{-}OH + CF_3COOH$	−6.18(1.98)

[a]In aqueous solution: standard state for water is the pure liquid with unit activity.
[b]Calculated from the free energy of formation data in Table 2.

value for the free energy of transfer was calculated from the group contributions reported by Hine and Mookerjee, with the inclusion of the 'distant polar interaction' which they report for ethylene glycol. This is equivalent to the assumption that in both ethylene glycol and pinacol monoformate an intramolecular hydrogen bond is present in the gas phase. In the second method, the assumption was made that the free energy of hydrolysis of pinacol monoformate was the same as for *tert*-butyl formate. This assumption involves the subsidiary assumption that the second hydroxyl in pinacol does not affect the stability of the ester in a strongly hydrogen bonding solvent such as water. The agreement between the two methods is good (see Table 4). The free energy of formation (in aqueous solution) for pinacol monotrifluoroacetate was calculated using the assumption that the free energy of hydrolysis for this ester was the same as for *tert*-butyl trifluoroacetate. The latter value was calculated from the heat of hydrolysis determined in this work.

The free energies of formation for **3** and **11** were calculated from those for **1** and **2**, and **10** respectively. The free energy of formation of **10** was calculated from that for **9** making the assumption that the free energy change for

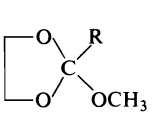

1 R = H
2 R = CH_3
3 R = CF_3

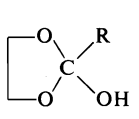

4 R = H
5 R = CH_3
6 R = CF_3

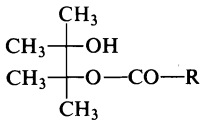

7 R = H
8 R = CF_3

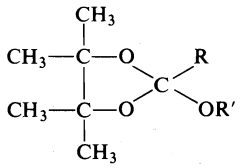

9 R = H; R′ = C_2H_5
10 R = H; R′ = CH_3
11 R = CF_3; R′ = CH_3
12 R = H; R′ = H
13 R = CF_3; R′ = H

TABLE 5. Differences in free energy of formation between 2-methoxy dioxolanes and the corresponding trimethyl orthoesters[a]

Trimethyl orthoester	ΔG_f^0	Dioxolane	ΔG_f^0	$\Delta\Delta G_f^{0b}$
$HC(OCH_3)_3$	−87.22(0.20)	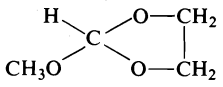	−84.99(1.49)	2.23(1.50)
$CH_3C(OCH_3)_3$	−89.05(0.20)	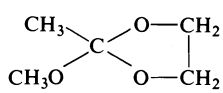	−87.97(1.49) (av.)	1.08(1.50) 1.65(1.06)
$CF_3C(OCH_3)_3$	−231.00(1.3)	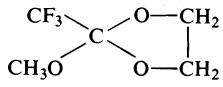	−229.35(1.68)[c]	1.65[d]
$HC(OCH_3)_3$	−87.22(0.20)	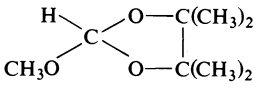	−89.56(2.44)	−2.34(2.45)
$CF_3C(OCH_3)_3$	−231.00(1.30)	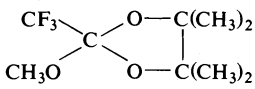	−233.34(2.75)[c]	−2.34[d]

[a]In aqueous solution at 25°C; kcal mol^{-1}.
[b]$\Delta\Delta G_f^0 = \Delta G_f^0$ dioxolane − ΔG_f^0 orthoester.
[c]Calculated using the appropriate value for $\Delta\Delta G$.
[d]Assumed.

reaction [4] was zero. Advantage was taken of the small, and within experimental error constant, magnitude of the difference in free energy of formation of **1** and trimethyl orthoformate, or **2** and trimethyl orthoacetate (see Table 5). The corresponding quantity for the trifluoroacetates was also assumed to be constant. This assumption is equivalent to the assumption of group additivity; the particular method employed has the advantage of using a small difference in free energies of formation. Similarly the free energy of formation of **11** was calculated making the assumption that the difference in free energies of formation of **11** and trimethyl orthotrifluoroacetate was the same as that for **10** and trimethyl orthoformate.

[4] 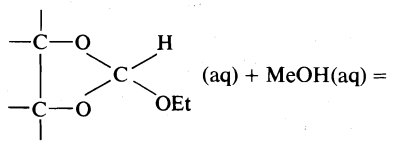 (aq) + MeOH(aq) =

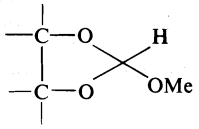 (aq) + EtOH(aq)

Finally, the free energies of formation of **4**, **5**, **6**, **12**, and **13** were calculated from those for **1**, **2**, **3**, **9**, and **11** by the methods previously described (10).

Thermodynamic data for all the compounds discussed in this paper are found in Table 2. Further details of the calculation procedure are to be found in the Experimental.

In principle, all of the group equivalents (and most of the steric interaction corrections) necessary to calculate $\Delta H_f^0(g)$, $S^0(g)$, and ΔG_t for the compounds considered in this paper are available, either from the tabulations in Benson (17, 18) and Hine (14), or from other work. In order to test the predictive power of these methods, and also as a check on the calorimetric determinations, values were calculated for many of the compounds in Table 2. In the case of hydroxy compounds, no correction to $\Delta H_f^0(g)$ was made for hydrogen bond formation (since the heat of hydrogen bond formation in the gas phase is unknown), and therefore the 'distant polar interactions' correction to ΔG_t was that for

RO—C—C—OR and not for HO—C—C—OH (14). The values so calculated are also found in Table 2. The agreement is quite satisfactory, and indicates that the group contributions approximation is quite satisfactory for these compounds, provided that adequate corrections can be made for steric interactions. In the case of the pinacol orthoesters and monoesters, the magnitudes of the steric corrections necessary were not obvious, and experimental measurements were obligatory.

Equilibrium constants for the cyclization reactions are found in Table 6, which compares the thermochemical and experimental values. Despite the fact that the thermochemical values were necessarily calculated in a rather roundabout way the agreement is satisfactory.

Discussion

Thermochemical Quantities

Several of the heat of formation values upon which this work is based are less reliable than would be desired: the values for methoxyethanol and pinacol are old (pre 1930 (15)), and could be in error by several kilocalories (although the pinacol value is consistent with values calculated by the group additivity scheme, the value for methoxyethanol is in disagreement by 14 kcal/mol, whether the calculated value is estimated directly or indirectly, starting with an estimated value for methoxyethyl formate, and using the experimental value for the heat of hydrolysis). Although this introduces a systematic error of unknown magnitude into the enthalpies and free energies of formation of each series of esters and orthoesters, it does not affect the relative values within each series, nor the absolute values of the free energy changes for the cyclization reactions.

Steric Interactions

Several of the compounds studied in this work are subject to significant crowding; for these compounds comparison of the observed free energies of formation with those calculated by the group additivity method permits an evaluation of the magnitude of this interaction (subject to possible systematic errors resulting from the uncertainty in the heat of formation of pinacol).[3]

For *tert*-butyl formate, the observed strain is 2.53 ± 2.13 kcal/mol; for *tert*-butyl trifluoroacetate the observed strain is 3.39 ± 2.72 kcal/mol. These values are indistinguishable within experimental error, and therefore it seems probable that both esters adopt the same conformation, **14**, with the carbonyl eclipsing the

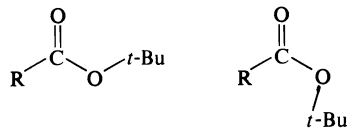

14 **15**

tert-butyl group rather than **15**, since the latter conformation would show a significant increase in crowding when R changes from H to CF_3.[4]

For pinacol the observed strain is 2.13 ± 2.85 kcal/mol; for pinacol monoformate the strain is higher, 6.95 ± 3.07 kcal/mol; the strain in **9** is only 2.07 ± 2.92 kcal/mol, which is within experimental error the same as for pinacol. Cyclization of pinacol monoformate to the orthoester apparently provides considerable relief of strain.

Free Energies of Cyclization

In Table 6 are summarized the thermochemically derived free energies of cyclization which were the object of this investigation, as well as the experimental values of Hine *et al.* (5) which permit a test of the thermochemical approach.

In calculating the probable errors for Table 6, it was necessary to perform a complete error analysis to determine the terms which actually contributed to the uncertainty in the change in free energy for cyclization. The uncertainties in free energy of formation in Table 2 are not independent quantities for related orthoesters and glycol monoesters. Consequently the uncertainties reported are in some cases significantly smaller than would be obtained directly from Table 2.

For the monoformates and monoacetates of ethylene glycol, the free energies of cyclization are quite unfavorable (and in fact are only about 3 kcal/mol more favorable than for the analogous intermolecular reaction of methanol with the methyl esters (7)), so that these reactions

[3]The effect of alkyl substituents upon the ease of ring formation (the *gem*-dialkyl effect) has been shown to result from both enthalpic and entropic contributions (44) for the case of six-membered rings. The 'strain energies' evaluated in this section will likewise contain both enthalpic and entropic contributions.

[4]Esters normally adopt the *s-trans* (*Z*) conformation **14** (45), but for *tert*-butyl esters it seemed quite possible that there might be a shift to the *E* conformation **15**, particularly in the case of the formate. This appears not to have happened.

TABLE 6. Free energies of cyclization for glycol monoesters

Reaction	ΔG^{0a} Calculated	ΔG^{0a} Experimental
$CH_2(OH)CH_2OCHO \rightleftharpoons$ 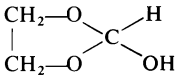	7.54(2.19)	
$CH_2(OH)CH_2OCOCH_3 \rightleftharpoons$ 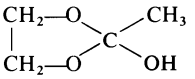	10.72(2.19)	
$(CH_3)_2C(OH)CH_2OCHO \rightleftharpoons$ 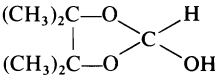	3.21(1.73)	
$CH_2(OH)CH_2OCOCF_3 \rightleftharpoons$ 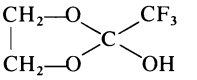	2.83(1.98)	+(various solvents)[c]
$CH_2(O^-)CH_2OCOCF_3 \rightleftharpoons$ 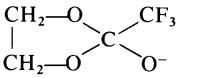	−4.82(2.80)[b]	−(ethylene glycol)[c]
$(CH_3)_2C(OH)CH_2OCOCF_3 \rightleftharpoons$ 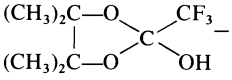	−3.38(2.75)	−0.24 (CCl_4)[c] −0.56 (benzene)[c] −1.75 (dioxane)[c] −1.75 (acetonitrile)[c]

[a]In kcal mol^{-1}.
[b]Calculated using pK_a values estimated (by methods described in ref. 8) as 14.4(1.0) for $HOCH_2CH_2OCOCF_3$ and 8.8(1.0) for **6**.
[c]Reference 5; although no equilibrium constant could be measured for cyclization of $HOCH_2CH_2OCOCF_3$ or its anion, it was demonstrated that some **6** was present in neutral solutions, and that extensive cyclization occurred in basic solutions.

are essentially unobservable by any direct method. Pinacol monoformate shows a much greater tendency to cyclize, although the equilibrium is still sufficiently unfavorable that the noncyclic form predominates overwhelmingly, and is the only species observable in the nmr spectrum. Comparison of Tables 6 and 7 shows that the greater tendency for pinacol monoformate to cyclize, relative to ethylene glycol monoformate, may be attributed to relief of steric compression involving the methyl groups of pinacol. It would be of interest to see if molecular mechanics calculations predict an effect of this magnitude, but unfortunately no calculation for the appropriate tetramethyl cyclopentane appears to have been done.

Ethylene glycol monotrifluoroacetate shows the expected (7) increase in cyclization tendency resulting from the electron withdrawing acyl substituent, but the equilibrium is still unfavorable for the neutral compound. The thermochemical prediction is in accord with experiment, since Hine *et al.* (5) report that none of the cyclic form could be detected, although enough of this rather acidic hydroxyl compound was present to be trapped by diazomethane. Using pK_a values estimated using ρ^*–σ^* correlations (7), the free energy of cyclization of the anion of ethylene glycol monotrifluoroacetate can be estimated as -4.82 ± 2.80 kcal/mol, which is consistent with the observation that addition of this ester to a solution of sodium 2-hydroxyethoxide in ethylene glycol leads to rapid formation of a less basic species, presumed to be the conjugate base of **6**, followed by a slower decomposition (5).

When both of the effects which favor cyclization (electron withdrawing acyl substituent and steric compression by methyl substituents) operate together, as in pinacol monotrifluoro-

TABLE 7. Strain energy for crowded compounds

Compound	ΔG_f^0(aq)[a] Ideal	ΔG_f^0(aq)[a] Experimental	$\Delta\Delta G_f^0$(aq)[a]
$(CH_3)_3C—OCHO$	−76.69(1.64)	−74.16(1.36)	2.53(2.13)
$(CH_3)_2C(OH)—C(OH)(CH_3)_2$	−84.56(1.64)	−82.43(2.34)	2.13(2.85)
$(CH_3)_2C(OCHO)—C(OH)(CH_3)_2$	−116.41(1.64)	−109.46(2.59)	6.95(3.07) [4.82][b]
	−93.06(1.64)[c]	−90.99(2.42)	2.07(2.92)
$(CH_3)_3C—OCOCF_3$	−216.48(1.64)	−213.09(2.18)	3.39(2.72)

[a]In kcal mol^{-1}; no corrections for *gauche* interactions.
[b]Difference in strain between pinacol monoformate and pinacol.
[c]Calculated including a correction for ring strain (ref. 16), but no corrections for steric interactions.

acetate, the cyclization of the neutral ester becomes favored. The calculated value of -3.38 ± 2.75 kcal/mol, aqueous solution, is in satisfactory agreement with the observed value of -1.75 kcal/mol in dioxane or acetonitrile.[5]

The results in Table 6 show that predictions based upon the thermochemical method developed in this laboratory for calculating the free energies of formation of tetrahedral intermediates are in satisfactory agreement with the available data for cyclization of glycol monoesters, and provide a means to calculate the equilibrium constant for cyclization in cases where direct measurement is impossible. The results in this paper constitute a further test of the method, which demonstrably had led to valid results in those cases where comparison with experiment has been possible, and therefore may be assumed to be a reliable guide when no other source of information is available, as is the case for almost all tetrahedral intermediates in acyl transfer reactions.

Furthermore, the results in Table 2 show that the free energies of formation of the orthoesters could be calculated quite successfully by the group additivity methods of Benson and coworkers (17, 18) and Hine and Mookerjee (14) in the absence of severe steric interactions. For many classes of organic compounds calculations by these methods deserve to be considered competitive with experiment as sources of thermodynamic information. Calculations of this sort coupled with extrathermodynamic relations of the sort used to obtain free energies of formation of tetrahedral intermediates from free energies of formation of orthoesters (7–10) are potentially a very powerful source of information otherwise unobtainable concerning the energetics of reaction intermediates. It is the thesis of this paper that these calculational methods deserve to be included in the standard armamentarium of the physical organic chemist engaged in studying the mechanisms of reactions in solution.

[5]Although an experimental value for the free energy of cyclization for pinacol monotrifluoroacetate in aqueous solution would be extremely desirable, it is likely to be extremely difficult to measure, if it is ever possible, because of the rapid and irreversible hydrolysis of trifluoroacetate esters (28). The solvent effect has been attributed (5) to the need for a hydrogen bond accepting solvent to stabilize the cyclic hemiorthoester, which cannot form an intramolecular hydrogen bond as can the acyclic tautomer. However, the well known insensitivity of hydrogen bond strength to acceptor basicity (46), which is borne out by the identity of equilibrium constants in dioxane and acetonitrile, despite the very different basicities of the solvents, suggests that the equilibrium constant in water will be very similar to that in acetonitrile.

Experimental

Materials

Ethylene glycol, methoxyethanol, triethyl orthoformate, trimethyl orthoformate, trifluoroacetic acid, and *tert*-butyl alcohol were reagent grade chemicals, redistilled before use if necessary. Pinacol was freed of water by azeotropic distillation with benzene and recrystallized from benzene – petroleum ether and then pentane; mp 41.5–44°C; lit. (19) mp 42.5–44.5°C.

Methoxyethyl formate was prepared by the method of van Es and Stevens (20) for alkyl formates; bp 126.5–128.5°C; lit. (21*a*) bp 131°C. Methoxyethyl acetate was

prepared from methoxyethanol and acetic anhydride; bp 64–66°C (12 Torr); lit. (21*b*) bp 144°C. **1** and **2** were prepared by exchange reactions from the trimethyl orthoester and ethylene glycol (21*c*); bp (**1**) 126–129°C; lit. (21*b*) 129.5°C; (**2**) 129°C; lit. (22) 132–134°C. **9** was prepared from triethyl orthoformate and pinacol by the method of Crank and Eastwood (23); bp 78–80°C (12 Torr); lit. (23) bp 72–75°C (17 Torr); 168–172°C. **7** was prepared from **9** by partial hydrolysis (23); **9** was dissolved in 0.001 *N* HCl, allowed to stand a few minutes, neutralized with bicarbonate, and extracted repeatedly with ether; bp 80–82.5°C (12 Torr); lit. (24) bp 84–85°C (18 Torr). *Tert*-Butyl formate was prepared by the method of Stevens and van Es (20, 25); bp 82°C, lit. (25) bp 83°C. *tert*-Butyl acetate was prepared by the method of Hauser *et al.* (26); bp 96°C; lit. (26) bp 97°C. *tert*-Butyl trifluoroacetate was prepared by the method of Bourne *et al.* (27); bp 84.5°C; lit. (27) bp 85–86°C. All compounds were checked for purity by nmr spectroscopy.

Methods

Heats of reaction and solution were measured using a simple Dewar calorimeter of the kind previously described (9). Solubilities were measured as previously described (7), by nmr analysis of equilibrated samples, integrating relative to suitable internal standards. In this way were measured the following solubilities in water at 25 ± 2°C: **1**, ca. 3 *M*; **2**, ca. 2 *M*; *tert*-butyl formate, 0.30 ± 0.3 *M*; *tert*-butyl acetate, 0.043 ± 0.004 *M*; **9**, 0.104 ± 0.001 *M*; methoxyethyl formate and acetate were miscible with water as was **7**. Since *tert*-butyl trifluoroacetate hydrolyzes rapidly (28), its solubility was estimated from that of *tert*-butyl acetate using the relationship between solubility and hydrophobicity (measured by Hansch π values (29)) (30) and the π values for CH_3 and CF_3 bound to carbonyl groups (31).

The stoichiometry of the hydrolysis of **1**, **2**, or **9** was determined by nmr analysis of a solution obtained from 100 μl of the orthoester in 1.0 ml of 0.001 *N* HCl. A lower concentration of HCl than in the calorimetric measurements was used to slow the hydrolysis of the esters which are the immediate products of hydrolysis from the orthoesters. Error analysis shows that the final results are insensitive to errors in the stoichiometry.

Equilibrium constants for ester formation were determined by dissolving weighed amounts of acid and alcohol, with 1 ml of 1 *N* HCl in a known total volume (made to 10 ml with water). After standing overnight at room temperature (24 ± 1°C), the solutions were analyzed by nmr. If the acid and ester peaks were not resolved, a portion of the equilibrium solution was titrated to p*H* 7 (p*H* meter) using saturated aqueous Na_3PO_4. Ionization of the carboxylic acid caused a chemical shift sufficient for easy resolution of the ester and 'acid' peaks.

For this work, the literature value of the heat of formation of solid pinacol was used. The heat of vaporization was estimated from the available boiling point data (bp 173°C at 762 Torr, bp 85°C at 21 Torr) by fitting to the Antoine equation

$$\log p = A - B/(t + C)$$

with $C = 230$. Empirically this equation has been found to correlate vapor pressure data for a wide range of compounds remarkably well (16). The heat of vaporization of the liquid was then calculated from the derivative of this equation; the value so obtained was 14.08 kcal/mol. The heat of melting was estimated by assuming that the entropy of melting is the same as that for *tert*-butyl alcohol, i.e. 5.32 eu (15). Then from the melting point (41°C), the heat of melting is 1.67 kcal/mol, and the heat of sublimation is 15.75 kcal/mol. For methoxyethanol, the heat of formation employed for calculations was that derived from the heat of hydrolysis of methoxyethyl formate, starting with the heat of formation of the ester estimated by the group additivity method.

Calculations

Vapor pressures were calculated from the normal boiling point using heats of vaporization estimated using the Wadsö equation (32), and an average value of -12 cal deg^{-1} mol^{-1} for the heat capacity of vaporization (33). When the only available boiling point was at reduced pressure, the normal boiling point was estimated by iterative solution of the equation obtained by substituting the Wadsö equation into the integrated equation for ln *p* as a function of *T*.[6]

Free energies of transfer were calculated from vapor pressure and solubility data as previously described (8).

Entropy Values

Wherever possible, entropy values were taken from standard compilations (15, 34); where no literature values were available, the entropies were estimated by accepted procedures, using, in order of preference, the methods of substitution (15), starting with the analogous hydrocarbon (for **1**), the method of group contributions (18) (for methoxyethanol, **2**, *tert*-butyl formate, methoxyethyl acetate, pinacol, pinacol monoformate, and **9**), and the method of atomic contributions (17) (for *tert*-butyl trifluoroacetate).

Acknowledgments

I thank the National Research Council of Canada and the Alfred P. Sloan Foundation for financial support of this research, and Dana Zendrowski and Patricia A. Cullimore for technical assistance.

1. (*a*) S. L. Johnson. Adv. Phys. Org. Chem. **5**, 237 (1967); (*b*) W. P. Jencks. Catalysis in chemistry and enzymology. McGraw-Hill, New York, NY. 1968. pp. 463–554; (*c*) T. C. Bruice and S. J. Benkovic. Bioorganic mechanisms. Vol. 1. W. A. Benjamin, New York, NY. 1966. pp. 1–211.
2. (*a*) J. Hine. Physical organic chemistry. 2nd ed. McGraw-Hill, New York, NY. 1962. Chapt. 12; (*b*) A. Williams and K. T. Douglas. Chem. Rev. **75**, 627 (1975).
3. R. H. de Wolfe. Carboxylic ortho acid derivatives. Academic Press, New York, NY. 1970.
4. R. B. Woodward. Pure Appl. Chem. **9**, 49 (1964).
5. J. Hine, D. Ricard, and R. Perz. J. Org. Chem. **38**, 110 (1973).
6. M. L. Bender. J. Am. Chem. Soc. **75**, 5986 (1953).
7. J. P. Guthrie. Can. J. Chem. **54**, 202 (1976).
8. J. P. Guthrie. J. Am. Chem. Soc. **95**, 6999 (1973).
9. J. P. Guthrie. J. Am. Chem. Soc. **96**, 3608 (1974).
10. J. P. Guthrie. Can. J. Chem. **53**, 898 (1975).

[6]J. P. Guthrie. Unpublished results.

11. J. L. KURZ and D. N. WEXLER. J. Am. Chem. Soc. **97**, 2255 (1975).
12. A. HALASZ and S. ROVIRA. Bull. Soc. Chim. Fr. **8**, 185 (1941).
13. S. D. ROSS and M. FINKELSTEIN. J. Org. Chem. **22**, 847 (1957).
14. J. HINE and P. K. MOOKERJEE. J. Org. Chem. **40**, 292 (1975).
15. D. R. STULL, E. F. WESTRUM, JR., and G. C. SINKE. The chemical thermodynamics of organic compounds. Wiley, New York, NY. 1969.
16. R. R. DREISBACH. Pressure–volume–temperature relationships of organic compounds. 3rd ed. Handbook Publishers, Inc., Sandusky, OH. 1952.
17. (*a*) H. K. EIGENMANN, D. M. GOLDEN, and S. W. BENSON. J. Phys. Chem. **77**, 1687 (1973); (*b*) S. W. BENSON and J. H. BUSS. J. Chem. Phys. **29**, 546 (1958).
18. S. W. BENSON. Thermochemical kinetics. Wiley, New York, NY. 1968.
19. (*a*) L. FIELD and J. E. LAWSON. J. Am. Chem. Soc. **80**, 838 (1958); (*b*) H. S. KING and W. W. STEWART. Proc. Trans. Nova Scotian Inst. Sci. **17**, 262 (1930); Chem. Abs. **25**, 1799 (1931).
20. A. VAN ES and W. STEVENS. Recl. Trav. Chim. **84**, 704 (1965).
21. (*a*) Beilstein, Handbuch der organischen Chemie. Springer-Verlag, Berlin. Vol. 2(2). p. 19; (*b*) Vol. 2(4). p. 214; (*c*) H. BAGANZ and L. DOMARSCHKE. Ber. **91**, 650 (1958).
22. S. M. MCELVAIN and M. J. CURRY. J. Am. Chem. Soc. **70**, 3781 (1948).
23. G. CRANK and F. W. EASTWOOD. Aust. J. Chem. **17**, 1392 (1964).
24. W. J. HICKINBOTTOM, D. R. HOGG, D. PETER, and D. G. M. WOOD. J. Chem. Soc. 4400 (1954).
25. W. STEVENS and A. VAN ES. Recl. Trav. Chim. **83**, 1287 (1964).
26. C. R. HAUSER, B. E. HUDSON, B. ABRAMOVICH, and J. C. SHRIVERS. Org. Synth. Coll. Vol. III, 142 (1955).
27. E. J. BOURNE, M. STACEY, J. C. TATLOW, and R. WORRALL. J. Chem. Soc. 3268 (1958).
28. J. G. WINTER and J. M. W. SCOTT. Can. J. Chem. **46**, 2887 (1968).
29. T. FUJITA, J. IWASA, and C. HANSCH. J. Am. Chem. Soc. **86**, 5175 (1964); M. S. TUTE. Adv. Drug Res. **6**, 1 (1971).
30. C. HANSCH, J. E. QUINLAN, and G. L. LAWRENCE. J. Org. Chem. **33**, 347 (1968).
31. C. HANSCH and N. CORNELL. Arch. Biochem. Biophys. **151**, 351 (1972).
32. I. WADSÖ. Acta Chem. Scand. **20**, 544 (1966).
33. S. W. BENSON and G. D. MENDENHALL. J. Am. Chem. Soc. **98**, 2046 (1976).
34. (*a*) F. D. ROSSINI, D. D. WAGMAN, W. H. EVANS, S. LEVINE, and I. JAFFE. U.S. Natl. Bur. Stand. Circ. No. 500 (1952); (*b*) J. D. COX and G. PILCHER. Thermochemistry of organic and organometallic compounds. Academic Press, New York, NY. 1970.
35. J. KONICEK and I. WADSÖ. Acta Chem. Scand. **25**, 1541 (1971).
36. E. M. ARNETT and D. R. MCKELVEY. *In* Solute–solvent interactions. *Edited by* J. F. Coetzee and C. D. Ritchie. Marcel Dekker, New York, NY. 1969.
37. H. K. HALL, JR. and J. H. BALDT. J. Am. Chem. Soc. **93**, 140 (1971).
38. S. W. BENSON, F. R. CRUICKSHANK, D. M. GOLDEN, G. R. HAUGEN, H. E. O'NEAL, A. S. RODGERS, R. SHAW, and R. WALSH. Chem. Rev. **69**, 279 (1969).
39. S. W. BENSON and H. E. O'NEAL. Kinetic data on gas phase unimolecular reactions. National Standard Reference Data Series, National Bureau of Standards (U.S.), 21, 1970.
40. J. HINE and A. W. KLUEPPEL. J. Am. Chem. Soc. **96**, 2924 (1974).
41. K. KUSANO and I. WADSÖ. Acta Chem. Scand. **25**, 219 (1971).
42. K. KUSANO, J. SUURKUUSK, and I. WADSÖ. J. Chem. Thermodyn. **5**, 757 (1973).
43. K. KUSANO and I. WADSÖ. Acta Chem. Scand. **24**, 2037 (1970).
44. N. L. ALLINGER and V. ZALKOW. J. Org. Chem. **25**, 701 (1960).
45. T. C. BRUICE and S. J. BENKOVIC. Bioorganic mechanisms. Vol. 1. W. A. Benjamin, New York, NY. 1968. p. 21.
46. E. M. ARNETT, E. J. MITCHELL, and T. S. S. R. MURTY. J. Am. Chem. Soc. **96**, 3875 (1974).

Metal-ion oxidations in solution. Part XX.[1] The mechanism of the reaction of thallium(III) with 2-mercaptosuccinic acid in perchlorate media

ZAHID AMJAD, JOHN G. CHAMBERS, AND ALEXANDER MCAULEY[2]

Department of Chemistry, The University of Victoria, Victoria, B.C., Canada V8W 2Y2

and

Department of Chemistry, The University of Glasgow, Glasgow G12 8QQ, Scotland

Received March 7, 1977

ZAHID AMJAD, JOHN G. CHAMBERS, and ALEXANDER MCAULEY. Can. J. Chem. **55**, 3575 (1977).

The oxidation of 2-mercaptosuccinic (thiomalic) acid (HRSH) by thallium(III) proceeds via an inner sphere mechanism. Spectrophotometric and kinetic evidence are provided for the formation of a sulphur-bonded thallium(III) intermediate. The data are consistent with the reaction scheme

$$TlOH^{2+} + HRSH \underset{}{\overset{K_2}{\rightleftharpoons}} [TlSRH]^{2+} \xrightarrow{k_2} Tl(II) + HRS^{\cdot}$$

in which the complex decomposes via a one-electron intramolecular transfer $k_2 = 3.8 \times 10^{-4}$ s^{-1} at 25°C, with $K_2 = 1650\ M^{-1}$. The enthalpy of activation $\Delta H_2^{\ddagger}$ for the redox reaction (11.8 ± 1.2 kcal/mol) is considerably smaller than for other systems of this type and reflects the greater ease of reaction. Comparison is made of possible one- and two-electron transfer pathways.

ZAHID AMJAD, JOHN G. CHAMBERS et ALEXANDER MCAULEY. Can. J. Chem. **55**, 3575 (1977).

L'oxydation de l'acide mercapto-2 succinique (thiomalique) (HRSH) par le thallium(III) procède selon un mécanisme "sphère interne". Les résultats des mesures spectrophotométriques et cinétiques sont en faveur de la formation d'un complexe intermédiaire présentant une liaison soufre–thallium(III). Ces résultats sont en accord avec le schéma réactionnel suivant:

$$TlOH^{2+} + HRSH \underset{}{\overset{K_2}{\rightleftharpoons}} [TlSRH]^{2+} \xrightarrow{k_2} Tl(II) + HRS^{\cdot}$$

dans lequel le complexe intermédiaire se décompose par transfert intramoléculaire d'un électron ($k_2 = 3.8 \times 10^4\ s^{-1}$ et $K_2 = 1650\ M^{-1}$ à 25°C). L'enthalpie d'activation $\Delta H_2^{\ddagger}$ pour la réaction d'oxydation–réduction (11.8 ± 1.2 kcal mol^{-1}) est considérablement plus petite que pour d'autres systèmes du même genre et reflète une plus grande réactivité. On fait une comparaison entre la possibilité d'un processus par transfert d'un ou de deux électrons.

[Traduit par le journal]

Thallium(III) has recently been used as a mild oxidant in the reactions of a variety of organic compounds (2, 3). Most of these oxidations have been carried out in acetate media owing to solubility problems associated with more polar media. In some instances, nitrate, sulphate, and chloride salts have been investigated in aqueous solutions but difficulties in interpretation arise from the presence of several reactant Tl(III) complexes (4). The situation is somewhat clearer in perchloric acid media where there is less tendency for complexation between Tl^{3+} and ClO_4^- to occur.

Recently, the stopped-flow technique has been used to investigate the oxidation of catechol and other 1,2- and 1,4-dihydroxybenzenes (5–7). In these reactions there is no spectroscopic or kinetic evidence for any precursor complex formation prior to the electron transfer step except in the case of the adrenaline oxidation (7) where kinetic parameters are suggestive of the existence of an intermediate. Spectrophotometric evidence for complex formation in Tl(III) oxidations of this type was first provided by Halvarson and Halpern (8) in the reaction with formic acid. Kinetic analysis of the reaction with phosphorous acid (9) is also consistent with an initial preequilibrium.

The oxidation of sulphur-containing substrates by various metal ions has been the subject of

[1]For Part XIX, see ref. 1.

[2]Present address: Department of Chemistry, University of Victoria, Victoria, B.C., Canada V8W 2Y2.

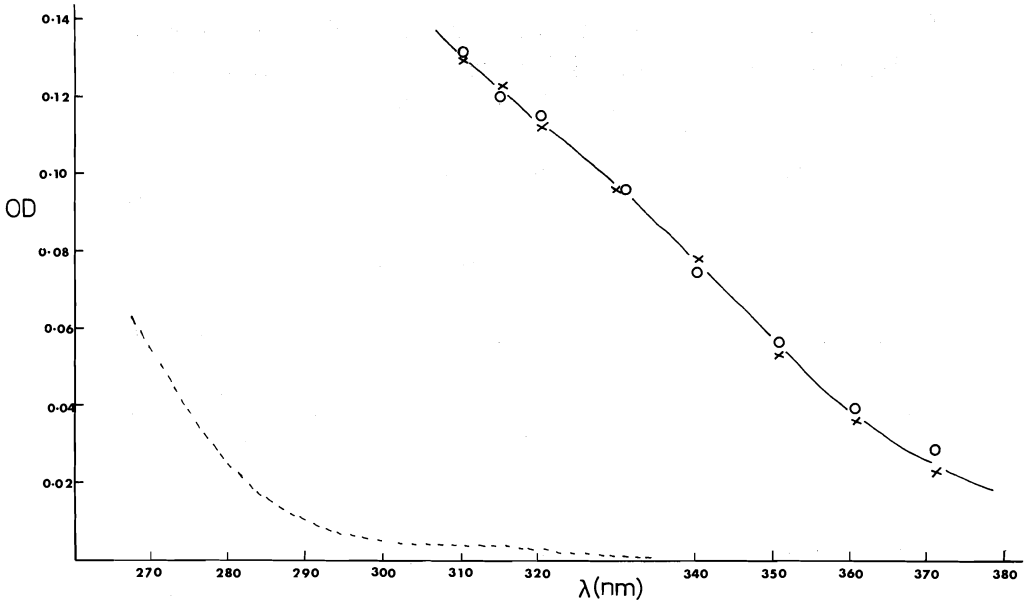

FIG. 1. Spectrum of Tl(III)–thiomalic acid intermediate. $T = 25°C$; $[H^+] = 1.00\ M$; $I = 2.00\ M$. (○) $[Tl(III)] = 3 \times 10^{-4}\ M$, [thiomalic acid] $= 3 \times 10^{-4}\ M$; (×) $[Tl(III)] = 3 \times 10^{-4}\ M$, [thiomalic acid] $= 3 \times 10^{-3}\ M$; (-) $[Tl(III)] = 3 \times 10^{-4}\ M$.

numerous investigations and in many instances (e.g. with Fe(III) (10), V(V) (11), Cr(VI) (12)) intermediates have been characterized from initial absorbance changes. There are, however, no data available on the reactions of thallium(III) with thiols and it is of interest to examine whether Tl(III)–sulphur bonded complexes have any significant thermodynamic stability in aqueous media. In the present study, the reaction with thiomalic acid (2-mercaptosuccinic acid) has been investigated at various ligand and hydrogen ion concentrations using stopped-flow and conventional methods.

Experimental

Thallium(III) perchlorate was prepared by dissolution of Tl_2O_3 (Koch-Light 99.99% pure) in 5–7 M $HClO_4$ at 60–70°C over a period of 6–8 h. An alternative approach was also used where after reaction of Tl_2CO_3 with excess $HClO_4$, the washed acidified slurry of thallium(I) perchlorate was electro-oxidized at room temperature until all the metal ion was dissolved. The thallium(III) concentration was determined by dilution of a known volume of the stock to yield a solution less than 0.5 M in $HClO_4$. Addition of 2% KI was followed by titration against sodium thiosulphate. The end point was marked by the change from dirty blue to the clear yellow of the precipitate of thallium(I) iodide. The thallium(I) content of the stock was determined following addition of HCl by titration with potassium iodate with chloroform as indicator. The analytical hydrogen ion concentration was determined by dilution, reaction with H_2O_2 to reduce the metal ion and after cooling, titration with standard base, due account being taken of the protons liberated in the peroxide reduction. Freshly prepared $Tl(ClO_4)_3$ solution (ca. 0.225 M Tl^{3+} in 6.39 M $HClO_4$) was found to contain less than 0.1% Tl(I) and storage at ~5°C in a dark bottle showed a content of <0.3% after 3 months.

Thiomalic acid (Evans Chemetics or Koch-Light (pure)) was used. In some instances material re-crystallized from ethanol was also reacted. The preparation and standardization of sodium perchlorate, lithium perchlorate, and perchloric acid have been described previously (10).

The product disulphide was identified spectroscopically. Whereas the thiol shows only a broad band in the range 200–230 nm, the disulphide exhibits a peak at 215 nm. On reacting solutions of Tl(III) and thiol in 0.5 M $HClO_4$ the spectrum produced was identical to that obtained on treatment of a solution of the thiol with hydrogen peroxide which is known to yield the disulphide.

Kinetic Measurements

The reactions were investigated in an excess of thiomalic acid in order to maintain the disulphide as product and to minimize any overoxidation which has been observed previously in reactions of this type (13). A modified two-jet mixer stopped-flow system incorporated into a Unicam SP800 spectrophotometer was used for most kinetic runs although at low temperatures either a SP800 or Cary 17 spectrometer with thermostatted cell holder was used to monitor the absorbance changes directly. In a typical experiment, reactant solutions were prepared immediately prior to use. Comparison of optical densities at $\lambda = 280$ nm of 'blank' solutions in which Tl(III) was diluted with acid perchlorate solution with those where thiomalic acid was present indicated the formation of a complex within the time of mixing. Data derived under

TABLE 1. Observed rate constants at various mercaptosuccinic acid (HRSH) acid hydrogen ion concentrations, [Tl(III)] = 3.0×10^{-4} *M*, $I = 2.00$ *M*, $\lambda = 308$ nm. Slopes (*S*) and intercepts (*I*) were derived from plots according to eq. 11[a]

T/°C	[H⁺]/*M*	10^2[HRSH]/*M*	$10^4 k_{obs}/s^{-1}$	*S*/(*M* s)	$10^{-3}I$/s
7.8	0.25	0.6	0.617		
		1.2	0.751	33.5 ±0.03	10.65±0.005
		2.4	0.833		
20.7	0.25	0.625	2.02		
		1.25	2.31	8.22±0.22	3.64±0.02
		1.876	2.45		
		2.50	2.53		
	0.50	1.25	1.99		
		1.876	2.22	16.1 ±1.1	3.65±0.06
		2.50	2.31		
		3.75	2.43		
	0.75	1.25	1.79		
		1.876	2.05	24.4 ±1.5	3.62±0.08
		2.50	2.14		
		3.75	2.35		
	1.00	1.25	1.67		
		1.876	1.89	29.4 ±1.2	3.67±0.06
		2.50	2.06		
		3.75	2.26		
25.0	0.25	1.25	3.03[b]		
		2.50	3.35	6.83±0.9	2.74±0.05
		3.75	3.40		
	0.50	0.75	2.41[c]		
		1.25	2.74	11.3 ±0.7	2.67±0.06
		2.50	3.19		
		3.75	3.40		
	1.00	0.75	1.78[d]		
		1.25	2.32[e], 2.36	22.7 ±1.2	2.53±0.10
		2.50	2.92		
		3.75	3.12		
30.0	0.50	0.625	3.72[e], 3.74		
		1.25	4.74	6.34±0.5	1.64±0.05
		1.875	5.15		
		3.125	5.29		
	0.75	0.625	3.19[e], 3.16		
		1.25	3.98	8.52±0.3	1.80±0.04
		2.50	4.69		
	1.00	1.25	3.73		
		1.875	4.15	10.8 ±0.46	1.82±0.03
		3.125	4.63		

[a]Unweighted least-squares treatment.
[b]$\lambda = 330$ nm.
[c]$\lambda = 290$ nm.
[d]$\lambda = 350$ nm.
[e]Using degassed solutions.

differing sets of conditions are presented as the spectrum of the intermediate in Fig. 1. In previous reactions where complexes have been identified it has been possible, in some instances where the equilibrium constant is low, to evaluate *K* from the initial absorbance changes (10). Attempts to derive this information by this method were unsuccessful probably owing to a fairly high formation constant with consequent virtual total complexing of the metal present (*vide infra*). The subsequent redox reactions were monitored at $\lambda = 290$–350 nm. The [H⁺] range studied was 0.25–1.00 *M* at a total ionic strength of 2.00 *M*. All experiments were conducted in the presence of air which was shown to have no detectable effect on the observed rate constants Reactions carried out under nitrogen with solutions previously de-gassed yielded the observed rate constants to within experimental error (Table 1). Although air sensitivity has been found for the Np(VI) oxidation of thiols, this has not been shown to be the case for the corresponding cerium(IV) oxidations (14).

Results and Discussion

The stoichiometry of the reaction was determined by spectrophotometric titration of the unreacted thiomalic acid present in the mixture (14). Typical reaction conditions were [Tl(III)] = 5–12 $\times 10^{-5}$ *M*, [thiol] = 5.2×10^{-4} *M*,

$[H^+] = 1.2\ M$ and three evaluations yielded a ratio of 2.1 ± 0.3 mol of thiomalic acid (HRSH) reacting per mole of metal ion, consistent with the reaction

[1] $Tl(III) + 2HRSH \rightarrow Tl(I) + HRSSRH + 2H^+$

The overall kinetics may be adequately represented by the following reaction scheme

[2] $$Tl^{3+} + H_2O \underset{}{\overset{K_h}{\rightleftharpoons}} TlOH^{2+} + H^+$$

[3] $$Tl^{3+} + HRSH \overset{K_1}{\rightleftharpoons} [TlHRSH]^{3+}$$

[4] $$TlOH^{2+} + HRSH \overset{K_2}{\rightleftharpoons} [TlSRH]^{2+} + H_2O$$

[5] $$[TlHRSH]^{3+} \overset{K_3}{\rightleftharpoons} [TlSRH]^{2+} + H^+$$

[6] $$[TlHRSH]^{3+} \xrightarrow{k_1} Tl(II) + HRS^{\cdot} + H^+$$

[7] $$[TlSRH]^{2+} \xrightarrow{k_2} Tl(II) + HRS^{\cdot}$$

[8] $$[Tl(II)] + HRSH \xrightarrow{k_3} Tl(I) + HRS^{\cdot} + H^+$$

[9] $$2HRS^{\cdot} \xrightarrow{k_4} HRSSRH$$

Further hydrolysed species of Tl(III) and the proton-dissociated carboxylate anion form of the ligand are also possible reactants but at the hydrogen ion concentrations used, the amounts of such species present in solution would be very low.

Providing the protolytic reactions are fast, and the electron transfer sufficiently slow such that $k_3, k_4 \gg k_1, k_2$ then in an excess of substrate the decrease of Tl(III) may be described as

[10] $$\frac{-d[Tl(III)]_{tot}}{dt} = k_1[TlHRSH]^{3+} + k_2[TlSRH]^{2+}$$

and using the above scheme, the observed rate constant, k_{obs}, may be expressed in the form

[11] $$k_{obs}^{-1} = \frac{([H^+] + K_h)}{(k_1K_1[H^+] + k_2K_2K_h)[HRSH]} + \frac{K_1[H^+] + K_2K_h}{(k_1K_1[H^+] + k_2K_2K_h)}$$

Kinetic runs showed good linearity of first order plots to 80–90% reaction. Measured values at various $[H^+]$ and [HRSH] are presented in Table 1.

The inverse hydrogen ion dependence may be correlated with the hydrolytic equilibrium of Tl_{aq}^{3+} and using a hydrolysis constant $K_h = 0.073\ M$ (15), the aquated metal ion Tl_{aq}^{3+} is present, under the experimental conditions used, to the extent of 78–94%. An alternative origin of the effect may derive from equilibrium 5 where $K_1K_3 = K_2K_h$. It is impossible to distinguish kinetically between reaction combinations [2] and [4], and [3] and [5] as to the route for formation of $[TlSRH]^{2+}$. An equilibrium similar to [5] has been favoured, however, in the oxidation of H_2O_2 (16) and hypophosphorous acid (9).

According to [11] at constant $[H^+]$, plots of k_{obs}^{-1} against $[HRSH]^{-1}$ should be linear and this is observed. Using the slope (S) and intercept (I) values derived (Table 1) the following equations may be evaluated

[12] $$\frac{([H^+] + K_h)}{S} = k_1K_1[H^+] + k_2K_2K_h$$

and

[13] $$\frac{([H^+] + K_h)}{S} I = K_1[H^+] + K_2K_h$$

In order to calculate the rate and equilibrium parameters, accurate values for K_h are required. There appears to be little dependence of this equilibrium constant on ionic strength (15, 17, 18) and the data used in this study are extrapolated from those at various temperatures (17) at 1.00 M. Evaluation of the left-hand side of eq. 13 showed the values to be independent of $[H^+]$ (Table 2). It would thus appear that only one complex, namely $[TlSRH]^{2+}$, predominates in

TABLE 2. Determination of equilibrium constants using eq. 13

T/°C	$[H^+]/M$	$([H^+] + K_h)I/S$
7.8	0.25	84.7 ± 1.4
20.7	0.25	133 ± 3
	0.50	125 ± 6
	0.75	119 ± 5
	1.00	131 ± 6
25.0	0.25	127 ± 4
	0.50	136 ± 5
	1.00	125 ± 6
30.0	0.50	178 ± 20
	0.75	186 ± 5
	1.00	189 ± 8

TABLE 3. Equilibrium and rate constants and thermodynamic parameters

T/°C	K_2K_h	$10^{-3}K_2/M^{-1}$	$10^4k_2/s^{-1}$
7.8	84.7±1.4	5.13	0.939±0.04
20.7	127 ±6	2.34±0.09	2.76 ±0.05
25.0	129 ±8	1.65±0.15	3.78 ±0.16
30.0	184 ±9	1.50±0.09	5.61 ±0.23
	$\Delta H_2 = -4.4\pm1.0$ kcal/mol $\Delta S_2 = 0\pm3$ cal deg^{-1} mol^{-1}	$\Delta H_2^{\neq} = 5.98\pm1.2$ kcal/mol $\Delta S_2^{\neq} = -7\pm6$ cal deg^{-1} mol^{-1}	

the rate determining redox step. The spectrum shown in Fig. 1 probably closely approximates that of a Tl(III)—S bonded complex. The value at 25°C of the equilibrium constant for the reaction

$$Tl^{3+} + HRSH \rightleftharpoons [TlSRH]^{2+} + H^+$$

may be computed to be 129 ± 8.

Modification of eq. 11 to exclude terms involving k_1 and K_1, which are negligible under the experimental conditions, thus allows for the evaluation of the redox rate constant k_2. Values at various temperatures together with associated thermodynamic data are presented in Table 3. The associated activation enthalpy is 11.8 ± 1.2 kcal/mol. This value is substantially lower than that for reaction of the oxygen bonded complexes: 26.0 (formic acid) (8), and 27.8 kcal/mol (oxalic acid) (19) respectively. This may be the result of a greater degree of electron delocalization in the Tl—S bond compared with that in Tl—O.

Unfortunately there are few data available with which to make comparisons. Also, the reaction is too slow to allow for detection of radical intermediates of this substrate. With the one-electron oxidants Fe(III) (20) and Cu(II) (21) a rate determining dimerisation provides a low-energy pathway for electron transfer via a four-centre M_2S_2 system which yields disulphide without radical formation. In cases where two-electron transfer reactions have been encountered (e.g. Cr(VI) + cysteine (12) or thioureas (22)) 2 mol of thiol are generally incorporated in the transition state. Since there is no evidence for any second-order kinetic term in reductant (and little change in the uv spectrum in the presence of a 10-fold excess of mercaptosuccinic acid confirms the absence of significant build-up of 1:2 complexes, see Fig. 1) it may be assumed that the rate determining reaction is a one-electron transfer to Tl(II) and the organic radical. Tl(II) has been shown recently to be a powerful oxidant (23) and a rapid second reaction to produce Tl(I) with formation of another RS$^{\bullet}$ species would be consistent with the observed stoichiometry. It is considered unlikely that thallium(III) is a sufficiently strong oxidant to undergo a two-electron reaction to give RS^+ which could react with a second mole of thiol to yield the disulphide. More data are required on reactions of this type especially to enable comparisons to be made of Tl(III)—O and Tl(III)—S bond types. Attempts are currently underway to measure the reaction rates of the initial complex formation in order to provide much needed detail on the reactivity of Tl(III) aquo-ions.

Acknowledgements

One of us (Z.A.) wishes to thank the University of Glasgow for the award of a Demonstratorship. Support from the Science Research Council (U.K.) and the National Research Council of Canada is acknowledged.

1. A. McAuley and M. A. Olatunji. Can. J. Chem. **55**, 3335 (1977).
2. A. McKillop, B. P. Swann, M. E. Ford, and E. C. Taylor. J. Am. Chem. Soc. **95**, 3641 (1973).
3. J. E. Byrd and J. Halpern. J. Am. Chem. Soc. **95**, 2586 (1973).
4. K. S. Gupta and Y. K. Gupta. Inorg. Chem. **14**, 2000 (1975).
5. E. Mentasti, E. Pelizzetti, E. Pramauro, and G. Givaudi. J. Inorg. Nucl. Chem. **37**, 537 (1975); E. Mentasti, E. Pelizzetti, and E. Pramauro. J. Inorg. Nucl. Chem. **37**, 1733 (1975).
6. E. Pelizzetti, E. Mentasti, M. E. Carlotti, and G. Girandi. J. Chem. Soc. Dalton Trans. 794 (1975).
7. E. Pelizzetti, E. Mentasti, E. Pramauro, and M. E. Carlotti. Gazz. Chim. Ital. **105**, 307 (1975).
8. H. N. Halvorson and J. Halpern. J. Am. Chem. Soc. **78**, 5562 (1956).
9. K. S. Gupta and Y. K. Gupta. J. Chem. Soc. A, 256 (1970).
10. A. G. Lappin and A. McAuley. J. Chem. Soc. Dalton Trans. 1564 (1975).

11. W. F. PICKERING and A. MCAULEY. J. Chem. Soc. A, 1173 (1968).
12. J. P. MCCANN and A. MCAULEY. J. Chem. Soc. Dalton Trans. 783 (1975).
13. C. J. WESCHLER, J. C. SULLIVAN, and E. DEUTSCH. Inorg. Chem. **13**, 2360 (1974).
14. D. K. LAVALLEE, J. C. SULLIVAN, and E. DEUTSCH. Inorg. Chem. **12**, 1440 (1973).
15. G. BIEDERMAN. Ark. Kemi, **6**, 527 (1964).
16. P. D. SHARMA and Y. K. GUPTA. J. Chem. Soc. Dalton Trans. 81 (1975).
17. B. M. THAKURIA and Y. K. GUPTA. J. Chem. Soc. Dalton Trans. 77 (1975).
18. T. E. ROGERS and G. M. WAIND. Trans. Faraday Soc. **57**, 1360 (1961).
19. L. B. MONSTEAD, O. MONSTEAD, and G. NORD. Trans. Faraday Soc. **66**, 936 (1970).
20. K. J. ELLIS, A. G. LAPPIN, and A. MCAULEY. J. Chem. Soc. Dalton Trans. 1930 (1974).
21. A. G. LAPPIN and A. MCAULEY. Unpublished data.
22. M. A. OLATUNJI and A. MCAULEY. J. Chem. Soc. Dalton Trans. 683 (1975).
23. B. FALCINELLA, P. D. FELGATE, and G. S. LAWRENCE. J. Chem. Soc. Dalton Trans. 1367 (1974).

Metal-ion oxidations in solution. Part XXI.[1] Kinetics and mechanism of the reaction of ascorbic acid, hydroquinone, and catechol with 12-tungstocobaltoate(III)

ZAHID AMJAD, JEAN-CLAUDE BRODOVITCH, AND ALEXANDER MCAULEY[2]
Department of Chemistry, The University of Victoria, Victoria, B.C., Canada V8W 2Y2
and
Department of Chemistry, The University of Glasgow, Glasgow G12 8QQ, Scotland
Received March 7, 1977

ZAHID AMJAD, JEAN-CLAUDE BRODOVITCH, and ALEXANDER MCAULEY. Can. J. Chem. **55**, 3581 (1977).

The mechanisms of oxidation of the three di-hydroxy substrates in the title reactions have been investigated in acid media [$HClO_4$] = 0.04–1.00 *M*, at an ionic strength of 1.0 *M* [$LiClO_4$] over the temperature range 5–35°C using the stopped-flow method. In contrast to the reactions of hydroquinone (k_2(25°C) = 1.43×10^4 M^{-1} s^{-1}, $\Delta H^{\ddagger} = 3.6 \pm 0.4$ kcal mol^{-1}, $\Delta S^{\ddagger} = -34 \pm 8$ cal deg^{-1} mol^{-1}) and catechol (k_2(25°C) = 9.5×10^2 M^{-1} s^{-1}, $\Delta H^{\ddagger} = 5.9 \pm 0.9$ kcal mol^{-1}, $\Delta S^{\ddagger} = 27 \pm 8$ cal deg^{-1} mol^{-1}) where no hydrogen ion dependence is observed over the range studied, the rate variations of oxidation of ascorbic acid (H_2A) are consistent with two reactions involving H_2A ($k_5 = 77.4$ M^{-1} s^{-1}, $\Delta H^{\ddagger} = 4.5 \pm 0.6$ kcal mol^{-1}, $\Delta S^{\ddagger} = -35 \pm 5$ cal deg^{-1} mol^{-1}) and HA^- ($k_6 = 2.41 \times 10^5$ M^{-1} s^{-1}, $\Delta H^{\ddagger} = 2.0 \pm 1$ kcal mol^{-1}, $\Delta S^{\ddagger} = -17 \pm 6$ cal deg^{-1} mol^{-1}). The dissociation constant of ascorbic acid has been redetermined over the temperature range studied. Solvation effects are considered important in these outer-sphere systems, which may be discussed in terms of the Marcus relationship. Comparisons with related reactions are discussed.

ZAHID AMJAD, JEAN-CLAUDE BRODOVITCH et ALEXANDER MCAULEY. Can. J. Chem. **55**, 3581 (1977).

On étudie par la méthode du flux stoppé les mécanismes d'oxydation des trois substrats dihydroxylés figurant dans le titre, en milieu acide [$HClO_4$] = 0.04–1.00 *M*, pour une force ionique de 1.0 *M* [$LiClO_4$] et dans un écart de température de 5–35°C. En comparaison avec les réactions de l'hydroquinone (k_2(25°C) = 1.43×10^4 M^{-1} s^{-1}, $\Delta H^{\ddagger} = 3.6 \pm 0.4$ kcal mol^{-1}, $\Delta S^{\ddagger} = -34 \pm 8$ cal deg^{-1} mol^{-1}) et du catéchol (k_2(25°C) = 9.5×10^2 M^{-1} s^{-1}, $\Delta H^{\ddagger} = 5.9 \pm 0.9$ kcal mol^{-1}, $\Delta S^{\ddagger} = 27 \pm 8$ cal deg^{-1} mol^{-1}) ou il n'y a pas de dépendance avec l'acidité du milieu dans l'écart étudié, les variations de la vitesse d'oxydation de l'acide ascorbique (H_2A) sont en accord avec les deux réactions impliquant les espèces H_2A ($k_5 = 77.4$ M^{-1} s^{-1}, $\Delta H^{\ddagger} = 4.5 \pm 0.6$ kcal mol^{-1}, $\Delta S^{\ddagger} = -35 \pm 5$ cal deg^{-1} mol^{-1}) et HA^- ($k_6 = 2.41 \times 10^5$ M^{-1} s^{-1}, $\Delta H^{\ddagger} = 2.0 \pm 1$ kcal mol^{-1}, $\Delta S^{\ddagger} = -17 \pm 6$ cal deg^{-1} mol^{-1}). La constante de dissociation de l'acide ascorbique est recalculée pour les conditions expérimentales indiquées ci-dessus. Les effets de solvatation semblent être importants pour ces systèmes à sphères extérieures lesquels peuvent être interprétés selon la théorie de Marcus. Une comparaison avec d'autres réactions similaires est présentée.

[Traduit par le journal]

Although the 12-heteropoly-acids and their salts were first described in 1933 (2), relatively little is known of the mechanism of their reactions in solution. The 12-tungstocobaltate(II) $[Co(II)O_4 \cdot W_{12}O_{36}]^{6-}$ and 12-tungstocobaltate-(III) $[Co(III)O_4 \cdot W_{12}O_{36}]^{5-}$ ions, hereafter described as [Co(II)] and [Co(III)], have been shown (3, 4) to be examples of complexes in which both the oxidized and reduced forms of the metal are located within CoO_4 tetrahedra. Indeed, in the case of the cobalt(III) complex it is one of the few instances of this metal ion in a tervalent state in a tetrahedral site. Unlike many octahedral cobalt(III) complexes the metal centre in the tungstocobaltiate ion is reduced reversibly. Brubaker and Rasmussen (5) have described the kinetics of the electron exchange between [Co(II)] and [Co(III)] using ^{60}Co tracer techniques. From the structure and stability of these anions it appears that the tungstate groups are substitutionally inert and species of this type

[1]For Part XX, see ref. 1.
[2]Present address: The University of Victoria, Victoria, B.C., Canada V8W 2Y2.

represent ideal complexes for the study of outer-sphere electron transfer in solution.

In many studies of the oxidation of ligands by metal ions the possibility exists for transient complex formation. Intermediate cobalt(III) species have been identified in several instances (6–8). In the present study, using [Co(III)], such interactions between oxidant and reductant would be expected to be weak and this enables the investigation of other factors in electron transfer reactions of this type.

The oxidation of L-ascorbic acid has been studied using a variety of reagents and conditions. An intermediate complex has been identified with vanadium(V) (9), the redox decomposition involving the formation of an ascorbate radical rather than a two-electron transfer to the diketone. Similar radical formation has also been established in the reactions with iron(III)–EDTA complexes (10) and hexacyanoferrate(III) (11). In a recent study (12) the rates of oxidation of ascorbic acid by tris(1,10-phenanthroline)iron(III) and its derivatives have been discussed in terms of free energy changes using the Marcus theory (13). The reaction of benzene 1,2- and 1,4-diols by hexaquo-cobalt(III) (14) may also involve some outer-sphere character. In the case of hydroquinone particularly, there is conflicting evidence as to the reaction mechanism. Davies (15) has suggested, from a comparison of reactivity of several substrates, that an outer-sphere process is operative but this conflicts with the data of Wells (16). Later investigations (14) support the former suggestion with no evidence for any reaction intermediates. Studies with the heteropolyacid system may help to resolve this problem and for this reason the investigations were extended to include both hydroquinone and catechol.

Experimental

Potassium 12-tungstocobaltiate was prepared by the method of Baker and McCutcheon (3) either from the 12-tungstodicobaltoate by oxidation with persulphate or by electrolysis of the 12-tungstocobaltoate complex. The uv-visible spectrum was monitored and it was found that no changes in absorbance were evident over the hydrogen ion concentration range $pH \sim 5.5$–0. At 388 nm, $\varepsilon = 1150 \pm 5\ M^{-1}\ cm^{-1}$.

Stock solutions of L-ascorbic acid (Hopkin and Williams) and hydroquinone (B.D.H. reagent) and catechol (Fisher, resublimed) were prepared prior to use. Details of preparation and standardisation of other solutions have been published previously (17).

Stoichiometry

Spectrophotometric titrations were used to determine reaction stoichiometries. Spectra of solutions containing various concentrations of organic substrate ($0.7–15 \times 10^{-4}\ M$) at a constant oxidant concentration in the range $1.0–4.5 \times 10^{-4}\ M$ at $[H^+] \sim 0.5\ M$ (ascorbic acid), $[H^+] = 0.04\ M$ (catechol and hydroquinone) were measured after reaction had occurred.

Dissociation Constants

In the hydrogen ion concentration ranges used ($[H^+] = 0.04–1.00\ M$) any proton dissociation of the phenol groups was considered to be negligible ($pK > 6$) (18). Ascorbic acid, however, is known to act as a monobasic acid and since data are few (11, 19) on the value for the dissociation constant at the ionic strength used in this study and over a range of temperatures, it was decided to measure this value precisely. Since the kinetic data (*vide infra*) are insensitive to Cl^- ions, solutions were prepared using this anion since better reproducibility was obtained in glass electrode measurements when compared to perchlorate solutions. Accurate dilutions of $[H^+] \sim (4.00 \times 10^{-4} - 5.00 \times 10^{-2}\ M)$ were made in 1.00 M LiCl solutions and a reference slope derived from measurements using a glass electrode/saturated calomel system. Hydrogen ion concentrations of ascorbic acid solutions in acid/base titrations were thus obtained directly. The concentration quotient $K_a = [H^+][HA^-]/[H_2A]$ was measured (reproducibility $\pm 6\%$) over the temperature range 3.8–35.0°C.

Kinetic Measurements

The reactions were studied either at 388 nm (decrease of [Co(III)]) or 625 nm (formation of [Co(III]) under conditions of excess reductant. The latter wavelength was used specifically in the reaction with catechol where there was evidence for a slower secondary process (interpreted as hydrolysis of the ketonic product) which interfered with infinity readings. Measurements were made using the stopped-flow apparatus described previously (20) and a modified Applied Photophysics instrument. The hydrogen concentration range employed was $[H^+] = 0.04–1.00\ M$ at a total ionic strength of 1.00 M ($LiClO_4$). The presence of a sufficient excess of reductant ensured pseudo-first order reaction conditions and plots were linear to at least 85–90% reaction. In the case of catechol, however, interference from the secondary reaction was noted at higher temperatures. Replicate measurements agreed to $\pm 3\%$. Studies were carried out in the presence of air which was found to have no detectable effect on the observed rate constant.

Results and Discussion

(*a*) *Stoichiometry*

In all three systems studied, the spectrophotometric titrations showed oxidant–reductant ratios of $(2.01 \pm 0.02):1$ (ascorbic acid), $(2.00 \pm 0.03):1$ (hydroquinone), and $(2.09 \pm 0.05):1$ (catechol). The overall reaction may thus be written in the form

[1] $2[Co(III)] + R(OH)_2 \longrightarrow 2[Co(II)] + R(=O)_2 + 2H^+$

where 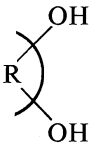 represents the dihydroxy substrate.

(b) Dissociation Constant of Ascorbic Acid

The data from acid–base titrations using the known $[H^+]$ of each solution were treated in the manner suggested by Speakman (21). The data at several temperatures are presented in Table 1 where there is seen to be only a small variation in K_a over the range studied. Determinations in both chloride and nitrate media indicate that the values derived in the present study are slightly higher at lower temperatures than those obtained recently (12). The agreement at room temperature and above, however, is excellent. Dissociation constants are known to vary markedly with temperature over wide ranges and for many systems the values pass through a minimum at or near room temperature (22). The position of this minimum is dependent on solvation and electrostatic effects. In the present conditions ($I = 1.0\ M$), however, over the temperature range studied, the best representation of all the available data is of a linear relationship between pK_a and temperature. This line was used in the interpolations to yield the dissociation constants at the appropriate temperatures.

(c) Kinetics and Mechanism

The linearity of first order plots confirmed the reaction order as unity with respect to the oxidant and data over a wide range of reductant concentrations established a first order dependence. Data at 25°C are presented in Fig. 1 for the systems studied. The rate law may thus be expressed in the form (H_2L = reductant)

$$-d[Co(III)]/dt = 2k_2[Co(III)][H_2L]$$

TABLE 1. Dissociation constant[a] for ascorbic acid at various temperatures, $I = 1.00\ M$ LiCl, or $1.0\ M$ $NaNO_3$

T/°C	10^5K_a	T/°C	10^5K_a
3.80	9.8	20.0	9.3[c]
3.80	8.6[b]	24.76	9.6
6.0	6.6[c]	29.70	11.0
11.0	8.4[b]	35.0	13.0[c]
14.0	10.0		

[a]Mean errors of individual constants (±6%) based on 10 measurements at each temperature.
[b]Nitrate media.
[c]Reference 12, $NaClO_4$ solutions.

The second order rate constants k_2 were found to be independent of wavelength of investigation, [Co(II)], oxygen, and added chloride ion. Extinction coefficients obtained by extrapolation to $t = 0$ were identical to those obtained in the absence of reductant. Values for k_2 for hydroquinone and catechol showed no variation with $[H^+]$ over a 25-fold concentration range and rate constants are presented in Table 2. The data are thus consistent with the reaction scheme

$$[2]\quad [Co(III)] + H_2L \xrightarrow{k_2} [Co(II)] + H^+ + HL^\cdot$$

$$[3]\quad [Co(III)] + HL^\cdot \xrightarrow{\text{fast}} [Co(II)] + L + H^+$$

The reaction with ascorbic acid, however, showed a marked hydrogen ion dependence on the rate. In this case the data may be represented by the scheme

$$[4]\quad H_2L \xrightarrow{K_a} HL^- + H^+$$

$$[5]\quad [Co(III)] + H_2L \xrightarrow{k_5} [Co(II)] + H^+ + HL^\cdot$$

$$[6]\quad [Co(III)] + HL^- \xrightarrow{k_6} [Co(II)] + HL^\cdot$$

$$[7]\quad Co(III) + HL^\cdot \xrightarrow{\text{fast}} [Co(II)] + L + H^+$$

where H_2L and HL^- represent the protonated and dissociated forms of ascorbic acid. Assuming the pre-equilibrium to be rapidly established, and allowing for the overall stoichiometry, the reaction rate may be written as

$$[8]\quad -d[Co(III)]/dt = \frac{2\{k_5 + k_6K_a/[H^+]\}[Co(III)][H_2L]_t}{(1 + K_a/[H^+])}$$

TABLE 2. Second order rate constants for reactions of [Co(III)] with hydroquinone and catechol, $I = 1.0\ M$ $LiClO_4$, $[H^+] = 0.04\ M$, $[Co(III)] = 1\text{–}3 \times 10^{-4}\ M$

T/°C	$10^3k_2/(M^{-1}\ s^{-1})$[a]	T/°C	$10^2k_2/(M^{-1}\ s^{-1})$[a]
Hydroquinone		Catechol	
5.0	8.84	11.47	5.65
12.0	10.4	19.0	7.90
19.0	12.8	25.0	9.50
25.0	14.3	30.0	11.58
30.0	16.5	35.0	13.50
$\Delta H^* = 3.6 \pm 0.4$ kcal mol^{-1}		$\Delta H^* = 5.9 \pm 0.9$ kcal mol^{-1}	
$\Delta S^* = -34 \pm 8$ cal $deg^{-1}\ mol^{-1}$		$\Delta S^* = -27 \pm 8$ cal $deg^{-1}\ mol^{-1}$	

[a]Each constant quoted represents the mean value of at least five separate determinations over the ligand concentration range $0.6\text{–}10 \times 10^{-3}\ M$.

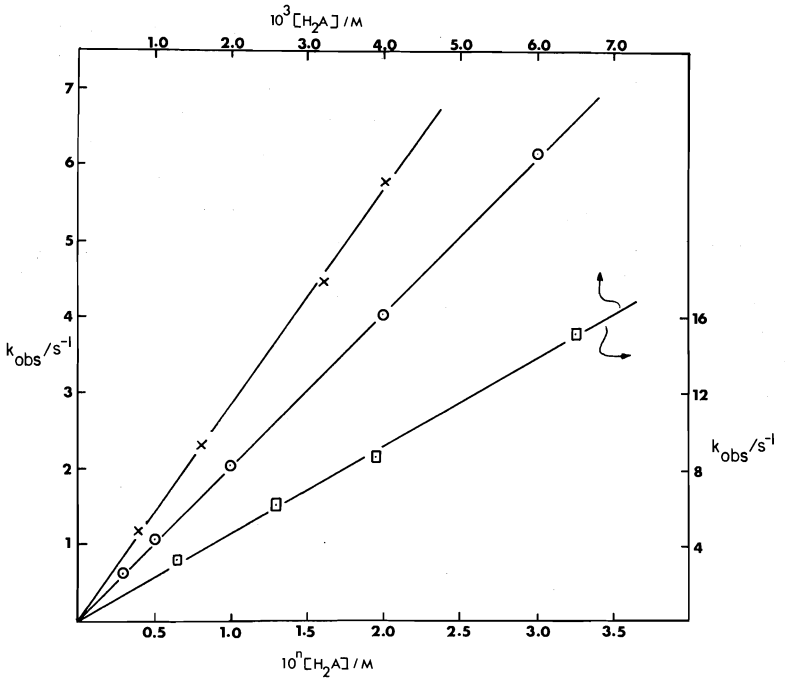

FIG. 1. Plots of k_{obs} against $[H_2A]$. (⊙) Ascorbic acid [0.3–3.0 × 10^{-2} M], [Co(III)] = 3.0 × 10^{-4} M, $[H^+]$ = 0.50 M, T = 15.1°C. (×) Hydroquinone [2.4–20 × 10^{-4} M], [Co(III)] = 4.06 × 10^{-5} M, $[H^+]$ = 0.04 M, T = 25.0°C (10^{-4} k_{obs}). (⊡) Catechol [1.3–6.50 × 10^{-3} M], [Co(III)] = 1.64 × 10^{-4} M, $[H^+]$ = 0.04 M, T = 25.0°C (upper and right hand coordinates).

TABLE 3. Second order rate constants at various $[H^+]$ and temperatures for the ascorbic acid reaction; [Co(III)] = 1.85 × 10^{-4} M, λ = 388 nm, I = 1.0 M ($LiClO_4$)

T/°C	$[H^+]/M$	$10^{-2}k_2/(M^{-1}\ s^{-1})$	T/°C	$[H^+]/M$	$10^{-2}k_2/(M^{-1}\ s^{-1})$
8.8	0.050	3.84	25.0	0.20	2.21
	0.20	1.34		0.40	1.48
	0.40	0.925		0.50	1.40
	0.50	0.84		0.60	1.225
	0.60	0.77		0.80	1.125
	0.80	0.69			
15.1	0.10	2.86	30.1	0.30	1.97
	0.30	1.33		0.50	1.58
	0.50	1.03		0.70	1.37
	0.70	0.91		0.90	1.27
	0.90	0.825			

where $[H_2L]_t = [H_2L] + [HL^-]$. Under the experimental conditions used, $[H^+]$ = 0.04–1.00 M, $K_a/[H^+] \ll 1$ (Table 1), the second order rate constants may be expressed in the form

$$[9] \quad \frac{k_{obs}}{2[H_2L]} = k_2 = (k_5 + k_6K_a/[H^+])$$

Treatment of the data (Table 3) according to eq. 9 yielded straight lines at all temperatures studied, with slopes and intercepts equal to k_2K_a and k_1 respectively. The rate constants for the various reactions studied are presented in Table 4. Since there is no change in the nature of the oxidant over the hydrogen ion concentration range studied (confirmed both spectroscopically and by a lack of any $[H^+]$ dependence in the reactions of the benzene diols) it is possible to assign the reaction pathways unambiguously. It is of interest to note that although the oxidant carries a large negative charge, the anionic form

TABLE 4. Dependence of rate constants on temperature

T/°C	$k_5/(M^{-1}\,s^{-1})$	k_6K_a/s^{-1}	pK_a[a]	$10^{-5}k_6/(M^{-1}\,s^{-1})$
8.8	49.1	17.0	4.065	1.97±0.07
15.1	58.2	22.3	4.025	2.36±0.11
25.0	77.4	28.3	3.96	2.58±0.17
30.1	93.1	31.5	3.935	2.71±0.21

$\Delta H_5^{\ddagger} = 4.5 \pm 0.6$ kcal/mol $\quad \Delta H_6^{\ddagger} = 2.0 \pm 2$ kcal M^{-1}

$\Delta S_5^{\ddagger} = -34.7 \pm 5$ cal deg^{-1} M^{-1} $\quad \Delta S_6^{\ddagger} = -29 \pm 5$ cal M^{-1} deg^{-1}

[a]Data interpolated from Table 1.

TABLE 5. Reaction rates of metal complexes with ascorbate anion at 25°C

Oxidant	$10^{-3}k_2/(M^{-1}\,s^{-1})$	$\Delta H_2^{\ddagger}$/(kcal M^{-1})	$\Delta S_2^{\ddagger}$/(cal deg^{-1} M^{-1})	Ref.
$CoW_{12}O_{40}^{5-}$	241	2.0	−29	This work
Fe(III)(h EDTA)	21.5	5.0	−21	21
Fe(III)·EDTA$^-$	4.0	4.5	−27	21
Fe(III)–CDTA	1.3	4.3	−30	21
Fe(III)–DPTA	0.88	4.1	−32	21
$Fe(CN)_6^{3-}$	0.37	—	—	11

of the ascorbic acid in fact is substantially more reactive than the undissociated substrate. Second order rate constants for reaction 6 were calculated using the K_a values interpolated at the appropriate temperatures. The increased reactivity of the ascorbate anion has been observed previously in the reactions with anionic iron(III) chelates (23) (Table 5) where unlike the present study there is no evidence for any pathway corresponding to k_5. An analysis of the data presented in the paper by Mushran and coworkers (11) indicates (Fig. 2 of ref. 11) that a hydrogen ion dependence similar to that observed with the cobalt complex is shown in the reaction with hexacyanoferrate(III). Also, interestingly, the ratio of k_6/k_5 rate constants in the $Fe(CN)_6^{3-}$ system is $\sim 1.25 \times 10^3$ which is not too markedly different from the corresponding ratio of 3.1×10^3 observed in the present study. For the reaction with HA^-, however, the rate constants obtained are very much ($\sim 10^6$) lower than those derived for the reaction of the cationic $Fe(phen)_3^{3+}$ oxidants (12). This may reflect the importance of electrostatic parameters in these reactions.

The activation parameters for the various reactions investigated are very similar and possibly indicate common reaction features, especially for the three dihydroxy species, hydroquinone, catechol, and undissociated ascorbic acid. It is interesting to note that the more rapid reaction of the ascorbate ion is associated with the only species among those studied here for which no proton solvation is required.

An attempt was made to interpret these data using the LFER proposed by Marcus (13) as applied by Pelizzetti and Mentasti (12). For an outer-sphere transition complex, one would expect the activation to be given by the expression

$$[10]\quad \Delta G^*_{12} = w_r + \frac{\lambda_{12}}{4} + \frac{\Delta G^{\phi\prime}_{12}}{4} + \frac{(\Delta G^{\phi\prime}_{12})^2}{4\lambda_{12}}$$

where $\lambda_{12} = 2(\Delta G^*_{11} - w_{11} + \Delta G^*_{22} - w_{22})$, and $\Delta G^{\phi\prime}_{12} = \Delta G^{\phi}_{12} + w_p - w_r$. The terms ΔG^*_{11} and ΔG^*_{22} represent the free energies of activation of the self-exchange reaction and ΔG^{ϕ}_{12} the standard free energy of the reaction. The different work terms, w_{11}, w_{22}, w_p, w_r, required to bring the reactants and products together are considered to provide only a small contribution at this ionic strength and were neglected (24).

Equation 10 is usually written in the form

$$[11]\quad \Delta G^*_{12} - \frac{\lambda_{12}}{4} - \frac{\Delta G^{\phi}_{12}}{4\lambda_{12}} = \tfrac{1}{2}\,\Delta G^{\phi}_{12}$$

A plot of the left-hand side of eq. 11 against ΔG^{ϕ}_{12} should have a slope of $\frac{1}{2}$ and zero intercept.

All the parameters required for such a plot were either available (5, 12, 24) or could be inferred. For the Co(III)/Co(II) self-exchange

TABLE 6. Evaluation of free energy parameters

	E_0/V	$k_2/(M^{-1}\ s^{-1})$	ΔG^0/(kcal mol^{-1})	Q^d/(kcal mol^{-1})	λ_{12}	ΔG^*_{12}/(kcal mol^{-1})
HA^-	0.93[a]	1.58×10^5	−2.08	−1.505	38.72	8.20
H_2Q	1.08[b]	1.43×10^4	1.39	0.359	43.72	11.30
H_2Cat	1.17[b]	1.16×10^4	3.46	0.512	43.72	11.51
H_2A	1.31[c]	7.74×10^1	6.58	1.593	43.72	12.70

[a]Reference 12.
[b]Reference 24.
[c]Extrapolated value from plot log k_2 vs. E_0 for other three species.
[d]$Q=\Delta G^*_{12}-(\lambda_{12}/4)-((\Delta G^0_{12})^2/4\lambda_{12})$.

reaction the value $\Delta G^*_{11} = 15.36$ kcal/mol was obtained by extrapolating to 1.0 M ionic strength the data of Rasmussen and Brubaker (5). The corresponding parameter $\Delta G^*_{22} = 6.5$ kcal/mol for the $H_2L/HL^\bullet$ couples was assumed to be constant for all the dihydroxy forms of the reductants (24). For the ascorbate ion the value $\Delta G^*_{22} = 4$ kcal/mol for $HA^-/HA^\bullet$ was used (12). The ΔG^*_{12} values were obtained from the experimental activation parameters. The redox potentials were identical to those quoted previously (24), except for that of the couple $H_2A/HA^\bullet$. In this case by extrapolating from a plot of log k_2 against E^0 for the three dihydroxy substrates under investigation the value $E^0 = 1.31$ V for $H_2A/HA^\cdot$ was determined.

Table 6 includes the values of the terms involved in eq. 11. When plotted these data gave a slope of 0.34 ± 0.07 and an intercept of -0.56 ± 0.6 kcal/mol. Considering the relative scarcity of data and the precision with which all the various parameters are known, these results show at least a good qualitative agreement with the theory. More definitive statements must await written data using the same oxidant but with different reducing species encompassing a wide range of E_0 values.

Acknowledgements

One of us (Z.A.) wishes to thank the University of Glasgow for the award of a Demonstratorship. Support from the National Research Council of Canada and the University of Victoria is also acknowledged.

1. Z. AMJAD, J. G. CHAMBERS, and A. MCAULEY. Can. J. Chem. This issue.
2. J. F. KEGGIN. Nature, **131**, 908 (1933); Proc. R. Soc. London Ser. A, **144**, 75 (1934).
3. L. C. W. BAKER and T. P. MCCUTCHEON. J. Am. Chem. Soc. **78**, 4503 (1956).
4. L. C. W. BAKER and V. E. SIMMONS. J. Am. Chem. Soc. **81**, 4745 (1959).
5. P. G. RASMUSSEN and C. H. BRUBAKER. Inorg. Chem. **3**, 977 (1964).
6. J. HILL and A. MCAULEY. J. Chem. Soc. A, 1169 (1968).
7. T. J. CONOCCHIOLI, G. H. NANCOLLAS, and N. SUTIN. Inorg. Chem. **5**, 1 (1966).
8. R. G. SANDBERG, J. J. AUBORN, E. M. EYRING, and K. O. WATKINS. Inorg. Chem. **11**, 1952 (1972).
9. K. KUSTIN and D. A. TOPPEN. Inorg. Chem. **12**, 1404 (1973).
10. R. R. GRINSTEAD. J. Am. Chem. Soc. **82**, 3464 (1960).
11. U. S. MEHROTRA, M. C. AGRAWAL, and M. P. MUSHRAN. J. Phys. Chem. **73**, 1996 (1969).
12. E. PELIZZETTI, E. MENTASTI, and E. PRAMAURO. Inorg. Chem. **15**, 2898 (1976).
13. R. A. MARCUS. J. Phys. Chem. **72**, 891 (1968).
14. E. PELIZZETTI, E. MENTASTI, and E. PRAMAURO. J. Chem. Soc. Dalton Trans. 23 (1976).
15. G. DAVIES and K. O. WATKINS. J. Phys. Chem. **74**, 3388 (1970).
16. C. F. WELLS and L. V. KURITSYN. J. Chem. Soc. A, 2930 (1969).
17. A. G. LAPPIN and A. MCAULEY. J. Chem. Soc. Dalton Trans. 1564 (1975).
18. Handbook of chemistry and physics. *Edited by* C. D. Hodgman. Chemical Rubber Company, Cleveland, Ohio. 1961.
19. M. M. TAQUI-KHAN and A. E. MARTELL. J. Am. Chem. Soc. **89**, 4176 (1967).
20. K. J. ELLIS and A. MCAULEY. J. Chem. Soc. Dalton Trans. 1533 (1973).
21. J. C. SPEAKMAN. J. Chem. Soc. 855 (1940).
22. R. W. GURNEY. Ionic processes in solution. Dover, New York. 1953. p. 128.
23. M. M. TAQUI-KHAN and A. E. MARTELL. J. Am. Chem. Soc. **90**, 3386 (1968).
24. E. PELIZZETTI and E. MENTASTI. J. Chem. Soc. Dalton Trans. 2222 (1976).

Nonexistence of the alleged isobindone. The aldol–retroaldol reaction of 1,3-indandione

ALFRED TAURINS
Department of Chemistry, McGill University, Montreal, P.Q., Canada H3A 2K6

Received April 4, 1977

ALFRED TAURINS. Can. J. Chem. **55**, 3587 (1977).

The existence of the alleged isobindone has been disproved. The compound, mp 330°C, formed as a byproduct in the aldol–retroaldol condensation reaction of 1,3-indandione is not isobindone but 1-(1,3-indandionyl-2)-3-(1,3-indandionyliden-2)indene. The compound, mp 337°C, formed from bindone in pyridine solution has the composition $C_{36}H_{18}O_5$.

ALFRED TAURINS. Can. J. Chem. **55**, 3587 (1977).

On réfute l'existence de la soi-disante isobindone. Le composé qui fond à 330°C et qui se forme comme produit secondaire dans la condensation aldolique–rétroaldolique de l'indandione-1,3, n'est pas l'isobindone mais le (indandione-1,3 yl-2)-1 (indandione-1,3 ylidène-2)-3 indène. Le composé formé à partir de la bindone en solution pyridinique, et qui a un point de fusion de 337°C, possède la composition $C_{36}H_{18}O_5$.

[Traduit par le journal]

In 1931, Fischer and Wanag (1) claimed that bindone (**1**) possessed an isomer, 'isobindone', of structure **2**. They studied the transformation of bindone to 'isobindone' and a reverse reaction under various conditions and considered these processes as isomerization (1, 2). Thirty years later an ir and uv investigation (3) did not provide support for the structure **2**; however, no further work on this subject appeared.

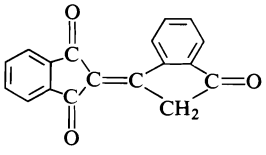

1

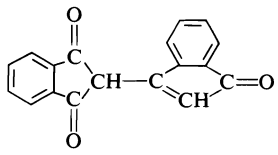

2

Despite the closely related structural formulas for bindone (**1**) and isobindone (**2**) there are striking differences in their chemical and physical properties indicating the inadequacy of the structure **2**.

Bindone; mp 210°C. Soluble in hot glacial acetic acid. Aqueous sodium hydroxide forms a violet solution of the Na-salt of **1**. Ultraviolet spectrum of the Na-salt of **1**: $\lambda_{max}(H_2O)$ 305, 355.5, 525 nm (log ε 1.58, 1.17, 1.38) (3). Dry K_2CO_3 in hot toluene forms a dark green K-salt of isobindone (2).

'*Isobindone*'; mp 330°C. Insoluble in hot glacial acetic acid. Methanolic 0.5% sodium methoxide forms a dark-green solution of the Na-salt of 'isobindone'. Ultraviolet spectrum of the Na-salt: $\lambda_{max}(CH_3OH)$ 420, 655 nm (log ε 1.45, 1.05) (3). Hot aqueous sodium hydroxide (0.1 *N*) forms a violet solution of the Na-salt of bindone.

Comparison of the spectral properties of the salts of bindone and 'isobindone' (see above) leads to the conclusion that the latter has a more extended chromophore and, in order to accommodate the more extended chromophore, it is likely to be a larger molecule.

An additional sign of the inadequacy of formula **2** for 'isobindone' is the existence of 2,2′-dimethylisobindone (**3**) (4) (systematic name: 2,2′-dimethyl-2,3′-biindenyl-1,1′,3(2H)-trione). Both formulas **2** and **3** possess the same basic

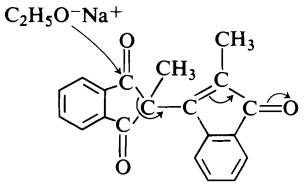

3

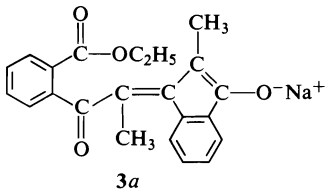

3a

structure. The only difference between them is that the structure **2** has hydrogens on C-2 and C-2′ while in **3** the same carbon atoms carry methyl groups. Therefore, one could expect that if 'isobindone' had the structure **2**, its physical properties should be similar to those of compound **3**. However, that is not the case, since compound **3** is volatile *in vacuo* and has mp 198°C (4), significantly lower than the mp of 'isobindone' (see above).

Despite the fact that compound **3** has no —CH_2CO— groups, and consequently cannot enolize, it very easily forms a blue solution with ethanolic sodium ethoxide (4). Therefore, we postulate that the reaction involves the ring opening (**3** → **3***a*).

Reinvestigation of the alleged 'isobindone' showed definitely that it has the formula $C_{27}H_{14}O_4$, formed by the aldol condensation of three molecules of 1,3-indandione. The proof was provided by elemental analysis and mass spectrometry. *Anal.* calcd. for $C_{27}H_{14}O_4$ (mw 402.41): C 80.6, H 3.5; found: C 80.7, H 3.8. Mass spectra for $C_{27}H_{14}O_4$: *m/e* 402 (M^+), 374 ($M^+ - CO$), 358 ($M^+ - CO - O$; HR $C_{26}H_{14}O_2$), 346 ($M^+ - 2CO$), 329 ($M^+ - 2CO - OH$; HR $C_{25}H_{13}O$), 289 ($M^+ - 4CO - H$; HR $C_{23}H_{13}$); ms for bindone, $C_{18}H_{10}O_3$ (mw 274.28): *m/e* 274 (M^+), 246 ($M^+ - CO$), 219 ($M^+ - 2CO + H$; HR $C_{16}H_{10}O$), 189 ($M^+ - 3CO - 1H$; HR $C_{15}H_9$), 163 (HR $C_{13}H_7$), 114 (HR C_9H_6).

In order to obtain compound $C_{27}H_{14}O_4$ in the pure state, it is essential to crystallize it from a low boiling solvent, like chloroform, but not from nitrobenzene as suggested by Fischer and Wanag (1). In boiling nitrobenzene the compound undergoes a chemical change resulting in blackening of the solution from which only a part of the solute of varying composition can be recovered. Fischer and Wanag (1) claimed that they established the composition of 'isobindone' by elemental analysis and cryoscopic mw determination in phenol (mw found: 246, 265; calcd. for $C_{18}H_{10}O_3$: 275). Obviously, their samples were not the right ones, and their oversight arose from the fact that they did not recognize the true nature of the transformation: bindone ⇄ 'isobindone' as being an aldol–retroaldol reaction which occurred also during the crystallization of the sample from nitrobenzene and mw determination in phenol.

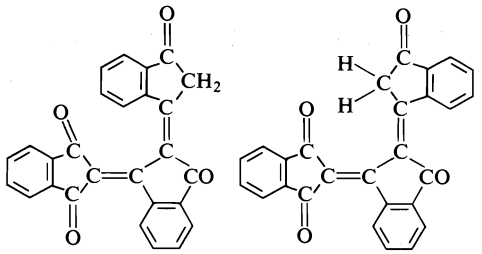

4 **5**

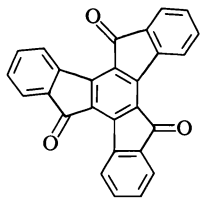

6

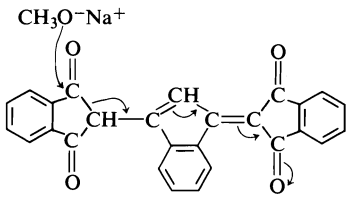

7

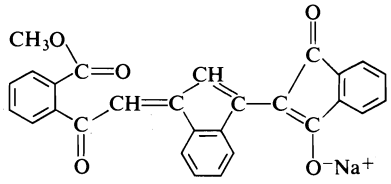

8

For compound $C_{27}H_{14}O_4$ (mp 330°C) structures **4** and **5** must be excluded on steric grounds and, therefore, the most probable structure could correspond to 1-[1,3-indandionyl-2]-3-[1,3-indandionyliden-2]indene (**7**). Examination of space-filling molecular models for bindone and compound $C_{27}H_{14}O_4$, containing two or three 1,3-indandionyl units, respectively, shows that the molecules cannot be planar at the C=C bonds due to interference of a C=O group with a hydrogen atom on the neighboring benzene

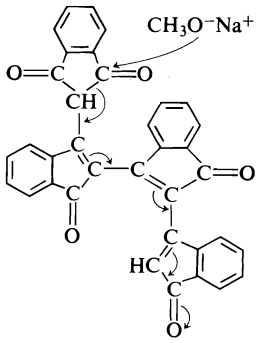

9

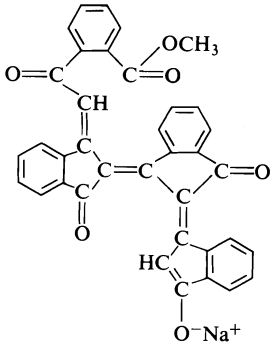

ring. The twist of the double bond could be ~30° resulting in decrease of the overlapping of π-electrons and the decrease in the double-bond character. The structure **4** is the most crowded while the structure **5** could lead to the formation of truxenquinone (**6**). It is believed that the reaction of compound **7** with 0.5% methanolic sodium methoxide is not based on enolate formation, but is analogous to the reaction of compound **3** forming a dark-green salt (**8**) by the ring opening and increasing the number of conjugated double bonds.

In conclusion, the name 'isobindone' must be removed from the literature.

The condensation product of bindone (**1**) in pyridine solution which has been described either as $C_{45}H_{24}O_7$ (5) or $C_{27}H_{14}O_4$ (1), actually is $C_{36}H_{18}O_5$. It melts at 337°C and is slowly soluble in 1.5% methanolic sodium methoxide solution with a dark-blue color. For this compound the structure **9** is proposed possessing single bonds between the indandionyl units. These bonds allow the existence of a non-planar structure. The incorrect results by the previous workers have been apparently obtained by crystallizing the compound **9** from nitrobenzene. In this work, compound **9** was obtained in pure state by precipitating it from the solution in sodium methoxide with dilute HCl, washing with water and methanol, and drying. *Anal.* calcd. for $C_{36}H_{18}O_5$ (mw 530.54): C 81.5, H 3.4; found: C 81.5, H 3.7; ms: *m/e* 530 (M^+), 513 ($M^+ - OH$), 502 ($M^+ - CO$), 485 ($M^+ - CO - OH$), 474 ($M^+ - 2CO$), 460 ($M^+ - 2CO - CH_2$), 460 ($M^+ - C_6H_4(CO)_2$) + 2H. Ultraviolet visible spectrum of the Na-salt of **9**: $\lambda_{max}(CH_3OH)$ 283, 312, 345, 378, 538, 605, 625 nm (log ε 4.39, 4.29, 4.13, 4.06, 4.07, 4.13, 4.12).

Acknowledgment

This research was supported by the National Research Council of Canada. Elemental analyses were performed by Dr. C. Daessle, Microanalytical Laboratory, Montreal, Quebec.

1. W. M. Fischer and G. Wanag. Lieb. Ann. **489**, 97 (1931).
2. G. Vanags. Acta Univ. Latv. Kim. Ser. **2**, 153 (1931); Chem. Abstr. **26**, 1921 (1932).
3. R. Zhagata, J. Stradins, A. Grinvalde, and G. Vanags. Dokl. Akad. Nauk SSSR, **135**, 77 (1960); Chem. Abstr. 13396*d* (1961).
4. H. Simonis and G. Wojack. Chem. Ber. **70**, 1837 (1937).
5. M. Jonescu. Chem. Ber. **60**, 1233 (1927).

Influence de la coordination du thallium sur la cinétique de décomposition du composé d'oxythallation: C_6H_5—$CH(OCH_3)$—$CH_2Tl(OAc)_2$

LOUISE NADON ET MIKLOS ZADOR
Département de chimie, Université de Montréal, C.P. 6210, Montréal (Qué.), Canada H3C 3V1

Reçu le 17 février 1977

LOUISE NADON et MIKLOS ZADOR. Can. J. Chem. **55**, 3590 (1977).

L'influence de la coordination du thallium sur la vitesse de décomposition du composé d'oxythallation C_6H_5—$CH(OCH_3)$—CH_2TlX_2($R'TlX_2$) a été étudiée en milieu eau–méthanol. En présence de faibles concentrations d'ions Cl^-, la vitesse de décomposition oxydante diminue à cause de la formation d'espèces $R'TlCl^+$ et $R'TlClOH$, ces deux dernières étant moins réactives que l'espèce $R'Tl^{2+}$. A haute concentration en ions Cl^-, il y a formation d'espèces $R'TlCl_2$ ou $R'TlCl_3^-$; on observe alors la décomposition en réactifs de départ, soit le styrène et le Tl(III), similairement observée pour les organomercuriques.

Le mécanisme des réactions est discuté en termes de changement du caractère électrophile du thallium dû à la coordination par le ligand.

LOUISE NADON and MIKLOS ZADOR. Can. J. Chem. **55**, 3590 (1977).

The effect of coordination of thallium was studied on the rate of decomposition in methanol–water of the product of oxythallation, C_6H_5—$CH(OCH_3)$—CH_2TlX_2($R'TlX_2$). At low Cl^- ion concentrations, the rate of the oxidative decomposition decreased because of the formation of $R'TlCl^+$ and $R'TlClOH$, both of which are less reactive than $R'Tl^{2+}$. At high Cl^- ion concentration, $R'TlCl_2$ or $R'TlCl_3^-$ are formed and a decomposition to the starting materials, namely styrene and Tl(III), was observed; this is analogous to the behaviour of organomercurials.

The mechanism of the reactions is discussed in terms of the electrophilic character of thallium effected by the coordination by ligand.

[Journal translation]

Introduction

Le mécanisme de décomposition d'organothalliques du type $R_1R_2C(OR_3)$—CH_2TlX_2 ($R'TlX_2$) présente un intérêt particulier étant donné que ces composés se forment comme intermédiaires dans l'oxydation d'oléfines par les sels thalliques (1).

Les études précédentes ont permis de montrer que les principales formes réactives sont $R'Tl^{2+}$ et $R'TlOH^+$ et que la réactivité de $R'Tl^{2+}$ est beaucoup plus grande que celle de $R'TlOH^+$ (2, 3).

Dans ce travail on présente les résultats d'une étude de l'influence de quelques ligands sur la vitesse de décomposition de C_6H_5—$CH(OCH_3)$—$CH_2Tl(OAc)_2$.

Partie expérimentale

Réactifs et produits

La méthode de synthèse de C_6H_5—$CH(OCH_3)$—$CH_2Tl(OAc)_2$ ainsi que l'analyse des produits d'oxydation ont été décrites précédemment (2). Les réactifs utilisés sont de qualité analytique.

Méthodes cinétiques

Les réactions sont suivies par la mesure de la variation de l'absorbance. La méthode expérimentale a été décrite auparavant (2). Les résultats de flux stoppé sont traités par un système d'acquisition et de traitement de données de notre construction (4). Les constantes de vitesse sont obtenues directement par un programme de régression approprié à l'aide d'une calculatrice programmable Tektronix 31. Les constantes de vitesse sont, en général, les moyennes de cinq expériences et la reproductibilité des résultats est d'environ ±5%.

Résultats et discussion

La décomposition oxydative de l'organothallique $R'Tl(OAc)_2$ se fait d'après l'éq. 1.

$$[1]\quad C_6H_5—CH(OCH_3)—CH_2Tl(OAc)_2 \xrightarrow{ROH} C_6H_5—CH_2—CH(OCH_3)(OR) + Tl^+ + OAc^- + HOAc$$

Elle implique la migration du groupe phényle et conduit à un acétal ou un aldéhyde suivant la nature de R (2).

En solution eau–méthanol (75% v/v – 25% v/v) il a été montré (2) qu'à des $pH < 5$ et à des concentrations en $R'Tl(OAc)_2 \leq 10^{-3}$ M, celui-ci se dissocie et les espèces dominantes en solution sont reliées par l'équilibre 2.

$$[2]\quad R'TlOH^+ + H^+ \overset{K_1}{\rightleftharpoons} R'Tl^{2+} + H_2O$$

L'acidité influence cet équilibre et, partant, la nature et la concentration des espèces éventuelles se formant en présence de ligands.

Influence de faibles concentrations en ions Cl^-

En l'absence d'acide fort ajouté ($pH \simeq 5.0$) l'addition d'ions Cl^- entraîne la diminution de la vitesse de réaction, comme l'indiquent les résultats du tableau 1. Ceci est attribué, en se basant sur les connaissances acquises sur l'affinité du Tl^{3+} pour les halogénures, à la formation d'espèces telles $R'TlCl_n^{2-n}$, moins réactives que $R'Tl^{2+}$. Les résultats indiquent que, pour un rapport $[R'Tl]/[Cl^-] = 1$ la vitesse ne diminue que d'un facteur de 0.7 et qu'il faut la présence de grands excès de Cl^- pour avoir une diminution de vitesse appréciable.

A une acidité plus élevée où l'équilibre 2 est plus déplacé vers la formation de $R'Tl^{2+}$, l'influence des ions chlorure est plus prononcée (voir tableau 2).

TABLEAU 1. Influence des ions Cl^- en absence d'acide fort*

$[Cl^-]$ (M)	$10^4 \times k_{exp}$ (s^{-1})	$10^4 \times k_{calc}$ (s^{-1})
—	17.8	19.5
2.0×10^{-4}	17.2	18.2
4.0×10^{-4}	15.8	16.9
6.0×10^{-4}	13.2	15.8
8.0×10^{-4}	13.6	14.8
1.0×10^{-3}	12.3	13.9
1.5×10^{-3}	11.0	12.2
2.0×10^{-3}	11.1	10.8
4.0×10^{-3}	7.9	7.6
6.0×10^{-3}	6.5	6.0
8.0×10^{-3}	6.1	5.0
1.0×10^{-2}	5.3	4.4
5.0×10^{-2}	2.3	2.0

*$T = 25°C$; $[R'Tl(OAc)_2] = 1.0 \times 10^{-3}$ M; $[H^+] = 1.7 \times 10^{-5}$ M; solvant: H_2O–CH_3OH 75%–25% (v/v); $\mu = 0.5$ M.

TABLEAU 2. Influence des ions Cl^- en présence de $HClO_4$*

$[Cl^-]$ (M)	$10^2 \times k_{exp}$ (s^{-1})	$10^2 \times k_{calc}$ (s^{-1})
—	29	32
1.0×10^{-5}	24	26
3.0×10^{-5}	19	18
5.0×10^{-5}	14	13
1.0×10^{-4}	5.6	7.0
1.5×10^{-4}	4.5	4.7
2.0×10^{-4}	3.1	3.5
1.0×10^{-2}	0.12	0.10

*$T = 25°C$; $[R'Tl(OAc)_2] = 2.5 \times 10^{-5}$ M; $[H^+] = 0.025$ M; solvant: H_2O–CH_3OH 75%–25% (v/v); $\mu = 0.5$ M.

Pour interpréter l'ensemble des résultats il a fallu tenir compte des équilibres 3 et 4.

$$[3] \qquad R'Tl^{2+} + Cl^- \overset{K_2}{\rightleftharpoons} R'TlCl^+$$

$$[4] \qquad R'TlOH^+ + Cl^- \overset{K_3}{\rightleftharpoons} R'TlClOH$$

La vitesse de réaction est donnée par l'éq. 5.

$$[5] \quad V = k_{exp}[R'Tl]_{total} = k_1[R'Tl^{2+}] + k_2[R'TlOH^+] + k_3[R'TlCl^+]$$

Ces hypothèses conduisent à l'éq. 6.

$$[6] \quad k_{exp} = \frac{k_1K_1[H^+] + k_2 + k_3K_1K_2[H^+][Cl^-]}{1 + K_1[H^+] + K_1K_2[H^+][Cl^-] + K_3[Cl^-]}$$

La détermination des paramètres de l'éq. 6 a été faite par une méthode d'itération en utilisant, en première approximation les valeurs de K_1, k_1 et k_2 obtenues précédemment (2).

Le calcul des concentrations des diverses expèces à l'équilibre a été fait en admettant des valeurs de K_2 et K_3 raisonnables compte tenu de l'affinité de Tl^{3+} pour l'ion Cl^-. L'affinement des résultats consiste à optimiser les valeurs de K_2, K_3 et k_3. Les valeurs suivantes des paramètres ont été obtenues: $k_1 = 0.36$ s^{-1}, $k_2 = 1.5 \times 10^{-4}$ s^{-1}, $k_3 = 3.0 \times 10^{-4}$ s^{-1}, $K_1 = 300$ M^{-1}, $K_2 = 5 \times 10^4$ M^{-1} et $K_3 = 300$ M^{-1}.

La constante de vitesse calculée à l'aide de ces paramètres est en accord satisfaisant avec les résultats obtenus aux deux acidités (tableaux 1 et 2).

Les valeurs des paramètres indiquent que la coordination de $R'Tl^{2+}$ par le Cl^- entraîne une diminution des réactivité ($k_1/k_3 = 1200$) du même ordre que la coordination par OH^- ($k_1/k_2 = 2400$). Les deux ligands entraînement donc une diminution similaire du caractère électrophile du Tl, et du carbone adjacent ce qui rend la migration du groupe phényle lors de la rupture hétérolytique du lien C—Tl, moins favorisée.

La constante d'équilibre de formation de $R'TlCl^+$, K_3 est d'au plus un ordre de grandeur inférieure à la constante similaire du Tl(III) ($TlCl^{2+} + Cl^+ \rightleftharpoons TlCl^{2+}$, $K_{1,2} = 1.5 \times 10^5$ M^{-1} (5)); ceci montre que le thallium conserve son affinité pour ce ligand dans l'organothallique.

Il y a une espèce 1:2, R'TlOHCl, qui intervient dans l'interprétation des résultats. Sa concentration est relativement importante à

p$H \sim 5.0$, ce qui est dû au fait que $R'TlOH^+$ est l'espèce qui domine, par rapport à $R'Tl^{2+}$, dans ces conditions. Sa contribution à la vitesse n'est pas significative mais elle pourrait l'être à p$H > 5$; toutefois, il y a alors formation d'un précipité, ce qui rend l'étude impossible. A acidité plus élevée ($>10^{-2}$ M) sa concentration devient négligeable.

L'hypothèse impliquant la formation d'une autre espèce 1:2, $R'TlCl_2$, n'améliore pas de façon significative l'accord entre résultats expérimentaux et calculés.

Influence des hautes concentrations en ions Cl^-

A hautes concentrations en ions chlorures (≥ 0.1 M) et à acidité plus élevée (≥ 0.1 M) un phénomène nouveau apparaît. En effet, au lieu de la diminution habituelle d'absorbance, on observe une augmentation. L'étude de la nature des produits a permis de montrer que dans ce cas l'organothallique se décompose pour redonner les réactifs de départ:

$$C_6H_5—CH(OCH_3)—CH_2TlX_2 \rightarrow C_6H_5CH=CH_2 + Tl(III) + CH_3OH$$

Dans ces conditions il n'y a pas de disparition de thallium d'état d'oxydation 3+, tel que montré par le dosage iodométrique, dans lequel l'organothallique se comporte comme le Tl(III) (voir plus loin). L'analyse chromatographique en fin de réaction, correspondant à l'arrêt de la variation de l'absorbance, indique que le styrène s'est regénéré quantitativement à l'exclusion des produits d'oxydation habituels.

Il apparaît donc, que dans le schéma habituel de l'oxydation thallique:

$$[7] \qquad Tl(III) + \text{oléfine} \underset{k_{-1}}{\overset{k_1}{\rightleftharpoons}} \text{organothallique}$$

$$[8] \qquad \text{organothallique} \xrightarrow{k_2} \text{produits d'oxydation}$$

l'étape correspondante au retour vers les réactifs de départ (k_{-1}) devient prépondérante.[1] En tenant compte de l'ensemble des résultats, on peut expliquer ce phénomène (au point de vue dynamique) comme suit. (*i*) L'augmentation de la concentration en Cl^- entraîne la formation d'espèces telles $R'TlCl_2$, $R'TlCl_3^-$. (*ii*) L'électronégativité du thallium ainsi coordiné est nettement diminuée; ceci cause une diminution de la polarisation du lien C—Tl et la diminution ou même la disparition du caractère électrophile du carbone lié au thallium. (*iii*) La rupture hétérolytique du lien C—Tl pour conduire aux produits d'oxydation est empêchée ou du moins drastiquement ralentie. (*iv*) En même temps, l'attaque électrophille par H^+ est favorisée et le retour vers les réactifs de départ est accéléré.

Au point de vue thermodynamique l'explication est également assez cohérente avec les connaissances acquises. Pour Tl^{3+} l'équilibre 7 est déplacé complètement vers la droite. Toutefois, en présence de 0.1 M en ion Cl^-, la concentration du Tl^{3+} libre est d'environ 10^{-12}% de celle du Tl(III) total, compte tenu des constantes de stabilité des complexes avec Cl^- (5) ce qui explique le renversement de la situation.

La réaction de décomposition en réactifs de départ est d'ordre un en organothallique. La constante k_{-1} varie linéairement avec la concentration en H^+, mais elle est indépendante de la concentration en Cl^- (voir fig. 1).

Ces résultats sont compatibles avec le méca-

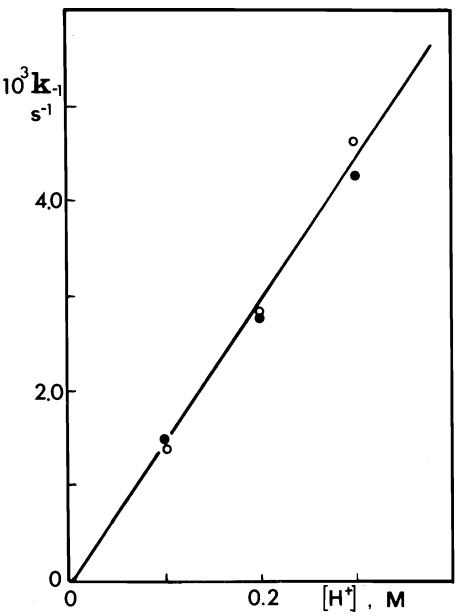

FIG. 1. Décomposition de l'organothallique en réactifs de départ. $T = 25°C$; $[R'Tl(OAc)_2] = 2.5 \times 10^{-5}$ M; solvant: H_2O–CH_3OH 75%–25% (v/v); $\mu = 0.5$ M. ○, $[Cl^-] = 0.1$ M; ●, $[Cl^-] = 0.5$ M.

[1]A des concentrations en H^+ et en Cl^- inférieures à 0.1 M les étapes 7 et 8 interviennent simultanément, leur importance et vitesse relatives dépendant des conditions.

nisme suivant:

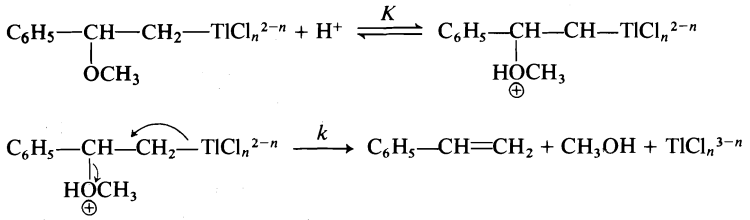

avec $k_{-1} = kK[H^+]$ et $kK = 1.5 \times 10^{-2} M^{-1} s^{-1}$ à 25°C

Dans le cas de la décomposition des organomercuriques dans le méthanol un mécanisme légèrement différent a été proposé; il implique une attaque concertée par un acide halogéné, HX (6):

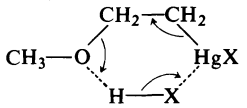

Dans notre cas l'ion Cl^- coordine le métal avant l'attaque de H^+, et son rôle consiste à rendre le thallium moins électrophile. Le fait que la vitesse de réaction soit indépendante de la concentration en Cl^- (0.1 *M* à 0.5 *M*) indique[2] que la coordination ne change pas dans ce domaine ou, si elle change (e.g. $R'TlCl_2 + Cl^- \rightleftharpoons R'TlCl_3^-$), ce changement n'a pas d'influence appréciable sur la vitesse de décomposition. A cause de la gamme de concentration limitée, il n'est pas possible d'avoir plus d'information sur la nature exacte des expèces.

Il est à remarquer que l'influence des ions Cl^- observée dans ce cas est très différente de celle observée dans la décomposition des diacetoxyalkylthallium (e.g. $CH_3Tl(OAc)_2$). Cette réaction est accélérée par les ions Cl^- (7). Ceci est expliqué en admettant que Cl^- agit comme réactif nucléophile dans l'attaque S_N2 sur le carbone portant le thallium (8). Ce changement du mécanisme d'intervention des ions Cl^- montre l'importance de la participation ou la migration des groupes en position β (H, alkyle, aryle, OH, OR, OOCR) lors de la rupture du lien C—Tl dans le cas des composés d'oxythallation.

[2]A acidité constante, l'augmentation de la concentration en Cl^- entraîne l'augmentation de la très faible quantité de HCl non-dissocié Il ne semble donc pas que le mécanisme concerté puisse avoir une contribution majeure.

L'influence d'ions I^- et de l'éthylènediamine

La décomposition de l'organothallique en présence d'ions I^- se fait d'après l'éq. 9.

[9] $C_6H_5—CH(OCH_3)—CH_2Tl^{2+} + 3I^- \rightarrow C_6H_5—CH=CH_2 + CH_3OH + TlI + I_2$

La quantité de I_2 formé correspond à la quantité de[3] RTl^{2+} et le styrène est régénéré quantitativement, à l'exclusion de tout produit d'oxydation.

La cinétique de cette réaction rapide n'a pas pu être étudiée par flux stoppé, dû aux problèmes causés par la précipitation de TlI. Par analogie au cas des ions Cl^-, il est logique d'admettre qu'il y a d'abord coordination conduisant à $R'TlI_n^{2-n}$, qui se décompose ensuite par le mécanisme discuté plus haut. Dans ce cas, l'équilibre 7 est déplacé vers la formation du styrène à cause de la réduction du Tl(III) formé par I^-.

Nous avons voulu étudier l'influence de divers ligands azotés. Deux limitations ont été rencontrées, soit l'absorption par les bases aux longueurs d'onde utilisées et, l'influence faible (e.g. NH_3) due à la protonation des bases en milieu acide.

A pH = 5.0, l'influence de l'éthylènediamine (en) a été étudiée. Dans ce cas on observe encore une diminution de la vitesse de décomposition oxydative (voir fig. 2). Ceci est attribué à la coordination du thallium entraînant une baisse importante de la réactivité.

Le Tl(III) forme divers complexes avec l'éthylènediamine (9). En solution aqueuse on admet la formation d'un complexe 1:1 d'après l'équation: $Tl(OH)_2^+ + en \rightleftharpoons Tl(OH)_2 \cdot en^+$, avec une constante de $1 \times 10^{13} M^{-1}$ (10). Par

[3]Cette réaction peut être utilisée pour le dosage de l'organothallique par iodométrie.

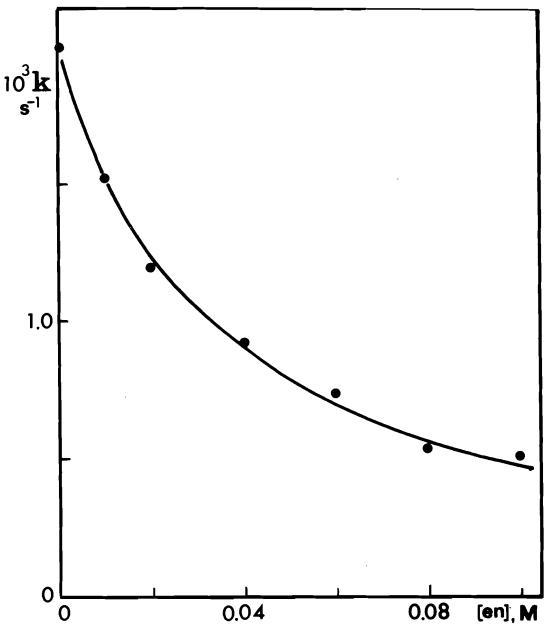

FIG. 2. Influence de l'éthylènediamine. $T = 25°C$; $[R'Tl(OAc)_2] = 1.0 \times 10^{-3}$ M; $[H^+] = 1.7 \times 10^{-5}$ M; solvant: H_2O–CH_3OH 75%–25% (v/v); $\mu = 0.5$ M. Courbe calculée; points expérimentaux.

analogie, il est probable que dans notre cas il s'agisse de la formation de $R'TlOH{\cdot}en^+$.

L'interprétation des résultats, en admettant que le complexe formé n'a pas de contribution à la vitesse[4], conduit à un accord satisfaisant entre résultats expérimentaux (points) et la courbe calculée de la fig. 2, d'après l'éq. 10.

$$[10] \quad k_{exp} = \frac{k_1 K_1[H^+] + k_2}{1 + K_1[H^+] + K_{en}[en]_{total}}$$

On obtient une constante de formation apparente[5] de $K_{en} = 30$ M^{-1}. En utilisant les valeurs de pK_a de l'éthylènediamine dans l'eau ($pK_{a_1} = 7.5$, $pK_{a_2} = 10.8$) on peut estimer la valeur de la constante d'équilibre pour la réaction: $R'TlOH^+ + en \rightleftharpoons R'TlOH{\cdot}en^+$ à $\sim 10^{10}$ M^{-1}.

La stabilité de $R'TlOH{\cdot}en^+$ est donc d'un facteur d'environ 10^3 inférieure à celle de $Tl(OH)_2{\cdot}en^+$. Ceci permet de comprendre les résultats à une acidité plus élevée ($[H^+] = 0.025$ M à l'équilibre); dans ces conditions, Tl(III) est complexé significativement (10), malgré la faible concentration de l'éthylènediamine non-protonée, mais RTlOH ne l'est plus et on n'observe pas d'effet mesurable sur la vitesse.

Conclusion

L'étude de la cinétique de formation du composé d'oxythallation a déjà permis de montrer que la coordination du Tl^{3+} par l'ion Cl^- entraîne une baisse de sa réactivité (11). Les résultats présents montrent, que la vitesse de décomposition oxydative de l'organothallique formé dépend, de façon encore plus marquée, de la coordination du thallium dans $R'Tl^{2+}$. De plus, dans ce composé, l'affinité du Tl pour divers ligands (OH^-, Cl^-, éthylènediamine) est comparable à celle de Tl^{3+}.

La réactivité de $R'Tl^{2+}$ est beaucoup plus grande que celle de $R'TlOH^+$ et $R'TlCl^+$, tandis que celle de R'TlOHCl n'est pas mesurable dans les conditions expérimentales. La diminution du caractère électrophile du Tl entraîne la polarisation moindre du lien C—Tl et la migration du groupe phényle est défavorisée.

La formation d'espèces, telles $R'TlCl_2$ ou $R'TlCl_3^-$ amplifie encore ce phénomène et la vitesse de décomposition oxydative devient négligeable. Par contre, elle favorise l'attaque électrophile par H^+ sur le groupe méthoxy, conduisant de façon semblable aux cas des organomercuriques à la décomposition de l'organothallique pour régénérer le styrène et le Tl(III).

En conclusion, l'influence des ligands affecte de façon déterminante la vitesse relative des étapes de l'oxydation thallique et l'ensemble doit être considéré lorsqu'on interprète les résultats obtenus pour des sels thalliques différents.

Remerciements

Les auteurs remercient le Conseil national de recherches du Canada pour la bourse d'études graduées (L.N.) et la subvention de recherches (M.Z.) octroyées.

1. P. M. HENRY. J. Am. Chem. Soc. **87**, 990 (1965); **87**, 4423 (1965); J. E. BYRD et J. HALPERN. J. Am. Chem. Soc. **95**, 2586 (1973).

[4]A des concentrations en ligand > 0.1 M un phénomène parasite, identifié comme une réaction secondaire des produits avec l'éthylènediamine interfère dans les variations d'absorbance. Ceci empêche l'étude plus poussée, pouvant conduire à la détermination de la constante de vitesse, très faible, de cette espèce.

[5]La constante est obtenue en considérant la concentration totale en ne tenant pas compte de la protonation de l'éthylènediamine.

2. L. NADON et M. ZADOR. Can. J. Chem. **52**, 2667 (1974).
3. C. BEAUDRY et M. ZADOR. J. Organomet. Chem. **102**, 265 (1975).
4. K. THAMMAVONG et M. ZADOR. J. Phys. E, **9**, 1041 (1976).
5. D. PESCHANSKI et S. VALLADAS-DUBOIS. Bull. Soc. Chim. Fr. 1170 (1956); S. AHRLAND, L. GRENTHE, L. JOHANSSON et B. NOREN. Acta Chem. Scand. **17**, 1567 (1963).
6. O. W. BERG, W. P. LAY, A. RODGMAN et F. G. WRIGHT. Can. J. Chem. **36**, 358 (1958).
7. H. KUROSAWA et R. OKAWARA. J. Organomet. Chem. **10**, 211 (1967).
8. U. POHL et F. HUBER. J. Organomet. Chem. **116**, 141 (1976).
9. F. YA. KUL'BA, A. V. BARSUKOV et YU. S. VARSHAVSKII. Russ. J. Inorg. Chem. **13**, 237 (1968).
10. B. I. LOBOV, F. YA. KUL'BA et V. E. MIRONOV. Russ. J. Inorg. Chem. **12**, 176 (1967).
11. L. NADON, M. TARDAT, M. ZADOR et S. FLISZAR. Can. J. Chem. **51**, 2366 (1973).

Consecutive reactions in the thermal decomposition of phenylalkyldiazirines

MICHAEL T. H. LIU AND BARRY M. JENNINGS

Department of Chemistry, University of Prince Edward Island, Charlottetown, P.E.I., Canada C1A 4P3

Received May 5, 1977

MICHAEL T. H. LIU and BARRY M. JENNINGS. Can. J. Chem. **55**, 3596 (1977).

The thermal decomposition of phenyl-*n*-butyldiazirine and of phenylmethyldiazirine in DMSO and in HOAc have been investigated over the temperature range 80–130°C. The intermediate diazo compounds, 1-phenyl-1-diazopentane and 1-phenyldiazoethane respectively have been detected and isolated. The decomposition of phenyl-*n*-butyldiazirine and the subsequent decomposition of its product, 1-phenyl-1-diazopentane, are an illustration of consecutive reactions. The kinetic parameters for the isomerization and decomposition reactions have been determined. The isomerization of phenylmethyldiazirine to 1-phenyldiazoethane is first order and probably unimolecular but the kinetics for the subsequent reactions of 1-phenyldiazoethane are complicated by several competing rate processes.

MICHAEL T. H. LIU et BARRY M. JENNINGS. Can. J. Chem. **55**, 3596 (1977).

On étudie la décomposition thermique entre 80 et 130°C du phényl-3 *n*-butyl-3 diazirine et du phényl-3 méthyl-3 diazirine dans le DMSO et l'acide acétique. Les composés diazo intermédiaires sont respectivement le phényl-1 diazo-1 pentane et le phényl-1 diazo-1 éthane. Ces derniers ont été détectés et isolés. La décomposition du phényl-3 *n*-butyl-3 diazirine et la décomposition ultérieure de son intermédiaire le phényl-1 diazo-1 pentane sont un bon exemple de réactions successives. On détermine les paramètres cinétiques pour les réactions d'isomérisation et de décomposition. L'isomérisation du phényl-3 méthyl-3 diazirine en phényl-1 diazo-1 éthane est d'ordre 1 et probablement unimoléculaire, mais les cinétiques des réactions ultérieures du phényl-1 diazo-1 éthane sont compliquées par plusieurs processus qui entrent en compétition.

[Traduit par le journal]

Introduction

The intermediacy of diazomethane in the decomposition of diazirine has been the subject of discussion for many years (1–3). While there is sufficient evidence for the diazomethane intermediate in the photolysis of diazirine (4), its presence in the thermal decomposition has only been implicated, and no diazomethane intermediate has ever been isolated from a diazirine pyrolysis experiment (5–8). In one report (9), the attempted synthesis of 3,3-diphenyldiazirine resulted in the formation of diphenyldiazomethane; however, the precursory existence of diazirine was never verified. Only in the case of 3-methyl-3-vinyldiazirine has the linear diazo isomer been observed (8) as its subsequent reaction product, 3-methylpyrazole. We have recently reported (10) the formation of 1-phenyl-1-diazopentane (**2**) as evidence for diazo intermediate in the thermolysis of phenyl-*n*-butyldiazirine (**1**). In this paper, we wish to report the complete kinetic data for the thermal decomposition of **1** and **2** as well as the data for the decomposition of phenylmethyldiazirine (**4**). Comparisons will be made in relation to the existing data for the thermal decomposition of methylvinyldiazirine and of various chlorodiazirines.

Results and Discussion

1. Decomposition of Phenyl-n-butyldiazirine (1)

The thermal decomposition of **1** in DMSO solutions (0.1 *M*) at 100°C gave nitrogen, *cis*- and *trans*-1-phenyl-1-pentenes (ratio *cis*:*trans* = 1:5) along with a small amount (<5%) of valerophenone. No azine was found. The formation of valerophenone was due to the oxidation of **2** by DMSO and the olefins were the rearrangement products of carbene **3**. When the reaction was followed by uv or ir spectroscopy, an intermediate species was observed to form rapidly and subsequently diminish, uv_{max} at 520 nm (low ε) and ir at 4.90 μ are consistent with this intermediate being assigned as 1-phenyl-1-diazopentane, **2**. The isolation of **2** was possible by interruption of the reaction after 1 h followed by extraction with petroleum ether. Compound **2** appears to be very stable, as the red petroleum ether solution remained unchanged at room temperature for several days. The above results serve to support a stepwise mechanism for the decomposition of the diazirine as in

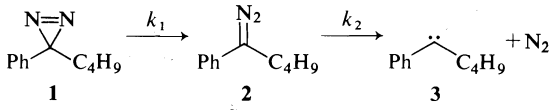

1 2 3

SCHEME 1

Scheme 1. The rates of decomposition of **1** in DMSO were studied over the temperature range 80–130°C by measuring the disappearance of its uv_{max} at 371 nm (k_1) and by measuring the evolved nitrogen during the decomposition (k_2). The first-order rate constants, k_1 and k_2, are presented in Table 1. The determination of k_2 in DMSO by the N_2 evolution method requires elaboration. The first-order plot from N_2 measurements does not give a straight line; in fact, there is a slight curvature (convex) during the first 20–30 min of the reaction. This curvature is due to the build-up of the diazo compound. After such time, N_2 evolution begins to approximate first-order behavior and it is in this portion of the graph that k_2 was taken. In order to confirm the value of k_2, we have synthesized 1-phenyl-1-diazopentane from a separate experiment, and its N_2 evolution in DMSO was measured. The first-order rate constants determined in this manner were within 3% of the values reported in Table 1. That the two measurements in DMSO solvent differ by a factor of 3 suggests that in fact two different rates are being measured; k_1 can therefore be taken as the rate of isomerization of **1** to **2**, while k_2 may be regarded as the rate of decomposition of **2** giving nitrogen and **3**. The assignment of k_1 and k_2 above finds further support in their measurement in acetic acid (Table 1). It is well established that diazirine decomposition is unaffected by acid (1) while the decomposition of diazomethanes is acid catalyzed (11). Thus in this case, the isomerization of **1** to **2** would be the rate determining step in the overall reaction and k_2 would be expected to equal k_1, which is the experimental observation. The data in Table 1 gave excellent Arrhenius plots from which equations 1 and 2 were obtained by least-squares analysis. R is taken as

TABLE 1. Rate constants for the thermal decomposition of phenyl-*n*-butyldiazirine (k_1) and 1-phenyl-1-diazopentane (k_2)

Solvent	T(°C)	$k_1 \times 10^4$(s^{-1})*	$k_2 \times 10^4$(s^{-1})*
DMSO	82.2	0.98±0.02	
	89.0	2.08±0.04	
	97.4	4.98±0.03	
	100.2	6.75±0.02	
	109.4	16.63±0.12	
	98.8		1.93±0.02
	100.2		2.23±0.16
	105.4		3.77±0.05
	111.4		5.64±0.09
	119.4		12.57±0.13
	126.5		24.49±0.22
HOAc	100.2	5.24±0.07	5.78±0.20

*All k_1 values were determined by uv and k_2 values by N_2 measurements.

[1] $k_1 = 10^{13.26\pm0.05} \exp((-28\,080 \pm 90)/RT)\ s^{-1}$

[2] $k_2 = 10^{12.03\pm0.54} \exp((-26\,810 \pm 950)/RT)\ s^{-1}$

1.987 cal mol^{-1} K^{-1} throughout this text. The errors quoted are standard deviations. The Arrhenius parameters for k_1 are in good agreement with reported values for decomposition of other diazirines (7). The parameters for k_2 compare well with those for the decomposition of diethyl diazosuccinate (11) (E = 27.31 kcal/mol, log A = 11.77) and for the decomposition of diphenyldiazomethane (12) (E = 27.9 kcal/mol, log A = 13.25).

Now the question arises whether the concerted elimination of N_2 from **1** to give carbene **3** can be completely ruled out. In order to answer this question and also to test the consistency of the rate constants (k_1 and k_2) assignment, the following experiments have been carried out. For a consecutive reaction of the type $A \xrightarrow{k_1} B \xrightarrow{k_2} C$, the concentration of B is given by [3] (13).

[3] $[B] = [A]_0 \frac{k_1}{k_2 - k_1}(e^{-k_1 t} - e^{-k_2 t})$

Thus by knowing the initial concentration of **1** and the values of k_1 and k_2 at the temperature of the experiment, the concentration of **2** can be determined at any time t. The concentration of **2** at a time t was determined by withdrawing an aliquot of reaction mixture and running it into a large excess of acetic acid to convert **2** to the ester, 1-phenyl-1-pentyl acetate. This mixture was then worked up in the usual manner and analyzed by vpc. When observed m mole ester vs. calculated m mole ester are plotted, a straight line with a slope of 0.90 is obtained. This indicates that 90% of the calculated amount of **2** is being accounted for in the measured ester. Owing to the number of manipulations required in the experimental procedure and analysis, a value for

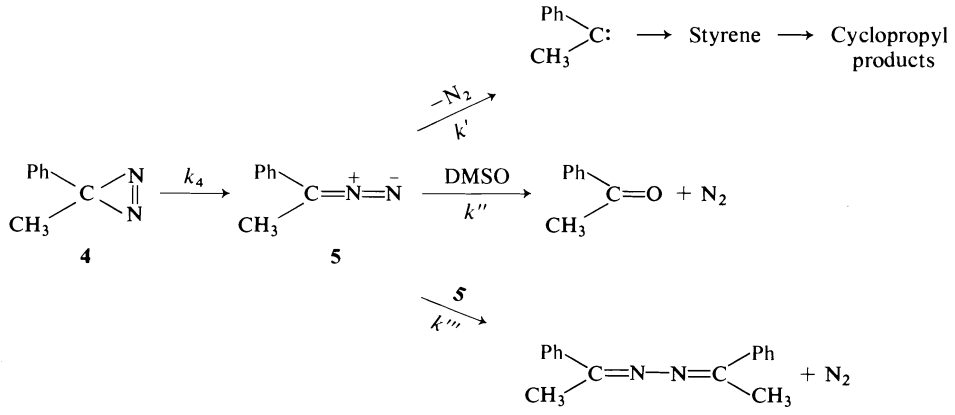

SCHEME 2

the experimental error of ±5–10% does not seem unreasonable. Hence, it is suggested that all diazirine **1** decomposes via the diazo isomer **2**.

2. Decomposition of Phenylmethyldiazirine (4)

Schmitz and Ohme (14) reported that the thermal decomposition of phenylmethyldiazirine **4** in nitrobenzene gave styrene. This is to be contrasted with Overberger and Anselme's results (15) for which they reported that the thermal decomposition of 1-phenyl-diazoethane **5** gave acetophenone azine as the only product. In our present work, the thermal decomposition of **4** in DMSO (0.1 *M*) gave the following products: styrene 10–15%, cyclopropyl products (carbene + styrene) 15%, acetophenone 45%, and acetophenone azine 10–15%. In addition, 1-phenyldiazoethane (**5**) has been isolated as evidence for a diazo intermediate during the decomposition of phenylmethyldiazirine (**4**). The decomposition pathways are summarized in Scheme 2. Further experimentation (16) shows that in the decomposition of diazirine **4**, the formation of **5** is not affected by the nature of the solvent, but its subsequent decomposition to stable products is dependent on solvent polarity and concentration. A separate study in the mechanism of azine formation (17) clearly indicates that azine could not be formed by the attack of carbene on **5**. It is interesting to note that the absence of azine formation in the decomposition of phenyl-*n*-butyldiazirine could well be explained in terms of a steric effect. It is because of this steric effect that the decomposition of **1** is truly an example of consecutive reactions. In the decomposition of **4**, the kinetics are complicated by the presence of several other competing reactions in the decomposition of **5**. However, the isomerization of **4** to **5** is still first order and probably unimolecular. Thus, rate constants in DMSO for the isomerization reaction were determined by uv spectroscopy and are listed in Table 2. The data gave a good Arrhenius plot from which [4] was obtained by least-squares analysis. When N_2

$$[4] \quad k_4 = 10^{13.45\pm0.46} \exp((-28\,500 \pm 790)/RT)\ s^{-1}$$

kinetics were attempted in DMSO, great curvature was evident in the first-order plots, thus confirming the complexity of the reaction. Since the rate of nitrogen formation is

$$[5] \quad V_{N_2} = k'[\mathbf{5}] + k''[\mathbf{5}][\text{DMSO}] + k'''[\mathbf{5}]^2$$

the order of the reaction should, in fact, be between first and second order in **5**. When **4** is decomposed in HOAc, the diazo compound **5** will immediately be removed by HOAc as the ester; hence, the rate constant obtained by uv measurements should be equal to the one obtained by N_2 measurement. This was observed experimentally. The activation energies for the thermal decomposition of the diazirines **1** and

TABLE 2. Rate constants for the thermal decomposition of phenylmethyldiazirine (k_4)

Solvent	T(°C)	$k_4 \times 10^4$(s^{-1})	Method
DMSO	83.6	0.98±0.02	uv
	92.1	2.70±0.04	uv
	99.6	6.44±0.05	uv
	108.6	14.40±0.31	uv
	116.0	28.03±0.55	uv
HOAc	99.6	4.20±0.08	uv
	99.6	4.79±0.03	N_2

4 as well as that of chlorophenyldiazirine (7*c*) in DMSO solvent are about 28 kcal/mol. It would appear that the energy of activation depends only on the presence of the phenyl ring. However, the relative rate for k(chlorophenyldiazirine)/k(**1** or **4**) at 100°C is approximately equal to 6.

Our earlier work (7*b*, *d*, *e*) on the thermal decomposition of chlorodiazirines suggests that the decomposition of diazirine occurs by a two-step mechanism. We have also inferred that the intermediate is similar to diazomethane in structure and the extent of polarization in this intermediate would depend on the substituent present in the diazirine ring (7*b*, *e*). Perhaps the most striking example for a polarized transition state is the 3-chloro-3-*p*-methoxyphenyldiazirine in which the positive charge on the carbon of the diazo group is stabilized by the *p*-methoxyphenyl substituent (7*b*). In the decomposition of **1**, the two measurements (by uv and N_2) in DMSO differ by a factor of 3, but in the decomposition of chlorophenyldiazirine in the same solvent, the rate constants obtained by either method are equal (7*c*). This implies that the chlorophenyldiazomethane intermediate decomposes rapidly as soon as it is formed. However, we are certain that there is a definite lifetime for the chlorophenyldiazomethane intermediate but the duration is too short to be detectable by conventional techniques. Several chlorodiazomethanes are also known to be unstable (18, 19).

In conclusion, all diazirines will isomerize (k_i) to the corresponding diazo intermediate with similar rate constants (hence similar E and A) since all reactions involve the ring opening process. However, the rate constants (k_d) for the subsequent reaction of the diazo intermediates differ in many powers of 10. In the case of phenyl-*n*-butyldiazirine, a value of 0.33 was obtained for k_d/k_i and in the case of methylvinyldiazirine (7*d*, 8, 20), a value of approximately 70 was found for k_d/k_i. It is reasonable to assume a value of $>10^3$ in the case of chlorophenyldiazirine. It is to be noted that the diazirines, which we have chosen in the above discussion, are all stable compounds (chlorophenyldiazirine has the least kinetic and thermodynamic stability) and they can be kept in the refrigerator (0°C) for several weeks without decomposition. Such stability is not observed for the corresponding diazo compounds. The indicated order of stability is as follows:

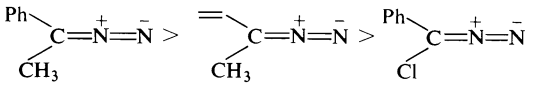

Experimental

The ir and nmr spectra were obtained with Perkin-Elmer Model 257 and Varian Associates, T60 instruments respectively. The chemical shifts are given in τ scale together with splitting pattern, relative integrated areas, and assignments. The uv spectra were measured with a Unicam SP 800 spectrophotometer and mass spectra with a Hitachi-Perkin-Elmer model RMS-4 spectrometer. The vpc analyses were carried out using a Perkin-Elmer model F 11 equipped with a hydrogen flame detector; the peak areas were integrated by a ball and disc integrator.

1. Synthesis of n-Butylphenylketimine

To a 1 ℓ, 3 neck flask equipped with magnetic stirrer, dropping funnel, and condenser was added 100 ml of anhydrous ether and 100 ml (0.22 mol) of 2.2 *M* *n*-butyllithium in hexane. With stirring, a solution of 20 g (0.2 mol) of benzonitrile in 100 ml ether was added dropwise. Considerable heat was evolved and the reaction mixture became dark in color. After complete addition, the reaction mixture was refluxed for 3 h, then allowed to cool. Anhydrous methanol (50 ml) was added dropwise and stirring was continued for an extra half hour. The mixture was then filtered and concentrated *in vacuo*, giving a dark oil, which was distilled (90–95°C, 0.8 Torr) to give 18.6 g (61%) of the product: ir 1620 cm^{-1} (C=N); nmr τ 0.7 (br m, 1, =NH), 2.4 and 2.7 (each m, total 5, aromatics), 7.4 (t, 2, J = 7 Hz, >C(=NH) —CH_2), 8.5 (br m, 4, methylenes), 9.05 (m, 3, methyl).

2. Synthesis of Phenyl-n-butyldiaziridine from n-Butylphenylketimine

A solution of 19 g (0.12 mol) of ketimine in 125 ml of methanol was added dropwise with stirring to 50 ml of liquid NH_3 at −50°C in a three neck 250 ml flask. After stirring for ½ h at −50°C, hydroxylamine-*O*-sulphonic acid (HOS, 25 g, 0.22 mol) was added in small portions. After stirring for 1 h at −50°C, the reaction mixture was allowed to warm up overnight. The mixture was added to 400 ml ether, filtered, washed with water, and dried. After filtering and removal of solvent, 21 g amber oil remained: ir 3450 cm^{-1} (N—H).

3. Synthesis of Phenyl-n-butyldiaziridine from Valerophenone (n-Butylphenylketone)

A mixture of valerophenone (13 g, 0.08 mol), benzylamine (13 g, 0.12 mol), *p*-toluenesulphonic acid (1 g), and benzene (100 ml) was heated to reflux for 68 h. The water formed during the reaction was trapped in a Dean Stark apparatus via benzene azeotrope. After this period, the theoretical quantity of water was collected and the reaction mixture was allowed to cool. After filtering the mixture the benzene solution was washed with saturated $NaHCO_3$, water, and was dried. Removal of benzene left a yellow oil which was distilled at 170–180°C (2 Torr) to give 16.43 g (82%) of *N*-benzyl-*n*-butylphenylketimine; ir 1625 cm^{-1} (C=N). This product was dissolved in 125 ml methanol and added dropwise to 75 ml of liquid ammonia at −30°C. After stirring at −30°C for 3 h, 18.65 g (0.165 mol) of HOS were added in small portions, and

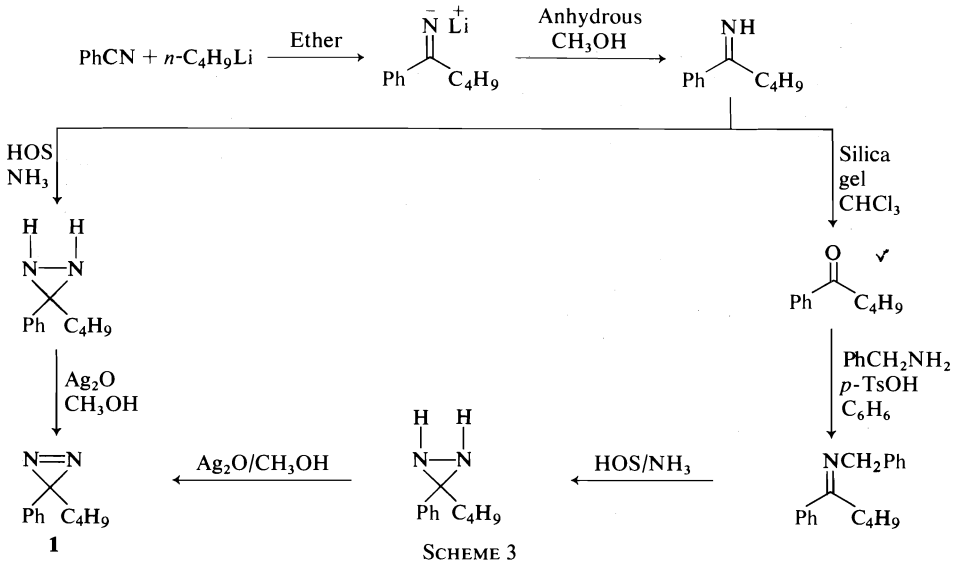

SCHEME 3

the procedure continued in the same manner as in part 2 above. Yield was 18.4 g of amber oil.

4. Synthesis of Phenyl-n-butyldiazirine (1) from Phenyl-n-butyldiaziridine

The crude diaziridine (11.45 g) prepared by either method above was dissolved in 150 ml methanol and added to a suspension of freshly prepared silver oxide in 50 ml methanol. After stirring for 2 h, during which time a heavy silver mirror coated the interior walls of the flask, the solution was filtered, added to 600 ml ether, washed with several portions of water, and dried. Removal of ether left 11.5 g of yellow oil which was chromatographed on 100 g silica gel (100–200 mesh) with CH_2Cl_2 – petroleum ether (1:6). This resulted in 4.0 g (this represents an overall yield of 35% with respect to either *n*-butylphenylketimine or *N*-benzyl-*n*-butylphenylketimine) of diazirine as a nearly colorless liquid: ir 1580 cm^{-1} (N=N); nmr τ 2.8 (m, 3, *meta* and *para* aromatics), 3.13 (m, 2, *ortho*), 8.07 (br t, J = 7 Hz, 2, 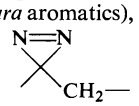), 8.7 (m, 4, methylenes), 9.1 (br t, 3, methyl); uv_{max} (petroleum ether) 372 (ε 235), 382 sh (ε 214); ms (70 eV) *m/e* 146 (parent − N_2). The synthetic procedures for phenyl-*n*-butyldiazirine are summarized in Scheme 3.

5. Product Analysis

a. Decompositions of 1 in DMSO

The reaction mixtures from two kinetic experiments were combined and diluted with 200 ml water. This was extracted with 2 × 25 ml ether and the combined ether extracts were washed with 50 ml water, dried and concentrated *in vacuo*, giving 340 mg of yellow oil. The vpc analysis on a 12 ft 20% Carbowax showed three components. Column chromatography (silica gel, 50% benzene–$CHCl_3$) resolved the mixture into two components. The minor fraction was identified as valerophenone (< 5%) while the major portion was a mixture of the other two components, which were identified as *cis* and *trans* (1:5) 1-phenyl-1-pentenes on the basis of identical retention times as authentic samples and nmr data: τ 2.8 (s, 5, aromatic), 3.8 (m, 2, olefinic) 7.9 (m, 2, allylic), 8.6 (m, 2, methylene), 9.1 (br, t, 3, methyl).

b. Decomposition of 1 in HOAc

The reaction mixture from one kinetic experiment was extracted as above to give 190 mg of oil. The vpc showed three components in a ratio of 1:5:19. Column chromatography on silica gel with CCl_4–$CHCl_3$ separated the mixture into two fractions. The first, 27 mg, was shown to be a mixture of *cis*- and *trans*-1-phenyl-1-pentenes. The second, 158 mg, was identified as 1-phenyl-1-pentyl-acetate on the basis of these spectral properties: ir 1745 cm^{-1} (ester C=O); nmr τ 2.77 (s, 5, aromatic), 4.35 (t, J = 6.5 Hz, 1, 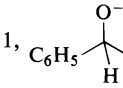), 8.04 (s, 3, acetate methyl), 8.2 (m, 2, methylenes), 8.7 (m, 4, methylenes), 9.13 (t, 3, J = 6 Hz, methyl); *m/e* parent 206; *Anal.* calcd. for $C_{13}H_{18}O_2$: C 75.69, H 8.80; found: C 75.33, H 8.76.

c. Isolation of 1-Phenyl-1-diazopentane (2)

Phenyl-*n*-butyldiazirine (0.5 g) in 20 ml DMSO was heated at 91°C for 2 h. At this time the now red mixture was added to 700 ml water at 10°C and the mixture was extracted with 2 × 50 ml petroleum ether. The combined petroleum ether fractions were washed with water, dried, and concentrated *in vacuo* to give 400 mg of dark-red oil. The ir of this material showed an intense band at 2040 cm^{-1} (diazo >C=N_2), plus indications of a little olefin and carboxyl material. The crude diazo mixture retained its color for several days at room temperature.

6. Photolysis of Phenyl-n-butyldiazirine (1) in Benzene; Isomerization to 1-Phenyl-1-diazopentane (2)

A solution of 400 mg diazirine in 100 ml benzene was degassed and was irradiated with light from a Hanovia 450 W type L lamp in a quartz immersion well, filtered through a 20 cm × 20 cm plate of Corning #5840 glass (transmit 330 < λ < 400 nm). The reaction was monitored by uv spectroscopy, which showed, after 1 h of irradiation, complete disappearance of the diazirine ab-

sorption and the appearance of a long band of low ε centered at about 520 nm (diazo isomer). Good isosbestic points were observed, indicating no other product was found. The solution was concentrated *in vacuo* giving 370 mg of a deep-red oil, the diazo compound.

7. Synthesis of Phenylmethyldiazirine (4)

Phenylmethyldiazirine, **4**, was synthesized from the *N*-benzylmethylphenylketimine in the manner of Schmitz and Ohme (14). The final yield of diazirine (colorless) was 23%, based on the starting ketimine. Spectral properties: ir 1600 cm^{-1} (N=N); nmr τ 2.8 (m, 3, *meta* and *para* aromatics), 3.2 (m, 2, *ortho*), 8.52 (s, 3, methyl) uv_{max} (methanol) 368 nm (ε 187).

8. Product Analysis

a. Decomposition of Phenylmethyldiazirine (4) in DMSO

The reaction mixtures from several DMSO kinetic experiments were combined and worked up as in part 5 above. The products were: styrene 10–15%, cyclopropyl products (carbene + styrene) 15%, acetophenone 45%, and acetophenone azine 10–15%.

b. Decomposition of 4 in Acetic Acid

The reaction mixtures from two kinetic experiments were combined and worked up as above. The product was identified as 1-phenyl-1-ethylacetate on the basis of the following spectral properties: ir 1745 cm^{-1} (ester C=O); nmr τ 2.76 (s, 5, aromatic), 4.22 (q, J = 6.5 Hz, 1, 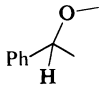 8.03 (s, 3, acetate methyl), 8.50 (d, 3, J = 6.5 Hz, methyl); ms (70 eV) parent 164; *Anal.* calcd. for $C_{10}H_{12}O_2$: C 73.15, H 7.37; found: C 72.81, H 7.38.

9. Isolation of 1-Phenyldiazoethane (5)

Phenylmethyldiazirine **4** (0.5 g) in 20 ml DMSO was heated at 90°C for 2 h. The solution turned red. The red material has a strong ir absorption at 2040 cm^{-1} and was isolated as in part 5*c* and identified as 1-phenyl-diazoethane (**5**).

10. Kinetic Procedure

The methods described previously (*7b*, *c*) were employed for 10 ml solutions of diazirine (0.1 M) in either DMSO or HOAc.

Acknowledgements

Grateful acknowledgement is made by M.T.H.L. for a grant-in-aid of research from the National Research Council of Canada and from the Senate Research Committee of U.P.E.I. We also wish to thank W. Y. Kwan for technical assistance.

1. E. Schmitz. Angew. Chem. Int. Ed. Engl. **3**, 333 (1964).
2. W. Kirmse. Carbene chemistry. Academic Press, New York, NY. 1971.
3. C. H. Bramford and C. F. H. Tipper. Comprehensive chemical kinetics. Vol. 5. Elsevier Publishing Company, New York, NY. 1972.
4. R. A. Smith and J. R. Knowles. J. Chem. Soc. Perkin Trans. II, 686 (1975); H. M. Frey. Adv. Photochem. **4**, 225 (1966).
5. E. Schmitz, C. Hörig, and C. Grundemann. Chem. Ber. **100**, 2093 (1967).
6. E. W. Neuvar and R. A. Mitsch. J. Phys. Chem. **71**, 1229 (1967).
7. (*a*) H. M. Frey and M. T. H. Liu. J. Chem. Soc. A, 1916 (1970); (*b*) M. T. H. Liu and K. Toriyama. Can. J. Chem. **50**, 3009 (1972); (*c*) M. T. H. Liu and K. Toriyama. J. Phys. Chem. **76**, 797 (1972); (*d*) M. T. H. Liu and K. Toriyama. Can. J. Chem. **51**, 2393 (1973); (*e*) M. T. H. Liu and D. H. T. Chien. J. Chem. Soc. Perkin Trans. II, 937 (1974); (*f*) M. T. H. Liu and D. H. T. Chien. Can. J. Chem. **52**, 246 (1974).
8. E. Schmitz. 23rd International Congress of Pure and Applied Chemistry. Vol. II. Butterworths, London. 1971. p. 283.
9. C. G. Overberger and J-P. Anselme. Tetrahedron Lett. 1405 (1963).
10. B. M. Jennings and M. T. H. Liu. J. Am. Chem. Soc. **98**, 6416 (1976).
11. M. T. H. Liu, O. Banjoko, Y. Yamamoto, and I. Moritani. Tetrahedron, 1645 (1975).
12. D. Bethell, D. Whitaker, and J. D. Callister. J. Chem. Soc. 2466 (1965).
13. K. J. Laidler. Chemical kinetics. McGraw-Hill Book Company, Inc., New York, NY. 1950.
14. E. Schmitz and R. Ohme. Ber. **94**, 2166 (1961).
15. C. G. Overberger and J-P. Anselme. J. Org. Chem. **29**, 1188 (1964)
16. M. T. H. Liu and K. Ramakrishnan. J. Org. Chem. Nov. (1977).
17. M. T. H. Liu and K. Ramakrishnan. Tetrahedron Lett. 3139 (1977).
18. G. L. Closs and J. J. Coyle. J. Am. Chem. Soc. **84**, 4350 (1962).
19. R. J. Bussey and R. C. Newman, Jr. J. Org. Chem. 1323 (1969).
20. A. Ledwith and D. Parry. J. Chem. Soc. B, 41 (1967).

Spin–lattice relaxation and hydrodynamical rotation of triphenylene

RODERICK E. WASYLISHEN
Department of Chemistry, University of Winnipeg, Winnipeg, Man., Canada R3B 2E9
AND
BRIAN A. PETTITT
Russell, Man., Canada R0J 1W0
AND
WERNER DANCHURA
Department of Chemistry, University of Manitoba, Winnipeg, Man., Canada R3T 2N2

Received February 7, 1977

RODERICK E. WASYLISHEN, BRIAN A. PETTITT, and WERNER DANCHURA. Can. J. Chem. **55**, 3602 (1977).

The viscosity and temperature dependence of ^1H, ^2H, and ^{13}C nmr relaxation rates of triphenylene were investigated. The observed η/T dependence of the reorientation correlation time, τ_c, is compared with that derived from the work of Hu and Zwanzig based on hydrodynamic rotation with 'stick' and 'slip' boundary conditions. In the hydrodynamic regime, $\tau_c = C\eta/T$. The observed slope, $C_{experimental}$, is 6.2 ± 2 ns K/cP and the calculated values are $C_{slip} = 4.1 \pm 0.6$ ns K/cP and $C_{stick} = 31.0 \pm 3.1$ ns K/cP. These data imply that the reorientation of triphenylene obeys a near-slip condition. That is, rotation in the plane of the molecule encounters little resistance, but rotation of the plane of the molecule is resisted by shear forces in the solvent displaced during rotation. Expressions are given for Boltzmann-averaged free rotation times and comparisons are made with the $\eta = 0$ intercept and the times for slightly hindered rotation.

RODERICK E. WASYLISHEN, BRIAN A. PETTITT et WERNER DANCHURA. Can. J. Chem. **55**, 3602 (1977).

On étudie par rmn ^1H, ^2H et ^{13}C l'effet de la viscosité et de la température sur les vitesses de relaxation du triphénylène. La dépendance observée η/T du temps corrélatif de réorientation τ_c est comparée avec celle obtenue des travaux de Hu et Zwanzig basée sur la rotation hydrodynamique dans des conditions limites "collantes" et "glissantes". Pour le régime hydrodynamique, $\tau_c = C\eta/T$. La pente observée $C_{expérimental}$ est 6.2 ± 2 ns K/cP et les valeurs calculées sont $C_{glissante} = 4.1 \pm 0.6$ ns K/cP et $C_{collante} = 31.02 \pm 3.1$ ns K/cP. Ces résultats impliquent que la réorientation du triphénylène suit une condition qui rapproche de la "glissante". Par exemple, on rencontre une petite résistance pour la rotation dans le plan de la molécule, mais la rotation du plan de la molécule est gênée par des forces de rupture développées au sein du solvant déplacé lors de la rotation. Des expressions sont présentées pour les temps de rotation libre moyens de Boltzmann et des comparaisons sont faites entre l'ordonnée $\eta = 0$ et les temps pour une rotation légèrement empêchée.

[Traduit par le journal]

Introduction

Recent calculations by Hu and Zwanzig (1) relating rotational friction coefficients of spheroids under two sets of boundary conditions have proved useful in the study of molecular rotations in liquids by nuclear magnetic relaxation methods (2). When combined with Woessner's theory (3), their results bring calculated rotational correlation times, τ_c, into line with those measured by nmr. The important equations can be summarized as

$$\tau_c = C\eta/T \quad [1]$$

where η is the shear viscosity and T the temperature of the liquid, and the two models predict very different slopes.

In this paper, the method is outlined for a restricted class of molecules and results are presented from a detailed study of triphenylene (Fig. 1) by proton, deuterium, and carbon-13 relaxation. An appendix presents a brief discussion of rotation in the inertial limit.

Theory

A spin–lattice relaxation time, T_1, is calculated by manipulating the equations of motion for the decay of nuclear magnetization into the form (4)

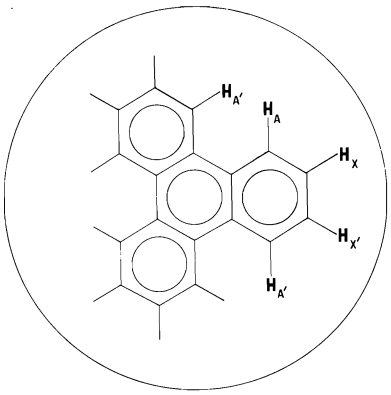

FIG. 1. Triphenylene within a circle of radius 6 Å.

$$[2] \quad \frac{d}{dt}\langle M_z\rangle = -\frac{1}{T_1}(\langle M_z\rangle - \langle M_z\rangle_0)$$

where $\langle M_z\rangle_0$ is the equilibrium value of $\langle M_z\rangle$. For quadrupolar and dipolar intramolecular relaxation in liquids, the time dependence of the spin–lattice interaction is a result of molecular rotation. Consequently, T_1 can be related to molecular parameters that characterize the dynamics of rotation; in particular, the rotational time τ_c. In the limit where rotational motion is much faster than the Larmor frequencies of the nuclei considered, the important relations for the molecules considered here are as follows.

(*a*) Carbon-13:

$$[3] \quad \frac{1}{T_1} = \frac{\gamma_H{}^2\gamma_C{}^2\hbar^2\,\tau_c}{r_{CH}{}^6}$$

(*b*) Protons:

$$[4] \quad \left(\frac{1}{T_1}\right)_i = \frac{3}{2}\gamma_H{}^4\hbar^2\tau_c\sum_j r_{ij}{}^{-6}$$

for proton i, where j is summed over other protons near enough to cause relaxation.

(*c*) Deuterium:

$$[5] \quad \frac{1}{T_1} = \frac{3\pi^2}{2}\left(\frac{e^2qQ}{h}\right)^2\tau_c$$

ignoring the asymmetry parameter for C—D bonds. Here $h = 2\pi\hbar \equiv$ Planck's constant; $\gamma_{H\text{ or }C} \equiv$ magnetogyric ratio of ^1H or ^{13}C; $r \equiv$ internuclear distance; and $e^2qQ/h \equiv$ quadrupolar coupling constant.

In the hydrodynamical model of molecular rotation (1, 3, 5–7), τ_c can be related to the components of the rotational friction tensor, $\bar{\bar{\zeta}}$, of the solid body representing the molecule in a continuous fluid. It is assumed that the molecule undergoes small, random jumps characterised by a rotational diffusion tensor, $\bar{\bar{R}}$. The elements of the diagonalized $\bar{\bar{R}}$ are defined such that the molecule diffuses through angles (rms)

$$[6] \quad \langle\Delta\theta_i{}^2\rangle^{1/2} = (2R_i\Delta t)^{1/2} \quad i = 1, 2, 3$$

in time Δt small on a macroscopic scale but large enough for several jumps to occur (8). Perrin (7*a*) has shown that, for small jumps at equilibrium,

$$[7] \quad R_i = kT/\zeta_i$$

For brevity, the equations of this model are restricted to those of spheroidal molecules ($R_1 = R_2 \neq R_3$) with all relevant internuclear vectors perpendicular to the symmetry axis (the 3 axis). Under the boundary condition that the fluid at the surface of the spheroid has the same velocity as the surface, the ζ's are (3)

$$[8] \quad \zeta_1 = \zeta_2 = \frac{32\pi\eta\,(c^4 - a^4)}{3\{(2c^2 - a^2)S - 2c\}}$$

$$\zeta_3 = \frac{32\pi\eta a^2(c^2 - a^2)}{3(2c - a^2S)}$$

where $a = b$ are the 1 and 2 semi-axes and c is the 3 semi-axis of the spheroid.

$$S = 2(a^2 - c^2)^{-1/2}\tan^{-1}\frac{(a^2 - c^2)^{1/2}}{c}$$

$$[9] \quad \text{for } a > c \text{ (oblate spheroid)}$$

$$S = 2(c^2 - a^2)^{-1/2}\ln\left(\frac{c + (c^2 - a^2)^{1/2}}{c}\right)$$

$$\text{for } a < c \text{ (prolate spheroid)}$$

Woessner's (3) calculation of τ_c then becomes

$$[10] \quad \tau_c = \frac{1}{24R_1} + \frac{3}{8(R_1 + 2R_3)} = \frac{\zeta_1}{24kT} + \frac{3\zeta_1}{8kT(1 + (2\zeta_1/\zeta_3))}$$

Inspection of [7], [8], and [10] shows that τ_c is proportional to η/T and the slope can be calculated from the size of the molecule.

Hu and Zwanzig (1) calculated the ζ_i's for spheroids under boundary conditions where the body slips through the fluid and resistive forces are due only to the displacement of fluid as the body rotates. Thus, $\zeta_3 = 0$ since

no fluid is displaced by rotation about the symmetry axis, and the viscosity dependence of T_1 is due to displacement of fluid by rotation of the symmetry axis. That is, as $\zeta_3 \rightarrow$ very small, $R_3 \rightarrow$ very large and τ_c of [10] is dominated by the first term

$$[11] \qquad \tau_c' = \zeta_1'/24kT$$

where the prime indicates that the calculation is done under 'slip' boundary conditions. Hu and Zwanzig tabulate their results in terms of the ratio

$$[12] \qquad \zeta_1'/\zeta_1 \equiv f(\rho)$$

where

$$\rho \equiv c/a \text{ for oblate spheroids}$$

$$\equiv a/c \text{ for prolate spheroids}$$

Hence,

$$[13] \qquad \tau_c' = f(\rho)\zeta_1/24kT$$

and $\tau_c' < \tau_c$ since $f(\rho) \leq 1$ and the contribution of the second term of [10] has been lost.

In precise terms, it is important to distinguish between hydrodynamical (continuum) and molecular (discrete) ideas, but the qualitative correspondence used here implies that the 'slip' condition is appropriate in the absence of attractive solute–solvent interactions, whereas the 'stick' condition requires these interactions to be strong. On this basis, the two types of boundary conditions would appear to represent lower and upper limits to τ_c. The 'stick' model is especially poor for large solvent molecules because the boundary is not even approximately hydrodynamical.

Experimental

Triphenylene was obtained from the Aldrich Chemical Company and from Dr. Herman Ziffer, N.I.H., Bethesda, Maryland. Triphenylene-d_{12} was obtained from Merck Sharp and Dohme. All solvents were available commercially. Non-deuterated solvents were all spectro-quality reagents.

Proton-decoupled ^{13}C nmr spectra were obtained on a Varian CFT-20 spectrometer (10 mm probe) using a sweep width of 500 Hz and a data acquisition time of 4.095 s. A co-axial tube containing D_2O provided the necessary deuterium lock for the CFT-20. Spin–lattice relaxation times were measured using the inversion–recovery pulse sequence ($d - 180° - t - 90°$), where d is a delay time ($d > 5T_1$) and t is a variable time. The 90° pulse was 18 μs. Nuclear magnetic resonance spectra were obtained for 11 different t values and T_1 was calculated from the slope of a plot of $\ln(\langle M_z\rangle_0 - \langle M_z\rangle)$ vs. t (9). All lines were broadened by approximately 3 Hz using a sensitivity enhancement factor. Approximately 1000 transients were required in order to obtain reasonable signal to noise. The nOe factors were measured using the gated proton decoupler on the CFT-20 ($d \simeq 10T_1$).

All triphenylene solutions used in the proton nmr studies were 0.02 M or less depending on the solubility of I. Solutions were degassed on a high vacuum gas line at least five times by the freeze–pump–thaw technique. All proton measurements were carried out on a Varian HR-200 MHz nmr spectrometer equipped with a Fourier transform accessory. No lock was required for this superconducting magnet therefore it was not necessary to add an internal reference to the solutions. The proton spectrum of triphenylene at 220 MHz is that of a typical AA′XX′ spin system. The H_A protons were typically 200 Hz or more downfield from H_X. Proton spin–lattice relaxation times were measured using non-selective pulses and the inversion recovery sequence. Spectra were obtained for at least 20 different values of t. Typically the 90° pulse was 40 μs while the 180° pulse was 80 μs. The data were accumulated, acquisition time 8 s, and the resulting free induction decay was weighted with an exponential weighting factor and Fourier transformed with a Varian 620L computer. The exponential weighting factor broadened all transitions by approximately 1.6 Hz at half height. Spin–lattice relaxation times were calculated from slopes of plots of $\ln(\langle M_z\rangle_0 - \langle M_z\rangle)$ vs. t. These plots were quite linear thus the recovery rates have been assumed describable in terms of a single exponential time constant (T_1) (see Figs. 2 and 3).

Deuteron relaxation rates of triphenylene-d_{12} were measured at 10 MHz on a Bruker B-KR322 variable frequency spectrometer. The inversion–recovery pulse sequence was used and T_1 was calculated from the slope of a plot of $\ln(\langle M_z\rangle_0 - \langle M_z\rangle)$ vs. t. The free induction decays were not Fourier transformed.

Results and Discussion

1. Geometric Considerations

a. τ_c from Carbon-13 Relaxation

For a 0.045 M solution of triphenylene in CCl_4 at 28.5 ± 2°C the value $T(^{13}C_{A,A'}) = T_1(^{13}C_{X,X'}) = 2.15 \pm 0.1$ s was observed. Equation 3, with a C—H bond length of 1.08 Å, gives $\tau_c = 20.5$ ps. For $C_{A,A'}$ and $C_{X,X'}$ the nOe's were 3.0 ± 0.1.

b. Proton–Proton Separations

To calculate τ_c for triphenylene from ^1H nmr spin–lattice relaxation rates and [4], it is necessary to know the various proton–proton separations. Only protons H_A and $H_{X'}$ are sufficiently proximate to H_X to be effective in its relaxation. Similarly, only $H_{A'}$ and H_X are effective in relaxing H_A. For a 0.02 M solution of triphenylene in CCl_4 at 28.5°C, $T_1(H_A) = 2.81$ s and $T_1(H_X) = 7.10$ s. Assuming $\tau_c = 20.5$ ps and $r_{AX} = r_{XX'}$, substitution into [4] gives $r_{AX} = r_{XX'} = 2.51$ Å and $r_{AA'} = 1.99$ Å.

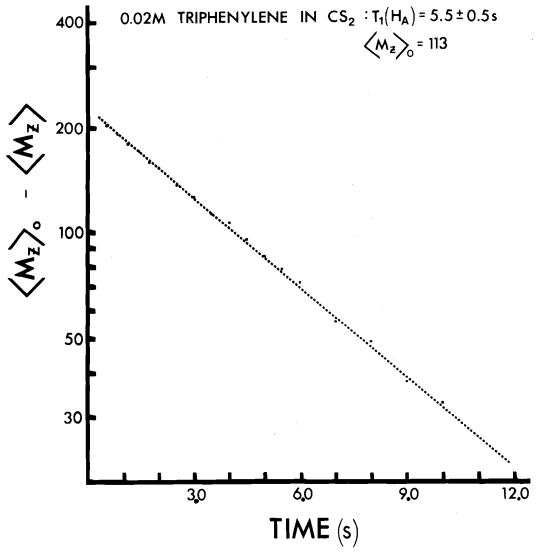

FIG. 2. Plot of $\ln(\langle M_z\rangle_0 - \langle M_z\rangle)$ vs. t for H_A.

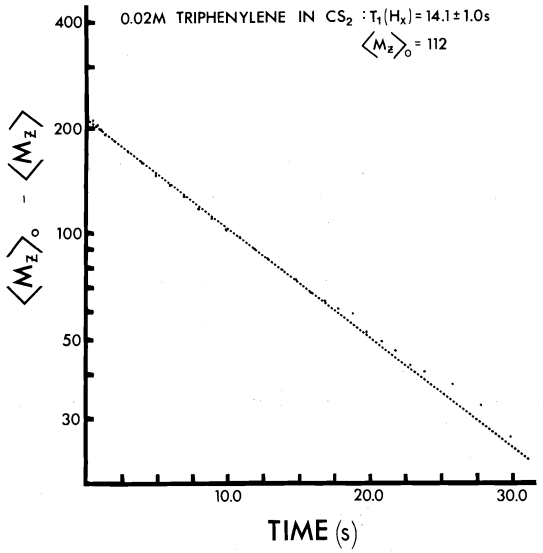

FIG. 3. Plot of $\ln(\langle M_z\rangle_0 - \langle M_z\rangle)$ vs. t for H_X.

These values of r_{HH} are used in all subsequent calculations of τ_c from proton T_1's of triphenylene.

From the carbon skeleton determined by X-ray crystallography (10) the values $r_{AX} = 2.46$ Å, $r_{XX'} = 2.48$ Å, and $r_{AA'} = 1.86$ Å were calculated assuming a planar molecule with all C—H bonds 1.08 Å and all CC_iC angles bisected by the C_i—H vectors. A neutron diffraction study (11) gave $r_{AA'} = 1.91$ Å.

Because we have ignored multi-spin effects (see footnote 1 in part 2*b*) the H—H separations obtained here may not be reliable.

c. Molecular Size

For the calculation of C_{slip} and C_{stick} from [11] and [10], an estimate of the size of triphenylene was necessary. The atomic volume increments given by Edward (12) give a molecular volume of 209.4 Å^3. X-ray data (10) indicate that the triphenylene ring planes are separated by 3.4 Å in the solid state (note: the accepted van der Waals radius for carbon is 1.65–1.7 Å). $V = 4/3\pi a^2 c = 209.4$ Å^3 and $c = 1.7$ Å gives $a = 5.42$ Å. This value for a was taken to be a lower limit. If the molecule is considered to extend one van der Waals radius (1.25–1.45 Å) beyond the periphery of the $H_{XX'}$ protons, then $a = 4.75 + 1.45 = 6.2$ Å can be regarded as an upper limit.

2. Comparison of Observed and Calculated η/T Dependence of τ_c

a. Proton Results

Proton spin–lattice relaxation times for 0.02 *M* solutions of triphenylene in a number of solvents at 20°C are given in Table 1. The observed ratio of $T_1(H_{X,X'})/T_1(H_{A,A'})$ is approximately constant, 2.61 ± 0.22 in all solutions. When a 0.1 *M* solution of triphenylene in CS_2 was saturated with oxygen, $T_1(H_A) = 1.94$ s and $T_1(H_X) = 2.23$ s. Intermolecular dipolar contributions to the proton T_1's were ignored on the basis of general agreement with the deuterium data, and measurements in benzene-d_6 (0.1 *M*) which were within the experimental error of the values in benzene-d_6 (0.02 *M*).

Proton T_1's were also measured for a 0.02 *M* solution of triphenylene in CCl_4 as a function of temperature. In Fig. 4, $\tau_c(H_X)$ is plotted vs. η/T (correlation coefficient = 0.994). A plot of approximately the same slope was obtained for $\tau_c(H_A)$ vs. η/T (correlation coefficient = 0.989). At temperatures greater than 60°C, the ratio $T_1(H_X)/T_1(H_A)$ appears to decrease slightly ($\simeq 2.34$ at 79°C).

b. Deuterium Results

Deuterium spin–lattice relaxation times and τ_c values for 0.1 *M* triphenylene-d_{12} in several solvents at 25°C are given in Table 2. A plot of τ_c vs. η gives a straight line with correlation coefficient = 0.996.

With the exception of the DMSO solutions, the τ_c values calculated for triphenylene and triphenylene-d_{12} are in good agreement. If inertial

TABLE 1. Proton spin–lattice relaxation times for 0.02 M solutions of triphenylene at 20°C

Solvent	Solvent viscosity η (cP)	$T_1(H_A)$ (s)	$T_1(H_X)$ (s)	$\tau_c(H_A)$ (ps)	$\tau_c(H_X)$ (ps)
Dimethylsulfoxide-d_6	2.203	0.91	2.45	64.0	59.7
Dioxane-d_8	1.306	1.56	4.31	37.3	34.0
Pyridine-d_5	0.974	2.34	6.05	24.9	24.2
Carbon tetrachloride	0.969	2.45	6.25	23.8	23.4
Cyclohexane-d_{12}	0.960	2.90	7.00	20.1	20.9
Tetrachloroethylene	0.870	2.51	7.10	23.2	20.6
Benzene-d_6	0.652	3.45	9.14	16.9	16.0
Toluene-d_8	0.590	3.44	8.67	16.9	16.9
Chloroform-d	0.580	3.27	8.58	17.8	17.1
Carbon disulfide	0.363	5.50	14.10	10.6	10.4
Acetone-d_6	0.326	4.50	11.30	12.9	12.9

TABLE 2. Deuterium spin–lattice relaxation times of 0.1 M triphenylene-d_{12} at 25°C

Solvent	Solvent viscosity η (cP)	$T_1(^2H)$ (ms)	τ_c (ps)
Dimethylsulfoxide	1.996	42.5	45.9
1,1,2,2-tetrachloroethane	1.637	47	41.6
Carbon tetrachloride	0.904	85	22.8
Benzene	0.603	130	15.0
Chloroform	0.542	122	16.0
Dichloromethane	0.415	152	12.8
Carbon disulfide	0.356	195	10.0

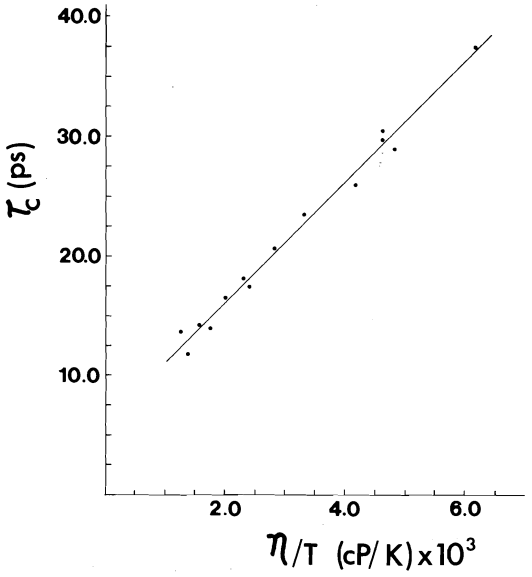

FIG. 4. $\tau_c(H_X)$ vs. η/T for 0.02 M solution of triphenylene in CCl_4 between −11°C and 95.5°C.

effects were important, the τ_c's for the deuterated molecule would be longer, but the errors in the T_1's preclude serious consideration of the differences. The ^1H data is less reliable than the ^2H data for the following reasons. (*1*) Because protons have longer T_1's than deuterons, they are more likely to be affected by intermolecular relaxation with traces of paramagnetic species such as O_2. (*2*) Cross-relaxation and cross-correlation terms may become significant for spin $\frac{1}{2}$ nuclei under certain circumstances (13). Such effects result in non-exponential recovery of $\langle M_z \rangle$ after a 180° pulse, and a description in terms of a single time constant is then incorrect. Near-exponential recovery[1] of $\langle M_z \rangle$ and the agreement between the τ_c's derived from the proton and deuterium data suggest that errors due to these effects are relatively small.

Experimental and calculated values of C are summarized in Table 3. Agreement is especially good between the experimental values obtained by varying the temperature in CCl_4

[1]Non-exponential behavior became most evident at times greater than the T_1's derived from the initial recovery rates. One referee has correctly pointed out that the linear three-spin correlation power density $J_{A'AX}$ is greater in magnitude than the direct A–X interactions ($J_{A'AX} > J_{AX}$). By using more concentrated solutions and/or signal averaging for longer periods of time it would probably be possible to demonstrate that the ^1H recovery curves are actually logarithmically bilinear. If the errors due to multi-spin effects are indeed relatively large, then the derived r_{HH} values in part 1*b* are not real proton–proton separations.

TABLE 3. Slopes of τ_c vs. η/T

	$C_{exp}\left(\frac{ns\ K}{cP}\right)$			$C_{calc}\left(\frac{ns\ K}{cP}\right)$	
	H_A	H_X	a (Å)	Stick	Slip
(*1*) Table 1	8.18	7.51	5.6	28.2	3.58
(*2*) Without dioxane and DMSO	5.27	5.12	5.8	31.0	4.08
(*3*) Figure 4	6.32	6.08	6.0	34.1	4.63
(*4*) Table 2	6.22		6.2	37.3	5.22

(proton T_1's) and varying the viscosity for the deuterium T_1's. If the highly polar solvents dioxane and dimethyl sulfoxide are omitted from the proton data, C is substantially decreased. C_{exp} is best regarded as 6.2 ± 2 ns K/cP. If the plane of the triphenylene ring is assigned a radius $a = 5.8 \pm 0.2$ Å, then $C_{slip} = 4.1 \pm 0.6$ ns K/cP and $C_{stick} = 31.0 \pm 3.1$ ns K/cP. These data imply that the reorientation of triphenylene obeys a near-slip condition. That is, rotation in the plane of the molecule encounters little resistance but rotation of the plane of the molecule is resisted due to shear forces in the solvent displaced during rotation. That is also the case for benzene (2*a*), and preliminary work in this laboratory on pyrene and coronene indicates that it is also true for those molecules.

The intercepts of τ_c vs. η/T plots have been regarded (2*b*, 14) as quantitatively representing inertial rotation on the basis of heuristic use of the equipartition theorem. In the Appendix the free rotar time, τ_{FR}, is given as an ensemble average and compared with the results of Moniz, Steele, and Dixon (15) for small (but non-zero) friction coefficients. The results of triphenylene and a few other molecules are presented in Table 4. Free rotation is slightly faster than the slightly hindered rotation and considerably faster than the experimental intercept. It is not a satisfactory procedure to extrapolate linearly out of the hydrodynamic regime, through the kinetic regime, and into the inertial limit.

TABLE 4. Free rotation times (ps)

	$\tau_{nmr}{}^0$	τ_{MSD}	τ_{FR}
Adamantane	1.4[a]	0.63	0.57
Benzene	0.75[b]	0.34	0.31
Triphenylene	2.6[c]	1.15	1.05
Coronene	5.6[d]	1.38	1.26

[a]Deuterium nmr in several solvents at 23.5°C.
[b]Reference 2*a*: 23°C.
[c]From results given in Table 2: 25°C.
[d]In pyridine-d_5 and CS_2 at 20°C.

Acknowledgements

We wish to thank Dr. Jim Visintainer for carrying out the deuterium nmr measurements, Valerie Wasylishen for analyzing proton T_1 data, and Drs. Edwin D. Becker, Ted Schaefer, and Ed Tomchuk for their support and encouragement. The support of the National Research Council of Canada is gratefully acknowledged. Also, we wish to thank one of the referees for several helpful comments.

1. C.-M. HU and R. ZWANZIG. J. Chem. Phys. **60**, 4354 (1974).
2. (*a*) D. R. BAUER, G. R. ALMS, J. J. BRAUMAN, and R. PECORA. J. Chem. Phys. **61**, 2255 (1974). (*b*) D. R. BAUER, J. J. BRAUMAN, and R. PECORA. J. Am. Chem. Soc. **96**, 6840 (1974).
3. D. E. WOESSNER. J. Chem. Phys. **37**, 647 (1962).
4. A. ABRAGAM. The principles of nuclear magnetism. Oxford University Press, London. 1961. Chapt. VIII.
5. (*a*) G. STOKES. Trans. Cambridge Philos. Soc. **9**, 5 (1856). (*b*) G. STOKES. Mathematical and physical papers. Cambridge. 1903. (*c*) D. EDWARDES. Q. J. Pure Appl. Math. **26**, 70 (1892). (*d*) G. B. JEFFREY. Proc. London Math. Soc. **14**, 327 (1915).
6. A. EINSTEIN. Investigations on the theory of the Brownian movement. Dover, New York, NY. 1956. pp. 19–34.
7. (*a*) F. PERRIN. J. Phys. Radium, **5**, 497 (1934). (*b*) F. PERRIN. J. Phys. Radium, **7** (1936).
8. W. T. HUNTRESS, JR. *In* Advances in magnetic resonance. Vol. 4. *Edited by* J. S. Waugh. Academic Press, N.Y., NY. 1970. p. 9.
9. T. C. FARRAR and E. D. BECKER. Pulse and Fourier transform NMR. Academic Press, New York, NY. 1971.
10. F. R. AHMED and J. TROTTER. Acta Crystallogr. **16**, 503 (1963).
11. G. FERRARIS, D. W. JONES, and J. YERKESS. Z. Kristallogr. **138**, S113 (1973).
12. J. T. EDWARD. J. Chem. Educ. **47**, 261 (1970).
13. (*a*) J. D. CUTNELL, S. B. W. ROEDER, S. L. TIGNOR, and R. S. SMITH. J. Chem. Phys. **62**, 879 (1975), and references contained therein. (*b*) J. D. CUTNELL and J. A. GLASEL. J. Am. Chem. Soc. **98**, 7542 (1976), and references contained therein. (*c*) I. D. CAMPBELL and

R. FREEMAN. J. Magn. Reson. **11**, 143 (1973). (*d*) L. G. WERBELOW and A. G. MARSHALL. Mol. Phys. **28**, 113 (1974), and references contained therein. (*e*) J. F. RODRIGUES DE MIRANDA and C. W. HILBERS. J. Magn. Reson. **19**, 11 (1975).
14. J. GRANDJEAN and P. LASZLO. Mol. Phys. **30**, 413 (1975).
15. W. B. MONIZ, W. A. STEELE, and J. A. DIXON. J. Chem. Phys. **38**, 2418 (1963).

Appendix: Inertial Rotation of Spheroids

With angular velocity $\bar{\omega}$, a molecule rotates through angle θ in time

$$[A:1] \qquad \tau = \theta\omega^{-1}$$

The average value of this quantity in a Boltzmann distribution of energies is

$$[A:2] \quad \tau_{FR} = \frac{\theta(I_1I_2I_3)^{1/2}}{(2\pi kT)^{3/2}} \int d^3\omega\, \omega^{-1} \times \exp\left\{-\frac{(I_1{\omega_1}^2 + I_2{\omega_2}^2 + I_3{\omega_3}^2)}{2kT}\right\}$$

where I_i (i = 1,2,3) are the principal moments of inertia. This expression results in the following.

1. Spheres: $I_1 = I_2 = I_3 \equiv I$

$$[A:3] \qquad \tau_{FR} = \theta(2I/\pi kT)^{1/2}$$

2. Oblate spheroids: $I_1 = I_2 < I_3$

$$[A:4] \quad \tau_{FR} = 2\theta\left[\frac{I_1I_3}{2\pi kT(I_3 - I_1)}\right]^{1/2} \times \tan^{-1}\left[\frac{I_3 - I_1}{I_1}\right]^{1/2}$$

3. Prolate spheroids: $I_1 = I_2 > I_3$

$$[A:5] \quad \tau_{FR} = \theta\left[\frac{I_1I_3}{2\pi kT(I_1 - I_3)}\right]^{1/2} \times \ln\left[\frac{1 + \left(\frac{I_1 - I_3}{I_1}\right)^{1/2}}{1 - \left(\frac{I_1 - I_3}{I_1}\right)^{1/2}}\right]$$

If the molecule is crudely treated as a sphere with average moment of inertia I_{av} given by

$$[A:6] \qquad \frac{1}{I_{av}} = \frac{1}{3}\left(\frac{1}{I_1} + \frac{1}{I_2} + \frac{1}{I_3}\right)$$

the method of Moniz, Steele, and Dixon (MSD) (15) gives

$$[A:7] \qquad \tau_{MSD} = \tfrac{1}{2}(\pi I_{av}/3kT)^{1/2}$$

for rotation through $\theta = \sqrt{3}/3$ rad ([6] with $\Delta t = \tau_c$ and $\tau_c = 1/6R$).

Nuclear charge dispersion studies in the light-mass region formed in the fission of ^{238}U by protons of energy 35–85 MeV[1]

J.-L. GALINIER, M. DIKŠIĆ, AND L. YAFFE

Department of Chemistry, McGill University, Montreal, P.Q., Canada H3A 2K6

Received May 25, 1977

J.-L. GALINIER, M. DIKŠIĆ, and L. YAFFE. Can. J. Chem. **55**, 3609 (1977).

Cross sections for the independent formation of ^{76}As and ^{78}As, for the partially cumulative formation of ^{77}As and ^{77}Ge, and the cumulative formation of ^{79}As, ^{78}Ge, and ^{75}Ge formed in the fission of ^{238}U by protons of energies 35–85 MeV have been determined. Charge dispersion curves have been obtained. Values of $(Z_A - Z_p)$ and full-widths at half-maximum of the curves show that the behaviour of these light-mass products is the same as their complementary fragment ($A \approx 152$). This is inconsistent with values found at $A = 96$.

J.-L. GALINIER, M. DIKŠIĆ et L. YAFFE. Can. J. Chem. **55**, 3609 (1977).

On mesure les sections efficaces pour la formation indépendante de ^{76}As et ^{78}As, la formation cumulative partielle de ^{77}As, ^{77}Ge, ainsi que pour la formation cumulative de ^{79}As, ^{78}Ge et ^{75}Ge issus de la fission de ^{238}U par des protons ayant des énergies comprises entre 35 et 85 MeV. Des courbes de distribution de charge sont ainsi obtenues. Les valeurs de $(Z_A - Z_p)$ et les largeurs à mi-hauteur de ces courbes indiquent que les produits ayant des masses légères se comportent de la même manière que leurs compléments lourds ($A \approx 152$). Ceci est en désaccord avec les valeurs trouvées à $A = 96$.

[Traduit par le journal]

Introduction

Charge distribution in the fission of heavy nuclei has been the object of numerous studies. In the 20–85 MeV range, the McGill group has produced a substantial body of experimental data, particularly for the proton fission of ^{238}U (1–7). Charge dispersion curves have been found to be adequately represented by a Gaussian distribution. The study of the dependence of charge distribution parameters on the excitation energy imparted to the target nucleus shows that, for a given mass chain, Z_p, the most probable charge, moves towards stability with increasing incident energy, whereas the width of the distributions increases correlatively. Both effects are found to be more pronounced in the heavy partner (1, 4) than in the light one (3) when one considers the type of asymmetric mass split which is most probable ($Z = 55$ and $Z = 38$ regions respectively). Symmetric mass divisions yield intermediate results so far as the rate of displacement of Z_p is concerned (6). Recent results obtained show that in the case of very asymmetric fission, changes in Z_p are less sensitive to increases in incident energy and that only narrow charge distribution curves are compatible with the experimental data (7). This was explained as due to energy transfers involving deposition of energies far below what one can expect from compound nucleus formation, or the fission of a nucleus having undergone substantial neutron evaporation. The rather broad curves obtained in the $Z = 55$ region were assumed to be the result of competition between neutron evaporation and fission at each successive step in the de-excitation of the initial cascade nucleus (8).

Very little information has been available concerning nuclear charge distribution in fission of ^{238}U for mass number regions below $A = 90$–93 (3). The present work was undertaken to supplement data obtained in the medium-energy range, particularly to study the behaviour of fission products complementary to the rare-earths nuclides previously investigated (7). We have, therefore, chosen to look at isotopes of germanium and arsenic produced in ^{238}U fission, covering a mass range $A = 75$–79.

Experimental

(A) Irradiations

The target assembly consisted of three uranium foils (134 mg/cm^2) carefully aligned, the center foil constituting the master target and the other two serving to compensate for recoil losses of fission products, and two copper foils (44 mg/cm^2) of the same size placed upstream of the uranium stack with respect to the proton beam.

[1]With financial assistance from the National Research Council of Canada.

The outer copper foil was used to monitor the beam by means of the reaction $^{65}Cu(p,pn)^{64}Cu$. The whole stack was wrapped in thin aluminum foil, fixed on to the end of the cyclotron probe, and irradiated in the internal beam of the McGill synchrocyclotron for 10 min. The beam energy degradation at the level of the master target was of the order of the uncertainty in the beam energy (± 2 MeV) and hence could be neglected. The bombarding energies ranged from 35 to 85 MeV in steps of 5 MeV.

(B) Chemical Separations

(i) Arsenic and Germanium

Following irradiation, the leading edge of the target assembly was sheared off and the middle uranium foil was selected for chemical treatment. Arsenic and germanium were separated by adaptation of standard radiochemical procedures (9–11). The uranium target was dissolved in 0.1 ml 10 *N* HCl in the presence of 0.1 ml of 30% H_2O_2, to which is added 20 mg of sodium arsenate carrier, 1 ml each of ^{74}As and ^{69}Ge tracer solutions (prepared beforehand by (p,n) reaction on ^{74}Ge and ^{69}Ga respectively), and 6 ml of H_2O. The solution was transferred to a separatory funnel containing 7 ml 7.2 *N* HI and 20 ml of benzene. The funnel was immediately shaken for 30 s and the time of phase separation recorded as the time for the isolation of arsenic from the germanium parent. The aqueous phase containing the fission products, among which is germanium, was drained and set aside for subsequent germanium separation. The arsenic was back-extracted twice with 8 ml H_2O and the combined aqueous fractions washed with 10 ml benzene for 10 s. Then 1.0 ml (10 mg) of sodium tellurate hold-back carrier and 7.0 ml 10 *N* HCl were added to the solution which was heated nearly to boiling and reduced with SO_2. After elementary tellurium was filtered, the supernatant solution was boiled to eliminate excess SO_2. The solution was cooled, 1 ml of antimony hold-back carrier and 20 ml 6 *N* HCl were added, and arsenic reduced to the elementary state by adding 100 mg KI and 1 g of sodium hypophosphite. Coagulation was completed on a water bath and the arsenic transferred to a fiber-glass disk, washed with ethanol and isopropyl ether, dried at 110°C, and mounted for activity measurements. The time elapsed between the end of bombardment and the end of the separation was typically 20 min, thus making the measurement of 9.0 min ^{79}As feasible.

To the aqueous phase containing germanium and the other fission products, 10 ml of 10 *N* HCl and 10 ml of saturated H_3BO_3 solution were added. GeS_2 was precipitated with 5 ml of saturated Na_2S solution and centrifuged. The supernate was discarded and the GeS_2 precipitate washed and transferred with 15 ml 4.5 *N* HCl to a distillation unit. $GeCl_4$ was distilled at 120°C and recovered in 10 ml 4.5 *M* HCl, saturated with H_2S, and placed in an ice bath. After 20 min, the GeS_2 precipitate thus obtained was filtered on a fiber-glass disk, washed with ethanol and isopropyl ether, dried at 110°C, and mounted for activity measurements.

(ii) Copper

The chemistry of copper separation followed the standard procedure of Kraus and Moore (12). The copper monitor foil was weighed, dissolved in 3 *N* HCl to which 2 drops of 30% H_2O_2 had been added, the solution was evaporated to dryness, and the residue transferred with a minimum amount of 4.5 *N* HCl to a 20.0 × 0.7 cm anion-exchange column loaded with Dowex-1X8 resin (100–200 mesh size) pretreated with 4.5 *N* HCl. After Zn, Co, and Fe were removed with 4.5 *N* HCl, Cu was eluted with 1.5 *N* HCl, the middle fraction of the eluate being retained. Cu^{2+} was reduced to Cu^+ by heating in the presence of $NaHSO_3$, CuSCN was precipitated by addition of 1 ml of 10% NH_4SCN solution, and a solid sample for activity measurements was prepared as described previously.

(C) Activity Measurements and Treatment of Data

Relevant properties of the nuclides measured in this work are shown in Table 1. The γ-radiations were measured with a calibrated 30 cm^3 Ge(Li) detector operated in conjunction with a 4096-channel pulse-height analyzer equipped with magnetic tape readout. In the case of ^{64}Cu, the solid samples were sandwiched between two aluminum absorbers sufficiently thick to ensure complete annihilation of the positrons within them. Portions of the γ-ray spectra containing the peaks of interest were analyzed with the spectrum-stripping program GAMANAL (20) to locate peaks and to calculate net-peak areas after subtraction of the Compton background. The counting rate of each nuclide was usually followed for several half-lives and then extrapolated to the time of end of bombardment, or separation time from parent (whichever was applicable), with the aid of the CLSQ least-squares analysis program (21). These extrapolated counting rates were converted to disintegration rates by making the usual corrections for chemical yields, branching ratios, and detector efficiencies, and used to calculate formation cross sections following standard procedures. The monitor cross sections used to that effect are shown in Table 2.

TABLE 1. Summary of the decay properties of observed nuclides

Nuclide	Half-life	γ rays measured (keV)	γ rays per 100 decays	Ref.
^{76}As	26.32 h	559.1	45	13
^{77}As	38.7 h	239.1	1.4	16
^{78}As	90.7 min	613.6	54	15
		695.4	18	
		827.8	7	
		1308.8	11	
^{79}As	9.01 min	95.5	9.37[a]	17
^{75}Ge	82.78 min	264.8	11.2	14
^{77}Ge	11.3 h	209.0, 211.0	52.9	16
		264.0	100	
		366	31	
		415	49	
		557	34	
^{78}Ge	87.0 min	277.3	96	15
^{64}Cu	12.74 h	511.0 β^+ annihilation	38	19

[a] E_3 transition. Total internal conversion coefficient $\alpha_T = 9.57$ (18).

TABLE 2. Cross sections for the reaction $^{65}Cu(p,pn)^{64}Cu$ (22)

E_p (MeV)	σ (mb)	E_p (MeV)	σ (mb)
35	250	65	162
40	245	70	155
45	194	75	150
50	187	80	144
55	178	85	141
60	170		

Results

The independent formation cross sections for ^{76}As and the cumulative cross sections ^{78}Ge, ^{77g}Ge, and ^{78}Ge were computed directly at each incident energy. The independent cross sections of ^{78}As were calculated using the cumulative ^{78}Ge cross sections simultaneously measured in order to correct for the parent contribution during irradiation and between the end of bombardment and the time of As–Ge separation. The same method was applied to the calculation of the partially-cumulative cross section of ^{77}As using the cumulative cross section of ^{77g}Ge (this cross section includes a 24% isomeric transition contribution from the cumulative cross section of ^{77m}Ge (19)). In the case of ^{79}As, the branching ratio for the highly-converted 95.5 keV γ-ray was corrected by a total internal conversion coefficient of 9.57 (18). All cross sections determined in this work appear in Table 3. The error quoted with each value is associated with monitor cross sections (5.4%), detector efficiencies (1%), chemical yield (4%), and target superficial density (2%). In the case of ^{78}As independent cross sections, an additional 5% error was added, due to uncertainties in the cross-section values of the precursor ^{78}Ge. No error was associated with uncertainties in decay schemes and half-lives. An additional uncertainty due to counting statistics was added for each individual determination, as given by the CLSQ program. In most measurements, it rarely exceeds 2%. However, in the case of ^{76}As, due to the extremely low formation cross sections at low bombarding energies, this type of error could amount to 15%. The total error was assessed for each measurement by taking the square root of the sums of the squares of individual errors outlined above. The error varies between ±13% and ±28%. Excitation functions for the nuclides studied are shown in Figs. 1 and 2.

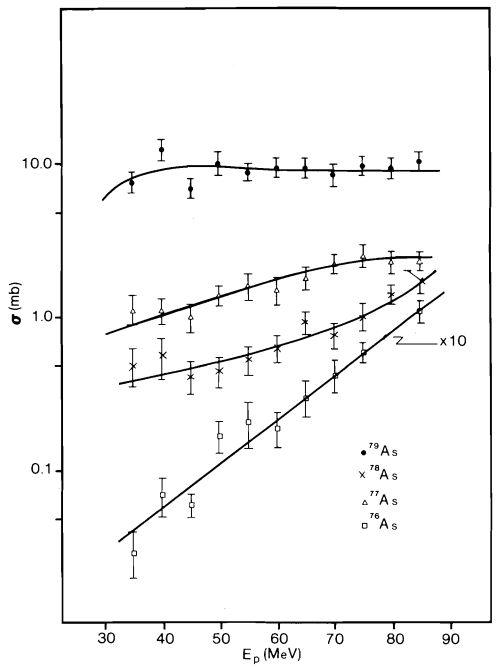

FIG. 1. Excitation functions for the cumulative formation cross section of ^{79}As and ^{77}As (partially), and the independent formation cross section of ^{76}As and ^{78}As.

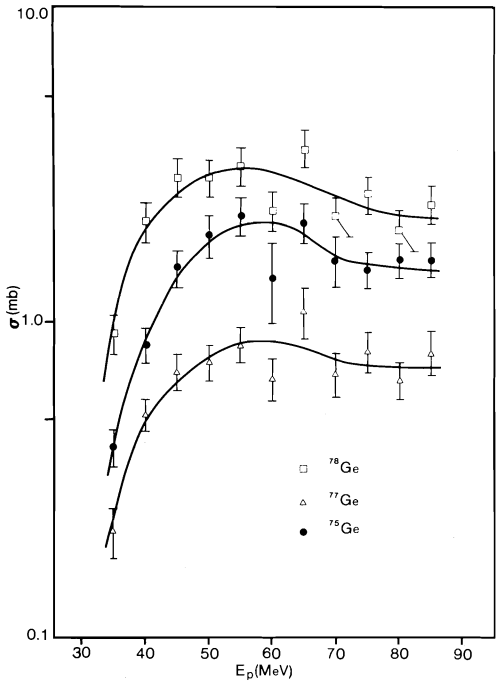

FIG. 2. Excitation functions for the cumulative formation cross section of ^{75}Ge, ^{77g}Ge, and ^{78}Ge.

TABLE 3. Experimental cross sections

E_p (MeV)	σ (mb) $^{76}As^a$ $N/Z=1.3030$	$^{77}As^b$ $N/Z=1.3333$	$^{78}As^a$ $N/Z=1.3636$	^{79}As $N/Z=1.3939$	^{75}Ge $N/Z=1.3438$	$^{77}Ge^c$ $N/Z=1.4063$	^{78}Ge $N/Z=1.4375$
35	0.003±0.001	1.1±0.3	0.49±0.14	7.7±1.0	0.41±0.05	0.22±0.04	0.94±0.12
40	0.007±0.002	1.1±0.2	0.57±0.18	12.5±1.6	0.86±0.11	0.52±0.06	2.1 ±0.3
45	0.006±0.001	1.0±0.2	0.42±0.10	7.0±0.9	1.5 ±0.2	0.71±0.09	2.9 ±0.4
50	0.017±0.004	1.4±0.2	0.45±0.10	10.0±1.4	1.9 ±0.3	0.76±0.10	2.9 ±0.4
55	0.021±0.007	1.6±0.3	0.53±0.11	8.8±1.1	2.2 ±0.3	0.87±0.11	3.2 ±0.4
60	0.019±0.005	1.5±0.3	0.62±0.12	9.4±1.2	1.4 ±0.4	0.67±0.10	2.3 ±0.3
65	0.030±0.008	1.8±0.3	0.92±0.15	9.3±1.3	2.1 ±0.3	1.1 ±0.2	3.6 ±0.5
70	0.042±0.010	2.2±0.3	0.76±0.14	8.4±1.4	1.6 ±0.3	0.70±0.11	2.2 ±0.3
75	0.059±0.009	2.5±0.4	1.0 ±0.2	9.6±1.3	1.5 ±0.2	0.83±0.12	2.6 ±0.3
80		2.3±0.4	1.4 ±0.2	9.1±1.2	1.6 ±0.2	0.67±0.09	2.0 ±0.3
85	0.108±0.016	2.3±0.3	1.7 ±0.3	10.1±1.4	1.6 ±0.2	0.82±0.13	2.4 ±0.3

[a]Independent cross section.
[b]Partially-cumulative cross section: ^{77}As (*i*) + 0.76 ^{77m}Ge (*c*).
[c]Partially-cumulative cross section: ^{77}Ge (*c*) + 0.24 ^{77m}Ge (*c*).

TABLE 4. Parameters of charge dispersion curves

E_p (MeV)	Peak position N/Z_p	A_p[a]	Z_A[b]	$Z_A - Z_p$	Full-width at half-maximum N/Z	Z
35	1.420	79.86	34.97	1.97	0.073	0.99
40	1.442	80.57	35.24	2.24	0.090	1.22
45	1.433	80.28	35.13	2.13	0.080	1.08
50	1.446	80.73	35.30	2.30	0.097	1.31
55	1.445	80.70	35.29	2.29	0.098	1.32
60	1.428	80.12	35.07	2.07	0.084	1.14
65	1.434	80.31	35.14	2.14	0.093	1.26
70	1.427	80.09	35.05	2.05	0.095	1.29
75	1.426	80.04	35.04	2.04	0.098	1.33
80	1.409	79.51	34.83	1.83	0.089	1.22
85	1.410	79.52	34.84	1.84	0.096	1.31

[a]Calculated from arsenic isotopic distribution.
[b]From Coryell (25).

The independent cross sections were converted into independent fractional chain yields for the purpose of constructing charge dispersion curves. The cumulative cross sections were used as a first estimate of the total chain yields for $A = 75$, 77, 78, 79, while for $A = 76$ the total chain yield value was estimated by interpolation. A first set of charge dispersion curves was thus generated with the help of the ORGLS program (23) using the usual constraint prescribed by Friedlander *et al.* (24). This in turn allowed for the adjustment of total chain yields to more realistic values. Two iterations were sufficient to arrive at the final results shown in Table 4. A representative sample of a charge dispersion curve is shown in Fig. 3.

The average precision on the most probable neutron-to-proton ratios (N/Z_p) and the full-widths at half-maximum (fwhm) in N/Z units is 2% and 3% respectively, as given by the ORGLS program. The most probable mass (A_p) was calculated, at each incident energy, for arsenic isotopic distribution and the corresponding Z_A values were deduced from Coryell (25). The precision on the resulting values of ($Z_A - Z_p$) and fwhm in Z units is, on the average, 3.5% and 8%, respectively, with the exception of the ($Z_A - Z_p$) value at 35 MeV which appears to be too low by ~15%, this being probably attributable to poor precision on ^{76}As and ^{78}As independent cross sections at that particular energy. The variation of ($Z_A - Z_p$) and fwhm as a

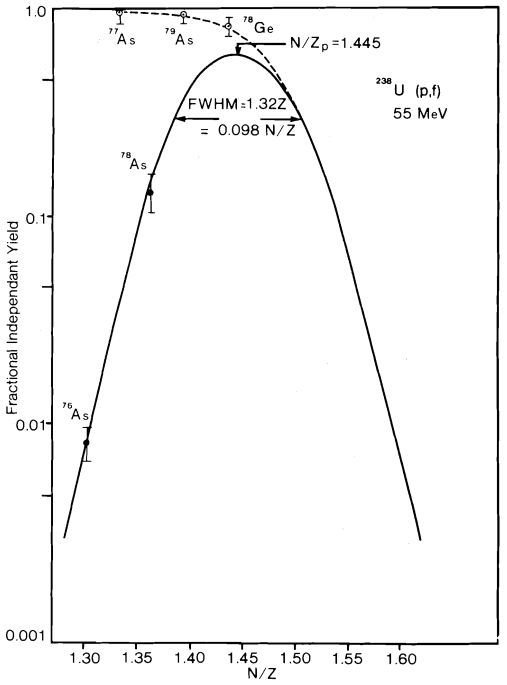

FIG. 3. Charge dispersion curve at 55 MeV.

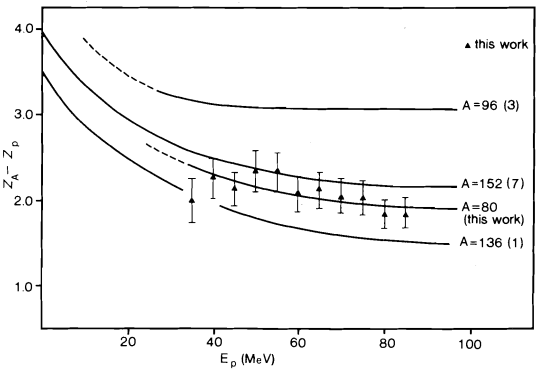

FIG. 4. Displacement of the most probable charge from stability as a function of incident energy.

function of bombarding energy is shown in Figs. 4 and 5 respectively, along with data of several other workers (1, 3, 5–7).

Discussion

The excitation functions of the independently formed nuclides ^{76}As and ^{78}As (Fig. 1) show a monotonic increase in the 35–85 MeV bombarding energy range, thus exhibiting, at least in this limited region, the classical behaviour of species close to the stability line found in medium-

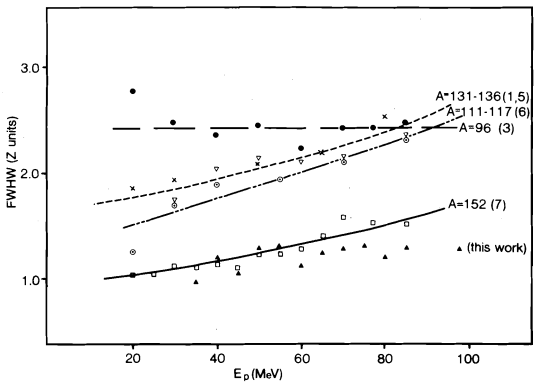

FIG. 5. Full-width at half-maximum of charge dispersion curves as a function of incident energy.

energy fission. The yield of ^{76}As (N/Z = 1.3030) increases by about 1.5 orders of magnitude, compared to a factor of ~4 for the more neutron-rich ^{78}As (N/Z = 1.3636). The scarcity of data at higher energy unfortunately does not allow for a precise determination of the incident energy at which these excitation functions would reach a maximum. However, the values of 0.8 mb at 170 MeV and 0.21 mb at 340 MeV reported respectively by Hagebø *et al.* (26) and Folger *et al.* (27) for the production of ^{76}As suggest that the excitation function of this particular nuclide goes through a broad maximum, or levels off, at an incident energy considerably lower (by about 1 order of magnitude) than the prediction from the systematics of Friedlander *et al.* (24) for nuclides in the vicinity of the cesium region. If this is the case, the light products appear to behave differently from their heavy partners. (For instance the excitation function for the production of independently formed ^{150}Pm is in accord with systematics by reaching its maximum at 100 MeV (7).) On the other hand, if we compare our data to those of Khan *et al.* (3) in the yttrium mass region, we observe a qualitative agreement (^{92}Y (N/Z = 1.3590) and ^{93}Y (N/Z = 1.3846) reach their maxima much below the predicted incident energy). However, one must await higher-energy data before drawing further conclusions.

The excitation functions for the cumulatively formed species ^{78}Ge, ^{77g}Ge, ^{78}Ge, and ^{79}As (Figs. 1 and 2) exhibit broad maxima shifting toward lower incident energies with increasing value of N/Z of the nuclide. The excitation function of ^{79}As (N/Z = 1.3939) is almost flat

within experimental uncertainties, while that of ^{75}Ge ($N/Z = 1.3438$) indicates a variation of cross sections of about a factor of 5 in the 35–85 MeV bombarding energy range. This trend agrees well with that found in the complementary mass region (7) and, again, as in the case of the heavier rare-earths, differs from that reported for heavy cumulatively formed products resulting from the most probable-fission mode (cesium region and its vicinity) where cross sections decrease sharply over the whole bombarding energy range (1, 2, 4, 5). This difference indicates that the displacement of the most probable charge along light isobaric chains plays a less prominent role in the decrease of cumulative cross sections with increasing bombarding energy.

The values of $(Z_A - Z_p)$ deduced in this work appear to be quite similar in magnitude to those found in the complementary mass region ($A = 152$) as shown in Fig. 4. A linear least-squares fit performed on the variation of Z_p (arbitrarily calculated for mass $A = 80$) against the variation of the average excitation energy E^* of the fissioning nucleus obtained by Dikšić *et al.* (5) using the Vegas Stepno code (28) followed by Monte Carlo evaporation (29, 30) gives a value of $\delta Z_p/\delta E^* = 0.0197\ \text{MeV}^{-1}$. This result is in excellent agreement with the value of 0.0208 MeV^{-1} found in the complementary mass region in the 20–85 MeV bombarding energy range (7), and the value of 0.0200 MeV^{-1} reported by Nethaway (31) in the excitation energy range 6.8–21.2 MeV for mass chain $A = 82$. However, our data differ considerably in magnitude from those reported at mass chain $A = 96$ (3), as seen in Fig. 4. This is a direct consequence of the very low values of N/Z_p found in the present work. Such a trend of sharply decreasing N/Z_p with mass below $A \sim 90$ has already been pointed out at higher energies by Hagebø *et al.* (26) and Pappas and Hagebø (32) at 170 MeV and Hogan and Sugarman (33) at 440 MeV. Wahl *et al.* (34) have also shown that, at thermal energies, ^{235}U fission gives rise to light products whose N/Z_p values are much below those of their complementaries (by about $\sim 0.05\ N/Z$ unit), even though these values do not seem to vary much below mass $A = 100$. Figure 6 shows the results of the McGill group (1–7) at 50 and 85 MeV, along with the curve constructed by Pappas and Hagebø (32) at 170 MeV. Both sets of data are in good agreement as far as trends are concerned. The reason as to why the light fission products exhibit such a sharp drop in N/Z_p values has been attributed, at 170 MeV, to fast fission events taking place at the highest excitation energy available (26). In our case, such an argument would contradict the conclusions drawn in the complementary mass region (7) where highly asymmetric mass divisions have been shown to be caused by low-deposition energy cascades, as demonstrated by the relatively small number of post-fission neutrons deduced from the variation of Z_p, using the method of McHugh and Michel (35). Our results on N/Z_p indicate also that the conclusion of Hagebø *et al.* (26) that the UCD hypothesis cannot be applied in its simple form to the fission reactions leading to light fragments at 170 MeV, may be extended to the lower excitation energy range involved in this work. This is also supported by the work of Lee *et al.* (36) on the isotopic distributions of rubidium and cesium formed in the fission of ^{238}U at 80 and 100 MeV. In order to explain the low N/Z_p value found for rubidium, these authors show that the ratio of the number of post-fission neutrons emitted by the heavy fragment to that emitted by its light partner should equal 0.78 if the UCD prescription is to describe the processes of charge division in an adequate fashion. This value is not consistent with the experimental findings of Cheifetz *et al.* (37) who report an experimentally measured ratio of 2.2 for the mass split, 1.5 in the 155 MeV proton-induced fission of ^{238}U, and Bishop *et al.* (38) who report ratios from 1.12 to 1.34 for similar mass divisions in the 11.5–22 MeV proton energy range. If we look at the

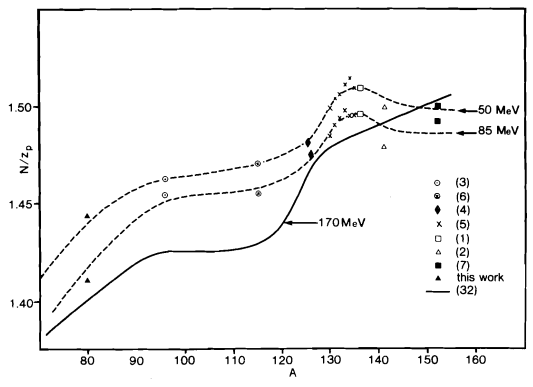

FIG. 6. Variation of the most probable neutron-to-proton ratio with the mass of the fission chains for three incident energies.

variation of the full-width at half-maximum as a function of bombarding energy (Fig. 5), we see that fission products of mass $A = 80$ behave virtually in the same fashion as their complementary partners, fwhm varying respectively from 0.99 to 1.31 Z units and 1.06 to 1.53 Z units (7). Again, we notice a large difference in magnitudes between the results of Khan *et al.* (3) at mass $A = 96$ and ours, as shown in Fig. 5. One qualitative explanation for both narrow widths and low N/Z_p could be that early members in the isobaric decay chains are likely to be delayed-neutron emitters. The occurrence of such a type of decay has indeed been observed in the vicinity of the mass region investigated, as reported by Kratz *et al.* (39), for nuclides such as ^{84}As, ^{85}As, and ^{86}As which are only 3 units of Z removed from the stability line. The extent to which delayed-neutron emission might alter the original charge dispersion features is, however, very difficult to assess as far as widths are concerned, while it probably contributes to substantial shift towards lower values in N/Z_p. It is then surprising to see that both N/Z_p and fwhm exhibit essentially the same variation in both the As–Ge and the rare-earths complementary mass regions. If this agreement is not to be fortuitous, it seems reasonable to assume that delayed-neutron emission superimposes itself to the de-excitation process of the primary fission fragments without masking the influence of increasing bombarding energy.

1. J. H. Davies and L. Yaffe. Can. J. Phys. **41**, 762 (1963).
2. S. S. Parikh, D. A. Marsden, N. T. Porile, and L. Yaffe. Can. J. Chem. **45**, 1863 (1967).
3. A. H. Khan, G. B. Saha, and L. Yaffe. Can. J. Chem. **48**, 1924 (1970).
4. L. D. Miller and L. Yaffe. J. Inorg. Nucl. Chem. **35**, 1805 (1973).
5. M. Dikšić, D. K. McMillan, and L. Yaffe. J. Inorg. Nucl. Chem. **36**, 7 (1974).
6. S. Sarkar and L. Yaffe. Can. J. Chem. **54**, 2349 (1976).
7. J.-L. Galinier and L. Yaffe. J. Inorg. Nucl. Chem. In press.
8. B. D. Pate, J. S. Foster, and L. Yaffe. Can. J. Chem. **36**, 1691 (1958).
9. A. Kjelberg and A. C. Pappas. J. Inorg. Nucl. Chem. **11**, 173 (1959).
10. R. J. Prestwood. *In* Collected radiochemical procedures. Los Alamos Rept. 1721. 1976. p. 229.
11. R. J. Prestwood. *In* Collected radiochemical procedures. Los Alamos Rept. 1721. 1976. p. 59.
12. K. A. Kraus and G. E. Moore. J. Am. Chem. Soc. **75**, 1460 (1953).
13. F. E. Bertrand and R. L. Auble. Nucl. Data Sheets, **19**(No. 4), 507 (1976).
14. D. J. Horen and M. B. Lewis. Nucl. Data Sheets, **16**(No. 1), 25 (1975).
15. P. P. Urone and F. E. Bertrand. Nucl. Data Sheets, **15**(No. 2), 107 (1975).
16. W. W. Bowman and K. W. MacMurdo. At. Data and Nucl. Data Tables, **13**(Nos. 2–3), 215 (1974).
17. P. P. Urone and D. C. Kocher. Nucl. Data Sheets, **15**(No. 3), 257 (1975).
18. R. S. Hager and E. C. Seltzer. Nucl. Data Tables, **A4**, 26–28 (1968).
19. C. M. Lederer, J. M. Hollander, and I. Perlman. Table of isotopes. 6th ed. Wiley, New York, NY. 1967.
20. R. Gunnink, R. A. Meyer, J. B. Niday, and R. P. Anderson. Nucl. Instrum. Methods, **65**, 26 (1968).
21. J. B. Cumming. U.S. Atomic energy report. Number NAS-NS 3107. 1962. p. 25.
22. D. Newton, S. Sarkar, L. Yaffe, and R. B. Moore. J. Inorg. Nucl. Chem. **35**, 361 (1973).
23. L. A. Busing and H. A. Levy. Oak Ridge National Laboratory Report. No. ORNL-TM-271. 1962. Unpublished.
24. G. Friedlander, L. Friedman, B. Gordon, and L. Yaffe. Phys. Rev. **129**, 1809 (1963).
25. C. D. Coryell. Ann. Rev. Nucl. Sci. **2**, 305 (1953).
26. E. Hagebø, A. C. Pappas, and P. Aagaard. J. Inorg. Nucl. Chem. **26**, 1639 (1964).
27. R. L. Folger, P. C. Stevenson, and G. T. Seaborg. Phys. Rev. **98**, 107 (1955).
28. K. Chen, Z. Fraenkel, G. Friedlander, J. R. Grover, J. M. Miller, and Y. Shimamoto. Phys. Rev. **166**, 949 (1968).
29. I. Dostrovsky, Z. Fraenkel, and P. Rabinowitz. Proceedings of the 2nd international conference on the peaceful uses of atomic energy. Vol. 15. United Nations, Geneva. 1958. p. 301.
30. I. Dostrovsky, Z. Fraenkel, and G. Friedlander. Phys. Rev. **116**, 683 (1959).
31. D. R. Nethaway. University of California Lawrence Livermore Laboratory. Report UCRL-51538. 1974.
32. A. C. Pappas and E. Hagebø. J. Inorg. Nucl. Chem. **28**, 1769 (1966).
33. J. J. Hogan and N. Sugarman. Phys. Rev. **182**, 1210 (1969).
34. A. C. Wahl, A. E. Norris, R. A. Rouse, and J. C. Williams. Second symposium on the physics and chemistry of fission. I.A.E.A., Vienna. 1969. Paper SM-122/116, p. 813.
35. J. A. McHugh and M. C. Michel. Phys. Rev. **172**, 1160 (1968).
36. J. K. P. Lee, G. Pilar, B. L. Tracy, and L. Yaffe. J. Inorg. Nucl. Chem. **37**, 2035 (1975).
37. E. Cheifetz, Z. Fraenkel, J. Galin, M. Lefort, J. Peter, and X. Tarrago. Phys. Rev. C, **2**, 256 (1970).
38. C. J. Bishop, R. Vandenbosch, R. Aley, R. W. Shaw, Jr., and I. Halpern. Nucl. Phys. A, **150**, 129 (1970).
39. J. V. Kratz, H. Franz, and G. Herrmann. J. Inorg. Nucl. Chem. **35**, 1407 (1973).

The reaction of iodine with lithium tri-*tert*-butoxyaluminohydride.[1] A reaction with variable stoichiometry unsuitable for analytical standardization

DONALD C. WIGFIELD AND FREDERICK W. GOWLAND
Department of Chemistry, Carleton University, Ottawa, Ont., Canada K1S 5B6

Received January 21, 1977

DONALD C. WIGFIELD and FREDERICK W. GOWLAND. Can. J. Chem. **55**, 3616 (1977).

Solutions of lithium tri-*tert*-butoxyaluminohydride (LTBA) have been standardized by reduction of cyclohexanone, followed by gas–liquid chromatography (glc) and/or spectral analysis of the extent of reaction. These results are compared with the standard titrimetric analysis of LTBA by iodine, to determine whether the standardizing equation is

[5] $$LiAl(OBu^t)_3H + I_2 \rightarrow HI + LiI + Al(OBu^t)_3$$

or

[3] $$LiAl(OBu^t)_3H + \tfrac{1}{2}I_2 \rightarrow \tfrac{1}{2}H_2 + LiI + Al(OBu^t)_3$$

It is clear that in fact both of these reactions occur, with [5] predominating at low hydride to iodine ratios, and [3] becoming increasingly significant when the hydride and iodine concentrations become comparable. The usual titrimetric method of standardizing LTBA is therefore essentially unusable.

DONALD C. WIGFIELD et FREDERICK W. GOWLAND. Can. J. Chem. **55**, 3616 (1977).

On étalonne des solutions de tri-*tert*-butoxyaluminohydrure de lithium (TBAL) par réduction de la cyclohexanone suivie par CPG ou par analyse spectrale du degré de réaction ou les deux à la fois. Ces résultats sont comparés à l'analyse titrimétrique étalonnée de (TBAL) par l'iode, afin de déterminer si l'équation de normalisation est:

[5] $$LiAl(OBu^t)_3H + I_2 \rightarrow HI + LiI + Al(OBu^t)_3$$

ou

[3] $$LiAl(OBu^t)_3H + \tfrac{1}{2}I_2 \rightarrow \tfrac{1}{2}H_2 + LiI + Al(OBu^t)_3$$

Il est clair qu'en fait les deux réactions se produisent, [5] étant prédominante à faibles rapports hydrure à iodure; [3] a un accroissement devenant important lorsque les concentrations en hydrure et en iodure deviennent comparables. La méthode titrimétrique habituelle pour étalonner (TBAL) est par conséquent inutilisable.

[Traduit par le journal]

Kinetics play a vital role in unravelling the mechanistic details of reductions of carbonyl compounds by complex metal hydrides (see, for example, ref. 3 and references cited therein). Since these reductions are generally first-order both in organic substrate and in hydride, an accurate knowledge of the concentration of the complex metal hydride in the reduction solution is required. Recently we have needed to measure the concentration of solutions of lithium tri-*tert*-butoxyaluminohydride (LTBA) for kinetic and other (4) studies; in doing so we have found that the currently used titrimetric method can give rise to anomalous results. We wish to report the unsuitability of this titrimetric method for LTBA analysis.

The Problem

Complex metal hydrides, such as lithium aluminum hydride (LAH), are generally analysed titrimetrically by reaction with iodine. The procedure involves two titrations: (*a*) titration of the iodine solution with thiosulfate (ref. 5, p. 453 *et seq.*); and (*b*) the addition of a deficient amount of lithium aluminum hydride to the same volume of iodine solution as in (*a*), followed by titration of the remaining iodine with thiosulfate. The difference between the two titrations clearly has equivalence to the quantity of hydride oxidized. Felkin (6) has shown that the following equation holds:

[1] $$LiAlH_4 + 2I_2 \rightarrow 2H_2 + LiI + AlI_3$$

[1]Often called lithium aluminum tri-*tert*-butoxyhydride. Related nomenclative problems occur for substituted borohydrides (1). Chemical Abstracts is currently (Vol. 83) referring to this compound as "aluminate (1-), hydrotris (2-methyl-2-propanolato) lithium". We have retained the name given to it by its discoverers (2).

This equation, in combination with the reaction of iodine with thiosulfate (ref. 5, p. 453 *et seq.*)

[2] $$2S_2O_3^{2-} + I_2 \rightarrow S_4O_6^{2-} + 2I^-$$

establishes the 1:4 equivalence between lithium aluminum hydride and sodium thiosulfate.

Direct extrapolation of the I_2–LAH reaction to LTBA gives the following equation

[3] $$LiAl(OBu^t)_3H + \tfrac{1}{2}I_2 \rightarrow \tfrac{1}{2}H_2 + LiI + Al(OBu^t)_3$$

This equation, in combination with [2], clearly implies a 1:1 equivalence between LTBA and thiosulfate. If the original titre of x ml of thiosulfate to reduce the iodine solution is diminished to z ml by the prior addition of y ml of LTBA solution, then the molarity of LTBA is given by:

[4] $$M_{LTBA} = M_{Na_2S_2O_3}\left(\frac{x - z}{y}\right)$$

This equation is equivalent to that suggested by Ayres *et al.* (7).

In the course of using [3] and resulting expressions, however, certain peculiarities led us to consider its basis more carefully. In the absence of further experimental data the alternative reaction (eq. 5), seemed equally plausible.

[5] $$LiAl(OBu^t)_3H + I_2 \rightarrow LiI + HI + Al(OBu^t)_3$$

This equation, in combination with [2], gives a 1:2 equivalence between LTBA and thiosulfate, and, retaining the same designation of the volumes x, y, and z, leads to [6].

[6] $$M_{LTBA} = M_{Na_2S_2O_3}\left(\frac{x - z}{2y}\right)$$

Equations 4 and 6 clearly differ by a factor of two, and an independent method of quantitative analysis is required to establish which of the two is correct. For this purpose we have chosen the reaction of LTBA with cyclohexanone, and evaluation of the extent of reduction. This reaction has the twofold advantage that, firstly, it is the reaction in which we are interested, and, secondly, that cyclohexanone is known to react with LTBA with a 1:1 stoichiometry (8).

Results and Discussion

In order to utilize the reduction of cyclohexanone as a measure of [LTBA], accurate assay of the extent of reduction is required. This was achieved with two independent methods.

The first of these methods involved glc determination of the relative amounts of cyclohexanol and unreacted cyclohexanone after reaction with a deficient amount of LTBA. With this method the molarity of a LTBA solution is given by

[7] $$[LTBA] = [Ketone]\left(\frac{q}{p}\right)\left(\frac{\%\ \text{reduction}}{100}\right)$$

where p and q are the volumes (ml) of the LTBA and ketone solutions, respectively. For the glc system used in this work a significant detector response differential between cyclohexanol and cyclohexanone was measured; the actual percent reduction was thus obtained by multiplying the apparent percent reduction by a factor of 0.92.

The second method involved the analysis of unreacted ketone by the absorbance of the n–π^* band at 288 nm. We have, in fact, utilized this method for following the kinetics of this reaction; this analytical application was somewhat simpler, involving only the initial absorbance and the absorbance after reaction was complete (~2 min). The molarity of a LTBA solution in this determination is given by

[8] $$[LTBA] = \left(\frac{A_0 - A_f}{a}\right)\left(\frac{q + p}{p}\right)$$

where A_f is the final absorbance value, A_0 is the initial absorbance value, already corrected for the change in volume that will occur on adding the LTBA solution, a is the molar absorptivity, and p and q are the volumes as indicated above. It was found that glc and spectral analyses were in close agreement.

Armed with reliable analyses of LTBA solutions, comparisons were made with the apparent analysis given by the iodine titration method using both [4] and [6]. From the results, summarized in Table 1, a number of points are evident.

1. At low hydride to iodine ratios, [5] apparently occurs and use of [6] gives reasonably good[2] agreement with the glc or spectral analysis. In fact these ratios were those actually used for our related kinetic work, and led us initially to believe that [5] was the chemistry involved.

2. At hydride concentrations comparable to the iodine concentration, [3] appears to occur and the use of [4] gives the correct analysis of the hydride concentration.

3. At most [hydride]:[iodine] ratios (i.e., those

[2]There is still a substantial error, however, due to the small quantity of iodine consumed and the crucial volume thus being a small difference between two large titres.

TABLE 1. Comparison of titration, gas–liquid chromatography, and spectral concentrations[a] of LTBA solutions

Titration		Gas–liquid chromatography	Spectral	Correct titration equation
Equation 4[b]	Equation 6[b]			
0.0144	0.0072	0.0074		6
0.0244	0.0122	0.0143		6
0.0394	0.0197	0.0183		6
0.0500	0.0250		0.0321	—
0.0532	0.0266	0.0336	0.0344	—
0.0554	0.0277	0.0355	0.0351	—
0.0572	0.0286		0.0419	—
0.0622	0.0311		0.0450	—
0.0702	0.0351		0.0424	—
0.0704	0.0352		0.0456	—
0.0750	0.0375		0.0540	—
0.0814	0.0407		0.0537	—
0.0868	0.0434		0.0542	—
0.0900	0.0450		0.0584	—
0.0932	0.0466		0.0650	—
0.0980	0.0495		0.0661	—
0.1054	0.0527		0.0750	—
0.1290	0.0645	0.1250		4
0.1404	0.0702	0.1274		4
0.1722	0.0861	0.1764		4

[a][LTBA], mol/ℓ.
[b]Iodine concentration 0.076 *M*.

lying between those covered in the above two cases), the true hydride concentration lies between the values obtained using [4] and [6]. Presumably, therefore, this corresponds to LTBA and iodine reacting by both [3] and [5].

4. The consequence of point *3* is that the iodine titration method for LTBA is an unreliable and almost useless analytical method. The stoichiometry is variable and unpredictable unless the concentration of LTBA is already known with sufficient accuracy to ensure that conditions for predominance of either [3] or [5] will be in effect.

These conclusions, although unexpected, are not unreasonable. Even if [3] were to occur, the first step of such a process would presumably be [5]. The second step would be

[9] $LiAl(OBu^t)_3H + HI \rightarrow H_2 + LiI + Al(OBu^t)_3$

From the data, therefore, it would appear that [9] is viable and the question of whether [3] or [5] is appropriate is essentially a question of competition between [5] and [9]. Clearly at low [hydride] to [iodine] ratios there will always be a predominance of I_2 over HI; [9] is effectively eliminated by this concentration effect, and the data will correspond to [5] and [6]. At higher hydride to iodine concentrations, more HI will be produced, [9] will compete more effectively with [5] to the point where [3] and [4] accommodate the data. We have attempted to illustrate this change of stoichiometry from the 1:1 of [5] to the 2:1 of [3] in the plot of Fig. 1.

The difference in chemistry between LTBA and LAH is worth considering. Clearly the reduction of HI by LAH competes more effectively with reduction of I_2 than it does in the LTBA case. One important difference between LAH and LTBA are the four hydrides of LAH compared to only one hydride of LTBA, and it is worth noting that after the reaction of LAH with I_2, the HI and the modified aluminum species (still containing three hydrides and still a reducing agent) are necessarily produced in the same vicinity. It is possible, therefore, that the efficient reduction of HI to H_2 by LAH is, at least in part, due to this local concentration or solvent cage effect. Such an effect, of course, would not be applicable in LTBA reductions.

Conclusions

The stoichiometry of the standardizing reaction between iodine and LTBA is variable, ranging from 1:1 to 1:2. This titrimetric method for determination of [LTBA] is therefore of no use unless the value of [LTBA] is already known with some accuracy beforehand. Data in the literature which may derive from this standard-

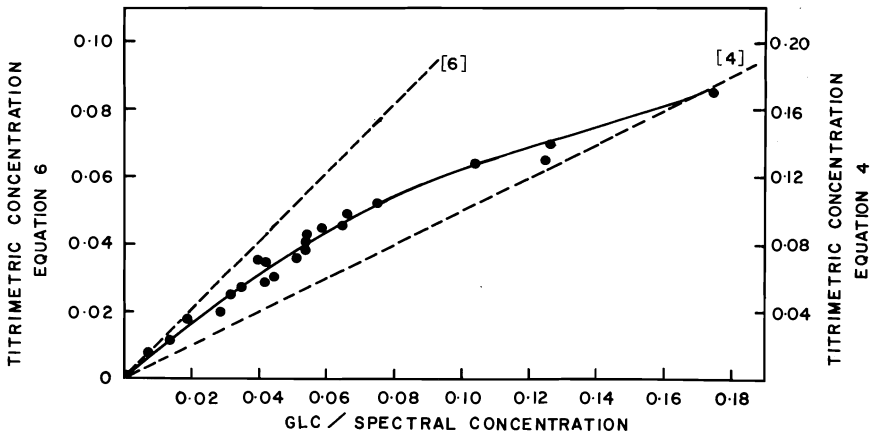

FIG. 1. Comparison of [LTBA] from glc/spectral determinations with apparent values from titrimetric analysis. The dashed lines correspond to [4] and [6], respectively.

izing reaction must therefore be regarded as suspect.

Experimental

Materials

Tetrahydrofuran (Fisher Certified) was distilled from lithium aluminum hydride (Ventron; Alfa Products) at atmospheric pressure, protecting the distillate from moisture. Benzene (Fisher) was distilled under nitrogen and stored over molecular sieves (Fisher; 4 Å). Iodine (Fisher), sodium thiosulphate (Baker), glacial acetic acid (Fisher), soluble starch (Fisher), cyclohexanone (Fisher), cyclohexanol (Fisher), diethyl ether (Mallinkrodt), and lithium tri-*tert*-butoxyaluminohydride (Ventron; Alfa Products) were used without further purification. Gas–liquid chromatography was performed on a Hewlett-Packard F and M 402 gas chromatograph equipped with a QF-1(5%) column. Carrier gas flow was 4 ml/min, oven 86°C, injector port 200°C, manifold 200°C. Peak areas were determined electronically with an Infotronics CRS-208 electronic integrator. The retention times for cyclohexanone and cyclohexanol were 2.9 and 5.8 min (9), respectively. Spectral analyses were performed on a Beckman 25 spectrophotometer at 288 nm.

Titrimetric Analysis

A typical determination follows; stock solutions of standardized sodium thiosulphate (ref. 5, p. 455 *et seq.*) (0.06382 *M*) and of iodine in benzene (6) (0.07605 *M*) were prepared. LTBA (0.05245 g) was dissolved in 10.0 ml of tetrahydrofuran; an aliquot (5.0 ml) of this solution was pipetted into a iodine flask containing 5.0 ml of the stock iodine solution. The flask was stoppered and swirled periodically (ca. 5 min). Glacial acetic acid (15 ml) was added and the solution was titrated against the standard thiosulphate solution to the starch indicator end point. A blank following the above outlined procedure was run omitting the hydride solution. The data were analyzed using [4] and [6], respectively.

Spectral Method

To 2.0 ml of hydride solution in a cuvette, which had been fitted with a cover, 1.0 ml of ketone solution of known concentration was injected. Simultaneously with injection the chart recorder was activated and the decay trace, characteristic of the second order reaction, was obtained. The limiting absorbance (A_f) was observed after 1–2 min. The initial absorbance (A_0) was obtained by dividing the absorbance of the ketone solution by three to allow for dilution.

Gas–Liquid Chromatography Method

To 5.0 ml of a stock cyclohexanone solution (0.05416 *M* in THF), 5.0 ml of the hydride solution was added and the vessel stoppered. After 2 days[3] at room temperature the solution was treated with 1 *M* HCl (1 ml), extracted with ether (2 ml), and analyzed by glc. In the glc system used (flame ionization detector), the detector response to cyclohexanol and cyclohexanone were found to be significantly (8%) different. Thus a correction to the cyclohexanol:cyclohexanone ratio needed to be applied in order to obtain the true amount of cyclohexanone remaining in the sample. Use of [7] then yielded the concentration of available hydride.

1. H. I. SCHLESINGER and H. C. BROWN. J. Am. Chem. Soc. **75**, 186 (1953).
2. H. C. BROWN and R. F. MCFARLIN. J. Am. Chem. Soc. **80**, 5372 (1958).
3. D. C. WIGFIELD and D. J. PHELPS. J. Org. Chem. **41**, 2396 (1976).
4. D. C. WIGFIELD, D. J. PHELPS, R. F. POTTIE, and R. SANDER. J. Am. Chem. Soc. **97**, 897 (1975).
5. D. A. SKOOG and D. M. WEST. Fundamentals of analytical chemistry. 2nd ed. Holt, Rinehart and Winston, Inc. 1969. p. 453 *et seq.*
6. H. FELKIN. Bull. Soc. Chim. Fr. 347 (1951).
7. D. C. AYRES, D. N. KIRK, and R. SAWDAYE. J. Chem. Soc. B, 505 (1970).
8. H. C. BROWN and H. R. DECK. J. Am. Chem. Soc. **87**, 5620 (1965).
9. D. C. WIGFIELD and D. J. PHELPS. J. Am. Chem. Soc. **96**, 543 (1974).

[3]The time is not critical, in the usual uv analysis procedure the absorbance had decreased to a finite value within 1–2 min under the conditions of our kinetic experiment.

Nuclear magnetic resonance studies on the self-association of adenosine 5′-triphosphate in aqueous solutions[1]

YIU-FAI LAM[2] AND GEORGE KOTOWYCZ

Department of Chemistry, The University of Alberta, Edmonton, Alta., Canada T6G 2G2

Received March 22, 1977

YIU-FAI LAM and GEORGE KOTOWYCZ. Can. J. Chem. **55**, 3620 (1977).

The self-association of adenosine 5′-triphosphate (ATP) in aqueous, basic solutions has been studied. The results indicate that the monomer–dimer–trimer equilibrium model for base association fits the data well, but so does a model which includes higher order species. This indicates that the ATP molecules in solution can undergo indefinite linear self-association. The average value of the association constant based on the ^1H and ^{31}P chemical shift measurements is 0.9 ± 0.3 M^{-1}. Longitudinal relaxation rates for the H8, H1′, and H2 protons of ATP were obtained as a function of the nucleotide concentration. The analysis of the viscosity-corrected proton H2 data yields an association constant of 5.1 ± 1.3 M^{-1}.

YIU-FAI LAM et GEORGE KOTOWYCZ. Can. J. Chem. **55**, 3620 (1977).

On a étudié l'auto-association du triphosphate-5′ d'adénosine (TPA) en solution aqueuse et basique. Les résultats indiquent que l'équilibre modèle monomère–dimère–trimère pour l'association basique se compare bien aux données, mais il en est de même pour un modèle qui inclut des espèces d'ordre supérieur. Ceci indique que les molécules TPA en solution donnent lieu à une auto-association linéaire indéfinie. La valeur moyenne de la constante d'association basée sur les mesures du déplacement chimique est de 0.9 ± 0.3 M^{-1}. Les vitesses de relaxation longitudinale pour le protons H8, H1′ et H2 du TPA sont obtenues comme étant fonction de la concentration du nucléotide. L'analyse des valeurs pour le proton H2 corrigées de la viscosité nous donne une constante d'association de 5.1 ± 1.3 M^{-1}.

[Traduit par le journal]

Adenosine 5′-triphosphate (ATP) self-associates in aqueous solutions (1–3) due to the base-stacking interactions which have been observed for many nucleotides (4–7). However, the exact nature of the complex or complexes formed in

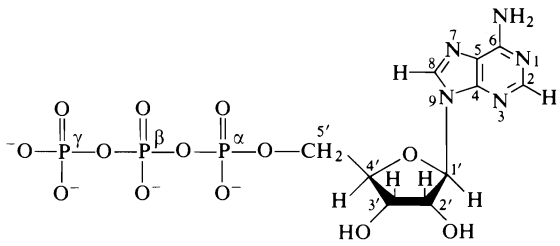

ATP

solution, especially at neutral or slightly basic p*H*, is still not known. On the basis of circular dichroism and uv measurements (2), an association constant of 8.2 M^{-1} at 25°C was obtained at a p*H* of 8.7 in a 1 *M* Tris HCl buffer with 0.5 *M* $MgCl_2$. The proposed model (2) is one with indefinite linear self-association and each step has the same equilibrium constant. Heyn and Bretz (2) could not assign a unique geometry for the ATP molecules in the stack but feel that head-to-tail association of the adenine bases is most likely. Further circular dichroism measurements (3) were interpreted in terms of a monomer–dimer model. At a p*H* of 2.8 and 20°C, a dimerization constant of 88 M^{-1} was obtained. In the complex, the charged phosphate of one ATP molecule interacts electrostatically with the charged adenine ring of the second ATP molecule. In this model, the two adenine rings are stacked head-to-tail and the ATP molecule is in the *anti* conformation (3). At basic p*H*'s, the model of Heyn and Bretz (2) was applied (3) and an association constant of 51 M^{-1} was obtained (20°C, p*H* 8.7) with no $MgCl_2$ present. Stacking interactions have also been studied in the presence of 0.154 *M* NaCl (1) and a monomer–dimer–trimer association model at acidic p*H*'s describes the data best of all.

Nuclear magnetic resonance (nmr) experiments also offer valuable information concerning the self-association of ATP. Based on the ring proton chemical shift studies carried out at a

[1]This is paper No. 8 in the Nuclear magnetic resonance studies of nucleotide – metal ion interactions.

[2]Postdoctoral fellow, 1975–1976. Present address: Department of Life Sciences, University of Pittsburgh, Pittsburgh, PA 15260, U.S.A.

pH of about 7 (9), a dimerization constant of about 5 M^{-1} was obtained (8) when higher order associations were neglected. In addition, nmr techniques have been applied in the study of stacking interactions of a related system, adenosine 5′-monophosphate (10–19), or 5′-AMP. A head-to-head base association model has been proposed (10) as well as the head-to-tail (11, 12, 19). Deuterium substitution is now being applied extensively in these studies (11, 16–20). Ellis and co-workers (19) have studied the stereospecificity of stacking interactions by measuring the proton relaxation times of 5′-AMP and 8-deuteroadenosine 5′-monophosphate. Their results indicate that the base stacking of 5′-AMP is stereospecific at 5°C and, from their calculated internuclear distances, they propose a head-to-tail stacking model. They also observe that, at 30°C, even though the molecules may stack, the stereospecificity is gone. Egan (16) has also studied intermolecular association in 8-deuteroadenosine 5′-monophosphate by monitoring the deuterium magnetic resonance relaxation times over the concentration range 0.01–1.0 m (pH 7.0). He observed that a plot of $(\eta T_1)^{-1}$ vs. the solute concentration is concentration dependent (η = viscosity) and this was attributed to the effect of stacking. An analysis of the data in terms of a monomer–dimer equilibrium yields a value for the equilibrium constant of 2.1 ± 0.7 (30°C) and the analysis also indicates that the association may proceed past the dimer stage.

The object of the present study is to determine the nature of the ATP association complex at a pH of 8.4. With this in mind, the chemical shifts of the H8, H2, and H1′ protons, as well as the α, β, and γ phosphorus nuclei have been measured as a function of the ATP concentration. In addition, longitudinal relaxation times of the H2 proton, which are extremely sensitive to intermolecular effects, were measured as a function of the nucleotide concentration. A viscosity correction is applied to these longitudinal relaxation times. The data are analyzed in terms of several association models. The monomer–dimer–trimer equilibrium model fits the data well, but so does a model which includes tetramers, pentamers, and higher order species.

Experimental

Sample Purification and Preparation

ATP (disodium salt) was purchased from Sigma Chemical Co. It was purified by passing a 0.1 M ATP solution through a Dowex-50 cation exchange resin and then freeze-dried. For all ^{1}H and ^{31}P nmr experiments, samples were then freeze-dried three times from D_2O and then dissolved in D_2O. For the proton homonuclear nuclear Overhauser effect (nOe) experiments, samples were degassed four times using the freeze–pump–thaw technique and then were sealed in nmr tubes. The pD of all the solutions was 8.4. All nucleotide concentrations were determined by uv techniques. Two sets of samples were prepared for all of the nmr experiments with the exception of the ^{31}P shift studies and the proton–proton nOe experiments. The first series contained purified ATP, whereas the second series also contained 2% EDTA (as a mole fraction of the ATP concentration) to check for the effects arising from any trace metal ion impurities (21). The nmr experiments were repeated with both sets of samples. The ^{31}P chemical shifts were measured on solutions containing only purified ATP, whereas the proton–proton nOe experiments were carried out on solutions that contained 2% EDTA.

Inosine 5′-triphosphate (ITP) was purchased from Sigma Chemical Co. and was purified using Chelex 100. The purified ITP was freeze-dried several times from D_2O and then two solutions were prepared in D_2O for the proton spin–lattice relaxation time measurements. The 2% EDTA (as a mole fraction of the ITP concentration) was added to both solutions and the pD was 6.4 and 7.2. The ITP was slightly hydrolyzed ($\sim$10%) but this does not affect the present conclusions.

Viscosity Measurements

Viscosities of ATP solutions at 27°C were measured both in D_2O (pD 8.4) and in H_2O (triply distilled) (pH 8.0) following standard procedures using an Ostwald viscometer. For the measurements in D_2O, 2% EDTA (as a mole fraction of the ATP concentration) was added to the solutions.

Proton Magnetic Resonance Experiments

Proton chemical shifts, as well as spin–lattice relaxation times, were measured at 27°C in the Fourier transform mode (100.0 MHz) using the Varian HA-100-15 nmr spectrometer interfaced with the Digilab FTS/NMR-3 Fourier transform system including the pulse unit (FTS/NMR 400-2) and the Nova 1200 computer. The temperature was controlled using the Bruker B-ST 100/700 temperature controller. The deuterium resonance from the solvent D_2O was used for the lock signal. Depending on the signal to noise ratio, 30–200 free induction decay signals were collected for each spectrum. The sweep width for each spectrum and the number of data points were chosen for a resolution of 0.25 Hz per data point. The spin–lattice relaxation times were measured using the (π–τ–$\pi/2$) two-pulse sequence (22, 23). The $\pi/2$ pulse width was 45 μs. The ATP proton H8, H2, and H1′ chemical shifts were calibrated with respect to three internal references: *tert*-butyl alcohol, *p*-dioxane, and DSS. Since the behaviour of the proton chemical shifts as a function of the ATP concentration was the same with respect to both *tert*-butyl alcohol and *p*-dioxane, the results are expressed with respect to *tert*-butyl alcohol. The concentration of each internal reference was 2 mM. When the common internal reference compound DSS was used (sodium-2,2-dimethyl-2-silopentane-5-sulphonate), it was found that this reference signal shifted with the ATP concentration. DSS is

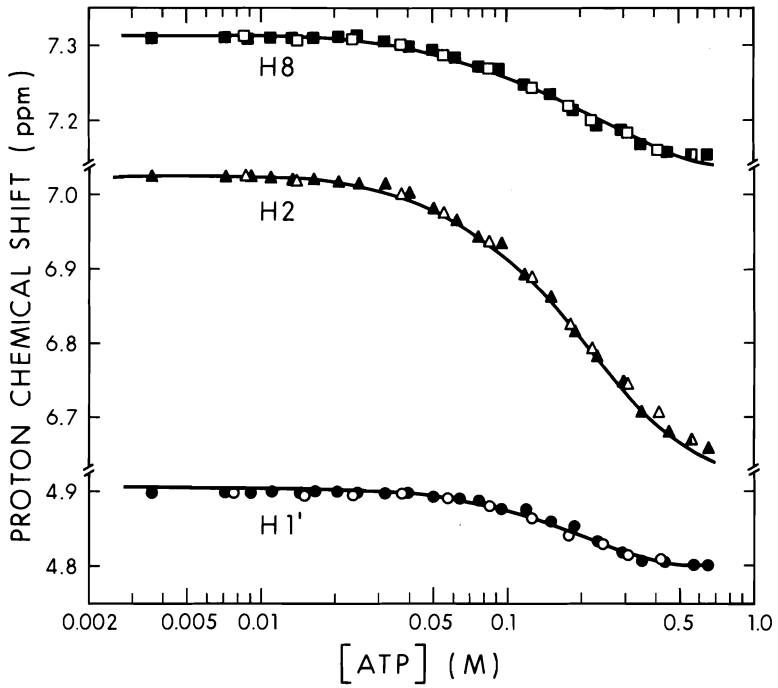

FIG. 1. Proton chemical shifts of protons H8, H2, and H1′ plotted as a function of the ATP concentration. All three protons experience a shift to high field with an increase in the ATP concentration. The data represented by the open symbols are for solutions without EDTA, whereas the solid symbols represent the data obtained for solutions with EDTA. The shifts are expressed in ppm to low field of internal *tert*-butyl alcohol. The experiments were carried out at 100.0 MHz at 27°C. Solutions were prepared in D_2O at a p*D* of 8.4. The solid curves represent the computer fit to the data based on the monomer–dimer–trimer equilibrium model.

therefore not a satisfactory reference compound for these studies (24).

^{31}P Nuclear Magnetic Resonance Experiments

Proton decoupled Fourier transform ^{31}P nmr spectra were obtained at 27°C using the Varian HA-100-15 nmr spectrometer (40.48 MHz) and the Digilab FTS/NMR-3 Fourier transform system, as was discussed in the preceding paragraph. One hundred free induction decay (fid) signals were collected for each spectrum and the resolution was 0.25 Hz per data point. The ^{31}P shifts for the α, β, and γ ATP resonances were calibrated with respect to an internal reference, Na_2HPO_4, and are expressed as ppm to high field of this reference.

Proton–Proton Nuclear Overhauser Effect Measurements

These experiments were carried out at 27°C in the Fourier transform mode using the Bruker WP-60 nmr spectrometer (60.0 MHz) and the Bruker temperature controller B-ST 100/700. The pulse angle was set at 20° less than the normal π/2 pulse angle, and the repetition rate was 8 s, which was sufficiently long for the nuclei to relax back to thermal equilibrium. The signal areas were integrated digitally. Throughout the experiments, the proton decoupler was on, except during the digitization of the fid signal. In the present experiments, protons H2′ and H3′ were separately irradiated. However, the chemical shift between these two protons was ~0.17 ppm with H2′ to lower field (12, 25). Consequently, irradiation of one of these protons may affect the other proton. The nOe is defined as $(A_2 - A_1)/A_1$ where A_2 is the area of the observed peak with irradiation while A_1 is the area of the same peak without irradiation.

Results

A plot of the H8, H2, and H1′ proton chemical shifts as a function of the ATP concentration is shown in Fig. 1. The results clearly indicate that, as the ATP concentration increases, the proton resonances shift to high field due to stacking and hence to ring-current shielding. Sigmoid curves are observed for the three proton chemical shifts and the largest high-field shift is observed for proton H2 (0.37 ppm). Excellent agreement is obtained when the results are compared with and without EDTA.

A plot of the ^{31}P chemical shifts for the α, β, and γ resonances is shown in Fig. 2. All three resonances shift to low field as the ATP concentration increases, an effect that is opposite to that observed for the proton chemical shifts.

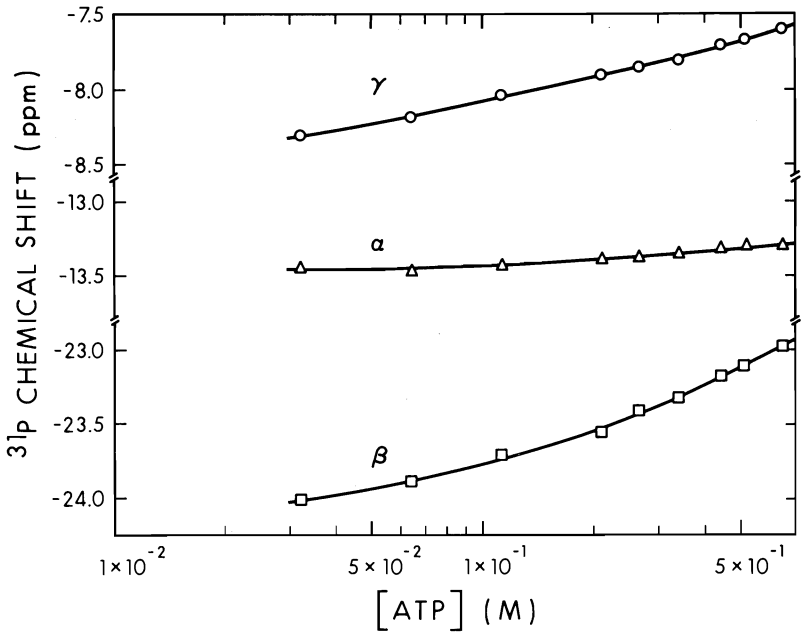

FIG. 2. ^{31}P chemical shifts of the α, β, and γ phosphorus nuclei plotted as a function of the ATP concentration. All three phosphorus nuclei experience a shift to low field with an increase in the ATP concentration. The shifts are expressed in ppm to high field of internal inorganic phosphate (~3 mM) so that shifts with the most positive value (in ppm) are to lowest field. The experiments were carried out at 40.48 MHz in the Fourier transform mode at 27°C. Solutions were prepared in D_2O at a pD of 8.4.

The greatest shift is observed for the β resonance (1 ppm) whereas the α phosphorus resonance is very slightly affected. No significant changes in the coupling constants between the phosphorus nuclei are observed. For 0.034 M ATP solutions, $J(\alpha,\beta) = 19 \pm 1$ Hz and $J(\beta,\gamma) = 19.5 \pm 1$ Hz. For 0.51 M ATP, $J(\alpha,\beta) = 18 \pm 1$ Hz and $J(\beta,\gamma) = 18.5 \pm 1$ Hz.

The results of the relaxation measurements on proton H2 are shown in Fig. 3, both in the absence and presence of 2% EDTA. Protons relax predominantly via the dipole–dipole relaxation mechanism which is given by the equation (26)

$$[1] \qquad \frac{1}{T_1}(^1\mathrm{H}) = \frac{3}{2}\gamma_H{}^4\hbar^2 \sum_i \langle r^{-6}\rangle_i \tau_{ci}$$

In [1], γ is the magnetogyric ratio of hydrogen, $\langle r^{-6}\rangle$ is the conformationally averaged value of the inverse sixth power of the distance and i represents the protons which affect the T_1 of the proton under consideration via the dipolar interaction. The average reorientational correlation time, τ_c, can be approximated by the Stokes or Einstein equation (27)

$$[2] \qquad \tau_c = \frac{4\pi\eta a^3}{3kT}$$

where η is the viscosity of the solution and k is the Boltzmann constant.

With this in mind, viscosities were measured on ATP solutions, at 27°C, both in H_2O and in D_2O. The results of these measurements are shown in Fig. 4. Applying the viscosity correction for the solvent D_2O, a plot of $[\eta T_1]^{-1}$ vs. the concentration of ATP for proton H2 is shown in Fig. 5. A significant change is observed up to a nucleotide concentration of about 0.20 M, and then the results are concentration independent. For protons H8 and H1′, T_1 measurements were also carried out, but the results are sensitive to the presence of EDTA (Fig. 6) and hence to the presence of trace metal ions in solution. In addition, since the relaxation of these protons is not due only to intermolecular dipole–dipole effects as is the case for proton H2, the data in Fig. 6 were not further analyzed in the study of intermolecular association equilibria.

In view of the results in Fig. 6, T_1 values for the H8, H2, and H1′ protons of purified ITP

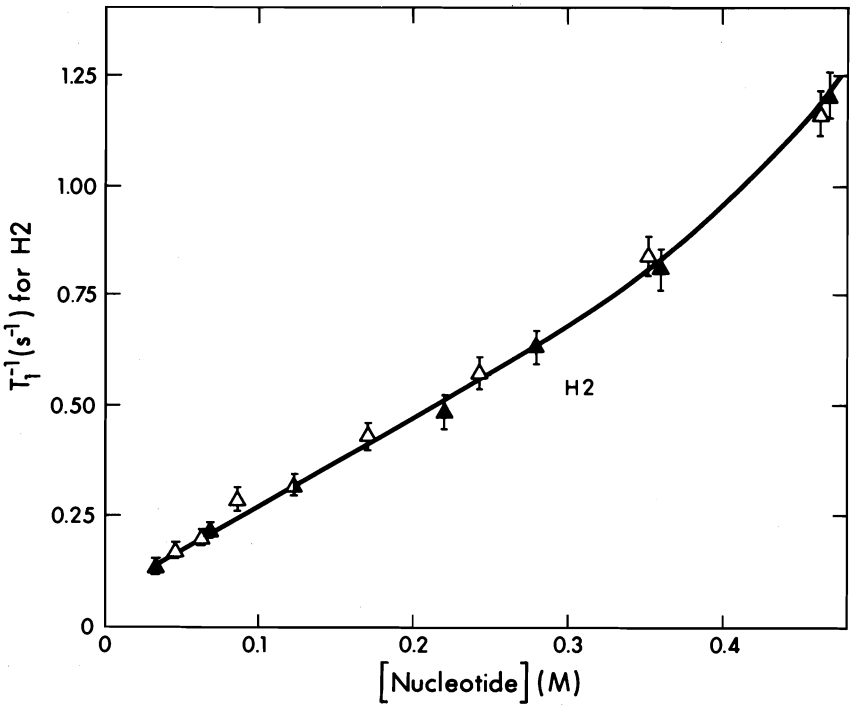

FIG. 3. The T_1^{-1} values for proton H2 of pure ATP are plotted as a function of the nucleotide concentration in solution. These T_1^{-1} measurements were carried out at 100.0 MHz in the Fourier transform mode (27°C) on samples prepared in D_2O at a pD of 8.4. The data represented by the open symbols are for solutions without EDTA, whereas the solid symbols represent the data obtained for solutions with EDTA.

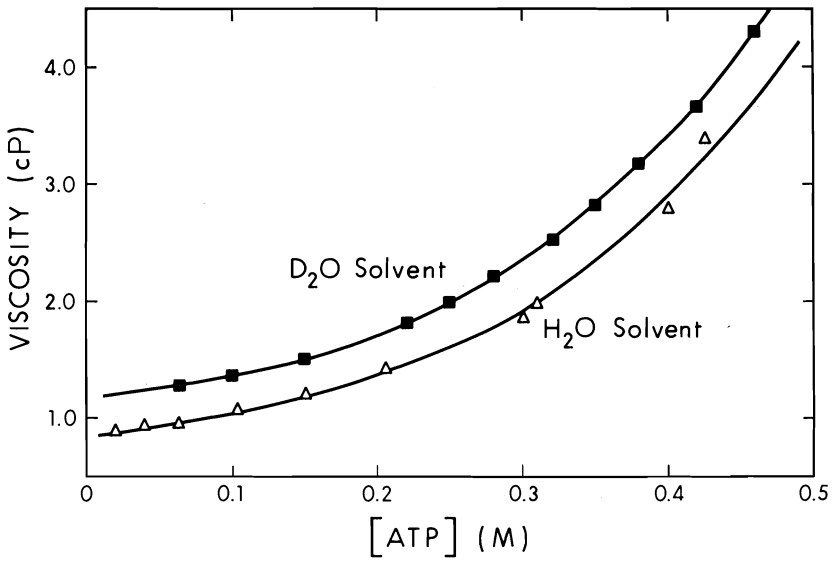

FIG. 4. A plot of the viscosities of ATP solutions measured in H_2O and D_2O as a function of the ATP concentration. The experiments were carried out at 27°C.

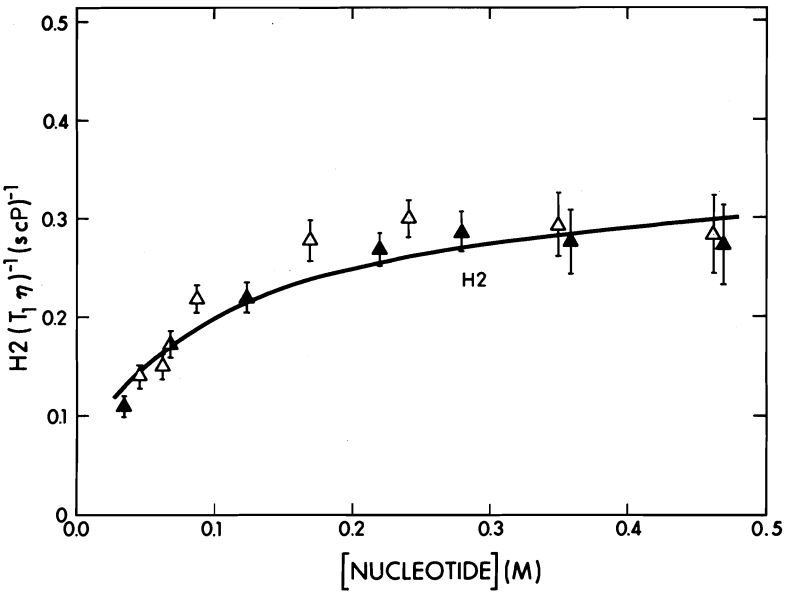

FIG. 5. A plot of the viscosity corrected relaxation rate $(T_1\eta)^{-1}$ for proton H2 of pure ATP plotted as a function of the nucleotide concentration in solution. As discussed in the caption to Fig. 3, the solid symbols represent the data obtained for solutions with EDTA, whereas the open symbols are for solutions without EDTA. The solid curves represent the best fit to the data based on the monomer–dimer–trimer equilibrium model.

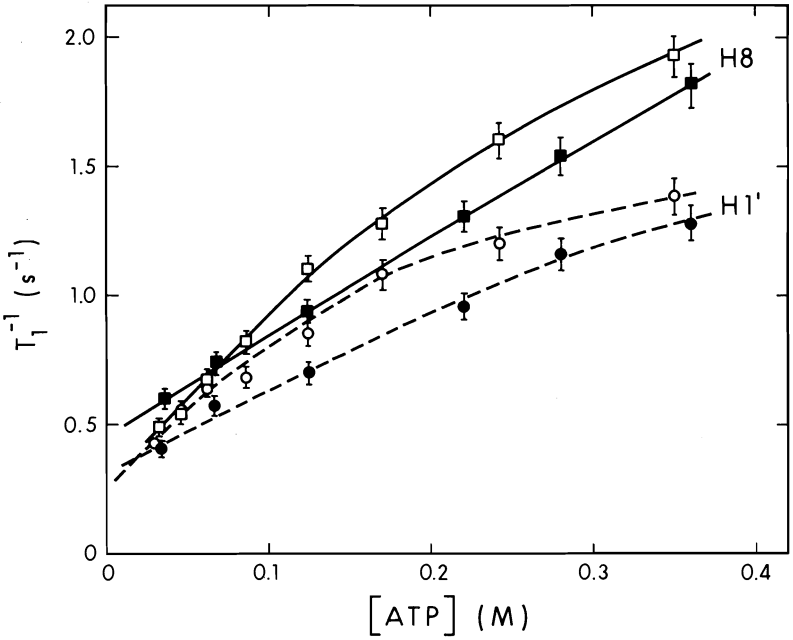

FIG. 6. A plot of the H8 and H1′ proton T_1^{-1} data as a function of the ATP concentration. The experiments were carried out at 100.0 MHz in the Fourier transform mode (27°C) on samples prepared in D_2O at a pD of 8.4. The data represented by the open symbols are for solutions without EDTA, whereas the solid symbols represent the data obtained for solutions with EDTA.

TABLE 1. The nuclear Overhauser effect observed for proton H8 upon irradiation of proton H2 and the ribose protons[a]

[ATP] (M)	H1′	H2′	H3′	H2
0.44	~0	0.15±0.03	0.15±0.03	0
0.22	~0	0.15±0.03	0.19±0.03	0
0.11	~0	0.15±0.03	0.11±0.03	0
0.056	0.05±0.03	0.15±0.03	0.13±0.03	0

[a]The samples were degassed, and the temperature was 27°C. The solutions were at a pD of 8.4 and contained 2% EDTA. In addition, the adenine H2 proton was not affected when the ribose protons were irradiated.

solutions (with 2% EDTA) were remeasured (28). For two ITP solutions prepared in D_2O with [ITP] = 0.20 ± 0.03 M and a pD of 6.4 and 7.2, the average values of the proton T_1 data are: H8 = 1.3 ± 0.15 s, H2 = 3.0 ± 0.3 s, and H1′ = 1.6 ± 0.2 s. These relaxation times are significantly longer than those previously reported (28), suggesting that in the earlier study, even though some EDTA was added, the relaxation times were shortened by paramagnetic impurities.

Proton–proton nOe experiments were carried out as a function of the ATP concentration. The results are tabulated in Table 1. Large enhancements are observed for proton H8 upon irradiation of protons H2′ and H3′. Since the ribose proton resonances are not well resolved at 60.0 MHz, the measured values of the nOe must be treated with caution.

Data Treatment

In order to decide on the nature of the intermolecular complex present in solution, the data were first analyzed as a function of the ATP concentration using multiple regression. The equation that was used is

$$[3] \qquad f(c)\ [\text{observed}] = \sum_{i=0}^{k} \alpha_i c^i$$

where k is the order of the polynomial, α_i is the ith regression coefficient, and c is the concentration. This relationship is, in general, applicable for studies of self-aggregating systems (2, 4, 29, 30). In carrying out the regression analysis, each set of data was fitted to a power series and k was varied (k = 2, 3 . . . 6). Then, the significance of each of the regression coefficients thus obtained was tested using the F test (30, 31). The results indicate that for the chemical shift data for protons H8, H2, and H1′, and for the β and γ phosphorus, the coefficients α_0, α_1, and α_2 are significant in the regression analysis when a confidence limit of 99% is applied. For the α-phosphorus shifts, which are not very sensitive to the ATP concentration, only the α_0 and α_1 coefficients are significant. In analyzing the viscosity corrected relaxation rates for H2, the α_3 coefficient was found to be significant. Values of the α_0 coefficient are listed in Table 2. These are important in the following analysis, as this coefficient corresponds to the values of the chemical shifts and to the relaxation rates for the ATP monomer in the limit of infinite dilution.

The nature of the intermolecular association may now be considered. The intermolecular stacking interactions in solution are analyzed in terms of the following equilibria in solution (4, 5):

$$[4] \qquad \begin{aligned} m_1 + m_1 &\overset{K_2}{\rightleftharpoons} m_2 \\ m_1 + m_2 &\overset{K_3}{\rightleftharpoons} m_3 \\ m_1 + m_{n-1} &\overset{K_n}{\rightleftharpoons} m_n \end{aligned}$$

The terms m_i and K_i are the concentration and the association constant, respectively. These terms are related by the equations

$$[5] \qquad c = \sum_{i=1}^{n} i m_i$$

TABLE 2. Limiting values of the parameters for the ATP monomer (α_0 coefficient) obtained from the multiple regression analysis[a]

Measurement	α_0 coefficient
H8 chemical shift	7.32 ppm
H2 chemical shift	7.04 ppm
H1′ chemical shift	4.91 ppm
α-P chemical shift	−13.5 ppm
β-P chemical shift	−24.1 ppm
γ-P chemical shift	−8.3 ppm
H2 viscosity corrected relaxation rate $(\eta T_1)^{-1}$	0.047 s^{-1} cP^{-1}

[a]The limiting values of the chemical shift parameters for the ATP monomer (α_0) were obtained by a multiple regression analysis of the data using the polynomial $Y_{obs} = \alpha_0 + \alpha_1 x + \alpha_2 x^2$. The ATP concentration is represented by x. For the viscosity corrected relaxation rates, the polynomial $Y_{obs} = \alpha_0 + \alpha_1 x + \alpha_2 x^2 + \alpha_3 x^3$ was used.

TABLE 3. Results of the calculations for the monomer–dimer equilibrium model

Measurement	Association constant (M^{-1})	Value of p_2[a] for the dimer	Standard error[b] of the fit
H8 chemical shift	1.08±0.15	6.91±0.03 ppm	7.99×10^{-2}
H2 chemical shift	0.74±0.09	5.91±0.08 ppm	1.33×10^{-2}
H1′ chemical shift	0.88±0.17	4.62±0.03 ppm	6.48×10^{-3}
α-P chemical shift	0.32±0.23	−12.6±0.4 ppm	1.85×10^{-2}
β-P chemical shift	0.53±0.08	−20.6±0.3 ppm	2.69×10^{-2}
γ-P chemical shift	0.75±0.19	−6.4±0.3 ppm	3.16×10^{-2}
H2 viscosity corrected relaxation rate $(\eta T_1)^{-1}$	5.0 ±1.5	0.45±0.04 s^{-1} cP^{-1}	2.29×10^{-2}

[a]In the analysis, the characteristic values of p_1 used for the monomer are the corresponding values of α_0 ($\equiv p_1$) listed in Table 2.
[b]The standard error of the fit was calculated using the equation

$$[(Y_{obs} - Y_{predicted})^2/(\text{No. of data points} - \text{No. of parameters})]^{1/2}$$

TABLE 4. Results of the calculations for the monomer–dimer–trimer equilibrium model

Measurement	Association constant (M^{-1})	Value of p_2[a] and p_3	Standard[b] error of the fit
H8 chemical shift	1.29±0.15	6.99±0.02 ppm	7.52×10^{-2}
H2 chemical shift	0.92±0.09	6.16±0.05 ppm	1.25×10^{-2}
H1′ chemical shift	1.08±0.18	4.68±0.02 ppm	6.25×10^{-3}
α-P chemical shift	0.43±0.26	−12.9±0.3 ppm	1.83×10^{-2}
β-P chemical shift	0.66±0.09	−21.4±0.2 ppm	2.55×10^{-2}
γ-P chemical shift	0.90±0.19	−6.8±0.2 ppm	3.06×10^{-2}
H2 viscosity corrected relaxation rate $(\eta T_1)^{-1}$	5.1 ±1.3	0.40±0.03 s^{-1} cP^{-1}	2.17×10^{-2}

[a]For the analysis, p_2 was chosen equal to p_3. The characteristic values of p_1 used for the monomer are the corresponding values of α_0 ($\equiv p_1$) listed in Table 2.
[b]The standard error of the fit was calculated using the equation

$$[(Y_{obs} - Y_{predicted})^2/(\text{No. of data points} - \text{No. of parameters})]^{1/2}$$

and

$$[6] \qquad K_i = \frac{m_i}{m_i m_{i-1}} \quad (i \geq 2)$$

Under conditions of fast exchange, the observed chemical shift or relaxation rate is given by the equation

$$[7] \qquad f(c)[\text{observed}] = \sum_{i=1}^{n} x_i p_i$$

where p_i is the chemical shift or the relaxation rate of a given nucleus in the species with i ATP molecules in a stack, x_i is the corresponding mole fraction ($x_i \equiv i m_i/c$), and n is the degree of association.

The proton H8, H2, and H1′ chemical shift data, as well as the ^{31}P chemical shifts and the H2 viscosity corrected relaxation rates, were fitted to [5], [6], and [7] using a nonlinear least-squares program (32, 33). All the data for proton H2 (Fig. 5) were used in the analysis. When the analysis was carried out including only the solutions containing EDTA, very similar results were obtained. The results of the simple monomer–dimer equilibrium model are given in Table 3. The data were also analyzed in terms of a monomer–dimer–trimer equilibrium model present in solution. In this analysis, however, since K_2 and K_3, as well as p_2 and p_3, are perfectly correlated, a fit to the data could only be achieved with $K_2 = K_3$ and $p_2 = p_3$. The results of this analysis are given in Table 4. In these analyses, p_1 was set equal to the corresponding α_0 value from Table 2. Equilibria involving higher order species were also tested, up to $n = 10$, with $K_i = K_{i+1}$ and $p_i = p_{i+1}$.

Discussion

X-ray studies by Kennard *et al.* (34) show the presence of two molecules of ATP, four sodium ions, and six water molecules in the asymmetric unit. The triphosphate chain is in the folded conformation in both ATP molecules, and the base to sugar conformation is *anti*. In one molecule (A) of ATP, the triphosphate chain is folded so as to form part of a left-handed helix, while in the second molecule (B), it forms part of

a right-handed helix. The ribose ring is in the C3′ *endo* conformation in molecule A and C2′ *endo* conformation in molecule B. In addition, it was observed that for the base stacking, the base planes are stacked almost parallel to each other with A and B molecules alternating, with an average separation of 3.40 Å. The degree of overlap was considerable, and the base stacking is head-to-tail. Theoretical calculations (35–37) support the folded triphosphate chain. The molecular orbital calculations (36) indicate that the free ATP molecule has an intrinsic tendency to adopt a folded conformation due to a possible hydrogen bonding between the terminal OH and the adenine N7 nitrogen. In addition, recent phosphorus–proton nOe experiments (0.1 *M* ATP in D_2O, p*D* 7.5) indicate that the γ phosphorus interacts spatially with the ribose protons in the H3′ and H4′ region (38).

The H8, H2, and H1′ proton chemical shifts (Fig. 1) are independent of concentration up to an ATP concentration of about 0.02 *M*. As the ATP concentration increases, a sigmoid dependence of the chemical shifts is observed, and all resonances shift to high field, due to intermolecular association and ring-current shielding effects. The largest concentration effect is observed for proton H2, followed by proton H8. The smallest shift is for proton H1′. This same order of concentration effects was observed for adenosine 5′-monophosphate (12), a system in which the adenine bases stack in a head-to-tail manner (11, 12, 19). The ATP proton chemical shifts are consistent with a head-to-tail adenine base stacking, in agreement with the solid state observations.

Brown *et al.* (39) carried out water proton relaxation time measurements on ATP solutions in the presence of paramagnetic Mn(II) ions. Their results are independent of the ATP concentration when concentrations of about 0.02 *M* and lower are studied. Consequently, the proton chemical shift data and the results of Brown *et al.* (39) are self-consistent and indicate that the degree of self-association is very small or negligible for ATP solutions less than 20 m*M*. This result indicates that in the cell where the ATP concentration is less than 10 m*M* (40), the ATP molecules probably do not self-associate.

A comparison of the proton chemical shifts in the monomer (Table 2) and those calculated for the aggregate (Table 4) yields values of +0.33, +0.88, and +0.23 ppm for protons H8, H2, and H1′ respectively. These data further support, in a qualitative manner, the head-to-tail stacking model. With the aid of the theoretical calculations for the ring current shielding areas for the adenine base (41), the observed and calculated chemical shifts due to the base stacking are self-consistent. By placing one adenine base in a head-to-tail fashion over another base at a separation of 3.4 Å, and locating C2 of the top base on the +1 ppm contour line of the bottom base, protons H2 and H8 are then in the +0.8 and +0.3 ppm shielding regions, respectively.

In solution, the nOe experiments (Table 1) indicate that comparable enhancements are observed for the adenine H8 proton when the ribose H2′ or H3′ protons are irradiated, while an enhancement was not observed for the adenine H2 proton. In addition, the measured enhancements are independent of the ATP concentration. Since the nOe is sensitive to the distance between the observed proton and the proton under irradiation, comparable nOe effects, within experimental error, for H8 upon irradiating H2′ or H3′ indicate that proton H8 is located predominantly near protons H2′ and H3′ whereas proton H2 is far removed. These results indicate (42) that the ATP molecules are predominantly in the *anti* conformation over the concentration range studied, as is observed in the solid state. However, the nOe is also sensitive to a variety of effects (42–45), so the conclusions reached from the present nOe data must be treated with caution. To determine precisely the exact conformations of the ATP molecules and the exact stereospecificity of the intermolecular base–base orientation, proton relaxation rates must be obtained for 8-deutero ATP and compared with those for pure ATP, at 5°C (11, 17, 18, 19).

The behavior of $(T_1\eta)^{-1}$ for H2 (Fig. 5) is very similar to that observed for D8 in 8-deuteroadenosine 5′-monophosphate (16) as a function of the nucleotide concentration. Hence both sets of data measure the degree of intermolecular association (16), since H2 proton is relaxed primarily by the H8 proton of the neighboring base in the head-to-tail base stacking model (11, 12, 19). However, proton H8 is relaxed via intermolecular dipole–dipole interactions with a neighboring base H2 proton as well as by intramolecular dipole–dipole interactions with the ribose protons of the same molecule (19). This is only a qualitative conclusion. It has been

observed that 5′-AMP (19) at 5°C is almost exclusively in the *anti* conformation. However, at 30°C, a simple two-state model, in which the purine ring spends 92% of its time in the *anti* conformer and only 8% of the time in the *syn* conformer, fits the data, and so does a model which allows large amplitude rotations about the pure *anti* position (19).

A comparison of the standard errors in Tables 3 and 4 indicates that the monomer–dimer–trimer equilibrium model in solution fits the data better than the monomer–dimer model. The constants given in Table 4 were used to plot the solid curves to the data in Figs. 1, 2, and 5. However, when higher order complexes were introduced into the analysis, very little improvement in the fit to the data was obtained and the equilibrium constants increased slightly. For example, for the proton H8 data, when tetramers are included in the analysis, $K = 1.40 \pm 0.16$ and when pentamers are also included, $K = 1.45 \pm 0.17$. Consequently, the present results suggest the presence of higher oligomers and indicate that the ATP molecules in solution can undergo indefinite linear self-association. This conclusion is in agreement with the stacking model proposed on the basis of uv and cd studies (2, 3), a model with indefinite linear self-association where each step has the same equilibrium constant.

The average value of the association constant based on the proton and phosphorus chemical shift data (Table 4) is $0.9 \pm 0.3\ M^{-1}$. However, for the viscosity corrected H2 relaxation rates $(\eta T_1)^{-1}$, the association constant is $5.1 \pm 1.3\ M^{-1}$. The relaxation measurements give a slightly larger value for the association constant than is obtained from the chemical shift data. This may be due to the large macroscopic viscosity correction that has been applied to the relaxation rates (16, 46), whereas the microscopic viscosity is really necessary. Secondly, the chemical shift data may be more sensitive to initial dimerization or trimerization with higher order species exerting less influence, whereas the $1/T_1$ relaxation data should be continuously proportional to aggregate size, due to the dependence on the correlation time.

Acknowledgements

The authors thank Dr. P. D. Ellis for valuable discussions, Dr. T. Nakashima, Mr. T. Brisbane and Mr. Glen Bigam for their assistance in carrying out some of the relaxation measurements, and the National Research Council of Canada for financial assistance.

1. W. E. Ferguson, C. M. Smith, E. T. Adams, Jr., and G. H. Barlow. Biophys. Chem. **1**, 325 (1974).
2. M. P. Heyn and R. Bretz. Biophys. Chem. **3**, 35 (1975).
3. T. J. Gilligan III and G. Schwarz. Biophys. Chem. **4**, 55 (1976).
4. P. O. P. Ts'o and S. I. Chan. J. Am. Chem. Soc. **86**, 4176 (1964).
5. S. I. Chan, M. P. Schweizer, P. O. P. Ts'o, and G. K. Helmkamp. J. Am. Chem. Soc. **86**, 4182 (1964).
6. P. O. P. Ts'o. The physicochemical basis of interactions of nucleic acid. *In* Molecular associations in biology. *Edited by* B. Pullman. Academic Press, New York, NY. 1968. pp. 39–75.
7. P.O.P. Ts'o. Bases, nucleosides, and nucleotides. *In* Basic principles in nucleic acid chemistry. Vol. I. *Edited by* P.O.P. Ts'o. Academic Press, New York, NY. 1974. pp. 453–584.
8. H. Sternlicht, D. E. Jones, and K. Kustin. J. Am. Chem. Soc. **90**, 7110 (1968).
9. H. Sternlicht, R. G. Shulman, and E. W. Anderson. J. Chem. Phys. **43**, 3133 (1965).
10. M. P. Schweizer, A. D. Broom, P. O. P. Ts'o, and D. P. Hollis. J. Am. Chem. Soc. **90**, 1042 (1968).
11. M. Guéron, C. Chachaty, and T.-D. Son. Ann. N.Y. Acad. Sci. **222**, 307 (1973).
12. T.-D. Son and C. Chachaty. Biochim. Biophys. Acta, **335**, 1 (1973).
13. I. C. P. Smith, H. H. Mantsch, R. D. Lapper, R. Deslauriers, and T. Schleich. *In* Conformation of biological molecules and polymers. *Edited by* E. D. Bergmann and B. Pullman. Academic Press, New York, NY. 1973. pp. 381–402.
14. W. D. Hamill, Jr., R. J. Pugmire, and D. M. Grant. J. Am. Chem. Soc. **96**, 2885 (1974).
15. H.-D. Ludemann and O. Roder. J. Am. Chem. Soc. **97**, 4402 (1975).
16. W. Egan. J. Am. Chem. Soc. **98**, 4091 (1976).
17. K. Akasaka, T. Imoto, S. Shibata, and H. Hatano. J. Magn. Reson. **18**, 328 (1975).
18. A. P. Zens, P. T. Fogle, T. A. Bryson, R. B. Dunlap, R. R. Fisher, and P. D. Ellis. J. Am. Chem. Soc. **98**, 3760 (1976).
19. A. P. Zens, T. A. Bryson, R. B. Dunlap, R. R. Fisher, and P. D. Ellis. J. Am. Chem. Soc. **98**, 7559 (1976).
20. H. Saito, H. H. Mantsch, and I. C. P. Smith. J. Am. Chem. Soc. **95**, 8453 (1973).
21. R. E. Wasylishen and J. S. Cohen. Nature, **249**, 847 (1974).
22. R. L. Vold, J. S. Waugh, M. P. Klein, and D. E. Phelps. J. Chem. Phys. **48**, 3831 (1968).
23. R. Freeman and H. D. W. Hill. J. Chem. Phys. **51**, 3140 (1969).
24. Y. F. Lam and G. Kotowycz. FEBS Lett. **78**, 181 (1977).
25. I. Feldman and R. P. Agarwal. J. Am. Chem. Soc. **90**, 7329 (1968).
26. I. Solomon. Phys. Rev. **99**, 559 (1955).
27. C. P. Poole, Jr., and H. A. Farach. Relaxation in

magnetic resonance. Academic Press, New York, NY. 1971. p. 229.
28. G. P. P. KUNTZ and G. KOTOWYCZ. Biochemistry, **14**, 4144 (1975).
29. R. F. STEINER. Arch. Biochem. Biophys. **39**, 333 (1952).
30. M. E. MAGAR. Data analysis in biochemistry and biophysics. Academic Press, New York, NY. 1972. pp. 216–257, 342–400.
31. G. W. SNEDECOR and W. G. COCHRAN. Statistical methods. 5th ed. Iowa State College Press, IA. 1956. pp. 246–247.
32. D. W. MARQUARDT. J. Soc. Ind. Appl. Math. **11**, 431 (1963).
33. P. D. LARK, B. R. CRAVEN, and R. C. L. BOSWORTH. The handling of chemical data. Pergamon Press, Toronto, Ont. 1968. pp. 207–267.
34. O. KENNARD, N. W. ISAACS, W. D. S. MOTHERWELL, J. C. COPPOLA, D. L. WAMPLER, A. C. LARSON, and D. G. WATSON. Proc. R. Soc. London Ser. A, **325**, 401 (1971).
35. M. SUNDARALINGAM. Biopolymers, **7**, 821 (1969).
36. D. PERAHIA, B. PULLMAN, and A. SARAN. Biochem. Biophys. Res. Commun. **47**, 1284 (1972).
37. O. E. MILLNER, JR. and J. A. ANDERSEN. Biopolymers, **14**, 2159 (1975).
38. P. A. HART. J. Am. Chem. Soc. **98**, 3735 (1976).
39. F. F. BROWN, I. D. CAMPBELL, R. HENSON, C. W. J. HIRST, and R. E. RICHARDS. Eur. J. Biochem. **38**, 54 (1973).
40. A. L. LEHNINGER. Biochemistry. 2nd ed. Worth Publishers, Inc., New York, NY. 1975. pp. 389–390.
41. C. GIESSNER-PRETTRE and B. PULLMAN. J. Theor. Biol. **27**, 341 (1970); Biochem. Biophys. Res. Commun. **70**, 578 (1976).
42. J. H. NOGGLE and R. E. SCHIRMER. The nuclear Overhauser effect, chemical applications. Academic Press, New York, NY. 1971. pp. 44–75.
43. T. D. SON, W. GUSCHLBAUER, and M. GUERON. J. Am. Chem. Soc. **94**, 7903 (1972).
44. P. BALARAM, A. A. BOTHNER-BY, and J. DADOK. J. Am. Chem. Soc. **94**, 4015 (1972).
45. W. EGAN, S. FORSEN, and J. JACOBUS. Biochemistry, **14**, 735 (1975).
46. L. W. REEVES and C. P. LEE. Can. J. Chem. **48**, 3307 (1970), and references therein.

Stereochemical basis of anticonvulsant drug action. VI. Crystal and molecular structure of diphenylsilanediol[1]

J. KEITH FAWCETT AND NORMAN CAMERMAN[2]

Department of Biochemistry, University of Toronto, Toronto, Ont., Canada M5S 1A8

AND

ARTHUR CAMERMAN

Departments of Medicine (Neurology) and Pharmacology, University of Washington, Seattle, WA 98195 U.S.A.

Received June 1, 1977

J. KEITH FAWCETT, NORMAN CAMERMAN, and ARTHUR CAMERMAN. Can. J. Chem. **55**, 3631 (1977).

The crystal and molecular structure of diphenylsilanediol, a compound with recently demonstrated anticonvulsant activity, has been determined and its stereochemistry compared with other antiepileptics. Crystals of diphenylsilanediol are triclinic, space group $P\bar{1}$, with cell dimensions $a = 9.912$, $b = 15.048$, $c = 14.519$ Å, $\alpha = 120.83$, $\beta = 99.95$, $\gamma = 100.84°$, $Z = 6$ molecules per cell (3 molecules per asymmetric unit). The structure was determined by Patterson and Fourier methods and refined to a final discrepancy value $R = 0.034$. The phenyl ring planes in the molecule are rotated by 80° with respect to each other, and the hydroxyl oxygen atoms are 2.66 Å apart. The molecular parameters help to delineate limits of stereochemical variation in these molecules with retention of anticonvulsant activity.

J. KEITH FAWCETT, NORMAN CAMERMAN et ARTHUR CAMERMAN. Can. J. Chem. **55**, 3631 (1977).

On a déterminé la structure cristalline et moléculaire du diphénylsilanediol, composé ayant démontré une activité anticonvulsive et sa stéréochimie est comparée à d'autres composés antiépileptiques. Les cristaux du diphénylsilanediol sont tricliniques de groupe spatial $P\bar{1}$ avec des dimensions de maille suivantes: $a = 9.912$, $b = 15.048$, $c = 14.519$ Å, $\alpha = 120.83$, $\beta = 99.95$, $\gamma = 100.84°$, $Z = 6$ molécules par maille (3 molécules par unité asymétrique). La structure est déterminée par les méthodes de Patterson et Fourier et affinée à une différence finale de $R = 0.034$. Les plans des cycles phényles dans la molécule sont tournés de 80° l'un par rapport à l'autre et les atomes d'oxygène des groupes hydroxyles sont à une distance de 2.66 Å. Les paramètres moléculaires aident à délimiter la variation stéréochimique dans ces molécules ayant une activité retenue et anticonvulsive.

[Traduit par le journal]

Introduction

In previous papers in this series (1–5) we have described X-ray crystallographic determinations of the molecular structures of chemically different agents which all possess clinical or laboratory demonstrated activities against grand mal epilepsy. These researches resulted in the discovery and identification of certain stereochemical features common to the structures of the different drugs, features which may be the basis of their one mutual pharmacological activity, anticonvulsant efficacy. Thus diphenylhydantoin (DPH), diazepam, procyclidine, trihexyphenidyl, and ethylphenacemide all possess two hydrophobic regions of structure, and when the drug conformations are compared so that these regions are maximally superposed, each compound has two electron-donor groups situated in similar orientations and positions with respect to each other and to the hydrophobic groups.

Recently, reports have appeared ascribing anticonvulsant properties to the silicon-containing compound diphenylsilanediol (DPSD). DPSD has been shown to inhibit electroshock and chemically induced seizures in laboratory tests (6) and to be of use in controlling idiopathic epilepsy in animals (6).[3] There is evidence that the mechanism of action of DPSD is similar to that of diphenylhydantoin. We have undertaken the determination of the structure of DPSD in order to compare its three-dimensional molecular conformation and stereochemistry with those of the other anticonvulsants. The

[1]For part V see ref. 1.

[2]To whom correspondence should be addressed.

[3]R. H. Rech. Personal communication.

quantitative description of the relative positions and orientation of the hydrophobic phenyl rings and the electron-donor hydroxyl moieties should prove valuable in further delineating the range of variation permitted for these features in drug structures with retention of anticonvulsant activity.

Experimental

Crystals of diphenylsilanediol, obtained by slow evaporation from ethanol–water solution, are colorless needles elongated along *a*. Unit cell parameters were determined by diffractometer measurement of 2θ values for 15 general reflections, and crystal data (Delaunay reduced cell) are:

$C_{12}H_{12}O_2Si$ fw = 216.31
Triclinic, $a = 9.912 \pm 0.002$, $b = 15.048 \pm 0.008$, $c = 14.519 \pm 0.008$ Å, $\alpha = 120.83° \pm 0.04°$, $\beta = 99.95° \pm 0.04°$, $\gamma = 100.84° \pm 0.04°$, $V = 1731$ Å^3, $Z = 6$, D_c 1.24 g cm^{-3}. Space group (confirmed by structure analysis) $P\bar{1}$. CuK_α radiation, $\lambda = 1.54178$ Å, $\mu(CuK_\alpha) = 15.8$ cm^{-1}.

The intensities of all independent reflections having $2\theta(CuK_\alpha) \leq 132°$ (corresponding to a minimum interplanar spacing $d = 0.84$ Å) were measured on an automated four-circle diffractometer with nickel-filtered CuK_α radiation using the 2θ–θ scan technique, with a scan range of 2° and stationary background counts at each end of the scan. The intensities were corrected for background and Lorentz and polarization factors applied; no absorption corrections were made. Three standard reflections monitored frequently showed no significant decrease in intensity during data collection. A total of 6048 unique reflections were measured of which 5506 (91%) had $I > 2\sigma(I)$ and were considered to be observed.

Structure Determination

The structure was determined using Patterson methods. Density calculations indicated that the triclinic unit cell probably contained either six molecules of diphenylsilanediol or fewer DPSD molecules plus some solvent. Two Patterson syntheses were calculated, one containing contributions from all observed reflections (5506) and the other including only those observed reflections having $\sin\theta/\lambda > 0.40$ Å^{-1} (3717). When peaks from the two maps were compared it was found that the three highest peaks *common to both maps* could represent cross-vectors between three silicon atoms in an asymmetric unit of a centrosymmetric unit cell. The corresponding three self-vectors were also present, but because of their size (half that of the cross-vectors) they did not stand out among the large number of other peaks. A weighted three-dimensional Fourier map, phased on the derived silicon positions, revealed one phenyl ring and parts of others. Two more weighted Fourier syntheses revealed the complete structure, which was found to have six molecules of diphenylsilanediol/unit cell with no solvent of crystallization. Three cycles of isotropic least squares, during which all 36 hydrogens were located on difference Fourier maps, resulted in the discrepancy index $R = 0.102$.

Five sets of least-squares cycles having three blocks/cycle (one molecule/block) completed the refinement. The heavy atoms were refined anisotropically; the hydrogen positions were refined and, after each set of cycles, the hydrogen isotropic *B*'s were made equal to the temperature factor of the atom to which they are attached. The 5506 observed reflections were used for the refinement. The function minimized was $\Sigma w(\Delta F)^2$; unit weights were employed and final residuals were $R = R_w = 0.034$. The maximum shift/error in the final cycle was 0.1 and the final $(\Sigma w(\Delta F)^2/(m-n))^{1/2} = 1.29$. Scattering factors used for silicon, oxygen, and carbon (7) and for hydrogen atoms (8) were as cited. Table 1 lists the fractional coordinates of the nonhydrogen atoms and Table 2 the hydrogen positional parameters.[4]

Results and Discussion

Molecular Structure

Figure 1 is a stereoscopic drawing of the three crystallographically independent DPSD molecules comprising the asymmetric unit of the crystal cell. The conformations of the three molecules are extremely similar, having only very small differences in torsional angles between comparable parts of the different molecules. The phenyl rings in each DPSD are in a nearly mutually perpendicular arrangement, the angles between normals to the two rings averaging 80° (±2°). The hydroxyl groups all participate maximally in an intricate hydrogen-bonding network which links molecules within each asymmetric triplet, as well as from triplet to triplet. There are two systems of H-bonds: (*1*) the even-numbered oxygens in a given triplet of DPSD molecules (O(2), O(4), O(6), the upper three in the stereoscopic drawing) form one end of a hydrogen-bonded chair of O atoms, the other being comprised of oxygens in a triplet related to these by a center of symmetry, i.e., resulting in a chair

O(2)...O(6)...O(4)...O(2′)...O(6′)...O(4′)
⋮.....⋮

with an average O...O distance of 2.74 Å; (*2*) the odd-numbered oxygen atoms (lower three in Fig. 1) in a DPSD triplet form a hydrogen-bonded chair of O atoms through alternating involvement with odd-numbered counterparts in molecules related by a different center of symmetry, i.e.,

O(1)...O(3′)...O(5)...O(1′)...O(3)...O(5′)
⋮.....⋮

average O...O distance is 2.70 Å.

Figure 2 shows the bond lengths and angles in DPSD, the values given being the averages over

[4]Tables of final observed and calculated structure factors and nonhydrogen atom thermal parameters are available, at a nominal charge, from the Depository of Unpublished Data, CISTI, National Research Council of Canada, Ottawa, Ont., Canada K1A 0S2.

TABLE 1. Fractional atomic coordinates

Atom	x	y	z	Atom	x	y	z
Si1	0.2876	0.1977	0.0156	C18	0.3560	0.0402	0.3948
O1	0.4278	0.1576	0.0266	C19	0.2361	−0.2142	0.1543
O2	0.1456	0.0906	−0.0383	C20	0.0987	−0.2684	0.1419
C1	0.3044	0.3092	0.1603	C21	0.0707	−0.3595	0.1454
C2	0.4401	0.3788	0.2392	C22	0.1791	−0.3986	0.1631
C3	0.4561	0.4658	0.3457	C23	0.3150	−0.3474	0.1748
C4	0.3371	0.4869	0.3767	C24	0.3435	−0.2566	0.1698
C5	0.2018	0.4195	0.3009	Si3	0.2466	−0.1735	−0.2166
C6	0.1852	0.3316	0.1941	O5	0.4226	−0.1161	−0.1669
C7	0.2835	0.2432	−0.0815	O6	0.1681	−0.1125	−0.1225
C8	0.2421	0.1660	−0.1978	C25	0.1991	−0.3165	−0.2558
C9	0.2430	0.1976	−0.2719	C26	0.1934	−0.3400	−0.1751
C10	0.2842	0.3052	−0.2327	C27	0.1577	−0.4461	−0.2038
C11	0.3252	0.3832	−0.1190	C28	0.1268	−0.5317	−0.3143
C12	0.3251	0.3524	−0.0432	C29	0.1338	−0.5114	−0.3954
Si2	0.2722	−0.0892	0.1545	C30	0.1699	−0.4047	−0.3667
O3	0.4163	−0.0778	0.1155	C31	0.1860	−0.1620	−0.3368
O4	0.1345	−0.0989	0.0657	C32	0.0536	−0.1476	−0.3623
C13	0.3077	0.0358	0.2961	C33	0.0088	−0.1371	−0.4508
C14	0.3050	0.1333	0.3081	C34	0.0929	−0.1434	−0.5175
C15	0.3520	0.2308	0.4150	C35	0.2227	−0.1594	−0.4958
C16	0.4006	0.2324	0.5098	C36	0.2698	−0.1675	−0.4058
C17	0.4025	0.1379	0.5007				
Standard deviations							
Si	0.00005	0.00004	0.00004		0.00005	0.00004	0.00004
O	0.0002	0.0001	0.0001		0.0002	0.0001	0.0001
C	0.0003	0.0002	0.0002		0.0003	0.0002	0.0002

TABLE 2. Fractional atomic coordinates for hydrogen atoms

Atom	x	y	z	Atom	x	y	z
HO1	0.462	0.144	−0.012	HC18	0.355	−0.026	0.387
HO2	0.080	0.089	−0.052	HC20	0.026	−0.238	0.136
HC2	0.520	0.367	0.216	HC21	−0.023	−0.394	0.135
HC3	0.548	0.515	0.396	HC22	0.159	−0.465	0.164
HC4	0.349	0.550	0.453	HC23	0.398	−0.375	0.186
HC5	0.116	0.434	0.324	HC24	0.445	−0.218	0.182
HC6	0.080	0.281	0.138	HO5	0.460	−0.128	−0.134
HC8	0.209	0.090	−0.226	HO6	0.165	−0.064	−0.106
HC9	0.214	0.141	−0.355	HC26	0.214	−0.281	−0.097
HC10	0.282	0.326	−0.291	HC27	0.154	−0.461	−0.149
HC11	0.353	0.458	−0.088	HC28	0.098	−0.606	−0.338
HC12	0.354	0.405	0.035	HC29	0.116	−0.568	−0.472
HO3	0.459	−0.021	0.135	HC30	0.177	−0.391	−0.423
HO4	0.138	−0.104	0.019	HC32	−0.004	−0.140	−0.312
HC14	0.265	0.130	0.239	HC33	−0.086	−0.128	−0.468
HC15	0.343	0.292	0.415	HC34	0.057	−0.133	−0.583
HC16	0.435	0.304	0.584	HC35	0.286	−0.164	−0.540
HC17	0.438	0.139	0.571	HC36	0.360	−0.183	−0.390
Standard deviations							
	0.003	0.002	0.002		0.003	0.002	0.002

equivalent parameters in all three independent molecules.[5] (The figure in brackets under each value indicates the number of independent determinations contributing to that averaged value.) The coordination around the silicon is tetrahedral, the angles between groups reflecting the relative degree of steric and/or electronic repulsion between them. The Si—OH distance of 1.633 Å agrees closely with Si—OCH_3 and

[5]Tables of individual bond lengths and angles have been deposited. See footnote 4.

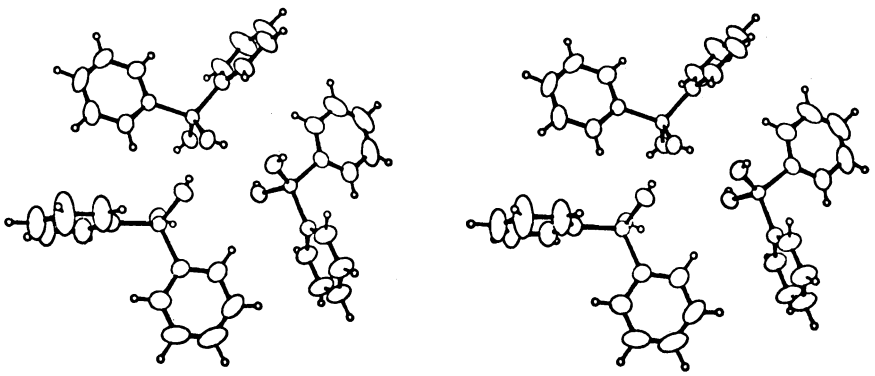

FIG. 1. Stereoscopic drawing of three molecules of DPSD comprising the asymmetric unit of the crystal cell.

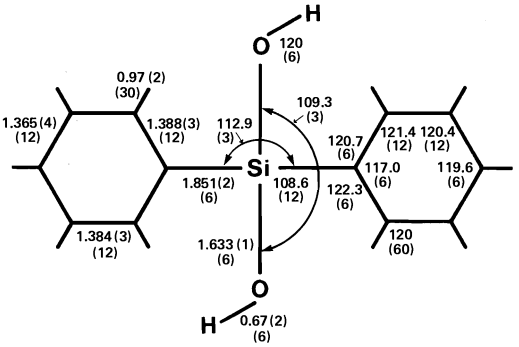

FIG. 2. Bond distances (Å) and valency angles (deg) averaged over equivalent parts of the independent DPSD molecules. Standard deviations of bond lengths are in parentheses. Standard deviations of angles are 0.1° for angles at Si and 0.2° for angles at C. The numbers in parentheses below the values are the number of independent measurements contributing to that averaged value.

Si—O(menthoxy) lengths of 1.636 and 1.630 Å in (+)-α-naphthylphenyl-1-menthoxymethoxysilane (9); the Si...C(phenyl) separation of 1.851 Å also compares closely to the value of 1.855 Å for a similar bond in that compound, and is a little shorter (though probably not significantly so) than an average of 1.866 Å for Si—C(phenyl) bonds in a number of phenylsilanes (10). The C—C bonds in the phenyl rings appear systematically shortened around the *para* carbon atoms; this is undoubtedly an artifact of the increased thermal vibrations at the distal ends of the rings. The significant decrease in C—C—C angle at the carbon bonded to silicon (117.0°) likely relieves intramolecular steric repulsions.

Comparisons With Other Anticonvulsants

In previous studies in this series we have shown that the molecular conformations of diphenylhydantoin, diazepam, procyclidine, trihexyphenidyl, and ethylphenacemide have stereochemical features in common. They all contain two bulky hydrophobic groups and two electron-donor functions, and when the drugs' three-dimensional structures are compared these entities occupy similar positions and orientations in space. These stereochemical similarities in chemically different anticonvulsants have led us to postulate that they may be the features responsible for antiepileptic activity (2).

The fact that DPSD has been reported to have anticonvulsant activity is further support for our postulation, as DPSD possesses *only* those stereochemical features common to the above drugs; i.e., it consists of a central silicon atom to which are bonded two phenyl rings (hydrophobic groups) and two hydroxyl groups (electron donors). Table 3 compares distances between these groups in DPSD with similar separations in diphenylhydantoin. The ring–ring separation is slightly larger in DPSD, but the main difference in dimensions in the two molecules involves the electronegative oxygen atoms.

TABLE 3. Distances (Å) between phenyl ring centroids and oxygen atoms in diphenylhydantoin (DPH) and diphenylsilanediol (DPSD)

	DPH	DPSD
Ring (1) – Ring (2)	4.84	5.43
Ring (1) – O(1)	5.68	4.09
Ring (1) – O(2)	3.97	
Ring (2) – O(1)	5.51	
Ring (2) – O(2)	4.23	
O(1) – O(2)	4.56	2.66

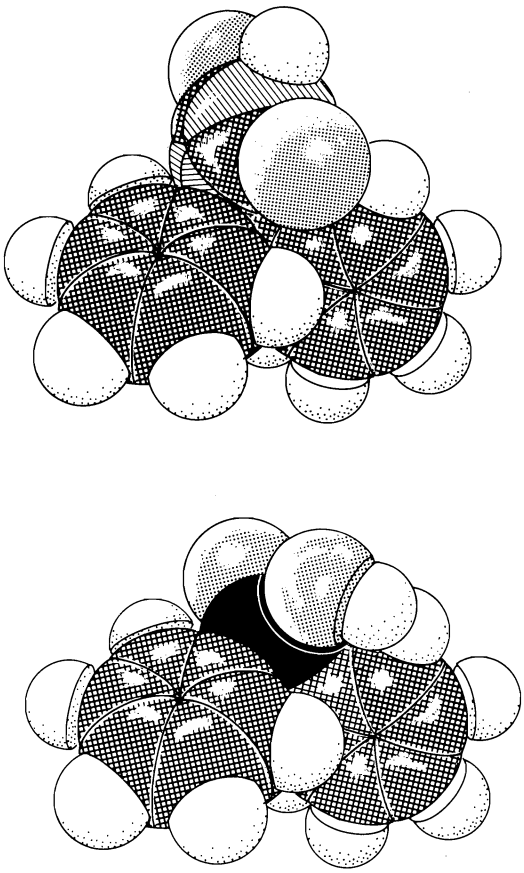

FIG. 3. Space filling models of diphenylhydantoin (top) and diphenylsilanediol.

Because both hydroxyls are on the same atom in DPSD, their separation is necessarily shorter than the distance between (ketonic) oxygens in DPH, 2.66 Å vs. 4.56 Å in DPH. This may indicate that either there is some flexibility in the receptor to accommodate electron donors of somewhat different separations, or that the groups on the receptor which interact with the electronegative atoms (—OH, $\diagdown$NH perhaps) $\diagup$ may do so by donating hydrogens in H-bond formation in the case of DPH and by accepting H-bonds from the hydroxyl oxygens of DPSD. There is slight evidence that either the latter possibility may be more likely, or that the oxygen...oxygen separation of 2.66 Å may be approaching a lower limit for retention of anticonvulsant action: the (ketonic) oxygen...oxygen separation of 2.45 Å in phenylbutansultam (1) is accompanied by only a weak anticonvulsant effect. (Figure 3 shows space filling models of DPH and DPSD and illustrates graphically the conformational similarities.) Because of the molecular symmetry of DPSD the ring...oxygen distances are all closely similar; the value of 4.09 Å in Table 3 represents the average of 12 independent measurements in the molecule (range = 4.01–4.19 Å).

Acknowledgements

This work was supported by United States Public Health Service Grant NS 09839 from the National Institute of Neurological and Communicative Disorders and Stroke and by the Medical Research Council of Canada. A.C. is the recipient of a Research Career Development Award NS 70801 from the National Institutes of Health (NINCDS).

1. A. CAMERMAN and N. CAMERMAN. Can. J. Chem. **53**, 2194 (1975).
2. A. CAMERMAN and N. CAMERMAN. Science, **168**, 1457 (1970); Acta Crystallogr. Sect. B, **27**, 2205 (1971); J. Am. Chem. Soc. **94**, 268 (1972).
3. N. CAMERMAN and A. CAMERMAN. Mol. Pharmacol. **7**, 406 (1971).
4. N. CAMERMAN and A. CAMERMAN. J. Am. Chem. Soc. **94**, 8553 (1972).
5. A. CAMERMAN and N. CAMERMAN. Proc. Natl. Acad. Sci. USA, **74**, 1264 (1977).
6. V. D. HULCE and R. H. RECH. Pharmacologist, **16**, 228 (1974); **17**, 178 (1975). (Abstracts.)
7. D. T. CROMER and J. B. MANN. Acta Crystallogr. Sect. A, **24**, 321 (1968).
8. R. F. STEWART, E. R. DAVIDSON, and W. T. SIMPSON. J. Chem. Phys. **42**, 3175 (1965).
9. J. A. KANTERS and A. M. VAN STEEN. Cryst. Struct. Commun. **2**, 261 (1973).
10. P. C. CHIEH and J. TROTTER. J. Chem. Soc. A, 1778 (1969); C. GLIDEWELL and G. M. SHELDRICK. J. Chem. Soc. A, 3127 (1971); J. P. VIDAL, J. L. GALIGNE, and J. FALGUEIRETTES. Acta Crystallogr. Sect. B, **28**, 3130 (1972); J. P. VIDAL, J. LAPASSET, and J. FALGUEIRETTES. Acta Crystallogr. Sect. B, **28**, 3137 (1972); D. CARLSTROM and G. FALKENBERG. Acta Chem. Scand. **27**, 1203 (1973).

Photolyse du *trans*-butène-2 vers 7.1 eV

ANDRZEJ WIĘCKOWSKI[1] ET GUY J. COLLIN

Département des Sciences pures, Université du Québec à Chicoutimi, Chicoutimi (Qué.), Canada G7H 2B1

Reçu le 16 juin 1977

ANDRZEJ WIĘCKOWSKI et GUY J. COLLIN. Can. J. Chem. **55**, 3636 (1977).

Nous avons étudié la photolyse du *trans*-butène-2 (*t*B-2) dans un système statique en utilisant une lampe à azote: 7.10–7.11 eV (174.5–174.3 nm). Les principaux modes de fragmentation de la molécule *t*B-2 photoexcitée sont la rupture de la liaison terminale C—C avec libération de radicaux CH_3 et CH_3CHCH ($\Phi = 0.33$) et l'élimination d'hydrogène (atomique ou moléculaire) avec formation concurrente de butadiène-1,3 ($\Phi = 0.27$). Le radical CH_3CHCH s'isomérise en radical allylique, qui à son tour se fragmente en allène et atome d'hydrogène. Cette dernière réaction est sensible à la pression, de telle sorte que vers 13 300 N m^{-2} (100 Torr), certains intermédiaires sont stabilisés par collision. On n'a en outre pas pu mettre en évidence la stabilisation de la molécule *t*B-2 photoexcitée. En particulier, on n'observe pas ou très peu d'isomérisation du *t*B-2 en *cis*-butène-2 à basse pression: $P \leq 133$ N m^{-2}.

ANDRZEJ WIĘCKOWSKI and GUY J. COLLIN. Can. J. Chem. **55**, 3636 (1977).

The photolysis of *trans*-2-butene (*t*B-2) was studied at 7.10–7.11 eV (174.5–174.3 nm) in a static system using a nitrogen lamp. The main primary photochemical processes are the C—C split leading to the formation of CH_3 and CH_3CHCH radicals, the primary quantum yield, $\Phi = 0.33$ and the molecular or/and atomic hydrogen elimination, $\Phi = 0.27$ with concurrent formation of 1,3-butadiene. The excited CH_3CHCH radicals isomerize, followed by allene formation, or are stabilized by collisions. The stabilization of the photoexcited *t*B-2 molecules is an inefficient process in the pressure region studied (10–20 000 N m^{-2}). Only small isomerization of *t*B-2 was observed below 133 N m^{-2} ($\simeq$1 Torr).

Introduction

La photolyse des oléfines dans la région de l'ultraviolet sous vide est bien connue (pour une revue, voir ref. 1). Dans le cas particulier du *t*B-2 il faut noter le travail de Borrell et coll. (2). A 184.9 nm on remarque qu'il est facile de stabiliser non seulement les radicaux intermédiaires provenant de la fragmentation de la molécule photoexcitée, mais également la molécule photoexcitée (2). A plus courte longueur d'onde, à 147 nm, nous avons montré qu'il est pratiquement impossible de stabiliser par collision quelle qu'espèce excitée que ce soit (3). En outre l'isomérisation est relativement importante à 184.9 nm, alors qu'elle est pratiquement absente à 147 nm. Enfin on note à 147 nm le bris de la liaison C—C d'une façon plus marquée qu'à 184.9 nm (2, 3). Nous avons repris cette étude en photolysant le *t*B-2 entre ces deux longueurs d'onde. Notre but est d'obtenir plus d'informations sur la fragmentation de la molécule photoexcitée, sur la nature et la qualité de ces fragments et, bien sûr, d'essayer de réconcilier ces importantes divergences entre les deux travaux mentionnés plus haut.

Partie expérimentale

La préparation de la lampe à azote a déjà été décrite (4, 5) et est munie d'une fenêtre en quartz. Son spectre d'émission enregistré à l'aide d'un monochromateur McPherson, GCA-235, d'un demi-mètre, montre les deux raies situées à 174.3–174.5 nm dans le rapport 1:0.5 respectivement. Ces deux raies sont entourées d'un certain nombre de raies provenant probablement d'impuretés. On a estimé d'après l'enregistrement du spectre (fente 30 μm; vitesse de 5 nm/min) que la lampe débite 15% de son intensité entre 165 et 170 nm, 70% entre 170 et 175 nm (raies de l'azote) et 15% au-dessus de 175 nm.

L'actinométrie est réalisée par comparaison avec la photochimie de l'éthylène. Le rendement en acétylène est pratiquement indépendant de la longueur d'onde entre 163.4 et 193 nm et de la pression de l'éthylène tout au moins entre 133 et 2660 N m^{-2} (1 à 20 Torr) (6, 7). On a admis que $\Phi(C_2H_2) = 0.75$ dans ces photolyses.

Le *t*B-2 est un produit "Matheson" et contient du *cis*-butène-2 (0.48%), du butane normal (0.25%) et du butadiène-1,3 (0.063%) comme impuretés et est utilisé après dégasage sous haut vide 10^{-3} N m^{-2}, système à vide en pyrex équipé de robinets en verre-téflon. Les autres détails sont indiqués ailleurs (3, 8).

L'imprécision sur les valeurs expérimentales indiquées est en générale plus petite que 10%, sauf dans le cas où les valeurs calculées sont la différence de deux valeurs élé-

[1]Adresse permanente: Département de chimie, Université de Varsovie, Varsovie, Pologne.

mentaires (voir plus loin à l'usage de HI). L'analyse du butane normale, du *cis*-butène-2 et du butadiene-1,3 a été limitée à des pressions inférieures ou égales à 133 N m^{-2} (1 Torr) à cause du taux d'impuretés.

Résultats

Les résultats détaillés sont rapportés dans la tableau et les figures qui suivent. En bref, le rendement en acétylène est indépendant de la pression entre 13 et 20 000 N m^{-2} (0.1 et 150 Torr). Le rendement en méthane est aussi insensible à la pression. Il en est de même des rendements en méthyl-3-butène-1, isopentane, *cis*- et *trans*-pentène-2 entre 150 et 13 300 N m^{-2}. L'addition d'oxyde nitrique (5%) ne modifie pas les rendements en acétylène, éthylène, propylène, propyne, allène et butadiène-1,3. Par contre la formation de l'éthane, de l'isopentane et des pentène-2 disparaît. L'addition de 10% de HI augmente fortement les rendements du méthane et du propène, légèrement celui de l'éthylène (tableau 1). La pression a un effet important sur les rendements (elle les diminue) en éthylène, éthane, allène et propène (voir les figures qui suivent).

Discussion

Réactions radicalaires

L'effet de l'addition de 5% de NO, ou de 10% de HI montre sans ambiguités la présence de radicaux libres qui participent à la formation des produits observés. L'éthane et les C_5, sur la base de l'effet de NO, sont le résultat de réactions radicalaires. La présence de radicaux méthyles est confirmée par l'effet de HI, de même que la présence de radicaux C_3H_5. Ces radicaux formés en présence de HI, réagissent avec celui-ci (9) (réaction 1). L'augmentation de produit RH en présence de HI, permet d'estimer le rendement $\phi(R) = \phi(RH)_{HI} - \phi(RH)_{NO}$. En particulier $\Phi(CH_3) \simeq 0.70$.

TABLEAU 1. Photolyse du *t*B-2 vers 174 nm; rendements quantiques obtenus à 133 N m^{-2}

Produits	*t*B-2 pur	+5% NO	+10% HI
Méthane	0.047[b]	0.028	0.71
Acétylène	0.070[b]	0.071	0.071
Ethylène	0.025	0.028	0.040
Ethane	0.125	0.00	0.01
Propène	0.16	0.16	0.36
Propyne	0.028[b]	0.028	0.028
Allène	0.036	0.04	0.040
Butadiène-1,3	0.34[a,b]	0.27	0.32
Butadiène-1,2	traces	traces	traces
n-Butane	0.0	0.0	0.15
Méthyl-3-butène-1	0.030[b]	0.0	0.0
Isopentane	0.13[b]	0.0	0.0
trans-Pentène-2	0.045[b]	0.0	0.0
cis-Pentène-2	0.02[b]	0.0	0.0

[a]En fait pic composite de butadiène-1,3, isobutène et butène-1.
[b]Rendement pratiquement indépendant de la pression entre 130 et 13 300 N m^{-2}.

[1] $$R + HI \rightarrow RH + I$$

Par contre, la formation de radicaux éthyles est très faible puisque le rendement en éthane en présence de HI est de l'ordre de 0.01. L'éthane est donc formé par combinaison de radicaux méthyles; l'isopentane l'est par combinaison de radicaux méthyles et butyles secondaires. Ces radicaux sont formés par addition d'atome d'hydrogène sur la double liaison. Le radical butyle formé est vibrationellement excité et se décompose s'il n'est pas stabilisé par collision (10)

[2] $$H + t\text{B-2} \rightarrow s\text{-}C_4H_9^*$$
$$\Delta H = -1.65 \text{ eV } (-38 \text{ kcal mol}^{-1})$$

[3] $$s\text{-}C_4H_9^* \rightarrow CH_3 + C_3H_6$$
$$\Delta H = 1.1 \text{ eV } (28 \text{ kcal mol}^{-1})$$

[4] $$s\text{-}C_4H_9^* + M \rightarrow s\text{-}C_4H_9 + M^*$$

Le rendement des radicaux méthyles décroît donc lorsque la pression augmente; celui des radicaux butyles secondaires au contraire augmente. Ces deux effets contraires expliquent partiellement l'insensibilité observée du rendement en isopentane avec la pression. Le rendement en propylène décroît rapidement avec la pression (fig. 1) conformément au mécanisme [2]–[4].

L'existence de radicaux butyles est définitivement prouvée par l'apparition de butane normal en présence de HI (tableau 1). Ce rendement constitue une limite inférieure du rendement en radicaux butyles dans la photolyse du *t*B-2 pur. En effet HI est un excellent intercepteur d'atome d'hydrogène. Des résultats de la littérature on peut estimer le rapport $k_2/k_5 \simeq 18$ (9, 11)

[5] $$H + HI \rightarrow H_2 + I$$

Ainsi dans le système pur, le rendement en radicaux butyles stables est égal à celui en butane normal observé en présence de 10% de HI multiplié par 2.8: $\Phi(C_4H_9) \simeq 0.42$. Le rendement de la réaction 2 est alors égal à la somme du rendement en radicaux butyles stables et de

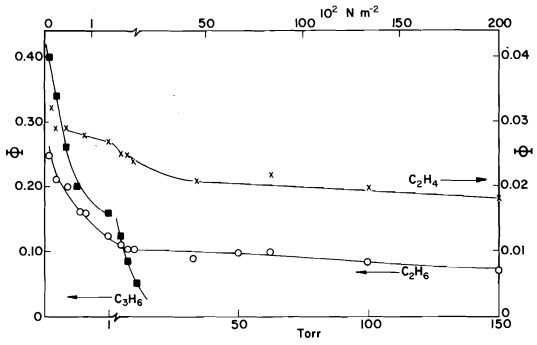

FIG. 1. Rendements quantiques du propène, de l'éthane et de l'éthylène obtenu dans la photolyse du *t*B-2 vers 7.1 eV en fonction de la pression.

celui de la réaction 3. Si le propène est entièrement formé dans le processus [3],[2] on obtient alors:

$$\Phi([2]) = \Phi([3] + \Phi(C_4H_9)) = 0.42 + 0.16 = 0.58$$

Pour obtenir le rendement en atomes d'hydrogène il faut à cette valeur ajouter participation de la réaction d'abstraction d'atome d'hydrogène:

[6] $$H + tB\text{-}2 \rightarrow H_2 + C_4H_7$$

En retenant pour le rapport k_6/k_2 une valeur proche de 0.08 (11, 13), le rendement de la réaction 6 peut être estimée: $\Phi([6]) \simeq 0.05$. Ce rendement est inférieur au rendement des produits insaturés en C_5 formés par combinaison des radicaux méthyles et C_4H_7, et explique donc partiellement leur formation. Au total le rendement $\Phi(H^{\cdot})$ est voisin de 0.63.

Enfin, une partie du pic composite de butadiène-1,3 (voir tableau 1) est sensible à la présence de NO. Bien que l'analyse complète de ce pic n'a pas été faite, il faut noter la présence de radicaux C_3H_5 dans ce système. Ceux-ci ont probablement la structure $CH_3\dot{C}HCH$ s'ils sont formés par fragmentation de la molécule *t*B-2 photoexcitée (2). Ils s'isomérisent probablement en radicaux allyliques comme cela est observé dans le cas du *cis*-butène-2 (8, 13).

[7] $$CH_3\dot{C}HCH^* \rightarrow \overline{CH_2CHCH_2}^*$$

La déduction du rendement $\Phi(C_3H_5)$ à partir de l'effet de HI n'est pas simple. Ce rendement est au moins égal au rendement en présence de HI, réaction 1, diminué de celui observé en présence de NO. Cependant, puisque HI intercepte facilement les atomes d'hydrogène (9), réaction 5, le rendement de la réaction 3, doit être diminué d'une valeur d'environ 0.10. Le rendement en radicaux C_3H_5 serait donc proche de 0.30 à 133 N m^{-2}. La réaction de combinaison des radicaux méthyles et $CH_3\dot{C}HCH$ d'une part et $\overline{CH_2\dot{C}HCH_2}$ d'autre part conduit respectivement au *cis*- ou au *trans*-butène-2 d'une part et au butène-1 d'autre part.

La nature du radical C_3H_5 peut-être davantage précisée sil l'on admet que les radicaux C_3H_5 sont partiellement excités lorsqu'ils sont formés (voir plus loin). Ceux qui ont la structure vinylique ne pouvant former l'allène, ceux ayant la structure allylique le formant.

[8] $$\overline{CH_2\dot{C}HCH_2}^* \rightarrow CH_2CCH_2 + H$$

[9] $$\overline{CH_2\dot{C}HCH_2}^* + M \rightarrow \overline{CH_2\dot{C}HCH_2} + M^*$$

Ce mécanisme de fragmentation–stabilisation par combinaison doit répondre à une équation de type Stern–Volmer. La fig. 2, montre que cela est le cas pourvu que la pression soit supérieure à 10 Torr. On peut même en déduire un rendement Φ' obtenu par extrapolation à pression nulle de l'ordre de 0.028. A basse pression la linéarité de l'équation Stern–Volmer est récupérée si l'on soustrait du rendement en allène, la valeur Φ' obtenue ci-haut, fig. 3. On peut en déduire une deuxième valeur Φ'' obtenue par extrapolation à pression nulle: $\Phi' = 0.037$. Cette façon de diviser l'échelle de pression en deux parties n'est pas nécessairement arbitraire. La linéarité observée dans les deux zones

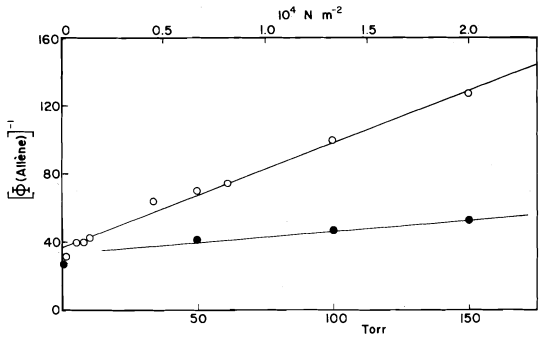

FIG. 2. Variation de $[\Phi(\text{allène})]^{-1}$ en fonction de la pression dans la photolyse du *t*B-2 pur entre 0 et 20 000 N m^{-2}, ○; et dans le système *t*B-2 (133 N m^{-2}) + hélium, ●.

[2]On n'a pas observé de formation de produit provenant de la réaction $CH_2 + tB\text{-}2 \rightarrow$ diméthylcyclopropane, même à haute pression (12). On peut donc en conclure que la fragmentation $tB\text{-}2^{**} \rightarrow C_3H_6 + CH_2$ est de peu d'importance dans ce système: $\Phi < 0.02$.

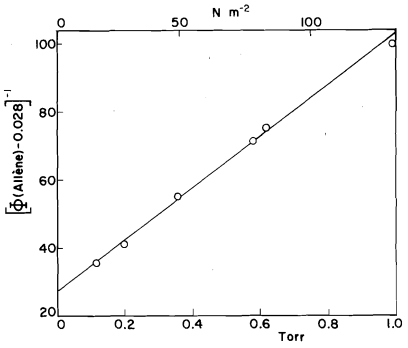

FIG. 3. Variation de $[\Phi(\text{allène}) - 0.028]^{-1}$ avec la pression dans la photolyse du *t*B-2 entre 0 et 133 N m^{-2}.

de pression peut indiquer l'existence de deux variétés de radicaux allyles, variétés différemment excitées. Ainsi la fragmentation de la molécule photoexcitée ne produirait pas des radicaux C_3H_5 avec une distribution d'énergie très large. Au contraire, cette distribution présenterait au moins deux "pics": ceux des radicaux ayant le plus d'énergie se décomposent même à haute pression; les autres ne se décomposant partiellement qu'à basse pression. Une observation supplémentaire qui sert à justifier le fait que le précurseur de l'allène qui est stabilisé n'est pas la molécule photoexcitée réside dans le fait que l'hélium et le *t*B-2 n'ont pas la même efficacité dans la stabilisation du précurseur (fig. 2) contrairement à ce qui est observé par Borrell et coll. à 184.9 nm (2).

Enfin, on observe la formation de radicaux éthyles et vinyles en faibles quantités et à travers le processus [1], on peut estimer le rendement $\Phi(C_2H_5) \simeq \Phi(C_2H_3) \simeq 0.01$.

Fragmentation de la molécule photoexcitée

A partir des données obtenues, il est tentant d'examiner la fragmentation de la molécule photoexcitée. Sur la base des produits obtenus en présence d'oxyde nitrique et de ceux en présence de HI, on peut reternir les processus suivants:

[10] $t\text{B-2} + h\nu \rightarrow t\text{B-2}^{**}$

[11] $t\text{B-2}^{**} \rightarrow C_4H_6 + 2H$ (ou H_2) $\quad \Phi \simeq 0.27$

[12] $t\text{B-2}^{**} \rightarrow C_2H_2 + 2CH_3 \quad \Phi = 0.07$

[13] $t\text{B-2}^{**} \rightarrow C_3H_4$(propyne) $+ CH_3 + H(CH_4)$ $\quad \Phi = 0.03$

[14] $t\text{B-2}^{**} \rightarrow C_3H_5^* + CH_3 \quad \Phi = 0.07$
$\hookrightarrow C_3H_4$(allène) $+ H$

[15] $t\text{B-2}^{**} \rightarrow C_3H_5 + CH_3 \quad \Phi = 0.26$

[16] $t\text{B-2}^{**} \rightarrow C_4H_7 + H$

Les rendements des réactions 11, 12, 13, 14 et 15 sont basées sur les rendements en butadiène-1,3, acétylène, propyne, allène (lorsque la pression est zéro), et en C_3H_5 (effet de HI) respectivement (la réaction 15 correspondant à la formation de radicaux C_3H_5 qui ne se décomposent pas à basse pression). Le rendement de la réaction 16 est difficilement appréciable. En admettant que les radicaux C_4H_7 réagissent avec les autres radicaux sur une base statistique, on obtient la relation,

$$\frac{k(CH_3 + C_4H_7)}{k(R + C_4H_7)} = \frac{\Phi(C_5H_{10})}{\Phi(RC_4H_7)} = \frac{\Phi(CH_3)}{\Phi(R)}$$

$\Phi(C_5H_{10})$ est égal à 0.025 (tableau 1), $\Phi(CH_3)$ à 1 Torr est voisin de 0.70 et $\Phi(R)$ est la somme des rendements de tous les radicaux: $\Phi(R) \simeq 1.8 \pm 10\%$. On obtient donc $\Phi(RC_4H_7) = 1.8 \times 0.095/0.70 \simeq 0.24 \pm 0.03$. De cette valeur qui est voisine du rendement $\Phi(C_4H_7)$, il faut soustraire le rendement de la réaction 6: $\Phi([16]) \simeq 0.19 \pm 0.05$.

Il faut ajouter que cette valeur est une valeur maximum, car si certains radicaux sont chauds, (H^*, CH_3^*) leur énergie interne favorise l'abstraction d'un atome d'hydrogène. Enfin le fait que les produits en C_5H_{10} aient des rendements insensibles avec l'augmentation de pression, montre que le radical C_4H_7 n'est pas le précurseur de l'allène ou de l'éthylène.

Ce dernier produit a un rendement qui suit la relation de Stern–Volmer: fig. 4. Ces résultats sont insuffisants pour proposer le mécanisme de formation ou tout au moins l'un de ces prédéces-

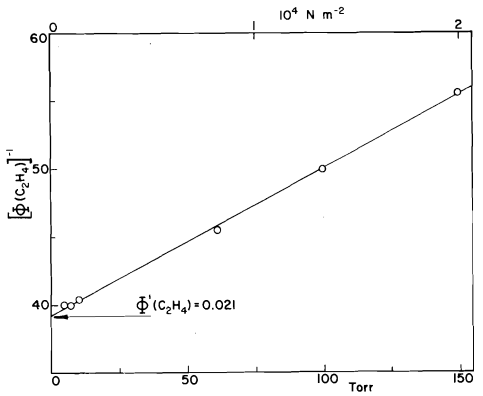

FIG. 4. Variation de $[\Phi(C_2H_4)]^{-1}$ avec la pression dans la photolyse du *t*B-2 entre 0 et 20 000 N m^{-2}.

seurs. A 184.9 nm, Borrell et coll. (2) montrent que la stabilisation de l'intermédiaire est insensible à la nature du stabilisant et en déduisent indirectement que l'espèce stabilisée est la molécule photoexcitée elle-même. Dans le cas du *cis*-butène-2 photolysé à 174 nm, nous avons récemment montré l'inverse (5). Ce qui tendrait à prouver qu'un fragment excité existe entre la molécule photoexcitée et la formation de l'éthylène. A 133 N m^{-2}, on trouve un rendement en radicaux éthyles et vinyles qui correspondraient assez bien à la faible stabilisation observée sur la fig. 4. On aurait donc:

[17] $$t\text{B-2}^{**} \rightarrow C_2H_3 + C_2H_5^*$$

[18] $$C_2H_5^* \rightarrow C_2H_4 + H$$

[19] $$C_2H_5^* + M \rightarrow C_2H_5 + M^*$$

La valeur obtenue par extrapolation à pression nulle donne un rendement maximum: $\Phi([17]) = 0.02$.

La somme des rendements de fragmentation: $\Phi([11] + \ldots [17])$ est égale à $0.91 \pm 10\%$. A l'imprécision expérimentale près, on a donc décomposition complète de la molécule photoexcitée, sans observer de stabilisation de celle-ci même à une pression en *t*B-2 de 20 000 N m^{-2} (150 Torr). Cette situation a été également observée avec le *cis*-butène-2 (5).

Ces résultats sont tout à fait différents de ceux observés par Borrell et James à 185 nm (15). La photochimie des butènes-2 y est expliquée en terme d'état Rydberg et d'état singulet π^*, π comme intermédiaires. L'état Rydberg se fragmente en une variété de produits à basse pression ou sont stabilisés par collision à haute pression avec retour dans l'état original: il n'y a pas d'isomérisation *cis–trans*. L'état singulet $V(\pi^*, \pi)$ conduit uniquement à l'isomérisation [15]. Ici, la longueur d'onde incidente correspond à peu près au maximum de l'absorption $V \leftarrow N$ (14) et en suivant l'argument présenté à Borrell et coll., on ne devrait observer que l'isomérisation contrairement à ce qui est observé. Il n'est pas interdit de penser à l'existence du mélange d'états Rydberg et d'états V, à moins que l'interprétation donnée par Borrell et coll. soit partiellement erronée [15].

Remerciements

Nous voulons exprimer notre gratitude au Ministère de l'Education du Québec (programme FCAC) et au Conseil national de recherches du Canada qui ont partiellement et conjointement financé cette étude.

1. G. J. Collin. J. Chim. Phys. 302 (1977).
2. P. Borrell, P. Cashmore, A. Cervenka et F. C. James. J. Chim. Phys. 229 (1970) et autres publications qui y sont citées.
3. G. J. Collin et P. M. Perrin. Can. J. Chem. **50**, 2823 (1972).
4. D. Davis et W. Brown. Appl. Optics, **7**, 2071 (1968).
5. A. Więckowski et G. J. Collin. Soumis pour publication.
6. P. Potzinger, L. C. Glasgow et G. Von Bünau. Z. Naturforsch. **27**, 628 (1972).
7. H. Hara et I. Tanaka. Bull. Chem. Soc. Jpn. **46**, 3012 (1973).
8. G. J. Collin, P. M. Perrin et C. M. Gaucher. Can. J. Chem. **50**, 2391 (1972).
9. G. J. Collin et K. Bukka. J. Photochem. **6**, 381 (1976/77).
10. B. S. Rabinovitch, R. F. Kubin et R. E. Harrington. J. Chem. Phys. **38**, 405 (1963).
11. K. R. Jennings et R. J. Cvetanović. J. Chem. Phys. **35**, 1233 (1961).
12. S. Krzysanowski et R. J. Cvetanović. Can. J. Chem. **45**, 665 (1967); T. W. Eder et R. W. Carr, Jr. J. Phys. Chem. **73**, 2064 (1969).
13. W. E. Falcone et W. A. Sunder. Int. J. Chem. Kinetics, **4**, 315 (1972).
14. W. M. Flicker, O. A. Mosher et A. Kuppermann. Chem. Phys. Lett. **36**, 56 (1975).
15. P. Borrell et F. C. James. Trans. Faraday Soc. **62**, 2452 (1966).

Characterization of natural gas hydrates by nuclear magnetic resonance and dielectric relaxation[1]

D. W. DAVIDSON, S. K. GARG, S. R. GOUGH, R. E. HAWKINS, AND J. A. RIPMEESTER

Division of Chemistry, National Research Council of Canada, Ottawa, Ont., Canada K1A 0R9

Received June 17, 1977

D. W. DAVIDSON, S. K. GARG, S. R. GOUGH, R. E. HAWKINS, and J. A. RIPMEESTER. Can. J. Chem. **55**, 3641 (1977).

Continuous-wave proton nmr spectra of the clathrate hydrates and/or deuteriohydrates of methane, ethane, propane, isobutane, and neopentane–D_2S have been recorded down to 2 K. Between 50 and 200 K each H_2O hydrate spectrum consists of a line 3 to 4 G wide from reorienting guest molecules and a broader band from rigid water molecules. Line shapes characteristic of non-rotating guests are obtained in D_2O hydrates at low temperatures, except for methane which gives a narrow line to 2 K. Neopentane, shown for the first time to be capable of enclathration, exhibits a Resing effect and other features related to its tetrahedral symmetry. Low-temperature dielectric absorption from reorienting guest-molecule dipoles has been measured in H_2S, propane, isobutane, and *n*-butane–H_2S hydrates. For steric reasons *n*-butane is encaged as a *gauche* rather than the *trans* isomer. Average barriers to reorientation estimated from nmr and dielectric data are 1.2 kcal/mol for ethane in type I hydrate and 0.6, 1.2, 1.4, and 0.8 kcal/mol for propane, isobutane, *n*-butane, and neopentane in type II.

D. W. DAVIDSON, S. K. GARG, S. R. GOUGH, R. E. HAWKINS et J. A. RIPMEESTER. Can. J. Chem. **55**, 3641 (1977).

On enregistre le spectre rmn du proton à onde continue des hydrates et des deutériohydrates de clathrate de méthane, éthane, propane, isobutane et néopentane jusqu'à une valeur inférieure de 2 K. Entre 50 et 200 K, chaque spectre hydrate H_2O consiste en une raie de largeur 3 à 4 G obtenue à partir de la réorientation des molécules encagées et d'une plus large bande obtenue à partir des molécules d'eau rigides. On obtient les courbes caractéristiques des molécules encagées qui ne tournent pas dans les hydrates D_2O à basse température, à l'exception du méthane qui donne une raie fine à 2 K. On montre pour la premiere fois que le néopentane a une aptitude à l'enclathration et manifeste un effet Resing et d'autres caractéristiques reliées à sa symétrie tétrahédrique. L'absorption diélectrique à basse température obtenue à partir de la réorientation des dipoles des molécules encagées est mesurée pour les hydrates de H_2S, le propane, l'isobutane et l'hydrate de *n*-butane–H_2S. Pour des raisons stériques, le *n*-butane est inséré sous forme d'isomère *gauche* plutôt que sous forme d'isomère *trans*. Les barrières moyennes d'énergie à la réorientation, évaluées à partir des données rmn et diélectriques, sont de 1.2 kcal/mol pour l'éthane sous la forme hydrate I et 0.6, 1.2, 1.4 et 0.8 kcal/mol pour le propane, l'isobutane, le *n*-butane et le néopentane sous la forme II.

[Traduit par le journal]

The discovery that natural gas occurs in the form of solid hydrate deposits in permafrost regions of the USSR (1, 2) and Canada (3) has revealed the need for more complete knowledge of the properties of natural gas hydrates. Practically all the numerous previous experimental studies of these hydrates (4, 5) have been concerned with thermodynamic properties and the determination of the temperature and pressure conditions of stability of hydrates in water–hydrocarbon systems.

Among the 91 molecular species now known (5, 6) to individually form gas hydrates are most of the common components of natural gas. Of the hydrocarbon components of natural gas, methane and ethane individually form hydrates of von Stackelberg's structure I, while propane and isobutane, which are too large for incorporation in the 12- and 14-hedral cages of structure I, form structure II hydrates in which they occupy the 16-hedral but not the 12-hedral cages.

Recent studies of a number of gas hydrates by nmr (5, 7) and dielectric (5, 8) techniques have shown the encaged or guest molecules in these clathrates generally to possess a remarkable degree of freedom of reorientation. We have now extended these studies to hydrates formed by

[1]NRCC No. 16178.

the components of natural gas. Wide-line proton magnetic resonance spectra have been recorded over wide temperature ranges for H_2O and/or D_2O hydrates of hydrocarbon molecules and hydrogen sulfide. In addition, low-temperature low-frequency dielectric absorption has been measured in the hydrates of H_2S and of slightly dipolar propane, isobutane, and *n*-butane molecules.

Although *n*-butane by itself is not known to form a gas hydrate, its presence is demonstrated in the 16-hedral cages of the double *n*-butane–H_2S hydrate, the hydrate being stabilized by the partial filling by H_2S of the 12-hedral cages of structure II. This result confirms the recent thermodynamic conclusions of Wu *et al.* (9) who found evidence of a double hydrate of *n*-butane and methane, with methane here serving as the 'Hilfsgas' (10). Likewise, our nmr measurements show neopentane (2,2-dimethylpropane) to form a double hydrate with H_2S, apparently the first evidence of the encagability of this relatively large molecule.

Experimental Methods

Preparation of Hydrates

Nominal purities of the gases employed were in excess of 99.5% except for ethane and neopentane which were 99.0+%.

Ethane hydrate (deuteriohydrate) was prepared over a period of about a month in a pressure vessel at 0°C (5°C) under 13 atm of ethane gas, the formation of hydrate being monitored by the fall in pressure. Propane and isobutane hydrates were prepared by condensing the liquid hydrocarbon onto cooled, powdered H_2O or D_2O ice and conditioning for a period of weeks at ~ -13°C. H_2S–*n*-butane double hydrate was formed from a cooled mixture of liquid butane and H_2O under H_2S gas at a pressure less than that required to form the single H_2S hydrate. This hydrate was nucleated in the melt by vigorous agitation with a Vortex mixer and grown at $\sim$2°C over several days until further uptake of H_2S became negligible. A similar procedure was used to prepare the neopentane–D_2S–D_2O hydrate, with a reaction temperature of 6°C. Three samples of CCl_4–H_2S hydrate of different H_2S content were prepared by shaking CCl_4–H_2O mixtures at 2°C in a large vessel containing H_2S gas. H_2S hydrate itself was grown at $\sim$22°C over a period of weeks in the dielectric cell itself (see below), which was placed in a pressure vessel and subjected to about 20 atm of H_2S. In most of the above cases, the samples were periodically cooled to low temperatures during the reaction period to crack the hydrate crust which tends to inhibit further hydrate formation.

The amount of unreacted hydrocarbon could be monitored by the intensity of the narrow liquid line in the nmr spectrum at temperatures above the hydrocarbon melting point. This showed none of the samples employed to contain more than a few percent of unreacted hydrate-former.

Nuclear Magnetic Resonance Measurements

Proton nmr spectra were recorded as the derivative of the absorption signal in a marginal oscillator circuit resonating at $\sim$21.4 MHz, with 84 Hz modulation and phase-sensitive detection using a PAR 124 lock-in amplifier. Samples in sealed glass tubes were set in a sample holder consisting of a coil wound on a threaded quartz tube which was mounted in an Andonian Associates liquid helium cryostat equipped with a tail-piece elongated to fit between the pole pieces of a Bruker electromagnet. Temperature control and measurement were as previously described (11).

Line widths were obtained as separations between the *extrema* of the recorded derivative curves. Second moments of absorption lines, corrected for small modulation broadening, were evaluated by a PDP8-E computer from spectra converted to digital form. No problems with signal saturation were encountered.

Dielectric Measurements

The brass dielectric cell used for the hydrocarbon hydrates was constructed with horizontal parallel plate electrodes, the lower electrode being provided with a concentric guard ring. The disc-shaped sample was held firmly between the electrodes by a bellows arrangement. Samples were finely ground in the cold vapour over liquid nitrogen and then pressed in a pre-cooled 1.9-cm diameter die under a pressure of about 1200 kg/cm^2. The sample disc was about 2 mm in thickness, thinner samples being found to be subject to cracking. The cell constant was calculated from the thickness of the sample measured at $\sim$77 K. As a result of uncertainty in cell constant and the effects of surface roughness and voids in the pressed samples, the measured low-temperature permittivities may be in error by as much as 5%.

H_2S hydrate was grown in a stainless-steel cylindrical dielectric cell similar in design and geometry to the brass cell used in previous low-temperature dielectric studies of ice (12).

Of the methods previously used (13) to measure the capacitance and conductance of gas hydrates, only the General Radio 1615A Bridge has resolution and sensitivity good enough to define the small dielectric loss associated with the reorientation of enclathrated propane, isobutane, and *n*-butane molecules. The conductance resolution of this bridge ($\Delta G = 10^{-12}\ \Omega^{-1}$) is associated with a limiting uncertainty $\Delta\varepsilon''$ in dielectric loss of $\pm\Delta G/(2\omega C_0)$, where ω is the angular frequency and C_0 the cell constant in farads. For our hydrocarbon hydrate samples C_0 was $\sim 10^{-12}$ F and measurements were undertaken only at frequencies of 1 kHz and greater, where $\Delta\varepsilon''$ was less than ± 0.0001.

Results

Dielectric Measurements

Dielectric absorption at sub-MHz frequencies has previously been observed at low temperatures in a number of hydrates of dipolar molecules (5, 13, 14). Since this absorption arises from reorientation of the dipole moment of the

guest molecule, it is expected to be absent in the hydrates of methane, nitrogen, carbon dioxide, and other components of natural gas which lack permanent dipole moments. This is true also of ethane in its centrosymmetric (staggered) form or in the presence of rapid rotation of the CH_3 groups with respect to one another. No low-temperature dielectric absorption was in fact found in ethane hydrate within the sensitivity of the measurements (~2% of the absorption shown by propane hydrate).

Figure 1 shows the temperature dependence of the real (ε′) and imaginary (ε″) parts of the complex permittivity of the structure II hydrates of propane (dipole moment 0.083 D) and isobutane (0.132 D), as measured at three frequencies. The maxima in the dielectric loss (ε″) curves associated with the reorientation of encaged propane molecules occur at temperatures less than half those of the corresponding absorption by isobutane and the two species are easily distinguished, even though the absorption associated with each is relatively broad. The corresponding dispersion of ε′ with temperature is likewise distinctive. (The difference in Fig. 1 between the absolute values of ε′ for the two hydrates is not experimentally significant.)

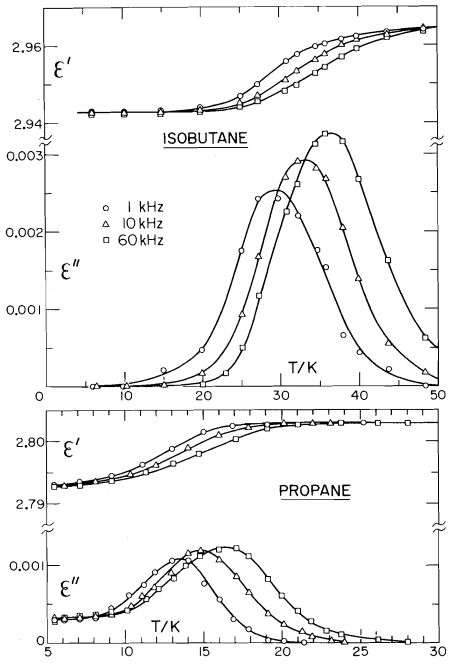

FIG. 1. Dispersion of permittivity (ε′) and dielectric loss (ε″) in propane and isobutane hydrates at low temperatures.

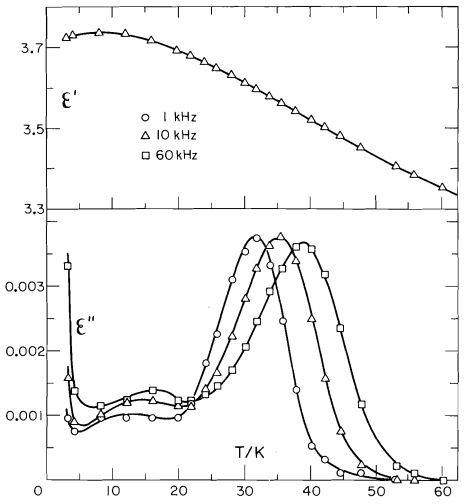

FIG. 2. Dielectric behavior of *n*-butane–H_2S hydrate at low temperatures.

Results for the double hydrate of *n*-butane and H_2S are shown in Fig. 2. The principal dielectric loss peaks from *n*-butane occur only 2 to 3 deg above those from isobutane at the same frequencies of measurement and these peaks would overlap in a hydrate containing both isomers. The secondary absorption region which occurs between 10 and 20 K for *n*-butane may serve to distinguish this guest from isobutane but propane also absorbs in this region. The relatively large value of ε′, its rise with decrease of temperature, and the sharp rise of ε″ below 4 K all arise from the presence of H_2S. Behavior of this kind has previously been observed for the structure II H_2S double hydrates of tetrahydrofuran and trimethylene oxide (13).

The structure I H_2S hydrate itself behaves as shown in Fig. 3. The maximum loss from reorienting H_2S molecules in both single and double hydrates occurs below 1.8 K even at 1 MHz. The extremely fast reorientation rate of enclathrated H_2S is unique among the polar guest molecules which have been studied.

Nuclear Magnetic Resonance Measurements

The formation of a H_2O clathrate by a hydrogen-containing species is generally to be recognized by a proton magnetic resonance spectrum which, at temperatures between roughly 50 and 200 K, consists of a narrow component 3 to 4 G wide arising from the protons of the 'rotating' guest species superimposed on a broad ice-like

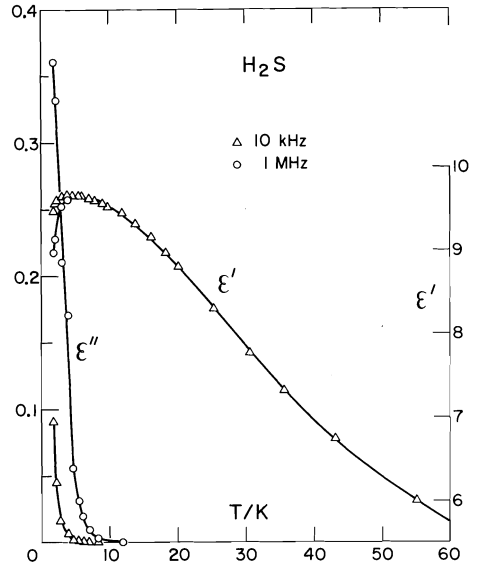

FIG. 3. Dielectric behavior of H_2S hydrate at low temperatures.

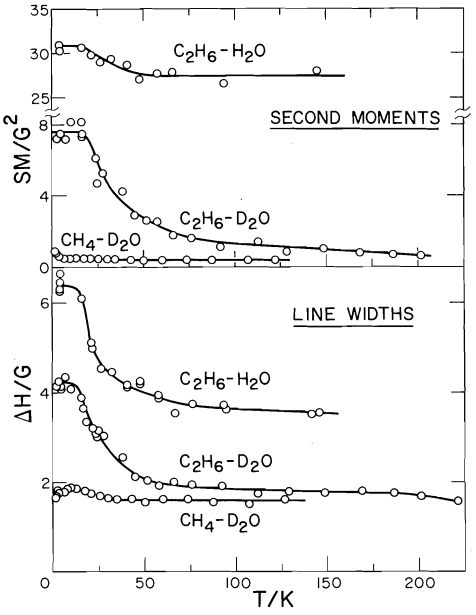

FIG. 4. The nmr line widths and second moments of structure I hydrocarbon hydrates.

resonance arising from 'rigid' water molecules (for examples, see refs. 15–17).

Most previous nmr studies of the motions of enclathrated molecules have been made in D_2O rather than H_2O lattices to eliminate the signal from the water protons (except for HDO impurity). This also greatly reduces the broadening effect of the magnetic nuclei of the host lattice on the spectrum of the guest molecule and more spectral detail is revealed at low temperatures (18).

In the present study of hydrocarbon hydrates more extensive measurements have been made in D_2O than in H_2O. Since deuteriation of the host lattice is likely to have a negligible effect on the motion of the guest molecules, it is normally possible to predict the hydrate spectrum from the deuteriohydrate spectrum of the same guest molecule.

Structure I Hydrates

The structure I hydrate of CH_4 in D_2O has previously been studied (19). At temperatures upward from 1.8 K there is a single structureless line whose width (Fig. 4) is 1.6 G and second moment 0.42 ± 0.02 G^2 between 30 K and 130 K. Although spectra of CH_4 in H_2O have not been obtained, it is anticipated from the D_2O results that these will resemble that shown for ethane hydrate at 146 K (Fig. 5), and remain unchanged over essentially the whole range of

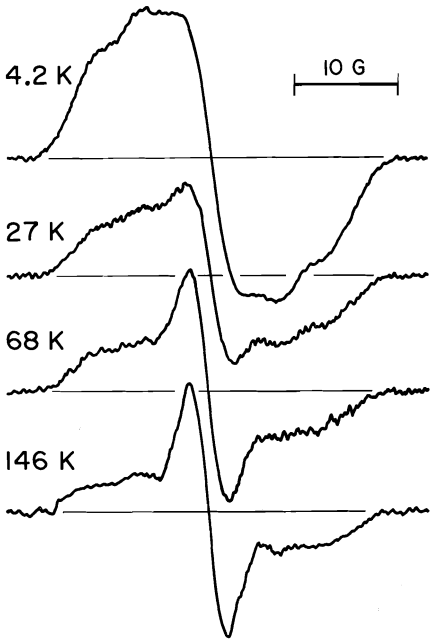

FIG. 5. Line shapes of ethane hydrate.

temperature between 1.8 and 200 K, the width of the narrow component being about 3.6 G.

Ethane has been studied in both D_2O and H_2O. Line shapes at a number of temperatures are shown in Figs. 5 and 6 and the temperature

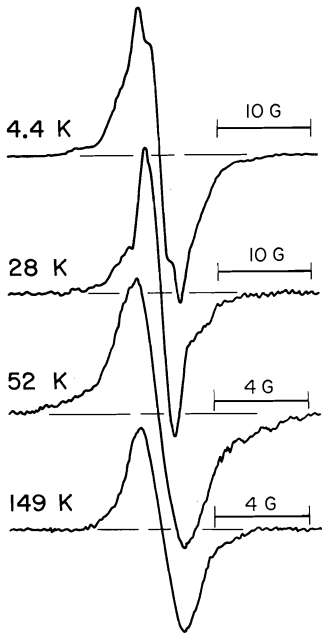

FIG. 6. Line shapes of ethane deuteriohydrate.

dependence of line width and second moment in Fig. 4. Below about 15 K the line shape of C_2H_6 in D_2O (and H_2O) is independent of temperature and shows the absence of overall reorientation of C_2H_6 molecules. The presence of tunnelling of the methyl groups, however, is clearly shown by a value of the low-temperature second moment ($7.6 \pm 0.5\ G^2$) of C_2H_6 deuteriohydrate which is much less than the value ($\sim 25\ G^2$ (20)) expected for rigid C_2H_6 molecules. With increase of temperature, narrowing occurs and the second moment falls to half its low-temperature value by about 36 K and thereafter with increasing slowness to $\sim 1.1\ G^2$ at 100 K and $\sim 0.75\ G^2$ at 200 K. The second moment of C_2H_6 in H_2O shows a corresponding fall which is less pronounced because this second moment is mostly determined by the protons of rigid H_2O molecules. There is overlap of the H_2O and C_2H_6 signals (Fig. 5) at very low temperatures where the widths of the narrow component plotted (Fig. 4) are only approximate.

Structure II Hydrates

Line shapes of the H_2O clathrates of propane and isobutane are illustrated in Fig. 7. Line widths and second moments of the deuteriohydrates are plotted in Fig. 8. The isotopically

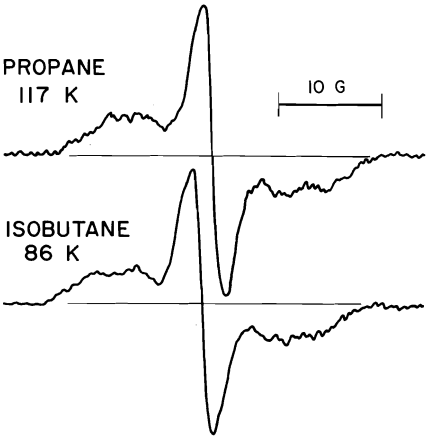

FIG. 7. Line shapes of propane and isobutane hydrates.

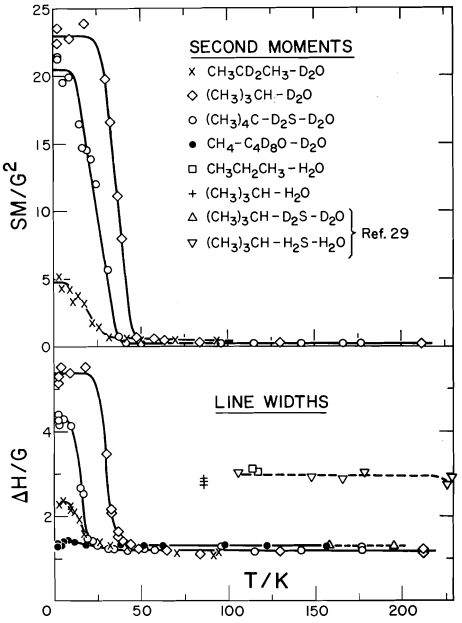

FIG. 8. Line widths and second moments of structure II hydrocarbon hydrates.

substituted $CH_3CD_2CH_3$ form was chosen for better definition of the low-temperature line shape of the CH_3 groups. The low temperature second moment of $5.0 \pm 0.5\ G^2$ (this would have been $\sim 8\ G^2$ for $CH_3CH_2CH_3$ in D_2O) falls to $2.5\ G^2$ at 18 K and to about $0.35\ G^2$ at 100 K. These values are not consistent with the very large second moments of $CH_3CH_2CH_3$ in D_2O previously reported above 77 K (21).

For $(CH_3)_3CH$ in D_2O the second moment is $22.4 \pm 1.5\ G^2$ below 25 K and falls to half

this value at ~37 K, to 0.30 G^2 at 90 K, and to 0.23 G^2 at 210 K. The line width of 1.20 ± 0.04 G between 60 and 210 K agrees with the width of 1.3 G reported by Chassonneau *et al.* (22) for the isobutane–D_2S–D_2O hydrate at two temperatures (see Fig. 8). (However, our second moments at comparable temperatures are only half the 0.55 ± 0.05 G^2 value obtained by these workers.) There is also agreement between their line width (3.0 G between 100 and 200 K) of the isobutane component in the isobutane–H_2S–H_2O system and our width (2.85 ± 0.10 G at 86 K) of isobutane in H_2O.

Line shapes of neopentane in the D_2S–D_2O double hydrate are illustrated in Fig. 9. The absorption begins to narrow at about 13 K, the second moment (Fig. 8) falling to half its low temperature value of 21.0 ± 1.5 G^2 at about 24 K and to about 0.30 G^2 at 50 K. Thereafter it shows little change with temperature, the second moment being 0.26 ± 0.03 G^2 between 60 and 180 K. The line width is 1.23 ± 0.04 G over this temperature range.

Any natural gas hydrate of structure II is likely to contain considerable quantities of methane, mainly in the 12-hedral cages. Previous measurements of the CH_4–tetrahydrofuran-d_8–D_2O type II hydrate (19) gave proton spectra rather similar to that of the structure I CH_4 deuteriohydrate itself, with second moments which hardly changed from 5 K upward. From these results one anticipates that the line width of the CH_4 absorption in a type II H_2O double hydrate should likewise remain independent of temperature above 5 K at a value of about 4.1 G. This width is estimated from the assumption that all CH_4 molecules occupy 12-hedra.

It does not seem possible to prepare for nmr study a sample of H_2S hydrate in D_2O because of the well-known rapid exchange of hydrogen atoms between water and hydrogen sulfide. Figure 10 shows a spectrum of a hydrate sample of approximate composition $0.9CCl_4 \cdot 0.40H_2S \cdot 17H_2O$. The narrow component, identified with H_2S from its variation with H_2S content, appears only as a central shoulder on the H_2O line which makes up 98% of the absorption intensity. It is inferred from the dielectric results that this line characteristic of rotating H_2S molecules should persist down to liquid helium temperatures.

We cannot agree with Chassonneau *et al.* (22) that the *very* narrow line (width <150 mG)

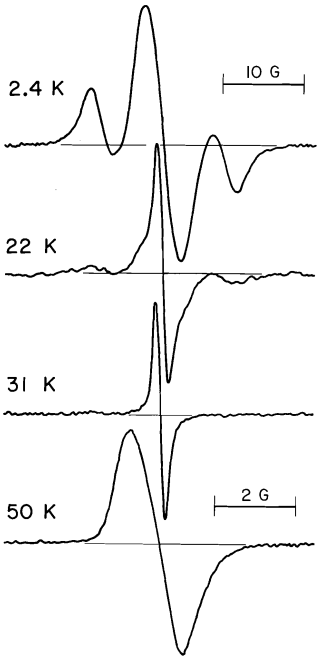

FIG. 9. Line shapes of neopentane in D_2O double hydrate with D_2S.

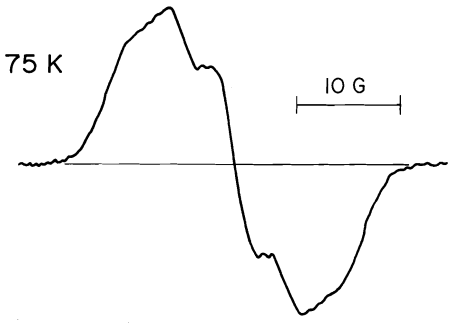

FIG. 10. Line shape of CCl_4–H_2S double hydrate at 75 K.

reported by them at all temperatures above 120 K in the H_2S double hydrates of CCl_4, tetrahydrofuran, isobutane, and thiophene is due to rapid reorientation *and diffusion* of encaged H_2S molecules. This line is much more likely to have arisen from the presence of liquid H_2S in their samples.

Discussion

Proton Nuclear Magnetic Resonance Line Shapes at Low Temperatures

None of the low-temperature proton spectra of the hydrocarbon deuteriohydrates show a line shape characteristic of either rigid CH_3

TABLE 1. Reorientational properties of guest molecules

Guest	Hydrate structure	Dielectric absorption: Temp. of max. ε'' at 100 kHz (K)	Dielectric absorption: E_A (kcal/mol)	Nuclear magnetic resonance line narrowing: $T_{1/2}$ (K)	Nuclear magnetic resonance line narrowing: V_0 (kcal/mol)
H_2S	I, II-double	<1.8			
CH_4	I, II-double			<1.8	
C_2H_6	I			36	1.17
C_3H_8	II	17.0	0.60	17	0.55
iso-C_4H_{10}	II	37.3	1.21	37	1.20
n-C_4H_{10}	II-double	39.6	1.41		
neo-C_5H_{12}	II-double			24	0.78

groups or, at the other extreme, of CH_3 groups which are undergoing rotation in the fast tunnelling limit (23). More detailed analysis of methyl-group line shapes in hydrocarbon and other enclathrated molecules will be presented elsewhere.

Reorientation Rates of Encaged Molecules

For hydrogen sulfide the average reorientation rate is greater than 1 MHz even at 1.8 K and for methane is also too fast to be definable by the present techniques in the sense that the proton spectrum remains a narrow line to below 2 K. For the remaining guests the general reorientation rates and their dependence on temperature may be derived from analysis of the nmr and dielectric data. It is emphasized that both line-narrowing and dielectric absorption show the presence of wide distributions of reorientation rates in all the hydrates studied. These distributions are a general characteristic of clathrate hydrates and are ultimately attributable to the 'frozen-in' orientational disorder of the lattice water molecules, as discussed elsewhere (5, 13, 17).

Average reorientation rates and 'activation energies' for reorientation are given in Table 1. For dipolar guest molecules the temperature of maximum dielectric absorption at 100 kHz is given along with an effective Arrhenius activation energy E_A derived from the dependence of the temperature of maximum absorption on frequency (Fig. 11).

With increasing temperature an nmr line begins to narrow at the temperature where the molecular reorientation rate becomes approximately equal to the width (in frequency units) of the unnarrowed line. For the present hydrocarbon deuteriohydrates, this width, as the square root of the second moment, is about

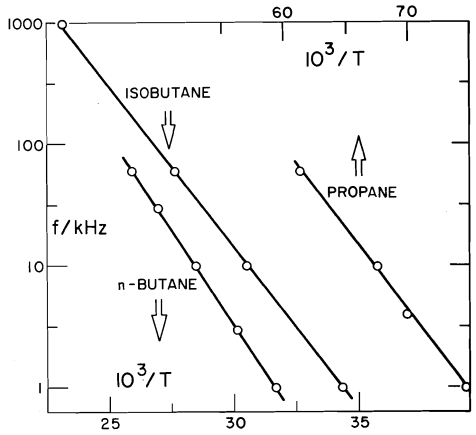

FIG. 11. Temperature dependence of the frequency of maximum ε'' in structure II hydrates.

10 kHz. For a single reorientation rate ν_c which varies with temperature according to $\nu_c = \nu_0 \exp(-V_0/RT)$, Waugh and Fedin (24) showed that, with 'normal' values of the rotational oscillation frequency ν_0 of about 10^{12} Hz, V_0 (kcal/mol) $\approx 37T_c$, where T_c is the temperature of the onset of narrowing. Where, as in the present cases, there is a wide distribution of reorientation rates, the temperature of initial narrowing not only loses its simple significance but is experimentally difficult to define. We have therefore chosen instead of T_c the temperature $T_{1/2}$ at which the second moment has fallen to one half its low temperature value. Under the assumption that the average reorientation rate is about 100 kHz at this temperature, the Waugh formula is modified to V_0 (kcal/mol) $\approx 32.4T_{1/2}$, the new factor being $37 - R \ln 10$. Values of V_0 estimated from this relationship are given in Table 1 where the $T_{1/2}$'s recorded are accurate to about ± 2 K.

There is good agreement between the activa-

TABLE 2. Contributions to proton second moments (G^2) of isotropically rotating guests in rigid D_2O lattices, SM(HDO–D_2O) = 0.89 G^2

Guest	SM(interguest)	SM(guest–D_2O)	SM(HDO–guest)
CH_4	0.216	0.117	1.51
C_2H_6	0.214	0.104	1.44
$CH_3CD_2CH_3$	0.065	0.077	0.46
C_3H_8	0.086	0.077	0.61
C_4H_{10}	0.108	0.077	0.77
C_5H_{12}	0.129	0.077	0.92

TABLE 3. Total second moments (G^2) for isotropically rotating guests in rigid D_2O lattices of different HDO content

	$x = 0, z = 0$	$x = 0.003$		$x = 0.010$	
Guest	SM(total)	z	SM(total)	z	SM(total)
CH_4	0.33	0.0088	0.36	0.0287	0.44
C_2H_6	0.32	0.0081	0.35	0.0266	0.42
$CH_3CD_2CH_3$	0.14	0.0167	0.17	0.0536	0.25
C_3H_8	0.16	0.0126	0.19	0.0408	0.26
C_4H_{10}	0.19	0.0101	0.21	0.0329	0.27
C_5H_{12}	0.21	0.0084	0.23	0.0276	0.29

tion energies E_A and V_0 derived from the two techniques for propane and isobutane hydrates.

Second Moments for Isotropically Rotating Guests

The second moments of proton absorption lines for isotropically rotating guest molecules in rigid D_2O lattices were calculated by the method given in the Appendix. The results are given in Table 3, where x is the atom fraction of H as impurity in the D_2O employed. The sensitivity of second moment to x is considerable, the effect of 1% HDO in the D_2O being to increase the second moment by one-third to three-quarters, depending on the hydrate.

Comparison of Table 3 with the experimental second moments of 0.40 ± 0.2 G^2 for CH_4 (30–130 K), 0.23 G^2 for $(CH_3)_3CH$ (210 K), and 0.26 ± 0.03 G^2 for $(CH_3)_4C$ (60–180 K) shows good agreement for somewhat less than 1 at.% H in the D_2O.

Effects of Cage Type and Guest-molecule Symmetry on Motional Averaging

For ethane in D_2O the second moment continues to fall with increasing temperature over the whole range of measurement (Fig. 4) and is well in excess of the value calculated for isotropic reorientation (Table 3) even at 200 K. This behavior probably results from the oblate shape of the 14-hedral cage which tends to favor orientations in which the long axis of the ethane molecule lies in and near the equatorial plane midway between opposite hexagonal rings of water molecules. The preference of ethane for equatorial configurations is likely to be somewhat greater than that already suggested (25), with some experimental support, for the smaller chlorine molecule in the same cage. With increase of temperature the motional averaging becomes somewhat more isotropic.

The 16-hedral cages occupied by the larger hydrocarbon molecules are much more spherical than the 14-hedra. The space average symmetry, or the symmetry averaged over the disordered orientations of the water molecules, is tetrahedral ($\bar{4}3m$). At temperatures below about 200 K the motion responsible for nmr line narrowing is reorientation within cages which are distorted from tetrahedral symmetry to an extent determined by the fixed (on an nmr time scale) positions of the hydrogen atoms of the cage water molecules. The variation of this distortion from cage to cage is mainly responsible for the distribution of reorientation rates of guest molecules in structure II hydrates. It may also lead to some residual lack of isotropy in the time averaged directions of the inter-proton magnetic fields of the guest molecules, even when the reorientation rates are very fast. The degree of this anisotropy varies with the geometry of the guest molecule, the greatest effect

on the proton second moment being observed for such relatively unsymmetrical molecules as tetrahydrofuran (17). The ^{19}F second moments of SF_6 and CF_4 encaged in H_2O and D_2O, on the other hand, show no residual anisotropy, even at temperatures down to ~ 20 K (19). Analysis shows that guest molecules of cubic symmetry (i.e., tetrahedral or octahedral molecules) in a cage *of any symmetry* should be characterized by a zero contribution to the second moment from interactions between magnetic nuclei within the guest molecule at all temperatures where the reorientation rates are sufficiently fast (say >1 MHz). It is only necessary that such a molecule undergo a thermally activated process which interchanges the σ equivalent orientations, where σ, the symmetry number, is 12 for tetrahedral and 24 for octahedral molecules. It is immaterial whether there is one or more distinguishable preferred orientations within the cage.

In agreement with these conclusions, the second moment of the tetrahedral neopentane molecule (Fig. 8) shows no change with temperature between 60 and 180 K and has a value indistinguishable from that for isotropic reorientation. Propane and isobutane on the other hand have, near 100 K, somewhat larger moments than the isotropic value.

The spectra of enclathrated neopentane recorded at seven temperatures between 14 and 35 K exhibit clearly the Resing 'apparent phase-change' effect (26) in the form of a superposition of the broad, structured 'rigid lattice' line and a narrow line of almost Gaussian shape, only the latter being observed above 50 K (cf. Fig. 9). This behavior is attributed to a broad distribution of correlation times τ_c such that at temperatures in the transition region $\omega_1\tau_c \gg 1$ (rigid molecules) or $\omega_1\tau_c \ll 1$ (rotating molecules) for most molecules and $\omega_1\tau_c \sim 1$ for relatively few, where ω_1 is approximately the square root of the rigid-lattice second moment ($\sim 2\pi \times 20$ kHz). For the reasons of symmetry already given, neopentane molecules which are rotating at all appear to do so isotropically. The temperature variation of the second moment may be analyzed in terms of a simple Gaussian distribution of activation energies E_c (or log-normal distribution of correlation times), as already described (19) for the Resing effect in SF_6 and CF_4 hydrates. For the mean correlation time $\tau_m = 10^{-12} \exp(E_m/RT)$ and the distribution $G(E_c) = \pi^{-\frac{1}{2}}A^{-1} \exp((E_c - E_m)/A)^2$, values of $E_m = 743$ and $A = 280$ cal/mol were found for the mean activation energy and width parameter, respectively.

Geometry of Encaged n-Butane

Of the two rotational isomers of *n*-butane which exist in the gaseous phase, the *trans* form is more stable than the *gauche* by about 760 cal/mol (27). The longest van der Waals dimension of the *trans* isomer is 7.9 Å if 2.0 Å is taken for the van der Waals radius of the CH_3 groups. This form is much too long for encagement in the structure II 16-hedron (5). Moreover, the *trans* isomer has zero dipole moment and cannot give rise to the dielectric absorption observed. The *gauche* form on the other hand is smaller (length 7.1 Å for the gas-phase dihedral angle of 62.3°) and has a finite dipole moment. The contribution of the interaction with the cage water molecules to the dependence of potential energy on dihedral angle will, in all probability, result in a smaller dihedral angle than in the gas, i.e., the geometry of encaged *n*-butane is likely to be intermediate between the *gauche* form of the gas and the *cis* form (length 6.7 Å).

The effect of the cage on the geometry of *n*-butane may have another consequence. The barrier to interchange of two *gauche* isomers via the *cis* form is considerably reduced by the interactions with the cage which favour the *cis* form and it is possible that the dielectric absorption observed (Fig. 2) between 10 and 20 K arises from this interchange, which would result in some dipole reorientation.

1. N. CHERSKY and Y. MAKOGON. Oil and Gas Int. **10**, No. 8, 82 (1970).
2. Y. F. MAKOGON. Gidraty prirodnykh gazov (Hydrates of natural gas). Nedra, Moscow. 1974.
3. C. BILY and J. W. L. DICK. Bull. Can. Pet. Geol. **22**, 340 (1974).
4. D. L. KATZ (*Editor*). Handbook of natural gas engineering. McGraw-Hill Book Co., New York. 1959. p. 189.
5. D. W. DAVIDSON. *In* Water: A comprehensive treatise. Vol. 2. Plenum Press, New York. 1973. p. 115.
6. J. A. RIPMEESTER and D. W. DAVIDSON. Mol. Cryst. Liq. Cryst. In press.
7. S. K. GARG and D. W. DAVIDSON. *In* Physics and chemistry of ice. *Edited by* E. Whalley. Roy Soc. Canada, Ottawa. 1973. p. 56.
8. S. R. GOUGH and D. W. DAVIDSON. *In* Physics and chemistry of ice. *Edited by* E. Whalley. Roy. Soc. Canada, Ottawa. 1973. p. 51.

9. B.-J. Wu, D. B. Robinson, and J.-J. Ng. J. Chem. Thermodyn. **8**, 461 (1976).
10. M. Von Stackelberg and W. Meinhold. Z. Elektrochem. **58**, 40 (1954).
11. S. K. Garg and D. W. Davidson. J. Chem. Phys. **58**, 1898 (1973).
12. S. R. Gough. Can. J. Chem. **50**, 3046 (1972).
13. S. R. Gough, R. E. Hawkins, B. Morris, and D. W. Davidson. J. Phys. Chem. **77**, 2969 (1973).
14. S. R. Gough, S. K. Garg, J. A. Ripmeester, and D. W. Davidson. Can. J. Chem. **52**, 3193 (1974); **53**, 2215 (1975).
15. S. K. Garg, B. Morris, and D. W. Davidson. J. Chem. Soc. Faraday Trans. II, **68**, 481 (1972).
16. Y. A. Majid, S. K. Garg, and D. W. Davidson. Can. J. Chem. **47**, 4697 (1969).
17. S. K. Garg, D. W. Davidson, and J. A. Ripmeester. J. Magn. Reson. **15**, 295 (1974).
18. S. K. Garg and D. W. Davidson. Chem. Phys. Lett. **13**, 73 (1972).
19. S. K. Garg, S. R. Gough, and D. W. Davidson. J. Chem. Phys. **63**, 1646 (1975).
20. W. H. Theis, G. E. Fredericks, and E. D. McCormick. J. Magn. Reson. **20**, 98 (1975).
21. C. A. McDowell and P. Raghunathan. J. Mol. Struct. **5**, 433 (1970).
22. M. A. Chassonneau, J. Dufourcq, and B. Lemanceau. C. R. Acad. Sci. Paris, **273**, 793 (1971).
23. F. Apaydin and S. Clough. J. Phys. C, **1**, 932 (1968).
24. J. S. Waugh and E. I. Fedin. Fiz. Tverd. Tela Leningrad, **4**, 2233 (1962).
25. D. W. Davidson. Can. J. Chem. **49**, 1224 (1971).
26. H. A. Resing. J. Chem. Phys. **43**, 669 (1965).
27. S. S. Chen, R. C. Wilhoit, and B. J. Zwolinski. J. Phys. Chem. Ref. Data, **4**, 859 (1975).

Appendix

Calculation of Second Moments of Isotropically Rotating Guests

These second moments include contributions from the absorption of protons present (mainly as HDO) as impurity in the D_2O as well as from the protons of the guest molecules:

$$[1]\quad \mathrm{SM(total)} = (1\text{-}z)\mathrm{SM(guest)} + z\mathrm{SM(HDO)}$$

where z is the fraction of the total number of protons which is present as impurity in the D_2O. The absorption by guest molecules is broadened by the magnetic fields of the protons of neighboring guests and by the deuterons (and protons) of the water lattice:

$$[2]\quad \mathrm{SM(guest)} = \mathrm{SM(interguest)} + \mathrm{SM(guest\text{–}host)}$$

where the second term depends on the atom fraction x of H in the D_2O according to

$$[3]\quad \mathrm{SM(guest\text{–}host)} = \mathrm{SM(guest\text{–}D_2O)} \times (1 + 34.8x)$$

Values of SM(interguest) and SM(guest–D_2O) were calculated (15) from the Van Vleck formula by taking the guest-molecule protons to be located at the cage centres and half deuterons to be distributed tetrahedrally around the oxygen atoms with OD bond lengths of 1.00 Å, one position lying on the radial extension of the position vector of each oxygen atom with respect to the cage centre (19).

The HDO impurity second moment is

$$[4]\quad \mathrm{SM(HDO)} = \mathrm{SM(HDO\text{–}host)} + \mathrm{SM(HDO\text{–}guest)}$$

where the first term is

$$[5]\qquad \mathrm{SM(HDO\text{–}D_2O)}\,(1 + 34.8x)$$

Since the second moments of both the structure I and structure II H_2O lattices are about 32 G^2 (5),

$$[6]\quad \mathrm{SM(HDO\text{–}D_2O)} = \frac{(4/15)I_D(I_D + 1)\gamma_D{}^2}{(3/5)I_H(I_H + 1)\gamma_H{}^2}32 = 0.89\ \mathrm{G}^2$$

where the I's are nuclear spin quantum numbers and the γ's gyromagnetic ratios. Values of SM(HDO–guest) were evaluated from the tetrahedral water molecule assumption, taking explicit account of the guest molecules in the four cages to whose walls each water molecule is common. The contribution of more distant guests was estimated as an additional 10%.

Complete occupancy of the large cages has been assumed for type II hydrates. For CH_4, 97.5% occupancy of cages of both sizes (corresponding to $CH_4 \cdot 5.9D_2O$) and for C_2H_6, 93.5% occupancy of the large cages ($C_2H_6 \cdot 8.2D_2O$), have been assumed.

The contributions for 100% D_2O are given in Table 2 and the total second moments for D_2O consisting of 100, 99.7, and 99.0 at.% D in Table 3.

The deprotonation and rearrangement of *N*-methyl methylphosphazenium quaternary salts: a novel synthetic route to cyclic azaphosphorins

RICHARD T. OAKLEY AND NORMAN L. PADDOCK[1]

Department of Chemistry, University of British Columbia, 2075 Wesbrook Place, Vancouver, B.C., Canada V6T 1W5

Received February 2, 1977

RICHARD T. OAKLEY and NORMAN L. PADDOCK. Can. J. Chem. **55**, 3651 (1977).

The *N*-methyl methylphosphazenium salts $(NPMe_2)_{3,4}\cdot MeI$ and $N_3P_3Ph_4Me_2\cdot MeI$ can be deprotonated by a variety of bases to yield the novel azaphosphorins $Me_{2n-1}(NHMe)P_nN_{n-1}CH$ (n = 3, 4) and $Me(NHMe)Ph_4P_3N_2CH$, formed by a rearrangement in which the methylated nitrogen atom is displaced from the PN ring by the initially produced exocyclic methylene group. The ^1H nmr spectra of the azaphosphorins indicate a rapid proton exchange between the endocyclic carbon and the exocyclic nitrogen, which can be slowed by the addition of an auxiliary base. When KO-*t*-Bu reacts with the quaternary salts, nucleophilic attack competes with proton removal, and the linear oxides $(NHMe)(PMe_2N)_nPMe_2O$ (n = 2–4) have been isolated from these reactions. The azaphosphorins $Me_{2n-1}(NHMe)P_nN_{n-1}CH$ (n = 3, 4) are hydrolysed in aqueous ethanol to give the cyclic oxides $Me_{2n-1}(O)P_nN_{n-1}CH_2$, and react with methyl iodide by a proton transfer reaction to give the hydroiodides $Me_{2n-1}(NHMe)P_nN_{n-1}CH\cdot HI$. Their reaction with benzoyl chloride leads to the derivatives $Me_7(NHMe)P_4N_3CCOPh$ and $Me_7(NMeCOPh)P_3N_2CCOPh$, the initial substitution on carbon indicating that it is the primary basic centre. Model calculations of π-electron energies suggest that both the azaphosphorin rearrangement and the proton exchange reactions depend on the relative orbital electronegativity of the ring and exocyclic atoms, the less electronegative atom being more stable in the endocyclic position.

RICHARD T. OAKLEY et NORMAN L. PADDOCK. Can. J. Chem. **55**, 3651 (1977).

Les sels de *N*-méthyl méthylphosphazénium $(NPMe_2)_{3,4}\cdot MeI$ et $N_3P_3Ph_4Me_2\cdot MeI$ peuvent être déprotonés par une variété de bases conduisant à de nouvelles azaphosphorines $Me_{2n-1}(NHMe)P_nN_{n-1}CH$ (n = 3, 4) et $Me(NHMe)Ph_4P_3N_2CH$, formées par réarrangement, où l'atome d'azote méthylé est déplacé du cycle PN par le groupe méthylène exocyclique formé initialement. Le spectre rmn ^1H des azaphosphorines indique un échange rapide de protons entre le carbone endocyclique et l'azote exocyclique, qui peut être ralenti par l'addition d'une base auxiliaire. Lorsque le KO-*t*-Bu réagit avec les sels quaternaires, une attaque nucléophile concurrence l'abstraction du proton et il résulte de ces réactions des oxydes linéaires $(NHMe)(PMe_2N)_nPMe_2O$ (n = 2–4). Les azaphosphorines $Me_{2n-1}(NHMe)P_nN_{n-1}CH$ (n = 3, 4) sont hydrolysées dans l'éthanol aqueux pour conduire aux oxydes cycliques $Me_{2n-1}(O)P_nN_{n-1}CH_2$, et elles réagissent avec l'iodure de méthyle par une réaction de transfert de protons pour conduire aux hydroiodures $Me_{2n-1}(NHMe)P_nN_{n-1}CH\cdot HI$. Elles réagissent avec le chlorure de benzoyle pour conduire aux dérivés $Me_7(NHMe)P_4N_3CCOPh$ et $Me_7(NMeCOPh)P_3N_2CCOPh$; la substitution initiale sur le carbone indique que celui-ci est le premier centre basique. Des calculs modèles des énergies pour les électrons-π suggèrent que tant le réarrangement des azaphosphorines que les réactions d'échange de protons dépendent de l'électronégativité relative des orbitales du cycle et des atomes exocycliques, l'atome le moins électronégatif étant plus stable en position endocyclique.

[Traduit par le journal]

Introduction

The formation of carbanions from methylphosphazenes by their reaction with strong bases (1) parallels the acidic behaviour of simple alkylphosphine oxides (2) and exemplifies the many chemical similarities that exist between cyclic phosphazenes $(X_2PN)_n$ and simple phosphoryl compounds X_3PO. In a further study of the acidic properties of the methylphosphazenes, we have investigated the reaction of *N*-methyl methylphosphazenium salts $(NPMe_2)_n\cdot MeI$ with bases (3). As expected, these salts can be deprotonated by a variety of bases, as are such phosphonium salts as $Me_2P(NMe_2)_2{}^+X^-$ (4). However, the final products of such reactions indicate the occurrence of an unusual skeletal rearrangement, thereby illustrating that although many properties of phosphazenes correspond to those of mononuclear phosphorus compounds, certain chemical features are di-

[1]Author to whom correspondence should be addressed.

rectly related to their cyclic structure. The reaction leads to several new azaphosphorin derivatives.

Results

Reactions of Quaternary Methylphosphazenium Salts with Bases

We have used chiefly the bases potassium *tert*-butoxide (KO-*t*-Bu) and sodium hexamethyldisilylamide. Both are appreciably soluble in hydrocarbons, which are the most convenient media for achieving a clean separation of the products, and both have been used successfully in the deprotonation of phosphonium salts (5–8). The reaction with the silylamide is the simpler. In boiling octane or toluene, $NaN(SiMe_3)_2$ reacts smoothly with the quaternary iodides $N_3P_3Me_6 \cdot MeI$ and *gem*-$N_3P_3Ph_4Me_2 \cdot MeI$, (**1**, R = Me, Ph) removing a proton from one of the P-methyl groups adjacent to the quaternized nitrogen atom. The final products are not the expected ylids **2**, but rather the novel azaphosphorins **4** (*a*, R = Me; *b*, R = Ph), formed from the ylids by a rearrangement in which the methylated nitrogen atom is displaced from the ring, the resulting exocyclic imine (**3**) then tautomerizing to give the aromatic amine form **4**. An exactly analogous reaction occurs with $N_4P_4Me_8 \cdot MeI$ (**5**), to give the azaphosphorin **8**.

Potassium *tert*-butoxide reacts both as a base, removing a proton from an exocyclic group, (as in Scheme 1), to form an azaphosphorin, and as a nucleophile attacking a phosphorus atom adjacent to the quaternized nitrogen atom, to form a linear oxophosphazene. The products obtained from the reactions of the monoquaternary salts $(NPMe_2)_{3,4} \cdot MeI$ and the diquaternary salt $(NPMe_2)_4 \cdot 2MeSO_3F$ with KO-*t*-Bu collectively demonstrate both possibilities, and indicate that the relative importance of the two processes is strongly dependent on the size and charge of the cyclic phosphazenium cation.

In the reaction of $(NPMe_2)_3 \cdot MeI$ with KO-*t*-Bu, proton abstraction does not occur. Instead, the *tert*-butoxide ion effects a nucleophilic attack on phosphorus, and cleaves the PN skeleton (Scheme 2). The subsequent elimination of isobutene or (less probably) an ether (9, 10) then produces the novel linear oxophosphazene $(NHMe)(PMe_2N)_2PMe_2O$ (**9**) in high yield (92%). The reaction of the tetrameric salt $(NPMe_2)_4 \cdot MeI$ with KO-*t*-Bu shows a marked contrast to the one just described. Nucleophilic

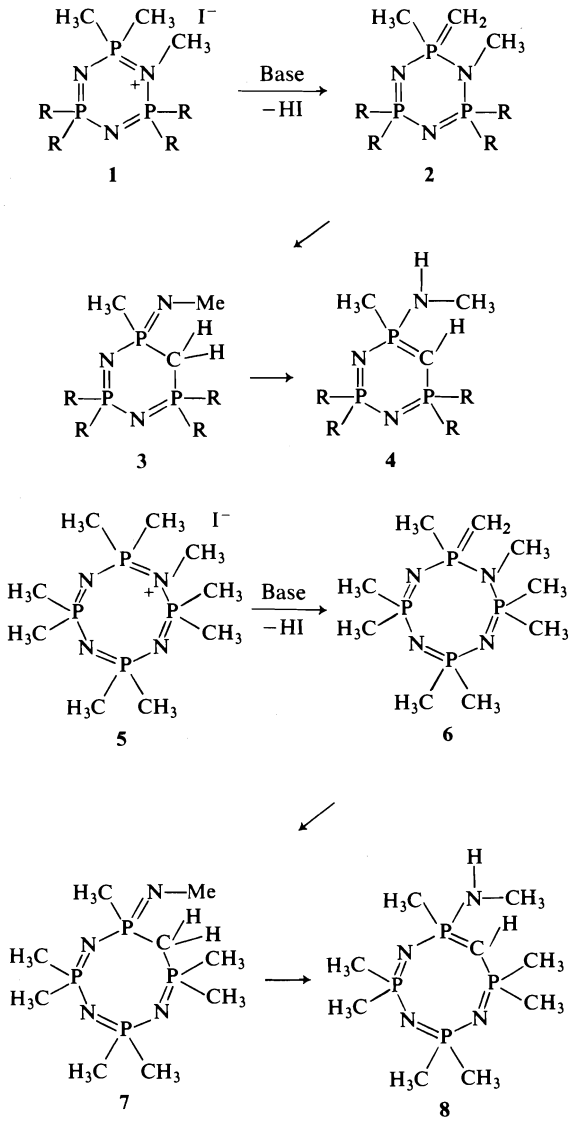

SCHEME 1

attack of *tert*-butoxide ion still occurs, to give the open chain oxide $(NHMe)(PMe_2N)_3PMe_2O$ (**10**) but the yield of this product is low (~5%). The principal product (~80%) is the cyclic azaphosphorin **8**, formed presumably by a deprotonation reaction and a phosphazene–azaphosphorin rearrangement. The reaction of the diquaternary ion $[(NPMe_2)_4 \cdot 2Me]^{2+}$ with KO-*t*-Bu reflects the effect of an increase in charge on the tetrameric ring. Nucleophilic attack on phosphorus now predominates, the only product of the reaction, the linear oxophosphazene

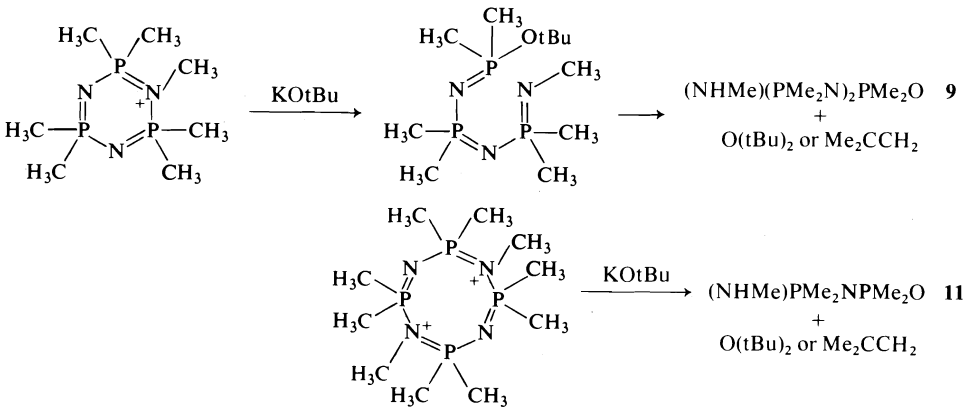

SCHEME 2

(NHMe)(PMe_2N)PMe_2O (**11**), indicating that ring cleavage occurs twice.

Spectra and Structures

The structures of the azaphosphorins **4** and **8** have been established spectroscopically (see Table 1 for numerical details). The ^1H nmr spectrum of **4***b* in benzene (Fig. 1*a*) shows the expected features, the resonances of the MeP, the MeN, the NH, and the CH protons all being clearly distinguishable. The *N*-methyl signal is similar in position and appearance to the equivalent resonance in $N_3P_3(NHMe)_6$ (δ_H(NMe) = 2.57 ppm (11)), for which no ^1H–^1H coupling is observed. The chemical shift of the CH proton is close to that found in other phosphorins (12, 13), and as such is at lower field than in C-alkyl ylids $R_3P{=}CHR'$ (δ_H(CH) = −0.5 to −1.0 ppm (14)) in which the anionic nature of the ylidic carbon atom has a large shielding effect on the CH proton. It is at higher field than in those ylids which are stabilized by electron withdrawing substituents on carbon (e.g. δ_H(CH) in $Ph_3P{=}CHC(O)Me$ is 3.68 ppm (15)).

The lack of resolution of the CH resonance into the expected triplet is explicable in terms of a rapid proton exchange between nitrogen and carbon, a process which has already been observed for methylene diphosphine dioxides in the presence of aniline (16), and which, in the present case, corresponds to the tautomeric change between the imine and amine forms **3** and **4**. Similar effects have been observed elsewhere; the sulphur ylid **12** has been shown to exist in solution in two tautomeric forms (17), and the azaphosphorin $MeS(NPPh_2)_2CH$ (**13**), whose broad CH singlet at δ_H 1.6 ppm is not resolved into the expected triplet even at −30°C (13), may well undergo a similar exchange.

In the present system, proton transfer is believed to be promoted by traces of acid, as is found for simple ylids (13, 14, 18, 19) and, as in

TABLE 1. ^1H nmr parameters[a] and vibrational frequencies[b] of azaphosphorin derivatives

Compound	**4***a*	**8**	**4***b*[g]
δ(MeN)	2.47(14.0)[c]	2.46(13.0)[c]	2.28(14.0)[c]
δ(MeP)	1.45(14.0)	~1.42[d]	1.43(14.5)
δ(Me_2P)	1.32(12.5)	~1.42[d]	[e]
	1.39(13.5)		
ν(N—H)	3180	3210	3195
ν(C—N)[f]	1081	1082	1067
ν(P=N)	1159, 1187	1153, 1185, 1209	1144, 1170, 1191

[a]δ(ppm) in C_6D_6, reference internal tetramethylsilane. *J*(PH) (Hz) in parentheses.
[b]ν(cm^{-1}) from Nujol mull spectra, assignments tentative.
[c]No ^1H–^1H coupling observed (at ambient temperature).
[d]Unresolved multiplet.
[e]δ(Phenyl) ~7.0–8.0 ppm.
[f]Assignment confirmed by ir spectrum of $Me_7(NHCD_3)P_4N_3CH$, ν(N—C)1037 cm^{-1}, cf. ν(N—C) in $MeNH_2$, 1044 cm^{-1}, CD_3NH_2, 973 cm^{-1} (52, 53).
[g]δ(CH) = 1.23, δ(NH) = 1.76 ppm (broad singlets).

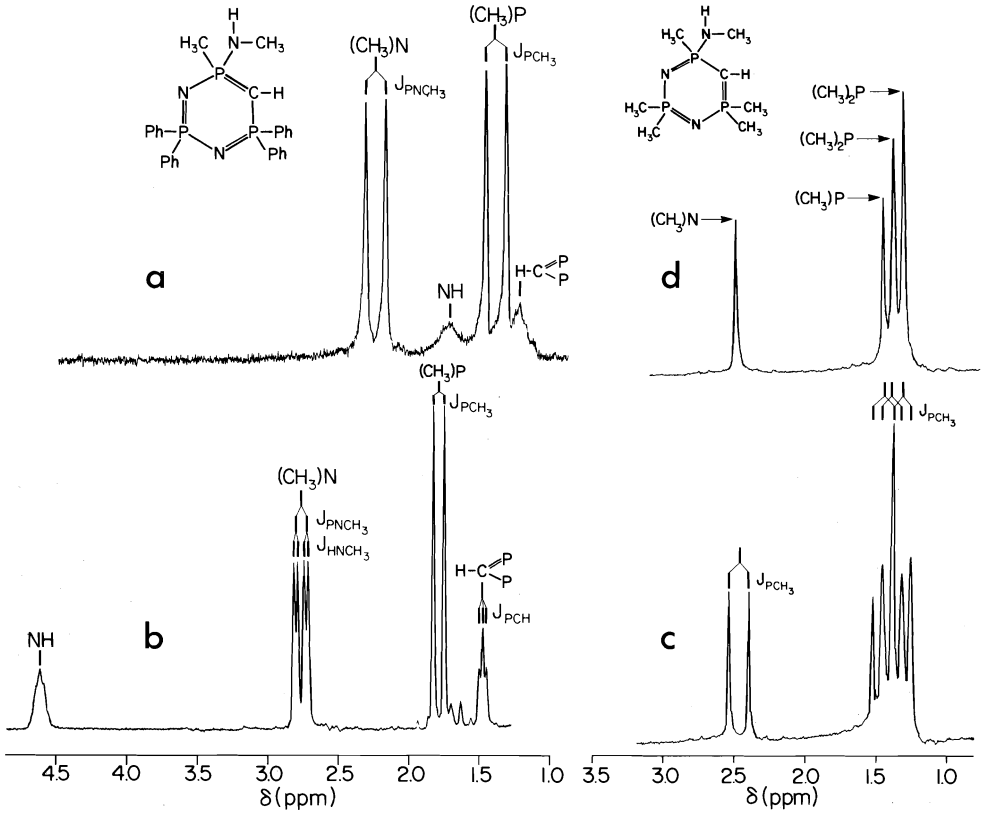

FIG. 1. ^{1}H nmr spectra of azaphosphorins **4***b*(*a*, 100 MHz, C_6D_6; *b*, 220 MHz, C_5D_5N) and **4***a*(*c*, 100 MHz, C_6D_6; *d*, 100 MHz, ^{31}P decoupled).

ylids (19), can be suppressed by the addition of an auxiliary base. For example, the ^{1}H nmr spectrum of **4***b* in pyridine (Fig. 1*b*) is better resolved than the same spectrum run in benzene (Fig. 1*a*), and shows clearly the ^{1}H–^{1}H coupling

[1]

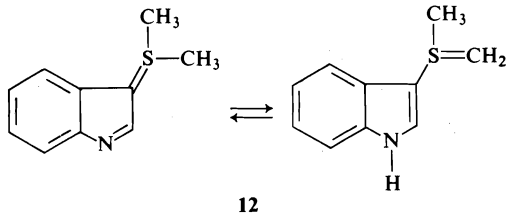

12

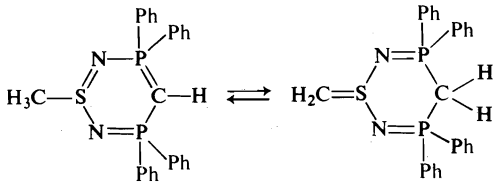

13

in the NHMe group and also the ^{1}H–^{31}P coupling of the CH proton.[2]

The corresponding methyl derivative **4***a* is more basic, sufficiently so to decompose chloroform, and proton exchange from carbon to nitrogen is consequently more rapid. Its ^{1}H nmr spectrum in benzene (Fig. 1*c* and *d*) shows no NH or CH signals, even when pyridine is added. The other structural features, however, are observed; the resonances of the PMe group, the two inequivalent PMe_2 groups, and the NMe group are readily distinguished. The NH and CH resonances are also absent from the ^{1}H nmr spectrum of the corresponding eight-membered ring compound **8** but, for all the azaphosphorins listed in Table 1, the presence of the NHMe group is confirmed by the observation of a

[2]The dependence of the chemical shifts of the NH and CH resonances on the nature of the solvent, and on temperature, is noteworthy. Further work is required to relate this dependence to the imine–amine equilibrium.

TABLE 2. $^{31}P^{a}$ and $^{1}H^{b}$ nmr parameters and vibrational frequencies[c] of linear oxophosphazenes $MeNH(PMe_2)_nPMe_2O$

n =	1	2	3
$\delta_P P_A$	81.7	98.0	101.8
$\delta_P P_B$	81.2	85.3	98.3
$\delta_P P_C$	—	80.9	87.3
$\delta_P P_D$	—	—	80.7
$\delta_H(Me_2P_A)$	1.22(13.5)[d]	1.20(13.5)[d]	1.18(13.0)[d]
$\delta_H(Me_2P_B)$	1.48(14.0)	1.37(12.0)[d]	1.36(13.0)[d]
$\delta_H(Me_2P_C)$	—	1.51(12.5)	1.41(15.0)
$\delta_H(Me_2P_D)$	—	—	1.50(15.0)
$\delta_H(MeN)$	2.51(13.0)	2.47(14.0)	2.49(14.0)
$J(HH)$ (MeNH)[e]	7.0	8.5	6.0
ν(P═N)	1205	1220	1190, 1220, 1260
ν(P═O)	1150	1135	1135
ν(N—H)	3110	3130	3103

[a]δ(ppm), $CDCl_3$, reference external P_4O_6. Phosphorus atoms lettered alphabetically from the oxygen atom. Positive shifts upfield of P_4O_6.
[b]δ(ppm), CD_3CN, reference internal TMS; J(PH)(Hz) in parentheses.
[c](cm^{-1}), Nujol mulls, assignments tentative.
[d]J(PH) (long range) ~1.0 Hz.
[e]In Hz.

ν(N—H) band in their infrared spectra. Its frequency (~3200 cm^{-1}) is similar to the value found for it in *N*-alkyl phosphoramidates (20). The high values of ν(N—C) indicate a single rather than a double exocyclic PN bond. In *N*-alkylphosphoramidates, for example, ν(N—C) is found in the region of 1020–1220 cm^{-1} (20), whilst in *N*-methyl phosphinimines (21, 22), its value is much lower (848 cm^{-1} in Ph_3PNMe (21)).

The ^{1}H and ^{31}P nmr spectra (Table 2) of the compounds $NHMe(PMe_2N)_nPMe_2O$ (n = 1, 2, 3) indicate an open chain structure, since all the phosphorus atoms, and PMe_2 protons, are inequivalent. Shielding of the phosphorus atoms is expected to decrease with increasing distance from oxygen, because of the polarization of charge towards the more electronegative end of the molecule, and, as in the analogous phenyl compounds (23), the δ_P values are so assigned. Hydrogen bonding is indicated for all the compounds listed in Table 2 by the low value of ν(P═O) (1170 cm^{-1} in Me_3PO (24)).

Reactions of Azaphosphorins

The chemical properties of the azaphosphorins reported here are primarily those of a strong base but, depending on the position of the equilibrium between the imine and amine tautomeric forms, the compounds can be regarded as being related either to phosphorus ylids R_3PCHR' or to imines R_3PNR'. In some respects their behaviour is similar to that of λ_5-phosphorins (25); they do not, for example, react with molecular oxygen (as do simple ylids (26, 27)), nor do they undergo the Wittig reaction, the P═C bond being insufficiently polar. In the reaction of **4***a* and **8** with aqueous ethanol, the exocyclic P—N bond is broken rather than the endocyclic P═C bond, to give the cyclic oxides **14**, **15**; the ready loss of the exocyclic methylamino group from these molecules is in contrast to the hydrolytic stability of aminophosphazenes. In related molecules, cleavage of the P═C bond can occur, as in the hydrolysis of the azaphosphorin $MeC(NPPh_2)_2CH$ (12). Both reaction paths are exemplified in the hydrolysis of the di-imine $PhN{=}PPh_2CH_2PPh_2P{=}NPh$. In basic solution, the expected diphosphine dioxide is produced, but acidic hydrolysis results in the cleavage of a central P—C bond, and the formation of the simple oxides $MePh_2PO$ and $(NHPh)Ph_2PO$ (28). The course of the reaction

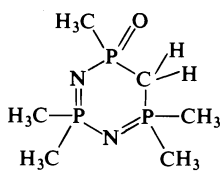

14

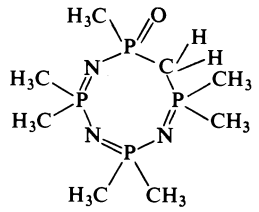

15

TABLE 3. ^{1}H nmr parameters[a] of cyclic phosphazene oxides **14, 15**

Compound	δ(CH_2)	δ(MeP)	δ(Me_2P)[b]	δ(Me_2P')[b]	δ(Me_2P'')[b]
14	1.95(13.5)[c] 2.11(13.5)	1.96(13.5)	1.61(14.0)	1.48(15.0)[d] 1.53(15.0)	—
15	2.31(12.5)	1.94(13.0)	1.63(14.0) 1.56(14.0)	1.54(13.0)[e] 1.47(13.0)	1.47(14.0)

[a]δ(ppm), $CDCl_3$, reference internal TMS. J(PH) (Hz) in parentheses.
[b]Ring positions of P, P′, P″ uncertain.
[c]ABXY pattern partially obscured by P-methyl resonances; J(PH) values approximate. $J(H_AH_B)$ = 13.5 Hz.
[d]Inequivalent geminal methyl groups displaying second order coupling.
[e]Inequivalent geminal methyl groups.

evidently depends sensitively on the conditions used.

Like their parent azaphosphorins, the oxides **14**, **15** can be represented by either of two tautomeric forms **16***a*, *b*. However, the appearance of

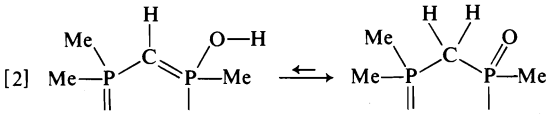

16*a* **16***b*

characteristic methylene signals in their ^{1}H nmr spectra (Table 3), and the absence of a ν(O—H) band from their infrared spectra, indicates that the equilibrium favours the oxide structure **16***b*. In the six-membered ring, the methylene protons are magnetically inequivalent, as expected, and give rise to an AB proton coupling pattern. In the eight-membered ring, the two protons are accidentally equivalent, and give rise to a simple triplet (Fig. 2).

Unlike other azaphosphorins (12), and simple ylids R_3PCHR' (14, 29–32), which react with methyl iodide to give C-methylated phosphonium salts, the azaphosphorins reported here react to give the corresponding C-hydroiodides, **17** and **18** (X = I). Presumably the initial

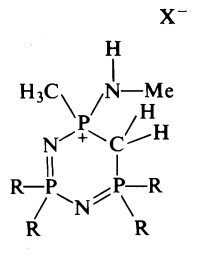

17

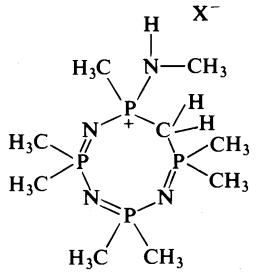

18

methylation is immediately followed by a proton transfer reaction with a second mole of azaphosphorin (eq. 3), as is found in the alkylation of

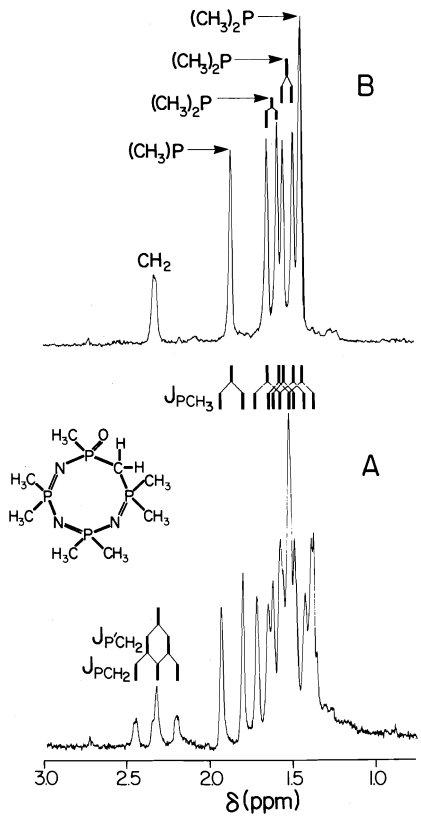

FIG. 2. ^{1}H nmr spectra of the phosphazene oxide **15** (100 MHz, $CDCl_3$); (*A*) direct, (*B*) ^{31}P decoupled.

phosphinimines (33). Protonation on carbon rather than on nitrogen is confirmed by the ^{1}H nmr spectra (Table 4) of the salts, which show a characteristic AB proton coupling pattern for the inequivalent methylene protons. The presence of a positive charge on the rings further facilitates the interpretation of their spectra; the charge distribution is less uniform than in the neutral compounds, and the various signals are better separated, as is illustrated in Fig. 3, which shows the ^{1}H nmr spectra of **17** (X = I).

TABLE 4. ^{1}H nmr parameters[a] of the azaphosphorin hydrohalides **17**, **18**

	17 (R = Me)		**18**		**17** (R = Ph)
Parameter	X = I	X = Cl	X = I	X = Cl	X = I[b]
δ(MeN)	2.65(13.5)	2.63(13.5)	2.62(13.0)	2.57(13.5)	2.19(14.5)
J(HH)	5.5	5.5	5.5	6.0	5.5
δ(HN)	5.85	6.03	4.24	5.37	4.51
δ(MeP)	1.99(13.0)	1.99(13.5)	1.96(13.5)	2.04(13.5)	1.83(14.5)
δ(Me_2P)[c]	1.86(13.5)	1.79(14.0)[d] 1.73(14.0)	1.79(13.5)	1.78(13.5)	—
δ(Me_2P')[c]	1.58(14.0)	1.53(14.0)	1.53(13.5)[d] 1.49(13.5)	1.58(15.0)[d] 1.51(15.0)	—
δ(Me_2P'')[c]	—	—	1.49(13.5)	1.51(15.0)	—
δ(CH_2)(H_A)[e]	3.74 (15.0, 11.0)	4.09 (14.0, 11.0)	3.75 (15.5, 12.5)	3.96 (15.0, 12.0)	3.77 [f]
δ(CH_2)(H_B)[e]	2.78 (13.5, 13.5)	2.27 (14.0, 13.5)	3.05 (15.5, 12.5)	2.86 (15.0, 13.0)	3.55 [f]
J(H_AH_B)[g]	15.5	15.0	15.5	15.0	15.0

[a]δ(ppm), $CDCl_3$, reference internal TMS; *J*(PH) (Hz) in parentheses.
[b]Phenyl region omitted.
[c]Relative positions of P, P′, P″ uncertain.
[d]Inequivalent methyl groups on same phosphorus atom.
[e]ABXY pattern, partially obscured; *J*(PH) approximate.
[f]*J*(PH) not assigned. In CD_3CN, $H_{A,B}$ equivalent, δ = 3.44 ppm, *J*(PH): 13.0 Hz.
[g]In Hz.

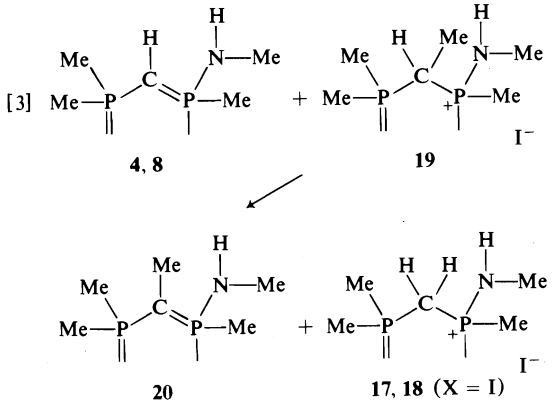

The appearance and position of the resonance of the *N*-methyl protons is similar to that found in aminophosphonium salts (34), exhibiting both ^{31}P–^1H and ^1H–^1H coupling. However, the addition of one drop of D_2O to a solution of **17** (X = I) in $CDCl_3$ brings about the immediate collapse of ^1H–^1H couplings, and the loss of the NH resonance (Fig. 3*B*), indicating that proton exchange between the solvent and the exocyclic nitrogen is rapid. The methylene protons are expected to be less acidic, and their exchange with protic solvents is consequently slower, but the effect is nonetheless observable. When **17** (X = I) is dissolved in D_2O, the methylene resonance appears as a simple triplet which, upon allowing the solution to stand, becomes less intense and finally vanishes (after about 2 h).

In the reaction of the azaphosphorins with methyl iodide, the neutral product **20** cannot be isolated. It apparently undergoes a second methylation and proton transfer reaction, the overall yield of hydroiodide being such that 3 mol of azaphosphorin are converted into 2 mol of hydroiodide. In order to determine the position of primary substitution on the azaphosphorin ring (carbon or nitrogen), the reactions of **4***a* and **8** with benzoyl chloride have been examined. In the case of the eight-membered ring, the reaction yields the C-benzoyl derivative **22**. The reaction of the six-membered ring is more vigorous and, as with its reaction with methyl iodide, cannot be stopped at the first stage. Instead, the initially formed C-benzoyl derivative reacts with a second mole of benzoyl chloride, to give the *N*-benzoyl C-benzoyl compound **21**.

As in the case of their parent azaphosphorins, the ^1H nmr spectra of the benzoylated derivatives **21** and **22** (Table 5) reveal very little separation of the P-methyl resonances, thereby indicating

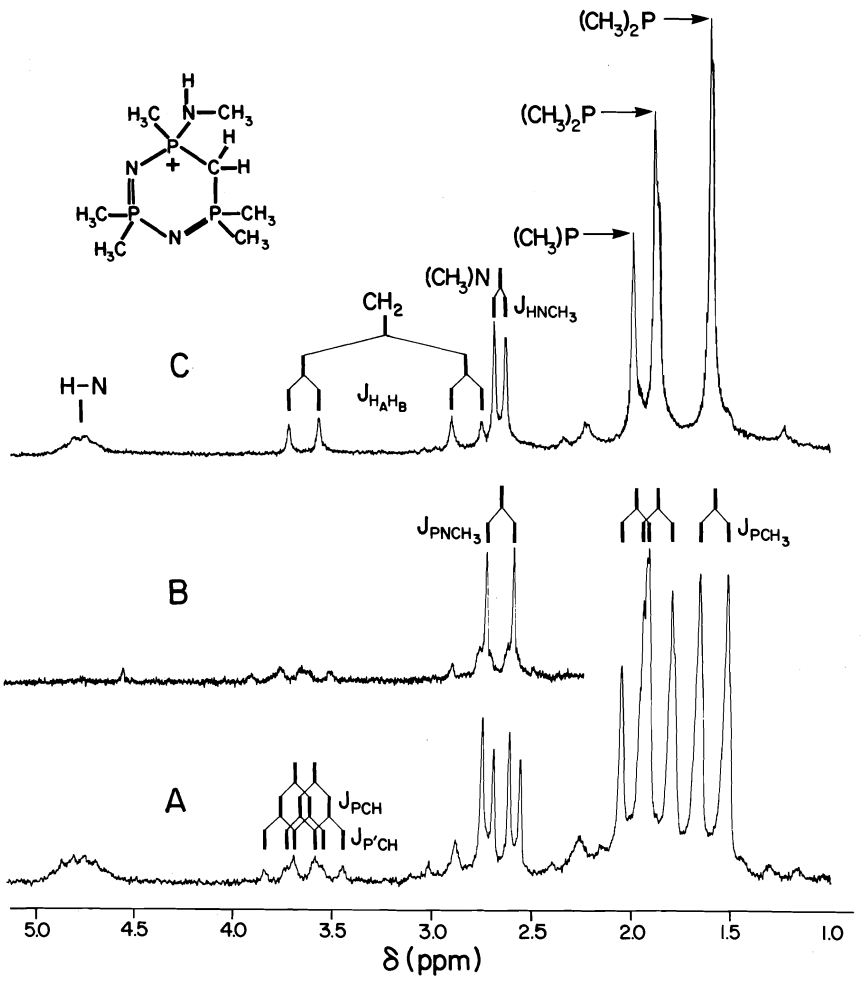

FIG. 3. ^1H nmr spectra (100 MHz) of the azaphosphorin hydroiodide **17** (X = I) in $CDCl_3$; (*A*) direct, (*B*) with one drop of D_2O added, (*C*) ^{31}P decoupled.

the uniformity of the charge distribution within the ring. For the tetrameric compound, ^1H–^1H coupling in the NHMe group is now observed (as it is in simple *N*-methyl amides); proton exchange is obviously suppressed by the low basicity of the nitrogen. The shielding of the *N*-methyl protons in **21** (δ_H(NMe) = 2.50 ppm) is greater than in *N*-methyl benzanilide (δ_H-(NMe) = 3.40 ppm, $CDCl_3$, reference internal TMS), suggesting that the diffusion of lone pair density from nitrogen to phosphorus is limited.

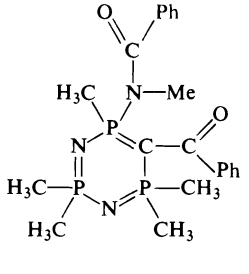

21

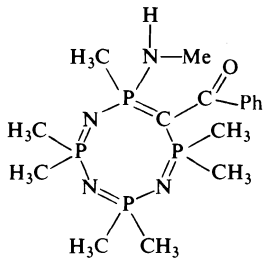

22

The infrared spectra of these compounds are too complex to allow a detailed interpretation, but their carbonyl stretching frequencies (Table 5) are well isolated and easily identified. For both the six- and the eight-membered ring, the low value of the carbonyl frequency is similar to that found in other acylated ylids (35–37), and reflects the extent to which resonance such as that depicted in eq. 4 weakens the C=O double bond. The lower frequency found in the six-

TABLE 5. ^{1}H nmr parameters[a] and carbonyl stretching frequencies[b] of azaphosphorin benzoyl derivatives **21**, **22**

Compound	δ(MeN)	δ(MeP)	δ(Me_2P)[c]	ν(C=O)
21	2.50(9.0)	1.70(15.0)	1.64(13.5), 1.60(13.0) 1.55(13.5), 1.48(13.0)	1502 1642
22	2.46(14.0)[d]	[e]	[e]	1530

[a]δ(ppm), $CDCl_3$, reference internal TMS; *J*(PH) (Hz) in parentheses.
[b]ν(C=O) (cm^{-1}), Nujol mull.
[c]No equivalent methyl groups.
[d]*J*(HH)(MeNH) = 5.5 Hz; δ(NH) = 2.70 ppm.
[e]Unresolved PMe, PMe_2 multiplet near δ = 1.55 ppm.

[4] 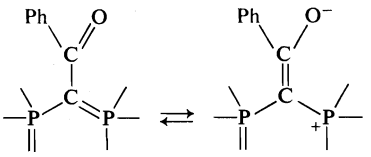

membered ring suggests that electron release onto the C-benzoyl group is greater for that ring size. The amide carbonyl frequency of **17** (1642 cm^{-1}) is similar to that found in simple tertiary amides (e.g. ν(C=O) in $PhCONMe_2$ is 1640 cm^{-1} (38), and in $PhCONMePh$[3] is 1653 cm^{-1}). In these latter compounds, the presence of an *N*-phenyl group increases ν(C=O), the competitive electron withdrawing effect of the aromatic ring reducing the influence of the ionic form $Ph—N^+\equiv C—O^-$ (40). The relatively low value of the amide carbonyl frequency in **17** is consistent with the ^{1}H nmr evidence indicating that conjugative interactions between phosphorus and the exocyclic nitrogen are limited.

Discussion

N-Ethyl phosphazenium salts (41), like their pyridine analogues, react with bases to yield the neutral compound and ethylene. Such an elimination reaction is not possible for the *N*-methyl compounds, and their principal reactions with bases are deprotonation and nucleophilic attack. In the pyridine series, a 2-methyl group is deprotonated to give a methide, which is alkylated on carbon rather than on nitrogen, thereby conserving ring aromaticity (42). When an electron-withdrawing substituent is present in the 2- (or 4-) position, the susceptibility of the molecule to nucleophilic attack at these positions is increased, and, in basic solutions, such salts are hydrolysed to pyridones (42), the stability of which is enhanced by the strength of the carbonyl bond.

In the reactions reported here, deprotonation and nucleophilic attack both occur, but the balance between them is determined by the reagent and by the ring size. Open chain oxides are produced when KO-*t*-Bu is used, primarily because the elimination of isobutene or dibutyl ether allows the formation of a strong phosphoryl bond. The size of the ring has a marked effect on the relative yield of cyclic and linear products. The ^{31}P nmr shifts of $(NPMe_2)_{3,4}\cdot MeI$ (43) suggest that the partial positive charge on the phosphorus atoms adjacent to the *N*-methyl group is greater in the six-membered ring compound, nucleophilic attack and the formation of the linear oxide being thereby promoted, as found.

Deprotonation of the *N*-methyl methylphosphazenium salts occurs, as expected, at the 2-position, and the consequent rearrangement is probably aided by the electrophilic character of the phosphorus atoms adjacent to the alkylated nitrogen atom. Although the detailed mechanism is unknown, it seems likely to involve a four-centre interaction (as shown) similar to that of

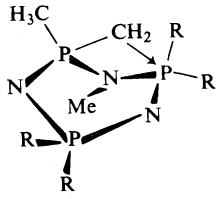

the Wittig reaction.[4] A related mechanism has been suggested (44) for the base catalyzed rearrangement of $(Me_3PCSiMe_2)_2$, in which a

[3]Present work, CCl_4 solution; Nujol mull, 1650 cm^{-1}; cf. 1641 cm^{-1} (39).

[4]The possibility that the reaction is bimolecular, so reducing strain in the transition state, has been suggested by a referee, and cannot at present be excluded.

methylene group enters the ring. A rearrangement in the opposite sense, but also involving a 4-centre mechanism, occurs during the ammonolysis of bis(diphenylphosphino)methane in carbon tetrachloride to give $(MePPh_2NPPh_2NH_2)Cl$ (12), and may account for the apparent migration of a methyl group during the chloramination of bis(diphenylphosphino)methylamine, which yields the salt $[NHMePPh_2NPPh_2NH_2]Cl$ (45).

In the latter two examples, the driving force of the reaction is probably the formation of the resonance stabilized $(P{=}N{=}P)^+$ cation. The phosphazene–azaphosphorin system is more complicated, in that both a cyclic π-system and an exocyclic π-bond are involved, but we can nevertheless understand the rearrangements that take place by simple model calculations of the π-energy changes. The three related molecular forms are shown in Fig. 4. which shows how the π-electron energies of the three forms depends on the assumed Coulomb parameter of carbon. Isomer *a* is the exocyclic ylid **6** formed by the deprotonation of the quaternary cation, *b* is the product of its direct rearrangement to an *exo*-imide **7**, and *c* results from the further proton migration to give the azaphosphorin **8**. Form *c* is unique in restoring the cyclic delocalization of the initial quaternary compound **5**.

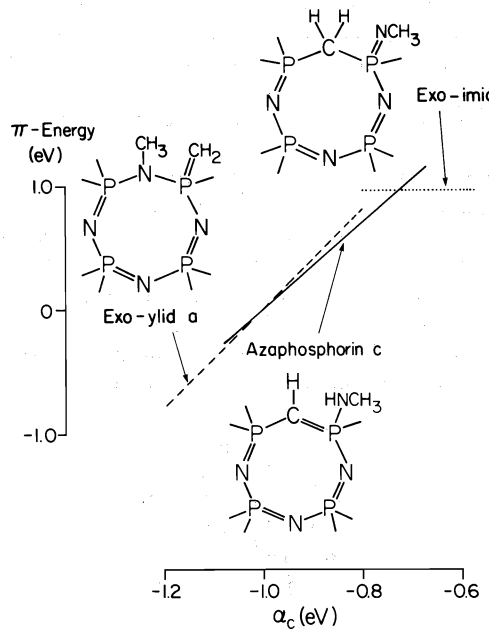

FIG. 4. π-Electron energies (eV, arbitrary zero) of the three isomers shown, as a function of the assumed Coulomb parameter of carbon. The values of α_P(2 eV) and α_N (−1 eV) used are not critical, but have been found useful for the description of other properties of $(NPMe_2)_n$. All resonance parameters were taken to be −1 eV, independent of overlap, in both out-of-plane and in-plane π-systems.

Although the energetic advantage of the delocalization may be important, the calculations show that it may be outweighed by a high localized π-energy in an exocyclic bond in *a* or *b*.

The general result is that the exocyclic position is favoured for the more electronegative atom. To take the extreme cases first, if $\alpha_C < -1$, (the value for nitrogen), *a* is the most stable form, and no rearrangement would be expected. On the other hand, if $\alpha_C < -0.7$ (approximately), rearrangement should take place, but should stop at the *exo*-imide stage *b*. In both cases the molecule is stabilized by a strong exocyclic π-bond. For intermediate values of α_C, the situation is more interesting. The azaphosphorin *c* is now slightly more stable than the *exo*-ylid *a*, because cyclic delocalization is now possible; if localized bonds are assumed, the azaphosphorin is never favoured over the *exo*-ylid. In terms of the simple model used, it is therefore possible to understand the azaphosphorin rearrangement as being driven by the increase of π-energy arising from the displacement of the more electronegative atom from the ring, and reinforced by the attainment of cyclic delocalization.[5]

Although the results of Fig. 4 are qualitative, the assumed parameters are realistic enough to show that the energy differences between the three forms are likely to be small, and it is not surprising that proton transfer between the endocyclic carbon and endocyclic nitrogen atoms of the azaphosphorins is fast enough to cause a collapse of the ^{31}P–^{1}H coupling of the CH signal. The results have another application. Since oxygen is more electronegative than nitrogen, the introduction of an exocyclic phosphoryl group in the cyclic oxophosphazenes **14**, **15** alters the equilibrium in favour of exocyclic π-bonding, lowering the energy of the *exo*-imide *b* without direct effect on the energies of *a* and *c*. It is consistent with this result that rapid proton

[5]In a reaction which is apparently similarly dependent on relative electronegativity, 2-arylaminopyrylium chlorides can be deprotonated to pyranimines, which then rearrange to pyridones in a reaction closely analogous to the azaphosphorin rearrangement described above. The corresponding reaction of the thiapyrylium iodides stops at the thiapyranimine stage (51).

migration is not observed in the cyclic oxophosphazenes described above. The general concepts are further supported by the structures of the phosphazenes $N_3P_3Ph_5(OH)$ and $N_4P_4Ph_6(OH)_2$ (non-geminal) for which hydroxy- rather than oxy-structures have been suggested (46, 47). From the present point of view, the potential tautomeric equilibrium is that between forms *b* and *c* of Fig. 4, N being substituted for CH in the ring, and O for NCH_3 in the exocyclic position. The increased electronegativity of the ring atom would tend, following the diagram, to stabilize the cyclically delocalized form *c*. The energy balance is sensitively dependent on the relative electronegativities of the relevant atoms. The same feature is found in pyridine chemistry; 2- and 4-hydroxy pyridines normally exist in the pyridone form, but when the oxygen is replaced by a less electronegative atom, as in 2-aminopyridine, the aromatic amino-form, rather than the exocyclic imide, is the more stable.

Experimental

Sodium metal, hexamethyldisilazane, methyl iodide, and benzoyl chloride were commercial products. Potassium *tert*-butoxide and methyl fluorosulphate were also obtained commercially. The former was purified by sublimation *in vacuo*, the latter by distillation under nitrogen. Hexane and octane were of reagent grade. Toluene, diethyl ether, and acetonitrile were dried by distillation from sodium, lithium aluminium hydride, and calcium hydride, respectively. All of the preparations were carried out under an atmosphere of nitrogen.

Quaternary Salts

The monoquaternary salts $(NPMe_2)_{3,4}\cdot MeI$ were prepared by the reaction of the neutral methylphosphazenes with methyl iodide (43). The preparation of the salt $(NPMe_2)_4\cdot 2MeCl$ by the reaction of Me_2PCl_3 and $MeNH_2\cdot HCl$ has already been reported (48); the diquaternary salt $(NPMe_2)_4\cdot 2MeSO_3F$ used here was prepared by treating $(NPMe_2)_4$ with two equivalents of $MeSO_3F$ in acetonitrile solution. The product was precipitated quantitatively from the solution by the addition of diethyl ether, and purified by recrystallization from acetonitrile: mp 231–233°C; ^1H nmr spectrum, 100 MHz (δ, $CDCl_3$, int. TMS), 2.84 (6H, triplet, J_{PH} = 11.5 Hz), 1.95 (24H, doublet, J_{PH} = 13.7 Hz); ir spectrum ν(P═N) 1275, 1330 cm^{-1}; ν(C—N), 1070 cm^{-1}. *Anal.* calcd. for $C_{10}H_{30}F_2N_4O_6S_2P_4$: C 22.7, H 5.7, N 10.6; found: C 22.9, H 5.9, N 10.6. *gem*-Dimethyltetraphenylcyclotriphosphazene $N_3P_3Ph_4Me_2$ was prepared by the reaction of $(NH_2PPh_2NPPh_2NH_2)Cl$ with Me_2PCl_3 (49) in chlorobenzene, the neutral compound being liberated from its hydrochloride by treatment with triethylamine; mp 142–144°C (lit. (50) 140–142°C). The methiodide was prepared from it by heating it in methyl iodide for 72 h. The precipitated salt was recrystallized from ethanol and dried at 60°C/0.01 Torr for 7 h to remove all the solvent: mp 226–227°C (dec.); ^{31}P nmr spectrum (δ, $CDCl_3$, ext. P_4O_6), 64.1 (1P, PMe_2), 81.0 (1P, PPh_2 adjacent to NMe), 93.5 (1P, remote PPh_2); ^1H nmr spectrum (δ, $CDCl_3$, int. TMS), 3.07 (3H, triplet, J_{PH} = 11.0 Hz), 2.22 (6H, doublet, J_{PH} = 14.0 Hz), 7.0–8.0 (20H, broad unresolved multiplet); ir spectrum; ν(P═N), 1220, 1260 cm^{-1}; ν(C—N), 1070 cm^{-1}. *Anal.* calcd. for $C_{27}H_{29}IN_3P_3$: C 52.7, H 4.75, I 20.6, N 6.8; found: C 52.9, H 5.0, I 20.4, N 6.8.

Reaction of $(NPMe_2)_4\cdot MeI$ with $NaN(SiMe_3)_2$

Sodium (0.20 g, 8.7 mmol) was added to a slurry of $(NPMe_2)_4\cdot MeI$ (3.54 g, 8.0 mmol) in 200 ml octane. About 0.5 ml of $HN(SiMe_3)_2$ was injected into the reaction mixture at the reflux temperature, and, to compensate for possible losses by evaporation, again at 24 h intervals to a total reaction time of 72 h. The mixture was cooled and filtered and the solvent distilled from the filtrate to leave a white solid, which was purified by sublimation at ~130°C/0.01 Torr and recrystallization from hot hexane to give colourless hygroscopic prisms of **8** (2.21 g, 7.0 mmol, 88%); mp 104–105°C. *Anal.* calcd. for $C_9N_{26}N_4P_4$: C 34.3, H 8.6, N 17.8; found C 34.4, H 8.5, N 17.6.

Reaction of $(NPMe_2)_3\cdot MeI$ with $NaN(SiMe_3)_2$

In a similar reaction, sodium (0.35 g, 15.3 mmol) and $(NPMe_2)_3\cdot MeI$ (5.11 g, 13.9 mmol) were allowed to react with $HN(SiMe_3)_2$ in octane (200 ml). After 96 h, the mixture was filtered while still hot and the solvent distilled from the filtrate. The white solid product was purified by sublimation at ~130°C/0.01 Torr and recrystallization from hot hexane to give colourless hygroscopic plates of **4***a*, (2.68 g, 11.2 mmol, 80%); mp 140–142°C. *Anal.* calcd. for $C_7H_{20}N_3P_3$: C 35.15, H 8.4, N 17.6; found: C 35.4, H 8.5, N 17.6.

Reaction of $Me_2Ph_4P_3N_3\cdot MeI$ with $NaN(SiMe_3)_2$

Sodium (0.06 g, 2.6 mmol), $Me_2Ph_4P_3N_3\cdot MeI$ (1.34 g, 2.2 mmol) dried as before to remove EtOH and $HN(SiMe_3)_2$ were allowed to react together in 60 ml boiling toluene for 24 h. The mixture was filtered and the solvent distilled off. The residual white solid was purified by recrystallization from benzene–octane to give colourless prisms of **4***b*, (0.95 g, 2.0 mmol, 93%); mp 147–149°C. *Anal.* calcd. for $C_{27}H_{28}N_3P_3$: C 66.1, H 5.3, N 8.9; found: C 65.9, H 5.55, N 8.65.

Reaction of $(NPMe_2)_4\cdot MeI$ with KO-t-Bu

Finely powdered $(NPMe_2)_4\cdot MeI$ (3.00 g, 6.8 mmol) was added to a slurry of KO-*t*-Bu (0.84 g, 7.4 mmol) in 100 ml hexane, and the mixture heated under reflux for 24 h. The solvent was distilled from the filtered solution to leave a white solid (1.82 g) which was sublimed at ~130°C/0.01 Torr on to a water cooled cold finger. The sublimate (**8**) was recrystallized from hot hexane (1.71 g, 5.4 mmol, 80%) and identified by comparison of its ir spectrum with that of an authentic sample, and by its mp, 104–105°C. The residual oil in the sublimation vessel solidified into a white solid, which was purified by recrystallization from hot hexane to give colourless hygroscopic cubes of **10** (0.11 g, 0.33 mmol, 5%); mp 72–74°C. *Anal.* calcd. for $C_9H_{28}N_4OP_4$: C 32.5, H 8.5, N 16.9; found C 32.6, H 8.6, N 16.9.

Reaction of $(NPMe_2)_3\cdot MeI$ with KO-t-Bu

Similarly, $(NPMe_2)_3\cdot MeI$ (1.38 g, 3.8 mmol) was

allowed to react with a slurry of KO-*t*-Bu (0.50 g, 4.5 mmol) in 50 ml boiling hexane. After 24 h, the mixture was filtered and the solvent removed from the filtrate to leave a colourless oil. Sublimation of this oil at ~130°C/0.01 Torr on to a cold finger at −78°C yielded **9** as a white hygroscopic solid (0.89 g, 3.4 mmol, 92%), which was recrystallized as colourless plates by cooling a concentrated solution of it in pentane to −23°C; mp 35–37°C. *Anal.* calcd. for $C_7H_{22}N_3OP_3$: C 32.7, H 8.6, N 16.3; found: C 32.6, H 8.5, N 16.0.

Reaction of $(NPMe_2)_4 \cdot 2MeSO_3F$ with KO-t-Bu

In a similar experiment, a slurry of KO-*t*-Bu (1.30 g, 11.6 mmol) and $(NPMe_2)_4 \cdot 2MeSO_3F$ (2.70 g, 5.1 mmol) was heated to reflux in 60 ml hexane. After 24 h, the solution was decanted from the pasty residue and the solvent distilled off to yield a white solid, which was recrystallized from hot hexane to give colourless feather-like crystals of **11** (0.93 g, 5.0 mmol, 50%); mp 73–75°C. *Anal.* calcd. for $C_5H_{16}N_2OP_2$: C 33.0, H 8.9, N 15.4; found: C 33.3, H 8.9, N 15.25.

Hydrolysis of Azaphosphorins 4a, 8

In separate experiments, samples of **4***a* and **8** (0.3–0.4 g) were dissolved in 25 ml of a 50/50 ethanol–water mixture. After 24 h, the solvent was removed at room temperature *in vacuo* to leave a white solid. Recrystallization from benzene of the solid from **4***a* gave colourless hygroscopic blocks of **14**, mp 184–186°C. *Anal.* calcd. for $C_6H_{17}N_2OP_3$: C 31.9, H 7.6, N 12.4; found: C 32.2, H 7.6, N 12.3. Recrystallization from hot hexane of the solid from **8** gave colourless feather-like crystals of **15**; mp 140–143°C. *Anal.* calcd. for $C_8H_{23}N_3OP_4$: C 31.9, H 7.7, N 13.95; found: C 32.1, H 7.9, N 14.0.

Reaction of Azaphosphorins 4a, b, 8, with Methyl Iodide

The addition of an excess of methyl iodide to a solution of **4***a* (1.04 g, 4.33 mmol) in ether resulted in the precipitation of the hydroiodide **17** (R = Me) (0.99 g, 2.7 mmol). Similarly, the azaphosphorins **4***b* (0.155 g, 0.32 mmol) and **8** (0.44 g, 1.4 mmol) yielded, respectively, the hydroiodides **17** (R = Ph) (0.14 g, 0.23 mmol) and **18** (0.43 g, 1.0 mmol). The neutral products of the transylidation reactions could not be isolated. The air-stable crystalline hydroiodides were recrystallized from acetonitrile–toluene: **17** (R = Me), mp 194–195°C. *Anal.* calcd. for $C_7H_{21}IN_3P_3$: C 22.9, H 5.8, I 34.6, N 11.45; found: C 23.0, H 5.9, I 34.2, N 11.3; **17** (R = Ph), mp 248–252°C. *Anal.* calcd. for $C_{27}H_{29}N_3P_3I$: C 52.7, H 4.75, N 6.8; found: C 52.7, H 4.75, N 6.9; **18**, mp 155–156°C. *Anal.* calcd. for $C_9H_{27}IN_4P_4$: C 24.45, H 6.15, I 28.7, N 12.7; found: C 24.5, H 6.3, I 28.55, N 12.6.

Reaction of Azaphosphorins 4a, 8, with Benzoyl Chloride

A solution of benzoyl chloride (0.21 g, 1.5 mmol) in 20 ml ether was added dropwise to a stirred solution of **4***a* (0.54 g, 2.25 mmol) in 100 ml ether. After 3 h the mixture was filtered, leaving the hydrochloride of **17** (R = Me) (0.45 g, 1.64 mmol): mp 194–197°C. *Anal.* calcd. for $C_7H_{21}ClN_3P_3$: C 30.5, H 7.7, Cl 12.9, N 15.2; found: C 30.2, H 7.8, Cl 12.6, N 15.0. Distillation of the solvent from the filtrate left the crude dibenzoyl derivative **21** (0.26 g, 0.59 mmol), which was recrystallized from hot benzene–octane as colourless blocks: (dec.) 181–184°C. *Anal.* calcd. for $C_{21}H_{28}N_3O_2P_3$: C 56.4, H 6.3, N 9.4; found: C 56.1, H 6.2, N 9.6.

In another experiment, a solution of benzoyl chloride (0.12 g, 0.9 mmol) in 10 ml ether was added dropwise to a stirred solution of the azaphosphorin **8** (0.56 g, 1.8 mmol) in 50 ml ether. A fine white precipitate was immediately formed. After 3 h the mixture was filtered, and the hygroscopic solid recrystallized from acetonitrile–benzene to give small colourless cubes of the hydrochloride of **18** (0.26 g, 0.7 mmol): mp 193–195°C. *Anal.* calcd. for $C_9H_{27}ClN_4P_4$: C 30.8, H 7.8, N 16.0; found: C 30.9, H 7.7, N 15.9. The solvent was distilled from the filtrate to leave a yellow oil which, on drying *in vacuo*, solidified to a yellow, air stable powder. Recrystallization of this solid from hot hexane yielded yellow mica-like plates of the benzoyl derivative **22**: mp 133–134°C. *Anal.* calcd. for $C_{16}H_{30}N_4OP_4$: C 46.0, H 7.2, N 13.4; found: C 45.7, H 7.3, N 13.1.

Acknowledgements

We are grateful to the National Research Council of Canada for financial support and for an NRCC Scholarship (to R.T.O.), and to Dr. A. A. Grey, of the Ontario Research Foundation, for the 220 MHz spectra.

1. H. P. Calhoun, R. H. Lindstrom, R. T. Oakley, N. L. Paddock, and S. M. Todd. Chem. Commun. 343 (1975).
2. J. R. Richard and C. V. Banks. J. Org. Chem. **28**, 123 (1963).
3. H. P. Calhoun, R. T. Oakley, and N. L. Paddock. Chem. Commun. 454 (1975).
4. K. Issleib and M. Lischewski. Synth. Inorg. Met.-Org. Chem. **3**, 255 (1973).
5. G. Märkl. Tetrahedron Lett. 807 (1961).
6. D. B. Denney and J. Song. J. Org. Chem. **29**, 495 (1964).
7. M. Schlosser and K. F. Christmann. Angew. Chem. Int. Ed. Engl. **3**, 636 (1964).
8. C. R. Krüger and E. G. Rochow. Angew. Chem. Int. Ed. Engl. **2**, 617 (1963).
9. M. Becke-Goehring and G. Koch. Chem. Ber. **92**, 1188 (1959).
10. M. Grayson and P. T. Keough. J. Am. Chem. Soc. **82**, 3919 (1960).
11. C. T. Ford, F. E. Dickson, and I. I. Bezman. Inorg. Chem. **4**, 890 (1965).
12. R. Appel, R. Kleinstuck, and K. D. Ziehn. Chem. Ber. **105**, 2476 (1972).
13. L. Siekmann, H. O. Hoppen, and R. Appel. Z. Naturforsch. **23**b, 1156 (1968).
14. H. Schmidbaur and W. Tronich. Chem Ber. **101**, 595 (1968); **101**, 604 (1968).
15. H. J. Bestmann and J. P. Snyder. J. Am. Chem. Soc. **89**, 3936 (1967).
16. V. N. Setkina, T. Ya. Medved, and M. I. Kabachnik. Izv. Akad. Nauk SSSR Ser. Khim. 1399 (1967).
17. G. D. Davies, Jr., W. R. Anderson, Jr., and M. V. Pickering. Chem. Commun. 301 (1974).

18. H. J. BESTMANN, H. G. LIBERDA, and J. P. SNYDER. J. Am. Chem. Soc. **90**, 2963 (1968).
19. P. CREWS. J. Am. Chem. Soc. **90**, 2961 (1968).
20. R. A. CHITTENDEN and L. C. THOMAS. Spectrochim. Acta, **22**, 1449 (1966).
21. W. WIEGRÄBE and H. BOCK. Chem. Ber. **101**, 1414 (1968).
22. J. BRAGIN, S. CHAN, E. MAZZOLA, and H. GOLDWHITE. J. Phys. Chem. **77**, 1506 (1973).
23. A. SCHMIDPETER and K. STOLL. Angew. Chem. Int. Ed. Engl. **10**, 131 (1971).
24. L. W. DAASCH and D. C. SMITH. J. Chem. Phys. **19**, 22 (1951).
25. G. MÄRKL. Angew. Chem. Int. Ed. Engl. **2**, 153 (1963); **2**, 479 (1963).
26. H. J. BESTMANN. Angew. Chem. **72**, 34 (1960).
27. H. J. BESTMANN and O. KRATZER. Chem. Ber. **96**, 1899 (1963).
28. A. M. AGUIR, H. J. AGUIAR, and T. G. ARCHIBALD. Tetrahedron Lett. 3187 (1966).
29. H. J. BESTMANN and H. SCHULZ. Tetrahedron Lett. No. 4, 5 (1960); Chem. Ber. **95**, 2921 (1962).
30. K. ISSLEIB and R. LINDNER. Justus Liebigs Ann. Chem. **707**, 120 (1967).
31. G. WITTIG and M. RIEBER. Justus Liebigs Ann. Chem. **562**, 177 (1949).
32. G. WITTIG, H. D. WEIGMANN, and M. SCHLOSSER. Chem. Ber. **94**, 676 (1961).
33. R. APPEL and A. HAUSS. Z. Anorg. Allg. Chem. **311**, 290 (1961).
34. F. KAPLAN, G. SINGH, and H. ZIMMER. J. Phys. Chem. **67**, 2509 (1963).
35. G. WITTIG and U. SCHOLLKOPF. Chem. Ber. **87**, 1318 (1954).
36. F. RAMIREZ and S. DERSHOWITZ. J. Org. Chem. **22**, 41 (1957).
37. T. A. MASTRYUKOVA, KH. A. SUERBAEV, E. I. FEDIN, P. V. PETROVSKII, E. I. MATRASOV, and M. I. KABACHNIK. J. Gen. Chem. USSR, **43**, 1185 (1973).
38. S. PINCHAS, D. SAMUEL, and M. WEISS-BRODAY. J. Chem. Soc. 3063 (1961).
39. A. R. KATRITZKY and R. A. JONES. J. Chem. Soc. 2067 (1959).
40. L. J. BELLAMY. The infrared spectra of complex molecules. 2nd ed. Chapman and Hall, London, England. 1958. p. 213.
41. T. N. RANGANATHAN. Ph.D. Thesis. University of British Columbia, Vancouver, B.C. 1970.
42. E. N. SHAW. *In* Pyridine and its derivatives. *Edited by* E. Klingsberg. Interscience, New York, NY. 1961. Chapt. 3.
43. H. T. SEARLE, J. DYSON, N. L. PADDOCK, and T. N. RANGANATHAN. J. Chem. Soc. Dalton Trans. 203 (1975).
44. W. MALISCH and H. SCHMIDBAUR. Angew. Chem. Int. Ed. Engl. **13**, 540 (1974).
45. D. F. CLEMENS, M. L. CASPAR, D. ROSENTHAL, and R. PELUSO. Inorg. Chem. **9**, 960 (1970).
46. C. D. SCHMULBACH and V. R. MILLER. Inorg. Chem. **5**, 1621 (1966).
47. D. L. HERRING and C. M. DOUGLAS. Inorg. Chem. **4**, 1012 (1965).
48. R. T. OAKLEY and N. L. PADDOCK. Can. J. Chem. **53**, 3038 (1975).
49. M. BERMANN and K. UTVARY. J. Inorg. Nucl. Chem. **31**, 271 (1969).
50. R. APPEL and G. SALEH. Chem. Ber. **106**, 3455 (1973).
51. A. S. AFRIDI, A. R. KATRITZKY, and C. A. RAMSDEN. Chem. Commun. 899 (1976).
52. A. P. GRAY and R. C. LORD. J. Chem. Phys. **26**, 690 (1957).
53. J. R. DURIG, S. F. BUSH, and F. G. BAGLIN. J. Chem. Phys. **49**, 2106 (1968).

Ab initio calculation of the vibrational structure in the electronic spectra of HCN and DCN between 1700 and 2000 Å

M. PERIĆ[1] AND S. D. PEYERIMHOFF

Lehrstuhl für Theoretische Chemie der Universität Bonn, Wegelerstraße 12, 53 Bonn, Germany

AND

R. J. BUENKER[2]

Institut für Physikalische Chemie der Universität Bonn, Wegelerstraße 12, 53 Bonn, Germany

Received February 11, 1977

M. PERIĆ, S. D. PEYERIMHOFF, and R. J. BUENKER. Can. J. Chem. **55**, 3664 (1977).

Ab initio SCF and CI calculations for the potential surfaces of HCN in ground and various $^1(\pi,\pi^*)$ excited states are carried out using an AO basis of double-zeta quality augmented with various polarization functions. These results are then combined with transition moment data to allow for a Franck-Condon analysis of the vibrational structure of the lowest three electronic transitions in both HCN and DCN. The resulting intensity distribution is then compared with the corresponding experimental data reported by Herzberg and Innes. This work confirms the earlier conclusion of Schwenzer *et al.* that the upper state in the $\alpha \leftarrow \tilde{X}$ band system is the $^1\Sigma^- - ^1A''$ species, and not the $^1\Delta$ as originally believed. In addition a detailed mechanism for the observed predissociation of the α state is outlined, in which the gradual conversion of the π^* MO of bent HCN into a pure hydrogenic $1s$ AO plays a key role. Arguments are also presented in favor of assigning the $\beta \leftarrow \tilde{X}$ transition seen in DCN to a $^1\Delta$–$2^1A'$ upper state with the same D + CN dissociation limit as for the $^1\Sigma^- - ^1A''$ species.

M. PERIĆ, S. D. PEYERIMHOFF et R. J. BUENKER. Can. J. Chem. **55**, 3664 (1977).

Les calculs *ab initio* SCF et CI pour les surfaces de potentiel de HCN à l'état fondamental et à différents états excités $^1(\pi,\pi^*)$ sont effectués en se basant sur des AO de qualité double-zêta augmentées avec diverses fonctions de polarisation. Ces résultats sont ensuite combinés avec les données du moment de transition pour permettre une analyse Franck-Condon de la structure de vibration des trois transitions électroniques les plus basses dans HCN et DCN. La répartition de l'intensité résultante de ces calculs est comparée avec les données expérimentales correspondantes rapportées par Herzberg et Innes. Ce travail confirme la conclusion postulée auparavant par Schwenzer et ses collaborateurs à savoir que l'état supérieur dans la bande $\alpha \leftarrow \tilde{X}$ est l'espèce $^1\Sigma^- - ^1A''$ et non $^1\Delta$ comme on le croyait initialement. En plus, on schématise un mécanisme détaillé pour la prédissociation de l'état α dans laquelle une conversion graduelle de π^* MO pour le HCN courbé en $1s$ AO purement hydrogénique joue un rôle principal. Il est aussi proposé que la transition $\beta \leftarrow \tilde{X}$ observée dans DCN implique un état supérieur $^1\Delta$–$2^1A'$ avec la même limite de dissociation D + CN que pour l'espèce $^1\Sigma^- - ^1A''$.

[Traduit par le journal]

1. Introduction

The ultraviolet spectrum of HCN has been recorded in considerable detail experimentally (1–4) between 1120 and 2000 Å. Although the high-energy absorption in this region is quite strong (1, 2), that observed in the near-ultraviolet between 2000 and 1700Å (3, 4) is much weaker; under high resolution the latter feature appears to consist of two distinct band systems with fine structure, referred to as $\alpha \leftarrow \tilde{X}$ and $\beta \leftarrow \tilde{X}$ respectively (4). The first of these is observed in both the HCN and DCN isomers and shows diffuseness (predissociation) toward shorter wavelengths; the $\beta \leftarrow \tilde{X}$ system, on the other hand, has only been reported for DCN (4). Vibrational and rotational analyses of these bands have led to the conclusion that the molecule is bent ($\measuredangle$HCN = 125°) in the α upper state and (with somewhat less certainty) also in the β state ($\measuredangle$HCN = 114.5°). In the original work both of these states have been concluded to possess $^1A''$ symmetry ($\pi^3\pi^*$ configuration), correlating with $^1\Delta(\alpha)$ and $^1\Sigma^-(\beta)$ states of the linear HCN geometry respectively. The much stronger absorption lines of a third system ($C \leftarrow \tilde{X}$) around 1500 Å and below is believed to

[1]Permanent address: Institut za Fizicku hermiju, Prirodno-matematicki fakultet, Studentski trg 12, 1100 Beograd, Jugoslavia.

[2]Present address: Gesamthochschule Wuppertal, Lehrstuhl Theoretische Chemie, D-5600 Wuppertal-Elberfeld, Gaußstraße 20.

correspond to a different upper state ($\measuredangle$HCN = 141°) of $^1A'$ symmetry which correlates with a $^1\Pi$ species in linear HCN. It should be noted that excitation from the $^1\Sigma^+$ ground state to the latter is allowed by the dipole selection rules, in contrast to the situation for the other states of $^1\Delta$ and $^1\Sigma^-$ symmetry.

Theoretical studies (5, 6) dealing with four HCN states of A' and three of A'' symmetry, on the other hand, predict that the second $^1A''$ state of this system should prefer a linear or nearly linear geometry. Furthermore this finding is in complete agreement with the qualitative predictions of molecular orbital theory (7, 8), but of course stands in strong contrast with the value of 114.5° derived by Herzberg and Innes (4) for the equilibrium internuclear angle of the β state. In addition the calculated excitation energies (5) to $2^1A''$ are seen to differ from the experimental ($\tilde{B}^1A''$) quantities by approximately 0.75 eV. More extensive theoretical treatments (6) have confirmed the originally calculated results and have also indicated that Rydberg characteristics are absent in all such $^1(\pi,\pi^*)$ states of this molecule.

In light of these discrepancies between the experimental inferences derived from the HCN spectrum and the above theoretical predictions it was decided to carry out a further theoretical study of the $^1(\pi,\pi^*)$ excited states of this system using the *ab initio* CI method. Such calculations (9) have recently been successful in reproducing and/or predicting details of the electronic spectra of a good number of molecular systems (water, hydrogen sulfide, ethane, diborane, formaldehyde, acetone, thioacetone, and butadiene, for example), quite generally leading to excitation energies which differ from their experimental values by no more than a few tenths of an eV. At the same time the vibrational structure of the HCN bands in question is also calculated using a priori methods, in a similar way as previously done for O_2 (10) and HSO (11), in order to allow for a more detailed theoretical comparison with the measured absorption spectrum than has heretofore been possible. The present paper reports the results of these investigations.

2. SCF Results for Excited States and Qualitative Aspects

The basis set employed in this study is essentially of double-zeta quality augmented by a few polarization functions, consisting of the lobe functions for N, C, and H derived by Whitten (12), i.e. 4*s* and 2*p* groups for each of the heavy atoms and two *s* groups for the hydrogen expansion with scaling factor $\eta^2 = 2.0$. In addition a one-component *p* function (exponent $\alpha = 0.735824$) is employed on H and one *s* Gaussian is located in each of the CN ($\alpha = 1.45$) and CH bonds ($\alpha = 1.54$) respectively. The influence of Rydberg functions on the lower-lying SCF states was tested (at $\measuredangle$HCN = 125°) and the conclusion reached earlier (6) was thereby supported, namely that such (π,π^*) states show no tendency to mix in Rydberg character; thus long-range Rydberg-like functions are omitted from the basis set in all further investigations. The total SCF energy obtained for the HCN ground state in this basis is −92.8467 hartree; this value is comparable with the −92.85738 hartree result obtained with a set of six contracted *s* and three contracted *p* functions on carbon and 3*s* groups on hydrogen (13), but is inferior to the same set including various *d*-type AO's (−92.90768 hartree (13)) or the double-zeta plus polarization value (−92.8897 hartree) of ref. 6. On the other hand, experience with a number of systems has shown that such additional polarization functions have a similar energy-lowering effect on both ground and excited states (14) (differences after CI have been observed to be generally less than 0.3 eV) and thus there is good reason to believe that the present basis should be capable of allowing for a sufficiently realistic description of the low-energy HCN spectrum.

For all calculations the HCN molecule is placed in the *xz* plane with the C—N bond lying on the *z* axis. Variations in the HCN internuclear angle and the corresponding CN and CH distances were then systematically undertaken relative to the experimental equilibrium ground state structure ($\measuredangle$HCN = 180°, CN = 2.1845 bohr, and CH = 2.0107 bohr).

The SCF calculations are carried out for all states accessible by the normal Roothaan procedure (15); the resulting angular potential curves are contained in Fig. 1. It is immediately seen that the SCF curves for the excited states do not correspond to states of pure symmetry in the linear nuclear arrangement; a very similar picture is also obtained for the corresponding states of isoelectronic HCO^+ (16). The lowest triplet states are thus expected to fall in the following energetic ordering: $^3\Sigma^+$ ($6a' \rightarrow 7a'$), $^3\Delta$ ($1a'' \rightarrow 2a''$, $1a'' \rightarrow 7a'$), and

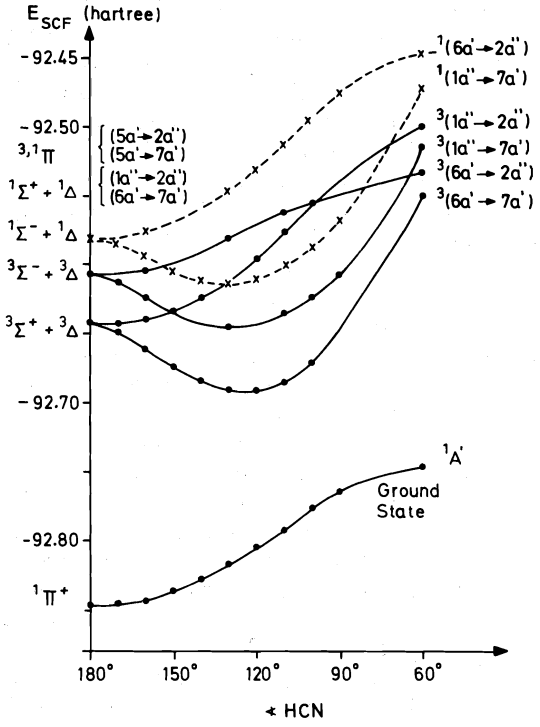

FIG. 1. SCF angular potential curves for various states of HCN. Note that at 180° the results obtained do not correspond to states of pure symmetry (CH = 2.0107 bohr, CN = 2.1845 bohr in all cases).

$^3\Sigma^-$ ($6a' \rightarrow 2a''$). Among the singlet states only ($1a'' \rightarrow 7a'$) and ($6a' \rightarrow 2a''$) are accessible in the SCF treatment, corresponding to a mixture of $^1\Sigma^- + {}^1\Delta$ species at 180°. The other pair, $6a' \rightarrow 7a'$ and $1a'' \rightarrow 2a''$, are in all likelihood *higher* in energy since the splitting between the corresponding singlet and triplet multiplets of such configurations (representing an excitation between orbitals lying *in the same plane*, i.e. with large exchange integral K) is considerably larger than for singlet–triplet states in which the two singly occupied MO's lie in different planes. The same situation is found in HCO^+ after CI is carried out (16), as well as in isoelectronic acetylene (17), for which the energy ordering of $\pi_u^3\,\pi_g$ states of $^3\Sigma_u^+ < {}^3\Delta_u < {}^3\Sigma_u^- \approx {}^1\Sigma_u^- < {}^1\Delta_u < {}^1\Sigma_u^+$ is well known (or alternatively upon inspection of the observed N_2 spectrum (18)).

It is also seen from Fig. 1 that occupation of the $7a'$ species (or the corresponding MO in acetylene), as found in many instances before (5, 7, 8, 16, 17), always results in a bent upper state, in complete agreement with qualitative MO theory. On the other hand, Fig. 1 also makes it clear that the shapes of the angular SCF potential curves may deviate considerably from the actual surfaces, particularly at large HCN angles, and thus that the SCF equilibrium data (especially force constants) for these $^1(\pi,\pi^*)$ states might thereby be in considerable error. From investigation of the charge density of the $7a'$ orbital it is also obvious that occupation of this MO promotes dissociation into H + CN, since (although it is a π^*-type MO at small C—H distances) it changes in bent geometries into a purely hydrogenic species at large internuclear separations. This behavior has been found in related molecules such as HCO^+ (16), HNO (19), HCO, HN_2 (18), HN_2^+ (20), and HNO^+ (21).

The variation of the SCF energy with CN and CH distances in various electronic states of this system is contained in Fig. 2 *a*, *b* (linear nuclear arrangement). A marked increase in the CN bond length is seen upon $\pi \rightarrow \pi^*$ excitation relative to the ground state, as one would expect; the corresponding potential curves for the various (π,π^*) states themselves are seen to bear a great similarity to one another, however. The results for CH stretching in the linear arrangement are not greatly different in ground and excited states, also as would be expected, but given the change in the $7a' - \pi^*$ component upon molecular bending discussed above, there is reason to believe that this uniform pattern may be broken in non-linear conformations.

To summarize then one expects the $^1\Sigma^-$–$^1A''$ state to be the lowest-lying singlet excited state of HCN, followed by the $^1\Delta$–($^1A''$,$^1A'$), i.e. the reverse ordering to what has been assumed in the original assignment of the observed band structure (4); vertical transitions to both states are dipole forbidden from the linear $^1\Sigma^+$ ground state. The remaining $^1(\pi,\pi^*)$ state ($^1\Sigma^+$) is not only less stable than $^1\Sigma^-$ and $^1\Delta$ but quite possibly even lies above $^1\Pi(\sigma \rightarrow \pi^*)$; transitions to both $^1\Sigma^+$ and $^1\Pi$ are dipole allowed. It thus seems clear that only the lowest three $^1(\pi,\pi^*)$ states, correlating with $^1\Sigma^-$ and $^1\Delta$ species, could be responsible for the relatively weak absorption observed in the 1700–2000 Å region of the HCN and DCN spectra and therefore the CI calculations to be discussed below will only consider electronic transitions to these upper states.

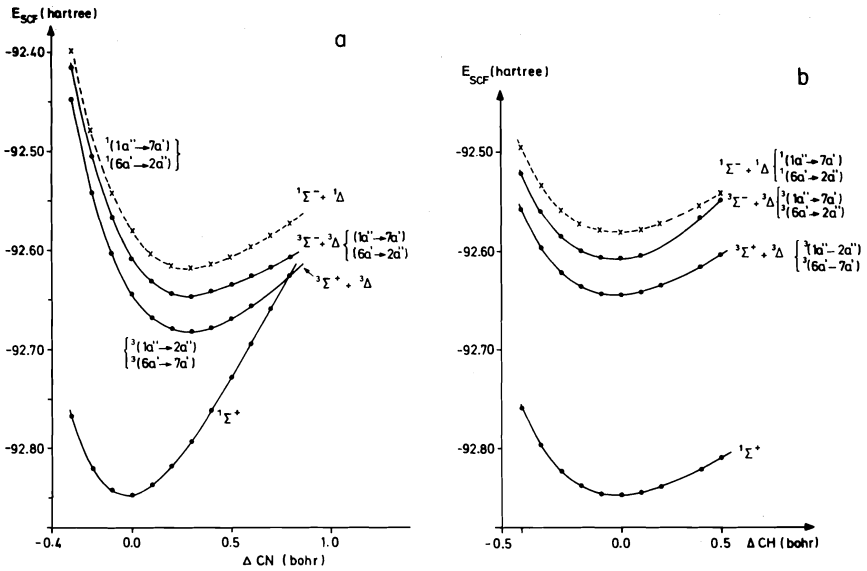

FIG. 2. SCF potential curves for CN stretch (*a*) and CH stretch (*b*) for various states of HCN. (Linear nuclear arrangement, CN = 2.1845 bohr, CH = 2.0107 bohr; the abscissa shows changes relative to the above values.)

3. CI Calculations and Potential Curves for the $^1\Sigma^+$–$\tilde{X}\,^1A'$, $^1\Sigma^-$–$^1A''$, and $^1\Delta$–$2^1A'$,$2^1A''$ (π,π^*) States

The CI calculations including configuration selection and energy extrapolation are carried out in the standard manner (9). In the present case four electrons are always kept in core, i.e. the inner shells of carbon and nitrogen are held doubly occupied, while the remaining electrons are allowed to variably occupy the other MO's in the basis. The natural orbitals of the lowest state of a given symmetry (i.e. $^1\Sigma^+$–$^1A'$ and $^1\Sigma^-$–$^1A''$) are employed for the construction of configurations; they are obtained in each instance by diagonalizing the first-order density matrix of a large-threshold CI (with a relatively small secular equation) for the lowest state. For the $^1A'$ space eight main configurations are used for constructing the configuration space and a 2-root selection procedure corresponding to $1^1A'$ and $2^1A'$ states is carried out. In order to represent the lowest two $^1A''$ states single- and double-excitation species with respect to *four* main configurations are generated, while configuration selection is based on the energy lowerings for both of these states. The same procedure (i.e. the same main configurations) is maintained for the construction of the entire potential curves. In this way 27 079 configurations are generated for the $^1A'$ space at each geometry and 15 007 for the $^1A''$ space; the orders of the secular equations actually solved in the energy extrapolation procedure fall between 1300 and 3000. Several examples for the expansion of the four states under consideration are contained in Table 1, always given at two different internuclear angles.

The angular potential curves thus obtained are given in Fig. 3. At $\measuredangle$HCN = 180° the two components of $^1\Delta$ are not entirely degenerate, primarily because in the $^1A'$ component two configurations with $|c_i| > 0.1$ are not included in the set of main configurations (see Table 1) and therefore this component lies too high compared to its $^1\Delta$–$^1A''$ counterpart by roughly 0.1 eV. At relatively small angles yet another configuration of $^1A'$ symmetry, correlating with $^1\Pi$ in linear geometry, makes a significant contribution to the $2^1A'$ (Table 1), and hence the repulsive part of this potential curve is probably calculated to be somewhat steeper than it would be in an exact treatment.

The first $^1A''$ state has a quite compact CI expansion in the NO basis employed, particularly for bent configurations. The $2^1A''$ state requires a larger number of reference species for

TABLE 1. Expansion coefficients ($|c_i| \geq 0.1$) and corresponding configurations for the four lowest HCN states at two different internuclear angles; 8 main, 2 root selection treatment for $^1A'$ and 4 main, 2 root selection for the $^1A''$ space

∠ HCN	State	c_i[a]	Configuration	
180°	$^1\Sigma^+(X^1A')$	0.951(1)	$\ldots 1a''^2\ 6a'^2$	$(\ldots \pi^4)$
		−0.121(2)	$1a''^2 \rightarrow 2a''^2$	
		−0.121(3)	$6a'^2 \rightarrow 7a'^2$	$(\pi^2 \rightarrow \pi^{*2})$
		0.123(4)	$1a''6a' \rightarrow 7a'2a''$	
	$^1\Delta(2^1A')$	0.66(5)	$1a'' \rightarrow 2a''$	$\pi \rightarrow \pi^*$
		−0.66(6)	$6a' \rightarrow 7a'$	
		0.148(7)	$1a'' \rightarrow 4a''$	$\pi \rightarrow 3\pi^*$
		−0.148(8)	$6a' \rightarrow 5a''$	
		0.116	$1a'' \rightarrow 5a''$	$\pi \rightarrow 4\pi^*$
		−0.116	$6a' \rightarrow 16a'$	
120°	X^1A'	0.945(1)	$\ldots 1a''^2\ 6a'^2$	
		−0.118(2)	$1a''^2 \rightarrow 2a''^2$	
		−0.157(3)	$6a'^2 \rightarrow 7a'^2$	
		−0.124(4)	$1a''6a' \rightarrow 7a'2a''$	
	$2^1A'$	0.730(6)	$6a' \rightarrow 7a'$	
		0.474(5)	$1a'' \rightarrow 2a''$	
		0.141(8)	$6a' \rightarrow 14a'$	
		0.104(7)	$1a'' \rightarrow 4a''$	
		−0.290	$4a' \rightarrow 7a'$	$\sigma \rightarrow \pi^*$
		0.130	$5a' \rightarrow 7a'$	origin
180°	$^1\Sigma^-(^1A'')$	0.802(1)	$1a'' \rightarrow 7a'$	$\pi \rightarrow \pi^*$
		−0.541(2)	$6a' \rightarrow 2a''$	
	$^1\Delta(2^1A'')$	0.547(1)	$1a'' \rightarrow 7a'$	$\pi \rightarrow \pi^*$
		0.785(2)	$6a' \rightarrow 2a''$	
		−0.140(4)	$6a' \rightarrow 4a''$	$\pi \rightarrow 3\pi^*$
120°	$1^1A''$	0.962(1)	$1a'' \rightarrow 7a'$	
		−0.123(2)	$6a' \rightarrow 2a''$	
	$2^1A''$	0.907(2)	$6a' \rightarrow 2a''$	
		−0.144(3)	$5a' \rightarrow 2a''$	
		−0.129(4)	$6a' \rightarrow 4a''$	
		0.117(1)	$1a'' \rightarrow 7a'$	
		−0.221	$4a' \rightarrow 2a''$	

[a]The numbers in parentheses always indicate the main configuration; no number denotes the fact that the corresponding species has not been included in the set of main configurations. Note that the basis set consists of NO's derived for the lowest state of a given irreducible representation in C_s symmetry.

a proper description. Despite the fact that the $4a' \rightarrow 2a''$ configuration appears with sizeable coefficient at 120° (Table 1), it was not included in the generating set of configurations since a value of 120° for the internuclear angle is already quite far from the minimum for this electronic state.

The CN stretch potential curves obtained in the CI calculations do not differ greatly from their SCF counterparts but a general tendency toward larger equilibrium bond lengths in all states treated is noted (Table 2). The ground state CH stretch curve has not been calculated since very little change from the SCF results already discussed (Fig. 2*b*) is expected, at least in the neighborhood of the equilibrium structure, which is critical for representation of the absorption spectrum. The situation for the lowest excited state of HCN is more interesting, however, because of the dissociative behavior of this species. The calculated CI potential curve for the $^1A''$ state (Fig. 4) shows a maximum near 3.20 bohr, reflecting an avoided crossing between the bound $^1(\pi,\pi^*)$ curve of HCN and that for the $H(^2S) + CN(^2\Pi)$ dissociation products. As discussed in section 2 this circumstance arises because of the fact that the $7a'$ component of the π^* MO correlates with a pure hydrogenic $1s$ AO at infinite separation (for bent nuclear arrangements). The calculated barrier height for

TABLE 2. Equilibrium data for the lowest electronic states of HCN obtained from the SCF and CI treatment. Comparison with previous theoretical predictions and the experimentally deduced values is also made. (Distances are given in bohr, angles in degrees.)

State	Method	CN	∠HCN	CH
Ground state	SCF	2.163	180	1.980
	CI	2.245	180	2.00
	INO, ref. 5	2.230	180	1.994
	Exptl. (ref. 4)	2.185	180	2.011
	SCF, ref. 12	2.1793	180	2.0026
$^1A''$	SCF	2.466(∠180°)	127	1.980
	CI	2.514(∠125°)	123	2.05
	INO, ref. 5	2.491	127.2	2.071
	α state, Exptl. (ref. 4)	2.451	125	2.154
	SCF, ref. 12	2.499	121.05	2.075
$2^1A''$	SCF	2.466	180	1.980
	CI	2.527	≈180	—
	INO, ref. 5	2.487	164.4	2.033
$2^1A'$	SCF	—	—	—
	CI	2.554	120	—
	Ref. 5	2.432	124.9	2.082
β State, Exptl.		2.521	114.5	2.15

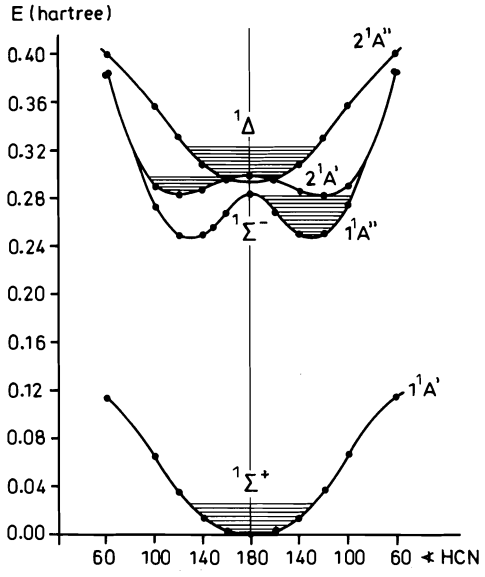

FIG. 3. Angular potential curves for the low-lying states of HCN obtained from the CI calculations. The calculated vibrational levels are also indicated.

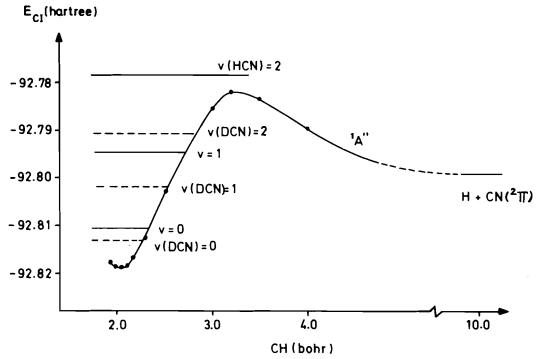

FIG. 4. Dissociative CH stretch potential curve for the $^1A''$ excited state obtained from the CI calculations (∠HCN = 125°, CN = 2.52 bohr). Corresponding vibrational levels for HCN and DCN are also indicated.

dissociation along this channel is 1.0 eV relative to the $^1A''$ energy minimum.

A summary of the various calculated equilibrium structural parameters obtained via polynomial fits to all the data points for each of the states under investigation is given in Table 2. If the various vibrational modes are allowed to be coupled (22) the calculated equilibrium distances are found to be slightly larger than those obtained under the assumption of separability of modes, while the $^1A''$ internuclear angle is calculated to be reduced in this more elaborate procedure. The present calculated values are in close agreement with those of earlier theoretical treatments (5); the latter values generally fall between those of the present SCF and CI calculations respectively.

In general the various theoretical results are seen to be in reasonably good accord with their corresponding experimentally reported values for the lowest two states of HCN, with the possible exception of the CH distance in the $^1A''$

TABLE 3. Calculated vibrational frequencies (under the assumption of uncoupled modes) for the various states of HCN and DCN employing SCF and CI potential curves. (Values are given in cm^{-1}.)

State	Potential	ν_3(CN)	ν_2(∠HCN)[a]	ν_1(CH)
HCN: Ground state	SCF	2396	691 F 707 H	3499
	CI	2046	600	3552
	Exptl. (ref. 4)	2097	712	3311
$^1A''$			1168 F	
	SCF	1624(∠180°)	1229 H	3549
	CI	1412(∠180°) 1547(∠125°)	1100	—
	Exptl. (ref. 4)	1506	949	—
$2^1A'$	SCF	1668(triplet)	—	3560(triplet)
	CI	1412	855 F 819 H	—
$2^1A''$			764 F	
	SCF	1621	765 H	3549
	CI	1500	552	—
DCN: Ground state	CI	2008	420	2517
$^1A''$		1386(∠180°)	878	$\approx 3549 \times 2^{-1/2}$
	CI	1518(∠125°)		
	Exptl. (ref. 4)	1506	735	—
$2^1A'$	CI	1384	606	$\approx 3560 \times 2^{-1/2}$
$2^1A''$	CI	1472	386	
β State (Exptl. (ref. 4))			(731)[b]	

[a]Two values are obtained, corresponding to the Fourier and Hermite type ($R_0\theta$) expansion of the vibrational wavefunction.
[b]Values given in ref. 4 for the state of DCN; however, since the v_2 numbering is unclear, this result may not correspond to the zeroeth vibrational level.

upper state, for which uniformly smaller results are obtained in the calculations than the 2.154 value deduced by Herzberg and Innes (4) for this quantity. As remarked earlier (5, 6), however, the calculations are in clear disagreement with the earlier experimental assignment of the β state (with a small equilibrium ∠HCN value of 114.5°) as the $2^1A''$ state. On the other hand, an assignment for this experimental species as the $2^1A'$ state instead of $2^1A''$ does appear to fit in reasonably well with the observed structural data for the upper state in question.

4. Vibrational Structure of the $^1(\pi,\pi^*)$ Transitions

In order to obtain the vibrational levels associated with the various electronic states of HCN it is assumed (in contrast to the ground state treatment (22) given earlier) that the various modes, namely CH stretching, CN stretching, and ∠HCN (ϕ) bending can be treated independently of one another. The corresponding CI energy curves are taken as the potential in which the nuclear motion occurs; the CN and CH stretching species are represented via a polynomial fit in the corresponding internal coordinate, while for the bending motion a Fourier series in $\cos 2n\phi$ is employed or alternatively a polynomial in the variable $R_0\phi$ (where R_0 is the CH distance). Thus the anharmonicity of the potential is taken into account in this treatment, but the various vibrational modes are left uncoupled therein. The vibrational wavefunctions are similarly expanded in a series of Hermite polynomials or in $\cos 2n\phi$ and $\sin 2n\phi$ series (23) and the corresponding energy levels and expansion coefficients are obtained using the variational method by solving the appropriate secular equation. Normally up to 25 terms are employed in each expansion; more details on the general procedure employed may be found elsewhere (22–24). The vibrational frequencies thus obtained are given in Table 3 and are compared with the best experimental values available for these quantities. It is found that these calculated results agree with the corresponding observed

values to within an error of 50–200 cm^{-1}; similar error limits have been noted in other applications of this method, as for example for HSO (11) and N_2H_2 (25), for which coupling between the vibrational modes is neglected.

In order to calculate the intensity distribution for the transitions between various vibrational levels of the different electronic states, the electronic transition moment is assumed to be independent of the CN stretching and CH stretching coordinate. The latter quantity is assumed to depend strongly on the angle HCN, however, since $\boldsymbol{R}_{e'e''}$ between the ground and all three upper states vanishes at 180° ($^1\Sigma^- - \tilde{X}^1\Sigma^+$, $^1\Delta - \tilde{X}^1\Sigma^+$) while it has a non-zero value in the non-linear H—C—N arrangement. The calculated variation of $\boldsymbol{R}_{e'e''}$ for the upper states under consideration is found in Fig. 5. The total transition moment between different vibrational levels is then approximated by the expression[3]

$$\boldsymbol{R}_{e'v'e''v''} = \langle\psi_{v_1'}|\psi_{v_1''}\rangle\langle\psi_{v_3'}|\psi_{v_3''}\rangle \times \langle\psi_{v_2'}|R_{e'e''}(\phi)|\psi_{v_2''}\rangle$$

For the lowest-energy $^1A'' \leftarrow \tilde{X}^1A'$ ($^1\Sigma^+$) transition the Franck-Condon factors between $\tilde{X}^1A'$ ($v_3'' = 0$) and the v_3' (CN) vibrational levels of the upper state are plotted in Fig. 6*a* for both the HCN and DCN isotopes; because of the increased CN bond length in the $^1(\pi,\pi^*)$ upper state the largest overlap is not found for the corresponding O—O transition but rather between $v_1'' = 0$ and the second and third energy level of the excited electronic state. The situation is even more drastic for the corresponding quantities in the angular distribution (Fig. 6*b*); the highest intensity is predicted between the $v_2'' = 0$ level and the $v_2' = 6$ species of the $^1A''$ state. At the same time it is seen from Fig. 3 that the depth of the $^1A''$ angular potential well is such that the $v_2' = 7$ level lies above the energy maximum at 180°, while all other lower-energy v_2' levels are still found within the well. For DCN the situation is slightly changed since 7 (almost 8) vibrational levels are indicated to lie within the angular potential well, whereupon it is calculated that the most intense transition in DCN should occur for somewhat larger angular quantum number ($v_2' = 8$) than for the lighter isotope. No significant intensity shift between

[3]The last integral in this expression is evaluated by fitting $R_{e'e''}(\phi)$ in the same basis as is used for the expansion of ψ_{v_2}.

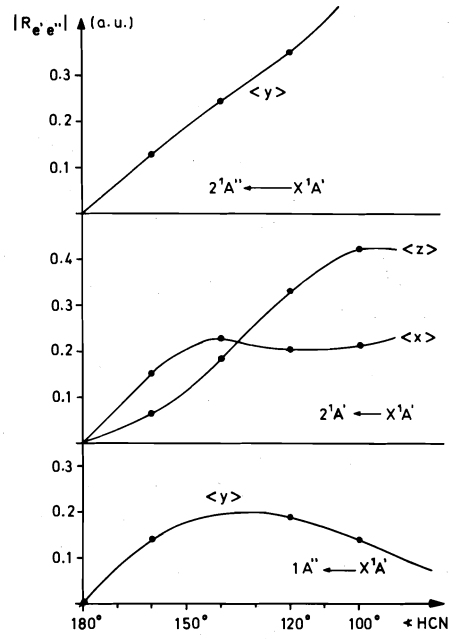

FIG. 5. Calculated electronic transition moments for various upper states of HCN as a function of internuclear angle. The direction of polarization is indicated in each instance.

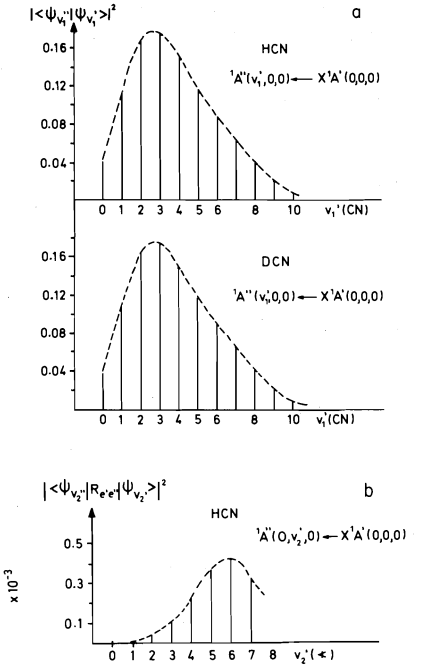

FIG. 6. Calculated Franck-Condon factors for various vibrational transitions in HCN and DCN; CN progressions are shown in part *a*, while a bending progression is given in part *b*.

HCN and DCN is expected for the CN vibrational pattern according to the present treatment, however (see also Table 3).

Finally, by far the largest Franck-Condon factor is calculated between the corresponding zeroeth CH vibrational levels of $\tilde{X}^1A'$ and α^1A''. It is also seen from Fig. 4 that excitation into higher-lying CH levels of the $^1A''$ state could lead effectively to dissociation into H + CN($^2\Pi$) via a tunnelling process.

The calculated results for the transition to the other bent $^1(\pi,\pi^*)$ upper state ($2^1A'$) are wholly analogous to those for $^1A''$, with the modification that the intensity maximum for ν_2 vibrations is shifted to somewhat smaller upper-state quantum numbers (4 or 5) compared to the latter case (since the depth of the angular well is found to be somewhat more shallow than for the $^1A''$ state). The $2^1A'$ species should also dissociate into H(^2S) + CN($^2\Pi$), and presumably with even greater facility since the absolute minimum in energy for this state lies above that of the $^1A''$ (see Fig. 3). Because the $2^1A''$ state is calculated to be linear, just as the ground state itself, the most intense vibrational transition in this case occurs for $v_2'' = 0$ to $v_2' = 1$, as required by the dipole forbiddenness of the corresponding electronic transition; also all higher-energy ν_2 vibrational transitions are calculated to be much weaker than the $1 \leftarrow 0$ species. The intensity distribution for the other two vibrational modes in this transition is found to be similar to that found for the $\alpha^1A'' \leftarrow \tilde{X}^1A'$ and $2^1A' \leftarrow \tilde{X}^1A'$ species. Finally it should be noted that, consistent with the results of Fig. 5, the overall intensity of the lowest-energy $^1A'' \leftarrow \tilde{X}^1A'$ transition is found to be markedly smaller than for either of the other two $^1(\pi,\pi^*)$ species calculated.

5. Comparison with Experiment

A. The $\alpha \leftarrow \tilde{X}(^1A'' \leftarrow \tilde{X}^1A')$ Transition

The calculated T_e and T_0 values for the various $^1(\pi,\pi^*)$ transitions of HCN treated in this study are compared with experiment and earlier theoretical findings in Table 4. The present CI treatment appears to overestimate the lowest T_0 value by some 0.25 eV, an error which is quite consistent with experience based on similar CI calculations for other small molecules. As noted above, however, this lowest $^1(\pi,\pi^*)$ species does not correlate with the $^1\Delta$ state in the linear nuclear arrangement but rather with $^1\Sigma^-$. The experimental data for this transition show a long bending progression, with an intensity maximum for $v_2' = 6$ (see Fig. 7*b*), which is rather faithfully represented in the calculated results of Fig. 6*b*. Similarly the shift of the maximum to $v_2' = 5$ in the corresponding hot bands [$\alpha(0,n,0)^0 \leftarrow \tilde{X}(0,1,0)$ and $\alpha(0,n,0)^2 \leftarrow \tilde{X}(0,1,0)$] for this transition is also mirrored in the calculated findings, which show $\langle\psi_{v_2'}|R^{\nu}_{e'e''}|\psi_{v_2''}\rangle$ values of 0.0652, 0.0654, and 0.0647 for the upper quantum numbers $v_2' = 4$, 5, and 6 respectively if the ground state $v_2'' = 1$ species replaces the $v_2'' = 0$ wavefunction. The results for DCN show quite similar behavior, except that the intensity maximum is shifted to higher v_2' quantum numbers because of the decreased magnitude in its vibrational frequency (Table 3).

The analogous findings for the ν_1 CN stretch progressions are not as easily understood, however, as can be seen by comparing calculated and experimental results in Figs. 6*a* and 7*a* respectively. The calculations show virtually no distinction between the intensity distributions in this vibrational species for the two isotopes HCN and DCN, a finding which seems reasonable in light of the small change in reduced mass which occurs for this mode upon deuteration. Yet the experimental spectrum shows a marked shift in both the overall shape and location of the maximum for the intensity distribution in such CN progressions in going from one isotope to the other. The calculated distribution for both systems is thus seen to agree reasonably well with the observed DCN spectral results, which show a maximum for $v_2' = 3$, but it is significantly less peaked than that reported for HCN. Whether a more nearly exact theoretical treatment of the vibrational structure of this transition can succeed in representing such a distinction between HCN and DCN remains to be seen, but at least at this point it is not immediately clear why the CN progressions of the two systems should appear so dissimilar.

In the higher-energy range of the $\alpha \leftarrow \tilde{X}$ transition the various absorption lines become increasingly diffuse, with this phenomenon setting in somewhat earlier in HCN than in DCN. In addition, in the latter isotope there is evidence of a second electronic transition, referred to as $\beta \leftarrow \tilde{X}$ by Herzberg and Innes (4) in this spectral region; the experimental intensity distribution for the strongest observed bending progression in this system is shown in Fig. 8.

TABLE 4. Relative energies (eV) calculated for the minima of the various states. (Ground state energy is −93.0700 hartree.)

	T_e	T_0 (HCN)	T_e (ref. 5)	T_0, Exptl. (ref. 4)
Ground state $^1\Sigma^+$	0.0	0.0	0.0	0.0
$^1A''$	6.76	6.73	6.48	6.48
$2^1A'$	7.55	7.52	6.78	[7.48][a]
$^1\Delta$–$2^1A''$	8.03	7.99	7.52	—
$CN(^2\Pi) + H(^2S)$	7.37(D_e)	7.12(D_0)	—	6.80(D_0)

[a]Deduced under the assumption that the $\beta(0,8,0) \leftarrow \tilde{X}(0,0,0)$ line of ref. 4 corresponds to the O—O transition (see text).

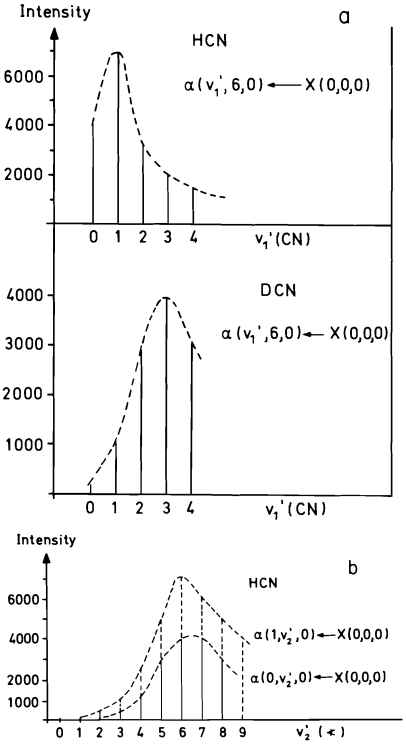

FIG. 7. Measured relative intensity values (taken from ref. 4) for various vibrational transitions in HCN and DCN. These results should be compared with the corresponding theoretical findings given in Fig. 6 *a*, *b* respectively.

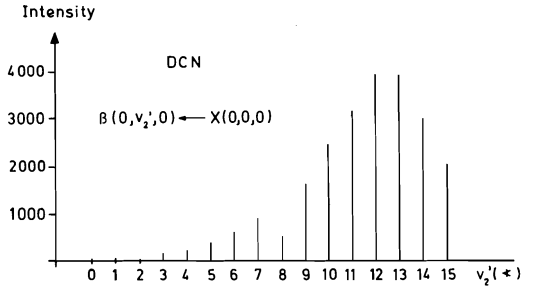

FIG. 8. Measured relative intensity values (taken from ref. 4) for a bending progression in the $\beta \leftarrow \tilde{X}$ transition.

Herzberg and Innes (4) have argued that the diffuseness in the $\alpha \leftarrow \tilde{X}$ bands is most likely caused by CH (or CD) predissociation, and this interpretation is certainly consistent with the calculated potential curve shown in Fig. 4. The D_0 value for dissociation of the upper state into $H(^2S) + CN(^2\Pi)$ is now believed to be 0.32 eV (4, 26), compared with the present calculated value of 0.40 eV (the energy of the dissociation products relative to that of the lowest ground state vibrational level is observed to be 6.80 eV, while the corresponding CI result is 7.12 eV; see Table 4). Because of the avoided crossing discussed in section 3, however, there is a barrier hindering this process which is approximately 1.0 eV in height. As indicated in Fig. 4 a potential well of this depth would allow for two stable CH vibrational levels in HCN and three such CD species in DCN. Tunnelling of H or D across the barrier obviously adds an additional instability factor to the overall physical situation, however, whereby Herzberg and Innes (4) have argued that distinctions in the masses of the hydrogenic isotopes and resultant differences in their ability to tunnel are at least partially responsible for the fact that diffuseness in the bands sets in at lower energies for the lighter HCN system.

B. The $\beta \leftarrow \tilde{X}$ *Transition*

Although the theoretical description of the $\alpha \leftarrow \tilde{X}$ transition fits in quite well with the corresponding experimental data (geometry, transition energy, intensity distribution, and predissociation features in HCN and DCN), the situation for the $\beta \leftarrow \tilde{X}$ band system at shorter wavelength is by no means clear. As indicated at the end of section 2, there seems to be general agreement that only the lowest three $^1(\pi,\pi^*)$ species of HCN fall in the energy range which corresponds to the $\alpha \leftarrow \tilde{X}$ and $\beta \leftarrow \tilde{X}$ absorption region. The observation that DCN is more

likely to possess a stable $v_3' = 1$ level in the $^1A''$ α state than HCN might lead to the conclusion that the $\beta \leftarrow \tilde{X}$ band system, which is only seen in the DCN spectrum, involves the same upper electronic state. On the other hand the calculated Franck-Condon factors of the previous section indicate that vibrational transitions to the $v_3' = 1$ level in the $\alpha \leftarrow \tilde{X}$ system should only be about 10% as intense as the corresponding $v_3' = 0$ species, whereas the observed $\beta \leftarrow \tilde{X}$ absorption lines are seen to be comparable in intensity to the *strongest* $\alpha \leftarrow \tilde{X}$ species found at longer wavelength. Thus when both energy and intensity results are considered, it does not appear that other than $v_3' = 0$ vibrational transitions are observed in the spectrum, and hence it seems best to conclude that the $v_3' = 1$ and higher species indicated to lie below the potential maximum in Fig. 4 for both isotopic species are in fact unstable relative to tunnelling across the corresponding barrier to dissociation; a similar conclusion has been reached earlier by Herzberg and Innes (4).

Consequently the list of choices for assignment to the β state can be narrowed down to the remaining two $^1(\pi,\pi^*)$ species, $2^1A'$ and $2^1A''$, but unfortunately there appear to be strong arguments against both of these possibilities as well. According to Herzberg and Innes (4) the β state is characterized by a strongly bent equilibrium geometry (~114.5°) and possesses $^1A''$ symmetry, the latter conclusion having been based on the appearance of the rotational fine structure in the $\beta \leftarrow \tilde{X}$ band. The present calculations find, on the other hand, that although one of these two states does show the desired (bent) geometrical characteristics, it is the $2^1A'$ species which does so and not the $2^1A''$, and thus there is clearly a conflict which needs to be resolved. Ordinarily a violation of selection rules is a more important consideration than the occurrence of such discrepancies in structural data but there is reason to believe the situation may not be so simple in the present case. First of all there is by now a large amount of evidence that *ab initio* calculations of the type employed in the present work are quite reliable for the prediction of such geometrical characteristics; both previous calculations as well as the conclusions based on qualitative MO theory agree with the present finding that the $2^1A''$ state is linear (or very nearly so (5)). Secondly there is some evidence that the operation of such rotational selection rules is unclear in the spectrum for a similar electronic transition in HO_2, namely in the 14 300 Å $^2A' \rightarrow {}^2A''$ band system.[4] In view of both these considerations it therefore seems worthwhile to look more closely into the possibility that the $2^1A'$ $^1(\pi,\pi^*)$ species is the upper state involved in the $\beta \leftarrow \tilde{X}$ absorption system observed by Herzberg and Innes (4).

Comparison of the observed intensity distribution in the bending progression of this transition (Fig. 8) with the calculated results of the previous section raises still further questions, however. The most intense lines in this progression are assigned by Herzberg and Innes (4) as $v_2' = 12$ and 13 respectively, for example, whereas the calculations suggest that the length of such bending progressions (in the $2^1A' \leftarrow \tilde{X}$ transition) from maximum to tail should actually be somewhat smaller than for the $\alpha \leftarrow \tilde{X}$ band (in which $v_{2'\,max} = 7$ or 8 for DCN; Fig. 3). On the other hand it seems possible that the observed group of vibrational transitions in question actually consists of two progressions, the weaker of which shows a maximum at $v_2' = 7$. Such an interpretation would then lead to an assignment for the origin of the stronger of the two progressions as the $\beta(0,8,0) \leftarrow \tilde{X}(0,0,0)$ member, thereby placing the absorption maximum for this system at $v_2' = 12$ (or 13) minus 8 = 4 (or 5), in much better agreement with the calculated results for the $2^1A' \leftarrow {}^1A'$ intensity distribution (see section 4).[5]

The fact that the $\beta \leftarrow \tilde{X}$ system can only be observed for the deuterated isotope of HCN also seems to be satisfactorily rationalized in terms of a $2^1A'$ assignment for the upper state. Both $2^1A'$ and $^1A''$ (α species) have the same dissociation limit, namely $H(^2S) + CN(^2\Pi)$, but the more stable $^1A''$ species appears to be some 0.8 eV

[4]In addition to $\Delta K = \pm 1$ the $\Delta K = 0$ line is observed to occur with relatively high intensity near the band centers (27).

[5]In support of this argument, it can be noted that there is also a plausible assignment for the lower-energy portion of the intensity distribution in Fig. 8, namely as a hitherto unassigned series of hot bands for the $\alpha \leftarrow \tilde{X}$ system. The cold bands for the $\alpha(2,v_2',0) \leftarrow \tilde{X}$ progression are relatively strong, with a maximum relative intensity of 3500 having been reported in the original paper (4). The latter species is assigned as $\alpha(2,7,0) \leftarrow \tilde{X}$ (0,0,0) and is found at 60 142 cm^{-1}, and hence one would expect the corresponding hot band species to occur some 500 cm^{-1} to the red thereof, with fairly substantial intensity; this description fits the previously assigned $\beta(0,7,0) \leftarrow \tilde{X}(0,0,0)$ member reasonably well, especially since the $\alpha(2,7,0) \leftarrow \tilde{X}(0,1,0)$ species remains unassigned in the original experimental interpretation.

more stable at their respective equilibrium geometries (Fig. 3). As a result it seems clear that the $2^1A'$ is marked by a relatively small potential barrier to dissociation (in the order of 2000 cm^{-1} according to the calculations), and hence, given the greater capacity of the proton to tunnel through this barrier (plus the fact that the zero-point energy of HCN is significantly greater than in DCN), it seems plausible that only the heavier isotope could be stable to predissociation in this electronic state.

The exact numbering of the individual members of the progression shown in Fig. 8 is very difficult to discern based on the relatively small range of wavelength over which the $\beta \leftarrow \tilde{X}$ band is actually observed. Consequently it appears impossible to locate the true T_0 value for the $\beta \leftarrow \tilde{X}$ transition. One of the most plausible alternatives from the standpoint of the present interpretation, however, is that the $\beta(0,8,0) \leftarrow \tilde{X}(0,0,0)$ line (at 60 350 cm^{-1}) in the original notation (see Fig. 8) corresponds to the O—O species and thus that T_0 is 7.48 eV for this DCN transition, which value in turn lies less than 0.1 eV below the corresponding calculated result of Table 4. If the latter vibrational species involves $v_1' = 1$ instead, the error between calculation and experiment would be greater by the amount of one additional ν_1' quantum, i.e. by roughly 0.15 eV (1300–1400 cm^{-1}). The earlier calculated T_0 result of Schwenzer *et al.* (5) is 0.7 eV below the present CI value (Table 4).

In summary it is found that the vibrational intensity distribution calculated for the $2^1A' \leftarrow {}^1A'$ transition appears to be in reasonably good agreement with the experimental observations for the $\beta \leftarrow \tilde{X}$ band, just as the results for the ${}^1A'' \leftarrow {}^1A'$ species are seen to satisfactorily reproduce the details of the measured spectrum for the $\alpha \leftarrow \tilde{X}$ system. Since such an assignment for the $\beta \leftarrow \tilde{X}$ species appears to be at odds with the rotational selection rules for such polyatomic systems there is still clearly a need to justify this interpretation in more detail, but in considering this point the difficulties with the alternative $2^1A'' \leftarrow {}^1A'$ assignment should not be overlooked. The presence of the rather long (and relatively intense) 500 cm^{-1} vibrational progression in the $\beta \leftarrow \tilde{X}$ transition of DCN needs to be explained in a manner which is consistent with the appearance of the associated rotational fine structure of this band system before it can be claimed that theory and experiment are fully reconciled in this instance, and the results of the present CI study indicate that none of the ${}^1A''$ states of this molecule possesses the type of potential surface required to account for such vibrational characteristics.

Acknowledgments

One of us (M.P.) wishes to thank the Deutsche Akademische Austauschdienst for the granting of a predoctoral fellowship. The services and computer time made available by the University of Bonn Computing Center are also gratefully acknowledged.

1. W. C. Price. Phys. Rev. **46**, 529 (1934).
2. W. C. Price and A. D. Walsh. Trans. Faraday Soc. **41**, 381 (1945).
3. H. J. Hilgendorff. Z. Phys. **95**, 781 (1935).
4. G. Herzberg and K. K. Innes. Can. J. Phys. **35**, 842 (1957).
5. G. M. Schwenzer, S. V. O'Neil, and H. F. Schaefer III. J. Chem. Phys. **60**, 2787 (1974).
6. G. M. Schwenzer, C. F. Bender, and H. F. Schaefer III. Preprint on publication.
7. A. D. Walsh. J. Chem. Soc. 2288 (1953).
8. R. J. Buenker and S. D. Peyerimhoff. Chem. Rev. **74**, 127 (1974).
9. R. J. Buenker and S. D. Peyerimhoff. Theor. Chim. Acta (Berl.), **39**, 217 (1975); **35**, 33 (1974).
10. R. J. Buenker, S. D. Peyerimhoff, and M. Perić. Chem. Phys. Lett. **42**, 383 (1976).
11. A. B. Sannigrahi, K. H. Thunemann, S. D. Peyerimhoff, and R. J. Buenker. Chem. Phys. **20**, 25 (1977).
12. J. L. Whitten. J. Chem. Phys. **44**, 359 (1966).
13. U. Wahlgren, J. Pacansky, and P. S. Bagus. J. Chem. Phys. **63**, 2874 (1975).
14. S. D. Peyerimhoff and R. J. Buenker. Adv. Quantum Chem. **9**, 69 (1975).
15. C. C. J. Roothaan. Rev. Mod. Phys. **32**, 179 (1960).
16. P. J. Bruna, S. D. Peyerimhoff, and R. J. Buenker. Chem. Phys. **10**, 323 (1975); P. J. Bruna. Astrophys. Lett. **16**, 107 (1975).
17. W. E. Kammer. Chem. Phys. Lett. **6**, 529 (1970).
18. S. D. Peyerimhoff and R. J. Buenker. Ber. Bunsenges. Phys. Chem. **78**, 119 (1974).
19. A. A. Wu, S. D. Peyerimhoff, and R. J. Buenker. Chem. Phys. Lett. **35**, 316 (1975).
20. K. Vasudevan, S. D. Peyerimhoff, and R. J. Buenker. Chem. Phys. **5**, 149 (1974).
21. C. Marian, P. J. Bruna, R. J. Buenker, and S. D. Peyerimhoff. Mol. Phys. **33**, 63 (1977).
22. M. Perić. Mol. Phys. To be published.
23. S. D. Peyerimhoff and R. J. Buenker. Theor. Chim. Acta (Berl.), **27**, 243 (1972).
24. M. Perić. Ph.D. thesis, University of Bonn, Bonn. 1976.
25. M. Perić, R. J. Buenker, and S. D. Peyerimhoff. Can. J. Chem. **55**, 1533 (1977).
26. G. Herzberg. Electronic spectra of polyatomic molecules. D. van Nostrand Co., Inc., New York, NY. 1966.
27. E. Fink. Abstracts of the Advanced Study Institute, Spectroscopy and Kinetics of Atmospheric Constituents. Arabba, March 1977.

Canadian Journal of Chemistry

Published by
THE NATIONAL RESEARCH COUNCIL OF CANADA

Volume 55 Number 21 November 1, 1977

Journal canadien de chimie

Publié par
LE CONSEIL NATIONAL DE RECHERCHES DU CANADA

Volume 55 numéro 21 1 novembre 1977

Preparation and fate of carbon monosulfide (CS). Ultraviolet photoelectron spectroscopic study of the thermolysis of 5,5-dimethyl-1-phenyl-Δ^3-1,3,4-triazoline-2-thione

DAVID C. FROST AND NICK P. C. WESTWOOD
Department of Chemistry, University of British Columbia, Vancouver, B.C., Canada V6T 1W5
AND
NICK HENRY WERSTIUK,[1] LUBOMIRA CABELKOVA-TAGUCHI, AND JOHN WARKENTIN[1]
Department of Chemistry, McMaster University, Hamilton, Ont., Canada L8S 4M1

Received June 17, 1977

DAVID C. FROST, NICK P. C. WESTWOOD, NICK HENRY WERSTIUK, LUBOMIRA CABELKOVA-TAGUCHI, and JOHN WARKENTIN. Can. J. Chem. **55**, 3677 (1977).

The results of an ultraviolet photoelectron spectroscopic study of the thermolysis of 5,5-dimethyl-1-phenyl-Δ^3-1,3,4-triazoline-2-thione (**1**) are presented. That CS_2 is one of the major products establishes that carbon monosulfide (CS) is formed as a reaction intermediate in the thermolysis. Other products of thermolysis of **1** are molecular nitrogen and isopropylidenephenylamine (**2**). The photoelectron spectrum of the latter is also reported. Thermolysis of **1** in solution also leads to CS, which polymerizes extensively in the absence of trapping agents but is partly converted to CS_2 in the presence of S_8 and to COS in the presence of cyclohexanone.

DAVID C. FROST, NICK P. C. WESTWOOD, NICK HENRY WERSTIUK, LUBOMIRA CABELKOVA-TAGUCHI et JOHN WARKENTIN. Can. J. Chem. **55**, 3677 (1977).

On présente les résultats d'une étude ups sur la thermolyse du diméthyl-5,5 phényl-1 Δ^3-triazoline-1,3,4 thione-2 (**1**). Le CS_2 étant l'un des produits principaux implique que le monosulfure de carbone se forme comme intermédiaire dans la réaction de thermolyse. Les autres produits de la thermolyse de **1** sont l'azote moléculaire et l'isopropylidènephénylamine (**2**). Le spectre photoélectronique de ce dernier est aussi présenté. La thermolyse d'une solution de **1** conduit aussi au CS qui polymérise considérablement en absence d'agents piégeurs mais se convertit partiellement en CS_2 en présence de S_8 et en COS, en présence de cyclohexanone.

[Traduit par le journal]

Ultraviolet photoelectron spectroscopy (ups) is a technique for measuring the ionization potential for removal of electrons from molecular orbitals. The results, through the use of Koopman's theorem, give information about the nature of bonding in molecules. Although ups thus far has been used predominantly in a conventional way to study bonding in appreciably volatile and stable molecules of known structure (1–3), clearly the technique could be used to identify highly reactive intermediates, unstable molecules, and their reaction products in the gas phase. At present there are few studies of the latter, unconventional application of photoelectron spectroscopy documented in the literature (4–8).

In this paper we describe an ups study of the products from vacuum thermolysis, at 225°C,

[1]Authors to whom enquiries should be addressed.

of 5,5-dimethyl-1-phenyl-Δ^3-1,3,4-triazoline-2-thione (**1**). Kinetics and products of thermolysis of **1** in chlorobenzene solution are also reported.

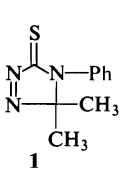

1

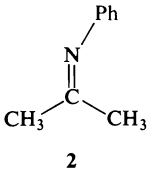

2

Experimental

Materials

Compound **1** was prepared from the 4-phenylthiosemicarbazone of acetone by oxidative cyclization on alumina (9). The sample used for this work was recrystallized from ethanol. It was homogeneous (tlc) and melted sharply at 170°C.

Ultraviolet Photoelectron Spectroscopy

The ups study was carried out with a versatile ups spectrometer of the design of Frost and co-workers (10). Thione (**1**) was sublimed ($P_{\text{initial}} = 10^{-6}$ Torr) into a pyrolysis tube (glass, $l = 10$ cm) maintained at 225 ± 10°C. The tube led through a U trap cooled to −100°C, directly into the photoionization chamber of the spectrometer. The spectrum[2] shown in Fig. 1*a* is that of the volatile thermolysis products that passed through the −100°C trap. That in Fig. 1*b* was obtained by warming the trap after pumping the volatiles out of the spectrometer.[2]

Kinetics

Thermolysis of **1** in chlorobenzene was followed by ^{1}Hmr. For a typical kinetics experiment, a solution of **1** (0.0268 *M*) in chlorobenzene containing toluene (0.0281 *M*) as internal standard for integration was degassed and sealed into an nmr tube. Five or more ^{1}Hmr spectra were recorded with a Varian HA-100 intrument before the tube was placed in an oil bath at 148 ± 0.1°C. The tube was removed at intervals, cooled quickly with liquid nitrogen, and warmed to room temperature before five or more spectra were recorded. Time outside the 148°C bath was not counted and the time scale was not corrected for warm-up and cooling periods which were short and partly cancelling.

As reaction progressed the intensity of the methyl singlet of **1** (1.2 δ) diminished and two new singlets of equal intensity appeared near 1.6 and 2.0 δ. A standard first-order plot of log (peak height at 1.2 δ, normalized with respect to that of the reference singlet) against time was a straight line with correlation coefficient in the range 0.9875 to 0.9983. The average first-order rate constant (seven runs) obtained from the slopes was $k_1 = 6.42 \times 10^{-5}$ s^{-1}.

Products

In spent solutions from kinetics runs the two product singlets, attributed to isopropylidenephenylamine (**2**), together accounted for more than 95% of the methyl groups of **1**. A gummy, brown solid qualitatively fitting the literature description of polymeric CS (11) was also obtained. Isopropylidenephenylamine (**2**) was prepared independently by the method of Kuhn and Jochims (12). The crude anil was vacuum redistilled twice: bp 80–81°C, ^{1}Hmr ($CDCl_3$) δ 2.05 (s, 3H), 1.70 (s, 3H), 3.0–7.4 (m, 5H). A sample of **2** isolated by gas chromatography (Varian Aerograph A90-P3, 5 ft × 1/4 in. column, 15% SE30 on 60–80 mesh Chromosorb P, 65°C) of the products from thermolysis of **1** had the identical ^{1}Hmr spectrum. Hydrolysis of either sample afforded acetone and aniline.

Trapping of CS with Sulphur

A sample of **1** (0.20 g) in chlorobenzene (35 ml) containing sulphur (1.5 g) was placed in a flask connected to a gas sampling bulb. The system was evacuated and purged with argon until the mass spectrum of a gas sample was free from air peaks. The system was then sealed off and heated at the reflux temperature for 6 h. The flask containing the solution was cooled to room temperature and then to Dry Ice temperature before a gas sample was taken for mass spectrometry. Major peaks at *m/e* 76 (CS_2), 40 (argon), and 28 (N_2) were recorded. A control experiment, run in the same way except for the absence of sulphur, gave a gas sample with large peaks at *m/e* 40 and 28 but a negligible signal at *m/e* 76.

Trapping of CS with Cyclohexanone

This experiment was analogous to the one described above. Compound **1** was decomposed in neat cyclohexanone and the gas phase was sampled for mass spectrometry. A signal at *m/e* 60, assigned to COS, was observed as well as masses 40 and 28. A control sample from decomposition of **1** in chlorobenzene under air instead of argon did not give a signal at *m/e* 60.

Results and Discussion

The spectrum[2] in Fig. 1*a* shows that CS_2 (IP 10.17, 12.80, 14.47, 16.16 eV) and N_2 (IP 15.57, 16.6–17.8 envelope, 18.73 eV) are the major volatile products from the gas phase thermolysis of **1** that pass through the −100°C trap. A small quantity of CS is indicated by the weak band at 11.28 ± 0.05 eV (13). Trace quantities of CO (IP 14.00 eV) are evident. The band at 8.62 eV and the broad bands centered at 10.44 and 12.30 eV cannot be assigned with confidence at this time. Their appearance and disappearance suggest that they arise from a single species and the band positions correspond to those of propanethione (14).

That CS_2 is one of the major products of the gas phase thermolysis of **1** is explained by invoking the intermediacy of CS. That CS is the source of CS_2 is supported by the work of Richardson and co-workers (15) who established that CS is converted to CS_2 at room temperature via a heterogeneous wall reaction.

When the volatiles were pumped off and the

[2]The thermolysis experiments and the resulting spectra were reproducible.

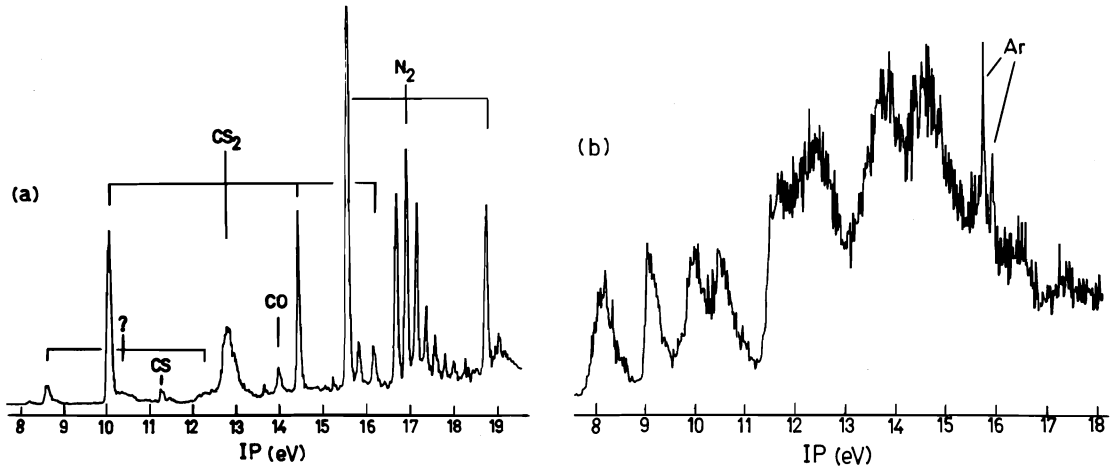

FIG. 1. *(a)* The He(I) photoelectron spectrum of the volatiles from the pyrolysis of **1**. *(b)* The He(I) photoelectron spectrum of **2**.

−100°C trap was warmed, an additional small amount of the unknown species[2] (IP 8.62, 10.44, and 12.30) was initially observed. At ambient temperature, the photoelectron spectrum[2] shown in Fig. 1*b* was obtained, which was assigned to isopropylidenephenylamine (**2**), the major product of the solution thermolysis of **1**. The first two IP's with maxima at 8.19 and 9.13 eV we assign, respectively, to the b_1 and a_2 type π MO's (local C_{2v} symmetry) which result from a separation of the degenerate π MO's (e_{1g}) upon substitution of benzene (16). As usual, the a_2 MO remains unperturbed since there is a node at the point of substitution and the b_1 MO is destabilized. The bands at 10.04 and 10.57 eV we assign to the C=N π MO and the nitrogen lone pair, respectively, on the basis of a comparison with other alkylidene alkyl and aryl amines (17, 18) and isoelectronic styrenes (19). This ordering could be reversed depending on the magnitude of the torsional angle about the phenyl–nitrogen single bond which determines the magnitude of the *n*–π separation (17).

The thermolysis chemistry of **1** in solution lends support to the conclusions drawn from the ups experiment. At 148°C, in chlorobenzene, decomposition of **1** is first order ($k_1 = 6.42 \times 10^{-5}$ s^{-1}) and isopropylidenephenylamine (**2**) accounts for more than 95% of the methyl and phenyl groups of **1**. Some attack by CS on **1** or on **2** probably accounts for the remaining 5%.

Several mechanisms for thermolysis of **1** have to be considered, including heterolytic and homolytic bond cleavages. The fact that an increase in solvent polarity decreases the rate constant ($k_{C_6H_5NO_2} = 0.53k_{C_6H_6}$ at 148°C) suggests that highly polar transition states and intermediates are not involved. Among homolytic pathways, stepwise decomposition via intermediate **3** is considered most likely because of growing evidence that some unsymmetric azo compounds thermolyze by the two-step mechanism (for examples and leading references see ref. 20). The

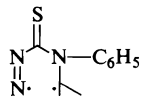

3

expected energy difference between C(sp^2)—N and C(sp^3)—N bonds should make **1** a strong candidate for stepwise decomposition. Further mechanistic conjecture is not warranted at this time.

Our brief ups study of the thermolysis of **1** illustrates the utility of the technique for studying the intermediates from gas phase organic reactions. The solution chemistry of **1** confirms that it is a thermal source of CS and suggests that it may be particularly useful for studies of the chemistry of that reactive intermediate in the liquid phase.

Acknowledgements

I (N.H.W.) wish to thank Professors D. C. Frost and C. A. McDowell and their colleagues for the hospitality afforded me during the course of my sabbatical leave at the University of

British Columbia. This work was supported by the National Research Council of Canada.

1. D. W. TURNER, A. D. BAKER, and C. R. BRUNDLE. Molecular photoelectron spectroscopy. Wiley, New York, NY. 1970.
2. A. D. BAKER and D. BETTERIDGE. Photoelectron spectroscopy. Pergamon Press, New York, NY. 1972.
3. J. H. D. ELAND. Photoelectron spectroscopy. Wiley, New York, NY. 1974.
4. A. B. CORNFORD, D. C. FROST, F. G. HERRING, and C. A. MCDOWELL. Discuss. Faraday Soc. **54**, 56 (1972).
5. W. JONATHAN, A. MORRIS, M. OKUDA, K. J. ROSS, and D. J. SMITH. Discuss. Faraday Soc. **54**, 48 (1972) and references quoted therein.
6. T. KOENIG, R. WIELESEK, W. SNELL, and T. BALLE. J. Am. Chem. Soc. **97**, 3225 (1975).
7. P. SOLOUKI, P. ROSMUS, and H. BOCK. J. Am. Chem. Soc. **98**, 6054 (1976).
8. E. BLOCK, H. BOCK, S. MOHMAND, P. ROSMUS, and B. SOLOUKI. Angew. Chem. Int. Ed. Engl. **15**, 383 (1976).
9. J. LANDQUIST. J. Chem. Soc. C, 63 (1970).
10. D. C. FROST, S. T. LEE, C. A. MCDOWELL, and N. P. C. WESTWOOD. J. Electron Spectrosc. In press.
11. M. A. P. HOGG and J. E. SPICE. J. Chem. Soc. 4196 (1958).
12. R. KUHN and R. JOCHIMS. Chem. Ber. **96**, 990 (1963); R. KUHN and H. SCHRETZMANN. Biokchimija, **22**, 173 (1957).
13. N. JONATHAN, A. MORRIS, M. OKUDA, D. J. SMITH, and K. J. ROSS. Chem. Phys. Lett. **13**, 334 (1972).
14. H. W. KROTO, B. M. LANDSBERG, R. J. SUFFOLK, and A. VODDEN. Chem. Phys. Lett. **29**, 265 (1974).
15. R. J. RICHARDSON, H. T. POWELL, and J. D. KELLEY. J. Phys. Chem. **77**, 2601 (1973).
16. A. D. BAKER, D. P. MAY, and D. W. TURNER. J. Chem. Soc. B, 22 (1968).
17. E. HASELBACH and F. HEILBRONNER. Helv. Chim. Acta, **53**, 684 (1970).
18. T. BALLY, E. HASELBACH, S. LANYLOVA, F. MARSCHNER, and M. ROSSI. Helv. Chim. Acta, **59**, 486 (1976).
19. J. P. MAIER and D. W. TURNER. Faraday Discuss. Chem. Soc. **55**, 197 (1973).
20. (*a*) K. K. SHEN and R. G. BERGMAN. J. Am. Chem. Soc. **99**, 1655 (1977); (*b*) N. A. PORTER and L. J. MARNETT. J. Am. Chem. Soc. **95**, 4361 (1973); (*c*) R. C. NEUMAN, JR. and E. W. ERTLEY. J. Am. Chem. Soc. **97**, 3130 (1975).

Substituent effects of phosphorus-containing groups on aromatic reactivity. Determination of substituent constants by ^{13}C nuclear magnetic resonance spectroscopy

TOMASZ A. MODRO

Department of Chemistry, University of Toronto, Toronto, Ont., Canada M5S 1A1

Received April 25, 1977

TOMASZ A. MODRO. Can. J. Chem. **55**, 3681 (1977).

^{13}C nmr spectra have been obtained for a series of benzene derivatives substituted with phosphorus-containing groups of the type PZ_2, $P(O)Z_2$, and $P(S)Z_2$. Inductive and resonance substituent constants were determined from the shielding of *meta* and *para* carbon atoms according to the dual-substituent parameter approach. Possible mechanisms of substituent effects of P^{III} and P^{V} derived functional groups are discussed and in some cases compared with effects of the analogous nitrogen derivatives.

TOMASZ A. MODRO. Can. J. Chem. **55**, 3681 (1977).

On a enregistré les spectres de résonance magnétique nucléaire ^{13}C d'une série de dérivés du benzène, substitués par des groupes d'atome central phosphore de types PZ_2, $P(O)Z_2$ et $P(S)Z_2$. Les constantes d'induction et de résonance des substituants sont déterminées à partir des effets de blindage des carbones *méta* et *para* selon l'approche paramètre substituant-double. Des mécanismes possibles pour l'effet des substituants du P^{III} et P^{V}, liés aux groupes fonctionnels, sont discutés et dans certains cas comparés aux effets de dérivés analogues de l'azote.

[Traduit par le journal]

The use of ^{13}C nmr spectroscopy in the elucidation of the electronic structure of organic molecules continues to increase (for a recent review see ref. 1). For aromatic systems, ring ^{13}C chemical shifts have been found to be a useful and sensitive probe in studies of the polar and resonance effects of substituents, particularly at the *para* and *meta* positions (2). Substituent-induced changes in ^{13}C chemical shifts have been correlated with various substituent constants, with a variable degree of success. It is now recognized that structural effects on the ^{13}C nmr chemical shift of the *para* and *meta* carbon atoms relative to benzene are best described by the dual-substituent parameter (dsp) approach (3). According to this approach, the relative change in shielding at a given position results from the contributions of inductive and resonance effects of the substituent, expressed in terms of σ_I and σ_R^0 constants:

$$[1] \qquad {}^{13}C\ \delta_X - {}^{13}C\ \delta_H = a\sigma_I + b\sigma_R^0$$

^{13}C nmr spectroscopy seems to be a particularly useful tool for investigations of substituent effects of phosphorus–containing groups. For both tervalent and tetravalent phosphorus derivatives $-PZ_2$ and $-P(Y)Z_2$, numerous structural variations are possible (in the nature of both Z and Y ligands) which modify the net electronic effect of the substituent. This effect is a function of various factors, such as the electronegativities of Z and Y, bond order at the P atom, donor properties of phosphorus non-bonding electrons (in case of PZ_2 substituents), and acceptor abilities of the vacant *d* orbitals on phosphorus. The evaluation of substituent effects by determination of the reactivities of a series of PZ_2 and $P(Y)Z_2$ substituted benzene derivatives can often be hindered by the high reactivity of the phosphorus-containing function itself (e.g. oxidation, hydrolysis, Arbuzov-type reactions, etc.).

^{13}C nmr spectra were employed by Retcofsky and Griffin (4) in determining the σ_p and σ_p^+ constants for some organophosphorus groups. The substituent constants derived could be used to compare the electron-withdrawing abilities of the related pairs of P^{III} and P^{V} functional groups, PZ_2 and $P(O)Z_2$. Although the $P(O)(OEt)_2$ substituent has been found to be more electronegative than $P(OEt)_2$ (σ_p values $+0.55$ and $+0.33$, respectively), according to Retcofsky and Griffin the substituent PPh_2 is *more* electron withdrawing than $P(O)Ph_2$ (σ_p values $+0.68$ and $+0.53$, respectively), and PCl_2 *more* electron withdrawing than $P(O)Cl_2$ (σ_p of $+0.61$ and $+0.43$). Such a conclusion (resulting most likely from erroneous ^{13}C chemical shift assignments)

TABLE 1. ^{13}C chemical shifts for phenyl carbon atoms of Ph—X (in ppm relative to $^{13}C_6H_6$, low field shifts positive) and (in parentheses) ^{13}C–^{31}P coupling constants (in Hz). Solvent CCl_4, unless indicated. Concentration ca. 0.5 *M*

No.	X	Position			
		ipso	*ortho*	*meta*	*para*
1	PMe_2[a]	—[b]	+2.53 (18.4)	+0.07 (5.8)	−0.33 (≃0)
2	PPh_2	+9.24 (12.6)	+5.51 (19.6)	+0.06 (6.2)	+0.22 (≃0)
3	P(Ph)Cl	+10.93 (33.0)	+3.53 (24.4)	+0.20 (7.0)	+1.80 (≃0)
4	PCl_2	+12.56 (51.8)	+1.95 (31.2)	+0.57 (8.0)	+4.20 (≃0)
5	PF_2	—[c]	+1.43 [d]	+0.31 [d]	+4.64 [d]
6	$P(OEt)_2$	+13.90 (23.2)	+1.57 (18.4)	−0.39 (5.0)	+1.02 (≃0)
7	$P(NEt_2)_2$[a]	—[c]	+2.91 (16.6)	−0.31 (2.8)	−1.20 (≃0)
8	$P(O)Me_2$	—[b]	+1.69 (8.8)	+0.10 (11.8)	+2.69 (2.2)
9	$P(O)Ph_2$	+5.78 (102.8)	+3.90 (9.6)	−0.10 (11.6)	+2.98 (1.8)
10	$P(O)Cl_2$	—[c]	+2.19 (13.6)	+0.72 (17.8)	+5.82 (3.8)
11	$P(O)(OEt)_2$	+1.57 (187.4)	+3.62 (10.0)	−0.17 (14.8)	+3.44 (3.0)
12	$P(O)(NEt_2)_2$	—[c]	+3.78 (8.6)	−0.22 (12.6)	+2.28 (3.2)
13	$P(S)Me_2$	+6.68 (82.0)	+2.03 (10.6)	+0.19 (11.8)	+2.85 (3.0)
14	$P(S)Ph_2$	+7.69 (85.0)	+4.17 (10.4)	−0.10 (10.8)	+2.76 (4.0)
15	$P(S)Cl_2$	—[c]	+2.12 (14.4)	+0.39 (17.6)	+5.17 (4.0)
16	$P(S)(OEt)_2$	+6.05 (152.4)	+2.82 (11.8)	−0.36 (15.0)	+3.37 (3.4)
17	NMe_2[e]	+22.60	−15.5	+1.00	−11.5
18	NPh_2	+19.77	−6.98	+0.92	−5.62
19	$N(O)Me_2$[f]	+26.22	−8.35	+0.83	+0.59

[a]In cyclohexane.
[b]No peak observed due to solubility limitation.
[c]Assignment uncertain.
[d]Determination of $J_{C,P}$ difficult because of additional ^{13}C–^{19}F coupling.
[e]Taken from ref. 9.
[f]In $CHCl_3$.

is not only counter to chemical intuition, but also is not in accord with known facts about structure–reactivity relationships in organophosphorus chemistry. Substituent constants derived by Schindlbauer and Prikoszovich (5) from ^{19}F nmr chemical shifts for a series of *meta* and *para* substituted fluorobenzenes clearly show that $P(O)Z_2$ is always more electron withdrawing than the corresponding PZ_2 group. Recently, Klabuhn *et al.* (6) demonstrated that in various reactions (base-catalyzed ester hydrolysis, aromatic nucleophilic substitution, S_N2 and S_N1 reactions), the *p*-$P(O)R_2$ substituent (R = phenyl, cyclohexyl) is significantly more electron withdrawing than the corresponding *p*-PR_2 group; the reactivity ratio varied from 1.6 to 380.

Unfortunately, Retcofsky and Griffin's results have recently been uncritically cited by Nelson and Williams in their review article (ref. 1, p. 247) as an illustration of the application of ^{13}C nmr spectroscopy in estimating substituent constants which have not been determined chemically.

In continuation of our interest in the substituent effects of phosphorus-containing groups upon the properties of an adjacent aromatic system (ref. 7, and preceding papers of this series), we have used ^{13}C nmr chemical shifts to monitor changes in the electron distribution of the benzene ring in a series of Ph—PZ_2, Ph—$P(O)Z_2$ and Ph—$P(S)Z_2$ derivatives (including compounds investigated by Retcofsky and Griffin). The chemical shifts obtained were used to evaluate substituent inductive and resonance constants, according to the dual-substituent parameter approach.

Results and Discussion

^{13}C chemical shifts for the ring carbon atoms in 16 derivatives of benzene, substituted with PZ_2, $P(O)Z_2$, or $P(S)Z_2$ groups, have been measured in CCl_4 or cyclohexane solutions. No common solvent could be used for all compounds studied, because of either insolubility in cyclohexane (compounds **8**, **9**, **13**, **14** of Table 1) or reaction with carbon tetrachloride (compounds **1**, **7**, and to some extent compound **6**). However, the differences in the chemical shift values obtained for a given compound in these two solvents never exceeded 0.03 ppm, and did not affect the derived values of substituent constants. The identical values of ^{13}C chemical shifts for various monosubstituted benzenes measured in CCl_4 and cyclohexane have been reported previously (8). Chemical shifts (and ^{13}C–^{31}P coupling constants) for the substituted benzenes of interest are shown in Table 1.

The values obtained for $\Delta\delta$ do not confirm Retcofsky and Griffin's observations; in all cases

TABLE 2. Estimated σ_I and σ_R^0 constants for organophosphorus substituents

Substituent	σ_I	σ_I (lit.[a])	σ_R^0	σ_R^0 (lit.[a])
PMe_2	+0.02	(+0.06)	−0.02	(−0.02)
PPh_2	+0.04	(+0.21)	0.00	(−0.01)
P(Ph)Cl	+0.18	—	+0.05	—
PCl_2	+0.49	(+0.44)	+0.11	(+0.17)
PF_2	+0.37	—	+0.16	—
$P(OEt)_2$	−0.17	—	+0.08	—
$P(NEt_2)_2$	−0.22	—	−0.02	—
$P(O)Me_2$	+0.17	(+0.35)	+0.10	(+0.15)
$P(O)Ph_2$	+0.08	(+0.37)	+0.14	(+0.14)
$P(O)Cl_2$	+0.65	(+0.65)	+0.17	(+0.25)
$P(O)(OEt)_2$	+0.06	(+0.21)	+0.16	(+0.17)
$P(O)(NEt_2)_2$	−0.02	—	+0.12	—
$P(S)Me_2$	+0.23	—	+0.10	—
$P(S)Ph_2$	+0.07	(+0.40)	+0.13	(+0.11)
$P(S)Cl_2$	+0.43	(+0.59)	+0.17	(+0.21)
$P(S)(OEt)_2$	−0.05	—	+0.18	—
NMe_2[b]		+0.06		−0.52
NPh_2	+0.25		−0.33	
$N(O)Me_2$	+0.54		(0.00)	

[a]Reference 5.
[b]Taken from Hine (13, Chapt. 3.3).

the carbon atom *para* to the $P(O)Z_2$ substituent is more deshielded than that *para* to the corresponding PZ_2 group.[1] In agreement with earlier results obtained for monosubstituted benzenes (10), the largest variation of shifts is found for the *ipso* carbon atom, and the smallest occur at the *meta* carbon. The variations at the *ipso* position, as well as at the *ortho* carbons, reflect not only polar, but also purely magnetic effects of the substituent and therefore cannot be used as reliable measures of substituent effects. The chemical shifts of the *meta* and *para* carbon atoms are believed to be essentially free of magnetic anisotropy effects of a substituent (11) and can be used without any correction in evaluating the appropriate substituent constants.

Inductive and resonance substituent constants of phosphorus-containing groups were calculated from the dsp fits for *meta* and *para* ^{13}C shifts, according to [2] and [3] (12). The

$$[2] \qquad \Delta\delta\,{}^{13}C_p = 3.98\sigma_I + 19.79\sigma_R^0$$

$$[3] \qquad \Delta\delta\,{}^{13}C_m = 1.54\sigma_I - 1.61\sigma_R^0$$

results are summarized in Table 2. Where possible, σ_I and σ_R^0 values are compared with those obtained by Schindlbauer and Prikoszovich (5) from the ^{19}F nmr chemical shifts for the *meta* and *para* substituted fluorobenzenes. Resonance parameters σ_R^0, calculated by Schindlbauer and Prikoszovich from the difference in shielding of the *para* and *meta* carbons, agree very well with our values obtained from [2] and [3]. The values of inductive substituent constants σ_I on the other hand are seriously different; in almost all cases the σ_I constants reported in ref. 5 are much more positive than our values obtained from the dsp approach. σ_I values were calculated by Schindlbauer and Prikoszovich according to the single substituent parameter approach ($\Delta\delta\ {}^{19}F_m = a\sigma_I + b$) and in our opinion these results tend to grossly overestimate the inductive electron-withdrawing properties of the organophosphorus groups studied. For example, their σ_I values for the PR_2 groups (R = Me, Ph) are almost identical with those for the corresponding NR_2 groups; a result not likely on the simple basis of the electronegativity difference of phosphorus and nitrogen. Similarly, it would be difficult to rationalize the stronger inductive effect of the $P(O)Me_2$ substituent ($\sigma_I = +0.35$ (5)) compared to that of the acetyl group ($\sigma_I = +0.28$ (13)).

The data presented in Table 2 permit one to arrange phosphorus-containing groups with respect to their electronic effects. As for the inductive effects, the electron-attracting properties decrease within each class of substituents in the following order of σ_I values.

For the PZ_2 type substituents:

[1]We believe that the values reported by Retcofsky and Griffin as *para* carbon shielding for the PPh_2, $P(O)Ph_2$, $P(O)Cl_2$, and $P(S)Cl_2$ groups probably represent the chemical shifts of the *ortho* carbon atoms.

$$PCl_2 > PF_2 > P(Ph)Cl > PPh_2 > PMe_2 > H > P(OEt)_2 > P(NEt_2)_2$$

For the $P(O)Z_2$ groups:

$$P(O)Cl_2 > P(O)Me_2 > P(O)Ph_2 > P(O)(OEt)_2 > H > P(O)(NEt_2)_2$$

For the $P(S)Z_2$ substituents:

$$P(S)Cl_2 > P(S)Me_2 > P(S)Ph_2 > H > P(S)(OEt)_2$$

The observed order of inductive withdrawal does not follow the order of decreasing electronegativity of atoms bonded to the phosphorus atom ($F > O > Cl \simeq N > C_{sp^2} > C_{sp^3}$). The effective charge density on the phosphorus results from the superimposition of the inductive withdrawal by groups Z (following the electronegativity scale) and the p_π–d_π electron back-donation from the groups Z to the vacant *d* orbitals of the phosphorus atom. Interestingly enough, the PF_2 group has a weaker inductive effect than the PCl_2 substituent, contrary to the significant difference in electronegativities of fluorine and chlorine.[2] This result remains, however, in agreement with the p_π–d_π electron feedback model; the 3*p* nonbonding orbitals of chlorine are less effective in resonance donation to the vacant *d* orbitals of phosphorus, relative to the 2*p* nonbonding electrons of fluorine (14*a*). In consequence, the less electronegative chlorine substituents increase the electron deficiency of phosphorus more than do the fluorine atoms. The high degree of the $2p_\pi$–d_π bonding between oxygen (or nitrogen) and the phosphorus atom is well documented for various organophosphorus systems (15). This effect results in a considerable net inductive electron donation (relative to hydrogen) of the ester and amide groups derived from the P^{III} atom (compounds **5** and **6**), as well as reducing the inductive electron withdrawal practically to zero for the phosphoryl and thiophosphoryl esters and amides (compounds **11**, **12**, and **16**).

Resonance effect parameters σ_R^0 are similar for all tetravalent phosphorus groups $P(O)Z_2$ and $P(S)Z_2$ (σ_R^0 range +0.10 to +0.18) and locate these substituents among strong, mesomerically electron-withdrawing groups such as nitro, cyano, or acetyl substituents. The resonance effects in this case are due to the p_π–d_π interactions between the P^V atom and the aromatic system; the σ_R^0 values indicate that this effect is of a similar order of magnitude to the p_π–p_π conjugation between the ring and the nitro or carbonyl functions. For the PZ_2 type groups, despite the presence of the nonbonding electrons on phosphorus, net conjugative *withdrawal* is observed for fluorine-, chlorine-, and alkoxy-substituted systems. In these cases, the high electronegativity of Z promotes the mesomeric electron withdrawal from the ring to the vacant *d* orbitals of phosphorus to an extent that is not counterbalanced by the p_π–p_π donation of the phosphorus lone pair.

According to the data in Table 2, the PR_2 substituents (R = Me, Ph) are weakly electron withdrawing by inductive effects and almost negligibly electron donating by resonance effects. This should result in total electronic effects for these substituents upon reactivity which are weak in magnitude and possibly variable in direction, depending on the relative response of the reaction center to inductive and resonance effects. In reactions studied by Klabuhn *et al.* (6), the PR_2 (R = cyclohexyl, phenyl) behaves in ester hydrolysis as a weakly electron-withdrawing (by a factor of ca. 2) and in S_N1 reaction as a weakly electron-donating (by a factor of ca. 3) substituent. Dissociation measurements for the *meta*- and *para*-PR_2 substituted benzoic acids (16) and phenols (17) demonstrate the weak electron-accepting properties of phosphorus-containing substituents, and therefore suggest greater importance of inductive effects upon the acidity of phenolic and carboxyl groups. On the other hand, the relative reactivity of P^{III} derivatives in Arbuzov-type reactions seems to follow the order of resonance electron release of the phosphorus moiety. These reactions involve nucleophilic attack of the phosphorus nonbonding electrons at saturated carbon atoms, and the relative reactivity of the system Z_3P decreases in the order Z = alkyl > aryl > alkoxyl (14*b*, 18), following the order of decreasing values of σ_R^0 constants.

There is little structural parallel between organic compounds of phosphorus and nitrogen; nevertheless the substituent effects of the few phosphorus-containing groups investigated can be directly compared with those of the nitrogen analogues. Such comparisons can involve tertiary phosphines and their oxides; substituent con-

[2]The difluoromethyl group is, as expected, more electron withdrawing than the dichloromethyl group, as can be demonstrated by the values of their Taft's substituent constants σ^* (+2.05 and +1.94, respectively) (13, Chapt. 3.6).

stants for the corresponding nitrogen derivatives are included at the bottom of Table 2. Comparison of σ values of MZ_2 groups (M = P, N; Z = Me, Ph) clearly demonstrates fundamental differences in electronic properties of phosphorus and nitrogen. While the inductive electron withdrawal, due to the higher electronegativity, is significantly greater for amino groups, the NZ_2 substituents show (relative to the negligible effects of the PZ_2 groups) powerful electron-donating resonance effects (−0.52 vs. −0.02 and −0.33 vs. 0.00, respectively). This reflects the dramatic difference in the conjugative abilities of the nitrogen 2*p* and phosphorus 3*p* nonbonding electrons with respect to an aromatic π system. In *N*,*N*-dimethylaniline-*N*-oxide (**19**), the substituent effect (if the hyperconjugative electron-release is ignored) operates solely via the inductive mechanism; consequently similar deshielding of the *meta* and *para* positions is observed.[3] The inductive effect of the $N(O)Me_2$ group is again much greater than that of the $P(O)Me_2$, because of the electronegativity difference, and also because oxygen lone pair back-donation is not possible for the nitrogen-containing substituent.

Experimental

Substrates **2**, **3**, **4**, **9**, **10**, **14**, **15**, and **18** were commercial products and were recrystallized or distilled where necessary. Substrates **1**, **5**, **6**, **7**, **8**, **11**, **12**, **13**, **16**, and **19** were synthesized according to standard procedures.

^{13}C chemical shifts were determined on a Varian CFT-20 spectrometer operating in pulsed Fourier transform mode at a probe temperature of 35–40°C. A capillary containing 80% D_2O – 20% dioxan was used as a lock in each case. The ^{13}C chemical shifts were measured relative to the internal solvent resonance and are reported relative to the chemical shift of benzene measured in the same solvent. Solutions of 0.5 *M* were used, solubility permitting. In a few cases chemical shifts were measured for various substrate concentration (0.5–0.1 *M*); no change in chemical shift values was observed. Chemical shift values are reproducible to better than ±0.02 ppm.

^{13}C chemical shift assignments were based upon relative intensities, off-resonance decoupling experiments, and values of ^{13}C–^{31}P coupling constants in related systems. The assignment of the C_{ipso} and C_{para} carbon atom resonances is simplified by the absence of a nuclear Overhauser effect for the quaternary C_{ipso} carbon atom, and therefore by its much lower intensity relative to the C_{para} signal. The assignment of the C_{meta} and C_{ortno} (and also of C_{ipso} and C_{para}) resonances was based upon the magnitude of the $J(^{13}C^{31}P)$ coupling. For all four ring carbon atoms the following ranges of the $J(^{13}C^{31}P)$ coupling constants were found (in Hz): P^V derivatives: C_{ipso} (82–187), C_{ortho} (8.6–14.4), C_{meta} (10.8–17.8), C_{para} (1.8–4.0): P^{III} derivatives: C_{ipso} (12.6–51.8), C_{ortho} (8.8–31.2), C_{meta} (2.8–8.0), C_{para} (~0). Some of the observed $J(^{13}C^{31}P)$ coupling constants could be compared with the available literature data; excellent agreement was found for both P^V (20) and P^{III} (21) derivatives.

[3]The NH_3^+ and NMe_3^+ groups give the identical deshielding of *meta* and *para* carbon atoms in the corresponding benzene derivatives (19).

Acknowledgements

The financial assistance of the National Research Council of Canada is gratefully acknowledged.

1. G. L. Nelson and E. A. Williams. Prog. Phys. Org. Chem. **12**, 229 (1976).
2. G. C. Levy and G. L. Nelson. Carbon-13 NMR for organic chemists. Wiley-Interscience, New York. 1972. Chapt. 4.
3. R. T. C. Brownlee and R. D. Topsom. Tetrahedron Lett. 5187 (1972).
4. H. L. Retcofsky and C. E. Griffin. Tetrahedron Lett. 1975 (1966).
5. H. Schindlbauer and W. Prikoszovich. Chem. Ber. **102**, 2914 (1969).
6. B. Klabuhn, H. Goetz, P. Steirl, and D. Alscher. Tetrahedron, **32**, 603 (1976).
7. T. A. Modro, W. F. Reynolds, and E. Skorupowa. J. Chem. Soc. Perkin Trans. II. (1977). In press.
8. G. L. Nelson, G. C. Levy, and J. C. Cargioli. J. Am. Chem. Soc. **94**, 3089 (1972).
9. J. B. Stothers. Carbon-13 nmr spectroscopy. Academic Press, New York. 1972. Chapt. 4.
10. H. Spiesecke and W. G. Schneider. J. Chem. Phys. **35**, 731 (1961).
11. G. E. Maciel and J. J. Natterstad. J. Chem. Phys. **42**, 2427 (1965).
12. W. J. Hehre and R. W. Taft. Prog. Phys. Org. Chem. **12**, 159 (1976).
13. J. Hine. Structural effects on equilibria in organic chemistry. Wiley-Interscience, New York. 1975. (*a*) Chapt. 3.7; (*b*) Chapt. 3.6.
14. A. J. Kirby and S. G. Warren. The organic chemistry of phosphorus. Elsevier. Amsterdam. 1967. (*a*) Chapt. 1.2(a); (*b*) Chapt. 2.2(a)
15. J. R. Van Wazer and J. H. Letcher. Topics in phosphorus chemistry. Vol. 5. Interscience, New York. 1967. Chapt. 3.III.
16. I. G. Maklakhova, E. N. Tsvetkov, D. I. Lobanov, and M. I. Kabachnik. J. Gen. Chem. USSR, **41**, 2837 (1971).
17. E. N. Tsvetkov, M. M. Makhamatkhanov, D. I. Lobanov, and M. I. Kabachnik. J. Gen. Chem. USSR, **42**, 761 (1972).
18. R. F. Hudson. Structure and mechanism in organophosphorus chemistry. Academic Press, London. 1965. p. 137.
19. W. F. Reynolds, I. R. Peat, M. H. Freedman, and J. R. Lyerla. Can. J. Chem. **51**, 1857 (1973).
20. T. A. Albright, W. J. Freeman, and E. E. Schweizer. J. Org. Chem. **40**, 3437 (1975).
21. H. J. Jakobsen and O. Manscher. Acta Chem. Scand. **25**, 680 (1971); G. M. Bodner and M. Gaul. J. Organomet. Chem. **101**, 63 (1975).

A comparison of substituent effects on vicinal proton–proton and carbon–proton coupling constants

T. P. FORREST AND S. SUKUMAR

Department of Chemistry, Dalhousie University, Halifax, N.S., Canada B3H 4J3

Received April 28, 1977

T. P. FORREST and S. SUKUMAR. Can. J. Chem. **55**, 3686 (1977).

Vicinal carbon–proton coupling constants have been determined for a series of *tert*-butyl derivatives and compared to the vicinal proton–proton coupling constants in the analogous series of isopropyl derivatives. In both series coupling constants were found to decrease with electronegativity of substituent, with $^3J_{C,H}$ decreasing more rapidly than $^3J_{H,H}$. The relationship between the two types of coupling was found to be $J_{C,H} = 1.2J_{H,H} - 3.5$. The regular change in the ratio of $J_{C,H}$ to $J_{H,H}$ indicates that substituent effects can be useful in predicting carbon–proton coupling constants from proton–proton models.

T. P. FORREST et S. SUKUMAR. Can. J. Chem. **55**, 3686 (1977).

Les constantes de couplage vicinales carbone–proton sont mesurées pour une série de dérivés *tert*-butylés et comparées aux constantes de couplage vicinales proton–proton obtenues pour une série analogue de dérivés isopropylés. Dans les deux séries, les constantes de couplage semblent diminuer avec l'électronégativité du substituant avec $^3J_{C,H}$ diminuant plus rapidement que $^3J_{H,H}$. La relation entre les deux types de couplage est établie comme étant $J_{C,H} = 1.2J_{H,H} - 3.5$. Le changement régulier dans le rapport de $J_{C,H}$ à $J_{H,H}$ indique que l'effet des substituants peut être utile dans la prédiction des valeurs des constantes de couplage carbone–proton à partir des modèles proton–proton.

[Traduit par le journal]

Proton–proton coupling constants are used much more frequently than carbon–proton coupling constants in structural and stereochemical analysis because of the well developed correlations between the coupling constants and molecular structure in the former case, and the greater ease with which the proton–proton couplings may in general be obtained. However, for many compounds the carbon–proton couplings are easily measured, yet the lack of an extensive background of structural correlations limits their usefulness. Because the major contributing mechanism, the Fermi contact mechanism, is the same for both couplings, attempts have been made to develop correlations between $J_{C,H}$ and $J_{H,H}$ in order that predictions of carbon–proton coupling sizes in particular structures might be made from proton–proton models. In the case of vicinal couplings, parallel behavior of $^3J_{C,H}$ and $^3J_{H,H}$ with respect to dihedral angle is suggested by several investigations which indicate that vicinal carbon–proton couplings have an angular dependence similar to the Karplus relationship found for proton–proton systems (1–3). The conclusions regarding the electronic effect of substituents on $^3J_{C,H}$ seem somewhat more equivocal. Attempts to correlate substituent electronegativity with $^3J_{C,H}$ have led to the conclusion that definite correlations were not easily made but electronegativity effects did not appear to be very important (4, 5). Other results indicate that the electronic effect is quite large (6–8).

A recent report (9) describes the correlation of proton–proton couplings with carbon–proton couplings in analogous compounds in which the proton is replaced by a carboxylic acid group. For the series of 20 pairs of coupling constants, which include ^2J, ^3J, ^4J, and ^5J values, through aliphatic, aromatic, and olefinic systems, a plot of $J_{C,H}$ values against the corresponding $J_{H,H}$ values gave a 'straight line' (correlation coefficient 0.95). Although the average value of the ratio of $J_{C,H}$ to $J_{H,H}$ was 0.76, the ratio of individual pairs of compounds varied between 0.45 and 1.64. It would appear that the use of a simple ratio for predicting $J_{C,H}$ values from $J_{H,H}$ values would not yield reliable results, and that the different stereoelectronic effects of groups on $J_{C,H}$ and $J_{H,H}$ must be taken into account. In this investigation we have attempted to compare the effect of substituent electronegativity on $^3J_{C,H}$ and $^3J_{H,H}$ while as much as possible maintaining other factors constant. For this purpose $^3J_{C,H}$ values have been determined for a series of *tert*-butyl derivatives and compared to $^3J_{H,H}$ values

of the isopropyl analogues. This yields a comparison of a methyl group vs. a proton in identical situations. In each case the observed coupling would be the average of three coupling constants, two *gauche*, ${}^{g}J^{H,X}$ and ${}^{g}J^{H,C}$, and one *anti*, ${}^{a}J$ (Fig. 1).

In order that no factor might be introduced due to conformer population differences, the substituents were restricted to groups with axial symmetry, i.e. the halogens, hydrogen, and the methyl group. The results (Table 1) indicate that the ${}^{3}J_{C,H}$ values follow the trend of the ${}^{3}J_{H,H}$ values, decreasing with increasing electronegativity of the substituent.

Figure 2 shows plots of $J_{C,H}$, $J_{H,H}$, and their ratios against electronegativity, all showing monotonic decreases with increasing electronegativity. A plot of $J_{C,H}$ against $J_{H,H}$ (Fig. 3) gives a straight line (correlation coefficient 0.991) fitting eq. 1.

$$[1] \qquad {}^{3}J_{C,H} = 1.2\,{}^{3}J_{H,H} - 3.5$$

The results indicate a parallel behavior of the carbon–proton and proton–proton couplings toward substituent electronegativity, with the carbon–proton coupling appearing to be slightly more sensitive to the electronegativity effect (Fig. 3, slope = $dJ_{C,H}/dJ_{H,H} = 1.2$). This parallel behavior of the two types of couplings should not be projected to situations in which the substituent is in different positions or orientations relative to the coupled atoms. The electronegativity effect

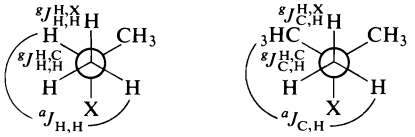

FIG. 1. Subscripts refer to the coupling atoms; superscripts refer to the atoms *anti* to the coupling atoms.

TABLE 1. Nuclear magnetic resonance data for isopropyl and *tert*-butyl derivatives

Substituent	E^a	${}^{3}J_{C,H}$	${}^{3}J_{H,H}$	Ratio
D	2.2	5.27	7.38[b]	0.714
CH_3	2.6	4.62	6.8[c]	0.679
I	2.65	4.45	6.69	0.665
Br	2.95	4.22	6.54	0.645
Cl	3.15	4.08	6.43	0.635
F	3.9	3.81	6.10	0.625

[a]Huggins electronegativity values (10).
[b]Reference 12.
[c]Reference 13.

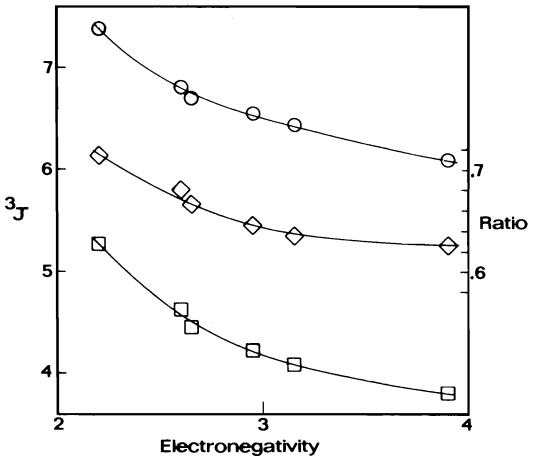

FIG. 2. Plot of ${}^{3}J_{H,H}$ (○), ${}^{3}J_{C,H}$ (□), and ${}^{3}J_{C,H}/{}^{3}J_{H,H}$ (◇) against Huggins (10) electronegativity values.

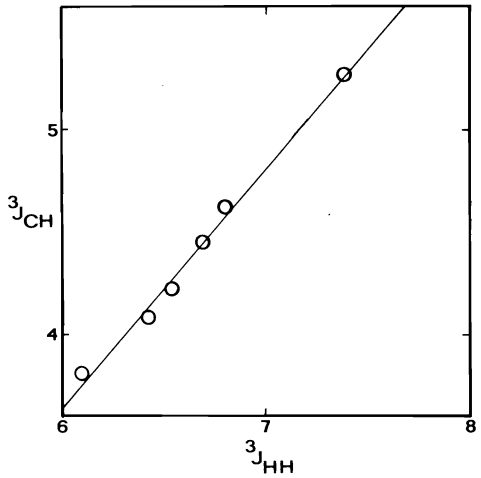

FIG. 3. Plot of vicinal proton–proton coupling constants from isopropyl derivatives against vicinal carbon–proton coupling constants in the *tert*-butyl analogues.

has been shown in the proton–proton case to be greatest when the substituent is *anti* to the proton (11). This effect has not been tested in this investigation since the electronegative substituent has always been *anti* to the proton in the compounds used. Furthermore, it has been reported (4, 8) that when the electronegative substituent is directly attached to the coupled carbon the size of the coupling constant increases with increasing electronegativity, although there seems to be some inconsistency in this trend.

Experimental

The coupling constants were obtained from ^{1}H spectra and natural abundance ^{13}C spectra, determined on a

Varian CFT 20 spectrometer using 65% v/v solutions in deuterochloroform at ambient temperature.

Acknowledgments

We are grateful to the National Research Council of Canada for financial assistance, to S. Sternhell in whose laboratories some of this work was conducted, and to G. Brophy and J. L. Nemorin for determining some of the spectra.

1. L. T. J. DELBAERE, M. N. G. JAMES, and R. U. LEMIEUX. J. Am. Chem. Soc. **95**, 7866 (1973).
2. J. A. SCHWARCZ, N. CYR, and A. S. PERLIN. Can. J. Chem. **53**, 1872 (1975).
3. R. WASYLISHEN and T. SCHAEFER. Can. J. Chem. **50**, 2710 (1972).
4. G. K. KARABATOS, J. D. GRAHAM, and F. M. VANE. J. Am. Chem. Soc. **84**, 37 (1962).
5. G. K. KARABATOS and C. E. ORZECH, JR. J. Am. Chem. Soc. **86**, 3574 (1964).
6. A. S. PERLIN and J. SCHWARCZ. Can. J. Chem. **50**, 3667 (1972).
7. R. U. LEMIEUX, T. NAGABHUSHAN, and B. PAUL. Can. J. Chem. **50**, 773 (1972).
8. C. A. KINGSBURY, D. DRONEY, A. SEPCHIK, W. RISSLER, and D. DURHAM. J. Org. Chem. **41**, 3863 (1976).
9. J. L. MARSHALL and R. SEIWELL. Org. Magn. Reson. **8**, 419 (1976).
10. M. L. HUGGINS. J. Am. Chem. Soc. **75**, 4123 (1953).
11. D. H. WILLIAMS and N. S. BHACCA. J. Am. Chem. Soc. **86**, 2742 (1964).
12. R. E. WASYLISHEN and T. SCHAEFER. Can. J. Chem. **52**, 3247 (1974).
13. J. S. WAUGH and F. W. DOBBS. J. Chem. Phys. **31**, 1235 (1959).

Application de la spectrométrie infrarouge, Raman et résonance magnétique nucléaire à l'étude des complexes en solution aqueuse. Al^{3+}–$H_2C_2O_4$

M. Jaber,[1] F. Bertin et G. Thomas-David

Laboratoire de Chimie Analytique II, Université de Lyon I, 43 boulevard du 11 Novembre 1918 69621 Villeurbanne, France

Reçu le 11 janvier 1977

M. Jaber, F. Bertin et G. Thomas-David. Can. J. Chem. **55**, 3689 (1977).

L'étude par spectrométrie Raman du système Al^{3+}–$H_2C_2O_4$ en solution aqueuse en fonction du degré d'acidité de solutions et du rapport t = [métal]/[coordinat] montre très nettement la formation successive de complexes $Al(C_2O_4)^+$, $Al(C_2O_4)_2^-$ et $Al(C_2O_4)_3^{3-}$. La formation de l'espèce $Al(C_2O_4)^+$ qui avait été rejetée par certains auteurs est confirmée ici et l'on peut identifier facilement ses fréquences caractéristiques ainsi que celles de l'espèce $Al(C_2O_4)_2^-$. La rmn de deux noyaux ^{27}Al et ^{13}C confirme ces résultats et permet d'identifier chaque complexe par un signal bien caractéristique. De plus cette étude nous a permis de rejeter l'hypothèse d'une formation de complexes hydroxydés du moins en quantité importante.

Nous avons pu également utiliser les hauteurs de bandes de diffusion Raman aux huit fréquences sélectionnées caractéristiques des espèces $Al(C_2O_4)^+$, $Al(C_2O_4)_2^-$ et $Al(C_2O_4)_3^{3-}$ pour déterminer leur distribution en fonction de l'acidité de la solution.

M. Jaber, F. Bertin, and G. Thomas-David. Can. J. Chem. **55**, 3689 (1977).

A study by Raman spectrometry of the system Al^{3+}–$H_2C_2O_4$ in aqueous solution as a function of the acidity of the solution and of the ratio t = [metal]/[ligand] shows very clearly the successive formation of the complexes $Al(C_2O_4)^+$, $Al(C_2O_4)_2^-$, and $Al(C_2O_4)_3^{3-}$. The formation of the species $Al(C_2O_4)^+$, which had been rejected by some authors, is confirmed and it was easily possible to identify its characteristic frequencies as well as those of the species $Al(C_2O_4)_2^-$. The ^{27}Al and ^{13}C nmr spectra confirm these results and allow the identification of each complex by means of a clearly characteristic signal. Moreover, the results of this study permit the rejection of the hypothesis of the formation of hydroxylated complexes, at least in important quantities.

It also was possible to use the intensities of the Raman scattering bands at eight selected characteristic frequencies of the species $Al(C_2O_4)^+$, $Al(C_2O_4)_2^-$, and $Al(C_2O_4)_3^{3-}$ to determine their distribution as a function of the acidity of the solution.

[Journal translation]

Introduction

Dans un travail antérieur appliqué à l'acide oxalique (1), nous avons mis au point une méthode de détermination des concentrations des différentes espèces en équilibre: $H_2C_2O_4$, $HC_2O_4^-$ et $C_2O_4^{2-}$ en mesurant les hauteurs des bandes Raman caractéristiques de chaque espèce, et nous en avons déduit les constantes de formation de l'acide oxalique. Les résultats obtenus, en bon accord avec ceux de la méthode classique de pH, nous ont convaincu de l'utilité de la spectrométrie Raman pour suivre des équilibres se formant en milieu très acide, là où la potentiométrie ne peut pas donner des renseignements précis.

Nous avons étudié le système $H_2C_2O_4$–Al^{3+} pour lequel certains travaux mettent en évidence la présence de deux complexes seulement: $Al(C_2O_4)_2^-$ et $Al(C_2O_4)_3^{3-}$, et donnent des valeurs pour les constantes successives K_2 et K_3 (2) ou globales β_2 et β_3 (3, 4). Dutt et Sur (2) en particulier affirment que le complexe $Al(C_2O_4)^+$ ne se forme pas, la complexation conduisant directement à l'espèce $Al(C_2O_4)_2^-$. Seul Babko et Dubovenko (5) ont mis en évidence par spectrophotométrie d'absorption uv l'existence de trois espèces successives, mais les valeurs obtenues pour K_2 et K_3 diffèrent beaucoup de celles obtenues par Dutt. Enfin signalons que Zolotukhin (4) a remarqué la formation des complexes hydroxydés sans indiquer leur nature.

Devant ce nombre restreint de résultats et leur discordance, nous avons tenté de reprendre l'étude de ce système d'abord par la méthode de pH, mais celle-ci s'avère inadéquate car les complexes se forment en milieu trop acide; la courbe de formation de Bjerrum que nous avons obtenue pour ce système n'est pas exploitable

[1]Boursier du C.N.R.S. Libanais.

(1). Par contre l'évolution, en fonction du pH, des spectres Raman de solutions contenant le coordinat acide oxalique et les ions Al^{3+} permet de suivre les équilibres de formation de complexes et ce sont les résultats de cette étude que nous présentons ici. Jusqu'à présent seul le spectre de diffusion d'une solution aqueuse de $K_3Al(C_2O_4)_3$ a intéressé plusieurs auteurs (6–10, 14).

Parallèlement, nous avons examiné nos solutions par la résonance magnétique nucléaire de deux noyaux ^{27}Al et ^{13}C, afin de dénombrer et de caractériser les espèces en présence. Dans ce domaine, seule la rmn de ^{27}Al a été étudiée par Haraguchi et Fujiwara (11) et Toy et coll. (12); ces auteurs montrent l'existence d'une seule raie attribuée au composé $Al(C_2O_4)_3^{3-}$ mais de déplacement chimique nul par rapport à la raie de l'espèce $Al(H_2O)_6^{3+}$ (11).

Conditions expérimentales

Les solutions étudiées sont de concentration 0.50 M en acide oxalique avec des concentrations en Al^{3+} telles que le rapport (métal)/(coordinat): $t = \frac{1}{6}, \frac{1}{3}, \frac{1}{2}$ et 1. On fixe l'acidité des solutions qui sont absentes de sel de fond par addition de potasse 10 M ou d'acide chlorhydrique Prolabo R.P. L'acidité est exprimée soit par le pH, soit par la concentration équivalente en acide chlorhydrique mesurée par l'intermédiaire d'un potentiomètre Metrohm E 388, au moyen de la chaîne suivante: electrode en verre/solution titrée/NaCl saturé/Hg_2Cl_2–Hg, préalablement étalonnée.

Toutefois la précision sur la mesure du pH est faible compte tenu de la valeur élevée et variable de la force ionique, c'est pourquoi on donne les valeurs du pH à 0.1 unité près.

Le domaine d'étude est limité pour chaque rapport par le début de précipitation de l'hydroxyde d'aluminium: p$H \sim 3.0$ pour $t = 1$, p$H \sim 4$ pour $t = \frac{1}{2}$ et p$H \sim 6.4$ pour $t = \frac{1}{3}$. Dans l'ensemble une cinquantaine de spectres sont enregistrés afin de suivre de façon systématique l'évolution des spectres en fonction de l'acidité donc de la complexation.

Les solutions deutériées aux différentes acidités sont préparées à partir de l'oxalate de sodium et de chlorure d'aluminium, produits Merck, par addition de DCl ~ 7.8 N dont la teneur en D_2O est 99.5%.

Les spectres Raman sont enregistrés à la température ordinaire (20°C) dans un domaine de fréquences compris entre 1800 et 150 cm^{-1} avec un spectromètre Coderg modèle PHO équipé d'un laser à argon ionisé Spectra-physics. La longueur d'onde de la raie excitatrice est de 488 nm. L'échantillon à examiner est contenu dans une petite cuve en verre parallélépipédique de 0.3 ou 1 ml. Les spectres ir sont enregistrés dans un domaine de fréquences compris entre 2000 et 700 cm^{-1} avec un spectromètre Perkin-Elmer 457. L'épaisseur des cellules en Irtran II utilisées est de 27 μm.

Les spectres de rmn, sont enregistrés à la température ordinaire avec le spectromètre Varian XL 100 du centre de rmn (Fédération des Centres Lyonnais de Mesures et d'Analyses) à la fréquence de 25.2 MHz. Pour le ^{13}C, le champ est stabilisé grâce aux noyaux de deutérium de C_6D_6 utilisé également comme référence externe; l'enregistrement est effectué après une accumulation de 10^4 passages environ. Dans l'étude du noyau ^{27}Al, il est impossible d'utiliser la même technique de stabilisation; nous ne disposions pas, d'autre part, de lock externe. Néanmoins, le champ était suffisamment stable pour que les résultats obtenus soient très reproductibles. L'enregistrement est réalisé avec une accumulation de 10^2 passages; la référence est constituée par les ions $Al(H_2O)_6^{3+}$ contenus dans la solution, ou introduits en référence externe (solution de $AlCl_3$ à p$H \sim 0$) quand tous les ions Al^{3+} de la solution étudiée sont complexés.

Résultats de la spectrométrie Raman

L'évolution des spectres Raman en fonction de l'acidité des solutions pour différents rapports [métal]/[coordinat] est présentée dans les tableaux 1 et 2 où sont indiquées les bandes des spectres Raman les plus caractéristiques pour les trois rapports étudiés en donnant les fréquences et leur intensité relative par rapport à la bande de l'eau située à 1640 cm^{-1} (1).

L'observation globale des spectres Raman des solutions d'oxalatoaluminate, pour $t = \frac{1}{3}$, nous permet de distinguer trois domaines principaux (tableau 1).

Au degré d'acidité $[HCl_{eq}] = 4.8$ N le spectre comporte les bandes de l'acide oxalique situées à 456, 590, 848, 1335, 1460 et 1750 cm^{-1} et la bande de l'ion $Al(H_2O)_6^{3+}$ à 523 cm^{-1} (1). Pour $4.8\ N > [HCl_{eq}] > 1.7\ N$, ces bandes diminuent régulièrement en intensité et la formation des complexes se manifeste par l'apparition de bandes intenses situées aux fréquences: 373, 573, 915, 1423, 1698 et 1727 cm^{-1} qui augmentent d'intensité au fur et à mesure de la neutralisation.

Dans l'intervalle suivant jusqu'à p$H \sim 0.5$, les bandes du coordinat continuent à diminuer, celles des complexes situées à 373, 573, 1698 et 1727 cm^{-1} se déplacent progressivement pour atteindre les fréquences 370, 580, 1689 et 1732 cm^{-1} à p$H = 0.4$, tandis que les deux bandes 915 et 1423 cm^{-1} maintiennent leurs positions initiales. Les intensités relatives des bandes se modifient nettement.

Pour les solutions de $0.5 <$ p$H < 2.1$, nous remarquons la diminution d'intensité des bandes dues à $H_2C_2O_4$ et de la bande de $HC_2O_4^-$ apparue à 868 cm^{-1} et qui disparait complète-

TABLEAU 1. Spectres Raman des oxalates complexes de Al^{3+} dans un rapport $t = \frac{1}{3}$ à différentes acidités

$[HCl_{eq}] = 4.9\ N$		$[HCl_{eq}] = 3.1\ N$		$[HCl_{eq}] = 2.1\ N$		$pH \sim 0$		$pH = 0.5$		$pH = 0.8$		$pH = 1.5$		$pH = 2.3$		$pH = 6.3$	
Fréq.	h_v	Fréq.	h_v	Fréq.	h_v	Fréq.	h_v	Fréq.	h_v	Fréq.	h_v	Fréq.	h_v	Fréq.	h_v	Fréq.	h_v
										273?		273	0.13	273	0.13	273	0.15
				373	0.07	370	0.34	371	0.43	371	0.37	369	0.32	369	0.31	369	0.34
455	0.79	455	0.65	456	0.62	456	0.36							433?		433?	
523		523						460	0.25	462	0.20	468	0.13	473	0.12	473	0.11
		573	0.10	573	0.25	580	0.89	582	1.25	582	1.35	583	1.46	583	1.93	583	1.93
				608		608		608		608		608		608	0.33	608	0.34
								811		811		811		811		811	0.03
846	1.51	846	1.43	848	1.35	848	0.70	848	0.35	848	0.20						
						858		859	0.41	859	0.31	859	0.18	859	0.18	859	0.15
								868		868		868?					
		915		915	0.15	915	0.60	916	0.88	917	1.00	917	1.20	918	1.68	918	1.68
						1278		1278		1278		1278		1278		1278	
1335?																1308	0.05
										1408?		1408	1.39	1408	1.50	1408	1.43
		1423	0.14	1423	0.44	1423	1.38	1426	1.98	1427	2.30	1428	2.96	1429	3.42	1429	3.45
1460	0.08	1460	0.09	1460	0.09											1486	0.05
				1698		1693		1690		1688		1686		1686		1686	
		1727	1.28	1727	1.41	1732	1.72	1733	1.70	1733	1.50	1732		1723		1723	
								1746?		1746?		1746	1.46	1746	1.71	1746	1.61
1750	1.88	1750	1.83	1750	1.70	1750	1.01										

TABLEAU 2. Spectres Raman des oxalates complexes de Al^{3+} dans des rapports $t = 1$ et $t = \frac{1}{2}$ à différentes acidités

$t = 1$								$t = \frac{1}{2}$											
$[HCl_{eq}] = 3.9$		$[HCl_{eq}] = 2.00$		$pH = 0.00$		$pH = 3.0$		$[HCl_{eq}] = 3.2\,N$		$[HCl_{eq}] = 1.9\,N$		$[HCl_{eq}] = 1.1\,N$		$pH = 0.6$		$pH = 1.9$		$pH = 3.6$	
Fréq.	h_v	Fréq.	h_v	Fréq.	h_v	Fréq.	h_v	Fréq.	h_v	Fréq.	h_v	Fréq.	h_v	Fréq.	h_v	Fréq.	h_v	Fréq.	h_v
																273?		273	
373	0.02	373	0.26	373	0.46	373	0.48	373		373	0.18	372	0.36	370	0.59	370	0.57	370	0.62
456	0.51	455	0.24	455	0.05	453	0.06	456	0.60	455	0.42	455	0.24	463	0.12	473	0.08	473	0.09
523		523						523											
573	0.11	574	0.72	576	1.12	577	1.43	573	0.22	573	0.56	578	0.95	580	1.51	580	1.57	580	1.64
		608		608		608		608		608		608		608		608		608	
																811?		811?	
848	1.13	848	0.48					848	1.25	848	0.90	848	0.47	848					
				859	0.16	859	0.14					859		859	0.19	859	0.15	859	0.16
915	0.09	915	0.42	915	0.74	915	0.92	915	0.10	915	0.33	915	0.61	915	0.98	915	1.11	915	1.19
1278		1278		1278		1278				1278		1278		1278		1278		1278	
																1408?		1408	
1423	0.28	1423	1.14	1423	1.73	1423	1.96	1423	0.31	1423	0.80	1423	1.42	1423	2.13	1424	2.48	1424	2.47
1460	0.10							1460	0.11	1460	0.11								
1698		1698		1698		1696		1698		1698		1696		1689		1689		1689	
1727	1.11	1727	1.63	1727	1.92	1727	1.83	1727	1.22	1727	1.49	1729	1.70	1731	1.69	1732	1.80	1732	1.66
																		1746	
1750	1.52	1750	0.81					1750	1.62	1750	1.22	1750	0.77						

ment à pH = 1.4. Les fréquences de vibration des complexes situées à 370, 580, 915, 1423 et 1689 cm^{-1} migrent respectivement vers 369, 583, 918, 1429 et 1686 cm^{-1} avec une modification considérable d'intensité. La bande à 1732 cm^{-1} tend à disparaître et il se forme dans ce domaine de fréquences une bande située à 1746 cm^{-1}; la présence simultanée de ces deux bandes se voit très nettement sur les spectres correspondants aux pH 0.8, 0.9, 1.2 et 1.5. En même temps cinq raies nouvelles situées à 273, 473, 811, 1408 et 1723 cm^{-1} sont observées.

Pour les valeurs du pH > 2.1, les positions et les intensités des bandes restent constantes. Deux raies de très faible intensité dues à l'ion $C_2O_4^{2-}$ en solution (1) apparaissent vers 1308 et 1486 cm^{-1} pour les pH > 5 (le pH varie brusquement par addition de soude de pH 2.3 à 5).

Pour $t = \frac{1}{2}$ (tableau 2), les spectres des solutions d'acidité 4.9 N > $[HCl_{eq}]$ > 1.9 N présentent les bandes déjà observées dans la première étape du rapport $t = \frac{1}{3}$. Les bandes des complexes augmentent d'intensité sans modification des fréquences. Dans l'intervalle $[HCl_{eq}] = 1.9\ N - pH < 0.6$ les bandes de $H_2C_2O_4$ diminuent pour disparaître complètement; celles des complexes qui augmentent d'intensité subissent la même modification importante signalée dans la deuxième étape du rapport $t = \frac{1}{3}$. Et pour des pH > 0.6, les bandes des complexes gardent des fréquences constantes, leurs intensités augmentent légèrement et il apparait une bande supplémentaire à 473 cm^{-1} attribuable aux complexes; enfin juste avant la précipitation de l'hydroxyde d'aluminium on aperçoit deux bandes très faibles situées à 273 et 811 cm^{-1} et deux épaules faibles aussi vers 1408 et 1746 cm^{-1}, intenses sur les spectres du rapport $t = \frac{1}{3}$ à pH > 0.5.

Pour $t = 1$ (tableau 2), les complexes commencent à se former dans un milieu très acide, à une concentration en $[HCl_{eq}] = 4.9\ N$. La neutralisation des solutions entraîne la même évolution observée pour $t = \frac{1}{3}$, dans le domaine 4.8 N > $[HCl_{eq}]$ > 1.7 N et pour $t = \frac{1}{2}$, 4.9 N > $[HCl_{eq}]$ > 1.9 N. Les bandes des complexes augmentent d'intensité sans changer de fréquence sur toute la gamme d'acidité à l'exception de celle à 573 cm^{-1} qui commence à se déplacer légèrement pour $[HCl_{eq}] \sim 1.8\ N$ pour atteindre 577 cm^{-1} à pH 0.2. A cette valeur de pH les bandes dues à $H_2C_2O_4$ et à $Al(H_2O)_6^{3+}$ ont disparu et il n'apparait aucune bande caractéristique de l'ion $HC_2O_4^-$.

Discussion

1. Mise en évidence des espèces $Al(C_2O_4)^+$, $Al(C_2O_4)_2^{2-}$ et $Al(C_2O_4)_3^{3-}$ par spectrométrie Raman

Pour le rapport $t = 1$ quelle que soit l'acidité de la solution, les fréquences observées pour les complexes ont une position constante à l'exception de la bande à 573 cm^{-1} qui se déplace légèrement. Ces mêmes fréquences étant observées pour les rapports $t = \frac{1}{2}$ et $t = \frac{1}{3}$ aux fortes acidités, on peut penser que dans ces domaines le complexe $Al(C_2O_4)^+$ est prépondérant, ses fréquences caractéristiques sont 373, 453, 573, 608, 859, 915, 1278, 1423, 1698 et 1727 cm^{-1}.

Pour le rapport $t = \frac{1}{3}$ à pH > 2.1, les bandes du coordinat ayant complètement disparu, le complexe en solution ne peut être que $Al(C_2O_4)_3^{3-}$ dont les fréquences de vibration caractéristiques sont 273, 369, 473, 583, 608, 811, 859, 918, 1278, 1408, 1429, 1686, 1723 et 1746 cm^{-1}. Notons que ces fréquences sont tout à fait comparables à celles observées pour le complexe $K_3Al(C_2O_4)_3 \cdot 3H_2O$ cristallisé (1). Par contre le déplacement très net de certaines bandes dans l'intervalle $[HCl_{eq}] < 1.7\ N - pH < 0.5$ pour le même rapport caractérise la présence d'une nouvelle espèce vraisemblablement $Al(C_2O_4)_2^-$. En effet une telle modification spectrale n'est pas attribuable à l'existence simultanée des deux espèces $Al(C_2O_4)^+$ et $Al(C_2O_4)_3^{3-}$ car on devrait constater simultanément une migration des deux bandes 915 et 1423 cm^{-1} vers 918 et 1429 cm^{-1}, d'autant plus que ces dernières possèdent des coefficients de diffusion beaucoup plus grands que les premières; de plus l'existence du composé $Al(C_2O_4)_3^{3-}$ doit se manifester par l'apparition des deux bandes fortes situées à 1408 et 1746 cm^{-1} ce qui n'est pas le cas. Les mêmes modifications se produisent pour le rapport $t = \frac{1}{2}$ dans l'intervalle d'acidité $[HCl_{eq}] < 1.9\ N - pH < 0.6$ confirmant une telle attribution. L'existence de deux espèces $Al(C_2O_4)_2^-$ et $Al(C_2O_4)_3^{3-}$ en solution pour $t = \frac{1}{3}$ se manifeste à pH = 0.9 par la juxtaposition très nette de deux bandes 1732 et 1746 cm^{-1}. Donc les fréquences de vibration dues à l'espèce $Al(C_2O_4)_2^-$ se situent à 370, 473, 580, 608, 859, 915, 1278, 1423, 1689 et 1732 cm^{-1}.

Il est à noter que dans le cas du rapport $t = 1$, pour les pH élevés, l'espèce $Al(C_2O_4)_2^-$ doit être présente en quantité non négligeable puisqu'on constate un déplacement de fréquence de la bande à 573 cm^{-1} vers 577 cm^{-1}. De même la présence du complexe $Al(C_2O_4)_3^{3-}$ en faible concentration, à des pH élevés dans un rapport $t = \frac{1}{2}$ explique l'apparition des bandes très faibles vers 273, 811, 1408 et 1746 cm^{-1}.

Sur la fig. 1, on donne les spectres des oxalatoaluminates enregistrés dans des conditions telles que chaque complexe est majoritaire. On observe nettement les modifications d'intensité relative des bandes reportée à la même intensité de la bande de l'eau, en passant d'une espèce à une autre. Les tableaux 1 et 2 montrent plus clairement la différence en fréquences.

Le spectre que nous attribuons au complexe $Al(C_2O_4)_3^{3-}$ en solution est très proche de celui obtenu récemment par Vaisserman et Gouteron avec toutefois quelques écarts dans les fréquences et une bande supplémentaire située à 811 cm^{-1} observée également par Murata.

On remarquera que la formation des complexes hydroxydés, si elle existe, ne peut avoir lieu en forte proportion car on devrait sans doute assister à une modification progressive du spectre pour les pH élevés surtout pour les rapports $t = 1$, et $t = \frac{1}{2}$, ce qui n'est pas le cas; de plus la concentration en ion oxalate calculée sur les deux bandes 1308 et 1486 cm^{-1} garde une valeur très faible.

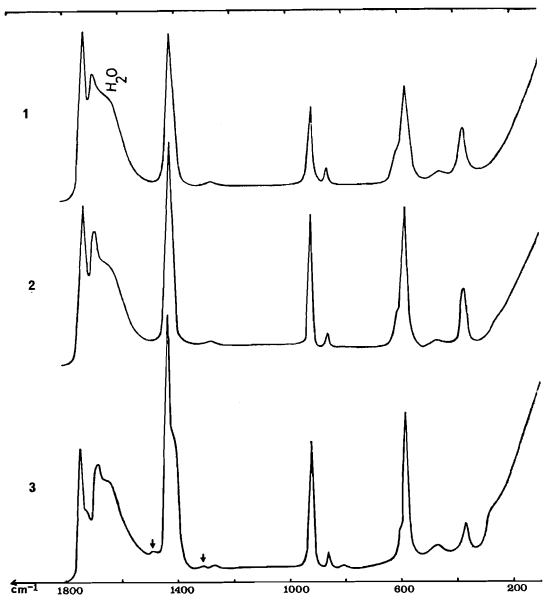

FIG. 1. Spectres Raman des oxalatoaluminates en solution aqueuse. (*1*) $t = 1$, p$H = 2.5$; (*2*) $t = \frac{1}{2}$, p$H = 1$; (*3*) $t = \frac{1}{3}$, p$H = 6.4$. (↓) Bandes de $C_2O_4^{2-}$ en solution.

2. Confirmation apportée par les spectres infrarouge

L'évolution des spectres ir des oxalatoaluminates à différentes acidités nous permet, pour un rapport $t = \frac{1}{3}$, de distinguer deux étapes différentes.

La première caractérise une espèce individuelle prépondérante à p$H > 2.1$ où les bandes du coordinat ont disparu. Puisque la précipitation de l'hydroxyde d'aluminium n'a lieu qu'à p$H \sim 6.4$ les ions Al^{3+} sont complexés et l'espèce ne peut être que $Al(C_2O_4)_3^{3-}$ caractérisée par les fréquences d'absorption ir 810, 825, 912, 1270, 1290, 1405, 1450?, 1690 et 1720 cm^{-1}, qui sont analogues à celles observées pour le complexe $K_3Al(C_2O_4)_3 \cdot 3H_2O$ à l'état cristallisé (7, 9, 14).

La seconde étape s'étend du $[HCl_{eq}] = 4.8\ N$ jusqu'à p$H \sim 0.5$; elle est caractérisée, outre les bandes du coordinat libre, par les fréquences 820, 912, 1280, 1415, 1440?, 1695 et 1725 cm^{-1}; ces fréquences sont observées aussi pour le rapport $t = 1$ sur toute la gamme d'acidité étudiée, elles correspondent donc au complexe $Al(C_2O_4)^+$, par analogie aux résultats de la spectrométrie Raman.

Les spectres ir ne subissent pratiquement pas des modifications résultant du passage de l'espèce $Al(C_2O_4)^+$ à $Al(C_2O_4)_2^-$. D'ailleurs pour le rapport $t = \frac{1}{2}$ à p$H \sim 3$ le spectre est analogue à celui du rapport $t = 1$, à ceci près qu'il présente deux bandes à 1720 et 810 cm^{-1} dues à la présence d'une quantité importante de complexe $Al(C_2O_4)_3^{3-}$ (1).

3. Confirmation obtenue par résonance magnétique nucléaire des noyaux ^{27}Al et ^{13}C

3.1. Résonance magnétique nucléaire du ^{27}Al

Les résultats obtenus sont schématisés sur la fig. 2. Pour les deux rapports $t = \frac{1}{3}$ et $t = \frac{1}{6}$ à pH 5, un seul signal symétrique est obtenu (*a*); il est caractéristique du composé $Al(C_2O_4)_3^{3-}$ et se situe à 405 Hz du signal de $Al(H_2O)_6^{3+}$ pris comme référence. Pour le rapport $t = 1$ et une acidité $[HCl_{eq}] \sim 1.5\ N$, le spectre comporte aussi un seul signal large, symétrique (*d*) situé à 160 Hz de la référence; quand on neutralise la solution par la potasse, ce signal s'éloigne de la

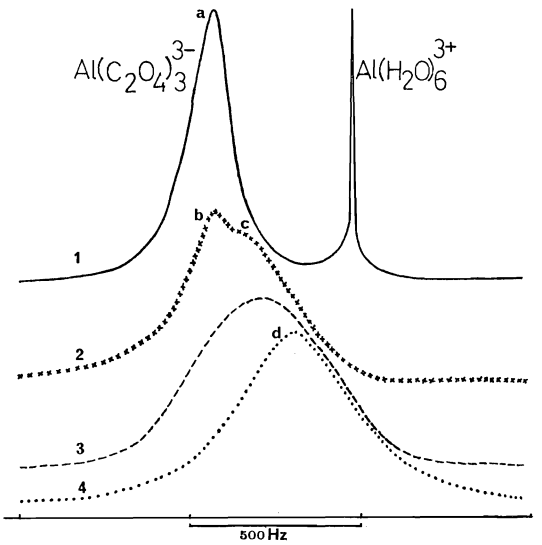

FIG. 2. Spectres rmn du noyau ^{27}Al des oxalatoaluminates à différentes acidités et pour différents rapports. (*1*) $t = \frac{1}{3}$, p$H = 5$; (*2*) $t = \frac{1}{2}$, p$H = 2$; (*3*) $t = \frac{1}{2}$, p$H =$ 0.1; (*4*) $t = 1$, p$H \sim 0$.

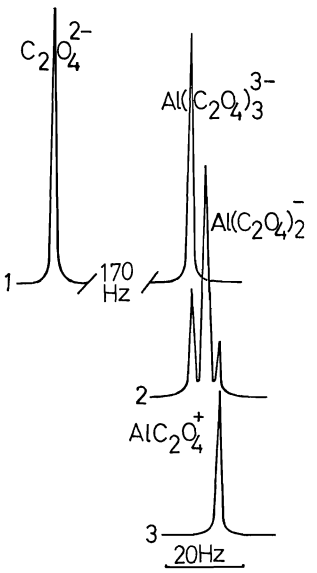

FIG. 3. Spectres rmn du noyau ^{13}C des oxalatoaluminates en solution. (*1*) $t = \frac{1}{6}$, p$H = 6$; (*2*) $t = \frac{1}{2}$, p$H = 3$; (*3*) $t = 1$, p$H \sim 0.1$.

référence tout en gardant sa symétrie sur toute la gamme d'acidité.

L'étude systématique du rapport $t = \frac{1}{2}$ en fonction du degré d'acidité conduit en milieu très acide aux mêmes résultats que ceux obtenus pour le rapport $t = 1$. L'augmentation du pH entraîne un déplacement régulier du signal sans changement de symétrie (exemple: courbe *3*) puis on observe dans l'intervalle $0.6 <$ p$H <$ 4 un dédoublement de la raie: une des deux raies se trouve à la fréquence caractéristique de $Al(C_2O_4)_3^{3-}$ (405 Hz) (*b*); la deuxième (*c*) qui se trouve à environ 330 Hz de la référence est due très probablement à l'espèce $Al(C_2O_4)_2^{-}$; il semble que la raie large observée aux fréquences intermédiaires résulte de l'échange des noyaux ^{27}Al entre les deux espèces $Al(C_2O_4)^{+}$ et $Al(C_2O_4)_2^{-}$ dont les concentrations relatives varient avec le pH.

3.2. Résonance magnétique nucléaire du ^{13}C

On donne sur la fig. 3 certains spectres caractéristiques. Pour le rapport $t = \frac{1}{6}$ à p$H \sim 5$, les spectres rmn comportent deux signaux de même intensité, l'un caractéristique de $C_2O_4^{2-}$, présent en excès, à 1170 Hz l'autre situé à 970 Hz est attribué à $Al(C_2O_4)_3^{3-}$. Pour le rapport $t = \frac{1}{3}$ on observe seulement le signal dû à $Al(C_2O_4)_3^{3-}$; ceci implique que tous les carbones de ce composé résonnent à la même fréquence.

Pour un rapport $t = 1$ à $[HCl_{eq}] = 1.5\ N$, on observe un seul pic situé à 965 Hz, qui ne peut être dû qu'à l'espèce $Al(C_2O_4)^{+}$. Pour un rapport $t = \frac{1}{2}$ à p$H \sim 3$, le spectre présente trois signaux voisins, les deux extrêmes se trouvent aux fréquences caractéristiques des espèces $Al(C_2O_4)^{+}$ et $Al(C_2O_4)_3^{3-}$, le troisième situé au milieu (967 Hz), le plus intense est certainement dû à $Al(C_2O_4)_2^{-}$ en solution. Cette attribution est confirmée par les variations d'intensité relative des trois raies en fonction du pH sur le même rapport. Plusieurs spectres d'un même échantillon enregistrés en faisant varier le temps d'acquisition et le temps d'attente entre deux passages montrent que les phénomènes de relaxation n'influencent pratiquement pas les intensités relatives des trois pics.

Les résultats de la rmn de deux noyaux ^{27}Al et ^{13}C recoupent ceux que nous avions observés par spectrométrie Raman; mais l'interférence des pics et la faible différence des déplacements chimiques, 2 et 3 Hz, ne permettent pas une mesure directe des concentrations en espèces.

4. Méthode de détermination des concentrations, par spectrométrie Raman, des différents complexes formés

4.1. Choix des bandes

Après avoir mis en évidence par Raman et rmn la présence de trois espèces en solution et identifié les bandes de diffusion propres à

chacune, nous tentons d'exploiter les hauteurs de ces bandes pour déterminer la concentration des oxalatoaluminates complexes; cette exploitation est d'autant plus difficile que ces espèces sont simultanément présentes en solution et que les bandes interfèrent entre elles.

Pour déterminer la concentration de deux espèces $H_2C_2O_4$ et $HC_2O_4^-$ on utilise la hauteur des bandes à 848 et 868 cm^{-1} caractéristiques de ces espèces et qui sont peu influencées par la bande très faible des complexes, située à 859 cm^{-1}; les deux bandes 1308 et 1486 cm^{-1} sont utilisées pour calculer $[C_2O_4^{2-}]$.

Pour calculer la concentration des trois complexes $Al(C_2O_4)^+$, $Al(C_2O_4)_2^-$ et $Al(C_2O_4)_3^{3-}$ on peut utiliser les hauteurs des bandes aux fréquences 369, 373, 573, 583, 915, 918, 1423 et 1429 cm^{-1} qui n'interfèrent pas avec les fréquences de vibration propres au coordinat, en particulier les deux dernières bandes ne sont certainement pas influencées par le triplet 1380–1410–1444 cm^{-1}, dû à $HC_2O_4^-$: l'intensité de ce triplet doit en effet être très faible puisque la bande à 868 cm^{-1} caractéristique de cette même espèce et dont le coefficient de diffusion est trois fois supérieur à celui du triplet (1) n'est visible que pour un rapport $t = \frac{1}{3}$ et dans un domaine de pH étroit.

Pour tous les calculs, la bande de l'eau est utilisée comme étalon interne, dans les mêmes conditions que précédemment (1).

4.2. Principe de la méthode de calcul des concentrations

Les symboles utilisés ont la signification suivante: X, Y et Z sont respectivement les concentrations de $H_2C_2O_4$, $HC_2O_4^-$ et $C_2O_4^{2-}$; A_ν, B_ν et C_ν sont les coefficients de diffusion respectifs à la fréquence ν, déterminés dans un travail antérieur (1). P, Q et R sont les concentrations de $Al(C_2O_4)^+$, $Al(C_2O_4)_2^-$ et $Al(C_2O_4)_3^{3-}$, D_ν, E_ν et F_ν leurs coefficients de diffusion (paragraphe 4.3). h_ν représente à la fréquence ν l'intensité relative, par rapport à la bande de l'eau 1640 cm^{-1}, d'une bande qui peut être due à la contribution de plusieurs espèces. C_L et C_M sont respectivement les concentrations analytiques du ligand et du métal en solution.

Le principe de la méthode de calcul est le suivant: les bandes 848, 868, 1308 et 1486 cm^{-1} permettent de déterminer la concentration du coordinat libre selon les relations:

$$[1] \quad h_{848} = XA_{848} + YB_{848}$$

$$[2] \quad h_{868} = XA_{868} + YB_{868}$$

$$[3] \quad h_{1308} = ZC_{1308}; \quad h_{1486} = ZC_{1486}$$

Les relations de bilan pour le coordinat et le métal sont:

$$[4] \quad C_L = X + Y + Z + P + 2Q + 3R$$

$$[5] \quad C_M = [Al^{3+}] + P + Q + R$$

Etant donné l'interférence des bandes de diffusion dues aux trois complexes pour chacune des huit fréquences sélectionnées, on peut écrire huit relations du type:

$$[6] \quad h_\nu = PD_\nu + QE_\nu + RF_\nu$$

Ayant déterminé de proche en proche les coefficients de diffusion D_ν, E_ν, et F_ν un programme intitulé SPECTRAL, analogue au programme SPECTRAM (1) utilisé précédemment, permet de calculer par moindres carrés les concentrations optimales P, Q et R.

4.3. Calcul des coefficients de diffusion D_ν, E_ν et F_ν à différentes fréquences

On se place d'abord dans des conditions telles que $Al(C_2O_4)^+$ est le seul complexe présent en solution, ceci est réalisé pour les différents rapports t en milieu suffisamment acide. Les relations 1 et 2 donnent facilement le bilan du coordinat non engagé et par conséquent la valeur de P, d'après l'éq. 4. D_ν est ensuite calculé suivant la relation 6. Les résultats obtenus sont rassemblés dans le tableau 3.

On utilise ensuite les spectres obtenus dans un rapport stoechiométrique $t = \frac{1}{3}$ et dans un domaine de pH élevé, compris entre 2.5 et 6.4 où la formation du complexe $Al(C_2O_4)_3^{3-}$ est pratiquement totale, les bandes dues aux complexes gardent une intensité pratiquement constante; les bandes à 1308 et 1486 cm^{-1} du coordinat libre donnent une estimation de $Z \sim 0.01$ M soit 2% de C_L. Etant donné la grande stabilité du trioxalatoaluminate, on peut considérer P et $[Al^{3+}]$ comme pratiquement nulles et les éqs 4 et 5 entraînent:

$$R = C_M - Z; \quad Q = Z$$

Si de plus on néglige, en première approximation, l'influence du complexe $Al(C_2O_4)_2^-$ on peut calculer directement les différents co-

TABLEAU 3. Coefficients de diffusion D_v

Rapport t	$[HCl_{eq}]$	$X + Y$	P	D_{369}	D_{373}	D_{573}	D_{583}	D_{915}	D_{918}	D_{1423}	D_{1429}
1	3.1	0.26	0.16	0.52	0.45	2.01	1.57	1.08	1.02	2.74	2.40
1	2.0	0.14	0.33	0.66	0.75	2.15	1.83	1.18	1.10	3.24	2.82
$\frac{1}{2}$	3.2	0.32	0.09	0.50	0.40	1.97	1.66	0.91	0.78	2.76	2.16
$\frac{1}{2}$	2.6	0.31	0.12	0.51	0.65	2.21	1.65	1.18	0.93	3.13	2.39
Moyenne				0.5 ±0.1	0.6 ±0.2	2.1 ±0.1	1.7 ±0.1	1.1 ±0.1	1.0 ±0.2	3.0 ±0.3	2.4 ±0.4

TABLEAU 4. Coefficients de diffusion F_v

pH	F_{369}	F_{373}	F_{573}	F_{583}	F_{915}	F_{918}	F_{1423}	F_{1429}
2.1	1.81	1.68	4.69	11.47	8.74	10.10	17.86	21.79
4.9	1.87	1.75	4.72	11.29	8.62	9.84	16.81	20.83
5.5	1.79	1.74	4.08	11.67	7.50	9.82	15.93	20.81
6.1	1.96	1.81	4.39	11.56	8.46	10.00	15.80	20.75
6.4	1.94	1.74	5.18	11.96	8.09	9.87	15.21	19.56
Moyenne	1.87 ±0.09	1.74 ±0.07	4.6 ±0.6	11.6 ±0.4	8.3 ±0.8	9.9 ±0.2	16.0 ±1	21 ±1

TABLEAU 5. Coefficients de diffusion E_v

Rapport t	pH	$X + Y = Q$	R	E_{369}	E_{373}	E_{573}	E_{583}	E_{915}	E_{918}	E_{1423}	E_{1429}
$\frac{1}{3}$	0.5	0.13	0.02	2.76	2.69	5.10	6.60	4.37	4.24	10.35	9.43
$\frac{1}{3}$	0.7	0.11	0.05	2.69	2.76	4.72	5.85	3.81	3.34	9.73	7.86
$\frac{1}{3}$	0.8	0.09	0.07	2.40	2.58	4.20	5.22	3.51	2.94	10.26	7.87
$\frac{1}{3}$	0.9	0.07	0.09	2.71	2.62	5.19	5.24	4.41	2.60	10.80	7.94
Rapport t	pH	$X + Y = P$	Q	E_{369}	E_{373}	E_{573}	E_{583}	E_{915}	E_{918}	E_{1423}	E_{1429}
$\frac{1}{2}$	0.1	0.13	0.12	2.84	2.85	6.26	6.58	4.94	4.21	10.56	9.22
$\frac{1}{2}$	0.2	0.08	0.16	2.66	2.62	5.07	6.25	4.46	4.00	9.81	8.29
$\frac{1}{2}$	0.6	0.03	0.21	2.54	2.52	4.90	6.16	4.18	3.71	8.96	7.73
$\frac{1}{2}$	0.7	0.02	0.21	2.55	2.53	4.86	6.23	4.55	4.08	9.77	8.43
Moyenne				2.6 ±0.2	2.7 ±0.2	5.0 ±1	6.0 ±0.8	4.3 ±0.8	3.6 ±0.9	10.0 ±1	8 ±1

efficients F_v, par la relation 6 en mesurant les hauteurs relatives h_v sur les spectres.

L'utilisation de ces valeurs approchées de F_v permet d'estimer la valeur des E_v dont le calcul précis est difficile car il est impossible d'isoler un domaine d'acidité où l'espèce $Al(C_2O_4)_2^-$ est seule. Pour le rapport $t = \frac{1}{3}$ et dans un domaine de $0.1 < pH < 0.5$ nous pouvons considérer que $[Al^{3+}]$ et P sont nulles. En appliquant les relations 1 et 2 on détermine $(X + Y)$; les relations 4 et 5 donnent Q et R et par conséquent E_v d'après la relation 6 en utilisant les coefficients F_v approchés. Ces premières valeurs de E_v permettent de corriger les résultats obtenus pour F_v en tenant compte de la présence du complexe $Al(C_2O_4)_2^-$. Les résultats définitifs pour F_v sont présentés dans le tableau 4 et permettent de recalculer les valeurs de E_v.

A titre de vérification nous avons également déterminé E_v en nous plaçant dans un rapport $t = \frac{1}{2}$ et dans un domaine de $0 < pH < 0.5$ conditions dans lesquelles nous pouvons supposer que $[Al^{3+}]$ et R sont négligeables; seules P et Q sont prépondérantes; D_v étant donné.

Le tableau 5 résume toutes les valeurs obtenues pour E_v à différents pH et dans les deux rapports.

L'examen des tableaux montre que les coefficients D_v, E_v et F_v sont bien caractéristiques des différentes espèces aux huit fréquences

TABLEAU 6. Constantes de stabilité des oxalates complexes d'aluminium(III)

Auteurs	Log K_1	Log K_2	Log K_3	Log β_2	Log β_3	Methode
Lacroix (3)				13	16.3	Solubilité
Babko et Dubovenko (5)	7.26	4.85	1.31			Spectrométrie uv
Dutt et Sur (2)		5.45	3.69			Potentiométrie
Zolotukhin (4)				13	16.79	Fluorimétrie
Nos valeurs (1)	6.1±0.2	5.0±0.1	3.87±0.06	11.1	15.0	Potentiométrie
	7.3	6.0	3.87	13.3	17.2	Spectrométrie Raman

choisies. La déviation moyenne rend compte de l'imprécision sur la mesure des hauteurs de bandes des complexes et du coordinat libre (bandes 848 et 868 cm^{-1}).

4.4. Détermination des concentrations des complexes, répartition des différentes espèces en fonction du degré d'acidité de la solution et calcul des constantes de stabilité

Connaissant les coefficients de diffusion de trois espèces aux huit fréquences sélectionnées, nous avons, à l'aide du programme SPECTRAL, utilisant les concentrations du coordinat engagé et les hauteurs des bandes aux fréquences choisies, calculé la concentration optimale des espèces présentes en solution et déterminé l'écart quadratique sur chaque concentration. Les concentrations ainsi obtenues pour les rapports $t = \frac{1}{2}$ et $t = \frac{1}{3}$ sont présentées dans la fig. 4 en fonction du pH ou [HCl_{eq}].

Enfin ces valeurs de P, Q et R obtenues pour les rapports $t = 1$, $\frac{1}{2}$ et $\frac{1}{3}$ sont utilisées pour déterminer les valeurs optimales des constantes des équilibres de formation des complexes:

$$Al^{3+} + C_2O_4^{2-} \rightleftarrows Al(C_2O_4)^+ \qquad \beta_1$$

$$Al^{3+} + 2C_2O_4^{2-} \rightleftarrows Al(C_2O_4)_2^- \qquad \beta_2$$

$$Al^{3+} + 3C_2O_4^{2-} \rightleftarrows Al(C_2O_4)_3^{3-} \qquad \beta_3$$

L'affinement par moindres carrés est réalisé à l'aide d'un programme intitulé AFFIBETA, variante du programme AFFIPLNE mis au point ultérieurement (13). AFFIBETA est construit en remplaçant la fonction $\bar{n} = f(pH)$ du programme AFFIPLNE par les paramètres P, Q et R exprimés en fonction du pH et en utilisant les dérivées $\partial P/\partial\beta_1$, $\partial Q/\partial\beta_2$ et $\partial R/\partial\beta_3$ au lieu de $\partial\bar{n}_i/\partial K_j$.

L'affinement est effectué à partir de 17 points expérimentaux situés dans un domaine de p$H > 0.5$. Une variation de 0.2 unité sur la valeur numérique du pH n'a pas d'influence sensible sur la valeur des constantes:

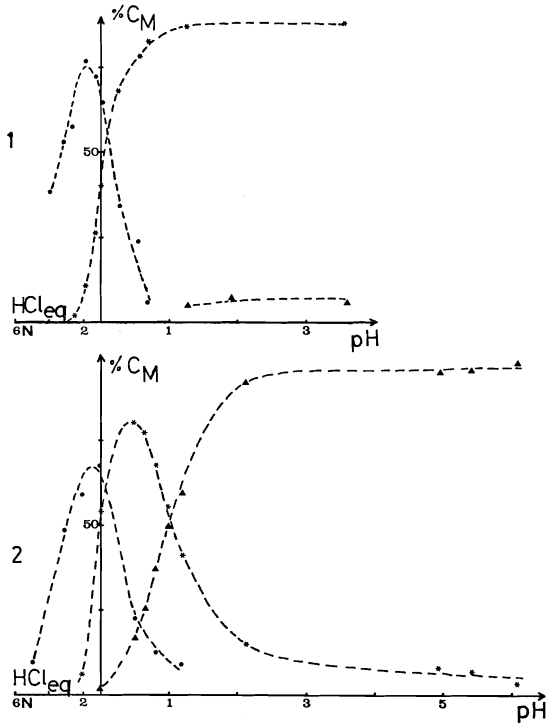

FIG. 4. Courbes de répartition de l'aluminium engagé dans chaque complexe par rapport à la concentration analytique C_M pour (*1*) $t = \frac{1}{2}$ et (*2*) $t = \frac{1}{3}$. (●) $AlC_2O_4^+$; (*) $Al(C_2O_4)_2^-$; (▲) $Al(C_2O_4)_3^{3-}$.

$$\beta_1 = 1.15 \times 10^7 \quad \beta_2 = 3.11 \times 10^{13} \quad \beta_3 = 3.37 \times 10^{17}$$

soit:

$$K_1 = 1.15 \times 10^7 \quad K_2 = 2.70 \times 10^6 \quad K_3 = 1.08 \times 10^4$$

Les constantes ont été utilisées pour tracer la courbe de répartition des complexes par le programme CALCON; on a constaté alors que pour les p$H < 0.5$ les points expérimentaux ne sont pas placés exactement sur cette courbe calculée; ceci est dû certainement au domaine étroite du

pH utilisé pour l'affinement. C'est pourquoi nous avons tenté de calculer une série de courbes de répartition en modifiant les valeurs des constantes successives K_1 et K_2, K_3 étant maintenue à la valeur précise obtenue par la méthode du pH ($K_3 = 7.53 \times 10^3$) de façon à obtenir la meilleure concordance possible entre les concentrations expérimentales et les courbes calculées. Les valeurs ainsi obtenues sont données dans le tableau 6 ainsi que celles déterminées par différents auteurs.

1. M. JABER. Thèse, Université de Lyon, Lyon. 1975.
2. N. DUTT et B. SUR. Zh. Anorg. Chem. **293**, 195 (1957).
3. S. LACROIX. Ann. Chim. **4**, 25 (1949).
4. V. ZOLOTUKHIN. J. Inorg. Chem. USSR, **13**, 367 (1968).
5. A. K. BABKO et L. I. DUBOVENKO. Zh. Neorg. Khim. **2**, 1294 (1957).
6. H. MURATA et K. KAWAI. J. Chem. Phys. **25**, 796 (1956).
7. R. GAUFRES et J. MATHIEU. C.R. Acad. Sci. **248**, 81 (1959).
8. V. SAHINI, R. BELDIE et M. DAMASCHIN. Rev. Roum. Chim. **11**, 1361 (1966).
9. J. VAISSERMAN. C.R. Acad. Sci. (Paris) Ser. B, **270**, 948 (1970).
10. R. HESTER et R. PLANE. Inorg. Chem. **3**, 513 (1964).
11. H. HARAGUCHI et S. FUJIWARA. J. Phys. Chem. **73**, 10 (1969); **73**, 3467 (1969).
12. A. D. TOY, T. D. SMITH et J. R. PILBROW. Aust. J. Chem. **26**, 1889 (1973).
13. G. DUC, F. BERTIN et G. THOMAS-DAVID. Bull. Soc. Chim. Fr. **3–4**, 495 (1975).
14. J. GOUTERON. J. Inorg. Nucl. Chem. **38**, 55 (1976).

Additivity schemes permitting the estimation of partial molar heat capacities of organic compounds in aqueous solution

J. PETER GUTHRIE[1]

Department of Chemistry, University of Western Ontario, London, Ont., Canada N6A 5B7

Received March 9, 1977

J. PETER GUTHRIE. Can. J. Chem. **55**, 3700 (1977).

The available $\bar{C}_{p_2}$ values for neutral organic compounds in aqueous solution can be fitted with useful precision by additivity schemes based on atomic, bond, or group contributions. For the set of 132 compounds these schemes require 11, 14, or 49 parameters and give weighted average deviations of 14, 9, or 6 J K^{-1} mol^{-1}. For acyclic molecules the atomic contributions scheme permits chemically useful estimates of $\bar{C}_{p_2}$ to be made for compounds of C, H, O, and N.

J. PETER GUTHRIE. Can. J. Chem. **55**, 3700 (1977).

Les données disponibles pour les valeurs de $\bar{C}_{p_2}$ de composés organiques neutres en solution aqueuse peuvent être ajustées avec une bonne précision grâce à des schémas d'additivité basés sur des contributions atomiques, de liaison et de groupe. Pour une série de 132 composés, ces schémas demandent 11, 14 ou 49 paramètres et conduisent à des écarts de moyenne pondérée de 14, 9 ou 6 J K^{-1} mol^{-1}. Pour des molécules acycliques, le schéma des contributions atomiques permet d'établir une bonne évaluation chimique des valeurs $\bar{C}_{p_2}$ qui peut être appliquée aux composés contenant les atomes C, H, O et N.

[Traduit par le journal]

Introduction

In the course of another investigation a need was found for free energies of transfer from gas to solution for some small, water miscible organic compounds. Although free energies of transfer are readily determined for sparingly soluble compounds, the determination becomes more difficult for very soluble materials. Experimental activity coefficient data (equivalent to free energies of transfer) are frequently available at the boiling point, so that it would be advantageous to be able to correct these data to room temperature. Since the temperature difference is considerable, and the change in heat capacity from gas to aqueous solution is large (1), one may not assume that the enthalpy of transfer is temperature independent. Provided that heats of solution and vaporization were available, the remaining requirement if free energies at 25°C were to be calculated from data at higher temperatures was that a value for the change in heat capacity from gas to aqueous solution be available.

In the past decade there has been a marked increase in the quantity and quality of heat capacity determinations for aqueous solutes (2–10). Nevertheless, the number of compounds for which data are available is small compared to the number which might be studied. Benson *et al.* (11) have shown that heat capacities of gaseous molecules can be estimated quite successfully by various additivity schemes, and has reported tables of parameters for atom, bond, and group contributions (11, 12); this procedure has recently been extended to liquid hydrocarbons (13). It seemed worthwhile to investigate whether, and to what extent, such estimation procedures could be applied to partial molar heat capacities for solutes in water.

Several authors (4–6, 8–10) have considered the question of additivity of group contributions and Wadso and co-workers (10) in particular have analyzed their data in this way. All schemes published to date are, however, very limited in their range of applicability.

We wish to report here that partial molar heat capacities in aqueous solution, $\bar{C}_{p_2}$, can be estimated quite well using the atom, bond, or group contributions schemes (with increasing precision as one goes from atom contributions to group contributions), and in particular that estimates of useful reliability can be obtained using atom contributions. In the course of this investigation several additional $\bar{C}_{p_2}$ values were evaluated by analysis of published data.

Calculational Methods

Heat Capacities From Activity Data

Literature data (5, 14) in the form of ln (p/c) were fitted (16) to the equation

[1]Alfred P. Sloan Fellow, 1975–1977.

$$\ln\left(\frac{p}{c}\right) = -\frac{\Delta G_\theta{}^0}{R\theta} + \frac{\Delta H_\theta{}^0}{R}\left(\frac{1}{\theta} - \frac{1}{T}\right) + \frac{\Delta C_{p\theta}{}^0}{R}\left(\frac{\theta}{T} - 1 + \ln\frac{T}{\theta}\right)$$

(where θ is the reference temperature, here 298 K) by means of a nonlinear least squares (17) program. $C_p{}^0$(g) was estimated by Benson's group contributions method (12*a*) where experimental values were not available. Although this treatment permitted the evaluation of $\bar{C}_{p_2}$ values for several ketones, the values are of low precision. There is a clear need for more measurements on different carbonyl compounds.

Heat Capacities of Benzoic Acids

Partial molal heat capacities of sodium benzoate, sodium *m*-hydroxybenzoate, and sodium *p*-hydroxybenzoate have been reported (4). The corresponding $\bar{C}_{p_2}$ values for the carboxylic acids may be calculated using values of ΔC_p for ionization (18), and the $\bar{C}_{p_2}$ values for Na^+ and H^+ (19). Because of the indirect way these were calculated, and the necessity for using ΔC_p of ionization values derived as second derivatives from equilibrium data, the $\bar{C}_{p_2}$ values for benzoic acid were assigned an estimated precision of ± 25 J K^{-1} mol^{-1}.

Determination of Parameter Values

The $\bar{C}_{p_2}$ data were fitted to the equation

$$\bar{C}_{p_2 j} = \sum_i A_i X_{ij}$$

where A_i is the parameter for the *i*th structural feature and X_{ij} is the number of times the *i*th structural feature appears in compound *j*, by means of a least squares program. Initially the full set of data was employed, and then the set was restricted so that only parameters defined by three or more compounds were included. For the bond and group contributions, the set was further restricted by eliminating compounds for which calculated and observed values differed markedly. Compounds which were not included in the least squares fitting are indicated in Table 1.

The remaining parameters were evaluated for each scheme by taking the parameters determined by least squares as given and fitting the remaining compounds, one parameter at a time. As far as possible values for parameters determined this way were calculated from the set of compounds for which the new parameter was the only one needed besides the set already determined. Since the parameter values which were not determined by least squares are based upon small numbers of compounds they can only be regarded as provisional.

Results and Discussion

Atomic Contributions

The $\bar{C}_{p_2}$ data employed comprise a set of 132 compounds (see Table 1).[2] For the atomic contributions approach, different parameters were employed for H bonded to C, to O, or to N, and atoms were classed as to hybridization state. The rationale for this approach is that $\bar{C}_{p_2}$ contains a large contribution reflecting the interaction of water with the solute, or the effect of solute upon the organization of water molecules (10, 20). Thus it seemed important to choose parameters in a way which reflected the ability of groups to hydrogen bond to water; this leads to a larger set of parameters than Benson employed for gaseous molecules. This scheme seems justified because the different parameters for a given atom were assigned different value by the least square program. Thus H_C is 75 ± 3 while H_O is 60 ± 3 and H_N is 64 ± 3. Similarly C_4 is -68 ± 7 while C_3 is -14 ± 3 (all in J K^{-1} mol^{-1}).

Strictly speaking benzene ring carbons should be treated separately since, as will be seen below, cyclization normally leads to a significant change in $\bar{C}_{p_2}{}^0$. Initially, following Benson (11), C_B was used as a distinct parameter, incorporating one sixth of the cyclization effect. However C_B and C_3 (the parameter for an ethylenic or other sp_2 hybridized carbon) were indistinguishable and so in the final least squares calculation all sp_2 carbons were treated alike. For saturated cyclic molecules the fit was markedly poorer than for the acyclic compounds, so that the cyclic compounds were omitted from the least squares calculations. The fit was somewhat improved by the addition of parameters for five- or six-membered rings, but these parameters were ill defined and the fit remained poor. No obvious way to improve the fit with a small increase in the number of parameters presented itself.

For acyclic compounds or benzene derivatives the fit is really quite good, with a weighted average deviation (calculated as $(\Sigma(\bar{C}_{p_2}\text{(obs.)} - \bar{C}_{p_2}\text{(calc.)})^2/(\sigma\bar{c}_{p_2}\text{(obs.)})^2/(\text{degrees of freedom}))^{1/2}$)

[2]A few additional compounds containing new structural features (such as triple bonds (2) or seven-membered rings (21)) were not included in order to avoid introducing still more parameters.

TABLE 1. Partial molar heat capacities

Compound	Experimental[a]			Calculated					
				Atom		Bond		Group	
	$\bar{C}_{p_2}$[b]	σ[c]	Ref.	$\bar{C}_{p_2}$[b]	Δ[d]	$\bar{C}_{p_2}$[b]	Δ[d]	$\bar{C}_{p_2}$[b]	Δ[d]
Methane	262	0.8	3, 10	232	30	241	21	[j]	
Ethane	304	6	3, 10	315	−11	327	−22	324	−20
Propane	366	10	3, 10	397	−31	413	−47	408	−42
n-Butane	399	4	3, 10	479	−80	498[i]	−99	492[i]	−93
n-Pentane	572	70	10	561	11	584	−12	575	−3
n-Hexane	635	45	10	643	−8	670	−35	659	−24
Benzene	361	5	10	369	−8	361	0	361	0
Toluene	430	13	10	451	−21	445	−15	430	0
Ethylbenzene	504	13	10	533	−29	531	−27	517	−13
n-Propylbenzene	606	25	10	615	−9	616	−10	601	5
Ethylene	243	8	1	273	−30	244[i]	−1	244[i]	−1
Methanol	158.2	0.1	9, 10	175	−17	173	−15	158	0
Ethanol	260.3	0.1	9, 10	258	2	259	1	260	0
n-Propanol	352.9	0.2	9, 10	340	13	345	8	244	9
n-Butanol	437.0	0.5	9, 10	422	15	430	7	427	10
n-Pentanol	523.8	0.3	9, 10	504	20	516	8	511	13
n-Hexanol	611	23	10	586	25	602	9	595	16
n-Heptanol	737	23	10	668	69	688	49	679[i]	58
i-Propanol	359	16	10	340	19	345	14	385[i]	−26
i-Butanol	432.5	0.4	10	422	11	430	3	428[i]	5
tert-Butanol	464.0	0.6	10	422	42	430	34	472[i]	−8
s-Butanol	498	20	2	422	76	430	68	469[i]	29
tert-Pentanol	564	20	2	504	60	516	48	556[i]	8
Neopentanol	503.5	0.7	10	504	0	516	−12	506	−2
2,2-Dimethyl-1,3 propanediol	432.3	0.3	10	447	−15	448	−16	442	−10
1,1,1-Tris (hydroxymethyl)-ethane	373.3	0.2	10	390	−17	380	−7	377	−4
Pentaerythrytol	328.8	0.2	10	333	−4	312	16	313	16
Glycerol	253	27	10[e]	226	27	209	44	255[i]	−2
1,2-Ethanediol	192	1	10	200	−9	191	1	196	−4
1,3-Propanediol	269	4	10	283	−14	277	−8	280	−11
1,4-Butanediol	347	1	10	365	−18	362	−15	363	−16
1,5-Pentanediol	439	6	10	447	−8	448	−9	447	−8
1,6-Hexanediol	522	1	10	529	−7	534	−12	531	−9
Benzyl alcohol	396	2	10	398	−2	377	19	[j]	
2-Phenylethanol	462	3	10	480	−18	463	−1	453	9
3-Phenylpropanol	530	4	10	562	−32	548	−18	537	−7
Allyl alcohol	357	15	2	298	59	301[i]	50	357[i]	0
Crotyl alcohol	403	22	2	381	22	437	−34	403[i]	0
3-Buten-1-ol	400	20	2	381	19	393[i]	7	375[i]	25
4-Penten-1-ol	434	22	2	463	−29	479[i]	−45	459[i]	−25
2-Methoxyethanol	290	4	10	298	−8	291	−1	285	5
2-Ethoxyethanol	387	5	10	380	7	377	10	386	1
2-Propoxyethanol	468	5	10	462	6	463	5	470	−2
2-Butoxyethanol	556	7	10	544	12	549	8	554	2
1,2-Dimethoxyethane	380	7	10	395	−15	392	−12	374	6
1-Ethoxy-2-methoxyethane	463	7	10	477	−14	477	−14	476	−13
1-Propoxy-2-methoxyethane	563	7	10	559	3	563	0	559	4
1-Butoxy-2-methoxyethane	652	10	10	641	10	649	3	643	9
1,2-Diethoxyethane	569	7	10	560	9	563	0	577	−8
Phenol	310	2	10	316	−6	303[i]	7	311[i]	−1
p-Cresol	384	2	10	394	−10	384[i]	0	380	4
p-Ethylphenol	465	10	10	476	−11	470[i]	−5	500[i]	−35
2-Phenoxyethanol	459	2	10	434	25	465[i]	−6	[j]	

TABLE 1 (*Continued*)

Compound	Experimental[a]			Calculated					
				Atom		Bond		Group	
	$\bar{C}_{p_2}$[b]	σ[c]	Ref.	$\bar{C}_{p_2}$[b]	Δ[d]	$\bar{C}_{p_2}$[b]	Δ[d]	$\bar{C}_{p_2}$[b]	Δ[d]
Acetaldehyde	146	21	22	207	−61	164	−18	146[i]	0
Acetone	241	1	6	242	−1	242	−1	241[i]	0
Isobutylmethylketone	426	63	14[f]	536	−110	499	−73	500[i]	−74
Dipropylketone	422	62	15[f]	618	−196	585	−163	593[i]	−171
Dipropylketone	416	59	15[f]	618	−202	585	−169	589[i]	−173
Methyl *n*-pentylketone	438	29	15[f]	618	−180	585	−147	583[i]	−145
Formic acid	96	1	10	68	28	93	3	96[i]	0
Acetic acid	165	3	10	150	15	171	−6	175[i]	−10
Propanoic acid	253	3	10	232	21	257	−4	265[i]	−12
Butanoic acid	337	3	10	314	22	343	−6	349[i]	−12
Pentanoic acid	432	7	10	397	35	428	3	433[i]	−1
Isobutyric acid	334	2	10	315	19	343	−9	351[i]	−17
Pivalic acid	417	9	10	397	20	429	−12	417[i]	21
Succinic acid	225	4	10	150	75	188	37	206[i]	19
Glutaric acid	271	4	10	232	39	273	−2	290[i]	−19
Adipic acid	336	10	10	314	22	359	−23	374[i]	−38
Pimelic acid	410	5	10	397	13	445	−35	458[i]	−48
Benzoic acid	372	25	[h]	280	85	375[i]	−3	371[i]	1
m-Hydroxybenzoic acid	306	25	[h]	230	76	327[i]	−21	322[i]	−16
p-Hydroxybenzoic acid	337	25	[h]	230	107	327[i]	10	322[i]	15
Methylamine	155	1	10	165	−10	168	−13	157	−2
n-Propylamine	327	5	10	330	−3	339	−12	335	−8
n-Butylamine	422	4	10	412	10	425	−3	419	3
n-Pentylamine	515	5	10	494	21	511	4	503	12
n-Hexylamine	604	4	10	576	28	596	8	586	18
i-Propylamine	342	18	10	330	12	339	3	342[i]	0
i-Butylamine	416	9	10	412	4	425	−9	420[i]	−4
tert-Butylamine	403	7	10	412	−9	425	−22	431[i]	−28
Dimethylamine	261	2	10[e]	259	2	258	3	260	1
Ethylmethylamine	331	20	10	341	−10	344	−13	386[i]	−55
Diethylamine	487	18	10	423	63	430	57	481	6
Ethylpropylamine	570	8	10	506	64	516	54	575	−5
Dipropylamine	652	6	10, 7	587	64	601	51	669	−17
Trimethylamine	398	2	10[e]	353	45	349	49	357[i]	41
Diethylmethylamine	533	21	10	367	166	52	12	545	−12
Triethylamine	609	5	10	599	10	606	3	639[i]	−30
1,2-Ethanediamine	185	2	10	181	4	180	5	179	6
1,3-Propanediamine	256	3	10	263	−7	266	−10	262	−6
1,4-Butanediamine	340	4	10	345	−5	352	−12	346	−6
Aniline	307	2	10	302	5	307[i]	0	[j]	
Benzylamine	375	2	10	384	−9	371	4	[j]	
2-Phenylethylamine	445	2	10	466	−21	457	−12	445	0
3-Phenylpropylamine	516	5	10	549	−33	543	−26	579	−13
Tris(hydroxymethyl)-amino methane	268	[g]	10	241	27	221	47	236[i]	32
Formamide	82	1	10	98	−16	83	−1	80[i]	2
N-Methylformamide	164	2	10	191	−27	173	−9	164[i]	0
Acetamide	162	2	10[e]	180	−18	161	1	168[i]	−6
N-Methylacetamide	258	3	10	273	−15	252	6	252	6
N-Ethylacetamide	343	5	10	355	−12	338	5	346[i]	−3
N-Propylacetamide	437	5	10	437	0	423	14	430[i]	7
N-Butylacetamide	516	1	10	520	−4	509	7	514[i]	2
N-Methylpropanamide	334	4	10	355	−21	338	−4	342[i]	−8
N-Methylbutanamide	434	5	10	437	−3	423	11	426[i]	8
N-Methylpentanamide	524	4	10	520	4	509	15	510[i]	14

TABLE 1 (*Concluded*)

Compound	Experimental[a]			Calculated					
				Atom		Bond		Group	
	$\bar{C}_{p_2}$[b]	σ[c]	Ref.	$\bar{C}_{p_2}$[b]	Δ[d]	$\bar{C}_{p_2}$[b]	Δ[d]	$\bar{C}_{p_2}$[b]	Δ[d]
N-Methylisobutyramide	431	6	10	437	−6	423	8	428[i]	3
N-Isopropylacetamide	441	5	10	437	4	423	18	437[i]	4
N-Methylpivalamide	476	7	10	520	−43	573	−97	473[i]	3
N-(*tert*-Butyl)acetamide	498	5	10	530	−21	573	−75	526	−28
Lactamide	225	[g]	23	204	21	178	47	[j]	
Urea	88	1	6	70	18	80	8	97[i]	−9
N,*N*-Dimethylurea	248	1	5	257	−9	262	−14	257[i]	−9
N,*N*′-Dimethylurea	274	1	5	257	17	262	12	265[i]	9
Tetramethylurea	435	1	5	444	−9	443	−8	417[i]	18
Cyclopentanol	488	18	2	423[i]	65	407[i]	81	488[i]	0
Tetrahydrofuran	295	25	10	356[i]	−61	334[i]	−39	315[i]	−20
2-Methyltetrahydrofuran	435	8	10	438[i]	−3	420[i]	15	441[i]	−6
Pyrrolidine	333	8	10	353[i]	−20	322[i]	11	345[i]	−12
N-Methylpyrrolidine	450	12	10	446[i]	4	413[i]	37	410[i]	40
1,3-Dioxolane	175	8	10	232[i]	−57	194[i]	−19	[j]	
Cyclohexane	516	30	10	523[i]	−7	533[i]	−17	541[i]	−25
Cyclohexylamine	481	3	10	467[i]	14	462[i]	19	475[i]	6
Cyclohexanol	521	19	2	466[i]	55	466[i]	55	475[i]	3
Piperidine	405	1	8, 10	396[i]	9	381[i]	24	407[i]	−2
Tetrahydropyan	385	1	8, 10	399	−14	393[i]	−8	377[i]	8
1,4-Dioxane	222	1	8, 10	275[i]	−53	253[i]	−31	213[i]	9
Piperazine	264	1	8, 10	269[i]	−5	229[i]	35	273[i]	−9
Morpholine	239	1	8	332	−93	291[i]	−2	293[i]	−9
Glucose	251	[g]	24	196[i]	55	144[i]	107	[j]	
Sucrose	633	[g]	10	353[i]	280	241[i]	392	[j]	

[a]Reference 10 collects data from many sources; for compounds included in ref. 10 individual references are made only where one of several reported values was chosen as best and used for regression analysis.
[b]J deg^{-1} mol^{-1}.
[c]Uncertainty in the experimental value.
[d]Difference, observed − calculated.
[e]Average of two reported values; σ is |value-average|.
[f]Determined by least squares analysis of solubility data from the references cited.
[g]No indication of experimental error was given in the original reference.
[h]Calculated from $\bar{C}_{p_2}$ for the sodium salt (4), $\bar{C}_{p_2}$ for Na^+ and H^+ (19), and $\Delta\bar{C}_p$ for ionization of the acid (18).
[i]Not included in the regression analysis.
[j]This compound contains a unique group.

equal to 10.7 J K^{-1} mol^{-1} or 2.6 cal K^{-1} mol^{-1}. In terms of the precision commonly attainable experimentally this is really quite good, and in terms of the original motivation for this investigation, namely to allow extrapolation of data at 100°C to 25°C, it is more than adequate. Error analysis shows that the contribution of uncertainties in ΔC_p to uncertainties in ΔG_θ is

$$\theta\left|\frac{\theta}{T}-1+\ln\frac{T}{\theta}\right|\sigma_{\Delta C_p}$$

For $\theta = 298$, $T = 373$ K; this amounts to $7.0 \times \sigma_{\Delta C_p}$ (in kcal mol^{-1}), so that for errors in ΔC_p to contribute less than 0.1 kcal to the error in ΔG, $\sigma_{\Delta C_p}$ must be less than 4 cal K^{-1} mol^{-1}, a condition which is easily satisfied by the atomic contributions estimates.

In Table 1 may be found calculated values of $\bar{C}_{p_2}$ for all compounds used in this study as well as the differences between observed and calculated values; the parameters are given in Table 2.

Bond Contributions

For this approach the parameters were chosen in the manner employed by Benson and Buss (11) with C═O treated as a bivalent atom, C═C treated as a tetravalent atom (so that C_d—X includes a contribution for the carbon–carbon double bond) and a benzene ring treated as a hexavalent atom (so that C_B—X includes a contribution for the ring). The least squares analysis included 102 compounds and 12 parameters, with a weighted average deviation of 8 J K^{-1} mol^{-1}. The compounds containing ethylenic bonds were omitted from this cal-

TABLE 2. Atomic contributions to $\bar{C}_{p_2}$

Atom[a]	Parameter value (J K^{-1} mol^{-1})	Atom[a]	Parameter value (J K^{-1} mol^{-1})
H_C	75(3)	N_2	−80(4)
H_O	60(3)	O_2	−42(4)
H_N	64(3)	O_1	−12(4)
C_4	−68(7)	Five-membered ring	70(47)
C_3	−14(3)	Six-membered ring	31(41)
N_3	−119(8)		

[a]H_C is hydrogen bonded to carbon; H_O is hydrogen bonded to oxygen, H_N is hydrogen bonded to nitrogen; C_4 is tetracoordinate (sp^3) carbon, etc.; N_3 is tricoordinate (sp^3) nitrogen, etc.; O_2 is dicoordinate (sp^3) oxygen, etc.

TABLE 3. Bond contributions to $\bar{C}_{p_2}$

Bond[a]	Parameter value (J K^{-1} mol^{-1})	Bond[a]	Parameter value (J K^{-1} mol^{-1})
C—H	60(1)	CO—C	−60(2)
C—C	−35(2)	CO—C_B	20(16)[b]
C_B—H	60(6)	CO—O	14(2)
C_B—C	−37(32)	N—H	26(1)
C_d—H	61[b]	C—N	−64(2)
C_d—C	11(40)[b]	CO—N	−11(2)
O—H	36(4)	C_B—N	−45[b]
C—O	−44(4)	Five-membered ring	44(25)[b]
C_B—O	−24(14)[b]	Six-membered ring	17(35)[b]
CO—H	43(3)		

[a]C_B represents a benzene ring carbon: the ring is treated as a hexavalent atom; C represents an ethylenic carbon; the double bond is treated as a tetravalent atom; CO is treated as a divalent atom.
[b]Not fitted in the regression analysis.

culation because the parameters involved (C_d—H and C_d—C) were not well determined by the data, as were compounds containing C_B—O or C_B—N bonds, and all saturated cyclic compounds. The remaining parameters were calculated separately, taking the parameters determined by least squares as given. The ring compounds were not satisfactorily treated at the bond level of approximation, although corrections for five- or six-membered rings improved the fit; the parameters are given in Table 3.

Group Contributions

This approach requires a much larger set of parameters, and consequently a much larger data base if they are to be evaluated. When the condition was imposed that each parameter be determined by at least three compounds, only 12 parameters could be evaluated by least squares, from a set of 48 compounds. For this set the weighted standard deviation of calculated from observed values was 6 J K^{-1} mol^{-1}. The remaining parameters were evaluated (to give preliminary values) by taking the well determined set of 12 as given, and calculating the value required to fit a compound with one more parameter. This allowed a further 9 parameters to be determined. Then the process was repeated taking the 21 parameters as given to determine the final set of 28 parameters. When ring contributions were calculated as before there remained serious discrepancies between observed and calculated values. This situation could be considerably improved by introducing a 'ring parameter', and a 'heteroatom-in-ring parameter' for each of five- and six-membered rings. By using these four parameters, the cyclic compounds could be fitted about as well as the acyclic compounds. Clearly $\bar{C}_{p_2}$ for a cyclic molecule is much more sensitive to subtle steric efforts and solvation interactions than is $\bar{C}_{p_2}$ for an acyclic molecule, since the latter is satisfactorily fitted even by atomic contributions, whereas the former requires that the degree of substitution of each atom be taken into account, *and* that the presence of a heteroatom in a ring, rather than in a side chain, be explicitly allowed for. At the earlier levels of approximation the various contributions to $\bar{C}_{p_2}$ for cyclic compounds were not taken account of in a way which permitted any improvement when the presence or absence of heteroatoms in the rings was included as a parameter.

Several groups are specified by only one compound; such groups have been included in Table 4 only when $\bar{C}_{p_2}$ for the compound is reasonably precise, i.e. probably known to within less than 20 J K^{-1} mol^{-1}.

For the full set of 132 compounds for which $\bar{C}_{p_2}$ values were available, the atomic contributions scheme required 11 parameters to give a weighted average deviation of 14 J K^{-1} mol^{-1}; the bond contributions scheme required 19 parameters to give a weighted average deviation of 9 J K^{-1} mol^{-1}; and the group contributions scheme required 49 parameters to give a weighted average deviation of 6 J K^{-1} mol^{-1}. Although the group contributions scheme is superior, it requires a dramatically larger set of parameters, and is only markedly superior for ring compounds.

TABLE 4. Group contributions to $\bar{C}_{p_2}$

Group[a]	Parameter value (J K^{-1} mol^{-1})	Group[a]	Parameter value (J K^{-1} mol^{-1})
$CH_3(X)$	162(2)[b]	CO(O)(C)	−99[c]
$CH_2(C)_2$	84(1)[b]	$CH_2(C)(CO)$	90(8)
$CH(C)_3$	7(4)	$CH(C)_2(CO)$	14(7)
$C(C)_4$	−78(5)[b]	$C(C)_3(CO)$	−103(30)
CdH_2	122[c]	$CO(C)_2$	−83[c]
CdH(C)	6[c]	$C_B(CO)$ + $CO(O)(C_B)$	−41(16)
$CH_2(C)(C_d)$	150(25)	$NH_2(C)$	−5(4)[b]
C_BH	60(6)[b]	$NH(C)_2$	−32(5)[b]
$C_B(C)$	−33(3)[b]	$N(C)_3$	−129(35)
$CH_2(C)(C_B)$	87(24)[b]	$CH_2(C)(N)$	94(4)[b]
OH(C)	−4(5)[b]	$CH(C)_2(N)$	23[c]
$CH_2(C)(O)$	101(4)[b]	$C(C)_3(N)$	−50(29)
$CH(C)_2(O)$	65(28)	$NH_2(C_B)$ + $C_B(N)$	7[c]
$C(C)_3(O)$	−10(8)	$NH_2(CO)$	96[c]
O(C)	−76(6)[b]	NH(C)(CO)	18[c]
$CH_2(O)_2$	174[c]	$N(C)_2(CO)$	−68(9)
$CH_2(O)(C_d)$	233[c]	CO(C)(N)	−90(6)
$OH(C_B)$	−4(5)[d]	$CO(N)_2$	−95(9)
$CH_2(O)(C_B)$	134[c]	Five-membered ring	91[c]
$C_B(O)$	15(3)	Six-membered ring	32(17)
$O(C)(C_B)$	−46[c]	Heteroation in five-membered ring	−70(27)
HCO(Y)	−16[c]	Heteroation in six-membered ring	−34(10)
OH(CO)	112[c]		

[a]This list does not include several groups for which only one $C_{p_2}^0$ value of low precision is available. Following Benson (12) and Hine (25), $CH_3(X)$ has been assigned the same value for all X; C, C_d, C_B, O, N, CO; similarly HCO(Y) has been assigned the same value for all Y; C, O, N. The number in parentheses is the estimated standard deviation of the parameter, where this could be estimated.
[b]Determined by least squares analysis.
[c]Based on only one compound for which this was the new contribution.
[d]$OH(C_B)$ was assigned the same value as OH(C).

Conclusions

It appears clear from the results reported above that for acyclic compounds $\bar{C}_{p_2}$ can be estimated with a precision which is not only good enough to be useful, but competitive with all but the best experimental determinations. As reliable data for more classes of compounds become available it will be possible progressively to replace the atomic by the bond and finally the group contributions schemes. At present it will most often be necessary to employ the atomic contributions scheme to estimate an unknown $\bar{C}_{p_2}$ value because the higher order schemes lack parameter values.

Acknowledgements

I thank the National Research Council of Canada and the Alfred P. Sloan Foundation for financial support of this work.

1. F. FRANKS and D. S. REID. *In* Water, a comprehensive treatise. Vol. 2. *Edited by* F. Franks. Plenum Press, New York. 1973. Chapt. 5.
2. E. M. ARNETT, W. B. KOVER, and J. V. CARTER. J. Am. Chem. Soc. **91**, 4028 (1969).
3. D. M. ALEXANDER, D. J. T. HILL, and L. R. WHITE. Aust. J. Chem. **24**, 1143 (1971).
4. J. E. DESNOYERS, R. PAGÉ, G. PERRON, J-L. FORTIER, P. A. LEDUC, and R. F. PLATFORD. Can. J. Chem. **51**, 2129 (1973).
5. P. R. PHILIP, G. PERRON, and J. E. DESNOYERS. Can. J. Chem. **52**, 1709 (1974).
6. O. KIOHARA, G. PERRON, and J. E. DESNOYERS. Can. J. Chem. **53**, 3263 (1975).
7. S. BERGSTRÖM and G. OLOFSSON. J. Solution Chem. **4**, 535 (1975).
8. O. KIOHARA, G. PERRON, and J. E. DESNOYERS. Can. J. Chem. **53**, 2591 (1975).
9. C. JOLICOEUR and G. LACROIX. Can. J. Chem. **54**, 624 (1976).
10. N. NICHOLS, R. SKÖLD, C. SPINK, J. SUURKUUSK, and I. WÄDSO. J. Chem. Thermodyn. **8**, 1081 (1976).
11. S. W. BENSON and J. H. BUSS. J. Chem. Phys. **29**, 546 (1958).
12. (*a*) S. W. BENSON. Thermochemical kinetics. Wiley, New York, NY. 1968; (*b*) H. K. EIGENMANN, D. M. GOLDEN, and S. W. BENSON. J. Phys. Chem. **77**, 1687 (1973).
13. M. LURIA and S. W. BENSON. J. Chem. Eng. Data, **22**, 90 (1977).
14. P. GROSS, J. C. RINTELEN, and J. H. SAYLOR. J. Phys. Chem. **43**, 197 (1939).
15. J. H. SAYLOR, V. J. BAXT, and R. P. GROSS. J. Am. Chem. Soc. **64**, 2742 (1942).
16. E. C. W. CLARKE and D. N. GLEW. Trans. Faraday Soc. **62**, 539 (1966).
17. (*a*) W. E. WENTWORTH. J. Chem. Educ. **42**, 96 (1965); **42**, 162 (1965); (*b*) W. E. DEMING. Statistical adjustment of data. Dover Publications, New York, NY. 1964.
18. J. W. LARSON and L. G. HEPLER. *In* Solute–solvent interactions. *Edited by* J. F. Coetzee and C. D. Ritchie. Marcel Dekker, New York. 1969. p. 11.
19. H. L. FRIEDMAN and C. V. KRISHNAN. *In* Water, a comprehensive treatise. Vol. 3. *Edited by* F. Franks. Plenum Press, New York. 1973. p. 72.
20. C. TANFORD. The hydrophobic effect. Wiley-Interscience, New York. 1973.
21. S. CABANI, G. CONTI, A. MARTINELLI, and E. MATTEOLI. J. Chem. Soc. Faraday Trans. I, **69**, 2112 (1973).
22. J. L. KURZ. J. Am. Chem. Soc. **89**, 3524 (1967).
23. F. T. GUCKER and T. W. ALLEN. J. Am. Chem. Soc. **64**, 191 (1942).
24. J. T. EDSALL. J. Am. Chem. Soc. **57**, 1506 (1935).
25. J. HINE and P. K. MOOKERJEE. J. Org. Chem. **40**, 292 (1975).

Pyridine nitrosazones and their cobalt(III) chelates

AHMAD SAMI SHAWALI[1] AND IKHLASS M. ABBASS
Department of Chemistry, Faculty of Science, University of Cairo, Giza, Egypt

Received May 3, 1977

AHMAD SAMI SHAWALI and IKHLASS M. ABBASS. Can. J. Chem. **55**, 3707 (1977).

Nitrosation of pyridine aldehyde *p*-tolylhydrazones **2** with amyl nitrite gives rise to *p*-toluneazopyridine aldoximes **4** which form stable tris chelates with cobalt(III). Spectral data (ir, uv, and ^{1}Hmr) indicate that the ligands exist mainly in the assigned azooxime structure **4**, and that their chelates have five-membered ring structure **7**. Also, the ^{1}Hmr spectra imply *mer*-configuration **9** for the chelates examined. No evidence for the tautomeric nitrosohydrazone structure **3** for the ligands and the *fac*-configuration **8** for Co(III) chelates could be obtained. Using the HMO method, the azooxime form **4** for the ligand was shown to be more stable than the nitrosohydrazone structure **3**. Also, good agreement was obtained between observed transition energies and those calculated by the HMO method. The acid dissociation constants of the ligands in 50 vol% ethanol–water at 25°C and ionic strength of 0.1 were determined spectrophotometrically.

AHMAD SAMI SHAWALI et IKHLASS M. ABBASS. Can. J. Chem. **55**, 3707 (1977).

La nitrosation de *p*-tolylhydrazones aldéhydiques de pyridine **2** par le nitrite d'amyle conduit à des aldoximes *p*-toluèneazopyridine **4** lesquels forment des chélates stables avec le cobalt(III). Les données spectrales (ir, uv et rmn) indiquent que les ligands existent principalement sous la forme azooxime **4** et leurs chélates possèdent une structure comportant un cycle à cinq membres **7**. De plus, les spectres rmn suggèrent une configuration *mer* **9** pour les chélates étudiés. On ne peut obtenir de preuves évidentes pour une structure tautomère nitrosohydrazone **3** pour les ligands et d'une configuration *fac* **8** pour les chélates Co(III). En utilisant la méthode HMO, on peut démontrer que la forme azooxime **4** pour le ligand est plus stable que la structure nitrosohydrazone **3**. Un bon accord est aussi obtenu entre les énergies de transition observées et celles calculées par la méthode HMO. Les constantes de dissociation acide des ligands dans une solution à 50% par volume éthanol–eau à 25°C à une force ionique de 0.1 sont déterminées spectrophotométriquement.

[Traduit par le journal]

Various nitrosazones of type **1** (X = H, alkyl, or aryl and Ar = substituted phenyl) have been described (1–4). However, nitrosazones in which X (in **1**) is a heterocyclic group have so far not been reported. In this paper we describe the synthesis of three heterocyclic nitrosazones, namely **4***a* to **4***c*, and report on their spectroscopic and acid dissociation properties. We have also probed the synthesis, structure, and stereochemistry of cobalt(III) chelates with these

X—C(:NOH)N:NAr
1

heterocylic nitrosazones, and the results are described in this report. The present investigation was undertaken to see the effect of the presence of a heteronitrogen atom in the X group on the tautomeric structure of **1**, and to establish the relative stability of the possible tautomeric forms of **1** within the framework of the Huckel molecular orbital method (HMO). Also, it was our intention to examine the effect of such a heteroatom on the structure and the stereochemical pattern of the Co(III) chelates with **1**.

[1]Author to whom all correspondence should be addressed.

Results and Discussion

Treatment of pyridinealdehyde *p*-tolylhydrazones **2***a* to **2***c* with amyl nitrite in methanol in the presence of sodium methoxide gives the corresponding nitrosation products. The spectral characteristics of the latter products indicate that they exist exclusively in the azooxime structure **4**. No evidence for the tautomeric nitrosohydrazone structure **3** could be obtained. The latter form is probably first formed in the nitrosation of **2**, and immediately tautomerises to **4**.

In ethanol each compound exhibits two characteristic bands: a weak n–π^* maximum ($\log \varepsilon < 4$) near 430 nm, and a strong π–π^* band ($\log \varepsilon > 4$) at 323 nm (Table 1). Such an electronic absorption pattern is similar to that reported (5) for *trans* azo compounds, and

TABLE 1. Spectral characteristics of the compounds

Compound	λ_{max}(EtOH) (nm) (log ε)	$\bar{\nu}$ (cm^{-1}) (assignment) (KBr)	δ[a] ($CDCl_3$) (Cps) $ArCH_3$	NH(OH)[b]
2*a*	362(4.347), 305(3.834), 242(3.977)	3200–3280(NH)[d]	136	[c]
2*b*	365(4.246), 303(3.961), 248(3.993)	3220–3240(NH)[d]	138	[c]
2*c*	372(4.348), 302(3.544), 247(4.184)	3140–3260(NH)[d]	136	[c]
4*a*	435(3.600), 320(4.369)	3200–2300(OH), 1025(NO)	133, 130	(789)
4*b*	436(3.422), 322(4.413)	3200–2500(OH), 1050(NO)	145, 140	(780)
4*c*	430(2.536), 320(4.388)	3100–2300(OH), 1043(NO)	135, 133	(790)
4*d*	430(2.659), 315(4.168)	3400–3000(OH), 1032(NO)	144, 142	(705)
7*a*	460(4.298), 325(4.811), 260(4.678)	1245(NO)	135, 133, 130	
7*b*	480(5.066), 328(4.940), 260(4.763)	1255(NO)	145, 139, 137	
7*c*	475(4.127), 329(5.037), 260(4.845)	1220(NO)	135, 130, 128	
7*d*	480(4.059), 325(4.821), 265(4.801)	1230(NO)	139, 135, 133	

[a]From tetramethylsilane at 60 MHz in $CDCl_3$; aromatic protons give multiplet signal in the region 6.80–8.90 ppm.
[b]Center of a broad signal.
[c]Overlapped by aromatic proton multiplet.
[d]Weak.

accordingly is in support of the assigned azo-oxime structure **4**.

Infrared spectra of the compounds **4***a* to **4***c* in the solid state and in solution (CCl_4) show an intense band near 1040 ± 10 cm^{-1} assignable to the N—O stretch. Simple monoximes usually exhibit their N—O stretch in the region 930–960 cm^{-1}. The higher frequency position of the NO band in **4** might be due to the possible contribution of the resonance structure **5**, as was suggested for quinone monoximes ($\bar{\nu}_{NO}$ = 975–1007 cm^{-1}) (6). Furthermore, the spectra of **4** in the solid state (KBr) and in solution (CCl_4) show a broad band in the 2800–3150 cm^{-1}, due to the hydrogen bonded OH group. The parent hydrazones **2***a* to **2***c* exhibit a weak NH band near 3200 cm^{-1}. The solution phase of **4** shows an additional sharp band near 3500 cm^{-1} whose intensity is concentration dependent. Most probably the latter band arises from a free OH group.

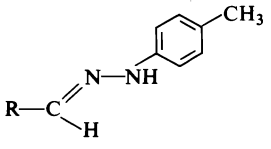

2

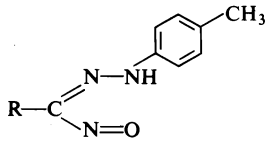

3

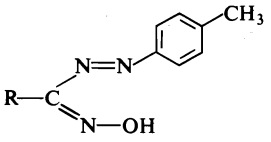

4

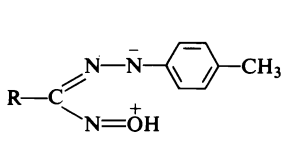

5

a R = 2-Pyridyl
b R = 3-Pyridyl
c R = 4-Pyridyl
d R = Phenyl

The ^{1}Hmr spectra of **4***a* to **4***c* also support their assigned structure. Thus, in $CDCl_3$ all compounds exhibit a one proton broad signal at δ 12.6–13.6 ppm (disappeared on shaking the solution with D_2O) assignable to =NOH. The Ar—CH_3 protons in **4** show two distinct but overlapping signals (Table 1). This observation suggests that each of the compounds exists in solution as a mixture of the *EE* and *ZE* isomers. Unsymmetrical ketoximes exhibit solution equilibria of isomers which can be identified by their ^{1}Hmr spectra (7). The arylazooximes (R = H, alkyl, or aryl) show a parallel behaviour (3, 4).

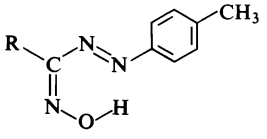

EE

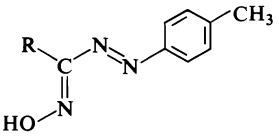

ZE

To establish the relative stability of the azooxime and nitrosohydrazone tautomers of the compounds prepared within the framework of the Huckel molecular orbital (HMO) method (8), use has been made of the concept of bonding energy, defined by the equation:

$$BE = W - W'$$

where W is the total π-electrons localized on atomic orbitals. That is

$$W' = \sum_{i=1}^{n} s_i a_i$$

where n is the number of atomic centres, s_i is the number of electrons contributed by atom i to the π system, and a_i is the Coulomb integral for

atom *i*. For a given tautomeric pair, the tautomer with the greater bonding energy is expected to have the greater stability.

In the application of the HMO method, the standard convention was adopted for heteroatoms (X) in which h_X and k_{CX} were related, respectively, to the Coulomb integral (a_X) and the resonance integral (β_{CX}) by the relationships:

$$a_X = a_0 + h_X\beta_0$$

$$\beta_{CX} = k_{CX}\beta_0$$

The values used in this work are based on those given by Streitwieser (8); the values for the azo group have been successfully used by Block (9). In Table 2 are summarized the values of the heteroatom parameters used.

Bonding energies were calculated for the tautomers of compounds studied (**3***a* to **3***d*) and the values of ΔBE_{AO-NH} are given in Table 3. As shown for all the compounds, the ΔBE value is positive indicating greater stability for the azooxime form. The results are in agreement with the spectral evidence presented above. The energies for the first electronic transitions were also calculated and the results are given in Table 3 together with the observed transition energies. The good agreement between the two sets of values substantiates further the azooxime structure assigned.

The acid dissociation constants of the nitrosazones **3***a* to **3***c* together with that of *p*-tolueneazobenzaldoxime (**3***d*) were determined spectrophotometrically in 50 vol% ethanol–water solution at 25.0 ± 0.1°C and ionic strength μ of 0.10. At p*H* < 7, each compound exhibits an intense π–π* band near 325 nm. In alkaline medium the ambident anion, RC(NO$^-$)N:NAr ↔ RC(NO):NN̄Ar shows an intense π–π* band at 350 ± 5 nm. Spectra recorded at different p*H* values showed an isosbestic point near 330 nm. The absorbance values of freshly prepared solution measured at λ_{max} of the anion plotted against p*H* showed a dependence in the shape of a dissociation curve of a monobasic acid. From the p*H*-absorbance data, the pK_a values for **3***a* to **3***d* were calculated. At least two independent runs were conducted for each compound. The pK_a values were reproducible to ±0.02 p*K* unit in different titrations, and the average values thus obtained are listed in Table 3. The data show that the heterocyclic nitrosazones **3***a* to **3***c* are more acidic than *p*-toluneazobenzaldoxime **3***d*. The low values of pK_a for **3***a* to **3***c* are due to the electron withdrawing character of the heterocyclic substituent (10).

TABLE 2. The HMO heteroatom parameters used in the study of azooxime–nitrosohydrazone tautomerism

Azooxime		Nitrosohydrazone	
h_N	0.50	h_{NH}	1.50
h_O	2.00	h_N	0.50
k_{C-N}	0.90	h_O	0.50
k_{NN}	1.00	k_{NN}	0.70
k_{N-OH}	0.90	k_{C-NH}	0.70
$k_{C=N}$	1.10	$k_{C=N}$	1.10
		k_{C-NO}	0.80
		$k_{N=O}$	0.70

Arylazooximes **4***a* to **4***c*, like **4***d*, combine quite readily with cobalt(II) acetate in aqueous ethanolic solution and the tris arylazooximato cobalt(III) separates out as dark-red crystals from such solutions. Analysis of the complexes synthesized substantiates the assigned composition. It is known (11) that cobalt(II) undergoes very fast oxidation by aerial oxygen in presence of nitrosazones.

Hunter *et al.* (4) described the cobalt(III) complexes of arylazobenzaldoximes and assigned them the six-membered ring formulation **6** on the basis of analogy with tris-(2-arylazophenolato)-Co(III). On the other hand Kalia *et al.* (11), on the basis of infrared spectra, assigned the five-membered ring structure **7** for such complexes. The infrared spectra of the complexes of this study seem to be compatible with the five-membered ring structure **7**. Thus, in their ir

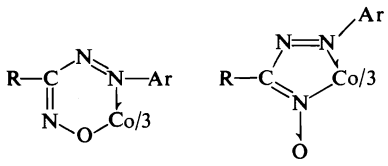

6 **7**

spectra each compound exhibits its N—O band at a frequency which is about 200 cm^{-1} higher than that of the corresponding ligand. This large increase in ν_{NO} indicates that in the chelate the ligand does not exist in the oxime form. *N*-Oxides and nitrones exhibit their N—O bands at much higher frequency ranges than that of oxomes (12). It is assumed that the arylazooximes, by analogy with some oximes (11, 13), probably react momentarily in the nitrone form.

On the basis of the five-membered ring

TABLE 3. Acid dissociation constants, bonding energy differences between azooxime and nitrosohydrazone tautomers of nitrosazones, and observed and calculated transition energies

Compound	ΔBE_{AO-NH}[b] β[a]	Major tautomer	λ_{max}(EtOH) (nm)	E_{max}[c] (eV)	Calcd.[d] transition energies β[a]	Calcd.[d] transition energies eV	pK_a
4*a*	0.901	AO	435	2.850	0.857	2.845	9.61
4*b*	0.899	AO	436	2.843	0.848	2.815	9.54
4*c*	0.900	AO	430	2.883	0.864	2.868	9.45
4*d*	0.799	AO	430	2.883	0.846	2.809	9.99

[a]The HMO resonance integral.
[b]AO = azooxime; NH = nitrosohydrazone.
[c]Transition energy in electron volts.
[d]Calculated transition energy for azooxime form in units of β, and in electron volts using the conversion factor of 3.32 eV/β (15).

structure **7**, the Co(III) chelates can have the *fac*- and/or the *mer*-configurations, **8** and **9** respectively. To identify the exact configuration of such chelates, their ^{1}Hmr spectra in $CDCl_3$ were examined. The spectral data are summarized in Table 1. As shown, each chelate exhibits

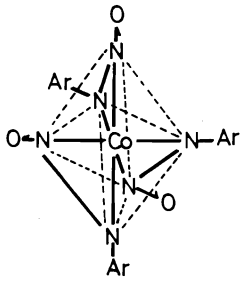

8

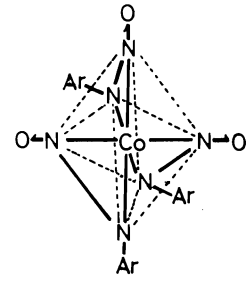

9

three signals of equal intensity for the *p*-methyl protons. This observation indicates that the complexes have the *mer*-configuration, **9**. This is because the *mer*-isomer **9** has no symmetry element and this makes the three chelate rings magnetically unequivalent, and accordingly the *p*-tolyl groups would have different chemical shifts. On the other hand, the *fac*-form, **8**, has a threefold axis of symmetry and this renders all three chelate rings magnetically equivalent. This difference has been used to determine the configuration of several tris-chelates of Co(III) (14). That the complexes prepared take up the *mer*-formulation **9** rather than the *fac*-structure **8** seems to be due to the lower degree of steric crowding in **9** than in **8**. Thus, in the *fac*-isomer three *p*-tolyl groups project from corners of one of the faces of the octahedron, whereas in the *mer*-form a maximum of two *p*-tolyl groups project on each face. This difference renders the *mer*-isomer to be sterically more favourable than the *fac*-form.

Experimental

Melting points are uncorrected and were measured on a Gallenkamp electrothermal instrument model 1A6301. The ^{1}Hmr spectra were recorded on a Varian T60-A spectrometer. Electronic and vibration spectra were measured on Unicam SP8000 and SP1000 spectrophotometers respectively. Elemental analyses were performed by Alfred Bernhardt Mikroanalytisches Laboratorium, West Germany.

Hydrazones (2a to 2c)

The *p*-tolylhydrazones **2***a* to **3***c* were prepared by adding the appropriate aldehyde (0.01 mol) to *p*-tolylhydrazine hydrochloride (0.01 mol) in methanol (70 ml). In each case, the mixture was refluxed for 3 h, and working it up gave the corresponding hydrazone in 80–90% yield, which was crystallized from methanol. *Anal.* calcd. (found) for **2***a*: mp 177°C; $C_{13}H_{13}N_3$; C 73.90 (73.88), H 6.20 (6.20), N 19.89 (19.90); for **2***b*: mp 160°C; $C_{13}H_{13}N_3$; C 73.90 (73.79), H 6.20 (6.18), N 19.89 (18.87); for **2***c*: mp 182°C; $C_{13}H_{13}N_3$; C 73.90 (73.95), H 6.20 (6.19), N 19.89 (19.89).

Synthesis of Nitrosazones (4a to 4d)

These were prepared by allowing the appropriate hydrazone to react with excess *n*-amyl nitrite following the procedure as previously described by Bamberger (3). All compounds were crystallized from methanol. *Anal.* calcd. (found) for **4***a*: mp 139–140°C; $C_{13}H_{12}N_4O$; C 64.98 (64.54), H 5.03 (4.95), N 23.32 (23.28); for **4***b*: mp 164–165°C, $C_{13}H_{12}N_4O$; C 64.98 (65.02), H 5.03 (5.10), N 23.32 (23.30); for **4***c*: mp 180°C, $C_{13}H_{12}N_4O$; C 64.98 (64.82), H 5.03 (4.94), N 23.32 (23.31); for **4***d*: mp 110–111°C (lit. (2) 111°C).

Cobalt(III) Chelates: General Method

Nitrosazone (0.007 mol) was dissolved in ethanol (20 ml) and to it was added cobalt(II) acetate·$4H_2O$ (0.002 mol) dissolved in water (6 ml) at room temperature. The reaction mixture, which turned immediately deep pink in colour, was stirred for 2 h, left overnight at room temperature, diluted with water, and extracted with chloroform. The extract was dried ($MgSO_4$) and filtered. The solvent in the filtrate was removed and the residue

left was crystallized from benzene – petroleum ether. *Anal.* calcd. (found) for **7***a*: mp 194–195°C; $C_{39}H_{33}N_{12}O_3Co$; C 60.31 (60.15), H 4.28 (4.30), N 21.64 (21.49), Co 7.58 (7.32); for **7***b*: mp 218–219°C; $C_{39}H_{33}N_{12}O_3Co$; C 60.31 (60.04), H 4.28 (4.36), N 21.64 (21.63), Co 7.58 (7.67); for **7***c*: mp 205–207°C; $C_{39}H_{33}N_{12}O_3Co$; C 60.31 (60.50), H 4.28 (4.47), N 21.64 (21.51), Co 7.58 (7.36); for **7***d*: mp 145–146°C (lit. (4) 145°C).

*Acid Dissociation Constants of the Ligands **4**a to **4**d*

These were determined spectrophotometrically in 50 vol% ethanol–water at ionic strength of 0.10 and 25 ± 0.1°C as previously described (1). p*H* measurements were made using a Radiometer p*H* meter model 63, and the observed p*H* values (*B*) were corrected to hydrogen ion concentration using the relation: $-\log [H^+] = B + \log U_H$ where $\log U_H$ is the correction factor for the medium used (1). The pK_a values are given in Table 3.

HMO Calculations

These were carried out on Hewlett-Packard calculator, model 9830A.

1. A. S. Shawali and B. Altahou. Can. J. Chem. **54**, 3260 (1976).
2. K. C. Kalia and A. Chakravorty. J. Org. Chem. **35**, 223 (1970).
3. E. Bamberger and W. Pemsel. Ber. **36**, 85 (1903).
4. L. Hunter and C. B. Roberts. J. Chem. Soc. 823 (1941).
5. A. E. Gillams and E. S. Stern. Electronic absorption spectroscopy. Edward Arnold, London. 1960. p. 271.
6. D. Hadzi. J. Chem. Soc. 2725 (1956).
7. E. Lustig. J. Phys. Chem. **65**, 491 (1961).
8. A. Streitwieser. Molecular orbital theory for organic chemists. John Wiley & Sons, New York. 1961; N. C. Baird and M. A. Whitehead. Can. J. Chem. **45**, 2059 (1967).
9. H. Bock. Angew. Chem. Int. Ed. Engl. 457 (1965).
10. M. Simonetta and G. Favini. Gazz. Chim. Ital. **84**, 566 (1954); **85**, 1026 (1955).
11. K. C. Kalia and A. Chakravorty. Inorg. Chem. **7**, 2016 (1968).
12. R. Blink and D. Hadzi. J. Chem. Soc. 4539 (1950); K. Burger, I. Ruff, and F. Ruff. J. Inorg. Nucl. Chem. **27**, 179 (1965); L. E. Godycki and R. E. Rundle. Acta Crystallogr. **6**, 487 (1953); E. Frasson, R. Bardi, and S. Bezzi. Acta Crystallogr. **12**, 201 (1959).
13. P. Pfeiffer and J. Richarz. Ber. **61**, 103 (1928); P. Pfeiffer. Ber. **63**, 1811 (1930); N. J. Patel and B. C. Halder. J. Inorg. Nucl. Chem. **29**, 1037 (1967).
14. A. Chakravorty and K. C. Kalia. Inorg. Nucl. Chem. Lett. **3**, 319 (1967) and the references cited therein.
15. J. K. Elwood. J. Org. Chem. **38**, 2430 (1973).

Spectra of the 1:1 and 3:1 solid complexes of coronene–TCNQ

KIM DOAN TRUONG AND ANDRÉ D. BANDRAUK

Département de chimie, et Groupe de recherche sur les semiconducteurs et les diélectriques, Université de Sherbrooke, Sherbrooke (Qué.), Canada J1K 2R1

Received May 31, 1977

KIM DOAN TRUONG and ANDRÉ D. BANDRAUK. Can. J. Chem. **55**, 3712 (1977).

Two new solid TCNQ complexes have been isolated, coronene–TCNQ 1:1 and 3:1. The infrared and electronic absorption spectra are presented for the two different stoichiometries. From these spectra we infer that the complexes are covalent in the ground state with a charge transfer band appearing at 730 nm. The out of plane vibrations of the individual molecules are noticeably perturbed upon complexation.

KIM DOAN TRUONG et ANDRÉ D. BANDRAUK. Can. J. Chem. **55**, 3712 (1977).

Deux nouveaux complexes de TCNQ ont été isolés à l'état solide, coronène–TCNQ 1:1 et 3:1. Les spectres d'absorption infrarouge et électronique sont présentés pour les deux stoichiométries. Nous avons établi que ces complexes sont covalents à l'état fondamental avec une bande de transfert de charge située à 730 nm. Les vibrations de déformation des molécules sont perceptiblement perturbées par la complexation.

Introduction

Much attention is presently being focused upon charge transfer complexes as these offer alternative possibilities for semiconductor materials (1). In particular, complexes with TCNQ as an acceptor have given rise to interesting systems, ranging from insulators to one-dimensional conductors. These latter complexes fall in the category of π-molecular charge transfer crystals and have unusual electrical properties (1, 2).

We have recently discovered a new stoichiometric form of perylene–TCNQ, i.e., its 3:1 modification (3). Together with the 1:1 form, they present interesting examples of solid state solutions of organic molecules. Of note was the fact that the vibrational structure of the absorption band of pure solid perylene (4) remained intact in the 3:1 complex but was completely broadened in the 1:1 complex. Furthermore, the charge transfer band of both complexes showed no room temperature structure. To our knowledge there is only one confirmed observation of vibrational structure in the organic solid state charge transfer band (5).[1] As it is generally believed that the mechanism of charge carrier formation in these crystals is associated with the charge transfer interaction between donor and acceptor molecules (1), the study of crystal spectra of these complexes is interesting in connection with the nature of their charge transfer excitons (6). These are thought to be responsible for the photoconductor properties of charge transfer systems (1).

In this work we present the synthesis and spectroscopic characterization of a system similar to the perylene–TCNQ system. We have obtained crystals of coronene–TCNQ in 1:1 and 3:1 stoichiometric ratios. In Fig. 1 we illustrate the structure of the individual molecules. Of note is the fact that perylene and coronene have very similar dimensions. In addition, TCNQ fits right into the middle of perylene. It is not surprising therefore that the crystal structure of perylene–TCNQ (1:1) shows an alternation of donor–acceptor in linear stacks (7). Furthermore, perylene in its β form (8) and coronene (9) have similar crystal structures. Both crystals are

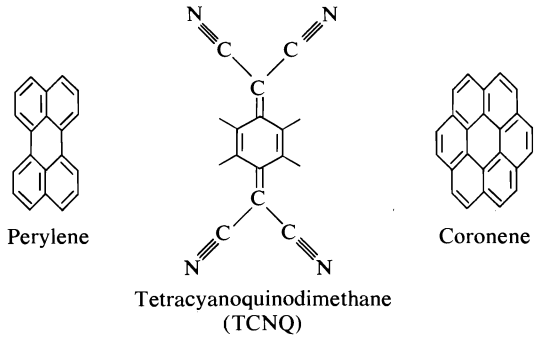

FIG. 1. Structures of perylene, tetracyanoquinodimethane (TCNQ), and coronene.

[1]Recently, Haarer (5) has observed a zero phonon transition for a charge transfer crystal. We thank the referee for this observation.

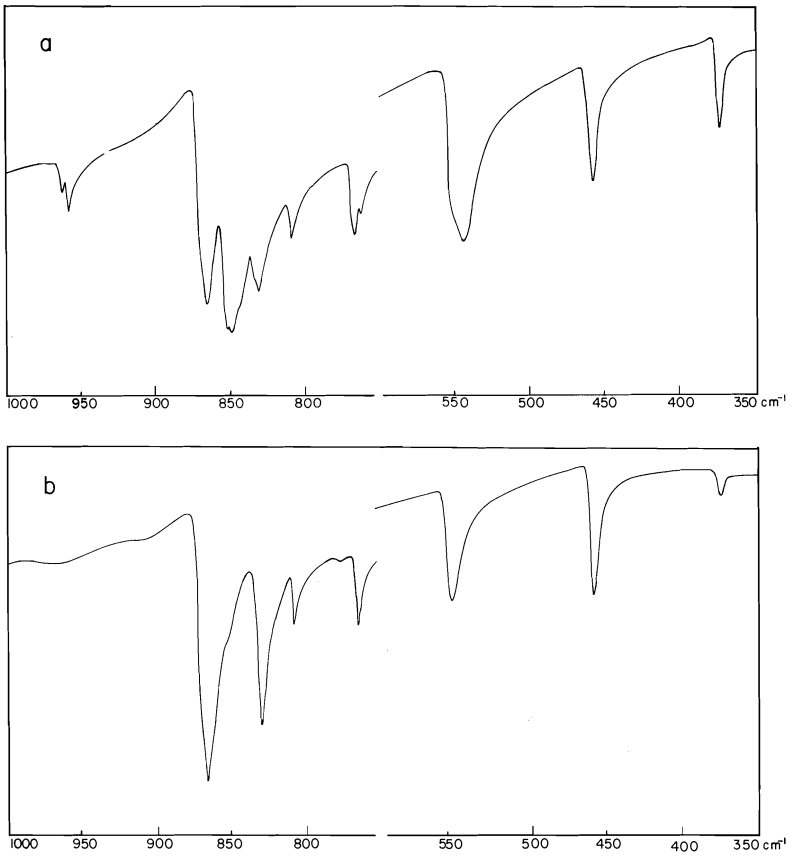

FIG. 2. Infrared spectra of: (*a*) 3:1 complex; (*b*) 1:1 complex.

monoclinic with nearly perpendicular linear stacks of molecules. Considering the similar structure both for the isolated molecules and their crystals, it is not surprising these form analogous complexes with TCNQ. We should add that we were unable to synthesize 3:1 crystals of pyrene with TCNQ. Although pyrene has physical similarities to perylene and coronene, its crystal structure (10), although monoclinic, shows four molecules per unit cell as opposed to two molecules for perylene and coronene. Thus a slight geometrical disparity seems to be important in controlling the stoichiometries of these charge transfer systems.

Experimental

Commercial coronene was recrystallized from benzene whereas pure TCNQ was obtained from acetonitrile solution. The purified coronene (0.001 mol) was dissolved in hot benzene. Purified TCNQ (0.003 mol) was also dissolved in hot benzene in a different flask. The two solutions were then mixed hot. An exothermic reaction was observed immediately and the solution became green. The solution was cooled overnight at room temperature. Green needles were found to precipitate. The same crystals were found when prepared by the diffusion method as described in ref. 11. Elemental analysis gives the following result (theoretical values in parentheses) for the 3:1 complex: C 91.28 (91.30), H 3.92 (3.62), N 4.87 (5.08).

The 1:1 complex was prepared as above but using equimolar ratios. Deep blue-black crystals were found after crystallization. Elemental analysis gives the following: C 85.72 (85.71), H 3.16 (3.17), N 10.9 (11.12).

Electronic absorption spectra were taken in KBr with a Varian Techtron 635 spectrometer. Infrared spectra were recorded on a Perkin-Elmer 621 model with a range of 200–4000 cm^{-1}. Spectra were taken in both Nujol mulls and KBr. Little difference was observed between the two media.

Infrared Spectra

In Fig. 2 we present the infrared spectra of the two different stoichiometric complexes. Table 1 also gives a résumé of the more important frequencies including measurements on pure TCNQ and coronene. The interpretation of these results will be based on the infrared and

TABLE 1. Infrared frequencies (cm^{-1})[a]

Coronene–TCNQ 3:1	TCNQ	Coronene	Coronene–TCNQ 1:1
2223(m)	2224(s)		2222(m)
1616(w)		1618(w)	1616(w)
1608(m)		1608(m)	1608(m)
1540(m)	1540(s)		1540(m)
1485(w)	1402(w)	1476(w)	1485(w)
1354(m)	1354(s)		1354(m)
1314(s)		1314(s)	1314(s)
1134(m)		1132(w)	1134(m)
1125(m)	1120, 1130(m)	1125(w)	1125(m)
962(m)	960(m)	962(w)	
957(m)		957(w)	
865(s)		848(s)	865(s)
854(s)	856(s)		
831(s)			831(s)
809(s)		810(w)	809(m)
766(m)	771(w)	768(m)	765(m)
545(s)		545(s)	553(s)
457(m)	473(s)		457(s)
375(m)		375(m)	375(w)

[a]s = strong, m = medium, w = weak.

Raman study of TCNQ by Takenaka (12) where detailed calculations and assignments of TCNQ vibrational modes have been made. The vibrational spectra of coronene are less complete and here we rely on the partial assignments of Babkov *et al.* (13, 14).

A perusal of Table 1 for the high frequency modes reveals that these modes are little perturbed when compared to the isolated molecular frequencies. Thus the characteristic C=C vibration of TCNQ at 1540 cm^{-1} is essentially undisplaced with respect to pure TCNQ in the 1:1 and 3:1 complexes. Similarly the very strong absorption of coronene at 1314 cm^{-1} also remains unchanged in the complexes. The one slight difference between the complexes is the accentuation of an absorption at 1190 cm^{-1} in the 3:1 complex. This line occurs in pure TCNQ (1200 cm^{-1}) albeit weak (12) but is also accentuated in the 3:1 perylene TCNQ complex (3). Thus in the region of 800–1600 cm^{-1}, one can infer that one has superpositions of unperturbed TCNQ and coronene molecules.

The low frequency region of Fig. 2, 1000–700 cm^{-1}, shows more clearly the effect of the formation of the complexes. In particular the band in the region 900–800 cm^{-1} is quite different for the two stoichiometries. Thus the TCNQ and coronene C—H out of plane bending vibrations with corresponding frequencies at 856 and 848 cm^{-1} (12, 14) are visibly perturbed in the 3:1 complex. Thus the shoulder at 850 cm^{-1} in the 1:1 complex separates off in the 3:1 complex from the vibrations at 865 and 831 cm^{-1} and seems to be split into two components. We attribute the 865 cm^{-1} vibration to TCNQ, whereas the 831 cm^{-1} vibration would seem to belong to complexed coronene. The doublet at 854 cm^{-1} probably comes from a Davydov splitting occurring between two equivalent uncomplexed coronenes. This interpretation is supported by the fact that in the 1:1 complex the 865 and 831 cm^{-1} vibrations appear isolated. Of note is the fact that the same sort of behaviour occurs in the C—H region of the perylene–TCNQ complexes (3). As indicated in the Introduction, this is not surprising in view of the physical similarities between the two donors. We add, finally, that whereas the 962 cm^{-1} band of TCNQ is absent in the 1:1 complex, it reappears in the 3:1 complex.

Electronic Spectra

The infrared spectra in the previous section indicate that the complex is weak and therefore that one has hardly any charge transfer in the ground state. The charge transfer in fact occurs in the first excited state as shown in Fig. 3. A maximum occurs for both stoichiometries at 730 nm. This transition also appears in the solution spectrum of coronene with TCNQ observed at 740 nm by Beukers and Szent-Gyorgyi

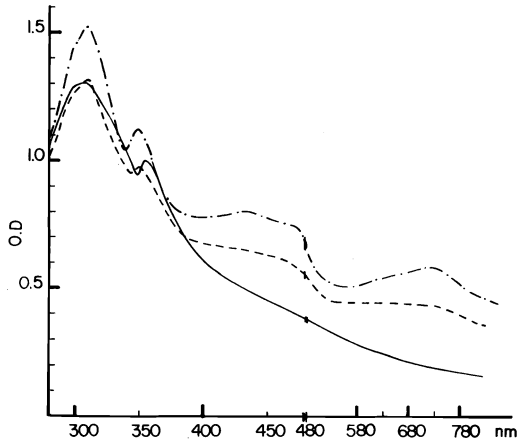

FIG. 3. Electronic spectra: (—) coronene; (---) 3:1 complex; (-·-) 1:1 complex.

(15). This corresponds to the charge transfer band. The maximum at 400 nm corresponds to TCNQ (16) whereas the maxima at 300 and 350 nm correspond to the characteristic β and *p* bands of coronene (17). In this region, the spectra of the individual moieties are well separated. Of interest is the fact that the *p* band of coronene remains virtually unchanged in pure coronene in the 1:1 and 3:1 complexes, as seen clearly in Fig. 3. This is in contrast to the perylene–TCNQ complexes, (3), where the vibrational structure of the perylene absorption persisted in the 3:1 complex but was completely broadened in the 1:1 complex. This aspect of the coronene spectra reinforces the suggestion that the *p* band is indeed a new electronic transition (17).

Returning once more to the charge transfer band at 730 nm, it must be noted that no vibrational structure is observed in the case of both 1:1 and 3:1 complexes. In the analogous perylene–TCNQ system this unstructured band appears at 930 nm. The difference in energy between the charge transfer bands of these two systems amounts to 0.36 eV. This corresponds precisely to the difference in ionization potentials of the last occupied molecular orbitals of the isolated perylene and coronene molecules as reported by Boschi *et al.* (18). Inasmuch as these orbitals are of a_u symmetry for perylene and of e_{2u} symmetry for coronene, one would expect some Jahn–Teller distortion in the charge transfer band of the coronene complexes. It would therefore be of interest to examine these bands at low temperature in order to resolve the vibrational structure and thus elucidate further the true nature of these charge transfer states.

Discussion

Our spectroscopic studies of the new 1:1 and 3:1 coronene–TCNQ complexes in the solid state show that both stoichiometric forms are weak complexes with a charge transfer band occurring at 730 nm. The infrared spectra of these complexes confirm the weak interaction in the ground state. In addition, it is observed that the C—H bending vibrations are perturbed in both stoichiometries. This phenomenon was also observed in the perylene–TCNQ analogous system (3). The crystal structure of the 3:1 modification of this system is now being investigated by Hanson[2] and this should help ascertain the cause of the splitting of these vibrations for that stoichiometry.

The coronene, perylene, and TCNQ systems deserve further study in view of the many similarities alluded to in the Introduction. In particular, there are phase transitions which occur in pure coronene (17, 19) and also in perylene (8). It will be interesting to see what is the effect of an acceptor such as TCNQ on these phase transitions. We are presently studying these by resonance Raman scattering experiments and plan to report these results shortly (20). Another outstanding problem in these systems is the vibronic couplings in the charge transfer bands. As mentioned in the previous section, the coronene cation should exhibit a Jahn–Teller distortion in the charge transfer state. This aspect and other problems will be examined at low temperatures to establish the true nature of charge transfer states in the solid state.

Acknowledgments

We thank the Defence Research Board for a grant to GRSD which financed this research. We further thank Dr. L. Caron, director of GRSD, for encouraging studies of the organic solid state.

1. H. MEIER. Monographs in modern chemistry. Vol. 2. Organic semiconductors. Verlag Chemie, Weinheim. 1974; R. FOSTER. Organic charge transfer complexes. Academic Press, New York, NY. 1969.
2. A. I. GARITO and A. J. HEEGER. Acc. Chem. Res. **7**, 232 (1974).
3. K. D. TRUONG and A. D. BANDRAUK. Chem. Phys. Lett. **44**, 232 (1976).

[2]A. W. Hanson. Private communication.

4. K. FUKE, K. KAYA, T. KAJIWARA, and S. NAGAKURA. J. Mol. Spectrosc. **63**, 98 (1976).
5. H. KURODA, T. KUNII, S. HIROMA, and H. AKAMATU. J. Mol. Spectrosc. **22**, 60 (1967); D. HAARER. Chem. Phys. Lett. **27**, 91 (1974).
6. R. L. BECKMAN, J. M. HAYES, and G. J. SMALL. Chem. Phys. **21**, 135 (1977).
7. I. J. TICKLE and C. K. PROUT. J. Chem. Soc. Perkin Trans. II, 726 (1973).
8. J. TANAKA. Bull. Chem. Soc. Jpn. **36**, 1237 (1963).
9. J. M. ROBERTSON and J. G. WHITE. J. Chem. Soc. 607 (1947).
10. J. M. ROBERTSON and J. G. WHITE. J. Chem. Soc. 358 (1947).
11. G. T. POTT and J. KOMMANDEUR. Mol. Phys. **13**, 373 (1967).
12. T. TAKENAKA. Spectrochim. Acta, Part A, **27**, 1753 (1971).
13. L. M. BABKOV *et al.* Opt. Spectrosc. (USSR), **34**, 38 (1973).
14. L. M. BABKOV and M. A. KOVNER. Opt. Spectrosc. (USSR), **35**, 214 (1973).
15. R. BEUKERS and A. SZENT-GYORGYI. Recl. Trav. Chim. Pays-Bas, **81**, 255 (1962).
16. R. R. PENNELLY and C. J. ECKHARDT. Chem. Phys. **12**, 89 (1976).
17. K. OHNO, T. KAJIWARA, and H. INOGUCHI. Bull. Chem. Soc. Jpn. **45**, 996 (1972).
18. R. BOSCHI, E. CLAR, and W. SCHMIDT. J. Chem. Phys. **60**, 4406 (1974).
19. C. A. FYFE, B. A. DUNELL, and J. RIPMEESTER. Can. J. Chem. **49**, 3332 (1971).
20. A. D. BANDRAUK, K. D. TRUONG, H. J. BERNSTEIN, and V. SALARES. To be published.

Potential affinity and photoaffinity reagents for the membrane protein of human erythrocytes involved in glucose transport. Synthesis of 6-amino-6-deoxy derivatives of D-glucose[1]

MOHABIR RAMJEESINGH AND ARTHUR KAHLENBERG[2]

Laboratory of Membrane Biochemistry, Lady Davis Institute for Medical Research, Jewish General Hospital, Montreal, P.Q., Canada H3T 1E2

Received January 26, 1977

MOHABIR RAMJEESINGH and ARTHUR KAHLENBERG. Can. J. Chem. **55**, 3717 (1977).

From 1,2-*O*-isopropylidene-α-D-glucofuranose **1**, the 6-amino-6-deoxy-1,2:3,5-di-*O*-isopropylidene-α-D-glucofuranose **6** was prepared in a four-step sequence in an overall 50% yield. The conversion of **6** to the 6-bromoacetamido-6-deoxy **10**, 6-deoxy-6-isothiocyanato **11**, and 6-(*p*-azido-*o*-nitroanilino)-6-deoxy **12** derivatives of D-glucose is described.

MOHABIR RAMJEESINGH et ARTHUR KAHLENBERG. Can. J. Chem. **55**, 3717 (1977).

On prépare l'amino-6 déoxy-6 di-*O*-isopropylidène-1,2:3,5 α-D-glucofurannose (**6**) à partir du *O*-isopropylidène-1,2 α-D-glucofurannose (**1**) dans une synthèse comportant quatre étapes et de rendement global de 50%. On décrit la transformation de **6** en dérivés bromoacétamido-6 déoxy-6 (**10**), déoxy-6 isothiocyanato-6 (**11**) et (*p*-azido *o*-nitro-anilino)-6 déoxy-6 du D-glucose.

[Traduit par le journal]

The stereospecific transport of D-glucose across the human erythrocyte membrane represents a typical example of facilitated diffusion, mediated, apparently, by a membrane protein possessing one or more sugar binding sites (1, 2). However, the results of recent attempts to identify this D-glucose transport protein have been neither definitive nor in agreement (2–8). The application of the methods of affinity or photoaffinity labelling, currently in widespread use for the attachment of covalent labels at the active-site of protein molecules (9, 10), would aid in establishing the identity of the D-glucose transport protein and would allow subsequent investigation of its properties. In this paper we wish to report the synthesis of three potential substrate-directed alkylating agents of the D-glucose transport protein, namely 6-bromoacetamido-6-deoxy-D-glucose **10**, 6-deoxy-6-isothiocyanato-D-glucose **11**, and 6-(*p*-azido-*o*-nitroanilino)-6-deoxy-D-glucose **12**. Based on previous studies of the structural requirements and bulk tolerance for substituents on the D-glucose molecule for binding to the D-glucose transport protein (11, 12), these glucose derivatives should prove to be successful alkylating substrates for this transport protein. The bromoacetamido moiety of **10** is a well-known alkylating group for proteins by virtue of the facile displacement of the bromine atom by amino groups (13). The isothiocyano moiety of **11** is known to react readily with amino and sulfhydryl groups of proteins yielding thioureas and dithiocarbamic esters, respectively (14). Upon photolysis, the *p*-azido-*o*-nitroanilino moiety of **12** is converted into a nitrene derivative capable of insertion into neighbouring C—H bonds (15). Moreover the absorption maximum (452 nm) of **12** enables photolysis to be effected without damage to the protein.

Selective mesylation of 1,2-*O*-isopropylidene-α-D-glucofuranose **1** gave the methylsulfonate **2** (16). Treatment of **2** with acetone–dimethoxypropane in the presence of *p*-toluenesulfonic acid gave, after 2 days of refluxing, the diacetone derivative **3**. Displacement of the mesyloxy group of **3** with sodium azide in refluxing acetone–water yielded the azide **5** in good yield. Alternatively, displacement of the mesyloxy group of **2** with sodium azide gave **4** (17) which was then converted to **5** using acetone–dimethoxy-propane and a catalytic amount of *p*-toluenesulfonic acid. Reduction of **5** by either catalytic hydrogenation with 10% palladium on charcoal or excess sodium borohydride in refluxing isopropanol gave the syrupy amine **6** in good yield. The amine **6** had been obtained pre-

[1]Supported by a grant (MT-3120) from the Medical Research Council of Canada.

[2]To whom inquiries should be addressed.

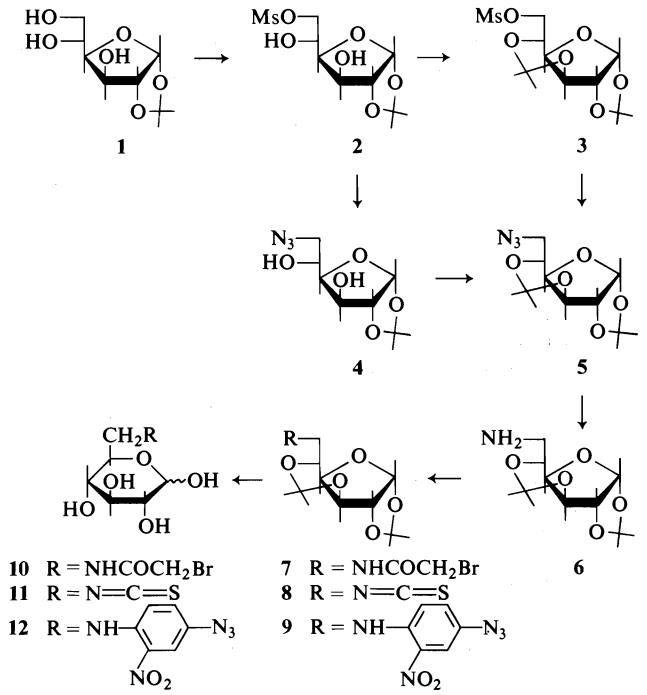

viously and characterized as its crystalline *p*-toluenesulfonate salt by Grosheintz and Fischer (20) and by Ohle and v. Vargha (21).

Reaction of the amine **6** with bromoacetic anhydride in dimethylformamide gave the crystalline bromoacetamido-D-glucofuranose derivative **7**. Treatment of **7** with 50% aqueous trifluoroacetic acid gave the 6-bromoacetamido-6-deoxy-D-glucose **10**, mp 115–119°C.

Treatment of the amine **6** with dicyclohexylcarbodiimide and carbon disulfide in tetrahydrofuran (18) at −10°C yielded the crystalline isothiocyanate **8**. Mild cleavage of the diacetonide with 50% aqueous trifluoroacetic acid at 10°C gave the oily 6-deoxy-6-isothiocyanato-D-glucose **11**.

Upon treatment of the amine **6** with 4-azido-1-fluoro-2-nitrobenzene (19) in ethanol at 60°C for 24 h, 6-(*p*-azido-*o*-nitroanilino)-6-deoxy-1,2:3,5-di-*O*-isopropylidene-α-D-glucofuranose **9** was obtained as bright red crystals, mp 95°C. Cleavage of the diacetonide with 50% aqueous trifluoroacetic acid at room temperature gave the corresponding glucose derivative **12**, mp 180°C (dec.).

Experimental

Melting points were determined on a Mel-Temp block and are uncorrected. Mass spectra were obtained on a AE1-MS-902 mass spectrometer at 70 eV using a direct-insertion probe. Nuclear magnetic resonance spectra were recorded on a Varian Associates T-60 spectrometer using tetramethylsilane as an internal standard. Infrared spectra were obtained on a Unicam SP-200G Grating Spectrophotometer. Ultraviolet spectra were determined with a Beckman spectrophotometer Acta V. Microanalyses were carried out by C. Daessle, Montreal. Analytical thin layer chromatography was performed on silica gel coated plastic plates (Eastman Kodak) and on a preparative scale on silica gel (Merck $UV_{254,366}$) coated glass plates. Ascending paper chromatography was performed on Whatman No. 1 paper.

1,2-O-Isopropylidene-6-O-methylsulfonyl-α-D-glucofuranose **2**

The procedure of Freudenberg and v. Oertzen (16) was used with modifications in the work-up procedure. After the reaction was completed, the solvent was evaporated off and the residue dissolved in a small volume of chloroform was passed through a silica-gel column (act. III), using ethyl acetate as an eluent. The first several fractions collected gave the product as a clear viscous oil which crystallized on standing, mp 99°C (lit. (16) mp 99°C), yield 90%; ir (film) 1185, 1360 (—SO_2), 1385 (*gem*-dimethyl), 3500 cm^{-1} (OH); ^{1}Hmr($CDCl_3$) δ 1.30 (s, 3H, C—Me), 1.50 (s, 3H, C—Me), 3.06 (s, 3H, S—Me), 4.10 (2H, exchangeable, 2 OH), 4.15 (m, 2H), 4.48 (m, 3H), 4.52 (d, J = 3.5 Hz, H-2), 5.90 (d, J = 3.5 Hz, H-1).

1,2:3,5-Di-O-isopropylidene-6-O-methylsulfonyl-α-D-glucofuranose **3**

The mesylate **2** (6 g, 16.8 mmol) was heated under reflux in a mixture of acetone (50 ml) and dimethoxypropane (75 ml) containing *p*-toluenesulfonic acid (10 mg) with a Dean-Stark trap filled with molecular sieves. After 48 h, the mixture was evaporated to dryness and

purified on a silica-gel column (act. III) with ethyl ether – benzene (3:7) as eluent. The first fractions gave the oily diacetonide (4.8 g, R_f = 0.65, ether–benzene 3:7), yield 85%; ir (film) 1185, 1350, 3185 cm^{-1} (*gem*-dimethyl); ^{1}Hmr ($CDCl_3$) δ 1.30 (s, 3H, C—Me), 1.32 (s, 6H, C—Me_2), 1.44 (s, 3H, C—Me), 3.10 (s, 3H, S—Me), 4.06 (m, 2H), 4.48 (m, 3H), 4.60 (d, J = 3.5 Hz, H-2), 5.90 (d, J = 3.5 Hz, H-1).

6-Azido-6-deoxy-1,2:3,5-di-O-isopropylidene-α-D-glucofuranose ***5***

The diacetonide **3** (5 g, 14.8 mmol) was dissolved in acetone–water (80 ml, 5:3) and sodium azide (5 g) was added. The mixture was heated under reflux for 72 h. The solution was then evaporated down to dryness. Water (50 ml) and chloroform (25 ml) were added and the mixture transferred to a separatory funnel. The organic layer was collected and the aqueous layer was further extracted with chloroform (2 × 25 ml). Drying of the chloroform extract with sodium sulfate and evaporation gave the oily azido derivative **5**. The oil was chromatographed on a silica-gel column (act. III) with methylene chloride – hexane (3:2) as eluent. The first several fractions gave the oily azido derivative (3.4 g), yield 80%; ir (film) 1385 (*gem*-dimethyl), 2100 cm^{-1} (azide; ^{1}Hmr ($CDCl_3$) δ 1.32 (s, 3H, C—Me), 1.35 (s, 6H, C—Me_2), 1.52 (s, 3H, C—Me), 3.52 (m, 2H, H-6, 6′), 4.02 (m, 2H), 4.32 (1H), 4.50 (d, J = 3.5 Hz, H-2), 5.90 (d, J = 3.5 Hz, H-1).

Alternatively **5** can be prepared from **4** by refluxing the latter in a mixture of acetone (30 ml) and dimethoxypropane (45 ml) containing *p*-toluenesulfonic acid (10 mg) with a Dean Stark trap filled with molecular sieves. The work-up is the same as above giving **5** in good yield.

6-Azido-6-deoxy-1,2-O-isopropylidene-α-D-glucofuranose ***4***

The procedure of Cramer (17) was used for the preparation of **4**; ir (KBr disc) 1385 (*gem*-dimethyl), 2110 (azide), 3600 cm^{-1} (OH); ^{1}Hmr ($CDCl_3$) δ 1.32 (s, 3H, C—Me), 1.52 (s, 3H, C—Me), 3.52 (d, J = 2.5 Hz, H-6, 6′), 3.55 (b, 2H, OH), 4.04 (m, 2H), 4.32 (1H), 4.50 (d, J = 3.5 Hz, H-2), 5.90 (d, J = 3.5 Hz, H-1).

6-Amino-6-deoxy-1,2:3,5-di-O-isopropylidene-α-D-glucofuranose ***6***

The azide **5** (1 g, 3.5 mmol) was dissolved in absolute ethanol (50 ml) and hydrogenated at 2 atm pressure over 100 mg of 10% palladium on charcoal. After 16 h, the catalyst was filtered off, and the solvent was removed under reduced pressure to give a quantitative yield of the syrupy amine **6**.

Alternatively, to the azide **5** (1 g, 3.5 mmol) in isopropanol (50 ml) was added sodium borohydride (2.5 g) and the mixture refluxed for 14 h. The isopropanol was evaporated under reduced pressure, water (40 ml) added, and the aqueous solution extracted with methylene chloride (3 × 30 ml). Drying of the methylene chloride extract with sodium sulfate, and evaporation gave the amine (0.75 g), yield 82%; ir (film) 1385 (*gem*-dimethyl), 3350, 3410 cm^{-1} (NH); ^{1}Hmr ($CDCl_3$) δ 1.32 (s, 3H, C—Me), 1.35 (s, 6H, C—Me_2), 1.52 (s, 3H, C—Me), 2.90 (2H, exchangeable, NH_2), 3.52 (2H, H-6, 6′), 4.02 (m, 2H), 4.32 (1H, H-3), 4.50 (d, J = 3.5 Hz, H-2), 5.90 (d, J = 3.5 Hz, H-1).

The procedure of Grosheintz and Fischer (20) was used to prepare the crystalline *p*-toluenesulfonate derivative of the amine **6**; mp 172°C with heating at 10°C per minute (lit. (20) 171.5–172.5°C); $[\alpha]_D^{25}$ +30° (*c* 3.884, water). Ohle and v. Vargha (21) reported a rotation of +30.5° (*c* = 5.4, water).

6-Bromoacetamido-6-deoxy-1,2:3,5-di-O-isopropylidene-α-D-glucofuranose ***7***

The amine **6** (450 mg) was dissolved in dimethylformamide (5 ml). To this was added bromoacetic anhydride (460 mg) dissolved in dimethylformamide (2 ml). The reaction mixture was stirred overnight. The solvent was then evaporated off and the residue chromatographed on a silica-gel column (act. III). Elution with ethyl ether – petroleum ether (1:1) gave **7** (R_f = 0.5, ether – petroleum ether 1:1) which was recrystallized twice from ethyl ether, mp 152–154°C, $[\alpha]_D^{25}$ +12° (*c* 1.5, methanol), yield 95%; ir KBr (disc) 1385 (*gem*-dimethyl), 1550 (N—H), 1670 (amide), 3400 cm^{-1} (N—H); ^{1}Hmr ($CDCl_3$) δ 1.32 (s, 3H, C—Me), 1.35 (s, 6H, C—Me_2), 1.52 (s, 3H, C—Me), 2.92 (apparent d, J = 5 Hz, H-6, 6′), 3.58 (m, 2H), 3.82 (s, 2H, CH_2Br), 4.22 (m, 1H), 4.52 (d, J = 3.5 Hz, H-2), 5.90 (d, J = 3.5 Hz, H-1), 6.95 (1H, exchangeable, N—H). *Anal.* calcd. for $C_{14}H_{22}NO_6Br$: C 44.21, H 4.79, N 3.68, Br 21.05; found: C 44.32, H 5.71, N 3.79, Br 21.48.

6-Bromoacetamido-6-deoxy-D-glucose ***10***

Bromoacetamido-glucofuranose **7** (500 mg, 1.3 mmol) was added to 50% aqueous trifluoroacetic acid (10 ml) and the reaction mixture was stirred for 1 h. The solvent was then evaporated off under vacuum, leaving a solid residue which was dissolved in hot ethanol (15 ml). Addition of ethyl acetate (5 ml) and cooling gave the crystalline bromoacetamido-glucose **10**, mp 115–119°C, $[\alpha]_D^{25}$ +38° (after 2 h; *c* 4.425, water), yield 90%; ir (KBr disc) 1545 (N—H), 1655 (amide), 1640 (weak, aldehyde), 3450 cm^{-1} (broad, O—H); ^{1}Hmr (D_2O) δ 3.4–3.6 (3H), 3.90 (s, 2H, CH_2Br), 4.0 (m, 2H), 4.7 (1H, H-2), 5.18 (d, J = 2.5 Hz, C-1); mass spectrum (70 eV) *m/e* 265, 263 ($M^+ - 2H_2O$), 247, 245 ($M^+ - 3H_2O$), 166 ($M^+ - 3H_2O$ – Br), 139, 137. *Anal.* calcd. for $C_8H_{14}NO_6Br$: C 32.0, H 4.67, N 4.67, Br 26.67; found: C 31.75, H 4.62, N 4.57, Br 27.31.

6-Deoxy-1,2:3,5-di-O-isopropylidene-6-isothiocyanato-α-D-glucofuranose ***8***

The amine **6** (1.25 g, 4.8 mmol) dissolved in ethyl ether (10 ml) was added to an ethyl ether (25 ml) solution of dicyclohexylcarbodiimide (0.9 g, 0.9 mol. equiv.) and carbon disulfide (10 ml) stirred at −10°C. The reaction mixture was kept at −10°C for 1 h and then allowed to reach room temperature during 3 h. The solution was set aside at room temperature overnight after which the dicyclohexylthiourea was filtered off. The solution was evaporated to a small volume which was chromatographed on silica-gel plates eluting with ethyl ether – hexane (1:1). The band (R_f = 0.85, ethyl ether – hexane 1:1) was extracted with chloroform and evaporated to give an oil which crystallized on standing, mp 68°C, $[\alpha]_D^{25}$ +45° (*c* 2.1, acetone), yield 69%; ir (film) 1385 (*gem*-dimethyl), 2100 cm^{-1} (N=C=S); ^{1}Hmr ($CDCl_3$) δ 1.32 (s, 3H, C—Me), 1.38 (s, 6H, C—Me_2), 1.52 (s, 3H, C—Me), 3.24 (d of d, J_{AB} = 8 Hz, J = 2.5 Hz, H-6), 3.60 (d of d, J_{AB} = 8 Hz, J = 3 Hz, H-6′), 4.15 (m + s, 3H), 4.25 (d, J = 3.5 Hz, H-2), 5.92 (d, J = 3.5 Hz, H-1); uv λ_{max} (EtOH) 247 nm (ε = 1500). *Anal.* calcd. for $C_{13}H_{19}NO_5S$:

C 51.82, H 6.31, N 4.65, S 10.63; found: C 51.27, H 6.45, N 4.72, S 10.68.

6-Deoxy-6-isothiocyanato-D-glucose ***11***

The isothiocyanate **8** (600 mg, 2 mmol) was dissolved in 50% aqueous trifluoroacetic acid (15 ml) and stirred at 10°C for 1 h. The solvent was then evaporated off under vacuum leaving the 6-deoxy-6-isothiocyanato-D-glucose **11** as an oil. Paper chromatography had shown the product to be homogeneous with $R_f = 0.5$ (1-butanol–EtOH–H_2O, 6:4:3) and with $R_f = 0.75$ (EtOH–Py–H_2O, 6:4:3); ir (film) 2100 cm^{-1} (N=C=S); ^{1}Hmr (D_2O) δ 3.4–4.5 (5H), 4.7 (1H), 5.18 (d, $J = 2.5$ Hz, C-1). *Anal.* calcd. for $C_7H_{11}NO_5S$: C 38.05, H 4.98, N 6.33, S 14.48; found: C 37.92, H 5.02, N 6.31, S 14.30.

6-(p-Azido-o-nitroanilino)-6-deoxy-1,2:3,5-di-O-isopropylidene-α-D-glucofuranose ***9***

The amine **6** (250 mg, 1 mmol) and 4-azido-1-fluoro-2-nitrobenzene (550 mg, 3 mmol) were heated together at 60°C in ethanol for 48 h. Evaporation of ethanol gave a red residue which was chromatographed on silica-gel plates with benzene – methylene chloride (4:1) as eluent. The coloured band at $R_f = 0.55$ was extracted with chloroform. The oil so obtained was dissolved in hexane and refrigerated at 4°C to give the crystalline product, mp 98–100°C, $[\alpha]_D^{25}$ −142° (*c* 0.82, acetone), yield 65%; ir (KBr disc) 1385 (*gem*-dimethyl), 1520 (NO_2), 2100 (N_3), 3360 cm^{-1} (amine); ^{1}Hmr ($CDCl_3$) δ 1.32 (s, 3H, C—Me), 1.35 (s, 6H, C—Me_2), 1.54 (s, 3H, C—Me), 3.23 (m, 2H, H-6, 6′), 4.25 (m + s, 3H), 4.51 (d, $J = 3.5$ Hz, H-2), 5.90 (d, $J = 3.5$ Hz, H-1), 6.92 (1H, exchangeable, N—H), 7.7 and 8.82 (3H, aromatic protons). uv λ_{max} (EtOH) 252, 455 nm (ε = 28 200 and 4600). *Anal.* calcd. for $C_{18}H_{23}N_5O_7$: C 51.31, H 5.46, N 26.60; found: C 50.92, H 5.56, N 26.46.

6-(p-Azido-o-nitroanilino)-6-deoxy-D-glucose ***12***

The azido derivative **9** (150 mg) was stirred in 50% aqueous trifluoroacetic acid (10 ml) for 1 h in the dark. The reaction mixture was then evaporated to dryness. The residue after washing with methylene chloride (2 × 15 ml) was filtered giving 95 mg of the product, mp 192°C (dec.), yield 78%; ir (KBr disc) 1520 (NO_2), 1680 (C=O), 2110 (N_3), 3450 cm^{-1} (b, O—H); uv λ_{max} (EtOH) 252, 455 nm (ε = 28 000, 4600). *Anal.* calcd. for $C_{12}H_{15}N_5O_7$: C 42.23, H 4.40, N 20.53; found: C 41.24, H 4.45, N 19.86.

1. P. G. LeFevre. *In* Current topics in membranes and transport. Vol. 7. *Edited by* F. Bonner and A. Kleinzeller. Academic Press, New York, NY. 1975. p. 109.
2. C. Y. Jung. *In* The red blood cell. Vol. 2. *Edited by* D. MacN. Surgenor. Academic Press, New York, NY. 1975. p. 705.
3. S. Lin and J. A. Spudich. Biochem. Biophys. Res. Commun. **61**, 1471 (1974).
4. C. Y. Jung and L. M. Carlson. J. Biol. Chem. **250**, 3217 (1975).
5. A. Kahlenberg. J. Biol. Chem. **251**, 1582 (1976).
6. M. Kasahara and P. C. Hinkle. Proc. Natl. Acad. Sci. USA, **73**, 396 (1976).
7. C. Zala and A. Kahlenberg. Biochem. Biophys. Res. Commun. **72**, 866 (1976).
8. E. R. Batt, R. E. Abbott, and D. Schachter. J. Biol. Chem. **251**, 7184 (1976).
9. S. J. Singer. Adv. Protein Chem. **22**, 1 (1967).
10. J. R. Knowles. Acc. Chem. Res. **5**, 155 (1972).
11. A. Kahlenberg and D. Dolansky. Can. J. Biochem. **50**, 638 (1972).
12. J. E. G. Barnett, G. D. Holman, and K. A. Minday. Biochem. J. **131**, 211 (1973).
13. Weygand and Hilgetag. Preparative organic chemistry. *Edited by* G. Hilgetag and A. Martini. John Wiley and Sons, New York, NY. 1972. p. 448 and references cited there.
14. C. R. McBroom, C. H. Samanen, and I. J. Goldstein. Methods Enzymol. **28**, 212 (1972).
15. E. W. Thomas. Carbohydr. Res. **31**, 101 (1973).
16. K. Freudenberg and K. v. Oertzen. Ann. Chem. **574**, 37 (1951).
17. F. D. Cramer. Methods Carbohydr. Chem. **1**, 242 (1962).
18. J. C. Jochims and A. Seeliger. Angew. Chem. Int. Ed. Engl. **6**, 174 (1967).
19. G. W. J. Fleet, J. R. Knowles, and R. R. Porter. Biochem. J. **128**, 499 (1972).
20. J. M. Grosheintz and H. O. L. Fischer. J. Am. Chem. Soc. **70**, 1476 (1948).
21. H. Ohle and L. v. Vargha. Ber. **62**, 2432 (1929).

Modified MacInnes equation

BO-LONG POH
School of Chemical Sciences, Universiti Sains Malaysia, Penang, Malaysia

Received April 18, 1977

BO-LONG POH. Can. J. Chem. **55**, 3721 (1977).

A modified MacInnes equation is presented and its relationships with Taft and Brønsted equations discussed.

BO-LONG POH. Can. J. Chem. **55**, 3721 (1977).

On présente une équation modifiée de MacInnes; ses relations avec les équations de Taft et Brønsted sont discutées.

[Traduit par le journal]

Introduction

About 50 years ago MacInnes (1) found that the ionization constants of several homologous series of ω-substituted carboxylic acids could be expressed by

$$[1] \qquad pK_a = pK_\infty + S/n$$

where n is the number of methylene carbon atoms between the carboxylic acid group and the substituent and pK_∞ and S are empirical constants. Later, Greenstein (2) showed that the MacInnes equation could be modified to

$$[2] \qquad pK_a = pK_\infty + S'/l^2$$

where l is the distance between the carboxylic acid group and the substituent and S' is an empirical constant. In this paper we put forward a slightly modified MacInnes equation that encompasses [1] and [2] and discuss some interesting deductions from it.

Results and Discussion

The modified MacInnes equation has the form

$$[3] \qquad pK_a = pK_\infty + Sl_1^2/l^2$$

where l_1 refers to the distance between the carboxylic acid group and the substituent in the first member of the homologous series, namely XCH_2COOH. Equation 3 is similar to [2] with $S' = Sl_1^2$ and is also similar to [1] because the values of l_1^2/l^2 turn out to be close to the corresponding values of $1/n$ (see Table 1) when the fully extended conformation is used to calculate l in the usual manner (3). We suggest that those acids which give linear pK_a against $1/n$ plots are fully extended in conformation. Table 2 lists the acids that follow the MacInnes equation closely together with the calculated values of pK_∞, S, and the correlation coefficients. The results indicate that the dipolar and charged substituted acids listed in Table 2 are fully extended in

TABLE 1. Comparison of $1/n$ and l_1^2/l^2 for some $X(CH_2)_nCOOH$ and $X(CH_2)_n\overset{+}{N}H_3$

$1/n$		1	0.50	0.33	0.25	
l_1^2/l^{2*} for $X(CH_2)_nCOOH$	X = Cl	1	0.54	0.34	0.21	(3.39 Å)[a]
	X = Br	1	0.54	0.34	0.21	(3.43 Å)[a]
	X = I[b]	1	0.53	0.35	0.22	(3.49 Å)[a]
	X = OH[b]	1	0.54	0.33	0.19	(3.35 Å)[a]
	X = CN[b]	1	0.52	0.39	0.26	(4.18 Å)[a]
	X = COOH	1	0.52	0.41	0.29	(4.87 Å)[a]
l_1^2/l^{2*} for $X(CH_2)_n\overset{+}{N}H_3$	X = $\overset{+}{N}H_3$[c]	1	0.46	0.37	0.27	(3.02 Å)[a]
	X = COO^-	1	0.52	0.38	0.25	(3.97 Å)[a]
l_1^2/l^2 for free rotation conformation[d]		1	0.75	0.58	0.52	

NOTE: * indicates fully extended conformation.
[a]The ratios were calculated from data taken from ref. 3 unless otherwise stated. The values of l_1 are given in parentheses.
[b]Calculated in this work using the method in ref. 3.
[c]Calculated from data taken from ref. 22.
[d]Average l_1^2/l^2 value for free rotation conformation for X = Cl, Br, COOH, and $\overset{+}{N}H_3$ in $X(CH_2)_nCOOH$. Calculated from data taken from ref. 3.

water. Similar conclusions have been reached for charged substituted acids but the conclusions for the dipolar substituted acids are not in agreement with earlier ones which are, however, not clear cut (4, 5). The deviation of malonic acid (2) from such a plot can be explained in terms of the folded structure of its monoanion due to the presence of intramolecular H-bonding (6–8). A folded conformation gives a smaller value of l and thus a smaller pK_a value. This is indeed the case for malonic acid. Equation 3 was applied to three series of carboxylic acids with known structures, namely 4-substituted bicyclo[2.2.1]heptane-1-carboxylic acids, 4-substituted bicyclo-[2.2.2.]octane-1-carboxylic acids, and *trans*-4-substituted cyclohexane-1-carboxylic acids, to test its applicability in predicting their pK_a values in water. The values of pK_∞ and S used were taken from Table 2 and the values of l were calculated from the known geometries of the molecules. The results given in Table 3 show that the observed and calculated values are in good agreement.

From the close agreement in the pK_∞ values for different substituents and their closeness to the pK_∞ value for the unsubstituted series we may approximate [3] to

$$[4] \qquad pK_a - pK_0 = Sl_1^2/l^2$$

where K_0 is the ionization constant for the unsubstituted acid. Equation 4 is analogous to the Taft equation

$$[5] \qquad pK_a - pK_0 = -\sigma^*\rho^*$$

with S and l_1^2/l^2 analogous to $-\sigma^*$ and ρ^*, respectively. For the ionization of substituted acetic acids, XCH_2COOH, in water at 25°C with $\rho^* = 1.72$ and $l_1^2/l^2 = 1$, and using $\sigma_I = 0.45\sigma^*$ (9, 10), we expect $\sigma_I = -0.26S$ from [4] and [5]. A plot of σ_I against S (Fig. 1) is linear and yields a slope of -0.23 which is close to the predicted value of -0.26. Comparing [4] and [5] we expect the ratio of the S values for the aliphatic carboxylic acids and amine conjugate acids to be

TABLE 2. Calculated values of pK and S for some ω-substituted aliphatic carboxylic acids and amine conjugate acids, $X(CH_2)_nY$

X	S	pK_∞	n*	r**	Ref.
		Y = COOH			
H	−0.15	4.91	7	—	19*a*
Cl	−2.52	5.34	4	1.000	20
Br	−2.46	5.32	5	0.999	20
I	−2.19	5.30	4	0.992	20
OH	−1.38	5.20	4	0.999	20
COOH	−0.97	4.99	5	0.985	19*b*
COO^-	+0.34	5.03	5	0.987	19*b*
$\overset{+}{N}H_3$	−2.55	4.88	5	1.000	21
SO_3^-	−1.12	5.31	5	1.000	19*c*
C_6H_5	−0.83[a]	—	—	—	—
F	−2.57[a]	—	—	—	—
CH_3CO	−1.56[a]	—	—	—	—
CH_3S	−1.42[a]	—	—	—	—
H_2NCO	−1.50[a]	—	—	—	—
CH_3O	−1.61[a]	—	—	—	—
CN	−2.67[a]	—	—	—	—
NO_2	−3.46[a]	—	—	—	—
$\overset{+}{N}(CH_3)_3$	−3.31[a]	—	—	—	—
		Y = $\overset{+}{N}H_3$			
H	0.00	10.64	9	—	21
Br	−5.34	11.12	3	0.925	21
OH	−3.32	11.14	5	0.991	21
COO^-	−1.29	11.02	5	0.979	21
$\overset{+}{N}H_3$	−8.54	11.43	6	0.991	21
SO_3^-	−6.35	12.15	6	0.997	21
NH_2	−3.03	11.17	6	0.965	21
$COOC_2H_5$	−3.28	10.89	5	1.000	21
C_6H_5	−1.46	10.71	5	0.993	21
PO_4^{2-}	−1.31	11.35	4	0.981	21
CCl_3	−6.47	12.15	4	0.979	21
CF_3	−2.95[b]	—	—	—	—
CH_3S	−3.52[c]	—	—	—	—
CH_3O	−3.28[c]	—	—	—	—
CN	−5.91[b]	—	—	—	—
HC≡C	−3.10[b]	—	—	—	—

NOTE: Average $pK_\infty = 5.14 \pm 0.18$ for Y = COOH; 11.25 ± 0.50 for Y = $\overset{+}{N}H_3$. *Number of points used in the correlation. **Correlation coefficient.

[a]Calculated from the pK_a values of XCH_2COOH using [1] with $n = 1$ and $pK_\infty = 5.14$.

[b]Calculated from the pK_a values of $XCH_2\overset{+}{N}H_3$ using [1] with $n = 1$ and $pK_\infty = 11.25$.

[c]Calculated from the pK_a values of $X(CH_2)_2\overset{+}{N}H_3$ using [1] with $n = 2$ and $pK_\infty = 11.25$.

TABLE 3. Observed and calculated ionization constants of 4-substituted bicyclo[2.2.1]heptane-1-carboxylic acids, 4-substituted bicyclo[2.2.2]octane-1-carboxylic acids, and *trans*-4-substituted cyclohexane-1-carboxylic acids in water

Substituent	pK_a[a]	pK_a[b]	pK_a[c]
H	4.88(4.86)[d]	5.08(4.87)[d]	4.90(4.87)[d]
COO^-	4.98(4.92)	5.16(5.12)	5.06(5.12)
OH	—	—	4.69(4.83)
OCH_3	—	—	4.66(4.71)
$COOCH_3$	4.49(4.58)	4.76(4.67)	4.66(4.67)
COOH	4.50(4.68)	4.77(4.73)	4.67(4.73)
Cl	4.36[e](4.53)	4.62[e](4.66)	4.58(4.66)
CN	4.23(4.29)	4.55(4.92)	4.48(4.42)
$\overset{+}{N}(CH_3)_3$	3.72(4.08)	4.08(4.25)	—

[a]4-Substituted bicyclo[2.2.1]heptane-1-carboxylic acids, $l_1^2/l^2 = 0.32$; pK_a data taken from ref. 23.

[b]4-Substituted bicyclo[2.2.2]octane-1-carboxylic acids, $l_1^2/l^2 = 0.27$; pK_a data taken from ref. 23.

[c]*trans*-4-Substituted cyclohexane-1-carboxylic acids, $l_1^2/l^2 = 0.27$; pK_a data taken from ref. 24.

[d]Calculated values in parentheses.

[e]Br.

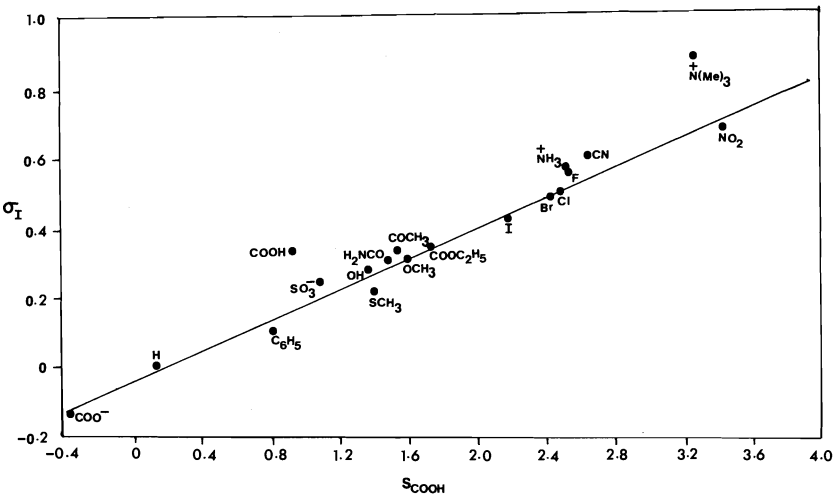

FIG. 1. σ_I vs. S(COOH).

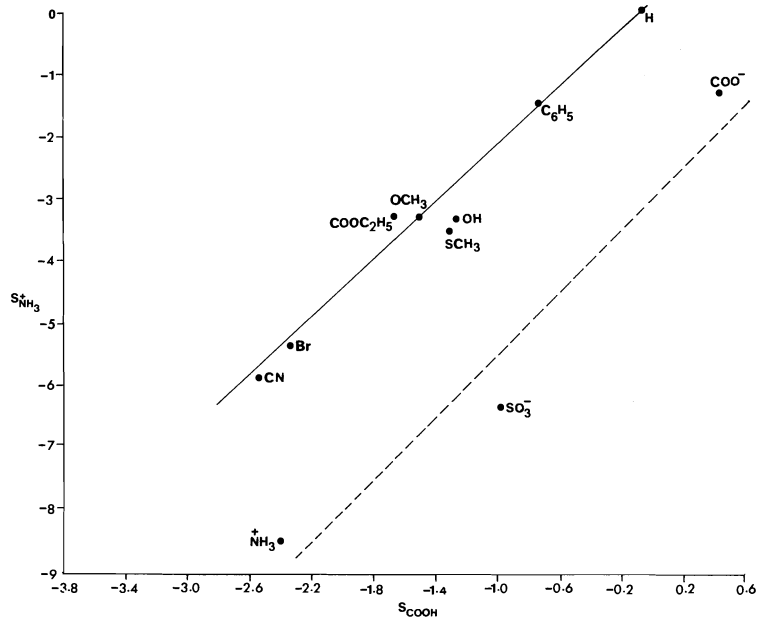

FIG. 2. $S(^+NH_3)$ vs. S(COOH).

equal to the ratio of their ρ* values. A plot of the two sets of S values yields a slope of 2.30 (solid line, Fig. 2) which is close to the ρ* ratio of 1.85 (11) for the two series $XCH_2\overset{+}{N}H_3$ and XCH_2COOH, and 1.87 (11) for the two series $ArCH_2\overset{+}{N}H_3$ and $ArCH_2COOH$. The reason that the charged substituents fall on a separate and almost parallel line (slope 2.48) is not clear (9, 10).

Since the Taft equation is applicable to rate constants, eq. 4 can similarly be modified by replacing the equilibrium constant K_a by the rate constant k_x. For a general acid-catalyzed reaction

$$[6] \qquad HA + B \rightleftharpoons \overset{\delta+}{B}\text{---}H\text{---}\overset{\delta-}{A} \rightleftharpoons \overset{+}{B}H + A^-$$

where HA is an acid and B a base, the charge developed on A in the transition state is only a fraction (α, the Brønsted coefficient) of that of the conjugate base A. Therefore, the equation correlating the rate constants is

TABLE 4. Anomalous and corrected Brønsted exponent (α)

Reaction series	α Reported	α Corrected[a]	Ref.
1. $ArCH_2NO_2 + \bar{O}H \xrightarrow{H_2O} ArCHNO_2^- + H_2O$	1.54	0.88	(14, 15)
2. $ArCH_2NO_2 + B \xrightarrow{H_2O} ArCHNO_2^- + BH^+$ (B = morpholine)	1.29	0.78	(14, 15)
3. $ArCH_2NO_2 + B \xrightarrow{H_2O} ArCHNO_2^- + BH^+$ (B = 2,6-lutidine)	1.30	0.78	(14, 15)
4. $ArCHMeNO_2 + \bar{O}H \xrightarrow{H_2O} ArCHMeNO_2^- + H_2O$	1.14	0.69	(14, 15)
5. $ArCHMeNO_2 + \bar{O}H \xrightarrow[\text{Dioxane}]{50\%\ H_2O} ArCHMeNO_2^- + H_2O$	1.17	0.70	(16)
6. $ArCHMeNO_2 + \bar{O}R \xrightarrow{50\%\ H_2O\text{–MeOH}} ArCHMeNO_2^- + ROH$	1.37	0.83	(17, 18)
7. $ArCH_2CHMeNO_2 + \bar{O}R \xrightarrow{50\%\ H_2O\text{–MeOH}} ArCH_2CMeNO_2^- + ROH$	1.61	0.89	(17, 18)

[a]The values of l that were used to calculate these numbers are given in the Appendix.

[7] $$-\log k_x = \alpha S l_1^2/l^2 - \log k_0$$

The combination of [4] and [7] yields

[8] $$\log k_x = m\alpha \log K_a + (\log k_0 - m\alpha \log K_0)$$

where $m = (l_e/l_r)^2$ and l_r and l_e denote the distances between the substituent and the center where the charge is located for the general acid-catalyzed reaction and the ionization equilibrium, respectively. When the charge is located on the same atom in both the transition state of the general acid-catalyzed reaction and in the conjugate base in the ionization equilibrium of the corresponding acid m is unity and [8] is reduced to the Brønsted (12) equation. The reactions that give anomalous α values (outside the range of zero to one) are those that do not have the charge located on the same atom in both the transition state of the general acid-catalyzed reaction and in the conjugate base in the ionization equilibrium of the corresponding acid. In such cases the reported α values should really be $m\alpha$ values. Table 4 gives a list of reactions which have anomalous α values (13). In the nitroalkane series the negative charge of fully formed nitronate ions is very probably largely delocalized onto the nitro group (13) whereas the partially developed negative charge in the transition state of the nitronate ions producing process is probably located on the α-carbon atom. By substituting the estimated l values the reported values were corrected and found to be normal (Table 4).

We are currently attempting to relate the modified MacInnes equation to the Kirkwood–Westheimer (3) equation. We hope to be able to explain why in the case of charged substituted acids their pK_a values are inversely proportional to the square of l in the modified MacInnes equation but are inversely proportional to l in the Kirkwood–Westheimer treatment.

Acknowledgements

The author wishes to thank Professor John T. Edward for reading the manuscript and offering some invaluable comments. Financial aid from the Universiti Sains Malaysia in the form of a Short Term Research Project Grant is gratefully acknowledged.

1. D. A. MACINNES. J. Am. Chem. Soc. **50**, 2587 (1928).
2. J. GREENSTEIN. J. Am. Chem. Soc. **58**, 1314 (1936).
3. F. H. WESTHEIMER and M. W. SHOOKHOOF. J. Am. Chem. Soc. **61**, 555 (1939).
4. J. T. EDWARD, P. G. FARRELL, and J. L. JOB. J. Chem. Phys. **57**, 5251 (1972).
5. J. T. EDWARD, P. G. FARRELL, and J. L. JOB. J. Phys. Chem. **77**, 2191 (1973).
6. J. JONES and F. G. SOPER. J. Chem. Soc. 133 (1936).
7. D. H. MCDANIEL and H. C. BROWN. Science, **118**, 370 (1953).
8. F. H. WESTHEIMER and O. T. BENFEY. J. Am. Chem. Soc. **78**, 5309 (1956).
9. C. D. RITCHIE and W. F. SAGER. Progress in physical organic chemistry. Vol. 2. Interscience, New York, NY. 1964.
10. R. W. TAFT, JR. J. Am. Chem. Soc. **75**, 4231 (1953).

11. O. EXNER. Advances in linear free energy relationships. Plenum Press, London. 1972. pp. 21–22.
12. J. N. BRØNSTED and K. PEDERSON. Z. Phys. Chem. **108**, 185 (1924).
13. A. J. KRESGE. Chem. Soc. Rev. London, **2**, 475 (1973).
14. F. G. BORDWELL and W. J. BOYLE, JR. J. Am. Chem. Soc. **93**, 511 (1971).
15. F. G. BORDWELL and W. J. BOYLE, JR. J. Am. Chem. Soc. **94**, 3907 (1972).
16. M. FUKUYAMA, P. W. K. FLANAGAN, F. T. WILLIAMS, JR., L. FRAINIER, S. A. MILLER, and H. SCHECHTER. J. Am. Chem. Soc. **92**, 4689 (1970).
17. F. G. BORDWELL, W. J. BOYLE, JR., J. A. HANTALE, and K. C. YEE. J. Am. Chem. Soc. **91**, 4002 (1969).
18. F. G. BORDWELL, W. J. BOYLE, JR., and K. C. YEE. J. Am. Chem. Soc. **92**, 5926 (1970).
19. R. P. BELL. The proton in chemistry. 2nd ed. Chapman and Hall, London. 1973. (*a*) p. 75; (*b*) p. 96; (*c*) p. 99.
20. W. S. SINGLETON. Fatty acids, their chemistry, properties, production, and uses. Part I. Interscience, New York, NY. 1960. p. 620.
21. D. D. PERRIN. Dissociation constants of organic bases in aqueous solution. Butterworth, London. 1965.
22. C. TANFORD. J. Am. Chem. Soc. **79**, 5348 (1957).
23. C. F. WILCOX and C. LEUNG. J. Am. Chem. Soc. **90**, 336 (1968).
24. S. SIEGEL and J. M. KOMARMY. J. Am. Chem. Soc. **82**, 2547 (1960).

Appendix

The values of l used in Table 4 were calculated from the following data using chlorine as the substituent.

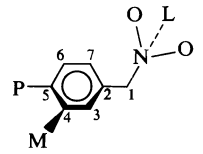

Arylnitromethanes

$l_r(para) = PC_1 = 5.18$ Å; $l_r(meta) = MC_1 = 5.12$ Å; $l_e(para) = PL = 6.46$ Å; $l_e(meta) = ML = 6.76$ Å; $m(para) = 1.56$; $m(meta) = 1.75$. Ring is at 90° to the NC_1C_2 plane; $C_4M = C_5P = 0.89$ Å; C—C(ring) = 1.38 Å; $C_1—C_2 = 1.53$ Å; $C_1—N = 1.44$ Å; angle $C_2—C_1—N = 120°$ for nitronate ion; negative charge is located at L, 0.62 Å beyond the N atom on the extension of the $C_1—N$ bond for the nitronate ion.

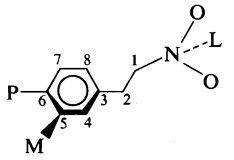

1-Arylnitroethanes

$l_r(para) = PC_1 = 5.86$ Å; $l_r(meta) = MC_1 = 5.78$ Å; $l_e(para) = PL = 7.90$ Å; $l_e(meta) = ML = 7.77$ Å; $m(para) = 1.82$; $m(meta) = 1.80$. Ring is at 90° to the NC_1C_2 plane; angle $C_1—C_2—C_3 = 109°$; others identical to those for arylnitromethanes.

Pyridine-catalyzed halogenation of aromatic compounds. III. Chlorination and the relative stabilities of trichloride and tribromide in chloroform

GERALD E. DUNN AND JAMES A. PINCOCK

Department of Chemistry, University of Manitoba, Winnipeg, Man., Canada R3T 2N2

Received June 7, 1977

GERALD E. DUNN and JAMES A. PINCOCK. Can. J. Chem. **55**, 3726 (1977).

The mechanism of catalysis of aromatic chlorination by pyridine was investigated by measuring the rates of chlorination of toluene in acetic acid with and without added pyridine, pyridinium nitrate, or lithium chloride. All three increase the rate of chlorination slightly and to about the same extent. The effect on the second-order rate constant for chlorination of *p*-chloranisole in chloroform was determined for pyridine, pyridinium chloride, *N*-ethylpiperidinium chloride, tetra-*n*-butylammonium chloride, and tetra-*n*-butylammonium perchlorate. Again, all additives increase the rate constant, with the increase being least for pyridine. It is concluded that, for chlorination in dilute solution, pyridine has no specific catalytic effect, but probably increases the rate by increasing the polarity of the medium. Tetra-*n*-butylammonium chloride was observed to have a decreasing accelerating effect on chlorination in chloroform as its concentration is increased. This was thought to be the result of complexation of chlorine as trichloride. The formation constant for tetra-*n*-butylammonium trichloride in chloroform was found by the Benesi–Hildebrand spectrophotometric method to be $17 \pm 3\ M^{-1}$. This, together with the previously determined value of $9 \times 10^4\ M^{-1}$ for the corresponding tribromide, shows that the order of stability of trihalides in nonaqueous solvents is $Br_3^- \gg Cl_3^-$, contrary to an earlier report.

GERALD E. DUNN et JAMES A. PINCOCK. Can. J. Chem. **55**, 3726 (1977).

On étudie le mécanisme catalytique de la pyridine dans la chloration de noyaux aromatiques, en mesurant les vitesses de chloration du toluène dans l'acide acétique avec ou sans addition de pyridine, nitrate de pyridinium ou chlorure de lithium. Ces derniers augmentent légèrement la vitesse de chloration et environ dans la même mesure. L'influence sur la constante de vitesse d'ordre 2 pour la chloration du *p*-chloroanisole dans le chloroforme est déterminée pour la pyridine, le chlorure de pyridinium, le chlorure de *N*-éthylpipéridinium, le chlorure et le perchlorate de tétra-*n*-butylammonium. Encore une fois, tous ces catalyseurs augmentent la constante de vitesse. Cette augmentation est moins marquée dans le cas de la pyridine. On en déduit que pour la chloration en solution diluée, la pyridine n'a pas un effet catalytique spécifique mais accroit probablement la vitesse en augmentant la polarité du milieu. On remarque que le chlorure de tétra-*n*-butylammonium a un effet d'augmentation de la vitesse de chloration dans le chloroforme qui diminue à mesure que sa concentration augmente. On pense que ceci soit le résultat d'une complexation du chlore sous forme de trichlorure. La constante de formation du trichlorure de tétra-*n*-butylammonium dans le chloroforme déterminée par la méthode spectrophotométrique de Benesi–Hildebrand est de $17 \pm 3\ M^{-1}$. Cette valeur avec celle déterminée antérieurement de $9 \times 10^4\ M^{-1}$ pour le tribromure correspondant montre que l'ordre de stabilité des trihalogénures dans des solvants nonaqueux est $Br_3^- \gg Cl_3^-$ et en opposition avec un rapport antérieur.

[Traduit par le journal]

Introduction

In 1908 Cross and Cohen (1) reported the use of pyridine as a catalyst for aromatic halogenation, and its use for this purpose is still occasionally recommended (2, 3). Part I of this series examined the effect of pyridine upon the bromination of mesitylene in dilute solutions in chloroform or acetic acid and reported that, while pyridine and its salts increase the rate of bromination, the effect is no larger than those of several other electrolytes, so that under these conditions it appears to be no more than a simple salt effect (4). The present report concerns chlorination, which Cross and Cohen also found to be catalyzed by pyridine.

Results

Preliminary Experiments

Cross and Cohen (1) passed chlorine gas into benzene containing a few drops of pyridine at 50°C and isolated a 42% yield of chlorobenzene together with a little dichlorobenzene. When we attempted to repeat this procedure the only product isolated was α-benzenehexachloride, either in daylight or in the dark. On the other hand, when benzene was saturated with chlorine

TABLE 1. Second-order rate constants for the chlorination of toluene in acetic acid at 25°C

$[Cl_2] \times 10^2$ (M)	$[C_7H_8]$ (M)	Catalyst	$k \times 10^4$ (M^{-1} s^{-1})	Ref.
2.5	0.10	—	5.0	5
0.7–2.7	0.1–0.4	—	6.5	6
3.1–3.4	0.19	—	5.3	7
9.3	0.16	—	5.3	8
14.2	0.83	—	3.8	8
4.28	0.127	—	5.05	This work
2.58	0.170	—	4.65	This work
6.44	0.235	—	4.95	This work
6.31	0.233	—	4.96	This work
6.16	0.377	—	4.46	This work
8.99	0.375	—	4.55	This work
9.71	0.391	—	4.66	This work
9.34	0.389	Pyridine, 0.0228 M	5.62	This work
5.96	0.354	Pyridinium nitrate, 0.0313 M	6.36	This work
9.14	0.371	Lithium chloride, 0.0313 M	5.45	This work

at room temperature, then thermostated at 60°C in the dark and analyzed by gas chromatography, chlorobenzene was found. In the absence of pyridine the yield after 19 h was about 4% based on chlorine, whereas in the presence of 1–2% of pyridine the yield was about 85% after 6 h. Thus it is evident that pyridine does catalyze the chlorination of benzene even though we were unable to repeat Cohen's preparation.

Rate Studies

Many of the earlier kinetic studies of aromatic chlorination were done on methylbenzenes in acetic acid solution (5–8), so we began with toluene in acetic acid. The earlier workers reported the reaction to give exclusively nuclear substitution and to be first order with respect to each of aromatic hydrocarbon and chlorine (5–8). We followed the disappearance of chlorine iodimetrically and obtained good second-order plots over at least two half-lives. Table 1 shows the reproducibility of the rate constant at different initial concentrations of chlorine and toluene, and compares the results with literature values. It also shows that both pyridine and pyridinium nitrate increase the rate constant for chlorination, but the effect is small and not significantly larger than that of lithium chloride.

In an attempt to approach Cohen's nonpolar, aprotic reaction conditions more closely, attention was turned to other solvents. Chloroform was chosen because in the bromination studies it was found to be the least polar solvent which dissolves pyridinium salts and does not react with halogen (4). *p*-Chloroanisole was chosen as substrate because in chloroform solution it gives convenient rates and a single product, 2,4-dichloroanisole. The disappearance of chlorine was followed spectrophotometrically with the aromatic substrate in large excess, so that pseudo-first-order kinetics were expected. However, first-order plots were found to have a distinct accelerating curvature, as shown in Fig. 1, line A. On the other hand, when the concentrations of chlorine and substrate were varied, the initial rates measured over the first 10% of reaction show the reaction to be first-order with respect to each of chlorine and aromatic substrate. Table 2 shows the constancy and reproducibility of the second-order constant calculated from initial pseudo-first-order rate constants and *p*-chloroanisole concentrations. It also shows that pyridine increases the initial second-order rate constant by a factor of 4–5, but not in proportion to the concentration of pyridine.[1]

From the facts that pseudo-first-order plots of chlorination in chloroform are curved, although initial rates suggest that the reaction is first order with respect to chlorine, it was suspected that the curvature in the rate plots is due to acceleration by the HCl produced in the reaction. This was confirmed when the chlorination was carried out in the presence of an initial concentration of HCl in excess of that produced during the reaction. Figure 1, line B, shows that under these conditions a good first-order plot can be obtained, and Table 3 shows that the second-

[1]A referee makes the very reasonable suggestion that the apparent pyridine catalysis is due in large part to the pyridinium chloride formed from the HCl produced in the reaction, and that this explains why the catalysis is independent of the initial amount of pyridine.

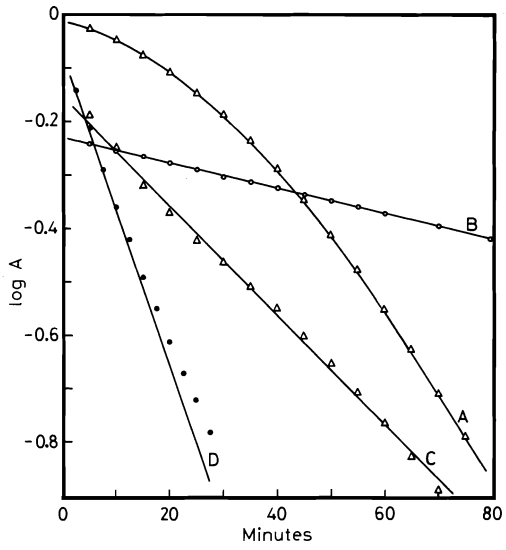

FIG. 1. Chlorination of *p*-chloroanisole in chloroform at 25°C. (A) *p*-Chloroanisole 0.947 *M*, chlorine 6.1 × 10^{-2} *M*. (B) *p*-Chloroanisole 0.142 *M*, chlorine 5.74 × 10^{-3} *M*, hydrogen chloride 4.34 × 10^{-2} *M*; the plot continues straight to log $A = -0.85$. (C) Data from line A plotted as eq. 2; the ordinate for this line is 10^{-3} log $A/(k_2 + k_3$ [HCl]). (D) *p*-Chloroanisole 0.163 *M*, chlorine 0.906 × 10^{-2} *M*, TBACl 1.85 × 10^{-2} *M*.

TABLE 2. Initial second-order rate constants for the chlorination of *p*-chloroanisole in chloroform at 25.0°C

[*p*-Chloroanisole] (*M*)	$[Cl_2] \times 10^2$ (*M*)	[Pyridine] × 10^2 (*M*)	$k \times 10^4$ (M^{-1} s^{-1})
1.45	2.1	—	1.05
1.34	1.6	—	0.93
1.30	1.85	—	1.11
1.29	1.33	—	1.03
1.01	3.7	—	1.03
0.946	3.32	—	0.98
0.946	3.27	—	0.98
0.946	3.22	—	0.93
0.909	3.20	—	1.13
0.900	2.30	—	1.00
0.864	2.9	—	1.06
0.578	5.3	—	0.96
0.519	4.5	—	1.09
0.494	4.1	—	0.93
0.326	0.672	8.11	4.85
0.326	0.672	9.95	4.51
0.326	0.672	15.4	4.06

order rate constant is proportional to the concentration of HCl. This could be interpreted as meaning that the reaction is third order (first order with respect to each of *p*-chloroanisole, chlorine, and hydrogen chloride), which suggests that the runs without added HCl should obey a rate law of the form:

$$[1] \quad -d[Cl_2]/dt = k_2[Ar][Cl_2] + k_3[Ar][Cl_2][HCl]$$

Integration of [1] with the assumption that absorbance A is proportional to $[Cl_2]$ yields [2].

$$[2] \quad -\log A = \frac{[Ar]}{2.3}(k_2 + k_3\,[HCl])t - \log A_0$$

Figure 1, line C, shows a plot of log $A/(k_2 + k_3$ [HCl]) vs. t in which k_2 is taken to be the rate constant for the initial reaction with no added HCl (Table 2), k_3 is the third-order rate constant in the presence of added HCl (Table 3), and [HCl] is calculated from the decrease in chlorine concentration. The fit is reasonably good, confirming that the downward curve in the ordinary rate plot is caused by the HCl produced as the chlorination proceeds.

That HCl exerts its effect as a specific reactant, however, is made doubtful by the observation that similar effects are produced by various other electrolytes. Table 3 shows that the second-order rate constants for chlorination of *p*-chloroanisole in chloroform are proportional to the concentration of each of hydrogen chloride, pyridinium chloride, *N*-ethylpiperidinium chloride (NEPCl), and tetra-*n*-butylammonium perchlorate ($TBAClO_4$). The first three of these contain chloride and an acidic cation, either of which could conceivably participate in the chlorination reaction, but the fourth contains neither, so it seems highly unlikely that any of these reagents are direct participants in the mechanism. It is more likely that their effect is on the polarity of the medium. That the effect should be linear in concentration of electrolyte is somewhat surprising, but perhaps the range of concentration of electrolytes available in chloroform is not large enough to reveal a deviation from linearity.

Tetra-*n*-butylammonium chloride (TBACl) behaves differently from the other electrolytes in two respects. Figure 1, line D, shows that the pseudo-first-order rate constant of a run using this salt decreases as the run progresses, so that the rate constants given in Table 3 are initial rates only. Furthermore, these initial rate constants are not directly proportional to the concentration of TBACl, as is the case with the other electrolytes, but increase much less rapidly than the salt concentration. This behavior is reminiscent of bromination in chloroform solution, where most electrolytes have an accelerating

TABLE 3. Chlorination of *p*-chloroanisole in chloroform in the presence of various additives at 25°C

Additive	[*p*-Chloroanisole] (*M*)	$[Cl_2] \times 10^2$ (*M*)	[Additive] $\times 10^2$ (*M*)	$\frac{k\ (M^{-1}\ s^{-1})}{\text{[Additive]}\ (M)} \times 10^2$
Hydrogen chloride	0.167	2.70	3.85	1.45
	0.142	5.74	4.34	1.45
	0.344	2.89	5.42	1.36
	0.274	2.70	7.06	1.36
	0.283	2.87	8.79	1.50
Pyridinium chloride	0.272	1.35	1.15	7.8
	0.544	0.675	2.30	8.3
	0.271	1.78	2.63	8.5
	0.541	0.898	5.26	7.3
NEPCl	0.325	0.356	2.87	2.63
	0.325	0.356	3.42	2.66
	0.650	0.178	5.74	2.68
TBACl	0.163	0.453	1.85	32.6
	0.163	0.906	1.85	34.5
	0.325	0.453	3.70	23.6
	0.407	0.906	4.64	21.0
	0.813	0.453	9.27	11.1
$TBAClO_4$	0.218	0.672	1.28	10.3
	0.436	0.336	2.56	11.3
	0.218	0.672	2.70	12.3
	0.436	0.336	4.60	10.8

effect but bromides retard bromination, with the retardation being greater for tetra-*n*-butylammonium bromide than for pyridinium or *N*-ethylpiperidinium bromides (4). The retardation was found to be caused by complexation of bromine as tribromide ion, with the formation constant of tribromide increasing with the size and symmetry of the accompanying cation. If the formation constants for trichloride ion show a similar dependence on cation, it is possible that the formation of trichloride could produce a retarding effect at high concentrations of TBACl but not with the other chlorides of Table 3. We therefore examined the formation constant for tetra-*n*-butylammonium trichloride.

Formation Constant

That TBACl does indeed form a complex with chlorine is indicated by the following observations. In the spectral region 250–400 nm chlorine in chloroform solution shows a single broad absorption maximum at 330 nm ($\varepsilon = 100$), whereas a mixture of chlorine with a 30-fold excess of TBACl shows a single sharper absorption maximum at 257 nm ($\varepsilon = 6.6 \times 10^2$ based on chlorine concentration). That the new absorption arises from interaction of chlorine with chloride rather than tetra-*n*-butylammonium ion is shown by the fact that a 30-fold excess of $TBAClO_4$ produces no change in the chlorine absorption in this region.

To determine the formation constant for $TBACl_3$ in chloroform the Benesi–Hildebrand spectrophotometric method (9) was used with slight modification. The form of the equation and the conditions used are the same as those described earlier for pyridinium tribromide (4). The absorbance data at 305 nm are given in Table 4 and plotted in Fig. 2. From a least-squares treatment of the data it was calculated that *K* (the formation constant) = $17 \pm 3\ M^{-1}$

TABLE 4. Absorbance at 305 nm of $TBACl_3$ solutions in chloroform at 25.0°C

$[TBACl] \times 10^2$ (*M*)	$[Cl_2] \times 10^4$ (*M*)	Absorbance
3.24	4.54	0.305
4.75	4.66	0.412
6.19	4.98	0.578
7.27	4.56	0.544
8.35	4.66	0.564
10.1	4.07	0.551
10.4	4.87	0.693
13.0	4.67	0.639
16.8	4.49	0.734

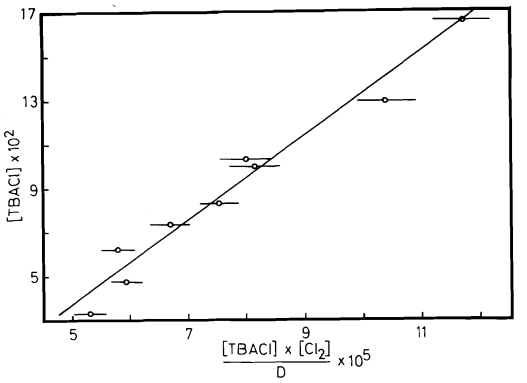

FIG. 2. Benesi–Hildebrand plot for determining the formation constant of $TBACl_3$. $D = A - \varepsilon_{TBACl}$ [TBACl] $- \varepsilon_{Cl_2}$ [Cl_2].

and ε_c (the absorptivity of the complex) $= 1.9 \times 10^2\ M^{-1}\ cm^{-1}$.

Discussion

Rate Studies

Table 1 shows that pyridine, pyridinium nitrate, and lithium chloride at similar concentrations in acetic acid solvent all produce similar small increases in the rate of chlorination of toluene. Consequently, there seems no need to ascribe any specific catalytic role to pyridine other than the salt effect it (as pyridinium acetate) shares with the other electrolytes listed.

In chloroform the effects are larger. It is difficult to compare the effect of pyridine (Table 2) with those of other electrolytes (Table 3) because their concentration dependences vary, but interpolation or extrapolation of the data in Tables 2 and 3 give the following approximate factors for the increase in second-order rate constant produced by an $8.0 \times 10^{-2}\ M$ concentration of each additive: pyridine 4.8, hydrogen chloride 11, pyridinium chloride 64, NEPCl 21, and $TBAClO_4$ 90. It appears that the more ionic the additive, the larger is its effect. As in acetic acid solution, the results are consistent with a medium effect (larger in chloroform than in acetic acid because of the smaller polarity of chloroform). Certainly there is no evidence of any special catalytic effect by pyridine.

In general, then, the results for chlorination agree with those for bromination: although pyridine has an accelerating effect on the rates of aromatic halogenation by both bromine and chlorine in dilute solutions in either acetic acid or chloroform, the effect is of the same order of magnitude as that produced by soluble salts. Since the effect increases in less polar solvents, it is possible that it could be great enough to account for Cohen's results using the aromatic substrate (benzene) as solvent. Also, for each halogen, addition of the corresponding halide (particularly with tetra-*n*-butylammonium cation) causes a decrease in rate of halogenation by complexation of some of the halogen as trihalide.

Tetra-n-butylammonium Trichloride

There has been considerable disagreement in the literature about the relative stabilities of the trihalides in nonaqueous solvents. In 1964 Nelson and Iwamoto (10) reported the formation constants of the three trihalides in acetonitrile to be $10^{6.6}$, 10^7, and 10^{10} for I_3^-, Br_3^-, and Cl_3^-, respectively, thus indicating that the order of stabilities is the reverse of that in water. Subsequent investigators have disagreed with these results, finding trichloride to be much less stable than tribromide or triiodide in nitromethane, acetonitrile (11), and sulfolane (12). The values of the stability constants vary somewhat from one investigator to another. Using polarographic methods, Manchon (11) did not detect any trichloride in nitromethane or acetonitrile, whereas Benoit *et al.* (12) found a formation constant of $10^{3.1}$ for trichloride in sulfolane. Giordano *et al.* (13), using a vapor pressure method, found formation constants of trichloride in acetonitrile to vary from 107 at ionic strength 0.0095 to 7 at ionic strength 0.365. In view of our observation that stability constants of tribromide and trichloride in chloroform depend to some extent upon the accompanying cation, it may be that the different values obtained for trichloride formation by different workers are due in part to the different cations used: tetraethyl (11), tetra-*n*-butyl (10), and lithium (13).

However that may be, our results are in qualitative agreement with those which find trichlorides to be less stable than tribromides in nonaqueous solvents, just as in water. The formation constant for $TBABr_3$ is so large ($9 \times 10^4\ M^{-1}$) that addition of TBABr nearly stops bromination of mesitylene (4), whereas TBACl has only a small retarding effect on the chlorination of *p*-chloroanisole.

Experimental

Materials

Pyridine (Karl Fischer reagent), chlorobenzene, and 2,4-dichloroanisole were commercial products (Eastman) used without further purification. Chlorine and hydrogen

chloride (Matheson) were passed from the suppliers' cylinders through two concentrated sulfuric acid bubblers. Benzene and toluene were purified by the method of Fieser (14). Chloroform, acetic acid, TBACl, $TBAClO_4$, NEPCl, and pyridinium chloride were prepared as previously described (4). *p*-Chloroanisole (Eastman) was purified by distillation through a 90-plate column, collecting the fraction boiling at 89.0°C, 21 Torr.

Rate Measurements

The rate of disappearance of chlorine in acetic acid solutions was followed iodimetrically. Solutions of known concentrations of chlorine and toluene (or toluene plus salt) were mixed in a thermostat at 25.0 ± 0.1°C and aliquots were withdrawn for titration over periods up to three half-lives. Solutions containing only chlorine showed no concentration change over this period.

In chloroform solution the disappearance of chlorine was followed spectrophotometrically at a wavelength between 330 and 400 nm chosen to give initial absorbances in the range 0.5–1.0 and to keep the absorbance of salts below 0.05. Solutions containing only chlorine showed no change in absorbance over 24 h. Slow reactions were run in a thermostat with aliquots withdrawn at intervals for absorbance measurements. Faster reactions were carried out in the cuvette of a Beckman DK-1 spectrophotometer thermostated at 25.0 ± 0.1°C by circulating water from a constant temperature bath. Initial concentrations of chlorine and hydrogen chloride were obtained by titration of the stock solutions before mixing.

The product of chlorination of *p*-chloroanisole was determined by allowing a run to proceed for 10 half-lives or more, then injecting samples into a gas chromatograph (30% Apiezon-L on Chromosorb-W) at 180°C. Only two peaks were found: *p*-chloroanisole and 2,4-dichloroanisole, identified by comparison with authentic samples. Yields of 2,4-dichloroanisole ranged from 84 to 99%.

Formation Constants

Under conditions of high TBACl concentration and low chlorine concentration it was found that the absorbance of mixtures of the two in chloroform decreased with time. Stock solutions of known concentrations of TBACl and chlorine were mixed in the thermostated cuvette (25.0 ± 0.1°C) of the Beckman DK-1 spectrophotometer and absorbance readings were recorded over a 20 min period. Extrapolation to zero time gave initial absorbances with a spread of ±3% over several repetitions. Including the error in transferring small amounts of chloroform solutions, we estimate the overall error at ±5%. This gives rise to the error bars in Fig. 2.

Acknowledgment

The authors are grateful to the National Research Council of Canada for financial support.

1. W. E. Cross and J. B. Cohen. Proc. Chem. Soc. London, 15 (1908).
2. A. I. Vogel. Elementary practical organic chemistry. Part I. Small scale preparations. 2nd ed. Longmans, London. 1965. p. 253.
3. P. B. D. de la Mare and J. H. Ridd. Aromatic substitution. Butterworth Scientific Publications, London. 1959. p. 109.
4. G. E. Dunn and B. J. Blackburn. Can. J. Chem. **52**, 2552 (1974).
5. P. B. D. de la Mare and P. W. Robertson. J. Chem. Soc. 279 (1943).
6. R. M. Keefer and L. J. Andrews. J. Am. Chem. Soc. **79**, 4348 (1957).
7. H. C. Brown and L. M. Stock. J. Am. Chem. Soc. **79**, 5175 (1957).
8. P. B. D. de la Mare and M. Hassam. J. Chem. Soc. 1519 (1958).
9. H. A. Benesi and J. H. Hildebrand. J. Am. Chem. Soc. **71**, 2703 (1949).
10. I. V. Nelson and R. T. Iwamoto. J. Electroanal. Chem. **7**, 218 (1964).
11. J. C. Marchon. C. R. Acad. Sci. Ser. C, **267**, 1123 (1968).
12. R. L. Benoit, M. Guay, and J. Desbarres. Can. J. Chem. **46**, 1261 (1968).
13. M. C. Giordino, V. A. Macagro, and L. E. Sereno. Anal. Chem. **45**, 205 (1973).
14. L. F. Fieser. Experiments in organic chemistry. 3rd ed., revised. D. C. Heath and Co., Boston, MA. 1957.

Concerning the nonexistence of the intramolecular hydrogen bond in 2-nitrothiophenol

TED SCHAEFER AND WILLIAM J. E. PARR[1]

Department of Chemistry, University of Manitoba, Winnipeg, Man., Canada R3T 2N2

Received June 13, 1977

TED SCHAEFER and WILLIAM J. E. PARR. Can. J. Chem. **55**, 3732 (1977).

The long-range spin–spin coupling constants between the sulfhydryl proton and the ring protons in 2-nitrothiophenol in $CDCl_3$ and C_6D_6 solutions suggest the presence of two conformers in which the S—H bond prefers the benzene plane. The conformer in which the S—H bond lies *trans* to the nitro group is favoured over the *cis* conformer by a free energy difference of 0.5 ± 0.2 kcal/mol at 305 K. Apparently any intramolecular hydrogen bond is very weak compared to that in 2-nitrophenol.

TED SCHAEFER et WILLIAM J. E. PARR. Can. J. Chem. **55**, 3732 (1977).

Les constantes de couplage spin–spin à longue distance entre le proton sulfhydryle et les protons du cycle aromatique du nitro-2 thiophénol dans des solutions $CDCl_3$ et C_6D_6 suggèrent la présence de deux conformères dans lesquels le lien S—H s'oriente dans le plan du cycle. Le conformère dans lequel la liaison S—H se situe *trans* au groupe nitro est favorisé par rapport au conformère *cis* par une différence d'énergie libre de 0.5 ± 0.2 kcal/mol à 305 K. Il apparait qu'une liaison hydrogène intramoléculaire quelconque est vraiment faible comparée à celle observée dans le nitro-2 phénol.

[Traduit par le journal]

Introduction

The energy of the intramolecular hydrogen bond in *o*-nitrophenol has never been directly determined (1). Indirect methods based on the chemical shift of the hydroxyl proton (2, 3) and on the torsional frequency of the hydroxyl group (4, 5) yield the energy as 6.7 ± 0.2 kcal/mol. These methods apparently work for weaker hydrogen bonds as well, agreeing with the measured enthalpy of formation of −1.4 kcal/mol for the intramolecular hydrogen bond in *o*-fluorophenol (5). Furthermore, the predictions based on chemical shifts and torsional frequencies are in accord with the deduction, from the contact shifts of hydroxyl protons induced by the di-*tert*-butyl nitroxide radical (5), that the intramolecular hydrogen bond in *o*-nitrophenol is somewhat weaker than in salicylaldehyde.

Another method for the determination of the relative energies of conformers such as **1***a* and **1***b* depends on the well-known stereospecificity

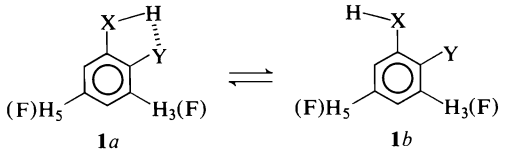

1*a* **1***b*

X = O, S

of the nuclear spin–spin coupling constants over five bonds, $^5J^{H,H(F)}$, between the proton on the sidechain, XH, and the protons or ^{19}F nuclei in the positions *meta* to XH. For example, in **1***a*, $^5J_m^{H,H_3} \equiv {}^5J_c \sim 0$ Hz and $^5J_m^{H,H_5} \equiv {}^5J_t \sim 0.6$ Hz in a variety of phenol derivatives (6, 7).

Now, if Y = NO_2 and if the energy of the hydrogen bond is as large as 6 to 7 kcal/mol, then **1***b* is negligibly populated at ambient temperatures; so that $^5J_c \sim 0$ Hz, in agreement with the observed spectra for 3-fluoro-6-nitrophenol and other nitrophenol derivatives (7). For *o*-dihalophenol derivatives, on the other hand, ^5J_c and ^5J_t have comparable magnitudes and ΔG^0 is a few hundred calories per mole at room temperature (6).

The enhanced intensity of the infrared band, corresponding to the S—H stretching frequency, of *o*-nitrothiophenol relative to thiophenol has been attributed to an intramolecular hydrogen bond; although, in contrast to the phenols, the shift in frequency is remarkably small (8). The dipole moment in benzene solution of *o*-nitrothiophenol has been interpreted as arising from 76 + 4% abundance of the hydrogen bonded form, **1***a*, the apparent increased population of the nonbonded conformer being attributed to intermolecular S—H...π bonding (8).

The small shift in the S—H stretching frequency does suggest a small proportion of the

[1]Postdoctoral fellow, 1974–1976.

TABLE 1. Proton chemical shifts and spin–spin coupling constants for 2-nitrothiophenol

Parameter	Value[a] C_6D_6–$CDCl_3$[b]	Value $CDCl_3$[c]	Parameter	Value C_6D_6–$CDCl_3$[b]	Value $CDCl_3$[c]
ν_{SH}	339.812(5)	403.54	$^5J_{36}$	0.412(14)	0.44
ν_3	778.391(4)	821.56	$^4J_o^{H,SH}$	−0.518(9)	−0.46
ν_4	654.568(9)	726.48	$^5J_m^{H_3,SH}$	0.462(6)	0.45
ν_5	667.489(7)	742.23	$^5J_m^{H_5,SH}$	0.242(9)	0.22
ν_6	659.800(9)	743.41	$^6J_p^{H,SH}$	−0.031(8)	−0.02
$^3J_{34}$	8.347(14)	8.41	Rms deviation	0.0152	0.0238
$^3J_{45}$	7.263(8)	7.32	Transitions calculated	88	91
$^3J_{56}$	8.022(10)	8.00	Peaks observed	51	44
$^4J_{35}$	1.456(9)	1.41	Transitions assigned	65	71
$^4J_{46}$	1.323(7)	1.28			

[a]In Hz at 100 MHz at 305 K to low field of internal tetramethylsilane, numbers in parentheses giving the standard deviation in the last place.
[b]Five mol% in 4:1 v/v C_6D_6–$CDCl_3$ solution.
[c]Five mol% in $CDCl_3$ solution.

intramolecularly bonded form. Therefore a measurement of ^5J_c and/or ^5J_t is indicated for *o*-nitrothiophenol. Recent work (9) has demonstrated that intermolecular proton exchange can be retarded, leading to multiplet structure in the proton magnetic resonance spectra of the sulfhydryl proton in thiophenol and some of its derivatives.

Experimental

The 2-nitrothiophenol was prepared and purified by the method of Foster and Reid (10). A 5 mol % solution in $CDCl_3$, containing a small amount of tetramethylsilane (TMS), was carefully degassed by the freeze-pump-thaw technique. The proton magnetic resonance spectrum was calibrated in the frequency sweep mode at sweep rates of 0.02 and 0.01 Hz/s on an HA 100 spectrometer. The probe temperature was 305 K. Decoupling experiments ascertained the presence of all splittings in the ring proton spectrum caused by spin–spin coupling to the sulfhydryl proton.

Another sample, consisting of a 5 mol% solution in 1:4 v/v $CDCl_3/C_6D_6$ was also calibrated by reading sweep and manual oscillator frequencies at approximately 5 Hz intervals.

Results and Discussion

Spectral Analysis

The spectrum of 2-nitrothiophenol in $CDCl_3$ solution was analyzed as a five spin system by means of the computer program LAME (11, 12). It turned out that the protons at positions 5 and 6 were very tightly coupled. The relative chemical shift is 0.8 Hz and the coupling constant is 8 Hz. The sulfhydryl proton, SH, couples to these two protons and also to that at position 3, H_3, leading to extensive overlap of peaks in its own spectral region. In consequence, the spectral parameters became imprecise, the couplings to SH being known to an estimated accuracy of 0.04 Hz.

However, the solution containing about 80% v/v of C_6D_6 yielded spectra with larger internal chemical shifts and could be analyzed satisfactorily. The results are given in Table 1. Note, however, that the couplings to SH from the ring protons are equal in the two solutions, to within experimental error.

The calculated and observed SH resonance peaks are displayed in Fig. 1 for both solutions.

The Conformational Populations

$^6J_p^{H,SH}$ and the Coplanarity of the SH and Benzene Moieties

$^6J_p^{H,OH}$ in phenol is less than 0.03 Hz, and $^6J_p^{H,SH}$ is -0.33 ± 0.02 Hz in thiophenol (13, 14). The nonzero value in the latter compound reflects the much smaller barrier to internal rotation in the thiophenol; ^6J being proportional to $\langle \sin^2\theta \rangle$, where θ is the angle by which the S—H bond twists away from the aromatic plane (14). The barrier in phenol is about 3.5 kcal/mol (15) but drops to about 1 kcal/mol in thiophenol (14). However, in *p*-nitrothiophenol the internal barrier to rotation about the C—S bond rises to about 2.5 kcal/mol (16), attributable to increased double-bond character induced by conjugation with the nitro group.

As the barrier increases, $\langle \sin^2\theta \rangle$ approaches zero. The observation that $^6J_p^{H,SH}$ in 2-nitrothiophenol is -0.03 ± 0.02 Hz (Table 1) suggests a barrier to internal rotation of greater than 3 kcal/mol (14) for the SH group. Of course, the barrier is no longer twofold in this compound, but it is reasonable to conclude that

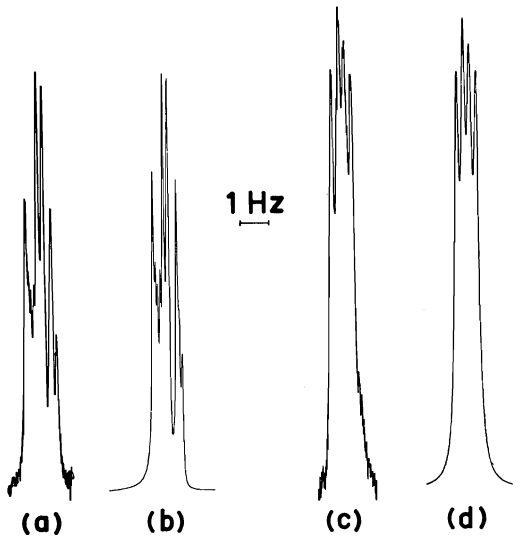

FIG. 1. In *a* and *b* the observed and calculated spectra of the sulfhydryl proton of 2-nitrothiophenol as a 5 mol% solution in 1:4 v/v $CDCl_3$–C_6D_6 solution are given; similarly in *c* and *d* for a 5 mol% solution in $CDCl_3$. The spectral parameters in Table 1 are used to calculate the spectra. The different appearance in the two solutions arises not from large differences in the couplings to the sulfhydryl proton, but from the different internal chemical shifts of the ring protons.

nonplanar conformations are inappreciably populated and that 2-nitrothiophenol can be discussed in terms of conformations **1***a* and **1***b*. This is not to say that the nitro group necessarily lies in the plane of the benzene ring.

The Populations of 1a and 1b

If nonplanar forms of 2-nitrothiophenol can be ignored, the σ–π mechanism does not contribute to $^5J_m^{H,SH}$ (16). If this coupling displays the stereospecificity of $^5J_m^{H,OH}$, then $^5J_c^{H,SH}$ is 0.0 Hz, i.e., $^5J^{H_3,SH}$ is zero in **1***a* and $^5J^{H_5,SH}$ vanishes in **1***b*. With these assumptions it follows that the free energy difference between **1***a* and **1***b* is 0.4 kcal/mol at 305 K, i.e., the *trans* form, **1***b* is approximately twice as abundant as the form **1***a*. Within experimental error, this conclusion applies to both solvents, $CDCl_3$ and C_6D_6.

On the other hand, if ^5J_c is as large as 0.1 Hz, then $^5J_t = 0.6$ Hz, and two equations can be written for the populations of **1***a* and **1***b*. The *trans* form is then 2.9 times as abundant as the *cis* form, corresponding to a free energy difference of 0.65 kcal/mol.

A third possibility, in which ^5J_t in **1***b* is somewhat smaller than ^5J_t in **1***a*, the most likely situation[2] if the electronegative nitro group polarizes the bonds in the coupling path in **1***b*, involves an even larger preponderance of the *trans* form, **1***b*.

Small Intermolecular Hydrogen Bonding

Strong intermolecular hydrogen bonding of the sulfhydryl group would favor form **1***b*. However, the equilibrium constant for the association of benzenethiol itself in CCl_4 is only 0.011 ℓ/mol (18), while infrared data on a variety of thiophenol derivatives suggest that noticeable intermolecular association occurs only at concentrations exceeding 1 *M* in CCl_4 (19).

The concentration of 2-nitrothiophenol in $CDCl_3$ is only ca. 0.6 *M*. The chemical shift of the sulfhydryl proton, ν_{SH}, of a 2 mol% solution of 4-nitrothiophenol in $CDCl_3$ is 3.73 ppm[3] and is 4.04 ppm for the 2-nitro isomer (Table 1). The relatively small shift to low field of 0.3 ppm can arise simply from the proximity of the nitro group in conformer **1***a* and is not an indication of intermolecular hydrogen bonding. Rather, when compared to the very large downfield shift of the hydroxyl proton caused by an *ortho* nitro substituent (3), the observed ν_{SH} in 2-nitrothiophenol is consistent with the conclusions based on $^5J_m^{H,SH}$ above.

In the presence of C_6D_6, ν_{SH} moves to high field, but no more so than the shifts of nearby ring protons (Table 1).

Conclusions

Contrary to the interpretation of infrared and dipole moment data, the present work implies that the S—H bond in 2-nitrothiophenol prefers to lie *trans* to the nitro substituent in $CDCl_3$ and C_6D_6 solutions. The *trans* form is favored over the *cis* form by a free energy difference of 0.5 ± 0.2 kcal/mol at 305 K. Any tendency to intramolecular hydrogen bond formation is clearly rather weak. Furthermore, the S—H bond apparently prefers the benzene plane in both forms and, as indicated by van der Waals radii, the nitro group may well twist out of the benzene plane so as to relieve steric strain.

Acknowledgment

We are grateful to the National Research Council of Canada for financial support.

[2]INDO MO FPT calculations, containing parameters for divalent sulfur (17), did not converge. However, previous calculations on 2-fluorophenol (7) suggest the possibility discussed above.

[3]Unpublished data from this laboratory.

1. U. KOELLE and S. FORSÉN. Acta Chem. Scand. Ser. A, **28**, 531 (1974).
2. I. GRÄNACHER. Helv. Phys. Acta, **34**, 372 (1961).
3. L. W. REEVES, E. A. ALLEN, and K. O. STROMME. Can. J. Chem. **38**, 1249 (1960).
4. W. G. FATELEY, G. L. CARLSON, and F. F. BENTLEY. J. Phys. Chem. **79**, 199 (1975).
5. T. SCHAEFER. J. Phys. Chem. **79**, 1888 (1975).
6. J. B. ROWBOTHAM and T. SCHAEFER. Can. J. Chem. **52**, 3037 (1974).
7. J. B. ROWBOTHAM, M. SMITH, and T. SCHAEFER. Can. J. Chem. **53**, 986 (1975).
8. T. KOBAYASHI, A. YAMASHITA, Y. FURUYA, R. HORIE, and M. HIROTA. Bull. Chem. Soc. Jpn. **45**, 1494 (1972).
9. T. SCHAEFER and W. J. E. PARR. Can. J. Chem. **55**, 552 (1977).
10. D. G. FOSTER and E. E. REID. J. Am. Chem. Soc. **46**, 1936 (1924).
11. S. CASTELLANO and A. A. BOTHNER-BY. J. Chem. Phys. **41**, 3863 (1964).
12. C. W. HAIGH and J. M. WILLIAMS. J. Mol. Spectrosc. **32**, 398 (1969).
13. T. SCHAEFER, J. B. ROWBOTHAM, and K. CHUM. Can. J. Chem. **54**, 3666 (1976).
14. W. J. E. PARR and T. SCHAEFER. J. Magn. Reson. **25**, 171 (1977).
15. E. MATHIER, D. WELTI, A. BAUDER, and Hs. H. GUNTHARD. J. Mol. Spectrosc. **37**, 63 (1971).
16. T. SCHAEFER and W. J. E. PARR. Can. J. Chem. **55**, 552 (1977).
17. V. GALASSO. Theor. Chim. Acta, **34**, 137 (1974).
18. S. H. MARCUS and S. I. MILLER. J. Am. Chem. Soc. **88**, 3719 (1966).
19. J. G. DAVID and H. E. HALLAM. Spectrochim. Acta, **21**, 841 (1965).

The reaction of 2-aminopyridine 1-oxides with thiophosgene. 2*H*-[1,2,4]Oxadiazolo[2,3-*a*]pyridin-2-thiones

DANIELLE ROUSSEAU[1] AND ALFRED TAURINS[2]

Department of Chemistry, McGill University, Montreal, P.Q., Canada H3A 2K6

Received April 14, 1977

DANIELLE ROUSSEAU and ALFRED TAURINS. Can. J. Chem. **55**, 3736 (1977).

2-Aminopyridine 1-oxides react with thiophosgene in ethanol solution in the presence of sodium bicarbonate to produce 2*H*-[1,2,4]oxadiazolo[2,3-*a*]pyridin-2-thiones. The products are stable at room temperature, however, they explode on being heated at the temperature range 121 to 137°C.

DANIELLE ROUSSEAU et ALFRED TAURINS. Can. J. Chem. **55**, 3736 (1977).

Les oxydes d'amino-2 pyridine réagissent avec le thiophosgène en solution éthanolique en présence de bicarbonate de sodium pour conduire à des [2H]-oxadiazolo-[1,2,4] pyridine-[2,3-*a*] thiones-2. Les produits sont stables à la température de la pièce cependant, ils explosent par chauffage dans un écart de température se situant entre 121 et 137°C.

[Traduit par le journal]

2*H*-[1,2,4]Oxadiazolo[2,3-*a*]pyridin-2-one (**1**) has been prepared by heating ethyl *N*-2-pyridylcarbamate 1-oxide (**2**) at 150°C (1), and by treatment of 2-aminopyridine 1-oxide with phosgene (2, 3). Since compound **1** exhibited in its ir spectrum a carbonyl band at 1773 cm^{-1}, in the range for γ-lactones (~1770 cm^{-1}), it was concluded that it has a normal C=O group within a five-membered ring. It showed considerable stability towards heat (3), and underwent pyrolysis at 600°C (4).

An isomeric compound, 1,3,4-oxadiazolo[3,2-*a*]pyridin-2(3*H*)-one (**3**) was prepared by treating 1-amino-2(2*H*)-pyridone (**4**) with phosgene (3). Its ir spectrum showed bands at 1745 and 1785 cm^{-1}, a region assigned to *meso*-ionic carbonyl stretching.

On treatment with ethanol or ammonia, compound **1** yielded pyridine 1-oxide derivatives: *N*-2-pyridylcarbamate 1-oxide (**2**) and *N*-2-pyridylurea 1-oxide (**5**), respectively, whereas compound **3** with the same reagents gave 2-pyridone derivatives: ethyl *N*-[2(2*H*)-pyridon-1-yl]carbamate (**6**) and *N*-[2(2*H*)pyridon-1-yl]urea (**7**), respectively.

In this paper, the formation and properties of sulfur analogs of compounds **1** and **3** are described. When an ether solution of thiophosgene was mixed with an ethanolic solution of 2-aminopyridine 1-oxide in the presence of sodium bicarbonate, a cream colored solid was immediately deposited. On being heated to 132°C in a melting point tube, this product unexpectedly exploded. Its ir spectrum did not show any bands characteristic of the isothiocyanate group. The elemental analysis, nmr and mass spectra of the new compound agreed with the structure of 2*H*-[1,2,4]oxadiazolo[2,3-*a*]pyridin-2-thione (**8**). The compound reacted slowly at room temperature with methanol or ethanol by losing sulfur and deoxygenation of the N—O bond to give methyl or ethyl *N*-2-pyridylcarbamates. However, there was no reaction between ammonia and compound **8**. It has a low solubility in other organic solvents, except dimethylsulfoxide, from which it could be successfully recrystallized.

A number of methyl substituted 2*H*-[1,2,4]oxadiazolo[2,3-*a*]pyridin-2-thiones (**9**–**13**) were prepared from 2-amino-*x*-methylpyridine 1-oxides and thiophosgene, and all of them possessed the

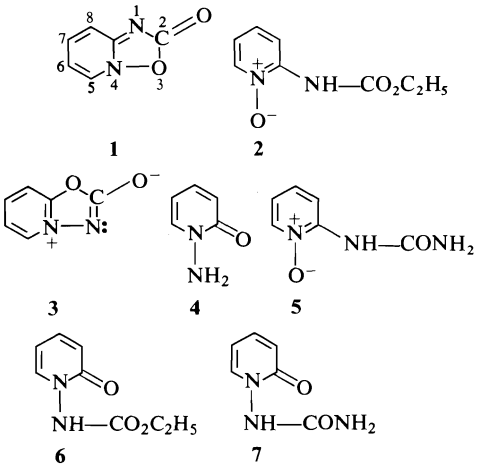

1 **2** **3** **4** **5** **6** **7**

[1]NRCC Scholarship holder 1967–1972.

[2]Author to whom correspondence should be addressed.

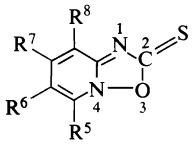

8 $R^5, R^6, R^7, R^8 = H$
9 $R^5 = CH_3$; $R^6, R^7, R^8 = H$
10 $R^6 = CH_3$; $R^5, R^7, R^8 = H$
11 $R^7 = CH_3$; $R^5, R^6, R^8 = H$
12 $R^8 = CH_3$; $R^5, R^6, R^7 = H$
13 $R^5, R^7 = CH_3$; $R^6, R^8 = H$

ability to explode on heating. The nature of the products formed during the explosion is being studied. In addition, it is necessary to mention that all 2*H*-[1,2,4]oxadiazolo[2,3-*a*]pyridin-2-thiones are stable at room temperature and do not decompose on standing in closed containers.

It was found that 2*H*-[1,2,4]oxadiazolo[2,3-*a*]pyridin-2-thiones are formed not only in the reaction of thiophosgene with 2-aminopyridine 1-oxides, but also with 2-acetamidopyridine and ethyl *N*-2-pyridylcarbamate 1-oxides. On the basis of this evidence the mechanism for this reaction must differ from that suggested for the analogous reaction of phosgene with 2-aminopyridine 1-oxide (3). In the latter mechanism, the first step involves the interaction of the amino group with phosgene to form an isocyanate group, followed by the attack of the N-oxide group on the isocyanate group and the ring closure. The mechanism of the thiophosgene reaction (Scheme 1) indicates that the oxygen

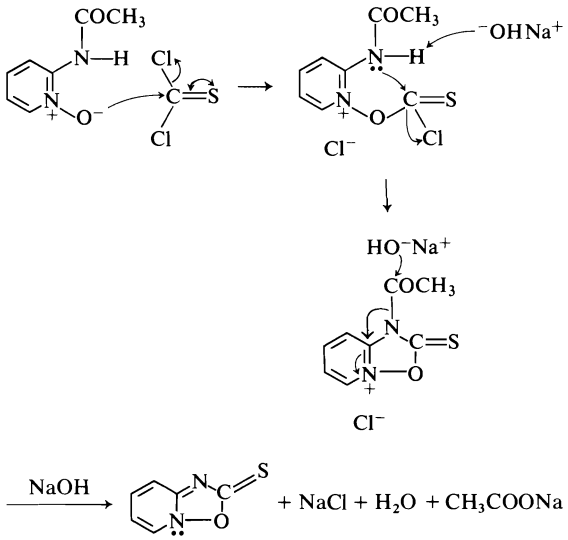

SCHEME 1. Reaction of 2-acetamidopyridine 1-oxide with thiophosgene.

atom of the N-oxide group initiates the reaction by attacking the carbon of the thiophosgene molecule to form a C—O bond. Since the reaction occurs in slightly basic solution, the hydroxyl ions are involved in establishing the N—C bond and eliminating the proton or acetyl group, respectively.

That this mechanism (Scheme 1) requires a free access by thiophosgene to the N-oxide group to initiate the reaction, is obvious from the fact that *N,N'*-diethoxycarbonylaminopyridine 1-oxide (**14**) does not react with thiophosgene, presumably because of the steric hindrance by the two bulky ethoxycarbonyl groups near the N-oxide oxygen.

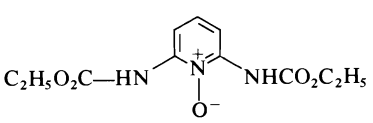

14

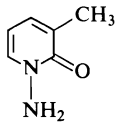

15

The previously proposed (3) formation of 2-isocyanatopyridine 1-oxide with phosgene is doubtful for the following reason. Since it is known that Hofmann degradation of acid amides involves the formation of intermediate isocyanates (6) one should expect a fast interaction between $-\overset{+}{N}-O^-$ and $-N=C=O$ groups, and formation of 2*H*-[1,2,4]oxadiazolo-[2,3-*a*]pyridin-2-one in the degradation of 2-pyridinecarboxamide 1-oxide. However, the only product observed in this reaction was 2-aminopyridine 1-oxide (7). In addition, compound **1** is stable toward prolonged alkaline hydrolysis.

Thiophosgene reacted also with 1-amino-3-methyl-2(2*H*)-pyridone (**15**), in a reaction analogous to that of phosgene (3) to give 8-methyl-[1,3,4]oxadiazolo[3,2-*a*]pyridin-2-thione (**16**) melting at 249–250°C without exploding (Scheme 2). Its mass spectrum revealed the presence of a molecular ion of *m/e* 166. The composition of compound **16** was confirmed by the high resolution mass spectrum. *Exact Mass* calcd. for $C_7H_6N_2OS$: 166.0201; found: 166.0200.

Experimental

2H-[1,2,4]Oxadiazolo[2,3-a]pyridin-2-thione, 8

(*a*) To 2-aminopyridine 1-oxide (0.5 g, 5 mmol) dissolved in 10 ml of water in presence of sodium bicarbonate (0.85 g, 10 mmol) was added gradually a solution of thiophosgene (0.6 g, 5 mmol) in 15 ml of ethyl ether. A white solid was immediately formed. The mixture was stirred for 2 h at 20°C, then filtered to give 0.660 g (87.5%) of 2*H*-[1,2,4]oxadiazolo[2,3-*a*]pyridin-2-thione

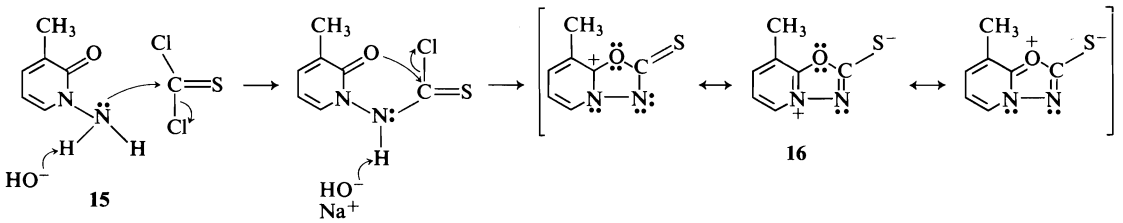

SCHEME 2. Reaction of 1-amino-3-methyl-2(2*H*)-pyridone (**15**) with thiophosgene.

(**8**), exploding at 132–133°C in the melting point tube. After recrystallization from DMSO it exploded at 134°C; nmr (DMSO-d_6): δ 9.59 (s, H-5), 7.75 (s, H-6), 8.47 (s, H-7), 8.08 (s, H-8); uv (C_2H_5OH): λ_{max} 289, 331.5 nm (log ε 4.27, 3.72); ir (KBr): 1619 (vs), 1577 (m), 1485 (s), 1449 (vs), 1400 (vs), 1382 (vs), 1290 (vs), 1146 (s), 1123 (m), 903 (m), 851 (m), 763 (vs), 623 (m), 434 (m) cm^{-1}. *Anal.* calcd. for $C_6H_4N_2OS$: C, 47.4, H, 2.6, N 18.4; found: C 47.1, H 2.9, N 18.2.

(*b*) A mixture of 2-acetamidopyridine 1-oxide (1.037 g, 6.8 mmol) and sodium bicarbonate (1.28 g, 15.2 mmol) in aqueous ethanol (25 ml) was treated with thiophosgene (0.88 g, 7.7 mmol) in 15 ml of ether. The mixture was stirred for 1 h and filtered to give 0.61 g (58.5%) of **8**, exploding at 134°C (recrystallized from dimethylsulfoxide), and showing the spectral characteristics mentioned under (*a*).

Compound **8** and ethanol produced ethyl *N*-2-pyridylcarbamate which was identified by its melting point, infrared spectrum (band at 1722 cm^{-1}), and mass spectrum (*m/e* 166). Treatment of **8** with refluxing methanol for 2.5 h gave colorless needles of methyl *N*-2-pyridylcarbamate, mp 128°C, lit. (5) 128–129°C.

5-Methyl-2H-[1,2,4]oxadiazolo[2,3-a]pyridin-2-thione, ***9***

(*a*) 2-Amino-6-methylpyridine 1-oxide hydrochloride (1.50 g, 9.3 mmol), thiophosgene (1.15 g, 10 mmol) and sodium bicarbonate afforded 1.286 g (81%) of **9**. Recrystallization from dimethylsulfoxide–benzene mixture produced cream-colored crystals, exploding at 134°C; uv (ethanol): λ_{max} 287, 333.5 nm (log ε 4.20, 3.61); ir (KBr): 1623 (m), 1569 (m), 1502 (m), 1413 (s), 1370 (s), 1322 (vs), 1255 (m), 1159 (m), 1086 (m), 1020 (m), 799 (s), 622 (vw), 427 (w) cm^{-1}. *Anal.* calcd. for $C_7H_6N_2OS$: C 50.5, H 3.6, N 16.9, S 19.3; found: C 50.2, H 3.7, N 16.8, S 18.9.

(*b*) By reacting 2-acetamido-6-methylpyridine 1-oxide (9.12 g, 54.9 mmol), thiophosgene (6.6 g, 57.4 mmol) and sodium bicarbonate in ethanol, 7.77 g (85.2%) of **9** was obtained, exploding at 134°C (dimethylsulfoxide–benzene).

6-Methyl-2H-[1,2,4]oxadiazolo[2,3-a]pyridin-2-thione, ***10***

(*a*) Treatment of 2-amino-5-methylpyridine 1-oxide hydrochloride (1.01 g, 6.2 mmol) with thiophosgene (0.81 g, 7 mmol) and sodium bicarbonate in ethanol gave 0.585 g (56.4%) of **10** as beige needles, exploding at 121°C (dimethylsulfoxide); uv (ethanol): λ_{max} 288, 330 nm (log ε 4.20, 3.65); nmr (DMSO-d_6): δ 9.50 (s, H-5), 8.33 (d, H-7), 8.00 (d, H-8). 2.77 (s, CH_3-6); ir (KBr): 1622 (m), 1503 (s), 1418 (vs), 1387 (vs), 1322 (vs), 1266 (s), 1024 (m), 819 (s), 733 (w), 559 (w) cm^{-1}. *Anal.* calcd. for $C_7H_6N_2OS$: C 50.5, H 3.6, N 16.9; found: C 50.7, H 3.9, N 16.6.

(*b*) Similarly, 2-acetamido-5-methylpyridine 1-oxide (7.04 g, 42.4 mmol), thiophosgene (5.1 g, 44.3 mmol), and sodium bicarbonate in ethanol gave 5.1 g (72.3%) of **10**, exploding at 121.5°C.

Compound **10** and refluxing ethanol gave ethyl (5-methyl-2-pyridyl)carbamate, mp 143°C; lit. (5) 144–145°C.

7-Methyl-2H-[1,2,4]oxadiazolo[2,3-a]pyridin-2-thione, ***11***

(*a*) By treatment of 2-amino-4-methylpyridine 1-oxide hydrochloride (1.06 g, 6.6 mmol) with thiophosgene (0.76 g, 6.6 mmol) and sodium bicarbonate in ethanol, 0.84 g (76.3%) of **11** was obtained. Colorless needles (dimethylsulfoxide–benzene) were obtained, exploding at 131.5°C; uv (ethanol): λ_{max} 289, 326 nm (log ε 4.28, 3.83); nmr (DMSO-d_6): δ 9.47 (d, H-5), 7.60 (d, H-6), 7.91 (s, H-8), 2.88 (s, CH_3-7). *Anal.* calcd. for $C_7H_6N_2OS$: C 50.5, H 3.6, N 16.9; found: C 49.9, H 3.7, N 16.7.

(*b*) Similarly, reaction of 2-acetamido-4-methylpyridine 1-oxide (8.09 g, 48.7 mmol) with thiophosgene (5.94 g, 51.6 mmol) afforded 70% of **11**, exploding at 132°C.

(*c*) The treatment of ethyl *N*-(4-methyl-2-pyridyl)carbamate 1-oxide (0.63 g, 3.2 mmol) with thiophosgene (0.36 g, 3.2 mmol) and sodium bicarbonate gave 0.48 g (90%) of **11**, exploding at 132°C.

8-Methyl-2H-[1,2,4]oxadiazolo[2,3-a]pyridin-2-thione, ***12***

In similar fashion, a mixture of 2-acetamido-3-methylpyridine 1-oxide (3.57 g, 21.5 mmol) gave upon treatment with thiophosgene (2.63 g, 22 8 mmol) and sodium bicarbonate in ethanol 2.69 g (75.4%) of **12** as a cream-colored precipitate. Colorless needles (dimethylsulfoxide–benzene) were obtained, exploding at 134°C; uv (ethanol): λ_{max} 287.5, 336 nm (log ε 4.16, 3.63); nmr (DMSO-d_6): δ 9.44 (d, H-5), 8.28 (d, H-7), 7.46 (t, H-6), 2.87 (s, CH_3-8); ir (KBr): 1607 (s), 1497 (s), 1440 (m), 1428 (m), 1388 (vs), 1310 (s), 1278 (s), 1064 (m), 1002 (m), 809 (s), 780 (s), 741 (m), 626 (w) cm^{-1}. *Anal.* calcd. for $C_7H_6N_2OS$: C 50.5, H 3.6, N 16.9, S 19.2; found: C 50.4, H 3.8, N 16.6, S 19.2.

5,7-Dimethyl-2H-[1,2,4]oxadiazolo[2,3-a]pyridin-2-thione, ***13***

2-Amino-4,6-dimethylpyridine 1-oxide hydrochloride (2.44 g, 14 mmol), thiophosgene (1.73 g, 15 mmol), and sodium bicarbonate in ethanol gave 1.87 g (74.4%) of **13**. Cream-colored crystals (dimethylsulfoxide–benzene were obtained), exploding at 137°C; nmr (DMSO-d_6): δ 7.71 (s, H-8), 7.10 (s, H-6), 2.74 (s, CH_3-5), 2.61 (s, CH_3-7); ir (KBr): 1628 (s), 1569 (s), 1418 (vs), 1381 (s), 1335 (s), 1271 (s), 1027 (m), 848 (s), 798 (m), 728 (w), 534 (w) cm^{-1}; ms no molecular ion of *m/e* 180 was present; the strongest peak at *m/e* 148 ($M^{\ddagger}$ − S) was

assigned to 4,6-dimethyl-2-pyridyl isocyanate. *Anal.* calcd. for $C_8H_8N_2OS$: C 53.3, H 4.4, N 15.5, S 17.8; found: C 53.0, H 4.4, N 15.8, S 17.8.

8-Methyl-[1,3,4]oxadiazolo[3,2-a]pyridin-2-thione, ***16***

1-Amino-3-methyl-2-pyridone (0.2 g) (**15**) (3) was dissolved in aqueous ethanol (10 ml) in the presence of sodium bicarbonate (0.5 g) and treated with a solution of thiophosgene (0.5 g) in ether (10 ml). The precipitate was filtered off and extracted with boiling ethanol. The evaporation of the ethanolic extract left 0.245 g of the product **16**, mp 249–250°C (short colorless needles after crystallization from dimethylsulfoxide) (Scheme 2).

Low resolution mass spectrum: *m/e* 166 is the $M^{\cdot+}$, in agreement with the composition of compound **16**. A fragment ion of *m/e* 109 may be assigned to 3-methyl-2-pyridone whose presence may be rationalized as being created by the expulsion of SCN from the molecular ion. High resolution mass spectrum: *Exact Mass* calcd. for $C_7H_6N_2OS$: 166.0201; found: 166.0200. The nmr spectrum (DMSO-d_6): δ 9.16 (d, H-5), 7.94 (t, H-6), 8.42 (d, H-7), 2.87 (s, CH_3-8).

1. A. R. KATRITZKY. J. Chem. Soc. 2063 (1956).
2. J. H. BOYER, R. BORGERS, and L. T. WOLFORD. J. Am. Chem. Soc. **79**, 678 (1957).
3. K. HOEGERLE. Helv. Chim. Acta, **41**, 548 (1958).
4. H. R. SNYDER and M. M. ROBINSON. J. Am. Chem. Soc. **74**, 549 (1952).
5. A. R. KATRITZKY. J. Chem. Soc. 4385 (1957).
6. E. S. WALLIS and JOHN F. LANE. Organic reactions. Vol. 3. *Edited by* R. Adams. J. Wiley and Sons, New York, NY. 1946. p. 268.
7. G. T. NEWBOLD and F. S. SPRING. J. Chem. Soc. S133 (1949).

The acid-catalyzed hydrolysis of phosphinates. III. The mechanism of hydrolysis of methyl and benzyl dialkylphosphinates[1]

KHAMIS A. ABBAS AND ROBERT D. COOK[2]

Department of Chemistry, American University of Beirut, Beirut, Lebanon and Department of Chemistry, Memorial University of Newfoundland, St. John's, Nfld., Canada A1C 5S7

Received April 5, 1977

KHAMIS A. ABBAS and ROBERT D. COOK. Can. J. Chem. **55**, 3740 (1977).

The rates of the acid-catalyzed hydrolysis of methyl dimethyl-, diethyl-, diisopropyl-, and di-*tert*-butylphosphinate in D_2SO_4–D_2O and of *p*-methoxybenzyl, *p*-chlorobenzyl, *p*-nitrobenzyl, and benzyl diethylphosphinate in H_2SO_4 – 70% w/w DMSO–H_2O have been studied. The bell-shaped p*H*-rate profiles, the Bunnett–Olsen ϕ (0.91 to 1.28), Bunnett w (2.28 to 3.52) and w^* (−0.94 to +0.17), and Yates-McClelland r (0.61 to 2.6) values, and the entropies of activation (−18 to −24 eu) all support an A2 mechanism for the methyl esters. The suggested mechanism for the benzyl esters is a unimolecular hydrolysis ($A_{al}1$). This conclusion is supported by the p*H*-rate profiles, the ϕ_r values (−0.12 to −0.29) and the entropies of activation (−4 to −7 eu). The pK_a's of the esters are also reported and they range between −2.4 to −3.3.

KHAMIS A. ABBAS et ROBERT D. COOK. Can. J. Chem. **55**, 3740 (1977).

On étudie les vitesses d'hydrolyse catalysées par un acide du diméthyl-, diéthyl-, diisopropyl- et di-*tert*-butylphosphinate de méthyle dans une solution D_2SO_4–D_2O ainsi que pour les diéthylphosphinates de *p*-méthoxybenzyle, *p*-chlorobenzyle, *p*-nitrobenzyle et benzyle dans une solution H_2SO_4 – 70% w/w DMSO–H_2O. Les courbes obtenues en forme de cloche du p*H*-vitesse d'hydrolyse, les valeurs ϕ (0.91 à 1.28) de Bunnett–Olsen, de w (2.28 à 3.52) et w^* (−0.94 à +0.17) de Bunnett et les valeurs de r (0.61 à 2.6) de Yates-McClelland ainsi que les entropies d'activation (−18 à −24 ue) sont favorables à un mécanisme de type A2 pour les esters méthyliques. On propose un mécanisme d'hydrolyse unimoléculaire ($A_{al}1$) pour les esters benzyliques. Cette conclusion est appuyée par l'allure des courbes (p*H*-vitesse d'hydrolyse), les valeurs ϕ_r (−0.12 à −0.29) ainsi que les entropies d'activation (−4 à −7 ue). On présente aussi les valeurs des pK_a des esters qui se situent entre −2.4 et −3.3.

[Traduit par le journal]

Introduction

Because of their biological importance, the hydrolysis reactions of phosphates (1), and to a lesser extent, phosphonates (2), have been extensively studied. Although phosphinates do not occur in nature, their hydrolysis reactions have also been the subject of several reports. Most of these studies have been carried out in alkaline medium (3). It has been shown that, in general, phosphinates hydrolyze via a mechanism involving attack of hydroxide on phosphorus and subsequent cleavage of the P—O bond. A few esters, *p*-nitrophenyl diphenylphosphinate (**1**) (4), some methyl methylarylphosphinates (**2***a–c*) (5), some l-arylethyl diphenylphosphinates (**3***a–d*) (6) and some alkyl phenylethylphosphinates (**4***a–e*) (7) have been studied in acid medium. There are four general possibilities for the hydrolysis of phosphinates in acid medium. These possibilities are: (*i*) water not involved in the rate-determining step and P—O bond cleavage ($A_{ac}l$); (*ii*) water not involved and C—O bond cleavage ($A_{al}1$); (*iii*) water involved and P—O bond cleavage ($A_{ac}2$); (*iv*) water involved and C—O bond cleavage ($A_{al}2$). An A2 mechanism with P—O bond cleavage as shown by O-18 studies has been proposed for the hydrolysis of **1** (4). A similar mechanism was suggested for compounds **2***a–c*; however, no evidence was presented to support P—O bond cleavage (5). Subsequently, McClelland has shown by O-18 experiments that compounds **2***a–c* undergo acid-catalyzed hydrolysis with approximately 90% P—O bond cleavage (8). A unimolecular ($A_{al}1$) pathway has been proposed for compounds **3***a–c* (6). Compounds **4***a* and **4***b* hydrolyze by an A2 mechanism with 49% and 65% C—O bond cleavage respectively (7). In this paper we report our results on the hydrolysis of methyl dimethyl- (**5***a*), diethyl- (**5***b*), diisopropyl- (**5***c*), and di-*tert*-butylphosphinate (**5***d*)

[1]Taken from the Ph.D. dissertation of K. A. Abbas, American University of Beirut (1975). For Part II, see ref. 30.

[2]Address correspondence to this author at the American University of Beirut, Beirut, Lebanon.

TABLE 1. Rate constants for the hydrolysis of methyl dialkylphosphinates[a] ($R_2PO_2CH_3$) in D_2SO_4–D_2O at 75°C[b]

R = CH_3		R = C_2H_5		R = i-C_3H_7		R = t-C_4H_9	
D^+ M[c]	k[d]	D^+ M[c]	k[d]	D^+ M[c]	k[d]	D^+ M[c]	k[d]
1.85	6.34[l]	1.20	1.19[l]	1.00	0.41[n]	1.05	0.85[l]
2.50	7.53[l]	1.90	1.97[l]	1.20	0.68[l]	1.50	1.12[l]
3.25	10.45[l]	2.58	2.96[l]	1.75	0.99[n]	1.80	1.35[l]
3.40	11.09[l]	3.20	4.68[l]	1.80	1.09[l]	2.20	1.51[l]
3.95	14.49[l]	3.90	5.43[n]	2.50	1.53[l]	2.65	2.14[l]
4.85	20.18[l]	4.85	6.08[l]	3.20	1.98[l]	3.05	2.21[l]
6.07	26.03[l]	5.60	6.65[l]	3.85	2.93[l]	3.36	2.75[l]
6.65	30.14[l]	6.10	8.30[m]	3.90	3.05[m]	3.90	2.97[m]
7.45	32.68[m]	7.20	9.02[l]	5.60	3.53[l]	4.00	3.17[m]
7.65	33.43[l]	7.50	8.39[l]	6.55	4.10[l]	4.70	3.34[m]
8.45	37.62[m]	8.45	7.73[l]	7.05	4.13[l]	5.25	3.41[l]
9.25	34.41[l]	8.50	7.74[n]	8.00	3.82[l]	6.40	3.38[l]
9.75	30.20[m]	10.58	5.11[l]	8.30	3.47[l]	7.10	3.19[l]
9.85	27.36[m]	13.10	4.59[n]	8.90	2.54[l]	7.75	3.05[l]
11.40	23.43[m]	15.18	3.30[l]	10.50	1.75[l]	8.45	2.22[l]
13.05	20.35[l]	8.45[e]	2.09[l]	12.80	1.59[l]	10.60	1.11[l]
14.25	18.27[l]	8.50[i]	0.74[m]	15.45	0.53[l]	12.80	0.55[m]
15.55	17.14[l]			8.00[e]	1.46[l]	15.30	0.29[l]
16.82	16.50[l]			8.00[i]	0.27[n]	16.60	0.19[l]
18.70	7.29[m]					18.50	0.00
7.64[e]	9.19[l]					7.73[j]	7.40[l]
7.60[f]	2.86[l]					7.74[j]	8.39[l]
16.85[g]	1.38[l]					7.73[k]	19.60[l]
16.84[h]	6.13[l]					7.76[k]	20.80[l]

[a]Ester = 0.15–0.21 m [b]T = 75.4 ± 0.4°C, unless indicated. [c]The molarity, determined from a calibration curve which was prepared by titration. [d]$k \times 10^6$ s^{-1}; obtained from a least squares computer analysis; correlation coefficients given in *l*, *m*, and *n*. [e]T = 62.7°C. [f]T = 52.8°C. [g]T = 52.0°C. [h]T = 67.5°C. [i]T = 50.8°C. [j]T = 84.8°C. [k]T = 95.8°C. [l]Correlation coefficient, $r > 0.99$. [m]$0.99 > r > 0.98$. [n]$r < 0.98$.

in D_2O–D_2SO_4 solution as well as our results for the hydrolysis of *p*-methoxybenzyl (**6***a*), benzyl (**6***b*), *p*-chlorobenzyl (**6***c*), and *p*-nitro benzyl diethylphosphinate (**6***d*) in H_2SO_4 – 70% w/w dimethylsulfoxide–water solution.

p-$NO_2C_6H_4O(O)P(C_6H_5)_2$ **1**

p-$XC_6H_4(CH_3)P(O)OCH_3$ **2**

a X = H
b X = CH_3
c X = Cl

p-$XC_6H_4(CH_3)CHO(O)P(C_6H_5)_2$ **3**

a X = H
b X = CH_3
c X = Cl
d X = NO_2

$C_6H_5(C_2H_5)P(O)OR$ **4**

a R = CH_3
b R = C_2H_5
c R = $C_2H_4OCH_3$
d R = i-C_3H_7
e R = i-C_4H_9

$R_2P(O)OCH_3$ **5**

a R = CH_3
b R = C_2H_5
c R = i-C_3H_7
d R = t-C_4H_9

p-$XC_6H_4CH_2O(O)P(C_2H_5)_2$ **6**

a X = OCH_3
b X = H
c X = Cl
d X = NO_2

Results

Rate Data

The observed first-order rate constants for the hydrolysis of compounds **5***a–d* and **6***b–c* at different acid strengths[3] (C_{D^+} or C_{H^+}) are given in Tables 1 and 2 respectively. In subsequent correlations the Hammett acidity functions D_0 and H_0 are also used. The D_0 values are corrected for temperature (9, 10); however, the H_0 values are for 25°C (11). Rate–pH profiles are given in Figs. 1–3.

Basicity Data

The basicity measurements as determined by the nmr method (12) for compounds **5***a–d*, **6***b–d* and for ethyl diethyl- and isopropyl diethylphosphinate are given in Table 3. A typical plot of the nmr chemical shift versus the appropriate acidity function for methyl dimethylphosphinate (**5***a*) is given in Fig. 4. The value of M in Table 3 is the slope of the plot of $\log_{10}$

[3]C_{D^+} and C_{H^+} are the deuterium and hydrogen ion concentrations and were determined from calibration curves which were prepared by titrating weighted samples.

TABLE 2. Rate constants for the hydrolysis of *p*-chlorobenzyl and benzyl diethylphosphinate[a] in H_2SO_4 – 70% DMSO–H_2O

$(C_2H_5)_2PO_2CH_2C_6H_5$[b]		*p*-$ClC_6H_4CH_2O_2P$-$(C_2H_5)_2$[c]	
H^+ M[d]	$k \times 10^6$ (s^{-1})[e]	H^+ M[d]	$k \times 10^6$ (s^{-1})[e]
1.75	2.73[i]	1.82	1.41[j]
2.50	4.47[i]	2.46	2.42[j]
3.10	7.88[i]	3.10	3.21[i]
3.70	10.34[i]	3.45	4.30[i]
3.80	10.20[i]	4.15	6.19[i]
4.60	31.68[i]	4.80	10.06[i]
5.78	10.18[i]	5.70	42.36[i]
1.70[f]	10.94[k]	1.90[f]	4.76[j]
1.80[g]	26.99[i]	1.85[g]	13.63[j]
1.75*h*	62.61[i]	1.85[h]	37.78[i]

[a]Ester = 0.30–0.35 *m*. [b]T = 50.2°C unless indicated. [c]T = 50.5°C unless indicated. [d]The molarity; determined from a calibration curve which was prepared by titration. [e]Obtained from a least squares computer analysis; correlation coefficients given in *i*, *j*, and *k*. [f]T = 60.1°C. [g]T = 70.0°C. [h]T = 77.7°C. [i]r = (correlation coefficient) > 0.99. [j]0.99 > r > 0.98. [k]0.98 > r > 0.97.

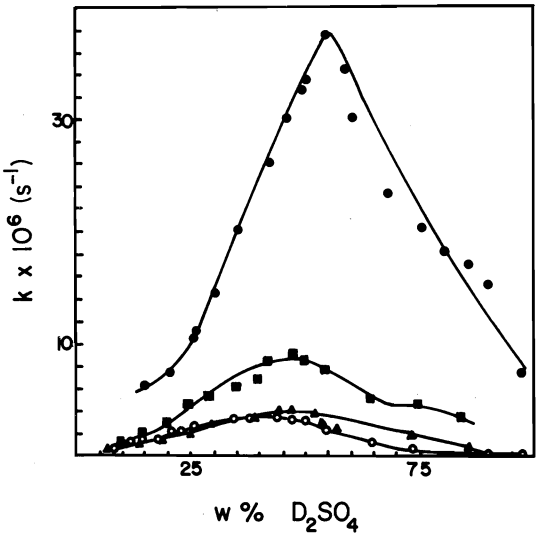

FIG. 1. Rate profiles for methyl dialkylphosphinate hydrolysis in D_2SO_4 at 75°C; (●) methyl; (■) ethyl; (▲) isopropyl; (○) *tert*-butyl.

C_{SD^+}/C_S versus $-D_0$ and represents the deviation of the substrate from Hammett basicity[4] (eq. 1) (12).

$$[1] \quad \log_{10} C_{SD^+}/C_S = M\,(pK_{SD^+} - D_0)$$

Activation Parameters

The values of the activation parameters calculated for the acid-catalyzed hydrolysis of compounds **5***a–d*, **6***b*, and **6***c* are given in Table 4.

[4]C_S and C_{SD^+} are the concentrations of ester and protonated ester respectively.

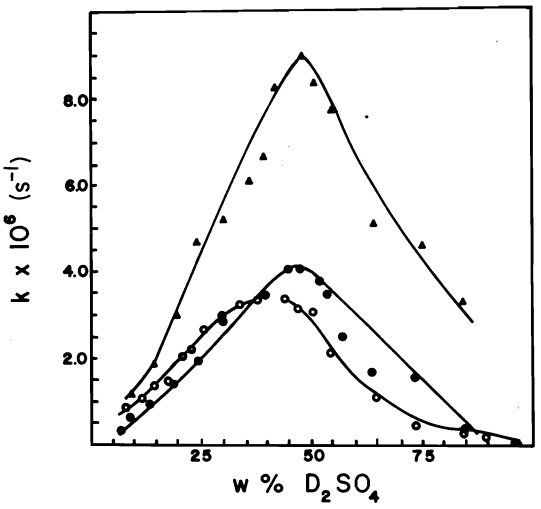

FIG. 2. Expanded rate profiles for methyl dialkylphosphinate hydrolysis in D_2SO_4 at 75°C; (▲) ethyl; (●) isopropyl; (○) *tert*-butyl.

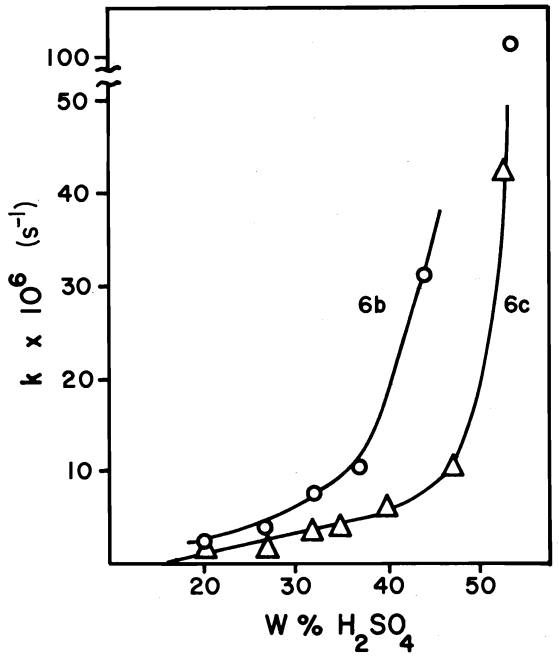

FIG. 3. Rate profiles for benzyl (**6***b*) and *p*-chlorobenzyl (**6***c*) diethylphosphinate hydrolysis in H_2SO_4 – 70% DMSO–H_2O at 50°C.

Treatment of the Kinetic Data

Bunnett w and w Equations (13)*

The equations used for determining the w and w^* values are the appropriate ones for when the substrate is appreciably protonated (eqs. 2 and

TABLE 3. Basicity of phosphinates as determined by the nmr method[a]

Compound	Half protonation[d]	pK_a[e]	M value[e]	r[e]
Methyl dimethylphosphinate[b]	−3.07	−3.14	0.49	0.993
Methyl diethylphosphinate[b]	−3.27	−3.56	0.51	0.988
Methyl diisopropylphosphinate[b]	−3.15	−3.29	0.51	0.998
Methyl di-*tert*-butylphosphinate[b]	−3.05	−3.11	0.62	0.994
Ethyl diethylphosphinate[b]	−3.04	−3.21	0.50	0.985
Isopropyl diethylphosphinate[b]	−2.41	−2.41	0.68	0.994
Benzyl diethylphosphinate[c]	−2.95	−2.81	0.78	0.989
p-Chlorobenzyl diethylphosphinate[c]	−3.25	−3.16	0.50	0.999
p-Nitrobenzyl diethylphosphinate[c]	−2.75	−2.62	0.49	0.999

[a]Reference 12.
[b]In D_2SO_4–D_2O.
[c]In H_2SO_4 – 70% DMSO–H_2O.
[d]Taken from plot of chemical shift versus $-D_0$ or $-H_0$.
[e]Obtained from the least squares analysis of the plot of log [SH$^+$]/[S] versus $-D_0$ or $-H_0$; r = correlation coefficient.

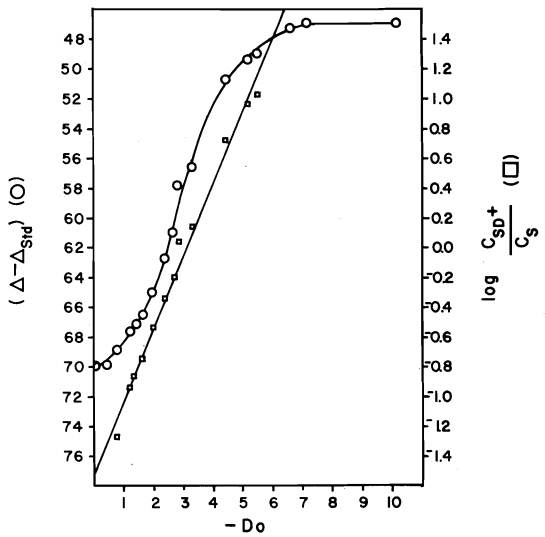

FIG. 4. Protonation of methyl dimethylphosphinate as measured by chemical shift and the dependence of log C_{SD^+}/C_S on D_0.

3).[5] The results of the application of these equations to the rate data obtained for compounds **5***a–d* are given in Table 5. All the

$$[2]\quad \log_{10} k_{obs} - \log_{10} d_0/(d_0 + K_{SD^+}) = w \log_{10} a_{D_2O} + C$$

[5]In [2] and [3] and the following equations the a_{D_2O} values (activity of deuterium oxide) are for 20°C (14) and $-\log_{10} d_0 = D_0$.

$$[3]\quad \log_{10} k_{obs} - \log_{10} C_{D^+}/(d_0 + K_{SD^+}) = w^* \log_{10} a_{D_2O} + C'$$

w plots are curved as is predicted when data obtained over a wide range of acid strength are used (13). The w^* plots give better correlations. However, if the rate data obtained in a medium range of acidities is used then that section of the w plot is relatively linear (see correlation coefficients). Figure 5 gives the w and w^* plots for compound **5***a*.

Bunnett and Olsen ϕ Approach (15)

Bunnett and Olsen suggested that the linear free energy relationship (lfer) represented by [4] would be useful in determining the mechanism of acid-catalyzed reactions when a wide range of acidities is used (15). The ϕ values obtained are composites of ϕ_e, which relates to the equilibrium protonation step, and ϕ_r, which relates to the reaction step. The values for ϕ_e and ϕ_r can be obtained from [5] and [6] respectively. Equation 6 represents the proper form of the Bunnett–Olsen lfer for a moderately basic substrate. The values obtained for ϕ, ϕ_e, and ϕ_r are given in Table 5. A typical ϕ plot is given

$$[4]\quad \log_{10} k_{obs} + D_0 = \phi(D_0 + \log_{10} C_{D^+}) + C''$$

TABLE 4. Activation parameters obtained for the acid-catalyzed hydrolysis of phosphinates

Compound	Weight % acid	Slope[c]	r	E_a (kcal/mol)	$\Delta H^{\ddagger}$ (kcal/mol)	$\Delta G^{\ddagger}$ (kcal/mol)	$\Delta S^{\ddagger}$ (eu)
5*a* Methyl dimethylphosphinate[a]	50.5[d]	−4.81	1.000	22.1	21.5	27.7	−18±3
	90.5	−4.93	0.998	22.7	22.0	28.3	−18±3
5*b* Methyl diethylphosphinate[a]	55[d]	−4.60	0.999	21.1	20.5	28.8	−24±3
5*c* Methyl diisopropylphosphinate[a]	52.5[d]	−5.21	0.986	23.8	23.1	29.3	−18±3
5*d* Methyl di-*tert*-butylphosphinate[a]	50[d]	−5.11	1.000	23.5	22.8	29.5	−19±3
6*b* Benzyl diethylphosphinate[b]	14.7	−5.50	0.997	25.3	24.6	27.4	−7±3
6*c* *p*-Chlorobenzyl diethylphosphinate[b]	15.5	−5.89	0.999	27.1	26.4	27.9	−4±3

[a]In D_2SO_4–D_2O at 75°C.
[b]In H_2SO_4 – 70% DMSO–H_2O at 77.7°C.
[c]Obtained from a least squares computer analysis of the plot of log k versus $1/T$; r = correlation coefficient.
[d]Acid strength where the substrates are half-protonated.

TABLE 5. Results of the analyses of the kinetic data by the Bunnett, Bunnett–Olsen, and Yates–McClelland equations

	w values[a]				w^* values[a]				ϕ_e values[f]			
Compounds	Weight % D_2SO_4	Pts.	w	r[b]	Weight % D_2SO_4	Pts.	w^*	r[b]	Weight % D_2SO_4	Pts.	ϕ_e	r[b]
	15–26[c]	5	6.74	0.994								
5*a*	26–51[d]	7	2.28	0.991	26–51[d]	7	−0.94	0.995				
	15–61[e]	14	1.88	0.956	25–58[e]	11	−1.2	0.982	15–85	18	0.58	0.998
	10–35[c]	7	4.53	0.988								
5*b*	30–50[d]	6	3.00	0.989	30–50[d]	6	−0.18	0.689				
	10–55[e]	11	3.30	0.987	10–55[e]	11	−0.31	0.832	15–85	14	0.56	0.993
	7–30[c]	8	5.71	0.990								
5*c*	30–48[d]	5	3.19	0.996	30–48[d]	5	−0.04	0.198				
	7–54[e]	13	3.33	0.986					15–74	14	0.60	0.998
	8–35[c]	10	6.26	0.987								
5*d*	26–48[d]	7	3.52	0.992	26–48[d]	7	+0.17	0.802				
	8–55[e]	15	3.64	0.978					8–90	19	0.47	0.999

	ϕ_r values[g]				ϕ values[h]					Yates–McClelland r values[i]			
Compounds	Weight % D_2SO_4	Pts.	ϕ_r	r[b]	Weight % D_2SO_4	Pts.	ϕ	r[b]	$\phi_e+\phi_r$	Weight % D_2SO_4	Pts.	Y–M r	r[b]
5*a*	26–51	7	0.09	0.899	26–51	7	0.91	0.999					
	15–90	19	0.13	0.963	15–90	19	1.10	0.998	0.71	15–56[e]	14	0.61	0.972
5*b*	30–50	6	0.32	0.980	30–50	6	1.05	0.998					
	25–65	10	0.36	0.996	10–55	11	1.01	0.997	0.92	10–55[e]	11	1.16	0.949
5*c*	30–48	5	0.35	0.994	30–48	5	1.12	0.999					
	25–86	12	0.32	0.986	25–86	12	1.24	0.999	0.92	7–54[e]	13	1.11	0.988
5*d*	26–48	7	0.56	0.999	26–48	7	1.22	0.994					
	8–74	17	0.48	0.995	8–74	17	1.28	0.998	0.95	9–55[e]	15	2.60	0.995

[a]Reference 13. [b]r = Correlation coefficient; from a least squares computer analysis. Low values of r are expected if the slope value is close to zero. [c]Low acidity range. [d]Medium acidity range. [e]All points for which a_{D_2O} values are known; for w^*, low acidity points are ignored because of scatter. [f]Reference 15*a*, eq. 5. [g]Reference 15*b*, eq. 6. [h]Reference 15*b*, eq. 4. [i]Reference 16*a*.

$$[5]\quad \log_{10} C_{SD^+}/C_S + D_0 = \phi_e(D_0 + \log_{10} C_{D^+}) + C'''$$

$$[6]\quad \log_{10} k_{obs} \times (C_S + C_{SD^+})/C_{SD^+} = \phi_r(D_0 + \log_{10} C_{D^+}) + C^*$$

for compound **5***d* in Fig. 6. The ϕ plots are linear over the entire range of acidities studied even though [4] strictly applies only to very weakly basic substrates.

Yates–McClelland Equation (16)

In order to eliminate the problems created by

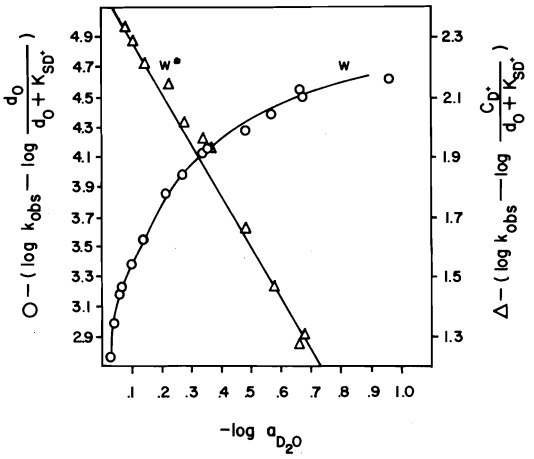

FIG. 5. Bunnett w and w^* plots of the rate data obtained for methyl dimethylphosphinate hydrolysis.

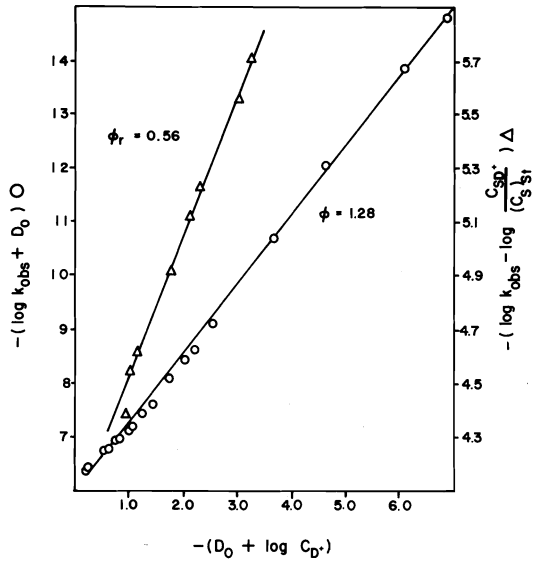

FIG. 6. Bunnett–Olsen ϕ and ϕ_r plots of the rate data obtained for methyl di-*tert*-butylphosphinate hydrolysis.

the non-cancellation of the activity coefficient ratios when analyzing the rate data of the acid-catalyzed hydrolysis of a non-Hammett substrate, Yates and McClelland suggested that the appropriate acidity function for that substrate be used (16). In order to avoid defining new acidity functions for every new type of substrate it was suggested that the Hammett acidity function be modified as in [7] (the M value comes

$$[7] \qquad H_{\text{phosphinates}} = MH_0$$

from [1]). The form of the Yates–McClelland equation used is given in [8]. The values obtained for r, which represents the number of water molecules involved in the rate-determining step, are given in Table 5. A typical r plot is given in Fig. 7.

$$[8] \quad \log_{10} k_{\text{obs}} - \log_{10} d_0^M/(d_0^M + K_{SD^+}^M) = r \log_{10} a_{D_2O} + C^\dagger$$

Discussion

Methyl Esters: General Comments

The pH-rate profiles for compounds 5*a–d* are given in Fig. 1 and an expanded profile for compounds **5***b–d* is given in Fig. 2. The rates of hydrolysis of these compounds show both acid catalysis and at higher acidities acid inhibition of reaction. The bell-shaped curves that are obtained are typical of acid-catalyzed reactions where water is involved in the rate-determining step (17). The acid-catalyzed portion of the curve represents an increase in reactivity due to increasing amounts of protonated ester while the acid-inhibited part is due to a decrease in the activity of water in more concentrated acid solution. The four esters are approximately 40% protonated at their maximum rate. Further proof for an A2 mechanism can be found in the application of the Bunnett w and w^* equations (13) as well as the Bunnett–Olsen ϕ (15) and Yates–McClelland r-value (16) approaches to the study of acid-catalyzed reactions (see next section).

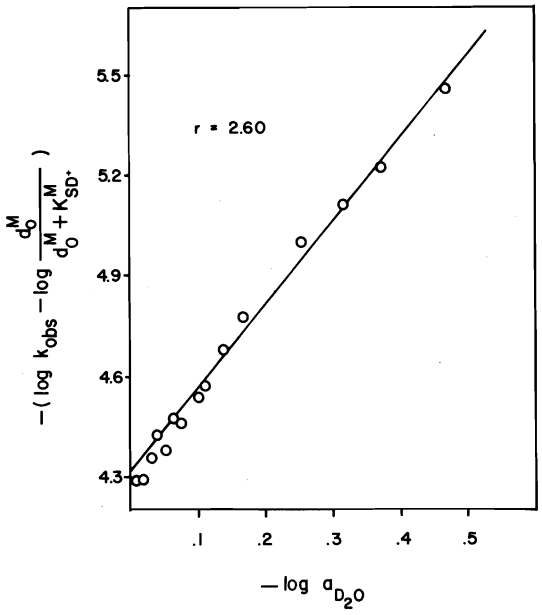

FIG. 7. Yates–McClelland r plot of the rate data obtained for methyl di-*tert*-butylphosphinate hydrolysis.

It is also important to note that the p*H*-rate profiles show no upward curvature at high acid concentrations unlike several acetate esters (16). These acetates, for example methyl acetate, have bell-shaped p*H*-rate profiles which at concentrations above 85% sulfuric acid show slight increases of rate. These upward tails have been explained as a change of mechanism from $A_{ac}2$ to $A_{ac}1$, that is, rate-determining formation of an acylium ion (16). The analogous species for phosphinates would be a phosphinylium ion ($R_2P(O)^+$). There is evidence from studies on the hydrolysis of phosphinyl chlorides that such species are not very stable (18) and therefore in the acid-catalyzed hydrolysis of phosphinates an $A_{ac}1$ pathway is most likely of high energy. An $A_{al}1$ mechanism in the case of the methyl esters is equally unlikely because of the instability of the methyl carbonium ion.

Treatment of the Kinetic Data

The hydrolysis of esters **5***a–d* has been studied over nearly the entire range of sulfuric acid concentration. Because of this factor, the *w* plots, as predicted, are curved, that is, the value of *w* is dependent on the concentration range of acid. If a medium concentration range is used (25–50% D_2SO_4), the values of *w* range from 2.28–3.52 increasing from **5***a* to **5***d*. These values are indicative of an A2 mechanism with water acting as a nucleophile or as a proton transfer agent in the rate-determining step. The *w** plots give straighter lines over a wider acid concentration range than those for *w* and again the results support an A2 mechanism. This mechanism is also suggested by the results obtained from the Bunnett–Olsen lfe relationship (ϕ values). The ϕ_e and ϕ_r values were also determined. Because the substrates are moderately weak bases the proper form of the Bunnett–Olsen relationship is that which is represented by [6] (ϕ_r). The ϕ_r values support a rate-determining step in which water participates as a nucleophile. The appropriate form of the Yates–McClelland equation (eq. 8) gives *r* values which range from 0.6 to 2.6. The value of *r* represents the number of water molecules needed in the rate-determining step. Clearly, for these methyl esters, at least one molecule of water is necessary.

Underlying all these results is the interesting relationship between solvation as represented by the value of *M* and the range of values for the different parameters *w*, *w**, and *r*. Further work is needed in this area although some progress has been achieved by the group of McClelland, Yates and co-workers (19).

Activation Parameters

The entropies of activation of compounds **5***a–d* are in the range of −17 to −24 eu. These values are typical of A2 reactions (20). The entropy of activation was also calculated for compound **5***a* from the rate data in 90.5% D_2SO_4 and the value obtained is the same as that in 50.5% acid. This result also supports the conclusion drawn from the p*H*-rate profiles that the mechanism does not change at very high acidities.

Relative Rate and Point of Cleavage

The relative rate values for a number of different ester systems under varying conditions of p*H*, solvent, and temperature are given in Table 6. The rates of acid-catalyzed hydrolysis of phosphinates are much less sensitive to the size of the substituents on phosphorus than are the corresponding rates in alkaline medium. This result is similar to that obtained for carboxylic esters. The mechanism for carboxylic ester hydrolysis in acid or base involves attack at carbonyl carbon to form a tetrahedral intermediate. It has also been shown that in the alkaline hydrolysis of phosphinates attack takes place on phosphorus with resultant cleavage of the P—O bond (3). However, in acid, water attacks both phosphorus and carbon leading to cleavage of both the P—O and C—O bonds (7, 8). The place of attack appears to be very sensitive to conditions, to the nature of the nucleophile, and to the size of the substituents on phosphorus. For example, compound **2***a* hydrolyzes in 1.0 *M* $HClO_4$ with 90% P—O bond cleavage (8) and compound **4***a* hydrolyzes in 3 *M* $HClO_4$ with 51% P—O bond cleavage (7).

It is likely that the energy barriers to attack at phosphorus and to attack at carbon are very similar and that these esters hydrolyze via both pathways with C—O cleavage becoming more favourable as the size of the alkyl groups on phosphorus increase.

At very high acid concentration hydrolysis does take place, although very slowly. The activity of water at these acid concentrations is extremely low and therefore, it is possible that HSO_4^- is the nucleophile affecting reaction (21). Above 85% H_2SO_4 the concentration of HSO_4^-

TABLE 6. Relative rates of ester hydrolysis

Reaction	R				Ref.
	CH_3	C_2H_5	i-C_3H_7	t-C_4H_9	
$R_2PO_2CH_3 + D^+$	3.6	1.5	0.8	1	[a]
$R_2PO_2CH_3 + D^+$	11	2.5	1.2	1	[b]
$R_2PO_2CH_3 + D^+$	40	9	3	1	[c]
$C_6H_5(C_2H_5)PO_2R + H^+$	1.6	1	—	—	[d]
$C_6H_5(C_2H_5)PO_2R + H^+$	1.5	1	13	—	[e]
$R_2PO_2CH_3 + OH^-$	1700	33	1	—	[f]
$RCO_2C_2H_5 + OH^-$	100	47	10	1	[g]
$RCO_2H + H^+ (C_2H_5OH)$	40	33	11	1	[h]

[a]In D_2SO_4–D_2O; $D_0 = -1$, at 75°C. This work.
[b]In D_2SO_4–D_2O; $D_0 = pK_{SD^+}$, at 75°C. This work.
[c]In D_2SO_4–D_2O; $D_0 = -5.8$, at 75°C. This work.
[d]Reference 7. 3.01 M $HClO_4$ (H_2O) at 100°C.
[e]Reference 7. 2.31 M $HClO_4$ in 40% dimethoxyethane–water at 100°C; relative rates for R = $CH_3OCH_2CH_2$—, 0.31 and R = $(CH_3)_2CHCH_2$—, 0.2.
[f]Reference 3. 60% Dimethoxyethane–water at 75°C.
[g]Reference 28. 88% Ethanol–water at 30°C.
[h]Reference 29. Esterification in HCl at 14.3°C.

is more than 100 times greater than that of H_2O and this would more than offset their nucleophilicity difference (22).

In McCoy's study of the acid-catalyzed alcoholysis of phosphinates **4***a* and **4***b* with methanol and isobutyl alcohol, ethers were isolated as products (greater than 95% attack of alcohol on carbon) (7). In our hydrolysis experiments dimethyl ether is formed in the reactions run in acid strengths above 25% D_2SO_4. Although under these experimental conditions the product of our reaction, methanol, dehydrates, one cannot rule out the possibility that some of the ether is formed in an alcoholysis reaction similar to that observed by McCoy.

In conclusion it can be stated that the evidence clearly suggests an A2 mechanism for the hydrolysis of compounds **5***a–d*.

Benzyl Esters

Noyce and Virgilio (6) have studied the solvolysis of l-arylethyl diphenylphosphinates (**3***a–d*) in 80% ethanol–water at 75°C. The evidence clearly supports their suggested $A_{al}1$ mechanism. The title compounds, **6***a–d*, are less sterically hindered than **3***a–d* toward attack of water (associative mechanism) and they would give rise to a slightly less stable carbonium ion (dissociative mechanism), therefore the possibility of either an A2 or A1 mechanism exists for the hydrolysis of these compounds.

The methoxy ester (**6***a*) hydrolyzes too quickly for the determination of either the pK_{SH^+} or accurate rate constants. The nitro ester (**6***d*), on the other hand, only shows appreciable hydrolysis in solutions containing more than 60% H_2SO_4. The pH-rate profiles for compounds **6***b* and **6***c* are given in Fig. 3. These compounds show a continuous increase in rate with increasing acid concentration. Such profiles are indicative of hydrolysis reactions where water is not involved in the rate-determining step, i.e. dissociative mechanisms.

The ϕ values obtained for compounds **6***b* and **6***c* are positive (0.45 and 0.53 respectively) but the ϕ_r values are negative (−0.12 and −0.29 respectively). The positive values for ϕ would indicate the involvement of water; however, very little is known about the effect of organic solvents on the value of ϕ (15) and, in any case, the values do not take into consideration the amount of protonated substrate as do the ϕ_r values. Negative values of ϕ_r are consistent with an A1 mechanism.

The strongest evidence for a dissociative mechanism comes from the values of the entropy of activation. The $\Delta S^{\neq}$ values for compounds **6***b* and **6***c* at 77°C are −7 and −4 eu respectively. These values fall between the ranges of entropies of activation expected for an A1 and A2 reaction (20); however, there are several examples of A1 reactions which have small negative entropies (20). Tommila and Murto (23) have also found that the $\Delta S^{\neq}$ for the hydrolysis of ethyl acetate in HCl–DMSO–H_2O is smaller than the $\Delta S^{\neq}$ in HCl–H_2O (22). This result indicates that the $\Delta S^{\neq}$ values for com-

pounds **6***b* and **6***c* might even be slightly positive if the reaction were carried out in H_2SO_4–H_2O only.

The substrate which is least likely to undergo dissociation to a carbonium ion is the *p*-nitro ester (**6***d*). This compound undergoes hydrolysis at a reasonable rate only at an acid concentration where the activity of water is very low and beyond the point where the compound is completely protonated. Therefore it is reasonable to assume that this compound also hydrolyzes by a dissociative $A_{al}1$ mechanism. An $A_{ac}1$ mechanism cannot be completely ruled out but it is less likely given the apparent instability of the phosphinylium ion (18).

A Hammett ρ value was calculated for the reaction using relative rate data taken from the reaction half-lives at 40% H_2SO_4 and 50°C.[6] The value obtained using σ^+ was −3.5. This result also supports a unimolecular reaction involving carbonium ion formation. The ρ value obtained by Noyce and Virgilio for compounds **3***a–d* is −5.1 (6). Therefore, an $A_{al}1$ mechanism is suggested for compounds **6***a–d*.

Basicity of Phosphinates

Because of the similarity between the protonation behaviour of phosphine oxides and phosphinates, protonation undoubtedly takes place, in the latter compounds, on the oxygen of the P=O group. There appears to be no correlation between the pK_a of the phosphinates and the nature of the carbon groups attached to phosphorus. However, the methyl-, ethyl-, and isopropyl diethylphosphinates have pK_a values which decrease appreciably with the decreasing size of the alkyl group in the alcohol part of the ester (−3.56, −3.21, and −2.41 respectively). A possible explanation for this trend is to postulate that interaction of the type shown in structure **7** is important. As the R group becomes more electron donating the interaction as depicted in structure **7** will become more important and the ester would be expected to be more basic. Supporting evidence for this point comes from the large polar substituent effect of the R group in the alkaline hydrolysis of the identical esters (ρ* = 8) (3).

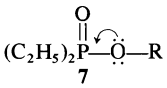

7

[6]Approximate calculated rate constants were used for compounds **6***a* and **6***d*.

The values of *M* given in Table 3 indicate how different phosphinates are from anilines (Hammett bases). The lower the *M* value the more that substrate is solvated. All the phosphinates have approximately the same *M* value (0.5) except for methyl di-*tert*-butylphosphinate and isopropyl diethylphosphinate. For these compounds there appears to be some steric inhibition of solvation. Phosphinates should be more highly solvated than anilines because of the presence of two oxygens each with two pairs of non-bonding electrons. Oxygen is also a harder base than nitrogen and therefore should interact better with the proton (12).

The results for benzyl diethylphosphinate are difficult to explain. The *M* value is 0.78, considerably higher than all of the other esters studied. One possible explanation would be that the compound is undergoing reaction even in the short time needed for the nmr measurement. Of all the compounds for which the pK_a was determined this ester is the most reactive.

Experimental

General

Elemental analyses were performed by E. Pascher, Bonn, Germany. Melting points were taken in capillary tubes and are uncorrected. All nuclear magnetic spectra were taken on a Varian model A60D spectrometer and infrared spectra were taken on a Perkin-Elmer model 257 spectrophotometer.

Synthesis of Esters

The synthesis and the physical and spectral data for compounds **5***a–c* as well as for ethyl diethyl- and isopropyl diethylphosphinate have been previously reported (3 and references therein). Benzyl diethylphosphinate has been synthesized by a method different from that reported here but the compound was not characterized (24). For all compounds nmr and infrared spectra were consistent with structural assignments. The elemental analyses and boiling points for the previously unreported esters are given in Table 7.

Methyl di-tert-Butylphosphinate

The ester was prepared by addition of diazomethane to a methanol solution of di-*tert*-butylphosphinic acid. The methanol was removed and the ester distilled. The acid was prepared by refluxing the acid chloride with aqueous 1 *N* sodium hydroxide for 48 h (25); mp 205–207°C (lit. 201°C (25), 208–210°C (26)). The di-*tert*-butylphosphinyl chloride was synthesized from *tert*-butyldichlorophosphine by a procedure similar to that of Crofts and Parker (25). The phosphinyl chloride (101–105°C/5 Torr) was recrystallized from petroleum ether; mp 80–81.5°C (lit. 82.5°C (25), 80.1–80.9°C (27)). The *tert*-butyldichlorophosphine was prepared by a method similar to that of Voskuil and Arens (27).

Benzyl and Substituted Benzyl Diethylphosphinates

Into a four-necked round bottom flask equipped with

TABLE 7. Physical constants and C, H, and P analyses

Compound	bp	Analysis					
		Calculated			Found		
		C	H	P	C	H	P
5*d*	76–77/0.7 Torr	51.43[a]	10.95	14.77	51.76	10.55	14.94
6*a*[c]	Not distillable[b]	—	—	—	—	—	—
6*b*	Not distillable[b] (133–35/0.5 Torr)[d]	62.25	8.07	14.60	61.41	8.12	14.18
6*c*	Not distillable[b]	53.56	6.54	12.56	53.64	6.56	12.46
6*d*	Not distillable[b]	51.35	6.27	12.04	50.82	6.17	12.11

[a]Analyzes for the monohydrate, $C_9H_{12}PO_2 \cdot H_2O$.
[b]The benzyl and substituted benzyl esters were purified by chromatography.
[c]Elemental analysis not performed.
[d]Reference 24.

a stirrer, a condenser, a dropping funnel, and a thermometer were placed diethylphosphinyl chloride (0.1 mol) and 100 ml of dry ether. The flask was cooled to 5°C and a solution of the appropriate alcohol (0.15 mol) and freshly distilled triethylamine (0.15 mol) in 100 ml of ether was added with stirring over a period of 3 h. A second portion of alcohol (0.5 mol) was then added over a period of 1 h and the reaction was stirred for a further 4 h at 5°C. The mixture was allowed to come to room temperature and stand overnight. The triethylammonium chloride was filtered and the filtrate was washed first with 1% HCl and then with 5% sodium bicarbonate. The ether layer was finally washed with water, dried over sodium sulfate, and concentrated at room temperature on a rotatory evaporator. The separation of the alcohols from the esters was achieved by column chromatography using silica gel. The alcohols were eluted with a 4:1 benzene–chloroform solution and the esters with a 5:1 chloroform–methanol solution. The chromatogram was followed by thin-layer chromatography on silica gel with chloroform as solvent. When benzyl diethylphosphinate was distilled at 110–112°C/0.05 Torr, nmr showed that the ester had partially decomposed into acid and alcohol. Henning *et al.* (24) have prepared the benzyl ester by a transalkylation reaction of ethyl diethylphosphinate and benzyl chloride using a catalytic amount of triphenylphosphine. The ir and nmr spectra were not reported; however, the authors mentioned that the compound decomposed at 180°C. The crude yield for the preparation of the benzyl esters by the method reported in this paper is 85–90%.

Kinetic Measurements

The hydrolyses of compounds **5***a–d* were run in dideuterosulfuric acid – deuterium oxide solution and the hydrolyses of compounds **6***a–d* were run in solutions of sulfuric acid and 70% w/w dimethylsulfoxide–water. The molarities of the acids were determined from calibration curves. The calibration curves were prepared by titrating weighted samples of the acid solutions. The dimethylsulfoxide was purified by distillation.

The rates were followed by nmr spectroscopy. Aliquots of the reaction mixtures were capped in nmr tubes which were immersed in a bath at appropriate temperatures. The nmr spectra were recorded at different time intervals. Two runs were carried out in sealed nmr tubes. Identical results were obtained from the kinetic experiments with sealed and capped tubes. In the nmr the decrease in the intensity of the CH_3 of the OCH_3 or the CH_2 of the p-$XC_6H_4OCH_2$ of the esters and the increase in the intensity of the same groups in the respective alcohols were followed. Each aliquot was integrated 10–16 times and the results were averaged. The chemical shift difference between these resonances is between 20 and 24 Hz. At the higher concentrations of acid another peak appears; this peak was shown to be due to ether formation. Samples of methanol and *p*-methoxybenzyl alcohol were placed in acid under reaction conditions and after a period of time another peak appeared at a chemical shift difference equal to the shift difference observed during hydrolysis. This conclusion is also supported by nmr studies on mixtures of methanol and dimethyl ether (Matheson) in acid solution.

The spectra of ethyl diethyl- and isopropyl diethylphosphinate are too complex to be integrated properly and therefore the kinetics of hydrolysis of these compounds were not studied.

By plotting $\log_{10}$ (unhydrolyzed ester/original ester) versus time, straight lines were obtained. The slopes of the plots were obtained by a least squares computer analysis. The rate constant, k_{obs}, is then equal to 2,303 (slope)/3600 s^{-1}.

Measurement of pK_a's

The pK_a's of the esters were measured using the procedure of Haake *et al.* (12). The pK_a's of compounds **5***a–d* were measured in D_2SO_4–D_2O solution (concentration of the ester was approximately 0.1 *M*) and those for **6***a–d* were measured in H_2SO_4 – 70% w/w DMSO–H_2O solution. Trimethylammonium chloride was used as an internal standard.

Acknowledgment

The authors are indebted to the Research Committee of the Faculty of Arts and Sciences of the American University of Beirut for financial support.

1. F. H. WESTHEIMER. Acc. Chem. Res. **1**, 70 (1968); S. J. BENKOVIC. *In* Comprehensive chemical kinetics. Vol. 10. *Edited by* C. H. Bamford and C. F. H. Tipper. Elsevier, London. 1972.
2. R. F. HUDSON and L. KEAY. J. Chem. Soc. 2463

(1956); L. KEAY. J. Org. Chem. **28**, 1426 (1963); L. KEAY. Can. J. Chem. **43**, 2637 (1965); G. AKSNES and J. SONGSTAD. Acta Chem. Scand. **19**, 893 (1965); H. CHRISTOL, M. LEVY, and C. MARTY. J. Organomet. Chem. **12**, 459 (1968); H. CHRISTOL and C. MARTY. J. Organomet. Chem. **12**, 471 (1968); J. I. G. CADOGAN, D. EASTLICK, F. HAMPSON, and R. K. MACKIE. J. Chem. Soc. B, 144 (1969); V. E. BEL'SKII, G. Z. MOTYGULLIN, and O. N. GRISHINA. Izv. Akad. Nauk SSSR Ser. Khim. **12**, 2813 (1969).

3. R. D. COOK, C. E. DIEBERT, W. SCHWARZ, P. C. TURLEY, and P. HAAKE. J. Am. Chem. Soc. **95**, 8088 (1973).
4. P. HAAKE and G. HURST. J. Am. Chem. Soc. **88**, 2544 (1966).
5. J. F. BUNNETT, J. O. EDWARDS, D. V. WELLS, H. J. BRASS, and R. CURCI. J. Org. Chem. **38**, 2703 (1973).
6. D. S. NOYCE and J. A. VIRGILIO. J. Org. Chem. **37**, 2643 (1972).
7. V. E. MCCOY, JR. Ph.D. Dissertation, Harvard University, Cambridge, MA. 1965.
8. R. A. MCCLELLAND. J. Chem. Soc. Chem. Commun. 226 (1976).
9. E. HOGFELDT and J. BIGELEISEN. J. Am. Chem. Soc. **82**, 15 (1960); J. SIERRA, M. OJEDA, and P. A. H. WYATT. J. Chem. Soc. B, 1570 (1970).
10. P. TICKLE, A. G. BRIGGS, and J. M. WILSON. J. Chem. Soc. B, 65 (1970); C. D. JOHNSON, A. R. KATRITZKY, and S. A. SHAPIRO. J. Am. Chem. Soc. **91**, 6654 (1969).
11. K. YATES and G. WELCH. Can. J. Chem. **50**, 1513 (1972).
12. P. HAAKE, R. D. COOK, and G. HURST. J. Am. Chem. Soc. **89**, 2650 (1967).
13. J. F. BUNNETT. J. Am. Chem. Soc. **83**, 4956; **83**, 4968; **83**, 4973; **83**, 4978 (1966).
14. J. BUS, H. STEINBERG, and TH.J. DE BOER. Recl. Trav. Chim. **87**, 609 (1968).
15. J. F. BUNNETT and F. P. OLSEN. Can. J. Chem. (*a*) **44**, 1899 (1966); (*b*) **44**, 1917 (1966).
16. (*a*) K. YATES and R. A. MCCLELLAND. J. Am. Chem. Soc. **89**, 2686 (1967); (*b*) K. YATES. Acc. Chem. Res. **4**, 136 (1971).
17. M. LILER. Reaction mechanisms in sulfuric acid. Academic Press, New York, NY. 1971. p. 183.
18. P. HAAKE and P. S. OSSIP. J. Am. Chem. Soc. **93**, 6924 (1971).
19. R. A. MCCLELLAND, T. A. MODRO, M. F. GOLDMAN, and K. YATES. J. Am. Chem. Soc. **97**, 5223 (1975).
20. L. L. SCHALEGER and F. A. LONG. Adv. Phys. Org. Chem. **1**, 1 (1963).
21. R. A. COX. J. Am. Chem. Soc. **96**, 1059 (1974).
22. C. G. SWAIN and A. S. ROSENBERG. J. Am. Chem. Soc. **83**, 2154 (1961).
23. E. TOMMILA and M. L. MURTO. Acta Chem. Scand. **17**, 1957 (1963).
24. H. G. HENNING, G. HILGETAG, and G. BUSSE. J. Prakt. Chem. **33**, 188 (1970).
25. P. C. CROFTS and D. M. PARKER. J. Chem. Soc. C, 332 (1970).
26. P. C. CROFTS and G. M. KOSOLOPOFF. J. Am. Chem. Soc. **75**, 3379 (1959).
27. W. VOSKUIL and J. F. ARENS. Recl. Trav. Chim. **82**, 302 (1963).
28. K. KINDLER. Ber. **69B**, 2792 (1936).
29. C. K. INGOLD. Structure and mechanism in organic chemistry. 2nd. ed. Cornell University Press, Ithaca, NY. 1969. p. 1135.
30. K. A. ABBAS and R. D. COOK. Tetrahedron Lett. 3559 (1975).

Open-chain nitrogen compounds. Part III.[1] The formation of triazenes in the reaction of diazonium salts with α-aminoacetonitrile and related α-substituted alkylamines

THERESA A. DANIELS, SHIRAZ SIDI, AND KEITH VAUGHAN[2]

Department of Chemistry, Saint Mary's University, Halifax, N.S., Canada B3H 3C3

Received April 4, 1977

THERESA A. DANIELS, SHIRAZ SIDI, and KEITH VAUGHAN. Can. J. Chem. **55**, 3751 (1977).

Several triazenes of type $Ar{\cdot}N{=}N{\cdot}NH{\cdot}CH_2Y$, where Y is electron withdrawing, have been prepared by reaction of the diazonium salts $X{\cdot}C_6H_4N_2^+$ (X = H, *p*-NO_2, *p*-CO_2Me, *p*-COPh, and *o*-COPh) with the α-substituted alkylamines NH_2CH_2Y (Y = CN, CO_2Et, COPh, and $CH(OCH_3)_2$) in aqueous solution, without prior isolation of the diazonium salt. In all cases, the diazonium ion attacks at the NH_2 moiety exclusively and the methylene group in NH_2CH_2Y shows no tendency to compete for the diazonium ion.

THERESA A. DANIELS, SHIRAZ SIDI et KEITH VAUGHAN. Can. J. Chem. **55**, 3751 (1977).

Plusieurs triazènes de types $Ar{\cdot}N{=}N{\cdot}NH{\cdot}CH_2Y$, où Y est un groupe attracteur d'électrons, sont préparés, en solution aqueuse, par réaction de sels diazonium $X{\cdot}C_6H_4N_2^+$ (X = H, *p*-NO_2, *p*-CO_2Me, *p*-COPh et *o*-COPh) avec des alkylamines α-substituées NH_2CH_2Y (Y = CN, CO_2Et, COPh et $CH(OCH_3)_2$) sans isolation préalable des sels diazonium. Dans tous les cas, l'ion diazonium attaque exclusivement le site NH_2 et le groupe méthylène dans NH_2CH_2Y montre aucune tendance à entrer en compétition vis-à-vis de l'ion diazonium.

[Traduit par le journal]

Introduction

The reaction of diazonium salts with proteins has been extensively used as a structural probe, typically in the elucidation of the topography of the active sites of enzymes (2). The azo-proteins formed in this way arise largely from diazo-coupling with the activated aromatic rings of tyrosine and histidine residues and the ε-amino group of lysines (3). The reaction of diazonium salts at the α-amino group of free amino acids leads to deamination of the amino acid (4, 5), via the unstable triazenes, $ArN{=}N{\cdot}NH{\cdot}CHR{\cdot}CO_2H$, but the rate of this *N*-diazo coupling is independent of the pK_a of the acid (6). By contrast, *N*-diazo coupling with glycine ethyl ester affords stable triazenes (5, 7, 8), which usefully decompose under acid catalysis to give ethyl diazoacetate, $N_2CH{\cdot}CO_2Et$ (7).

In part II (1) of this series, the preparation and characterisation of a number of monomethyltriazenes, $X{\cdot}C_6H_4{\cdot}N{=}N{\cdot}NH{\cdot}Me$, were described; the formation of triazenes by the reaction of aqueous diazonium salts with methylamine was favoured by the presence of an electron-withdrawing substituent (X) in the aryl group. It was of interest to us to extend the previous work by looking at the reaction of diazonium ions with amines of type NH_2CH_2Y (where Y is electron withdrawing), to examine the triazenes arising therefrom (eq. 1) and to assess the possibility of competitive coupling at the activated CH_2 group (eq. 2).

[1] $$ArN_2^+ + NH_2CH_2Y \longrightarrow ArN{=}N{\cdot}NH{\cdot}CH_2Y$$

[2] $$ArN_2^+ + CH_2\begin{matrix}NH_2\\Y\end{matrix} \longrightarrow Ar{\cdot}NH{-}N{=}C\begin{matrix}NH_2\\Y\end{matrix}$$

Discussion

Previous reports of the formation of triazenes of type **1** (7, 9) employed diazonium fluoroborates as starting materials, with an organic solvent or an aqueous–organic mixture as the medium. Since methylamine couples readily in aqueous solution with diazonium salts substituted with electron-withdrawing groups (1), it seemed worthwhile to attempt reaction of the same diazonium salts with α-substituted alkylamines in purely aqueous solution. Indeed, direct coupling of the diazonium salts, $X{\cdot}C_6H_4N_2^+$ (X = H, *p*-NO_2, *p*-CO_2Me, *p*-COPh, and *o*-COPh) with aminoacetonitrile, NH_2CH_2CN, in aqueous solution, in the presence of sodium acetate, proved to be most successful

[1]For part II see ref. 1.

[2]To whom all correspondence should be sent.

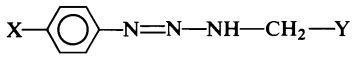

1

a X = H, Y = CN
b X = NO_2, Y = CN
c X = CO_2Me, Y = CN
d X = Ac, Y = CN
e X = NO_2, Y = CO_2Et
f X = CO_2Me, Y = CO_2Et
g X = CO_2Me, Y = COPh
h X = NO_2, Y = COPh
i X = NO_2, Y = $-CH(OCH_3)_2$

and afforded the triazenes (**1***a–d* and **2***a*) in moderate to excellent yields. Similarly, reaction of the diazonium salts, *p*-X·$C_6H_4N_2^+$ (X = NO_2 and CO_2Me) with glycine ethyl ester gave high yields of the *N*-arylazoglycine ethyl esters (**1***e* and *f*). However, attempts to couple the diazonium salts from aniline and *p*-aminoacetophenone with glycine ethyl ester under identical conditions were unsuccessful.

The structures of the cyanomethyltriazenes (**1***a–d* and **2***a*) are corroborated by elemental analysis and spectroscopic data. The ir spectra all display NH absorption in the range 3200–3250 cm^{-1}; **1***c* displays ester-carbonyl absorption at 1695 cm^{-1} and **1***b* exhibits the nitro-group bands at 1530 and 1350 cm^{-1}. However, absorption due to the C≡N group is either absent, or extremely weak at 2260–2300 cm^{-1}, as in the ir spectra of **1***b* and **1***d*. Although the absence of strong cyano bands suggests that these triazenes may exist in a cyclic iminotriazoline form, the open-chain nature of the cyanomethyltriazenes is clearly demonstrated by the nmr spectral data. The *N*-methylene proton resonance appears consistently as a singlet in the range δ 4.53–4.68 ppm; NH proton resonance is observed in the spectrum of the ester (**1***c*) at δ 9.3 ppm. Preliminary studies of the chemistry of the cyanomethyltriazenes suggests that cyclization may be initiated by heating in ethanol and affords 5-arylaminotriazoles (**3**); the scope and synthetic use of this reaction are under further investigation. The spectral characteristics of the *N*-arylazoglycine ethyl esters (**1***e* and *f*) are also consistent with open-chain structures. Significant broadening of the *N*-methylene and aromatic proton resonance is seen in the nmr spectrum of **1***e*, suggesting that this triazene, like the monomethyl analogue (**1**, X = NO_2, Y = H), is in a state of rapid tautomeric equilibrium at room temperature (10).

Whereas the reaction of *p*-nitrobenzene diazonium tetrafluoroborate with α-aminoacetaldehyde dimethyl acetal (which, unlike the free aldehyde, is readily available) in acetonitrile at −10°C gave only dark red oils, aqueous coupling of diazotized *p*-nitroaniline with the dimethyl acetal gave a low yield of the solid triazene (**1***i*). Treatment of the *p*-nitrobenzene diazonium salt with ω-aminoacetophenone in aqueous solution afforded the keto-triazene (**1***h*), which, on the basis of spectroscopic evidence, exists exclusively as the cyclic 5-hydroxytriazoline (**4**), as proposed previously (9, 11). Carbonyl absorption is absent from the ir spectrum of **4**, whereas a broad band at 3200 cm^{-1} probably arises from the hydroxyl group. On the other hand the *p*-methoxycarbonylphenyltriazene (**1***g*), obtained in low yield in an analogous manner, appears to exist in the open-chain form, since the ir spectrum displays a keto-carbonyl band at 1660 cm^{-1}, in addition to NH and ester-carbonyl bands at 3350 and 1720 cm^{-1} respectively.

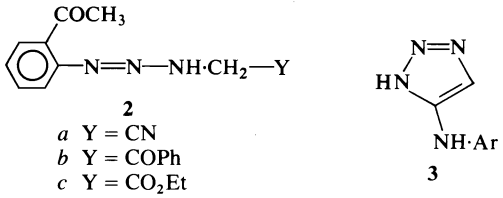

2

a Y = CN
b Y = COPh
c Y = CO_2Et

3

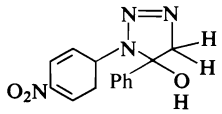

4

o-Acetylphenyltriazenes, e.g. **2***b* and **2***c*, are potential precursors of 4-methylenebenzotriazines, since other *o*-acetylphenyltriazenes cyclize over alumina (12). However, the keto-triazene (**2***b*) was unstable and decomposed in contact with alumina to give a mixture of *o*-aminoacetophenone and diazoacetophenone, $N_2CH·COPh$. The formation of the diazoketone was indicated by ir absorption at 2100 cm^{-1} and by methine proton resonance at δ 5.9 ppm in the nmr spectrum; analogous fragmentation of the *p*-nitrophenyltriazene (**1***h*) has been reported (9). Diazotization of *o*-aminoacetophenone, followed by treatment with glycine ethyl ester, is strangely anomalous and affords an unstable, bright red solid, which does not appear to be the expected triazene (**2***c*).

Considerable interest in the pharmacology of triazenes has been aroused by the potential of dialkyltriazenes ($ArN{=}NNR_2$) to act as anti-tumour agents (13). Recent studies have demonstrated the importance of monomethyltriazenes in the metabolism of these anti-tumour agents (14), and therefore it is important to establish the biological effects of the monoalkyltriazenes described here. Dialkyltriazenes display selective action against a broad spectrum of tumours, including plasma cell tumours and the R1 and TLX5 lymphomas (13). However, the nitrophenyltriazenes (**1***b* and **1***e*) were found to be inactive towards TLX5 lymphoma cells in in vivo tests, and the cyanomethyltriazenes (**1***b* and **1***c*) were inactive towards the P388 tumour in vivo. The inactivity of these triazenes suggests that they cannot metabolize to produce monomethyltriazenes, which is not an unexpected result.

In conclusion, it is evident that diazonium salts may be coupled with certain α-substituted alkylamines in aqueous media to afford monoalkyltriazenes directly from the reaction mixture. Isolation of the diazonium fluoroborate, prior to coupling, is certainly not always necessary, and may in some cases be less desirable than aqueous coupling. In all cases studied here, the diazonium ion attacks at the NH_2 moiety and shows no tendency to attack at the activated CH_2 (in NH_2CH_2Y), which would give rise to hydrazone formation (eq. 2). Although such hydrazone formation is well known (15) in the case of bifunctional methylene compounds, the methylene group in NH_2CH_2Y does not compete successfully for the diazonium ion and triazene formation is exclusive.

Experimental

Melting points were obtained on a hot stage apparatus and are uncorrected. Infrared spectra were recorded with Nujol mulls on Perkin-Elmer Infracord and 467 grating spectrophotometers, and nmr spectra were obtained in deuteriochloroform, with tetramethylsilane as internal standard, on a Varian EM 360 60 MHz spectrometer. Microanalyses were conducted by Chemalytics Inc., Tempe, Arizona.

Reaction of Diazonium Salts with Glycine Ethyl Ester or Aminoacetonitrile or α-Aminoacetophenone

General Procedure

The aromatic amine (0.013 mol) was dissolved in 2 *M* hydrochloric acid (30 ml), diluted with water (40 ml), and diazotized at 0°C with sodium nitrite (0.013 mol) in a minimum volume of water. A solution of *either* glycine ethyl ester hydrochloride *or* aminoacetonitrile hydrochloride *or* α-aminoacetophenone hydrochloride (0.013 mol) in water was added slowly to the diazonium salt solution. The mixture was stirred for 1 h at 0°C, whereupon the solution was normally clear. The clear solution was treated with a large excess of sodium acetate (25–30 g). and the triazene precipitated slowly from the reaction mixture. Precipitation was normally evident after 15 min, and was usually complete within 24 h after warming slowly to room temperature. (Note: addition of the diazonium salt solution *to* a solution of the amine hydrochloride, containing sodium acetate, did not decrease the time required for full precipitation of the triazene, but did increase the yield in one case.) This procedure afforded the following triazenes, which usually recrystallized from hexane or benzene or a mixture of the two solvents.

1-Phenyl-3-(α-cyanomethyl-)triazene (*1a*)—Yield 22%; mp 92–95°C; ν_{max} 3200, 1600 cm^{-1}; δ ($CDCl_3$) 4.53 (s, 2H, CH_2), 7.27 (s, 5H, aromatic), and 7.5 (br s, 1H, NH). *Anal.* calcd. for $C_8H_8N_4$: C 60.0, H 5.03, N 34.98; found: C 59.99, H 4.99, N 34.56.

1-(p-Nitrophenyl-)3-(α-cyanomethyl-)triazene (*1b*)—Yield 94%; mp 95–96°C (dec.); ν_{max} 3250, 2300(w), 1610, 1530, and 1350 cm^{-1}; δ ($CDCl_3$) 4.67 (s, 2H, CH_2), 7.33 (d, 2H, aromatic), and 8.23 (d, 2H, aromatic). *Anal.* calcd. for $C_8H_7N_5O_2$: C 46.80, H 3.41, N 34.15; found: C 46.65, H 3.40, N 34.29.

1-(p-Methoxycarbonylphenyl-)3-(α-cyanomethyl-)triazene (*1c*)—Yield 94%; mp 132.5–135.5°C; ν_{max} 3250, 1695, and 1610 cm^{-1}; δ ($CDCl_3$) 3.88 (s, 3H, O—Me), 4.59 (s, 2H, CH_2), 7.21 (d, 2H, aromatic), 7.99 (d, 2H, aromatic), and approx. 9.3 (v br s, 1H, NH). *Anal.* calcd. for $C_{10}H_{10}N_4O_2$: C 55.04, H 4.60, N 25.70; found: C 55.22, H 4.72, N 25.75.

1-(p-Acetylphenyl-)3-(α-cyanomethyl-)triazene (*1d*)—Yield 36%; mp 86–88°C; ν_{max} 3220, 2260(w), 1656, and 1620 cm^{-1}; *Anal.* calcd. for $C_{10}H_{10}N_4O$: C 59.40, H 4.98; found: C 59.72, H 4.66.

1-(o-Acetylphenyl-)3-(α-cyanomethyl-)triazene (*2a*)—Yield 78%; mp 80–82°C; ν_{max} 3180 (broad) and 1640 cm^{-1}; δ ($CDCl_3$) 2.66 (s, 3H, acetyl Me), 4.68 (s, 2H, CH_2), 6.8–8.0 (m, 5H, aromatic and NH). *Anal.* calcd. for $C_{10}H_{10}N_4O$: C 59.40, H 4.98, N 27.71; found: C 59.41, H 4.82, N 27.67.

N-(p-Nitrophenylazo-)glycine Ethyl Ester (*1e*)—Yield 80%; mp 98–99°C (lit. (9) 96–98°C); ν_{max} 3300, 1710, 1600(w), 1510, and 1340 cm^{-1}; δ ($CDCl_3$) 1.30 (t, 3H, CH_3), 4.30 (q, 2H, CH_2—O), 4.50 (br s, 2H, CH_2—N), 7.4 (br d, 2H, aromatic), 8.13 (d, 2H, aromatic), and 9.3 (br s, 1H, NH). *Anal.* calcd. for $C_{10}H_{12}N_4O_4$: C 47.62, H 4.80, N 22.21; found: C 47.47, H 4.73, N 22.18.

N-(p-Methoxycarbonylphenylazo-)glycine Ethyl Ester (*1f*)—Yield 84%; mp 70–71°C; ν_{max} 3320, 1720, 1708, and 1597 cm^{-1}; δ ($CDCl_3$) 1.23 (t, 3H, CH_3), 3.87 (s, 3H, O—CH_3), 4.2 (q, 2H, O—CH_2), 4.4 (br s, 2H, N—CH_2), 7.3 (d, 2H, aromatic), 8.0 (d, 2H, aromatic), and 9.5 (br s, 1H, NH). *Anal.* calcd. for $C_{12}H_{15}N_3O_4$: C 54.30, H 5.66, N 15.85; found: C 53.95, H 5.63, N 15.42.

1-(p-Methoxycarbonylphenyl-)3-phenacyltriazene (*1g*)—Yield 6%; mp 145–148°C; ν_{max} 3250, 1710, and 1660 cm^{-1}. *Anal.* calcd for $C_{16}H_{15}N_3O_3$: C 64.65, H 5.05; found: C 64.29, H 5.06.

1-p-Nitrophenyl-5-hydroxy-5-phenyl-Δ^2*-1,2,3-triazoline*

(*4*)—Yield 76%; mp 118–120°C, ν_{max} 3200 (br), 1595, 1520, and 1340 cm^{-1}.

This product was identical with material obtained by treatment of a mixture of *p*-nitrobenzene diazonium tetrafluoroborate and ω-aminoacetophenone hydrochloride, in suspension in ethanol, with aqueous sodium carbonate at 0°C, according to the method of McGarrity (9).

1-(p-Nitrophenyl-)3-(β,β-dimethoxyethyl-)triazene (*1i*)—*p*-Nitroaniline (1.78 g) was diazotized as described above and treated with α-aminoacetaldehyde dimethyl acetal (1.36 g). The mixture was stirred for 1 h, filtered to remove cloudiness, and the clear filtrate treated with a solution of sodium acetate (25 g). After stirring for a further 0.75 h, the yellow precipitate was separated to afford the triazene (0.55 g, 17%), mp 62–63°C; ν_{max} 3150, 1595, 1540, and 1330 cm^{-1}; δ ($CDCl_3$) 2.13 (s, 6H, O—Me), 2.60 (d, 2H, N—CH_2), 3.40 (t, 1H, CH), 6.0 (br d, 2H, aromatic), 6.8 (d, 2H, aromatic), and 8.2 (br s 1H, NH). *Anal.* calcd. for $C_{10}H_{14}N_4O_4$: C 47.20, H 5.50, N 22.00; found: C 46.40, H 5.10, N 21.50.

Acknowledgements

The authors are extremely grateful to the Saint Mary's University Senate Research Committee for financial support, and to Dr. D. L. Hooper, Dalhousie University, and Dr. M. F. G. Stevens, University of Aston, for helpful discussions and comments. We are also indebted to the Chester Beatty Research Institute, London, and the National Institutes of Health, Bethesda, Maryland, for determination of anti-tumour activity.

1. T. P. Ahern, H. Fong, and K. Vaughan. Can. J. Chem. **55**, 1701 (1977).
2. M. F. G. Stevens. Prog. Med. Chem. **13**, 211 (1976).
3. M. Tabachnik and H. Sobotka. J. Biol. Chem. **234**, 1726 (1959); J. H. Phillips, Jr., S. A. Robrish, and C. Bates. J. Biol. Chem. **240**, 699 (1965).
4. H. Eagle and C. Vickers. J. Biol. Chem. **114**, 193 (1936).
5. H. Zahn, B. Wollerman, and O. Waschka. Z. Physiol. Chem. **294**, 100 (1953).
6. M. Remes, J. Divis, V. Zverina, and M. Matrka. Coll. Czech. Chem. Commun. **41**, 2566 (1976).
7. R. J. Baumgarten. J. Org. Chem. **32**, 484 (1967).
8. Y. F. Shealy and C. A. Krauth. J. Med. Chem. **9**, 34 (1966).
9. J. F. McGarrity. Chem. Commun. 558 (1974).
10. K. Vaughan. J. Chem. Soc. Perkin Trans. II, 17 (1977).
11. C. E. Olsen and C. Pedersen. Acta Chem. Scand. Ser. B, **27**, 2279 (1973).
12. H. Fong and K. Vaughan. Can. J. Chem. **53**, 3714 (1975).
13. R. C. S. Audette, T. A. Connors, H. G. Mandel, K. Merai, and W. C. J. Ross. Biochem. Pharm. **22**, 1855 (1973).
14. T. A. Connors, P. M. Goddard, K. Merai, W. C. J. Ross, and D. E. V. Wilman. Biochem. Pharm. **25**, 241 (1976).
15. E. J. Gray, M. F. G. Stevens, G. Tennant, and R. J. S. Vevers. J. Chem. Soc. Perkin Trans. I, 1496 (1976).

Reductive desulfurization using tributyltin hydride[1]

JOHN M. MCINTOSH AND CALVIN K. SCHRAM

Department of Chemistry, University of Windsor, Windsor, Ont., Canada N9B 3P4

Received June 6, 1977

JOHN M. MCINTOSH and CALVIN K. SCHRAM. Can. J. Chem. **55**, 3755 (1977).

Reaction of tributyltin hydride with a variety of organic sulfides gives results which depend on the structure of the starting material. Acyclic sulfides undergo desulfurization leading to hydrocarbons in varying yields. However, 2,5-dihydrothiophenes give dienes and 3,6-dihydro-2*H*-thiopyrans are inert.

JOHN M. MCINTOSH et CALVIN K. SCHRAM. Can. J. Chem. **55**, 3755 (1977).

La réaction de l'hydrure de tributylétain avec une variété de sulfures organiques donne des résultats qui dépendent de la structure du produit de départ. Les sulfures acycliques subissent une désulfuration conduisant à des hydrocarbures avec un rendement variable. Cependant, les dihydro-2,5 thiophènes conduisent aux diènes tandis que les dihydro-3,6 2*H*-thiopyrannes sont inertes.

[Traduit par le journal]

For the past several years, we have been engaged in a study of the preparation and use of 2,5-dihydrothiophenes (**1**) (1) and 3,6-dihydro-2*H*-thiopyrans (**2**) (2) and as part of these investigations we considered a reductive desulfurization (Scheme 1). Considering the ease of

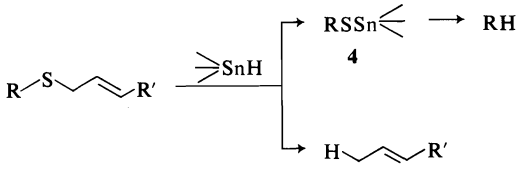

SCHEME 1

formation of **1** and **2**, a ready desulfurization which proceeded without isomerization would afford an operationally simple stereo- and regiospecific preparation of *cis*-olefins, which would have application in the area of pheromone synthesis.

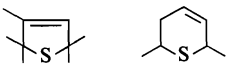

1 **2**

Of the many reagents that have been used to effect desulfurizations of sulfides, Raney Nickel has been most commonly employed (3), but this reagent suffers from the concomitant reduction of other sites of unsaturation (4). More recently lithium in ethylamine (5) alone or in combination with Raney Nickel (6) has given excellent results in some cases. However, we felt that another method for effecting this transformation which would tolerate a wider range of functionality would be beneficial.

The well-known ability of divalent sulfur atoms to enter into radical reactions suggested that a reducing agent that functions by a radical mechanism might effect the desired reaction. One of the most common reagents of this type is the trialkyltin hydride (**3**) (7). We now report the results of a brief survey of the use of this reagent for reductive desulfurization.

Prior to our work, scattered reports on the use of **3** on divalent sulfur-containing products had appeared (8) which suggested that desulfurization would occur. However, two interfering reactions, viz. hydrostannylation and double-bond reduction, can occur when using olefinic substrates **1** or **2** and for that reason we began our investigations with saturated and aromatic substrates. When these were completed several olefinic substrates and two thioketals were examined.

Results and Discussion

The results of the reactions are summarized in Table 1. All reactions were carried out using tri-*n*-butyltin hydride (**3***a*) as the reducing agent and products were identified by comparison with authentic samples.

As can be seen, the results fall into three distinct categories. Most simple acyclic carbon–sulfur bonds are cleaved to some extent. As expected, allylic and benzylic bonds appear to cleave more easily than aliphatic ones. It must be noted that our work-up procedure (see Experi-

[1]Presented in part at the Annual Conference, Chemical Institute of Canada, Montreal, P.Q., June 1977.

TABLE 1. Desulfurization experiments[a,b]

Run	Sulfide	Reference	Products	% product
1	$(PhCH_2)_2S$		$PhCH_3$	76
2	n-$C_7H_{15}SCH_2Ph$		$PhCH_3 + C_7H_{16}$	85, 49
3	$(n$-$C_8H_{17})_2S$		C_8H_{18}	8[c]
4		9	$PhCH_3$ + 	63, 37
5	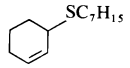		C_7H_{16} + 	38, 62
6	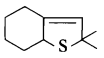	1*b*	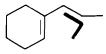	44
7	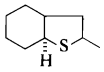	1*b*	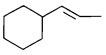	15
8		2	No reaction[d]	
9		2	No reaction[d]	
10		10	C_6H_{12}	44
11	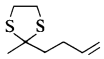		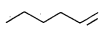	<10

[a]See Experimental section for details.
[b]$(C_4H_9)_3SnH$ used in all reactions.
[c]90% based on unconsumed sulfide.
[d]Starting material quantitatively recovered after all hydride consumed.

mental section) would not detect non-volatile hydrostannylated products, and therefore in cases where an olefinic product is formed, which may react further with **3***a* (runs 4–7 and 11), the yields indicated represent minimum values for the actual cleavage process.

Inspection of Table 1 further suggests that cleavage of a carbon–sulfur bond in a sulfide may be more difficult than that in which one of the sulfur bonds is joined to tin as in the presumed intermediate **4** (Scheme 1). Thus, the yield of alkanes in runs 2 and 5 (40–50%) is much larger than that in run 3.

We are unable to account satisfactorily for the complete inertness of thiopyrans **2** (runs 8 and 9). These were recovered quantitatively from the reaction mixtures. In view of the results of runs 4 and 5, it seems unlikely that both reductive desulfurization and hydrostannylation would be completely suppressed by an electronic interaction between the sulfur atom and the π-bond electrons. On the other hand, the presence of some degree of steric interference in the form of methyl group(s) at the α-position also seems insufficient to cause the observed results.

Reduction of dihydrothiophenes **1** (runs 6 and 7) resulted in a completely different reaction. The diene products obtained are identical with those obtained from the cheletropic sulfur dioxide elimination from the corresponding sulfone (1*a*). At this time, we are unable to say whether this reaction is concerted. In run 7, the sole product obtained is the E-isomer but while this is formally the result of a disrotatory ring opening, it is also the most stable product and its formation may simply reflect the preferred thermodynamic orientation. The low yield of product also makes any mechanistic conclusions tenuous at best.

Conclusion

It is clear from these rather limited results that we have not achieved our original goals of a viable olefin synthesis. At present we are considering other ways this might be achieved and will report any developments at a later date.

Experimental

Nuclear magnetic resonance spectra were run on a JEOL C60 HL spectrometer in $CDCl_3$ solution with

Me_4Si as internal standard: infrared spectra were run on a Beckman IR 12 in chloroform solution. Gas–liquid chromatographic analyses were run on an F & M Model 720 instrument using a 10 ft × 0.375 in. column packed with 20% SE-30 on Chromosorb W.

Materials

Starting materials for all runs except 2, 5, and 11 were purchased or prepared as outlined in the literature. Hydride **3***a* was routinely prepared by reduction of bis(tri-*n*-butyltin)oxide with polymethylhydrosiloxane (11).

Reduction Procedure

A mixture of 0.01 mol of the sulfide, 0.022 mol of **3***a*, and a catalytic amount of azobisisobutyronitrile (VAZO) was placed in a round-bottom flask fitted with a magnetic stirrer, and a condenser with a nitrogen inlet. The system was purged with dry nitrogen and heated at 80°C (oil bath temperature) for 8 h. In cases where more than 2.2 mol equivalents of **3***a* were used (in runs 10 and 11, 4.4 equiv. of **3***a* were used) the remainder of the hydride was added at intervals during the reflux period. Additional initiator was added occasionally to these reactions. The cooled solution was diluted with 20 ml of diglyme and distilled at atmospheric pressure to a head temperature of 162°C. The distillate was added to 10 ml of water, the organic phase separated, washed with an additional 10 ml of water and dried. Gas–liquid chromatographic analysis gave the ratio of products formed, which when multiplied by the weight of organic product gave the percentage yields. These were confirmed by nmr analysis. Products were identified by comparison of their retention times and nmr spectra with authentic samples. In the case of runs 6 and 7, the infrared and mass spectra were also identical to authentic samples (1*b*).

Heptyl Benzyl Sulfide

n-Heptyl mercaptan (6.6 g, 0.05 mol) was titrated to the phenolphthalein endpoint with a 1.0 *N* solution of sodium ethoxide. Benzyl chloride (6.3 g, 0.05 mol) was added dropwise with stirring at room temperature and then the mixture was stirred overnight. After filtration and evaporization of the filtrate, the remaining yellow oil was taken up in methylene chloride, dried and evaporated. Distillation afforded 9.6 g (86%) of a colourless oil, bp 174–180°C (17 Torr); nmr 7.25–7.30 (s, 5), 3.60–3.55 (s, 2), 2.45–2.18 (t, 2, J = 6 Hz), 1.65–1.05 (m, 12), 0.95–0.65 (t, 3, J = 4 Hz); ir($CHCl_3$) 3080, 3020, 2960, 2920, 2860, 2840, 1450, 700 cm^{-1}; n_D^{20} = 1.5204. *Anal.* calcd for $C_{14}H_{22}S$: C 75.61, H 9.97; found: C 75.77, H 9.88.

3-Cyclohexen-1-yl Heptyl Sulfide

3-Cyclohexen-1-yl heptyl sulfide was prepared by the same general procedure using 0.05 mol of 3-bromocyclohexene (12) and *n*-heptyl mercaptan. Distillation gave 8.0 g (76%) of a colourless oil, bp 92–96°C (0.04 Torr); nmr 5.90–5.80 (m, 2), 3.62–3.30 (m, 1), 2.84–2.52 (t, 2, J = 8 Hz), 2.30–1.75 (m, 6), 1.65–1.15 (m, 12), 1.05–0.85 (t, 3, J = 4 Hz); ir($CHCl_3$) 3020, 2970, 2950, 2850, 1465, 1455, 1440 cm^{-1}; n_D^{20} = 1.4951. *Anal.* calcd for $C_{13}H_{24}S$: C 73.51, H 11.39; found: C 73.35, H 11.55.

2-(3-Buten-1-yl)-2-methyl-1,3-dithiolane

A mixture of 10 g (0.1 mol) of allylacetone, 15 g (0.16 mol) of ethane dithiol, and 1 g of *p*-toluenesulfonic acid in 150 ml benzene was refluxed for 8 h under a Dean-Stark water separator. The cooled solution was washed with an equal volume of 1 *N* potassium hydroxide, once with water, and then was dried. Evaporation of the solvent and chromatographing the residue on basic alumina (pentane) gave 80% of a colourless liquid, bp 114–116 (14 Torr); nmr 6.05–5.5 (m, 1), 5.15–4.75 (m, 2), 3.30 (s, 4), 2.45–1.85 (m, 4); ir 3100, 2960, 2940, 2870, 2860, 1652, 1460, 925 cm^{-1}. *Anal.* calcd. for $C_8H_{14}S_2$: C 55.12, H 8.09; found: C 55.33, H 8.19.

1. (*a*) J. M. McIntosh and G. M. Masse. J. Org. Chem. **40**, 1294 (1975); (*b*) J. M. McIntosh, H. B. Goodbrand, and G. M. Masse. J. Org. Chem. **39**, 202 (1974); J. M. McIntosh and R. S. Steevensz. Can. J. Chem. **55**, 2442 (1977).
2. J. M. McIntosh and H. Khalil. Can. J. Chem. **54**, 1923 (1976).
3. G. R. Pettit and E. E. van Tameln. Organic reactions. Vol. 12. Wiley, New York, NY. 1962. p. 356.
4. G. Stork and P. L. Stotter. J. Am. Chem. Soc. **91**, 7780 (1969).
5. J. F. Biellmann and J. B. Ducep. Tetrahedron, **27**, 5861 (1971).
6. P. L. Stotter and R. E. Hornish. J. Am. Chem. Soc. **95**, 4444 (1973); K. Kondo, A. Negishi, K. Matsui, D. Tunemoto, and S. Masamune. Chem. Commun. 1311 (1972).
7. H. G. Kuivila. Acc. Chem. Res. **1**, 299 (1968).
8. (*a*) J. L. Brokenshire and K. U. Ingold. Int. J. Chem. Kin. **3**, 343 (1971); (*b*) M. Pang and E. I. Becker. J. Org. Chem. **29**, 1948 (1964); (*c*) J. G. Noltes and G. J. M. van der Kirk. Chem. Ind. 294 (1959).
9. J. Morganstern and R. Mayer. J. Prakt. Chem. **34**, 116 (1966).
10. H. Fuhrer and H. H. Guenthard. Helv. Chim. Acta, **45**, 2036 (1962).
11. K. Hayashi, J. Iyoda, and I. Shiihara. J. Organomet. Chem. **10**, 81 (1967).
12. A. C. Cope and L. L. Estes. J. Am. Chem. Soc. **72**, 1128 (1950).

Mise en évidence d'un nouvel acide tungstique en solution. Filiations avec d'autres polytungstates

JEAN LEMERLE ET JEAN LEFEBVRE

Laboratoire de Chimie III, Université Pierre et Marie Curie, 4, place Jussieu, 75230 Paris, Cedex 06, France

Reçu le 10 février 1977

JEAN LEMERLE et JEAN LEFEBVRE. Can. J. Chem. **55**, 3758 (1977).

Un nouvel acide tungstique est préparé en solution aqueuse par échange d'ions. A la température ambiante les solutions se gélifient en quelques heures, puis 3 à 4 jours plus tard précipitent l'oxyde jaune WO_3. En solution aqueuse, cet acide est constitué de tétramères des motifs élémentaires $W_6O_{19}^{2-}$, s'associant par la suite pour donner le gel. Isolé à l'état solide cet acide est amorphe aux rayons X. En milieu hydroorganique, l'acide tungstique est stabilisé en solution, mais existe alors en équilibre avec les ions tungstique Y et hexatungstique mis en évidence par Fuchs. La condensation de l'acide Y et d'une des formes réduites est discutée. Les formes acides des ions hexatungstique (Fuchs) et tungstique Y ont été préparées à l'état pur en solution et à l'état solide.

JEAN LEMERLE and JEAN LEFEBVRE. Can. J. Chem. **55**, 3758 (1977).

A new tungstic acid has been prepared in aqueous solutions by ion exchange. At room temperature gelation occurs in solutions in a few hours, and 3 or 4 days after, the yellow oxide WO_3 precipitates. In aqueous solutions, this acid is formed by tetramers of $W_6O_{19}^{2-}$ units, which give a gel after association. X-ray analyses of tungstic acid in the solid state demonstrate the absence of crystallinity. In hydroorganic medium, tungstic acid is stabilized in solution, but exists in equilibrium with the Y tungstic and hexatungstic (Fuchs) anions. The condensation of the Y acid and one of its reduced forms is discussed. The pure acid forms of hexatungstic (Fuchs) and Y ions are obtained in solutions and in the solid state.

Introduction

L'acidification de l'ion tungstate par un acide fort conduit à de nombreux polytungstates dont la nature et les propriétés dépendent du degré d'acidification (1). La préparation en solution d'acides tungsto VI antimoniques V pyrochlores (2) nous a amenés à préparer des solutions tungstiques où le seul cation présent est le proton (l'acide antimonique est floculé ou gélifié par de nombreux cations). Cette préparation d'acide tungstique conduit à un nouveau type de polymère que nous appellerons acide tungstique α et que nous précisons dans ce travail.[1]

Caractéristiques de l'acide tungstique α

Les solutions aqueuses d'acide tungstique α à la concentration voisine de 0.1 mol/ℓ en tungstène ne sont stables à la température ambiante ($t \simeq 20°C$) qu'une dizaine d'heures. Après ce temps elles deviennent opalescentes, se gélifient au bout d'une vingtaine d'heures, puis après 3 à 4 jours précipitent totalement l'oxyde $WO_3 \cdot H_2O$ jaune (caractérisé par son diffractogramme X). Cette évolution peut être ralentie, voire stoppée par l'addition de solvants organiques (DMSO) dès la préparation (50% de DMSO suffisent pour maintenir la solution indéfiniment limpide).

Les solutions aqueuses sont caractérisées par des spectres d'absorption dans l'uv présentant un épaulement vers 275 nm (fig. 1). Diluées à basse température elles suivent la loi de Beer. Par contre si les solutions sont préparées diluées, un épaulement apparaît vers 325 nm et se transforme en maximum pour les fortes dilutions ($[W] < 4.6 \times 10^{-3}$ mol/ℓ) (fig. 1). Ce maximum est caractéristique du décatungstate (3), qui dans ces conditions de concentration doit se former en quantité non négligeable. L'étude de l'acide tungstique α est donc conduite sur des solutions de concentration supérieure à 6×10^{-2} mol/ℓ en tungstène.

Pendant la période où les solutions aqueuses d'acide α sont limpides, celles-si sont constituées pour l'essentiel d'espèces contenant 24 atomes de tungstène. Il faut néanmoins noter la présence de particules très condensées, d'abord en quantité négligeable, dont la proportion croît au cours de l'évolution et devenant prépondérantes quand l'acide se gélifie.

[1]Lorsque l'acidification d'un anion conduit immédiatement à un acide bien défini mais instable, on désigne généralement par la lettre α cette forme initiale instable, souvent soluble dans l'eau, et par la lettre β la forme stable. Exemples: acides stanniques et acides antimoniques α et β.

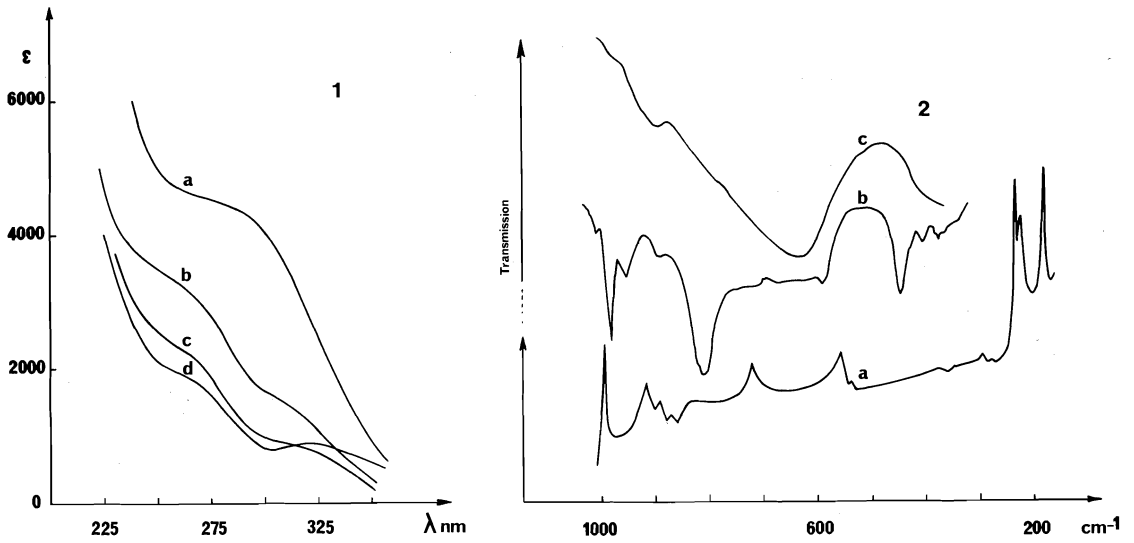

FIG. 1. Spectre uv des solutions aqueuses d'acide tungstique α dès la préparation. (*a*) [W] = 10^{-1} mol/ℓ; (*b*) [W] = 4.4×10^{-2} mol/ℓ; (*c*) [W] = 2×10^{-2} mol/ℓ; (*d*) [W] = 4.6×10^{-3} mol/ℓ.

FIG. 2. (*a*) Spectre raman de l'acide hexatungstique; (*b*) spectre ir de l'acide hexatungstique; (*c*) spectre ir de l'acide tungstique α.

D'autre part en solution hydroorganique (eau–DMSO 50%), la condensation apparente de l'acide tungstique α n'est plus que de 6. Néanmoins la baisse de condensation apparente en solution hydroorganique ne se produit pas immédiatement après l'addition de DMSO. On peut penser que l'édifice de base est constitué par un ion contenant six atomes de tungstène, pouvant s'associer dans l'eau, pour donner aux concentrations voisines de 0.1 mol/ℓ un ensemble soluble de quatre motifs élémentaires. L'association dans l'eau ne doit cependant pas procéder uniquement par liaisons hydrogène, car elles seraient rompues immédiatement par l'addition de DMSO. Au cours du vieillissement des solutions aqueuses l'association se poursuit pour donner le gel, et doit s'accompagner d'une déshydratation pour conduire à l'oxyde $WO_3 \cdot H_2O$ jaune.

L'addition d'un grand excès d'ions Li^+, Na^+ ou K^+ à une solution d'acide tungstique α provoque la précipitation de son sel.[2] On sépare alors par centrifugation un solide gommeux amorphe aux rayons X. La composition des solides est résumée au tableau 1. Ces précipités sont en tous points comparables à l'acide tungstique α solide obtenu par congélation rapide de la solution dès la préparation, et insolubilisé par l'éthanol au cours de la fusion à 0°C du glaçon dans ce solvant. Ils ont même spectre ir (fig. 2) et sont tous amorphes aux rayons X.

TABLEAU 1. La composition des solides

Cation (M^+)	[H^+] combiné/[W]	[M^+]/[W]
Li^+	1.59–1.61	0.26–0.28
Na^+	1.62–1.66	0.33–0.34
K^+	1.63–1.66	0.30–0.34

D'autre part les titrages protométriques rapides des solutions fraîchement préparées présentent deux points équivalents, l'un vers p*H* 5, l'autre vers p*H* 9. Le premier (p*H* ≃ 5) correspond à 0.37 [H^+]/[W]. Le spectre uv de la solution obtenue à ce p*H* n'est pas modifié par rapport à celui de l'acide initial. Il y a donc bon accord entre le nombre de protons titrables immédiatement et celui des cations contenus dans le sel de l'acide. Le polyion est donc porteur d'une charge négative pour trois atomes de tungstène. La formation du motif élémentaire peut se résumer ainsi:

$$6WO_4^{2-} + 10H^+ \rightleftharpoons W_6O_{19}^{2-} + 5H_2O$$

L'acide tungstique α n'est pas réductible à l'électrode à goutte de mercure. D'autre part le nombre de protons titrés, soit à p*H* 5, soit à

[2]L'addition d'ions Cs^+ ou $N(CH_3)_4^+$ provoque la précipitation d'un autre polytungstate (décatungstate) qui sera étudiée plus loin.

p*H* 9 varie avec le temps d'évolution de la solution (tableau 2).

La dégradation de l'acide tungstique α en WO_4^{2-} peut avoir comme intermédiaire l'ion paratungstique A, $HW_6O_{21}^{5-}$, comme c'est souvent le cas pour les polytungstates. Ceci peut être obtenu en ajoutant 0.8 $[OH^-]/[W]$ à l'acide, soit après 24 h de contact avec la base si l'acide α est utilisé en solution, soit dès la dissolution (quelques minutes) de l'acide α à l'état solide (obtenu par congélation) dans la base. La présence du paratungstate A seul dans ces conditions est mise en évidence par électrophorèse, centrifugation analytique et spectre ir du sel d'argent.

L'acide tungstique α est donc un isomère de l'ion hexatungstique isolé par Jahr, Fuchs et coll. (4–6) mais dont la forme solide est amorphe aux rayons X. Il est donc de composition très différente de celle annoncée par Richardson (7). Le problème pouvait se poser de savoir s'il était très différent d'un autre polytungstate formé rapidement dans ce domaine d'acidité: le ψ métatungstate. Le spectre ir du solide et la condensation de l'acide α en solution prouvent que ces deux tungstates sont bien différents.

Transformations de l'acide tungstique α en acide décatungstique

Le principe de cette transformation consiste à faire agir les ions $N(CH_3)_4^+$ ou Cs^+ en milieu aqueux sur une solution d'acide tungstique α. On obtient alors rapidement, avec un rendement de 90%, du décatungstate (tungstate Y) (3), caractérisé par le spectre ir du solide, le spectre uv et le polarogramme de la solution diluée.

A partir d'une solution hydroorganique (eau–DMSO 50%) de décatungstate de tétraméthylammonium ($[W] \simeq 10^{-2}$ mol/ℓ) on peut obtenir par échange $(N(CH_3)_4^+/H^+)$ dans une résine Dowex 50 WX2, une solution d'acide décatungstique. Après évaporation de celle-ci sous pression réduite à chaud, on isole l'acide décatungstique à l'état solide sous forme d'une poudre jaune bleuissant très rapidement à la lumière.

TABLEAU 2. Variation avec le temps d'évolution des solutions

Age de l'acide tungstique évolué à 20°C (h)	$[H^+]$ titré/[W]		
		p*H* 9	
	p*H* 5	Immédiatement	A t_∞ à p*H* constant
0	0.37	1	2
2	0.35	1	1.90
19	0.25	1.34	1.70
20	0.25	1.42	1.69
72	0.20	1.66	1.73

Le tungstate Y mis en évidence par Glemser et coll. (3) a été l'objet de controverses quant à sa masse molaire. Boyer et coll. (8, 9) ont montré que les propriétés électrochimiques de ce tungstate étaient en accord avec une dodécacondensation. Plus récemment Fuchs et coll. (10) ont déterminé la structure du sel de tributylammonium montrant qu'il s'agit d'un décatungstate. Les solutions aqueuses de tungstate Y ne sont stables qu'à basse température ($t \simeq 0$°C). Par contre l'addition de 20 à 30% de DMSO stabilise les solutions plusieurs jours à la température ambiante. Quelle que soit la préparation (tungstate Y de tétraméthylammonium ou forme acide obtenue à partir de l'acide α, tungstate Y de sodium (11) ou de potassium (12)), la condensation du polytungstate (déterminée par centrifugation analytique) est toujours la même dans le domaine de concentration étudié ($2 \times 10^{-3} \leq [W] \leq 8 \times 10^{-2}$ mol/ℓ). Elle est comprise entre 8 et 9 et le soluté est moléculairement homogène. Par contre le dérivé correspondant au premier stade de réduction de ce polytungstate est dodécacondensé. La masse molaire du tungstate Y en solution est donc plus en faveur de celle déterminée par Fuchs (décatungstate), mais la réduction doit s'accompagner d'une modification de structure du polyanion.

Transformation de l'acide tungstique α en acide hexatungstique

L'acide tungstique Y est alors préparé en dissolvant préalablement le tungstate de sodium (WO_4^{2-}) dans un mélange eau–DMSO 50% puis en réalisant l'échange Na^+/H^+ dans une résine Dowex 50 WX2 (réfrigérée à 2°C). Par évaporation sous pression réduite, à chaud, d'une solution récente d'acide tungstique α en milieu eau–DMSO 50% on recueille un solide jaune cristallisé ayant même spectre ir que l'hexatungstate de Fuchs et coll. (6). La solution dans le méthanol a un spectre uv présentant un maximum à 275 nm caractéristique de ce polytungstate. La condensation, déterminée par ultracentrifugation analytique en solution méthanolique est égale à 6. Par dissolution dans l'eau cet acide se transforme en acide décatungstique. En

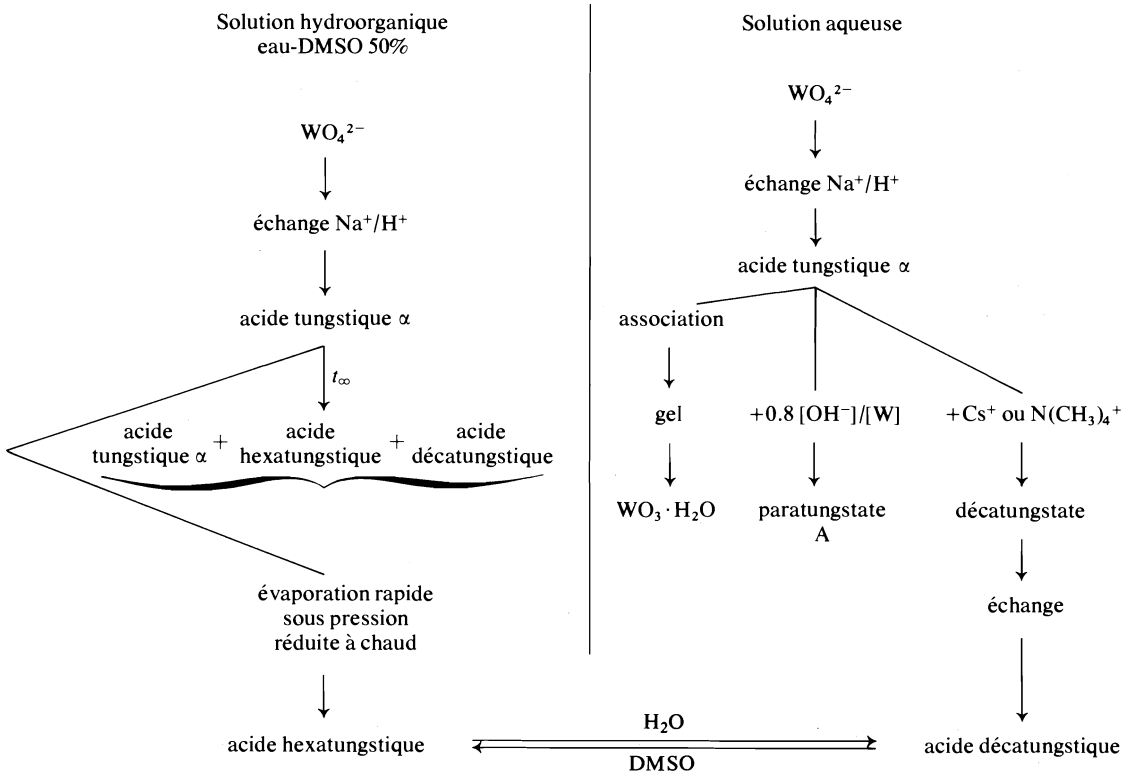

SCHÉMA 1

effet en suivant l'évolution des spectres uv après dissolution dans l'eau à basse température, on constate l'apparition de deux points isosbestiques à 268 nm et 303 nm. Le spectre final présente le maximum caractéristique du tungstate Y à 325 nm.

Par contre une solution hydroorganique (eau–DMSO 50%) d'acide tungstique α, âgée de plusieurs mois a un spectre uv présentant un épaulement à 325 nm indice de la présence de décatungstate. Cette solution peut être précipitée par différents cations. L'argent précipite l'acide α tandis que l'ion $N(CH_3)_4^+$ précipite l'hexatungstate (caractérisés par leur spectre ir). Dans les deux cas le spectre uv du filtrat présente un maximum très marqué à 325 nm. L'ion $P(C_6H_5)_4^+$ précipite un mélange de décatungstate et d'hexatungstate. Par contre le filtrat ne présente plus de maximum à 325 nm. On peut donc envisager la présence en solution de trois espèces tungstiques. La transformation en milieu eau–DMSO 50% aboutit aux équilibres:

[1] acide tungstique α ⇌ acide hexatungstique ⇌ acide décatungstique

On peut considérer qu'à l'équilibre on obtient 75% du tungstène sous forme de décatungstate. Par contre la proportion d'hexatungstate et de tungstate α est difficile à préciser.

Si certaines transformations de l'acide tungstique α en solution hydroorganique peuvent s'expliquer à partir du déplacement de l'équilibre, d'autres en contradiction, peuvent être expliquées par des considérations cinétiques.

L'évaporation à chaud d'une solution fraîchement préparée d'acide α enrichit le solvant en DMSO, donc favorise la formation de l'hexatungstate plutôt que celle du décatungstate (11). Par contre lorsqu'on évapore une solution d'acide décatungstique obtenu par échange en milieu eau–DMSO, le solvant s'enrichissant en DMSO, on devrait obtenir uniquement l'hexatungstate. Le fait que l'on obtienne de l'acide décatungstique pur peut s'expliquer par une vitesse d'évaporation du solvant organique beaucoup plus rapide que la transformation décatungstate → hexatungstate. Ceci a été confirmé en chauffant à reflux une solution de décatungstate dans le DMSO. On observe alors la transformation, mais dans un temps infiniment

plus long que celui mis pour l'évaporation conduisant à l'acide décatungstique solide.

On peut donc résumer les différentes filiations entre les ions polytungstiques par le schéma 1.

Partie expérimentale

Préparations des solutions

L'acide tungstique α est préparé par échange d'ions dans une résine Dowex 50 WX2, 100–200 mesh sous forme H^+ à partir d'une solution de tungstate de sodium. La colonne dans laquelle a lieu l'échange et le récipient recueillant l'acide sont thermostatés par une circulation d'alcool à 2°C.

Dosage des éléments

Les cations alcalins sont dosés par spectrophotométrie d'absorption atomique (appareil Jobin Yvon type Delta). Le tungstène est dosé par colorimétrie à 400 nm du complexe W réduit – KSCN (13). Le nombre de protons combinés est déterminé en mesurant la quantité de base nécessaire à la dégradation totale du polyion en WO_4^{2-} à p*H* 9 (combititreur Métrohm 3D).

Les différents composés obtenus sont caractérisés par: (*a*) leur spectre uv visible (spectrophotomètre Beckman Acta V); (*b*) leur spectre ir (échantillonnage en micropastilles de KBr, spectrophotomètre Perkin-Elmer modèle 457); (*c*) leur spectre Raman (spectromètre Coderg type PHO); (*d*) leur diffractogramme X (générateur Philips PW 1008 équipé d'une chambre Debye-Scherrer de 114 mm de diamètre (rayonnement utilisé: raie K_α du cuivre; filtre de nickel)); (*e*) leur mobilité électrophorétique (appareil LKB Multiphor); (*f*) leur masse molaire (ultracentrifugation analytique).

L'ultracentrifugation analytique est réalisée à l'aide d'une centrifugeuse Beckman modèle E équipée des optiques schlieren et à absorption, avec monochromateur et scanner. La masse molaire de l'acide tungstique α est déterminée à basse température ($t = 10$°C), selon la technique de transition vers l'équilibre de sédimentation (14) à 36 000 et 48 000 tours min^{-1} et à la concentration en tungstène égale à 7×10^{-2} mol/ℓ, en présence de divers solvants: solutions aqueuses $HClO_4$, LiCl, ou solutions hydroorganiques (eau–DMSO 50%) de HCl et NaCl. Tous les électrolytes sont à la concentration 0.1 mol/ℓ et sont ajoutés au moment de la mesure. Dans ces conditions aucune précipitation n'a lieu.

La condensation de l'acide décatungstique est déterminée à l'équilibre de sédimentation (vitesse de rotation 10 000, 15 000, 20 000, 22 000 tours min^{-1}) dans une cellule à six canaux. Un témoin de métatungstate à la même concentration que l'échantillon étudié est introduit dans l'un des compartiments de la cellule. Pour ce tungstate la dodécacondensation a toujours été vérifiée. Toutes ces déterminations sont faites en milieu eau–DMSO 30%.

Les volumes spécifiques partiels sont déterminés par picnométrie (15).

1. P. Souchay. Ions minéraux condensés. Masson, Paris. 1969.
2. J. Lemerle et J. Lefebvre. Bull. Soc. Chim. **3**, 409 (1976).
3. O. Glemser, W. Holznagel, W. Höltje et E. Schwarzmann. Z. Naturforsch. Teil A, **20**, 725 (1965).
4. K. F. Jahr, J. Fuchs et R. Oberhauser. Chem. Ber. **101**, 477 (1968).
5. J. Fuchs et K. F. Jahr. Z. Naturforsch. Teil B, **23**, 1380 (1968).
6. R. Mattes, H. Bierbusse et J. Fuchs. Z. Anorg. Allg. Chem. **385**, 230 (1971).
7. E. Richardson. J. Inorg. Nucl. Chem. **12**, 79 (1959).
8. M. Boyer. J. Electroanal. Chem. **31**, 441 (1971).
9. M. Boyer et P. Souchay. Rev. Chim. Miner. **8**, 591 (1971).
10. J. Fuchs, H. Hartl, W. Schiller et U. Gerlach. Acta Crystallogr. Sect. B, **32**, 740 (1976).
11. P. Courtin et J. Lefebvre. Bull. Soc. Chim. **9–10**, 1983 (1975).
12. F. Chauveau, M. Boyer et B. Lemeur. C.R. Acad. Sci. **268**, 479 (1969).
13. G. Charlot. Analyse quantitative minérale. Masson, Paris. 1961.
14. W. J. Archibald, J. Phys. Colloid Chem. **51**, 1204 (1947).
15. F. Sécheresse, J. Lemerle et J. Lefebvre. Bull. Soc. Chim. **11**, 2423 (1974).

The synthesis, thermochromism, and cycloadditive properties of an *o*-methylenethioquinone system

P. DE MAYO AND H. Y. NG

Photochemistry Unit, Department of Chemistry, University of Western Ontario, London, Ont., Canada N6A 3K7

Received May 27, 1977

P. DE MAYO and H. Y. NG. Can. J. Chem. **55**, 3763 (1977).

The irradiation of 4,5-benzo-1,2-dithiole-3-thione (**1**) in the presence of cyclopentene and of tetramethylethylene gives 1:1 adducts. In solution these adducts are in equilibrium with eight-membered-ring dimers. The thermodynamic parameters for this equilibrium have been determined. The available evidence suggests a head-to-head configuration. These same monomeric adducts give Diels–Alder addition products with normal dienophiles, but also react similarly with simple thiones (adamantanethione, norbornanethione, cyclohexanethione) to give thioorthoesters. The structures of the latter substances have been demonstrated both spectroscopically and, chemically, by hydrolysis to a thiosalicylic acid derivative. The thioorthoesters have been shown to undergo stereoisomerization on acid catalysis. Of the two mechanisms considered for this process (reversal to thiones and ion-pair formation) the former has been excluded.

P. DE MAYO et H. Y. NG. Can. J. Chem. **55**, 3763 (1977).

L'irradiation du benzo-4,5 dithiol-1,2 thione-3 (**1**) en présence de cyclopentène et de tétraméthyléthylène conduit à des adduits 1:1. En solution, ces adduits sont en équilibre avec des dimères cycliques à huit chaînons. On détermine les paramètres thermodynamiques pour ces équilibres. L'indice connue est en faveur d'une configuration tête à tête. Ces mêmes adduits monomères donnent des produits d'addition Diels–Alder avec des diénophyles normaux, mais ils réagissent d'une manière analogue avec des thiones simples (adamantanethione, norbornanethione, cyclohexanethione) pour conduire à des thioorthoesters. On détermine la structure de ces derniers spectroscopiquement et chimiquement en les hydrolysant en dérivés d'acide thiosalicylique. Les thioorthoesters démontrent une tendance à la stéréoisomérisation lors d'une catalyse acide. Deux mécanismes sont envisagés pour ce processus; l'inversion en thiones et la formation d'une paire d'ions; seul le dernier est retenu.

[Traduit par le journal]

Substances containing the *o*-quinonoid moiety are of considerable general interest because of the wide variety of chemical transformations of which they are capable (1, 2). Frequently they, or their derivatives, are so reactive that their ephemeral existence has only been detected by chemical trapping (see, for example, refs. 3–6) or by the nature of further transformation products (e.g. refs. 7–10). Our object, deriving from a general interest in the fundamental photochemistry of thiones, was to prepare an *o*-methylene thioquinone derivative, a species at that time unknown.

The photochemistry of 1,2-dithiole-3-thiones had previously been investigated (11–13) and the results obtained by Okazaki, Inamoto, and their collaborators and by ourselves suggested a route to such *o*-methylene thioquinones. This was successful; the present paper describes the preparation of two examples of such a system and an account of their unusual properties.[1]

[1]After our preliminary communication of part of this work (14) Okazaki and Inamoto described related and independent work which was, in part, complementary (15).

Irradiation of 4,5-benzo-1,2-dithiole-3-thione (**1**) in the presence of cyclopentene or of tetramethylethylene gave the desired quinonoid system (**2**) directly.

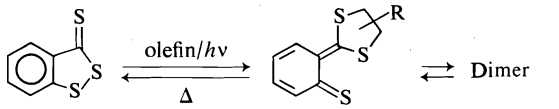

1 **2***a* R = $(CH_2)_3$ **3***a* R = $(CH_2)_3$
b R = $(CH_3)_4$ *b* R = $(CH_3)_4$

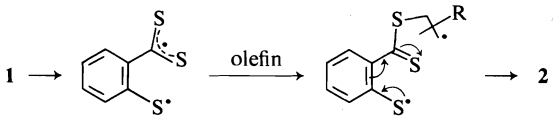

A **B**

The formation of **2** may be envisaged as occurring, formally, via A and B (11–13).

The adduct **2***a*, obtained with cyclopentene, when refluxed in carbon tetrachloride for 12 h regenerated **1** in high yield. This adduct was obtained as a colourless solid which was, at the time, surprising, and certainly incompatible with the monomeric formulation **2***a*: this, having a conjugated thione function, should be deep blue.

The solid adduct **2***b* obtained with tetramethylethylene, was, indeed, blue, but pale. Both substances, however, gave blue solutions whose intensities were temperature dependent, to the extent that in the case of **2***a* a solution in benzene became colourless near 5°C. The quite striking Prussian Blue colour was regenerated on warming to blood temperature and, in the absence of oxygen, the cycle would be repeated, apparently indefinitely (the substance evidently had potential use for magicians and others). In both cases, then, the supposed monomers **2** were in an equilibrium which was temperature dependent with some other species, **3**, which was colourless: the nature of this equilibrium will be discussed later.

The Monomer Structures, 2

The ready reversibility of the formation of **2***a* (together with its mode of formation) (11–13) strongly suggested that no deep seated rearrangement involving carbon–carbon bonds was involved. Presuming, therefore, that the blue entity, **2***a*, was the desired species, whatever its further and reversible transformation, a Diels–Alder addition was attempted with *N*-phenylmaleimide and with acetylenedicarboxylic acid, dimethyl ester. The adducts **4** and **5** were obtained.

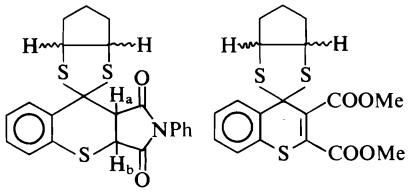

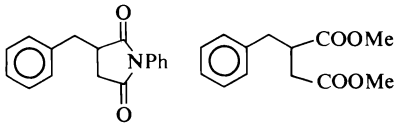

The ^{1}Hmr of **4** was consistent with that of a 1:1 adduct, and this was confirmed by the mass spectrum. Aside from the nine aromatic protons a singlet at 4.93 ppm for two protons was also present. In view of the different environments of H_a and H_b this was puzzling, but the coincidental identity of the chemical shifts was revealed by the resolution into two doublets (J = 9 Hz) on the addition Eu(fod)$_3$. Although two stereoisomers are possible the crystalline adduct appeared to be a single isomer (80°C). The structure assigned to **4** was further confirmed by total desulfurization with Raney nickel to benzyl-*N*-phenylsuccinimide, **6**.

The acetylene adduct, on the other hand, was not obtained crystalline. The mass spectrum of the amorphous solid nonetheless indicated a 1:1 adduct, and the infrared spectrum (ν_{max} 1721 cm^{-1}) the presence of the conjugated ester functions. Desulfurization gave, as expected, **7**.

In a similar manner **2***b* was allowed to react with *N*-*n*-propylmaleimide, *N*-phenylmaleimide, and acetylene dicarboxylic acid, dimethyl ester. The structures of the adducts (**8**–**10**) were confirmed in a similar way.

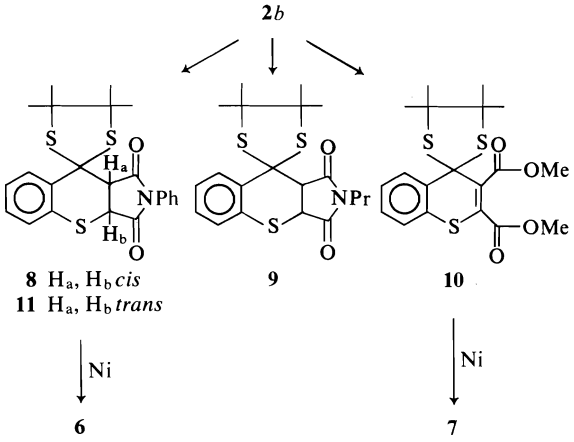

Attempted desulfurization of **8** with a vintage, 4 year old, sample of Raney nickel yielded **11**. This substance resembled **8** closely in its mass spectrum and infrared spectrum. It was, therefore, presumed to be the *trans* adduct, isomerisation having been induced by the basic catalyst. The coupling constant for the methine protons is 9 Hz in **8** and 19 Hz in **11**. There figures are in good accord with those for the corresponding protons in **12** (16).

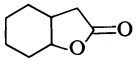

12

The ^{1}Hmr spectra of **8**, **9**, and **11** all showed four singlets for the nonequivalent methyl groups. With the ester **10** two six-proton singlets were observed, as expected for a rapid boat–boat interconversion of the central ring. Determination of the spectrum in carbon disulphide between +30°C and −110°C indicated a coalescence temperature near −70°C. Below this

temperature four peaks were seen to be partly resolved. These did not sharpen at −110°C, probably because of the high viscosity. The activation energy for the inversion, on the assumption that the above interpretation is correct, is 10.0 ± 1.0 kcal/mol (17, 18). The large uncertainty is partly due to the imprecision in the coalescence temperatures and the values of the chemical shifts.

The total of the above evidence suggests that the adducts are adequately represented by the *o*-methylene quinonoid structures, and this is consistent with the visible and ultraviolet absorption spectra. Both **2***a* and **2***b* showed intense absorption at 585 nm. Most conjugated thiones show absorption in this region (19–22), indicative of transitions of $\pi^* \leftarrow n$ type, but there is no doubt that the present absorption has a different origin: the molar extinction coefficients observed are far too high for what is a symmetry forbidden transition. It is, therefore, almost certainly a $\pi^* \leftarrow \pi$ transition, the $\pi^* \leftarrow n$ absorption submerged and unresolved. There cannot be much ct (charge-transfer) contribution to this transition in view of the very slight solvent dependence of the absorption (Table 1). This is to be contrasted with the large shift observed for Michler's thione (22) where there is a large ct contribution. In fact, the extended π system, together with the effect of sulphur substitution (23–25) could be sufficient to account for the position of the $\pi^* \leftarrow \pi$ band. Thus the parent *o*-xylylene absorbs at 373 nm (26) and the corresponding thione would be expected at longer wavelength (compare 3-methylenecholest-4-ene (239 nm, ref. 24) with **13** (296 nm, ref. 19)).

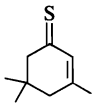

13

Single sulphur substitution in enones results in displacements of ~85 nm (24).

The fact that the presently noted properties of the monomeric species **2***a* and **2***b* are adequately described by those representations does not exclude the possibility of the existence of an additional equilibrium with the cyclized valence tautomers of type **14**. Such equilibria have been

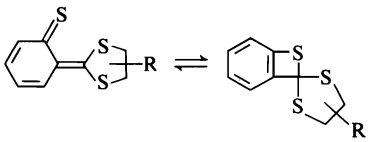

14

proposed for ketene imines and ketene thiones (27–29), but in the present case we have no evidence for its existence.

TABLE 1. Solvent effect on λ_{max} of **2***a*

Solvent	λ_{max} (nm)
Acetonitrile	580
Methanol	583
Chloroform	585
Methylene chloride	585
Benzene	585

The Structure of the Dimers

The reversible equilibria observed with **2** were not, in themselves, indicative of dimerization. The first hypothesis, in fact, was that it represented something of the type **14**. That it represented a reversible dimerization was shown in two ways.

The first was by the establishment of the concentration dependence of the average molecular weight. The molecular weight, determined cryoscopically in benzene for **2***a* was 496 ± 10: that calculated for a dimer was 502. However, the molecular weights determined osmometrically in chloroform yielded the results shown in Fig. 1. Here, a concentration dependence is clearly indicated though, regrettably, values at very low concentrations could not be determined.

The second was by the use of optical method for measuring monomer concentration. With this technique (see Appendix) equilibrium constants (K_c) could be determined at various concentrations at constant temperature. Only for the system

$$A_2 \rightleftharpoons 2A$$

was the equilibrium 'constant', in fact, constant. The values are indicated in Table 2 for **2***a* and **2***b*; in addition, values for other conceivable equilibria for **2***a* are included to indicate the changes in K_c.

Given that the equilibrating species was a dimer, a number of possibilities existed for the actual structures. Diels–Alder addition, though known with such systems (see following section) and in general with *o*-quinonoid systems (for instance, refs. 26, 30–32), could be eliminated on spectroscopic grounds. The dimers were transparent above 300 nm: any $(2_\pi + 2_\pi)$ or $(2_\pi + 4_\pi)$ addition must leave a conjugated absorbing

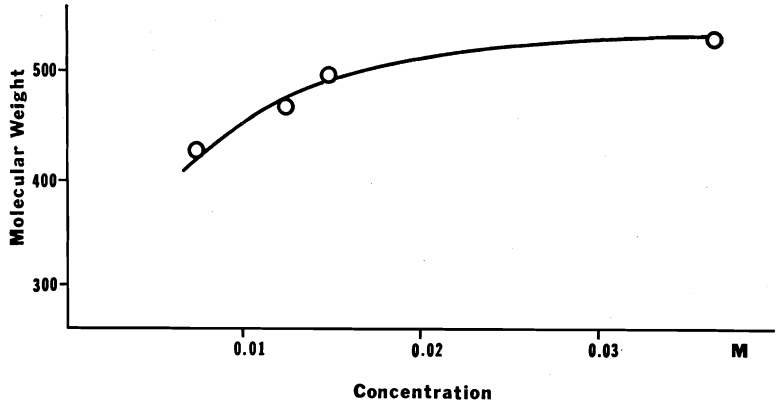

FIG. 1. Concentration dependence of the molecular weight of **2***a* in chloroform as determined osmometrically.

TABLE 2. Equilibrium constants at 24.5°C

[**2***a*] (mg/5 ml)	$K(M)$ ($\times 10^6$)	[**2***b*] (mg/5 ml)	$K(M)$ ($\times 10^4$)	K_1[a]	K_2[b] ($\times 10^8$)	K_3[c] ($\times 10^5$)
3.38	8.45	3.43	1.89	0.82	3.34	8.94
2.08	8.83	2.05	1.90	1.16	2.35	12.2
0.406	8.75	1.23	1.87	1.64	1.6	17.2
0.161	8.89	0.37	2.02	4.5	0.71	54.4
0.027	8.46	0.074	1.73	16.0	0.13	157.0
0.00108	9.14					
(0.000065	6.50)					

[a]For **2***b* assuming the equilibrium $A \rightleftharpoons A'$.
[b]For **2***b* assuming the equilibrium $A_2 \rightleftharpoons 3A$.
[c]For **2***b* assuming the equilibrium $2A_3 \rightleftharpoons 3A_2$.

system, **15** detectable above 300 nm (33), or contain a spectroscopically recognizable thione group. In addition, the latter type of addition was excluded by the ^1H and ^{13}C nmr spectra

15

which clearly indicated symmetry and the lack of unsaturation aside from the aromatic rings. The ^{13}C spectrum of **2***b*, for instance, contained by 13 signals. The most probable structures were thus eight-membered rings **16***a,b* or **17***a,b*. An eight-membered ring has been reported for dithietenes. This is also an equilibrium, but requires higher temperatures (34). On desulphurization with Raney nickel at 40–60°C a small yield of bibenzyl (4%) was obtained. At face value this suggested **16***a* for the dimer structure, but the possibility of a *trans*-annular coupling (28) cannot be completely excluded, nor the formation of bibenzyl from monomeric precursors.

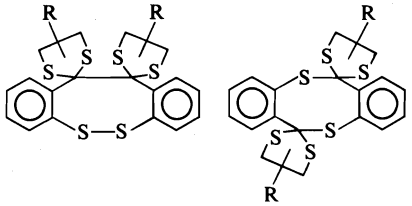

16*a* R = $(CH_2)_3$ **17***a* R = $(CH_2)_3$
b R = $(CH_3)_4$ *b* R = $(CH_3)_4$

Another argument may be adduced to support the same structure. It seems most probable that **3***a* and **3***b* should have the same regiospecificity. If that be accepted, then were the *trans* arrangement **17***a,b*, that obtaining the equilibrium for the two pairs might be expected to be very similar. In fact (section following) there is a free energy difference of 3.3 kcal/mol which should be steric in origin. Such an effect is hard to rationalize without involving **16***a,b*.

The Equilibrium

The position of the equilibrium was dependent on the polarity of the medium, the monomer

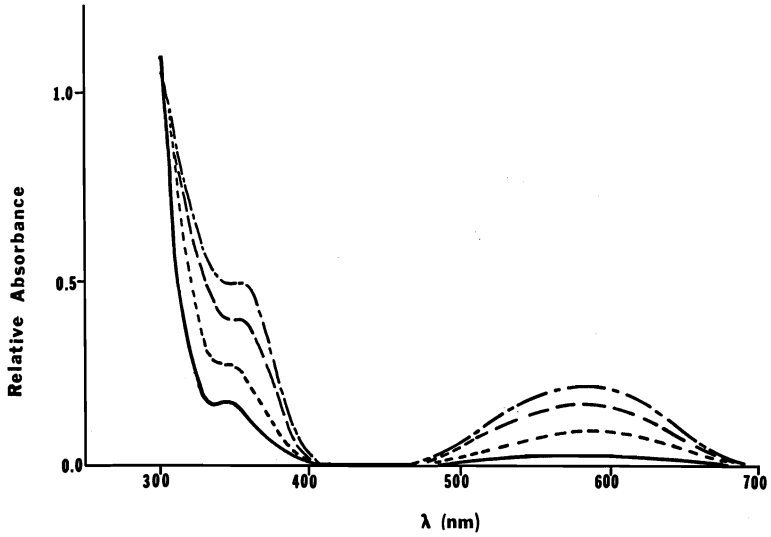

FIG. 2. Solvent effect on the absorption of **2***a*: (—) CH_2Cl_2–hexane 1:4; (---) 2:3; (——) 3:2; (····) pure CH_2Cl_2.

being favoured with increasing polarity (Fig. 2). In a particular solvent the position of the equilibrium was also temperature dependent. For a methylene chloride solution the change over the range $-16°C$ to $+33°C$ is shown in Fig. 3. Similar displacements could also be achieved by brief irradiation at both 254 nm and at 585 nm (Fig. 4). On removal of the light the original equilibrium was slowly restored.

Equilibrium constants (K_c) were measured at 585 nm (see Appendix) in benzene and chloroform over a range of $\sim 40°$. The values of K_c were obtained and plots of ln K_c against reciprocal temperatures are shown in Fig. 5. The values of ΔH^0 and ΔS^0 were computed (least squares) and are shown in Table 3. The value of ΔH^0 for **2***a* is about 2 kcal/mol larger than that of **2***b* in both solvents. We interpret this, as stated, in terms of steric crowding in **16**, but we recognize that the argument is not conclusive. It is interesting that in the recent extension to the naphthalene series (35) the isolation of the monomers has been reported without there being evidence for equilibria with dimers.

Cycloaddition Reactions

In the characterization of the monomers normal dienophiles were used. At a stage when Diels–Alder structures for the dimers were still thought possible the addition of **2***a* and **2***b* to alicyclic thiones was also attempted as a model reaction. Adducts were obtained and the chemistry thereof is here reported.[2]

The thiones selected were adamantanethione, norbornanethione, cyclohexanethione, and thiocamphor. From the first three substances and **2***a* pure adducts were obtained at room temperature. In the case of norbornanethione only one isomer could be obtained crystalline. With thiocamphor 3 days were necessary before the colour of the thione was discharged, and on attempted isolation **2***a* was regenerated. Similar experiments were performed with **2***b*, but only in the case of cyclohexanethione could an adduct be isolated.

The structure of the **2***a*–adamantanethione adduct followed from the evidence to be described. Similarity of analytical and spectral data allowed that of the other adducts to be allocated by analogy.

Two adducts were obtained from **2***a* and adamantanethione. These were 1:1 adducts and the four possibilities **18***a,b*, **19***a,b* were to be considered. Since the mass spectral fragmentation patterns for the two isomers were identical the choice lay between **18** and **19**: it seemed unlikely that structural isomers could behave so similarly. This view was supported by the isomerization to be described. Only one isomer was formed from

[2]For the addition of thiones to dienes, see refs. 36–38. For the use of α,β-unsaturated thiones as dienes, see refs. 35, 39–44.

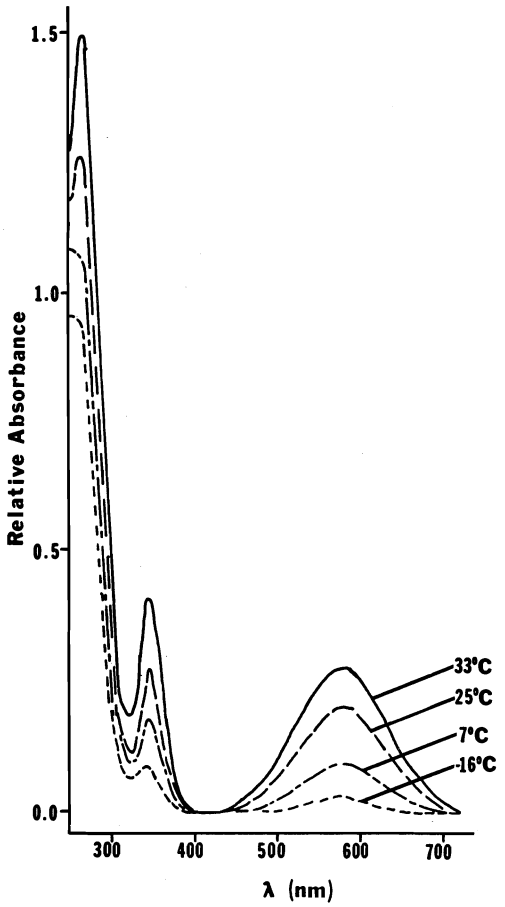

FIG. 3. Temperature effect on absorption of **2***a* in methylene chloride.

2*b* and cyclohexanethione, in agreement with this view.

The chemical distinction between **18** and **19** is that **19** is a thioorthoester whereas **18** is a disulphide. Under conditions of reduction with lithium aluminium hydride when a disulphide would be expected to be cleaved there was no reaction (45). This, though negative evidence, appeared to favour **19**, as did the reversibility of the Diels–Alder formation. Accordingly, the hydrolysis of the thioorthoester was undertaken. Stirring a mixture of **19** with mercuric oxide in the presence of boron trifluoride at 0°C gave adamantanone in 50% yield. In addition, the mercaptide chloride, **20**, of *o*-mercaptobenzoic acid was obtained in similar yield.

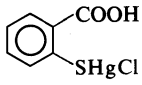

20

The possibility that the thiosalicylic acid was formed in some way from **2***a* itself was eliminated by showing that the adduct was thermally stable under the conditions used. Only isomerization occurred (see below).

The Adduct Isomerization

It was observed that a pure isomer of **19** showed a single methine proton signal at $\delta = 4.4$ ppm ($CDCl_3$). After 12 h the signal for the other isomer ($\delta = 4.0$ ppm) was also visible, and the presence of the second isomer was confirmed by isolation. The equilibrium could be approached from both sides, and the final ratio was ~1:1. The same isomerization could be achieved in benzene at 80°C but was slow and needed over 3 days.

The adduct of **2***a* with norbornanethione behaves similarly: in methylene chloride-d_2 – acetonitrile-d_3 (2:1) at 40°C 20% conversion of the δ 4.4 isomer to the other was achieved in 4 days. In carbon tetrachloride no change was observed in 4 days.

Since more polar solvents appeared to favour the isomerization and since chloroform frequently contains acid, it seemed likely that the process was heterolytic. This was confirmed when a solution of the **2***a* – cyclohexanethione adduct (mixture, major isomer $\delta = 4.4$, ratio 4:1) in carbon tetrachloride, which had been stable for at least 58 h, when acidified with dry hydrogen chloride equilibrated (final ratio: 2:1) in 1 h.

Two general possibilities existed for the inversion: a reversion of the adducts to starting materials, followed by recombination; or a cleavage of a single bond (C—S) of the thio-

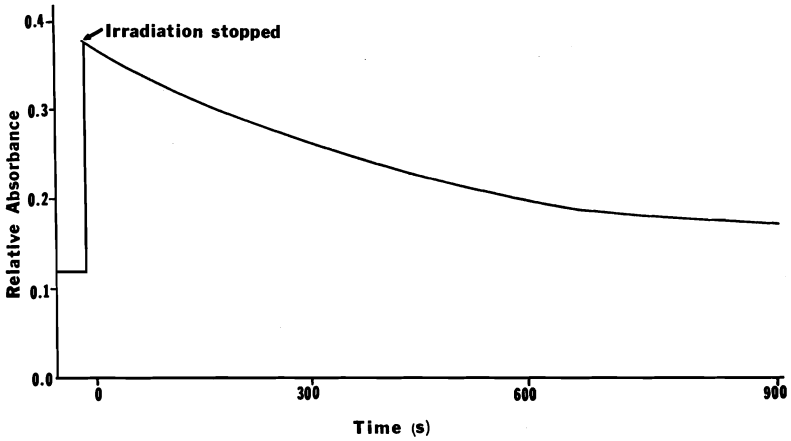

FIG. 4. Effect of light on the **2***a*–**3***a* equilibrium.

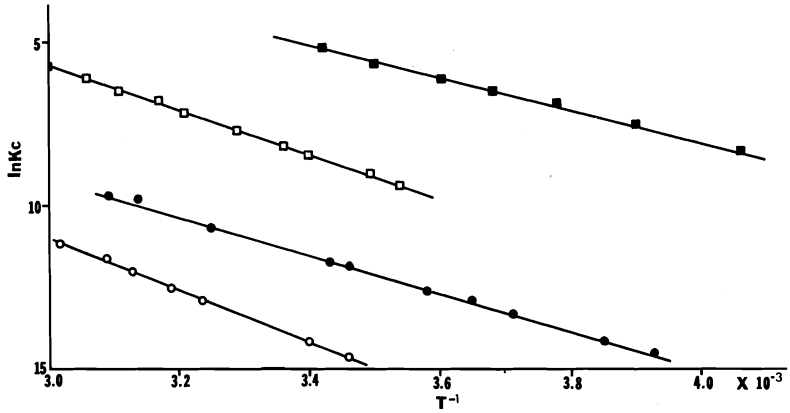

FIG. 5. Plot of ln K_c of (○) **2***a* in benzene, (●) **2***a* in $CHCl_3$, (□) **2***b* in benzene, (■) **2***b* in $CHCl_3$ as a function of the reciprocal absolute temperature.

TABLE 3. Thermodynamic parameters

	2*a*		**2***b*	
	Dimer ⇌ Monomer		Dimer ⇌ Monomer	
Solvent	C_6H_6	$CHCl_3$	C_6H_6	$CHCl_3$
ΔH^0 (kcal/mol)	15.8±1.0	11.5±0.4	14.1±0.3	9.4±0.2
ΔS^0 (eu)	25.6±2.0	16.1±1.2	31.1±0.8	21.8±0.8

orthoester, followed by rotation and recombination (Scheme 1). If the first be not occurring in a solvent cage from which there is no escape, then the mechanisms are distinguishable. To reveal the distinction the isomerization of the norbornanethione – **2***a* adduct was carried out in benzene at 80°C in the presence of norbornanethione-α,α-d_2. The recovered, but partly isomerized, adduct contained no deuterium, as shown by mass spectrometry. Further, permitting the isomerization to occur in the presence of the powerful dienophile, *N*-phenylmaleimide both in benzene and chloroform, gave none of the adduct **4**. The route via the dithiolenium ion is thus preferred.

The allocation of the stereochemistry of the isomers may be reasonably made on the following grounds. The relevant protons are either *syn*

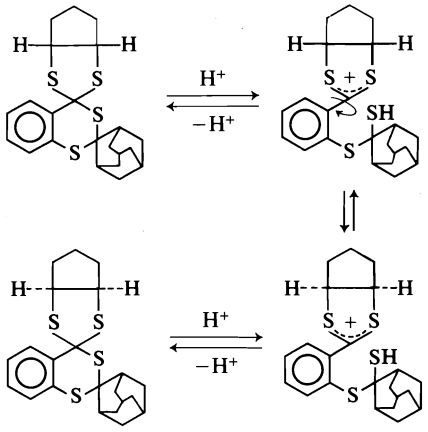

SCHEME 1

or *anti* to the aromatic ring. The higher field protons would, from the inspection of models, be expected to be those *syn* to the aromatic ring. To confirm this the adducts from **21** (13) and adamantanethione were prepared. Both were observed in solution but only one isomer could be isolated. However, both isomers, as shown by integration, had the relevant proton signals at 4.5 ppm.

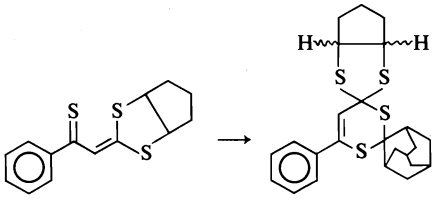

21

Experimental

Melting points were determined on a Reichert hot stage apparatus. Cyclopentene and tetramethylethylene were refluxed over zinc dust and distilled. Benzene was purified by irradiation with chloranil for 7 days and fractionally distilled. Boron trifluoride etherate was purified according to Fieser (47). 4,5-Benzo-1,2-dithiole-3-thione was prepared according to the method of Lozac'h (48).

2-Benzyl-N-phenylsuccinimide

This was prepared according to Arcona (49) from 2-benzylsuccinic acid (0.4 g) and aniline (0.18 g) at 180°C, mp 128–130°C; ν_{max}: 1778, 1714 cm^{-1}. *Exact Mass* calcd. for $C_{17}H_{15}O_2N$: 265.1102; found (ms): 265.1090.

*Irradiation of **1** with Cyclopentene*

It was established optically that no reaction occurred between these substances in ethereal solution in the dark in several hours. Exposure to room light led to reaction.

A mixture of **1** (99 mg), cyclopentene (1 ml), and ether (30 ml) was irradiated with a 450 W medium pressure lamp until the solution turned deep blue (ca. 2 h). After evaporation of the solvent the residue was chromatographed (silica gel, 9 g; light petroleum (60–80°C) – benzene, 2:3) to give **2***a* as a white solid, recrystallized from methylene chloride – methanol, mp 158–160°C (dec.), 112 mg (80%); δ: 3.95 (m, ca. 1.5H, S—$(CH_2)_2$—S), 4.40 (m, ca. 0.5H, S—$(CH_2)_2$—S); λ_{max} (benzene, 5.24 × 10^{-3} *M*) 585 (24.8), 351 (139); (acetonitrile, 6.61 × 10^{-4} *M*) 580 (348), 346 (620); (methylene chloride, 5.02 × 10^{-3} *M*) 585 (97), 347 (136), 260 (3590).

When a solution of **2***a* (20 mg) in carbon tetrachloride (5 ml) was refluxed for 12 h the product showed one spot on tlc and crystallization (hexane) gave **1** in quantitative yield.

*Desulphurization of **2a***

The compound (1.08 g) and Raney nickel (10 g) was heated in benzene at 40°C for 20 h. Starting material remained, and the temperature was raised to 60°C for 4 h. From the mixture, by tlc, was isolated bibenzyl (4%) and benzyl alcohol (13.5%) both identified by comparison with authentic specimens.

*Reaction of **2a** with N-Phenylmaleimide*

The thione (39 mg) and imide (29 mg) in benzene (10 ml) were stirred at room temperature in the dark. The tlc yielded the adduct **4** (53 mg, 80%) crystallized from ethyl acetate, mp 93–95°C; ν_{max}($CHCl_3$): 1770, 1710 cm^{-1}; δ: 1.5–2.4 (m, 6H), 4.1–4.4 (m, 2H), 4.93 (s, 2H), 6.80–8.13 (m, 9H). When Eu(fod)$_3$ (53 mg) was added the peak at 4.93 became a pair of doublets (J = 9 Hz); λ_{max}(MeOH): 283 (sh) nm (ε = 300). *Anal.* calcd. for $C_{22}H_{19}NO_2S_3$: C 62.11, H 4.50, N 3.29; found: C 62.11, H 4.56, N 3.30.

Desulfurization of the adduct (300 mg) with Raney nickel (3 g) in benzene by refluxing for 24 h gave (ethanol–water, 1:1) the benzyl-*N*-succinimide **6** (142 mg, 77%), mp and mixture mp 128–130°C, further identified by ir, ^{1}Hmr, and mass spectrum.

The adduct with acetylene dicarboxylic acid, dimethyl ester prepared in the same way could not be obtained in crystalline form though apparently it was homogeneous on tlc. The ^{1}Hmr spectrum was consonant with the assigned structure; λ_{max}(CH_2Cl_2): 318 (3900), 253 nm (8400). Desulfurization gave dimethyl benzylsuccinate identified by ir and mass spectrum.

*Irradiation of **1** with Tetramethylethylene*

The irradiation was performed as with cyclopentene. From 90 mg **1** was obtained (methylene chloride – methanol) **2***b* as pale blue crystals (135 mg, 90%), mp 136–138°C (dec.); δ (220 MHz, CD_2Cl_2 at −50°C): 1.2 (s, 3H), 1.33 (s, 3H), 1.59 (s, 3H), 1.80 (s, 3H); λ_{max}(C_6H_6) (2.59 × 10^{-4} *M*) 585 nm (2270); ^{13}Cmr (CD_2Cl_2): 148.6 (s), 139.4 (d), 134.19 (s), 129.52 (d), 128.67 (d), 128.07 (s) (aromatic), 77.60 (s), 66.23 (s), 66.12 (s), 28.32 (q), 26.93 (q), 23.48 (q), 23.31 (q). *Exact Mass* calcd. for $C_{13}H_{16}S_3$: 268.0409; found (ms): 268.0405. *Anal.* calcd. for $C_{13}H_{16}S_3$: C 58.20, H 6.01, S 35.79; found: C 58.33, H 6.19, S 34.88.

The molecular weight determined at 5.8 mg/ml at 38°C by osmometry was 496. This is equivalent to the presence of 7.4% monomer. Determined by absorption at 585 nm a value of 9.7% was obtained.

*Reaction of **2b** with N-Phenylmaleimide*

A solution of **2***b* (500 mg) and the imide (400 mg) in benzene for 24 h yielded the adduct **8**, mp 242–245°C

(700 mg, 85%), from ethyl acetate; $\lambda_{max}(CHCl_2)$: 1775, 1710 cm^{-1}; ^{1}Hmr δ: 1.36 (s, 3H), 1.46 (s, 3H), 1.58 (s, 3H), 1.70 (s, 3H), 4.405 (s, 1H), 4.415 (s, 1H). After the addition of Eu(fod)$_3$ (28 mg) the signals at 4.41 were replaced doublets at 4.83 and 5.9 (J = 9 Hz). *Anal.* calcd. for $C_{23}H_{23}NO_2S_3$: C 62.58, H 5.25, N 3.17, S 21.75; found: C 63.28, H 5.55, N 3.20, S 21.55.

Desulfurization of **8** with Raney nickel (12 g) of **2***b* (500 mg) gave 2-benzyl-*N*-phenylsuccinimide (230 mg), mp and mixture mp 128–130°C. Attempted desulfurization of **8** with vintage (4 year old: stored in alcohol) Raney nickel in absolute alcohol (22 h, reflux) gave material which was separated by tlc. Aside from the adduct **8** recovered there was obtained the isomer **11**, mp 225–227°C (119 mg); ^{1}Hmr ($CHCl_3$) δ: 1.46, 1.55, 1.60, 166 (all s, all 3H), 3.34 (d, J = 19 Hz), 4.11 (d, J = 19 Hz); uv $\lambda_{max}(CH_2Cl_2)$: 298 nm (2500). *Anal.* calcd. for $C_{23}H_{23}NO_2S_3$: C 62.58, H 5.25, N 3.17, S 21.75; found: C 62.62, H 5.13, N 3.27, S 21.72.

Reaction of 2b with N-n-Propylmaleimide

The thione (100 mg) and the imide (50 mg) in benzene (30 ml) gave, in 30 min at room temperature, the adduct **9**, 128 mg (79%), mp 213–214°C; ν_{max}: 1724 cm^{-1}; ^{1}Hmr ($CDCl_3$): 0.4 (t, J = 4 Hz), 0.9–1.3 (m, 2H), 1.26, 1.46, 1.53, 1.70 (s, 3H each), 3.20 (t, 2H J = 4 Hz), 4.20 (s, 2H). *Anal.* calcd. for $C_{20}H_{25}NO_2S_3$: C 58.96, H 6.18, N 3.44, S 23.56; found: C 58.96, H 6.09, N 3.41, S 23.79.

Reaction of 2b with Acetylene Dicarboxylic Acid, Dimethyl Ester

The thione (100 mg) and ester (0.5 ml) in benzene (10 ml), after 12 h at room temperature gave, after tlc, the adduct **10** (67%, 95 mg) from methanol, mp 94–97°C; $\lambda_{max}(CHCl_3)$: 1721; ^{1}Hmr ($CDCl_3$): 1.4 (s, 6H), 1.54 (s, 6H), 3.94 (s, 3H), 3.96 (s, 3H). The spectrum was scanned (CS_2) from +30 to −110°. The separation of the resolved peaks at low temperature was 160 ± 15 Hz. *Anal.* calcd. for $C_{19}H_{22}O_4S_3$: C 55.61, H 5.40, S 23.39; found: C 56.10, H 5.70, S 22.88.

The ester was desulfurized to give dimethyl 2-benzylsuccinate by Raney nickel (15%).

Determination of Molar Extraction Coefficients

A Gilford spectrophotometer 240 was used with a double set of thermospacers with matched 1.0 and 10.0 cm cells at 24.5 ± 0.2°C. For variable temperature measurements a Kryothermat Haake model KT-62 constant temperature circulator with a cell in a Cary 14 was used. The temperature was measured with an iron–constantan thermocouple. One hour minimum was allowed for equilibration.

Thionorbornanone

This was prepared by the method described by Greidanus (50) for adamantanethione. The final product was distilled at 55–60°C/0.02 Torr. *Exact Mass* calcd. for $C_7H_{10}S$: 126.0503; found (ms): 126.0509.

Thionorbornane-d_2

Sodium metal (0.5 g) was added to a solution of methanol-*d* (10 g) and was stirred until all the metal had dissolved. Norcamphor (1 g) was added and the mixture refluxed 24 h. Deuterated water was added and the mixture extracted with ether. The residue, after removal of the solvent, was reacted with phosphorus pentasulfide to give the thione. The ratio $d_0:d_1:d_2$ was 1.1:1.0:1.9.

Diels–Alder Addition with Thiones

The following procedure is typical. A solution of a **2***a* (420 mg, 1.67 mmol) and adamantanethione (320 mg; 2.0 mmol) in benzene (20 ml) was kept in the dark at room temperature for 24 h. After removal of solvent the residue was separated by preparative tlc (light petroleum (60–80°C) – methylene chloride, 1:1). The adduct thus obtained, if containing two stereoisomers, was further separated by tlc using cyclohexane (4 cycles).

In the present instance one isomer (higher R_f) was obtained as a white solid (280 mg; 51%), mp 188–189°C (from ethyl acetate); λ_{max}: 298 (sh, 1500). *Anal.* calcd. for $C_{22}H_{26}S_4$: C 63.15, H 6.26, S 30.59; found: C 63.10, H 6.18, S 30.33.

The slower-moving material (109 mg, 22%) had mp 145–146°C (from ethyl acetate). *Anal.* calcd. for $C_{22}H_{26}S_4$: C 63.15, H 6.26, S 30.59; found: C 63.64, H 6.41, S 30.19.

With thionorbornanone the faster-moving compound was obtained in 63.5% yield (132 mg) from 120 mg of **2***a*. It had mp 143–145°C (from ethyl acetate); $\lambda_{max}(CH_2Cl_2)$: 300 (sh, 1200). *Anal.* calcd. for $C_{19}H_{22}S_4$: C 60.31, H 5.86; found: C 60.41, H 6.10. The slower-moving component could not be induced to crystallize.

With cyclohexanethione (51) **2***a* (92 mg) gave 79 mg (64%) of faster-moving material, mp 106–108°C; $\lambda_{max}(CH_2Cl_2)$: 296 (sh, 2750); ms (*m/e*): 366 (M^+, 9%) 252 (20), 184 (100), 120 (35), 114 (25), 67 (35). *Anal.* calcd. for $C_{18}H_{22}S_4$: C 59.01, H 6.05, S 35.94; found: C 59.45, H 5.74, S 35.08. The slower-moving isomer (31 mg, 25%) had mp 143–145°C; $\lambda_{max}(CH_2Cl_2)$: 270 (sh, 4000); ms (*m/e*): 366 (M^+, 10%) 252 (25), 184 (100), 120 (35), 114 (23), 67 (35). *Anal.* calcd. for $C_{18}H_{22}S_4$: C 59.01, H 6.05, S 35.94; found: C 59.21, H 6.01, S 35.02.

With cyclohexanethione and **2***b* a single adduct was obtained in 88% yield (250 mg), mp 142–144°C (from ethyl acetate); $\lambda_{max}(CH_2Cl_2)$: 270 (sh, 2000). *Anal.* calcd for $C_{19}H_{26}S_4$: C 59.67, H 6.85, S 33.47; found: C 60.20, H 7.01, S 33.08.

With adamantanethione and thionorbornanone the colour of **2***b* was discharged in 3 days. On evaporation of the solvent at 35°C reversion to the starting material occurred. With thiocamphor there was no reaction.

The Reaction of 21 and Adamantanethione

This was carried out as in the previous examples. Two isomers were obtained in about 25% total yield based on 28 mg thione. The ratio of isomers, based on singlets at 6.27 and 6.29 in the ^{1}Hmr spectrum, was 3:1. One isomer was separated by tlc and had mp 136–138°C (from ethyl acetate); δ: 4.5 (m, 2H), 6.29 (s, 1H); ms (*m/e*): 278 (M^+, 6%) 210 (80), 166 (100), 145 (60), 91 (45), 77 (20), 67 (25). *Anal.* calcd. for $C_{24}H_{28}S_4$: C 64.85, H 6.35; found: C 64.99, H 6.35.

Hydrolysis of 19 with Mercuric Oxide

A cooled solution of **19** (20 mg) in tetrahydrofuran (5 ml) was added to a stirred mixture of red mercuric oxide (2 mol equiv.) and boron trifluoride etherate (2 mol equiv.) in aqueous tetrahydrofuran (15%, 15 ml). After 30 min, diethyl ether was added and the precipitate filtered off.

The filtrate was washed (saturated $NaHCO_3$, saturated aqueous NaCl). The residue, after evaporation of the solvent gave adamantanethione, mp 258–259°C (3 mg, 50%), characterized as the 2,4-dinitrophenylhydrazone,

mp 219–220°C (52). The original precipitate from the hydrolysis was stirred with concentrated hydrochloric acid for 3 h at room temperature. The white solid (10 mg) was collected and washed with water. This compound was soluble in K_2CO_3 solution and had the same R_f as thiosalicylic acid mercaptide chloride on an Eastman 6060 sheet using isopropanol–triethylamine–water (2:1:1), mp 270°C (sub.); ν_{max}(KBr): 3400 (b), 1680 (vs), 1470, 1422, 1300, 1270, 745 cm^{-1}.

Isomerization of ***19***

A solution of each pure isomer (12 mg in 0.3 ml $CDCl_3$) was examined in an nmr tube over 48 h at the end of which both isomers were present in ~1:1 ratio. The reaction was also performed in a sealed nmr tube in benzene at 80°C.

Exchange Experiments

A solution of the **2***a*–norbornanethione adduct (12 mg) and deuterated norbornanethione (10 mg) in benzene (2 ml) was sealed under N_2 in a glass tube and kept at 80°C for 4 days. Under these conditions the thione itself is stable except for isomerization. The reaction mixture which contained only the starting materials was separated. The M, $M+1$, $M+2$ ratios were 100:24:17. The undeuterated material was 100:24:21. The minimum exchange detectable was estimated to be ~4%. Similar experiments using *N*-phenylmaleimide instead of the thionorbornanone at room temperature or in benzene solution at 80°C gave no trace of the adduct **4**.

1. R. Gompper. Angew. Chem. Int. Ed. **8**, 312 (1969).
2. H. U. Wagner and R. Gompper. *In* The chemistry of the quinoid compounds. *Edited by* S. Patai. Wiley-Interscience, New York, NY. 1974.
3. M. P. Cava and A. A. Deana. J. Am. Chem. Soc. **81**, 4266 (1959).
4. R. K. Smalley and H. Suschitzky. Tetrahedron Lett. 3465 (1966).
5. O. L. Chapman and C. L. McIntosh. Chem. Commun. 383 (1971).
6. K. Salisbury. Tetrahedron Lett. 737 (1971).
7. M. P. Cava and R. L. Shirley. J. Am. Chem. Soc. **82**, 654 (1960).
8. C. M. Bowes, D. F. Montecalvo, and F. Sondheimer. Tetrahedron Lett. 3181 (1973).
9. M. S. Ao and E. M. Burgess. J. Am. Chem. Soc. **93**, 5298 (1971).
10. R. S. Becker and J. M. Michl. J. Am. Chem. Soc. **88**, 5931 (1966).
11. P. de Mayo and H. Y. Ng. Tetrahedron Lett. 1561 (1973).
12. R. Okazaki, K. Okawa, and N. Inamoto. Chem. Commun. 843 (1971).
13. R. Okazaki, F. Ishii, K. Ozawa, and N. Inamoto. Chem. Lett. 9 (1972).
14. P. de Mayo and H. Y. Ng. J. Chem. Soc. Chem. Commun. 877 (1974).
15. R. Okazaki and N. Inamoto. Chem. Lett. 1439 (1974).
16. H. O. House, H. Babad, R. B. Toothill, and A. W. Noltes. J. Org. Chem. **27**, 4141 (1962).
17. H. S. Gutowsky and C. H. Holm. J. Chem. Phys. **25**, 1228 (1956).
18. I. C. Calder and P. J. Garratt. J. Chem. Soc. 660 (1967).
19. P. Metzner and J. Vialle. Bull. Soc. Chim. Fr. 3138 (1972).
20. M. J. Janssen. Rec. Trav. Chim. **79**, 464 (1960).
21. K. J. Rosengren. Acta Chem. Scand. **16**, 2284 (1962).
22. D. S. L. Blackwell, C. C. Liao, R. O. Loutfy, P. de Mayo, and S. Paszyc. Mol. Photochem. **4**, 171 (1972).
23. R. S. Becker and J. Kolc. J. Phys. Chem. **72**, 997 (1968).
24. A. I. Scott. Interpretation of the ultraviolet spectra of natural products. Pergamon Press, Oxford, England. 1964.
25. C. C. Price and S. Oae. Sulfur bonding. Ronald Press, New York, NY. 1962.
26. C. R. Flynn and J. Michl. J. Am. Chem. Soc. **96**, 3280 (1974).
27. P. Ahern, T. Navratil, and K. Vaughan. Tetrahedron Lett. 4547 (1973).
28. O. L. Chapman and C. L. McIntosh. J. Am. Chem. Soc. **92**, 7001 (1970).
29. A. O. Pedersen, S. O. Lawesson, P. D. Klemmensen, and J. Kolc. Tetrahedron, **26**, 1157 (1970).
30. J. S. Bornstein, J. E. Shields, and J. H. Supple. J. Org. Chem. **32**, 1499 (1967).
31. M. S. Chanhan, F. D. Dean, D. Matkin, and M. L. Robinson. J. Chem. Soc. Perkin Trans. I, 120 (1973).
32. G. Catterall. J. Chem. Soc. Chem. Commun. 41 (1974).
33. W. J. Bailey and R. A. Raylouny. J. Org. Chem. **27**, 3476 (1962).
34. C. G. Krespan. J. Am. Chem. Soc. **83**, 3434 (1961).
35. R. Okazaki, K. Sunagawa, M. Kotera, and N. Inamoto. Tetrahedron Lett. 3815 (1976).
36. W. J. Middleton. J. Org. Chem. **30**, 1390 (1965).
37. A. Schönberg and B. König. Tetrahedron Lett. 3361 (1965).
38. A. Ohno, Y. Ohnishi, and G. Tsuchihashi. Tetrahedron, **25**, 871 (1969).
39. G. Jacqmin, J. Nasielski, G. Billy, and M. Remy. Tetrahedron Lett. 3655 (1973).
40. D. B. J. Easton, D. Leaver, and T. J. Rawlings. J. Chem. Soc. Perkin Trans. I, 41 (1972).
41. J. C. Meslin and H. Quiniou. Bull. Soc. Chim. Fr. 2517 (1972).
42. M. Bard, J. C. Meslin, and H. Quiniou. J. Chem. Soc. Chem. Commun. 672 (1973).
43. R. Okazaki, A. Kitamura, and N. Inamoto. J. Chem. Soc. Chem. Commun. 257 (1975).
44. F. Ishii, R. Okazaki, and N. Inamoto. Tetrahedron Lett. 4283 (1976).
45. R. C. Arnold, A. P. Lien, and R. M. Alm. J. Am. Chem. Soc. **72**, 731 (1950).
46. J. V. Keussler and W. Lüttke. Z. Electrochem. **63**, 614 (1959).
47. L. F. Fieser and M. Fieser. Reagents for organic synthesis. J. Wiley, New York, NY. 1967.
48. L. Legrand, Y. Mollier, and N. Lozac'h. Bull. Soc. Chim. Fr. 327 (1953).
49. A. Arcoria, H. Lumbroso, and R. Passerini. Bull. Soc. Chim. Fr. 754 (1959).
50. J. W. Greidanus. Can. J. Chem. **48**, 3530 (1970).
51. D. C. Sen. J. Indian Chem. Soc. **13**, 268 (1936).
52. P. von R. Schleyer and R. D. Nicholas. J. Am. Chem. Soc. **83**, 182 (1961).

TABLE 4. Molar absorbance variation with concentration

Compound	Concentration (M as monomer)	Absorbance	Solvent
2*a*	2.48×10^{-4}	652	$CHCl_3$
	1.61×10^{-4}	832	
	3.22×10^{-5}	1675	
	1.28×10^{-5}	2427	
	5.36×10^{-6}	3060	
	2.14×10^{-6}	4020	
	8.58×10^{-7}	4730	
	5.14×10^{-8}	5440	
	0.00 (extrap.)	5456 ± 150	
2*b*	2.56×10^{-4}	2269	Benzene
	1.53×10^{-4}	2690	
	9.21×10^{-5}	3105	
	2.76×10^{-5}	4097	
	5.53×10^{-6}	4705	
	0.00 (extrap.)	5004 ± 100	
2*b*	2.47×10^{-4}	4635	$CHCl_3$
	9.88×10^{-5}	4959	
	4.94×10^{-5}	5101	
	2.47×10^{-5}	5180	
	0.00 (extrap.)	5254 ± 100	

Appendix

Optical Measurements

The absorption spectrum of the dimer of **2***a* could be obtained at low temperature in ether (no absorption at 585 nm). The spectrum of the pure monomer could not be obtained, but peaks at 346 and 585 and a shoulder at 260 nm were found in a wide variety of solvents and are attributed to the monomer. The molar extinctions for the monomers were obtained, at 585 nm, by the method of Keussler and Lüttke (46) used for nitroso compound association.

The dimer dissociation constant is

$$[1] \qquad K_c = C_m^2/C_d$$

where C_m and C_d are the molar concentrations. C, the total molar concentration is $C_m + 2C_d$. If α is the monomeric fraction

$$[2] \qquad K_c = 2C\alpha^2/(1-\alpha)$$

The effective molar absorbancy, ε, is given by

$$[3] \qquad \varepsilon = \alpha\varepsilon_m + \frac{(1-\alpha)\varepsilon_d}{2}$$

where ε_m and ε_d are the absorption extinctions for monomer and dimer. But since at 585 nm, the monitoring wavelength, $\varepsilon_d = 0$, then $\alpha = \varepsilon/\varepsilon_m$ where eq. 2 becomes

$$[4] \qquad K_c = \frac{2C(\varepsilon/\varepsilon_m)^2}{1-(\varepsilon/\varepsilon_m)}$$

or

$$[5] \qquad (\varepsilon_m - \varepsilon)K_c = 2C\varepsilon^2/\varepsilon_m$$

or

$$[6] \qquad \varepsilon = K\varepsilon^2 C + \varepsilon_m$$

where

$$K = -2/(\varepsilon_m K_c)$$

Hence ε_m at 585 nm could be obtained by plotting ε vs. $\varepsilon^2 C$ and extrapolating to zero concentration. The molar extinction coefficients were determined in benzene and chloroform at 24–25°C. The results are given in Table 4. The low degree of dissociation of **2***a* in benzene precluded the obtention of a reliable value. It was assumed that the same ratio held in this solvent as did for **2***a*/**2***b* in chloroform, giving $\varepsilon = 5250$.

Migration of hydroxyl in secondary systems during solvolysis in acid solution[1]

ROBERT C. CATHCART, JOHN W. BOVENKAMP, AND ROBERT Y. MOIR
Department of Chemistry, Queen's University, Kingston, Ont., Canada K7L 3N6
AND
ROBERT A. B. BANNARD AND ALFRED A. CASSELMAN
Defence Research Establishment Ottawa, Ottawa, Ont., Canada K1A 0Z4

Received October 1, 1976[2]

ROBERT C. CATHCART, JOHN W. BOVENKAMP, ROBERT Y. MOIR, ROBERT A. B. BANNARD, and ALFRED A. CASSELMAN. Can. J. Chem. **55**, 3774 (1977).

A system of compounds has been prepared which is well adapted for displaying the role of *trans* vicinal, secondary hydroxyl in solvolysis. On methanolysis in acid solution, compounds **5**, **7***a*, and **8***a* all gave the same products, **9***a* and **10***a*, and in practically the same proportions, suggesting that at least one intermediate was common to all three reactions. These intermediates were such that **7***a* and **8***a* were not interconverted during the solvolysis, a fact in support of **6** as a common intermediate. Several alternative explanations were shown to be untenable, largely by taking advantage of the remarkable differences between hydroxyl and methoxyl. The work provides the most decisive evidence available for the covalent participation of hydroxyl as a neighbor group in the solvolysis of secondary systems, and contributes also to the study of the reverse reaction, the acid-catalyzed scission of epoxides.

ROBERT C. CATHCART, JOHN W. BOVENKAMP, ROBERT Y. MOIR, ROBERT A. B. BANNARD, et ALFRED A. CASSELMAN. Can. J. Chem. **55**, 3774 (1977).

On prépare un système de composés lequel est bien adapté pour mettre en évidence le rôle du groupe hydroxyle *trans* vicinal dans des réactions de solvolyse. La méthanolyse en solution acide des composés **5**, **7***a* et **8***a* conduit aux mêmes produits **9***a* et **10***a* et essentiellement aux mêmes proportions suggérant qu'au moins un intermédiaire est commun aux trois réactions. Ces intermédiaires sont de telle sorte que **7***a* et **8***a* ne sont pas convertis l'un dans l'autre pendant la solvolyse, ce qui est en accord avec l'hypothèse que **6** soit un intermédiaire commun. Plusieurs interprétations ne peuvent être soutenues, essentiellement parce qu'elles ne tiennent pas compte des grandes différences entre un groupe hydroxyle et méthoxyle. Ce travail apporte l'évidence très nette de la participation covalente du groupe hydroxyle comme groupe voisin dans la solvolyse de systèmes secondaires et contribut aussi à l'étude de la réaction inverse, la scission catalysée par un acide des époxydes.

[Traduit par le journal]

The role of neighboring hydroxyl in the solvolysis of secondary systems is still not clear. As shown later, there seems little prospect of demonstrating its participation by isolating or trapping a bridged intermediate under the acid conditions needed to prevent confusion with another reaction.[3] Less direct and less compelling evidence has often been offered. The observed steric course for solvolysis has been said to be evidence for covalent participation by hydroxyl (1), but it is obviously not sufficient, since the similar methoxyl group has the same configura-

[1]Most of the work is taken from the Ph.D. Theses (Queen's University) by (*a*) J. W. Bovenkamp, November, 1973, and (*b*) R. C. Cathcart, September, 1975.

[2]Revision received June 22, 1977.

[3]Oxides have been demonstrated as intermediates (or by-products) in the solvolysis of tertiary systems (3*c*, 3*d*, 5), but as the authors point out, the nonacidic conditions were such that at least some participation by the conjugate anion of hydroxyl was to be suspected. Aside from this difficulty there would be little doubt that hydroxyl is capable of migration in tertiary systems, since in them even methoxyl has been observed to migrate (3*a*, 3*b*). A secondary oxide, *cis*-cyclooctene oxide, has been isolated (8*c*) in the solvolysis of the corresponding *trans*-bromohydrin with acetic acid and sodium acetate. One may infer from the contexts (8) that the authors suspected oxyanion intervention in this system also. Although epoxides have been demonstrated as 'intermediate by-products' in the acid-catalyzed pinacolic rearrangement of tetraphenylethylene glycols (13*a*), solvolysis of the similar 1,1,2-triphenyl-2-bromoethanol does not proceed through the epoxide (13*b*). Epoxides have been established as intermediates in one route for ketone–ketone rearrangements (14), and recently Ganem (15) has described the attack of *trans*-hydroxyl groups upon neighboring chloronium ions, in certain addition reactions of olefins.

tion-holding effect (2), and is, at least in secondary systems (3) at the vicinal position (4), known to show little or no covalent participation (5–7).[4] Rate enhancement by *trans, vicinal* hydroxyl is of course stronger evidence for participation (1, 8–11) but the fact that the net effect of hydroxyl is nearly always inhibitory (1) may be sufficient to indicate the difficulty of dissecting the effect due to covalent participation from the inductive effects, from steric effects, and from effects due to 'internal solvation' or 'ion-dipole stabilization' (1, 5, 8, 10–12). Ingenious but even less direct methods for detecting participation have been suggested (1, 8–11).

Much the most convincing practically available evidence would be the demonstration of hydroxyl wandering during the solvolysis of secondary systems. The only example[3] known to us is that reported by Dicko and Bodot (11) who showed that hydrolysis of **1** gave **2**, and pointed out that the most probable explanation is that the reaction proceeds through the intermediate **3**. Two reservations are possible. The reaction may not be typical, since **3** cannot be formed from the locked structure **1** through the usual chair-like conformations (16). Secondly, it is possible that the route may have lain partly through **4**, which is much more reactive than **1**, and hence difficult to detect. The suggested possible conversion of **1** to **4**, by way of a doubly-bridged transition state, or by anion migration within an intermediate ion-pair, is analogous to mechanisms most familiar in the equilibration of locked diaxial and diequatorial dibromides, or in the self-racemization of 2-norbornyl brosylate (17), but frequently proposed for other neighbor groups, including hydroxyl (13, 14, 18–21).

A more decisive approach is obtained by focusing attention upon the oxide **5** and its protonated form **6**. If a protonated epoxide is an intermediate in solvolysis with neighboring *trans* hydroxyl, then **6** is the common intermediate in the solvolyses of **5**, **7***a*, and **8***a*. In previous work we had shown (22) that the acid-catalyzed methanolysis of **5** gave two products, **9***a* and **10***a*, the former predominating greatly. If a protonated epoxide is an intermediate, *then methanolysis of the oxide* **5** *and of each of the tosylates* **7***a and* **8***a should give both* **9***a and* **10***a*. In this paper it is shown that not only does the indicated migration

[4]The strongest evidence for this lies in the success of Haworth's method for determining the structures of carbohydrates (7).

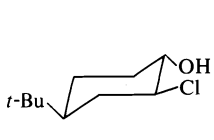

1

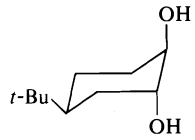

2

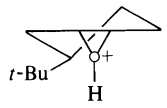

3

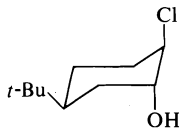

4

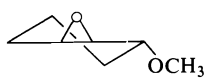

5

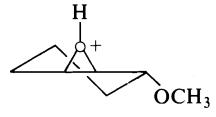

6

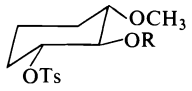

7*a* R = H
7*b* R = Ac

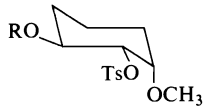

8*a* R = H
8*b* R = Ac

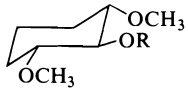

9*a* R = H
9*b* R = Ac

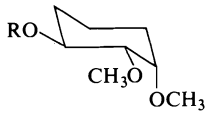

10*a* R = H
10*b* R = Ac

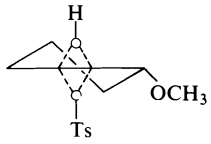

11

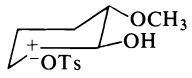

12

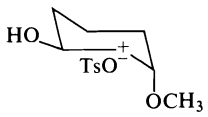

13

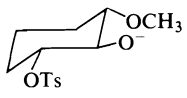

14

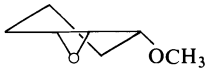

15

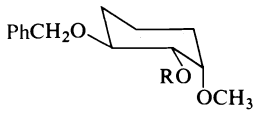

16*a* R = H
16*b* R = Ts
16*c* R = CH_3

TABLE 1. Gas–liquid chromatographic analyses of solvolyses products[a] (see footnote 14)

Run No.[b]	Substrate	Reaction time	Relative area[c,d,e] of peak due to **10***b* (%)
i	Tosylate **7***a*	200 h	3.4(0.07)[d]
ii	Tosylate **7***a*	300 h	3.3(0.07)
viii	Tosylate **8***a*	500 h	4.2(0.19)
ix	Tosylate **8***a*	587 h	4.0(0.19)
—	Epoxide **5**	(few min.)	4.0(0.10)

[a]As their acetates.
[b]For referral to Experimental and to Table 2.
[c]As 100 (area due to **10***b*)/(total area due to **9***b* and **10***b*).
[d]Figures in parentheses are standard deviations of the mean for 5 or 6 successive injections of the sample into the chromatograph.
[e]Calibration of the method (isolation, acetylation, and injection) was done in the previous work (see footnote 1*a*) using the same detector, integrator, column packing, and nearly the same ratio **9***b*/**10***b*, but with somewhat different conditions of temperature and loading. Applying this calibration to the present results gives, for a peak area ratio of 4.0:96.0, a molar ratio of 6.5:93.5, and for a peak area ratio of 3.4:96.6, a molar ratio of 5.6:94.4. As a check, extrapolation of the value obtained in previous work (see footnote 1*a*) for the solvolysis of **5** in aqueous methanolic perchloric acid at 2.4°C gives the molar ratio 7.6:92.4 at 64°C under the condition $\Delta^2 S^{\ddagger} = 0$ (unpublished data). These corrections, unnecessary for the discussion of Scheme 1, are useful for Scheme 2 and for later papers.

of hydroxyl occur in the solvolyses of both **7***a* and **8***a*, but in addition, **7***a* and **8***a* each give the products **9***a* and **10***a* in approximately the same ratio as that observed for the oxide **5** (Table 1). When considered together with the kinetic evidence obtained by others (1, 8–11), these results seem to us to be direct evidence for the covalent participation of hydroxyl. This view has also been strengthened by an experimental investigation of the likely alternatives.

Methanolysis, catalyzed by perchloric acid at 64°C, was complete in a few minutes when the oxide **5** was the substrate, but was only about three-fourths complete after 200 h when the tosylate **7***a* was used, and was less than half complete in 500 h when **8***a* was used. Clearly, if Scheme 1 represents the mechanism there is no

Tosylate $\rightleftharpoons$ Protonated epoxide (**6**) $\rightarrow$ Products

(**9***a* and **10***a*)

SCHEME 1

prospect of verification by direct isolation of the epoxide. Mousseron, Bodot, and co-workers (10, 11) have used the reversibility of the first step in Scheme 1 (that is, the *external return* of the nucleophile) in gaining indirect evidence for the presence of intermediates analogous to **6**. Under the conditions of our solvolyses, this reversibility was suppressed, along with the consequent rearrangement pathway (22, 23):

$$\mathbf{7}a \xleftarrow{\text{TsOH}} \text{Protonated epoxide } \mathbf{6} \xrightarrow{\text{TsOH}} \mathbf{8}a$$

Indeed, no such rearrangement of either tosylate was observed during the solvolyses. By attempting to fit reaction profiles to the sheaf of possibilities crudely represented by **11** (as transition state or intermediate, with varying degrees of concertedness, and with **12** and **13** as possible co-intermediates), one can therefore rule out the possibility of any important contribution from all those pathways,[5,6] alternative to Scheme 1, which involve the internal migration of tosylate:

Product $\leftarrow$ Tosylate **7***a* $\rightleftharpoons$ Tosylate **8***a* $\rightarrow$ Product

Another set of pathways alternative to Scheme 1 involve the anions[3] of the tosylates (e.g. **14**). Previous workers have felt that these routes could not have been important in their rate studies, on the basis of the curious method used to follow the kinetics of the reactions.[7] In spite

[5]If routes involving internal **7***a* $\rightleftharpoons$ **8***a* are a main contributor to the solvolyses, then the energy barrier between **7***a* and **8***a* must at the same time be very low, in order to allow each of them to give the same product ratio, and very high, in order to prevent appreciable equilibration between **7***a* and **8***a*; this is impossible of course. Competition between these routes and Scheme 1 gives rise to the following system, which as a limit problem can be solved exactly:

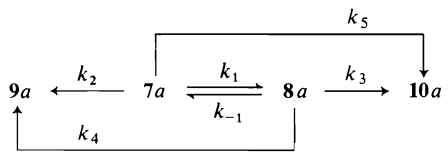

In the solvolyses, no rearranged tosylate was seen, though it would have been detected with certainty if it had amounted to as little as 3% of the reactant. Consequently the maximum possible intervention of **7***a* $\rightleftharpoons$ **8***a*, consistent with this, in the solvolysis of **7***a* can easily be shown to have entirely negligible results. However, calculations also show that the maximum intervention of **7***a* $\rightleftharpoons$ **8***a* in the solvolysis of **8***a* might cause its observed half-life to be as much as 20% lower than that appropriate to Scheme 1 alone; there might also be a very small effect upon the product ratio obtained from **8***a* (see footnote 14). There is of course no positive evidence for any of these effects.

[6]Corresponding internal migrations in other systems (13, 14, 17–21) have been supposed to occur easily. By far the simplest explanation for the failure of the migration in the present system lies in the preferred production of the protonated epoxide **6** either directly from **7***a* or **8***a*, or by a very rapid internal attack of hydroxyl upon its neighboring centre in **12** or **13**.

[7]The reactions were allowed to begin at neutrality and proceed to high acidity at the end, being followed by titration of aliquots. 'Straight line' plots have been reported both for derivatives of ethane (24) and of cycloalkanes (1, 8).

TABLE 2. Methanolysis of the tosylates **7***a* and **8***a*

Run No.[a]	Procedure[b]	Tosylate	Acid[c] added (ml)	Time of heating (h)	Crude[d] yield (mg)	P/R[e] ratio	Yield[d] of crude acetate (mg)
i	*a*	**7***a*	5.00	200	91	(5)	108
ii	*a*	**7***a*	5.00	300	86	(12)[f]	142
iii	*b*	**7***a*	0.5	125	75[g]	1.1	
iv	*b*	**7***a*	2.5	125	72[g]	1.2	
v	*b*	**7***a*	0.5	200	78	3.0	
vi	*b*	**7***a*	2.5	200	79	2.4	43[d]
vii[h]	—	**7***a*	0.00	95	—	0.7?[h]	
viii	*a*	**8***a*	5.00	500	138[i]	0.44	140
ix	*a*	**8***a*	5.00	587	139[i]	0.56[j]	102
x	*b*	**8***a*	0.5	500	90	0.42	
xi	*b*	**8***a*	2.5	500	82	—	

[a]For reference to text and Table 1.
[b]See Experimental.
[c]Of 0.100 *M* methanolic perchloric acid. Total volume in procedure *a* was about 30 ml, and in *b* 15.00 ml at room temperature.
[d]From 0.20 g tosylate in procedure *a*, 0.10 g in *b*.
[e]The molar ratio **9***a*/tosylate, estimated by nmr, the less accurate values in parentheses, the ratio **9***a*/**8***a* being much more accurately estimated than **9***a*/**7***a*. From these ratios the apparent solvolysis rate constants *k* may be calculated (i.e. $k_3 = k_4 = 0$, Scheme 2) and compared with the titration value (see Experimental). The effect of nonzero values of k_3 and k_4 is to move the values of *k* for **7***a* and **8***a* closer together and closer to the ratio observed for the alkali-catalyzed reactions of the corresponding chlorohydrins. See Footnote 1*a*.
[f]Interrupted at 95 h, this run gave a P/R value of 0.89.
[g]Semi-solid products.
[h]Titration experiment; see Experimental.
[i]Almost completely solid products.
[j]Interrupted at 95 h, this run showed (nmr) little reaction.

of certain difficulties in the argument,[8] we believe their conclusions to be correct. To guard against the possible intervention of the anions of the tosylates, all but one of our solvolyses were conducted at high acidities, and in addition it was shown that large changes in the acidity had little effect upon the rates of solvolysis of **7***a* and **8***a* (see Table 2). Finally, a tedious but obvious analysis showed that at least in the present system, the small or zero effect on the rates, caused by changes in the acidity, could not be due to approximately offsetting catalysis by both acid and base.

Direct intervention of free anions such as **14** was therefore negligible. Nevertheless the great driving force available in routes involving the alkoxide anions such as **14** (5) would appear to be partially realized through general base catalysis by the solvent, that is, by hydrogen bonding through the hydrogen of the hydroxyl group. No other explanation seems possible for two facts brought to light by the careful work of Roberts and co-workers (1, 8). The ability of hydroxyl to

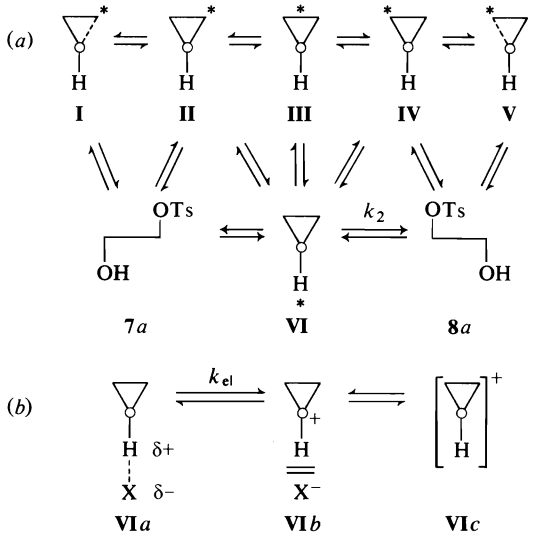

FIG. 1. Condensed illustration of ion-pair (and other) routes in acid-catalyzed epoxide scissions and in solvolyses with neighboring *trans*-hydroxyl. (*a*) The asterisks are meant to show the approximate position of the counterion, when appropriate. All possible routes are not shown, and in particular the separate positions, in the sequences, of the three subspecies are not shown. (*b*) Illustration of the three subspecies for one of the above ions; each of **I**–**V** is also supposed to possess forms *a*, *b*, and *c*, that is, tight, solvent-separated, and 'free', respectively. In particular, the process k_{el} connecting **VI***a* and **VI***b* has been supposed (31) to be rate-determining in certain epoxide scissions.

[8]Curvature has been reported in other plots, and attributed either to salt effects (10*c*), or to the reversibility of Scheme 1 (10). However, the much larger curvature due to base catalysis could not have been missed, and when rate constants are available both for the neutral and the base-catalyzed reaction (24, 25), it is clear that the latter is negligible at low p*H*.

participate was found to be very sensitive to the solvent used; paradoxically, the more nucleophilic the solvent, the more effective was the (nucleophilic) participation by hydroxyl. Alternative explanations[9] (based on the then current view that unaided solvolysis was nearly limiting in mechanism (26)) showed difficulty in coping with the second fact: while hydroxyl's effect on the rate was very sensitive to the solvent used, that of the very similar methoxyl was uniformly inhibiting in all solvents. These results are obviously in agreement with methoxyl's inability to respond to general base catalysis.[10]

The remaining alternatives to Scheme 1 are presented in condensed form in Fig. 1, which also serves to unite the chemistry of our previous (22, 23, 27, 28) and following (e.g. 29) papers on the mechanisms of epoxide scission and formation. Discussion of the ion-pair mechanisms (26, 30) is made easier by the recent application of these concepts to oxide scissions by Wylde and his co-workers (31, 32[11]). Figure 1 is essentially their scheme, considerably modified to allow for the two secondary centres and for the necessary stereochemical prescriptions.

Each of the species **I** to **VI** in Fig. 1(*a*) appears in the three forms of tight ion-pairs, solvent separated pairs, and 'free' (i.e., solvated) ions, as indicated for **VI** in Fig. 1(*b*). For example, **12** is a conventionalized drawing of **I***a*, **13** of **V***a*, and the free ions **II***c*, **III***c*, **IV***c*, and **VI***c* are identical to each other. The asterisks in Fig. 1(*a*) are meant to show the approximate positions of the counter ions; in all but **VI** they are *trans* to hydroxyl and (according to current theory) block their attached, but perhaps not their vicinal, positions from direct attack by outside reagents. Since the vicinal hydroxyl is a very effective block on the other side, the chemistry of oxide-related ion-pairs may actually be much simpler than those of more conventional ions, in spite of the following additional complexities. The number of ions is almost doubled because of the two possible counter-ions, and nearly doubled again on account of the stereochemistry about oxygen (33). According to the general theory, any of the 54 ionic species of Fig. 1 may lie either in a linear sequence of reactions, in a side-branch, or in loops; any of the species may be a true intermediate, a transition state, or simply an approximation to an ordinary point on the reaction profile, and which of these it is may vary with the environment. For example, the scission of **VI***c* to form **8***a* might proceed either through a route in which **IV***a* is a true intermediate, or by the process labelled k_2 in Fig. 1(*a*), in which **IV***a* might represent fairly well a transition state with some charge separation, that is, the 'borderline S_N2' favored in the past by most authors (32, 34). Only experiment can distinguish among the possibilities. Obviously, even when the experiments are brilliantly designed and executed, as by Shiner and co-workers (35), the rate constants (23 in the model (35) on which Wylde (31) based his mechanisms) will be hopelessly underdetermined, and the results will have to be interpreted with a long series of assumptions, a general procedure obviously subject to astronomically large errors (35, 36).

Fortunately, large simplifications are possible. In the first place, there is no need to consider other ionic species, such as those with 'free' hydroxyl groups (more open than **I** and **V**). This is shown by the strong configuration-holding effect of hydroxyl (1, 8, 11, 37, and present work). Confirmation is afforded (*a*) by the relative rates of solvolysis reported here for **7***a* and **8***a*, the inhibition of the rate caused by neighboring methoxyl being much less than that observed

[9]Some holders of the view that hydroxyl does not participate have been driven to the clearly wrong conclusion that the solvent acts by altering the inductive effect of hydroxyl (cf. methoxyl). Better versions of this view can be constructed, and operational distinctions between these versions and Scheme 1 can again be had in the contrast between methoxyl and hydroxyl as neighbors. Whereas methoxyl binds tightly enough to the reaction centre to enforce retention of configuration, during solvolysis (1, 2), it seems to have no rate-enhancing effect (5, 6) and, in secondary systems, it does not wander (7). Hydroxyl, besides possessing the same steric control and a modest rate-enhancing effect, clearly wanders with ease, passing through a symmetrical structure, which whether a true intermediate or not, clearly has hydroxyl covalently bonded to both reactive centres.

[10]Titration experiments, showing how easily **7***a* was converted to **5**, via **14**, by base, made it imperative to show that the base used in the isolation of the products had no appreciable effect on the results. This was done in two ways. The more reactive tosylate (**7***a*) was recovered unchanged when subjected to the process of isolation. The results obtained were unaffected either by the use of a weaker base or by subjecting the isolated product of an interrupted solvolysis to further reaction. Further formation of **9***a* and **10***a* during isolation was in any case impossible, since the half-life of **5** under more severe conditions of base catalysis is known to be about 30 h (27).

[11]Reference expressing a cautionary or contradictory opinion.

by Roberts *et al.* (8) in the absence of hydroxyl; (*b*) by the rate-enhancing effects observed for neighboring hydroxyl by Roberts (1); and (*c*) by the agreement of product distributions from **7***a* and **8***a* with that formerly seen for the epoxide **5** (28). Unlike the situation in the phenonium ion series (26*b*), the solvent in this system is unable to compete with the neighbor group for initial possession of the reactive centre. Finally, the fact that if ions with 'free' hydroxyl did exist, their only fate was collapse to more bonded systems, was shown by the failure of a careful search for reaction products typical of the 'free-hydroxyl' structures (i.e. from attack by solvent or by neighboring methoxyl). This search was conducted through proton magnetic resonance spectroscopy of both crude and acetylated reaction products, and by the more sensitive method of gas–liquid chromatography, the latter supported[1a] by the previous study of the retention times of a large number of related compounds (38).

A second simplification results from the clear requirement (Table 1) that there must be at least one common intermediate in the solvolyses of **7***a* and **8***a*. Intervention of any of the 34 ions **II**, **III**, **IV**, or **VI** as intermediate would be the equivalent of Scheme 1, and the only remaining alternative to Scheme 1 is that **I** and **V** exist as pairs of intermediates, with the more symmetrical systems **II**, **III**, **IV**, and **VI** existing at most as mere transition states. This alternative can only be held with the further postulate that **I** and **V** must be in rapid equilibrium with each other, in order to explain the fact that **7***a* and **8***a* give essentially the same product mixture. At first sight, therefore, the alternatives of Scheme 1 or of the rapidly interchanging pairs **I** and **V** would seem to involve the same difficulty as that in the controversy over nonclassical ions (26, 30).[12] However, in all probability, the corresponding ion (**6**) is both stable and easily reached. The results of Table 1 show that solvolysis of the epoxide **5** must involve intermediates which, except possibly for the counter-ion, are the same[13] as those involved in the solvolysis of the tosylates. The non-classical ion of hydroxyl-assisted solvolysis (e.g. **6**) is therefore merely the conjugate acid of a well-known and stable compound (e.g. **5**); furthermore there is some physical evidence (33, 42) for the existence of stable cyclic oxonium ions. There are excellent reasons (22, 28, 32) for the almost universal acceptance (34) of the cyclic protonated epoxide as an intermediate in epoxide scissions. Even those (43; see also 31) who look upon analogues of **I** and **V** as reactive intermediates postulate analogues of **6** as the structures for the protonated epoxides present in considerable amounts in their solutions.

While Scheme 1 is thus undoubtedly the main mechanism of solvolysis of the tosylates, intermediates such as **I** and **V** might still occur as small notches in the reaction profile. Partition at such intermediates might make them detectable. Indeed the results of Table 1 suggest that an intermediate resembling **I** may be a reality, since relatively more **9***a* is formed from **7***a* than from **5** or from **8***a*. According to the very careful standardization of the analytical method (29) in the previous work,[1a] the difference in product ratios (Table 1) is significant. Two constant errors, nearly always ignored in previous work, fortunately proved to be small in the present system. The first error, due to a possible side reaction, was estimated as mentioned previously,[5,14] while the second error (due to differential survival of the products under sol-

$$\text{Tosylate} \begin{cases} \xrightarrow{k_1} \mathbf{9}a \xrightarrow{k_3} \text{Further products} & k = k_1 + k_2 \\ \xrightarrow{k_2} \mathbf{10}a \xrightarrow{k_4} \text{Further products} & \Delta k = k_3 - k_4 \end{cases}$$

SCHEME 2

[12]Serious difficulties arise in the alternative hypothesis. Two of these will be clear to the reader from the initial considerations given already (see footnotes 6 and 9). A third stems from the hypothesis, not necessarily true (21, but see 39) though deeply embedded in recent interpretations of ion-pair theory (35*a*, 40; however, see 35*b*), that substrate (e.g. **7***a*) and intermediate (e.g. **I***a*) are in rapid pre-equilibrium. With the further requirement (in the alternative mechanism) that **I** and **V** are also approximately in equilibrium, **7***a* and **8***a* should interconvert, but they do not. Obviously, the easiest and most convincing escape from this dilemma lies in postulating the existence of a third intermediate, **6**.

[13]The agreement in product ratios between epoxide and tosylates (Table 1) cannot be a coincidence. Whether **9***a* and **10***a* are formed from a rapidly equilibrating pair such as **I** and **V**, or by direct attacks upon a protonated epoxide (e.g. **6**), the product ratios will be governed by Curtin–Hammett theory (28, 41). Diagrams will quickly show that both conformational and polar effects would result in much less **10***a* being formed from **I** and **V** than directly from **6**, and that it is impossible to escape the conclusion that oxide and tosylate must solvolyze in the same way.

volysis conditions) was determined by calculations based on the approximate mechanism shown in Scheme 2.[14] It was easily shown that the methods used previously for the purpose lacked the necessary accuracy. Neither correction had any important effect upon the results of Table 1.[14] Theory would also lead one to expect that structure **I** would be more important than structure **V** (Fig. 1). The polar effect of neighboring methoxyl is unfavorable to **V**, and the conformational effects favorable to **I**, each in comparison with routes involving pure S_N2. Nevertheless, in view of the difficulty of the experiments, it seems safer to say that while there may be some evidence for partition at an intermediate resembling **I**, at least three-fourths of **7***a* must solvolyze by Scheme 1. The proportions for **5** and for **8***a* must be even larger. These estimates are satisfactory for certain further applications of Curtin–Hammett theory.

The work was made possible by a new synthesis devised for **8***a* and **10***a*. Formerly **10***a* had been obtained (22) in very low yields after a difficult separation, from the direct methanolysis of **5**. In the new route, treatment of the stereoisomeric epoxide **15** with benzyl alcohol gave as the only product compound **16***a*, which was easily converted either to its tosylate **16***b* or its methyl ether **16***c*. Catalytic hydrogenation of **16***b* gave **8***a*, the benzyl group being removed in preference to the somewhat sensitive tosyl group (23). Hydrolysis of **16***c* with concentrated hydrochloric acid gave a good overall yield of **10***a*.

Experimental

Infrared spectra were recorded on a Perkin-Elmer model 180 grating spectrometer. Proton magnetic resonance spectra (nmr) were determined on a calibrated Brüker HFX 60 spectrometer or on a Varian T 60 spectrometer; some were repeated at the Canadian 220 MHz Centre. The apparent chemical shifts are reported in parts per million downfield from an internal TMS standard for solutions in chloroform-*d* and the apparent coupling patterns and constants (Hz) are taken directly from the spectra. Elemental analyses were performed by Alfred Bernhardt Microanalytisches Laboratorium, Bonn, liquid samples being homogeneous to glc. Analyses by glc were carried out with a Jarrell Ash Model 700 analytical gas chromatograph fitted with a strontium-90 detector and a recorder fitted with a mechanical integrator. The column, aluminum tubing of 6.35 mm outside diameter and length 366 cm, was packed for half its length with 4% diethylene glycol sebacate, and for the other half with 4% silicone fluid QF 1, both on Chromosorb G (70–80 mesh, acid washed, and treated with DMCS (Chromatographic Specialties, Brockville, Ontario). Melting points marked (p) are corrected (44); others were determined on a Koffler hotstage. *Trans*- and *cis*-3-methoxycyclohexene oxides (**5** and **15**) (22, 23) were shown by glc to be at least 99.5% pure.

*(±)-(1RS,2RS,3RS)-1-O-Benzyl-3-O-methyl-1,2,3-cyclohexanetriol (**16***a*)

Sodium (0.55 g) was dissolved in benzyl alcohol (6 ml) and the mixture was added to a solution of *cis*-3-methoxycyclohexene oxide (**15**) (5.15 g) in benzyl alcohol (40 ml, previously fractionated), heated on a steam bath for 70 h, and then neutralized with acetic acid. Most of the benzyl alcohol was then distilled away (0.04 Torr) through a micro-fractionating column. The organic product was separated from the residue by solution in ether, the ether was removed, and the oil distilled in a Späth apparatus. The fraction distilling at 58–115°C (bath temperature) and 0.004 Torr, yield 7.81 g, slowly crystallized on standing. One washing with light petroleum (bp 30–60°C) and one recrystallization from this solvent yielded 5.72 g of crystals (61%); mp 51.6–52.5°C (p). Five more recrystallizations gave the analytical sample; mp 53.4–53.6°C (p). *Anal.* calcd. for $C_{14}H_{20}O_3$: C 71.16, H 8.53; found: C 71.15, 71.21, H 8.82, 8.85.

The *p-nitrobenzoate*, after one recrystallization from ethanol, had mp 81.8–82.2°C (p); nmr (T-60): 8.22 (aromatic, 4H), 7.24 (aromatic, 5H, narrow), 5.34 (geminal to nitrobenzoxyl, 1H, dd, *J*, 2.7 and 6.6), 4.60 (benzyl methylene, 2H, sharp), 3.80 (2H, overlapped), 3.34 (methyl). *Anal.* calcd. for $C_{21}H_{23}O_6N$: C 65.44, H 6.02, N 3.63; found: C 65.28, 65.34, H 6.01, 5.97, N 3.64, 3.72.

*(±)-(1RS,2RS,3RS)-1-O-Benzyl-2,3-di-O-methyl-1,2,3-cyclohexanetriol (**16***c*)

The general method is that of Diner *et al.* (45). The benzyl methyl ether (**16***a*) (2.86 g, made as just above) was dissolved in dry 1,2-dimethoxyethane (7.06 ml) together with methyl iodide (2.00 g). While the mixture was magnetically stirred, sodium hydride (0.376 g) was added in 5 equal portions during 30 min. Another portion (0.3 ml) of methyl iodide was added, the stirring was continued for 2.5 h, and the volume was then reduced to one-third by distillation. Dry ether (10 ml) was added to the residue, and the insoluble salts were washed with more ether. Evaporation of the dried ether filtrates gave a light yellow oil which after redistillation in the Späth apparatus was colorless, b.p. 96–97°C, bath temperature at 0.005 Torr; yield 2.56 g (85%). Comparison by nmr with starting material showed the disappearance of hydroxyl, and the appearance of a second methoxyl at 3.46 ppm. *Anal.*

[14]From the product-survival experiments, Δk was found to be 0.00023 h^{-1}. Calculations based on Scheme 2 showed that correction for product losses required only very small changes in the relative peak areas of Table 1 (to 3.2 from **7***a*, and to 3.8 from **8***a*). These experiments also showed that **9***a* and **10***a* were not equilibrated during the solvolysis. Further correction to remove the effects of intervention of routes involving internal **7***a* $\rightleftharpoons$ **8***a* (see footnote 5) was shown to require the value from **8***a* to move from that from **7***a* by an amount proportional to their difference. For example, the difference given in Table 1 implies that the corrected value for **8***a* should be moved upward by an amount not greater than 0.1, i.e. at the most from 3.8 to 3.9.

calcd. for $C_{15}H_{22}O_3$: C 71.97, H 8.86; found: C 71.94, 71.87, H 8.85, 8.86.

*(±)-(1RS,2SR,3RS)-1,2-Di-O-methyl-1,2,3-cyclohexanetriol (**10a**) (22), and Derivatives*

The benzyl dimethyl ether (**16c**) (2.91 g, made as just above) was stirred 1.5 h with concentrated hydrochloric acid (34 ml) at 95°C. The mixture was neutralized with sodium bicarbonate and then repeatedly extracted with ether (10 × 30 ml). Careful fractionation of the oil recovered from the dried ethereal solution yielded 0.953 g (51%) of a colorless oily product (b.p. 72–106°C, bath temperature at 14 Torr in the Späth apparatus). Analysis by glc showed the absence of starting material and the presence of an unknown impurity (0.2–0.4%); nmr (T-60): 3.81 (overlapped, 2H, b), 3.38 (methyl), 3.46 (methyl), 2.97 (geminal to 2-methoxyl, 1H, dd, *J*, 2.8, 9.1), 2.92 (hydroxyl, 1H, exchanged with D_2O). *Anal.* calcd. for $C_8H_{16}O_3$: C 59.96, H 10.07; found: C 59.82, 59.88, H 9.91, 9.96.

Unlike its isomers, the *p-nitrobenzoate* of **10***a* formed with difficulty. The alcohol (0.160 g) and *p*-nitrobenzoyl chloride (0.1865 g) were heated on the steam bath for 3 h with dry pyridine (0.8 ml). Water (0.25 ml) and a little potassium carbonate were added, and the complete solution subjected to Späth distillation. A solid subliming at 90°C bath temperature (20 Torr) was discarded, and a colorless oil, 0.053 g, was collected, b.p. 175°C at 0.6 Torr; nmr (T-60): 8.29 (aromatic, 4H, narrow), 5.44 (geminal to *p*-nitrobenzoxyl, 1H, m), 3.74 (overlapped, 2H), 3.53 (methyl), 3.46 (methyl). Two recrystallizations of the oil from aqueous ethanol gave crystals, 18 mg, mp 70.0–70.8°C (p) (lit. (22) 71.2–71.8°C).

The *acetate* (**10***b*) was obtained as a pure oil (glc), bp 77.5–78°C, bath temperature at 15 Torr, after two careful fractionations in the Späth apparatus; nmr (220 MHz): 5.13 (geminal to acetoxyl, 1H, dt, *J* 4.05 and 7.35), 3.33 (geminal to 2-methoxyl, 1H, dd, *J* 2.90 and 7.25), 3.62 (geminal to 1-methoxyl, 1H, m), 3.37 and 3.45 (methoxyls), 2.05 (acetate methyl). *Anal.* calcd. for $C_{10}H_{18}O_4$: C 59.39, H, 8.97; found: C 59.24, 59.40, H 8.85, 8.85.

*(±)-(1RS,2RS,3RS)-1-O-Benzyl-3-O-methyl-2-O-p-toluenesulfonyl-1,2,3-cyclohexanetriol (**16b**)*

Crude crystalline benzyl methyl ether **16***a* (6.35 g, made as above from the *cis*-oxide) was warmed 1 h on the steam bath with dry pyridine (15 ml) and *p*-toluenesulfonyl chloride (6.3 g). When this mixture was poured into water, an oil separated which crystallized when stirred. After being recovered, washed with water, extracted with light petroleum (bp 60–110°C) and then recrystallized from this solvent, the product was obtained in a yield of 5.8 g (36%). Its mp (88–92°C) was raised to 91–92°C by two further recrystallizations; nmr (Brüker): 7.50 (aromatic, 4H, A_2B_2), 7.25 (aromatic, 5H, narrow), 4.56 (geminal to tosyloxyl, 1H, dd, *J* 2.6 and 7.2), 4.46 (benzyl methylene, 2H, narrow), 3.75 (2H, hump), 3.20 (methoxyl), 2.38 (aromatic methyl). *Anal.* calcd. for $C_{21}H_{26}O_5S$: C 64.59, H 6.71; found: C 64.68, H 6.84.

*(±)-(1RS,2SR,3RS)-1-O-Methyl-2-O-p-toluenesulfonyl-1,2,3-cyclohexanetriol (**8a**) (the '2-Tosylate')*

The benzyl ether (**16***b*) (2.90 g, mp 91–92°C, prepared as above) was shaken with absolute ethanol (200 ml) and palladized charcoal (0.13 g, 10%) for 28 h under a hydrogen pressure of 70 psi. The crude product (2.49 g) gave 2.11 g (95%) of feathery needles, mp 88.5–89°C, after two recrystallizations from ethanol – light petroleum (1:1); nmr (Brüker): 7.43 (aromatic, 4H, A_2B_2), 4.37 (geminal to tosyloxyl, 1H, dd, *J* 8.8 and 2.8), 3.98 (geminal to methoxyl, 1H, m), 3.65 (geminal to hydroxyl, 1H, hump), 3.20 (methoxyl), 2.43 (aromatic methyl). *Anal.* calcd. for $C_{14}H_{20}O_5S$: C 55.98, H 6.71; found: C 56.04, H 6.75.

The *acetate* (**8***b*) was obtained in 92% yield as colorless, feathery needles, mp 86.5–88°C. One recrystallization from light petroleum gave the analytical sample, whose mp (88.5–89.5°C) was similar to that of its isomer (**7***b*) (23). The nmr (Brüker) was distinctive: 7.57 (aromatic, 4H, A_2B_2), 5.1 (geminal to acetoxyl, 1H, broad m), 4.56 (geminal to tosyloxyl, 1H, dd, *J* 9.0 and 2.8), 3.92 (geminal to methoxyl, 1H, b m), 3.29 (methoxyl), 2.45 (aromatic methyl), 1.82 (acetate methyl). *Anal.* calcd. for $C_{16}H_{22}O_6S$: C 56.12, H 6.48; found: C 56.08, H 6.57.

*1,3-Di-O-methyl-r-1,t-2,c-3-cyclohexanetriol (**9a**) and its Acetate (**9b**)*

The alcohol (**9***a*) (22, 23, 27), available in the pure state (glc) from previous work, was recognizable in the nmr chiefly by its very sharp single methoxyl peak, appearing in spectra of the pure compound at 3.39 (T-60) or 3.40 (cal. A-60), but in spectra of synthetic mixtures with its isomer (**10***a*) overlapping the downfield methoxyl of the latter. Also characteristic were single small peaks on either side of the methoxyl peak, representing the outlying members of the triplet due to hydrogen geminal to hydroxyl. Its *acetate* (**9***b*), mp 68.5–68.9°C (p) (lit. (23) 65.5–66.5°C), pure to glc, had a much more distinctive spectrum (220 MHz): 4.85 (geminal to acetoxyl, 1H, t, *J* 9.35), 3.33 (methoxyls, 6H), 3.14 (geminal to methoxyl, 2H, m), 2.10 (acetate methyl). *Anal.* calcd. for $C_{10}H_{18}O_4$: C 59.39, H 8.97; found: C 59.28, 59.40, H 8.67, 8.80.

*(±)-(1RS,2SR,3SR)-1-O-Methyl-3-O-p-toluenesulfonyl-1,2,3-cyclohexanetriol (**7a**) (the '1-Tosylate')*

This compound, made from the *trans*-oxide (**5**) as previously described (23), was obtained after two recrystallizations as colorless, poorly formed crystals, mp 129–130.5°C (lit. (23) 127.5–129°C); nmr (Brüker): 7.61 (aromatic, 4H, A_2B_2), 4.37 (geminal to tosyloxyl, 1H, unresolved m), 3.48 (geminal to hydroxyl, 1H, t, *J* 9.0), 3.40 (methoxyl), 3.0 (geminal to methoxyl, 1H, hump), 2.85 (hydroxyl, 1H, sharp), 2.44 (aromatic methyl). The *acetate* (**7***b*) of this tosylate, made as previously described (23), showed in particular a characteristic triplet at 5.10 ($J = 9$).

Solvolysis Experiments

Each solvolysis was carried out in a flask equipped with reflux condenser and drying tube, and heated under reflux, with stirring, in an oil bath. In particular, the five experiments reported in Table 1 were performed together under exactly the same conditions, using reagents from the same sources.

*Methanolysis of the trans-Oxide (**5**)*

The oxide (0.128 g) was dissolved in dry methanol (10.0 ml) and heated to reflux. In another flask, 0.1 *M* methanolic perchloric acid (made by dilution of 72% perchloric acid with dry methanol, thus introducing a trace of water) (5.00 ml) and methanol (15.0 ml) were heated to reflux, the hot oxide solution rapidly added, and the combined solutions heated an additional 5 min

under reflux. Most of the solvent was removed by rotary evaporation at room temperature, and then ethyl ether (15.0 ml) and an excess of sodium carbonate were added. The mixture was filtered, the solid washed with ether, and the combined ether extracts were evaporated to yield a pale yellow oil (0.243 g), the analysis of which is described later.

Methanolysis of the Tosylates (7a and 8a)

Procedure (a)—The tosylate (0.20 g) was dissolved in reagent methanol (25.0 ml) and 0.1 *M* methanolic perchloric acid (5.00 ml) was added. The mixture was heated for the prescribed time (Table 2), and the crude solvolysis product isolated as described for the product from the oxide, but usually with further purification (i.e. separation from small amounts of polymers) by extraction into light petroleum. Results are given in Table 2.

Procedure (b)—The tosylate (0.10 g) was treated with 0.1 *M* methanolic perchloric acid (amounts in Table 2), the volume made up to 15.0 ml with dry methanol, and the mixture was heated for the times shown in Table 2. After being cooled, the mixture was treated with sodium acetate in amounts equivalent to the *added* acid (0.050–0.25 mmol), the volume was reduced to about 1 ml by rotary evaporation under reduced pressure, the residue was treated with sodium carbonate (0.05 or 0.25 mmol), the rest of the solvent removed, and the residue extracted with light petroleum. Evaporation of the extract gave the pale yellow solvolysis product in yields given in Table 2.

Nuclear Magnetic Resonance Spectra of the Crude Solvolysis Products

The spectra from the reaction products of **7***a* were, except in the proportions of the contributors, all remarkably alike, and could be regarded as due to mixtures of the 1,3-dimethyl ether (**9***a*) and the unreacted '1-tosylate' (**7***a*), the latter distinguished by its aryl, aryl methyl, and methoxyl peaks, the last 0.05 ppm upfield from that of **9***a*. A total absence of signals near 3.78 showed that even moderate amounts of other likely compounds (rearranged reactant or product or diols from hydrolysis) could not be present, as their signals from H geminal to hydroxyl were absent. A more sensitive test for the absence of the rearranged tosylate (**8***a*) lay in the absence of its methoxyl signal in a clear region of the spectrum, so that as little as 2–3% would have been seen. The signal envelope from the methylene ring protons had the shape characteristic of 1,2,3-tri-equatorially substituted cyclohexanes. Not all impurities would have been as apparent as the rearranged tosylate; for example no certain sign of the 1,2-dimethyl ether (**10***a*), known to be present to the extent of about 5% (see glc results), could be detected. In synthetic mixtures of **10***a* with **9***a*, one of the methoxyl signals of **10***a* was resolved from that of its neighbor, but at much less than one-third the apparent area at equal concentrations. P/R ratios (see Table 2) were usually calculated by comparing the area of the aryl methyl signal with that from the 'methoxyl' region, the error being larger than that for **8***a*.

The spectra of the solvolyses products from **8***a* (runs *viii–x*, Table 2) were extremely similar to each other, and to that of a synthetic mixture containing '1-tosylate' (**7***a*) (3 mg), '2-tosylate' (**8***a*) (30 mg), and the 1,3-dimethyl ether (**9***a*) (6.5 mg). In the spectrum of the synthetic mixture *no trace of signal due to the 1-tosylate could be discerned*, showing the need for the separation described below. However, because the methoxyl peak of the '2-tosylate' (**8***a*) was well separated from those of the ethers **7***a* and **9***a*, it *was* possible to say that the lack of a second methoxyl peak from the ethers ruled out the presence of any considerable amounts of the direct product of solvolysis (**10***a*). This peak separation also allowed much more accurate determinations of the P/R ratios than for **7***a*.

Separation of Reactant and Product; Demonstration of Rearrangement in the Latter and Its Lack in the Former

The crude product from the methanolysis of the '2-tosylate' (**8***a*) from run *x* (Table 2) was dissolved in ethyl acetate (3 ml), and extracted twice with water (10 ml portions). The material from the organic layer was much enriched in the '2-tosylate', as shown by nmr, and two more similar extractions left in the organic layer a material whose nmr spectrum (compared to that of authentic **8***a*) showed it to be almost pure '2 tosylate', containing a trace of **9***a*. Comparison with a spectrum of **7***a*, and with a spectrum of a mixture of '2-tosylate' (30 mg) and '1-tosylate' (**7***a*) (3 mg), showed that as little as 2–3% of **7***a* would have been detectable in the spectrum of the extract, but none was seen.

The aqueous extracts were evaporated to small volume, taken up in ethyl acetate, dried over magnesium sulphate, and again evaporated to leave a residue (13 mg) whose nmr spectrum consisted mainly of a very large methoxyl signal shown to belong to **9***a* by comparison with the very small residual peaks of **8***a* that remained. This residue was heated at 110°C for 14 h with acetic anhydride (0.5 ml), the excess anhydride was destroyed with ethanol, and the solvents were removed. The residue (11 mg) showed in nmr the pattern decisive for **9***b* (23): absence of aromatic peaks; 4.85 (t, $J = 9.5$), 3.34 (methoxyl singlet), 2.04 (half the area of the methoxyl peak; acetate methyl, singlet). Fairly large shoulders on the methyl and methoxy peaks, as well as a small signal near the triplet, pointed to the presence of impurities. Distillation of the sample in the Späth apparatus (at 60°C *in vacuo*) gave a distillate (5 mg) which partly solidified. Its nmr spectrum showed that the feature near the triplet had been removed and the shoulders (due to unacetylated material **9***a*) much reduced, in comparison with the peaks due to **9***b*.

Solvolysis with No Added Acid; Rate by Titration

The '1-tosylate' (**7***a*) (0.201 g) was heated under reflux 95 h with dry methanol (30.0 ml). After being cooled, the solution was made up to 50.00 ml with methanol, and 10 ml aliquots were titrated with standard aqueous sodium hydroxide (0.01000 *N*, Fisher Scientific Certified). Equal amounts of bromthymol blue and phenol red were used as the mixed indicator (46), giving a sharp color change. The alkali consumptions (6.66 and 6.62 ml) in duplicates suggested the reaction had proceeded to 49.7% completion. (The titration procedure was checked by using *p*-toluenesulphonic acid as substrate.) However, the nmr spectrum of the product differed from those of runs *i–vi* (Table 2) in having a large water peak and in showing the presence of an impurity, likely *p*-toluenesulphonic acid, which made the regular procedure for determining P/R inapplicable. It was altered as follows. Quite satisfactory linear plots were obtained, from the other runs, for two different peak height ratios versus P/R; use of these gave

a P/R ratio for the present experiment of 0.7. The titrations had to be done with care; end-point colors faded quickly, and if pursued, the unknowns (or a test sample of pure reactant **7***a*) consumed, within a few minutes at room temperature, an amount of alkali equal to 100% reaction of **7***a* (showing its rapid conversion to **5**). This was the *only* result if bromthymol blue was used as the sole indicator, the color change then being insufficiently sharp.

Stability of the Reactant during Isolation

The '1-tosylate' (**7***a*) (76 mg) was dissolved in methanolic perchloric acid (2.5 ml of 0.1 *M* made up to 15.0 ml with methanol). The mixture was then worked up immediately according to procedure *a*, care being taken to make the conditions slightly more rigorous than those of the solvolysis. The product (76.5 mg), nearly all crystalline, showed in its nmr spectrum only peaks due to the reactant, except for extremely small peaks due to solvent impurities well downfield from the peak due to H geminal to tosyloxy in **7***a*.

Relative Stability of the Reaction Products towards the Conditions of Solvolysis

The nmr spectra were recorded for separate solutions of **9***a* (76.0 mg) and **10***a* (76.65 mg), each in $CDCl_3$ (1 ml). The two solutions were then mixed and made up to a total volume of 10 ml in chloroform; the resulting solution was accurately divided in two, and the solvent removed from each portion. One half was kept for reference; the other half of the mixture was treated with methanol (31.25 ml) and 0.100 *M* methanolic perchloric acid (6.25 ml of a solution made by adding 250 ml of methanol and 3.49 g of 72% aqueous perchloric acid). After the solution had been heated under reflux for 210 h, it was treated with an excess of solid sodium bicarbonate and then filtered. Solvent was removed on the rotary evaporator near room temperature, the residue was stirred with ether (50 ml) and magnesium sulfate, and the solid and solvent successively removed once more to yield a clear oil (67 mg, or 88%). (In a preliminary trial, using procedure *a*, the yield was 102%.) Infrared spectra of product and reference samples showed a band centered near 1713 cm^{-1} in both. In a preliminary trial, this band was considerably more intense for the product, but in the main experiment, using a different instrument, the reference sample gave the more intense band. In none of the spectra was there any band near 2700 cm^{-1} (aldehyde C—H stretch, to be expected from rearrangement products). The nmr spectra for $CDCl_3$ solutions of product and reference samples (taken with forward and backward scans, and with or without prior treatment of the solutions with D_2O) were alike, except for minor variations in the hydroxyl peak and in the degree of deuteration. Especially notable was the survival of the prominent quartet, upfield from the methoxyl signals, due to **10***a*, and of the outer parts of the triplet due to **9***a*, straddling the methoxyl signals. (In the preliminary, 200 h trial these bands were especially well resolved, and similar in product and reference). Methoxyl peak height ratios (5 trials each) were found to be 2.51 ± 0.03 for the product, and 2.53 ± 0.03 for the reference standard, in forward scans observed after treatment of the samples with D_2O. (It is noteworthy that this degree of accuracy is insufficient.) Each sample was then acetylated by the procedure described below, the reaction period being 4 h, and the excess acetic anhydride being removed with ethanol. The crude acetates so obtained (83 mg from the heated product, 92 mg from the reference standard) were then subjected to glc analysis, using the '4% DEGS' column and the instrument and conditions previously described (38), the analyses being performed in succession on the same day. The reference standard (5 trials) showed peak areas for **9***b*/**10***b* of 1.000:0.795 ± 0.002 and the reaction product (6 trials), 1.000:0.835 ± 0.002, respectively, the errors quoted being standard deviations of the means. The peaks due to **9***b* and **10***b* were identified by their retention times, 8.13 and 4.89 min, respectively, and also by successive additions of authentic **9***b* and **10***b*. The standard sample showed two small peaks, one at 9.95 min, 4% of the total integrated area, the other, smaller and broad, at approx 10.7 min, due to impurities in the original **9***a*; these persisted unchanged in position and relative area in the heated material, and likely represent diacetates, as suggested below. The glc of the heated sample showed two new peaks, one very small and broad, the other, 2% of the total integrated area (4 peaks) at 5.92 min. Successive injection of **9***a* and **10***a* showed that it was *not* due to unacetylated materials, so that the peaks identified as such in the solvolysis products (see below) probably also include a small proportion of this unknown by-product. The nmr spectra showed the expected three methoxyl and two acetate peaks, similar in product and reference standard.

Analyses by Gas–Liquid Chromatography of the Solvolysis Products

Lack of Interference by Tosylates

Trial acetylations of **7***a* and **8***a* under the conditions described below for the solvolysis products showed (nmr) no detectable products due to acetolysis; **7***a* was, however, incompletely acetylated. Heated at 180–200°C, compound **8***b* rapidly gave a blue-black tar. When the decomposition was followed at a lower temperature, no rearrangement products could be detected (nmr). A similar decomposition of **8***b* occurred at the injection port of the gas–liquid chromatograph, giving rise to small peaks reported below.

Acetylations of Samples prior to Analysis

The crude sample from solvolysis was heated overnight in an oil bath at 94°C with acetic anhydride (3 ml), the anhydride then being destroyed by the addition, and removal under reduced pressure, of successive portions (5 ml) of water, or in later runs, ethanol. Yield (from the solvolysis product of the oxide) 0.181 g or 90% based on the oxide **5**. Samples from the tosylates were treated in the same way, dark products being purified by re-extraction into light petroleum. Yields are given in Table 2. In one experiment (run *vi*, Table 2) the acetylated product from the solvolysis of **7***a* showed (nmr) the presence of **9***b* (the main product), **9***a*, and **7***a*; lines of **7***b*, if present, would have been hidden. Rearranged product **10***b* was possibly represented by one small peak on the side of a much larger acetate–methyl peak. An acetylated product from the solvolysis of the '2-tosylate' **8***a* (run *xi*, Table 2), gave a very well resolved spectrum (nmr) which showed, aside from aqueous acetic acid, the presence only of **8***b*, **9***a*, and **9***b*, the major product, thus confirming the lack of major side reactions already deduced from the spectra of unacetylated materials.

Gas–Liquid Chromatography

All analyses were performed under exactly the same conditions, an argon gas pressure of 40 psi and an oven temperature of 190°C being maintained. All five solvolysis samples were analyzed successively on the same day, and special care was taken to ensure that samples of the same size were taken for each injection, so that the highest peak on each chromatogram reached at least 80% of the maximum recorder reading. (Otherwise the nonlinearity of the detector had noticeable effects on the results for minor products.) Smaller peaks were read at 10× amplification. At least five injections were made for each sample. The principal results are given in Table 1, minor peaks being reported below. (In all cases, the peak due to **9***b* had at least 7 times the area of any other.)

The product from the trans-oxide (**5**) gave a peak due to the unacetylated alcohols (**9***a* and **10***a*), 8% of the total area, and two minor peaks, at 1.7 and 2.0 min, each less than 0.5% of the largest peak. The *product from the* '*1-tosylate*' **7***a* gave a peak due to **9***a* and **10***a*, 10% and 11% of the total area, and three small peaks, all less than 0.5% of the largest peak, at 1.6 min and at 6.0 and 8.4 min (diacetates). Preliminary trials were useful in showing that little or no bias was introduced by incomplete acetylation at the levels experienced. Successive acetylations of a sample gave products showing peak areas due to **9***a* of 15.0, 13.6, and 8% of the total, and area ratios 100 × (**10***b*)/(**9***b* + **10***b*) of 2.9, 3.0, and 3.3%, respectively. Much of this small bias appeared to be due to a slight tailing of the unacetylated material. The *product from the* '*2-tosylate*' **8***a* gave peaks due to unacetylated material, 3.2% of the total area in run *viii*, 7.4% in run *ix*. Two other peaks occurred at times characteristic of the decomposition of the '2-tosylate' or its acetate (**8***b*), that at 2.1 min amounting to 5.3% of the total in run *viii*, 7.4% in run *ix*, and that at 5.9 min, 3.5% in run *viii*, 11.3% in run *ix*. Two very small peaks, at 1.4 and 1.7 min, amounted to less than 0.5% of the largest peak in both runs.

Standard retention times were determined with purified samples under the conditions of the analyses: the acetate **9***b* of the 1,3-dimethyl ether, 4.7 min; its isomer **10***b*, 3.2 min; both unacetylated ethers (**9***a* and **10***a*), 2.6 min; from injection of the '2-tosylate' (**8***a*), 1.7 and 1.4 min (small peak); of its acetate (**8***b*), 2.1, 1.7 (small peak), and 5.9 min (trace). These times served not only for recognition of the peaks described in the analysis, but also by calibrating the times observed with those of the previous work[1a] (38) to eliminate from consideration the far wider range of possibilities previously studied.

Acknowledgements

The aid of the National Research Council of Canada, in financial support of the work, and in the grant of Scholarships to one of us (J.W.B.) is acknowledged. A special scholarship (to R.C.C.) from Queen's University is also acknowledged. We wish to thank Dr. A. Grey and the Canadian 220 MHz NMR Centre for obtaining the 220 MHz spectra mentioned.

1. D. D. ROBERTS. J. Org. Chem. **33**, 118 (1968).
2. S. WINSTEIN and R. B. HENDERSON. J. Am. Chem. Soc. **65**, 2196 (1943).
3. (*a*) S. WINSTEIN, C. R. LINDEGREN, and L. L. INGRAHAM. J. Am. Chem. Soc. **75**, 155 (1953); (*b*) S. WINSTEIN, E. ALLRED, R. HECK, and R. GLICK. Tetrahedron, **3**, 1 (1958); (*c*) S. WINSTEIN and L. L. INGRAHAM. J. Am. Chem. Soc. **74**, 1160 (1952); (*d*) S. WINSTEIN and L. GOODMAN. J. Am. Chem. Soc. **76**, 4368 (1954).
4. D. S. NOYCE and B. N. BASTIAN. J. Am. Chem. Soc. **32**, 1246 (1960).
5. S. WINSTEIN and E. GRUNWALD. J. Am. Chem. Soc. **70**, 830 (1948).
6. A. STREITWIESER. Solvolytic displacement reactions. McGraw-Hill, New York, NY. 1962.
7. (*a*) M. L. WOLFROM. Organic chemistry. Vol. 2. *Edited by* H. Gilman. Wiley and Sons, New York, NY. 1938. p. 1399; (*b*) H. HIBBERT, M. E. PLATT, and N. M. CARTER. J. Am. Chem. Soc. **51**, 3641 (1929).
8. (*a*) D. D. ROBERTS and W. HENDRICKSON. J. Org. Chem. **34**, 2415 (1969); (*b*) D. D. ROBERTS and J. G. TRAYNHAM. J. Org. Chem. **32**, 3177 (1967); (*c*) J. G. TRAYNHAM and J. SCHNELLER. J. Am. Chem. Soc. **87**, 2398 (1965).
9. H. S. GOLINKIN, D. M. PARBHOO, and R. E. ROBERTSON. Can. J. Chem. **48**, 1296 (1970).
10. (*a*) H. BODOT, J. JULLIEN, and M. MOUSSERON. C. R. Chim. Fr. 1101 (1958); 1110 (1958); (*b*) J. JULLIEN, M. MOUSSERON, and A. PEYRON. Bull. Soc. Chim. Fr. 1093 (1958); (*c*) G. BODENNEC, H. BODOT, and A. NATTAGHE. Bull. Soc. Chim. Fr. 876 (1967).
11. D. DICKO and H. BODOT. Tetrahedron, **27**, 1761 (1971).
12. (*a*) J. H. ROLSTON and K. YATES. J. Am. Chem. Soc. **91**, 1469 (1969); **91**, 1477 (1969); **91**, 1483 (1969); (*b*) J. A. PINCOCK and K. YATES. Can. J. Chem. **48**, 2944 (1970); (*c*) K. YATES and R. S. MCDONALD. J. Am. Chem. Soc. **93**, 6297 (1971); (*d*) K. YATES, R. S. MCDONALD, and S. A. SHAPIRO. J. Org. Chem. **38**, 2460 (1973).
13. (*a*) Y. POCKER and B. P. RONALD. J. Am. Chem. Soc. **92**, 3385 (1970); (*b*) J. F. LANE and D. R. WALTERS. J. Am. Chem. Soc. **73**, 4234 (1951).
14. (*a*) A. E. FAVORSKII and A. CHILINGAREN. Compt. Rend. **182**, 221 (1926); (*b*) A. FRY, M. EBERHARDT, and I. OOKUNI. J. Org. Chem. **25**, 1252 (1960); (*c*) T. E. ZALESSKAYA and T. B. REMIZOVA. J. Gen. Chem. USSR, **35**, 29 (1965).
15. B. GANEM. J. Am. Chem. Soc. **98**, 858 (1976).
16. S. J. ANGYAL. Chem. Ind. London, 1230 (1954).
17. (*a*) D. N. KIRK and M. P. HARTSHORN. Steroid reaction mechanisms. Elsevier, Amsterdam. 1968. p. 363; (*b*) P. L. BARILI, G. BELLUCCI, F. MAIRONI, A. MARSILI, and I. MORELLI. J. Chem. Soc. Perkin Trans. II, 58 (1972); (*c*) C. A. GROB and S. WINSTEIN. Helv. Chim. Acta, **35**, 782 (1952); (*d*) S. WINSTEIN and D. TRIFAN. J. Am. Chem. Soc. **74**, 1154 (1952).
18. R. M. NOYES and E. KORÖS. Acc. Chem. Res. **4**, 233 (1971).
19. N. C. G. CAMPBELL, D. M. MUIR, R. R. HILL, J. H. PARISH, R. M. SOUTHAM, and M. C. WHITING. J. Chem. Soc. B, 355 (1968).
20. K. OKAMOTO, S. SAITO, and H. SHINGU. Bull. Soc. Chem. Jpn. **43**, 3008 (1970).
21. H. L. GOERING and R. W. THIES. J. Am. Chem. Soc. **90**, 2967 (1968); **90**, 2968 (1968).
22. R. A. B. BANNARD, A. A. CASSELMAN, E. J.

LANGSTAFF, and R. Y. MOIR. Can. J. Chem. **46**, 35 (1968).
23. R. U. LEMIEUX, R. K. KULLNIG, and R. Y. MOIR. J. Am. Chem. Soc. **80**, 2237 (1958).
24. (*a*) C. L. MCCABE and J. C. WARNER. J. Am. Chem. Soc. **70**, 4031 (1948); (*b*) H. D. COWAN, C. L. MCCABE, and J. C. WARNER. J. Am. Chem. Soc. **72**, 1194 (1950).
25. A. A. FROST and R. G. PEARSON. Kinetics and mechanism. 2nd ed. J. Wiley and Sons, New York, NY. 1961. p. 301.
26. (*a*) S. R. HARTSHORN. Aliphatic nucleophilic substitution. Cambridge University Press, London. 1973; (*b*) C. J. LANCELOT, D. J. CRAM, and P. v. R. SCHLEYER. Carbonium ions. Vol. 3. *Edited by* G. A. Olah and P. v. R. Schleyer. Wiley and Sons, New York, NY. 1972. p. 1347.
27. J. A. MCRAE, R. Y. MOIR, J. W. HAYNES, and L. G. RIPLEY. J. Org. Chem. **17**, 1621 (1952).
28. E. J. LANGSTAFF, R. Y. MOIR, R. A. B. BANNARD, and A. A. CASSELMAN. Can. J. Chem. **46**, 3649 (1968).
29. J. W. BOVENKAMP, R. Y. MOIR, and R. A. B. BANNARD. Can. J. Chem. In press.
30. (*a*) D. J. RABER, J. A. HARRIS, and P. v. R. SCHLEYER. Ions and ion pairs in organic reactions. *Edited by* M. Szwarc. Wiley and Sons, New York, NY. 1974. Chapt. 2; (*b*) D. J. RABER and J. M. HARRIS. J. Chem. Educ. **49**, 60 (1972).
31. G. LAMATY, R. MALEQ, C. SELVE, A. SIVADE, and J. WYLDE. J. Chem. Soc. Perkin Trans. II, 1119 (1975).
32. J. BIGGS, N. B. CHAPMAN, and V. WRAY. J. Chem. Soc. B, 71 (1971).
33. J. B. LAMBERT and D. H. JOHNSON. J. Am. Chem. Soc. **90**, 1350 (1968).
34. (*a*) R. E. PARKER and N. S. ISAACS. Chem. Rev. **59**, 737 (1959); (*b*) J. G. BUCHANAN and H. Z. SABLE. Selective organic transformations. Vol. 2. *Edited by* B. S. Thyagaraja. Wiley and Sons, New York, NY. 1972. p. 1.
35. (*a*) V. J. SHINER. Isotope effects in chemical reactions. *Edited by* C. J. Collins and N. S. Bowman. ACS Monograph 167, Van Nostrand-Reinhold, New York, NY. 1970. p. 90; (*b*) K. HUMSKI, V. SENDIJAREIRĆ, and V. J. SHINER. J. Am. Chem. Soc. **95**, 7722 (1973).
36. F. HOYLE. Galaxies, nuclei, and quasars. Harper and Row, New York, NY. 1965. p. 85.
37. S. WINSTEIN and R. BUCKLES. J. Am. Chem. Soc. **64**, 2787 (1942).
38. J. W. BOVENKAMP, R. Y. MOIR, A. A. CASSELMAN, and R. A. B. BANNARD. J. Chromatogr. **118**, 345 (1976).
39. A. F. DIAZ, I. LAZDINS, and S. WINSTEIN. J. Am. Chem. Soc. **90**, 1904 (1968).
40. J. M. W. SCOTT. Can. J. Chem. **48**, 3807 (1970).
41. (*a*) E. L. ELIEL. Stereochemistry of carbon compounds. McGraw Hill, New York, NY. 1962; (*b*) D. Y. CURTIN. Rec. Chem. Prog. (Kresge-Hooker Sci. Lib.), **15**, 111 (1954).
42. G. A. OLAH and P. J. SZILAGYI. J. Org. Chem. **36**, 1121 (1971).
43. (*a*) J. G. PRITCHARD and F. A. LONG. J. Am. Chem. Soc. **78**, 2667 (1956); (*b*) J. G. PRITCHARD and I. A. SIDDIQUI. J. Chem. Soc. Perkin Trans. II, 452 (1973).
44. F. C. MERRIAM. Anal. Chem. **20**, 1246 (1948).
45. U. E. DINER, F. SWEET, and R. K. BROWN. Can. J. Chem. **44**, 1591 (1966).
46. M. PÁNKOVÁ, J. SICHER, M. TICHÝ, and M. C. WHITING. J. Chem. Soc. B, 365 (1968).

Reductive acylation of the aliphatic diazo function. *N*-(2-Diazo-3-oxoalkanoyl)-glycine esters as synthetic precursors of [γ-(aryloxy)threonyl]glycine derivatives[1]

JAMES H. LOOKER, JAMES W. CARPENTER, AND NORTON P. PEET[2]

Department of Chemistry, The University of Nebraska-Lincoln, Lincoln, NE 68588, U.S.A.

Received February 4, 1977

JAMES H. LOOKER, JAMES W. CARPENTER, and NORTON P. PEET. Can. J. Chem. **55**, 3786 (1977).

Catalytic reduction of several *N*[2-diazo-3-oxo-4-(aryloxy)alkanoyl]glycine esters gives *N*-[2-hydrazono-3-oxo-4-(aryloxy)alkanoyl]glycine esters. A pyrazine is obtained by catalytic reduction in ethanolic hydrogen chloride of *N*-[2-diazo-3-oxo-4-(phenoxy)butanoyl]glycine ethyl ester. A two-step procedure involving reductive acetylation or trifluoroacetylation of the diazo function, and subsequent borohydride reduction of the keto group yields the corresponding acylamino alcohol derivatives.

JAMES H. LOOKER, JAMES W. CARPENTER et NORTON P. PEET. Can. J. Chem. **55**, 3786 (1977).

La réduction catalytique de plusieurs esters *N*-[diazo-2 oxo-3(aryloxy) alkanoyl-4] glycine conduit aux esters *N*-[hydrazono-2 oxo-3(aryloxy) alkanoyl-4] glycine. Une pyrazine est obtenue par réduction catalytique dans une solution éthanolique de chlorure d'hydrogène de l'ester éthylique *N*-[diazo-2 oxo-3(phénoxy) butanoyl-4] glycine. Une technique comportant deux étapes et impliquant une acétylation ou trifluoroacétylation par réduction de la fonction diazo et une réduction subséquente par le borohydrure du groupe carbonyle conduit aux amino-alcools acylés.

[Traduit par le journal]

Introduction

4-Phenoxyl derivatives of *N*-(2-diazo-3-oxobutanoyl)glycine esters are readily available from the interaction of *N*-(diazoacetyl)glycine ethyl ester (DGEE) with the appropriate acid chloride (1). Reduction under suitable conditions would lead to novel [γ-(aryloxy)threonyl]glycine derivatives. Previous studies of aroyldiazoacetic esters have shown that catalytic reduction over palladium–charcoal (2*a*) or platinum-on-carbon (2*b*, 2*c*) yields arylserines. Chemical reduction of aroyldiazoacetic esters gave nitrogen-free products. Because catalytic reduction procedures do not lead to threonylglycine derivatives (sequel), chemical reduction procedures were reexamined. Of particular interest were the observations of Albertson and co-workers (3*a*), who devised a procedure for the reductive acetylation of α-oximinoacetoacetic ester, of Regitz (3*b*), who effected the reductive acetylation of phenylbenzoylketazine, and of Pfister and co-workers (3*c*), whose synthesis of threonine utilized a reductive acetylation step.

In the present paper, we report both catalytic and chemical reduction studies of *N*-(2-diazo-3-oxoalkanoyl)glycine ester derivatives.

[1]Dedicated to the memory of Herbert Dorr.

[2]National Institutes of Health Predoctoral Fellow, 1968–1970.

Results and Discussion

Catalytic reduction of aroyldiazoacetic esters is a useful route to arylserines (2). Its extension to previously described (1) 4-phenoxy derivatives of *N*-(2-diazo-3-oxobutanoyl)glycine esters has been investigated. Reduction at atmospheric pressure of esters **1**–**4** in aqueous acetic acid with 1.2 to 1.4 mol of hydrogen over 10% palladium-on-charcoal results in *N*-[2-hydrazono-3-oxo-4 (or 5)-(aryloxy)alkanoyl]glycine esters **5**, **7**, **8**, and **9** (eq. 1). In reduction of **1**, use of platinum-on-carbon, and a hydrogen pressure of 3 atm also gives **5**. Insolubility of product hydrazones accounts in part for their ready isolation. The resistant nature of the aliphatic carbonyl group in **1**–**4**, and **5**, **7**, **8**, and **9** towards reduction over palladium catalysts is not surprising (4). In our hands, platinum-on-carbon also is an ineffective catalyst for reduction of the carbonyl group in keto peptides. Data for catalytic reduction of **1** and **3** are given in Table 1.

In ethanolic hydrogen chloride, hydrogenation of **1** over palladium-on-charcoal leads to pyrazine **6**. Presumably **6** results from an intermediate 2-amino-3-oxo-alkanoylglycine ester (**10**) which undergoes dimeric condensation to a dihydropyrazine, which is oxidized to **6** (eq. 2). No reduction of **3** occurred over palladium-on-charcoal in ethanol in absence of added acid.

TABLE 1. Catalytic hydrogenation of *N*-[2-diazo-3-oxo-4-(aryloxy)butanoyl] glycine ethyl esters (**1**) (**3**)

Substrate	Solvent	Catalyst	Product (% yield)
1	70% HOAc	10% Pd/C[a]	Hydrazone (50.5)
1	Gl. HOAc	5% Pt/C[a]	Hydrazone (42.3)
1	EtOH–HCl	10% Pd/C[a]	Pyrazine (22.3)
1	Gl. HOAc	10% Pd/C[b]	Hydrazone (66)
1	80% HOAc	5% Pt/C[b]	Hydrazone (47.5)
3	EtOAc	5% Rh/C[b]	Hydrazone (28.5)[c]

[a]Atmospheric pressure, room temperature.
[b]Pressure 40 psig, room temperature.
[c]An 18% yield of an oil tentatively identified as *N*-[3-oxo-4-(*o*-methoxyphenoxy)butanoyl]glycine ethyl ester, from loss of nitrogen, also was isolated.

In previous studies (**5**, **6**) reduction of hydrazones to β-amino alcohols has been effected. An attempt to hydrogenate **5** in glacial acetic acid over palladium-on-charcoal at approximately 3 atm pressure gave no hydrogen uptake; 83% of **5** was recovered.

[1] $ArO\text{-}(CH_2)_nCOCN_2CONHCH_2CO_2C_2H_5$

1, **2**, **3**, and **4**

1 and **5** Ar = C_6H_5, $n = 1$
2 and **7** Ar = p-F-C_6H_4, $n = 1$
3 and **8** Ar = o-$(CH_3O)C_6H_4$-, $n = 1$
4 and **9** Ar = o-$(CH_3O)C_6H_4$-, $n = 2$

Pd/C, $HOAc–H_2O$, H_2

$ArO\text{-}(CH_2)_nCOC(=NNH_2)CONHCH_2CO_2C_2H_5$

5, **7**, **8**, and **9**

[2] **1** → (Pd/C, HCl–EtOH, H_2) → $[C_6H_5OCH_2COCH(NH_2)CONHCH_2CO_2C_2H_5]$

10 → [Dihydropyrazine] → (O_2, Air) → **6**

6: R = $C_6H_5OCH_2$-, R′ = -$CONHCH_2CO_2C_2H_5$

[3] **3** / **11** → ($Zn–HOAc$, Ac_2O) → $ArOCH_2COCH(NHCOCH_3)CONHCH_2CO_2C_2H_5$

12 **13**

3 and **12** Ar = o-$(CH_3O)C_6H_4$-
11 and **13** Ar = p-$(CH_3O)C_6H_4$-

[4] **3** / **11** → ($Zn–TFA$, TFAA) → $ArOCH_2COCH(NHCOCF_3)CONHCH_2CO_2C_2H_5$

14 Ar = o-$(CH_3O)C_6H_4$-
15 Ar = p-$(CH_3O)C_6H_4$-

[5] **14** / **15** → ($NaBH_4$, CH_3OH) → $ArOCH_2CH(OH)CH(NHCOCF_3)CONHCH_2CO_2C_2H_5$

16 Ar = o-$(CH_3O)C_6H_4$-
17 Ar = p-$(CH_3O)C_6H_4$-

[6] **3** → (Zn, AcOH) →

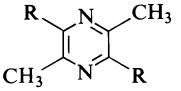

18 R = -$CONHCH_2CO_2C_2H_5$

Catalytic reduction of α-diazo ketones of this study proceeds with addition of hydrogen to yield the hydrazone, or hydrogenolysis of a reduced diazo function of undetermined nature to give the amino ketone. The latter dimerizes even in strongly acidic medium.

An alternative to catalytic reduction involves a modification of reductive acetylation procedures cited (3). Diazo keto derivatives **3** and **11** from interaction of the appropriate acid chloride with DGEE can be purified without column chromatography. Reductive acetylation of **3** and **11** (eq. 3) yields [2-acetamido-3-oxo-4-(*o*-methoxyphenoxy)butanoyl]glycine ethyl ester (**12**) and the *p*-methoxy isomer (**13**) in 77% and 32% yields, respectively. Inasmuch as the trifluoroacetyl blocking group is useful in peptide synthesis, because of its ready removal in dilute base (7–9), treatment of **3** and **11** with zinc, trifluoroacetic acid, and trifluoroacetic anhydride has been carried out, and gives the trifluoroacetyl analogs **14** and **15** (eq. 4). Either the acetyl or the trifluoroacetyl blocking group is effective in preventing pyrazine formation.

In order to obtain the threonine or allothreonine amino alcohol unit, the *N*-acylamino ketones **12**, **14**, and **15** were reacted with sodium borohydride in methanol, in a procedure pre-

viously shown to effect reduction of a keto group without significant attack at an ester carbonyl function (10). The borohydride reduction product of **12** possessed a wide melting range, and could not be purified by crystallization. However, the [γ-(aryloxy)threonyl]glycine derivatives **16** and **17** were obtained (eq. 5) from **14** and **15** upon borohydride reduction in 71 and 40% yields, respectively. One stereoisomer, of unassigned configuration (*erythro* or *threo*), was isolated in each instance. Stereoselectivity for the reduction procedure was not in evidence, however.

Simultaneous removal of the *N*-trifluoroacetyl group and saponification of the carboethoxy function of **16** were attempted with alcoholic sodium hydroxide by the procedure of Schallenberg and Calvin (9). The infrared spectrum of the hygroscopic product did not possess ester and trifluoroacetamido carbonyl bands, but did have a band at 1660 cm^{-1}, tentatively attributed to the peptide amide carbonyl group. The product formed both hydrochloride and hydrobromide salts, also extremely hygroscopic.

Chemical reduction of **3** with zinc – acetic acid gives a low yield of 2,5-dimethyl-3,6-bis-carboethoxymethylcarbamoylpyrazine (**18**) (eq. 6). Formation of a pyrazine in acetic acid is not surprising. However, cleavage of the phenoxymethyl group during chemical reduction is noteworthy.

Experimental

All melting points are uncorrected, and were determined by the capillary tube method on a Mel-Temp apparatus. Elemental analyses were performed by A. Bernhardt, Mülheim, Germany, or by Micro-Tech Laboratories, Skokie, Illinois. Nuclear magnetic resonance spectra were recorded on a Varian A60 spectrometer with tetramethylsilane as internal standard. Infrared spectra were obtained with a Perkin-Elmer model 237 spectrophotometer. Mass spectra were recorded on a Hitachi RMU-6D spectrometer.

N-[2-Hydrazono-3-oxo-4-(phenoxy)butanoyl]glycine Ethyl Ester **5**

One gram of *N*-[2-diazo-3-oxo-4-(phenoxy)butanoyl]-glycine ethyl ester (**1**), prepared as previously described (1), was dissolved in 24.5 ml glacial acetic acid. Water (10.5 ml) and 50 mg of 10% palladium-on-charcoal were added, and hydrogenation carried out immediately. Hydrogen uptake was 101 ml over 47 min. A colorless precipitate appeared after 15 min and 23 ml of hydrogen uptake. The reduction mixture was filtered over Celite on a sintered glass funnel. The mixture of catalyst and insoluble organic material then was washed with methylene chloride until no organic solid remained in admixture with the catalyst. The filtrate was concentrated and cooled to give 0.51 g, (50.5%) of colorless crystalline **5**, mp 173.6–174.0°C; ir (CH_2Cl_2) 3460 (NH), 3310 (NH), 3150 (NH), 1750 (ester CO), 1678 (amide CO), 1642 (keto CO) cm^{-1}. *Anal.* calcd. for $C_{14}H_{17}N_3O_5$: C 54.72, H 5.58, N 13.68; found: C 54.79, H 5.62, N 13.54.

Hydrogenation of 0.54 g of **1** in 35 ml, of glacial acetic acid with 30 mg of 5% platinum-on-carbon resulted in uptake of 233 ml of hydrogen over 5.5 h. Catalyst removal by filtration, followed by solution of the total filtrate in methylene chloride, extraction of acetic acid with water (extract discarded), drying, and solvent removal gave a white residue. Crystallization of the latter from methylene chloride gave 0.23 g (42.3%) of **5**, mp 169–170°C.

N-[2-Hydrazono-3-oxo-4-(p-fluorophenoxy)butanoyl]glycine Ethyl Ester, 7

One gram of *N*-[2-diazo-3-oxo-4-(*p*-fluorophenoxy)butanoyl]glycine ethyl ester (**2**) in 35 ml of 70% acetic acid, with 50 mg of 10% palladium-on-charcoal, was hydrogenated with 111 ml of hydrogen over 53 min (room temperature, 1 atm). Product isolation was as described for **5**. Hydrazone **7** was removed from catalyst with methylene chloride and methanol. The extract was dried, concentrated, and cooled to yield 1.08 g of **7**, mp 183–184°C. Recrystallization from 60 ml of hot methanol gave colorless needles, yield 0.98 g (97%), mp 183–184.5°C; ir (KBr) 3395 (NH), 3360 (NH), 3160 (NH), 1740 (ester CO), 1680 (amide CO), 1650 (keto CO) cm^{-1}. *Anal.* calcd. for $C_{14}H_{16}N_3O_5F$: C 51.69, H 4.96, N 12.92, F 5.84; found: C 51.96, H 5.06, N 12.87, F 5.98.

N-[2-Hydrazono-3-oxo-4-(o-methoxyphenoxy)butanoyl]glycine Ethyl Ester, 8

One gram of *N*-[2-diazo-3-oxo-4-(*o*-methoxyphenoxy)-butanoyl]glycine ethyl ester (**3**) in 80 ml of 62% acetic acid, with 50 mg of 10% palladium-on-charcoal was hydrogenated with 102 ml of hydrogen (room temperature, 1 atm). The mixture was filtered and water added to the filtrate. The substance resulting was collected and dried *in vacuo*; yield 0.64 g (63.6%), mp 117–120°C. Recrystallization from ether – methylene chloride gave colorless needles of **8** (540 mg), mp 119.8–120°C; ir (CH_2Cl_2) 3465 (NH), 3320 (NH), 3155 (NH), 1747 (ester CO), 1677 (amide CO), 1645 (keto CO) cm^{-1}. *Anal.* calcd. for $C_{15}H_{19}N_3O_6$: C 53.40, H 5.68, N 12.46; found: C 53.30, H 5.73, N 12.30.

N-[2-Hydrazono-3-oxo-5-(o-methoxyphenoxy)pentanoyl]glycine Ethyl Ester, 9

N-[2-Diazo-3-oxo-5-(*o*-methoxyphenoxy)pentanoyl]-glycine ethyl ester (**4**) (160 mg) in 10 ml of 70% acetic acid with 10 mg of 10% palladium-on-charcoal was reacted with 14 ml of hydrogen over 18 min (room temperature, 1 atm). The mixture was filtered, and the mixture of catalyst and product washed with methylene chloride and methanol as for **7**. Filtrate was heated to effect complete solution, then cooled to yield 40 mg of **9** (24.8%), mp 143–144°C; ir (KBr) 3408 (NH), 3264 (NH), 3148 (NH), 1740 (ester CO), 1650 (amide CO), 1617 (keto CO?), 1600 (phenyl) cm^{-1}. *Anal.* calcd. for $C_{16}H_{21}N_3O_6$: C 54.69, H 6.02, N 11.96; found: C 54.52, H 5.95, N 12.00.

2,5-Bis-phenoxymethyl-3,6-bis-(carboethoxymethyl)carbamoylpyrazine, 6

N-[2-Diazo-3-oxo-4-(phenoxy)butanoyl]glycine ethyl

ester (650 mg) in 50 ml of absolute ethanol was added to 2.5 ml of 17% anhydrous hydrogen chloride in absolute ethanol. Hydrogenation over 200 mg of 10% palladium-on-charcoal (room temperature, 1 atm) gave 119 ml of hydrogen uptake (3 h). The reaction mixture was filtered, solvents removed by flash evaporation of the filtrate, and the colorless residue heated with 50 ml of ethyl acetate. A trace of insoluble material was removed by filtration and discarded. Filtrate concentration gave a light yellow oil (660 mg), which in methylene chloride solution was chromatographed on 65 g of silicic acid – Celite 545 (5:1 w/w). The column was eluted successively with 90 ml benzene, 235 ml of benzene – methylene chloride (1:1 v/v), 345 ml of benzene – methylene chloride (9:1 v/v), and methylene chloride – ethyl acetate (9:1 v/v). Removal of solvent from the latter eluate gave 131 mg of solid residue, recrystallized from ethyl ether – methylene chloride to give **6**, mp 133–136°C; ir (CH_2Cl_2) 3400 (NH), 1755 (ester CO), 1690 (amide CO), 1605 (phenyl) cm^{-1}; ^{1}Hmr ($CDCl_3$) δ 1.28 (t, 6H, CH_3 groups), 4.02–4.28 (m, 8H, carboethoxymethyl and ester CH_2 groups), 5.83 (s, 4H, phenoxymethyl CH_2 groups), 6.83–7.30 (m, 10H, aromatic), 7.93–8.23 (s, 2H, NH). *Anal.* calcd. for $C_{28}H_{30}N_4O_8$: C 61.08, H 5.49, N 10.18; found: C 60.79, H 5.59, N 10.18.

N-[2-Diazo-3-oxo-4-(p-methoxyphenoxy)butanoyl]glycine Ethyl Ester, ***11***

To 38.36 g of *N*-diazoacetylglycine ethyl ester (1, 11) in 500 ml of methylene chloride was added a solution of 22.49 g of *p*-methoxyphenoxyacetyl chloride in 100 ml of methylene chloride over 35 min. The reaction mixture was stirred for 43 h, washed with 100 ml water, dried, and solvent volume reduced to 100 ml. Addition of 200 ml ethyl ether and cooling yielded colorless **11** which was collected and air-dried; yield 17.78 g (47.3%), mp 86–88°C; ir (CH_2Cl_2) 3310 (NH), 2140 (CN_2), 1745 (ester CO), 1675 (amide CO), 1625 (keto CO) cm^{-1}; ^{1}Hmr ($CDCl_3$) δ 1.30 (t, J = 7.2 Hz, 3, ester CH_3), 3.82 (s, 3, OCH_3), 4.18 (d, J = 5.5 Hz, 2, glycine CH_2), 4.27 (q, J = 7.2 Hz, 2, ester CH_2), 4.91 (s, 2, ether CH_2), 6.93 (s, 4H, aromatic), 8.78 (b m, 1, NH). *Anal.* calcd. for $C_{15}H_{17}N_3O_6$: C 53.73, H 5.11, N 12.53; found: C 53.58, H 4.94, N 12.68.

N-[2-Acetamido-3-oxo-4-(o-methoxyphenoxy)butanoyl]glycine Ethyl Ester, ***12***

N-[2-Diazo-3-oxo-4-(*o*-methoxyphenoxy)butanoyl]glycine ethyl ester (**3**) (5.00 g), prepared as previously described (1), was dissolved in acetic acid (52.5 ml) and acetic anhydride (17.5 ml) added. Zinc dust (3.75 g) was added over 30 min; when the temperature rose to 35°C, the reaction mixture was maintained at 30–35°C. The reaction mixture was stirred for an additional 10 min, and then 52.5 ml of water added over 60 min. The reaction mixture was stirred 18 h, filtered, and extracted with methylene chloride (50 ml, ×5). The extract was washed with 100 ml of water, dried, and solvent removed. Trituration of residual oil with petroleum ether (bp 30–60°C) yielded colorless **12**, mp 131–133°C, yield 4.21 g (77.2%); ir (CH_2Cl_2) 3390 (NH), 3340 (NH), 1740 (ester CO), 1650–1685 (b, amide and keto CO) cm^{-1}; ^{1}Hmr ($CDCl_3$) δ 1.21 (t, J = 7.2 Hz, 3, ester CH_3), 2.08 (s, 3, acetyl CH_3), 3.88 (s, 3, OCH_3), 4.01 (d, J = 5.5 Hz, 2, glycine CH_2), 4.15 (q, J = 7.2 Hz, 2, ester CH_2), 4.82 (s, 1, ether CH_2), 4.86 (s, 1, ether CH_2), 5.79 (d, J = 6.5 Hz, 1, amide CH), 6.95 (s, 4, aromatic), 7.17 (b d, J = ~5.5 Hz, 1, acetamido NH), 8.08 (b t, J = ~6.5 Hz, 1, peptide NH). *Anal.* calcd. for $C_{17}H_{22}N_2O_7$: C 55.73, H 6.05, N 7.65; found: C 55.67, H 5.98, N 7.75.

N-[2-Acetamido-3-oxo-4-(p-methoxyphenoxy)butanoyl]glycine Ethyl Ester, ***13***

The title compound was prepared in 31.9% yield from 1.87 g of **11** as described for **12**. The product **13** melted at 137.5–139°C; ir (CH_2Cl_2) 3410 (b, NH), 1745 (ester CO), 1685 (b, amide and keto CO) cm^{-1}; ^{1}Hmr ($CDCl_3$) δ 1.23 (t, J = 7.2 Hz, 3, ester CH_3), 2.15 (s, 3, $COCH_3$), 3.73 (s, 3, OCH_3), 3.96 (d, J = 5.5 Hz, 2, glycine CH_2), 4.14 (q, J = 7.2 Hz, 2, ester CH_2), 4.79 (s, 2, ether CH_2), 5.56 (d, J = 6.5 Hz, 1, amide CH), 6.82 (s, 4, aromatic), 7.09 (b d, J = ~6.5 Hz, 1, acetamido NH), 7.46 (t, J = 5.5 Hz, 1, peptide NH). *Anal.* calcd. for $C_{17}H_{22}N_2O_7$: C 55.73, H 6.05, N 7.65; found: C 56.01, H 6.09, N 7.66.

N-[2-Trifluoroacetamido-3-oxo-4-(o-methoxyphenoxy)butanoyl]glycine Ethyl Ester, ***14***

N-[2-Diazo-3-oxo-4-(*o*-methoxyphenoxy)butanoyl]glycine ethyl ester (**3**) (3.79 g) was added to a mixture of trifluoroacetic acid (18 ml) and trifluoroacetic anhydride (6 ml) which had been precooled to 0°C. Zinc dust (3.0 g) was added over 35 min, when the temperature rose to 26°C. Methylene chloride (200 ml) was added, then 20 ml water over 10 min. The reaction mixture was filtered, and the aqueous phase washed with methylene chloride (30 ml, ×4). The extracts were washed with 75 ml water, dried, and solvent removed. The residual solid was recrystallized twice from methylene chloride – petroleum ether (bp 30–60°C) to give 1.81 g (38.3%) of colorless **14**, mp 133.5–134.5°C; ir (CH_2Cl_2) 3350 (NH), 1740 (ester CO), and 1685–1650 (b, amide and keto CO) cm^{-1}; ^{1}Hmr ($CDCl_3$) δ 1.93 (t, J = 7.2 Hz, 3, ester CH_3), 3.93 (s, 3, OCH_3), 4.07 (d, J = 5.5 Hz 2, glycine CH_2), 4.17 (q, J = 7.2 Hz, 2, ester CH_2), 4.83 (s, 2, ether CH_2), 5.93 (d, J = 6.5 Hz, 1, amide CH), 7.02 (m, 4, aromatic), 7.86 (b d, J = ~6.5 Hz, 1, trifluoroacetamido NH), 8.30 (b, t, J = ~5.5, 1, peptide NH). *Anal.* calcd. for $C_{17}H_{19}F_3N_2O_7$: C 48.58, H 4.56, F 13.56, N 6.66; found: C 48.52, H 4.70, F 13.78, N 6.60.

N-[2-Trifluoroacetamido-3-oxo-4-(p-methoxyphenoxy)butanoyl]glycine Ethyl Ester, ***15***

The title compound was prepared in 53.4% yield from 3.45 g of **11** as described for **14**, and melted at 136–137°C; ir (CH_2Cl_2) 3370 (b, NH), 1745 (ester CO), 1720 (trifluoroacetamido CO), 1690 (b, peptide and keto CO) cm^{-1}; ^{1}Hmr ($CDCl_3$) δ 1.27 (t, J = 7.2 Hz, 3, ester CH_3), 3.78 (s, 3, OCH_3), 4.04 (d, J = 5.5 Hz, 3, glycine CH_2), 4.20 (q, J = 7.2 Hz, 2, ester CH_2), 4.78 (s, 1, ether CH_2), 4.81 (s, 1, ether CH_2), 5.68 (d, J = 6.5 Hz, 1, amide CH), 6.98 (s, 4, aromatic), 7.42 (b t, J = ~5.5, 1, peptide NH), 7.86 (b d, J = ~6.5 Hz, 1, trifluoroacetamido NH). *Anal.* calcd. for $C_{17}H_{19}F_3N_2O_7$: C 48.58, H 4.56, F 13.56, N 6.66; found: C 48.72, H 4.75, F 13.88, N 6.67.

N-[2-Trifluoroacetamido-3-hydroxy-4-(o-methoxyphenoxy)butanoyl]glycine Ethyl Ester, ***16***

N-[Trifluoroacetamido-3-oxo-4-(*o*-methoxyphenoxy)-butanoyl]glycine ethyl ester (**14**) (1.81 g) was dissolved in dry methanol (250 ml) and the solution cooled to 10°C. Sodium borohydride (0.091 g) was added, and the re-

sulting mixture stirred in an ice bath for 3.75 h. Water (250 ml) was added and the aqueous solution extracted with methylene chloride (50 ml, ×6). The extracts were dried, solvent removed, and viscous residual oil triturated with petroleum ether (bp 30–60°C) to give a white solid. Recrystallization of the latter from methylene chloride – petroleum ether (bp 30–60°C) gave **16**, mp 121–123°C, in 1.30 g yield (71.5%); ir (CH_2Cl_2) 3575 (free OH), 3385 (b, NH and H-bonded OH), 1730 (ester CO), 1685 (b, amide CO groups) cm^{-1}; ^{1}Hmr ($CDCl_3$) δ 1.22 (t, J = 7.2 Hz, 3, ester CH_3), 3.83 (s, 3, OCH_3), ca. 4.15 (m, 8, ester, glycine and ether CH_2 groups, CHOH), 4.87 (m, 1, amide CH), 6.89 (s, 4, aromatic), 7.70 (b t, J = ~5.5 Hz, 1, peptide NH), 8.08 (b d, J = ~8.0 Hz, trifluoroacetamido NH). *Anal.* calcd. for $C_{17}H_{21}F_3N_2O_7$: C 48.34, H 5.01, F 13.49, N 6.63; found: C 48.20, H 5.19, F 13.13, N 6.52.

N-[Trifluoroacetamido-3-hydroxy-4-(p-methoxyphenoxy)butanoyl]glycine Ethyl Ester, ***17***

The title compound was prepared in 40.0% yield from 1.05 g of **15**, as described for **16**, and melted at 126–128°C; ir (CH_2Cl_2) 3575 (free OH), 3385 (b, NH groups and H-bonded OH), 1735 (ester CO), 1685 (b, amide CO groups) cm^{-1}; ^{1}Hmr ($CDCl_3$) δ 1.22 (t, J = 7.2 Hz, 3, ester CH_3), 3.75 (s, 3, OCH_3), ca. 4.15 (m, 8, ester, glycine and ether CH_2 groups, CHOH), 4.86 (m, 1, amide CH), 6.81 (s, 4, aromatic), 7.47 (b t, J = ~5.5, 1, peptide NH), 8.04 (b d, J = ~8.0, 1, trifluoroacetamide NH). *Anal.* calcd. for $C_{17}H_{21}F_3N_2O_7$: C 48.34, H 5.01, F 13.49, N 6.63; found: C 48.35, H 4.92, F 13.21, N 6.62.

2,5-Dimethyl-3,6-bis-carboethoxymethylcarbamoylpyrazine, ***18***

N-[2-Diazo-3-oxo-4-(*o*-methoxyphenoxy)butanoyl]glycine ethyl ester (**3**) (1.60 g) was dissolved in 20 ml of acetic acid. Zinc dust (2.5 g) was added over 30 min with external cooling (temperature at 30–35°C). The mixture was stirred for an additional 20 min, then 20 ml of water added over 30 min. The mixture was stirred for 1.5 h, filtered, and the filtrate extracted with methylene chloride (40 ml ×3). The extracts were washed with 25 ml of 5% sodium bicarbonate, dried, and solvent removed. Trituration of residual oil with a small amount of ether gave a yellow solid, which was recrystallized from methylene chloride – petroleum ether (bp 30–60°C) to give **18** in 41 mg yield, mp 169–170.5°C; ir (CH_2Cl_2) 3410 (NH), 1740 (ester CO), 1675 (amide CO) cm^{-1}; ^{1}Hmr ($CDCl_3$) δ 1.33 (t, J = 7.2 Hz, 6, ester CH_3 groups), 2.97 (s, 6, pyrazine 2,5-methyl groups), 4.24 (d, J = 5.5 Hz, 4, carboethoxymethyl groups), 4.29 (q, J = 7.2 Hz, 4, ester CH_2 groups), 8.55 (b t, J = ~5.5 Hz, 2, NH); ms *m/e* calcd. for $C_{16}H_{22}N_4O_6$: 366; found: 366. *Anal.* calcd. for $C_{16}H_{22}N_4O_6$: C 52.45, H 6.05, N 15.29; found: C 52.33, H 6.24, N 15.18.

Acknowledgements

This investigation was supported by grants CA-04750 from the National Cancer Institute and 5-F01 GM 39522-02 from General Medical Sciences Institute of the U.S. Public Health Service. Mass spectra were determined by David L. von Minden.

1. J. H. Looker and J. W. Carpenter. Can. J. Chem. **45**, 1727 (1967).
2. (*a*) J. H. Looker and D. N. Thatcher. J. Org. Chem. **23**, 403 (1958); (*b*) K. Kronberger. Ph.D. Thesis. University of Nebraska, Lincoln, NE, U.S.A. 1967; (*c*) B. Cho. Ph.D. Thesis. University of Nebraska, Lincoln, NE, U.S.A. 1966.
3. (*a*) N. F. Albertson, B. F. Tullar, J. A. King, B. B. Fishburn, and S. Archer. J. Am. Chem. Soc. **70**, 1151 (1948); (*b*) M. Regitz. Chem. Ber. **98**, 1210 (1965); (*c*) K. Pfister III, C. A. Robinson, A. C. Shabica, and M. Tishler. J. Am. Chem. Soc. **71**, 1101 (1949).
4. E. Breitner, E. Roginski, and P. N. Rylander. J. Org. Chem. **24**, 1855 (1959).
5. L. Birkofer. Chem. Ber. **80**, 83 (1947).
6. R. Pfleger and F. Reinhardt. Chem. Ber. **90**, 2404 (1957).
7. F. Weygand and E. Csendes. Angew. Chem. **64**, 136 (1952).
8. F. Weygand and E. Leising. Chem. Ber. **87**, 248 (1954).
9. E. F. Schallenberg and M. Calvin. J. Am. Chem. Soc. **77**, 2779 (1955).
10. H. O. House, H. Babad, R. B. Toothill, and A. W. Noltes. J. Org. Chem. **27**, 4141 (1962).
11. T. Curtius and A. Darapsky. Chem. Ber. **39**, 1373 (1906).

Reactions of bishalomethylarenes with superoxide

L. H. DAO, A. C. HOPKINSON, AND E. LEE-RUFF
Department of Chemistry, York University, Downsview, Ont., Canada M3J 1P3
AND
J. RIGAUDY
Laboratoire de Chimie Organique de l'ESPCI, 10 rue Vauquelin, Paris V^e, France

Received May 31, 1977

L. H. DAO, A. C. HOPKINSON, E. LEE-RUFF, and J. RIGAUDY. Can. J. Chem. **55**, 3791 (1977).

1,2-Dioxenes **2**, **7**, and **14** are obtained from the reactions of potassium superoxide with 1,2-bishalomethylarenes. Rearrangement products are also formed in competition with the cyclization reaction. The relative yields of dioxenes depend on the relative concentration of superoxide to substrate as well as reaction conditions. Mechanisms for the formation of the rearrangement products are proposed.

L. H. DAO, A. C. HOPKINSON, E. LEE-RUFF et J. RIGAUDY. Can. J. Chem. **55**, 3791 (1977).

Les dioxènes-1,2 (**2**, **7** et **14**) sont obtenus par réaction du superoxyde de potassium avec les bis-halogénométhyl-1,2 arènes. Des produits de réarrangement sont aussi formés par une réaction compétitive avec celle de cyclisation. Les rendements relatifs en dioxène dépendent de la concentration relative du superoxyde aussi bien que des conditions de réaction. On propose des mécanismes pour la formation des produits de réarrangement.

[Traduit par le journal]

During the past decade there has been good evidence for the production of superoxide ion (O_2^-) in the reduction of O_2 by several enzymes including some present in mitochondria and in the endoplasmic reticulum (1–3). This ion radical has been implicated to intervene in lipid peroxidation processes involving production of allylic hydroperoxides during the early stages of the reaction (2). It is not known whether O_2^- is directly involved or whether it acts as a precursor to other reactive species (e.g. singlet oxygen) in such processes. Non-enzymatic formation of alkyl and acyl peroxides and hydroperoxides using free superoxide with alkyl and acyl halides, and sulphonate esters have been reported (4–6). It was further shown that superoxide is a moderately active nucleophile in displacement reactions of alkyl and electrophilic aryl halides (6–9). With the idea of extending these reactions to include alkyl dihalides and the preparation of cyclic peroxides, we embarked on an investigation of the reactivity of a series of bishalomethylarenes with O_2^-. In this paper we wish to report the synthesis of the hitherto unknown *o*-xylylene peroxide (**2**) (a potential precursor to the theoretically interesting *o*-xylylene) and derivatives of **2** along with competitive rearrangements in the reactions of O_2^- with 1,2-bishalomethylarenes **1***a*, *b*.

Results

The reactions of 1,2-bishalomethylbenzenes **1***a* and *b* with potassium superoxide (KO_2) complexed with dicyclohexyl crown-6 resulted in the formation of two products **2** and **3** with relative yields depending on relative concentration of KO_2 and substrate, nature of solvent, and reaction times. The yield of *o*-xylylene peroxide **2** was a maximum when the reaction was carried out in dimethylformamide (DMF) and stopped after 2–3 h using about a 2:1 equiv. ratio of KO_2 to substrate. Attempted isolation of **2** from solution led *inevitably to violent explosions*. The identity of **2** was inferred

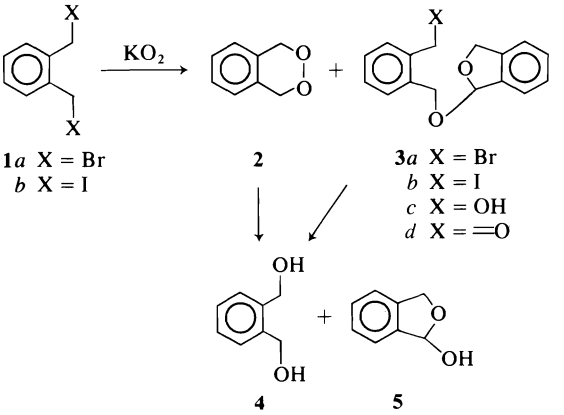

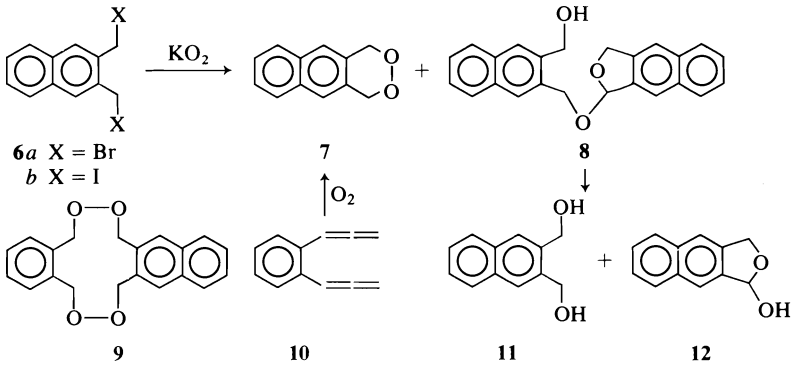

from the following observations: Purified **2** (in solution) gave a positive test for peroxide with I^-. Reduction of **2** with lithium aluminum hydride (LAH) gave the diol **4** (16) which was prepared independently by complete reduction of *o*-phthalaldehyde with LAH as well as hydrolysis of either **1***a* or *b* with hydroxide ion. The nmr spectrum of **2** exhibited two signals (δ 7.15(m), 5.12(s)) of equal intensities. Indirect evidence that **2** was not dimeric was gathered from the following experiment. Reaction of an equimolar mixture of dihalides **1** and **6** resulted in an equimolar mixture of peroxides **2** and **7**, in addition to acetals **3** and **8**. After separation of the more stable **7** from the mixture there was no evidence for the presence of the mixed peroxide **9** as seen by thin-layer chromatography and nmr spectrum of the mixture. The identity of acetals **3***a–c* was established by its acidic hydrolysis to a mixture of phthalanol **5** and diol **4** as well as by analysis of its spectral data (^1H, ^{13}C nmr, ir, and mass spectra). Acetals **3***c* and **3***d* appeared to be secondary products from subsequent oxidation of **3***a* and *b*. Reaction of dihalides **6***a* and *b* with crown ether complexed KO_2 resulted in similar products **7** (10–30%) and **8** (40–90%). The physical and spectral properties of **7** were identical to those reported for the product obtained from oxygenation of 1,2-bisallenylbenzene (**10**). The structure of acetal **8** was established by its hydrolysis to a mixture of **11** and **12** which were independently synthesized. The ^1H nmr spectra of derivatives **3**, **5**, **8**, and **12** all exhibited long range coupling between the methyne proton and one of the benzylic protons across the acetal bridge (J = 2 Hz). This phenomenon has been observed in other substituted naphthalans (10).

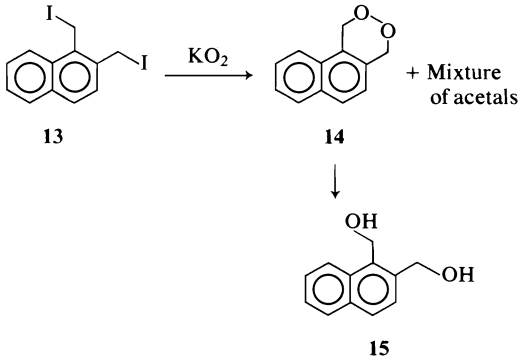

Extension of these reactions to dihalide **13** resulted in lower yields of the cyclic peroxide **14** (10–15%) along with an inseparable mixture of acetals inferred from the analysis of the spectral data and comparison with spectral data of acetals **3** and **8**. The structure of **14** was shown by analysis of its spectral data and reduction to the diol **15** as well as its positive test with I^- for peroxide.

Discussion

Formation of cyclic peroxides **2**, **7**, and **14** is presumed to follow a similar mechanism as in the case of acyclic peroxides, namely double nucleophilic substitution of O_2^- with the intervention of a peroxyl radical (4) (Scheme 1). Yields of peroxides were highly dependent on reaction times and relative concentration of O_2^-. It was found that peroxides **2** and **7**, when subjected to reaction conditions identical to those of their synthesis, underwent decomposition to a complex mixture over an extended period of time. On the other hand 9,10-diphenylanthracene-9,10-peroxide (**16**) was reduced by superoxide to diol **17**. Similar observations were made by San-Filippo and co-workers (12) in the reduction of diacyl peroxides to carboxylic acids in the presence of superoxide. These transformations may involve initial formation of an alkoxy

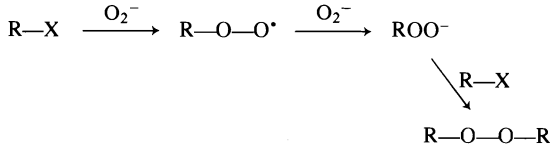

SCHEME 1

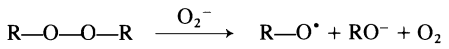

SCHEME 2

radical according to Scheme 2. Such radicals may undergo hydrogen abstraction or be further reduced by O_2^- yielding another equivalent of alkoxide. Precedent for such a mechanism was demonstrated by Peters and Foote (13) in the reduction of *tert*-butyl hydroperoxide to the *tert*-butoxyl radical.

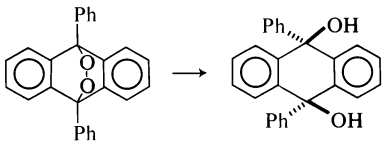

16 **17**

Two mechanisms (Scheme 3) can be envisaged leading to cyclic acetals **3** and **8**: (*A*) *o*-xylylene peroxides **2** and **7** may be involved as intermediates to these acetals via hemiacetal anion **18** or (*B*) competitive formation of a dihaloperoxide **19** undergoing base-catalyzed disproportionation to **20** and **21** which upon recoupling generates the observed acetal **3**. Base-catalyzed rearrangements of cyclic peroxides possessing an α-hydrogen have been reported to generate hydroxycarbonyl products (14). However, it does not appear that mechanism *A* plays an important role in these transformations. The sodium salt of **18** was generated independently from phthalanol **12** and shown not to undergo nucleophilic substitution with **1** under identical conditions. Furthermore nucleophilic substitutions by alkoxide on **1** was found to be quite inefficient. The most stable conformation of **1** is likely to be such that both halogens occupy the *exo* positions as shown here.

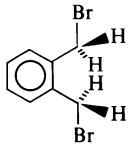

1

Thus bimolecular nucleophilic substitutions would require the nucleophile to approach the substrate from the more hindered *endo* side. On the other hand such steric constraints would not be as important for the linear and smaller O_2^- ion.

From our results it would appear that alicyclic peroxides can be obtained in moderate to good yields using superoxide. The advantage in using superoxide to hydroperoxy anion or peroxide is that O_2^- being a weaker base (22) will minimize competitive base-catalyzed reactions such as dehydrohalogenations and rearrangements of base sensitive peroxides.

We are extending these reactions to include 1,3- and 1,2-alkyl dihalides to explore the potential use of O_2^- in the synthesis of more strained peroxides such as dioxetanes. We are also exploring the nature of peroxides **2**, **7**, and **14** as potential sources of *o*-quinodimethanes. Derivatives of **2** have been obtained previously by oxygenation of the photoenols of *o*-toluylaldehyde and ketones (15).

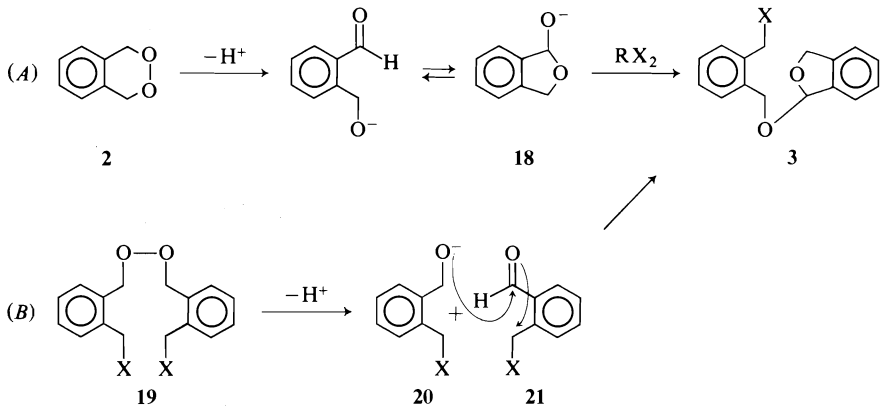

2 **18** **3** **19** **20** **21**

SCHEME 3

Experimental

α,α-Xylylene dibromide was obtained from Aldrich Chemicals. 2,3- and 1,2-bisbromomethylnaphthalenes were obtained from bromination of 2,3- and 1,2-dimethyl naphthalenes according to the method of Wittig (20). The bisiodomethylarenes were prepared by reaction of the dibromides with sodium iodide in acetone and recrystallization of the resultant precipitate from chloroform. All of the diiodides gave correct analyses.

1,4-Dihydro-2,3-benzodioxin, 2

o-Xylene dibromide (2.64 g, 10 mmol) was added to a vigorously stirred mixture of powdered potassium superoxide (1.42 g, 20 mmol) in dry DMF (70 ml) at 25°C. The resulting mixture was allowed to stir for 2 h, then cautiously poured onto 100 ml ice-water, and extracted with three 50-ml portions of ether. The ethereal solution was washed with three 30-ml portions of ice-water and evaporated to dryness to give 1.05 g of a crude liquid which was purified by tlc (benzene as eluant); yield 0.60 g (44%); ir (neat) 2900, 1505, 1460, 1430, 1363, 1040, 1018, 977, 865 cm^{-1}; nmr (CCl_4) δ 5.12 (4H, s), 7.00–7.30 (4H, m); ms *m/e* 254 (M^+).[1] Positive iodine test. It was the only time we isolated **2** pure enough. Other attempts resulted in explosion or vigorous decomposition.

Reduction of 1,4-Dihydro-2,3-benzodioxin, 2

A solution of **2** in ether was added slowly to a stirred mixture of $LiAlH_4$ in ether at −50°C. The resulting mixture was stirred at −50°C for 30 min and 2 h at 25°C. A solution of 10% aqueous sodium hydroxide was added slowly until a clear solution had formed. The precipitate was filtered and washed with ether. The combined washings and filtrate were washed with water, dried over H_2SO_4, and concentrated to give an oily paste. Recrystallization of the product from benzene gave pure 1,2-bishydroxymethylbenzene, mp 65–66°C, which had ir and nmr spectra identical to those of authentic material prepared by reduction of phthalide with $LiAlH_4$ or hydrolysis of *o*-xylene dibromide **1***a* (16).

Phthalanyl Ethers 3

o-Bromomethylbenzenemethyl 1-Phthalanyl Ether, 3a

Potassium superoxide (250 mg, 3.52 mmol) in dry benzene (5 ml) or dry THF was carefully crushed with a glass rod. Dicyclohexyl-18-crown-6 (200 mg) and *o*-xylene dibromide (250 mg, 0.95 mmol) were added slowly. The resulting mixture was protected from moisture with a $CaCl_2$ drying tube and was stirred vigorously. Instant evolution of gas was observed and the reaction was followed by tlc. After 2 h at room temperature, the solid was filtered and washed with dry benzene. The filtrate was stripped to a pale yellow residue. The residue was applied to tlc and eluted with 1:1 v/v benzene–hexene. Starting material (153 mg) was isolated besides **3***c* and 61 mg (40%) of **3***a*; nmr ($CDCl_3$) δ 4.55 (s, 2H), 4.75 (s, 2H), 5.05–5.15 (2H, m, ABX), 6.30 (d, 1H), 7.10–7.40 (m, 8H); ir (neat) 3075, 1460, 1363, 1255, 1220, 1065, 1000, 905 cm^{-1}.

When the reaction was left for a longer period **3***a* was completely transformed to **3***c*.

o-Iodomethylbenzenemethyl 1-Phthalanyl Ether, 3b

The *o*-xylene diiodide **16** was converted to **3***b* and **3***c* as described above. **3***b* was purified by preparative tlc (benzene as eluant); nmr ($CDCl_3$) δ 4.62 (2H, s), 4.80 (2H, s), 5.15–5.30 (2H, ABX, m), 6.44 (1H, d), 9.25–7.55 (8H, m); ^{13}C nmr (ref. TMS) 140, 138, 137, 135 ppm (q. C's), 130–121 ppm (8 peaks, aromatic), 106 ppm (methine C), 73 ppm (methylene C), 66 ppm (methylene C), 4 ppm (methylene C).

o-Hydroxymethylbenzenemethyl 1-Phthalanyl Ether 3c

1*a* or **1***b* (10 mmol) was added to a stirred mixture of powdered potassium superoxide (1.42 g, 20 mmol) in dry DMF (70 ml) at 25°C.[2] After 15 h, the mixture was poured into 100 ml ice-water and worked up as for **2**. After purification by tlc, a pale yellow oil was obtained (0.768 g, 60%); nmr ($CDCl_3$) δ 4.85 (2H, s) 5.12 (2H, s), 5.10–5.20 (2H, ABX), 6.35 (1H, d), 7.20–7.50 (8H, m); ir (neat) 3500, 1616, 1460, 1365, 1257, 1075, 1000 cm^{-1}; ms (30 eV) 256 (M^+), 238 ($M - H_2O^+$), 135 (100%).

Hydrolysis of 3a, b, c

3*a*, *b*, *c* (2 mmol) were dissolved in 10 ml EtOH 95%. Concentrated H_2SO_4 (1 ml) was added and the mixture was refluxed for 1 h. The cooled solution was neutralized carefully with aqueous NaOH (20%), saturated with NaCl, and extracted with ether. The ethereal solution was dried over $MgSO_4$ and concentrated to an oil (the nmr spectra showed an equimolar mixture of **4** and **5**), which gave after separation by preparative tlc **4** and **5** (17).

5 was independently prepared by reduction of phthalide in toluene at −78°C under N_2 with diisopropyl aluminium hydride; nmr (CCl_4) δ 5.00–5.15 (2H, ABX) 6.15 (1H, d, J = 2 Hz), 7.15–7.40 (4H, m); ir (neat) 3480, 1465, 1365, 1100, 1075, 1000 cm^{-1}.

o-Formylbenzenemethyl 1-Phthalanyl Ether, 3d

1*a* (6.5 g, 24.6 mmol) was added to a stirred suspension of powdered potassium superoxide (3.0 g, 42.2 mmol) in dry DMSO (150 ml) at 25°C. After 2 h, the mixture was poured in ice-water and worked up in the usual way to give 2.0 g of yellow oil which was purified by preparative tlc ($CHCl_3$–benzene 80:20) to give 1.60 g of pure **3***d*; nmr (CCl_4) δ 5.00–5.25 (2H, m), 5.12 (2H, s), 6.28 (1H, d), 7.10–8.00 (8H, m), 10.10 (1H, s); ir (neat) 3490, 1770, 1700, 1600, 1480, 1367, 1287, 1220, 1050, 1000 cm^{-1}; ms (70 eV) 254 (M^+), 253 ($M - 1^+$).

3*d* (0.50 g, 1.96 mmol) was dissolved in 10 ml of 95% EtOH. H_2SO_4 (2 ml) was added and the mixture was refluxed for 1 h, cooled, neutralized with 20% NaOH, saturated with NaCl and extracted with ether. The ethereal solution was dried and concentrated to give exclusively pure **5**.

1,4-Dihydro-2,3-naphtho[2,3]dioxin, 7

To a suspension of potassium superoxide (220 mg, 3.1 mmol) in dry THF (10 ml) was added dicyclohexyl-16-crown-18 (150 mg) and diiodide **6***b* (614 mg, 1.5 mmol). The mixture was stirred for 3 h, filtered, and filtrate concentrated to a residue (300 mg) which gave by tlc 100 mg of **6***b*, 20 mg (7%) of **7**, mp 170–172°C (lit. (11) 166–167°C), which had nmr and uv spectra identical to those of

[1]The ms exhibited an identical fragmentation pattern as **3***d*. It was shown (see following) that **2** was thermally labile.

[2]If benzene or THF were used as solvent in presence of crown ether, the mixture was concentrated and directly purified by tlc to give **3***c*.

authentic material (11). A polar compound **8** was also isolated.

The dibromide **6***a* was converted to **7** and **8** in benzene and crown ether as described above.

*2-Hydroxymethylnaphthalene-3-methyl 2,3-Naphthalanyl Ether, **8***

The dibromide **6***a* (1.68 g, 5 mmol) was added to a stirred suspension of potassium superoxide (1.42 g, 20 mmol) in dry DMF (100 ml). After 20 h, the mixture was worked up with ether to give after purification by tlc pure **8** (200 mg, 25%), mp 135–136°C; nmr ($CDCl_3$) δ 4.88 (2H, s), 5.20 (2H, s), 5.00–5.25 (2H, m), 6.45 (1H, d), 7.40–7.90 (12H, m); ir (KBr) 3400, 1668, 1600, 1500 cm^{-1}, ms (70 eV) 356 (M^+).

*Hydrolysis of **8***

To dimer **8** (190 mg, 0.53 mmol) in 5 ml of 95% EtOH was added 1 ml H_2SO_4. The mixture was refluxed for 1 h, neutralized with NaOH 20%, saturated with NaCl, and extracted with ether. The ethereal solution was concentrated and the residue separated by tlc to give **11** (75 mg, 75%), mp 158–160°C (lit. (16) 159–160°C), and **12** (55 mg, 56%).

12 was oxidized by CrO_3 to naphthalide, mp 206°C (lit. (18) 206°C).

*1,4-Dihydro-2,3-Naphtho[1,2]dioxin, **14***

The diiodide **13** (600 mg) was added to a suspension of powdered KO_2 in 20 ml of dry tetrahydrofuran. The solution was stirred at room temperature for 48 h. The excess KO_2 was filtered off and the filtrate evaporated. The residue was chromatographed on five plates (benzene) to give 20 mg of peroxide **14**, mp 54–56°C; nmr ($CDCl_3$) δ: 8–7.1 (6H, m), 5.64 (2H, s), 5.33 (2H, s); *m/e* 186; positive iodine test.

*Reduction of **14***

To a solution of peroxide **14** (15 mg) in 5 ml THF was added 20 mg of $LiAlH_4$. The solution was stirred at room temperature for 10 min. Water (0.5 ml) was slowly added. The solution was filtered and the filtrate washed neutral with water, dried with anhydrous $MgSO_4$, and evaporated to yield a solid material (15 mg); mp ($CHCl_3$) 123–124°C (lit (21) 126°C).

*meso-9,10-Dihydroxy-9,10-diphenyl Anthracene, **17***

Peroxide **16** (1.0 g, 2.76 mmol) was added to a stirring mixture of potassium superoxide (2.4 g, 34 mmol) in dry DMF (100 ml) under N_2. After 5 days, the mixture was poured into ice-water and worked up with ether. The ethereal solution, after concentration, gave 1 g of crude product which recrystallized in chloroform–benzene to give 0.80 g of pure **17**, mp 255–256°C (lit. (19) 256°C).

*Reaction of **2** and **7** with KO_2*

Peroxide **2** (or **7**) was added to a stirring mixture of potassium superoxide in dry DMF. The reaction was followed by tlc. After complete reaction of **2** (or **7**), the mixture was poured in ice-water and extracted by ether. The work-up of the ethereal solution gave a complex mixture of products as seen by the nmr spectrum of the product.

*Dynamic Studies of **1** and **6** with KO_2 in Crown Ether – THF by Nuclear Magnetic Resonance*

Dibromide **1***a* (26.4 mg, 0.1 mmol) was added to a suspension of potassium superoxide (14.2 mg, 0.2 mmol) and dicyclohexyl-crown ether 6 (20 mg) in 0.5 ml dry THF in a nmr tube. The reaction was followed by ^1H nmr. After 10 min, there was a formation of ~10% of **2**. The percentage of **2** did not increase with the time (the same after 10 h). With the time (about 30 min after mixing) **3** slowly formed to reach the maximum (~30%) after 10 h. The proportions of **1***a*, **2**, and **3** did not change with the time. More KO_2 was added (14.2 mg, 0.2 mmol) and in 5 min, all starting material **1** was consumed, raising the yield of **3**, but in the same time all of **2** was destroyed to an unidentified product (dec.).

The same observation was made with **6** in a similar reaction.

*Reaction of **7** with KO_2 in the Presence of Silica Gel*

Peroxide **7** in chloroform was added to a mixture of KO_2, crown ether, and silica gel in chloroform. The mixture was stirred for 30 min and passed through a short column of silica gel – chloroform. The chloroform solution was concentrated to give naphthalide, mp 206–207°C (recrystallization benzene) (lit. (18) 206°C); nmr ($CDCl_3$) δ 5.50 (2H, s), 7.50–8.50 (6H, m); ir (KBr) 1770, 1640, 1610, 1470, 1330, 1230 cm^{-1}; ms (70 eV) 184 (M^+).

*Thermal Stability of **2** and **7***

Peroxide **7** (40 mg) in CCl_4 in a nmr tube was heated in a CCl_4 bath. The reaction was followed by nmr. **7** was unchanged after 4 days.

Peroxide **2** in CCl_4 in a nmr tube was heated in a CCl_4 bath. After 15 h, 70% of **2** was consumed (by following the decrease of the integration of the CH_2 signal of **2** and formation of new signals in the aromatic area). After 5 days, all of the CH_2 signal had vanished. Only the aromatic signal was observed.

*Attempts to Prepare **3a** and **3b***

NaH (50%) in oil (350 mg, 7 mmol) was added to a solution of phthalanol **5** (0.610 g, 4.5 mmol) in dry THF (20 ml) under nitrogen. The mixture was stirred and refluxed overnight. Dibromide **1***a* (1.18 g, 4.5 mmol) in 5 ml THF was slowly added and the mixture refluxed for 10 h. The mixture was then worked up to give, after separation by tlc, starting materials.

Different attempts were made in benzene, ether, and chloroform but without success.

Acknowledgements

We gratefully acknowledge financial support from the National Research Council of Canada and the Centre National de Recherche Scientifique (CNRS), France.

1. P. F. Knowles, J. F. Gibson, F. M. Pick, and R. C. Bray. Biochem. J. **111**, 53 (1969).
2. T. C. Pederson and S. D. Aust. Biochem. Biophys. Res. Commun. **48**, 789 (1972).
3. I. Fridovich. Biochem. Soc. Trans. **1**, 48 (1973).
4. R. A. Johnson and E. G. Nidy. J. Org. Chem. **40**, 1680 (1975).

5. R. A. JOHNSON. Tetrahedron Lett. 331 (1976).
6. E. J. COREY, K. C. NICOLAOU, M. SHIBASEK, Y. MACLUDA, and C. S. SHINER. Tetrahedron Lett. 3183 (1975).
7. T. YAMAGUCHI and H. C. VAN DER PLAS. Rec. Trav. Chim. Pays-Bas, **96**, 89 (1977).
8. A. FRIMER and I. ROSENTHAL. Tetrahedron Lett. 2809 (1976).
9. P. F. LEVONOWICH, H. P. TANNENBAUM, and R. C. DOUGHERTY. J. Chem. Soc. Chem. Commun. 597 (1975).
10. R. R. FRASER and R. N. RENAUD. Can. J. Chem. **49**, 755 (1971).
11. C. M. BOWES, D. F. MONTECALVO, and F. SONDHEIMER. Tetrahedron Lett. 3181 (1973).
12. J. S. SAN-FILIPPO, L. J. ROMANO, C. I. CHERN, and J. S. VALENTINE. J. Org. Chem. **41**, 586 (1976).
13. J. W. PETERS and C. S. FOOTE. J. Am. Chem. Soc. **98**, 875 (1976).
14. R. N. MOORE and R. V. LAWRENCE. J. Am. Chem. Soc. **81**, 458 (1959).
15. D. M. FINDLAY and M. F. TCHIR. J. Chem. Soc. Chem. Commun. 154 (1976).
16. W. RIED. Chem. Ber. **89**, 708 (1956).
17. E. HESSERT. Chem. Ber. **10**, 1448 (1877).
18. F. MAYER, W. SCHAEFER, and J. ROSENBACH. Arch. Pharm. Weinheim, Ger. 584 (1929).
19. A. MUSTAFA. J. Chem. Soc. 2435 (1952).
20. G. WITTIG and H. LUDWIG. Ann. Chem. Paris, **589**, 55 (1954).
21. F. WEYGAND, K. G. KINKEL, and D. TIETJEN. Chem. Ber. **83**, 394 (1950).
22. D. BEHAR, G. CZAPSKI, J. RABANI, L. M. DORFMAN, and H. A. SCHWARZ. J. Phys. Chem. **74**, 3209 (1970).

Preparation of *N,N,N′,N′*-tetramethylphosphorodiamidate intermediates for reductive deoxygenation of alcohols using *N,N*-dimethylphosphoramidic dichloride

HSING-JANG LIU, SING PING LEE, AND WING HONG CHAN

Department of Chemistry, University of Alberta, Edmonton, Alta., Canada T6G 2G2

Received May 17, 1977

HSING-JANG LIU, SING PING LEE, and WING HONG CHAN. Can. J. Chem. **55**, 3797 (1977).

Treatment of alcohols with *n*-butyllithium and *N,N*-dimethylphosphoramidic dichloride followed by addition of dimethylamine gave rise to *N,N,N′,N′*-tetramethylphosphorodiamidates, intermediates involved in a process for reductive deoxygenation of alcohols. This procedure should prove especially useful for alcohols in which the hydroxyl group is sterically hindered.

HSING-JANG LIU, SING PING LEE et WING HONG CHAN. Can. J. Chem. **55**, 3797 (1977).

Le traitement d'alcools avec le *n*-butyllithium et du *N,N*-diméthyl amidodichlorophosphate suivi d'une addition de diméthylamine conduit aux *N,N,N′,N′*-tétraméthyl phosphorodiamidates qui sont des intermédiaires impliqués dans un processus de déoxygénation des alcools. Cette procédure peut s'affirmer spécialement dans le cas des alcools ayant un groupement hydroxyle stériquement encombré.

[Traduit par le journal]

Recently, Ireland and his co-workers (1) reported an elegant method for replacing a hydroxyl group with a hydrogen, a process which is often required in organic synthesis. They showed that alcohols could be readily converted to the corresponding *N,N,N′,N′*-tetramethylphosphorodiamidates (TMPDA) by reacting the alkoxide anion with *N,N,N′,N′*-tetramethyldiamidophosphorochloridate and that subsequent treatment of the TMPDA derivatives with lithium–ethylamine resulted in reductive cleavage of the carbon–oxygen bond to give the deoxygenation products in high yields (Scheme 1). During the course of our synthetic studies on 5-epikessane (**1**), it became necessary to remove the hydroxyl group of alcohol **2**[1] and therefore the preparation of its TMPDA derivative was attempted. Apparently due to the steric congestion of the hydroxyl group, **2** was found to be completely unreactive towards *N,N,N′,N′*-tetramethyldiamidophosphorochloridate; under both the reported reaction conditions and modified conditions, the starting material was recovered intact. As a consequence of these findings an alternative method for preparing the TMPDA derivative of **2** was required. We wish to report a procedure for the formation of TMPDA from alcohols, which *should prove especially useful* for

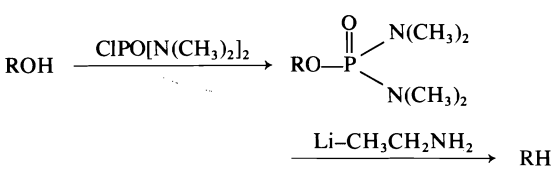

SCHEME 1

those alcohols in which the hydroxyl group is *highly hindered.*

The present procedure involves the use of the more reactive *N,N*-dimethylphosphoramidic dichloride (DMPADC) (2) as the phosphorylating reagent. In contrast to its observed lack of reactivity towards *N,N,N′,N′*-tetramethyldiamidophosphorochloridate, the anion of **2** generated by *n*-butyllithium reacted smoothly with DMPADC in 1,2-dimethoxyethane and *N,N,N′,N′*-tetramethylethylenediamine. At room temperature, the phosphorylation was found to be complete within 16 h. The resulting monochloride **3**, which was shown by thin-layer chromatography to be the sole product, was conveni-

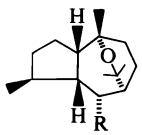

1 R = H
2 R = OH
3 R = $OPO(Cl)N(CH_3)_2$
4 R = $OPO[N(CH_3)_2]_2$

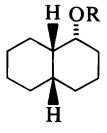

5 R = H
6 R = $PO[N(CH_3)_2]_2$
7 R = $PO(Cl)N(CH_3)_2$

[1]Preparation of **2** will be reported elsewhere in connection with the total synthesis of **1**.

TABLE 1. Preparation of TMPDA from alcohols $ROH \xrightarrow[(3)\ (CH_3)_2NH]{(1)\ n\text{-BuLi};\ (2)\ PO(Cl)_2N(CH_3)_2} ROPO[N(CH_3)_2]_2$

Alcohol	Reaction time (h): Before addition of $(CH_3)_2NH$	Reaction time (h): After addition of $(CH_3)_2NH$	Isolated yield of TMPDA (%)	Physical data of TMPDA: Infrared (neat) (cm^{-1})	Physical data of TMPDA: Nuclear magnetic resonance (CCl_4) δ	Physical data of TMPDA: Analysis
2	16	1	95	990, 1230, 1460[c]	1.02 (d, 3H, J = 6.5 Hz), 1.16 (s, 3H), 1.28 (s, 3H), 1.50 (s, 3H), 2.66 (d, 12H, J = 10 Hz), 4.65 (m, 1H)	ms M^+ 372.2545 (calcd. for $C_{19}H_{37}N_2O_3P$: 372.2548)
5	3	0.5	81	750, 990, 1225, 1305, 1460	2.55 (d, 12H, J = 10 Hz), and 4.14 (m, 1H)	ms M^+ 288.1968 (calcd. for $C_{14}H_{29}N_2O_2P$: 288.1967). *Anal.* calcd.: C 58.31, H 10.14, N 9.71; found C 58.58, H 10.24, N 9.43
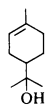	16	0.5	52[a]	760, 990, 1235, 1310, 1460	1.40 (s, 6H), 1.62 (s, 3H), 1.92 (m, 4H), 2.54 (d, 12H, J = 10 Hz), 5.32 (m, 1H)	ms m/e (M − 152) 136.1251 (calcd. for $C_{10}H_{16}$: 136.1252). *Anal.* calcd. for $C_{14}H_{29}N_2O_2P$: C 58.31, H 10.14; found C 58.34, H 10.41
$CH_3(CH_2)_{21}OH$	16	0.5	77	750, 980, 1225, 1300, 1460	0.89 (t, 3H, J = 5 Hz), 1.25 (b s, 40H), 2.57 (d, 12H, J = 10 Hz,) 3.78 (dd, 2H, J = 13, J' = 7.5 Hz)	ms M^+ 460.4153 (calcd. for $C_{26}H_{57}N_2O_2P$: 460.4157)
$CH_3(CH_2)_{15}OH$	5	0.5	80	760, 990, 1230, 1300, 1465	0.88 (t, 3H, J = 6 Hz), 1.25 (b s, 28H), 2.60 (d, 12H, J = 11 Hz), 3.83 (dd, 2H, J = 13, J' = 7.5 Hz)	ms M^+ 376.3226 (calcd. for $C_{20}H_{45}N_2O_2P$: 376.3218). *Anal.* calcd.: C 63.79, H 12.05, N 7.44; found: C 63.51, H 12.15, N 7.32
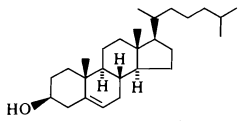	16	0.5	100[b]	905, 995, 1310 1470[c]	0.67 (s, 3H), 0.86 (d, 6H, J = 6 Hz), 0.90 (d, 3H, J = 6 Hz), 1.00 (s, 3H), 2.55 (d, 12H, J = 10 Hz), 4.00 (m, 1H), 5.37 (m, 1H)	ms m/e (M − 152) 368.3431 (calcd. for $C_{27}H_{44}$: 368.3442). *Anal.* calcd. for $C_{31}H_{57}N_2O_2P$: C 71.50, H 11.03, N 5.38; found: C 71.69, H 11.10, N 5.11

[a]A small amount of dehydration products was also obtained.
[b]The product was obtained as a solid. Recrystallization from petroleum ether gave a constant mp of 136–137°C.
[c]The spectrum was taken in chloroform.

ently converted to the TMPDA **4** by addition of dimethylamine prior to the work-up of the reaction. The material thus obtained was virtually free of impurities and a rapid column chromatography afforded a 95% yield of **4**[2]. The synthetic applicability of this procedure is further illustrated with decalol **5**. While **5** was found also unreactive with *N,N,N′,N′*-tetramethyldiamidophosphorochloridate, its reaction with DMPADC resulted in total consumption of the starting material in 3 h and its TMPDA derivative **6**[2] was isolated in 81% yield after brief treatment of the phosphorylation product **7** with dimethylamine. The procedure is apparently a general one. Additional examples are to be found in Table 1 which also summarizes the physical data of the TMPDA prepared by this method.

On the basis of the mode of reactions, monochlorides such as **3** and **7** could be logically assumed to be involved as the first-stage products (i.e. products formed before the addition of dimethylamine) in the described transformation $ROH \rightarrow ROPO[N(CH_3)_2]_2$. Experimentally, it was verified as follows. Treatment of **5** with DMPADC without the subsequent addition of dimethylamine (*vide supra*) gave rise, as expected, to **7**[3,4], the structure of which was clearly indicated by its nmr [(CCl_4) δ 2.65 (d, 6H, J = 10 Hz, $-N(CH_3)_2$) and 4.48 (m, 1H, —CHO—)] and mass spectra [M^+ 279.1153 and 281.1128 (Anal. calcd. for $C_{12}H_{23}ClNO_2P$: 279.1155 and 281.1126)].

Experimental

General and Material

Elemental analyses were performed by the microanalytical laboratory of this department. Melting points were determined on a Kofler hot stage apparatus and are uncorrected. Infrared (ir) spectra were recorded on a Perkin-Elmer model 457 or 257 grating infrared spectrophotometer. Nuclear magnetic resonance spectra were recorded on Varian A-60, 90 MHz Perkin-Elmer 32 and HR-100 spectrometers using tetramethylsilane as internal standard. The following abbreviations are used: s = singlet, d = doublet, t = triplet, and m = multiplet. Mass (ms) spectra were recorded on an AEI MS-50 mass spectrometer.

With the exception of **2**[1] and **5**[5], commercially available alcohols were used without purification. DMPADC was prepared according to a reported procedure (2).

Preparation of TMPDA Derivatives of Alcohols

Other than reaction time (see Table 1), the conditions used for the transformation of the six alcohols studied to their TMPDA derivatives were identical to those illustrated below with 1-hexadecanol. Physical data and yields of all the products are compiled in Table 1.

To a solution of 1-hexadecanol (485 mg, 2 mmol) in 1,2-dimethoxyethane–*N,N,N′,N′*-tetramethylethylenediamine (4:1; 8 ml) was added a 2.38 *M* solution of *n*-butyllithium in hexane (1.3 ml; 3 mmol) under a nitrogen atmosphere. After stirring at room temperature for 15 min, DMPADC (1.619 g, 10 mmol) was introduced. Stirring was continued for 5 h at which time complete disappearance of the starting material was observed (thin-layer chromatography). An excess of dimethylamine (ca. 5 ml) was added at 0°C and after 30 min the reaction mixture was poured into water and extracted with ether. The extracts were washed three times with saturated aqueous sodium chloride solution, combined, dried with magnesium sulfate, and filtered. Concentration of the solution gave an oil which was subjected to silica gel column chromatography. Elution with ether afforded 590 mg of the corresponding TMPDA.

Acknowledgments

We are grateful to the National Research Council of Canada and the University of Alberta for financial support.

1. R. E. Ireland, D. C. Muchmore, and U. Hengartner. J. Am. Chem. Soc. **94**, 5098 (1972).
2. E. N. Walsh and A. D. F. Toy. Inorg. Synth. **7**, 69 (1963).
3. Z. Skrowaczewska and P. Mastalerz. Rocz. Chem. **27**, 443 (1953); Chem. Abstr. **49**, 3876 (1955).

[2]Upon treatment with lithium–ethylamine, both TMPDA **4** and **6** underwent smoothly the reductive cleavage of the C—O bond. Under the reported conditions (1), **6** afforded *cis*-decalin in 70% yield and a 75% yield of 5-epikessane (**1**) was obtained from **4**.

[3]This compound was found to be rather unstable. Satisfactory yield (55%) of the pure material was obtained by rapid column chromatography of the crude product on silica gel with ether–benzene (1:9) elution.

[4]Several *N,N*-dimethylphosphoramidic chlorides have previously been prepared by the reaction of DMPADC with sodium alkoxide – phenoxide (see ref. 3 for example). We are grateful to one of the referees for drawing our attention to this aspect.

[5]We wish to thank Professor W. A. Ayer for a generous gift of this alcohol.

Amino group acidity in aminopyridines and aminopyrimidines[1]

MADELEINE G. HARRIS AND ROSS STEWART

Department of Chemistry, University of British Columbia, Vancouver, B.C., Canada V6T 1W5

Received March 28, 1977

MADELEINE G. HARRIS and ROSS STEWART. Can. J. Chem. **55**, 3800 (1977).

The acidities of the amino group in 18 heterocyclic compounds, nine pyridines, eight pyrimidines, and one triazine, have been measured. The pK_{HA} values (standard state water) were calculated using the Bunnett–Olsen and Marziano–Cimino–Passerini extrapolative techniques from ultraviolet spectral changes accompanying ionization of the amino group in aqueous DMSO containing base. These compounds, together with seven anilines previously studied, constitute a well-behaved Hammett system (σ dependency) with a ρ value of 5.20, provided compounds containing nitro groups *ortho* or *para* to the amino group are excluded. The acid-strengthening effect of aza groups is additive and appears to be primarily due to induction rather than resonance, in contrast to the behaviour of the nitro group.

MADELEINE G. HARRIS et ROSS STEWART. Can. J. Chem. **55**, 3800 (1977).

On mesure les acidités du groupe aminé de 18 composés hétérocycliques: neuf pyridines, huit pyrimidines et une triazine. Les valeurs de pK_{HA} (l'état fondamental, l'eau) sont calculées en utilisant les techniques d'extrapolation Bunnett–Olsen et Marziano–Cimino–Passerini à partir des variations du spectre ultraviolet accompagnant l'ionisation du groupe aminé dans une solution aqueuse de DMSO contenant une base. Ces composés, réunis avec sept anilines étudiées antérieurement, constituent un système se comportant selon Hammett (dépendant de σ) avec une valeur de ρ de 5.20; on ne peut admettre des composés contenant des groupes nitro en *ortho* ou *para* du groupe aminé. L'effet qui renforce l'acidité des groupes aza est additif et semble être causé principalement par de l'induction plutôt que par de la résonance en opposition avec le comportement du groupe nitro.

[Traduit par le journal]

Introduction

During the past 15 years polar aprotic solvents such as dimethyl sulfoxide (DMSO), sulfolane, and hexamethylphosphoramide have been widely used to increase the basicity of hydroxide ion towards carbon and nitrogen acids (1). We have previously developed acidity functions for such systems and determined acidity constants of a number of anilines and diphenylamines (2). We now turn our attention to the amino group acidity in amino-substituted nitrogen-containing heterocyclic systems. There are two reasons for so doing. First, useful information can be obtained regarding the effect of aza substitution on reactivity. Secondly the amino-substituted heterocycles adenine, guanine, and cytosine are of great biological interest, since the amino groups of these nucleotide bases participate in hydrogen-bonding in the double-stranded DNA helix. Indeed, the rate of hydrogen exchange in DNA has been linked to the acidity of the amino hydrogens in such compounds (3).

The present paper is concerned with a determination of the pK_{HA} values of the amino group in 18 aza-substituted anilines (nine aminopyridines, eight aminopyrimidines, and one aminotriazine) together with an analysis of the effect of the aza group on acidity. The following paper (36) deals with the acidities of the nucleotide bases, which, because of the smaller spectral changes that accompany ionization, present special difficulties in the determination of pK.

Although pK_{HA} is defined in terms of simple proton dissociation (1, 2) the reaction that takes place in the systems described herein can be illustrated as follows.

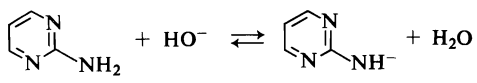

Competition from what is presumed to be hydroxide addition occurred in a few instances.

Experimental

Preparation of Compounds

Compounds **1–5**, **8**, **11–14**, **17**, and **19** (Table 1) were obtained commercially and purified by recrystallization or sublimation. Where discrepancies (usually minor) were noted with literature properties elemental and spectral analyses were performed.

[1]Taken in part from the Ph.D. Thesis of Madeleine G. Harris, University of British Columbia, Vancouver, B.C. 1976.

TABLE 1. Spectral data for neutral and anionic forms of **1–19**

Compound[d]	Neutral molecule[a] λ_{max} (nm)	Neutral molecule[a] log ε	Anion[b] λ_{max} (nm)	Anion[b] log ε
1 2-Aminopyridine	298.5	3.58	378	3.39
2 2-Amino-5-chloropyridine	314	3.54	395	3.31
3 2-Amino-3,5-dichloropyridine	321	3.72	397	3.54
4 2-Amino-3-nitropyridine	398	3.86	523	3.96
5 2-Amino-5-nitropyridine	362	4.22	445	4.46
6 2-Amino-3-chloro-5-nitropyridine	359	4.20	439	4.46
7 2-Amino-3,5-dinitropyridine	375(sh)	3.94	489	4.02
8 4-Aminopyridine	275(sh)	3.25	291	4.18
9 4-Amino-3-nitropyridine	368	3.69	468	3.84
10 4-Amino-3,5-dinitropyridine	383	3.85	[c]	
11 2-Aminopyrimidine	298	3.52	373	3.30
12 2-Amino-4-chloropyrimidine	300	3.57	360	3.63
13 2-Amino-4,6-dichloropyrimidine	301	3.60	351	3.38
14 2-Amino-5-nitropyrimidine	333	4.16	412	4.38
15 4-Aminopyrimidine	274	3.49	324	3.27
16 4-Amino-2-chloropyrimidine	277	3.60	319	3.35
17 4-Amino-2,6-dichloropyrimidine	278	3.55	320	3.27
18 4-Amino-2-chloro-5-nitropyrimidine	348	3.78	430	3.76
19 2-Amino-*s*-triazine	266	3.29	316	3.06

[a]In DMSO.
[b]In 96–99.5% DMSO containing hydroxide or *tert*-butoxide ion.
[c]Initial red colour fades within seconds to yellow, owing probably to Meisenheimer adduct formation (35). Acidification restores spectrum of neutral **10**.
[d]The numbering of the pyridine, pyrimidine, and triazine rings is as follows:

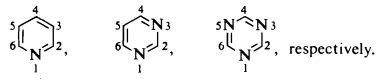

respectively.

*2-Amino-3-chloro-5-nitropyridine (**6**)*

2-Amino-5-nitropyridine (1.39 g) in ethanol (100 ml) was treated with chlorine gas for a few minutes at 0°C until the solution turned bright orange. Evaporation of the solvent gave an orange oil. Addition of 20 ml water effected the precipitation of a rust-coloured solid, which was collected, washed with water, and dried. Two-fold recrystallization from ethanol (charcoal), then from ethanol alone, gave light yellow needles, mp 207–209.5°C (lit. (4) 211–213°C; (5) 205–206°C). *Anal.* calcd. for $C_5H_4N_3O_2Cl$: C 34.60, H 2.32, N 24.22; found: C 34.54, H 2.42, N 23.93.

*2-Amino-3,5-dinitropyridine (**7**)*

2-Amino-3-nitropyridine was converted to 2-nitramino-3-nitropyridine by the method of Talik and Talik (6). It isomerized to the dinitro compound upon standing in concentrated sulfuric acid for 24 h. Recrystallization from ethanol gave orange–yellow needles, mp 189.5–190.5°C (lit. (7) 190–191°C).

*4-Amino-3-nitropyridine(**9**)*

A modification of the procedure of Koenigs *et al.* (8) was used. A suspension of 4-aminopyridine (5 g) and 20 ml of concentrated sulfuric acid was kept at 0–10°C while fuming nitric acid (3.5 g) was added over a period of 30 min. The mixture was brought to room temperature, stirred for 60 min, and then poured onto ice. After overnight storage the mixture was filtered and the filtrate treated with concentrated aqueous ammonia. The resulting precipitate was crystallized from water to give yellow needles of 4-nitraminopyridine, mp 235°C (violent dec.). This compound (2 g) was added carefully to concentrated sulfuric acid (10 ml) to form a dark red solution, which was maintained at 90°C for 1 h. The solution was cooled to room temperature, left overnight, then poured onto crushed ice, and made just neutral with concentrated aqueous ammonia. Upon standing at 0°C, a granular dark brown solid precipitated. Recrystallization once from 80% ethanol, then twice from water (charcoal) gave a chartreuse-coloured powder, mp 203–204.5°C (lit (9) 200°C (dec.); (10) 200–202°C; (11) 204°C). *Anal.* calcd. for $C_5H_5N_3O_2$: C 43.16, H 3.63, N 30.21; found: C 43.14, H 3.81, N 30.24. (An elemental analysis was conducted because of discrepancies between observations made during the synthesis and those reported in the literature (8).)

*4-Amino-3,5-dinitropyridine (**10**)*

Prepared by the method of Koenigs *et al.* (9), but using an excess of sulfuric and nitric acids: light yellow needles, mp 169–171°C (lit. (9) 170–171°C; (12) 168–169°C).

*4-Aminopyrimidine (**15**)*

Kindly supplied by D. J. Brown; mp 149.5–151.5°C.

*4-Amino-2-chloropyrimidine (**16**)*

This compound was prepared from 2,4-dichloropyrimidine and ammonia by the method of Ballweg (13). Sublimation and recrystallization from water gave colourless needles, mp ~200°C, with decomposition to a red tar (lit. (14) 206–207°C; (15) 219–220°C; (16) 209–210°C). A satisfactory nmr spectrum was obtained.

*4-Amino-2-chloro-5-nitropyrimidine (**18**)*

Purified 2,4-dichloro-5-nitropyrimidine was treated

with 1.5 *M* aqueous ammonia at 0°C. The resulting solid was recrystallized from water to give white crystals, mp 217.5–218°C after coloration at 206°C (lit. colours, 205°C, mp (17) 217°C; (18) 220–221°C).

Preparation of Solutions

Solutions containing up to 90 mol% DMSO were prepared as previously described (2). Those in the range 90–100% were prepared by adding anhydrous DMSO (purified over calcium hydride, distilled, and then subjected to zone-freezing) to reagent bottles in a nitrogen-filled dry box; the bottles were sealed with a rubber serum cap, removed from the dry box, and various volumes of water added by syringe through the serum cap. The bottles were stored in a desiccator when not in use. Karl Fischer analysis of the anhydrous DMSO indicated a water content of less than 0.005% by weight.

Tetramethylammonium hydroxide was added either as a 10% by weight aqueous solution, or as the solid pentahydrate in the dry box. Anhydrous solutions containing base tended to turn yellow within 1–2 days if care was not taken to exclude light and traces of air. Potassium *tert*-butoxide solutions were also prepared in the dry box using the pure solid. Titration with acid was used in all cases to determine the concentration of base present. A DMSO solution of the amino compound to be studied was injected by syringe to a serum-capped uv cell containing the DMSO solution and the spectrum recorded.

Treatment of Data

Substantial changes in their uv spectra accompany the conversion of most of the aminopyridines and aminopyrimidines to their anions (Table 1). As the mole fraction of DMSO is increased the wavelength maxima of both the un-ionized and ionized forms of all the indicators studied shift to the red. The λ_{max} of the neutral form usually shifts 1–2 nm and λ_{max} of the anion 3–5 nm over the region of 10–90% ionization, although shifts in the latter are as much as 10 nm in some cases. Furthermore the ε_{max} of the un-ionized and ionized forms generally increase with increasing DMSO content.

Medium effects on the spectrum of HA and A^- were corrected for using a combination of the methods of Hammett *et al.* (19) and Katritzky and co-workers (20). Measurements of ε were made at λ_{A^-} max observed for each DMSO–water solution examined. Occasionally, in solutions where the indicator was partially ionized, the spectrum of HA overlapped that of A^- to the extent that λ_{A^-} max could not be determined with certainty. It was observed experimentally, however, that λ_{A^-} max varied linearly with the acidity function H_- (determined using aromatic amines (2*a*)) for nearly all the indicators studied. Assuming that the rate of lateral shift of λ_{A^-} is the same within and without the region of ionization, values of λ_{A^-} max where $\varepsilon_{HA} = 0$ were plotted against H_- and the least squares straight line extrapolated to give λ_{A^-} max in the desired solution.

Values of ε thus obtained were plotted against H_- yielding good sigmoidal titration curves in every case. The inflection point was estimated by eye and was taken to correspond to 50% ionization. To ensure that the values of ε_{A^-} on the arm of the titration curve corresponded to values greater than 99% ionization, only values of ε_{A^-} in solutions of H_- at least three units greater than H_- at half-ionization were used. (Plots of log *I* vs. mol% DMSO for the aminopyridines and pyrimidines rose less steeply than similar plots for the anilines and diphenylamines used to define the H_- function.) Extrapolation of the linear arm of the titration curve (ε_{A^-} vs. H_-) gave the value of ε_{A^-} in each solution where the indicator was partially ionized.

When using DMSO–water solutions ε_{HA} may be directly determined in each solution by injecting a volume of water equal to the volume of base into the cell, or by omitting the injection of extra water altogether with an appropriate correction in ε_{HA} due to the changed concentration. In practice, however, values of ε_{HA} were smoothed out by plotting against H_-. The ionization ratio *I* was then calculated for each solution using the equation $I = [A^-]/[HA] = \varepsilon - \varepsilon_{HA}/\varepsilon_{A^-} - \varepsilon$, where ε is the measured extinction coefficient at λ_{A^-}, and ε_{HA} and ε_{A^-} are the corrected extinction coefficients at this wavelength of the neutral and anionic species, respectively.

Acidity function studies often make use of ionization ratio data and we have deposited such data for the compounds described herein with the Depository of Unpublished Data,[2] together with sundry observations of the spectral changes that accompany ionization.

Results

The compounds studied in this work did not obey H_-, the acidity function derived using anilines and diphenylamines (2*a*). Although plots of log *I* of the indicators against H_- were invariably linear, the slopes were usually less than unity. The pK_{HA} of a given indicator may be arrived at without the construction of an appropriate acidity function by using two extrapolative procedures: the Bunnett–Olsen method (21) (the B.O. method) and the Marziano–Cimino–Passerini method (22) (the M.C.P. method). Both of these methods, originally derived for acid systems, have been adapted to basic DMSO–water systems by Cox *et al.* (23).

It was observed that, for most of the compounds studied in this work, log *I* varies linearly with mol% DMSO. (This data is also deposited with the Depository of Unpublished Data.[2]) Non-linear plots were observed only for indicators ionizing at high mol% DMSO. These observations suggest that log *I* values of the indicators are linear functions of one another as the DMSO content is varied.

The equations used to calculate pK_{HA} by the B.O. method is [1], and that used in the M.C.P. method is [2].

$$[1]\quad H_- - \log I = \phi(H_- - pK_w - \log [HO^-] + \log a_{H_2O}) + pK_{HA}$$

[2]Complete set of tabular data is available, at a nominal charge, from the Depository of Unpublished Data, CISTI, National Research Council of Canada, Ottawa, Canada K1A 0S2.

TABLE 2. Acidity constants[a] determined by the B.O. and M.C.P. methods

Compound	B.O. method		M.C.P. method			
	ϕ	pK_{HA}	Correlation coefficient	m^*	pK_{HA}	pK_{HA} (average)
			Pyridines			
1	−0.150	23.50	0.992	0.924	23.48	23.5
2	−0.184	21.74	0.999	0.905	21.88	21.8
3	+0.010	20.87	0.991	1.037	20.65	20.8
4	−0.195	16.65	0.999	0.887	16.76	16.7
5	−0.272	15.69	0.999	0.803	15.84	15.8
6	−0.062	14.84	0.999	1.009	14.99	14.9
7	−0.087	13.75	0.999	1.143	13.87	13.8
8	−0.156	22.26	0.990	0.927	22.33	22.3
9	−0.068	15.82	0.999	1.046	16.08	15.9
			Pyrimidines			
11	−0.353	19.78	0.992	0.885	21.24	20.5
12	−0.308	18.20	0.999	0.715	18.07	18.1
13	−0.268	16.61	0.998	0.809	16.77	16.7
14	−0.179	14.60	0.999	0.881	14.72	14.7
15	−0.265	18.53	0.996	0.724	18.18	18.4
16	−0.322	16.34	0.995	0.741	16.45	16.4
17	−0.328	15.07	0.999	0.760	15.29	15.2
18	−0.407	13.33	0.996	0.608	13.36	13.3
19	−0.542	14.91	0.998	0.492	14.94	14.9

[a] $K_{HA} = [H^+][ArNH^-]/[ArNH_2]$ in standard state, water.

H_- is a suitable acidity function, that determined for aromatic amines in the present case, and K_w and a_{H_2O} are the dissociation constant and activity (23, 24), respectively, of water.

$$[2] \quad pK_w + \log [HO^-] - \log a_{H_2O} - \log I = m^* \log (f_{A^-*}/f_{HA*} f_{HO^-}) + pK_{HA}$$

Here f_{A^-*} and f_{HA*} are the activity coefficients of a reference acid, in this case 2,4,4′-trinitrodiphenylamine. Using [1] the quantity $H_- - \log I$ is plotted against $(H_- - pK_w - \log [HO^-] + \log a_{H_2O})$ to give pK_{HA} as the intercept and ϕ as the slope. In analogous fashion [2] gives pK_{HA} as intercept and m^* as slope. The value of pK_w at 25°C has been taken as 13.996 (23). Table 2 contains the values of the acidity constants of the aminopyridines and aminopyrimidines determined by the B.O. method and the ϕ values obtained.

Table 2 also contains the pK_{HA} values obtained by the M.C.P. procedure, the values of log $(f_{A^-*}/f_{HA*} f_{HO^-})$ being taken from the values determined by Cox and Stewart (23*a*). The correlation coefficients are remarkably high for most of the compounds studied. (Correlation coefficients have little significance in the B.O. treatment when ϕ is small and they have accordingly not been given in Table 2.) It can be seen that the B.O. and M.C.P. methods give values in good agreement for all compounds except **11**.

Could these acidity constants have been determined using the standard acidity function approach? If the pyridines and pyrimidines were perfectly behaved indicators with respect to the aniline scale H_-, one would simply read off the H_- value at half-ionization to obtain pK_{HA}. In fact, the pyridines and pyrimidines give highly linear plots of log I against H_-, but the slopes vary between 0.8 and 1.1, most of them being less than unity. Not surprisingly, in several instances H_- at half-ionization is more than one pK unit different from the average values recorded in Table 2.

There are sufficient data available from the present work to enable an acidity function to be determined that would better reflect the ionization behaviour of pyridines and pyrimidines than does H_-, and such a function is described (reluctantly) in the accompanying paper (36).

Discussion

Cox and Stewart (23*a*) have proposed that a given set of indicators form an adequate acidity function set if their m^* values lie within a range of $m_{av}^* \pm 0.100$. Applying this criterion, the aminopyridines form such a set, $m_{av}^* = 0.962$

$\pm$ 0.084, if 2-amino-5-nitropyridine, **5**, and 2-amino-3,5-dinitropyridine, **7**, are omitted. The 2- and 4-aminopyrimidines, with the exception of 4-amino-2-chloro-5-nitropyrimidine, **18**, form another set, $m_{av}^* = 0.788 \pm 0.097$.

The value of m_{av}^* for the mono-aza compounds, the pyridines, is only slightly less than unity, but that for the di-aza compounds, the pyrimidines, is markedly less. More significant, perhaps, is the fact that the tri-aza compound, **19**, has a m^* value of only 0.492 (Table 2). Clearly, insertion of nitrogen atoms in the aromatic ring causes deviations from normal behaviour, using H_- and aromatic amines as the standard for comparison, and it is worthwhile speculating upon the reasons for this effect.

It can be readily shown that a less-than-unit value of m^* results from activity coefficient behaviour in the mixed solvent of the following type,

$$f_{A^-}/f_{HA^*} < f_{P^-}/f_{HP}$$

where HP and P represent the aza compounds and HA* and A* represent the reference compound and, hence, the entire aniline and diphenylamine series. Such behaviour can be associated with the extent of delocalization of charge in the anion of the compounds undergoing dissociation. Those with small degrees of charge delocalization, alcohols and to a lesser extent, phenols, will have small values of m^* (again using anilines as the reference), which corresponds to a flat acidity function vs. solvent composition curve. (This analysis ignores the contribution of changes in the activity coefficient of the neutral compounds with changing medium, a common but not always reliable practice (25).)

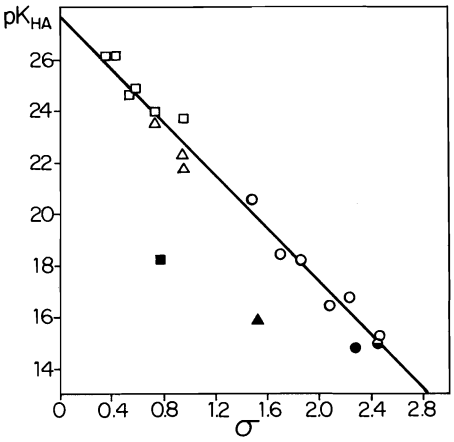

FIG. 1. Hammett plot for the acidity of pyridines (triangles), pyrimidines (circles), anilines (squares), and triazine (half-filled circle). The filled symbols represent compounds in which a nitro group is *para* to the anionic centre. In order of decreasing acidity the compounds are **14**, **19**, **17**, **5**, **16**, **13**, **12**, 4-nitroaniline, **15**, **11**, **2**, **8**, **1**, 3,4,5-trichloroaniline, 3,5-dichloroaniline, 3,4-dichloroaniline, 3-cyanoaniline, 3-trifluoromethylaniline, and 3-chloroaniline; the pK_{HA} values of the named compounds come from ref. 23*a*. The substituent constants come from refs. 27 and 31 The rho value is 5.20 (correlation coefficient 0.992), neglecting the *para* nitro compounds.

Consider the two compounds 4-nitroaniline, p*K* 18.2 (23*a*), and 4-aminopyrimidine, p*K* 18.4, both of which are measurably ionized in 70 mol% DMSO containing 0.01 *M* hydroxide ion. The lower value of m^* for the latter compound (0.724, compared to 0.958 (23*a*)) suggests that there is less formal delocalization of charge in the pyrimidine anion X than in the nitrophenyl anion Y, despite the presence of two loci for such charge dispersal in the former case.

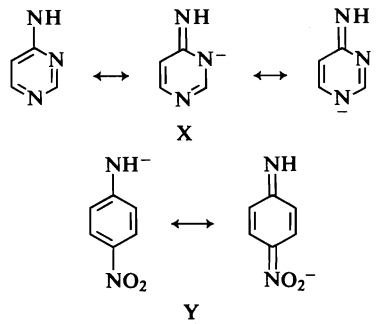

X

Y

Previous work indicated that a *para* nitro substituent was extraordinarily proficient at dispersing negative charge in nitrogen and carbon anions, as revealed by the requirement for a greatly exalted value of σ^- for this group (26). On the other hand, as shown below, the aza substituent does not even require the use of the σ^- constant to correlate acidities, and this suggests that the aza substituent operates mainly by induction, in agreement with the activity coefficient argument delineated above.

Substituent constants for the aza group have been determined by Deady and co-workers (27) using the basic hydrolysis rates of methyl pyridine carboxylates in 85% methanol at 25°C, and a ρ value of 2.26, established for the basic hydrolysis of methyl benzoates using the same reaction conditions. The values for the aza substituent were $\sigma_{2N} = 0.75$, $\sigma_{3N} = 0.65$, and

$\sigma_{4N} = 0.96$, in good agreement with the σ_N values obtained previously using data for the basic hydrolysis of ethyl benzoates (28). (The steric effect of an aza substituent is negligible and for this reason the 2-aza group is better behaved than are ordinary *ortho* substituents.)

The additivity of aza substituent constants has been demonstrated by Deady *et al.* (29) using the basic hydrolysis rates of six methyl diazine carboxylates in 85% methanol at 10°C. Excellent correlations were obtained, even when the aza groups were adjacent to each other. Such additivity is consistent with the results of Chan and Miller (30) on the rate of nucleophilic substitution of chlorodiazines with *p*-nitrophenoxide ion.

The acidities of *meta* and *para* substituted anilines and their aza derivatives (including the 2-aza substituent) have been correlated with the substituents' Hammett σ values (31) in Fig. 1. An excellent correlation is obtained (correlation coefficient 0.992), provided *para* nitro substituted compounds are neglected. This substituent, of course, is able to conjugate directly with the negatively charged site, and we have previously observed that a greatly exalted value (considerably larger than σ^-) would be required to represent its acid-strengthening effect in aromatic amines. The enormous anion-stabilizing property of the nitro group that so affects the 4-nitroaniline equilibrium is very greatly reduced in the aza compounds. Indeed, in 2-amino-5-nitropyrimidine, **14**, the deviation in the Hammett plot is so modest that were σ^- to be used for the nitro group *para* to the amino group the conjugative effect would be overcompensated for.

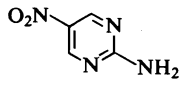

14

It is interesting to note that the aza group, to which the nitro group is sometimes compared (32, 33), shows no such tendency. That is, the effect of an additional aza group is essentially unaffected by the number of aza groups already present in the molecule. Substituting a single nitro group at the 4-position of aniline has a much greater acid-strengthening effect than does the substitution of an aza group at this position ($pK_{HA} = 18.2$ for 4-nitroaniline (23*a*) and 22.3 for 4-azaaniline, **8**). Indeed, two aza groups are required to roughly equal the effect of one nitro group; the pK_{HA} of 2,4-diazaaniline, **15**, is 18.4. However, addition of a third aza group produces a slightly *greater* increase in acidity than does the addition of a second nitro group, 3.5 p*K* units compared to ~3 for the nitro compounds (2*b*). This effect is reminiscent of the differing effects of nitro and cyano groups on the acidities of alkanes (26*a*, 34).

Included in Fig. 1 are all substituted anilines for which data is available, except 4-cyanoaniline. The cyano group is in direct conjugation with the anionic site and it has been omitted, although its degree of deviation is not particularly great.

The plot in Fig. 1, covering some 11 p*K* units, extrapolates to a value of 27.8, in reasonable agreement with the value of 27.3 previously estimated for the pK_{HA} of aniline (2*a*).[3] The slope of the line, 5.20, is somewhat larger than the ρ value for diphenylamines, 4.07 (2*a*). This result is not unexpected, since in the latter case two rings are involved in charge dispersal.

The fact that an excellent linear correlation between p*K* and σ is obtained over a range of some 11 p*K* units using compounds with multiple substituents shows not only that substituent effects in these systems are additive, but also that the aza group transmits effects through the ring to essentially the same extent as does trigonal carbon. That is, benzene and heterocyclic nuclei are similar in their ability to transmit electronic effects.

Acknowledgment

The financial support of the National Research Council is gratefully acknowledged.

1. (*a*) C. H. ROCHESTER. Acidity functions. Academic Press, London, England. 1970; (*b*) K. BOWDEN. Chem. Rev. **66**, 119 (1966).
2. (*a*) D. DOLMAN and R. STEWART. Can. J. Chem. **45**, 911 (1967); (*b*) R. STEWART and J. P. O'DONNELL. Can. J. Chem. **42**, 1681 (1964); (*c*) R. STEWART and J. P. O'DONNELL. J. Am. Chem. Soc. **84**, 493 (1962); (*d*) A. ALBAGLI, J. R. JONES, and R. STEWART. Can. J. Chem. **52**, 1059 (1974); (*e*) A. ALBAGLI, A. BUCKLEY,

[3]The pK_{HA} values used in the correlation in Fig. 1 are the average values listed in Table 2, together with the aniline values from ref. 23*a*. If the B.O. values are used a slightly higher correlation coefficient is obtained (0.993 compared to 0.992 for the average values), whereas the M.C.P. values give a slightly poorer correlation coefficient, 0.989. It is not possible to state at this point if the rather small difference in correlation coefficient obtained by the two methods is significant.

A. M. LAST, and R. STEWART. J. Am. Chem. Soc. **95**, 4711 (1973).
3. (*a*) M. P. PRINTZ and P. H. VON HIPPEL. Biochemistry, **7**, 3194 (1968); (*b*) M. P. PRINTZ and P. H. VON HIPPEL. Proc. Natl. Acad. Sci. U.S.A. **53**, 363 (1965).
4. A. H. BERRIE, G. T. NEWBOLD, and F. S. SPRING. J. Chem. Soc. 2590 (1951).
5. M. G. BYSTRITSKAYA and A. W. KIRSSANOW. J. Gen. Chem. USSR, **10**, 1827 (1940); Chem. Abstr. **35**, 4380 (1941).
6. T. TALIK and Z. TALIK. Rocz. Chem. **41**, 483 (1967).
7. A. E. TSCHITSCHIBABIN and A. W. KIRSSANOW. Chem. Ber. **61**, 1223 (1928).
8. E. KOENIGS, G. KINNE, and W. WEISS. Chem. Ber. **57**, 1172 (1924).
9. E. KOENIGS, M. MIELDS, and H. GURLT. Chem. Ber. **57**, 1179 (1924).
10. A. ALBERT and G. B. BARLIN. J. Chem. Soc. 5156 (1963).
11. J. W. CLARK-LEWIS and R. P. SINGH. J. Chem. Soc. 2379 (1962).
12. H. GRABOYES and A. R. DAY. J. Am. Chem. Soc. **79**, 6421 (1957).
13. H. BALLWEG. Annalen, **673**, 153 (1964).
14. S. GABRIEL. Chem. Ber. **38**, 1689 (1905).
15. G. E. HILBERT and T. B. JOHNSON. J. Am. Chem. Soc. **52**, 1152 (1930).
16. M. M. STIMSON. J. Am. Chem. Soc. **71**, 1470 (1949).
17. O. ISAY. Chem. Ber. **39**, 250 (1906).
18. F. S. OKAMURA, H. KUSAKA, and T. TAKEMATSU. Bull. Chem. Soc. Jpn. **33**, 1471 (1960).
19. L. A. FLEXSER, L. P. HAMMETT, and A. DINGWALL. J. Am. Chem. Soc. **57**, 2103 (1935).
20. (*a*) A. R. KATRITZKY, A. J. WARING, and K. YATES. Tetrahedron, **19**, 465 (1963); (*b*) C. D. JOHNSON, A. R. KATRITZKY, B. J. RIDGEWELL, N. SHAKIR, and A. M. WHITE. Tetrahedron, **21**, 1055 (1965).
21. J. F. BUNNETT and F. P. OLSEN. Can. J. Chem. **44**, 1899 (1966).
22. N. C. MARZIANO, G. M. CIMINO, and R. C. PASSERINI. J. Chem. Soc. Perkin Trans. II, 1915 (1973).
23. (*a*) R. A. Cox and R. STEWART. J. Am. Chem. Soc. **98**, 488 (1976); (*b*) R. A. COX, R. STEWART, M. J. COOK, A. R. KATRITZKY, and R. A. TACK. Can. J. Chem. **54**, 900 (1976).
24. S. Y. LAM and R. L. BENOIT. Can. J. Chem. **52**, 718 (1974).
25. R. A. COX, A. M. LAST, and R. STEWART. J. Chem. Soc. Perkin Trans. II, 1678 (1974).
26. (*a*) R. STEWART and D. DOLMAN. Can. J. Chem. **45**, 925 (1967); (*b*) R. STEWART and D. J. KROEGER. Can. J. Chem. **45**, 2173 (1967).
27. (*a*) A. D. CAMPBELL, S. Y. CHOOI, L. W. DEADY, and R. A. SHANKS. Austr. J. Chem. **23**, 203 (1970); (*b*) L. W. DEADY and R. A. SHANKS. Austr. J. Chem. **25**, 431 (1972).
28. H. H. JAFFE and H. LLOYD JONES. *In* Advances in heterocyclic chemistry. *Edited by* A. R. Katritzky. Academic Press, New York, NY. 1964. p. 209.
29. L. W. DEADY, D. J. FOSKEY, and R. A. SHANKS. J. Chem. Soc. B, 1962 (1971).
30. T. L. CHAN and J. MILLER. Austr. J. Chem. **20**, 1595 (1967).
31. C. D. JOHNSON. The Hammett equation. Cambridge University Press, Cambridge, England. 1973.
32. J. CLARK and D. D. PERRIN. Q. Rev. Chem. Soc. **18**, 295 (1964).
33. A. ALBERT. Heterocyclic chemistry. 2nd ed. Athlone Press, London, England. 1968.
34. D. J. CRAM. Fundamentals of carbanion chemistry. Academic Press, New York, NY. 1965. Chapt. 1.
35. F. TERRIER, A.-P. CHATROUSSE, and R. SCHAAL. J. Org. Chem. **37**, 3010 (1972).
36. R. STEWART and M. G. HARRIS. Can. J. Chem. This issue.

Amino group acidity in nucleotide bases[1]

ROSS STEWART AND MADELEINE G. HARRIS
Department of Chemistry, University of British Columbia, Vancouver, B.C., Canada V6T 1W5

Received March 28, 1977

ROSS STEWART and MADELEINE G. HARRIS. Can. J. Chem. **55**, 3807 (1977).

The acidities (standard state, water) of the amino groups in 17 *N*-alkylated derivatives of adenine, guanine, cytosine, and isocytosine have been determined in aqueous DMSO containing base. Adenine methylated at the 9-position is a weaker acid than its 7-methylated isomer by 2.0 pK units and this difference is explained in terms of the known stabilities of the parent tautomers. A similar situation exists with 1- and 3-methylcytosine ($\Delta pK = 3.3$). The position of alkylation of the isocytosine and guanine systems has a small or negligible effect on acidity, again consistent with known tautomeric effects. A modified ribosyl group attached to the 1-position of cytosine has an acid-strengthening effect of 1.9 units, relative to methyl. Of the amino groups involved in nucleotide base-pairing, that in the methyl derivative of guanine has the highest acidity, $pK_{HA} = 14.6$; those in the cytosine and adenine derivatives have identical acidities, 16.7. An acidity function for purines and pyrimidines is reported for aqueous DMSO containing 0.011 *M* tetramethylammonium hydroxide (H_-^P).

ROSS STEWART et MADELEINE G. HARRIS. Can. J. Chem. **55**, 3807 (1977).

On détermine les acidités (l'état fondamental, l'eau) du groupe aminé de 17 dérivés *N*-alkylés de l'adénine, guanine, cytosine et isocytosine dans une solution aqueuse de DMSO contenant une base. L'adénine méthylée en position 9 est un acide plus faible que son isomère méthylé en position 7 par 2.0 unités de pK. Cette différence est expliquée en termes de stabilités connues pour les tautomères parents. Une situation analogue existe dans le cas de la méthyl-1 et méthyl-3 cytosine ($\Delta pK = 3.3$). La position du groupe alkyle dans l'isocytosine et la guanine, a peu ou très peu d'effet sur l'acidité et compatible avec les effets tautomères connus. Un groupe ribosyle modifié, fixé à la position 1 de la cytosine a un effet qui renforce l'acidité de 1.9 unités par rapport au méthyle. De tous les groupes aminés impliqués dans l'appariement d'une nucléotide avec une base, c'est le dérivé méthylé de la guanine qui possède la plus grande acidité $pK_{HA} = 14.6$; pour les dérivés de la cytosine et adénine, ceux-ci ont des acidités identiques de 16.7. On décrit une fonction d'acidité pour les purines et pyrimidines dans une solution aqueuse de DMSO contenant 0.011 *M* d'hydroxyde de tétraméthylammonium (H_-^P).
[Traduit par le journal]

Introduction

In the accompanying paper we examined the acidity of the amino group in some substituted aza-benzenes: pyridines, pyrimidines, and *s*-triazine (1). Herein we extend the work to another important group of heterocyclic compounds, the nucleotide bases. The amino groups in such compounds are involved in the base-pairing interaction that is responsible for the replicating ability of nucleic acids and, indeed, the acidity of the amino hydrogens is believed to determine to a considerable extent the strength of the base-pairing interaction (2).

Of the four main nucleotide bases, cytosine **1**, uracil **2**, adenine **3**, and guanine **4**, only uracil does not possess an amino group, and hence it is not included in this study.

The other three compounds all have one or more acidic centres in addition to the amino group and to avoid interfering with the measurement of the latter's acidity the other centres have been alkylated. This has the further advantage of increasing the resemblance to the naturally occurring nucleosides, in which a ribose unit replaces the acidic hydrogen at such locations.

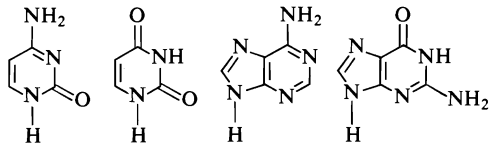

1 **2** **3** **4**

The 18 compounds studied in this work include two derivatives of cytosine, three of isocytosine **5**, eight of adenine, two of guanine, one of isoguanine **6**, and a cytidine **7**.

Most of the compounds display only modest spectral changes upon deprotonation, generally much less than for pyridines and pyrimidines,

[1]Taken in part from the Ph.D. thesis of Madeleine G. Harris, University of British Columbia, Vancouver, B.C. 1976.

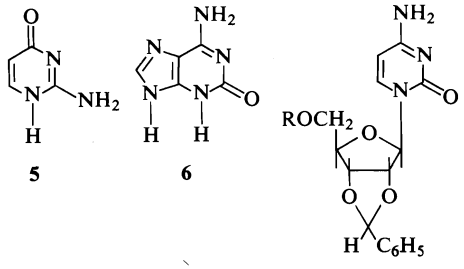

5 6

7, R = trityl

and special techniques were needed to determine their degrees of dissociation.[2] As before, aqueous dimethyl sulfoxide (DMSO) solutions containing added hydroxide ion were used to produce the basic media required to effect the deprotonation of the amino groups.

Experimental

Preparation of Compounds

Compounds **8**, **10**, **17**, **21**, and **22** (Table 1) were obtained from commercial sources and were purified by recrystallization. Elemental analyses were performed as checks on identity and purity.

*1-Methyl-5-bromocytosine (**9**)*

Prepared by bromination of 1-methylcytosine following the method of Doub and Krolls for the methyl analog (3). The compound was purified by chromatography on alumina to give yellow crystals, mp 210–211.5°C. *Anal.* calcd. for $C_5H_6N_3OBr \cdot \frac{1}{2}H_2O$: C 28.18, H 3.28, N 19.73, Br 37.50; found: C 28.25, H 3.30, N 19.51, Br 37.33. A complex of this compound has been previously reported (4).

*1-Methylisocytosine (**11**)*

Prepared by methylation of isocytosine with methyl iodide, essentially as described by Brown and Jacobsen (5); mp 280°C (dec.) (lit. (5) 283–285°C; (6) 275–280°C).

*3-Methylisocytosine (**12**)*

Kindly supplied by D. J. Brown; mp 257–260°C (lit. (5) 257–260°C).

*9-Methyladenine (**13**)*

Prepared from adenine and tetramethylammonium hydroxide (7). Sublimation and recrystallization gave white crystals, mp 305–306°C (lit. (7) 301–302°C).

*2-Chloro-9-methyladenine (**14**)*

2,6-Dichloropurine was methylated in DMSO with methyl iodide in the presence of potassium carbonate to give a mixture of the 7- and 9-methyl isomers (8). Separation of the isomers was best effected by chromatography over neutral alumina with ethyl acetate as eluant. The recrystallized 2,6-dichloro-9-methylpurine thus obtained was aminated (9) to give 2-chloro-9-methyladenine. Recrystallization from water gave white crystals which were dried *in vacuo* at 100°C before analysis. The compound turns yellow near 270°C but does not melt below 300°C; nmr δ 3.70 (s, 3H), 7.68 (m, 2H), 7.97 (s, 1H). *Anal.* calcd. for $C_6H_6N_5Cl$: C 39.23, H 3.27, N 38.15; found: C 39.26, H 3.14, N 38.45.

*2-Chloro-8-methoxy-9-methyladenine (**15**)*

2,8-Dichloro-9-methyladenine (0.05 g) was dissolved in 30 ml of warm methanol and a solution of 0.5 g of sodium hydroxide in 25 ml methanol added. The solution was refluxed for 5 h, then cooled to room temperature, and allowed to stand overnight. Recrystallization of the granular precipitate from 95% ethanol gave white crystals which were dried at 100°C *in vacuo* for 24 h before analysis, mp 270–270.5°C (dec.); nmr δ 3.43 (s), 4.12 (s), 7.28 (m). *Anal.* calcd. for $C_7H_8N_5OCl$: C 39.36, H 3.77, N 32.78; found: C 39.57, H 3.90, N 32.96.

*2,8-Dichloro-9-methyladenine (**16**)*

Uric acid was converted to 2,6,8-trichloropurine (10) and then methylated with methyl iodide (11). Treatment with ethanolic ammonia gave the product (12). White crystals, mp 266–268°C (lit. (12) 260–261°C).

*2-Chloro-7-methyladenine (**18**)*

Theobromine was converted to 2,6-dichloro-7-methylpurine (13) which was selectively aminated to the desired product as follows. A saturated solution of ammonia in methanol was heated in a sealed tube with 0.9 g of the dichloro compound at 90–100°C for 19 h. After work-up with base and then acid, followed by recrystallization, white needles were obtained; mp 284.5°C (gas evolution) (lit. (14, 15) 284°C (gas evolution)). Satisfactory elemental analyses and nmr spectra were obtained.

*2-Chloro-7-methyl-8-methoxyadenine (**19**)*

Prepared using Fischer's method (16) from **20**. White crystals which, upon heating, turn yellow at 227°C and melt at 248.5°C with gas evolution, nmr δ 3.67 (s, 3H), 4.12 (s, 3H), 7.03 (m, 2H). *Anal.* calcd. for $C_7H_8N_5OCl$: C 39.36, H 3.77, N 32.78; found: C 39.43, H 3.83, N 32.58.

*2,8-Dichloro-7-methyladenine (**20**)*

Prepared from theobromine according to the method of Fischer (14, 17). White needles which, upon heating, turn yellow near 270°C but do not melt below 300°C (17). Satisfactory elemental analyses and nmr spectra were obtained.

*3,7-Dimethylisoguanine (**23**)*

Prepared from theobromine, essentially by the method of Nikolaeva and Golovchinskaya (18). White needles, mp 350°C (dec.) (lit. (18) 360°C).

*2,3-Dihydro-1H-5-oxoimidazo(1,2-c)pyrimidine (**24**) Hydrochloride*

Prepared from uracil by the method of Ueda and Fox (19). Does not melt upon heating; a satisfactory elemental analysis was obtained.

2′,3′-O-Benzylidene-5′-O-tritylcytidine (7)

Kindly supplied by R. C. Lord and used without further purification.

Measurements and Treatment of Data

Spectral measurements were made in DMSO containing tetramethylammonium hydroxide as previously described (1, 20). Most of the nucleotide bases show spectra comprising two or more transitions for both the un-ionized and ionized forms. For example, the spectrum of **20** in the neutral form can be reconstructed with a Dupont 310 Curve Resolver using a minimum of five Gaussian transitions; the ionized form required three such functions. With the exception of **10**, **12**, **21**, and **22** the un-ionized and ionized spectra, though markedly

[2]The method of characteristic vector analysis, very recently described (40) might also be used to advantage in such cases.

TABLE 1. Spectral data for neutral and anionic forms

Compound	Neutral molecule[a]		Anion[b]	
	λ_{max} (nm)	log ε	λ_{max} (nm)	log ε
7 2′,3′-O-Benzylidene-5′-O-tritylcytidine	—	—[c]	275(sh)	3.89
8 1-Methylcytosine	276	3.85	288	3.82
9 1-Methyl-5-bromocytosine	291	3.84	297	3.77
10 3-Methylcytosine	293	4.07[d]	307	4.00
11 1-Methylisocytosine	258	3.67	285	3.25[e]
12 3-Methylisocytosine	288	3.88	318	3.84
13 9-Methyladenine	262	4.18	286	3.99
14 2-Chloro-9-methyladenine	266	4.15	282	4.17
15 2-Chloro-8-methoxy-9-methyladenine	267	4.15	274	4.16
16 2,8-Dichloro-9-methyladenine	270	4.22	285	4.05
17 7-Methyladenine	271	4.01	300	4.06
18 2-Chloro-7-methyladenine	278	4.01	289	4.07
19 2-Chloro-7-methyl-8-methoxyadenine	275	4.07	278	4.13
20 2,8-Dichloro-7-methyladenine	279	4.01	291	4.02
21 1,9-Dimethylguanine	258	4.15	311	3.80
22 1,7-Dimethylguanine	285	3.84	343	3.72
23 3,7-Dimethylisoguanine	289	3.99	293	4.02
24 2,3-Dihydro-1*H*-5-oxoimidazo(1,2-*c*)pyrimidine	297	4.01[d]	323	3.89

[a]In 30–55 mol% aqueous DMSO, except where noted.
[b]In 86–96 mol% aqueous DMSO, except where noted.
[c]No absorption maximum above 260 nm.
[d]In water at p*H* 10.0.
[e]In 63 mol% aqueous DMSO.

different in shape from each other, overlap to a large extent and, because of medium effects on spectra, the ionization ratio *I* cannot be evaluated accurately using the approach taken with the pyridines and pyrimidines (1). In such cases no one method of correcting for medium effects appears to be entirely satisfactory and we have found it useful to exploit the spectral peculiarities of the individual indicator to calculate *I*. In one case, **23**, the spectral change with the medium is about the same as the change caused by ionization, too small for any meaningful estimate of *I* to be made.

Even though the shift in λ_{max} that accompanies ionization is quite small for most of the compounds under consideration the areas under the spectral curves of the neutral molecule and anion are sufficiently different in many cases to allow good estimates of *I* to be made.

The values of *I* so obtained were compared to those obtained using several other approaches, including that of Katritzky and co-workers (21) which makes use of measurements at a single wavelength, and the details are given elsewhere (22). With one exception, **8**, the values obtained by the area method and that of Katritzky and co-workers are quite close. Since the change in area that accompanies ionization of **8** is quite small the method of Katritzky and co-workers was used to calculate *I*, and similarly with **13**, **24**, **11**, and **7**, although in the latter cases the two methods give similar results. For **10**, **12**, **21**, and **22**, the method used previously was employed (1).

The equation used to calculate the ionization ratio *I* by the area method is [1], which is analogous to the equation using extinction coefficients used previously (1).

$$[1] \qquad I = [A^-]/[HA] = Z - P/Q - Z$$

Z is the area under the total spectral curve for the mixture of A^- and HA in any given solvent mixture; *P* is the area under the curve for a solution of HA in the same solvent mixture in the absence of base; and *Q* is the area for A^- determined by extrapolation from data obtained in the presence of base and higher concentrations of DMSO, the extrapolation being made by plotting area against H_- (20) and reading off the area for the H_- corresponding to the solvent mixture.

A difficulty with the area method (23, 24) arises from the fact that usually not all of the spectral transitions under consideration lie above 260 nm, the effective cut-off wavelength when DMSO is used. There are two alternative methods which were felt to be appropriate for choosing the wavelength ranges. The first is to use as much of the unobscured spectrum as possible by measuring the area from 260 nm to longer wavelengths. The second is to employ the area from the isosbestic point, defined by the two curves closest to 50% ionization (25), to longer wavelengths. These two methods were investigated for two representative compounds **18** and **20** and we have concluded that *I* does not depend significantly on the choice of wavelength cut-off, provided *Q* and *P* differ significantly (preferably by a factor of 1.5), a condition that was met by many of the compounds studied. For reasons of simplicity of operation we have used the 260 nm cut-off method. Areas were measured using a planimeter. Since the ionization data were to be converted to p*K* by an extrapolative procedure it was necessary to avoid as much as possible errors at the extrema. Accordingly, only log *I* values between +0.80 and −0.80 were, in general, used.

All compounds reacted instantaneously and reversibly with base and we have assumed, as before (20), that proton loss rather than hydroxide addition takes place.

The ionization ratio data for the compounds described

TABLE 2. Acidity constants[a] determined by the B.O. and M.C.P. methods

Compound	B.O. method		M.C.P. method			pK_{HA} (average)
	ϕ	pK_{HA}	Corr. coeff.	m^*	pK_{HA}	
7	−0.624	14.75	0.990	0.405	14.78	14.8
8	−0.411	16.69	0.999	0.641	16.77	16.7
9	−0.294	15.03	0.997	0.789	15.25	15.1
10	−0.226	13.37	0.999	0.800	13.42	13.4[b]
11	−0.294	14.22	0.999	0.775	14.36	14.3
12	−0.315	14.28	0.999	0.734	14.37	14.3
13	−0.479	16.74	0.996	0.554	16.73	16.7
14	−0.406	15.61	0.992	0.667	15.79	15.7
15	−0.353	16.66	0.999	0.714	16.80	16.7
16	−0.374	15.10	0.997	0.704	15.27	15.2
17	−0.539	14.67	0.998	0.511	14.78	14.7
18	−0.313	14.02	0.989	0.797	14.24	14.1
19	−0.421	14.62	0.996	0.629	14.70	14.7
20	−0.259	13.61	0.987	0.793	13.69	13.7
21	−0.462	14.46	0.998	0.617	14.65	14.6
22	−0.515	14.91	0.999	0.547	15.06	15.0
24	−0.246	12.42	0.998	0.802	12.50	12.5

[a] $K_{HA} = [H^+][ArNH^-]/[ArNH_2]$ in standard state, water.
[b] See also ref. 19.

herein have been deposited with the Depository of Unpublished Data.[3]

Results and Discussion

The pK_{HA} values were calculated from ionization data by the extrapolative procedures of Bunnett and Olsen (B.O.) and Marziano, Cimino, and Passerini (M.C.P.), as described previously (1, 26–28). These values are given in Table 2, together with rounded-off averages that will be used in subsequent discussion.

The Cytosine and Isocytosine Systems

Compounds **8**, **10**, **11**, and **12** are all much stronger acids than the aminopyrimidines (1), reflecting the considerable acid-strengthening effect of the carbonyl group.

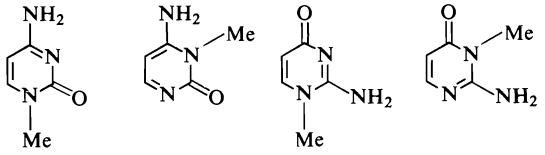

8 (pK = 16.7) **10** (pK = 13.4) **11** (pK = 14.3) **12** (pK = 14.3)

There is an interesting difference between the cytosine system, **8** and **10**, and the isocytosine system, **11** and **12**, the latter two compounds having identical acidities whereas the former pair differ by 3.3 pK units. Acid-strengthening or acid-weakening effects in organic acids are usually rationalized in terms of electronic effects in the acid anion. One looks in vain, however, at the anionic structures of the four compounds for such a rationale. They are all isomeric species with apparently very similar charge distributions. On the other hand the neutral compounds **8** and **10** must differ markedly in stability; indeed, by an amount equivalent to about 3 pK units, provided that the same difference in stability exists as for the de-methylated compounds (29, 30, 31).

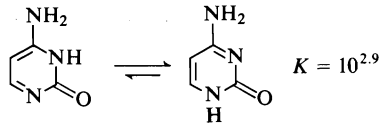

Katritzky and Waring (30) used a related argument based on *basicity* differences to determine this quantity. The greater acidity (and basicity) of **10** than of **8** is thus due to lower stability of the neutral molecule.[4]

[3] Complete set of tabular data is available, at a nominal charge, from the Depository of Unpublished Data, CISTI, National Research Council of Canada, Ottawa, Canada K1A 0S2.

[4] It is unfortunate that **8** is the one compound studied in this work that gives I values that depend significantly on the method used. The area method gives a pK of 15.5, which were it correct would mean that the ΔpK between **8** and **10** is 2.1 instead of 3.3. We believe that the larger value is the more reliable, partly because the ionization data determined using a single wavelength (see Experimental) leads to a well-behaved Hammett indicator plot (Fig. 2).

Are the identical acidities of the isocytosines **11** and **12** also consistent with the known tautomeric constants of the corresponding de-methylated species? Yes, for it has been shown that isocytosine is a mixture of the two tautomers, both in aqueous solution and in the solid state, where, indeed, a 1:1 ratio exists (29, 32, 33).

The Adenine and Guanine Systems

9-Methyladenine **13** is 2.0 pK units weaker than the 7-methyl isomer **17** and similar differences, 1.5–2.0 units, exist for the three pairs of derivatives **14–16** and **18–20**.

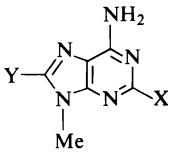

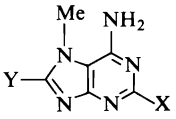

13, X = Y = H
14, X = Cl, Y = H
15, X = Cl, Y = MeO
16, X = Y = Cl

17, X = Y = H
18, X = Cl, Y = H
19, X = Cl, Y = MeO
20, X = Y = Cl

Like the cytosine and isocytosine systems discussed earlier the anionic charge distribution is much the same in the 9- and 7-methyl series except that here the anions of the weaker acids, those belonging to the 9-methyl series, have an additional contributing structure **13***a* that is not present in the anions of the 7-methyl series.

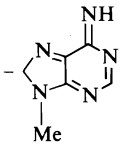

13*a*

Structure **13***a* has the negative charge on carbon and would not be expected to have a great effect on the ion's stability. Nonetheless, whatever influence it exerts would produce an effect in the opposite direction to that observed.

The difference in acidity of the two series can again be traced to the stabilities of the neutral molecules. Eastman's estimate for the tautomeric constant favouring the 9- over the 7-system in adenine is 16 (34, 29) corresponding to a difference of 1.2 pK units in the correct direction in the acid strengths of the alkylated derivatives, assuming there is no difference in the stabilities of the anions.

The guanines **21** and **22** differ in acidity by only 0.4 pK units and although precise data for the tautomeric constant of the parent compound is not available it has been suggested that guanine, itself, as we might now expect, exists in solution as a mixture of the 9- and 7-tautomeric forms, corresponding to the de-methylated forms of **21** and **22** (ref. 29, p. 523).

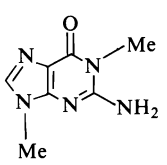

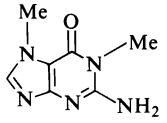

21 (pK = 14.6) **22** (pK = 15.0)

Substitution of chlorine at the 2-position in the two adenine systems produces an expected increase in acid strength, compare **13** and **14**, and **17** and **18**, although the effect is smaller than in the pyrimidine series (1). Further chlorine substitution at the 8-position, as in **16** and **20**, produces an additional, but smaller, increase in acidity. The smaller effect of the second group appears to be a consequence of the resonance effect exerted by +R groups in this position. This follows from a consideration of the 2-chloro-8-methoxy compounds **15** and **19**. The effect of a 2-chloro group (largely inductive and acid-strengthening) is cancelled by the effect of an 8-methoxy group (largely resonance and acid-weakening).

Effect of an Imidazole Ring

Fusing a methylated imidazole ring to 4-aminopyrimidine produces the adenines **13** and **17**. These are, respectively, 1.7 and 3.7 units stronger than the pyrimidine, an effect that can be attributed largely to the inductive effect of the sp^2 nitrogen atom in the five-membered ring. On the other hand, fusing a methylated imidazole ring to 3-methylisocytosine produces the guanines, **21** and **22**, which are 0.3 and 0.7 units *weaker* acids than the isocytosine. Presumably, the conjugation of the sp^3 nitrogen atom of the imidazole ring with the carbonyl group in the six-membered ring greatly reduces the latter group's acid-strengthening effect with the result that the imidazole's net effect becomes one of electron donation.

Ribonucleoside Acidity

The compounds studied in this work possess a methyl group at the position occupied by the ribose moiety in ribonucleosides and it is of interest to determine the effect of such substitution on amino group acidity. Fox and Van Praag

used a 5-nitro substituent to increase the acid strength of 1-methylcytosine and cytidine so that their acidities could be directly compared in aqueous solution (35, 36). They found the pK to be 10.55 for the 1-methyl compound and 9.12 for the cytidine, a 1.4 pK unit acid-strengthening effect of ribosyl over methyl. It was suggested that hydrogen bonding occurs between the unionized 2′-OH group and the carbonyl group of the pyrimidine ring since spectral changes in the pyrimidine spectrum accompanied hydroxyl ionization (37). No such shifts were observed in 2′-deoxyribosyl derivatives where the 2′-OH group is replaced by a proton.

Since we are able to measure the acidities of very weak acids we should be able to compare the effects of ribosyl and methyl groups in the absence of such acid-strengthening groups as nitro. Unfortunately, ionization of the hydroxyl groups in the ribosyl unit (37) occurs at lower basicities than those required to ionize the amino group and we have had to block the hydroxyl functions for this reason. The cytidine **7**, which has the interfering hydroxyls blocked with a benzylidine and a trityl group, has a pK_{HA} of 14.8 (half-ionized in 51.0 mol% DMSO), considerably lower than the value of 16.7 found for 1-methylcytosine **8** (half-ionized in 65.0 mol% DMSO).

This increase in acidity of 1.9 pK units is comparable to the 1.4 pK unit increase found by Fox *et al.* (35, 37) for the nitro-substituted compound. It is significant that **7** does not possess a 2′-hydroxyl group and, hence, the increased acidity cannot be attributed to the presence of such a group. We believe the ribosyl group's acid-strengthening effect is a result of the cumulative inductive effect of the oxygen atoms in the ribosyl group, particularly that in the ring.

It is difficult to give a very precise estimate of the acidity of the amino group in adenosine but it will certainly be greater than that of 9-methyladenine, whose pK is 16.7. Since the ribosyl and amino groups are further away from one another than in cytidine the inductive effect will be less and one might expect a value near 16 for the amino group in adenosine.

The pertinence of amino group acidity to the matter of base-pairing in nucleotide chains was alluded to in the Introduction. It is curious that the amino groups in 9-methyladenine **13** and 1-methylcytosine **8** have identical acidities, pK = 16.7 (although following the argument in the previous paragraph the ribosyl effect will be greater in cytidine than in adenosine). The amino group in adenine, of course, base-pairs with thymine and that in cytosine with guanine (Fig. 1). Each pair has, in addition, a link that does not involve an amino group, and the cytosine–guanine pair has a third link through guanine's 2-amino group. It is noteworthy that the latter appears to be the most acidic of the three amino groups under consideration (pK_{HA} of **21** is 14.6). Provided amino group acidity in the methylated bases is indeed related to hydrogen-bonding ability in the nucleotides, guanine can be assumed to have a more effective hydrogen-bonding amino unit than either adenine or cytosine.

An Acidity Function for Purines and Pyrimidines

The compounds studied in this work and most of the pyrimidines and pyridines studied previously are not well-behaved Hammett indicators with respect to the H_- scale previously developed using aromatic amines (20). In most cases the increase in ionization with increasing

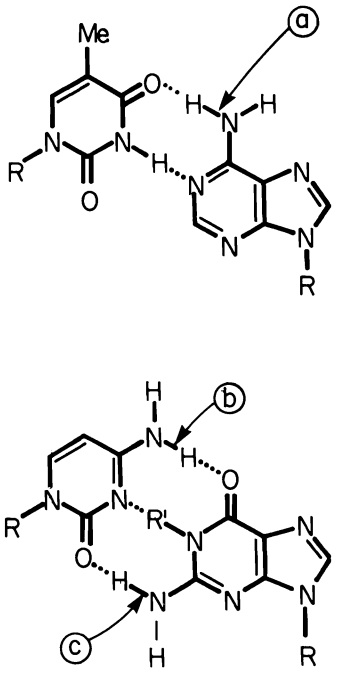

FIG. 1. The base-pairing arrangements in nucleotides, R = nucleotide attachment, R′ = H. Upper pair: thymine–adenine; lower pair: cytosine–guanine. The bonds whose acidities have been measured in the unpaired molecules with R = R′ = methyl are identified: pK_{HA} values are *a*, 16.7; *b*, 16.7; *c*, 14.6.

DMSO content is smaller than would be expected and the probable origins of this effect were described previously (1). We have made use of the B.O. and M.C.P. extrapolative techniques since, when sufficient ionization data is available, reliable pK values can be determined regardless of the adherence or lack thereof to an acidity function. The alternative approach to pK determination in mixed solvents is to attempt to construct an acidity function using the compounds in question (38). We have sufficient data to construct such a scale to which, it turns out, most of the pyrimidines and purines adhere satisfactorily. We are reluctant to inflict upon the body scientific yet another acidity function but we feel obliged to do so since it may be of use in examining acidities of compounds of related structure for which sufficient, accurate, ionization data have not or cannot be obtained to enable the extrapolative techniques to be used. In such cases estimating the DMSO concentration in which the compound is half ionized allows one to calculate a pK, on the assumption that the compound follows the acidity function constructed using compounds of similar structure. Such an operation is preferable to using the B.O. or M.C.P. techniques when only a few imprecisely determined values of the ionization ratio are available.

The scale has been anchored in the standard state water using **24**, whose pK_{HA} has been reported to be 12.6 (19). Our potentiometric measurements in water at 25°C give a value near this, 12.43, and we have used the latter value in our calculations.

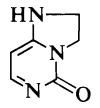

24

A plot of log I for **24** against mol% DMSO is parallel to those for the slightly weaker acids 3-methylcytosine **10** and 2,8-dichloro-7-methyladenine **20**. An attempt was made to use **20** to anchor the scale by using a high enough concentration of hydroxide ion to enable the ionization ratio to be determined in water. This could be done using 0.1 M tetramethylammonium hydroxide. Plots of log I vs. mol% DMSO in 0.1 and 0.011 M base are parallel, but, unfortunately, the value of Δ log I is 1.12, appreciably larger than the value expected from the difference in base concentration (39).

TABLE 3. Acidity function for pyrimidines and purines in the system DMSO – H_2O – 0.011 M tetramethylammonium hydroxide

Mol% DMSO	H_-[a,b]
0.3	12.0
1.0	12.1
3.0	12.3
5.0	12.5
10.0	12.9
15.0	13.3
20.0	13.8
25.0	14.2
30.0	14.6
40.0	15.5
50.0	16.3
60.0	17.0
70.0	17.7
80.0	18.5
85.0[c]	19.0
87.6	19.3

[a]Interpolated and rounded-off values (22).
[b]Determined using indicators of Fig. 2.
[c]H_- value is 21.2 (20).

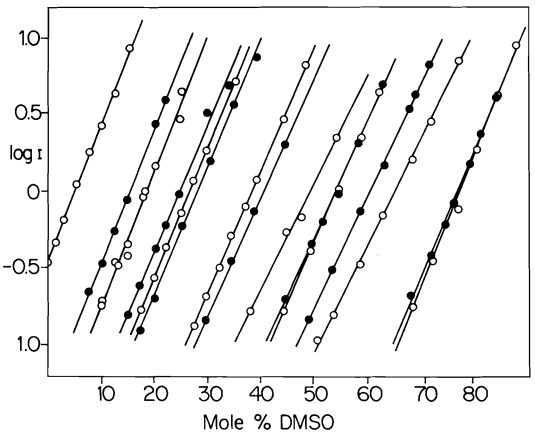

FIG. 2. Ionization ratio as a function of solvent composition. From left to right the compounds are **24, 10, 20, 18, 11, 12,** 4-amino-2,6-dichloropyrimidine (1), **16, 14,** 4-amino-2-chloropyrimidine (1), 2-amino-4,6-dichloropyrimidine (1), **15, 8,** 2-amino-4-chloropyrimidine (1), and 4-aminopyrimidine (1).

Table 3 gives values for aqueous DMSO of the scale, designated H_-^P where P signifies pyrimidine or purine. Figure 2 shows the excellent parallelism in the ionization plots of the indicators used to determine the scale. In the case of other purines or pyrimidines not used in constructing the scale, deviations between H_-^P at half-ionization and the pK determined by the B.O. and M.C.P. methods amounted in two cases, **13** and **17**, to as much as one pK unit.

Acknowledgments

We thank Drs. D. J. Brown and R. C. Lord for gifts of compounds, Dr. P. H. von Hippel for helpful discussions, and the National Research Council of Canada for financial support.

1. M. G. Harris and R. Stewart. Can. J. Chem. This issue.
2. M. P. Printz and P. H. von Hippel. Biochemistry, **7**, 3194 (1968); P. H. von Hippel. Fed. Proc., Fed. Am. Soc. Exp. Biol. **24**, 1458 (1965); M. P. Printz and P. H. von Hippel. Proc. Natl. Acad. Sci. U.S.A. **53**, 363 (1965).
3. L. Doub and U. Krolls. J. Heterocycl. Chem. **7**, 527 (1970).
4. H. M. Sobell, K. Tomita, and A. Rich. Proc. Natl. Acad. Sci. U.S.A. **49**, 885 (1963).
5. D. J. Brown and N. W. Jacobsen. J. Chem. Soc. 3172 (1962).
6. R. B. Angier and W. V. Curran. J. Org. Chem. **26**, 1891 (1961).
7. T. C. Myers and L. Zeleznick. J. Org. Chem. **28**, 2087 (1963).
8. A. G. Beaman and R. K. Robins. J. Org. Chem. **28**, 2310 (1963).
9. R. Falconer, J. M. Gulland, and L. F. Story. J. Chem. Soc. 1784 (1939).
10. J. Davoll and B. A. Lowy. J. Am. Chem. Soc. **73**, 2936 (1951).
11. E. Y. Sutcliffe and R. K. Robins. J. Org. Chem. **28**, 1662 (1963).
12. E. Fischer. Chem. Ber. **32**, 267 (1899).
13. G. Ya. Uretskaya, E. I. Rybkina, and G. P. Men'shikov. J. Gen. Chem. USSR, **30**, 350 (1960).
14. E. Fischer. Chem. Ber. **28**, 2480 (1895).
15. T. Itai and G. Ito. Chem. Pharm. Bull. (Tokyo), **10**, 1141 (1962).
16. E. Fischer. Chem. Ber. **30**, 1846 (1897).
17. E. Fischer. Chem. Ber. **31**, 104 (1898).
18. L. A. Nikolaeva and E. S. Golovchinskaya. Pharm. Chem. J. (USSR), **2**, 206 (1968).
19. T. Ueda and J. J. Fox. J. Am. Chem. Soc. **85**, 4024 (1963).
20. D. Dolman and R. Stewart. Can. J. Chem. **45**, 911 (1967).
21. A. R. Katritzky, A. J. Waring, and K. Yates. Tetrahedron, **19**, 465 (1963); C. D. Johnson, A. R. Katritzky, B. J. Ridgewell, N. Shakir, and A. M. White. Tetrahedron, **21**, 1055 (1965).
22. M. G. Harris. Ph.D. Thesis, University of British Columbia, Vancouver, B.C. 1976.
23. R. S. Ryabova, I. M. Medvetskaya, and M. I. Vinnik. Russ. J. Phys. Chem. **40**, 339 (1966).
24. C. T. Davis and T. A. Geissman. J. Am. Chem. Soc. **76**, 3507 (1954).
25. L. A. Flexser, L. P. Hammett, and D. Dingwall. J. Am. Chem. Soc. **57**, 2103 (1935).
26. J. F. Bunnett and F. P. Olsen. Can. J. Chem. **44**, 1899 (1966).
27. N. C. Marziano, G. M. Cimino, and R. C. Passerini. J. Chem. Soc. Perkin Trans. II, 1915 (1973).
28. R. A. Cox and R. Stewart. J. Am. Chem. Soc. **98**, 488 (1976); R. A. Cox, R. Stewart, M. J. Cook, A. R. Katritzky, and R. A. Tack. Can. J. Chem. **54**, 900 (1976).
29. J. Elguero, C. Marzin, A. R. Katritzky, and P. Linda. The tautomerism of heterocycles. Academic Press, New York, NY. 1976.
30. A. R. Katritzky and A. J. Waring. J. Chem. Soc. 3046 (1963).
31. M. Dreyfus, O. Bensaude, G. Dodin, J. E. Dubois. J. Am. Chem. Soc. **98**, 6338 (1976).
32. C. Helene and P. Douzou. C. R. Acad. Sci. **259**, 4387 (1964); **259**, 4853 (1964).
33. B. D. Sharma and J. F. McConnell. Acta Crystallogr. **19**, 797 (1965).
34. J. W. Eastman. Ber. Bunsenges. Phys. Chem. **73**, 407 (1969).
35. J. J. Fox and D. Van Praag. J. Org. Chem. **26**, 526 (1961).
36. M. Hirata. Chem. Pharm. Bull. (Tokyo), **16**, 430 (1968).
37. J. J. Fox, L. F. Cavalieri, and N. Chang. J. Am. Chem. Soc. **75**, 4315 (1953).
38. C. H. Rochester. Acidity functions. Academic Press, London, England. 1970.
39. K. Bowden. Chem. Rev. **66**, 119 (1966).
40. J. T. Edward and S. C. Wong. J. Am. Chem. Soc. **99**, 4229 (1977).

Canadian Journal of Chemistry

Published by
THE NATIONAL RESEARCH COUNCIL OF CANADA

Journal canadien de chimie

Publié par
LE CONSEIL NATIONAL DE RECHERCHES DU CANADA

Volume 55 Number 22 November 15, 1977

Volume 55 numéro 22 15 novembre 1977

Failure of the scaling laws in the thermal explosion of methyl isocyanide

JOHN L. COLLISTER AND HUW O. PRITCHARD
Chemistry Department, York University, Downsview, Ont., Canada M3J 1P3

Received October 19, 1976[1]

JOHN L. COLLISTER and HUW O. PRITCHARD. Can. J. Chem. **55**, 3815 (1977).

Thermal explosions of methyl isocyanide have been studied in spherical reaction vessels with volumes in the range 300–5000 ml. The normal inverse dependence of the explosion limit on the square of the radius appears to hold over limited ranges, e.g. from 300–1000 ml and from 2000–3000 ml, but the explosion limits at 1000 ml and 2000 ml are characterized by markedly different values of the critical parameter δ_c. Temperature measurements were made at and near the vessel walls, but they do not reveal any abnormalities which could be used to explain these results.

An appendix reports measurements of the thermal conductivities of methyl cyanide and methyl isocyanide from 200–350°C

JOHN L. COLLISTER et HUW O. PRITCHARD. Can. J. Chem. **55**, 3815 (1977).

L'explosion thermique de l'isocyanure de méthyle a fait l'objet d'une étude dans différents vases réactionnels sphériques de volumes compris entre 300–5000 ml. L'expression de la dépendance normale inverse de la limite d'explosion sur le rayon au carré semble être valable au delà des écarts délimités, e.g. à partir de 300 à 1000 ml puis de 2000 à 3000 ml, mais les limites d'explosion à 1000 ml et 2000 ml sont caractérisées par nettement différentes valeurs du paramètre critique δ_c. Les mesures de la température sont faites à et près de la paroie du récipient, mais celles-ci ne révèlent pas d'anomalies qui pourraient être utilisées pour expliquer les résultats.

Un appendice rapporte les mesures de conductivité thermique du cyanure et isocyanure de méthyle à partir de 200 jusqu'à 350°C.

[Traduit par le journal]

It was suggested some time ago that the thermal isomerization of methyl isocyanide might be a good reaction with which to test the theory of explosions (1); principally, the kinetics of the isomerization are well understood, and since it is not a chain reaction, the usual problems of variable inhibition by impurities are absent. We have recently made an extensive study of the rate of this isomerization over wide ranges of both temperature and pressure (2) and we now report an attempt to use this reaction to make a test of thermal explosion theory over a wide range of one parameter, the radius of the vessel.

The experimental technique is simple and well known (1–4): methyl isocyanide is admitted to a spherical vessel held in a constant temperature air bath by momentarily opening an electrically operated valve; the temperature at the centre of the vessel is monitored using a fine thermocouple, and the pressure using a pressure transducer attached to the neck. If the pressure of isocyanide admitted is below the critical explosion pressure, a temperature rise of less than 40°C is recorded at the centre of the vessel,

[1]Revision received July 27, 1977.

whereas above this critical pressure, the temperature at the centre rises very markedly, and at the same time a peak appears in the pressure trace (1): the critical pressure is located by trial and error for each bath temperature and for each reaction vessel.

Experimental

The original aim of this experiment was to establish the precision of the scaling law by performing very accurate experiments in 500, 1000, and 2000 ml vessels. The reaction vessels were enclosed in an air thermostat, stirred by a large high-speed fan, and controlled by electronic proportionating devices fed with a primary signal from a Hewlett-Packard 2802A platinum resistance thermometer; the fine control heaters had a thermal time constant of less than 1 s, and the platinum resistance element was calibrated at the melting point of lead. For these three vessels (and also for the 300 ml vessel), both the spatial homogeneity and the resettability were of the order of ± 0.1°C. However, in later work, a 5000 ml vessel was used, which was rather too large to be properly accommodated in the furnace: in this case, the resettability was still ± 0.1°C, but the spatial homogeneity was no better than ± 0.5°C.

The electrically operated valve (Leybold–Hereaus NW10) was the same as has been used in previous work (1) and was held open for the required length of time by a 50 V dc square-wave pulse. The forepressure of methyl isocyanide was adjusted before each experiment to within 0.01 Torr using a Texas Instruments quartz spiral gauge: by this technique, and profiting from the fact that the methyl isocyanide isomerization is insensitive to both impurity and surface effects, it was an easy matter to locate the critical explosion pressure with high precision. However, it very quickly became apparent that the scaling law (eq. 1 below) failed disastrously between the 1000 and 2000 ml vessels and, thereafter, we were content to bracket the explosion limit with a critical and a subcritical experiment differing by less than 1% in pressure. Thus, the values of P_c listed in Table 1 may be regarded as being accurate to $\pm 1\%$ or ± 0.03 Torr, whichever is the greater.

In previous work, it had been thought that convective effects, signalled by a discontinuity in the temperature rise at the centre of the vessel (1), were important for Rayleigh numbers in excess of 400. We chose, therefore, to limit our experiments to cases having low Rayleigh numbers[2] and (with two inadvertent exceptions) the Rayleigh numbers for all experiments listed in Table 1 are less than 400, accounting for the absence of data for most sizes of vessel below either 320 or 300°C. We also imposed a high-temperature limit on these experiments of 360°C because we did not feel that it was possible to extrapolate the reaction rate data accurately in the fall-off region (2) beyond this point.

[2]A Rayleigh number of 400 does not, of course, correspond to the complete absence of convection. Ra = 400 corresponds to a Nusselt number ($Nu = 0.3(Ra)^{1/4}$) of about 1.3, and hence about 25% of the heat transport is by convection at this limit.

Results and Discussion

The results are reduced to non-dimensional form in Table 1, using rate constants derived from our own measurements (2) and thermal conductivities given in the Appendix. The explosion limits are characterized by the critical value of δ, δ_c, where δ is dimensionless and is given by (5)

$$[1] \qquad \delta = \frac{E}{RT_0^2}\frac{Q}{\lambda}r^2\frac{k_{uni}P}{RT_0}$$

E is the activation energy, T_0 is the vessel temperature, r is the vessel radius, λ is the thermal conductivity, Q is the (exothermic) heat of reaction, P is the pressure, and k_{uni} is the (fallen-off) rate constant for that pressure; for a spherical vessel, in the absence of diffusion effects, δ_c should have a value of between about 4 and 4.5 for this reaction ($B \simeq 60$ and $\varepsilon \simeq 0.01$ in the notation of ref. 5), and if anything, because both B and ε are temperature dependent, there should be a slight increase in δ_c as T_0 increases (cf. Table II of ref. 5).

First, we notice that for a fixed radius, the values of δ_c are approximately constant, but the magnitudes of the variations are disappointingly large. If the lack of constancy in δ_c for a given r were due to errors in the thermal conductivity, then each row of δ_c in Table 1 should show the same trends, which is not the case. Since the temperature in each experiment was stable and reproducible to within ± 0.1°C and each critical pressure was accurate to within $\pm 1\%$, we can only conclude that the fairly large scatter of δ_c within one row is inherent in the nature of the experiment. Since the reaction is in its fall-off region, and is almost second order at the lowest values of P_c, the value of δ_c contains (in effect) a power P_c^y where y approaches 2; this causes a relatively small magnification ratio but, with the precision in the temperature and pressure measurements attained in this work, should present no difficulties.

Second, we notice that in general the values of δ_c appear to be much greater than the predicted value of between 4 and 4.5 whereas, previously, values near 5 had been found (1): the agreement found previously was fortuitous, since it was based on an assumed value for Q of 15 kcal mol^{-1}; using the recently determined value of $Q = 23.7$ kcal mol^{-1} (6), together with our new thermal-conductivity data, the previous results

TABLE 1. Thermal explosion limits for methyl isocyanide as a function of vessel radius and temperature*

T (°C)		260	280	300	320	340	360
λ (cal (cm °C s)$^{-1} \times 10^5$)		5.4	5.8	6.2	6.5	7.0	7.3
$V = 300$	P_c (Torr)				23.5	12.1	9.1
	k (s^{-1})				8.2×10^{-2}	1.6×10^{-1}	3.4×10^{-1}
	δ_c				**11.5**	**9.8**	**13.6**
$V = 500$	P_c (Torr)				19.1	10.8	6.8
	k (s^{-1})				7.4×10^{-2}	1.5×10^{-1}	2.7×10^{-1}
	δ_c				**11.4**	**11.0**	**10.9**
$V = 1000$	P_c (Torr)				13.3	7.6	5.1
	k (s^{-1})				6.3×10^{-2}	1.2×10^{-1}	2.2×10^{-1}
	δ_c				**11.4**	**10.7**	**11.0**
$V = 1500$	P_c (Torr)			28.6	13.0	7.3	4.6
	k (s^{-1})			2.9×10^{-2}	6.2×10^{-2}	1.2×10^{-1}	2.0×10^{-1}
	δ_c			**18.0**†	**14.9**	**13.7**	**12.5**
$V = 2000$	P_c (Torr)			11.8	6.8	4.2	2.8
	k (s^{-1})			2.0×10^{-2}	4.3×10^{-2}	8.2×10^{-2}	1.4×10^{-1}
	δ_c			**5.5**	**5.8**	**6.0**	**5.8**
$V = 3000$	P_c (Torr)			10.3	6.0	3.3	2.4
	k (s^{-1})			1.9×10^{-2}	4.0×10^{-2}	7.0×10^{-2}	1.2×10^{-1}
	δ_c			**6.8**	**6.9**	**5.7**	**6.5**
$V = 5000$	P_c (Torr)	22.0	7.7	4.6	2.7	1.4	1.2
	k (s^{-1})	2.3×10^{-3}	4.6×10^{-3}	1.1×10^{-2}	2.5×10^{-2}	3.4×10^{-2}	6.9×10^{-2}
	δ_c	**3.3**†	**1.9**	**2.4**	**2.7**	**1.6**	**2.4**

*Comparison between nominal and actual volumes:

Nominal volume (ml)	300	500	1000	1500	2000	3000	5000
Actual volume (ml)	305	481	1043	1657	1922	3280	5240
Mean radius $(3V/4\pi)^{1/3}$ (cm)	4.18	4.86	6.29	7.34	7.71	9.22	10.78

†These two cases have Ra > 400.

would now correspond to values of $\delta_c = 10.1$, 9.0, and 8.1 at 299, 323, and 351°C respectively. We note that there is a discrepancy between our values for δ_c in the 1000 ml vessel of 11.0 $\pm$ 0.4 and the previous ones, obtained in a 1200 ml vessel (1), which could be accounted for by an error in one or other of the temperature or pressure calibrations. We have checked very extensively both our temperature and pressure measurements, and found them to be accurate; unfortunately, it is not possible to reconstruct the original apparatus (1) to check for calibration errors there, so we cannot reconfirm their correctness; however, we note that the data in Table 1 show large changes to occur in the value of δ_c between the 1000 and 2000 ml vessels, so that the existence of this discrepancy does not necessarily imply any error.

Examining Table 1 in closer detail, we notice that the data from the 500 and 1000 ml flasks conform well to the scaling law, but the observed value of δ_c is almost a factor of 3 too large; the data from the 300 ml flask also conform, more-or-less, to the scaling law. Similarly the data from the pair of 2000 and 3000 ml flasks also scale reasonably well, and the corresponding value of δ_c is only some 20–50% larger than the theoretical value. Thus, it would appear that some kind of transition in the scaling behaviour occurs between 1000 and 2000 ml, and the earlier data (1) from a 1200 ml flask (as recalculated above) would actually fit in with the observed trend. We hoped to understand this trend better by performing experiments in another size of vessel ($V = 1500$ ml), but this vessel yielded a totally inconsistent set of δ_c values, usually the highest of any observed at each temperature in these experiments.[3] Finally, we decided to examine the explosion limits in a 5000 ml flask, the largest

[3]Although 1.5 ℓ spherical flasks are no longer commercially available, we were able to locate a 1.5 ℓ flat-bottomed flask, which we had blown into a sphere by hand; the radius of this flask varies by $\pm$1.5 mm, which is considerably more variation than is exhibited by the other (machine made) flasks; normally, this departure from roundness would be of only minor importance, but in view of the unexplained nature of the behaviour we have found, we note it here. We did not equip this particular flask with a thermocouple.

our furnace could accommodate, and found yet another unexpected result, a value of δ_c less than the theoretical value, which means that in this flask, the explosion takes place more readily than can be explained by the thermal theory. It is relatively easy to conceive of mechanisms which will dampen the explosion but there are few effects which could cause the explosion to become easier than expected.

We have carried out the following diagnostic tests in order to try to elucidate the cause or causes of these failures in the scaling law.

(*i*) As before (2) we tested for radical chain effects, which were shown to be absent previously at smaller volumes (2), by adding 1% of propylene to the reactant gas; again, δ_c was only slightly affected and it seems that this is not the problem.

(*ii*) Tests were made for spurious admission heating effects (7): different neck diameters were used, the time the electrically operated value was held open (normally 0.2 s) was varied from 0.05 to 0.4 s, and for the largest vessel (where such effects are normally the most prevalent) the geometry of the flow was altered; none of these tests revealed any spurious heating effects as the gas entered the vessels.

(*iii*) The temperature-rise profiles at the centre of the various vessels were always[4] normal in the sense that they approached 40°C (1) as the critical pressure was approached, and once above the critical pressure the induction times became progressively shorter the greater the excess pressure.

(*iv*) The observation, noted above, that in the 5000 ml flask the explosion is initiated more readily than thermal theory would predict is disturbing and so we decided to examine the assumption of infinitely rapid heat dissipation at the walls. Consequently, we constructed two flasks, 500 ml and 5000 ml, with a second thermocouple placed about 0.5 mm away from the wall, and compared the behaviour in the two vessels. In the subcritical range, we could detect no temperature rise near the wall in either vessel. However, in explosions whose initial pressures were within 2% of P_c, there was a significant difference in behaviour: in the 500 ml flask, temperature rises near the wall were still only of the order of 0.3–0.5°C whereas in the 5000 ml flask, they were 5–7°C. If the walls can be assumed to remain at the furnace temperature throughout, this observation shows no more than that once an explosion has occurred, the convective cooling is much more rapid in the smaller flask where the pressure is higher.[5]

Since it is important to know whether there is any change in temperature at the walls, we vacuum-coated the inside of two flasks (3000 and 5000 ml) with platinum. Electrical contact was established at two points about 10 cm apart such that the resistance of the platinum film was about 15 Ω, and using this as one arm of a conventional resistance bridge, we could detect a change of between 0.1 and 0.2°C in the mean wall temperature. In the 3000 ml vessel, there was no detectable change in resistance either below or above the explosion limit. In the 5000 ml vessel, we could not detect any temperature rise in subcritical experiments; however, when an explosion occurred, there appeared to be a consistent temperature rise of about 0.25°C at the wall, but this is so little in excess of our noise level during the explosion that it may not be significant.[6] Thus, the validity of this assumption of constant wall temperature appears to be confirmed.

In summary, we have been unable to find any experimental reason for the surprising variation of the critical parameter δ_c for this explosion from vessel to vessel at constant temperature, or for the same vessel at different temperatures; these variations far exceed our experimental precision. There is one theoretical possibility we have not yet examined, however: we have used in the calculation of our δ values the normal equilibrium thermal conductivity of methyl isocyanide and methyl cyanide. But newly formed methyl cyanide molecules are rather far from being equilibrium molecules, for although their translational temperature will be the same as that of the reactant molecules from which they were formed, they have in excess of 62 kcal mol^{-1} of internal energy: the validity of using equilibrium thermal conductivities (for molecules having about 3 kcal mol^{-1} of internal energy) under these conditions needs to be considered.

[4]Except in the 1500 ml flask, where they were not measured.

[5]We are indebted to Dr. B. J. Tyler and a referee for pointing this out.

[6]In these experiments, an opaque platinum film was deposited fairly evenly over the spherical part of the vessel: since the explosion limit remained unchanged, we can also rule out any hypotheses involving radiation losses.

Acknowledgments

This work was supported by the National Research Council of Canada; we would also like to acknowledge assistance from R. D. Ketcheson and Miss G. Seifried in performing many of these experiments.

1. H. O. PRITCHARD and B. J. TYLER. Can. J. Chem. **51**, 4001 (1973).
2. J. L. COLLISTER and H. O. PRITCHARD. Can. J. Chem. **54**, 2380 (1976).
3. D. H. FINE, P. GRAY, and R. MACKINVEN. Proc. R. Soc. London, Ser. A, **316**, 223 (1970).
4. N. G. GERRI and F. KAUFMAN. Tenth Symposium (International) on Combustion. The Combustion Institute. 1965. p. 227.
5. B. J. TYLER and T. A. B. WESLEY. Eleventh Symposium (International) on Combustion. The Combustion Institute. 1967. p. 1115.
6. M. H. BAGHAL-VAYJOOEE, J. L. COLLISTER, and H. O. PRITCHARD. Can. J. Chem. **55**, 2634 (1977).
7. D. H. FINE, P. GRAY, and R. MACKINVEN. Nature, **223**, 393 (1969).
8. S. H. P. CHEN and S. C. SAXENA. High Temp. Sci. **5**, 206 (1973).
9. B. J. JODY and S. C. SAXENA. Phys. Fluids, **18**, 20 (1975).
10. J. L. COLLISTER. Ph.D. Thesis. York University, Toronto, Ont. 1976.

Appendix

The thermal conductivities of methyl cyanide and methyl isocyanide were measured using the hot-wire column technique described by Chen, Jody, and Saxena (8, 9). The column used was a Pyrex tube 1 m long ($2L$), 6.061 mm in internal diameter ($2b$) and with a platinum wire of 0.204 mm in diameter ($2a$) stretched along the axis: the outer wall was water-cooled and maintained at 12°C, and the experiment consisted of determining the electric power dissipation (Q_H) required to maintain the platinum wire at a series of known temperatures (T_H); thence the thermal conductivity at the wire temperature is (8)

$$\lambda = \frac{\ln (b/a)}{4\pi L} \frac{dQ_H}{dT_H}$$

The method is very simple to use, especially so in the region of temperatures of interest in explosion studies, and of acceptable accuracy (say, within 10%) with a minimum of sophistication in instrumentation: the apparatus was tested out on He, Ar, N_2, and CO_2 and gave results within about 5% of the best accepted values; further details are available in thesis form (10) and in the original publications (8, 9). Table A1 summarizes the results of these measurements which are probably accurate to within ±10%: our values are about 30% lower at 300°C than those estimated previously (1), and somewhat less temperature dependent; slow decomposition of methyl isocyanide at 400°C and above to give noncondensable gases causes the thermal conductivity to rise abruptly, so results are quoted only up to 350°C.

TABLE A1. Thermal conductivity of methyl isocyanide

T (°C)	200	250	300	350
λ (mW cm^{-1} deg^{-1})	0.17	0.22	0.26	0.30

Using this technique, the measured thermal conductivity values for methyl cyanide are indistinguishable from those for methyl isocyanide, as given in Table A1.

Partial tosylation of 1,5-anhydro-D-glucitol[1]

YÔTARO KONDO, KAZUYOSHI YABUUCHI, AND SHIGEHIRO HIRANO
Department of Agricultural Chemistry, Tottori University, Tottori 680, Japan

Received May 10, 1977

YÔTARO KONDO, KAZUYOSHI YABUUCHI, and SHIGEHIRO HIRANO. Can. J. Chem. **55**, 3820 (1977).

Dimolar tosylation of 1,5-anhydro-D-glucitol (**1**) in pyridine yielded the 2,6-di-*O*-tosylate (**6**) (35%) as the major product, along with the tetra-*O*-tosylate (**2**) (1%), the 3,4,6-tri-*O*- (**3**) (1%), 2,4,6-tri-*O*- (**4**) (8%), and 2,3,6-tri-*O*-tosylate (**5**) (6%), and the 3,6-di-*O*- (**7**) (4%) and 4,6-di-*O*-tosylate (**8**) (6%). The order of the relative reactivity of the hydroxyl groups in **1** towards tosyl chloride was predicted as 6-OH > 2-OH > 4-OH > 3-OH.

YÔTARO KONDO, KAZUYOSHI YABUUCHI et SHIGEHIRO HIRANO. Can. J. Chem. **55**, 3820 (1977).

La tosylation dimolaire de l'anhydro-1,5 D-glucitol (**1**) dans la pyridine conduit à un mélange contenant principalement le di-*O*-tosylate-2,6 (**6**) 35%, puis du tétra-*O*-tosylate (**2**) 1%, du tri-*O*-tosylate-3,4,6 (**3**) 1%, -2,4,6 (**4**) 8% et -2,3,6 (**5**) 6%, du di-*O*-tosylate-3,6 (**7**) 4% et -4,6 (**8**) 6%. L'ordre relatif de réactivité des groupements hydroxyles dans **1** vis-à-vis le chlorure de tosyle a été établi comme étant 6-OH > 2-OH > 4-OH > 3-OH.

[Traduit par le journal]

Systematic studies of selective sulfonylation of monosaccharides have been reported and the orientation of aglycon was found to greatly affect the reactivity of the ring hydroxyl groups (1–9). Selective sulfonylation of monosaccharides having no aglycon has received little attention. This communication describes dimolar tosylation of 1,5-anhydro-D-glucitol (**1**).

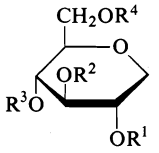

1 $R^1 = R^2 = R^3 = R^4 = H$
2 $R^1 = R^2 = R^3 = R^4 = Ts$
3 $R^1 = H, R^2 = R^3 = R^4 = Ts$
4 $R^1 = R^3 = R^4 = Ts, R^2 = H$
8 $R^1 = R^2 = H, R^3 = R^4 = Ts$
10 $R^1 = R^3 = R^4 = Ts, R^2 = Ac$
14 $R^1 = R^2 = Ac, R^3 = R^4 = Ts$

Treatment of **1** (10) with 2 mol equiv. of tosyl chloride in pyridine gave a mixture which was fractionated by column chromatography on silica gel to afford the tetra-*O*-tosylate **2** (1%), the 3,4,6-tri-*O*-tosylate (**3**) (1%), a mixture of the 2,4,6-tri-*O*- (**4**) (8%) and 2,3,6-tri-*O*-tosylate (**5**) (6%), and the 2,6-di-*O*- (**6**) (35%), 2,4-di-*O*- (**7**) (4%) and 2,3-di-*O*-tosylate (**8**) (6%). Tri-*O*-tosylates **4** and **5** could not be separated by column chromatography.

In order to determine the position of tosyl groups in the tri-*O*-tosylate **3** and a mixture of **4** and **5**, and in the di-*O*-tosylates **6**, **7**, and **8**, the respective compound was converted into the corresponding mono-*O*-acetyl-tri-*O*-tosyl derivatives **9** and a mixture of **10** and **11**, and di-*O*-acetyl-di-*O*-tosyl derivatives **12**, **13**, and **14**. Compound **9** was identical with 2-*O*-acetyl-1,5-anhydro-3,4,6-tri-*O*-tosyl-D-glucitol which was obtained by the sequential acetylation, debenzylidenation, and pertosylation of 1,5-anhy-

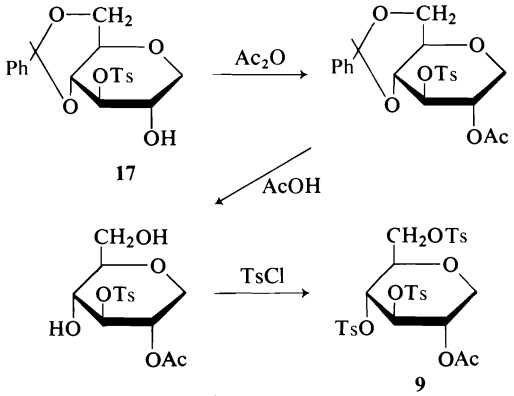

SCHEME 1

[1]Presented at the Annual Meeting of the Agricultural Chemical Society of Japan, April 1, 1977, Yokohama, Japan.

dro-4,6-*O*-benzylidene-3-*O*-tosyl-D-glucitol (**17**) (Scheme 1). Crystallization of the mixture of **10** and **11** gave 4-*O*-acetyl-1,5-anhydro-2,3,6-tri-*O*-tosyl-D-glucitol (**11**) which had physical constants in good agreement with those of the authentic sample prepared by successive debenzylidenation followed by preferential tosylation at the 6-OH group and acetylation of 1,5-anhydro-4,6-*O*-benzylidene-2,3-di-*O*-tosyl-D-glucitol (**15**) (11) (Scheme 2). The ^{1}Hmr spectrum of **11** showed the methyl proton of the acetoxyl group at τ 8.22. In the ^{1}Hmr spectrum of the

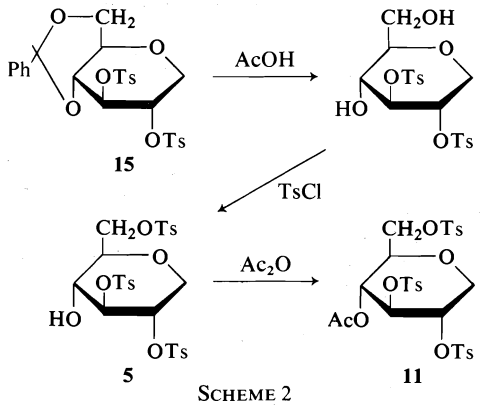

SCHEME 2

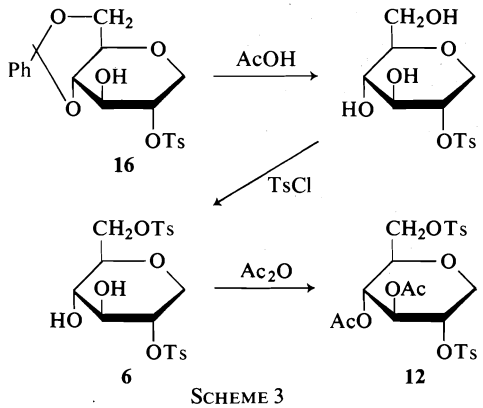

SCHEME 3

mixture of **10** and **11**, the signals of the methyl proton of the acetoxyl group appeared at τ 8.22 and 8.30 with relative proton intensities of 4:3. Therefore, the resonance at τ 8.30 was assigned to the acetyl-methyl proton signal of 3-*O*-acetyl-1,5-anhydro-2,4,6-tri-*O*-tosyl-D-glucitol (**10**). This indicates the ratio of **10** to **11** in the mixture to be 4:3.

The structures of **12** and **13** were determined as 3,4-di-*O*-acetyl-1,5-anhydro-2,6-di-*O*-tosyl-D-glucitol and 2,4-di-*O*-acetyl-1,5-anhydro-3,6-di-*O*-tosyl-D-glucitol by comparison of their physical properties with those of the authentic samples prepared from 1,5-anhydro-4,6-*O*-benzylidene-2-*O*-tosyl-D-glucitol (**16**) (12) and 1,5-anhydro-4,6-*O*-benzylidene-3-*O*-tosyl-D-glucitol (**17**), respectively, by sequential acetylation, debenzylidenation, 6-*O*-tosylation, and acetylation (Schemes 3 and 4). Accordingly, the remaining compound **14** must be the structure of 2,3-di-*O*-acetyl-1,5-anhydro-4,6-di-*O*-tosyl-D-glucitol.

In the dimolar tosylation of **1**, the preponderance of the 2,4,6-tri-*O*-tosylate **4** over **3** and **5** and that of the 2,6-di-*O*-tosylate **6** over **7** and **8** shows that the order of the relative reactivity of the hydroxyl groups in **1** is 6-OH > 2-OH > 4-OH > 3-OH.

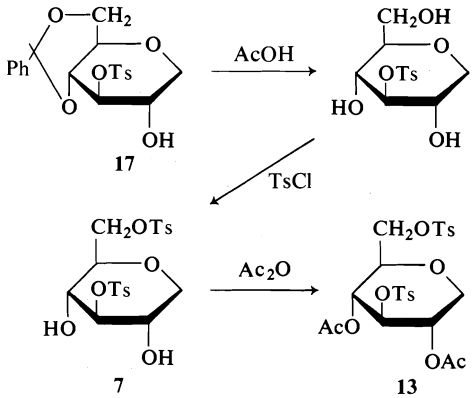

SCHEME 4

In the sulfonylation of methyl α-D-glucopyranoside (5, 8) and methyl α-D-xylopyranoside (6), the relative reactivity order of the secondary hydroxyl groups was reported as 2-OH > 4-OH > 3-OH. The finding that the 2-OH groups are the most reactive of the ring hydroxyl groups is in agreement with the results of selective benzoylation (3, 9) of these compounds. Intramolecular hydrogen bonding between the 2-OH group and the glucosidic oxygen atom at C-1 has been invoked to rationalize the enhanced reactivity of the 2-OH group (3). In the sulfonylation of methyl β-D-glucopyranoside (5) and methyl 6-deoxy-β-D-glucopyranoside (7), the 4-OH groups are the most reactive of the secondary hydroxyl groups. The relative reactivity to sulfonylation of methyl β-D-xylopy-

ranoside (6) was in the order 4-OH > 3-OH > 2-OH. It is of interest to note that the 4-OH groups are the most reactive to sulfonylation of methyl β-D-glucopyranoside and methyl 6-deoxy-β-D-glucopyranoside since the 4-OH group in the latter is the least reactive to benzoylation (4). The lowest reactivity of the 4-OH group towards benzoyl chloride was interpreted (3, 4) as steric hindrance with the 5-benzoyloxymethyl (or 5-methyl) group. On the other hand, the greater reactivity to sulfonylation of the 4-OH group compared with the 3-OH group in methyl α- and β-D-glucopyranosides, methyl 6-deoxy-β-D-glucopyranoside, and **1** may be explained by the inductive effect (7) of the 5-tosyloxymethyl (or 5-methyl) group (sulfonylation at the primary hydroxyl group being assumed to occur first) or a hydrophobic interaction between the 5-tosyloxymethyl (or 5-methyl) group and the methylphenyl group of the incoming sulfonyl reagent. However, it is shown (7) that the tosyloxy group in the sugar ring has no substantial accelerating effect on the neighboring hydroxyl groups; the rate of tosylation is decelerated. It is noteworthy that the 4-OH group in methyl β-D-xylopyranoside and the 2-OH group in **1** are the most reactive of the secondary hydroxyl groups. The 2-OH group in **1** cannot take part in hydrogen bonding. This indicates that deoxygenation has an activating effect on a neighboring hydroxyl group.

From the results reported for sulfonylation of methyl α- and β-D-glucopyranosides and methyl 6-deoxy-β-D-glucopyranoside, it is clear that intramolecular hydrogen bonding is rather more important than the electronic effects to account for the difference in the reactivity of the secondary hydroxyl groups. The order of the reactivity of methyl α- and β-D-xylopyranosides to sulfonylation suggest that an accelerating effect of hydrogen bonding on the rate of sulfonylation is stronger than the stereochemical effect caused by the introduction of the deoxy group into C-5. The result in the present study on the sulfonylation of **1** indicates that this stereochemical factor is more important than the electronic effects.

Accordingly, the above argument suggests that the order of the factors governing the relative reactivity of the secondary hydroxyl groups to sulfonylation is intramolecular hydrogen bonding > stereochemical factors (whether or not hydroxyl groups are adjacent to deoxy groups, $—CH_2—$) > electronic effects. From this order it may be possible to predict the order of the relative reactivity of the secondary hydroxyl groups in methyl glycopyranosides with *gluco-* and *xylo*-configurations.

Experimental

Melting points were determined on a Yanagimoto micro hot-stage apparatus and are uncorrected. Optical rotations were measured with a Yanagimoto OR-50 polarimeter and ^{1}Hmr spectra were recorded on a Hitachi R-24 60 MHz instrument using chloroform-*d* with tetramethylsilane as an internal standard.

*Dimolar Tosylation of 1,5-Anhydro-D-glucitol (**1**)*

Tosyl chloride (2.555 g, 2.2 mol equiv.) was added portionwise to a solution of 1,5-anhydro-D-glucitol (10) (**1**, 1 g) in anhydrous pyridine (20 ml) at 0°C. The solution was kept at 0°C for 24 h and stirred at 5°C for 48 h, and then extracted with chloroform. The extract was washed with dilute sulfuric acid, saturated sodium bicarbonate, and water, and dried over Na_2SO_4. The residual syrup after evaporation of the solvent was subjected to a silica gel column (70–230 mesh, Merck). Elution with benzene–acetone (9:1 (v/v)) gave 1,5-anhydro-2,3,4,6-tetra-*O*-tosyl-D-glucitol (**2**, 34 mg, 0.7%), which was crystallized from chloroform, mp 212–213°C, $[\alpha]_D^{16}$ − 1.8° (*c* 4.4 in pyridine). *Anal.* calcd. for $C_{34}H_{36}O_{13}S_4$: C 52.29, H 4.66, S 16.42; found: C 52.11, H 4.38, S 16.13.

Benzene–acetone (4:1 (v/v)) eluted a mixture (541 mg, 14.1%) of 1,5-anhydro-2,4,6-tri-*O*-tosyl-D-glucitol (**4**) and 1,5-anhydro-2,3,6-tri-*O*-tosyl-D-glucitol (**5**), and 1,5-anhydro-3,4,6-tri-*O*-tosyl-D-glucitol (**3**, 32 mg, 0.8%). Benzene–acetone (2:1 (v/v)) eluted 1,5-anhydro-3,6-di-*O*-tosyl-D-glucitol (**7**, 124 mg, 3.6%). Benzene–acetone (1:1 (v/v)) eluted 1,5-anhydro-2,6-di-*O*-tosyl-D-glucitol (**6**, 1.168 g, 34.5%) and 1,5-anhydro-4,6-di-*O*-tosyl-D-glucitol (**8**, 197 mg, 5.8%). The above syrupy tosylates could not be crystallized.

*1,5-Anhydro-4,6-O-benzylidene-D-glucitol 2-O-Tosylate (**16**) and 3-O-Tosylate (**17**)*

1,5-Anhydro-4,6-*O*-benzylidene-D-glucitol (11) (965 mg) was partially tosylated with tosyl chloride (869 mg, 1.2 mol equiv.) in pyridine (8 ml) according to the method of Newth (12). Usual work-up afforded the crystalline residue which was chromatographed on silicic acid (100 mesh, Mallinkrodt) and eluted with benzene – ethyl acetate (9:1 (v/v)) to give 1,5-anhydro-4,6-*O*-benzylidene-2,3-di-*O*-tosyl-D-glucitol (**15**, 202 mg, 9.4%), mp 193–195°C, $[\alpha]_D^{22}$ − 40.8° (*c* 1.0 in chloroform) (lit. (11) mp 185–189°C, $[\alpha]_D^{20}$ − 48.5° (*c* 1.5 in chloroform)); ^{1}Hmr data τ 4.78 (s. 1H, ϕCH), 5.16 (t, 1H, $J_{2,3} = J_{3,4} =$ 8.5 Hz, H-3), 7.58, 7.78 (2s, 6H, $CH_3\phi$). Elution with benzene – ethyl acetate (4:1 (v/v)) gave 1,5-anhydro-4,6-*O*-benzylidene-2-*O*-tosyl-D-glucitol (**16**, 637 mg, 41.0%), mp 177–178°C, $[\alpha]_D^{24}$ − 15.8° (*c* 1.4 in chloroform) (lit. (12) mp 174–175°C); ^{1}Hmr data τ 4.52 (s, 1H, ϕCH), 7.23 (b s, 1H, OH exchanges in D_2O), 7.53 (s, 3H, $CH_3\phi$). Elution with benzene – ethyl acetate (2:1 (v/v)) gave 1,5-anhydro-4,6-*O*-benzylidene-3-*O*-tosyl-D-glucitol (**17**,

106 mg, 6.8%), mp 145–146°C, $[\alpha]_D^{22}$ − 42.3° (*c* 0.7 in chloroform); ^{1}Hmr data τ 4.45 (s, 1H, ϕCH), 6.53 (b s, 1H, OH exchanges in D_2O), 7.61 (s, 3H, $CH_3\phi$). *Anal.* calcd. for $C_{20}H_{22}O_7S$: C 59.10, H 5.46; found: C 58.71, H 5.48. Finally the starting material (247 mg, 25.6%) was eluted with ethyl acetate.

*2-O-Acetyl-1,5-anhydro-3,4,6-tri-O-tosyl-D-glucitol (**9**)*

Procedure A

Acetic anhydride (1 ml) was added to a solution of compound **3** (31 mg) in pyridine (1 ml) and the mixture was stirred overnight at room temperature. The reaction mixture was extracted with chloroform and the extract was washed with water. The residual syrup after evaporation of the solvent was crystallized from ethanol to give the title compound (33 mg, 96.7%), mp 181–182°C, $[\alpha]_D^{20}$ + 27.0° (*c* 0.2 in chloroform); ^{1}Hmr data τ 7.59 (s, 9H, $CH_3\phi$), 8.18 (s, 3H, CH_3CO). *Anal.* calcd. for $C_{29}H_{32}O_{12}S_3$: C 52.08, H 4.83, S 14.38; found: C 52.38, H 4.74, S 14.42.

Procedure B

1,5-Anhydro-4,6-*O*-benzylidene-3-*O*-tosyl-D-glucitol (**17**, 115 mg) was acetylated with acetic anhydride (1 ml) in pyridine (2 ml) in the usual way. The reaction mixture was extracted with chloroform, and the extract was washed with water, dried over Na_2SO_4, and concentrated. The residual syrup was dissolved in acetic acid – water (4:1 (v/v), 5 ml), and the solution was heated at 80°C for 1 h, and repeatedly evaporated after addition of water to afford a syrup. The debenzylidenated product was treated with tosyl chloride (650 mg) in pyridine (2 ml) at 40°C for 4 days. The reaction mixture was worked-up in the usual way and the resulting residue was recrystallized from ethanol to yield compound **3** (113 mg, 59.2%) which was identical with the substance prepared by procedure A.

*4-O-Acetyl-1,5-anhydro-2,3,6-tri-O-tosyl-D-glucitol (**11**)*

Procedure A

Acetylation of a mixture of **4** and **5** (540 mg) with acetic anhydride (3 ml) in pyridine (3 ml) in the usual way, followed by normal work-up, gave a syrup (522 mg, 90.6%) which on crystallization from ethanol yielded the title compound (200 mg, 34.7%), mp 132–134°C, $[\alpha]_D^{20}$ + 3.1° (*c* 1.0 in chloroform); ir data ν_{max} (KBr) 3450 cm^{-1} (hydrate); ^{1}Hmr data τ 7.55 (s, 9H, $CH_3\phi$), 8.22 (s, 3H, CH_3CO). *Anal.* calcd. for $C_{29}H_{32}O_{12}S_3 \cdot H_2O$: C 50.71, H 5.00, S 14.00; found: C 50.58, H 4.93, S 13.88.

Procedure B

A solution of 1,5-anhydro-4,6-*O*-benzylidene-2,3-di-*O*-tosyl-D-glucitol (**15**, 100 mg) in acetic acid – water (4:1 (v/v), 3 ml) was heated at 80°C for 1 h. The residual syrup after evaporation was treated with tosyl chloride (33 mg, 1 mol equiv.) in pyridine (2 ml) at 0°C. The mixture was stirred at the same temperature for 1 h, at room temperature for 1 h, and then at 40°C for 1.5 h. Acetic anhydride (1 ml) was added to the solution which was stirred overnight. The reaction mixture was extracted and purified as described above to give a syrup. Crystallization from ethanol yielded compound **11** (95 mg, 79.0%) which was identical with the substance prepared by procedure A.

*3,4-Di-O-acetyl-1,5-anhydro-2,6-di-O-tosyl-D-glucitol (**12**)*

Procedure A

Compound **6** (900 mg) was treated with acetic anhydride (5 ml) in pyridine (6 ml) overnight. Usual work-up followed by crystallization from ethanol gave the title compound (942 mg, 89.0%), mp 149–150°C, $[\alpha]_D^{20}$ +68.3° (*c* 1.4 in chloroform); ^{1}Hmr data τ 7.57 (s, 6H, $CH_3\phi$), 8.08, 8.27 (2s, 6H, CH_3CO). *Anal.* calcd. for $C_{24}H_{28}O_{11}S_2$: C 51.78, H 5.08, S 11.52; found: C 51.91, H 4.93, S 11.30.

Procedure B

1,5-Anhydro-4,6-*O*-benzylidene-2-*O*-tosyl-D-glucitol (**16**, 343 mg) was debenzylidenated with acetic acid – water (4:1 (v/v), 15 ml) in the usual way. The resulting syrup was tosylated with tosyl chloride (155 mg, 1 mol equiv.), and the reaction mixture was extracted with chloroform and the extract was washed with water, and dried over Na_2SO_4. Evaporation and acetylation with acetic anhydride (2 ml) in pyridine (3 ml) afforded compound **12** (305 mg, 59.8%) which was identical with the substance prepared by procedure A.

*2,4-Di-O-acetyl-1,5-anhydro-3,6-di-O-tosyl-D-glucitol (**13**)*

Procedure A

Acetylation of compound **7** (95 mg) with acetic anhydride (2 ml) in pyridine (2 ml) gave the title compound (109 mg, 97.3%), mp 167–168°C, $[\alpha]_D^{20}$ + 38.8° (*c* 1.1. in chloroform); ^{1}Hmr data τ 7.58 (s, 6H, $CH_3\phi$), 8.06, 8.15 (2s, 6H, CH_3CO). *Anal.* calcd. for $C_{24}H_{28}O_{11}S_2$: C 51.78, H 5.08, S 11.52; found: C 51.89, H 5.04, S 11.61.

Procedure B

1,5-Anhydro-4,6-*O*-benzylidene-3-*O*-tosyl-D-glucitol (**17**, 93 mg) was debenzylidenated with acetic acid – water (4:1 (v/v), 4 ml) and treated with tosyl chloride (44 mg, 1 mol equiv.) in pyridine (2 ml) at 0°C. The solution was stirred at 0°C for 1 h and at room temperature for 4 h, extracted with chloroform, and the extract was concentrated. The residual syrup was treated with acetic anhydride (1 ml) in pyridine (2 ml) to give compound **13** (90 mg, 65.0%) which was identical with the substance prepared by procedure A.

*2,3-Di-O-acetyl-1,5-anhydro-4,6-di-O-tosyl-D-glucitol (**14**)*

Compound **8** (196 mg) was treated with acetic anhydride (2 ml) in pyridine (2 ml) overnight. The reaction mixture was worked-up in the usual way to yield the title compound (219 mg, 94.8%) as a syrup which could not be crystallized, $[\alpha]_D^{20}$ + 20.2° (*c* 1.0 in chloroform); ir data ν_{max}(film) 3500 cm^{-1} (hydrate); ^{1}Hmr data τ 7.60 (s, 6H, $CH_3\phi$), 8.08, 8.12 (2s, 6H, CH_3CO). *Anal.* calcd. for $C_{24}H_{28}O_{11}S_2 \cdot 2H_2O$: C 48.63, H 5.45, S 10.82; found: C 48.52, H 5.21, S 10.45.

1. A. H. Haines. Adv. Carbohydr. Chem. Biochem. **33**, 11 (1976).
2. R. W. Jeanloz and D. A. Jeanloz. J. Am. Chem. Soc. **79**, 2579 (1957).
3. J. M. Williams and A. C. Richardson. Tetrahedron, **23**, 1369 (1967).
4. Y. Kondo, K. Miyahara, and N. Kashimura. Can. J. Chem. **51**, 3272 (1973).

5. R. C. CHALK, D. H. BALL, and L. LONG, JR. J. Org. Chem. **31**, 1509 (1966).
6. R. C. CHALK and D. H. BALL. Carbohydr. Res. **28**, 313 (1973).
7. J. STANÉK, JR., K. ĆAPEK, and J. JARÝ. Collect. Czech. Chem. Commun. **40**, 3370 (1975).
8. H. B. SINCLAIR. Carbohydr. Res. **50**, 247 (1976).
9. T. SIVAKUMARAN and J. K. N. JONES. Can. J. Chem. **45**, 2493 (1967).
10. R. K. NESS, H. G. FLETCHER, JR., and C. S. HUDSON. J. Am. Chem. Soc. **72**, 4547 (1950).
11. E. ZISSIS and N. K. RICHTMYER. J. Am. Chem. Soc. **77**, 5154 (1955).
12. F. H. NEWTH. J. Chem. Soc. 2717 (1959).

Polyol–Water interactions. Apparent molal heat capacities and volumes of aqueous polyol solutions

GIUSEPPA DIPAOLA[1] AND BERNARD BELLEAU[2]

Department of Chemistry, McGill University, Montreal, P.Q., Canada H2A 2K6

Received April 28, 1977

GIUSEPPA DIPAOLA and BERNARD BELLEAU. Can. J. Chem. **55**, 3825 (1977).

Volumetric specific heats (25°C) and densities (24°C) were measured with a flow microcalorimeter and flow densimeter for 12 polyols in water (0.05 to 2 *m*), and for NaCl and *n*-Bu_4NBr in 1 *m* aqueous alditol solutions. The infinite dilution properties (ϕ_c^0 and ϕ_v^0) of the polyols show specificities in polyol–water interactions which are discussed in terms of the compatibility of the polyol stereochemistry and the existing water environment. The derived heat capacities and volumes of transfer of hydrophobic and hydrophilic probes to aqueous solutions of homologous polyols suggest that structural interactions are reduced in these systems as compared to pure water.

GIUSEPPA DIPAOLA et BERNARD BELLEAU. Can. J. Chem. **55**, 3825 (1977).

On mesure les chaleurs spécifiques volumétriques (25°C) et densités (24°C) à l'aide d'un microcalorimètre et densimètre dynamiques de 12 polyols dans l'eau (0.05 à 2 *m*), et du NaCl et *n*-Bu_4Br dans des solutions aqueuses d'alditol 1 *M*. Les propriétés de dilution infinie (ϕ_c^0 et ϕ_v^0) des polyols démontrent des spécificités pour les interactions polyol–eau qui sont interprétées en termes de compatibilité stéréochimique du polyol et de l'environnement aqueux existant. Les capacités calorifiques et volumiques dérivées du transfert de sondes hydrophobiques et hydrophiliques aux solutions aqueuses des polyols homologues suggèrent que les interactions structurales sont réduites dans ces systèmes en comparaison avec l'eau pure.

[Traduit par le journal]

Introduction

In a previous publication (1) we reported results of a study of apparent molal volumes and heat capacities of various 'structural' probes in aqueous glycerol solutions. We now wish to describe the results of similar studies for the case of alditols and related polyols in aqueous solution (2) in order to determine whether there exists a correlation between polyol–water interactions and the stabilizing effects of polyols on biological systems (1).

Thermodynamical studies giving information on the infinite dilution properties of hydrophilic solutes have been limited mainly to some measurements of heats of solution (3–5). Recently, standard apparent molal heat capacities were obtained for a number of low molecular weight alcohols and polyols (6). A number of volumetric studies of solutions of monosaccharides have also been reported (4, 6, 7).

[1]Holder of a Centennial Predoctoral Scholarship of the National Research Council of Canada; present address: Department of Chemistry, University of Toronto, Toronto, Ontario, Canada M5S 1A1.

[2]Author to whom correspondence may be addressed.

Experimental

Heat capacities were measured with a flow microcalorimeter capable of detecting differences between the volumetric specific heat of a solution and that of a reference solvent to $\pm 3 \times 10^{-5}$ J K^{-1} cm^{-3}. Densities were determined with a flow digital densimeter sensitive to $\pm 3 \times 10^{-6}$ g cm^{-3}. Details of the experimental procedure have been published previously (1). Apparent molal quantities (ϕ_c, ϕ_v) were calculated in the usual way (1).

Reagent grade polyhydric alcohols were used without further purification: glycerol (Fisher Certified Spectranalyzed); ethylene glycol and 1,2-propanediol (Matheson, Coleman and Bell, Chromatoquality); 1,3-propanediol (Eastman Kodak Reagents); D-arabitol, D-xylitol, ribitol (Nutritional Biochemicals); D-mannitol, D-sorbitol, *myo*-inositol, sucrose (Fisher Certified Reagents); and *meso*-erythritol (Aldrich).

Results

Binary Systems

Relative densities (24°C) and volumetric heat capacities were measured for several alditols and other related polyhydroxy compounds in water in the concentration range of 0.05 to 2 *m*.[3]

[3]Complete sets of tabular data for d_0/d, σ/σ_0, ϕ_v, and ϕ_c are available, at a nominal charge, from the Depository of Unpublished Data, CISTI, National Research Council of Canada, Ottawa, Ont., Canada K1A 0S2.

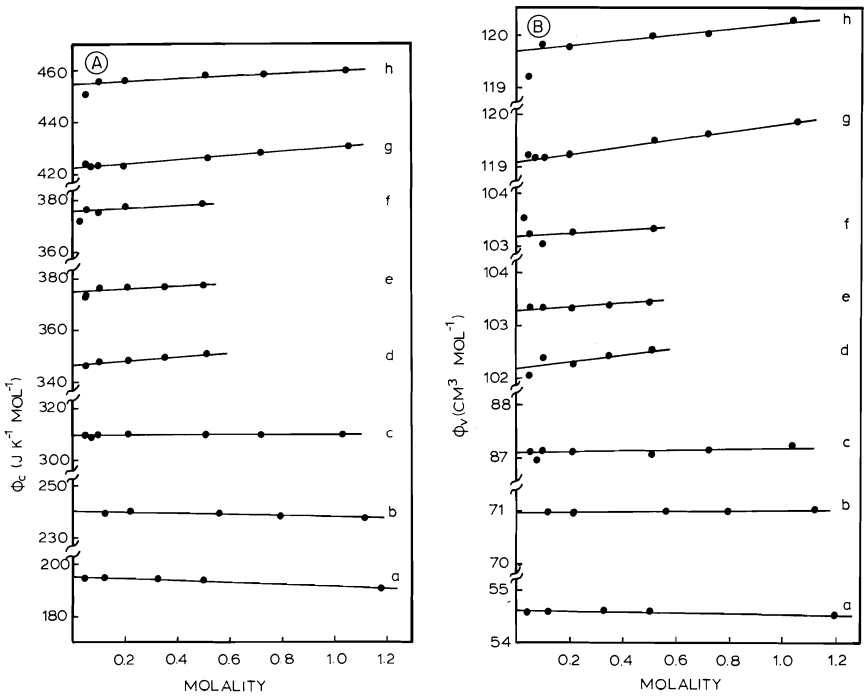

FIG. 1. Concentration dependence of the apparent molal quantities of the alditols [CH_2OH-$(CHOH)_nCH_2OH$] in water: (*a*) ethylene glycol; (*b*) glycerol; (*c*) *meso*-erythritol; (*d*) D-xylitol; (*e*) D-arabitol; (*f*) ribitol; (*g*) D-sorbitol; (*h*) D-mannitol. (*A*) ϕ_c at 25°C. (*B*) ϕ_v at 24°C. This temperature was selected because of the experimental set-up. The error introduced by taking the density ratios at 24 rather than 25°C is vanishingly small.

The derived ϕ_c and ϕ_v values for the alditols exhibit a linear concentration dependence (Fig. 1). These results were fitted by linear regression analysis to equations of the form

$$[1] \qquad \phi_x = \phi_x^0 + B_x m$$

where m represents the molal concentration of the polyol, and ϕ_x represents the appropriate apparent molal quantity. The resulting excess coefficients (B_c, B_v) are collected in Table 1, which also includes the limiting apparent molal quantities (ϕ_c^0, ϕ_v^0) for the 12 polyols studied. The estimated uncertainties on ϕ_v^0 and ϕ_c^0 are ± 0.1 cm^3 mol^{-1} and $\pm(1\text{–}2)$ J K^{-1} mol^{-1}. For most of the excess coefficients, only the magnitude is significant, owing to the limited number of data points (5–9 points were obtained in duplicate in the concentration range quoted for each polyol). A comparison of ϕ_c^0 and ϕ_v^0 data with earlier results (from the literature) shows excellent agreement for those few cases where such measurements have been previously undertaken (Table 1).

The present results reveal several interesting features.

(*1*) The replacement of a hydrogen atom (C—H) by an —OH group (for example, compare 1,3-propanediol and glycerol results) sharply reduces the apparent molal heat capacity, but only slightly affects the volume. This is in agreement with the results of Jolicoeur and Lacroix (6) and Franks *et al.* (4, 8).

(*2*) The limiting thermodynamic properties show significant differences between stereoisomeric molecules. For example, the ϕ_c^0 and ϕ_v^0 values for sorbitol are 32 J K^{-1} mol^{-1} and 0.55 cm^3 mol^{-1} lower than the corresponding values for mannitol. Similar trends in the volumetric properties of this stereoisomeric pair have also been observed by Franks *et al.* at 5°C (4).

Such specificity implies non-additivity of group contributions to the overall measured property. One must therefore exercise caution

TABLE 1. Apparent molal volumes and heat capacities of various polyols in water at 24°C and 25°C respectively

Polyol	ϕ_v^0 (cm^3 mol^{-1})	B_v	ϕ_c^0 (J K^{-1} mol^{-1})	B_c	Concentration range (m)
Ethylene glycol[a]	54.60	−0.06	195.0	−3.4	0.03–3.05
1,2-Propanediol	75.77	−0.01	312.9	−4.7	0.06–5.14
1,3-Propanediol	71.91	−0.27	268.6	−8.3	0.03–1.08
Glycerol	70.95	0.05	240.2	−1.8	0.12–4.49
meso-Erythritol	87.10	0.13	310.0	−0.03	0.04–1.04
D-Xylitol	102.14	0.76	346.4	8.8	0.05–0.51
D-Arabitol	103.31	0.21	374.6	5.6	0.05–0.50
L-Arabitol[b]	103.33	(0.58)	372.8	(11.5)	0.09–0.52
Ribitol	103.11	0.45	375.6	6.8	0.04–0.51
D-Mannitol	119.71	0.52	455.4	4.7	0.09–1.05
D-Sorbitol	119.16	0.60	423.1	6.9	0.05–2.10
Sucrose[a]	211.82	0.92	649.4	13.1	0.05–1.02

[a]Literature values of ϕ_c^0 data for aqueous polyols at 25°C: ethylene glycol 191.9 J K^{-1} mol^{-1} (6); $B_c = -5.5$. Literature values of ϕ_v^0 data at 25°C: for ethylene glycol 54.63 cm^3 mol^{-1} (6); $B_v = -0.08$. Sucrose 211.124 ml mol^{-1} (7); $B_v = 1.997$, sucrose 211.49 ml mol^{-1} (see reference cited in ref. 7).
[b]Data shown in parentheses are considered unreliable due to the limited number of points investigated (3 points).

when using group contributions for predicting solution behavior.

(*3*) There is no apparent difference in the limiting solution behavior of D- and L-configurations of the alditols, e.g. identical results (within experimental uncertainty for D- and L-arabitol.

(*4*) Both the B_c and B_v coefficients exhibit the same trends, i.e. negative signs which reach zero in the case of glycerol or *meso*-erythritol and become increasingly positive for the higher molecular weight polyols.[4] Monohydric alcohols and diols have negative B_v coefficients which decrease as the size of the hydrocarbon group increases (6). The corresponding B_c coefficient for α,ω-alcohols becomes positive with increasing chain length (6). It therefore appears difficult to draw any definite conclusions about the nature of polyol–polyol interactions from the excess coefficients.

Ternary Systems

Apparent molal volumes and heat capacities of transfer of 0.1 m NaCl and 0.1 m n-Bu_4NBr to 1 m aqueous alditol solutions are summarized in Table 2. The heat capacities of transfer are negative for the hydrophobic 'structure-maker' n-Bu_4NBr, and positive for NaCl. The volumes of transfer are positive, except in the case of the transfer of n-Bu_4NBr to glycerol and erythritol solutions. The electrostrictive structure-breaker, NaCl, appears to be more effective (as judged by the absolute magnitude of the transfer functions) than n-Bu_4NBr in differentiating the structural effects of stereoisomeric molecules.[5]

Discussion

Binary Systems

The polyhydroxy compounds studied behave ideally, i.e. the apparent molal quantities in water exhibit only a marginal concentration dependence (0.05–2 m), indicating the absence of any marked solute–solute interactions (no long-range interactions) in these systems.

It is interesting to examine a plot of the standard apparent molal quantities vs. the number of carbon atoms of the alditols (general formula $CH_2OH(CHOH)_nCH_2OH$, where $n = 0$ to 4) (Fig. 1). The experimental points for glycerol, *meso*-erythritol, arabitol, ribitol, and mannitol fall on a straight line (linear correlation coefficient 0.99). However, xylitol and sorbitol show marked negative deviations from such a line;

[4]It is interesting to note that ΔH_s also changes sign at the same crossover point, i.e. lower homologs show exothermic behavior; the higher molecular weight polyols show endothermic behavior (3–5).

[5]Although the dielectric constant of glycerol–water mixtures is similar to that of water, the difference in dipole moments could be significant in ion–solvent interactions with the smaller ions. This could be a possible reason for the better discrimination of NaCl as compared to n-Bu_4NBr towards various polyols (C. Jolicoeur, personal communication).

TABLE 2. Apparent molal volumes (24°C) and heat capacities (25°C) of transfer of 0.1 *m* NaCl and *n*-Bu_4NBr from water to 1 *m* aqueous alditol solutions[a]

Solvent	NaCl		*n*-Bu_4NBr	
	$\Delta\phi_{c\ tr}$ ($J\ K^{-1}\ mol^{-1}$)	$\Delta\phi_{v\ tr}$ ($cm^3\ mol^{-1}$)	$\Delta\phi_{c\ tr}$ ($J\ K^{-1}\ mol^{-1}$)	$\Delta\phi_{v\ tr}$ ($cm^3\ mol^{-1}$)
Glycerol	10	0.5	−50	−0.55
meso-Erythritol	8	0.31	−53	−0.74
D-Arabitol	20	1.10	−47	−0.02
Ribitol	18	1.34	−44	−0.15
D-Xylitol	27	1.65	−45	0.72
D-Mannitol	13	−0.01	−53	0.04
D-Sorbitol	41	3.34	−50	0.65

[a]The estimated uncertainties on $\Delta\phi_{c\ tr}$ and $\Delta\phi_{v\ tr}$ are $\pm 2\ J\ K^{-1}\ mol^{-1}$ and $\pm 0.15\ cm^3\ mol^{-1}$. Salt concentrations are expressed on the aquamolality concentration scale. Transfer functions are defined as $\Delta\phi_{x\ tr} = \phi_{x(soln)} - \phi_{x(H_2O)}$, where ϕ_x represents the appropriate molal quantity at a specific concentration.

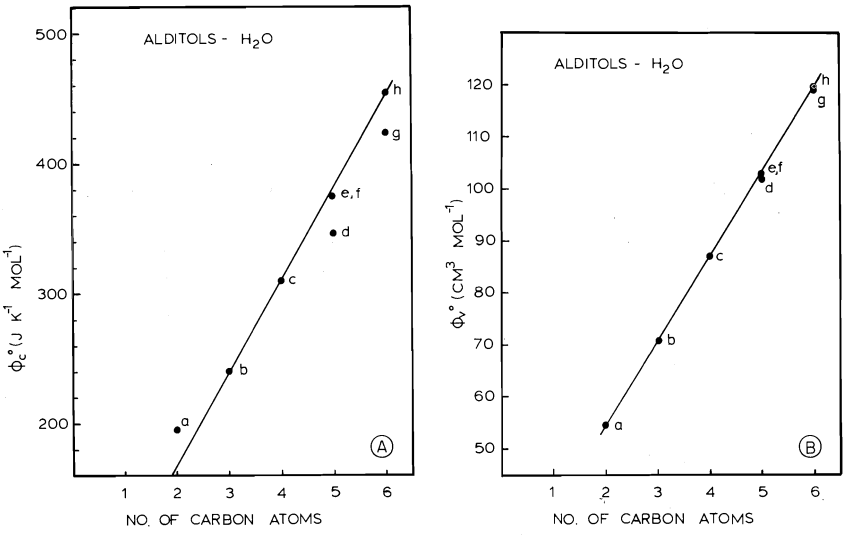

FIG. 2. Standard apparent molal quantities of the alditols in water: (*a*) ethylene glycol; (*b*) glycerol; (*c*) *meso*-erythritol; (*d*) D-xylitol; (*e*) D-arabitol; (*f*) ribitol; (*g*) D-sorbitol; (*h*) D-mannitol. (*A*) ϕ_c^0 at 25°C. (*B*) ϕ_v^0 at 24°C. This temperature was selected because of the experimental set-up. The error introduced by taking the density ratios at 24 rather than 25°C is vanishingly small.

conversely ethylene glycol shows a marked positive deviation from the line.

The present results can be explained in terms of the adaptability of the particular alditol molecule to its water environment. A consideration of alditol (solution) stereochemistry may be the key to a possible explanation. Nuclear magnetic resonance studies have shown that the most stable conformation of an acyclic polyhydric alcohol in solution is a planar, zig-zag arrangement of the carbon chain (9, 10), in which the O. . .O separation corresponding to C_n—O, $C_{(n+2)}$—O bonds is 2.50 Å (9, 11). If any 1–3 (OH—OH) unfavorable non-bonded interactions exist in the planar zig-zag form, then the molecule assumes a bent or 'sickle' conformation which is generated from the zig-zag form through a 120° rotation about an internal C—C bond (12–15). The polyols that fall on the line (Fig. 2) exist in the planar zig-zag conformation,[6]

[6]Ribitol seems to be an exception. Although it exists in the bent conformation (12–15), it appears to fall on the line. However, a careful examination of the data reveals that the numerical values for ribitol are considerably lower than those for arabitol, even if this difference is sometimes within the limit of experimental uncertainty.

whereas the others would assume the bent conformation. An excellent correlation thus exists between differences in the solution conformation of the alditols, and their limiting thermodynamic properties (ϕ_c^0, ϕ_v^0).

The lower standard apparent molal heat capacities of sorbitol and xylitol, as compared to the values for mannitol and sorbitol, suggest that sorbitol and xylitol are relatively more disruptive of the solvent structure than the corresponding stereoisomers.[7] Wilson (16) has reached the same conclusion from studies of heats of transfer of NaCl to the aqueous hexitols.

The steric discrimination effects, and the structure-altering characteristics shown by the polyols in water may be understood in terms of an observation made by Warner (17). If a hypothetical alcohol molecule could adopt a conformation in which the projected O—O distances were approximately 4.8 Å apart (corresponding to the second nearest neighbor oxygen distance in water), then the solvent would experience a minimum disturbance. However, if the polyol has negligible hydrophobic character, and if the orientation of the hydroxyl groups on the carbon chains is unable to assume a conformation completely compatible with the solvent, then the polyol would act as a 'structure-breaker'. The amount of structure-breaking would be determined by the compatibility of the polyol conformation with the solvent structure.

Studies supporting the present proposals include spectroscopic (7, 18) and thermodynamic measurements (7, 19) on the mutarotation equilibria of sugars, and volumetric studies (7, 20) on solutions of monosaccharides.

The present results are in accord with a specific hydration model (18) in which the structural emphasis is placed not only on the potential solute hydration sites, but also on their relative conformations.

Ternary Systems

Since the dielectric properties of dilute polyol–water solutions (4) do not differ greatly from those of water (21), transfer functions can be used to obtain information on structural hydration interactions. The heat capacities of transfer of NaCl and *n*-Bu_4NBr (Table 2) suggest that there is a decrease in structural order in solutions of the higher molecular weight polyols. The apparent molal volumes of transfer are consistent with the explanation centered on structural compatibility between glycerol and water (1), and the increasing incompatibility of the higher homologs (because of their greater rotational flexibility) and water. The anomaly in the sign of $\Delta\phi_{v\ tr}$ observed for transfers of hydrophobic probes to aqueous glycerol (1) disappears as the structural compatibility decreases. This is illustrated by the positive volumes of transfer of *n*-Bu_4NBr to aqueous solutions of the pentitols and hexitols (Table 2).

The results show that structural hydration effects for a homologous series of polyols in water are not too different from what was previously observed with aqueous glycerol systems (1). This work therefore further substantiates the hypothesis that an effect other than a simple alteration of water structure would be implicated in the stabilizing effect of polyols on biological macromolecules (i.e. proteins).

[7]The interpretation is based on structural hydration-interaction arguments.

Acknowledgement

This work was generously supported by the National Research Council of Canada.

1. G. DiPaola and B. Belleau. Can. J. Chem. **53**, 3452 (1975) and references cited therein.
2. G. DiPaola. Ph.D. thesis. McGill University, Montreal, P.Q., Canada. 1976.
3. F. Franks. Water: a comprehensive treatise. Vol. 4. *Edited by* F. Franks. Plenum Press, New York, NY. 1975.
4. F. Franks, D. S. Reid, and A. Suggett. J. Solution Chem. **2**, 99 (1973).
5. G. S. Parks and K. E. Manchester. J. Am. Chem. Soc. **74**, 3435 (1952).
6. C. Jolicoeur and G. Lacroix. Can. J. Chem. **54**, 624 (1976).
7. J. Sangster, T. T. Teng, and F. Lenzi. J. Solution Chem. **5**, 575 (1976).
8. F. Franks, M. A. J. Quickenden, D. S. Reid, and B. Watson. Trans. Faraday Soc. **66**, 582 (1970).
9. S. A. Barker, E. J. Bourne, and D. H. Whiffen. J. Chem. Soc. C, 3865 (1952).
10. D. Horton and M. J. Miller. J. Org. Chem. **30**, 2457 (1965).
11. G. A. Jeffrey and J. S. Kim. Carbohydr. Res. **14**, 207 (1970).
12. D. Horton and J. D. Wander. Carbohydr. Res. **15**, 271 (1970).
13. H. S. El Khadem, D. Horton, and T. F. Page, Jr. J. Org. Chem. **33**, 734 (1968).
14. W. S. Chilton and R. C. Krahm. J. Am. Chem. Soc. **90**, 1318 (1968).
15. D. Horton and J. D. Wander. Carbohydr. Res. **10**, 279 (1969).

16. D. P. WILSON. Ph.D. thesis. Clark University, Worcester, MA, U.S.A. 1974; D. P. WILSON and W.-Y. WEN. J. Phys. Chem. **80**, 431 (1976).
17. D. T. WARNER. Nature, **196**, 1055 (1962).
18. M. J. TAIT, A. SUGGETT, F. FRANKS, S. ABLETT, and P. A. QUICKENDEN. J. Solution Chem. **1**, 131 (1972).
19. F. FRANKS. Hydrogen-bonded solvent systems. *Edited by* A. K. Covington and P. Jones. Taylor and Francis, London, England. 1968. p. 31.
20. F. FRANKS, J. R. RAVENHILL, and D. S. REID. J. Solution Chem. **1**, 3 (1972).
21. D. EISENBERG and W. KAUZMANN. The structure and properties of water. Oxford University Press, Oxford, England. 1969.

Ammonium salts of benzoic acid and the crystal structure of ammonium hydrogen bisbenzoate[1]

IAN A. OXTON, T. STANLEY CAMERON, AND OSVALD KNOP
Department of Chemistry, Dalhousie University, Halifax, N.S., Canada B3H 4J3
AND
ARCHIBALD W. MCCULLOCH
Atlantic Regional Laboratory, National Research Council of Canada, Halifax, N.S., Canada B3H 3Z1

Received June 6, 1977

IAN A. OXTON, T. STANLEY CAMERON, OSVALD KNOP, and ARCHIBALD W. MCCULLOCH. Can. J. Chem. **55**, 3831 (1977).

The ir spectrum of the isotopically isolated NH_3D^+ ion was used to deduce the possible site symmetries of the NH_4^+ ion in ammonium benzoate, NH_4PhCOO, and ammonium hydrogen bisbenzoate, $NH_4H(PhCOO)_2$. The NH_4^+ ion in both crystals is strongly hydrogen-bonded, one of the two isotopically isolated ND frequencies in ammonium benzoate being the lowest such frequency reported to date. The site symmetry C_2 of NH_4^+ in $NH_4H(PhCOO)_2$ has been confirmed by determining the crystal structure of this compound. The O···H···O bond in the dibenzoate ion, $(PhCOO\cdots H\cdots OOCPh)^-$, is short, 2.46(1) Å, and probably symmetric.

IAN A. OXTON, T. STANLEY CAMERON, OSVALD KNOP et ARCHIBALD W. MCCULLOCH. Can. J. Chem. **55**, 3831 (1977).

On a utilisé le spectre ir du NH_3D^+ isolé isotopiquement pour déduire les symétries de site possibles de l'ion NH_4^+ dans le benzoate d'ammonium, NH_4PhCOO, et dans le bisbenzoate d'ammonium et d'hydrogène, $NH_4H(PhCOO)_2$. L'ion NH_4^+ dans les deux cristaux est fortement lié par des ponts hydrogènes, et une des deux fréquences ND isotopiquement isolée dans le benzoate d'ammonium est la plus basse fréquence de ce type rapportée à date. La symétrie de site C_2 du NH_4^+ dans le $NH_4H(PhCOO)_2$ est confirmée par une détermination de la structure cristalline de ce composé. Le lien O···H···O dans l'ion dibenzoate $(PhCOO\cdots H\cdots OOCPh)^-$ est court, 2.46(1) Å, et probablement symétrique.

[Traduit par le journal]

The original aim of this investigation was to deduce the symmetry of the ammonium ion(s) in ammonium benzoate (AB), a compound of unknown crystal structure, using the dilute NH_3D^+ ion as an ir spectroscopic probe (1). This method has given correct results when applied to some structurally well-characterized ammonium salts (2), and we now wished to show that a prediction of the site symmetry of an ammonium ion can be made in a complete absence of structural information.

For compounds that are recoverable without change from aqueous solution, recrystallization from water containing 1–2% D_2O is the standard method of preparing suitable material. However, it was found that the crystals obtained from a hot aqueous solution of AB on cooling were not AB but ammonium hydrogen bisbenzoate (AHB), $NH_4H(PhCOO)_2$, or a mixture of AHB and hydrated AB. A closer investigation showed that under various conditions the products of recrystallization from aqueous media, including aqueous ammonia, might be AHB, AB, $AB\cdot H_2O$, or mixtures of these. The monohydrate has not been described previously, but hydrates of the alkali salts, $PhCOOLi\cdot H_2O$, $PhCOONa\cdot H_2O$, and $PhCOOK\cdot 3H_2O$, as well as $PhCOONH_4\cdot 1.5$-MeOH have been reported (3).

Very little information is available in the literature on the properties of AHB (cf. ref. 3), but salts of the type $K^+(XHX)^-$ (X = carboxylate ion) have been the subject of a number of studies (4–8; data compiled by J. C. Speakman in Table 5-4 of ref. 9), with much of the discussion centering on the nature of the X···H···X hydrogen bond. We therefore took advantage of the availability of AHB to make a prediction of the NH_4^+ site symmetry in this compound as well as in AB, and to verify the prediction from a determination of the crystal structure of AHB, with a view to providing, in addition, what information might be obtainable from the X-ray study about the O···H···O bond.

Experimental

The ammonium benzoate used in this work was from two sources: Mallinckrodt and Eastman. One supply was 25 years old and appeared to consist entirely of AHB.

[1]NRCC No. 16209.

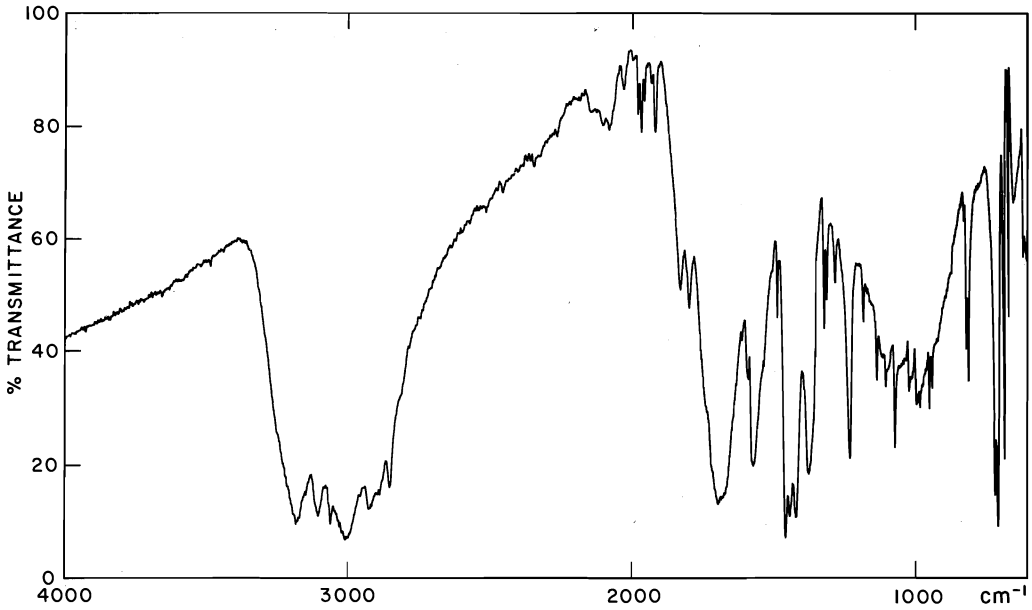

FIG. 1. Infrared spectrum of ammonium hydrogen bisbenzoate (AHB) at 77 K.

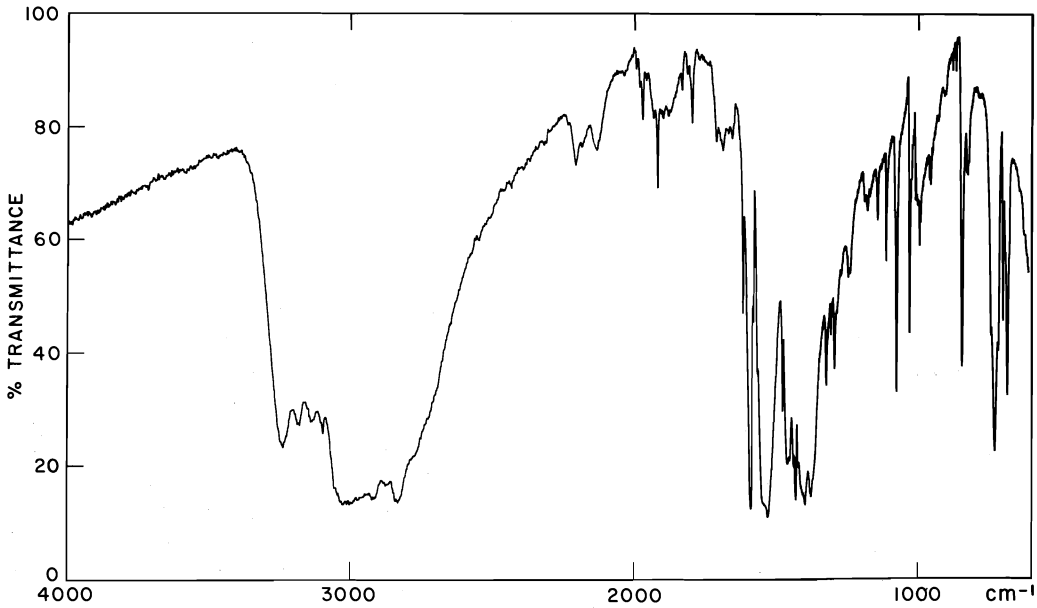

FIG. 2. Infrared spectrum of ammonium benzoate (AB) at 77 K.

The solubility of AB appeared to increase appreciably on heating, but it is not clear whether this is due to an intrinsic increase in the solubility of AB or to partial or complete conversion to AHB. Recrystallization of the fresh supply of commercial AB from hot aqueous solution usually resulted in a mixture of AHB and AB, the latter frequently hydrated; the proportion of AHB increased with the period of heating. Recrystallization of material from either source from concentrated ammonia solution produced AB alone (see below). Samples of the salts containing 1% D were prepared in a similar manner with the addition of an appropriate quantity of D_2O to the solvent.

Infrared spectra of Nujol and Fluorolube mulls were recorded with a Perkin-Elmer model 180 spectrophotometer fitted with a variable-temperature cryostat. No visible changes in the spectra accompanied cooling of the sample from room temperature to liquid-nitrogen temperature (Figs. 1 and 2) other than band sharpening and small frequency shifts. Vibrational frequencies are accurate to ± 1.0 cm^{-1}.

The ^{1}H nmr spectra were recorded at a concentration of 65 mg per 0.5 g of anhydrous dimethylsulfoxide-d_6, using a Varian A-60A spectrometer and Me_4Si as internal standard.

The crystal data of AHB are as follows:

$C_{14}H_{15}O_4N$ fw = 261.28
Monoclinic, $B2/b$, a = 29.301(8), b = 11.439(3), c = 3.901(1) Å, γ = 94.93(1)°, V = 1302 Å^3, ρ_o = 1.298 (flotation), Z = 4, ρ_c = 1.332 (18 ± 2°C); CuKα_1, λ = 1.54051 Å (carbon monochromator), μ = 7.73. $F(000)$ = 552 e.

Because of the high vapour pressure of AHB the single crystal that was used for the intensity measurements was sealed inside two concentric Lindemann-glass capillary tubes.[2] A Picker FACS 1 four-circle diffractometer was used to determine the unit-cell dimensions, from 12 general reflections with 2θ in the range of 50–60°, and to measure (ω–2θ scan) the intensities of 296 independent reflections (26% of those observable) with $I > 3\sigma$ and 2θ values between 4 and 120°. The minimum base width was 3.5°. Three standard reflections were measured every 60 reflections. The intensities of these three reflections decreased steadily throughout the data collection but could be adjusted to a standard scale from a least-squares fit (σ = 0.032) to a first-order decay; from the counting statistics the esd of these standard reflections was 2.2%. The data were reduced to $|F_o|$ by the routine procedure. No absorption or extinction corrections were applied. The scattering factors for neutral atoms were taken from ref. 10. Fifty reflections with $|E| > 1.0$ were used to solve the structure by an application of the tangent formula that examined $128 = 2^7$ sets of starting phases and successively eliminated all but the most likely. This program is part of an X-ray system written by Sheldrick (11). From the E map with the lowest Karle R factor (12) the positions of all non-hydrogen atoms could be found.

The structure was refined by full-matrix least squares, $\Sigma(\Delta|F|)^2$ = min., with isotropic temperature factors on all the atoms.[3] When the conventional R factor was 0.13 the H atoms of the ammonium ion and phenyl groups were located from a difference Fourier synthesis. The H atom of the carboxyl group could not be found. The final R factor with the H atoms included was 0.08; there were no significant features on the difference Fourier map calculated at this stage. The least-squares weights were calculated from $w = 1/(\sigma^2|F_o| - 0.001|F_o|^2)$. The positional parameters are given in Table 1, and interatomic distances and inter-bond angles in Table 2.

TABLE 1. Final atomic parameters in AHB* (× 10^4 for C, O, and N; × 10^3 for H)

Atom	x	y	z	U (Å^2)
C(1)	3850(5)	−433 (12)	3050(42)	417
C(2)	3720(5)	−1598 (12)	3815(50)	463
C(3)	3276(5)	−2056 (14)	3263(59)	573
C(4)	2968(6)	−1391 (15)	1741(56)	621
C(5)	3087(5)	−235 (13)	920(51)	536
C(6)	3524(5)	246 (13)	1538(52)	490
C(10)	4318(5)	118 (12)	3757(50)	535
O(1)	4404(4)	1211 (9)	3417(36)	638
O(2)	4625(3)	−553 (8)	4589(29)	524
N(1)	½†	¼†	−975(63)	626
H(2)	398(3)	−201 (8)	503(29)	26
H(3)	317(4)	−295 (12)	421(41)	36
H(4)	264(4)	−168 (10)	175(36)	48
H(5)	284(5)	30 (12)	−3(52)	73
H(6)	361(4)	117 (10)	121(31)	71
H(10)	468(2)	224 (9)	−26(31)	68
H(11)	513(4)	181 (7)	−211(34)	87

*Note the disparity in the unit-cell dimensions (see Experimental).
†This value has not been multiplied by 10^4.

Results and Discussion

Characterization and Relative Stabilities of AB and AHB

The crystals obtained on cooling a hot aqueous solution of commercial AB were usually plate-like. Their ir spectrum is shown in Fig. 1. That this compound was AHB is apparent from its ^{1}H nmr spectrum which showed a six-proton multiplet (*meta* and *para*) at δ 7.43, a four-proton multiplet (*ortho*) at δ 7.98, and a broad singlet at δ 8.52 (exchangeable protons) integrating for five hydrogens.

However, the crystals freshly prepared from a strongly basic aqueous ammonia solution were laths which tended to be hygroscopic. After only brief drying they were dissolved in DMSO-d_6, with some difficulty; their ^{1}H nmr spectrum in this solution showed a three-proton multiplet at δ 7.35, a two-proton multiplet at δ 7.95, and a broad singlet at δ 6.12 (6.2 H). On this evidence the briefly-dried crystals were $AB{\cdot}H_2O$. Upon further drying anhydrous AB was obtained, but prolonged drying resulted in gradual loss of ammonia. This was reflected by increasing solubility in DMSO, a gradual downfield shift of the averaged signal for the exchangeable hydrogens and an obvious change in the relative integral for the latter. The end product of the decomposition was AHB.[4]

The ^{1}H nmr spectrum of anhydrous AB showed a multiplet for the *meta* and *para* ring hydrogens centred at δ 7.33. The broad singlet (δ 8.09) for the hydrogens of the ammonium ion was superposed on the multiplet (δ 7.92) for the remaining aromatic hydrogens. The spectrum integrated correctly for the normal salt AB. The ir spectrum of AB is shown in Fig. 2.

[2]The vapour pressure (presumably of NH_3) was sufficient to burst a single capillary tube after the crystal inside it had been irradiated for about 2 days.

[3]A list of the structure factors (Table 3) is available, at a nominal charge, from the Depository of Unpublished Data, CISTI, National Research Council of Canada, Ottawa, Ont., Canada K1A 0S2.

[4]Berzelius reported as early as 1805 that on evaporation of an aqueous solution of AB ammonia is liberated, with the formation of an acid salt (3).

TABLE 2. Interatomic distances (Å) and inter-bond angles (deg) in AHB*

Bond	Distance (Å)	Bonds	Angle (deg)
C(1)—C(2)	1.39(1)	C(6)—C(1)—C(2)	118(1)
C(1)—C(6)	1.41(1)	C(2)—C(1)—C(10)	122(1)
C(1)—C(10)	1.49(1)	C(6)—C(1)—C(10)	119(1)
C(2)—C(3)	1.38(1)	C(1)—C(2)—C(3)	120(1)
C(3)—C(4)	1.37(2)	C(2)—C(3)—C(4)	120(1)
C(4)—C(5)	1.38(2)	C(3)—C(4)—C(5)	121(1)
C(5)—C(6)	1.37(2)	C(4)—C(5)—C(6)	120(1)
C(10)—O(1)	1.26(1)	C(5)—C(6)—C(1)	120(1)
C(10)—O(2)	1.27(1)	C(1)—C(10)—O(1)	120(1)
O(2)···O(2′)	2.46(1)	C(1)—C(10)—O(2)	118(1)
N(1)···O(1)	2.78(1)	O(1)—C(10)—O(2)	122(1)
N(1)···O(2″)	2.93(1)	H(10)—N(1)—H(10‴)	148(10)
N(1)—H(10)	1.00(1)	H(10)—N(1)—H(11)	107(3)
N(1)—H(11)	1.00(1)	H(11)—N(1)—H(11‴)	128(10)
H(10)···O(1)	1.99(5)	N(1)—H(10)···O(1)	135(6)
H(11)···O(2″)	1.93(8)	N(1)—H(11)···O(2)	176(6)

*NOTE: ′ $1-x, -y, 1-z$; ″ $1-x, -y, -z$; ‴ $1-x, \frac{1}{2}-y, z$.

The ir spectrum of AHB (Fig. 1) is very similar to those of $KH(PhCOO)_2$ (13) and $KH(PhCH_2COO)_2$ (5) with the NH_4^+ absorptions added. The main differences between the spectra of AB and AHB are summarized in Table 4. No band which could be satisfactorily assigned to the OH stretching mode was observed. This also seems to be the case in several other compounds of this type (5, 13), although in AHB such a band could be obscured by the NH stretching bands of NH_4^+.

Although AB appears to decompose into AHB fairly readily, AHB may not itself be very stable in view of the observation[2] that it dissociates in the X-ray beam, presumably into benzoic acid and ammonia.

Isotopically Isolated NH_3D^+ Ions in AHB and AB

The ND stretching region of the isotopically isolated NH_3D^+ ion in AHB, at liquid-nitrogen temperature, is shown in Fig. 3. Two sharp bands are observed which are separated in frequency by about 100 cm^{-1} (Table 5). Of the two components of $\nu_1(NH_3D^+)$ that at the lower frequency is somewhat more intense. This is not surprising in view of the difference in hydrogen-bond strength implied by the frequency difference (cf. below). Assuming that only one set of equivalent NH_4^+ ions is present in the crystal the observed spectrum is consistent with an NH_4^+ ion of an effective (1) symmetry C_{2v} or C_2 and hence with the existence of two pairs of nonequivalent N—H bonds.

The corresponding region in the spectrum of AB (1% D) is complicated by the presence of an underlying absorption (see Fig. 2) but it seems more than likely that the absorption arising from the NH_3D^+ ion again consists of two sharp bands (Fig. 4, Table 5); overtone and combination modes may frequently appear with greater intensity than $\nu_1(NH_3D^+)$ when the NH_3D^+ ion is present at a 1% concentration level. The characteristically pronounced sharpening of this mode upon cooling (14) is often extremely useful in assisting assignment where interference from other absorptions occurs.

Upon the above assumption, and using the

TABLE 4. Infrared frequencies (cm^{-1}) of ammonium benzoate (AB) and ammonium hydrogen benzoate (AHB) at 77 K

Assignment	AB	AHB
ν(OH)	—	*
ν(C═O)	—	1690
ν(C═O), asym.	1535	—
ν(C═O), sym.	†	—
δ(OH), in-plane	—	†
ν(C—O)	—	1229
δ(OH), out-of-plane	—	~950

*Not observed.
†Not assigned because of proximity of $\nu_4(NH_4^+)$.

TABLE 5. Infrared frequencies (cm^{-1}) of the isotopically dilute NH_3D^+ ion in AB and AHB at 77 K

	$\nu_1(NH_3D^+)$	$\Delta\nu_{1/2}$
AB	2271.9	8.0
	2195.7	*
AHB	2340.1	6.0
	2246.0	7.0

*Half-width uncertain because of underlying combination band.

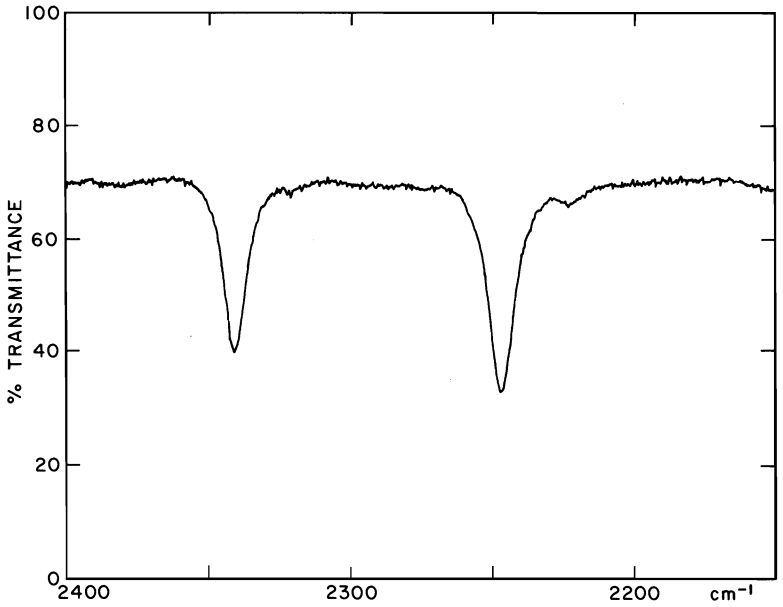

FIG. 3. The ND stretching region of the ir spectrum of the isotopically isolated NH_3D^+ ion in AHB at 77 K.

nomenclature of ref. 1, the possible site symmetries S of the ammonium ion in AHB and AB may be deduced as

$E'(NH_3D^+)$	$E(NH_4^+)$	$S(NH_4^+)$
$C_s(2)$, $C_s(2)$	C_{2v}	C_{4v}, D_{2h}, C_{2v}
	or	
$C_1(2)$, $C_1(2)$	C_2	C_4, C_{2h}, C_2

The spectra in both salts are indicative of strongly hydrogen-bonded ammonium ions. This is especially true of the lower-lying of the two absorptions in each compound. In fact, the isotopically isolated ND stretching frequency of 2195.7 cm^{-1} observed in AB is the lowest such frequency reported to date.

Crystal Structure of AHB

AHB is practically isostructural with $KH(PhCOO)_2$ (6) except that the ammonium ions in the AHB structure form with the dibenzoate ions $(PhCOO\cdots H\cdots OOCPh)^-$ hydrogen-bonded helices which lie in the zone of the b axis (Figs. 5 and 6). One hydrogen bond is between the centrosymmetrically related carboxyl oxygens O(2) and O(2′) of the dibenzoate ion and another between O(2) and N(1). The N(1) atom is located on a twofold axis and therefore able to propagate the helix through a hydrogen bond to a diad-related benzoate unit (Fig. 6). Adjacent helices are linked through hydrogen bonds between O(1) and N(1) to form a layer parallel to the (100) plane. The hydrogen-bonded distances O(2)···O(2′), N(1)···O(1), and N(1)···O(2) are 2.46(1), 2.78(1), and 2.93(1) Å, respectively.

Of the two non-equivalent H atoms of the ammonium ion, H(10) is clearly defined in the difference Fourier synthesis and forms an angle H(10)—N(1)—H(10′) of 148(10)° with its twofold-related atom. This large deviation from the tetrahedral angle could be the result of strong hydrogen bonding. H(11) is poorly defined, with H(11)—N(1)—H(11′) of 129(10)°. Both hydrogens are located about 1.0 Å from N(1).

There was no trace at, or near, the centre of symmetry in the difference Fourier synthesis, of the H atom that forms the bond between the benzoate units in the dibenzoate ion. Attempts to place and refine a hydrogen atom in all the reasonable positions produced a very large isotropic temperature factor. The O···O contact is short (15), comparable with the corresponding O···O separations in acid salts of other organic acids (9), and represents a strong hydrogen bond. The two C—O bond lengths in the carboxyl group are not significantly different: C(10)—O(1), 1.26(1) Å, and C(10)—O(2), 1.27(1) Å. They are similar to those found in $KH(PhCOO)_2$, 1.22(4) and 1.24(4) Å (6), and in the benzoate ion itself, in a thallous benzoate thiourea complex (16), where the ion has C_{2v} symmetry and a C—O bond length of 1.25(2) Å. It thus seems

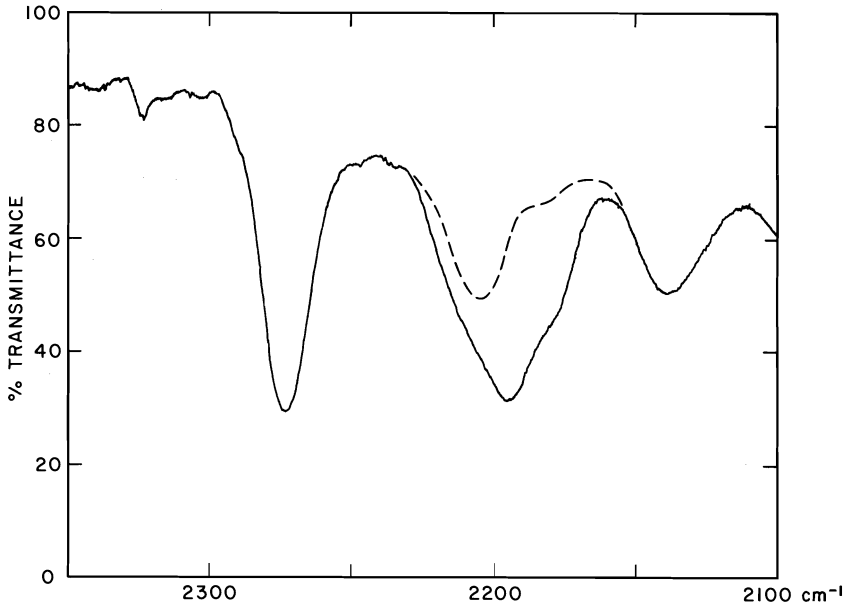

FIG. 4. The ND stretching region of the ir spectrum of the isotopically isolated NH_3D^+ ion in AB at 77 K. The dashed line corresponds to the estimated contour of the underlying absorption (see text).

unlikely that the proton in AHB is closely associated with either carboxyl oxygen in the O···H···O bond. The dimensions of the rest of the anion are unexceptional and there are no other unusually short inter-ion contacts.

Additional Observations

We have not investigated the structural features of AB in any detail beyond the effective symmetry of the NH_4^+ ion. Some statements are nevertheless possible when the information available in the literature is examined. The only crystallographic data are derived from optical-goniometer and optical measurements (3, 17, 18).[5] According to these the crystal symmetry of AB is *mmm*, with an axial ratio of 0.9873:1:2.1504 and a measured density (3) of 1.260, 1.262, or 1.213 g/cm^3, and there is perfect cleavage along (001). Assuming this point-group symmetry and the composition AB to be correct, the site symmetry of the NH_4^+ ion will be one of the following: D_{2h}, C_{2v}, C_{2h}, or C_2 (see above). Steinmetz (18) pointed out the similarity of the axial ratios of AB and benzoic acid[6] when the largest term in the ratio for AB is doubled; this would suggest that $Z(AB) = 4$. On this additional, reasonable assumption a symmetry $S = D_{2h}$ at the NH_4^+ site could only occur in space group no. 69; $S = C_{2v}$ only in nos. 63, 65, 67, 71, or 74; $S = C_{2h}$ only in nos. 63–67, 72, or 74; and $S = C_2$ only in nos. 48–58 or 60.

The unit cell of AHB shows dimensional and space-group similarity not only to $KH(PhCOO)_2$ (6) but also to $KH(PhCH_2COO)_2$ (4, 7).

Adducts of Na benzoate with two and three molecules of benzoic acid, NaB·2HB and NaB·3HB, have been reported (3). It would be of interest to establish whether ammonium analogues of these compounds exist.

Conclusions and Summary

Under different conditions of crystallization and drying, three salts (ammonium benzoate AB, ammonium benzoate monohydrate $AB·H_2O$, and ammonium hydrogen bisbenzoate AHB) have been obtained from solutions of commercial ammonium benzoate. Both AB and $AB·H_2O$ are readily converted to AHB.

Infrared spectra of the isotopically dilute NH_3D^+ ion in AB and AHB were used to predict that the effective symmetries E of the NH_4^+ ion in these crystals are C_{2v} (corresponding to site symmetries $S = C_{4v}$, D_{2h}, or C_{2v}) or C_2 (corresponding to $S = C_4$, C_{2h}, or C_2). This prediction was confirmed, for AHB, by a determination of the crystal structure of this com-

[5]Some of these are due to de Marignac and date as far back as 1857 (3).

[6]The axial ratio quoted in ref. 18 for benzoic acid is in fact the ratio of the unit-cell dimensions.

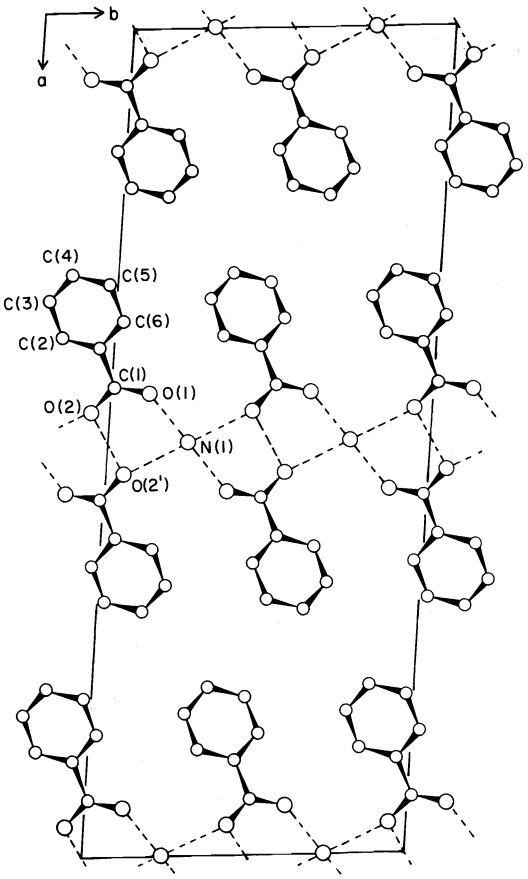

FIG. 5. The unit cell of AHB projected perpendicular to the *c*-axis.

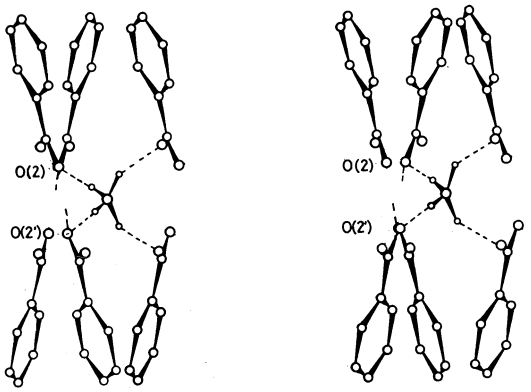

FIG. 6. Environment of the ammonium ion in AHB viewed along the *b*-axis.

pound. It is found that the single set of equivalent NH_4^+ ions occupies sites of C_2 symmetry. The NH_4^+ and $(PhCOO\cdots H\cdots OOCPh)^-$ ions form hydrogen-bonded layers whilst short O···H···O bonds link together the benzoate units in the centrosymmetric dibenzoate ions. AHB is essentially isostructural with its potassium analogue.

The N—H···O bonds in AB and AHB are strong. The isotopically isolated ND stretching frequency of NH_3D^+ in AB, 2195.7 cm^{-1}, is the lowest such frequency reported to date.

Placing a H atom at, or close to, the centre of the dibenzoate ion resulted in very large isotropic temperature factors for this atom when the structure of AHB was refined on this hypothesis. This finding is similar to that obtained by Bacon and Curry (7) in their neutron-diffraction study of the crystal structure of $KH(PhCH_2COO)_2$. While the O···H···O bond in AHB is *formally* symmetric, no definite conclusion can be made, in static terms, about the location of this hydrogen atom from the present evidence.

Acknowledgment

This investigation was supported by research grants from the National Research Council of Canada to O.K. and T.S.C.

1. I. A. OXTON, O. KNOP, and M. FALK. J. Phys. Chem. **80**, 1212 (1976).
2. I. A. OXTON, O. KNOP, and M. FALK. Can. J. Chem. **53**, 2675 (1975); **53**, 3394 (1975); **54**, 892 (1976).
3. Beilsteins Handbuch d. org. Chemie. 4th ed. Vol. 9. Main work, 1926. p. 107; 1st suppl. 1932. pp. 59–60; 2nd suppl. 1949. pp. 83–84; 3rd suppl. 1970. p. 375.
4. J. C. SPEAKMAN. J. Chem. Soc. 3357 (1949).
5. M. DAVIES and W. J. ORVILLE-THOMAS. J. Chem. Soc. 2858 (1951).
6. J. M. SKINNER, G. M. D. STEWART, and J. C. SPEAKMAN. J. Chem. Soc. 180 (1954).
7. G. E. BACON and N. A. CURRY. Acta Crystallogr. **10**, 524 (1957); **13**, 717 (1960).
8. R. BLINC and D. HADŽI. Spectrochim. Acta, **16**, 852 (1960).
9. W. C. HAMILTON and J. A. IBERS. Hydrogen bonding in solids. W. A. Benjamin, Inc., New York, NY. 1968. p. 182.
10. J. A. IBERS and W. C. HAMILTON (*Editors*). International tables for X-ray crystallography. Vol. IV. The Kynoch Press, Birmingham, England. 1974.
11. G. SHELDRICK. X-Ray system report. University Chemical Laboratory, Lensfield Road, Cambridge, England. 1976.
12. J. KARLE and I. L. KARLE. Acta Crystallogr. **21**, 849 (1966).
13. D. HADŽI and A. NOVAK. Nuovo Cimento, **11**, Suppl. No. 3, 715 (1955).
14. I. A. OXTON, O. KNOP, and M. FALK. J. Mol. Struct. **37**, 69 (1977).
15. I. D. BROWN, M. C. BROWN, and F. C. HAWTHORNE. BIDICS 1975. Inst. for Materials Res., McMaster University, Hamilton, Ont. 1976. pp. 77–79.
16. L. H. W. VERHOEF and J. C. A. BOEYENS. Acta Crystallogr. B, **25**, 607 (1969).
17. H. ZIRNGIEBL. Z. Kristallogr. **36**, 117 (1902).
18. H. STEINMETZ. Z. Kristallogr. **53**, 463 (1914).

Mass and infrared spectra of some S_4N_4 complexes of group VIII metals[1]

IAN S. BUTLER AND TSUTOMU SAWAI

Department of Chemistry, McGill University, 801 Sherbrooke St. West, Montreal, P.Q., Canada H3A 2K6

Received April 4, 1977

IAN S. BUTLER and TSUTOMU SAWAI. Can. J. Chem. **55**, 3838 (1977).

The mass and ir spectra of the complexes formed between S_4N_4 and MCl_2 (M = Ni, Co, Pd) in methanol solution have been investigated. The mass spectral data indicate that the stoichiometry of the complexes is $M(S_2N_2H)_2$ and the principal fragmentation is the stepwise loss of SN units, as is the case for S_4N_4 itself. The ir spectra of the complexes show the presence of N—H groups and suggest *cis*-planar configurations for the S_2N_2H chelating ligands.

IAN S. BUTLER et TSUTOMU SAWAI. Can. J. Chem. **55**, 3838 (1977).

On étudie les spectres de masse et infrarouge de complexes formés dans une solution méthanolique entre S_4N_4 et MCl_2 (M = Ni, Co, Pd). Les données obtenues à partir du spectre de masse indiquent que la stoichiométrie des complexes est $M(S_2N_2H)_2$ et que la principale fragmentation est la perte successive des unités SN comme pour le cas de S_4N_4. Le spectre infrarouge des complexes montre la présence de groupes N—H et suggère une configuration planaire *cis* pour les ligands de chélation S_2N_2H.

[Traduit par le journal]

Introduction

In 1953, the isolation of the first transition metal thionitrosyl complex, $Ni(NS)_4$, from the reaction of $Ni(CO)_4$ with S_4N_4 in benzene was reported (1). Following this, it was quickly established that monomeric $M(NS)_4$ complexes could be synthesized by three main routes: heating anhydrous MCl_2 (M = Ni, Co, Pd) with S_4N_4 in alcohols (2); reaction of metal carbonyls (e.g., $Co_2(CO)_8$ (3) and $Fe(CO)_5$ (4)) with S_4N_4; shaking finely divided metal powders (Ni, Co, Pd) with S_2N_2 in tetrahydrofuran (5). The analogous platinum derivative, $Pt(NS)_4$, was prepared by the reaction of H_2PtCl_6 with S_4N_4 in dimethylformamide–H_2O (6). Surprisingly, an X-ray analysis of $Pt(NS)_4$ revealed the presence of two S_2N_2 bidentate chelating ligands instead of the four coordinated NS groups expected and these chelating ligands were arranged in a *cis*-planar configuration (7):

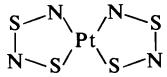

Concurrent with this X-ray study, Piper was investigating the ir and nmr spectra of the complex obtained from the reaction of anhydrous $NiCl_2$ with S_4N_4 in methanol (8, 9) and he was able to show the presence of two N—H groups. Subsequent research on derivatives of $Ni(S_2N_2H)_2$ established that $Ni(S_2N_2Me)_2$ has a *trans*-planar configuration (10), while a *cis*-planar structure is preferred for $Ni(S_2N_2H)$-$[S_2N_2(CONHPh)]$ (11). In both cases, the substituent groups, H, Me, and CONHPh, are attached to the nitrogen atoms which are bonded directly to the central nickel atom. The *trans* stereochemistry for $Ni(S_2N_2Me)_2$ was rationalized on the basis of steric considerations and it was concluded that the *cis*-planar structure shown below was the most likely for $Ni(S_2N_2H)_2$, assuming that no rearrangement took place during the reactions. Furthermore, the analogous complexes of other group VIII metals were presumed to have the same structure. However, this has never been established definitively.

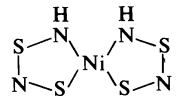

In this paper, we report the mass and ir spectra of the complexes formed by the reactions of MCl_2 (M = Ni, Co, Pd) with S_4N_4 in methanol. Our objectives were to verify the presence of N—H groups and, if possible, to determine the structures of the complexes. The products obtained from the reaction of H_2PtCl_6 with S_4N_4 in dimethylformamide–H_2O were also investigated.

Experimental

Tetrasulphur tetranitride (S_4N_4) was prepared according to the literature method (12). Other materials were obtained from the sources indicated: anhydrous $NiCl_2$

[1]Taken in part from the Ph.D. thesis of T.S., McGill University, Montreal, P.Q. 1973. Presented in part at the 173rd National Meeting of the American Chemical Society, New Orleans, LA, March, 1977.

and $CoCl_2$ (Alfa Inorganics, Inc.); anhydrous $PdCl_2$ and $H_2PtCl_6 \cdot 6H_2O$ (Research Organic/Inorganic Chemical Corp.); acid-washed alumina (Fisher Scientific Co.). The nickel, cobalt, and palladium complexes were prepared as described previously (2, 9). Complete details of these syntheses are contained in ref. 13. The synthesis of $Pt(S_2N_2H)_2$ according to the method of Fluck *et al.* (6) was attempted 10 times but no product analysing as $Pt(S_2N_2H)_2$ could be obtained. In every case, a white precipitate was formed which was identified by ir and elemental analysis as $(NH_4)_2SO_4$. *Anal.* calcd for $H_8N_2O_4S$: H 6.1, N 21.2, S 24.3; found: H 6.2, N 20.8, S 24.0.

Infrared spectra were recorded on a Perkin-Elmer model 521 grating spectrophotometer as KBr disks. The spectra were calibrated against the bands of polystyrene (accuracy ca. $\pm 2\ cm^{-1}$). Mass spectra were measured on an AEI MS-902 spectrometer under the following conditions: 70 eV electron energy, 145–180°C inlet temperature, 8 kV acceleration voltage, and resolution of 1000. The samples were introduced into the ion source using a direct insertion probe. The most important fragments observed, their relative intensities, and the proposed assignments for S_4N_4 and the nickel, cobalt, and palladium complexes are given in Figs. 1–4, respectively. The assignments for the complexes are based on the principal metal isotopes present: ^{58}Ni, ^{59}Co, and ^{106}Pd. A least-squares computer program was written to decompose the observed peak intensities into the intensities associated with the various fragment ions concerned, e.g., FH_2^+, FH^+, and F^+ where F = a metal-containing fragment.

Results and Discussion

The proposed fragmentation scheme for the mass spectrum of S_4N_4 is shown in Fig. 1. The principal fragmentation is the loss of SN units to give species such as $S_3N_3^+$; the transient SN molecule has been identified by microwave spectroscopy (14). One of the main peaks corresponds to $S_2N_2^+$; the S_2N_2 molecule is known to exist as a highly reactive species (5). Other reasonably abundant ions are $S_3N_2^+$, S_3N^+, S_2N^+, S_2^+, N_4^+, and the doubly charged species $S_3N_2^{2+}$. There is a major peak at *m/e* 76 which cannot be attributed to any of the $S_xN_y^+$ species; this peak is assigned tentatively to SN_2O^+ formed by combination with residual oxygen present in the mass spectrometer.

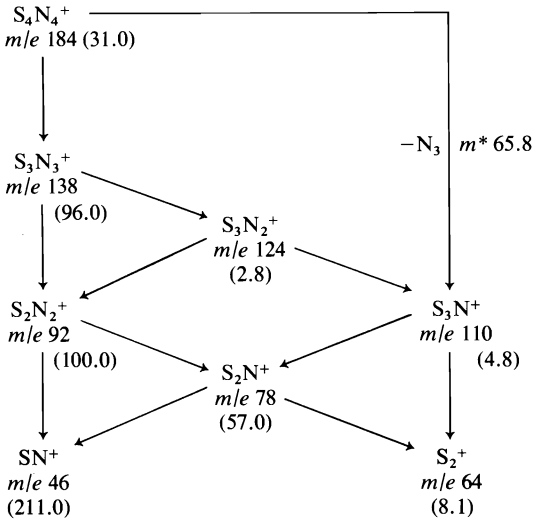

FIG. 1. Proposed mass spectral fragmentation scheme for S_4N_4.

There are several common features in the mass spectra of the nickel, cobalt, and palladium complexes. First, all three complexes exhibit parent molecular ions in which there are two hydrogen atoms present, thus confirming the previously assumed $M(S_2N_2H)_2$ stoichiometry of the species. Second, the successive loss of SN groups is the predominant fragmentation process. In particular, the loss of the first SN group from each of the parent molecular ions is verified by the appearance of the expected metastable ion. This behaviour is reminiscent of S_4N_4 itself. The final feature in common is the loss of hydrogen atoms from the various fragment ions throughout the spectra. Table 1 gives the ratios of the abundances of the fragment ions FH_2^+, FH^+, and F^+ (e.g., $MS_4N_4H_2^+$, $MS_4N_4H^+$, and $MS_4N_4^+$, respectively) calculated from the observed peak intensities assuming that they are sums of the intensities of the different fragments present. In the case of the nickel complex, the parent molecular ion, $NiS_4N_4H_2^+$ (*m/e* 244), is the dominant species, while the palladium complex apparently readily loses its two hydrogen atoms and $PdS_4N_4^+$ (*m/e* 290) is the most abun-

TABLE 1. Calculated ratios of abundances of fragment ions in the mass spectra of $M(S_2N_2H)_2$ complexes (M = Co, Ni, Pd)

		Relative ratio of fragment ions[a]		
Fragment ion	*n*	Co	Ni	Pd
$MS_4N_4H_n^+$	2	100	100	1.8
	1	31	0	1.3
	0	0	0	96
$MS_3N_3H_n^+$	2	57	43	0
	1	42	20	5.8
	0	8.3	0	69
$MS_2N_2H_n^+$	2	12	60	0
	1	35	50	21
	0	37	38	21
$MSNH_n^+$	2	0	0	5.7
	1	28	22	14
	0	50	89	35

[a]Ratio derived from the relative abundances in the mass spectra.

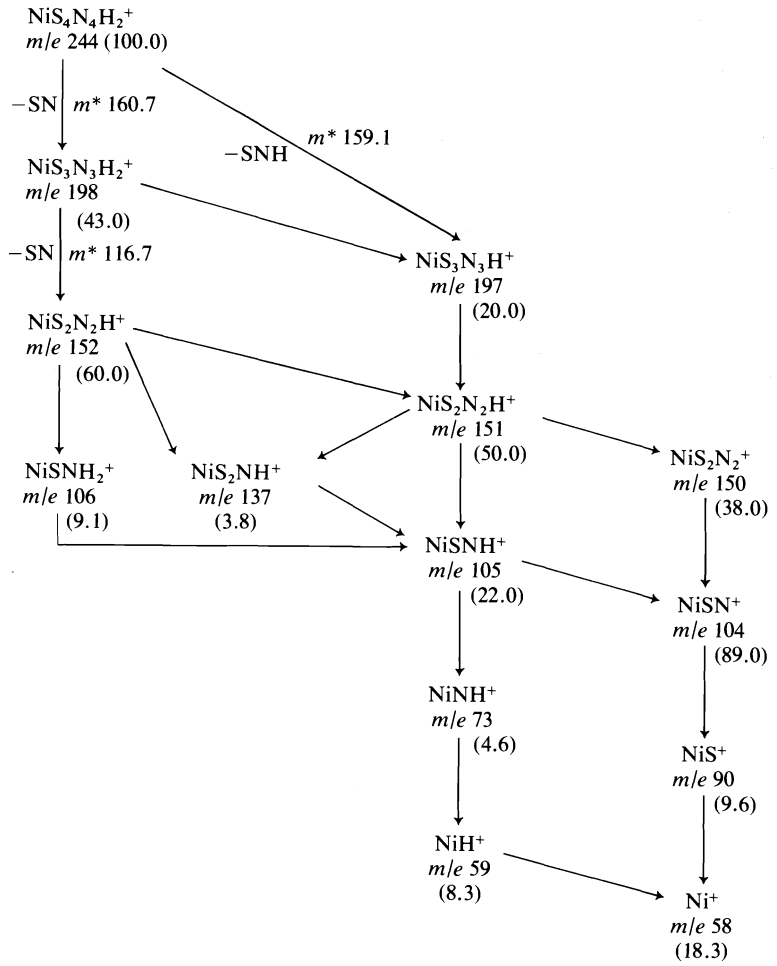

FIG. 2. Proposed mass spectral fragmentation scheme for $Ni(S_2N_2H)_2$.

dant of the $PdS_4N_4H_n^+$ ($n = 2, 1, 0$) ions. The cobalt complex lies in between these two extremes. These mass spectral observations are in accord with the nickel complex being generally considered to be the most stable of the three.

In the case of $NiS_4N_4H_2^+$, there is also a metastable peak corresponding to the release of an SNH group. Thus, bond rupture within the chelate ring seems to take place rather indiscriminantly. In contrast to the cobalt derivative, there is no evidence for the loss of S_2N_2 from any of the fragment ions nor is the dehydrogenated species, $NiS_4N_4H^+$, formed. The appearance of the expected metastable peak confirms the loss of SN from $NiS_3N_3H_2^+$ (*m/e* 198) to give $NiS_2N_2H_2^+$ (*m/e* 152).

The chief observation of Piper in his study of the ir spectrum of the nickel complex was the appearance of N—H stretching modes at 3235 and 3095 cm^{-1} (8, 9). He was apparently unable to deduce any more structural information but he favoured a *trans*-planar arrangement of the S_2N_2H chelating ligands with the location of the N—H groups being unknown. However, as mentioned in the Introduction, the structures of the substituted nickel complexes, $Ni(S_2N_2Me)_2$ (10) and $Ni(S_2N_2H)[S_2N_2(CONHPh)]$ (11), have since been determined by X-ray diffraction and these complexes adopt *trans*- and *cis*-planar structures, respectively. In both cases, the S_2N_2 chelate rings, the nickel atom, and the carbon atoms attached to the nitrogen atoms of the rings share the same plane. On the basis of these results and Piper's ir data, it is generally accepted that the parent $Ni(S_2N_2H)_2$ complex has two N—H groups bonded to the central nickel atom

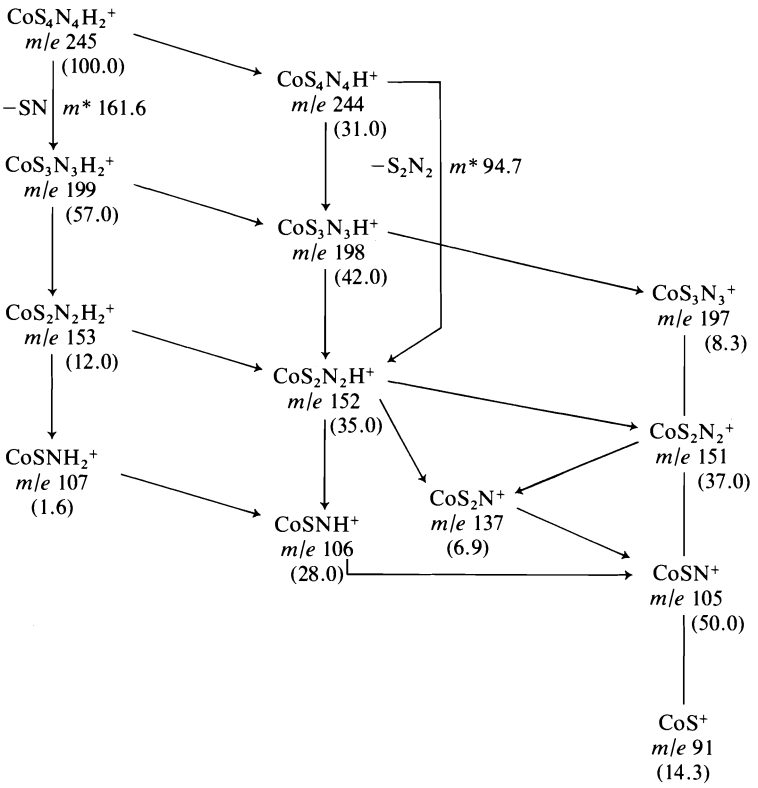

FIG. 3. Proposed mass spectral fragmentation scheme for $Co(S_2N_2H)_2$.

with the hydrogen atoms lying in the same plane as the chelate rings. Although the structure of $Pt(S_2N_2H)_2$ has been determined as *cis*-planar (7), it has yet to be established whether or not the other $M(S_2N_2H)_2$ (M = Ni, Co, Pd) complexes have the same structure.

The two possible geometrical isomers for the $M(S_2N_2H)_2$ complexes are shown below. From symmetry considerations, there are 23 ir-active vibrations ($10a_1 + 9b_1 + 4b_2$) for the *cis*-C_{2v} structure and 15 ($5a_u + 10b_u$) for the *trans*-C_{2h}

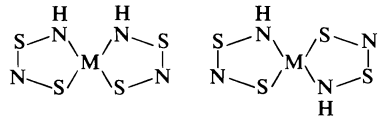

cis-C_{2v} *trans*-C_{2h}

structure. Moreover, two ir-active N—H stretching vibrations ($a_1 + b_1$) are expected for the *cis* isomer, while only one mode (b_u) should be observed for the *trans* isomer. The ir spectra of the nickel, cobalt, and palladium complexes are very similar and the data are compared in Table 2. There are two distinct N—H stretching bands observed for each complex observed at ~3265 and ~3145 cm^{-1}. Since the energy difference between these absorptions (~120 cm^{-1}) is too large to be attributable to site or factor group splitting, the *cis* structure is favoured. Furthermore, the close similarity of the ir spectra suggests that all three complexes adopt the same structure. On the basis of the number of bands in the spectra, the *cis* structure is again favoured because there are about 15 bands which may reasonably be considered as fundamentals, even ignoring the region below 300 cm^{-1} where some low energy modes are expected to absorb.

For comparative purposes, the ir data for S_4N_4 and $TiCl_4 \cdot S_4N_4$ (15) are also given in Table 2. The spectrum observed for S_4N_4 is in good agreement with that reported by Lippincott and Tobin (16). There is little coincidence between the spectra of the group VIII complexes and that of S_4N_4, while the spectrum of $TiCl_4 \cdot S_4N_4$ is quite similar to that of S_4N_4. This is consistent with the fact that the original S_4N_4 is not held intact in the complexes being considered in the present work.

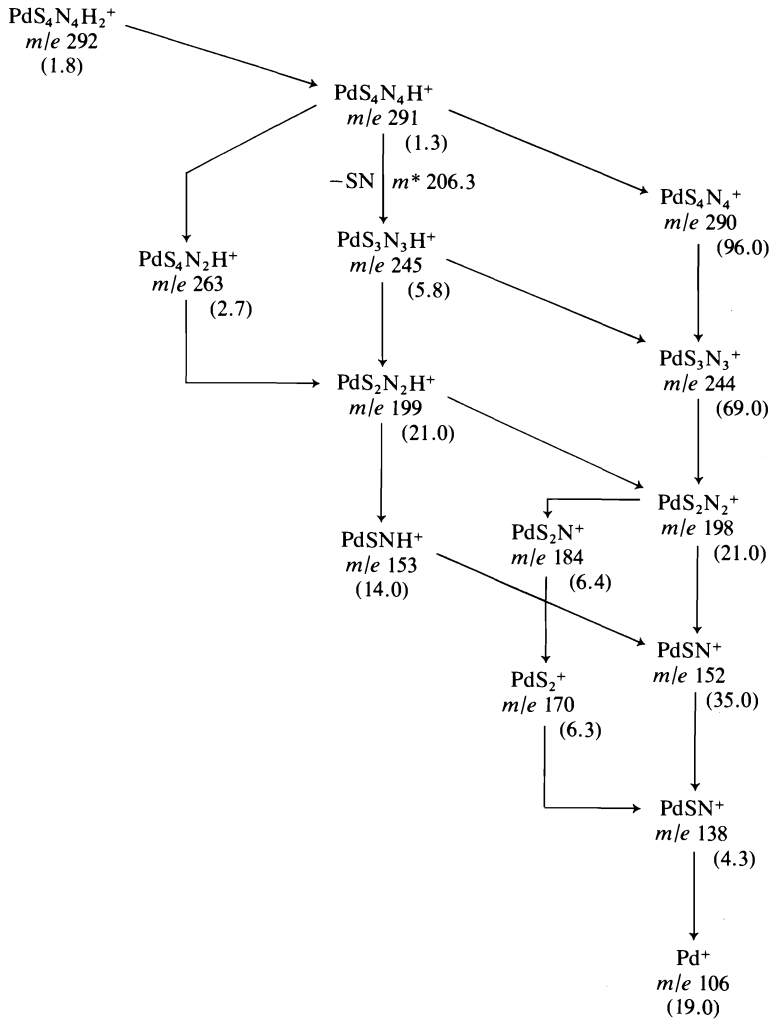

FIG. 4. Proposed mass spectral fragmentation scheme for $Pd(S_2N_2H)_2$.

Since only small amounts of the complexes were obtained from the syntheses, no far-ir spectra were recorded. Attempts were made to measure the Raman spectra using Kr^+ (647.1 nm) laser excitation, but these failed owing to the poor scattering properties of the dark-red–violet complexes. In view of this, it is pointless to give detailed vibrational assignments for the ir spectra, but some general assignments can be made and these have been included in Table 2.

The N—H bending modes in $S_4N_4H_4$ occur at $\sim 1300\ cm^{-1}$ (16), i.e., considerably lower in energy than those for saturated secondary amines (1580–1490 cm^{-1}) (17). In the present study, the very weak, broad bands observed in the 1400–1200 cm^{-1} range are assigned tentatively to the N—H bending modes. Banister *et al.* have examined the relationship between ν(S—N) and the S—N bond length (18). For example, the S—N bond length in S_4N_4 is 1.616 Å, and Banister *et al.*'s prediction for ν(S—N) is $\sim 940\ cm^{-1}$; the observed value for ν(S—N) is 925 cm^{-1}. From the X-ray study (7) on $Pt(S_2N_2H)_2$, the average S—N bond length is ~ 1.59 Å and accordingly the ir bands for the group VIII complexes appearing at $\sim 1030\ cm^{-1}$ have been assigned to ν(S—N) vibrations.

As part of our study on the structures of the group VIII metal S_4N_4 complexes, we attempted to prepare $Pt(S_2N_2H)_2$ according to the literature method but all our efforts proved in vain. Copious amounts of $(NH_4)_2SO_4$ and, in some cases, small quantities of a dark-violet compound could be isolated. Unfortunately, we

TABLE 2. Infrared spectra of $M(S_2N_2H)_2$ and related complexes (cm^{-1})

S_4N_4	$TiCl_4 \cdot S_4N_4$[a]	$Co(S_2N_2H)_2$	$Ni(S_2N_2H)_2$	$Pd(S_2N_2H)_2$	Assignment
		3278 w			
		3267 m,sp	3274 m,sp	3262 s,sp	N—H stretching
		3136 m,br	3147 m,br	3134 s,br	
				1629 m,br	
		1399 vvw,br	1401 vvw,br	1399 s	N—H bending and combination modes
			1234 vvw,br	1205 s,br	
		1164 w,br	1158 m	1150 s,sh	
		1123 w,br		1117 s,br	
	1040 s	1037 m	1033 ms	1057 s	
	1020 m,sh	1028 m,sh	1024 m,sh	1019 s	S—N stretching
	950 s	1000 ms		969 m	
925 vs					
		898 sh	894 m,sh	892 m	
		890 w	887 m		
		860 ms			
763 w,br	785 s	834 ms			
	760 m				
723 ms	720 w,sh	719 s	714 s		
703 s,sh		704 s	704 s,sh		
697 s	680 w		697 s	678 s	Skeletal modes of chelate rings
		643 m	630 w,br	634 s,sh	
625 vw	625 w	624 w,br		620 s	
		579 sh	585 w	575 w	
551 vs	567 w				
546 vs	545 vw				
525 w,m		525 w	520 m	537 w,br	
		516 sh		487	
		456 m	447 w,br	442 vw	
	410 s				
	375 s				
	365 s				Skeletal modes and metal–ligand modes
340 s	345 s	338 ms			
			329 s	317 ms	
		321 w	311 w,sp		

[a]Data from ref. 15

could not obtain a reproducible elemental analysis for this dark-violet compound. The formation of $(NH_4)_2SO_4$ is presumably the result of the acid-catalysed (H_2PtCl_6) reaction of S_4N_4 with water. The mass spectrum of the dark-violet product is complex but $Pt(S_3N)_2$ and a trace of $Pt(S_2N_2H)(S_3N)$ appear to be present. The ir spectrum (KBr disk) shows the presence of one N—H stretching absorption at ~3120 cm^{-1}. Complexes of the compositions, $M(S_3N)_2$ and $M(S_2N_2H)(S_3N)$, have been reported previously for nickel (9), and cobalt and palladium (19), but not for platinum.

In conclusion, the stoichiometry of the $M(S_2N_2H)_2$ (M = Ni, Co, Pd) complexes has been verified and it appears that all three complexes adopt a *cis*-planar geometry. These complexes are certainly not thionitrosyls and it is worth mentioning here that the first authentic thionitrosyls, $Mo(NS)(S_2CNR_2)$ (R = Me, Et, etc.), have only recently been reported (20). Finally, in view of the considerable current interest in polymeric sulphur nitride, $(SN)_x$, because of its metallic behaviour (21), we anticipate that there will be renewed interest in the chemistry of the $M(S_2N_2H)_2$ species and their derivatives as these complexes may well prove to be convenient precursors to $(SN)_x$ and related polymers.

Acknowledgements

This research was generously supported by the National Research Council of Canada and the Quebec Department of Education.

1. M. GOEHRING and A. DEBO. Z. Anorg. Allg. Chem. **273**, 319 (1953).
2. M. GOEHRING, K.-W. DAUM, and J. WEISS. Z. Naturforsch. Teil B, **10**, 298 (1955).
3. K.-W. DAUM, M. GOEHRING, and J. WEISS. Z. Anorg. Allg. Chem. **278**, 260 (1955).

4. M. GOEHRING and K.-W. DAUM. Z. Anorg. Allg. Chem. **282**, 83 (1955).
5. M. GOEHRING and D. VOIGT. Naturwissenschaften, **40**, 482 (1953).
6. E. FLUCK, M. GOEHRING, and J. WEISS. Z. Anorg. Allg. Chem. **287**, 51 (1956).
7. I. LINDQVIST and J. WEISS. J. Inorg. Nucl. Chem. **6**, 184 (1958).
8. T. S. PIPER. Chem. Ind. (London), 1101 (1957).
9. T. S. PIPER. J. Am. Chem. Soc. **80**, 30 (1958).
10. J. WEISS and M. ZIEGLER. Z. Anorg. Allg. Chem. **322**, 184 (1963).
11. J. WEISS and U. THEWALT. Z. Anorg. Allg. Chem. **343**, 274 (1966).
12. M. VILLENA-BLANCO and W. L. JOLLY. Inorg. Synth. **9**, 98 (1967).
13. T. SAWAI. Ph.D. Thesis, McGill University, Montreal, P.Q. 1973.
14. D. CHAPMAN and T. C. WADDINGTON. Trans. Faraday Soc. **58**, 1679 (1962) and references cited therein.
15. P. J. ASHLEY and E. G. TORRIBLE. Can. J. Chem. **47**, 2587 (1969).
16. E. R. LIPPINCOTT and M. C. TOBIN. J. Chem. Phys. **21**, 1559 (1953).
17. R. T. CONLEY. Infrared spectroscopy. Allyn & Bacon, Inc., Boston, MA. 1966.
18. A. J. BANISTER, L. F. MOORE, and J. S. PADLEY. Spectrochim. Acta, Part A, **23**, 2705 (1967).
19. J. WEISS. Fortschr. Chem. Forsch. **5**, 635 (1965).
20. J. CHATT and J. R. DILWORTH. J. Chem. Soc., Chem. Commun. 508 (1975).
21. M. J. COHEN, A. F. GARITO, A. J. HEEGER, A. G. MACDIARMID, C. M. MIKULSKI, M. S. SARAN, and J. KLEPPINGER. J. Am. Chem. Soc. **98**, 3844 (1976) and references cited therein.

Fluorine exchange between four-, five-, and six-coordinate silicon compounds[1]

RONALD KIRK MARAT AND ALEXANDER F. JANZEN

Department of Chemistry, University of Manitoba, Winnipeg, Man., Canada R3T 2N2

Received June 2, 1977

RONALD KIRK MARAT and ALEXANDER F. JANZEN. Can. J. Chem. **55**, 3845 (1977).

Intermolecular fluorine exchange in the systems SiF_4–SiF_5^-, $MeSiF_3$–$MeSiF_4^-$, $PhSiF_3$–$PhSiF_4^-$, SiF_5^-–SiF_6^{2-}, SiF_4–SiF_6^{2-}, and $MeSiF_3$–SiF_6^{2-} has been studied by fluorine and proton nmr spectroscopy. Exchange is postulated to involve fluorine-bridged intermediates; alternative pathways of exchange, such as fluoride dissociation or impurity (HF and H_2O) catalyzed exchange, have been eliminated. Addition of NH_3 to SiF_5^-–SiF_6^{2-} slows down exchange whereas addition of Et_2NH to $MeSiF_3$ promotes exchange.

RONALD KIRK MARAT et ALEXANDER F. JANZEN. Can. J. Chem. **55**, 3845 (1977).

On étudie par rmn du proton et du fluor l'échange intermoléculaire du fluor dans les systèmes SiF_4–SiF_5^-, $MeSiF_3$–$MeSiF_4^-$, $PhSiF_3$–$PhSiF_4^-$, SiF_5^-–SiF_6^{2-}, SiF_4–SiF_6^{2-} et $MeSiF_3$–SiF_6^{2-}. On fait l'hypothèse que l'éxchange implique des intermédiaires à fluor ponté; on élimine la possibilité d'un autre mode d'échange comme la dissociation du fluor ou de l'échange catalysée par une impureté (HF et H_2O). L'addition de NH_3 au système SiF_5^-–SiF_6^{2-} a pour effet de ralentir l'échange; par contre l'addition de Et_2NH à $MeSiF_3$ la favorise.

[Traduit par le journal]

Introduction

On the basis of our study of catalyzed intermolecular fluorine exchange in the $MeSiF_4^-$ anion (1), we concluded that HF is a very effective fluorine transfer reagent and that any reagents such as H_2O or MeOH, which react with $MeSiF_4^-$ to liberate HF, can promote fluorine exchange, whereas reagents such as Pr_4NF or $(Me_3Si)_2NH$, which remove HF from solution, can inhibit fluorine exchange. Since the presence of HF and H_2O impurities could be monitored and their concentration reduced, it became feasible to study intermolecular fluorine exchange between four-, five-, and six-coordinate silicon fluorides without interference from impurity catalyzed processes.

Five- and six-coordinate silicon fluorides are known, e.g. SiF_5^-, $RSiF_4^-$, SiF_4:base, SiF_6^{2-}, $SiF_4(C_2O_4)^{2-}$, $SiF_2(C_2O_4)_2^{2-}$, $RSiF_5^{2-}$, SiF_4:2base, SiF_5:base$^-$ (2–9); however, less is known about the mechanism of exchange in silicon fluorides than about exchange processes in the analogous tin (10), phosphorus (11), antimony (12), or boron (13) fluorides.

Previously, we suggested that six-coordinate intermediates and four-center reactions may be important in reaction mechanisms of silicon and phosphorus compounds (1, 14). In this paper, we we wish to describe the effect that changes in the coordination number of silicon have on the intermolecular fluorine transfer process in systems such as SiF_4–SiF_5^-, $MeSiF_3$–$MeSiF_4^-$, $PhSiF_3$–$PhSiF_4^-$, SiF_5^-–SiF_6^{2-}, SiF_4–SiF_6^{2-}, $MeSiF_3$–SiF_6^{2-}, NH_3–SiF_5^-–SiF_6^{2-}, and $NHEt_2$–$MeSiF_3$.

[1]Presented at the 2nd Joint CIC–ACS Conference, Montreal, Canada, May 29 – June 2, 1977.

Experimental

General

Dichloromethane (Fisher), CH_3SiF_3 (PCR), $SiCl_4$ (M.C.B.), ammonia (Matheson), 49% hydrofluoric acid (Fisher), and 10% aqueous $(n\text{-}C_3H_7)_4NOH$ (Eastman) were used without further purification. SiF_4 was prepared from $SiCl_4$ and SbF_3 in a stainless steel cylinder. $C_6H_5SiF_3$ was prepared from $C_6H_5SiCl_3$ and SbF_3 in tetramethylene sulfone solvent (15). $(n\text{-}C_3H_7)_4NF$ (16), $(n\text{-}C_3H_7)_4N^+SiF_5^-$ (2), $(n\text{-}C_3H_7)_4N^+CH_3SiF_4^-$ (1, 3), and $(n\text{-}C_3H_7)_4N^+C_6H_5SiF_4^-$ (3) were prepared by literature methods and characterized by their mp, ir, and nmr spectra. $[(n\text{-}C_3H_7)_4N]_2SiF_6$ was prepared by neutralization of 10% aqueous $(n\text{-}C_3H_7)_4NOH$ with 3% aqueous HF followed by addition of an equimolar quantity of $(n\text{-}C_3H_7)_4N^+SiF_5^-$; water was evaporated with the addition of methanol and the product recrystallized from 1:1 chloroform – ethyl acetate in 77% yield. The white needle-like crystals, mp 75–77°C, had an ir spectrum characteristic of the SiF_6^{2-} anion (17).

Nuclear Magnetic Resonance Spectra

The nmr spectra were recorded on Varian A-56/60A and HA-100-D spectrometers at 56.4 and 100 MHz for fluorine and proton, respectively; proton decoupled ^{13}C nmr spectra were recorded on a Bruker WH90 spectrometer at 22.63 MHz. Temperatures were calibrated by the method of Van Geet (18) and are considered accurate to ±1°C. Calculated spectra for the SiF_5^-–SiF_6^{2-} system were produced with the program DNMR-3

TABLE 1. Chemical shifts of some fluorides

Compound	Solvent and concentration	^{19}F chemical shift (ppm)
CH_3SiF_3	CH_2Cl_2, 1 *M*	134.6
SiF_4	1:2 v/v CH_3CN–CH_2Cl_2, 0.5 *M*	162
$C_6H_5SiF_3$	CH_2Cl_2, 1 *M*	143.1
$(n\text{-}C_3H_7)_4N^+SiF_5^-$	CH_2Cl_2, 0.65 *M*	137.4
$(n\text{-}C_3H_7)_4N^+CH_3SiF_4^-$	CH_2Cl_2, 0.66 *M*	111.0
$(n\text{-}C_3H_7)_4N^+C_6H_5SiF_4^-$	CH_2Cl_2, 0.54 *M*	118.7
$[(n\text{-}C_3H_7)_4N]_2SiF_6$	CH_2Cl_2, 0.39 *M*	127.4
$(n\text{-}C_3H_7)_4NF$	CH_2Cl_2, 0.96 *M*	114.6
$(n\text{-}C_3H_7)_4N^+FHF^-$	CH_2Cl_2, 0.1 *M*[a]	149.4
HF	1:1 v/v CH_3CN–CH_2Cl_2, 3 *M*	170[b]

[a]The bifluoride ion is observed as an impurity peak in the tetrapropylammonium fluoride sample.
[b]The chemical shift and line width of HF vary with solvent and temperature.

(19) using the Fortran H compiler on an IBM 370-158 computer. Calculated spectra for the CH_3SiF_3–$CH_3SiF_4^-$ system were produced as described previously (1). The pseudo-first-order rate constants for exchange were obtained by visual comparison of the calculated and experimental spectra and are considered accurate to ±10%.

The nmr samples were prepared by weighing solid reagents, recrystallized and dried under vacuum, directly into dry nmr tubes. Dichloromethane (0.5 ml) was added and nmr tubes degassed and sealed under vacuum. Small quantities (10 μl)) of C_6F_6 were added to produce a convenient internal chemical shift and line width standard. Table 1 lists the chemical shifts and coupling constants of compounds used in this study. Chemical shifts were converted to the $CFCl_3$ scale by adding the chemical shift of a dilute $C_6F_6/CFCl_3$ mixture in CH_2Cl_2 (162.87 ppm). All chemical shifts in Table 1 are reported to high field of $CFCl_3$; they agree well with literature values obtained under different conditions (1, 3, 8, 20).

Results and Discussion

It was essential to verify that impurities such as HF, H_2O, F^-, FHF^-, etc. were not the cause of the rapid intermolecular fluorine exchange processes observed in this study. This was accomplished in several ways: firstly, by observing ^{29}Si–F or F–Si–CH_3 coupling in all starting materials; secondly, by noting the effect on the nmr spectra of reagents, e.g. $(Me_3Si)_2NH$, which are known to react with trace amounts of HF; thirdly, by diluting the sample (an increase in the rate of exchange might be caused by impurities in the solvent whereas a decrease would be consistent with a bimolecular exchange mechanism).

Exchange between Four- and Five-coordinate Silicon Fluorides

The fluorine nmr spectra of $MeSiF_4^-$ (Fig. 1*A*) and $MeSiF_3$ (Fig. 1*B*) show well-resolved quartets with retention of F–Si–CH_3 coupling, thereby confirming that impurity catalyzed intermolecular exchange is not occurring in the

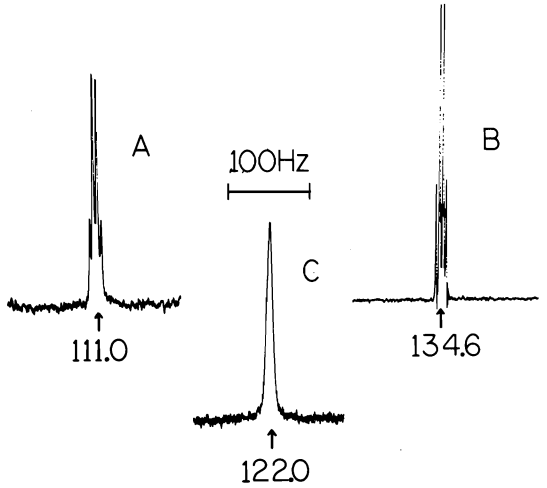

FIG. 1. Fluorine nmr spectra of 0.66 *M* $(n\text{-}C_3H_7)_4N^+CH_3SiF_4$ (1*A*) and 0.66 *M* CH_3SiF_3 (1*B*) in CH_2Cl_2 solution. Figure 1*C* shows mixture of samples 1*A* and 1*B* at +41°C.

starting materials. On mixing $Pr_4N^+MeSiF_4^-$ (0.66 *M*) and $MeSiF_3$ (0.66 *M*), the quartets are replaced by a single peak of half-height width ~20 Hz at +122.0 ppm (Fig. 1*C*). The proton nmr spectrum shows a single sharp peak at −0.2 ppm, assigned to the methyl group of rapidly exchanging $MeSiF_4^-$ and $MeSiF_3$.

The temperature dependent proton nmr spectrum, from −50 to +33°C, of a sample containing $Pr_4N^+MeSiF_4^-$ (0.49 *M*) and $MeSiF_3$ (1.8×10^{-3} *M*) was analyzed by the method described previously (1) and gave an activation energy $E_a = 5.4 \pm 1.1$ kcal/mol. Attempts to determine the order in $MeSiF_3$ were unsuccessful, mainly because of the difficulty of measuring and condensing small quantities of $MeSiF_3$ into nmr tubes (the addition of as little as 2.5×10^{-7}

mol of $MeSiF_3$ to 2.45×10^{-4} mol of Pr_4N^+-$MeSiF_4^-$ in 0.5 ml dichloromethane produced coalescence).

In a similar experiment, the fluorine nmr spectrum of a mixture of SiF_4 (0.66 *M*) and $Pr_4N^+SiF_5^-$ (0.64 *M*) was recorded at −51°C. A single peak of half-height width ~10 Hz was observed at +152.3 ppm and only minor changes occurred in the spectrum from −51° to +40°C; for example, at −11°C the single fluorine peak shifted to +149.5 ppm (towards SiF_5^-), the half-height width increased to ~20 Hz and the intensity decreased slightly, suggesting that the concentration of SiF_4 in solution decreased slightly at higher temperature, thus slowing down the rate of fluorine exchange.

The $PhSiF_3$–$PhSiF_4^-$ system also showed rapid intermolecular fluorine exchange, as verified by ^{19}F and ^{13}C nmr.

Rapid intermolecular fluorine exchange between four- and five-coordinate silicon fluorides in the systems SiF_4–SiF_5^-, $MeSiF_3$–$MeSiF_4^-$, and $PhSiF_3$–$PhSiF_4^-$ is readily explained in terms of coordination changes Si 4 ⇌ 5, F 1 ⇌ 2, and intermediate (i) **1**.

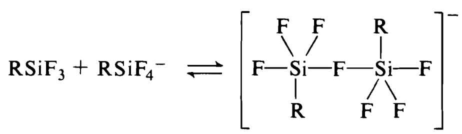

i-**1**

R = F, Me, Ph

Five- and Six-coordinate Silicon Fluorides

The reagents $Pr_4N^+SiF_5^-$ and $(Pr_4N)_2SiF_6$ gave single sharp peaks in the fluorine nmr spectra (Table 1) with retention of ^{29}Si–F coupling. On mixing $Pr_4N^+SiF_5^-$ (0.5 *M*) and $(Pr_4N)_2SiF_6$ (0.5 *M*), the ^{29}Si–F coupling was lost and two broad peaks were observed at +41°C, with half-height width of 210 Hz for SiF_5^- and 150 Hz for SiF_6^{2-}. Coalescence of the peaks occurred at about +80°C. The Arrhenius plot over the temperature range −40 to +80°C was reasonably linear and gave an activation energy $E_a = 5.1 \pm 0.2$ kcal/mol (Fig. 2).

Intermolecular fluorine exchange can be explained in terms of coordination changes Si 5 ⇌ 6, F 1 ⇌ 2, and intermediate **2**. Dilution of the SiF_5^-–SiF_6^{2-} sample produced a decrease in the exchange rate, consistent with the postulated bimolecular mechanism; however, the

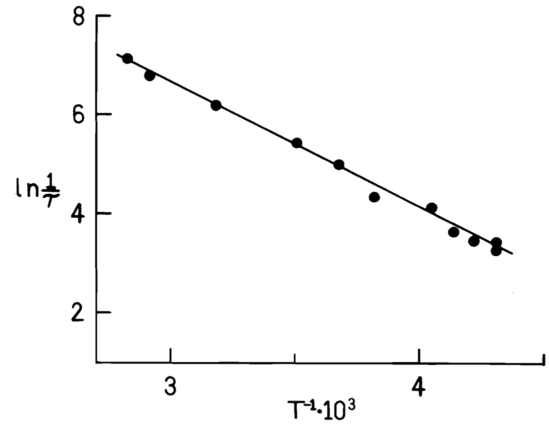

FIG. 2. Plot of ln $1/\tau$ vs. $1/T$. Sample contained $(n\text{-}C_3H_7)_4N^+SiF_5^-$ (0.5 *M*) and $[(n\text{-}C_3H_7)_4N]_2SiF_6$ (0.5 *M*) in CH_2Cl_2 (0.4 ml).

fact that both free ions are in equilibrium with ion-pairs or aggregates precludes a more definitive kinetic analysis. The addition of a small amount of $(Me_3Si)_2NH$ (3 µl) had no noticeable effect upon the exchange rate.

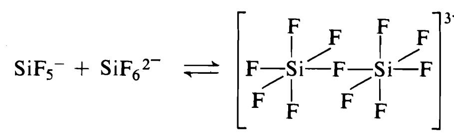

i-**2**

A comparison of the SiF_5^-–SiF_6^{2-} and $RSiF_3$–$RSiF_4^-$ systems shows that coalescence in the SiF_5^-–SiF_6^{2-} system occurs at higher temperature and higher concentration of reagents. This difference probably resides in the unfavourable dissociation of $Pr_4N^+SiF_5^-$ and $(Pr_4N)_2SiF_6$; hence, the concentration of free SiF_5^- and SiF_6^{2-} ions in solution is probably quite low as compared to the concentration of $RSiF_3$.

Four- and Six-coordinate Silicon Fluorides

A mixture of SiF_4 (0.49 *M*) and $(Pr_4N)_2SiF_6$ (0.49 *M*) showed a broadened peak at +136.6 ppm, close to the chemical shift of pure Pr_4N^+-SiF_5^- (Table 1). The reaction was repeated on a larger scale using 1.2 mmol SiF_4 and 0.14 mmol $(Pr_4N)_2SiF_6$. Evaporation of the solution and recrystallization gave pure $Pr_4N^+SiF_5^-$ as confirmed by comparison of its melting point, infrared, and nmr spectrum with that of an authentic sample.

Similarly, a mixture of $MeSiF_3$ (1.0 *M*) and $(Pr_4N)_2SiF_6$ (0.49 *M*) showed two broad peaks

in the region expected for $MeSiF_4^-$ and SiF_5^-. Evaporation and infrared and nmr examination of the white residue showed it to be a mixture of $MeSiF_4^-$ and SiF_5^-.

These reactions may be summarized by coordination changes Si $4 \rightleftharpoons 5 \rightleftharpoons 6$, F $1 \rightleftharpoons 2$, and intermediate **3**. They demonstrate that the

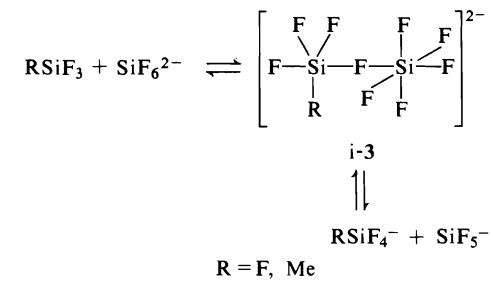

formation of five-coordinate silicon fluorides is thermodynamically and kinetically favoured in the SiF_4–SiF_6^{2-} and $MeSiF_3$–SiF_6^{2-} systems; therefore, simply mixing four- and six-coordinate silicon fluorides represents a convenient way of preparing five-coordinate silicon fluorides.[2] $(Pr_4N)_2PhSiF_5$ was also prepared (9) for this study; however, attempts to recrystallize the compound and remove impurities such as HF and FHF^- were not successful, therefore, we could not distinguish between impurity catalyzed or bimolecular fluorine exchange.

Base and Intermolecular Fluorine Exchange

The results discussed above demonstrate that intermolecular fluorine exchange is rapid, on the nmr time scale, if the coordination number of silicon in the exchanging species is different. Conversely, fluorine transfer is extremely slow between silicon fluorides of the same coordination number, i.e. exchange is not observed in the systems SiF_4–SiF_4, $RSiF_3$–$RSiF_3$, SiF_5^-–SiF_5^-, $RSiF_4^-$–$RSiF_4^-$, and SiF_6^{2-}–SiF_6^{2-}.

The relationship between coordination number and intermolecular fluorine exchange may also be investigated by using a Lewis base, rather than a fluorine ligand, to vary the coordination number of silicon. In such an experiment it was found that addition of a large excess of NH_3 (10 *M*) to a sample containing $Pr_4N^+SiF_5^-$ (0.5 *M*) and $(Pr_4N)_2SiF_6$ (0.5 *M*) inhibited fluorine exchange, presumably because SiF_5^- is converted to $SiF_5(NH_3)^-$ (7, 8) and intermolecular fluorine exchange between six-coordinate $SiF_5(base)^-$ and SiF_6^{2-} is slow on the nmr time scale.

Base may also promote exchange, as illustrated by the addition of $NHEt_2$ (0.2 *M*) to a non-exchanging sample of $MeSiF_3$ (1.6 *M*) which produced single peaks in the ^{19}F and ^1H nmr spectra at +41°C with loss of F–Si–CH_3 coupling. In this case, the addition of base presumably facilitates fluorine transfer between the four-, five-, and six-coordinate silicon species $MeSiF_3$, $MeSiF_3$(base), and $MeSiF_3(base)_2$.

Intramolecular Axial–Equatorial Exchange

Intramolecular axial–equatorial exchange in SiF_5^-, $MeSiF_4^-$, and $PhSiF_4^-$ was found to be rapid on the nmr time scale under all experimental conditions. Although this study provides no direct evidence related to the mechanism of axial–equatorial exchange, the postulate that exchange occurs via intermediates **4** or **5** is consistent with our previous suggestion that the lowest energy pathway of axial–equatorial exchange in trigonal bipyramidal molecules involves Lewis acid–base interactions and rapid equilibration of five- and six-coordinate geometries (8). Since SiF_5^- samples do not exhibit

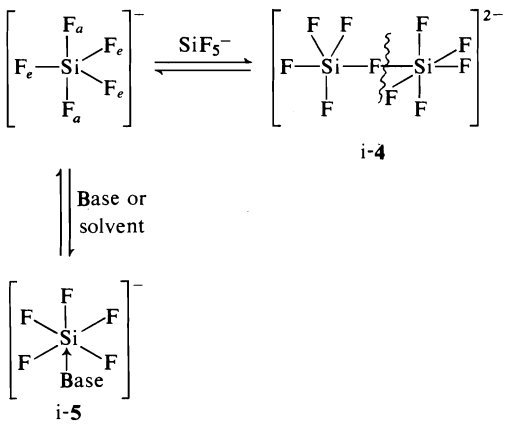

intermolecular fluorine exchange (in the absence of impurities (8)) it must be concluded that cleavage at six-coordinate Si in i-**4** is faster than at five-coordinate Si, hence, fluorine transfer will not occur despite the formation of i-**4**. Any Lewis base or solvent may also induce rapid coordination changes Si $5 \rightleftharpoons 6$ via i-**5** and lead to axial–equatorial exchange.

[2]It is of historical interest that Berzelius prepared SiF_6^{2-} salts from SiF_4 and metal fluorides in 1828 (*cited in* ref. 21). Perhaps the facile addition of ionic fluoride to SiF_5^-, combined with the volatility of SiF_4, prevented earlier detection of SiF_5^-.

Acknowledgement

The financial assistance of the National Research Council of Canada is gratefully acknowledged.

1. R. K. MARAT and A. F. JANZEN. Can. J. Chem. **55**, 1167 (1977).
2. H. C. CLARK, K. R. DIXON, and J. G. NICOLSON. Inorg. Chem. **8**, 450 (1969).
3. F. KLANBERG and E. L. MUETTERTIES. Inorg. Chem. **7**, 155 (1968).
4. L. TANSJÖ. Acta Chem. Scand. **18**, 456 (1964); **18**, 465 (1964); J. J. MOSCONY and A. G. MACDIARMID. Chem. Commun. 307 (1965); R. MÜLLER and C. DATHE. Chem. Ber. **98**, 235 (1965); R. MÜLLER, C. DATHE, and D. MROSS. Chem. Ber. **98**, 241 (1965); K. LICHT, C. PEUKER, and C. DATHE. Z. Anorg. Allg. Chem. **380**, 293 (1971).
5. P. A. W. DEAN and D. F. EVANS. J. Chem. Soc. A, 2569 (1970).
6. N. MILLER. Nature, **158**, 950 (1946); C. J. WILKINS and D. K. GRANT. J. Chem. Soc. 927 (1953); A. D. ADLEY, D. F. R. GILSON, and M. ONYSZCHUK. Chem. Commun. 813 (1968).
7. I. WHARF and M. ONYSZCHUK. Can. J. Chem. **50**, 3450 (1972).
8. J. A. GIBSON, D. G. IBBOTT, and A. F. JANZEN. Can. J. Chem. **51**, 3203 (1973).
9. R. K. MARAT and A. F. JANZEN. J. Chem. Soc. Chem. Commun. In press.
10. P. A. W. DEAN and D. F. EVANS. J. Chem. Soc. A, 1154 (1968).
11. S. BROWNSTEIN and J. BORNAIS. Can. J. Chem. **46**, 225 (1968).
12. P. A. W. DEAN, R. J. GILLESPIE, R. HULME, and D. A. HUMPHREYS. J. Chem. Soc. A, 341 (1971); P. A. W. DEAN and R. J. GILLESPIE. J. Am. Chem. Soc. **91**, 7260 (1969); **91**, 7264 (1969).
13. S. BROWNSTEIN and J. PAASIVIRTA. Can. J. Chem. **43**, 1645 (1965); S. BROWNSTEIN. J. Inorg. Nucl. Chem. **35**, 3567 (1973); J. S. HARTMAN and P. STILBS. J. Chem. Soc. Chem. Commun. 566 (1975); M. AZEEM, M. BROWNSTEIN, and R. J. GILLESPIE. Can. J. Chem. **47**, 4159 (1969).
14. R. E. WASYLISHEN, G. S. BIRDI, and A. F. JANZEN. Inorg. Chem. **15**, 3054 (1976).
15. W. J. E. PARR, T. SCHAEFER, and K. MARAT. Can. J. Chem. **55**, 3243 (1977).
16. E. J. COREY and A. VENKATESWARLU. J. Am. Chem. Soc. **94**, 6190 (1972).
17. R. D. PEACOCK and D. W. A. SHARP. J. Chem. Soc. 2762 (1959).
18. A. L. VAN GEET. Anal. Chem. **42**, 679 (1970).
19. D. A. KLEIER and G. BINSCH. Program 165, Quantum Chemistry Program Exchange, 1970.
20. E. L. MUETTERTIES and W. D. PHILLIPS. J. Am. Chem. Soc. **81**, 1084 (1959); J. S. MARTIN and F. Y. FUJIWARA. Can. J. Chem. **49**, 3071 (1971).
21. Gmelins Handbuch der anorganischen Chemie. 8th ed. Silicon. Part B. Verlag Chemie, Weinheim/Bergstrasse. 1959. p. 630.

Limiting equivalent conductances for selected substituted ammonium ions in water

SHEILA TERESA LOBO AND ROSS ELMORE ROBERTSON
Department of Chemistry, The University of Calgary, Calgary, Alta., Canada T2N 1N4
Received March 7, 1977

SHEILA TERESA LOBO and ROSS ELMORE ROBERTSON. Can. J. Chem. **55**, 3850 (1977).

The temperature dependence of the limiting equivalent conductances of the ions 2-methoxyethylammonium, bis-2-methoxyethylammonium, 3-methoxypropylammonium, piperidinium, quinuclidinium, cyclohexylammonium, and diethylammonium have been determined over the range 5–45°C. The probable effect of these ions on the adjacent water structure has been explored in terms of an approach used by Kay and co-workers and the behaviour in water has been compared with that of other alkylammonium ions.

SHEILA TERESA LOBO et ROSS ELMORE ROBERTSON. Can. J. Chem. **55**, 3850 (1977).

On étudie l'influence de la température sur les conductances équivalentes limites des ions méthoxy-2 éthylammonium, bis-méthoxy-2 éthylammonium, méthoxy-3 propylammonium, pipéridinium, quinuclidinium, cyclohexylammonium et diéthylammonium dans l'écart de température de 5 à 45°C. L'effet probable de ces ions sur la structure de l'eau adjacente est étudié en profondeur en fonction d'une approche utilisée par Kay et ses collaborateurs et le comportement dans l'eau de ces ions est comparé avec celui d'autres ions alkylammonium.
[Traduit par le journal]

Introduction

In our pK_b studies of various substituted amines in water, such as simple alkylamines (1, 2), cyclic amines (3), and aminoethers (4, 5)[1] by the Shedlovsky–Kay method (6), limiting equivalent conductances, Λ_0, of the corresponding amine hydrochlorides (BH^+Cl^-) were determined as a function of temperature between 5 and 45°C.

These experimental $\Lambda_0(BH^+Cl^-)$ can easily be dissected into their contributory ionic $\lambda_0(BH^+)$ and $\lambda_0(Cl^-)$ values. The $\lambda_0(BH^+)$ values, thus obtained, in combination with the viscosity of water, η, permit the calculation of the Walden product, $\lambda_0\eta$. Káy and co-workers (7–9) have used $\lambda_0\eta$ and its temperature dependence in classifying the effect of tetraalkylammonium ions, alkali metal, and halide ions on the surrounding water in terms of structure-making or -breaking. The various substituted ammonium ions studied by us lend themselves to such an analysis.

These ions are amphiphilic, consisting of a polar ionic part, i.e., $—NH_3^+$, NH_2^+, NH^+ and a nonpolar hydrocarbon part. The interaction of these two parts with the adjacent water structure is necessarily different. The ionic part of the solute will be hydrated electrostrictively, whereas the alkyl hydrocarbon part will be subjected to hydrophobic hydration to the extent permitted by the adjacent charge. The balance between these two types of hydration will determine whether a particular ion appears to be a water structure-breaker or -maker.

Most of the $\lambda_0(BH^+)$ values obtained here have not been reported before and the temperature dependence of these values as far as we know have never been examined. It is proposed in the present work to correlate λ_0, $\lambda_0\eta$, and $d(\lambda_0\eta)/dT$ of the ions studied with those available in the literature and determine their net effect on the neighbouring water structure. We examine as well the effect of variation in the structure of the ammonium ion, i.e. RNH_3^+, $R_2NH_2^+$, R_3NH^+, and R_4N^+, where R = Me, Et, *n*-Pr, on the above-mentioned physical quantities.

Experimental

The conductance method for determining Λ_0 of the amine hydrochlorides required the utmost care with respect to the purity of the salts and water, temperature control during measurements, and accuracy of conductance–concentration data. The experimental set-up and technique have been described previously (1) and were designed to achieve these standards.

The hydrochlorides were prepared from commercially available amines, which were purified prior to the preparation of the salt. Quinuclidine was available as quinuclidine hydrochloride (Eastman White Label) which was converted to the free base by the method of Brown and Eldred (10). The purity of the amines was checked by gc

[1]Tables reporting K_b as a function of temperature report $\Lambda_0(BH^+Cl^-)$ instead of $\Lambda_0(BH^+OH^-)$; this comment applies to refs. 3 and 4 as well.

and mass spectral analysis. The hydrochlorides of the amines were prepared by passing dry hydrogen chloride gas (Matheson of Canada Ltd.) through an ethereal solution of the purified amine. The salt was washed with ether and dried under vacuum over silica gel. The aminoether hydrochlorides presented added problems in that they were deliquescent. In these cases, after removal of most of the ether and water, the last trace impurities were removed by short path distillation under high vacuum. The bis-2-methoxylamine hydrochloride was recrystallized from a toluene–ethanol mixture, under anhydrous conditions.

Potassium chloride used for cell-constant determinations was of analytical grade, recrystallized from conductivity water twice, and fused in a platinum boat (11). $\Lambda_0(BH^+Cl^-)$ was determined as a function of temperature between 5 and 45°C at 10° intervals.

Results

The conductance–concentration data[2] were fitted by a linear least-squares fit to the Onsager equation, modified by Robertson and co-workers (1) to correct for any errors peculiar to our system of measurement, i.e. zeroing the titrimeter capable of delivering fixed concentration of salt solutions to the cell, possible adsorption on the walls of the cell at lower concentrations, and a check on the water correction. The equation used was

$$[1]\quad \frac{1000C_k\left[\frac{1}{R_i}-\frac{1}{R_0}\right]}{c_i - c_0} = \Lambda_0 - \frac{A[c_i^{3/2} - c_0^{3/2}]}{c_i - c_0}$$

where R_i and R_0 are resistances of the solution measured at concentrations c_i (c_i being between 10 and 15 values) and c_0, respectively, the concentration of the chloride being determined gravimetrically. A is the limiting slope, C_k is the cell constant, and Λ_0 is the intercept of the Λ vs. concentration plot. The concentration of the stock solution was approximately 0.05 M so that the concentration range used in determining Λ_0 was between 0.00015 M and 0.003 M. Since Λ_0 of the amine hydroxides (BH^+OH^-) was of interest in obtaining the basic dissociation constants, K_b, of amines, the Λ_0 values of the hydrochlorides (BH^+Cl^-) were converted into those of the corresponding hydroxides by using the Kohlrausch equation

$$[2]\quad \Lambda_0(BH^+OH^-) = \Lambda_0(BH^+Cl^-) + \lambda_0(OH^-) - \lambda_0(Cl^-)$$

$\lambda_0(Cl^-)$ used in [2] was from Harned and Owen (12), who fitted λ_0 vs. temperature data to the cubic equation

$$[3]\quad \lambda_0{}^t = \lambda_0{}^{25} + A(t - 25) + B(t - 25)^2 + C(t - 25)^3$$

Similarly $\lambda_0{}^t(OH^-)$ vs. temperature values from Robinson and Stokes (13, p. 465) were fitted to a cubic equation as above, to obtain the required constants (1) of [3] needed for interpolation.

The $\Lambda_0(BH^+OH^-)$ values vs. temperature data were fitted to a cubic equation by linear least squares. Although the standard deviation ($\sigma\Lambda$, cf. last column of Table 1) of the equivalent conductance vs. concentration plot is better than 0.03% for individual Λ_0 determinations, the reproducibility (precision) of the Λ_0 values at any given temperature may show somewhat larger errors (cf. column 4 of Table 1). Λ_0 vs. temperature data for bis-2-methoxyethylamine hydroxide are reported in Table 1 as a typical illustration of the type of results obtained. The table contains the observed $\Lambda_0(BH^+OH^-)$ values as a function of temperature, the difference between observed and calculated values, the latter obtained from the cubic equation used to fit the data, and the standard deviation of $\sigma\Lambda$ for individual Λ_0 determinations from plots of equivalent conductance vs. concentration. Table 2 contains values of the parameters A, B, C, and D of the cubic equation

$$[4]\quad \Lambda_0 = A + Bt + Ct^2 + Dt^3$$

used to fit $\Lambda_0(BH^+OH^-)$ vs. temperature data for all the amine hydroxides studied here. These parameters are useful for interpolating any desired Λ_0 value in the range 5–45°C.

Since the hydrochlorides examined here are salts of a weak base and strong acid, the possibility that hydrolysis might have a significant effect on the value of $\Lambda_0(BH^+Cl^-)$ was considered, particularly with respect to salts of the weaker amines, 2-methoxyethylamine and bis-2-methoxyethylamine (pK_a = 9.390 and 8.609, respectively). In the absence of the correction for hydrolysis, the experimental Λ_0 values will be higher, because ammonium ions are replaced by hydrogen ions of higher mobility.

The hydrolysis correction has been determined

[2]The original conductance data are available, at a nominal charge, from the Depository of Unpublished Data, CISTI, National Research Council of Canada, Ottawa, Ont., Canada K1A 0S2.

TABLE 1. Limiting equivalent conductance (Λ_0) vs. temperature for bis-2-methoxyethylammonium hydroxide in water

T (°C)	Λ_0(obsd.)[a] ($cm^2\ \Omega^{-1}\ mol^{-1}$)	Λ_0(calcd.) ($cm^2\ \Omega^{-1}\ mol^{-1}$)	Λ_0(obsd.) − Λ_0(calcd.) ($cm^2\ \Omega^{-1}\ mol^{-1}$)	$\sigma\Lambda$
4.993	150.96	150.94	+0.02	0.02
5.000	150.96	150.96	−0.002	0.01
15.002	188.99	189.09	−0.09	0.02
15.004	189.10	189.09	+0.008	0.02
24.986	229.05	228.92	+0.13	0.04
25.008	229.00	229.00	−0.004	0.02
35.000	269.98	270.00	−0.02	0.04
35.013	269.99	270.01	−0.07	0.03
44.997	311.55	311.51	+0.04	0.03
44.998	311.49	311.51	−0.02	0.03

[a]Not corrected for hydrolysis.

TABLE 2. Constants of eq. 4

Hydroxide	A	B	$C \times 10^3$	$D \times 10^5$
2-Methoxyethylammonium	137.782	3.8234	8.4623	−2.400
Bis-2-methoxyethylammonium	132.737	3.5596	0.13527	−0.1058
3-Methoxypropylammonium	138.718	3.8729	9.1429	−1.935
Cyclohexylammonium	132.135	4.2798	−0.13572	+0.2288
Piperidinium	136.873	3.7793	8.5587	—
Quinuclidinium	135.540	3.8461	6.0898	—
Diethylammonium[a]	235.974	4.1939	6.2265	−6.129

[a]$t = (t - 25)$.

by taking into consideration the equilibrium

[5] $$BH^+ + H_2O \rightleftharpoons B + H_3O^+$$

and the procedure followed is essentially that of Campbell and Bock (14). The corrected conductance (Λ_{corr}) can be calculated by

[6] $$\Lambda_{obsd} = (1 - x)\Lambda_{corr} + x\Lambda_{0\ HCl}$$

where $\Lambda_{0\ HCl}$ values were obtained from Robinson and Stokes (13, p. 465), and x is the degree of hydrolysis. It was found that for 2-methoxyethylammonium hydroxide, the maximum difference in the observed and corrected Λ_0 values was 0.1% and for bis-2-methoxyethylammonium hydroxide 0.3%. It was therefore not necessary to correct for Λ_0 values of the hydroxides of 3-methoxypropylamine, cyclohexylamine, piperidine, quinuclidine, or diethylamine, all of which are salts of stronger bases than methoxyethylamine and bis-2-methoxyethylamine. The effect of hydrolysis on Λ_0 is illustrated for bis-2-methoxyethylammonium hydroxide in Table 3.

TABLE 3. Limiting equivalent conductance (Λ_0) vs. temperature for bis-2-methoxyethylammonium hydroxide in water

T (°C)	Λ_0(obsd.) ($cm^2\ \Omega^{-1}\ mol^{-1}$)	Λ_0(corr. for hydrolysis) ($cm^2\ \Omega^{-1}\ mol^{-1}$)
4.993	150.96	150.87
5.000	150.96	150.84
15.002	188.99	188.74
15.004	189.10	188.85
24.986	229.05	228.59
25.008	229.00	228.54
35.000	269.98	269.29
35.013	269.99	269.40
44.997	311.55	310.71
44.998	311.49	310.61

Discussion

The problems associated with estimating and interpreting solute–solvent interactions are varied and to a considerable degree dependent on the experimental method. It is well known that water, as a solvent, presents special problems in such studies because of its peculiar structure. The latter may be described in terms of a mixture model or a continuous model but each will treat bulk water as possessing, to a greater or lesser degree, three-dimensional hydrogen bonded structures. These structures are modified by the solute, as indicated by measurement of various physical properties of the solute–water system. In the case of ionic solutes the evaluation of the value of the physical property for the ion of

TABLE 4. Limiting ionic conductances (λ_0) of selected substituted ammonium ions in water for a series of temperatures[a]

Ion	Temperature (°C)					
	5	10	15	25	35	45
Cyclohexylammonium	22.43	24.17	28.12	35.04	42.07	50.86
Piperidinium	25.19	25.89	29.56	37.52	46.59	57.04
Quinuclidinium	24.13	24.98	28.67	36.32	44.57	53.72
2-Methoxyethylammonium	26.32	27.21	31.03	39.10	47.90	57.56
3-Methoxypropylammonium	27.52	28.71	32.87	41.77	51.60	62.52
Bis-2-methoxyethylammonium	20.07	19.95	22.89	29.35	36.31	43.43
Ethylammonium (1)	30.52	32.34	36.58	46.60	57.00	66.97
Diethylammonium	21.51	25.07	28.81	36.79	45.43	54.65
Triethylammonium[b]	18.38	21.42	24.56	31.29	38.83	47.61
Trimethylammonium (2)	28.39	32.52	37.06	46.94	57.38	67.65

[a]Units of λ_0: $cm^2\ \Omega^{-1}\ mol^{-1}$.
[b]D. Northcott and R. E. Robertson. Unpublished data.

TABLE 5. Walden products ($\lambda_0\eta$) of selected substituted ammonium ions in water for a series of temperatures[a]

Ion	Temperature (°C)					
	5	10	15	25	35	45
Cyclohexylammonium	0.3407	0.3159	0.3203	0.3120	0.3027	0.3031
Piperidinium	0.3826	0.3384	0.3367	0.3341	0.3352	0.3400
Quinuclidinium	0.3674	0.3265	0.3266	0.3234	0.3206	0.3202
2-Methoxyethylammonium	0.3998	0.3556	0.3534	0.3481	0.3446	0.3431
3-Methoxypropylammonium	0.4180	0.3752	0.3744	0.3719	0.3712	0.3726
Bis-2-methoxyethylammonium	0.3049	0.2607	0.2607	0.2613	0.2612	0.2588
Ethylammonium	0.4636	0.4227	0.4166	0.4149	0.4101	0.3991
Diethylammonium	0.3267	0.3277	0.3281	0.3296	0.3268	0.3257
Triethylammonium	0.2792	0.2800	0.2797	0.2786	0.2793	0.2842
Trimethylammonium	0.4312	0.4250	0.4221	0.4180	0.4128	0.4032

[a]Units of $\lambda_0\eta$: $cm^2\ \Omega^{-1}\ mol^{-1}$ P.

interest and, specifically, its effect on water structure may not be simple nor satisfactory, due to the inability of separating out the contribution of the counter-ion.

Conductance measurements offer the advantage in that accurate estimates of single ion limiting equivalent conductances, λ_0, can be obtained without introducing arbitrary assumptions. However, λ_0 alone does not give as satisfactory a parameter for determining the effect of an ion on water structure as the Walden product, $\lambda_0\eta$, and its temperature dependence. These have been used by Kay and co-workers (7–9) to classify ions as structure-breakers or -makers.

In order to obtain λ_0 values for the ions studied here, λ_0 values of the substituted ammonium ions are obtained from $\Lambda_0(BH^+OH^-)$ (cf. Table 2) and $\lambda_0(OH^-)$ values (13, p. 465) and η values have been taken from ref. 15. λ_0 and $\lambda_0\eta$ for all the substituted ammonium ions studied here are listed in Tables 4 and 5, repectively. For the sake of comparison, values for ethylammonium (1), trimethylammonium (2), and triethylammonium[3] ions are also included.

Figure 1 illustrates the temperature dependence of $\lambda_0\eta$ of the ions listed in Tables 4 and 5. As rationalized by Kay and Evans (8), structure-breakers usually have high Walden products. These values tend to decrease with increasing temperature, because there is less water structure to break at higher temperatures.

Such ions as $n\text{-}Pr_4N^+$ and $n\text{-}Bu_4N^+$, which show a positive temperature coefficient of $\lambda_0\eta$, are judged to be structure-makers since the hydrophobic cage-like structures formed by such ions melt with increasing temperature, producing smaller faster moving entities. From Fig. 1,[4] if we ignore the 5°C points, we conclude

[3]D. Northcott and R. E. Robertson. Unpublished data.

[4]The 5°C points for most of the compounds investigated here appear to be anomalous; however, we found no justifiable reason to ignore these data (cf. last column of Table 1).

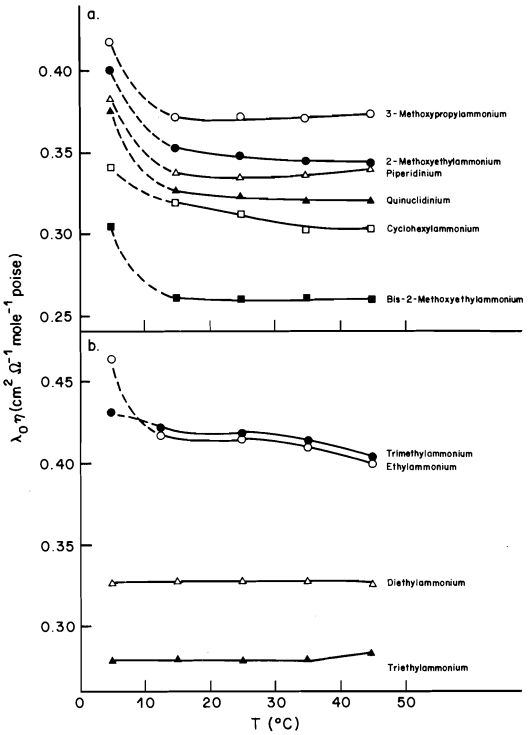

FIG. 1. Temperature dependence of Walden products for selected ammonium ions: (*a*) cyclic and methoxy substituted ammonium ions; (*b*) simple aliphatic ammonium ions.

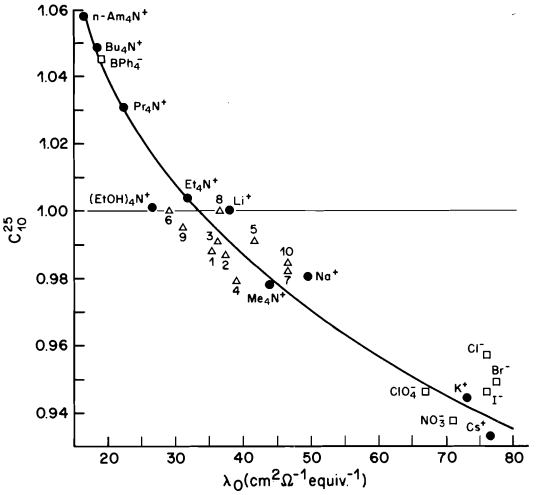

FIG. 2. Plot of C_{10}^{25} vs. λ_0^{25}: *1*, cyclohexylammonium; *2*, piperidinium; *3*, quinuclidinium; *4*, 2-methoxyethylammonium; *5*, 3-methoxypropylammonium; *6*, bis-2-methoxyethylammonium; *7*, ethylammonium; *8*, diethylammonium; *9*, triethylammonium; *10*, trimethylammonium.

that 2-methoxyethylammonium, cyclohexylammonium, quinuclidinium, ethylammonium, and trimethylammonium ions are structure-breakers. By the same criterion the piperidinium ion is seen to be a weak structure-maker. Bis-2-methoxyethylammonium, 3-methoxypropylammonium, triethylammonium, and diethylammonium ions appear to have no net effect on water structure. That the latter four ions should have no net effect on water structure is unexpected. Intramolecular hydrogen bonding in the case of 3-methoxypropylammonium ion may affect its structure-breaking ability. However, the secondary ammonium ions also appear to show anomalous behaviour. Rather than rely solely on the temperature dependence of $\lambda_0\eta$ of these ions, we have used a plot of C_{10}^{25} vs. λ_0^{25} for distinguishing between structure-breakers and -makers, as suggested by Kay (9). We have superimposed our values on Kay's original plot (9), Fig. 2. The results of this plot are interesting.

In Fig. 2, structure-making ions have high C_{10}^{25} values and lie in the upper left-hand corner of the plot, whereas structure-breakers lie in the lower right-hand corner of the plot. Ions that have both these features balanced have a C_{10}^{25} value of unity and lie on the centre of the plot. Thus the alkylammonium ions and the cyclic ammonium ions studied here lie slightly below the centre of the plot and indicate an overall structure-breaking effect, although it is not very strong. The bis-2-methoxyethylammonium ions and diethylammonium ions have no net effect on water structure, the reason, as mentioned earlier, not being obvious. Thus, although a smooth correlation is possible for the tetraalkylammonium ions, small variations are noted for the partially substituted ammonium ions.

In order to determine if these deviations are related to the size of the ion, we recall the Stokes relation (13, p. 125), which for univalent ions is

$$[7]\quad \lambda_0\eta = \frac{15.4}{6\pi r_s} = \frac{15.4}{6\pi}\left(\frac{4\pi N}{3}\right)^{1/3}\left(\frac{1}{\bar{V}^0}\right)^{1/3}$$

where r_s is the radius in aqueous solution, N is Avogadro's number, and $\bar{V}^0$ is the partial molar volume. If [7] is obeyed, the plot of $\lambda_0\eta$ vs. $(1/\bar{V}^0)^{1/3}$ should give a straight line. In Fig. 3 the well-known fact that the hypothetical line is not in accord with the experimental facts for small ions is of less significance here than the systematic deviations evident in the case of alkylammonium ions. The larger the alkyl groups and the more insulated the charge, the closer the

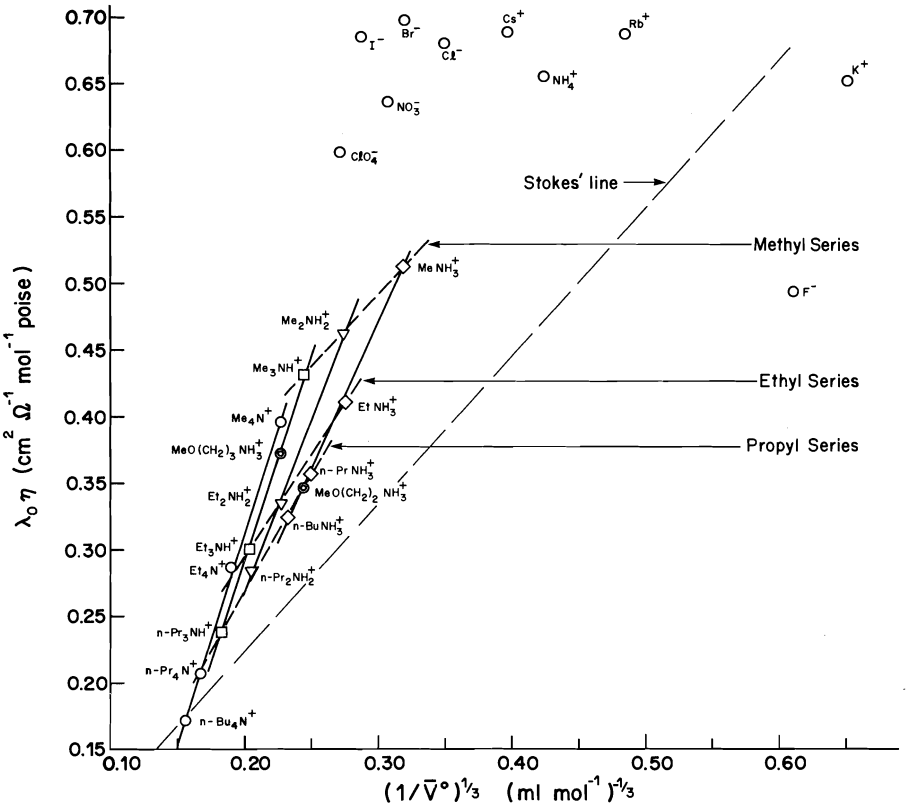

FIG. 3. Plot of $\lambda_0\eta$ vs. $(\bar{V}^0)^{-1/3}$ at 25°C. λ_0 and $\bar{V}^0$ data are taken from Kay (18) and Friedman and Krishnan (19) and this work, except for λ_0 of $MeNH_3^+$ (20), $EtNH_3^+$ (20), *n*-$PrNH_3^+$ (20), *n*-$BuNH_3^+$ (20), *n*-$Pr_2NH_2^+$ (16), Et_3NH^+ (16) and $\bar{V}^0$ of $MeO(CH_2)NH_3^+$ (17), $MeO(CH_2)_3NH_3^+$ (17).

adherence to the above relation (cf. Bu_4N^+). This trend has been explained by Kay (18). It appears that each category of ions, i.e. primary, secondary, tertiary, and quaternary ammonium ions, is well correlated by straight lines, although each series deviates from the Stokes line in the direction of higher mobility, with the quaternary ammonium ions deviating the most. The Me, Et, Pr, and Bu series are correlated among themselves, although in the case of the Me series, Me_4N^+ deviates from the line, but as we progress to the Bu series the deviation of the quaternary ammonium ion vanishes. Thus in any given series, be it type of ion or the type of substituent, size of the ion is related to the Walden product, and $\bar{V}^0$. No apparent correlation, dependent on size, is found for the ethyl substituted ammonium ions (the only series for which C_{10}[25] values are available, Fig. 2) and unfortunately no volumetric data are available for all the cyclic ammonium ions studied here. Neither are accurate conductance data available for all the members of the methyl, propyl, and butyl series to draw any firm conclusions about the scatter of points in the structure-breaking region in Fig. 2. As for the methoxyalkylammonium ions (cf. Fig. 3), $MeO(CH_2)_2NH_3^+$ falls on the line of the primary ammonium ions and its $\lambda_0\eta$ value appears to be related to size. However, $MeO(CH_2)_3NH_3^+$ deviates in the direction of larger $\lambda_0\eta$ although its size is close to that of *n*-$BuNH_3^+$. If this ion does break water structure in its immediate vicinity so as to have a higher mobility, one would naturally expect its apparent size in aqueous solution to be smaller. That the effective size of the ion in solution governs the magnitude of λ_0 and $\bar{V}^0$ is seen in Fig. 3. This was observed also by Desnoyers and co-workers (20) for ions of the type RNH_3^+.

Although on the basis of the above analysis, the ions studied here are classified as weak water structure-breakers, we must admit that the concept of structure-makers and -breakers is not entirely satisfactory, because it is not known

specifically what type of water structure is made or broken. However, we tend to agree with Kay and Evans (8) that analysis of λ_0 values based on the model of structure-breaking and -making properties of ions in aqueous solution is preferable to that based solely on the approach of electrostrictive hydration and arbitrary corrections to Stokes' law.

Acknowledgement

Financial help from the National Research Council of Canada is gratefully acknowledged.

1. W. VAN DER LINDE, D. NORTHCOTT, W. REDMOND, and R. E. ROBERTSON. Can. J. Chem. **47**, 279 (1969).
2. D. NORTHCOTT and R. E. ROBERTSON. J. Phys. Chem. **73**, 1559 (1969).
3. S. T. LOBO, T. S. S. R. MURTY, and R. E. ROBERTSON. Can. J. Chem. **54**, 3607 (1976).
4. S. T. LOBO and R. E. ROBERTSON. Can. J. Chem. **54**, 3600 (1976).
5. S. T. LOBO. Ph.D. Dissertation. The University of Calgary, Calgary, Alta. 1975.
6. T. SHEDLOVSKY and R. L. KAY. J. Phys. Chem. **60**, 151 (1956).
7. D. F. EVANS and R. L. KAY. J. Phys. Chem. **70**, 366 (1966).
8. R. L. KAY and D. F. EVANS. J. Phys. Chem. **70**, 2325 (1966).
9. R. L. KAY. Adv. Chem. Ser. **73**, 1 (1968).
10. H. C. BROWN and N. R. ELDRED. J. Am. Chem. Soc. **71**, 445 (1949).
11. T. SHEDLOVSKY. J. Am. Chem. Soc. **54**, 1411 (1932).
12. H. S. HARNED and B. B. OWEN. The physical chemistry of electrolytic solutions. 3rd ed. Reinhold Publishing Co., New York, NY. 1958. p. 233.
13. R. A. ROBINSON and R. H. STOKES. Electrolyte solutions. 2nd ed. Butterworth's Publications Ltd., London. 1965. p. 465.
14. A. N. CAMPBELL and E. BOCK. Can. J. Chem. **36**, 330 (1958).
15. R. C. WEAST (*Editor*). Handbook of chemistry and physics. 51st ed. Chemical Rubber Publishing Company, Cleveland. p. F-36.
16. T. S. MOORE and T. F. WINMILL. J. Chem. Soc. 1635 (1912).
17. S. CABANI, V. MOLLICA, L. LEPORI, and S. T. LOBO. J. Phys. Chem. Accepted for publication.
18. R. K. KAY. *In* Water, a comprehensive treatise. Vol. 3. *Edited by* F. Franks. Plenum Press, New York, NY. 1973.
19. H. L. FRIEDMAN and C. V. KRISHNAN. *In* Water, a comprehensive treatise. Vol. 3. *Edited by* F. Franks. Plenum Press, New York, NY. 1973.
20. J. E. DESNOYERS, M. AREL, and P.-A. LEDUC. Can. J. Chem. **47**, 547 (1969).

A radiochemical study of the kinetics of ion-exchange on zirconium antimonate

JOHN MATHEW AND SHIV NATH TANDON
Department of Chemistry, University of Roorkee, Roorkee – 247672, India

Received April 6, 1977

JOHN MATHEW and SHIV NATH TANDON. Can. J. Chem. **55**, 3857 (1977).

This paper reports the radiochemical study of the kinetics of ion-exchange of Rb^+ and Cs^+ with H^+ on zirconium antimonate. The slow step which determines the rate of exchange of these ions is diffusion through the particle. Values for the diffusion coefficients, energy of activation, and entropy of activation have been calculated. The data obtained have been compared with those reported for other organic and inorganic exchangers.

JOHN MATHEW et SHIV NATH TANDON. Can. J. Chem. **55**, 3857 (1977).

Cet article rapporte l'étude radiochimique de la cinétique de l'échange ionique de Rb^+ et Cs^+ avec H^+ sur de l'antimonate de zirconium. L'étape lente qui détermine la vitesse de l'échange de ces ions est la diffusion à travers la particule. On a calculé des valeurs pour les coefficients de diffusion, l'énergie d'activation et l'entropie d'activation. On a aussi comparé les valeurs obtenues avec celles rapportées pour d'autres échangeurs organiques et inorganiques.

[Traduit par le journal]

Introduction

The rate-controlling step in ion-exchange was first shown by Boyd *et al.* (1) to be diffusion either in the exchanger particles itself ('particle diffusion') or in an adherent stagnant liquid layer ('film diffusion'); in an intermediate range of conditions both mechanisms may affect the rate. Though many studies of the kinetics of ion-exchange on organic resins have been reported, rather less information exists on the kinetics of exchange on inorganic ion-exchangers. Nancollas and Paterson (2) have found particle diffusion to be the slow step which determines the rate of exchange on zirconium phosphate. Similar observations have also been made on some hydrous oxides (2–4) and tantalum arsenate (5). However, with less concentrated solutions, the rate-determining step for exchange on zirconium phosphate involves both film and particle diffusion (6).

Recently, we reported (7) the ion-exchange characteristics of zirconium antimonate and showed the utility of the material by demonstrating various separations of analytical and radiochemical interest. It was observed that Rb^+ and Cs^+ exchange stoichiometrically with this exchanger. In the present report, a radiochemical study of the kinetics of the exchange of Rb^+ and Cs^+ with H^+ on zirconium antimonate is described, and the thermodynamic parameters for the exchange are calculated. The data obtained for this material are compared with those for organic resins and other inorganic exchangers.

Experimental

Reagents and Apparatus

Zirconium oxychloride (Riedel, A. R.) and potassium pyroantimonate (E. Merck, G. R.) were used. All other chemicals were of analytical grade. ^{86}Rb ($t_{1/2}$ = 18.8 d) and ^{134}Cs ($t_{1/2}$ = 2.19 y) obtained from BARC, Bombay, were employed as tracers.

All radiometric determinations were done by scintillation counting, by means of a NaI/Tl well-type crystal employing a counter together with a single-channel analyser (ECIL, Hyderabad).

Kinetic Measurements

The synthesis of the exchanger is described elsewhere (7) and the sample No. 4A which has the highest exchange capacity was chosen for the study. The air-dried material was converted to the H^+ form by treatment with 1 *M* HCl. Finally, it was washed several times with deionised water and dried over saturated ammonium chloride solution (relative humidity 79%). The exchange capacities determined by a radiotracer technique (8) for Rb^+ and Cs^+ were 0.61 and 0.55 mequiv./g, respectively.

The radius of the particle of the sieved fractions was determined by measuring the diameter of 100 particles with a micrometer microscope. The mean radius of the particle measured was 6.42×10^{-3} cm for the smaller-sized fractions and 1.20×10^{-2} cm for the larger-sized fractions.

Rates of exchange were determined by the 'limited bath technique'. Twenty millilitres of the labelled metal chloride solutions (total ionic strength $\mu = 0.11$ *N*) were shaken in a thermostatic bath at the desired temperature. Then 0.2 g of the exchanger in the H^+ form was added. At preset time intervals, samples of the supernatent solution were removed for analysis to determine the extent of exchange. The experiments were conducted at 20, 30, 40, and 50°C (±0.5°C).

Analytical Procedures

Rubidium and cesium solutions were analysed radiometrically. The results are expressed in terms of the

TABLE 1. B values as a function of particle size and temperature

System	Particle size r (cm)	B values (s^{-1}) 20°C	30°C	40°C	50°C
Rb^+/H^+	1.20×10^{-2}	2.78×10^{-4}	3.33×10^{-4}	3.96×10^{-4}	4.76×10^{-4}
	6.42×10^{-3}	8.33×10^{-4}			
Cs^+/H^+	1.20×10^{-2}	1.67×10^{-4}	2.22×10^{-4}	2.78×10^{-4}	3.63×10^{-4}
	6.42×10^{-3}	5.55×10^{-4}			

exchange fraction F, with time according to the following expression

$$F = (S_0 - S_t)/(S_0 - S_\infty)$$

where F = fraction exchanged at time t, S_0 = counts s^{-1} ml^{-1} at $t = 0$, S_t = counts s^{-1} ml^{-1} at $t = t$, S_∞ = counts s^{-1} ml^{-1} at equilibrium.

The data obtained were analysed by the least-squares method (9). The estimated errors were within 5% for each measured value of the diffusion coefficient and other thermodynamic parameters.

Results and Discussion

The conditions of the present experiment were set to study the particle diffusion mechanism only. As the limited bath technique was employed, the equation developed by Boyd *et al.* (1) and improved by Reichenberg (10) can be used. If the rate-determining step is diffusion through the exchanger, then the following equation is valid.

$$[1] \qquad F = 1 - \frac{6}{\pi^2}\sum_{n=1}^{\infty}\frac{1}{n^2}\exp(-n^2Bt)$$

where F is the fractional attainment of equilibrium, n is an integer, $B = \pi^2\bar{D}/r^2$, in which $\bar{D}$ is the effective diffusion coefficient of the exchanging ion inside the exchanger and r is the radius of the particle.

According to the above equation, F is a function of B and t only and is thus independent of the concentration of the external solution. Experimental results may be tested to determine whether they conform to the above equation by plotting values of Bt (calculated from the experimentally determined values of F) against corresponding values of t; Bt values are taken from Reichenberg's table (10).

The values of F as function of time for different concentrations of Rb^+ and Cs^+ on zirconium antimonate are shown in Fig. 1. The plots of Bt vs. t for the Cs^+/H^+ system are linear and pass through the origin with constant diffusion coefficients within experimental error only for

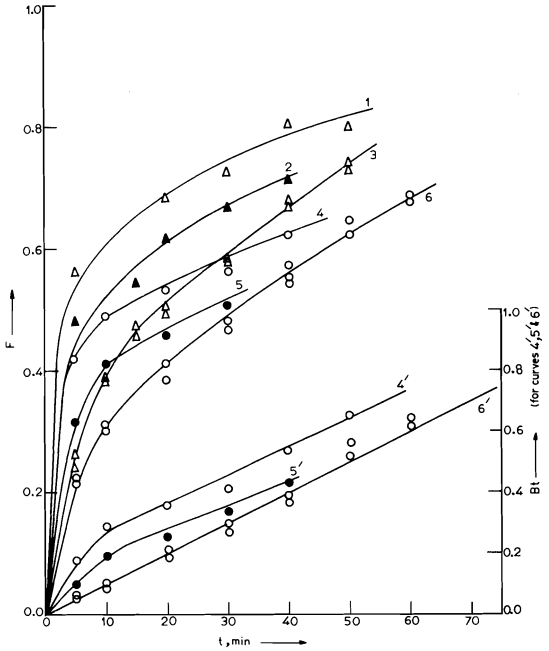

FIG. 1. Effect of the concentration of Rb^+ and Cs^+ on the rate of exchange on zirconium antimonate. (▲, △) Rb^+: *1*, 0.02 *M*; *2*, 0.05 *M*; *3*, 0.1 and 0.2 *M*. (●, ○) Cs^+: *4* and *4′*, 0.02 *M*; *5* and *5′*, 0.05 *M*; *6* and *6′*, 0.1 and 0.2 *M*.

concentrations above 0.1 *M*. Similar plots were obtained for the Rb^+/H^+ system. These results suggest that in the initial stages of the exchange, diffusion of Rb^+ and Cs^+ is not controlled by particle diffusion alone for 0.02 and 0.05 *M* solutions, while at concentrations $\geq$ 0.1 *M*, the slow step which determines the exchange is particle diffusion.

The results of the variation of particle size of the exchanger on the rate of exchange of Rb^+ and Cs^+ on zirconium antimonate are given in Table 1. For the Rb^+/H^+ system at 20°C, the ratio of the squares of the radii is 3.49 which agrees within experimental error with the inverse

ratio of the B values, 3.0, as required by [1]. Similarly, for the Cs^+/H^+ system at 20°C, the ratio of the squares of the radii is 3.49 and the inverse ratio of B values is 3.32. Thus the proportionality of B to r^{-2} is confirmed within experimental error and an effective diffusion coefficient can be calculated.

The rate of exchange increased with an increase in temperature from 20 to 50°C, suggesting that the mobility of these ions increases with increasing temperature. As a typical example, a plot of Bt vs. t obtained at different temperatures for the Rb^+/H^+ system is shown in Fig. 2; the values of B are tabulated in Table 1.

The resolution of the McKay plot (11), given in Fig. 3, in the case of the Rb^+/H^+ as well as the Cs^+/H^+ system indicates that the resulting graphs are curves similar to those of independently decaying activities. A complex exchange reaction likely occurs due to the presence of more than one type of functional site, or to the presence of $[Sb(OH)_6]^-$ bound in different ways. A similar exchange mechanism has already been observed in the isotopic exchange kinetics of phosphate ions between aqueous solution and solid zirconium phosphate (12).

When log D is plotted against $1/T$ (Fig. 4), straight lines are obtained, enabling the energy of activation (E_a) and the pre-exponential constant (D_0) to be estimated from an Arrhenius equation $D = D_0 \exp(-E_a/RT)$. The entropy of activation (ΔS^*) can then be calculated from D_0 by substituting in the equation proposed by Barrer *et al.* (13)

$$D_0 = 2.72(kTd^2/h) \exp(\Delta S^*/R)$$

where k = Boltzmann constant, T = 273 K, d = average distance between two successive positions in the process of diffusion, taken as equal to 5 Å, h = Planck's constant, R = gas constant.

The values of the diffusion coefficient obtained

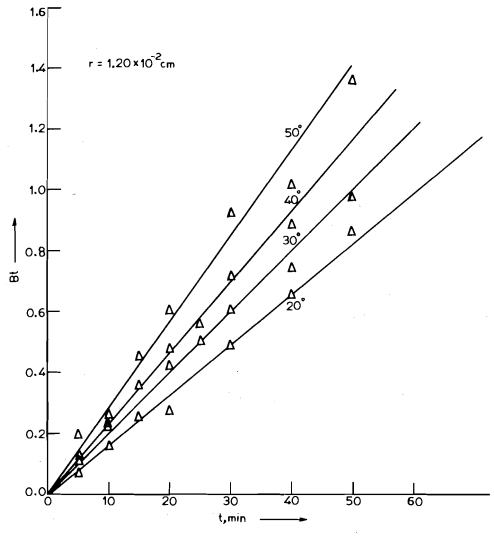

FIG. 2. Plot of Bt vs. t for Rb^+ at different temperatures.

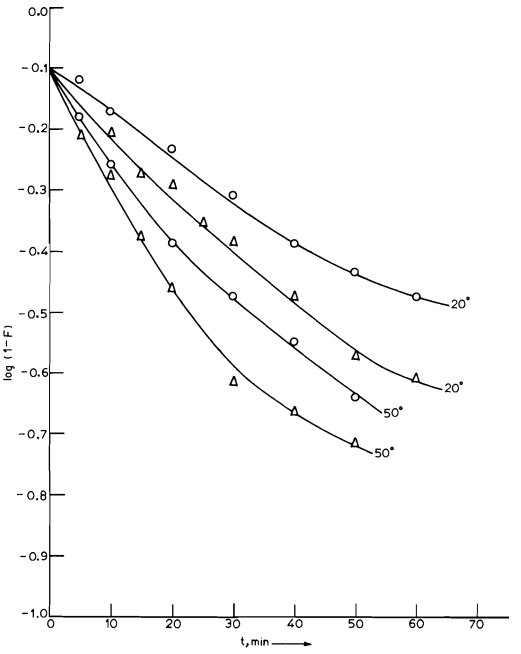

FIG. 3. McKay plot for the Rb^+/H^+ and Cs^+/H^+ systems on zirconium antimonate (△, Rb^+; ○, Cs^+).

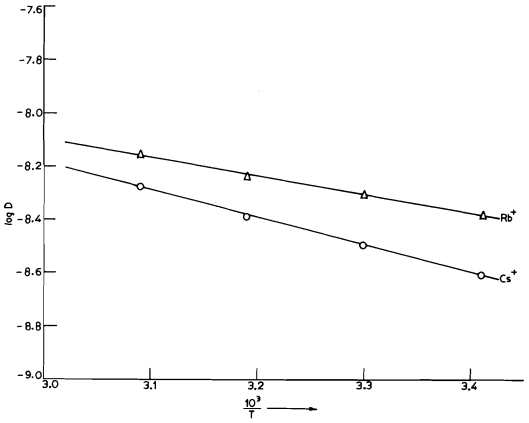

FIG. 4. Plot of log D vs. $1/T$.

TABLE 2. Diffusion coefficients and other thermodynamic parameters calculated for the exchange of Rb^+ and Cs^+ on zirconium antimonate

System	Particle size r (cm)	Diffusion coefficients D (cm^2/s)				D_0 (cm^2/s)	E_a (kcal/mol)	ΔS^* (cal deg^{-1} mol^{-1})
		20°C	30°C	40°C	50°C			
Rb^+/H^+	1.20×10^{-2}	4.06×10^{-9}	4.86×10^{-9}	5.78×10^{-9}	6.95×10^{-9}	7.71×10^{-7}	3.0	−21.50
	6.42×10^{-3}	3.64×10^{-9}						
Cs^+/H^+	1.20×10^{-2}	2.44×10^{-9}	3.24×10^{-9}	4.06×10^{-9}	5.30×10^{-9}	4.43×10^{-6}	4.4	−18.02
	6.42×10^{-3}	2.32×10^{-9}						

(Table 2) for Rb^+ and Cs^+ on zirconium antimonate are much less than those obtained for strongly cationic resins, but appreciably higher than those for zeolites. On Dowex 50-8.6X, $\bar{D}$ for rubidium and cesium ions are reported to be 13.8×10^{-7} and 13.7×10^{-7} cm^2/s respectively (14). For zeolites, however, the values of the effective diffusion coefficients are much smaller and are of the order of 10^{-12}–10^{-16} cm^2/s (15). The $\bar{D}$ value of Cs^+ at 20°C on zirconia, given by Hallaba *et al.* (4), is 2.2×10^{-9} cm^2/s and on zirconium phosphate (16) the reported value is 1.1×10^{-8} cm^2/s. Thus, a comparison of the values of the diffusion coefficient reported herein with that of inorganic resins and other exchangers indicates that zirconium antimonate shows rates of exchange approaching those of organic resins as well as some inorganic exchangers.

Energies of activation show an increase in magnitude with increase in ionic size. This is analogous to the behaviour of alkali metal ions migrating through analcite (17), where the diffusion coefficient decreases with increasing ionic size and energies of activation increase with increasing ionic size. It may therefore be said that rubidium and cesium ions suffer from a certain degree of dehydration while diffusing into the pores of zirconium antimonate and this may presumably explain why D for the Rb^+/H^+ system is higher than that for the Cs^+/H^+ system. The coefficient $\bar{D}_0$ also shows the trend of being higher in value with increasing covalent ionic size (18). A negative value for the entropy of activation suggests that upon exchange of these cations, no significant structural change occurs in zirconium antimonate.

Acknowledgements

The financial assistance of the Council of Scientific and Industrial Research, New Delhi, to one of us (J.M.) is gratefully acknowledged. Thanks are also due to Mr. N. J. Singh for helping with some of the experiments.

1. G. E. BOYD, A. W. ADAMSON, and L. S. MYERS. J. Am. Chem. Soc. **69**, 2836 (1947).
2. G. H. NANCOLLAS and R. PATERSON. J. Inorg. Nucl. Chem. **22**, 259 (1961).
3. C. HEITNER-WIRGUIN and A. ALBU-YARON. J. Appl. Chem. **15**, 445 (1965).
4. E. HALLABA, N. Z. MIZAK, and H. N. SALAMA. Indian J. Chem. **11**, 580 (1973).
5. J. P. RAWAT and P. S. THIND. J. Phys. Chem. **80**, 1384 (1976).

6. C. B. AMPHLETT, L. A. MCDONALD, and M. J. REDMAN. J. Inorg. Nucl. Chem. **6**, 220 (1958).
7. J. MATHEW and S. N. TANDON. J. Radioanal. Chem. **27**, 315 (1975).
8. L. ZSINKA and L. SZIRTES. Acta Chim. Budapest, **69**, 249 (1971).
9. D. L. HARNETT. Introduction to statistical methods. Addison-Wesley Publishing Company, Inc., MA. 1970.
10. D. REICHENBERG. J. Am. Chem. Soc. **75**, 589 (1953).
11. H. MCKAY. Nature London, **142**, 977 (1938).
12. M. K. RAHMAN and J. BARRETT. J. Inorg. Nucl. Chem. **36**, 1899 (1974).
13. R. M. BARRER, R. F. BARTHOLOMEW, and L. V. C. REES. J. Phys. Chem. Solids, **21**, 12 (1961).
14. G. E. BOYD and B. A. SOLDANO. J. Am. Chem. Soc. **75**, 6091 (1953).
15. V. I. GORSHKOV, G. M. PANCHENKOV, and T. V. IVANOVA. Zh. Fiz. Khim. **36**, 19690 (1962).
16. C. B. AMPHLETT. Inorganic ion exchangers. Elsevier Publishing Company, Amsterdam. 1964. p. 129.
17. R. M. BARRER and L. V. C. REES. Trans. Faraday Soc. **56**, 709 (1960).
18. L. PAULING. The nature of the chemical bond. 2nd ed. Cornell University Press, Ithaca, NY. 1948. p. 350.

Raman spectrum of solid CH_4 in phase II

A. Cabana and Nguyen Dinh Thé

Département de Chimie, Université de Sherbrooke, Sherbrooke (Qué.), Canada J1K 2R1

Received June 10, 1977

A. Cabana and Nguyen Dinh Thé. Can. J. Chem. **55**, 3862 (1977).

The Raman spectrum of crystalline CH_4 in phase II has been obtained. The ν_1, ν_2, and ν_3 bands have been observed as well as two weak bands in the lattice vibration region. The spectrum is found to be consistent with the structure originally proposed by James and Keenan. There is excellent agreement between a theoretical model proposed by Yamamoto and co-workers and the spectra presented here.

A. Cabana et Nguyen Dinh Thé. Can. J. Chem. **55**, 3862 (1977).

On a enregistré le spectre Raman du CH_4 cristallin dans la phase II. Les bandes ν_1, ν_2 et ν_3 ont été observées de même que deux bandes faibles dans la région des vibrations de réseau. On a pu conclure que le spectre peut être interprété sur la base de la structure proposée par James et Keenan. Il existe un accord excellent entre un modèle théorique proposé par Yamamoto et ses collaborateurs et les spectres présentés ici.

The infrared (1–3) and Raman (4) spectra of CH_4 in noble gas matrices were found to exhibit some fine structure which has been tentatively assigned to various rotation–vibration features. A suitable model for the hindered rotation of the molecule in the matrices was developed later (5, 6) and the assignment proposed by the experimentalists proved to be qualitatively correct.

The infrared spectra of neat CH_4 crystals have also been reported by several investigators (see ref. 7). Chapados and Cabana (7) compared the spectrum of the neat solid in phase II with the spectrum of the molecule in a krypton matrix and recognized that the spectrum is consistent with the theoretical model proposed by James and Keenan (8), a model which was confirmed later by Press (9) from a coherent neutron diffraction experiment of CD_4. The Raman spectra of the neat crystals have also been reported (10, 11). Only Anderson and Savoie (11) have obtained the spectrum of the solid in phase II. Considering that these investigators worked before the advent of powerful gas lasers their spectra were very satisfactory, and the phase I spectrum we have obtained is no different from theirs. However, the phase II spectrum lacked the resolution now available and is not good enough to reveal the weaker features that provide convincing evidence for rotation in that phase. We report here the Raman spectrum recorded with the higher resolution obtainable using the equipment and techniques described previously (12, 13), and discuss the spectrum in terms of the recent calculations of the ν_3 and ν_4 infrared and Raman bands reported by Yamamoto and co-workers (14). Their calculations have provided a quantitative basis for the assignment of the infrared data.

Of the four fundamental vibrations, ν_1, ν_2, and ν_3 have been observed, but ν_4 has not been found although the appropriate region was carefully scanned at wide slits and high gains. The spectrum of the neat crystal is shown in Figs. 1 (ν_3), 2 (ν_1), and 3 (ν_2) and the Raman shifts are collected in Tables 1 and 2. The weak band on the low frequency side of ν_1 has been assigned to the strong ν_1 band of C_2H_6 present at low concentration in our sample of CH_4.

Phase II CH_4 very likely belongs to space group O_h^6 (*Fm*3*c*). In this structure there are eight molecules per primitive cell of which six, occupying sites of D_{2d} (42*m*) symmetry, are ordered and two, occupying sites of *O* (432) symmetry, are free to rotate. Therefore, the molecules at sites of symmetry *O* should lead to rotational features in the spectrum whereas molecules at sites of symmetry D_{2d} could lead to site and factor group splittings as predicted from group theory (7). It is to be noted that the centrosymmetric structure imposes that all of the ir active components should be Raman inactive and vice-versa. The infrared spectrum (7) did not reveal any site or factor group splittings. It is likely that these splittings are too small to be resolvable; the same appears to be applicable to the Raman spectrum. Three lattice modes, of which one is of rotational origin, are expected for

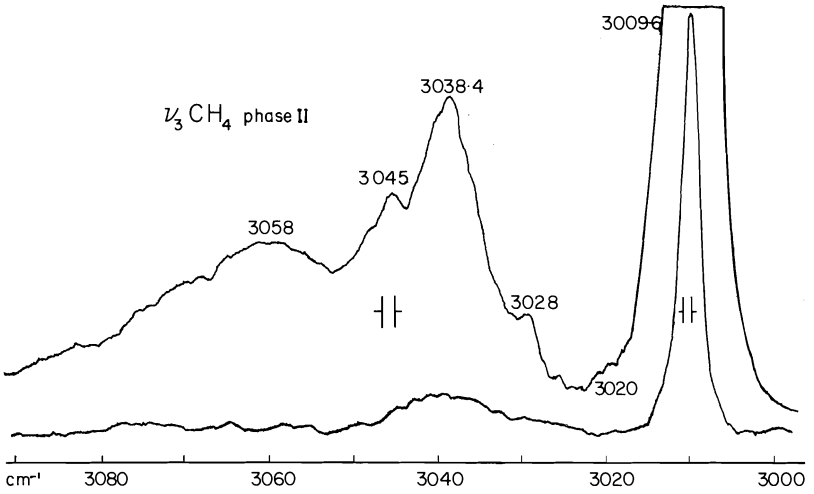

FIG. 1. The Raman spectrum of the ν_3 vibration region of CH_4 recorded at 9 K in phase II.

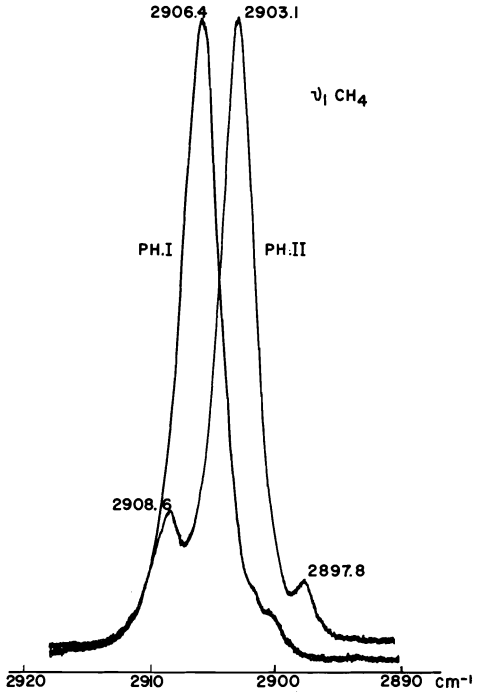

FIG. 2. The ν_1 Raman bands of CH_4 recorded at 9 K in phase II. The low frequency band at 2897.8 cm^{-1} arises from C_2H_6 present at low concentration in our sample. The phase I spectrum was obtained just above the transition temperature.

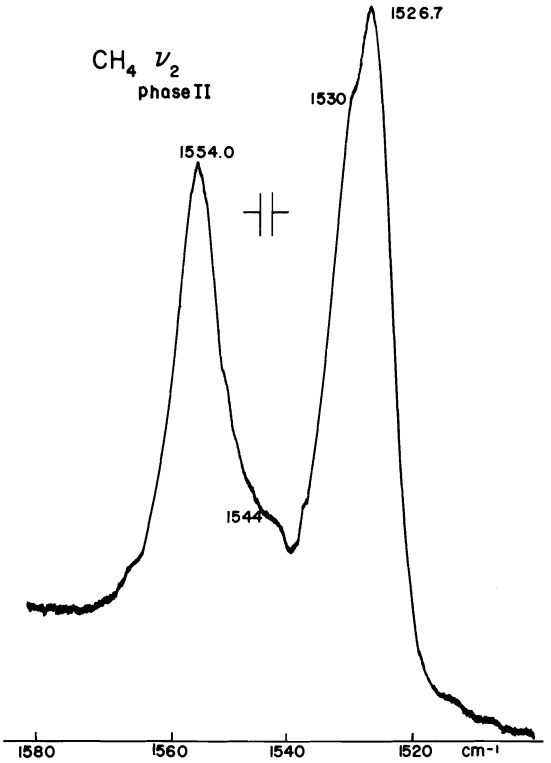

FIG. 3. The ν_2 Raman band of CH_4 recorded at 9 K in phase II.

the D_{2d} molecules in the Raman as well as in the infrared spectrum (see Table 6, ref. 7) but only two of these have been observed in either the infrared (7) or the Raman spectrum (Table 2).

The ν_1 band of CD_4 at low concentration in crystalline CH_4 phase II has been recorded and is shown in Fig. 4. The vibrations of the guest CD_4 molecule should, under these conditions, be largely uncoupled from those of the host molecules such that factor group splitting

TABLE 1. Observed and calculated Raman shifts in the ν_3 band of CH_4 crystal phase II

Frequencies (cm^{-1})[c]		
Observed	Calculated[a]	Assignments[a,b]
	2990.6 w	$O(2)T$
	2999.1 w	$P(2)T$
	2999.8 w	$P(2)E$
3009.6 vs	3008 vs	D_{2d}, ν_3
3013 w, sh	3011.7 w	$Q(2)T$
	3011.7 w	$Q(2)E$
	3012.0 w	$Q(2)T$
	3012.4 m	$Q(1)$
3020 vw	3019.5 w	$Q(2)E$
	3019.5 w	$Q(2)T$
3028 w	3024.6 m	$R(1)$
	3025.1 m	$R(1)$
3038.4 m, br	3032.5 m	$R(1)$
	3034.3 s	$S(0)$
	3037.8 w	$Q(2)T$
3045 m	3041.5 s	$S(0)$
3058 m, br	3049.9 m	$R(1)$
	$\simeq$3050 br	D_{2d}

[a]Reference 14.
[b]Assignments are for molecules at sites of symmetry O_h, unless otherwise noted.
[c]v = very, s = strong, w = weak, sh = shoulder, m = medium, br = broad.

TABLE 2. Observed and calculated Raman shifts for crystalline CH_4 phase II

Frequencies (cm^{-1})			
Observed	Calculated[a]	Tentative assignment	
41 vw		D_{2d}	Lattice
52 vw		D_{2d}	
1526.7		D_{2d}	
1530 m, sh	1530.0[b]	$Q(1)$ of O_h	ν_2
1544 m, sh	1542.6	Mainly $R(1)$ of O_h	
1554 s	1551.5	Mainly $S(0)$ of O_h	
2903.1 v, s		D_{2d}, ν_1	ν_1
2908.6 m		Q of O_h	

[a]Frequencies calculated from ref. 14.
[b]$Q(1)$ of O_h molecules is adjusted to the experimentally measured wave number.

should be absent. Therefore, the component of lower intensity found at the higher frequency (2095.9 cm^{-1}) should arise from the rotating molecules. Since in the ν_1 band only $\Delta J = 0$ transitions are expected, this band should be mainly due to the $Q(1)$ and $Q(2)$ transitions. Several transitions due to the rotating molecules are identified in the ν_3 band of the neat crystal where agreement between theory and experiment is satisfactory (see Fig. 1 and Table 1). In the ν_1 band of the neat crystal it is very likely that the component of lower intensity found at the higher frequencies is also attributable to rotating

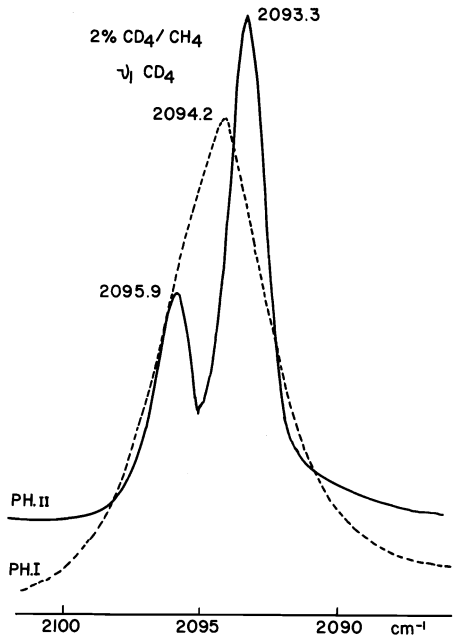

FIG. 4. The ν_1 Raman band of CD_4 at low concentration in CH_4 phase II at 9 K. The phase I spectrum was obtained just above the transition temperature.

molecules (see Fig. 2 and Table 2). Several features are also tentatively assigned to rotating molecules in the ν_2 band of the neat crystal (see Fig. 3 and Table 2). The two main components (1554.0 and 1526.7 cm^{-1}) are certainly too far apart to arise from site or factor group splitting. Although the assignment proposed here for some of the weaker lines is uncertain, the main features of these Raman spectra are found consistent with the structure generally accepted for the solid in phase II. The ν_3 Raman band, calculated by Yamamoto and co-workers (14), is certainly in good agreement with the experiment.

Acknowledgments

Financial support provided by the Ministère de l'Education de la Province de Québec and by the National Research Council of Canada is gratefully acknowledged. The authors wish to thank Professor Yamamoto for providing the results of the calculations prior to their publication.

1. A. CABANA, G. B. SAVITSKY, and D. F. HORNIG. J. Chem. Phys. **39**, 2942 (1963).
2. F. H. FRAYER and G. E. EWING. J. Chem. Phys. **46**, 1994 (1967); **48**, 781 (1968).
3. A. CHAMBERLAND, R. BELZILE, and A. CABANA. Can. J. Chem. **48**, 1129 (1970).

4. A. CABANA, A. ANDERSON, and R. SAVOIE. J. Chem. Phys. **42**, 1122 (1965).
5. K. NISHIYAMA and T. YAMAMOTO. J. Chem. Phys. **58**, 1001 (1973).
6. K. KOBASHI, Y. KATAOKA, and T. YAMAMOTO. Can. J. Chem. **54**, 2154 (1976).
7. C. CHAPADOS and A. CABANA. Can. J. Chem. **50**, 3521 (1972).
8. H. M. JAMES and T. A. KEENAN. J. Chem. Phys. **31**, 12 (1959).
9. W. PRESS. J. Chem. Phys. **56**, 2597 (1972).
10. M. F. CRAWFORD, H. L. WELSH, and J. H. HARROD. Can. J. Phys. **30**, 81 (1952).
11. A. ANDERSON and R. SAVOIE. J. Chem. Phys. **43**, 3468 (1965).
12. A. CABANA. *In* Vibrational spectra and structure. *Edited by* J. R. Durig. Elsevier, Amsterdam, The Netherlands. 1975. Chapt. 2, pp. 49, 50.
13. R. P. FOURNIER, R. SAVOIE, NGUYEN DINH THÉ, R. BELZILE, and A. CABANA. Can. J. Chem. **50**, 35 (1972).
14. K. KOBASHI, K. OKADA, and T. YAMAMOTO. To be published.

Interactions solutés–solvants dans les mélanges eau – alcool *tert*-butylique. VIII. Volumes molaires apparents des benzoates halogéno-substitués[1]

NICOLE DOLLET, LEVON AVEDIKIAN ET JEAN JUILLARD

Laboratoire d'Etude des Interactions Solutés–Solvants, Université de Clermont II, Les Cézeaux, B.P. 45, 63170, Aubière, France

Reçu le 6 avril 1977

NICOLE DOLLET, LEVON AVEDIKIAN et JEAN JUILLARD. Can. J. Chem. **55**, 3866 (1977).

Les volumes molaires apparents du benzoate de potassium et de quelques benzoates *para*-substitués (−F, −Cl, −I, $-CH_3$) ont été déterminés dans les mélanges eau – alcool *tert*-butylique pour des teneurs en alcool comprises entre 0 et 40% en poids. Des variations importantes de volume sont observées en milieu riche en eau. L'effet de la taille des substituants sur ces variations et la situation des maxima de volume apparent sont discutés en relation avec la structure des mélanges solvants.

NICOLE DOLLET, LEVON AVEDIKIAN, and JEAN JUILLARD. Can. J. Chem. **55**, 3866 (1977).

Apparent molal volumes of potassium salts of *para*-substituted (−F, −Cl, −I, $-CH_3$) and unsubstituted benzoic acids in water – *tert*-butyl alcohol mixtures (0–40% by weight) are reported. Large volume changes are observed in media rich in water. Substituents size effects on both the location and the amplitude of the volume maxima are discussed in terms of the structure of the mixed solvents.

Les mélanges eau – alcool *tert*-butylique (TBA) sont parmi les plus étudiés des mélanges hydro-alcooliques. En effet, cet alcool apparait comme le type même des cosolvants promoteurs de la structure de l'eau. En particulier, l'addition de TBA à une solution aqueuse détermine souvent des variations spectaculaires des propriétés des solutés. De nombreux résultats concernant les propriétés thermodynamiques de solutés variés (halogénures alcalins, sels d'ammonium quaternaires, acides carboxyliques et leurs sels) ont été accumulés ces dernières années. Dans un mémoire récent (2) nous avons traité des enthalpies de transfert des benzoates *para* halogéno-substitués. L'étude de l'effet de substituant nous a permis de souligner l'existence d'un effet de taille et d'un effet spécifique dans la solvatation de ces composés, l'effet de taille déterminant l'existence de maxima endothermiques de l'enthalpie de transfert pour une composition bien définie ($x \approx 0.051$) des mélanges. Ce travail a été poursuivi et nous présentons aujourd'hui des résultats concernant les volumes molaires apparents des mêmes espèces dans ces mélanges. Une étude préliminaire (3) des *p*-bromobenzoate et benzoate de potassium nous a déjà permis de noter que l'effet de substituant est le plus notable pour une composition voisine de 0.055 en fraction molaire. Nous avons mesuré ici, dans des conditions expérimentales plus satisfaisantes, les masses volumiques de solutions de benzoate, *p*-fluoro, -chloro et -iodobenzoates de potassium dans des mélanges contenant de 0 à 40% de TBA. Nous avons aussi déterminé les volumes apparents et les enthalpies de transfert du *p*-méthylbenzoate, résultats utiles pour la discussion sur la nature des effets de substituants.

[1]Article précédent dans cette série, réf. 1.

Partie expérimentale

La préparation des sels et la purification des solvants: eau et TBA, sont effectuées selon les procédures déjà décrites (2, 4). Les masses volumiques des solutions sont mesurées à 25.00 ± 0.01°C à l'aide d'un densimètre à flux SODEV, modèle 0ID, conformément à la technique décrite par Picker *et al.* (5). Pratiquement, les masses volumiques des solutions de benzoates sont comparées à celle du mélange solvant correspondant, elle-même déterminée par rapport à celle de l'eau ($\rho = 0.997047$ g/cm³ à 25°C (6)). Compte tenu des conditions opératoires relatives à l'appareillage et à la nature des solutions, les masses volumiques sont connues à $\pm 1 \times 10^{-5}$ g cm^{-3} près.

La détermination des enthalpies de dissolution du *p*-méthylbenzoate de potassium dans les mélanges eau–TBA est faite selon la méthode utilisée précédemment (2).

Résultats

Les volumes molaires apparents ϕ_v se déduisent simplement des masses volumiques ρ et ρ_0, respectivement des solutions et du mélange solvant correspondant:

$$\phi_v = \frac{M}{\rho} - \frac{1000\,(\rho - \rho_0)}{\rho\rho_0 m}$$

TABLEAU 1. Volumes molaires apparents ϕ_v en cm^3 pour une molalité de 0.08 des benzoates de potassium dans les mélanges eau–TBA à 298.15 K

X^a	Benzoate de potassium	*p*-Fluorobenzoate de potassium	*p*-Chlorobenzoate de potassium	*p*-Iodobenzoate de potassium	*p*-Méthylbenzoate de potasssium
0	96.7	99.7	109.3	121.1	112.8
5.0	96.4	98.3	108.0	120.0	111.1
7.0	95.1	98.2	108.1	120.1	111.0
10.0	95.5	98.9	109.2	121.8	111.5
12.0	96.2	100.0	110.7	124.1	112.4
15.0	98.1	102.9	115.2	129.6	114.8
18.0	100.2	106.8	120.1	134.7	118.1
20.0	101.7	108.6	122.2	136.7	120.1
22.0	102.5	109.6	123.0	136.7	121.1
25.0	103.2	110.2	122.8	135.9	121.4
30.0	103.6	110.1	121.9	134.6	121.2
35.0	103.7	109.6	120.4	132.7	121.0
40.0	103.6	109.2	119.2	131.6	121.2

[a]Pourcentage en poids de TBA.

où M est la masse molaire du soluté et m la molalité de la solution.

La variation avec la concentration est donnée par la relation de Redlich et Meyer (7):

$$\phi_v = \phi_v^0 + S_v\sqrt{c} + b_v c$$

où c est la molarité de la solution, b_v une constante empirique et S_v la pente limite de Debye–Hückel. Celle-ci ne dépend pas de la nature de l'électrolyte mais seulement de sa valence, de la température et des propriétés du milieu solvant (constante diélectrique D et son coefficient de pression $\partial D/\partial P$, compressibilité isotherme β_t).

La méthode expérimentale ne permettant pas d'atteindre le domaine des très faibles concentrations, une extrapolation à concentration nulle de ϕ_v en fonction de $\sqrt{c}$ ne saurait conduire à une valeur acceptable de ϕ_v^0, c'est-à-dire au volume molaire partiel à dilution infinie V^0. De plus, il n'existe pas de données sur la variation avec la pression de la constante diélectrique des mélanges étudiés, ce qui ne permet pas le calcul de S_v et donc l'extrapolation de $\phi_v - S_v\sqrt{c}$ en fonction de c. Ceci nous a conduit à ne considérer dans chaque solvant étudié, que les volumes molaires apparents des sels pour une molalité déterminée (0.08 m). Ces volumes apparents sont donnés dans le tableau 1. Notons à ce propos que, pour des solutions de NaCl dans les mêmes mélanges, ϕ_v et V^0 varient de façon analogue avec la composition du milieu solvant (8).

Sur le tableau 2 sont rapportées les enthalpies molaires de dissolution du *p*-méthylbenzoate pour une molalité de 10^{-2} environ dans tous les mélanges étudiés, ainsi que l'effet, sur les enthalpies de transfert, du substituant *p*-méthyl.

TABLEAU 2. Enthalpies molaires de dissolution ΔH_s et effet de substituant sur les enthalpies molaires normales de transfert $\delta_R\Delta H_t^{0a}$ du *p*-méthylbenzoate de potassium dans les mélanges eau–TBA à 298.15 K (ΔH_s et $\delta_R\Delta H_t^0$ en kJ mol^{-1})

X	ΔH_s	$\delta_R\Delta H_t^0$
0	7.20	0.00
5.0	11.20	0.80
10.0	16.90	1.80
15.0	24.90	3.55
18.0	28.95	4.30
20.0	30.15	4.15
25.0	28.75	2.70
30.0	26.20	1.80
35.0	24.10	1.10
40.0	22.30	0.75

[a]Calculées en utilisant les valeurs des enthalpies molaires normales de transfert du benzoate de potassium provenant de la réf. 2.

Discussion

Les volumes apparents de transfert sont portés sur la fig. 1. Toutes les courbes obtenues ont une allure analogue. On observe un minimum de volume molaire en milieu très riche en eau ($x \approx 0.02$), puis un accroissement brutal, enfin une décroissance après passage par un maximum. L'augmentation de la taille du substituant correspond à une augmentation rapide de l'amplitude du maximum et de façon moins sensible, à son déplacement vers les milieux plus riches en eau. On observe donc, mis à part l'existence du premier minimum, une allure des courbes comparable à celle des enthalpies de transfert.

L'analogie est encore plus frappante si l'on considère les effets de substituant sur ces gran-

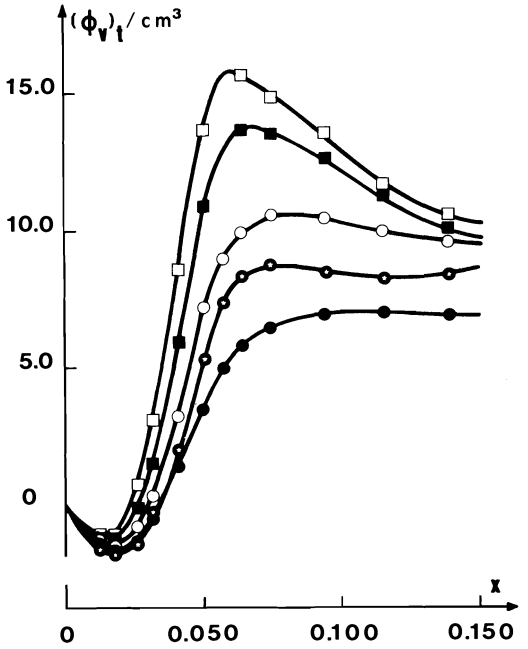

FIG. 1. Volumes apparents de transfert $(\phi_v)_t$ à 298.15 K des benzoates de potassium, de l'eau aux mélanges eau–TBA en fonction de la fraction molaire en TBA: ●, benzoate de K; ○, *p*-fluorobenzoate de K; ■, *p*-chlorobenzoate de K; □, *p*-iodobenzoate de K; ✪, *p*-méthylbenzoate de K.

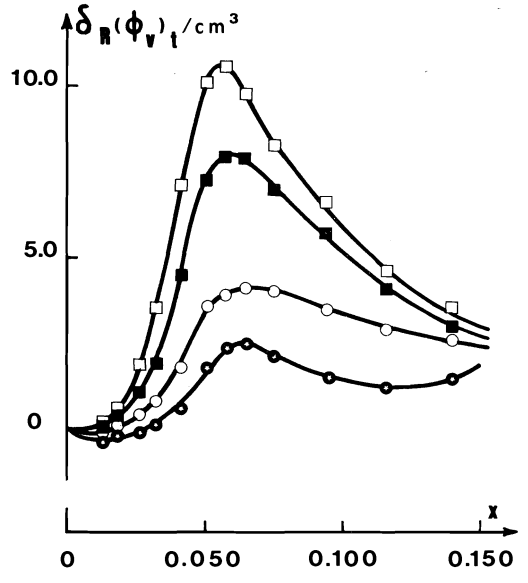

FIG. 2. Effets de substituants, à 298.15 K, sur les volumes apparents de transfert, des *p*-fluoro (○), *p*-chloro (■), *p*-iodo (□) et *p*-méthyl (✪) benzoates en fonction de la fraction molaire en TBA.

deurs de transfert:

$$\delta_R(\phi_v)_t = (\phi_v)_t(\text{benzoate substitué}) - (\phi_v)_t(\text{benzoate})$$

$\delta_R(\phi_v)_t$ traduit l'effet de la présence du substituant sur le volume de transfert de l'anion, celui du cation potassium étant éliminé dans la soustraction.

Les minima à $x \approx 0.02$ disparaissent sur ces courbes (fig. 2) et l'on obtient des maxima situés ici, à des compositions un peu plus riches en TBA que pour les enthalpies ($x \approx 0.06$).

On observe d'autre part, pour une composition quelconque des mélanges, une certaine corellation entre effets de substituant sur les enthalpies et les volumes de transfert des différents benzoates. Les effets observés ici semblent donc, comme dans le cas des enthalpies, directement liés à la taille du substituant. Toutefois, au seul vu des résultats concernant les benzoates halogéno-substitués, il n'est pas possible d'éliminer à priori l'hypothèse d'effets de substituant de type Hammett, ces effets variant pour ces substituants dans le même sens que la taille. Les résultats concernant le substituant *p*-méthyl dont le σ de Hammett est négatif, incitent à penser qu'il s'agit bien d'un effet de taille, encore qu'une correlation rigoureuse entre taille du substituant et amplitude du maximum impliquerait des effets plus voisins des substituants *p*-CH_3 et *p*-Cl.

Nous avons suggéré dans le travail précédent (2) l'existence de deux effets principaux dans la solvatation des solutés en mélange eau–TBA: un effet de solvatation spécifique et un effet de taille. Cet effet serait dominant dans les différences entre benzoate et benzoates substitués. Ces différences peuvent être estimées à partir des grandeurs thermodynamiques de formation de cavité pour les solutés correspondants. Des calculs utilisant la théorie des particules calibrées (scaled particle theory) sont exclus dans la mesure où il n'est pas possible de déterminer de façon simple les diamètres de sphère rigide de ces solutés. Par contre, la formule d'Eley (voir réf. 9) permet de calculer, à partir des volumes des benzoates, les enthalpies de formation de cavité: $\Delta H_c = T\gamma_v V^\theta$ où ΔH_c est l'enthalpie de formation d'une cavité de taille molaire à température et pression constantes, V^θ le volume molaire du soluté et γ_v le coefficient thermique de pression du milieu solvant:

$$\gamma_v = (\partial P/\partial T)_v = \alpha_P/\beta_T$$

Un exemple des résultats obtenus, comparés aux valeurs expérimentales, est donné sur la fig. 3 où nous avons porté, d'une part les différences calculées entre ΔH de transfert du benzoate et du *p*-iodobenzoate de potassium (en utilisant les valeurs de γ_v interpolées, aux concentrations considérées, à partir de celles données par Macdonald et Hyne (10)), et d'autre part, les différences expérimentales. La correspondance est acceptable jusqu'à $x = 0.05$ mais la formule de Eley ne permet pas de prévoir la décroissance brusque de la grandeur étudiée au-delà de cette fraction molaire en alcool *tert*-butylique.

En fait, la présence de maxima aigus, particulièrement sur les différences entre benzoates substitués et non-substitués pour des fractions molaires en alcool comprises entre 0.05 et 0.06, nous incite à interpréter l'effet de volume à l'aide du modèle des "cages fluctuantes" de Baumgartner et Atkinson (11). Ce modèle établit une analogie entre la structure des hydrates solides: clathrate de molécules organiques, et la structure des solutions aqueuses de ces molécules à température ordinaire, analogie déjà suggérée par divers auteurs (12). Compte tenu de la taille de l'alcool *tert*-butylique, il s'agit d'un clathrate de type II. Un clathrate de ce type stabilisé par une inclusion d'acide sulfhydrique (17 H_2O, 1 TBA, 2 H_2S) a d'ailleurs été signalé et étudié par Glew *et al.* (13). Baumgartner et Atkinson ont proposé (11) de considérer que les solutions aqueuses pourraient conserver partiellement, à l'état liquide, la structure de l'hydrate solide, celle-ci étant soumise toutefois à des fluctuations notables. Dans ces conditions la fraction molaire $1/18 \approx 0.055$ en TBA correspondrait au maximum de structuration des mélanges. Le minimum de compressibilité adiabatique est d'ailleurs observé sensiblement pour cette composition (11). Dans l'hypothèse d'une telle structure "quasi-clathrate" des solutions, les solutés d'une certaine taille ne pourraient entrer dans l'édifice qu'en le brisant ce qui correspondrait aux maxima endothermiques d'enthalpie. Ceux-ci seraient obtenus pour la composition 1–17 des mélanges et leur amplitude serait fonction de la taille des solutés.

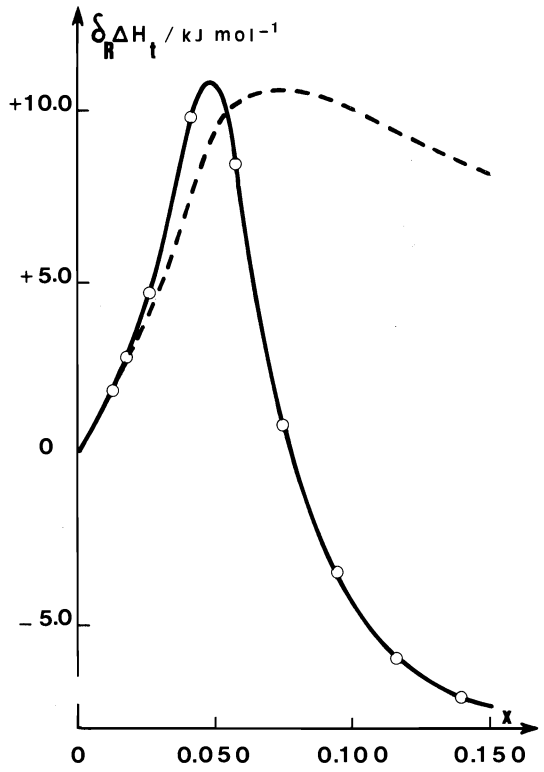

FIG. 3. Effet de substituant expérimental (—) et effet de substituant calculé (---) par la formule d'Eley sur les enthalpies de transfert du *p*-iodobenzoate à 298.15 K.

C'est bien ce que l'on observe avec des solutés volumineux tels que les sels de tétraphénylborate (14, 15) par exemple. L'effet de taille constaté précédemment sur les enthalpies de transfert des benzoates halosubstitués et confirmé ici par l'étude du méthylbenzoate s'explique bien dans ce cadre, l'introduction de substituants de plus en plus volumineux correspondant à un accroissement de l'amplitude des maxima d'enthalpie, maxima situés à une composition des mélanges voisine de $x \approx 0.055$.

On peut raisonnablement supposer que le bris de la structure détermine aussi un accroissement local de volume dans la solution, accroissement reflété par une augmentation du volume apparent des solutés. Cet accroissement serait le plus net pour le milieu le plus structuré et fonction de la taille du soluté introduit. L'addition de substituants de plus en plus volumineux correspond bien à un accroissement de volume molaire de plus en plus net, accroissement maximal pour une composition des mélanges de plus en plus proche de celle de la composition de "pseudo-clathrate" (fig. 2). Il convient de noter d'ailleurs, à propos de la situation exacte des maxima tant d'enthalpie que de volume de transfert, que celle-ci est difficile à préciser; les grandeurs mesurées: volumes

et enthalpies, le sont pour des concentrations finies; une correction de dilution convenable entrainerait sans doute de légers glissements. Il est clair toutefois que les maxima d'effet de substituant ici considérés sont observés pour des concentrations très voisines de la fraction molaire 1/17.

En conclusion donc, les résultats rapportés ici sont parfaitement compatibles avec le modèle "des cages fluctuantes" proposé par Baumgartner et Atkinson (11) pour rendre compte de la structure de certains mélanges hydro-organiques et en particulier des solvants mixtes eau – alcool *tert*-butylique.

1. Y. POINTUD, J.-P. MOREL et J. JUILLARD. J. Phys. Chem. **80**, 2381 (1976).
2. N. DOLLET et J. JUILLARD. J. Solution Chem. **5**, 77 (1976).
3. N. DOLLET et J. JUILLARD. J. Chim. Phys. **70**, 1733 (1973).
4. L. AVEDIKIAN, J. JUILLARD, J.-P. MOREL et M. DUCROS. Thermochim. Acta, **6**, 283 (1973).
5. P. PICKER, E. TREMBLAY et C. JOLICOEUR. J. Solution Chem. **3**, 377 (1974).
6. G. S. KELL. J. Chem. Eng. **12**, 66 (1967).
7. O. REDLICH et D. M. MEYER. Chem. Rev. **64**, 221 (1964).
8. L. AVEDIKIAN, G. PERRON et J. E. DESNOYERS. J. Solution Chem. **4**, 331 (1975).
9. E. A. MOELWYN HUGHES. The chemical statics and kinetics of solutions. Academic Press, London, England. 1971. p. 509.
10. D. D. MACDONALD et J. B. HYNE. Can. J. Chem. **49**, 2636 (1971).
11. E. K. BAUMGARTNER et G. ATKINSON. J. Phys. Chem. **75**, 2336 (1971).
12. E. M. ARNETT. Physico-chemical processes in mixed aqueous solvents. *Edité par* F. Franks. Hennemann Educational Book, London, England. 1967. p. 105.
13. D. N. GLEW, H. D. MAK et N. S. RATH. Hydrogen-bonded solvent systems. *Edité par* A. K. Covington et P. Jones. Taylor and Francis, London, England. 1968. p. 195.
14. E. ARNETT et D. R. MCKELVEY. J. Am. Chem. Soc. **87**, 1393 (1965).
15. L. L. BRIGHT et R. JEZOREK. J. Phys. Chem. **79**, 800 (1975).

The effects of counter ion nature on the adsorption of nitrate ion at the mercury/solution interface

W. Ronald Fawcett and James B. Sellan

Guelph–Waterloo Centre for Graduate Work in Chemistry (Guelph Campus), Department of Chemistry, University of Guelph, Guelph, Ont., Canada N1G 2W1

Received May 25, 1977

W. Ronald Fawcett and James B. Sellan. Can. J. Chem. **55**, 3871 (1977).

The adsorption of nitrate ion at mercury has been studied from two systems at constant ionic strength, namely, x *M* $NaNO_3$ + $(0.2 - x)$ *M* NaF and x *M* KNO_3 + $(0.2 - x)$ *M* KF. The surface excess due to adsorbed nitrate ions was determined from differential capacity data using a modified version of the Hurwitz–Parsons analysis which takes into consideration variation in ionic activity coefficients with solution composition. The amount of adsorbed nitrate ion at a given electrode charge density and bulk nitrate ion concentration is shown to depend markedly on both ionic strength and the nature of the counter ion at the outer Helmholtz plane; when the charge in the diffuse layer is positive, an increase in ionic strength results in more anion adsorption and vice versa. A change in the cation from Na^+ to K^+ also results in increased anion adsorption. The effects observed are discussed in terms of the Stern–Grahame–Levine model for ionic adsorption which is based on an electrostatic description of the charged interface with consideration of discreteness-of-charge effects.

W. Ronald Fawcett et James B. Sellan. Can. J. Chem. **55**, 3871 (1977).

On étudie l'adsorption de l'ion nitrate par le mercure dans deux systèmes à force ionique constante à savoir x *M* $NaNO_3$ + $(0.2 - x)$ *M* NaF et x *M* KNO_3 + $(0.2 - x)$ *M* KF. L'excès de surface dû aux ions nitrate adsorbés est déterminé à partir des résultats sur la capacité différentielle en utilisant une version modifiée de l'analyse Hurwitz–Parsons qui tient compte de la variation des coefficients d'activité ionique avec la composition de la solution. La quantité d'ion nitrate adsorbé à une électrode de densité de charge donnée et à une concentration en ions nitrate donnée semble dépendre nettement de la force ionique et de la nature de l'ion opposé au plan Helmholtz de l'extérieur; lorsque la charge dans la couche diffuse est positive, un accroissement de force ionique produit une plus grande adsorption d'anion et vice versa. Un changement de nature de cation Na^+ à K^+ occasionne aussi un accroissement d'adsorption d'anion. Les effets observés sont interprétés en termes d'un modèle de Stern–Grahame–Levine pour l'adsorption ionique lequel est basé sur une description électrostatique de l'interface chargé tout en tenant compte des effets de caractère discret de charge.

[Traduit par le journal]

Introduction

In a recent experimental study of the adsorption of iodide ion at mercury from solutions of constant ionic strength (1), it was shown that the amount of adsorbed iodide ion depends on the nature of the cation in the solution. More specifically, the adsorbed charge density increased for constant electrode charge density and bulk iodide concentration when the cation was changed from Na^+ to K^+. This result was rationalized on the basis of a model in which the thickness of the inner region of the double layer and the average potential profile as a function of distance from the electrode/solution interface depends on the nature of the counter ion forming the boundary of the inner region at the outer Helmholtz plane (oHp). Since the adsorption of iodide ion is strong, the field at the oHp is negative under normal experimental conditions and the counter ion is always a cation. On the other hand, the adsorption of nitrate ion at mercury is of intermediate strength (2, 3). Payne has shown (2, 3) that the parameters of the nitrate adsorption isotherm depend greatly on ionic strength. When nitrate adsorption is studied from solutions containing only an alkali metal nitrate salt, the magnitude of the adsorbed charge density, $|\sigma_a|$, at a positive electrode is greater than the electrode charge density, σ_m for bulk nitrate concentrations in the range 0.01 to 1 *M* (3). However, when the ionic strength is maintained at a high level by adding an indifferent electrolyte such as an alkali metal fluoride, the influence of the diffuse layer is reduced and $|\sigma_a|$ falls below σ_m at lower bulk nitrate concentrations (2). As a result, the field at the oHp for

a given positive electrode charge density changes from positive to negative and the nature of the counter ion at this plane from anion to cation. Thus, the variation of inner layer properties with the nature of the counter ion at the oHp may be investigated more extensively in this system.

The adsorption of nitrate ion and of some other polyatomic anions such as perchlorate (4) and hexafluorophosphate (5) can be characterized as anomalous with respect to the behaviour of most other anions (6). A particularly striking feature of their behaviour is the fact that the slopes of Christie plots, that is, plots of the potential drop across the inner layer against adsorbed charge density, decrease markedly with increase in electrode charge density becoming negative when σ_m is large and positive (2, 6). According to Grahame's electrostatic model of the inner layer (7), the slope of the Christie plot is equal to the reciprocal of the integral capacity of the region between the adsorption or inner Helmholtz plane (iHp) and the oHp. Thus, a negative slope cannot easily be rationalized on the basis of the electrostatic model. Furthermore, analysis of nitrate adsorption on the basis of an isotherm model which accounts for diffuse layer effects (8, 9) would lead to an adsorption isotherm at constant σ_m characterized by attractive interaction between adsorbed anions on the iHp. Damaskin (10, 11) has argued on the basis of data for anion adsorption from concentrated solutions that adsorbed nitrate and perchlorate anions are separated from the electrode by a layer of water molecules. If this interpretation is correct, then the iHp and oHp could be very close to one another; furthermore, Grahame's model of the inner layer could be inapplicable to these systems. On the other hand, the data for anion adsorption from solutions of constant ionic strength may be complicated by concomitant adsorption of fluoride ion at high positive electrode charge densities (5).

The present study was undertaken in an attempt to resolve the anomalous features of nitrate adsorption at mercury outlined above. The systems studied were $NaNO_3$ + NaF and KNO_3 + KF at constant ionic strength (0.2 *M*). The low ionic strength was chosen in order to minimize possible effects of fluoride ion adsorption and problems connected with defects in the Gouy–Chapman model used to estimate diffuse layer properties.

Experimental

Differential capacity against potential data for the mercury/aqueous solution interface were measured for 18 systems of composition x *M* $NaNO_3$ + (0.2 − x) *M* NaF and x *M* KNO_3 + (0.2 − x) *M* KF where x had the values 0, 0.01, 0.016, 0.025, 0.04, 0.063, 0.1, 0.14, and 0.20 *M*. The capacity data were obtained with an ac bridge at a frequency of 1000 Hz and at 50 mV increments in potential of the mercury electrode with respect to a saturated calomel reference electrode. The counter electrode was a platinum cyclinder whose area was much larger than that of the mercury drop. Procedures for operation of the bridge and determination of drop area at balance and of the potential of zero charge were those given by Hills and Payne (12). The experiments were carried out at 25.0 ± 0.1°C.

Variation in nitrate ion activity with solution composition was estimated from previously reported activity coefficients for the pure salts (13) as described previously (1). The analysis of the capacity against potential data was the same as described earlier (1).

Results

Capacity against potential curves for the $NaNO_3$–NaF system are shown in Fig. 1. As reported previously (2, 3), a pronounced capacity maximum is observed at potentials just positive of the potential of zero charge (pzc); as the bulk

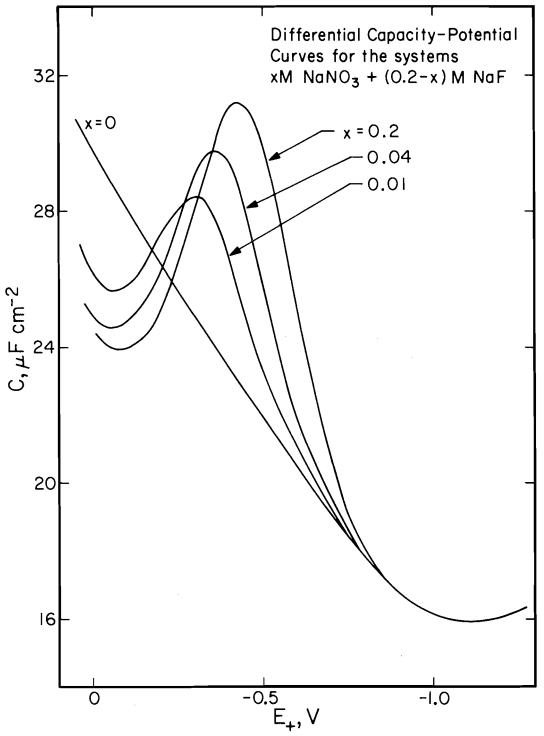

FIG. 1. Differential capacity against electrode potential curves for a mercury electrode in contact with aqueous solutions of x *M* $NaNO_3$ + (0.2 − x) *M* NaF at 25°C. The concentration of $NaNO_3$ is indicated for each curve.

concentration of nitrate ion increases, the position of the maximum shifts to more negative potentials with the pzc and its height increases. Capacity curves for the KNO_3–KF system are qualitatively similar. At potentials positive of the pzc there is negligible difference between capacities in the two systems at a given potential; at negative potentials, the capacity is somewhat higher in the K^+ system with a value of 16.25 μF cm^{-2} at the capacity minimum (−1.1 V), the corresponding value in the Na^+ system being 15.95 μF cm^{-2}.

The experimental potential scale was converted to one of thermodynamic significance corresponding to the potential of the polarizable electrode against a reference electrode reversible to the cation in the system, E_+ in the following way. Individual cationic activity coefficients in the mixed electrolyte were assumed to be given by

$$[1]\quad \ln \gamma_M = \frac{-A\mu^{1/2}}{1 + \beta \mathring{a}_M \mu^{1/2}} + \beta_{MNO_3} c_{NO_3} + \beta_{MF} c_F$$

where A and B are the Debye–Hückel constants, $\mathring{a}_M$, the ion size parameter for cation M^+ (Na^+ or K^+), μ, the ionic strength, β_{MX}, the interaction coefficient between cation M and anion X, and c_X, the concentration of anion X; anionic activity coefficients were assumed to be independent of solution composition (1). If β_{MNO_3} is significantly different from β_{MF}, one might expect γ_M to vary with solution composition at constant ionic strength. From the data reported by Robinson and Stokes (13), $\gamma_\pm(NaF) = 0.710$, $\gamma_\pm(NaNO_3) = 0.703$, $\gamma_\pm(KF) = 0.727$, and $\gamma_\pm(KNO_3) = 0.663$ at $\mu = 0.2\ M$. Since $\gamma_\pm(NaF) \simeq \gamma_\pm(NaNO_3)$, one may assume that $\beta_{NaF} \simeq \beta_{NaNO_3}$. The difference $(\beta_{KNO_3} - \beta_{KF})$ can be estimated from the following ratio

$$[2]\quad \ln \left(\frac{\gamma_\pm(KNO_3)}{\gamma_\pm(KF)} \frac{\gamma_\pm(NaF)}{\gamma_\pm(NaNO_3)} \right) = (\beta_{KNO_3} - \beta_{KF} + \beta_{NaF} - \beta_{NaNO_3})\mu$$

From the above data, $\beta = (\beta_{KNO_3} - \beta_{KF})\mu \simeq -0.082$. The corresponding shift in the thermodynamic potential scale E_+ with respect to that measured against a constant reference electrode E_r is given by (1)

$$[3]\quad dE_+ = dE_r - (\beta/f)dx$$

where $x = c_{NO_3}/(c_{NO_3} + c_F)$ and $f = F/RT$. According to this analysis, the potential scale shifts by 2 mV when the electrolyte is changed from 0.2 M KF to 0.2 M KNO_3. Although the above correction is small it is important that activity effects be carefully considered in the present context where the relatively minor effect of counter ion nature on ionic adsorption isotherms is being studied.

The capacity–potential data were twice integrated from negative potentials ($E_+ = -1.669$ V at $\sigma_m = -22$ μC cm^{-2} for the $NaNO_3$–NaF system, and $E_+ = -1.640$ V at $\sigma_m = -22$ μC cm^{-2} for the KNO_3–KF system) where anion adsorption could be assumed negligible. $\Delta\xi_+$, the value of Parsons' function ξ_+ at any charge density with respect to its value at $\sigma_m = -22$ μC cm^{-2} was calculated for integral increments in σ_m using well established techniques modified to take into account the variation in γ_{K^+} in the KNO_3–KF system as described previously (1). The adsorbed charge density due to NO_3^- ion, σ_a, was calculated according to the equation

$$[4]\quad \frac{f}{(1 + \beta x)} \left(\frac{\partial \Delta\xi_+}{\partial \ln x} \right)_{\sigma_m} = \sigma_a + \sigma_x^d \frac{\beta x}{(1 + \beta x)}$$

where σ_x^d is the surface excess of anions in the diffuse layer. The derivative $(\partial\Delta\xi_+/\partial \ln x)_{\sigma_m}$ was estimated using a least-squares fit of a cubic equation to $\Delta\xi_+$ against $\ln x$ data over the total experimental range (14). σ_x^d was estimated from the Gouy–Chapman theory according to which

$$[5]\quad \sigma_x^d = -\Theta\mu^{1/2} - \frac{(\sigma_m + \sigma_a)}{2} - \frac{[(\sigma_m + \sigma_a)^2 + 4\Theta^2\mu]^{1/2}}{2}$$

where $\Theta = (RT\varepsilon/2\pi)^{1/2}$, ε being the dielectric constant of the pure solvent. Initially, it was assumed that $\sigma_x^d \simeq -\Theta\mu^{1/2}$; the estimate was improved using an iterative technique, successive approximations for σ_a and σ_x^d being obtained by solving eqs. 4 and 5 for σ_a and σ_x^d respectively.

Adsorption isotherms for the $NaNO_3$–NaF and KNO_3–KF systems at constant charge density are shown in Fig. 2. When σ_m is positive, $|\sigma_a|$ falls below σ_m at low bulk nitrate concentrations but is greater than σ_m when the nitrate concentration is high. A similar result was obtained by Payne (2) for the case of adsorption from solutions of composition $x\ M$ NH_4NO_3 + $(1 - x)\ M$ NH_4F. The value of σ_a in the K^+ system is approximately the same as that in the Na^+ system when $|\sigma_a| < \sigma_m$ but significantly larger when $|\sigma_a| \geq \sigma_m$. Although one does not

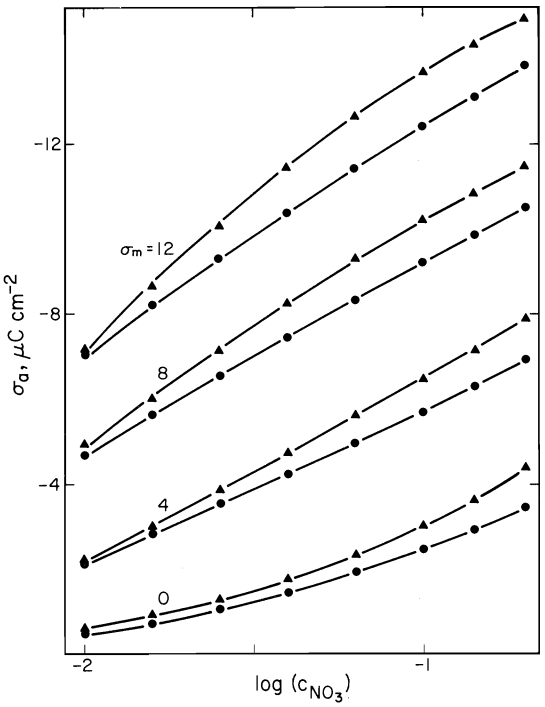

FIG. 2. Plots of adsorbed charge density due to NO_3^-, σ_a, against the logarithm of NO_3^- concentration in the bulk, log c_{NO_3}, for various constant charge densities on the electrode (indicated by the integers adjacent to each curve) for adsorption from the $NaNO_3$–NaF (●) and KNO_3–KF (▲) systems.

expect ionic adsorption isotherms to be congruent in either electrode potential or charge density on the basis of the electrostatic model for ionic adsorption (1, 8, 9), Payne (2, 3) was able to fit data for nitrate adsorption to a simple Frumkin isotherm congruent in electrode charge density. Examination of the present data on the basis of tests described by Parsons (15) showed that the interaction parameter in the adsorption isotherm varies significantly with electrode charge density. More specifically, plots of $1/C - 1/C_0$ against σ_a at constant charge density, where C is the differential capacity and C_0 that in the solution containing no nitrate, showed a maximum whose position and height depended on σ_m. Thus, there is no merit in fitting these data to a simple congruent isotherm, since any parameters derived would not be subject to direct interpretation.

The effects on ionic strength on nitrate adsorption at positive σ_m are illustrated in Fig. 3. At low nitrate ion concentration where $|\sigma_a| < \sigma_m$, the field at the oHp is positive. When the ionic strength is increased, the potential drop across the diffuse layer ϕ^d becomes less positive and the diffuse layer has a smaller enhancing effect on anion adsorption; thus, $|\sigma_a|$ decreases when the ionic strength increases. On the other hand, when bulk nitrate concentration is sufficiently high that $|\sigma_a| > \sigma_m$, ϕ^d is negative, and anions are repelled from the double layer. When the ionic strength is increased, $|\phi^d|$ decreases in magnitude and the amount of specifically adsorbed anion increases at constant electrode charge density and bulk anion concentration.

Plots of the potential drop across the inner layer, ϕ^{md}, against the adsorbed charge density σ_a at constant σ_m are shown for the $NaNO_3$–NaF system in Fig. 4. The plots are linear with positive slopes for lower values of σ_m. However, as σ_m becomes more positive, the slope decreases and eventually becomes negative. It should also be noted that the latter plots possess some curvature such that the slope increases with increase in σ_a. This observation would undoubtedly not have been made if the value of ϕ^{md} for $\sigma_a = 0$ had not been included. Indeed, these data are often missing in previously published Christie plots for systems studied at constant ionic strength so that their interpretation is subject to some doubt. The fact that the average slope of the Christie plots changes with $\sigma_m = 0$ is further support of the conclusion reached above, namely, that the adsorption of nitrate ion cannot be described by an isotherm congruent in either electrode potential or charge density. The average slope of the plots of ϕ^{md} against σ_a was determined by fitting the data to a straight line by least squares. The results for both the $NaNO_3$–NaF and KNO_3–KF systems are shown in Fig. 5. The behavior of both systems is qualitatively similar in that the average slope decreases with increase in σ_m. However, the average slope for the K^+ system is consistently smaller as was observed previously for the corresponding iodide systems (1).

The present data were tested to determine whether the variation in adsorbed charge density with bulk activity at constant electrode charge density could be described by a simple non-congruent adsorption isotherm. Since the nitrate ion concentration was limited to 0.2 M, the maximum adsorbed charge density, σ_{am}, could not be determined; it was assumed to be -25 μC cm^{-2}, the value obtained by Payne from analysis of nitrate adsorption data at bulk concentrations up to 1 M at both constant and varying ionic strength (2, 3). According to the Frumkin iso-

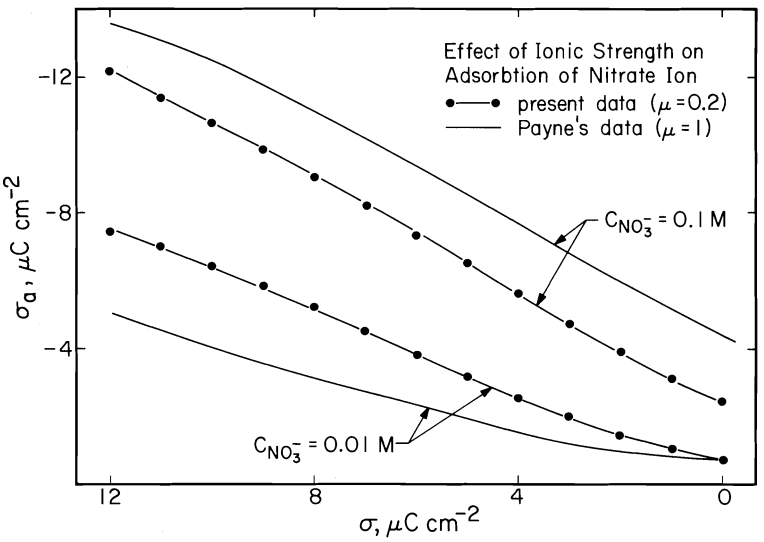

FIG. 3. Plots of adsorbed charge density due to NO_3^-, σ_a, against electrode charge density, σ_m, for bulk NO_3^- concentrations of 0.01 and 0.1 *M* at varying ionic strength μ; the data at $\mu = 0.2$ *M* are for the x *M* $NaNO_3$ + (0.2 − x) *M* NaF system and those at $\mu = 1$ *M* for the x *M* NH_4NO_3 + (1 − x) *M* NH_4F system (2).

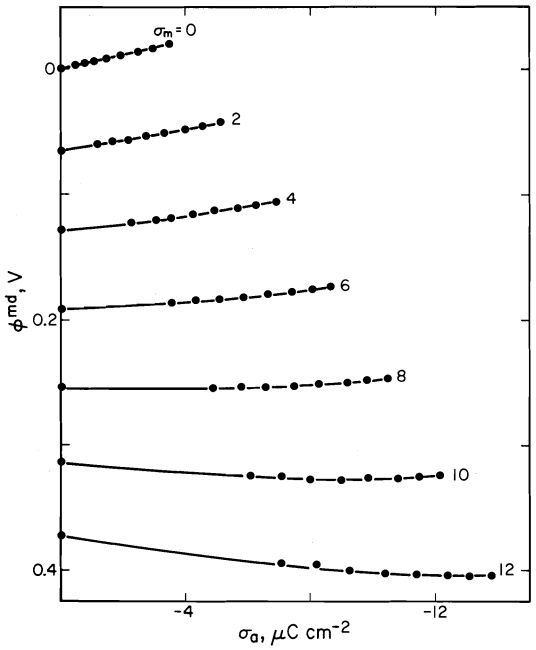

FIG. 4. Plots of the potential drop across the inner layer, ϕ^{md}, against the adsorbed charge density due to NO_3^-, σ_a, at constant electrode charge density σ_m (indicated by the integer adjacent to each plot) for adsorption from the system x *M* $NaNO_3$ + (0.2 − x) *M* NaF.

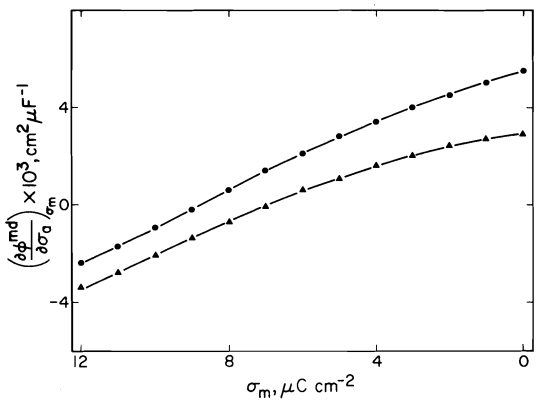

FIG. 5. Plots of the average slope of Christie plots, $(\partial\phi^{md}/\partial\sigma_a)_{\sigma_m}$, against electrode charge density, σ_m, for the $NaNO_3$–NaF (●) and KNO_3–KF (▲) systems.

therm, plots of ln $(-\sigma_a/c_{NO_3})$ − ln $(\sigma_a - \sigma_{am})$ against σ_a at constant electrode charge density σ_m should be linear with a slope independent of σ_m if the isotherm is congruent in σ_m. The corresponding plots for the $NaNO_3$–NaF system are shown in Fig. 6; it is apparent that, although the plots are approximately linear, their slope varies markedly with σ_m. Closer examination of the data at σ_m = 10 and 12 μC cm^{-2} shows that the corresponding plots are somewhat curved; however, the curvature could be due to errors in σ_a at the lowest and highest bulk concentrations where the numerical differentiation procedure used in the data analysis is least accurate (14). According to the electrostatic theory of ionic adsorption (1, 8, 9) which assumes Grahame's model of the inner layer, the Frumkin isotherm should contain a term in

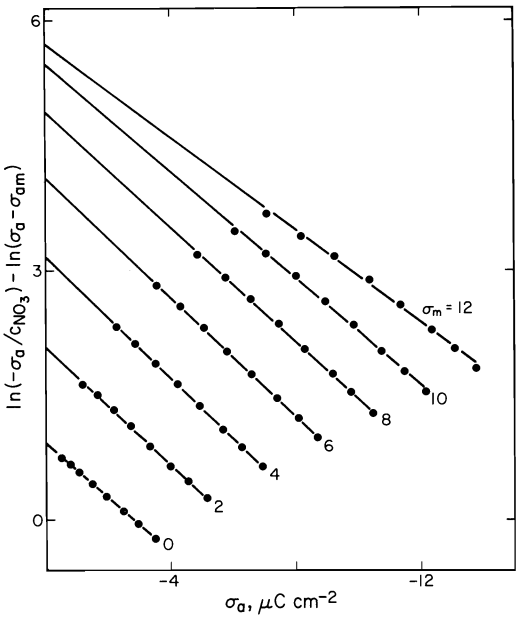

FIG. 6. Plots of adsorption data for the $NaNO_3$–NaF system at constant electrode charge density according to the Frumkin isotherm (eq. 13).

ϕ^d, the potential drop across the diffuse layer. Plots of $\ln(-\sigma_a/c_{NO_3}) - \ln(\sigma_a - \sigma_{am}) - f\phi^d$ against σ_a were constructed for the same data, ϕ^d being calculated from the Gouy–Chapman model of the diffuse layer. The slope of these plots was much less than those shown in Fig. 6. For $\sigma_m = 0$, 2, and 4, the slope was approximately zero. At higher electrode charge densities, the plots had a negative slope at low σ_a which decreased to zero with increase in σ_a. It is important to note that since $\sigma_a + \sigma_m$ is close to zero, ϕ^d varies markedly with $\sigma_a + \sigma_m$. Since $f\phi^d$ is not negligible in comparison with $\ln(-\sigma_a/c_{NO_3}) - \ln(\sigma_a - \sigma_{am})$, small errors in σ_a will result in large errors in ϕ^d, and thus, large errors in the isotherm plots. On the other hand, if the negative slope observed at higher electrode charge densities is not due to experimental error, a naive interpretation of these plots is that ion–ion interactions on the iHp are attractive for these conditions. However, as is argued below, the results obtained can also be attributed to a significant change in inner layer properties with increase in adsorbed charge density. Because of the curvature, the isotherm plots according to the electrostatic model could not be used to determine the variation in standard free energy of adsorption with σ_m and, therefore, they are not presented. Qualitatively similar results were obtained for the KNO_3–KF system, the principal difference being that the slopes of the isotherm plots were lower at a given electrode charge density.

Discussion

Effects of Activity Coefficient Variation

As argued previously (1), the activity coefficients of anions in a mixed salt solution containing a single cation may be assumed to be constant to a first approximation. This follows from the fact that the nature of the counter ion atmosphere around a given anion does not change when solution composition is changed. On the basis of experimental mean ionic activity coefficients, and assuming that the effective radii of the ions in the present systems are approximately equal (16), one may assume that the activity of nitrate ion in a 0.2 *M* KNO_3 solution is less than that in a 0.2 *M* $NaNO_3$ solution. Thus, other factors ignored, one would expect less adsorption from the KNO_3–KF system at a given bulk nitrate ion concentration and electrode charge density. The fact that the opposite is observed must be attributed to other effects.

The parameter β, which accounts for the change in metal ion activity when F^- is substituted by NO_3^-, is negative in the KNO_3–KF system. In this case failure to account for the variation in γ_K with solution composition would result in $|\sigma_a|$ being underestimated by about 8% at the highest nitrate ion concentration. It is interesting to note that if the data analysis had been carried out without the correction described above, the derived charge densities for adsorbed nitrate ion would still be greater in the K^+ system than in the Na^+ system at higher bulk concentrations. In conclusion, the observed dependence of σ_a on the nature of the cation in the system cannot be attributed to bulk activity effects, or to the model used to account for variation in individual ionic activity coefficients with solution composition.

The Properties of the Inner Layer

According to Grahame's model, the potential drop across the inner layer is given by

$$[6] \qquad \phi^{md} = (\sigma_m/K_{md}) + (\sigma_a/K_{ad})$$

where K_{md} is the integral capacity of the inner layer and K_{ad}, the integral capacity of the region between the iHp and oHp. If K_{md} and K_{ad} are

constant for a fixed value of σ_m, then the slope of the Christie plot is equal to $1/K_{ad}$. It is apparent from Fig. 4, that this condition holds at lower values of σ_m where $\sigma_a + \sigma_m < 0$ over most of the experimental range. Then, the predominant counter ion at the oHp is the cation Na^+ and the thickness and dielectric properties of the inner layer may be assumed to be approximately independent of adsorbed charge density, σ_a. At higher values of σ_m, $\sigma_a + \sigma_m$ is positive for low values of σ_a and eventually becomes negative. Accordingly, the counter ion at the oHp changes from anion to cation, and variation in both the thickness and dielectric properties of the inner layer with σ_a is possible. In general, the slope of the Christie plot is given by

$$[7] \quad \left(\frac{\partial \phi^{md}}{\partial \sigma_a}\right)_{\sigma_m} = \frac{1}{K_{ad}} + \sigma_m \left(\frac{\partial(1/K_{md})}{\partial \sigma_a}\right)_{\sigma_m} + \sigma_a \left(\frac{\partial(1/K_{ad})}{\partial \sigma_a}\right)_{\sigma_m}$$

It seems reasonable to assume that the derivatives defining changes in K_{md} and K_{ad} with σ_a are approximately constant for a given value of σ_m. Since the slopes decrease with increasing σ_m for constant σ_a, one may assume that $(\partial(1/K_{md})/\partial\sigma_a)_{\sigma_m}$ is negative. Therefore, the inner layer capacity, K_{md}, decreases with increasing adsorption when the counter ion defining the boundary of the inner layer changes from anion to cation. Similarly, for fixed σ_m, the slope of plots at higher σ_m increases with increase in $|\sigma_a|$ indicating that $(\partial(1/K_{ad})/\partial\sigma_a)_{\sigma_m}$ is also negative; this change corresponds to a decrease in K_{ad} with increasing adsorption. Since a change in the nature of the counter ion will chiefly affect the properties of the outer region of the inner layer, K_{ad} is expected to vary much more than K_{md}.

Although variation in the nature of the counter ion at the oHp could affect the local dielectric constant of the solvent through its influence on solvent dipole orientation, it is probably valid to assume that the chief effect is a variation in thickness of the inner region with solvated size of the counter ion when the concentration of these ions on the oHp is low. Since the average slope of the Christie plots for the K^+ system are lower than those for Na^+ (Fig. 5), one may assume that K_{ad} is higher when K^+ is the counter ion. This corresponds to the inner layer being less thick when the more weakly solvated K^+ ion forms its boundary on the solution side. The fact that K_{ad} decreases when the counter ion at the oHp changes from anion to cation can be attributed to an increase in thickness of the inner layer when a weakly solvated anion is replaced by a more strongly solvated cation. Since the dependence of the slopes of the Christie plots on σ_a and σ_m is qualitatively similar for the K^+ system, one may assume that the thickness of the inner layer with K^+ ions at the oHp is greater than with anions. In the region where $\sigma_m + \sigma_a$ is positive, F^- is the predominant anion in the mixed electrolyte system. Thus, the anomalous behaviour of the Christie plots for the present systems can be rationalized if it is assumed that the thickness of the inner layer, x_d depends on the nature of the predominant counter ion at the oHp in the order $x_d(F^-) < x_d(K^+) < x_d(Na^+)$.

The form of the Christie plots observed in the present case is qualitatively similar to that observed by Payne for the system $x\ M\ NH_4NO_3 + (1 - x)\ M\ NH_4F$ (2), with the exception that no curvature was noted. This could be due to the fact that the value of ϕ^{md} in the limit $\sigma_a \to 0$ was not considered but it could also reflect smaller changes in K_{ad} with counter ion nature at higher ionic strength where diffuse layer screening is more effective. The behaviour of Christie plots for NO_3^- adsorption from KNO_3 solutions of varying ionic strength is entirely different (3). As pointed out by Payne (3), these plots appear to have a constant slope independent of σ_m. For the range of bulk concentrations involved, $\sigma_a + \sigma_m$ is negative so that the counter ion at the oHp is always the cation. Interpretation of these data is much more difficult since imaging conditions and the effective thickness of the inner layer probably change with ionic strength. It is undoubtedly true that the Christie plots would be curved in this case if data were available at very low nitrate ion concentrations.

Payne (2, 3) argued that one should consider the contribution to ϕ^{md} of solvent dipoles removed from the inner layer in the adsorption process. He also suggested that the decrease in average slope of the Christie plots with increase in σ_m could be attributed to the fact that water molecules compete more effectively for adsorption sites under these conditions. According to the above analysis, a change in the number and orientation of water dipoles with σ_a would effect the dielectric constant distribution in the inner

layer and lead to curved Christie plots. As pointed out by Levine (8), this effect is quantitatively accounted for by eq. 6 and does not require the addition of an explicit term to account for the potential drop across oriented solvent dipoles. However, it is much more difficult to rationalize the large difference in adsorption behaviour for single and mixed electrolyte solutions on the basis of more effective water adsorption at high σ_m; if this were important, one would also expect the slopes of the Christie plots in the single electrolyte system to decrease with increase in σ_m.

It is instructive to compare the present results with those obtained for the adsorption of chloride ion at Hg from solutions of constant ionic strength (17). Since Cl^- adsorption is moderate, the magnitude of σ_a falls below σ_m for the low bulk Cl^- concentrations. Thus for positive values of σ_m, the sign of the charge in the diffuse layer changes from negative to positive and the counter ion at the oHp, from anion to cation, when the bulk Cl^- concentration is increased at constant σ_m. However, in this case the Christie plots are not curved and have positive slopes over the range of values of σ_m studied. The lack of curvature can be interpreted as evidence that the distances of closest approach of a non-adsorbed Cl^- ion and the cation, in this case K^+, are approximately equal so that K_{ad} is independent of the nature of the counter ion at constant σ_m. The decrease in the slopes of these plots with increase in σ_m can be attributed to a change in dielectric properties of the inner region which results in an increase in K_{ad} and K_{ma}. This increase may well be associated with a break up of water clusters in the inner region with increase in σ_m (18). Another important difference between the present data and those for Cl^- adsorption (17) is that the integral capacity K_{ad} is significantly smaller in the Cl^- system. This suggests that the iHp is closer to the oHp in the NO_3^- system so that small changes in the distance of closest approach of the counter ion have a large effect on the integral capacity of the outer region of the inner layer. If the adsorption of NO_3^- does not result in displacement of water molecules next to the electrode, one would indeed expect the iHp to be further from the electrode than it is for halide ions which are assumed to interact directly with the Hg electrode. Thus, the present interpretation of inner layer properties in the presence of adsorbed NO_3^- is in agreement with that of Damaskin *et al.* (10), which was based on an analysis of thermodynamic data obtained at very high bulk NO_3^- concentrations.

Tilak and Devanathan (28) presented a detailed model for nitrate ion adsorption on the basis of a study of adsorption from NH_4NO_3 solutions in the concentration range 0.05 to 11.23 *M*. However, in their data analysis they failed to consider the fact that the experimentally derived relative surface excess is significantly different from the absolute surface excess for concentrated solutions (10, 11). Thus, the values of σ_a reported by these authors cannot be considered reliable. It is undoubtedly true that some of the apparent anomalies discussed in ref. 28 are due to the erroneous data analysis. Any assessment of their model for nitrate adsorption must await reanalysis of the data.

The Adsorption Isotherm

According to the electrostatic model for ionic adsorption (8, 9), the adsorption isotherm may be written

$$[8]\quad \ln(-\sigma_a) - \ln(\sigma_a - \sigma_{am}) = \Phi + \ln a_{NO_3} + f\phi^d + a\sigma_a + b\sigma_m$$

where a_{NO_3} is the bulk nitrate ion activity, a and b, parameters relating the change in free energy of adsorption to changes in σ_a and σ_m, respectively, and Φ, a parameter related to the standard free energy of adsorption. Φ, a, and b depend on the electrical state of the interface which is determined by the value of σ_m, but they are normally assumed to be independent of a_{NO_3} and thus, σ_a. When discreteness-of-charge effects are estimated on the basis of the cutoff-disc model, the following expressions for a and b are obtained (8):

$$[9]\quad a = \frac{f}{K_{ad}}\left(1 - g\frac{K_{md}}{K_{ma}}\right)$$

where K_{ma} is the integral capacity of the region between the metal and the iHp, and g, a dimensionless parameter which is often assumed to be close to unity (19), and

$$[10]\quad b = f/K_{ad}$$

According to the Gouy–Chapman–Stern model, the potential drop across the diffuse layer in the presence of specific adsorption is given by

$$[11]\quad \phi^d = \frac{2}{f}\sinh^{-1}\left(\frac{\sigma_m + \sigma_a}{2\Theta\mu^{1/2}}\right)$$

When $\sigma_m + \sigma_a < \Theta\mu^{1/2}$, $f\phi^d$ is given to a good approximation by

$$[12] \qquad f\phi^d = (\sigma_m + \sigma_a)/\Theta\mu^{1/2}$$

For the present systems $\Theta\mu^{1/2} = 2.62\ \mu C\ cm^{-2}$; examination of the data in Fig. 4 reveals that the sum $\sigma_m + \sigma_a$ is indeed small and that the limiting expression for $f\phi^d$ may be applied to the data over most of the experimental range. The adsorption isotherm may now be written

$$[13] \quad \ln(-\sigma_a) - \ln(\sigma_a - \sigma_{am}) = \Phi + \ln a_{NO_3} + \left[\frac{f}{K_{ad}}\left(1 - g\frac{K_{md}}{K_{ma}}\right) + \frac{1}{\Theta\mu^{1/2}}\right]\sigma_a + \left(\frac{f}{K_{ad}} + \frac{1}{\Theta\mu^{1/2}}\right)\sigma_m$$

Equation 12 is of the form of the Frumkin isotherm but gives explicit expressions for the interaction parameter and the variation in free energy of adsorption with σ_m.[1]

According to the data shown in Fig. 6, the Frumkin interaction parameter as determined from the slopes of the adsorption isotherm plots at constant σ_m varies from 0.36 $cm^2\ \mu C^{-1}$ at $\sigma_m = 0$ to 0.28 $cm^2\ \mu C^{-1}$ at $\sigma_m = 12\ \mu C\ cm^{-2}$. Since $1/\Theta\mu^{1/2} = 0.382\ cm^2\ \mu C^{-1}$, the term $f(1 - gK_{md}/K_{ma})/K_{ad}$ must be negative. Considering the fact that all parameters involved are positive by definition, it is concluded that $K_{ma} < gK_{md}$ for the present system over the range of values of σ_m considered. Furthermore, since the integral capacity of any portion of the inner layer must be greater than the total integral capacity of the inner layer, K_{md}, it is apparent that the dimensionless parameter g is greater than unity. Levine and Robinson (19, 21) have calculated g on the basis of models which assume both discontinuous (19) and continuous variations (21) of the dielectric constant ε with distance from the electrode. It is clear from these calculations that one expects g to depend significantly on the relative positions of the iHp and oHp. If the planar nitrate ion is adsorbed flat on the Hg surface without an intervening water molecule, then the iHp would be about 2 Å from the metal surface. Assuming the inner layer has a thickness of 5.5 Å when the counter ion is Na^+, this spatial arrangement of iHp and oHp would lead to values of g which are less than unity, independent of the model chosen for ε (19, 21). On the other hand, if adsorbed nitrate ions are separated from the electrode by an intervening layer of water molecules, the iHp would be approximately 5 Å from the electrode, and thus much closer to the oHp. Under these circumstances g is greater than unity and can reach values sufficiently large that the parameter a is negative (eq. 9) when ϕ^d is small (19, 21). Physically, these conditions are such that the individual charge centres on the iHp are very efficiently screened by their local ionic atmospheres in the diffuse layer.

Although analysis of the isotherm parameters at high values of σ_m would be complicated by variation in K_{ad} with σ_a, an approximate analysis can be carried out for the data obtained in the region $0 \leq \sigma_m \leq 4\ \mu C\ cm^{-2}$. From the Christie plot, $K_{md} = 30.3\ \mu F\ cm^{-2}$ and $K_{ad} = 222\ \mu F\ cm^{-2}$ at $\sigma_m = 2\ \mu C\ cm^{-2}$ in the Na^+ system. From the slope of the isotherm plot, $a = -0.02\ cm^2\ \mu C^{-1}$ and on the basis of eq. 9, $g = 1.3$. This parameter is constant in the given range of σ_m, and falls within the range of values of g estimated by Levine and Robinson (19, 21). Examination of the equivalent data for the K^+ system reveals that $K_{ad} = 417\ \mu F\ cm^{-2}$, $K_{md} = 30.8\ \mu F\ cm^{-2}$, and $a = -0.13\ cm^2\ \mu C^{-1}$ at $\sigma_m = 2\ \mu C\ cm^{-2}$. The corresponding value of g, 2.6, falls outside of the range considered in analysis of the discreteness-of-charge model but undoubtedly it indicates that the iHp is very close to the oHp. The fact that K_{ad} for the K^+ system is approximately twice that for the Na^+ system indicates that the distance between the iHp and oHp, x_{ad}, decreases by approximately a factor of two when the counter ion is changed from Na^+ to K^+.

On the basis of the above analysis, one can distinguish two factors which account for the increase in nitrate adsorption when the counter ion is changed from Na^+ to K^+. Firstly, the average potential drop across the region between the iHp and oHp, ϕ^{ad} which is given by

$$[14] \qquad \phi^{ad} = (\sigma_m + \sigma_a)/K_{ad}$$

becomes less negative as K_{ad} increases in magnitude ($\sigma_m + \sigma_a < 0$). Since ϕ^d is independent of counter ion nature to a first approximation, the average potential on the adsorption plane is less

[1]It should be noted that some variation in Φ with σ_m is expected due to a corresponding variation in the polarization and self-image energies of the adsorbed species (20).

negative and the concentration of nitrate ions increases. Secondly, as x_{ad} decreases, the screening of adsorbed ions by the diffuse layer becomes more effective so that the difference between the micro-potential at an adsorption site and the average potential on the iHp becomes more positive; accordingly, discreteness-of-charge effects also contribute to $|\sigma_a|$ being larger in the K^+ system. The effect is sufficiently large in the present system that the interaction parameter a in the Stern–Grahame–Levine isotherm (eq. 8) is positive, that is, attractive.

An alternative explanation of the increase in $|\sigma_a|$ in going from the Na^+ to the K^+ system is that alkali metal cations are weakly adsorbed, the extent of adsorption increasing with cation atomic number (22, 23). However, the field assisting possible cation adsorption is much weaker in the present case, than in systems where anion adsorption is strong, such as iodide (1). The fact that the differences in amounts adsorbed between the Na^+ and K^+ systems are quantitatively similar for NO_3^- and I^- adsorption suggests that cation adsorption is not the cause of the dependence of σ_a on the counter ion nature. As pointed out previously (24), the general features of Cs^+ adsorption estimated on the basis of double layer data for the system $x\,M$ CsCl + $(1 - x)\,M$ LiCl can be attributed to a dependence of the thickness of the inner layer on solvated cation size. More generally stated, the Gouy–Chapman theory does not account for differences in the sizes of ions present in the diffuse layer. For this reason the detailed arguments based on this model used by Damaskin (25) in support of alkali metal cation adsorption are subject to doubt. It is clear that further clarification of the possible role of cation adsorption must await the development of a model for the diffuse layer which properly accounts for finite ion size.

Finally, Hills and Reeves (5) have argued that the differences in adsorption behaviour observed for moderately adsorbed anions in solutions of varying and constant ionic strength can be attributed to coadsorption of F^- anion from the mixed electrolyte system at high positive values of σ_m. However, these authors did not consider the effect of ionic strength on ionic adsorption so that their conclusions are subject to some doubt. Schiffrin (26) showed that small but significant specific adsorption of F^- could be detected at Hg for $\sigma_m \geq 6\ \mu C\ cm^{-2}$ and $c_F \geq 0.1\ M$ at 15°C. When F^- ion specific adsorption is significant, the measured surface excess due to adsorbed anions is actually given by

$$[15] \qquad \sigma_a = \sigma_a(NO_3^-) - \frac{c_{NO_3}}{c_F}\,\sigma_a(F^-)$$

where $\sigma_a(NO_3^-)$ and $\sigma_a(F^-)$ are the adsorbed charge densities due to nitrate and fluoride ions, respectively. The effect of possible F^- ion adsorption would be greatest for $c_{NO_3^-} = c_{F^-} = 0.1\ M$; at lower F^- ion concentrations, $\sigma_a(F^-)$ goes to zero, and at higher concentrations, $c_{NO_3^-}/c_{F^-}$ is less than unity. Neglect of F^- ion adsorption leads to underestimation of the adsorbed charge density due to nitrate ions and would result in the Christie plots being less curved. It is extremely difficult to assess the role of F^- ion adsorption since errors in the analysis of the interfacial thermodynamic data for single fluoride salt solutions can be large (26) and the role of defects in the Gouy–Chapman theory used in data analysis very important (24). However, when one compares the present results with those for the PF_6^-–F^- system studied by Hills and Reeves (5), it is clear that F^- adsorption is much less important in the present case. If, as suggested by Baugh and Parsons (27), the adsorbed fluoride ion retains its primary hydration shell, it may be excluded from its adsorption plane when that plane is already occupied by the more strongly adsorbed NO_3^- ion.

Acknowledgement

This work was supported by a grant from the National Research Council of Canada.

1. W. R. Fawcett and T. A. McCarrick. J. Electrochem. Soc. **123**, 1325 (1976).
2. R. Payne. J. Phys. Chem. **69**, 4113 (1965).
3. R. Payne. J. Electrochem. Soc. **113**, 999 (1966).
4. R. Payne. J. Phys. Chem. **70**, 204 (1966).
5. G. J. Hills and R. M. Reeves. J. Electroanal. Chem. **31**, 269 (1971).
6. R. Payne. J. Electroanal. Chem. **41**, 277 (1973).
7. D. C. Grahame. J. Am. Chem. Soc. **80**, 4201 (1958).
8. S. Levine. J. Colloid Interface Sci. **37**, 619 (1971).
9. W. R. Fawcett. J. Electroanal. Chem. **84**, 303 (1977).
10. B. B. Damaskin, V. F. Ivanov, N. I. Melekhova, and L. F. Maiorova. Elektrokhimiya, **4**, 1342 (1968).
11. B. B. Damaskin, A. N. Frumkin, V. F. Ivanov, N. I. Melekhova, and V. F. Khonina. Elektrokhimiya, **4**, 1336 (1968).
12. G. J. Hills and R. Payne. Trans. Faraday Soc. **61**, 316 (1965).

13. R. A. ROBINSON and R. H. STOKES. Electrolyte solutions. Butterworths, London. 1955.
14. W. R. FAWCETT and J. E. KENT. Can. J. Chem. **48**, 47 (1970).
15. R. PARSONS. J. Electroanal. Chem. **7**, 136 (1964).
16. J. KIELLAND. J. Am. Chem. Soc. **59**, 1675 (1937).
17. R. PAYNE. Trans. Faraday Soc. **64**, 1638 (1968).
18. R. PARSONS. J. Electroanal. Chem. **59**, 229 (1975).
19. S. LEVINE and K. ROBINSON. J. Electroanal. Chem. **41**, 159 (1973).
20. S. LEVINE, G. M. BELL, and D. CALVERT. Can. J. Chem. **40**, 518 (1962).
21. K. ROBINSON and S. LEVINE. J. Electroanal. Chem. **47**, 395 (1973).
22. A. N. FRUMKIN, B. B. DAMASKIN, and N. V. NIKOLAEVA-FEDOROVICH. Doklady Akad. Nauk SSSR, **115**, 751 (1957).
23. B. B. DAMASKIN, N. V. NIKOLAEVA-FEDOROVICH, and A. N. FRUMKIN. Doklady Akad. Nauk SSSR, **121**, 129 (1958).
24. W. R. FAWCETT. J. Electroanal. Chem. **39**, 474 (1972).
25. B. B. DAMASKIN. J. Electroanal. Chem. **65**, 799 (1975).
26. D. J. SCHIFFRIN. Trans. Faraday Soc. **67**, 3318 (1971).
27. L. M. BAUGH and R. PARSONS. J. Electroanal. Chem. **40**, 407 (1972).
28. B. V. K. S. R. A. TILAK and M. A. V. DEVANATHAN. J. Phys. Chem. **73**, 3582 (1969).

Direct electrochemical synthesis of neutral and anionic chloro- and bromo-complexes of titanium, zirconium, and hafnium

JACOB J. HABEEB, FAROUQ F. SAID, AND DENNIS G. TUCK
Department of Chemistry, University of Windsor, Windsor, Ont., Canada N9B 3P4

Received June 13, 1977

JACOB J. HABEEB, FAROUQ F. SAID, and DENNIS G. TUCK. Can. J. Chem. **55**, 3882 (1977).

Electrochemical oxidation of titanium, zirconium, or hafnium(IV) in the presence of a solution of chlorine or bromine (X) in acetonitrile (L) leads to direct synthesis of MX_4L_2 species in good yield. These compounds are easily transformed into other neutral adducts. On addition of tetraalkylammonium salts to the solution phase, the products are the salts $(R_4N)MCl_5$ or $(R_4N)_2MBr_6$, except that with titanium Et_4NTiBr_4 was also formed under some conditions. The advantages of this method are discussed, and a possible reaction mechanism proposed.

JACOB J. HABEEB, FAROUQ F. SAID et DENNIS G. TUCK. Can. J. Chem. **55**, 3882 (1977).

L'oxydation électrochimique du titane, du zirconium ou de l'hafnium(IV) en présence d'une solution de chlore ou de brome (X) dans l'acétonitrile (L) conduit à la synthèse direct d'espèces MX_4L_2 avec de bons rendements. On peut facilement transformer ces composés dans d'autres adduits neutres. Par addition de sels de tétraalkylammonium à la phase en solution, les produits sont les sels $(R_4N)MCl_5$ ou $(R_4N)_2MBr_6$, excepté avec le titane alors que le Et_4NTiBr_4 se forme aussi suivant quelques conditions. On discute des avantages de cette méthode et on propose un mécanisme possible pour la réaction.

[Traduit par le journal]

Introduction

The complexes of the elements titanium, zirconium, and hafnium, and in particular the neutral adducts of the tetrahalides, form one of the best explored topics in classical coordination chemistry. The parent tetrahalides are key compounds in the preparation of these derivatives, many of which have been obtained by direct reaction of the two components in non-aqueous solution (1). Various methods are available for the preparation of the tetrahalides themselves. Direct combination of the metal and halogen is not recommended for $TiCl_4$, which, like the bromide, is obtained by the high temperature (200–1250°C) treatment of TiO_2 by various chlorinated species. Direct bromination of the metal at 300–600°C yields $TiBr_4$. Similar methods have been used for tetrahalides of zirconium and hafnium (2).

We have now shown that the tetrachlorides and tetrabromides of these three chemically inert metals can be prepared at room temperature by electrochemical oxidation of the metal in a cell containing an organic solution phase. The products are either the adducts $MX_4 \cdot 2CH_3CN$, which can readily be converted to other adducts, or the anionic M(IV) halogeno complexes, depending on the composition of the solution. Only in the case of titanium were complexes of the M(III) state obtained, a pattern which parallels that established in the electrochemical preparation of β-diketonate complexes of these elements (3). This work completes a series of electrochemical preparations of anhydrous halides of the top row transition metals, work which has resulted in the production of VX_2 (X = Cl, Br, I) (4), $CrBr_3$ (5) and mono- or dihalides of Mn, Fe, Co, Ni, Cu, and Zn (6). Anionic bromo-complexes of these and other metals (7) have also been prepared in good yield at room temperature by direct electrochemical syntheses.

Experimental

Materials

The metals titanium (foil, 0.67 mm thick, m2N7), zirconium (foil, 0.25 mm thick, M3N), and hafnium (wire, 1 mm diameter, m3N7) were used as supplied (Alfa Inorganics). Solvents were dried over molecular sieve (acetonitrile, methanol) or sodium (benzene), and distilled under nitrogen before use.

Preparative Procedures

The electrochemical method was essentially that used in earlier work (5, 7). Samples of metal formed the anode of a cell containing an organic solvent phase with a platinum wire (0.5 mm diameter) as the counter electrode. The detailed experimental conditions are given in Table 1.

In certain specific cases noted below, we determined the current efficiency expressed as moles of metal dissolved per Faraday, in experiments of relatively short duration (1–2 h), during which time the current was held

TABLE 1. Experimental conditions for electrochemical preparation of Group IVA halide complexes

Elements	Solution phase composition (volumes in cm^3)	R_4NX added (g)	Initial Voltage (V)	Initial Current (mA)	Time of electrolysis (h)	Weight metal dissolved (g)
		Neutral complexes				
Ti/Cl	CH_3CN 50; $Cl_{2(g)}$	0	20	150	8.0	0.53
Zr/Cl	CH_3CN 50; $Cl_{2(g)}$	0	10	100	6.0	[e]
Hf/Cl	CH_3CN 50; $Cl_{2(g)}$	0	20	150	8.0	0.71
Ti/Br	CH_3CN 50; Br_2 2	0	10	200	4.5	1.34
Zr/Br	CH_3CN 50; Br_2 2	0	10	170	4.5	[e]
Hf/Br	CH_3CN 50; Br_2 2	0	15	200	3.0	1.21
		Anionic complexes				
Ti/Cl	$SOCl_2$ 50; $Cl_{2(g)}$	0.5[c]	30	150	6.0	0.63
Zr/Cl	$SOCl_2$ 50; $Cl_{2(g)}$	1.0[c]	30	150	10.0	0.54
Hf/Cl	$SOCl_2$ 50; $Cl_{2(g)}$	1.0[c]	50	25	8.0	0.72
Ti/Br[a,b]	C_6H_6 60; Br_2 2	1.0[d]	30	130	0.5	0.21
Ti/Br[b]	C_6H_6 15; Br_2 3	1.0[d]	15	400	3.0	[e]
Zr/Br[a,b]	C_6H_6 20; Br_2 2	1.0[d]	15	350	3.0	0.07
Hf/Br[a,b]	C_6H_6 15; Br_2 2	1.0[d]	15	150	4.0	0.15

[a]Two phases; reaction apparently occurs only in lower, conducting, layer.
[b]See text for details.
[c]R = C_3H_7.
[d]R = C_2H_5.
[e]Not recorded.

constant. The chemical efficiency of the system, expressed as mole of complex obtained per mole of metal dissolved, was generally in the range 80–95%. In view of these high yields from room temperature experiments lasting 1–10 h, no attempt was made to study the effect of electrode size, current, temperature, etc., on the overall chemical efficiency.

The electrochemical preparation affords the bisacetonitrile adduct of the tetrachlorides and bromides, except in those cases where gram quantities of tetraethylammonium halide were present, when the appropriate anionic halogeno complexes were obtained. Thionyl chloride proved to be the most satisfactory solvent for the preparation of the anionic chlorocomplexes (see Table 1).

The bisacetonitrile adducts are soluble in acetonitrile, and the resultant solutions have been the starting point for the synthesis of other neutral adducts. The results of these experiments are in some respects at variance with the existing literature, and we return to this point below.

Analytical and Spectroscopic Methods

Halogen analysis was by the Volhard method. Titanium was determined by titration against ethylenediamine tetraacetic acid (EDTA, disodium salt). The sample was dissolved in nitric acid and oxidized with hydrogen peroxide; after addition of excess EDTA, and neutralization, the solution was titrated with standard bismuth(III) nitrate, using xylenol orange as indicator. A similar method was used for zirconium and hafnium, with solutions prepared by dissolving the sample in sulphuric acid plus sodium sulphate (8).

Infrared spectra were obtained on a Perkin-Elmer IR-12 instrument, and served to identify the presence of neutral ligands or substituted ammonium cations in the solids prepared.

Results and Discussion

Neutral Halides

The experimental conditions detailed in Table 1 allowed us to produce gram quantities of $MX_4 \cdot 2CH_3CN$ (M = Ti, Zr, Hf; X = Cl, Br) within a few hours. The presence of two *cis*-acetonitrile ligands was confirmed by doublet absorptions in the $\nu(C{\equiv}N)$ region of the infrared spectrum (Table 2). The frequencies are in good agreement with those previously reported (9) for these compounds, confirming the formulation based on the analytical results. Thus the first conclusion from our work is that these

TABLE 2. Infrared absorptions of $MX_4 \cdot 2CH_3CN$ adducts (M = Ti, Zr, Hf; X = Cl, Br)[a]

Compound	$\nu(C{\equiv}N)$
$TiCl_4 \cdot 2CH_3CN$	2286, 2310
$TiBr_4 \cdot 2CH_3CN$	2280, 2305
$ZrCl_4 \cdot 2CH_3CN$	2284, 2306
$ZrBr_4 \cdot 2CH_3CN$	2260, 2285
$HfCl_4 \cdot 2CH_3CN$	2275, 2303
$HfBr_4 \cdot 2CH_3CN$	2280, broad

[a]Frequencies in cm^{-1}; samples run as Nujol mulls between potassium bromide plates.

complexes are now readily available in high yield by a room temperature synthetic route which uses the metals as the accessible source of high purity element.

We have not been able to prepare any of the tetraiodo complexes of these elements (nor any anionic iodo-complexes), despite the fact that iodides of a number of other transition metals have been obtained by electrochemical synthesis (6). A range of experimental conditions was investigated, varying such factors as voltage, current, composition, metal surface pre-treatment, and the use of Br_2–I_2 mixtures, all without success, in that in no case were we able to isolate MI_4, or MI_4L_2 species. By monitoring the weight of the anode, we showed that appreciable quantities (0.5–0.05 g) of titanium (and zirconium) dissolved, and in some cases solids of indeterminate composition were obtained. For example, electrolysis of titanium (anode) with a solution of iodine in acetonitrile yielded a product containing 7.4% Ti, 32.5% I, and having no ν(C≡N) absorption in the infrared. In another case, zirconium was electrolytically dissolved (0.38 g) into a benzene–methanol solution of iodine and *n*-Pr_4NI; the final solid contained 36.7% Zr, 26.5% I. No explanation for these and similar results is forthcoming, and further work on this topic is planned.

Adducts of MX_4

The literature on the adducts of the tetrachlorides and tetrabromides of Group IVA is very extensive (1). Our experiments have revealed one aspect of the chemistry of these compounds not apparently reported, namely that bidentate ligands such as ethylenediamine and 2,2′-bipyridine may form both 1:1 and 1:2 adducts with $TiBr_4$. The existing literature on the preparation of the adducts of such ligands (10, 11) refers to experiments carried out in benzene solution, from which compounds such as $TiBr_4$·bipy precipitate. Our earliest preparations used electrochemically prepared solutions of MBr_4 in benzene–methanol (3:1); excess bromine was removed from the solution with a stream of nitrogen, and ethylenediamine (also in benzene–methanol) added dropwise until precipitation occurred. The resultant solids were shown to be the 1:1 adduct MBr_4·en (M = Ti, Zr, Hf: see Table 3). Later experiments used $TiBr_4 \cdot 2CH_3CN$ as the starting material, and acetonitrile as the reaction medium. Typical conditions would involve 50–100 mg of $TiBr_4 \cdot 2CH_3CN$ in 10 cm^3 acetonitrile; a solution of 50 mg of 2,2′-bipyridine in 15 cm^3 of the same solvent was added dropwise until yellow precipitation occurred. The product was collected and dried *in vacuo*. Under such conditions, we obtained the compounds $TiBr_4$·2en (12) and $TiBr_4$·2bipy, of which the latter does not appear to have been reported previously. Solvent dielectric constant may be the critical factor in these preparations; benzene may favour the neutral six-coordinate MX_4L, while in acetonitrile an ionic species $[MX_2L_2]X_2$ could be formed. Further investigation of this problem is planned.

Anionic Complexes

Although benzene–methanol proved to be a satisfactory reaction medium for the electrochemical preparation of a number of transition metal anionic bromo-complexes (7), we were not able to use it for the preparation of anionic complexes of Group IVA metals. For the chlorides, thionyl chloride proved very useful, and the electrochemical oxidation of titanium, zirconium, or hafnium in the presence of chlorine in this solvent (Table 1) containing tetra-*n*-propylammonium chloride leads to the formation of the salt *n*-$Pr_4N[MCl_5]$ in each case. With the two heavier metals, the compound precipitated from the solution as the electrolysis proceeded; for titanium, addition of diethylether to the final reaction solution resulted in precipitation of the salt. In cells containing benzene, bromine, and tetraethylammonium bromide, two different experimental conditions applied. For relatively low bromine concentrations (those marked [a] in Table 1), two phases are present; only the lower of these had any significant conductivity, and the cell was arranged so that both electrodes (and especially the Group IV metal of the anode) were immersed in this layer. As the electrolysis proceeded, precipitation of the $(Et_4N)_2MBr_6$ salts occurred, with the reaction visibly taking place in the lower phase.

The MCl_5^- and MBr_6^{2-} salts (or their analogues with other cations) have been reported previously, with one exception. The salt $Et_4N[TiCl_5]$ results from the reaction of Et_4NCl and $TiCl_4$ in dichloromethane (13) and a solvated salt $Et_4N[ZrCl_5]CH_3CN$ has been reported by Feltz (14). The hexabromo complexes of the Group IVA metals were prepared by Clark and co-workers (15), who also analysed the vibrational spectra. Thus only the salt

TABLE 3. Analytical results for neutral and anionic Group IVA halide complexes

Compound	Colour	Found (%)		Calculated (%)	
		Metal	Halogen	Metal	Halogen
Electrochemical syntheses					
$TiCl_4 \cdot 2CH_3CN$	Yellow	17.7	52.2	17.7	52.2
$ZrCl_4 \cdot 2CH_3CN$	Colourless	28.8	45.1	28.9	45.1
$HfCl_4 \cdot 2CH_3CN$	Colourless	44.2	35.1	44.4	35.3
$TiBr_4 \cdot 2CH_3CN$	Red	10.8	71.1	10.7	71.1
$ZrBr_4 \cdot 2CH_3CN$	Orange	18.4	64.8	18.5	64.9
$HfBr_4 \cdot 2CH_3CN$	Orange	30.1	54.8	30.8	55.1
$(C_3H_7)_4NTiCl_5$	Yellow	11.7	43.1	11.7	43.1
$(C_3H_7)_4NZrCl_5$	Colourless	20.4	38.9	20.2	38.8
$(C_3H_7)_4NHfCl_5$	Colourless	32.5	32.6	32.8	32.8
$(C_2H_5)_4NTiBr_4$	Blue–black	9.4	63.7	9.5	63.2
$[(C_3H_5)_4N]_2TiBr_6$	Red	6.0	60.3	6.1	60.9
$[(C_2H_5)_4N]_2ZrBr_6$	Pale yellow	10.6	56.7	10.7	56.7
$[(C_2H_5)_4N]_2HfBr_6$	Pale yellow	19.1	51.0	19.0	51.4
Neutral addition compounds[a]					
$TiBr_4 \cdot en$	Colourless	11.2	74.0	11.2	74.4
$TiBr_4 \cdot 2en$	Pale yellow	9.6	65.1	9.8	65.5
$TiBr_4 \cdot 2bipy$	Yellow	7.2	46.8	7.1	47.0
$ZrBr_4 \cdot en$	Colourless	19.2	67.3	19.3	67.9
$HfBr_4 \cdot en$	Colourless	30.5	57.4	31.9	57.4

[a]en = ethylenediamine; bipy = 2,2′-bipyridyl.

n-$Pr_4N[HfCl_5]$ represents a new complex, and one which completes a group of lighter analogues. In view of the extensive literature on the structure and vibrational spectra of these anions, we have not carried out any further investigation of the compounds prepared.

If the bromine content is increased in the benzene–Br_2–Et_4NBr system, prepared by adding Et_4NBr to a solution of bromine in benzene, the two phases eventually coalesce; in the present case, this occurred when the benzene–bromine ratio was approximately 5:1 (v/v). Electrolytic oxidation of titanium in this solution, produced not titanium(IV), but the known titanium(III) salt (16) $Et_4N[TiBr_4]$. We discuss below a possible explanation of the anomaly that an increase in the concentration of the apparent oxidizing agent in solution (i.e. Br_2) results in a decrease in the oxidation state of titanium in the final product. Two relevant precedents for this synthesis can be noted immediately. Firstly, the electrochemical oxidation of titanium in the presence of β-diketonates and similar ligands results in the formation of titanium(III) TiL_3 complexes, which can be subsequently oxidized to $TiOL_2$. Zirconium and hafnium form only ML_4 species under such conditions (3). Secondly, the electrochemical oxidation of other top row transition metals to form anhydrous bromide under conditions similar to those used in the present work yields low oxidation state compounds, including vanadium(II) (4) and copper(I) (6). The formation of the $TiBr_4^-$ anion is therefore part of this pattern; we were not able to produce the M(III) states of either zirconium or hafnium, again in keeping with our results with diketonates.

We conclude that the electrochemical method of these various complexes represents a rapid and convenient synthesis which avoids the synthesis and isolation of the MX_4 intermediates.

Reaction Mechanism

In an earlier discussion of the electrochemical synthesis of other transition metal halides (6), it was pointed out that measurement of the current efficiency gives a good indication of the possible reaction mechanism. In the present work, we have carried out such experiments over short periods of time (1–2 h) at constant current (40–50 mA) for the M–Br_2 in benzene system. The measured current efficiencies were 1.1 mol Ti F^{-1}, 2.7 mol Zr F^{-1}, and 1.25 mol Hf F^{-1}, in terms of weight of metal dissolved. These values are somewhat lower than the range of 2–10 mol F^{-1} reported earlier (6), but higher than can be

accounted for by a primary process $M \rightarrow M^{4} + 4e^{-}$, for which the current efficiency should be 0.25 mol F^{-1}.

The proposed mechanism envisages the first step as being the formation of Cl_2^- or Br_2^-

[1] $$Br_2 + e^- \rightarrow Br_2^-$$

and the anode process is believed to be

[2] $$Br_2^- + M \rightarrow MBr + Br + e^-$$

with subsequent reactions

[3] $$MBr + Br \rightarrow MBr_2$$

[4] $$MBr + Br_2 \rightarrow MBr_3$$

[5] $$MBr_2 + Br_2 \rightarrow MBr_4$$

Other reactions are also possible; the main point of [3], [4], and [5] is to show that different oxidation states of a given metal may be produced in such systems. Reactions such as the sequence

[6] $$MBr + Br_2 \rightarrow MBr_2 + Br$$

[7] $$M + Br \rightarrow MBr$$

can be invoked to explain current efficiencies higher than 1 mol metal dissolved per Faraday.

In all but one case, the oxidation sequence obviously produces compounds in which the M(IV) oxidation state is stabilized. The exception is the oxidation of titanium in the presence of high concentrations of Br_2 and Br^- (and hence Br_3^-). This may point to the importance of [4] under such conditions. Certainly the stability of the M(III) state is significantly higher in titanium than in the heavier metals, and this, coupled with the observed precipitation of a salt that is insoluble and therefore kinetically resistant to oxidation, serves to rationalize the experimental result. Thus while the present results do nothing to bolster the previous arguments quantitatively, the information of an intermediate oxidation state does support a mechanism involving stepwise oxidation of the metal in these electrochemical experiments.

Acknowledgement

This work was supported in part by Operating Grants from the National Research Council of Canada.

1. R. J. H. Clark. The chemistry of titanium and vanadium. Elsevier, Amsterdam, The Netherlands, 1968; R. J. H. Clark. *In* Comprehensive inorganic chemistry. Vol. 3. Pergamon Press, Oxford, England. 1973. p. 408; D. C. Bradley and P. Thornton. *In* Comprehensive inorganic chemistry. Vol. 3. Pergamon Press, Oxford, England. 1973. p. 434.
2. R. Colton and J. H. Canterford. Halides of the first row transition metals. Eilwy-Intersciences, New York, NY. 1969. p. 40.
3. J. J. Habeeb, D. G. Tuck, and F. H. Walters. To be published.
4. J. J. Habeeb, L. Neilson, and D. G. Tuck. Can. J. Chem. **55**, 2631 (1977).
5. J. J. Habeeb and D. G. Tuck. Inorg. Synth. In press.
6. J. J. Habeeb, L. Neilson, and D. G. Tuck. To be published.
7. J. J. Habeeb, L. Neilson, and D. G. Tuck. Synth. React. Inorg. Met. Org. Chem. **6**, 105 (1976).
8. T. S. West. Complexometry with EDTA and related reagents. BDH Chemicals Ltd., Poole, U.K. 1969. pp. 210, 217.
9. Y. Kawano, Y. Hase, and O. Sala. J. Mol. Struct. **30**, 45 (1976) and references cited therein.
10. R. J. H. Clark. J. Chem. Soc. 1377 (1963).
11. G. W. A. Fowles and R. A. Walton. J. Less-Common Met. **5**, 510 (1963).
12. S. Prasad and J. B. P. Tripathi. J. Indian Chem. Soc. **34**, 749 (1957).
13. J. A. Creighton and J. H. S. Green. J. Chem. Soc. A, 808 (1968).
14. A. Feltz. Z. Anorg. Chem. **358**, 21 (1968).
15. W. Van Bronswyk, R. J. H. Clark, and L. Maresca. Inorg. Chem. **8**, 1395 (1969).
16. G. W. A. Fowles and B. J. Russ. J. Chem. Soc. A, 517 (1967).

A new method for the macro- and microdetermination of tri- and tetrathionate

K. A. IDRISS, I. M. ISSA, AND M. R. MAHMOUD

Chemistry Department, Faculty of Science, Assiut University, Assiut, Egypt

Received December 22, 1976[1]

K. A. IDRISS, I. M. ISSA, and M. R. MAHMOUD. Can. J. Chem. **55**, 3887 (1977).

A rapid and precise method is described for the determination of tri- and tetrathionate. It is based on oxidation of $S_3O_6^{2-}$ or $S_4O_6^{2-}$ with $KMnO_4$ in sulphuric acid medium in the presence of fluoride, required for preventing the formation of insoluble oxides of manganese. The optimum conditions for both the visual and potentiometric end-point detection are 0.1–0.16 *M* H_2SO_4 and 0.24–0.38 *M* NaF. Trithionate is oxidized to sulphate as an end product, whereas the oxidation product of tetrathionate comprises dithionate and sulphate according to

$$3MnO_4^- + S_4O_6^{2-} + 6HF_2^- + 2H^+ \rightleftharpoons 3MnF_4^- + S_2O_6^{2-} + 2SO_4^{2-} + 4H_2O$$

Examination of the potentiometric titrations and the spectrophotometric scans of samples being titrated showed the presence of intermediate equilibria in solution. The species produced are identified and a theory is given for the net reactions. The method is thoroughly dependable for the determination of amounts of $S_3O_6^{2-}$ or $S_4O_6^{2-}$ corresponding to 0.1–10 mg of sulphur.

K. A. IDRISS, I. M. ISSA et M. R. MAHMOUD. Can. J. Chem. **55**, 3887 (1977).

On présente une méthode rapide et précise pour la détermination de tri- et tétrathionates. Cette technique est basée sur l'oxydation des espèces $S_3O_6^{2-}$ ou $S_4O_6^{2-}$ par le $KMnO_4$ en milieu acide sulfurique et en présence d'ions fluorure nécessaires pour prévenir la formation d'oxydes de manganèse insoluble. Les conditions optimums pour la limite de détection visuelle et potentiométrique sont: 0.1–0.16 *M* H_2SO_4 et 0.24–0.38 *M* NaF. Le trithionate est oxydé jusqu'au sulfate tandis que le produit d'oxydation du tétrathionate comprend le dithionate et le sulfate. Ce processus est représenté par l'équation suivante:

$$3MnO_4^- + S_4O_6^{2-} + 6HF_2^- + 2H^+ \rightleftharpoons 3MnF_4^- + S_2O_6^{2-} + 2SO_4^{2-} + 4H_2O$$

L'examen des titrations potentiométriques et des enregistrements spectrophotométriques des échantillons montrent la présence d'équilibres intermédiaires en solution. Les espèces produites sont identifiées et une théorie est proposée pour les réactions globales. La méthode est totalement précise et permet la détermination d'une quantité d'espèces $S_3O_6^{2-}$ ou $S_4O_6^{2-}$ pouvant correspondre à 0.1–10 mg de soufre.

[Traduit par le journal]

Introduction

The determination of macro-amounts of polythionates have been investigated by oxidation with vanadate (1), iodate, bromate (2), and periodate (3). The reaction of polythionates ($S_nO_6^{2-}$) where $n = 3$–5, with mercuric chloride was applied by Jay (4) for their analysis. The acidity produced from the reaction was measured. Nietzel and DeSesa (5) described a spectrophotometric method for determining as little as 5 mg/ℓ of $S_4O_6^{2-}$ based on the reduction of tetrathionate with cyanide to form thiocyanate, and the latter was determined colorimetrically with an excess of Fe(III) ions.

No method has yet been given involving the oxidation of tri- or tetrathionate with permanganate. The reaction in acid medium, however, is beset with difficulties due to its sluggishness and the precipitation of insoluble oxides of manganese. In the present method, this difficulty is overcome by carrying out the oxidation in a sulphuric acid medium in the presence of fluoride, since the latter is capable of capturing trivalent manganese as complex anions (6). The method is simpler than those given before and includes both the visual and potentiometric titration of thionate solution with MnO_4^- and vice versa. It is also planned to investigate the application of the method as an analytical procedure for the determination of micro-amounts of tri- and tetrathionate and to put forward a mechanism for the reactions involved.

Experimental

Solutions

Potassium permanganate solutions were prepared by a method similar to that of Stamm (7) and standardized with sodium oxalate (8). Sodium trithionate and tetrathionate solutions were prepared and standardized according to recommended procedures (3). Other solutions included ~2% *M* sodium fluoride, 2 *M* sulphuric acid, and 0.25 *M* copper sulphate.

[1]Revision received July 9, 1977.

Equipment

The emf of the titration cell was measured by a direct reading millivoltmeter of the Radiometer (28 Mb) type, using a Pt electrode with a saturated calomel electrode as reference half-cell. The uv and visible absorption spectra of solutions were recorded using a Unicam S.P. 8000 spectrophotometer within the wavelength range 200–600 nm using 1 cm matched silica cells.

Titration Procedure

A volume of tri- or tetrathionate solution containing 0.1–10 mg of sulphur was placed in a titration vessel and mixed with the required volume of 2 *M* H_2SO_4 to give an acidity of 0.2–0.32 *N* and also with 50 ml of 2% NaF solution. The mixture was diluted to 100 ml with twice-distilled water and then titrated with $KMnO_4$ solution. If a visual end-point was desired, an appropriate amount of 0.25 *M* $CuSO_4$ solution was added.

Results and Discussion

The reaction of both $S_3O_6^{2-}$ and $S_4O_6^{2-}$ with permanganate in the presence of fluoride proceeds less rapidly at the beginning of the titration, needing 2–3 min for attainment of equilibrium. However, as the volume of $KMnO_4$ consumed exceeds one-half that required for complete reaction, the oxidation process becomes rapid. It therefore appears that the oxidation of tri- or tetrathionate includes an intermediate equilibria. The stoichiometry of the reactions involved is proposed and the species produced in each case has been identified and confirmed by recording the spectrophotometric scans of the titrated solutions.

The results of the potentiometric titration are not affected by addition of Cu(II) which is essential for the detection of the end-point in the visual titration (9, 10) (to mask the pink colour of the MnF_4^- complex). The visual end-point method is suitable in the presence of copper sulphate solutions containing 0.07–1 g Cu.

Determination of Trithionate

Titration of Trithionate with Permanganate

From the results obtained the reaction appears to proceed quantitatively in accordance with the equation:

$$[1]\quad 2MnO_4^- + S_3O_6^{2-} + 4HF_2^- \rightleftharpoons 2MnF_4^- + 3SO_4^{2-} + 2H_2O$$

The potentiometric titration curves possess two inflections (Fig. 1), the first being due to the reduction of MnO_4^- to Mn(II) and the second to the formation of Mn(III). Trithionate is oxidized to dithionate in the first step, whereas in the second step an induced coupled reaction

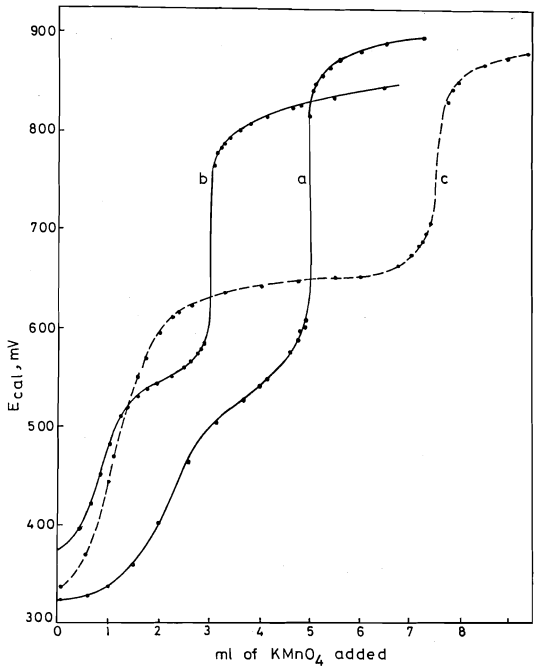

FIG. 1. Titration of $S_3O_6^{2-}$ with $KMnO_4$. (*a*) Titration of 2 ml 0.025 *M* $S_3O_6^{2-}$ with 0.02 *M* MnO_4^- in the presence of 0.12 *M* H_2SO_4 and 0.24 *M* NaF. (*b*) Titration of 1 ml 0.0020 *M* $S_3O_6^{2-}$ with 0.00124 *M* MnO_4 in the presence of 0.12 *M* H_2SO_4 and 0.24 *M* NaF. (*c*) Titration of 3 ml 0.025 *M* $S_3O_6^{2-}$ with 0.02 *M* MnO_4^- in the presence of 0.16 *M* H_2SO_4 and 0.24 *M* NaF.

of Mn(II) and $S_2O_6^{2-}$ with permanganate occurs.

As shown from data obtained in Table 1 and the spectrograms *a* and *b* in Fig. 2, the first inflection corresponds to reaction 2 and the second inflection to reaction 3.

$$[2]\quad 2MnO_4^- + 2S_3O_6^{2-} + 4H^+ \rightleftharpoons 2Mn^{2+} + 3S_2O_6^{2-} + 2H_2O$$

$$[3]\quad 2MnO_4^- + 2Mn^{2+} + 3S_2O_6^{2-} + 8HF_2^- \rightleftharpoons 4MnF_4^- + 6SO_4^{2-} + 2H_2O + 4H^+$$

The conversion of trithionate to SO_4^{2-} according to eq. 3 presumably takes place due to the presence of Mn(II) in solution. The stoichiometry of reaction 3 can be obtained from the following equations.

$$[3a]\quad MnO_4^- + 10HF_2^- + 4Mn^{2+} \rightleftharpoons 5MnF_4^- + 2H^+ + 4H_2O \text{ (ref. 11)}$$

$$[3b]\quad MnO_4^- + 2HF_2^- + 2S_2O_6^{2-} \rightleftharpoons MnF_4^- + 4SO_4^{2-} + 2H^+$$

TABLE 1. Potentiometric titration of $S_3O_6^{2-}$ with $KMnO_4$, total volume made up to 100 ml with water

Titration medium	Experimental end-point (ml) (*i*)	Experimental end-point (ml) (*ii*)	Theoretical end-point (ml) (*i*)	Theoretical end-point (ml) (*ii*)	Error (%) (*i*)	Error (%) (*ii*)
(*a*) In the presence of 0.24 *M* NaF and varying concentrations of H_2SO_4						
1. No acid added	Yellowish turbidity					
2. 0.04 *M* H_2SO_4	Slow reaction					
3. 0.06 *M* "	3.02	5.82	3.0	6.0	+0.67	−1.33
4. 0.10 *M* "	2.96	5.96	3.0	6.0	−1.33	0.67
5. 0.12 *M* "	2.94	6.0	3.0	6.0	−2.0	Nil
6. 0.14 *M* "	2.94	6.0	3.0	6.0	−2.0	Nil
7. 0.16 *M* "	2.88	5.96	3.0	6.0	−2.67	−0.66
8. 0.20 *M* "	2.85	5.88	3.0	6.0	−4.0	−2.0
9. 0.08 *M* "	3.18	6.32	3.2	6.4	−0.63	−1.25
10. 0.12 *M* "	3.15	6.38	3.2	6.4	−1.67	−0.31
11. 0.20 *M* "	3.08	6.28	3.2	−4.0	−1.88	
(*b*) In the presence of 0.12 *M* H_2SO_4 and varying concentrations of NaF						
0.24 *M* NaF	2.86	5.85	3.0	6.0	−4.66	−2.5
0.30 *M* "	2.94	5.98	3.0	6.0	−2.0	0.33
0.36 *M* "	2.95	5.98	3.0	6.0	−1.66	0.33
No NaF added	Reaction slow and brown precipitate formed					

(*c*) In the presence of 0.12 *M* H_2SO_4 and 0.24 *M* NaF	$S_3O_6^{2-}$ ml	$S_3O_6^{2-}$ *M*	Sulphur content (mg)						
1.	4	0.025	9.6	4.5	9.95	5.0	10.0	−10.0	−0.5
2.	2	0.025	4.8	2.42	5.0	2.5	5.0	−3.2	Nil
3.	2	0.012	2.3	1.18	2.4	1.2	2.4	1.7	Nil
4.	5	0.0042	2.02	4.88	9.4	4.72	9.44	1.27	0.42
5.	2	0.0042	0.81	1.86	3.78	1.89	3.78	1.58	Nil
6.	2	0.002	0.38	3.15	6.38	3.2	6.4	1.56	0.31
7.	2	0.001	0.19	1.56	3.18	1.6	3.2	2.5	0.62

NOTES: (*i*) Mn(VIII) → Mn(II); (*ii*) Mn(VII) → Mn(III); (*a*) Nos. 1–8, 5 ml 0.012 *M* $S_3O_6^{2-}$ titrated with 0.02 *M* $KMnO_4$, 9–11, 2 ml of 2×10^{-3} *M* $S_3O_6^{2-}$ titrated with 1.25×10^{-3} *M* $KMnO_4$; (*b*) 5 ml of 0.012 *M* $S_3O_6^{2-}$ titrated with 0.02 *M* $KMnO_4$; (*c*) Nos. 1–3, using 0.02 *M* $KMnO_4$ as titrant, 4–5, using 8.9×10^{-3} *M* $KMnO_4$ as titrant, 6–7, using 1.25×10^{-3} *M* $KMnO_4$ as titrant.

The overall reaction 1 can be obtained by combining [2] and [3]. Figure 2 reveals the absence of an absorption band for MnF_4^- (12) in the spectrum of the reaction mixture at the first inflection but it is present in the spectrum of the solution at the second step. It is apparent also that the absorption band due to Mn(II) and $S_2O_6^{2-}$ (10) disappears when the second end-point is attained.

Optimum Experimental Conditions

Reasonable accuracy in either the visual or potentiometric end-point detection is attained at acidities ranging from 0.1–0.18 *M* sulphuric acid in the presence of 0.24 *M* NaF. At low acidities (<0.04 *M*) the solution becomes slightly turbid owing to partial production of higher manganese oxides. At higher acidities the end-point occurs too early owing to the sluggishness of reaction 3.

The results obtained indicate that the fluoride concentration can be varied from 0.24–0.38 *M* at a constant concentration of sulphuric acid (0.12 *M*) without causing appreciable errors. The visual titration was found to be favourable for the determination of amounts of $S_3O_6^{2-}$ containing 0.3–8 g of sulphur, whereas the potentiometric procedure is applicable for amounts of $S_3O_6^{2-}$ containing 0.09–10 mg S. With higher trithionate concentrations the reaction becomes less rapid and the titration medium slightly turbid owing to hydrolysis of Mn(III) to

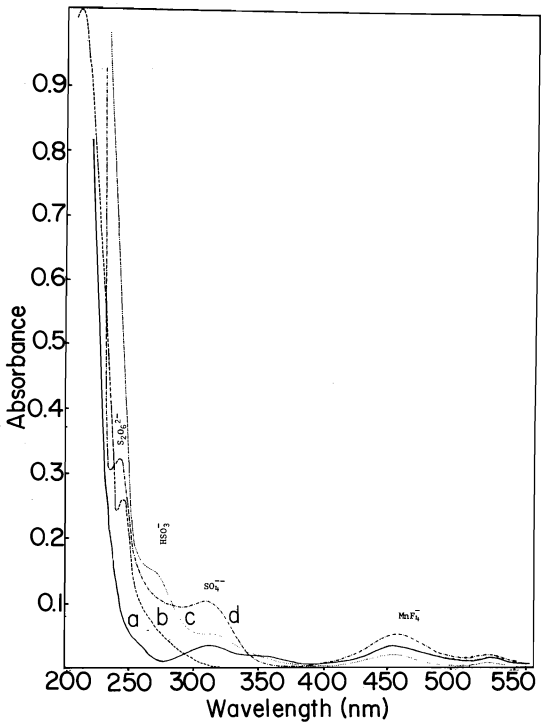

FIG. 2. Spectrophotometric scans of the reaction mixtures (blank solution contains the same concentration of sodium fluoride and sulphuric acid) at the first and second oxidation steps. (*a*) Reaction of 3 ml 2.5 × 10^{2-} *M* $S_3O_6^{2-}$ with 0.01 *M* MnO_4^- in the presence of 0.12 *M* H_2SO_4 and 1% NaF at the second step. (*b*) Reaction of 10 ml 4.2 × 10^{-3} *M* $S_3O_6^{2-}$ with 0.01 *M* MnO_4^- in the presence of 0.12 *M* H_2SO_4 and 1% NaF at the first step. (*c*) Reaction of 5 ml 1.343 × 10^{-2} *M* $S_4O_6^{2-}$ with 0.0096 *M* MnO_4^- in the presence of 0.16 *M* H_2SO_4 and 1% NaF at the first step. (*d*) Reaction of 5 ml 1.343 × 10^{-2} *M* $S_4O_6^{2-}$ with 0.0096 *M* MnO_4^- in the presence of 0.16 *M* H_2SO_4 and 1% NaF at the second step.

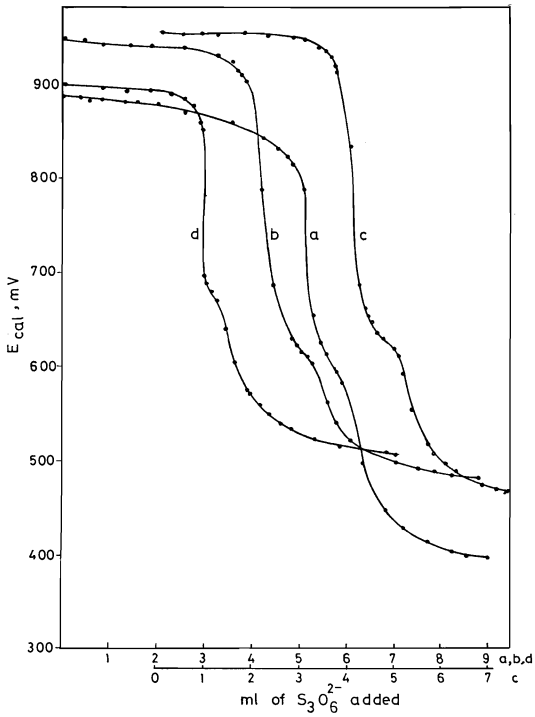

FIG. 3. Titration of $KMnO_4$ with trithionate. (*a*) Titration of 5 ml 0.02 *M* $KMnO_4$ with 0.012 *M* $S_3O_6^{2-}$ in the presence of 0.06 *M* H_2SO_4 and 0.24 *M* NaF. (*b*) Titration of 5 ml 0.02 *M* MnO_4^- with 0.012 *M* $S_3O_6^{2-}$ in the presence of 0.1 *M* H_2SO_4 and 0.24 *M* NaF. (*c*) Titration of 5 ml 0.02 *M* MnO_4^- with 0.012 *M* $S_3O_6^{2-}$ in the presence of 0.14 *M* H_2SO_4 and 0.24 *M* NaF. (*d*) Titration of 10 ml 0.00124 *M* MnO_4^- with 0.0021 *M* $S_3O_6^{2-}$ in the presence of 0.12 *M* H_2SO_4 and 0.24 *M* NaF.

Mn_2O_3 (11). The error is generally <0.7% when the optimum conditions are adopted. The curves obtained on titrating $KMnO_4$ solution with $S_3O_6^{2-}$ are shown in Fig. 3.

Determination of Tetrathionate

The reaction of tetrathionate with permanganate in acid solution containing fluoride proceeds relatively slowly at the start, needing ~3 min between each addition of titrant. As the end-point is approached the electrode equilibration becomes very rapid. The results obtained indicate that the reaction proceeds quantitatively in accordance with the equation:

[4] $3MnO_4^- + S_4O_6^{2-} + 6HF_2^- + 2H^+ \rightleftharpoons 3MnF_4^- + 2SO_4^{2-} + S_2O_6^{2-} + 4H_2O$

Titration of Tetrathionate with Permanganate

The titration curves obtained when tetrathionate solutions are titrated with MnO_4^- (cf. Fig. 4) are characterised by two inflections, the first of which corresponds to the equation

[5] $2MnO_4^- + S_4O_6^{2-} + 4HF_2^- + H^+ \rightleftharpoons 2MnF_4^- + 3HSO_3^- + SO_4^{2-} + H_2O$

The volume of MnO_4^- consumed at the first inflection, as well as the appearance of the absorption bands characterising HSO_3^- and MnF_4^- (10) in the spectrum of the reaction mixture at the first inflection, provides support for eq. 5.

Reaction 5, however, is experimentally verified by choosing the suitable p*H* range within which the solutions can be titrated successfully. The quantitative course of the reaction is achieved at p*H* 2.5–4.0. This range is suitable for the

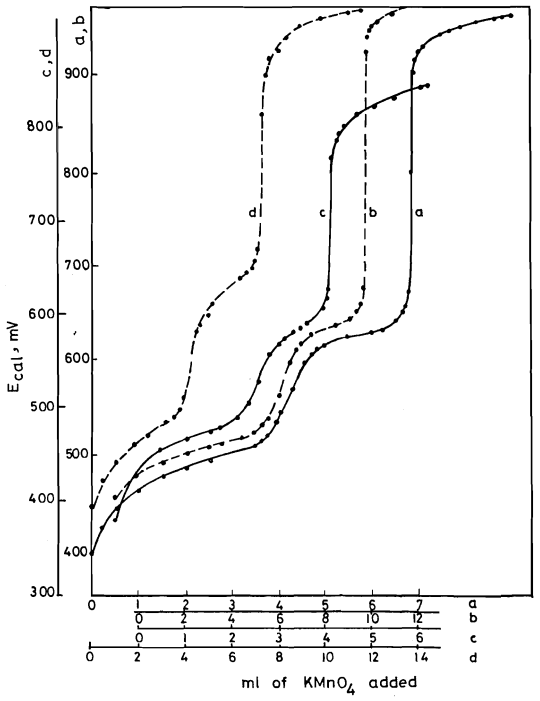

FIG. 4. Titration of $S_4O_6^{2-}$ with $KMnO_4$. (*a*) Titration of 5 ml 0.0091 *M* $S_4O_6^{2-}$ with 0.02 *M* $KMnO_4$ in the presence of 0.1 *M* H_2SO_4 and 0.24 *M* NaF. (*b*) Titration of 8 ml 0.0091 *M* $S_4O_6^{2-}$ with 0.02 *M* $KMnO_4$ in the presence of 0.1 *M* H_2SO_4 and 0.24 *M* NaF. (*c*) Titration of 2 ml 1.4×10^{-3} *M* $S_4O_6^{2-}$ with 1.8×10^{-3} *M* $KMnO_4$ in the presence of 0.1 *M* H_2SO_4 and 0.24 *M* NaF. (*d*) Titration of 5 ml 0.0091 *M* $S_4O_6^{2-}$ with 0.02 *M* $KMnO_4$ in the presence of 0.2 *M* H_2SO_4 and 0.24 *M* NaF.

quantitative reaction of HSO_3^- with MnO_4^- without decomposition of the sulphur compound to yield SO_2 (10). This intermediate oxidation product (HSO_3^-) is then further oxidized along the second step, according to the reaction

$$[6] \quad MnO_4^- + 3HSO_3^- + 2HF_2^- + H^+ \rightleftharpoons MnF_4^- + S_2O_6^{2-} + SO_4^{2-} + 3H_2O \text{ (ref. 10)}$$

The formation of dithionate is confirmed by the presence of an absorption band at 242 nm (10) in the spectrum of the reaction mixture at the second inflection (Fig. 2*d*), and by its analysis using the method of Murthy (13). Reaction 6 is also realized by determining the concentration of the MnF_4^- complex produced at the second end-point using the spectral data and comparing the results with theoretical values. It was found that the concentration of the MnF_4^- produced at the second inflection, as well as the volume of permanganate consumed at that step, each represent one-third of the total as given by the overall eq. 4. This verifies the validity of the suggested mechanism.

It is noteworthy that the end product in the oxidation of $S_4O_6^{2-}$ differs from that obtained in the case of $S_3O_6^{2-}$. Tetrathionate produces a mixture of $S_2O_6^{2-}$ and SO_4^{2-}. The production of $S_2O_6^{2-}$ can be attributed to the absence of Mn(II) necessary for the catalytic oxidation of dithionate according to eq. 3. If Mn(II) were added to a solution of $S_4O_6^{2-}$ prior to titration, SO_4^{2-} would be the only sulphur containing product. This can be shown by doing the following experiment.

A known excess of Mn(II) is added to a solution of tetrathionate (varying concentration), followed by the addition of the appropriate amount of 1 *M* sulphuric acid and 0.5 *M* NaF. The mixture is then titrated with $KMnO_4$.

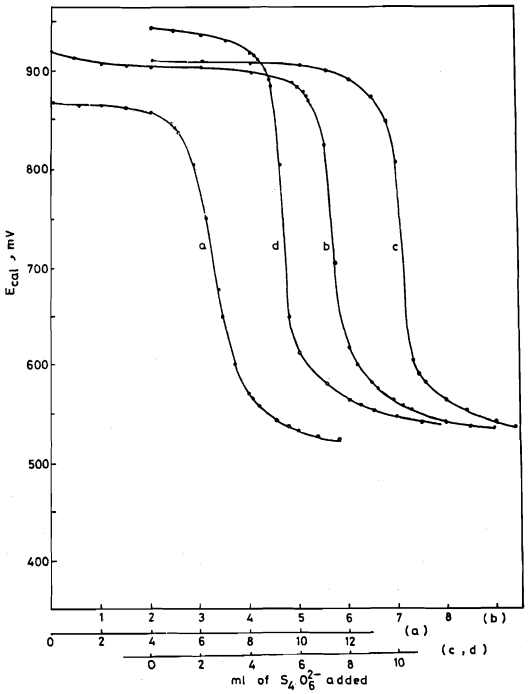

FIG. 5. Titration of $KMnO_4$ with $S_4O_6^{2-}$. (*a*) Titration of 8 ml 0.0058 *M* $KMnO_4$ with 0.0028 *M* $S_4O_6^{2-}$ in the presence of 0.08 *M* H_2SO_4 and 0.24 *M* NaF. (*b*) Titration of 8 ml 0.0059 *M* $KMnO_4$ with 0.0028 *M* $S_4O_6^{2-}$ in the presence of 0.12 *M* H_2SO_4 and 0.24 *M* NaF. (*c*) Titration of 15 ml 0.0188 *M* $KMnO_4$ with 0.00908 *M* $S_4O_6^{2-}$ in the presence of 0.12 *M* H_2SO_4 and 0.24 *M* NaF. (*d*) Titration of 8 ml 0.0188 *M* $KMnO_4$ with 0.00908 *M* $S_4O_6^{2-}$ in the presence of 0.15 *M* H_2SO_4 and 0.24 *M* NaF.

TABLE 2. Potentiometric titration of $S_4O_6^{2-}$ with $KMnO_4$

Titration medium	Experimental end-point (ml) (*i*)	Experimental end-point (ml) (*ii*)	Theoretical end-point (ml) (*i*)	Theoretical end-point (ml) (*ii*)	Error (%) (*i*)	Error (%) (*ii*)
(*a*) In the presence of 0.24 *M* NaF and varying concentrations of H_2SO_4						
No acid added	Yellowish turbidity					
0.03 *M* H_2SO_4	Slow reaction					
0.08 *M* "	4.35	6.84	4.55	6.76	− 4.4	+1.18
0.1 *M* "	4.32	6.78	4.55	6.76	− 5.17	+0.3
0.12 *M* "	4.25	6.76	4.55	6.76	− 6.6	Nil
0.16 *M* "	4.15	6.72	4.55	6.76	− 8.8	−0.59
0.20 *M* "	4.08	6.68	4.55	6.76	−10.33	−1.18
0.22 *M* "	3.95	6.60	4.55	6.76	−14.3	−2.37

(*b*) In the presence of 0.1 *M* H_2SO_4 and 0.24 *M* 2% NaF

$S_4O_6^{2-}$ titrated ml	$S_4O_6^{2-}$ titrated *M*	Sulphur content (mg)						
1. 8	0.0091	9.32	6.98	10.84	7.28	10.80	−4.1	+0.37
2. 3	0.0091	3.49	2.67	4.06	2.73	4.05	−2.2	+0.24
3. 2	0.0045	0.93	0.86	1.35	0.90	1.35	−4.4	Nil
4. 2	0.0014	0.36	2.98	4.64	3.11	4.66	−4.11	−0.43
5. 2	0.0004	0.10	1.29	1.98	1.33	2.0	−3.0	−0.5

NOTES: (*i*) At the first step; (*ii*) at the second step; (*a*) 5 ml of 0.0091 *M* $S_4O_6^{2-}$ titrated with 0.02*M* $KMnO_4$; (*b*) Nos. 1–3, using 0.02 *M* $KMnO_4$ as titrant, 4–5, using 1.8×10^{-3} *M* $KMnO_4$ as titrant.

By knowing the amount of permanganate consumed in reaction with Mn(II), the amount of $KMnO_4$ necessary for the oxidation of $S_4O_6^{2-}$ can be evaluated. The results obtained indicate that the oxidation of $S_4O_6^{2-}$ takes place in accordance with

$$[7]\quad 7MnO_4^- + 2S_4O_6^{2-} + 14HF_2^- + 2H^+ \rightleftharpoons 7MnF_4^- + 8SO_4^{2-} + 8H_2O$$

The last equation can be deduced, however, by combining eqs. 5, 6, and 3*b*. This leads to the opinion that the role played by Mn(II) to convert $S_2O_6^{2-}$ produced in reaction 6 can be represented stoichiometrically as given in eq. 3.

On the other hand, the catalytic effect of Mn(II) in the conversion of tetrathionate to sulphate as an end product is evidenced by performing titrations of mixtures of tri- and tetrathionate containing large amounts of $S_3O_6^{2-}$ (≥ 5 mg). The stoichiometry of the tetrathionate reaction does not remain the same as for the reaction carried out individually but proceeds according to eq. 7 and yields SO_4^{2-}. Thus the method can be applied under such conditions to determine the sum of $S_3O_6^{2-}$ and $S_4O_6^{2-}$ on the basis that the two reductants are oxidized to sulphate. However, this method cannot be used to determine either tri- or tetrathionate in a mixture of the two.

Optimum Experimental Conditions

Reasonable accuracy is obtained on titrating tetrathionate solutions with $KMnO_4$ at acidities ranging from 0.1–0.18 *M* sulphuric acid in the presence of 0.24 *M* sodium fluoride. At higher acidities, early end-points are obtained owing to the instability of tetrathionate under such conditions. At low acid concentrations (<0.08 *M* H_2SO_4), the reaction becomes rather slow or alternatively yields partially Mn(IV) as MnO_2. The fluoride concentration can be varied from 0.24–0.38 *M* when the acidity of the medium is kept constant at 0.12 *M* H_2SO_4. Table 2 indicates that when the optimum acidity and fluoride content are adopted, amounts of $S_4O_6^{2-}$ corresponding to 0.1–10 mg sulphur can be titrated either visually or potentiometrically with an error less than 1%. Figure 5 demonstrates the titration of permanganate with $S_4O_6^{2-}$.

1. A. KURTENACKER and K. BITTNER. Z. Anorg. Allg. Chem. **142**, 119 (1925).
2. R. LANGE and A. KURTENACKER. Z. Anal. Chem. **123**, 169 (1942).
3. R. KAUSHIK and P. RAJENDRA. Indian J. Chem. **8**, 462 (1970).
4. R. R. JAY. Anal. Chem. **25**, 288 (1953).
5. O. A. NIETZEL and M. A. DESESA. Anal. Chem. **27**, 1839 (1955).
6. I. M. ISSA, A. EL-SAMAHY, and M. M. GHONEIM. Electrochim. Acta, **16**, 1655 (1971).
7. H. STAMM. Z. Angew. Chem. **47**, 791 (1934).
8. R. A. FOWLER and H. B. BRIGHT. J. Res. Natl. Bur. Stand. **15**, 493 (1935).
9. I. M. ISSA, A. EL-SAMAHY, and M. M. GHONEIM. J. Egypt. Chem. **12**, 175 (1969).
10. I. M. ISSA, K. A. IDRISS, and M. M. GHONEIM. Talanta, **22**, 249 (1976).
11. I. M. ISSA and M. M. GHONEIM. Talanta, **20**, 517 (1973).
12. I. M. ISSA, M. M. GHONEIM, A. EL-SAMAHY, and M. THARWAT. Electrochim. Acta, **17**, 1252 (1972).
13. A. R. MURTHY. Curr. Sci. India, **22**, 371 (1953).

A new route to ring-fused tetrahydrofurans: reaction of Δ^4-unsaturated alcohols with phenylselenenyl chloride

DERRICK L. J. CLIVE,[1] GIM CHITTATTU, AND C. K. WONG

Department of Chemistry, University of Alberta, Edmonton, Alta., Canada T6G 2G2

Received May 4, 1977

DERRICK L. J. CLIVE, GIM CHITTATTU, and C. K. WONG. Can. J. Chem. **55**, 3894 (1977).

Δ^4-Olefinic alcohols react with phenylselenenyl chloride to produce tetrahydrofurans with a phenylseleno-group *trans* and β to the ether oxygen. The [4.3.0] and [3.3.0] oxabicyclic systems produced have *cis* ring fusion as in **5** and **7**.

DERRICK L. J. CLIVE, GIM CHITTATTU et C. K. WONG. Can. J. Chem. **55**, 3894 (1977).

Les alcools Δ^4-oléfiniques réagissent avec le chlorure de phénylsélénényle produisant des tétrahydrofurannes ayant un groupe phénylséléné *trans* et en position β de l'hétéroatome. Les systèmes oxabicycliques [4.3.0] et [3.3.0] produits, ont une fusion de cycle *cis* comme pour **5** et **7**.

[Traduit par le journal]

The introduction of selenium into organic molecules as, for example, PhSe, is an important process since the resulting phenyl alkyl selenides have considerable utility in synthesis because they can be converted into olefins in high yield (e.g. ref. 1).

One route to selenides that is extremely rapid and gentle is the stereospecific addition across double bonds of species formally represented as PhSeZ, where Z can be CF_3COO (2), CH_3COO (3*a*), MeO (3*a*, 3*b*), EtO (3*b*), or Pr^iO (3*b*). This reaction is a clean *anti* addition (2, 3) but is characterized by poor regioselectivity (2, 3*b*, 4). The observations (2*a*, 3*b*) summarized by [1] are

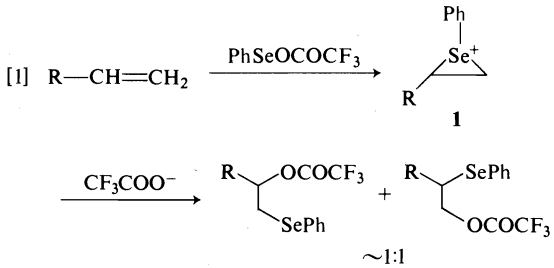

typical, so that any refinement of the process that makes it regiospecific would constitute a useful synthetic method. The product distribution of [1] results from attack at both electrophilic carbons (5) in the intermediate **1** but we have found that strict regiochemical control is possible by arranging for the intermediate (see **1**) to be captured in an intramolecular process. Of several ring systems that should be accessible in this way we have examined the preparation of tetrahydrofurans because of the widespread occurrence among natural products of structures with five-membered rings incorporating oxygen. Our route to these heterocycles (eqs. 2–4) involves

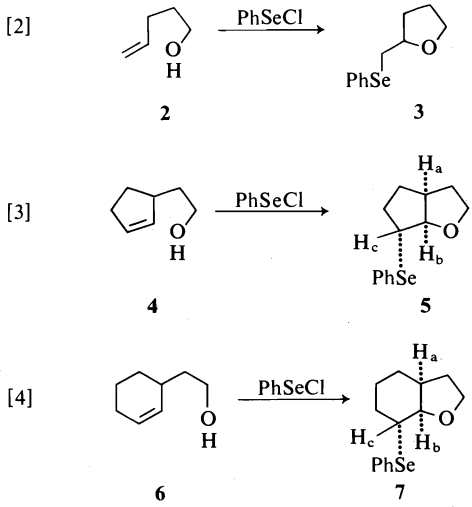

treating a Δ^4-olefinic alcohol with phenylselenenyl chloride (PhSeCl).

If the reaction is regarded as a trigonal cyclisation (see Scheme 1) then the empirically based rules for ring closure (6) suggest that both 5-*exo*- and 6-*endo*-trigonal pathways may be followed, leading, in the case of pent-4-enol **2** to the tetrahydrofuran **3** and the tetrahydropyran **8** (see Scheme 1). If the intermediate is of type **9** both modes of cyclisation are again allowed but production of a five-membered ring is expected

[1] Author to whom correspondence should be addressed.

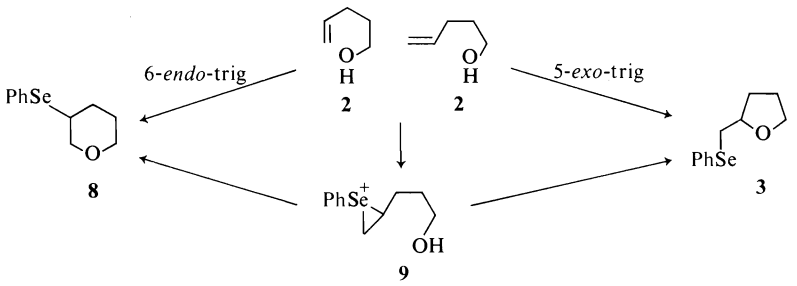

SCHEME 1

(7) to be preferred. It is known that ring closure of pent-4-enol with halogens leads to tetrahydrofurans (8) but that cyclisation with lead tetraacetate gives both five- and six-membered heterocycles (9).

In order to establish the preferred pathway with selenium reagents we treated pent-4-enol in ethyl acetate, with 1 equiv. of phenylselenenyl chloride and found that it is rapidly transformed into the tetrahydrofuran **3**, which can be isolated in 75% yield.[2] The proton magnetic resonance spectrum defines the structure of **3**, and, as expected, mass spectral analysis shows the production of fragments corresponding to $(PhSeCH_2)^+$, $(PhSe)^+$, and $(M—PhSeCH_2)^+$.

In order to have synthetic utility this cyclisation must be applicable to ring-fused ethers and should proceed in a clearly defined stereochemical fashion. Therefore, we examined the substrates **4** and **6**.

Compound **4** was converted cleanly into the bicyclic ether **5** which was isolated in 84% yield. Mass measurement on the molecular ion defined the elemental composition of **5**, and the stereochemistry shown at each of the asymmetric centres was evident from the proton magnetic resonance spectrum. The signal for H_b, which is centred at 4.36 ppm, is a doublet of doublets in which the smaller coupling is barely resolved. The larger coupling is 6.5 Hz. For *cis* ring fusion the dihedral angle between H_a and H_b is estimated from Dreiding models to be less than 20° and a value of ca. 7 Hz is therefore anticipated for J_{ab}. The small value of J_{bc} establishes that the PhSe-group is *trans* to the ether oxygen. For *trans* ring fusion neither relative orientation of the PhSe-group would make J_{bc} vanishingly small.

Compound **6** was cyclised in the same way and gave **7** in 77% yield. Mass measurement served to define the constitution of **7** and the stereochemistry of the ring fusion was established chemically by hydrogenolysis with Raney nickel (10) to the known (11) *cis*-perhydrobenzofuran. The proton magnetic resonance spectrum (270 MHz) of **7** shows a quartet (J = 5.1 Hz) due to H_c. This pattern is the result of three equal (or nearly equal) vicinal couplings as would be experienced by an equatorial hydrogen in a chair conformation of cyclohexane.[3] We have found a close analogy, using the same electrophile, for supporting the stereochemical assignment made to **7**. The olefinic acid **10** can be cyclised to the lactone **11** by treatment with phenylselenenyl chloride and the structure of the product **11**, in which H_c gives rise to a quartet with J = 4 Hz, was established by unambiguous synthesis from the known (13) epoxide **12** (14).

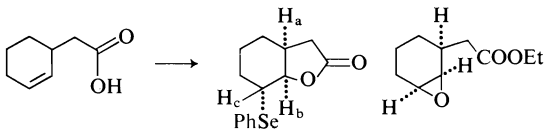

10 **11** **12**

13 **14**

In the preparation of the tetrahydrofurans **3**, **5**, and **7** the minimum reaction time was not established but small scale spectroscopic runs described below showed that cyclisation is very rapid. *A priori* it was possible that the first stage in these reactions is addition of phenylselenenyl chloride to the double bond to produce

[2]During preparation of this manuscript we received a report (19) of cyclisation of a *symmetrical* hydroxy olefin and of hydroxy olefins of the type shown in [3].

[3]1-Chloro-2-phenylselenocyclohexane exists at room temperature largely (60%) in the diaxial conformation (12).

a β-chloroselenide which is converted into the cyclic ether if the phenylseleno-group is *trans* to the hydroxyalkyl side chain. If the relationship is *cis* then chloroselenide formation would have to be a reversible process (15). When phenylselenenyl chloride was mixed (using CD_2Cl_2 solutions) at −80°C with 1 equiv. of **4** then low temperature (−60°C) ^1H nmr measurements, made within 5 min of mixing, showed no olefinic protons. The spectra obtained correspond to the cyclised product but the presence of at least some β-chloroselenide cannot be excluded. Evidently the ring closure is a very rapid process.

In order to establish whether formation of β-chloroselenides is easily reversible we heated compound **13** (16) in $CDCl_3$ at 60°C in the presence of an excess of cyclohexene. The cyclohexyl derivative **14** (12) was not formed and no change was seen during 16 h.

Although halogen-induced ring closures (*8a*) and cyclisations in tellurium chemistry (17) provide analogies for the reactions reported here, the examples in the selenium series allow advantage to be taken of the mildness with which selenides (18) can be subjected to further synthetic transformations.

Experimental

All reactions were conducted under nitrogen using oven-dried apparatus. Ethyl acetate was refluxed over phosphorus pentoxide (2 h) and then distilled from the mixture. Phenylselenenyl chloride was used as supplied by Aldrich. Pent-4-enol (**2**), 2-(2-cyclopenten-1-yl)ethanol (**4**), and 2-(2-cyclohexen-1-yl)ethanol (**6**) were prepared by the methods cited. Nuclear magnetic resonance spectra were run in $CDCl_3$ on a 100 MHz instrument, unless otherwise stated. Thin layer and preparative layer chromatography employed Merck Silica Gel PF-254 and the plates were activated at 110°C for 1 h before use. Merck Silica Gel 60 (particle size 0.063–0.200 mm) was used for column chromatography.

2-(Phenylselenomethyl)tetrahydrofuran ***3***

Phenylselenenyl chloride (382 mg, 1.99 mmol) in ethyl acetate (3 ml) was injected over 5 min into a cooled and magnetically stirred ethyl acetate solution (3 ml; internal temperature −77°C) of pent-4-enol (172 mg, 1.99 mmol). A further portion (0.5 ml) of ethyl acetate was used to wash residual reagent from the addition syringe into the reaction mixture. Within 5 min after the end of the addition the cold reaction mixture had become colourless and none of the alcohol could be detected by tlc (silica, ethyl acetate – 2,2,4-trimethylpentane (1:4 by volume)). The solvent was evaporated (water pump vacuum, room temperature) 15 min after the end of the addition and the resulting oil was chromatographed over silica gel (20 × 1.4 cm) with a mixture of ethyl acetate and 2,2,4-trimethylpentane (1:4 by volume). Appropriate fractions (tlc) were combined and evaporated. Bulb to bulb distillation (bath temperature 82°C; 0.01 Torr) gave compound **3** (362 mg, 75.1%) as a colourless oil that was chromatographically homogeneous (silica, ethyl acetate – 2,2,4-trimethylpentane (1:4 by volume); R_f 0.5); ir ν_{max} (neat) 1580, 1480, 1437, 735 cm^{-1}; ^1H nmr δ 1.45–2.14 (m, 4H), 2.8–3.2 (m, 2H), 2.55–4.2 (m, 3H), 7.1–7.3 (m, 3H), 7.35–7.65 (m, 2H); ms 242 $(M)^{+\cdot}$, 172 $(C_6H_5SeCH_2)^+$, 157 $(C_6H_5Se)^+$, 171 $(M - C_6H_5SeCH_2)^+$. *Anal.* calcd. for $C_{11}H_{14}OSe$: C 54.77, H 5.80, O 6.63; found: C 54.73, H 5.89, O 6.79. *Mol. Wt.* calcd. for $C_{11}H_{14}OSe$: 242.0204; found: 242.0210.

8-exo-Phenylseleno-2-oxabicyclo[3.3.0]octane ***5***

Phenylselenenyl chloride (382 mg, 1.99 mmol) in ethyl acetate (4 ml) was injected over 5 min into a cooled and magnetically stirred ethyl acetate solution (4 ml; internal temperature −78°C) of 2-(2-cyclopenten-1-yl)-ethanol (224 mg, 1.99 mmol). A further portion (0.5 ml of ethyl acetate was used to wash residual reagent from the addition syringe into the reaction mixture. After 1 h at −78°C the temperature was raised to 25°C during 30 min and kept at 25°C for 3 h. The reaction vessel was then immersed for 30 min in an oil bath preheated to 80°C by which time no alcohol remained (tlc control). The product was then isolated exactly as described above except that the solvent for chromatography was a 3:7 (by volume) mixture of ethyl acetate and 2,2,4-trimethylpentane. Compound **5** was obtained, after bulb to bulb distillation (bath temperature 104°C, 0.01 Torr), as a pale yellow oil (450 mg, 84.3%) that was chromatographically homogeneous (silica, ethyl acetate – 2,2,4-trimethylpentane (3:7 by volume); R_f 0.5); ir ν_{max} (neat) 1580, 1480, 1067, 1042, 1025 cm^{-1}; ^1H nmr δ 1.2–2.35 (m, 6H), 2.6–3.0 (m, 1H), 3.45–3.95 (m, 3H), 4.36 (d, J = 6.5 Hz; each signal broad, 1H), 7.0–7.38 (m, 3H), 7.38–7.65 (m, 2H); ms 268 $(M)^{+\cdot}$, 157 $(C_6H_5Se)^+$. *Anal.* calcd. for $C_{13}H_{16}OSe$: C 58.43, H 6.04, O 5.99; found: C 58.56, H 6.11, O 5.99. *Mol. Wt.* calcd. for $C_{13}H_{16}OSe$: 268.0366; found: 268.0357.

5-exo-Phenylseleno-7-oxabicyclo[4.3.0]nonane ***7***

Phenylselenenyl chloride (382 mg, 1.99 mmol) in ethyl acetate (5 ml) was injected over 45 min into a cooled and magnetically stirred ethyl acetate solution (5 ml, internal temperature −65°C) of 2-[2-cyclohexen-1-yl]ethanol (252 mg, 1.99 mmol). A further portion (1 ml) of ethyl acetate was used to wash residual reagent from the addition syringe into the reaction mixture. After the addition the cooling bath was removed and the mixture was stirred at room temperature for 18 h (with protection from light). The solvent was then evaporated (water pump vacuum at room temperature) and the residual oil, in dichloromethane (1.5 ml), was applied to two preparative layer silica plates (20 × 60 × 0.1 cm) which were developed once with benzene–ethylacetate (5:1 by volume). The product band (located under uv light) was extracted with ether. Removal of the solvent and bulb to bulb distillation (bath temperature 110°C, 0.005 Torr) gave compound **7** (431 mg, 77%) as a pale yellow oil that was chromatographically homogeneous (silica, benzene–ethylacetate (5:1 by volume); R_f 0.6); ir ν_{max} (neat) 1583, 1480, 1458, 1439, 1305, 1164, 1070, 1023, 1000, 967, 935, 737, 688 cm^{-1}; ^1H nmr (270 MHz) δ 1.25–1.80 and 1.86–2.07 (m, 8H), 2.36 (m, $W_{1/2}$ = 21 Hz, 1H), 3.50 (q, J = 5.1 Hz, 1H), 3.8–4.1 (m, 3H), 7.2 (m, 3H), 7.4 (m, 2H); ms 282

$(M)^{+\cdot}$, 157 $(C_6H_5Se^+)^+$, 125 $(M - C_6H_5Se)^+$. *Anal.* calcd. for $C_{14}H_{18}OSe$: C 59.79, H 6.41, O 5.69; found: C 59.64, H 6.49, O 5.91. *Mol. Wt.* calcd. for $C_{14}H_{18}OSe$: 282.0523; found: 282.0524.

Conversion of 5-exo-Phenylseleno-7-oxabicyclo[4.3.0]-nonane into 2-Oxabicyclo[4.3.0]nonane

Raney nickel (1 ml of settled W-2 catalyst, stored under ethanol) was rinsed under a nitrogen atmosphere with several portions of ether and was then covered with ether (5 ml). Compound **7** (281 mg, 1 mmol) in ether (1 ml) was injected and a further portion (0.5 ml) of ether was used as a rinse. The nitrogen atmosphere above the reaction mixture was replaced by hydrogen and the mixture was stirred at room temperature under hydrogen for 21 h. At this stage no starting material was left (tlc control). The catalyst was filtered off and washed with ether (4 × 10 ml). The combined organic extract was evaporated (water pump vacuum, room temperature) and the residual oil (96 mg) was applied in dichloromethane (1 ml) to a preparative layer silica plate (20 × 60 × 0.1 cm) which was developed once with chloroform–ethyl-acetate (9:1 by volume). The required band, located by spraying one edge of the plate with iodine vapour, was extracted with ether. Removal of the solvent under vacuum gave an oil (31.5 mg, 25%) identical with an authentic (11) specimen of *cis*-7-oxabicyclo[4.3.0]nonane.

Acknowledgements

Acknowledgement is made to the National Research Council of Canada and to the Donors of the Petroleum Research Fund, administered by the American Chemical Society, for the support of this research.

1. G. Stork and S. Raucher. J. Am. Chem. Soc. **98**, 1583 (1976); D. L. J. Clive. Chem. Commun. 695 (1973).
2. (*a*) D. L. J. Clive. Chem. Commun. 100 (1974); (*b*) H. J. Reich. J. Org. Chem. **39**, 428 (1974).
3. (*a*) K. B. Sharpless and R. F. Lauer. J. Org. Chem. **39**, 429 (1974); (*b*) A. Toshimitsu, S. Uemura, and M. Okano. Chem. Commun. 166 (1977).
4. N. Miyoshi, S. Furui, S. Murai, and N. Sonoda. Chem. Commun. 293 (1975).
5. G. H. Schmid and D. G. Garratt. Tetrahedron Lett. 3991 (1975).
6. (*a*) J. E. Baldwin. Chem. Commun. 734 (1976); (*b*) J. E. Baldwin. Chem. Commun. 738 (1976); (*c*) J. E. Baldwin and J. A. Reiss. Chem. Commun. 77 (1977).
7. G. Stork and J. F. Cohen. J. Am. Chem. Soc. **96**, 5271 (1974).
8. (*a*) D. L. H. Williams. Tetrahedron Lett. 2001 (1967); (*b*) A. Bresson, G. Dauphin, J.-M. Geneste, A. Kergomard, and A. Lacourt. Bull. Soc. Chim. Fr. 1080 (1971).
9. M. Lj. Mihailović and Z. Cerković. Synthesis, 209 (1970).
10. M. Sevrin, D. Van Ende, and A. Krief. Tetrahedron Lett. 2643 (1976).
11. Y. Yamamototo, R. J. Gargiulo, and D. S. Tarbell. J. Org. Chem. **36**, 846 (1971).
12. N. S. Zefirov, L. G. Gurvich, A. S. Shashkov, and V. A. Smit. J. Org. Chem. USSR, **10**, 1800 (1974).
13. Yu. A. Arbuzov, V. T. Ivanov, M. N. Kolosov, Yu. A. Ovchinnikov, and M. M. Shemyakin. J. Gen. Chem. USSR, **34**, 1031 (1964).
14. D. L. J. Clive and G. Chittattu. Chem. Commun. 484 (1977).
15. G. H. Schmid and P. H. Fitzgerald. J. Am. Chem. Soc. **93**, 2547 (1971).
16. E. G. Kataev, T. G. Mannafov, E. A. Berdnikov, and O. A. Komarovskaya. J. Org. Chem. USSR, **9**, 1998 (1973).
17. M. de Moura Campos and N. Petragnani. Tetrahedron Lett. 11 (1959).
18. K. B. Sharpless, K. M. Gordon, R. F. Lauer, D. W. Patrick, S. P. Singer, and M. W. Young. Chemica Scripta, **8**A, 9 (1975).
19. K. C. Nicolaou and Z. Lysenko. Tetrahedron. Lett. 1257 (1977).

Synthesis and crystal structure of thiosemicarbazidedichloromercury(II)

CHUNG CHIEH AND DIANNA H. COWELL

Guelph–Waterloo Centre for Graduate Work in Chemistry, Department of Chemistry, University of Waterloo, Waterloo, Ont., Canada N2L 3G1

Received June 13, 1977

CHUNG CHIEH and DIANNA H. COWELL. Can. J. Chem. **55**, 3898 (1977).

Thiosemicarbazidedichloromercury(II) was synthesized in an ethanol–water solution by keeping the molar ratio of $HgCl_2$ and thiosemicarbazide (tsc) at 1:1. The crystal is monoclinic: a = 8.966(11), b = 6.817(9), c = 12.092(14) Å, β = 100.3(1)°, and space group $P2_1/c$ with four molecules per unit cell. The tsc is a bidentate ligand in this complex with Hg—S = 2.417(6) Å, Hg—N = 2.51(2) Å. The mercury atom is trigonal pyramidally four-coordinated, with two Hg—Cl distances of 2.366(6) and 2.770(5) Å. When the tsc is coordinated to the mercury(II) ions, the chemical shift of the ^1H atoms on the NH_2 and NH groups shift to a lower field.

CHUNG CHIEH et DIANNA H. COWELL. Can. J. Chem. **55**, 3898 (1977).

On a synthétisé la thiosemicarbazide de dichloromercure(II) dans une solution éthanol–eau en maintenant un rapport molaire de $HgCl_2$ et de thiosemicarbazide (tsc) à 1:1. Les cristaux sont monocliniques a = 8.966(11), b = 6.817(9), c = 12.092(14) Å, β = 100.3(1)° et groupe d'espace $P2_1/c$ avec quatre molécules par maille; tsc est un ligand bidentate dans ce complexe avec Hg—S = 2.417(6) Å, Hg—N = 2.51(2) Å. L'atome de mercure est tétracoordonné dans une pyramide trigonale avec deux distances Hg—Cl de 2.366(6) et 2.770(5) Å. Lorsque le tsc est coordonné aux ions de mercure(II), le déplacement chimique des atomes ^1H sur les groupes NH_2 et NH se déplace vers les bas champs.

[Traduit par le journal]

Introduction

During the synthesis of bisthiosemicarbazidedichloromercury(II) a thin needle-like crystalline product was formed at first (1). Those needles disappeared in the reaction in which the molar ratio of $HgCl_2$ to thiosemicarbazide (tsc) is 1 to 2. When the molar ratio was kept at 1:1, thiosemicarbizidedichloromercury(II) was synthesized and the crystals became prismatic as they grew. A similar complex was found with zinc(II) (2) instead of mercury(II) but the two compounds are not isostructural. The crystal structure and nmr spectra of $HgCl_2$(tsc) are described in this paper.

Experimental

Preparation of $HgCl_2$(tsc)

The chemicals used in this study are the same as those of ref. 1. To an ethanol–water solution containing 2 mM of tsc, 2 mM of $HgCl_2$ crystals were added. A new kind of needle-like crystal started to form and the crystals were visible in 10 min. The solution was covered and the reaction proceeded slowly at room temperature, 25 ± 3°C, overnight. The crystals were collected by filtration. There was a trace of black material due to decomposition and the sample appeared silvery.

The nmr spectra were measured on a WP-60 (Bruker) in DMSO-d_6 with TMS as standard.

Crystallographic Measurements

Photographic methods were used for space group determination. Cell constants were estimated from film data and then refined by the least-squares method from the 2θ values of 34 reflections measured on a G.E. XRD-6 diffractometer. Crystal data are:

$CCl_2H_5HgN_3S$ fw = 362.7

Monoclinic, a = 8.966(11), b = 6.817(9), c = 12.092(14), β = 100.3(1)°. V = 727.1 Å^3, D_o = 3.31 (by flotation), Z = 4, D_c = 3.313 g cm^{-3}, mp = 182°C. Systematic absences: $h0l$, $l = 2n + 1$, $0k0$, $k = 2n + 1$; space group $P2_1/c$, μ(MoKα) = 225.1 cm^{-1}.

The crystal used for intensity measurements had {0, 1, 1} and {1, 1, 1} faces developed. It was cut out of a prism perpendicular to a and a face (100) was included as boundaries for absorption correction which was done by a revised version of the program written by Coppens *et al.* (3). The dimensions of the crystal along a, b, and c are 0.14, 0.10, and 0.11 mm respectively. Among 1268 independent reflections with 2θ < 50° measured, 1031 reflections having $I > 3\sigma(I)$ were considered observed. The stability of the crystal and instrument were monitored by four standard reflections as described in ref. 1. Data reduction was also similar.

In the Patterson map, there was an intense (0.9 × origin) peak at (0, ½, ½). This led us to think that the mercury was located at a special position. However, the measured density corresponds to four molecules per unit cell; therefore, the intense peak was treated as one on a Harker line. The solution was then straightforward.

The atomic scattering factors from Cromer and Waber

(4) were used with anomalous dispersion coefficients for Hg from Cromer (5). At the final stage a weighting function $w = (\sigma(F^2))^{-1}$ was used and the R ($= \Sigma||F_o| - |F_c||/\Sigma|F_o|$) and R_w ($=(\Sigma w^2[|F_o| - |F_c|]^2/\Sigma wF_o^2)^{1/2}$) were 0.068 and 0.065. The difference Fourier at this stage showed only ripples around the mercury atom. The atomic coordinates are given in Table 1.[1] Refinement using data without absorption corrections gave R of 0.12 and some atoms had negative temperature factors.

Results and Discussion

The crystal consists of individual molecules. Bond lengths and angles are given in Fig. 1, which shows two molecules that are related to each other by a center of symmetry. The mercury is four coordinated with a trigonal pyramidal geometry. A least-squares plane calculated for Hg, S, N(3), and Cl(2) has a maximum deviation of 0.21 Å. The mercury atom is 0.30 Å above the plane containing S, N(3), and Cl(2). This coordination geometry is different from that of thiosemicarbazidedichlorozinc(II), in which the two crystallographically independent molecules are tetrahedrally coordinated.

However, the large angle found for ∠Cl(2)-HgS, 157.3°, indicated the preference of diagonal coordination in many mercury complexes (6). An alternative description is 'two plus two coordination'. There are two strong and nearly linear S—Hg—Cl bonds and two weak Cl—Hg—N bonds. The Hg—Cl bonds are not equivalent. The attraction between the two molecules is surprisingly weak with a Hg···S distance of 3.65 Å in contrast to the interaction found in other compounds (7).

The five-membered chelating ring is relatively flat; the maximum deviation from the least-squares plane is 0.14 Å. The ∠NNC and ∠NCS angles are greater than 120° for both the mercury and zinc complexes, but values for these angles in nickel complexes and the free tsc are close to 120° (8). The bond lengths for the tsc ligand are normal. The planarity, however, is not as good as that of free tsc or tsc in $HgCl_2(tsc)_2$ (1). The dihedral angle for NNCS is 5.5° for $HgCl_2(tsc)$.

The molecules are held together by very weak N—H···Cl hydrogen bonds. The significant short intermolecular distances are: Cl(1)···N(2) = 3.20(2), Cl(1)···N(1) = 3.22(2), Cl(2)···N(3) = 3.27(2), and Cl(2)···N(1) = 3.40(2) Å.

[1]Copies of the tables of structure factors and temperature parameters may be obtained, at a nominal charge, from the Depository of Unpublished Data, CISTI, National Research Council of Canada, Ottawa, Ont., Canada K1A 0S2.

TABLE 1. Final atomic parameters with estimated standard deviations $\pm(x, y, z; x, \frac{1}{2} - y, \frac{1}{2} + z)$

Atom	x	y	z
Hg	0.1440(1)	−0.0109(2)	0.17906(6)
Cl(1)	0.4236(6)	0.0113(1)	0.3196(4)
Cl(2)	0.0033(7)	−0.0826(10)	0.3219(5)
S	0.2025(8)	0.1461(10)	0.0127(5)
N(1)	0.3686(19)	0.0052(46)	−0.1278(15)
N(2)	0.3080(25)	−0.2215(33)	−0.0057(17)
N(3)	0.2316(21)	−0.2960(36)	0.7067(15)
C	0.2985(21)	−0.0378(35)	−0.0431(15)

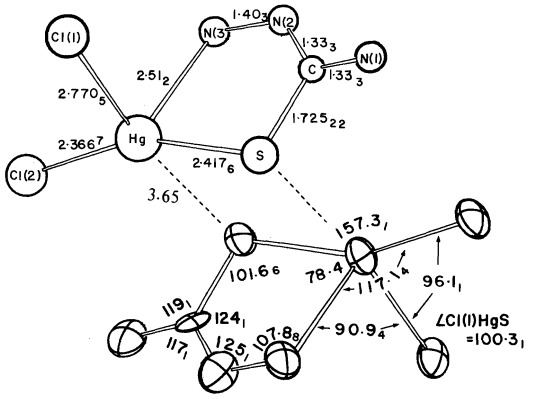

FIG. 1. Bond lengths and angles for thiosemicarbazidedichloromercury(II). The two molecules are related to each other by a center of symmetry. The estimated standard deviations are given by the small numbers referred to the last digits.

The chemical shifts, τ, of the hydrogens for tsc, $HgCl_2(tsc)$, and $HgCl_2(tsc)_2$ are given in Table 2. The assignment was made in comparison with the nmr spectra of thioacetamide, *N*-methylthiourea, and 4-methylthiosemicarbazide (9). Upon complexing, the CNH_2 and NH protons shift down field. In $HgCl_2(tsc)$, the protons of the bonded NH_2 group gave a very broad peak which overlapped with the also

TABLE 2. Chemical shifts, τ, of mercuric chloride and thiosemicarbazide complexes (ppm)

Bond	tsc	$HgCl_2$·tsc	$HgCl_2(tsc)_2$
N—NH_2	4.51	4.6[a]	4.78
C—NH_2	7.30	8.46	8.32
N—H	8.58	10.00	9.62

[a]A very broad peak due to NH_2 overlapped with the peak of the impurity in DMSO-d_6.

broadened peak due to H_2O present as impurity in DMSO. It is not clear whether the NNH_2 group is coordinated to the mercury in DMSO solution, since the solvent interacts rather strongly with the mercuric ion. The small net chemical shift for the NNH_2 proton in $HgCl_2$-(tsc) reflects this tendency.

1. C. CHIEH. Can. J. Chem. **55**, 1583 (1977).
2. L. CAVALCA, M. NARDELLI, and G. BRANCHI. Acta Crystallogr. **13**, 688 (1968).
3. P. COPPENS, L. LEISEROWITZ, and D. ROBINOVICH. Acta Crystallogr. **18**, 1035 (1965).
4. D. T. CROMER and J. T. WABER. Acta Crystallogr. **18**, 104 (1965).
5. D. T. CROMER. Acta Crystallogr. **18**, 17 (1965).
6. D. GRDENIC. Q. Rev. **19**, 303 (1965).
7. C. CHIEH and L. P. C. LEUNG. Can. J. Chem. **54**, 3077 (1976).
8. R. G. HAZELL. Acta Chem. Scani. **22**, 2171 (1968); **22**, 2809 (1968).
9. C. J. POUCHERT. The Aldrich library of nmr spectra. Vol. 3. Aldrich Chemical Co. Inc., WI. 1974. pp. 144–145.

Etude conformationnelle par spectroscopie photoélectronique de sulfures de bithiényle

P. MEUNIER

Laboratoire de Polarographie Organique (LA 33), Faculté des Sciences Gabriel, Bd Gabriel, 21000, Dijon, France

ET

G. PFISTER-GUILLOUZO[1]

Laboratoire de Chimie Organique Physique, I.U.R.S., Avenue Philippon, 64000 Pau, France

Reçu le 11 mai 1977

P. MEUNIER et G. PFISTER-GUILLOUZO. Can. J. Chem. **55**, 3901 (1977).

Les sulfures de bithiényle-3,3′ et de bithiényle-2,2′ ont fait l'objet d'une étude par spectroscopie photoélectronique. L'analyse de ces données expérimentales a permis de proposer pour ces composés des conformations privilégiées de nature différente selon l'orientation des substituants.

P. MEUNIER and G. PFISTER-GUILLOUZO. Can. J. Chem. **55**, 3901 (1977).

3,3′-Bithienyl and 2,2′-bithienyl sulfides have been studied by photoelectron spectroscopy. Experimental data allow one to suggest different preferential conformations according the orientation of the substituents.

Introduction

Les oxyde et sulfure de biphényle, substitués ou non, ont fait l'objet d'études conformationnelles nombreuses. Divers travaux effectués par dipolemétrie (1–4), diffraction de rayons X (5–9), spectroscopie d'absorption dans l'ultraviolet (10, 11) et diffraction électronique (12) ont permis à leurs auteurs de conclure sans ambiguïté à la prédominance de formes non planes, l'existence privilégiée d'une forme asymétrique semblant, en revanche, beaucoup moins bien établie.

Récemment, dans le cas du sulfure de bipyridyle-2,2′ Chachaty et coll. (13), par une étude en rmn, concluent à l'existence de formes symétriques, twistées de 36° par rapport au plan CSC central.

Dans la série des sulfures de bithiényle, aucune étude n'a, à notre connaissance, été entreprise. Nous avons tenté d'aborder ce problème, comme dans le cas des bithiényles (14) et certains de leurs dérivés hétéropontés (15) à l'aide de la spectroscopie photoélectronique, en étudiant, parallèlement aux sulfures de bithiényle eux-mêmes, des dérivés dibromés susceptibles, a priori, de présenter des conformations hautement privilégiées.

Sulfure de bithiényle-3,3′ et dérivés

Spectres expérimentaux

Les spectres sont reproduits dans les figs 1–3,

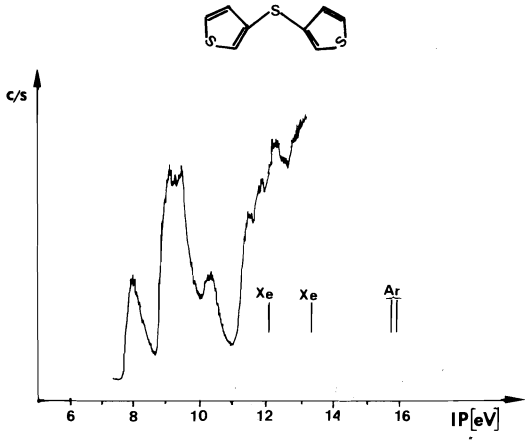

FIG. 1. Spectre photoélectronique du sulfure de bithiényle-3,3′.

et les valeurs des potentiels d'ionisation sont indiquées dans le tableau 1.

Le spectre photoélectronique du sulfure de bithiényle-3,3′ présente, entre 8 et 11 eV, trois bandes: (*a*) une première bande, peu intense, à 8.06 eV; (*b*) une deuxième bande, très intense, pour laquelle on observe distinctement deux potentiels à 9.16 et 9.50 eV; (*c*) une troisième bande, peu intense, à 10.40 eV.

Les spectres des deux dérivés dibromés étudiés sont assez semblables à celui du sulfure de bithiényle lui-même. La seule différence notable est l'écart sensiblement plus important observé entre les troisième et quatrième potentiels d'ionisation dans le cas du dérivé dibromé en 2,2′.

[1]A qui toute demande d'information devra être adressée.

TABLEAU 1. Potentiels d'ionisation (verticaux) du sulfure de bithiényle-3,3′ et de ses dérivés dibromés en 2,2′ et 4,4′

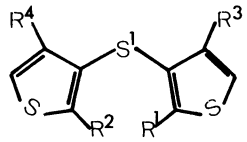

Attribution	$\pi_{C=C}$	π_S	$\pi_{C=C}$	π_S	π_{S1}	σ_{Br}*	π_{Br}*
$R^1=R^2=R^3=R^4=H$	8.06	9.16		9.50	10.40		
$R^1=R^2=Br$; $R^3=R^4=H$	8.10	8.80	9.00	9.55	10.40	10.85	11.40
$R^1=R^2=H$; $R^3=R^4=Br$	8.20	9.00		9.40	10.30	10.80	11.45

*Pour tous les composés examinés l'interaction entre le système π des cycles thiophéniques et la paire du brome de même symétrie conduit à une stabilisation nette de cette dernière.

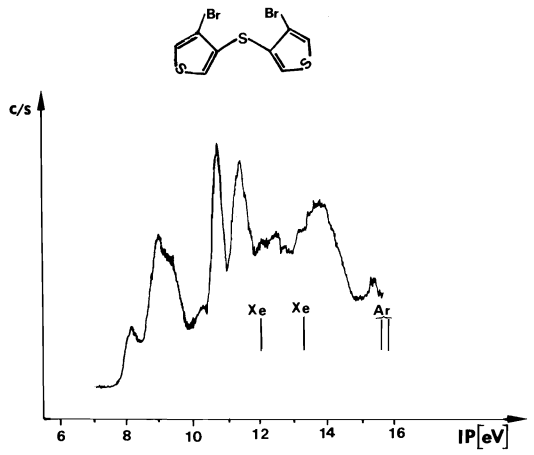

FIG. 2. Spectre photoélectronique du dibromo-4,4′ sulfure de bithiényle-3,3′.

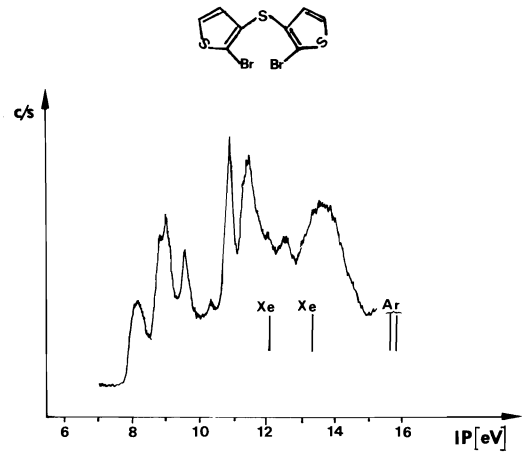

FIG. 3. Spectre photoélectronique du dibromo-2,2′ sulfure de bithiényle-3,3′.

Dans le cas des sulfures de bithiényles, les interactions entre le groupement sulfure et les noyaux thiophéniques seront très différenciées selon l'angle entre la paire π de l'atome de soufre et les deux cycles thiophéniques et selon la conformation de la molécule. En effet, pour une molécule plane ou présentant une certaine symétrie, l'influence du soufre ne se traduira que par une interaction destabilisante sur les orbitales totalement symétriques. Par contre, cette influence sera, pour une conformation dissymétrique, non négligeable pour tous les potentiels d'ionisation considérés.

On note dans les spectres des trois composés étudiés des bandes aux environs de 9 et 9.5 eV, valeurs très proches de celles observées pour le thiophène, le bromo-2 thiophène et le bromo-3 thiophène.

Ceci ne s'interprète que dans le cadre des hypothèses suivantes: (*a*) interaction négligeable entre les deux noyaux thiophéniques et quasi dégénérescence des combinaisons antisymétrique et symétrique des orbitales A_2 et $2B_1$ du thiophène; (*b*) interaction nulle entre les combinaisons antisymétriques des orbitales A_2 et $2B_1$ du thiophène et l'orbitale π du soufre du groupement sulfure.

On est donc conduit à penser que ce sulfure de bithiényle existerait plutôt sous une conformation pseudo-symétrique présentant une rotation des deux cycles en sens opposés, c'est-à-dire l'une ou l'autre des deux conformations suivantes.

L'ensemble du spectre s'interprète ainsi compte tenu des seules interactions entre la paire π de l'atome de soufre du groupement sulfure et les combinaisons symétriques des orbitales A_2 et $2B_1$ des noyaux thiophéniques (fig. 4).

TABLEAU 2. Potentiels d'ionisation calculés pour le sulfure de bithiényle-3,3′ (conformation **1**)

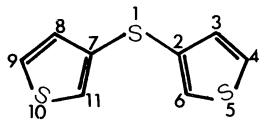

Potentiels d'ionisation (verticaux) expérimentaux (eV)	Valeurs théoriques (eV)	Contribution des orbitales atomiques (%)	Nature	Symétrie
8.06	9.30	$S_1=26$; $C_2=C_7=8$; $C_4=C_9=5$; $S_5=S_{10}=2$; $C_6=C_{11}=10$	π	B
9.16	10.45	$S_1=10$; $C_3=C_8=11$; $C_4=C_9=6$; $S_5=S_{10}=14$; $C_6=C_{11}=2$	π	B
9.16	10.50	$C_2=C_7=4$; $C_3=C_8=6$; $C_4=C_9=13$; $C_6=C_{11}=14$	π	A
9.50	10.80	$C_2=C_7=6$; $C_3=C_8=5$; $S_5=S_{10}=25$	π	A
10.40	11.85	$S_1=49$; $C_2=C_7=2$; $C_4=C_9=2$	π	B

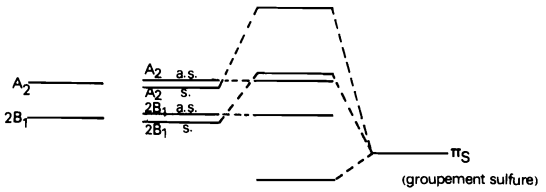

FIG. 4. Interactions orbitalaires mises en jeu: sulfure de bithiényle-3,3′.

Les considérations précédentes ne permettent pas de définir la conformation adoptée préférentiellement par les molécules de sulfure de bithiényle-3,3′; afin de chercher à préciser ce point, nous avons examiné les spectres des dérivés dibromés en 4,4′ et 2,2′.

Dans les deux cas on peut remarquer tout d'abord que, contrairement à ce qui a été signalé pour les dibromobithiényles (14) (qui pourtant présentent un angle de rotation important des deux cycles thiophéniques) on n'observe pas d'éclatement entre les paires libres des atomes de brome. Ce fait peut être attribué à un éloignement beaucoup plus grand entre ces deux atomes.

Dans le cas du dibromo-4,4′, un tel éloignement ne peut se concevoir que pour une conformation de type **1** assez "twistée." La stabilisation du premier potentiel (alors qu'on attend un effet destabilisant du brome) et la destabilisation du cinquième potentiel conduisent par rapport aux dérivé non substitué à conclure à une interaction légèrement plus faible entre le soufre central et les noyaux thiophéniques et donc à l'existence d'une conformation plus twistée.

Dans le cas du dibromo-2,2′, le maximum d'éloignement entre les deux atomes de brome ne peut être obtenu que pour une conformation de type **2**, assez fortement "twistée."

Nous avons cherché à confirmer les hypothèses précédemment formulées par une comparaison des données expérimentales avec les résultats tirés de calculs CNDO/S (tableaux 2 et 3) pour une conformation de type **1** et une conformation de type **2** (chaque noyau thiophénique faisant un angle de 30° avec le plan du groupe sulfure). Nous n'avons indiqué la contribution relative des orbitales atomiques que pour la conformation **1**, les résultats obtenus pour la conformation **2** étant très voisins. A noter que les deux structures choisies pour effectuer les calculs correspondent sensiblement à un contact de van der Waals entre les hydrogènes H_2 et $H_{2'}$ (conformation **1**) et H_4 et $H_{4'}$ (conformation **2**), ce type de conformation préférentielle ayant souvent été mis en évidence dans des problèmes du même type (13, 16, 17).

L'examen des tableaux 2 et 3 conduit aux remarques suivantes: (*a*) les spectres calculés

TABLEAU 3. Potentiels d'ionisation calculés pour le sulfure de bithiényle-3,3′ (conformation **2**)

Potentiels d'ionisation (verticaux) expérimentaux (eV)*	Valeurs théoriques (eV)	Nature	Symétrie
8.10	9.60	π	B
8.80	10.30	π	B
9.00	10.40	π	A
9.55	10.90	π	A
10.40	11.80	π	B

*Dérivé dibromé en positions 2 et 2′.

pour les deux conformations sont assez semblables, ce qui correspond bien aux spectres expérimentaux; (*b*) toutefois on constate sur les spectres calculés un écart entre les deux premiers potentiels d'ionisation plus faible (0.7 eV) pour une conformation de type **2** que pour celle de type **1** (1.1 eV).

Cette constatation s'accorde bien avec l'expérience, et ce compte tenu de la différence d'effet d'un atome de brome en α et en β.

L'étude des spectres photoélectroniques amène donc à proposer une structure de type **1** pour le sulfure de bithiényle lui-même et son dérivé dibromé en 4,4′, le dibromo-2,2′ présentant par contre une conformation privilégiée de type **2**.

Le fait que le sulfure de bithiényle-3,3′ présente des conformations différentes selon la substitution est d'ailleurs confirmé par l'allure nettement différenciée des spectres électroniques de ces mêmes dérivés.[2] En effet, pour le dérivé dibromé en 4,4′, les deux bandes de moyenne intensité à 271 et à 259 nm dans le *n*-heptane sont à rapprocher de celles observées à 278 et à 249 nm pour le dérivé non substitué. Au contraire, pour le dérivé dibromé en 2,2′ on observe une bande à 292 nm et un massif très intense aux environs de 240 nm.

Sulfure de bithiényle-2,2′ et dérivés

Spectres expérimentaux

Les spectres sont reproduits dans les figs 5–7 et les valeurs des potentiels d'ionisation sont rassemblées dans le tableau 4.

On constate que ces spectres sont assez semblables pour tous les composés considérés et comprennent: (*a*) une première bande, peu intense, aux environs de 8.5 eV; (*b*) une deuxième bande, très intense, entre 9 et 9.5 eV qui apparaît plus ou moins résolue selon le composé considéré; celle-ci résulte sans doute du recouvrement de plusieurs ionisations; (*c*) enfin, une dernière bande peu intense aux environs de 10.2 eV; celle-ci apparaissant sous forme d'un épaulement dans le cas du sulfure de bithiényle lui-même.

Discussion des résultats

Comme dans le cas du sulfure de bithiényle-3,3′: (*a*) on retrouve dans le spectre deux bandes aux environs de 9 et 9.5 eV; (*b*) on n'observe pas d'éclatement des paires libres des atomes de brome, ce qui nous incite à proposer une

[2]P. Meunier. Travaux non publiés.

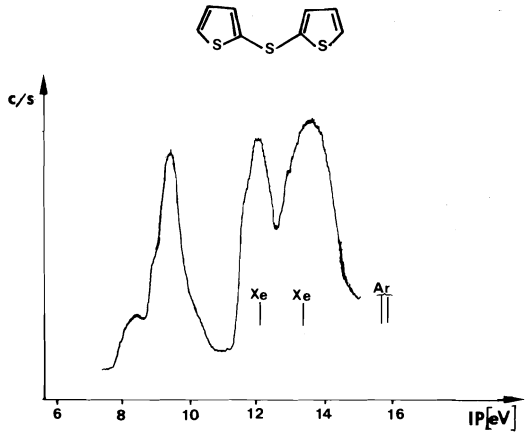

FIG. 5. Spectre photoélectronique du sulfure de bithiényle-2,2′.

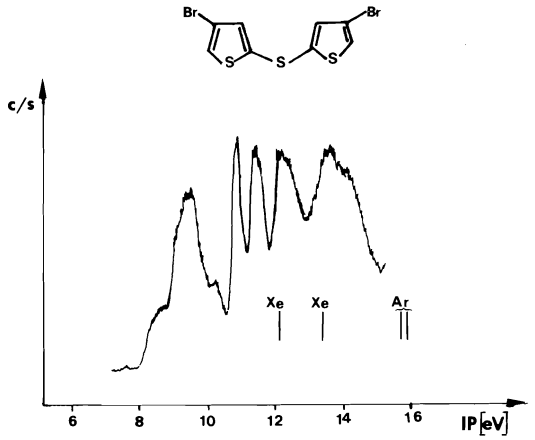

FIG. 6. Spectre photoélectronique du dibromo-4,4′ sulfure de bithiényle-2,2′.

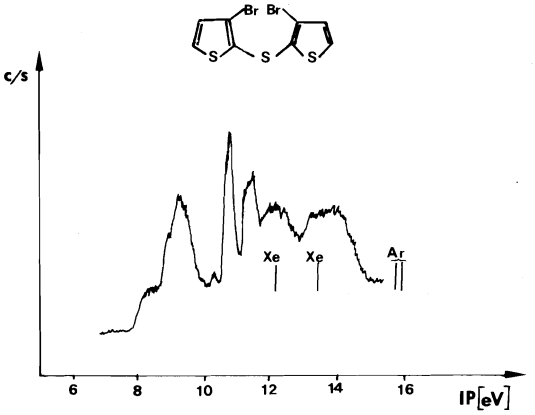

FIG. 7. Spectre photoélectronique du dibromo-3,3′ sulfure de bithiényle-2,2′.

TABLEAU 4. Potentiels d'ionisation (verticaux) du sulfure de bithiényle-2,2′ et de ses dérivés dibromés en 4,4′ et 3,3′

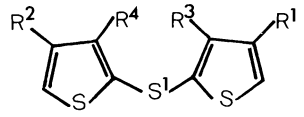

Attribution	$\pi_{C=C}$	$\pi_{C=C}$	π_S	π_S	π_{S1}	σ_{Br}*	π_{Br}*
$R^1=R^2=R^3=R^4=H$	8.40	8.95	9.45		10.15		
$R^1=R^2=Br$, $R^3=R^4=H$	8.60	9.00	9.25	9.50	10.20	10.90	11.45
$R^1=R^2=H$, $R^3=R^4=Br$	8.50	8.95	9.15	9.45	10.30	10.70	11.45

*Confer tableau 1.

conformation pseudo-symétrique correspondant à une rotation en sens inverse des deux cycles thiophéniques.

De plus, étant donné la position même du premier potentiel d'ionisation, il semblerait que les interactions schématisées dans la fig. 8, entre la paire libre du soufre du groupement sulfure et les deux combinaisons symétriques des orbitales A_2 et $2B_1$ soient faibles. Ceci correspondrait ainsi, pour l'une ou l'autre des deux conformations envisageables **3** ou **4**, à un angle de rotation relativement important.

Nous avons enregistré également le spectre d'un dérivé plus encombré stériquement: celui du diiodo-3,3′ sulfure de bithiényle-2,2′. Bien que, dans ce cas, il y ait superposition partielle des ionisations dues aux atomes d'iode avec celles des cycles thiophéniques, les valeurs observées pour les cinq premiers potentiels d'ionisation sont très voisines de celles signalées pour son analogue bromé. Ceci semble indiquer que la conformation préférentielle d'un dérivé disubstitué en 3,3′ doit être celle pour laquelle les deux substituants sont le plus éloignés possible. Cette conformation, compatible avec l'encombrement relatif des atomes de soufre, doit être de type **3**.

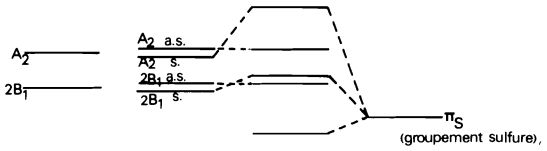

FIG. 8. Interactions orbitalaires mises en jeu: sulfure de bithiényle-2,2′.

Pour cette conformation remarquons que les atomes de soufre thiophéniques sont au contact de van der Waals pour un angle de chacun des deux cycles avec le plan CSC d'environ 50°.

Si l'on compare le dérivé dibromé en 4,4′ (pour lequel, on peut raisonnablement ne considérer que l'effet électronique) avec le dibromo-3,3′ (où intervient de plus l'effet stérique des substituants), on constate pour le composé le plus encombré, une destabilisation de 0.1 eV des premier et troisième potentiels d'ionisation et une stabilisation à peu près équivalente du potentiel d'ionisation associé à l'orbitale π du groupement sulfure. Cet effet peut être attribué à une interaction sensiblement plus grande entre les cycles et le soufre central.

Si l'on supposait que tous les composés examinés présentent une disposition spatiale du même type, la destabilisation observée lors de la substitution en 3,3′ ne pourrait s'expliquer que par un angle moins grand, entre les deux cycles, ce qui est tout à fait contradictoire avec l'effet stérique apporté par deux atomes de brome, *a fortiori* par deux atomes d'iode.

Il est vraisemblable au contraire que la substitution en position stériquement encombrée a un effet similaire à celui observé pour le sulfure de bithiényle-3,3′, c'est-à-dire modifie la conformation privilégiée de la molécule. On est donc tout naturellement amené à proposer pour le sulfure de bithiényle-2,2′ et son dérivé dibromé en 4,4′, une conformation du type **4**, avec un angle de torsion du même ordre que celui proposé pour la conformation de type **3**.

Nous avons rassemblé dans les tableaux 5 et 6 les résultats obtenus par la méthode CNDO/S pour les deux conformations **3** et **4** comme pour le sulfure de bithiényle-3,3′, nous n'avons indiqué les contributions des orbitales atomiques que pour l'une des deux conformations (chaque

TABLEAU 5. Potentiels d'ionisation calculés pour le sulfure de bithiényle-2,2′ (conformation **4**)

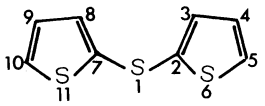

Potentiels d'ionisation (verticaux) expérimentaux (eV)	Valeurs théoriques (eV)	Contribution des orbitales atomiques (%)	Nature	Symétrie
8.40	9.40	$S_1=25$; $C_2=C_7=10$; $C_3=C_8=5$; $C_5=C_{10}=8$	π	B
8.95	10.45	$C_2=C_7=10$; $C_3=C_8=3$; $C_4=C_9=7$; $C_5=C_{10}=10$	π	A
9.45	10.78	$S_1=5$; $C_3=C_8=6$; $C_4=C_9=4$; $S_6=S_{11}=16$	π	B
9.45	10.90	$C_3=C_8=7$; $C_4=C_9=3$; $S_6=S_{11}=22$	π	A
10.15	11.10	$S_1=46$; $C_4=C_9=3$; $C_5=C_{10}=3$; $S_6=S_{11}=6$	π	B

TABLEAU 6. Potentiels d'ionisation calculés pour le sulfure de bithiényle-2,2′ (conformation **3**)

Potentiels d'ionisation (verticaux) expérimentaux (eV)*	Valeurs théoriques (eV)	Nature	Symétrie
8.50	9.40	π	B
8.95	10.40	π	A
9.15	10.55	π	B
9.45	11.10	π	A
10.30	11.20	π	B

*Dérivé dibromé en positions 3 et 3′.

noyau thiophénique faisant un angle de 50° avec le plan CSC central).

On constate tout d'abord une assez bonne concordance entre les valeurs théoriques et les valeurs expérimentales, concordance qui se traduit d'ailleurs par deux spectres théoriques assez voisins parallèlement à ce qui est observé expérimentalement.

De plus, on remarque dans le spectre théorique, pour la conformation **3**, une destabilisation du troisième potentiel d'ionisation et une stabilisation du cinquième potentiel d'ionisation. Ces constatations sont en excellent accord avec les caractéristiques spectrales signalées pour les deux dérivés dibromés.

Dans ce cas également l'hypothèse avancée de deux conformations différentes selon la substitution est confirmée par l'allure des spectres électroniques. Les dérivés substitués en positions 3 et 3′ présentent en effet un massif unique aux environs de 260 nm alors que les absorptions du produit non substitué et de son dérivé dibromé en 4,4′ correspondent à deux bandes à 270 et 240 nm.

Partie expérimentale

Synthèses

Les dibromo et diiodo thiophènes ont été obtenus selon les données de la littérature citées en référence: dibromo-2,4 thiophène: p $éb_{70}$: 120–125°C (litt. (19) p $éb_{9-10}$ 83–85°C); dibromo-3,4 thiophène: p $éb_{20}$: 115–120°C (litt. (20) p $éb_{12}$ 94–95°C); diiodo-2,3 thiophène: p $éb_{15}$: 160–163°C (litt. (21) p $éb_{11}$ 135–140°C). Le bromo-3 iodo-2 thiophène a été synthétisé par action du mélange iode – acide iodique sur le bromo-3 thiophène selon les modalités décrites pour la synthèse des bromoiodo thiéno(2,3-*b*) thiophènes (22). Au départ de 163 g (1 mol) de bromo-3 thiophène, on isole 260 g (rdt 90%) de dérivé bromoiodé: p $éb_{0.5}$ 87–90°C. *Anal.* calc. pour C_4H_2SBrI: C 16.63, H 0.70, S 11.10, Br 27.66, I 43.92; trouvé: C 16.9, H 0.8, S 11.3, Br 27.5, I 43.7. Caractéristiques rmn ($CDCl_3$): H_β: d/1, δ 6.92 ppm; H_α: d/1, δ 7.43 ppm; $J_{\alpha\beta}$ = 4.8 Hz.

Les sulfures de bithiényle ont été obtenus par action du sulfure de bis-phényl sulfonyle sur les thiényl-2 et thiényl-3 lithium selon les modalités opératoires proposées par De Jong et Janssen (23). Les sulfures ainsi obtenus ont été purifiés par chromatographie en phase gazeuse.

Sulfure de bithiényle-2,2′—Température de la colonne 235°C; temps de rétention 8.6 min; débit d'hélium 200 cm^3/min.

Sulfure de bithiényle-3,3′—Température de la colonne 255°C; temps de rétention 6.9 min; débit d'hélium 200 cm^3/min.

Les sulfures de bithiényles dihalogénés ont pour la plupart été synthétisés par action à −70°C d'une demi-mol de dichlorure de soufre ou de sulfure de bisphényl-sulfonyle sur l'organolithien obtenu par action de 1 mol de *n*-butyllithium sur 1 mol de dihalogéno thiophène convenable. Les caractéristiques des réactions sont rassemblées dans le tableau 7.

Quant au dibromo-2,2′ sulfure de bithiényle-3,3′, il a été obtenu par action du *N*-bromo succinimide sur le sulfure de bithiényle-3,3′ selon le mode opératoire suivant: 4 g (0.02 *M*) de sulfure de bithiényle-3,3′ sont

TABLEAU 7. Obtention des sulfures de dihalogeno bithiényles

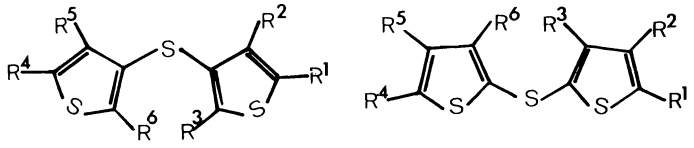

Thiophène substitué	Réactif utilisé après action du *n*-butyllithium	Produit obtenu	Méthodes de purification	Solvant de recristallisation	Rdt (%)
I-2,Br-3	SCl_2 $S(C_6H_5SO_2)_2$	**1** $R^3=R^6=Br$ $R^1=R^2=R^4=R^5=H$	Chromatographie sur gel de silice (éther de pétrole, 40–65°C)	Pentane	41 70
diBr-2,4	$S(C_6H_5SO_2)_2$	**1** $R^2=R^5=Br$ $R^1=R^3=R^4=R^6=H$	Chromatographie sur gel de silice (éther de pétrole)	Pentane	54
diBr-3,4	$S(C_6H_5SO_2)_2$	**2** $R^2=R^5=Br$ $R^1=R^3=R^4=R^6=H$	Distillation puis chromatographie en phase vapeur*		68
diI-2,3	SCl_2 $S(C_6H_5SO_2)_2$	**1** $R^3=R^6=I$ $R^1=R^2=R^4=R^5=H$	Chromatographie sur gel de silice (éther de pétrole)	Ether de pétrole	46 72

*Température de colonne 265°C; temps de rétention 7.9 min; débit d'hélium 250 cm³/min.

TABLEAU 8. Caractéristiques des composés obtenus

Composés	Caractéristiques physiques		Analyse (%)						Caractéristiques rmn
	Ce travail	Litt.	Calc. ou Tr.	C	H	S	Br	I	
				Sulfures de bithiényle-2,2′					
DiBr-3,3′	pf 56°C	pf 54–55°C (23)							H_2,H_6: d/2 δ=7.30 ($CDCl_3$) H_3,H_7: d/2 δ=6.95 $J_{2,3}$=5.3 Hz Litt. (23) (CD_3COCD_3) H_2,H_6: d/2 δ=7.63 H_3,H_7: d/2 δ=7.10 $J_{2,3}$=5.2 Hz
DiBr-4,4′	pf 29–30°C		Calc. Tr.	26.98 26.7	1.13 1.1	27.01 26.8	44.88 44.8		H_2,H_6: d/2 δ=7.20 (CCl_4) H_4,H_8: d/2 δ=7.08 $J_{2,4}$=1.5 Hz
DiI-3,3′	pf 87°C		Calc. Tr.	21.33 21.2	0.89 1.0	21.37 21.3		56.41 56.3	H_2,H_6: d/2 δ=7.35 ($CDCl_3$) H_3,H_7: d/2 δ=7.05 $J_{2,3}$=5.5 Hz
				Sulfures de bithiényle-3,3′					
DiBr-2,2′	Huile		Calc. Tr.	26.98 27.1	1.13 1.1	27.01 26.9	44.88 45.0		H_2,H_6: d/2 δ=7.12 (CCl_4) H_3,H_7: d/2 δ=6.77 $J_{2,3}$=5.4 Hz
DiBr-4,4′	p $éb_{0.07}$ 180°C	p $éb_{0.06}$ 164–165°C (23)							H_2,H_6: d/2 δ=7.25 (CCl_4) H_5,H_9: d/2 δ=7.05 $J_{2,5}$=3.5 Hz Litt. (23) (CD_3COCD_3) H_2,H_6: d/2 δ=7.68 H_5,H_9: d/2 δ=7.33 $J_{2,5}$=3.4 Hz

dissous dans 50 cm³ de chloroforme anhydre. A cette solution vigoureusement agitée sont ajoutés par petites fractions 7.1 g (0.04 *M*) de *N*-bromo succinimide. Le milieu réactionnel est maintenu 5 h à température ambiante puis traité par 30 cm³ d'eau. Le mélange est extrait au chloroforme et les phases organiques sont séchées, évaporées et le résidu obtenu est chromatographié sur gel de silice (éluant éther de pétrole). On isole 4.5 g (rdt 63%) d'une huile incolore. La purification est complétée par chromatographie en phase gazeuse: température de la colonne 235°C; temps de rétention 7.1 min; débit d'hélium 250 cm³/min. Les caractéristiques des sulfures dihalogénés synthétisés sont rassemblées dans le tableau 8.

Spectroscopie photoélectronique

L'étude spectroscopique a été réalisée sur un appareil Perkin-Elmer PS 18 muni d'une source à hélium I (21.21 eV ou 584 Å). Les spectres ont été calibrés à l'aide des pics associés aux doublets $^2P_{1/2}$ et $^2P_{3/2}$ de l'argon (15.755 et 15.933 eV), et du xénon (12.127 et 13.427 eV). Les potentiels d'ionisation sont estimés à ± 0.02 eV près.

Chromatographie en phase gazeuse

L'appareil utilisé était un chromatographe Aerograph Autoprep 700. La colonne présentait les caractéristiques suivantes: longueur 609.6 cm; diamètre 9.5 mm; phase stationnaire Chromosorb WAW, 45–60 mesh imprégné de SE30 à 15%.

Calculs

Ils ont été effectués à l'aide de la méthode CNDO/S étendue à la troisième période avec intervention des orbitales *d* (24). Les géométries utilisées ont été déduites des valeurs expérimentales indiquées pour le thiophène (25) et de celles couramment utilisées pour les dérivés sulfurés: longueur C—S = 1.76 Å (9), angle CSC = 100.0° (18).

1. K. Higasi et S. Uyeo. Bull. Chem. Soc. Jpn. **14**, 87 (1939).
2. M. Gomel, H. Lumbroso, N. Marziano et R. Passerini. Bull. Soc. Chim. Fr. 1908 (1959).
3. M. Aroney, R. J. W. Le Fevre et J. D. Saxby. J. Chem. Soc. 1167 (1963).
4. R. J. W. Le Fevre et J. S. Saxby. J. Chem. Soc. B, **11**, 1064 (1966).
5. J. Toussaint. Mem. Soc. R. Sci. Liège, **12**, 1 (1952).
6. K. Plieth. Z. Naturforsch. Teil A, **2**, 409 (1927).
7. J. Toussaint. Bull. Soc. R. Sci. Liège, **15**, 96 (1948).
8. N. E. Blackmore et S. Abrahams. Acta Crystallogr. **8**, 329 (1955).
9. J. Toussaint. Bull. Soc. Chim. Belge, **54**, 319 (1945).
10. A. Mangini et R. Passerini. J. Chem. Soc. 1168 (1952).
11. C. C. Price et H. Morita. J. Am. Chem. Soc. **75**, 4747 (1953).
12. K. Higasi, S. Uyeo et S. Yamaguchi. Bull. Inst. Phys. Chem. Res. **23**, 506 (1947).
13. C. Chachaty, G. C. Pappalardo et G. Scarlata. J. Chem. Soc. Perkin Trans. II, **11**, 1234 (1976).
14. P. Meunier, M. Coustale, C. Guimon et G. Pfister-Guillouzo. J. Mol. Struct. **36**, 233 (1977).
15. P. Meunier et G. Pfister-Guillouzo. Can. J. Chem. Sous presse.
16. A. Almenningen, O. Bastiansen et P. Svendsas. Acta Chem. Scand. **12**, 1671 (1958).
17. M. Grimaud, M. Loudet, R. Royer et G. Pfister-Guillouzo. Bull. Soc. Chim. **5–6**, 1161 (1974).
18. E. Pai. Indian J. Phys. **9**, 121 (1934).
19. S. O. Lawesson. Ark. Kemi. **11**, 317 (1957).
20. S. Gronowitz. Acta Chem. Scand. **13**, 1045 (1959).
21. S. Gronowitz et V. Vilks. Ark. Kemi. **21**, 191 (1963).
22. P. Meunier et P. Fournari. Bull. Soc. Chim. **3–4**, 587 (1974).
23. F. de Jong et M. J. Janssen. J. Org. Chem. **36**, 1645 (1971).
24. C. Guimon, D. Gonbeau et G. Pfister-Guillouzo. Tetrahedron, **29**, 3399 (1973).
25. B. Bak, D. Christensen, L. Hansen-Nygard, et J. Rastrup-Andersen. J. Mol. Spectrosc. **7**, 56 (1961).

Studies of reagents for spectrophotometric measurement of ionic magnesium

DENNIS G. MCMINN

Department of Chemistry, Gonzaga University, Spokane, WA 99258, U.S.A.

AND

BYRON KRATOCHVIL

Department of Chemistry, University of Alberta, Edmonton, Alta., Canada T6G 2G2

Received December 22, 1976[1]

DENNIS G. MCMINN and BYRON KRATOCHVIL. Can. J. Chem. **55**, 3909 (1977).

Four mono-azo aryl dyes having the *o*-carboxy-*o'*-hydroxy functionality were investigated as reagents for the measurement of ionic Mg^{2+} in solutions containing complexing ligands. 2-(2'-Carboxyl-1'-benzeneazo)-1,8-dihydroxynaphthalene-3,6-disulfonic acid came closest to the ideal of having absorbance unaffected by p*H* over the p*H* range of interest and of differentiating between Ca^{2+} and Mg^{2+} complex formation. Ligand acid dissociation constants and formation constants for the metal–ligand complexes were measured.

DENNIS G. MCMINN et BYRON KRATOCHVIL. Can. J. Chem. **55**, 3909 (1977).

On a étudié quatre colorants mono-azo aryles ayant une fonction *o*-carboxy *o'*-hydroxy comme réactif pour la mesure de Mg^{2+} ionique dans des solutions contenant des ligands complexants. L'acide (carboxy-2' benzèneazo-1')-2 dihydroxy-1,8 naphthalène disulfonique-3,6 est celui qui se rapproche le plus de l'état idéal où l'absorption n'est pas affectée par le p*H* à des valeurs de p*H* intéressantes et où il est possible d'effectuer une différentiation entre la formation de complexes de Ca^{2+} et de Mg^{2+}. On a mesuré les constantes de dissociation acide des ligands et les constantes de formation des complexes métal–ligand.

[Traduit par le journal]

The measurement of free, or ionic, calcium and magnesium levels in biological systems is important because often the ionic concentration is of greater clinical significance than the total metal concentration. However, free metal ion levels (that is, aquated but not complexed to other species) are often difficult to determine in physiological fluids. The most widely used method of determining ionic calcium is the membrane ion selective electrode that, although of use in blood serum analysis, does not provide reliable results in urine. A corresponding ion selective electrode for magnesium is not yet available.

A second approach to the determination of ionic calcium or magnesium is by a spectrophotometric procedure involving formation of a weak but highly absorbing metal–ligand complex in a manner analogous to the measurement of p*H* by an indicator. The requirements of an indicator ligand for measurement of free metal ion concentration have been outlined by Scarpa (1). These include: (*a*) a small conditional formation constant for the metal ion of interest, but negligible tendency to complex other metals; (*b*) a large molar absorptivity for the metal–indicator complex at a wavelength free of interference from the uncomplexed ligand or other components of the sample; and (*c*) minimal side effects on the properties of the system under measurement. It is also advantageous if the spectrum and conditional formation constant of the metal–ligand complex undergo no appreciable change over a broad range of p*H*. In this way prior p*H* adjustment, which may shift equilibria and change ionic metal levels, can be avoided.

This approach has seen use in the determination of ionic concentrations of only two metals, calcium and magnesium. For calcium, murexide and tetramethylmurexide have been used as indicator ligands for measurements in urine and other biological systems (2). Tetramethylmurexide is the better of the two, but both have the disadvantage that the spectra of the free indicator and the calcium complex overlap extensively, and that the absorbance of the calcium complex fades relatively rapidly. Also, high concentrations of sodium interfere. For magnesium the most studied compounds have been of the *o,o'*-dihydroxyazoaryl class because the magnesium complexes of these ligands have high

[1]Revision received August 6, 1977.

molar absorptivities and are more stable than the corresponding calcium analogs. Eriochrome Blue SE and Calmagite (1, 3) have been investigated for this purpose; in each case calcium forms a complex of sufficient stability to interfere, and absorbance readings at two wavelengths are necessary to correct for the calcium present. Eriochrome Black T has also been studied (4); its properties and range of applicability are similar to the other two dyes.

Diehl and Ellingboe, in a study of the properties of a large number of azo dyes, demonstrated that complexation with calcium and magnesium occurs if one of the *ortho* positions in an azoaryl system is occupied by a hydroxyl group and the other by either a hydroxyl or carboxyl group (5). Further, they showed that conditional formation constants for calcium and magnesium are both smaller by a factor of about 100 when the second *ortho* position contains a carboxyl group. The hydroxyl–carboxyl combination is more attractive as a system for measuring ionic magnesium concentrations because a small formation constant minimizes disruption of equilibria already established in the system to be measured. Also, the larger acid dissociation constant of a carboxyl group increases the p*H* range over which the ligand possesses the same degree of protonation and the same spectral properties, which may permit measurement over a wider p*H* range without correction. In this work three compounds containing the *o*-carboxyl-*o'*-hydroxyl functionality were studied to obtain more information about the role of ligand structure in optimization of the measurement of ionic magnesium.

Experimental

Apparatus and Materials

Anthranilic acid (BDH) was purified by recrystallization from water using Norit-A (Fisher) and washing with cold water. Sodium 2-naphthol-6-sulfonate was purified by precipitation from water by bubbling in HCl gas, filtering, and washing with 30% aqueous HCl; brilliant white crystals were obtained (6). 2-Naphthol (British Drug House), chromotropic acid (practical grade, Eastman P-230 as disodium salt with two waters of hydration), and 3-methyl-1-phenyl-2-pyrazolin-5-one (Eastman 1397) were used as received.

Ammonia buffer, $\mu = 0.10$, was used for measurements at p*H* 10.1. A 0.0334 *M* solution of $MgCl_2$ was prepared and standardized by titration with standard 0.01 *M* EDTA. Stock solutions ($\sim 10^{-4}$ *M*) of sulfonated compounds were prepared in water; non-sulfonated compounds were dissolved in 98% ethanol. All solutions of the ligands were protected from light. Absorption spectra were obtained on a Unicam SP 1700 recording spectrophotometer. p*H* measurements were made on an Orion Model 801 digital p*H* meter. The meter and glass electrode were standardized with NBS standard buffers. Melting points were determined on a Fisher-Johns melting point apparatus and are uncorrected. Microanalyses were performed in the Microanalytical Laboratory, Department of Chemistry, University of Alberta, Edmonton, Alta. Thin layer chromatography (tlc) was performed on precoated Silica Gel 60 F-254 plates (Brinkmann) in a presaturated chamber (Gelman Model 51325) with 98% ethanol as eluting solvent.

The acid dissociation constants for the hydroxylic and carboxylic protons were determined by potentiometric titration with NaOH or by spectrophotometry. Values of pK_1 for the non-sulfonated ligands could not be determined in water because of insolubility at low p*H*. Formation constants for the magnesium and calcium complexes of the four ligands at p*H* 10.1 and $\mu = 0.10$ were determined by pipetting 1.0 ml of stock solution[2] of dye and an aliquot of stock solution of metal ion into a volumetric flask, adding KCl as necessary to adjust ionic strength, then diluting the solution to volume with NH_3–NH_4Cl buffer. Absorption measurements were made immediately after mixing because solutions of the complexes decompose slowly with time, especially when exposed to light. Calculations of the conditional formation constants were performed by the method of Ramette (7), using a BASIC computer program supplied by the author and modified for use on a Digital Equipment Corporation PDP-11 computer. In all cases the 'initial' metal ion concentrations were adjusted to take account of complexation by the ammonia present in the buffer solution. No spectrophotometric evidence for formation of ML_2 or higher complexes was found.

Preparation of Dyes

(*a*) 1-(2'-Carboxyl-1'-benzeneazo)-2-hydroxynaphthalene (**1**) was prepared according to the published method (5) and recrystallized from acetic acid: mp 275–277°C (lit. (8) 268°C; (9) 278°C; (5) 273.5–274.5°C). Thin-layer chromatography showed one spot ($R_f = 0.21$).

(*b*) 1-(2'-Carboxyl-1'-benzeneazo)-2-hydroxynaphthalene-6-sulfonic acid (**2**) (C.I. 15975) was prepared in an analogous manner from diazotized anthranilic acid and purified sodium 2-hydroxynaphthalene-6-sulfonate. It was isolated by bubbling in gaseous HCl, filtering the slurry as much as possible (sintered glass), then transferring to acetone. The suspension was warmed until the solid dissolved, then benzene added until precipitation began. The material was cooled, filtered, and washed with cold benzene. The hard brick-red solid was removed from the filter and dried under vacuum. Elemental analysis indicated the product was a mixture of the free acid and the sodium salt. Thin-layer chromatography showed one colored band which stretched from near the origin to

[2]In the approach used here the initial ligand concentration, and therefore the presence of non-complexing impurities in the dye, is not crucial since only differences in absorbances are necessary to measure the formation constant. Measurements of molar absorptivities of the ligand–metal complexes do, however, require knowledge of the analytical concentrations of both the ligand and the metal ion.

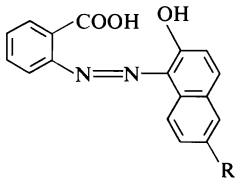

1, R = H
2, R = SO_3H

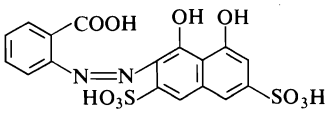

3

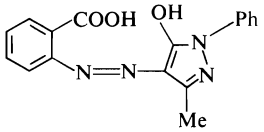

4

$R_f \sim 0.28$, and small spots of three colorless impurities at slightly higher R_f.

(*c*) 2-(2′-Carboxyl-1′-benzeneazo)-1,8-dihydroxynaphthalene-3,6-disulfonic acid (**3**) was prepared by slow addition of a cooled solution of diazotized anthranilic acid (7.25 mmol) to a solution of chromotropic acid (7.25 mmol) in 25 ml of 0.1 *M* NaOH. When the resulting solution was acidified with gaseous HCl a dark red solid precipitated. This material was filtered, washed with 30% aqueous HCl followed by a few drops of cold water, dried over calcium chloride, and ground to give a brick-red powder. The powder was taken up in methanol and added to the top of a 1.5 × 10 cm column containing 7.5 g of Amberlyst 15 strongly acidic cation exchange resin (Rohm and Haas, 120–325 mesh, de-fined). The resin had been converted previously into the hydrogen form by washing with HCl until free of sodium (flame test), with water until neutral, and finally with methanol until transparent in uv light. Elution of the dye mixture with additional methanol gave a dark eluate; a faint purple band remained on the column. The solid obtained on evaporation of the solvent from the eluate showed no sodium (flame test), no halogen (Beilstein test), and gave a ^1H nmr spectrum showing no aliphatic protons. Attempts to establish unambiguously the site of coupling on the chromotropic acid by ^{13}C and ^1H nmr were unsuccessful, but from reaction of other azo compounds with chromotropic acid the predicted position is *ortho* to one of the hydroxyl groups. Duplicate samples (82.7 mg and 77.2 mg) upon titration with NaOH gave equivalent weights of 184.6 and 186.7. From these results a formula $C_{17}H_{12}N_2O_{10}S_2 \cdot 5H_2O$ is proposed (equiv. wt. 186.2 based on three titrated protons). Thin-layer chromatography showed one spot ($R_f = 0.47$) plus a faint residue which remained at the origin. *Anal.* calcd. for $C_{17}H_{12}N_2O_{10}S_2 \cdot 5H_2O$: C 36.55, H 3.97, N 5.02, S 11.48; found (duplicate elemental analysis): C 36.36, 36.39, H 3.27, 3.09, N 4.51, 4.55, S 11.13, 10.08.

(*d*) 4-(2′-Carboxyl-1′-benzeneazo)-3-methyl-1-phenyl-2-pyrazolin-5-one (**4**) (C.I. 18690) was prepared by coupling diazotized anthranilic acid (7.25 mmol) to 3-methyl-1-phenyl-2-pyrazolin-5-one (7.25 mmol) dissolved in 25 ml of 0.3 *M* NaOH. Reaction was immediate at 5°C. The compound was isolated by filtration and recrystallized from ethanol–water giving fluffy orange crystals: mp 278–279°C. *Anal.* calcd. for $C_{17}H_{14}N_4O_3$: C 63.35, H 4.38, N 17.38; found (duplicate elemental analysis): C 62.10, 62.25, H 4.38, 4.36, N 17.04, 17.33.

Results

Figure 1 shows the absorption spectra for the four ligands studied, along with spectra of solutions of the ligand plus calcium or magnesium. In Fig. 2 are shown plots of spectral dependence on p*H* measured at selected wavelengths for each ligand. Table 1 summarizes the absorption data and Table 2 gives the experimentally determined acid dissociation constants and the conditional formation constants for the complexes of the four ligands with Mg^{2+} and Ca^{2+}. From these data equilibrium constants were calculated using the formula $K = K'\alpha_{ML}/\alpha_M\alpha_L$, where K is the equilibrium constant at $\mu = 0.10$; K' the conditional formation constant at $\mu = 0.10$, p*H* 10.1; α_{ML} the fraction of complex present in 1:1 ratio; α_M the fraction of uncomplexed metal present as aquated species; and α_L the fraction of uncomplexed dye present in the form available for complexing (10).

The value of α_L in each case was calculated from knowledge of K_a for the second acid dissociation constant of L and the p*H* at which K' was measured. α_{ML} was taken as 1.0, since no evidence for formation of other than 1:1 complexes was reported by Diehl and Ellingboe (5), nor was any detected in the present study. The other significant metal complex present, $M(NH_3)^{2+}$, was accounted for in determining the 'initial' metal concentration so α_M was also taken as 1.0. This could be done because the fraction of the total metal present that was converted to the metal ligand complex was less than 1% in all cases, and the ratio of the concentration of free M^{2+} to $M(NH_3)^{2+}$ was little affected by the addition of ligand. The results are tabulated in Table 2.

Discussion

Compounds **1–4** were synthesized and studied to provide information on the properties of azo dyes that might lead to improved reagents for the measurement of ionic magnesium levels over

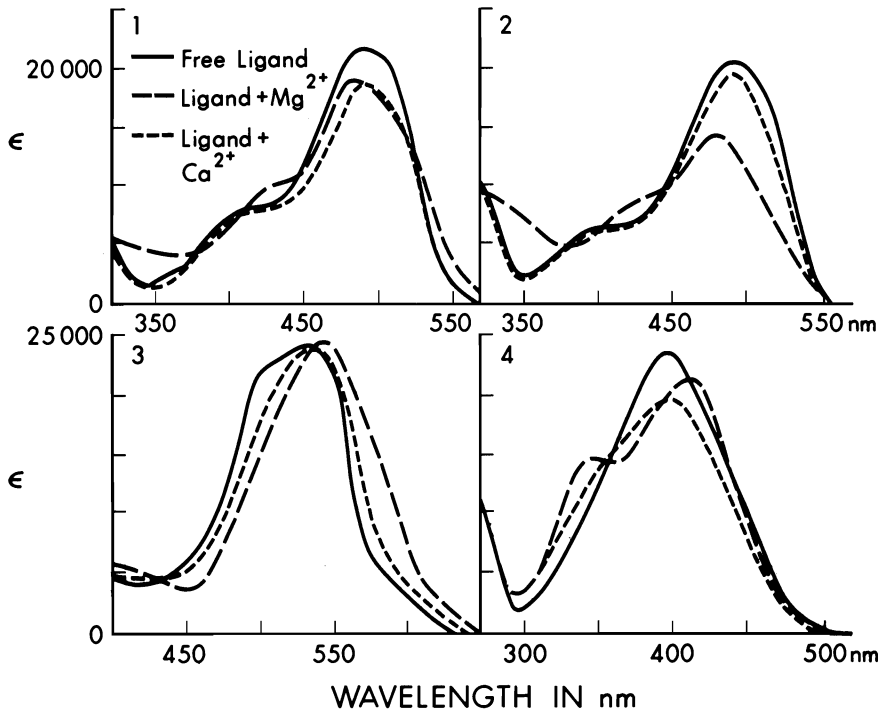

FIG. 1. Absorption spectra of ligand, ligand + Mg^{2+}, and ligand + Ca^{2+} ($[M^{2+}] \sim 10^{-3}$ *M*) at p*H* 10.1 and ionic strength 0.10. (*a*) 5×10^{-5} *M* **1**; (*b*) 2.7×10^{-5} *M* **2**; (*c*) 9.4×10^{-6} *M* **3**; (*d*) 1.8×10^{-5} *M* **4**.

a range of p*H*, particularly in the region of physiological p*H*. To achieve this goal the absorbance of the ligand must be independent of p*H* over the range of interest. All three of the *o*-carboxyl-*o'*-hydroxyl systems met this criterion over the range of p*H* 5 to 9. A second requirement is that the conditional formation constant for the magnesium–ligand complex not vary significantly over the p*H* range encountered in samples. Since K' depends on α_L, the p*K* of the hydroxyl group is the major factor determining the usable p*H* range. Thus compound **3**, which has the lowest p*K* for the hydroxyl group of the compounds studied, gives a spectral response to changes in Mg^{2+} concentration at lower p*H* values than do the other three compounds. Thirdly, the conditional formation constant between ligand and magnesium should be on the order of only a few hundred so that equilibria between ionic magnesium and other components of the sample are not greatly affected.

Diehl and Ellingboe (5) found the formation constants for complexes of the *o,o'*-substituted azoaryl ligands with magnesium to be greater than those for calcium. This was the case for all the compounds studied here except compound **1**. The uncertainty in measuring K' for the complex between Ca^{2+} and either **1** or **2** is large because spectra of the ligand and the metal–ligand complex are highly similar.

The ligands investigated so far for measurement of ionic magnesium in biological systems require careful p*H* adjustment during measurement because they undergo acid dissociation and corresponding spectral changes of the free ligand over the physiologically important p*H* range of 6.5 to 8. The free ligand properties are important because overlap of the spectra of uncomplexed ligand and complex make correction for free ligand absorbance necessary. With compounds **2** and **3**, overlap of the spectra of the free and complexed ligands still is present, but wavelengths can be chosen where absorbance of the free ligand is unaffected by p*H* over a relatively wide range. For these systems the factor limiting the usable p*H* range is that complexation with magnesium is too small at p*H* values below about 9 for **2** and 7 for **3** (three p*H* units below p*K*(OH)) for the systems to be useful analytically.

In an effort to reduce interference from calcium the pyrazole system **4** was investigated.

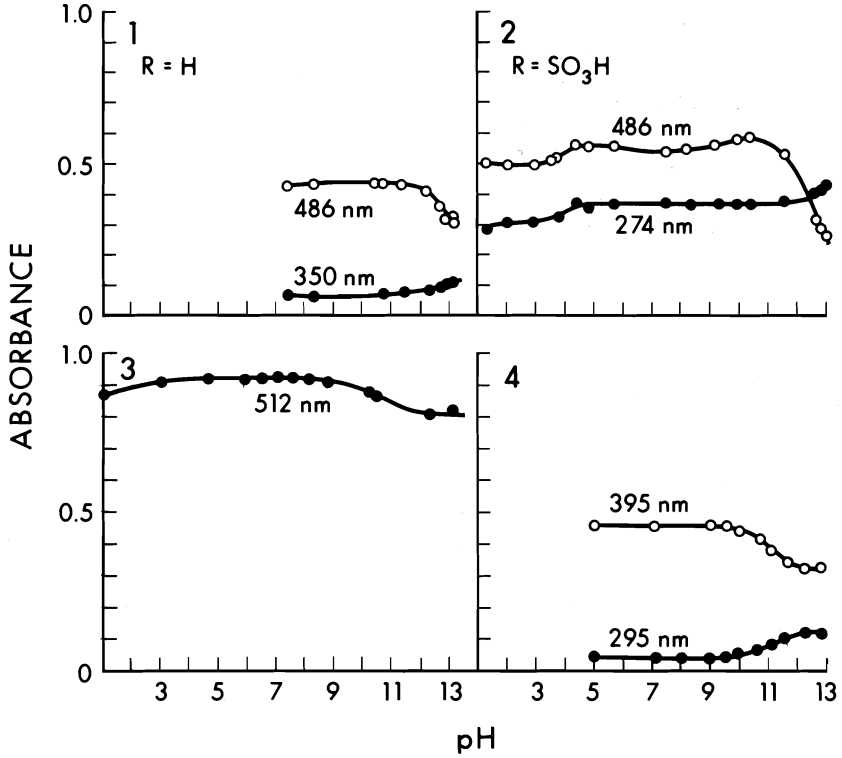

FIG. 2. Plots of absorbance of ligand vs. p*H* for ligands **1**–**4** at selected wavelengths.

TABLE 1. Spectral data for ligands and their magnesium and calcium complexes at p*H* 10.1

	λ_{max}			log ε^a		
Compound	Free ligand	Ligand + Mg^{2+}	Ligand + Ca^{2+}	Free ligand	Ligand + Mg^{2+}	Ligand + Ca^{2+}
1	490	480[b]	490	4.33	4.13	4.21
2	486	480[b]	486	4.32	4.09	4.24
3	532	552	540	4.39		
	512 (sh)			4.36[c]	4.26[c]	4.28[c]
4	395	412	395	4.37	4.29	4.25

[a]Measured at λ_{max} of free ligand.
[b]Estimate, since λ_{max} is dependent on $[Mg^{2+}]$.
[c]Measured at 512 nm, p*H* 10.2.

TABLE 2. Acid dissociation constants of ligands, conditional equilibrium constants for magnesium and calcium complexes at p*H* 10.1, $\mu = 0.10$, and thermodynamic equilibrium constants at $\mu = 0.10$

			Mg^{2+}		Ca^{2+}	
Compound	p*K*(COOH)	p*K*(OH)	log *K'* (p*H* 10.1)	log *K*	log *K'* (p*H* 10.1)	log *K*
1	—[a]	12.3[b]	1.85[b]	4.05	2.38[b]	4.58
2	3.6[c], 4.6[d]	12.2	2.54	4.65	2.18	4.29
3	3.5[d]	10.2	4.02[e]	4.32	3.20[e]	3.50
4	—[a]	10.9	2.82	3.69	2.36	3.23

[a]Insoluble below p*H* 5.
[b]Reported: $pK_2 = 12.0$, log *K'* $(Mg^{2+}) = 2.10$ at $\mu = 0.10$, p*H* 10.1, no complex formation with Ca^{2+} (4).
[c]From spectrochemical data.
[d]From potentiometric titration.
[e]Measured at p*H* 10.2.

Snavely *et al.* reported an appreciable difference between Mg^{2+} and Ca^{2+} complex formation constants for the similar compound 4-(2′-hydroxyl-1′-benzeneazo)-3-methyl-1-phenyl-2-pyrazolin-5-one (log K' for Mg^{2+}, 10.94; for Ca^{2+}, 8.72 in 75% dioxane) (11). However, although the formation constant for magnesium with **4** is in the right range, that for calcium is too close to be useful in selective measurements. Also, the complexes are yellow, which would further hamper their use for the direct determination of ionic magnesium in some applications, as in urine.

Of the compounds synthesized, **3** appears the most useful for measurement of ionic magnesium. This compound is similar in structure to many analytically useful azo dyes, but has not been reported previously. The widely separate pK_a values of 3.5 and 10.2 make possible a wide variation in p*H* without accompanying spectral changes due to changes in concentration of HL^-, and the conditional formation constant with magnesium makes the system usable over a p*H* range of about 7 to 10. However, it shares with previously studied compounds the disadvantages that the free ligand absorbs significantly at the same wavelength as the magnesium complex, and the formation constant for calcium, while smaller than that of magnesium, is sufficiently large to cause some interference.

We conclude that the *o*-carboxyl-*o*′-hydroxyl azo function is not likely to provide a reagent capable of complexing magnesium and not calcium. The reagents previously proposed, Eriochrome Blue SE, Eriochrome Black T, and Calmagite, along with compound **4** discussed here, are similar in complexing properties; all require a correction for calcium. This correction is best done by recording the difference in absorbance readings at two wavelengths (1).

Acknowledgements

We thank Peter Jeremy for preparation of **1**, and Dr. Fred Cantwell for supplying the resin in the form used in this study. Financial support of the National Research Council of Canada and the University of Alberta is gratefully acknowledged.

1. A. Scarpa. Biochemistry, **13**, 2789 (1974).
2. J. Raaflaub. Z. Physiol. Chem. **288**, 288 (1951); **328**, 198 (1967).
3. A. Scarpa. Ion Enzyme Electrodes Biol. Med., Int. Workshop. *Edited by* M. Kessler. University Park Press, Baltimore, MD. 1976. p. 252.
4. (*a*) M. Walser. Anal. Chem. **32**, 711 (1960); (*b*) R. D. Berlin. Anal. Biochem. **14**, 135 (1966).
5. H. Diehl and J. Ellingboe. Anal. Chem. **32**, 1120 (1960).
6. K. H. Engel and A. W. Hutchinson. J. Am. Chem. Soc. **52**, 211 (1930).
7. R. W. Ramette. J. Chem. Educ. **44**, 647 (1967).
8. H. D. K. Drew and J. K. Landquist. J. Chem. Soc. 292 (1938).
9. G. Schetty and W. Kusler. Helv. Chim. Acta, **44**, 2193 (1961).
10. H. A. Laitinen and W. E. Harris. Chemical analysis. 2nd ed. McGraw-Hill, New York, NY. 1975. p. 195.
11. F. A. Snavely, W. C. Fernelius, and B. E. Douglas. J. Soc. Dyers Col. **73**, 491 (1957). *From* H. Zollinger (*Trans. by* H. E. Nursten). Azo and diazo chemistry – aliphatic and aromatic compounds. Interscience, New York, NY. 1961. p. 356.

Un exemple d'isomérisation radicalaire en chaînes: la photoinduction de l'isomérisation *cis–trans* de la pentène-3 one-2

ARMEL RIOUAL, ANDRÉ DEFLANDRE ET JACQUES LEMAIRE

Laboratoire de Photochimie, U.E.R. Sciences Exactes et Naturelles, Université de Clermont II, Clermont-Ferrand, France

Reçu le 26 janvier 1977[1]

ARMEL RIOUAL, ANDRÉ DEFLANDRE et JACQUES LEMAIRE. Can. J. Chem. **55**, 3915 (1977).

Une étude des variations des rendements quantiques initiaux de l'isomérisation *cis–trans* photosensibilisée de la pentène-3 one-2 en fonction des concentrations initiales du donneur et de l'accepteur, de la longueur d'onde d'excitation, de la nature du donneur et du solvant permet de proposer des mécanismes de sensibilisation n'impliquant pas seulement des transferts d'énergie triplet–triplet. Les donneurs carbonylés (acétophénone, benzophénone, acétone) sont susceptibles d'induire une isomérisation radicalaire en chaînes dans les solvants où le sensibilisateur est réduit; l'exemple de l'acétophénone est particulièrement significatif. Dans les solvants qui ne conduisent pas à la photoréduction du donneur (comme le benzène ou le CCl_4), le mécanisme classique du transfert d'énergie triplet–triplet permet d'expliquer les résultats obtenus. L'isomérisation sensibilisée par les donneurs aromatiques (benzène, mésitylène) s'interprète par un double mécanisme: à faible concentration d'accepteur, les transferts d'énergie (triplet–triplet) sont prépondérants, alors qu'à forte concentration, il se forme un exciplexe entre l'aromatique excité dans son niveau singulet et la cétone; cet exciplexe se désactive en se dissociant et en provoquant l'isomérisation de la cétone α,β insaturée.

ARMEL RIOUAL, ANDRÉ DEFLANDRE, and JACQUES LEMAIRE. Can J. Chem. **55**, 3915 (1977).

Mechanisms of the photosensitized *cis–trans* photoisomerization of 3-penten-2-one which do not imply only classical triplet–triplet energy transfer are proposed; they are based upon measurements of the variations of initial quantum yields of isomerization with the initial donor and acceptor concentrations, the wavelength of excitation, and the nature of the donor and of the solvent. Carbonyl donors (acetophenone, benzophenone, acetone) induce a radical isomerization by a chain process in reducing solvents; the example of acetophenone is specially interesting. In solvents in which the donor is not photoreduced (as benzene or CCl_4) classical triplet–triplet energy transfers occur. Sensitization with aromatic donors (benzene, mesitylene) proceeds through triplet–triplet energy transfer at low concentrations of the acceptor. At higher concentrations of acceptor, an exciplex is formed between the ketone and the aromatic in its singlet excited state; this exciplex is deactivated by dissociation and by causing the isomerization of the α,β-unsaturated ketone.

De très nombreuses mesures du rendement quantique de transition inter-systèmes sont basées sur des isomérisations *cis–trans* photosensibilisées, tant en phase gazeuse (1) qu'en solution (cf. par exemple réfs 2–7). Les auteurs admettent alors que l'interaction entre la molécule à étudier et l'accepteur isomérisable peut se réduire à un transfert d'énergie triplet–triplet dans un domaine convenable de concentration de cet accepteur. Mais s'il est facile d'exclure la participation de l'état excité singulet d'un donneur fluorescent, il est parfois plus difficile d'assurer que le niveau triplet du donneur ne participe qu'à un transfert d'énergie.

Dans le cadre d'une étude des aspects quantitatifs du comportement photochimique des cétones α,β insaturées (8, 9), nous avons été amenés à examiner les processus d'isomérisation *cis–trans* sensibilisée de la pentène-3 one-2. Comme nous allons le rapporter plus loin, les résultats expérimentaux obtenus nous amènent à proposer d'autres mécanismes d'isomérisation que ceux impliquant de simples transferts d'énergie triplet–triplet.

[1]Revision reçue le 27 juillet 1977.

Techniques expérimentales

Préparation et purification des pentènes-3 ones-2 trans et cis

Les formes *trans* et *cis* de la pentène-3 one-2 sont extraites d'un produit technique Aldrich. La forme *trans* est séparée par une bidistillation sur une colonne à bande tournante Nester-Faust, suivie d'une chromatographie préparative en phase vapeur sur un appareil Hupe et Busch APG 402 (équipé d'une colonne à 5% de Carbowax 20M). La pentène-3 one-2 ainsi obtenue contient 4% de méthyl-4 pentène-3 one-2. Nous avons vérifié que la présence de ce dernier composé, que nous avons précédemment étudié (8), ne perturbait pas le comportement photochimique de la pentène-3 one-2 *trans*. La pentène-3

one-2 *cis* est ensuite préparée par irradiation de la forme *trans*. Après une nouvelle séparation par chromatographie préparative, l'isomère *cis* obtenu contient 6% de forme *trans* et environ 10% de pentène-4 one-2 et il doit être conservé à l'obscurité, à 0°C. La pentène-4 one-2 ne peut être excitée dans le mélange, ni par absorption directe, ni par transfert d'énergie, et nous avons vérifié qu'elle ne modifiait pas les processus photochimiques des pentènes-3 ones-2.

Techniques d'irradiation

Deux dispositifs d'irradiation monochromatique ont été utilisés: une lampe à vapeur de mercure type "basse pression" à résonance (Philips TUV 15 W) et une lampe à vapeur de mercure type "très haute pression" (Osram HBO 200 W) associée à un monochromateur Bausch et Lomb haute intensité. Les réacteurs sont en quartz Suprasil et l'oxygène dissous peut être éliminé par les cycles classiques congélation, pompage sous vide dynamique, liquéfaction. L'intensité lumineuse disponible est mesurée par des actinométries basées soit sur la photolyse de l'acide oxalique sensibilisée par les ions uranyles (10) soit sur la photoréduction de ferrioxalate (11) soit encore sur l'isomérisation *cis–trans* de l'azobenzène (12, 13).

Techniques analytiques

Les solutions diluées de pentène-3 one-2 *cis* ou *trans* ont été dosées soit par spectrophotométrie uv (Jobin et Yvon Monospac) soit par chromatographie en phase vapeur à l'aide d'un appareil Varian série 1400 équipé d'une colonne à 10% de Carbowax 20M de 10 pieds de longueur. Quelques dosages ont été également réalisés par spectroscopie infrarouge à l'aide d'un spectrophotomètre Perkin-Elmer modèle 180. Les spectres de fluorescence ont été enregistrés sur un appareil Perkin-Elmer-Hitachi MPF 3.

Expériences préliminaires sous excitation directe et photosensibilisations

Nous avons déjà rapporté l'essentiel des résultats acquis en excitation directe (9). Les rendements quantiques initiaux $\Phi^0_{c\to t}$ et $\Phi^0_{t\to c}$ mesurés et les régimes photostationnaires observés s'interprètent en admettant que le niveau triplet d'un isomère se désactive avec une égale probabilité vers les deux formes *cis* et *trans* de la pentène-3 one-2. Les principales propriétés des sensibilisateurs employés sont rassemblées dans le tableau 1.

Isomérisation *trans–cis* de la pentène-3 one-2 photosensibilisée par des composés carbonylés

Etude expérimentale de la sensibilisation par l'acétophénone

Le tableau 2 rassemble les rendements quantiques initiaux d'isomérisation *cis–trans* sensibilisée par l'acétophénone, mesurés dans diverses conditions expérimentales. Nous avons successivement examiné l'influence des concentrations initiales du donneur et de l'accepteur, l'influence de la longueur d'onde d'excitation et celle du solvant en milieu soigneusement dégazé. La présence d'oxygène provoque une nette diminution du rendement $(\Phi^S_{c\to t})^0$ (0.11 au lieu de 1.5 en milieu dégazé dans les mêmes conditions de concentration et d'irradiation). Il convient de noter les valeurs supérieures à l'unité des rendements quantiques mesurés dans le *n*-heptane. On a rapporté dans la littérature, des rendements quantiques d'isomérisation *cis–trans* du 2,4-hexadiène sensibilisée par la benzophénone, supérieurs à 160 (20); des mesures ultérieures ont ramené ces rendements à des valeurs plus habituelles (21). Le seul exemple non controversé concernerait l'isomérisation *cis–trans* du piperylène sensibilisée par la benzophénone, qui aux fortes concentrations (1 à 10 M), présente des rendements augmentant de 1 à 1.7 (22). Dans les solvants comme le tétrachlorure de carbone ou le benzène, les rendements quantiques initiaux d'isomérisation *cis–trans* de la pentène-3 one-2 reprennent des valeurs plus classiques. Dans le tableau 3, nous indiquons les valeurs du rendement $(\Phi^S_{c\to t})^0$ en solvant binaire (*n*-heptane–benzène) de composition variable.

Si la solution dans le *n*-heptane contient initialement la forme *trans*, le rendement quantique $(\Phi^S_{t\to c})^0$ reste toujours faible (0.02 dans une solution 2×10^{-2} M en acétophénone et 4×10^{-3} M en pentène-3 one-2).

Nous avons représenté, à titre d'exemple, sur la fig. 1, les variations des concentrations des formes *trans* et *cis* de la pentène-3 one-2 dans une solution contenant initialement 10^{-3} M de forme *cis*, 10^{-2} M d'acétophénone et irradiée à 313 nm. Ces courbes appellent trois remarques: (*a*) le rapport de la concentration de la forme *trans* à celle de la forme *cis* atteint des valeurs maximales aussi élevées que 7; (*b*) les processus d'isomérisation *cis* → *trans* sont accompagnés d'un processus de disparition irréversible de la pentène-3 one-2; nous avons rapporté dans le tableau 2 les rendements quantiques initiaux de ce processus; (*c*) l'acétophénone est susceptible d'être photoréduite par le solvant, mais la disparition du sensibilisateur ne devient mesurable que lorsque la concentration de pentène-3 one-2 n'est plus que de 10^{-4} M.

Etude expérimentale de la sensibilisation par la benzophénone

L'influence des paramètres macroscopiques usuels (concentrations initiales du donneur et de l'accepteur, longueur d'onde d'excitation, nature du solvant) sur les rendements quantiques initiaux d'isomérisation *cis* → *trans* de la pentène-3 one-2 sous forme *cis* a été à nouveau

TABLEAU 1. Caractéristiques des sensibilisateurs employés

Sensibilisateur (Références)	Acétophénone (14)	Benzophénone (14)	Acétone (14,15)	Benzène (6,14,16,17)	Mésitylène (14,17,18,19)
Energie du niveau T_1 kcal/mole	74	70	79-80	84,3	80,3
Rendement quantique de transition inter-systèmes $S_1 \rightarrow T_1$	1	1	1	0,25 à 0,71	0,60 à 0,55
Durée de vie de S_1 (ns)	-	0,02 0,005		30	37
Durée de vie de T_1 (μs)	100 (eau) 0,23(cyclohexane) 0,11(isopropanol)	20 (eau) 0,3 (cyclohexane) 0,04(isopropanol)	0,4 (n-hexane)	0,5 à 6×10^{-3}	-
ε (λ_{exc}) dans le n-heptane $mole^{-1}.l.cm^{-1}$	33 (297nm) 39 (313 nm) 6 (365nm)	116 (297nm) 73 (365nm)	9,5 (297nm, eau)	-	-

examinée et le tableau 4 rapporte les résultats de nos mesures. Nous avons également étudié les variations des concentrations des différents composants du mélange sous irradiation. Là encore, le rapport de la concentration de la forme *trans* à celle de la forme *cis* atteint des valeurs maximales très supérieures à l'unité (6 à 8 sous excitation à 297 ou à 313 nm, 4.2 sous excitation à 365 nm); les processus de disparition irréversible se superposent aussi à l'isomérisation de la pentène-3 one-2. Enfin, comme le montre la fig. 2, la benzophénone disparait dès les premiers instants de l'irradiation dans le *n*-heptane sans présenter la même "période d'induction" que l'acétophénone.

La benzophénone n'est pas susceptible de sensibiliser l'isomérisation *trans* → *cis* de la pentène-3 one-2 dans le *n*-heptane. Par contre, ce même donneur à 2×10^{-2} *M*, sensibilise cette isomérisation dans le tétrachlorure de carbone (cf. tableau 5); parallèlement, la phosphorescence, à température ambiante de la benzophénone dans le tétrachlorure de carbone est éteinte par la cétone insaturée selon une même loi de Stern–Volmer que l'isomérisation sensibilisée.

Etude expérimentale de la sensibilisation par l'acétone

L'acétone est un sensibilisateur d'emploi difficile; substance peu absorbante, elle doit être employée à des fortes concentrations où elle s'autodésactive. Mais ce donneur permet de comparer le comportement de la pentène-3 one-2 en solution aqueuse et en solution dans le *n*-heptane. Le tableau 6 rassemble les rendements quantiques initiaux dans ces deux solvants.

Interprétation des résultats expérimentaux

L'excitation de l'acétophénone dans un solvant pouvant participer à un processus de photoréduction du donneur provoque l'isomérisation *cis–trans* de la pentène-3 one-2 avec un rendement quantique initial très supérieur à 0.5. Un tel résultat ne peut être interprété par un transfert d'énergie rapide entre sensibilisateur et la cétone α,β insaturée. En effet, un sensibilisateur qui peuple totalement son niveau triplet peut

TABLEAU 2. Rendements quantiques initiaux des processus d'isomérisation et de disparition irréversible de la pentène-3 one-2 *cis* sensibilisées par l'acétophénone

Solvant	n-heptane						
λ_{exc} (nm)	297						365
$(\text{Pentène-3 one-2 cis})_o$ mole.l^{-1}	$5{,}2.10^{-2}$	$1{,}05.10^{-3}$			$5{,}2.10^{-3}$		
$(\text{Acétophénone})_o$ mole.l^{-1}	2.10^{-2}	$0{,}5.10^{-2}$	1.10^{-2}	2.10^{-2}	1.10^{-2}	2.10^{-2}	2.10^{-2}
$(\Phi^S_{c\to t})^o$	1,50	1,55	1,60	1,63	1,50-1,60	1,55	0,97
Φ^S_{disp}	0,19	0,145			0,065		

Solvant	CCl_4			benzène
λ_{exc} (nm)	297		365	313
$(\text{Pentène-3 one-2 cis})_o$ mole.l^{-1}	10^{-3}	5.10^{-3}	10^{-3}	10^{-3}
(Acétophénone) mole.l^{-1}	10^{-2}	10^{-2}	2.10^{-2}	10^{-2}
$(\Phi^S_{c\to t})$	0,19	0,19	0,20	0,30

TABLEAU 3. Rendement quantique initial d'isomérisation sensibilisée par l'acetophénone (10^{-2} *M*) en solvant binaire *n*-heptane–benzéne; [pentène-3 one-2 *cis*] = 10^{-3} mol ℓ^{-1}; λ_{exc} = 313 nm

Proportion de n-heptane	$(\Phi^S_{c\to t})^o$
0	0,30
0,20	0,51
0,50	0,80
0,80	1,05
1	1,50

provoquer au maximum la population quantitative du niveau triplet de la pentène-3 one-2; étant donné qu'en excitation directe, une population de 80 à 90% du niveau triplet de la forme *trans* ou *cis* conduit à un rendement quantique d'isomérisation de 0.40 à 0.45 (9), la population quantitative du niveau triplet de la pentène-3 one-2 permettrait d'obtenir un rendement maximum égal à 0.5. Cette situation se rencontre d'ailleurs dans les solvants qui ne peuvent participer à un processus de photoréduction du sensibilisateur, comme par exemple le benzène ou le tétrachlorure de carbone; il intervient alors un transfert d'énergie relativement rapide se manifestant par des rendements quantiques d'isomérisation sensibilisée inférieurs à 0.5 (cf. tableaux 2 et 4).

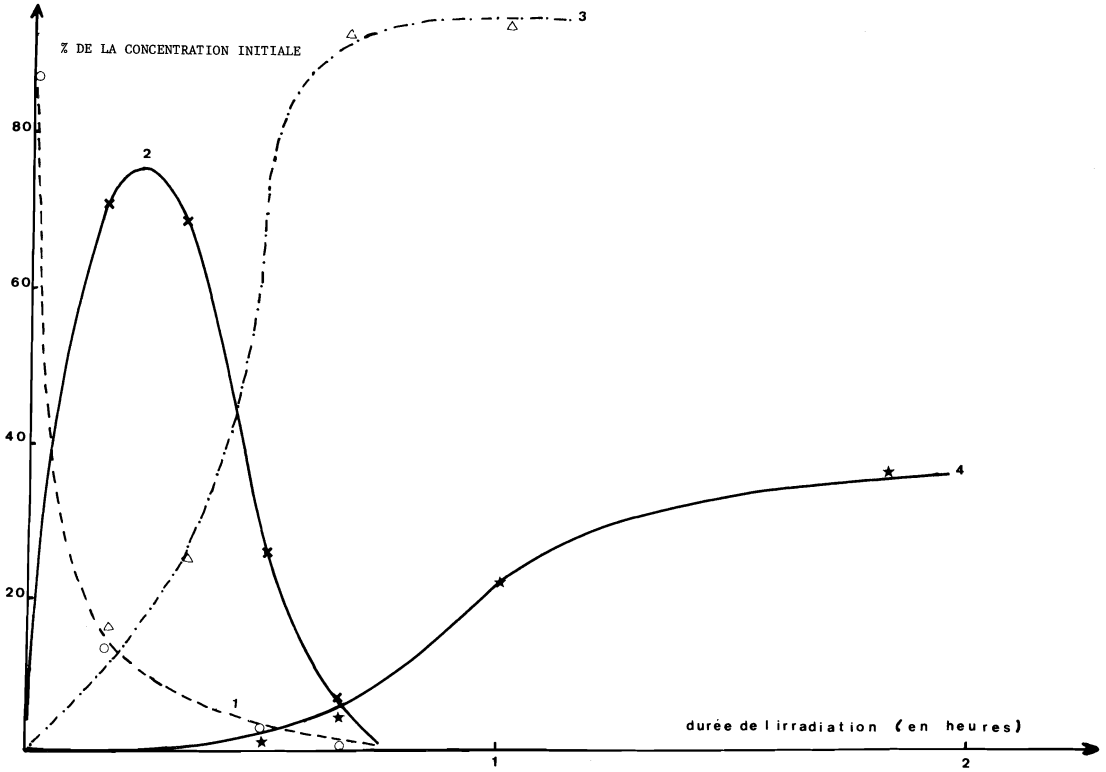

FIG. 1. Isomérisation de la pentène-3 one-2 *cis* (10^{-3} *M*) sensibilisée par l'acétophénone (10^{-2} *M*) (λ_{exc} = 313 nm; solvant: *n*-heptane dégazé): courbe 1: forme *cis*; courbe 2: forme *trans*; courbe 3: disparition de la pentène-3 one-2; courbe 4: disparition de l'acétophénone.

Il est à noter également que l'excitation de l'acétophénone ou de benzophénone dans un solvant réducteur ne conduit pas à l'isomérisation *trans–cis* de la pentène-3 one-2.

Par contre, dans un solvant non réducteur, un transfert d'énergie permet de sensibiliser tout aussi bien l'isomérisation *trans–cis* que l'isomérisation *cis–trans*. En particulier, l'étude effectuée dans le cas de la benzophénone le montre clairement (cf. tableau 5).

Il faut donc considérer que dans les solvants réducteurs, l'acétophénone est capable d'induire une isomérisation radicalaire de la forme *cis* et non de la forme *trans*. L'effet de solvant sur l'isomérisation sensibilisée de la forme *cis* montre que les radicaux responsables de l'isomérisation radicalaire ne sont pas issus d'une dissociation photochimique du sensibilisateur, mais plutôt d'un processus de photoréduction de ce sensibilisateur par le solvant SH.

$$(C_6H_5—CO—CH_3)_{T_1} + SH \rightarrow (C_6H_5—\underset{\displaystyle OH}{\overset{\displaystyle |}{\dot{C}}}—CH_3) + (S^{\cdot})$$

Une interprétation très analogue peut être proposée pour les résultats acquis en sensibilisation par la benzophénone, bien que l'isomérisation de la forme *cis* s'effectue avec un rendement $(\Phi^{S}_{c\rightarrow t})^{0} = 0.30$ suffisamment faible pour être interprétée en termes de transfert d'énergie. Deux remarques justifient le mécanisme d'induction radicalaire: (*i*) En solution dans le *n*-heptane le rendement quantique d'isomérisation sensibilisée par la benzophénone de la forme *trans* est nul et donc très inférieur à $(\Phi^{S}_{c\rightarrow t})^{0}$. Dans le benzène et le tétrachlorure de carbone où la sensibilisation implique un transfert d'énergie, les rendements quantiques $(\Phi^{S}_{c\rightarrow t})^{0}$ et $(\Phi^{S}_{t\rightarrow c})^{0}$ sont voisins. (*ii*) Le rapport [*trans*]/[*cis*] en régime photostationnaire est voisin de 1 dans le benzène ou le tétrachlorure de carbone, alors que dans le *n*-heptane ce rapport prend des valeurs maximales très supérieures à l'unité.

La benzophénone apparaît expérimentalement comme un inducteur moins efficace que l'acétophénone, alors que la population du niveau triplet de ces deux sensibilisateurs est

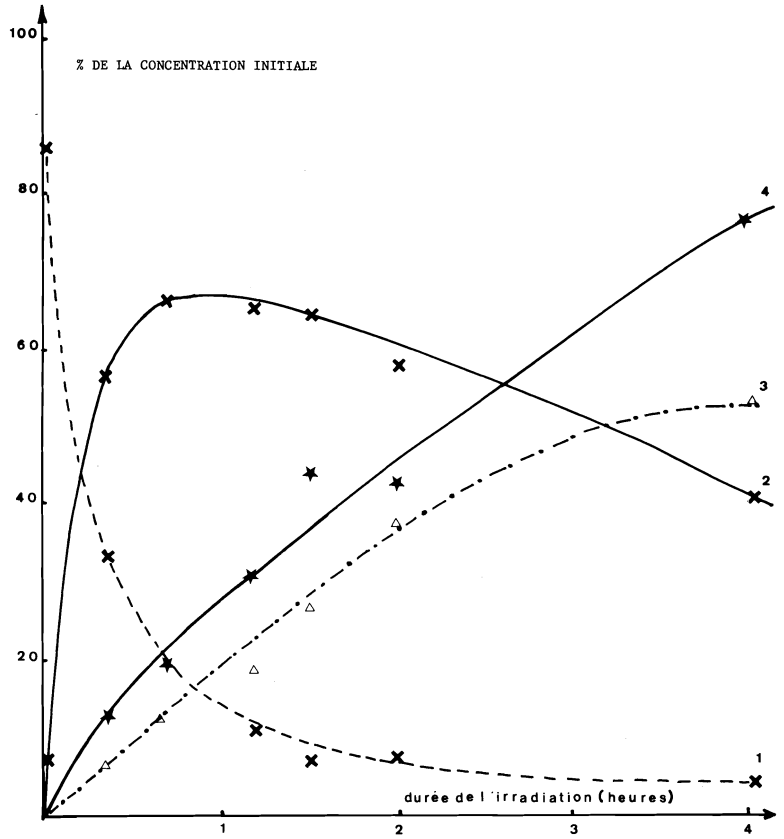

FIG. 2. Isomérisation de la pentène-3 one-2 *cis* (10^{-3} *M*) sensibilisée par la benzophénone (0.8×10^{-2} *M*) (λ_{exc} = 313 nm; solvant: *n*-heptane dégazé): courbe 1: forme *cis*; courbe 2: forme *trans*; courbe 3: disparition de la pentène-3 one-2; courbe 4: disparition de la benzophénone.

TABLEAU 4. Rendements quantiques initiaux des processus d'isomérisation et de disparition irréversible de la pentène-3 one-2 *cis* sensibilisées par la benzophénone

Solvant	n-heptane				benzène	
λ_{exc} (nm)	297		313	365	313	365
$(\text{Pentène-3 one-2 cis})_o$ mole.l^{-1}	10^{-3}	10^{-3}	10^{-3}	10^{-3}	10^{-3}	10^{-3}
$(\text{Benzophénone})_o$ mole.l^{-1}	5.10^{-3}	10^{-2}	$0{,}8.10^{-2}$	10^{-2}	10^{-2}	10^{-2}
$(\Phi^S_{c\to t})^o$	0,32	0,29	0,26	0,125	0,21	0,18
Φ^S_{disp}	0,03	0,03	0,029	0,013	-	-

TABLEAU 5. Rendement quantique initial d'isomérisation de la pentène-3 one-2 *trans* sensibilisée par la benzophénone (2×10^{-2} mol ℓ^{-1}) dans le tétrachlorure de carbone (sous excitation à 313 nm)

$(\text{Pentène-3 one-2 trans})_0$ mole.l^{-1}	2.10^{-4}	$1{,}35.10^{-3}$	2.10^{-3}	$3{,}4.10^{-3}$	$5{,}4.10^{-3}$	$1{,}08.10^{-2}$
$(\Phi^{S}_{t\to c})^0$	0,015	0,07	0,10	0,15	0,18	0,31

TABLEAU 6. Rendements quantiques initiaux des processus d'isomérisation et de disparition irréversible de la pentène-3 one-2 *cis* sensibilisées par l'acétone

Solvant	eau						n-heptane		
λ_{exc} (nm)	297						297		
$(\text{Pentène-3 one-2 cis})_0$ mole.l^{-1}	2.10^{-4}	2.10^{-4}	10^{-3}	10^{-3}	10^{-3}	5.10^{-3}	10^{-3}	5.10^{-3}	5.10^{-3}
$(\text{Acétone})_0$ mole.l^{-1}	$6{,}8.10^{-2}$	$2{,}75.10^{-1}$	$2{,}75.10^{-1}$	$5{,}5.10^{-1}$	$8{,}25.10^{-1}$	$5{,}5.10^{-1}$	$3{,}4.10^{-2}$	$3{,}4.10^{-2}$	$5{,}5.10^{-1}$
$(\Phi^{S}_{c\to t})^0$	0,13	0,088	0,30	0,20	0,11	0,18	0,69	0,69	0,34
Φ^{S}_{disp}	0,035	0,056	0,012	0,033	0,026	0,017	0,31	0,17	0,21

pratiquement totale et que leur photoréductibilité par le *n*-heptane reste voisine. La différence de comportement pourrait être attribuée à la nature des radicaux $C_6H_5—\dot{C}(OH)—C_6H_5$, plus encombrants que les radicaux issus de l'acétophénone.

L'induction radicalaire de l'isomérisation *cis–trans* de la pentène-3 one-2 par les deux cétones aromatiques employées peut s'interpréter par le mécanisme en chaînes suivant (schéma 1).

Amorçage photochimique

[1] $C_6H_5COR + n\text{-}C_7H_{16} \xrightarrow{\Phi_r I_a} C_6H_5\dot{C}(OH)R + n\text{-}C_7H_{15}$

$R = CH_3$ ou C_6H_5

Propagation

[2] $C_6H_5\dot{C}(OH)R$ + 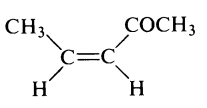 $\xrightarrow{k_2}$ $C_6H_5C(OH)R$ 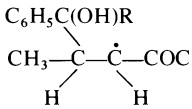 ou $C_6H_5C(OH)R$ 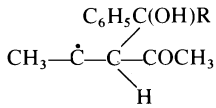 (radicaux r$^{\cdot}$)

[3] r$^{\cdot}$ $\xrightarrow{k_3}$ $(1-\alpha)$ 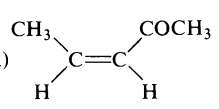 + α 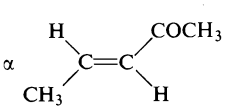 + $C_6H_5—\dot{C}(OH)—R$

Rupture

$C_6H_5—\dot{C}(OH)R + C_6H_5—\dot{C}(OH)R \xrightarrow{k_4}$
$C_6H_5—\dot{C}(OH)R + r^{\cdot} \xrightarrow{k_4'}$ produits
$r^{\cdot} + r^{\cdot} \xrightarrow{k_4''}$

SCHÉMA 1

TABLEAU 7. Variations du rendement quantique $(\Phi^{S}_{c\rightarrow t})^{0}$ en fonction de l'intensité lumineuse absorbée

Sensibilisateur	λ_{exc} (nm)	297	313	365
Acétophénone	$(I_a)^{1/2}$ (photon/cm^3.s)$^{1/2}$	$(2,2\pm0,2).10^7$	-	$(3,8\pm0,1).10^7$
	$(\Phi^{S}_{c\rightarrow t})^{0}$	1,50±0,10	-	0,97±0,05
Benzophénone	$(I_a)^{1/2}$ (photon/cm^3.s)$^{1/2}$	$(2,6\pm0,1).10^7$	$(3\pm0,1).10^7$	$(6,6\pm0,2).10^7$
	$(\Phi^{S}_{c\rightarrow t})^{0}$	0,32±0,03	0,26±0,03	0,12±0,01

Ce schéma appelle les remarques suivantes: (*a*) La catalyse par atomes libres ou radicaux de l'isomérisation *cis–trans* du dideuterioéthylène, du butène-2 et du stilbène a déjà été rapportée dans la littérature (23). (*b*) Les cétones aromatiques en se photoréduisant ne peuvent pas induire l'isomérisation de la forme *trans* de la pentène-3 one-2; ceci s'interprète en admettant que les radicaux $C_6H_5\dot{C}(OH)R$ ne peuvent réagir, pour des raisons stériques, avec l'isomère *trans*. On peut aussi supposer que la forme *trans*, plus stable que l'isomère *cis*, peut capturer les radicaux $C_6H_5\dot{C}(OH)R$ en donnant des radicaux (r′), non dissociatifs, disparaissant par recombinaison. (*c*) Si le processus de rupture prépondérant intervient par recombinaison des radicaux (r′), le schéma cinétique conduit aux relations suivantes:

$$[4] \qquad [r'] = (\Phi_r I_a/2k_4'')^{1/2}$$

$$[5] \qquad (\Phi^{S}_{c\rightarrow t})^{0} = \frac{k_3\Phi_r\alpha}{(2k_4'')^{1/2}}\frac{1}{I_a^{1/2}}$$

Si le processus de rupture prépondérant implique les radicaux $C_6H_5\dot{C}(OH)R$, de même

$$[6] \qquad [C_6H_5\dot{C}(OH)R] = (\Phi_r I_a/2k_4)^{1/2}$$

$$[7] \qquad (\Phi^{S}_{c\rightarrow t})^{0} = \frac{k_2\Phi_r\alpha}{(2k_4)^{1/2}}\frac{[\text{pentène-3 one-2}]}{I_a^{1/2}}$$

Seule la relation 5 est compatible avec nos résultats expérimentaux; en effet, les rendements quantiques d'isomérisation $(\Phi^{S}_{c\rightarrow t})^{0}$ sont indépendants de la concentration de pentène-3 one-2. Même à faible concentration, la cétone capte tous les radicaux $C_6H_5\dot{C}(OH)CH_3$ formés. La relation 5 nous permet en outre d'interpréter l'influence apparente de la longueur d'onde sur les rendements quantiques mesurés. Nous rapportons dans le tableau 7 les valeurs de la racine carrée des intensités lumineuses absorbées $I_a^{1/2}$ lors de nos mesures à différentes longueurs d'onde: on vérifie alors que les rendements quantiques sont inversement proportionnels à $I_a^{1/2}$.

Dans les solvants où le mécanisme de l'isomérisation sensibilisée implique un processus moléculaire de transfert d'énergie, les rendements quantiques apparaissent être très normalement indépendants de l'intensité lumineuse absorbée et donc aussi de la longueur d'onde d'excitation.

L'influence de l'oxygène se manifeste par une inhibition importante de l'isomérisation *cis* → *trans* induite radicalairement. L'oxygène peut réagir avec les radicaux présents dans le milieu pour donner naissance à des radicaux peroxydiques; ces radicaux oxygénés ne seraient donc plus susceptibles de s'additionner sur la double liaison de la pentène-3 one-2 et disparaitraient par duplication. L'oxygène est, en outre, susceptible de désactiver l'état triplet du sensibilisateur.

Au mécanisme radicalaire proposé doit, en fait, se superposer un mécanisme moléculaire mettant en jeu des transferts d'énergie entre le sensibilisateur et l'accepteur. De tels transferts provoquent une désactivation partielle du niveau

triplet du sensibilisateur, ce qui peut se manifester expérimentalement par l'inhibition de la photoréduction du sensibilisateur (comme dans le cas de l'acétophénone). Cependant, même dans la phase où la photoréduction du sensibilisateur par le *n*-heptane est inhibée par la pentène-3 one-2, nos résultats expérimentaux montrent que le mécanisme radicalaire en chaînes d'isomérisation reste prépondérant devant celui impliquant le transfert d'énergie. Le rendement $(\Phi^{S}_{c\rightarrow t})^{0}$ est toujours supérieur à $(\Phi^{S}_{t\rightarrow c})^{0}$; tout se passe comme si seule l'isomérisation *cis–trans* était possible. A des temps d'irradiation de plus en plus longs, le rapport [*trans*]/[*cis*] doit donc prendre des valeurs de plus en plus élevées et tendre vers l'infini. Mais à l'isomérisation se superpose une disparition de la penténone. La concentration de *trans* passe ainsi par un maximum pour ensuite décroître jusqu'à la disparition complète du réactif.

Enfin, dans le cas de l'acétone en solution aqueuse, l'existence du phénomène d'autodésactivation du sensibilisateur est facilement mise en évidence. A même concentration de pentène-3 one-2, un accroissement de la concentration d'acétone se manifeste par une diminution du rendement quantique d'isomérisation. Les radicaux formés au cours de ce processus d'autodésactivation ne peuvent donc pas initier une isomérisation radicalaire. L'isomérisation sensibilisée mise en évidence ne peut alors être qu'un processus moléculaire par transfert d'énergie.

En solution dans le *n*-heptane, le rendement quantique d'isomérisation $(\Phi^{S}_{c\rightarrow t})^{0}$ peut être supérieur à 0.5, et les rendements de disparition sont plus élevés qu'en solution aqueuse. Un transfert d'énergie entre l'acétone et la pentène-3 one-2 ne permet pas, à lui seul, de justifier ces valeurs; l'isomérisation est donc, au moins partiellement initiée par les radicaux issus de la photoréduction.

Une différence apparait cependant entre les valeurs du rendement quantique d'isomérisation sensibilisée d'une part par l'acétophénone, et d'autre part par l'acétone. En effet, alors que les rendements quantiques de l'isomérisation sensibilisée par l'acétophénone ne dépendent pas des concentrations du donneur et de l'accepteur dans le domaine étudié, les rendements de l'isomérisation sensibilisée par l'acétone dépendent de la concentration d'acétone. Cette difference de comportement peut signifier que l'autodésactivation de l'acétone est plus rapide que celle de l'acétophénone.

Parallèlement à l'isomérisation, une disparition importante est mesurée. Cette disparition peut être initiée par les radicaux issus de la photoréduction, mais également par les radicaux issus de l'autodésactivation; le rendement de disparition augmente avec la concentration d'acétone. Or l'acétone présente des coefficients d'extinction molaire plus faibles que l'acétophénone ou la benzophénone et doit alors être utilisée à concentration plus forte; l'autodésactivation, et par conséquent la disparition, sont favorisées au détriment de l'isomérisation.

Isomérisation *trans–cis* de la pentène-3 one-2 photosensibilisée par le benzène et le mésitylène

Par opposition aux "sensibilisateurs" carbonylés induisant des isomérisations radicalaires, en solution dans les alcanes, les sensibilisateurs aromatiques devraient impliquer uniquement des transferts d'énergie. Les résultats que nous rapportons ici montrent que les mécanismes d'interaction entre aromatiques excités et pentène-3 one-2 ne sont pas aussi simples.

Etude expérimentale de la sensibilisation par le benzène et le mésitylène

Nous avons d'une part mesuré les rendements quantiques initiaux d'isomérisation *trans* → *cis* et *cis* → *trans* de la pentène-3 one-2 sensibilisée par le benzène ou le mésitylène excité à 253.7 nm (cf. tableau 8) et d'autre part le degré d'extinction de fluorescence de ces donneurs par la cétone insaturée en solvant dégazé (cf. tableau 9).On peut observer l'apparition de régimes photostationnaires avec l'un ou l'autre des donneurs; ces régimes sont caractérisés par un rapport [*trans*]/[*cis*] voisin de l'unité.

Interprétation des résultats expérimentaux

A 10^{-2} *M* de pentène-3 one-2 *trans*, l'extinction de la fluorescence du benzène et du mésitylène atteint respectivement 77 et 83%. Si l'on se réfère à nouveau à l'excitation directe, on s'attend à mesurer un rendement quantique d'isomérisation sensibilisée par transfert d'énergie triplet–triplet respectivement égal à $0.23 \times 0.25 \times 0.50 = 0.03$ et à $0.17 \times 0.55 \times 0.50 = 0.05$ avec les deux donneurs envisagés (le rendement quantique de la transition $S_1 \rightarrow T_1$ du benzène en solution diluée est pris égal à 0.25 et celui du mésitylène à 0.55). Les rendements quantiques effectivement mesurés montrent que

TABLEAU 8. Rendements quantiques initiaux des processus d'isomérisation de la pentène-3 one-2 *cis* et *trans* sensibilisées par le benzène et le mésitylène

Nature du sensibilisateur: BENZENE

(Sensibilisateur) mole.l^{-1}	2,95.10^{-2}	5,9.10^{-2}	5,9.10^{-2}	5,7.10^{-2}	8,85.10^{-2}	10^{-2}	10^{-2}	2,5.10^{-2}	2,5.10^{-2}	2,5.10^{-2}	5.10^{-2}
(Pentène-3 one-2 trans) mole.l^{-1}	5.10^{-3}	10^{-3}	5.10^{-3}	10^{-2}	5.10^{-3}						
(Pentène-3 one-2 cis) mole.l^{-1}						10^{-3}	5.10^{-3}	2.10^{-3}	5.10^{-3}	9.10^{-3}	5.10^{-3}
$(\Phi^{S}_{t\to c})^{0}$	0,145	0,105	0,15	0,17	0,145						
$(\Phi^{S}_{c\to t})^{0}$	-	-	-	-	-	0,097	0,085	0,105	0,105	0,095	0,100

Nature du sensibilisateur: MESITYLENE

(Sensibilisateur) mole.l^{-1}	2,90.10^{-2}	2,9.10^{-2}	2,9.10^{-2}	2,9.10^{-2}	2,9.10^{-2}	2,9.10^{-2}	2,9.10^{-2}
(Pentène-3 one-2 trans) mole.l^{-1}	5.10^{-4}	10^{-3}	5.10^{-3}	10^{-2}			
(Pentène-3 one-2 cis) mole.l^{-1}					2,72.10^{-2}	5,00.10^{-3}	9,00.10^{-3}
$(\Phi^{S}_{t\to c})^{0}$	0,13	0,16	0,223	0,225			
$(\Phi^{S}_{c\to t})^{0}$					0,15	0,15	0,145

l'isomérisation ne résulte pas exclusivement d'un transfert triplet–triplet. En outre, il faut exclure un transfert singulet–singulet qui devrait, à la limite, provoquer la même isomérisation qu'en excitation directe. Pour interpréter nos résultats expérimentaux, nous devons alors proposer un mécanisme d'isomérisation sensibilisée impliquant une espèce instable justifiant de l'extinction de la fluorescence et conduisant à l'isomérisation de la pentène-3 one-2; cette espèce instable introduite pour les seules raisons cinétiques pourrait être un exciplexe conduisant à l'isomérisation de la pentène-3 one-2 lors de sa désactivation dissociative.

$$D(S_1) + A_{trans}(S_0) \rightarrow (A{-}D)^1 \text{ (D donneur aromatique)}$$

$$(A{-}D)^1 \rightarrow D(S_0) + (1 - \Phi^{e}_{tc})A_{trans}(S_0) + \Phi^{e}_{tc}A_{cis}(S_0)$$

Le calcul du rendement quantique d'isomérisation sensibilisée $(\Phi^{S}_{t\to c})^{0}$ peut être effectué à partir du mécanisme classique où interviendrait la formation d'un exciplexe et un transfert

TABLEAU 9. Extinction de la fluorescence du benzène ou du mésitylène par la pentène-3 one-2 *trans*

(Pentène-3 one-2 trans) mole.l^{-1}	0	10^{-3}	2.10^{-3}	6.10^{-3}	10^{-2}
Intensité de fluorescence du benzène (mesurée à 277,5 nm)	72,5	44	39	24,5	16,8
Intensité de fluorescence du mésitylène (mesurée à 290 nm)	98	74	47,5	26,5	16,7

TABLEAU 10. Importance des deux voies compétitives d'isomérisation de la pentène-3 one-2 *trans* sensibilisées par le benzène et le mésitylène

Sensibilisateur	Benzène					Mésitylène				
(Pentène-3 one-2 trans) mole.l^{-1}	10^{-2}	6.10^{-3}	5.10^{-3}	2.10^{-3}	10^{-3}	10^{-2}	6.10^{-3}	2.10^{-3}	10^{-3}	5.10^{-4}
$\frac{I_F}{I_F^0}$	0,23	0,34	/	0,54	0,61	0,17	0,27	0,485	0,755	/
$\Phi^e_{t\to c}(1-\frac{I_F}{I_F^0})$	0,135	0,115	/	0,080	0,070	0,175	0,155	0,110	0,051	0,026*
$(\Phi^S_{t\to c})^0_{exp}$	0,17		0,15		0,105	0,225	/	/	0,16	0,13
Pourcentage de l'isomérisation via l'exciplexe	80%		72%		67%	77%	≃ 67%*	≃ 57%*	32%	20%

d'énergie triplet–triplet; il conduit à l'expression suivante:

$$(\Phi^S_{t\to c})^0 = \Phi^e_{tc}\left(1 - \frac{I_F}{I_F^0}\right) + \Phi_{S_1\to T_1}\frac{k_T(A)}{k_d + k_T(A)}\Phi^t_{tc}\frac{I_F}{I_F^0}$$

où Φ^e_{tc} est la probabilité d'isomérisation issue de l'exciplexe, I_F^0 et I_F sont les intensités de fluorescence du donneur mesurées en l'absence et en présence de pentène-3 one-2, $\Phi_{S_1\to T_1}$ rendement de transition inter-systèmes du donneur, k_T est la constante de vitesse du transfert d'énergie triplet–triplet, k_d est la somme des constantes de tous les autres processus de désactivation du niveau triplet du donneur, Φ^t_{tc} est le rendement quantique de l'isomérisation consécutive à une population totale du niveau triplet de l'accepteur.

Une expression analogue peut être écrite pour

$(\Phi^{S}_{c\rightarrow t})^{0}$. A forte concentration de pentène-3 one-2, le terme $k_T(A)/(k_d + k_T(A))$ tend vers l'unité et il est alors possible de calculer $\Phi^{e}_{t\rightarrow c}$ (0.177 dans le cas du benzène, 0.21 dans le cas du mésitylène). On peut alors calculer la part de l'isomérisation issue du transfert d'énergie et celle impliquant l'exciplexe (cf. tableau 10).

Cette interprétation fait intervenir l'existence des deux mécanismes concurrents et complémentaires que sont la formation d'exciplexe et le transfert d'énergie triplet–triplet. Il permet d'interpréter les rendements quantiques d'isomérisation de la pentène-3 one-2 sensibilisée par le benzène et le mésitylène.

1. R. B. CUNDALL, F. J. FLETCHER et D. G. MILNE. J. Chem. Phys. **39**, 3536 (1963); Trans. Faraday Soc. **60**, 1146 (1964); R. B. CUNDALL et A. DAVIES. Trans. Faraday Soc. **62**, 1151 (1966).
2. A. A. LAMOLA et G. S. HAMMOND. J. Chem. Phys. **43**, 2129 (1961).
3. R. B. CUNDALL et W. TIPPET. Trans. Faraday Soc. **66**, 350 (1970).
4. R. R. HENTZ et L. M. PERKEY. J. Phys. Chem. **74**, 3407 (1970).
5. R. B. CUNDALL, L. C. PEREIRA et D. A. ROBINSON. Chem. Phys. Lett. **13**, 253 (1972).
6. R. R. HENTZ et R. M. THIBAULT. J. Phys. Chem. **77**, 1105 (1973).
7. R. B. CUNDALL et S. McD. OGILVIE. Organic molecular photophysics. *Rédigé par* J. B. Birks. J. Wiley, New York, NY. 1973. p. 33.
8. F. BONNET et J. LEMAIRE. Bull. Soc. Chim. Fr. 1185 (1973).
9. A. DEFLANDRE, A. LHEUREUX, A. RIOUAL et J. LEMAIRE. Can. J. Chem. **54**, 2127 (1976).
10. L. J. HEIDT, G. W. TREGAN et F. A. MIDDLETON. J. Phys. Chem. **74**, 1876 (1970).
11. C. A. PARKER et C. G. HATCHARD. J. Phys. Chem. **22**, 63 (1959).
12. J. RONAYETTE, R. ARNAUD, P. LEBOURGEOIS et J. LEMAIRE. Can. J. Chem. **52**, 1848 (1974).
13. G. GAUGLITZ. J. Photochem. **5**, 41 (1976).
14. S. L. MUROV. Handbook of photochemistry. *Rédigé par* Dekker. M. Dekker, New York, NY. 1973.
15. J. C. SCIANO. J. Photochem. **2**, 81 (1973/74).
16. K. SANDROS. Acta Chem. Scand. **23**, 2815 (1969).
17. J. KLEIN, F. HEISEL, H. LAMI et G. LAUSTRIAT. Communication au Congrès International de Luminescence, Budapest. 1966.
18. F. A. CARROL et F. M. QUINA. J. Am. Chem. Soc. **94**, 6246 (1972).
19. F. A. CARROL et F. M. QUINA. J. Am. Chem. Soc. **98**, 1 (1976).
20. H. L. HYNDMAN, B. M. MONROE et G. S. HAMMOND. J. Am. Chem. Soc. **91**, 2852 (1969).
21. J. SALTIEL, L. METIS et M. WRIGHTON. J. Am. Chem. Soc. **91**, 5684 (1969).
22. R. HURELY et A. C. TESTA. J. Am. Chem. Soc. **92**, 211 (1970).
23. S. PATAI (*Rédacteur*). The chemistry of alkenes. Vol. 1. Interscience Publ., New York, NY. 1964. p. 391; J. ZABICKY (*Rédacteur*). The chemistry of alkenes. Vol. 2. Interscience Publ., New York, NY. 1970. p. 970.

Catalytic asymmetric hydrogenation using ruthenium(II) complexes with chelating chiral sulfoxide ligands

BRIAN R. JAMES AND RODERICK S. MCMILLAN

Department of Chemistry, University of British Columbia, Vancouver, B.C., Canada V6T 1W5

Received May 30, 1977

BRIAN R. JAMES and RODERICK S. MCMILLAN. Can. J. Chem. **55**, 3927 (1977).

A chelating sulfoxide ligand, (2*R*,3*R*)-2,3-*O*-isopropylidene-2,3-dihydroxy-1,4-bis(methyl sulfinyl)butane monohydrate, or 'dios', containing chiral carbons has been synthesized. A corresponding bis(benzyl sulfinyl) compound, 'bdios', and an acetal-cleaved derivative, 'ddios', are also reported. Ruthenium(II) neutral complexes have been made containing such ligands, which can bind via oxygen or sulfur; the complexes are active homogeneous catalysts for hydrogenation of prochiral olefinic acid substrates; optical purities of up to 25% were attained.

BRIAN R. JAMES et RODERICK S. MCMILLAN. Can. J. Chem. **55**, 3927 (1977).

On a synthétisé un ligand chélatant sulfoxyde, le monohydrate du (2*R*,3*R*) *O*-isopropylidène-2,3 dihydroxy-2,3 bis(méthylesulfinyl)-1,4 butane ou "dios", contenant des carbones chiraux. On rapporte aussi la préparation d'un composé correspondant bis(benzylsulfinyl), "bdios", et d'un dérivé dont l'acétal a été clivé, "ddios". On a préparé des complexes neutres du ruthénium(II) contenant de tels ligands qui se lient par l'intermédiaire d'un oxygène ou de soufre; les complexes sont des catalyseurs homogènes actifs pour l'hydrogénation de substrats acides oléfiniques prochiraux; on a obtenu des activités optiques allant jusqu'à 25%.

[Traduit par le journal]

Introduction

Our continuing interest in asymmetric homogeneous hydrogenation, especially using ruthenium(II) and rhodium(I) catalysts containing chiral phosphine and sulfoxide ligands (1–3), has led us to the development of three new chelating chiral sulfoxide ligands: (2*R*,3*R*)-2,3-*O*-isopropylidene-2,3-dihydroxy-1,4-bis(methyl sulfinyl)-butane monohydrate, the corresponding bis-(benzyl sulfinyl) derivative, and (2*R*,3*R*)-2,3-dihydroxy-1,4-bis(methyl sulfinyl)butane. We have named these ligands *dios*, *bdios*, and *ddios*, respectively, since they are patterned after the chelating phosphine derivative *diop*, developed by Kagan and Dang (4). Diop complexes of rhodium(I) and ruthenium(II) are known to be highly effective as catalysts for stereoselective hydrogenations (5–7).

Three complexes of ruthenium(II), $(RuCl_2(ddios)_2 \cdot 2H_2O$, $RuCl_2(dios)(ddios)$, and $RuCl_2(ddios)(dmso)(CH_3OH)$, where dmso = dimethylsulfoxide), have been synthesized and characterized, and have been tested as catalysts for asymmetric hydrogenation of some prochiral olefinic substrates. Although the dios-type sulfoxide ligands are prepared as a mixture of the diastereomers, the corresponding catalysts do induce a moderate degree of asymmetry in the hydrogenated substrates.

Results and Discussion

Sulfoxide Ligands

The dios and bdios ligands were prepared from L-(+)-tartaric acid, although the non-naturally occurring acid may also be used. Scheme 1 summarizes the synthetic procedures. The route to the dithiol (**I**) follows literature procedures (8). Treatment with methyl iodide or benzyl bromide in aqueous NaOH then gives the methyl or benzyl sulfide derivative; this displacement of the halide by the anion formed from the mercaptan (9) went smoothly, and the use of a N_2 atmosphere prevented formation of a dithioketal (8). The sulfides were extracted from the aqueous mixtures in high yield. Efficient oxidation to the sulfoxides was carried out using a stoichiometric amount of H_2O_2 in acetone (10). The overall yield of dios and bdios from tartaric acid was 15 and 13%, respectively. The oxidation process at the sulfur should be non-stereospecific, although we were unable to determine the ratio of diastereomers by nmr using a lanthanide chiral shift reagent (2). Carbon atoms 2 and 3 will remain *R* while the configuration at the sulfurs will be (*S*,*S*), (*R*,*R*), (*S*,*R*), and (*R*,*S*), the last two giving identical products.

The dios and bdios products both contain an associated H_2O molecule. Dios is a white, hygroscopic solid, soluble in common solvents

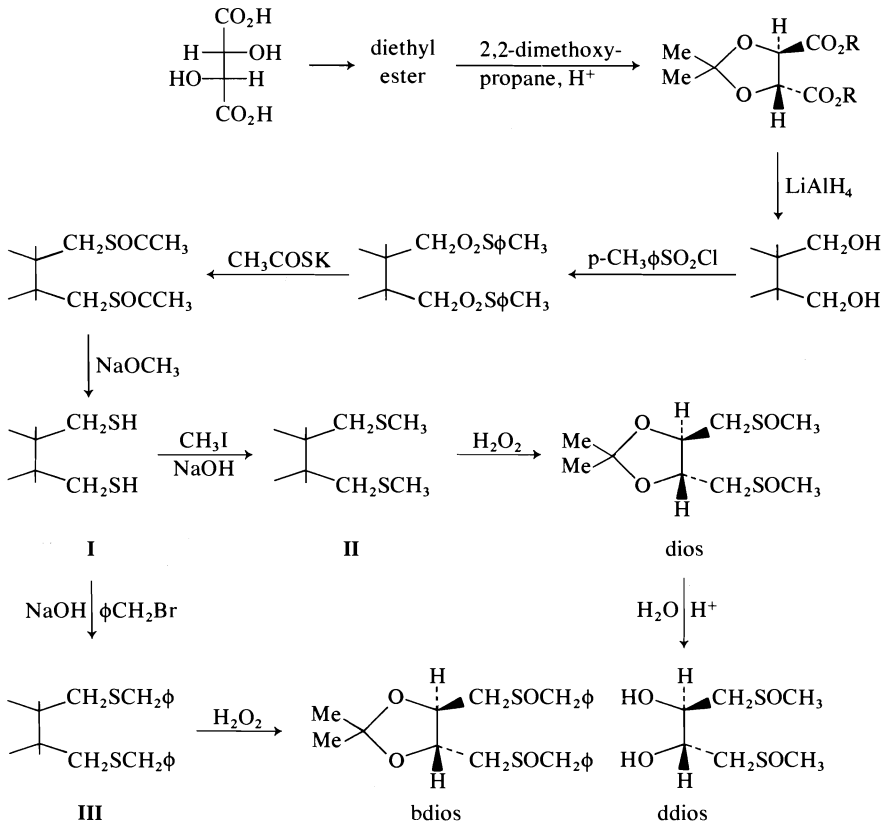

SCHEME 1. Synthetic scheme for dios, ddios, and bdios.

except hexanes in which it is slightly soluble; bdios is a white, non-hygroscopic solid showing similar solubility characteristics although it is insoluble in hexanes and is only slightly soluble in benzene and diethyl ether.

The ddios ligand was originally detected during synthesis of the ruthenium complexes, and results from acid cleavage of the acetal; the acetone by-product is readily detected. Ddios will again be a mixture of diastereomers.

Dichlorobis(ddios)ruthenium(II) Dihydrate, ***1***

This complex was prepared by (*a*), the addition of dios to the 'blue solution' formed on refluxing $RuCl_3 \cdot 3H_2O$ in methanol under 1 atm H_2 (11, 12); and by (*b*), sulfoxide exchange with *cis*-$RuCl_2(dmso)_4$ (13) in methanol. Compound **1**, which gives the correct elemental analysis, is a yellow solid, insoluble in acetone, slightly soluble in alcohols, and more soluble in water and *NN*-dimethylacetamide (dma), in which it is non-ionic.

The ir shows ν(SO) of S-bonded sulfoxide at 1095 cm^{-1}, and a 970 cm^{-1} band is assigned to a methyl rocking mode (14); broad bands centred at 3370 and 1630 cm^{-1} are attributed to H_2O. A poorly resolved far ir region precludes assignment of ν(Ru—Cl).

The nmr spectra in dmso-d_6 and in D_2O show closely spaced narrow resonance peaks at δ 3.25–3.70 due to the methylene and methyl protons of S-bonded ddios (14), and broad absorbances from δ 3.70–4.30 due to methine and hydroxyl protons. No absorption due to O-bonded or free sulfoxide is present in the region δ 2.00–3.00 (14), and there are no peaks at δ 1.00–2.00 due to isopropylidene methyl protons of a coordinated dios (see Experimental). A narrow resonance at δ 3.25 in dmso-d_6 decreased in height on addition of molecular sieve, and is attributed to H_2O.

The spectral data show that the four sulfoxide moieties are all S-bonded, which contrasts with $RuCl_2(dmso)_4$ where one dmso is O-bonded, presumably due to steric reasons (13). The water molecules must be those of solvation, or be

H-bonded to the ligand alcohol groups. A *cis* geometry of chlorides is favoured on comparison with the *cis* yellow tetrakis(dmso) complex; the pale green solid observed during the synthesis of **1** (see Experimental) could be the *trans* isomer. There remains the uncertainty of the configuration at the sulfurs.

Dichloro(dios)(ddios)ruthenium(II), 2

The neutral yellow complex, synthesized from *cis*-$RuCl_2(dmso)_4$ by an exchange reaction with dios in $CHCl_3$, analyzes correctly and is soluble in polar and halogenated solvents, and is insoluble in ether and alkanes. Aqueous solutions are air-sensitive and become green, probably due to formation of ruthenium(III).

A strong ir band at 1100 cm^{-1} is assigned to ν(SO), S-bonded, and a medium band at 932 cm^{-1} could be ν(SO), O-bonded. Bands at 3500 and 1065 cm^{-1} are due, respectively, to ν(OH) and tentatively ν(CO) of the diol. A medium doublet at 1104 and 1113 cm^{-1} is assigned to the C—H bending mode of a geminal dimethyl group (15). The far ir region is not well resolved but a 335 cm^{-1} band could be ν(Ru—Cl).

The ^1H nmr of **2** in $CDCl_3$ shows a singlet at δ 1.42 due to the six isopropylidene methyl protons, and a singlet at δ 2.58 due to protons of a methyl group α to an uncoordinated sulfur; between δ 2.61–2.90 are multiplet resonances due to the protons of a methyl and a methylene group α to an uncoordinated or 'O-bonded' sulfur atom; between δ 3.07–3.80 and δ 3.90–4.70 are multiplets due to the remaining protons of S-bonded dios and ddios ligands. The integration ratios for the S-bonded, O-bonded, free sulfoxide methyl and methylene protons show that in $CDCl_3$ three of the four sulfoxides are S-bonded, the other O-bonded one is partly dissociated, and the amount of dios and ddios is equal. The nmr spectrum is essentially the same in D_2O; addition of DCl–D_2O rapidly removes the δ 1.42 singlet, and generates a singlet at δ 2.05 attributed to acetone. These data show the cleavage of the isopropylidene groups of coordinated dios to form ddios and acetone.

Apparently two dios ligands are not readily chelated, while cleavage to give one ddios likely increases the ligand flexibility and decreases the size, allowing coordination of one dios and one ddios. Even then, coordination through one sulfoxide oxygen atom appears necessary to decrease steric interactions. The dios ligand is considered more likely to coordinate through oxygen, and thus a probable structure involves a bidentate S-bonded ddios and a bidentate dios coordinated through one sulfur and one oxygen. The complex in $CDCl_3$ behaves like *cis*-$RuCl_2(dmso)_4$ in that the single O-bonded sulfoxide here also partly dissociates (16). In water, the O-bonded dmso of $RuCl_2(dmso)_4$ dissociates completely (17); a chelate effect presumably reduces the effective lability of the 'dangling O-atom' in complex **2**.

Dichloro(ddios)(dmso)(CH_3OH)ruthenium(II), 3

Exchange of dios with *cis*-$RuCl_2(dmso)_4$ in a 1:1 mole ratio in refluxing methanol resulted in the neutral complex **3**, which is soluble in water, and dma, and slightly soluble in alcohols. The ir shows bands at 3400 cm^{-1} ν(OH); 1123 and 1100 cm^{-1} ν(SO), S-bonded; a number of bands including a sharp one at 1018 cm^{-1} could be ν(CO) stretches of the alcohol groups. Bands at 325 and 305 cm^{-1} are tentatively assigned to ν(Ru—Cl), implying a *cis*-dichloride structure.

The ^1H nmr in D_2O shows sharp closely spaced resonances (perhaps singlets) at δ 3.52, 3.60, 3.63, and 3.75, and are due to the 12 methyl protons of S-bonded ddios and dmso, the three methyl protons of methanol, and the four methylene protons of ddios. A pair of broad peaks between δ 3.9–4.1 and 4.2–4.4 are due to methine protons (ddios) and alcohol protons (ddios, methanol). An integration ratio of the sharp to broad peaks is ~4:1, consistent with the assignments. Resonances due to O-bonded or free ddios or dmso (δ 2.0–3.0), or the isopropylidene methyl protons of dios (δ ~ 1.45) are not observed. The labile methanol is almost certainly displaced by the water (17).

Considering the nature of complexes **1** and **2**, the 1:1 exchange reaction was expected to produce $RuCl_2(ddios)(dmso)_2$ with one O-bonded sulfoxide (possibly of a dmso) to limit steric interactions, but clearly the methanol competes effectively for coordination. The ruthenium(II) cluster ($Ru_3(CO_2CH_3)_6(CH_3OH)_3$) features an ir band at 996 cm^{-1} (18); this and the 1018 cm^{-1} peak of **3** could be the ν(CO) of coordinated methanol.

Catalytic Asymmetric Hydrogenation

The results of some hydrogenations catalyzed by complexes **1**, **2**, and **3**, are summarized in Table 1.

TABLE 1. Asymmetric hydrogenation results using dios and ddios ruthenium(II) complexes in dma[a]

Catalyst[b]	$[Ru^{II}]$ (M)	Substrate	Molarity of substrate	H_2 (psi)	T (°C)	t (h)	% hydrogenation	Enantiometric excess[c] (%)
1	0.007	Diethyl itaconate	0.5	1800	60	288	100	3.8(*R*)[d]
1	0.015	Itaconic acid	1.8	45	42	144	0	—
2[e]	0.013	Itaconic acid	0.5	44	55	168	49	25.2(*R*)
2[f]	0.013	Itaconic acid	0.5	50	71	168	100	8.1(*R*)
2[e]	0.016	Atropic acid	0.6	46	52	144	17	4.1(*S*)
2[e]	0.016	2-Acetamidoacrylic acid	0.5	47	55	240	62	7.2(*S*)
3	0.016	Itaconic acid	0.6	48	63	240	29	5.4(*R*)

[a]5–10 ml solutions.
[b]**1**, $RuCl_2(ddios)_2{\cdot}2H_2O$; **2**, $RuCl_2(dios)(ddios)$; **3**, $RuCl_2(ddios)(dmso)(MeOH)$.
[c]Predominant enantiomer in parenthesis; ee's are based on the specific rotation of the chiral acid; (*S*)-*N*-acetylalanine, $([\alpha]_D^{26} = -66.5°$; C 2, $H_2O)$ ref. 19, (*R*)-α-methylsuccinic acid, $([\alpha]_D^{20} = +17.09°$; C 10, absolute EtOH) ref. 20, and (*S*)-2-phenylpropanoic acid, $([\alpha]_D^{25} = +76.1°$, C 8, $CHCl_3)$ ref. 20.
[d]0.006 *M* proton sponge added, some metal present at the end of the reaction; the succinate diester product was hydrolyzed to the diacid to determine ee.
[e]Initial yellow solutions became orange by the end of the reaction.
[f]Initial yellow solution became red by the end of the reaction.

In water or dma, 10^{-2} *M* solutions of $RuCl_2(ddios)_2{\cdot}2H_2O$ containing ~0.5 *M* olefinic substrate (e.g. acrylamide, itaconic acid) were unreactive toward 3 atm H_2 at 60°C. Similar solutions containing cationic derivatives of **1** (chloride being removed by filtering after treatment with $AgPF_6$) reacted extremely slowly with H_2. Addition of 'proton sponge' (the strong base 1,8-bisdimethylaminonaphthalene) enhanced these hydrogenation reactions somewhat, presumably by promoting formation of intermediate hydrides via a reaction such as [1] (21),

$$[1] \qquad Ru^{II}Cl + H_2 \rightleftharpoons Ru^{II}H + H^+ + Cl^-$$

Diethyl itaconate was completely hydrogenated using such a catalyst system at high H_2 pressure (Table 1) to give (*R*)-α-methylsuccinate in low but significant enantiomeric excess (ee); some metal precipitated during the hydrogenation and the extent of contribution from a heterogeneous process is uncertain.

The $RuCl_2$(dios)(ddios) catalyst without proton sponge effected homogeneous hydrogenation of itaconic, atropic, and 2-acetamidoacrylic acids under 3 atm H_2 with different degrees of stereoselectivity (Table 1); a maximum 25% ee was attained with itaconic acid. $RuCl_2$(ddios)(dmso)-(CH_3OH) was less effective.

All three catalyst systems give predominantly the *R* enantiomer of α-methylsuccinic acid, and data using **2** indicate decreasing asymmetric induction with increasing temperature; this might result from greater ligand dissociation, and hence less stereoselective catalytic species present with concomitant less restriction on motion of coordinated substrate. The higher rates observed (**2** > **1**) are probably due to the greater lability of the O-bonded sulfoxide present in **2**. The stereoselectivity sequence (**2** > **3**) parallels the number of bulky chiral chelated sulfoxides. The lower optical yields (using **2**) obtained for reduction of atropic and 2-acetamidoacrylic acids compared to itaconic acid likely result from differences in substrate bonding. This could include π-bonding, carboxylate coordination, and H-bonding (—COOH or $\rangle$NH with sulfoxide oxygen or —OH of ddios); for example, see ref. 5. The additional carboxyl acid group of itaconic acid almost certainly plays a role.

The high pressures necessary to effect catalysis, plus the effect of added base, suggest that activation of H_2 is a rate-determining step (eq. 1);

whether olefin is coordinated prior to or after this step cannot be ascertained without kinetic data.

Experimental

General

Dried, degassed reagent grade solvents were used throughout. Ru complexes were made under H_2, Ar, or N_2 atmospheres using schlenk-tube techniques. Spectra were run on a Perkin-Elmer 457 (ir, Nujol mulls between CsI), and a Varian T60 (^{1}H nmr using as references TMS in $CDCl_3$, acetone, and sodium 2,2-dimethyl-2-silapentane-5-sulfonate in D_2O). Optical rotations were recorded on a Perkin-Elmer 421 polarimeter at room temperature using a 10 cm path length microcell. Uncorrected melting points were measured on a Gallenkampt using evacuated capillary tubes. Microanalyses were done by P. Borda of this department.

Itaconic acid (Eastman) and 2-acetamidoacrylic acid (Fluka) were CP grade; atropic acid was prepared according to the literature (22). Ruthenium(III) trichloride trihydrate was obtained as $RuCl_3 \cdot 3H_2O$ (41.83% Ru) from Johnson Matthey Limited.

Sulfoxide Ligands

2,3-O-Isopropylidene-1,4-dithio-L-threitol, I

A preparation (8) from 104 g of L-(+)-tartaric acid ($[\alpha]_D^{25} = +12.8$, C 17, H_2O) gave 42 g (32%) of the colourless liquid **I**, bp 60°C (0.10 mm); $[\alpha]_D^{24} = -13.3°$, C 3.3, $CHCl_3$; δ_{TMS} (neat) 1.38 (singlet, 6H, CMe_2), 1.74 (triplet, $J = 8$ Hz, 2H, —SH), 2.58–2.95 (multiplet, 4H, —CH_2—), 3.76–4.05 (multiplet, 2H, —CH) (lit. (8) $[\alpha]_D^{23} = -13.0°$, C 3.2, $CHCl_3$; δ_{TMS} (neat) as observed).

(2R,3R)-(−)-2,3-Isopropylidene-2,3-dihydroxy-1,4-bis(methylthio)butane, II

To a 250 ml three-necked flask equipped with a gas-inlet tube, a reflux condenser, an addition funnel, and internal stirring, was added 12.7 g (0.32 mol) of NaOH in 75 ml of water. Compound **I** (30 g, 0.15 mol) was added slowly to the vigorously stirred, N_2-flushed solution (a white solid precipitated). Iodomethane (43.8 g, 0.31 mol) was then added as rapidly as the resulting exothermic reaction would allow, and the stirred reaction mixture was refluxed for 4 h. The sulfide layer was separated, washed with water, 10% sodium hydroxide, and finally water before drying with $CaCl_2$. The aqueous layer was extracted with petroleum ether (4 × 100 ml), washed with water, 10% sodium hydroxide, water, and the solvent then stripped off. The liquid residue was washed with 10% sodium hydroxide, water, and dried over calcium chloride. The two dried sulfide fractions were combined and vacuum-distilled to give 20.6 g (60%) of clear colourless liquid, bp 66°C (0.02 mm). $[\alpha]_D^{25} = -6.8°$, C 4.9, $CHCl_3$; δ_{TMS} (CCl_4) 1.37 (singlet, 6H, CMe_2), 2.17 (singlet, 6H, —CH_3), 2.58–2.80 (multiplet, 4H, —CH_2—), 3.77–4.05 (multiplet, 2H, —CH).

(2R,3R)-(−)-2,3-O-Isopropylidene-2,3-dihydroxy-1,4-bis(methyl sulfinyl)butane·H_2O; dios

Compound **II** (20.2 g, 0.09 mol) and 50 ml of acetone were placed in a 250 ml flask. Thirty percent hydrogen peroxide (9.6 ml, 0.18 mol) was added slowly to the cooled (5°C), stirred solution. After stirring overnight, the solvent was flash-evaporated with the final traces of water removed at the vacuum pump. The resulting clear oil solidified over a period of one week, to give 18.9 g (82%) of a hygroscopic white solid, mp 63–85°C; $[\alpha]_D^{23} = -85.8°$, C 5.2, $CHCl_3$; δ_{TMS} ($CDCl_3$) 1.43 (singlet, 6H, CMe_2), 2.66 (singlet, 6H, —CH_3), 2.90–3.35 (multiplet, 4H, —CH_2—), 4.05–4.02 (multiplet, 2H, —CH); δ_{TMS} (acetone-d_6) 3.0 (singlet, 2H, H_2O); ν(SO) 1042 cm^{-1}. *Anal.* calcd. for $C_9H_{20}O_5S_2$: C 39.68, H 7.40; found: C 39.24, H 7.05.

(2R,3R)-(−)-2,3-O-Isopropylidene-2,3-dihydroxy-1,4-bis(benzylthio)butane, III

Compound **I** (11.3 g, 0.06 mol) was added to 4.76 g (0.12 mol) NaOH in 30 ml H_2O in a N_2-purged 100 ml three-necked flask equipped with an addition funnel, reflux condenser, gas-inlet tube, and internal stirring. After dissolution was complete, 19.9 g (0.12 mol) of α-bromotoluene was added with vigorous stirring, and the reaction mixture heated to reflux for 3 h when the sulfide layer formed. Diethyl ether (400 ml) was added to the cooled reaction mixture to dissolve the sulfide. The ether layer was separated, and the aqueous layer further extracted with ether (3 × 75 ml). The ether fractions were combined, washed with water, 10% sodium hydroxide, and water, and dried over anhydrous $CaCl_2$. Removal of the ether gave a white solid, which could be recrystallized from CCl_4; 18.3 g (84%), mp 86–88°C. $[\alpha]_D^{25} = -56.7°$, C 2.7; $CHCl_3$; δ_{TMS} ($CDCl_3$) 1.38 (singlet, 6H, CMe_2), 2.50–2.70 (multiplet, 4H, —CH_2—), 3.65–3.95 (multiplet, 2H, —CH), 3.72 (singlet, 4H, $ArCH_2$—), 7.22 (singlet, 10H, Ar—H).

(2R,3R)-(−)-2,3-O-Isopropylidene-2,3-dihydroxy-1,4-bis(benzyl sulfinyl)butane·H_2O; bdios

Compound **III** (15.9 g 0.043 mol) and 50 ml acetone were placed in a 100 ml flask. Thirty percent H_2O_2 (9.0 ml, 0.086 mol) was added slowly to the cooled (5°C), stirred solution. The white solid which precipitated overnight was filtered, and the mother liquor flash-evaporated to give a colourless oil, which on addition of 50 ml diethyl ether gave more white precipitate. The ether precipitates were combined, washed with petroleum ether, and vacuum dried; 10.5 g (50%), mp 158–168°C (dec.); $[\alpha]_D^{25} = -15.0$, C 1.5, $CHCl_3$; ν(cm^{-1}) 1021 (SO), 1605 1591 (C=C); δ_{TMS} (acetone-d_6) 1.30–1.50 (multiplet 6H, CMe_2), 2.90–3.10 (multiplet, 6H, —CH_2—, H_2O), 4.0–4.5 (multiplet, 2H, —CH), 4.0–4.1 (multiplet, 4H, $ArCH_2$—), 7.32 (singlet, 10H, Ar—H). *Anal.* calcd. for $C_{21}H_{28}O_5S_2$: C 59.41, H 6.65; found: C 59.51, H 6.71.

Ruthenium Compounds

cis-$RuCl_2$(dmso)$_4$

A literature preparation was used (13, 16).

Dichlorobis[(2R,3R)-2,3-dihydroxy-1,4-bis(methyl sulfinyl)butane]ruthenium(II) Dihydrate; Dichlorobis(ddios)ruthenium(II) Dihydrate, I

To the blue solution, formed by refluxing 0.75 g $RuCl_3 \cdot 3H_2O$ in 50 ml CH_3OH under 1 atm H_2, was added 1.56 g dios. Refluxing under H_2 was continued for another 12 h, when a faint green solid precipitated (0.90 g, 46%) and this was filtered and washed with methanol. The filtrate was concentrated (10 ml) and a yellow precipitate filtered off (0.52 g, 27%). Combination of the solids and precipitation from a water solution with acetone yielded 1.33 g (68%) of pale yellow solid: δ_{DSS} (D_2O) 3.25–4.30 (multiplet, 26H, ddios); ir (see text). *Anal.* calcd. for $C_{12}H_{32}Cl_2O_{10}RuS_4$: C 22.6, H 5.07, Cl 11.14; found:

C 22.70, H 4.62, Cl 11.30. Compound **1** was also prepared from $RuCl_2(dmso)_4$ (0.50 g) and dios (0.63 g) by allowing them to react in refluxing methanol (40 ml) overnight, when a yellow precipitate formed. Concentration to 15 ml and cooling to 3°C, yielded, after washing with acetone and drying *in vacuo*, 0.45 g (69%) of product.

*Dichloro[(2R,3R)-(−)-2,3-O-isopropylidene-2,3-dihydroxy-1,4-bis(methyl sulfinyl)butane][(2R,3R)-2,3-dihydroxy-1,4-bis(methyl sulfinyl)butane]ruthenium(II); Dichloro(dios)(ddios)ruthenium(II), **2***

$RuCl_2(dmso)_4$ (0.94 g) and dios (0.80 g) in $CHCl_3$ (50 ml) were refluxed for 120 h; the solution changed from yellow to golden. Removal of the $CHCl_3$ left a residue which dissolved in acetone (15 ml). After filtering, addition of ether (50 ml) precipitated a light yellow solid, which was filtered off, washed with ether and vacuum-dried, 0.57 g (46%); δ_{TMS} ($CDCl_3$) 1.42 (singlet, 6H, CMe_2), 2.58 (singlet, 3H, S—CH_3, uncoordinated), 2.61–2.90 (multiplet, 5H, —CH_2SCH_3), 3.07–3.80 (multiplet, 17H, —CH_2SCH_3, —OH), 3.90–4.70 (multiplet, 4H, —CH); λ_{max} ($CHCl_3$) (log ε); 309 nm (2.67), 356 nm (2.74); ir (see text). *Anal.* calcd. for $C_{15}H_{32}Cl_2O_8RuS_4$: C 28.12, H 5.03, Cl 11.07; found: C 28.30, H 5.13, Cl 11.04.

*Dichloro[(2R,3R)-2,3-dihydroxy-1,4-bis(methyl sulfinyl)butane][dimethyl sulfoxide][methanol]ruthenium(II); Dichloro(ddios)(dmso)(MeOH)ruthenium(II), **3***

$RuCl_2(dmso)_4$ (1.0 g) and dios (0.57 g) were refluxed in 50 ml of methanol; after 42 h the reaction mixture was cooled and the yellow powder filtered off, washed with methanol and ether, and vacuum dried to yield 0.90 g (88%). Recrystallization from dma gave yellow microcrystals: δ_{DSS} (D_2O) 3.52, 3.60, 3.63, 3.75 (singlets, 19H, CH_3S—CH_2, CH_3S, CH_3O), 3.9–4.1, 4.2–4.4 (multiplets, 5H, OH, CH); ir (see text). *Anal.* calcd. for $C_9H_{24}Cl_2O_6RuS_3$: C 21.77, H 4.87, Cl 14.24; found: C 21.69, H 4.68, Cl 14.57.

Hydrogenation Procedures

The procedure for following H_2-uptake at 1 atm has been described previously (23). Hydrogenations at about 50 psi were performed in a Vortex apparatus; reactions at 1800 psi were carried out in a stainless steel Parr high pressure bomb (3000 psi). Solutions containing catalyst and substrate were prepared under Ar. The final reaction mixtures were filtered through celite, and the filtrate pumped to dryness. For the itaconic and atropic acid systems, the residue was dissolved in 10% aqueous NaOH; this was filtered, and the filtrate extracted with $CHCl_3$ to remove sulfoxide and catalyst and then made just acidic with aqueous HCl. The hydrogenated products and unreacted substrates were then extracted with ether, and the ether solution dried over anhydrous $MgSO_4$; reduction in volume yielded the acids. For the 2-acetamidoacrylic acid system, the dry residue was dissolved in water; filtering, extraction with $CHCl_3$, and removal of the water left a brown oil which on addition of ice-cold ether gave crystals of *N*-acetylalanine and unreacted substrate.

The composition of the product mixtures was determined by ^1H nmr, and the optical rotations measured in the appropriate solvent (see Table 1).

Acknowledgments

We thank the National Research Council of Canada for financial support and Johnson Matthey Limited for loan of ruthenium.

1. B. R. James, R. H. Morris, and K. J. Reimer. Can. J. Chem. **55**, 2353 (1977).
2. B. R. James, R. S. McMillan, and K. J. Reimer. J. Mol. Catal. **1**, 439 (1976).
3. B. R. James and D. K. W. Wang. Inorg. Chim. Acta, **19**, L17 (1976).
4. H. B. Kagan and T. P. Dang. J. Am. Chem. Soc. **94**, 6429 (1972).
5. W. S. Knowles, M. J. Sabacky, and B. D. Vineyard. Adv. Chem. Ser., **132**, 274 (1974).
6. B. R. James and D. Mahajan. Isr. J. Chem. In press.
7. B. R. James, D. K. W. Wang, and R. F. Voigt. Chem. Commun. 574 (1975).
8. M. Carmack and C. J. Kelley. J. Org. Chem. **33**, 2171 (1969); P. W. Feit. J. Med. Chem. **7**, 14 (1964).
9. D. T. McAllan, T. V. Cullum, R. A. Dean, and F. A. Fidler. J. Am. Chem. Soc. **73**, 3627 (1951).
10. S. Hünig and O. Boes. Ann. Chem. **579**, 23 (1953).
11. J. D. Gilbert, D. Rose, and G. Wilkinson. J. Chem. Soc. A, 2765 (1970).
12. B. R. James and R. S. McMillan. Inorg. Nucl. Chem. Lett. **11**, 837 (1975).
13. A. Mercer and J. Trotter. J. Chem. Soc. Dalton, 2480 (1975); B. R. James, E. Ochiai, and G. L. Rempel. Inorg. Nucl. Chem. Lett. **7**, 781 (1971).
14. R. S. McMillan, A. Mercer, B. R. James, and J. Trotter. J. Chem. Soc. Dalton, 1006 (1975).
15. J. R. Dyer. Applications of absorption spectroscopy of organic compounds. Prentice-Hall, Englewood Cliffs, NJ. 1965. p. 33.
16. I. P. Evans, A. Spencer, and G. Wilkinson, J. Chem. Soc. Dalton, 204 (1973).
17. K. I. Hardcastle, D. O. Skovlin, and A. H. Eidawad. Chem. Commun. 190 (1975).
18. A. Spencer and G. Wilkinson. J. Chem. Soc. Dalton, 1570 (1972).
19. S. M. Birbaum, L. Levintow, R. B. Kingsley, and J. P. Greenstein. J. Biol. Chem. **194**, 455 (1952).
20. R. E. Burnett. Ph.D. Thesis. University of New Hampshire, Durham, New Hampshire. 1971.
21. B. R. James, A. D. Rattray, and D. K. W. Wang. Chem. Commun. 792 (1976).
22. L. Horner, H. Winkler, A. Repp, A. Mentrupka, and P. Beck. Tetrahedron Lett. 965 (1963).
23. B. R. James and G. L. Rempel. Discuss. Faraday Soc. **46**, 48 (1968).

Electron scavenging by COS in the radiolysis of supercritical *cis*- and *trans*-2-butene

MASARU NISHIKAWA, KAZUO IMAI, AND YUKO SOMA

Department of Pure and Applied Sciences, University of Tokyo, Komaba, Meguro-ku, Tokyo 153, Japan

Received June 10, 1977

MASARU NISHIKAWA, KAZUO IMAI, and YUKO SOMA. Can. J. Chem. **55**, 3933 (1977).

The electron scavenging reaction with COS was studied in γ-irradiated supercritical butenes in the density range 0.24–0.48 g/cm^3 at 170 ± 1°C and in the liquid phase at room temperature. $G(CO)_{fi}$ estimated by means of the 'square root' model at each density studied agreed within experimental accuracy with $G(N_2)_{fi}$ obtained previously. In liquid butenes, $G(CO)_{fi}$, as well as $G(N_2)_{fi}$, agreed with G_{fi} obtained by electrical measurements. Rate constants estimated from the reactivity parameters for reactions with COS were less than 1/10 of those with N_2O at each density studied except at $d = 0.48$ g/cm^3 in *trans*-2-butene.

MASARU NISHIKAWA, KAZUO IMAI et YUKO SOMA. Can. J. Chem. **55**, 3933 (1977).

On a étudié les réactions de piégeages d'électrons avec COS dans des butènes à l'état supercritique irradiés par des radiations γ à des densités allant de 0.24–0.48 g/cm^3 à 170 ± 1°C et dans une phase liquide à température de la pièce. A l'intérieur des limites expérimentales les valeurs de $G(CO)_{fi}$ estimées par le modèle de la "racine carrée" à chacune des densités étudiées sont en bon accord avec les valeurs de $G(N_2)_{fi}$ obtenues antérieurement. Dans les butènes liquides $G(CO)_{fi}$ de même que $G(N_2)_{fi}$ sont en bon accord avec les G_{fi} obtenues par des mesures électriques. Les constantes de vitesses estimées à partir des paramètres de réactivité pour les réactions avec COS sont moins que 10 fois plus petites que celles de N_2O à chacune des densités étudiées excepté à $d = 0.48$ g/cm^3 dans le butène-2 *trans*.

[Traduit par le journal]

Introduction

Electron scavenging reactions by N_2O have recently been studied in several supercritical hydrocarbons, and it has been established that they are quantitatively described by the 'square root' model (1). The treatment of the data by the model has allowed one to estimate the free ion yields (G_{fi}) and the kinetic parameters for the reaction of electrons with N_2O in supercritical hydrocarbons. The present work extends the observation to the system of COS in supercritical butenes. The objective of the study is to test the applicability of and the interpretation by the model in a system other than N_2O–hydrocarbon mixtures.

Experimental

Phillips Research Grade *cis*-2-butene (99.90%) and *trans*-2-butene (99.78%) were passed through a 1 m column of activated silica gel and were degassed. They were further purified by circulating overnight through traps filled with crushed potassium hydroxide and (bubbling through) Na–K alloy, respectively, by means of an electromagnetically operated pump. Matheson Research Grade carbonyl sulfide (96.0%) was used after passing through a trap filled with potassium hydroxide and bulb-to-bulb distillation.

Methods of sample preparation and irradiation in a ^{60}Co source were described previously (1). The irradiation was carried out at 170 ± 1°C; the critical temperatures are 160.0°C and 155.0°C for *cis*-2-butene and *trans*-2-butene, respectively. The dose rate was 4.66×10^{18} eV g^{-1} h^{-1} in Fricke solution and appropriate corrections were made for the electron density ratios. Total dose for most samples did not exceed 5×10^{18} eV/g, but it was ca. 1×10^{19} eV/g for the liquid.

The method of product analysis was essentially the same as described previously (1), except that a 50 cm column of Molecular Sieve 5A was used at 60°C and the whole contents of the irradiated cell was introduced into a gas chromatograph for the samples of lower density.

Results and Discussion

Carbonyl sulfide has been found to give carbon monoxide upon electron capture (2–4). Although the detailed mechanism is not yet known, some secondary reactions subsequent to electron capture by COS appear to be present in liquid benzene when the COS concentration is sufficiently high (3). Sato *et al.* (3) maintain that COS behaves in a quite similar manner to N_2O in the radiolysis of liquid benzene solutions.

The yields of CO from the γ-radiolysis of *cis*-2-butene–, and *trans*-2-butene–COS mixtures in the supercritical state over the density range 0.24–0.48 g/cm^3 and in the liquid phase can be adequately described by the square root model

$G(CO) = G(CO)_{fi} + G(CO)_{gi}(A[COS])^{1/2}$ in the lower concentration range (Figs. 1 and 2). $G(CO)_{fi}$ obtained as the intercepts in the square root plots agree within experimental accuracy with the values of $G(N_2)_{fi}$ previously observed with N_2O as the electron scavenger (1*c*) at each density studied in both isomeric butenes. The agreement, together with the fact that both $G(N_2)_{fi}$ and $G(CO)_{fi}$ obtained in the liquid butenes at room temperature agree quite well with G_{fi} determined by electrical measurements (5), supports our interpretation that secondary reactions are unimportant in the concentration range studied (<0.01 *M*) and there is a one-to-one ratio between the product and the electron captured both by N_2O and COS.

From the slope of the plot and assuming $G_{fi} + G_{gi} = 100/W = 4.2$ (5), one can calculate the reactivity parameter *A* (Table 1). At each density studied the value of *A* obtained in *trans*-2-butene is much larger than that in *cis*-2-butene. The trend has been observed previously with N_2O as the electron scavenger (1*c*). However, the magnitude of *A* for N_2O is always much larger in both hydrocarbons. The ratio of *A* for COS and N_2O ranges from 0.045, in *trans*-2-butene at $d = 0.36$ g/cm^3 to 0.08 in *trans*-2-butene at $d = 0.61$ g/cm^3 (liquid, 23°C), with an exception at $d = 0.48$ g/cm^3 where it is 0.16 (Table 1).

The parameter *A* is given by

$$A = k_s/\lambda$$

where k_s is the rate constant for charge scavenging, and λ a constant for a given solvent, representing the rate of geminate recombination (6). Since the ratio of *A*'s is taken at the same density, the values of λ should be the same. Hence, it is actually the ratio of the rate constants for charge scavenging by COS and N_2O. Thus, it is concluded that dissociative electron capture takes place with a much slower rate with COS in liquid and supercritical butenes.

Sato *et al.* argue that the rate constants for N_2O and for COS are equal in liquid benzene (3). The disparity is not unexpected since it is known that the reactivity of a solute for electrons is different in different media (8). Moreover, their argument is based on a competition study where complications such as charge transfer might be present. Recently determined values of electron affinities (4*b*, 7) suggest such a possibility. In addition, the concentration range of their study is much too high ($\gtrsim 0.4$ *M*) and a reaction mechanism including sequences of secondary reactions has to be constructed. In contrast, the present method offers a much simpler and less ambiguous way of determining relative k_s values for charge scavenging.

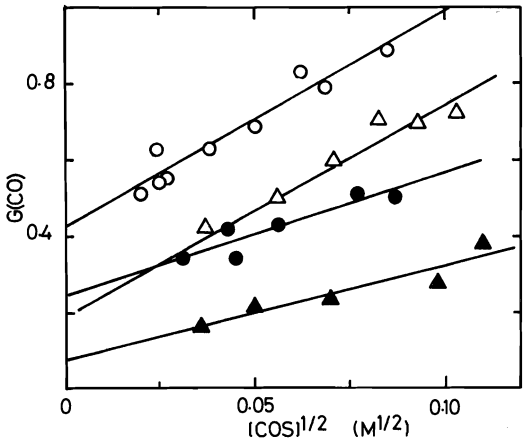

FIG. 1. Yields of CO from *trans*-2-butene–COS mixtures at 170°C as a function of the square root of the molar concentration of COS: ○, 0.24 g/cm^3; ●, 0.36 g/cm^3; △, 0.48 g/cm^3; ▲, 0.61 g/cm^3 (liquid, 23°C).

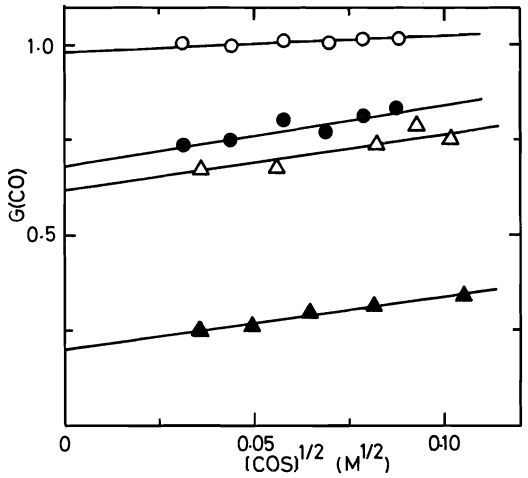

FIG. 2. Yields of CO from *cis*-2-butene–COS mixtures at 170°C as a function of the square root of the molar concentration of COS: ○, 0.24 g/cm^3; ●, 0.36 g/cm^3; △, 0.48 g/cm^3; ▲, 0.62 g/cm^3 (liquid, 23°C).

The variation in *A* ratios, i.e. k_s ratios, is difficult to understand until individual values of k_s and other information are obtained. However, perhaps it could be accounted for in terms of the relationship noted in liquid hydrocarbon between k_s and the energy of the electron in its conducting state V_0, or $V_0 - 0.8P_-$, P_- being

TABLE 1. G_{fi}, electron ranges, and kinetic parameter values

Density (g/cm³)	$G(CO)_{fi}$	$G(N_2)_{fi}$[a]	b[b] (Å)	A_{cos} (M^{-1})	A_{cos}/A_{N_2O}[c]	f[d]
			trans-2-Butene			
0.24±0.01	0.42	0.48	103	2.29	0.065	0.05
0.36±0.01	0.24	0.34	71	0.66	0.045	0.04
0.48±0.01	0.19	0.25	50	1.86	0.16	0.27
0.61 (liq. 23°C)	0.07	0.08	47	0.35	0.080	0.08
			cis-2-Butene			
0.24±0.01	0.97	1.06	171	0.41	0.060	0.002
0.36±0.01	0.68	0.75	116	0.21	0.058	0.003
0.48±0.01	0.62	0.60	105	0.17	0.052	0.003
0.62 (liq. 23°C)	0.20	0.22	69	0.12	0.067	0.008

[a]Reference 1*c*.
[b]The most probable range for ion–electron separation estimated from

$$G_{fi} = G_{tot}\int_0^\infty f(r)\exp(-r_c/r)\,dr$$

where $f(r)$ was taken to be a Gaussian with a power function tail (1*c*).
[c]Values for A_{N_2O} were taken from ref. 1*c*.
[d]The encounter efficiency for the reaction $COS + e^- \rightarrow CO$.

the polarization energy of the anion formed upon electron capture; the peak position in the k_s vs. V_0 or $V_0 - 0.8P_-$ curve may be different for N_2O and for COS (8, 9).

The encounter efficiency (f) of a reaction defined as the ratio of k_s to that in the diffusion-controlled case, $4\pi RD_e$, where R is the reaction radius and D_e the diffusion coefficiency of electrons, has been shown to be

$$f = 3Ar_c/4\pi R(6\times 10^{20})b^3$$

where r_c is the Onsager distance, $e^2/\varepsilon kT$, and b is the most probable distance of ion–electron separation, when the Nernst–Einstein relationship is assumed for geminate recombination of ion–electron pairs (1*c*). By taking $R = 5$ Å and by using b values estimated from $G(CO)_{fi}$ by the method previously described (1*c*), one can calculate f values for the electron reaction of COS. The salient features one notes in the f values summarized in Table 1 are: (*1*) the values in *trans*-2-butene are larger by an order of magnitude except at $d = 0.48$ g/cm³ than those in *cis*-2-butene, and (2) they are smaller approximately by an order of magnitude than the corresponding values observed for N_2O (1*c*). The trend (*1*) has been observed also for N_2O, though the nature of the behavior is not yet understood. Very small f values for COS may indicate that the reaction involves some processes which require large activation energies and/or negative entropies of activation.

1. (*a*) Y. YAMAGUCHI and M. NISHIKAWA. J. Chem. Phys. **59**, 1298 (1973); (*b*) M. NISHIKAWA, Y. YAMAGUCHI, and K. FUJITA. J. Chem. Phys. **61**, 2356 (1974); (*c*) M. NISHIKAWA and Y. YAMAGUCHI. Can. J. Chem. **55**, 2088 (1977).
2. S. HIROKAMI, S. SHISHIDO, and S. SATO. Bull. Chem. Soc. Jpn. **43**, 973 (1970).
3. S. SATO, K. HOSOYA, S. SHISHIDO, and S. HIROKAMI. Bull. Chem. Soc. Jpn. **45**, 2308 (1972).
4. (*a*) J. P. ZIESEL, G. J. SCHULZ, and J. MILHAUD. J. Chem. Phys. **62**, 1936 (1975); (*b*) R. N. COMPTON, P. W. REINHARDT, and C. D. COOPER. J. Chem. Phys. **63**, 3821 (1975).
5. J.-P. DODELET, K. SHINSAKA, U. KORTSCH, and G. R. FREEMAN. J. Chem. Phys. **59**, 2376 (1973).
6. S. J. RZAD, P. P. INFELTA, J. M. WARMAN, and R. H. SCHULER. J. Chem. Phys. **52**, 3971 (1970).
7. D. G. HOPPER, A. C. WAHL, R. C. C. WU, and T. O. TIERNAN. J. Chem. Phys. **65**, 5474 (1976).
8. A. O. ALLEN, T. E. GANGWER, and R. A. HOLROYD. J. Phys. Chem. **79**, 25 (1975).
9. (*a*) A. HENGLEIN. Can. J. Chem. **55**, 2112 (1977); (*b*) R. A. HOLROYD. Ber. Bunsenges. Phys. Chem. **81**, 298 (1977).

Proton and fluorine magnetic resonance studies of some benzoyl fluoride derivatives. Sensitivity of the fluorine shifts to intramolecular van der Waals interactions and steric effects

TED SCHAEFER, KIRK MARAT, KALVIN CHUM, AND ALEXANDER F. JANZEN

Department of Chemistry, University of Manitoba, Winnipeg, Man., Canada R3T 2N2

Received June 13, 1977

TED SCHAEFER, KIRK MARAT, KALVIN CHUM, and ALEXANDER F. JANZEN. Can. J. Chem. **55**, 3936 (1977).

The syntheses and the analyses of the high resolution proton and fluorine magnetic resonance spectra of the 3-fluoro-4-methyl-, 2-fluoro-5-chloro-, 2-fluoro-6-chloro-, 2,6-difluoro-, and of the pentafluorobenzoyl fluorides are reported. The spin–spin coupling constants over five bonds between the sidechain fluorine-19 and the ring protons are sensitive to intrinsic substituent perturbations. Their use in the deduction of conformational preferences is much more problematical than is the use of the corresponding proton–proton couplings in benzaldehyde derivatives. The 2-fluoro-6-chloro compound is nonplanar, as indicated by a finite magnitude of the long-range proton–fluorine coupling over six bonds. The nonplanarity is also indicated by a comparison of the through-space fluorine–fluorine coupling to those in the other compounds. The chemical shift of the sidechain fluorine moves to low field by over 35 ppm as the size of the two *ortho* substituents increases. The individual shifts are discussed in terms of intramolecular van der Waals interactions and of out-of-plane twisting of the COF group.

TED SCHAEFER, KIRK MARAT, KALVIN CHUM et ALEXANDER F. JANZEN. Can. J. Chem. **55**, 3936 (1977).

On rapporte la synthèse et l'analyse des spectres de résonance magnétique nucléaire du proton et du fluor des fluorures du fluoro-3 méthyl-4, du fluoro-2 chloro-5, du fluoro-2 chloro-6, du difluoro-2,6 et du pentafluorobenzoyle. Les constantes de couplage spin–spin à travers cinq liaisons entre le fluor-19 de la chaîne latérale et les protons du cycle sont sensibles à des perturbations intrinsèques du substituant. Leur utilisation dans la déduction des conformations préférentielles est beaucoup plus problématique que l'usage des constantes correspondantes de couplage proton–proton dans les dérivés du benzaldéhyde. Le fluorure du fluoro-2 chloro-6 benzoyle n'est pas planaire tel qu'indiqué par une grandeur finie du couplage à longue distance à travers six liens entre le proton et le fluor. Il y a aussi une indication de non planarité par une comparaison du couplage fluor–fluor à travers l'espace avec celui observé dans d'autres composés. Les déplacements chimiques du fluor de la chaîne latérale se déplacent vers les bas champs par environ 35 ppm à mesure que l'encombrement des deux substituants *ortho* augmente. On discute des déplacements individuels en termes d'interactions de van der Waals intramoléculaires et de torsion hors plan du groupe COF.

[Traduit par le journal]

Introduction

The long-range coupling constants between the aldehydic proton and ring protons or fluorine nuclei in benzaldehyde (1) and its derivatives (2–7) indicate that $^5J_m^{H,CHO}$, the coupling involving protons in the *meta* position to the aldehyde group, is not very sensitive to intrinsic substituent effects but that it is highly stereospecific. In **1**,

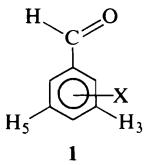

1

$^5J_m^{H_3,CHO}$ apparently lies between 0.76 and 0.96 Hz depending on the nature and position of groups X, and there is no evidence that $^5J_m^{H_5,CHO}$ is other than zero (4). The observed $^5J_m^{H,CHO}$ values are never smaller than the 0.38 Hz in benzaldehyde.

In benzaldehyde itself, $^6J_p^{H,CHO}$ is perhaps −0.04 Hz (1), in agreement with a σ–π mechanism (8) which yields a nonzero $^6J_p^{H,CHO}$ for a nonplanar geometry. The barrier to internal rotation in benzaldehyde is at least 4.6 kcal/mol (9, 10), so that nonplanar conformations are not appreciably populated at ambient temperatures. However, when *ortho* substitution forces the aldehyde group out of the benzene plane, as in 2,6-dichloro- and 2,6-dinitrobenzaldehydes (11), $^6J_p^{H,CHO}$ becomes as large as 0.2 Hz in magnitude.

In benzoyl fluoride, $^4J_o^{H,CFO}$ is −0.60 Hz,

$^5J_m^{H,CFO}$ is 1.33 Hz, and $^6J_p^{H,CFO}$ is undetectably small (1). In *p*-chloro- and in *p*-methylbenzoyl fluoride (12), the first two couplings change by only about 0.05 Hz from their values in benzoyl fluoride, suggesting that $^4J^{H,CFO}$ and $^5J^{H,CFO}$ might be useful as indicators of conformational populations. In this paper we report a full analysis of the proton or fluorine magnetic resonance spectra of five derivatives of benzoyl fluoride, **1** to **5**. The long-range couplings to ^{19}F in the sidechain are discussed in terms of their stereospecificities and their substituent dependence. The ^{19}F chemical shift in COF is very sensitive to the presence of *ortho* substituents and is rationalized in terms of short-range interactions.

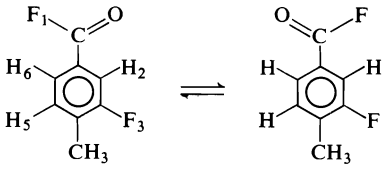

1*a* **1***b*

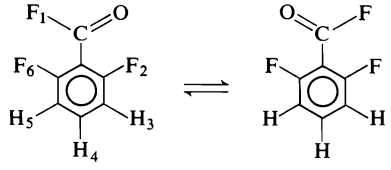

2*a* **2***b*

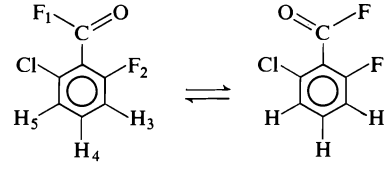

3*a* **3***b*

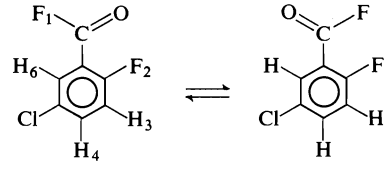

4*a* **4***b*

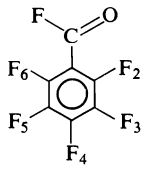

5

Experimental

Compounds

Fluorination of the commercial benzoic acid derivatives with SF_4 (13) yielded the corresponding benzoyl fluorides (13, 14). Product identity was confirmed by mass, ^1H, and ^{19}F spectra and by analysis (A. Bernhardt) for C, H, and F in **2**, **3**, and **4** which, respectively, had mp 30°C, bp 45°C/0.5 Torr, and bp 64°C/2 Torr; **5** had bp 35°C/5 Torr. **1** was a by-product of the synthesis of 3-fluoro-4-methyl benzotrifluoride and was separated from the mixture by gc on a 5 ft × ¼ in. 3% SE-30 column. The bp was not recorded. The yields ranged from 83% for **4** to 45% for **5**.

Spectral Work

Solutions of **1**, 5 mol% in C_6D_6; **2**, 20 mol% in $CDCl_3$; **3**, 20 mol% in CS_2; **4**, 25 vol.% in CF_3CCl_3; and **5**, 20 vol.% in CF_3CCl_3, were degassed and sealed into 5 mm sample tubes. Internal TMS or CF_3CCl_3 served as sources of lock signals.

Proton magnetic resonance spectra were calibrated at 5 Hz intervals in the frequency sweep mode on an HA100 spectrometer at 32°C. Fluorine magnetic resonance spectra were similarly calibrated on a DA60I spectrometer at 29°C. The manual oscillator in this spectrometer was replaced by an external HP 4204A audio-oscillator and either the high-field (for ring fluorines) or the low-field (for COF) sidebands of CF_3CCl_3 were used as lock signals. The resonance of internal $CFCl_3$ occurs at 82.2 ppm to low-field of CF_3CCl_3 (14).

Extensive double resonance experiments (15, 16) or standard spectral analysis procedures gave the signs of F,F and H,F coupling constants relative to known F,F or H,F couplings between nuclei on the benzene ring.

Results and Discussion

Spectral Analysis

These were performed in the usual manner by means of the computer program LAME (17, 18). Separate iterations were carried out for the proton spectra at 100 MHz and for the fluorine-19 spectra at 56.4 MHz. Table 1 presents the ensuing spectral parameters for 3-fluoro-4-methylbenzoyl fluoride. The standard deviations were ≤ 0.006 Hz, and a comparison between those parameters obtainable from both sets of spectra suggests an accuracy of 0.02 Hz in the coupling constants (except perhaps for $^4J_{12}$).

For reasons of space, somewhat briefer sets of spectral data for **2** to **5** are given in Tables 2 and 3. The previous data for **5** in CCl_4 gave no signs of the couplings to the sidechain fluorine nucleus (19) and gave $^4J_{35}$ as $<|0.6|$ Hz, whereas we find -0.54 Hz. Figure 1 shows the observed and calculated spectra for F_3 and F_5 (*meta* position).

Note that spectra were calibrated in the frequency sweep mode, so that, in the tables, a 'shift to low field' from the internal lock is taken as equivalent to a frequency higher than the lock frequency and vice versa.

TABLE 1. Proton and fluorine-19 spectral parameters for 3-fluoro-4-methylbenzoyl fluoride,* **1**, (5 mol% in benzene-d_6)

Parameter	1	1	Parameter	1	1
ν_1†	5608.254(2)†	—	$^5J_{25}$	0.361(3)*	—
ν_2	750.383(2)	—	$^4J_{26}$	1.720(3)	—
ν_3	−1844.100(2)	—	$^4J_{34}$	2.120(4)	2.119(3)§
ν_4	234.516(2)	—	$^4J_{35}$	7.329(4)	7.310(5)
ν_5	729.374(2)	—	$^5J_{36}$	−0.519(5)	−0.531(6)
ν_6	763.917(2)	—	$^4J_{45}$	−0.782(2)	—
$^4J_{12}$	−0.444(4)‡	−0.481(5)§	$^3J_{46}$	0.388(2)	—
$^5J_{13}$	—	4.516(3)	$^3J_{56}$	7.897(2)	—
$^7J_{14}$	<0.03	—	Rms deviation		0.021 Hz
$^5J_{15}$	1.550(4)	1.563(5)	Peaks observed‖		162
$^4J_{16}$	−0.589(5)	−0.592(5)	Transitions		
			Calculated‖		650
$^3J_{23}$	9.497(4)	9.516(6)	Assigned‖		586
$^5J_{24}$	0.428(2)	—			

*The numbering of the nuclei is as in **1** of the text.
†The proton chemical shifts in Hz to low-field of internal TMS at 100 MHz and 32°C; the fluorine-19 shifts in Hz to low-field of internal CF_3CCl_3 at 56.443 MHz and 29°C.
‡The numbers in parentheses are the standard deviations in the last place. The couplings in this column are obtained from iteration on proton peaks at 100 MHz.
§The couplings in this column are obtained from iteration on the ^{19}F peaks at 56.4 MHz. The average deviation between the two sets of couplings is 0.015 Hz, with one large deviation of 0.037 Hz (J_{12}).
‖Summed over both spectra.

TABLE 2. Proton and fluorine-19 spectral parameters for 2-fluoro-5-chlorobenzoyl fluoride,* **4**, and for 2-fluoro-6-chlorobenzoyl fluoride,† **3**

Parameter	4	3	Parameter	4	3
ν_1‡	6397.3	7526.9	$^3J_{23}$	9.76	9.30
ν_2	−1521.3	−1415.5	$^4J_{24}$	4.11	5.83
ν_3	716.75	709.95	$^5J_{25}$	—	−1.43
ν_4	760.40	749.38	$^4J_{26}$	5.95	—
ν_5	—	727.66	$^3J_{34}$	8.91	8.53
ν_6	784.70	—	$^4J_{35}$	—	0.99
$^4J_{12}$	43.56§	30.60	$^5J_{36}$	0.36	—
$^5J_{13}$	0.89	0.76	$^3J_{45}$	—	8.17
$^6J_{14}$	<0.03	−0.29	$^4J_{46}$	2.75	—
$^5J_{15}$	—	0.82	$^3J_{56}$	—	—
$^4J_{16}$	−0.68	—			

*25 vol.% in CF_3CCl_3.
†20 mol% in CS_2.
‡Proton chemical shifts in Hz at 100 MHz to low-field of internal TMS at 32°C; fluorine-19 shifts in Hz at 56.4 MHz to low-field (positive numbers) of CF_3CCl_3 at 29°C.
§The coupling constants are accurate to 0.03 Hz, iterating on the spectra from ^1H and F_2.

Ring Proton and Fluorine Chemical Shifts and Coupling Constants within the Ring

These parameters have been repeatedly discussed (1, 4, 12, 19–21) for related compounds and nothing really new can be added here. This is not to say that the parameters are fully understood.

Proton Couplings to Fluorine in the COF Group Over Five and Four Bonds

From the $^5J_{15}$ and $^5J_{13}$ values for **1** to **4** in the Tables, it is clear that, in general, $^5J_m^{H,COF}$ displays an appreciable intrinsic substituent dependence, i.e. this coupling does not depend only on whether the C—H and C—F bonds lie *cis* ($^5J_{cis}$) or *trans* ($^5J_{trans}$) to one another. $^5J_m^{H,COF}$ varies between 0.76 and 1.55 Hz.

In benzaldehyde derivatives in which, for example, an *ortho* hydroxyl group holds the aldehyde group firmly in one conformation, $^5J_{cis}^{H,CHO}$ is zero (2, 4, 5). Unfortunately, this situation cannot be attained for benzoyl fluoride derivatives; reaction of phenols with SF_4 gave unidentifiable products. INDO MO FPT calculations appear to be of dubious validity for the purpose of finding whether $^5J_{cis}^{H,CFO}$ is zero (22). It is conceivable that $^5J_{cis} < 0$; a negative $^5J_{cis}^{F,OH}$ of −0.35 Hz exists in a *m*-fluorophenol derivative (23).

With these difficulties in mind, perusal of

TABLE 3. Spectral parameters for 2,6-difluorobenzoyl fluoride,* **2**, and for pentafluorobenzoyl fluoride,† **5**

Parameter	2	5	Parameter	2	5
ν_1‡	7291.5	7297.0	$^3J_{23}=^3J_{56}$	9.63	−20.64
$\nu_2=\nu_6$	−1343.4	−2965.5	$^4J_{24}$	6.03	7.88
$\nu_3=\nu_5$	704.76	−4422.4	$^4J_{26}$	0.51	−8.57
ν_4	764.10	−3483.6	$^3J_{34}=^3J_{45}$	8.56	−19.60
$^4J_{12}$	37.53§	38.84	$^4J_{35}$	1.01	−0.54
$^5J_{13}=^5J_{15}$	1.00	2.59	$^5J_{25}=^5J_{36}$	−1.32	8.92
$^6J_{14}$	<0.03	1.13			

*20 mol% in $CDCl_3$.
†20 vol% in CF_3CCl_3.
‡Chemical shifts as in Tables 1 and 2, negative sign indicating to high-field of CF_3CCl_3.
§Coupling constants in Hz to an accuracy of 0.02 Hz for 2 and to 0.04 Hz for 5. The average difference between parameters derived from ^1H and ^{19}F spectra was 0.01 Hz for 2.

$^5J_m^{H,COF}$ and $^4J_o^{H,COF}$ in the tables suggests that a study of other accessible substitution patterns can hardly lead to regularities from which reliable estimates of conformer populations can be made.

These discouraging conclusions stand in sharp contrast to those reached for benzaldehyde derivatives (4, 6) or for fluorophenol derivatives (23). In the latter, $^5J_m^{F,OH}$ is a precise and accurate indicator of conformer populations.

Over Six Bonds, $^6J_p^{H,COF}$

As has been argued previously for phenol (24) and benzaldehyde (11), in which $^6J_p^{H,OH}$ and $^6J_p^{H,COH}$ are probably less than 0.04 Hz in magnitude, the unobservably small $^6J_p^{H,COF}$ in benzoyl fluoride is consistent with a barrier to internal rotation of greater than 4 kcal/mol. The argument depends on the assumption that ^6J is proportional to $\sin^2\theta$, where θ is the angle by which the COF group twists out of the benzene plane, i.e. that ^6J is transmitted via a σ–π mechanism (8, 25). If so, then in **1** $^7J_p^{CH_3COF}$ should be very nearly equal to $-^6J_p^{H,COF}$ in benzoyl fluoride (25). Indeed, these two couplings are less than 0.03 Hz in both compounds.

$^6J_p^{H,COF}$ is also <0.03 Hz in **2** and **4**, indicating planarity, or a very small twist, of the COF group, in the presence of one or two *ortho* fluorine substituents. On the other hand, in **3**, $^6J_p^{H,COF}$ is -0.29 ± 0.03 Hz, somewhat smaller in magnitude than the −0.37 Hz observed in 2,6-dimethylbenzoyl fluoride (22) for which an angle of twist of about 25° has been estimated. It is assumed here that $^6J_p^{H,COF}$ has an appreciable magnitude only when the COF group lies out of the aromatic plane. This assumption leads to no inconsistencies of interpretation, although it cannot be proved that intrinsic substituent effects will not give rise to a nonzero ^6J for a coplanar conformation. It may be noted that in 2,6-dinitro- and 2,6-dichlorobenzaldehydes the COH group very likely twists away from the aromatic plane (11).

The planarity of **1**, **2**, **4**, and **5**, and the nonplanarity of **3** and of 2,6-dimethylbenzoyl fluoride are in congruence with the large through-space $^4J_o^{F,CFO}$ values as well as with the peculiar chemical shifts of the COF fluorine nucleus to be discussed below.

Through-space F,F Couplings and the Chemical Shift of ^{19}F in COF

F,F Couplings

Through-space or proximate F,F couplings, arising from direct interactions between the orbitals centered on the fluorine atoms (26), are exceedingly sensitive to the internuclear distance, r_{FF}. For example, the empirical equation $J^{F,F}$ (Hz) $= 6800 \times \exp(-1.99\ r_{FF}(\text{Å}))$, apparently valid between 2.2 and 4.0 Å (27), roughly reproduces the observed $^4J^{F,F}$ values in 2-fluorobenzotrifluoride derivatives.

If, in the *trans* arrangement of the C—F bonds in **2**, $^4J^{F,F}$ is only about 1.5 Hz (28), a COF geometry based on microwave data on acetyl fluoride (29) and benzoyl fluoride (10) and on a regular benzene geometry entails $^4J^{F,F}$ as 69.6 Hz in the *cis* arrangement on the basis of the above equation. If the assumed rigid geometry is altered to change r_{FF} from 2.30 Å to 2.275 Å, exact agreement with the observed 37.5_3 Hz in **2** is achieved: (1.5 + 73.5)/2. Of course, this result does not prove the planar geometry of **2**, indicated by the near zero value of $^6J_p^{H,COF}$ above.

The increase of 1.3 Hz in $^4J^{FF}$ for **5** can be simply rationalized by a decrease of 0.01 Å in r_{FF} relative to **2**, arising perhaps from slightly greater crowding in the C_6F_5 compared to the $C_6F_2H_3$ moiety. Writing $^4J^{F,F} = 43.5_6$ Hz =

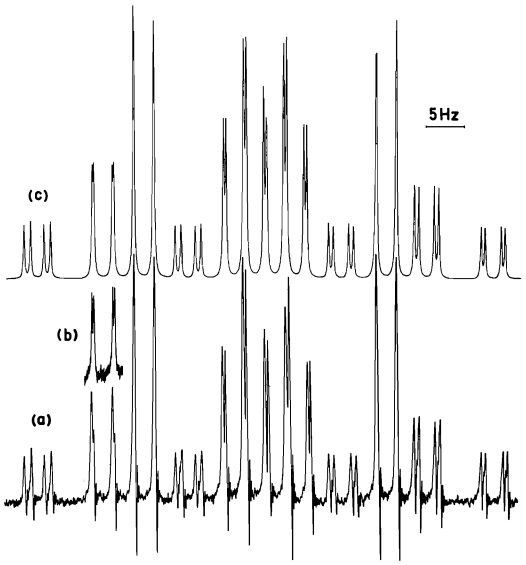

FIG. 1. The observed and calculated spectra at 56.443 MHz of the fluorine nuclei *meta* to COF in pentafluorobenzoyl fluoride, **5**, as a 20 vol.% solution in CF_3CCl_3 at 29°C. The observed spectrum was recorded at a sweep rate 0.1 Hz/s, clearly too large for a clean resolution of some of the small splittings. The inset shows a set of peaks recorded at a sweep rate of 0.02 Hz/s, used in calibration procedures.

$73.5p_{cis} + 1.5p_{trans}$, and $p_{cis} + p_{trans} = 1$, yields $p_{cis} = 0.5_8$ for **4**, i.e. **4***b* is probably somewhat more highly populated than **4***a*.

$^4J^{F,F}$ is 30.6 Hz in **3**, which is indicated as nonplanar by the finite magnitude of $^6J_p^{H,COF}$. An average increase of rather less than 0.1 Å in r_{FF} for the *cis* conformation accounts for the decrease in $^4J^{F,F}$, and is consistent with an average angle of twist of about 20° of the COF group.

The ^{19}F Shift in COF

The magnetic nuclei in the $^{13}C^1H^{17}O$ and $^{13}CO^{19}F$ groups are less shielded than are their counterparts in most other organic functional groupings (1, 20, 30, 31), perhaps as a consequence of low-lying excited electronic states in the C=O bond. Of interest here is the large shift to low-field caused by the *ortho* substituents in benzoyl fluoride derivatives. The shifts are, in Hz at 56.443 MHz relative to internal CF_3CCl_3: 5608 (H,H), 6397 (H,F), 7291 (F,F, **2**), 7297 (F,F, **5**), 7529 (F,Cl), and 7629 (CH_3,CH_3, (ref. 22)). Allowing for differential internal solvent shifts of up to 30 Hz (20, 32), the shielding range of near 2000 Hz, or about 35 ppm, is remarkable.

The change in shielding is clearly not a strong function of the mesomeric or inductive properties of the ring substituents. For example, **2** and **5** are characterized by almost identical $CO^{19}F$ shifts, whereas two *ortho* methyl groups cause the largest low-field shift (although the shifts were measured in different solvents, the shift difference between **1** and *p*-methylbenzoyl fluoride (12) is apparently only about 0.4 ppm (25 Hz)).

Large decreases in shielding in the presence of proximate atomic groupings have been interpreted (20, 33–36) either in terms of intramolecular van der Waals forces or in terms of steric effects. The distinction between these mechanisms rests on the 'distance', *r*, between the atomic groupings. The former are proportional to r^{-6} and are attractive forces, whereas steric effects come about when the electron clouds overlap and cause mutual distortion of the electron clouds or small changes in molecular geometry. The quantitative calculations of shielding changes from these two mechanisms are problematical (20, 36), although it appears certain that the van der Waals interactions cause deshielding and there is some evidence (35) that steric interactions do the same.

In Fig. 2, the observed $CO^{19}F$ shift is plotted versus the mean of the van der Waals radii of the two *ortho* substituents. Indications from $^6J_p^{H,COF}$ are that the molecule is planar for H,H,

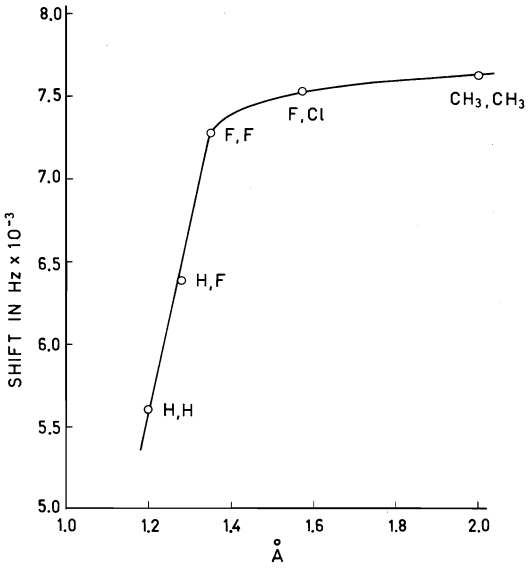

FIG. 2. The shift in Hz at 56.443 MHz to low-field of internal CF_3CCl_3 of the $CO^{19}F$ group is plotted versus the mean of the van der Waals radii in Å of the substituents *ortho* to COF.

H,F, and F,F substituents, suggesting that steric effects, as described above, are still relatively small or, in any event, not large enough to cause appreciable twisting about the partial double bond between the benzene ring and the COF group.

The use of microwave data for the geometry of the COF group suggests an overlap of at least 0.2 Å between the van der Waals radii of the fluorine atoms situated in the COF group and the ring C—F bonds, leading us to believe that the shift of ca. 30 ppm to low-field caused by two *ortho* F,F substituents may well contain a contribution from the steric effects.

The F,Cl and CH_3,CH_3 pairs induce a substantial out-of-plane twist of the COF moiety, as indicated by $^6J_p^{H,COF}$, the twist being largest for CH_3,CH_3. The curvature of the plot in Fig. 2 implies that further large down-field shifts by large substituents, like I,I, will be relatively small because overlap of electron clouds can be relieved by twisting of the COF group.

It may be noted that the ^{19}F shift in alkyl COF compounds lies to low-field of C_6H_5COF (37–39) and that therefore at least part of the observed low-field shifts caused by the F,Cl and CH_3,CH_3 pairs may arise from partial inhibition of conjugation with the benzene ring.

The resonance of $(CH_3)_3COF$ occurs at about 200 Hz to low field of that in C_6H_5COF. On the assumptions that this shift arises from conjugation and that it depends on the square of the cosine of the angle of twist in C_6H_5COF, an estimated angle of twist of 25° in 2,6-dimethylbenzoyl fluoride (22) would lead to a low-field shift of about 40 Hz in the latter compound. Apparently, the shift due to partial loss of conjugation is only a small fraction of the observed shift changes.

Acknowledgements

We are grateful to the National Research Council of Canada for financial support.

1. R. J. Kostelnik, M. P. Williamson, D. E. Wisnosky, and S. M. Castellano. Can. J. Chem. **47**, 3313 (1969).
2. S. Forsén, B. Åkermark, and T. Alm. Acta Chim. Scand. **18**, 2313 (1964).
3. G. J. Karabatsós and F. M. Vane. J. Am. Chem. Soc. **85**, 3886 (1963).
4. R. Wasylishen and T. Schaefer. Can. J. Chem. **49**, 3216 (1971).
5. D. G. DeKowalewski and S. Castellano. Mol. Phys. **16**, 567 (1969).
6. W. Danchura, T. Schaefer, J. B. Rowbotham, and D. J. Wood. Can. J. Chem. **52**, 3986 (1974).
7. S. S. Danyluk, C. L. Bell, and T. Schaefer. Can. J. Chem. **47**, 4005 (1969).
8. C. Heller and H. M. McConnell. J. Chem. Phys. **32**, 1535 (1960).
9. W. G. Fateley, R. K. Harris, F. A. Miller, and R. E. Witkowski. Spectrochim. Acta, **21**, 231 (1965).
10. R. K. Kakar. J. Chem. Phys. **56**, 1189 (1972).
11. C. L. Bell, S. S. Danyluk, and T. Schaefer. Can. J. Chem. **47**, 3529 (1969).
12. H. Bildsøe and K. Schaumburg. J. Magn. Reson. **14**, 223 (1974).
13. W. C. Smith. Angew. Chem. Int. Ed. Engl. **1**, 467 (1962).
14. J. Feeney, L. H. Sutcliffe, and S. M. Walker. Mol. Phys. **11**, 117 (1966).
15. J. P. Maher and D. F. Evans. Proc. Chem. Soc. 208 (1961).
16. R. Freeman and W. A. Anderson. J. Chem. Phys. **37**, 2053 (1962).
17. S. Castellano and A. A. Bothner-By. Mellon Institute Publication, Pittsburgh, PA. 1967; J. Chem. Phys. **41**, 3863 (1964).
18. C. W. Haigh and J. M. Williams. J. Mol. Spectrosc. **32**, 398 (1969).
19. L. N. Pushkina, A. P. Stepanov, V. S. Zhukov, and A. D. Naumov. Org. Magn. Reson. **4**, 607 (1972).
20. J. W. Emsley and L. Phillips. Prog. Nucl. Magn. Reson. Spectrosc. **7**, 1 (1971).
21. R. Wasylishen and T. Schaefer. Can. J. Chem. **49**, 94 (1971).
22. T. Schaefer, K. Chum, K. Marat, and R. E. Wasylishen. Can. J. Chem. **54**, 800 (1976).
23. J. B. Rowbotham, M. Smith, and T. Schaefer. Can. J. Chem. **53**, 986 (1975).
24. T. Schaefer, J. B. Rowbotham, and K. Chum. Can. J. Chem. **54**, 3666 (1976).
25. R. Wasylishen and T. Schaefer. Can. J. Chem. **50**, 1852 (1972).
26. J. Hilton and L. H. Sutcliffe. Prog. Nucl. Magn. Reson. Spectrosc. **10**, 27 (1975).
27. J. Hilton and L. H. Sutcliffe. Spectrochim. Acta, Part A, **32**, 201 (1976).
28. S. Ng and C. H. Sederholm. J. Chem. Phys. **35**, 1243 (1961).
29. R. W. Kilb, C. C. Lin, and E. B. Wilson. J. Chem. Phys. **26**, 1695 (1957).
30. J. B. Stothers. Carbon-13 NMR spectroscopy. Academic Press, New York, NY. 1972.
31. H. A. Christ. Helv. Phys. Acta, **33**, 572 (1960).
32. G. Filipovich and G. V. D. Tiers. J. Phys. Chem. **63**, 761 (1959).
33. T. Schaefer, W. F. Reynolds, and T. Yonemoto. Can. J. Chem. **41**, 2969 (1963).
34. N. Boden, J. W. Emsley, J. Feeney, and L. H. Sutcliffe. Mol. Phys. **8**, 133 (1964); G. L. Caldow. Mol. Phys. **11**, 71 (1966).
35. Y. Momura and Y. Takeuchi. J. Chem. Soc. Chem. Commun. 259 (1970).
36. W. T. Raynes. Nucl. Magn. Reson. Spec. Per. Rep. Chem. Soc. London, **1**, 1 (1972).
37. A. A. Nemysheva and I. L. Knunyants. Dokl. Akad. Nauk SSSR, **177**, 856 (1967).
38. K. Schaumburg. J. Magn. Reson. **7**, 177 (1972).
39. C. Brown, M. Murray, and R. Schmutzler. J. Chem. Soc. C, 878 (1970).

Réactions avec le diazométhane d'esters cinnamylidène maloniques ou cyanacétiques méthylés ou phénylés en γ des groupements fonctionnels et des malononitriles correspondants. Thermolyse des pyrazolines obtenues

J. MARTELLI ET R. CARRIÉ

Groupe de Recherches de Physicochimie Structurale, ERA No 389, Université de Rennes, B.P. 25 A, 35031 Rennes, Cedex, France

Reçu le 6 avril 1977

J. MARTELLI et R. CARRIÉ. Can. J. Chem. **55**, 3942 (1977).

La synthèse d'esters cinnamylidène maloniques ou cyanacétiques méthylés ou phénylés en γ des groupements fonctionnels est réalisée. Les configurations des divers isomères obtenus sont déterminées et les conformations discutées. Le diazométhane s'additionne exclusivement sur la double liaison α,β de ces dipolarophiles selon une orientation unique. La thermolyse des pyrazolines-1 obtenues est étudiée.

J. MARTELLI and R. CARRIÉ. Can. J. Chem. **55**, 3942 (1977).

The syntheses of cinnamylidene malonic or cyanacetic esters, bearing a methyl or a phenyl group in the position γ to the withdrawing groups, were achieved. The configurations of the various isomers were established and the conformations are discussed. Diazomethane adds exclusively to the α,β double bond of these dipolarophiles in only one orientation. The thermolysis of the resulting 1-pyrazoline was studied.

Dans le cadre de recherches expérimentales et théoriques sur l'addition des dipoles 1,3 à des dipolarophiles présentant plusieurs sites d'addition potentiels, l'étude de l'addition de diazocomposés à divers diènes conjugués *gem* diactivés a été entreprise (1). Afin de compléter

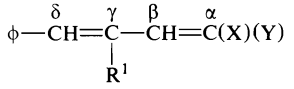

I

les résultats relatifs aux esters cinnamylidène maloniques, cyanacétiques et aux malononitriles correspondants (2) nous avons été conduit à préparer les composés I et à préciser leur comportement vis à vis du diazométhane dans le but de discuter l'influence d'un groupement en γ des substituants activants sur la réactivité des deux sites dipolarophiles et sur l'orientation de l'addition. Les composés I sont susceptibles d'exister sous différentes formes isomères géométriques qui sont quelquefois isolées et dans tous les cas caractérisées à l'aide des données spectroscopiques uv et de rmn. Le diazométhane est additionné à ces oléfines; les monocycloadduits obtenus sont étudiés ainsi que leurs produits de thermolyse.

Synthèse et étude structurale des diènes I (1 à 8)

Ils sont préparés par condensation de l'aldéhyde cinnamique substitué et du composé à méthylène actif correspondant; quatre formes isomères géométriques peuvent exister (**1** à **4** avec $R^1 = CH_3$, $R^2 = H$, **5** à **8** avec $R^1 = \phi$, $R^2 = H$).

Les condensations conduisent (*1*) lorsque $R^1 = CH_3$, à l'isomère **1** avec **2** à l'état de traces et (*2*) lorsque $R^1 = \phi$, au mélange des isomères **5** et **6** qui peuvent être séparés dans certains cas.

L'irradiation des composés **1**, **5** ou **6** en solution les isomérise au niveau soit de la double liaison γδ seulement lorsque le solvant est le méthanol soit à la fois des liaisons αβ et γδ si l'on opère dans le benzène pendant un temps suffisamment long. Ainsi, en solution benzénique, après 4 h d'irradiation à la température

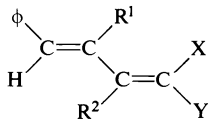

1, 5, 11, 15

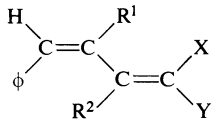

2, 6, 12, 16

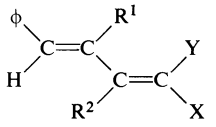

3, 7, 13, 17

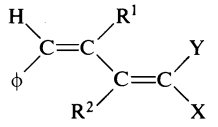

4, 8, 14, 18

1 à **4** $R^1 = CH_3$, $R^2 = H$
5 à **8** $R^1 = \phi$, $R^2 = H$
11 à **14** $R^1 = CH_3$, $R^2 = CH_3$
15 à **18** $R^1 = \phi$, $R^2 = CH_3$

a X = CN, Y = CO_2CH_3
b X = CN, Y = $CO_2C_2H_5$
c X = Y = CN
d X = Y = CO_2CH_3

d'ébullition du solvant, on obtient, à partir de **1***a*, le mélange: **1***a* (41%); **2***a* (31%); **3***a* + **4***a* (28%) (détermination rmn).

Les divers composés sont isolés cristallisés ou caractérisés à l'aide de la rmn; leurs caractéristiques figurent au tableau 1.

Les composés **1** et **2** (**5** et **6**) sont des isomères de configuration au niveau de la double liaison γδ. En effet, l'isomérisation dans le méthanol des composés **1** donne **1** + **2** (**5** ou **6** donne **5** + **6**) et ceci est vérifié avec **1***c*, **1***d*, **6***c*, **6***d* pour lesquels il ne peut y avoir d'isomérisation au niveau de αβ. De plus les caractéristiques spectroscopiques uv des composés **1** (**5**) sont trop différentes de celles des composés **2** (**6**) pour qu'il puisse s'agir d'une isomérisation de configuration αβ.

Ces caractéristiques sont, dans le cas des composés **1**, tout à fait comparables à celles des esters cinnamylidène cyanacétiques, maloniques et des malononitriles correspondants non substitués en β et γ ou uniquement méthylés en β, que la configuration au niveau de αβ soit *E* ou *Z* (2); la double liaison γδ est donc de type *E* pour **1** et *Z* pour **2**.

Bien que la différence de valeur du couplage ^4J (du proton en δ et du substituant méthyle en γ) entre le composé **1** et le composé **2** correspondant ne soit pas suffisante pour prouver à elle seule la configuration de la double liaison γδ (3), les valeurs observées, ^4J = 1.3 à 1.5 Hz (cisoïd) > ^4J = 1.1 à 1.2 Hz (transoïd), sont en accord avec les structures proposées.

Lorsque l'étude rmn est effectuée en solution dans $CDCl_3$, les signaux dûs aux protons du substituant aromatique sont des singulets pour **1***a* à **1***d* et des multiplets plus ou moins larges pour **2***a* à **2***c*; or il est bien connu qu'un tel substituant s'il est coplanaire avec la double liaison (et en l'absence d'autres effets dûs éventuellement au reste de la molécule) donne un multiplet alors que le signal est singulet si la double liaison porte en *cis* du phényle un autre substituant stériquement important (4–7).

Enfin la proximité du phényle en *cis* de H_β dans les composés **2** explique le déblindage de ce proton par rapport à celui du composé **1** correspondant. Un déblindage semblable est observé par Pattenden et Weedon (8) pour les méthyl-2 phényl-5 pentadiènoates de méthyle correspondants.

Les données spectroscopiques uv et plus particulièrement les valeurs des coefficients d'extinction moléculaire des composés **5** et **6** pour les maxima d'absorption de plus grande longueur d'onde (respectivement $\varepsilon_M \simeq 14\,000$ et $\varepsilon_M' \simeq 30\,000$) rappellent celles des *cis* et *trans* stilbènes diversement substitués (9, 10). La configuration *Z* au niveau γδ (les deux φ sont en *cis* l'un de l'autre, composé **5**) entraîne la non coplanéïté des phényles et de la double liaison éthylénique d'où un abaissement important de ε_M. L'aspect des signaux rmn dûs aux phényles est également en accord avec les configurations γδ proposées.

Au niveau de la configuration de la double liaison αβ les attributions de structure sont en accord avec les données spectroscopiques de rmn: comme pour tous les méthylène cyanacétates étudiés jusqu'à présent (11, 2), l'ester en *cis* de H_β rend compte du déblindage plus élevé de **1***a* et **1***b*, **2***a* et **2***b* comparativement à **1***c* et **2***c*; de même pour les composés phénylés en γ **5** et **6** on constate un déblindage d'environ 0.40 à 0.50 ppm du proton H_β de l'ester nitrile par rapport à celui du dinitrile correspondant.

On note enfin la quasi identité des déplacements chimiques de H_β des composés phénylés **6***a* à **6***d* et des méthylés en γ de structure correspondante **2***a* à **2***d*.

Les composés **3***a* ou **4***a*, **7***a* et **8***a* obtenus photochimiquement sont des isomères de configuration au niveau de la double liaison αβ respectivement de **1***a* ou **2***a*, **5***a* et **6***a*, le proton H_β de ces derniers (H_β en *cis* du groupement ester en α) est déblindé par rapport au H_β des premiers. Pour ces composés de configuration *Z* au niveau de la double liaison αβ une interaction d'origine stérique au niveau de l'ester en α et du substituant en γ est susceptible d'expliquer leur obtention difficile dans l'éventualité d'une conformation S *trans*.

La conformation des diènes **1** à **8** est délicate à établir (absence de couplage $^3J_{\beta\gamma}$) cependant la similitude des caractéristiques spectroscopiques uv et de rmn des composés **1** avec celles des diènes du même type non substitués en γ (dont la structure est établie) (2, 8) suggère une conformation privilégiée S *trans*. Il est logique de penser que la conformation privilégiée des composés **2** reste voisine de S *trans*, au moins pour **2***a*, **2***b* et **2***c* (H_β nettement déblindé par le phényle en δ).

De même, une conformation S *trans* privilégiée, voisine de la planéïté, semble pouvoir être attribuée aux composés **6**: la comparaison des

TABLEAU 1. Caractéristiques des diènes de **1** à **8**, $R^2 = H$

					uv (éthanol)		rmn $CDCl_3$ ou (C_6D_6)[a]					
No	R^1	X	Y	pf (°C)	λ_M (nm)	ε_M	H_β	H_δ	$R^1 = CH_3$	CO_2CH_3 ou $CO_2CH_2CH_3$	C_6H_5[b] (aspect)	$^4J(H_\delta—R^1)$
1*a*		CN	CO_2CH_3	108	340	30 600	7.96	7.15	2.41	3.88	s	
							(7.72)	(6.50)	(2.14)	(3.40)		(1.1)
2*a*		CN	CO_2CH_3	60	343	17 950	8.20	7.10–7.45	2.41	3.83	m	
							(8.15)	(6.64)	(2.19)	(3.36)		(1.3)
3*a* ou **4***a*		CN	CO_2CH_3	[c]			(6.73)[d]	(6.34)	(1.79)	(3.26)		
1*b*		CN	$CO_2C_2H_5$	81	340	30 600	7.94	7.14	2.40	4.33	s	
2*b*	CH_3			[c]			8.18	—	2.40	4.28	m	
1*c*		CN	CN	129	347	32 700	7.42	7.12	2.38		s	
							(6.38)	(6.18)	(1.85)			(1.2)
2*c*		CN	CN	[c]	350	20 300[e]	7.64		2.38		m	
							(6.46)	(7.04–7.26)	(1.89)			(1.5)
1*d*		CO_2CH_3	CO_2CH_3	50–52	314	30 000	7.44	6.92	1.99	3.56	s	
							(7.52)	(6.64)	(1.91)	(3.44)		(1.1)
2*d*		CO_2CH_3	CO_2CH_3	[c]	315	13 800[f]	7.69	6.83	1.99	3.56	s	
							(7.88)	(6.59)	(1.91)	(3.35)		(1.4)
5*a*		CN	CO_2CH_3	[c]	356	13 680[g]	8.40	7.0–7.5		3.81	s, me	
							(8.40)			(3.35)		
6*a*		CN	CO_2CH_3	151	352	32 000	8.10	7.0–7.5		3.79	mL, mL	
							(8.00)	(6.86)		(3.31)		
7*a*		CN	CO_2CH_3	[c]	354	13 370[h]	7.62	7.10		3.22	s, me	
										(2.83)		
8*a*	C_6H_5	CN	CO_2CH_3	[c]			7.1–7.5	6.80		3.70		
							(6.56)			(3.07)		
5*b*		CN	$CO_2C_2H_5$	148			8.38	7.15		4.36	s, me	
6*b*		CN	$CO_2C_2H_5$	78	348	32 500	8.11	7.0–7.5		4.34	mL, mL	
5*c*		CN	CN	[c]			7.92	7.0–7.6				
								(1H à 6.59)				
6*c*		CN	CN	176	358	33 500	7.1–7.6	7.1–7.6			mL, mL	
								(6.58 et 6.33)				
5*d*		CO_2CH_3	CO_2CH_3	81–83	334	15 200	7.96	7.02		3.11 3.81	s, s	
							(8.11)	(6.80)		(2.99) (3.40)		
6*d*		CO_2CH_3	CO_2CH_3	138	327	29 800	7.67	7.1 ou 7.3		3.14 3.76	mL, mL	
							(7.74)	(6.71)		(2.99) (3.40)		

[a]Les déplacements chimiques sont exprimés en ppm (référence interne TMS) et les constantes de couplage en hertzs. Il en sera ainsi dans la suite de l'exposé.
[b]s, singulet; m, multiplet; e, étroit; L, large.
[c]Isomère non purifié.
[d]L'un seulement des isomères est caractérisé avec certitude.
[e]Déterminé à partir d'un mélange **1***c* + **2***c*.
[f]Déterminé à partir d'un mélange **1***d* + **2***d*.
[g]Déterminé à partir d'un mélange **5***a* + **6***a*.
[h]Déterminé à partir d'un mélange **5***a* + **7***a*.

déplacements chimiques de H_β des composés **6** et **2** correspondants indique une analogie structurale.

Action du diazométhane

Le diazométhane s'additionne d'une manière stéréospécifique sur la double liaison αβ des composés I. De même que pour les composés non substitués en γ la vitesse de l'addition et la stabilité du monoadduit formé sont très différentes suivant la nature des substituants X et Y, nous envisagerons deux cas.

Composé I dinitriles et esters nitriles

Les composés I de configuration *E* en αβ conduisent quantitativement, par action d'une quantité stoechiométrique de dipôle, aux composés β-méthylés correspondants. Partant d'un mélange d'isomères géométriques au niveau de la double liaison γδ (en proportions connues), les deux isomères β-méthylés sont obtenus dans les mêmes proportions. La méthylation s'effectue (schéma 1) par l'intermédiaire d'une pyrazoline-1 instable qui est mise en évidence dans deux cas: **9***a* et **10***a* (X = CN, Y = CO_2CH_3), en opérant l'addition du diazométhane à −20°C sur **1***a* et **6***a* respectivement.

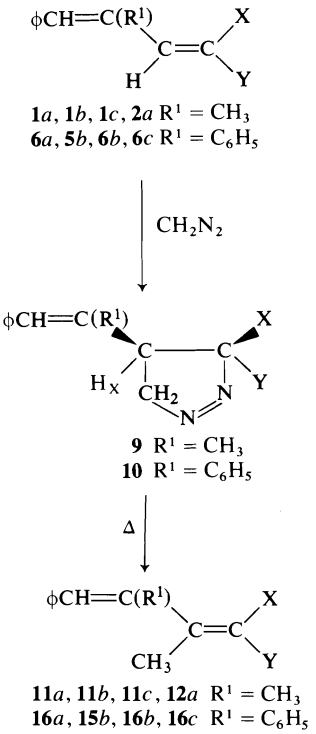

1*a*, **1***b*, **1***c*, **2***a* $R^1 = CH_3$
6*a*, **5***b*, **6***b*, **6***c* $R^1 = C_6H_5$

9 $R^1 = CH_3$
10 $R^1 = C_6H_5$

11*a*, **11***b*, **11***c*, **12***a* $R^1 = CH_3$
16*a*, **15***b*, **16***b*, **16***c* $R^1 = C_6H_5$

SCHÉMA 1

Le site et l'orientation de cette cycloaddition sont établis à l'aide de la rmn (système ABX). Les caractéristiques des pyrazolines **9***a* et **10***a* sont les suivantes (rmn $CDCl_3$): **9***a*: 6.46 (s élargi, φCH=), 1.67 (s élargi, $R^1 = CH_3$), 3.92 (s, CO_2CH_3); système ABX: $H_A = 5.19$, $H_B = 4.95$, $H_X = 3.50$; $J_{AB} = 18.2$, $J_{AX} = 3.2$, $J_{BX} = 7.8$. **10***a*: 6.44 (φCH=), 3.37 (s, CO_2CH_3); système ABX $H_A = 5.28$, $H_B = 4.97$; $J_{AB} = 17.8$, $J_{AX} = 7.7$, $J_{BX} = 7.8$.

Comme les diènes dont ils dérivent, les composés β-méthylés $R^1 = CH_3$ et $R^1 = \phi$ peuvent exister sous quatre formes isomères géométriques **11** à **18**.

L'isomérisation au niveau de la double liaison αβ seule, se produit lorsque le composé **11** ou **12** ($R^1 = CH_3$, X ≠ Y) est abandonné en solution éthérée. Un mélange photostationnaire de deux (X = Y = CN) ou quatre (X = CN, Y = CO_2R) isomères est obtenu lorsqu'on irradie une solution méthanolique ou benzénique des composés **11**, **12** ($R^1 = CH_3$), **15** ou **16** ($R^1 = \phi$). Les composés obtenus par perte d'azote à partir des monoadduits **9** ou **10** ont la même configuration que les diènes dont ils dérivent, cette caractéristique de la méthylation par le diazométhane est tout à fait conforme aux observations antérieures (12, 2).

Les attributions de structures sont effectuées sur les considérations spectroscopiques uv et de rmn développées pour les diènes précurseurs. Les résultats figurent au tableau 2.

L'aspect des signaux des protons aromatiques: singulet lorsque le phényle δ est en *cis* de $R^1 = \phi$ (**15** et **17**) ou $R^1 = CH_3$ (**11**); les couplages $^4J(H_\delta, CH_{3\gamma})$ lorsque $R^1 = CH_3$ (*J* cisoïd > *J* transoïd); l'examen des déplacements chimiques du méthyle β déblindé par le groupement ester en *cis* pour les composés **11**, **12**, **15** et **16** comparativement à **13**, **14**, **17** et **18**; la similitude des variations relatives (suivant les isomères considérés) de CH_3 en β et du H_β des diènes dont ils dérivent; enfin des comparaisons pouvant être effectuées avec les données spectroscopiques citées dans la littérature (3, 13, 14) permettent d'établir la structure des diènes β-méthylés.

A l'exclusion des composés **11** auxquels une structure S *trans EE* voisine de la planéïté peut encore être attribuée (Wiley et coll. ont montré que l'acide diméthyl-3,4 phényl-5 pentadiènoïque est S *trans EE* (13, 14)), les composés β-méthylés obtenus **12** à **18** ne semblent pas pouvoir être

TABLEAU 2. Caractéristiques des diènes **11** à **18**, X = CN

				uv éthanol		rmn $CDCl_3$, (C_6D_6)					
No	R^1	Y	pf (°C)	λ_M (nm)	ε_M	$R^2 = CH_3$	H_δ	$R^1 = CH_3$	CO_2CH_3 ou $CO_2CH_2CH_3$	C_6H_5 (aspect)	$^4J(H_\delta—R^1)$
11*a*		CO_2CH_3	[a]			2.48	6.63	2.06	3.83	s	1.3
12*a*		CO_2CH_3	[a]			2.44	6.41	2.06	3.74		1.5
13*a*		CO_2CH_3	[a]			2.37	6.22	2.03	3.75	me	1.3
14*a*		CO_2CH_3	[a]			2.22	6.30	2.01	3.70		
11*b*	CH_3	$CO_2C_2H_5$	[a]			2.46	6.65	2.08	4.27	s	
12*b*		$CO_2C_2H_5$	[a]			2.45	6.42	2.10	4.30	m	
13*b*		$CO_2C_2H_5$	[a]			2.35	6.23	2.10			
14*b*		$CO_2C_2H_5$	[a]			2.23	6.29	2.10			
11*c*		CN	71	340	10 500	2.38 (1.78)	6.80 (6.53)	2.08 (1.59)		s	1.3
12*c*		CN	108–109	326	2 800	2.33 (1.64)	6.60 (6.18)	2.06 (1.48)		me	1.6
15*a*		CO_2CH_3	110	279	19 700[b]	2.54 (2.38)	6.96		3.80 (3.20)	s, s	
16*a*		CO_2CH_3	126–127	330	8 600	2.29 (2.11)	6.91		3.86 (3.41)	m, m	
17*a*		CO_2CH_3	[a]			2.39 (2.07)	6.87 (6.65)		3.55 (2.99)	s, s	
18*a*		CO_2CH_3	[a]			2.18	6.50		3.70		
15*b*		$CO_2C_2H_5$	125			2.54	6.94		4.25	s, s	
16*b*	C_6H_5	$CO_2C_2H_5$	134			2.28	6.89		4.30	m, m	
17*b*		$CO_2C_2H_5$	[a]			2.35	6.84		4.05	s, s	
18*b*		$CO_2C_2H_5$	[a]			2.16	6.50				
15*c*		CN	[a]			2.44	7.1–7.7			s, s	
16*c*		CN	109–111	350	12 200	2.25 (1.59)	7.0–7.4			s, m	

[a]Composé non purifié caractérisé à l'aide de la rmn.
[b]Absence de bande d'absorption dans la région 330–350 nm.

TABLEAU 3. Caractéristiques des composés **19–21**

No	R^1	—CH=	J	R^1	CO_2CH_3	H_A	H_B	H_X	J_{AB}	J_{AX}	J_{BX}	ϕ(aspect)
19	CH_3	6.27	1.2	1.67	3.67 et 3.82	4.90	4.76	—	18.1	4.8	7.8	m
20	CH_3	6.39	1.5	1.41	3.67 et 3.82		Système ABX non analysé					s
21	ϕ	6.28			3.70 et 3.82	5.08	4.91	3.98	18.5	4.1	8.8	

plans à cause de fortes interactions stériques s'exerçant au niveau du substituant en γ et d'un substituant en α d'une part, du phényle en δ et du méthyle en β d'autre part.

Composés I diesters

Le diazométhane s'additionne exclusivement (même en présence d'un gros excès de dipôle) sur la double liaison αβ de ces diesters et selon le sens indiqué (schéma 2); il y a formation de pyrazoline-1 stable à la température ambiante. L'addition du dipôle est beaucoup plus lente que dans le cas des esters nitriles correspondants. **5***d* ne réagit pas avec le diazométhane (il faut remarquer que **7***a*, ester nitrile de structure analogue, additionne lentement le dipôle).

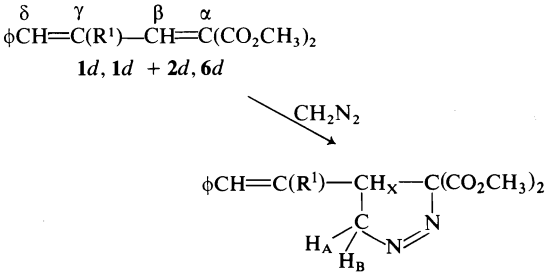

SCHÉMA 2

Les pyrazolines obtenues sont caractérisées à l'aide de la rmn. La valeur du déplacement chimique du méthyle ($R^1 = CH_3$), celle de la constante de couplage ^4J allylique sont des preuves de la conservation de la configuration de la double liaison au niveau de γδ. L'existence d'un système ABX donne l'orientation de l'addition.

Les caractéristiques de rmn ($CDCl_3$) des composés figurent au tableau 3.

Les pyrazolines-1 **19** et **21** sont décomposées thermiquement dans le xylène au reflux (schéma 3); elles conduisent respectivement aux oléfines **22** (65%) + **23** (35%) et **24** (65%) + **25** (26%) accompagnées d'un autre produit non identifié.

Les composés **22** à **25**, non isolés, sont caractérisés dans le mélange obtenu après thermolyse par leurs propriétés spectroscopiques (rmn) (tableaux 4 et 5).

Composés **22** et **24**: les trois protons éthyleniques (β, γ, ε) sont déblindés et le couplage avec $J_{\beta\gamma} = 15$ et 16 Hz, caractérise une stéréochimie *trans*. On observe un doublet correspondant au proton plus blindé porté par le carbone α substitué par deux esters dont les méthyles sont équivalents; on notera également la conservation, par rapport aux diènes de départ, de la forme des signaux dûs aux phényles et pour **22** le couplage du méthyle en δ avec H_ε.

Composés **23** et **25**: le dédoublement des signaux pour $CH_{3\gamma}$ et H_δ (**23**) est témoin d'un couplage ^4J entre ces protons; les deux esters ne sont pas équivalents, ce qui confirme l'existence d'une double liaison en αβ.

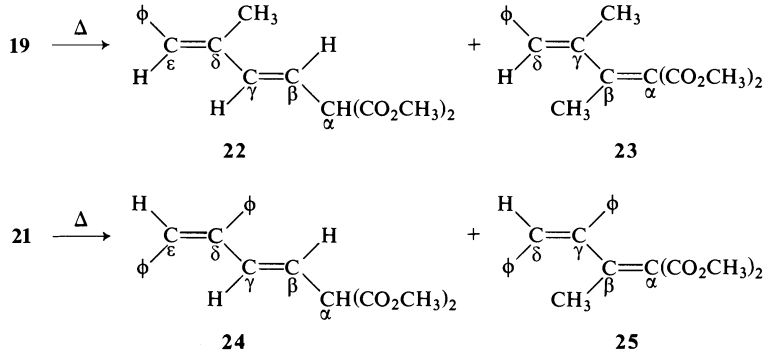

SCHÉMA 3

TABLEAU 4. Caractéristiques de rmn ($CDCl_3$) des composés **22** et **24**

No	H_ε	J	$CH_{3\delta}$	H_γ	$J_{\beta\gamma}$	H_β	$J_{\alpha\beta}$	H_α	CO_2CH_3	ϕ(aspect)
22	6.42	1.2	1.95	6.34	16	5.86	9	4.10	3.65	s
24	6.52			6.49	15	5.43	9	4.08	3.62	mm

TABLEAU 5. Caractéristiques de rmn ($CDCl_3$) des composés **23** et **25**

No	H_δ	J	$CH_{3\gamma}$	$CH_{3\beta}$	CO_2CH_3
23	6.25	1.2	1.95	2.19	3.58 et 3.65
25	*		—	2.04	3.71 et 3.50 à 3.62

*Signal masqué par ceux des protons aromatiques.

Dimérisation des diènes 1

Les composés **1***b*, **1***c* et **1***d* sont photosensibles à l'état solide. S'ils ne sont pas conservés à l'abri de la lumière, ils conduisent rapidement aux produits de dimérisation correspondants **26**, **27**, **28**, dont la structure est établie à l'aide

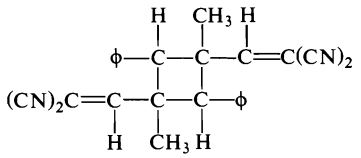

27

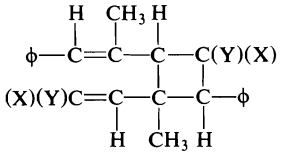

26 X = CN, Y = $CO_2C_2H_5$
28 X = Y = CO_2CH_3

de la rmn (la stéréochimie n'est pas précisée). **26** ($CDCl_3$): 0.80 et 1.34 (—CH_2—CH_3), 3.96 et 4.32 (—CH_2—CH_3), 1.46 (s, CH_3), 1.93 (s élargi, CH_3), 6.60 (s élargi, H), 8.47 (s, H), 4.20 (s élargi, H), 4.32 (s, H); ϕ aspect: deux multiplets étroits. **27** (DMSO-d_6): 8.30 (s, 2H), 1.48 (s, 6H), 4.39 (s, 2H); ϕ (aspects): deux multiplets étroits. **28** (C_6D_6): 4.27 (s, 1H), 4.95 (s, 1H), 6.61 (s élargi, 1H), 7.51 (s, 1H), 1.96 (d, 3H, J = 1.2), 1.73 (s, 3H), 3.06 (s, 6H, $2CO_2CH_3$ fortuitement équivalents), 3.26 (s, 3H, CO_2CH_3) et 3.29 (s, 3H, CO_2CH_3).

Conclusion

La synthèse d'esters cinnamylidène cyanacétiques ou maloniques γ substitués et des malononitriles correspondants est réalisée et leur stéréochimie discutée.

L'introduction d'une substitution en γ ne modifie pas le comportement de ces diènes vis à vis des diazocomposés: l'addition s'effectue exclusivement sur la double liaison $\alpha\beta$ et dans le sens attendu. Il convient cependant de noter la nette différence de réactivité entre certains isomères géométriques.

L'évolution thermique des pyrazolines-1 obtenues n'est pas non plus affectée par cette substitution en γ: lorsque l'un des groupements activants est un groupement nitrile la thermolyse, d'une manière quantitative et stéréospécifique, conduit à des diènes β-méthylés.

Les cycloadduits dérivés des diènes *gem*-diactivés par deux groupements esters se comportent différemment. Les oléfines résultant de la migration du groupe vinyle substitué sur le carbone 5 de la pyrazoline-1 sont principalement formées. Elles s'isomérisent par prototropie dans le milieu réactionnel.

Partie expérimentale

Les spectres de rmn sont réalisés avec un appareil JNM MH 100 (Jeolco) à 100 MHz. Les spectres uv sont obtenus à l'aide d'un appareil Unicam SP 700 à partir de solutions dans l'alcool à 95°. Les points de fusion sont pris au banc chauffant Kofler. Tous les composés pour lesquels le mot "analyse" est indiqué, suivi d'une formule moléculaire explicite, ont fourni des résultats analytiques correspondant à $\pm 0.4\%$ près, au plus, sur les éléments analysés (C, H, N) (Service de Microanalyse de l'Université de Rennes).

Le phényl-3 méthyl-2 propène-2 al est obtenu par crotonisation de l'aldéhyde benzoïque et de l'aldéhyde propionique en présence de méthylate de sodium selon la technique de Burton (15). L'aldéhyde phényl-2 cinnamique est également préparé par crotonisation suivant la méthode de Etienne et Weill-Reynal (16) décrite par Bargain (17).

Dienes 1 à 8

Les méthodes sont: *A*, condensation suivant Cope et coll. (18); *B*, condensation du type précédent modifiée

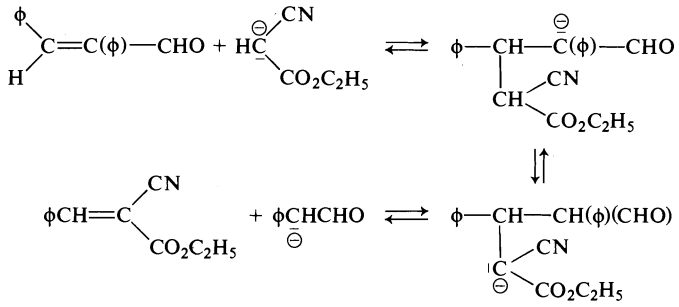

SCHÉMA 4

selon Mowry (19); *C*, condensation suivant Allen et Spangler (20).

1*a* (*A*, rdt 38%), pf 108°C (méthanol). Analyse $C_{14}H_{13}NO_2$.

1*b*, **2***b* (*A*, rdt 73%, mélange **1***b* (88%) + **2***b* (12%)) (intégration du signal rmn dû à H_β).

1*b*, pf 81°C (éthanol). Analyse $C_{15}H_{15}NO_2$.

1*c* (*B*, quantité de solvant doublée, rdt 55%), pf 129°C (éthanol). Analyse $C_{13}H_{10}N_2$.

1*d*, pf 50–52°C (éther). Analyse $C_{15}H_{16}O_4$.

5*a*, **6***a* (*A*, rdt 73%, mélange **5***a* (20%) + **6***a* (80%)).

6*a*, pf 151°C (éthanol). Analyse $C_{19}H_{15}NO_2$.

5*b*, **6***b*. La méthode *A* conduit avec un rendement global de 40% à un mélange des deux isomères dans des proportions relatives très variables suivant la manipulation. De l'huile obtenue à partir du produit brut de réaction après distillation du cyanacétate en excès, cristallisent les diènes par addition d'éthanol; du résidu distille, à 140°C sous 2 mm, un composé qui cristallise par refroidissement pf 50°C, c'est l'ester α-cyanocinnamique $\phi CH{=}C(CN)(CO_2C_2H_5)$, dont la formation résulte d'une addition de Michael de l'anion cyanacétate sur la double liaison de l'aldéhyde (schéma 4), il est identifié par comparaison avec un échantillon authentique (21).

5*b*, pf 148°C (éthanol). Analyse $C_{20}H_{17}NO_2$.

6*b*, pf 78°C (éthanol). Analyse $C_{20}H_{27}NO_2$.

5*c*, **6***c*. La méthode *B* conduit au mélange des deux isomères. Après distillation du solvant, on recueille 9 g de cristaux jaunes (pf 173°C) et 1 g d'une huile constituée du mélange des deux isomères.

6*c*, rdt 59%, pf 176°C (éthanol).

5*d*, **6***d*. La condensation (*C*) conduit à un mélange de deux isomères, ils cristallisent ensemble par addition de quelques cm^3 de méthanol à l'huile épaisse obtenue par distillation du solvant; rdt 64%. **6***d* cristallisé est obtenu à partir d'une solution benzénique concentrée du produit brut de la réaction en distillant partiellement le solvant.

5*d*, pf 81–83°C, est obtenu par cristallisation fractionnée d'un mélange enrichi en **5***d* par irradiation.

Isomérisation photochimique

Les composés **1** ou **6** sont isomérisés en solution (1 g dans 130 cm^3 de méthanol ou de benzène sec). La solution contenue dans un ballon de quartz surmonté d'un réfrigérant est irradiée au moyen d'une lampe Hanau (brûleur TQ 81) placée extérieurement; l'irradiation est effectuée à la température de reflux du solvant.

Action du diazométhane sur les oléfines

Le dipôle, préparé à partir de la nitrosométhylurée (22) (0.5 *M*) et le diène sont abandonnés en solution éthérée à 0°C; les composés β-méthylés ou les pyrazolines correspondants sont obtenus par simple distillation du solvant sous vide à basse température. Dans le cas des esters nitriles et dinitriles, la réaction est généralement totale après 24 h avec une quantité de dipôle égale ou légèrement supérieure à la stoechiométrie. On notera cependant une méthylation partielle dans un cas: **5***a* (18%) + **7***a* (82%) + CH_2N_2 (1.5 fois la quantité stoechiométrique) conduit après 24 h à une méthylation totale de **5***a* (**5***a* → **15***a*) et une méthylation partielle de **7***a* (**7***a* → **7***a* + **17***a*). L'addition du diazométhane aux diesters nécessite une plus grande proportion de dipôle (1.5 à 4 q.s.) et un temps de réaction plus long; dans ces conditions le dipôle est sans action sur **5***d*.

X = *CN*, *Y* = *CN ou* CO_2R (*R* = CH_3, C_2H_5)

Pyrazolines—Si la réaction d'addition du dipôle sur le diène est conduite à −20°C l'adduit obtenu est suffisamment stable à basse température, pour permettre une étude de ses caractéristiques de rmn.

Oléfines β méthylés—**11***c*, pf 71°C (éthanol). Analyse $C_{14}H_{12}N_2$. **12***c*, pf 108–109°C (éthanol). Analyse $C_{14}H_{12}N_2$. **15***a*, pf 110°C (éthanol). **16***a*, pf 126–127°C (éthanol). **15***b*, pf 125°C (éthanol). **16***b*, pf 134°C (éthanol). **16***c*, pf 109–111°C (éthanol). Analyse $C_{19}H_{14}N_2$.

X = *Y* = CO_2CH_3

Pyrazolines—Les pyrazolines-1 obtenues sont des huiles: **20** est étudiée à partir du mélange **19** + **20** dans lequel elle est minoritaire.

Photodimérisation des diènes 1

Les composés **1***b*, **1***c* et **1***d* abandonnés à la lumière du jour à l'état finement pulvérisé, conduisent en quelques jours aux dimères correspondants **26** à **28**.

26, analyse $C_{30}H_{30}N_2O_4$; pf 123°C (éthanol).

27, pf 264°C ($CHCl_3$, éther); très peu soluble.

28. La dimérisation est plus lente que pour les composés précédents (plusieurs semaines). Le produit résultant pf 95–100°C, trop soluble dans les solvants organiques usuels, n'a pu être recristallisé.

1. J. MARTELLI. Thèse, Université de Rennes, Rennes. 1976.
2. J. MARTELLI et R. CARRIÉ. Bull. Soc. Chim. Fr. A paraître.
3. H. ROTTENDORF, S. STERNHELL et J. R. WILMSHURST. Aust. J. Chem. **18**, 1759 (1965).
4. G. J. MARTIN et M. L. MARTIN. The stereochemistry of double bonds. *Dans* Progress in NMR spectroscopy. Vol. 8. *Rédigé par* J. W. Emsley, J. Feeney et L.

H. Sutcliffe. Pergamon Press, New York, NY. 1972. p. 163.
5. R. H. WILEY, T. H. CRAWFORD et C. E. STAPLES. J. Org. Chem. **27**, 1535 (1962).
6. M. GIRAUD. Thèse, Université de Paris, Paris. 1971.
7. J. C. DORÉ et C. VIEL. J. Chim. Phys. **10**, 1150 (1975).
8. G. PATTENDEN et B. C. L. WEEDON. J. Chem. Soc. 1997 (1968).
9. H. H. JAFFE et M. ORCHIN. Theory and applications of U.V. spectroscopy 3e ed. John Wiley and Sons, New York, NY. 1965. p. 277 et suivantes.
10. M. V. SARGENT et C. J. TIMMONS. J. Chem. Soc. 2222 (1964).
11. (*a*) D. E. MCGREER, R. S. MCDANIEL et M. G. VINJE. Can. J. Chem. **43**, 1389 (1965). (*b*) J. HAMELIN et R. CARRIÉ. Bull. Soc. Chim. Fr. 2162 (1968).
12. J. HAMELIN et R. CARRIÉ. Bull. Soc. Chim. Fr. 3000 (1968).
13. R. H. WILEY et C. E. STAPLES. J. Org. Chem. **28**, 3413 (1963).
14. R. H. WILEY, P. F. G. NAU, H. C. VAN DER PLAS et T. H. CRAWFORD. J. Org. Chem. **27**, 1991 (1962).
15. H. BURTON. J. Chem. Soc. 748 (1932).
16. A. ETIENNE et J. WEILL-REYNAL. Bull. Soc. Chim. Fr. 1142 (1953).
17. M. BARGAIN. Thèse d'Ingénieur-Docteur, Université de Rennes, Rennes. 1962.
18. A. C. COPE, C. M. HOFMANN, C. WYCKOFF et E. HARDENBERGH. J. Am. Chem. Soc. **63**, 3452 (1941).
19. D. T. MOWRY. J. Am. Chem. Soc. **65**, 991 (1943).
20. C. F. H. ALLEN et F. W. SPANGLER. Organic syntheses, collective volume III. John Wiley and Sons, New York, NY. 1967. p. 377.
21. H. LE MOAL, R. CARRIÉ, A. FOUCAUD, M. BARGAIN et C. SEVELLEC. Bull. Soc. Chim. Fr. 1033 (1966).
22. F. ARDNT. Organic syntheses, collective volume II. John Wiley and Sons, New York, NY. 1957. p. 165.

The mechanism of the thermal decarbonylation of 2,2-dimethyl-3-butenal

ROBERT J. CRAWFORD, STUART LUTENER, AND HIROKAZU TOKUNAGA
Department of Chemistry, The University of Alberta, Edmonton, Alta., Canada T6G 2G2

Received June 24, 1977

ROBERT J. CRAWFORD, STUART LUTENER, and HIROKAZU TOKUNAGA. Can. J. Chem. **55**, 3951 (1977).

The thermal decarbonylation of 2,2-dimethyl-3-butenal is shown to be an intramolecular extrusion of carbon monoxide concerted with the transfer of hydrogen (deuterium) to the γ-position. The reaction displays a kinetic isotope effect of 2.8 (at 296.9°C) and follows first order kinetics (E_a = 44.2 ± 0.2 kcal mol^{-1}, log A = 13.4 ± 0.3).

ROBERT J. CRAWFORD, STUART LUTENER et HIROKAZU TOKUNAGA. Can. J. Chem. **55**, 3951 (1977).

On démontre que la décarbonylation thermique du diméthyl-2,2 butène-3 al est une extrusion intramoléculaire de monoxyde de carbone concertée avec un transfert d'hydrogène (deutérium) vers la position γ. La réaction présente un effet isotopique cinétique de 2.8 (à 296.9°C) et suit une cinétique du premier ordre (E_a = 44.2 ± 0.2 kcal mol^{-1}, log A = 13.4 ± 0.3).
[Traduit par le journal]

Introduction

Recently we examined the thermolysis of 2-vinyloxirane (1) and concluded that one of the initial products was 3-butenal which, depending upon the surface of the vessel, was tautomerized to *E*- or *Z*-2-butenal or produced propylene and carbon monoxide. Traces of oxygen brought about a catalytic reaction and large amounts of CO and propylene were produced, but even after the most careful conditioning propylene and CO were present. We suggested that the decarbonylation of 3-butenal was both radical catalyzed and under oxygen free conditions proceeding via an intramolecular mechanism. To study this more thoroughly we have examined the thermolysis of the non-enolizable 2,2-dimethyl-3-butenal (**1**). There are few instances of decarbonylation of β,γ-unsaturated aldehydes. The most thoroughly studied is the work of Schaffner (2) where the singlet photosensitized decarbonylation of *R*-(+)-laurolenal (**2**) to *S*-(−)-1,2,3-trimethylcyclopentene (**3**) is observed.

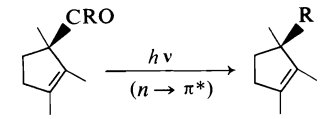

2 **3**

a R = H *a* R = H
b R = D *b* R = D

The stereochemistry in this, and other steroid cases (3), leads to the suggested skeletal mechanism wherein the hydrogen (or deuterium) is attached in the product to the same carbon to which the aldehyde carbon was attached in the reactant; this was accompanied by a small amount of allylic rearrangement.

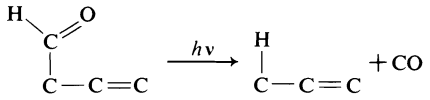

Synthesis of Deuterated 2,2-Dimethyl-3-butenals

We required for our mechanistic studies 2,2-dimethyl-3-butenal (**1**) and its deuterium labelled derivatives **1**-d_1, and **1**-d_3. The aldehyde **1** was conveniently prepared from the cyclohexylimine of tiglaldehyde using lithium diisopropylamide in tetrahydrofuran (THF) at −78°C and methylating the resulting anion with methyl iodide to

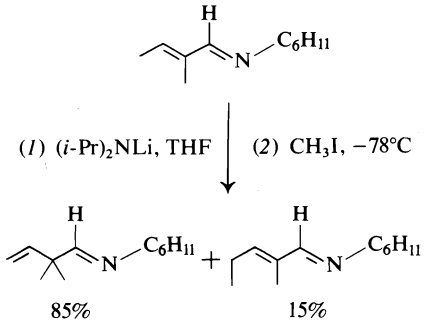

produce the imine of **1**. Methyl-d_3 iodide was used to produce **1**-d_3. The C(1) labelled aldehyde (**1**-d_1) was prepared using the method of Corey

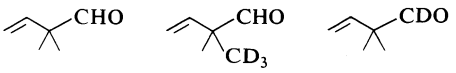

1 **1**-d_3 **1**-d_1

and Seebach (4) wherein the dithiane (**4**) is converted to its corresponding anion and deuterated. Mild hydrolysis (4) gave the aldehyde **1**-d_1 with less than 1% protium at C(1) as assessed by ^{1}H nmr.

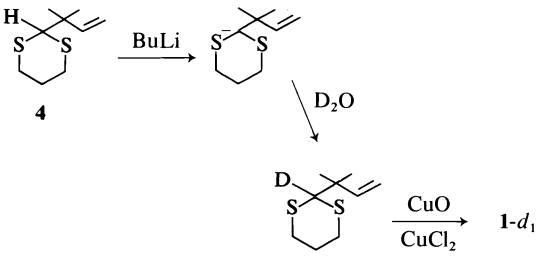

4

Kinetics

The rate of decarbonylation of **1** was followed by measuring the pressure increase as a function of time. The reaction vessel consisted of a 1 ℓ well-conditioned Pyrex sphere as described in our earlier paper (1) except that a side-arm was attached and extended through the wall of the thermostated vessel. A National transducer LX 3702 A reading 0–10 V was interfaced with a Hewlett-Packard 5150 A thermal printer equipped with a time interval control, thus pressure readings were taken automatically at regular intervals. That the reaction followed first order kinetics was established by measuring the rate at different pressures and finding the rate constant to be unchanged on going from 50 to 200 Torr initial pressure of **1**. Having observed a 1 to 2 min warm-up period from the time of injection of our sample we decided to use the method of Guggenheim (5) to obtain more precise values of the rate constants. While it is possible that the warm-up period was in fact an induction period for a chain reaction, samples of pentanal required the same length of time to come to temperature equilibrium, and with a thermocouple well extended to the centre of the reaction vessel we were able to observe a comparable initial temperature differential upon admission of any gas. The values of the rate constants obtained over the temperature range 282 to 302°C are listed in Table 1. Aliphatic aldehydes such as acetaldehyde undergo high temperature pyrolysis and under certain conditions can give rise to first order kinetics for the chain process outlined in eqs. 1–4 (6). We

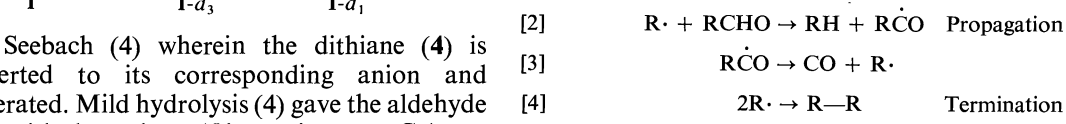

have examined the effect of two radical chain inhibitors, toluene and 1,4-cyclohexadiene, upon the reaction rate constant, and these data are presented in Table 2.

Product Studies

The thermolysis of **1**, **1**-d_1, and **1**-d_2 at 300°C leads to carbon monoxide and 2-methyl-2-butene with less than 0.5% of any other hydrocarbon present. The ^{1}H nmr spectra of **1**-$d_1$and **1**-d_3 indicate that the aldehydic hydrogen (deuterium) has been transferred to the C(4) position of the original butenal.

The reaction was shown to be intramolecular by attempted crossover experiments involving **1**-d_1 and **1**-d_3. The 2-methyl-2-butene produced was carefully examined by mass spectrometry for the presence of C_5H_{10}, C_5H_9D, $C_5H_7D_3$, and $C_5H_6D_4$. After correcting for the natural abundance of ^{13}C and deuterium incorporation level, we found no evidence for the crossover products C_5H_{10} and $C_5H_6D_4$. Our mass spectra were sufficiently reproducible that if either of these were present at the 0.5% level they would have been detected.

Discussion

The experimental data demonstrate that the thermal decarbonylation of **1** is an intramolecular, nonradical scavengeable process of a highly reproducible rate. These data are best interpreted in terms of a molecular mechanism involving the transfer of the aldehydic hydrogen to the γ-position as in **5**.

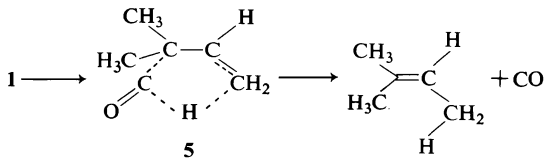

5

The reaction is very similar to that involving the decarboxylation of the corresponding car-

TABLE 1. Kinetic data for the rate of thermolysis of 2,2-dimethyl-3-butene at 0.3 atm pressure

Temperature (°C)	10^4k_1 (s^{-1})	
281.7±0.1	1.168±0.006	E_a=44.2±0.2 kcal mol^{-1}
286.7	1.668±0.004	log A=13.4±0.3
291.8	2.40 ±0.01	
	2.41 ±0.01	ΔH^*=43.1±0.2 kcal mol^{-1}
296.8	3.35 ±0.01	ΔS^*_{300}=+2.0±0.5 eu
301.9	4.74 ±0.01	

TABLE 2. Thermolysis of **1** in the presence of radical chain inhibitors, at 298.5°C

Pressure of **1** (atm)	Inhibitor	10^4k_1 (s^{-1})
0.4		3.55±0.02
0.3	0.04 atm toluene	3.54±0.01
0.3	0.04 atm 1,4-cyclohexadiene	3.41±0.01

boxylic acid, 2,2-dimethyl-3-butenoic acid (log A = 11.13, E_a = 36.6 kcal mol^{-1}) (7). The magnitude of the kinetic isotope effect, k_H/k_D = 2.8 at 296.9°C corresponds to a value of 7.2 at 25°C (see Table 3), indicates that the hydrogen is extensively transferred in the transition state; this coupled with the low activation energy in comparison with that normally associated with the thermolysis of RCO—H bonds (E_a 44.2 kcal mol^{-1} vs. bond dissociation energy of greater than 82 kcal mol^{-1} (6)) suggests that the process is highly concerted.

Experimental

All boiling points are uncorrected. Purifications by preparative gc were carried out on a Nester Faust model 850 'Prepkromatic'. The columns used were 6 ft biwall tubing packed with 20% Carbowax 1500 on Chromosorb W 30–60 mesh. The carrier gas was helium at a flow rate of 500 ml min^{-1}. The nuclear magnetic resonance (nmr) spectra were obtained using a Varian A 60 or HA 100 spectrometer.

Thermolysis Kinetics

Quantitative rate experiments were conducted in a static Pyrex vacuum system constructed as described earlier (1). The rates were followed by means of a pressure transducer (National LX 3702 A) attached to the cell via a 3 mm Pyrex tube. The transducer was mounted on the outside of the oven wall thus the dead space was less than 1% of the total reactor volume. The transducer was calibrated against a mercury manometer and was found to be linear over the desired pressure range. The output signal from the transducer (0–10 V range) was recorded at regular intervals on a Hewlett-Packard 5150 A thermal printer equipped with a time interval control.

All samples for kinetic runs were prepared from materials dried over 4A molecular sieves, transferred to breakseals, and degassed by standard procedures. At least 20 points were taken for each rate measured.

TABLE 3. Kinetic isotope effect for the thermolysis of **1** and **1**-d_1. Reactions run as pairs on same day at 296.9°C

Sample	10^4k_1 (s^{-1})	k_H/k_D
1	3.32±0.01	
1-d_1	1.18±0.01	2.81±0.04
1	3.33±0.01	
1-d_1	1.17±0.01	2.85±0.04

2,2-Dimethyl-3-butenal (1)

The aldehyde **1** was prepared by alkylation of the cyclohexylimine of tiglaldehyde which was prepared by adding cyclohexylamine (10.9 g, 0.11 mol) to a solution of tiglaldehyde (8.4 g, 0.11 mol) in benzene (125 ml). The solution was stirred and the water removed by azeotropic distillation using a Dean Stark trap (2 h). The benzene was then removed on a rotary evaporator and the residual liquid was essentially identical (nmr, ir) with that of an aliquot purified by distillation, bp 60–65°C/2 Torr (8). The undistilled residual liquid was used directly for the alkylation step.

A solution of *n*-butyllithium (21.4 ml, 52.5 mmol) was reduced to half volume under reduced pressure and dry tetrahydrofuran (THF) (50 ml) was added. After the addition of bipyridyl (12 mg) the solution was cooled to −50°C and diisopropylamine (5.30 g, 52.5 mmol) in THF (25 ml) was slowly added and the red solution cooled to −78°C. The afore-mentioned tiglaldehyde imine (8.25 g, 50 mmol) was dissolved in THF (25 ml) and added dropwise. The solution was maintained at −78°C and methyl iodide in THF was added in a titration-like procedure. The colour of the solution abruptly changed to pale yellow upon the addition of 1 equiv.; this was then followed by an additional 20%. The resulting solution was diluted with approximately three volumes of ether and poured into ice water (100 ml), washed with saturated NaCl solution, and the solvent evaporated. Gas chromatography (Carbowax, 1500, 150°C) indicated the residual product to be a 5:1 mixture of imines and an nmr spectrum of the crude indicated that the imine of 2,2-dimethyl-3-butenal was the major product and the imine of 2-methyl-2-pentanal was the isomer.

The imine derivatives were then placed in a flask with a solution of oxalic acid (40 g) in water (100 ml) and the

TABLE 4. Attempted crossover experiments at 248°C

Sample ratio **1**-d_1:**1**-d_3	Reaction time (h)	Initial pressure (atm)	Product ratio				
			d_0	d_1	d_2	d_3	d_4
1:0	6	0.42	3.16	100	0.03	—	—
0:1	6	0.42	—	—	1.23	100	—
1:1	6	0.42	3.34	100	1.35	108	—
1:1	6	0.42	3.44	100	1.23	101	0.02
1:1	6	1.12	3.11	100	0.87	85	0.3
1:1	3	0.42	3.67	100	1.30	106	0.0
1:1	12	0.42	3.16	100	1.31	108	0.0

aldehydes steam distilled. Extraction of the distillate with ether, followed by drying and distillation, resulted in two fractions, exclusive of solvent, bp 93–94°C/700 Torr, 2,2-dimethyl-3-butenal (2.6 g, 60%) (9) and bp 130–131°C/700 Torr 2-methyl-2-pentanal (0.4 g, 10%) (10). Yields were improved to 80% upon scaling up by fourfold.

*2-Methyl-2-trideuteriomethyl-3-butenal (**1**-d_3)*

The method of synthesis was the same as that above for **1** only that trideuteriomethyl iodide was used. The ^{1}H nmr spectrum displayed a peak at δ 1.21 which was three times the size of the peak at δ 9.39.

*1-Deuterio-2,2-dimethyl-3-butenal (**1**-d_1)*

The propanedithiol derivative of **1** was prepared in a 250 ml round bottom flask equipped with a magnetic stirrer, $CaCl_2$ drying tube, and a gas inlet. A solution of 2,2-dimethyl-3-butenal (11.0 g, 0.11 mol) and 1,3-propanedithiol (12.0 ml, 0.12 mol) was stirred and cooled to 0°C. Hydrogen chloride gas was bubbled through the solution for 5 min, after which the temperature rose to +5°C and fell back to zero. After work-up in the conventional manner a vacuum distillation on the residual oil gave 15.0 g, 73%, of a pale yellow oil, bp 103°C/2.5 Torr; ^{1}H nmr ($CDCl_3$) δ_{TMS}: 1.23 (s, 6H), 2.0 (m, 2H), 2.9 (m, 4H), 4.04 (s, 1H), 4.9–6.2 (m, 3H).

The dithiane (15 g, 96 mmol) was dissolved in dry THF and cooled to −40°C after which 1.2 equiv. of *n*-butyllithium in hexane was added over ½ h, and stirred for 2 h under a nitrogen atmosphere. The reaction was quenched with D_2O and the dithiane isolated as above: 15 g recovered, ^{1}H nmr same as above except for the signal at δ 4.04 which was less than 1% of its original intensity.

A solution of the dithiane (4.72 g, 25 mmol) in 200 ml acetonitrile containing 2 ml H_2O was warmed to 70°C on cupric oxide (7.9 g, 100 mmol), $CuCl_2$–$2H_2O$ (8.5 g, 50 mmol) was added, and the solution maintained at 70°C for an additional 30 min (4). The solution was then cooled and filtered, the precipitate washed with acetonitrile, the solution plus wash diluted with H_2O (150 ml) extracted with pentane and dried, and the aldehyde purified by distillation (2.3 g, 95%). The aldehydic signal at δ 9.39 was less than 0.005 times its original intensity.

Attempted Crossover Experiments

Sample tubes containing **1**-d_1, **1**-d_3, and mixtures of these were carefully degassed and then heated at 298°C. Table 4 gives the experimental conditions and the intensities corrected for ^{13}C for each of the runs.

Acknowledgements

We wish to thank Professor S. Masamune for helpful discussions concerning the dithiane hydrolysis and Dr. A. Hogg for the mass spectrometric measurements.

1. R. J. CRAWFORD, S. B. LUTENER, and R. D. COCKCROFT. Can. J. Chem. **54**, 3364 (1976).
2. K. SCHAFFNER. Chimia, **19**, 575 (1965); E. BAGGIOLINI, H. P. HAWLOW, and K. SCHAFFNER. J. Am. Chem. Soc. **92**, 4906 (1970).
3. J. IRIARTE, J. HILL, K. SCHAFFNER, and O. JEGER. Proc. Chem. Soc. London, 114 (1963); M. AKHTAR. Tetrahedron Lett. 4727 (1965).
4. E. J. COREY and D. SEEBACH. Angew. Chem. Int. Ed. Engl. **4**, 1075 (1965); **4**, 1077 (1965).
5. A. A. FROST and R. G. PEARSON. Kinetics and mechanism. 2nd ed. J. Wiley and Sons, Inc., New York, NY. 1961. p. 49.
6. M. B. COLBETT, III, D. W. NAEGELLI, and I. GLASSMAN. Int. J. Chem. Kinet. **7**, 223 (1975), and earlier references cited therein.
7. D. B. BIGLEY and R. W. MAY. J. Chem. Soc. B, 557 (1967).
8. J.-C. GAUTIER, S. RISSE, and J. WIEMANN. Ann. Chim. (Paris), 435 (1970).
9. M. JULIA and M. BAILLARGE. Bull. Soc. Chim. Fr. 734 (1966).
10. G. J. MARTIN and J. P. GOUSENARD. Bull. Soc. Chim. Fr. 2501 (1969).

Canadian Journal of Chemistry

Published by
THE NATIONAL RESEARCH COUNCIL OF CANADA

Journal canadien de chimie

Publié par
LE CONSEIL NATIONAL DE RECHERCHES DU CANADA

Volume 55 Number 23 December 1, 1977

Volume 55 numéro 23 1 décembre 1977

Simultaneous diffusion and chemical activation control of the kinetics of the binding of carbon monoxide to ferroprotoporphyrin IX in glycerol–water mixtures of high viscosity[1]

BRIAN B. HASINOFF

Department of Chemistry and the Faculty of Medicine, Memorial University of Newfoundland, St. John's, Nfld., Canada A1C 5S7

Received June 7, 1977

BRIAN B. HASINOFF. Can. J. Chem. **55**, 3955 (1977).

The kinetics of the reaction of ferroprotoporphyrin IX with CO have been studied in mixed glycerol–water solvents of high viscosity in order that the simultaneous influence of chemical activation and diffusion control of the reaction might be observed. Analyses of curved Arrhenius plots indicated that in the low temperature high viscosity limits the reaction is largely diffusion controlled. The deviation of the second order diffusion rate constants, from that predicted by simple theory for reaction between uniformly reactive spheres of equal radii, is a factor of 0.3 to 0.9, depending upon the solvent composition. A couple of other models for diffusion controlled reaction, ascribing these deviations to changes of steric requirements, were also examined.

BRIAN B. HASINOFF. Can. J. Chem. **55**, 3955 (1977).

On a étudié la cinétique de la réaction de la ferroprotoporphyrine IX avec le CO dans des solvants mixtes de glycérol–eau de grande viscosité de façon à pouvoir observer simultanément l'influence de l'activation chimique et du contrôle de la diffusion sur la réaction. L'analyse des courbes d'Arrhenius indique qu'aux limites de basse température et de haute viscosité la réaction est grandement contrôlée par la diffusion. La déviation des constantes de vitesse de diffusion du deuxième ordre par rapport à celles qui sont prédites par la théorie simple de la réaction entre des sphères réactives uniformes qui ont un rayon égal est d'un facteur de 0.3 à 0.9 dépendant de la composition du solvant. Une couple d'autres modèles pour une réaction contrôlée par la diffusion et attribuant ces déviations à des changements dans les facteurs stériques ont aussi été examinés.

[Traduit par le journal]

In a previous study (1) the reaction of ferroprotoporphyrin IX (heme) with carbon monoxide was studied by laser flash photolysis as a function of temperature and pressure in 100% glycerol and 80% v/v ethylene glycol – water. A comparison of the activation enthalpies and activation volumes with the viscosity activation parameters indicated that in 100% glycerol the kinetics are almost totally controlled by diffusion. From a consideration of $\Delta V^{\ddagger}$ (1), obtained in 80% v/v ethylene glycol – water, a dissociative mechanism was indicated.

This study extends the range of viscosities studied by using mixtures of glycerol and water, such that both chemical activation and diffusion control contribute to the kinetics. It is of interest to measure the kinetics in this region as a test of the applicability of the theory of diffusion controlled reactions. Glycerol–water solvent mixtures exhibit a wide range of viscosities (2) with large temperature coefficients so that the

[1]This work has been supported in part by a National Research Council of Canada Grant, No. A9430.

diffusion controlled region can be easily distinguished from the chemical activation controlled region of normally lower activation energy.

The theory of the effects of diffusion controlled rates on chemical kinetics is historically due to von Smoluchowshi (3) and has been reviewed and critically examined by Noyes (4). Since the classical theory is only strictly applicable to spherical molecules of uniform surface reactivity, a number of refinements to the basic theory have been proposed. The theory has been extended to molecules with orientation constraints due to limited accessibility of their active sites (5–9). Even moderate steric requirements (5–7) can produce drastic reductions in the diffusion controlled rate constants. A recent related study (10) of the binding of CO and O_2 to myoglobin in glycerol–water indicated the importance of diffusion control on these reactions.

For the reaction of spherical, uniformly reactive molecules in a homogeneous fluid the diffusion controlled second order rate constant, k_D is (4)

$$[1] \qquad k_D = 4\pi RD$$

where R is the sum of the radii of the reacting molecules ($r_A + r_B$) and D is the sum of the translational diffusion coefficients. Use of the Stokes–Einstein expression

$$[2] \qquad D = kT/6\pi r\eta$$

for r_A and r_B and eq. 1, with conversion to units of M^{-1} s^{-1}, gives

$$[3] \qquad k_D = \frac{2000RT}{3\eta}\frac{(r_A + r_B)^2}{r_A r_B}$$

where R is the gas constant in J K^{-1} mol^{-1}, η the viscosity in Pa s (1 Pa s $\equiv$ 1 kg m^{-1} s^{-1} $\equiv$ 10 P). If $r_A = r_B$ then

$$[4] \qquad k_D = 8000RT/3\eta$$

Note that eq. 4 has no adjustable parameters and depends only on T and η of the solvent. Modifying eq. 4 to include a factor, α, that is a measure of the departure of the reaction from that predicted for reaction between spheres of equal radii and uniform reactivity, yields

$$[5] \qquad k_D = \alpha(8000\ RT/3\eta)$$

The factor α may include steric, probability, interaction, and radius factors. With $\alpha = 1$ in eq. 5 for 100% glycerol at 20°C (η = 1.41 Pa s) $k_D = 4.6 \times 10^6\ M^{-1}$ s^{-1}, which compares to water at the same temperature (η = 1 mPa s) $k_D = 6.4 \times 10^9\ M^{-1}$ s^{-1}.

The activation enthalpy of a diffusion controlled reaction is (1)

$$[6] \qquad \Delta H_D^{\ddagger} = -R\,\partial \ln (k_D/T)/\partial T^{-1} = B$$

and for the solvent

$$[7] \qquad B = R\,\partial \ln \eta/\partial T^{-1}$$

where B is the viscosity activation energy in the empirical relationship

$$[8] \qquad \eta = \eta_0 \exp (B/RT)$$

In the more general case where there is simultaneous chemical activation and diffusion contributing to the observed kinetics (4, 6)

$$[9] \qquad k^{-1} = k_0^{-1} + k_D^{-1}$$

where k is the observed second order rate constant and k_0 is the rate constant that would be observed if diffusion effects were absent. In eq. 9, k_D represents the maximum rate at which an association reaction can proceed.

Experimental

Reagents

Heme (as hemin chloride, Eastman) was dissolved in 1 M aqueous NaOH on the day of use. The spectrophotometrically determined (1) heme solution in N_2 saturated glycerol–water of known composition was added to a serum cap sealed fluorescence cell containing a few crystals of sodium dithionite to reduce the iron. The final [NaOH] was either 0.01 or 0.02 M. The CO stock solution was prepared by bubbling C.P. CO through water for 20 min at a known temperature and pressure, and its concentration determined using Henry's Law (11). This CO saturated solution was then transferred to the reaction cell with a gas tight syringe. Using published densities, the weights of additions, and known dilutions, the final concentrations of the glycerol–water solution, heme, and CO were determined.

Apparatus

The flash photolysis apparatus, the spectrophotometric detection system, and the analog-to-digital data acquisition system have been described (10). The reaction of heme and CO was followed at a wavelength of 430 nm (7 nm band pass). The first order rate constants, k_{obs}, were obtained by fitting 256 digitized voltage–time values to a three parameter nonlinear least squares equation of the form $A = A_0 \exp(-k_{obs}t) + A_\infty$, where A, A_0, and A_∞ are the absorbances at time $t = t$, $t = 0$, and $t = \infty$ respectively. Only the last 10% of the reaction was followed for about 6 half-lives. Three or more values of k_{obs} were averaged, giving a relative standard deviation of 2–5%. The temperature of the reaction cell was held constant to ±0.03°C.

Results

Dependence of the Kinetics of the Heme + CO Reaction on Solvent Composition and Temperature

The recombination of heme with CO after flash photolysis may be represented by

$$\text{heme—CO} \xrightarrow{h\nu} \text{heme} + \text{CO} \qquad \text{(dissociation)}$$

$$\text{heme} + \text{CO} \xrightarrow{k} \text{heme—CO} \qquad \text{(recombination)}$$

The reaction has been well studied (1, 13, 14) and the rate has been shown to be proportional to [CO]. Upon flash photolysis of heme—CO in the presence of 15- to 30-fold excess ligand, recombination was first order where heme varied from 2.9 to 7.3 μM and k_{obs} fell in the range 25 to 480 s^{-1}. The second order rate constant was calculated from $k = k_{obs}/[CO]$. The variation of log k with T^{-1} is plotted in Fig. 1. The reaction was studied over a temperature range of 10 to 60°C which gave a variation in viscosity of 0.01 to 1.7 Pa s. Data from ref. 14 are plotted in Fig. 2. The curvature in the plots is ascribed to diffusion control. The magnitude of the curvatures makes it unlikely that this effect is due to a change in heat capacity of activation of the reactants.

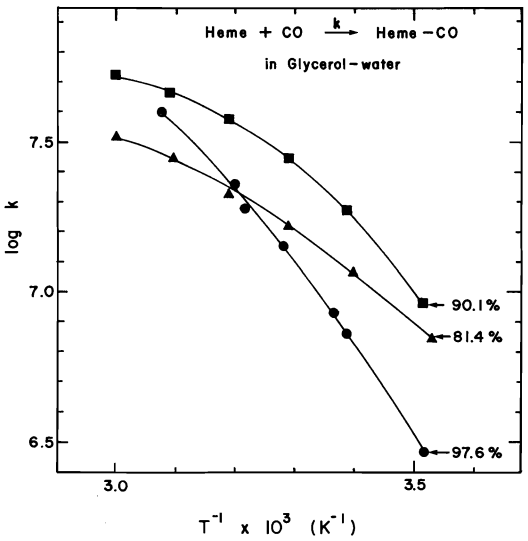

FIG. 1. Log k vs. T^{-1} in glycerol–water mixtures for the reaction of heme and CO. The curved solid lines are those calculated from the three parameter nonlinear least squares analysis of the rate and viscosity data in eq. 10. At the high temperature limit the reaction kinetics are controlled by chemical activation and by diffusion at the low temperature limit. At the highest and lowest viscosities studied the reaction is 92% and 18% diffusion controlled respectively.

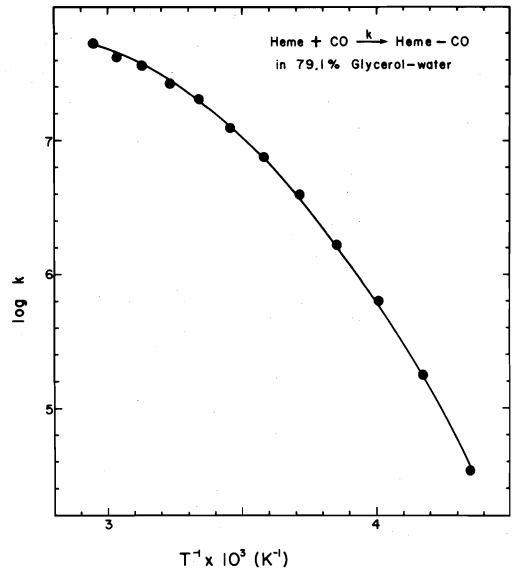

FIG. 2. Log k vs. T^{-1} for the reaction of heme and CO from the data of ref. 14 in 79.1 wt.% glycerol–water. Other comments as in Fig. 1.

The data were analyzed with eq. 5 in eq. 9 yielding

$$k^{-1} = k_0^{-1} + k_D^{-1}$$

$$[10] \quad k^{-1} = \left(\frac{kT}{h}\exp\frac{\Delta S^{\ddagger}}{R}\exp\frac{-\Delta H^{\ddagger}}{RT}\right)^{-1} + \left(\alpha\frac{8000RT}{3\eta}\right)^{-1}$$

where k_0 is assumed to have the usual temperature dependence.

Nonlinear least squares analysis (12) was used to obtain the three best fit parameters $\Delta H^{\ddagger}$, $\Delta S^{\ddagger}$, and α. The results are listed in Table 1 and plotted as the continuous curves in Figs. 1 and 2. Equation 10 has two independent variables, T and η; the latter was obtained from an empirical equation (10) at the appropriate temperature and solvent composition.

Also listed in Table 1 are values of $\Delta H_D^{\ddagger}$ obtained from a four parameter ($\Delta H_D^{\ddagger}$, $\Delta H^{\ddagger}$, $\Delta S^{\ddagger}$, and α/η_0) nonlinear least squares analysis of eqs. 5, 6, and 8 substituted in eq. 9. This analysis provides a semiquantitative independent test of eq. 9. Since B, the viscosity activation energy parameter, varies considerably with temperature (Table 1), the kinetically determined

TABLE 1. Diffusion and chemical activation control parameters for the reaction of heme with CO in glycerol–water mixtures[a]

Wt.% glycerol	$\Delta H^{\ddagger}$ (kcal mol^{-1})[b]	$\Delta S^{\ddagger}$ (cal K^{-1} mol^{-1})[b]	α[c]	$\Delta H_D^{\ddagger}$ (kcal mol^{-1})	Range of B (kcal mol^{-1})
97.6	3.1±2.7	−12.8±8.1	0.89±0.08	23±10	12–15
90.1	−0.7±0.5[f]	−25.0±1.5	0.79±0.03	13[g]	10–13
81.4	2.4±0.5	−16.8±1.4	0.26±0.03	13±6	8–11
79.1[d]	1.4±0.7	−18.7±2.1	0.21±0.01	16±1	7–15
—[e]	7.5±0.8	1.2±3	—	—	—

[a]Error values are standard deviations from nonlinear least squares analysis.
[b]Activation parameters for pure chemical control of reaction.
[c]From an analysis of eq. 10 and is the factor by which k_D departs from reaction between uniformly reactive spheres of equal radii; eq. 4.
[d]From a reanalysis of data in ref. 14.
[e]From ref. 1 in 80% v/v ethylene glycol – water containing 10 mM NaOH.
[f]When constrained to a positive value, a value of 0 was obtained with no significant difference in the standard deviation of the fit. The value of α was the same within its standard deviation.
[g]Indeterminate error.

$\Delta H_D^{\ddagger}$ would be expected to show only a rough correspondence. In general, it is seen that values of $\Delta H_D^{\ddagger}$ do approach the values of B at the low temperature limits where diffusion control is the greatest. Also since both the previously determined $\Delta H_D^{\ddagger}$ and $\Delta V_D^{\ddagger}$ in 100 wt.% glycerol (1) showed a close correpondence with both the temperature and pressure viscosity activation parameters, it is with some assurance that the results may be analyzed with the three parameter eq. 10.

The $\Delta H^{\ddagger}$ at the highest glycerol composition is not very well determined as the contribution from chemical activation ranges from only 8 to 45%. In general the values of $\Delta H^{\ddagger}$ are somewhat lower than for reaction in 80% v/v ethylene glycol – water (1) even though the $\Delta G^{\ddagger}$'s are similar.

Discussion

Interpretation of the Diffusion Controlled Reaction of Heme with CO

Clearly it is possible to write more complex reaction schemes to explain curved Arrhenius plots. In a temperature study (14) extending from 5 to 340 K, at a single glycerol–water composition, results were rationalized on the basis of a sequential mechanism with one bimolecular and three unimolecular steps. After making assumptions about the relative magnitudes of the observed rate constants, the data were interpreted in the high temperature limit, using three rate constants (six activation parameters). The effect of diffusion control on the kinetics was considered (14) and the conclusions reached agreed partly with results given in ref. 1. However, the situation was described as being different for the less viscous glycerol–water mixture as a correspondence with k_D was not achieved with the three-step mechanism. In the discussion given here the curved Arrhenius plots are ascribed to simultaneous chemical activation and diffusion control, with nonunity values of α being due to steric and other requirements. At the closest comparable solvent compositions of the two studies the rate constants agree absolutely within about 20% ($k = 3.3 \times 10^7\ M^{-1}\ s^{-1}$ in 81.4 wt.% glycerol at 60.1°C and $k = 4.2 \times 10^7\ M^{-1}\ s^{-1}$ in 79.1 wt.% glycerol at 56.8°C), which is fair considering the different solvent compositions and methods of preparation.

At the highest glycerol composition employed α is close to 1, indicating that the rate of the reaction is close to that predicted for reaction between uniformly reactive spheres of equal radii. Obviously heme and CO are not uniformly reactive spheres and their radii would be significantly different.[2]

With these considerations, taking a slightly more sophisticated model (17) and factoring α into components

$$[11]\quad \alpha = \tfrac{1}{4}\sigma_{CO}\sigma_{heme}\frac{(r_{heme} + r_{CO})(r_{heme} + r_{CO}^{S})}{r_{heme}r_{CO}^{S}}$$

where r_{CO}^{S} is the Stokes radius of CO, and σ_{CO} and σ_{heme} are steric factors on CO and heme which may be visualized as the fraction of the total surface area on each reactant over which reaction can occur. It is known that the radii of O_2 molecules in glycerol–water, calculated from eq. 2 and polarographically determined diffusion coefficients (18), are anomalously

[2]The radius of the heme molecule from X-ray data is estimated from the shortest in-plane dimension (15) on tetraphenylporphine to be ~4 Å. The radius of CO is estimated from gas viscosity data (16) to be 1.8 Å.

small (the Stokes radii vary from 0.15 Å in 80 wt.% glycerol to 0.086 Å in 92.5 wt.% glycerol). These radii are between 12 and 21 times smaller than might be reasonably expected. Conversely, the diffusion coefficients are abnormally large in these solvents. Similarly, for the diffusion of H_2O in glycerol–water (19) the Stokes radii have also been found to be anomalously small. Whatever the cause for the failure of the Stokes–Einstein expression, since eq. 3 is based on eq. 2, the contribution of the smaller Stokes radii should be considered in eq. 11. Assuming a value of σ_{CO} of $\frac{1}{2}$ (17), the values of σ_{heme}, calculated from the Stokes radii for O_2, physically reasonable radii for heme and CO[2], and experimentally determined values of α in eq. 11, are given in Table 2.

A reasonable independent approximation to σ_{heme} might be the ratio of the area of the binding site, considered to be equal to the cross-sectional area of a CO molecule, to the surface area of the heme considered as a sphere.[2] This ratio is $\sigma_{heme} = A_{CO}/A_{heme} = \pi r_{CO}^2/4\pi r_{heme}^2 = 0.05$. The experimental values range from 0.04 to 0.1 which is in good agreement, considering the model and its assumptions. These values of σ_{heme} are up to 26 times larger than corresponding values (10) found for the reaction of myoglobin and CO where, as might be expected, the steric requirements are more severe. The reasons for the decline in σ_{heme} or α with solvent composition cannot be explained with any certainty. Qualitative changes in the hydration shell from lowest to highest water compositions could conceivably change the steric requirements of the reactants. This change might come about through a change in the long range interaction potential (16) due to changes in the dielectric constant ($\Delta\varepsilon/\varepsilon \sim 25\%$ (2)) or charge distribution. Possibly the model is oversimplified in its assumptions.

In a more sophisticated theoretical treatment of diffusion controlled reactions (5–7), a model was employed that included the effects of both translational and rotational diffusion. This model made the following assumptions: (*1*) the center of the incoming ligand (a mobile orientatable sphere of radius r_{CO}) must lie on the surface of a small target hemisphere of radius r_T centered at a distance r_{CO} above the reactive site on the surface; (*2*) the reactive site vector must lie within the reaction cone of constraint (half cone angle θ); and (*3*) $\theta r_{CO} = r_T$ (θ in radians). From these considerations, an equation, said to be valid to better than 20%, was presented (5) that was not formally derived but rather inferred from the results of numerical integrations.

$$[12]\quad k_D = \frac{(1 - \cos\theta)\,\theta r_{CO}\,(r_{CO}^S + r_{heme})2000RT}{3r_{CO}^S\, r_{heme}\,\eta}$$

A feature of eq. 12 is its extreme sensitivity to θ, particularly at low θ. A measure of α as before may be obtained from eq. 12 by comparison with eq. 5.

$$[13]\quad \alpha = \frac{(1 - \cos\theta)\,\theta r_{CO}\,(r_{CO}^S + r_{heme})}{4r_{CO}^S\, r_{heme}}$$

From the experimental values of α and eq. 13, values of θ and r_T are given in Table 2. Both θ and r_T decrease at higher water compositions, which accords with the decrease in σ_{heme} in the previous model. The large values of θ indicate that the heme binding site does not have a high steric requirement. The values of θ obtained for the heme–CO reaction range approximately between 50% and a factor of six larger (depending on the solvent composition) than that found (10) for the reaction of myoglobin and CO. These differences undoubtedly reflect the increased accessibility of heme compared to myoglobin. One possible interpretation of the large θ's is that reaction with Fe^{2+} may even be from either side of the planar heme molecule. The size of the target radius is also quite reasonable, being about the same order as that of the CO molecule.[2] Probably this model should not be relied upon to give much better than order-of-magnitude estimates in k_D.

TABLE 2. Diffusion control and steric factors for the reaction of heme and CO in mixtures of glycerol–water

Wt.% glycerol	α	Radius factor[a]	σ_{heme}[b]	θ (°)[c]	r_T (Å)[d]
97.6	0.89	71	0.10	130	4.0
90.1	0.79	69	0.09	120	3.7
81.4	0.26	46	0.05	80	2.4
79.1	0.21	38	0.04	70	2.2

[a]Equal to $(r_{heme} + r_{CO})(r_{heme} + r_{CO}^S)/r_{heme}r_{CO}^S$ in eq. 11.
[b]Fraction of total surface area for reaction on heme. Compares to a calculated value of 0.05.
[c]Half cone angle of constraint for ligand entry.
[d]Target radius. Compares to $r_{CO} \simeq 1.8$ Å.[2]

1. E. F. CALDIN and B. B. HASINOFF. J. Chem. Soc. Faraday Trans. I, **71**, 515 (1975).
2. J. B. SEGUR. *In* Glycerol. *Edited by* C. S. Miner and N. N. Dalton. Reinhold Publishing, New York, NY. 1953. p. 238.

3. M. VON SMOLUCHOWSKI. Z. Phys. Chem. **92**, 129 (1917).
4. R. M. NOYES. Progress in reaction kinetics. Vol. 1. *Edited by* G. Porter. Pergamon Press, New York, NY. 1961. p. 129.
5. J. M. SCHURR and K. S. SCHMITZ. J. Phys. Chem. **80**, 1934 (1976).
6. J. M. SCHURR. Biophys. J. **10**, 700 (1970).
7. J. M. SCHURR. Biophys. J. **10**, 717 (1970).
8. M. DOI. Chem. Phys. **11**, 107 (1975).
9. K. SOLC and W. H. STOCKMAYER. Int. J. Chem. Kinet. **5**, 733 (1973).
10. B. B. HASINOFF. Arch. Biochem. Biophys. **183**, 176 (1977).
11. National Research Council. International critical tables. Vol. 3. McGraw-Hill, New York, NY. 1933. p. 254.
12. D. W. MARQUARDT. IBM SHARE Library Program SDA 3094. 1964.
13. M. H. SMITH. Biochem. J. **73**, 90 (1959).
14. N. ALBERDING, R. H. AUSTIN, S. S. CHAN, L. EISENSTEIN, H. FRAUENFELDER, I. C. GUNSALUS, and T. M. NORDLUND. J. Chem. Phys. **65**, 4701 (1976).
15. R. COUNTRYMAN, D. COLLINS, and J. L. HOARD. J. Am. Chem. Soc. **91**, 5166 (1969).
16. J. O. HIRSCHFELDER and C. F. CURTISS. *In* Molecular theory of gases and liquids. John Wiley, New York, NY. 1954. p. 1111.
17. A. WELLER. Progress in reaction kinetics. Vol. 1. *Edited by* G. Porter. Pergamon Press, New York, NY. 1961. p. 189.
18. J. JORDON, E. ACKERMAN, and R. L. BERGER. J. Am. Chem. Soc. **78**, 2979 (1956).
19. O. LAMM and G. SJOSTEDT. Trans. Faraday Soc. **34**, 1158 (1938).

Thermodynamics of transfer of *p*-nitroaniline from water to alcohol + water mixtures at 25°C and the structure of water in these media

KUMARDEV BOSE AND KIRON K. KUNDU[1]

Physical Chemistry Laboratories, Jadavpur University, Calcutta-700032, India

Received December 6, 1976[2]

KUMARDEV BOSE and KIRON K. KUNDU. Can. J. Chem. **55**, 3961 (1977).

Free energies (ΔG_t^0) and entropies (ΔS_t^0) of transfer at 25°C of the nonelectrolyte *p*-nitroaniline from water to various alcohol + water mixtures have been determined from solubility measurements at seven temperatures from 10–40°C. Increasing specific solute–solvent interactions have been proposed to interpret the nature of the ΔG_t^0-composition profiles and the enhanced structure of water in the water-rich mixed solvents has been correlated with maxima in the ΔS_t^0-composition profiles. The effectiveness of *p*-nitroaniline as a useful probe for studying solvent structure has been pointed out.

KUMARDEV BOSE et KIRON K. KUNDU. Can. J. Chem. **55**, 3961 (1977).

On a déterminé les énergies libres (ΔG_t^0) et les entropies (ΔS_t^0) de transfert à 25°C du nonélectrolyte *p*-nitroaniline de l'eau vers divers mélanges d'alcool + de l'eau; ces valeurs ont été déterminées à partir de mesures de solubilité à sept températures entre 10–40°C. On a proposé une augmentation spécifique des interactions soluté–solvant pour interpréter la nature des profils ΔG_t^0 des compositions et l'on a pu effectuer une corrélation entre l'augmentation d'orientation de l'eau dans des solvants mixtes riches en eau et les maxima dans les profils ΔS_t^0 composition. On a mis en évidence l'efficacité de la *p*-nitroaniline comme sonde utile pour étudier la structure de solvants.

[Traduit par le journal]

Introduction

From the study of a wide variety of processes in aqueous mixtures of simple monohydric alcohols (1–3), it is now a fairly well-established fact that small amounts of alcohols strengthen the three-dimensional structure of liquid water. In terms of Frank and Wen's "flickering clusters" (4), the average lifetime of such bulky ice-like clusters is extended; in other words, the equilibrium, bulky "icebergs" ↔ monomeric water, existing in pure water is shifted to the left in water-rich aquo-alcoholic mixtures.

The thermodynamic quantities, specifically the enthalpy and the entropy, of transfer of quite a number of inert nonelectrolytes have been used to glean structural information in aquo-organic mixtures (5–7). The determination of these transfer parameters is very simple, being obtainable from heat of solution and/or solubility data at different temperatures. These observations support the findings obtained by use of more direct techniques like nmr spectroscopy (8), ultrasonic absorption and relaxation (9), and X-ray diffraction (10), and may prove to be as valuable and as reliable probes to solvent-structure studies as any of the more sophisticated methods.

Recently, interpretation of entropies of transfer of hydrogen halides in terms of solvent structure has been attempted for a few solvent systems, notably ethylene glycol + water (11*a*,*b*), urea + water (11*c*), *tert*-butyl alcohol + water (12*a*), propan-2-ol + water (12*b*–*e*), and ethanol + water (12*c*–*e*). The ionic entropies of transfer obtained (11*b*) or guessed (11*c*) therefrom have proved useful but electrostatic contributions necessarily confuse the issue. In this regard, neutral nonelectrolytes should be better suited as structural probes. Furthermore, as pointed out by Arnett (5), the entropy, rather than the enthalpy, of transfer of these species should be considered to reflect structural features more accurately.

In this study the solute chosen by us is *p*-nitroaniline (*p*NA). Although it cannot accurately be called a nonelectrolyte, *p*NA, having a predominant resonance contribution from a zwitterionic structure (see Discussion), has an appropriately low solubility in alcohol + water solvents, yet a high enough optical molar extinction coefficient at 380 nm to be determined accurately by spectrophotometry. Saturated solubilities of *p*NA in water and in aqueous

[1]Author to whom correspondence should be addressed.
[2]Revision received July 13, 1977.

mixtures of methanol, ethanol, isopropanol, and *tert*-butyl alcohol were measured at seven equidistant temperatures ranging from 10 to 40°C and the free energies (ΔG_t^0) and entropies (ΔS_t^0) of transfer from water to the mixed solvents were obtained therefrom.

Experimental

The alcohols were purified by standard methods (13). The water used was distilled in an all-glass apparatus after prior de-ionization and distillation with alkaline permanganate. The *p*NA (Riedel) was recrystallized twice from 95% ethanol and dried *in vacuo*. The mixed solvents were prepared by mixing weighed quantities of alcohol and water. The aqueous mixtures of methanol and ethanol contained 10, 20, 30, 50, and 70% while those of isopropanol and *tert*-butyl alcohol contained 10, 20, 30, and 50% by weight of alcohol. The measurement of solubilities at each temperature in the various solvents was essentially similar to that described previously for ethylene glycol + water (14*a*) and methanol + propylene glycol mixtures (14*b*) at 25°C. In order to restrict the absorbance values within the range 0.100–0.800 the saturated solutions were diluted (200–5000 times) with water. Optical absorbances of the diluted solutions were measured by a Beckmann DU model G 2400 spectrophotometer at 380 nm. The molar extinction coefficient of *p*NA in water was taken to be 12 800 (15). Saturation at a given temperature was attained in all solvents within 7–10 days. The error in measuring solubility was about ±2%.

Results

Molar solubilities (S_s) of *p*NA in the aquo-alcoholic solvents as well as in pure water at different temperatures, expressed as $-\log S_s$ are available elsewhere.[3] The free energies of solution (ΔG_s^0) on the molar scale were calculated for each solvent using [1]

$$[1] \qquad \Delta G_s^0 = -RT \ln S_s$$

and fitted by the method of least squares to an equation of the form

$$[2] \qquad \Delta G_s^0 = a_s + b_s T + c_s T \ln T$$

where T is the absolute temperature. The values of the coefficients a_s, b_s, and c_s are listed in Table 1. The free energies (ΔG_t^0) and entropies (ΔS_t^0) of transfer at 25°C were calculated using [3] and [4]

$$[3] \quad \Delta G_t^0 = (a_s - a_w) + (b_s - b_w)T_0 + (c_s - c_w)T_0 \ln T_0$$

$$[4] \quad \Delta S_t^0 = -[(b_s - b_w) + (c_s - c_w) + (c_s - c_w) \ln T_0]$$

where $T_0 = 298.15$ K, and the subscript w indicates quantities for water. ΔG_t^0 and ΔS_t^0 values are given in Table 1; the maximum uncertainties in these quantities as calculated by Please's method (16) are ±0.06 kJ mol^{-1} and ±4.0 J K^{-1} mol^{-1} respectively.

Discussion

As seen from Fig. 1, ΔG_t^0 for *p*NA decreases as the proportion of alcohol in the solvent increases, while ΔS_t^0 passes through a maximum for all alcohols. Since the *p*NA molecule is a resonance hybrid and the most important contributor is the zwitterionic form

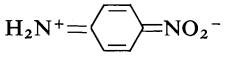

the observed behaviour will be dictated by the solvation of the hydrocarbon nucleus as well as of the charged ends relative to their solvation in pure water.

It has been observed by various workers (1, 5, 11, 17) that entropies of transfer of various electrolytes, polar nonelectrolytes, and neutral nonelectrolytes pass through maxima at certain critical compositions of alcohol + water mixtures. In our recent papers (12) we have attempted to explain the ΔS_t^0 values for hydrogen halides in these mixtures in terms of a four-step mechanism proposed earlier (11*a–c*). Lately, this approach has been rationalized by a semi-quantitative treatment of the transfer process (12*e*). The same approach may be used, with some modifications, to deal with the present problem concerning ΔS_t^0's of *p*NA. As will be shown, the same formulation of the process provides a satisfactory interpretation of ΔG_t^0 as well.

The hydrophobic effect (18, 19) of the aromatic nucleus in *p*NA is a characteristic feature of all such solutes possessing a bulky organic group and provides the key to the understanding of the problem. It has been suggested by Parker and co-workers (20) that water molecules around a hydrophobic solute form a hydrogen-bonded network among themselves and the formation of such a highly ordered surface or 'skin' contributes appreciably to the ΔS_t^0 of the solute.

The model we adopt for discussion of the solvated state of the *p*NA molecule is shown in Fig. 2. The general amphiphilic solute molecule

[3] Complete set of the actual experimental data is available, at a nominal charge, from the Depository of Unpublished Data, CISTI, National Research Council of Canada, Ottawa, Canada K1A 0S2.

TABLE 1. Coefficients of [2] and free energies and entropies of transfer of *p*-nitroaniline from water to alcohol + water mixtures at 25°C

Alcohol	Mol% alcohol	a_s/ (kJ mol^{-1})	b_s/ (kJ mol^{-1} K^{-1})	c_s/ (kJ mol^{-1} K^{-1})	ΔG_t^0/ (kJ mol^{-1})	ΔS_t^0/ (J K^{-1} mol^{-1})
Methanol	5.88	−35.50	1.5184	−0.23810	−0.67	11
	12.33	152.47	−2.6065	0.37437	−2.10	34
	19.43	−64.89	2.2701	−0.35421	−3.18	37
	35.99	10.06	0.4363	−0.07836	−6.38	23
	50.00	−0.66	0.5988	−0.10171	−8.32	17
	56.76	70.40	−1.0649	0.14804	−9.01	8
Ethanol	4.17	−12.67	1.0314	−0.16604	−0.64	15
	8.91	87.58	−1.1087	0.14979	−1.94	40
	14.36	51.43	−0.2594	0.02083	−3.94	54
	28.13	34.84	−0.1358	0.00676	−7.58	25
	40.00	31.25	−0.1762	0.01511	−9.02	10
	47.73	−124.37	3.3365	−0.51011	−9.55	15
Isopropanol	3.23	54.35	−0.3704	0.04039	−0.87	34
	6.98	92.14	−1.1170	0.14797	−2.94	60
	11.39	−3.74	0.8274	−0.13851	−5.76	35
	20.00	44.66	−0.4537	0.05640	−8.21	10
	23.08	−85.47	2.4614	−0.37879	−8.49	10
tert-Butyl alcohol	2.63	−21.42	1.3943	−0.22474	−0.90	45
	5.73	297.30	−5.7697	0.84341	−3.58	55
	9.44	24.44	0.1164	−0.03055	−6.15	15
	15.00	−22.76	1.0574	−0.16889	−7.81	8
	19.57	−38.93	1.3586	−0.21252	−8.31	−1
Water		39.55	−0.2139	0.02215	—	—

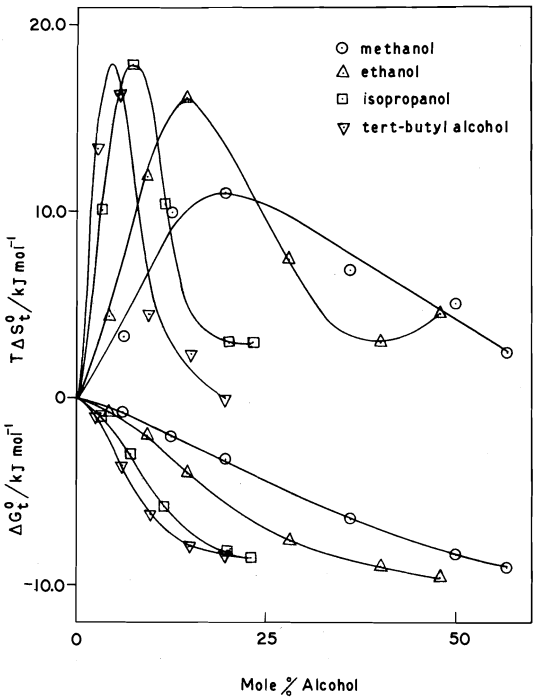

FIG. 1. Variation of ΔG_t^0 and $T\Delta S_t^0$ of *p*-nitroaniline at 25°C on the molar scale with alcohol mole percent.

M is represented by R (X_1,X_2...), where R is the hydrophobic moiety and X_1,X_2... are hydrophilic groups capable of undergoing hydrogen-bonded interactions with water or any other suitable solvent. In pure water as well as in a mixed aqueous solvent, M is enclosed by the hydrophobically created skin and X_1,X_2... enter into hydrogen-bonding with water or cosolvent molecules at the skin surface. If the cosolvent is an amphiphilic molecule R′Z (R′ = hydrophobic part, Z = hydrophilic part), in the mixed solvent R′Z molecules may enter the cavity and participate in two types of interactions: (*i*) dispersion interaction between R′ and R, (*ii*) hydrogen-bonded interaction between Z and the skin surface. Collectively, these interactions may be called 'buffer bonds', as the R′Z molecule acts as a buffer, so to speak, between the R group and the skin.

The transfer of the molecule M from water to the mixed solvent, i.e. from state (*a*) to state (*b*) (Fig. 2) may be considered to take place in four successive steps: (*1*) rupture of the H-bonds between X_1,X_2... and the skin surface, followed by the removal of M from the cavity; (*2*) collapse of the skin to form normal water structure; (*3*)

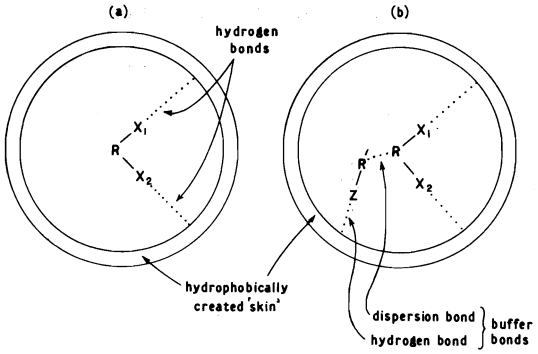

FIG. 2. An amphiphilic molecule in (*a*) water, (*b*) mixed aqueous solvent. In the transfer process, (*a*) is the initial state and (*b*) is the final state.

creation of a suitable cavity inside the mixed solvent; (*4*) introduction of M into the solvent cavity and formation of buffer bonds.

The change of any standard thermodynamic function X^0 (free energy, enthalpy, heat capacity, etc.) in the overall process will then be given by

$$[5] \qquad \Delta X_t^0 = \sum_{i=1}^{4} \Delta X_i$$

with

$$[6a] \qquad \Delta X_1 = -\Delta X_{HB}{}^w$$

$$[6b] \qquad \Delta X_2 = X_b{}^w - X_a{}^w$$

$$[6c] \qquad \Delta X_3 = X_a{}^s - X_b{}^s$$

$$[6d] \qquad \Delta X_4 = \Delta X_{HB}{}^s + \Delta X_{BB}$$

where the subscripts a and b respectively signify states of solvent molecules in the 'skin phase' and in the 'bulk phase', the superscripts w and s refer to pure water and mixed solvent respectively, and ΔX_{HB} and ΔX_{BB} are the thermodynamic functions of formation of the total number of hydrogen bonds and buffer bonds respectively.

Combining [6*a*]–[6*d*] with [5], we get

$$[7] \quad \Delta X_t^0 = (X_a{}^s - X_a{}^w) + (X_b{}^w - X_b{}^s) + (\Delta X_{HB}{}^s - \Delta X_{HB}{}^w) + \Delta X_{BB}$$

This equation is quite general and may be used to predict the behaviour of ΔX_t^0 for any amphiphilic solute in aquo-organic solvents. In the present case where M = *p*NA and the cosolvent is an alcohol R′OH, the analysis of ΔG_t^0 and ΔS_t^0 in terms of [7] is as follows.

Free Energies of Transfer

The skin phase is a more compact and more stable structure in pure water than in a mixed solvent, because steric inhibition (by R′) and fewer H-bonding sites in R′OH discourage strong solvent–solvent interactions when R′OH is present in that phase. With the increasing addition of R′OH, the skin phase becomes more and more loosely bound, which means that the term $(G_a{}^s - G_a{}^w)$ is increasingly positive. In the mixed solvent as compared to water, the strength of individual H-bonds in the bulk phase increases while their total number decreases (17). Consequently, the change in the total interaction energy in the bulk solvent with increasing proportions of alcohol should be small, i.e. the term $(G_b{}^w - G_b{}^s)$ is small, whatever its sign may be, at least when the alcohol content is not too high.

The term $(\Delta G_{HB}{}^s - \Delta G_{HB}{}^w)$ relates to the H-bonding interactions of the NH_2 and NO_2 groups with the skin surface. The positively charged NH_2 group is likely to be solvated preferentially by the more 'basic' alcohol molecules and the negatively charged NO_2 group by the more 'acidic' water molecules (21). Thus, out of the four H-bonds formed, two are progressively strengthened and two weakened with increasing proportions of R′OH. It follows that the value of $(\Delta G_{HB}{}^s - \Delta G_{HB}{}^w)$ should remain approximately zero with changing solvent composition.

With increasing alcohol content, dispersion interactions between R′ and the hydrocarbon nucleus of *p*NA grow increasingly strong causing ΔG_{BB} to assume increasingly large negative values.

The sharp fall of ΔG_t^0 in water-rich compositions arises from the predominance of ΔG_{BB} over the other terms in these regions. With further amounts of added alcohol, dispersion interactions reach saturation and the term $(G_a{}^s - G_a{}^w)$ becomes sufficiently large to cause a flattening out of the ΔG_t^0 curve, as observed. The observed order in $|\Delta G_t^0|$: *tert*-butyl alcohol > isopropanol > ethanol > methanol, is a consequence of the increasing strength of dispersion interactions with increasing size of R′.

Entropies of Transfer

For reasons cited above, the skin phase is a more ordered region in pure water than in a mixed solvent, hence $(S_a{}^s - S_a{}^w)$ is a positive quantity which increases in magnitude with increasing alcohol mole percent.

Small quantities of alcohol are known to extend and reinforce the hydrogen-bonded three-

dimensional structure of water (17). The 'supernormal' structure in water-rich compositions is rapidly broken up by further addition of alcohol, with the commencement of formation of alcohol–water H-bonded associates, the so-called two-dimensional structure (17). In the region where the supernormal structure is being built up, order is being created in the bulk solvent and $(S_b^w - S_b^s)$ is increasingly positive. In the region of structural collapse and destruction of bulk order, the positive value of this term decreases. This means that $(S_b^w - S_b^s)$ should pass through a maximum at the point of maximum structure promotion.

The third term at [7], $(\Delta S_{HB}^s - \Delta S_{HB}^w)$, is even less important than the corresponding free energy term, since the change in configuration and disposition of the H-bonds formed by the NH_2 and the NO_2 group is hardly significant to cause appreciable changes in entropy.

The formation of buffer bonds in the mixed solvent leads to an ordering effect of a kind which slightly increases with increasing alcohol content; ΔS_{BB} is thus increasingly negative, although the increase is slow.

In water-rich compositions of alcohol + water mixtures, the behaviour of ΔS_t^0 ought to be guided almost exclusively by the bulk structure term $(S_b^w - S_b^s)$ since the opposing smaller effects of the skin phase term $(S_a^s - S_a^w)$ and the buffer-bond term are likely to neutralize each other. At higher alcohol contents, where these terms are of comparable magnitude, the observed ΔS_t^0 contains a significant contribution from each. Since the bulk structure term first increases and then decreases, the appearance of a maximum near the region of maximum solvent structuredness is an expected feature of the ΔS_t^0 curves in alcohol + water mixtures.

The position, height, and sharpness of the maximum depends on the structure-forming propensity of the alcohol concerned. Indeed, as Fig. 1 shows, ΔS_t^0 for *tert*-butyl alcohol not only reaches the highest maximum and reaches it the earliest, but also falls away the most rapidly. This is because, of all the hydrocarbon groups (R′), the *tert*-butyl group is the largest and hence the most effective in promoting water structure. As R′ decreases in size, the maximum shifts towards higher alcohol mole percents, becoming shorter and broader at the same time, till at methanol, it is only a smooth hump. The maximum appears for *tert*-butyl alcohol at 0.04, for isopropanol at 0.07, for ethanol at 0.15, and for methanol at 0.20 mole fraction of alcohol. These positions agree more or less with those obtained from other studies (1) and seem to represent the solvent composition at which the highest degree of water structure prevails.

It may be questioned whether it is justified to ignore the effect of simple electrostatic solvation in our discussion, since *p*NA has a predominantly zwitterionic structure. In mixed solvents having dielectric constants less than that of water, the electrostatic contributions to ΔG_t^0 and ΔS_t^0 of a pair of ions, as estimated tentatively by the Born equation, may be shown (12) to have positive and negative values respectively. This would mean that after correcting for this effect, ΔG_t^0 values will become more negative and ΔS_t^0 values more positive, while their essential behaviour remains unaltered, and the present model still explains the observed trends satisfactorily.

Acknowledgement

Acknowledgement is due to the National Council of Educational Research and Training for providing an N.S.T.S. scholarship to one of us (K.B.).

1. S. Rajender and R. Lumry. Biopolymers, **9**, 1125 (1970).
2. R. L. Kay, G. P. Cunningham, and D. F. Evans. *In* Hydrogen-bonded solvent systems. *Edited by* A. K. Covington and P. Jones. Taylor and Francis, London. 1968. p. 249; T. L. Broadwater and R. L. Kay. J. Phys. Chem. **74**, 3802 (1970).
3. J. A. Lanning, M. J. Pikal, and J. Q. Chambers. J. Phys. Chem. **78**, 70 (1974).
4. H. S. Frank and W. Y. Wen. Discuss. Faraday Soc. **24**, 133 (1957).
5. E. M. Arnett, W. G. Bentrude, J. J. Burke, and P. McC. Duggleby. J. Am. Chem. Soc. **87**, 1541 (1965); E. M. Arnett. *In* Physico-chemical processes in mixed aqueous solvents. *Edited by* F. Franks. Heinemann, London. 1967. p. 105.
6. G. L. Bertrand, F. J. Millero, C. H. Hu, and L. G. Hepler. J. Phys. Chem. **70**, 699 (1966).
7. A. Ben-Naim. J. Phys. Chem. **71**, 4002 (1967); A. Ben-Naim and S. Baer. Trans. Faraday Soc. **60**, 1736 (1964); A. Ben-Naim. *In* water and aqueous solutions. *Edited by* R. A. Horne. Wiley-Interscience, New York, NY. 1972. p. 425.
8. D. N. Glew, R. D. Mak, and N. S. Rath. Chem. Commun. 264 (1968); M. Ageno and P. L. Indovina. Proc. Natl. Acad. Sci. USA, **57**, 1158 (1967); J. Clifford and B. A. Pethica. Trans. Faraday Soc. **61**, 182 (1965).
9. C. J. Burton. J. Acoust. Soc. Am. **20**, 186 (1948); L. R. O. Storey. Proc. Phys. Soc. **65**, 943 (1952); M. J. Blandamer and D. Waddington. J. Phys. Chem.

74, 2569 (1970); M. C. R. SYMONS and M. J. BLANDAMER. *In* Hydrogen-bonded solvent systems. *Edited by* A. K. Covington and P. Jones. Taylor and Francis, London. 1968. p. 211.
10. F. CINNEMO and E. TARTAGLIONE. Nuovo Cimento, **11**, 401 (1959).
11. (*a*) K. K. KUNDU. Indian J. Chem. **10**, 303 (1972); (*b*) K. K. KUNDU, D. JANA, and M. N. DAS. Electrochim. Acta, **18**, 95 (1973); (*c*) K. K. KUNDU and K. MAZUMDAR. J. Chem. Soc. Faraday Trans. I, **69**, 806 (1973); **71**, 1422 (1975).
12. (*a*) K. BOSE, A. K. DAS, and K. K. KUNDU. J. Chem. Soc. Faraday Trans. I, **71**, 1838 (1975); (*b*) **72**, 1633 (1976); (*c*) K. DAS, K. BOSE, and K. K. KUNDU. J. Chem. Soc. Faraday Trans. I, **73**, 655 (1977); (*d*) K. DAS, K. BOSE, A. K. DAS, and K. K. KUNDU. Electrochim. Acta. In press; (*e*) K. BOSE, K. DAS, A. K. DAS, and K. K. KUNDU. J. Chem. Soc. Faraday Trans. I. In press.
13. Technique of organic chemistry. 2nd ed. Vol. VII. *Edited by* A. Weissberger. Interscience, New York, NY. 1965.
14. (*a*) K. K. KUNDU, A. L. DE, and M. N. DAS. J. Chem. Soc. Perkin Trans. II, 2063 (1972); (*b*) J. Chem. Soc. Dalton Trans. 386 (1972).
15. E. A. BRAUDE and E. S. STERN. J. Chem. Soc. 1976 (1948).
16. N. W. PLEASE. J. Biochem. **56**, 196 (1954).
17. F. FRANKS and D. J. G. IVES. Q. Rev. Chem. Soc. **20**, 1 (1966).
18. C. TANFORD. The hydrophobic effect: formation of micelles and biological membranes. Wiley-Interscience, New York, NY. 1973.
19. H. S. FRANK and M. W. EVANS. J. Chem. Phys. **13**, 507 (1945).
20. B. G. COX, G. R. HEDWIG, A. J. PARKER, and D. W. WATTS. Aust. J. Chem. **27**, 477 (1974); A. J. PARKER. Electrochim. Acta, **21**, 671 (1976).
21. (*a*) D. FEAKINS and P. WATSON. J. Chem. Soc. 4734 (1968); (*b*) D. FEAKINS. *In* Physico-chemical processes in mixed aqueous solvents. *Edited by* F. Franks. Heinemann, London. 1967. p. 71.

Carbonyl stretching frequencies in acyl- and aryl-substituted phenyl benzoates

AHMAD SAMI SHAWALI[1]
Department of Chemistry, Faculty of Science, University of Cairo, Giza, Egypt
AND
NAMEK FARAHAT EWEISS
Department of Chemistry, Faculty of Science, University of Kuwait, Kuwait

Received June 2, 1977

AHMAD SAMI SHAWALI and NAMEK FARAHAT EWEISS. Can. J. Chem. **55**, 3967 (1977).

The infrared carbonyl stretching frequencies of acyl-substituted *p*-tolyl, phenyl, and *p*-chlorophenyl benzoates, $XC_6H_4COOC_6H_4Y$, have been determined in carbon tetrachloride. Each of the substituted phenols generated an independent $\bar{\nu}$–σ plot which was correlated precisely with the Hammett equation (r = 0.999–0.998). The values of ρ_X so obtained show no tendency to vary with the structure of the parent phenol and are all within $\pm$0.202 of the mean value of 13.899. Similar correlations were obtained with the Hammett plots made by varying the aryl moieties of the esters while holding the acyl portions constant. For the four sets (**4**–**8**) studied, the mean value of ρ_Y is 8.964 $\pm$ 0.266. Using the slopes of $\bar{\nu}_{C=O}$ vs. σ correlations in the series studied, the transmissive factor for the ether bridge in carbon tetrachloride was calculated (π' = 0.64). An expression relating substituents in both acyl and aryl moieties to the monosubstituted compounds suggests that substituents on the two different groups act reasonably independently of each other; $\Delta\bar{\nu}_{XY} = 1.021\ (\pm 0.031)\ (\Delta\bar{\nu}_X + \Delta\bar{\nu}_Y) - 0.44\ (\pm 0.254)$. For all esters studied the equation $\bar{\nu}_{XY} = 127.215\ (\pm 1.444)\ ((\sigma_X/\rho_Y) + (\sigma_Y/\rho_X)) + 1734.9\ (\pm 0.078)$ was found to hold with r = 0.998.

AHMAD SAMI SHAWALI et NAMEK FARAHAT EWEISS. Can. J. Chem. **55**, 3967 (1977).

On a déterminé, dans le tétrachlorure de carbone, les fréquences d'élongation du carbonyle dans l'infrarouge de benzoates de *p*-tolyle, de phényle et de *p*-chlorophényle, substitués dans la portion acyle, $XC_6H_4COOC_6H_4Y$. Chacun des phénols substitués génère une courbe $\bar{\nu}/\sigma$ indépendante qui présente une corrélation précise avec l'équation de Hammett (r = 0.999–0.998). Les valeurs de ρ_X ainsi obtenues ne présentent aucune tendance de variation avec la structure du phénol de base et sont toutes à l'intérieur de $\pm$0.202 de la valeur moyenne de 13.899. On a pu obtenir des corrélations semblables avec les courbes de Hammett en faisant varier la portion arylée des esters et en maintenant les portions acylées constantes. Pour les quatre séries (**4**–**8**) étudiées, la valeur moyenne de ρ_Y est de 8.964 $\pm$ 0.266. Utilisant les pentes de $\bar{\nu}_{C=O}$ vs. σ dans les séries étudiées, le facteur de transmission du pont éthéré dans le tétrachlorure de carbone a pu être calculé (π' = 0.64). Une expression reliant les substituants à la fois des portions acylés et arylés avec les composés monosubstitués suggère que les substituants sur les deux groupes différents agissent d'une façon raisonablement indépendante l'un de l'autre $\Delta\bar{\nu}_{XY} = 1.021\ (\pm 0.031)\ (\Delta\bar{\nu}_X + \Delta\bar{\nu}_Y) - 0.44\ (\pm 0.254)$. Pour tous les éthers étudiés l'équation: $\bar{\nu}_{XY} = 127.215\ (\pm 1.444)\ ((\sigma_X/\rho_Y) + \sigma_Y/\rho_X)) + 1734.9\ (\pm 0.078)$ est suivie avec r = 0.998.

[Traduit par le journal]

Linear correlation of the infrared group frequencies in *meta*- and *para*-substituted benzene derivatives with the Hammett σ constant have been reported by several workers (1). The relation is usually expressed by a Hammett-type equation,

$$[1] \qquad \bar{\nu} = \rho\sigma + \bar{\nu}_0$$

A survey of literature indicates that the sensitivity, as measured by ρ, of the group frequency to substituents in structurally related compounds seems to exhibit little, if any, change with the structure of the parent compounds. For example, the values of ρ reported for ethyl benzoates (2) and acetophenones (3) in carbon tetrachloride are 14.81 and 15.9, respectively. To shed more light on this problem, the carbonyl stretching frequencies of phenyl benzoates (**1**–**8**), which were substituted in both the acyl and aryl moieties, were determined in carbon tetrachloride. Each aryl derivative was used to generate an independent Hammett plot by systematic substitutions on the acyl groups. The present infrared investigation was also undertaken to obtain quantitative information pertinent to the effectiveness of the transmission of electronic

[1]Author to whom all inquiries should be addressed.

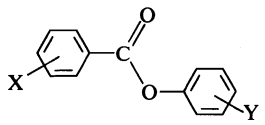

1 X = *p*-OCH_3, *p*-CH_3, H, *p*-Cl, *m*-Cl, *m*-NO_2, *p*-NO_2; Y = H
2 X = H, *p*-Cl, *p*-NO_2, *m*-Cl, *m*-NO_2; Y = *p*-CH_3
3 X = H, *p*-CH_3, *p*-Cl, *m*-NO_2, *p*-NO_2; Y = *p*-Cl
4 X = H; Y = *p*-CH_3, H, *p*-Cl, *m*-Cl, *p*-Ac, *m*-NO_2, *p*-NO_2
5 X = *p*-Cl; Y = *m*-Cl, *p*-Cl, H, *p*-CH_3
6 X = *p*-NO_2; Y = *p*-Cl, *p*-Me, *m*-Cl, H
7 X = *p*-Me; Y = *m*-NO_2, *p*-Cl, *p*-NO_2, H
8 X = *m*-NO_2; Y = *p*-Cl, H, *p*-Me

effects through the ether bridge, and to examine the effects of multisubstitution.

Results and Discussion

The Effect of Substituents on the Acyl Moiety

The carbonyl stretching frequencies (cm^{-1}) obtained for the esters studied in carbon tetrachloride are listed in Table 1. As can be seen in the table, electron attracting groups shift the absorption band to higher frequency values (cm^{-1}), as compared with the unsubstituted compound, in the three series (**1–3**) studied. An opposite shift is observed in the compounds with substituents that supply electrons. The values of $\bar{\nu}_{C=O}$ (cm^{-1}) have been correlated with the σ constants as taken from Ritchie and Sager (4). A computer program was written to carry out the least-squares and statistical treatment of the data with the σ constants according to the method of Jaffe (5). The results of the computation for the three series of esters are given in Table 2. It is obvious that there is no apparent tendency of the ρ values to vary as the pK_a of the phenol changes. All of the ρ values are within one standard deviation from the mean value of 13.899. The ρ value of ~13.90 obtained for phenyl benzoates should be compared with the value of 14.81 obtained from a similar study on ethyl benzoates (2). The ratio of these ρ values, being close to unity, further substantiates the foregoing conclusion that the value of ρ appears to be independent of the nature of the alcohol portion of the ester molecule.

In order to get a further estimate of the relative importance of resonance (*R*) and field (*F*) effects, the treatment reported by Swain and Lupton (6) has been employed using the equation

$$[2] \qquad \bar{\nu} = \alpha F + \beta R + \bar{\nu}_0$$

where α and β represent the sensitivity of C=O stretching frequency to the field and resonance effects, respectively. The equation that fits the data for phenyl benzoates, **1**, is

$$\bar{\nu} = 7.76(\pm 0.344)F + 14.518(\pm 0.688)R + 1735.225; \quad r = 0.999$$

The value for the resonance contribution, % *R*, to the correlation is ca. 45 (7).[2] Comparison of this value with that reported for benzophenones (% *R* = 43) (3) indicates that sensitivity of the carbonyl stretching frequencies to resonance effects in these two series of compounds is approximately the same.

The Effect of Substituents on the Aryl Moiety

In 1960, Freedman (7) observed that the C=O stretching frequencies of aryl acetates failed to correlate with σ for the *para*-substituents. To explain this behaviour, he concluded that the frequency was dependent only on the inductive component of σ. In 1973, Cohen and Takahashi (8) determined the absorption frequencies of the C=O group in a series of 48 mono- and polysubstituted phenyl hydrocinnamates in CCl_4, and found the values to correlate well with σ^0 (or $\Sigma\sigma^0$) constants for the ring substituents. They concluded that the carbonyl frequency is thus dependent on the electronic effects (inductive and resonance) that the substituent group would exercise on the C-1 bearing the acyloxy group. More recently, do Amaral and do Amaral (9) observed that the values of the carbonyl group absorption frequencies for three series of phenyl esters of allylacetic, diphenylacetic, and allyldiphenylacetic acids in CCl_4 are satisfactorily correlated with σ as well as σ^0 constants.

In the present study, the application of Hammett's equation for the carbonyl group absorption frequencies of the four sets of aryl benzoates, **4** to **7**, using σ as well as σ'' and σ^0 constants was tried. Values of σ, σ'', and σ^0 were taken from the compilation of Ritchie and Sager (4). The results of the statistical analysis of the data by the least-squares method are given in Table 3. It can be seen that for a given set of esters the values of ρ, ρ'', and ρ^0 are in very close agreement, and that the values of the correlation coefficients do not permit a judgement as to

[2]Percent resonance contribution was calculated as indicated in ref. 6; ϕ and ψ were calculated internally, based upon the number of points used in the correlation.

TABLE 1. Carbonyl stretching frequencies (cm^{-1}) and characterization of phenyl benzoates, $XC_6H_4COOC_6H_4Y$

Acid substituent X	Phenol substituent Y	$\bar{\nu}_{C=O}$[a]	$\Delta\bar{\nu}$	mp (lit. mp) (°C)	Ref.
4-OCH_3	H	1731	−4.0	85–86(87)	12
4-CH_3	H	1733	−2.0	82(83)	13
H	H	1735	0.0	71(68)	10
4-Cl	H	1738.5	3.5	108(107)	15
3-Cl	H	1739.5	4.5	58(56)	10
3-NO_2	H	1744.5	9.5	98–99(97–98)	16
4-NO_2	H	1746	11.0	128(128–129)	10
H	4-CH_3	1733.5	−1.5	72(70–71)	10
H	4-Cl	1737	2.0	89(88–89)	10
H	3-Cl	1738.5	3.5	72(71–72)	17
H	4-$COCH_3$	1739	4.0	135(132–133)	18
H	3-NO_2	1741.5	6.5	96(95)	14
H	4-NO_2	1742.5	7.5	142(142–143)	10
4-CH_3	3-NO_2	1739	4.0	106(106–107)	10
4-CH_3	4-Cl	1734.5	−0.5	91(91–92)	19
4-CH_3	4-NO_2	1739.5	4.5	122(120–121)	10
4-Cl	3-Cl	1741.5	6.5	94(95)	20
4-Cl	4-Cl	1740	5.0	96(96–96.5)	10
4-Cl	4-CH_3	1736.5	1.5	98(97.5–98.5)	10
4-NO_2	4-Cl	1748	13.0	171(171–172)	10
4-NO_2	4-CH_3	1744	9.0	98(98–99)	10
4-NO_2	3-Cl	1749	14.0	162–163(164–165)	20
3-Cl	4-CH_3	1738.5	3.5	78(75.1–76)	21
3-NO_2	4-Cl	1747	12.0	124(124.5)	17
3-NO_2	4-CH_3	1743	8.0	76(77–78)	22

[a]Measured in carbon tetrachloride.

TABLE 2. Correlation between the carbonyl frequencies (cm^{-1}) of acyl-substituted phenyl benzoates in CCl_4 and the Hammett substituent constants[a]

Series	Best-fit linear equation	r	S_ρ[b]	S_i[b]	n
1	$\bar{\nu}=13.703\sigma+1734.98$	0.998	0.395	0.177	7
2	$\bar{\nu}=13.803\sigma+1733.23$	0.999	0.316	0.161	5
3	$\bar{\nu}=14.191\sigma+1736.90$	0.999	0.134	0.065	5

[a]Hammett's ρ value is dimensionless. In this work it has the dimension of cm^{-1} as is common in the literature in spectroscopic comparison.
[b]Standard deviations in the slope (S_ρ) and intercept (S_i).

which one of the σ value series our results fit best. This probably results from the fact that the values of σ, σ^n, and σ^0 for the substituents examined are so similar that a statistically valid distinction becomes impossible. The mean values of ρ, ρ^n, and ρ^0 for the four sets of esters are 8.966, 9.274, and 8.836 and the mean standard errors are ±0.266, ±0.674, and ±0.473, respectively.

These data also show that the ρ value appears to be insensitive to the nature of the acyl portion of the esters over the range studied. This result is in accord with the finding of Kirsch *et al.* (10) that the values of ρ obtained for the rates of alkaline hydrolysis of acyl-substituted *p*-nitrophenyl, *m*-nitrophenyl, *p*-chlorophenyl, phenyl, and *p*-tolyl benzoates show no tendency either to increase or decrease with the intrinsic reactivity of the parent phenol. All values are within ±0.040 of the mean of 2.021.

A comparison of the results reported in Tables 2 and 3 reveals that the stretching frequency of the ester carbonyl group is more sensitive to substituent effects in the acyl portion than in the phenolic moiety. This greater sensitivity is obvious in terms of the vibrating CO group being one bond closer to the acyl substituent than it is to the phenol. Taft and Lewis (11) have shown,

TABLE 3. Correlation between the carbonyl frequencies (cm^{-1}) of substituted phenyl benzoates in CCl_4 and the Hammett substituent constants

Best-fit linear equation	r	S_ρ	S_i	n
	Aryl benzoates, **4**			
$\bar{\nu}=9.226\sigma+1735.0$	0.996	0.360	0.171	7
$\bar{\nu}=9.425\sigma''+1734.8$	0.996	0.507	0.219	5
$\bar{\nu}=9.305\sigma^0+1734.9$	0.998	0.252	0.121	5
	Aryl *p*-chlorobenzoates, **5**			
$\bar{\nu}=8.849\sigma+1738.2$	0.993	0.725	0.169	4
$\bar{\nu}=8.890\sigma''+1738.04$	0.972	2.110	0.338	3
$\bar{\nu}=8.757\sigma^0+1738.05$	0.982	1.173	0.283	4
	Aryl *p*-nitrobenzoates, **6**			
$\bar{\nu}=9.204\sigma+1745.8$	0.995	0.663	0.148	4
$\bar{\nu}=10.289\sigma''+1745.6$	0.998	1.563	0.251	3
$\bar{\nu}=9.186\sigma^0+1745.6$	0.993	0.787	0.189	4
	Aryl *p*-toluates, **7**			
$\bar{\nu}=8.584\sigma+1732.8$	0.998	0.384	0.207	4
$\bar{\nu}=8.490\sigma''+1732.8$	0.996	0.705	0.332	3
$\bar{\nu}=8.098\sigma^0+1732.7$	0.994	0.868	0.432	4

empirically, from a consideration of substituent effects upon the dissociation constants of acids, that the transmission of electronic effects through saturated atoms falls off according to the equation $\rho \simeq (2.8 + 0.5)^{1-i}$, where i = the number of saturated atoms between the benzene ring and the reaction centre.

The correlation of the data for series **4** with F and R constants gave the relation

$$\bar{\nu}_4 = 5.450(\pm 0.515)F + 8.230(\pm 1.510)R + 1734.83(\pm 0.302)$$

and a value of 34% for the resonance contribution to the correlation was obtained. This value suggests that the ether bridge can transmit resonance effects.

Using the ρ values obtained for acyl-substituted phenyl benzoates and aryl-substituted phenyl benzoates (cf. Tables 2 and 3) we calculated the transmissive factor of the electronic effects for the ether bridge, π_0', from the equation

$$[3] \qquad \pi_0' = \rho_Y/\rho_X$$

where ρ_X and ρ_Y are the slopes of the $\Delta\bar{\nu}$ vs. σ_X and $\Delta\bar{\nu}$ vs. σ_Y linear free-energy relationships, respectively. The average value of π_0' obtained from the different series studied was found to be 63.97 ($\pm$2.358)%. This value is, within statistical limits, close to the value of 62% calculated from the reaction constants of alkaline hydrolysis of substituted phenyl benzoates (12).

Substitution in Acyl and Aryl Moieties

In an attempt to gain further information as to the influence of a substituent on the acyl group or of a substituent on the phenolic ring, the disubstituted phenyl benzoates in Table 1 were examined. If an acyl substituent has the same effect on the carbonyl frequency, regardless of the substituent on the aryl group, then a plot of the sum of $\Delta\bar{\nu}$ values for the two monosubstituted compounds vs. the $\Delta\bar{\nu}$ value for the corresponding disubstituted compound should give a linear relationship. Least-squares analysis of the data provides eq. 4, with correlation coefficient, $r = 0.995$.

$$[4] \quad \Delta\bar{\nu}_{XY} = 1.021(\pm 0.031) \sum (\Delta\bar{\nu}_X + \Delta\bar{\nu}_Y) - 0.44(\pm 0.0254)$$

The good correlation obtained (Fig. 1) suggests that substituents on the phenolic ring influence the carbonyl stretching frequency in a manner which is reasonably independent of substituents on the benzoyl group and vice versa. This observation suggests, therefore, that the effect of substituents on the carbonyl stretch ing frequency of aryl aroate would be correlated by

$$[5] \qquad \Delta\bar{\nu}_{XY} = \rho_X\sigma_X + \rho_Y\sigma_Y$$

A similar equation was proposed by Jaffe (5) for compounds containing two substituted benzene rings that are not symmetrically placed with respect to the reaction site. To test the

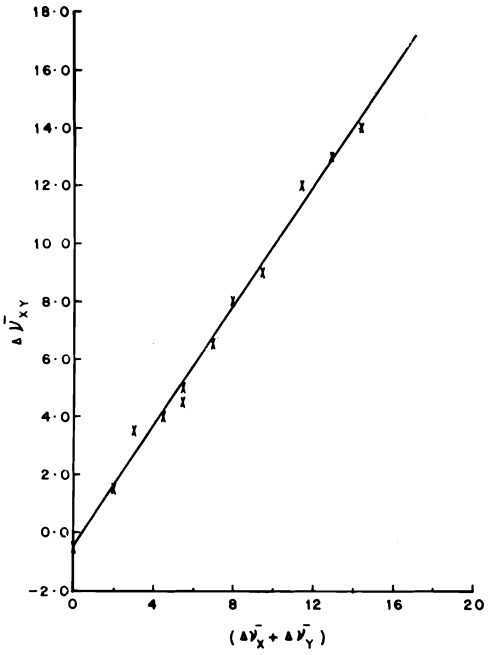

FIG. 1. Correlation of $\Delta\bar{\nu}_{XY}$ (cm^{-1}) for disubstituted phenyl benzoates with ($\Delta\bar{\nu}_X + \Delta\bar{\nu}_Y$) for the monsubstituted analogs.

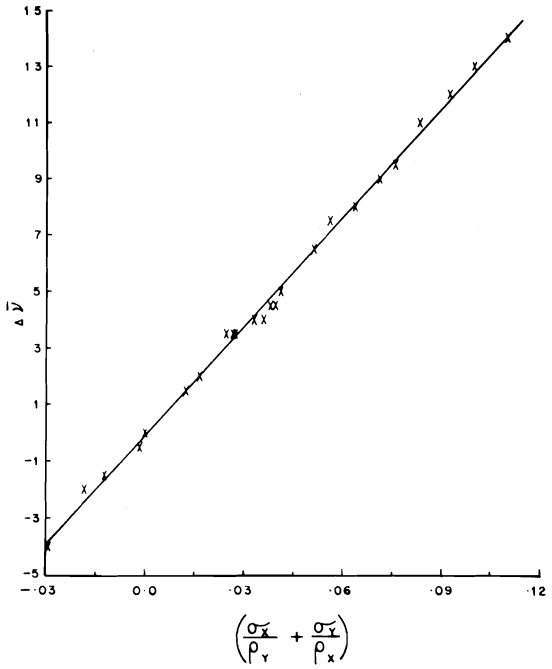

FIG. 2. Hammett plot of the carbonyl stretching frequency (cm^{-1}) versus the combined substituent effects for mono- and polysubstituted phenyl benzoates.

applicability of this equation, its linear form (eq. 6) was used.

$$[6] \qquad \Delta\bar{\nu}_{XY} = \rho_X\rho_Y\left(\frac{\sigma_X}{\rho_Y} + \frac{\sigma_Y}{\rho_X}\right)$$

In Fig. 2 are plotted the $\Delta\bar{\nu}$ values for the CO absorption (cm^{-1}) of the 25 compounds in the series studied as ordinate and the $(\sigma_X/\rho_Y) + (\sigma_Y/\rho_X)$ function as abscissa. It is seen that all mono- and disubstituted esters follow this Hammett relation closely. The equation of the straight line in Fig. 2,

$$\bar{\nu}_{XY} = 127.215(\pm 1.444)\left(\frac{\sigma_X}{\rho_Y} + \frac{\sigma_Y}{\rho_X}\right) - 1734.9(\pm 0.078)$$

(with correlation coefficient, r, of 0.998) can be used to predict the $\bar{\nu}_{C=O}$ stretching frequencies of other substituted phenyl benzoates.

Experimental

Materials

The substituted phenyl benzoates were generally prepared by the interaction of equivalent amounts of aroyl chloride and phenol in 10% sodium hydroxide solution or in pyridine while stirring as previously described (12). The products precipitated were collected by filtration, washed with 5% sodium carbonate solution, crystallized from ethanol until a constant melting point was obtained, and then dried over P_2O_5 in a vacuum desiccator. Table 1 lists the uncorrected melting points obtained with an electrothermal melting point apparatus (Gallenkamp 1A6301), and literature references for compounds prepared.

Infrared Frequencies

The ir stretching frequencies for all the esters were determined in spectral grade carbon tetrachloride using a Beckman IR-12 grating spectrometer operated in the expanded scale mode at a scan rate of 8 cm^{-1}/min, chart speed of 1 in./min, and period setting of 2. Calibration and paper alignment difficulties were minimized by recording the 1583.1 cm^{-1} polystyrene band on each spectrum. The carbonyl absorption band had a symmetric shape that simplified the determination of its position in the spectrum. The band frequencies were taken at the half-width of the half-height. All frequencies reported were obtained from averaging at least three different scans, all of which gave frequencies which were within 0.3 cm^{-1} of one another. The estimated relative error in frequencies is approximately 0.5 cm^{-1}.

Calculations

The least-squares treatment, the multiple regression analysis, and other statistical computations (5) were performed using a Hewlett-Packard calculator model 9830A.

Acknowledgments

We wish to thank Professor J. F. Ogilvie for

providing the computer program, and Mr. A. El-Moussa for assistance in recording the spectra.

1. (*a*) M. St. C. Flett. Trans. Faraday Soc. **44**, 767 (1948); (*b*) N. Fuson, M. L. Josien, and E. M. Shelton. J. Am. Chem. Soc. **76**, 2526 (1954); (*c*) R. N. Jones, W. F. Farbes, and W. A. Mueller. Can. J. Chem. **35**, 504 (1957); (*d*) H. C. Brown and Y. Okamoto. Can. J. Chem. **36**, 4979 (1958).
2. H. W. Thompson, R. W. Needham, and D. Jameson. Spectrochim. Acta, **9**, 208 (1957).
3. N. L. Silver and D. W. Boykin, Jr. J. Org. Chem. **35**, 759 (1970).
4. C. D. Ritchie and W. F. Sager. Prog. Phys. Org. Chem. **2**, 323 (1964).
5. H. H. Jaffe. Chem. Rev. **53**, 191 (1953).
6. C. G. Swain and E. C. Lupton, Jr. J. Am. Chem. Soc. **90**, 4328 (1968).
7. H. H. Freedman. J. Am. Chem. Soc. **82**, 2454 (1960).
8. L. A. Cohen and S. Takahashi. J. Am. Chem. Soc. **95**, 443 (1973).
9. A. T. do Amaral and L. do Amaral. J. Org. Chem. **41**, 1623 (1976).
10. J. F. Kirsch, W. Clewell, and A. Simon. J. Org. Chem. **33**, 127 (1968).
11. R. W. Taft, Jr. and I. C. Lewis. J. Am. Chem. Soc. **80**, 2436 (1958).
12. F. M. Irvine and J. C. Smith. J. Chem. Soc. 74 (1927).
13. A. W. Titherley and L. Stubbs. J. Chem. Soc. **105**, 299 (1914).
14. G. Neumann. Ber. **19**, 2979 (1886).
15. K. Nakazawa and S. Baba. J. Pharm. Soc. Jpn. **75**, 378 (1955).
16. A. L. Bernoulli and A. St. Goar. Helv. Chim. Acta, **9**, 751 (1926).
17. W. J. Wohlleben. Ber. **42**, 4371 (1909).
18. Y. Akahori. Chem. Pharm. Bull. Tokyo, **13**, 368 (1965).
19. M. Neeman, A. Modiano, and Y. Shor. J. Org. Chem. **21**, 671 (1956).
20. T. Matsukawa, S. Ban, and T. Imada. J. Pharm. Soc. Jpn. **71**, 477 (1951).
21. R. C. Huston and K. R. Robinson. J. Am. Chem. Soc. **73**, 2483 (1951).
22. S. B. Hanggi. Helv. Chim. Acta, **4**, 25 (1921).

Effect of an external electric field on the yield of trapped electrons in a γ-irradiated hydrocarbon glass

NORIYUKI KATO, TOYOAKI KIMURA, AND KENJI FUEKI

Department of Synthetic Chemistry, Faculty of Engineering, Nagoya University, Chikusa-ku, Nagoya, Japan

Received May 9, 1977

NORIYUKI KATO, TOYOAKI KIMURA, and KENJI FUEKI. Can. J. Chem. **55**, 3973 (1977).

Trapped electron yields were measured by means of optical absorption spectroscopy for a hydrocarbon glass γ-irradiated at 77 K in the presence of an external electric field. It was observed that the yield of trapped electrons increased in the presence of an external electric field as compared with that in the absence of an external electric field. The experimental results were analyzed theoretically and interpreted as due to overall effects involving changes in geminate recombination times which were caused by an external electric field.

NORIYUKI KATO, TOYOAKI KIMURA et KENJI FUEKI. Can. J. Chem. **55**, 3973 (1977).

On a mesuré les rendements d'électrons piégés—en faisant appel à la spectroscopie d'absorption optique—dans un verre hydrocarboné irradié par des radiations γ à 77 K en présence d'un champ électrique externe. On a observé que le rendement des électrons piégés augmente en présence d'un champ électrique externe par comparaison avec l'absence d'un tel champ. On a analysé les résultats expérimentaux d'une façon théorique et on les a interprétés en fonction d'effects globaux impliquant des changements dans les temps de recombinaison géminale qui sont causés par un champ électrique externe.

[Traduit par le journal]

Introduction

The properties of trapped electrons in organic glasses at low temperatures have extensively been investigated in the last decade (1–3). It is now well established that trapped electrons can be produced with significant yields in γ-irradiated organic glasses. Trapped electron yields produced in γ-irradiated nonpolar hydrocarbon glasses at 77 K were reported by several investigators (4–10). The largest yield of trapped electrons (e_t^-) in γ-irradiated hydrocarbon glasses was obtained for 2-methylpentane (2MP) glass in which $G(e_t^-)$ was reported to be 1.1 at 77 K (10).

The effect of an external electric field on the yield of trapped electrons in a γ-irradiated 2MP glass at 77 K was first observed in the present work. By applying high voltages during γ-irradiation, the yield of trapped electrons produced in 2MP glass was increased almost linearly with increasing external electric field strength under our experimental conditions. In order to interpret the experimental results, we have calculated theoretically the yield of trapped electrons in the presence of an external electric field by applying the Nernst–Einstein relation to the motion of thermalized electrons in the Coulombic field and assuming a modified exponential distribution function for thermalized electrons.

Experimental

2-Methylpentane was used as a hydrocarbon matrix which forms a clear glass at 77 K and yields the most trapped electrons among hydrocarbon matrices reported hitherto. Tokyo Kagaku Seiki standard pure 2MP was dried over calcium hydride and purified with freshly activated molecular sieve (13X 1/16) pellets in vacuum. The sample preparation was carried out by distilling purified solvent into a quartz cell on a vacuum line. The cell was of a rectangular type (10 mm × 20 mm) with Suprasil windows and two stainless steel mesh electrodes separated by 1 mm from each other. A Fluke Model 410B power supply was used to apply a high voltage between the electrodes during γ-irradiation. The sample was γ-irradiated at 77 K at a dose rate of 4.5×10^5 rad h^{-1} to a dose of 1.5×10^5 rad. The range of external electric field strengths was 10–80 kV cm^{-1}. The relative yield of trapped electrons at 77 K was determined by optical absorption measurements with a Hitachi Model 323 recording spectrophotometer; the analyzing light was passed through the cell in the direction perpendicular to the electrode plane and the bleaching light from a slide projector was passed through the cell in the direction parallel to the electrode plane. The optical absorption measurements were made in such a way that the optical absorption of trapped electrons at 1700 nm was measured 5 min after the termination of γ-irradiation.

Results and Discussion

The experimental results are given in Figs. 1 and 2. Figure 1 shows optical absorption spectra of trapped electrons produced in 2MP glass γ-irradiated at 77 K in the absence (curve *1*) and

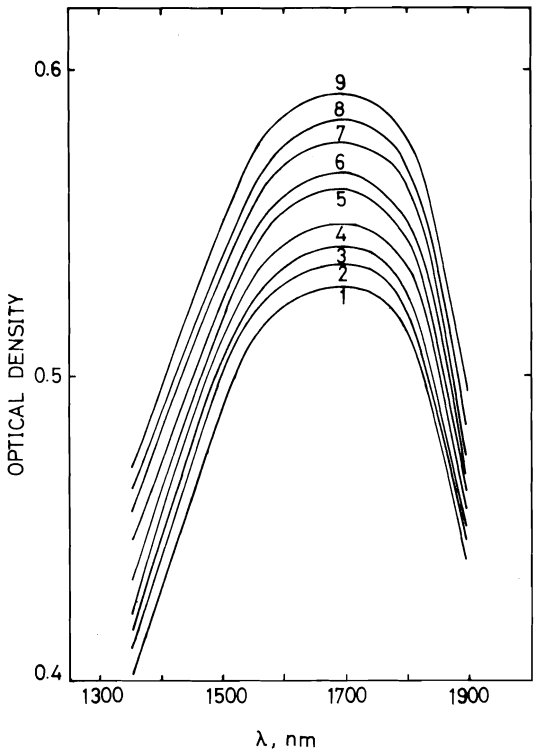

FIG. 1. Optical absorption spectra of trapped electrons in 2-methylpentane glass γ-irradiated at 77 K in the presence and absence of an external electric field: *1*, $E = 0$; *2–9*, $E = 10$, 20, 30, 40, 50, 60, 70, and 80 kV/cm, respectively.

presence (curves *2–9*) of an external electric field. It can be seen in Fig. 1 that the optical absorption increases in intensity with increasing applied voltage, but the shape and position of the absorption spectra remain essentially the same. Figure 2 shows the optical density ratio, OD^E/OD^0, plotted against the applied electric field, E. Here OD^E and OD^0 are, respectively, the optical densities at 1700 nm of the trapped electron absorption observed for the samples γ-irradiated in the presence and absence of an external electric field. The experiments were repeated several times at each applied field. As a result, it was found that the values of OD^E/OD^0 given in the present paper were somewhat smaller than those in the previous communication (11). The values of OD^E/OD^0 represented by vertical bars in Fig. 2 indicate the range of reproducibility in the experiments.

Our theoretical analysis of the experimental results is based on an estimation of changes in recombination times of thermalized electrons by

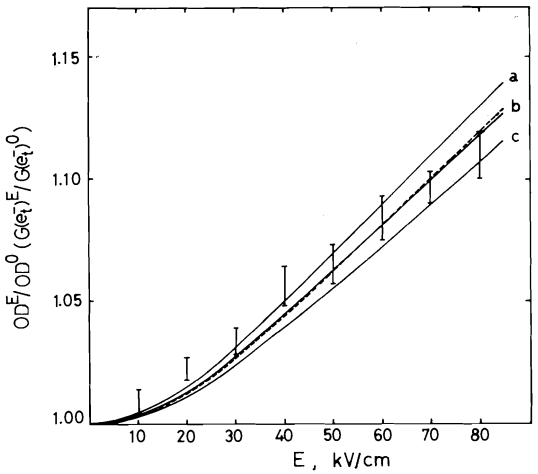

FIG. 2. Plots of observed OD^E/OD^0 at 1700 nm and calculated $G(e_t^-)^E/G(e_t^-)^0$ versus applied electric field strength: (—) $n = 1.0$: $b = 75$ (a), 72 (b), and 70 (c) Å; (---) $n = 0.1$: $b = 55$ Å.

the presence of an external electric field which would affect the efficiency of electron trapping in the matrix. Figure 3 shows the potential energy, $U(r)$, of an electron versus the separation distance, r, between a positive ion and an electron. The potential energy in the presence of an external electric field is given by eq. 1.

$$[1] \qquad U(r) = (-e^2/\varepsilon r) + eEr\cos\theta$$

Here e is the electronic charge, ε the dielectric constant of the matrix, E the applied field strength, and θ the angle between the direction joining the electron to the positive ion and that

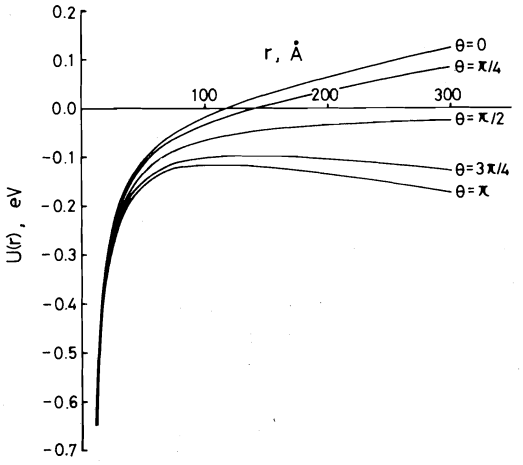

FIG. 3. Potential energy curves of an electron in the presence of an external electric field. $E = 50$ kV/cm; $\varepsilon = 2.2$.

of the external electric field. Figure 3 illustrates the potential energy curves for several values of θ at $E = 50$ kV cm^{-1}. The curve for $\theta = \pi/2$ is identical to that in the absence of an external electric field. The potential energy increases monotonously with increasing separation distance for $0 \leqq \theta \leqq \pi/2$, and it goes through a maximum for $\pi/2 \leqq \theta \leqq \pi$, where the distance, r_m, at which the potential energy is maximum, depends on θ. The recombination times, τ_1 and τ_2, of thermalized electrons with positive ions can be calculated separately in the two regions of potential energies corresponding to $0 \leqq \theta \leqq \pi/2$ and $\pi/2 \leqq \theta \leqq \pi$, respectively. The motion of thermalized electrons at 77 K can be described to a good approximation by the Nernst–Einstein relation, neglecting the random diffusion of electrons due to their thermal motion. The Nernst–Einstein relation is given by eq. 2.

$$[2] \qquad \frac{\partial r/\partial t}{-\partial U(r)/\partial r} = \frac{D}{kT}$$

where D, k, and T are the diffusion constant of an electron, Boltzmann's constant, and the absolute temperature, respectively. The diffusion constant is related to the electron mobility, μ, by $D = kT\mu/e$. The value of μ was taken as 0.1 cm^2 V^{-1} s^{-1}, which was the measured electron mobility in 3-methylpentane glass at 77 K (12). Equation 3 gives $-\partial U(r)/\partial r$ under an external electric field.

$$[3] \qquad -\partial U(r)/\partial r = (-e^2/\varepsilon r^2) - eE\cos\theta$$

Substituting eq. 3 into eq. 2, we get

$$[4] \qquad \partial r/\partial t = (D/kT)[(-e^2/\varepsilon r^2) - eE\cos\theta]$$

The recombination time, τ, of the thermalized electron with the positive ion can be written as eq. 5 by integrating eq. 4.

$$[5] \qquad \tau = -\frac{kT\varepsilon}{De^2}\int_r^0 \frac{dr}{(1/r^2) + (\varepsilon E\cos\theta/e)} = -\frac{kT\varepsilon}{De^2}(e/\varepsilon E\cos\theta)\int_r^0 \left[1 - \frac{(e/\varepsilon E\cos\theta)}{(e/\varepsilon E\cos\theta) + r^2}\right] dr$$

Performing the integration of eq. 5, we get eqs. 6 and 7 for the two regions of θ, respectively.

$$[6] \qquad \tau_1 = \left(\frac{1}{Dr_c}\right)\left(\frac{e}{\varepsilon E\cos\theta}\right)[r - \sqrt{e/\varepsilon E\cos\theta}\,\tan^{-1}(\sqrt{\varepsilon E\cos\theta/e}\,r)] \qquad \text{for } 0 \leqq \theta \leqq \pi/2$$

$$[7] \qquad \tau_2 = \left(\frac{1}{Dr_c}\right)\left(\frac{e}{\varepsilon E\cos\theta}\right)\left[r + \tfrac{1}{2}\sqrt{-e/\varepsilon E\cos\theta}\,\ln\frac{\sqrt{-e/\varepsilon E\cos\theta} - r}{\sqrt{-e/\varepsilon E\cos\theta} + r}\right]$$
$$\text{for } \pi/2 \leqq \theta \leqq \pi,\ r \leqq r_m$$

where $r_c = e^2/\varepsilon kT$ ($\varepsilon = 2.2$). It is assumed that all the thermalized electrons at $\pi/2 \leqq \theta \leqq \pi$ and initial separation distances $r > r_m$ have escaped from the positive ion, since in this case $\partial U(r)/\partial r < 0$. Thus, the theoretical yield of trapped electrons in the presence of an external electric field can be expressed as

$$[8] \qquad G(e_t^-)^E = G_t\left[\int_0^{\pi/2}\int_0^{\infty} f(r)\{1 - \exp(-k_T\tau_1)\}2\pi\sin\theta\, d\theta\, r^2\, dr + \int_{\pi/2}^{\pi}\int_0^{r_m} f(r)\{1 - \exp(-k_1\tau_2)\}2\pi\sin\theta\, d\theta\, r^2\, dr + \int_{\pi/2}^{\pi}\int_{r_m}^{\infty} f(r)2\pi\sin\theta\, d\theta\, r^2\, dr\right]$$

where $r_m = \sqrt{-e/\varepsilon E\cos\theta}$; k_T represents the electron trapping rate, which was determined by equating the theoretical value of $G(e_t^-)^0$ in eq. 8 to the experimental value of $G(e_t^-)^0 = 1.1$ in the absence of an external electric field; G_t is the total yield of thermalized electrons. The value of G_t in hydrocarbon glasses is not known at present. Since the glass and the liquid are both disordered systems and the density of glasses is only slightly higher than that of liquids, electron energy loss processes, leading to ionization, in glasses would be similar to those in liquids. Therefore, it seems reasonable to assess the value of G_t in hydrocarbon glasses on the basis of the value of G_t in hydrocarbon liquids. Although the value of G_t in hydrocarbon liquids is not exactly known, it is considered to lie in the range 4–5 from several investigations (13–18). Thus, we have assumed $G_t = 4.2$ in the present calculations. This value is also close to the gas

phase value. $f(r)$ is the initial spacial distribution function of thermalized electrons. In the present calculations we have used a modified exponential distribution function (eq. 9).

$$[9] \quad f(r) = \frac{n+1}{4\pi n b r^2} \times [1 - \exp(-nr/b)] \exp(-r/b)$$

where b and n are adjustable parameters, and $\int_0^\infty f(r) 4\pi r^2 \, dr = 1$. This function behaves like a simple exponential distribution function $f(r) = (1/4\pi b r^2) \exp(-r/b)$ for large values of r, and the value of $4\pi r^2 f(r)$ becomes zero at $r \fallingdotseq 0$. The property of this function appears to be more realistic than that of the simple exponential distribution function at $r = 0$. Equation 9 reduces to the simple exponential distribution function for $n \to \infty$. The mean range, $\bar{r}$, of thermalized electrons can be derived from eq. 9 as

$$[10] \quad \bar{r} = \left(\frac{n+2}{n+1}\right) b$$

A number of studies have been made on the spacial distribution function of thermalized electrons in liquid hydrocarbons (19–22). Gaussian functions and exponential functions are the most representative types of electron distribution functions used in such studies. A one-parameter Gaussian function gives too low values for G_t when its parameter is adjusted so that the theoretical curves best fit the experimental curves for the electric field dependence of free ion yields (22). On the other hand, a one-parameter simple exponential function gives too high values for G_t (22). A Gaussian-power function gives better theoretical results, but still somewhat too low values for G_t (22). Our two-parameter modified exponential function can well account for the electric field dependence of free ion yields in several liquid hydrocarbons with reasonable values of G_t.[1] Thus, we have applied the modified exponential distribution function to thermalized electrons in a hydrocarbon glass.

The first term of eq. 8 represents the yield of trapped electrons arising from the region $0 \leqq \theta \leqq \pi/2$, and the second and third terms give the trapped electron yield from the region $\pi/2 \leqq \theta \leqq \pi$. It can be shown that the calculated relative yield of trapped electrons reproduces well the observed relative yield of trapped electrons at each applied field strength by using the two common parameters, b and n, of the electron distribution function.

[1]T. Kimura and K. Fueki. Unpublished results.

TABLE 1. Electron trapping rate and the mean range of the thermalized electron distribution in 2-methylpentane at 77 K

n	b (Å)	$\bar{r}$ (Å)	k_T (s^{-1})
1.0	75	113	3.2×10^9
1.0	72	108	3.6×10^9
1.0	70	105	4.0×10^9
0.1	55	105	3.9×10^9

Comparison of the calculated trapped electron yield with the experimental one is made in Fig. 2. The curves show the calculated $G(e_t^-)^E/G(e_t^-)^0$ plotted against the applied electric field, where $G(e_t^-)^E$ and $G(e_t^-)^0$ are the trapped electron yields in the presence and absence of an external electric field, respectively. The solid curves a, b, and c show the theoretical curves for $n = 1.0$ and for $b = 75$, 72, and 70 Å, respectively. The dashed curve was obtained for $n = 0.1$ and $b = 55$ Å. It can be seen from Fig. 2 that the calculated $G(e_t^-)^E/G(e_t^-)^0$ increases almost linearly with increasing applied field strength except at low field strengths, and this is in accord with the experimental results. The solid curve b and the dashed curve best fit the experimental data. Table 1 shows the calculated values of the mean range, $\bar{r}$, of the initial electron distribution and the electron trapping rate, k_T, determined so as to be consistent with the observed yield of trapped electrons. The average time required for electron trapping in 2MP glass may be given by $1/k_T$ which is $\sim 3 \times 10^{-10}$ s. The mean range, $\bar{r}$, is 100–110 Å for both values of $n = 1.0$ and 0.1. In a paramagnetic relaxation study of trapped electrons, Lin and Kevan (5) concluded that the average distance of trapped electrons from other paramagnetic species in 3-methylpentane glass at 77 K was greater than 130 Å. It should be noted, however, that the mean range obtained in the present work is associated with the initial distribution of thermalized electrons, while the trapped electron distribution as studied by paramagnetic relaxation is associated with the distribution of stably trapped electrons. Therefore, it is reasonable that our value of the electron range is somewhat less than that ob-

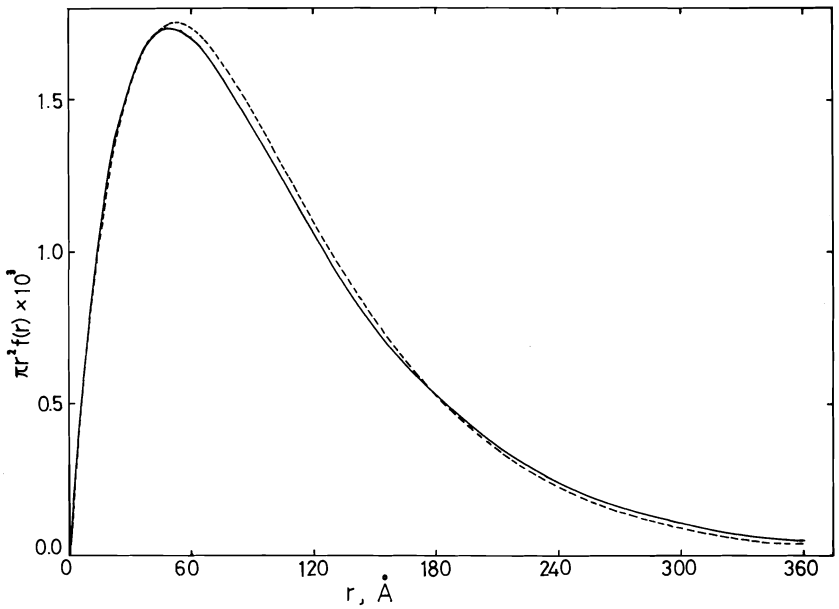

FIG. 4. Distribution functions of thermalized electrons: (—) $n = 1.0$, $b = 72$ Å, (---) $n = 0.1$, $b = 55$ Å.

tained by Lin and Kevan. It is interesting to note that the shape of the electron distribution function is almost the same, in spite of the large difference in the n values used. Figure 4 shows the electron distribution functions used to calculate the yield of trapped electrons which agree well with the experimental results, where the parameters $n = 1.0$ and $b = 72$ Å (solid curve) and $n = 0.1$ and $b = 55$ Å (dashed curve) are used. The close similarity of the electron distribution functions in Fig. 4 indicates that the electron distribution function obtained in the present calculation is appropriate for describing the spacial distribution of thermalized electrons within the framework of the modified exponential distribution function.

Acknowledgement

This work was partially supported by the Nagoya University Computing Center.

1. W. H. HAMILL. *In* Radical ions. *Edited by* E. T. Kaiser and L. Kevan. Wiley-Interscience, New York, NY. 1968. Chapt. 9.
2. J. E. WILLARD. *In* Fundamental processes in radiation chemistry. *Edited by* P. Ausloos. Wiley, New York, NY. 1968. Chapt. 9.
3. L. KEVAN. *In* Advances in radiation chemistry. Vol. 4. *Edited by* M. Burton and J. L. Magee. Wiley-Interscience, New York, NY. 1974. pp. 181–305.
4. D. R. SMITH and J. PIERONI. J. Phys. Chem. **70**, 2379 (1966).
5. D. P. LIN and L. KEVAN. J. Chem. Phys. **55**, 2629 (1971).
6. M. SHIROM, R. F. CLARIDGE, and J. E. WILLARD. J. Chem. Phys. **47**, 286 (1969).
7. M. A. BONIN, J. LIN, K. TSUJI, and F. WILLIAMS. Adv. Chem. Ser. **82**, 269 (1968).
8. J. LIN, K. TSUJI, and F. WILLIAMS. J. Am. Chem. Soc. **90**, 2766 (1968).
9. C. CHACHATY. J. Chim. Phys. **64**, 614 (1967).
10. T. KIMURA, N. BREMER, and J. E. WILLARD. J. Chem. Phys. **66**, 1127 (1977).
11. N. KATO, T. KIMURA, and K. FUEKI. J. Chem. Phys. **65**, 5020 (1976).
12. Y. MARUYAMA and K. FUNABASHI. J. Chem. Phys. **56**, 2342 (1972).
13. J. M. WARMAN, K.-D. ASMUS, and R. H. SCHULER. J. Phys. Chem. **73**, 931 (1969).
14. J. M. WARMAN and S. J. RZAD. J. Chem. Phys. **52**, 485 (1970).
15. S. J. RZAD and K. M. BANSAL. J. Phys. Chem. **76**, 2374 (1972).
16. N. H. SAGERT, J. A. REID, and R. W. ROBINSON. Can. J. Chem. **47**, 2655 (1969).
17. M. TANAKA and K. FUEKI. J. Phys. Chem. **77**, 2524 (1973).
18. G. R. FREEMAN and T. E. M. SAMBROOK. J. Phys. Chem. **78**, 102 (1974).
19. W. F. SCHMIDT and A. O. ALLEN. J. Phys. Chem. **72**, 3730 (1968).
20. J.-P. DODELET, K. SHINSAKA, U. KORTSCH, and G. R. FREEMAN. J. Chem. Phys. **59**, 2376 (1973).
21. G. G. ABELL and K. FUNABASHI. J. Chem. Phys. **58**, 1079 (1973).
22. J. CASANOVAS, R. GROB, D. BLANC, G. BRUNET, and J. MATHIEU. J. Chem. Phys. **63**, 3673 (1975).

Synthetic applications of the photochemically induced addition of oxycarbinyl species to α-enones. Part I. The addition of simple alcohols[1,2]

BERT FRASER-REID, NEVILLE LEWIS HOLDER, DAVID ROY HICKS, AND DAVID LOUIS WALKER

Guelph-Waterloo Centre for Graduate Work in Chemistry, Waterloo Campus, University of Waterloo, Waterloo, Ont., Canada N2L 3G1

Received April 11, 1977

BERT FRASER-REID, NEVILLE LEWIS HOLDER, DAVID ROY HICKS, and DAVID LOUIS WALKER. Can. J. Chem. **55**, 3978 (1977).

The photochemically induced conjugate addition of simple alcohols to a variety of α-enones has been investigated. With hex-2-enopyranosid-4-uloses (**1**), the alkylations occur from the less-hindered side and are completely stereo- and regioselective. The resulting 1,4-ketoalcohols (**2**) are readily cyclized to α-cyclopropyl ketones which have been prepared by alternative, less desirable routes. Alkylative additions of hex-1-enopyran-3-uloses occur also although less readily and without stereospecificity, giving *C*-glycosides. 2-Cyclohexenone and carvone are also photoalkylated by methanol giving moderate yields of the 1,4-ketols. In the case of carvone, carvone camphor was not detected as a by-product. Steroidal α-enones and mesityl oxide both fail to be photoalkylated by methanol.

BERT FRASER-REID, NEVILLE LEWIS HOLDER, DAVID ROY HICKS et DAVID LOUIS WALKER. Can. J. Chem. **55**, 3978 (1977).

L'addition conjuguée photochimiquement induite d'alcools simples à une variété d'énones-α est étudiée. L'alkylation des hexéno-2 pyrannosiduloses-4 (**1**) a lieu sur le côté le moins encombré de la molécule et est complètement stéréo et régiosélective. Les cétoalcools-1,4 (**2**) résultants sont ensuite cyclisés en α-cyclopropyl cétones lesquelles ont été préparées par des routes moins désirables. L'addition par alkylation des hexéno-1 pyrannuloses-3 se produit aussi quoique moins facilement et sans stéréospécificité, conduisant à des *C*-glycosides. La cyclohexène one-2 et la carvone sont aussi photoalkylées par le méthanol conduisant avec un rendement moyen aux cétols-1,4. Dans le cas de la carvone, la carvone-camphre n'est pas détectée comme produit secondaire. Les énones-α dans la série des stéroïdes ainsi que l'oxyde de mésityle ne sont pas photoalkylés par le méthanol.

[Traduit par le journal]

The ready availability in recent years of carbohydrate α-enones (1) has prompted the use of these versatile compounds in a variety of syntheses (see for example ref. 2). Conjugate-addition–alkylation of these enones offers simple access to biologically important branched-chain sugars, and hence we undertook an examination of a number of such reactions (3). In an accompanying paper (4) we report our results on the stereochemical course of copper-induced addition of organometallic reagents to some carbohydrate enones. In this and the following paper (5) we describe the photoinduced addition of oxycarbinyl species to these enone receptors.

The photoinduced addition of alcohols to α-enones is not popular, although it dates back to 1957 when, in connection with a synthesis of terebic acid, Schenck *et al.* added isopropanol to maleic acid (6). The reaction has been of interest to photochemists (7) but prior to our own work (3) there was only one recorded investigation of its synthetic utility (8), and the results therefrom were not encouraging. In this and the accompanying paper (5), it will be shown that the photoalkylation reaction is a simple and highly promising method of carbon–carbon bond formation. Experiments to determine some mechanistic aspects of these reactions are currently underway and will be reported in the future.

Additions to Alkyl Hex-2-enopyranosid-4-uloses (1)

Photoalkylation was effected by irradiating the enones (**1**) derived from D-glucose in methanol[3] containing benzophenone at 350 nm. In the case of the keto alcohol **1***a*, a single 1,4-

[1]For preliminary accounts of this work see ref. 3.

[2]Taken in part from the Ph.D. Theses (University of Waterloo) of N.L.H. (1972) and D.R.H. (1975), and the M.Sc. Thesis of D.L.W. (1975).

[3]For the addition of species other than methanol see the accompanying paper (5).

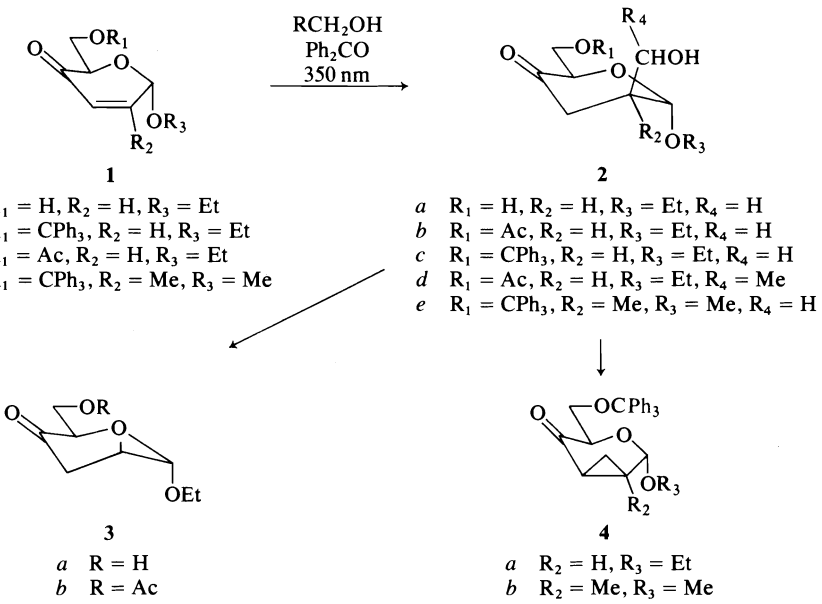

SCHEME 1

adduct, **2***a*, was isolated in 66% yield after chromatography. For characterization **2***a* was (*i*) acetylated and converted to the 2,4-dinitrophenylhydrazone, (*ii*) converted to a di-*p*-nitrobenzoate, and (*iii*) converted to a di-*O*-trityl derivative.

The tritylated (**1***b*) and acetylated (**1***c*) enones were similarly photoalkylated with methanol to give **2***c* (75% yield) and **2***b* (50% yield) respectively, and the adducts were readily correlated with those described in the preceding paragraph. In all cases there were variable amounts (5–16%) of carbohydrate-aromatic contaminants which were removed during the chromatographic separation.

Addition of ethanol to the enone acetate **1***c* gave a 50% yield of the adduct **2***d* which was characterized by formation of a crystalline derivative.

In order to correlate the stereochemistries of the products of photoalkylation with those obtained from cuprate additions (4), the primary alcohol in the adduct **2***b* was converted to a methyl group via tosylation, iodinolysis, and hydrogenolysis. The resulting acetate **3***b* was prepared alternatively by acetylation of the cuprate adduct **3***a* described in the accompanying paper (4).

Thus both modes of alkylation proceeded with the same stereoselectivity. However the ^{1}H nmr spectrum did not allow an unambiguous assignment of orientation. Thus in compound **2***a*, H-1 was located around 4.8 ppm with a coupling constant, $J_{12} \cong 4.0$ Hz. This value seemed to indicate *cis* hydrogens (i.e. axial H-2) as in α-D-*gluco* derivatives (9).[4] However, when the primary hydroxyl group in **2***c* was tosylated and the product treated with base, the *lyxo*-cyclopropyl ketone **4***a* was formed rapidly and in virtually quantitative yield. Compound **4***a* and the related *ribo* diastereomer (cf. **7**) have both been prepared in this laboratory (10).

The effect of substitution at the β-carbon upon the course of the photoalkylation was assessed by use of enone **1***d*. Addition of methanol gave a 61% yield of **2***e* which was cyclized to **4***b* in the previously described manner. In order to confirm the structure of **4***b* the diastereomer **7** was synthesized as shown in Scheme 2. In view of the stereochemistry of Simmons–Smith cyclopropanation of olefins such as **5** (11), *ribo* configuration of **7** is assured. Thus the presence of a β-substituent on the α-enone system does not affect the stereochemistry of the photoalkylation.

Additions to Hex-1-enopyran-3-uloses (8–11)

In view of the successful experiments detailed above, we decided to examine additions to the hex-1-enopyran-3-uloses since, if the reactions

[4]This conclusion was reached erroneously in our preliminary communication (3*a*).

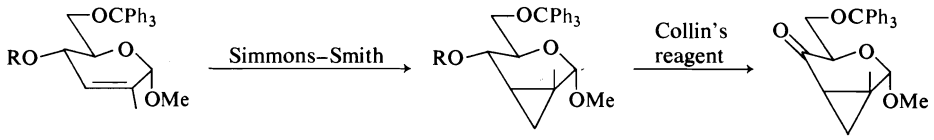

5
a R = H
b R = Ac

6
a R = H
b R = Ac

7

SCHEME 2

proceeded with the same degree of regioselectivity, this would offer a simple entry into *C*-glycosyl compounds.[5] The latter are of current interest for the elaboration of biologically important nucleoside analogues (for reviews see ref. 13).

The enones **8–11** required in this study had been synthesized previously either by Collins *et al.* (14) and (or) ourselves (15).

Irradiation of enone **8** in methanol containing benzophenone for 6 h afforded two polar products (**12** + **13**) which were isolated as a mixture by chromatography. The formation of a trityl ether indicative of a primary alcohol suggested that the desired photoalkylation had occurred, but the yield of material was low (~45%) and there seemed to be little hope of resolving the two products.

The isopropylidene analogue **9** proved even less encouraging in that the mixture of alcohols was obtained in 25% yield.

The conformationally mobile systems **10** and **11** were next investigated.[6] Enone **10** yielded only ~40% of a substance which could have been an addition product of methanol. However, the results with **11** were more encouraging. Thus the product from irradiation of **11** in methanol for 12 h was chromatographed, and a crystalline material was obtained in 65% yield. The mass spectrum showed a molecular ion at *m/e* 460 as expected for the methanol adduct. However, the melting point range (157–165°C) suggested a mixture (**14***a* + **15***a*). This was supported by the presence, in the nmr spectrum, of two overlapping doublets ($\delta \sim 5.5$) assignable to H-6 of the proposed structures.

In an attempt to achieve fractionation, the mixture was detritylated and, in order to remove any confusion arising from acetyl migration, the product was converted to the triacetates (**14***b* + **15***b*), but these also were unresolved on thin layer chromatograms.

Attempts to obtain the triols by deacetylation of the triacetate mixture revealed that the compounds in this series (**14** and **15**) are labile to base. Reduction of the ketone gave base-stable products but the reduction was not stereoselective and therefore of little use. A mode of base-induced fragmentation which necessitates a carbonyl group at C-4 is expressed in **16**.

Finally resolution of **14***a* + **15***a* was achieved using the method of 'short-fat' column chromatography (16). Recovery from the column was only 80%, but components **14***a* and **15***a* were obtained as crystalline substances, mp 171–173°C and 175–177°C respectively, in the ratio 7:3.

Structural assignments were made by studying the signals for H-2, H-3*a* and H-3*e* in the 220 MHz spectra of the derived acetates **14***c* and **15***c*, the coupling constants being determined by double irradiation. In each case, the *geminal* H-3 protons were identified as two double doublets with common coupling constants of 16.0 Hz in **14***c*, and 14.4 Hz in **15***c*. For the latter isomer H-3*a* should show an additional large coupling for $J_{2,3a}$, while H-3*e* should show a corresponding small coupling. Accordingly the signal with the additional coupling $J_{2,3a}$ of 12.0 Hz at 2.72 ppm was ascribed to H-3*a*, while that with the smaller coupling ($J_{2,3e}$) of 2.8 Hz at 2.58 ppm was ascribed to H-3*e*.

Similar reasoning when applied to the major photoproduct **14***c* gives H-3*a* at 2.94 ppm ($J_{2,3a}$ = 7.0 Hz), and H-3*e* at 2.53 ppm ($J_{2,3e}$ = 2.5 Hz), $J_{3a,3e}$ being 16.0 Hz.

Further evidence substantiating the above assignment was obtained from the ^{13}C nmr spectra of the triacetates **14***b* and **15***b*. Carbons 2, 3, and 5 are α, β, and δ, respectively, to the C-1 substituent and should be more shielded in the axial than in the equatorial adduct. Accord-

[5]For some other syntheses of *C*-glycosyl compounds see ref. 12.

[6]Possible effects of conformational mobility of these receptors in photoalkylation reactions are currently being examined and will be discussed in future publications.

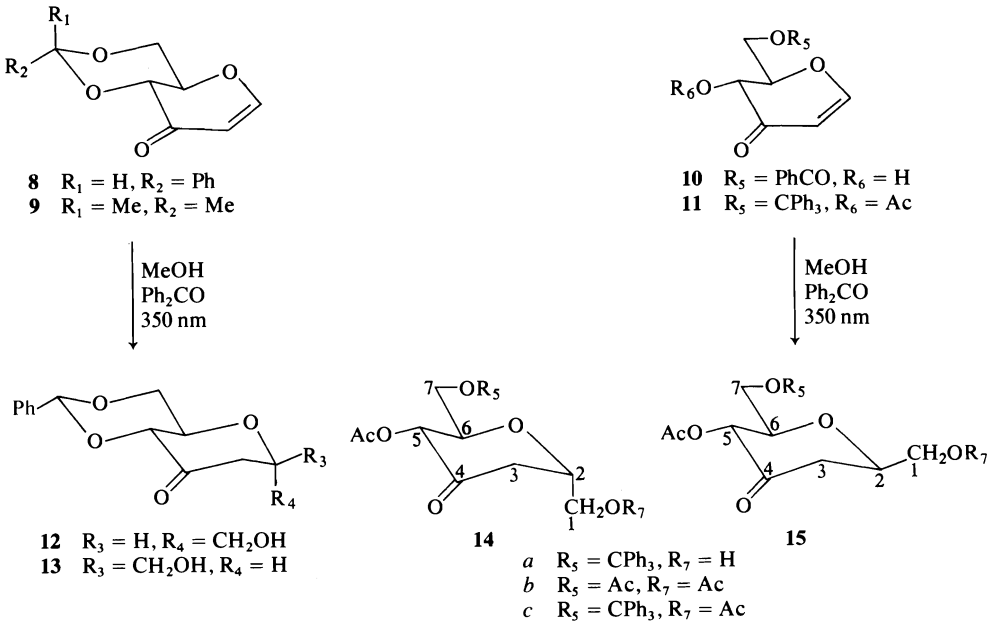

SCHEME 3

ingly, the resonances for C-2, -3, and -5 are at 72.4, 41.6, and 73.0 ppm respectively in **14***b* and, at 75.2, 43.5, and 77.2 ppm in **15***b*.

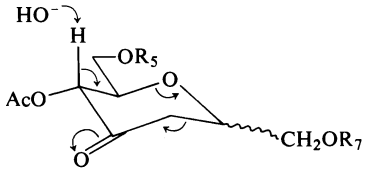

16

Photoalkylation of Some Noncarbohydrate Enones

There have been only a few reported instances where the photoinduced alkylation described herein has been applied to carbocyclic enones. Following Schenck *et al.*'s addition of isopropanol to maleic acid (6), the same alcohol was added to cyclopentenone (7*a*), a steroidal enone (8), and addition of methanol (7*e*) or ethanol (8) has been observed only rarely. Following upon our initial report (3*a*), Bundy (17) and Wissner (18) added methanol and *n*-octanol, respectively, to substituted cyclopentenones in connection with synthetic studies in the prostaglandin area.

In view of the foregoing successful additions to the carbohydrate enones, a sampling of noncarbohydrate enones was investigated.

Although benzophenone sensitized irradiation of 2-cyclohexenone in methanol was still incomplete after 25 h, the reaction was stopped because a large number of products was evident on tlc. The major product was isolated by chromatography in 33% yield and shown to be the known 3-hydroxymethylcyclohexanone, **17** (19).

With ethanol, the addition was complete within 24 h and there seemed to be fewer by-products. The keto alcohol **18** was isolated as a mixture of epimers in 33% yield and oxidized to the diketone **19** for characterization (20).

Carvone **20** was regarded as an interesting test case because of the ease with which cycliza-

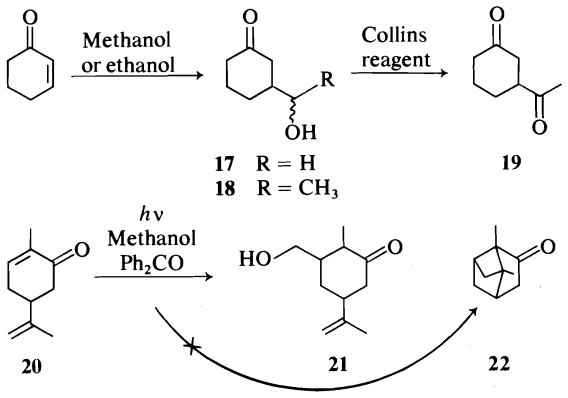

SCHEME 4

tion to carvone camphor, **22**, occurs in polar solvents (21). In fact the product mixture from the reaction of carvone with methanol showed no trace of carvone camphor prepared independently (21), judging from glc. Instead chromatographic fractionation afforded a 58% yield of keto alcohols judged to be a mixture of the diastereomers of **21** because of the overlapping doublets for the 2-methyl groups. Repeated careful fractionation afforded one of these diastereomers as a crystalline substance. Elemental analysis and spectroscopic data indicated the gross structure to be **21**, although the stereochemistry was not deduced.

Noteworthy failures in the alkylation with ethanol or methanol were the 1- and 4-cholestene-3-ones. The enones were consumed in both cases and a number of products were formed. However, these did not contain a hydroxyl group, judging from the infrared spectrum. Crotonaldehyde and mesityl oxide similarly failed to give any evidence of photoalkylation.

Experimental

Melting points were determined in capillary tubes in a Mel-Temp block and are uncorrected. Elemental analyses were performed by Micro-analyses Laboratory, Toronto, Ontario. The nmr spectra ($CDCl_3$, TMS) were determined on a Varian T-60, a Varian HA 100, or a Varian HR-220 spectrometer, the J values quoted being the spacing measured directly from the spectra. Infrared spectra were determined on a Beckman model IR-10 spectrometer using 0.1 mm sodium chloride solution cells (chloroform as solvent). Optical rotations were determined on a Carl Zeiss model LEP nür 370740 Lichtelektrishes Prazision polarimeter at 23°C.

Thin-layer chromatography was performed on glass plates coated with silica gel (HF-254, E. Merck) to a thickness of 0.3 mm. The following solvent systems were used to develop the plates; ethyl acetate – petroleum ether (30–60°C) (1:4); ethyl acetate – petroleum ether (30–60°C) (1:1); ethyl acetate; or benzene. For column chromatography E. Merck silica gel (0.063–0.20 mm, 70–230 mesh A.S.T.M.) was used.

General Conditions for Photoalkylation Reactions

The apparatus used was a Rayonet Photochemical Reactor (model RPR-100). A solution of the enone (1.0 mmol) and benzophenone (0.16 mmol) in the alcohol-addend (80 ml) was placed in a Pyrex photolysis cell equipped with a cold finger through which cold water was circulated. Nitrogen gas was bubbled into the solution through a glass capillary for 1 h to remove oxygen, and then the lamps (350 nm) were switched on, the gas flow being maintained. The reaction was monitored by tlc and when it was completed, the solvent was removed, and the residue chromatographed on a silica gel column in order to isolate the product.

Ethyl 2,3-Dideoxy-2-C-hydroxymethyl-α-D-threo-hexopyranosid-4-ulose, **2a**

A solution of enone **1a** (1.54 g, 8.9 mmol) (1*b*) and benzophenone (0.255 g, 1.44 mmol) in methanol (720 ml) was irradiated as described in the general procedure above. After 5 h the reaction was finished and chromatography on silica afforded compound **2a** (1.1 g, 66%) as a syrup. There were small amounts of slow-running material showing features of aromatic and carbohydrate compounds which were discarded. $R_f = 0.4$ in ethyl acetate; ir 3367, 1720 cm^{-1}; nmr (60 MHz) δ: 5.05 (d, 1, H-1, $J_{12} = 4.0$ Hz), 2.1–2.7 (m, 3, H-2, H-3*a*, H-3*e*), 4.20 (m, 1, H-5, $J_{56} = J_{56'} = 4.0$), 3.42–3.90 (m, 2, H-6, H′-6).

For the di-*p*-nitrobenzoate of **2a**: mp 134.5–135°C; $[\alpha]_D^{23}$ +75.04° (*c* 5, $CHCl_3$). *Anal.* calcd. for $C_{23}H_{22}N_2O_{11}$: C 54.97, H 4.41, N 5.57; found: C 54.85, H 4.13, N 5.06.

For the ditritylate of **2a**: mp 180.5–181°C; $[\alpha]_D^{23}$ +79.2° (*c* 2.5, $CHCl_3$). *Anal.* calcd. for $C_{47}H_{44}O_5$: C 81.94, H 6.43; found: C 81.57, H 6.60.

Ethyl 6-O-Acetyl-2,3-dideoxy-2-C-hydroxymethyl-α-D-threo-hexopyranosid-4-ulose, **2b**

The acetylated enone **1c** (1.73 g, 8.94 mmol) (1*b*) and benzophenone (0.255 g, 1.4 mmol) in methanol (720 ml) was irradiated as described in the general procedure for 5 h. Chromatographic fractionation on silica using ethyl acetate – petroleum ether (30–60°C) (1:1) afforded the major product **2b** (1.1 g, 50%) as well as slower-running material showing aromatic and carbohydrate features.

$R_f = 0.46$ in ethyl acetate – petroleum ether (1:1); nmr (60 MHz) δ: 5.01 (d, 1, H-1, $J_{12} = 4.0$ Hz), 2.2–2.9 (m, 3, H-2, H-3*a*, H-3*e*), 4.1–4.3 (m, 3, H-5, H-6, H′-6), 3.5–3.9 (m, 4, OCH_2CH_3 and OCH_2OH), 1.1 (t, 3, OCH_2CH_3).

For characterization, **2b** was acetylated and converted to the 2,4-dinitrophenylhydrazone, mp 146–148°C. *Anal.* calcd. for $C_{19}H_{24}N_4O_{10}$: C 48.72, H 5.16, N 11.96; found: C 48.87, H 4.94, N 12.21.

Ethyl 2,3-Dideoxy-2,3-C-methylene-6-O-triphenylmethyl-α-D-lyxo-hex-2-enopyranosid-4-ulose, **5a**

(*a*) The tritylated enone **1b** (1*b*) (2.5 g) was irradiated with benzophenone (500 mg) in methanol (400 ml) for 8.5 h in the usual manner described above. Fractionation on a silica column using ethyl acetate – petroleum ether (30–60°C) (1:1) afforded 1.97 g (75% yield) of **2c**. (This compound was identified by tritylation to the above-described ditritylate of **2a**).

A portion of the photoproduct **2c** (900 mg) was treated with a twofold excess of *p*-toluenesulfonyl chloride (800 mg) in pyridine (20 ml) and methylene chloride (10 ml) at 0°C overnight. Customary work-up gave the expected tosylate ($R_f = 0.68$ in 50% ethyl acetate – petroleum ether (30–60°C) which showed signs of being unstable.

The tosylate (0.81 g, 1.35 mmol) was dissolved in dry THF (50 ml) and a solution of diazabicyclononene (0.20 g, 1.6 mmol) in THF (10 ml) was added. After 0.5 h the solution was poured into ice water (50 ml) and extracted three times with chloroform. The chloroform was washed successively with dilute hydrochloric acid, water, and saturated sodium bicarbonate and then dried. The solu-

tion yielded **4***a* (0.53 g, 92%) having identical nmr spectra to the previously described material (10).

(*b*) Alternatively the tosylate described in (*a*) (180 mg) was refluxed in butanone (1.5 ml) with sodium iodide (310 mg) for 1.5 h when tlc indicated completion. The derived iodide (R_f = 0.76 in 50% ethyl acetate – petroleum ether (30–60°C)) (0.17 g) was dissolved in dry pyridine (4 ml), and silver fluoride (0.17 g) was added with stirring. The solution turned black immediately and a silvery mirror was deposited within minutes. Thin-layer chromatography (petroleum ether (30–60°C) – ethyl acetate (4:1)) after 5 min showed the absence of the starting iodide (R_f = 0.52) and one product of lower R_f (0.35). The reaction mixture was poured into ice water (10 ml) and extracted with diethyl ether (2 × 15 ml). The combined ether layers were washed with 5% hydrochloric acid (until the aqueous layer remained acidic), a sodium bicarbonate solution, and then dried over sodium sulphate. Subsequent evaporation afforded **4***a* (0.061 g, 36%).

(*c*) Silver fluoride (0.10 g, 4.25 mmol) was added to a stirred acetonitrile (5 ml) solution of the iodide described in (*b*) (0.105 g). The reaction was monitored by tlc (petroleum ether (30–60°C) – ethyl acetate (4:1)) and after 20 h was complete. The solution was filtered and evaporated and the resulting residue taken up in diethyl ether (20 ml) and filtered again. Evaporation of the ether after decolourization gave **4***a* (0.060 g, 78%).

Ethyl 6-O-Acetyl-2,3-dideoxy-2-C-[(R,S)-hydroxy(methyl)methyl]-α-D-threo-hexopyranosid-4-ulose, **2***d*

A solution of the ketoacetate, **1***c* (1.5 g, 7.73 mmol) and benzophenone (0.200 g, 1.12 mmol) in ethanol (720 ml) was irradiated for 7 h when tlc indicated completion. The photoadduct **2***d* was isolated in the usual way (see general procedure above) and characterized by mesylation and then conversion to the 2,4-dinitrophenylhydrazone. For the latter derivative: mp 138–140°C; $[\alpha]_D^{23}$ +72.22° (*c* 5.2, $CHCl_3$). *Anal.* calcd. for $C_{19}H_{26}N_4SO_{11}$: C 44.09, H 4.86, N 10.82, S 6.19; found: C 44.07, H 5.10, N 10.72, S, 6.01.

The nmr spectrum of **2***d* shows two doublets ~5.0 ppm (J = 4 Hz for both), corresponding to the (*R*) and (*S*) configurations at the secondary alcohol.[7]

Methyl 2,3-Dideoxy-2-C-hydroxymethyl-2-C-methyl-6-O-triphenylmethyl-α-D-threo-hexopyranosid-4-ulose, **2***e*

A solution of enone **1***d* (0.246 g, 0.59 mmol) and benzophenone (0.020 g, 0.1 mmol) dissolved in methanol (50 ml) was irradiated in the manner described above. After 5.5 h tlc indicated that no starting material remained and that a new compound, R_f 0.24 in ethyl acetate – petroleum ether (30–60°C) (1:4), had been formed. After evaporation of the solvents the residue was chromatographed on a silica gel column using the same solvent mixture. Compound **2***e* (0.163 g, 61%) was recovered as a syrup; $[\alpha]_D^{23}$ +27.4° (*c* 2.08, $CHCl_3$); ir ν_{max}: 3430 (OH), 1720 (C=O) cm^{-1}; ms *m/e*: 369 (M^+ − Ph), 203 (M^+ − Tr); nmr (60 MHz) δ: 5.56 (s, 1, H-1), 2.0–2.35 (m, 2, H-3*a*, H-3*e*), 4.20 (m, 1, H-5), 3.5–3.8 (m, 2, H-6, H′-6), 0.98 (s, 3, CCH_3), 3.5–3.8 CH_2OH.

Methyl 2,3-Dideoxy-2-C-methyl-2,3-C-methylene-6-O-triphenylmethyl-α-D-lyxo-hexopyranosid-4-ulose, **4***b*

The tritylated photoproduct **2***e* (0.122 g, 0.25 mmol) was dissolved in dry pyridine (5 ml) and *p*-toluenesulphonyl chloride (0.190 g, 1.0 mmol) was added. The reaction mixture was placed in an oil bath (45°C) and stirred for 4 h. At this time, no starting material remained (tlc) and a new compound, R_f = 0.42 in ethyl acetate – petroleum ether (30–60°C) (1:4), had been formed. The cooled reaction mixture was poured into ice water (50 ml) and extracted with ether (50 ml). The ether layer was washed successively with a 5% hydrochloric acid solution (50 ml), a saturated sodium bicarbonate solution (50 ml), and water (50 ml) and then dried over sodium sulphate. The residue obtained upon evaporation of the solvent weighed 0.068 g (65%). Compound **4***b* was a syrup which gave the following data: ir ν_{max}: 1695 (ketone conjugated to cyclopropyl ring) cm^{-1}; ms *m/e*: 351 (M^+ − Ph), 185 (M^+ − Tr); nmr δ: 0.9–1.3 (m, 2, cyclopropyl methylene), 1.25 (s, 3, C—CH_3) 1.90 (m, 1, H-3), 3.41 (s, 3, OCH_3), 3.40–3.80 (m, 2, H-6, -6′), 4.0 (t, 1, $J_{5,6}$ = $J_{5,6'}$ = 6.0 Hz, H-5), 4.95 (s, 1, H-1), 7.2–7.8 (m, 15, phenyl).

Methyl 2,3-Dideoxy-2-C-methyl-2,3-C-methylene-6-O-triphenylmethyl-α-D-ribo-hexopyranosid-4-ulose **7**

The alcohol **5***a* (1*a*) (1.0 g, 2.4 mmol) was dissolved in dry pyridine (10 ml) and cooled to 0°C in an ice bath. Acetic anhydride (1 ml) was added and the reaction mixture stirred for 6 h at 0°C. At this time, tlc indicated the formation of a new compound, R_f = 0.60 in ethyl acetate – petroleum ether (30–60°C) (1:4), and no starting material. The reaction mixture was worked up in the usual manner and afforded the syrupy acetate **5***b* (0.950 g, 86%). Significant nmr features were: δ 1.75 (m, 3, C—CH_3), 1.90 (s, 3, $OCOCH_3$), 3.2–3.4 (m, 2, H-6, -6′), 3.58 (s, 3, —OCH_3), 3.90–4.2 (m, 1, H-5), 4.8 (s, 1, H-1), 5.2–5.4 (m, 1, H-4), 5.58 (m, 1, H-3), 7.2–7.8 (m, 15, phenyl). The material (**5***b*) was used directly as follows.

Zinc/copper couple (0.500 g), methylene iodide (0.72 ml), one crystal of iodine, and dry diethyl ether (5 ml) were placed in a dry 25 ml round bottom flask. The acetate **5***b* (0.900 g, 1.96 mmol) dissolved in dry diethyl ether (5 ml) was added. After 24 h at reflux the starting material had all been consumed and tlc indicated that a new product, R_f = 0.18 in ethyl acetate – petroleum ether (30–60°C) (1:10), had been formed. The reaction mixture was diluted with ether (20 ml), washed with a saturated ammonium chloride solution (2 × 20 ml), a saturated sodium bicarbonate solution (20 ml), water (20 ml), and dried over sodium sulphate. The residue obtained upon evaporation of the solvent was chromatographed on a silica gel column to afford **6***b* (0.256 g, 28.4%). Significant nmr features were: δ 1.21 (s, 3, C—CH_3), 1.05–1.55 (m, 3, cyclopropyl), 1.85 (s, 3, —$OCOCH_3$), 3.10–3.85 (m, 3, H-5, -6, -6′), 3.50 (s, 3, —OCH_3), 4.87 (s, 1, H-1), 5.08 (dd, 1, $J_{4,5}$ = 10.0 Hz, $J_{3,4}$ = 5.0 Hz, H-4), 7.18–7.80 (m, 15, phenyl).

The crude cyclopropyl acetate **6***b* (0.225 g, 0.49 mmol) was dissolved in methanol (10 ml) and sodium carbonate

[7]For other examples and further discussion, see the accompanying paper (5).

(0.126 g) was added. The reaction mixture was stirred at room temperature for 4 h. At this time, tlc indicated that deacetylation was complete and a new product, $R_f = 0.21$ in ethyl acetate – petroleum ether (30–60°C) (1:4), had been formed. The reaction mixture was filtered and the residue obtained upon evaporation of the solvent was extracted with ethyl acetate. The ethyl acetate solution was filtered and evaporated to afford **6***a* (0.187 g, 89%). Compound **6***a* exhibited the following nmr features: δ 0.92–1.35 (m, 3, cyclopropyl), 1.05 (s, 3, C—CH_3), 1.96 (bs, 1, OH), 3.1–3.5 (m, 3, H-5, -6, -6′), 3.40 (s, 3, —OCH_3), 3.82 (dd, 1, $J_{4,5} = 10.0$ Hz, $J_{3,4} = 6.0$ Hz, H-4), 4.65 (s, 1, H-1), 7.10–7.6 (m, 15, phenyl).

The cyclopropyl alcohol **6***a* (0.175 g, 0.4 mmol) was dissolved in methylene chloride (10 ml). To this vigorously stirred solution was added the chromium trioxide – dipyridine complex (1.05 g, 4.0 mmol). After 1 h at room temperature tlc indicated the reaction was complete and a new compound $R_f = 0.37$ in ethyl acetate – petroleum ether (30–60°C) (1:4) had been formed. The reaction mixture was diluted with ether (40 ml) and stirred for an additional 15 min. The solution was then filtered through a bed of Celite. The filtrate was washed with a 5% hydrochloric acid solution (30 ml), a saturated sodium bicarbonate solution (30 ml), and water (30 ml). The organic layer was then decolourized, dried over anhydrous sodium sulphate, and evaporated to give **7** (0.142 g, 83%). Compound **7** was a syrup which gave the following data: ir ν_{max}: 1690 (ketone conjugated to cyclopropyl ring) cm^{-1}; ms *m/e*: 351 ($M^+ - Ph$), 185 ($M^+ - Tr$); nmr δ: 1.0–1.4 (m, 2, cyclopropyl methylene), 1.35 (s, 3, C—CH_3), 1.95 (m, 1, H-3), 3.40 (s, 3, OCH_3), 3.4–4.0 (m, 2, H-6, -6′), 4.2 (m, 1, H-5), 5.35 (s, 1, H-1), 7.2–7.8 (m, 15, phenyl).

*5-O-Acetyl-2,6-anhydro-3-deoxy-7-O-triphenylmethyl-*D*-arabino-hept-4-ulose,* ***14c*** *and 5-O-Acetyl-2,6-anhydro-3-deoxy-7-O-triphenylmethyl-*D*-ribo-hept-4-ulose,* ***15c***

4-*O*-Acetyl-6-*O*-triphenylmethyl-D-*erythro*-pyran-3-ulose **11** (2.0 g, 4.67 mmol) (16), and benzophenone (0.32 g, 1.7 mmol) were dissolved in methanol (800 ml) and irradiated in the usual manner for 12 h at which time tlc (ethyl acetate – petroleum ether (30–60°C) (1:1)) showed completion. The solvent was removed under reduced pressure and the resultant residue chromatographed to yield **14***a* and **15***a* as a mixture (1.35 g, 65%).

A portion of this product (0.70 g) was eluted through a short column (20 cm × 2.5 cm) of tlc silica gel using petroleum ether (30–60°C) – ethyl acetate (3:2). Upon identification of resultant fractions (nmr) **14***a* (0.397 g) and **15***a* (0.158 g) were isolated in a total recovery of 80%. Compound **15***a* constituted 30% of the mixture (20% yield from photolysis), **14***a* constituting 70% (45% yield from photolysis). Both **14***a* and **15***a* were recrystallized from cold ethanol.

For compound **14***a*: mp 171–173°C; $[\alpha]_D^{23}$ +168.2° (*c* 1.46, chloroform); *Anal.* calcd. for $C_{28}H_{28}O_6$: C 73.03, H 6.13; found: C 72.83, H 6.29.

For compound **14***c*: nmr (220 MHz) δ: 2.53 (dd, 1, $J_{3a,3e} = 16.0$ Hz, $J_{2,3e} = 2.5$ Hz, H-3*e*), 2.94 (dd, 1, $J_{2,3a} = 7.0$ Hz, H-3*a*), 3.13 (dd, 1, $J_{7e,7a} = 9.8$ Hz, $J_{6,7e} = 3.9$ Hz, H-7*e*), 3.48 (dd, 1, $J_{6,7a} = 2.0$ Hz, H-7a), 4.08 (dd, 1, $J_{1e,1a} = 12.2$ Hz, $J_{1e,2} = 3.8$ Hz, H-1*e*), 4.18 (m, 1, H-6), 4.45 (dd, 1, $J_{1a,2} = 7.0$ Hz, H-1*a*), 4.75 (m, 1, H-2), 5.50 (d, 1, $J_{5,6} = 10.0$ Hz, H-5).

For compound **15***a*: mp 171–173°C; $[\alpha]_D^{23}$ +293.4° (*c* 1.85, chloroform). *Anal.* calcd. for $C_{28}H_{28}O_6$: C 73.03, H 6.13; found: C 73.18, H 6.28.

For compound **15***c*: nmr (220 MHz) δ: 2.58 (dd, 1, $J_{3a,3e} = 14.4$ Hz, $J_{2,3e} = 2.8$ Hz, H-3*e*), 2.72 (dd, 1, $J_{2,3a} = 12.0$ Hz, H-3*a*), 3.12 (dd, 1, $J_{7e,7a} = 10.3$ Hz, $J_{6,7e} = 3.8$ Hz, H-7*e*), 3.49 (dd, 1, $J_{6,7a} = 1.7$ Hz, H-7*a*), 3.75 (dq, 1, H-6), 3.95 (m, 1, H-2), 4.30 (d, 2, $J_{1,2} = 4.6$ Hz, H-1*a*, H-1*e*), 5.47 (d, 1, $J_{5,6} = 10.0$ Hz, H-5).

Photoadditions to 2-Cyclohexenone. Compounds ***17*** *and* ***18***

2-Cyclohexenone (1.1g), benzophenone (150 mg), and methanol (600 ml) were irradiated for 24 h in the usual manner. The crude oily product was chromatographed on a silica gel column using ethyl acetate – petroleum ether (30–60°C) (1:1). Unreacted starting material (410 mg) was recovered, as well as the adduct **17** ($R_f = 0.21$), 308 mg (33% corrected for unreacted starting material).

In agreement with the literature (19*b*), the nmr spectrum of compound **17** shows (CCl_4) δ_{TMS}: 3.72 (d, 2, CH_2OH), 1.4–2.5 (m, 10, ring protons and O*H*); ir: 3400, 1705 cm^{-1}.

Similar reaction of 2-cyclohexenone (1.5 g), benzophenone (200 mg), and ethanol (800 ml) for 24 h, and subsequent chromatographic fractionation with ethyl acetate – petroleum ether (30–60°C) (1:1) afforded **18** (880 mg, 33%), $R_f = 0.47$. The 220 MHz nmr spectrum ($CDCl_3$) showed δ_{TMS}: 3.5 (m, 1 C*H*-OH), 2.0–2.46 (m, 4, CH_2COCH_2); ir: 3400, 1705 cm^{-1}. Compound **18** was oxidized to 3-acetyl cyclohexanone (20).

*Photoaddition of Methanol to Carvone (****20****)*[8]

Carvone (**20**) (1.26 g) and benzophenone (255 mg) were dissolved in methanol (700 ml) and irradiated for 34 h in the usual manner. Under these conditions carvone camphor (**22**) prepared independently (21) was not formed, judging by glc; however, if benzophenone was excluded, **22** was formed (21). The crude photoproduct was chromatographed on a silica column using ethyl acetate – petroleum ether (30–60°C) (1:2) in order to remove aromatic substances. A fraction (700 mg, 58%) was obtained which was consistent with the gross structure, **21** judging from nmr evidence. Refractionation afforded a pure isomer of **21**, which was crystallized from ether–hexane, mp 104.5–105°C; nmr (60 MHz, $CDCl_3$) δ_{TMS}: 4.78 (bs, 2, CH_2=C), 3.6 (m, 2 CH_2OH), 1.68 (bs, 3, CH_3—C=), 1.0 (d, 3, CH_3CH); ir: 3500 cm^{-1} (OH), 3090 (=CH_2), 1645 (C=C). *Anal.* calcd. for $C_{11}H_{18}O_2$: C 72.49, H 9.95; found: C 72.44, H 9.95.

Acknowledgements

We are very pleased to acknowledge financial support from the National Research Council of Canada, Environment Canada, and Bristol Laboratories (Syracuse).

[8]We are indebted to Mr. D. E. Iley for these experiments.

1. (*a*) D. R. HICKS and B. FRASER-REID. Can. J. Chem. **53**, 2017 (1975); (*b*) B. FRASER-REID, A. MCLEAN, E. W. USHERWOOD, and M. YUNKER. Can. J. Chem. **48**, 2877 (1970); (*c*) E. F. L. J. ANET. Carbohydr. Res. **1**, 348 (1966); (*d*) K. BOCK and C. PEDERSEN. Tetrahedron Lett. 2983 (1969); (*e*) O. ACHMATOWICZ, JR., P. BUKOWSKI, B. SZECHNER, Z. ZWEIZCHOWSKA, and A. ZAMOJSKI. Tetrahedron, **22**, 1973 (1971); (*f*) P. KOLL, T. SCHULTEK, and R.-W. RENNECKE. Chem. Ber. **109**, 337 (1976).
2. D. L. WALKER and B. FRASER-REID. J. Am. Chem. Soc. **97**, 6251 (1975); R. M. SRIVASTAVA, B. J. CARTHY, and B. FRASER-REID. Tetrahedron Lett. 2175 (1974); J. CLEOPHAX, S. D. GERO, and J. LEBOUL. J. Chem. Soc. Chem. Commun. 710 (1973); J. CLEOPHAX, J. LEBOUL, A. OLESKER, and S. D. GERO. Tetrahedron Lett. 4911 (1973).
3. (*a*) B. FRASER-REID, N. L. HOLDER, and M. B. YUNKER. J. Chem. Soc. Chem. Commun. 1286 (1972); (*b*) D. L. WALKER, B. FRASER-REID, and J. K. SAUNDERS. J. Chem. Soc. Chem. Commun. 319 (1974).
4. M. B. YUNKER, D. E. PLAUMANN, and B. FRASER-REID. Can. J. Chem. This issue.
5. B. FRASER-REID, R. C. ANDERSON, D. R. HICKS, and D. L. WALKER. Can. J. Chem. This issue.
6. G. O. SCHENCK, G. KOLTZENBURG, and H. GROSSMANN. Angew. Chem. **69**, 177 (1957).
7. (*a*) R. DOLOU, M. VILKHS, and M. PFAU. C. R. Acad. Sci. Ser. C. **249**, 429 (1959); (*b*) M. PFAU, R. DOLOU, and M. VILKHS. C. R. Acad. Sci. Ser. C, **254**, 1817 (1962); (*c*) P. DE MAYO, J. P. PETE, and M. TCHIR. Can. J. Chem. **46**, 2535 (1968); (*d*) D. BELLUS, D. R. KEARNS, and K. SCHAFFNER. Helv. Chim. Acta, **52**, 971 (1969); (*e*) W. C. AGOSTA and A. B. SMITH III. J. Am. Chem. Soc. **93**, 5513 (1971); (*f*) S. WOLFF, W. L. SCHREIBER, A. B. SMITH III, and W. C. AGOSTA. J. Am. Chem. Soc. **94**, 7797 (1972).
8. P. BLADON and I. A. WILLIAMS, J. Chem. Soc. C, 2032 (1967).
9. R. U. LEMIEUX, R. K. KULLNIG, H. J. BERNSTEIN, and W. G. SCHNEIDER. J. Am. Chem. Soc. **81**, 6098 (1958).
10. B. FRASER-REID and B. J. CARTHY. Can. J. Chem. **50**, 2928 (1972).
11. B. FRASER-REID and B. RADATUS. Can. J. Chem. **50**, 2909 (1972); H. E. SIMMONS and R. D. SMITH. J. Am. Chem. Soc. **80**, 5323 (1958); W. G. DAUBEN and G. H. BEREZIN. J. Am. Chem. Soc. **85**, 468 (1963); S. WINSTEIN and J. SONNENBERG. J. Am. Chem. Soc. **83**, 3235 (1961).
12. J. G. BUCHANAN, A. D. DUNN, and A. R. EDGAR. J. Chem. Soc. Perkin Trans. I, 68 (1976); H. OHRUI, G. H. JONES, J. G. MOFFATT, M. L. MADDOX, A. T. CHRISTENSEN, and S. K. BRYAN. J. Am. Chem. Soc. **97**, 4602 (1975); S. HANESSIAN and A. G. PERNET. Can. J. Chem. **52**, 1266 (1974); **52**, 1280 (1974); L. KALVODA, J. FARKAS, and F. SORM. Tetrahedron Lett. 2297 (1970); A. ROSENTHAL and H. J. KOCH. Can. J. Chem. **43**, 1375 (1965); K. MATSUURA, K. NISHIYAMA, K. YAMEDA, Y. ARAKI, and Y. ISHIDO. Bull. Chem. Soc. Jpn. **46**, 2538 (1973).
13. K. GERZON, D. C. DE LONG, and J. C. CLINE. Pure Appl. Chem. **28**, 489 (1971); R. J. SUHADOLNIK. Nucleoside antibiotics. Wiley-Interscience, New York, NY. 1970.
14. P. M. COLLINS, P. GUPTA, and R. IYER. J. Chem. Soc. C, 1670 (1972).
15. B. FRASER-REID, D. L. WALKER, S. Y.-K. TAM, and N. L. HOLDER. Can. J. Chem. **51**, 3950 (1973).
16. B. J. HUNT and W. RIGBY. Chem. Ind. London, 1868 (1967).
17. G. L. BUNDY. Tetrahedron Lett. 1957 (1975).
18. A. WISSNER. J. Org. Chem. **42**, 356 (1977).
19. (*a*) G. STORK and J. FICINI. J. Am. Chem. Soc. **83**, 4678 (1961); (*b*) C. ALEXANDRE and F. ROUESSAC. Bull. Chim. Soc. Fr. 1837 (1971).
20. E. J. COREY and L. S. HEGEDUS. J. Am. Chem. Soc. **91**, 4928 (1969); E. J. COREY and D. CROUSE. J. Org. Chem. **33**, 298 (1968); D. BILLUS, D. KEARNS, and K. SCHAFFNER. Helv. Chim. Acta, **52**, 971 (1969).
21. G. BUCHI and I. M. GOLDMAN. J. Am. Chem. Soc. **79**, 4741 (1957); J. MEINWALD and R. S. SCHNEIDER. J. Am. Chem. Soc. **87**, 5218 (1965).

Synthetic applications of the photochemically induced addition of oxycarbinyl species to α-enones. Part II.[1] The addition of ketals, aldehydes, and polyfunctional species[2,3]

BERT FRASER-REID, ROBERT CHARLES ANDERSON, DAVID ROY HICKS, AND DAVID LOUIS WALKER

Guelph-Waterloo Centre for Graduate Work in Chemistry, Waterloo Campus, University of Waterloo, Waterloo, Ont., Canada N2L 3G1

Received April 11, 1977

BERT FRASER-REID, ROBERT CHARLES ANDERSON, DAVID ROY HICKS, and DAVID LOUIS WALKER. Can. J. Chem. **55**, 3986 (1977).

Alcohols possessing an α-hydrogen, acetals, and aldehydes undergo photochemically induced conjugate addition to a variety of α-enones to give 1,4-ketols, 1,4-keto ketols and 1,4-diketones respectively. It appears that the aldehydes frequently succeed where acetals and alcohols fail, and acetals where alcohols fail. It is therefore possible to employ polyfunctional addenda and achieve addition at only one of the activated sites. The reactions are always regiospecific and are frequently completely stereoselective.

BERT FRASER-REID, ROBERT CHARLES ANDERSON, DAVID ROY HICKS et DAVID LOUIS WALKER. Can. J. Chem. **55**, 3986 (1977).

Les alcools possédant un hydrogène en α, les acétals et les aldéhydes subissent une addition conjuguée photochimiquement induite avec une variété d'énones-α pour conduire respectivement à des cétols-1,4, céto-cétols-1,4 et dicétones-1,4. Il apparait fréquemment que les aldéhydes réussissent où les acétals et alcools échouent, puis les acétals où les alcools échouent. Il est maintenant possible d'employer des produits polyfonctionnels fixés par addition et d'effectuer l'addition seulement à l'un des sites actifs. Les réactions sont toujours régiospécifiques et sont souvent complètement stéréosélectives.

[Traduit par le journal]

In the accompanying paper (1), we report several examples of the photochemically induced conjugate addition – alkylation of α-enones by simple alcohols. Other projects in our laboratory (2) required that the synthetic potential of these reactions be explored. In contemplating the utility of these products we were mindful of the recent work of Schlessinger and co-workers (3) who have shown that 1,4-dicarbonyl species can be extremely versatile synthons. Differentiation of the two hydroxyl groups could, at times, be advantageous as has been ably demonstrated by Stork and Jung (4). The appeal of the photoadducts is therefore apparent since, being at different oxidation levels, the 1,4-functionalities lend themselves to selective manipulation.

In view of the excellent promise of this simple, economical procedure in synthetic organic chemistry, we wondered whether more complex addenda could be attached in an equally undemanding experimental operation. In this paper we describe some results of these investigations.

In the previous studies (1), the reacting alcohol also served as the solvent, a requirement which obviously posed a severe limitation. However, it was found that cyclohexane or acetonitrile were excellent solvents, even though the ratio of addend to substrate still had to be very high (~40:1) for the reaction to proceed at a useful rate. For purposes of solubility, acetonitrile is our preferred solvent.

The readily prepared enone **1** (5) was our favorite substrate primarily because its photoalkylation reactions had been found to go with complete stereoselectivity (1), yielding the axial adduct at carbon-2.

Ethylene glycol, propane-1,3-diol, methyl hydracrylate, and methyl glycollate were chosen as polyfunctional alcohols for the studies summarized in Table 1 (entries 1–4). With ethylene glycol and the enone **1***a*, the ketodiol **3***a* was

[1]For Part I, see ref. 1.

[2]For preliminary accounts of this work, see refs. 9 and 12.

[3]Taken in part from the Ph.D. Thesis (University of Waterloo) of D.R.H. (1975) and M.Sc. Thesis of D.L.W. (1975).

TABLE 1. Benzophenone-induced addition of oxycarbinyl species to α-enones

Entry	Substrate	Addend	Time (h)	Product	Percent yield (after chromatography)
1	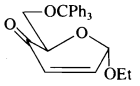 **1***a*	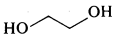	4	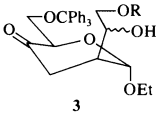 **3** *a* R = H *b* R = CPh_3	75–79
2	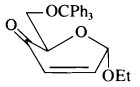 **1***a*	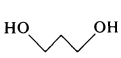	5	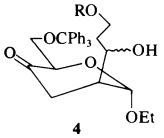 **4** *a* R = H *b* R = CPh_3	49
3	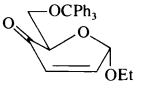 **1***a*	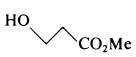	5.5	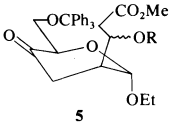 **5** *a* R = H *b* R = THP	32 R = H 74 R = THP
4	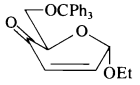 **1***a*	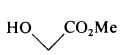	—	No adduct	
5	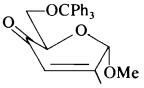 **2**	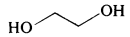	7	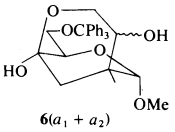 **6**(a_1 + a_2)	38 + 33
6	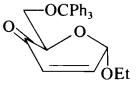 **1***a*	 **11**	2	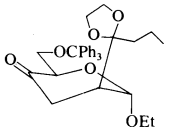 **12**	62
7	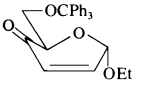 **1***a*	 **20**	4	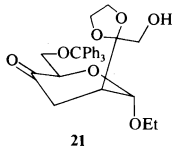 **21**	42
8	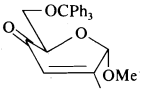 **2**	 **20**	48	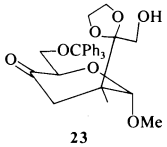 **23**	46
9	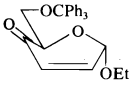 **1***a*	CH_3CHO	5	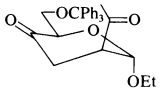 **24**	67

TABLE 1 (*Concluded*)

Entry	Substrate	Addend	Time (h)	Product	Percent yield (after chromatography)
10	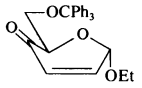 **1a**	PhCHO	2	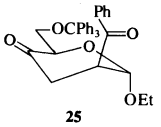 **25**	58
11	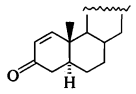 **27**	CH_3CHO	12	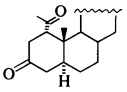 **28**	42
12		CH_3CHO	2	 **29**	31

obtained in 75–79% yield after chromatography. Similarly the photoadduct **4***a* was obtained in 49% yield.

The adduct with methyl hydracrylate (**5***a*) decomposed during silica column chromatography, and as a result the isolated yield was low (32%). If, however, the crude photoproduct was protected as the tetrahydropyranyl ether prior to chromatography, the adduct **5***b* could be isolated in 74% yield.

There was no evidence for photoaddition when methyl glycollate was used under the usual conditions (Table 1, entry 4).

The photoadducts **3***a*, **4***a*, and **5***a* showed hydroxyl and strong carbonyl absorptions in the infrared indicating that internal hemiacetal formation had not occurred. In support of this **3***a* and **4***a* were converted readily at room temperature to the ditritylates **3***b* and **4***b*. The photoproducts were, as expected, epimeric at the newly created secondary alcohol (C-7) and this was apparent from the presence of two doublets ~5 ppm for two anomeric protons, $J_{12} \cong 4.5 \pm 0.5$ Hz. The epimers were not resolved in any of these cases but oxidation of **3***b*, **4***b*, and **5***a* give the diketones **7**, **8**, and **9** respectively which now showed only one doublet ~5 ppm, $J_{12} \doteq 4.5$ Hz.

The photoproduct of enone **2** with ethylene glycol provided a contrast in that chromatography afforded two substances **6***a*$_1$ and **6***a*$_2$ in 38 and 33% yields respectively. These compounds were assigned hemiacetal structures because of the absence of ketonic absorption in the infrared and the fact that tritylation did not proceed at room temperature. However, at 50°C, reaction occurred slowly, requiring 36 h for complete formation of the corresponding ditritylates **6***b*$_1$ and **6***b*$_2$ as amorphous solids.

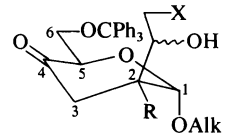

	Alk	R	X
3*a*	Et	H	OH
3*b*	Et	H	$OCPh_3$
4*a*	Et	H	CH_2OH
4*b*	Et	H	CH_2OCPh_3
5*a*	Et	H	CH_2CO_2Me
6*b*, **6***b*$_1$	Me	Me	$OCPh_3$

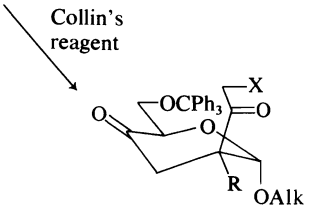

	Alk	R	X
7	Et	H	$OCPh_3$
8	Et	H	CH_2OCPh_3
9	Et	H	COOMe
10	Me	Me	$OCPh_3$

SCHEME 1

Each of the ditritylates **6***b*$_1$ and **6***b*$_2$ upon oxidation gave the same amorphous diketone **10** (Scheme 1).

In contemplating alternative methods for differentiating the 1,4-functionalities in the photo-

adducts we recalled the photosensitized addition of dioxolane to olefins, a reaction first demonstrated by Rosenthal and Elad (6). Its utility in the synthesis of branched-chain sugars has been explored by Jewel and Szarek (7) and Matsuura and co-workers (8). However, with these simple olefins, the additions are usually neither regio- nor stereoselective.

To our knowledge, there were no instances of alkylation of α-enones with acetals prior to our preliminary report (9). However, an example of *acid catalyzed intra*molecular addition (the outcome of which was a six-membered ring component of a linear tetracyclic molecule) had been reported by Barton and co-workers (10).

Attempts to alkylate **1***a* with dioxolane as solvent were abandoned because of the formation of a heavy oily residue from which the photoproduct could not be extricated. This problem was not encountered when 2-propyl-1,3-dioxolane (**11**) was used as a reagent (Table 1, entry 6). The ketone **12** was the sole product, its stereo- and regiochemistry being apparent from the appearance of the H-1 signal (5.12 ppm, $J_{12} = 4.0$ Hz).

However, the dioxolane could conceivably add to the receptor **1***a* either at the dioxycarbinyl site *a* giving **12**, or at the monoxycarbinyl site *b* giving an adduct such as **13** (Scheme 2). Had the latter been formed the nmr spectrum would have shown a signal of ~5 ppm for the acetal proton of the dioxolane residue. This was not observed.

Chemical proof for this aspect was desirable but the carbohydrate adducts were not suitable because of their lability to acid hydrolysis. Consequently it was decided to examine the reactions of 2-cyclohexenone (routes *d*, *e*, *f*) summarized in Scheme 3. Addition of ethanol to 2-cyclohexenone (**14**) gave a 40% yield of the previously described keto alcohol **15** (1) which upon oxidation gave a substance whose nmr data were identical to those published by Corey and co-workers (11) for the diketone **18**.

Alternatively addition of the dioxolane **16** gave a 54% yield of a substance judged to be **17** on the basis of nmr and mass spectral data. Furthermore acid hydrolysis gave the same diketone, **18**, obtained in route *d*. In order to detect whether a product such as **13** had been formed, the total photoproduct from reaction of **14** and **16** was hydrolyzed, and the crude

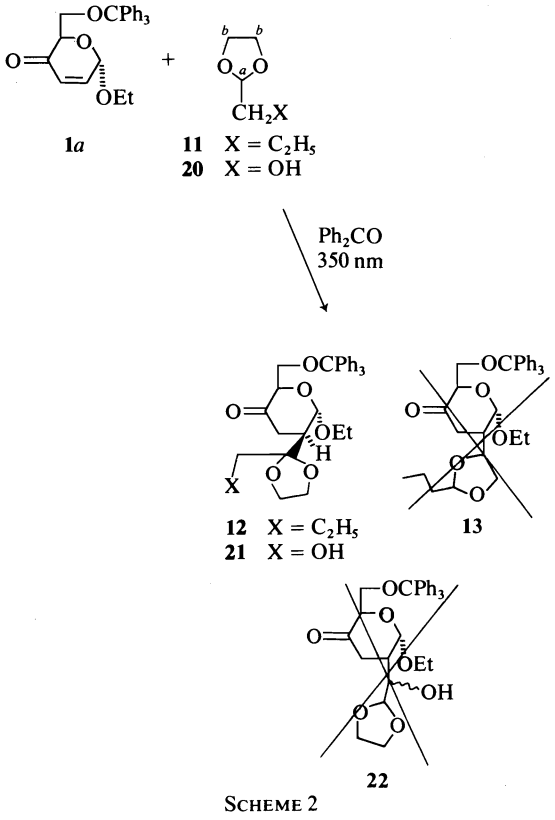

SCHEME 2

hydrolysate examined for the presence of a glycol (such as **19**) by periodate oxidation. A negative result indicated that addition at site *b* of the dioxolane ring had not occurred.

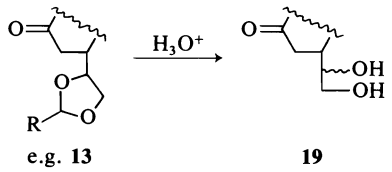

The interesting acetal **20**, prepared as indicated in Scheme 4, added equally selectively at the 2-position, giving the highly functionalized substance **21** (Table 1, entry 7), in 42% yield after chromatography. Again addition at the alternate carbinyl sites *a* or *c* (Scheme 2) to give structures such as **13** or **22** respectively were ruled out by the presence of only one acetal proton in the nmr spectrum.

Addition of **20** to enone **2** (Table 1, entry 8) proved understandably more difficult, considering the fact that a maximally substituted

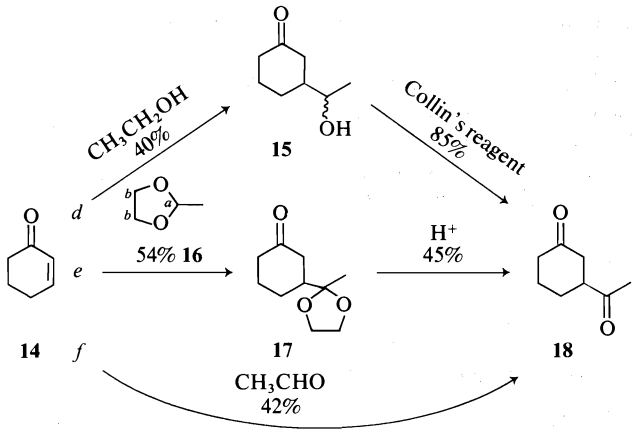

SCHEME 3

carbon–carbon bond is being forged in **23**. After being allowed to go 10 times longer than with **1***a*, the reaction was still incomplete. However, it was stopped, since there was evidence of decomposition of the product. The isolated yield of **23** was 46%, based on unrecovered starting material.

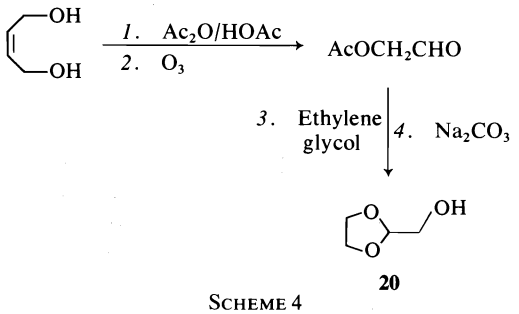

SCHEME 4

The success with the acetals suggested that it might be possible to add aldehydes directly to the enones in cases where differentiation of the carbonyl groups was not desired (12). We were encouraged by the work of Stockmann involving free-radical addition of acetaldehyde to norbornene (13).

The enone **1***a* was irradiated under the usual conditions using acetaldehyde as the addend (Table 1, entry 9). The diketone **24** was obtained in 67% yield after chromatography. Similarly, benzaldehyde was added to **1***a* to give **25** in 58% yield (Table 1, entry 10).

The stereochemistry and identity of aldehyde addition were established as shown in Scheme 5 via the previously described keto alcohol **26** (1).

Some noncarbohydrate enones were also found to react moderately well with aldehydes. Thus 2-cyclohexenone and acetaldehyde afforded a 42% yield of diketone **18** completing the series shown in Scheme 3.

The results with 1-cholesten-3-one **27** and 4-cholesten-3-one are interesting (Scheme 6). The latter fails to give a photoadduct with alcohols, acetals, or aldehydes; with the former (**27**) we have had success *only* with acetaldehyde. Thus the diketone **28** was obtained in 42% yield after chromatography.

Assignment of configuration of the acetyl group in **28** is based on our interpretation of the 220 MHz nmr spectrum in which H-1 appears as a doublet of doublets with spacing of 1.8 and 6.0 Hz. These values suggest that H-1 is equatorially oriented and coupled to two *gauche* protons. Furthermore we have noted (1)

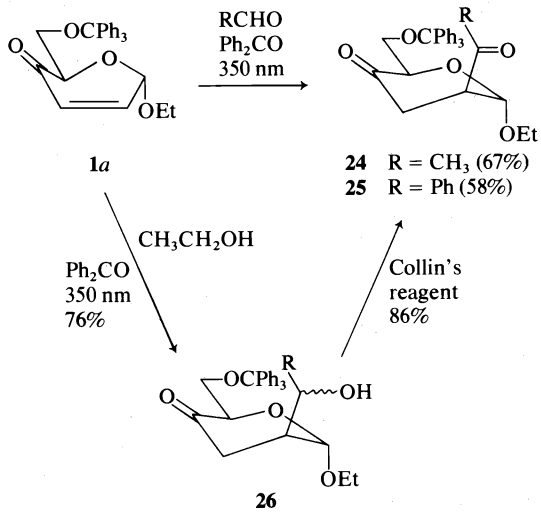

SCHEME 5

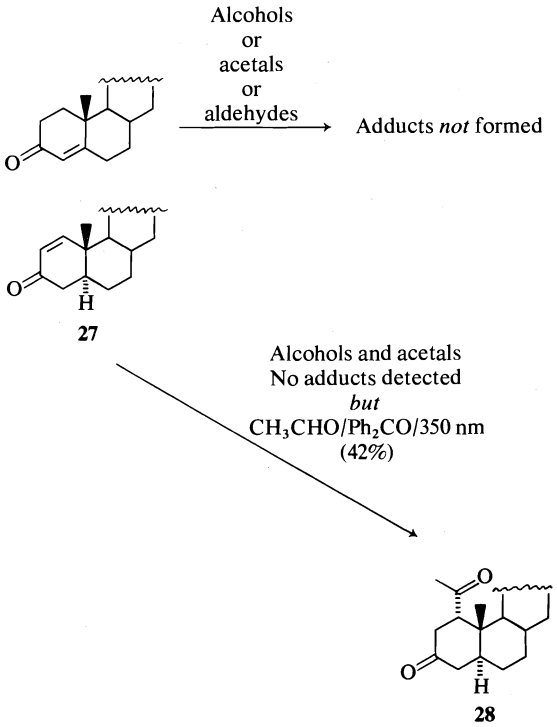

SCHEME 6

that these photoalkylations like cuprate additions are very sensitive to steric effects; hence the incoming addend should add *anti* to the C-19 methyl group.

The alkylation of mesityl oxide (Table 1, entry 12) is noteworthy since other additions (i.e. of alcohols and acetals) to acyclic systems have usually been unsuccessful. However, the addition of acetaldehyde was complete within 2 h, the yield after isolation of the known diketone (**29**) (13) being 31%.

The results in this and in the accompanying paper (1) indicate a wide disparity between the success of various α-enones as receptors in the photoalkylation reactions. An understanding of the factors responsible for these differences is obviously desirable and studies aimed at this objective are continuing in our laboratories.

Experimental

Materials and methods used have already been given in ref. 1.

General Conditions for Photoalkylation Reactions

Method A

A solution of the enone (1.0 mmol) and benzophenone (0.16 mmol) dissolved in the solvent-addend (80 ml) was placed in a Pyrex photolysis tube. The reaction mixture was cooled by means of a cold finger extending into the solution. Nitrogen gas was bubbled into the solution throughout the length of the irradiation by means of a glass capillary tube. The reaction was photolyzed at 350 nm in a Rayonet Photochemical reactor (model RPR-100) until tlc indicated the reaction was complete. At this time the solvent was removed and the residue chromatographed on a silica gel column in order to isolate the product.

Method B

A solution of the enone (1.0 mmol), benzophenone (0.16 mmol), and the addend (40 mmol) was dissolved in either hexane or acetonitrile (80 ml) and photolyzed as above. The reaction mixture was worked up as above except that in cases where the addend was a high boiling liquid it was removed by high vacuum distillation.

Ethyl 2,3-Dideoxy-2-C-(R,S)-hydroxy(hydroxymethyl)-methyl)-6-O-triphenylmethyl-α-D-threo-hexo-pyranosid-4-ulose, 3a

The enone **1***a* (1.0 g, 2.42 mmol) and benzophenone (0.12 g, 0.68 mmol) were dissolved in acetonitrile (40 ml) and ethylene glycol (400 ml) and the solution was photolyzed in the usual manner (method B). Thin-layer chromatography (diethyl ether – benzene (1:1)) after 4 h showed no starting material and one spot of lower R_f (0.16). The solvents were evaporated under reduced pressure and the resulting residue was chromatographed on a silica column to yield **3***a* (0.79 g, 69%) as a thick colourless oil. The nmr spectrum of the oil showed two doublets at 5.28 ppm (J_{12} = 4.1 Hz) and 5.08 ppm (J_{12} = 5.0 Hz) in 2:1 ratio; ir: 1730 cm^{-1} (saturated ketone).

Ethyl 2,3-Dideoxy-2-C-(oxo(triphenylmethoxymethyl)-methyl)-6-O-triphenylmethyl-α-D-threo-hexo-pyranosid-4-ulose, 7

The photoproduct from the preceding experiment, **3***a* (0.79 g, 1.66 mmol) was tritylated in pyridine (20 ml) with trityl chloride (1.38 g, 5.0 mmol) over 5 days. Normal work-up and subsequent column chromatography (petroleum ether (30–60°C) – ethyl acetate (4:1)) afforded the ditritylate **3***b* (0.81 g, 97%) as a thick oil. This oil was dissolved in methylene chloride (30 ml) and chromium trioxide – dipyridine (4.0 g, 1.55 mmol) was added with vigorous stirring. At 1 h the solution was diluted with diethyl ether (100 ml), stirred for an additional 5 min, and then filtered through Celite. The filtrate was washed with 5% hydrochloric acid and then a saturated solution of sodium bicarbonate, dried over anhydrous sodium sulphate, and decolourized with activated charcoal. Evaporation under reduced pressure gave **7** (0.68 g, 85%) which crystallized on standing. Recrystallization from diethyl ether gave fine white fibers; mp 180–181.5°C; $[\alpha]_D^{23}$ +90.8° (*c* 1.31, chloroform); ir ν_{max}: 1730 cm^{-1}; nmr (60 MHz) shows one doublet δ 5.27 (J_{12} = 5.0 Hz).[4] *Anal.* calcd. for $C_{48}H_{44}O_6$: C 80.42, H 6.18; found: C 80.35, H 6.22.

Ethyl 2,3-Dideoxy-2-C ((R,S)-hydroxy(β-hydroxyethyl)-methyl)-6-O-triphenylmethyl-α-D-threo-hexo-pyranosid-4-ulose, 4a

A solution of the enone **1***a* (0.82 g, 1.98 mmol) and benzophenone (0.16 g, 0.88 mmol) in acetonitrile (40 ml) and 1,3-propanediol (300 ml) was irradiated in the usual

[4]For characteristic nmr features of these systems see the analysis of the 220 MHz spectrum of **8**.

way (method B) for 5 h. Thin-layer chromatography (diethyl ether – benzene (1:1)) at this time showed only photoproduct (R_f 0.14). The solvents were evaporated under reduced pressure (0.01 Torr and bath temperature of 94°C to remove propanediol). Column chromatography of the resulting residue afforded **4***a* (0.470 g, 49%) as an oil; ir: 1730 cm^{-1} saturated ketone; nmr (60 MHz) shows two doublets δ 5.24 (J_{12} = 50) and 5.08 (J_{12} = 4.2) in 2:1 ratio.

Ethyl 2,3-Dideoxy-2-C-(oxo(β-triphenylmethoxyethyl)-methyl)-6-O-triphenylmethyl-α-D-threo-hexo-pyranosid-4-ulose, ***8***

The photoproduct from the preceding experiment, **4***a* (0.287 g, 0.58 mmol), was tritylated in pyridine (5 ml) with trityl chloride (0.65 g, 2.34 mmol) over 72 h. Normal work-up and column chromatography (petroleum ether (30–60°C) – ethyl acetate (4:1)) gave the ditritylate **4***b* (0.225 g, 53%). This ditritylate was oxidized in methylene chloride (20 ml) with chromium trioxide – dipryidine (1.1 g, 4.3 mmol) for 0.5 h. The solution was diluted with diethyl ether (80 ml) and filtered through Celite. The filtrate was processed in the usual manner to afford **8** (0.210 g, 93%). Recrystallization from diethyl ether gave needles, mp 140–141°C; $[\alpha]_D^{23}$ +99.8° (*c* 1.96, chloroform); nmr (HR-220) δ: 2.42 (dd, 1, $J_{2,3e}$ = 4.2 Hz, $J_{3e,3a}$ = 15.2 Hz, H-3*e*) 2.64–2.92 (m, 3, H-3*a*, 8, 8′), 3.05 (m, 1, $J_{2,3a}$ = 12.2 Hz, H-2), 3.38 (dd, 1, $J_{5,6e}$ = 6.1 Hz, $J_{6e,6a}$ = 10.0 Hz, H-6*e*), 3.49 (dd, 1, $J_{5,6a}$ = 2.9 Hz, H-6*a*), 3.30–3.50 (m, 2, H-9, 9′), 4.20 (dd, 1, H-5), 5.25 (d, 1, $J_{1,2}$ = 5.5 Hz, H-1). *Anal.* calcd. for $C_{49}H_{46}O_6$: C 80.52, H 6.34; found: C 80.49, H 6.42.

Ethyl 2,3-Dideoxy-2-C-((R,S)-hydroxy(carbomethoxy-methyl)methyl)-6-O-triphenylmethyl-α-D-threo-hexo-pyranosid-4-ulose, ***5a***, *and Its Tetrahydropyranyl Derivative* ***5b***

(*a*) A solution of the enone **1***a* (0.25 g, 0.60 mmol) and benzophenone (0.03 g, 0.17 mmol) in methyl 3-hydroxy propionate (90 ml) was irradiated for 5.5 h in the usual manner (method A). Thin-layer chromatography (petroleum ether (30–60°C) – ethyl acetate (13:7)) revealed the absence of enone (R_f 0.60) and the production of **5***a* (R_f 0.32). The methyl 3-hydroxy propionate was evaporated at 0.01 Torr with a bath temperature of 60°C. Column chromatography of the resulting residue gave **5***a* (0.112 g, 32%) as a yellow oil.

(*b*) A solution of enone **1***a* (1.50 g, 3.62 mmol) and benzophenone (0.18 g, 0.99 mmol) in methyl 3-hydroxy propionate (600 ml) was irradiated for 6 h in the usual manner (method A). The methyl 3-hydroxy propionate was evaporated off as described in (*a*) and the resultant residue was treated with 3,4-dihydropyran (3.0 g, 35 mmol) and toluenesulphonic acid (0.020 g, 0.10 mmol) in methylene chloride (40 ml) at −10°C for 0.75 h. The reaction mixture was poured into a sodium bicarbonate solution and the methylene chloride layer separated, washed with water, dried over sodium sulphate, and evaporated. Compound **5***b* (1.62 g, 74% from **1***a*) was isolated after column chromatography (petroleum ether (30–60°C) – ethyl acetate (4:1)) of the resulting oil. R_f 0.30 in petroleum ether (30–60°C) – ethyl acetate (4:1); ir: 1730 cm^{-1}. Treatment of **5***a* (prepared in (*a*)) with dihydropyran gave an identical derivative.

Ethyl 2,3-Dideoxy-2-C-(oxo(carbomethoxymethyl)-methyl)-6-O-triphenylmethyl-α-D-threo-hexo-pyranosid-4-ulose, ***9***

The photoproduct **5***a* (0.090 g, 0.17 mmol) was treated with chromium trioxide – dipyridine (0.80 g, 3.14 mmol) in methylene chloride (10 ml) for 0.5 h. The reaction mixture was then diluted with diethyl ether (30 ml) and filtered through Celite. The filtrate was washed with 5% hydrochloric acid and then a saturated sodium bicarbonate solution. Evaporation, after drying over sodium sulphate gave **9** (0.031 g, 34%) as an oil; nmr (HR-220) δ: 2.50 (dd, 1, $J_{2,3e}$ = 4.4 Hz, $J_{3e,3a}$ = 15.6 Hz, H-3*e*), 2.85 (dd, 1, $J_{2,3a}$ = 12.5 Hz, H-3*a*), 3.18 (m, 1, H-2), 3.39 (dd, 1, $J_{5,6e}$ = 6.1 Hz, $J_{6e,6a}$ = 9.6 Hz, H-6*e*), 3.49 (dd, $J_{5,6a}$ = 2.5 Hz, H-6*a*), 3.60 (s, 2, H-8, 8′), 3.73 (s, 3, OMe), 4.24 (dd, 1, H-5), 5.23 (d, 1, $J_{1,2}$ = 5.8 Hz, H-1).

Methyl 2,3-Dideoxy-2-C-(R,S)-hydroxy(hydroxymethyl)-methyl)-2-C-methyl-6-O-trityl-α-D-threo-hexo-pyranosid-4-uloses, ***6a***$_1$ *and* ***6a***$_2$*, and Their Ditrityl Derivatives,* ***6b***$_1$ *and* ***6b***$_2$

The enone **2** (1.242 g, 3.0 mmol) and benzophenone (0.087 g, 0.48 mmol) were dissolved in ethylene glycol (240 ml) and photolyzed in the usual manner (method A). After 7 h tlc indicated that the reaction was complete and that two new products had been formed. Evaporation of the solvent and chromatographic separation afforded **6***a*$_1$ (0.810 g, 38%) (R_f 0.16, in petroleum ether (30–60°C) – ethyl acetate (4:1)) which on tlc charred red on spraying with sulphuric acid, and **6***a*$_2$ (0.70 g, 33%) (R_f 0.20, same solvent mixture) which on tlc charred black on spraying with sulphuric acid.

The diol **6***a*$_1$ (or **6***a*$_2$) (0.500 g, 1.05 mmol) was dissolved in dry pyridine (10 ml) and trityl chloride (0.836 g, 3.0 mmol) was added. The reaction mixture was placed in an oil bath (50°C) and stirred for 36 h. At this time tlc indicated that the starting material had been consumed and a new compound had been formed. Conventional work-up and chromatography of the reaction product afforded **6***b*$_1$ (or **6***b*$_2$) (0.653 g, 91%).

Compound **6***b*$_1$ was an amorphous solid: R_f 0.57 in petroleum ether (30–60°C) – ethyl acetate (4:1); ir ν_{max}: 3600, 3440 (OH), 1735 (saturated ketone) cm^{-1}; ms *m/e*: 463 (M^+ − Tr); nmr (220 MHz) δ: 0.88 (s, 3, C—CH_3), 1.77 (d, 1, $J_{3e,3a}$ = 12.0 Hz, H-3*e*), 2.14 (d, 1, H-3*a*), 2.91, 3.27, 3.45, 3.82, 4.09 (set of multiplets (2 ABM systems), 6, H-5, -6, -6′ and H-7, -8, -8′), 3.09 (s, 3, OCH_3), 5.70 (s, 1, H-1), 7.2–7.8 (m, 30, phenyl).

Compound **6***b*$_2$ was a syrup: R_f 0.64 in petroleum ether (30–60°C) – ethyl acetate (4:1); ir ν_{max}: 3440 (OH), 1735 (saturated ketone) cm^{-1}; ms *m/e*: 463 (M^+ − Tr); nmr (220 MHz) δ: 0.83 (s, 3, C—CH_3), 1.75 (d, 1, $J_{3e,3a}$ = 11.5 Hz, H-3*e*), 2.0 (d, 1, H-3*e*), 3.05, 3.45, 3.77, 4.05 (set of multiplets (2 ABM systems), 6, H-5, -6, -6′, and H-7, -8, -8′), 3.25 (s, 3, OCH_3), 5.55 (s, 1, H-1), 7.2–7.8 (m, 30, phenyl).

Methyl 2,3-Dideoxy-2-C-(oxo(triphenylmethoxymethyl)-methyl)-2-C-methyl-6-O-trityl-α-D-threo-hexo-pyranosid-4-ulose, ***10***

(*a*) The ditritylated alcohol **6***b*$_1$ (0.350 g, 0.49 mmol) was dissolved in methylene chloride (10 ml) and the chromium trioxide – dipyridine complex (2.1 g, 8.1 mmol)

was added to the vigorously stirred solution. After 1 h at room temperature a tlc of the reaction mixture indicated that all of the starting material had been consumed and a new slower-running compound had been produced. The reaction mixture was diluted with ether (40 ml) and stirred an additional 15 min. The solution was then filtered through a bed of Celite and the filtrate was washed successively with a 5% hydrochloric acid solution (20 ml), a saturated sodium bicarbonate solution (20 ml), and water (20 ml). The organic layer was then decolourized, dried over sodium sulphate, and evaporated to afford **10** (0.312 g, 89%).

(*b*) The ditritylated alcohol **6**b_2 (0.320 g, 0.45 mmol) when subjected to the same reaction as above afforded **6**b_1 (0.272 g, 85%).

The compounds produced in parts (*a*) and (*b*) had the same R_f 0.52 in petroleum ether (30–60°C) – ethyl acetate (4:1) and gave identical ir and nmr spectra.

The diketone **10** was a noncrystalline foam which gave the following data: ir ν_{max}: 1730 (saturated ketone) cm^{-1}; ms *m/e*: 461 ($M^+ - Tr$); nmr (220 MHz) δ: 1.07 (s, 3, C—CH_3), 2.34 (d, 1, $J_{3e,3a}$ = 16.0 Hz, H-3*e*), 2.73 (d, 1, H-3*a*), 3.40 (m(ABX), 2, $J_{6,6'}$ = 11.0 Hz, $J_{5,6}$ = 7.0 Hz, $J_{5,6'}$ = 2.5 Hz, H-6, -6′), 3.45 (s, 3, OCH_3), 3.96 (s, 2, H-8, -8′), 4.03 (dd, 1, H-5), 5.05 (s, 1, H-1), 7.2–7.8 (m, 30, phenyl).

Ethyl 2,3-Dideoxy-2-C-(2-propyl-1,3-dioxolan-2-yl)-6-O-trityl-α-D-threo-hexopyranosid-4-ulose, ***12***

The enone **1***a* (0.248 g, 0.6 mmol), benzophenone (0.018 g, 0.1 mmol), and 2-propyl-1,3-dioxolane (2.80 g, 24 mmol) were dissolved in acetonitrile (70 ml) and photolyzed in the usual manner (method B). After 2 h tlc indicated that the reaction was complete and a new product (R_f 0.33, petroleum ether (30–60°C) – ethyl acetate (4:1)) had been formed. The residue obtained after evaporation of the solvents was chromatographed on a silica gel column using the same solvent system and afforded **12** (0.197 g, 62%). Compound **12** was a syrup which gave the following data: ir ν_{max}: 1730 (saturated ketone) cm^{-1}; ms *m/e*: 485 ($M^+ - OEt$), 287 ($M^+ - Tr$); nmr δ: 0.7–1.9 (m, 10, —CH_2CH_3, alkyl side chain), 2.2–2.75 (m, 3, H-2, -3*e*, -3*a*), 3.3–4.4 (m, 9, H-5, -6, -6′, —CH_2CH_3, ketal methylene), 5.12 (d, 1, $J_{1,2}$ = 4.0 Hz, H-1), 7.2–7.8 (m, 15, phenyl).

2-(3-Oxocyclohexyl)-2-methyl-1,3-dioxolane, ***17***

2-Cyclohexenone (5 g, 0.05 mol), benzophenone (600 mg, 3.3 mmol), and 2-methyl dioxolane (50 ml) in cyclohexane (800 ml) was irradiated in the usual manner (method B) for 57 h. The product was fractionated on a silica column using petroleum ether (30–60°C) – ethyl acetate (4:1) and the material of R_f 0.19 was collected (5.2 g, 54%). Compound **17** gave the following data: ir ν_{max}: 1730 (saturated ketone) cm^{-1}; ms *m/e*: 183 ($M^+ - 1$); nmr (60 MHz) δ: 1.2 (s, 3, CH_3), 1.4–2.5 (m, 9, ring protons), 3.87 (s, 4, ketal methylene).

2-Hydroxymethyl-1,3-dioxolane, ***20*** *(Scheme 5)*

Acetic anhydride (118 ml, 1.25 mol) and acetic acid (120 ml, 2.1 mol) were refluxed in a 500 ml flask while *cis*-2-butene-1,4-diol (44.0 g, 0.5 mol) was added dropwise. The reaction mixture was refluxed for 24 h. At this time the reflux condenser was replaced by a Vigreux column (30 cm) and the reaction mixture was fractionally distilled under aspirator vacuum. The product, 1,4-di-*O*-acetyl-*cis*-2-butene-1,4-diol, was collected by high vacuum distillation after the acetic anhydride and acetic acid had been removed: yield 66.0 g, bp 75–80°C (1.5 Torr).

The diacetate (10.0 g, 0.058 mol) was dissolved in ethyl acetate (100 ml) and cooled to 0°C in an ice bath. Ozone was bubbled through the solution until the starting olefin had been consumed (tlc). Pd/C (5%) (0.5 g) was added and the reaction mixture was hydrogenated at atmospheric pressure at 0°C. The crude product obtained upon filtration and evaporation was dissolved in benzene (20 ml). Ethylene glycol (1.86 g) and *p*-toluenesulphonic acid (0.018 g) were added and the reaction mixture was refluxed using a Dean–Stark trap to remove the water formed during the reaction. After 6 h the reaction mixture was poured into a separatory funnel and diluted with ether (20 ml). The organic layer was washed with a saturated sodium bicarbonate solution (20 ml) and water (20 ml), dried over sodium sulphate, and evaporated. The residue was fractionally distilled to give 2-acetoxymethyl-1,3-dioxolane: yield 5.1 g; bp 49–51°C, 0.4 Torr; R_f 0.44 (petroleum ether (30–60°C) – ethyl acetate (1:1)); nmr δ: 2.03 (s, 3, —$OCOCH_3$), 3.90 (m, 4, —CH_2CH_2—), 4.0 (d, 2, J = 4.0 Hz, —CH_2CH—), 5.03 (t, 1, J = 4.0 Hz, acetal proton).

The acetylated acetal (5.0 g, 0.034 mol) was dissolved in methanol (30 ml) and sodium carbonate (4.25 g, 0.051 mol) was added. The reaction mixture was stirred at room temperature for 4 h, filtered through a bed of Celite, and evaporated to dryness. The residue was extracted with chloroform and filtered. The filtrate was evaporated to dryness and the resulting oil was distilled under high vacuum to give **20**: yield 2.9 g; bp 44–48°C, 0.5 Torr; R_f 0.18 (petroleum ether (30–60°C) – ethyl acetate (1:1)); nmr δ: 2.9 (bs, 1, OH), 3.68 (d, 2, J = 3.0 Hz, —CH_2OAc), 4.0 (m, 4, —CH_2CH_2—), 5.05 (t, 1, J = 3.0 Hz, acetal proton).

Ethyl 2,3-Dideoxy-2-C-(2-hydroxymethyl-1,3-dioxolan-2-yl)-6-O-trityl-α-D-threo-hexopyranosid-4-ulose, ***21***

The tritylated enone **1***a* (0.620 g, 1.5 mmol) and the acetal **20** (6.0 g, 60 mmol) were dissolved in acetonitrile (140 ml) and photolyzed in the usual manner (method B). After 4 h the reaction was complete (tlc) and a new product had been formed, R_f 0.23 in petroleum ether (30–60°C) – ethyl acetate (2:1). The residue obtained after normal work-up was chromatographed on a silica gel column using the same solvent system as eluant to afford **21** (0.319 g, 42%). Compound **21** was a syrup which gave the following data: ir ν_{max}: 3460 (OH), 1735 (saturated ketone) cm^{-1}; ms *m/e*: 487 ($M^+ - CH_2OH$), 441 ($M^+ - Ph$); nmr δ: 1.26 (t, 3, J = 7.0 Hz, CH_2CH_3), 2.3–2.9 (m, 3, H-2, -3*e*, -3*a*), 3.3–4.4 (m, 10, H-5, -6, -6′, ketal methylene, —CH_2OH), 5.15 (d, 1, $J_{1,2}$ = 4.0 Hz, H-1), 7.2–7.8 (m, 15, phenyl).

Methyl 2,3-Dideoxy-2-C-(2-hydroxymethyl-1,3-dioxolan-2-yl)-2-C-methyl-6-O-trityl-α-D-threo-hexopyranosid-4-ulose, ***23***

The tritylated enone **2** (0.435 g, 1.05 mmol), the acetal **20** (4.2 g, 42 mmol), and benzophenone (0.032 g, 0.18 mmol) were dissolved in acetonitrile (100 ml) and photolyzed in the usual manner. The reaction was stopped after 48 h. At this time tlc indicated that a new product had been formed, R_f 0.21 in petroleum ether (30–60°C) –

ethyl acetate (4:1). Some starting material was still present, and some decomposition had occurred. After the usual work-up the residue was chromatographed on a silica gel column using the same solvent system, whereby unreacted starting material (0.152 g) was obtained. On this basis the yield of compound **23** (0.163 g) was 46%. Compound **23** was a syrup which gave the following data: ir ν_{max}: 3450 (OH), 1720 (saturated ketone) cm^{-1}; ms *m/e*: 487 ($M^+ - OCH_3$) or ($M^+ - CH_2OH$); nmr δ: 0.85 (s, 3, C—CH_3), 1.92 (m, 2H, H-3*e*, -3*a*), 3.22 (s, 3, OCH_3), 3.3–4.5 (m, 10, H-5, -6, -6′, ketal methylenes, —CH_2OH), 4.88 (s, 1, H-1), 7.2–7.8 (m, 15, phenyl).

Ethyl 2-C-Acetyl-2,3-dideoxy-6-O-trityl-α-D-threo-hexo-pyranosid-4-ulose, ***24***

(*a*) The enone **1***a* (0.465 g, 1.12 mmol), benzophenone (0.036 g, 0.2 mmol), and acetaldehyde (6.3 ml, 0.112 mol) were dissolved in acetonitrile (90 ml) and photolyzed in the usual manner (method B). The reaction was complete in 5 h (tlc) and a new compound had been formed (R_f 0.40 in petroleum ether (30–60°C) – ethyl acetate (4:1)). The residue obtained after evaporation of the solvents was chromatographed on a silica gel column in the same solvent system to afford compound **24** (0.344 g, 67%).

(*b*) The enone **1***a* (1.5 g, 3.72 mmol) and benzophenone (0.113 g, 0.62 mmol) were dissolved in ethanol and photolyzed in the usual manner (method A). After 7 h tlc indicated that the reaction was complete and a new product had been formed (R_f 0.20 in petroleum ether (30–60°C) – ethyl acetate (4:1)). The residue obtained after the usual work-up was chromatographed on a silica gel column and afforded **26** (1.29 g, 76%) as a mixture of epimers. The material (0.59 g, 1.3 mmol) was dissolved in methylene chloride (35 ml) and the chromium trioxide – dipyridine complex (1.8 g) was added to the vigorously stirred solution. After 1 h tlc indicated that the starting material had all been consumed and a new product had been formed. The reaction mixture was diluted with ether (100 ml) and stirred for an additional 15 min. The solution was then filtered through a bed of Celite, decolourized, and dried over sodium sulphate. Compound **24** (0.515 g, 86%) was recovered when the solvents were evaporated.

Compound **24** after crystallization from ethanol gave the following data: mp 107–108°C; $[\alpha]_D^{23}$ +150° (*c* 1.0, $CHCl_3$); ms *m/e*: 381 (M^+ – Ph), 215 (M^+ – Tr); nmr δ: 1.3 (t, 3, J = 8.0 Hz, CH_2CH_3), 2.21 (s, 3, —$COCH_3$), 2.47 (m, 1, H-3*e*), 2.79 (m, 1, H-3*a*), 3.03 (m, 1, H-2); 3.3–4.2 (m, 5, H-5, -6, -6′, —CH_2CH_3), 5.32 (d, 1, $J_{1,2}$ = 5.0 Hz, H-1); 7.20–7.70 (m, 15, phenyl). *Anal.* calcd. for $C_{29}H_{30}O_5$: C 75.96, H 6.59; found: C 75.98, H 6.53.

Ethyl 2-C-Benzoyl-2,3-dideoxy-6-O-trityl-α-D-threo-hexo-pyranosid-4-ulose, ***25***

The enone **1***a* (0.464 g, 1.12 mmol), benzophenone (0.036 g, 0.2 mmol), and benzaldehyde (10 ml) were dissolved in acetonitrile (80 ml) and photolyzed in the usual manner (method B). After 2 h tlc indicated that the starting material had all been consumed and a new product had been formed R_f 0.41 in petroleum ether (30–60°C – ethyl acetate (4:1)). The residue obtained upon evaporation of the solvents was dissolved in ether (50 ml) and washed successively with a saturated sodium bisulphite solution (3 × 50 ml) and water (50 ml). The solution was then dried over sodium sulphate and evaporated to dryness. The residue was separated on a silica gel column using the same solvent system and afforded **25** (0.338 g, 58%). Compound **25** was crystallized from ether–hexane and gave the following data: mp 127–128°C; $[\alpha]_D^{23}$ +178.7° (*c* 1.83, $CHCl_3$); nmr δ: 1.3 (t, 3, J = 7.0 Hz, —CH_2CH_3), 2.4–3.0 (m, 3, H-2, -3*a*, -3*e*), 3.2–4.4 (m, 5, H-5, -6, -6′, —CH_2CH_3); 5.4 (d, 1, $J_{1,2}$ = 5.0 Hz, H-1), 7.2–8.3 (m, 20, phenyl). *Anal.* calcd. for $C_{34}H_{32}O_5$: C 78.44, H 6.20; found: C 78.50, H 6.17.

3-Acetylcyclohexanone, ***18***

(*a*) 2-Cyclohexenone (0.432 g, 4.5 mmol), benzophenone (0.136 g, 0.75 mmol) and acetaldehyde (40 ml) were dissolved in acetonitrile (320 ml) and photolyzed in the usual manner (method B). After 10 h an nmr spectrum of the crude reaction mixture indicated that the reaction was complete. The residue was chromatographed on a silica gel column and afforded compound **18** (0.317 g, 42%); R_f 0.23 in petroleum ether (30–60°C) – ethyl acetate (4:1). The structure of **18** was confirmed by comparison of its nmr and ir spectra with published data for the compound prepared by another route (11).

(*b*) 3-(-1-Hydroxyethyl)cyclohexane (1) (0.564 g) was dissolved in methylene chloride (20 ml) and treated with 3.0 g of chromium trioxide – dipyridine complex. After 1 h, the reaction was worked up as described above for **10** and the material was purified by column chromatography: R_f 0.31 in benzene–ether (1:1); nmr (60 MHz) δ: 1.4–2.4 (m, 8, ring protons), 2.10 (s, 3, CH_3), 2.5–3.0 (m, 1, methine). These data were in excellent agreement with those described for compound **18** (11).

(*c*) The ketal **17** (500 mg) was dissolved in dioxane (5 ml) and 1 *N* sulfuric acid (5 ml) added. The solution was stirred at room temperature and after 1 h, tlc in benzene–ether (1:1) indicated that the hydrolysis was complete. Customary work-up and chromatography afforded 300 mg of **18**. (The ketal **17** on standing at room temperature decomposes to diketone **18**.)

1-Acetyl-3-cholestanone, ***28***

1-Cholesten-3-one **27** (0.431 g, 1.1 mmol), benzophenone (0.036 g, 0.2 mmol), and acetaldehyde (10 ml) were dissolved in acetonitrile (100 ml) and irradiated for 12 h in the usual manner (method B). The product was chromatographed on a silica column using diethyl ether – benzene (1:9) and the substance having R_f 0.22 was recovered (0.192 g, 42%) and recrystallized from methanol; mp 139–140°C; ms *m/e*: 428 (M^+), 413 ($M^+ - CH_3$), 385 (M^+ – Ac), 385 (M^+ – (Ac + CH_3)); 315 ($M^+ - C_8H_{17}$); nmr δ: 2.00–2.31 (m, 3, H-2 ax., H-4 eq., H-4 ax.), 2.21 (s, 3, $COCH_3$), 2.40 (q, 1, H-2 eq.), 3.26 (dd, 1, H-1). *Anal.* calcd. for $C_{29}H_{28}O_2$: C 81.25, H 11.29; found: C 81.28, H 11.12.

3,3-Dimethyl-2,5-hexanedione, ***29***

Mesityl oxide (0.440 g, 5.1 mmol), benzophenone (0.154 g, 0.85 mmol), and acetaldehyde (40 ml) were dissolved in acetonitrile (320 ml) and photolyzed in the usual manner (method B). After 2 h an nmr spectrum of the crude reaction mixture obtained upon evaporation of the solvents indicated that the starting material had all

been consumed. The residue was chromatographed on a silica gel column using petroleum ether (30–60°C) – ethyl acetate (4:1). One fraction (R_f 0.33) which was detected by exposing the tlc plate to iodine vapor, gave compound **29** (0.205 g, 31%) as a light yellow oil. The nmr spectrum of **29** exhibited the following: δ: 1.25 (s, 6, C—CH_3), 2.12 (s, 3, $COCH_3$), 2.18 (s, 3, $COCH_3$), 2.8 (s, 2, CH_2). Compound **29** was characterized as its bis-2,4-nitrophenylhydrazone, mp 216–217°C, (lit. (13) 217–218°C).

Acknowledgements

We are very pleased to acknowledge financial support from the National Research Council of Canada, Environment Canada, and Bristol Laboratories (Syracuse).

1. B. Fraser-Reid, N. L. Holder, D. R. Hicks, D. L. Walker, and M. B. Yunker. Can. J. Chem. This issue.
2. D. L. Walker and B. Fraser-Reid. J. Am. Chem. Soc. **97**, 6251 (1975).
3. J. L. Herrmann, J. E. Richman, and R. H. Schlessinger. Tetrahedron Lett. 3267 (1973); 3271 (1973); 3275 (1973); R. J. Cregge, J. L. Herrmann, and R. H. Schlessinger. Tetrahedron Lett. 2603 (1973); R. J. Cregge, J. L. Herrmann, J. E. Richman, R. F. Romanet, and R. H. Schlessinger. Tetrahedron Lett. 2595 (1973).
4. G. Stork and M. E. Jung. J. Am. Chem. Soc. **96**, 3683 (1973).
5. B. Fraser-Reid, A. McLean, E. W. Usherwood, and M. Yunker. Can. J. Chem. **48**, 2877 (1970).
6. J. Rosenthal and D. Elad. Chem. Commun. 684 (1968); J. Rosenthal and D. Elad. J. Org. Chem. **33**, 805 (1968).
7. J. S. Jewell and W. A. Szarek. Tetrahedron Lett. 43 (1969).
8. K. Matsuura, S. Maeda, Y. Araki, Y. Ishido, and A. Murai. Tetrahedron Lett. 2869 (1970); K. Matsuura, K. Nishiyama, K. Yamada, Y. Araki, and Y. Ishido. Bull. Chem. Soc. Jpn. **46**, 2538 (1973).
9. B. Fraser-Reid, D. R. Hicks, D. L. Walker, D. E. Iley, M. B. Yunker, S. Y-K. Tam, and R. C. Anderson. Tetrahedron Lett. 297 (1975).
10. D. H. R. Barton, D. L. J. Clive, P. D. Magnus, and G. Smith. J. Chem. Soc. C, 2193 (1971); D. H. R. Barton, P. D. Magnus, and J. I. Okogun. J. Chem. Soc. Perkin Trans. I, 1103 (1972).
11. E. J. Corey and L. S. Hegedus. J. Am. Chem. Soc. **91**, 4928 (1969); E. J. Corey and D. Crouse. J. Org. Chem. **33**, 298 (1968).
12. D. R. Hicks, R. C. Anderson, and B. Fraser-Reid. Synth. Commun. **6**, 417 (1976).
13. H. Stockmann. J. Org. Chem. **29**, 245 (1964).
14. L. Crombie and K. Mackenzie. J. Chem. Soc. 4417 (1958).

Synthetic routes to 2′,3′-cyclopropanated and 2′,3′-unsaturated nucleosides[1]

STEVE YIK-KAI TAM[2] AND BERT FRASER-REID

Guelph-Waterloo Centre for Graduate Work in Chemistry, Waterloo Campus, University of Waterloo, Waterloo, Ont., Canada N2L 3G1

Received April 11, 1977

STEVE YIK-KAI TAM and BERT FRASER-REID. Can. J. Chem. **55**, 3996 (1977).

Cyclopropyl glycopyranosides which solvolyze via a stabilized cyclopropyl carbinyl-oxocarbonium ion react under neutral conditions with nucleoside bases in nitromethane at 200°C to give good yields of the corresponding cyclopropanated nucleosides. Under similar conditions hex-2-enopyranosides (which solvolyze by allyl-oxocarbonium ions) do not react. However, under catalysis by mercuric bromide or acetic acid, the corresponding 2′,3′ unsaturated nucleosides are formed although accompanied by appreciable amounts of 1′,2′-unsaturated-3′-nucleosides. Formation of the latter may be avoided if the hex-2-enopyranosides are first converted to the hex-2-enopyranosyl acetates by treatment with boron trifluoride and acetic anhydride. The derived acetates react with the nucleoside bases without catalysis to give anomeric mixtures of nucleosides, there being no trace of the unwanted 3′-nucleosides.

STEVE YIK-KAI TAM et BERT FRASER-REID. Can. J. Chem. **55**, 3996 (1977).

Les cyclopropyl glycopyrannosides lesquels se solvolysent via un ion cyclopropyl-oxocarbonium stabilisé, réagissent dans des conditions de neutralité avec des bases nucléosides dans le nitrométhane à 200°C pour conduire avec de bons rendements au nucléoside cyclopropylé correspondant. Dans des conditions similaires, les hexéno-2 pyrannosides (lesquels se solvolysent par un ion allyl-oxocarbonium) ne réagissent pas. Par contre, ces réactions catalysées par le bromure mercurique ou l'acide acétique conduisent aux nucléosides 2′,3′-insaturés correspondants quoique accompagnés d'une quantité appréciable de nucléosides-3′ 1′,2′-insaturés. La formation de ce dernier peut-être évitée si on transforme en premier lieu les hexéno-2 pyrannosides en acétate d'hexéno-2 pyrannosyle par action du trifluorure de bore et de l'anhydride acétique. Ces acétates réagissent, sans catalyseur, avec les bases nucléosides pour conduire à des mélanges anomériques de nucléosides. On n'observe aucune trace des nucléosides-3′ non désirés.

[Traduit par le journal]

Introduction

In a previous paper from our laboratory, the synthesis and chemistry of some cyclopropyl glycopyranosides (e.g. **1** and **2**) were described (1). The fact that the glycosides, **1** and **2**, were readily hydrolyzed by boiling water to the carboxaldehyde **4** was attributed to the remarkable stability of the intermediate cyclopropylcarbinyl-oxocarbonium ion (**3**)[3] (2, 3), the existence of which was supported by the exclusive formation of **4** in the silver-ion assisted hydrolysis of the homoallyl iodide **5** (1, 5). Further study of the solvolysis of the cyclopropyl compounds revealed that in **3** the stabilization of the anomeric cation by the ring oxygen completely overwhelms that by the cyclopropyl ring (4). Thus the stabilized ion **3** may be regarded as an 'activated' intermediate for carbonium ion reactions occurring at the anomeric center. In this paper we report that this stable intermediate (Scheme 1) may be exploited for the preparation of 2′,3′-cyclopropanated nucleosides which proceed via an anomeric cation (for a review see ref. 6), and as an extension of this study we have developed a new approach to the synthesis of 2′,3′ unsaturated nucleosides by making use of stabilized allyl-oxocarbonium ions (**6**) (7).

Results and Discussion

Condensation of **1** with 6-chloropurine was effected by heating the reactants in nitromethane without any added catalyst (Scheme 2). After 6 h of reaction, a 1:1 anomeric mixture of the 2′,3′-cyclopropanated nucleosides **7** was isolated in 71% yield. The anomers could be partially separated by silica gel column chromatography,

[1]Cyclopropylcarbinyl-oxocarbonium ions, Part VIII. For Part VII see ref. 4.

[2]Taken from the Ph.D. Thesis of S. Y-K. Tam. Present address: Sloan Kettering Institute for Cancer Research, 145 Boston Post Road, Rye, New York, NY 10580, U.S.A.

[3]An alternative name for **3** is cyclopropyl(oxo)methylium ion (4).

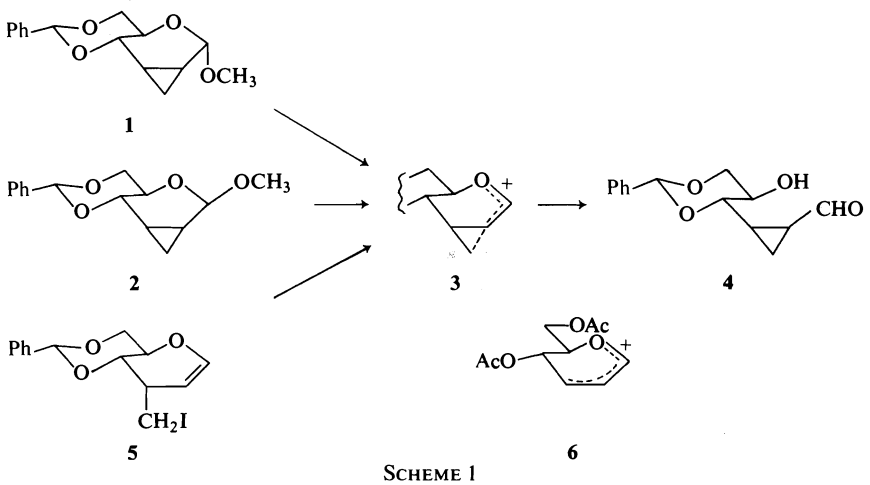

SCHEME 1

and anomeric configurational assignments were made by comparing their ^{1}H nmr spectra to those of their glycosidic counterparts **1** and **2** (1) (Table 1). Thus α-configuration was assigned to the anomer showing the larger $J_{1',2'}$ value.

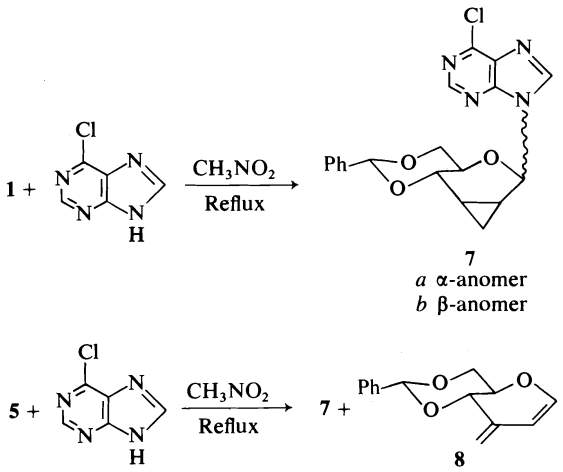

SCHEME 2

The position of substitution on the purine residue was determined to be N-9 by the uv data in ethanol: 263 nm (ε = 10 383) and 257 nm (ε = 9161). These values are closer to those usually observed for N-9 substitution (8, 9) than to those (278–283 nm, ε = 7400) for N-7 substitution (10).

Reaction of the homoallyl iodide **5** with 6-chloropurine under the agency of silver nitrate and sodium carbonate afforded the same mixture of the anomers of **7** in 58% yield. In the latter reaction the previously described (3, 4) diene **8** resulting from elimination of hydrogen iodide was isolated in 20% yield.[4]

The reaction of the 2,3-unsaturated glycopyranoside **9** with 6-chloropurine in refluxing nitromethane was very slow in comparison to the cyclopropyl glycopyranoside **1**, and **9** remained largely unreacted even after 1 day. Addition of mercuric bromide or acetic acid to the reaction mixture resulted in formation of a significant amount of the unwanted 3′-nucleosides, **11**, identifiable by characteristic (see for example ref. 11) ^{1}H nmr signals, ~6.6 and ~5.0 ppm for the glycal protons H′-1 and H′-2.

We suspected that the formation of **11** might be due to the acidic catalyst employed and consequently decided to examine a substrate which would not require such catalysis. Thus the glycoside **9** was first converted to the glycosyl acetate **12** by treatment with acetic anhydride in the presence of a catalytic amount of boron trifluoride etherate (Scheme 3), and **12** was then reacted with 6-chloropurine in refluxing nitromethane. This alteration proved advantageous since a 1:1 anomeric mixture of **10** was obtained in 48% yield, and **11** was not detected in the reaction mixture. Interestingly, small amounts of glycal sugars, **13** and **14**, were also formed in the boron trifluoride – acetic anhydride reaction of **9**. However, these were recovered unreacted in the nucleoside-formation reaction.

[4]Attempts were made to obtain the free nucleosides from **7**. Since the usual methods of debenzylidenation, viz. hydrogenolysis and acid hydrolysis, were incompatible with the cyclopropane ring, the Hanessian–Hular reaction (22) was attempted, but this led to a complex mixture.

TABLE 1. Proton magnetic resonance parameters for 6-chloro-9-(4′,6′-*O*-benzylidene-2′,3′-dideoxy-2′,3′-*C*-methylene-(α and β)-D-allopyranosyl)purine and their methyl glycoside analogues*

		Chemical shifts (τ values)									
Compound	Anomer	H-1′	H-2′	H-3′	H-4′	H-5′	H-6′	H-6″	H-7′*exo*	H-7′*endo*	Base
7	α	3.38	7.83	8.05	5.68	6.50	6.28	5.53	8.96	8.58	1.64 and 1.19
1†	α	5.00	8.35	8.49	5.92	6.53	6.32	5.78	9.25	8.74	
7	β	3.67	8.29	8.08	5.54	6.50	6.28	5.74	8.85	8.61	1.64 and 1.19
2†	β	5.23	9.00	8.88	5.70	6.71	6.29	5.78	9.14	8.93	

		Coupling constants (Hz)											
Compound	Anomer	$J_{1'2'}$	$J_{2'3'}$	$J_{2'7'exo}$	$J_{2'7'endo}$	$J_{3'4'}$	$J_{3'7'exo}$	$J_{3'7'endo}$	$J_{4'5'}$	$J_{5'6'}$	$J_{5'6''}$	$J_{6'6''}$	$J_{7'endo}$ $J_{7'exo}$
7	α	6.0	9.0	8.0	5.5	5.0	8.0	5.5	9.5	10.0	4.5	−10.5	−5.5
1†	α	6.0	9.0	8.0	5.5	5.0	8.0	5.5	9.5	10.0	4.5	−10.5	−5.5
7	β	1.0	9.0	8.0	5.5	5.0	8.0	5.5	9.5	10.0	4.5	−10.5	−5.5
2	β	1.0	9.0	8.0	5.5	5.0	8.0	5.5	9.5	10.0	4.5	−10.5	−5.5

*Determined at 220 MHz in $CDCl_3$ (TMS). *J* values were read directly from spectra run at 250 Hz sweep width.
†See ref. 5.

TABLE 2. Proton magnetic resonance parameters for some 2′,3′-unsaturated nucleosides

			Chemical shifts (τ values)										
Compound	Anomer	Solvent	H-1′	H-2′	H-3′	H-4′	H-5′	H-6′	H-6″	Base		$[\alpha]_D^{23}$	Ref.
10	α	$CDCl_3$	3.35	3.76	3.60	4.52	6.05	5.75	5.90	1.18	1.67	59.9	8
10	α	$CDCl_3$	3.35	3.78	3.59	4.52	6.07	5.70	5.90	1.16	1.67	65.7	This work
15	α	$CDCl_3$	3.42	3.81	3.60	4.58	6.08	5.8		1.71		10.5	9
10	β	$CDCl_3$	3.24	3.89	3.70	4.44	5.78	5.72	5.74	1.16	1.68	85.6	8
10	β	$CDCl_3$	3.27	3.95	3.70	4.45		5.66–6.00		1.18	1.72	80.5	This work
15	β	C_6D_6	4.02	4.87	4.25	4.63	6.38	5.9		2.42		45	9

		Coupling constants (Hz)										
Compound	Anomer	$J_{1'2'}$	$J_{1'3'}$	$J_{1'4'}$	$J_{2'3'}$	$J_{2'4'}$	$J_{3'4'}$	$J_{4'5'}$	$J_{5'6'}$	$J_{5'6''}$	$J_{6'6''}$	Ref.
10	α	3.0	−2.0	1.6	10.2	−2.0	2.0	9.0	5.3	2.6	−12.1	8
10	α	2.0	−1.5	1.5	10.2	*	2.0	9.0	5.3	2.6	−12.2	This work
15	α	3.0	−1.5	1.2	10.0	−1.7	1.7	8.5	*	*	*	9
10	β	1.8	−2.2	2.6	10.2	−1.6	1.8	8.4	4.7	3.3	−12.2	8
10	β	2.0	−2.0	2.2	10.2	−2.0	1.8	8.6	*	*	*	This work
15	β	1.5	−2.0	2.2	10.0	−2.2	2.0	9.0	*	*	*	9

*Values not determined.

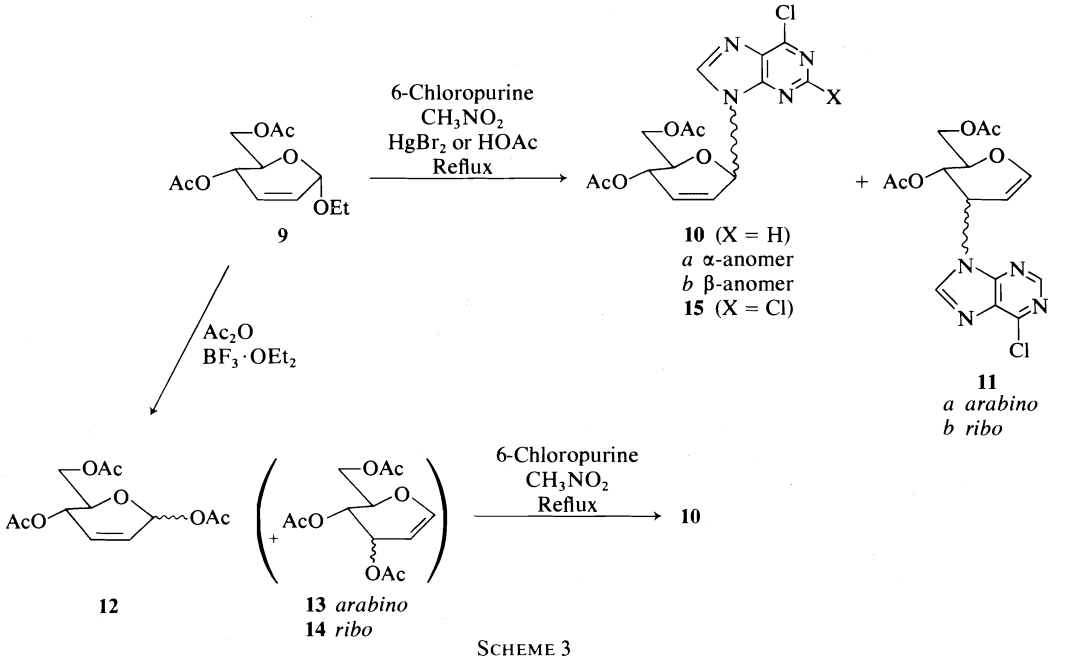

SCHEME 3

The anomers of **10** could be partially separated by silica gel column chromatography. The ^1H nmr parameters and optical rotation values (Table 2) of the pure anomers are in good agreement with the reported data for the authentic anomers, which were obtained by Garcia-Munoz and co-workers, from the reaction of triacetylglucal with 6-chloropurine (8). Accordingly, the β-anomer was identified as the isomer showing the larger homoallyl coupling ($J_{1',4'}$) and smaller $J_{1',2'}$ value. For purposes of comparison, the parameters of the 2,6-dichloropurine derivatives (**15**) which were prepared by Ferrier and Ponpipom (9) are also included in Table 2.

When the same sequence of reactions (Scheme 4) was applied to the 6-deoxy olefinic sugar **17** obtained from **16** (12), an overall yield of 33% of the 6′-deoxy-2′,3′-unsaturated nucleosides **18** was obtained. In this case, the β-anomer (**18***b*) could be fractionally crystallized from the anomeric mixture. Again, no trace of nucleosides of the glycal type (e.g. **11**) was detected.

Summary

Compound **7** is the first example of a 2′,3′-cyclopropanated nucleoside. Its formation from **1** without the need for acid catalysis demonstrates once again the exceptional stability of the cyclopropylcarbinyl-oxocarbonium ion[3] intermediate (**3**) which results upon cleavage of the glycoside bond (5). The formation of **7** from the homoallyl iodide **5** further confirms the intervention of **3** in these reactions. The comparatively slower

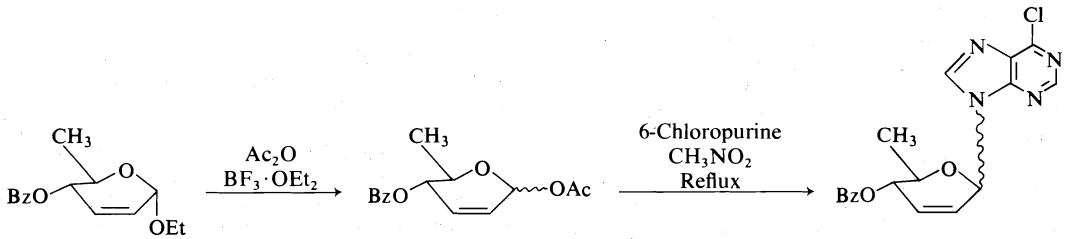

Bz = PhCO
SCHEME 4

reaction of the 2,3-unsaturated glycopyranoside **9** parallels the previously observed differences in the rate of hydrolysis of **1** and **9** (13). All these results indicate that **3** is a more highly stabilized carbonium ion than the allyl-oxocarbonium ion, **6**.

Conversion of the glycoside, **9**, to the glycosyl acetate, **12**, facilitated the formation of the ion **6** for obvious reasons. This approach to the synthesis of 2′,3′-unsaturated nucleosides from a 2,3-unsaturated hexopyranoside via the corresponding acetate, offers at least one advantage over the existing and most commonly used 'glycal approach' (8, 9, 14–16). The method provides exclusively the 2′,3′-unsaturated nucleosides, whereas the 'glycal approach' furnishes the 1′,2′-unsaturated 3′-nucleosides (17, 18) and/or 2′-deoxy nucleosides (8, 19–21) as side products, thereby increasing the difficulty in isolating the desired product. Further experiments to test the generality of the method are underway and will be reported in due course.

Experimental

General

Melting points were determined on a Fischer-Johns heating stage or a Mel-Temp apparatus, and are uncorrected. The nmr spectra were determined, unless otherwise stated, in deuteriochloroform containing 1% tetramethylsilane as internal standard with either a Varian T-60, a Varian HA 100, or a Varian HR 220 spectrometer. Coupling constants were obtained by measuring spacings of spectra judged to be first order.

Thin-layer chromatography (tlc) was performed on glass plates coated with silica gel (HF-254, E. Merck) to a thickness of 0.3 mm and developed with petroleum ether (35–60°C) – ethyl acetate (1:1) unless otherwise stated. The chromatograms were first viewed under ultraviolet light, then exposed to iodine vapor, and finally sprayed with concentrated sulfuric acid. Heating in an oven is required for complete visualisation.

For column chromatography, E. Merck silica gel (0.05–0.20 mm, 70–325 mesh A.S.T.M.) was used.

6-Chloro-9-(4′,6′-O-benzylidene-2′,3′-dideoxy-2′,3′-C-methylene-(α and β)-D-allopyranosyl)purine, **7**

(*a*) 6-Chloropurine (2 g, 12.9 mmol) was dissolved in 95 ml freshly dried nitromethane and methyl 4,6-*O*-benzylidene-2,3-dideoxy-2,3-*C*-methylene-α-D-allopyranoside **1** (1) (2 g, 7.3 mmol) was added. After refluxing vigorously under anhydrous conditions for 6 h, the reaction mixture was allowed to cool. Evaporation of the solvent afforded a solid residue the nmr spectrum of which indicated the presence of unreacted starting material and a 50:50 mixture[5] of **7**α and **7**β. The product mixture was fractionated on a column of silica with 50% ethyl acetate in petroleum ether (30–60°C) as irrigating solvent. The chromatogram afforded 550 mg of starting material (**1**), 60 mg of pure **7**β, 1.45 g of a mixture of the two anomers (**7**β (R_f 0.29) and **7**α (R_f 0.22)) and about 0.9 g of 6-chloropurine. The total yield of nucleosides was thus calculated to be 71% based on the recovered starting material. A further amount (32 mg) of **7**β could be crystallized out from the mixture with ethyl acetate – petroleum ether as solvent.

(*b*) 6-Chloropurine (200 mg, 1.3 mmol) was dissolved in 20 ml of hot nitromethane and then treated with sodium carbonate (400 mg), silver nitrate (100 mg), and 4,6-*O*-benzylidene-1,2,3-trideoxy-3-*C*-iodomethyl-D-*ribo*-hex-1-enopyranose, **5** (200 mg, 0.56 mmol). After refluxing vigorously under anhydrous conditions for 6 h, the reaction mixture was allowed to cool. Evaporation of the solvent afforded a solid residue, the nmr spectrum of which showed the complete disappearance of the starting material and the presence of the known (3, 4) diene **8** and a 50:50 mixture[4] of **7**α and **7**β. Column chromatography afforded 22 mg of the diene **8** (20% yield) and 125.1 mg of a mixture of **7**α and **7**β (58% yield). A small amount of unreacted 6-chloropurine was also recovered.

For compound **7**β after recrystallization from methanol: mp 222.0–224.5°C; $[\alpha]_D^{23}$ +23.54° (*c* 1, $CHCl_3$); uv λ_{max} (EtOH): 263 nm (ε 10 383) and 257 nm (ε 9161). The nmr parameters are presented in Table 1. *Anal.* calcd. for $C_{19}H_{17}O_3N_4Cl$: C 59.31, H 4.45, N 14.56, Cl 9.21; found: C 59.30, H 4.62, N 14.25, Cl 9.73.

Compound **7**α has not been obtained completely free of **7**β. The nmr parameters shown in Table 1 were obtained on a slightly impure sample.

6-Chloro-9-(4′,6′-di-O-acetyl-2′,3′-dideoxy-(α and β)-D-erythro-hex-2′-enopyranosyl)purine, **10**

Ethyl 4,6-di-*O*-acetyl-2,3-dideoxy-α-D-*erythro*-hex-2-enopyranoside **9** (2 g, 7.7 mmol) was dissolved in a mixture of acetic anhydride (9 ml) and dry benzene (20 ml) and then boron trifluoride etherate (0.02 ml) was added. After stirring at room temperature for 8 h, the light brown solution mixture was poured into ice-cold sodium bicarbonate solution (50 ml) and stirred for 0.5 h. The mixture was then extracted with ether and washed with water. The dried (Na_2SO_4) solution on evaporation afforded a thick syrup from which methanol was evaporated a few times to remove acetic acid. The final syrupy product weighed 1.98 g and showed, on tlc, two overlapping spots of R_f 0.45 and 0.40. The latter was later shown to be the glycosyl acetate **12** and the former was a mixture of the unreacted starting material **9** and the glycal side products **13** and **14**. The nmr spectrum of the product showed that **12** constituted 77% of the mixture and since fractionation could not be effected the mixture was used directly for the following synthesis.

The syrupy mixture containing **12** (1.4 g) was dissolved in nitromethane (50 ml), and 6-chloropurine (1.0 g) was added. The mixture was then refluxed vigorously for 8 h. After removal of the solvent, the solid residue was fractionated on a silica column with 40% ether in benzene as eluant. The first zone afforded 325 mg of a mixture of **13**, **14**, and unreacted **12**. The second zone afforded a pure syrupy sample of the β-nucleoside **10**β (25 mg), and the third a (50:50) mixture of **10**α and **10**β (883 mg). The pure α-nucleoside **10**α (24 mg) was obtained from

[5]Nuclear magnetic resonance estimate based on relative intensity of the (H-1′)'s of (**7**α) and (**7**β) at τ 3.39 and 3.67 respectively.

the fourth zone. The total yield of the nucleosides was thus calculated to be 48% based on compound **9**, or 66% based on the glycosyl acetate **12**.

For **10**α: $[\alpha]_D^{23}$ +65.7° (*c* 1, $CHCl_3$); λ_{max} (EtOH): 263 nm.

For **10**β: $[\alpha]_D^{23}$ +80.5° (*c* 0.5, $CHCl_3$); λ_{max} (EtOH): 263 nm.

Nuclear magnetic resonance parameters are shown in Table 2. The physical constants of **10**α and **10**β are in good agreement with published data for the compounds prepared by another route (8).

*6-Chloro-9-(4′-O-benzoyl-2′,3′,6′-trideoxy-(*α *and* β*)-*D*-erythro-hex-2′-enopyranosyl)purine,* ***18***

Methyl 4-*O*-benzoyl-2,3,6-trideoxy-α-D-hex-2-enopyranoside **16** (12) (1 g) was dissolved in a mixture of acetic anhydride (4.5 ml) and dry benzene (10 ml), and boron trifluoride etherate (0.01 ml) was added. The mixture was stirred at room temperature for 5 h and then worked up as described above for **12**. The syrupy product weighed about 1 g and appeared to be homogeneous on tlc (R_f 0.69 in 50% ether in benzene), although the nmr spectrum showed that there were some glycal derivatives (cf. **13** *and* **14**) in addition to **17**.

The syrupy product mixture (1 g) was dissolved in 30 ml of nitromethane and 6-chloropurine (600 mg) was added. The mixture was then heated in a Wood's alloy bath at a temperature of 200°C for 7 h. After removal of the solvent, the solid residue was fractionated on a silica column with 50% ether in benzene as eluant to afford 154 mg of a mixture of **17** and glycal impurities. The nucleosides obtained from the column had a total weight of 489 mg. The nmr spectrum of the mixture closely resembled that of **10**α and **10**β (Table 2). The composition of the α and β anomers of **18** in the mixture was about 50:50 based on the relative intensity of the signals centered at τ 8.62 and 8.70 for the methyl doublets. The yield of the anomeric mixture of **18** was calculated to be 33% based on compound **16**.

Fractional crystallization of the mixture with hexane afforded 135 mg of pure **18**β: mp 186–188°C; $[\alpha]_D^{23}$ +162.3° (*c* 1, $CHCl_3$); λ_{max} (EtOH): 263 and 232 nm. *Anal.* calcd. for $C_{18}H_{15}O_3N_4Cl$: C 58.31, H 4.08, N 15.11, Cl 9.56; found: C 58.27, H 4.26, N 15.21, Cl 9.53.

Acknowledgements

We are very pleased to acknowledge financial support from the National Research Council of Canada, Environment Canada, and Bristol Laboratories (Syracuse).

1. B. RADATUS and B. FRASER-REID. Can. J. Chem. **50**, 2909 (1972).
2. B. FRASER-REID and B. RADATUS. Can. J. Chem. **47**, 4095 (1969).
3. B. FRASER-REID and B. RADATUS. Can. J. Chem. **48**, 2146 (1970).
4. B. FRASER-REID and B. RADATUS. J. Chem. Soc. Perkin Trans. I, 1872 (1975).
5. B. FRASER-REID and B. RADATUS. Can. J. Chem. **50**, 2919 (1972).
6. K. A. WATANABE, D. H. HOLLENBERG, and J. J. FOX. J. Carbohydr. Nucleosides, Nucleotides, **1**, 1 (1974).
7. R. J. FERRIER. J. Chem. Soc. 5443 (1964).
8. M. FUERTES, G. GARCIA-MUNOZ, F. G. DE LAS HERAS, R. MADRONERO, M. STUD, and M. RICO. Tetrahedron, **28**, 4099 (1972).
9. R. J. FERRIER and M. M. PONPIPOM. J. Chem. Soc. C, 553 (1971).
10. A. G. BEAMAN and R. K. ROBINS. J. Org. Chem. **28**, 2310 (1963).
11. L. D. HALL and L. F. JOHNSON. Tetrahedron, **20**, 883 (1964); B. FRASER-REID, B. J. CARTHY, and B. RADATUS. Tetrahedron, **28**, 2741 (1972).
12. M. B. YUNKER, S. Y-K. TAM, D. R. HICKS, and B. FRASER-REID. Can. J. Chem. **54**, 2411 (1976).
13. B. FRASER-REID and B. RADATUS. J. Am. Chem. Soc. **92**, 5288 (1970).
14. J. J. K. NOVAK and F. SORM. Experientia, **18**, 213 (1962).
15. E. E. LEUTZINGER, R. K. ROBINS, and L. B. TOWNSEND. Tetrahedron Lett. 4475 (1968).
16. T. KONDO, H. NAKAI, and T. GOTO. Tetrahedron, **29**, 1801 (1973).
17. E. E. LEUTZINGER, R. K. ROBINS, and C. B. TOWNSEND. Tetrahedron Lett. 3751 (1970).
18. T. KONDO and T. GOTO. Agric. Biol. Chem. **35**, 912 (1971).
19. N. NAGASAWA, I. KUMASHIRO, and T. TAKENISHI. J. Org. Chem. **32**, 251 (1967).
20. E. E. LEUTZINGER, W. A. BOWLES, R. K. ROBINS, and L. B. TOWNSEND. J. Am. Chem. Soc. **90**, 127 (1968).
21. G. J. LOURENS and A. JORDAAN. J. Heterocycl. Chem. **9**, 975 (1972).
22. S. HANESSIAN. Methods Carbohydr. Chem. **6**, 183 (1972).

The stereochemistry of conjugate addition of lithium dialkyl cuprate reagents to some carbohydrate α-enones

MARK BERNARD YUNKER,[1] DIETER ERNEST PLAUMANN, AND BERT FRASER-REID

Guelph-Waterloo Centre for Graduate Work in Chemistry, Waterloo Campus, University of Waterloo, Waterloo, Ont., Canada N2L 3G1

Received April 11, 1977

MARK BERNARD YUNKER, DIETER ERNEST PLAUMANN, and BERT FRASER-REID. Can. J. Chem. **55**, 4002 (1977).

Conjugate addition–alkylation reactions of lithium dialkyl cuprates to hex-2-enopyrano-4-ulosides (**1**), hex-3-enopyrano-2-ulosides (**2**), and hex-1-enopyrano-3-uloses (**3**) have been investigated. Extensive studies with **1** show that the homogeneous system using the soluble tri-*n*-butylphosphine copper(I) complex is less satisfactory than the heterogeneous medium in which copper(I) iodide is used. The use of Grignard reagents versus alkyl lithiums has also been investigated, the latter being found preferable. 1,2-Addition was observed in some cases, but conditions were developed to avoid formation of these side products.

With α-enones **1** and **2** alkylation is completely stereoselective, the newly introduced alkyl group being in axial orientation. With **3** a complex mixture is obtained from which equatorial and axial adducts can be isolated in approximately equal amounts.

MARK BERNARD YUNKER, DIETER ERNEST PLAUMANN et BERT FRASER-REID. Can. J. Chem. **55**, 4002 (1977).

On étudie les réactions conjuguées d'addition–alkylation des dialkyl cuprates de lithium aux hexéno-2 pyrannoulosides-4 (**1**), hexéno-3 pyrannoulosides-2 (**2**) et hexéno-1 pyrannoulose-3 (**3**). Une étude développée sur **1** montre que le système homogène utilisant le complexe soluble tri-*n*-butylphosphine–cuivre(I) est moins satisfaisant que le milieu hétérogène dans lequel l'iodure de cuivre(I) est utilisé. On étudie aussi l'utilisation des réactifs de Grignard par rapport aux alkyllithiums, ces derniers ayant été trouvés préférables. Dans quelques cas, on observe une addition-1,2, mais les conditions sont développées de façon à avoir le moins de ces produits secondaires.

Avec les énones-α **1** et **2**, l'alkylation est entièrement stéréosélective et le groupement alkyle introduit a une orientation axiale. En utilisant **3**, un mélange complexe est obtenu dans lequel des adduits axiaux et équatoriaux peuvent être isolés dans des quantités approximativement égales.

[Traduit par le journal]

A programme of research in this laboratory involves the preparation of unsaturated derivatives of sugars and investigation of their usefulness for introducing new functionality into the pyranose ring (1). In pursuing this objective we have developed efficient syntheses of the α-enones **1** (2), **2** (3), **3** (4), and **4** (5), each of which opens the possibility for attaching new substituents at one, two, or three different sites of the molecule. Carbon–carbon branched sugars are of particular importance in view of their omnipresence among the major antibiotics. As a result we have investigated the stereochemical course of alkylation of enones **1**, **2**, and **3** and we report our findings herein. In accompanying papers (6, 7) we describe some photoalkylation reactions of these receptors.

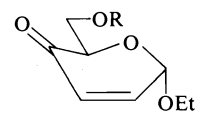

1

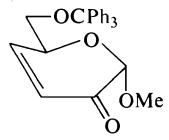

2

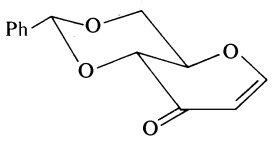

3

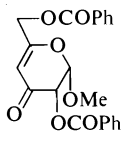

4

Lithium dialkyl copper(I) complexes are the preferred reagents for achieving conjugate-addition–alkylation of α-enones (8) and although the mechanism of the reaction has not been established firmly (9), it is apparent that the course of addition is strongly influenced by steric factors (10).

The reagent may be generated in either

[1]Taken in part from the Ph.D. Thesis of M. B. Yunker, University of Waterloo, 1975. Holder of NRCC Studentships 1972–1975. Present address: Chemistry Department, University of Victoria, Victoria, B.C., Canada.

TABLE 1. Copper(I) induced addition of alkyl residues to some carbohydrate α-enones

Entry	Substrate	Organoalkyl (4 equiv.)	Equivalents of nBu$_3$PCuI	1,4-Adduct (% yield)[a]	1,2-Adduct (% yield)[a]
1	**1***a*	MeMgI	2.00	**5***a* (50)	**6***a* (trace)
2	**1***a*	MeLi	0.02	**5***a* (29)	**6***a* (19 and 7)
3	**1***a*	MeLi	2.00	**5***a* (79)	**6***a* (trace)
4	**1***b*	MeMgI	2.00	**5***b* (88)	**6***b* (2 and 1)
5	**1***b*	MeLi	0.02	**5***b* (64)	**6***b* (16 and 21)
6	**1***b*	MeLi	2.00	**5***b* (94)	None
7	**1***b*	C_2H_3MgBr	2.00	**5***c* (40)	**6***c* (10)
8	**1***b*	$LiMe_2Cu$	—	**5***b* (84)	None
9	**2**	$LiMe_2Cu$	—	**12** (83)	None

[a]After isolation by column chromatography.

homogeneous or heterogeneous systems (9) and we decided to examine both.[2]

Additions to Alkyl Hex-2-enopyranosid-4-uloses (1)

Enone **1**, being the most accessible of the three, was used for our preliminary studies. The results in Table 1 show that with the homogeneous systems, the best yields of conjugate addition were achieved with alkyl lithiums rather than Grignards as the organometallic reagents. Also evident from the results is the fact that substantial amounts of the soluble copper complex must be used, and entries 1–3 versus 4–8 indicate the general superiority of the tritylated enone **1***b* for producing **2***b*.

With the heterogeneous system, the yield of adduct was somewhat less (Table 1, entry 8). However, this method is preferable since (*a*) preparation of the phosphine complex and (*b*) chromatography of the reaction product to remove the liberated phosphine are both avoided.

In either case the reaction gave a single 1,4-adduct (Scheme 1). The methyl **5***a* and vinyl **5***c* adducts were characterized as their 2,4-dinitrophenylhydrazones. Adduct **5***b* was detritylated and found to be identical to **5***a*.

The additions are therefore completely stereoselective and because of the sensitivity to steric effects (10), we had anticipated that addition would occur on the side opposite to the aglycon of **1**. However, the nmr spectra of **5** did not allow an unambiguous assignment of orientation. Thus in **5***a*, H-1 was located at 4.71 ppm with an observed spacing, J_{12} = 4.0 Hz. This value seemed consistent with *cis* hydrogens (i.e. axial H-2) as in α-D-*gluco* derivatives (11), implying that the addition had occurred from the *most* hindered side.

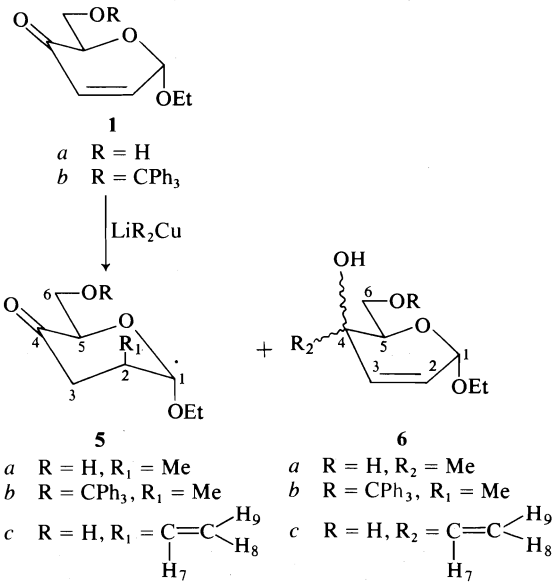

SCHEME 1

In order to gain clarification of this question, **5***a* was reduced with lithium aluminium hydride (Scheme 2). The product, **7**, was evidently a mixture of epimers judging from the elongated 'spot' on thin-layer chromatograms. Although the epimers could not be resolved, the 220 MHz nmr spectrum showed two anomeric protons at 4.47 and 4.57 ppm in the ratio 2:3 respectively, and with associated coupling constants J_{12} = 0.0 and 2.6 Hz. The value of these couplings is definitive evidence (12, 13) for a diequatorial relationship of H-1 and H-2.[3]

[2]Since this work was initially done (14) another soluble copper complex, Me_2S–CuBr, has been developed which is reported to be superior to Bu_3P–CuI (20).

[3]Additional, more rigorous proof for the stereochemistry at C-2 of **5***a* was obtained by correlation with the product from the photochemical addition of methanol to **1** (6, 14).

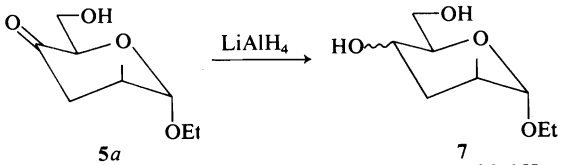

5*a*
J_{12} = 4.0 Hz

7
J_{12} = 0.0 and 2.6 Hz

SCHEME 2

It is evident that changing the hybridization at C-4 from sp^2 (in **5***a*) to sp^3 (in **7**) affects significantly the magnitude of J_{12}. Special caution in making assignments on systems such as these is therefore advisable, particularly since the value, $J_{12} \cong 4$, is usually diagnostic (11, 12) of axial–equatorial protons as in **9**. Thus with the epimers **8** and **9** prepared recently in connection with the

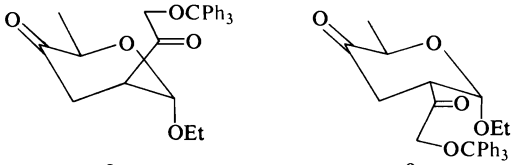

8
J_{12} = 5.2 Hz

9
J_{12} = 4.6 Hz

synthesis of pillarose (15), the J_{12} values are 5.2 Hz for the equatorial–equatorial hydrogens, and 4.6 for the equatorial–axial pair (16).

As indicated in Table 1, (entries 2 and 5) 1,2-addition products were also obtained, especially when smaller amounts of catalyst were employed. These products were recognized by their polar nature on thin-layer chromatograms and, after isolation, by their nmr spectra which showed olefinic signals and their infrared spectra which showed hydroxyl absorptions.

The epimeric tertiary alcohols **6** were usually isolated from chromatograms as syrupy, unstable mixtures. However, one epimer of **6***a* was obtained in sufficient quantity and purity (Table 1, entry 2) to be characterized as its *p*-nitrobenzoate.

There was only one vinyl adduct **6***c* obtained, and it was characterized by its nmr spectrum. The complex olefinic region consisted of superimposed AB(H-2,3) and ABM(H-7,8,9) patterns, and this analysis was verified by computer simulation (Fig. 1).

The orientation of the vinyl group in **6***c* is assigned as equatorial by comparison with the epimeric pair of allylic alcohols **10** and **11** prepared by Walker and Fraser-Reid in connection with the synthesis of pillarose (15). From the nmr data for **6***c*, **10**, and **11** shown in Table 3, it is

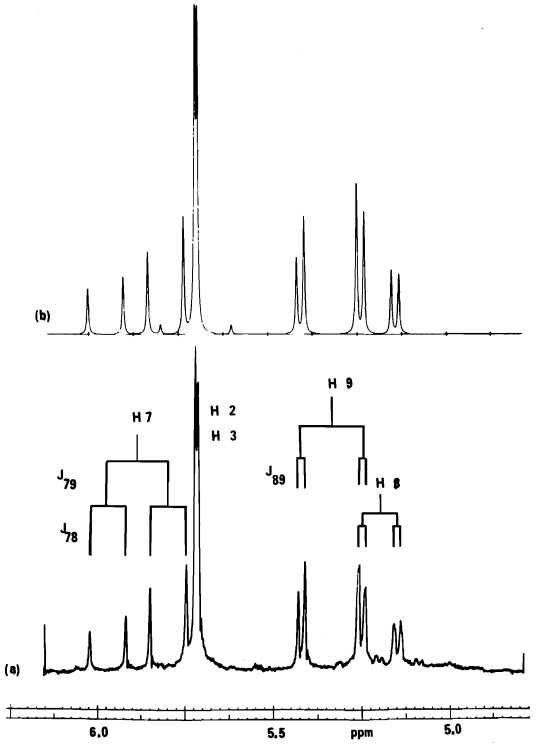

FIG. 1. (*a*) 220 MHz nmr spectrum of ethyl 2,3-dideoxy-4-*C*-vinyl-α-D-*threo*-hex-2-enopyranoside, **6***c*; (*b*) simulated spectrum (see also Table 3).

evident that those of **10** and **6***c* are closer than those of **11** and **6***c*.

It is seen from Table 1 (entries 6 and 8), that by judicious choice of reagent and substrate, the occurrence of 1,2-addition products may be obviated.

Additions to Hex-3-enopyranosid-2-uloses, 2

With the foregoing evidence from enone **1**, we turned our attention to enone **2**. Alkylation using the heterogeneous method (Scheme 3) gave

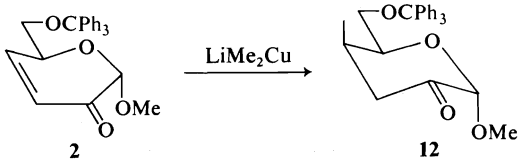

2 **12**

SCHEME 3

a single product, **12**, obtained in 83% yield, there being no evidence of a 1,2-adduct.

The structure of **12** was deduced from its 100 MHz ^{1}H nmr spectrum; data from this spectrum are shown in Table 2. Assignment of the stereochemistry at C-4 rests on information obtained, with the aid of decoupling experiments,

TABLE 2. Nuclear magnetic resonance data for some 1,4- and 1,2-adducts of enones **1**, and **2**[a]

	Chemical shifts in ppm (TMS, $CDCl_3$)									
Adduct	H-1	H-2		H-3eq	H-3ax	H-4	H-5	H-6	H′-6	Alkyl
5*a*[b]	4.71	2.17		2.63	2.29	—	4.16	3.90		CH_3 = 1.25
5*b*[c]	4.70			2.0–2.3		—	4.24	3.50		CH_3 = 1.06
5*c*[b]	4.84	2.80		2.55	2.50	—	4.19	3.90		H-7 5.85 H-8 5.18 } [a] H-9 5.14
6*a*[d] (R_f 0.13)	5.02	5.65		5.92	—	—		3.5–4.2		CH_3 = 1.18
6*a*[d] (R_f 0.07)	5.07		5.85		—	—		3.1–4.2		CH_3 = 1.25
6*b*[d] (R_f 0.29)	4.87	5.57		5.82	—	—		3.1–4.2		CH_3 = 1.26
6*b*[d] (R_f 0.18)	5.03		5.77		—	—	4.19	3.42–3.90		CH_3 = 1.28
12[c]	4.54			2.98	2.20	2.50	~4.5	3.42	3.10	CH_3 = 0.84

	Coupling constants (Hz)[e]								
Adduct	J_{12}	J_{23ax}	J_{23eq}	J_{3ax3eq}	J_{34}	J_{45}	J_{56}	$J_{56'}$	$J_{66'}$
5*a*[b]	3.6	4.0	8.0	15.0	—	—	4.3	[f]	12.0
5*b*[c]	4.0	[f]	[f]	[f]	—	—	3.0	5.5	[f]
5*c*[b]	4.0	5.0	8.0	15.3	—	—	4.5	[f]	11.5

[a]For additional data see Tables 3 and 4, and Experimental. [b]220 MHz. [c]100 HMz. [d]60 MHz. [e]Read directly from the spectra. [f]Not determined.

TABLE 3. Nuclear magnetic resonance data for some 4-*C*-vinyl pyranosides[a]

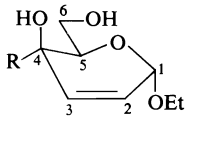

6*c*

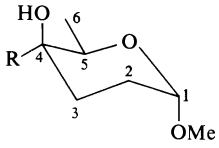

10

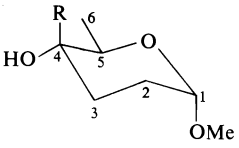

11

R =

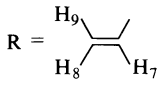

Compound	Chemical shifts (ppm)[b]			Coupling constants[c]		
	H-7	H-8	H-9	J_{78}	J_{89}	J_{79}
6*c*	5.88	5.21	5.35	10.5	1.8	17.1
10[d]	5.80	5.14	5.35	10.0	2.5	15.2
11[d]	6.37	5.31	5.41	10.0	2.5	18.5

[a]For additional data see Experimental.
[b]$CDCl_3$, TMS.
[c]Read directly from 220 MHz spectra run at 250 Hz sweep width.
[d]See refs. 15 and 16.

from the C-3 of methylene protons. Usually with a geminal pair of protons, the equatorial one occurs at lower field than the axial. This trend is increased in **12** by the anisotropy of the carbonyl group (17). Hence H-3 equatorial occurs at 2.98 ppm while H-3 axial is at 2.20 ppm. The signal for H-3 axial appears as a doublet of doublets $J = 15.0$ and 2.5 Hz, the former value being obviously the geminal coupling. The small value of 2.5 Hz is consistent only with an equatorial H-4 proton. The signal for H-3 equatorial is also a doublet of doublets with $J = 15.0$ and 6.0.

Additions to Hex-1-enopyran-3-uloses, 3

With the α-enone **3**, reaction with lithium dimethyl cuprate using either the homogeneous or heterogeneous system (Scheme 4) gave a complex

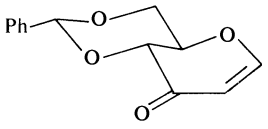

3

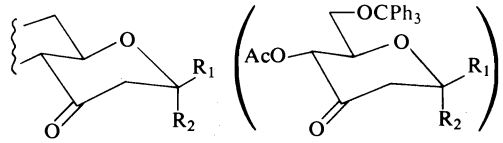

13

a $R_1 = H, R_2 = Me$
b $R_1 = Me, R_2 = H$

14

a $R_1 = H, R_2 = CH_2OAc$
b $R_1 = CH_2OAc, R_2 = H$

SCHEME 4

mixture from which two conjugate addition products **13***a* and **13***b* were isolated by column chromatography in 18 and 20% yields respectively. There was no evidence for 1,2-addition in the other components of the complex mixture.

The stereochemistries of the epimeric pair **13***a* and **13***b* were assigned by comparison with the pair of *C*-glycosides **14***a* and **14***b* prepared by Walker and co-workers (6, 16). The data in Table 4 show that in the case of the equatorial congeners, **13***b* and **14***b*, H-2 resonates at 4.0 and 3.95 ppm respectively while with the axial pair, **13***a* and **14***a*, H-2 is at lower field, 4.6 and 4.76 ppm respectively. Similarly, in **13***b* and **14***b*, H-3 axial is ~2.5 and 2.72 ppm respectively, while in **13***a* and **14***a*, this proton is at 2.93 and 2.94 ppm respectively.

In summary, in the alkylation of enones **1** and **2**, the products of conjugate addition are exclusively axial. This is in agreement with the usually observed course of addition to 2-cyclohexenones (9, 10), as well as the observations of Gero and co-workers on the direction of kinetically controlled addition of nucleophiles to **1** (18). With enone **3**, however, this rule is apparently not obeyed.

Experimental

Melting points were determined in capillary tubes in a Mel-Temp block and are uncorrected. Elemental analyses were performed by Micro-analyses Laboratory, Toronto, Ontario. The nmr spectra ($CDCl_3$, TMS) were determined on a Varian T-60 a Varian HA 100, or a Varian HR-220 spectrometer, the *J* values quoted being the spacing measured directly from the spectra. Infrared spectra were

TABLE 4. Nuclear magnetic resonance data for some *C*-glycopyran-4-ulosides[a]

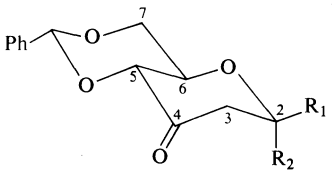

13

a $R_1 = H, R_2 = Me$
b $R_1 = Me, R_2 = H$

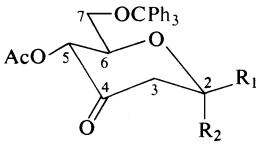

14

a $R_1 = H, R_2 = CH_2OAc$
b $CH_2OAc, R_2 = H$

	Chemical shifts (ppm)[b]			Coupling constants[c]		
Compound	H-2	H-3ax	H-3eq	J_{23ax}	J_{23eq}	J_{3ax3aq}
13*a*	4.60	2.93	2.35	6.0	1.5	14
14*a*	4.76	2.94	2.53	7	2.5	14
13*b*	4.00	2.50			Unresolved	
14*b*	3.95	2.72	2.58		Unresolved	

[a]For additional data see Experimental.
[b]$CDCl_3$, TMS.
[c]Read directly from 220 MHz spectra run at 250 Hz sweep width.
[d]See ref. 6.

determined on a Beckman model IR-10 spectrometer using 0.1 mm sodium chloride solution cells (chloroform as solvent). Optical rotations were determined on a Carl Zeiss model LEP nür 370740 Lichtelektrishes Präzision polarimeter at 23°C.

Thin-layer chromatography was performed on glass plates coated with silica gel (HF-254, E. Merck) to a thickness of 0.3 mm. The following solvent systems were used to develop the plates. Ethyl acetate – petroleum ether (30–60°C) (1:4); ethyl acetate – petroleum ether (30–60°C) (1:1); ethyl acetate; benzene. For column chromatography E. Merck silica gel (0.063–0.20 mm, 70–230 mesh A.S.T.M.) was used.

Ethyl 2,3-Dideoxy-2-C-methyl-α-D-threo-hexopyranosid-4-ulose (5a) and Its 6-O-Triphenylmethyl Derivative (5b)

The procedure in part (*b*) is generally preferred since chromatography is not needed for obtaining pure product.

(*a*) Methyl iodide (0.75 ml, 12 mmol) was added to a suspension of dry magnesium (0.296 g, 12 mmol) in anhydrous ether (20 ml) containing a crystal of iodine, an N_2 atmosphere and efficient stirring being maintained throughout. The mixture was then refluxed until the magnesium had all reacted, after which the solution was cooled to −78°C in a Dry Ice – acetone bath. The desired amount of tri-*n*-butylphosphine copper(I) iodide (19) (see Table 1) was added in ether (~15 ml) to give a bright yellow suspension.

Alternatively, the ethereal solution of tri-*n*-butylphosphine copper(I) iodide was added to methyl lithium at −78°C and diluted with ether to give a bright yellow solution.

In either case, after 15 min the enone **1***a* or **1***b* (3.0 mmol) (2) in ether (30 ml) was added dropwise. The mixture was stirred for 25 min and then poured into stirred saturated aqueous ammonium chloride (0.25 ℓ). The ether layer was separated, the aqueous layer extracted several times with ether, and the ether phases combined and dried. The residue resulting after evaporation was chromatographed on a silica column.

Results of various experiments using differing concentrations of the phosphine catalyst are shown in Table 1.

For compound **5***a* $R_f = 0.34$ in ethyl acetate – petroleum ether (30–60°C) (1:1); nmr data additional to those in Table 2; δ 3.56 and 3.85 (m, 2, $OCH_AH_BCH_3$, $J_{AB} = 9.5$ Hz), 1.25 (t, 3, OCH_2CH_3, $J = 7.0$), 1.11 (d, 3, CH—CH_3, $J = 6.0$).

For the 2,4-dinitrophenylhydrazone of **5***a* recrystallized from ethyl acetate, mp 188.5–189°C; $[\alpha]_D^{23} + 203°$ (*c* 0.51, $CHCl_3$). *Anal.* calcd. for $C_{15}H_{20}N_4O_7$: C 48.91, H 5.47, N 15.21; found: C 48.80, H 5.62, N 15.34.

Compound **5***b* was characterized by detritylation to **5***a*. For **5***b*, $R_f = 0.46$ in ethyl acetate – petroleum ether (30–60°C) (1:4); nmr data for **5***b* additional to those in Table 2: 3.3–4.1 (m, 2, OCH_2, CH_3), 1.24 (t, 3, OCH_2, CH_3, $J = 7.0$ Hz), 1.06 (d, 3, CH—CH_3, $J = 6.5$), 7–7.6 aromatic.

(*b*) Into a dry three-necked round bottom flask equipped with a nitrogen inlet and stirring bar were placed cuprous iodide (22.4 g, 0.118 mol) and anhydrous ether (500 ml). The suspension was cooled to −78°C and methyl lithium (0.238 mol) was added dropwise giving, eventually, a yellow solution. After 0.5 h the enone **1***b* (24.0 g, 0.0585 mol) (1*b*) dissolved in the minimum amount of ether was added dropwise and then stirring was continued for 1 h. The mixture was poured into saturated aqueous ammonium chloride and the product isolated by ether extraction in the usual way. The residue remaining after evaporation (21.0 g, 84%) was usually chromatographically pure **5***b* described above.

Ethyl 2,3-Dideoxy-4-C-methyl-α-D-hex-3-enopyranoside, 6a and its 6-O-Trityl Derivative 6b

If in the reaction described in (*a*), the reactant ratios in entries 3 and 7 (Table 1) were used, quantities of the epimeric tertiary alcohols **6***a* or **6***b* were obtained. These were readily recognized since they moved more slowly on tlc than the major products **5***a* or **5***b* respectively.

For the epimers **6***a*: $R_f = 0.13$ and 0.07 in ethyl acetate – petroleum ether (30–60°C) (1:1).

For component of $R_f = 0.13$: ir 3600 cm^{-1}, no car-

bonyl; nmr data additional to those in Table 2: δ 3.5–4.2 (m, 2, OCH_2—CH_3), 1.25 (t, 3, OCH_2—CH_3), 1.18 (s, 3, C—CH_3) exchangeable OH, J_{12} = 2 Hz, J_{23} = 10 Hz.

p-Nitrobenzoate derivative recrystallized from ether – petroleum ether (30–60°C), mp 83.5–84°C; $[\alpha]_D$ +29.0° (*c* 1.88, in $CHCl_3$). *Anal.* calcd. for $C_{10}H_{19}NO_7$: C 56.97, H 5.68, N 4.15; found: C 56.88, H 5.64, N 4.22.

For component of R_f = 0.07: ir 3600 cm^{-1}, no carbonyl; nmr data additional to those in Table 2: δ 3.3–4.1 (m, 2, OCH_2CH_3), 1.22 (t, 3, OCH_2CH_3), 1.25 (s, 3, C—CH_3) exchangeable OH.

For the epimers of **5***b*: R_f = 0.29 and 0.18 in ethyl acetate – petroleum ether (30–60°C) (1:4).

For compound of R_f = 0.29: ir 3600 cm^{-1}, no carbonyl; nmr data additional to those in Table 2: δ 3.1–4.2 (m, 2, OCH_2CH_3), 1.25 (t, 3, OCH_2CH_3), 1.26 (s, 3, CCH_3), aromatic and exchangeable OH, J_{12} = 3 Hz, J_{23} = 10 Hz.

For component of R_f = 0.18: ir 3600 cm^{-1}, no carbonyl; nmr data additional to those in Table 2: δ 3.2–4.2 (m, 2, OCH_2CH_3), 1.32 (t, 3, OCH_2CH_3), 1.28 (s, 3, CCH_3), aromatic and exchangeable OH.

Ethyl 2,3-Dideoxy-2-C-vinyl-α-D-threo-hexopyranosid-4-ulose, **5***c*

A few crystals of iodine were added to dry magnesium (0.483 g, 20 mmol) in dry tetrahydrofuran (25 ml) and vinyl bromide (1.4 ml, 20 mmol) was added, and the mixture was brought to reflux under a nitrogen atmosphere and with constant stirring. It was necessary to use a Dry Ice–isopropanol condenser during the reflux. After 1 h the magnesium had all reacted. The solution was cooled to −78°C, and tri-*n*-butylphosphine copper(I) iodide (see Table 1) dissolved in ether (~20 ml) was added. Enone **1***a* (0.86 g, 5 mmol) (1b) in ether (40 ml) was added dropwise and the stirring continued for 0.5 h. After the usual work-up procedure (see above) the residue was fractionated on a silica column using ethyl acetate – petroleum ether (30–60°C) (1:1).

For compound **5***c*: R_f = 0.52 in ethyl acetate – petroleum ether (30–60°C) (1:1); nmr data additional to those in Table 2: δ 3.60 and 3.85 (m, 2, $OCH_AH_BCH_3$, J_{AB} = 9.5 Hz), 1.25 (t, 3, OCH_2CH_3, *J* = 7.0 Hz). For —CH_7=CH_8H_9: δ 5.85 (m, 1, H-7, J_{27} = 6.5 Hz, J_{78} = 10 Hz, J_{79} = 17 Hz), 5.18 (d, 1, H-8, J_{89} = 1.25 Hz), 5.14 (d, 1, H-9).

2,4-Dinitrophenylhydrazone of **5***c* was recrystallized from ethyl acetate, mp 175–175.5°C; $[\alpha]_D^{23}$ +144° (*c* 1.13, $CHCl_3$). *Anal.* calcd. for $C_{16}H_{20}N_4O_7$: C 50.53, H 5.30, N 14.73; found: C 50.37, H 5.39, N 14.59.

Ethyl 2,3-Dideoxy-4-C-vinyl-α-D-threo-hex-2-enopyranoside, **6***c*

The chromatographic fractionation described immediately above (see also Table 1) afforded compound **6***c*, R_f 0.19 in ethyl acetate – petroleum ether (1:1); ir 3600 cm^{-1}, no carbonyl; nmr data additional to those in Table 3: δ 3.6–4.2 (m, 2, OCH_2CH_3), 1.25 (t, 3, OCH_2CH_3). For —CH_7=CH_8H_9: δ 5.88 (dd, 1, H-7, J_{78} = 10.25, J_{79} = 17.13), 5.21 (dd, 1, H-8, J_{89} = 1.80), 5.35 (dd, 1, H-9).

Methyl 3,4-Dideoxy-4-C-methyl-6-O-triphenylmethyl-α-D-threo-hexopyranosid-2-ulose, **12**

Into a dry three-necked flask equipped with a stirrer, nitrogen inlet, and dropping funnel was placed 9.0 g (0.047 mol) of cuprous iodide and dry ether (250 ml). The suspension was cooled to −78°C in a Dry Ice – acetone bath, and to it was added dropwise 79 ml of 1.3 *M* methyl lithium (0.102 mol). The solution became clear and a trace of yellow material remained in suspension. After 10 min, a solution of enone **2** (9.5 g, 0.023 mol) in the minimum amount of dry ether was added dropwise. Once the addition was completed, the solution was stirred for a further 45 min and was then poured into aqueous saturated bicarbonate solution (2 ℓ) and stirred for 1 h. The solution was then poured into a separatory funnel and the ether layer was recovered. The aqueous layer was washed with chloroform (2 × 150 ml) and the organic phases were combined and dried (Na_2SO_4). Evaporation under reduced pressure yielded 9.5 g of crude product which was eluted down a column of silica gel using 50% ethyl acetate – petroleum ether (30–60°C). Compound **12** (8.1 g, 83%) was a crystalline substance, mp 164–165°C; $[\alpha]_D^{23}$ +4.6° (*c* 3.10, chloroform); nmr data for **12** additional to those in Table 2: δ 3.56 (s, 3, OCH_3). 7.25–7.60 (m, 15, aromatic), $J_{12} \cong 0$, J_{3ax4} = 2.5, J_{3eq4} = 6.0, J_{3ax3eq} = 15.0, J_{56} = 6.0, $J_{56'}$ = 7.0, $J_{66'}$ = 12.0. *Anal.* calcd. for $C_{26}H_{28}O_4$: C 77.86, H 6.71; found: C 77.98, H 6.71.

2,6-Anhydro-5,7-benzylidene-1,3-dideoxy-D-arabino-hept-4-ulose, **13***a*, *and 2,6-Anhydro-5,7-benzylidene-1,3-dideoxy-D-ribo-hept-4-ulose*, **13***b*

Conjugate addition of methyl to the enone **3** (0.230 g, 1.0 mmol) (4) was carried out as described above for preparation of **5***a*. The two products **13***a* and **13***b* were isolated by silica column chromatography, 0.044 g (20%) and 0.043 g (18%) respectively, using ethyl acetate – petroleum ether (30–60°C) (1:1); R_f = 0.36 and 0.42 respectively.

For compound **13***a*: nmr (60 MHz) δ: 1.32 (d, 3, J_{12} = 8.0 Hz, H-1), 4.60 (ddq, 1, H-2), 2.93 (dd, 1, J_{3a3e} = 14 Hz, J_{23a} = 6, H-3*a*), 2.35 (dd, 1, J_{23e} = 1.5, H-3*e*), 3.5–4.5 (m, 4, H-5, H-6, H-7, H′-7), 5.5–6 (s, 1, H-8), 7.1–7.5 (m, 5, aromatic).

2,4-Dinitrophenylhydrazone: mp 243–243.5°C; $[\alpha]_D^{23}$ −58° (*c* 0.34, $CHCl_3$). *Anal.* calcd. for $C_{20}H_{20}N_4O_7$: C 56.07, H 4.71, N 13.08; found: C 56.04, H 4.62, N 13.09.

For compound **13***b*: nmr (60 MHz) δ: 1.32 (d, 3, J_{12} = 7.0 Hz, H-1), 4.0 (m, 1, H-2), 2.5 (m, 2, H-3*a*, H-3*e*), 3.5–4.7 (m, 4, H-5, H-6, H-7, H′-7), 5.56 (s, 1, H-8), 7.2–7.6 (m, 5, aromatic).

2,4-Dinitrophenylhydrazone: mp (sealed tube) 256–257°C. $[\alpha]_D^{23}$ −128° (*c* 0.20, $CHCl_3$). *Anal.* calcd. for $C_{20}H_{20}N_4O_7$: C 56.07, H 4.71; found: C 55.94, H 4.80.

Acknowledgements

We are very pleased to acknowledge financial support from the National Research Council of Canada, Environment Canada, and Bristol Laboratories (Syracuse).

1. B. Fraser-Reid. Acc. Chem. Res. **8**, 192 (1975).
2. B. Fraser-Reid, A. McLean, E. W. Usherwood, and M. Yunker. Can. J. Chem. **48**, 2877 (1970).
3. N. L. Holder and B. Fraser-Reid. Can. J. Chem. **51**, 3357 (1973).

4. B. FRASER-REID, D. L. WALKER, S. Y.-K. TAM, and N. L. HOLDER. Can. J. Chem. **51**, 3950 (1973).
5. M. B. YUNKER. Ph.D. Thesis, University of Waterloo, Waterloo, Ontario. 1975.
6. B. FRASER-REID, N. L. HOLDER, D. R. HICKS, and D. L. WALKER. Can. J. Chem. This issue.
7. B. FRASER-REID, R. C. ANDERSON, D. R. HICKS, and D. L. WALKER. Can. J. Chem. This issue.
8. H. O. HOUSE, W. L. RESPESS, and G. M. WHITESIDES. J. Org. Chem. **31**, 3128 (1966).
9. G. H. POSNER. Org. React. **19**, 1 (1972).
10. J. A. MARSHALL and H. ROEBKE. J. Org. Chem. **33**, 840 (1968); E. PIERS, W. DE WAAL, and R. W. BRITTON. Can. J. Chem. **47**, 4299 (1969); E. PIERS, W. M. PHILLIPS-JOHNSON, and C. BERGER. Can. J. Chem. **53**, 1291 (1975); C. J. SIH, R. G. SALOMON, P. PRICE, R. SOOD, and G. PERUZZOTTI. J. Am. Chem. Soc. **97**, 857 (1975).
11. R. U. LEMIEUX, R. K. KULLNIG, H. J. BERNSTEIN, and W. G. SCHNEIDER. J. Am. Chem. Soc. **81**, 6098 (1958).
12. G. KOTOWYCZ and R. U. LEMIEUX. Chem. Rev. **73**, 669 (1973).
13. B. COXON. Methods Carbohydr. Chem. **6**, 513 (1972).
14. B. FRASER-REID, N. L. HOLDER, and M. B. YUNKER. J. Chem. Soc. Chem. Commun. 1286 (1972).
15. D. L. WALKER and B. FRASER-REID. J. Am. Chem. Soc. **97**, 6251 (1975).
16. D. L. WALKER. M.Sc. Thesis, University of Waterloo, Waterloo, Ontario. 1975.
17. R. H. BIBLE. Interpretation of NMR spectra. Plenum Press, New York, NY. 1965. Chapt. 3.
18. J. CLEOPHAX, S. D. GERO, E. JEGOU-AUMONT, J. LEBOUL, and D. MERCIER. J. Chem. Soc. Chem. Commun. 11 (1975); J. CLEOPHAX, S. D. GERO, and J. LEBOUL. J. Chem. Soc. Chem. Commun. 710 (1973).
19. G. B. KAUFFMAN and R. P. PINAREL. Inorg. Synth. **6**, 3 (1960).
20. H. O. HOUSE, C-Y. CHU, J. M. WILKINS, and M. J. UMEN. J. Org. Chem. **40**, 1460 (1975).

Analyse de quelques processus photophysiques chez les dérivés diphénylés en position 4 du γ-pyranne et du γ-thiopyranne

GABRIEL LORD,[1] LUC FOISY, LUCIE BARIL,
DENIS GRAVEL ET GILLES DUROCHER

Département de chimie, Université de Montréal, C.P. 6210, Succ. A, Montréal (Qué.), Canada H3C 3V1

Reçu le 5 avril 1977

GABRIEL LORD, LUC FOISY, LUCIE BARIL, DENIS GRAVEL et GILLES DUROCHER. Can. J. Chem. **55**, 4010 (1977).

L'étude des processus photophysiques ainsi que de la photolyse des dérivés diphénylés en position 4 du γ-pyranne (**1**) et du γ-thiopyranne (**2**) est discutée dans cet article. Les effets de solvants, de températures et de variations dans l'intensité de la source photolytique sont parmi les paramètres expérimentaux utilisés lors de cette étude. Il est démontré que la première transition électronique singulet–singulet chez les molécules (**1**) et (**2**) est de nature ππ*. Les chromophores divinyléther et divinylthioéther contribuent à la première transition électronique de ces molécules et également ils participent à la désactivation non-radiative de l'état premier singulet excité de ces molécules. Par ailleurs, l'énergie de l'état triplet ππ* inférieur semble surtout localisée dans les groupements phénylés.

Il est également démontré que la photolyse du diphényl-4,4 pyranne (**1**) s'effectue suivant un mécanisme monomoléculaire pour produire une photoaldéhyde qui à son tour est décomposée sous l'effet du rayonnement. Il est de plus montré que cette aldéhyde est un photoproduit secondaire dans la séquence photoréactionnelle du diphényl-4,4 pyranne.

GABRIEL LORD, LUC FOISY, LUCIE BARIL, DENIS GRAVEL, and GILLES DUROCHER. Can. J. Chem. **55**, 4010 (1977).

The photophysical processes along with the photolysis of 4,4-diphenyl-γ-pyran (**1**) and 4,4-diphenyl-γ-thiopyran (**2**) are discussed in this paper. The solvent effect, the temperature effect, and the photolytic source intensity dependence of the yield of the secondary photoproduct are all among the experimental parameters investigated. It is shown that the first singlet–singlet electronic transition in molecules **1** and **2** is ππ* in nature. The divinyl ether and divinyl thioether chromophore play a role in this transition and also directly contribute to the radiationless deactivation of the first excited singlet states of these molecules. On the other hand the energy of the first triplet ππ* state seems to be more localized in the phenyl groups of the molecules **1** and **2**.

It is also shown that the photolysis of molecule **1** occurs by a monomolecular mechanism to produce a photoaldehyde which is also photolysed under prolonged irradiation. This aldehyde has also been shown to be a secondary photoproduct in the photoreaction sequence of 4,4-diphenyl-γ-pyran.

Introduction

Dans le cadre plus général de l'étude des propriétés photophysiques et photochimiques de systèmes divinyliques cycliques substitués par différents hétéro atomes en position 1 du cycle, nous rapportons dans ce travail le comportement photophysique de deux molécules types: le diphényl-4,4 γ-pyranne (**1**) et le diphényl-4,4 γ-thiopyranne (**2**).

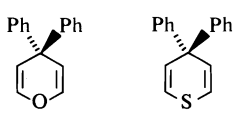

1 **2**

[1]Etudiant au doctorat, boursier du Ministère de l'éducation du Québec.

Alors que peu de réactions photochimiques ont été étudiées aussi intensément que le réarrangement di-π-méthane surtout par le groupe de Zimmerman et ses collaborateurs (1–3), on ne relève que deux études dans la littérature sur les dérivés disubstitués en position 4 du pyranne et ce sont des substitutions de type aryl-benzyl (4, 5). Récemment, Gravel et coll. ont publié la synthèse de même qu'une étude photochimique du diphényl-4,4 γ-pyranne (6). A notre connaissance, aucune étude spectroscopique ni photophysique des dérivés disubstitués en position 4 du pyranne et du thiopyranne n'a été publiée jusqu'à ce jour. Ce travail s'insère dans le projet d'étude de la photochimie et de la spectroscopie des chromophores du type —C—C—O—C—C— et —C—C—S—

C—C—. Deux articles sur ces derniers ont déjà été publiés (7, 8).

Conditions expérimentales

Produits chimiques

Le diphényl pyranne (**1**) et le diphényl thiopyranne (**2**) ont été synthétisés puis purifiés par recristallisation et sublimation par Gravel et coll. (6). Le méthyl-3 pentane utilisé comme solvant était de marque "Pure grade" de la compagnie Phillips Petroleum. Il a été traité sur H_2SO_4, distillé, neutralisé puis redistillé sur sodium. L'éthanol 95% de marque commerciale a été distillé sur H_2SO_4 puis redistillé sur sodium. Ces deux solvants ainsi traités formaient de beaux verres à 77 K dans des tubes cylindriques de 3 mm de diamètre intérieur ou encore dans des cellules rectangulaires de 2 mm de parcours optique. De plus l'intensité de l'émission provenant des impuretés résiduelles étaient nettement inférieure par un facteur 10 environ à l'intensité des émissions provenant des molécules **1** et **2**.

Mesures spectrales

Les spectres d'absorption ont été enregistrés à la température ambiante ainsi qu'à 77 K sur un spectrophotomètre Cary 17 et également dans quelques cas (pour les cinétiques) sur un appareil Spectronic 505 de Bausch and Lomb. Les spectres de fluorescence et de phosphorescence ont été enregistrés à l'aide d'un spectrofluorophosphorimètre Aminco-Bowman à focalisation ellipsoïdale; la correction des spectres en unité de quanta s^{-1} a été décrite antérieurement de même que le module expérimental pour l'observation de la phosphorescence (9). Une lampe xénon a été utilisée à l'excitation avec un arrangement de fentes nous procurant une bande passante de 3 nm.

La méthode d'obtention des rendements quantiques de fluorescence à la température ambiante a déjà été décrite en utilisant le diphényl-9,10 anthracène (DPA) comme substance étalon (10). Alors que l'on continue dans la littérature de référer à deux valeurs bien distinctes pour le rendement quantique de la DPA en solution diluée ($< 5 \times 10^{-5}\ M$) dans le cyclohexane soit 0.83 (11) et 1.0 (12), nous avons utilisé la première valeur pour des raisons déjà énumérées précédemment (10). Les solutions ont d'abord été dégazées et le pourcentage de désactivation de la fluorescence par l'oxygène a été obtenu et utilisé à nouveau pour d'autres solutions, la reproductibilité s'est avérée très bonne. Le rendement quantique de fluorescence à 77 K des molécules **1** et **2** a été obtenu par comparaison des surfaces sous les bandes de fluorescence à la température ambiante et à 77 K. Nous avons alors tenu compte de la variation dans l'indice de réfraction des solvants entre les deux températures de même que de la variation dans la densité optique à la longueur d'onde d'irradiation (13).

Les rendements quantiques de phosphorescence à 77 K des composés **1** et **2** ont été obtenus à l'aide de deux substances étalons différentes avec le même résultat compte-tenu de la précision expérimentale de l'ordre de 15% dans les rendements de phosphorescence. La fluorescence de la DPA à 77 K avec un rendement quantique de 0.83, a été utilisée puisqu'il a été démontré que ce rendement quantique ne dépend pas de la température (13). La phosphorescence du naphtalène à 77 K avec un rendement quantique de 0.06 a également été utilisée (14). Pour chacune des substances étalons la densité optique à 77 K a été ajustée à celle du produit dont le rendement était inconnu à la longueur d'onde d'excitation.

Photolyse

Les irradiations à 2537 Å ont été effectuées avec deux montages différents: *1.* Une lampe au mercure basse pression (Hanovia "Flat Spiral" Z1500-203) a été utilisée dans toutes les mesures de cinétique d'apparition des photoproduits observés. Un dispositif a été conçu pour intercaler des filtres de densité neutre entre le faisceau lumineux produit par cette lampe et l'échantillon à photolyser. Ces filtres de densité neutre faits en grillage métallique possédaient les pourcentages de transmission suivants: 75, 64.6, 50.1 et 27.5%. *2.* D'autres séries d'expériences ont été effectuées dans un réacteur Rayonet.

Résultats et discussion

(1) Spectres d'absorption

Les spectres d'absorption des molécules **1** et **2** sont tracés sur les figs 1 et 2 et cela pour un solvant non polaire et un solvant polaire. Comme on peut le constater l'effet de solvant est minime sur l'énergie du premier système de bandes, un faible effet bathochrome est observé en passant d'un solvant non polaire à un solvant polaire comme l'éthanol. Le second système de bandes à énergie plus élevée est davantage influencé par le solvant, ce qui contribue à expliquer le recouvrement plus marqué des deux premiers systèmes de bandes électroniques de ces molécules dans un solvant comme l'éthanol. Par ailleurs les spectres d'émission sont tout à fait identiques lorsqu'enregistrés dans les solvants polaires et non polaires. Ceci est caractéristique d'une transition $\pi^* \leftarrow \pi$ faiblement permise comme celle observée chez le benzène ($^1B_{2u} \leftarrow {}^1A_g$).

Les coefficients d'extinction molaire confirment également cette dernière attribution. Par soustraction du deuxième système de bandes, nous avons été amenés à mesurer les coefficients d'extinctions molaires (ε) au maximum d'absorption de la première transition électronique de ces molécules: la molécule **1** montre un ε de 440 M^{-1} cm^{-1} à 38 460 cm^{-1} (2600 Å) dans le méthyl-3 pentane (3MP) pour lequel le recouvrement entre les deux systèmes est réduit à son minimum. Par ailleurs ils nous a fallu utiliser l'approximation de la bande de type gaussien à 41 kK pour en déduire un ε de 540 M^{-1} cm^{-1} à 34 250 cm^{-1} dans le 3MP pour la molécule **2**. Les énergies des transitions électroniques pures ($\bar{\nu}_{00}$) ont été évaluées en faisant la moyenne arithmétique

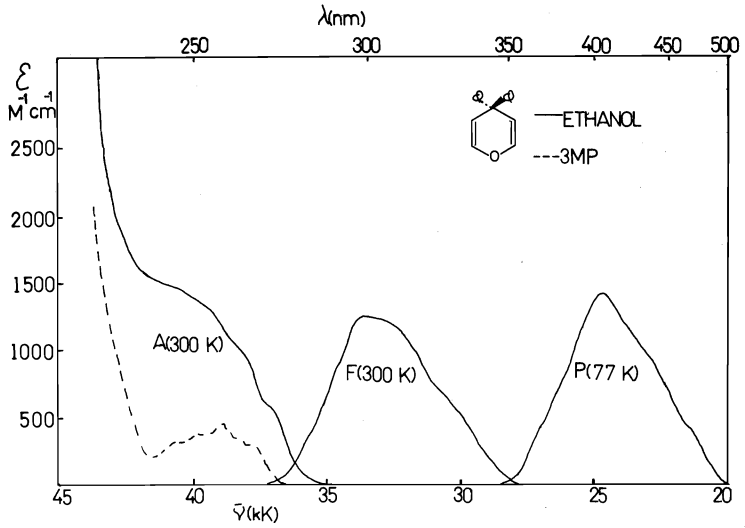

FIG. 1. Spectres d'absorption, de fluorescence et de phosphorescence du diphényl-4,4 pyranne (**1**) dans l'éthanol et dans le méthyl-3 pentane. Les spectres d'émission sont corrigés et tracés en unités relatives de quanta $cm^{-3}\ s^{-1}$ en ordonnée.

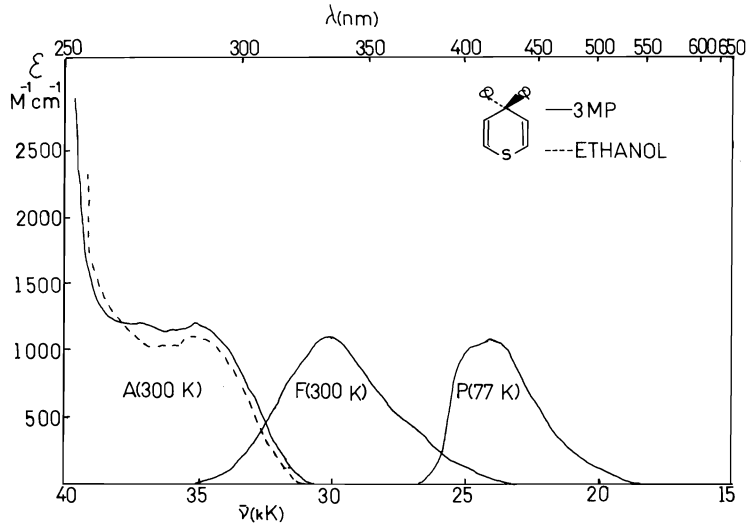

FIG. 2. Spectres d'absorption, de fluorescence et de phosphorescence du diphényl-4,4 thiopyranne (**2**) dans l'éthanol et le méthyl-3 pentane. Les spectres d'émission sont corrigés et tracés en unités relatives de quanta $cm^{-3}\ s^{-1}$ en ordonnée.

entre les maxima en absorption et en fluorescence puisque l'image miroir entre les deux spectres, telle que calculée par la méthode de Birks et Dyson (22), est bonne. En conséquence nous croyons que la configuration électronique des molécules **1** et **2** dans l'état électronique premier singulet excité (S_1) doit s'apparenter à celle dans l'état fondamental (S_0). Les énergies des transitions électroniques pures évaluées sont données dans le tableau 1.

Dans le même tableau nous retrouvons la valeur de la constante radiative théorique k_F telle que calculée à partir des spectres d'absorption des molécules **1** et **2** dans le 3MP. Par examen des spectres corrigés pour le recouvrement, ces valeurs de k_F ne seraient que peu modifiées dans un solvant comme l'éthanol. La méthode de calcul de k_F proposée par Birks et Dyson (11, 15) a été utilisée et ses limites ont été discutées dans un article antérieur (10). Etant donné le recouvrement assez important des deux premiers systèmes de bandes pour la

TABLEAU 1. Paramètres de l'état premier singulet excité (S_1) des diphényl-4,4 pyranne et thiopyranne

	$\bar{\nu}_{max}$[a] (cm^{-1})	ε_{max} ($M^{-1}\,cm^{-1}$)	$\bar{\nu}_{0,0}(S_0-S_1)$ (cm^{-1})	$k_F \times 10^{-6}$ (s^{-1})	$\phi_F \times 10^{3}$[b]	$k_{nr} \times 10^{-9}$[b] (s^{-1})	$\phi_F \times 10^{3}$[c]	$k_{nr} \times 10^{-9}$[c] (s^{-1})
Diphényl-4,4 pyranne (**1**)	38 460	440	35 740	11	1.2	9.2	37	0.29
Diphényl-4,4 thiopyranne (**2**)	34 250	540	32 030	7	1.5	4.7	1.1	6.4

[a]Absorption.
[b]En solution fluide à 300 K, $\lambda_{exc} = 260$ nm.
[c]En matrice vitreuse à 77 K, $\lambda_{exc} = 260$ nm.

molécule **2** surtout, la précision sur ces constantes est de $\pm 2 \times 10^6\ s^{-1}$, ce qui implique que les deux molécules **1** et **2** possèdent la même probabilité intrinsèque d'émettre des photons en fluorescence.

En conclusion, la première transition électronique dans les molécules **1** et **2** semble être de nature $\pi^* \leftarrow \pi$ et de type benzénoïde. L'effet de solvant, la valeur des coefficients d'extinction molaire ainsi que la comparaison des spectres d'absorption et de fluorescence jouent en faveur d'une telle interprétation. Cependant, alors que le benzène absorbe à 38 400 cm^{-1} (bande 0–0) dans un solvant non polaire, la première transition de la molécule **1** a subit un déplacement bathochrome de 2660 cm^{-1} et celle de la molécule **2** a subit un déplacement bathochrome de 6370 cm^{-1} par rapport au benzène. Nous croyons que ceci démontre une participation du chromophore divinyléther à la première transition électronique de ces molécules. Bien qu'il soit généralement admis que les électrons *d* du soufre ne jouent pratiquement pas de rôle dans l'énergie de la transition $\pi\pi^*$ de chromophores semblables —C=C—S—C=C— (7, 16), l'électronégativité du soufre étant identique à celle du carbone, il a été proposé que chez le thiophène la délocalisation des électrons p–π du soufre sur le noyau aromatique puisse expliquer le déplacement bathochrome de 6000 cm^{-1} de la première transition $\pi\pi^*$ du thiophène comparé à celle du furane qui est l'analogue oxygéné (17, 18). La participation du chromophore divinyléther semble donc être impliquée dans la première transition électronique des molécules **1** et **2**. Une preuve irréfutable serait obtenue si les spectres du diphényl tétrahydropyranne et tétrahydrothiopyranne étaient disponibles.

(2) Spectres d'émission et rendements quantiques

(A) Fluorescence

Les spectres de fluorescence et de phosphorescence des molécules **1** et **2** sont reproduits aux figs 1 et 2. Ces spectres sont totalement indépendants du solvant qu'il soit polaire ou non polaire et ceci aussi bien en ce qui concerne l'énergie des transitions que pour les rendements quantiques. Le spectre d'action corrigé de ces fluorescences se superposent en tout point aux spectres d'absorption. Les spectres de fluorescence forment une image en miroir avec le spectre d'absorption dans des conditions de résolution spectrale identiques. Ceci nous permet d'utiliser avec une bonne approximation la constante de désactivation radiative théorique k_F comme paramètre dans l'étude cinétique de l'état S_1 de ces molécules (10). Les rendements quantiques de fluorescence sont rapportés au tableau 1 pour une excitation à 260 nm dans l'éthanol. Ce sont des valeurs corrigées pour l'effet géométrique et l'effet de concentration et donc obtenues par extrapolation à une densité optique nulle. Etant donné la faible valeur des rendements, l'erreur relative sur la reproductibilité se situe à 25%. Les rendements ϕ_F sont donc identiques pour les deux molécules étudiées dans les conditions de précision expérimentale actuelle.

Compte-tenu de la définition du rendement quantique de fluorescence: $\phi_F = k_F(k_F + k_{nr})^{-1}$, la constante de désactivation non radiative (k_{nr}) de l'état premier singulet excité des molécules **1** et **2** est rapportée dans le tableau 1. Cette constante non radiative globale est en fait la somme de trois constantes du premier ordre correspondant aux processus de conversion interne $S_1 \rightsquigarrow S_0(k_c)$, d'intercombinaison $S_1 \rightsquigarrow T_1(k_i)$ et de réaction photochimique à l'état $S_1(k_{RS})$. A température ambiante dans un milieu fluide, la conversion interne peut en toute probabilité compétitionner aussi bien avec l'intercombinaison qu'avec la photochimie d'autant plus que les spectres d'absorption de même que les constantes radiatives k_F démontrent claire-

TABLEAU 2. Paramètres de l'état triplet (T_1) des diphényl-4,4 pyranne et thiopyranne

	$\bar{\nu}_{max}$[a] (cm^{-1})	$\bar{\nu}_{0,0}(S_0-T_1)$ (cm^{-1})	$\phi_p \times 10^3$	τ_p (s)
Diphényl-4,4 pyranne (**1**)	24 500	(27 200)	3.2	1.8
Diphényl-4,4 thiopyranne (**2**)	24 000	(26 700)	2.2	2.1

[a]Phosphorescence.

ment l'influence des groupements phényliques dans cette première transition électronique. Examinons l'effet du milieu sur la constante non radiative k_{nr}.

(A.1) Effet de la température et/ou de la rigidité du milieu sur les rendements de fluorescence—Alors que les intensités intégrées des spectres d'absorption des molécules **1** et **2** ne sont pas modifiées en passant d'un milieu fluide à température ambiante à un milieu vitreux à 77 K, le rendement quantique de fluorescence du dérivé oxygéné (**1**) est augmenté par un facteur 30 à 77 K pendant que le rendement ϕ_F du dérivé soufré (**2**) n'est pas affecté par la température ou la rigidité du milieu comme le démontre les résultats au tableau 1. Etant donné que la formation du photoproduit primaire est probablement l'étape cinétique lente dans le processus de décomposition de la molécule (**1**), et étant donné que nous avons vérifié que la vitesse d'apparition du photoproduit aldéhydique (voir sect. 3) sous l'effet de la photolyse à 2537 Å est à peu de chose près inchangée lorsque l'on travaille à la température ambiante ou en matrice vitreuse à 77 K, la variation obtenue dans le rendement quantique ϕ_F de la molécule **1** pourrait surtout être attribuée à l'un ou à l'autre des phénomènes de conversion interne ou d'intercombinaison, bien que l'on ne puisse exclure à coup sur une influence possible de la température sur k_{RS}. Comme il est peu vraisemblable que la probabilité d'intercombinaison diminue par un facteur 30 à 77 K étant donné que l'énergie de la première transition électronique S_0–S_1 dans ces molécules est très peu modifiée par l'abaissement de la température, nous attribuons la variation du rendement ϕ_F surtout à une diminution de la constante k_c dans la molécule **1** lorsque cette molécule est piégée dans une matrice vitreuse. Cette hypothèse possède cependant son corollaire sur la cinétique de la molécule **2**. Ou bien la conversion interne dans cette dernière molécule est constante en fonction de la température (car ϕ_F est constant en fonction de T) ou encore, l'intercombinaison dans la molécule **2** est beaucoup plus probable que dans la molécule **1** rendant $k_c \ll k_i$ aussi bien à 300 K qu'à 77 K. Pour que la deuxième hypothèse soit valable, il faudrait que k_i (**2**) $\geq 10\, k_i$ (**1**) de façon à pouvoir expliquer la compétition entre k_c (**1**) et k_i (**1**) à température ambiante.

(B) Phosphorescence

Les spectres de phosphorescence des molécules **1** et **2** sont représentés aux figs 1 et 2 respectivement. Même si ces spectres de phosphorescence sont pratiquement au même endroit (une différence de 500 cm^{-1} existe entre les deux), il a été vérifié que leurs spectres d'action corrigés correspondent bien aux spectres d'absorption des molécules **1** et **2** à 77 K. La transition (0, 0) en phosphorescence a été évaluée en prenant le nombre d'onde qui correspond au dixième de l'intensité maximale du spectre. Cette valeur ne peut qu'être approximative et elle est exprimée entre parenthèses dans le tableau 2 à côté du nombre d'onde correspondant au maximum Franck–Condon de la transition.

Les rendements quantiques de phosphorescence de même que les durées de vie sont également indiqués au tableau 2. Tout comme pour les rendements de fluorescence, une erreur de 25% sur la reproductibilité de ces rendements a été observée. L'erreur sur la durée de vie n'est cependant que de ± 0.1 s. Les rendements ϕ_p et les temps de vie τ_p des molécules **1** et **2** sont donc pratiquement identiques.

Les spectres de phosphorescence ainsi que la cinétique de l'état T_1 démontrent 1° que l'état triplet de plus basse énergie dans les molécules **1** et **2** est de nature $\pi\pi^*$ et que 2° la phosphorescence de ces molécules est de nature benzénoïde et doit prendre son origine dans l'un ou l'autre des noyaux aromatiques sans être influencée par les hétéroatomes de ces molécules.

Le rendement quantique de phosphorescence est défini comme suit:

$$[1] \qquad \phi_p = \frac{k_i}{k_F + k_{nr}} \frac{k_p}{k_p + k_{ip} + k_{RT}}$$

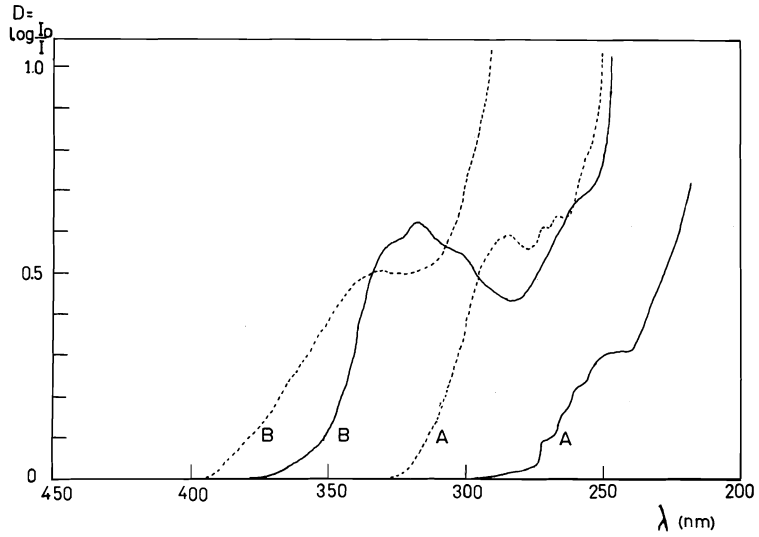

FIG. 3. Spectres d'absorption avant (A) et après (B) un temps de photolyse (2 min pour la molécule (**1**) et 7 min pour la molécule (**2**)) du diphényl-4,4 pyranne (trait continu) et du diphényl-4,4 thiopyranne (trait discontinu) dans le méthyl-3 pentane à température ambiante.

où k_p est la constante de désactivation radiative de l'état triplet, k_{ip} est la constante de désactivation non radiative pour l'intercombinaison $T_1 \rightsquigarrow S_0$ et k_{RT} est la constante de désactivation de l'état triplet par le processus photochimique réactionnel. Du fait que la durée de vie de phosphorescence $\tau_p = (k_p + k_{ip} + k_{RT})^{-1}$, des tableaux 1 et 2 et appliquant [1] aux deux molécules **1** et **2** à 77 K on tire que:

$$[2] \qquad \frac{k_i(\mathbf{2})/k_p(\mathbf{2})}{k_i(\mathbf{1})/k_p(\mathbf{1})} = 13$$

Etant données les valeurs identiques de ϕ_p et de τ_p pour les deux molécules, aucun effet d'atome lourd interne ne peut être mis en évidence (19) et il est alors très probable que $k_p(\mathbf{2}) \simeq k_p(\mathbf{1})$. Ainsi donc, le rapport des constantes pour l'intercombinaison serait de l'ordre $k_i(\mathbf{2}) \cong 10k_i(\mathbf{1})$. Ce résultat vient confirmer la deuxième hypothèse discutée à la sect. A.1 à l'effet que le processus d'intercombinaison $S_1 \rightsquigarrow T_1$ est beaucoup plus probable dans le dérivé soufré que dans le dérivé oxygéné.

En conclusion des parties 1 et 2, les spectres d'absorption ainsi que les cinétiques de l'état S_1 des molécules **1** et **2** semblent démontrer la participation du chromophore divinyléther à la première transition électronique $S_0 \rightarrow S_1$ de type $\pi\pi^*$ de ces molécules. Par ailleurs la transition $T_1 \rightarrow S_0$ semble être indépendante du chromophore divinyléther dans les mêmes molécules. Les spectres de phosphorescence, les rendements de phosphorescence ainsi que les temps de vie semblent démontrer une localisation de l'énergie triplet au niveau des groupements phényliques.

(3) Photolyse et étude du photoproduit aldéhydique

Lorsque l'on irradie à l'aide de lampes "basse pression" (appareil Rayonet) à 2537 Å les molécules **1** et **2** dans le méthyl-3 pentane ou dans l'éthanol, un nouveau système d'absorption électronique apparaît centré à 3180 Å pour la molécule **1** et à 3330 Å approximativement pour la molécule **2** dans le 3MP comme l'indique la fig. 3.

(A) Nature de la transition à 3180 Å

Il a été démontré par Gravel et coll. (6) que l'un des photoproduits secondaires était l'aldéhyde suivant

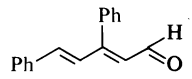

3, diphényl-3,4 pentadiène-2,3 al
(+ isomères géométriques)

Ce produit a été isolé et caractérisé par rmn (6). Il montre un spectre d'absorption tout à fait identique à celui observé sur la fig. 3 avec un maximum à 3180 Å dans le 3MP et une structure fine vibrationnelle assez bien définie dans le même solvant. Cette transition électronique centrée à 3180 Å subit un effet bathochrome dans

un solvant polaire comme l'éthanol et le maximum de la bande se retrouve à 3340 Å soit un déplacement de 1510 cm^{-1}. La photolyse de la molécule **1** en matrice vitreuse de 3MP fait également apparaître avec à peu près la même vitesse la bande du produit aldéhydique qui est cependant déplacée vers le rouge (3300 Å) comparativement au spectre à température ambiante, le déplacement est de 1150 cm^{-1}.

Le fait que la réaction photochimique s'effectue avec approximativement la même facilité en milieu fluide et en milieu rigide démontre que l'apparition de l'aldéhyde doit s'effectuer par l'intermédiaire d'un mécanisme monomoléculaire. D'autre part, les effets de solvant sur la position de la bande d'absorption de l'aldéhyde démontre que cette transition est de nature $\pi\pi^*$. Dans le cas de la molécule **2**, la réaction photochimique semble procéder par le même mécanisme, la bande dont le maximum est mal défini vers 3400 Å serait la bande caractéristique de la première transition $\pi\pi^*$ de la thioaldéhyde correspondante. La bande s'étend jusque dans la région du visible et doit englober la transition $n \rightarrow \pi^*$ aux plus grandes longueurs d'onde (20).

*(B) Cinétique d'apparition et de disparition de l'aldéhyde (**3**)*

A l'aide d'une lampe au mercure "basse pression" (Hanovia flat spiral) focalisée sur une des faces d'une cellule rectangulaire de 1 cm de parcours optique, nous avons observé la variation de la densité optique à 3180 Å en fonction du temps de photolyse de la molécule **1** dans le 3MP. La figure 4 montre cette variation pour deux échelles différentes des temps de photolyse. Le graphique démontre clairement que l'aldéhyde une fois formé est détruite sous l'effet du rayonnement à 2537 Å. Il est évident sur la fig. 3 que l'aldéhyde absorbe fortement à 2537 Å, région correspondante à une transition $\pi\pi^*$ supérieure. La cinétique d'apparition de l'aldéhyde est du premier ordre aux temps de photolyse courts, dans l'intervalle de temps où la décomposition n'affecte pas encore la cinétique de montée. Entre 150 et 400 s de photolyse, l'aldéhyde disparaît en suivant également une loi cinétique du premier ordre pour atteindre un palier aux temps plus longs, ce qui semble démontrer que le produit formé de la photolyse de l'aldéhyde absorbe également à 2537 Å. Ceci confirme que l'apparition de l'aldéhyde est un phénomène monomoléculaire ainsi que sa disparition.

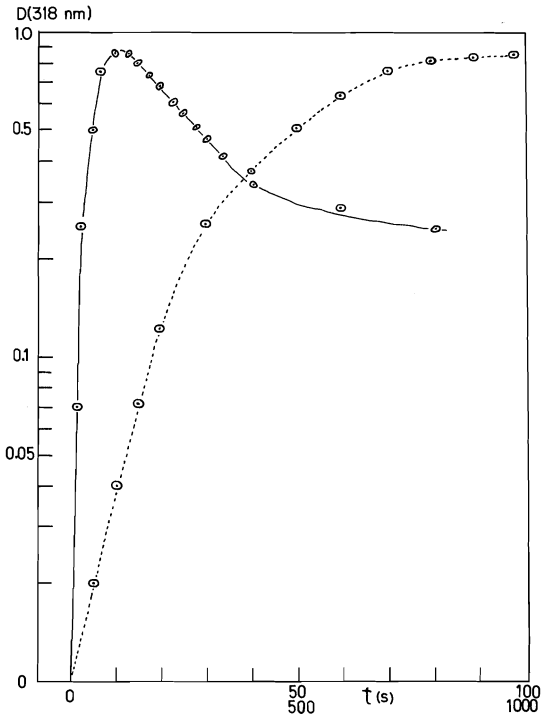

FIG. 4. Variation du logarithme de la densité optique du photoproduit aldéhydique (**3**) en fonction du temps de photolyse de la molécule (**1**) dans le méthyl-3 pentane ($C = 1.22 \times 10^{-4}$ *M*) avec la raie du mercure à 2537 Å. (---) correspond à l'échelle 0–100 s en abscisse; (—) correspond à l'échelle 0–1000 s en abscisse.

*(C) Effet de l'intensité de la lampe photolytique sur la vitesse d'apparition de l'aldéhyde (**3**)*

Des filtres de densité neutre décrits à la partie expérimentale ont été intercalés entre la source photolytique et la cellule optique. La densité optique de l'aldéhyde à 3180 Å a été mesurée pour un temps de photolyse fixe de 20 s, temps où l'apparition de l'aldéhyde obéit à une loi cinétique du premier ordre comme en fait foi la fig. 4. Une solution fraîche (1.22×10^{-4} *M*) du produit **1** a été photolysée pour chacun des quatre filtres utilisés. De la relation générale existant entre la vitesse d'une réaction photochimique et l'intensité de la lumière absorbée (I_a), on tire pour de faibles densités optiques que $D = aI_0^n$ où I_0 est l'intensité de la lumière excitatrice (21). Une valeur de $n = 1.9 \pm 0.1$ a été obtenue montrant bien que deux photons à 2537 Å sont nécessaires pour produire une molécule d'aldéhyde **3**. L'aldéhyde est donc un photoproduit secondaire provenant d'un photoproduit primaire suite à l'irradiation de la molécule **1**.

Gravel et coll. (6) ont récemment isolé et caractérisé les produits secondaires suite à une irradiation de la molécule **1** à 2537 Å en plus de mettre en évidence l'unique photoproduit primaire de la réaction. La séquence réactionnelle proposée est la suivante dans l'alcool *t*-butylique comme solvant:

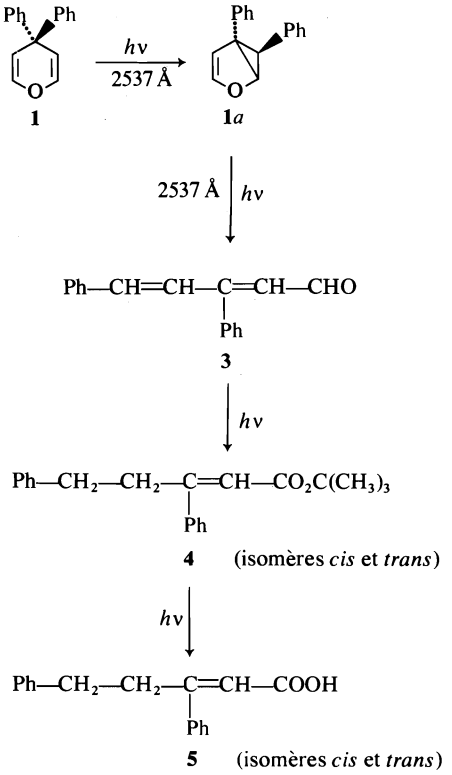

Le diphényl-5,6 bicyclo [3.1.0] oxa-2 hexène-3 *trans endo* (**1***a*) est en fait l'unique photoproduit primaire formé à la suite du réarrangement di-π-méthane (6). Les autres produits isolés: **3**, **4** et **5** ainsi que les isomères géométriques résulteraient de l'irradiation du photoproduit primaire et de l'irradiation subséquente des sous-produits secondaires. Etant donné que les molécules **1***a*, **4** et **5** absorbent dans la région de 2800–2300 Å, la spectroscopie ultraviolette ne peut en aucun cas les caractériser. Cependant l'étude cinétique effectuée sur l'aldéhyde **3** et décrite plus haut confirme en tout point cette séquence réactionnelle. En effet l'apparition du photoproduit **3** doit obéir à une loi cinétique du premier ordre et de plus sa vitesse d'apparition doit être proportionnelle au carré de l'intensité de la lumière absorbée par la molécule **1** c'est-à-dire proportionnelle au carré de l'intensité de la source de photolyse aux faibles densités optiques du produit **1**. Par ailleurs, nous avons aussi montré que la molécule **3** se décompose également par un mécanisme cinétique de premier ordre au cours de l'irradiation continue à 2537 Å confirmant ainsi que les molécules **4** et **5** sont des photoproduits secondaires obtenus de la photodécomposition de l'aldéhyde **3**.

Remerciements

Cette étude a été subventionnée par le Conseil national de recherches du Canada et par le Ministère de l'éducation du Québec. L'un de nous (G.L.) a bénéficié de l'octroi d'une bourse du Ministère de l'éducation du Québec.

1. H. E. Zimmerman, R. J. Boettcher, N. E. Buehler, G. E. Keck et M. G. Steinmetz. J. Am. Chem. Soc. **98**, 7680 (1976).
2. C. Santiago, K. N. Houk, R. A. Snow et L. A. Paquette. J. Am. Chem. Soc. **98**, 7443 (1976).
3. S. S. Hinson, P. S. Mariano et H. E. Zimmerman. Chem. Rev. **73**, 531 (1973).
4. K. Dimroth, K. Wolf et H. Kroke. Ann. Chem. **678**, 183 (1964).
5. N. K. Cuong, F. Fournier et J. J. Basselier. C. R. Acad. Sci. Ser. C, **271**, 1626 (1970); N. K. Cuong, F. Fournier et J. J. Basselier. Bull. Soc. Chim. Fr. 2117 (1974).
6. D. Gravel, C. Leboeuf et S. Caron, Can. J.Chem. **55**, 2373 (1977).
7. A. A. Planckaert, J. Doucet et C. Sandorfy. J. Chem. Phys. **60**, 4846 (1974).
8. G. Leduc et Y. Rousseau. Can. J. Chem. **53**, 483 (1975).
9. D. Muller, M. Ewald et G. Durocher. Can. J. Chem. **52**, 407 (1974).
10. Y. Beauchamp et G. Durocher. Spectrochim Acta, Part A, **32**, 269 (1976).
11. J. B. Birks. J. Res. Nat. Bur. Stand., Sect. A, **80**, 389 (1976).
12. W. R. Ware et W. Rothman. Chem. Phys. Lett. **39**, 449 (1976).
13. W. N. Mantulin et J. R. Huber. Photochem. Photobiol. **17**, 139 (1973).
14. H. M. Rosenberg et S. D. Carson. J. Phys. Chem. **72**, 3531 (1968).
15. J. B. Birks et D. J. Dyson. Proc. R. Soc. London, Ser. A, **275**, 135 (1963).
16. R. A. W. Johnstone et S. D. Ward. Tetrahedron, **25**, 5485 (1969).
17. H. C. Longuet-Higgins. Trans. Faraday Soc. **45**, 173 (1949).
18. H. H. Jaffe et M. Orchin. Theory and applications of ultraviolet spectroscopy. John Wiley & Sons, New York, NY. 1962.
19. V. L. Ermolaev et K. K. Suitashev. Opt. Spectrosc. **7**, 399 (1959).
20. E. S. Stern et C. J. Timmons. Electronic absorption spectroscopy in organic chemistry. 3è éd. St. Martins's Press, New York, NY. 1970. p. 56.
21. J. G. Calvert et J. N. Pitts, Jr. Photochemistry. John Wiley & Sons Inc., New York, NY. 1967. p. 651.
22. J. B. Birks et D. J. Dyson. Proc. R. Soc. London, Ser. A, **275**, 135 (1963).

Salt effects on adsorbed nonelectrolytes

ROBERT AVEYARD AND SYED M. SALEEM
Department of Chemistry, The University, Hull, HU6 7RX, England

Received May 9, 1977

ROBERT AVEYARD and SYED M. SALEEM. Can. J. Chem. **55**, 4018 (1977).

An approach to the study of the influence of electrolytes on adsorbed nonelectrolytes at liquid surfaces is described. The adsorption of tetrabutylammonium bromide (Bu_4NBr) from aqueous solution to the interfaces with octane, decanol, and air has been determined. Results are presented for the effects of some inorganic salts (NaCl, NH_4Br, and Na_2CO_3), and of Bu_4NBr on monolayers of butanol at the air – aqueous solution interface, and of Bu_4NBr on dodecanol adsorbed at the octane – aqueous solution interface. The interfacial salt effects differ from the bulk effects in the cases studied. The inorganic salts, which salt-out butanol (and alkanols generally) in aqueous solution, have little or no effect on adsorbed butanol. On the other hand, Bu_4NBr which salts-in alkanols in bulk aqueous solution has a strong salting-out effect on dodecanol at the liquid–liquid interface; a similar but less marked effect is observed for butanol at the liquid–vapour surface. Salting-in of alkanols by Bu_4NBr in bulk has previously been ascribed to hydrophobic interactions between cations and alkyl groups of the alkanol, whereas the surface effect is assumed to result from interactions between alcoholic OH groups and cations.

ROBERT AVEYARD et SYED M. SALEEM. Can. J. Chem. **55**, 4018 (1977).

On décrit une manière d'approche à l'étude de l'influence des électrolytes sur les nonélectrolytes adsorbés à la surface des liquides. L'adsorption du bromure de tétrabutylammonium (Bu_4NBr) provenant d'une solution aqueuse aux interfaces avec l'octane, le décanol et l'air est déterminée. On présente les résultats de l'effet de quelques sels inorganiques (NaCl, NH_4Br et Na_2CO_3), et du Bu_4NBr sur les monocouches de butanol à l'interface air – eau de la solution ainsi que celui du Bu_4NBr sur le dodécanol adsorbé à l'interface octane – eau de la solution. Dans les cas étudiés, les effets interfaciales de sels diffèrent des effets de masse. Les sels inorganiques relarguant le butanol (généralement un alkanol) en solution aqueuse, ont peu ou très peu d'effet sur le butanol adsorbé. D'un autre côté, le Bu_4NBr qui absorbe les alkanols en solution concentrée dans l'eau a un grand effet relarguant sur le dodécanol à l'interface liquide–liquide; un effet similaire mais moins marqué est observé pour le butanol à la surface liquide–vapeur. L'absorption des alkanols par Bu_4NBr en solution concentré a été attribuée antérieurement aux interactions hydrophobiques entre les cations et les groupes alkyles de l'alcanol, tandis que l'effet de surface semble résulter des interactions entre les groupes hydroxyles (des alcools) et les cations.

[Traduit par le journal]

Introduction

A considerable body of literature exists stretching back over several decades, concerning the ways in which electrolytes, both organic and inorganic, influence the chemical potential of nonionic solutes in aqueous solution. Much of the current interest centres on effects of salts on proteins. Frequently the solutes studied have been polar and, to some extent, surface-active (1, 2). The question naturally arises as to what effect electrolyte has on the solute adsorbed at an interface, particularly if the electrolyte itself is surface-active. Only a very limited amount has been reported on interfacial salt effects (3, 4) even though they are intrinsically as interesting as bulk effects, and are likely to be of relevance in a variety of systems, including some of biological and of industrial importance. Of course, there have been many investigations into the effects of inorganic salts on adsorbed *ionic* surfactants in connection with electrical double layer theory (*5a*). In such studies the much smaller effects of the kind reported here are usually neglected.

We have previously studied the ways in which some simple inorganic electrolytes influence alkane–water interfacial tensions (6) and decanol–water interfacial tensions (3). In addition we have considered the effects of NaCl on very dilute adsorbed films of alkanols at the dodecane – aqueous solution interface (3). In the present work we propose an approach to the study of surface salt-effects, and extend previous investigations to take in adsorbed films at air–

solution interfaces, and to include a surface-active organic electrolyte, tetra-*n*-butylammonium bromide, Bu_4NBr.

We are unable at this stage to view our results in terms of theory, as we were in recent studies on bulk salt effects on alkanols (7, 8). Our main aim has been to obtain experimental results to ascertain the magnitude and nature of the effects. Nonetheless, interesting empirical observations emerge which may prove of value in the surface and colloid chemistry of systems involving interfaces which contain polar organic surfactants.

Experimental

Measurement of Surface and Interfacial Tensions

Surface and interfacial tensions were determined, as described in ref. 9, using the drop-volume technique in conjunction with the smoothed correction factors of Harkins and Brown (10). The apparatus was immersed in a water thermostat maintained at the required temperature to within ± 0.01 K. All necessary densities were determined to within $\pm 2 \times 10^{-4}$ g cm^{-3} using a 25 cm^3 density bottle. Surface tensions were reproducible to better than ± 0.10 mN m^{-1}, and interfacial tensions to better than ± 0.05 mN m^{-1}.

Distribution of Bu_4NBr between Water and Decanol

This salt is soluble in decanol, and in order to calculate equilibrium concentrations in the aqueous phase, as required for the determination of adsorption at the decanol–solution interface, we have determined distribution ratios, K, defined as (salt molality in water)/(salt molality in decanol). Weighed amounts of decanol, water, and Bu_4NBr were placed in stoppered conical flasks and immersed in a water thermostat at 25°C for at least 24 h, with frequent shaking of the flasks. Weighed amounts of aqueous phase were then withdrawn and analysed for Bu_4NBr, in terms of Br^- concentration using the Volhard method. The amount of salt in the decanol phase was estimated by mass balance. The values of K, given in Table 1, cannot be regarded as being very precise since in the presence of Bu_4NBr the mutual low solubilities of water and decanol may be enhanced, and this has not been allowed for. As far as this system is concerned, however, we have only sought to obtain rough adsorption values, as mentioned later

Materials

Two samples of *n*-octane, *puriss* grade from Newton-Maine (England), were passed over chromatographic alumina before use, and each had a purity (estimated, as were other quoted purities, by glc) of >99.5%. One sample had an interfacial tension against water at 20°C of 51.55 mN m^{-1}, and the other 51.71 mN m^{-1}. Dodecanol (*puriss* grade from Koch-Light, England) was redistilled using a spinning band fractionating column, and had a purity >99.9%. A Fluka *puriss* sample of butanol was found to have a purity $\simeq$99.8% and was used without further treatment.

The inorganic salts (NaCl, NH_4Br, and Na_2CO_3) were all 'Analar' grade from Hopkin and Williams, England, and were treated as described in ref. 6. Tetrabutylammonium bromide was obtained from Eastman, with a quoted purity (by titration) of at least 98%. It was further purified in the way described by Conway *et al.* (11).

All water used was twice distilled, the second time using an all-Pyrex glass still. The best test of purity in the present context is the surface tension. Our values of 72.67, 71.89, and 71.14 $\pm$ 0.10 mN m^{-1} at 20, 25, and 30°C, respectively, are in very good agreement with those (72.75, 71.97, and 71.18 $\pm$ 0.05 mN m^{-1} respectively) quoted in the International Critical Tables (12).

TABLE 1. Values of K for Bu_4NBr distributed between water and decan-1-ol at 25°C, for various aqueous phase molalities, m, of salt

K	$10m$	K	$10m$
2.78	0.600	0.86	1.717
2.72	0.702	0.76	2.188
1.70	1.002	0.72	3.234
1.68	1.051	0.73	3.251
0.84	1.594	0.68	5.162

Results

Adsorption of Tetrabutylammonium Bromide

Unlike the inorganic salts discussed later, Bu_4NBr is positively adsorbed at the interfaces of present interest, and it is the *adsorbed* salt which gives rise to the salt effects on adsorbed nonelectrolytes. We have therefore determined the extent of adsorption at the octane–solution (o–s), air–solution (a–s), and decanol–solution (d–s) interfaces, using interfacial tensions measured in the present work,[1] in conjunction with the Gibbs equation.

The Gibbs adsorption equation for an i-component system is

$$[1] \quad -d\gamma = \sum_i \Gamma_i \, d\mu_i = \Gamma_o \, d\mu_o + \Gamma_w \, d\mu_w + \Gamma_{A^+} \, d\mu_{A^+} + \Gamma_{Br^-} \, d\mu_{Br^-}$$

where γ is the interfacial tension and Γ_i the surface excess of i; subscripts o, w, and A^+ refer to the organic liquid (octane or decanol), water, and Bu_4N^+ respectively. Terms for H^+ and OH^- arising from dissociation of water are negligible, and are omitted from eq. 1.

[1]These interfacial tensions, and others referred to subsequently, are available, at a nominal charge, from the Depository of Unpublished Data, CISTI, National Research Council of Canada, Ottawa, Ont. Canada K1A 0S2.

In octane + water systems $d\mu_o \ll d\mu_{A^+}, d\mu_{Br^-}$ and so $\Gamma_o d\mu_o$ is negligible. For the decanol + water system, where higher concentrations of Bu_4NBr (which is soluble in decanol) are employed, the approximation of neglecting $\Gamma_o d\mu_o$ will be less valid, but in the present context this is probably not important. Choosing a Gibbs dividing surface such that $\Gamma_w = 0$, eq. 1 becomes (*5b*)

$$[2] \quad \Gamma^w_{A^+Br^-} = (0.5/RT)(d\pi/d \ln a_\pm) = (0.5a_\pm/RT)(d\pi/da_\pm)$$

where π is the surface pressure, defined as the lowering of interfacial tension caused by adsorption (so that $-d\gamma = d\pi$), and $a_\pm$ is the mean activity of the electrolyte. For strong adsorption as at the o–s and a–s interfaces, $\Gamma^s_{A^+Br^-}$, the *total* surface concentration of Bu_4NBr, does not differ much from the excess $\Gamma^w_{A^+Br^-}$.

The molal activity $a_\pm$ is equal to $mf_\pm$; m is the molality of electrolyte, and $f_\pm$ the mean molal activity coefficient. For dilute solutions of salt (such as those used for adsorption to the o–s and a–s interfaces) $f_\pm$ differs only slightly from the mean *molar* activity coefficient, $y_\pm$, and hence can be obtained to a very good approximation using an equation of Guntelberg (see ref. 13):

$$[3] \quad f_\pm \simeq y_\pm = \exp\left\{-\frac{4.2021 \times 10^6 c^{1/2}}{(\varepsilon T)^{3/2}(1 + c^{1/2})}\right\}$$

in which c is the salt molarity and ε the relative permittivity of the solution, taken here to be equal to that of water at the appropriate temperature (14). Values of $f_\pm$ from eq. 3 are very close to those obtained by interpolation of the experimental data of Lindenbaum and Boyd (15).

The π–$a_\pm$ data for the various temperatures between 17 and 30°C are, within experimental errors, superimposable both for the o–s and for the a–s interfaces, and can be expressed, for the o–s interface, by

$$[4] \quad \pi/(\text{mN m}^{-1}) = 4.11747 \times 10 + 9.93776 \ln a_\pm + 6.24598 \times 10^{-1} (\ln a_\pm)^2$$

for $m \leq 1 \times 10^{-2}$ mol kg^{-1}, and for the a–s interface by

$$[5] \quad \pi/(\text{mN m}^{-1}) = 6.33503 \times 10^{-2} + 4.55516 \times 10^2 a_\pm - 1.30563 \times 10^4 a_\pm^2$$

for $m \leq 0.9 \times 10^{-2}$ mol kg^{-1}. Combination of [4] or [5] with the appropriate form of [2] yields surface excesses.

In the case of the d–s interface at 25°C we have fitted interfacial tensions to

$$[6] \quad \gamma/(\text{m}M\ \text{m}^{-1}) = -0.66932 - 4.10705 \ln a_\pm - 0.45568 (\ln a_\pm)^2$$

for m (aqueous phase) ≤ 0.33 mol kg^{-1}. In this system both phases contain all three components, and higher concentrations of salt have been used. Values of $a_\pm$ for Bu_4NBr in the aqueous phase have been interpolated directly from the results of Lindenbaum and Boyd (15), and no account has been taken of the effect of decanol in the aqueous phase on $a_\pm$. For this, and other reasons mentioned earlier, surface excesses of Bu_4NBr at the d–s interface are less reliable than those obtained for the o–s and a–s interfaces.

Tamaki (16) has studied the adsorption of Bu_4NX (X = Cl, Br, I) at the a–s and hexane–solution interfaces. The results are not fully reported, however, and are only given in graphical form so that comparisons with our data have not been possible.

Adsorption of Dodecanol at the Octane – Aqueous Bu_4NBr Interface

Dodecan-1-ol, mole fraction x in dilute solution in octane, has been adsorbed to interfaces with aqueous Bu_4NBr of varying molality m at 20°C, and to the interface with 1.26×10^{-3} m Bu_4NBr at several temperatures between 17 and 30°C.

Standard free energies of adsorption, $\Delta_a\mu^\ominus$, for dodecanol have been obtained from the interfacial tensions by use of the expression (*5c*)

$$[7] \quad \mu^{\ominus,\sigma} - \mu^{\ominus,l} = \Delta_a \mu^\ominus = -RT \ln (\lim_{x \to 0} [\pi/x])$$

where $\mu^{\ominus,\sigma}$ and $\mu^{\ominus,l}$ are standard chemical potentials of alcohol in surface and bulk (alkane) respectively, and π is the surface pressure of adsorbed alkanol. The standard states are unit π for the surface and unit x for bulk, both assumed ideal. In the range of x studied, π is a rectilinear function of x (see Fig. 1*a*) and $\lim_{x \to 0} [\pi/x]$ is equal to the slope of this line. Values of $\Delta_a\mu^\ominus$ are given in Table 2, and their significance is discussed later.

A mean standard enthalpy, $\Delta_a h^\ominus$, and entropy, $\Delta_a s^\ominus$, of adsorption of dodecanol from octane to the interface with 1.26×10^{-3} m Bu_4NBr have been obtained, in the range 17 to 30°C, using

$$[8] \quad \Delta_a\mu^\ominus = \Delta_a h^\ominus - T\Delta s^\ominus$$

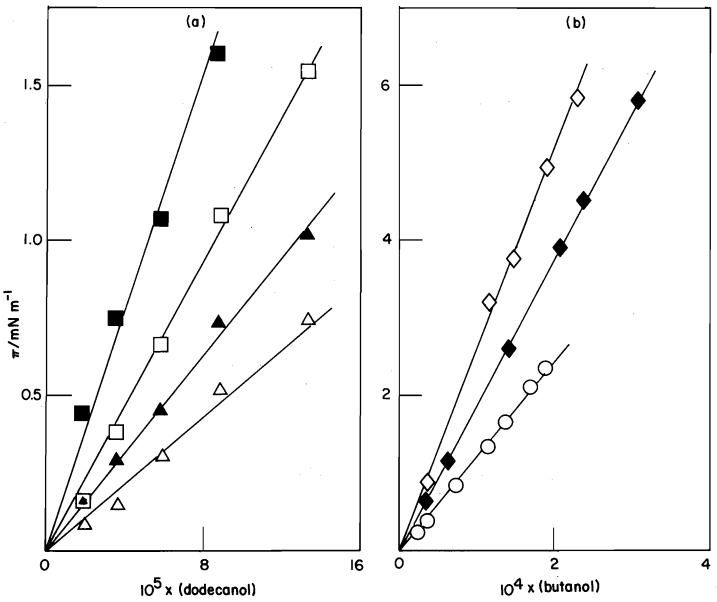

FIG. 1. Surface pressures, π, of alkanol monolayers as a function of mole fraction, x, of alkanol in bulk, at 20°C. (*a*) Dodecanol films adsorbed from octane to the interface with aqueous Bu_4NBr; molality zero (■), 1.31×10^{-3} (□), 7.64×10^{-3} (▲), 2.05×10^{-2} (△). (*b*) Butanol films adsorbed from aqueous NaCl to the air–solution interface; salt molalities are zero (○), 0.907 (◆), 1.578 (◇).

TABLE 2. Standard free energies of adsorption, $\Delta_a\mu^{\ominus}$, of dodecanol from octane to interfaces with aqueous Bu_4NBr

(*a*) Aqueous Bu_4NBr, molality m, at 20°C

$10^3 m$/(mol kg^{-1})	$-\Delta_a\mu^{\ominus}$/(kJ mol^{-1})	$10^3 m$/(mol kg^{-1})	$-\Delta_a\mu^{\ominus}$/(kJ mol^{-1})
0	23.64	7.640	21.81
1.313	22.89	13.245	21.23
2.839	22.33	20.464	21.14
5.761	22.01		

(*b*) 1.26×10^{-3} *m* Bu_4NBr at various temperatures

Temp./°C	$-\Delta_a\mu^{\ominus}$/(kJ mol^{-1})	Temp./°C	$-\Delta_a\mu^{\ominus}$/(kJ mol^{-1})
17.0	22.79	25.0	23.01
20.0	22.83	27.8	22.88
22.5	22.94	30.0	22.94

The $\Delta_a\mu^{\ominus} - T$ data, plotted in Fig. 2*a*, were treated by the method of least squares, yielding the values for $\Delta_a h^{\ominus}$ and $\Delta_a s^{\ominus}$ given in Table 3.

There is a contribution to the variation of $\Delta_a\mu^{\ominus}$ with T from the variation of $\Gamma^w_{A^+Br^-}$ with T, but by assuming $d\Delta_a\mu^{\ominus}/d\Gamma^w_{A^+Br^-}$ is independent of T in the range studied, we have allowed for the very small contribution from this source, and the $\Delta_a\mu^{\ominus}$ used are 'corrected' values.

Adsorption of Butanol from Aqueous Electrolyte to the Air–Solution Interface

Aqueous Solutions of Bu_4NBr

Surface tensions of various solutions containing Bu_4NBr and butanol have been determined, and standard free energies of adsorption of butanol, given in Table 4, have been calculated using eq. 1, where $\mu^{\ominus,1}$ is now a standard chemical potential of the alcohol in the aqueous phase. The mean standard enthalpy and standard

TABLE 3. Values of $\Delta_a X^{\ominus}$ and $\Delta X^{\ominus,\sigma}$ for dodecanol at the o–s interface and for butanol at the a–s interface, at 20°C

	o – water or a – water		o – salt solution or a – salt solution				
	$\Delta_a h^{\ominus}$	$\Delta_a s^{\ominus}$	$\Delta_a h^{\ominus}$	$\Delta_a s^{\ominus}$	$\Delta\mu^{\ominus,\sigma}$	$\Delta h^{\ominus,\sigma}$	$\Delta s^{\ominus,\sigma}$
Dodecanol	−31.1[a]	−25.4[a]	−19.5	+11.5	+0.82	+11.6	+36.9
Butanol	−1.5[b]	+73[b]	−4.1	+64.0	+0.10	−2.6	−9

[a]From ref. 18.
[b]From ref. 19. Free energy and enthalpy changes given in kJ mol^{-1} and entropy changes in J mol^{-1} K^{-1}. The salt solution is 1.26×10^{-3} *m* Bu_4NBr giving a surface excess of 3.2×10^{-7} mol m^{-2} at the o–s interface and 1.1×10^{-7} mol m^{-2} at the a–s interface.

TABLE 4. Standard free energies of adsorption, $\Delta_a\mu^{\ominus}$, of butanol from aqueous Bu_4NBr to the air–solution interface

(*a*) Aqueous Bu_4NBr, molality *m*, at 20°C

$10^3 m$/(mol kg^{-1})	$-\Delta_a\mu^{\ominus}$/(kJ mol^{-1})	$10^3 m$/(mol kg^{-1})	$-\Delta_a\mu^{\ominus}$/(kJ mol^{-1})
0.645	22.94	6.532	22.66
1.262	22.89	8.961	22.63
3.084	22.84		

(*b*) 1.26×10^{-3} *m* Bu_4NBr at various temperatures

Temp./°C	$-\Delta_a\mu^{\ominus}$/(kJ mol^{-1})	Temp./°C	$-\Delta_a\mu^{\ominus}$/(kJ mol^{-1})
20.0	22.89	27.5	23.69
22.5	23.10	30.0	23.55
25.0	23.23		

entropy of adsorption of butanol from 1.26×10^{-3} *m* Bu_4NBr to the a–s interface were calculated using eq. 8 (see Fig. 2*b*) and the values are given in Table 3.

Aqueous Solutions of Inorganic Salts

We have previously studied the bulk salt effects of various inorganic salts, including NH_4Br, NaCl, and Na_2CO_3, on butanol. These salts influence the chemical potential of butanol to widely different extents and for that reason we have chosen them for the present study.

Adsorption free energies for butanol, obtained from the appropriate surface tensions (see Fig. 1*b*), are given in Table 5. Three concentrations of NaCl have been studied and $\Delta_a\mu^{\ominus}$ for butanol is a linear function of salt molality. Only one concentration each has been used for Na_2CO_3 and NH_4Br, both concentrations being close to 1 *m*.

Discussion

Thermodynamic Parameters Associated with Surface Salt Effects

It is convenient to discuss the effects which salts have on adsorbed nonelectrolytes in terms of the parameters $\Delta X^{\ominus,\sigma}$ (where $X^{\ominus,\sigma}$ = standard chemical potential $\mu^{\ominus,\sigma}$, partial molar enthalpy $h^{\ominus,\sigma}$, or partial molar entropy $s^{\ominus,\sigma}$ of nonelectrolyte in an infinitely dilute film), defined as

$$[9]\quad \Delta X^{\ominus,\sigma} = X^{\ominus,\sigma}(\text{Salt present}) - X^{\ominus,\sigma}(\text{Salt absent})$$

These quantities are in turn related to the adsorption parameters $\Delta_a X^{\ominus}$ (see eq. 7) by

$$[10]\quad \Delta_a X^{\ominus}(\text{Salt present}) - \Delta_a X^{\ominus}(\text{Salt absent}) = \Delta(\Delta_a X^{\ominus}) = \Delta X^{\ominus,\sigma} - \Delta_{tr} X^{\ominus}$$

The quantity $\Delta_{tr} X^{\ominus}$ is defined by

$$[11]\quad \Delta_{tr} X^{\ominus} = X^{\ominus,1}(\text{Salt present}) - X^{\ominus,1}(\text{Salt absent})$$

it being understood that the bulk standard state is the same for adsorption and bulk transfer.

There are two special, but important cases. First, in the event that the nonelectrolyte is adsorbed from (*a*) an organic solvent in which the electrolyte is insoluble, or (*b*) an aqueous phase in which the bulk salt effect on the nonelectrolyte is negligible, eq. 10 becomes

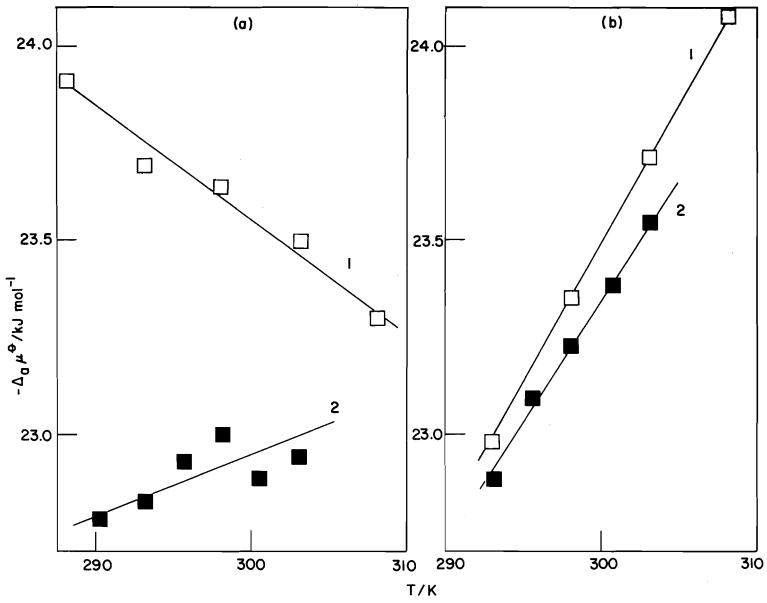

FIG. 2. Plots of free energies of adsorption, $\Delta_a\mu^{\ominus}$, against T for (*a*) dodecanol at (1) octane–water, (2) octane – Bu_4NBr solution interface, and (*b*) butanol at (1) air–water, (2) air – Bu_4NBr solution interface. The salt solution is 1.26×10^{-3} *m*, and at 20°C the surface excess is 3.2×10^{-7} mol m^{-2} at the o–s interface and 1.1×10^{-7} mol m^{-2} at the a–s interface.

TABLE 5. Standard free energies of adsorption, $\Delta_a\mu^{\ominus}$, of butanol from aqueous inorganic salts, molality *m*, to the air–solution interface at 20°C

	H_2O	NaCl	NaCl	NaCl	Na_2CO_3	NH_4Br
m/(mol kg^{-1})	—	0.518	0.907	1.578	1.002	1.008
$-\Delta_a\mu^{\ominus}$/(kJ mol^{-1})	23.05	23.62	23.98	24.77	25.91	23.61

[12] $$\Delta(\Delta_a X^{\ominus}) = \Delta X^{\ominus,\sigma}$$

Second, if the surface salt effect is negligible eq. 10 reduces to

[13] $$\Delta(\Delta_a X^{\ominus}) = -\Delta_{tr} X^{\ominus}$$

Positive values of $\Delta\mu^{\ominus,\sigma}$ correspond to salting-out, and negative values to salting-in.

Much of the data for bulk effects is reported in terms of so-called salting constants k (2). It may be useful to define a similar quantity for surface effects to facilitate comparisons in future work. By analogy with the treatment of bulk effects, we may define a salting constant, k^{σ}, for the surface in a system where $\Delta\mu^{\ominus,\sigma}$ is a linear function of *m*, such that

[14] $$\Delta\mu^{\ominus,\sigma}(m = 1) = 2.303RTk^{\sigma}$$

The constant k^{σ} is in turn related to an activity coefficient, f^{σ}, for adsorbed nonelectrolyte, by

[15] $$k^{\sigma} = \log f^{\sigma}(m = 1)$$

If $\Delta\mu^{\ominus,\sigma}$ and *m* are not linearly related then

[16] $$k^{\sigma} = [\mathrm{d} \log f^{\sigma}/\mathrm{d}m]_{m=0}$$

The activity coefficient is a distribution ratio for the nonelectrolyte between the surface of water and of salt solution, the activity coefficient on water being unity.

In the case of surface-active electrolytes one might choose to define k^{σ} and f^{σ} in terms of *surface* concentrations of electrolyte rather than bulk concentration.

Systems Containing Inorganic Salts

The inorganic salts studied are negatively adsorbed at both the o–s and a–s interfaces, and from the point of view of surface or interfacial tensions, the systems behave as if there were a salt-free layer of water at the interface of the

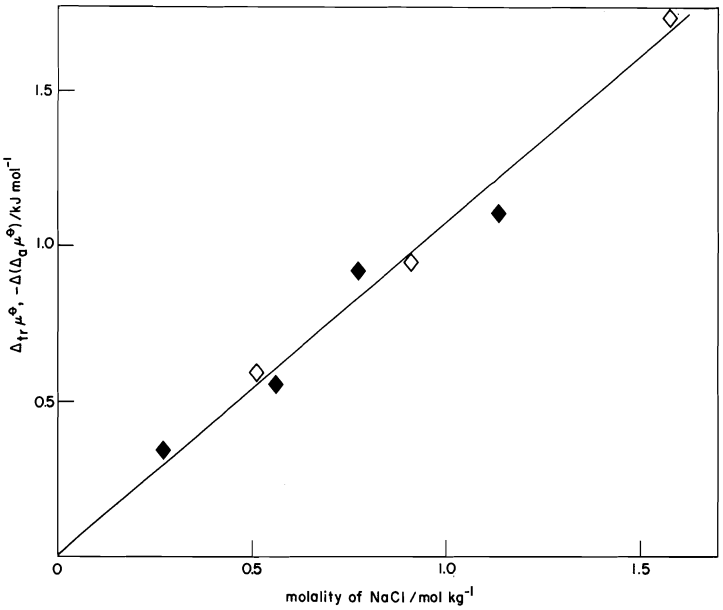

FIG. 3. Effects of NaCl on butanol at the a–s interface (◇), the o–s interface (◆), and in bulk aqueous solution (full line).

order of 0.3 to 0.6 nm thick (6). If ions in the vicinity of the surface are to interact with adsorbed alcohol molecules it must therefore be from below the salt-free layer. We have shown elsewhere (3) that NaCl up to bulk concentrations of about 2 mol kg^{-1} in water has a negligible effect on the free energy of adsorption of dodecanol from dodecane so that, since NaCl is insoluble in the alkane, $\Delta\mu^{\ominus,\sigma}$ is negligible (see eq. 12). On the other hand $\Delta_a\mu^{\ominus}$ for the adsorption of butanol from aqueous NaCl to the dodecane solution interface is significantly dependent on salt concentration. In this case it was found that $\Delta(\Delta_a\mu^{\ominus})$ is equal to $-\Delta_{tr}\mu^{\ominus}$, so that again NaCl has no effect on the chemical potential of adsorbed alkanol (eq. 13).

From the present results for butanol at the a–s interface we find that for NaCl up to concentrations of about 1.5 mol kg^{-1}, $-\Delta(\Delta_a\mu^{\ominus})$ is within experimental errors equal to $\Delta_{tr}\mu^{\ominus}$, so that here too $\Delta\mu^{\ominus,\sigma}$ is zero. This can be appreciated from Fig. 3 where we show $-\Delta(\Delta_a\mu^{\ominus})$ for butanol adsorbed from aqueous NaCl to the a–s interface, together with $\Delta_{tr}\mu^{\ominus}$ for transfer of butanol from water to aqueous NaCl; the latter results are taken from ref. 8. Also included are the results for the adsorption of butanol from aqueous NaCl to the dodecane–solution interface (3); all three sets of data are coincident.

We thus have the rather surprising result that NaCl up to quite high concentrations does not affect the properties of surface water, at the o–s or a–s interface, in any way which alters the chemical potential of adsorbed alkanol. We note that butanol is salted-out by NaCl in bulk aqueous solution (8), but that the OH group gives a salting-in contribution to the overall effect (17). The values of $\Delta_{tr}\mu^{\ominus}$ for 1 *m* NaCl are, for butanol 1.07 kJ mol^{-1} (at 20°C), and for OH -0.17 kJ mol^{-1} (at 25°C).

For NH_4Br and Na_2CO_3, $-\Delta(\Delta_a\mu^{\ominus})$ for butanol adsorption at the a–s interface (0.56 and 2.86 kJ mol^{-1} respectively from Table 5) differs slightly from $\Delta_{tr}\mu^{\ominus}$ (0.42 and 3.14 kJ mol^{-1} for the molalities shown in Table 5), indicating a slight salting-out of adsorbed butanol by NH_4-Br and a slight salting-in by Na_2CO_3.

Systems Containing Bu_4NBr

Adsorption of Bu_4NBr

As mentioned, Bu_4NBr is positively adsorbed from dilute aqueous solution at the interfaces of present interest. Results are presented in Fig. 4 as plots of ln ($\Gamma^{w}_{A^+Br^-}/a_{\pm}$) vs. π for 25°C; the plots are linear and limiting values of ln ($\Gamma^{w}_{A^+Br^-}/a_{\pm}$) at $\pi = 0$ have been obtained by extrapolation. The extent of adsorption at the interfaces increases in the order d–s < a–s < o–s, the ratios of ($\Gamma^{w}_{A^+Br^-}/a_{\pm}$) at infinite dilution being 1:11:48. The standard free energy of adsorption of Bu_4NBr is therefore more

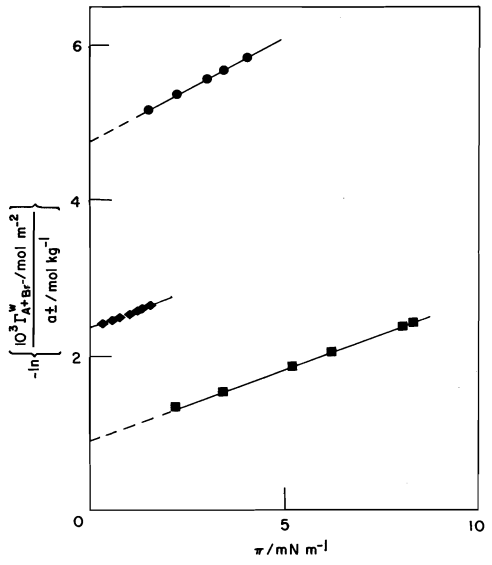

FIG. 4. Adsorption of Bu_4NBr at decanol–water (●), air–water (◆), and octane–water (■) interfaces at 25°C.

negative for the o–s interface than for the a–s interface by an amount $RT \ln (48/11) = 3.67$ kJ mol^{-1} at 25°C. For straight chain homologues the standard free energy of adsorption of the methylene group from water is more negative by about 0.5 kJ mol^{-1} for the o–s interface than for the a–s interface (*5d*). Assuming the same to be true for CH_2 groups in Bu_4N^+, and that the cation is immersed in water to the same extent at the o–s and a–s interfaces, we may say as a rough estimate that 3.67/0.5 ($\simeq$7) CH_2 groups per Bu_4N^+ ion leave the aqueous phase on adsorption. That is, the adsorbed cation is a little over half immersed in water, as might be expected intuitively.

In a relative sense adsorption of Bu_4NBr at the d–s interface is weak. We have reported elsewhere (3) that of the three types of interface studied here, alkali halides are *least desorbed* at the d–s interface. Thus it is probably not a simple charge effect that causes the relatively low adsorption of Bu_4NBr. The effect may originate in the nature of the different kinds of hydration layers around the alcoholic OH groups and the alkyl groups of the cation. This point is mentioned again later.

Effect of Bu_4NBr on Dilute Adsorbed Layers of Alkanols

We first remark that alkanols are salted-in (i.e., $\mu^{\ominus,1}$ made more negative) by Bu_4NBr in bulk aqueous solution, the effect being greater the greater the alkanol chain length (7). Here we consider the effect of *adsorbed* Bu_4NBr on (*i*) dodecanol at the o–s interface and (*ii*) butanol at the a–s interface.

The free energy for the adsorption of dodecanol from octane to the o–s interface is shown as a function of both molality and the surface excess of Bu_4NBr in Fig. 5*a*. The relationship involving the surface excess is rectilinear. Since the salt is insoluble in octane eq. 12 is applicable and we find that $d\mu^{\ominus,\sigma}/d\Gamma^w_{A^+Br^-} = 0.256$ kJ mol^{-1}/10^{-7} mol m^{-2}. Similar results for butanol at the a–s interface are shown in Fig. 5*b*, and again the plot of $\Delta_a\mu^{\ominus}$ vs. surface excess of salt is linear, but of smaller slope. For the concentrations of salt used ($m < 0.9 \times 10^{-2}$ mol kg^{-1}) it is known that $\Delta_{tr}\mu^{\ominus}$ for butanol is negligible (7) and so eq. 12 is again applicable and $d\mu^{\ominus,\sigma}/d\Gamma^w_{A^+Br^-} = 0.094$ kJ mol^{-1}/10^{-7} mol m^{-2}.

Earlier, we quoted standard heats and entropies of adsorption of butanol and dodecanol to interfaces involving 1.26×10^{-3} *m* aqueous Bu_4NBr (Fig. 2 *a*,*b*; Table 3). Also included in Figs. 2*a* and *b* are corresponding plots of $\Delta_a\mu^{\ominus}$ vs. *T* for adsorption to the interfaces with water, the data being taken from refs. 18 and 19. Various relevant free energy, enthalpy, and entropy changes are presented in Table 3, and referred to below.

Contrary to the situation for bulk solutions, adsorbed alkanols are salted-out by adsorbed Bu_4NBr. The bulk effects have been attributed to hydrophobic interactions between alkyl chains of alkanol and cation (7). At the surface, however, the OH groups of the alcohol are constrained in a way which they are not in bulk, to come into close proximity with the hydrophobic cations. The salting-out of dodecanol at the o–s interface is about 3 times greater than that of butanol at the a–s interface. For dodecanol it is likely that the major part of the salt effect results from interactions occurring on the water side of the interface since all the materials on the alkane side consists of hydrocarbon groups. Thus, we believe that interactions between alcoholic OH groups and adsorbed ions, probably Bu_4N^+ ions but possibly to some extent Br^- ions, are responsible for the salting-out. In this connection we recall that Bu_4NBr is absorbed much less strongly to the d–s interface than either the a–s or o–s interfaces.

The values of $\Delta h^{\ominus,\sigma}$ and $T\Delta s^{\ominus,\sigma}$ for dodecanol at the o–s interface (where $\Gamma^w_{A^+Br^-} = 3.2 \times 10^{-7}$ mol m^{-2}), given in Table 3, are both large

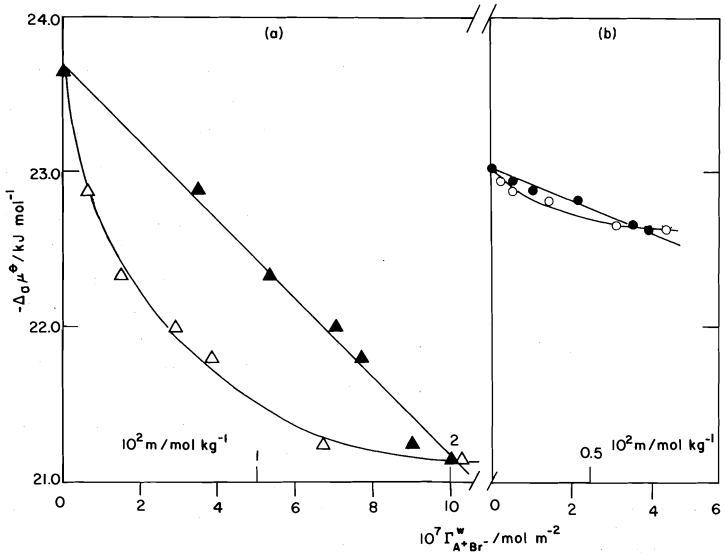

FIG. 5. Standard free energies of adsorption of alkanols to interfaces containing Bu_4NBr at 20°C. (*a*) Adsorption of dodecanol from octane to octane – Bu_4NBr solution interface as a function of surface excess of salt (▲), and molality of salt (△). (*b*) Adsorption of butanol from salt solution to air – Bu_4NBr solution interface as a function of surface excess of salt (●), and molality of salt (○).

and *positive*, almost compensating, giving the relatively small positive free energy change. It is not possible at present to account quantitatively for these results. If however, salting-out does result in the main from interactions between 'incompatible' hydration shells around OH and Bu_4N^+, it appears likely from the sign of $\Delta h^{\ominus,\sigma}$ and $\Delta s^{\ominus,\sigma}$ that a net disruption of water structure occurs in the salting-out process.

Similar interactions between OH and Bu_4N^+ presumably also exist in films of butanol at the a–s interface, and yet butanol is less strongly salted-out than dodecanol. It appears then that there is an additional salting-in component for butanol; this could result from interactions between the alkyl chains of the alcohol and those chains of the Bu_4N^+ which are not immersed in water. Values of $\Delta h^{\ominus,\sigma}$ and $T\Delta s^{\ominus,\sigma}$ for butanol (with $\Gamma^w_{A^+Br^-} = 1.1 \times 10^{-7}$ mol m^{-2}) are *negative* and almost compensating. The salting-in component clearly gives rise to a large negative contribution to both $\Delta h^{\ominus,\sigma}$ and $\Delta s^{\ominus,\sigma}$ which is to be expected for a quasi-condensation process for alkyl chains.

In conclusion, we have established an approach to the study of salt effects on adsorbed nonelectrolytes. Only a limited number of what might be called 'model' systems have been investigated, and there is much scope to consider more complex nonelectrolytes such as might be of direct technical or biological importance, together with a wider range of electrolytes. It is clear, however, from the present findings that, for a given nonelectrolyte and surface-active salt, surface salt effects can be quite different at different kinds of interfaces, and that the effects can operate in an opposite sense to those in bulk. For the salts which are desorbed, the surface salt effects are small or zero, even though the salt-free layer of water at the surface is only a few Å thick, and the bulk effects are sizeable. It is probable that in the case of alcohol films at the alkane–water interface however, the surface salt effect should really be compared with the effect on the OH group in bulk, rather than on the whole molecule, since the alkyl chain of the adsorbed alcohol is presumably 'dissolved' in alkane.

Acknowledgment

The authors express their gratitude to the Science Research Council (Colloid Science) for the provision of a maintenance grant for one of them (S.M.S).

1. V. F. SERGEEVA. Russ. Chem. Rev. **34**, 309 (1965).
2. F. LONG and W. MCDEVIT. Chem. Rev. **51**, 119 (1952).
3. R. AVEYARD and S. M. SALEEM. J. Chem. Soc. Faraday Trans. I, **73**, 84 (1977).
4. J. RALSTON and T. W. HEALY. J. Colloid Interface Sci. **42**, 629 (1973).

5. R. AVEYARD and D. A. HAYDON. Introduction to the principles of surface chemistry. Cambridge University Press. 1973. (*a*) p. 40 *et seq.*; (*b*) p. 108; (*c*) p. 107; (*d*) p. 105.
6. R. AVEYARD and S. M. SALEEM. J. Chem. Soc. Faraday Trans. I, **72**, 1609 (1976).
7. R. AVEYARD and R. HESELDEN. J. Chem. Soc. Faraday Trans. I, **70**, 1953 (1974).
8. R. AVEYARD and R. HESELDEN. J. Chem. Soc. Faraday Trans. I, **71**, 312 (1975).
9. R. AVEYARD and D. A. HAYDON. Trans. Faraday Soc. **61**, 2255 (1965).
10. W. D. HARKINS and F. E. BROWN. J. Am. Chem. Soc. **41**, 499 (1919).
11. B. E. CONWAY, R. E. VERRALL, and J. E. DESNOYERS. Trans. Faraday Soc. **62**, 2738 (1966).
12. International critical tables. Vol. IV. McGraw-Hill, New York, NY. 1928. p. 447.
13. R. A. ROBINSON and R. H. STOKES. Electrolyte solutions. Butterworth, London. 1955.
14. R. C. WEAST (*Editor*). Handbook of chemistry and physics. Chemical Rubber Co., Cleveland, OH. 1970. E-67.
15. S. LINDENBAUM and G. E. BOYD. J. Phys. Chem. **68**, 911 (1964).
16. K. TAMAKI. Bull. Chem. Soc. Jpn. **40**, 38 (1967).
17. F. L. WILCOX and E. E. SCHRIER. J. Phys. Chem. **75**, 3757 (1971).
18. R. AVEYARD and B. J. BRISCOE. J. Chem. Soc. Faraday Trans. I, **68**, 478 (1972).
19. J. H. CLINT, J. M. CORKILL, J. F. GOODMAN, and J. R. TATE. J. Colloid Interface Sci. **28**, 522 (1968).

Metal complexation by α-mercapto-β-aryl acrylic acids

JOSEPH WAGNER,[1] PIERRE VITALI, JOSIANE SCHOUN, AND EUGENE GIROUX[2]

Centre de Recherche Merrell International, 16, rue d'Ankara, 67084 Strasbourg, Cedex, France

Received June 21, 1977

JOSEPH WAGNER, PIERRE VITALI, JOSIANE SCHOUN, and EUGENE GIROUX. Can. J. Chem. **55**, 4028 (1977).

Protonation constants of several α-mercapto-β-aryl acrylic acids and constants for formation of complexes between these ligands and bivalent metal cations were determined by computer-assisted analysis of p*H*-titration data. Ligand–metal ion mixtures in 50% (v/v) dioxane–water and in water, $I = 0.1$ *M* ($NaClO_4$) were titrated at 25°C with sodium hydroxide. Initial estimates of complex formation constants were refined with the SCOGS program. The ligands were shown to complex zinc(II) and nickel(II) metal ions avidly. These ligands potently inhibited the metal-dependent enzymes alkaline phosphatase, carboxypeptidase A, coeruloplasmin, and thermolysin. Partition of zinc(II) between aqueous and *n*-butanol or *n*-octanol phases was enhanced in favor of the organic phase by several of these complexants.

JOSEPH WAGNER, PIERRE VITALI, JOSIANE SCHOUN et EUGENE GIROUX. Can. J. Chem. **55**, 4028 (1977).

Les constantes de protonation et les constantes de formation de complexes de métaux bivalents avec une série d'acides α-mercapto-β-aryl acryliques ont été déterminées par analyse à l'ordinateur des courbes de titration p*H*-métriques. Les titrations ont été effectuées sur des mélanges de ligand et du cation métallique dans des solutions de 50% (v/v) dioxane–eau et dans l'eau, $I = 0.1$ *M* ($NaClO_4$) à 25°C avec de la soude. Les valeurs initiales des constantes ont été déterminées à partir des courbes de formation et ont été affinées par utilisation du programme SCOGS. Les constantes obtenues montrent que les ligands présentent une grande affinité spécialement pour le zinc(II) et le nickel(II). Ces ligands inhibent fortement les metalloenzymes, phosphatase alcaline, carboxypeptidase A, ceruloplasmine et thermolysine. Plusieurs de ces ligands augmentent l'extraction du zinc dans la phase organique dans des essais de partition du zinc(II) entre l'eau et le *n*-butanol ou le *n*-octanol.

Introduction

Some β-aryl derivatives of α-mercaptoacrylic acid influence the distribution and metabolism of zinc in the rat. Following administration of a single dose of α-mercapto-β-(2-furyl) acrylic acid or α-mercapto-β-phenyl acrylic acid, blood plasma zinc concentration increased many-fold within a few hours and remained elevated for as long as 5 days (1). Evidence for formation of a ternary complex of plasma albumin, zinc, and the furyl derivative was obtained (2). While the complexation of metal ions by many α- and β-mercapto acids and amino acids has been well studied (3), few data of a similar nature are available for the α-mercapto-β-aryl acrylic acids. Foye and Lo (4) reported stability constant data for complexes of the phenyl derivative with Al^{3+}, Cu^{2+}, and Fe^{3+}; they also found this compound to have antimicrobial activity. In this report we present data characterizing complexation by several α-mercapto-β-aryl acrylic acids of zinc and of other metal cations and data on the inhibition of four metal-dependent enzymes by these ligands and other metal-complexing agents.

Experimental

Syntheses

The α-mercapto-β-aryl acrylic acids depicted in Scheme 1 were prepared by alkaline hydrolysis of the corresponding rhodanine derivatives obtained from the condensation of the appropriate aldehyde with rhodanine, following the procedure of Campaigne and Cline (5). Melting points were determined on a Kofler hot stage apparatus and are uncorrected. The nmr spectra were recorded on a Varian T60 using tetramethylsilane (TMS) or 3-(trimethylsilyl)-1-propane sulfonic acid as internal standards. Chemical shifts are given in ppm (δ, TMS = 0) and coupling constants in Hz. The abbreviations s, d, m, and br refer to singlet, doublet, multiplet and broadened, respectively. Compounds **1**, **2**, **5**, **6**, **7**, and **10**, already described in the literature (6–9) presented analytical data in agreement with their structure.[3] Thiosalicylic acid **9** (Fluka) was recrystallized from methanol.

[1]Author to whom correspondence should be addressed.

[2]Present address: Merrell-National Laboratories, Cincinnati, OH 54215, USA.

[3]These data have been deposited in the Depository of Unpublished Data. Copies may be obtained, at a nominal charge, from the Depository of Unpublished Data, CISTI, National Research Council of Canada, Ottawa, Canada K1A 0S2.

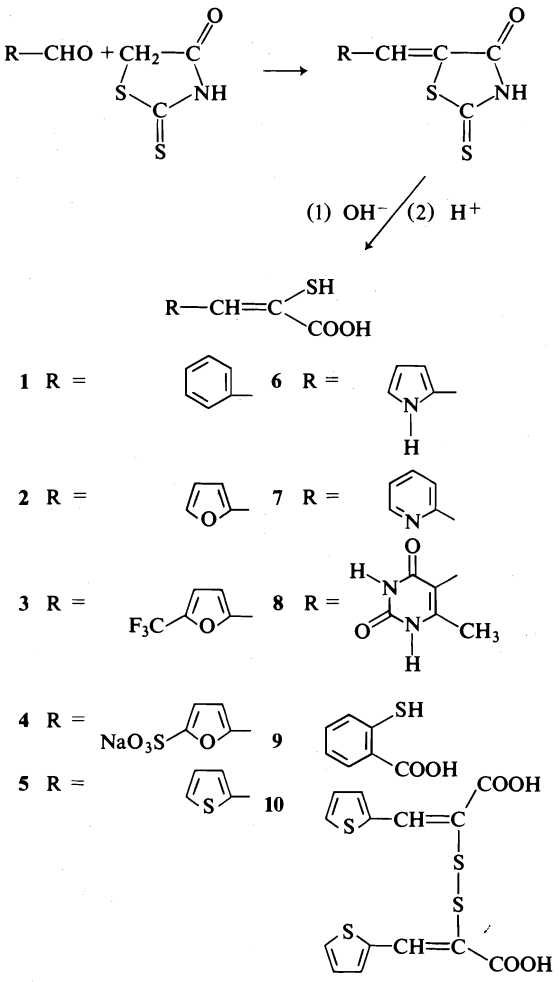

SCHEME 1

5-(5-Trifluoromethyl-2-furylmethylene) Rhodanine

5-Trifluoromethyl-2-furfural (3.4 g, 2.1 mmol) (10), rhodanine (2.92 g, 2.2 mmol), and dry sodium acetate (5.16 g) in 35 ml of glacial acetic acid were stirred together and heated to reflux. After 10 min, a precipitate occurred and heating was continued for 2 h. The reaction mixture was cooled, 30 ml of water was added, and the precipitate was filtered, washed with water, and dried. Chromatography over silica gel (eluent CH_2Cl_2), followed by recrystallization in dichloromethane–pentane yielded 3.7 g (63%) of yellow crystals, mp 174°C; nmr ($CDCl_3$): 6.80 (m, 2H, ring protons), 7.38 (s, 1H, exocyclic —CH=). *Anal.* calcd. for $C_9H_4F_3NO_2S_2$: C 38.71, H 1.44, N 5.01, S 22.96; found: C 38.70, H 1.56, N 5.10, S 22.91.

α-Mercapto-β-(5-trifluoromethyl-2-furyl) Acrylic Acid (3)

5-(5-Trifluoromethyl-2-furylmethylene) rhodanine (1.58 g, 5.66 mmol), 25 ml of 1 *N* sodium hydroxide solution, and 25 ml of water were stirred under nitrogen at room temperature for 10 h. After cooling and acidification at p*H* 1.5 with concentrated hydrochloric acid, a precipitate was recovered by filtration. The material was washed by stirring with 50 ml of water under nitrogen at room temperature, acidified with concentrated hydrochloric acid and filtered to yield 0.8 g (60%) of slightly brown crystals, mp 158°C; nmr (acetone-d_6): 7.1 (m, 2H, ring protons), 7.6 (s, 1H, exocyclic —CH=). *Anal.* calcd. for $C_8H_5F_3O_3S$: C 40.34, H 2.11, S 13.46; found: C 40.26, H 2.11, S 13.60.

5-(5-Sodiumsulfonate-2-furylmethylene) Rhodanine

5-Sodiumsulfonate-2-furanaldehyde was converted as above to the rhodanine derivative. Recrystallization in water gave yellow crystals (73% yield), mp 280°C (dec.); nmr (DMSO-d_6): 6.62 (d, J = 3, 1H, ring proton), 7.03 (d, J = 3, 1H, ring proton), 7.4 (s, 1H, exocyclic —CH=). *Anal.* calcd. for $C_8H_4NO_5S_3Na$: C 30.67, H 1.29, N 4.47; found: C 30.63, H 1.32, N 4.51.

α-Mercapto-β-(5-sodiumsulfonate-2-furyl) Acrylic Acid (4)

This compound was obtained from the corresponding rhodanine derivative (89% yield); mp >220°C (dec.); nmr (D_2O): 6.88 (s, 2H, ring protons), 7.45 (s, 1H, exocyclic —CH=). *Anal.* calcd. for $C_7H_5O_6S_2Na$: C 30.88, H 1.85; found: C 30.69, H 1.81.

5-(1,2,3,4-Tetrahydro-6-methyl-2,4-dioxo-5-pyrimidylmethylene) Rhodanine

This compound was obtained from 5-carbaldehyde-6-methyluracil (11) (83% yield); orange crystals, mp >260°C; nmr (DMSO-d_6): 2.33 (s, 3H, CH_3), 7.21 (s, 1H, exocyclic —CH=), 11.46 (s, 1H, NH), 12.33 (b s, 1H, NH). *Anal.* calcd. for $C_9H_7N_3O_3S_2$: C 40.13, H 2.62, N 15.60; found: C 40.20, H 2.74, N 15.64.

α-Mercapto-β(1,2,3,4-tetrahydro-6-methyl-2,4-dioxo-5-pyrimidyl) Acrylic Acid (8)

This compound was obtained from the preceding compound (68% yield); yellow crystals, mp 240°C (dec.); nmr (DMSO-d_6): 2 (s, 3H, CH_3), 7.2 (s, 1H, —CH=), 11.1 (b s, 3H, NH, COOH). *Anal.* calcd. for $C_8H_8N_2O_4S$: C 42.09, H 3.54, N 12.27; found: C 41.99, H 3.72, N 12.31.

Potentiometric Titrations

Water with greater than 10 MΩ cm^{-1} resistivity was prepared using a Millipore 'Milli-Q' system. Dioxane (Baker AR) was refluxed 48 h over sodium and distilled through a Vigreux column. Solutions (0.1 *M*) of sodium perchlorate, zinc(II) nitrate, nickel(II) chloride (all from E. Merck) or of the perchlorates of cobalt(II), iron(II), manganese(II), nickel(II), or zinc(II) (all from Pierce Chemical) in water or in 50% (v/v) dioxane–water were slightly acidified with perchloric acid (p*H* = 3) to suppress hydrolysis; concentrations were determined by Schwarzenbach's procedure (12). Sodium hydroxide solutions were standardized by titration with hydrochloric acid (Titrisol, E. Merck). Solutions (0.1 *M*) of ligands in 50% (v/v) dioxane–water were prepared by dissolving the ligands in 5 ml of dioxane (degassed by bubbling of nitrogen) and adjusting to 10 ml with degassed water. One half equivalent of $HClO_4$ was added in preparation of solutions of ligands **1**, **2**, **5**, and **9**. Ligand solutions were stored under nitrogen at 5°C. Fresh stock was prepared each day, as some ligands in solution, especially **6** and **7**, oxidized to disulfide (5–10%) after 6–10 h.

Mixtures (20 ml) of ligand and metal ion were titrated

with NaOH (0.3 *M* in water, or in 50% (v/v) dioxane–water). At each of two ligand concentrations (2 and 4 m*M*), metal ion concentrations were employed to yield ligand–metal stoichiometries of 8:1, 4:1, and 2:1. Ligand solutions also were titrated in the absence of metal ion. All titrations were carried out in a water-jacketed vessel thermostated at 25 ± 0.1°C. The titration cell was tightly covered and nitrogen saturated with solvent was bubbled through the solution.

A Mettler semi-automatic titration system consisting of modules DK 10, 12, 13, and 15 connected to a DV 11 burette and equipped with a Metrohm glass electrode EA 109 and an E 430 saturated calomel electrode was used. The electrodes and p*H* meter were calibrated to read p*H* with four aqueous buffer solutions (p*H* = 4.01 to 10.01). For measurements in 50% aqueous dioxane, the glass electrode was conditioned for several days in the mixed solvent (13). The sleeve-type calomel electrode was refilled with saturated KCl after five to six titrations. The p*H* values were measured to ±0.01 unit.

Protonation and Formation Constants

Formation constants β_{pqr} correspond to the general equation

$$[1]\quad pL^{2-} + qM^{2+} + rH^{+} \rightleftharpoons (L_pM_qH_r)^{(-2p+2q+r)+}$$

'Practical' protonation constants of the ligands are

$$[2]\qquad \beta_{101} = [HL^{-}]/(H^{+})\,[L^{2-}]$$

$$[3]\qquad \beta_{102} = [H_2L]/(H^{+})^2[L^{2-}]$$

Initial estimates for β_{101} and β_{102} were obtained from titration curves and formation curves ($\bar{n}_H = f(pH)$) and were refined using the computer program SCOGS (14) on a UNIVAC 1110 computer. For the calculation of H^+ and OH^- concentrations from H^+ activities as measured by the glass electrode, a correction factor of -0.06 ± 0.02 was determined by titrating at a constant ionic strength of 0.1 at 25°C a 0.01 *M* solution of HCl in 50% (v/v) dioxane–water with a solution of NaOH in 50% (v/v) dioxane–water. The pK_w was calculated to be 15.38 ± 0.02, in agreement with previous results (15, 16). For measurements in water, the mean activity coefficient $f_{\pm}$ was taken as 0.79 and the pK_w as 13.996 (17) at 25°C and $I = 0.1$ *M* ($NaClO_4$). Approximate values of formation constants β_{110} and β_{210} were obtained at $\bar{n} = f(pL)$, given by [4] and [5]. C_M and C_L are total ligand and

$$[4]\quad \bar{n}_L = \frac{C_L - [L^{2-}][1 + \beta_{101}(H^{+}) + \beta_{102}(H^{+})^2]}{C_M}$$

$$[5]\quad [L_2^{-}] = \frac{2C_L + [EX_{acid}] - [H^{+}] + [OH^{-}] - C_{base}}{\beta_{101}(H^{+}) + 2\beta_{102}(H^{+})^2}$$

metal concentrations, respectively, $[EX_{acid}]$ is the excess of perchloric acid added in preparation of stock solutions and C_{base} is the concentration of added base. Constants were refined over the entire range of experimental data by the use of the SCOGS program. If by adding other species, no further reduction in the standard deviation of titre could be achieved, the last set of values was retained. Experimental and calculated formation curves were compared on a Hewlett-Packard 9820 desk calculator fitted with a HP 9862 plotter.

Ligands and Zinc Partition Experiments

Two millilitres of a solution of zinc sulfate (33.5 μ*M*), prepared in 0.05 *M* 3-(*N*-morpholino)propanesulfonic acid, 0.15 *M* NaCl, p*H* 6.0, was shaken with complexant and *n*-octanol (8 ml) or *n*-butanol (2.5 ml). The complexant (4 mol/mol $ZnSO_4$) was freshly dissolved either in the organic solvent or in the zinc sulfate solution. After 5 min of contact the phases were separated by centrifugation. Zinc concentration in the aqueous phase was determined by atomic absorption spectroscopy. Zinc standards were prepared by dilution of Titrisol standard (E. Merck), using aqueous solvent contacted with organic solvent. Each partition mixture was analyzed in triplicate.

Inhibition of Enzymes by Complexants

E. Coli alkaline phosphatase (E.C.3.1.3.1., Sigma Chemical) was assayed spectrophotometrically (18), using the kit supplied by Boehringer-Mannheim. Enzyme was incubated with inhibitor (freshly dissolved in dimethylsulfoxide or in buffer) for 15 min at 30°C in p*H* 10.5 buffer before initiation of the enzymatic reaction by addition of substrate. In all assays dimethylsulfoxide was present at a final concentration of 5% (v/v). Bovine carboxypeptidase A (E.C.3.4.12.2, Sigma Chemical) was assayed by a p*H*-stat technique (19). Enzyme was incubated with inhibitor (freshly dissolved in polyethylene glycol 300 or in buffer) for 10 min at 30°C at p*H* 7.5 before initiation of the enzymatic reaction by addition of substrate, hippuryl-D,L-β-phenyllactic acid (Fox Chemical). The final concentration of polyethylene glycol 300 was 5% (v/v). The p*H* of the reaction mixture was maintained at 7.5 with a Mettler titration system. Human coeruloplasmin (E.C.1.16.3.1., Sigma Chemical) was assayed spectrophotometrically using *o*-dianisidine (Sigma Chemical) as substrate (20). The rate of reaction was determined after preincubation of enzyme with inhibitor (freshly dissolved in ethanol; final ethanol concentration 2.5% (v/v)) for 15 min at 30°C in p*H* 5.0 buffer. Assay mixtures contained 0.1 m*M* disodium EDTA (21) to suppress enhancement of activity due to traces of iron. The possibility of decolorization of the assay mixture by inhibitor was checked by the method of Curzon and Cumings (22). Thermolysin (E.C.3.4.24.4., Sigma Chemical) was assayed fluorimetrically using enzyme freed of low molecular weight contaminants by gel chromatography on Sephadex G-25 (Pharmacia Fine Chemicals). Enzyme solution was stored at −25°C and thawed prior to assay. An aliquot was diluted to 1.8 ml with a buffer of 10 m*M* 5,5-diethylbarbituric acid, 90 m*M* NaCl, p*H* 7.5. (23). To the enzyme solution was added inhibitor freshly dissolved in buffer or in ethanol (a total of 0.1 ml ethanol in all assay tubes). The mixture was heated for 10 min in a water bath at 40°C. The enzymatic reaction was initiated by addition of 0.1 ml of a 20 m*M* solution of carbobenzoxyglycyl-L-leucineamide (Protein Research Foundation, Osaka, Japan) in ethanol. The reaction mixture was maintained at 40°C and six aliquots of 0.2 ml were removed at 5 min intervals. Hydrolysis of the peptide bond was measured in these samples by the fluorescamine technique (24).

In all inhibition studies the effect of four or more con-

centrations of a given inhibitor was assessed. Remaining enzyme activity was plotted as a function of inhibitor concentration. From a smooth curve drawn through the data, the concentration of inhibitor necessary to reduce activity to 50% of the control value was obtained by interpolation.

Results

Protonation Constants

Computer-refined values of protonation constants of the thiol and carboxyl groups of the ligands are presented in Table 1. In the series of α-mercapto-β-aryl acrylic acids the nature of the aryl substituent did not influence strongly the ionization of the carboxyl group, but ionization of the thiol group was influenced by the electron donation ability (25) of the aryl group (compare **1**, **2**, and **5**). For the furan derivatives, ionization of the carboxyl and thiol groups varied in the same order as the inductive effect of the substituent (26) in position 5 of the furan ring (compare **2**, **3**, and **4**). The pK_a values found for ligands **1** and **9** are in agreement with those of other workers (4, 27, 28) if we take into account that our results are 'practical' pK_a values.

Metal Complex Formation Constants

Computer-refined values of formation constants of metal–ligand complexes are presented in Table 2. An emphasis was placed upon the study of zinc complexes because of the effect these ligands have upon zinc metabolism. In Fig. 1 are illustrated titration curves of two concentrations of α-mercapto-β-furyl acrylic acid **2** in the absence and in the presence of zinc(II) at ligand–metal ratios of 8:1, 4:1, and 2:1. Similar curves were prepared for the other ligands. The formation curves ($\bar{n}$ versus log $[L^{2-}]$) corresponding to the titration curves of Fig. 1 for $C_L = 4$ mM were all superimposable. This indicated that for the zinc(II)–ligand system only the mononuclear species ZnL and ZnL_2^{2-} were present. Approximate values of the stability constants log β_{110} (11.1) and log β_{210} (20.5) obtained at $\bar{n} = 1/2$ and $\bar{n} = 3/2$ were refined with the SCOGS program over the entire pH range (2.8–9.7) to an estimated standard deviation in titre of 4.1×10^{-3} (6 curves and 161 points). The value found for the estimated standard deviation of titre in calculation of the protonation constants was 3.8×10^{-3}. Qualitatively similar conclusions were reached for all ligands listed in Table 2: only mononuclear zinc(II) complexes appeared to be formed.

Only mononuclear complexes appeared to form between nickel(II) and the ligands. Titration curves obtained with α-mercapto-β-thienyl acrylic acid **5** and several bivalent metal ions at a ligand–metal ratio of 2:1 are illustrated in Fig. 2. In titrations with iron(II) and manganese(II), hydrolysis occurred at high pH values, especially at lower ligand–metal ratios. Attempts to titrate ligand–copper(II) mixtures failed; dark-colored solutions occurred upon adding copper(II) salt to carefully degassed ligand solutions, indicating, presumably, oxidation–reduction involving the thiol group (29). Cadmium(II) and lead(II) precipitated with ligands **1** to **8** in the mixed solvent when the pH was raised to 3–5. No formation constants were obtained. The values obtained for formation of calcium(II)–ligand **5** complexes indicated, as expected, that affinity of these ligands for alkaline earth cations was relatively low.

Using data in Tables 1 and 2, species distributions in metal–ligand systems were calculated as a function of pH. In Fig. 3 are illustrated concentrations across the pH range of zinc ion, ligand **2** species, and zinc–ligand complexes in 50% aqueous dioxane at two ligand–metal ratios. In Fig. 4 are illustrated species distributions of the zinc ion – ligand **4** system in two media, an aqueous and a mixed solvent. Under any of these conditions essentially all of the metal is complexed by these ligands at neutral pH.

TABLE 1. Protonation constants (β_{pqr}) of ligands at 25°C and $I = 0.1$ M ($NaClO_4$) in 50% (v/v) aqueous dioxane

Ligand	Log $\beta_{pqr} \pm \sigma$[a]			
	β_{101}	β_{102}	n[b]	m[c]
1[d]	10.29±0.01	15.19±0.01	108	4
2	9.89±0.01	14.80±0.01	93	3
3	9.02±0.01	13.50±0.01	58	3
4	9.13±0.01	13.73±0.01	73	3
4[e]	7.37±0.01	10.55±0.01	73	3
5	9.25±0.01	14.07±0.01	106	4
6	9.62±0.01	14.90±0.01	47	2
7	10.77±0.01	16.31±0.02	43	2
8	9.39±0.01	13.98±0.01	74	3
9[f]	10.29±0.01	15.39±0.01	84	3
10	6.19±0.01	11.73±0.01	56	2

[a] β_{pqr} refers to the general complex $L_pM_qH_r$, where L = ligand, M = metal, and H = proton; σ is the standard deviation.
[b] Number of experimental observations.
[c] Number of titration curves analyzed.
[d] $pK_{a1} = 10.22$, $pK_{a2} = 4.72$ in 50% ethanol–water at 25°C (4).
[e] Values determined in aqueous medium.
[f] $pK_{a1} = 4.93$, $pK_{a2} = 9.96$ in 50% (v/v) dioxane–water at 25°C, $I = 0.1$ M ($NaClO_4$) (27). $pK_{a1} = 6.50$, $pK_{a2} = 11.95$ in 75% (v/v) dioxane–water at 30°C, $I = 0.02$ (KCl) (stoichiometric stability constants) (28).

TABLE 2. Formation constants (β_{pqr}) of metal(II) cation–ligand complexes at 25°C and $I = 0.1$ *M* ($NaClO_4$) in 50% (v/v) aqueous dioxane

Ligand	Metal	Log $\beta_{pqr} \pm \sigma$[a]			
		β_{110}	β_{210}	n[b]	m[c]
1	Zn^{2+}	11.28±0.01	20.85±0.02	153	6
	Ni^{2+}	10.96±0.04	22.36±0.01	160	6
2	Zn^{2+}	11.15±0.01	20.55±0.01	161	6
	Ni^{2+}	10.53±0.02	21.53±0.01	177	6
3	Zn^{2+}	10.33±0.02	18.89±0.03	96	5
4	Zn^{2+}	10.61±0.02	19.53±0.02	122	6
4[d]	Zn^{2+}	8.26±0.02	15.22±0.01	94	4
5	Zn^{2+}	11.00±0.01	19.82±0.03	166	6
	Ni^{2+}	10.06±0.03	20.79±0.01	178	6
	Co^{2+}	9.22±0.01	16.70±0.02	86	3
	Fe^{2+}	8.23±0.01	14.73±0.03	80	6
	Mn^{2+}	6.26±0.02	10.41±0.06	65	3
	Ca^{2+}	3.28±0.04	—	60	4
6	Zn^{2+}	10.93±0.02	19.87±0.02	123	6
	Ni^{2+}	10.36±0.03	20.89±0.01	132	6
7	Zn^{2+}	12.82±0.06	19.61±0.01	37	3
	Ni^{2+}	12.61±0.06	19.56±0.15	60	3
8	Zn^{2+}	10.36±0.01	19.29±0.01	140	6
9	Zn^{2+}[e]	9.09±0.03	17.10±0.04	70	3
	Ni^{2+}[f]	8.09±0.04	16.00±0.03	72	3
10	Zn^{2+}	3.49±0.01	—	94	4

[a] β_{pqr} refers to the general complex $L_pM_qH_r$, where L = ligand, M = metal, and H = proton; σ is the standard deviation.
[b] Number of experimental observations.
[c] Number of titration curves analyzed.
[d] Values determined in aqueous medium.
[e] Log $\beta_1 = 9.95$; log $\beta_2 = 18.52$ in 75% (v/v) dioxane–water at 30°C, $I = 0.02$ *M* (KCl) (28).
[f] Log $K_1 = 8.1$; log $K_2 = 5.25$ in 50% (v/v) dioxane–water at 25°C, $I = 0.1$ *M* ($NaClO_4$) (27).

Partition Studies of Zinc(II)–Ligand Complexes

Data on extraction of zinc(II) from an aqueous phase into immiscible alcohols are presented in Table 3. In the absence of complexant, little zinc (added as zinc sulfate) partitioned into the organic phase. Some water-soluble complexants such as EDTA did not induce transfer of zinc into either alcohol. Other complexants did solubilize zinc(II) in the alcohols. Alcohol-soluble species were presumably those in which complexation was involved, although complexant concentration was not determined in any phase. Ligands **1**, **2** and **5** appeared to extract zinc ion well, relative to most of the complexants tested.

Inhibition of Metalloenzymes

Also presented in Table 3 are data on inhibition by complexants of enzymatic activity of the zinc-dependent enzymes, alkaline phosphatase and carboxypeptidase A, and the copper-dependent enzyme, coeruloplasmin. The tabled values were obtained from plots of inhibition vs. concentration curves, but the precision with which such concentrations were determined was not evaluated by statistical techniques, since in several cases the curves appeared to indicate complex inhibition kinetics. However, the mercapto acrylic acids were judged to be potent inhibitors. Results of the study of inhibition of thermolysin, a zinc-dependent enzyme, are plotted in Fig. 5, in which the concentration of complexant necessary to inhibit half of the total enzymatic activity appears related to the value of the formation constant of the 1:1 complex of zinc ion and inhibitor.

Discussion

Compared to many α- and β-mercapto acids and amino acids described in the literature (3), α-mercapto-β-aryl acrylic acids complex bivalent metal cations with relatively high affinity. Results obtained for β_{210} complexes of α-mercapto-β-thienyl acrylic acid **5** with several metals showed that the affinity of complexation followed the Irving–Williams order, $Mn^{2+} < Fe^{2+} < Co^{2+} < Ni^{2+} > Zn^{2+}$. With a given metal ion, but different α-mercapto-β-aryl acrylic acids, values of the complex formation constants varied with values of the protonation constants, as expected. Protonation constants of ligand **4** in aqueous solvent and in 50% (v/v) aqueous

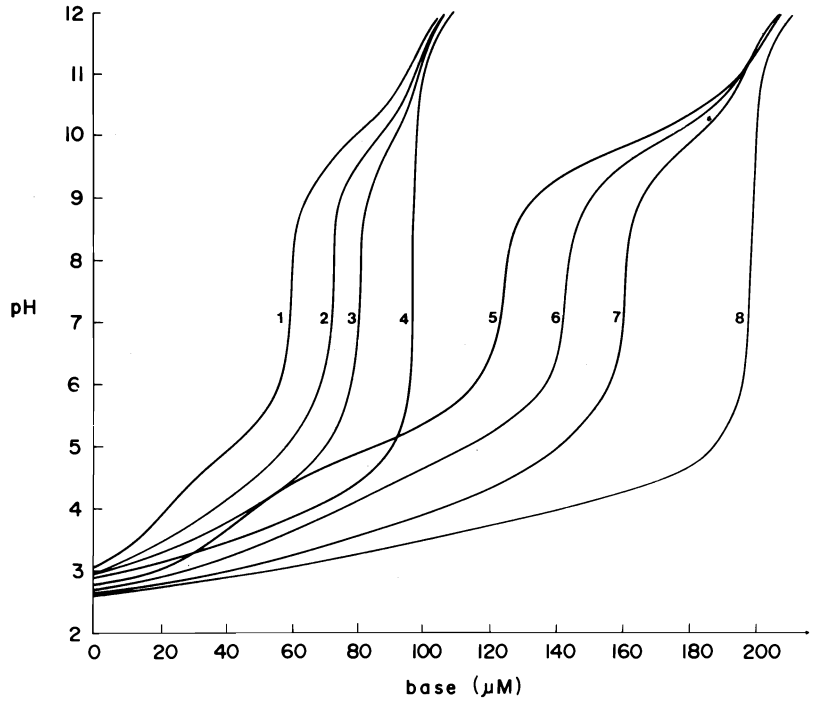

FIG. 1. Titration curves for α-mercapto-β-furyl acrylic acid – $Zn(NO_3)_2$ in 0.1 *M* $NaClO_4$ in 50% (v/v) dioxane water. Curve *1*, C_L = 2.0 m*M*, C_M = 0.0 *M*; *2*, C_L = 2.0 m*M*, C_M = 0.25 m*M*; *3*, C_L = 2.0 m*M*, C_M = 0.5 m*M*; *4*, C_L = 2.0 m*M*, C_M = 1.0 m*M*; *5*, C_L = 4.0 m*M*, C_M = 0.0 *M*; *6*, C_L = 4.0 m*M*, C_M = 0.5 m*M*; *7*, C_L = 4.0 m*M*, C_M = 1.0 m*M*; *8*, C_L = 4.0 m*M*, C_M = 2.0 m*M*.

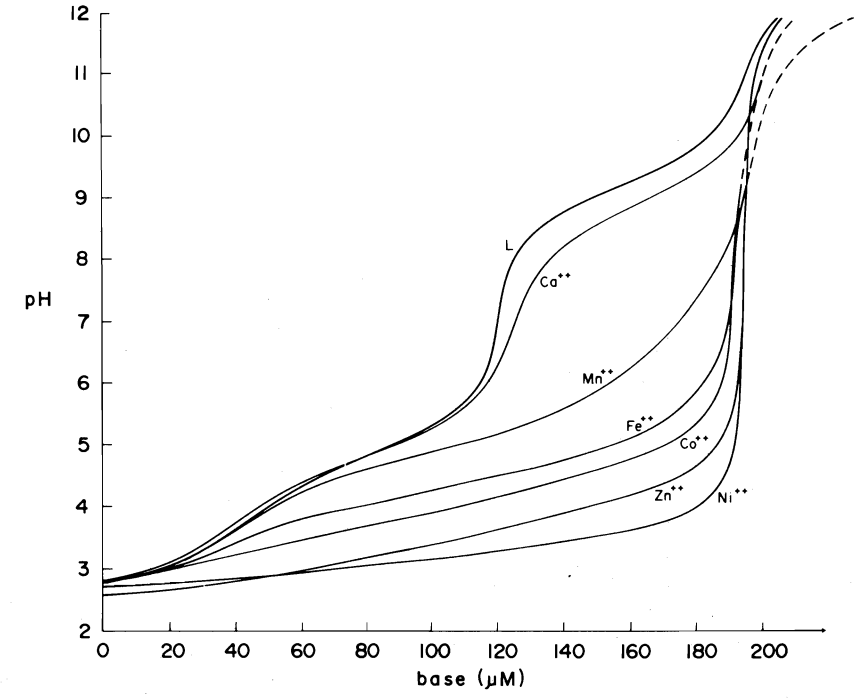

FIG. 2. Titration curves for α-mercapto-β-thienyl acrylic acid alone (L) and in the presence of cations in 50% (v/v) dioxane–water. C_L = 4.0 m*M*; C_M = 2.0 m*M*.

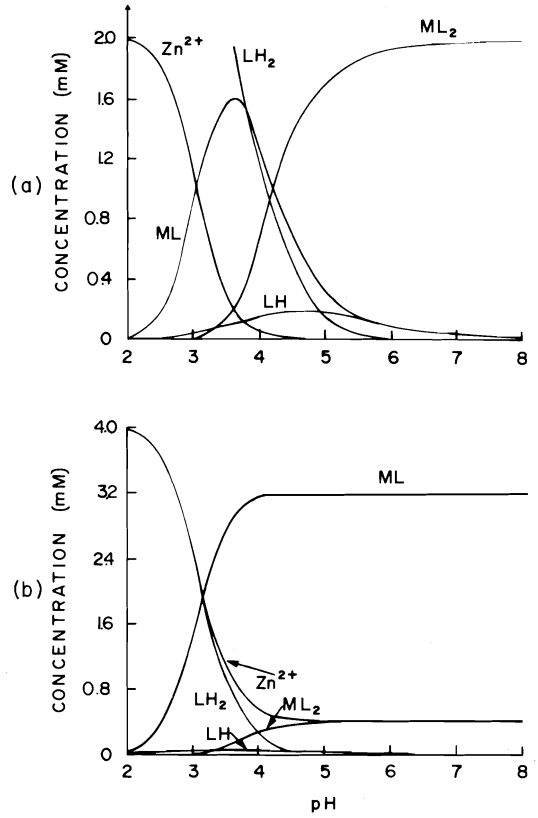

FIG. 3. Computed species distribution as a function of pH for solutions of α-mercapto-β-furyl acrylic acid (4.0 mM) with (*a*) Zn^{2+} (2.0 mM) and (*b*) Zn^{2+} (4.0 mM) in 50% (v/v) dioxane–water.

dioxane indicated increases in pK_a of 1.4 and 1.75 units in passing to the mixed solvent. One may compare pK_a values of ligand **4** in aqueous solution for dissociation of the carboxyl and thiol groups, 3.2 and 7.35, respectively, with those for a molecule such as α-mercapto acetic acid, 3.5 and 10.2, respectively (29). The more facile ionization is due in part to the double bond in the α position and the inductive effect of the aryl substituent. This characteristic underlies the potent complexation of metal ions by these compounds at physiological pH. Lipid solubility of zinc – mercapto acrylic acid complexes may be another important feature underlying their physiological effects. **1** and **2** were among the most effective ligands in enhancing the alcohol solubility of zinc, compared to many ligands previously studied in the aqueous buffer – butanol system (30).

Consistent with the generalizations drawn from the potentiometric study of complex formation, results of the study of inhibition of metalloenzymes were compatible with avid complexation of metals by mercapto acrylic acids. Alkaline phosphatase contains two zinc atoms per enzyme molecule (31) and coeruloplasmin contains at least six copper atoms (32). Carboxypeptidase contains a single zinc atom per molecule, but hydrolysis by the enzyme of the ester substrate does not follow simple Michaelis-Menten kinetics (33). Thermolysin contains a single zinc atom (34).

Relative differences in inhibitory potency may reflect characteristics of the interaction of enzyme with inhibitor, or they may reflect less profound properties such as the stability of the compound in the assay milieu. The four enzymes were assayed at acid pH (coeruloplasmin), at neutral pH (carboxypeptidase and thermolysin), and at alkaline pH (alkaline phosphatase). At micromolar concentrations of total zinc, ranking of the degree to which zinc would be complexed

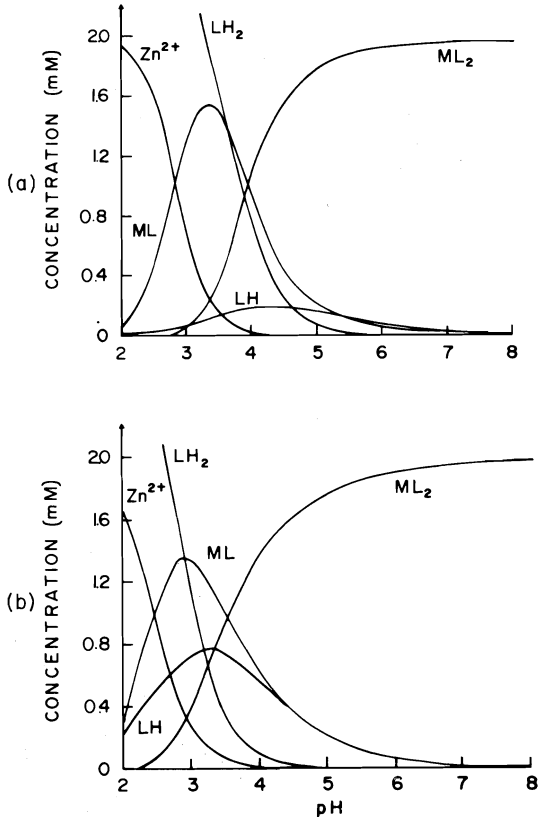

FIG. 4. Computed species distribution as a function of pH for solutions of α-mercapto-β-(5-sodiumsulfonate-2-furyl) acrylic acid (4.0 mM) and Zn^{2+} (2.0 mM) in (*a*) 50% (v/v) dioxane–water and (*b*) aqueous solvent.

TABLE 3. Effect of complexants on partition of zinc(II) between aqueous and organic phases and as inhibitors of metalloenzymes

Ligand	Pc[a]		Ligand concentration (mM) for 50% inhibition		
	Butanol	Octanol	Alkaline phosphatase	Carboxy peptidase A	Coerulo-plasmin
1	5.9	0.75	0.018	0.23	0.010
2	1.1	0.06	0.030	0.054	0.010
5	—	0.19	0.067	0.26	0.010
6	—	0.03	0.17	—	—
7	—	0.04	0.13	—	[d]
9	0.42	0.04	1.5	0.21	[d]
Na_2EDTA	[b]	[b]	0.057	0.32	>1
8-Thioquinoline	0.98	[c]	—	—	[d]
8-Hydroxyquinoline	0.48	[b]	0.12	—	0.038
1,10-Phenanthroline	—	[b]	0.14	0.073	>1
Mercapto acetic acid	0.13	[b]	0.15	1.0	—

[a]Pc = concentration of zinc in organic phase/concentration of zinc in aqueous phase.
[b]More than 90% of total zinc in aqueous phase.
[c]Less than 10% of total zinc in aqueous phase.
[d]Decolorisation (22) of reaction mixture.

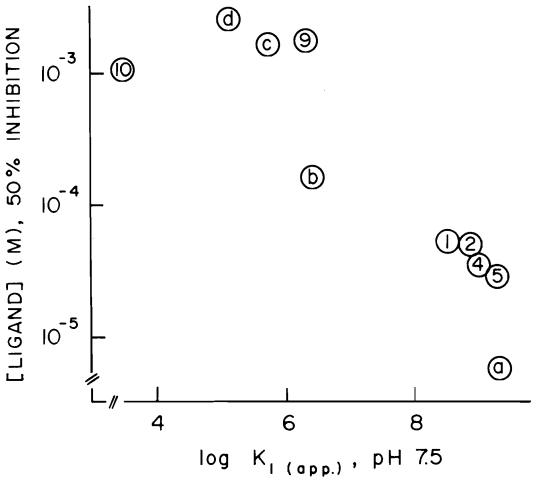

FIG. 5. Ligand concentration calculated for 50% inhibition of activity of thermolysin versus apparent formation constant at pH 7.5 for the ML complex. Formation constants of reference inhibitors were taken from the literature: a = 8-thioquinoline (35); b = 1,10-phenanthroline (36); c = 8-hydroxyquinoline (37); d = mercapto acetic acid (29).

at neutral pH by a considerable excess of ligand was calculated to be **5** > **4** > **2** > **3** > **6** > **8** > **1** > **7** > **9**. This order bears some relationship to that observed in the inhibition studies.

We have demonstrated that mercapto acrylic acids form complexes with a variety of metal cations. Yet in rats, these compounds affect zinc metabolism most markedly. While α-mercapto-β-furyl acrylic acid **2**, for example, raised zinc concentration in serum 10- to 15-fold, it had little or no effect on serum copper and iron concentration (1). Presumably the avidity of metal complex formation, the lipid solubility of the complexes, the stability of the complexant, and other features as well are involved in the effects of these compounds on trace metal metabolism.

Acknowledgements

We wish to express appreciation to Miss E. Friderich for her valuable assistance with the syntheses and to Dr. G. Letertre for the preparation of ligands **1** and **2**. We acknowledge helpful discussions with Prof. J. M. Lehn and Dr. N. J. Prakash and we thank Prof. D. R. Williams for a copy of the program SCOGS.

1. N. J. PRAKASH, P. J. SCHECHTER, E. GIROUX, and A. SJOERDSMA. Clin. Exp. Pharmacol. Physiol. **4**, 17 (1977).
2. E. GIROUX, N. J. PRAKASH, and P. J. SCHECHTER. Clin. Exp. Pharmacol. Physiol. **4**, 27 (1977).
3. L. G. SILLEN and A. E. MARTELL. Chem. Soc. Spec. Publ. No. 17 (1964); No. 25 (1971).
4. W. O. FOYE and J. R. LO. J. Pharm. Sci. **61**, 1209 (1972).
5. E. CAMPAIGNE and R. E. CLINE. J. Org. Chem. **21**, 32 (1956).
6. M. NISHIO and T. ITO. Agric. Biol. Chem. **29**, 732 (1965); **29**, 1119 (1965).
7. T. H. HASKELL, F. E. PETERSON, D. WATSON, N. R. PLESSAS, and T. CULBERTSON. J. Med. Chem. **13**, 697 (1970).
8. W. HERZ and K. DITTMER. J. Am. Chem. Soc. **70**, 503 (1948).
9. B. M. FERRIER and N. CAMPBELL. Chem. Ind. 1089 (1958).

10. R. E. BAMBURY, H. K. YAKTIN, and K. K. WYCKOFF. J. Heterocycl. Chem. **5**, 95 (1968).
11. R. BROSSMER and D. ZIEGLER. Chem. Ber. **102**, 2877 (1969).
12. G. SCHWARZENBACH and H. FLASCHKA. Complexometric titrations. 5th German ed. Ferdinand Enke Verlag, Stuttgart. 1965. pp. 125–233.
13. KWAN-KIT MUI, W. A. E. MCBRYDE, and E. NIEBOER. Can. J. Chem. **52**, 1821 (1974).
14. I. G. SAYCE. Talanta, **15**, 1397 (1968).
15. S. TAKAMOTO, Q. FERNANDO, and H. FREISER. Anal. Chem. **37**, 1249 (1965).
16. L. G. VAN UITERT and C. G. HAAS. J. Am. Chem. Soc. **75**, 451 (1953); L. G. VAN UITERT and W. C. FERNELIUS. J. Am. Chem. Soc. **76**, 5887 (1954).
17. R. G. BATES. Determination of p*H*. 2nd ed. John Wiley and Sons, New York, NY. 1973. pp. 47–49 and 448–450.
18. O. A. BESSEY, O. H. LOWRY, and M. J. BROCK. J. Biol. Chem. **164**, 321 (1946).
19. P. H. PETRA. *In* Methods in enzymology. Vol. XIX. *Edited by* G. E. Perlmann and L. Lorand. Academic Press, New York, NY. 1970. pp. 460–503.
20. K. H. SCHOSINSKY, H. P. LEHMANN, and M. F. BEELER. Clin. Chem. **20**, 1556 (1974).
21. P. O. GUNNARSSON and G. PETERSON. Eur. J. Biochem. **27**, 564 (1972).
22. G. CURZON and J. N. CUMINGS. *In* The biochemistry of copper. *Edited by* J. Peisach, P. Aisen, and W. E. Blumberg. Academic Press, New York, NY. 1966. pp. 545–557.
23. G. VOORDOUW, C. MILO, and R. S. ROCHE. Anal. Biochem. **70**, 313 (1976).
24. S. UDENFRIEND, S. STEIN, P. BOHLEN, W. DAIRMAN, W. LEIMGRUBER, and M. WEIGELE. Science, **178**, 871 (1972).
25. M. DAVIS, R. LAKHAN, and B. TERNAI. J. Org. Chem. **41**, 3591 (1976).
26. O. EXNER and W. SIMON. Coll. Czech. Chem. Commun. **29**, 2016 (1964); O. EXNER. Coll. Czech. Chem. Commun. **31**, 65 (1966).
27. S. V. LARIONOV, V. M. SCHUL'MAN, and L. A. PODOL'SKAYA. Russ. J. Inorg. Chem. **9**, 1264 (1964).
28. N. S. AL-NIAIMI and B. M. AL-SAADI. J. Inorg. Nucl. Chem. **36**, 1617 (1974).
29. D. D. PERRIN and I. G. SAYCE. J. Chem. Soc. A, 82 (1967); 53 (1968).
30. E. GIROUX and N. J. PRAKASH. J. Pharm. Sci. **66**, 391 (1977).
31. D. J. PLOCKE, C. LEVINTHAL, and B. L. VALLEE. Biochemistry, **1**, 373 (1962).
32. L. RYDEN and I. BJORK. Biochemistry, **15**, 3411 (1976).
33. R. C. DAVIES, J. F. RIORDAN, D. S. AULD, and B. L. VALLEE. Biochemistry, **7**, 1090 (1968).
34. S. A. LATT, B. HOLMQUIST, and B. L. VALLEE. Biochem. Biophys. Res. Commun. **37**, 333 (1969).
35. K. DEALEY and H. FREISER. Anal. Chem. **38**, 1577 (1966).
36. I. M. KOLTHOFF, D. L. LEUSSING, and F. S. LEE. J. Am. Chem. Soc. **73**, 390 (1951).
37. R. L. STEVENSON and H. FREISER. Anal. Chem. **39**, 1354 (1967).

The electro-deposition of silver on stationary and rotating glassy carbon discs

REMIGIO GERMANO BARRADAS, STEPHEN FLETCHER, AND SANDOR SZABO[1]

Department of Chemistry, Carleton University, Ottawa, Ont., Canada K1S 5B6

Received June 3, 1977

REMIGIO GERMANO BARRADAS, STEPHEN FLETCHER, and SANDOR SZABO. Can. J. Chem. **55**, 4037 (1977).

The deposition of silver onto glassy carbon is described. The solution consisted of 10^{-2} *M* $AgClO_4$ in 1.0 *M* $HClO_4$. Experiments reveal the difficulties in trying to separate nucleation and growth phenomena from mass transport effects. A simple semi-quantitative model is proposed to explain the experimental data. It is also shown that the deposition reaction is not completely reversible under certain experimental conditions.

REMIGIO GERMANO BARRADAS, STEPHEN FLETCHER et SANDOR SZABO. Can. J. Chem. **55**, 4037 (1977).

On décrit le dépôt de l'argent sur du carbone vitreux. La solution est formée de $AgClO_4$ 0.01 *M* dans du $HClO_4$ 1.0 *M*. Des expériences montrent les difficultés qui existent lorsque l'on veut séparer les phénomènes de nucléation et de croissance des effets de transport de masse. On propose un modèle simple semi-quantitatif pour expliquer les données expérimentales. On montre aussi que la réaction de déposition n'est pas complètement réversible sous certaines conditions expérimentales.

[Traduit par le journal]

Introduction

The electrochemical formation of new phases on foreign substrates is of considerable importance in electrocatalysis. Modification of catalysts by metal deposition reactions is now commonplace. Studies of metal deposition on glassy carbon are of particular interest in work of this kind because the carbon remains inert during the deposition reaction. This is in sharp contrast to most metal surfaces, for which complex surface area changes accompany the reaction proper. Also, bulk metals have oxide layers, adsorbed molecules, crystal defects, intergrain boundaries, etc. which further complicate the interpretation of data. Avoidance of these complications can usually be realized on metal-amalgam substrates (1), or else on specially prepared single-crystal electrodes, as has been demonstrated for the deposition of Ag^+ on Ag (2). In the latter case, it is possible to observe the propagation of steps of monomolecular height across the electrode surface accompanied by two-dimensional nucleation.

Although glassy carbon is superior to metals in many respects, its structure is still little understood. It is believed, however, to consist of a network of ribbon stacks obtained by pyrolysis of a polymeric material; possibly a phenolic resin (3). Consequently, even a highly polished surface must exhibit local inhomogeneities related to the carbon structure. A second minor difficulty is that glassy carbon has a high resistivity, and this contributes to ohmic problems in the measurement of accurate current–voltage and current–time relationships. Nevertheless, glassy carbon is an excellent material for the study of metal deposition reactions.

In the present investigation the principal techniques employed were the linear potential sweep and the single and double potential step methods. These were chosen because they allowed straightforward measurement of the processes occurring, while at the same time ensuring some degree of separation between nucleation and growth phenomena and the influence of mass transport from the bulk of solution. Rotating disc electrodes were also employed for the same reasons.

Experimental

The glassy carbon used in the present work was purchased directly from the Tokai Electrode Manufacturing Co. Ltd. (Japan). Rotating disc electrodes were sealed in Araldite and machined into small cylinders. Before use, the surfaces were polished with ceric oxide to a mirror finish and washed many times with double-distilled water. It was observed that further polishing with tissue paper resulted in a hydrophobic surface; this procedure was therefore avoided.

[1]On leave from Central Research Institute for Chemistry of the Hungarian Academy of Sciences, H-1525/17, Budapest, Hungary.

The cell used in voltammetric measurements was divided by a glass frit, while the counter electrodes were made of platinized platinum sheets of large surface area. An adjustable-luggin reference probe was included in the cell design in order to minimize the solution component of the total ohmic resistance in the measuring circuit. All potentials are quoted with respect to the hydrogen electrode in the same solution.

Unless otherwise stated, the plating solution consisted of 10^{-2} *M* silver perchlorate in 1.0 *M* (Aristar) perchloric acid. The constant potential source was a PAR 170, and experimental data were recorded directly on the same instrument. Deoxygenation was achieved by flushing the solution with purified nitrogen.

Results

Figure 1 shows the results of applying linear scans of potential to a freshly prepared glassy carbon electrode, over the potential range +800 mV to +400 mV. For clarity, only the deposition reaction is shown, while the reverse reaction is omitted. It is immediately apparent that the second and subsequent scans (curve B) are displaced from the original data (curve A) by a factor of approximately 60 mV. Removal of the electrode, followed by polishing with ceric oxide, resulted in the regeneration of curve A upon repeating the experiment. This remarkable behaviour may be explained in terms of residual nuclei of electrodeposited silver on the electrode surface after the first potential scan. The presence of these nuclei obviates the need for nucleation on the carbon surface in the second and successive scans. This hypothesis could be tested in three ways. Firstly, examination of the electrode surface *in situ* with bright illumination clearly indicated the presence of a silvery white deposit remaining on the electrode surface at +800 mV. Secondly, removal of the electrode at this potential, followed by examination using scanning electron microscopy, indicated the presence of a large number of residual silver nuclei associated with minute scratches on the electrode surface (Fig. 2). Thirdly, the chemical identity of the nuclei could be confirmed by switching the electrode to open circuit. After a few minutes, the electrode assumed the equilibrium potential of bulk silver in the same solution. The conclusion, therefore, is that the Ag^+/Ag deposition reaction is not entirely reversible at the glassy carbon electrode in 1.0 *M* $HClO_4$ (cf. ref. 4).

A similar conclusion may be achieved by repeatedly cycling the electrode potential until a pseudo steady state is reached. The results of

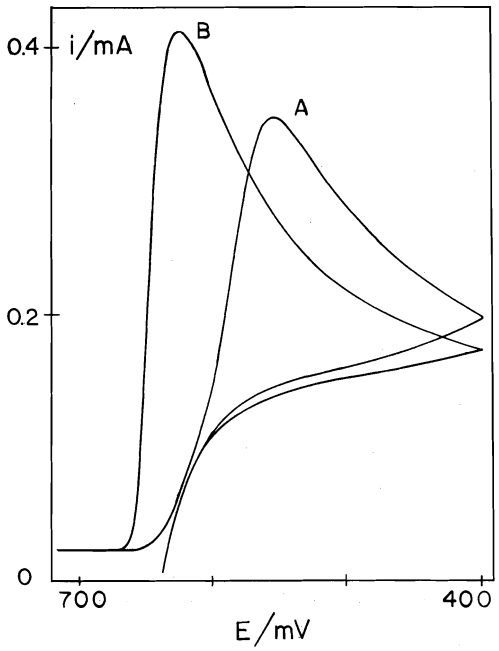

FIG. 1. 1 *M* $HClO_4$, 10^{-2} *M* $AgClO_4$, glassy C electrode. Linear potential scan from +800 mV to +400 mV. $v = 10$ mV s^{-1}, $\omega = 0$. (A) Clean surface, (B) second and successive cycles.

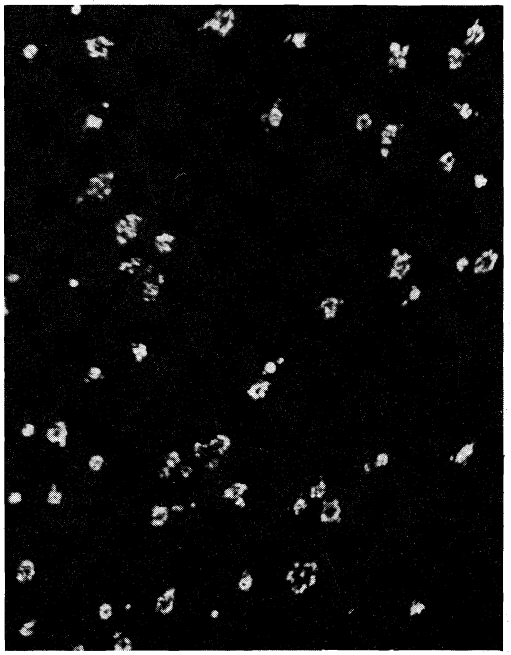

FIG. 2. Electrode surface viewed by scanning electron microscopy. Magnification 1000×, showing residual silver nuclei after 2 cycles between +800 mV and +400 mV at 50 mV s^{-1}.

this procedure are illustrated in Fig. 3. The voltammogram obtained is complex, and may not be analysed in a completely quantitative way. This is because the curves contain contributions from both the deposition reaction and from the relaxation of diffusion zones associated with mass transport from the bulk of solution. What is clear, however, is that a residual current is observed at +800 mV. The lack of complete reversibility therefore appears to be kinetic in origin, rather than being an intrinsically thermodynamic phenomenon.

The presence of the complicating features described above was of fundamental importance in designing further experiments. Because of surface roughness considerations, it was decided that the use of freshly prepared surfaces for every measurement might introduce small irregularities into the experimental data of a purely random nature. These irregularities would particularly influence the nucleation phenomena, and so this approach was rejected. Instead, it was decided to bring the electrode surface to a standard state prior to making any measurements. This could easily be carried out by linearly scanning the applied potential in the manner of Fig. 3, so that throughout the present work a large number of 'seed' nuclei were already present on the glassy carbon substrate. After this process, the electrode was also rotated before each measurement to ensure that the bulk concentration of Ag^+ extended to the electrode surface.

Investigation of Nucleation Processes

The transient response of the pretreated electrode following the application of a single potential step is illustrated in reduced variable form in Fig. 4. The transient exhibits a t^2 rise of current, which reaches a maximum and then decays as $t^{-1/2}$. The reaction is therefore proceeding via a nucleation and growth mechanism which at longer times is dominated by mass transport from the bulk of solution. In the limit the well-known equation for semi-infinite linear diffusion is obeyed

$$[1] \qquad i = nFA_sC_b(D_0/\pi t)^{1/2}$$

where i (mA) is the transient current, t (s) the transient time, D_0 ($cm^2\ s^{-1}$) the diffusion coefficient, C_b (mol cm^{-3}) concentration, and A_s surface area of electrode, respectively. Equation 1

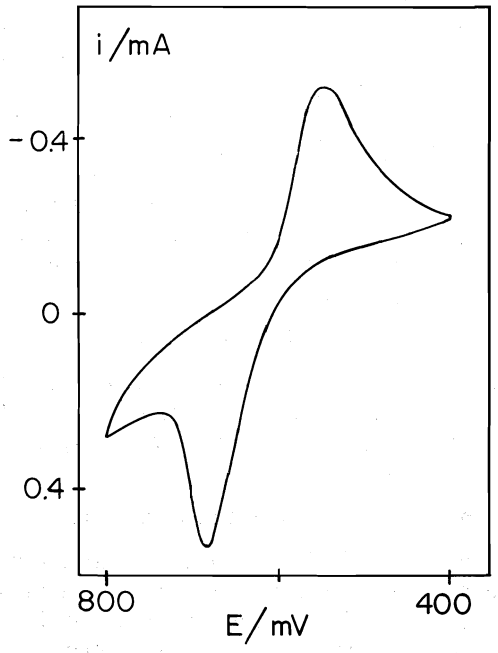

FIG. 3. 1 *M* $HClO_4$, 10^{-2} *M* $AgClO_4$, glassy C electrode. Continuous cycling linear potential scans from +800 mV to +400 mV. $\nu = 100$ mV s^{-1}, $\omega = 0$. Note residual current at +800 mV.

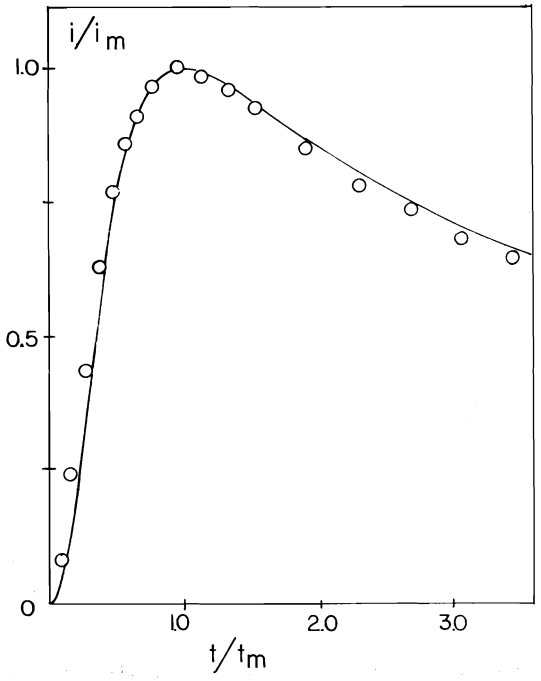

FIG. 4. Reduced variable test for complete experimental transient. Single potential step from +800 mV to +620 mV. Solid line is the theoretical shape according to eq. 9.

indicates that any diffusion zones surrounding the original nuclei have expanded and overlapped. The rising sections of the transients are tested in Fig. 5. The t^2 dependence is closely obeyed, in agreement with the data of Harrison (5, 8). Also, from the gradients of Fig. 5, it is possible to calculate the rate of growth of the deposit as a function of potential. This is shown in Fig. 6, where a very extreme dependence on potential is noted, about 5 mV per decade.

The use of the double potential step technique proved to be particularly interesting. A small pre-step (+450 mV for 40 ms) was first applied, followed by a second step on the time scale of seconds. In this case the current rises as t^1, while it decays as $t^{-1/2}$. Investigation of the rising transients as a function of potential is shown in Fig. 7. The linear dependence of current on time is observed at each potential, although extrapolation shows that the lines do not pass through the origin. This effect is quite usual with the double pulse technique, merely indicating that the current from the first step has not entirely decayed before the onset of growth at the lower overpotential. The gradients of the linear portions of the current–time curves (Fig. 7) are shown plotted versus potential in Fig. 8. As expected, an extreme dependence (~6.5 mV decade^{-1}) is noted in accord with the single step results (Fig. 6).

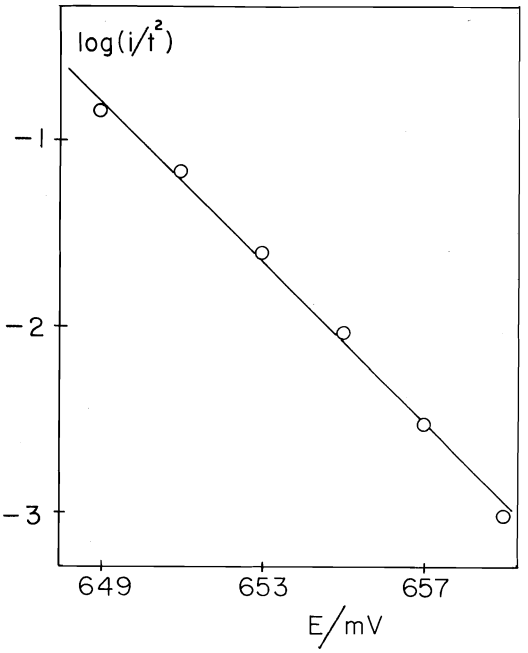

FIG. 6. Potential dependence of the function i/t^2 from single potential step experiments.

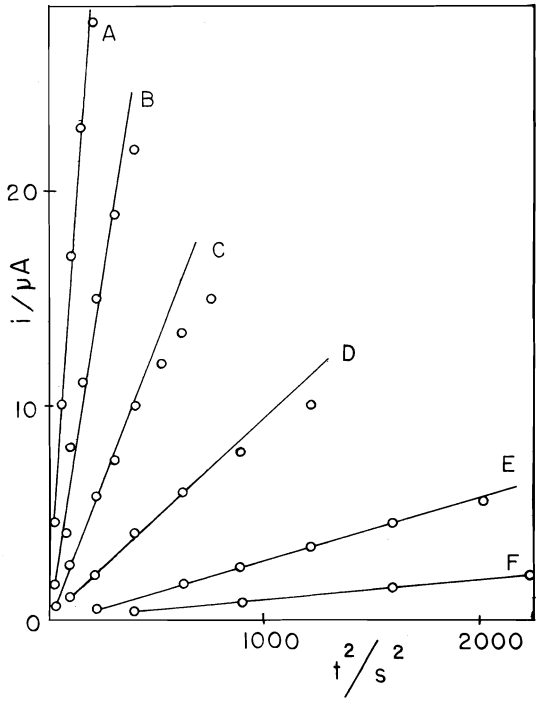

FIG. 5. 1 M $HClO_4$, 10^{-2} M $AgClO_4$, glassy C electrode. Single potential steps from +800 mV to (A) +649 mV, (B) +651 mV, (C) +653 mV, (D) +655 mV, (E) +657 mV, (F) +659 mV. Note t^2 dependence of current. Data recorded at short times, $\omega = 0$.

It is apparent from comparison of the single and double potential step results that the short-time behaviour of the current depends upon t^2 in the former case and upon t^1 in the latter instance. These two limiting cases may be understood on the assumption of a first-order nucleation law (1) of the form

$$[2] \qquad N = N_0[1 - \exp(-At)]$$

where N is number of nuclei and A (nuclei cm^{-2} s^{-1}) nucleation rate constant, respectively. At short times the exponential term may be expanded so that

$$[3] \qquad N \simeq N_0At \text{ (progressive nucleation)}$$

Alternatively, if N_0 is intrinsically large (or is enhanced by the double potential step technique) then $N \simeq N_0$. Consequently, the additional time dependence of the single step results may be explained on this basis.

However, a contradiction arises here because the pretreatment of the electrode indicates that

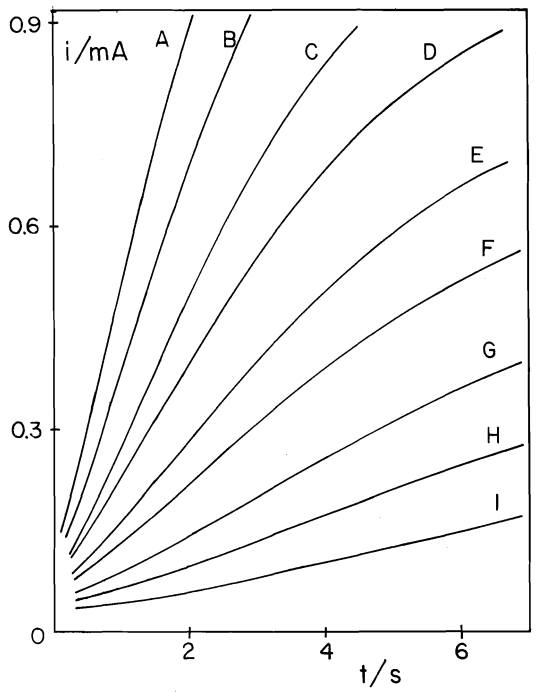

FIG. 7. Transients obtained by the double potential step method. Electrode potential switched from +800 mV to +400 mV (10 ms) then to (A) +662 mV, (B) +663 mV, (C) +664 mV, (D) +665 mV, (E) +666 mV, (F) +667 mV, (G) +668 mV, (H) +669 mV, (I) +670 mV. Note the linear dependence of i on t at short times.

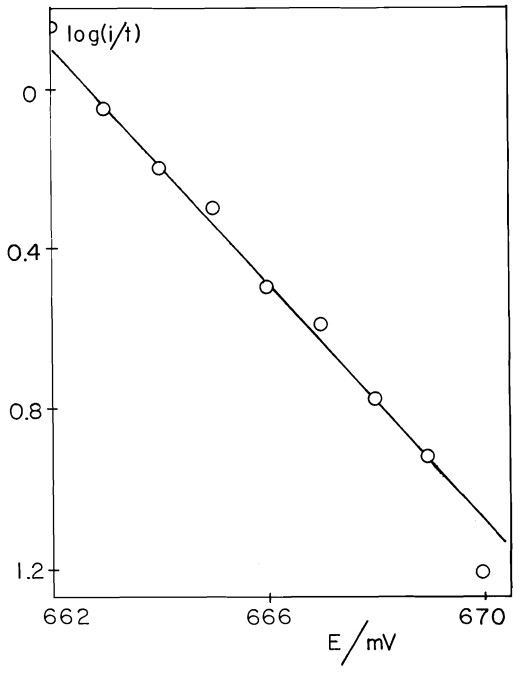

FIG. 8. Potential dependence of the function i/t from double step experiments.

N_0 should always be large, so that progressive nucleation will not be possible. The only realistic resolution of this dilemma is that the number of 'seed' nuclei on the carbon substrate must indeed be considered fixed by the pretreatment process, whereas progressive nucleation occurs at the same site during deposition at higher overpotentials.

This hypothesis is tested by scanning electron microscopy in Fig. 9. Although it is seen that nucleation is indeed occurring at the same sites, about four times as many 'seed' nuclei are present at +500 mV as compared to the electrode pretreatment (Fig. 2). This does not seriously invalidate the assumption of a constant number of seed nuclei, however, because (*a*) the overpotential used in obtaining Fig. 9 was much larger than that employed in the accumulation of the single-step data and (*b*) the nucleation rates observed at the sites of the 'seed' nuclei exhibit an extreme dependence on overpotential, and this is not detected by scanning electron microscopy.

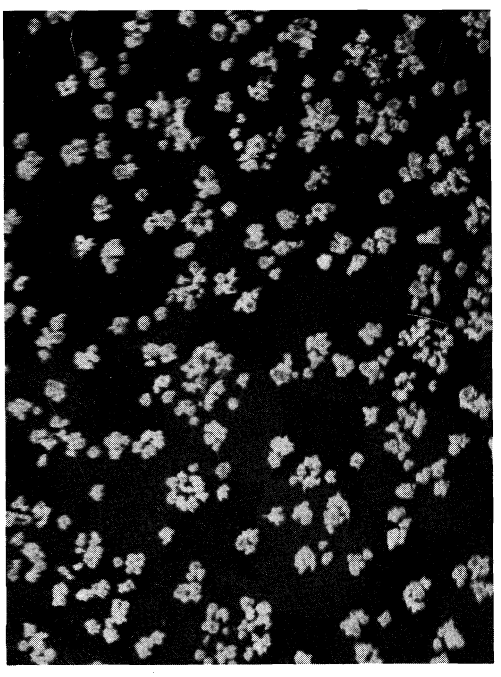

FIG. 9. Electrode surface viewed by scanning electron microscopy. Magnification 1000×, showing silver nuclei after potential step from +800 mV to +500 mV for 28 s.

The Influence of Mass Transport on the Nucleation Processes

The influence of mass transport on the nucleation processes is best observed by the use of rotating disc electrodes. Figure 10 shows a typical Levich plot for the deposition reaction, data being obtained from limiting currents observed during slow linear potential scans at various electrode rotation speeds. The experimental result is distinctive and highly reproducible. The unusual divergence from linearity at 0.2 $Hz^{-1/2}$ is noteworthy; it arises because of complex surface area changes during the growth of the electrodeposit. Thus

$$[4] \qquad i = 0.62nFA_sC_bD_0^{2/3}\nu^{-1/6}\omega^{1/2}$$

where A_s is the actual surface area of the electrode, ν kinematic viscosity, and ω (Hz) electrode rotation speed, respectively. Under these circumstances a well-developed Nernst diffusion layer must be present at the electrode surface, so that

$$[5] \qquad \delta = 1.62D^{1/3}\nu^{1/6}\omega^{-1/2}$$

where δ (cm) is diffusion layer thickness. It is of interest to conduct single and double potential step measurements under these circumstances. The results of single step experiments are shown in Fig. 11 for various rotation speeds. Once again a t^2 dependence is noted (cf. $\omega = 0$), but the absolute rate of reaction is related to the flux of Ag^+ to the electrode surface. That the flux occurs through a semi-infinite linear diffusion zone, rather than a hemispherical diffusion zone, is shown in Fig. 12. The current is obviously proportional to $1/\delta$.

The response of the rotating electrodes to the double potential step technique complicates the picture even further. Figure 13 shows a typical current–time plot obtained at $\omega = 25$ Hz. At short times $i \propto t^{1/2}$, rather than t^1 when $\omega = 0$ Hz. This implies that the flux of Ag^+ from the bulk of solution is having a profound effect upon the growth mechanism.

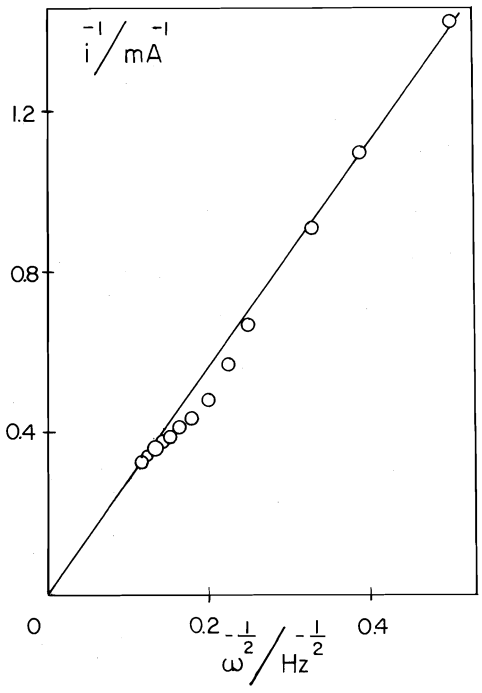

FIG. 10. 1 *M* $HClO_4$, 10^{-2} *M* $AgClO_4$, glassy C electrode. Limiting current versus $\omega^{1/2}$ for the deposition reaction. Linear potential scans from +800 mV to +400 mV, $\nu = 10$ mV s^{-1}, ω = various.

Discussion

When the Nernst diffusion zone hypothesis is applicable, a simple model for the growth of the electrodeposit may be proposed. Written for

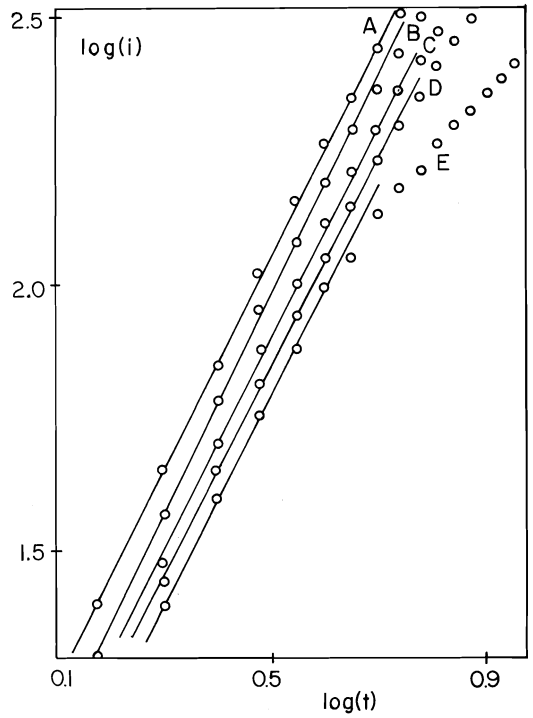

FIG. 11. Transient response to single potential step (+800 mV to +635 mV) with electrode rotation. (A) 60 Hz, (B) 50 Hz, (C) 40 Hz, (D) 30 Hz, (E) 10 Hz. The gradient $\simeq$ 2.0.

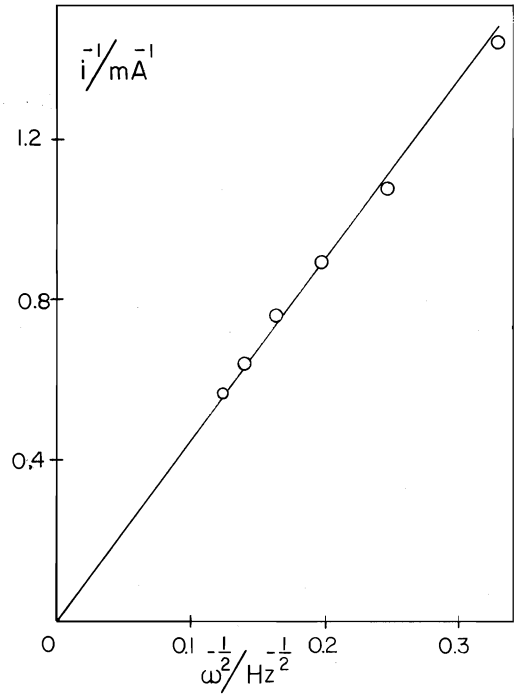

FIG. 12. Rotation speed dependence of growth transients measured at short times (t = 6.25 s). Double potential step, +800 mV to +400 mV (10 ms) then to +640 mV.

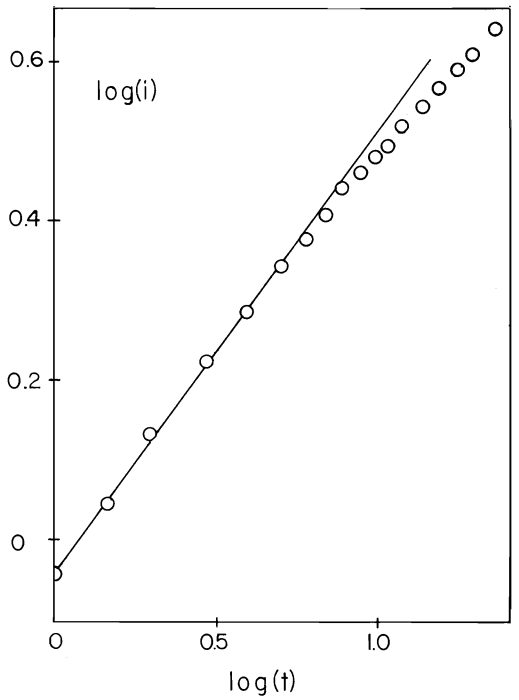

FIG. 13. Growth transient obtained from double potential step method with electrode rotation. Data recorded at short times. Potential switched from +800 mV to +400 mV (10 ms), then to +646 mV. ω = 25 Hz. Gradient $\simeq$ 0.50.

instantaneous nucleation

$$[6] \qquad \frac{i}{A_s} = \frac{N_0 A'}{A_s} nF \frac{D_0}{\delta}(C_b - C_s)$$

where A' is the 'effective' area of the Nernst diffusion layer per nucleus experiencing linear flux, and δ is the diffusion layer thickness. This equation therefore predicts $i_{growth} \propto \omega^{1/2}$ for a rotating disc electrode. Also, at long times, $N_0 A' \simeq A_s$ so that a $t^{-1/2}$ dependence of the current is predicted (eq. 1). At short times at a stationary laminar electrode, however, the problem is considerably more complex because it involves the overlap of individual hemispherical diffusion zones around each nucleus as well as the possible overlap of nuclei themselves. Various models for this type of growth have been proposed by Harrison and co-workers (6, 9, 10). In the present case, the observed results (Fig. 4) suggest

$$[7] \qquad \frac{1}{i/A_s} = \left(\frac{1}{i/A_s}\right)_{t\to 0} + \left(\frac{1}{i/A_s}\right)_{t\to \infty}$$

That is, the growth of the electrodeposit and the relaxation of the diffusion layer may be considered to be consecutive processes

$$[8] \qquad 1/i = (a/t^x) + (b/t^{-1/2})$$

where x represents the time dependence of the growth process at short times. In reduced variable form

$$[9] \qquad \frac{i}{i_m} = \frac{1 + 2x}{(t/t_m)^{-x} + 2x(t/t_m)^{1/2}}$$

where i_m (mA) is the current maximum in experimental transient and t_m time taken to achieve i_m respectively. This equation is shown in Fig. 14 as a function of x. Experimental data are in close agreement with this formulation (Fig. 4) although explanation of x in terms of models is still far from satisfactory (6).

An interesting conclusion follows from eq. 9. This is that accurate observation of growth transients at short times may only be achieved for currents below $\sim i_m/10$. This is because the influence of the falling section of the transient makes itself apparent above this value.

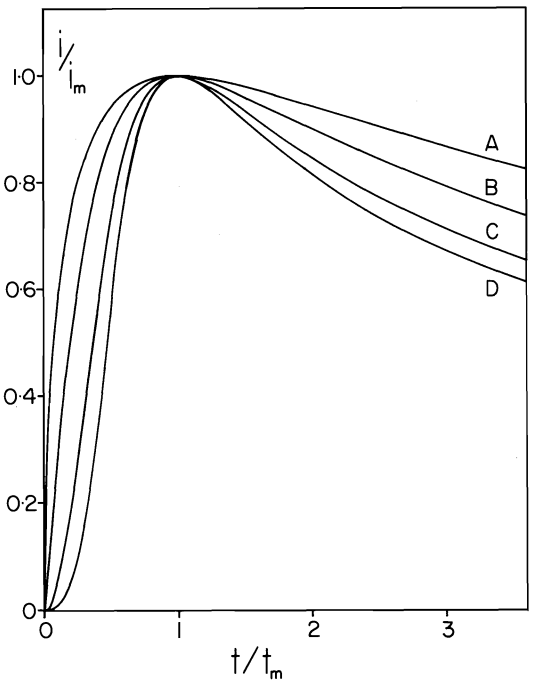

FIG. 14. Graphical representation of eq. 9. x = (A) 0.5, (B) 1.0, (C) 2.0, (D) 3.0.

Although a more complete model for the growth of Ag on glassy carbon cannot as yet be proposed, inspection of the experimental data shows that two types of nucleation are occurring. Firstly an approximately constant number of 'seed' nuclei are created by the pretreatment process. Secondly, new nuclei of silver are created on top of the seed nuclei progressively in time.

It should be noted that the three-dimensional silver deposits created on the electrode surface were rather amorphous in structure, and were crudely hemispherical in shape. Consideration of the crystallographic orientation of the deposits was therefore precluded. What was clear, though, was that the nuclei almost certainly grew into hemispherical diffusion zones emanating from the seed nuclei, and that at longer times these diffusion zones overlapped to create a condition of semi-infinite linear diffusion.

According to Frank (7) the growth of a three-dimensional deposit into a hemispherical diffusion zone should follow an equation of the form

$$[10] \qquad i = N_0 AnF(\rho/M)\pi S^3 D_0^{3/2} t^{1/2}$$

where S is a constant defined by Frank (6), M (g) gram-molecular weight, and ρ (g cm^{-3}) density of deposited material, respectively. However, in the present work the $t^{1/2}$ dependence is not observed (Fig. 7). The reason for this is somewhat obscure, although two possibilities present themselves. Either the mass transport has an unpredicted influence on the growth mechanism (e.g. the nucleation rate may be determined in part by the flux) or else the establishment of diffusion zones occurs so rapidly that overlap takes place on the time scale of the experimental data acquisition.

Acknowledgement

This work has been supported by a grant from the National Research Council of Canada.

1. J. A. HARRISON and H. R. THIRSK. Electroanal. Chem. **5**, 67 (1971).
2. E. B. BUDEVSKI. Progress in surface and membrane science. Vol. 11. *Edited by* D. A. Cadenhead and J. F. Danielli. 1976. p. 71.
3. G. M. JENKINS and K. KAWAMURA. Nature, **231**, 175 (1971).
4. M. KOPANICA and F. VYDRA. J. Electroanal. Chem. **31**, 175 (1971).
5. D. J. ASTLEY, J. A. HARRISON, and H. R. THIRSK. Trans. Faraday Soc. **64**, 192 (1968).
6. W. DAVISON and J. A. HARRISON. J. Electroanal. Chem. **44**, 213 (1973).
7. F. C. FRANK. Proc. R. Soc. London, Ser. A, **201**, 586 (1950).
8. J. A. HARRISON. J. Electroanal. Chem. **36**, 71 (1972).
9. M. F. BELL and J. A. HARRISON. J. Electroanal. Chem. **43**, 305 (1973).
10. J. A. HARRISON, R. P. J. HILL, and J. THOMPSON. J. Electroanal. Chem. **44**, 445 (1973).

The interaction of pulsed CO_2-laser radiation with common monomers[1]

A. GANDINI

Division of Chemistry, National Research Council of Canada, Ottawa, Ont., Canada K1A 0R6

Received July 20, 1977

A. GANDINI. Can. J. Chem. **55**, 4045 (1977).

Several monomers were submitted to pulsed TEA-CO_2 laser radiation. In the condensed phase neither polymerization nor decomposition was observed. In the vapour phase, polymerization did not take place but extensive decomposition occurred, mainly through molecular elimination reactions. Possible reasons for the lack of polymerization are discussed.

A. GANDINI. Can. J. Chem. **55**, 4045 (1977).

On a soumi plusieurs monomères à la radiation d'un laser à CO_2 à impulsions. En phase condensée ces monomères n'ont polymérisé ni souffert aucune décomposition. En phase vapeur on n'a observé que des importantes réactions de fragmentation moléculaire. On propose des interprétations visant à expliquer l'absence de polymérisation.

The recent development of high-power infrared lasers has promoted a number of studies dealing with the interaction of this intense radiation with organic and inorganic substrates. The often selective character of the excitation, which can lead to isotope enrichment (1), and other unique features of this new type of photochemistry (2–5) have already been recognised and are attracting considerable interest.

Following a report by Chin (6) that ethylene can be partly converted into low molecular-weight paraffins by pulsed radiation from a TEA-CO_2 laser, we decided to investigate the susceptibility of various monomers to polymerization by this technique.

The monomers were purified by standard procedures and stored under conditions which guaranteed the absence of thermal or photo-induced polymerization.

Experimental

Condensed-phase Experiments

Monomers in the liquid and solid phase were introduced into a test-tube type cell (3.5 cm id) provided with a side arm and a NaCl window. After purging the cell contents with pure nitrogen, irradiation with the appropriate line of a Lumonics 103 TEA tunable CO_2 laser was started. The beam could be focused onto the monomer surface with a NaCl lens (7.5 cm focal length). Typically, a reaction would last 30 to 60 min, at a pulse rate of about 1 Hz. Power densities of 1 to 3 MW/cm^2 were measured for the unfocused beams. The search for polymers at the end of the experiments consisted of pouring a portion of the liquid monomer (or a solution of the solid monomer) into an excess of a precipitant for the polymer in question. Another portion of the monomer was vacuum distilled at room temperature to search for possible residual oligomers. Infrared and nmr spectra of the monomers before and after the experiments were also taken to look for nonpolymeric products arising from the interaction.

Acrylonitrile

The liquid was irradiated with the 10.247 μm line (focused and unfocused) both at room temperature and at −78°C.The monomer slowly turned yellow and its temperature was raised by about 15°C. However, no polymer was obtained nor was any appreciable quantity of other products detected.

Methyl Methacrylate

The liquid was irradiated at room temperature with the 10.653 μm line with focused and unfocused beams. Warming was observed (to about 40°C). No polymer or any other products were obtained. Experiments at −78°C and −196°C with the solid monomer were equally unsuccessful.

Vinyl Acetate

The liquid was irradiated at room temperature and at −78°C with the 10.532 μm line (focused and unfocused). No products were formed in detectable quantities.

Styrene

The 10.220 μm line was used to irradiate the liquid at room temperature and the solid at −78°C. The monomer was recovered unchanged in both experiments.

N-Vinylcarbazole

The solid crystalline monomer was irradiated at room temperature with the 10.532 μm line. During irradiation some monomer crystals melted. Some polymerization was observed, but the yields were very small (less than 1% in 30 min). The same results were obtained with annealed, glassy monomer.

Acenaphthylene

The solid monomer (crystalline and glassy) was irradiated at room temperature with the 9.271 μm line. As in the case of *N*-vinylcarbazole the monomer sublimed in part to the side walls of the vessel. Traces of a brown product precipitated from *n*-pentane, but the yield was so small that no analysis could be carried out.

Gas-phase Experiments

Experiments with vapours were conducted with a

[1]NRCC No. 16239.

cylindrical cell provided with NaCl windows (8 cm optical path, 3.5 cm diameter). Following evacuation, a known pressure of the monomer vapour was introduced and an infrared spectrum taken. The cell was then placed in front of the CO_2 laser (Lumonics 101 TEA-CO_2 laser) and its contents submitted to pulsed radiation at 10.57 μm with a frequency of 1.2 Hz. The beam was focused in the middle of the cell, using a germanium lens (10 cm focal length). Infrared spectra were taken periodically to follow the appearance of products. At the end of each run the volatile products were analyzed by mass spectrometry after a rough separation based on vapour pressure. The solid products (if any) were analyzed by infrared spectroscopy.

Acrylonitrile (70-80 Torr)

The first 20–25 pulses produced an intense plasma. Thereafter the breakdown was less frequent and towards the end of the experiments (500–700 pulses) it was very sporadic. After 50 pulses a faint brown deposit was noticed on the cell walls and windows. This increased as the reactions proceeded. After 50 pulses the ir spectrum showed appreciable amounts of acetylene and HCN. After 200 pulses at least 50% of the acrylonitrile had been consumed and the only products detected by ir were acetylene and HCN. After 700 pulses there was little monomer left in the cell. The concentration of acetylene and HCN had increased correspondingly. Mass spectra of the products confirmed the predominance of these two compounds among the products, but also revealed the presence of smaller amounts of acetylene dimers, benzene, and hydrogen. The brown polymeric material deposited during the irradiation was *not* polyacrylonitrile; its aspect and ir spectrum suggested that it could be polyacetylene of low molecular weight.

Methyl Methacrylate (30 Torr)

Breakdown in the vapour was very infrequent and absent during the first 50 pulses. The formation of several products could be followed by taking ir spectra. Already after 50 pulses the presence of acetylene, methane, CO_2, and CO could be assessed. As the reaction proceeded, the concentration of methyl methacrylate decreased and, correspondingly, the typical bands of these four major products increased. After 1600 pulses more than 90% of the monomer had been consumed and a slight brown deposit was visible on the walls. Mass spectra of the final mixture confirmed the importance of the four major products and also indicated the presence of hydrogen, diacetylene, benzene, and probably isobutylene. No polymethylmethacrylate was deposited in the cell.

Vinyl Acetate (70 Torr)

Breakdown with this vapour occurred at every pulse for the first 100 pulses, then became less frequent. Extensive decomposition was noticed. The formation of CO, acetylene, methane, and CO_2 was followed by taking ir spectra during the reaction. After 300 pulses more than 70% of the monomer had been consumed. Mass spectra confirmed the predominance of CO, acetylene, and methane among the products. CO_2 and other products were also present. No polyvinylacetate was formed.

Vinyl Choride (50–500 Torr)

Irradiation of this monomer did not produce any plasma. Extensive decomposition into acetylene and hydrochloric acid occurred and as conversion increased a slight brown deposit began to form on the cell walls and windows. No polyvinylchloride was formed in these reactions. The decomposition of vinyl chloride also occurred with unfocused pulsed radiation of 10.611 μm and 9.603 μm from a tunable Lumonics 103 TEA-CO_2 laser. Again, no polymerization of the substrate occurred.

Discussion

From the experiments in the condensed phase it is obvious that, despite the fact that the radiation was strongly absorbed by the monomers, the concentration of free radicals generated by the pulse must have been minimal in all the systems studied, i.e., insufficient to induce a significant amount of chain initiation. It can be argued that either the energy absorbed is rapidly dissipated into the medium as heat or the interaction produces chemical changes of a non-radical nature, i.e., molecular decomposition processes giving volatile products. No important reaction forming aggregation products can be involved, since such products would have remained in the substrate and been detected.

The experiments in the gas phase indicate that decomposition of monomer molecules indeed occurs and without any appreciable polymerization. These fragmentation reactions seem to take place essentially through molecular elimination processes, the initial characteristic step being

$$CH_2{=}CHX \rightarrow CH{\equiv}CH + HX$$

Acrylonitrile and vinyl chloride follow this simple mechanism and only at high conversions other products, arising from the pyrolysis of acetylene, become important. Vinyl acetate probably produces acetic acid which in turn decomposes into methane, CO, and CO_2. The decomposition of methyl methacrylate is more complex, but the products again suggest the predominance of molecular splits.

It can be concluded that in the conditions selected for this work the energy from a high-power CO_2 laser is not effective in promoting polymerization. This has been attributed to a failure to produce radicals in sufficient concentration. Another explanation which might be considered is that radicals are formed after each pulse but the transient temperature attained *in the reaction zone* is higher than the ceiling temperature for the system and thus chain growth is thermodynamically precluded. If during thermal equilibration the radicals decay by other pro-

cesses, then the net result would be the absence of aggregation products.

Ethylene oligomerization seems to take place under high pressure (6). However, the very low yields of paraffins obtained (<0.1%) indicate that chain processes are not favoured. Although in that study (6) no search for other products was made, it is known that CO_2 laser radiation induces the decomposition of ethylene, to give mainly acetylene and hydrogen (7). Thus, in the experiments described by Chin (6) most of the energy absorbed is channelled into pathways which do not involve chain-propagation reactions with the substrate. It seems therefore inappropriate to consider the behaviour of that system as typical of a polymerization process.

1. R. V. AMBARTZUMIAN and V. S. LETOKHOV. Acc. Chem. Res. **10**, 61 (1977).
2. D. F. DEVER and E. GRUNWALD. J. Am. Chem. Soc. **98**, 5055 (1976).
3. W. BRAUN and W. TSANG. Chem. Phys. Lett. **44**, 354 (1976).
4. R. V. AMBARTZUMIAN, N. V. CHEKALIN, V. S. DOLJIKOV, V. S. LETOKHOV, and V. N. LOKHMAN. J. Photochem. **6**, 55 (1976/77).
5. J. M. PRESES, R. E. WESTON, JR., and G. W. FLYNN. Chem. Phys. Lett. **46**, 69 (1977).
6. S. L. CHIN. Can. J. Chem. **54**, 2341 (1976).
7. J. BASTIAENS, D. DE KEUSTER, and X. DE HEMPTINNE. Bull. Soc. Chim. Belg. **85**, 833 (1976).

Ligand effects upon the reactions of Ni(II) with sodium tetrahydroborate: Ni(I) complexes of bipyridyl and 1,10-phenanthroline

DAVID G. HOLAH, ALAN N. HUGHES, AND BENJAMIN C. HUI

Department of Chemistry, Lakehead University, Thunder Bay, Ont., Canada P7B 5E1

Received May 18, 1977

DAVID G. HOLAH, ALAN N. HUGHES, and BENJAMIN C. HUI. Can. J. Chem. **55**, 4048 (1977).

The reactions between $NaBH_4$ and Ni(II) have been studied in the presence of a variety of ligands in an effort to determine (*a*) the conditions under which reduction occurs, (*b*) the extent of the reduction (e.g. to Ni(I), Ni(0) complexes, or to Ni metal or boride), and (*c*) whether intermediate Ni complexes can be isolated.

With ligands having no π-bonding capabilities (NH_3, ethylenediamine, edta, citrate), reduction depends upon the Ni:ligand ratio and, in the presence of an excess of the ligand, reduction of Ni(II) is very slow. When vacant coordination sites exist on the metal through dissociation of, for example, $Ni(NH_3)_6^{2+}$, allowing for the interaction of the BH_4 group with the metal, then rapid reduction to the metal (or boride) takes place.

With the π-bonding N-donor ligands 1,10-phenanthroline (phen) and 2,2′-bipyridyl (bipy) reduction of the stable ML_3^{2+} complexes probably occurs via an outer-sphere electron transfer mechanism but, in these cases, new species of the type NiL_2X (L = phen, bipy; X = BH_4, PF_6, BPh_4), which formally contain Ni(I), have been isolated.

DAVID G. HOLAH, ALAN N. HUGHES et BENJAMIN C. HUI. Can. J. Chem. **55**, 4048 (1977).

On a étudié la réaction entre $NaBH_4$ et Ni(II) en présence d'une variété de ligands afin de déterminer (*a*) les conditions permettant la réduction, (*b*) le niveau de la réduction (par exemple jusqu'à des complexes de Ni(I), Ni(0) ou vers le Ni métallique ou le borure) et (*c*) si l'on peut isoler des complexes intermédiaires de Ni.

Lorsque les ligands n'ont pas de capacité de liaisons π (NH_3, éthylènediamine, edta, citrate), la réduction dépend du rapport Ni:ligand et, en présence d'un excès de ligand, la réduction de Ni(II) est très lente. Quand des sites de coordination vacants existent sur le métal par l'intermédiaire d'une dissociation, par exemple de $Ni(NH_3)_6^{2+}$, permettant une interaction du groupe BH_4 avec le métal, il y a alors une réduction rapide conduisant au métal (ou borure).

Avec des ligands donneurs par l'azote et pouvant créer des liens π comme la phénanthroline-1,10 (phen) et bipyridyl-2,2′ (bipy) la réduction des complexes stables ML_3^{2+} se produit probablement par l'intermédiaire d'un mécanisme de transfert électronique au niveau de la sphère extérieure mais dans ces cas on peut isoler de nouvelles espèces du type NiL_2X (L = phen, bipy; X = BH_4, PF_6, BPh_4) qui contiennent d'une façon formelle du Ni(I).

[Traduit par le journal]

Introduction

It is known that the presence of certain ligands prevents the rapid reduction by $NaBH_4$ of metal salts to the metal or to the insoluble borides (1). Without doubt, reactions between $NaBH_4$ and transition metal complexes containing phosphines are best documented and, in the case of nickel, these proceed by two different routes.

$$NiCl_2L_2 + BH_4^- \rightarrow NiHClL_2 \rightarrow NiH(BH_4)L_2$$

or

$$NiCl_2, L, BH_4^- \rightarrow NiClL_3 \rightarrow Ni(BH_4)L_3 \rightarrow NiL_2$$

depending on the nature of the phosphine (1–4).

The extent to which other ligands such as N-, O-, C-, or S-donors are able to prevent the reduction of metal salts by $NaBH_4$ has not been well studied. In the case of N-donors, Ni(II) in liquid ammonia (5) or in the presence of an excess of concentrated ammonia (6, 7) is not reduced by $NaBH_4$, the product being $Ni(NH_3)_6(BH_4)_2$. The reaction of $NaBH_4$ with $Nien_3Cl_2$ (en = ethylene diamine) in concentrated ammonia produces $Nien_3(BH_4)_2$ (6), while $Nien_2Cl_2$ is rapidly reduced to the metal or boride (8). Also, $NaBH_4$ does not reduce a variety of Ni(II) – cyclic nitrogen base complexes (9) even at 60°C.

Other ligands allow the incomplete reduction of metal ions. Thus Co(I) (10, 11) and Rh(I) (10) complexes of 1,10-phenanthroline (phen) and 2,2′-bipyridyl (bipy) have been obtained from $NaBH_4$ reductions (Ni(II) has not been studied) and the presence of dimethylglyoxime ($DMGH_2$) stabilizes a Co(I)–DMGH complex from Co(III)–$NaBH_4$ reactions (12, 13). Of industrial importance is the reaction of $NaBH_4$ with Ni(II)

and Co(II) in the presence of CN^- to produce $Ni_2(CN)_6^{4-}$ and $HCo(CN)_5^{3-}$, which catalyze the $NaBH_4$ reduction of dyes (14). Both the Ni and Co systems have been extensively studied in the homogeneous hydrogenations of a variety of unsaturated substances (15). Also, $NaBH_4$ solutions are used in electroless metal plating, where amines are usually present in solution (16).

In view of the considerable industrial interest in the use of $NaBH_4$, the object of this work is to study the effects that influence the course of Ni(II)–ligand–$NaBH_4$ reactions. These include the nature and electronic properties of the ligand, the stereochemistry of the starting metal complex, the molar ratios of the reactants, the time of the reaction, and the nature of the solvent.

Results and Discussion

I. Reactions With Nickel Complexes Containing N-donor Ligands

We have investigated the reactions between $NaBH_4$ and Ni(II) salts in the presence of a range of NH_3 and en concentrations in air and under nitrogen and find that the ability of these ligands to stabilize Ni(II) depends on the Ni:ligand ratio in solution. For example, aqueous solutions of $Ni(NH_3)_6Cl_2$ are rapidly reduced to the metal (or boride) while from aqueous or more concentrated ammonia solutions, the known (5–7) $Ni(NH_3)_6(BH_4)_2$ can be isolated. Only traces of metal (or boride) are formed when aqueous $Nien_3Cl_2$ is treated with $NaBH_4$ (reflecting the greater stability of $Nien_3^{2+}$ over $Ni(NH_3)_6^{2+}$) and reduction is suppressed completely in 50% en solutions. However, $Nien_2Cl_2$ is rapidly reduced (8).

The complexes $Ni(NH_3)_6(BH_4)_2$ and $Nien_3(BH_4)_2$ both slowly decompose in air, but no intermediate reduced-Ni complex could be isolated.

Reduced-Ni Complexes

In air, reactions between Ni(II) and $NaBH_4$ in the presence of phen and bipy lead initially to the complexes $NiL_3(BH_4)_2$ (L = phen, bipy) although decomposition generally occurs on drying and only $Nibipy_3(BH_4)_2 \cdot 3H_2O$ was isolated in reasonable purity ($\nu_{BH_4^-}$ at 2200 cm^{-1}). As decomposition occurs, the solids turn to the deep purple color typical of reduced-Ni complexes (see later) but all attempts to extract such species into organic solvents accelerated decomposition. In air, the decomposition products are slowly reoxidized to the tris(ligand)Ni(II) ions.

Under N_2, however, aqueous solutions of $Niphen_3Cl_2$ react with an excess of $NaBH_4$ to precipitate the air sensitive $Niphen_2BH_4 \cdot H_2O$ (Table 1). Solutions of this complex also result from similar reactions in alcohol. When $Niphen_2BH_4 \cdot H_2O$ is stirred in ethanol with $NaPF_6$ or $NaBPh_4$, the complexes α-$Niphen_2PF_6$ and $Niphen_2BPh_4$ precipitate. The former complex is converted into a second form, β-$Niphen_2PF_6$, when recrystallized from acetone while the latter is unchanged on recrystallization (Table 1). Reactions between $NaBH_4$ and $NiCl_2$–phen mixtures (1:2 and 1:1) in water produce $Niphen_2BH_4 \cdot H_2O$ and a blue solid (possibly $NiphenBH_4 \cdot H_2O$?), respectively.

The Ni:ligand ratio is also important in similar reactions involving bipy. Thus, reductions by $NaBH_4$ of aqueous Ni–bipy mixtures where the ratio is 1:6 result in no reduction, where the ratio is 1:3 a mixture of Ni(I) and Ni(II) is obtained, while a ratio of 1:2 produces $Nibipy_2BH_4 \cdot 2H_2O$. In ethanol, the reduction of $Nibipy_3Cl_2$ by $NaBH_4$ produces a dark blue solution. The only solid that could be isolated from this reaction (unlike the corresponding phen reaction) is an unstable pyrophoric solid, tentatively identified as $NibipyPF_6$, obtained after the addition of $NaPF_6$. This proved so difficult to handle that no further work on it was carried out. However, similar reductions in the presence of an excess of bipy produce solutions (of $Nibipy_2BH_4$) from which $Nibipy_2PF_6$ and $Nibipy_2BPh_4$ can be isolated (Table 1). The former complex can be recrystallized unchanged from acetone while the BPh_4^- complex is much less stable in organic solvents and, in acetonitrile for example, readily disproportionates to $Nibipy_3(BPh_4)_2$ and metal. The extreme air sensitivity of these complexes renders good analytical data difficult to obtain, but the close agreement of analyses and the magnetic and spectroscopic data leave little doubt that the structure assignments are correct.

Attempts to Prepare NiL_3^+ (L = Phen, Bipy)

It has not been possible to synthesize complexes containing the NiL_3^+ ion and indeed there appear to be no reports in the literature of six-coordinated Ni(I) complexes. Reactions between $Niphen_3Cl_2$ and $NaBH_4$ in the presence of an excess of ligand result in the formation of $Niphen_2BH_4 \cdot H_2O$. Decomposition of the initially formed pink precipitate (presumably $Niphen_3(BH_4)_2$) formed from $NiCl_2$–phen–$NaBH_4$ reactions in alcohol in the presence of an excess of

TABLE 1. Analytical data

Complex	Color	Analyses (%) N Found	N Calcd.	C Found	C Calcd.	H Found	H Calcd.
$Niphen_2BH_4 \cdot H_2O$	Blue	12.3	12.4	63.4	63.8	4.5	4.9
$Nibipy_2BH_4 \cdot 2H_2O$*	Blue	12.8	13.3	55.5	56.9	5.0	5.7
α-$Niphen_2PF_6$	Purple	10.1	9.9	51.7	51.1	3.4	2.9
β-$Niphen_2PF_6$	Blue	9.7	9.9	51.6	51.1	3.2	2.9
$Nibipy_2PF_6$	Violet	10.4	10.9	44.5	46.6	3.1	3.1
$Niphen_2BPh_4$	Purple	7.7	7.6	77.1	78.1	5.3	4.9
$Nibipy_2BPh_4$	Blue	7.5	8.1	77.2	76.7	5.5	5.3
$NiphenBH_4 \cdot H_2O$	Purple	10.0	10.3	53.5	53.0	4.2	5.2
$NibipyPF_6$†	Dark blue	7.8	7.8	33.8	33.4	2.6	2.2
$Nibipy_3(BH_4)_2 \cdot 3H_2O$	Pink	14.0	13.8	59.0	59.0	5.6	6.3

*Ni: found 13.9%, calculated 13.9%.
†Ni: found 16.5%, calculated 16.3%.

phen produces, after ~4 h, $Niphen_2BH_4 \cdot H_2O$, which on longer stirring (3–4 days) reacts to form a purple solution. Addition of $NaPF_6$ or $NaBPh_4$ to this produces α-$Niphen_2PF_6$ and $Niphen_2BPh_4$, respectively. In the absence of free phen, $Niphen_3(BH_4)_2$ decomposes in alcohol to a pyrophoric purple solid tentatively identified as $NiphenBH_4 \cdot H_2O$. Recrystallization of α-$Niphen_2PF_6$ from acetone in the presence of an excess of phen produces only the β complex, which does not react with either pyridine or PPh_3. Reactions between $Niphen_2BH_4 \cdot H_2O$ and $NaBPh_4$ in ethanol in the presence of an excess of phen result in the slow production of $Niphen_3(BPh_4)_2$, probably formed by the oxidation of the Ni(I) compound by water (17).

Attempts to synthesize $Niphen_3^+$ as the perchlorate salt from $Niphen_3(ClO_4)_2$ and $NaBH_4$ in a similar manner to that used in making $Cophen_3(ClO_4)$ (11) were also unsuccessful. No reaction was observed after 8 h at −5°C in 10% ethanol–water and at room temperature impure $Niphen_2BH_4$ is produced. Also, reactions between $Niphen_3X_2$ (X = BPh_4, PF_6) in THF and $NaBH_4$ lead only to the (slightly impure) $Niphen_2X$ complexes.

Similarly, no evidence for $Nibipy_3^+$ has been observed even from reactions involving a 10-fold excess of bipy. Indeed, the fact that $Nibipy_2^+$ can only be produced in the presence of an excess of ligand suggests that dissociation of $Nibipy_3^+$ and even of $Nibipy_2^+$ is more extensive than in the case of phen.

Physical Data

In the absence of single crystal X-ray data, it has proved difficult to assign structures to these Ni(I) complexes and to account satisfactorily for their electronic properties. Spectroscopic, magnetic, and electrical conductivity measurements are recorded in Tables 2 and 3 and some spectra are also illustrated in Figs. 1 and 2. Room temperature magnetic moments (Table 2) are, in general, consistent with one unpaired electron, although the moments of the $Nibipy_2X$ (X = PF_6 and BPh_4) are somewhat high. These values are reproducible and there is no evidence for the presence of small amounts of either paramagnetic Ni borides or, less likely, Ni(II) impurities.

Regarding electronic spectra, the complexes appear to fall into three clear structural types. There is obviously a close resemblance between the structures of $Niphen_2BH_4 \cdot H_2O$ and α-$Niphen_2PF_6$, as shown from their reflectance spectra (Fig. 1, Table 2). These spectra show no similarities with those of either tetrahedral (4, 18) or square planar (19) Ni(I) complexes and are probably therefore due either to five-coordinated metal, to which the spectra have some similarities (20), or to extensively distorted 6-coordinated structures. In either case, the weakly interacting, BH_4^- or PF_6^- groups dissociate in dilute solutions producing the 1:1 electrolytes $[Niphen_2]^+$-BH_4^- and β-$[Niphen_2]^+PF_6^-$. The infrared spectrum of the solid BH_4^- complex shows the B—H deformation and stretching frequencies at 1080 cm^{-1}, and 2150 sh, 2230, and 2300 cm^{-1} respectively, not inconsistent with very weakly coordinated BH_4 groups (4, 2). (It is interesting to note in passing that $Cobipy_2(ClO_4)$ is thought (10) to contain coordinated perchlorate.)

TABLE 2. Spectroscopic and magnetic properties

Complex		Spectrum (cm^{-1})*				μ_{eff} (B.M.)
$Niphen_2BH_4 \cdot H_2O$	Reflectance	7 140	10 900	17 200	23 000	2.06
	DMSO (5.39×10^{-4} *M*)		14 300(w,b,sh)	17 500	21 700(sh)	
			—	(1 224)	(1 280)	
	DMSO (1.82×10^{-3} *M*)			7 700		
	Sat. with $NaBH_4$			(~203)		
$NiphenBH_4 \cdot H_2O$	DMSO (4.91×10^{-3} *M*)			7 870		1.95
				(234)		
α-$Niphen_2PF_6$	Reflectance	9 800(sh)	11 100	16 900	24 800	2.33
β-$Niphen_2PF_6$	Reflectance	11 100(w,sh)	~14 300(w,sh)	18 200	24 400	2.38
	Acetone (1.42×10^{-3} *M*)		14 000sh	18 520	24 400	
			(~233)	(1 545)	(2 740)	
$Niphen_2BPh_4$	Reflectance		14 100(sh)	17 900	24 400	2.37
	Acetone (1.0×10^{-3} *M*)		14 100(sh)	18 900	24 400	
			(~211)	(1 505)	(2 410)	
$Nibipy_2BH_4 \cdot 2H_2O$	Reflectance			17 500(vb)	25 000	2.19
$Nibipy_2PF_6$	Reflectance			~20 000(vb)	26 000	2.37
	Acetone (3.99×10^{-3} *M*)			~20 000‡		
$Nibipy_2BPh_4$†	DMSO (1.72×10^{-3} *M*)			~20 000‡		2.37

*Molar extinction coefficients in parentheses.
†Insoluble in acetone, soluble with decomposition in DMSO.
‡ε values difficult to estimate because of charge transfer transition.

TABLE 3. Electrical conductivities, 25°C

Compound	Solvent	Concentration ($M \times 10^3$)	Molar conductance ($ohm^{-1}\,cm^2\,mol^{-1}$)
$Niphen_2BH_4 \cdot H_2O$	EtOH	0.78	37.2
	DMSO	2.43	20.4
$Nibipy_2BH_4 \cdot 2H_2O$	DMSO	3.09	18.1
β-$Niphen_2PF_6$	DMSO	1.73	32.9
	CH_3NO_2	0.79	98.3
	CH_3CN	0.77	179.3
	Acetone	1.67	166.2
$Nibipy_2PF_6$	DMSO	3.99	36.7
$Niphen_2BPh_4$	DMSO	1.12	29.9
$Nibipy_2BPh_4$	DMSO	1.52	27.8
$NiphenBH_4 \cdot H_2O$	DMSO	2.95	20.76
Reference compounds			
Ph_4PCl (1:1)	EtOH	1.10	31.2
	DMSO	5.0	21.6
	CH_3NO_2	1.19	74.3
	CH_3CN	0.96	148.8
$NaBPh_4$ (1:1)	DMSO	3.29	23.9
$NaPF_6$ (1:1)	Acetone	7.05	162.7
$NiCl_2 \cdot 6H_2O$ (1:2)	DMSO	5.64	52.1
$Ni(ClO_4)_2 \cdot 6H_2O$ (1:2)	DMSO	6.47	68.8
$Niphen_3(BPh_4)_2$ (1:2)	DMSO	0.92	61.1
$Cophen_3(ClO_4)_3$	DMSO	1.64	115.8

The second group of complexes having similar electronic spectra include β-$Niphen_2PF_6$, $Niphen_2BPh_4$, $Nibipy_2X$ ($X = BH_4^-$, PF_6^-, BPh_4^-), and dilute solutions of $Niphen_2BH_4 \cdot H_2O$, although measurement of the reflectance spectra of the bipy complexes is complicated by exceptionally high background absorption in the visible and near ir regions (see Table 2 and some representative spectra in Fig. 2). These spectra are all characterized by a band or shoulder in the ~20 000 cm^{-1} region ($\varepsilon \sim 1500$), which compares very favorably with the spectra of other

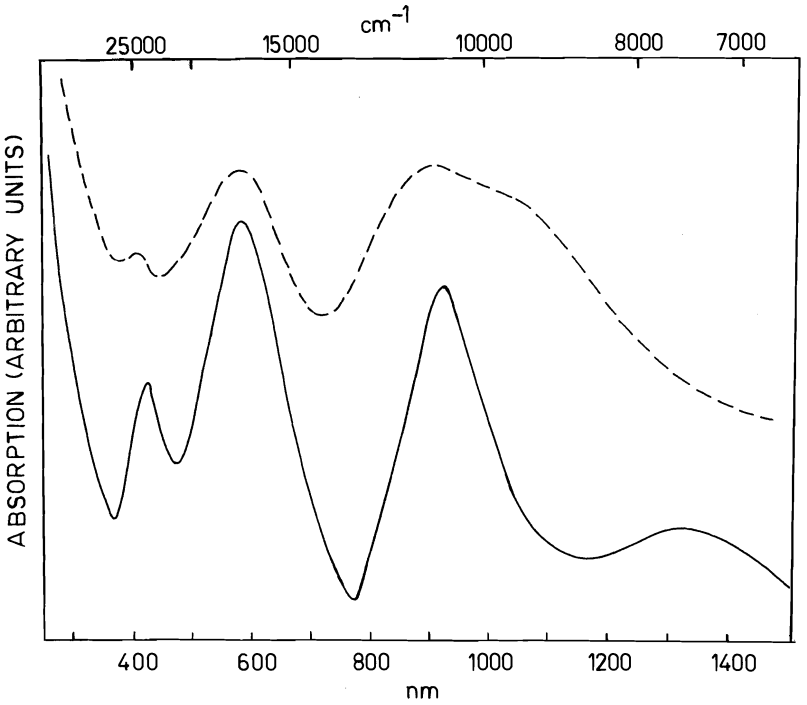

FIG. 1. Electronic spectra: — $Niphen_2BH_4 \cdot H_2O$ (reflectance); --- α-$Niphen_2PF_6$ (reflectance).

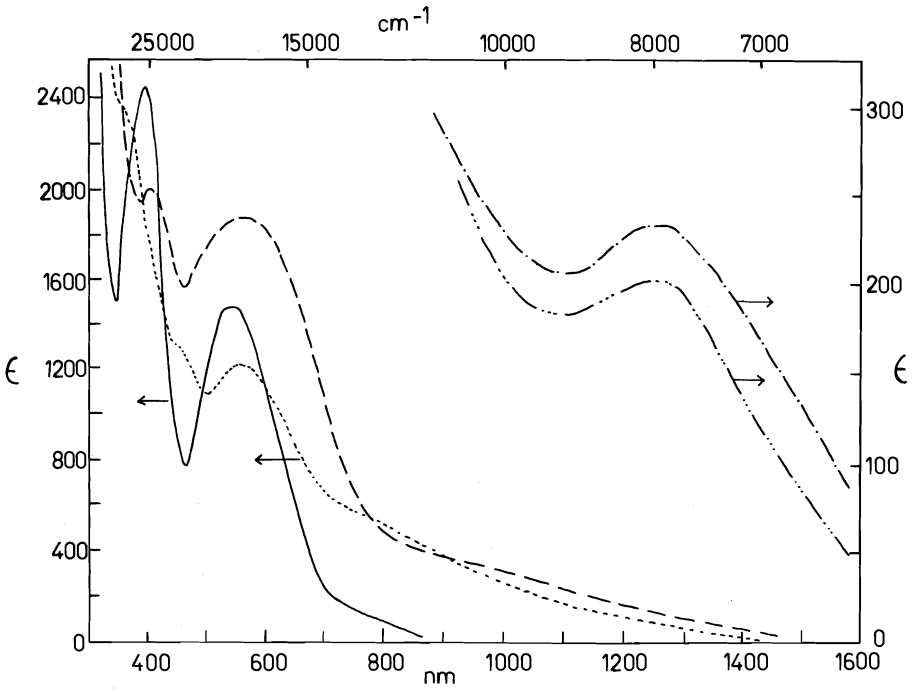

FIG. 2. Electronic spectra: — $Niphen_2BPh_4$, 1.78×10^{-3} *M* in acetone; – – – $Niphen_2BPh_4$, reflectance; --- $Niphen_2BH_4 \cdot H_2O$, 5.39×10^{-4} *M* in DMSO; ----- $Niphen_2BH_4 \cdot H_2O$, 8.88×10^{-3} *M* in DMSO saturated with $NaBH_4$; –·–·– $NiphenBH_4$, 4.91×10^{-3} *M* in DMSO.

square planar Ni(I) compounds (19) and with that of $Agbipy_2^{2+}$, which shows a band at $\sim 20\,000\ cm^{-1}$ ($\varepsilon \sim 1500$) (22). The absorption in the $25\,000\ cm^{-1}$ ($\varepsilon \sim 2500$) region in these complexes is probably due to an electron transfer band. A band similar to the weak low energy shoulder ($\sim 14\,000\ cm^{-1}$), which is particularly noticeable in the solution spectra of the $Niphen_2X$ ($X = PF_6^-$, BPh_4^-) complexes, has also been observed previously (20).

The reflectance spectrum of β-$Niphen_2PF_6$, after only one recrystallization, still shows the very weak remains of the $9800\ cm^{-1}$ band of the α compound, although this is totally absent in the solution spectrum. All the complexes in the group are 1:1 electrolytes in $\sim 10^{-3}$ *M* DMSO solutions (Table 3).

The remaining structural type is shown by $NiphenBH_4 \cdot H_2O$, which in DMSO solution shows (Table 2) a band at $7810\ cm^{-1}$ ($\varepsilon \sim 234$), although in more dilute DMSO solutions the compound dissociates to a 1:1 electrolyte. The above absorption spectrum is typical of a tetrahedral d^9 configuration (4, 18), and the ir spectrum of the solid is consistent with bidentate BH_4^- (21), having bands at 1970 (b), 2150, 2220, 2380, and $2480\ cm^{-1}$. It has already been mentioned that, in DMSO solution, $Niphen_2BH_4 \cdot H_2O$ changes to the square planar $[Niphen_2]^+$ species, but in the presence of an excess of $NaBH_4$, a further reaction occurs. This is probably the Ni(I) catalyzed decomposition of BH_4^- with the liberation of H_2 gas, and in the course of the reaction the solution develops a spectrum with a maximum at $7870\ cm^{-1}$ ($\varepsilon \sim 203$) very similar to that of $NiphenBH_4 \cdot H_2O$ (Table 2). The dissociation

$$Niphen_2BH_4 \rightleftharpoons NiphenBH_4 + phen$$

is probably involved. The analogous treatment of α-$Niphen_2PF_6$ with an excess of $NaPF_6$ in DMSO immediately produces $Niphen_3(PF_6)_2$.

Preliminary studies show that $Niphen_2BH_4 \cdot H_2O$ is an extremely active catalyst in the tetrahydroborate reductions of various functional groups. For example, $NaBH_4$, in the presence of a suspension of the above complex in methanol, reacts with acetonitrile and nitromethane (the latter reaction is extremely vigorous) to produce the corresponding amines, which were identified by mass spectrometry and by their odor. ($NaBH_4$ alone does not reduce either of these compounds.) The complex itself reacts with both compounds, although less extensively than with added $NaBH_4$.

Finally, attempts to use the above complex as a starting material to synthesize other Ni(I) complexes (of, for example, $DMGH_2$ and *N*,*N*-diethyldithiocarbamate (dtc)) resulted in oxidation to the corresponding Ni(II) derivatives.

Throughout this discussion the complexes have been presented in terms of Ni(I) species, with the unpaired electron localized on the metal. While we feel that this is the most reasonable arrangement, especially in view of results obtained from closely related Ni(II)–$NaBH_4$–phosphine reductions (23), the unpaired electron cannot be unambiguously located without epr results and even then some confusion exists in terms of the interpretation of the data (see, for example, ref. 24). The complexes could be formulated as Ni(II) species with one ligand present as a radical anion (it is difficult to explain why only one ligand would be reduced in reactions where such a large excess of $NaBH_4$ was used) or as Ni(III) species containing two one-electron reduced ligands. Such phenomena have been observed in electrochemically reduced Ni macrocyclic amine complexes (25, 26) where epr has proved useful (25) in establishing the location of the unpaired electrons.

II. Reactions with Ni Complexes Containing C, O, and S Donor Ligands

Reactions between $NaBH_4$ and Ni(II) in the presence of a variety of other ligands, such as edta, citrate (used in the preparation of high surface area heterogeneous catalysts of Co and Ni (27)), DMGH, dtc, and CN^- have been studied. In no case has any Ni(I) complex been isolated even from reactions where large cations, e.g. Ph_4P^+, had been added. Reduction of Ni(II) is prevented by edta and metal production is very slow in the presence of an excess of citrate. Reduction of $Ni(CN_4)^{2-}$ occurs, as has been observed previously (28), probably via the formation of an intermediate BH_4 complex, which would be facilitated by the lability and rapid exchange of CN groups in $Ni(CN)_4^{2-}$. On the other hand, the complexes $Nidtc_2$ and $Ni(DMGH)_2$ (non-labile ligands) are remarkably stable towards $NaBH_4$, even on heating, and metal production is very slow. These data are consistent with the results obtained from reactions between $NaBH_4$ and cationic Ni(II) complexes of cyclic tetramines and non-cyclic

tetradentate amines (9) and it seems that five-coordinated BH_4 complexes do not readily form under these conditions.

Conclusions

With the Ni(II) complexes of ligands with no π-bonding capabilities (edta, en, NH_3), the first step in the reduction appears to be the formation of a Ni–BH_4 link, which is facilitated by a vacant coordination site on the octahedral metal ion. This is related both to the stability constants for a given M–L system (edta > phen > bipy > en > NH_3 (29)) and to the lability and ease of dissociation of the ligands. When dissociation is prevented, reduction does not occur (or is dramatically slowed down), but with more dilute ligand concentrations, reduction to the metal or boride is rapid and complete.

Reductions by $NaBH_4$ of the very stable $Niphen_3^{2+}$ and $Nibipy_3^{2+}$ ions probably occur via an outer-sphere electron transfer mechanism, the π-bonding properties of the ligands enabling the Ni(I) species to be isolated.

With square planar Ni(II) complexes (DMGH, dtc) there appears to be a marked reluctance for BH_4 to interact in the axial positions. $Ni(CN)_4^{2-}$ is reduced, but in this case, the CN groups are extremely labile. It appears, however, that square planar cationic bidentate phosphine–Ni(II) species, unlike the cyclic amine complexes mentioned earlier, can interact with BH_4^- to produce Ni(I) complexes (23).

Experimental

Materials

All chemicals were reagent grade and were used without purification. Solvents were purified in the usual way, degassed, and stored over molecular sieves (4A).

$Ni(NH_3)_6Cl_2{\cdot}2H_2O$, $Nien_3Cl_2{\cdot}2H_2O$, $Nibipy_3Cl_2{\cdot}6H_2O$, $Niphen_3Cl_2{\cdot}7H_2O$, $Niphen_3(ClO_4)_2$, $Niphen_3(BPh_4)_2$, $Ni(DMGH)_2$, $Ni(dtc)_2$, $Na_2[Ni(edta)]$, and $K_2[Ni(CN_4)]$ are well known compounds and were prepared according to literature methods.

Physical Measurements

Physical measurements were carried out as previously described (4).

Syntheses

$NiL_3(BH_4)_2$ (L = Phen, Bipy)

The addition of aqueous solutions of $NaBH_4$ (10 *M* excess) to aqueous solutions of NiL_3Cl_2 caused the rapid precipitation of pink solids, which are probably $NiL_3(BH_4)_2$. Both solids decomposed and became dark purple when dried under a stream of dry N_2 or by pumping under reduced pressure. When dried over concentrated H_2SO_4, $Nibipy_3(BH_4)_2{\cdot}3H_2O$ was obtained but the phen complex again decomposed to a brown residue. This bipy complex turned to a pink paste and then to a purple solid under reduced pressure.

Aqueous suspensions of the above pink solids reacted further with $NaBH_4$ and produced green (bipy) or blue (phen) solutions with the liberation of H_2. Reactions left exposed to air continued to develop a surface pink layer, which disappeared on shaking, until all the BH_4^- was consumed when both solutions finally became pink. Heating speeded up this process and the Ni(II) starting materials were obtained from such solutions.

The following syntheses were carried out in a glove box under nitrogen.

$Niphen_2BH_4{\cdot}H_2O$

A solution of $NaBH_4$ (~0.5 g) in water (5 ml) was added to a stirred solution of $Niphen_3Cl_2{\cdot}7H_2O$ (1 g) dissolved in water (20 ml). The initially formed pink precipitate slowly turned first to green and then, after 2 h, to blue. The blue precipitate was filtered off, washed with water and, when almost dry, washed again with benzene and ether before being dried under high vacuum for ~5 h. The complex is insoluble in water, slightly soluble in ethanol, and soluble in DMSO. Solvents such as nitromethane and acetonitrile cause rapid decomposition (oxidation).

$Nibipy_2BH_4{\cdot}2H_2O$

A solution of $NaBH_4$ (0.65 g) in water (~10 ml) was added very slowly to a suspension of $Nibipy_2Cl_2$ (1.0 g) in water (~10 ml). A large volume of gas was evolved as the mixture became dark blue. The solution was stirred for ~15 min when the blue precipitate was filtered off, washed with water and, when almost dry, with ether, before high-vacuum drying.

$Niphen_2PF_6$

$Niphen_2BH_4{\cdot}H_2O$ was stirred with a 5 *M* excess of $NaPF_6$ in ethanol for 4 days to yield α-$Niphen_2PF_6$, which was filtered off, washed with ethanol, water–ethanol, ethanol, and finally ether, and then vacuum dried.

Alternatively, $NiCl_2{\cdot}6H_2O$ (0.67 g) and phen (3.16 g) were heated in ethanol (~40 ml). The mixture was cooled to room temperature and a suspension of $NaBH_4$ (0.53 g) in ethanol (~10 ml) was added dropwise. The mixture slowly turned green and after 2 days, became purple. After filtration, $NaPF_6$ (0.77 g) dissolved in ethanol (~10 ml) was added to the purple filtrate; the dark purple α-form precipitated immediately. Recrystallization from acetone–ethanol produced β-$Niphen_2PF_6$.

$Niphen_2BPh_4$, $Nibipy_2X$ (X = PF_6, BPh_4)

These complexes were prepared in a manner similar to that used for $Niphen_2PF_6$. A suspension of $NaBH_4$ in ethanol was added to a mixture of $NiCl_2{\cdot}6H_2O$ and the ligand (1:6). In the case of the bipy complexes, the anions were added after the mixture was stirred for ~24 h.

$NiphenBH_4{\cdot}H_2O$

$NiCl_2{\cdot}6H_2O$ (0.72 g) and phen (2.15 g) were heated together briefly in EtOH (~25 ml). After cooling the mixture, $NaBH_4$ (1.06 g) was added as an EtOH suspension. The mixture slowly turned purple on stirring overnight. A small amount of $NaBH_4$ (~0.2 g) was then added and the mixture was again stirred for ~30 min before the purple solid was separated, washed with EtOH, H_2O, EtOH, and ether.

$NibipyPF_6$

$Nibipy_3Cl_2{\cdot}6H_2O$ (0.71 g) was dissolved in EtOH

(~15 ml) and $NaBH_4$ (0.11 g) was added as an EtOH suspension. The solution became blue quickly. It was stirred for ~2 h before the solution was filtered. To the filtrate, $NaPF_6$ (0.71 g) in EtOH (~5 ml) was added, when a blue solid precipitated instantaneously. The product was filtered and washed with EtOH, H_2O, EtOH, and ether.

Acknowledgements

We thank the National Research Council of Canada and the Ventron Corporation, Beverly, Massachusetts for generous financial support of this work.

1. R. C. WADE, D. G. HOLAH, A. N. HUGHES, and B. C. HUI. Catal. Rev. **14**, 211 (1976).
2. M. L. H. GREEN, T. SAITO, and P. J. TANFIELD. J. Chem. Soc. A, 152 (1971).
3. M. L. H. GREEN, H. MUNAKATA, and T. SAITO. J. Chem. Soc. A, 469 (1971).
4. D. G. HOLAH, A. N. HUGHES, B. C. HUI, and K. WRIGHT. Can. J. Chem. **52**, 2990 (1974).
5. P. W. SCHENK and W. MULLER. Angew. Chem. **71**, 457 (1959).
6. E. ZIRNGIEBL and A. BURGER. U.S. Patent No. 3,298,798 (1967).
7. V. I. MIKHEEVA, N. N. MAL'TSEVA, and Z. K. STERLYADKINA. Russ. J. Inorg. Chem. **10**, 1292 (1965).
8. S. J. LIPPARD and P. S. WELCKER. Chem. Commun. 515 (1970).
9. N. F. CURTIS. J. Chem. Soc. 924 (1965).
10. B. MARTIN, W. R. MCWHINNIE, and G. M. WAIND. J. Inorg. Nucl. Chem. **23**, 207 (1961).
11. N. MAKI, M. YAMAGAMI, and H. ITATANI. J. Am. Chem. Soc. **86**, 514 (1964).
12. K. AOKI and A. MAYAKI. Jpn. Patent No. 7,021,284 (1970); Chem. Abstr. **73**, 98355 (1970).
13. M. GREEN and G. SWINDEN. Inorg. Chim. Acta, **5**, 49 (1971).
14. D. GOERRIG. U.S. Patent No. 3,273,955 (1966).
15. B. R. JAMES. Homogeneous hydrogenation. J. Wiley, New York, NY. 1973.
16. H. NIEDERPRÜM. Angew. Chem. Int. Ed. **14**, 614 (1975).
17. D. BINGHAM and M. G. BURNETT. J. Chem. Soc. A, 2165 (1970).
18. L. SACCONI and S. MIDOLLINI. J. Chem. Soc. Dalton Trans. 1213 (1972).
19. B. CORAIN, M. BRESSAN, P. RIGO, and A. TURCO. Chem. Commun. 509 (1968); M. ARESTA, C. F. NOBILE, and A. SACCO. Inorg. Chim. Acta, **12**, 167 (1975).
20. L. SACCONI, P. DAPPORTO, and P. STOPPIONI. J. Am. Chem. Soc. **97**, 5595 (1975); L. SACCONI, A. ORLANDINI, and S. MIDOLLINI. Inorg. Chem. **13**, 2850 (1974).
21. T. J. MARKS and J. R. KOLB. Chem. Rev. **77**, 263 (1977).
22. R. S. BANERJEE and S. BASU. J. Inorg. Nucl. Chem. **26**, 821 (1964).
23. D. G. HOLAH, A. N. HUGHES, B. C. HUI, and C. T. KAN. In preparation.
24. Y. SAITO, J. TAKEMOTO, B. HUTCHINSON, and K. NAKAMOTO. Inorg. Chem. **11**, 2003 (1972).
25. N. TAKVORJAN, K. FARMERY, V. KATOVIC, F. V. LOVECCHIO, E. S. GORE, L. B. ANDERSON, and D. H. BUSCH. J. Am. Chem. Soc. **96**, 731 (1974); F. V. LOVECCHIO, E. S. GORE, and D. H. BUSCH. J. Am. Chem. Soc. **96**, 3109 (1974).
26. D. C. OLSEN and J. VASILEVSKIS. Inorg. Chem. **8**, 1611 (1969).
27. J. A. SHROPSHIRE. U.S. Patent No. 3,548,830 (1970).
28. T. MIZUTA, H. SAMEJIMA, and T. KWAN. Bull. Chem. Soc. Jpn. **41**, 727 (1968).
29. J. C. BAILAR, JR., H. J. EMELEUS, R. S. NYHOLM, and A. F. TROTMAN-DICKENSON (*Editors*). Comprehensive inorganic chemistry. Vol. 3. Pergamon Press, New York, NY. 1973. p. 1139.

Déplacements chimiques de la résonance magnétique nucléaire ^{13}C dans les complexes carbonylés octaédriques des métaux de transition du groupe VIB. Effet écran produit par les électrons *d* non-liants du métal[1]

DANIEL COZAK

Anorganisch-Chemisches Institut des Technischen Universität München, 8000 Munich 2, R.F. Allemande

ET

IAN S. BUTLER

Département de Chimie, Université McGill, Montréal (Qué.), Canada H3A 2K6

Reçu le 26 mai 1977

DANIEL COZAK et IAN S. BUTLER. Can. J. Chem. **55**, 4056 (1977).

L'effet écran dû à la circulation paramagnétique des électrons *d* non-liants du métal de transition a été calculé pour la rmn ^{13}C des complexes octaédriques hexacarbonylés $M(CO)_6$ du groupe VIB. On trouve que les seules contributions d'importance au déplacement chimique de ces complexes produit par le remplacement du métal sont à l'opposé du déplacement observé expérimentalement. Le déplacement chimique produit par le remplacement d'un ligand carbonyle est discuté en fonction de la structure électronique du métal et de la distance métal–carbonyle des complexes $M(CO)_5L$.

DANIEL COZAK and IAN S. BUTLER. Can. J. Chem. **55**, 4056 (1977).

The ^{13}C nmr shielding effect at the carbonyl ligands due to the paramagnetic current in the non-bonding *d* orbitals of the metal in the group VIB $M(CO)_6$ complexes has been evaluated. For these complexes, the only contribution of significant importance to the chemical shielding calculated for the carbonyl ligands is opposite to that observed experimentally. The carbonyl chemical shift produced by substitution of one of the carbonyl ligands is discussed in terms of electronic structure of the metal and the metal–carbonyl bond lengths in the $M(CO)_5L$ complexes.

Introduction

Depuis l'utilisation de la résonance magnétique nucléaire du carbone (rmn ^{13}C) pour caractériser les fragments organiques des complexes organométalliques, l'interaction électronique des métaux de transitions avec le ligand a été le plus souvent invoquée pour rendre compte des déplacements chimiques observés. Par exemple, Cooper *et al.* (1) dans leurs études spectroscopiques de la rmn ^{13}C des ligands oléfiniques et allyliques complexés au platine(II) et au paladium(II) ont attribué le déplacement chimique des carbones complexés au métal a l'effet écran produit par les électrons *d* des orbitales libres de celui-ci. C'est-à-dire à un blindage paramagnétique qui résulterait de la circulation des électrons non-liants sur le métal. Depuis, plusieurs autres chercheurs ont candidement fait allusions à cet effet pour rendre compte, du moins en partie, du déplacement chimique observé pour la rmn ^{13}C des groupes carbonyles des séries de complexes homologues tel que $M(CO)_6$ et $M(CO)_5L$ (M = Cr, Mo, W; L = ligand donneur de deux électrons) (2–4). Dans tous les cas, ces attributions ont été très contreversées et demeurent jusqu'à date incertaines (5–7).

Les complexes carbonylés des métaux de transition du groupe VIB $M(CO)_6$ et $M(CO)_5L$, en ce qui concerne leurs structures, sont comparables au cas hypothétique des hydrures octaédriques des métaux de transition ayant une configuration électronique d^6 et à partir duquel le déplacement chimique à champ fort de la rmn ^1H fut interprété de la théorie et avec brio par Buckingham et Stephens (8). Il est bien connu que le pouvoir acide des orbitales π^* des groupes carbonyles a pour effet d'augmenter le nombre d'oxydation du métal, modifiant ainsi en quelque sorte la configuration d^6 de celui-ci. Cependant, la rmn ^1H des complexes carbonylés étudiée à date ex. $(\eta^6\text{–}C_6H_6)CrH(CO)_2L$ (9), $(\eta^5\text{–}C_5H_5)WH(CO)_3$ (10) et $(\eta^5\text{–}C_5H_5)$-$MnH(CO)_2L$ (11) indique un déplacement chimique à champ fort du proton hydrure. Alors, il est raisonnable de croire que malgré

[1]Cette communication fut extraite de la thèse de doctorat présentée par D.C., Université McGill, Montréal (Qué.), Canada, 1977.

l'interaction d–π^* entre le métal et ses ligands, le courant paramagnétique des électrons d du métal pourrait aussi dominer le blindage des ligands liés au métal même dans les complexes carbonylés.

Nous avons effectué les calculs nécessaires pour évaluer cet effet pour la liaison M—C(O) dans les complexes de la forme $M(CO)_6$ de symétrie O_h et $M(CO)_5L$ de symétrie C_{4v} (M = Cr, W) en se basant sur la théorie exposée par Buckingham et Stephens (8, 12) et revue par Lipscomb (13). Nous présentons ici nos résultats ainsi que les conclusions qui en découlent pour le déplacement chimique de la rmn ^{13}C des ligands carbonylés dans les complexes en question.

Partie expérimentale

Les équations utilisées pour le blindage sont indentiques à celles données par Buckingham et Stephens (8) pour les nombres quantiques principaux $n = 3$ et $n = 5$ correspondant ici, respectivement, au cas du chrome et du tungstène. Les calculs ont été effectués sur un ordinateur IBM 360-75 et les graphiques de σ vs. k ont été tracés à l'aide d'un programme PLOTON pour des incréments de l'abscisse k égales à 0.2 unités à partir de $k = 0.4$. Dans nos calculs la valeur approximative de l'énergie moyenne des niveaux électroniques excités ΔE figurant dans l'équation du blindage a été choisie comme étant égale à la plus basse transition singulet d–d du métal pour $M(CO)_6$. La seule qui soit permise d'après les règles de sélection de symétrie O_h pour les opérateurs du moment angulaire du blindage est la transition $^1A_1(t_{2g}^6e_g^0) \rightarrow {}^1T_{2g}(t_{2g}^5e_g^1)$. Beach et Gray (14) dans leurs études spectroscopiques des complexes $Cr(CO)_6$ et $W(CO)_6$ ont attribué les bandes à 32 500 et 33 500 cm^{-1}, respectivement, à cette transition. La longueur du lien metal–carbonyle R utilisée comme valeur représentative est la longueur du lien M—C(O) rapportée pour l'état solide de $Cr(CO)_6$, 1.92 Å et de $W(CO)_6$, 2.06 Å (14, 15). La valeur de l'exposant k de la fonction d'onde atomique de Slater $r^{(n-1)} \exp(-kr)$ (16) calculée d'après les règles du même auteur est de 1.6 pour les orbitales $3d$ du chrome complexées (i.e. configuration d^6 à spin bas). De façon semblable, en prenant la valeur du rayon covalent du chrome ou la valeur estimée à partir de la longueur du lien Cr—C(O),[2] on trouve $k = 1.3$. Il faut cependant mentionner que les fonctions d'ondes atomiques de Slater représentent mieux la distribution électronique radiale lorsque k est supérieur à la valeur calculée par ses règles (18). Alors, dans la discussion qui suit k sera considéré comme étant supérieur à 1.6 pour les orbitales d du chrome et du tungstène.

Résultats

L'effet écran du courant paramagnétique métallique sur les ligands carbonyles a été

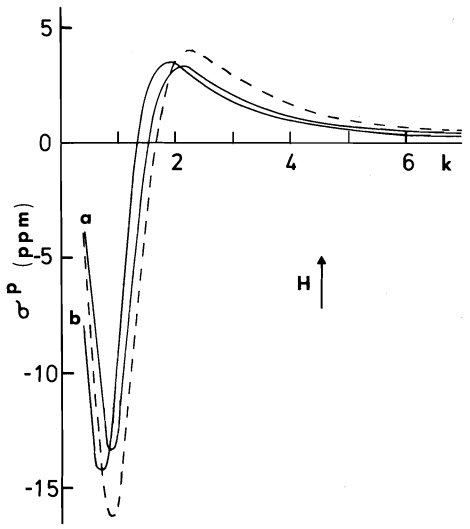

FIG. 1. Graphe de σ^p vs. k pour $\Delta E = 32\,000\ cm^{-1}$: (*a*) $W(CO)_6$, — $R = 2.06$ Å, --- $R = 1.92$ Å; (*b*) $Cr(CO)_6$, $R = 1.92$ Å.

évalué pour le cas plus général des complexes $M(CO)_6$ de symétrie O_h. Pour les complexes correspondants $M(CO)_5L$ de symétrie C_{4v}, l'expression mathématique du blindage demeure la même à l'exception des termes ΔE comme nous le verrons ici.

M(CO)₆

Les calculs effectués pour différentes valeurs de R indiquent que le blindage paramagnétique σ^p est très sensible aux variations de ce paramètre.[3] Comme le démontre les courbes de la fig. 1, une diminution de R égale à 0.14 Å entraine pour $W(CO)_6$ une augmentation de l'intercepte de la courbe avec l'abscisse k de 0.1 unité. Bien que les minima se trouvent à la même valeur de k, le fond du puits de la courbe se trouve déplacé de 3 ppm à champ faible et le maximum de la courbe ($R = 1.92$ Å) de 0.8 ppm à champ fort. Parallèlement, pour le complexe, on observe pour cette diminution de R une augmentation du blindage diamagnétique σ^d de 1.4 ppm ($k = 1.6$) (cf. fig. 2). L'ampleur de ses déplacements est liée au choix de la valeur de ΔE pour σ^p seulement. Par exemple, le minimum de la courbe σ^p de $W(CO)_6$ passe de -12.7 ppm à -13.9 ppm pour $\Delta E = 33\,000$ et $30\,000\ cm^{-1}$, respectivement. Les mêmes observations ont été notées pour $Cr(CO)_6$, mais les déplacements étaient plus petits.

[2]L'orbitale coordinante 5σ de CO peut être considérée comme étant un hybride *sp* du carbone (17).

[3]Dans cette ouvrage les termes σ^p et σ^d se rapportent qu'à l'effet écran étudié.

L'examen de la fig. 1 nous révele qu'un déplacement chimique significatif à champ faible des carbonyles de $W(CO)_6$ par rapport à ceux de $Cr(CO)_6$ est à prevoir pour les valeurs de k entre 1.6 et 2.0. Dans la fig. 2, malgré la du lien métal–carbonyle plus grande dans $W(CO)_6$, on constate que le blindage diamagnétique des carbonyles de ce dernier est plus important. Ainsi, par rapport à leur analogues du chrome les groupes carbonyles de $W(CO)_6$ se trouvent déblindés de ~ 4 ppm dû à σ^p et blindés de ~ 2 ppm dû à σ^d. Un déplacement chimique total $\sigma = \sigma^p + \sigma^d$ de l'ordre de 2 ppm à champ faible est à prévoir, pour une même valeur de k, entre le blindage des carbonyles de ces deux complexes. D'autre part, pour les valeurs de $k > 2$ un déplacement chimique total σ du même ordre de grandeur, à champ fort, est prévu à cause des contributions positives de σ^p et de σ^d (cf. figs 1 et 2).

$M(CO)_5L$

Pour les complexes monosubstitués $M(CO)_5L$ il est possible de prédire la direction et l'intensité de la contribution paramagnétique du métal σ^p sur les groupes carbonyles en considérant les valeurs calculées pour $M(CO)_6$. L'état électronique excité $^1T_{1g}(t_{2g}{}^5e_g{}^1)$ du métal pour la symétrie O_h se scinde en deux composantes pour la symétrie C_{4v} de $M(CO)_5L$, soit $^1E(b_2{}^2e_g{}^3a_1{}^1)$ et $^1A_2(b_2{}^1e_g{}^4b_1{}^1)$ comme indiqué dans la fig. 3. La transition électronique $^1A_1 \rightarrow {}^1E$ n'est compatible qu'avec la symétrie de l'opérateur du moment angulaire l_{xx} et l_{yy}, et la transition $^1A_1 \rightarrow {}^1A_2$ qu'avec celle de l_{zz}. Ainsi, les équations du

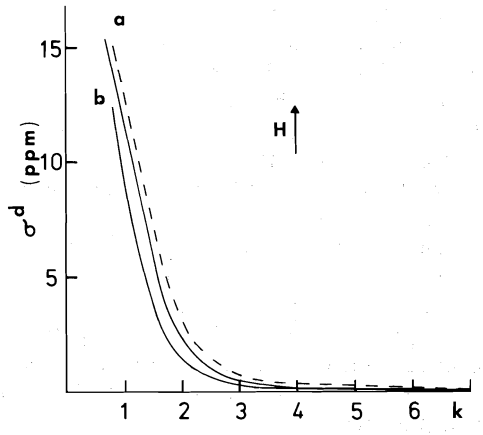

FIG. 2. Graphe de σ^d vs. k: (*a*) $W(CO)_6$, — R = 2.06 Å, --- R = 1.92 Å; (*b*) $Cr(CO)_6$, R = 1.92 Å.

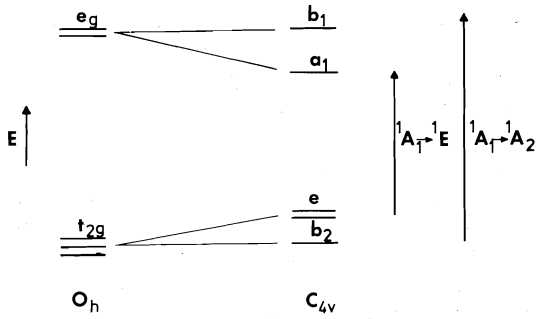

FIG. 3. Diagramme d'orbitales moléculaires pour les orbitales *d* dans un champ de symétrie O_h et C_{4v}.

blindage σ^p prennent la forme (8):

$$[1] \qquad \sigma_{xx}{}^p = \sigma_{yy}{}^p = \frac{A}{R^3\Delta E(E)}F(R)$$

$$[2] \qquad \sigma_{zz}{}^p = -\frac{4A}{R^3\Delta E(A_2)}G(R)$$

où A est une constante, $F(R)$ et $G(R)$ des fonctions de R, $\Delta E(E) = E(E) - E(^1A_1)$ et $\Delta E(A_2) = E(^1A_2) - E(^1A_1)$, respectivement. Pour les complexes octaédriques neutres $M(CO)_5L$, l'énergie $\Delta E(E)$ est de beaucoup inférieur à celle de la transition $\Delta E(A_2)$ (19). Donc, nous avons $|\sigma_{xx}{}^p + \sigma_{yy}{}^p|$ (pour $M(CO)_5L$) $> |\sigma_{xx}{}^p + \sigma_{yy}{}^p|$ (pour $M(CO)_6$) et $|\sigma_{zz}{}^p|$ (pour $M(CO)_5L$) $> |\sigma_{zz}{}^p|$ (pour $M(CO)_6$) pour $k >$ 1.6 étant donné que $\Delta E > \Delta E(A_2) > \Delta E(E)$. La figure 4 montre les courbes du blindage paramagnétique indépendant de l'énergie, soit $\sigma_{xx}{}^p\Delta E$ et $\sigma_{zz}{}^p\Delta E$ ainsi que $\sigma^p\Delta E = (\frac{2}{3}\sigma_{xx}{}^p + \frac{1}{3}\sigma_{zz}{}^p)\Delta E$ pour $W(CO)_6$. A l'aide de ces courbes et des eqs 1 et 2 un déplacement chimique à champ fort pour $\sigma_{xx}{}^p$ de $M(CO)_5L$ par rapport à $M(CO)_6$ est prévu étant donné son signe positif ($k > 1.6$) et un déplacement, moins important que celui de $\sigma_{xx}{}^p$, à champ faible pour $\sigma_{zz}{}^p$. Donc, une augmentation du blindage due à l'énergie est prévue pour les carbonyles des composés monosubstitués par rapport au composé hexacarbonylé correspondant.

Les variations de R, comme pour $M(CO)_6$, sont très importantes à la fois pour σ^d et σ^p. De façon générale les liaisons M—C(O) des dérivés monosubstitués $M(CO)_5L$ sont égales ou inférieures à celles du complexe parent et le lien du carbonyle-*trans* est le plus court, $R > R_{cis} > R_{trans}$ (15, 20). Donc, l'effet de R est sans équivoque d'accroître le blindage des carbonyles par le biais des blindages accrus de σ^p et

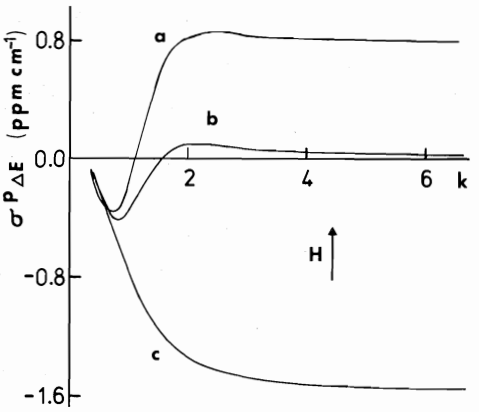

FIG. 4. Graphe du blindage paramagnétique indépendent de l'énergie pour $W(CO)_6$ (R = 2.06 Å) vs. k; (*a*) $\sigma_{xx}{}^p\Delta E$; (*b*) $\sigma^p\Delta E$; (*c*) $\sigma_{zz}{}^p\Delta E$.

σ^d pour $k > 2$. Etant donnée une différence très nette entre R_{cis} et R_{trans} le carbonyle-*trans* sera le plus affecté. Cependant, comme le démontre les courbes de la fig. 1, pour les valeurs de k inférieures au pointe d'intercepte des deux courbes de $W(CO)_6$ les carbonyles sont déblindés et l'ordre relatif des carbonyles-*cis* et -*trans* se trouve renversé.

Discussion

Le déplacement chimique de 20 ppm à champ fort observé (21) pour la rmn ^{13}C des carbonyles de $W(CO)_6$ par rapport à ceux de $Cr(CO)_6$ ne peut pas être expliqué que par l'effet considéré ici. Au maximum un déplacement de 2–5 ppm dans cette direction pourait être obtenu pour des valeurs appropriées de k, R et ΔE. Si nous considérons les valeurs de k comprisent entre 1.3 et 2.0, l'effet écran calculé prévoit un déblindage total de 2 ppm pour les ligands carbonyles. Bien que les valeurs de k inférieures à 2.0 peuvent être un choix discutable[4] pour les métaux de groupe VIB, il n'en demeure pas moins que la valeur de k = 1.3 calculée ici est une approximation du même ordre et tout aussi valable que les fonctions d'onde atomique de Slater qui ont servi au calcul du blindage chimique. Ce déplacement chimique ne demeure cependant pas sans explication. Selon Mann (6), il serait attribuable au nombre croissant de la charge nucléaire du métal du transition et aux orbitales d plus diffusent des métaux plus lourds, réduisant ainsi l'interaction liante d–π^* du métal avec les carbonyles. De même Mahnke *et al.* (22) ont calculé que le déplacement chimique de la rmn ^{13}C, observé lorsque la molécule diatomique CO est complexée à un atome métallique, était lier principalement à l'interaction d–π^* et par conséquent au terme ΔE du ligand. En plus vient s'ajouter le blindage diamagnétique du carbone qui est directement proportionnel au nombre atomique du métal (23). Notons que ces explications sont en accord avec le déplacement à champ fort observé lorsque CO est complexée à des métaux de transition du groupe IB (24).

Le déplacement chimique de la rmn ^{13}C à champ faible observé pour les complexes octaédriques monosubstitués $M(CO)_5L$ (21) des métaux du groupe VIB ainsi la position relatif des carbonyles-*cis* et -*trans* est l'opposé du déplacement prévu ici pour $k > 2.0$. Cependant, pour les valeurs de k entre 1.3 et 2.0 l'ordre relative *cis*/*trans* est consistant avec les résultats expérimentaux (i.e. le carbonyle-*trans* est à champ faible par rapport aux *cis*). Il est intéressant de noter que même si les complexes octaédriques neutres des métaux de transition des groupes VIIB et VIII ne sont pas encore connus. La résonance observée pour le carbonyle-*trans* des complexes $M(CO)_5X$ (M = Mn (25); M = Re (26)) et *cis*-$M(CO)_4X_2$ (M = Fe, Ru, Os (27)) où X = ligand donneur de 1 électron, se trouve à champ fort par rapport aux carbonyles-*cis*.

Le déplacement des carbonyles à champ fort prévu ici dans les complexes monosubstitués est dû principalement à la séquence des niveaux électroniques des orbitales d du métal tel qu'il est indiqué dans la fig. 3. Cette représentation des niveaux ènergitiques des orbitales d est celle généralement admise pour le fragment $M(CO)_5$ de symétrie C_{4v} (19, 28). Cotton *et al.* (29) pour expliquer l'énergie plutôt faible des transitions d–d observées des spectres uv des complexes $Cr(CO)_5$(amine), ont utilisé un diagramme où l'ordre des orbitales moléculaires a_1 et b_1 serait inverti par rapport à celui utilisé ici. Evans *et al.* (30) et dernièrement Fenske (31), ont démontré dans leurs études photoélectroniques des complexes $Mn(CO)_5X$ et $Re(CO)_5X$ que l'ordre des niveaux électroniques supérieurs remplis de symétrie e et b_2 varie selon le caractère acid/base du ligand X. Dans l'éventualité d'un tel renversement la valeur de $\Delta E(A_2)$ serait plus petite

[4]Voir la discussion traitant de ce sujet aux réfs 8 et 12.

que celle de $\Delta E(E)$ et un déblindage des carbonyles en résulterait par rapport au composé hexacarbonylé.

Remerciements

Nous tenons à remercier le Gouvernement du Québec et le Conseil national de recherches du Canada pour leur aide financière.

1. D. E. Cooper, R. P. Hughes et J. Powell. J. Am. Chem. Soc. **94**, 9244 (1972).
2. J. A. Connor, E. M. Jones, E. W. Randall et E. Rosenberg. J. Chem. Soc. Dalton Trans. 2419 (1972).
3. D. L. Cronin, J. R. Wilkinson et L. J. Todd. J. Magn. Reson. **17**, 353 (1975).
4. P. S. Braterman, D. W. Milne, E. W. Randall et E. Rosenberg. J. Chem. Soc. Dalton Trans. 1027 (1973).
5. L. E. Manzer. Inorg. Chem. **15**, 2354 (1976).
6. B. E. Mann. Adv. Organomet. Chem. **12**, 135 (1974).
7. J. Evans et J. R. Norton. Inorg. Chem. **13**, 3042 (1974).
8. A. D. Buckingham et P. J. Stephens. J. Chem. Soc. 2747 (1964).
9. D. N. Kursanov, V. N. Setkina, P. V. Petrovskii, V. I. Zdanovich, N. K. Baranetskaya et I. D. Rubin. J. Organomet. Chem. **37**, 339 (1972).
10. M. C. McIvor. J. Organomet. Chem. **27**, C59 (1971).
11. B. V. Lokshin, A. E. Ginzburg, V. N. Sektina, D. N. Kursanov et I. B. Nemirovskaya. J. Organomet. Chem. **37**, 347 (1972).
12. A. D. Buckingham et P. J. Stephens. J. Chem. Soc. 4583 (1964).
13. W. L. Lipscomb. Adv. Magn. Reson. **2**, 137 (1966).
14. N. A. Beach et H. B. Gray. J. Am. Chem. Soc. **90**, 5313 (1968).
15. J. A. Connor et O. S. Mills. J. Chem. Soc. A, 334 (1969).
16. J. C. Slater. Phys. Rev. **361**, 57 (1930).
17. R. K. Nesbet. J. Chem. Phys. **40**, 3619 (1964); **43**, 4403 (1965); W. M. Huo. J. Chem. Phys. **43**, 624 (1965).
18. J. W. Richardson, W. C. Niewpoort, R. R. Powell et W. F. Edgell. J. Chem. Phys. **36**, 1057 (1962).
19. M. Wrighton. Inorg. Chem. **13**, 905 (1974).
20. H. J. Plastas, J. M. Stewart et S. O. Grim. J. Am. Chem. Soc. **91**, 4326 (1969).
21. L. J. Todd et J. R. Wilkinson. J. Organomet. Chem. **77**, 1 (1974).
22. H. Mahnke, R. K. Sheline et H. W. Spiess. J. Chem. Phys. **61**, 55 (1974).
23. W. H. Flygare et J. Goodisman. J. Chem. Phys. **49**, 3122 (1968).
24. Y. Souma, J. Iyoda et H. Sano. Inorg. Chem. **15**, 968 (1976).
25. L. J. Todd et J. R. Wilkinson. J. Organomet. Chem. **80**, C31 (1974).
26. J. L. Webb et W. A. G. Graham. J. Organomet. Chem. **95**, 119 (1975).
27. L. Vancea, R. K. Pomeroy et W. A. G. Graham. J. Am. Chem. Soc. **97**, 1407 (1976).
28. M. Elian et R. Hoffmann. Inorg. Chem. **14**, 1058 (1975); R. N. Perutz et J. J. Turner. J. Am. Chem. Soc. **97**, 4791 (1975).
29. F. A. Cotton, W. T. Edwards, F. C. Rauch, M. A. Graham, R. N. Perutz et J. J. Turner. J. Coord. Chem. **2**, 247 (1973).
30. S. Evans, J. C. Green, M. L. H. Green, A. F. Orchard et D. W. Turner. Discuss. Faraday Soc. **47**, 112 (1969).
31. R. F. Fenske. Progress in inorganic chemistry. Vol. 21. *Edité par* S. J. Lippard. Interscience Publ., New York, NY. 1976.

Isolation of intermediates in the rearrangement of 4-cyano-4,5-dihydroazepines to furo[2,3-*b*]pyridine derivatives

BRIAN GREGORY,[1] ERIC BULLOCK, AND TENG-SONG CHEN

Department of Chemistry, Memorial University of Newfoundland, St. John's, Nfld., Canada A1C 5S7

Received June 24, 1977

BRIAN GREGORY, ERIC BULLOCK, and TENG-SONG CHEN. Can. J. Chem. **55**, 4061 (1977).

4-Cyano-4,5-dihydroazepines, when treated with an acidic ion-exchange resin in aqueous alcohol, undergo hydrolytic cleavage to a cyanooctanedionediester. The cyanooctanedionediester and its thermal cyclization product, a 4,7-dihydrofuro[2,3-*b*]pyridine, are shown to be intermediates in the rearrangement of cyanodihydroazepines to furo[2,3-*b*]pyridines by aqueous alcoholic silver nitrate. The mechanism of this rearrangement and the role of silver(I) are discussed. Ethyl 2-(2-cyanoethyl)acetoacetate cyclizes to a 1,2,3,4-tetrahydro-2-oxopyridine when refluxed with silver nitrate in aqueous ethanol.

BRIAN GREGORY, ERIC BULLOCK et TENG-SONG CHEN. Can. J. Chem. **55**, 4061 (1977).

Le traitement de cyano-4 dihydro-4,5 azépines par une résine échangeuse d'ions acide en milieu alcool aqueux provoque une hydrolyse conduisant à un cyanooctanedionediester. Cet ester et son produit de cyclisation thermique, une dihydro-4,7 furo[2,3-*b*] pyridine sont des intermédiaires dans le réarrangement des cyanodihydroazépines en furo[2,3-*b*] pyridine par le nitrate d'argent en solution alcoolique aqueuse. On discute du mécanisme de ce réarrangement et du rôle de l'argent(I). Le (cyano-2 éthyl)-2 acétoacétate d'éthyle se cyclise en tétrahydro-1,2,3,4 oxo-2 pyridine lorsqu'on le porte au reflux avec du nitrate d'argent dans l'éthanol aqueux.

[Traduit par le journal]

Earlier we have shown that the 4-cyano-4,5-dihydroazepine **3** gave a mixture of the furo[2,3-*b*]pyridine **8** and the pyrrolo[2,3-*b*]pyridine **9** when refluxed with silver nitrate in aqueous ethanol (1). It was suggested that the mechanism may involve acid-catalyzed hydrolytic ring-opening to give the acyclic vinylogous urethanes **11** and **13** and further hydrolysis to the octanedionediester **15**, followed by cyclization, dehydration, and oxidation to give **8** (1). The pyrrolopyridine **9** was thought to arise in a similar manner from **11** or **13**. In agreement with this hypothesis it was shown that aqueous nitrous acid gave only **8**, and that the characteristic ultraviolet absorption spectrum of **3** was rapidly lost in acidic media. Further indirect support was provided by Johnson and co-workers who showed that a dihydroazepine lacking the 4-cyano group was hydrolyzed to an octanedionediester (2) and that the reaction of an *N*-methyl-4-chloromethyldihydropyridine with potassium cyanide gave, after chromatography on silica gel, the furopyridine **4** and other products (3). We now report the isolation of intermediates and by-products which provide very strong evidence in support of the suggested mechanism, and suggest new potential synthetic applications of silver(I).

The lability of vinylogous urethanes to aqueous acid is well documented. Thus Robinson showed that ethyl 3-aminocrotonate is hydrolyzed in aqueous acid to ethyl acetoacetate and postulated that this involves protonation on the carbon atom situated β to the nitrogen (4). Similar protonation of Hantsch dihydropyridines (5) and esters of tetrahydronicotinic acid (6) has been suggested. Experimental support for β-protonation of vinylogous urethanes has been obtained using infrared (7), ultraviolet (6), and nuclear magnetic resonance spectroscopy (8). Protonation of **1** at C-3 or C-6 followed by attack of water on the resulting iminium salt would give the acyclic vinylogous urethanes **10** and **12**, which could either cyclize or be hydrolyzed further to the cyanooctanedionediester **14**. Early attempts to hydrolyze **1** to **14** using mineral acid gave very complex mixtures. Careful hydrolysis, using aqueous methanol in the presence of an acid-form ion exchange resin under an inert atmosphere, afforded a colorless oil, $C_{13}H_{17}NO_6$, which exhibited properties consistent with structure **14**. In particular, the posi-

[1]Author to whom all correspondence should be addressed.

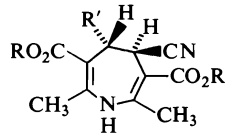

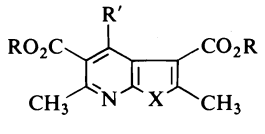

1 R′ = H, R = CH_3
2 R′ = R = CH_3
3 R′ = H, R = CH_2CH_3

4 R′ = H, R = CH_3, X = O
5 R′ = H, R = CH_3, X = NH
6 R′ = CH_3, R = CH_3, X = O
7 R′ = CH_3, R = CH_3, X = NH
8 R′ = H, R = CH_2CH_3, X = O
9 R′ = H, R = CH_2CH_3, X = NH

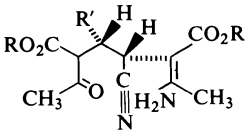

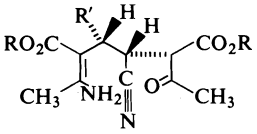

10 R′ = H, R = CH_3
11 R′ = H, R = CH_2CH_3

12 R′ = H, R = CH_3
13 R′ = H, R = CH_2CH_3

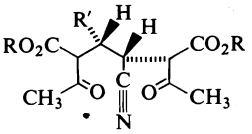

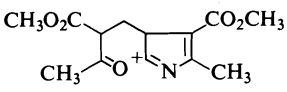

14 R′ = H, R = CH_3
15 R′ = H, R = CH_2CH_3

16

tive ferric chloride test and the shift and intensification of its ultraviolet absorption band in basic media are consistent with the presence of a β-ketoester moiety. The infrared spectrum showed the presence of cyano, saturated ester, and saturated ketone groups and additional peaks at 3474 and 1657 cm^{-1} which were assigned to hydroxyl and chelated carbonyl of an enol form of **14**. The infrared spectrum showed many similarities with that reported for the closely related dimethyl 2,7-octanedione-3,6-dicarboxylate (2). The mass spectrum showed fragments typical of a β-ketoester (9) and was entirely consistent with the structure **14**. In addition to compound **14**, traces of the furopyridine **4** and the pyrrolopyridine **5** were also isolated, and were identical with the products formed when the cyanodihydroazepine **1** was refluxed with aqueous methanolic silver nitrate. The furopyridine **4** was also formed by exposure of solutions of the cyanooctanedionediester **14** to air in the presence of a trace of acid, or to aqueous methanolic silver nitrate. It is therefore clear that in acidic media the furopyridine **4** is formed via **14**. When aqueous methanolic silver nitrate was used, silver(I) cation functioned as a dehydrogenating agent in the penultimate step (see below). This resulted in the drop in p*H* which was observed during the course of the reaction. It is not clear whether the ring opening occurs entirely by acid catalysis or whether silver cation can itself catalyze hydrolysis.

Attempts have been made to decide whether the cyclization of dimethyl 4-cyano-2,7-octanedione-3,6-dicarboxylate **14** involves nucleophilic attack by the nitrile nitrogen on a ketone carbonyl or by enolic hydroxyl on the nitrile carbon, and how silver(I) is involved. Attack by the nitrile group on the 2- or 7-ketone groups would give, after loss of water, the nitrilium ions **16** or **17**. Although cyclization to give **16** would appear to be precluded by the failure to find pyrrole or pyrrolopyran derivatives in the reaction product, the involvement of **17**, which could cyclize to give a dihydrofuropyridine, is supported by the nature of the final product and by the isolation, from a related system **2**, of a 1,2,3,4-tetrahydro-2-oxopyridine (see below). Further, the cyclization of δ-ketonitriles in acid media to give 1,2,3,4-tetrahydro-2-oxopyridines is well known (10–12) and has been postulated to proceed via nitrilium ions (10). In particular, ethyl 2-(2-cyanoethyl)acetoacetate is known to give ethyl 6-methyl-1,2,3,4-tetrahydro-2-oxopyridine-5-carboxylate (13) in the presence of hydrochloric acid, and we have shown that this cyclization can also be accomplished using silver nitrate in refluxing ethanol.

Cyclization by attack of enolic hydroxyl at C-7, on the 4-cyano group to give the iminopyran **19**, or a tautomer, is not considered to be involved in view of the absence of pyrrolopyran[2] derivatives in the reaction product. However, similar attack by the enolic hydroxyl at C-2 would give, after tautomerism, the 2-aminofuran **20**.[3] The coordination of silver(I) with the nitrogen of the nitrile[4] should render the nitrile carbon more susceptible to nucleophilic attack,[5] e.g. by the enolic hydroxyl, thus facilitating the formation of **20**. However, compound **14**,

[2]In the Knoevenagel reaction of malononitrile with cyclic β-ketoesters, iminopyran derivatives have been considered to be intermediates in the formation of alkoxypyridinols (14).

[3]Temnikova and co-workers (15) have observed the formation of 2-aminofurans from γ-ketonitriles in basic media.

[4]The formation of complexes between silver(I) and nitriles, e.g. $2AgNO_3 \cdot C_2H_4(CN)_2$, is well known (16–19).

[5]During the hydration of the nitrile function of 2-cyano-1,10-phenanthroline, transition metal ions are believed to function as general acid catalysts (20). Homogeneous hydration of nitriles may be catalyzed by transition metal derivatives and is believed to involve attack of hydroxide ion on the carbon of a coordinated nitrile (21).

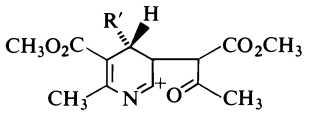

17 R′ = H
18 R′ = CH_3

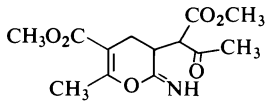

19

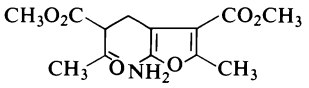

20

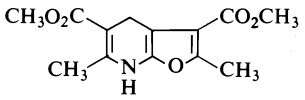

21

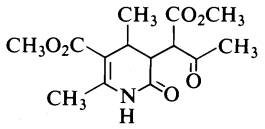

22

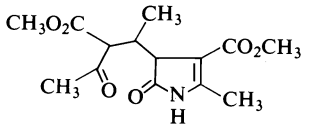

23

when heated alone at 160°C, slowly solidified to give a product $C_{13}H_{15}NO_5$ whose spectroscopic properties were in accord with the 4,7-dihydrofuropyridine structure **21** and which was easily oxidized by air, silver nitrate, or nitrous acid to the furopyridine **4**. Thus the cyclization of **14** can be accomplished in the absence of protons or silver(I). This is in contrast to ethyl 2-(2-cyanoethyl)acetoacetate which was recovered unchanged after prolonged heating at 160°C and from refluxing aqueous ethanol. In this latter case, silver(I) or proton catalysis would appear to be essential. This difference in behaviour may indicate that the formation of **21** from **14** proceeds by attack of the enolic hydroxyl group on the cyano carbon to give the 2-aminofuran **20** which then cyclizes to give **21**.

The action of silver nitrate in refluxing aqueous methanol on the 4-cyanodihydroazepine **2**[6] resulted in the formation of the expected furopyridine **6** and pyrrolopyridine **7** and, in addition, a third product, $C_{14}H_{19}NO_6$. The structure of this latter compound follows from its spectroscopic properties. Thus the presence of a methyl acetoacetate moiety was suggested by the presence of saturated ester and ketone carbonyl absorptions in the infrared spectrum, the presence of singlets at δ 2.28 (methyl of acetyl) and 3.78 (methyl ester) in the nmr spectrum, and the loss of methyl acetoacetate by McLafferty rearrangement in the mass spectrum (base peak at *m/e* 181). The ultraviolet spectrum (cf. ref. 22) was reminiscent of unsaturated γ- or δ-lactam ester chromophores. As a result of these observations structures **22** and **23** were considered. The latter structure was, however, eliminated by the absence of a band in the infrared spectrum at 1724–1730 cm^{-1} (cf. ref. 22) and, more significantly, by the nmr spectrum which showed a double doublet at δ 3.57. The structure was confirmed when **22** gave the furopyridine **6** when treated with concentrated sulfuric acid. The formation of the 2-oxo-1,2,3,4-tetrahydropyridine **22** from **2** may be the result of nucleophilic attack by water, rather than enolic hydroxyl, on some intermediate such as **18**, although silver(I) catalyzed hydration of the nitrile and cyclization (cf. refs. 11, 12) of the resulting amide cannot be excluded.

The foregoing results establish that the rearrangement of the cyanodihydroazepine **1** to the furopyridine **4** involves the intermediates **14** and **21**. Although the cyclization of **14** to **21** would appear to be initiated by nucleophilic attack of enolic hydroxyl on the cyano carbon, the present work does not eliminate completely the participation of nitrilium ion **17**. The possibility that coordination of a nitrile nitrogen with silver(I) renders the nitrile carbon more susceptible to nucleophilic attack under conditions near neutral p*H* has many synthetic implications, some of which are under investigation and will be reported in a subsequent communication.

Experimental

All details concerning spectral measurements, analyses, etc. are provided in an earlier publication (23). Ethyl 2-(2-cyanoethyl)acetoacetate was prepared by the method

[6]The preparation of this compound will be described in a forthcoming publication.

of Albertson (24) and has bp 123–125°C/1 Torr (lit. (24) 121°C/2 Torr).

The Reaction of Dimethyl 4-Cyano-4,5-dihydro-2,7-dimethylazepine-3,6-dicarboxylate ***1*** *with Silver Nitrate*

A solution of the cyano compound **1** (2.0 g) and silver nitrate (1.4 g) in methanol (30 ml) and water (2 ml) was heated under reflux for 2 days. The deposited silver was filtered off and the filtrate evaporated *in vacuo*. The residue was dissolved in chloroform and chromatographed on basic alumina using benzene and ethyl acetate as eluent. The first fraction yielded, after removal of solvent, dimethyl 2,6-dimethylfuro[2,3-*b*]pyridine-3,5-dicarboxylate **4** as white needles (1.32 g, 66%), mp 122–123°C (lit. (3) 122.5–124°C); ms *m/e*: 263(100, M^+), 232(96), 231(70), 203(46). The product had ir, uv, and nmr spectra which were identical with those of an authentic specimen prepared by the method of Childs and Johnson (3).

The second fraction yielded dimethyl 2,6-dimethylpyrrolo[2,3-*b*]pyridine-3,5-dicarboxylate **5** as fine white crystals (0.22 g, 11%), mp 250–251°C; ir ν_{max}: 3426 (NH str.), 1709 cm^{-1} (aryl ester); uv λ_{max}: 235.5 nm (ε 35 400), 255 nm (infl. ε 16 500), 298 nm (ε 8250); ^{1}Hmr (DMSO-d_6) δ: 2.67 and 2.75 (each s, methyls at C-2, -6), 3.84 and 3.88 (each s, methyl esters), 8.70 (s, H at C-4); ms *m/e*: 262 (99.5, M^+), 231(100), 230(43), 202(43), 171(49). *Anal.* calcd. for $C_{13}H_{14}N_2O_4$: C 59.54, H 5.38, N 10.68; found: C 59.49, H 5.38, N 10.51.

The Acid-catalyzed Hydrolysis of the 4-Cyano-4,5-dihydroazepine, ***1***

A mixture of the cyano compound **1** (2.0 g) and Dowex 50W-X8 (15 g) in methanol (60 ml) and water (10 ml) was stirred at 45°C for 4 h under a nitrogen atmosphere. After cooling, the resin was filtered off and the solvent removed under reduced pressure. The residue was transferred to a sublimation apparatus and distilled at 135–140°C (oil bath temperature) under 0.02–0.03 Torr to give dimethyl 4-cyano-2,7-octanedione-3,6-dicarboxylate **14** as a colorless viscous oil (1.74 g, 81%); ir ν_{max}: 3474 (enol OH), 2252 (C≡N str.), 1752 (saturated ester), 1729 (saturated ketone), 1657 (chelated carbonyl of enol form); uv (95% ethanol) λ_{max}: 218 nm (ε 1350), 260 nm (ε 1700); (0.01 *M* sodium hydroxide in 95% ethanol) λ_{max}: 275 nm (ε 27 000); ms *m/e*: 283 (1.5, M^+) 263(3), 241(3), 210(9), 168(7), 167(5), 155(22), 129(20), 117(15), 116(12), 112(5), 98(5), 97(20), 87(28), 85(5), 59(5), 55(16), 43(100). *Anal.* calcd. for $C_{13}H_{17}NO_6$: C 55.12, H 6.05, N 4.95; found: C 55.13, H 6.14, N 5.13.

Compound **14** was quantitatively converted to dimethyl 2,6-dimethylfuro[2,3-*b*]pyridine-3,5-dicarboxylate **4**, mp 122–123°C, when refluxed with silver nitrate in aqueous methanol.

Dimethyl 4,7-Dihydro-2,6-dimethylfuro[2,3-b]pyridine-3,5-dicarboxylate, ***21***

Dimethyl 4-cyano-2,7-octanedione-3,6-dicarboxylate **14** (1 g) was sealed under vacuum in a tube and heated at 160°C for 24 h. The oil gradually solidified to give a pale yellow product which was rapidly recrystallized twice from chloroform–ether – petroleum ether to give dimethyl 4,7-dihydro-2,6-dimethylfuro[2,3-*b*]pyridine-3,5-dicarboxylate **21** as pale yellow crystals (0.54 g, 58%); ir ν_{max}(KBr): 3297 (NH), 1720 (aryl ester), 1686 (unsaturated ester), 1654 cm^{-1} (C=C); uv λ_{max}: 223 nm (ε 9400), 347 nm (ε 8550); ^{1}Hmr (DMSO-d_6) δ: 2.20 (d, $J_{homoallyl}$ 0.5 Hz, CH_3 at C-6), 2.47 (s, CH_3 at C-2), 3.60 (q, $J_{homoallyl}$ 0.5 Hz, protons at C-4), 3.65, 3.78 (s, s, methyl esters), 9.48 (s, NH); ms *m/e*: 265 (50, M^+), 264(35), 250(100), 234(24), 232(33), 206(19), 204(35), 190(20). *Anal.* calcd. for $C_{13}H_{15}NO_5$: C 58.84, H 5.70, N 5.28; found: C 58.86, H 5.49, N 5.05.

Compound **21** was quantitatively oxidized to the furopyridine **4** by the action of silver nitrate in boiling aqueous methanol.

The Reaction of Dimethyl 4-Cyano-4,5-dihydro-2,5,7-trimethylazepine-3,6-dicarboxylate, ***2*** *with Silver Nitrate*

A solution of the cyano compound **2** (2.0 g) and silver nitrate (1.4 g) in methanol (30 ml) and water (2 ml) was heated under reflux for 2 days. The deposited silver was filtered off and the filtrate was evaporated *in vacuo*. The residue was dissolved in benzene and chromatographed on silica gel H using benzene – ethyl acetate as eluent. The first fraction yielded, after evaporation and recrystallization from aqueous dioxane, dimethyl 2,4,6-trimethylfuro[2,3-*b*]pyridine-3,5-dicarboxylate **6** as colorless prisms (0.39 g, 19.5%), mp 98–98.5°C; ir ν_{max}: 1727 (aryl ester); uv λ_{max}: 218 nm (ε 23 800) 251 nm (ε 9150), 260.5 nm (infl. ε 8000), 287 nm (ε 8500); ^{1}Hmr δ: 2.55, 2.64, and 2.71 (s, s, s, CH_3's at C-2, C-5, and C-6), 3.91 and 3.97 (s, s, methyl esters); ms *m/e*: 277(100, M^+), 246(84), 245(63), and 217(44). *Anal.* calcd. for $C_{14}H_{15}NO_5$: C 60.64, H 5.45, N 5.05; found: C 60.52, H 5.58, N 4.89.

The second fraction was recrystallized four times from benzene to give white prisms of methyl 3-(1-methoxycarbonyl-2-oxopropyl)-4,6-dimethyl-2-oxo-1,2,3,4-tetrahydropyridine-5-carboxylate **22** (0.37 g, 17%), mp 151–153°C; ir ν_{max}: 3395 (NH, free), 3218 (NH, bonded), 1753 (saturated ester), 1714 (ketone), 1701 (unsaturated ester), 1641 (lactam); uv λ_{max}: 214 nm (ε 3200), 279.5 (ε 11 500); ^{1}Hmr δ: 0.94 (d, *J* 7.0 Hz, CH_3 at C-4), 2.28 (s, acetyl), 2.45 (s, CH_3 at C-6), 3.09 (m, *J* 7.0 and 5.5 Hz, H at C-4) 3.57 (d d, *J* 11.4 and 5.5 Hz, H at C-3), 3.78 and 3.81 (s, s, methyl esters), 4.01 (d, *J* 11.4 Hz, H at C-1 of side chain), 8.63 (s, NH); ms *m/e*: 297 (14, M^+), 182(34), 181(100), 180(39), 142(56), 110(46), and 43(58). *Anal.* calcd. for $C_{14}H_{19}NO_6$: C 56.56, H 6.44, N 4.71; found: C 56.44, H 6.47, N 4.52.

The third fraction was recrystallized from ether – petroleum ether and yielded white prisms of dimethyl 2,4,6-trimethylpyrrolo[2,3-*b*]pyridine-3,5-dicarboxylate **7** (0.82 g, 41%), mp 157.5–159°C; ir ν_{max}: 3435 (NH, free), 3205 (NH, bonded), 1727 (aryl ester at C-3), 1709 (aryl ester at C-5); uv λ_{max}: 228 nm (ε 24 900), 250 nm (infl. ε 15 500), 294 nm (ε 11 000); ^{1}Hmr δ: 2.58, 2.65, and 2.68 (s, s, s, CH_3's at C-2, C-4, and C-6), 3.89 and 3.97 (s, s, methyl esters), 12.05 (s, NH); ms: *m/e*: 276 (100, M^+), 245(83), 244(35), 216(48), and 107(20). *Anal.* calcd. for $C_{14}H_{16}N_2O_4$: C 60.86, H 5.84, N 10.14; found: C 60.73, H 5.99, N 10.10.

The Reaction of Methyl 3-(1-Methoxycarbonyl-2-oxopropyl)-4,6-dimethyl-2-oxo-1,2,3,4-tetrahydropyridine-5-carboxylate, ***22****, with Sulfuric Acid*

Compound **22** (20 mg) in concentrated sulfuric acid (1 ml) was stirred at room temperature for 3 h and then

poured into ice water (30 ml). The acidic solution was neutralized with dilute sodium hydroxide and extracted with ether (3 × 20 ml). The ether extract was washed with water and dried over $MgSO_4$. After evaporation of the solvent, the residue was recrystallized from aqueous methanol to give prisms (6 mg, 32%), mp 95–96°C. This substance had uv and ms which were identical with those of authentic **6** and its mp was undepressed on admixture with **6**.

Reactions of Ethyl 2-(2-Cyanoethyl)acetoacetate

(*a*) Freshly distilled ethyl 2-(2-cyanoethyl)acetoacetate (0.454 g) was heated at 160°C in a sealed, evacuated tube for 12 h. Although the oil acquired a slight yellow color, it was found to be homogeneous by tlc and identical with starting material by ir, ms, and nmr and contained no ethyl 6-methyl-2-oxo-1,2,3,4-tetrahydropyridine-5-carboxylate.

(*b*) Freshly distilled ethyl 2-(2-cyanoethyl)acetoacetate (0.343 g) and silver nitrate (1.119 g) in ethanol (8 ml) and water (4 ml) were refluxed for 32 h. The solution was then filtered and concentrated to remove most of the ethanol. The aqueous mother liquors were extracted using chloroform (3 × 10 ml) and the chloroform extract washed with water (5 ml), dried with $MgSO_4$, filtered, and evaporated. The colorless slightly oily solid (330 mg) was recrystallized from ethanol to give ethyl 6-methyl-2-oxo-1,2,3,4-tetrahydropyridine-5-carboxylate (290 mg, 85%), mp 156–157°C (lit. (13) mp 154–156°C), which had ir, ms, and ^{1}Hmr spectra identical with those of an authentic sample.

When ethyl 2-(2-cyanoethyl)acetoacetate was refluxed in aqueous ethanol under the above conditions but lacking silver nitrate, no ethyl 6-methyl-2-oxo-1,2,3,4-tetrahydropyridine-5-carboxylate was detected using tlc or nmr after 37 h.

Acknowledgements

Financial aid from the National Research Council of Canada and Memorial University of Newfoundland is gratefully acknowledged. One of us (T.S.C.) wishes to thank Memorial University for the award of a Fellowship.

1. E. Bullock, B. Gregory, and A. W. Johnson. J. Chem. Soc. 1632 (1964).
2. M. Anderson and A. W. Johnson. J. Chem. Soc. 2411 (1965).
3. R. F. Childs and A. W. Johnson. J. Chem. Soc. C, 1950 (1966).
4. R. Robinson. J. Chem. Soc. 1038 (1916).
5. E. A. Braude, J. Hannah, and R. Linstead. J. Chem. Soc. 3249 (1960).
6. E. Wenkert, K. G. Dave, F. Haglid, R. G. Lewis, T. Oishi, R. V. Stevens, and M. Terashima. J. Org. Chem. **33**, 747 (1968).
7. B. Witkop. J. Am. Chem. Soc. **78**, 2873 (1956).
8. H. Wamhoff. Tetrahedron, **26**, 3849 (1970).
9. H. Budzikiewicz, C. Djerassi, and D. H. Williams. Mass spectrometry of organic compounds. Holden-Day, San Francisco, CA. 1967.
10. A. I. Meyers and J. C. Sircar. *In* The chemistry of the cyano group. *Edited by* Z. Rappoport. Interscience, London. 1970. p. 341.
11. F. Brody and P. R. Ruby. *In* Pyridine and its derivatives. Part I. *Edited by* E. Klingsberg. Interscience, New York, NY. 1960. p. 99.
12. H. Meislich. *In* Pyridine and its derivatives. Part III. *Edited by* E. Klingsberg. Interscience, New York, NY. 1962. p. 509.
13. N. F. Albertson. J. Am. Chem. Soc. **74**, 3816 (1952).
14. J. L. van der Baan and F. Bickelhaupt. Tetrahedron, **30**, 2447 (1974).
15. S. N. Semenova, N. F. Bondar, and T. I. Temnikova. Zh. Org. Khim. **9**, 2127 (1973).
16. K. B. Yatsimirski and V. D. Korableva. Zh. Neorg. Khim. **9**, 357 (1957).
17. A. P. Zuur and W. L. Groenveld. Recl. Trav. Chim. Pays-Bas, **86**, 1089 (1967).
18. J. Reedijk, A. P. Zuur, and W. L. Groenveld. Recl. Trav. Chim. Pays-Bas, **86**, 1127 (1967).
19. M. Kubota, D. L. Johnston, and I. Matsubar. Inorg. Chem. **5**, 386 (1966).
20. R. Breslow, R. Fairweather, and J. Keana. J. Am. Chem. Soc. **89**, 2135 (1967).
21. M. A. Bennett and T. Yoshida. J. Am. Chem. Soc. **95**, 3030 (1973).
22. J. H. Atkinson, R. S. Atkinson, and A. W. Johnson. J. Chem. Soc. 5999 (1964).
23. E. Bullock, R. A. Carter, R. M. Cochrane, B. Gregory, and D. C. Shields. Can. J. Chem. **55**, 895 (1977).
24. N. F. Albertson. J. Am. Chem. Soc. **72**, 2594 (1950).

The synthesis of methyl 2-*O*-benzoyl-3,4-*O*-(*S*)- and methyl 2-*O*-benzoyl-3,4-*O*-(*R*)-benzylidene- β-L-ribopyranoside

DAVID M. CLODE

Department of Chemistry, University of Cape Coast, Cape Coast, Ghana

Received June 16, 1977

DAVID M. CLODE. Can. J. Chem. **55**, 4066 (1977).

Benzylidenation of methyl β-L-arabinopyranoside, by the method of Oldham and Honeyman, followed by benzoylation, gave methyl 2-*O*-benzoyl-3,4-*O*-(*S*)-benzylidene-β-L-arabinopyranoside (**1**). Selective acid hydrolysis of a 1:1 mixture of the diastereomeric forms of methyl 2-*O*-benzoyl-3,4-*O*-benzylidene-β-L-arabinopyranoside gave the (*R*)-isomer (**3**). Debenzoylation of **1** and **3** gave methyl 3,4-*O*-(*S*)-and methyl 3,4-*O*-(*R*)-benzylidene-β-L-arabinopyranoside (**2** and **4**) respectively. Oxidation of **2**, followed by reduction and benzoylation, gave methyl 2-*O*-benzoyl-3,4-*O*-(*S*)-benzylidene-β-L-ribopyranoside (**7**). A similar reaction sequence with **4** gave methyl 2-*O*-benzoyl-3,4-*O*-(*R*)-benzylidene-β-L-ribopyranoside (**8**).

DAVID M. CLODE. Can. J. Chem. **55**, 4066 (1977).

La benzylidénation du β-L-arabinopyrannoside de méthyle par le méthode de Oldham et Honeyman, suivie par une benzoylation, conduit au *O*-benzoyl-2 *O*-(*S*)-benzylidène-3,4 β-L-arabinopyrannoside de méthyle (**1**). Une hydrolyse acide sélective de mélange 1:1 des formes diastéréoisomères du *O*-benzoyl-2 *O*-benzylidène-3,4 β-L-arabinopyrannoside de méthyle fournit l'isomère (*R*) (**3**). Les débenzoylations de **1** et de **3** conduisent respectivement aux *O*-(*S*)-benzylidène-3,4 et au *O*-(*R*)-benzylidène-3,4 β-L-arabinopyrannoside de méthyle (**2** et **4**). L'oxydation de **2** suivit par une réduction et une benzoylation fournit le *O*-benzoyl-2 *O*-(*S*)-benzylidène-3,4 β-L-ribopyrannoside de méthyle (**7**). Une séquence similaire de réaction avec **4** fournit le *O*-benzoyl-2 *O*-(*R*)-benzylidène-3,4 β-L-ribopyrannoside de méthyle (**8**).

[Traduit par le journal]

Introduction

In order to study the condensation of methyl β-D-ribopyranoside with benzaldehyde (following paper) it was considered necessary to prepare an *O*-benzylidene-ribopyranoside of known structural configuration. A suitable starting material for such a derivative is methyl 3,4-*O*-benzylidene-β-D-arabinopyranoside which by inversion of the configuration at C-2 would give methyl 3,4-*O*-benzylidene-β-D-ribopyranoside.

Using the Gerhardt (3) method of benzylidenation Oldham and Honeyman (1) isolated the two diastereomers of methyl 3,4-*O*-benzylidene-β-L-arabinopyranoside as their benzoates. They found that an old sample of methyl 3,4-*O*-benzylidene-β-L-arabinopyranoside, which had been freed from methyl β-L-arabinopyranoside, gave an acid stable (hot 0.05 *N* hydrochloric acid in aqueous acetone) benzoate, mp 126–127°C. This was probably a pure diastereomer. They also found that benzoylation of a freshly prepared sample of the acetal gave a mixture of benzoates having mp 100–102°C. The predominant isomer was acid labile (0.05 *N* hydrochloric acid) and fractionation of this mixture gave what was probably a second pure diastereomer, mp 120–122°C. No other physical measurements were made.

Baggett *et al.* (2) benzylidenated methyl β-L-arabinopyranoside, using Oldham and Honeyman's method (1), and the crude product showed benzyl proton signals at δ 5.70 and 5.44 with integrated areas in the ratio ca. 1:2.5. Benzoylation of this mixture gave a product, with benzyl proton signals at δ 5.82 and 5.47, from which was separated a benzoate, mp 119–120°C, with a single benzyl proton signal at δ 5.49. This benzoate was assigned the structure methyl 2-*O*-benzoyl-3,4-*O*-(*S*)-benzylidene-β-L-arabinopyranoside(**1**).

Results and Discussion

Benzylidenation of methyl β-L-arabinopyranoside, using Oldham and Honeyman's method (1), and benzoylation of the product, gave **1**. Debenzoylation of **1** gave methyl 3,4-*O*-(*S*)-benzylidene-β-L-arabinopyranoside (**2**). In subsequent reactions it was possible to crystallize out the (*S*)-isomer **2** directly from the initial product of the benzylidenation. Benzoylation of the mother liquors from this fractional crystallization gave a crystalline product **A** whose nmr spectrum showed two benzyl protons of equal

integrated area. This benzoate **A** was evidently an equimolar mixture of diastereomers. From the work of Oldham and Honeyman (1) it is apparent that the (*S*)-benzoate isomer **1** (mp 120–122°C) is acid labile, compared with the (*R*)-benzoate isomer **3** (mp 126–127°C). Thus **A** was treated with acid and the hydrolysis of the (*S*)-isomer was followed by nmr spectroscopy.

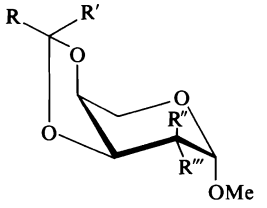

1 R = H, R′ = Ph, R″ = H, R‴ = OBz
2 R = H, R′ = Ph, R″ = H, R‴ = OH
3 R = Ph, R′ = H, R″ = H, R‴ = OBz
4 R = Ph, R′ = H, R″ = H, R‴ = OH
5 R = H, R′ = Ph, R″ = H, R‴ = OCH_2SCH_3
6 R = Ph, R′ = H, R″ = H, R‴ = OCH_2SCH_3
7 R = H, R′ = Ph, R″ = OBz, R‴ = H
8 R = Ph, R′ = H, R″ = OBz, R‴ = H

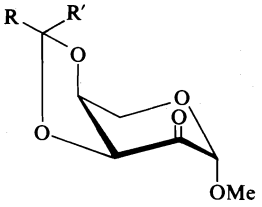

9 R = H, R′ = Ph
10 R = Ph, R′ = H

Initially the behaviour of the isomers, with acid, under essentially anhydrous (i.e., non-hydrolysing) conditions, was examined. The benzoate **A** was dissolved in chloroform-*d* containing *p*-toluenesulphonic acid (4%) and the signals in the benzyl region of the nmr spectrum were examined at intervals. After 24 h there was no change observed in the initial spectrum indicating that the 1:1 mixture of isomers was an essentially equilibrium mixture,[1] a result which agreed with the findings of Baggett *et al.* (2). This is in contrast to recent work by Buchanan and Edgar (4), on the acid-catalyzed ethylidenation of some methyl pentopyranosides, where they show that there is a strong preference for the isomer in which the methyl group has the *endo* configuration. A drop of water was then added and the high-field benzyl proton signal, corresponding to the (*S*)-isomer, slowly decreased in size. After 21 h and the addition of more acid this signal could no longer be detected. The reaction mixture was then processed in the normal way and methyl 2-*O*-benzoyl-3,4-*O*-(*R*)-benzylidene-β-L-arabinopyranoside (**3**) was isolated. In subsequent large scale reactions dioxan was used as the solvent and 5 *N* hydrochloric acid was added dropwise. Debenzoylation of **3** gave methyl 3,4-*O*-(*R*)-benzylidene-β-L-arabinopyranoside (**4**).[2]

Oxidation of **2** with methyl sulphoxide – acetic anhydride (5) gave methyl 3,4-*O*-(*S*)-benzylidene-β-L-*erythro*-pentopyranosidulose (**9**) directly in 32% yield. Fractionation of the mother liquors gave more of the ketone **9** (13%) plus methyl 3,4-*O*-(*S*)-benzylidene-2-*O*-(methylthio)methyl-β-L-arabinopyranoside (**5**), an expected by-product from these reactions (6). In a similar manner oxidation of **4** gave the ketone **10** in 60% yield and a syrupy product which was considered to be the (methylthio)methyl derivative **6**.

Reduction of **9** with sodium borohydride in aqueous ethanol, following the general method of Theander (7), gave a syrupy product **B** whose nmr spectrum showed two benzyl proton signals at δ 5.91 and 5.83 with integrated areas in the ratio 3:17. Part of this product was hydrolysed and examination of the hydrolysate by paper chromatography showed two components corresponding to reference standards of L-arabinose and D-ribose, and clearly different from D-lyxose and D-xylose. The ribose component appeared to be the major product. The riboside has been shown (8) to be the major product of the reduction of methyl 3,4-*O*-isopropylidene-β-L-*erythro*-pentopyranosidulose. A similar result was obtained from the reduction of **10** and the nmr spectrum of the syrupy product **C** showed two benzyl proton signals at δ 6.17 and 6.04 with integrated areas in the ratio 14:3.

Benzoylation of **B** and **C** gave crystalline benzoates, in good yield, which were clearly

[1]A similar treatment of methyl 3,4-*O*-(*S*)-benzylidene-β-L-arabinopyranoside (**2**) (benzyl proton signal δ 5.75) resulted in the rapid appearance of a second signal at δ 6.03 in the nmr spectrum. After 3 min the two signals had equal integrated areas, which did not alter during a further 18 h, indicating that an equilibrium mixture of two diastereomers had been formed. The addition of a drop of water to this mixture resulted in the rapid disappearance (10 min) of the signal at δ 5.75.

[2]Compound **4** could also be isolated, following the selective hydrolysis of a 1:1 mixture of **2** and **4** (dioxan and 5 *N* hydrochloric acid), but this procedure was less satisfactory.

TABLE 1. Nuclear magnetic resonance data for compounds **2, 4–10**

Compound[a]	Chemical shifts (δ) (first-order couplings, Hz, in parentheses)[c]										
	H-1 ($J_{1,2}$)	H-2 ($J_{2,3}$)	H-3 ($J_{3,4}$)	H-4 ($J_{4,5}$)	H-5	$-CH_2$-SCH$_3$	Aryl	PhCH	OCH$_3$	SCH$_3$	OH
2	4.65d (3.5)	←	3.60 —	4.40m →			7.37m	5.84s	3.39s		2.87s
4	4.77d (4.0)	←	3.60 —	4.60m →			7.37m	6.17s	3.42s		2.82d (7.5)
5	4.78d (4.0)	←	3.80 —	4.60m →		4.78s	7.43m	5.90s	3.43s	2.05s	
6	←		3.70 —	5.00m →			7.33m	6.17s	3.40s	2.16s	
7[b]	←	4.10 —	5.20m →		3.78m		7.00–8.20m	5.64s	3.38s		
8[b]	←	4.10 —	5.20m →		3.86m		6.90–8.10m	6.08s	3.34s		
9	4.65–4.90m		4.65–4.90m (6.5)	4.56dt (1.5)	4.22m		7.41m	5.89s	3.47s		
10	4.77s		4.93d (5.5)	4.53dt (1.5)	4.15m		7.34m	6.12s	3.48s		

[a]In chloroform-*d*, unless otherwise stated.
[b]In carbon tetrachloride.
[c]Abbreviations for nmr: s, singlet; d, doublet; t, triplet; and m, multiplet.

different from the arabinoside isomers **1** and **3**. These benzoates were thus methyl 2-*O*-benzoyl-3,4-*O*-(*S*)-benzylidene-β-L-ribopyranoside (**7**) and methyl 2-*O*-benzoyl-3,4-*O*-(*R*)-benzylidene-β-L-ribopyranoside (**8**) respectively.

Experimental

All melting points are uncorrected. Evaporations were performed under diminished pressure with a bath temperature below 40°C. Light petroleum refers to the fraction boiling at 60–80°C. Thin-layer chromatography was performed with Silica Gel G (E. Merck, Darmstadt, Germany), activated at 110°C, and components were detected with iodine vapour or vanillin – sulphuric acid solution, as appropriate. Column chromatography was conducted with Silica Gel 7734 (70–325 mesh ASTM, E. Merck). Solvent systems A, B, C, D, and E, used in the above chromatography, refer to the following systems of carbon tetrachloride – ethyl acetate 9:1, 8:2, 7:3, 6:4, and 1:1 respectively. Paper chromatography was carried out by downward irrigation, using Whatman No. 1 paper, and sugars were detected with alkaline silver nitrate. The nmr spectra were measured at 60 MHz with a Perkin-Elmer R-10 instrument. Chemical shifts refer to an internal standard of tetramethylsilane (δ = 0.00) and are recorded, together with spin-coupling values (Hz), in Table 1. The ir spectra were measured with a Perkin-Elmer model 257 ir spectrometer.

Methyl 2-O-Benzoyl-3,4-O-(S)-benzylidene-β-L-arabinopyranoside (1) (1, 2)

A mixture of methyl β-L-arabinopyranoside (3.5 g, 21.34 mmol) and benzaldehyde (20 ml) was heated for 4 h at 135°C with removal of water as described by Oldham and Honeyman (1). Excess of benzaldehyde was then removed by distillation and the syrupy residue was poured into benzene. Unchanged starting material (0.53 g) was filtered off and the filtrate was shaken with 2% sodium hydroxide solution, washed with water, dried ($MgSO_4$), and evaporated. The syrupy product was benzoylated during 18 h with benzoyl chloride (5 ml) in anhydrous pyridine (10 ml) to give a syrup which crystallized from chloroform – light petroleum. Recrystallization from ethanol – light petroleum gave **1** (1.4 g, 20%), mp 123–124°C; $[\alpha]_D^{25}$ +224° (*c* 1.0, $CHCl_3$) (lit. (2) mp 119–120°C, $[\alpha]_D^{20}$ +224° in $CHCl_3$); ν_{max} 1712 cm^{-1} (C=O).

Methyl 3,4-O-(S)-Benzylidene-β-L-arabinopyranoside (2)

Sodium (catalytic quantity) was added to a solution of **1** (1 g, 2.81 mmol) in anhydrous methanol (50 ml) and the reaction mixture was kept overnight at room temperature. A few drops of water were added to the reaction mixture and carbon dioxide was bubbled through it for 15 min. The solution was then evaporated and the resulting syrup was dissolved in ethyl acetate. The solution was filtered and the filtrate evaporated to give a syrup which crystallized. Recrystallization from ethyl acetate – light petroleum gave **2** (0.49 g, 64%), mp 81°C; $[\alpha]_D^{25}$ +162° (*c* 1.0, $CHCl_3$). *Anal.* calcd. for $C_{13}H_{16}O_5$: C 61.9, H 6.4; found: C 62.0, H 6.5.

In another experiment methyl β-L-arabinopyranoside (9 g) was benzylidenated as above and **2** (3 g, 19%) was isolated directly by fractional crystallization, with the aid of a seed crystal.

Methyl 2-O-Benzoyl-3,4-O-(R)-benzylidene-β-L-arabinopyranoside (3)

The mother liquors from the above fractional crystallization were evaporated and the resulting syrup was

benzoylated during 18 h with benzoyl chloride (3.5 ml) in anhydrous pyridine (5 ml) to give a solid product. Recrystallization from ethanol – light petroleum gave mixture **A** (6.4 g) whose nmr spectrum (CCl_4) showed two benzyl proton signals at δ 5.81 and 6.17 of equal integrated area.

Fused *p*-toluenesulphonic acid (5 mg) was added to a solution of **A** (120 mg, 0.34 mmol) in chloroform-*d* and the signals in the benzyl proton region of the nmr spectrum were examined at intervals. After 24 h there was no change in the initial spectrum, with signals at δ 5.80 and 6.12, and a drop of water was then added. After 4 h the signals had integrated areas in the ratio ca. 1:2, but in another 12 h there was no further change. More acid (5 mg) was added and after another 5 h only the signal at δ 6.12 was detected. The solution was then diluted with chloroform, washed with saturated aqueous sodium hydrogen carbonate and water, dried ($MgSO_4$), and evaporated. The resulting syrup crystallized and was recrystallized from ethanol to give **3** (20 mg, 17%), mp 125–127°C; $[\alpha]_D^{25}$ +168° (*c* 1.0, $CHCl_3$); (lit. (1) mp 126–127°C; $[\alpha]_D^{18}$ +174° in $CHCl_3$); ν_{max} 1725 cm^{-1} (C=O).

In subsequent large scale reactions **A** was dissolved in dioxan and 5 *N* hydrochloric acid was added dropwise. Aliquots were withdrawn at intervals and the benzyl proton region of the nmr spectrum examined. The reaction was complete when the initial signals at δ 5.54 and 5.90 were replaced by a single signal at δ 5.90, and was processed as above to give **3** in 35–40% yield.

*Methyl 3,4-O-(R)-Benzylidene-β-L-arabinopyranoside (**4**)*

Sodium (catalytic quantity) was added to a solution of **3** (0.91 g, 2.56 mmol) in anhydrous methanol (50 ml) and the reaction mixture was kept overnight at room temperature. The reaction was processed in the normal manner to give **4** (0.43 g, 66%), mp 72–74°C; $[\alpha]_D^{25}$ +173° (*c* 0.6, $CHCl_3$). *Anal.* calcd. for $C_{13}H_{16}O_5$: C 61.9, H 6.4; found: C 62.1, H 6.3.

*Methyl 3,4-O-(S)-Benzylidene-β-L-erythro-pentopyranosidulose (**9**)*

Acetic anhydride (40 ml) was added to a solution of **2** (2 g, 7.94 mmol) in methyl sulphoxide (60 ml) and the reaction mixture was stirred for 21 h at room temperature. The solution was then diluted with water, neutralized with aqueous potassium carbonate solution, and extracted with chloroform. The chloroform extract was washed with water, dried ($MgSO_4$), and evaporated. The resulting syrup crystallized on the addition of diisopropyl ether and recrystallization from the same solvent gave **9** (0.64 g, 32%), mp 106–107°C; $[\alpha]_D^{25}$ +136° (*c* 1.0, $CHCl_3$); ν_{max} 1757 cm^{-1} (C=O). *Anal.* calcd. for $C_{13}H_{14}O_5$: C 62.4, H 5.6; found: C 62.4, H 5.8.

The tlc (solvent B) examination of the mother liquors showed two components, the slower moving corresponding to **9**. This material was placed on a column of silica gel (100 g) and eluted with solvent B, collecting 100 ml fractions. The fractions were examined by tlc and fractions 5 and 6, containing the faster moving component, were evaporated to give a syrup (0.36 g, 14.5%) which crystallized on standing. Recrystallization from ethanol gave methyl 3,4-*O*-(*S*)-benzylidene-2-*O*-(methylthio)methyl-β-L-arabinopyranoside (**5**), mp 45–47°C; $[\alpha]_D^{25}$ +67° (*c* 2.0, $CHCl_3$). *Anal.* calcd. for $C_{15}H_{20}O_5S$: C 57.7, H 6.4, S 10.3; found: C 57.8, H 6.2, S 10.5.

Fractions 9–14, containing the slower moving component, were evaporated to give more **9** (0.26 g, 13%).

*Methyl 3,4-O-(R)-Benzylidene-β-L-erythro-pentopyranosidulose (**10**)*

Compound **4** (0.4 g, 1.59 mmol) was oxidised as described above to give a syrup that showed two major components by tlc (solvent B). The syrup was placed on a column of Silica Gel (34 g) and eluted with solvent B, collecting 25 ml fractions. The fractions were examined by tlc and fractions 8–12, containing the slower moving component, were evaporated. The crystalline residue was recrystallized from ether – light petroleum to give **10** (0.24 g, 60%), mp 74–75°C; $[\alpha]_D^{25}$ +122° (*c* 1.0, $CHCl_3$); ν_{max} 1745 cm^{-1} (C=O). *Anal.* calcd. for $C_{13}H_{14}O_5$: C 62.4, H 5.6; found: C 62.2, H 5.6.

Fractions 4 and 5, containing the faster moving component, were evaporated to give syrupy **6** (68 mg, 14%), $[\alpha]_D^{25}$ +45° (*c* 1.2, $CHCl_3$).

*Methyl 2-O-Benzoyl-3,4-O-(S)-benzylidene-β-L-ribopyranoside (**7**)*

Sodium borohydride (100 mg) was added to a solution of **9** (100 mg, 0.40 mmol) in 70% aqueous ethanol (40 ml) and the reaction mixture stirred for 4 h at room temperature. Water (15 ml) was then added and the solution was extracted with ethyl acetate (8 × 15 ml). The extract was dried ($MgSO_4$) and evaporated to give a syrup **B** (81 mg, 80%). The nmr spectrum (chloroform-*d*) showed two benzyl proton signals at δ 5.91 and 5.83 with integrated areas in the ratio 3:17; tlc (9:1 benzene–methanol) showed two components, the minor corresponding to **2**.

Treatment of **B** (80 mg) with 1 *N* sulphuric acid (15 ml) at 100°C and examination of the neutralized (barium carbonate) hydrolysate by paper chromatography (8:2:1 ethyl acetate – pyridine–water), with D-xylose, D-ribose, L-arabinose, and D-lyxose as standards, showed two components corresponding to ribose and arabinose, the former predominating.

Benzoylation of **B** (150 mg) with benzoyl chloride (0.15 ml) in anhydrous pyridine (0.3 ml) during 18 h gave a syrupy product that solidified after 2 days. Recrystallization from ethanol gave **7** (105 mg, 50%), mp 106–107°C; $[\alpha]_D^{25}$ +170° (*c* 0.6, $CHCl_3$); ν_{max} 1720 cm^{-1} (C=O). *Anal.* calcd. for $C_{20}H_{20}O_6$: C 67.4, H 5.7; found: C 67.7, H 5.4.

*Methyl 2-O-Benzoyl-3,4-O-(R)-benzylidene-β-L-ribo-pyranoside (**8**)*

Compound **10** (50 mg, 0.20 mmol) was reduced as described above to give a syrup **C** (34 mg, 65%). The nmr spectrum (chloroform-*d*) showed two benzyl proton signals at δ 6.17 and 6.04 with integrated areas in the ratio 14:3.

Hydrolysis of **C** as described above and examination of the neutralized hydrolysate by paper chromatography showed two components corresponding to ribose and arabinose, the former predominating.

Benzoylation of **C** (155 mg) with benzoyl chloride (0.15 ml) in anhydrous pyridine (0.3 ml) during 18 h gave a syrupy product that solidified after 2 weeks. Recrystal-

lization from ether–pentane gave **8** (90 mg, 41%), mp 83–85°C; $[\alpha]_D^{25}$ +57° (*c* 0.6, $CHCl_3$); ν_{max} 1724 cm^{-1} (C=O). *Anal.* calcd. for $C_{20}H_{20}O_6$: C 67.4, H 5.7; found: C 67.3, H 5.6.

Acknowledgements

The Department of Chemistry, Birmingham University, England, is gratefully acknowledged for financial support and for providing the necessary research facilities. The author thanks Drs. J. M. Webber and N. Baggett for helpful discussions and Dr. J. A. Montgomery for a sample of methyl 5-*O*-benzoyl-β-D-ribofuranoside.

1. M. A. OLDHAM and J. HONEYMAN. J. Chem. Soc. 986 (1946).
2. N. BAGGETT, K. W. BUCK, A. B. FOSTER, and J. M. WEBBER. J. Chem. Soc. 3401 (1965).
3. W. GERHARDT. Ger. Patent No. 253 083 (1910); Chem. Zentralbl. **83**, 1953 (1912).
4. J. G. BUCHANAN and A. R. EDGAR. Carbohydr. Res. **49**, 999 (1976).
5. J. D. ALBRIGHT and L. GOLDMAN. J. Am. Chem. Soc. **87**, 4214 (1965).
6. J. D. ALBRIGHT and L. GOLDMAN. J. Am. Chem. Soc. **89**, 2416 (1967).
7. O. THEANDER. Acta Chem. Scand. **18**, 2209 (1964).
8. P. M. COLLINS and W. G. OVEREND. J. Chem. Soc. 3448 (1965).

The acid-catalyzed rearrangement of methyl 3,4-*O*-benzylidene-β-D-ribopyranoside

DAVID M. CLODE

Department of Chemistry, University of Cape Coast, Cape Coast, Ghana

Received June 16, 1977

DAVID M. CLODE. Can. J. Chem. **55**, 4071 (1977).

Methyl 3,4-*O*-(*R*)-benzylidene-β-D-ribopyranoside (**2**) rapidly rearranged, under anhydrous acidic conditions, to give methyl 2,3-*O*-(*R*)-benzylidene-β-D-ribopyranoside (**6**). Further rearrangement of **2** and **6** gave the (*S*)-isomers **4** and **8**, an equilibrium mixture of the four pyranoside acetals **2**, **4**, **6**, and **8** resulting. At higher acid concentrations, the rearrangement proceeded, with ring contraction, to give the diastereomeric forms of methyl 2,3-*O*-benzylidene-β-D-ribofuranoside (**11** and **13**) as the sole product. Treatment of methyl 3,4-*O*-(*S*)-benzylidene-β-D-ribopyranoside (**4**) with acid resulted in the immediate formation of the equilibrium mixture of pyranoside acetals. On increasing the acid concentration this mixture again underwent ring contraction to give the diastereomers **11** and **13** as the final product. The rearrangement of **2** and **4** was monitored by following the change in signals in the benzyl proton region of the nmr spectrum.

DAVID M. CLODE. Can. J. Chem. **55**, 4071 (1977).

Le *O*-(*R*)-benzylidène-3,4 β-D-ribopyrannoside de méthyle (**2**) se réarrange rapidement dans des conditions acide anhydre pour conduire au *O*-(*R*)-benzylidène-2,3 β-D-ribopyrannoside de méthyle (**6**). Des réarrangements subséquents de **2** et de **6** fournissent les isomères (*S*) **4** et **8**; il en résulte un mélange à l'équilibre des quatre acétals des pyrannosides **2**, **4**, **6** et **8**. A des concentrations plus élevées d'acide, le réarrangement se produit avec une contraction de cycle pour conduire aux formes diastéréoisomères des *O*-benzylidène-2,3 β-D-ribofurannoside de méthyle (**11** et **13**) comme seuls produits. Le traitement acide du *O*-(*S*)-benzylidène-3,4 β-D-ribopyrannoside de méthyle (**4**) par de l'acide conduit à la formation immédiate d'un mélange à l'équilibre d'acétals de pyrannoside. Par augmentation de la concentration d'acide, ce mélange subit à nouveau une contraction de cycle pour conduire aux diastéréoisomères **11** et **13** comme produits finals. On a suivi le réarrangement de **2** et **4** en surveillant le changement dans les signaux des protons benzyliques dans le spectre de résonance magnétique nucléaire.

[Traduit par le journal]

Introduction

Levene and Stiller (1) isolated methyl 2,3-*O*-isopropylidene-D-ribofuranoside following the condensation of acetone with methyl D-ribopyranoside. They also isolated a second product which they considered to be methyl 2,3-*O*-isopropylidene-D-ribopyranoside. Barker *et al.* (2) reexamined this reaction and showed that methylation of the mixed products, followed by hydrolysis, yielded 2-, 4-, and 5-*O*-methyl-D-ribose. This suggested that both methyl 2,3- and methyl 3,4-*O*-isopropylidene-D-ribopyranoside are products of the condensation. It was subsequently shown (3) that the supposed methyl 2,3-*O*-isopropylidene-4-*O*-*p*-toluenesulphonyl-D-ribopyranoside, obtained by Levene and Stiller (1), was in fact methyl 3,4-*O*-isopropylidene-2-*O*-*p*-toluenesulphonyl-D-ribopyranoside. It was concluded by Levene *et al.* (4) that, since methyl D-ribopyranoside is normally formed from the furanoside under acidic conditions, the ring contraction must have taken place after condensation with acetone. This reaction has recently been reinvestigated by Hughes and Maycock (5) who showed that the formation of methyl 2,3-*O*-isopropylidene-D-ribofuranoside probably arose from the presence of methyl D-ribofuranoside in the starting material and not from a ring contraction.

Barker *et al.* (2) also reported that the benzylidenation of methyl β-D-ribopyranoside gave a syrupy methyl 2,3-*O*-benzylidene-D-ribofuranoside of unspecified configuration. In this reaction, because pure methyl β-D-ribopyranoside was used, the formation of the furanoside acetal must have been the result of a ring contraction. The present work describes an examination of this ring contraction as part of a programme concerned with the formation and migration of cyclic acetals of carbohydrates.

Results and Discussion

It seems reasonable to assume that benzylidenation of methyl β-D-ribopyranoside gives an

initial product consisting of a mixture of the diastereomeric forms of methyl 2,3- and methyl 3,4-*O*-benzylidene-β-D-ribopyranoside. Rearrangement of these pyranoside acetals, to give the thermodynamically most stable product, a methyl 2,3-*O*-benzylidene-D-ribofuranoside, then occurs. The driving force for the reaction is the formation of the favourable *cis*-fused system of two five-membered rings (6). In order to test this proposition it was proposed to treat an *O*-benzylidene-ribopyranoside of known structural configuration, under anhydrous acidic conditions, in an attempt to promote a ring contraction.

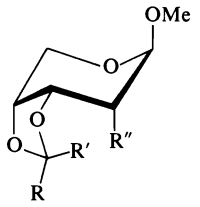

1 R = H, R′ = Ph, R″ = OBz
2 R = H, R′ = Ph, R″ = OH
3 R = Ph, R′ = H, R″ = OBz
4 R = Ph, R′ = H, R″ = OH

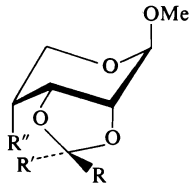

5 R = H, R′ = Ph, R″ = OBz
6 R = H, R′ = Ph, R″ = OH
7 R = Ph, R′ = H, R″ = OBz
8 R = Ph, R′ = H, R″ = OH
9 R = R′ = CH_3, R″ = OBz

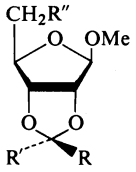

10 R = H, R′ = Ph, R″ = OBz
11 R = H, R′ = Ph, R″ = OH
12 R = Ph, R′ = H, R″ = OBz
13 R = Ph, R′ = H, R″ = OH

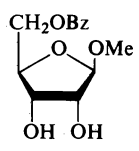

14

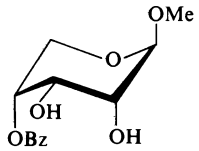

15

Methyl 2-*O*-benzoyl-3,4-*O*-(*R*)- and methyl 2-*O*-benzoyl-3,4-*O*-(*S*)-benzylidene-β-D-ribopyranoside, (**1**) and (**3**) respectively, were prepared as described in the preceding paper for the L-enantiomer, starting with D-arabinose. Debenzoylation of **1** gave methyl 3,4-*O*-(*R*)-benzylidene-β-D-ribopyranoside (**2**) as a homogeneous (tlc and nmr spectroscopy) syrup. The rearrangement of **2**, under anhydrous acidic conditions, was then followed by nmr spectroscopy. A solution of **2** in chloroform-*d* was treated with acidic chloroform (chloroform containing ca. 0.2% hydrogen chloride) and aliquots were removed at various intervals and the signals in the benzyl proton region of the nmr spectrum examined. After 10 min a new benzyl proton signal at δ 5.88 had appeared with a corresponding diminution of the initial signal at δ 5.80. There was no further change in the nmr spectrum and so after 30 min more acidified chloroform was added. A third benzyl proton signal at δ 6.32 then appeared and after 1 h the three signals at δ 5.80, 5.88, and 6.32 had integrated areas in the ratio 13:8:15, which did not alter during a further 24 h with the addition of more acid.

Since a significant amount of **2** still remained in the mixture, it appeared that this isomer had rearranged to give an equilibrium mixture of pyranoside acetals but that no ring contraction had occurred. This suggested that the acidic conditions may not have been drastic enough to effect a change in ring size and, therefore, anhydrous hydrogen chloride was bubbled directly into the reaction mixture. An immediate change in the benzyl proton signals was observed; the signals at δ 5.80 and 5.88 merged to form a broad hump and two new signals at δ 5.75 and 5.98 appeared. After 30 min only the new signals at δ 5.75 and 5.98 remained. These were of approximately equal size and the difference in chemical shift was consistent (7, 8) with their being the benzyl protons corresponding to the diastereomeric forms of methyl 2,3-*O*-benzylidene-β-D-ribofuranoside (**11** and **13**) (2, 9).

Acetal migration is a fairly well established phenomenon. One of the earliest examples was observed by Hibbert and co-workers (10) who found that the isomeric methylidene, benzylidene, and *p*-nitrobenzylidene cyclic acetals of glycerol were readily interconverted in the presence of hydrogen chloride. Acetal migration has more recently been studied (11, 12) by following the change in the signal pattern in the

benzyl proton region of the nmr spectrum. Other examples include the observation made by Williams (13) that methyl 2,3-*O*-isopropylidene-β-D-allofuranoside and methyl 2,3:5,6-di-*O*-isopropylidene-β-D-allofuranoside were two of the products obtained during the acid-catalyzed methanolysis of 1,2:5,6-di-*O*-isopropylidene-α-D-allofuranose. This rearrangement has also been studied by Haga *et al.* (14) who showed that treatment of the above di-*O*-isopropylidene-allofuranose with acidic acetone resulted in the formation, in good yield, of the 2,3:5,6-di-*O*-isopropylidene derivative. Closely related to the above is the rearrangement of 5-*O*-benzoyl-1,2-*O*-isopropylidene-3-*C*-methyl-α-D-ribofuranose to the 2,3-*O*-isopropylidene derivative in acidic methanol solution (15).

Migration of an *O*-isopropylidene group on a pyranose ring is also known; thus the 2,3-*O*-isopropylidene derivative is formed as an intermediate in the hydrolysis, in aqueous acetic acid, of 1,6-anhydro-3,4-*O*-isopropylidene-β-D-talopyranose (16). Inch (17) has shown that methyl 4,6-*O*-benzylidene-2-deoxy-2-halogeno-α-D-altropyranoside undergoes facile, acid-catalyzed, acetal migration to give methyl 3,4-*O*-(*S*)-benzylidene-2-deoxy-2-halogeno-α-D-altropyranoside. It was also shown that the (*S*)-isomer is the thermodynamically more-stable form of this compound since a sample of the (*R*)-isomer rearranged into this isomer under acidic conditions. Closely related to the rearrangement of **2** is the observation (18) that 1,2:4,5-di-*O*-isopropylidene-D-psicopyranose rearranges in acidic acetone to give 1,2:3,4-di-*O*-isopropylidene-D-psicofuranose. In this case it is reasonable to assume that we have migration of the 4,5-*O*-isopropylidene group to the 3,4-position prior to ring contraction.

Treatment of **2** with acid had resulted in the rapid formation of an isomer with a benzyl proton signal at δ 5.88. Previous work on the correlation of configuration of substituted derivatives of 2-phenyl-1,3-dioxan and 2-phenyl-1,3-dioxolan with the chemical shifts for the benzyl proton signals in the nmr spectra (7,8), and also a mechanistic interpretation of the formation and migration of benzylidene acetals, enabled this signal to be assigned to the benzyl proton of methyl 2,3-*O*-(*R*)-benzylidene-β-D-ribopyranoside (**6**). The benzyl proton signal at δ 6.32, which had appeared more slowly, was tentatively assigned to the benzyl proton signal of **4**. It was, however, considered possible that the benzyl proton signal of methyl 2,3-*O*-(*S*)-benzylidene-β-D-ribopyranoside (**8**) might also have the same chemical shift.

To confirm these assigned structures the various acetals present in the early stages of the rearrangement were isolated and characterized. Thus the rearrangement was repeated and the reaction terminated after 4.5 h before the direct introduction of anhydrous hydrogen chloride. Fractionation of the product gave three homogeneous (tlc) syrups **A**, **B**, and **C**, in order of elution. Compounds **B** and **C** had identical nmr spectra to **4** and **2** respectively and the structure of these products was proved conclusively by converting them into their known crystalline benzoates **3** and **1**. Syrup **A** showed benzyl proton signals at δ 5.88 and 6.32 which were considered to belong to the benzyl protons of the diastereomers **6** and **8** respectively, the signal at δ 6.32 in the rearrangement thus representing the signal from the benzyl proton of both **4** and **8**. This assignment of structure for **A** was confirmed by the following sequence of reactions. Mixture **A** was converted into syrupy methyl 4-*O*-benzoyl-2,3-*O*-benzylidene-β-D-ribopyranoside (**5** and **7**) and hydrogenolysis of this benzoate gave homogeneous (tlc) syrupy methyl 4-*O*-benzoyl-β-D-ribopyranoside (**15**). Isopropylidenation of **15** gave methyl 4-*O*-benzoyl-2,3-*O*-isopropylidene-β-D-ribopyranoside (**9**), in fair overall yield, which had physical properties in agreement with those of a sample of the L-enantiomer prepared by a benzoate displacement reaction on methyl 2,3-*O*-isopropylidene-4-*O*-*p*-toluenesulphonyl-α-D-lyxopyranoside. Displacement at C-4 in D-lyxoside derivatives with various nucleophiles is known (19–21) and these give the corresponding 4-substituted L-riboside derivatives. It was noted, however, that attempted displacement at C-4 in D-rhamnose derivatives, with a variety of nucleophiles, resulted in ring contraction to give 5-substituted furanosides (22).

As pointed out earlier in the discussion, the first product of the rearrangement (benzyl proton signal δ 5.88) was assigned the structure **6**. This compound was isolated by termination of the reaction, when only the starting material (benzyl proton signal δ 5.80) and compound **6** (benzyl proton signal δ 5.88) were present, and fractionation of the mixture. Benzoylation of **6** gave a crystalline product whose nmr spectrum (Table 1) was consistent with its being methyl

TABLE 1. Nuclear magnetic resonance data for compounds **2**, **4–10**, **12**, **14**, and **15**

Compound[a]	Chemical shifts (δ) (first-order couplings, Hz, in parentheses)[b]									
	H-1 ($J_{1,2}$)	H-2 ($J_{2,3}$)	H-3 ($J_{3,4}$)	H-4 ($J_{4,5}$)	H-5	Aryl	PhCH	OCH_3	OH	CCH_3
2	4.68d (6.0)	← 3.55 — 4.60m →				7.42m	5.80s	3.42s	2.93s	
4	4.69d (5.0)	← 3.60 — 4.60m →				7.40m	6.32s	3.43s	2.90s	
5	← 3.80 — 4.90m →				5.65m	3.80–4.90m	7.00–8.30m	5.91s	3.49s	
6	4.73d (3.5)	← 3.60 — 4.60m →				7.47m	5.88s	3.45s	2.56s	
5, 7	← 3.80 — 5.80m →					7.20–8.40m	5.91s; 6.32s (ratio 6:4)	3.49s		
A (6, 8)	← 3.50 — 5.00m →					7.40m	5.88s; 6.32s (ratio 7:4)	3.43s	2.58s	
9	← 3.80 — 4.80m →				5.54m	3.80–4.80m	7.30–8.40m		3.49s	1.37s; 1.50s
10, 12	← 3.90 — 5.00m →						6.80–8.00m	5.53s; 5.80s (ratio 1:1)	3.15s	
14	4.87s	← 3.90 — 4.70m →					7.20–8.30m		3.29s	3.66s
15	4.76d (3.0)	← 3.60–4.40m →			5.25m	3.60–4.40m	7.20–8.40m		3.42s	3.37s

[a]In chloroform-*d*.
[b]Abbreviations for nmr: s, singlet; d, doublet; and m, multiplet.

4-*O*-benzoyl-2,3-*O*-(*R*)-benzylidene-β-D-ribopyranoside (**5**). Compound **5** had the same mobility (tlc) as the slower moving component of the mixture **5** and **7**, prepared by the benzoylation of **A**.

The final product of the rearrangement was expected to be the diastereomeric forms of methyl 2,3-*O*-benzylidene-β-D-ribofuranoside (**11** and **13**) and this was proved by the following reaction sequence. Benzoylation of the above product gave methyl 5-*O*-benzoyl-2,3-*O*-benzylidene-β-D-ribofuranoside (**10** and **12**) (23). Hydrogenolysis of this benzoate gave, in good yield, methyl 5-*O*-benzoyl-β-D-ribofuranoside (**14**), identical with an authentic sample, confirming the assigned structures. The formation of the furanoside isomers **11** and **13** from the acid-catalyzed rearrangement of **2** may be attributed to the thermodynamic stability of the system of two *cis*-fused, oxygen-containing, five-membered rings (6). The ring contraction proceeded with retention of configuration at the glycosidic centre since only the benzyl proton signals at δ 5.75 and 5.98, corresponding to methyl 2,3-*O*-benzylidene-β-D-ribofuranoside (**11** and **13**), were observed in the nmr spectrum. Retention of configuration at the glycosidic centre has been observed (24) during the acid-catalyzed conversion of methyl 3,6-anhydro-α-D-glucopyranoside into the α-furanoside. Methyl 3,6-anhydro-β-D-glucopyranoside underwent a similar conversion to give the β-furanoside derivative. Closely related is the recently reported (25) rearrangement of 3,6:3′,6′-dianhydro-α,α-trehalose into the difuranoid form. Other examples of the opening of the sugar ring accompanying acetal migration are known. Thus 1,2-*O*-isopropylidene-α-D-apio-L-furanose and its 5-thio analogue rearrange, in the presence of anhydrous methanolic hydrogen chloride, to give the respective methyl 2,3-*O*-isopropylidene-β-D-apio-D-furanoside derivative (26, 27). In the latter product the oxygen atom of the hemiacetal ring has been replaced by a sulphur atom. Extensive studies by Maeda *et al.* (28) on the acetalation mechanism of L-sorbose have confirmed that a pyranose to furanose ring conversion takes place following condensation with acetone. These workers have postulated that this change in ring size takes place via keto-form intermediates. Treatment of 1,2:4,5-di-*O*-isopropylidene-D-psicopyranose with acidic acetone resulted in migration of the 4,5-acetal and ring opening to

give 1,2:3,4-di-*O*-isopropylidene-D-psicofuranose (18). From the results obtained and from the above discussion it is clear that the change in ring size observed by Barker *et al.* (2) probably occurred after condensation of the methyl β-D-ribopyranoside with benzaldehyde. The pyranoside acetals, which would be formed initially, isomerize to give the final product, methyl 2,3-*O*-benzylidene-β-D-ribofuranoside.

The rearrangement of methyl 3,4-*O*-(*S*)-benzylidene-β-D-ribopyranoside (**4**) under anhydrous acidic conditions, was again conveniently followed by observing the change in the benzyl proton signals in the nmr spectrum. After 25 min two new benzyl proton signals at δ 5.80 and 5.88 had appeared with an accompanying decrease in the size of the initial signal at δ 6.32. These two new signals increased in size until after 3 h the three signals at δ 5.80, 5.88, and 6.32 had integrated areas in the ratio 7:4:9, which did not alter during a further 24 h. Anhydrous hydrogen chloride was then introduced directly into the reaction mixture. An identical change in the benzyl proton signals, to that noted at the corresponding point in the rearrangement of **2**, was observed and after 2 h only the two new signals at δ 5.75 and 5.98 remained. No change in this pattern was observed during another 24 h. The reaction mixture was then neutralized and the isolated product had identical nmr, ir, and chromatographic properties to methyl 2,3-*O*-benzylidene-β-D-ribofuranoside (**11** and **13**).

It is thus obvious than an essentially identical rearrangement, to that observed for the (*R*)-isomer **2**, had occurred and that the (*S*)-isomer **4** had rearranged ultimately to give a mixture of the diastereomers **11** and **13**. It is also clear, however, that in the early stages of this rearrangement there are some significant differences. In the above rearrangement we observed the simultaneous appearance of benzyl proton signals at δ 5.80 and 5.88 which may be assigned to **2** and **6** respectively. It is also probable that the benzyl proton signal for **8** appeared at the same time; however, it could not be observed since it had the same chemical shift as **4**. Thus from the start of the rearrangement we were observing the formation of an equilibrium mixture of pyranoside acetals. There did not appear to be any kinetic phase in this reaction. In contrast we did observe an initial kinetic phase in the rearrangement of the (*R*)-isomer **2**, where we have the selective formation of **6**, equilibration then taking place to give **4** and **8**. This initial kinetic control must reflect the low energy barrier for the conversion of the (*R*)-isomer **2** into the (*R*)-isomer **6**, compared with that for the conversion of **2** into the (*S*)-isomer **4** or **8**.

Experimental

The general methods are described in the preceding paper. Acidified chloroform refers to chloroform which has been shaken with water, dried ($MgSO_4$), and stood over anhydrous calcium chloride for 2 days. The chloroform solution was then filtered and anhydrous hydrogen chloride was bubbled through it for ca. 2 min. This procedure gave a chloroform solution containing ca. 0.2% of hydrogen chloride.

Methyl 3,4-O-(R)-Benzylidene-β-D-ribopyranoside (2)

Methyl 2-*O*-benzoyl-3,4-*O*-(*R*)-benzylidene-β-D-ribopyranoside (**1**), mp 109–110°C; $[\alpha]_D^{25}$ −168° (*c* 0.6, $CHCl_3$), was prepared as for the L-enantiomer (see preceding paper) starting with D-arabinose.

Sodium (catalytic quantity) was added to a solution of **1** (0.8 g, 2.25 mmol) in anhydrous methanol (75 ml) and the reaction mixture was kept overnight at room temperature. The reaction was then processed in the normal manner to give a syrup contaminated with methyl benzoate. Column chromatography with Silica Gel and elution with solvent C gave pure syrupy methyl 3,4-*O*-(*R*)-benzylidene-β-D-ribopyranoside (**2**) (567 mg, 99%), $[\alpha]_D^{25}$ −100° (*c* 1.6, $CHCl_3$).

Methyl 3,4-O-(S)-Benzylidene-β-D-ribopyranoside (4)

Methyl 2-*O*-benzoyl-3,4-*O*-(*S*)-benzylidene-β-D-ribopyranoside (**3**), mp 84–85°C, $[\alpha]_D^{25}$ −43° (*c* 0.6, $CHCl_3$), was prepared as for the L-enantiomer (see preceding paper) starting with D-arabinose.

Sodium (catalytic quantity) was added to a solution of **3** (0.3 g, 0.84 mmol) in anhydrous methanol (35 ml) and the reaction mixture was kept overnight at room temperature. The reaction was processed as above to give pure syrupy methyl 3,4-*O*-(*S*)-benzylidene-β-D-ribopyranoside (**4**) (167 mg, 79%), $[\alpha]_D^{25}$ −107° (*c* 1.1, $CHCl_3$).

Rearrangement of Methyl 3,4-O-(R)-Benzylidene-β-D-ribopyranoside (2)

(*a*) Acidified chloroform (0.1 ml) was added to a solution of **2** (0.5 g, 1.98 mmol) in chloroform-*d* (2.5 ml). Aliquots were removed at various intervals and the signals in the benzyl proton region of the nmr spectrum examined. After 10 min the initial benzyl proton signal (δ 5.80) had been replaced by two signals at δ 5.80 and 5.88, with integrated areas in the ratio 9:4, which did not alter during a further 20 min. More acidified chloroform (0.1 ml) was added and a third signal then appeared at δ 6.32. After 1 h the three signals at δ 5.80, 5.88, and 6.32 had integrated areas in the ratio 13:8:15, which did not alter during a further 24 h and with the addition of more acid (0.1 ml after 3 h and 8 h); tlc (solvent E) showed three components (R_F ca. 0.5), respectively, having the same mobilities as **2** and **4**, and a third component of higher mobility.

Anhydrous hydrogen chloride was then bubbled through the reaction mixture (ca 30 s) and after 30 min the three benzyl proton signals had been replaced by two

new signals at δ 5.75 and 5.98 with integrated areas in the ratio 5:6. This ratio did not change during a further 24 h. The reaction mixture was then poured into saturated aqueous sodium hydrogen carbonate and extracted with chloroform. The chloroform extract was washed with water, dried ($MgSO_4$), and evaporated to give syrupy methyl 2,3-*O*-benzylidene-β-D-ribofuranoside (**11** and **13**) (2, 9) (0.3 g, 60%); tlc (solvent D) showed two components (R_F ca. 0.5) which did not correspond to any of the three components observed previously. The nmr spectrum (9) *inter alia* two benzyl proton signals at δ 5.75 and 5.98 with integrated areas in the ratio 5:6.

Benzoylation of **11** and **13** (300 mg, 1.19 mmol) with benzoyl chloride (0.2 ml) in anhydrous pyridine (0.8 ml) during 18 h gave syrupy methyl 5-*O*-benzoyl-2,3-*O*-benzylidene-β-D-ribofuranoside (**10** and **12**) (23) (320 mg, 80%); ν_{max} 1724 cm^{-1} (C=O); tlc (solvent A) showed two components.

(*b*) In a second experiment acidified chloroform (0.1 ml) was added to a solution of **2** (0.87 g, 3.45 mmol) in chloroform-*d* (4.5 ml) and the reaction terminated after 3.5 h. The reaction was processed as before to give a syrup (0.78 g, 90%). The nmr spectrum showed benzyl proton signals at δ 5.80, 5.88, and 6.32 with integrated areas in the ratio 14:7:12 and tlc (solvent E) showed components, respectively, having the same mobilities as **2** and **4**, and a third component of higher mobility. Separation of this product by column chromatography on Silica Gel and elution with solvent C gave three homogeneous (tlc) syrups **A**, **B**, and **C**, in order of elution.

Compound **C** (208 mg, 0.83 mmol), whose nmr spectrum was identical with that of **2**, gave a crystalline benzoate (129 mg, 44%) that was indistinguishable from authentic **1**.

Compound **B** (100 mg, 0.40 mmol), whose nmr spectrum was identical with that of **4**, gave a crystalline benzoate (60 mg, 42%) which was identical with authentic **3**.

Syrup **A** (100 mg, 0.40 mmol) was benzoylated in the normal manner with benzoyl chloride (0.07 ml) in anhydrous pyridine (0.5 ml) during 18 h to give syrupy methyl 4-*O*-benzoyl-2,3-*O*-benzylidene-β-D-ribopyranoside (**5** and **7**) (128 mg, 88%) which showed two components by tlc (chloroform).

(*c*) In a third experiment acidified chloroform (0.1 ml) was added to a solution of **2** (0.63 g, 2.50 mmol) in chloroform-*d* (3 ml) and the reaction terminated after 30 min. The reaction was processed as before to give a syrup (0.47 g, 75%). The nmr spectrum showed benzyl proton signals at δ 5.80 and 5.88 with integrated areas in the ratio 17:7 and tlc (solvent E) showed two components, the slower moving corresponding to **2** and the faster to **A**. Fractionation of this mixture gave **2** (285 mg), which on benzoylation gave the crystalline benzoate **1** (287 mg, 71%) and methyl 2,3-*O*-(*R*)-benzylidene-β-D-ribopyranoside **6** (123 mg).

Benzoylation of **6** (123 mg, 0.49 mmol) with benzoyl chloride (0.09 ml) in anhydrous pyridine (1.0 ml) during 18 h gave a solid that was recrystallized from ethanol to give methyl 4-*O*-benzoyl-2,3-*O*-(*R*)-benzylidene-β-D-ribopyranoside (**5**) (108 mg, 62%), mp 78–79°C; $[\alpha]_D^{25}$ +7.5° (*c* 0.8, $CHCl_3$); ν_{max} 1724 cm^{-1} (C=O). *Anal.* calcd. for $C_{20}H_{20}O_6$: C 67.4, H 5.7; found: C 66.8, H 5.7.

Rearrangement of Methyl 3,4-O-(S)-Benzylidene-β-D-ribopyranoside (4)

Acidified chloroform (0.1 ml) was added to a solution of **4** (0.15 g, 0.60 mmol) in chloroform-*d* (0.8 ml) and the signals in the benzyl proton region of the nmr spectrum were examined at intervals. After 25 min two new signals at δ 5.80 and 5.88 had appeared and after 3 h the three signals at δ 5.80, 5.88, and 6.32 had integrated areas in the ratio 7:4:9 which did not alter during a further 24 h; tlc (solvent E) showed components, respectively, having the same mobilities as **2**, **4**, and **A**.

Anhydrous hydrogen chloride was then bubbled through the reaction mixture (ca. 30 s). After 2 h the three benzyl proton signals had been replaced by two new signals at δ 5.75 and 5.98 with integrated areas in the ratio 7:8 which did not change during a further 24 h. The reaction was worked up as in the preceding experiment to give a syrupy product (106 mg, 71%) that had identical nmr, ir, and chromatographic properties to methyl 2,3-*O*-benzylidene-β-D-ribofuranoside (**11** and **13**).

Methyl 5-O-Benzoyl-β-D-ribofuranoside (14)

Methyl 5-*O*-benzoyl-2,3-*O*-benzylidene-β-D-ribofuranoside (**10** and **12**) (320 mg, 0.90 mmol) was dissolved in ethanol (100 ml) and 5% palladium-on-charcoal (100 mg) was added. The reaction mixture was then shaken at room temperature, with hydrogen, at a pressure slightly greater than atmospheric, for 24 h, when the theoretical quantity of hydrogen (40 ml) had been absorbed. The catalyst was then filtered off and the filtrate evaporated to give a syrup which rapidly crystallized. Recrystallization from ether–pentane gave **14** (133 mg, 60%) indistinguishable from an authentic sample.

Methyl 4-O-Benzoyl-2,3-O-isopropylidene-β-L-ribopyranoside

(*a*) Methyl 2,3-*O*-isopropylidene-4-*O*-*p*-toluenesulphonyl-α-D-lyxopyranoside, mp 105–106°C, $[\alpha]_D^{25}$ −12° (*c* 1.85, EtOH) (lit. (29) mp 96–97°C, $[\alpha]_D^{22}$ −10.2° in EtOH), was prepared by the method of Kent and Ward (29).

(*b*) Sodium benzoate (4 g, 27.8 mmol) was added to a solution of methyl 2,3-*O*-isopropylidene-4-*O*-*p*-toluenesulphonyl-α-D-lyxopyranoside (1 g, 2.79 mmol) in dimethylformamide (200 ml) and the reaction mixture was stirred for 70 h at 130°C; tlc (solvent B) showed two components, the slower corresponding to the starting material. The reaction mixture was then poured into water (400 ml) and the aqueous solution was extracted with chloroform. The chloroform extract was washed with water, dried ($MgSO_4$), and evaporated. The syrupy product was placed on a column of Silica Gel (75 g) and eluted with solvent A, collecting 10 ml fractions. The fractions were examined by tlc and fractions 17–20, containing the faster moving component, were evaporated to give a crystalline residue (113 mg, 13%) which was recrystallized from ethanol–water to give methyl 4-*O*-benzoyl-2,3-*O*-isopropylidene-β-L-ribopyranoside, mp 53–55°C; $[\alpha]_D^{25}$ +56° (*c* 1.0, $CHCl_3$); ν_{max} 1716 cm^{-1} (C=O). *Anal.* calcd. for $C_{16}H_{20}O_6$: C 62.3, H 6.5; found: C 62.0, H 6.8. Fractions 23–32, containing the slower moving component, were evaporated to give the starting material (311 mg, 31%).

Methyl 4-O-Benzoyl-β-D-ribopyranoside (15)

Syrupy methyl 4-*O*-benzoyl-2,3-*O*-benzylidene-β-D-ribopyranoside (**5** and **7**) (170 mg, 0.48 mmol) was dissolved in ethanol (100 ml) and 5% palladium-on-charcoal (100 mg) was added. The reaction mixture was then shaken at room temperature with a slight overpressure of hydrogen. After 21 h the uptake of hydrogen (21 ml) was complete and the catalyst was removed by filtration; tlc (solvent E) showed a single component and the filtrate was evaporated to give a syrup (**15**) (111 mg, 78%).

Methyl 4-O-Benzoyl-2,3-O-isopropylidene-β-D-ribopyranoside (9)

Syrupy **15** (100 mg, 0.37 mmol) was dissolved in anhydrous acetone (10 ml) and concentrated sulphuric acid (0.5 ml) was added. The reaction mixture was shaken for 24 h at room temperature and then neutralized with anhydrous sodium carbonate. The mixture was filtered and the filtrate, which showed two components by tlc (solvent B), the minor corresponding to the starting material, was evaporated to give a syrup which crystallized. Recrystallization from ethanol–water gave **9** (58 mg, 53%), mp 53–55°C; $[\alpha]_D^{25}$ −58° (*c* 0.38, $CHCl_3$). The ir spectrum was identical with the methyl 4-*O*-benzoyl-2,3-*O*-isopropylidene-β-L-ribopyranoside prepared earlier.

Acknowledgements

The Department of Chemistry, Birmingham University, England, is gratefully acknowledged for financial support and for providing the necessary research facilities. The author thanks Drs. J. M. Webber and N. Baggett for helpful discussions and Dr. J. A. Montgomery for a sample of methyl 5-*O*-benzoyl-β-D-ribofuranoside.

1. P. A. Levene and E. T. Stiller. J. Biol. Chem. **106**, 421 (1934).
2. G. R. Barker, T. M. Noone, D. C. C. Smith, and J. W. Spoors. J. Chem. Soc. 1327 (1955).
3. G. R. Barker and J. W. Spoors. J. Chem. Soc. 2656 (1956).
4. P. A. Levene, A. L. Raymond, and R. T. Dillion. J. Biol. Chem. **95**, 699 (1932).
5. N. A. Hughes and C. D. Maycock. Carbohydr. Res. **35**, 247 (1974).
6. J. A. Mills. Adv. Carbohydr. Chem. **10**, 1 (1955).
7. N. Baggett, K. W. Buck, A. B. Foster, M. H. Randall, and J. M. Webber. J. Chem. Soc. 3394 (1965).
8. N. Baggett, K. W. Buck, A. B. Foster, and J. M. Webber. J. Chem. Soc. 3401 (1965).
9. S. Hanessian and N. R. Plessas. J. Org. Chem. **34**, 1053 (1969).
10. H. S. Hill, M. S. Whelen, and H. Hibbert. J. Am. Chem. Soc. **50**, 2235 (1928); H. Hibbert and N. M. Carter. J. Am. Chem. Soc. **50**, 3120 (1928); **50**, 3376 (1928).
11. F. S. Al-Jeboury, N. Baggett, A. B. Foster, and J. M. Webber. Chem. Commun. 222 (1965).
12. N. Baggett, K. W. Buck, A. B. Foster, B. H. Rees, and J. M. Webber. J. Chem. Soc. C, 212 (1966).
13. J. M. Williams. Carbohydr. Res. **13**, 281 (1970).
14. M. Haga, M. Takano, and S. Tejima. Carbohydr. Res. **14**, 237 (1970).
15. R. F. Nutt, M. J. Dickinson, F. W. Holly, and E. Walton. J. Org. Chem. **33**, 1789 (1968).
16. N. A. Hughes. Carbohydr. Res. **7**, 474 (1968).
17. T. D. Inch. Carbohydr. Res. **21**, 37 (1972).
18. K. James, A. R. Tatchell, and P. K. Ray. J. Chem. Soc. C, 2681 (1967).
19. R. L. Whistler, W. E. Dick, T. R. Ingle, R. M. Rowell, and B. Urbas. J. Org. Chem. **29**, 3723 (1964).
20. E. J. Reist, D. E. Gueffroy, and L. Goodman. J. Am. Chem. Soc. **86**, 5658 (1964).
21. E. J. Reist, D. E. Gueffroy, R. W. Blackford, and L. Goodman. J. Org. Chem. **31**, 4025 (1966).
22. C. L. Stevens, R. P. Glinski, K. G. Taylor, P. Blumbergs, and F. Sirokman. J. Am. Chem. Soc. **88**, 2073 (1966).
23. S. Jacobsen and C. Pedersen. Acta Chem. Scand. Ser. B, **28**, 866 (1974).
24. W. N. Haworth, L. N. Owen, and F. Smith. J. Chem. Soc. 88 (1941).
25. G. Birch, C. K. Lee, and A. C. Richardson. Carbohydr. Res. **19**, 119 (1971).
26. M. H. Halford, D. H. Ball, and L. Long, Jr. Carbohydr. Res. **8**, 363 (1968).
27. D. H. Ball, F. H. Bissett, I. L. Klundh, and L. Long, Jr. Carbohydr. Res. **17**, 165 (1971).
28. T. Maeda, Y. Miichi, and K. Tokuyama. Bull. Chem. Soc. Jpn. **42**, 2648 (1969) and references cited therein.
29. P. W. Kent and P. F. V. Ward. J. Chem. Soc. 416 (1953).

Preparative synthesis of 1-deoxy-D-*erythro*-2-pentulose and some of its derivatives[1]

JEAN-CLAUDE FISCHER, DEREK HORTON, AND WOLFGANG WECKERLE
Department of Chemistry, The Ohio State University, Columbus, OH 43210, U.S.A.

Received April 5, 1977

JEAN-CLAUDE FISCHER, DEREK HORTON, and WOLFGANG WECKERLE. Can. J. Chem. **55**, 4078 (1977).

Methyl 4,6-*O*-benzylidene-2-deoxy-α-D-*erythro*-hexopyranosid-3-ulose (**1**) was converted, by means of lithium hydroxide in a two-phase system, into 3,5-*O*-benzylidene-1-deoxy-*keto*-D-*erythro*-2-pentulose (**2**) in 55% yield. Compound **2** was further characterized as its (2,4-dinitrophenyl)hydrazone **3**, its 4-acetate **4**, and the 4-benzoate **5**. The configurational assignment for the corresponding pentitol derivatives (**6** and **8**) of **2** was achieved by ^{1}Hmr analysis of the cyclic carbonates **11** (from **6**) and **13** (from **8**) and confirmed by comparing the physical constants of the 1-deoxypentitols having the D-*ribo* (**12**) and D-*arabino* (**14**) configurations with literature data. Hydrolysis of **2** with mild acid afforded the title ketose (**9**) as a syrup that gave a crystalline (2,4-dinitrophenyl)hydrazone (**10**), and an acyclic triacetate (**15**) as an oil. A mechanism for the chain degradation of compound **1** to give **2** is proposed.

JEAN-CLAUDE FISCHER, DEREK HORTON et WOLFGANG WECKERLE. Can. J. Chem. **55**, 4078 (1977).

On a préparé le *O*-benzylidène-3,5 déoxy-1 *céto*-D-*érythro*-pentulose-2 (**2**) avec un rendement de 55% en faisant réagir l'hydroxyde de lithium dans un système à deux phases sur le *O*-benzylidène-4,6 déoxy-2 α-D-*érythro*-hexopyranosidulose-3 de méthyle (**1**). Le composé **2** a également été converti en ses dérivés caractéristiques; le dinitro-2,4 phénylhydrazone (**3**), l'acétate-4 (**4**) et le benzoate-4 (**5**). La configuration absolue des composés **6** et **8**, dérivés des pentitols de **2**, a été établie par analyse rmn des carbonates cycliques **11** (de **6**) et **13** (de **8**) puis confirmée par comparaison des constantes physiques de déoxy-1 pentitols de configuration D-*ribo* (**12**) et D-*arabino* (**14**) avec les données de la littérature. L'hydrolyse acide douce de **2** a donné une cétose sirupeuse **9** qui a été convertie en sa dinitro-2,4 phénylhydrazone cristalline (**10**) et en son triacétate acyclique se présentant sous forme huileuse (**15**). On propose un mécanisme pour la dégradation du composé **1** en **2**.

Introduction

In an earlier publication (1) it was reported that scaled-up experiments of the reaction of butyllithium with methyl 2,3:4,6-di-*O*-benzylidene-α-D-mannopyranoside initially led to a complex mixture containing a wide range of products accompanying the methyl 4,6-*O*-benzylidene-2-deoxy-α-D-*erythro*-hexopyranosid-3-ulose (**1**) that was desired as an intermediate in a proposed synthesis of daunosamine (1) and related sugars (2). From the mixture, a crystalline product was isolated in relatively low yield and subsequently identified as the 3,5-benzylidene acetal **2** of the title ketose. As compound **2** is synthetically interesting in its own right, a more practical procedure for its synthesis was considered a desirable objective and is described in the present article. This compound (**2**) has been obtained before by Overend and his coworkers (3) from the ketone **1** via its trimethylhydrazone iodide, but attempts to effect the direct conversion resulted in decreased yields of **2** and gave other unidentified and apparently unstable products.

The parent sugar of **2**, 1-deoxy-D-*erythro*-2-pentulose (**9**), constitutes one of the two possible, to the best of our knowledge thus far unknown, 1-deoxy analogs derived from (D or L)-*erythro*-pentulose ('ribulose') and the *threo* epimer ('xylulose'), although **9** must have been the (unidentified) intermediate in a study (4) correlating the configuration of 2-*C*-methyl-D-ribonic acid ('α'-D-glucosaccharinic acid) with 1-deoxy-D-arabinitol. The tribenzoate of 1-deoxy-L-*threo*-pentulose has been prepared (5), but attempted saponification failed to give the free sugar.

The value of **2** as precursor in the synthesis of

[1]Portions of this work were presented at the 171st National Meeting of the American Chemical Society, New York, NY, March 1976, CARB-3, and the Joint Meeting of the American Chemical Society and the Chemical Institute of Canada, Montreal, Canada, May 1977, CARB-39.

compounds of potential interest is demonstrated by the convenient preparation of the uniquely protected epimeric 1-deoxypentitols having D-*ribo* (**6**) and D-*arabino* (**8**) configurations in high yields. A synthesis, utilizing **2** as key intermediate, of optically pure analogs of atrolactic aldehyde is the topic of another report (for a preliminary report see ref. 6). These aldehydes constitute precursors of dioxolane derivatives that may exhibit anticholinergic activity (7).

Results and Discussion

The unexpected formation of the *O*-benzylidenepentulose **2** in the aforementioned reaction of methyl 2,3:4,6-di-*O*-benzylidene-α-D-mannopyranoside with butyllithium was traced to decomposition of the ketone **1** as the initial product under the strongly alkaline conditions of the original (8) isolation procedure. Consequently, the ketone **1** was treated with base under a wide variety of conditions, as by altering the nature and proportion of alkaline reagent, changing the solvent(s), and examining the mode of addition of the reagent to the substrate (or *vice versa*). From an estimated yield of **2** as low as 5–10% in the crude, complex mixture obtained under the original conditions (8), the procedure could be effectively improved by using a two-phase system of water and ether and employing stoichiometric amounts of lithium hydroxide as the base. The product **2** could then be isolated pure in 55% yield simply by recrystallization without recourse to chromatographic purification; further improvement in net yield was realized by processing the mother liquor.

The structure of **2** was corroborated from its elemental composition as well as from its spectral (ir, strong OH and C=O absorption bands; ms, M^{+}, $M - \cdot OH$, $M - Ac\cdot$) behavior, and especially from the ^{1}Hmr data. The complex, poorly resolved spectrum in chloroform-*d* (compare ref. 3) was rendered essentially first order by using benzene-d_6 as the solvent. In particular, the spectrum displayed (Table 1) a noteworthy multiline pattern for H-4 that collapsed to a six-line signal after the hydroxyl proton had been exchanged by deuterium. The physical constants of **2** were in fair agreement with those reported by Overend and co-workers (3) for the same compound obtained by an independent route.

The reactions exhibited by **2** provided additional evidence for the proposed structure. The presence of the carbonyl group was confirmed by the formation of a (2,4-dinitrophenyl)hydrazone (**3**) and by the reduction to the epimeric pentitols (**6** and **8**), discussed in more detail in the next paragraph. Chemical evidence for a free hydroxyl group was obtained by formation of the acetate **4** (as a distillable oil) and the crystalline benzoate **5**, both of which gave (Table 1) well-resolved ^{1}Hmr spectra in chloroform-*d*, in contrast to **2**, as a result of the anticipated downfield shift of the H-4 signal.

Treatment of the *O*-benzylidenepentulose **2** with sodium borohydride led to a semicrystalline product that was shown by tlc analysis to consist of two components (**6** and **8**), which were readily separated, without recourse to chromatography, by exploiting the very low solubility of **8** in cold toluene to isolate crystalline **8**, essentially quantitatively, from syrupy **6**. Conventional acetylation of the latter gave the crystalline diacetate **7**.

Configurational assignment at the newly formed, secondary alcoholic centers in **6** and **8** was accomplished by analysis of the spin-coupling interactions exhibited by H-2 in the ^{1}Hmr spectra of the corresponding 2,4-carbonates **11** and **13**. Carbonates were chosen for the formation of the cyclic derivatives instead of more common protecting groups (such as benzylidene or isopropylidene acetals) to achieve adequately dispersed ^{1}Hmr spectra (Figs. 1 and 2). Inspection of these figures and Table 1 shows that the multiplet attributable to H-2 (readily identified by double irradiation at the position of the methyl resonance) appears at lowest field in both instances, and is well separated from the doubled doublet for H-3. In the spectrum of **11** (Fig. 1), the large $J_{2,3}$ value (9.2 Hz) clearly indicates the *trans*-diaxial disposition of the protons at C-2 and C-3, thereby unequivocally establishing the D-*ribo* stereochemistry for the parent pentitol.

The other product (**13**) must, therefore, be the D-*arabino* isomer. The $J_{2,3}$ value (6.2 Hz) determined from its spectrum (Fig. 2), although still within the usual range (9*a*; for extensive studies on pyranoid sugar systems see ref. 9*b*) for the interaction of axially–equatorially disposed, vicinal protons on a six-membered ring, is somewhat larger than anticipated. This may be explained by the well-known (10) tendency of the chair form of the 1,3-dioxane ring to be additionally puckered in the O—C—O region and at the same time flattened in the C—C—C

TABLE 1. The 100-MHz ^{1}H nuclear magnetic resonance data for compounds **2–8, 11, 13,** and **15**

	Chemical shifts (δ)[a] (first-order couplings, Hz, in parentheses)									
Compound[b]	H-1 ($J_{1,2}$)	H-2 ($J_{2,3}$)	H-3 ($J_{3,4}$)	H-4 ($J_{4,5'}$)	H-5 ($J_{4,5}$)	H-5′ ($J_{5,5'}$)	Aryl	*PhC*-H	4-OR ($J_{4,OH}$)	Others[c] ($J_{2,OH}$)
2[d]	1.87 s	—	3.50 d (9.3)	3.73 m (9.8)	4.19 dd (4.8)	3.38 dd (10.0)	7.60–7.10 m	5.16 s	3.44 d (2.4)	
3[e]	2.17 s	—	4.31 d (8.2)	4.14 m_8 (9.0)	4.42 dd (4.8)	3.71 dd (9.8)	7.30—7.58 m	5.61 s	2.55 d (5.0)	7.23 s (NH)
4	2.34 s	—	4.17 d (9.7)	5.18 m_6 (9.7)	4.42 dd (5.3)	3.78 dd (10.7)	7.60–7.30 m	5.60 s	2.10 s	
5	2.33 s	—	4.38 d (9.9)	5.41 m_8 (10.0)	4.60 dd (5.3)	3.90 t (10.8)	8.15–7.38 m	5.68 s	8.15–7.38 m	
6[f]	1.48 d (6.3)	←		4.60–3.75 m		→	7.94–7.60 m	5.84 s	5.51 d (3.2)	5.06 d (2-OH) (5.3)
7	1.33 d (6.5)	5.10 dq (2.3)	3.93 dd (10.0)	4.94 m_6 (10.0)	4.36 dd (5.8)	3.60 t (11.0)	7.30–7.12 m	5.49 s	2.05 s	2.01 s (Ac)
8[f]	1.51 d (6.2)	4.43 m (2.2)	3.65 dd (8.8)	4.08 m (9.8)	4.50 dd (4.6)	3.83 t (9.6)	7.94–7.63 m	5.84 s	5.42 d (5.0)	4.66 d (2-OH) (7.0)
11[f]	1.67 d (6.3)	5.06 dq (9.2)	4.26 t (9.2)	←—4.96–4.62 m—→		4.19 t (10.0)	7.75 m	6.10 s	—	
13[f]	1.71 d (6.5)	5.31 m_5 (6.2)	4.72 dd (9.8)	4.99 m_6 (10.0)	4.74 dd (4.8)	4.22 t (10.0)	7.76 m	6.11 s	—	
15[d]	2.02 s	—	5.34 d (3.7)	5.56 m	←—4.27 m—→		—	—	1.84 s	1.79 s (Ac) 1.71 s (Ac)

[a]Signal multiplicities: s, singlet; d, doublet; t, triplet; q, quartet; m, multiplet; m_x, sextet, septet, etc.
[b]In chloroform-*d*, unless otherwise stated.
[c]Assignments in parentheses.
[d]In benzene-d_6.
[e]Additional signals at δ 9.10 (1 H, d, $J_{3',5'}$ 2.2 Hz, H-3′), 8.33 (1 H, dd, $J_{5',6'}$ 9.2 Hz, H-5′), 7.85 (1 H, d, H-6′).
[f]In methyl sulfoxide-d_6.

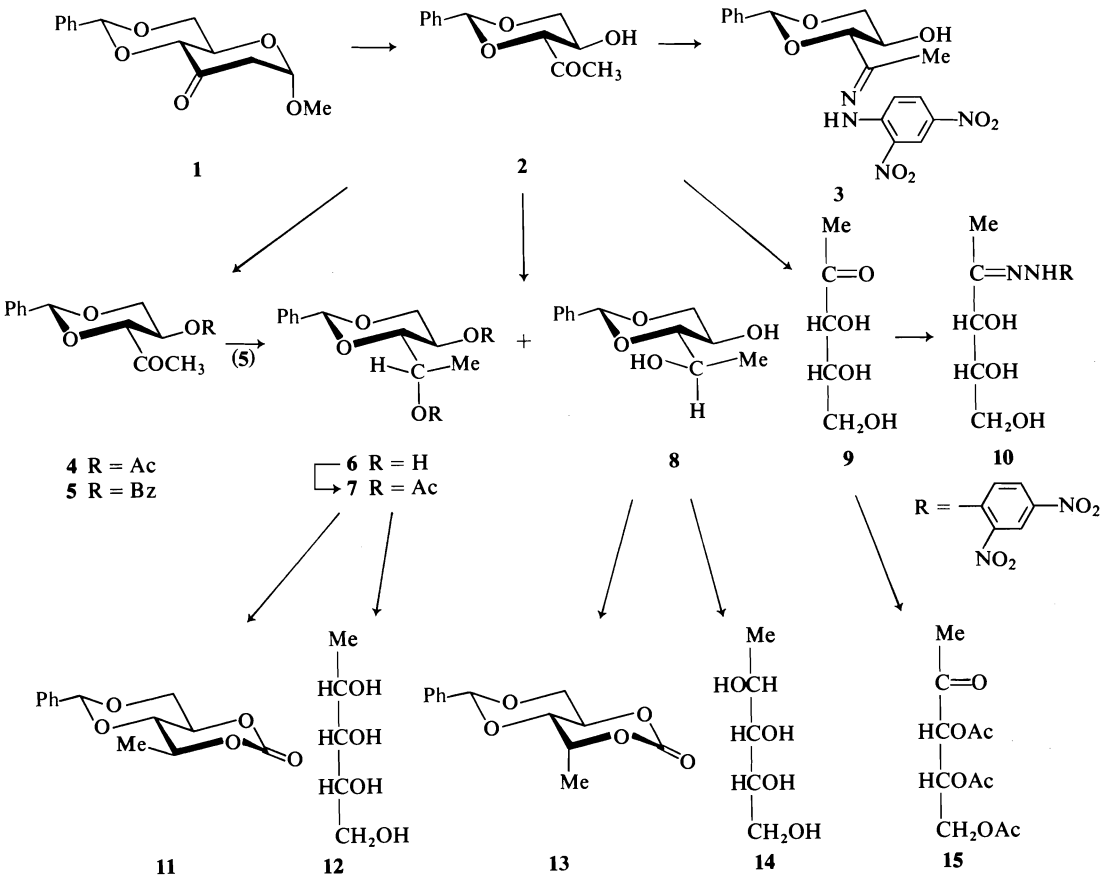

SCHEME 1

region. Such flattening leads to diminution of the H-2e–H-3a torsional angle and, in accordance with the Karplus equation, the $J_{2,3}$ value should consequently be larger.[2]

Further evidence for the configurational assignments made for **6** and **8** was provided by comparing the physical data of the parent pentitols with values for these compounds recorded in the literature. Mild acidic hydrolysis of **6** furnished crystalline 1-deoxy-D-ribitol (5-deoxy-L-ribitol, **12**), mp 69°C and $[\alpha]_D$ +15° in water. This product has been described (11) as having mp 74–75°C and $[\alpha]_D$ +9° in water. The physical characterization of the enantiomer of **12** in the literature is somewhat ambiguous; mp 77–80°C for a product containing solvent of recrystallization, 65–69°C for the solvent-free compound (12), and mp 80–85°C (13) have been reported.

Likewise, acidic hydrolysis of **8** led to the crystalline 1-deoxy-D-arabinitol (5-deoxy-D-lyxitol, **14**) whose physical constants (mp 130°C, $[\alpha]_D$ +1.4° in water) are in excellent agreement with data given in the literature for **14** (14) and (allowing for the sign of the specific rotation) for its enantiomer (14, 15).

The ratio between the products **6** and **8** in the borohydride reduction of **2** was determined by ^{1}Hmr spectroscopy to be 3:4 in favor of the crystalline D-*arabino* isomer **8**. When the benzoate **5** was treated with the same reducing agent, with subsequent debenzoylation, the overall high yielding (91%) sequence gave a slightly higher proportion of **8** (2:1 ratio of **8**:**6**). A noteworthy change in favor of **8** was observed, however, when catalytic hydrogenolysis of the *O*-benzylidenepentulose **2** was attempted under

[2]The same holds true for adjacent diaxial protons (as in **11**), but the respective spin-coupling interaction is not very sensitive to small decreases of this angle (compare ref. 10).

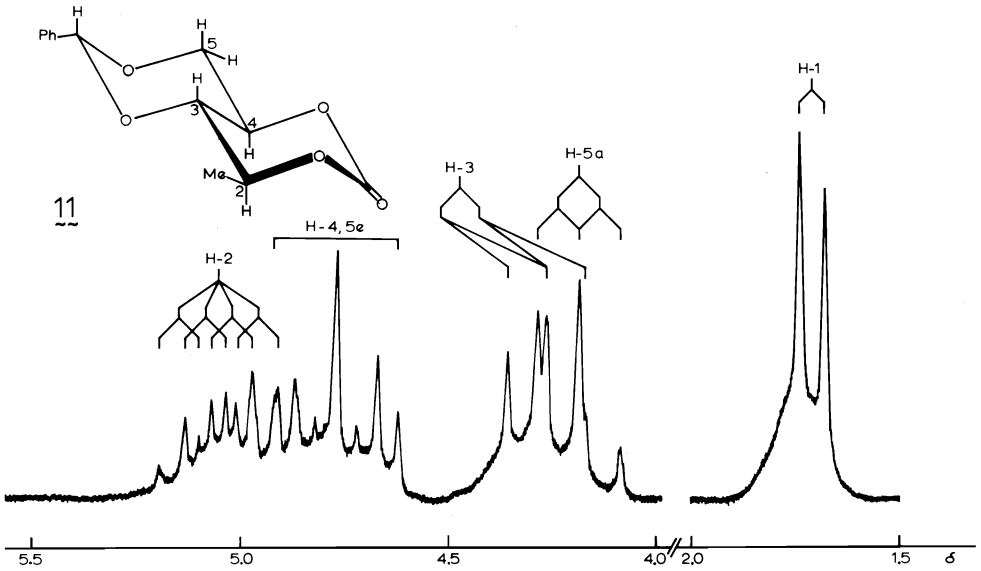

FIG. 1. Partial 100-MHz ^{1}Hmr spectrum of 3,5-*O*-benzylidene-2,4-*O*-carbonyl-1-deoxy-D-ribitol (**11**) in methyl sulfoxide-d_6.

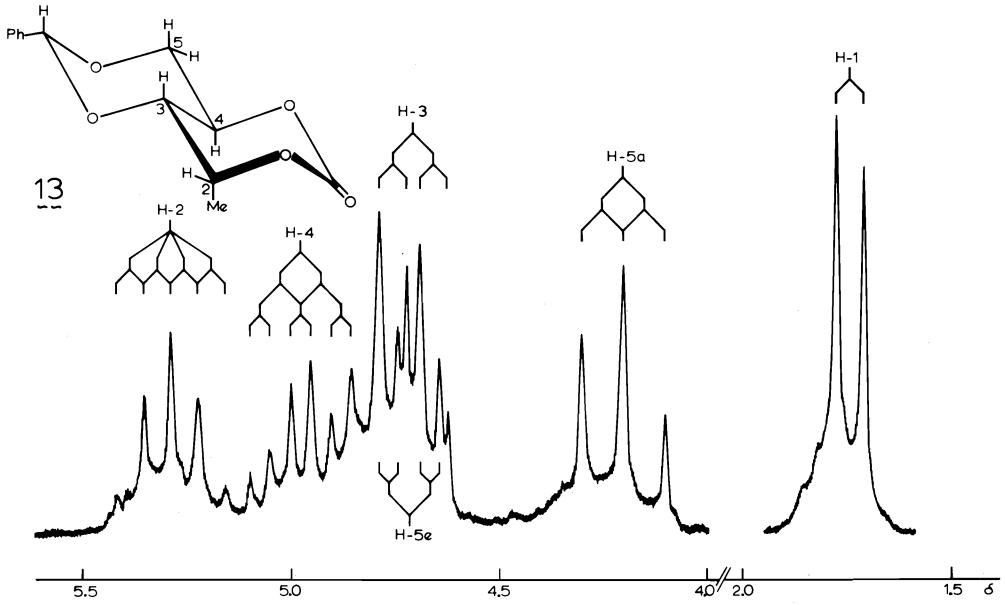

FIG. 2. Partial 100-MHz ^{1}Hmr spectrum of 3,5-*O*-benzylidene-2,4-*O*-carbonyl-1-deoxy-D-arabinitol (**13**) in methyl sulfoxide-d_6.

conditions under which the carbonyl function was anticipated to be stable. Originally envisaged for the conversion of **2** into the free ketose **9**, no reaction occurred at all during 24 h under atmospheric pressure, and under more-forcing conditions (1 kg cm^{-2} pressure of hydrogen) scarcely any debenzylidenation took place but, instead, the deoxypentitols **6** and **8** were formed in good net yield, the ratio being 1:5 in favor of **8**.

The conversion of **2** into 1-deoxy-D-*erythro*-2-pentulose (**9**) was achieved by mild acidic hydrolysis. The syrupy ketose **9** was isolated in good yield and was further characterized as its

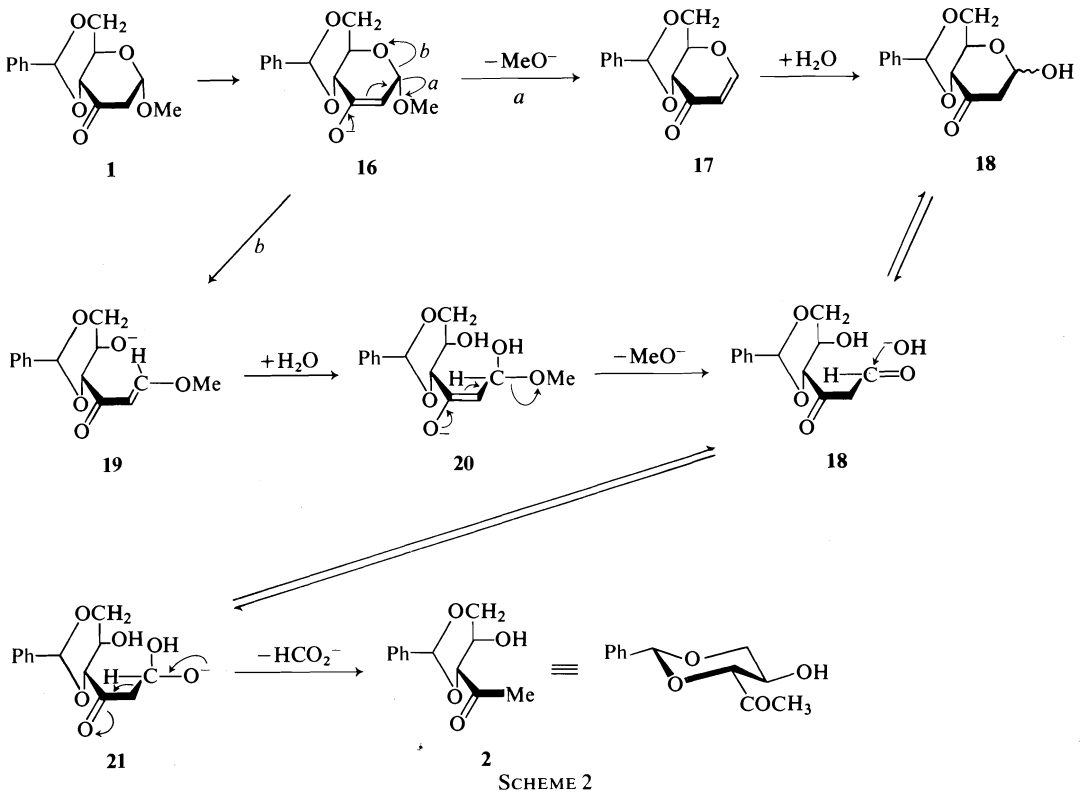

SCHEME 2

(2,4-dinitrophenyl)hydrazone **10**. Compound **9** may be assumed to exist mainly in the open-chain form, as a strong carbonyl-stretching absorption is evident at 1705 cm^{-1} in its ir spectrum. In solution, considerable proportions of the anomeric furanoses coexist with the open-chain form, as manifested by the ^{1}Hmr spectrum in methyl sulfoxide-d_6; the spectrum displayed three signals for the methyl group, having estimated intensities of 1:1:2.

Finally, the pentulose triacetate **15** was prepared, as it was needed as precursor for the dithioacetal of **9** that was required in ongoing studies (for reviews see ref. 16) in this laboratory. Compound **15** was prepared by acetylating **9** with acetic anhydride – zinc chloride and was obtained as a chromatographically homogeneous, colorless syrup that could be distilled *in vacuo*.

A plausible mechanism for the formation of **2** is illustrated in Scheme 2. Under basic conditions the corresponding enolate (**16**) of **1** may eliminate (route *a*) the glycosidic methoxyl group to give the enulose **17**. Hydration of this product and subsequent attack on **18** by hydroxide ion would lead, with elimination of formate, to the pentulose derivative **2**. The reaction does require a stoichiometric amount of base, together with an excess of water, to afford the product. The idea of elimination of the glycosidic group (route *a*) was supported by the fact that **1** anomerizes readily (Scheme 3) under alkaline conditions in anhydrous, methanolic solution, and gives an approximately equimolar ratio of the two anomers **1** and **22**; no degradation product **2** could be detected under these conditions. The β anomer **22** was isolated by column chromatography and was fully characterized.

In a further effort to support the foregoing mechanism, the enulose **17** (17) was prepared. When subjected to alkaline treatment in absolute methanol (Scheme 3), the anomeric glycosides **1** and **22** were indeed formed. However, when treated under the conditions used for the conversion of **1** into **2**, only minor proportions of the degradation product **2** could be detected, together with unchanged **17**, even after an extended period of reaction. This observation parallels a report by Garegg and Norberg (18) on the reaction of methyl 4-*O*-benzyl-2,6-dide-

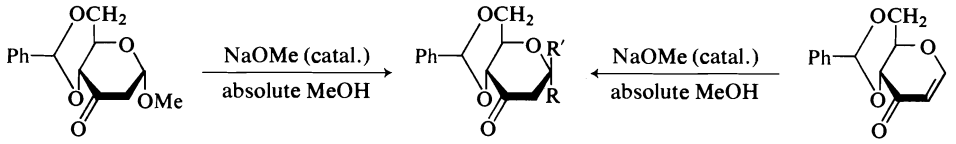

1 **1** R′ = H; R = OMe; **22** R′ = OMe; R = H; **17**

SCHEME 3

oxy-α-L-*threo*-hexopyranosid-3-ulose with methyllithium, which afforded an enulose analogous to **17**. Obviously, once this product is formed, it is fairly stable, even under the strongly alkaline conditions of the isolation procedure.

Therefore, route *a*, although conceptually appealing, cannot constitute the major avenue for the chain degradation, and an alternative mechanistic course must be available. A proposal is presented in Scheme 2 (route *b*): the enolate **16** may rearrange with cleavage of the C-1–O-5 bond to form the enone **19**. β-Addition of a hydroxyl ion to this product, and subsequent expulsion of the methoxyl group would lead to the glycosulose **18**. This intermediate, common to both possible pathways, would be transformed by the route outlined before, to give **2**. Route *b* is, of course, in accord with the requirements mentioned before (presence of water and a stoichiometric amount of base), but is difficult to prove.

Experimental

General Methods

Evaporations were performed under diminished pressure at a bath temperature below 50°C. Melting points were determined with a Thomas-Hoover apparatus and are uncorrected. A Perkin-Elmer model 141 polarimeter and 1-dm tubes were used for measurement of specific rotations in chloroform, unless otherwise stated. Infrared spectra were recorded on a Perkin-Elmer model 457 grating ir spectrometer with solids dispersed in potassium bromide and syrups as film on sodium chloride discs. The ^{1}Hmr spectra were recorded at 100 MHz with a Varian HA-100 spectrometer; chemical shifts refer to an internal standard of tetramethylsilane (δ = 0.00), and are listed together with first order spin-coupling values (Hz) in Table 1. The assignments were confirmed in most instances by decoupling experiments. Thin layer chromatography was performed on precoated plates of Silica Gel 60 (E. Merck, Darmstadt); zones were detected by uv light and by spraying with sulfuric acid and subsequent heating. Solvent volumes are v/v; petroleum ether refers to the fraction boiling at 65–110°C. Column chromatography was performed with silica gel (Merck No. 7734; 63–200 μm). Microanalyses were performed by W. N. Rond. Mass spectra were recorded by C. R. Weisenberger with an AEI MS-9 double-focusing, high resolution spectrometer operating at an ionizing potential of 70 eV and an accelerating potential of 8 kV; the source temperature (direct-inlet system) was 120°C. Data and probable assignments for compounds **9**, **10**, **12**, **14**, and **15** are summarized in Table 2. The spectra of all benzylidene acetals displayed intense peaks of aromatic ions (*m/e* 107, 106, 105, 91, 79, and 77); the notations h_1 and h_2 in the assignments refer to the *h*-rupture process proposed by Chizhov *et al.* (20). X-ray powder diffraction data give interplanar spacings, Å, for CuKα radiation. The camera diameter was 114.59 mm. Relative intensities were estimated visually: m moderate, s strong, v very, w weak. The strongest lines are numbered (1, strongest); double numbers indicate approximately equal intensities.

*3,5-O-Benzylidene-1-deoxy-keto-*D*-erythro-2-pentulose (2)*

To a suspension of methyl 4,6-*O*-benzylidene-2-deoxy-α-D-*erythro*-hexopyranosid-3-ulose (1) (**1**, 50 g, 189 mmol) in ether (2 ℓ) was added a solution of lithium hydroxide monohydrate (8 g, 191 mmol) in water (1200 ml) and the mixture was vigorously stirred at ~20°C for 16 h, after which time tlc (4:1 ether – petroleum ether) indicated that all **1** had reacted. The organic layer was separated and the aqueous, yellow phase was extracted with ether. The combined extracts were washed with ice–water and evaporated to give a white, crystalline residue (~28 g). Recrystallization from 10 parts of 1:4 ethyl acetate – petroleum ether afforded the title compound **2** as fine needles; yield 23.2 g (55%), mp 82.5°C, $[\alpha]_D^{23}$ +40.5° (*c* 1) (lit. (3) mp 76.5–78.5°C, $[\alpha]_D$ +38.7° in chloroform); ν_{max}(KBr) 3430 (OH), 1710 cm^{-1} (C=O); *m/e* (rel. intensity) 222 (0.6, M$^{+\cdot}$), 205 (0.7, *M* − •OH), 180 (12, *M* − ketene), 179 (100, M − Ac•), 149 (6, h_2), 107 (100, PhCHOH$^+$; m* at 64.0, calcd. for 179 → 107: 63.96), 106 (50, PhCO$^+$; m* at 75.4, calcd. for 149 → 106: 75.41), 91 (21, PhCH$_2^+$; m* at 46.3, calcd. for 179 → 91: 46.26), 71 (5; m* at 33.8, calcd. for 149 → 71: 33.83), 43 (74, Ac$^+$); X-ray powder diffraction data: 9.25 m (3), 6.06 vw, 5.84 s (1), 5.50 m, 4.47 m, 4.36 s (2), 3.85 m, 3.77 m, 3.66 m, 3.55 m, 3.41 w, 2.59 w and 2.44 vw. *Anal.* calcd. for $C_{12}H_{14}O_4$ (222.24): C 64.85, H 6.35; found: C 64.99, H 6.42.

*3,5-O-Benzylidene-1-deoxy-*D*-erythro-2-pentulose (2,4-Dinitrophenyl)hydrazone (3)*

To a solution of the pentulose derivative **2** (150 mg, 0.68 mmol) in methanol (5 ml) was added (2,4-dinitrophenyl)hydrazine (150 mg, 0.76 mmol) and the mixture was kept for 15 h at ~25°C. The solvent then was distilled off, and the residue triturated with ether. The extract was filtered and evaporated to afford a yellow solid that was shown by tlc (4:1 ether – petroleum ether) to be a mixture of two components. The slower moving, major product was obtained pure by preparative tlc and was recrystallized from ethanol – petroleum ether; yield 120 mg (44%), mp 180°C, $[\alpha]_D^{21}$ +13.1° (*c* 0.4); ν_{max}(KBr)

TABLE 2. Major fragment ions[a] (% of base peak) observed in the electron-impact mass spectra of acyclic pentulose derivatives

Compound					
9[b] $R^1, R^2 = O$ $R^3 = H$	**10** $R^1, R^2 = NNHC_6H_3(NO_2)_2$ $R^3 = H$	**12**[c] $R^1, R^3 = H$ $R^2 = OH$	**14**[d] $R^1 = OH$ $R^2, R^3 = H$	**15**[e] $R^1, R^2 = O$ $R^3 = Ac$	Assignment
134 (0.1)	314 (9)	136 (—)	136 (—)	260 (—)	$M^{+\cdot}$
133 (0.8)	315 (1.4)	137 (0.11)	137 (0.4)	262 (0.3)	$M \pm 1/+2$
					Me | R^1CR^2
119 (0.18)	299 (0.5)	121 (—)	121 (—)	245 (—)	
43 (100)	223 (2.3)	45*(100)	45*(100)	43 (100)	
91 (8)	91 (7.2)	91 (2.6)	91 (2.4)	217 (0.3)	$HCOR^3$
73 (12)	253 (25)	75 (28)	75 (52)	115 (4)	
61 (33)	61 (18)	61*(50)	61 (44)	145 (1.8)	$HCOR^3$
103 (3)	283 (1)	105 (1.3)	105 (1.5)	187 (0.3)	
31 (16)	31 (16)	31*(31)	31 (46)	73 (3.5)	CH_2OR^3
117 (2.8)	297 (0.6)	119 (0.15)	119 (1.2)	158 (9)	Others
$M - \cdot OH$	$M - \cdot OH$	$M - \cdot OH$	$M - \cdot OH$	$M - Ac_2O$	
116 (1.4)	265 (1.8)	118 (0.17)	118 (0.3)	98 (13)	
$M - H_2O$	$283 - H_2O$	$M - H_2O$	$M - H_2O$	158 − ketene	
86 (3.2)	73 (8)	87*(6.4)	87 (5.7)		
$103 - \cdot OH$	$91 - H_2O$	$105 - H_2O$	$105 - H_2O$		
	43 (100)				

[a]Prominent metastable fragments observed in the spectra are indicated by an asterisk at the daughter ion of the process involved.
[b]Metastable ions were observed for the following transitions: 61 → 43 (calcd. 30.31/found 30.3); $M^{+\cdot}$ → 74 (60%; 40.87/40.9); 74 → 56 (22%; 42.38/42.4); 91 → 73 (58.56/58.5).
[c]Additional metastable ions were found for the following transitions: 74 (77%) → 56 (73%; 42.38/42.3); 75 → 57 (38%; 43.32/43.3).
[d]Additional metastable ions were recorded for the following transitions: 119 → 60 (11%, 30.25/30.3); 74 (70%) → 56 (67%; 42.38/42.4); 75 → 57 (48%; 43.32/43.3); 137 → 119 (103.36/103.3).
[e]Subsequent fragmentation of *m/e* 217 leads (19) to ions of the *CC series*: 157 (1%, CC_2), 115 (4%, CC_3), and 73 (3.5%, CC_4).

3500 (OH), 3330 (NH), 1625 (C=N), 1600 and 1505 (phenyl), 1525 and 1340 cm^{-1} (NO_2); *m/e* (rel. intensity) 402 (11, $M^{+\cdot}$), 265 (6), 253 (18, h_1), 220 (3, $M - \cdot NHC_6H_3(NO_2)_2$), 205 (9), 183 (9, $(NO_2)_2C_6H_3NH_2^{+\cdot}$), 179 (7, $M - \cdot C(Me)=NNHC_6H_3(NO_2)_2$), 163 (19), 150 (12), 149 (100, h_2), 117 (11), and 43 (34); X-ray powder diffraction data: 11.04 m (3), 9.02 w, 7.34 w, 6.91 m, 6.48 s (2), 5.50 m, 4.96 m, 4.58 w, 4.27 m, 3.87 w, 3.55 m (4), and 3.41 vs (1). *Anal.* calcd. for $C_{18}H_{18}N_4O_7$ (402.37): C 53.73, H 4.51, N 13.92; found: C 53.54, H 4.72, N 13.93.

4-O-Acetyl-3,5-O-benzylidene-1-deoxy-D-*erythro-2-pentulose (4)*

The pentulose derivative **2** (300 mg, 1.35 mmol) was treated with 1:2 acetic anhydride – pyridine (6 ml) for 18 h at ~25°C. Methanol (5 ml) was then added with cooling and, after 1 h, the mixture was evaporated. Pyridine and then toluene (two 10 ml portions each) were added to and evaporated from the residue to afford syrupy **4** in theoretical yield (360 mg). To secure an analytical sample, a portion was distilled under diminished pressure (5 mTorr, bath temperature ~150°C); $[\alpha]_D^{23}$ +26.6° (*c* 1); ν_{max}(film) 1750 (ester C=O) and 1730 cm^{-1} (C=O); *m/e* (rel. intensity) 264 (0.1, $M^{+\cdot}$), 221 (24, $M - Ac\cdot$), 204 (0.3, $M - HOAc$), 149 (2.4, h_2), 115 (100, 221 − PhCHO; m* at 59.9, calcd. 59.84), 43 (80, Ac^+; m* at 16.1, calcd. for 115 → 43: 16.08). *Anal.* calcd. for $C_{14}H_{16}O_5$ (264.28): C 63.63, H 6.10; found: C 63.74, H 6.21.

4-O-Benzoyl-3,5-O-benzylidene-1-deoxy-D-*erythro-2-pentulose (5)*

To a mixture of the pentulose derivative **2** (6.0 g, 27 mmol) in pyridine (30 ml) was added benzoyl chloride (5 ml, 43.3 mmol). After 18 h at ~25°C, the mixture was poured into ice–water (500 ml) saturated with potassium carbonate. The crystalline precipitate was collected, washed with water, dried, and recrystallized from ether (or ethyl acetate) – petroleum ether to give pure **5**; yield 7.98 g (91%); mp 95–96°C, $[\alpha]_D^{22}$ −23.1° (*c* 1); ν_{max}(KBr) 1730 (ester C=O), 1715 (C=O), 1600 and 1580 cm^{-1} (monosubstituted phenyl); *m/e* (rel. intensity) 326 (0.3, $M^{+\cdot}$), 283 (22, $M - Ac\cdot$), 221 (0.1, $M - PhCO\cdot$), 220

(0.1, M − PhCHO), 204 (0.7, M − $PhCO_2H$), 178 (17, 283 − PhCO•), 177 (100, 283 − PhCHO; m* at 110.7, calcd. 110.70), 149 (5, h_2), 122 (6, $PhCO_2H^{+\cdot}$), 105 (89, $PhCO^+$; m* at 90.3, 62.3, and 33.8, calcd. for 122 → 105: 90.37, for 177 → 105: 62.29, and for 326 → 105: 33.82), 43 (22, Ac^+); X-ray powder diffraction data: 11.78 s (3), 9.66 w, 8.07 vw, 7.62 vw, 7.10 m, 5.60 m, 5.26 m, 5.01 m, 4.79 m, 4.54 s (2), 4.34 vw, 4.18 w, 3.79 s (1), 3.61 w, 3.43 vw, 3.15 vw, and 3.04 m. *Anal.* calcd. for $C_{19}H_{18}O_5$ (326.35): C 69.93, H 5.56; found: C 70.14, H 5.70.

*3,5-O-Benzylidene-1-deoxy-*D*-ribitol (**6**) and its* D*-Arabino Analog **8***

*From **2** with Sodium Borohydride*

Sodium borohydride (1.7 g, 44.9 mmol) was added to a cooled (0°C) solution of the pentulose derivative **2** (4 g, 18 mmol) in aqueous methanol (95%, 60 ml) and the mixture was kept for 18 h at ~25°C. Methanol was then distilled off and the residue was dissolved in dichloromethane (150 ml) and washed with water. The aqueous phase was extracted again with dichloromethane, and the combined organic solutions were dried (magnesium sulfate) and evaporated. The resultant, semicrystalline residue (3.46 g, 86%) was shown by ^{1}Hmr spectroscopy to be a 3:4 mixture of **6** and **8**. Recrystallization from toluene (90 ml) afforded the pure D-*arabino* isomer **8** as light, fluffy crystals; yield 1.97 g (49%); mp 138–139°C, $[\alpha]_D^{21}$ −17.3° (*c* 1); R_F 0.17 (ether); *m/e* (rel. intensity) 224 (12, $M^{+\cdot}$), 180/179 (9/36, M − $CH_3CHO\bullet$/$CH_3CH(OH)\bullet$; m* at 144.6/143.0, calcd. 144.65/143.04), 162 (0.9, 180 − H_2O/179 − •OH), 119 (1.5, M − PhCO•), 108 (18, $PhCH_2OH^{+\cdot}$; m* at 64.8, calcd. for 180 → 108: 64.80), 107 (100, $PhCHOH^+$; m* at 64.0, calcd. for 179 → 107; 63.96), 91 (14, $PhCH_2^+$; m* at 46.3, calcd. for 179 → 91: 46.26), 73 (9, $\overset{1}{CH_3}—\overset{2}{CH(OH)}—\overset{3}{CO^+}$), 45 (16), 44 (9), 43 (25); X-ray powder diffraction data: 10.77 w, 9.06 w, 6.73 s (2), 6.28 s (1), 5.43 m, 4.55 m, 4.21 s, 4.04 m, 3.78 s (3), 3.59 s, and 3.28 s. *Anal.* calcd. for $C_{12}H_{16}O_4$ (224.26): C 64.27, H 7.19; found: C 64.05, H 7.04.

Evaporation of the mother liquor after separation of **8** gave the D-*ribo* isomer **6** as an essentially pure syrup that solidified to an opaque glass after keeping for several days *in vacuo* over paraffin; yield 1.49 g (37%). For analytical purposes, a sample was further purified by column chromatography on silica gel with ether as eluant: $[\alpha]_D^{21}$ −28.6° (*c* 1.8); R_F 0.26 (ether); *m/e* (rel. intensity) 224 (20, $M^{+\cdot}$), 181/180/179 (4.6/10.5/3.7, M − Ac•/$CH_3CHO\bullet$/$CH_3CH(OH)\bullet$; m* at 146.2/144.7/143.0, calcd. 146.25/144.65/143.04), 162 (1, 180 − H_2O/179 − •OH), 119 (1.3, M − PhCO•; m* at 63.3, calcd. 63.22), 108 (12.2, $PhCH_2OH^{+\cdot}$; m* at 64.8, calcd. for 180 → 108: 64.80), 107 (100, $PhCHOH^+$; m* at 64.0, calcd. for 179 → 107: 63.96), 91 (7.8, $PhCH_2^+$; m* at 46.3, calcd. for 179 → 91: 46.26), 73 (5, $\overset{1}{CH_3}—\overset{2}{CH(OH)}—\overset{3}{CO^+}$), 45 (8), 43 (9). *Anal.* calcd. for $C_{12}H_{16}O_4$ (224.26): C 64.27, H 7.19; found: C 64.26, H 6.99.

*From **2** by Catalytic Hydrogenation*

The pentulose derivative **2** (2 g, 90 mmol) in methanol (40 ml) was hydrogenated under pressure (1 kg cm^{-2}) in the presence of 5% palladium-on-charcoal (200 mg). After 20 h, tlc (ether or 2:3 benzene–acetone) revealed that scarcely any debenzylidenation had occurred, but that the epimeric deoxypentitols **6** and **8** had been formed instead. The catalyst was filtered off and the filtrate evaporated. The resulting residue was dissolved in chloroform and the solution processed as described in the preceding section to afford a 1:5 mixture (as estimated from ^{1}Hmr data) of compounds **6** and **8**, identical with the products isolated by the first procedure; yield 1.52 g (75%).

*From **5** with Sodium Borohydride*

A cooled (−15°C) solution of sodium borohydride (2 g, 52.8 mmol) in 9:1 methanol–water (40 ml) was added to a cooled solution of the benzoate **5** (7.9 g, 24.5 mmol) in a mixture of methanol (150 ml) and ethyl acetate (50 ml). The solution was kept for 3 h at −15°C, water (100 ml) was then added, and the organic solvent was distilled off. To the remaining turbid, aqueous phase was added a 4 *M* solution of potassium hydroxide in 2:3 water–methanol (50 ml). After 4 h at ~20°C, water (100 ml) and acetic acid (10 ml) were added and the product was extracted with chloroform. Processing as described in the previous sections gave a 1:2 mixture (as judged from ^{1}Hmr data) of the epimers **6** and **8**, yield 5 g (91%). Fractional crystallization afforded the pure, crystalline *arabino* derivative **8** (3.17 g, 58%) and the syrupy *ribo* analog **6** (1.7 g, 31%); both products were indistinguishable from those prepared by the previous procedures.

*2,4-Di-O-acetyl-3,5-O-benzylidene-1-deoxy-*D*-ribitol (**7**)*

The benzylidene acetal **6** (400 mg, 1.78 mmol) was treated with 1:2 acetic anhydride – pyridine (9 ml) for 18 h at ~25°C. After conventional processing, the crystalline product (480 mg, 88%) was recrystallized from hexane: mp 62–63°C, $[\alpha]_D^{21}$ −72.7° (*c* 1.1); ν_{max}(KBr) 1725 (C═O), 745 and 695 cm^{-1} (aryl); *m/e* (rel. intensity) 308 (3.7, $M^{+\cdot}$), 265 (0.3, M − Ac•), 248 (1.2, M − HOAc), 231 (0.4, M − Ph•), 221 [4.5, M − •$CH(CH_3)$-OAc], 205 (0.3, M − HOAc − Ac•), 203 (0.25, M − PhCO•), 186 (1.9, M − $PhCO_2H$), 149 (6.7, h_2), 142 (10, M − PhCHO − HOAc), 115 (55, $OCH—\overset{+}{(CH_3)C}═OAc$), 43 (100, Ac^+); X-ray powder diffraction data: 9.30 s, 7.79 s, 6.30 s (3), 5.11 w, 4.94 m, 4.41 m, 4.29 vs (1), 4.17 w, 3.98 vs (2), 3.57 m, and 3.45 w. *Anal.* calcd. for $C_{16}H_{20}O_6$ (308.33): C 62.33, H 6.54; found: C 62.18, H 6.45.

*1-Deoxy-*D*-erythro-pentulose (**9**)*

A solution of the pentulose derivative **2** (4 g, 18 mmol) in acetic acid (30 ml) and water (70 ml) was heated for 1 h on a water bath whereupon tlc (2:3 benzene–acetone) indicated that deacetalation was complete. The solution was concentrated and small portions of toluene and then 2-propanol were repeatedly distilled from the residue. A solution of the remaining, yellow syrup in water (50 ml) was extracted with ether, and then lyophilized, to give **9** as a chromatographically homogeneous, colorless syrup; yield 1.76 g (73%), $[\alpha]_D^{21}$ −37° (equil., *c* 1.3, water); ν_{max}(film) 3500–3200 (OH), 1705 cm^{-1} (C═O); for ms data see Table 2; ^{1}Hmr (methyl sulfoxide-d_6; hydroxyl protons exchanged by deuterium) δ 4.60–3.70 (4 H, complex m, H-3,4,5,5′), 2.59, 2.57, 2.55 (total integrated peak area 3 h, 3 s, estimated ratio 1:1:2, H-1). *Anal.* calcd. for $C_5H_{10}O_4$ (134.13): C 44.77, H 7.51; found: C 44.64, H 7.19.

After being kept for several days, the product turned yellow, and fast-moving, uv light-absorbing compounds could be detected by tlc.

1-Deoxy-D-erythro-pentulose (2,4-Dinitrophenyl)hydrazone (10)

A mixture of the pentulose **9** (1.1 g, 8.2 mmol) and (2,4-dinitrophenyl)hydrazine (2 g, 10.1 mmol) in aqueous ethanol (95%, 50 ml) was heated for 6 h on a water bath. Thin layer chromatography (2:3 benzene–acetone) of the residue obtained after evaporation of the solvent revealed the presence of two products (R_F 0.30 and 0.36) as well as unchanged reagent that was present in excess. Column chromatography on silica gel, with 1:1 benzene–acetone as eluant, furnished the slower-moving, major product **10**; yield 1.47 g (57%). After recrystallization from ethyl acetate it had mp 116–118°C, $[\alpha]_D^{21}$ −53.7° (*c* 0.3, acetone); ν_{max}(KBr) 3500–3300 (OH, NH), 1615 (C=N), 1595 and 1500 (phenyl), 1515 and 1340 cm^{-1} (NO_2); for ms data, see Table 2; X-ray powder diffraction data: 11.94 vw, 10.39 w, 7.08 m, 5.88 m, 5.01 w, 4.56 m, 4.27 s (2), 3.95 m, and 3.63 s (1). *Anal.* calcd. for $C_{11}H_{14}N_4O_7$ (314.26): C 42.04, H 4.49, N 17.83; found: C 42.03, H 4.62, N 17.60.

3,5-O-Benzylidene-2,4-O-carbonyl-1-deoxy-D-ribitol (11)

To a cooled (0°C) solution of the pentitol derivative **6** (450 mg, 2 mmol) in pyridine (20 ml) was added a solution of phosgene in benzene (12.5%, w/v, 10 ml, 12.6 mmol). After 1 h at ~25°C the excess of phosgene was decomposed by adding a saturated solution of sodium hydrogen carbonate (100 ml), and the mixture was extracted with dichloromethane. Evaporation of the dried (magnesium sulfate) extract and removal of residual pyridine by evaporating a little toluene from the residue gave crystalline **11**; yield 490 mg (98%). After recrystallization from ethanol, it had mp 181–183°C, $[\alpha]_D^{21}$ +5.3° (*c* 0.8); ν_{max}(KBr) 1750 (C=O), 750 and 700 cm^{-1} (aryl); *m/e* (rel. intensity) 250 (63, M$^{+\cdot}$), 251/249 (6/16, *M* ± 1), 206 (3.3, *M* − CO_2; m* at 169.8, calcd. 169.74), 191 (1.1, 206 − Me•), 173 (1.2, *M* − Ph•), 163 (1.4, 206 − Ac•), 149 (1.6, h_2), 145 (3.8, *M* − PhCO•), 144 (15, *M* − PhCHO), 134 (1.5, *M* − CO_2 − Ac• − CHO•; m* at 71.8, calcd. 71.82), 115 (1, 145 − CH_2O) 105 (100, PhCO$^+$; m* at 44.1, calcd. for 250 → 105: 44.10), 71 (11.5, 115 − CO_2), 57 (57, $\overset{3}{O}CH—\overset{2}{C}H—\overset{1}{C}H_3]^+$), 43 (16, Ac$^+$); X-ray powder diffraction data: 7.13 m, 6.10 s (2), 5.08 s (3, 3), 4.64 s (3, 3), 3.81 w, 3.60 s (1), 3.22 w, and 3.07 w. *Anal.* calcd. for $C_{13}H_{14}O_5$ (250.23): C 62.39, H 5.64; found: C 62.28, H 5.58.

1-Deoxy-D-ribitol (5-Deoxy-L-ribitol, 12)

A solution of the benzylidene acetal **6** (1.7 g, 7.6 mmol) in acetic acid (15 ml) and water (35 ml) was heated for 90 min on a water bath. The solvent then was evaporated off and 1-propanol (three 10 ml portions) was added to and distilled from the residue to remove last traces of benzaldehyde. The resulting white solid was recrystallized from acetonitrile (15 ml) to afford **12**; yield 880 mg (85%), mp 69°C, $[\alpha]_D^{21}$ +15° (*c* 0.9, water) and +11.8° (*c* 1, methanol); R_F 0.35 (3.17 methanol–ether); for ms data, see Table 2; X-ray powder diffraction data: 10.39 vs (2, 2), 8.00 vs (2, 2), 6.73 vw, 6.19 vw, 5.12 w, 4.95 s, 4.61 w, 4.35 w, 4.12 m, 3.93 vs (1), and 3.78 m. *Anal.* calcd. for $C_5H_{12}O_4$ (136.15): C 44.11, H 8.88; found: C 44.10, H 8.69.

For this compound, Foster and co-workers (11) reported mp 74–75°C, $[\alpha]_D$ +9° in water; the enantiomorph of **12** has been reported (12) to have mp 77–80°C (for a product containing solvent of recrystallization) and 65–69°C (solvent-free), $[\alpha]_D$ −10.6° in water, and (13) mp 80–85°C, $[\alpha]_D$ −11.2° in methanol.

3,5-O-Benzylidene-2,4-O-carbonyl-1-deoxy-D-arabinitol (13)

Treatment of the benzylidene acetal **8** (500 mg, 2.2 mmol) in pyridine (20 ml) with phosgene (12.5% w/v solution in benzene, 12 ml, 15.2 mmol) afforded, after processing as described for **11**, crude, crystalline **13**; yield 540 mg (97%). After recrystallization from ethanol, it had mp 158–159°C, $[\alpha]_D^{21}$ +99.7° (*c* 0.7); ν_{max}(KBr) 1750 (C=O), 748 and 700 cm^{-1} (aryl); *m/e* (rel. intensity) 250 (39, M$^{+\cdot}$), 251/249 (55/15, *M* ± 1), 206 (5, *M* − CO_2), 191 (1.4, 206 − Me•), 173 (1.1, *M* − Ph•), 163 (1, 206 − Ac•), 149 (2, h_2), 145 (5.7, *M* − PhCO•; m* at 84.1, calcd. 84.10), 144 (18, *M* − PhCHO), 134 (6, *M* − CO_2 − Ac• − CHO•; m* at 71.9, calcd. 71.82), 115 (2.7, 145 − CH_2O), 71 (7, 115 − CO_2) 57 (12, $\overset{3}{O}CH—\overset{2}{C}H—\overset{1}{C}H_3]^+$), 43 (20, Ac$^+$); X-ray powder diffraction data: 7.19 m, 6.10 m, 5.15 s (3), 4.68 s (2), 3.82 vw, 3.70 s (1), and 3.16 m. *Anal.* calcd. for $C_{13}H_{14}O_5$ (250.25): C 62.39, H 5.64; found: C 62.11, H 5.44.

1-Deoxy-D-arabinitol (5-Deoxy-D-lyxitol, 14)

The benzylidene acetal **8** (2.8 g, 12.5 mmol) was hydrolyzed in the way already described for the *ribo* analog **6**. Recrystallization from ethanol gave **14** as white crystals; yield 1.48 g (87%), mp 130°C, $[\alpha]_D^{21}$ +1.4° (*c* 1.2, water) and −0.6° (*c* 2.3, methanol); R_F 0.25 (3.17 methanol–ether); for ms data, see Table 2; X-ray powder diffraction data: 7.16 vs (1), 6.58 vw, 4.82 vs (2), 4.63 vs (3), 4.15 vw, 3.86 m, 3.55 m, 3.33 vw, 3.27 vw. 3.10 vw, 2.92 m, 2.74 m, and 2.49 m. *Anal.* calcd. for $C_5H_{12}O_4$ (136.15): C 44.11, H 8.88; found: C 44.41, H 8.71.

For this compound, Bollenback and Underkofler (14) found 131–132°C, $[\alpha]_D$ +2.46° in water, and, for the enantiomorph, mp 129–131°C, $[\alpha]_D$ −1.46° in water; for the latter the mp 131–133°C has also been reported (15).

3,4,5-Tri-O-acetyl-1-deoxy-keto-D-erythro-pentulose (15)

A mixture of the pentulose **9** (2.1 g, 15.7 mmol) and powdered, anhydrous zinc chloride (500 mg) in acetic anhydride (50 ml) was kept for 18 h at 0°C. After a further 15 h at ~20°C, the mixture was poured into ice-water (250 ml) saturated with sodium hydrogencarbonate. The product was extracted with dichloromethane (three 50 ml portions), the extract washed with aqueous sodium hydrogencarbonate, dried (magnesium sulfate), and evaporated. Pyridine and toluene (two 10 ml portions each) were successively added to and evaporated from the residue to give crude **15** as a pale yellow syrup; yield 3 g (74%). To secure an analytical sample, a portion was distilled under diminished pressure (0.05 Torr, bath temperature ~120°C); $[\alpha]_D^{21}$ −8° (*c* 2.3); ν_{max}(film) 1740 cm^{-1} (C=O); for ms data, see Table 2. *Anal.* calcd. for $C_{11}H_{16}O_7$ (260.25): C 50.77, H 6.20; found: C 51.09, H 6.15.

Treatment of Methyl 4,6-O-Benzylidene-2-deoxy-α-D-erythro-hexopyranosid-3-ulose (1) with Base under Anhydrous Conditions

To the glycoside **1** (400 mg, 1.5 mmol), dissolved in absolute tetrahydrofuran (10 ml), was added 30 m*M* sodium methoxide (5 ml) and the solution was kept at ~25°C for 24 h, whereupon tlc (4:1 ether – petroleum ether) revealed the presence of another product (R_F 0.38) accompanying **1** (R_F 0.27) in the mixture. The solution was poured with vigorous mechanical stirring into ice–water (100 ml) containing ammonium chloride (5 g). Extraction with dichloromethane (two 40 ml portions) and evaporation of the dried (magnesium sulfate) extract furnished a crystalline residue (340 mg, 85%) that was shown by ^{1}Hmr to be a 1:1 mixture of the anomeric methyl hexulosides **1** and **22**. Separation was effected by column chromatography on silica gel using the tlc solvent as eluant. The component having R_F 0.38 crystallized upon evaporation of the solvent and was recrystallized from ethanol to give pure *methyl 4,6-O-benzylidene-2-deoxy-β-D-erythro-hexopyranosid-3-ulose* (**22**); mp 194–195°C, $[\alpha]_D^{21}$ −51.3° (*c* 0.8); ν_{max}(KBr) 1725 (C=O), 750 and 690 cm^{-1} (aryl); *m/e* (rel. intensity) 264 (3, M$^+$), 233/232 (1.2/2.2, *M* − MeO•/MeOH), 204 (2, *M* − HCO_2Me), 190 (4.5, 232 − ketene; m* at 155.6, calcd. 155.60), 177 (19, *M* − OCH—CH_2—HC—OMe; m* at 118.7, calcd. 118.67), 161 (3, 204 − Ac•), 149 (100, h_2; m* at 84.1, calcd. 84.09), 145 (12), 129 (18, *M* − PhCO• − CH_2O), 115 (18, h_1), 97 (11), 87 (76, h_1 − CO), 59 (43, 87 − CO; m* at 40.0, calcd. 40.01), 58 (82), 43 (21, Ac$^+$); ^{1}Hmr (chloroform-*d*) δ 7.64–7.28 m (5 H; m, aryl), 5.56 (1 H, s, PhC*H*), 4.75 (1 H, dd, $J_{1,2a}$ 7.6 Hz, H-1), 4.45 (1 H, dd, $J_{5,6}$ 4.3 Hz, H-6), 4.32 (1 H, d, $J_{4,5}$ 9.4 Hz, H-4), 3.89 (1 H, t, $J_{6,6'}$ 10 Hz, H-6′), 3.68 (1 H, dt, $J_{5,6'}$ 10 Hz, H-5), 3.51 (3 H, s, OMe), 2.84 (1 H, dd, $J_{1,2e}$ 3.7 Hz, H-2e), 2.64 (1 H, dd, $J_{2e,2a}$ 15 Hz, H-2a); X-ray powder diffraction data: 11.86 w, 10.52 m, 8.54 s (3), 7.79 w, 6.13 s (2), 4.82 w, 4.38 m, 4.18 m, 3.97 s (1), 3.89 m, 3.73 m, 3.59 m, 3.25 m, and 3.07 w. *Anal.* calcd. for $C_{14}H_{16}O_5$ (264.28): C 63.63, H 6.10; found: C 63.56, H 6.06.

The second fraction (R_F 0.27) was indistinguishable (by mixture mp and spectroscopic data) from the starting material **1**.

1,5-Anhydro-4,6-O-benzylidene-2-deoxy-D-erythro-hex-1-eno-3-ulose (17)

1,5-Anhydro-4,6-*O*-benzylidene-2-deoxy-D-*ribo*-hex-1-enitol (4,6-*O*-benzylidene-D-allal, 780 mg, 3.3 mmol) (21) was oxidized with the chromium trioxide – dipyridine complex as described by Collins (17) to afford the title compound **17**; yield 520 mg (67%). After recrystallization from 2-propanol, **17** was obtained as white, cottonlike crystals: mp 128–129°C, $[\alpha]_D^{21}$ +170° (*c* 0.8) (lit. (17) mp 128–129°C, $[\alpha]_D$ +189° in chloroform); ν_{max}(KBr) 1685 and 1590 (C=C—C=O), 750 and 695 cm^{-1} (aryl); *m/e* (rel. intensity) 232 (5, M$^+$), 204 (4.5, *M* − CO), 190 (3.3, *M* − ketene), 162 (3.6, *M* − CO − ketene), 160 (1, 204 − CH_3CHO; m* at 125.5, calcd. 125.49), 145 (15, 162 − •OH; m* at 110.7, calcd. for 190 → 145: 110.66), 105 (100, PhCO$^+$; m* at 68.1, calcd. for 162 → 105: 68.06), 97 (20, O(CH=CH)$_2$C=OH$^+$), 71 (23, OCH—CH_2—CO$^+$); ^{1}Hmr (chloroform-*d*) δ 7.60–7.25 (5 H, m, aryl), 7.19 (1 H, d, $J_{1,2}$ 5.9 Hz, H-1), 5.52 (1 H, s, PhC*H*), 5.37 (1 H, d, H-2), 4.50–3.80 (4 H, m, H-4,5,-6,6′); X-ray powder diffraction data: 10.27 s, 5.82 s, 5.57 s, 5.14 m, 4.95 w, 4.68 w, 4.50 s, 4.20 vs (1), 2.83 s, 3.60 s (3), and 3.48 vs (2). *Anal.* calcd. for $C_{13}H_{12}O_4$ (232.24): C 67.23, H 5.21; found: C 67.18, H 5.42.

When the glycenulose **17** was treated with catalytic amounts of sodium methoxide in absolute methanol – tetrahydrofuran, approximately equal amounts of the anomers **1** and **22** were formed (detected by tlc).

For the attempted conversion into **2**, a mixture of the enulose **17** (200 mg, 0.86 mmol), dissolved in ether (20 ml), was shaken with 100 m*M* aqueous solution of lithium hydroxide (10 ml) for 48 h at ~20°C. Thin layer chromatography (4:1 ether – petroleum ether) of the ethereal phase then revealed that unchanged **17** (R_F 0.29) was mostly still present, together with small amounts of the pentulose derivative **2** (R_F 0.36; estimated yield 10%) and minor, unidentified side-products

Acknowledgment

This work was supported, in part, by Grant No. GM-11976 (The Ohio State University Research Foundation Project 1820) from the National Institute of General Medical Services, National Institutes of Health, U.S. Public Health Service, Bethesda, MD 20014, U.S.A.

1. D. Horton and W. Weckerle. Carbohydr. Res. **44**, 227 (1975).
2. D. Horton, T.-M. Cheung, and W. Weckerle. Carbohydr. Res. **58**, 139 (1977); D. M. Clode, D. Horton, and W. Weckerle. Carbohydr. Res. **49**, 305 (1976), and earlier papers in this series, cited therein.
3. P. M. Collins, D. Gardiner, and W. G. Overend. Carbohydr. Res. **32**, 203 (1974).
4. J. C. Sowden and D. R. Strobach. J. Am. Chem. Soc. **82**, 3707 (1960).
5. R. B. Bennett. Ph.D. Thesis, The Ohio State University. 1958; cf. Chem. Abstr. **63**, 8467d (1965).
6. J.-C. Fischer and D. Horton. Abstracts of Papers Am. Chem. Soc. Meet. **171**, CARB-29 (1976).
7. T. D. Inch. Adv. Carbohydr. Chem. Biochem. **27**, 191 (1972).
8. A. Klemer and G. Rodemeyer. Chem. Ber. **107**, 2612 (1974).
9. (*a*) F. A. Bovey. Nuclear magnetic resonance spectroscopy. Academic Press, New York. 1969. p. 132 and p. 355; (*b*) P. L. Durette and D. Horton. Org. Magn. Reson. **3**, 417 (1971) and references cited therein.
10. J. F. Stoddart. Stereochemistry of carbohydrates. Wiley-Interscience, New York. 1971. Chapter 5.5; E. L. Eliel and Sr. M. C. Knoeber. J. Am. Chem. Soc. **90**, 3444 (1968).
11. K. W. Buck, A. B. Foster, B. H. Rees, J. M. Webber, and F. E. Hardy. Carbohydr. Res. **2**, 115 (1966).
12. L. Hough, J. K. N. Jones, and D. L. Mitchell. Can. J. Chem. **36**, 1720 (1958).
13. A.-M. Sepulchre, A. Gateau, and S. D. Gero. Carbohydr. Res. **24**, 311 (1972).
14. G. M. Bollenback and L. A. Underkofler. J. Am. Chem. Soc. **72**, 741 (1950).

15. A. N. DE BELDER and H. WEIGEL. Chem. Ind. London, 1689 (1964).
16. D. HORTON and J. D. WANDER. Adv. Carbohydr. Chem. Biochem. **32**, 16 (1976); D. HORTON. Pure Appl. Chem. **42**, 301 (1975); D. HORTON, P. L. DURETTE, and J. D. WANDER. Ann. N.Y. Acad. Sci. **222**, 884 (1973); P. L. DURETTE, D. HORTON, and J. D. WANDER. Adv. Chem. Ser. **117**, 147 (1973).
17. P. M. COLLINS. Carbohydr. Res. **11**, 125 (1969); compare R. E. ARRICK, D. C. BAKER, and D. HORTON. Carbohydr. Res. **26**, 441 (1973).
18. P. J. GAREGG and T. NORBERG. Acta Chem. Scand. Ser. B, **29**, 507 (1975).
19. N. K. KOCHETKOV and O. S. CHIZHOV. Adv. Carbohydr. Chem. **21**, 39 (1966).
20. O. S. CHIZHOV, L. S. GOLOVKINA, and N. S. WULFSON. Carbohydr. Res. **6**, 138 (1968).
21. A. A. J. FEAST, W. G. OVEREND, and N. R. WILLIAMS. J. Chem. Soc. 7378 (1965); M. SHARMA and R. K. BROWN. Can. J. Chem. **44**, 2825 (1966); R. U. LEMIEUX, E. FRAGA, and K. A. WATANABE. Can. J. Chem. **46**, 61 (1968).

The yellow pigments of *Beauveria* species. Structures of tenellin and bassianin[1]

CHI-KIT WAT,[2] A. GAVIN MCINNES, AND DONALD G. SMITH

Atlantic Regional Laboratory, National Research Council of Canada, Halifax, N.S., Canada B3H 3Z1

AND

JEFFREY L. C. WRIGHT AND LEO C. VINING

Biology Department, Dalhousie University, Halifax, N.S., Canada B3H 4J1

Received May 19, 1977

CHI-KIT WAT, A. GAVIN MCINNES, DONALD G. SMITH, JEFFREY L. C. WRIGHT, and LEO C. VINING. Can. J. Chem. **55**, 4090 (1977).

Tenellin and bassianin are deduced from chemical and spectroscopic evidence to be the 3-[(*E*,*E*)-4,6-dimethylocta-2,4-dienoyl] and 3-[(*E*,*E*,*E*)-6,8-dimethyldeca-2,4,6-trienoyl] derivatives of 1,4-dihydroxy-5-(*p*-hydroxyphenyl)-2(1*H*)-pyridone. Spin–spin coupling information in the ^{1}H and ^{13}C nuclear magnetic resonance spectra after biosynthetic enrichment of tenellin with ^{13}C and ^{15}N isotopes was a valuable aid in elucidating the structure.

CHI-KIT WAT, A. GAVIN MCINNES, DONALD G. SMITH, JEFFREY L. C. WRIGHT et LEO C. VINING. Can. J. Chem. **55**, 4090 (1977).

A partir des indications chimiques et spectroscopiques, il apparait que la ténelline et la bassianine sont les dérivés [(*E*,*E*) diméthyl-4,6 octadiène-2,4 oyl]-3 et [(*E*,*E*,*E*) diméthyl-6,8 décatriène-2,4,6 oyl]-3 de la dihydroxy-1,4 (*p*-hydroxyphényl)-5 (1*H*)-pyridone-2. L'information sur le couplage spin–spin tirée des spectres de résonance magnétique nucléaire du ^{1}H et ^{13}C de la ténelline par un enrichissement biosynthétique préalable en isotopes ^{13}C et ^{15}N est d'un grand intérêt dans l'élucidation de la structure.

[Traduit par le journal]

Introduction

Cultures of the insect pathogenic fungi *Beauveria bassiana* (Bals.) Vuill. and *B. tenella* (Delacroix) Siem. often develop a yellow color which is due to the formation of a mixture of related pigments (1, 2). Two of these substances, tenellin (**1**) and bassianin (**8**), have been isolated; their structures were reported in a preliminary communication (3) and we present here the evidence that establishes them as members of a new group of fungal biochromes. A related compound, ilicicolin H, has recently been isolated as an antifungal antibiotic from the imperfect fungus *Cylindrocladium ilicicola* (4).

Results and Discussion

Molecular formulae for tenellin, $C_{21}H_{23}NO_5$, and bassianin, $C_{23}H_{25}NO_5$, were determined by elemental analyses and high resolution mass spectroscopy. A terminal *sec*-butyl substituent in **1** was indicated by characteristic signals in the ^{1}Hmr spectrum (Table 1), and confirmed by double resonance experiments (vicinal coupling of H-13 to H-12 and H-14, and of H-12 to H-15). The chemical shift of the methine hydrogen H-12, and its vicinal coupling to an olefinic hydrogen H-11, required the *sec*-butyl group to be attached to a double bond. Double resonance studies also showed H-11 to be long-range coupled to the hydrogens (H-16) of a vinylic methyl group, and to one (H-9) of a pair of vinylic protons (H-8, H-9) which were *trans* vicinally coupled, and gave an AB sub-spectrum. Thus tenellin possesses an (*E*,?)-3,5-dimethyl-1,3-heptadienyl residue.

Since the ^{1}H and ^{13}C nmr spectra of **1** and its methylated derivative **2** were essentially indistinguishable, except for differences associated with replacement of a hydroxyl by a methoxyl substituent (Tables 1 and 2), the structural, stereochemical, and conformational features of **1** must be retained in **2**. Consequently a complete description of the stereochemistry of double bonds in the alkenyl substituent obtained by a nuclear Overhauser enhancement (nOe) study on **2** applies equally to **1**. The nOe measurements for **2** (irradiated proton(s) in parentheses) gave H-9 (H-11) 22%, H-8 (H-16) 20%, H-8 (H-11)

[1]NRCC No. 16189

[2]National Research Council of Canada Postdoctorate Fellow, 1969–1971. Present address: Botany Department, University of British Columbia, Vancouver, B.C.

TABLE 1. Proton magnetic resonance data (100 MHz) for tenellin (**1**), some derivatives (**2–7**), and bassianin (**8**)*

Compound	R_1	R_2	R_3	H-2′,H-6′, H-3′,H-5′†	H-6	H-8, H-9	H-11	H-12	H-13	H-14	H-15	H-16
1	11.67(bs)	9.48(s)	16.98(s)	7.07 (AA′BB′) $\Delta\nu_{AB}$ 49.6, N 8.6	8.10(s)	7.78 (AB) $\Delta\nu_{AB}$ 50.4, J_{AB} 15.3	5.92(bd) $J_{11,12}$ 9.6	2.40(m)	1.38(m)	0.85(t)	1.01(d) $J_{12,15}$ 6.3	1.88(bs)
2	3.98(s)	9.51(s)	17.40(s)	7.06 (AA′BB′) $\Delta\nu_{AB}$ 52.1, N 8.6	8.26(s)	7.74(AB) $\Delta\nu$ 40.3, J_{AB} 15.3	5.96(bd) $J_{11,12}$ 9.6	2.50(m)	1.36(m)	0.83(t)	0.99(d) $J_{12,15}$ 6.3	1.86(bs)
3	4.02(s)	3.79(s)	17.48(s)	7.24 (AA′BB′) $\Delta\nu_{AB}$ 47.7, N 8.6	8.34(s)	7.67 (AB) $\Delta\nu_{AB}$ 41.0, J_{AB} 15.4	5.98(bd) $J_{11,12}$ 9.4	2.52(m)	1.34(m)	0.84(t)	0.99(d) $J_{12,15}$ 6.4	1.86(bs)
4	3.98(s)	3.77(s)	3.41(s)	7.18 (AA′BB′) $\Delta\nu_{AB}$ 39.8, N 8.8	8.07(s)	6.76 (AB) $\Delta\nu_{AB}$ 81.1, J_{AB} 15.9	5.88(bd) $J_{11,12}$ 9.5	2.44(m)	1.30(m)	0.81(t)	0.96(d) $J_{12,15}$ 6.3	1.86(bs)
5‡	2.22(s)		17.1(s)	7.33 (AA′BB′) $\Delta\nu_{AB}$ 41.2, N 8.7	8.13(s)	7.88 (AB) $\Delta\nu_{AB}$ 50.8, J_{AB} 15.0	5.90(bd) $J_{11,12}$ 9.5	2.55(m)	1.40(m)	0.88(t)	1.02(d) $J_{12,15}$ 6.3	1.92(d) $J_{11,16}$ 0.1
6‡			16.0(s)	7.02 (AA′BB′) $\Delta\nu_{AB}$ 52.5, N 8.6	8.00(s)	3.23(t)	H-9 through H-16 in envelope, 0.8 → 2.0					
7	10.7(bs)	8.4(bs)	15.9(s)	7.02 (AA′BB′) $\Delta\nu_{AB}$ 52.8, N 8.6	8.00(s)		$\frac{CH_3CO}{2.70(s)}$					
8	10.8(bs)	8.5(bs)	17.08(s)	7.03 (AA′BB′) $\Delta\nu_{AB}$ 53.7, N 8.6	7.96(s)	7.88 (AB) $\Delta\nu_{AB}$ 48.2, J_{AB} 15.0						

	H-10, H-11	H-13	H-14	H-15	H-16	H-17	H-18
	6.60 (AB) $\Delta\nu_{AB}$ 26.2, J_{AB} 15.0, $J_{9,10}$ 10.2	5.58(bd) $J_{13,14}$ 9.6	2.49(m)	1.34(m)	0.85(t)	0.98(d) $J_{14,17}$ 6.6	1.84(d) $J_{13,18}$ 1.1

*Chemical shifts are given in ppm relative to tetramethylsilane (average value for complex multiplets). Coupling constants (J) and shift differences ($\Delta\nu_{AB}$) are given in Hz. Multiplicities are denoted by b = broad, d = doublet, m = multiplet, s = singlet, t = triplet. Spectra for compounds **1–4** were recorded in dimethylsulfoxide-d_6, and for **5–8** in tetrahydrofuran-d_8.

†These four protons formed an AA′BB′ system typical of a *para*-disubstituted benzene ring. $N = J_{AB} + J_{AB'}$, with $J_{AB'}$ probably < 0.5 Hz (5).

‡The hydroxy proton signals (R_2 in **5**, and R_1, R_2 in **6**) were too broad to detect.

TABLE 2. ^{13}C chemical shifts (δ_c TMS) and ^{13}C—^{1}H coupling constants (^nJ Hz) for tennelin (**1**), its mono-, di-, and trimethyl ethers (**2**, **3**, **4**), and bassianin (**8**)†

Carbon	1	2	3	4	Carbon	8
2	157.5(d) (^3J 5.5)	156.8(d) ($^3J\sim$5.5)	156.8(d) (^3J 4.6)	155.9(d) (^3J 5.1)	2	157.5(d) (^3J 5.0)
3	105.9(d) (^3J 5.5)	106.5(d) ($^3J\sim$4.5)	106.5(d) (^3J 6.1)	115.6(bd)	3	105.9(d) (^3J 5.1)
4	173.0(dd) (^3J 8.9 ^4J 3.8)	175.1(dd) (^3J 8.5 $^4J\sim$3)	175.1(dd) (^3J 9.0 ^4J 4.0)	162.6(m)	4	173.3(dd) (^3J 10.1 ^4J 2.5)
5	110.9(bs)	112.2(bs)	111.8(bs)	119.7(bs)	5	110.9(bs)
6	140.0(d) (^1J 183.6)	140.9(d) (^1J 184.4)	141.1(d) (^1J 184.5)	135.8 (^1J 185.8)	6	140.3(d) (^1J 183.5)
7	193.8(t) (^2J 5.0 ^3J 5.0)	193.7(t) ($^2J\sim{}^3J\sim$5)	193.7(t) (^2J 5.3 ^3J 5.3)	192.2(t) ($^2J\sim{}^3J\sim$5)	7	193.2(t) (^2J 5.2 ^3J 5.2)
8	123.1(dd) (^1J 167.5 ^2J 4.6)	122.8(dd) (^1J 167.6 ^2J 5.0)	122.8(dm) (^1J 166.4)	126.0(dd) (^1J 152.9 ^2J 5.5)	8	127.0(dm) (^1J 167.5)
9	149.7(dm) (^1J 159.1)	150.2(dm) ($^1J\sim$158)	150.2(dm) ($^1J\sim$158)	149.8(dm)*	9	145.8(dm) ($^1J\sim$157)
					10	125.3(dm) ($^1J\sim$155)
					11	146.1(dm) ($^1J\sim$158)
10	132.6(m)	132.6(m)	132.7(m)	131.9(m)	12	133.0(m)
11	150.8(dm) (^1J 154.8)	151.2(dm) ($^1J\sim$152)	151.2(dm) ($^1J\sim$154)	150.1(dm)*	13	148.6(dm) ($^1J\sim$155)
12	34.6(dm) (^1J 125.4)	34.6(dm)	34.6(dm)	34.4(dm)	14	34.2(dm)
13	29.4(tm) (^1J 126.0)	29.3(tm)	29.4(tm)	29.3(tm)	15	29.6(tm)
14	11.7(qm) (^1J 125.2)	11.7(qm)	11.7(qm)	11.7(qm)	16	11.7(qm)
15	19.8(qm) (^1J 125.8)	19.8(qm)	19.8(qm)	19.8(qm)	17	20.1(qm)
16	12.3(qm) (^1J 126.2)	12.3(qm)	12.3(qm)	12.2(qm)	18	12.3(qm)
1′	122.8(dt) (^3J 7.4, 3.5)	122.5(dt) (^3J 7.6, 4.0)	124.2(dt) (^3J 7.4, 3.2)	125.3(dt)	1′	122.8(dt) (^3J 8.1, 3.5)
2′,6′	130.2(dd) (^1J 160.0 ^3J 7.3)	130.3 (^1J 160.1 ^3J 7.2)	130.3(dd) (^1J 161.1 ^3J 7.2)	130.1(dd) (^1J 160.8 ^3J 7.2)	2′,6′	130.2(dd) (^1J 159.9 ^3J 7.4)
3′,5′	115.0(dd) (^1J 160.0 $^3J\sim$3)	115.0(dd) (^1J 159.4 $^3J\sim$4)	113.6(dd) (^1J 160.9 ^3J 4.5)	113.9(dd) (^1J 160.9 ^3J 4.4)	3′,5′	115.0(dd) (^1J 159.9 ^3J 3.2)
4′	156.9(t) (^3J 8.8)	157.0(t) ($^3J\sim$8.5)	158.8(m)	158.8(m)	4′	156.9(t) (^3J 9.1)
1-OCH_3		64.7(q) (^1J 146.7)	64.7(q) (^1J 146.8)	64.7(q) (^1J 146.8)		
4′-OCH_3			55.1(q) (^1J 144.2)	55.1(q) (^1J 144.2)		
4-OCH_3				60.5(q) (^1J 146.5)		

*Values may be interchanged. Multiplets were not resolved in the high resolution spectrum.

†Pulse Fourier transform spectra recorded at 30°C on 0.3–0.4 *M* solutions in dimethylsulfoxide-d_6 at 25.16 MHz, acquisition time 0.8 s, data accuracy ±0.6 Hz, spectra width 5120 Hz, flip angle 40°, internal ^2H pulse lock to solvent, proton noise decoupling $\gamma H_2/2\pi$, ca. 3800 Hz. Multiplicities (high resolution spectra) are denoted by b = broad, d = doublet, m = multiplet, q = quartet, s = singlet, t = triplet. Multiplet signals from carbons 12 through 16 in the high resolution spectra of **2**, **3**, **4**, and carbons 14 through 18 in **8** were not resolved sufficiently to estimate coupling constants to ±0.6 Hz. Separations were in the range of 126 ± 2 Hz. Values for carbons which are shown as approximations are probably within ±1 Hz. ^{13}C—H couplings in 2(1*H*)-pyridone involving H-6 were $^2J_{5,6}$ 3.3; $^3J_{2,6}$ 7.5; $^3J_{4,6}$ 8.6 Hz (11).

0%, and H-9 (H-16) 0%, establishing the presence of an (*E,E*)-3,5-dimethyl-1,3-heptadienyl unit.

Pulse Fourier transform ^{13}C nmr studies provided further structural information. The ^{13}C spectral data were obtained from proton noise decoupled (pnd) and high resolution (hr) spectra; assignment of resonances arising from carbons bonded to hydrogen were aided by off-resonance decoupling (ord) experiments which permitted the ^{1}H and ^{13}C spectra to be correlated (6). In some cases isotopic labelling with ^{13}C facilitated assignments. Thus splitting of resonances due to ^{13}C–^{13}C spin–spin coupling ($^{1}J_{CC}$) in the pnd ^{13}C spectrum of **1** enriched with [1,2-^{13}C]acetate (90% ^{13}C) showed that five pairs of carbons had been incorporated as intact two carbon units. Four of these pairs were C-7,C-8 ($^{1}J_{CC}$ 55.9 Hz); C-9,C-10 ($^{1}J_{CC}$ 53.6 Hz); C-11,C-12 ($^{1}J_{CC}$ 43.2 Hz); and C-13,C-14 ($^{1}J_{CC}$ 34.4 Hz). As resonances for the carbons bonded to hydrogen (C-8 and C-9, and C-11 through C-16) were readily assigned the results of the [1,2-^{13}C]acetate experiment enabled C-7 (δ_c 193.8) to be identified as a ketone carbonyl carbon, permitted the resonance for the quaternary olefinic carbon C-10 (δ_c 132.6) bonded to the vinylic methyl (C-16) group to be assigned, and, together with the ^{1}Hmr data, proved the carbon skeleton of the fragment C-7 through C-14 in structure **1**. The combined evidence establishes the presence of an *E,E*-4,6-dimethyl-octa-2,4-dienoyl unit in tenellin.

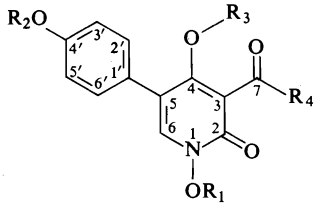

1 $R_1 = R_2 = R_3 = H$; R_4 = 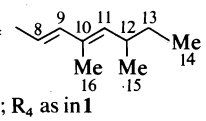

2 $R_1 = CH_3$; $R_2 = R_3 = H$; R_4 as in **1**

3 $R_1 = R_2 = CH_3$; $R_3 = H$; R_4 as in **1**

4 $R_1 = R_2 = R_3 = CH_3$; R_4 as in **1**

5 $R_1 = COCH_3$; $R_2 = R_3 = H$; R_4 as in **1**

6 $R_1 = R_2 = R_3 = H$; R_4 = 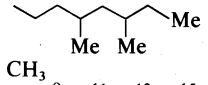

7 $R_1 = R_2 = R_3 = H$; $R_4 = CH_3$

8 $R_1 = R_2 = R_3 = H$; R_4 = 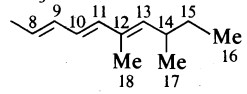

Chemical evidence also supported the above conclusion. Treatment of **1** under retro-aldol conditions gave a mixture of volatile aldehydes which were characterized as ethanal, propanal, 2-methylbutanal, and 2,4-dimethylhex-2-enal. The other fragment was isolated as the non-volatile crystalline compound **7**, which had a molecular formula $C_{13}H_{11}NO_5$, and gave a ^{1}Hmr spectrum which closely resembled that of **1** with signals for H-8 through H-16 replaced by an acetyl methyl (δ 2.70) resonance. Proton magnetic resonance evidence (Table 1) also showed that the double bonds of the acyl group in **1** could be selectively reduced by catalytic hydrogenation to give a tetrahydro derivative **6**, which lacked the strong ultraviolet absorption maximum exhibited by tenellin at 340 nm (2).

Apart from replacement of the A(H-8)B(H-9) system of **1** by an A(H-8)B(H-9)M(H-10)N(H-11) sub-spectrum, the ^{1}Hmr spectrum of bassianin (**8**) matched that of tenellin very closely (Table 1). The magnitudes of the three vicinal coupling constants, obtained by analysis of the ABMN system, indicated that adjacent olefinic hydrogens in **8** were *trans*-oriented (7). The ^{13}C nmr spectrum of **8** differed from that for **1** only by the presence of two additional resonances arising from the vinylic methine carbons C-10 and C-11 (Table 2). Consequently, related acyl groups must account for the structural difference between the metabolites, and by analogy bassianin must contain an (*E,E,E*)-6,8-dimethyl-deca-2,4,6-trienoyl unit. This is consistent with the bathochromic shift of maxima seen when the ultraviolet and visible absorption spectra of bassianin are compared with those of tenellin (2).

Another structural fragment was identified when oxidation of tenellin with alkaline hydrogen peroxide gave *p*-hydroxybenzoic acid. Three other more volatile acidic reaction products which gave molecular ions of *m/e* 168, 156, or 142 on mass spectral analysis were identified as C_{10}, C_9, and C_8 acids derived by cleavage of the acyl substituent. The *p*-hydroxyphenyl group accounted for the typical A(H-2′)A′(H-6′)B(H-3′)B′(H-5′) multiplets in the ^{1}Hmr spectra of **1** and **8**, and for four distinctive resonances in their corresponding ^{13}C nmr spectra. Two of these ^{13}C signals arose from the chemically equivalent pairs of carbons C-2′,C-6′ and C-3′,C-5′, which were characteristically one- and three-bond ^{13}C—H coupled and gave the

most intense ^{13}C signals. The signals for the hydrogens and carbons at the 3′- and 5′-positions occurred at higher field because they were shielded by the neighbouring phenolic hydroxy group. Typical deshielding by this group combined with three-bond ^{13}C—H coupling (**1**, $^3J_{CH}$ 8.8 Hz; **8**, $^3J_{CH}$ 9.1 Hz) to a pair of chemically equivalent aromatic hydrogens (H-2′, H-6′) permitted the triplet resonance occurring at δ_c 156.9 for both metabolites to be assigned to C-4′. Consistent with this assignment, the resonance at δ_c 158.8 for the corresponding carbon in derivative **3** (see below) was a multiplet (triplet of quartets) due to additional coupling with the hydrogens of the methoxyl substituent which had replaced the phenolic hydroxy group of **1**. Distinctive three-bond coupling (**1**, $^3J_{CH}$ 7.4 Hz; **8**, $^3J_{CH}$ 8.1 Hz) to another pair of chemically equivalent hydrogens (H-3′, H-5′) identified the resonance (δ_c 122.8) for C-1′ in both **1** and **8**, although the carbon was also coupled ($^3J_{CH}$ 3.5 Hz) to another hydrogen (H-6). Remaining unidentified resonances for quaternary carbons (C-2, C-3, C-4, and C-5 in Table 2) could not be confused with those for C-1′ and C-4′ since they had different multiplicities.

Three hydroxyl groups in **1** gave rise to resonances in the ^{1}Hmr spectrum (δ 9.48, δ 11.67, and δ 16.98) which had clear counterparts (δ 8.50, δ 10.80, and δ 17.08) in the corresponding spectrum of **8** (chemical shifts were temperature dependent, and signals disappeared when hydrogens exchanged with the deuterium of D_2O). The groups were progressively methylated with methyl iodide and silver oxide to yield derivatives with one (**2**), two (**3**) or three (**4**) methoxyl groups (Tables 1 and 2). Differences observed in the chemical shifts of corresponding hydroxyl groups in the two metabolites were largely due to the use of different solvents (**1**, DMSO-d_6; **8**, THF-d_6). The *p*-hydroxyphenyl hydroxyl group in **1** (δ 9.48), and **2** (δ 9.51), was easily identified because its replacement by a methoxyl substituent in **3** (δ 3.79, δ_c 55.1) was accompanied by the extra three-bond ^{13}C—H coupling to C-4′ referred to above.

The remaining structural fragment of tenellin and bassianin, accommodated by the partial formula $C_5H_3NO_3$, contained the unassigned sp^2 carbons C-2 through C-6 and the two unidentified hydroxyl groups (**1**, δ 11.67, δ 16.98; **8**, δ 10.8, δ 17.08). High resolution mass spectral studies together with precursor ion experiments showed that a major fragmentation pathway for both metabolites involved initial loss of an oxygen atom; in contrast the methyl ether derivatives **2**, **3**, and **4** lost CH_2O. These uncommon reactions suggested that the metabolites possessed a cyclic hydroxamic acid unit (8), and the combination of mass spectral and nmr results established that the hydroxamate hydroxyl group (δ 11.67) of **1** was methylated preferentially. Similarly, the monoacetate derivative (acetyl methyl δ 2.22, Table 1) was assigned structure **5** because the acetoxyl substituent was clearly not on C-4 (OH, δ 17.1), and a hydroxamic acid hydroxyl group, like those of the aspergillic acids (9), should be preferentially acetylated because of its acidic properties.

Carbons in and adjoining the hydroxamic acid group were identified with the aid of ^{15}N-labelling. Tenellin was 95% enriched with ^{15}N by supplying potassium nitrate-^{15}N as the sole nitrogen source for cultures of *B. bassiana*. Intense satellite resonances arising from ^{15}N—H($^nJ_{NH}$) and ^{15}N—^{13}C($^nJ_{NC}$) spin–spin coupling (10) in the ^{1}Hmr and pnd ^{13}C spectra of the labelled metabolite revealed that the nitrogen atom was directly bonded to C-6 (δ_c 140.0; $^1J_{NC}$ 15.0 Hz) and C-2 (δ_c 157.5; $^1J_{NC}$ 11.0 Hz), and geminal to C-3 (δ_c 105.9; $^2J_{NC}$ 9.2 Hz) and the only coupled hydrogen H-6 (δ 8.10; $^2J_{NH}$ 1.0 Hz). For all compounds in Table 2 spin–spin coupling between C-6 and H-6 ($^1J_{CH}$ 183–186 Hz) was similar to that in 2-pyridone ($^1J_{CH}$ 179.7 Hz).[3] Also C-2 and C-3 were identified as the fifth pair introduced as an intact unit ($^1J_{CC}$ 75.3 Hz) in the study with doubly labelled acetate (12) mentioned above. The high $^1J_{CC}$ value suggested that one of these carbons belonged to a carbonyl group (13). High ^{13}C-enrichments permitted coupling to be observed between adjacent ^{13}C—^{13}C units (C-3,C-7, $^1J_{CC}$ 65 ± 2; C-8,C-9, $^1J_{CC}$ 70 ± 2; C-10,C-11, $^1J_{CC}$ 70 ± 2; C-12,C-13, $^1J_{CC}$ 37 ± 2 Hz) in the [1,2-^{13}C]acetate study, and between C-2 and C-7 ($^2J_{CC}$ 4.6 ± 0.3 Hz) and C-3 and C-8 ($^2J_{CC}$ 7.7 ± 0.3 Hz) when **1** was labelled with [1-^{13}C]- and [2-^{13}C]acetates (12). Besides establishing the positions of C-2, C-3, and C-6 (hence H-6) relative to nitrogen, these results placed the acyl substituent on the shielded quaternary carbon C-3, and enabled the low-field C-2 resonance to be assigned to the hydroxamate carbonyl carbon.

[3]A. G. McInnes and J. A. Walter. Unpublished results.

Further nOe measurements on **2** showed that the *p*-hydroxyphenyl and methoxyl substituents were both in a vicinal relationship to H-6: H-6 (H-2′,-6′) 26%; H-2′,-6′ (H-6) 10%; H-3′,-5′ (H-6) 0%; H-6 (>$NOCH_3$) 8%. This implied that the carbon (C-5, δ_c 110.9) bearing the *p*-hydroxyphenyl substituent in **1** was shielded by a β-nitrogen, and that the remaining carbon (C-4, δ_c 173.0), which must carry the only unidentified hydroxyl group (δ 16.98), was attached to both C-3 and C-5. The conclusion, that tenellin possesses a 1-hydroxy-2(1*H*)-pyridone ring substituted as shown in structure **1**, was supported by the following observations.

Replacing the hydroxyl group common to **1** (δ 16.98), **2** (δ 17.40), and **3** (δ 17.48) with a methoxyl substituent (δ 3.41, δ_c 60.5) in **4** increased the multiplicity of the C-4 resonance due to additional ^{13}C—H coupling with the methoxyl hydrogens (Table 2), locating this hydroxyl group on C-4 of **1**. The deshielding of C-3 (≈9 ppm), and slight shielding of C-7 (≈1 ppm), accompanying this exchange of substituents was similar to the chemical shift trends exhibited by analogous carbons in juglone and its derivative (14). Moreover, a β-diketone system in enol form containing C-4, C-3, and C-7 in **1**, **2**, **3**, and **8** was consistent with the chemical shifts observed for these carbons, and the characteristic resonance for a strongly hydrogen-bonded hydroxyl group appearing at lowest field in the ^1Hmr spectrum. The chelate ring in structures **1**, **2**, **3**, and **8**, due to hydrogen bonding of the C-4 hydroxyl and C-7 carbonyl groups, restricts the conformational mobility of the acyl substituent and places H-8 in the deshielding region of the C-2 carbonyl group. This explains why H-8 (δ 8.03) was unexpectedly at lower field than H-9 (δ 7.54). The AB system for the corresponding hydrogens in **4**, on the other hand, was at appreciably higher field. Decoupling experiments indicated that H-11 in **4** was coupled to the hydrogen at H-9 (δ 7.17) giving rise to the low-field component of the AB system, as in the case of **1** ($J_{9,11} \leq 0.5$ Hz). In addition a 25% nOe of the high-field component (H-8; δ 6.36) was observed on irradiating the vinylic methyl hydrogens (H-16). The results indicated that methylation of the C-4 hydroxyl group caused a marked change in orientation of the acyl substituent, thereby removing H-8 from the deshielding effect of the C-2 carbonyl group. The chemical shifts of C-4 (δ_c 173–176) in **1**, **2**, and **3** were similar to those for the carbonyl carbons (≈δ_c 176) of 4-pyridones (15, 16), whereas the corresponding carbon in **4** (δ_c 162.6) and C-4 (δ_c 164.9) of 4-methoxypyridine (15) was considerably more shielded. This suggested considerable double bond character in the bond between C-4 and oxygen in **1**, **2**, and **3**, but not **4**, as a result of electron delocalization in the chelate ring of the β-diketone system (17). Published ^{13}C nmr data on 2-pyridones (15, 16) permitted the chemical shifts of the other carbons in the 1-hydroxy-2(1*H*)-pyridone ring to be rationalized when the probable effects of the acyl and aromatic substituents were taken into account. Furthermore, ^{13}C—H spin–spin couplings between H-6 and the carbons in the heterocyclic ring of the metabolite and its derivatives were similar to those observed for 2(1*H*)-pyridone (see footnote † to Table 2).

The mass spectral fragmentation patterns observed for tenellin and bassianin were consistent with the proposed structures. Most of the reaction sequences depicted in Fig. 1 to account for the more abundant fragment ions from tenellin were indicated by metastable ions or were established by precursor ion experiments. Alkyl fragments were lost in a stepwise and predictable manner but there was some branching of reaction pathways because tenellin, as well as the intermediate ions formed from it, were susceptible to the loss of a single oxygen atom from the hydroxamate grouping. The product ions then underwent further fragmentation in the alkyl moiety leading eventually to bond scission between C-7 and C-8, which gave rise to the relatively stable ion at *m/e* 230.

Biosynthetic labelling experiments have shown that C-4 and C-6 of **1** are enriched by [1-^{13}C]- and [2-^{13}C]phenylalanine, respectively (12). A structural unit consisting of C-4, C-5, C-6, and the aromatic substituent of **1** accounts for all of the amino acid carbons if it is assumed that the carboxyl carbon of phenylalanine migrates to the carbon adjacent to the aromatic ring at some stage in the biosynthetic process. The contiguous relationship of C-4 and C-5 and the nature of the intramolecular rearrangement have been confirmed in a more recent study (18) which demonstrated that only these two carbons were ^{13}C—^{13}C coupled ($^1J_{CC}$ 62 Hz) in the pnd ^{13}C spectrum of **1** enriched with [1,3-^{13}C]phenylalanine.

It follows that tenellin is 3-(4,6-dimethyl-*E*,*E*-

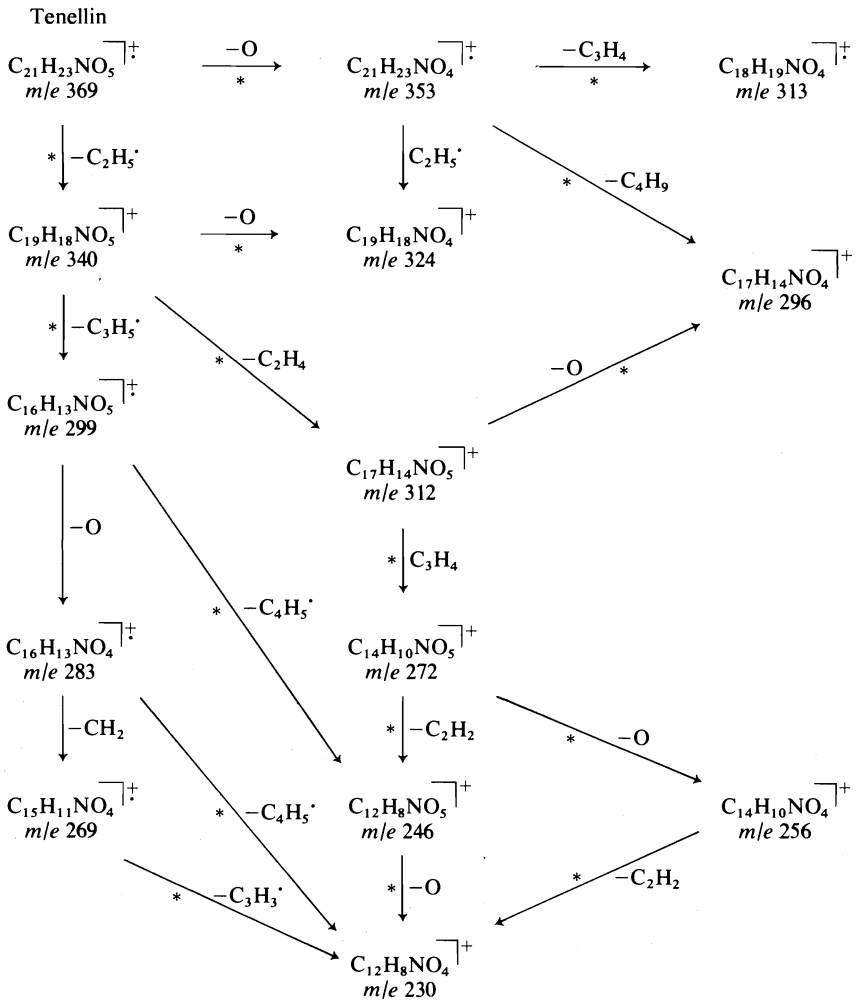

FIG. 1. Fragment ions in the mass spectrum of tenellin. Pathways marked with an asterisk were demonstrated by precursor ion experiments or deduced from the presence of metastable ions.

octa-2, 4-dienoyl)-1, 4-dihydroxy-5-(*p*-hydroxyphenyl)-2(1*H*)-pyridone, and bassianin is 3-(6,8-dimethyl-*E,E,E*-deca-2,4,6-trienoyl)-1,4-dihydroxy-5-(*p*-hydroxyphenyl)-2(1*H*)-pyridone.

Experimental

Melting points were measured with a Fisher-Johns hot plate and are uncorrected. Ultraviolet and infrared absorption spectra were recorded with Beckman model DK-2 and Perkin-Elmer model 237 spectrophotometers respectively. Mass spectra were obtained with a Dupont model 21-110B double-focusing spectrometer used in the electrical detection mode with 8 kV accelerating voltage and 70 eV electron energy. Accurate mass measurements were made by peak matching against a perfluorokerosene reference. In precursor ion measurements the ion accelerating voltage was varied while the voltage applied to the plates of the energy-focusing sector was kept constant (10).

A Varian Associates model HA 100 spectrometer was used to measure ^1H nmr spectra, and a Varian Associates model XL 100 was used to record the pulse Fourier transform ^{13}C nmr spectra. Operating conditions are given in the footnotes to Tables 1 and 2.

Biosynthetic Enrichment with Isotopes

Methods of culturing *B. bassiana* HLX 83 are described in detail elsewhere (2). The fungus was grown in a medium containing D mannitol (5%), potassium nitrate (0.5%), potassium dihydrogen phosphate (0.1%), magnesium sulfate heptahydrate (0.05%), sodium chloride (0.01%), calcium chloride (0.01%), and a trace mineral solution (1% v/v) containing zinc sulfate heptahydrate (880 mg), cupric sulfate pentahydrate (40 mg), manganous sulfate tetrahydrate (7.5 mg), boric acid (6 mg), and ammonium molybdate monohydrate (4 mg) per litre of water. To

obtain ^{15}N-enriched tenellin potassium (^{15}N) nitrate (95% enriched) replaced the usual nitrogen source at the same (0.5%) concentration. Sodium (^{13}C)acetate (90% enriched) was added to the cultures as a sterile aqueous solution, on the 3rd day after inoculation to give a concentration of 10 m*M* in the broth. In each experiment the volume of cultures grown was 500 ml.

Tenellin

Samples were isolated and purified as described previously (2). Measurements of the optical activity gave $[\alpha]_D^{24} - 44.0°$ (1%, acetone). The mass spectrum showed M^+ at *m/e* 369 (15% of base peak) and fragment ions at *m/e* 353 (2.5%), 340 (0.8%), 334 (1.2%), 324 (0.8%), 313 (19.6%), 312 (100%), 299 (0.7%), 296 (6.9%), 283 (0.7%), 272 (4.7%), 269 (0.4%), 246 (23.9%), and 230 (11.9%). Selected ions were accurately mass measured as *m/e* 369.1576 ($C_{21}H_{23}NO_5$ calcd.: 369.1576), 353.1626 ($C_{21}H_{23}NO_4$ calcd.: 353.1630), 312.0874 ($C_{17}H_{14}NO_5$ calcd.: 312.0872), 272.0561 ($C_{14}H_{10}NO_5$ calcd.: 272.0559). Metastable ions were present at *m/e* 312 (369 → 340), 264 (340 → 299) and 279 (353 → 313). Precursor ion measurements showed the following ion fragmentation pathways: *m/e* 369 → 353, 353 → 324, 353 → 296, 340 → 324, 340 → 312, 312 → 296, 312 → 272, 272 → 246, 299 → 246, 283 → 230, 269 → 230, 246 → 230.

Methylation

To a mixture of potassium carbonate (1.2 g) in acetone (20 ml), tenellin (185 mg) and methyl iodide (10 ml) were added. The reaction vessel was flushed with nitrogen and the contents were stirred in the dark for 2 h. Chloroform was added and the filtered solution evaporated. Examination of the greenish residue by thin-layer chromatography (tlc) on silica gel F_{254} (E. Merck, Darmstadt) in methanol–chloroform (1:20) showed unreacted tenellin (R_f 0.16) and three less polar components (R_f 0.30, 0.44, and 0.76) as quenching zones under ultraviolet light. The material was fractionated by tlc on preparative plates (500 × 20 × 2 mm) using methanol–chloroform (1:50) as solvent; zones were scraped off the plate and eluted with ethyl acetate or chloroform.

The product with R_f 0.30 yielded tenellin monomethyl ether as a greenish yellow solid (125 mg), mp (194°C; *m/e* at 383 (13.2%), 353 (12.3%), 326 (100%), 296 (73.6%), 260 (17.5%), and 230 (50%); accurate measurement of M^+ gave *m/e* 383.1731 ($C_{22}H_{25}NO_5$ calcd.: 383.1726). The upper zone with R_f 0.76 by tlc afforded tenellin dimethyl ether as a greenish yellow solid (40 mg), mp 96–98°C; *m/e* at 397 (23%), 381 (3%), 367 (9%), 340 (100%), 310 (43%), 274 (19%), 261 (28%), 244 (44%), 231 (18%), and 230 (25%). Accurate mass measurements gave *m/e* 397.1876 ($C_{23}H_{27}NO_5$ calcd.: 397.1889), 274.0713 ($C_{14}H_{12}NO_5$ calcd.: 274.0715), 244.0611 ($C_{13}H_{10}NO_4$ calcd.: 244.0610). From the middle zone (R_f 0.44 by tlc) a small amount of tenellin trimethyl ether was obtained as a gum (10 mg).

With methyl iodide and silver oxide as the methylating system higher yields of the trimethyl ether could be achieved by extending the reaction time. Thus when tenellin (100 mg) was shaken for 18–20 h with silver oxide (200 mg) and methyl iodide (30 ml) and the filtered and evaporated reaction mixture fractionated by preparative tlc the trimethyl ether was the main product (80 mg), *m/e* at 411 (5.9%), 397 (9.1%), 395 (7.36%), 340 (41.2%), 261 (100%), 231 (40.3%), 230 (48.3%), and 219 (82.4%); accurate measurement of M^+ gave 411.2052 ($C_{24}H_{29}NO_5$ calcd.: 411.2038).

Acetylation

Tenellin (100 mg) and acetic anhydride (1.5 ml) in pyridine (0.1 ml) were allowed to react at ambient temperature for 18 h. Chromatography of the product on a column of silicic acid – Celite with chloroform as eluant gave two fractions, one of which was recrystallized from chloroform–ether as orange-yellow needles (82 mg) mp 175–177°C, ν_{max} (carbon tetrachloride) at 1770, 1645 cm^{-1}; λ_{max} (ethanol) at 254 and 343 nm (log ε 4.31 and 4.35); *m/e* at 411 (8.8%), 354 (100%), 338 (21.6%), 312 (18.6%), 288 (12.7%), 272 (8.8%), 246 (13.2%), and 230 (10.8%); R_f (tlc, silica gel, and chloroform) 0.11.

The second fraction, R_f (tlc, silica gel, and chloroform) 0.24, was not purified but showed ν_{max} (potassium bromide) 1775, 1750, 1660, and 1645 cm^{-1}; M^+ at *m/e* 453.

Hydrogenation

Tenellin (80 mg) in methanol (35 ml) was reduced with hydrogen over 5% palladized charcoal. Hydrogen uptake (2.3 mol/mol) ceased after 1 min. The product was crystallized from aqueous methanol as cream needles, mp 145–147°C, λ_{max} (ethanol) at 254, 285 (inflection) and 358 nm (log ε, 4.37, 4.09, and 3.71); ν_{max} (potassium bromide) at 1650, 1620 cm^{-1}; M^+ at *m/e* 373.1873 ($C_{21}H_{27}NO_5$ calcd.: 373.1889), *m/e* at 373 (36.1%), 356 (11.5%), 274 (100%), 261 (61.5%), 246 (26.4%), and 230 (16.3%).

The same product was obtained when tenellin was hydrogenated under acidic conditions (a 1:1 mixture of methanol – acetic acid containing 1.2% (v/v) of concentrated hydrochloric acid) for 18 h; tlc of the crude reaction product showed no evidence of a deoxy derivative.

Retro-aldol Cleavage

Tenellin (55 mg) was heated under reflux in a slow stream of nitrogen with 2 *N* potassium hydroxide solution (10 ml) for 2 h. Volatile aldehydes from the reaction were trapped in a 0.3% solution of 2,4-dinitrophenylhydrazine in 2 *N* hydrochloric acid, and the precipitated hydrazones chromatographed on a column of silicic acid developed with benzene – petroleum ether (bp 60–80°C). Four orange-colored zones separated and the products, in order of elution, were characterized as: ethanal-2,4-dinitrophenylhydrazone (1 mg), mp 168°C, M^+ at *m/e* 224; propanal-2,4-dinitrophenylhydrazone (13 mg), mp 153°C, M^+ at *m/e* 238; 2-methylbutanal-2,4-dinitrophenylhydrazone (13 mg), mp 128.5–129°C, M^+ at *m/e* 266.1019 ($C_{11}H_{14}N_4O_4$ calcd.: 266.1015), δ (chloroform-*d*) at 1.00 (t, 3H), 1.20 (d, 3H), 1.56 (m), 2.48 (m), 7.45 (d), 8.13 (AB part of ABX, J_{AX} 2.5 Hz), 9.14 (X part of ABX), and 10.99 (bs) ppm; 2,4-dimethylhex-2-enal-2,4-dinitrophenylhydrazone (16 mg), mp 160–161°C, M^+ at *m/e* 306, δ (chloroform-*d*) at 0.88 (t, 3H), 1.03 (d, 3H), 1.42 (m), 1.97 (d, 3H), 2.60 (m), 5.75 (bd), 7.73 (s), 8.11 (AB part of ABX, J_{AX} 2.7 Hz), 9.11 (X part of ABX), and 11.08 (bs) ppm. The derivatives of ethanal, propanal, and 2,4-dimethylhex-2-enal were identified by melting point measurements after admixture with authentic specimens.

The reference sample of (+)2,4-dimethylhex-2-enal-2,4-dinitrophenylhydrazone derived from sclerotiorin (11) was a gift from Dr. W. B. Whalley, School of Pharmacy, University of London.

A nonvolatile product was removed from the acidified reaction mixture by extraction with ether. After sublimation *in vacuo* at 145–160°C and crystallization from methanol–ether it was obtained as cream-colored needles (8.5 mg), mp 230–231°C; λ_{max} (ethanol) at 254, and 360 nm (log ε 4.19 and 3.64); ν_{max} (potassium bromide) 1655, 1620 cm^{-1}; $M^{\ddagger}$ at *m/e* 261 (50% of base peak) and fragment ions at *m/e* 245 (100%) and 230 (72%). Accurate mass measurements gave *m/e* 261.0635 ($C_{13}H_{11}NO_5$ calcd.: 261.0637) and 245.0682 ($C_{13}H_{11}NO_4$ calcd.: 245.0688).

Oxidation with Alkaline Peroxide

Tenellin (100 mg) was heated with hydrogen peroxide (3 ml of a 3% solution) in 0.1 *N* sodium hydroxide (40 ml) on a steam bath for 6 h. Ether extraction of the acidified reaction mixture and sublimation in high vacuum gave two main fractions: at 30–90°C, a viscous liquid (6 mg) which was separated by gas–liquid chromatography using FFAP as liquid phase into three components; A (trace) $M^{\ddagger}$ at *m/e* 168; B, $M^{\ddagger}$ at *m/e* 156.1148 ($C_9H_{16}O_2$ calcd.: 156.1150); and C, $M^{\ddagger}$ at *m/e* 142.0992 ($C_8H_{14}O_2$ calcd.: 142.0994); the second fraction (12 mg) subliming at 100–125°C gave, after resublimation, *p*-hydroxybenzoic acid, mp 213–214°C, identified by comparison with an authentic specimen.

Acknowledgements

We thank Dr. W. B. Whalley, for a specimen of (+)2,4-dimethylhex-2-enal-2,4-dinitrophenylhydrazone. We are also grateful to Dr. G. P. Arsenault, Dr. W. D. Jamieson, and Mr. D. Embree of the National Research Council of Canada for mass spectral measurements and to Mr. J. Berrigan for technical assistance.

1. D. M. MacLeod. Can. J. Bot. **32**, 818 (1954).
2. S. H. El Basyouni, D. Brewer, and L. C. Vining. Can. J. Bot. **46**, 441 (1968).
3. A. G. McInnes, D. G. Smith, Chi-Kit Wat, L. C. Vining, and J. L. C. Wright. J. Chem. Soc. Chem. Commun. 281 (1974).
4. M. Matsumoto and H. Minato. Tetrahedron Lett. 3827 (1976).
5. J. Martin and B. P. Dailey. J. Chem. Phys. **37**, 2594 (1962).
6. B. Birdsall, N. M. J. Birdsall, and J. Feeney. J. Chem. Soc. Chem. Commun. 316 (1972).
7. F. A. Bovey. Nuclear magnetic resonance spectroscopy. Academic Press, New York, NY. 1969. p. 358.
8. R. T. Coutts and K. W. Hindmarsh. Org. Mass Spectrom. **2**, 681 (1969).
9. J. C. MacDonald. Can. J. Biochem. **48**, 1165 (1970).
10. R. L. Lichter. *In* Determination of organic structures by physical methods. *Edited by* F. C. Nachod and J. J. Zuckerman. Academic Press, New York, NY. 1971. p. 195.
11. R. A. Eade, H. Page, A. Robertson, K. Turner, and W. B. Whalley. J. Chem. Soc. 4913 (1957).
12. J. L. C. Wright, L. C. Vining, A. G. McInnes, D. G. Smith, and J. A. Walter. Can. J. Biochem. **55**, 678 (1977).
13. J. B. Stothers. Carbon-13 NMR spectroscopy. Academic Press, New York, NY. 1972. p. 370.
14. M. Kobayashi, Y. Terni, K. Tori, and N. Tsuji. Tetrahedron Lett. 619 (1976).
15. L. Stefaniak. Tetrahedron, **32**, 1065 (1976).
16. I. W. J. Still, N. Plavac, D. M. McKinnon, and M. S. Chauhan. Can. J. Chem. **54**, 280 (1976).
17. N. N. Shapet'ko, S. S. Berestova, G. M. Lukovkin, and Yu. S. Bogachev. Org. Magn. Reson. **7**, 237 (1975).
18. E. Leete, N. Kowanko, R. A. Newmark, L. C. Vining, A. G. McInnes, and J. L. C. Wright. Tetrahedron Lett. **47**, 4103 (1975).

Décharge triboélectrique dans le système propane – vapeur d'eau

JAN A. HERMAN
Département de Chimie, Université Laval, Québec (Qué.), Canada G1K 7P4

Reçu le 29 décembre 1976[1]

JAN A. HERMAN. Can. J. Chem. **55**, 4099 (1977).

Le propane gazeux additionné de quantités variables de vapeur d'eau est soumis à la décharge triboélectrique dans un système verre borosilicaté-mercure. Le taux de décomposition du propane semble être indépendant de la présence de la vapeur d'eau jusqu'à $p(H_2O) \approx 2$ Torr. Au-delà de cette valeur de la pression du H_2O la décharge disparaît. La composition relative en produits de décomposition du propane varie en fonction de la concentration de la vapeur d'eau.

JAN A. HERMAN. Can. J. Chem. **55**, 4099 (1977).

Gaseous propane containing various amounts of water vapour was subjected to a triboelectric discharge in an apparatus of mercury in borosilicate glass. The extent of decomposition of propane appeared not to depend on the presence of water vapour below a partial pressure of about 2 Torr. Above this pressure of H_2O the discharge disappeared. The relative composition of the products of the propane decomposition varied with the concentration of water vapour.

[Journal translation]

Introduction

L'étude des effets chimiques résultant de la décharge triboélectrique nous a conduit à examiner de plus près l'influence de la vapeur d'eau sur une telle décharge. En effet, il n'est pas facile de contrôler la teneur, surtout en trace, de la vapeur d'eau, aussi bien dans l'échantillon que celle adsorbée sur les parois du récipient. Or, il est reconnu que d'une part certaines réactions ioniques sont très sensibles à la présence de la vapeur d'eau, et d'autre part parmi les facteurs intervenant sur la triboélectrisation la nature de la surface joue un rôle très important (1, 2). Ces deux aspects liés à la présence éventuelle de la vapeur d'eau justifient la présente étude.

L'influence sur l'électrisation par contact de la vapeur d'eau adsorbée sur les parois est mal définie en raison de facteurs structuraux des matériaux utilisés et de la présence d'autres contaminants (au sens de la triboélectrisation) qui peuvent, selon les prétraitements des surfaces, modifier ou masquer la participation éventuelle des couches adsorbées de l'eau (3, 4). Kunkel (5), par exemple, a montré qu'un changement d'humidité n'affecte pratiquement pas la formation des charges électriques par friction à 20°C de la poudre de quartz.

Dans le cas qui nous préoccupe la présence de l'eau dans le système peut se manifester de deux manières: (*1*) son influence sur l'accumulation de charges électrostatiques sur les surfaces dans l'électrisation de contact, et (*2*) sa présence en phase gazeuse modifiant le caractère de la décharge (tribo)électrique. Dans le premier cas son influence pourrait se faire sentir au niveau de l'intensité de la décharge à travers le gaz en raison de l'importance de la charge superficielle. Dans le deuxième cas la présence des molécules de vapeur d'eau dans le gaz peut jouer un rôle modérateur de l'énergie cinétique (moyenne) des électrons accélérés par le champ électrique. De plus la présence de la vapeur d'eau influencera les réactions ioniques, mais cet aspect ne sera pas abordé dans ce travail.

L'examen partiel de ces deux aspects de l'influence de la vapeur d'eau sur la décharge triboélectrique est essayé sur le système $C_3H_8 + H_2O$, où la pression du propane est maintenue constante, tandis que celle de la vapeur d'eau est variable.

Procédure expérimentale

Les cellules de réactions de forme cylindrique (volume: 232 ± 15 cm^3) sont en verre borosilicate (Pyrex). Elles sont équipées de pointes cassables.

L'électrisation de contact étant très sensible à la qualité de la surface nous avons adopté une procédure rigoureuse de nettoyage des réacteurs (6). La cellule propre est soudée à une rampe à vide (limite du vide $\sim 10^{-5}$ Torr) et chauffée pendant 12 h à environ 350°C dans un four amovible. Simultanément dans un dispositif approprié connecté au système à vide au-dessus du réacteur on chauffe à reflux à environ 250°C pendant

[1]Révision reçue le 2 août 1977.

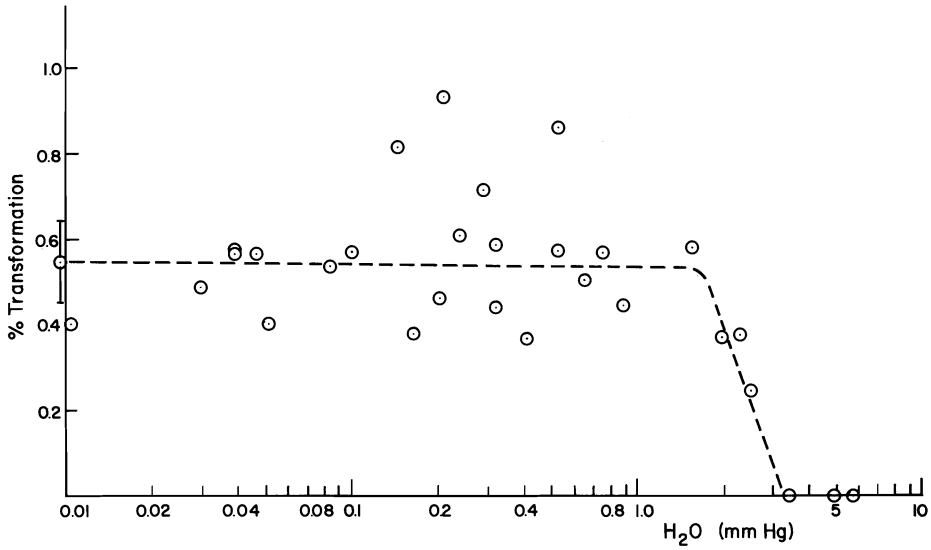

FIG. 1. Taux de décomposition du propane dans une décharge triboélectrique en présence de la vapeur d'eau. Le point à gauche de l'axe des ordonnées se rapporte au propane sec.

2 à 3 h sous haut vide ($\sim 10^{-5}$ Torr) 130 g de mercure. Une connection articulée permet de transvaser le mercure dans le réacteur sans détérioration du vide établi dans le système. Cette opération de transvasement du mercure dans le réacteur est exécutée après refroidissement à la température ambiante et juste avant l'admission d'une quantité contrôlée de vapeur d'eau et de propane. Ensuite le réacteur est scellé et mis en rotation autour de l'axe longitudinale du récipient pendant 60 min à une vitesse linéaire d'envion 21 cm s^{-1} (72 révolutions/min). Toutes les expériences sont faites à la température ambiante, soit 23 ± 2°C.

La provenance des réactifs et la procédure analytique sont déjà décrites (6). Précisons cependant que la présence du propane masque sur le chromatogramme le propyne et l'allène. L'hydrogène, les composés alkylmercuriques et les produits oxygénés (aldéhydes, alcools) n'ont pas été analysés systématiquement, cependant on n'a pas détecté de méthanol parmi les produits formés.

Résultats et discussion

La pression du propane est maintenue constante à 9.6 Torr pendant toutes les expériences, tandis que la pression partielle de la vapeur d'eau est variable. Les résultats de la décomposition du propane dans la tribodécharge sont présentés dans les figs 1 à 3. La fig. 1 montre le taux de décomposition du propane en fonction de la pression partielle du H_2O. Les figs 2 et 3 présentent les variations de la composition relative des produits provenant de la décomposition du C_3H_8 en fonction de la teneur en H_2O. Dans toutes ces figures l'échelle des pressions partielles du H_2O (axe des abscisses) est logarithmique. Les points se rapportant à la décomposition du *propane sec* (séché sur du sodium métallique) sont rapportés en dehors et à gauche de l'axe des ordonnées. On a indiqué par un segment vertical l'écart moyen des mesures, qui est de l'ordre de 20% pour les valeurs de la composition relative.

Le taux de décomposition du C_3H_8 (fig. 1) est calculé suivant l'expression $-\Delta(C_3H_8) = 0.33C_1 + 0.66\Sigma C_2 + (C_3H_6) + 1.33\Sigma C_4$. Pour nos conditions expérimentales ce taux de décomposition du *propane sec* est de 0.55 ± 0.10% pour tous les réacteurs utilisés. Pour des pressions partielle <2 Torr de la vapeur d'eau les résultats du taux de décomposition du C_3H_8 fluctuent dans une large zone et ne manifestent pas de tendance précise. Cela résulte des particularités propres de chacun des réacteurs utilisés. Certains réacteurs affichaient systématiquement des taux de décomposition du C_3H_8 plus élevés que d'autres. De plus, au fur et à mesure que les nettoyages des réacteurs se succèdent il apparaît un effet favorable à l'électrisation de contact résultant selon toute vraisemblance d'une modification irréversible de la surface du verre. On peut conclure prudemment que jusqu'à $p(H_2O) < 2$ Torr l'adsorption de la vapeur d'eau ne semble pas diminuer en moyenne la capacité triboélectrique du système. Mais au-delà de cette valeur de pression du H_2O la décharge diminue progressivement pour dis-

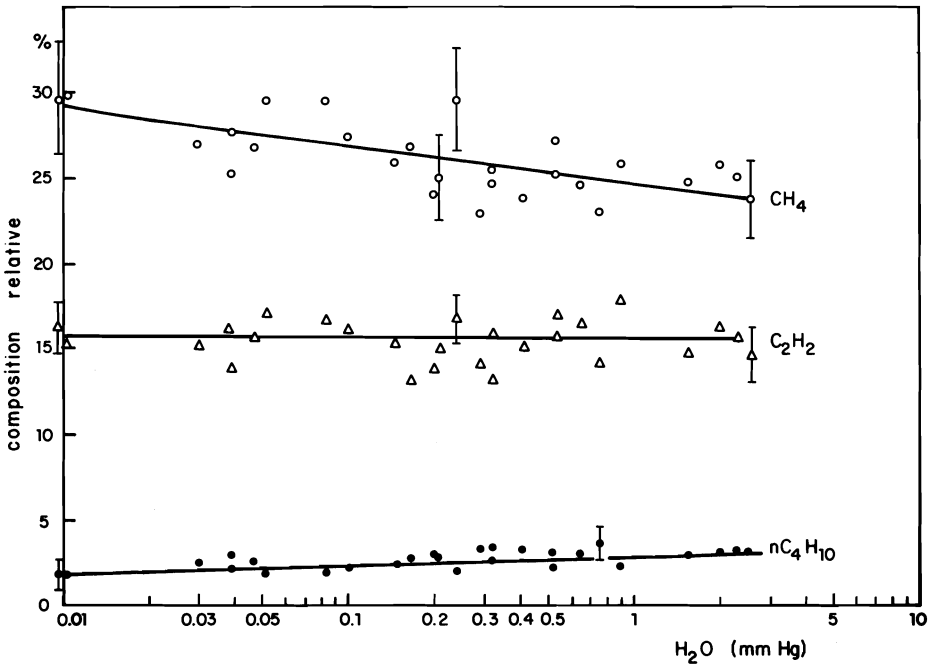

FIG. 2. Variation de la composition relative du méthane, de l'acétylène et du *n*-butane dans une décharge triboélectrique en présence de la vapeur d'eau. Les points à gauche de l'axe des ordonné se rapportent au propane sec.

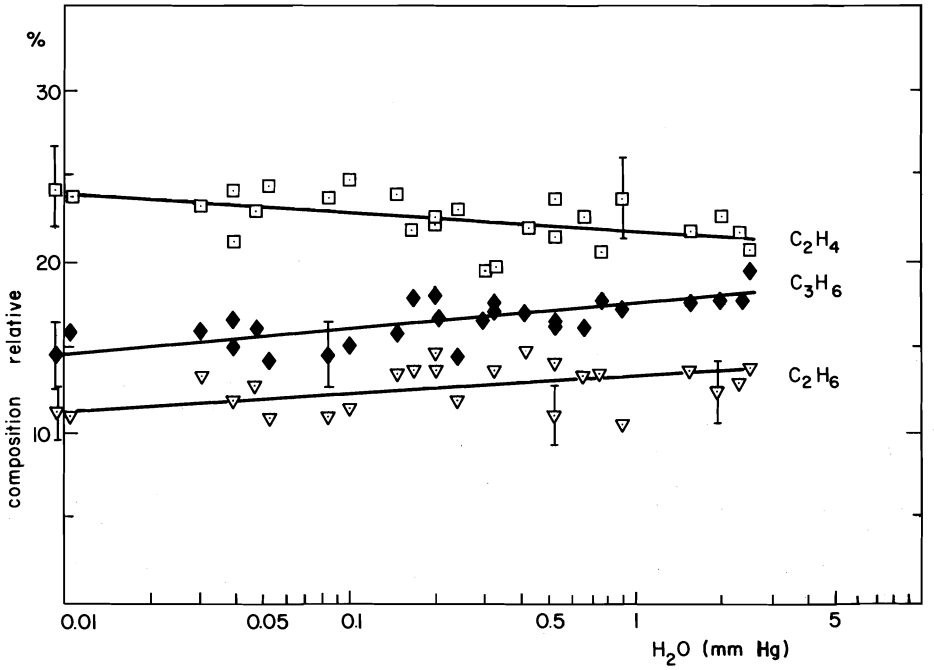

FIG. 3. Variation de la composition relative de l'éthylène, de l'éthane et du propène dans une décharge triboélectrique en présence de la vapeur d'eau. Les points à gauche de l'axe des ordonnées se rapportent au propane sec.

paraître complètement vers environ 3 Torr. Les causes de la diminution jusqu'à disparition complète de la décharge peuvent être multiples, p.ex. recombinaison des charges par migration superficielle sur les parois humides, blocage des sites préférentielles à la formation des charges, extinction "chimique" de la décharge électrique, etc.

Les compositions relatives des produits formés dans la tribodécharge du C_3H_8 en fonction de la pression partielle du H_2O (figs 2 et 3) montrent des écarts de l'ordre de 20% par rapport à la valeur moyenne, ce qui est normal pour ce genre d'expériences (6). Ici on peut déceler nettement des tendances: (*a*) les concentrations en CH_4 et C_2H_4 diminuent progressivement avec l'augmentation de la pression de la vapeur d'eau, (*b*) le pourcentage en C_2H_2 ne semble pas être influencé par la présence du H_2O, et (*c*) tous les autres produits analysés C_2H_6, C_3H_6, *n*-C_4H_{10} et iso-C_4H_{10} (ce dernier coïncide en grandeur à peu de chose près avec le *n*-butane) augmentent leur proportion avec la teneur de vapeur d'eau.

L'attachement d'électrons à la vapeur d'eau explique les diminutions progressives des concentrations des produits dont la formation exige l'existence de précurseurs hautement excités. En effet, il est reconnu que le principal mécanisme de perte d'électrons dans une décharge à travers le gaz est l'attachement d'électrons. L'attachement dissociatif d'électrons à la vapeur d'eau est bien établi et on connaît deux pics de résonance de l'ion H^- à 6 et 8 eV et deux pics de l'ion O^- à 9 et 11 eV (7). Malheureusement, on ne connaît pratiquement rien en ce qui concerne l'attachement d'électron au propane, ce qui rend toute comparaison avec H_2O impossible. Le "refroidissement" des électrons accélérés dans le champ par attachement à H_2O entraînera une augmentation de collisions inélastiques moins énergétiques entre les électrons et le propane, de sorte que les produits de décomposition tels le C_3H_6 et les radicaux méthyl et propyl seront favorisés au détriment de produits moléculaires du genre C_2H_4 ou CH_4, ou ceux formés par réactions avec le radical CH_2, dont la formation exige des précurseurs excités à des niveaux d'énergie plus élevés. La comparaison des spectres par impact électronique du H_2O et du C_3H_8 va dans le même sens. Celui de la vapeur d'eau montre une bande d'absorption située entre 6.8 et 8.7 eV et centrée sur $\sim$7.4 eV (transition $1b_1 \rightarrow 3s$) (8, 9), laquelle empiète à peine sur le début du spectre d'excitation électronique du propane commençant à 7.5 eV (10). Par contre les potentiels d'ionisation de la vapeur d'eau et du propane sont respectivement 12.6 et 11.1 eV (11), donc si l'ionisation comptait pour le principal mode de perte d'énergie c'est le propane qui en subirait la plus grande partie.

La formation de l'acétylène échappe apparemment à ce mécanisme. La concentration constante en C_2H_2 est, soit le résultat d'une réaction ion–molécule, soit d'une réaction hétérogène, par exemple la décomposition du propane adsorbé sur les sites d'où s'initie ou se termine la décharge.

En conclusion on peut dire que des faibles quantités de vapeur d'eau ne semblent pas influencer de manière appréciable les phénomènes chimiques accompagnant la décharge triboélectrique.

Remerciements

Nous remercions Mme M. Villard-Pittion pour l'aide apportée dans l'analyse des échantillons gazeux. Nos remerciements vont aussi au Conseil national de recherches du Canada et au Ministère de l'education du Québec (Octroi FCAC) pour l'aide financière.

1. L. B. Loeb. Static electrification. Springer-Verlag, Berlin, Germany. 1958.
2. W. H. Harper. Contact and frictional electrification. Clarendon Press, Oxford, England. 1967.
3. J. W. Peterson. J. Appl. Phys. **25**, 501 (1954); **25**, 907 (1954).
4. P. E. Wagner. J. Appl. Phys. **27**, 1300 (1956).
5. W. B. Kunkel. J. Appl. Phys. **21**, 820 (1950).
6. J. A. Herman, G. Mayrand et H. Tarki. Can. J. Chem. **55**, 454 (1977).
7. M. Cottin. J. Chim. Phys. **56**, 1025 (1959).
8. R. S. Mulliken. J. Chem. Phys. **3**, 506 (1935).
9. G. Herzberg. Trans. Faraday Soc. **27**, 402 (1931).
10. E. N. Lassettre, A. Skeberle et M. A. Dillon. J. Chem. Phys. **49**, 2382 (1968).
11. J. L. Franklin et coll. Natl. Stand. Ref. Data Ser., Natl. Bur. Stand. 26, 1969.

Pyrrole chemistry. XVI. Acylation of the pyrrolyl ambident anion

NAM-CHIANG WANG AND HUGH J. ANDERSON

Department of Chemistry, Memorial University of Newfoundland, St. John's, Nfld., Canada A1C 5S7

Received May 19, 1977

NAM-CHIANG WANG and HUGH J. ANDERSON. Can. J. Chem. **55**, 4103 (1977).

An investigation of the acylation of the pyrrolyl ambident anion has been carried out. The results have been rationalized in terms of the 'principle of hard and soft acids and bases.' The metal cation, solvent or complexing agent, halide of the pyrrole Grignard reagent, and temperature were varied. As well, the reactions of acylating agents of the carbonyl, cyanide, and carbimine type with the pyrrole Grignard reagent were studied to determine N/C acylation ratios under the same conditions. Several new products were isolated and identified.

NAM-CHIANG WANG et HUGH J. ANDERSON. Can. J. Chem. **55**, 4103 (1977).

On a effectué une étude de l'acylation de l'anion ambivalent pyrrolyle. On a rationalisé les résultats en termes du principe des acides et des bases durs et mous. On a fait varier le cation métallique, le solvant ou l'agent de complexation, l'halogénure du réactif de Grignard pyrrole et la température. On a de plus étudié les réactions des agents acylants de type carbonyle, cyanure et carbimine avec le réactif de Grignard pyrrole afin de déterminer les rapports d'acylation N/C dans les mêmes conditions. On a isolé et identifié plusieurs nouveaux produits.

[Traduit par le journal]

Introduction

The reactivity of the N-hydrogen of pyrrole and many of its C-substituted derivatives has made it possible to prepare numerous metal salts, including those of the Grignard type (1). Modern physical evidence has confirmed that it is the N-hydrogen which exchanges with methylmagnesium halide (2), that the proton magnetic resonance spectra of pyrrolylsodium and pyrrolylmagnesium chloride are similar, and that bonding to these metals is through the nitrogen (3). However, reaction products from these and other metal derivatives often include both N- and C-substitution products. The proportions of these products change with solvent, temperature, metal cation, reactant, and other factors (1*a*). Thus, these metal derivatives show ambident anion behaviour.

In his review of ambident anion reactivity, Shevelev (4) provides a thorough discussion of the reactions of metal derivatives of pyrrole with alkylating agents. Much less is known of their reactions at unsaturated carbon during acylations. We have been interested in the latter reactions because they serve to introduce functional groups at either carbon or nitrogen. The fact that pyrrolylmagnesium bromide reacts in ethyl ether with ethyl carbonate to give almost entirely N-acylation, but with ethyl dithiolcarbonate to give only C-acylation (5), suggested a need for further study and an attempt to provide a rationalization.

The 'principle of hard and soft acids and bases' (hsab) of Pearson (6) was used by Shevelev in his review (4) and appeared to us to provide a satisfactory method for attempting to rationalize the observed results. However, as Shevelev points out, there are complicating factors. The hardnesses of the various unsaturated carbons may be modified by coordination of the nucleophilic part of the acylating agent with the metal cation and the electrophilic part with the metal – ambident anion pair.

The nitrogen of the pyrrolyl anion is more electronegative, less polarizable, and a harder base, while the carbon (usually C-2, sometimes C-3) is less electronegative, more polarizable, and a softer base. Thus, the hard electrophilic carbon of an attacking carbonyl group would be expected to attack nitrogen, and does so when pyrrolylmagnesium bromide reacts in ethyl ether with ethyl carbonate. When the carbonyl carbon is softened, as in ethyl dithiolcarbonate, acylation is on carbon under the same conditions (5).

To rationalize pyrrole acylations, we have varied the metal, solvent, temperature, concentration, and acylating agent. In addition, complexing agents have also been employed in some experiments. Through these alterations various

TABLE 1. The reaction of magnesium and alkali metal salts of pyrrole with ethyl chloroformate in ethyl ether

Cation	1-Ester (%)	2-Ester (%)	1,1′-Ketone (%)	1,2-Diester (%)	N/C ratio	Total yield (%)
Mg^{2+}	13	21	0	19	25:75	53
Li^+	39	0	16	0	100:0	55
Na^+	87	0	0	0	100:0	87
K^+	64	0	0	0	100:0	64

TABLE 2. The reaction of pyrrolylmagnesium bromide and ethyl chloroformate in the presence of added reagents

Added reagent for 0.100 mol Grignard	1-Ester (%)	2-Ester (%)	1,2-Diester (%)	1,2′-Ketone (%)	N/C ratio	Total yield (%)
(Ether)	13	21	19	0	25:75	53
1,4-Dioxane (0.150 mol)	6	7	22	0	17:83	35
Dimethoxyethane (0.150 mol)	13	2	65	0	16:84	80
TMED* (0.100 mol)	51	5	0	2	89:11	58
(0.150 mol)	76	1	0	1	98:2	78

*TMED = *N,N,N′,N′*-tetramethylethylenediamine.

N- and C-acylated mixtures have been obtained. The results have been used to establish trends in behaviour and to correlate these with the hsab principle. Some experiments in alkylation will be reported separately (7).

Discussion

1. The Metal Cation

Alkylation studies of pyrrole and indole metal salts and Grignard reagents (8–10) suggested that a decreasing coordinating ability of the metal (or other) cation leads to increasing dissociation of the ion pair and to an increasing N/C ratio. Shevelev has equated the trend with the decreasing hardness of $Mg^{2+} > Li^+ > Na^+ > K^+ > R_4N^+$, leading to lowered association with the hard centre (N) and decreased hindrance to attack at that position.

Previous acylation experiments (11, 12) have usually involved a single comparison of the Grignard reagent with another metal derivative in reaction with a single reagent and appear to follow the expected pattern. Treibs and Dietl (13) made somewhat wider comparisons in both alkylation and acylation reactions. Many of their observations fit the expected pattern, although their report of mainly C-acylation of pyrrolyllithium by ethyl chloroformate in ethyl ether was neither confirmed by Hodge and Rickards (11) nor by us.

Our observation (Table 1) was that in ethyl ether, pyrrolylmagnesium bromide and ethyl chloroformate gave more C- than N-acylation while the K^+, Na^+, and Li^+ salts all gave exclusively N-acylation under comparable conditions. Similarly, ethyl chlorothiolformate gave mainly C-acylation with the pyrrole Grignard and entirely N-acylation with the lithium salt.

2. The Solvent

The most important factor for ambident anion reactions is the capacity of the solvent to solvate cations (4). Increased solvation of the cation weakens the attraction between the metal cation and the harder center of the ambident ion permitting attack by the alkylating or acylating agent on the nitrogen. In solvents other than ethyl ether, the Schlenk equilibrium may also be involved (14).

We have carried out a series of acylations of pyrrolylmagnesium bromide in ethyl ether, with ethyl chloroformate, to which was added $1\frac{1}{2}$ mol

TABLE 3. The reaction of pyrrolylmagnesium bromide with ethyl chlorothiolformate in ether in the presence of different ratios of TMED*

Ratio TMED/ Grignard	1-Thiol-ester (%)	2-Thiol-ester (%)	1,1′-Ketone (%)	1,2′-Ketone (%)	*S,S*-Diethyl dithiol-carbonate† (%)	N/C ratio	Total yield of pyrroles (%)
0:1	3	42	0	Trace	2	6:94	45
1:1	3	31	0	Trace	35	10:90	34
1.5:1	16	35	0	0	64	32:68	51
2:1	34	23	Trace	Trace	55	60:40	57
3:1	46	10	6	0	35	84:16	62
4:1	41	1	4	2	42	96:4	48
5:1	51	1	7	0	34	99:1	59

*TMED = *N,N,N′,N′*-tetramethylethylenediamine.
†Based on the quantity of the ethyl chlorothiolformate used.

TABLE 4. The reaction of pyrrolylmagnesium halides with ethyl chlorothiolformate in the presence of TMED in ether*

Pyrrolyl-MgX	1-Ester (%)	2-Ester (%)	1,1′-Ketone (%)	1,2′-ketone (%)	*S,S*-Diethyl dithiol-carbonate† (%)	N/C ratio	Total yield of pyrroles (%)
Cl	52	6	0	0	38	89:11	58
Br	34	23	Trace	Trace	55	60:40	57
I	10	28	0	5	27	28:72	43

*The ratio of TMED to pyrrolylmagnesium halides was 2:1.
†Based on the ethyl chlorothiolformate used.

equiv. of dioxane or of 1,2-dimethoxyethane. As shown in Table 2, neither of these caused a significant change in the N/C acylation ratio of about 1:4. However, the addition of 1½ mol equiv. of tetramethylethylenediamine (TMED) produced almost exclusive N-acylation. When ethyl chlorothiolformate was the acylating agent in ethyl ether there was a small amount of N-acylation. The N/C ratio increased steadily as the proportion of TMED was increased (Table 3), becoming mostly N-acylation above about 2:1 TMED–Grignard reagent, and almost completely N-acylation at about 4:1. The results of acylation were consistent with those for alkylation under like conditions (7). The harder solvating agent probably displaced the coordinated ether molecules from the metal cation first, then caused a further separation of the ion pair and increased N-attack.

3. The Halide of the Grignard Reagent

In order to determine whether acylation is sensitive to alterations in halide ion, we added 2 mol equiv. of TMED to the ethereal pyrrole Grignard solution and then acylated with ethyl chlorothiolformate. As shown in Table 4 there was a marked decrease in the N/C ratio going from the chloride to bromide to iodide that almost exactly paralleled the results of Reinecke *et al.* (10) in methylations of the indole Grignard where HMPA (hexamethylphosphoric triamide) was their added reagent. Our rationalization is: the softer the halide, the softer the magnesium becomes, weakening its coordinating ability. Thus the ion pair is less separated by TMED or HMPA complexing and less N-attack occurs. An alternative explanation is that ethyl chlorothiolformate exchanges halide ion with Br^- and I^- to form increasingly soft acylating agents which increasingly attack carbon. There is no evidence that such exchange occurs, however.

4. Temperature

A few alkylations of the pyrrolyl anion are known where the temperature has been varied from the normal 0–35°C range (8, 15, 16). We found that while pyrrolyllithium was N-acylated by ethyl carbonate in dioxane at room tempera-

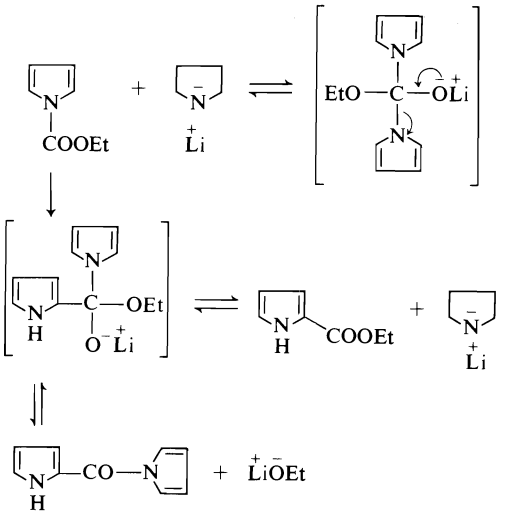

SCHEME 1

ture, there was a substantial amount of C-acylation at the boiling point. Closer examination of this reaction suggested that the kinetically formed 1-ester was slowly converted to the thermodynamically more favorable 2-ester under these conditions (see Scheme 1). These observations agree with the proposition that when a reversible reaction permits thermodynamic control of products, the electrophilic reagent forms a bond preferentially with the atom of an ambident anion that is most basic in relation to the proton, and here C is more basic than N (17). No such rearrangement took place when 1-butylpyrrole was refluxed with the pyrrole Grignard in ethyl ether (18).

5. Substituent Groups

The presence of substituent groups on the ambident pyrrolyl anion produced predictable results. It would be expected that electron withdrawing groups would stabilize the ambident anion and aid in dissociation of the N-metal bond while electron donor substituents would reduce this dissociation. While ethyl chloroformate with pyrrolylmagnesium bromide in ethyl ether gave both C- and N-acylation, it gave only C-acylation with 2-methylpyrrolylmagnesium bromide (19). Treibs (13) acylated the potassium salt of 2,4-dimethylpyrrole in xylene with ethyl chloroformate and obtained only the N-ester in moderate yield, while the corresponding lithium salt gave only the C-ester in unspecified yield. We found that the Grignard reagent from ethyl 2-pyrrolecarboxylate in ethyl ether was N-acylated by ethyl chloroformate in high yield under the usual conditions.

6. The Acylating Agent

The reaction of pyrrolylmagnesium bromide in ethyl ether with a variety of acylating agents was studied. We determined the N/C ratios for each under identical reaction conditions. Some of the initial products reacted further, so it was necessary to realize that a 1,2-(or 1,3-)disubstituted product could only arise from an initially C-acylated product which had undergone metal–hydrogen interchange with more pyrrolylmagnesium bromide. While N-acylated pyrroles do react with pyrrolylmagnesium bromide it is not by loss of a proton from the ring but by addition to the carbonyl leading to 1,2′-dipyrrolyl ketone (20).

Table 5 shows our results, supplemented by others in the literature, in a sequence to demonstrate that the N/C ratio depends on the hardness of the carbonyl carbon when all other parameters are constant. Thus, the hardest carbonyl compound examined was the carbonate ester where two hard ether oxygens are bonded to it. When one of these was replaced by softer atoms the N/C ratio fell. Our observation is that the order of decreasing hardness is O > C=O > Cl ~ CH_3 ~ SEt ~ H. When both ether oxygens were replaced by softer groups the amount of N-substitution was very small.

The much softer thiocarbonyl group of $(EtO)_2C{=}S$ gave only C-acylated pyrroles, while the much harder C=N— of dicyclohexylcarbodiimide gave only N-substitution. The behavior of the cyanides was closely similar to that of the carbonyl compounds.

There are two possible rationalizations for these N/C ratios. First, the carbonyl group of the acylating agent may have displaced a coordinated ether molecule from the metal cation, altering the degree of hardness of the metal, and the degree of separation of the ion pair. Second, there may be a difference in the reactivity of the carbonyl group itself toward the metal cation – ambident anion combination in a solvent whose bonding to metal remains constant. In any case, the hsab principle may be conveniently used to rationalize and to predict.

7. Products from Acylations

(*a*) When pyrrolylmagnesium bromide reacted

TABLE 5. Acylation of pyrrolylmagnesium bromide with various acylating agents in ether

Reactions		N/C	References
Pyrrolylmagnesium bromide in ethyl ether	+ 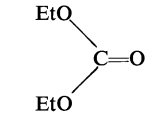	97:3	
	+ 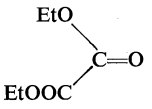	46:54	
	+ 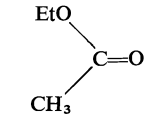	24:76	
	+ 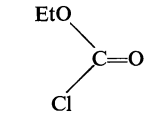	25:75	
	+ 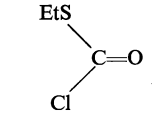	6:94	
	+ 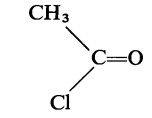	3:97	
	+ 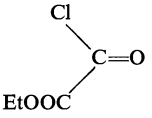	Mostly C	21
	+ 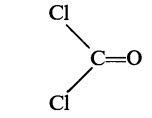	All C	22
	+ 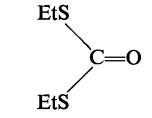	All C	5
	+ 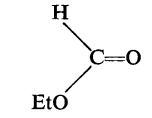	All C	23
	+ R—N=C=N—R	All N	
	+ Me_2N—C≡N	All N	
	+ R—C≡N	All C	24
	+ EtS—C≡N	All C	5
	+ Ph—N=C=O	80:20	12*a*
	+ Ph—N=C=S	75:25	12*b*

with ethyl acetate in ether, only 1- and 2-acetylpyrroles were obtained in modest yield under our conditions. However, in the presence of 1.5 mol equiv. of TMED a new compound, 1-acetoacetylpyrrole, was obtained as the major product. The compound could be obtained in good yield by adding ethylmagnesium bromide to a solution of 1-acetylpyrrole in the same ether–TMED solution, followed by ethyl acetate. So, the most acidic proton of 1-acetylpyrrole is on the acetyl group. A similar acylation of substituted pyrroles using an acyl halide and sodium hydride in THF gave 1-acylation followed by (*i*) in some examples O- and C-acylation of that group and (*ii*) in others exclusively O-acylation (25).

(*b*) The reaction with ethyl oxalate gave a mixture of ethyl 1-pyrrolylglyoxylate and the known ethyl 2-pyrrolylglyoxylate (21).

(*c*) The reaction with dicyclohexylcarbodiimide gave an excellent yield of *N,N'*-dicyclohexyl-1-pyrrolylcarbamidine (**1**). The lithium aluminum hydride reduction of this compound gave a good yield of *N,N'*-dicyclohexylformamidine (**2**) (26), confirming that the pyrrole N was the position attacked by the hard reagent, R—N=C=N—R.

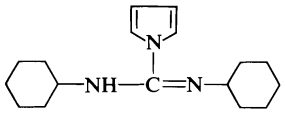

1

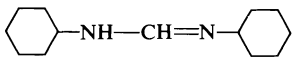

2

(*d*) The reaction with dimethylcyanamide gave exclusively *N,N*-dimethyl-1-pyrrolylcarbamidine (**3**) in low yield. The same product, also in low yield, was obtained from pyrrolyllithium and dimethylcyanamide.

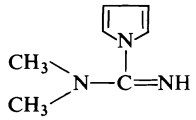

3

(*e*) The reaction with methyl thiocyanate, as reported before (5), gave only the 2-nitrile. However, using pyrrolyllithium a mixture of 1,1'-dipyrrolyl *N*-methylthioketimine (**4**) and

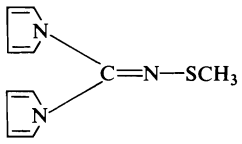

4

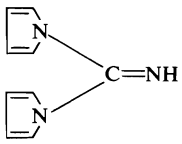

5

1,1'-dipyrrolyl ketimine (**5**) was isolated instead of the 1-nitrile.

(*f*) The reaction with ethyl chlorothiolformate gave the usual 1- and 2-thiolesters as well as traces of 1,2'-dipyrrolyl ketone and *S,S*-diethyl dithiocarbonate (**6**). The latter product probably arises from the reactions shown in Scheme 2.

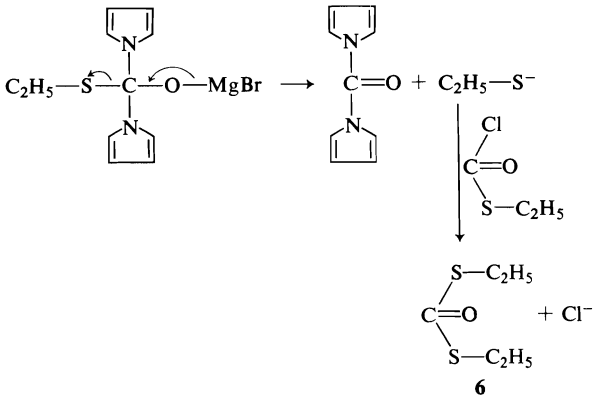

6

SCHEME 2

(*g*) As reported in Section 4, the reaction of pyrrolyllithium with ethyl carbonate in boiling dioxane gave a lower N/C ratio than reaction at 35°C. Refluxing a mixture of pyrrolyllithium and the 1-ester in dioxane resulted in its conversion to the 2-ester and much 1,2'-dipyrrolyl ketone. On the other hand, subjecting the 2-ester to this treatment gave only the 1,2'-dipyrrolyl ketone and none of the 1-ester. It was also found that lithium ethoxide acted on 1,2'-dipyrrolyl ketone under these conditions to give only the 2-ester. These observations are consistent with Scheme 1.

Experimental

The instrumental and related data are described in ref. 5. Analysis of reaction mixtures was carried out as follows. Each product was dried, the volume reduced to 50 ml or 100 ml, and a 1 ml sample retained for analysis. The rest of the solution was used for isolation and identification of products. A standard solution of an authentic sample of each compound to be analyzed by gas chromatography was prepared and used to select the analytical conditions. Suitable attenuation enabled selection of peaks of appropriate size to be cut and

weighed. In this way calibration and the percentage composition of mixtures could be determined.

1. Pyrrolylmagnesium Bromide

A solution of ethylmagnesium bromide was prepared under nitrogen from ethyl bromide (11.99 g, 0.110 mol), magnesium (2.43 g, 0.100 mol) in absolute ethyl ether (60 ml). After 1 h reflux, pyrrole (6.70 g, 0.100 mol) was added slowly followed by a further 1 h reflux.

2. Pyrrolyllithium

Following the method of Hodge and Rickards (11), a solution of butyllithium (0.100 mol) in ethyl ether (40 ml) was stirred under nitrogen at 0°C while a solution of pyrrole (7.37 g, 0.110 mol) in absolute ether (40 ml) was added. The mixture was stirred at room temperature a further ½ h.

3. Pyrrolylsodium

In a procedure similar to that of Hobbs *et al.* (8), a solution of pyrrole (8.41 g, 0.125 mol) in absolute tetrahydrofuran (10 ml) was added slowly to a suspension of sodium hydride (2.40 g, 0.100 mol) in tetrahydrofuran (75 ml). After 4 h reflux, the solvent was removed under vacuum and the residue flushed with dry nitrogen. Absolute ether (100 ml) was added and the suspension refluxed ½ h.

4. Pyrrolylpotassium

In a procedure similar to that of Clemo and Ramage (27), a solution of pyrrole (8.41 g, 0.125 mol) in absolute ether (25 ml) and absolute ethanol (2 drops) was added to potassium (3.91 g, 0.100 mol) and absolute ether (75 ml) under nitrogen. The reaction mixture was refluxed until all potassium had reacted.

5. Acylation with Ethyl Chloroformate and Ethyl Chlorothiolformate

(*a*) The Grignard solution (0.100 mol) was cooled to −20°C and a solution of ethyl chloroformate (10.9 g, 0.100 mol) in absolute ether (90 ml) was added over 1½ h. The cold mixture was stirred ½ h and then hydrolyzed with 1 *M* aqueous ammonium chloride (200 ml). When all solid had dissolved, the layers were separated and the aqueous layer extracted twice with equal volumes of ether. The combined ether extracts were washed twice with water and dried ($MgSO_4$). The volume was reduced to 100 ml and 1 ml was used for gc analysis.

After removal of ether, the residue was vacuum distilled to give ethyl 1-pyrrolecarboxylate (2.74 g, 19%), bp 78–81°C/14 Torr, and ethyl 2-pyrrolecarboxylate (5.97 g, 44%), bp 86–87°C/1 Torr. These are known compounds (28), possessing spectral properties in accord with the methyl esters (11).

(*b*) The reaction between pyrrolyllithium (0.100 mol) and ethyl chloroformate (0.100 mol) was carried out in ether (80 ml) at room temperature over 17 h. Hydrolysis was with ether saturated with water, while cooling, to yield ethyl 1-pyrrolecarboxylate (39%) and 1,1′-dipyrrolyl ketone (11%), bp 78–81°C/1 Torr; uv (ethanol): 243 nm (ε 16 700); ir (KCl): 1725 cm^{-1}; nmr τ: 2.70 (2H, t, αH), 3.65 (2H, t, βH). *Anal.* calcd. for $C_9H_8N_2O$: C 67.49, H 5.03, N 17.49; found: C 67.62, H 4.96, N 17.44.

(*c*) Following procedure 5(*b*), reaction of pyrrolylsodium (0.100 mol) and ethyl chloroformate (0.100 mol) gave only ethyl 1-pyrrolecarboxylate (87%).

(*d*) Reaction between pyrrolylpotassium suspension (0.100 mol) and ethyl chloroformate (0.100 mol) was carried out at reflux for 1½ h. Work-up was as described in 5(*b*). Only ethyl 1-pyrrolecarboxylate (64%) was obtained.

(*e*) As described in 5(*a*) a solution of ethyl chlorothiolformate (12.46 g, 0.100 mol) was added to the cold ether solution of pyrrolylmagnesium bromide (0.100 mol). After stirring 3 h the mixture was worked up to give ethyl 1-pyrrolethiolcarboxylate (3%) and ethyl 2-pyrrolethiolcarboxylate (42%) (5).

Ethyl 1-pyrrolethiolcarboxylate was also prepared by the addition of ethyl iodide (25.0 g, 0.150 mol) to 1-pyrrolylthiocarboxanilide (12*b*) (23.0 g, 0.120 mol) in aqueous 6 *M* sodium hydroxide (100 ml) followed by stirring at 100°C for 1 h. After cooling and separation of layers the aqueous layer was extracted twice with ether and the combined organic layers washed with water. The ether was removed and the residue heated to 100°C for 1 h with 6 *M* aqueous sulfuric acid (100 ml). After cooling, the ether extract was washed with 10% aqueous sodium bicarbonate and dried ($MgSO_4$). After removal of ether the product was distilled to give ethyl 1-pyrrolethiolcarboxylate (6.25 g, 24%), bp 105–106°C/10 Torr; uv (ethanol): 248 nm (ε 12 300); ir (film): 1680 cm^{-1}; nmr τ: 2.72 (2H, t, αH), 3.73 (2H, t, βH), 6.92 (2H, q, S—CH_2) 8.63 (3H, t, —CH_3). *Anal.* calcd. for C_7H_9NOS: C 54.19, H 5.85, N 9.03, S 20.65; found: C 54.32, H 5.79, N 9.13, S 20.78.

(*f*) Following procedure 5(*b*) but using ethyl chlorothiolformate, the products were ethyl 1-pyrrolethiolcarboxylate (4.85 g, 31%), 1,1′-dipyrrolyl ketone (1.11 g, 14%), and a trace of ethyl 2-pyrrolethiolcarboxylate. In addition, diethyl dithiolcarbonate (1.48 g), bp 105–109°C/42 Torr, was obtained. The infrared spectrum was identical to that of an authentic sample prepared by the literature method (29).

6. Solvents and Coordinating Agents

(*a*) After 1,2-dimethoxyethane (13.0 g, 0.150 mol) had been added to the solution of pyrrolylmagnesium bromide (0.100 mol), reaction 5(*a*) was repeated (see Table 2).

(*b*) Procedure 6(*a*) was followed, after adding dioxane (13.2 g, 0.150 mol) (see Table 2).

(*c*) After N,N,N′,N′-tetramethylethylenediamine (11.6 g, 0.100 mol) had been added to the solution of pyrrolylmagnesium bromide (0.100 mol), the mixture was refluxed 3 h, cooled, and treated as in 5(*a*). Products obtained were ethyl 1-pyrrolecarboxylate (7.09 g, 51%), ethyl 2-pyrrolecarboxylate (0.71 g, 5%), and 1,2′-dipyrrolyl ketone (0.18 g, 2%), mp 60–61°C (petroleum) (lit. (5) mp 58–60°C), mixture mp undepressed.

(*d*) Procedure 6(*c*) was followed, using TMED (0.150 mol) (see Table 2).

(*e*) After adding various molar ratios of TMED to the solution of pyrrolylmagnesium bromide (0.100 mol), reaction 6(*c*) was repeated using ethyl chlorothiolformate (0.100 mol) (see Table 3).

7. Pyrrolylmagnesium Halide Changes

(*a*) Pyrrolylmagnesium chloride was prepared from butylmagnesium chloride. After addition of TMED (2 mol equiv.), the mixture was refluxed 3 h. The procedure 5(*a*) was then followed (see Table 4).

(*b*) Procedure 7(*a*) was followed, using pyrrolylmagnesium bromide (see Table 4).

(*c*) Pyrrolylmagnesium iodide was prepared from

ethylmagnesium iodide, then 7(*a*) was followed (see Table 4).

8. Temperature Changes

(*a*) Pyrrolyllithium was prepared as usual but in absolute dioxane. To this solution was added an equimolar quantity of ethyl carbonate in dioxane and the reaction mixture stirred at 36°C (oil bath) for 36 h. After removal of much dioxane under reduced pressure and addition of ether, the mixture was worked up in the usual manner. The products isolated were ethyl 1-pyrrolecarboxylate (41%) and ethyl 2-pyrrolecarboxylate (1%). The N/C ratio was 98:2.

(*b*) Procedure 8(*a*) was followed; the reaction mixture was kept at reflux for 13 h. The products isolated were ethyl 1-pyrrolecarboxylate (37%), ethyl 2-pyrrolecarboxylate (16%), and 1,2′-dipyrrolyl ketone (19%). The N/C ratio was now 65:35.

(*c*) Equimolar quantities of pyrrolyllithium and ethyl 1-pyrrolecarboxylate were refluxed in dioxane for 24 h. After the usual work-up the products were found to be ethyl 2-pyrrolecarboxylate (32%) and 1,2′-dipyrrolyl ketone (22%).

(*d*) A solution of ethyl 2-pyrrolecarboxylate in dioxane was refluxed with 2½ times its molar equivalent of pyrrolyllithium for 24 h. After work-up, 1,2′-dipyrrolyl ketone (62%) was isolated. No ethyl 1-pyrrolecarboxylate was detected.

(*e*) A mixture of lithium ethoxide (1.04 g, 0.020 mol) and 1,2′-dipyrrolyl ketone (1.60 g, 0.01 mol) was refluxed in dioxane (100 ml) for 24 h. After work-up, ethyl 2-pyrrolecarboxylate (0.47 g, 34%) was isolated. No ethyl 1-pyrrolecarboxylate was detected. About 20% of the ketone was recovered.

9. Acylation of the 2-Ester

A solution of ethyl 2-pyrrolecarboxylate (6.95 g, 0.050 mol) in ethyl ether (30 ml) was added slowly to ethylmagnesium bromide (0.05 mol) in ether (50 ml). Heat was evolved as well as large quantities of gas, and a white precipitate was observed. After 30 min reflux, the solution was cooled in a bath to about −20°C. To the cold solution, ethyl chloroformate (5.43 g, 0.050 mol) in ether (60 ml) was added over about 1½ h. Then the reaction was stirred at room temperature 17 h, hydrolyzed with saturated aqueous ammonium chloride, and worked up as usual. The product was ethyl 1,2-pyrroledicarboxylate (8.80 g, 83%), bp 86–87°C/1 Torr.

10. Reactions of Pyrrolylmagnesium Bromide

(*a*) Ethyl acetate (8.81 g, 0.100 mol) in absolute ether (90 ml) was added to a cold (−20°C) solution of pyrrolylmagnesium bromide (0.100 mol) in ethyl ether (60 ml) over 1½ h. The reaction mixture was stirred ½ h longer at −10°C. After the usual work-up, the product mixture was analyzed. Unreacted starting material was distilled, followed by 1-acetylpyrrole (0.69 g, 6%), bp 80–81°C/12 Torr, identical in physical properties to a sample prepared by the method of Reddy (30). The residue was cooled and recrystallized from cyclohexane to give 2-acetylpyrrole, mp 89–90°C (2.03 g, 19%), identical to authentic material (31).

(*b*) When this reaction was repeated with stirring at room temperature for 17 h there was no significant change in yield or ratio of products.

(*c*) When reaction 10(*a*) was repeated in the presence of a 1½:1 molar ratio of TMED – pyrrolylmagnesium bromide, and the product hydrolyzed with 6 *M* hydrochloric acid, the organic extract gave 1-acetylpyrrole (3%), 2-acetylpyrrole (1%), and 1-acetoacetylpyrrole (80%), bp 80–84°C/1 Torr; mp (cyclohexane) 49–51°C; uv (ethanol): 350 nm (ε 30 700); ir (KCl): 1710, 1685, 1625 cm^{-1}; nmr (CCl_4) τ: 0.24 (0.6H, s, —OH), 2.80 (2H, t, αH), 3.80 (2H, t, βH), 4.45 (0.6H, s, C=CH), 6.24 (0.8H, s, $—CH_2—$), 7.75 (1.2H, s, $—CH_3$), 7.95 (1.8H, s, $—CH_3$). *Anal.* calcd. for $C_9H_8NO_2$: C 63.57, H 6.00, N 9.27; found: C 63.67, H 5.98, N 9.25. A pink color was obtained with aqueous $FeCl_3$.

(*d*) To a solution of ethylmagnesium bromide (0.050 mol) and TMED (0.075 mol) in ethyl ether (40 ml) was added a solution of 1-acetylpyrrole (0.050 mol) in ethyl ether (20 ml) at such a rate as to keep at reflux. Following 1 h at reflux, the solution was cooled to room temperature and ethyl acetate (4.84 g, 0.055 mol) in absolute ether (40 ml) was added over a period of 1 h. After 17 h stirring at room temperature it was worked up as in 10(*c*) and, after removal of solvent, 1-acetoacetylpyrrole (60%) was isolated by vacuum distillation.

(*e*) Reaction 10(*a*) was repeated using acetyl chloride (7.85 g, 0.100 mol). After removal of the 1-acetylpyrrole (0.10 g, 1%) and 2-acetylpyrrole (4.08 g, 35%) by vacuum distillation, the residue was taken up in 1:1 ether – carbon tetrachloride. This solution was warmed to evaporate some of the ether causing 3-acetylpyrrole to crystallize, mp 113–114°C (0.43 g, 4%), identical in physical properties to an authentic specimen (32).

(*f*) Following the procedure of 10(*a*), reaction with ethyl carbonate gave ethyl 1-pyrrolecarboxylate (13.76 g, 70%) and ethyl 2-pyrrolecarboxylate (0.20 g, 2%).

(*g*) A solution of 1,1′-dipyrrolyl ketone (1.60 g, 0.010 mol) in ethyl ether (20 ml) was added slowly to pyrrolylmagnesium bromide (0.025 mol) in ethyl ether (40 ml). After ½ h reflux, the product was worked up as usual to give 1,2′-dipyrrolyl ketone (1.13 g, 70%). No 1,1′-dipyrrolyl ketone was recovered.

(*h*) Following procedure 10(*a*) reaction with ethyl oxalate (14.61 g, 0.100 mol) gave ethyl 1-pyrrolylglyoxylate ((3.10 g, 19%), bp 70–71°C/1 Torr; ir (KCl): 1760, 1725 cm^{-1}; nmr ($CDCl_3$) τ: 2.60 (2H, t, αH), 3.62 (2H, t, βH), 5.55 (2H, q, $—CH_2—$), 8.59 (3H, t, $—CH_3$). *Anal.* calcd. for $C_8H_9NO_3$: C 57.48, H 5.43, N 8.38; found: C 57.57, H 5.53, N 8.45) and ethyl 2-pyrrolylglyoxylate ((3.69 g, 22%), bp 105–109°C/1 Torr, mp 39–40°C (lit. (21) mp 44.5°C); ir (film): 1730, 1645 cm^{-1}; nmr ($CDCl_3$) τ: 2.77 (1H, m, H_5), 2.92 (1H, m, H_2), 3.80 (1H, m, H_4), 5.71 (2H, q, $—CH_2—$), 8.72 (3H, t, $—CH_3$)).

(*i*) The procedure of 10(*a*) was followed using N,N′-dicyclohexylcarbodiimide (20.63 g, 0.100 mol). After stirring at room temperature for 17 h, the reaction mixture was worked up in the usual manner. Vacuum distillation gave N,N′-dicyclohexyl-1-pyrrolylcarbamidine (25.5 g, 93%) at 140–141°C/1 Torr; mp 42–44°C; uv (ethanol): 223 nm (ε 13 400); ir (KCl): 1640 cm^{-1}; nmr ($CDCl_3$) τ: 3.25 (2H, t, αH), 3.86 (2H, s, βH), 6.00 (1H, b s, NH), 6.78 (2H, s, N—CH), 8.5 (20H, m, 10-CH_2—). *Anal.* calcd. for $C_{17}H_{27}N_3$: C 74.68, H 9.95, N 15.37; found: C 74.48, H 10.11, N 15.25.

(*j*) The procedure of 10(*a*) was repeated with dimethylcyanamide (7.00 g, 0.100 mol). Following 17 h of stirring

at room temperature, the customary work-up gave unreacted pyrrole, dimethylcyanamide, and N,N′-dimethyl-1-pyrrolylcarbamidine (1.03 g, 8%), bp 109–110°C/15 Torr; uv (ethanol): 224 nm (ε 13 000); ir (film): 1635 cm^{-1}; nmr ($CDCl_3$) τ: 3.15 (2H, t, αH), 3.83 (2H, t, βH), 3.90 (1H, b s, NH), 7.20 (6H, s, NCH_3). *Anal.* calcd. for $C_7H_{11}N_3$: C 61.29, H 8.08, N 30.63; found: C 61.06, H 8.04, N 30.57. This reaction was repeated using an ether solution of pyrrolyllithium (0.100 mol) together with TMED (0.200 mol) and the product hydrolyzed with water and worked up to give N,N′-dimethyl-1-pyrrolylcarbamidine 1.30 g (10%). As well, starting materials were recovered.

(*k*) A solution of pyrrolyllithium (0.100 mol) in ethyl ether (40 ml) and TMED (0.200 mol) was treated at about −20°C with methyl thiocyanate (7.30 g, 0.100 mol) in ether (40 ml) over ½ h, and stirred at this temperature a further 1 h before the usual work-up. Vacuum distillation gave two products. The first was 1,1′-dipyrrolyl ketimine (3.97 g, 25%), bp 84–88°C/1 Torr, mp 47–48.5°C (petroleum bp 30–50°C); uv (ethanol): 238 nm (ε 17 800): ir (KCl): 3240, 1660 cm^{-1}; nmr ($CDCl_3$) τ: 2.34 (1H, b s, NH), 2.92 (2H, t, αH), 3.70 (2H, t, βH). *Anal.* calcd. for $C_9H_9N_3$: C 67.91, H 5.70, N 26.40; found: C 68.03, H 5.79, N 26.26. The second product was 1,1′-dipyrrolyl *N*-methylthioketimine (5.69 g, 28%), bp 105–110°C/1 Torr, mp 41–42°C (petroleum, bp 30–50°C); uv (ethanol): 239 nm (ε 9300), 296 nm (ε 11 400); ir: 1640, 1625 cm^{-1}; nmr ($CDCl_3$) τ: 3.80 (2H, t, αH), 3.71 (2H, t, βH), 7.32 (3H, s, —SCH_3). *Anal.* calcd. for $C_{10}H_{11}N_3S$: C 58.53, H 5.40, N 20.84, S 15.59; found: C 58.50, H 5.51, N 20.38, S 15.66.

11. Reduction of Compound ***1***

A mixture of N,N′-dicyclohexyl-1-pyrrolylcarbamidine (**1**) (3.22 g, 0.012 mol) and lithium aluminum hydride (0.88 g, 0.024 mol) in ethyl ether (200 ml) was refluxed for 26 h. The mixture was cooled in ice and hydrolyzed with water-saturated ether (200 ml). The organic solution was filtered, washed with water, and dried ($MgSO_4$). After filtration and solvent removal, the residue was vacuum distilled to give N,N′-dicyclohexylformamidine (1.38 g, 56%), bp 120–121°C/1 Torr, mp 102–104°C (lit. (26) mp 106°C). Other physical properties were consistent with this structure.

Acknowledgements

The continued financial support of the National Research Council of Canada and the Memorial University of Newfoundland is gratefully acknowledged. The authors are also indebted to Drs. C. E. Loader, A. R. Stein, and M. J. Newlands for many helpful discussions.

1. (*a*) H. Fischer and H. Orth. Die chemie des pyrrols. Vol. I. Akademische Verlagsgesellschaft, Leipzig. 1943. p. 120; (*b*) A. Gossauer. Die chemie der pyrrole. Springer Verlag, Berlin, Heidelberg, New York. 1974. p. 169.
2. G. P. Bean. Ph.D. Thesis. The Pennsylvania State University, University Park, PA. 1962.
3. M. G. Reinecke, H. W. Johnson, Jr., and J. F. Sebastian. J. Am. Chem. Soc. **85**, 2859 (1963).
4. S. A. Shevelev. Russ. Chem. Rev. **39**, 844 (1970).
5. C. E. Loader and H. J. Anderson. Can. J. Chem. **49**, 45 (1971).
6. (*a*) R. G. Pearson. J. Chem. Educ. **45**, 581 (1968); **45**, 643 (1968); (*b*) R. G. Pearson. Survey of progress in chemistry. Vol. 5. *Edited by* A. F. Scott. Academic Press, New York and London. 1969. pp. 1–52; (*c*) T. L. Ho. Chem. Rev. **75**, 1 (1975).
7. N. C. Wang, K. E. Teo, and H. J. Anderson. Can. J. Chem. This issue.
8. C. F. Hobbs, C. K. McMillin, E. P. Papadopoulos, and C. A. VanderWerf. J. Am. Chem. Soc. **84**, 43 (1962).
9. G. P. Bean. J. Org. Chem. **32**, 228 (1967).
10. M. G. Reinecke, J. F. Sebastian, H. W. Johnson, Jr., and C. Pyun. J. Org. Chem. **37**, 3066 (1972).
11. P. Hodge and R. W. Rickards. J. Chem. Soc. 2543 (1963).
12. (*a*) E. P. Papadopoulos and H. A. Habiby. J. Org. Chem. **31**, 327 (1966); (*b*) E. P. Papadopoulos. J. Org. Chem. **31**, 3060 (1966).
13. A. Treibs and A. Dietl. Justus Liebigs Ann. Chem. **619**, 80 (1958).
14. E. C. Ashby, J. Laemmle, and H. M. Neumann. Acc. Chem. Res. **7**, 272 (1974).
15. G. Ciamician and P. Silber. Ber. **17**, 1437 (1884).
16. E. P. Papadopoulos and K. I. Y. Tabello. J. Org. Chem. **33**, 1299 (1968).
17. R. Gompper. Angew. Chem. Int. Ed. **3**, 560 (1964).
18. A. J. Castro, J. F. Deck, N. C. Ling, J. P. Marsh, Jr., and G. E. Means. J. Org. Chem. **30**, 344 (1965).
19. P. Hodge and R. W. Rickards. J. Chem. Soc. 459 (1965).
20. C. E. Loader and H. J. Anderson. Can. J. Chem. **49**, 1064 (1971).
21. B. Oddo. Gazz. Chim. Ital. **50**, 258 (1920); Chem. Abstr. **15**, 2096 (1921).
22. V. V. Chelintzev and D. K. Skvortzov. J. Russ. Phys. Chem. Soc. **47**, 170 (1915); Chem. Abstr. **9**, 1472 (1915).
23. N. Potokhin. J. Russ. Phys. Chem. Soc. **59**, 761 (1927); Chem. Abstr. **22**, 3409 (1928).
24. J. McConnel, V. Petrow, and B. Sturgeon. J. Chem. Soc. 3332 (1953).
25. M. W. Moon, L. T. Bell, and D. M. Webster. J. Org. Chem. **39**, 315 (1974).
26. C. Grundmann and A. Kreutzberger. J. Am. Chem. Soc. **77**, 6559 (1955).
27. G. R. Clemo and G. R. Ramage. J. Chem. Soc. 49 (1931).
28. F. K. Signaigo and H. Adkins. J. Am. Chem. Soc. **58**, 1122 (1936).
29. G. Bulmer and F. G. Mann. J. Chem. Soc. 666 (1945).
30. G. S. Reddy. Chem. Ind. 1426 (1965).
31. H. J. Anderson and L. C. Hopkins. Can. J. Chem. **44**, 1831 (1966).
32. C. E. Loader and H. J. Anderson. Tetrahedron, **25**, 3879 (1969).

Pyrrole chemistry. XVII. Alkylation of the pyrrolyl ambident anion

NAM-CHIANG WANG, KANG-ER TEO, AND HUGH J. ANDERSON
Department of Chemistry, Memorial University of Newfoundland, St. John's, Nfld., Canada A1C 5S7

Received May 19, 1977

NAM-CHIANG WANG, KANG-ER TEO, and HUGH J. ANDERSON. Can. J. Chem. **55**, 4112 (1977).

A series of experiments were carried out to find optimum conditions for C- and N-alkylation of the pyrrolyl ambident anion. While almost total C-alkylation could be obtained, isolation of a single alkylation product was not feasible. However, N-alkylation of pyrrole and several 2-substituted pyrroles was readily achieved by phase transfer catalysis with primary alkyl halides.

NAM-CHIANG WANG, KANG-ER TEO et HUGH J. ANDERSON. Can. J. Chem. **55**, 4112 (1977).

On a effectué une série d'expériences afin de trouver les conditions optimales pour la C- et la N-alkylation de l'anion ambivalent pyrrolyle. Alors que l'on peut obtenir une C-alkylation presque totale, il n'est pratiquement pas possible d'isoler un seul produit d'alkylation. Toutefois la N-alkylation du pyrrole et de plusieurs pyrroles substitués en position 2 peut être réalisée par une catalyse de transfert de phase avec des halogénures d'alkyles primaires.

[Traduit par le journal]

In the course of our investigation of the acylation of the pyrrolyl ambident anion under various conditions (1) it seemed desirable to use the information gained to establish the simplest possible preparative methods for *C*- and *N*-alkylpyrroles. It has been necessary to extend earlier work by others as well as to repeat some of it under conditions comparable to those of our acylations.

The review by Shevelev (2) has related, among many other reactions, most of the known alkylation experiments on the pyrrolyl and indolyl ambident anions to the 'hard and soft acids and bases principle' (3). Thus alkylation of the pyrrolyl and indolyl salts of the hardest cations give the lowest N/C ratio.

The work of Hobbs *et al.* (4) has established that the order of increasing N/C ratio for allyl, crotyl, and benzyl halides is $Li^+ < Na^+ < K^+ < NR_4^+$, with the hardest ion, Li^+, giving most C-substitution, as expected. The even harder Mg^{2+} of Grignard reagents leads to almost exclusive C-substitution by allyl bromide (5). The saturated alkyl is harder than the allyl group and gives a higher N/C ratio under comparable conditions (6). Nevertheless, the amount of N-alkylation is very small with Grignard reagents (7).

Another factor is that the N/C ratio changes with the changing polarity of aprotic solvents. For example, the change from ethers to arenes and alkanes in the reaction of pyrrolylpotassium with allyl halides caused a decrease from 4:1 to 1:6 in the N/C ratio (4). The stepwise addition of the strongly coordinating dipolar aprotic solvent, hexamethylphosphoric triamide (HMPA), to the tetrahydrofuran solution of indolylmagnesium halide caused a regular increase in the N/C ratio of methylation products (8). In ethyl ether and tetrahydrofuran (THF), pyrrolylmagnesium bromide gave almost entirely C-methylation, but in pure HMPA gave only N-methylation (5). This hard coordinating agent strongly associates with the hard metal and separates the ion pair.

In an attempt to establish an experimentally convenient approach to preparative N-alkylation (Table 1) we first added 2 mol equiv. of HMPA to the ethyl ether solution of 1 mol equiv. of pyrrolylmagnesium bromide. While a rise in temperature and the appearance of a white precipitate was observed, there was no N-methylation with methyl iodide nor any significant change in the distribution of C-substituted products. Although our results were similar to those of Reinecke *et al.* (8), at lower ratios of HMPA to Grignard reagent we did not obtain in the pyrrole series the complete change to N-methylation they observed in the indole series. Because alkylation in pure HMPA required preparation of the Grignard reagent in ether and replacement of it by HMPA (5), this was not considered a satisfactorily simple approach to the preparation of *N*-alkylpyrroles.

Griffin and Obrycki (9) found little change in

TABLE 1. Methylation of pyrrolylmagnesium bromide

Ratio HMPA / Pyrrolyl–MgBr	1-Methyl (%)	2-Methyl (%)	3-Methyl (%)	2,3-Dimethyl (%)	2,5-Dimethyl (%)	2,3,5-Trimethyl (%)	N/C* ratio
Methyl iodide							
0:1	0.0	7.4	4.9	10.9	1.3	5.9	0:100
2:1	0.0	10.3	5.4	4.6	3.8	6.9	0:100
3:1	0.7	8.6	5.0	3.8	3.8	6.1	6:94
4:1	12.2	7.0	4.5	3.8	2.2	4.7	36:64
5:1	21.8	4.8	3.6	2.1	0.9	0.8	66:34
Dimethyl sulfate							
2:1	16.5	6.1	5.0	2.1	0.6	0.0	56:44
Methyl *p*-toluenesulfonate							
2:1	28.8	3.5	2.9	1.5	0.4	0.0	78:22
4:1	49	Trace	Trace	—	—	—	99:1

*About 30–40% of unchanged pyrrole was recovered from each reaction.

the small N/C ratio when pyrrolylmagnesium bromide in ethyl ether reacted with methyl iodide, bromide, sulfate, phosphate, or *p*-toluenesulfonate. However, using the softer allyl group, Papadopoulos and Tabello (6) obtained a greater N/C ratio for alkali metal salts of pyrrole with allyl *p*-toluenesulfonate than with allyl bromide. Thus, the harder leaving group does seem to have an effect under favorable conditions.

Reinecke *et al.* (8) had found that the addition of 2 mol equiv. of HMPA before treatment with methyl iodide permitted observation of decreasing N/C ratios for indolylmagnesium chloride, bromide, and iodide in THF solution. We added 2 mol equiv. of HMPA of pyrrolylmagnesium bromide and found it possible to observe that while no N-methylation took place with methyl iodide, there was a substantial proportion with methyl sulfate and *p*-toluenesulfonate. That is, the harder the alkylating agent the more the N-attack, provided the Mg is coordinated with a strongly polar aprotic reagent. We have also used tetramethylethylenediamine (TMED) in this way to observe the N/C ratios in some acylations (1).

It is not easy to alter the Grignard reaction to obtain nearly all N-alkylation by changes in solvent, complexing agent, or alkylating agent. The traditional use of alkali metal salts for N-alkylation requires anhydrous conditions and considerable care. One simple approach appeared to be the use of phase transfer catalysis which has recently been used successfully to N-alkylate indole and to benzylate pyrrole (10). The only other methods available require the formation of the relatively expensive thallium(I) salt of pyrrole (11) or the use of potassium hydroxide – dimethyl sulfoxide (12).

The phase transfer catalysis method makes use of the very soft quaternary ammonium salt of the ambident anion. The choice of a suitable tetraalkylammonium cation enables transfer of its ion pair with the pyrrolyl anion from the aqueous phase into an organic one of low polarity where it can react with the alkyl halide (13) at the harder (N) centre.

Our results for alkylations of pyrrole itself are recorded in Table 2. In each example the product was isolated by distillation and was found to show a ^{1}Hmr spectrum free of C-alkylated product except for the allyl halide reaction. There the ^{1}Hmr spectrum integration showed both 1- and 2-allylpyrroles in a ratio of about 1:4. So, once again the softer allyl halide tended to give a lower N/C ratio than did the alkyl halides (10*b*). The results were of preparative utility for primary alkyl halides, and did not require the alkyl iodides used by others (11, 12). They were not as satisfactory for the secondary (isopropyl) halide, and failed for the tertiary (*tert*-butyl) halide in common with the other methods (11, 12). For reasons that are not clear, butyl bromide gave superior yields to butyl chloride. Iodides are generally not satisfactory in the phase transfer method (13) as they give the softest alkylating reagent. The harder reagents, methyl sulfate and methyl *p*-toluenesulfonate, were more successful than methyl, ethyl, or butyl iodides.

The phase transfer method was also satisfactory for the methyl sulfate methylation of pyr-

TABLE 2. Phase transfer alkylation of pyrrole

Alkylating agent	Pyrrole isolated	% yield	Boiling or melting range (°C/Torr) Present study	Lit. (ref.)
Methyl iodide	1-Methyl-	30		
Methyl sulfate	1-Methyl-	68	113–114	114–115/747 (16*a*)*
Methyl *p*-toluenesulfonate	1-Methyl-	72		
Ethyl iodide	1-Ethyl-	28	129–130	129–130/762 (16*a*)*
Ethyl bromide	1-Ethyl-	84		
Propyl bromide	1-Propyl-	70	145–146	145.5–146.5 (16*a*)*
Butyl iodide	1-Butyl-	33		
Butyl bromide	1-Butyl-	84	166–169	170–171/760 (16*a*)*
Butyl chloride	1-Butyl-	25		
Pentyl bromide	1-Pentyl-	81	42–43/0.5	80–82/15 (16*b*)
Hexyl bromide	1-Hexyl-	70	50/0.5	210–215 (16*c*)
Isopropyl bromide	1-Isopropyl-	5	152–155	49–51/21 (16*d*)*
tert-Butyl chloride		N.R.		
Benzyl bromide	1-Benzyl-	67	88–90/0.8–0.9	248 (mp 15°C) (16*a*)*
3-Chloropropionitrile	1-Cyanoethyl-	71	93–94/0.5	132–133/10 (16*e*)

*^{1}Hmr spectra agree with ref. 17.

TABLE 3. Phase transfer methylation of substituted pyrroles with methyl sulfate

Substrate	Product	% yield	Boiling range (°C/Torr) Present study	Lit. (ref.)
2-Methylpyrrole	1,2-Dimethylpyrrole	25	140–141/760	139–141/760 (17*a*)
2-Acetylpyrrole	1-Methyl-2-acetylpyrrole	94	30–31/0.5	75–76/15 (17*b*)
2-Pyrrolecarbaldehyde	1-Methyl-2-pyrrolecarbaldehyde	77	30–31/0.5	75–76/12 (17*c*)
2-Pyrrolecarbonitrile	1-Methyl-2-pyrrolecarbonitrile	76	35–37/0.5	86–88/11 (17*d*)

roles having an electron withdrawing group at position-2. However, 2-methylpyrrole gave a poor yield of 1,2-dimethylpyrrole (see Table 3).

While alkylation of the pyrrole Grignard gives entirely C-substituted products, it can be seen from Table 1 that the method is not suitable for the preparation of 2- or 3-methylpyrrole. Most authors found (5, 7, 9) that the C-alkylated product was a mixture from which no single component was easily obtained in a yield of preparative value, or that the overall yield was low (14). No simple modification of the procedure has improved this situation so far. It appears that 2- and 3-alkylpyrroles are still best prepared through reduction of the corresponding acylpyrroles as suggested by Skell and Bean (15).

Preparation of the Grignard reagents from 2- and 3-methylpyrroles and 2,5-dimethylpyrrole and their reactions with methyl iodide helped to confirm the structures of the methylation products as well as to confirm that only C-methylation occurred in each case.

Experimental

Instruments and conditions were as described in ref. 19. Analysis of reaction mixtures was carried out on a Varian 1520B gas chromatograph equipped with a 12 ft column packed with 30% Carbowax 20M on Chromosorb W (80–100 mesh) with helium as carrier gas. Each product was dried, the volume reduced to a fixed volume, and a 1 ml sample retained for analysis as described in ref. 1. The rest of the solution was used for isolation and identification of products.

Pyrrolylmagnesium Bromide

This compound was prepared as described in ref. 1. All Grignard reagents were prepared and reacted under dry nitrogen.

Reaction with Methyl Iodide

Pyrrolylmagnesium bromide (0.400 mol) in absolute ether (800 ml) was cooled in ice, and methyl iodide (113 g, 0.800 mol) in absolute ether (100 ml) was added slowly with stirring. The reaction mixture was stirred overnight at room temperature, cooled in ice, and cold water added until the product was distributed between two layers. After two further ether extractions of the aqueous layer, the combined extracts were washed twice with water, flushed with nitrogen, and dried (K_2CO_3).

The dried product was reduced to 500 ml and analyzed by gas chromatography using authentic samples of pyrrole: 1-, 2-, and 3-methylpyrrole; 2,3- and 2,5-dimethylpyrrole; and 2,3,5-trimethylpyrrole for comparison. Distillation enabled separation into: (*a*) unreacted pyrrole, bp 129–131°C/760 Torr; (*b*) a mixture of 2- and 3-methylpyrrole, bp 147–149°C/760 Torr; (*c*) a mixture of 2,3- and 2,5-dimethylpyrrole, bp 65–67°C/10 Torr; and (*d*) a mixture of 2,3-, 2,5-dimethylpyrrole and 2,3,5-trimethylpyrrole, bp 72–75°C/10 Torr. Percentages are listed in Table 1. These fractions were used as well to compare nmr (and ir of fractions (*a*) and (*d*)) spectra with authentic samples. The physical properties of these compounds are given by Hinman and Theodoropulos (18*a*).

Reactions with Methyl Iodide in the Presence of HMPA

A solution of hexamethylphosphoric triamide (21.5 g, 0.120 mol) in absolute ether (10 ml) was added slowly to the pyrrolylmagnesium bromide (0.040 mol) in absolute ether (50 ml) at room temperature. The reaction mixture was refluxed 30 min, then cooled in ice. The reaction with methyl iodide (5.68 g, 0.040 mol), work-up, and analysis are described above, except that an earlier fraction, 1-methylpyrrole, bp 113–114°C, was collected and identified.

Results of experiments using varying proportions of HMPA are given in Table 1.

Reactions with Methyl p-Toluenesulfonate and Methyl Sulfate in the Presence of HMPA

These reactions were carried out, worked up, and analyzed as before. The results are given in Table 1.

Reaction of 2-Methylpyrrolylmagnesium Bromide with Methyl Iodide

The Grignard reagent was prepared from 2-methylpyrrole (0.040 mol) and reacted with methyl iodide (0.04 mol) in the manner described for pyrrole. Work-up and analysis was as before, giving 2,5-dimethylpyrrole (0.55 g, 17%), 2,3-dimethylpyrrole (0.43 g, 11%) and 2,3,5-trimethylpyrrole (0.33 g, 8%).

Reaction of 3-Methylpyrrolylmagnesium Bromide with Methyl Iodide

The Grignard reagent from 3-methylpyrrole (0.0070 mol) reacted with methyl iodide (0.0070 mol) gave, after the usual treatment, 2,3-dimethylpyrrole (0.13 g, 22%) and 2,3,5-trimethylpyrrole (0.17 g, 24%).

Reaction of 2,5-Dimethylpyrrolylmagnesium Bromide with Methyl Iodide

The Grignard reagent from 2,5-dimethylpyrrole (0.010 mol) reacted with methyl iodide (0.010 mol) gave, after the usual treatment, 2,3,5-trimethylpyrrole (0.22 g, 20%).

Typical Phase Transfer Catalysis Alkylation

A 50% aqueous solution of sodium hydroxide (5 ml) was added to a solution containing pyrrole (0.67 g, 0.010 mol), butyl bromide (1.5 g, 0.011 mol), and tetrabutylammonium bromide (0.32 g, 0.0010 mol) in methylene chloride (10 ml) with external cooling. The mixture was then stirred and gently refluxed for 20 h. The resulting mixture was diluted with water and extracted with methylene chloride. The combined extracts were washed with 2 *M* HCl, water, saturated brine solution, and dried ($MgSO_4$). The solvent was removed *in vacuo* at a temperature <40°C. A crude yield of brown liquid (1.14 g, 93%) was obtained. The crude product was then distilled at reduced pressure to give pure 1-butylpyrrole (1.03 g, 84%); the bp (Table 2) was in accord with the literature (16*a*) and its pmr and mass spectrum in agreement with the structure.

See Table 2 for other alkylations.

Reactions of 2-substituted pyrroles were carried out similarly. (Table 3). Some alkylations were checked for yield on a 10 × scale.

Acknowledgment

The continued financial support of the National Research Council of Canada and the Memorial University of Newfoundland is gratefully acknowledged.

1. N.-C. Wang and H. J. Anderson. Can. J. Chem. This issue.
2. S. A. Shevelev. Russ. Chem. Rev. **39**, 844 (1970).
3. (*a*) R. G. Pearson. J. Chem. Educ. **45**, 581 (1968); **45**, 643 (1968); (*b*) R. G. Pearson. *In* Survey of progress in chemistry. Vol. 5. *Edited by* A. F. Scott. Academic Press, New York and London. 1969. pp. 1–52.
4. C. F. Hobbs, C. K. McMillin, E. P. Papadopoulos, and C. A. VanderWerf. J. Am. Chem. Soc. **84**, 43 (1962).
5. G. Casnati and A. Pochini. Chim. Ind. Milan, **48**, 262 (1966).
6. E. P. Papadopoulos and K. I. Y. Tabello. J. Org. Chem. **33**, 1299 (1968).
7. G. P. Bean. J. Org. Chem. **32**, 228 (1967).
8. M. G. Reinecke, J. F. Sebastian, H. W. Johnson, Jr., and C. Pyun. J. Org. Chem. **37**, 3066 (1972).
9. C. E. Griffin and R. Obrycki. J. Org. Chem. **29**, 3090 (1964).
10. (*a*) A. Barco, S. Benetti, G. P. Pollini, and P. G. Baraldi. Synthesis, 124 (1976); (*b*) V. Bocchi, G. Casnati, A. Dossena, and F. Villani. Synthesis, 414 (1976); (*c*) A. Jonczyk and M. Makosza. Rocz. Chem. **49**, 1203 (1975).
11. C. F. Candy and R. A. Jones. J. Org. Chem. **36**, 3993 (1971).
12. H. Heaney and S. V. Ley. J. Chem. Soc. Perkin Trans. I, 499 (1973).
13. (*a*) E. V. Dehmlow. Angew. Chem. Int. Ed. Engl. **13**, 170 (1974); (*b*) M. Makosza. Pure Appl. Chem. **43**, 439 (1975); (*c*) J. Dockx. Synthesis, 441 (1973).
14. A. J. Castro, J. F. Deck, N. C. Ling, J. P. Marsh, Jr., and G. E. Means. J. Org. Chem. **30**, 344 (1965).
15. P. S. Skell and G. P. Bean. J. Am. Chem. Soc. **84**, 4655 (1962).
16. (*a*) H. Fischer and H. Orth. Die chemie des pyrroles. Vol. 1. Akademische Verlagsgesellschaft, Leipzig. 1943. pp. 28, 29; (*b*) H. Adkins and L. G. Lundsted. J. Am. Chem. Soc. **71**, 2964 (1949); (*c*) R. J. Zellner. U.S. Patent No. 3 008 965 (1961); Chem. Abstr. **57**, p5895 (1962); (*d*) C. F. Candy, R. A. Jones, and P. H. Wright. J. Chem. Soc. C, 2563 (1970); (*e*) J. M. Patterson, J. Brasch, and P. Drenchko. J. Org. Chem. **27**, 1652 (1962).
17. C. F. Candy and R. A. Jones. J. Org. Chem. **36**, 3993 (1971).

18. (*a*) R. L. HINMAN and S. THEODOROPULOS. J. Org. Chem. **28**, 3052 (1963); (*b*) H. FISCHER and H. ORTH. Die chemie des pyrroles. Vol. 1. Akademische Verlagsgesellschaft, Leipzig. 1943. p. 207; (*c*) H. FISCHER and H. ORTH. Die chemie des pyrroles. Vol. 1. Akademie der Verlaggesellschaft, Leipzig. 1943. p. 174; (*d*) H. J. ANDERSON. Can. J. Chem. **37**, 2053 (1959).
19. H. J. ANDERSON and H. NAGY. Can. J. Chem. **50**, 1961 (1972).

Stereospecific syntheses of the α-patchoulene and α-cedrene skeletons from a common intermediate

PIERRE DESLONGCHAMPS, JACQUES LAFONTAINE, LUC RUEST, AND PIERRE SOUCY

Laboratoire de synthèse organique, Département de chimie, Université de Sherbrooke, Sherbrooke (Qué.), Canada J1K 2R1

Received June 28, 1977

PIERRE DESLONGCHAMPS, JACQUES LAFONTAINE, LUC RUEST, and PIERRE SOUCY. Can. J. Chem. **55**, 4117 (1977).

The synthesis of the cyclopropane diketone **3** and its specific conversion into the tricyclic enedione **4** (cedrene skeleton) under kinetic control and into the tricyclic enedione **5** (patchoulene skeleton) under thermodynamic control is reported.

PIERRE DESLONGCHAMPS, JACQUES LAFONTAINE, LUC RUEST et PIERRE SOUCY. Can. J. Chem. **55**, 4117 (1977).

On rapporte la synthèse de la dicétone cyclopropanique **3** et sa transformation spécifique en ènedione tricyclique **4** (squelette du cédrène) sous contrôle cinétique et en ènedione tricyclique **5** (squelette du patchoulène) sous contrôle thermodynamique.

The sesquiterpenes α-cedrene and α-patchoulene are known to possess the structures **1** (1) and **2** (2) respectively (Scheme 1). If both structures are rewritten and represented by formulas **1***A* and **2***A*, it is interesting to note that α-cedrene and α-patchoulene have rings A and B identical (except for the configuration of the secondary methyl group) and that they differ by the attachment of one of the bonds of ring C. Ring C is attached to C-1 in cedrene and to C-5 in α-patchoulene. Both structures differ also by the position of the methyl group in ring C which is at C-8 in **1***A* and at C-10 in **2***A*. This analysis led us to imagine a synthetic route which could potentially produce both skeletons via a single intermediate. We wish to report the synthesis of the cyclopropane diketone **3**, a common intermediate lacking only the methyl group of ring C, and its specific conversion into the tricyclic enediones **4** (cedrene skeleton) or **5** (patchoulene skeleton) respectively.

Synthesis of the Cyclopropane Diketone 3

The synthetic route chosen to build **3** is described in Scheme 2. Both epimeric diacetate anhydrides **10***A* (R = H, R′ = OAc) and **10***B* (R = OAc, R′ = H) have been obtained pure and were individually transformed into **3**. The key steps from **10** are the formation of the tetrasubstituted olefins (**10** → **12**), the Arndt–Eistert homologation of the side chain (**12** → **16**), and the formation of the cyclopropane intermediates (**16** → **19**) (3) which were then converted into **3** by oxidation of the cyclopropane alcohols **20** and **21**. The details of these transformations which occurred in good yield in both epimeric series are described in the Experimental. The pyrolysis of the epimers **11** (*A* and *B*) was carried at 200–210°C under nitrogen at atmospheric pressure and this interesting elimination reaction proceeded well in both cases.[1]

The epimeric mixture (at carbon-2) **9** is known; it is one of the intermediates in the synthesis of α-cedrene carried out by Stork and Clarke (7). In their original synthesis, alkylation of the β-ketoester **6** with benzyl α-bromopropionate gave **7** (X = $OCH_2C_6H_5$) which was then converted (into the methyl ketone **8**) in five operations by the successive transformation of the benzyl ester group into a carboxylic acid (**7**, X = OH), an acid chloride (**7**, X = Cl), a diazoketone (**7**, X = CHN_2), an α-chloroketone (**7**, X = CH_2Cl), and a methyl ketone (**8**).

We have repeated this sequence of reactions and have obtained only one epimer (at carbon-6)

[1]This reaction does not proceed by elimination of acetic acid (Scheme 3) to give the intermediate **22** which could then undergo a retroene decarboxylative elimination (4), since the pyrolysis of **11** (COOH = COOD) did not give **12** (X = D) containing a deuterium. It is therefore either a direct elimination which could occur via an eight-membered transition state **23** (5) or an indirect one, via internal anhydride formation **24** followed by β-lactone **25** and loss of CO_2 (6).

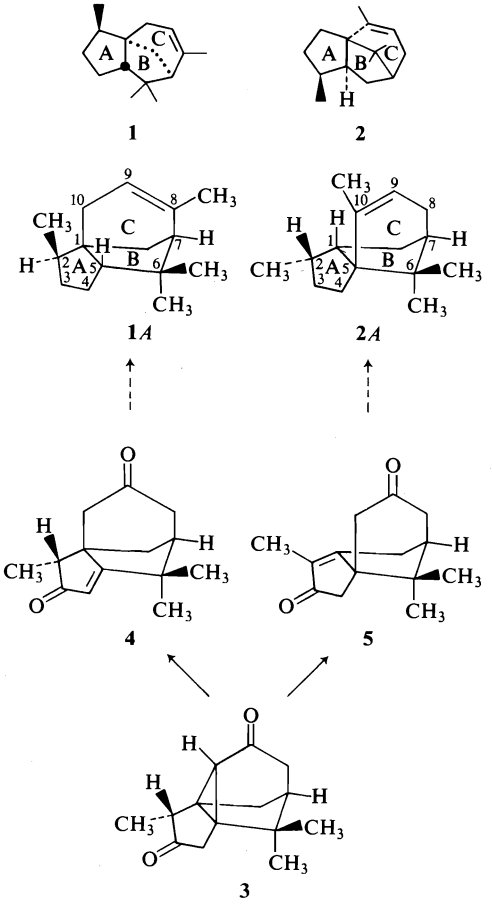

SCHEME 1

of diketone **8**. Treatment of that pure epimer of **8** with potassium *tert*-butoxide in *tert*-butanol gave a mixture of epimers **9**.

We have found that the same mixture of epimers **9** could be obtained in two steps from the β-ketoester **6**. Alkylation of **6** with 3-bromo-2-butanone gave an epimeric mixture (at carbon-6) of diketone **8** which was then converted into the same mixture of epimers **9**.

The reduction of crude **9** with sodium borohydride in ethanol followed by hydrolysis with aqueous potassium hydroxide and treatment with acetic anhydride in the presence of *p*-toluenesulfonic acid in benzene, gave a crystalline mixture of the epimers **10** which were separated by fractional crystallization.

Configuration of Epimers 10A and 10B

With the epimer **10***A*, a nuclear Overhauser effect (8) was not observed between the secondary methyl group and the proton H_3 (Scheme 4). This result was taken as evidence that the secondary acetate group is *cis* to the secondary methyl group. In the case of the epimer **10***B*, a 12% increase in the intensity of the signal for the proton H_3 was observed by irradiation of the secondary methyl group. This result was taken as evidence that the secondary methyl group is *trans* to the secondary acetate group in **10***B*.

The following series of transformations (Scheme 4) constitute a chemical proof that compounds **10***A* and **10***B* are epimeric at carbon-3 only. Basic hydrolysis of **10***B* followed by treatment with diazomethane gave the crystalline diol diester **26** which was then oxidized by the chromium trioxide – pyridine reagent (9) to give the ketoalcohol diester **27**. Reduction of **27** with sodium borohydride in methanol gave a mixture of the dihydroxy dimethyl esters **26** (66%) and **28** (34%) which were separated by preparative thin-layer chromatography. Oxidation of **28** with the chromium trioxide – pyridine reagent gave back **27**. Finally, basic hydrolysis of **26** and **28** followed by acetylation gave the epimers **10***B* and **10***A* respectively. The fact that the epimers **20** and **21** (Scheme 2) are both converted to the same cyclopropane diketone **3** by oxidation with the chromium trioxide – pyridine reagent further confirms that compounds of the *A* and the *B* series have different configurations at carbon-3 only.

The relative configurations of the secondary methyl and acetate groups of ring A with the anhydride and the tertiary acetate groups in compounds **10** could be determined by proton nmr and infrared spectroscopic analysis. The signal of the hydrogen at carbon-3 appears at a much lower field in **10***A* (5.41 δ) than in **10***B* (4.84 δ) indicating that this hydrogen must be *cis* to the anhydride function in **10***A* (Scheme 4) and *trans* in **10***B*. It appears reasonable to assume that the carbonyl group of an anhydride function properly oriented could have a deshielding effect (10). The secondary methyl groups have virtually the same chemical shift in both epimers (**10***A* = 1.02 δ and **10***B* = 1.08 δ) and the value corresponds to that expected for a methyl group not subject to strong deshielding or shielding effects. In support of this assignment, the secondary methyl group of norcedrene dicarboxylic acid anhydride (**29**)[2] appears at 1.34 δ (11). Thus the methyl group cannot be *cis* to the anhydride function in **10***A* and **10***B*.

[2]We are grateful to Professor Gilbert Stork for his generous gift of norcedrene dicarboxylic acid anhydride.

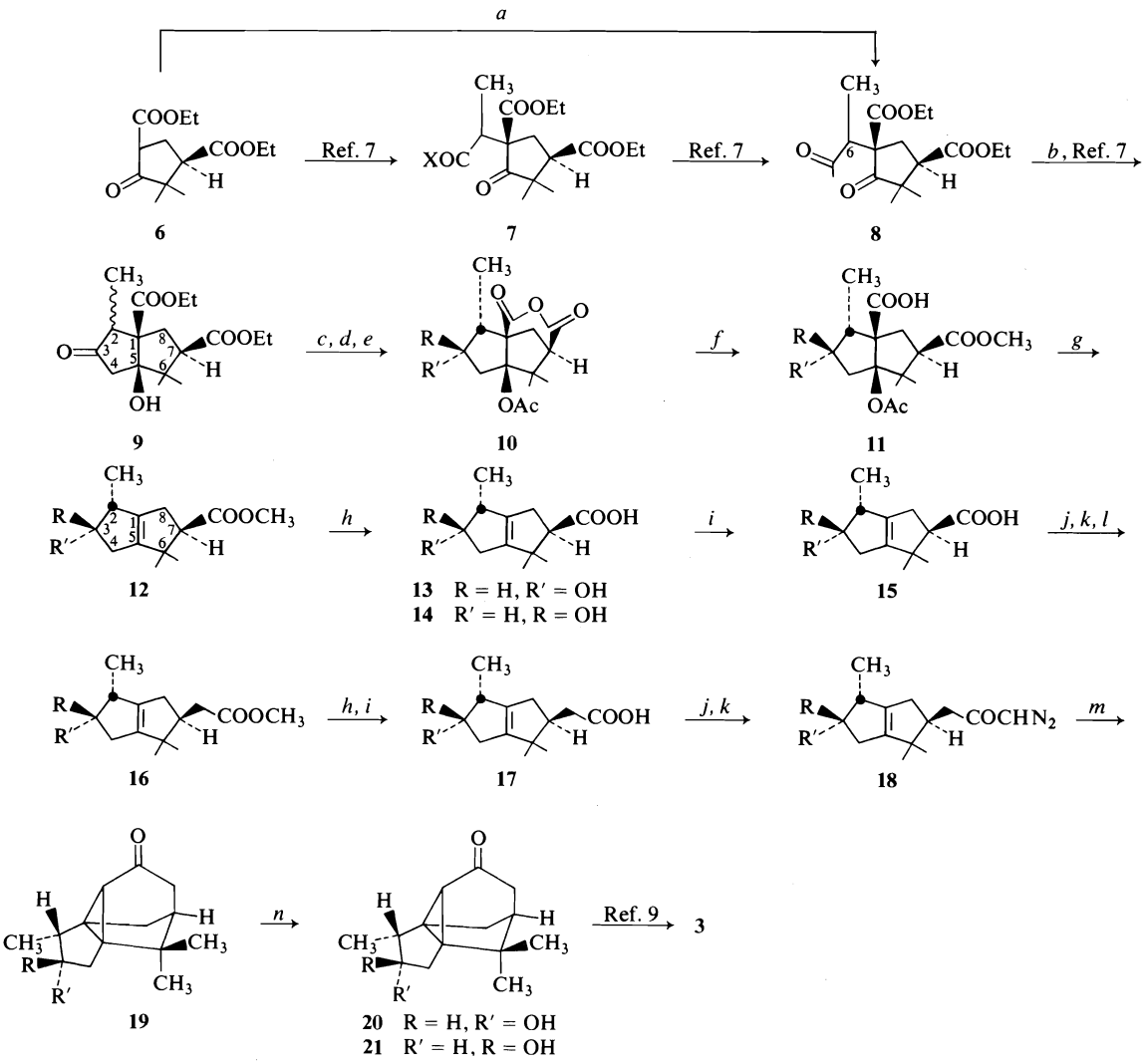

Series *A*: R = H, R' = OAc Series *B*: R' = H, R = OAc

(*a*) LiH, DME; 3-bromo-2-butanone; (*b*) *t*-BuOK, *t*-BuOH; (*c*) $NaBH_4$, EtOH; (*d*) KOH, H_2O; (*e*) $(CH_3CO)_2O$, *p*-toluenesulfonic acid; (*f*) CH_3ONa, CH_3OH; (*g*) pyrolysis, 200–210°C; (*h*) NaOH, H_2O; (*i*) $(CH_3CO)_2O$, pyridine; (*j*) oxalyl chloride, pyridine, benzene; (*k*) CH_2N_2, ether; (*l*) Ag_2O, CH_3OH; (*m*) copper, benzene (3); (*n*) NaOH, H_2O, THF.

SCHEME 2

A study of the hydroxyl absorption by infrared spectroscopy at high dilution of compounds **26**, **27**, and **28** indicates clearly that the hydroxyl groups are *cis* in **26** and *trans* in **28**. Compound **26** showed hydrogen bonded hydroxyl groups only (3460 and 3515 cm^{-1}) while the isomer **28** had both bonded and nonbonded hydroxyl frequencies (3470 and 3650 cm^{-1}). Ketone **27** was also studied as a model and it showed only bonded hydroxyl group frequency (3470 cm^{-1}).

These results indicate that the alternative structures **30** and **31** for **26** and **28** can be eliminated.

Reactivity of the Cyclopropane Diketone 3

Treatment of the tetracyclic diketone **3** with three equiv. of sodium methoxide in methanol

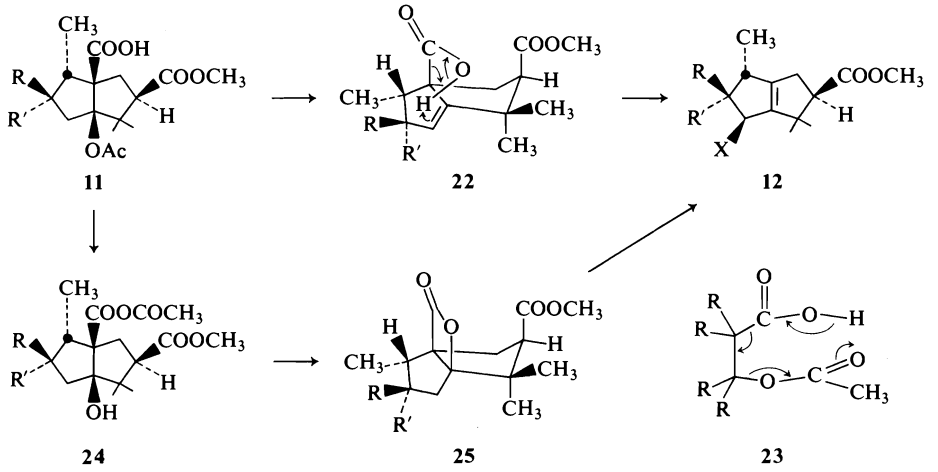

SCHEME 3

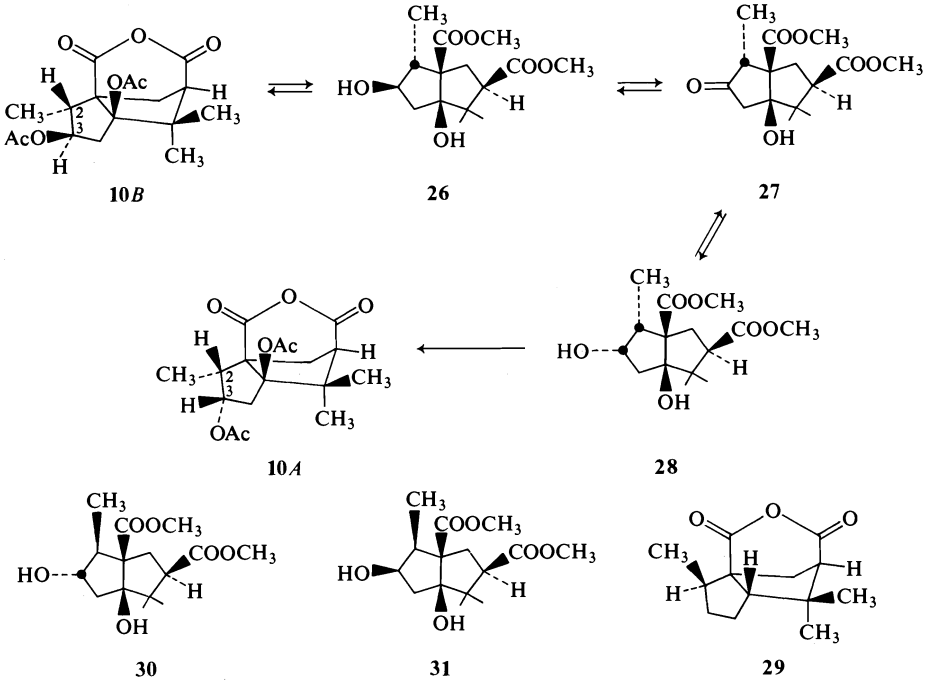

SCHEME 4

at room temperature for a period of 20 min gave a single product which was identified as the tricyclic enedione **4**[3] (12). When the same reaction was carried out for a period of 12 h, a single new substance was formed which was identified as the isomeric enedione **5**. Clearly, **4** is a kinetic product while **5** is the result of a reaction under thermodynamically controlled conditions.

These interesting results can be rationalized in the following way. It is reasonable to assume that enolization of **3** should be faster at the less hindered carbon-4 (Scheme 5), generating the kinetic enolate **32** which would then undergo a cyclopropane ring opening via a retro Michael addition reaction to give the tricyclic enolate **33** which yields **4** on protonation.

[3]With a catalytic amount of sodium methoxide, the same product **4** was obtained, but the reaction takes 68 h.

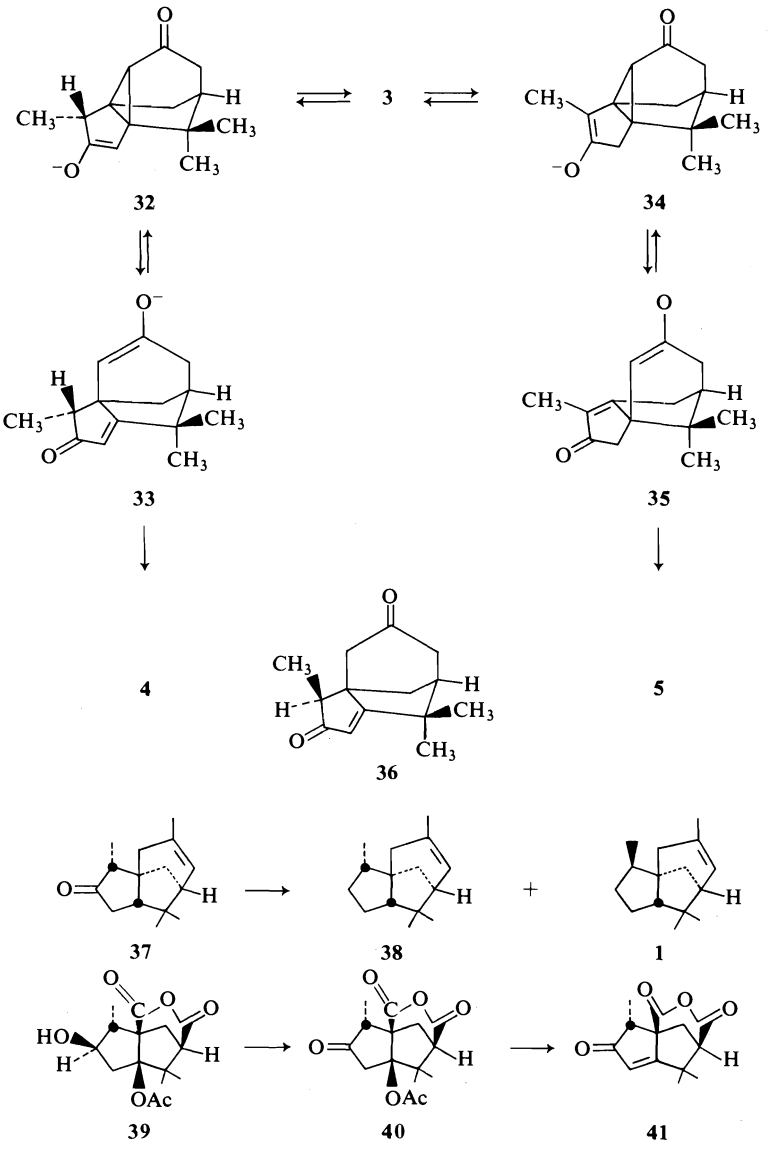

SCHEME 5

Formation of the other isomer **5** clearly indicates that **4** is in equilibrium under basic conditions with the tetracyclic dione **3** although the equilibrium is much in favor of **4**. It also indicates that **3** can also enolize at the more hindered carbon-2, although at a lower rate than at carbon-4, to give the more substituted enolate **34** which fragments to give the tricyclic enolate **35** which gives **5** on protonation.

The isomerization of **4** into **5** represents an interesting rearrangement which occurs via a cyclopropane intermediate **3** through a Michael – retro Michael addition reaction mechanism (12, 13).

It is in principle possible that the enedione **4** could possess the isomeric structure **36**. However, we believe that it is very unlikely that **4** could have completely isomerized to **36**. Demole *et al.* (14) have shown that the Wolff–Kischner reduction of **37** under equilibrating conditions gave a mixture of *epi*-α-cedrene **38** (65%) and α-cedrene (**1**) (35%) (Scheme 5).

During the course of this work, the pure tricyclic enone anhydride **41** was also prepared

(Scheme 5). Basic hydrolysis of **10***B* under mild conditions gave the alcohol **39** which was oxidized by the chromium trioxide – pyridine reagent to give crude ketoacetate **40**. Attempted crystallization of **40** resulted in the formation of pure enone **41**.

The conversion of **5** into α-patchoulene as well as the transformation of **4** into α-cedrene was not investigated.

Experimental

The ir spectra were taken on a Perkin-Elmer 257 spectrophotometer. The ultraviolet (uv) spectra were registered on a Varian Techtron 635 spectrophotometer. Vapor-phase chromatographic (vpc) analyses were carried out on a Varian aerograph instrument model 90-P. Proton nmr spectra were recorded on a Varian A-60 instrument. Chemical shifts are reported in δ values relative to tetramethylsilane as internal standard. The mass spectra were taken on a Hitachi-Perkin-Elmer RMU-6 mass spectrometer. Microanalyses were carried out by Mr. J. Tamas, Laboratoire de microanalyse, Université de Sherbrooke, and by Dr. C. Daessle, Organic Microanalyses, Montréal. Anhydrous magnesium sulfate was used as the drying agent in working up reactions. Low boiling petroleum ether (bp 30–60°C) was used.

Benzyl Ester **7** *(X = $OCH_2C_6H_5$)*

Following the experimental procedure of Stork and Clarke (7), the β-ketoester **6** (43 g, 0.17 mol) was alkylated with benzyl α-bromopropionate. Distillation gave the benzyl ester **7** (X = $OCH_2C_6H_5$) (33 g, 75%); bp 125°C/1.5 Torr (lit. (7) bp 132–133°C/0.01 Torr); ir ν_{max} ($CHCl_3$): 3300 and 1725 cm^{-1}; nmr ($CDCl_3$) δ: 7.26 (5H, s, C_6H_5), 5.02 (2H, m, $CH_2C_6H_5$), 4.0 (4H, q, 2 OCH_2CH_3), and 1.6–0.6 (15H, 5 CH_3).

Diester Diketone **8**

(a) From Benzyl Ester **7** *(X = $OCH_2C_6H_5$)*

Following the experimental procedure of Stork and Clarke (7), the benzyl ester **7** (X = $OCH_2C_6H_5$) (25 g, 0.06 mol) gave the carboxylic acid **7** (X = OH) (10 g, 53%); mp 113–114°C (lit. (7) mp 113–115°C); ir ν_{max} ($CHCl_3$): 3250 (br) and 1725 cm^{-1}; nmr ($CDCl_3$) δ: 4.25 (4H, q, J = 6 Hz, 2 OCH_2CH_3), 1.44–1.18 (12H, m), and 0.92 (3H, s, CH_3—C_5).

The carboxylic acid **7** (X = OH) (5 g, 15 mmol) was then transformed into **7** (X = CH_2Cl) (2.2 g, 44%); mp 72–73°C (lit. (7) mp 72–73°C); ir ν_{max} ($CHCl_3$): 1715 cm^{-1}; nmr ($CDCl_3$) δ: 4.22 (4H, q, J = 6 Hz, 2 OCH_2CH_3), 4.22 (2H, s, CH_2Cl), 1.4–1.1 (12H, 4 CH_3), and 0.95 (3H, s, 1 CH_3—C_5).

Compound **7** (X = CH_2Cl) (2.2 g, 6 mmol) was finally converted into the diester diketone **8** (1.8 g, 91%); mp 68–69°C (from petroleum ether) (lit. (7) mp 55–60°C); ir ν_{max} ($CHCl_3$): 1725 cm^{-1}; nmr ($CDCl_3$) δ: 4.15 (4H, q, J = 6 Hz, 2 OCH_2CH_3), 2.08 (3H, s, CH_3CO), 1.6–1.0 (12H, m, 4 CH_3), and 0.82 (3H, s, 1 CH_3—C_5).

(b) From β-Ketone Ester **6**

The β-ketone ester **6** (150 g, 0.60 mol) in dry dimethoxyethane (450 ml) was added to a suspension of lithium hydride (4.88 g, 0.61 mol) in dry dimethoxyethane (600 ml). After refluxing for 12 h under nitrogen, the mixture was decanted and the lithium hydride residue was washed with dry dimethoxyethane. To the combined dimethoxyethane solution was added 3-bromo-2-butanone (95.4 g, 0.63 mol) in dry dimethoxyethane (30 ml) and the mixture heated at reflux for 50 h under nitrogen. The solution was evaporated *in vacuo* and the solid removed by filtration. The filtrate was diluted with ether, washed with 10% aqueous sodium carbonate and water, and dried over sodium sulfate. The solvents were evaporated and the resulting oil was purified by chromatography on Florisil to yield the diester diketone **8** (121 g, 64%); ir ν_{max} ($CHCl_3$): 1725 cm^{-1}; nmr ($CDCl_3$) δ: 4.15 (4H, q's, OCH_2CH_3), 2.16 and 2.08 (3H, 2 s's (ratio 1:1), CH_3CO), and 1.45–0.84 (15H, m's, 5 CH_3).

Ketoalcohol Diester **9**

Following the experimental procedure of Stork and Clarke (7), the diketone diester **8** (34.7 g, 0.106 mol) was added to a cold solution (0°C) of potassium *tert*-butoxide (from 12.8 g, 0.33 mol, of potassium in 650 ml *tert*-butanol). The stirred solution was allowed to come to room temperature over 50 min, and then poured into a mixture of ether and water. The aqueous phase was extracted twice with ether and the combined ether phase was washed with a saturated sodium chloride solution. Drying and evaporation of the solvent yielded the ketoalcohol diester **9** as an oil (24.7 g, 71%) which was not further purified; ir ν_{max} ($CHCl_3$): 3450 and 1725 cm^{-1}; nmr ($CDCl_3$) δ: 4.15 (4H, q's, OCH_2CH_3) and 1.48–0.80 (15H, m's, 5 CH_3).

The same reaction was carried out with the pure epimer **8** (mp 68–69°C) and it gave the same epimeric mixture of the ketoalcohol diester **9**.

Diacetate Anhydrides **10***A and* **10***B*

A solution of crude ketoalcohol diester **9** (170 g, 0.52 mol) in absolute ethanol (200 ml) was added slowly to a suspension of sodium borohydride (31.4 g, 0.85 mol) in absolute ethanol (1.3 ℓ). After 4 h at 0°C, the mixture was acidified with dilute hydrochloric acid to pH 5. The mixture was concentrated and then extracted several times with ether. Drying and evaporation of the solvent gave an oily residue of crude diol diester (159 g, 93%). The crude diol diester (165 g, 0.506 mol) was heated at reflux with potassium hydroxide (123 g, 2.19 mol) in water (600 ml). After cooling, the solution was extracted with ether, the aqueous phase was acidified with dilute hydrochloric acid to pH 5, saturated with sodium chloride, then extracted several times with ether. Drying and evaporation of the solvent gave the diol diacid as an oil (110 g, 85%). A solution of the crude diol diacid (110 g, 0.405 mol), acetic anhydride (600 ml), and *p*-toluenesulfonic acid (800 mg) was heated at 60–70°C for 24 h. The acetic anhydride was removed *in vacuo* and the residue dissolved in ether. The organic phase was washed several times with water, dried, and evaporated to yield a viscous oil. Crystallization from chloroform gave the mixture of diacetate anhydrides **10***A* and **10***B* (36 g, 26%). Fractional crystallization from chloro-

form–pentane (1:2) afforded the diacetate anhydrides **10***A* and **10***B* in a ratio of 1:2.

*Diacetate Anhydride **10A***: mp 215–216°C (from chloroform–pentane); ir ν_{max} ($CHCl_3$): 1815, 1768, and 1740 cm^{-1}; nmr ($CDCl_3$) δ: 5.41 (1H, m, H_3), 2.08 (3H, s, CH_3CO), 2.00 (3H, s, CH_3CO), 1.37 (3H, s, CH_3—C_6), 1.17 (3H, s, CH_3—C_6), and 1.02 (3H, d, J = 7 Hz, CH_3—C_2); ms *m/e*: 338 (M^+). *Anal.* calcd. for $C_{18}H_{22}O_7$: C 60.35, H 6.51; found: C 59.98, H 6.35.

*Diacetate Anhydride **10B***: mp 158–160°C (from chloroform–pentane); ir ν_{max} ($CHCl_3$): 1835, 1790, and 1760 cm^{-1}; nmr ($CDCl_3$) δ: 4.84 (1H, q, J = 7.5 Hz, H_3), 2.06 (3H, s, CH_3CO), 2.03 (3H, s, CH_3CO), 1.38 (3H, s, CH_3—C_6), 1.16 (3H, s, CH_3—C_6), and 1.08 (3H, d, J = 7 Hz, CH_3—C_2); ms *m/e*: 338 (M^+). *Anal.* calcd. for $C_{18}H_{22}O_7$: C 60.35, H 6.51; found: C 59.68, H 6.30.

*Diacetate Anhydride **10A** from Diol Diester **28***

A solution of diol diester **28** (33 mg, 0.11 mmol) in tetrahydrofuran and sodium hydroxide (*N*, 0.33 ml, 0.33 mequiv.) was heated at reflux for 10 h. The solution was concentrated by evaporation *in vacuo* and extracted with ether. The aqueous phase was acidified with dilute hydrochloric acid (*N*) and extracted several times with ether. Drying and evaporation of the organic phase gave a product (crude diol diacid) which was dissolved in acetic anhydride (5 ml) containing *p*-toluenesulfonic acid (1 mg). This solution was heated at reflux for 6 h and evaporated to dryness and the product obtained was dissolved in ether. The organic phase was washed with water, dried, and evaporated to dryness to give the diacetate anhydride **10***A* (22 mg, 60%); mp 215–216°C.

*Diacetate Anhydride **10B** from Diol Diester **26***

Using the above experimental procedure, the diol diester **26** (34 mg, 0.11 mmol) was converted into the diacetate anhydride **10***B* (27 mg, 70%); mp 158–160°C.

*Acid Ester **11A***

The diacetate anhydride **10***A* (10.0 g, 30 mmol) in dry methanol (100 ml) was added to a solution of sodium (690 mg, 0.030 mol) in methanol (100 µl). The mixture was stirred at room temperature for 1 h, acidified with dilute hydrochloric acid to p*H* 6 and extracted several times with chloroform. The organic phase was washed with water, dried, and evaporated to give acid ester **11***A* (10.2 g, 93%); mp 111.5–112.5°C (from ether–pentane); ir ν_{max} ($CHCl_3$): 3500 (br), 1732, and 1698 cm^{-1}; nmr ($CDCl_3$) δ: 9.99 (1H, COOH), 5.47 (1H, m, H_3), 3.73 (3H, s, OCH_3), 2.08 (3H, s, CH_3CO), 1.98 (3H, s, CH_3CO), 1.28 (3H, s, CH_3—C_6), 0.97 (3H, s, CH_3—C_6), and 0.92 (3H, d, J = 7 Hz, CH_3—C_2); ms *m/e*: 328 (M^+ − 42). *Anal.* calcd. for $C_{18}H_{26}O_8$: C 58.38, H 7.02; found: C 58.43, H 6.96.

*Acid Ester **11B***

Using the above experimental procedure, the diacetate anhydride **10***B* (5.0 g, 15.0 mmol) was converted into acid ester **11***B* (5 g, 92%); mp 171–172°C (from chloroform–pentane); ir ν_{max} ($CHCl_3$): 3500 (br), 1732, and 1702 cm^{-1}; nmr ($CDCl_3$) δ: 10.34 (1H, COOH), 4.63 (1H, m, H_3), 3.73 (3H, s, OCH_3), 2.06 (3H, s, CH_3CO), 1.97 (3H, s, CH_3CO), 1.39 (3H, s, CH_3—C_6), 0.96 (3H, d, CH_3—C_2), and 0.93 (3H, s, CH_3—C_6); ms *m/e*: 328 (M^+ − 42). *Anal.* calcd. for $C_{18}H_{26}O_8$: C 58.38, H 7.02; found: C 57.95, H 6.92.

*Ester Acetate **12A***

The acid ester **11***A* (2.0 g, 5.4 mmol) was heated under nitrogen in a distillation apparatus and a mixture of an oil and acetic acid distilled at 200–210°C. The acetic acid was evaporated *in vacuo* and the oily ester acetate **12***A* was purified by successive microdistillations (1.38 g, 96%); ir ν_{max} ($CHCl_3$): 1747 cm^{-1}; nmr ($CDCl_3$) δ: 5.59 (1H, m, H_3), 3.71 (3H, s, CH_3O), 2.07 (3H, s, CH_3CO), 1.26 (3H, s, CH_3—C_6), 0.95 (3H, d, J = 7.5 Hz, CH_3—C_2), and 0.89 (3H, s, CH_3—C_6); ms *m/e*: 235 (M^+ − 31) and 223 (M^+ − 43). *Anal.* calcd. for $C_{15}H_{22}O_4$: C 67.67, H 8.27; found: C 67.47, H 8.40.

*Ester Acetate **12B***

Using the above experimental procedure, the acid ester **11***B* (2.0 g, 5.4 mmol) was transformed into the oily acetate ester **12***B* (1.4 g, 97%); ir ν_{max} ($CHCl_3$): 1725 cm^{-1}; nmr ($CDCl_3$) δ: 5.08 (1H, m, H_3), 3.71 (3H, s, CH_3O), 2.05 (3H, s, CH_3CO), 1.23 (3H, s, CH_3—C_6), 1.10 (3H, d, J = 7.0 Hz, CH_3—C_2), and 0.91 (3H, s, CH_3—C_6); ms *m/e*: 235 (M^+ − 31). *Anal.* calcd. for $C_{15}H_{22}O_4$: C 67.67, H 8.27; found: C 67.68, H 8.26.

*Alcohol Acid **13***

A solution of acetate ester **12***A* (3.35 g, 0.013 mol) and sodium hydroxide (*N*, 27 ml, 0.027 mol) in water (15 ml) was heated at reflux for 2 h. After cooling and extracting with ether, the aqueous phase was acidified to p*H* 4 with dilute hydrochloric acid, saturated with sodium chloride, and extracted several times with ether. Drying and evaporation of the solvent yielded the alcohol acid **13** as a viscous oil (2.68 g, 100%); ir ν_{max} ($CHCl_3$): 3600, 3500 (br), and 1702 cm^{-1}; nmr ($CDCl_3$) δ: 7.25 (1H, br, COOH), 4.65 (1H, m, H_3), 1.25 (3H, s, CH_3—C_6), 1.01 (3H, d, J = 7 Hz, CH_3—C_2), and 0.95 (3H, s, CH_3—C_6); ms *m/e*: 210 (M^+).

*Alcohol Acid **14***

Using the above experimental procedure, the acetate ester **12***B* (3.31 g, 13.0 mmol), gave the alcohol acid **14** (2.2 g, 84%); mp 157–158°C (from acetone); ir ν_{max} ($CHCl_3$): 3600, 3500 (br), and 1702 cm^{-1}; nmr ($CDCl_3$) δ: 5.25 (1H, br, COOH), 4.32 (1H, m, H_3), 3.12 (1H, t, J = 8.5 Hz, H_7), 1.25 (3H, s, CH_3—C_6), 1.08 (3H, d, J = 7 Hz, CH_3—C_2), and 0.96 (3H, s, CH_3—C_6); ms *m/e*: 210 (M^+). *Anal.* calcd. for $C_{12}H_{18}O_3$: C 68.57, H 8.57; found: C 68.39, H 8.76.

*Acetate Acid **15A***

The alcohol acid **13** (2.68 g, 0.012 mol) was dissolved in a mixture of acetic anhydride (19.5 ml) and pyridine (19.5 ml). After 3 h at room temperature, the mixture was cooled at 0°C and methanol (19.5 ml) was added dropwise. The reaction mixture was left to warm up to room temperature (1 h) and it was diluted with ether. The organic phase was washed several times with dilute hydrochloric acid and water. Drying and evaporation of the solvent yielded an oil which gave pure acetate acid **15***A* (2.25 g, 70%); mp 151–153°C (from dichloromethane–ether–pentane); ir ν_{max} ($CHCl_3$): 3600, 3500 (br), 1724, and 1707 cm^{-1}; nmr ($CDCl_3$) δ: 10.88 (1H, br, COOH), 5.61 (1H, m, H_3), 2.07 (3H, s, CH_3CO), 1.28

(3H, s, CH_3—C_6), 1.0 (3H, s, CH_3—C_6), and 0.95 (3H, d, J = 7 Hz, CH_3—C_2); ms *m/e*: 193 ($M^+ - 59$) and 192 ($M^+ - 60$). *Anal.* calcd. for $C_{14}H_{20}O_4$: C 66.64, H 7.99; found: C 66.57, H 8.23.

*Acetate Acid **15B***

Using the above experimental procedure, the alcohol acid **14** (3.0 g, 14 mmol) was converted into acetate acid **15*B*** (2.52 g, 70%); mp 105–107°C (from dichloromethane – petroleum ether); ir ν_{max} ($CHCl_3$): 3600, 3500 (br), 1727, and 1707 cm^{-1}; nmr ($CDCl_3$) δ: 12.65 (1H, br, COOH), 5.15 (1H, m, H_3), 3.20 (1H, m, H_7), 2.07 (3H, s, CH_3CO), 1.27 (3H, s, CH_3—C_6), 1.09 (3H, d, J = 7.5 Hz, CH_3—C_2), and 1.02 (3H, s, CH_3—C_6); ms *m/e*: 193 ($M^+ - 59$) and 192 ($M^+ - 60$). *Anal.* calcd. for $C_{14}H_{20}O_4$: C 66.64, H 7.99; found: C 66.45, H 8.23.

*Acetate Ester **16A***

A solution of acetate acid **15*A*** (1.08 g, 4.3 mmol) in pyridine (0.88 ml, 10.9 mmol) and anhydrous benzene (100 ml) was added dropwise during 1.5 h to a cooled solution (0°C) of oxalyl chloride (0.768 ml, 9.0 mmol) in anhydrous benzene (72 ml). The reaction mixture was left for 1.5 h at room temperature. After filtration, the solution was slowly added to a vigorously stirred cold (≃ −30°C; Dry Ice – acetone bath) solution of diazomethane (≃15 mg of CH_2N_2/ml) in ether (250 ml). The reaction mixture was left for 1 h at room temperature and the solvent was removed by evaporation *in vacuo* to yield a crude diazoketone (1.33 g, ≃100%) which was not further purified; ir ν_{max} ($CHCl_3$): 3110, 2110, 1720, and 1630 cm^{-1}.

A solution of the crude diazoketone (1.32 g, 4.3 mmol) in anhydrous methanol (70 ml) containing silver oxide (600 mg, 2.4 mequiv.) was heated to reflux during 12 h under nitrogen atmosphere. The solution was then filtered through Celite and evaporated to dryness. Chromatography with Florisil gave the pure oily acetate ester **16*A*** (818 mg, 68%); ir ν_{max} ($CHCl_3$): 1738 cm^{-1}; nmr ($CDCl_3$) δ: 5.58 (1H, m, H_3), 3.70 (3H, s, OCH_3), 2.07 (3H, s, CH_3CO), 1.06 (3H, s, CH_3—C_6), 0.95 (3H, d, J = 7.5 Hz, CH_3—C_2), and 0.83 (3H, s, CH_3—C_6); ms *m/e*: 221 ($M^+ - 59$) and 220 ($M^+ - 60$). This compound was found to decompose slowly at room temperature.

*Acetate Ester **16B***

Using the above experimental procedure, the acetate acid **15*B*** (1.16 g, 4.6 mmol) was converted into the corresponding diazoketone (1.26 g, ≃100%); ir ν_{max}: 3110, 2110, 1720, and 1630 cm^{-1}.

The crude diazoketone (1.26 g, 4.6 mmol) was then transformed into the oily acetate ester **16*B*** (842 mg, 65.4%); ir ν_{max} ($CHCl_3$): 1725 cm^{-1}; nmr ($CDCl_3$) δ: 5.11 (1H, m, H_3), 3.70 (3H, s, OCH_3), 2.05 (3H, s, CH_3CO), 1.09 (3H, d, J = 6.5 Hz), 1.03 (3H, s, CH_3—C_6), and 0.85 (3H, s, CH_3—C_6); ms *m/e*: 221 ($M^+ - 59$) and 220 ($M^+ - 60$). This compound was found to decompose slowly at room temperature.

*Acetate Acid **17A***

A solution of acetate ester **16*A*** (2.05 g, 7.3 mmol) in sodium hydroxide (0.5 *N*, 40 ml) was heated at reflux during 2 h. After cooling, the aqueous solution was extracted with ether, acidified with dilute hydrochloric acid to p*H* 5, saturated with sodium chloride, and extracted several times with ether. Drying and evaporation of the organic phase gave the corresponding alcohol acid (1.28 g, 78%); mp 111.5–112.5°C (from acetone – petroleum ether); ir ν_{max} ($CHCl_3$): 3640, 3500 (br), and 1705 cm^{-1}; nmr ($CDCl_3$) δ: 5.80 (1H, br, COOH), 4.64 (1H, m, H_3), 1.07 (3H, s, CH_3—C_6), 1.0 (3H, d, J = 8 Hz, CH_3—C_2), and 0.84 (3H, s, CH_3—C_6); ms *m/e*: 224 (M^+). *Anal.* calcd. for $C_{13}H_{20}O_3$: C 69.61, H 8.99; found: C 69.34, H 8.80.

A solution of the alcohol acid (1.00 g, 4.4 mmol) in acetic anhydride (13.2 ml) and pyridine (13.2 ml) was left for 2.5 h at room temperature. The mixture was cooled at 0°C and then methanol (13.2 ml) was added dropwise. The reaction mixture was left to warm up at room temperature (1 h) and it was diluted with ether. The organic phase was washed several times with dilute hydrochloric acid and water. Drying and evaporation of the solvent yielded an oil which gave pure acetate acid **17*A*** (944 mg, 80%); mp 91–92.5°C (from ether – petroleum ether); ir ν_{max} ($CHCl_3$): 3500 (br), 1725, and 1710 cm^{-1}; nmr ($CDCl_3$) δ: 10.25 (1H, br, COOH), 5.61 (1H, m, H_3), 2.07 (3H, s, CH_3CO), 1.09 (3H, s, CH_3—C_6), 0.95 (3H, d, J = 7.5 Hz, CH_3—C_2), and 0.84 (3H, s, CH_3—C_6); ms *m/e*: 207 ($M^+ - 59$) and 206 ($M^+ - 60$). *Anal.* calcd. for $C_{15}H_{22}O_4$: C 67.65, H 8.33; found: C 67.35, H 8.39.

*Acetate Acid **17B***

Using the above experimental procedure, the acetate ester **16*B*** (1.67 g, 6.0 mmol) gave the corresponding alcohol acid (1.07 g, 80%); mp 119–120°C (from acetone – petroleum ether); ir ν_{max} ($CHCl_3$): 3500 (br) and 1708 cm^{-1}; nmr ($CDCl_3$) δ: 7.50 (1H, br, COOH), 4.15 (1H, m, H_3), 1.05 (3H, d, J = 6.5 Hz, CH_3—C_2), 1.05 (3H, s, CH_3—C_6), and 0.85 (3H, s, CH_3—C_6); ms *m/e*: 224 (M^+). *Anal.* calcd. for $C_{13}H_{20}O_3$: C 69.61, H 8.99; found: C 69.34, H 8.80.

This crystalline alcohol acid (775 mg, 3.4 mmol) was then converted into the acetate acid **17*B*** (885 mg, 95%); mp 90–91°C (from ether–pentane); ir ν_{max} ($CHCl_3$): 3500 (br) and 1715 (br) cm^{-1}; nmr ($CDCl_3$) δ: 11.93 (1H, br, COOH), 5.14 (1H, m, H_3), 2.07 (3H, s, CH_3CO), 1.12 (3H, d, J = 7.0 Hz, CH_3—C_2), 1.07 (3H, s, CH_3—C_6), and 0.88 (3H, s, CH_3—C_6); ms *m/e*: 207 ($M^+ - 59$) and 206 ($M^+ - 60$). *Anal.* calcd. for $C_{15}H_{22}O_4$: C 67.65, H 8.33; found: C 67.42, H 8.20.

*Diazoketone **18A***

The acetate acid **17*A*** (300 mg, 1.13 mmol) dissolved in a mixture of pyridine (0.264 ml, 3.1 mmol) and anhydrous benzene (60 ml) was added dropwise during a period of 2 h to a cooled (0°C) solution of oxalyl chloride (0.228 ml, 2.7 mmol) in benzene (48 ml) under nitrogen atmosphere. The mixture was left at room temperature for 1 h. After filtration, the solution was slowly added to a vigorously stirred, cold (≃ −30°C, Dry Ice – acetone bath), solution of diazomethane (≃15 mg of CH_2N_2/ml) in ether (120 ml). The reaction mixture was left at room temperature for 1 h and evaporation of the solvent *in vacuo* yielded the crude diazoketone **18*A*** (320 mg, 100%) which was not further purified because of its instability; ir ν_{max} ($CHCl_3$): 2120, 1740, and 1640 cm^{-1}; nmr ($CDCl_3$) δ: 5.58 (1H, m, H_3), 5.40 (1H, s, $COCHN_2$), 2.08 (3H, s, CH_3CO), 1.07 (3H, s, CH_3—C_6), 0.93 (3H, d, J = 7 Hz, CH_3—C_2), and 0.84 (3H, s, CH_3—C_6).

Diazoketone 18B

Using the above experimental procedure, the acetate acid **17***B* (560 mg, 2.1 mmol) was converted into the crude diazoketone **18***B* (609 mg, ≃100%); ir ν_{max} ($CHCl_3$): 2120, 1740, and 1640 cm^{-1}; nmr ($CDCl_3$) δ: 5.33 (1H, s, $COCHN_2$), 5.05 (1H, m, H_3), 2.05 (3H, s, CH_3CO), 1.06 (3H, d, J = 7 Hz, CH_3—C_2), 1.03 (3H, s CH_3—C_6), and 0.84 (3H, s, CH_3—C_6).

Cyclopropane Acetate 19A

A solution of the crude diazoketone **18***A* (340 mg, 1.2 mmol) in anhydrous benzene (60 ml) containing copper (Fisher Co., 1.14 g) was heated at reflux during 3.75 h under a nitrogen atmosphere. The solution was filtered under Celite and evaporated to dryness. The crude product was purified by chromatography with Florisil to yield the oily cyclopropane acetate **19***A* (186 mg, 61%) which was not purified further because of its instability; ir ν_{max} ($CHCl_3$): 1730 and 1680 cm^{-1}; nmr ($CDCl_3$) δ: 5.10 (1H, m, H_3), 2.07 (3H, s, CH_3CO), 1.14 (3H, s, CH_3—C_6), 1.03 (3H, s, CH_3—C_6), and 0.93 (3H, d, J = 7.5 Hz, CH_3—C_2); ms *m/e*: 262 (M^+); vpc one peak at 9.5 min (5 ft, ¼ in., SE-30-5% on Chromosorb W, 200°C).

Cyclopropane Acetate 19B

Using the above experimental procedure, the crude diazoketone **18***B* (609 mg, 2.1 mmol) was converted to the oily cyclopropane acetate **19***B* (216 mg, 40%), after chromatography; ir ν_{max} ($CHCl_3$): 1725 and 1680 cm^{-1}; nmr ($CDCl_3$) δ: 5.07 (1H, m, H_3), 2.02 (3H, s, CH_3CO), 1.12 (3H, d, J = 8 Hz, CH_3—C_2), 1.10 (3H, s, CH_3—C_6), and 1.01 (3H, s, CH_3—C_6); ms *m/e*: 262 (M^+); vpc one peak at 12.6 min (5 ft, ¼ in., SE-30-5% on Chromosorb W, 181°C).

Cyclopropane Alcohol 20

A solution of crude cyclopropane acetate **19***A* (314 mg, 1.2 mmol) in tetrahydrofuran (15 ml), sodium hydroxide (*N*, 1.2 ml, 1.2 mmol), and water (3 ml) was heated at reflux for 2.5 h. The solution was concentrated by evaporation *in vacuo* and diluted with water (10 ml). It was then extracted several times with ether. Drying and evaporation of the organic phase yielded the cyclopropane alcohol **20** (240 mg, 75%); mp 118–119°C (from ether – petroleum ether); ir ν_{max} ($CHCl_3$): 3620, 3450, 1684, and 1667 cm^{-1}; nmr ($CDCl_3$) δ: 4.31 (1H, m, H_3), 1.12 (3H, s, CH_3—C_6), 1.02 (3H, s, CH_3—C_6), and 0.99 (3H, d, J = 7.2 Hz, CH_3—C_2); ms *m/e*: 220 (M^+). *Anal.* calcd. for $C_{14}H_{20}O_2$: C 76.33, H 9.15; found: C 75.56, H 8.91.

Cyclopropane Alcohol 21

Using the above experimental procedure, the crude cyclopropane acetate **19***B* (204 mg, 0.8 mmol) was converted into the cyclopropane alcohol **21** (165 mg, 96%); mp 120.5–121.5°C (from dichloromethane–ether); ir ν_{max} ($CHCl_3$): 3620, 3440, and 1675 cm^{-1}; nmr ($CDCl_3$) δ: 4.26 (1H, m, H_3), 1.09 (3H, s, CH_3—C_6), 1.04 (3H, d, J = 6 Hz, CH_3—C_2), and 0.99 (3H, s, CH_3—C_6); ms *m/e*: 220 (M^+). *Anal.* calcd. for $C_{14}H_{20}O_2$: C 76.33, H 9.15; found: C 75.94, H 8.97.

Cyclopropane Diketone 3

(a) From Cyclopropane Alcohol 20

Chromium trioxide (88 mg, 0.924 mmol) was added to a solution of pyridine (145 mg, 1.85 mmol) in dry dichloromethane (7 ml) and the mixture was stirred at room temperature for 15 min. A solution of cyclopropane alcohol **20** (33 mg, 0.154 mmol) in dichloromethane (5 ml) was added and the mixture was stirred for 15 min at room temperature. The solution was decanted and the residue was washed with dichloromethane. The organic phase was evaporated, ether was added, and the solution was filtered through Celite. Evaporation of the solvent gave cyclopropane diketone **3** (30 mg, 90%); mp 97–98°C (from ether – petroleum ether); ir ν_{max} ($CHCl_3$): 1750 and 1700 cm^{-1}; nmr ($CDCl_3$) δ: 2.93–1.45 (9H, m's), 1.18 (3H, d, J = 8 Hz, CH_3—C_2), 1.15 (3H, s, CH_3—C_6), and 1.09 (3H, s, CH_3—C_6); ms *m/e*: 218 (M^+); vpc one peak at 9.8 min (5 ft, ¼ in., SE-30-5% on Chromosorb W, 175°C). *Anal.* calcd. for $C_{14}H_{18}O_2$: C 77.03, H 8.31; found: C 76.71, H 8.06.

(b) From Cyclopropane Alcohol 21

Using the above experimental procedure, the cyclopropane alcohol **21** (100 mg, 0.46 mmol) was converted into the cyclopropane diketone **3** (92 mg, 90%); mp 97–98°C.

Tricyclic Enedione 4

A solution of the cyclopropane diketone **3** (33 mg, 0.15 mmol) in dry methanol (5 ml) containing sodium methoxide (30 mg, 0.45 mmol) was left at room temperature during 20 min. The solution was concentrated by evaporation *in vacuo*, diluted with water (10 ml), and acidified with dilute hydrochloric acid. The aqueous phase was extracted several times with ether. Drying and evaporation of the organic phase gave the tricyclic enedione **4** (33 mg, ≃100%); mp 160.5–162°C (from dichloromethane–ether); ir ν_{max} ($CHCl_3$): 1710 and 1630 cm^{-1}; nmr ($CDCl_3$) δ: 5.83 (1H, s, H_4), 3.05–1.08 (8H, m's), 1.24 (6H, s, $(CH_3)_2$—C_6), and 1.13 (3H, d, J = 7.5 Hz, CH_3—C_2); uv λ_{max} (EtOH): 237 nm (ε = 39 800); ms *m/e*: 218 (M^+); vpc one peak at 10.8 min (5 ft, ¼ in., SE-30-5% Chromosorb W, 175°C). *Anal.* calcd. for $C_{14}H_{18}O_2$: C 77.03, H 8.31; found: C 76.71, H 8.06.

If a catalytic amount of sodium methoxide (2 mg) is used, the tricyclic enedione **4** was obtained after 68 h of reaction time.

Tricyclic Enedione 5

A solution of the cyclopropane diketone **3** (70 mg, 0.32 mmol) in methanol (10 ml) containing sodium methoxide (50 mg, 0.92 mmol) was left at room temperature during 12 h. The solution was concentrated by evaporation *in vacuo*, diluted with water (10 ml), and acidified with dilute hydrochloric acid. The aqueous phase was extracted several times with ether. Drying and evaporation of the organic phase gave the tricyclic enedione **5** (70 mg, ≃100%); mp 96.0–96.5°C (from dichloromethane–ether–pentane); ir ν_{max} ($CHCl_3$): 1705 and 1665 cm^{-1}; nmr ($CDCl_3$) δ: 3.20–1.75 (9H, m's), 1.69 (3H, t, J = 2 Hz (homoallylic coupling), CH_3—C_2), 1.29 (3H, s, CH_3—C_6), and 0.89 (3H, s, CH_3—C_6); uv λ_{max} (EtOH): 243 nm (ε = 36 000); ms *m/e*: 218 (M^+); vpc one peak at 8.6 min (5 ft, ¼ in., SE-30-10% Chromosorb W, 178°C). *Anal.* calcd. for $C_{14}H_{18}O_2$: C 77.03, H H 8.31; found: C 76.77, H 8.11.

Diol Ester 26

A solution of diacetate anhydride **10***B* (1.0 g, 3.0 mmol) in tetrahydrofuran (30 ml) and sodium hydroxide (*N*,

15 ml, 15.0 mequiv.) was heated to reflux for 72 h. The solution was concentrated by evaporation *in vacuo* and extracted with ether. The aqueous phase was acidified with dilute hydrochloric acid and extracted several times with ether. After drying and evaporation of the solvent, it was dissolved in ether and a large excess of diazomethane in ether was added. Evaporation of the solvent gave the diol diester **26** (777 mg, 96%); mp 124–126°C (from dichloromethane–ether); ir ν_{max} ($CHCl_3$): 3540 (br), 1720, and 1695 cm^{-1}; nmr ($CDCl_3$) δ: 4.97 (1H, s, OH), 3.78 (3H, s, OCH_3), ≃3.75 (1H, m, H_3), 3.72 (3H, s, OCH_3), 1.14 (3H, s, CH_3—C_6), 1.02 (3H, d, J = 7 Hz, CH_3—C_2), and 0.78 (3H, s, CH_3—C_6); ms *m/e*: 300 (M^+). *Anal.* calcd. for $C_{15}H_{24}O_6$: C 59.98, H 8.05; found: C 60.02, H 7.99.

Ketoalcohol Diester 27

(a) From Diol Diester 26

Chromium trioxide (352 mg, 3.6 mmol) was added to a solution of pyridine (580 mg, 7.2 mmol) in dry dichloromethane (20 ml) and the mixture was stirred at room temperature for 30 min. A solution of the diol diester **26** (180 mg, 0.6 mmol) in dichloromethane (20 ml) was added and the mixture was stirred at room temperature for 20 min. The solution was decanted and the residue was washed with dichloromethane. The organic phase was evaporated, ether was added, and the solution was filtered through Celite. Evaporation of the solvent gave the ketoalcohol diester **27** (154 mg, 88%); mp 68–70°C (from ether–pentane); ir ν_{max} ($CHCl_3$): 3450, 1735, and 1700 cm^{-1}; nmr ($CDCl_3$) δ: 5.37 (1H, s, OH), 3.87 (3H, s, OCH_3), 3.73 (3H, s, OCH_3), 3.33–1.28 (6H, m's), 1.17 (3H, s, CH_3—C_6), 1.07 (3H, d, J = 7 Hz, CH_3—C_2), and 0.76 (3H, s, CH_3—C_6); ms *m/e*: 298 (M^+). *Anal.* calcd. for $C_{15}H_{22}O_6$: C 60.39, H 7.43; found: C 59.61, H 7.08.

(b) From Diol Diester 28

Using the above experimental procedure, the diol diester **28** (22 mg, 0.073 mmol) was converted into the ketoalcohol diester **27** (18 mg, 81%); mp 68–70°C.

Diol Diester 26 and 28 from Ketoalcohol Diester 27

A solution of ketoalcohol diester **27** (133 mg, 0.44 mmol) in methanol (5 ml) was added to a solution of sodium borohydride (34 mg, 0.88 mmol) in methanol (5 ml) and the mixture was left at 0°C for 2 h. The mixture was then acidified with dilute hydrochloric acid to p*H* 6 and concentrated by evaporation *in vacuo*. The resulting solution was extracted several times with dichloromethane. After drying and evaporation of the solvent, two products were obtained and separated by thin-layer chromatography on silica gel. The more polar product was identified as the diol ester **26** (56 mg); mp 124–126°C. The less polar product was identified as the diol diester **28** (34 mg); mp 127–128°C (from dichloromethane–ether); ir ν_{max} ($CHCl_3$): 3620, 3450, 1720, and 1690 cm^{-1}; nmr ($CDCl_3$) δ: 5.08 (1H, s, OH), 4.36 (1H, m, H_3), 3.81 (3H, s, OCH_3), 3.72 (3H, s, OCH_3), 2.93–2.12 (7H, m's), 1.13 (3H, s, CH_3—C_6), 1.04 (3H, d, J = 7 Hz, CH_3—C_2), and 0.73 (3H, s, CH_3—C_6); ms *m/e*: 300 (M^+). *Anal.* calcd. for $C_{15}H_{24}O_6$: C 59.98, H 8.05; found: C 60.21, H 8.05.

Alcohol Anhydride 39

A solution of diacetate anhydride **10***A* (1.5 g, 4.5 mmol) in tetrahydrofuran (50 ml), sodium hydroxide (*N*, 14 ml, 14.0 mequiv.) was heated at reflux for 12 h. The solution was concentrated by evaporation *in vacuo* and extracted with dichloromethane. The aqueous phase was acidified with dilute hydrochloric acid and extracted several times with ether. Drying and evaporation of the organic phase gave a product (diacid) which was dissolved in acetic anhydride (50 ml) and heated at reflux for 20 min. Evaporation of the solvent gave the alcohol anhydride **39** (1.10 g, 84%); mp 165–167°C (from acetone); ir ν_{max} ($CHCl_3$): 3480, 1810, 1760, and 1710 cm^{-1}; nmr ($CDCl_3$) δ: 3.93 (1H, m, H_3), 1.98 (3H, s, CH_3CO), 1.37 (3H, s, CH_3—C_6), 1.10 (3H, s, CH_3—C_6), and 1.07 (3H, d, J = 7 Hz, CH_3—C_2); ms *m/e*: 237 (M^+ − 59) and 236 (M^+ − 60). *Anal.* calcd. for $C_{15}H_{20}O_6$: C 60.80, H 6.80; found: C 60.48, H 6.77.

Tricyclic Enone Anhydride 41

Chromium trioxide (599 mg, 6.0 mmol) was added to a solution of pyridine (949 mg, 1.2 mmol) in dry dichloromethane (20 ml) and the mixture was stirred at room temperature for 30 min. A solution of the alcohol anhydride **39** (272 mg, 1.0 mmol) in dichloromethane (30 ml) was added and the mixture was stirred for 20 min at room temperature. The solution was decanted and the residue was washed with dichloromethane. The organic phase was evaporated, ether was added, and the solution was filtered through Celite. Evaporation of the solvent gave crude **40** as shown by nmr (no olefinic hydrogen) which by attempted crystallization gave the tricyclic enone anhydride **41** (212 mg, ≃100%); mp 156–160°C (from dichloromethane–ether); ir ν_{max} ($CHCl_3$): 1815, 1770, 1730, and 1635 cm^{-1}; nmr ($CDCl_3$) δ: 6.03 (1H, s, H_4), 3.35 (2H, m's), 2.3 (2H, m's), 1.44 (6H, s, $(CH_3)_2$=C_6), and 1.15 (3H, d, J = 7.5 Hz, CH_3—C_2); uv λ_{max} (EtOH): 235 nm (ε = 34 950); ms *m/e*: 234 (weak, M^+) and 190 (M^+ − 44).

Acknowledgements

Support for this work by the National Research Council of Canada, and by the Ministère de l'Education, Québec, is gratefully acknowledged.

1. G. Stork and R. Breslow. J. Am. Chem. Soc. **75**, 3291 (1953); P. A. Plattner, A. Fürst, A. Eschenmoser, W. Keller, H. Klaui, S. Meyer, and M. Rosner. Helv. Chim. Acta, **36**, 1845 (1953).
2. G. Buchi, R. E. Erickson, and N. Wakabayashi. J. Am. Chem. Soc. **83**, 927 (1961).
3. G. Stork and J. Ficini. J. Am. Chem. Soc. **83**, 4678 (1961).
4. G. Stork, J. E. Davies, and A. Meisels. J. Am. Chem. Soc. **81**, 5516 (1959); **85**, 3419 (1963); S. W. Pelletier, L. B. Hawley, Jr., and K. W. Gopinath. J. Chem. Soc. Chem. Commun. 97 (1966).
5. A. Viola, S. Madhavan, R. J. Proverb, B. L. Yates, and J. Larrahondo. J. Chem. Soc. Chem. Commun. 842 (1974), and references quoted therein.

6. G. W. MOERSCH and A. R. BURKETT. J. Org. Chem. **36**, 1149 (1971); W. ADAM, J. BUEZA, and JU-CHAO LIU. J. Am. Chem. Soc. **94**, 2000 (1972).
7. G. STORK and F. H. CLARKE, JR. J. Am. Chem. Soc. **77**, 1072 (1955); **83**, 3114 (1961).
8. J. H. NOGGLE and R. E. SCHIRMER. *In* The nuclear Overhauser effect: chemical applications. Academic Press, New York, NY. 1971.
9. R. RADTCLIFFE and R. RODEHORST. J. Org. Chem. **25**, 4000 (1970).
10. J. W. APSIMON and H. BEIERBECK. Can. J. Chem. **49**, 1328 (1971).
11. P. A. PLATTNER, G. W. KUSSEROW, and H. KLÄUI. Helv. Chim. Acta, **25**, 1345 (1942).
12. C. F. KOELSCH. J. Org. Chem. **26**, 1003 (1961); S. JULIA and G. LINSTRUMELLE. Bull. Soc. Chim. Fr. 3490 (1966).
13. S. DANISHEFSKY, M. Y. TSAI, and J. DYNAK. J. Chem. Soc. Chem. Commun. 7 (1975).
14. E. DEMOLE, P. ENGGIST, and C. BORER. Helv. Chim. Acta, **54**, 1845 (1971).

Individual rate constants of methyl radical reactions in the pyrolysis of dimethyl ether

ANDREW M. HELD, KIM C. MANTHORNE, PHILIP D. PACEY, AND HOWARD P. REINHOLDT

Department of Chemistry, Dalhousie University, Halifax, N.S., Canada B3H 4J3

Received June 1, 1977

ANDREW M. HELD, KIM C. MANTHORNE, PHILIP D. PACEY, and HOWARD P. REINHOLDT. Can. J. Chem. **55**, 4128 (1977).

Dimethyl ether was pyrolyzed in a flow system at 10 to 80 Torr and 1005 K. The average concentration of CH_3 radicals in the reactor was measured by ultraviolet absorption spectroscopy. Product yields were measured by gas chromatography. The system was simulated using a computer program, taking into account the warm-up of the entering gas and the occurrence of secondary reactions. Rate constants were varied to find values consistent with experimental observations. The limiting, high pressure rate constant for the recombination of CH_3 was estimated to be $10^{10.15\pm0.5}$ ℓ mol^{-1} s^{-1}. Estimated rate constants for the reactions

$$CH_3 + CH_3OCH_3 \rightarrow CH_4 + CH_2OCH_3 \text{ and } CH_3 + CH_2O \rightarrow CH_4 + CHO$$

were $10^{7.12\pm0.2}$ ℓ mol^{-1} s^{-1} and $10^{7.5\pm0.4}$ ℓ mol^{-1} s^{-1}, respectively.

ANDREW M. HELD, KIM C. MANTHORNE, PHILIP D. PACEY et HOWARD P. REINHOLDT. Can. J. Chem. **55**, 4128 (1977).

On a effectué la pyrolyse de l'éther diméthylique dans un système à flux entre 10 et 80 Torr à 1005 K. On a mesuré la concentration moyenne des radicaux CH_3 dans le réacteur par spectroscopie d'absorption ultraviolet. On a mesuré les rendements de produits par chromatographie en phase gazeuse. On a simulé le système en faisant appel à un programme d'ordinateur en tenant compte de la période de réchauffement du gaz qui entre et de l'existance de réactions secondaires. On a fait varier les constantes de vitesse pour trouver des valeurs en accord avec les observations expérimentales. On a estimé que la constante de vitesse à la limite de hautes pressions pour la recombinaison des radicaux CH_3 est de $10^{10.15\pm0.5}$ ℓ mol^{-1} s^{-1}. On a estimé que les constantes de vitesse des réactions

$$CH_3 + CH_3OCH_3 \rightarrow CH_4 + CH_2OCH_3 \text{ et } CH_3 + CH_2O \rightarrow CH_4 + CHO$$

sont respectivement de $10^{7.12\pm0.2}$ ℓ mol^{-1} s^{-1} et $10^{7.5\pm0.4}$ ℓ mol^{-1} s^{-1}.

[Traduit par le journal]

This paper reports measurements of the rate constants at 1005 K for two types of methyl radical reactions, the recombination reaction (see Table 1 for list of reactions),

[6] $$2CH_3 \rightarrow C_2H_6$$

and the abstraction reactions, particularly the reaction with dimethyl ether,

[5] $$CH_3 + C_2H_6O \rightarrow CH_4 + C_2H_5O$$

Abstraction reactions involving methyl radicals are of interest because several studies have reported curvature of the Arrhenius plots (1–3). With one exception (1), however, these studies have not reported direct measurements of the rate constants, but, instead, measurements relative to the rate constant of reaction 6.

Since the early work of Ingold and Lossing (4), there have been only two measurements of the rate constant of reaction 6 at high temperatures (>500 K). Clark, Izod, and Kistiakowsky (1) used mass spectrometry to follow the disappearance of methyl radicals in a shock tube at 1120 to 1400 K; Glanzer, Quack, and Troe (5) used ultraviolet absorption spectroscopy at similar temperatures. The rate constants measured differed by a factor of three. Knowledge of the temperature dependence of this reaction is important, both because the reaction is used as a reference reaction for studying abstractions, like [5], and because the temperature dependence provides a sensitive test for theoretical treatments of recombination reactions. Most Rice–Ramsperger–Kassel–Marcus (RRKM) calculations, which place the activated complex atop a rotational barrier at a point on the reaction coordinate with potential energy near its maximum value, predict a strong increase in rate with increasing temperature (5). Theories which place the critical configuration at lower energies, such as the adiabatic open channel (5), minimum state density (6), or maximum free energy theo-

ries (7), predict little or no temperature dependence.

In this work reactions 5 and 6 were studied in the pyrolysis of dimethyl ether. Methyl radical concentrations were measured by ultraviolet absorption spectroscopy; product concentrations, by gas chromatography. In an earlier gas chromatographic study (2), it was shown that reaction 6 was the only major source of C_2H_6; the rate constant, k_6, has been determined herein from measurements of the concentration of CH_3 and of the rate of formation of C_2H_6. Reaction 5 is believed to be the main source of CH_4 in the early stages of pyrolysis (2); k_5 has been determined herein from $[CH_3]$ and the rate of formation of CH_4.

Higher temperatures have been used than in the earlier work to increase ultraviolet absorption by CH_3 to a measureable level. The rate constant of the initiation reaction,

[1] $$CH_3OCH_3 \rightarrow CH_3 + OCH_3$$

determined in the earlier work from yields of C_2H_6, the main termination product, has been redetermined at these higher temperatures. Because of the higher temperatures, overall reaction rates and conversions were greater and secondary reactions of the products became significant. Interpretation of the experiments has been assisted by a computer simulation, taking into account secondary reactions and the temperature profile in the reactor. It has been possible to place limits on the rate constant of one secondary reaction,

[9] $$CH_3 + CH_2O \rightarrow CH_4 + CHO$$

Experimental

The experimental system was described previously (8), except for the changes that follow.

Dimethyl ether (Matheson, 99.87%) was degassed and allowed to flow at a controlled rate through a 1 cm inside diameter quartz reactor, heated externally by a nichrome wire resistance furnace. Temperatures were measured using a moveable Pt – Pt–15% Rh thermocouple in a 2 mm inside diameter quartz tube attached to the outside of the reactor. By a method described previously (9), average reaction temperatures were calculated.

Light from a McKee-Pedersen MP-1035 deuterium lamp was focussed and directed along the axis of the reactor. A portion of the light entered a McKee-Pedersen MP-1018A monochromator, which had been altered by decreasing the height of the entrance slit and covering all but a 3 mm diameter circle of the parabolic mirror behind this entrance slit. These alterations ensured that light from the side walls of the reactor could not reach the grating and the R372 photomultiplier. The slit function of the altered monochromator was studied using the 253.7 nm line from an Hg lamp. With the 1.6 mm slit width used, the slit function could be fitted to within 1% of the peak height by a Gaussian curve with full width at half height of 1.44 nm.

In most experiments, samples of product gases were injected directly into an on-line gas chromatograph. In some experiments, products were collected and analyzed on an external gas chromatograph. Columns and detectors have been described previously (2).

Results

Curves *a* and *b* of Fig. 1 are traces of a photomultiplier signal as a function of wavelength for experiments in which 10 Torr of dimethyl ether was passed through the reactor at temperatures of 850 and 1002 K, respectively. The curvature of the upper trace was caused by the optical system, as the dimethyl ether absorption continuum was found to be featureless at these wavelengths and the methyl radical concentration would be too small to contribute. The extra dip in curve *b* was interpreted as being caused by absorption by CH_3.

This interpretation was tested in several ways. Curve *c* of Fig. 1 shows the shape of the CH_3 peak calculated for the conditions of these experiments using a computer program[1] based on the theoretical model of Glanzer *et al.* (10). This model was shown (10) to match observations of the CH_3 spectrum at room temperature and at 1400 K. The computer program has also been used to calculate the extinction coefficient (2730 ℓ mol^{-1} cm^{-1}) at the absorption maximum and the oscillator strength (7.0×10^{-3}) of the main band (214.3 to 220.0 nm) for the conditions of this work.

Over 100 traces, like *b* in Fig. 1, have been made; peak heights have been calculated by comparing heights at the absorption maximum (216.5 nm) and minima (214.3 and 220.0 nm) with traces, like *a* in Fig. 1, at the same pressure but at 800 to 900 K. Average CH_3 concentrations in the reactor, calculated from peak heights, the extinction coefficient, and the length of the hot zone of the reactor, were reproducible, with standard deviations of about 10%.

Radical concentrations have also been calculated from peak areas and the oscillator strength; the average ratio of the CH_3 concentrations obtained by the two methods was 0.99 ± 0.11. When the band was traced with narrow slits,

[1]Copies of this and other original computer programs are available from the authors on request.

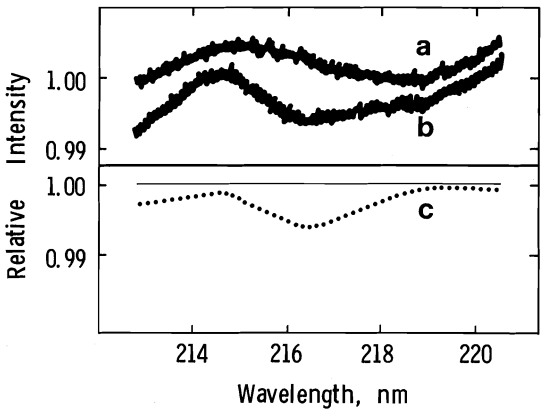

FIG. 1. Recorder traces of photomultiplier output with 10 Torr of $(CH_3)_2O$ in the reactor at 850 K (*a*) and 1002 K (*b*). Trace *a* has been raised 0.002 units for clarity. Curve *c* shows the theoretically predicted spectrum of CH_3 for the condition of curve *b*.

the characteristic double peak of the CH_3 spectrum appeared, as was reported previously (8). Variation of the pressure at room temperature indicated that absorption by dimethyl ether obeyed the Beer–Lambert law. Because the concentration of CH_3 varied along the reactor, there was no straightforward way of testing this law for this species.

Ethylene was found to absorb near 216 nm. At 1000 K, 10^{-5} mol ℓ^{-1} of C_2H_4 contributed an absorption dip from 214 to 220 nm of 0.5%. During pyrolysis experiments, average C_2H_4 concentrations in the reactor were kept at least an order of magnitude less than this to minimize interference.

Over 300 gas chromatographic analyses have been performed for reactor pressures from 10 to 80 Torr at reactor temperatures from 1000 to 1012 K.[2] H_2, CH_4, C_2H_6, and C_2H_4 were determined in most cases, CO and C_2H_6O in a few. As in previous work (2), C_2H_4 appeared to be formed mainly from an impurity; it will be given limited weight in subsequent discussions. The similarity of analyses performed with the D_2 lamp on and off showed that photochemical reactions were not significant.

Logarithms of the rates of formation of CH_4, H_2, and C_2H_6 are shown as a function of reactor residence time at 10 and 80 Torr reactor pressure in Figs. 2 and 3, respectively. Spectroscopically

[2]Tables of data are available, at a nominal charge, from the Depository of Unpublished Data, CISTI, National Research Council of Canada, Ottawa, Ont., Canada K1A 0S2.

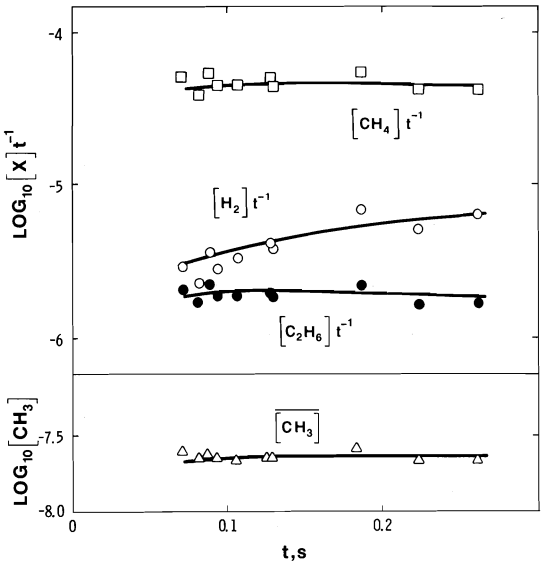

FIG. 2. Logarithms of the rates of formation of CH_4, H_2, and C_2H_6 (mol ℓ^{-1} s^{-1}) and of the average concentrations of CH_3 (mol ℓ^{-1}) as a function of reactor residence time at 1005 K and 10 Torr. Points are experimental; lines were predicted by the computer simulation.

determined average concentrations of methyl radicals are also shown.

Discussion

Computer Simulation

A computer simulation was used to assist in interpreting the experiments. The program, modelled after one described in ref. 11, integrated the rate equations for the system using a Runge–Kutta–Gill procedure. The reactions taken into account (numbered consistently with ref. 2) are listed in Table 1 with the corresponding rate constants.

Other reactions, as follows, were considered for inclusion in the program, but were estimated to make little contribution and were omitted. Alternative reactions of CH_3O and of C_2H_5 were considered in ref. 2 and shown to be negligible. Reactions of CH_2OCH_3 radicals were shown (2) to be possible minor contributors to termination at 784 K; because of the higher activation energy of reaction 4 compared to reaction 5, CH_2OCH_3 termination reactions would be even less able to compete with reaction 6 at higher temperatures. The recombination alternative to reaction 16 was not included, as acetaldehyde has not been observed as a product of dimethyl ether pyrolysis. Rates of the reverses of the reactions in Table 1 (except [−6] and

TABLE 1. Reactions and rate constants used in computer simulation

	Reaction	Log k at 1005 K (ℓ mol^{-1} s^{-1} or s^{-1})	E_A (kcal mol^{-1})	Sources or references
[1]	$C_2H_6O \rightarrow CH_3 + CH_3O$	See Table 2	77.	This work, 2
[2]	$CH_3O \rightarrow CH_2O + H$	[a]		
[3]	$H + C_2H_6O \rightarrow H_2 + CH_2OCH_3$	9.1	4.7	12
[4]	$CH_2OCH_3 \rightarrow CH_2O + CH_3$	[a]		
[5]	$CH_3 + C_2H_6O \rightarrow CH_2OCH_3 + CH_4$	See Table 2	15.	This work, 2
[6]	$2CH_3 \rightarrow C_2H_6$	See Table 2	0	This work
[−6]	$C_2H_6 \rightarrow 2CH_3$	Log k_6 − 12.8	91.	13, 14
[9]	$CH_3 + CH_2O \rightarrow CH_4 + CHO$	7.4	6.2	This work, 15
[10]	$H + CH_2O \rightarrow H_2 + CHO$	9.55	3.76	16, 17
[11]	$CHO + M \rightarrow H + CO + M$	8.0	14.7	18
[12]	$CH_3 + C_2H_6 \rightarrow CH_4 + C_2H_5$	6.6	21.5	This work, 9
[13]	$H + C_2H_6 \rightarrow H_2 + C_2H_5$	9.1	9.4	19
[14]	$C_2H_5 \rightarrow C_2H_4 + H$	[a]		
[15]	$CH_3 + H_2 \rightarrow CH_4 + H$	7.1	14.	20
[−15]	$H + CH_4 \rightarrow CH_3 + H_2$	8.4	15.	13
[16]	$CH_3 + CHO \rightarrow CH_4 + CO$	10.6	0	This work
[17]	$2CHO \rightarrow 2CO + H_2$	10.0	0	Estimate
[18]	$H + CHO \rightarrow H_2 + CO$	10.3	0	Estimate
[19]	$H + CH_3 \rightarrow CH_4$	9–9.7[b]	0	21

[a]Assumed to follow automatically whenever the respective radical was formed.
[b]Assumed pressure dependent.

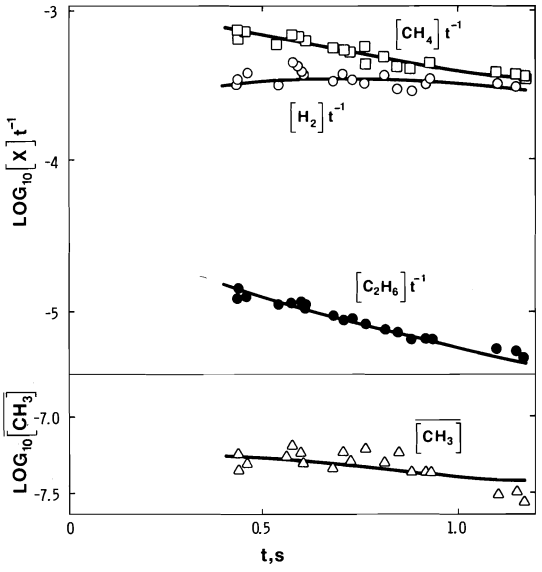

FIG. 3. Logarithms of the rates of formation of CH_4, H_2, and C_2H_6 (mol ℓ^{-1} s^{-1}) and of the average concentrations of CH_3 (mol ℓ^{-1}) as a function of reactor residence time at 1007 K and 80 Torr. Points are experimental; lines were predicted by the computer simulation.

[−15]) were calculated using thermochemistry (13) and were found to be negligible. Other reactions, such as the unimolecular decomposition of CH_2O or addition of radicals to C_2H_4 or CH_2O, could be eliminated by considering rate constants and thermochemistry in the literature (18, 22). Surface reactions were neglected because no effect of surface to volume ratio was observed in ref. 2.

The concentration of CH_3 was assumed to be zero at the reactor entrance and was allowed to relax toward its steady state value as the reaction progressed. At 10 Torr the relaxation time for this process was found to be 7% of the shortest experimental residence time. Use of the steady state assumption throughout the reactor would have led to an error in predicted product yields and average CH_3 concentration of about 7%. Because of their smaller concentrations, the corresponding relaxation times for H and CHO were at least an order of magnitude faster, justifying the use of the steady state assumption for these species.

To observe reaction rates which were as close as possible to the initial rates, faster reagent flow rates were used in these experiments than in ref. 2. As a result the reagent would have proceeded farther down the reactor before it was heated to the same temperature as the reactor wall. This problem has been considered by Mulcahy and Pethard (23), who described the average temperature of the gas, T_x, a distance x from the furnace entrance by the formula

$$[20] \quad T_x = T_s - 0.82(T_s - T_0) \times \exp(-3.658Ktx/R^2L)$$

where T_s and T_0 are the temperatures of the wall and the entering gas, respectively; K is the thermal diffusivity; t, the residence time; R, the tube radius; and L, the length of the furnace. The thermal diffusivity was estimated from the thermal conductivity (24) and heat capacity (22) of the similar molecule, ethanol, to be $3 \times 10^{-3}[C_2H_6O]^{-1}$ cm^2 s^{-1}. Temperatures within the reactor were calculated from eq. 20. Rate coefficients at each distance, x, could be calculated using the activation energies in Table 1. The rate equations were then integrated. This modification required changes in k_1 and k_6 of up to 10%.

Mulcahy and Pethard (23) have also considered the errors that arise because the flow velocity has a parabolic profile instead of the plug flow profile assumed by our program. For a first order reaction occurring at the conditions of this work, the error would be 0.5%. Although not all reactions in the present system are first order, these errors have been neglected.

Reactions -6, 17, 18, and 19 did not affect the simulations, even when increased by an order of magnitude. They could have been omitted. Reactions 13, 15, and -15 were only significant at the higher pressures.

The computer simulation was initially attempted using values of k_{12} from ref. 9, but this model predicted greater concentrations of C_2H_4 than observed at 80 Torr and long residence times. To correct this, k_{12} was reduced, although reducing k_{13}, increasing k_3 and k_{10}, or including reactions to remove C_2H_4 would have had a similar result.

The value of k_9 was chosen to give agreement with observed H_2 concentrations at 10 and 20 Torr.

Reaction 16 was a minor contributor to chain termination at high pressures and long residence times. The value of k_{16} was chosen to match the downward slopes of Figs. 2 and 3. This could also have been accomplished by adjusting k_{11}.

The rates of reactions 1, 5, and 6 were then varied at each pressure to match the $[CH_4]/t$, $[C_2H_6]/t$, and $[\overline{CH_3}]$ observations. The results for 10 and 80 Torr are shown as the solid lines in Figs. 2 and 3. Agreement at the other pressures used was also within experimental uncertainty. The coefficients, k_1, k_5, and k_6, used at each pressure, are shown in Table 2. Both k_1 and k_6 generally increase as pressure increases, as expected for dissociation–recombination reactions in their pressure dependent region. Values of k_5 were almost independent of pressure, as expected.

TABLE 2. Rate constants determined by computer simulation

Pressure (Torr)	$k_1 \times 10^2$ (s^{-1})	$k_5 \times 10^{-7}$ (ℓ mol^{-1} s^{-1})	$k_6 \times 10^{-9}$ (ℓ mol^{-1} s^{-1})
10	1.7±0.4	1.31±0.10	3.5
20	1.6±0.6	1.20±0.20	4.1
40	2.8±1.1	1.24±0.28	4.2
60	4.4±2.3	1.33±0.28	4.6
80	4.9±2.3	1.57±0.45	6.1

The rate constants in Table 1 were varied by factors of two in various combinations to find the sensitivity of k_1, k_5, and k_6 to changes in the model. Uncertainties in k_1, k_5, and k_6 determined in this way were combined with estimates of the scatter of the data. Uncertainties in the extinction coefficient and the thermal diffusivity, which have a similar effect at all pressures, were not included at this point.

The uncertainties in k_1, shown in Table 2, were greater than in the earlier work (2), because of the greater conversions. Using the experimentally determined Arrhenius parameters from ref. 2 ($\log A = 15.2$, $E_A = 77$ kcal mol^{-1}), the high pressure rate constant at 1005 K would be predicted to be 3.1×10^{-2} s^{-1}, within the uncertainty limits of the high pressure values in Table 2.

Recombination Reaction

The acceptable ranges for k_6 are shown, plotted as a function of the logarithm of pressure, by the vertical bars in Fig. 4. Curve *a* was calculated from the equilibrium constant (from Table 1) and from the RRKM model[3] used by Clark and Quinn (25) to reproduce their data for k_{-6} at 838 K. Curve *b* was calculated by the method of van den Bergh (26), using reduced Kassel curves and a collision efficiency for deactivation of excited C_2H_6 of 0.29. This model, with a smaller collision efficiency for deactivation by argon, was fitted to the data of Glanzer *et al.* (5) at 1350 K. Both curves can be seen to be somewhat steeper than, though compatible with, the pressure dependence observed in this work.

Extrapolating the data of this work to high

[3]State densities and sums were calculated using a program by W. L. Hase and D. L. Bunker, Quantum Chemistry Program Exchange, No. 234, Indiana University, Bloomington, IN, U.S.A.

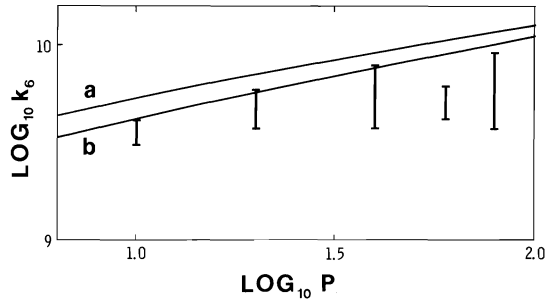

FIG. 4. Dependence of k_6 (ℓ mol^{-1} s^{-1}) on reactor pressure (Torr). The vertical bars show the range of values compatible with the present experiments for a fixed extinction coefficient. Curve *a* was calculated from the theoretical treatment of ref. 25; *b*, from ref. 26.

pressures would place too much emphasis on the less reliable 40 and 80 Torr results. Instead, comparisons have been made with curves *a* and *b*, which are based on more extensive and precise results. The experimental values of k_6 were, on the average, seven tenths of the values from curve *b*. If this proportion were retained, the limiting high pressure rate constant, $k_{6,\infty}$, for this work would be 1.4×10^{10} ℓ mol^{-1} s^{-1}, compared to the value, 2×10^{10} ℓ mol^{-1} s^{-1}, of curve *b*. By a similar comparison with curve *a*, again $k_{6,\infty}$ was found to be 1.4×10^{10} ℓ mol^{-1} s^{-1}. Values of k_6 from ref. 5 (the basis of curve *b*) depend directly on the extinction coefficient, whereas values from this work depend on its square. The uncertainty in the extinction coefficient quoted in ref. 5 was $\pm 30\%$. If the upper limit were taken, the values of $k_{6,\infty}$ from these sources would agree with each other and with most values measured at room temperature (27). The threefold disagreement between ref. 5 and the mass spectrometric measurements of refs. 1 and 4 would be narrowed but would not disappear. When the uncertainties in the extinction coefficient and the extrapolation are combined with the uncertainties in Fig. 4, we estimate that individual values of k_6 from the present work are reliable within about a factor of two and $k_{6,\infty}$ is reliable within a factor of three.

The present results tend to support the conclusion of Glanzer *et al.* that $k_{6,\infty}$ is no greater at high temperatures than at room temperature. The results then favour the adiabatic open channel or minimum state density theories.

Abstraction Reactions

Calculated values of k_5 were directly proportional to the extinction coefficient chosen, but almost independent of the thermal diffusivity. Uncertainties from other sources are shown in Table 2. This rate constant has not previously been measured individually, but only as the quotient $k_5 k_{6,\infty}^{-1/2}$. Calculating this quotient from Arrhenius parameters determined at 782–936 K in ref. 2 and taking $k_{6,\infty} = 1.4 \times 10^{10}$ ℓ mol^{-1} s^{-1} from this work led to a predicted value of k_5 at 1005 K of 1.36×10^7 ℓ mol^{-1} s^{-1}, in excellent agreement with the average, $1.33 \pm 0.14 \times 10^7$ ℓ mol^{-1} s^{-1}, from Table 2. Taking Arrhenius parameters from photolysis experiments at 407–523 K (28), a similar calculation led to $k_5 = 1.5 \times 10^6$ ℓ mol^{-1} s^{-1}, one ninth the observed value. Choice of a different source for $k_{6,\infty}$ would not have removed this difference. The difference cannot be caused by strong curvature of the Arrhenius plot for reaction 6, which has a similar rate constant at 300 K (27), 450 K (26), and high temperatures. Thus we conclude that reaction 5 exhibits a strongly curved Arrhenius plot.

Including the uncertainty in extinction coefficient, log k_5 would become 7.12 ± 0.2, in ℓ mol^{-1} s^{-1} units.

Values of k_9 of $3.0 (\pm 1.3) \times 10^7$ ℓ mol^{-1} s^{-1} were consistent with the observed H_2 yields. Including the uncertainty in the extinction coefficient, log $k_9 = 7.5 \pm 0.4$. Combining Arrhenius parameters for $k_9 k_{6,\infty}^{-1/2}$ from photolysis experiments at 357–453 K (15) and $k_{6,\infty}$ from this work led to a predicted value of k_9 of 4.5×10^6 ℓ mol^{-1} s^{-1} at 1005 K, one sixth of the experimental value. This reaction also appears to have a curved Arrhenius plot.

Since this article was submitted, a report (29) of a gas chromatographic study of dimethyl ether pyrolysis between 1063 and 1223 K has appeared. Extrapolation of the higher temperature data to 1005 K leads to the following predictions: $k_1 = 4.7 \times 10^{-2}$ s^{-1} at 1 atm, in satisfactory agreement with the present work; $k_9 = 2.5 \times 10^8$ ℓ mol^{-1} s^{-1}, almost an order greater than the present results. Reaction 9 merits further work.

Acknowledgements

The authors wish to thank the National Research Council of Canada for a grant in support of this research and Dr. Martin Quack for providing a copy of ref. 10 before publication.

1. T. C. CLARK, T. P. J. IZOD, and G. B. KISTIAKOWSKY. J. Chem. Phys. **54**, 1295 (1971).
2. P. D. PACEY. Can. J. Chem. **53**, 2742 (1975).

3. P. CAMILLERI, R. M. MARSHALL, and J. H. PURNELL. J. Chem. Soc. Faraday Trans. I, **71**, 1491 (1975).
4. K. U. INGOLD and F. P. LOSSING. J. Chem. Phys. **21**, 1135 (1953).
5. K. GLANZER, M. QUACK, and J. TROE. Chem. Phys. Lett. **39**, 304 (1976).
6. W. L. HASE. J. Chem. Phys. **64**, 2442 (1976).
7. K. J. LAIDLER and J. C. POLANYI. Progress in reaction kinetics. Vol. 3. *Edited by* G. Porter. Pergamon, Oxford. 1965.
8. P. D. PACEY. Chem. Phys. Lett. **23**, 394 (1973).
9. P. D. PACEY and J. H. PURNELL. J. Chem. Soc. Faraday Trans. I, **68**, 1462 (1972).
10. K. GLANZER, M. QUACK, and J. TROE. 16th International Symposium on Combustion, 949 (1977).
11. P. D. PACEY and J. H. PURNELL. Ind. Eng. Chem. Fundam. **11**, 233 (1972).
12. J. F. MEAGHER, P. KIM, J. H. LEE, and R. B. TIMMONS. J. Phys. Chem. **78**, 2650 (1974).
13. D. R. STULL, H. PROPHET *et al.* JANAF thermochemical tables. 2nd ed. National Bureau of Standards, Washington, DC. 1970.
14. AMERICAN PETROLEUM INSTITUTE. Selected values of properties of hydrocarbons and related compounds. Vol. A-72. Texas A & M University, College Station, Texas. 1975.
15. S. TOBY and K. O. KUTSCHKE. Can. J. Chem. **37**, 672 (1959).
16. R. R. BALDWIN and D. W. COWE. Trans. Faraday Soc. **58**, 1768 (1962).
17. A. A. WESTENBERG and N. DEHAAS. J. Phys. Chem. **76**, 2213 (1972).
18. H. G. SCHECKER and W. JOST. Ber. Bunsenges. Phys. Chem. **73**, 521 (1969).
19. P. CAMILLERI, R. M. MARSHALL, and J. H. PURNELL. J. Chem. Soc. Faraday Trans. I, **70**, 1434 (1974).
20. P. C. KOBRINSKY and P. D. PACEY. Can. J. Chem. **52**, 3665 (1974).
21. C. J. CHEN, M. H. BACK, and R. A. BACK. Can. J. Chem. **53**, 3580 (1975).
22. S. W. BENSON and H. E. O'NEAL. Kinetic data on gas phase unimolecular reactions. National Bureau of Standards, Washington, DC. 1970.
23. M. F. R. MULCAHY and M. R. PETHARD. Aust. J. Chem. **16**, 527 (1963).
24. Y. S. TOULOUKIAN, P. E. LILEY, and S. C. SAXENA. Thermophysical properties of matter. Vol. 3. IFI/Plenum, New York, NY. 1970.
25. J. A. CLARK and C. P. QUINN. J. Chem. Soc. Faraday Trans. I, **72**, 706 (1976).
26. H. E. VAN DEN BERGH. Chem. Phys. Lett. **43**, 201 (1976).
27. D. A. PARKES, D. M. PAUL, and C. P. QUINN. J. Chem. Soc. Faraday Trans. I, **72**, 1935 (1976).
28. P. GRAY and A. A. HEROD. Trans. Faraday Soc. **64**, 2723 (1968).
29. D. ARONOWITZ and D. NAEGELI. Int. J. Chem. Kinet. **9**, 471 (1977).

The use of polymer supports in organic synthesis. XII. The total stereoselective synthesis of *cis* insect sex attractants on solid phases

THOMAS M. FYLES[1] AND CLIFFORD C. LEZNOFF[2]
Department of Chemistry, York University, Downsview, Ont., Canada M3J 1P3
AND
JOHN WEATHERSTON
Forest Pest Management Institute, Sault St. Marie, Ont., Canada P6A 5M7
Received May 9, 1977

THOMAS M. FYLES, CLIFFORD C. LEZNOFF, and JOHN WEATHERSTON. Can. J. Chem. **55**, 4135 (1977).

A 2% crosslinked divinylbenzene–styrene copolymer, incorporating trityl chloride groups (**2**) was used in the synthesis of insect sex attractants of Lepidoptera by a two-step alkyne coupling route. Polymer **2** reacted with the symmetrical diols, 1,8-octanediol and 1,10-decanediol, to give the monoblocked polymer-bound diols **5** and **6** respectively. Mesylation of **5** and **6** gave the polymer-bound monomesylates **7** and **8** which on coupling with lithioacetylide gave the polymer-bound terminal alkynes **9** and **10** respectively. Acid cleavage of **9** and **10** provide 9-decyn-1-ol and 11-dodecyn-1-ol respectively. A second coupling step was performed by lithiation of **9** and **10** with *n*-butyllithium or *tert*-butyllithium followed by treatment with *n*-butyl bromide or ethyl bromide to give polymer-bound internal alkynes, which on acid hydrolysis gave 9-tetradecyn-1-ol (**22**), 11-hexadecyn-1-ol (**23**), and 11-tetradecyn-1-ol (**24**). If **10** had been lithiated with *n*-butyllithium and coupled with ethyl bromide, some translithiation occurred to liberate *n*-butyl bromide which entered into the coupling reaction eventually giving a mixture of **23** and **24**. This problem was resolved by the use of *tert*-butyllithium in the lithiation step. Attempts were made to reduce polymer-bound internal alkynes stereoselectively to *cis*-alkenes with 9-borabicyclononane, diisobutylaluminum hydride, and catechol borane but all these reagents proved inadequate due to incomplete reduction, overreduction, hydrogenolysis of the alkyne from the polymer, and non-selectivity. Polymer-bound internal alkynes were quantitatively reduced exclusively to *cis* insect sex attractants using disiamylborane without concurrent overreduction or hydrogenolysis.

THOMAS M. FYLES, CLIFFORD C. LEZNOFF et JOHN WEATHERSTON. Can. J. Chem. **55**, 4135 (1977).

On a utilisé un copolymère divinylbenzène–styrène réticulé à 2% et incorporant des groupes chlorure de trityle (**2**) pour réaliser la synthèse de l'attirant sexuel du Lepidoptera en faisant appel à un schéma de couplage d'alcynes impliquant deux étapes. Le polymère **2** réagit avec les diols symétriques octanediol-1,8 et décanediol-1,10 pour conduire suivant le cas aux diols monobloqués **5** et **6** liés au polymère. La mésylation de **5** et **6** fournit les monomésylates **7** et **8** liés au polymère qui, par couplage avec l'acétylure de lithium, conduisent respectivement aux alcynes terminales **9** et **10** liés au polymère. Une scission acide de **9** et **10** conduit respectivement aux décyn-9 ol-1 et dodécyn-11 ol-1. Une nouvelle étape de couplage, effectuée par la lithiation de **9** et **10** avec le *n*-butyllithium ou le *tert*-butyllithium, suivie par un traitement avec le bromure de *n*-butyle ou le bromure d'éthyle conduit aux alcynes internes liés au polymère qui par hydrolyse acide fournissent le tétradécyn-9 ol-1 (**22**), l'hexadécyn-11 ol-1 (**23**) et le tétradécyn-11 ol-1 (**24**). Si l'on avait effectué la lithiation de **10** avec du *n*-butyllithium et si on l'avait couplé avec du bromure d'éthyle, il se serait produit un peu de translithiation pour libérer du bromure de *n*-butyle qui peut entrer éventuellement dans la réaction du couplage pour conduire à un mélange de **23** et de **24**. On a résolu ce problème par l'utilisation du *tert*-butyllithium dans l'étape de lithiation. On a effectué des essais pour réduire d'une façon stéréosélective les alcynes internes liés au polymère afin d'obtenir des alcènes *cis*; à cette fin on a fait appel au 9-borabicyclononane, à l'hydrure de diisobutylaluminium et au catéchol-borane mais tous ces réactifs s'avèrent inadéquats à cause soit d'une réduction incomplète, d'une réduction trop grande, d'une hydrogénolyse de l'alcyne du polymère ou à cause de la non-sélectivité. On a pu réduire quantitativement les alcynes internes liés au polymère et obtenir exclusivement les attractants sexuels des insectes *cis* en faisant appel au disiamylborane sans obtenir de réduction supplémentaire ou d'hydrogénolyse.

[Traduit par le journal]

[1]Holder of NRCC Studentships 1974–1977.
[2]Author to whom correspondence should be addressed.

Introduction

Recently, we have reported the preparation of insect sex attractants (shown below) of Lepidop-

$$CH_3(CH_2)_mCH{=}CH(CH_2)_nOAc$$

cis

where $m = 1$–3 and $n = 6, 8$–10

tera on solid phases by an alkyne coupling route and by two different Wittig sequences (1, 2). The yields of reactions on solid phases, the use of symmetrical starting materials (3), the simplicity of solid phase reactions (4, 5), and the potential for synthesis in an automated procedure (6) showed distinct promise over solution phase methods, but several problems remained to be solved for the complete stereoselective synthesis of insect sex attractants (7) on solid phases. The use of expensive terminal alkynes in the coupling step can be construed as a disadvantage in both solid phase and solution methods of synthesis. Furthermore, in our previous syntheses on solid phases via the alkyne coupling route, the polymer-bound alkyne was cleaved from the polymer before stereoselective reduction to *cis* insect sex attractants was attempted. The stereoselective reduction was then achieved using 9-borabicyclononane (9-BBN) in solution (2, 8). A complete solid phase synthesis of *cis* insect sex attractants would require that the stereoselective *cis* reduction of an internal alkyne be accomplished directly on the polymer support. In this report we describe the synthesis of insect sex attractants on solid phases by a two-step alkyne coupling route using only acetylene and alkyl halides (9, 10). In addition, the stereoselective reduction of a polymer-bound alkyne to a polymer-bound *cis*-alkene by an examination of a variety of soluble reducing agents is described.

Results and Discussion

The Two-step Alkyne Route

A 2% crosslinked divinylbenzene (DVB)-styrene copolymer, incorporating trityl alcohol functional groups (**1**) (11, 12), was prepared by our direct lithiation method (12) and converted to a polymer-bound trityl chloride (**2**) (11, 12). Polymer **2** was treated with 1,8-octanediol (**3**) and 1,10-decanediol (**4**) for 48 h in pyridine at room temperature to give the monoprotected polymer-bound diols **5** and **6** respectively. Mesylation of **5** and **6** in benzene–pyridine (3:1) gave the polymer-bound symmetrical diol monomesylates **7** and **8** respectively. The amounts of diols bound to **5** and **6** and the yields of monomesylates derived from **7** and **8** were determined by acid cleavage as previously described (2) and are recorded in Table 1.

Monolithioacetylide can now be readily prepared in large quantities (13). Treatment of **7** and **8** with monolithioacetylide in tetrahydrofuran – hexamethylphosphoric triamide (THF–HMPT) (14) gave the polymer-bound terminal alkynes **9** and **10** respectively. Cleavage of **9** and **10** with HCl in dioxane as usual (2) gave 9-decyn-1-ol (**11**) and 11-dodecyn-1-ol (**12**) respectively in high conversion (Table 1) and some recovered **3** and **4** respectively. Lithiation of **9** with *n*-butyllithium (**13**) and **10** with **13** or *tert*-butyllithium (**14**) yielded the polymer-bound lithioalkynes **15** and **16** respectively. Coupling in THF–HMPT (14) of **15** with *n*-butyl bromide (**17**) and **16** with **17** or ethyl bromide (**18**) yielded the polymer-bound alkynes **19–21** respectively as shown in Scheme 1. Polymer-bound alkynes **19** and **21** had been previously prepared by a one-step alkyne coupling route from **7** and 1-lithio-1-hexyne and from **8** using 1-lithio-1-butyne respectively. Acid cleavage of **19–21** gave 9-tetradecyn-1-ol (**22**), 11-hexadecyn-1-ol (**23**), and 11-tetradecyn-1-ol (**24**) in high conversion from the symmetrical diols **3** and **4** (Table 1). All yields in Table 1 are calculated on products purified by preparative thin layer chromatography (tlc).

When a terminal alkyne is lithiated in a normal solution reaction (9, 10), equivalent amounts of *n*-butyllithium can be used to effect the lithiation. On polymer supports it is usually necessary to use excess reagents to drive reactions to completion and hence in our experiments on polymer **10**, excess **13** was used. Thus, in the coupling reaction of **16** with ethyl bromide (**18**), some excess **13** was present, which could and did exchange with **18** to give ethyllithium and some *n*-butyl bromide (**17**). The coupling of **16** prepared from *n*-butyllithium (**13**) with **18** thus led to a mixture of **20** and **21**, which on acid cleavage gave a mixture of the alkynols **23** and **24**. Analysis of this mixture, as their acetates, by high pressure liquid chromatography (hplc) showed that **24** was contaminated by about 15% of **23** (Table 2). The problem of translithiation was overcome by using *tert*-butyllithium (**14**) for the lithiation step and **24** could be prepared free of **23** (Table 2).

Conditions necessary for the conversion of **9**

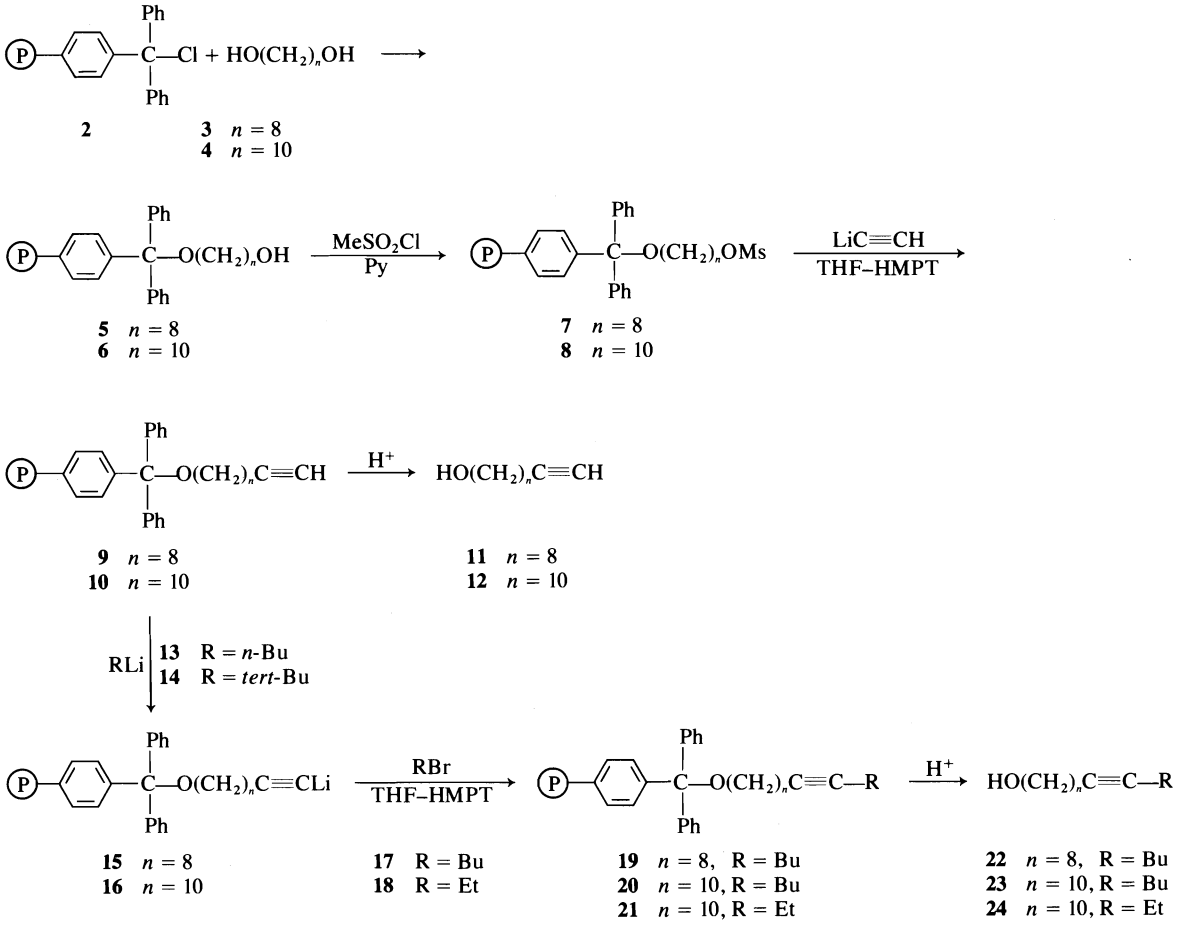

SCHEME 1

and **10** to **22–24** according to Scheme 1 could be readily monitored by hplc analysis of crude **22–24** prepared via solid phases. In practice, the alkyne fraction, containing internal and sometimes terminal alkyne, was separated by preparative tlc from recovered diol and the alkyne fraction and converted to their acetates which were analyzed by hplc. By this method, the amounts of terminal alkyne in **22–24** could be accurately determined (Table 2).

cis Reductions of Polymer-bound Alkynes

Although we had previously reduced internal alkynes to *cis*-alkenes in solution by catalytic hydrogenation over a Lindlar-type catalyst (2), the results were not completely stereoselective in that less than 85% of the pure *cis* isomers were produced. In addition, the use of an *insoluble* palladium oxide catalyst would be incompatible with insoluble polymer supports in any attempt to reduce polymer-bound alkynes to *cis*-alkenes. It had been shown (2, 8) that internal alkynes can be reduced stereoselectively to *cis*-alkenes with *soluble* 9-BBN. After experimenting with a variety of soluble reducing agents (see below), disiamylborane (15) was found to be ideal for the job of reducing polymer-bound alkynes stereoselectively to polymer-bound *cis*-alkenes. Thus, the polymer-bound internal alkynes, **19** and **21**, that had been prepared, in fact, by the one-step alkyne coupling route (2), were treated with a large excess of 0.5 *M* disiamylborane ($(Sia)_2BH$) in THF at 0°C for 4 h. Protonolysis with acetic acid yielded the polymer-bound *cis*-alkenes **25** and **26**, which on acid cleavage and acetylation yielded, according to Scheme 2, *cis*-9-tetradecen-1-yl acetate (**27**) (10), the sex attractant of *Spodoptera frugiperda* (J. E. Smith), and *cis*-11-tetradecen-1-yl acetate (**28**) (16), the sex attractant of *Argyrotaenia velutinana* (Walker), in high

TABLE 1. Yields of alkynols and intermediates prepared on solid phases via the two-step alkyne route

Internal alkynol	Quantity of diol initially bound to polymers 5 and 6[a] (mmol/g)	Quantity of diol monomesylate bound to polymers 7 and 8[b] (mmol/g)	Quantity of recovered diol[b] (mmol/g)	Quantity of terminal alkynol bound to polymers 9 and 10[c] (mmol/g)	Quantity of recovered diol[c] (mmol/g)	Quantity of internal alkynol bound to polymers 19–21[d] (mmol/g)	Quantity of recovered diol[d] (mmol/g)	Overall yield of internal alkynols (%)	Overall conversion to internal alkynols[e] (%)
22	0.58	0.29	0.23	0.22	0.30	0.21	0.29	36[f]	73
23	0.69	0.35	0.33	0.30	0.35	0.29	0.34	42	83
24	0.69	0.35	0.33	0.30	0.35	0.28	0.31	41[g]	74

[a]Determined by acid cleavage of **5** and **6**.
[b]Determined by acid cleavage of **7** and **8**.
[c]Determined by acid cleavage of **9** and **10**.
[d]Determined by acid cleavage of **19–21**.
[e]Yield if diol recovered from acid cleavage of **19–21** is recycled.
[f]Solution yield from ref. 10 is 36% based on 8-chloro-1-octanol.
[g]Prepared using **14** as the lithiating agent (Scheme 1).

conversion (Table 3). Attractants **27** and **28** were examined by hplc and vapour phase chromatography (vpc) for isomeric purity about the double bond and were found to have *cis*:*trans* ratios of 99:1 and 90:10 respectively (Table 4).

Earlier attempts to reduce **21** to **26** using excess 9-BBN at 50°C gave complete reduction but some hydrogenolysis (cleavage from the polymer) occurred and the reduction was *not* completely stereoselective even though it was completely stereoselective in solution (Tables 3 and 4). Less vigorous conditions resulted in incomplete reduction of the alkyne (Table 4). Catechol borane (17) has been recently recommended for the stereoselective reduction of alkynes to *cis*-alkenes in solution, but treatment of **21** with catechol borane in dioxane under normal conditions (17) led to complete hydrogenation and hydrogenolysis to 1-tetradecanol, analyzed by hplc as its acetate (Table 4). In THF under reflux, however, only partial reduction of **21** to **26** occurred. In addition, some hydrogenolysis from the polymer took place and product **26** exhibited a *cis*:*trans* ratio of only 2:3 and hence reduction took place in a non-stereoselective manner (Tables 3 and 4). Diisobutylaluminum hydride (DIBAH) has been used for the stereoselective *cis* reduction of alkynes (18). Treatment of **21** in THF with a slight excess of 1 *M* DIBAH in hexane at room temperature overnight gave little reaction. With excess DIBAH at 60°C reduction to alkene was still incomplete. Under reflux conditions in benzene, reduction was complete, but hydrogenolysis from the polymer was also complete (Tables 3 and 4). In addition, some 1-tetradecanol, analyzed as its acetate was detected in the filtrate of the polymer, showing that overreduction had occurred. The reductions were not completely stereospecific in that **28** exhibited a *cis*:*trans* ratio of 85:15.

As shown in Table 3 the stereoselective reductions of **19** and **21** leading to **27** and **28** using $(Sia)_2BH$ are virtually quantitative. The analogous reaction in solution described by Holan and O'Keefe (15) proceeded very well in 90% yield but was not quite as good as described herein. We have noticed this phenomenon before in which polymer-bound reactions *appear* to be consistently 5–20% better than their solution analogs (2) although documentation and strict comparisons are difficult to make as, by their very nature, polymer-bound reactions are not

TABLE 2. High pressure liquid chromatographic analysis of the alkynol fractions,[a] obtained under a variety of conditions via **9** and **10** according to Scheme 1

Polymer bound terminal alkyne	Lithiation agent[b]	Alkylating agent[c]	T (°C)	Relative yield of terminal alkynol[a] (%)	Relative yield of internal alkynol[a] (%)	Solvent for hplc analysis[d]
9	**13**	**17**	0	65[e]	35[f]	A
9	**13**	**17**	20–30	20	80	A
9	**13**	**17**	60–70	0	100	A
10	**13**	**17**	20–30	15[g]	85[h]	B
10	**13**	**17**	60–70	0	100	B
10	**13**	**18**	0	50	40[i]	B
10	**13**	**18**	60–70	0	85[j]	B
10	**14**	**18**	0	40	60	B
10	**14**	**18**	60	0	100	B

[a]Obtained by acid cleavage of **19–21**, separated from starting diol, and acetylated for hplc analysis.
[b]The period of lithiation was 0.5–0.75 h.
[c]The period of alkylation was 3–4 h.
[d]Solvent A is water–acetonitrile, 2:3, and solvent B is water–acetonitrile, 3:7.
[e]9-Decyn-1-yl acetate has a retention volume (V_T) of 9.3 ml.
[f]9-Tetradecyn-1-yl acetate has a V_T = 29.8 ml.
[g]11-Dodecyn-1-yl acetate has a V_T = 9.5 ml.
[h]11-Hexadecyn-1-yl acetate has a V_T = 25.6 ml.
[i]11-Tetradecyn-1-yl acetate has a V_T = 15.6 ml and is contaminated with 10% of 11-hexadecyn-1-yl acetate (V_T = 25.6 ml).
[j]11-Tetradecyn-1-yl acetate (V_T = 15.6 ml) is contaminated with 15% of 11-hexadecyn-1-yl acetate (V_T = 25.6 ml).

identical to their solution analogs in all respects. We make this observation because for this particular reduction a possible explanation is available. In the solution reaction the vinyl borane intermediate, hydrolyzed by protonolysis with acetic acid, yields boron-containing impurities which must be removed by treatment with hydrogen peroxide (15). In the analogous reductions of **19** and **21** leading to **25** and **26**, the boron-containing impurities are removed by simple filtration, as the desired products are bound to the insoluble support, and the products **27** and **28** are thus not subjected to treatment with hydrogen peroxide.

Elemental Analysis as a Diagnostic Tool for the Determination of Polymer-bound Products

We had previously stated that elemental analyses of polymer-bound products are unreliable guides to the purity of polymer-bound products (2), because, as in all reactions, side products are often obtained along with the desired product and hence polymer-bound products are unlikely to be pure. We prefer to base our yields of reactions on pure products isolated after cleavage from the polymer. Relles and Schluenz partially addressed this problem in discussing polymer-bound phosphine dichlorides (19). Firstly, they mention that elemental analysis of polymer-bound phosphorous is unreliable and irreproducible and, secondly, they quantify the amount of reagent bound to the polymer by the job it does and not by the phosphorous content of the polymer, which we feel is reasonable. In our own work in this paper, for example, elemental analysis of one batch of **8** for S (1.65%) shows a sulfur content corresponding to 0.52 mmol of 1,10-decanediol monomesylate/g, but acid cleavage yields only 0.29 mmol of 1,10-decanediol

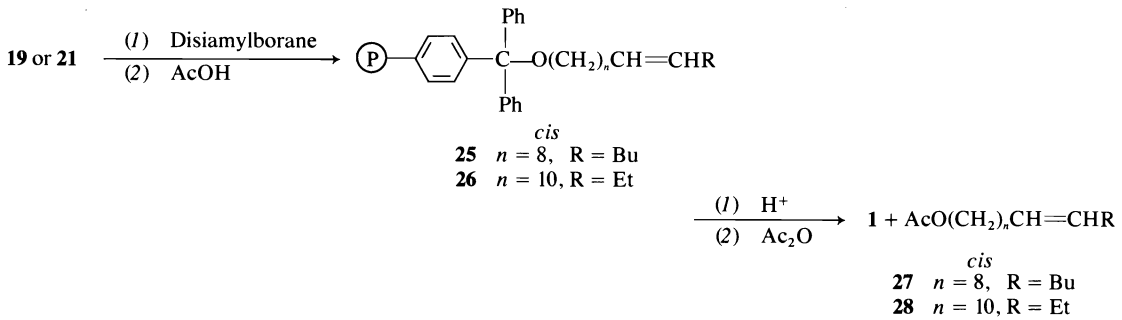

SCHEME 2

TABLE 3. Yields of sex attractants prepared by reduction of polymer-bound alkynes using various soluble reducing agents

Attractant	Quantity of diol initially bound to polymers 5 and 6[a] (mmol/g)	Quantity of diol monomesylate bound to polymers 7 and 8[b] (mmol/g)	Quantity of recovered diol[b] (mmol/g)	Quantity of internal alkynols bound to polymers 19 and 21[c] (mmol/g)	Quantity of recovered diol[c] (mmol/g)	Reducing agent	Quantity of alkenol bound to polymers 25 and 26[d] (mmol/g)	Quantity of recovered alkynol[d] (mmol/g)	Quantity of recovered diol[d] (mmol/g)	Overall yield (%)	Overall conversion[e] (%)
27	0.45	0.22	0.22	0.18	0.22	$(Sia)_2BH$	0.18	0	0.20	40[f]	72
28	0.46	0.22	0.24	0.18	0.24	$(Sia)_2BH$	0.17	0	0.23	37	74
28	0.65	0.30	0.32	0.25	0.35	9-BBN	0.10[g,h]	0	0.27[g,h]	15	42
28	0.65	0.30	0.32	0.25	0.35	Catechol borane	0.12[g]	0.07[g]	0.30[g]	19	34
28	0.65	0.30	0.32	0.25	0.35	DIBAH	0.14[g,h]	0.06[g,h]	0.29[g,h]	21	39

[a]Determined by acid cleavage of 5 and 6.
[b]Determined by acid cleavage of 7 and 8.
[c]Determined by acid cleavage of 19 or 21.
[d]Determined by acid cleavage of 25 or 26.
[e]Yield if diol recovered from acid cleavage of 25 or 26 is recycled.
[f]Solution yield from ref. 10 is 30% based on 8-chloro-1-octanol.
[g]Isolated as their acetates.
[h]The reducing agent caused partial hydrogenolysis in these cases and products were isolated from the filtrate of the reduction of 19 or 21.

monomesylate/g of **8**. Indeed recycled polymer **1** contained 0.06 mmol S (0.2%)/g which indicates that a small amount of sulfur-containing product or impurities become permanently bound to the polymer, while a larger fraction of sulfur-containing impurities are washed out during the acid cleavage step or during the procedure used for cleaning recycled **1**.[3] Thus elemental analysis of **8** is an unreliable guide to the quantity of 1,10-decanediol monomesylate bound to **8**, but does, of course give a maximum possible value. On the other hand elemental analysis for N, of freshly prepared **1** exhibited 0.78 mmol N (1.1%)/g of **1**, while recycled **1** still showed 0.29 mmol N (0.41%)/g. Undoubtedly, the nitrogen comes from the *N,N,N'N'*-tetramethylethylenediamine used in the preparation of **1** (12), but the nature and consequences of these irreversibly bound polymer-bound nitrogen-containing impurities is unclear at this time. Recycled **1** also contains 0.42 mmol Cl (1.49%)/g of **1**, probably derived from the conversion of **1** to **2** with acetyl chloride, but possibly due to multiple cleavages with HCl in dioxane. Since we can separately analyze for benzylic and trityl chloride by the Volhard method (20) and for aliphatic chloride (2) using potassium *tert*-butoxide, and these methods show no residual chloride for recycled **1**, we feel that the residual chloride in recycled **1**[4] results from chloride bound to the phenyl rings of **1**. Perhaps the surprising aspect of these analytical results lies in the fact that these irreversibly bound impurities do not appear to affect the success of polymer-bound syntheses, although an understanding of these processes will make polymer-bound syntheses even more attractive.

Conclusions

A total stereoselective synthesis of *cis* insect sex attractants on solid phases has been achieved by a two-step alkyne coupling route using very inexpensive symmetrical diols, acetylene, and alkyl halides. Disiamylborane proved to be the

[3]Bio-Beads SX-2 were used in all reactions. Chemical analysis of the beads as purchased showed 0.91% Cl, 0.68% N, and 0.84% S, while washed beads still showed 0.73% Cl, 0.36% N, and 0.41% S. Thus, non-exhaustive washing procedures do not reduce all of the Cl, N, and S content of the initial polymer, which contribute to unreliable analyses at a later stage.

[4]Polymer **1** has been recycled over 25 times without degradation or significant loss of capacity to bind symmetrical diols.

TABLE 4. High pressure liquid chromatographic analysis[a] of insect attractants,[b] obtained by reduction of polymer-bound alkynes in THF overnight with an excess of various reducing agents at different temperatures

Polymer bound alkyne	Reducing agent	T (°C)	Relative yield of unreduced alkynol[b] (%)	Relative yield of attractant[b] (%)	*cis*:*trans* ratio of attractant
19	$(Sia)_2BH$	0	0	100[c]	99:1[d]
21	$(Sia)_2BH$	0	0	100[e]	90:10[d]
21	9-BBN[f]	20–30	99.5	0.5	—
21	9-BBN	20–30	17	83	73:27
21	9-BBN	50	0	100	67:33
21	Catechol[f] borane	100[g]	0	0.5[h]	—
21	Catechol borane	65	37	63	40:60
21	DIBAH[f]	20–30	94	6	100:0
21	DIBAH	60	26	74	80:20
21	DIBAH[i]	80	0	75[h,j]	85:15

[a]Solvent B is used (see Table 2, footnote *d*).
[b]Obtained by cleavage of **25** or **26**, separated from starting diol, and acetylated for hplc or vpc analysis.
[c]This entry refers to **27**.
[d]These ratios were determined by vpc and hplc analysis. The retention volume (V_T) of *cis*-**27** is 24.2 ml, *trans*-**27** 26.2 ml, *cis*-**28** 26.0 ml, and *trans*-**28**, 27.4 ml.
[e]This and all lower entries in this column refer to **28**.
[f]Only a small excess of reducing agent was used.
[g]This reduction was done in dioxane.
[h]The remaining product was tetradecan-1-yl acetate produced by overreduction.
[i]In benzene.
[j]Complete hydrogenolysis from the polymer occurred and the product was isolated from the filtrate.

only effective reagent capable of converting a polymer-bound alkyne to a *cis* polymer-bound alkene in almost quantitative yield and high stereoselectivity. The polymer-bound products proved to be easier to purify and provided higher yields than reductions performed in solution. Elemental analysis cannot be used to provide quantitative information about polymer-bound products but can provide useful clues to possible side reactions and the presence of polymer-carried impurities.

Experimental

A Bausch and Lomb Abbé 3L refractometer was used to record the refractive indices. Infrared spectra were recorded on a Unicam SP1000 ir spectrophotometer as neat films between NaCl discs unless otherwise specified. Nuclear magnetic resonance spectra were recorded on a Varian EM360 spectrometer using deuteriochloroform as solvent and tetramethylsilane as internal standard. Mass spectra were recorded on a Perkin-Elmer-Hitachi RMU6E mass spectrometer. Silica gel was used for all thin and preparative layer chromatography. Fractions were extracted with ether in a Soxhlet extractor. Filtration was done under vacuum through sintered glass Buchner funnels. Filtration under an inert atmosphere was done as previously described (2). Microanalyses were performed by G. Gygli of Toronto.

Vapour phase chromatograms were run with a Perkin Elmer 990 instrument using a 15 ft × $\frac{1}{8}$ in. column of 10% Silar C on Gaschrom Q(60/80) at a temperature of 170°C and a nitrogen flow rate of 15 ml/min. High pressure liquid chromatograms were run with a Waters Associates Model 440 instrument, with an R-400 refractive index detector. A 30 × 0.4 cm reverse phase μ Bondapak C-18 column using water–acetonitrile mixtures as solvent was used at a flow rate of 1.0 ml/min. Spectral and analytical data are given for all new compounds and for known compounds where data are unreported.

Preparation of Polymer-bound Diol Monomesylates ***7*** *and* ***8***

The polymer-bound monomesylates **7** and **8** were prepared as previously described (2) except that benzene–pyridine, 3:1, was used as solvent instead of pure pyridine in the mesylation steps. This change gives a cleaner, less brown, polymer than previously described.

Preparation of Polymer-bound Terminal Alkynes ***9*** *and* ***10***

In a typical experiment, 10.8 ml (25 mmol) of a 2–3 *M* solution of *n*-butyllithium in 100 ml of dry THF was cooled in a Dry Ice – acetone bath under argon. Dry, acetone free, acetylene was bubbled into the solution for 0.5 h and the solution was stirred for a further 20 min at the Dry Ice bath temperature. To this solution 5 g of **7** or **8**, containing 0.25–0.35 mmol of diol monomesylate/g of polymer was added followed by the further addition of 100 ml of HMPT. The mixture was warmed to room temperature and stirred overnight. The black mixture was hydrolyzed with 20 ml of water. The polymer was filtered and washed with three 50 ml portions of ethanol, five 50 ml portions of water, three 25 ml portions of ethanol, and two 50 ml portions of benzene. The polymer, wet with benzene, was transferred to a thimble in a Soxhlet extractor in which molecular sieves (3A) had been placed in a second thimble or in the round bottom flask of the extractor, and the polymer was extracted with benzene for 4 h under reflux conditions. The polymer was washed

free of benzene with dry ether and dried *in vacuo* at 0.2 Torr for 0.5 h. The ir spectra of **9** and **10** exhibited a weak band at 3400 cm^{-1} (C≡C—H) and no absorptions at 1360 and 1180 cm^{-1} due to residual mesylate.

*Preparation of 9-Decyn-1-ol (**11**) and 11-Dodecyn-1-ol (**12**) and Their Acetates*

A suspension of 1.0 g of **9** in 40 ml of a 0.35 *M* HCl dioxane solution was stirred at room temperature for 48 h. The polymer residue was washed as previously described (12) and the filtrate diluted with water. As the product was somewhat soluble in water it was necessary to isolate the product from the aqueous solution in a liquid–liquid extractor using ether as the organic phase. The ether phase was dried over $MgSO_4$ and evaporated to yield 95 mg of crude material. Purification by preparative tlc (eluant, ether–benzene 2:3) afforded, from the slowest moving band (R_f, 0.15), 47 mg of recovered **3** and, from the faster moving band (R_f, 0.55), 34 mg of pure 9-decyn-1-ol (**11**), in 38% yield, as an oil; n_D^{25} 1.4851; ir: 3500 (O—H), 3400 (≡C—H), 2100 (C≡C) and 1050 cm^{-1} (C—O); nmr δ: 3.6 (t, 2, J = 7 Hz, CH_2OH), 2.2 (m, 2, $CH_2C{\equiv}C$), 1.9 (t, 1, J = 1.5 Hz, C≡C—*H*), and 1.7–1.2 (m, 12, $(CH_2)_6$). *Anal.* calcd. for $C_{10}H_{18}O$: C 77.87, H 11.76; found: C 76.98, H 11.88.

Acetylation of **11** with acetic anhydride in pyridine yielded 9-decyn-1-yl acetate as an oil; ir: 3400 (≡C—H), 2100 (C≡C), 1740 (ester C=O) and 1250 cm^{-1} (C—O); nmr δ: 4.0 (t, 2, J = 7 Hz, CH_2O), 2.2 (m, 2, $CH_2C{\equiv}C$), 2.0 (s, 3, CH_3CO), 1.9 (t, 1, J = 1.5 Hz, C≡C—*H*), and 1.8–1.2 (m, 12, $(CH_2)_6$); ms (70 eV) *m/e* (relative intensity): 196 (2.6) (M^+), 136 (10) ($M^+ - CH_3CO_2H$), 43 (100). *Anal.* calcd. for $C_{12}H_{20}O_2$: C 73.43, H 10.27; found: C 73.23, H 10.19.

Similarly (except that liquid–liquid extraction need not be used in this example), **10** yielded 61 mg of recovered **4** and 56 mg of 11-dodecyn-1-ol (**12**), in 43% yield, as an oil (lit. (21) $bp_{0.005}$ 83–86°C): n_D 1.4899 (lit. (21) n_D 1.4898); ir: 3500 (O—H), 3400 (≡C—H), 2100 (C≡C), and 1050 cm^{-1} (C—O); nmr δ: 3.6 (t, 2, J = 7 Hz, CH_2O), 2.2 (m, 2, $CH_2C{\equiv}C$), 1.9 (t, 1, J = 1.5 Hz, C≡C—*H*), and 1.8–1.2 (m, 16, $(CH_2)_8$).

Acetylation of **12** as before yielded 11-dodecyn-1-yl acetate as an oil; ir: 3400 (≡C—H), 2100 (C≡C), 1740 (ester C=O), and 1250 cm^{-1} (C—O); nmr δ: 3.6 (t, 2, J = 7 Hz, CH_2O), 2.2 (m, 2, $CH_2C{\equiv}C$), 2.0 (s, 3, CH_3CO), 1.8 (t, 1, J = 1.5 Hz, C≡C—*H*), and 1.8–1.2 (m, 16, $(CH_2)_8$); ms (70 eV) *m/e* (relative intensity): 224 (1) (M^+), 164 (9) ($M^+ - CH_3CO_2H$), and 43 (100). *Anal.* calcd. for $C_{14}H_{24}O_2$: C 74.95, H 10.78; found: C 74.61, H 10.75.

*Preparation of Polymer-bound Internal Alkynes **19–21***

In a typical experiment, 1.25 g of **10**, containing 0.4 mmol of **12** was suspended in 20 ml of dry THF at 60–70°C under argon. The mixture was treated with *n*-butyllithium (**13**) (3.5 ml of a 0.5 *M* solution in hexane, 8 mmol) and stirred at 60–70°C for 0.5 h. To the suspension was added 5 ml of *n*-butyl bromide (**17**) and 20 ml of HMPT and the mixture was stirred for 4 h at 60–70°C. The polymer was filtered, washed successively with 10 ml portions of ethanol (three times), water (three times), ethanol (three times), dioxane (three times), and ether (three times), and air dried to give the polymer-bound internal alkyne **20**.

The polymer-bound alkynes did not exhibit absorptions at 2100–2200 cm^{-1} (C≡C) in their ir spectra.

The formation of **19–21** was achieved to some extent under a variety of conditions and reagents based on the above procedure. These variations are outlined in Table 2.

*Preparation of Alkyn-1-ols **22–24** and Their Acetates*

Acid cleavage of 1.0 g of **20** as previously described (12) and filtration and washing of the polymer as before gave a filtrate which was neutralized and evaporated to a mixture of salts and oil. Organic material was extracted with ether dried over $MgSO_4$ and evaporated to give an oil. Preparative tlc as before gave 59 mg of recovered **4** and 69 mg of 11-hexadecyn-1-ol (**23**) as an oil; n_D 1.4687; ir: 3500 (O—H) and 1050 cm^{-1} (C—O); nmr δ: 3.6 (t, 2, J = 8 Hz, CH_2O), 2.2 (m, 4, $CH_2C{\equiv}CCH_2$), 1.8–1.2 (m, 20, aliphatic H), and 0.9 (t, 3, J = 7.5 Hz, CH_3CH_2). *Anal.* calcd. for $C_{16}H_{30}O$: C 80.61, H 12.68; found: C 80.91, H 12.68.

Acetylation of **23** as before yielded 11-hexadecyn-1-yl acetate as an oil; n_D 1.4645; ir: 1740 (ester C=O) and 1250 cm^{-1} (C—O); nmr δ: 4.0 (t, 2, J = 8 Hz, CH_2O), 2.2 (m, 4, $CH_2C{\equiv}CCH_2$), 2.0 (s, 3, CH_3CO), 1.8–1.2 (m, 20 aliphatic H), 0.9 (t, 3, J = 8 Hz, CH_3CH_2); ms (70 eV) *m/e* (relative intensity): 280 (22) (M^+), 220(11) ($M^+ - CH_3CO_2H$), and 43 (100). *Anal.* calcd. for $C_{18}H_{32}O_2$: C 77.09, H 11.50; found: C 77.50, H 11.58.

The yields of **23** and the previously reported (2) **22** and **24** are recorded in Table 1. The yields of **22–24** relative to recovered **11** and **12** under different reaction conditions were determined by hplc analysis of their acetates as shown in Table 2.

*Preparation of Polymer-bound cis-Alkenes **25** and **26** Using Disiamylborane and Other Reducing Agents*

A suspension of 1.25 g of **21**, containing 0.3 mmol **24** of **21** was treated with 20 mmol of a 0.5 *M* THF solution of $(Sia)_2BH$. The mixture was stirred at −10 to 0°C under argon for 4 h, treated with 5 ml of acetic acid, and stirred for a further 0.5 h at 0–10°C. The polymer-bound *cis*-alkene **26** was filtered, washed with 15 ml portions of water (three times), ethanol (three times), dioxane (three times), and ether (three times), and air dried.

The formation of **25** and **26** was achieved to some extent under a variety of conditions using soluble reducing agents such as 9-BBN, catechol borane, and DIBAH based essentially on the procedure outlined above. The variations on the above conditions are outlined in Table 4.

*Preparation of cis-9-Tetradecen-1-yl and Acetate (**27**) and cis-11-Tetradecen-1-ol and Acetate (**28**)*

Insect attractants **27** and **28** were isolated as previously described (2) by acid cleavage of **25** and **26** respectively followed by acetylation. The yields of **27** and **28** prepared by different reduction methods are outlined in Table 3. The isomeric purity of **27** and **28** obtained under different reaction conditions was determined by hplc analysis given in Table 4.

Acknowledgements

This research was supported by grants from the National Research Council of Canada, the Canadian Forestry Service of Environment Canada, and the Ontario Ministry of the Environment.

1. C. C. LEZNOFF and T. M. FYLES. J. Chem. Soc. Chem. Commun. 251 (1976).
2. C. C. LEZNOFF, T. M. FYLES, and J. WEATHERSTON. Can. J. Chem. **55**, 1143 (1977).
3. C. C. LEZNOFF. Chem. Soc. Rev. **3**, 65 (1974).
4. R. B. MERRIFIELD. J. Am. Chem. Soc. **85**, 2149 (1963).
5. R. L. LETSINGER and M. J. KORNET. J. Am. Chem. Soc. **85**, 3045 (1963).
6. R. B. MERRIFIELD, J. M. STEWART, and N. JERNBERG. Anal. Chem. **38**, 1905 (1966).
7. D. A. EVANS and C. L. GREEN. Chem. Soc. Rev. **2**, 75 (1973).
8. E. F. KNIGHTS and H. C. BROWN. J. Am. Chem. Soc. **90**, 5281 (1968); G. G. SCOUTEN. Ph.D. Thesis, Purdue University, Lafayette, IN. 1976.
9. N. GREEN, M. JACOBSON, T. J. HENNEBERRY, and A. N. KISHABA. J. Med. Chem. **10**, 533 (1967).
10. D. WARTHEN. J. Med. Chem. **11**, 371 (1968).
11. L. R. MELBY and D. R. STROBACH. J. Am. Chem. Soc. **89**, 450 (1967); F. CRAMER and H. KÖSTER. Angew. Chem. Int. Ed. Engl. **7**, 473 (1968); J. M. J. FRÉCHET and K. E. HAQUE. Tetrahedron Lett. 3055 (1975).
12. T. M. FYLES and C. C. LEZNOFF. Can. J. Chem. **54**, 935 (1976).
13. M. M. MIDLAND. J. Org. Chem. **40**, 2250 (1975).
14. H. NORMANT. Angew. Chem. Int. Ed. Engl. **6**, 1046 (1967); M. SCHWARZ and R. M. WATERS. Synthesis, 567 (1972).
15. H. C. BROWN and G. ZWEIFEL. J. Am. Chem. Soc. **83**, 3834 (1961); G. HOLAN and D. F. O'KEEFE. Tetrahedron Lett. 673 (1973).
16. W. L. ROELOFS and H. ARN. Nature, **219**, 513 (1968).
17. H. C. BROWN and S. K. GUPTA. J. Am. Chem. Soc. **97**, 5249 (1975).
18. J. J. EISCH and W. C. KASKA. J. Am. Chem. Soc. **88**, 2213 (1966).
19. H. M. RELLES and R. W. SCHLUENZ. J. Am. Chem. Soc. **96**, 6469 (1974).
20. J. M. STEWART and J. D. YOUNG. Solid phase peptide syntheses. W. H. Freeman Ltd., San Francisco, CA. 1969. p. 58.
21. W. W. CHRISTIE and R. T. HOLMAN. Chem. Phys. Lipids, **1**, 407 (1967).

The competitive scissions of cycloalkane oxiranes by charged and neutral nucleophiles in acidic aqueous methanol

JOHN W. BOVENKAMP[1] AND ROBERT Y. MOIR
Department of Chemistry, Queen's University, Kingston, Ont., Canada K7L 3N6
AND
ROBERT A. B. BANNARD
Defence Research Establishment Ottawa, Ottawa, Ont., Canada K1A 0Z4

Received May 19, 1977

JOHN W. BOVENKAMP, ROBERT Y. MOIR, and ROBERT A. B. BANNARD. Can. J. Chem. **55**, 4144 (1977).

Six related oxiranes (the *cis* and *trans* isomers derived from 3-methoxycyclopentene and from 3-methoxycyclohexene, as well as the oxiranes from the corresponding unsubstituted olefins) were each treated under the same conditions with an acidic solution containing charged and uncharged nucleophiles (chloride ion, water, and methanol). The corresponding perchloric acid catalyzed scissions were also carried out. Accurate and reproducible methods of product analysis for the reaction mixtures were developed. In this way, nucleophilic attacks upon different oxiranes were compared directly. Attacks by different nucleophiles upon the same oxirane, or by a single nucleophile upon different positions of the same oxirane, were compared in the very same solution. The results are considered to provide the most extensive demonstration of the effects of charge orientation yet available. The synthesis of some new isomeric 1,2,3-trisubstituted diols and dimethoxyalcohols are reported.

JOHN W. BOVENKAMP, ROBERT Y. MOIR et ROBERT A. B. BANNARD. Can. J. Chem. **55**, 4144 (1977).

Six oxirannes de même type (les isomères *cis* et *trans* du méthoxy-3 cyclopentène et du méthoxy-3 cyclohexène, aussi bien que les oxirannes provenant des oléfines non-substituées) sont traités individuellement dans les mêmes conditions par une solution acide contenant des nucléophiles chargés et non-chargés (ion chlorure, eau et méthanol). On réalise aussi les scissions correspondantes catalysées par l'acide perchlorique. On met au point des méthodes d'analyse précises et reproductibles des produits provenant du mélange réactionnel. De cette façon, les attaques nucléophiles sur les différents oxirannes sont comparées directement. Les attaques de différents nucléophiles sur le même oxiranne, ou par un seul nucléophile à différentes positions du même oxiranne, sont comparées dans la même solution. Les résultats semblent apporter la démonstration la plus marquée connue jusqu'à maintenant sur les effets d'orientation de charge. On rapporte la synthèse de quelques nouveaux diols trisubstitués-1,2,3 isomères et de diméthoxyalcools.

[Traduit par le journal]

The mechanism of oxirane[2] opening and the stereo- and regioselectivity of the nucleophilic addition have been topics of great interest (1–8). In these laboratories, we have expended a good deal of effort in this area due to our interest in conformational factors and the interaction of substituents in the cyclopentane and cyclohexane ring systems (see refs. 7–10 and references cited therein). In fact, it was the availability of compounds synthesized during these studies (for example most of **1–19**) (see Figs. 1*a* and 1*b*) which allowed us to proceed with the experiments described in this paper.

Although several papers deal with the scission of 3-substituted cyclohexene or cyclopentene oxides (see, for example, refs. 7, 8, and 11–15), these report almost exclusively either the attack of a charged nucleophile in an inert solvent or the acid or base catalyzed opening by the solvent. In several instances, the effect of the 3-substituent on stereo- and regioselectivity has been studied by comparing nucleophilic scissions which have been conducted under widely varying conditions. Although these interpretations are useful in a qualitative sense, the derivation of quantitative

[1]Present address: Defence Research Establishment Ottawa, Ottawa, Ont., Canada K1A 0Z4.

[2]For the remainder of this paper oxiranes will be designated as epoxides or cycloalkene oxides. These designations have been in use for many decades.

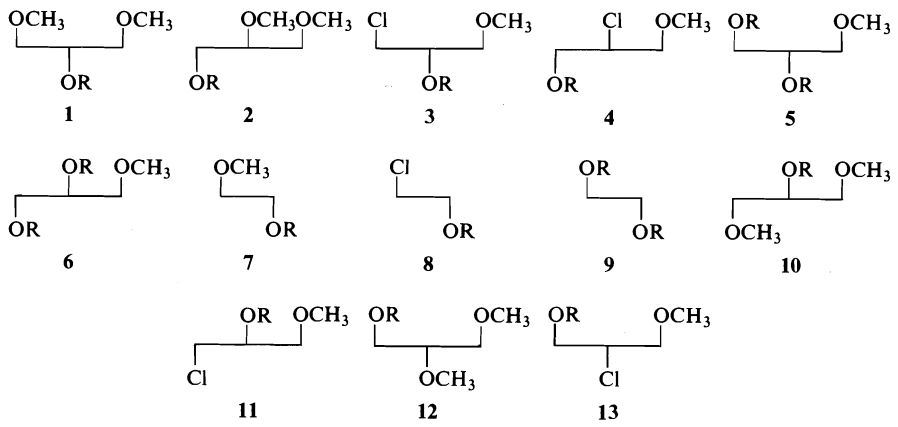

a R = H; cyclohexane series
b R = $COCH_3$; cyclohexane series
c R = H; cyclopentane series
d R = $COCH_3$; cyclopentane series

FIG. 1*a*. Structures of the 1,2-di- and 1,2,3-trisubstituted cycloalkanes. To conserve space, the unsubstituted ring methylenes are not shown.

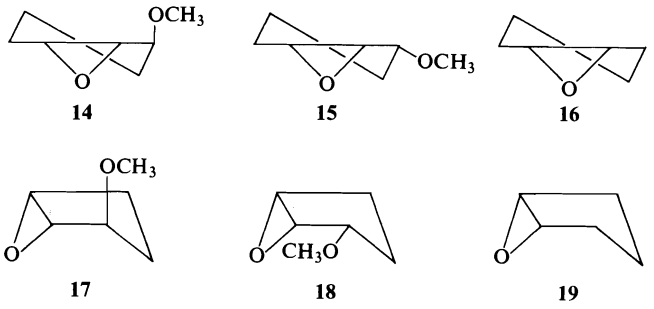

FIG. 1*b*. Oxirane structures.

data from which direct comparisons are possible demands careful standardization of experimental conditions.

In this paper are described the results obtained when the six epoxides **14–19** are subjected to scission under the same reaction conditions (2.43°C) in 50 wt.% aqueous methanol containing hydrochloric acid. A comparison is thus possible for charged and uncharged nucleophiles in terms of the presence and orientation of the 3-methoxyl substituent as well as in terms of the five- and six-membered ring systems.[3] The corresponding scissions using perchloric acid as the catalyst were also carried out.

Many years ago, Parker and Isaacs (1) strongly emphasized the need to carry out accurate product analyses in epoxide scission reactions. This requirement has clearly been met in this paper. In Table 1 are given the product analyses found in the cyclohexane series, while the corresponding figures for the cyclopentane series are found in Table 2.

Immediately apparent from Table 1 is the profound effect of the orientation of the methoxyl substituent on the proportion of chlorohydrin produced. In the scission of *trans*-3-methoxycyclohexene oxide (set 2), the total amount of chlorohydrin formed is 12.9%. Almost four times as much chlorohydrin (46.5%) is formed from the *cis* isomer under the same conditions (set 6). Less chlorohydrin is formed from cyclohexene oxide than from the *cis*-3-methoxycyclohexene oxide (compare sets 8 and 4; 5.2:7.2 respectively). A similar trend is found in the cyclopentane series (Table 2). As observed and discussed

[3]A number of papers have dealt with the comparison of charged and neutral nucleophiles in straight chain epoxides (1). In fact as early as 1929, Brönsted *et al.* (16) compared the attack of chloride ion and water upon ethylene oxide under acidic conditions.

TABLE 1. Composition of the reaction mixtures from cyclohexene oxides[a,b,c]

Set	Reagent concentrations (*M*)	Percent scission at epoxide carbons 1 and 2					
		CH_3OH		HCl		H_2O	
		C-1	C-2	C-1	C-2	C-1	C-2
		trans-3-Methoxycyclohexene oxide (**14**)					
		1*a*	**2***a*	**3***a*	**4***a*	**5***a*	**6***a*
1	0.15 $HClO_4$ 0.065 $NaClO_4$	45.9	2.19	—	—	49.2	2.65
2[d]	0.15 HCl 0.065 $NaClO_4$	40.9	1.91 ±0.01	11.9 ±0.3	0.97	41.9 ±0.03	2.44 ±0.07
		cis-3-Methoxycyclohexene oxide (**15**)					
		10*a*		**11***a*		**6***a*	
3[e]	0.015 $HClO_4$ 0.2 $NaClO_4$	43.4 ±0.9		—		56.6 ±0.9	
4	0.015 HCl 0.2 $NaClO_4$	(40.2)		7.2		(52.6)	
5	0.015 HCl 0.035 NaCl 0.165 $NaClO_4$	(34.3)		20.9		(44.8)	
6	0.15 HCl 0.065 $NaClO_4$	(23.2)		46.5		(30.3)	
		Cyclohexene oxide (**16**)					
		7*a*		**8***a*		**9***a*	
7[e]	0.015 $HClO_4$ 0.2 $NaClO_4$	45.8 ±0.7		—		54.2 ±0.7	
8	0.015 HCl 0.2 $NaClO_4$	(43.4)		5.2		(51.4) 51.0 by $NaIO_4$ ox.	
9	0.015 HCl 0.035 NaCl 0.165 $NaClO_4$	(38.4)		16.1		(45.5) 45.1 by $NaIO_4$ ox.	

[a]Initial ionic strength for each experiment was 0.215 *M*. Epoxide concentration was initially 0.06 *M* in all runs. The solvent was a 50:50 wt. % solution of methanol and water. Reaction temperature was 2.43°C.

[b]The percentages in parentheses are calculated using the assumption that the ratio of water to methanol scission is not significantly affected by whether the acid used is hydrochloric or perchloric. This assumption was shown to be true in two ways. First, in sets 1 (perchloric) and 2 (hydrochloric) (both sets analyzed by glc), the ratio of water to methanol scission product was 51.9:48.1 and 50.9:49.1 respectively. Also in Table 2, set 10 (perchloric acid) and set 11 (hydrochloric acid) were analyzed by glc and again the methanol–water product ratios were close (44.8 in set 10 and 44.4 in set 11). Secondly, the percentages of diol in sets 8 and 9 were calculated to be 51.4 and 45.5 from the methanol to water scission ratio of set 7. These were very close to the values of 51.0 and 45.1 found by sodium periodate oxidation.

[c]When the methanol and water scission figures are given in parenthesis, the amount of chlorohydrin formed was determined by the amount of hydrochloric acid consumed (all titrations carried out in triplicate).

[d]In the glc determinations, all of the peaks were well separated except in set 2 where the peaks for **4***a* and **1***a* completely overlapped. However, **4***a* could be obtained from the difference between the amount of hydrochloric acid consumed and the value found for **3***a*. This allowed the calculation of **1***a*. Two complete product analyses determinations were carried out for set 2. The values for set 1 were so close (on a percentage basis) to those of set 2 that only one determination was done.

[e]Average of three determinations.

previously for single nucleophilic scissions (7), a small but significant amount of minor isomer (C-2 scission) is formed from *trans*-3-methoxycyclohexene oxide **14** while no minor isomer formation was detected for the corresponding *cis* oxide **15**. As for single nucleophilic scissions, the very interesting reversal in minor isomer formation between the cyclohexane and the cyclopentane series is also found under the present conditions. In the cyclohexane series, C-2 attack is observed in the *trans* but not in the *cis* oxide while the reverse is found in the cyclopentane series. This phenomenon has been interpreted previously in terms of transition state geometries (8).

The most interesting comparisons in this type of study are those from which the energetics of the transition states may be deduced. Second- and third-order differences are the significant quantities in such a study and the main advantage of our approach is the accuracy with which these differences may be obtained. Nucleophilic attacks upon *different oxides* were performed as nearly as possible under exactly the same conditions of solvent, temperature, and ionic strength. Attacks by *different nucleophiles* upon the same oxide, or by a single nucleophile upon *different positions* of the same oxide, were compared in the very same solution. Finally, the comparisons made in this paper of different rates of reaction

TABLE 2. Composition of the reaction mixtures from cyclopentene oxides[a]

Set	Reagent concentrations (M)	Percent scission at epoxide carbons 1 and 2					
		CH_3OH		HCl		H_2O	
		C-1	C-2	C-1	C-2	C-1	C-2
		trans-3-Methoxycyclopentene oxide (**17**)					
		1*c*		**3***c*		**5***c*	
10[b]	0.15 $HClO_4$ 0.065 $NaClO_4$	55.2 ±1.0	—	—	—	44.8 ±1.0	—
11[b]	0.15 HCl 0.065 $NaClO_4$	46.8 ±0.4	—	15.8 ±0.1	—	37.4 ±0.3	—
		Cyclopentene oxide (**19**)					
		7*c*		**8***c*		**9***c*	
12[c]	0.015 $HClO_4$ 0.2 $NaClO_4$	52.8 ±1.1		—		47.2 ±1.1	
13	0.015 HCl 0.2 $NaClO_4$	(50.3)		4.8		(45.0)	
		cis-3-Methoxycyclopentene oxide (**18**)					
		10*c*	**12***c*	**11***c*	**13***c*	**6***c*	**5***c*
14	0.15 $HClO_4$ 0.065 $NaClO_4$	(47.8)	(2.54)	—	—	(47.9)	(1.76)
15[b]	0.15 HCl 0.065 $NaClO_4$	24.7 ±0.2	1.31 ±0.02	44.7 ±0.2	3.60 ±0.08	24.8 ±0.1	0.91 ±0.005

[a]See footnotes *a*, *b*, and *c* to Table 1.
[b]Two determinations.
[c]Four determinations.

are based upon analytical results only and are free from the errors inherent in kinetic measurements. Although a high order of accuracy was achieved in the free energy differences discussed below, likely more convincing is the fact that the conclusions reached are supported by the obviously substantial and significant differences in product composition reported in Tables 1 and 2.

In the reaction of a nucleophile N_1 with an epoxide E_1, several ground state energies remain in the expression [1] for the free energy[4] of the transition state ${F_{1,1}}^{\ddagger}$:

$$[1]\quad {F_{1,1}}^{\ddagger} = \Delta {F_{1,1}}^{\ddagger} + {F^0}_{E_1} + {F^0}_{H^+} + {F^0}_{N_1}$$

If we wish to compare attack of N_1 at carbons C-1 and C-2 of the same epoxide, then we have the familiar Curtin–Hammett equation (17)

$$[2]\quad \Delta^2 F^{\ddagger} = {F_{1,1}}^{\ddagger}(\text{C-1}) - {F_{1,1}}^{\ddagger}(\text{C-2}) = \Delta {F_{1,1}}^{\ddagger}(\text{C-1}) - \Delta {F_{1,1}}^{\ddagger}(\text{C-2})$$

In a previous paper (7), we have applied this equation to the results of oxide scissions under varied conditions of temperature and solvent composition.

[4]The symbol F is used in these papers for the Gibbs' free energy in order to avoid confusion with the symbol G used in conformational analysis for the free energy due to *gauche* effects.

If E_2 represents a second oxide which reacts with nucleophile N_1 and we wish to compare it with the attack of the same nucleophile on the first oxide, then

$$[3]\quad \Delta^2 F^{\ddagger} = {F_{2,1}}^{\ddagger} - {F_{1,1}}^{\ddagger} = (\Delta {F_{2,1}}^{\ddagger} - \Delta {F_{1,1}}^{\ddagger}) + ({F^0}_{E_2} - {F^0}_{E_1})$$

Equation 3 is only useful if one can gain some idea of the differences in the standard ground state free energies (${F^0}_{E_2}$ and ${F^0}_{E_1}$) of the two oxides. Because the theoretical explanation of these $\Delta^2 F^{\ddagger}$ values is complex, the discussion has been left to the paper on the kinetics of the reactions.

Ground state energies may be removed in another way, which leads to the most interesting conclusions of this paper. If we consider the reaction of two nucleophiles, N_1 and N_2, upon two epoxides, E_1 and E_2, then

$$[4]\quad \Delta^3 F^{\ddagger} = ({F_{2,2}}^{\ddagger} - {F_{2,1}}^{\ddagger}) - ({F_{1,2}}^{\ddagger} - {F_{1,1}}^{\ddagger}) = (\Delta {F_{2,2}}^{\ddagger} - \Delta {F_{2,1}}^{\ddagger}) - (\Delta {F_{1,2}}^{\ddagger} - \Delta {F_{1,1}}^{\ddagger})$$

by subtraction involving the appropriate eqs. 1. In [4] all ground state energies have disappeared. The second-order difference $\Delta^3 F^{\ddagger}$ has an immediate physical meaning. It is a measure of the

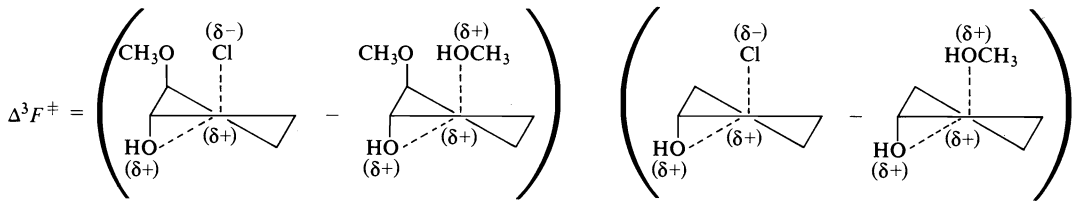

FIG. 2. The physical picture (it is the free energies of these transition states in the cyclopentane series which are being compared) of $\Delta^3F^{\ddagger}$ for one set of transition states in the cyclopentane series.

difference in the ability of two oxides to discriminate between two nucleophiles.[5] Thus in Fig. 2, $\Delta^3F^{\ddagger}$ represents the difference in the free energies of the transition states for chloride and methanol attack on position-1 of *trans*-3-methoxycyclopentene oxide as compared with the difference of the corresponding transition states in the scission of unsubstituted cyclopentene oxide.

The calculation of the values of $\Delta^3F^{\ddagger}$ from the product analysis data of Tables 1 and 2 is complicated by the fact that methanol and chloride attack the oxides in reactions of different apparent kinetic orders.

As pointed out by Lamaty *et al.* (6) for ethylene oxide, the equation for chlorohydrin (C) formation is given by

$$[5] \qquad \frac{dC}{dt} = \frac{1}{K}k_c[E][H^+][Cl^-]$$

where K is the equilibrium constant for the protonation of the epoxide (E). The corresponding equation for the product due to methanol attack (M) is

$$[6] \qquad \frac{dM}{dt} = \frac{1}{K}k_m[E][H^+]$$

Now $[Cl^-] = A_0 + S_0 - C$, where A_0 is the initial concentration of hydrochloric acid and S_0 is the concentration of sodium chloride. On dividing [5] by [6] we obtain

$$[7] \qquad \frac{k_c}{k_m}dM = \frac{dC}{A_0 + S_0 - C}$$

Integration of [7] gives

$$[8] \qquad \frac{k_c}{k_m} = \frac{1}{M}\ln\left\{\frac{A_0 + S_0}{A_0 + S_0 - C}\right\}$$

When the reaction is complete, then A_f, the final acidity, is equal to $A_0 - C_f$ and [8] becomes

$$[9] \qquad \frac{k_c}{k_m} = \frac{1}{M_f}\ln\left\{\frac{A_0 + S_0}{A_f + S_0}\right\}$$

Consider the most complicated case where $\Delta^3F^{\ddagger}$ (Cl^- vs. MeOH; epoxide **14** (set 2) vs. epoxide **16** (set 8) (Table 1)) is calculated for position-1 attack on an epoxide where position-2 is also attacked. For epoxide **14**, let the amount of chlorohydrin formed by position-1 attack be C_1 and by position-2 attack be C_2. Also let M_1 and M_2 represent the products due to methanol attack at positions-1 and -2 respectively. Thus, the rate constants for position-1 attack on **14** are

$$[9a] \qquad k_{c_1} = \frac{C_1}{C_1 + C_2}k_c$$

and

$$[9b] \qquad k_{m_1} = \frac{M_1}{M_1 + M_2}k_m$$

From [4]:

$$[10] \qquad \Delta^3F^{\ddagger} = \left(-RT\ln\frac{k_{c_1}h}{KT} + RT\ln\frac{k_{m_1}h}{KT}\right) - \left(-RT\ln\frac{0.5k_c'h}{KT} + RT\ln\frac{0.5k_m'h}{KT}\right)$$

The prime refers to values for the unsubstituted oxide **16**. Substitution of [9*a*] and [9*b*] into [10] results in

$$[11] \qquad \Delta^3F^{\ddagger} = RT\ln\frac{k_c'}{k_m'} - RT\ln\left(\frac{k_c}{k_m}\frac{C_1}{(C_1 + C_2)}\frac{(M_1 + M_2)}{M_1}\right)$$

[5]The theoretical analysis leading to [3] and [4] is subject to an error caused by partition at 'hidden' intermediates. Such an intermediate may be thought of as occupying a notch in the reaction profile, and the size of the resulting error as a function of the difference in height of the two sides of the notch, reaching a maximum when the two sides are equal in height. The error is negligible for intermediates such as protonated epoxides. At the time of writing, it is believed (3*c*, 6, 10, 18) that the error caused by ion-dipole or ion-pair intermediates is negligible for substitutions at secondary centres in highly nucleophilic solvents, and to some extent at least the errors will cancel in comparative studies like the present. Nevertheless, the large effect of barely perceptible valleys in the reaction profile near the rate-limiting transition state must be kept in mind in all applications of the Curtin–Hammett theory (19).

TABLE 3. Relative abilities of epoxides to discriminate between pairs of nucleophiles in acid catalyzed scissions[a,b] (symbols and relations from [4])

Epoxide E_2	Epoxide carbon attacked	Nucleophiles N_1	Nucleophiles N_2	$\Delta^3F^{\ddagger}$ (kcal/mol)[b]
		Cyclohexane series		
trans-3-Methoxy[c] (**14**)	1	Cl^-	MeOH	0.87
		H_2O	MeOH	0.05
	2	Cl^-	MeOH	0.56
		H_2O	MeOH	−0.01
cis-3-Methoxy[c] (**15**)	1	Cl^-	MeOH	−0.24
		H_2O	MeOH	−0.05
		Cyclopentane series		
Unsubstituted[c] (**19**)		Cl^-	MeOH	−0.14
		H_2O	MeOH	−0.15
trans-3-Methoxy[d] (**17**)	1	Cl^-	MeOH	0.61
		H_2O	MeOH	+0.05
cis-3-Methoxy[d] (**18**)	1	Cl^-	MeOH	−0.32
		H_2O	MeOH	−0.06
	2	Cl^-	MeOH	−0.55
		H_2O	MeOH	+0.14

[a]Reaction conditions are in footnote *a*, Table 1. The values of the initial and final acidities used in these calculations were obtained from titrations carried out in triplicate.
[b]Values of $\Delta^3F^{\ddagger}$ are calculated from [12] and [13]. The standard deviation in $\Delta^3F^{\ddagger}$ is approximately 0.01 kcal (depending on the example being considered). The average standard error (as a percent of the actual value) in the product analysis determinations was 1.34. The value of $\Delta^3F^{\ddagger}$ for position-1 attack on the *cis* epoxide **15** can vary from −0.22 to −0.27 kcal depending on which of sets 4, 5, or 6 are used for the *cis* oxide or whether set 8 or 9 is used for the unsubstituted oxide. This range shows that there is some error in the replacement of sodium perchlorate by hydrochloric acid and sodium chloride at the moderate ionic strength of 0.215 *M*; however, a higher ionic strength results in less chlorohydrin formation.
[c]E_1 is cyclohexene oxide (set 8).
[d]E_1 is cyclopentene oxide (set 13).

Substituting [9] into [11] and rearranging gives

$$[12]\quad \Delta^3F^{\ddagger} = -RT\ln\left\{\frac{\dfrac{C_1}{M_1(C_1+C_2)}\ln\dfrac{A_0+S_0}{A_f+S_0}}{\dfrac{1}{M_f'}\ln\dfrac{A_0'+S_0'}{A_f'+S_0'}}\right\}$$

The equations required when only one epoxide carbon is attacked ($C_2 = 0$) or when no sodium chloride is added ($S_0 = 0$) can be obtained directly from [12].

The calculation of $\Delta^3F^{\ddagger}$ for water versus methanol attack is much simpler. Since all of the products obtained from the perchloric acid catalyzed runs are of the same kinetic order, then $\Delta^3F^{\ddagger}$ can be calculated using [4] from product analysis only. Thus for water versus methanol attack upon position-1 for epoxides **14** vs. **16** (sets 1 and 7), eq. 4 becomes

$$[13]\quad \Delta^3F^{\ddagger} = -RT\ln((W_1/M_1)(M_1'/W_1'))$$

The calculated values of $\Delta^3F^{\ddagger}$ (see Table 3) indicate the ability of the substituted epoxides to discriminate between pairs of nucleophiles as compared to that of the corresponding unsubstituted epoxides. Other comparisons may be made by suitable combinations of the entries. From the table, it is seen that cyclopentene oxide discriminates between chloride ion and methanol, or between water and methanol, by about the same amount compared to cyclohexene oxide. In terms of yields, the differences of −0.14 and −0.15 kcal/mol are significant (compare set 8 (Table 1) with set 13 (Table 2)).

The most important result of Table 3 is the clear demonstration of the large variation in polar effects with orientation. In Fig. 3, comparison of **20** and **21** shows how unfavourable a *syn*-1,3-diaxial orientation of chloride and methoxyl (in **20**) is in comparison with the similar orientation of the two methoxyl groups (in **21**). The *gauche* arrangement of the same groups is only moderately less unfavourable to attack by chloride (compare **24** and **25**). In both these examples, it is not possible to distinguish between field effects and the effects of hydrogen bonding of the incoming methanol with the methoxyl substituent (in **21** and **25**); however, even though hydrogen bonding between 1,2 and *cis*-1,3 substituents has been shown to be important (9, 20 and references cited therein) under certain conditions, the extent to which bonding

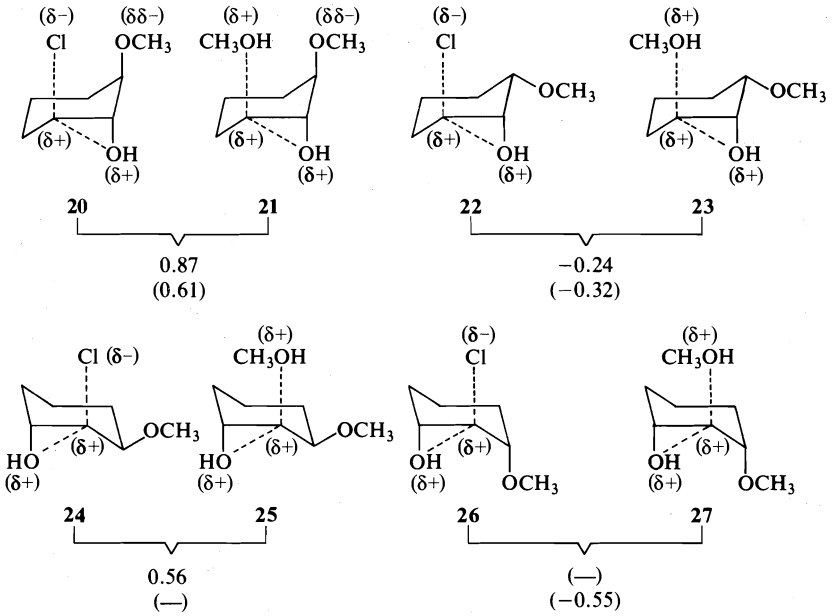

FIG. 3. Effect of dipole orientation on the relative selectivities of epoxides towards nucleophiles. (*1*) Values of Δ^3F^+ with respect to unsubstituted epoxides are given in kcal/mol, the values for the corresponding cyclopentane compounds being given in parentheses (see [4] and Table 3). NOTE: The numbers do not represent the difference in free energy between the transition states shown. Instead, for example, the non-parenthetical number joining **20** and **21** implies that introduction of a methoxyl group at the *trans*-3-position in cyclohexene oxide has made attack by chloride ion more unfavourable by 0.87 kcal/mol with respect to attack by methanol, than it was in cyclohexene oxide itself. (*2*) The transition states **20, 21, 24,** and **25** are obtained from the *trans* epoxides while those for **22, 23, 26,** and **27** are obtained from the *cis* epoxides. (*3*) For examples of the corresponding cyclopentane transition states, see Fig. 2. These distorted twist conformations and the orientation of the substituents in them has been presented in ref. 8.

takes place in strongly hydrogen bonding solvents is difficult to ascertain. In fact, Tichý (21) has concluded that, in a hydroxylic solvent, internal hydrogen bonding in the *trans*-1,2-amino alcohols studied by him does not play an important role.

That the field effects are certainly large is beautifully shown by the comparisons in which hydrogen bonding cannot have the same relative importance. In the anticlinal arrangement of nucleophile and substituent shown in **22** and **23**, or still more in the *anti* arrangement of **26** and **27** (Fig. 3), the electrical situation (of nucleophile versus substituent) has been reversed, and in agreement with this both are more favourable to attack by chloride than by methanol, in comparison with the unsubstituted oxides which lack the methoxyl dipole. The results strongly support the correctness of the chair-like[6] transition states pictured in Fig. 3 and thus is in agreement with the proposal made earlier (8) that the transition state of the nucleophilic attack on protonated epoxides is more similar to the products than to the reactants.[7,8]

In specifically comparing the results in Fig. 3 for the cyclohexane series (non-parenthetical values) with those of the cyclopentane series (parenthetical values), it is seen that for **20** vs. **21**, the value of 0.61 for the cyclopentane transition states would seem to indicate a deviation from

[6]Paulsen and Koebernick (22) have recently shown for the ground state that a 1,3-diaxial interaction must be large indeed in order to cause the cyclohexane ring to predominate in the boat conformation.

[7]This assumption has more recently (11) been applied in the nucleophilic attack on epibromonium ions.

[8]The residual contribution (not cancelled in the comparisons) of ordinary conformational *A*, *Z*, and *G* effects (17) to the Δ^3F^+ differences given in Table 3 and in Fig. 3 is essentially zero in the comparisons **22–23** and **26–27** and negligible in the comparison **24–25** (difference of two similar steric *gauche* effects). Since the charge-related and hydrogen bonding effects must be larger in the comparison **20–21** than in **24–25** it follows from the values given, that the ordinary *A*, *Z*, and *G* contributions to the differences **20–21** (Fig. 3) must be small also and perhaps negligible.

TABLE 4. The effect of ionic strength on the amount of chlorohydrin formed from cyclohexene oxide[a] (**16**)

	Concentration of reagents (*M*)			
Identification	HCl	$NaClO_4$	NaCl	% chlorohydrin
a	0.015	0.0	0.0	9.4
b	0.03	0.0	0.0	16.2
c	0.015	0.03	0.0	7.8
d[b]	0.015	0.2	0.0	5.2
e[c]	0.015	0.165	0.035	16.1

[a]Solvent in all entries was methanol–water (50:50 wt. %) and the concentration of cyclohexene oxide was 0.06 *M*.
[b]Set 8 of Table 1.
[c]Set 9 of Table 1.

the *syn*-1,3-diaxial arrangement of substituent and nucleophile; however, the size of the interaction remaining would indicate that the deviation is small. The difference between **22** and **23** for the two series is small and thus indicates that the orientation of the methoxyl dipole is not significantly different in the two series. In comparing the transition states for position-1 attack on the *cis* epoxide for the cyclopentane equivalents of **22** and **23** with that for position-2 attack (cyclopentane equivalents of **26** and **27**), it is seen that the methoxyl dipole stabilizes the transition state for chloride attack (relative to that for methanol scission at position-2) by 0.23 kcal/mol. The results presented here are in total agreement with the transition states proposed previously to explain isomer distributions for chloride attack on the four positions of the *cis*- and *trans*-3-methoxycyclopentene oxides (8). It appears that the results of Table 3 provide the most extensive demonstration of the effect of charge orientation yet available.

In Table 4 are figures showing how the yield of chlorohydrin can be controlled by the opposing mass law and ionic strength effects. For example, adding 0.2 mol/ℓ of $NaClO_4$ to the reaction solution (a vs. d) nearly halves the amount of chlorohydrin formed. The synthetic usefulness of such a relationship is readily apparent. A similar effect has been observed previously for much simpler epoxides (16, 23).

Table 5 compares the relative rates of attack upon the six epoxides studied by methanol and by water. The trend from the *trans* to unsubstituted to *cis* oxide is the same in both the cyclohexane and the cyclopentane systems. This behaviour is intelligible in terms of the dipole effect discussed above if (as expected) the positive charge on the nucleophilic oxygen in the transition state is less dispersed for methanol than for water. Another

TABLE 5. Comparison of methanol and water scission in the six epoxides

Epoxide	% scission by methanol[a]
trans-3-Methoxycyclohexene oxide	48.1
Cyclohexene oxide	45.8
cis-3-Methoxycyclohexene oxide	43.4
trans-3-Methoxycyclopentene oxide	55.2
Cyclopentene oxide	52.8
cis-3-Methoxycyclopentene oxide	50.4

[a]These figures are obtained from the perchloric acid catalyzed scissions listed in Tables 1 and 2. The remainder of the reaction product is that due to scission by water.

factor must be invoked to explain the constant 7% difference (Table 5) between corresponding members of the cyclohexane and cyclopentane series, the simplest explanation being that a difference in 'size' of the two reagents had different effects in the two series. In our solvent, which is 50% by weight aqueous methanol (or 36 mol% methanol), methanol is the better nucleophile with each of the epoxides studied. Newall and Eastham (24) have already pointed this out using ethylene oxide as the substrate. Interpolation of their results to the conditions of Table 5 suggests that ethylene oxide would show 44% scission by methanol, close to the value (46%) reported here for cyclohexene oxide.

All of the compounds required for this study from the cyclohexane series have been previously reported (7, 10 and references therein) except for the acetates **3***b* and **4***b* (see Table 6). In the cyclopentane series, the epoxides and chlorohydrins had been previously reported (8); however, several compounds in this series remained to be synthesized. The isomeric diols **5***c* and **6***c* were obtained from epoxides **17** and **18** respectively by acid catalyzed scission with water. The epoxide **17** gave **5***c* free of its isomer but the epoxide **18**

TABLE 6. Physical constants and analytical data for the acetates

Compound No.	Späth air bath boiling range (°C)	Refractive index (n_D^{25})	Elemental analysis					
			Calculated			Found		
			C	H	Cl	C	H	Cl
3*b*	mp 51.4–51.8		52.31	7.32	17.15	52.45, 52.47	7.42, 7.23	17.21, 17.03
4*b*	70–76(0.001 Torr)		52.31	7.32	17.15	52.12, 52.13	7.44, 7.45	17.02, 17.20
1*d*	74–86(9 Torr)	1.4393	57.43	8.57		57.26, 57.43	8.45, 8.50	
3*d*	69–80(5 Torr)	1.4556	49.88	6.80	18.40	49.83, 49.75	6.88, 6.76	18.21, 18.35
5*d*	80–86(4 Torr)	1.4431	55.55	7.46		55.45, 55.48	7.47, 7.38	
6*d*	74–86(4 Torr)	1.4457	55.55	7.46		55.42, 55.43	7.35, 7.45	
7*d*	38–50(15 Torr)	1.4337	60.73	8.92		60.52, 60.57	8.94, 8.77	
8*d*	68–78(15 Torr)	1.4533	51.70	6.82	21.80	51.89, 51.68	6.92, 6.83	21.75, 21.72
9*d*	67–78(11 Torr)	1.4400	58.05	7.58		57.90, 58.02	7.44, 7.49	
10*d*	68–78(12 Torr)	1.4397	57.43	8.57		57.19, 57.29	8.44, 8.45	
11*d*	70–77(10 Torr)	1.4559	49.88	6.80	18.40	49.85, 49.78	6.74, 6.71	18.24, 18.28
12*d*[a]	55–65(15 Torr)		57.43	8.57		57.60, 57.53	8.43, 8.42	
13*d*	65–77(9 Torr)	1.4546	49.88	6.80	18.40	49.74, 49.80	6.72, 6.80	18.65, 18.66

[a]This sample contained a small accurately determined amount of its isomer **10***d* (see Experimental).

gave a mixture of the diols with **6***c* predominating (93:7). The required diol **6***c* could be obtained pure by fractional distillation. This is in contrast to the situation in the cyclohexane series where **5***a* and **6***a* do not even begin to separate upon extensive fractional distillation and **5***a* must be obtained pure by conversion of the mixture of diols to the dibenzoates and recrystallization to purity (25).

The acid catalyzed scission of **17** with methanol gives the dimethoxy alcohol **1***c* free of its isomer. On opening **18** under the same conditions a mixture of **10***c* and **12***c* is obtained (90:10). Pure **10***c* was obtained after several tedious fractionations while the best that could be obtained for **12***c* was a mixture containing 83% of this isomer. The 11 cyclopentane acetates needed for the product analysis (**1***d*, **3***d*, **5***d*–**13***d*) have not been reported previously and their properties and elemental analyses are given in Table 6.

Experimental

Melting points were determined using a precision melting point apparatus (26) with calibrated Anschütz thermometers. Elemental analyses were conducted by the Alfred Bernhardt Microanalytisches Laboratorium of West Germany. Gas–liquid chromatographic (glc) analyses were carried out using a Jarrell-Ash (model 700) analytical gas chromatograph equipped with a strontium-90 detector and a Texas Instruments recorder (model FWS (Int.)) with a mechanical integration unit. The two principal columns used were: (*A*) a 6 ft by $\frac{1}{4}$ in. diameter (outside diameter) copper column packed with Embacel (60/100 mesh) impregnated with neopentyl glycol sebacate (10%) and (*B*) a 12 ft by $\frac{1}{4}$ in. diameter (outside diameter) aluminum column packed for half its length with 4% diethylene glycol sebacate and the other half with 4% silicone fluid QF-1 both on Chromosorb G (70/80 mesh, AW, DMCS treated). Column *A* was used to analyze compounds in the cyclohexane series, whereas column *B* was used to analyze compounds in the cyclopentane series as well as in all of the product analysis work.

Compounds Prepared Previously

The preparation of compounds used in this work, when not reported here, can be found in earlier papers (7, 8, 10 and references cited therein). Epoxides **14** and **15** and **17** and **18** were each free of their respective isomers and had a purity of better than 99.9%. The unsubstituted epoxides **16** and **19** were purer than 99.9 and 99.5% respectively.

Preparation of Acetates

The physical properties of newly prepared acetates are reported in Table 6. They were synthesized using essentially the same procedure as that described below for **5***d*.

(±)-1,2-Di-O-acetyl-3-O-methyl-(1,3/2)-1,2,3-cyclopentanetriol (5d)

To 1.05 g (7.9 mmol) of **5***c* in a round-bottom flask containing a stirring bar was added 3.27 g of acetic anhydride containing a drop of concentrated sulfuric acid. The solution which initially became hot was stirred at room temperature overnight. Water (8 ml) was added, the mixture was heated to 70°C for 15 min, and after being cooled was neutralized with sodium bicarbonate. The mixture was extracted with ether (3 × 25 ml). The combined extracts were dried with anhydrous magnesium sulphate, filtered, and the solvent removed to leave a light yellow oil. On distillation in a Späth tube, a clear colourless oil was obtained (1.55 g, 90%) at an air bath temperature of 80–86°C (4 Torr).

Preparation of Alcohols

(±)-1-O-Methyl-(1,3/2)-1,2,3-cyclopentanetriol (5c)

trans-3-Methoxycyclopentene oxide **17** (8.00 g, 0.070 mol) was added to water (20 ml) containing perchloric acid (three drops). The two phase system was stirred vigorously while being heated at 53°C. After 15 min, a

homogeneous solution resulted. After heating for a further 3 h at 53°C, the solution was neutralized (solid sodium bicarbonate), the bulk of the water removed at room temperature *in vacuo*, and the last traces of water were removed by azeotropic distillation with absolute ethanol. The resultant viscous oil was dissolved in ether and the solution was decanted from the small amount of precipitate. The solvent was removed *in vacuo* leaving a light yellow oil which was subjected to a Späth bulb distillation. A colourless viscous oil (7.89 g, 85%) (n_D^{25} 1.4755) was obtained at 87–100°C/0.02 Torr which gave a single peak by glc. *Anal.* calcd. for $C_6H_{12}O_3$: C 54.54, H 9.15; found: C 54.43, 54.38, H 9.08, 9.01.

(±)-1-O-Methyl-(1,2/3)-1,2,3-cyclopentanetriol (6c)

The *cis* epoxide **18** (10.0 g, 0.0878 mol) was treated with water (24 ml) containing three drops of perchloric acid in the manner described in the synthesis above for **5***c*. Unlike the *trans* isomer, the *cis* epoxide is soluble in the aqueous solutions. After work-up as for the synthesis of **5***c*, a clear, colourless, viscous oil was obtained (11.56 g, 99%). The crude oil showed two peaks on the glc with the minor peak having the same retention time as the diol (**5***c*) obtained from the *trans* epoxide. A small amount of this mixture was set aside for determination of the isomer percentages. (It was later shown by glc that 6.7% of the crude mixture was **5***c* while the remainder was **6***c*. This figure was obtained using the method of McNair and Bonelli (27), in which the glc areas were adjusted using correction factors obtained from a mixture of known composition.) The remainder was subjected to a careful fractionation using the Späth apparatus. After two fractionations, 4.67 g of **6***c* (bp 68–77°C/0.02 Torr; n_D^{25} 1.4757) was obtained free of its slightly higher boiling isomer. *Anal.* calcd. for $C_6H_{12}O_3$: C 54.54, H 9.15; found: C 54.45, 54.50, H 9.25, 9.16.

(±)-1,3-Di-O-methyl-(1,3/2)-1,2,3-cyclopentanetriol (1c)

trans-3-Methoxycyclopentene oxide (8.00 g, 0.0702 mol) was dissolved in methanol (20 ml) containing one drop of concentrated sulfuric acid. The solution was stirred at room temperature for 9 h, refluxed for 15 min, cooled, and neutralized with solid sodium bicarbonate. After removal of the methanol *in vacuo*, the residual clear colourless oil was distilled using the Späth apparatus. The first fraction (0.93 g, 8–9 Torr, bp ca. 60°C) was unreacted epoxide. The remainder (6.55 g, 64%) distilled at a bath temperature of 67–78°C/0.03 Torr and gave a single peak by glc (n_D^{25} 1.4523). *Anal.* calcd. for $C_7H_{14}O_3$: C 57,51, H 9.65; found: C 57.32, 57.38, H 9.46, 9.49.

(±)-1,3-Di-O-methyl-(1,2/3)-1,2,3-cyclopentanetriol (10c) and Its Isomer (12c)

cis-3-Methoxycyclopentene oxide **18** (10.03 g, 0.088 mol) was dissolved in methanol containing three drops of concentrated sulfuric acid. The solution was refluxed for 2.5 h, then neutralized with solid sodium bicarbonate. The oil obtained on removal of the methanol was dissolved in ether and dried (magnesium sulfate). On removal of the ether from the dried filtrate, a clear mobile oil was obtained (12.6 g, 98%).

This oil was shown by glc to contain three peaks: major peak (**10***c*), minor peak (**12***c*), and a trace impurity. A small sample of this mixture was shown later to contain 89.5% **10***c* and 10.5% **12***c*. These values were obtained after correcting the glc areas using correction factors obtained from a mixture of known composition (method of McNair and Bonelli (27)). After three careful Späth bulb fractionations of the crude oil, pure **10***c* was obtained (3.33 g, bp 65–77°C/9 Torr; n_D^{25} 1.4487). *Anal.* calcd. for $C_7H_{14}O_3$: C 57.51, H 9.65; found: C 57.35, 57.44, H 9.82, 9.68.

The minor isomer (**12***c*) and the unidentified impurity were in the higher boiling fractions. These were subjected to repeated fractionations in an attempt to obtain pure **12***c*. Eventually 0.30 g of a mixture (bp 64–70°C/9 Torr) was obtained which contained 83.2% **12***c*, 12.6% **10***c*, and 4.2% unidentified impurity. (In obtaining these figures, the glc peak areas for the minor (**12***c*) and major (**10***c*) isomers were corrected by adding a known amount of pure major isomer to a known amount of the mixture.) *Anal.* calcd. for $C_7H_{14}O_3$: C 57.51, H 9.65; found: C 57.28, 57.33, H 9.55, 9.55.

Standard Reaction Conditions for Epoxide Scissions

The epoxide scission reactions were conducted in a reaction vessel kept in an insulated Sargent bath maintained at 2.43 ± 0.005°C which contained a mixture of water and ethanol. A second bath was maintained at 22.0°C and it was at this temperature that the reaction solutions were made up (taking into account the contraction of the reaction solutions from 22.0°C to 2.43°C). The solvent for all the reactions was a 50:50 wt.% solution of methanol and water.

The required weight of epoxide was sealed into a thin walled glass bulb and placed in the reaction vessel in contact with the breaking tip of the end of a glass rod. The reaction solution was then pipetted in, a dilatometer[9] was attached to the reaction vessel, and equilibrated in the bath. The bulb was broken by tapping the glass rod, the mixture was stirred, and the solution was transferred into the dilatometer by the application of compressed air to an opening in the top of the reaction vessel.

Analysis of the Epoxide Scission Products

The main method used in the determination of the product composition was glc. This method is capable of giving the total composition of the reaction mixture. Two other methods which can account for only part of the reaction mixture and which can not distinguish between positional isomers were used as a check. These were periodate oxidation (to determine the amount of 1,2-diols formed) and the determination of the decrease in acidity during the reaction (to obtain the amount of chlorohydrin formed).

Product Analysis Using Gas–Liquid Chromatography

The retention times of the isomeric alcohols formed from **14** were too uniform for facile analysis. Therefore reaction products in the cyclohexane series were acetylated to provide the more readily separable derivatives. The reaction products in the cyclopentane series were also acetylated except for those formed from **18** in which the retention times of the isomeric acetates were unsuitably

[9]A manuscript which reports and discusses the kinetic results is being prepared. The main use of the dilatometer for the purpose of this paper was to indicate completion of the reaction.

close for quantitative analysis.[10] These were analyzed as mixtures of the alcohols which were well separated. Column *B* was used in the product analysis work. The only reaction mixture in which overlap between peaks occurred was that which resulted from opening the epoxide **14** with hydrochloric acid. In this case the acetates **4***b* and **1***b* completely overlapped; however, the percent of **4***b* (and consequently **1***b*) could be calculated from the amount of hydrochloric acid consumed and the percent of **3***b*.

All product analysis using the glc method were carried out as described below for the scission of **17** (0.06 *M* at 2.43°C) in aqueous methanol (50:50 wt.%; 0.15 *M* HCl; 0.065 *M* $NaClO_4$). From the hydrochloric acid titration, it was known that 15.7% of chlorohydrin had formed in the reaction. Also, from the corresponding run with perchloric acid, 37.8% of diol was expected and thus 46.5% of methanol scission product should be present. A mixture of this composition was weighed out and dissolved in 30 ml of the same solution that the epoxide had been reacted with to give a solution containing a total concentration of 0.0605 *M* of the alcohols. The solution of known composition and 30 ml of the epoxide scission solution were then treated in exactly the same manner as described below.

Solid sodium bicarbonate was added to neutralize the hydrochloric acid and the bulk of the solvent was then removed *in vacuo* (0.1 Torr). When the volume was reduced to 2–3 ml, two 50 ml portions of absolute ethanol were added and the residual water was removed by azeotropic distillation *in vacuo*. The residual oil was dissolved in chloroform and separated from the solid by filtration. After removal of the solvent, 5 ml of acetic anhydride was added to the residual mixture of the alcohols and the solution was heated under reflux for 4 h. The acetic anhydride and acetic acid were removed by successive addition and removal (at 0.1 Torr) of three 10 ml portions and then two 3 ml portions of absolute ethanol. The slightly yellowish oil was dissolved in chloroform (1.5 ml) and analyzed by glc. From the known mixture 0.384 g of acetates were obtained while 0.366 g were obtained from the epoxide scission solution. The peak areas of both mixtures were obtained by integration and the areas were then corrected with the factors obtained from the solution of known composition by the method of McNair and Bonelli (27). The diacetate or the major diacetate (when two were formed) was the compound which was assigned a correction factor of 1.0000.

In this manner the composition of the scission product of **17** was found to be 47.2% **1***c*, 37.1% **5***c*, and 15.7% **3***c*. A duplicate set gave values of 46.5% **1***c*, 37.7% **5***c*, and 15.9% **3***c*. The average value of 15.8% **3***c* agrees remarkably well with the amount of chlorohydrin calculated from hydrochloric acid consumption (15.7%). Also the average amount of diol **6***c* was 37.4% which was very close to that predicted (37.8%) from the amount of diol determined with the same epoxide when perchloric acid was used. The results of the product analysis are listed in Tables 1 and 2.

A Check of the Product Analysis Method Using Sodium Periodate Oxidation

The glc method of product analysis was checked for sets 8 and 9 (Table 1) by determining the amount of diol formed from cyclohexene oxide using sodium periodate oxidation. The procedure used was that of Dyer (28) with one modification. Since the sodium periodate reacts at a non-negligible rate with aqueous methanol, it was necessary to vary the volume of the solvent added to the blank with the expected concentration of diol in the reaction solution. That is, enough solvent was added to the blank so that the initial concentration of periodate was equal to that of the reaction solution after all of the diol had reacted. This method worked well since the reaction of the diol with the sodium periodate solution was rapid.

A check of the above method with a known mixture of the alcohols **7***a*, **8***a*, and **9***a* (in a ratio of 40.1:9.4:50.6 respectively; total molarity 0.0601) in aqueous methanol (50:50 wt.%) (0.015 *M* HCl) gave a value which was within 0.2% of the actual value of **9***a*. For set 8, the amount of cyclohexene oxide opened by water was determined to be 51.0 and for set 9 it was 45.1. These values compare very favourably with the values 51.4 and 45.5 respectively found by the glc method.

[10]For a detailed discussion of the retention time behaviour in these compounds see ref. 9.

Acknowledgement

The aid of the National Research Council of Canada, in financial support of this work, and in the grant of a studentship to one of us (J.W.B.), is gratefully acknowledged.

1. R. E. Parker and N. S. Isaacs. Chem. Rev. **59**, 737 (1959).
2. J. Biggs, N. B. Chapman, A. F. Finch, and V. Wray. J. Chem. Soc. B, 55 (1971).
3. (*a*) J. Biggs, N. B. Chapman, and V. Wray. J. Chem. Soc. B, 63 (1971); (*b*) 66 (1971); (*c*) 71 (1971).
4. H. Z. Sable and J. G. Buchanan. *In* Selective organic transformations. Vol. 2. *Edited by* B. S. Thyagarajan. Wiley-Interscience, New York, NY. 1972.
5. J. G. Pritchard and I. A. Siddiqui. J. Chem. Soc. Perkin Trans. II, 452 (1973).
6. G. Lamaty, R. Meleq, C. Selve, A. Sivade, and J. Wylde. J. Chem. Soc. Perkin Trans. II, 1119 (1975).
7. R. A. B. Bannard, A. A. Casselman, E. J. Langstaff, and R. Y. Moir. Can. J. Chem. **46**, 35 (1968).
8. E. J. Langstaff, R. Y. Moir, R. A. B. Bannard, and A. A. Casselman. Can. J. Chem. **46**, 3649 (1968).
9. J. W. Bovenkamp, R. Y. Moir, A. A. Casselman, and R. A. B. Bannard. J. Chromatogr. **118**, 345 (1976).
10. R. C. Cathcart, J. W. Bovenkamp, R. Y. Moir, R. A. B. Bannard, and A. A. Casselman. Can. J. Chem. **55**, 3774 (1977).
11. P. L. Barili, G. Bellucci, F. Marioni, and V. Scartoni. J. Org. Chem. **40**, 3331 (1975).
12. B. C. Hartman and B. Rickborn. J. Org. Chem. **37**, 4246 (1972).
13. B. Rickborn and W. E. Lamke II. J. Org. Chem. **32**, 537 (1967).
14. R. Steyn and H. Z. Sable. Tetrahedron, **25**, 3579 (1969).
15. J. C. Richer and C. Freppel. Can. J. Chem. **46**, 3709 (1968).
16. J. N. Brönsted, M. Kilpatrick, and M. Kilpatrick. J. Am. Chem. Soc. **51**, 428 (1929).

17. E. L. ELIEL, N. L. ALLINGER, S. J. ANGYAL, and G. A. MORRISON. Conformational analysis. Interscience Publishers, Inc., New York, NY. 1965.
18. A. F. DIAZ, I. LAZDINS, and S. WINSTEIN. J. Am. Chem. Soc. **90**, 1904 (1968).
19. E. L. ELIEL. Stereochemistry of carbon compounds. McGraw-Hill, New York, NY. 1962; D. Y. CURTIN. Record Chem. Prog. **15**, 111 (1954).
20. F. J. WINKLER and A. V. ROBERTSON. Chem. Ber. **109**, 633 (1976).
21. M. TICHÝ. Collect. Czech. Chem. Commun. **38**, 3631 (1973).
22. H. PAULSEN and H. KOEBERNICK. Chem. Ber. **109**, 112 (1976).
23. A. M. EASTHAM and G. A. LATREMOUILLE. Can. J. Chem. **30**, 169 (1952).
24. C. E. NEWALL and A. M. EASTHAM. Can. J. Chem. **39**, 1752 (1961).
25. E. J. LANGSTAFF, E. HAMANAKA, G. A. NEVILLE, and R. Y. MOIR. Can. J. Chem. **45**, 1907 (1967).
26. F. C. MERRIAM. Anal. Chem. **20**, 1246 (1948).
27. H. M. MCNAIR and E. J. BONELLI. Basic gas chromatography. 5th ed. Gow Mac Instrument Co., Walnut Breek, CA. 1969.
28. J. R. DYER. Methods of biochemical analysis. Vol. 3. *Edited by* D. Glick. Interscience, New York, NY. 1956. p. 127.

COMMUNICATION

Hydrogen/deuterium selectivity in the infrared laser photolysis of chloroethylene[1]

A. GANDINI, C. WILLIS, AND R. A. BACK

PIE Group, Division of Chemistry, National Research Council of Canada, Ottawa, Ont., Canada K1A 0R6

Received September 15, 1977

A. GANDINI, C. WILLIS, and R. A. BACK. Can. J. Chem. **55**, 4156 (1977).

The decomposition of chloroethylene to acetylene and hydrogen chloride induced by focused radiation from a CO_2 laser has been shown to be H/D isotopically selective at low pressures. As the pressure is reduced below 1 Torr, C—Cl bond scission appears to increase at the expense of molecular fragmentation and gives rise to radical processes which are isotopically non-selective.

A. GANDINI, C. WILLIS et R. A. BACK. Can. J. Chem. **55**, 4156 (1977).

On a montré que la décomposition du chloroéthylène en acétylène et acide chlorhydrique, provoquée par l'irradiation focalisée d'un laser à CO_2, est sélective vis-à-vis les isotopes H/D à des pressions faibles. En dessous de 1 Torr, la rupture de la liaison C—Cl devient un processus alternatif important par rapport à la fragmentation moléculaire et amorce des reactions radicalaires qui ne possèdent pas de sélectivité isotopique.

We wish to report some preliminary findings on the photolysis of chloroethylene and its monodeuterated homologues induced by infrared radiation from a high-power CO_2 TEA laser. This technique has been the subject of several recent reviews (1–3).

The gas-phase decomposition of chloroethylene has been studied under a variety of conditions (4–9). While in shock-tube pyrolysis (4, 5) molecular dehydrochlorination predominates ($CH_2{=}CHCl \rightarrow C_2H_2 + HCl$), the flash and steady-state ultraviolet photolyses (6–9) lead to two primary modes of fragmentation, viz. molecular dehydrochlorination and C—Cl bond rupture ($CH_2{=}CHCl \rightarrow C_2H_3 + Cl$), the latter process yielding ethylene as the major product. Berry (9) has thoroughly discussed the various aspects related to the photochemistry of this compound.

Chloroethylene was degassed on a vacuum line; only traces of acetylene were detected as impurity by glc analysis. A mixture of α- and β-monodeuterochloroethylenes was prepared by the photochemical addition of hydrogen chloride to monodeuteroacetylene. Mass spectra of the purified product at 13 eV gave the following composition: 8% chloroethylene, 6% dideuterochloroethylenes, and 86% monodeuterochloroethylenes. The line-tunable laser used, a Lumonics model 103, gave ~5 J pulses of 250 ns duration at 0.6 Hz. Reactions were conducted in cylindrical Pyrex cells, 40 to 50 mm id and 60 to 90 mm long, provided with NaCl windows. While for most of this work the laser beam was focused into the cell with a 50 mm focal length Ge lens, the effect of the unfocused beam (power density ~2 MW cm^{-2}) was also tested. The reaction progress was followed by mass spectrometry and by taking infrared spectra of the cell contents. Yields were determined at the end of each run by separating the residual reactants (chloroethylenes) at 113 K from the products (acetylene, HCl, and ethylene) and measuring their pressure ratio. The two fractions were then analysed by mass spectrometry and occasionally by glc. Isotopic ratios were measured before, during, and at the end of the reaction from mass spectra obtained at 10–13 eV.

Figure 1 shows the portion of the infrared spectra relevant to this study of both chloroethylene and the synthesized monodeuterochloroethylene mixture. From previously reported spectra (10–12) of individual homologues, the relative proportion of α and β derivatives in our mixture was estimated as approximately 1:1. Irradiation of 50 to 500 Torr of chloroethylene with various laser lines (focused and unfocused) produced appreciable yields of acetylene and HCl, as already reported (13).

At low chloroethylene pressures (<2 Torr) it

[1]NRCC No. 16344.

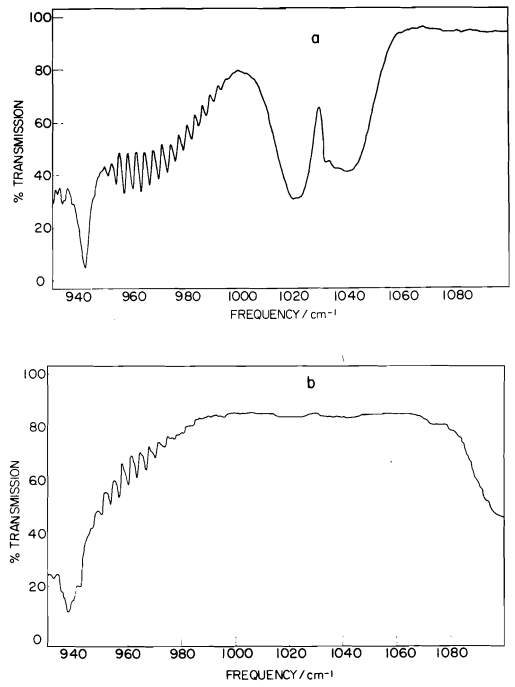

FIG. 1. Low-resolution infrared spectra of: (*a*) chloroethylene, 55 Torr; (*b*) mixture of monodeuterated chloroethylenes (see text), 40 Torr (the slight absorption around 1020 and 1040 cm^{-1} is due to 8% chloroethylene impurity). Optical path length 80 mm.

was possible to focus the beam without causing electrical breakdown, and decomposition was always observed provided the line selected matched an absorption feature of the substrate. As shown in Fig. 1, marked differences exist between the spectrum of chloroethylene and that of its monodeuterated homologues, suggesting that isotopically selective decomposition from mixtures of these two gases might be feasible. A mixture containing approximately equal amounts of chloroethylene and chloroethylenes-d_1 was therefore prepared and tested with different laser lines. Some of the results obtained are given in Table 1. Selective decomposition at 1041.34 and 1045.04 cm^{-1}, lines absorbed only by chloroethylene, produced enrichment in the deuterium content of the reactants. Conversely, selective decomposition at 1090.04 cm^{-1} resulted in deuterium enrichment in the products; the only absorbing molecule was α-deuterochloroethylene (10–12), and because β-deuterochloroethylene is transparent to that line, only about one half of the deuterium-containing substrate was in fact exposed to decomposition. The experiment at 1090.04 cm^{-1} with chloroethylene alone (No. 6, Table 1) clearly shows that no thermal reactions were induced in these systems if the substrate did not absorb the laser radiation. Focusing of the laser beam in the cell at substrate pressures higher than about 2 Torr resulted in electrical breakdown with abundant decomposition into acetylene (or acetylene-d_1) and HCl (or DCl) and no isotopic selectivity from H/D-containing mixtures.

The data in Table 1 show a decrease in selectivity with decreasing pressure, an unexpected result since in other systems the opposite has been observed (14–16). This gradual loss of selectivity with decreasing pressure was accompanied by the appearance of progressively larger proportions of ethylene (and to a minor degree of higher alkenes and alkynes) among the products. Thus, as the pressure is reduced, a second channel for decomposition, the homolytic cleavage of the C—Cl bond (6–9), becomes available to the vibrationally excited chloroethylenes and competes more and more successfully with the molecular elimination channel (final column, Table 1). While the activation energy for the latter process is 69 ± 3 kcal mol^{-1} (5), which is equivalent to about 23 photons of CO_2 radiation, the threshold energy required for C—Cl bond rupture in chloroethylene is about 90 kcal mol^{-1} ($\equiv D(C_2H_3—Cl)$ (17)), i.e., for this channel to become operative 7 more CO_2 photons must be absorbed by the chloroethylene molecule. The observation that bond scission becomes increasingly important as the pressure is reduced indicates that collisional deactivation is affecting the energy content of the decomposing molecules. The lifetime of molecules excited above the threshold for molecular elimination must be long enough to allow absorption of the additional photons required for bond scission, and in effect the decomposition must proceed from an assembly of molecules with a distribution of energies determined by the competition between absorption of laser radiation, collisional deactivation, and decomposition.

The onset of the second decomposition channel does not constitute a loss of primary isotopic selectivity, but the subsequent radical reactions involving the substrate are nonselective and thus cause a decrease in enrichment. Ways of circumventing this problem include the addition of radical scavengers and the reduction of pulse energy. These and other studies on the effect

TABLE 1. Experiments on the selective decomposition of mixtures of C_2H_3Cl and C_2H_2DCl with focused laser beams

Expt. No.	Initial % C_2H_3Cl	P_{tot}/Torr	ν/cm^{-1}	No. of pulses	% conv.[a]	Final % C_2H_3Cl	S^b	$\frac{C_2H_2^c}{C_2H_4}$
1	55	1.20	1045.04	6 000	34.0	37.5	8	>10
2	55	0.80	1041.34	11 000	33.4	32.0	>10	10
3	55	0.35	1041.34	16 000	~35	36.0	~8	4
4	55	0.12	1041.34	13 500	~46	37.0	~3	0.9
5	55	0.90	1090.04	11 000	10.5	61.5	>10	9
6	100	0.90	1090.04	10 000	0.0	100	—	—

[a]Conversions were calculated assuming molecular dehydrochlorination as the dominant fragmentation. When appreciable amounts of ethylene are formed (radical reactions) the values are approximate.
[b]For reactions 1–4: $S = [C_2H_3Cl]_{decomp}/[C_2H_2DCl]_{decomp}$. For reaction 5: $S = [C_2H_2DCl]_{decomp}/[C_2H_3Cl]_{decomp}$.
[c]Values obtained from mass spectra are uncorrected for relative sensitivity of the instrument.

of various parameters upon the quantitative behaviour of these systems are in progress.

1. M. J. BERRY. Annu. Rev. Phys. Chem. **26**, 259 (1975).
2. R. V. AMBARTSUMIAN and V. S. LETOKHOV. Acc. Chem. Res. **10**, 61 (1977).
3. S. KIMEL and S. SPEISER. Chem. Rev. **77**, 437 (1977).
4. P. CADMAN and W. J. ENGELBRECHT. Chem. Commun. 453 (1970).
5. F. ZABEL. Int. J. Chem. Kinet. **9**, 651 (1977).
6. M. G. BELLAS, J. K. S. WAN, W. F. ALEEN, O. P. STRAUSZ, and H. E. GUNNING. J. Chem. Phys. **68**, 2170 (1964).
7. T. FUJIMOTO, A. M. RENNERT, and M. H. J. WIJNEN. Ber. Bunsenges. Phys. Chem. **74**, 282 (1970).
8. P. AUSLOOS, R. E. REBBERT, and M. H. J. WIJNEN. J. Res. Natl. Bur. Stand. Sect. A, **77**, 243 (1973).
9. M. J. BERRY. J. Chem. Phys. **61**, 3114 (1974).
10. J. C. EVANS and H. J. BERNSTEIN. Can. J. Chem. **33**, 1792 (1955).
11. M. DE HEMPTINNE, G. GERMAIN-LEFEVRE, R. VAN RIET, and D. LANAERTS. Bull. Cl. Sci. Acad. R. Belg. **46**, 310 (1960).
12. S. ENOMOTO and M. ASAHINA. J. Mol. Spectrosc. **19**, 117 (1966).
13. A. GANDINI. Can. J. Chem. This issue.
14. R. V. AMBARTZUMIAN, I. A. GOROKHOV, V. S. LETOKHOV, G. N. MAKAROV, E. A. RYABOV, and N. V. TCHEKALIN. Kvantovaya Elektron. Moscow, **2**, 2197 (1975).
15. G. HANCOCK, J. D. CAMPBELL, and K. H. WELGE. Chem. Phys. Lett. **16**, 177 (1976).
16. M. C. GOWER and K. W. BILLMAN. Opt. Commun. **20**, 123 (1977).
17. S. W. BENSON. Thermochemical kinetics. John Wiley and Sons, New York, NY. 1976.

Canadian Journal of Chemistry

Published by
THE NATIONAL RESEARCH COUNCIL OF CANADA

Journal canadien de chimie

Publié par
LE CONSEIL NATIONAL DE RECHERCHES DU CANADA

Volume 55 Number 24 December 15, 1977

Volume 55 numéro 24 15 décembre 1977

Caerulomycins B and C, new 2,2′-dipyridyl derivatives from *Streptomyces caeruleus*[1]

A. G. McINNES AND D. G. SMITH

Atlantic Regional Laboratory, National Research Council of Canada, Halifax, N.S., Canada B3H 3Z1

AND

J. L. C. WRIGHT AND L. C. VINING

Department of Biology, Dalhousie University, Halifax, N.S., Canada B3H 4J3

Received August 3, 1977

A. G. McINNES, D. G. SMITH, J. L. C. WRIGHT, and L. C. VINING. Can. J. Chem. **55**, 4159 (1977).

Three new metabolites have been isolated from cultures of *Streptomyces caeruleus* and are related to caerulomycin, a known antibiotic metabolite of this organism now designated caerulomycin A. The structures of two of the new compounds, caerulomycins B and C, are shown to be 3-hydroxy-4-methoxy- and 3,4-dimethoxy-2,2′-dipyridyl-6-(*E*)-aldoxime.

A. G. McINNES, D. G. SMITH, J. L. C. WRIGHT et L. C. VINING. Can. J. Chem. **55**, 4159 (1977).

On a isolé trois nouveaux métabolites à partir de milieux de cultures des *Streptomyces caeruleus*; ces métabolites sont reliés à la caerulomycine, un métabolite antibiotique connu de ces organismes, qui est maintenant désigné sous le nom de caerulomycine A. Les structures de deux des nouveaux composés, les caerulomycines B et C, sont les hydroxy-3 méthoxy-4 et diméthoxy-3,4 dipyridyl-2,2′ aldoxime-6-(*E*).

[Traduit par le journal]

Streptomyces caeruleus, first described by Baldacci (1), belongs to a small group of alkaline-dependent actinomycetes investigated by Taber (2, 3). Cultures grown in starch-Czapek medium produce an antibiotic, caerulomycin, isolated in 1959 by Funk and Divekar (4), and henceforth referred to as caerulomycin A to distinguish it from a similarly named antibiotic, cerulomycin, isolated at approximately the same time from *Actinomyces caerulescens* (5). We have found that addition of 1 m*M* L-tryptophan to the medium modifies the *S. caeruleus* fermentation so that the product isolated is not the expected caerulomycin A, but a mixture of two related metabolites which are named caerulomycins B and C. Subsequent examination of cultures grown on unsupplemented starch-Czapek medium showed that the caerulomycin A that they produced was accompanied by small amounts of caerulomycins B and C as well as a fourth product which we refer to as caerulomycin D.

The structure of caerulomycin A was deduced from chemical and spectral evidence (6) to be 4-methoxy-2,2′-dipyridyl-6-(*E*)-aldoxime (**1***a*), and has been confirmed by synthesis (7). In this paper we present evidence that caerulomycins B and C have structures **2** and **3***a*, respectively. Caerulomycin D is a glycosidic derivative of 3,4-dihydroxy-2,2′-dipyridyl-6-(*E*)-aldoxime.[2]

[1]NRCC No. 16275.

[2]A. G. McInnes, D. G. Smith, J. A. Walter, J. L. C. Wright, G. P. Arsenault, and L. C. Vining. Unpublished results.

Isolation

Procedures described for the isolation of **1***a* from culture filtrates (4, 6) were modified to allow the recovery of only the ether-soluble basic fraction. High vacuum sublimation of the crude extract from cultures grown on starch-Czapek medium gave **1***a* mixed with small amounts of other caerulomycins, from which it was freed by several crystallizations from ethanol. Fractional crystallization of the unsublimed residue gave caerulomycin D. Caerulomycin C was the least soluble product but crystallized slowly from ethanol. It could be obtained pure by fractional crystallization of the crude caerulomycin mixture. This latter procedure applied to the crude extract from cultures grown in L-tryptophan-supplemented medium gave only caerulomycins B and C. In cultures grown on the unsupplemented medium caerulomycin B was a very minor component and could be separated only by preparative partition chromatography. Chromatography also provided an alternative and more satisfactory separation of the other three metabolites.

Properties

The molecular formulae of caerulomycins B and C were established by mass spectral and elemental analysis as $C_{12}H_{11}N_3O_3$ and $C_{13}H_{13}N_3O_3$. Caerulomycin B, but not C, gave a positive test for phenolic groups by coupling to stabilized diazonium salts. As with **1***a* (6), caerulomycin C could be converted to a monoacetate (**3***c*, ν_{max} 1760 cm^{-1}, δ 2.22 ppm) using a mild acetylating procedure, and to a nitrile (**3***b*, ν_{max} 2240 cm^{-1}) by eliminating the acetoxy group under more vigorous conditions. The mass spectra of caerulomycins B and C, like those of **1***a*, contained significant ion peaks corresponding to the loss of hydrogen, methyl, water, methoxyl, and aldoxime fragments. Caerulomycin C showed an initial loss of 30 mass units to generate an ion with *m/e* 229 equivalent to M^+ for **1***a* and giving rise to a similar series of fragment ions. In particular these included a second loss of 30 mass units and low abundance ions at *m/e* 155 (dipyridyl) and 78 (pyridyl). The spectrum of caerulomycin B lacked the *m/e* 155 ion but the peak at *m/e* 78 was relatively intense. The infrared spectra of the metabolites and their derivatives contained strong absorption bands in the same regions as those of 2,2′-dipyridyl and **1***a* (6). Also like 2,2′-dipyridyl and **1***a*, caerulomycins B and C gave a deep-red color in the presence of ferrous salts. The color given by 2,2′-dipyridyl is due to the complex Fe-$[(C_{10}H_8N_2)_3]^{2+}$ in which the pyridyl rings are *cis* coplanar (9), and steric hindrance due to substituents at the 3,3′- (10) or 6,6′-positions (11, 12) is known to partly or completely inhibit complex formation. In 2,2′-dipyridyl itself, both crystalline (13, 14) and in solution (9, 15, 16), the two rings are *trans* coplanar.

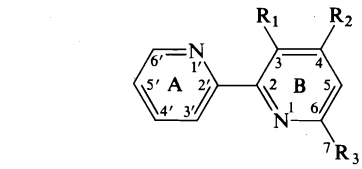

1*a*	R_1 = H	R_2 = OCH_3	R_3 = CH=NOH
b	R_1 = H	R_2 = OCH_3	R_3 = C≡N
c	R_1 = H	R_2 = OCH_3	R_3 = CH=NOAc
2	R_1 = OH	R_2 = OCH_3	R_3 = CH=NOH
3*a*	R_1 = OCH_3	R_2 = OCH_3	R_3 = CH=NOH
b	R_1 = OCH_3	R_2 = OCH_3	R_3 = C≡N
c	R_1 = OCH_3	R_2 = OCH_3	R_3 = CH=NOAc

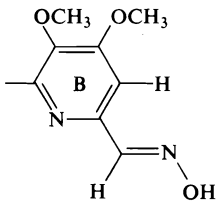

3*d*

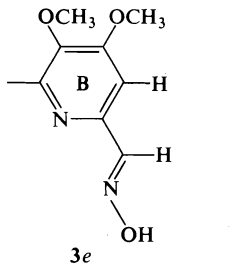

3*e*

2,2′-Dipyridyl (16) and **1***a* (4) show three principal absorbing bands in the ultraviolet region, with maxima at approximately 230, 260, and 280 nm. These bands are present in the spectrum of caerulomycin B, but the maxima are shifted to longer wavelengths by 13–48 nm, as would be predicted with the introduction of a hydroxyl group into a pyridine ring at position 3 (17). By hydrogen bonding to nitrogen of the adjacent ring this group should also maintain the *trans* coplanar conformation. Caerulomycin C and its derivatives show only two major ultraviolet absorption bands with maxima close to 230 and 260 nm. However, it is known that substitution of H-3 and H-3′ in 2,2′-dipyridyl shifts the weaker 280 nm band hypsochromically to the extent that it merges with that at 260 nm, and the shift is attributed to the steric effect of the substituents increasing the interplanar angle between the rings (16). These properties suggest that the two new metabolites contain a 2,2′-

TABLE 1. The ^{1}Hmr data for caerulomycin A (**1***a*), B (**2**), and C (**3***a*), caerulomycinonitrile A (**1***b*) and C (**3***b*), and caerulomycin C monoacetate (**3***c*) in DMSO-d_6*

Compound	H-3	H-5	H-7	H-3′	H-4′	H-5′	H-6′	3-OCH_3	4-OCH_3	NOH	CH_3CO	3-OH
1*a*	7.91	7.35	8.22	8.40	7.98	7.51	8.72		3.96	11.72		
1*b*	8.13	7.75		8.34	7.98	7.53	8.72		3.98			
2		7.39	8.06	8.54	8.13	7.56	8.67		3.94	11.41		14.62
3*a*†		7.49	8.05	7.69	7.92	7.43	8.67	3.76	3.98	11.60		
3*b*		7.96		7.71	7.96	7.49	8.70	3.80	4.02			
3*c*		7.63		7.70	7.94	7.50	8.70	3.78	4.01		2.22	

*H-3′, H-4′, H-5′, and H-6′ form an AMXY sub-spectrum which was analyzed with the Varian spin simulation program on a 620L data system associated with the model XL-100 spectrometer. The coupling constants for this system, and $J_{3,5}$ of **1***b*, are not given since they agreed within experimental error (±0.1 Hz) with values already reported for 2,2′-dipyridyl (20) and **1***a* (6).

†Nuclear Overhauser enhancement measurements for **3***a* were as follows: H-5 {4-OCH_3} 30%; H-7 {=NOH} 12%.

dipyridyl residue substituted at the 3- or 3′-position.

^{1}*H Nuclear Magnetic Resonance Spectra*

Proton assignments were confirmed by spin-decoupling experiments (19) and nuclear Overhauser enhancement (nOe) studies (20), while spectral simulation techniques were used to obtain relevant parameters from complex subgroups (see footnote to Table 1).

The ^{1}Hmr spectra of 2,2′-dipyridyl (9, 15, 18) in a variety of solvents including DMSO-d_6 (21), and the spectrum of **1***a* in $CDCl_3$ (6), have been reported. Known substituent effects in 2-substituted pyridines (22) account for spectral differences between **1***a* and its nitrile derivative (**1***b*). Thus H-3 and H-5 of **1***b* were deshielded by about 0.2 and 0.4 ppm, and signals for the oxime group of **1***a* at δ 8.22 and δ 11.72 ppm were absent. Signals corresponding to the ring A, oxime, and methoxyl hydrogens of **1***a* were also present in the ^{1}Hmr spectra of **2** and **3***a* (Table 1). Indeed, the spectra of **3***a* and **1***a* differed in only three respects. In the former the H-3 signal was replaced by one for a methoxyl group (δ 3.76), the H-5 resonance at δ 7.49 was a singlet, and H-3′ (δ 7.69) was shielded relative to the corresponding hydrogen of **1***a*.

In the *trans* coplanar conformation of 2,2′-dipyridyl, H-3 is close to the nitrogen atom of the adjacent ring and is deshielded by approximately 1.4 ppm as a result of contributions from the diamagnetic anisotropy of the neighbouring ring and dipolar fields associated with the nitrogen atom (9, 16). The remaining hydrogens are unaffected, and their chemical shifts are similar to those of pyridine (23). Introduction of a bulky substituent at C-3 would cause a conformational change (16) and so reduce the deshielding (particularly that associated with nitrogen) at H-3′. Thus, the upfield shift of H-3′ in caerulomycin C agrees with evidence from ultraviolet absorption and mass spectra, and indicates that this metabolite possesses a methoxyl substituent at C-3 and has structure **3***a*. Confirming this conclusion, irradiation at the resonance frequency of the low-field methoxyl group (δ 3.98) of **3***a* caused a 30% nOe of the H-5 singlet at δ 7.49. No nOe was obtained by irradiating the other methoxyl resonance at δ 3.76. Thus, the lone aromatic hydrogen is adjacent to the methoxyl group which has a chemical shift identical to that of the methoxyl substituent of **1***a*.

The ^{1}Hmr spectrum of the nitrile **3***b* was similar to that of **3***a* except that it contained no signals for an oxime group, and exhibited deshielding effects comparable to those noted in **1***b*. Of particular importance, the lone hydrogen at δ 7.49 in **3***a* was shifted by 0.47 ppm to δ 7.96 in **3***b*, which was similar to the deshielding of H-5 (δ 7.35 to δ 7.75) accompanying the conversion **1***a* to **1***b*. Thus, the substitution pattern at the 4-, 5-, and 6-positions of **1***a* is retained in **3***a*, and this in turn requires that the additional methoxyl group in **3***a* be attached to C-3.

Irradiation at the resonance frequency of the OH proton in **3***a* caused a 12% nOe of the H-7 signal, thus establishing an (*E*) configuration for the oxime group. Similar experiments showed that H-5 and H-7 do not contribute to each other's relaxation, which indicates that the oxime group is oriented as in partial structure **3***d* rather than **3***e*. A previous study using a different approach (6) established that the oxime group of **1***a* had an (*E*) configuration.

^{13}*C Nuclear Magnetic Resonance Spectra*

Further support for the proposed structure of caerulomycin C came from examination of the

TABLE 2. ^{13}C chemical shifts δ_c (TMS) for 2,2′-dipyridyl (**4**) and caerulomycins in DMSO-d_6*

Compound	C-2	C-3	C-4	C-5	C-6	C-7	C-2′	C-3′	C-4′	C-5′	C-6′	3-OCH_3	4-OCH_3
1*a*	156.9	106.5	166.6	105.5	153.4	148.8	154.6	120.7	137.2	124.4	149.2		55.5
1*b*	158.4	109.2	166.8	116.1	133.5	177.3	153.1	121.0	137.6	125.1	149.3		56.3
3*a*	151.0	143.8	159.4	103.5	148.2	148.5	155.9	124.0	136.3	123.1	148.7	61.0	56.0
3*b*	152.8	146.5	159.7	114.2	127.8	117.1	154.5	124.0	136.6	123.6	148.9	61.2	56.9
3*c*†	151.7	145.1	159.5	105.9	145.2	156.2	155.3	123.9	136.4	123.3	148.7	61.0	56.3
4							155.4	120.5	137.2	124.1	149.3		

*Pulse Fourier transform 8 K, sweep width 5120 Hz, data accuracy ±0.6 Hz.
†The signals for the acetyl group in this compound appeared at 19.2 and 167.9 ppm.

^{13}C nmr data in Tables 2 and 3 which list the proton noise decoupled (pnd) and high resolution (hr) spectral results. Assignments were aided by off-resonance decoupling (ord) experiments (23) and by the use of 2,2′-dipyridyl as a model compound. Apart from providing supporting evidence for the structure of caerulomycin C, these data are required for the structural elucidation[2] of caerulomycin D and for biosynthetic studies on ^{13}C-labeled **1***a*, now in progress, which rely upon correct interpretation of ^{13}C nmr spectra.

Assignment of resonances for 2,2′-dipyridyl and the ring-A carbons of **1***a* and **1***b* was straightforward, the ^{13}C—H spin–spin coupling data in Table 3 being similar to those observed for pyridine (24, 25) and 2-substituted pyridines (25, 26, 27). Typical deshielding by the directly bonded methoxyl substituent (28) and three-bond coupling to the methoxyl hydrogens (**1***a*, $^3J_{CH} \approx 3$ Hz; **1***b*, bm due to additional coupling with[2] H-5) identified C-4. Signals for ring-B carbons bonded to hydrogen (C-3, C-5) were assigned from differences in residual couplings in proton ord spectra. As expected, dehydration of the oxime was accompanied by considerable deshielding of C-5 (≈11 ppm), and to a lesser extent C-3 (≈3 ppm). Thus the oxime substituent in 2-pyridine aldoxime shields C-3 by 3.9 ppm but does not affect[3] C-5, whereas the nitrile group in 2-cyanopyridine (8) deshields both C-3 (4.7 ppm) and C-5 (3.3 ppm). Conversion to a nitrile also increased the spin–spin coupling between C-5 and H-5 from 165.2 to 171.8 Hz, in contrast to coupling between C-3 and H-3 which changed little. In **1***a* C-3 was also long-range coupled to H-5 ($^3J_{CH}$ 3.8 Hz), and C-5 to H-3 ($^3J_{CH}$ 3.6 Hz) and one additional hydrogen ($^nJ_{CH}$ 3.6 Hz). However, in **1***b* C-3 was still long-range coupled to H-5 whereas C-5 was coupled only to H-3 ($^3J_{CH}$ 3.8 Hz). Thus, the additional splitting in the C-5 resonance of **1***a* must have been due to H-7.

In the hr ^{13}C nmr spectrum of **1***a* one of the resonances due to the quaternary carbons C-2 and C-6 was a sharp singlet (δ_c 156.9); the other was a doublet (δ_c 153.4) with a spacing of 5.3 Hz. Since the latter signal was a sharp singlet in **1***b* it was assigned to C-6, because geminal coupling of H-7 to C-6 would be removed in the nitrile. The singlet at δ_c 156.9 was, therefore, assigned to C-2. The resonances for C-6 and C-2 in **1***b* appeared at δ_c 133.5 and δ_c 158.4, respectively, because conversion of the oxime to a nitrile would cause considerable shielding of C-6 (≈20 ppm) and a slight deshielding (≈1 ppm) of C-2. In pyridine-2-aldoxime C-2 is deshielded by 2.6 ppm and C-6 shielded by 0.4 ppm (28), whereas for 2-cyanopyridine C-2 is shielded by 16.3 ppm and C-6 deshielded by 1.1 ppm.[3]

Finally, the carbons of the oxime and nitrile groups (C-7) gave characteristic resonances at δ_c 148.8 and δ_c 117.3 (28[3]) and the methoxyl carbons at δ_c 55.5 (**1***a*) and δ_c 56.3 (**1***b*). The hr spectra showed that both the oxime carbon ($^3J_{CH}$ 7.7 Hz) and the nitrile carbon ($^3J_{CH}$ 3.8 Hz) were long-range coupled to H-5.

The ^{13}C nmr spectra of **3***a* and **3***b* were similar to those of **1***a* and **1***b*, with resonances at δ_c 148.5 and 117.1 ppm for the oxime and nitrile carbons. Five signals had chemical shifts and multiplicities in hr spectra that permitted them to be assigned to ring-A carbons. Of the two methoxyl groups in each compound (**3***a*, δ_c 56.0, δ_c 61.0; **3***b*, δ_c 56.9, δ_c 61.2) one had a chemical shift close to that of the methoxyl group in **1***a* (δ_c 55.5) or **1***b* (δ_c 56.3). Other differences were associated with the ring-B carbons and attributable to changes induced by the extra methoxyl

[3]A. G. McInnes, D. G. Smith, and J. A. Walter. Unpublished results.

TABLE 3. ^{13}C—H coupling constants ($^nJ_{CH}$) for the caerulomycins (**1***a*,*b*, **3***a*,*b*) and 2,2′-dipyridyl (**4**) in DMSO-d_6

Compound	C-2	C-3	C-4	C-5	C-6	C-7	3-OCH_3	4-OCH_3
1*a*	s	dd; ^1J 166.2 $^3J_{3,5}$ 3.8	bq; $^3J_{4,OCH_3} \approx 3$	dt; ^1J 165.2 $^3J_{5,3}=^3J_{5,7}$ 3.6	d; $^2J_{6,7}$ 5.3	dd; ^1J 167.5 $^3J_{7,5}$ 7.7		q; ^1J 145.8
1*b*	s	dd; ^1J 167.7 $^3J_{3,5}$ 3.8	bm	dd; ^1J 171.8 $^3J_{5,3}$ 3.8	s	d; $^3J_{7,5}$ 3.8		q; ^1J 146.4
3*a*	s	bm	q; $^3J_{4,OCH_3}$ 3.0	dd; ^1J 164.0 $^3J_{5,7}$ 2.2	d; $^2J_{6,7}$ 5.6	dd; ^1J 168.8 $^3J_{7,5}$ 9.2	q; ^1J 145.1	q; ^1J 146.5
3*b*	s	bm	bm	d; ^1J 170.0	s	d; $^3J_{7,5}$ 3.6	q; ^1J 146.1	q; ^1J 146.9

Compound	C-2′	C-3′	C-4′	C-5′	C-6′
1*a*	bm	dd; ^1J 166.5 $^3J_{3',5'}$ 6.6	dd; ^1J 165.3 $^3J_{4',6'}$ 6.1	ddd; ^1J 165.6 $^2J_{5',6'}$ 7.8; $^3J_{5',3'}$ 7.4	ddd; ^1J 179.0 $^2J_{6',5'}$ 3.6; $^3J_{6',4'}$ 7.0
1*b*	bm	dd; ^1J 166.5 $^3J_{3',5'}$ 7.2	dd; ^1J 165.8 $^3J_{4',6'}$ 6.0	ddd; ^1J 165.5 $^2J_{5',6'}$ 8.2; $^3J_{5',3'}$ 7.0	ddd; ^1J 179.7 $^2J_{6',5'}$ 3.5; $^3J_{6',4'}$ 7.0
3*a*	bm	dd; ^1J 165.7 $^3J_{3',5'}$ 7.1	dd; ^1J 164.9 $^3J_{4',6'}$ 6.3	ddd; ^1J 165.0 $^2J_{5',6'}$ 8.4; $^3J_{5',3'}$ 6.2	ddd; ^1J 178.3 $^2J_{6',5'}$ 3.8; $^3J_{6',4'}$ 7.3
3*b*	bm	dd; ^1J 165.8 $^3J_{3',5'}$ 5.6	dd; ^1J 165.6 $^3J_{4',6'}$ 6.3	ddd; ^1J 165.4 $^2J_{5',6'}$ 8.4; $^3J_{5',3'}$ 6.3	ddd; ^1J 179.5 $^2J_{6',5'}$ 3.4; $^3J_{6',4'}$ 6.9
4	bdd; $^3J_{2',4'}$ 6.9 $^3J_{2',6'}$ 10.4	ddd; ^1J 165.4 $^3J_{3',5'}$ 7.3; $^4J_{3',6'}$ 0.9	dd; ^1J 164.8 $^3J_{4',6'}$ 6.3	ddd; ^1J 165.2 $^2J_{5',6'}$ 8.5; $^3J_{5',3'}$ 6.5	ddd; ^1J 178.7 $^2J_{6',5'}$ 3.6; $^3J_{6',4'}$ 6.9

group. Many of the chemical shift trends and coupling characteristics noted for the ring-B carbons of **1***a* and **1***b* were observed in **3***a* and **3***b*.

The carbon bonded to hydrogen in ring B of **3***a* had a similar chemical shift to that of C-5 in **1***a* and both were almost equally deshielded upon conversion to the nitriles **3***b* and **1***b*. These conversions were also accompanied by similar increases in the $^1J_{CH}$ values. Furthermore the single aromatic proton in ring B was coupled to the oxime ($^3J_{CH}$ 9.2 Hz) and nitrile ($^3J_{CH}$ 3.6 Hz) carbons of **3***a* and **3***b* just as H-5 was coupled to these groups in **1***a* and **1***b*. In addition two ring-B quaternary carbons of **3***a* and **3***b* had similar spectral characteristics to C-6 and C-2 of **1***a* and **1***b*. One (δ_c 148.2) in **3***a* was geminally coupled to H-7 ($^2J_{CH}$ 5.6 Hz), whereas the corresponding carbon in **3***b* (δ_c 127.8) was characteristically shielded ($\approx$20 ppm) by the conversion of the oxime to a nitrile group. The other (δ_c 152.8) in **3***b* was slightly but typically deshielded relative to the corresponding carbon (δ_c 151.0) in **3***a*. Low intensity signals for the remaining carbons which bear methoxyl groups in **3***a* (δ_c 143.8, δ_c 159.4) and **3***b* (δ_c 146.5, δ_c 159.7) were easily recognized from their chemical shifts and from the broad multiplets which they gave in hr spectra as a result of coupling to the methoxyl hydrogens and a poor signal/noise ratio. The resonance at lowest field could be assigned to C-4 as the alternative would require the C-3 methoxyl to possess unreasonable shielding characteristics. The combined observations are, therefore, consistent only with the assignments given in Table 3, and with caerulomycin C having structure **3***a* and caerulomycinonitrile C structure **3***b*.

Caerulomycin C monoacetate must have structure **3***c*. In the ^{1}Hmr spectra, absence of an OH signal and a slight downfield shift of the resonances for H-5 and H-7 are the only differences from **3***a*. The ^{13}C spectrum of **3***c* was also similar to that of **3***a* apart from the presence of acetoxyl methyl (δ_c 19.2) and carbonyl (δ_c 167.9) signals, and a downfield shift of the oxime carbon resonance to δ_c 156.2.

It was also apparent from ^{1}Hmr evidence (Table 1) that replacement of the C-3 methoxyl group of **3***a* by a hydroxyl substituent in caerulomycin B was the only structural difference between the two metabolites. Thus caerulomycin B has structure **2**. Hydrogen bonding of this hydroxyl group with the nitrogen atom in ring A of **2** not only accounts for the low-field chemical shift of the hydroxyl proton (δ 14.62) but, in stabilizing the *trans* coplanar conformation of the dipyridyl ring system, ensures that H-3′ is deshielded as in **1***a*. Lack of material prevented ^{13}C nmr data being obtained for this metabolite.

Experimental

Melting points were measured on a hot stage and are uncorrected. Ultraviolet and infrared spectra were recorded with Unicam model SP 8000 and Perkin-Elmer model 237 spectrophotometers. Mass spectra were obtained with a Consolidated Electrodynamics Corporation model 110-B double-focusing spectrometer operated in the electrical mode. ^{1}H nuclear magnetic resonance spectra were obtained with a Varian Associates model HA-100 spectrometer. ^{13}C nuclear magnetic resonance spectra (25.16 MHz) were recorded with a Varian Associates model XL-100-15 pulsed Fourier transform spectrometer.

Isolation of Caerulomycins

Cultures of *Streptomyces caeruleus* were grown as described by Funk and Divekar in starch-Czapek medium (4), or in this medium supplemented with L-tryptophan at 1 m*M* concentration. The filtered broth was extracted with three half-volumes of ether and basic products were separated by extraction from the ether into *N* hydrochloric acid. They were recovered, after addition of excess sodium bicarbonate, by filtration and by back-extraction from the filtrate with ether. The crude residue from starch-Czapek cultures was sublimed at 105–130°C under high vacuum and the sublimate (mp 168–171°C) was recrystallized several times from ethanol to give caerulomycin A, mp 176–177°C.

Repeated recrystallization from ethanol of the unsublimed residue, collecting only the crop of fine colorless needles which formed immediately upon cooling, gave caerulomycin D, mp 241–242°C.

When a hot ethanolic solution of the crude caerulomycin from starch-Czapek medium was allowed to cool to room temperature the crop of needles deposited was a mixture of caerulomycin A with a smaller amount of caerulomycin D. The mother liquor slowly deposited a second crop of crystals consisting mainly of caerulomycin C (**3***a*). Recrystallization yielded colorless prisms, mp 208–210°C; λ_{max} in methanol at 229 and 263 nm (log ε 4.13 and 3.96); ν_{max} in potassium bromide at 3160, 1585, 1560, 1490, 1360, 1245, 1200, 1065, 995, 851, 800, and 712 cm^{-1}; *m/e* at 259 (15%), 258 (14%), 242 (100%), 229 (13%), 228 (10%), 214 (21%), 199 (14%), 155 (14%), 105 (17%), and 78 (31%). Accurate mass measurement of M$^+$, *m/e* 259.0952 (calcd. for $C_{13}H_{13}O_3N_3$: 259.09579); found: C 60.39, H 5.05, N 16.12 (calcd. for $C_{13}H_{13}O_3N_3$: C 60.23, H 5.01, N 16.21). Fractional crystallization in this manner of the extract from cultures grown on starch-Czapek medium containing L-tryptophan did not yield a first crop of needles. Caerulomycin C (25 mg/ℓ) separated slowly from the solution and was removed. When the mother liquor was concentrated caerulomycin B (**2**, 15 mg/ℓ) crystallized as feathery needles. These were sublimed in high vacuum at 110°C and recrystallized from methanol to give needles, mp 215–217°C; λ_{max} (log ε) in

ethanol at 249 (4.19), 273 (4.01) inflexion, 328 (3.75); ν_{max} in potassium bromide at 3250, 3160, 1565, 1472, 1374, 1280, 1200, 1165, 1050, 1040, 970, and 710 cm^{-1}; *m/e* at 245 (100%), 229 (67%), 228 (93%), 200 (22%), 171 (19%), 144 (22%), 105 (45%), 79 (26%), and 78 (42%). Accurate mass measurement of M^+ gave *m/e* 245.0797 (calcd. for $C_{12}H_{11}O_3N_3$: 245.0800).

Chromatography

Caerulomycins A, B, C, and D were separated qualitatively by thin-layer chromatography (tlc) on silica gel HF_{254} (Merck & Co., Darmstadt) using as solvent either a mixture of benzene – acetic acid – water (42:24:1) giving R_f values of 0.09, 0.05, 0.24, and 0.16, respectively, or a mixture of benzene–diethylamine (50:3) saturated with 10% aqueous ammonia giving R_f values of 0.39, 0.35, 0.31, and 0.21, respectively. Alternatively, the metabolites could be separated by circular chromatography on formamide-treated paper with benzene as mobile phase. The R_f values were 0.65, 0.57, 0.26, and 0.28, respectively. Caerulomycin zones were detected as quenching areas under light of 254 nm, and as red to purple areas after the plates had been sprayed with aqueous ferrous sulfate.

For the preparative separation of caerulomycins a column (90 × 2.6 cm) of Sephadex LH20 (Pharmacia, Uppsala) was equilibrated with the solvent system benzene – ethyl acetate – acetic acid – water (1:12:4:12). Crude caerulomycin (500 mg) in upper phase (5 ml) was applied and the column irrigated with upper phase while fractions (20 ml) were collected. Caerulomycins, eluted in the sequence B, A, D, C, were collected in fractions 24–29, 34–40, 42–103, and 140–142, respectively.

Caerulomycin C Monoacetate (3c)

Caerulomycin C (20 mg) was dissolved in acetic anhydride (3 ml) and kept at room temperature for 24 h. Ice was added to hydrolyze excess reagent and the solution evaporated *in vacuo* at 45°C. The product crystallized slowly from ether – petroleum ether (bp 60–80°C) as feathery needles (19 mg), mp 102–103°C; λ_{max} (log ε) in ethanol at 229 (4.13) and 265 (4.02) nm; λ_{max} in potassium bromide at 1760 cm^{-1}; M^+ at *m/e* 301.1063 (calcd. for $C_{15}H_{15}N_3O_4$: 301.1064).

Caerulomycinonitrile C (3b)

Caerulomycin C (25 mg) was heated under reflux with acetic anhydride (5 ml) for 3 h. The cooled solution was diluted with water and evaporated at 45°C *in vacuo* to a tan solid which crystallized from ethanol as colorless needles (16 mg), mp 114–116°C; λ_{max} (log ε) in ethanol at 227 (4.67) and 260 (3.81) nm; ν_{max} in chloroform at 2240 cm^{-1}; M^+ at *m/e* 241.0849 (calcd. for $C_{13}H_{11}N_3O_2$: 241.0851).

Acknowledgment

This work was supported in part by an operating grant from the National Research Council of Canada (to L.C.V.).

1. E. BALDACCI. Atti Ist. Bot. Univ. Pavia, **3**, 139 (1944).
2. W. A. TABER. Can. J. Microbiol. **5**, 335 (1959).
3. W. A. TABER. Can. J. Microbiol. **6**, 503 (1960).
4. A. FUNK and P. V. DIVEKAR. Can. J. Microbiol. **5**, 317 (1959).
5. M. G. BRAZHNIKOVA, I. N. KOVSHAROVA, G. F. GAUZE, M. A. SVESHNIKOVA, T. S. BOBKOVA, V. A. SHORIN, and O. K. ROSSOLIMO. Antibiotiki, **2**, 16 (1957).
6. P. V. DIVEKAR, G. READ, and L. C. VINING. Can. J. Chem. **45**, 1215 (1967).
7. S. RANGANATHAN, B. B. SINGH, and P. V. DIVEKAR. Can. J. Chem. **47**, 165 (1969).
8. H. L. RETCOFSKY and R. A. FRIEDEL. J. Phys. Chem. **72**, 2619 (1968).
9. S. CASTELLANO, H. GUNTHER, and S. EBERSOLE. J. Phys. Chem. **69**, 4166 (1965).
10. F. W. CAGLE and G. F. SMITH. J. Am. Chem. Soc. **69**, 1860 (1947).
11. W. W. BRANDT, F. P. DWYER, and E. C. GYATFAS. Chem. Rev. **54**, 959 (1954).
12. A. BERGH, P. O'D. OFFENHARTZ, P. GEORGE, and G. P. HAIGHT. J. Chem. Soc. 1533 (1964).
13. F. BERTINOTTI, A. M. LIQUORI, and R. PARISI. Gazz. Chim. Ital. **86**, 893 (1956).
14. L. L. MERRITT and E. D. SCHROEDER. Acta Crystallogr. **9**, 801 (1956).
15. F. A. KRAMER, JR. and R. WEST. J. Phys. Chem. **69**, 673 (1965).
16. T. McL. SPOTSWOOD and C. I. TANZER. Aust. J. Chem. **20**, 1227 (1967).
17. S. F. MASON. J. Chem. Soc. 1253 (1959).
18. V. M. S. GIL. Mol. Phys. **9**, 97 (1965).
19. R. A. HOFFMAN and S. FORSEN. Prog. Nucl. Magn. Reson. Spectrosc. **1**, 15 (1966).
20. J. H. NOGGLE and R. E. SCHIRMER. The nuclear Overhauser effect, chemical applications. Academic Press, New York, NY. 1971.
21. F. E. LYTLE, L. M. PETROSKY, and L. R. CARLSON. Anal. Chim. Acta, **57**, 239 (1971).
22. T. J. BATTERHAM. NMR spectra of simple heterocyclics. Wiley-Interscience, New York, NY. 1973. Chapt. 2.
23. G. C. LEVY and G. L. NELSON. Carbon-13 nuclear magnetic resonance for organic chemists. Wiley-Interscience, New York, NY. 1972.
24. G. MIYAJIMA, K. TAKAHASHI, and H. SUGIYAMA. Org. Magn. Reson. **6**, 181 (1974).
25. F. J. WEIGERT, J. HUSAR, and J. D. ROBERTS. J. Org. Chem. **38**, 1313 (1973).
26. Y. TAKEUCHI and N. DENNIS. J. Am. Chem. Soc. **96**, 3657 (1974).
27. Y. TAKEUCHI. Org. Magn. Reson. **7**, 181 (1975).
28. J. B. STOTHERS. Carbon-13 NMR spectroscopy. Academic Press, Inc., New York, NY. 1972. p. 197.

Synthesis and characterization of binuclear transition metal complexes incorporating the tridentate chelating ligand dimethyl (*N*,*N*-dimethylethanolamino)(1-pyrazolyl)gallate: crystal and molecular structure of bis-μ-pyrazolyl-(*N*(1),*N*(2))-bis[dimethyl (*N*,*N*-dimethylethanolamino)-(1-pyrazolyl)gallato(*N*(2),*O*,*N*)copper(II)]

KENNETH S. CHONG, STEVEN J. RETTIG, ALAN STORR, AND JAMES TROTTER

Department of Chemistry, University of British Columbia, 2075 Wesbrook Mall, Vancouver, B.C., Canada V6T 1W5

Received July 29, 1977

KENNETH S. CHONG, STEVEN J. RETTIG, ALAN STORR, and JAMES TROTTER. Can. J. Chem. **55**, 4166 (1977).

Details of the synthesis of the tridentate tris chelating ligand dimethyl(*N*,*N*-dimethylethanolamino)(1-pyrazolyl)gallate and the preparation and physical properties of the binuclear transition metal complexes incorporating this ligand are given. Crystals of bis-μ-pyrazolyl(*N*(1),*N*(2))-bis[dimethyl(*N*,*N*-dimethylethanolamino)(1-pyrazolyl)gallato(*N*(2),*O*,*N*)copper(II)] are monoclinic, $a = 12.018(2)$, $b = 10.390(1)$, $c = 13.568(3)$ Å, $\beta = 100.04(6)°$, $Z = 2$, space group $P2_1/c$. The structure was solved by direct methods and was refined by full-matrix least squares procedures to a final R of 0.045 and R_w of 0.058 for 2460 reflections with $I \geq 3\sigma(I)$. The centrosymmetric binuclear molecule features copper atoms having distorted square pyramidal coordination geometry. Three of the basal positions are occupied by the oxygen, pyrazolyl nitrogen, and amino nitrogen atoms of the tridentate tris-chelating ligand. The two remaining sites are occupied by bridging pyrazolyl groups, which provide a basal nitrogen atom to one copper atom and an apical nitrogen atom to the second copper centre. The gallium atoms have distorted tetrahedral coordination geometry. Important bond lengths (corrected for libration) are: Cu—O, 1.981(3), Cu—N(basal), 1.953(3)–2.143(4), Cu—N(apical), 2.173(3), Ga—O, 1.907(3), Ga—N, 1.991(4), and Ga—C, 1.962(7) and 1.977(7) Å.

KENNETH S. CHONG, STEVEN J. RETTIG, ALAN STORR et JAMES TROTTER. Can. J. Chem. **55**, 4166 (1977).

On rapporte les détails de la synthèse du ligand tridentate et trichélatant diméthyl(*N*,*N*-diméthyléthanolamino)(pyrazolyl-1)gallate et la préparation et les propriétés physiques de complexes binucléaires de métaux de transition incorporant ce ligand. Les cristaux du bis-μ-pyrazolyl(*N*(1),*N*(2))-bis[diméthyl(*N*,*N*-diméthyléthanolamino)(pyrazolyl-1)gallato(*N*(2),*O*,*N*)-cuivre(II)] sont monocliniques, $a = 12.018(2)$, $b = 10.390(1)$, $c = 13.568(3)$ Å, $\beta = 100.04(6)°$, $Z = 2$, groupe d'espace $P2_1/c$. On a résolu la structure par des méthodes directes et on l'a affinée par la méthode des moindres carrés (matrice complète) jusqu'à une valeur finale de R de 0.045 et de R_w de 0.058 pour 2460 réflexions avec $I \geq 3\sigma(I)$. La molécule binucléaire centrosymétrique comporte des atomes de cuivre dont la géométrie de coordination correspond à une pyramide carrée déformée. Trois des positions de base sont occupées par l'oxygène, l'azote du pyrazolyle et l'azote du groupe amino du ligand trichélatant et tridentate. Les deux autres sites sont occupés par les groupes pyrazolyles formant le pont; ils fournissent un atome d'azote de la base d'un des atomes de cuivre et un atome d'azote apical du second atome de cuivre. La géométrie de coordination des atomes de gallium correspond à un tétraèdre déformé. Les longueurs des liaisons importantes (corrigées pour la libration) sont: Cu—O, 1.981(3), Cu—N(base), 1.953(3)–2.143(4), Cu—N(apical), 2.173(3), Ga—O, 1.907(3), Ga—N, 1.991(4) et Ga—C 1.962(7) et 1.977(7) Å.

[Traduit par le journal]

Introduction

As part of an expanding investigation of pyrazolyl and related derivatives of gallium and aluminum, novel anionic tridentate chelating ligands have been synthesized and their coordinating abilities studied. Neutral dimeric molecules (1–4) and transition metal complexes derived from symmetrical anionic bidentate chelating ligands (5–8) have been reported. The present account describes the synthesis of the anionic ligand, dimethyl(*N*,*N*-dimethylethanolamino)-(1-pyrazolyl)gallate, $[Me_2Ga(OCH_2CH_2NMe_2)(N_2C_3H_3)]^-$, and its coordination properties with respect to the transition metal ions Co(II),

Ni(II), Cu(II), and Zn(II). The resulting binuclear transition metal complexes have distorted square pyramidal coordination geometry about the transition metal atoms. These atoms are bridged by two pyrazolyl groups and end-capped with the tridentate ligands.

Experimental

Air sensitive materials were handled in a glove box under an atmosphere of oxygen-free dry nitrogen or in a nitrogen-blanketed apparatus. Tetrahydrofuran (THF) was dried by refluxing over lithium aluminum hydride and was used immediately after distillation. Benzene was dried by refluxing over molten potassium followed by distillation. Pyrazole (K and K Laboratories) and sodium hydride (Alfa Inorganic) were used as supplied. *N,N*-dimethylethanolamine was refluxed over anhydrous $CaSO_4$ and distilled prior to use. Gallium trimethyl was prepared as previously described (9).

Sodium Dimethyl(N,N-dimethylethanolamino)(1-pyrazolyl)gallate, $Na^+[Me_2Ga(OCH_2CH_2NMe_2)(N_2C_3H_3)]^-$

$$[1]\quad NaH + N_2C_3H_4 \xrightarrow[N_2\ atm]{THF} Na^+N_2C_3H_3^- + H_2$$

$$[2]\quad Na^+N_2C_3H_3^- + Me_3Ga \xrightarrow[N_2\ atm]{THF} Na^+Me_3Ga(N_2C_3H_3)^-$$

$$[3]\quad Na^+Me_3Ga(N_2C_3H_3)^- + Me_2NCH_2CH_2OH \xrightarrow[N_2\ atm,\ reflux]{THF} Na^+[Me_2Ga(OCH_2CH_2NMe_2)(N_2C_3H_3)]^- + CH_4$$

Trimethyl gallium (4.28 g, 37.3 mmol) in THF was added to sodium pyrazolide (37.3 mmol) (made from sodium hydride (0.894 g, 37.3 mmol) and pyrazole (2.54 g, 37.3 mmol) in THF) in the same solvent. *N,N*-dimethylethanolamine (3.32 g, 37.3 mmol) was added to the resulting solution and on refluxing a slow evolution of methane occurred. The course of the reaction was monitored by ^1H nmr as well as by visual observation of gas evolution. The product solution exhibits a Ga–*Me* proton resonance 0.1 ppm to lower field than that from the starting material. There was a gradual appearance of the new signal at the expense of the original signal in the Ga–*Me* region of the spectrum. The reaction was complete after refluxing for 24 h. Aliquots of the resulting clear solution of the ligand were used in further experiments since attempts to isolate the sodium salt from the THF solution were not successful.

Attempted Preparation of $[Me_2Ga(OCH_2CH_2NMe_2)(N_2C_3H_3)]_2M$ (M = Co, Ni, Cu, Zn)

The experimental procedure is very similar for each case and can be illustrated by the preparation of the cobalt derivative. The transition metal starting materials for all of the preparations are listed in Table 1.

An aliquot of the ligand solution prepared above and containing $Na^+Me_2Ga(OCH_2CH_2NMe_2)(N_2C_3H_3)^-$

TABLE 1. Analytical data for $[Me_2Ga(OCH_2CH_2NMe_2)(N_2C_3H_3)_2M]_2$ complexes

Compound	Color	Melting point (°C)	Transition metal precursor	Analysis						Electronic spectra	
				Found (%)			Calculated (%)				
				C	H	N	C	H	N	ν_{max} (cm^{-1})	ε
M = Co	Purple	158–159	$CoCl_2$	37.8	5.8	18.4	37.8	5.8	18.4	20 325(sh)	177
										18 939(sh)	225
										17 762	316
										17 391(sh)	279
M = Ni	Green	197	$Ni(BF_4)_2{\cdot}6H_2O$	38.1	5.8	18.1	37.9	5.8	18.4	24 692	254
										21 765(sh)	93
M = Cu	Blue	139(dec.)	$CuBr_2$	37.1	5.8	18.1	37.4	5.7	18.1	15 385	249
M = Zn	White	138(dec.)	$ZnCl_2$	37.1	5.8	17.8	37.2	5.7	18.1		

(2.06 g, 7.43 mmol) was reacted with cobalt chloride, $CoCl_2$ (0.482 g, 3.71 mmol), dissolved in THF. A white precipitate (NaCl) formed and the color of the solution changed from pink to purple immediately. The precipitate was allowed to settle and the clear solution siphoned off prior to removal of the solvent. The resulting purple solid was recrystallized from benzene. The purple crystals were collected, washed with benzene, and subjected to physical measurements (see Table 1). Elemental analysis and mass spectral data show that instead of the expected mononuclear octahedral complex, the purple solid is a binuclear cobalt complex having the formulation $[Me_2Ga(OCH_2CH_2NMe_2)(N_2C_3H_3)_2Co]_2$, **1** (M = Co).

The nickel reaction produced, in addition to the green binuclear complex listed in Table 1, small amounts of orange and lilac crystalline materials. These were characterized by elemental analyses and mass spectrometry. The orange compound proved to be identical to the previously characterized (5, 6, 8) compound $[Me_2Ga(N_2C_3H_3)_2]_2Ni$. The lilac compound is a new complex having the formulation $[MeGa(N_2C_3H_3)_3]_2Ni$. The latter has since been synthesized in larger quantities by an alternate route and will be described in a forthcoming publication together with other compounds incorporating the tris-chelating anionic ligand $MeGa(N_2C_3H_3)_3^-$.

All four transition metal complexes are relatively stable in air as solids but solutions are rapidly oxidized on exposure to air. These oxidations may involve attack at the 'vacant' sixth coordination sites on the transition metals.

Spectra

Mass spectra were recorded on a Varian MAT CH4 mass spectrometer at 70 eV with an ion source temperature of 80–100°C. Data for the cobalt complex appear in Table 2.[1] Proton nmr spectra were recorded on Varian T60 and XL100 instruments, ir spectra on a Perkin-Elmer 457 spectrophotometer, and electronic absorption spectra (solutions) on a Cary 14 spectrometer using 1.0 cm solution cells.

X-Ray Crystallographic Analysis of Bis-μ-pyrazolyl(N(1),N(2))-bis[dimethyl(N,N-dimethylethanolamino)-(1-pyrazolyl)gallato(N(2),O,N)copper(II)]

The crystal chosen for study was mounted with (0, −1, 1) normal to the goniostat axis and had dimensions of ca. 0.09 × 0.45 × 0.64 mm. Unit-cell and space group data were obtained from film and diffractometer measurements. The unit-cell parameters were refined by a least squares on 2 sin θ/λ values for 30 reflections measured on a diffractometer with CuK_α radiation (λ = 1.5418 Å). Crystal data (at 22°C) are:

$C_{24}H_{44}Cu_2Ga_2N_{10}O_2$ fw = 771.20
Monoclinic, a = 12.018(2), b = 10.390(1), c = 13.568(3) Å, β = 100.04(6)°, V = 1668.2(6) Å^3, Z = 2, ρ_c = 1.535 g cm^{-3}, $F(000)$ = 788, $\mu(CuK_\alpha)$ = 37.7 cm^{-1}. Absent reflections: $0k0$, $k \neq 2n$, and $h0l$, $l \neq 2n$ define uniquely the space group $P2_1/c$ (C_{2h}^5, No. 14).

Intensities were measured with nickel-filtered CuK_α radiation on a Datex-automated General Electric XRD-6 diffractometer. A θ–2θ scan at 4 deg min^{-1} over a range of (1.80 + 0.86 tan θ) degrees in 2θ was employed. Background counts of 10 s were measured at each end of the scan. Data were measured to 2θ = 140°. The intensities of the check reflections, measured every 40 reflections throughout the data collection, decreased uniformly to final values that were 0.85 times the initial values. Lorentz and polarization corrections and batch check reflection scaling were applied, and the structure amplitudes were derived. An absorption correction was applied by a computer program using a Gaussian integration method (10, 11). Transmission factors ranged from 0.201 to 0.720. Of the 3165 independent reflections measured, 2472 (78%) had intensities greater than $3\sigma(I)$ above background where $\sigma^2(I) = S + B + (0.06S)^2$ with S = scan count and B = time averaged background count.

The structure was solved by direct methods (12). The positions of the metal atoms, the oxygen atom, and two nitrogen atoms were located on the E-map. Two cycles of full-matrix least squares refinement of the coordinates and isotropic thermal parameters of these five atoms gave R = 0.292. A difference map calculated at this point gave the position of the remaining non-hydrogen atoms. The non-hydrogen atoms were refined for two cycles with isotropic thermal parameters, then for two cycles with anisotropic thermal parameters, reducing R to 0.058. All 22 hydrogen atoms were located on a subsequent difference map and were included in the refinement with isotropic thermal parameters. The entire structure (270 variables) was refined for four cycles giving a final R of 0.045 and R_w of 0.058 for 2460 reflections with $I \geq 3\sigma(I)$ (12 reflections, which had $|F_o| - |F_c| > 3\sigma(F)$, were treated as unobserved in the final stages of refinement; instrumental error was suspected for these reflections, but it seemed unwise to bias the data by remeasuring them; none of the disagreements were exceptionally bad). For all 3165 reflections R = 0.059 and R_w = 0.066.

A correction for secondary extinction was approximated by basing the least squares refinement on the minimization of $\Sigma w[|F_o| - |F_c|/(1 + gI)|]^2$ where g is the extinction parameter and I the uncorrected intensity. The final value of g was 9.2 × 10^{-8}. The scattering factors of ref. 13 were used for the non-hydrogen atoms and those of ref. 14 for the hydrogen atoms. Anomalous scattering factors from ref. 15 were used for the Ga, Cu, O, and N atoms. The weighting scheme, $w = 1/\sigma^2(F)$, where $\sigma^2(F)$ is derived from the previously defined $\sigma^2(I)$, gave uniform average values of $w(|F_o| - |F_c|)^2$ over ranges of $|F_o|$ and was employed in the final stages of refinement.

On the final cycle of refinement the mean parameter shift was 0.07σ, the largest shift (0.84σ) being associated with the y coordinate of H(9c). The mean error in an observation of unit weight was 1.381. The final positional and thermal parameters appear in Tables 3 and 4,[1] respectively. Measured and calculated structure factors have been placed in the Depository of Unpublished Data.[1]

The ellipsoids of thermal motion for the non-hydrogen atoms are shown in Fig. 1. The thermal motion has been analysed in terms of the rigid-body modes of translation

[1]The structure factor table and Tables 2 (mass spectral data), 4 (thermal parameters), 5*b*, and 6*b* (bond lengths and angles involving hydrogen) are available, at a nominal charge, from the Depository of Unpublished Data, CISTI, National Research Council of Canada, Ottawa, Ont., Canada K1A 0S2.

TABLE 3. Final positional parameters (fractional × 10^4, Ga and Cu × 10^5, H × 10^3) with estimated standard deviations in parentheses

Atom	*x*	*y*	*z*
Ga	12078(4)	25976(5)	47580(5)
Cu	34102(5)	46909(5)	51842(4)
O	2488(2)	3294(3)	5614(2)
N(1)	1430(3)	3839(4)	3697(3)
N(2)	2309(3)	4690(4)	3877(3)
N(3)	4818(3)	3419(3)	5083(2)
N(4)	5935(3)	3664(3)	5102(3)
N(5)	3724(3)	5042(4)	6758(3)
C(1)	811(5)	4100(7)	2808(4)
C(2)	1282(6)	5115(7)	2390(4)
C(3)	2199(5)	5449(6)	3075(4)
C(4)	4704(4)	2131(4)	5070(4)
C(5)	5729(4)	1534(4)	5080(4)
C(6)	6482(4)	2529(4)	5098(4)
C(7)	2638(6)	3050(6)	6655(4)
C(8)	3661(6)	3748(6)	7171(4)
C(9)	−195(7)	3016(12)	5237(10)
C(10)	1554(7)	822(7)	4402(8)
C(11)	2811(8)	5866(8)	7016(6)
C(12)	4842(7)	5611(10)	7123(5)
H(1)	1(5)	353(5)	259(4)
H(2)	104(5)	545(5)	178(4)
H(3)	265(5)	604(6)	310(4)
H(4)	398(4)	173(4)	510(3)
H(5)	580(4)	60(5)	506(4)
H(6)	735(5)	255(4)	516(4)
H(7a)	277(6)	215(6)	687(5)
H(7b)	195(4)	343(5)	689(4)
H(8a)	439(5)	326(6)	701(4)
H(8b)	369(5)	379(5)	793(4)
H(9a)	−26(12)	268(11)	572(9)
H(9b)	−27(10)	356(11)	524(9)
H(9c)	−71(9)	302(10)	475(7)
H(10a)	194(7)	36(7)	508(6)
H(10b)	204(6)	82(7)	399(5)
H(10c)	108(9)	66(9)	402(7)
H(11a)	330(5)	667(6)	687(4)
H(11b)	298(6)	582(7)	767(5)
H(11c)	198(6)	542(6)	671(5)
H(12a)	502(5)	565(6)	783(4)
H(12b)	527(5)	492(6)	703(4)
H(12c)	493(9)	658(10)	672(7)

(T), libration (L), and screw (S) motion (16) using the computer program MGTLS. The rms standard error in the temperature factors σU_{ij} (derived from the least squares analysis) is 0.0030 Å^2. Analyses were successful for the 28 atom group consisting of Ga, Cu, O, N(1)–N(4), C(1)–C(7), and their symmetry related counterparts (rms ΔU_{ij} = 0.0059 Å^2) and the N(5) and Ga tetrahedra (rms ΔU_{ij} = 0.0019 and 0.0029 Å^2, respectively).

The appropriate bond distances have been corrected for libration (17, 18), using shape parameters q^2 of 0.08 for all atoms involved. Corrected bond lengths appear in Table 5 along with the uncorrected values. Changes in the bond angles were not significant; thus only the uncorrected bond angles appear in Table 6.

X-Ray film data indicate that the cobalt and nickel complexes are isomorphous with the copper complex.

Results and Discussion

The mass spectra of the binuclear transition metal complexes indicate high thermal stability. Signals due to the parent ions were observed in all cases. The major peaks in the mass spectrum of the cobalt complex (listed in Table 2[1]) provide an example of the fragmentation patterns observed. The isotopic patterns of the individual signals are in good agreement with those predicted from the isotopic distribution of metal atoms (^{69}Ga, 60%; ^{71}Ga, 40%; ^{59}Co, 100%). A further indication of the stability of the binuclear complexes is the presence of $M(N_2C_3H_3)_2M$ fragments, which can only arise after several fragmentation losses. The proton nmr spectrum of the diamagnetic zinc complex $[Me_2Ga(OCH_2CH_2NMe_2)(N_2C_3H_3)_2Zn]_2$ in C_6D_6 is consistent with a binuclear structure as found in the solid state for the copper complex. There are two unique equal intensity Ga–*Me* resonances at high field, as would be expected from the nonequivalent positions of these methyl groups in the structure. The N–*Me* resonances, although not as clearly resolved due to overlapping with the N—CH_2— signal, again occur at different positions in the spectrum as predicted from the solid state structure of the copper complex. The remainder of the spectrum was complicated by overlapping of signals but the overall integration gave the different protons in their expected intensity ratios.

The ir spectra of the four complexes are very similar and all display strong Ga—C symmetric and asymmetric stretching frequencies in the 530–540 and 570–580 cm^{-1} regions of the spectrum, respectively.

The visible spectra of the Co, Ni, and Cu complexes in benzene each consisted of one broad asymmetric absorption band. These are listed in Table 1 along with extinction coefficients. No assignment is attempted at this time but a magnetic moment study indicates that the compounds are high spin complexes. This is expected for five-coordinate complexes of this type involving N and O donor atoms (19). The cobalt complex, $[Me_2Ga(OCH_2CH_2NMe_2)(N_2C_3H_3)_2Co]_2$, gave a μ_{eff} value of 4.22 per cobalt ion at 298 K (corrected for ligand and metal diamagnetism). This is consistent with the presence of three unpaired electrons in a high spin

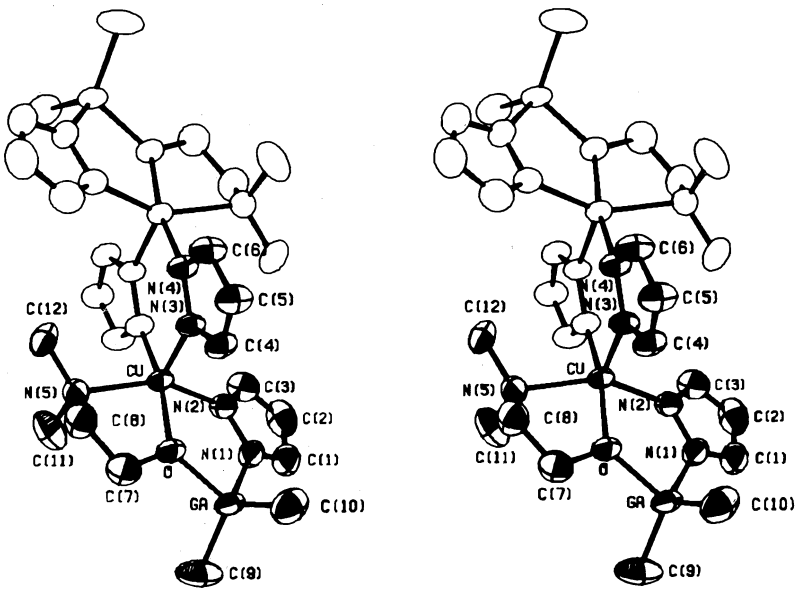

FIG. 1. A stereo view of the bis-μ-pyrazolyl(*N*(1),*N*(2))-bis[dimethyl(*N*,*N*-dimethylethanolamino)(1-pyrazolyl)gallato(*N*(2),*O*,*N*)copper(II)] molecule. Fifty percent ellipsoids are shown for the non-hydrogen atoms, hydrogen atoms are omitted for clarity.

TABLE 5. Bond lengths (Å) with estimated standard deviations in parentheses

(*a*) Non-hydrogen atoms*

	Length			Length	
Bond	Uncorr.	Corr.	Bond	Uncorr.	Corr.
Ga—O	1.902(3)	1.907	N(2)—C(3)	1.332(6)	1.332
Ga—N(1)	1.985(4)	1.991	N(3)—N(4)	1.361(4)	1.363
Ga—C(9)	1.958(7)	1.962	N(3)—C(4)	1.346(5)	1.346
Ga—C(10)	1.970(7)	1.977	N(4)—C(6)	1.350(5)	1.351
Cu—O	1.975(3)	1.981	N(5)—C(8)	1.464(6)	1.477
Cu—N(2)	2.019(4)	2.023	N(5)—C(11)	1.481(8)	1.486
Cu—N(3)	2.170(3)	2.173	N(5)—C(12)	1.473(7)	1.490
Cu—N(4)′	1.949(3)	1.953	C(1)—C(2)	1.366(9)	1.367
Cu—N(5)	2.134(4)	2.143	C(2)—C(3)	1.357(9)	1.357
O—C(7)	1.415(6)	1.420	C(4)—C(5)	1.377(6)	1.378
N(1)—N(2)	1.367(5)	1.370	C(5)—C(6)	1.371(6)	1.372
N(1)—C(1)	1.330(6)	1.330	C(7)—C(8)	1.492(8)	1.495

*Primed atoms at $1 - x$, $1 - y$, $1 - z$.

cobalt(II) ion having square pyramidal coordination geometry.

In previous studies (6–8), symmetric anionic ligands of the type $Me_2Ga(N_2C_3H_3)_2^-$ have been synthesized and their chelating properties towards transition metal ions studied. Substitution of pyrazole by a different active hydrogen compound in step 3 (see Experimental section) of the preparation of these ligands has led to a wide variety of asymmetric ligands of potentially higher denticity. The present study involves utilization of the active hydrogen compound *N*,*N*-dimethylethanolamine in step 3 of the ligand synthesis. This compound was of interest since it is known to react readily with Me_3Ga (20) to give the five-coordinate gallium complex $[Me_2NCH_2CH_2OGaMe_2]_2$, and thus should react easily with $Me_3GaN_2C_3H_3^-$ as in step 3. The ligand expected from this reaction, $[Me_2Ga(OCH_2CH_2NMe_2)(N_2C_3H_3)]^-$, may interact with transition metal ions in a number of ways as shown in **2**. The ligand may act a triden-

TABLE 6. Bond angles (deg) with estimated standard deviations in parentheses

(*a*) Non-hydrogen atoms*

Bonds	Angle (deg)	Bonds	Angle (deg)
O—Ga—N(1)	90.0(1)	Cu—N(2)—C(3)	132.4(4)
O—Ga—C(9)	111.4(4)	N(1)—N(2)—C(3)	105.9(4)
O—Ga—C(10)	108.9(3)	Cu—N(3)—N(4)	131.5(2)
N(1)—Ga—C(9)	109.2(4)	Cu—N(3)—C(4)	121.9(3)
N(1)—Ga—C(10)	111.7(3)	N(4)—N(3)—C(4)	106.5(3)
C(9)—Ga—C(10)	121.3(4)	Cu′—N(4)—N(3)	126.2(3)
O—Cu—N(2)	86.8(1)	Cu′—N(4)—C(6)	123.4(3)
O—Cu—N(3)	93.2(1)	N(3)—N(4)—C(6)	108.4(3)
O—Cu—N(4)′	166.0(1)	Cu—N(5)—C(8)	102.4(3)
O—Cu—N(5)	80.8(1)	Cu—N(5)—C(11)	109.1(4)
N(2)—Cu—N(3)	110.1(1)	Cu—N(5)—C(12)	113.4(4)
N(2)—Cu—N(4)′	92.9(1)	C(8)—N(5)—C(11)	110.5(5)
N(2)—Cu—N(5)	148.6(2)	C(8)—N(5)—C(12)	110.2(5)
N(3)—Cu—N(4)′	100.1(1)	C(11)—N(5)—C(12)	111.0(6)
N(3)—Cu—N(5)	99.4(1)	N(1)—C(1)—C(2)	109.1(5)
N(4)′—Cu—N(5)	92.4(1)	C(1)—C(2)—C(3)	105.0(5)
Ga—O—Cu	122.3(2)	N(2)—C(3)—C(2)	111.2(6)
Ga—O—C(7)	119.3(3)	N(3)—C(4)—C(5)	110.0(4)
Cu—O—C(7)	116.5(3)	C(4)—C(5)—C(6)	104.3(4)
Ga—N(1)—N(2)	119.2(3)	N(4)—C(6)—C(5)	109.8(4)
Ga—N(1)—C(1)	131.7(4)	O—C(7)—C(8)	109.4(4)
N(2)—N(1)—C(1)	108.9(4)	N(5)—C(8)—C(7)	111.1(5)
Cu—N(2)—N(1)	121.7(3)		

*Primed atoms at $1 - x, 1 - y, 1 - z$.

tate tris-chelating system, **2***a*; as a bidentate ligand to the metal atom M while coordinating back to the gallium (via the amino nitrogen atom) giving five-coordinate gallium as found in $[Me_2NCH_2CH_2OGaMe_2]_2$ (20), **2***b*; or (less likely) as a bidentate system via the pyrazolyl and amino nitrogen atoms, **2***c*. In the latter case the available lone electron pair on oxygen could then give some type of intermolecular association by donating to a second gallium atom, indicated by the dotted lines in **2***c*.

The X-ray crystallographic study of **1** (M = Cu) shows that the ligand is acting as a tridentate tris-chelating system as in **2***a* but that it is too bulky to enable accommodation of two ligands around the transition metal atom. Rather than the mononuclear complexes envisaged, the products isolated were binuclear complexes of the general formula $[Me_2Ga(OCH_2CH_2NMe_2)(N_2C_3H_3)_2M]_2$, which have two mononuclear $[Me_2Ga(OCH_2CH_2NMe_2)(N_2C_3H_3)]M$ fragments bridged by two pyrazolyl ($N_2C_3H_3$) groups. The formation of these compounds must involve decomposition of the ligand as this is the only source of pyrazolyl moieties. It is possible that once one ligand has been accommodated, a second ligand linked to the transition metal via its pyrazolyl nitrogen atom is unable to coordinate further and loses '$Me_2Ga(OCH_2CH_2NMe_2)$', which immediately forms the known dimer

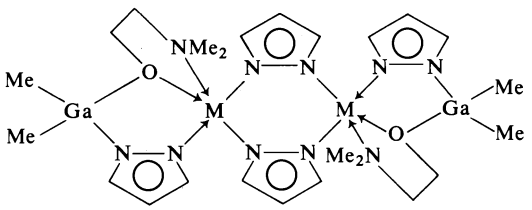

1

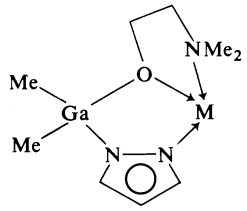

2*a*

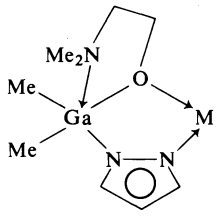

2*b*

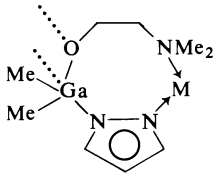

2*c*

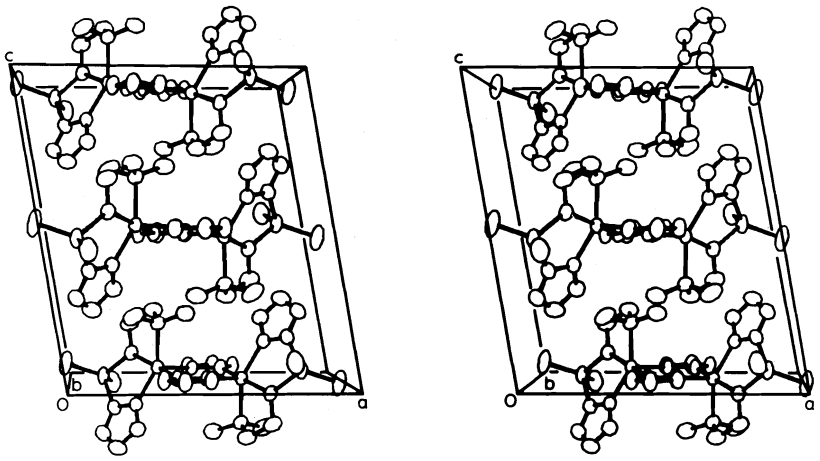

FIG. 2. The crystal structure of bis-μ-pyrazolyl(*N*(1),*N*(2))-bis[dimethyl(*N*,*N*-dimethylethanolamino)-(1-pyrazolyl)gallato(*N*(2),*O*,*N*)copper(II)] viewed along *b*.

$[Me_2NCH_2CH_2OGaMe_2]_2$ (20). This product occurred as a white residue obtained during recrystallization procedures and was identified by its characteristic mass spectrum. The resulting transition metal fragments then dimerize to give the observed binuclear transition metal products, **1**.

The crystal structure of the copper complex $[Me_2Ga(OCH_2CH_2NMe_2)(N_2C_3H_3)_2Cu]_2$ (Fig. 2) consists of discrete centrosymmetric binuclear molecules separated by normal van der Waals distances. The coordination geometry about copper in distorted square pyramidal with the copper atom displaced 0.362 Å toward the apical atom from the mean plane of the basal atoms. Three of the basal positions are occupied by the amino nitrogen, oxygen, and pyrazolyl nitrogen atoms of the tris-chelating ligand. The two remaining sites are occupied by the bridging pyrazolyl nitrogen atoms, which provide a basal atom to one copper atom and an apical atom to the second copper centre. The steric constraints imposed by ring formation are primarily responsible for distortion of the copper coordination group. The basal group itself is markedly non-planar. Bond angles at the copper atom between the apical and basal atoms range from 93.2(1) to 110.1(1)° and within the basal group *cis* angles range from 80.8(1) to 92.9(1)° while the *trans* angles are 148.6(2) and 166.0(1)°. The Cu—O and Cu—N bond lengths all lie within the normal range of distances observed for such bonds. The two basal Cu—N (pyrazolyl) distances (1.953(3) and 2.023(4) Å) are significantly different, the shorter distance being part of the less strained central $Cu_2(N_2C_3H_3)_2$ grouping, which was indicated by the mass spectrum to be a stable fragment. The apical Cu—N (pyrazolyl) bond (2.173(3) Å) is also part of this central grouping and is only 0.03 Å longer than the basal Cu—N (amino) bond (2.143(4) Å), which is lengthened by steric repulsion between the C(12) methyl group and one of the bridging pyrazolyl groups (H(12c)...N(3)′ = 2.51(9) and H(12c)...N(4)′ = 2.52(9) Å).[2]

The gallium atom has tetrahedral coordination geometry, distorted by the angle of 90.0(1)° in the five-membered chelate ring. The opposite angle, C(9)—Ga—C(10), is correspondingly expanded to 121.3(4)°. The bond lengths involving gallium are close to those in related molecules (1, 2–5, 7, 20–23).

The molecular framework consists of a system of nine fused rings, five of which are crystallographically unique. Torsion angles in the non-planar rings are listed in Table 7. The central Cu_2N_4 ring, situated about the molecular inversion centre, is significantly non-planar and has a flattened chair conformation. The Cu...Cu′ distance across this ring is 3.991(1) Å. The pyrazolyl ring that is fused to the central Cu_2N_4 ring is rigorously planar within experimental error ($\chi^2 = 0.24$) but both copper atoms are considerably displaced from the pyrazolyl mean plane (−0.1462(6) and 0.4158(6) Å for Cu and

[2]Here and elsewhere in this report primed atoms are related to those whose coordinates are listed in Table 3 by the molecular centre of symmetry at (1/2, 1/2, 1/2).

TABLE 7. Intra-annular torsion angles (deg)

Bond	Observed	Bond	Observed
Ga—O	−1.8(1)	Cu—O	−11.3(3)
O—Cu	2.2(1)	O—C(7)	−12.1(5)
Cu—N(2)	−2.0(2)	C(7)—C(8)	41.4(5)
N(2)—N(1)	1.3(3)	C(8)—N(5)	−47.4(4)
N(1)—Ga	0.2(2)	N(5)—Cu	31.4(3)
Cu—N(3)	16.8(2)		
N(3)—N(4)	−20.6(3)		
N(4)—Cu′	15.5(3)		

Cu′, respectively). As a result, the coordination about both N(3) and N(4) is significantly distorted from planarity (N(3) and N(4) are displaced 0.040(3) and 0.122(4) Å from their respective NCCu planes). The angle between normals to the mean planes of the Cu_2N_4 and N(3)N(4) pyrazolyl rings is 9.8°. The ethanolamine chelate ring (CuOC(7)C(8)N(5)) adopts a typical puckered conformation while the chelate ring (CuOGaN(1)N(2)) is nearly planar (mean and maximum deviations of atoms from the weighted least squares mean plane being 0.011 and 0.030(3) Å (for O), $\chi^2 = 136$). The $CuOGaN_2$ ring is also fused to a planar ($\chi^2 = 0.86$) pyrazolyl ring and as before the metal atoms are significantly displaced from the mean plane of the pyrazolyl ring (Cu by 0.0953(6) and Ga by 0.1313(6) Å) and the nitrogen coordination groups are not rigorously planar (N(1) being 0.041(4) Å from the GaNC plane and N(2) being 0.026(4) Å from the CuNC plane). The angle between normals to the $CuOGaN_2$ and N(1)N(2) pyrazolyl ring mean planes is 4.3°.

The trigonally coordinated oxygen atom lies 0.135(3) Å off the plane of its substituents and the Cu...Ga distance is 3.397(1) Å. The bond lengths and angles in the remainder of the molecule (see Tables 5 and 6) are generally as expected.

Acknowledgments

We thank the National Research Council of Canada for financial support and the University of British Columbia Computing Centre for assistance. We are grateful to Mr. J. Nip for mass spectra, Mr. P. Borda for C, H, N analyses, Dr. S. Chan for nmr spectra, and to Mr. R. Morrison for the magnetic susceptibility measurement.

1. D. F. RENDLE, A. STORR, and J. TROTTER. J. Chem. Soc. Dalton Trans. 2252 (1973).
2. A. ARDUINI and A. STORR. J. Chem. Soc. Dalton Trans. 503 (1974).
3. D. F. RENDLE, A. STORR, and J. TROTTER. Can. J. Chem. **53**, 2930 (1975).
4. D. F. RENDLE, A. STORR, and J. TROTTER. Can. J. Chem. **53**, 2944 (1975).
5. D. F. RENDLE, A. STORR, and J. TROTTER. J. Chem. Soc. Dalton Trans. 176 (1975).
6. F. G. HERRING, D. J. PATMORE, and A. STORR. J. Chem. Soc. Dalton Trans. 711 (1975).
7. D. J. PATMORE, D. F. RENDLE, A. STORR, and J. TROTTER. J. Chem. Soc. Dalton Trans. 718 (1975).
8. K. R. BREAKELL, D. J. PATMORE, and A. STORR. J. Chem. Soc. Dalton Trans. 749 (1975).
9. A. STORR and B. S. THOMAS. Can. J. Chem. **48**, 3667 (1970).
10. P. COPPENS, L. LEISEROWITZ, and D. RABINOVICH. Acta Crystallogr. **18**, 1035 (1965).
11. W. R. BUSING and H. A. LEVY. Acta Crystallogr. **22**, 457 (1967).
12. R. E. LONG. Ph.D. Thesis, University of California at Los Angeles, Los Angeles, CA. 1965.
13. D. T. CROMER and J. B. MANN. Acta Crystallogr. Sect. A, **24**, 321 (1968).
14. R. F. STEWART, E. R. DAVIDSON, and W. T. SIMPSON. J. Chem. Phys. **42**, 3175 (1965).
15. D. T. CROMER and D. LIBERMAN. J. Chem. Phys. **53**, 1891 (1970).
16. V. SCHOMAKER and K. N. TRUEBLOOD. Acta Crystallogr. Sect. B, **24**, 63 (1969).
17. D. W. J. CRUICKSHANK. Acta Crystallogr. **9**, 747 (1956); **9**, 754 (1956).
18. D. W. J. CRUICKSHANK. Acta Crystallogr. **14**, 896 (1961).
19. L. SACCONI. J. Chem. Soc. A, 248 (1970).
20. S. J. RETTIG, A. STORR, and J. TROTTER. Can. J. Chem. **53**, 58 (1975).
21. R. T. BAKER, S. J. RETTIG, A. STORR, and J. TROTTER. Can. J. Chem. **54**, 343 (1976).
22. S. J. RETTIG, A. STORR, and J. TROTTER. Can. J. Chem. **53**, 753 (1975).
23. K. S. CHONG, S. J. RETTIG, A. STORR, and J. TROTTER. Can. J. Chem. **55**, 2540 (1977).

L-Proline derivatives of gallium trimethyl and gallium triethyl: crystal and molecular structure of L-prolinatodimethylgallium

KENNETH R. BREAKELL, STEVEN J. RETTIG, ALAN STORR, AND JAMES TROTTER

Department of Chemistry, University of British Columbia, 2075 Wesbrook Mall, Vancouver, B.C., Canada V6T 1W5

Received July 8, 1977

KENNETH R. BREAKELL, STEVEN J. RETTIG, ALAN STORR, and JAMES TROTTER. Can. J. Chem. **55**, 4174 (1977).

Crystals of L-prolinatodimethylgallium are orthorhombic, $a = 10.624(2)$, $b = 10.567(4)$, $c = 8.2268(6)$ Å, $Z = 4$, space group $P2_12_12_1$. The structure was solved by direct methods and was refined by full-matrix least squares procedures to a final R of 0.029 and R_w of 0.035 for 1109 reflections with $I \geq 3\sigma(I)$. Details of the preparation and physical properties of L-prolinatodimethylgallium and L-prolinatodiethylgallium are given. The crystal structure of L-prolinatodimethylgallium consists of molecules each linked to two others by weak Ga—O bonds (2.695(3) Å) and N—H...O hydrogen bonds (N...O = 2.901(4) Å) to form a chain-like polymeric structure extending along the *b* axis. The gallium atom is five-coordinate and has distorted trigonal bipyramidal geometry. Important bond lengths are: Ga—O (axial), 2.044(3) and 2.695(3); Ga—N, 2.035(3); and Ga—C, 1.942(5) and 1.958(5) Å.

KENNETH R. BREAKELL, STEVEN J. RETTIG, ALAN STORR et JAMES TROTTER. Can. J. Chem. **55**, 4174 (1977).

Les cristaux du L-prolinatodiméthylgallium sont orthorhombiques, $a = 10.624(2)$, $b = 10.567(4)$, $c = 8.2268(6)$ Å, $Z = 4$, groupe d'espace $P2_12_12_1$. On a résolu la structure par des méthodes directes et on l'a affinée par la méthode des moindres carrés (matrice complète) jusqu'à une valeur finale de R de 0.029 et R_w de 0.035 pour 1109 réflexions avec $I \geq 3\sigma(I)$. On donne des détails concernant la préparation et les propriétés physiques de L-prolinatodiméthylgallium et de L-prolinatodiéthylgallium. La structure cristalline du L-prolinatodiméthylgallium est formée de molécules qui sont toutes liées avec deux autres par des liens Ga—O qui sont faibles (2.695(3) Å) et des liens hydrogènes N—H...O (N...O = 2.901(4) Å) pour former une structure en chaîne ressemblant à un polymère s'étendant le long de l'axe *b*. L'atome de gallium est pentacoordonné et possède une géométrie trigonale bipyramidale déformée. Les longueurs de liaisons importantes sont: Ga—O (axiale), 2.044(3) et 2.695(3); Ga—N, 2.035(3) et Ga—C, 1.942(5) et 1.958(5) Å.

[Traduit par le journal]

Introduction

Gallium trialkyls react readily with compounds containing 'active hydrogen', eliminating alkane to yield products containing either four- or five-coordinate gallium (1–11). These products are often associated and frequently occur as dimers. The present study involves the reaction of gallium trimethyl and gallium triethyl with the active hydrogen compound L-proline. The crystal structure of one of the products, L-prolinatodimethylgallium (**1**, R = Me), has been determined. This work is part of a continuing investigation of organogallium compounds in which the gallium atom is potentially five-coordinate.

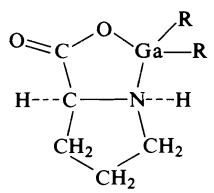

1

Experimental

All solvents were dried and distilled before use. Reactions involving gallium trialkyls were initiated in a glove box filled with dry nitrogen, with subsequent handling under a blanket of dry nitrogen or on a high vacuum line. Gallium trimethyl (12) and gallium triethyl (13) were prepared as previously described. L-Proline was used as supplied (Sigma Chemical Corporation).

L-Prolinatodimethylgallium

This compound was prepared by reacting gallium trimethyl (1.657 g, 14.44 mmol) with L-proline (1.610 g, 14.00 mmol) in refluxing benzene. The reaction mixture, initially milky in appearance, cleared as the reaction proceeded. At the completion of the reaction, when methane evolution had ceased, a clear benzene solution remained. Upon cooling this solution slowly to room temperature, large colorless crystals of the desired product were

deposited. The crystals were collected and dried. *Anal.* calcd. for $C_5H_8NO_2{\cdot}GaMe_2$: C 39.31, H 6.55, N 6.55; found: C 39.60, H 6.80, N 6.40.

L-Prolinatodiethylgallium

This compound was prepared by the reaction of gallium triethyl (2.540 g, 16.21 mmol) with L-proline (1.864 g, 16.21 mmol) in refluxing benzene. When evolution of ethane ceased, marking the completion of the reaction, the benzene solution was slowly cooled to room temperature yielding crystals of the desired product. The crystals were collected and dried. *Anal.* calcd. for $C_5H_8NO_2{\cdot}GaEt_2$: C 44.68, H 7.45, N 5.79; found: C 44.66, H 7.58, N 5.88.

Spectra

Mass spectra were recorded on a Varian MAT CH4 mass spectrometer at 70 eV with an ion source temperature of 80–100°C. Proton nmr spectra of $CDCl_3$ solutions were obtained on Varian T60 and XL100 instruments and ir spectra were recorded on a Perkin-Elmer 457 spectrophotometer as Nujol mulls.

X-ray Crystallographic Analysis of L-Prolinatodimethylgallium

The crystals chosen for study were mounted with b parallel to the goniostat axis and had dimensions of ca. 0.17 × 0.35 × 0.40 and 0.17 × 0.23 × 0.49 mm. Unit-cell and space group data were obtained from film and diffractometer measurements. The unit-cell parameters were refined by a least squares on 2 sin θ/λ values for 38 reflections measured on a diffractometer with CuK_α radiation (λ = 1.5418 Å). Crystal data (at 22°C) are:

$C_7H_{14}GaNO_2$ fw = 213.9

Orthorhombic, $a = 10.624(2)$, $b = 10.567(4)$, $c = 8.2268(6)$ Å, $V = 923.6(6)$ Å^3, $Z = 4$, $\rho_c = 1.538$ g cm^{-3}, $F(000) = 440$, $\mu(CuK_\alpha) = 40.2$ cm^{-1}. Absent reflections: $h00$, $h \neq 2n$, $0k0$, $k \neq 2n$, and $00l$, $l \neq 2n$ define uniquely the space group $P2_12_12_1$ (D_2^4, No. 19).

Intensities were measured with nickel-filtered CuK_α radiation on a Datex-automated General Electric XRD-6 diffractometer. A θ–2θ scan at 4° min^{-1} over a range of (1.80 + 0.86 tan θ) degrees in 2θ was employed. 10 s background counts were measured at each end of the scan. Data were measured to 2θ = 160°. The intensities of the check reflections, measured every 40 reflections throughout the data collection, decreased slowly and uniformly to values which were 0.94 times the initial values then dropped rapidly to 0.70 times the initial values. Data collected during the rapid drop in intensity of the check reflections were recollected using a second crystal. Intensities of the check reflections for the second crystal remained constant to within ±1% for this stage of the data collection. Lorentz and polarization corrections and batch check reflection scaling were applied, and the structure amplitudes were derived. An absorption correction was applied by a computer program using a Gaussian integration method (14, 15). Transmission factors ranged from 0.358 to 0.572 for crystal I and from 0.279 to 0.591 for crystal II. Of the 1180 independent reflections measured, 1117 (95%) had intensities greater than $3\sigma(I)$ above background where $\sigma^2(I) = S + B + (0.06S)^2$ with S = scan count and B = time averaged background count.

The structure was solved by direct methods (16, 17). All reflections with $|E| \geq 1.35$ were phased without the use of symbol phases. After tangent formula phase refinement (18) an E-map gave the positions of all 11 non-hydrogen atoms. Two cycles of full-matrix least squares refinement of the non-hydrogen atoms with isotropic temperature factors gave $R = 0.075$. Refinement with anisotropic temperature factors reduced R to 0.052. The coordinates of 10 of the 14 hydrogen atoms were determined from an electron density difference map calculated at this point. The remaining hydrogen atom positions were taken from subsequent difference maps. The entire structure (hydrogen atoms with isotropic thermal parameters) was refined for six cycles giving a final R of 0.029 and R_w of 0.035 for 1109 reflections with $I \geq 3\sigma(I)$ (8 reflections which had $|F_o| - |F_c| > 3\sigma(F)$ were treated as unobserved in the final stages of refinement; instrumental error was suspected for these reflections, but it seemed unwise to bias the data by remeasuring them; none of the disagreements were exceptionally bad). For all 1180 reflections R = 0.032 and $R_w = 0.037$.

A correction for secondary extinction was approximated by basing the least squares refinement on the minimization of $\Sigma w[|F_o| - |F_c|/(1 + gI)|]^2$ where g is the extinction parameter and I the uncorrected intensity. The final value of g was $6.2(9) \times 10^{-8}$. The scattering factors of ref. 19 were used for the non-hydrogen atoms and those of ref. 20 for the hydrogen atoms. Anomalous scattering factors from ref. 21 were used for the non-hydrogen atoms. The weighting scheme, $w = 1.0$ if $|F_o| < 20.0$, $w = (20.0/|F_o|)^2$ if $|F_o| \geq 20.0$, and $w = 0.38$ for the unobserved reflections, gave uniform average values of $w(|F_o| - |F_c|)^2$ over ranges of $|F_o|$ and was employed in the final stages of refinement.

The absolute configuration is fixed by the known chirality of the C(2) centre. As a result of coordination to gallium the proline nitrogen atom becomes chiral as well. The chirality of both centres (C(2) and N) is S. On the final cycle of refinement the mean parameter shift was 0.15σ and the largest shift (1.5σ) was associated with a hydrogen atom. The mean error in an observation of unit weight was 0.5172. A final difference map showed maximum fluctuations of ±0.75 e Å^{-3} near the gallium atom and ±0.24 e Å^{-3} elsewhere. The final positional and thermal parameters appear in Tables 1 and 2 respectively.[1] Measured and calculated structure factors have been placed in the Depository of Unpublished Data.[1]

The ellipsoids of thermal motion for the non-hydrogen atoms are shown in Fig. 1. The thermal motion has been analysed in terms of the rigid-body modes of translation (**T**), libration (**L**), and screw (**S**) motion (22) using the computer program MGTLS. The rms standard error in the temperature factors σU_{ij} (derived from the least squares analysis) is 0.0021 Å^2. Analysis of the entire molecule (rms $\Delta U_{ij} = 0.0044$ Å^2) yielded physically reasonable rigid-body parameters.

The appropriate bond distances have been corrected for libration (23, 24), using shape parameters q^2 of 0.08 for all atoms involved. Corrected bond lengths appear in Table 3 along with the uncorrected values. Corrected bond

[1]The structure factor table and Table 2 (thermal parameters) are available, at a nominal charge, from the Depository of Unpublished Data, CISTI, National Research Council of Canada, Ottawa, Ont., Canada K1A 0S2.

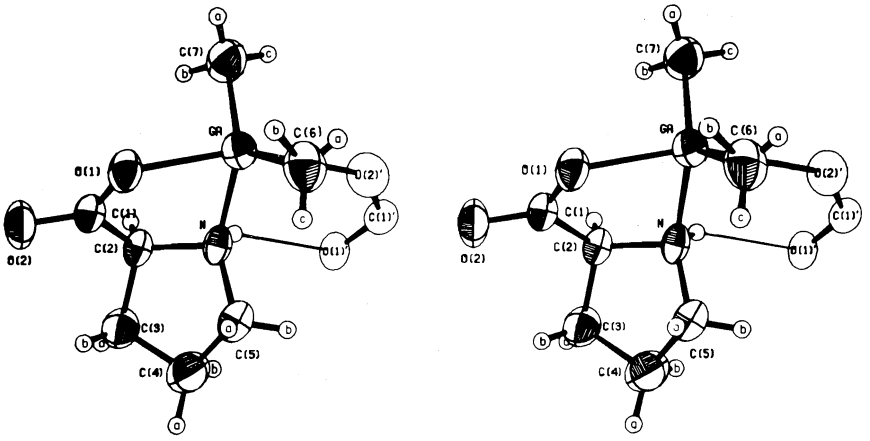

FIG. 1. A stereo view of the unique part of the L-prolinatodimethylgallium structure. Fine line represents a hydrogen bond. 50% ellipsoids are shown for the non-hydrogen atoms. Hydrogen atoms have been assigned artificially small thermal parameters for the sake of clarity.

TABLE 1. Final positional parameters (fractional × 10^4, Ga × 10^5, H × 10^3) with estimated standard deviations in parentheses

Atom	*x*	*y*	*z*
Ga	44112(5)	10881(5)	39254(6)
O(1)	5148(3)	−554(3)	3050(3)
O(2)	5954(4)	−1398(3)	808(5)
N	5554(4)	1800(3)	2177(4)
C(1)	5604(4)	−485(3)	1615(5)
C(2)	5708(4)	838(3)	871(4)
C(3)	6987(5)	1100(5)	79(6)
C(4)	7605(6)	2109(6)	1112(9)
C(5)	6857(5)	2128(4)	2664(6)
C(6)	5074(6)	1177(6)	6115(6)
C(7)	2673(5)	967(5)	3173(8)
H(N)	513(5)	233(5)	175(6)
H(2)	507(5)	94(6)	7(6)
H(3a)	714(6)	121(6)	−97(9)
H(3b)	746(8)	35(8)	30(10)
H(4a)	853(6)	203(6)	111(8)
H(4b)	735(11)	279(13)	74(17)
H(5a)	720(5)	155(6)	352(7)
H(5b)	687(6)	285(6)	325(7)
H(6a)	464(7)	143(8)	660(9)
H(6b)	492(8)	27(10)	665(10)
H(6c)	593(9)	117(8)	625(10)
H(7a)	221(6)	42(7)	371(9)
H(7b)	274(7)	67(8)	206(11)
H(7c)	215(11)	187(14)	302(15)

angles differ by less than 0.1° from the uncorrected values in Table 4.

Results and Discussion

Figure 1 shows a general view of the unique part of the structure with the crystallographic numbering scheme and Fig. 2 shows the structure viewed down the crystallographic *c* axis. Torsion angles defining the conformations of the five-membered rings are given in Table 5.

The crystal structure of L-prolinatodimethylgallium (Fig. 2) features an unusual chain-like association of monomer units extending along the *b* axis. Each molecular unit is linked to two others (related by the screw axis parallel to *b*) by two weak Ga—O bonds (2.695(3) Å) and two N—H...O(1)[$1 - x$, $1/2 + y$, $1/2 - z$] hydrogen bonds (N...O = 2.901(4), H...O = 2.27(5) Å, N—H...O = 137(4)°) to form a linear polymer which contains five-coordinate gallium atoms. Non-bonded distances between the parallel chains correspond to normal van der Waals interactions. Other five-coordinate gallium species consist of discrete molecular units; four of these are binuclear (9, 10, 25) while one is polynuclear (26) and one is mononuclear (27, 28).

The gallium atom has distorted trigonal bipyramidal coordination geometry. The equatorial positions are occupied by the nitrogen and two methyl carbon atoms and the axial sites by oxygen atoms. As in related compounds (9, 10, 25–28) the angles at the gallium atom are distorted from 'ideal' values by steric constraints imposed by chelate ring formation. The angle between axial substituents is 157.7(1)°, axial–equatorial angles range from 77.2(1) to 103.4(2)°, and the angles between the equatorial substituents range from 111.5(2) to 129.9(3)°. The gallium atom is displaced 0.2109(5) Å toward O(1) from the NC(6)C(7) plane.

The Ga—O(1) and Ga—C bond lengths are consistent with corresponding distances in the

TABLE 3. Bond lengths (Å) with estimated standard deviations in parentheses*

(*a*) Non-hydrogen atoms

Bond	Uncorr.	Corr.	Bond	Uncorr.	Corr.
Ga—N	2.027(3)	2.035	C(1)—C(2)	1.531(5)	1.538
Ga—O(2)′	2.695(3)	—	N—C(5)	1.482(6)	1.488
Ga—O(1)	2.036(3)	2.044	N—C(2)	1.488(4)	1.493
Ga—C(6)	1.936(5)	1.942	C(2)—C(3)	1.533(6)	1.538
Ga—C(7)	1.952(5)	1.958	C(3)—C(4)	1.514(8)	1.518
O(1)—C(1)	1.279(5)	1.283	C(4)—C(5)	1.505(8)	1.510
O(2)—C(1)	1.229(5)	1.232			

(*b*) Bonds involving hydrogen atoms

Bond	Length	Weighted mean
N—H	0.80(5)	—
C—H	0.67–1.11(5–14)	0.93(11)

*Primed atom at $1 - x, \frac{1}{2} + y, \frac{1}{2} - z$.

TABLE 4. Bond angles (deg) with estimated standard deviations in parentheses*

(*a*) Non-hydrogen atoms

Bonds	Angle (deg)	Bonds	Angle (deg)
O(1)—Ga—O(2)′	157.7(1)	Ga—N—C(2)	108.9(2)
O(1)—Ga—N	80.5(1)	Ga—N—C(5)	117.0(3)
O(1)—Ga—C(6)	103.4(2)	C(2)—N—C(5)	104.6(3)
O(1)—Ga—C(7)	101.3(2)	O(1)—C(1)—O(2)	124.7(4)
O(2)′—Ga—N	77.2(1)	O(1)—C(1)—C(2)	116.6(3)
O(2)′—Ga—C(6)	85.9(2)	O(2)—C(1)—C(2)	118.7(3)
O(2)′—Ga—C(7)	87.4(2)	N—C(2)—C(1)	109.1(3)
N—Ga—C(6)	115.1(2)	N—C(2)—C(3)	106.3(3)
N—Ga—C(7)	111.5(2)	C(1)—C(2)—C(3)	113.5(4)
C(6)—Ga—C(7)	129.9(3)	C(2)—C(3)—C(4)	105.8(4)
C(1)—O(1)—Ga	115.1(2)	C(3)—C(4)—C(5)	104.9(4)
Ga″—O(2)—C(1)	133.4(3)	N—C(5)—C(4)	105.1(4)

(*b*) Angles involving hydrogen atoms

Angle (deg)	Weighted mean (deg)
91–128(3–9)	109(8)

*Primed atoms at $1 - x, \frac{1}{2} + y, \frac{1}{2} - z$; double primed atom at $1 - x, y - \frac{1}{2}, \frac{1}{2} - z$.

other five-coordinate gallium structures (all of which have trigonal bipyramidal coordination geometry). The equatorial Ga—N bond (2.035(3) Å) is longer than those in $C_{24}H_{72}Ga_8N_{12}O_2$ (26) (1.949(3) and 1.999(3) Å) and the axial Ga—O(2)′ distance (2.695(3) Å) is the longest Ga—O bond yet observed. In most of the other five-coordinate gallium structures studied one of the axial bonds is relatively long, for example: Ga—O = 2.469(3) Å in the salicylaldehydatodimethylgallium dimer (10) and Ga—N = 2.779(3) Å in the polycyclic cage compound $C_{24}H_{72}Ga_8N_{12}O_2$ (26).

The conformation of the chelate ring is qualitatively equivalent to that in the related molecule L-prolinatodiphenylboron (29), the mean deviation between corresponding torsion angles being 3.3°. The steric and electronic differences between the tetrahedral boron and trigonal bipyramidal gallium complexes lead to small, but possibly significant, geometrical differences in the L-proline moieties. The C(1)—O(1) and C(1)—O(2) distances in the two complexes (1.300(3) and 1.219(3) Å for the boron and 1.283(5) and 1.232(5) Å for the gallium complex) reflect the relative weakness of the axial Ga—O(1) bond with respect to the B—O(1) bond as well as the effect of weak

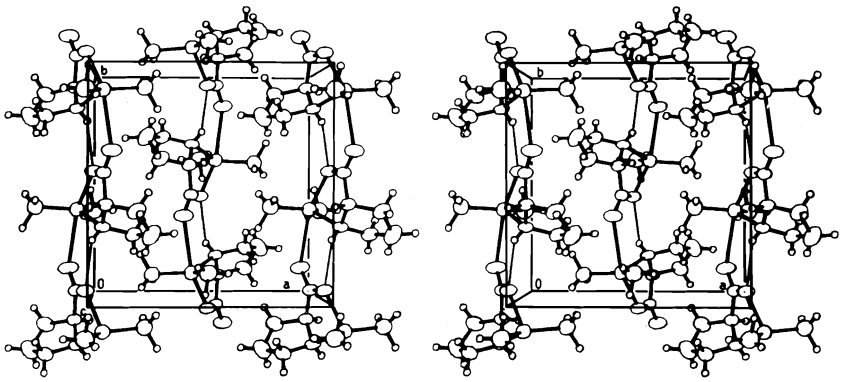

FIG. 2. The crystal structure of L-prolinatodimethylgallium viewed down *c*. Fine lines represent hydrogen bonds.

TABLE 5. Intra-annular torsion angles (deg)

Proline ring		Chelate ring	
Bond	Obs.	Bond	Obs.
N—C(2)	−27.1(4)	Ga—O(1)	−21.0(2)
C(2)—C(3)	7.2(4)	O(1)—C(1)	8.7(3)
C(3)—C(4)	15.2(5)	C(1)—C(2)	14.8(4)
C(4)—C(5)	−32.3(5)	C(2)—N	−30.2(3)
C(5)—N	37.0(4)	N—Ga	27.6(2)

coordination of the carbonyl oxygen atom, O(2), to the gallium atom.

The strongest signals in the mass spectra of the two L-prolinatodialkylgallium compounds were due to the parent ion minus one alkyl group. No signals with higher mass than the parent monomer ion were observed. In view of the weak association of monomer units in the solid (for the methyl derivative) the monomeric constitution in the gas phase is not surprising. Salicylaldehydatodimethylgallium was found to be monomeric in the gas phase but in the solid dimerizes through the formation of two weak Ga—O bonds (10). The parent monomer ion was only observed for the diethyl derivative, and then only at about 2% of the intensity of the strongest peak in the spectrum. The absence or low intensity of parent ion signals is common in this type of organogallium compound (2, 8). Other strong signals in the mass spectrum were due to $C_4H_8N{\cdot}GaR_2^+$, $C_4H_8N{\cdot}GaR^+$, GaR_2^+, Ga^+, and $C_4H_8N^+$ ions. The relative intensities of the peaks in the doublet signals of gallium containing ions agreed well with those predicted from the isotopic distribution of the metal atoms [^{69}Ga(60%), ^{71}Ga(40%)].

The proton nmr spectra of the two complexes in $CDCl_3$ solution showed similar patterns with the alkyl groups on gallium at high field and the L-prolinato proton resonances to lower field. The spectrum of L-prolinatodimethylgallium displayed the Ga–*Me* resonance as a sharp singlet, and a sharp triplet–quartet pattern was observed for the Ga–*Et* protons in L-prolinatodiethylgallium. These observations are somewhat surprising considering the different environments of the two methyl groups on gallium in the solid state structure of L-prolinatodimethylgallium.

The infrared spectra show strong Ga—C symmetric and asymmetric stretching vibrations in the 500–600 cm^{-1} region of the spectrum. In the dimethyl gallium compound these occur at 546 and 597 cm^{-1}, respectively, and in the diethyl gallium compound they are shifted to 516 and 563 cm^{-1}, respectively.

Acknowledgements

We thank the National Research Council of Canada for financial support and the University of British Columbia Computing Centre for assistance. We are grateful to Mr. J. Nip for mass spectra; Mr. P. Borda for C, H, N analyses; and Dr. S. Chan for nmr spectra.

1. A. STORR and B. S. THOMAS. J. Chem. Soc. A, 3850 (1971).
2. A. ARDUINI and A. STORR. J. Chem. Soc. Dalton Trans. 503 (1974).
3. D. F. RENDLE, A. STORR, and J. TROTTER. Can. J. Chem. **53**, 2930 (1975).
4. D. F. RENDLE, A. STORR, and J. TROTTER. Can. J. Chem. **53**, 2944 (1975).
5. K. R. BREAKELL, D. J. PATMORE, and A. STORR. J. Chem. Soc. Dalton Trans. 749 (1975).
6. D. F. RENDLE, A. STORR, and J. TROTTER. J. Chem. Soc. Dalton Trans. 176 (1975).
7. D. J. PATMORE, D. F. RENDLE, A. STORR, and J. TROTTER. J. Chem. Soc. Dalton Trans. 718 (1975).
8. R. T. BAKER, S. J. RETTIG, A. STORR, and J. TROTTER. Can. J. Chem. **54**, 343 (1976).
9. S. J. RETTIG, A. STORR, and J. TROTTER. Can. J. Chem. **53**, 58 (1975).
10. S. J. RETTIG, A. STORR, and J. TROTTER. Can. J. Chem. **54**, 1278 (1976).
11. K. S. CHONG, S. J. RETTIG, A. STORR, and J. TROTTER. Can. J. Chem. **55**, 2540 (1977).
12. A. STORR and B. S. THOMAS. Can. J. Chem. **48**, 3667 (1970).
13. A. W. LAUBENGAYER and W. F. GILLIAM. J. Am. Chem. Soc. **63**, 477 (1941).
14. P. COPPENS, L. LEISEROWITZ, and D. RABINOVICH. Acta Crystallogr. **18**, 1035 (1965).
15. W. R. BUSING and H. A. LEVY. Acta Crystallogr. **22**, 457 (1967).
16. J. KARLE and H. HAUPTMAN. Acta Crystallogr. **9**, 635 (1956).
17. J. KARLE and I. L. KARLE. Acta Crystallogr. **21**, 849 (1966).
18. M. G. B. DREW. Private communication (1969); see e.g. M. G. B. DREW, D. H. TEMPLETON, and A. ZALKIN. Acta Crystallogr. Sect. B, **25**, 261 (1969).
19. D. T. CROMER and J. B. MANN. Acta Crystallogr. Sect. A, **24**, 321 (1968).
20. R. F. STEWART, E. R. DAVIDSON, and W. T. SIMPSON. J. Chem. Phys. **42**, 3175 (1965).
21. D. T. CROMER and D. LIBERMAN. J. Chem. Phys. **53**, 1891 (1970).
22. V. SCHOMAKER and K. N. TRUEBLOOD. Acta Crystallogr. Sect. B, **24**, 63 (1969).
23. D. W. J. CRUICKSHANK. Acta Crystallogr. **9**, 747 (1956); **9**, 754 (1956).
24. D. W. J. CRUICKSHANK. Acta Crystallogr. **14**, 896 (1961).
25. S. J. RETTIG, A. STORR, and J. TROTTER. Can. J. Chem. **52**, 2206 (1974).
26. S. J. RETTIG, A. STORR, and J. TROTTER. Can. J. Chem. **53**, 753 (1975).
27. M. SHIRO and Q. FERNANDO. Anal. Chem. **43**, 1222 (1971).
28. K. DYMOCK and G. J. PALENIK. J. Chem. Soc. Chem. Commun. 884 (1973).
29. S. J. RETTIG and J. TROTTER. Can. J. Chem. **55**, 958 (1977).

The preparation and absolute configuration of *trans*-2-aminocyclopentanol enantiomers

ALEX A. BARR, IRENA FRENCEL,[1] AND J. BARRY ROBINSON[2]

Faculty of Pharmacy, University of Toronto, Toronto, Ont., Canada M5S 1A1

Received June 20, 1977

ALEX A. BARR, IRENA FRENCEL, and J. BARRY ROBINSON. Can. J. Chem. **55**, 4180 (1977).

A method is reported for the resolution of (±)-*trans*-2-benzylaminocyclopentanol using D- or L-dibenzoyltartaric acid as the resolving agent. Debenzylation of the enantiomeric bases gives the enantiomeric *trans*-2-aminocyclopentanols. These compounds have been converted to their quaternary ammonium acetate ester derivatives and the absolute configuration assigned by comparison of the ord spectra with the spectra of the appropriate cyclohexane derivatives.

ALEX A. BARR, IRENA FRENCEL et J. BARRY ROBINSON. Can. J. Chem. **55**, 4180 (1977).

On rapporte une méthode pour la résolution en antipodes optiques du (±)-benzylamino-2 cyclopentanol *trans* qui fait appel aux acides D- ou L-dibenzoyltartariques comme agent de résolution. La débenzylation des bases énantiomères conduit aux amino-2 cyclopentanols *trans* énantiomères. On a transformé ces composés en ester d'ammonium quaternaire et on a attribué leur configuration par comparaison de leur spectre ord avec les spectres des derivés appropriés de cyclohexane.

[Traduit par le journal]

Several distinct receptor types (preganglionic autonomic, postganglionic parasympathetic, somatic motor) have been identified as specific binding sites for the chemically simple molecule acetylcholine. However, the conformation of the acetylcholine molecule which becomes bound to each of these binding sites cannot currently be defined and one of the several possible approaches to this problem involves the synthesis of rigid and/or semirigid analogues of acetylcholine, of known stereochemistry, followed by evaluation of these compounds as acetylcholine-like agonists. (For a recent review, see ref. 1.)

The 1,2-disubstituted cycloalkanes of structure **1** have proved useful in such studies relating stereochemistry of the molecule to its acetylcholine-like pharmacological activity. Thus, the muscarinic agonist activity is found in the

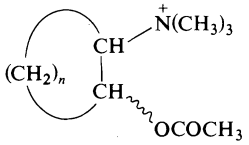

1 ($n = 1$–4)

(±)-*trans* isomers in the cyclohexane (**1**, $n = 4$) (2–4), cyclobutane (**1**, $n = 2$) (5), and cyclopropane (**1**, $n = 1$) (6–8) series. It is also the (±)-*trans* isomer which is a substrate for the enzyme acetylcholinesterase (acetylcholine hydrolase E.C. 3.1.1.7) in this series (3, 6, 9).

Within the cyclohexane and the cyclopropane series of compounds, the *trans* isomer has been resolved and both the muscarinic agonist activity and the enzyme catalyzed hydrolysis activity have been shown to be either a stereoselective (2–4) or a stereospecific phenomenon (6, 7).

Within the cyclopentyl series of compounds (**1**, $n = 3$), the relationships between stereochemistry and biological activity have not been as clearly demonstrated. An early preparation of (±)-*cis*- and (±)-*trans*-2-dimethylaminocyclopentylacetate methiodide (**1**, $n = 3$) (10) suggested that the (±)-*cis* isomer was a superior substrate for the enzyme acetylcholinesterase than either the (±)-*trans* isomer or acetylcholine. Subsequent studies of the muscarinic agonist activity among this series of compounds demonstrated the (±)-*cis* isomer to be only a weak partial agonist whereas the (±)-*trans* isomer was a more potent pure muscarinic agonist (11).

The above results stimulated a reinvestigation of the biological activity of the (±)-*cis* and (±)-*trans* isomers of the cyclopentyl series (**1**, $n = 3$). Enzyme substrate activity was found to be resident in the (±)-*trans* isomer only and we were thus further led to attempt the preparation

[1]Present address: Polish Academy of Science, Poznan, Poland.

[2]Author to whom correspondence should be addressed.

of the enantiomers of *trans*-2-dimethylaminocyclopentyl acetate methiodide and to determine the absolute configuration of each enantiomer. This study is the subject of the present communication. The biological data (enzyme activity and muscarinic agonist activity studies) will be the subject of a separate communication.

Synthesis

The preparation of (±)-*cis*- and (±)-*trans*-2-dimethylaminocyclopentyl acetate methiodide (**1**, $n = 3$) was accomplished using a previously reported method (10), the structure and stereochemistry of the products being checked, where appropriate, by infrared and proton magnetic resonance techniques. The physical properties of the products agreed well with reported literature data.

Although resolution of (±)-*trans*-2-aminocyclopentanol has been previously reported (12) using tartaric acid as the resolving agent, the requirement for performing all crystallizations at an elevated temperature was found to lead to poor control of the resolution process. In the present work, (±)-*trans*-2-benzylaminocyclopentanol was resolved using separately D- and L-dibenzoyltartaric acid. Decomposition of the stereoisomeric salts followed by hydrogenation of the extracted bases using palladium-on-charcoal gave the enantiomeric *trans*-2-aminocyclopentanols from which the enantiomeric *trans*-2-dimethylaminocyclopentyl acetate methiodides were separately prepared using conventional methods.

Absolute Configuration of the Enantiomers of *trans*-2-Dimethylaminocyclopentyl Acetate Methiodide

The absolute configuration of (−)-*cis*-2-dimethylaminocyclohexyl acetate methiodide has been previously established as (1*R*,2*S*) by unambiguous synthesis from (1*S*,2*R*)-(−)-*cis*-2-hydroxycyclohexane carboxylic acid (2). A similar method was also employed for the absolute configuration of (1*R*,2*R*)-(−)-*trans*-2-dimethylaminocyclohexyl acetate methiodide (4) and these conclusions were independently confirmed by circular dichroism studies of the cuprammonium complexes of the appropriate aminoalcohols (13).

In the present study the absolute configuration of the enantiomers of *trans*-2-dimethylaminocyclopentyl acetate methiodide was determined

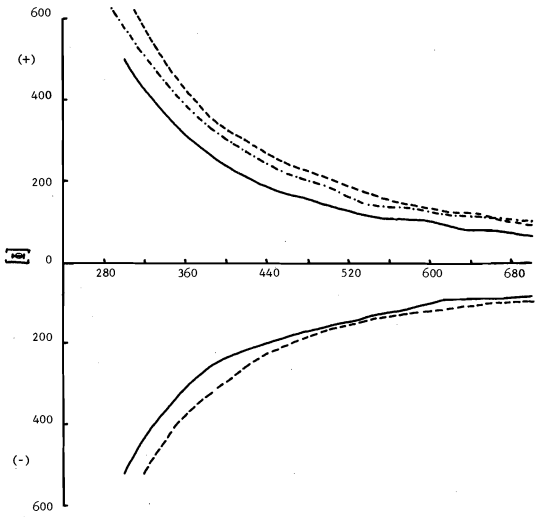

FIG. 1. Optical rotatory dispersion spectra in aqueous solution of 2-dimethylaminocycloalkyl acetate methiodide enantiomers: (—) *trans*-cyclopentyl derivatives; (--) *cis*-cyclohexyl derivatives; (-·-) *trans*-cyclohexyl derivative.

by comparison of the optical rotatory dispersion spectra of each of the enantiomers (recorded in aqueous solution between 700 and 250 nm) with the similarly recorded spectra of (1*S*,2*S*)-(+)-*trans*-, (1*R*,2*S*)-(−)-*cis*-, and (1*S*,2*R*)-(+)-*cis*-2-dimethylaminocyclohexyl acetate methiodide. Plain positive rotatory dispersion curves were shown by (1*S*,2*S*)-(+)-*trans*-2-dimethylaminocyclohexyl acetate methiodide, (1*S*,2*R*)-(+)-*cis*-2-dimethylaminocyclohexyl acetate methiodide and (+)-*trans*-2-dimethylaminocyclopentyl acetate methiodide (Fig. 1), thus indicating that they all possess the same absolute configuration at the C_1-atom (potential chromaphoric group). Thus, (+)-*trans*-2-dimethylaminocyclopentyl acetate methiodide has the (1*S*,2*S*) absolute configuration.

Experimental

All melting points were obtained using a Thomas-Hoover Uni-melt apparatus and are uncorrected. Infrared spectra were recorded on a Beckman IR-8 spectrophotometer and ^{1}Hmr spectra were recorded on a Varian T-60 spectrometer using CCl_4 as solvent and tetramethylsilane as external standard. Optical rotatory dispersion (ord) spectra were recorded on a Jasco ORD/UV-5 optical rotatory dispersion recorder. Combustion analyses were by Microanalysis Laboratory Ltd., Toronto.

(±)-2-Chlorocyclopentanone, (±)-2-dimethylaminocyclopentanone, (±)-*cis*- and (±)-*trans*-2-dimethylaminocyclopentanol, (±)-*cis*- and (±)-*trans*-2-dimethylaminocyclopentyl acetate and their methiodide salts were all prepared by known methods (10). Physical properties

were consistent with literature values and spectral properties were consistent with the proposed structures.

(±)-*cis*-2-Dimethylaminocyclopentyl acetate methiodide had mp 178.5–180°C (lit. (10) mp 177–178°C, (11) mp 176–177°C). *Anal.* calcd. for $C_{10}H_{20}INO_2$: C 38.35, H 6.44; found: C 38.4, H 6.5.

(±)-*trans*-2-Dimethylaminocyclopentyl acetate methiodide had mp 167–168°C (lit (10, 11) mp 166–167°C). *Anal.* calcd. for $C_{10}H_{20}INO_2 \cdot \frac{1}{2}H_2O$: C 37.3, H 6.5; found: C 37.25, H 6.5.

(±)-trans-2-Benzylaminocyclopentanol

To cyclopentene oxide (24.5 g) was added benzylamine (33.75 g) and water (5 ml) and the solution refluxed during 5 h. Water (50 ml) was added and the solution extracted with ether (5 × 50 ml), the extracts dried (Na_2SO_4), filtered, and evaporated. The residue was fractionally distilled, the fraction bp 110–113°C/0.1 Torr being collected. The product (33 g, 67%) crystallized on standing at room temperature overnight, mp 60–63°C; ^{1}Hmr ($CDCl_3$) δ: 7.33 (s, 5H, aromatic protons), 3.65–4.0 (m, with superimposed singlet at δ 3.8, total of 3H, C_2 methine proton and benzylic protons), 2.3–3.1 (m, 3H, C_1 methine proton, OH and NH, latter two displaced by D_2O), 1.1–2.2 (m, 6H, ring methylenes).

Resolution of (±)-trans-2-Benzylaminocyclopentanol

(±)-*trans*-2-Benzylaminocyclopentanol (54.5 g, 0.28 mol) was dissolved in absolute ethanol (300 ml) and added to a solution of dibenzoyl-D-tartaric acid monohydrate (mp 87–89°C) (113 g, 0.3 mol) in absolute ethanol (700 ml). The solution was allowed to stand at room temperature overnight and then at 4°C for a further 24 h. The crystals which deposited were collected and recrystallized three times from absolute ethanol to yield white needle crystals, mp 169–170°C; $[\alpha]_D^{20}$ −74° (*c* 0.16, ethanol), unchanged on further recrystallization. The product was dissolved in water, the solution made alkaline with KOH solution and extracted with chloroform (5 × 50 ml). The extracts were dried (Na_2SO_4), filtered, and the solvent evaporated. The residue was recrystallized from an acetone – petroleum ether (40–50°C) mixture to yield (−)-*trans*-2-benzylaminocyclopentanol (13.2 g) mp 74–75°C; $[\alpha]_D^{20}$ −52° (*c* 1.525, ethanol).

A sample of *trans*-2-benzylaminocyclopentanol enriched in the (+)-enantiomer was obtained by basification and extraction of the mother liquors from the above tartrate salt crystallizations. Reaction of this product with dibenzoyl-L-tartaric acid and crystallization as above yielded a salt, mp 169–170°C, $[\alpha]_D^{20}$ +75° (*c* 0.13, EtOH), from which (+)-*trans*-2-benzylaminocyclopentanol (7.3 g) was obtained, mp 76–77°C; $[\alpha]_D^{20}$ +59° (*c* 1.58, EtOH).

(−)-trans-2-Aminocyclopentanol

(−)-*trans*-2-Benzylaminocyclopentanol (6 g) was dissolved in ethanol (200 ml) and palladium-on-charcoal (2 g, 10%) added. The mixture was shaken over hydrogen at 20 lb/in.^{2} at room temperature until uptake of gas ceased. The reaction mixture was filtered, the filtrate acidified (HCl), and the solution evaporated to dryness under reduced pressure. The solid residue was recrystallized from an ethanol–ether mixture to yield white platelike crystals (3.5 g, 81%), mp 161–163°C; $[\alpha]_D^{20}$ −34.8° (*c* 1.6, H_2O) (lit (12) mp 155–156°C; $[\alpha]_D^{20}$ −29° (*c* 6.6, no solvent stated)). The above hydrochloride salt was dissolved in water, the solution made alkaline (KOH solution) and extracted with chloroform. The extracts were dried (Na_2SO_4), filtered, and the solvent evaporated. The residue was fractionally distilled, the fraction bp 104°C/8 Torr being collected as a viscous liquid which slowly solidified on standing; $[\alpha]_D^{20}$ −33.3° (*c* 1.7, EtOH) (lit. (12) bp 116–117°C/13 Torr; $[\alpha]_D^{20}$ −38° (concentration and solvent not stated)).

(+)-trans-2-Aminocyclopentanol

This compound was prepared in a similar manner as above but using (+)-*trans*-2-benzylaminocyclopentanol and had bp 100°C/8 Torr; $[\alpha]_D^{20}$ +36° (*c* 1.1, EtOH); hydrochloride salt, mp 160–162°C; $[\alpha]_D^{20}$ +32.2° (*c* 0.9, H_2O) (lit. (12) bp 116–117°C/13 Torr; $[\alpha]_D^{20}$ +38° (*c* 5.5, solvent not stated); hydrochloride salt, mp 155–156°C; $[\alpha]_D^{20}$ +29.3° (*c* 6.6, solvent not stated)).

(−)-trans-2-Dimethylaminocyclopentanol

(−)-*trans*-2-Aminocyclopentanol (2.75 g) was dissolved in formic acid (20 ml, 98%) and formaldehyde (20 ml, 40%) added and the solution warmed on a steam bath overnight. The reaction mixture was cooled, acidified with HCl, and concentrated to half volume under reduced pressure. The mixture was made alkaline (NaOH, 20% w/v) and continuously extracted with chloroform. The extracts were dried (Na_2SO_4), filtered, and the solvent evaporated. The residue was distilled, the fraction bp 90–93°C/10 Torr being collected (2 g); $[\alpha]_D^{20}$ —37°C (*c* 1.1 EtOH); ir and ^{1}Hmr spectra were identical to those of an authentic sample of (±)-*trans*-2-dimethylaminocyclopentanol.

(+)-trans-2-Dimethylaminocyclopentanol

The material was prepared in a similar manner from (+)-*trans*-2-aminocyclopentanol and had bp 90–93°C/10 Torr, $[\alpha]_D^{20}$ +40.5° (*c* 0.8, EtOH), and ir and ^{1}Hmr spectra identical to those of an authentic sample of the racemate.

(−)-trans-2-Dimethylaminocyclopentyl Acetate

This was prepared from (−)-*trans*-2-dimethylaminocyclopentanol by the method reported for the cyclohexane analogue (2). The product had bp 83–86°C/15 Torr, $[\alpha]_D^{20}$ −37.7° (*c* 0.76, EtOH), and spectral characteristics identical to those of the racemate.

(+)-trans-2-Dimethylaminocyclopentyl Acetate

This compound was prepared in a similar manner as above but using (+)-*trans*-2-dimethylaminocyclopentanol and had bp 83–85°C/15 Torr, $[\alpha]_D^{20}$ +43° (*c* 0.7, EtOH), and spectral characteristics identical to the racemate.

(−)-trans-2-Dimethylaminocyclopentyl Acetate Methiodide

Prepared from (−)-*trans*-2-dimethylaminocyclopentyl acetate by the method reported for the cyclohexane analogue (2), the product had mp 203–205°C. $[\alpha]_D^{20}$ −29.4° (*c* 0.61, EtOH). *Anal.* calcd. for $C_{10}H_{20}INO_2$: C 38.35, H 6.44; found: C 38.33, H 6.29.

(+)-trans-2-Dimethylaminocyclopentyl Acetate Methiodide

Prepared in a similar manner as above but using (+)-*trans*-2-dimethylaminocyclopentyl acetate, the product had mp 202–205°C, $[\alpha]_D^{20}$ +28° (*c* 1.14, EtOH). *Anal.* calcd. for $C_{10}H_{20}INO_2$: C 38.35, H 6.44; found: C 38.28, H 6.26.

Optical Rotatory Dispersion Spectra

The ord spectra of the quaternary ammonium ester salts (Fig. 1) were recorded in aqueous solution (approximately 5% w/v) using 1 cm path length cells.

Acknowledgments

The authors acknowledge the support of this project by the Medical Research Council of Canada, Grant MA-4033.

1. A. F. CASY. Prog. Med. Chem. **11**, 1 (1975).
2. J. B. KAY and J. B. ROBINSON. J. Chem. Soc. C, 248 (1969).
3. J. B. KAY, J. B. ROBINSON, B. COX, and D. POLKONJAK. J. Pharm. Pharmacol. **22**, 214 (1970).
4. J. B. ROBINSON. J. Pharm. Pharmacol. **22**, 222 (1970).
5. J. G. CANNON, T. LEE, V. SANKARAN, and J. P. LONG. J. Med. Chem. **18**, 1027 (1975).
6. C. Y. CHIOU, J. P. LONG, J. G. CANNON, and P. D. ARMSTRONG. J. Pharmacol. Exp. Ther. **166**, 243 (1969).
7. P. D. ARMSTRONG and J. G. CANNON. J. Med. Chem. **13**, 1037 (1970).
8. C. CHOTHIA and P. PAULING. Nature, **226**, 541 (1970).
9. J. B. ROBINSON. Can. J. Pharm. Sci. **11**, 112 (1976).
10. S. L. FRIESS and H. D. BALDRIDGE. J. Am. Chem. Soc. **78**, 2482 (1956).
11. G. LAMBRECHT. Cyclische Acetylcholine-Analoga. European University Papers, Series VIII, Div. A, Pharmacy, Vol. 4. H. Lang, Bern. 1974.
12. M. GODCHOT and M. MOUSSERON. Bull. Soc. Chim. Fr. **51**, 1270 (1932).
13. S. T. K. BUKHARI, R. D. GUTHRIE, A. I. SCOTT, and A. D. WRIXON. Tetrahedron, **26**, 3653 (1970).

^{13}C magnetic resonance studies 70.[1] The behavior of bicyclo[2.2.2]octenone under strongly basic conditions. A competition between retro Diels–Alder and Haller–Bauer cleavages

A. K. CHENG AND J. B. STOTHERS

Department of Chemistry, University of Western Ontario, London, Ont., Canada N6A 5B7

Received June 17, 1977

A. K. CHENG and J. B. STOTHERS. Can. J. Chem. **55**, 4184 (1977).

As a test for possible competitive α- and β-enolization in bicyclic ketones the behavior of bicyclo[2.2.2]octenone in *t*-BuO$^-$–*t*-BuOH at 185°C has been examined. The major reaction (~90%) involves Claisen condensation followed by retro Diels–Alder elimination of ethylene and Haller–Bauer cleavage. All acidic and phenolic components, accounting for 90% of the product, have been identified and characterized, primarily by their ^{13}Cmr spectra.

A. K. CHENG et J. B. STOTHERS. Can. J. Chem. **55**, 4184 (1977).

Afin de développer une méthode permettant d'évaluer des énolisations α et β en compétition dans les systèmes de cétones bicycliques, on a examiné le comportement de la bicyclo[2.2.2]-octénone en présence de *t*-BuO$^-$/*t*-BuOH à 185°C. La réaction principale (~90%) implique une condensation de Claisen suivie par une réaction de rétro Diels–Alder provoquant l'élimination d'éthylène et une coupure de Haller–Bauer. On a identifié et caractérisé tous les composants acides et phénoliques qui représentent 90% des produits; cette identification a été principalement effectuée par rmn du ^{13}C.

[Traduit par le journal]

It is well-established that proton abstraction from ketones can occur at positions more remote from the carbonyl group than the α-carbons to generate β-enolates in a variety of systems (1–3) and even γ-enolates in a few cases (1*a*, 4). Such enolates are potentially useful for synthesis since skeletal rearrangements can occur by protonation at sites other than that of the initial proton abstraction. It is therefore of interest to define the scope and limitations of these β- and γ-enolizations more precisely. One particular feature which merits attention is the possibility of remote enolization competing with α-enolate formation since a successful competition would enhance the synthetic utility of the former significantly. With few exceptions, the generation of β- and γ-enolates has been investigated with systems either lacking α-protons or having α-protons at bridgeheads thus generally rendering enolization difficult if not precluding it because of Bredt's rule. A notable exception is the isocamphanone–camphor system (1*a*) for which it was found that β-enolization dominated in terms of product composition since the α-enolates which are undoubtedly formed did not undergo Claisen condensation or other side reactions to appreciable extents; ketone recoveries were ~80%. Similarly β-enolization dominates in the cases of the bicyclo[3.2.1]octanones (3, 4*c*, 5); although these α-enolize at bridgehead carbons the resulting α-enolates are hindered, as are the available carbonyl sites and Claisen condensation was not observed (3, 4*c*, 5). From these earlier studies, we have shown that the α,α-dimethyl derivatives of bicyclo[2.2.2]octanone and bicyclo-[3.2.1]octan-6-one are interconvertible via β-enolization (3, 5) albeit very slowly. However, the corresponding derivatives of bicyclo[2.2.2]octenone (**1**), bicyclo[3.2.1]oct-2-en-6-one, and its Δ^3 isomer are readily isomerized (5) under typical β-enolization conditions, *t*-BuO$^-$–*t*-BuOH, 185°C. Since the half-life for equilibration of the latter ketones is a few hours, it was felt that this system would be suitable for examination of competitive α- and β-enolization. Since the [3.2.1] skeleton was expected to be the more stable from our results for the α,α-dimethyl derivatives (5), **1** was chosen for study and we wish to present the results in this paper. The major path involved Claisen condensation followed by retro Diels–Alder and Haller–Bauer cleavage. These products were identified largely by ^{13}Cmr spectroscopy; these data are presented and discussed.

Experimental

The general procedure described previously (3) was

[1]For part 69 see ref. 8.

employed for the reaction of **1** (6) but the nature of the reaction products necessitated changes in the work-up. After cooling, the individual reaction tubes were opened and the contents poured into water and ether. The ethereal layer was extracted 5 times with 20% sodium hydroxide solution and all aqueous solutions were combined. After acidification, the acidic reaction products were extracted with methylene chloride and the methylene chloride aliquots were combined and reextracted with 10% sodium carbonate solution. Acidification of the latter afforded the carboxylic acid products. A pure sample of the major component of this mixture was obtained by recrystallization from pentane–ether, mp 125–126°C. While the majority of the phenolic product was isolated by evaporation of the methylene chloride solution, some phenol was also present in the original 'neutral' mixture obtained by evaporation of the ether solvent. Gas chromatographic (gc) analyses were done with FFAP or diethylene glycol succinate (DEGS) columns. Preliminary gc analysis of the carboxylic acid fraction indicated that examination of these components as their methyl esters would be better. Consequently the total carboxylic acid fraction was esterified with diazomethane in the usual fashion. Analysis with FFAP columns revealed the presence of three major components in a ratio of 20:4:1; these were readily separated by preparative gc. The individual esters were characterized by their ir, uv, mass, ^{1}H, and ^{13}C spectra. Similarly, the products obtained by hydrogenation over PtO_2 and over Pd/C were identified and characterized. Hydrolyses to the parent carboxylic acids were also carried out in most cases. Precise mass measurements were obtained for most of these esters and acids. The phenolic product was a single compound, mp 56.5–57.5°C, and was found to be identical with authentic 2-phenylphenol by mixture melting point, ir, mass, ^{1}H, and ^{13}C spectra; ^{13}Cmr ($CDCl_3$) δ: 152.4(C-1), 128.2(C-2), 130.3(C-3), 120.8(C-4), 129.1(C-5), 115.9(C-6), 137.2(C-1, phenyl) 129.1(C-2, 3, 5, 6, phenyl), 127.7(C-4, phenyl). The neutral fraction, constituting $<10\%$ of the total product, was found to contain at least seven components on a DEGS column. One of these, present in distinctly larger amount than the others, exhibited the same retention time as **1**. Complete extraction of 2-phenylphenol from the neutral fraction was never realized but its retention time on the DEGS column was very long, more than 2 h longer than those of the other components. The combined yield of the isolated carboxylic acids and phenol was ca. 75%.

Hydrogenation Experiments

In an initial experiment, a pure sample of the major carboxylic acid (100 mg) was dissolved in ether containing PtO_2 (40 mg) and hydrogenated at 4 atm for 4 h. Proton and ^{13}C spectra showed the absence of olefinic and aromatic unsaturation in the product, while gc analysis on a 10% FFAP column after esterification revealed the presence of two components in essentially equal amounts. These were subsequently shown to be the methyl esters of the 4-cyclohexylmethylcyclohexanecarboxylic acids. An analogous hydrogenation using Pd/C was found to be much slower, but with the methyl ester of the major carboxylic acid (90 mg) in methanol containing 10% Pd/C (20 mg) hydrogenation occurred at 1 atm in 19 h to afford a 60:40 mixture of two compounds subsequently identified as the methyl esters of the 4-benzylcyclohexanecarboxylic acids **6** and **7**. After separation of these esters by gc on a 15% FFAP column, each was hydrolyzed to the parent acid by refluxing in 12% aqueous sodium hydroxide solution overnight. Acid **6** whose ester had the shorter retention time, melted at 93.5–94.5°C. Precise mass calcd. for $C_{14}H_{18}O_2$: 218.1306; found: 218.1311. Acid **7** melted at 87–8°C (lit. (7) 79–80°C); precise mass found: 218.1310. Similar hydrogenation experiments with the total acid product, after esterification, afforded the same two materials, establishing the isomeric nature of the three acids.

Spectra

The ^{13}C spectra were obtained with a Varian XL-100-15 system operating in the Fourier transform mode at 25.2 MHz with square-wave modulated decoupling or single frequency off-resonance decoupling at 100 MHz. The samples were examined as 5–10% (w/v) solutions in $CDCl_3$ and the data have an estimated precision of ± 0.05 ppm. Proton spectra were recorded with Varian T60 and XL-100 instruments using the same solutions.

Results

Preliminary experiments using our usual isolation procedure (3) quickly revealed the necessity for modifications. Initially the neutral fractions were relatively small indicating the presence of substantial proportions of acidic products. Acidification of the aqueous alkaline layer followed by methylene chloride extraction gave a product containing two major fractions with markedly different retention times on gc analysis. These were readily separated by reextraction of the methylene chloride solution with sodium carbonate solution. Evaporation of the methylene chloride furnished a low melting solid **2** (mp 56–57°C) which exhibited only sp^2 absorption in its ^{13}Cmr spectrum. Its precise mass, 170.0727, compared favorably with that calculated for $C_{12}H_{12}O$, 170.0731, and its infrared spectrum indicated the presence of hydroxyl absorption. Comparison of its physical properties (ir, ^{1}Hmr, ^{13}Cmr) and gc analysis with those for authentic 2-phenylphenol showed **2** to be identical with the latter.

The acidic product, soluble in Na_2CO_3 solution, was found by gc analysis to contain three components; samples of the major acid were isolated by recrystallization from pentane–ether. This acid (**3**) was examined by nmr spectroscopy. Its proton spectrum contained a complex multiplet centred at 7.2 ppm arising from six nuclei. The characteristic carboxyl proton absorption was evident at 10.40 ppm and a doublet due to two protons appeared at 2.61 ppm ($J \sim 7$ Hz). The infrared spectrum exhibited absorption characteristic of carboxylic acids and of aryl

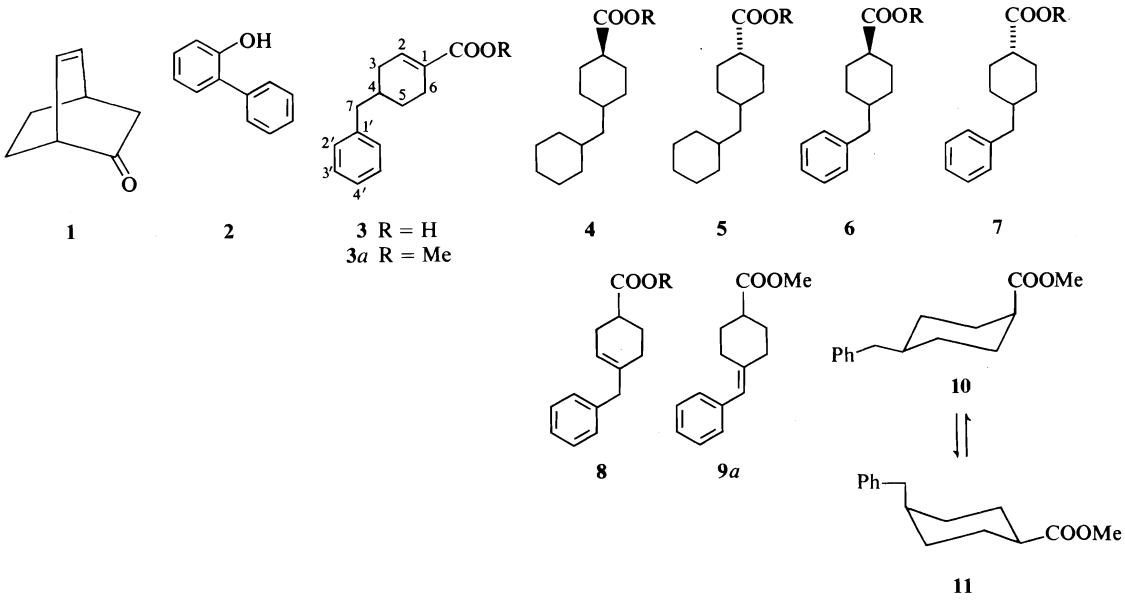

rings, with the carbonyl absorption at 1675 cm^{-1}. The ^{13}C spectrum exhibited signals typical of a phenyl group: 140.3(C-1), 129.1(C-2, 6), 128.3 (C-3, 5), and 126.0(C-4) ppm as well as the signals for a trisubstituted double bond: 141.7(CH) and 129.8 ppm. The carbonyl absorption appeared at 172.9 ppm. In the higher field region, methylene signals occurred at 23.7, 27.9, 32.3, and 42.4 ppm with a lone methine signal at 34.5 ppm. These data are consistent with the formulation of acid **3** as 4-benzylcyclohexene-1-carboxylic acid and a precise mass determination of 216.1133 agreed nicely with that calculated for $C_{14}H_{16}O_2$, 216.1149. Esterification with diazomethane furnished the methyl ester (**3***a*) which exhibited a similar ^{13}Cmr spectrum to that for **3** and its carbonyl absorption in the infrared occurred at 1705 cm^{-1}.

Preliminary attempts to hydrogenate the double bond of **3** over PtO_2 yielded a product totally lacking aryl and olefinic absorption in the ^1H and ^{13}C spectra. Esterification with diazomethane followed by gc analysis showed this product to contain two components in approximately equal amounts which were separable by preparative gc. Both esters **4***a* and **5***a* exhibited nine saturated carbon signals, four of which had twice the intensity of the others, in addition to the carbonyl and methoxyl absorptions near 176 and 51 ppm, respectively. The shieldings of ester **4***a*, having the shorter retention time, tended to be higher than those for **5***a*. The presence of four equivalent pairs of carbons confirmed that these esters contained a plane of symmetry. With Pd/C as catalyst, the hydrogenation of **3** proceeded sluggishly whereas with **3***a* a smooth conversion to a 2:3 mixture of two nonconjugated esters (**6***a*, **7***a*) was realized. These esters, after isolation by preparative gc, exhibited carbonyl absorption at 1727 and 1720 cm^{-1}, respectively, and both gave ^{13}C spectra containing signals characteristic of a phenyl group, a COOMe function, and five saturated carbon peaks, two of which had twice the intensity of the other three. As before, ester **6***a* with the shorter retention time had the somewhat more shielded carbon nuclei. Hydrolysis of each of these esters furnished samples of the corresponding acids as crystalline compounds. Acid **6** melted at 93–94°C while **7** melted at 87–88°C. The melting point for *trans*-4-benzylcyclohexanecarboxylic acid (**7**) has been reported (6) as 79–80°C but the earlier work did not describe a rigorous purification. We conclude that the earlier value refers to a sample contaminated with a small amount of the *cis* isomer **6**.

With these results in hand, attention was turned to characterization of the mixture of acids isolated by extraction with Na_2CO_3 solution. Initially, the mother liquors depleted in **3** were examined. Esterification with diazomethane furnished a mixture of three esters having distinctly different retention times upon gc analysis; that with the longest time was **3***a*. Hydrogenation of the mixture over PtO_2 and Pd/C gave the same

products as those found from the experiments with **3***a*. Thus the two unknown compounds differ from **3***a* only in the location of the double bond. Ester **8***a*, having the shortest retention time, exhibited carbonyl absorption at 1725 cm^{-1} in the infrared and λ_{max} of 250 nm (ε = 180) in the ultraviolet. The latter may be compared with the values of 260 nm (210) found for **3***a*. The ^{13}C spectrum of **8***a* contained, in addition to the phenyl and COOMe signals, those for a trisubstituted double bond, 121.1(CH) and 137.0 ppm, four methylene signals, 25.5, 27.3, 27.8, and 44.2 ppm, and a lone methine carbon at 39.3 ppm. These data indicate **8***a* to be the methyl ester of 1-benzylcyclohexene-4-carboxylic acid. This is supported by the appearance of a two-proton singlet at 3.20 ppm in the proton spectrum of **8***a* ascribable to a methylene group which is allylic and benzylic. The ^{13}C methylene signal at 44.2 ppm also strongly suggests the presence of a benzylic methylene carbon, tending to rule out the remaining double bond isomer having a trisubstituted olefinic bond. The third carboxylic acid (**9**) was found to be the latter isomer on the basis of the following observations. For the methyl ester in the ultraviolet spectrum, λ_{max} was 290 nm (400) and the proton spectrum contained, in addition to a five-proton multiplet at 7.20 ppm for the phenyl ring, a one-proton singlet at 6.23 ppm. These features are consistent with a styryl fragment. As in the cases of **3***a* and **8***a*, the ^{13}C spectrum for **9***a* consisted of four phenyl signals, those for a trisubstituted double bond, 123.3 (CH) and 138.0 ppm, four methylene signals, 27.8, 29.7, 30.4, and 35.8 ppm, and a methine carbon absorbing at 42.9 ppm. The absence of a methylene carbon near 44 ppm is good evidence against the presence of a benzylic methylene group. Thus the structures of the carboxylic acid products are **3**, **8**, and **9**. Precise mass measurements for all of the esters described above were obtained as well as the ^{13}C spectra. These data are tabulated in Table 1 together with the corresponding results for most of the carboxylic acids.

A series of runs for 5, 20, and 40 h reaction times were carried out and the product distribution was assessed by gc analysis. The product for the longer intervals was essentially unchanged from the results obtained for the shortest reaction periods. At least 90% of the product was in the acidic fractions with the total carboxylic acid fraction equal to the yield of phenol **2**. The neutral fraction constituted less than 10% of the

TABLE 1. ^{13}C shieldings[a] and precise mass measurements for acids and esters **3**–**9**

Cpd.	C-1	C-2	C-3	C-4	C-5	C-6	C-7	C-1′	C-2′	C-3′	C-4′	CO	OMe	Precise mass	
														Calcd.	Obsd.
3	129.8	141.7	32.3	34.5	23.7	27.9	42.4	140.3	129.1	128.3	126.0	172.9		216.1149	216.1133
3*a*	130.1	138.9	32.1	34.6	24.0	28.0	42.4	140.4	129.1	128.3	125.9	167.8	51.5	230.1305	230.1307
4	40.6	26.1	29.8	(32.4)	29.8	26.1	43.2	(34.5)	33.8	26.5	26.8	182.3		224.1775	224.1775
4*a*	40.7	26.2	29.8	(32.2)	29.8	26.2	43.0	(34.6)	33.7	26.5	26.8	175.9	51.4	238.1931	238.1938
5	43.5	28.9	32.6	(29.8)	32.6	28.9	45.3	(34.7)	33.8	26.5	26.8	182.9			
5*a*	43.6	29.1	32.7	(29.7)	32.7	29.1	45.3	(34.4)	33.7	26.4	26.8	176.6	51.4	238.1931	238.1935
6	40.3	26.0	29.1	38.0	29.1	26.0	42.0	141.1	129.1	128.2	125.7	182.2		218.1305	218.1306
6*a*	40.4	26.2	29.2	37.9	29.2	26.2	41.9	141.2	129.1	128.1	125.7	175.9	51.4	232.1462	232.1461
7	43.2	28.7	31.9	38.9	31.9	28.7	43.7	140.7	129.1	128.1	125.8	182.8			
7*a*	43.4	29.0	32.1	39.0	32.1	29.0	43.8	140.8	129.2	128.2	125.8	176.6	51.5	232.1462	232.1460
8	39.2	(27.2)	120.8	137.1	(27.5)	25.3	44.1	140.3	128.9	128.3	126.0	182.6			
8*a*	39.3	(27.3)	121.1	137.0	(27.8)	25.5	44.2	140.3	128.9	128.3	126.0	176.4	51.6	230.1305	230.1308
9*a*[b]	42.9	(29.7)	30.4	138.0	35.8	(27.8)	123.3	140.8	128.9	128.1	126.1	175.8	51.6		230.1310

[a]In ppm from internal TMS for $CDCl_3$ solutions; values in parentheses may be interchanged. For ease of comparison the numbering scheme shown for **3** has been followed.
[b]Carbon-3 is taken *cis* with respect to the phenyl ring.

material and was found to contain at least seven components by gc analysis. The three carboxylic acids were produced in a ratio of approximately 20:4:1 for **3**, **8**, and **9**, respectively. Although traces of a fourth acidic component constituting $<1\%$ of the acid fraction were detected by gc, this material was not isolated.

Discussion

The assignments for individual carbons listed in Table 1 follow from straightforward considerations. The carboxyl and methoxyl signals appear in characteristic regions while the phenyl absorptions are similarly readily identified, although the assignments for the *ortho* and *meta* carbons may be interchanged. The upfield shift for the carboxyl carbon in **3** relative to the others is a clear indication of its conjugated nature. The lack of a benzylic methylene signal in the spectrum of **9***a* near 44 ppm has already been noted as strong support for the assigned structure rather than that for the isomeric **8***a*. The slightly increased shieldings found for **4***a* vs. **5***a* and **6***a* vs. **7***a* point to the stereochemical assignments of *cis* vs. *trans*. In these cases, the *trans* isomers exist essentially as single conformations with both substituents in equatorial orientations. However, the *cis* isomers populate two axial–equatorial conformers, e.g. **10** and **11** for **6***a* but **10** should predominate since the conformational free energy of the carbomethoxyl group is smaller than that expected for the benzyl group, or, for **4***a*, the cyclohexylmethyl group. For **7***a*, the less shielded of the two methine carbon signals was assigned to C-1 because of its similarity to the corresponding signals in the spectra of methyl cyclohexanecarboxylate and its *trans*-4-*t*-butyl derivative, i.e. 43.4 vs. 43.1 and 43.4 ppm, respectively. Similar considerations led to the distinction between the C-2 and C-3 signals for **7***a*. In the *cis* isomer **6***a* each of these nuclei is expected to absorb at higher field because of the axial substituents and the listed assignments follow this reasoning. For **4** and **5**, as well as the corresponding methyl esters, specific methylene assignments presented a greater problem. For **5** and **5***a*, comparisons with the results for **7** and **7***a* pointed to the listed assignments for C-2(6) and C-3(5). For the *cis* isomers **4** and **4***a* these centres would be expected to be shielded. Some support for these methylene carbon assignments for the disubstituted cyclohexane ring is provided by the occurrence of two methylene signals, each due to two carbons, at 26.5 and 33.7 ppm in the spectra of **4**, **4***a*, **5**, and **5***a*; these are most readily assigned to C-3′(5′) and C-2′(6′) respectively, in the monosubstituted cyclohexane ring. These carbons may be expected to be essentially independent of the orientation of the cyclohexylmethyl group in these isomers. The assignments for C-3 and -5 for **9***a* followed from the fact that C-3, *cis* with respect to the phenyl ring, will be the more shielded, but the C-2 and -6 signals cannot be unequivocally distinguished.

The generation of the products obtained upon treatment of **1** with *t*-BuO^-–*t*-BuOH at 185°C is readily explained as shown in Scheme 1. The Claisen product **12** can reversibly dehydrate to **13** which will be in equilibrium with minor amounts of **14**. (Only one of the possible four isomers of **13** is included in the scheme for simplicity.) Irreversible loss of ethylene in a retro Diels–Alder reaction leads to **15**, the enol form of which can undergo a second retro Diels–Alder loss of ethylene to produce **2**. Hydroxide ion, formed from the dehydration step, attacking the carbonyl group of **15** leads to **16** with Haller–Bauer cleavage to generate **17** irreversibly. From the product distribution, **15** is partitioned approximately equally to **2** and **17**. Double bond migration to **3** is strongly favored by the formation of the conjugated system. Although **9** is also conjugated, it was found to be the minor component in the carboxylic acid mixture presumably because of steric destabilization arising from the close approach of the phenyl ring to the C-3 methylene group in a planar conjugated arrangement. Because of the symmetry of the system, **8** can be generated in two ways, increasing its probability of formation. Since the proportions of the three acids are independent of reaction time the observed ratios must represent the equilibrium concentrations. Presumably trace quantities of **17** may be present, as suggested by a small unidentified peak in gas chromatograms of the acid fraction.

Clearly Claisen condensation occurs readily in this system. Although this could be anticipated, the condensation is a series of equilibria and β-enolization of **1** to the more stable [3.2.1] skeleton could indeed occur in competition. The retro Diels–Alder process, however, is irreversible and clearly upsets the condensation equilibria by generating **15**. It follows, therefore, that β-

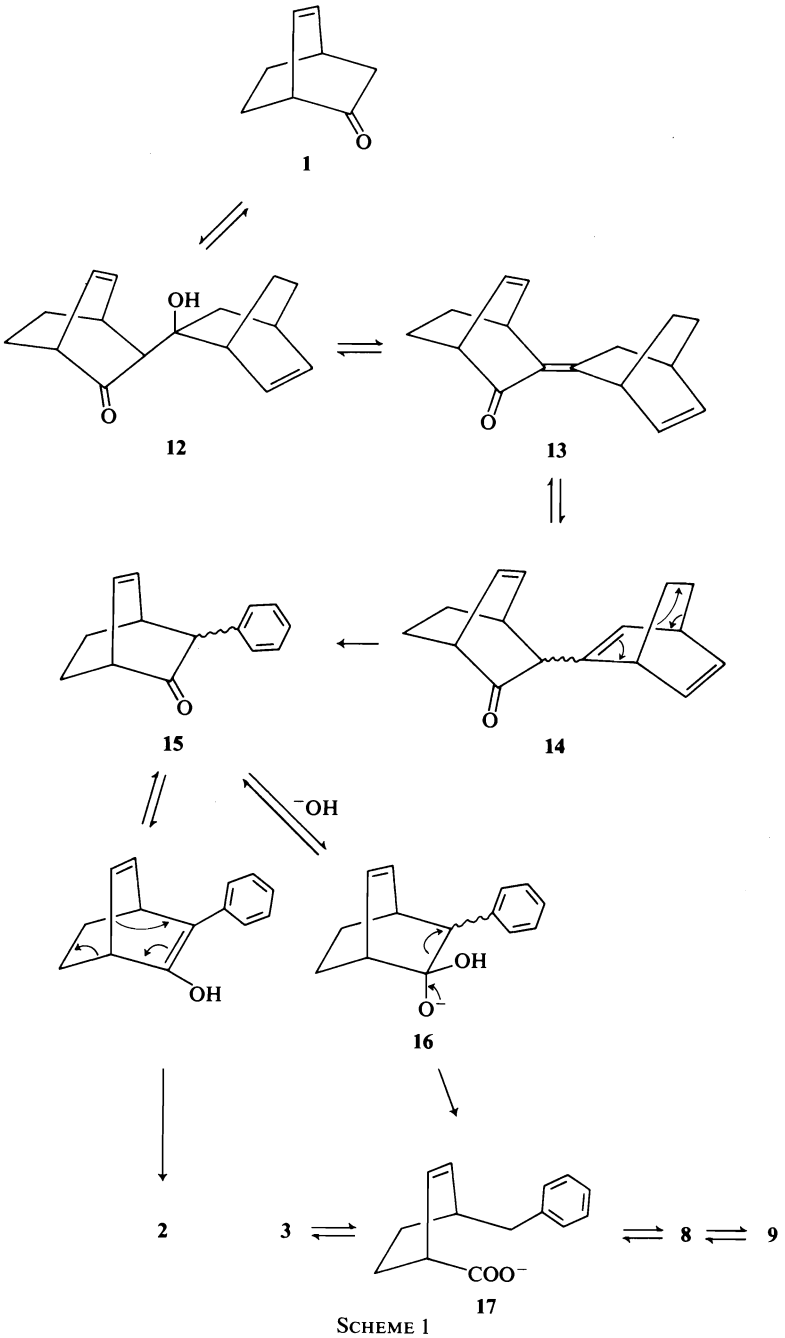

SCHEME 1

enolization is much slower and the retro Diels–Alder reaction removes **1** from the reaction mixture too rapidly for significant rearrangement via a β-enolate. Since, with few exceptions, the retro Diels–Alder process requires elevated temperatures, a successful competition between α- and β-enolization may be realized at significantly lower temperatures. Experiments to test this suggestion are under investigation.

Acknowledgements

We are grateful to the National Research

Council of Canada for financial support of this study and to Ms. Marlene Brown and D. Hairsine for technical assistance. We wish to thank Professor D. H. Hunter for valuable discussions.

1. (*a*) A. NICKON, J. L. LAMBERT, J. E. OLIVER, D. F. COVEY, and J. MORGAN. J. Am. Chem. Soc. **98**, 2593 (1976); (*b*) references cited therein.
2. M. B. RAMPERSAD and J. B. STOTHERS. J. Chem. Soc. Chem. Commun. 709 (1976).
3. A. K. CHENG, J. B. STOTHERS, and C. T. TAN. Can. J. Chem. **55**, 447 (1977).
4. (*a*) R. HOWE and S. WINSTEIN. J. Am. Chem. Soc. **87**, 915 (1965); (*b*) T. FUKUNAGA. J. Am. Chem. Soc. **87**, 916 (1965); (*c*) A. L. JOHNSON, N. O. PETERSEN, M. B. RAMPERSAD, and J. B. STOTHERS. Can. J. Chem. **52**, 4143 (1974).
5. D. M. HUDYMA, J. B. STOTHERS, and C. T. TAN. Org. Magn. Reson. **6**, 614 (1974).
6. P. K. FREEMAN, D. M. BALLS, and D. J. BROWN. J. Org. Chem. **33**, 2211 (1968).
7. T. INAZU and T. YOSHINO. Bull. Chem. Soc. Jpn. **41**, 652 (1968).
8. J. W. BLUNT and J. B. STOTHERS. Org. Magn. Reson. **9**, 439 (1977).

The chemistry of anions derived from tetracyanodiphenoquinodimethane (TCNDQ)

A. W. ADDISON, NAR S. DALAL, YUMIKO HOYANO, SYTZE HUIZINGA, AND LARRY WEILER

Department of Chemistry, University of British Columbia, Vancouver, B.C., Canada V6T 1W5

Received May 31, 1977

A.W. ADDISON, NAR S. DALAL, YUMIKO HOYANO, SYTZE HUIZINGA, and LARRY WEILER. Can. J. Chem. **55**, 4191 (1977).

Dihydro-TCNDQ was prepared from biphenyl. The dianion salts of TCNDQ with alkali metal and tetraalkylammonium counter ions were prepared and characterized by their nmr and uv-visible spectra. Solutions of these dianions undergo two one-electron oxidations at −0.31 and −0.15 V in DMF. The electrochemistry is complicated by a second chemical process involving the monoanion $TCNDQ^{\cdot-}$. This was postulated to involve a dimerization of $TCNDQ^{\cdot-}$ and this process was also implicated in the analysis of the uv-visible spectra of this anion. The $TCNDQ^{\cdot-}$ anion has a solution esr spectrum of over 25 lines which have been analyzed by a computer simulation of the spectrum.

A. W. ADDISON, NAR S. DALAL, YUMIKO HOYANO, SYTZE HUIZINGA et LARRY WEILER. Can. J. Chem. **55**, 4191 (1977).

On a préparé le dihydro-TCNDQ à partir du biphényle. On a pu préparer et caractériser par leurs spectres rmn et uv-visible les sels dianioniques du TCNDQ avec des ions de métaux alcalins ou de tétraalkylammonium comme contre ions. Des solutions de ces dianions subissent deux oxydations monoélectroniques à −0.31 et −0.15 V dans le DMF. L'électrochimie est compliquée par un deuxième processus chimique impliquant le monoanion $TCNDQ^{\cdot-}$. On a postulé que ce processus implique une dimérisation du $TCNDQ^{\cdot-}$ et on a aussi impliqué ce processus dans l'analyse du spectre uv-visible de cet anion. L'anion $TCNDQ^{\cdot-}$ a un spectre rpe en solution comprenant plus de 25 lignes qui ont pu être analysées par une simulation du spectre par ordinateur.

[Traduit par le journal]

Introduction

In the past few years there has been a great deal of interest in the synthesis and study of organic charge transfer complexes. Much of this interest arises from the novel transport properties of these materials, for example TTF·TCNQ (For a recent review of this field see ref. 1). A number of groups has been involved in the synthesis of new donors and acceptors to prepare

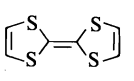

TTF

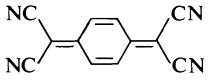

TCNQ

additional solid complexes and also to lead to a better understanding of the electronic properties of these materials. A range of donors has been prepared, the most promising of which appears to be HMTSF (2). However, none of the complexes of these donors has room temperature

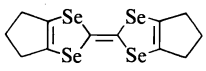

HMTSF

electrical conductivities substantially above that of TTF·TCNQ which is the original organic metal (3). Thus attention has turned to the synthesis of new acceptors. A number of studies have shown that substitution on the basic TCNQ skeleton usually produces an adverse effect on the conductivities of charge transfer solids with these acceptors (4, 11). Hence one is forced to investigate acceptors with a carbon skeleton different from that of TCNQ. The only successful venture in this area has been the preparation of TNAP (5) and its complex with TTF (6).

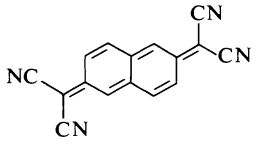

TNAP

An obviously attractive new acceptor would be tetracyanodiphenoquinodimethane (TCNDQ). The reduction potentials of the corresponding quinone (7) indicate that this basic carbon

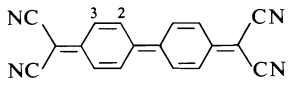

TCNDQ

skeleton is an excellent two electron acceptor. Unfortunately, attempts to prepare TCNDQ have led only to formation of a polymeric material (8*a*, *b*).[1] However, we have recently been able to prepare a number of salts of the anions of TCNDQ and study their physical properties.

Experimental

Visible and uv absorption spectra were obtained on Cary-14 and 17D instruments, and ^{1}H nmr spectra on a Varian Associates T60 spectrometer, with chemical shifts (δ) reported vs. internal TMS. Infrared spectra were obtained with a Perkin-Elmer 700, mass spectra from an AEI MS-9 spectrometer operating at 70 eV, and esr spectra on a Varian E3 instrument, calibrated with a ^{1}H nmr probe. Fluorescence spectra were recorded on an Aminco-Bowman instrument, at 0.5 mm slit widths, wavelength-calibrated with a mercury emission lamp.

Electrochemistry was performed at 25.0 ± 0.2°C with a three electrode cell, using apparatus incorporating a PAR-173 potentiostat and PAR-176 *i*/*E* converter. A Beckman rotating platinum disc electrode was used for dc polarography, and also served as a stationary electrode for cyclic voltammetry. Current vs charge plots were obtained by integration (McKee–Pedersen MP-1012A integrator) of the anodic current, and using the current and its integral as inputs for an X–Y recorder. The supporting electrolyte was G. F. Smith Chemical Co. polarographic grade tetraethylammonium perchlorate, dried *in vacuo* over P_4O_{10}. The reference electrode was a Ag|$AgClO_4$ (0.01 *M*), TEAP (0.1 *M*), CH_3CN half-cell, the potential of which we have measured as being 0.30 V positive of the sce, both in CH_3CN/TEAP at 25°C. Acetonitrile was distilled off P_4O_{10} under nitrogen before use, dimethylformamide was vacuum-distilled off P_4O_{10} or CaH_2, and 9,10-diphenylanthracene was recrystallized from acetonitrile, while other reagents were used as received.

4,4′-Biphenyldiacetonitrile (2)

Biphenyl was bisbromomethylated with HBr and paraformaldehyde in ca. 30% yield according to the procedure of Reynolds and Durham (9). This was converted into the bisnitrile (**2**) in ca. 90% yield by displacement of the bromide with NaCN in aqueous ethanol – dioxane (9). 4,4′-Biphenyldiacetonitrile (**2**) was characterized by the following data: mp 182–185°C (lit. (9) mp 185–187°C); ir ($CHCl_3$): 2280 cm^{-1}; nmr ($CDCl_3$) δ: 3.77 (s, 4H) 7.30 and 7.51 (AB quartet, J = 8 Hz, 8H).

Dimethyl 4,4′-Biphenyl-α,α,α′,α′-tetracyanodiacetate (3)

A mixture of freshly prepared sodium methoxide (56.5 mmol from 1.30 g of sodium) and 5.04 g (21.7 mmol) of bisnitrile (**2**) from above in ca. 300 ml of toluene was refluxed under nitrogen for 0.5 h to yield a clear solution. Then 25.4 g (283 mmol) of dimethyl carbonate were added and this mixture was refluxed for an additional 3 h. The solvents were then distilled from the reaction mixture until the temperature of the distillate reached 100°C. Finally, ca. 50 additional millilitres of toluene were distilled from the reaction mixture. The reaction mixture was cooled in ice and treated with 4.0 g (65 mmol) of cyanogen chloride in 20 ml of toluene. This mixture was heated to reflux for 1.5 h. Most of the solvents were distilled off and the residue was poured into a mixture of dilute aqueous acid and CH_2Cl_2. The aqueous layer was extracted with CH_2Cl_2 and the extracts were combined, washed with water, dried ($MgSO_4$), filtered, and the solvents removed to yield 9 g of crude product. This crude material was recrystallized from CH_2Cl_2–MeOH to yield 7.1 g (85%) of compound **3**: mp 160–162°C; ir ($CHCl_3$): 2280, 1770 cm^{-1}; nmr ($CDCl_3$): 3.90 (s, 6H), 7.7 (br s, 8H); ms *m*/*e* (relative intensity): 398 (0.3), 354 (2), 332 (6), 321 (8), 310 (6), 306 (12), 296 (8), 295 (10), 282 (12), 281 (11), 276 (21), 256 (16), 232 (35), 217 (100), 190 (70), 152 (20). *Anal.* calcd. for $C_{22}H_{14}N_4O_4$: C 66.32, H 3.54, N 14.07; found: C 66.18, H 3.61, N 14.14.

4,4′-Biphenyl-α,α′-dicyanodiacetonitrile (Dihydro-TCNDQ) (1)

(*a*) Chromatography of diester **3** on silica gel produced varying yields of dihydro-TCNDQ (1).

(*b*) Diester **3** (4 g, 0.010 mol) was dissolved in 10 ml of dioxane and 45 ml of 10% aqueous KOH. This solution was heated to 70°C for about 15 min, cooled to room temperature, and acidified with 6 *N* HCl to p*H* 2. The acid mixture was extracted with CH_2Cl_2. The extracts were combined, dried ($MgSO_4$), filtered, and the solvents evaporated to yield 2.3 g (82%) of purple solid, mp 172–179°C (lit. (8*a*) mp 176–181°C); ir ($CHCl_3$): 2260, 1495, 990 cm^{-1}; nmr ($CDCl_3$) δ: 5.1 (s, 2H), 7.6 (s, 8H).

Salts of the Dianion TCNDQ^{2-}

(*a*) Solutions of M_2^+ TCNDQ^{2-} were prepared by dissolving dihydro-TCNDQ (**1**) in an aqueous solution of NaOH or KOH, or by dissolving **1** in acetonitrile and treating with slightly more than 2 equiv. of NaH or KH. These solutions tended to oxidize quite rapidly; however, a trace of $NaBH_4$ stabilized the solutions for spectroscopic characterization, which included uv (CH_3CN) λ_{max}: 377 (5.1 × 10^4) and nmr (CD_3CN) δ: 6.83 (d, J = 8 Hz, 4H) and 7.22 (d, J = 8 Hz, 4H).

(*b*) The bistetraethylammonium and bistetra-*n*-butylammonium salts of TCNDQ^{2-} were prepared from the diester **3** or **1** by first forming solutions of the sodium salt of TCNDQ^{2-}. These solutions were obtained by dissolving **3** or **1** in aqueous NaOH, taking precautions to exclude oxygen. The solutions of TCNDQ^{2-} were filtered and treated with 2–3 equiv. of the tetraalkylammonium hydroxide, also in water. The bistetraalkylammonium salts precipitated in yields of 60–80%. The bistetraethylammonium TCNDQ^{2-} salt had mp ca. 70°C and resisted efforts at purification. However, the bistetra-*n*-butylammonium TCNDQ^{2-} salt was recrystallized from ethanol–water (1:3) to yield pure salt, mp 155–160°C; nmr (CD_3CN) δ: 1.1 (br t, J = 7 Hz, 24H) 1.6 (br m, 32H), 3.2 (br t, J = 8 Hz, 16H), 6.9 (d, J = 8 Hz, 4H), 7.3 (d, J = 8 Hz, 4H). *Anal.* calcd. for $C_{50}H_{80}N_6$: C 78.48, H 10.54, N 10.98; found: C 78.19, H 10.50, N 10.77.

[1]L. D. Pedersen and L. Weiler. Unpublished results.

Sodium Salt of TCNDQ$^{\cdot-}$

Poly-TCNDQ was prepared from dihydro-TCNDQ (**1**) and then converted into crude NaTCNDQ as outlined by Hertler (*8a*). This crude material was purified by continuous Soxhlet extraction with CH_3CN. Evaporation of the acetonitrile solution gave a black solid which could not be combusted in an elemental analysis. The solid was characterized by solution uv-visible and esr spectra. The solid also has an intense single esr line at $g = 2.0035$.

Results and Discussion

Synthesis of Dihydro-TCNDQ and its Anions

Dihydro-TCNDQ (**1**) was prepared as outlined in Fig. 1. Biphenyl was converted into 4,4′-biphenyldiacetonitrile (**2**) using the method of Reynolds and Durham (9). The anion of nitrile **2** was reacted with dimethyl carbonate followed by cyanogen chloride to yield dimethyl 4,4′-biphenyl-α,α,α′,α′-tetracyanodiacetate (**3**) according to the procedure of Sandman and Garito (10). Diester (**3**) was hydrolyzed and decarboxylated to yield dihydro-TCNDQ (**1**) by silica gel chromatography or by hydrolysis in aqueous base. A number of attempts to directly oxidize dihydro-TCNDQ (**1**) to TCNDQ were unsuccessful (8, 10).[1] Thus we turned to the preparation of the various salts of TCNDQ to study the metathetical reactions of these salts with salts of donors (D), for example eq. 1 (11).

[1] $M^+TCNDQ^- + D^+X^- \rightarrow D{\cdot}TCNDQ + MX$

$(M^+)_2TCNDQ^{2-} + D^{2+}(X^-)_2 \rightarrow D{\cdot}TCNDQ + 2MX$

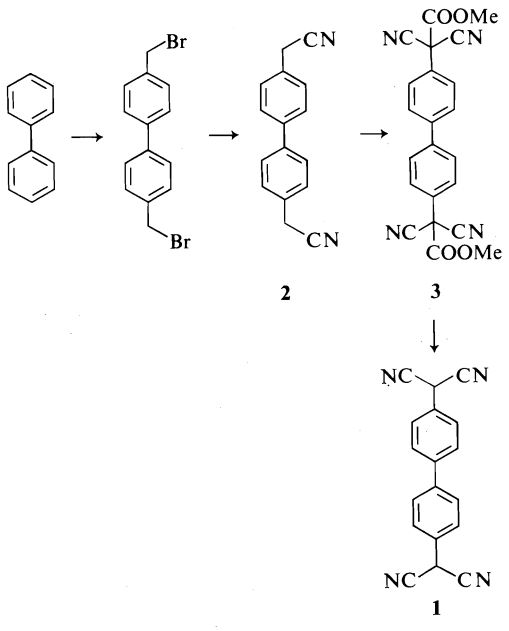

FIG. 1. Preparation of dihydro-TCNDQ (**1**).

The dianions of TCNDQ were prepared by deprotonation of dihydro-TCNDQ (**1**) with a variety of potassium and sodium bases to give $(M^+)_2TCNDQ^{2-}$. These salts were characterized by their nmr spectra and uv-visible spectra. The proton nmr spectrum of **1** in $CDCl_3$ has a two-proton singlet at δ 5.05 and an eight-proton singlet at δ 7.58. The nmr spectrum of the sodium salt of $TCNDQ^{2-}$ in acetonitrile shows an AB quartet at δ = 6.83 and 7.22 (J = 8 Hz). The disappearance of the signal at δ 5.05 in **1** and the upfield shift of the aromatic protons is consistent with the formation of $TCNDQ^{2-}$. As a result of our esr and molecular orbital (mo) studies (*vide infra*) we assign the signal at δ 6.83 to the protons on C-3. The mo calculations indicate that this carbon has a greater electron density than C-2 in the dianion. In addition the doublet at δ 6.83 in $TCNDQ^{2-}$ broadens noticeably when air is passed through the solution. This is attributed to formation of the radical anion $TCNDQ^-$ and the larger spin density on C-3 (*vide infra*) would lead to preferential broadening of this signal. This effect is reversed by the addition of $NaBH_4$.

Dihydro-TCNDQ (**1**) was converted into a polymer of TCNDQ with a number of oxidizing agents.[1] Treatment of the polymer with sodium iodide yielded crude NaTCNDQ (*8a*) which was purified via Soxhlet extraction with acetonitrile. This material was characterized as the radical ion salt, NaTCNDQ, by esr and uv-visible spectroscopy (*vide infra*).

Redox Chemistry of Anions of TCNDQ[2]

The TCNDQ redox system is not straightforward in its electrochemical behaviour, which is typified by the cyclic voltammagram in Fig. 2. Of three oxidation processes observable for $TCNDQ^{2-}$, in voltammetry the first two yield equivalent anodic currents, while the peak-to-peak potential separation of the lowest potential process (55–65 mV) is suggestive of an $n = 1$ redox step (13). With regard to this first oxidation process, it was also observed that (*i*) the voltammetric peak current function ($i_pc^{-1}v^{-1/2}$) in DMF is within 10% of that observed for the 1ē reduction (14) of 9,10-diphenylanthracene in DMF; (*ii*) the value of $n^{1/2}$ obtained from complementary voltammetry and chronoamperom-

[2]Abbreviations: TBA, tetra(*n*-butyl)ammonium; TEAP, tetraethylammonium perchlorate; DMF, *N*,*N*-dimethylformamide; rpe, rotating platinum electrode.

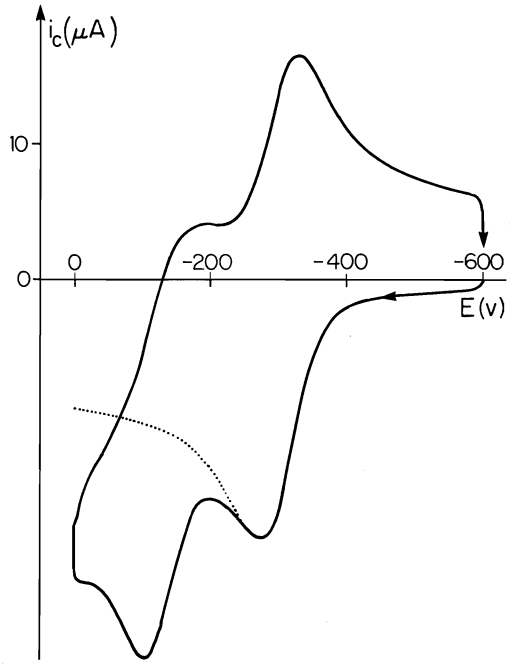

FIG. 2. Cyclic voltammagram of 0.23 mM $(TBA)_2$-(TCNDQ) in DMF–TEAP (0.1 M) at Pt-disc electrode, scan rate 0.167 V s^{-1}. The dashed curve is the extrapolated current decay of the first anodic peak (12).

etry at the same electrode (15) is 0.89 if reversibility is assumed; (*iii*) at the rpe (Fig. 3), good linearity of the $i_L:\omega^{1/2}$ plot (16) demonstrated the first oxidation to be diffusion controlled, while (*iv*) the ratio of the polarogram's slope at $E = E_{1/2}$ to the limiting current, $di/(i_L\, dE)$, was

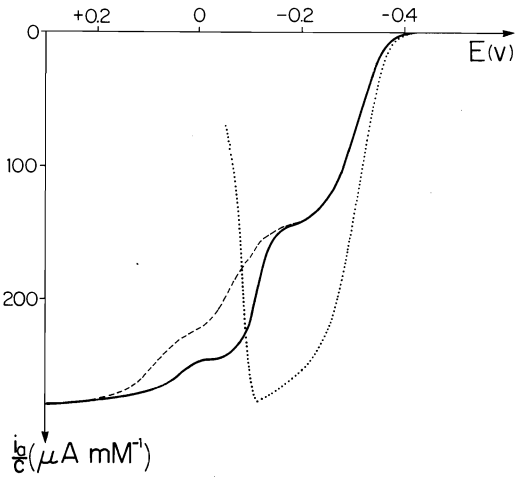

FIG. 3. Concentration-normalised rpe polarograms of $(TBA)_2(TCNDQ)$ at 30 revolutions s^{-1}: (*a*) 0.44 mM in DMF (—); (*b*) 2.0 mM in DMF (--); (*c*) 2.01 mM in CH_3CN) (· ·). Supporting electrolyte, 0.1 M TEAP.

close (9.9 V^{-1}) to the value (9.7 V^{-1}) expected for an $n = 1$ Nernstian process;[3] and (*v*) the limiting current was equivalent to that observed for the $n = 1$ 9,10-diphenylanthracene reduction. The $n = 1$ assignment was finally confirmed coulometrically (*vide infra*), and allows computation of the diffusion coefficient (Table 1) of $TCNDQ^{2-}$. As expected, the value is lower than that of TCNQ, while the $D\eta$ products (4.0×10^{-8} g cm s^{-2}) agree well with each other for the two solvents used, in which the redox process may be written as

$$TCNDQ^{2-} \rightleftharpoons TCNDQ^{\cdot-} + \bar{e}$$

The third oxidation step is resolved best in rpe polarography, which shows the second oxidation to be coupled with it, in the sense that the sum of the limiting currents of these second two waves is equal to the limiting current for the $TCNDQ^{2-} \rightarrow TCNDQ^{\cdot-}$ oxidation. This indicates that the oxidation of (nominally) $TCNDQ^{\cdot-}$ proceeds via two parallel pathways under our experimental conditions, to the product, nominally neutral TCNDQ. Precipitation (Fig. 3) of product on the electrode renders the system intractible with respect to more detailed electrochemical study, although observed dependences of the potentials of the second and third redox steps on $TCNDQ^{2-}$ concentration and on rpe rotation rate reiterate the non-Nernstian nature of the polarograms obtained for these oxidations, which are therefore observed only as steady-state results in a kinetically controlled system. The data of Table 1 are therefore derived by extrapolation to zero concentration and rotation rate where applicable. The two idealised processes

$$TCNDQ + \bar{e} \rightarrow TCNDQ^{\cdot-}$$

and

$$TCNDQ^{\cdot-} + \bar{e} \rightarrow TCNDQ^{2-}$$

are therefore separated by a potential difference (150–200 mV) considerably less than that for

[3]The usual relationship between current and potentia on a reversible polarogram

$$E = E^0 + \frac{RT}{nF} \ln\left(\frac{i_L - i}{i}\right)$$

on differentiation yields

$$\frac{di}{d\Delta} = -\frac{nF i_L e^{nF\Delta/RT}}{RT(1 + e^{nF\Delta/RT})^2}$$

where $\Delta = E - E^0 = E - E_{1/2}$ for $D_0 = D_R$. At $E = E_{1/2}$, the slope of the polarogram is $di/dE = -i_L nF/4RT$.

TABLE 1. Redox properties of TCNDQ and TCNQ[a]

Species	Solvent	E_1	E_2	D^b(cm^2 s^{-1})
$TCNDQ^{2-}$	CH_3CN	−0.31[c]		1.2×10^{-5}
$TCNDQ^{2-}$	DMF	−0.31[c]	−0.15[c,d]	5.0×10^{-6}
TCNQ	CH_3CN	−0.10[e]	−0.64[e]	1.3×10^{-5}

[a]Reduction potentials, in volts ± 10 mV, vs. Ag|$AgClO_4$ (0.01 *M*), TEAP (0.1 *M*), CH_3CN reference electrode, at 25°C.
[b]± 10%, computed from voltammetric peak currents (14).
[c]Oxidation of species.
[d]Lowest estimated limit; becomes more positive as concentration is increased.
[e]Reduction of species at Pt electrode (cyclic voltammetry).

TCNQ (17), but similar to that reported (7) for the structurally related 1,8-diphenoquinone. This is presumably a result of the increased delocalisation of, and thereby decreased coulombic interaction between, successive electrons added to the binuclear system.

From the measured potentials, a disproportionation constant can be calculated for the idealised reaction:

$$2TCNDQ^{\dot{-}} \rightleftharpoons TCNDQ + TCNDQ^{2-}$$

at a total TCNDQ concentration in the 1 m*M* region, $K = 2 \times 10^{-3}$, in 0.1 *M* TEAP. Hence the small potential difference between the successive process contains the implication that it is not possible to prepare solutions which contain pure $TCNDQ^{\dot{-}}$ without $TCNDQ^{2-}$ and/or TCNDQ present in these solvents.

Electrosynthesis of $TCNDQ^{\dot{-}}$ via anodic coulometry of $TCNDQ^{2-}$ was therefore performed firstly at the $E_{1/2}$ of the $TCNDQ^{2-}$/$TCNDQ^{\dot{-}}$ couple. Electrooxidation of 102 μmol of $(TBA)_2$(TCNDQ) at a platinum mesh anode at −0.31 V in 42 ml acetonitrile–TEAP resulted in the essentially linear current vs. charge plot shown in Fig. 4, intersecting the *q*-axis at 48 μF (0.47 F mol^{-1}). An rpe polarogram showed the solution to be 50 ± 5% through the first oxidation stage. Electrooxidation of 101 μmol of $(TBA)_2$(TCNDQ) in DMF–TEAP at +0.25 V was associated with the consumption of 1.93 F mol^{-1}, as judged from extrapolation of the *i* vs. *q* plot to $i = 0$. The orange solution eventually deposited a white precipitate of the (probably polymeric) neutral TCNDQ.

Electronic Spectra of Anions of TCNDQ

During electrooxidation of $TCNDQ^{2-}$ to $TCNDQ^{\dot{-}}$, the yellow solutions of the dianion became orange. A series of electrooxidation steps were carried out on a 2.3×10^{-5} *M* solution, in DMF–TEAP, and yielded the absorption spectral changes depicted in Fig. 5. The 377 nm band of $TCNDQ^{2-}$ decreased in intensity, and a structured band system appeared in the 500–550 nm region, with the spectra exhibiting an isosbestic point at 411 nm. The results obtained suggest that *both* $TCNDQ^{2-}$ and $TCNDQ^{\dot{-}}$ have absorption maxima near 375 nm, the latter with what we have deduced to be an approximately twofold decrease in intensity (Table 2). It would thus seem that the aromatic rings of $TCNDQ^{2-}$ and $TCNDQ^{\dot{-}}$ behave as electronically independent systems on the time scale of electronic absorption spectroscopy, which contrasts with our esr results below. That is, both results can be interpreted in terms of a twisted geometry with minimum interaction between the rings. Figure 6 shows that the dianion is luminescent in solution. The emission, which maximizes at 420 nm, is excited by the strong absorption in the 370 nm region, while its high intensity evidences that it is indeed fluorescence, and that a singlet ground state for $TCNDQ^{2-}$ is thereby confirmed.

When the 2.77 m*M* solution of $(TBA)_2$-TCNDQ in CH_3CN–TEAP was oxidized to

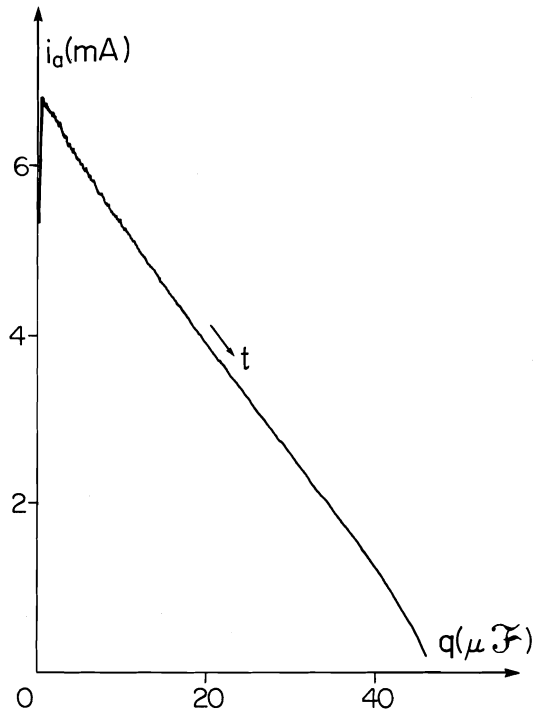

FIG. 4. Current vs. charge output from electrooxidation of $TCNDQ^{2-}$ in CH_3CN–TEAP at $E = E_{1/2}$ for first oxidation step. The current is capacitively damped.

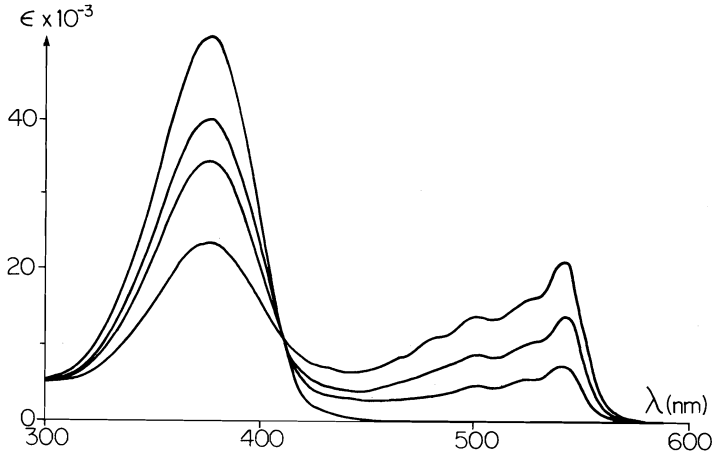

FIG. 5. Spectral changes accompanying electrooxidation of a DMF–TEAP solution of $(TBA)_2$-(TCNDQ) (2.3×10^{-5} *M*) to the radical anion, $TCNDQ^{\dot{-}}$. Decreasing absorbances near 370 nm correspond to approximately 0%, 40%, 65%, 90% oxidized respectively, as judged from application of the Nernst equation and the results of Fig. 4 to the reaction mixture at the attained potentials.

$E = E_{1/2}$, to form the $TCNDQ^{\dot{-}}/TCNDQ^{2-}$ equilibrium mixture, the acetonitrile solution showed the absorption band at ca. 375 nm and the structured band with $\varepsilon_{app} = 4200$ at 536 nm. When this solution was diluted with acetonitrile, the apparent molar absorptivity in the 375 nm region decreased, and the apparent molar absorptivity at 536 nm increased, to $\varepsilon = 73\,000$ when $[TCNDQ^{\dot{-}}] \simeq 6 \times 10^{-7}$ *M*. This concentration dependence is very suggestive of a self-association (e.g. dimerization) of the radical anion, with $TCNDQ^{\dot{-}}$ being the species exhibiting the structured absorption in the 500–550 nm region. Figure 5 shows, indeed, that electrosynthesized solutions of $TCNDQ^{\dot{-}}$ in DMF–TEAP also do not obey Beer's law, the apparent molar absorptivity at 540 nm again decreasing with increasing concentration of $TCNDQ^{\dot{-}}$. A similar phenomenon has been observed in the electronic spectrum of $TCNQ^{\dot{-}}$ in solution (17*b*), and we have previously observed strong self-association of organic radical ions in solution spectroelectrochemical studies (18). Furthermore, this postulate is consistent with our observations that (*i*) the peak voltammetric current function, $i_pC^{-1}v^{-1/2}$, for the second anodic maximum increases with decreasing scan rate, *v*, and (*ii*) the first oxidation step for $TCNDQ^{2-}$ has a peak current ratio $i_{p,c}/i_{p,a}$ greater than unity (19).

TABLE 2. Absorption spectra of TCNDQ anions and related compounds

	Solvent	λ_{max} (nm)	ε (ℓ mol^{-1} cm^{-1})
$\phi CH(CN)_2$	EtOH	255	2.25×10^2
$\phi C(CN)_2^-$	EtOH	288	6.1×10^3
H_2-TCNQ	EtOH	249	1.00×10^4
$TCNQ^{2-}$ (17*a*)	CH_3CN	330	3.1×10^4
		240	1.5×10^4
		210	3.1×10^4
$TCNQ^{\dot{-}}$ (17*b*)	CH_3CN	842	4.3×10^4
		420	2.4×10^4
H_2-TCNDQ	EtOH	360	2.82×10^3
		258	9.4×10^3
$TCNDQ^{2-}$	DMF[a]	377	5.1×10^4
		(220	3.3×10^4 in H_2O)
$TCNDQ^{\dot{-}}$	DMF[a]	542	2.4×10^4[b]
		375	2.25×10^4[b]

[a]0.1 *M* in TEAP.
[b]At a total TCNDQ anionic species concentration of 2.3×10^{-5} *M* of which 50% is monoanionic, 50% dianionic. Apparent ε given.

Finally, we have compared the electronic absorption spectra of TCNDQ with a number of related compounds given in Table 2. Ionization of H_2-TCNQ to yield the dianion of $TCNQ^{2-}$ produces a bathochromic shift of ca. 80 nm and indicates a strong interaction between the ring and substituents in a fully planar $TCNQ^{2-}$ ion. Phenylmalononitrile and H_2-TCNDQ on the other hand show much smaller bathochromic shifts on ionization. This would indicate that the dicyanomethylene groups in the anion of phenylmalononitrile and $TCNDQ^{2-}$ are not in the plane of the benzene ring. Also it is clear that the $TCNDQ^{2-}$ system is not fully planar (also *vide supra*). Twisting about the central CC bond and the exocyclic CC bonds is probably due to a

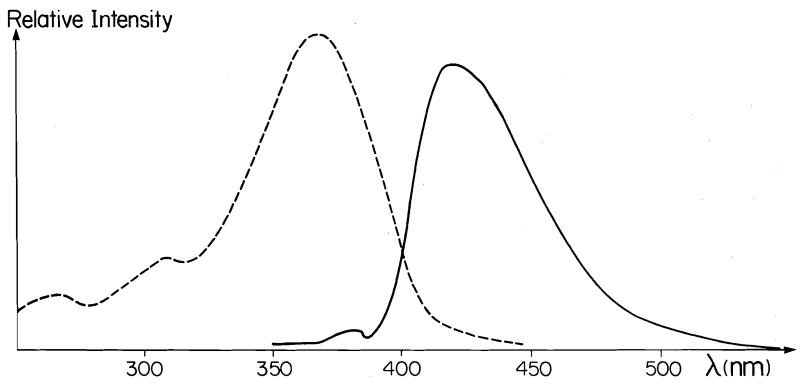

FIG. 6. Fluorescence emission (—) and excitation (--) spectra of a $\sim 2 \times 10^{-6}$ *M* solution of $(TBA)_2$-(TCNDQ) in acetonitrile. Spectra uncorrected for instrument spectral response.

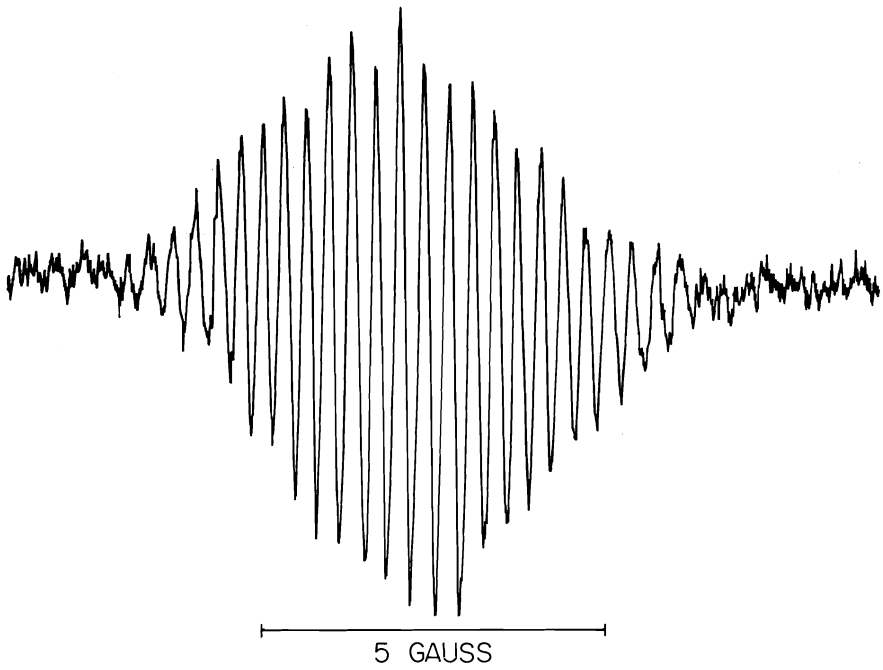

FIG. 7. Electron spin resonance spectrum of $TCNDQ^{\dot{-}}$ in DMF.

combination of steric and electrostatic effects. The bathochromic shift of the long wavelength band from $TCNDQ^{2-}$ to $TCNDQ^{\dot{-}}$ is also seen in the TCNQ anions. But the shift is much smaller in the former anions and again this is consistent with the proposal that the substituents are not conjugated in the TCNDQ system to the same extent that they are in the TCNQ system.

Electron Spin Resonance Spectra of $TCNDQ^{\dot{-}}$

The solution esr spectrum of other acceptor radical anions (20) and donor radical cations (18, 21) have been extremely useful in characterizing these species and studying aggregation (17*b*) and exchange (22) processes in solution. The esr spectrum of $TCNDQ^{\dot{-}}$ in DMF is shown in Fig. 7. The spectrum consists of over 25 lines with $g = 2.0032 \pm 0.0005$ in acetonitrile. The esr spectrum of $TCNQ^{\dot{-}}$ has over 45 lines and $g = 2.0026$ (20*a*). In acetonitrile solutions, the $TCNDQ^{\dot{-}}$ spectrum shows an asymmetry which has not been analyzed as yet. Spectra in acetone often show some signal broadening, possibly due to an exchange phenomenon. The *g* value is free-

electron like and consistent with the formulation of $TCNDQ^{\dot{-}}$ as a π radical anion.

A computer simulation of the spectrum agrees with the observed spectrum when $a_N = 0.7$ G, $a_{H_2} = 0.7$ G, and $a_{H_3} = 1.1$ G. Because of the complexity of the spectrum, small changes in these calculated values of the hyperfine constants might occur in a more detailed analysis of the spectrum. Although these values are consistent with the proposed structure of the radical anion, there is a difficulty in assigning the proton hyperfine couplings. In the radical anion of 4,4′-dinitrobiphenyl the assignments are $a_{H_2} = 0.20$ G and $a_{H_3} = 1.23$ G (23). However, the esr of the radical anion of 4,4′-dicyanobiphenyl is assigned as $a_{H_2} = 1.82$ G and $a_{H_3} = 0.30$ G (24). The difficulty in making these assignments has been stressed by Rieger and Fraenkel (23, 24); in addition, they suggest that a_{H_2} and a_{H_3} are mainly dependent on the electronegativity of the substituents at the 4 and 4′ positions (23). The dicyanomethylene group is probably between the nitro and cyano groups in electronegativity and this is reflected in the values of a_{H_2} and a_{H_3} in $TCNDQ^{\dot{-}}$ being between those of 4,4′-dinitrobiphenyl and 4,4′-dicyanobiphenyl. We have assigned a_{H_2} and a_{H_3} in TCNDQ on the basis of our extended Hückel calculations for the radical anion (*vide infra*).

It is well known that the McConnell relation, $a_H = Q_{CH}\rho_C$(25) is followed for a large number of organic π radicals. We have used the extended Hückel method of Hoffmann (26) to calculate the spin densities in $TCNQ^{\dot{-}}$ and $TCNDQ^{\dot{-}}$. From the calculated spin density in $TCNQ^{\dot{-}}$ and the observed proton hyperfine coupling, $a_H = 1.44$ G (27) we calculate a value of $Q = -24.4$ G, in good agreement with the values of Q obtained for other organic π radicals (28*a*). Using this value of Q and the calculated spin density[4] of $TCNDQ^{\dot{-}}$ we obtained $|a_{H_2}| = 0.86$ G and $|a_{H_3}| = 1.10$ G. Thus we suggest that the largest proton hyperfine coupling (1.1 G) be assigned to a_{H_3} and the smaller coupling (0.7 G) be assigned to a_{H_2}. This simple McConnell relation applies to neutral π radicals. Several workers have developed methods to include the effect of excess charge on the couplings in anions and cations (28*b*). However, this effect is usually small for anions and our value of Q calculated from the $TCNQ^{\dot{-}}$ spectrum partially corrects for this effect.

In addition, one can calculate the nitrogen hyperfine constants using the relation formulated by Rieger and Fraenkel (24) for cyano substituted π radicals. This relation is

$$a_N = \pm 29.7\ \rho_N{}^{\pi} \mp 13.3\ \rho_{C'}{}^{\pi}$$

The calculated nitrogen hyperfine coupling is 1.43 G in $TCNQ^{\dot{-}}$ compared with an observed value of 1.02 G (27). Similarly, the calculated nitrogen hyperfine coupling is 1.04 G in $TCNDQ^{\dot{-}}$ compared with an observed value of 0.7 G. In both cases the calculated value is about 50% higher than the observed a_N.

The observed esr spectrum is consistent with the formation of the $TCNDQ^{\dot{-}}$ radical anion and its serves to characterize the ion in solution. The assignment of the esr spectrum, although tentative, does allow us to probe the electronic nature of the highest occupied mo(homo) in $TCNDQ^{\dot{-}}$. As we have shown earlier, the homo in $TCNQ^{\dot{-}}$ is very important in understanding the conductivity (30) and solid state packing (31) in TCNQ salts. Our calculations indicate that the homo in $TCNDQ^{\dot{-}}$ has the same symmetry as that of $TCNQ^{\dot{-}}$. This is consistent with the observed esr spectrum and augurs well for the potential use of this acceptor.

The solid esr spectrum of powder NaTCNDQ has a very strong single line at $g = 2.0035$. This solid's esr signal is similar to that of the alkali metal salts of TCNQ (32).

[4]This calculation assumes a planar geometry for the radical anion and that the central double bond in TCNDQ is slightly longer than the other double bonds. The remaining bond lengths and angles were taken from those in TCNQ (29).

Acknowledgements

We are grateful to the National Research Council of Canada, University of British Columbia, and NATO for support of this work and to Dr. L. D. Pedersen for preliminary experimental results.

1. A. J. Berlinsky. Contemp. Phys. **17**, 331 (1976).
2. A. N. Block, D. O. Cowan, K. Bechgaard, R. E. Pyle, R. H. Banks, and T. O. Poehler. Phys. Rev. Lett. **34**, 1561 (1975).
3. A. F. Garito and A. J. Heeger. Acc. Chem. Res. **7**, 232 (1974).
4. R. C. Wheland. J. Am. Chem. Soc. **98**, 3926 (1976).
5. J. Diekmann, W. R. Hertler, and R. E. Benson. J. Org. Chem. **28**, 2719 (1963).
6. P. A. Berger, D. J. Dahm, G. R. Johnson, M. G. Miles, and J. D. Wilson. Phys. Rev. B, **12**, 4085 (1975).

7. M. E. PEOVER. J. Chem. Soc. 4540 (1962); M. E. PEOVER. Nature, **193**, 475 (1962).
8. (*a*) W. R. HERTLER. U.S. Patent No. 3 153 658 (1964); Chem. Abstr. **62**, 4145 (1965); (*b*) D. J. SANDMAN and A. J. GARITO. J. Org. Chem. **39**, 1165 (1974).
9. D. D. REYNOLDS and K. R. DURHAM. U.S. Patent No. 2 789 971 (1957).
10. D. J. SANDMAN and A. F. GARITO. J. Org. Chem. **28**, 1165 (1974).
11. R. C. WHELAND and J. L. GILLSON. J. Am. Chem. Soc. **98**, 3916 (1976).
12. S. PIEKARSKI and R. N. ADAMS. *In* Techniques of chemistry. Vol. 1, Pt. IIA. *Edited by* A. Weissberger and B. W. Rossiter. Wiley-Interscience, New York, NY. 1971. p. 541.
13. R. S. NICHOLSON and I. SHAIN. Anal. Chem. **36**, 706 (1964).
14. J. PHELPS, K. S. V. SANTHANAM, and A. J. BARD. J. Am. Chem. Soc. **89**, 1752 (1967).
15. T. R. MÜLLER and R. N. ADAMS. Anal. Chim. Acta, **25**, 482 (1961).
16. W. J. ALBERY. Electrode kinetics. Clarendon Press, Oxford. 1975. p. 57.
17. (*a*) M. R. SUCHANSKI and R. P. VAN DUYNE. J. Am. Chem. Soc. **98**, 250 (1976); (*b*) L. R. MELBY, R. J. HARDER, W. R. HERTLER, W. MAHLER, R. E. BENSON, and W. E. MOCHEL. J. Am. Chem. Soc. **84**, 3374 (1962); (*c*) P. H. RIEGER, I. BERNAL, W. H. REINMUTH, and G. K. FRAENKEL. J. Am. Chem. Soc. **85**, 683 (1963).
18. A. W. ADDISON, T. H. LI, and L. WEILER. Can. J. Chem. **55**, 766 (1977).
19. M. S. SHUMAN. Anal. Chem. **42**, 521 (1970).
20. (*a*) M. J. JONES and W. R. HERTLER. J. Am. Chem. Soc. **86**, 1881 (1964) and references therein; (*b*) L. R. MELBY. *In* The chemistry of the cyano group. *Edited by* Z. Rappaport. Interscience Publishers, New York, NY. 1970. p. 639.
21. F. WUDL, G. M. SMITH, and E. J. HUFNAGEL. Chem. Commun. 1453 (1970).
22. N. HARAN, Z. LUZ, and M. SHPORER. J. Am. Chem. Soc. **96**, 4788 (1974).
23. P. H. RIEGER and G. K. FRAENKEL. J. Chem. Phys. **39**, 609 (1963).
24. P. H. RIEGER and G. K. FRAENKEL. J. Chem. Phys. **37**, 2795 (1963).
25. H. M. MCCONNELL. J. Chem. Phys. **27**, 764 (1956).
26. R. HOFFMANN. J. Chem. Phys. **39**, 1397 (1963).
27. P. H. H. FISCHER and C. A. MCDOWELL. J. Am. Chem. Soc. **85**, 2694 (1963).
28. J. E. WERTZ and J. R. BOLTON. Electron spin resonance. McGraw-Hill Book Co., New York, NY. 1972. (*a*) p. 98; (*b*) p. 122.
29. R. E. LONG, R. A. SPARKS, and K. N. TRUEBLOOD. Acta Crystallogr. **18**, 932 (1965).
30. A. J. BERLINSKY, J. F. CAROLAN, and L. WEILER. Solid State Commun. **15**, 795 (1974).
31. A. J. BERLINSKY, J. F. CAROLAN, and L. WEILER. Solid State Commun. **19**, 1165 (1976).
32. T. HIBMA and J. KOMMANDEUR. Phys. Rev. B, **12**, 2608 (1975).

Phase-transfer catalyzed formation of cyanohydrin ethers and acetates[1]

JOHN M. MCINTOSH

Department of Chemistry, University of Windsor, Windsor, Ont., Canada N9B 3P4

Received July 4, 1977

JOHN M. MCINTOSH. Can. J. Chem. **55**, 4200 (1977).

In the presence of an allylic bromide, aldehydes, but not ketones, react with cyanide ion under phase-transfer catalysis to give cyanohydrin allyl ethers which can be converted to ketones. Other alkylating agents and nucleophiles give different results. Replacing the allylic bromide with acetic anhydride leads to cyanohydrin acetates.

JOHN M. MCINTOSH. Can. J. Chem. **55**, 4200 (1977).

En présence d'un bromure allylique, les aldéhydes mais non les cétones réagissent avec l'ion cyanure par catalyse de transfert de phase pour fournir des éthers mixtes d'allyl et de cyanohydrine qui peuvent être transformés en cétones. Des agents alkylant et des nucléophiles autres donnent des résultats différents. Le remplacement du bromure allylique par de l'anhydride acétique conduit aux acétates de cyanohydrine.

[Traduit par le journal]

Recently we have become interested in the interaction of nucleophiles with aldehydes and ketones under the influence of phase-transfer catalysis. This interest stems from our observations of 1,4-addition of various sulfur nucleophiles to conjugated aldehydes (1). In order to assess the generality of these reactions, we turned our attention to a well-studied nucleophile, cyanide ion, and we report here some of the interesting results observed.

The simplest reaction between carbonyl compounds and cyanide ion is an addition reaction leading to cyanohydrins. This process is known to be reversible and proceeds under general base catalysis (2). When an aqueous solution of potassium cyanide was stirred vigorously with a methylene chloride solution of cyclohexanone, 3-pentanone, or mesityl oxide, no cyanohydrin formation could be detected either with or without the addition of a catalytic amount of triethylbenzylammonium chloride (TEBAC). One possible rationale for this result was that the high p*H* of the cyanide solution did not permit protonation of the intermediate oxyanion **1** (eq. 1). Thus reversal of addition would occur. Conducting the reaction using tributylamine catalyst and an aqueous solution of hydrocyanic acid did lead to an equilibrium amount of **2**, but the possibility that this reaction did not involve phase-transfer catalysis led us to consider other alternatives for trapping **1**.

[1]

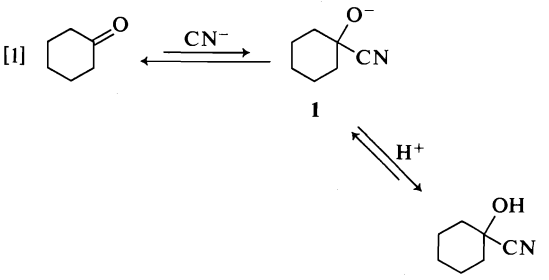

1 **2**

In this regard, the work of Cazes and Julia (3) is of interest. They have shown that preformed cyanohydrins derived from aldehydes can be alkylated with allylic halides under phase-transfer conditions. The products can be transformed into ketones via a [2,3] sigmatropic rearrangement. They point out that, under their conditions, the cyanohydrin may dissociate forming cyanide ion, and, in fact, they report minor amounts of allylic cyanide as by-products. It appeared to us that if cyanide ion was attacking the carbonyl ion in our reaction, allylic halides might trap **1** by an irreversible alkylation leading to products analogous to those observed by Cazes and Julia. The success of the reaction would depend on a preferential attack on the carbonyl group, rather than the well-known (4) attack at sp^3-hybridized carbon which would lead to nitriles.

Results and Discussion

Stirring a methylene chloride solution of butanal (**3***b*) and allyl bromide (**4***a*) with an

[1]Presented in part at the Annual Conference, Chemical Institute of Canada, Montreal, June 1977.

aqueous solution of potassium cyanide in the absence of a catalyst led to a rapid disappearance of the aldehyde, but only water soluble aldol-type oligomers of undetermined structure were produced. Incorporation of 4 mol% of TEBAC led to a smooth reaction to give cyanohydrin ether **6** (eq. 2). Repetition of this reaction using

[2] 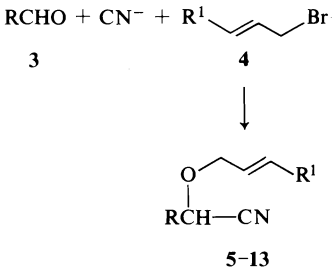

a variety of aliphatic aldehydes led to comparable results (Table 1). The only other products observed were unreacted starting materials and the previously mentioned water-soluble material. The latter material was obtained only when aldehydes possessing appreciable water solubility were employed (runs 1, 2, 4). All reactions were run on a 0.05 molar scale, using equimolar amounts of **3** and **4** and 1.5 equiv. of cyanide. When benzaldehyde (**3***e*) was used, small amounts of benzoin were also obtained (5). Noteworthy in all these examples is the near absence of allylic cyanides as determined by glc analysis of the crude reaction mixture. The ease with which compounds of type **5** can be obtained makes Cazes and Julia's ketone synthesis much more attractive.

Extension of the reaction to related systems led to unexpected results. Whereas replacing **4***a* with other primary allylic or benzylic bromides afforded the expected products, the less reactive allylic chlorides were completely inert (runs 9, 10) and only the water-soluble oligomers were obtained. The same result was obtained using 1-bromobutane (**4***d*) as the trapping reagent. Replacing the aldehydes with representative ketones (runs 11, 12) again changed the reaction and only allyl cyanide could be detected. The ketones could be quantitatively recovered after completion of the reaction. Thus it appears that the increased steric congestion present in ketones serves either to reduce the equilibrium amount of **1** or retards its reaction with **4** to a point where the desired reaction is very slow.

To examine this point in more detail, a more reactive trapping reagent was required and we turned our attention to the use of acetic anhydride. When the reaction of this with **3** was carried out in the usual fashion, a vigorous exotherm occurred, and only highly coloured products could be isolated. However, by carrying out the reaction at 0°C with slow addition of the organic reagents, a smooth conversion to the cyanohydrin acetate could be achieved (Table 2). In this case, a representative ketone (run 4) also gave the expected product although excess cyanide and acetic anhydride are required. Thus it appears that the failure of the reaction of ketones and **4***a* is due to an inefficient reaction between **1** and **4***a*. In view of the very rapid hydrolysis of acetic anhydride by aqueous cyanide solution, these reactions are quite remarkable. The current interest in cyanohydrin esters as synthetic pyrethroids (6) makes these latter reactions of some practical interest.

The reaction of conjugated carbonyl compounds with cyanide ion can occur either by 1,2- or 1,4-addition. Our previous work using sulfur nucleophiles (1) had led to products derived from 1,4-addition, although 1,2-addition may well be an undetected equilibrium side reaction. Very recent work by Liotta *et al.* (7) has shown that, using crown ether-catalyzed solid–liquid phase transfer conditions in the presence of a suitable proton source, 1,4-addition of cyanide ion to conjugated ketones can occur. The contrast between these results and those of Evans *et al.* (8) using silyl cyanides is noteworthy. Thus, we attempted to apply our conditions to this reaction.

Three different products can be envisaged (Scheme 1) depending on the mode of the initial cyanide attack. When crotonaldehyde or 2-cyclohexenone were reacted with cyanide ion and **4***a* (Table 1, runs 13, 14) under the usual conditions, only polymers were formed. However, the reac-

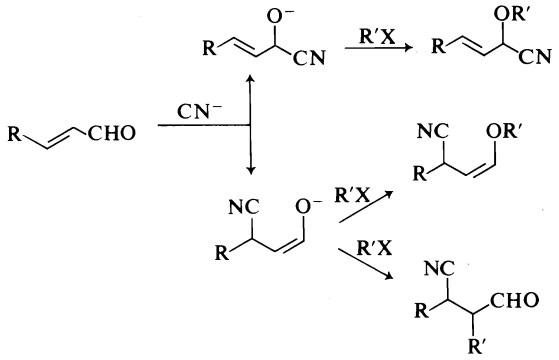

SCHEME 1

TABLE 1. Formation of cyanohydrin ethers and related reactions

Run no.	Carbonyl	RX	Anion	*T*	Product	Yield[a] (%)
1	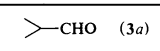 (3*a*)	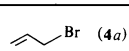 (4*a*)	CN^-	Ambient	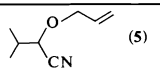 (5)	44 (70)
2	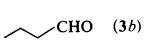 (3*b*)	**4*a***	CN^-	Ambient	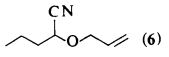 (6)	65 (70)
3	$C_8H_{17}CHO$ (3*c*)	**4*a***	CN^-	Reflux	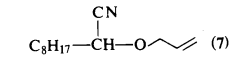 (7)	70 (84)
4	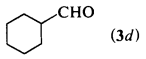 (3*d*)	**4*a***	CN^-	Reflux	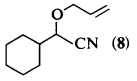 (8)	65 (84)
5	PhCHO (3*e*)	**4*a***	CN^-	Ambient	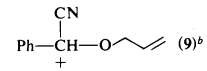 (9)[b] + benzoin	70[c] (88) 10
6	**3*a***	$PhCH_2Br$ (4*b*)	CN^-	Reflux	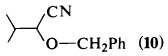 (10)	69 (92)
7	**3*d***	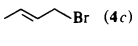 (4*c*)	CN^-	Reflux	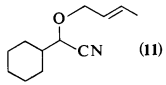 (11)	72 (83)
8	**3*b***	C_4H_9Br (4*d*)	CN^-	Ambient	Polymers	
9	**3*b***	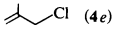 (4*e*)	CN^-	Ambient	Polymers	
10	**3*b***	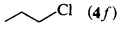 (4*f*)	CN^-	Ambient	Polymers	
11	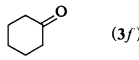 (3*f*)	**4*a***	CN^-	Ambient	 (12)	
12	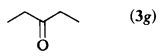 (3*g*)	**4*a***	CN^-	Reflux	**12**	
13	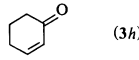 (3*h*)	**4*a***	CN^-	Ambient	Polymers	
14	(3*i*)	**4*a***	CN^-	Ambient	Polymers	

TABLE 1 (*Concluded*)

Run no.	Carbonyl	RX	Anion	*T*	Product	Yield[a] (%)
15	**3***a*	(**4***g*)	CN^-	Ambient	(**13**)	60 (88)
16	**3***a*	**4***a*	PhS^-	Ambient	(**14**)[d]	90 (100)
17	**3***a*	**4***a*	$AcS^{\ominus}$	Ambient	(**15**)[d]	91 (100)
18	**3***i*	**4***a*	$AcS^{\ominus}$	Ambient	**15** **3***i*	86 (100) 90

[a]Yields are distilled product unless otherwise noted; yields in parentheses are determined by glc.
[b]Reference 10.
[c]Corrected for unconsumed **3***e*.
[d]Reference 11.

tion of **3***i* with acetic anhydride did lead to a clean formation of the ester **19** derived from 1,2-addition of cyanide. Under the same conditions **3***h* was recovered quantitatively from the reaction.

We have also briefly investigated three other nucleophilic species which were chosen to obtain a less basic aqueous solution and thus minimize the formation of aldol-type polymers. When aqueous sodium azide was employed with **3***a* and **4***a*, no reaction of any kind occurred. However, the use of potassium thiophenoxide or thiolacetate led cleanly to the formation of the allylic sulfides **14** and **15**, with complete recovery of the carbonyl component (Table 1, runs 16–18). None of the previously described (9) attack on methylene chloride was observed. The contrast between the reaction of thiolacetate with **3***i* in the presence of **4***a* (formation of **15**) and in the absence of **4***a* (formation of **20**) (1) indicates how delicately balanced these reactions are.

14 **15** **20**

Finally, it should be noted that simple Michael acceptors do not effectively trap anions **1**, presumably due to a ready reversal of the reactions under the alkaline conditions. Thus, neither acrylonitrile nor ethyl acrylate afforded any useful products. We are currently investigating other variations of these reactions and the application of the products to synthesis. We will report on these in due course.

Experimental

Nuclear magnetic resonance spectra were recorded on a JEOL C60 HL spectrometer in deuterochloroform and are reported in parts per million downfield from TMS as internal standard. Infrared spectra were determined on a Beckman IR 12 instrument in chloroform solution. The drying agent used was anhydrous sodium sulfate and solvents were removed at reduced pressure. Gas chromatographic analyses were performed on either an F & M Model 720 or Hewlett-Packard Model 5750 instrument utilizing a 10 ft × 0.25 in. 20% SE 30 on Chromosorb W column. Mass spectra were determined on a Varian MAT CH 5-DF in the electron-impact mode. Microanalyses were performed by A. B. Gygli, Microanalysis Laboratory, Toronto.

General Procedure for Compounds 5–13

A solution of 4 g (0.06 mol) of potassium cyanide in 10 ml of distilled water was added to 20 ml of methylene chloride in a 100 ml round bottom flask fitted with a magnetic stirrer and reflux condenser. Four mol% (500

TABLE 2. Formation of cyanohydrin acetates

Run no.	Carbonyl	Product	Yield[a] (%)
1	**3***a*	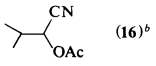 (16)[b]	56 (72)
2	$C_{10}H_{21}CHO$ (**3***j*)	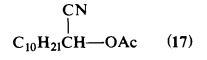 (17)	70 (85)
3	**3***f*	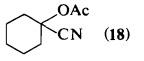 (18)	75 (88)
4	**3***i*	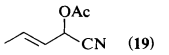 (19)	66 (80)
5	**3***h*	**3***h*	86

[a]Yields are distilled product; those in parentheses are determined by glc.
[b]See reference 12.

TABLE 3. Physical constants and nmr spectra of new compounds

Compound	bp (°C) (Torr)	n_D^{23}	Nuclear magnetic resonance[a]
5	58–60 (8.5)	1.4284	6.22–5.05(m, 3), 4.40–4.05(m, 2), 3.95(d, 1, J = 6 Hz), 2.04(h, 1, J = 6 Hz), 1.10(dd, 6, J = 2.6 Hz)
6	65–67 (7.4)	1.4263	6.30–5.16(m, 3), 4.42–3.80(m, 3), 2.30–1.35(m, 4), 1.01(t, 3, J = 7 Hz)
7	120–122 (2.7)	1.4395	6.20–5.61(m, 1), 5.60–5.10(m, 2), 4.51–3.75(m, 3), 2.00–0.50(m, 17)
8	86–88 (1.9)	1.4619	6.25–5.10(m, 3), 4.50–3.75(m, 3), 2.40–0.80(bm, 11)
10	96–98 (1.0)	1.4888	7.32(5, s), 4.65(AB quart., 2, J = 11 Hz), 3.90(d, 1, J = 6 Hz), 2.02 (h, 1, J = 6 Hz), 1.04(dd, 6, J = 3, 6 Hz)
11	102–104 (2.0)	1.4664	6.05–5.30(m, 2), 4.55–3.75(m, 3), 2.15–0.70(bm, 14)
13	142–144 (1.7)	1.5286	7.28(5, s), 6.80 and 6.52(half AB quart., 1, J = 16 Hz), 6.26 and 6.01 (half AB quart., 1, each dd, J = 5, 1.5 Hz), 4.37(dd, 2, J = 5, 2.5 Hz), 3.97(d, 1, J = 6 Hz), 2.00(h, 1, J = 6 Hz), 1.05(dd, 6, J = 6, 2 Hz)
16	72–76 (6.9)	1.4124	5.14(d, 1, J = 5 Hz), 2.14(s, 3), 2.50–1.90(m, 1), 1.10(dd, 6, J = 7, 2 Hz)
17	109–111 (0.25)	1.4360	5.31(t, 3, J = 6 Hz), 2.11(s, 3), 2.05–0.75(bm, 20)
19	81–83 (8.7)	1.4326	6.50–5.30(m, 3), 2.13(s, 3), 1.80(d, 3, J = 6 Hz)

[a]In $CDCl_3$ solution; tabulation follows the order: chemical shift (δ), multiplicity, number of protons, coupling constant.

mg) of TEBAC was added, the stirrer was started, and a mixture of the carbonyl compound (0.05 mol) and allylic bromide (0.05 mol) was added all at once through the condenser. A mild exotherm was noted. (Within 2 h, the phases had reversed, the aqueous phase being on top.) The reaction was stirred at ambient temperature or reflux (see Table 1) until glc analysis of the organic phase showed no further reaction was occurring. The phases were separated, the organic phase washed with 15 ml of water and evaporated. Ether was added to the residue to precipitate the catalyst. The ether solution was dried, filtered, and evaporated and the residue distilled to afford the products shown in Table 1. In the cases of **5** and **6** especially, considerable high-boiling material was left after distillation. Physical constants and spectral and analytical data for new compounds are given in Tables 3 and 4.[2]

[2]Copies of Table 4 are available, at a nominal charge, from the Depository of Unpublished Data, CISTI, National Research Council of Canada, Ottawa, Ont., Canada K1A 0S2.

Reactions using other nucleophiles or alkylating agents were run in exactly the same manner.

*General Procedure for Compounds **16–19***

A solution of 4 g (0.06 mol) of potassium cyanide in 10 ml of water was added to 10 ml of methylene chloride in a 100 ml three-necked round bottom flask fitted with a magnetic stirrer, addition funnel, and reflux condenser. Four mol% (500 mg) of TEBAC was added and the flask was cooled to 0°C in an ice bath. The stirrer was started and a mixture of 0.05 mol of each of the carbonyl compound and acetic anhydride in 15 ml of methylene chloride was added dropwise with stirring over a period of 20 min at 0°C. Stirring was continued at 0°C for 20 min and then at ambient temperature until glc indicated no further change in the composition of the mixture. Work-up was then effected in the same way as before and the products shown in Table 2 were isolated by distillation. Physical constants and spectral and analytical data for new compounds are given in Tables 3 and 4.

In the case of cyclohexanone, the yields given in Table

2 were obtained using 0.1 mol of cyanide and 0.1 mol of acetic anhydride.

Acknowledgements

The financial assistance of the National Research Council of Canada is gratefully acknowledged. Mr. Tom Hardy performed some of the preliminary experiments during a fourth-year research project.

1. J. M. McINTOSH and H. KHALIL. J. Org. Chem. **42**, 2123 (1977).
2. A. LAPWORTH. J. Chem. Soc. 1206 (1904).
3. B. CAZES and S. JULIA. Tetrahedron Lett. 2077 (1974).
4. C. M. STARKS and R. M. OWENS. J. Am. Chem. Soc. **95**, 3613 (1973).
5. C. M. STARKS. J. Am. Chem. Soc. **95**, 195 (1973).
6. Symposium on Synthetic Pyrethroids, Abstracts. American Chemical Society Convention, Sept. 1976, San Francisco,
7. C. L. LIOTTA, A. M. DABDOUB, and L. H. ZALKOW. Tetrahedron Lett. 1117 (1977).
8. D. A. EVANS, G. L. CARROLL, and L. K. TRUESDALE. J. Org. Chem. **39**, 914 (1974) and references therein.
9. A. W. HERRIOTT and D. PICKER. Synthesis, 447 (1975).
10. J. CAST, T. S. STEVENS, and J. HOLMES. J. Chem. Soc. 3521 (1960).
11. K. GRIESBAUM, A. A. OSWALD, E. R. QUIRAM, and W. NAEGELE. J. Org. Chem. **28**, 1952 (1963).
12. K. ICAIMURA and M. OHTA. Bull. Chem. Soc. Jpn. **43**, 1443 (1970).
13. J. P. COIC, P. ROLLIN, and R. SETTON. C. R. Acad. Sci. **272**, 1554 (1971).
14. L. J. BELLAMY. The infrared spectra of complex molecules. 3rd ed. Vol. I. Wiley, New York, NY. 1975. p. 297.

Crystal and molecular structure of hexamethylcyclotriphosphazene, $(NPMe_2)_3$

RICHARD T. OAKLEY, NORMAN L. PADDOCK, STEVEN J. RETTIG, AND JAMES TROTTER

Department of Chemistry, University of British Columbia, 2075 Wesbrook Mall, Vancouver, B.C., Canada V6T 1W5

Received July 5, 1977

RICHARD T. OAKLEY, NORMAN L. PADDOCK, STEVEN J. RETTIG, and JAMES TROTTER. Can. J. Chem. **55**, 4206 (1977).

Crystals of hexamethylcyclotriphosphazene are monoclinic, $a = 12.084(2)$, $b = 13.426(1)$, $c = 15.488(2)$ Å, $\beta = 102.92(2)°$, $Z = 8$, space group $C2/c$. The structure was solved by direct methods and was refined by full-matrix least squares procedures to a final R of 0.045 and R_w of 0.060 for 1922 reflections with $I \geq 3\sigma(I)$. The six-membered phosphazene ring is slightly nonplanar and has a distorted chair conformation. Important molecular dimensions (bond lengths are corrected for libration) are: P—N, 1.599(2)–1.612(2), P—C, 1.796(3)–1.823(4) Å, N—P—N, 115.7(1)–117.9(1), P—N—P, 122.1(1)–122.9(1), and C—P—C, 101.8(2)–103.1(2)°.

RICHARD T. OAKLEY, NORMAN L. PADDOCK, STEVEN J. RETTIG et JAMES TROTTER. Can. J. Chem. **55**, 4206 (1977).

Les cristaux de l'hexaméthylcyclotriphosphazène sont monocliniques: $a = 12.084(2)$, $b = 13.426(1)$, $c = 15.488(2)$ Å, $\beta = 102.92(2)°$, $Z = 8$, groupe d'espace $C2/c$. La structure a été résolue par des méthodes directes et a été affinée par la méthode des moindres carrés (matrice complète) jusqu'à une valeur finale de R de 0.045 et de R_w de 0.060 pour 1922 réflexions avec $I \geq 3\sigma(I)$. Le cycle a six chaînons du phosphazène n'est pas complètement planaire et assume une conformation chaise déformée. Les dimensions moléculaires importantes (longueurs de liaisons corrigées pour les librations) sont: P—N, 1.599(2)–1.612(2), P—C, 1.796(3)–1.823(4) Å, N—P—N, 115.7(1)–117.9(1), P—N—P, 122.1(1)–122.9(1) et C—P—C, 101.8(2)–103.1(2)°.
[Traduit par le journal]

Introduction

Hexamethylcyclotriphosphazene has been known for some time (1*a*), but its structure has not been determined. The X-ray crystallographic analysis of $(NPMe_2)_3$ has been prompted by the recent structure determinations of the methylphosphazenes $(NPMe_2)_{5-8}$ (2–5) in addition to the previously known structure of $(NPMe_2)_4$ (6). The structure of $(NPMe_2)_3$ is also of interest in relation to those known for other homogeneously substituted cyclotriphosphazenes $(NPX_2)_3$, where X = F (7–10), Cl (10–14), Br (15–18), C_6H_5 (19), $1/2[O_2C_6H_4]$ (20, 21), OC_6H_5 (22), NMe_2 (23), NCS (24), and $1/2[2,2'$-$OC_6H_4C_6H_4O]$ (25).

Experimental

Hexamethylcyclotriphosphazene was prepared by standard methods (1*b*). Crystals suitable for X-ray analysis were obtained by recrystallization from methylene chloride – toluene. The crystal chosen for study was mounted with a^* parallel to the goniostat axis and had dimensions of ca. 0.78 × 0.11 × 0.49 mm. Unit-cell and space group data were obtained from film and diffractometer measurements. The unit-cell parameters were refined by least squares on 2 sin θ/λ values for 36 reflections measured on a diffractometer with Cu K_α radiation ($\lambda = 1.5418$ Å). Crystal data (at 22°C) are:

$C_6H_{18}N_3P_3$ fw = 225.15

Monoclinic, $a = 12.084(2)$, $b = 13.426(1)$, $c = 15.488(2)$ Å, $\beta = 102.92(2)°$, $V = 2449.1(6)$ Å^3, $\rho_m = 1.21$ (flotation in aqueous KI), $Z = 8$, $\rho_c = 1.221$ g cm^{-3}, $F(000) = 960$, μ(Cu K_α) = 40.9 cm^{-1}. Absent reflections: hkl, $h + k \neq 2n$ and $h0l$, $l \neq 2n$. Space group $C2/c$ (C_{2h}^6, No. 15).

Intensities were measured with nickel-filtered Cu K_α radiation on a Datex-automated General Electric XRD-6 diffractometer. A θ–2θ scan at 4° min^{-1} over a range of (1.80 + 0.86 tan θ) degrees in 2θ was employed. 10 s background counts were measured at each end of the scan. Data were measured to $2\theta = 160°$. The intensities of the check reflections, measured every 50 reflections throughout the data collection, decreased uniformly to values which were 0.91 times the initial values. Lorentz and polarization corrections and batch check reflection scaling were applied, and the structure amplitudes were derived. An absorption correction was applied by a computer program using a Gaussian integration method (26, 27). Transmission factors ranged from 0.160 to 0.622. Of the 2686 independent reflections measured, 1931 (72%) had intensities greater than $3\sigma(I)$ above background where $\sigma^2(I) = S + B + (0.03S)^2$ with S = scan count and B = time averaged background count.

The structure was solved by direct methods (28). The positions of all the non-hydrogen atoms were determined from an E-map. Two cycles of full-matrix least squares refinement of the coordinates and isotropic thermal parameters of the non-hydrogen atoms, followed by two cycles with anisotropic thermal parameters, gave $R = 0.067$. The positions of all 18 hydrogen atoms were given

by an electron density difference map calculated at this point. The entire structure (including hydrogen atoms with isotropic thermal parameters) was refined for six cycles giving a final R of 0.045 and R_w of 0.060 for 1922 reflections with $I \geq 3\sigma(I)$ (9 reflections which had $|F_o| - |F_c| > 3\sigma(F)$ were treated as unobserved in the final stages of refinement; instrumental error was suspected for these reflections, but it seemed unwise to bias the data by remeasuring them; none of the disagreements were exceptionally bad). For all 2686 reflections $R = 0.063$ and $R_w = 0.064$.

A correction for secondary extinction was approximated by basing the least squares refinement on the minimization of $\Sigma w[|F_o| - |F_c|/(1 + gI)|]^2$ where g is the extinction parameter and I the uncorrected intensity. The final value of g was $3.2(9) \times 10^{-8}$. The scattering factors of ref. 29 were used for the non-hydrogen atoms and those of ref. 30 for the hydrogen atoms. Anomalous scattering factors from ref. 31 were used for the non-hydrogen atoms. The weighting scheme, $w = 1.0$ if $|F_o| < 20.0$, $w = (20.0/|F_o|)^2$ if $|F_o| \geq 20.0$, and $w = 0.09$ for the unobserved reflections, gave uniform average values of $w(|F_o| - |F_c|)^2$ over ranges of $|F_o|$ and was employed in the final stages of refinement.

On the final cycle of refinement the mean parameter shift was 0.04σ and no shift was greater than 0.32σ. The mean error in an observation of unit weight was 0.9013. The final positional and thermal parameters appear in Tables 1 and 2 respectively.[1] Measured and calculated structure factors have been placed in the Depository of Unpublished Data.[1]

The ellipsoids of thermal motion for the non-hydrogen atoms are shown in Fig. 1. The thermal motion has been analysed in terms of the rigid-body modes of translation (**T**), libration (**L**), and screw (**S**) motion (32) using the computer program MGTLS. The rms standard error in the temperature factors σU_{ij} (derived from the least squares analysis) is 0.0016 Å^2. Analysis of the entire molecule as a rigid body was unsuccessful, but each of the phosphorus tetrahedra was found to behave as a rigid body (rms $\Delta U_{ij} = 10$, 14, and 17×10^{-4} Å^2 for P(1), P(2), and P(3) respectively).

The appropriate bond distances have been corrected for libration (33, 34), using shape parameters q^2 of 0.08 for all atoms involved. Corrected bond lengths appear in Table 3 along with the uncorrected values. Corrected bond angles differ by less than 0.1° from the uncorrected values in Table 4.

Results and Discussion

Figure 1 shows a general view of the molecule with the crystallographic numbering scheme and Fig. 2 shows the packing arrangement viewed down a^*. Torsion angles in the six-membered ring are listed in Table 5. The mean structural parameters for $(NPMe_2)_3$ are compared with those of the methylphosphazenes, $(NPMe_2)_{4-8}$, and the homogeneously substituted cyclotriphosphazenes, $(NPX_2)_3$, in Table 6.[2]

TABLE 1. Final positional parameters (fractional: N and C $\times 10^4$, P $\times 10^5$, H $\times 10^3$) with estimated standard deviations in parentheses

Atom	x	y	z
P(1)	27858(6)	16684(5)	31964(4)
P(2)	26755(5)	26883(4)	16028(3)
P(3)	26644(6)	6007(4)	16357(4)
N(1)	2782(2)	2670(1)	2651(1)
N(2)	2780(2)	1631(1)	1151(1)
N(3)	2777(3)	645(1)	2682(1)
C(1)	4005(4)	1686(3)	4116(2)
C(2)	1606(4)	1689(4)	3732(3)
C(3)	3736(3)	3501(2)	1369(2)
C(4)	1399(3)	3308(3)	1064(3)
C(5)	3722(4)	−241(3)	1429(3)
C(6)	1362(4)	−10(3)	1124(3)
H(1*a*)	462(5)	177(4)	383(4)
H(1*b*)	400(3)	110(3)	447(3)
H(1*c*)	390(4)	232(3)	450(3)
H(2*a*)	99(4)	163(3)	327(3)
H(2*b*)	157(5)	104(5)	388(4)
H(2*c*)	151(6)	240(5)	395(4)
H(3*a*)	442(4)	325(3)	155(3)
H(3*b*)	362(3)	414(3)	161(2)
H(3*c*)	372(3)	350(3)	82(3)
H(4*a*)	91(4)	298(3)	115(3)
H(4*b*)	146(3)	403(3)	132(2)
H(4*c*)	135(4)	333(3)	44(3)
H(5*a*)	447(4)	8(4)	166(3)
H(5*b*)	369(3)	−25(3)	89(3)
H(5*c*)	365(3)	−93(3)	167(3)
H(6*a*)	76(5)	35(4)	129(4)
H(6*b*)	131(4)	−5(4)	46(3)
H(6*c*)	132(4)	−68(3)	139(3)

The crystal structure (Fig. 2) consists of well-separated molecules of hexamethylcyclotriphosphazene. The shortest intermolecular H...H and N...H contacts (2.43(8) and 2.70(4) Å respectively) correspond to normal van der Waals interactions.

At each phosphorus atom in the molecule, the two P—N and the two P—C distances are equal within experimental error. Small, but significant, differences in bond lengths and angles at the three independent phosphorus atoms result in a small distortion of the molecule from threefold symmetry which is probably a result of packing forces. The six-membered P_3N_3 ring is slightly, but significantly, non-planar, and has a distorted chair conformation; the mean and maximum

[1]The structure factor table and Table 2 (thermal parameters) are available, at a nominal charge, from the Depository of Unpublished Data, CISTI, National Research Council of Canada, Ottawa, Ont., Canada K1A 0S2.

[2]Here and elsewhere in this report mean values refer to weighted means with rms deviations from the mean in parentheses.

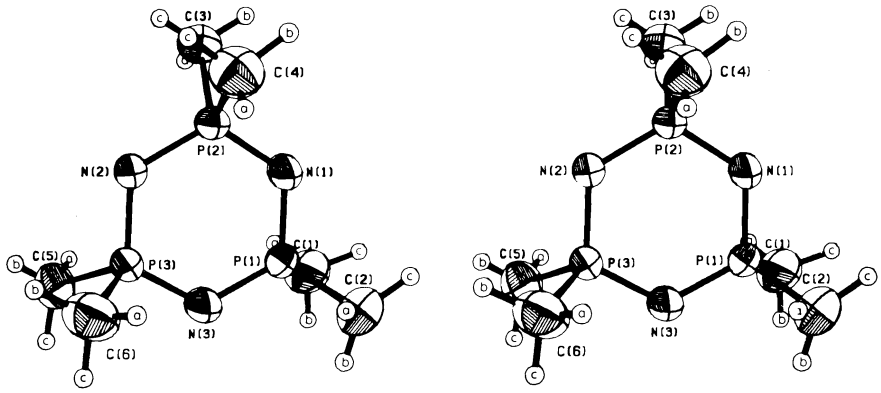

FIG. 1. A stereo view of the hexamethylcyclotriphosphazene molecule. 50% ellipsoids are shown for the non-hydrogen atoms. Hydrogen atoms have been assigned artificially small thermal parameters for the sake of clarity.

TABLE 3. Bond lengths (Å) with estimated standard deviations in parentheses

(*a*) Non-hydrogen atoms

Bond	Uncorrected (Å)	Corrected (Å)	Bond	Uncorrected (Å)	Corrected (Å)
P(1)—N(1)	1.587(2)	1.599	P(1)—C(1)	1.806(4)	1.823
P(1)—N(3)	1.588(2)	1.599	P(1)—C(2)	1.803(4)	1.821
P(2)—N(1)	1.600(2)	1.612	P(2)—C(3)	1.781(3)	1.796
P(2)—N(2)	1.600(2)	1.611	P(2)—C(4)	1.787(3)	1.804
P(3)—N(2)	1.594(2)	1.604	P(3)—C(5)	1.788(3)	1.803
P(3)—N(3)	1.597(2)	1.608	P(3)—C(6)	1.794(4)	1.811

(*b*) Bonds involving hydrogen atoms

Bond	Length (Å)	Weighted mean (Å)
C—H	0.77–1.06(4–7)	0.95(8)

TABLE 4. Bond angles (deg) with estimated standard deviations in parentheses

(*a*) Non-hydrogen atoms

Bonds	Angle (deg)	Bonds	Angle (deg)
N(1)—P(1)—N(3)	117.9(1)	C(3)—P(2)—C(4)	101.8(2)
N(1)—P(1)—C(1)	108.3(2)	N(2)—P(3)—N(3)	116.7(1)
N(1)—P(1)—C(2)	108.8(2)	N(2)—P(3)—C(5)	108.8(2)
N(3)—P(1)—C(1)	108.6(2)	N(2)—P(3)—C(6)	110.4(2)
N(3)—P(1)—C(2)	109.1(2)	N(3)—P(3)—C(5)	107.6(2)
C(1)—P(1)—C(2)	103.1(2)	N(3)—P(3)—C(6)	109.4(2)
N(1)—P(2)—N(2)	115.7(1)	C(5)—P(3)—C(6)	102.9(2)
N(1)—P(2)—C(3)	108.5(2)	P(1)—N(1)—P(2)	122.9(1)
N(1)—P(2)—C(4)	110.3(2)	P(2)—N(2)—P(3)	122.7(1)
N(2)—P(2)—C(3)	108.9(1)	P(3)—N(3)—P(1)	122.1(1)
N(2)—P(2)—C(4)	110.7(2)		

(*b*) Angles involving hydrogen atoms

Bonds	Angle (deg)	Weighted mean (deg)
P—C—H	101–113(2–4)	108(3)
H—C—H	92–142(3–5)	110(10)

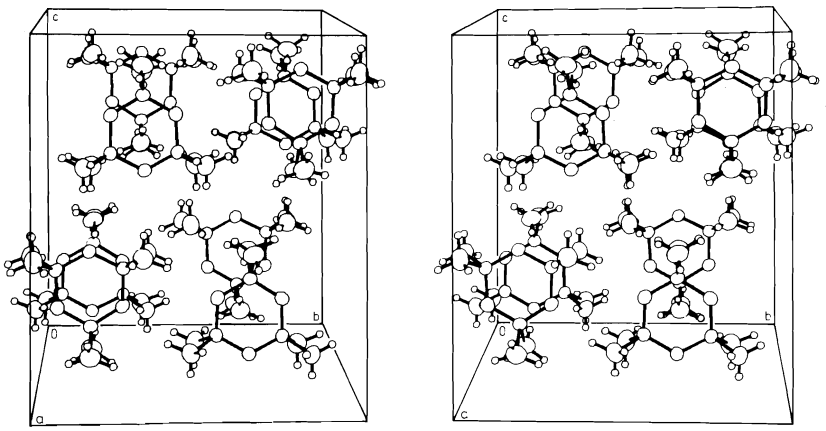

FIG. 2. The crystal structure of hexamethylcyclotriphosphazene viewed down a^*.

TABLE 5. Intra-annular torsion angles (deg)

Bond	Value
P(1)—N(1)	4.7(2)
N(1)—P(2)	−9.8(2)
P(2)—N(2)	15.8(1)
N(2)—P(3)	−16.3(2)
P(3)—N(3)	10.5(2)
N(3)—P(1)	−5.0(2)

deviations from the weighted least squares mean plane are 0.043 and 0.162(3) Å (N(2)).

Small deformations of P_3N_3 rings from planarity have been ascribed to intra- and intermolecular steric effects (12, 18, 19). In $(NPMe_2)_3$, the sum of the two independent mean ring angles is 0.6° less than the maximal 240°, and the resulting torsion angles (Table 5) would allow some steric relief of the methyl–methyl repulsion. The data of Table 6 suggest that there may also be an electronic effect. Electronegative substituents are known to decrease P—N bond lengths, as exemplified by the increase from 1.570 Å in $(NPF_2)_3$ to 1.605 Å in $(NPMe_2)_3$, the longest yet found in a trimeric phosphazene. There is evidently a related effect on angles, the N—P—N angle decreasing in the series F (119.6°) > Cl > Br > Ph > OPh > Me > NMe_2 (116.7°), in which the methyl group falls into the position expected chemically. The effect probably depends on the migration of bonding electron density which results from changes in the effective electronegativity of phosphorus.

In the larger cyclic methylphosphazenes, the steric constraints imposed by the six-membered

TABLE 6. Comparison of structural parameters (distances in Å and angles in degrees)

	P—N	P—C/X	N—P—N	P—N—P	C/X—P—C/X	Ref.
			Methylphosphazenes $(NPMe_2)_n$			
n = 3	1.605(6)	1.809(11)	116.8(11)	122.6(4)	102.6(7)	This work
4	1.596(5)	1.804(3)	119.8(2)	132.0(2)	104.1(2)	6
5	1.586(4)	1.801(4)	118.7(18)	132.9(17)	104.3(8)	2
6	1.593(6)	1.808(4)	118.3(18)	133.1(34)	104.2(5)	5
7	1.592(6)	1.804(11)	117.1(16)	132.9(20)	103.9(5)	3
8	1.590(13)	1.811(2)	117.2(20)	139.9(84)	103.5(10)	4
			Cyclotriphosphazenes $(NPX_2)_3$			
X = F	1.570(13)	1.529(4)	119.6(1)	120.4(8)	99.1(6)	9
Cl	1.581(5)	1.993(5)	118.4(1)	121.4(2)	101.4(2)	14
Br	1.576(9)	2.162(5)	118.2(8)	120.9(16)	102.1(1)	18
NCS	1.58(5)	1.63(1)	119(3)	121(4)	100(1)	24
C_6H_5	1.597(9)	1.804(5)	117.8(3)	122.1(7)	103.8(5)	19
OC_6H_5	1.575(2)	1.582(2)	117.3(5)	121.9(5)	98.1(28)	22
NMe_2	1.588(3)	1.652(4)	116.7(4)	123.0(4)	101.5(7)	23
$1/2(O_2C_6H_4)$	1.575(2)	1.594(2)	117.5(15)	122.5(5)	97.0(5)	20
$1/2(2,2'\text{-bi-}C_6H_4O)$	1.570(4)	1.584(4)	118.4(2)	121.0(2)	102.7(2)	25

ring are relaxed, and the angle at nitrogen can increase further. Associated secondary effects, such as changes in σ-hybridization, induce changes in the other mean structural parameters, most notably a decrease in P—N bond length from 1.605(6) Å to values ranging from 1.586(4) to 1.596(5) Å in $(NPMe_2)_{4-8}$.

Acknowledgments

We thank the National Research Council of Canada for financial support and the University of British Columbia Computing Centre for assistance.

1. (*a*) H. T. Searle. Proc. Chem. Soc. 7 (1959); (*b*) R. T. Oakley and N. L. Paddock. Can. J. Chem. **53**, 3035 (1975).
2. M. W. Dougill and B. Sheldrick. Acta Crystallogr. Sect. B, **33**, 295 (1977).
3. K. D. Gallicano, R. T. Oakley, N. L. Paddock, S. J. Rettig, and J. Trotter. Can. J. Chem. **55**, 304 (1977).
4. R. T. Oakley, N. L. Paddock, S. J. Rettig, and J. Trotter. Can. J. Chem. **55**, 2530 (1977).
5. R. T. Oakley, N. L. Paddock, S. J. Rettig, and J. Trotter.Can. J. Chem. **55**, 3118 (1977).
6. M. W. Dougill. J. Chem. Soc. 5471 (1961).
7. H. Jagodzinski, J. Langer, I. Oppermann, and F. Seel. Z. Anorg. Chem. **302**, 81 (1959).
8. H. Jagodzinski and I. Oppermann. Z. Kristallogr. **113**, 241 (1960).
9. M. W. Dougill. J. Chem. Soc. 3211 (1963).
10. M. I. Davis and J. W. Paul, Jr. J. Mol. Struct. **9**, 478 (1971).
11. L. O. Brockway and W. M. Bright. J. Am. Chem. Soc. **65**, 1551 (1943).
12. A. Wilson and D. F. Carroll. J. Chem. Soc. 2548 (1960).
13. E. Giglio. Ric. Sci. Suppl. **30**, 721 (1960).
14. G. J. Bullen. J. Chem. Soc. A, 1450 (1971).
15. H. Bode. Angew. Chem. Dtsch. **61**, 438 (1949).
16. P. DeSantis, E. Giglio, and A. Ripamonti. J. Inorg. Nucl. Chem. **24**, 469 (1962).
17. E. Giglio and R. Puliti. Acta Crystallogr. **22**, 304 (1967).
18. H. Zoer and A. J. Wagner. Acta Crystallogr. Sect. B, **26**, 1812 (1970).
19. F. R. Ahmed, P. Singh, and W. H. Barnes. Acta Crystallogr. Sect. B, **25**, 316 (1969).
20. L. A. Siegel and J. H. Van den Hende. J. Chem. Soc. A, 817 (1967).
21. H. R. Allcock, R. W. Allen, E. C. Bissell, L. A. Smeltz, and M. Teeter. J. Am. Chem. Soc. **98**, 5120 (1976).
22. W. C. Marsh and J. Trotter. J. Chem. Soc. A, 169 (1971).
23. S. J. Rettig and J. Trotter. Can. J. Chem. **51**, 1295 (1973).
24. J. B. Faught, T. Moeller, and I. C. Paul. Inorg. Chem. **9**, 1656 (1970).
25. H. R. Allcock, M. T. Stein, and J. A. Stanko. J. Am. Chem. Soc. **93**, 3173 (1971).
26. P. Coppens, L. Leiserowitz, and D. Rabinovich. Acta Crystallogr. **18**, 1035 (1965).
27. W. R. Busing and H. A. Levy. Acta Crystallogr. **22**, 457 (1967).
28. R. E. Long. Ph.D. Thesis. University of California at Los Angeles, Los Angeles, CA. 1965.
29. D. T. Cromer and J. B. Mann. Acta Crystallogr. Sect. A, **24**, 321 (1968).
30. R. F. Stewart, E. R. Davidson, and W. T. Simpson. J. Chem. Phys. **42**, 3175 (1965).
31. D. T. Cromer and D. Liberman. J. Chem. Phys. **53**, 1891 (1970).
32. V. Schomaker and K. N. Trueblood. Acta Crystallogr. Sect. B, **24**, 63 (1969).
33. D. W. J. Cruickshank. Acta Crystallogr. **9**, 747 (1956); **9**, 754 (1956).
34. D. W. J. Cruickshank. Acta Crystallogr. **14**, 896 (1961).

A study of the Osterberg–Sarkar–Kruck method for evaluating free metal and free ligand concentrations in solutions of complex equilibria

ROGER GUEVREMONT AND DALLAS L. RABENSTEIN

Department of Chemistry, University of Alberta, Edmonton, Alta., Canada T6G 2G2

Received April 21, 1977

ROGER GUEVREMONT and DALLAS L. RABENSTEIN. Can. J. Chem. **55**, 4211 (1977).

The method developed by Osterberg, Sarkar, and Kruck for obtaining the concentrations of free ions in solutions of complex equilibria from p*H* titration data has been studied to establish the conditions under which the method gives accurate values for free ligand and free metal concentrations in systems containing a variety of complexes, including protonated, hydroxy, mixed ligand, and polynuclear complexes. Simulated titration data have been used so that the true values of free ligand and free metal concentrations would be known. Calculation procedures are described for each step in the data evaluation, including procedures for extracting information about the stoichiometry of the complexes from the unique information provided by this method. The effect of various systematic and random errors is also considered.

ROGER GUEVREMONT et DALLAS L. RABENSTEIN. Can. J. Chem. **55**, 4211 (1977).

On a étudié la méthode développée par Osterberg, Sarkar et Kruck pour obtenir, à l'aide de données de titrations de p*H*, les concentrations en ions libres dans des solutions impliquant des équilibres complexes afin d'établir les conditions où la méthode fournit des valeurs précises pour les concentrations de ligands libres et de métaux libres dans des systèmes contenant une variété de complexes incluant des complexes des ligands protonés, hydroxylés et mixtes, et des complexes polynucléaires. On a utilisé des données de titrations simulées de façon à connaitre les valeurs réelles des concentrations de ligands libres et de métaux libres. On décrit des méthodes de calcul pour chacune des étapes dans l'évaluation des données incluant des méthodes pour extraire de l'information concernant la stoechiométrie des complexes à partir d'informations uniques fournies par cette méthode. On considère aussi l'effet de diverses erreurs systématiques et de celles dues au hasard.

[Traduit par le journal]

Introduction

Of the methods for determining the stability constants of metal complexes, those based on potentiometry with the glass electrode are used the most frequently and generally are considered to yield the best results. Several procedures can be used for extracting the stability constants from the experimental data, which usually consist of a series of p*H* titration curves for several combinations of the metal and ligand concentrations. If there are no protonated, deprotonated, hydroxy, or polynuclear complexes, the Bjerrum method (1) is the method of choice. However, if such species do form the stability constants are usually calculated by one of several elaborate computer-based evaluation methods, of which the more widely used are LETAGROP (2), GAUSS (3), SCOGS (4), and STEW (5).

Each of these computation methods makes use of the three mass balance equations for each experimental point.

$$[1] \quad C_H = [H] - [OH] + \sum q\beta_{pqr}\,[M]^p[H]^q[L]^r$$

$$[2] \quad C_M = [M] + \sum p\beta_{pqr}\,[M]^p[H]^q[L]^r$$

$$[3] \quad C_L = [L] + \sum r\beta_{pqr}\,[M]^p[H]^q[L]^r$$

where β_{pqr} and $\beta_{pqr}[M]_p[H]_q[L]_r$ are the stability constant and concentration, respectively, of the species $M_pH_qL_r$. In outline, the procedures generally involve systematic adjustments in the stability constants to minimize the function defined by eq. 4.

$$[4] \quad U = \sum(C_H^{exp} - C_H^{calc})^2$$

where the summation is over all experimental points. C_H^{calc} is obtained at each experimental point by first choosing a model for the solution equilibria and guessing values for the stability constants in this model. The guesses are substituted into eqs. 2 and 3, which are then solved simultaneously at each experimental point for [M] and [L]. These values and the guesses for the stability constants are then substituted into eq. 1 to give C_H^{calc}. Once U has been calculated for this set of stability constants, the constants are adjusted and the entire set of calculations is

repeated. This procedure is continued until U is apparently minimized. If the true minimum of the residual function has been found, the resulting stability constants are those which 'best' fit the experimental data, according to the criteria of least sum of the squares of the residuals, for the chosen model. Usually the stoichiometry of the complexes which form is not known, and this entire procedure is repeated with several models. Clearly, the values calculated for [M] and [L] at each experimental point, and thus the stability constants, depend on the model. It is disconcerting that different models can result in equivalent 'best' fits for the same chemical system.

Recently, a pH titration method has been described in which the free metal ion and the free ligand can be calculated simultaneously throughout the central titration of an appropriately designed set of titrations (6–8). This method is appealing in that the concentrations are obtained directly from the experimental data, without assuming any hypothesized collection of species for that system. The calculation of stability constants then reduces to a linear least-squares problem using any of the mass balance equations. If the stoichiometries of the complexes are not known, it still is necessary to postulate a model. It is to be expected, however, that fewer models will fit the data because the free ligand and free metal concentrations are known and not derived from the model.

We have undertaken a critical examination of this approach, to establish the conditions under which it gives accurate values for the free metal and free ligand concentrations in systems containing a variety of complexes. Our approach has been to analyze simulated titration data, so that the true values of free metal and free ligand concentration would be known. In addition, since this method provides information not available in the study of complex systems by other data evaluation procedures, we also consider ways in which this information can be used to provide guidance in the selection of a model.

Overview of the Method

The basic relationships in this method for determining the concentrations of free ions in solutions of complex equilibria[1] are

$$[5]\quad \mathrm{p[L]} = \mathrm{p[L]}_0 - \int_{\mathrm{p}H_0}^{\mathrm{p}H} \left(\frac{\mathrm{d}C_\mathrm{H}}{\mathrm{d}C_\mathrm{L}}\right)_{C_\mathrm{M},\mathrm{p}H} \mathrm{dp}H$$

$$[6]\quad \mathrm{p[M]} = \mathrm{p[M]}_0 - \int_{\mathrm{p}H_0}^{\mathrm{p}H} \left(\frac{\mathrm{d}C_\mathrm{H}}{\mathrm{d}C_\mathrm{M}}\right)_{C_\mathrm{L},\mathrm{p}H} \mathrm{dp}H$$

where C_H is the concentration of titrable proton, C_L and C_M are the total analytical concentrations of ligand and metal, and [L] and [M] are their free concentrations. For systems containing more components, equations analogous to [5] and [6] can be written for each component in the solution. For simplicity let us only consider the component L, remembering that the discussion is applicable to every component in the system.

The quantity $\mathrm{p[L]}_0$ is the negative logarithm of the concentration of free L at some initial pH_0. A pH_0 is usually chosen at which no complex is formed, and consequently $[\mathrm{L}]_0$ is equal to (or may be calculated from) C_L. The integral of $(\mathrm{d}C_\mathrm{H}/\mathrm{d}C_\mathrm{L})_{C_\mathrm{M},\mathrm{p}H}$ is evaluated from pH_0 to the pH at which p[L] is to be evaluated.

One experimental method for obtaining $(\mathrm{d}C_\mathrm{H}/\mathrm{d}C_\mathrm{L})_{C_\mathrm{M},\mathrm{p}H}$ as a function of pH is with a series of titrations where the total concentration of L is varied, while all the other components are at constant concentration. At a given pH, C_H is extracted from each of the titrations. The derivative $(\mathrm{d}C_\mathrm{H}/\mathrm{d}C_\mathrm{L})_{C_\mathrm{M},\mathrm{p}H}$ is the change in C_H with C_L, measured at C_L of the middle titration. In exactly this way the derivative at each pH throughout the titration is calculated. The values of $(\mathrm{d}C_\mathrm{H}/\mathrm{d}C_\mathrm{L})_{C_\mathrm{M},\mathrm{p}H}$ are then integrated from pH_0 to a given pH, and p[L] at that pH is calculated from [5]. The experiment is designed in such a way that, given a system of composition C_L and C_M, referred to as the composition of the middle titration, each component is in turn selectively varied. The FICS method will then provide [L] and [M] as a function of pH, for a solution of that overall composition.

The stability constants of the complexes are calculated by a linear least-squares fit of the [L] and [M] data into the mass balance equations. Any one mass balance is completely sufficient unless a given complex does not contain any of that particular component.

In the following section, the calculation procedures at each step in the method are considered.

Calculation Procedures in the FICS Method

C_H Calculations

The total concentration of titrable proton is

[1]For convenience, we will name this method FICS, for free ion concentrations in solution.

calculated from the relation

$$[7] \qquad C_H = (NTP \times C_L) + C_A - C_B$$

where NTP is the number of titrable protons on the ligand in the form used to prepare the solutions, and C_A and C_B are concentrations of added acid and base. Calculation of $(dC_H/dC_L)_{C_M,pH}$ requires that C_H be known at specific and closely spaced pH values throughout the series of titrations. Since this is difficult experimentally, some manipulation of the data is necessary. We have used a simple linear interpolation between data points. The linear interpolation is limited in that, first it does not use the entire body of data as a unit, and therefore does not have the smoothing potential which curve fitting procedures might have, and second it will bias the data in some cases. A bias to large C_H will result if the C_H vs. pH curve is concave upward, and to low C_H's if the curve is concave downward. However we have found that the linear interpolation provides very good estimates of C_H at the required pH's when data points are taken at pH intervals of 0.1 units or less. Efficient use of the experimental data requires that the pH interval used in the FICS procedure be approximately equal to that of the data.

The Derivative, $(dC_H/dC_L)_{C_M,pH}$

The reliability of the derivative depends strongly on several factors: (*1*) the accuracy of C_H, (*2*) the degree of curvature of the C_H vs. C_L function, (*3*) the number of titrations of varying C_L, and (*4*) the extent to which the concentrations of components other than C_L remain constant.

In Fig. 1 are plots of C_H vs. C_L at various pH values for a system containing a diprotic ligand and complexes ML, ML_2, ML_3, and $H_{-1}ML_2$, where $H_{-1}ML_2$ might be a hydroxy complex. The important characteristics to note are that C_H may vary over several orders of magnitude, under conditions of excess metal concentration C_H may be small, and there may be extreme curvature in the function of C_H vs. C_L.

The design of the experiment must avoid problems arising from the above factors. The quantity C_H has error associated with it, and if the absolute value of C_H is small the experimental data may not be sensitive enough to reflect the true behaviour of C_H with change in C_L. In this situation the derivative cannot have much significance. This will occur in systems where C_L is low, and in those containing excess metal.

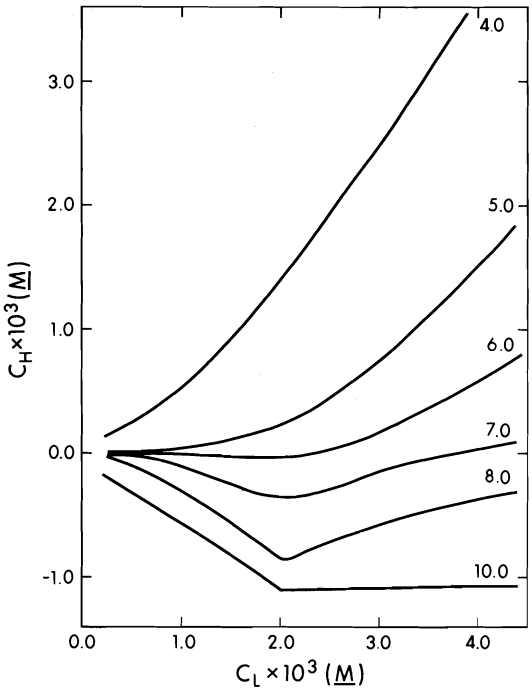

FIG. 1. C_H vs. C_L for a system containing a diprotic ligand and complexes ML, ML_2, ML_3, and $H_{-1}ML_2$. The overall ligand protonation constants are 1.0×10^6 and 1.0×10^{10}. The formation constants of the complexes are 1.0×10^6, 1.0×10^{11}, 1.0×10^{15}, and 1.0×10^4 respectively. C_M was constant at 1.0×10^{-3} M (see Tables 1 and 3).

Each point on a C_H vs. C_L plot represents data from a separate titration, and the numbers of points are therefore necessarily small. This imposes the requirement that the range of C_L be chosen so that C_H varies linearly with C_L. If this condition is met only two titrations are necessary, and more will provide increasingly reliable results. Reasonable random error is acceptable since a linear least-squares fit will tend to give better derivatives than the limit of accuracy of C_H might indicate possible. A linear variation in C_H with C_L can be achieved experimentally if the ligand to metal ratio is higher than the stoichiometric ligand to metal ratio of predominating complexes. The range of C_L must not be so wide as to extend into regions of curvature of the C_H vs. C_L function.

With a small number of data points, a least-squares polynomial fit will not solve the problem of curvature of C_H with C_L. First, if the function of C_H vs. C_L is in fact linear with ran-

dom error superimposed, the polynomial may try to fit even those errors. Second, if the function is nonlinear, it is not likely as simple as a polynomial of low degree, and systematic distortion of the actual relation will occur.

The Integral $\int_{pH_0}^{pH} \left(\frac{dC_H}{dC_L}\right)_{C_M,pH} dpH$

The values of $(dC_H/dC_L)_{C_M,pH}$ and $(dC_H/dC_M)_{C_L,pH}$ usually fall within the range $\pm n$, where n is the number of protons on the fully protonated ligand. Figure 2 shows the variation in these derivatives as a function of pH for the same system considered in Fig. 1.

The concentrations of free ligand and free metal at a particular pH are calculated by integrating the functions shown from pH_0 to that pH. We have chosen to evaluate the integral numerically from the tabulated function $(dC_H/dC_L)_{C_M,pH}$ using the trapezoid rule. This procedure, used at 0.1 pH intervals, gave as good accuracy as in most cases is appropriate. Alternatively, the entire set of $(dC_H/dC_L)_{C_M,pH}$ can be fit to a polynomial (7), and the integral evaluated by simple calculus.

All the series of simulated titration data presented in this paper were treated in exactly the manner described in the previous sections. Examples of free ligand and free metal concentrations derived using FICS are shown in Tables 1 and 2. Table 1 contains known and derived [L] and [M] corresponding to the system already referred to in Figs. 1 and 2. Table 2 presents results from which can be seen the effect of dilution on [L] and [M]. This is discussed in a later section on errors.

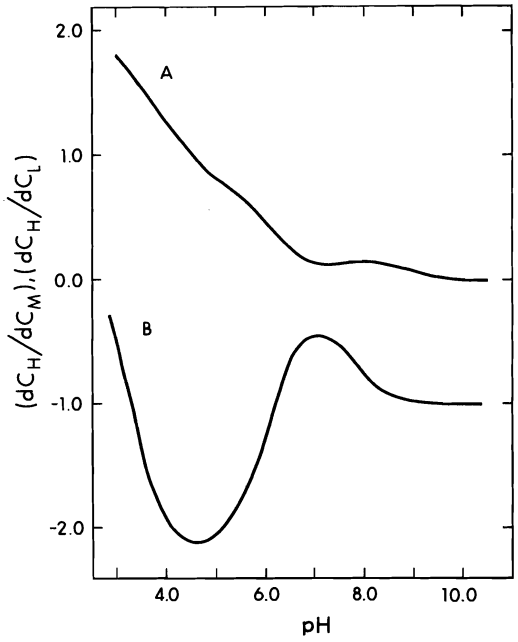

FIG. 2. $(dC_H/dC_L)_{C_M,pH}$, A, and $(dC_H/dC_M)_{C_L,pH}$, B, as a function of pH for the system of complexes defined in the legend of Fig. 1. $C_M = 1.0 \times 10^{-3}$ M, $C_L = 4.0 \times 10^{-3}$ M (see Tables 1 and 3).

Formation Constants

The FICS method provides free ligand and free metal concentrations as a function of pH. Formation constants can be extracted from a linear least-squares fit to the mass balance of each component in solution. The quantity U is minimized.

$$[8] \quad U = \sum(C_L - ([L] + \sum r\beta_{pqr}[M]^p[H]^q[L]^r))^2$$

In all the examples presented in this paper we have used a Gaussian elimination followed by matrix inversion to solve the simultaneous equations. Each mass balance is treated separately and no constants are given as knowns. The mass balance for protons, C_H, has not been used since weighting of the data would be necessary. For simplicity in this work, the mass balances for ligand and metal are shown as $\sum$[L] and $\sum$[M].

Some estimate of the accuracy of the FICS method is necessary. The simplest, though not the most reliable quantity, is the goodness of the fit of the model to the known total analytical concentrations of ligands and metals. The experimental values of [L] and [M] and the formation constants are inserted into [8] and the standard deviation of the fit is $[U/(n-1)]^{1/2}$, where n is the number of experimental points. The relative standard deviation of the fit, in percent, is used in this work.

The standard deviation calculation is limited in that it does not give any indication of the accuracy of the [L] and [M] data, rather it only estimates the fit of the hypothesized model to that data. For this reason a study of the evaluation of [L] and [M] by the FICS method using simulated titration data, where [L] and [M] are accurately known, is particularly important.

The suitability of a model describing the composition of complex species existing in solution may be checked several ways. It is expected that a good hypothesis will give a low standard deviation of the fit, and that the constants derived from one mass balance will agree

TABLE 1. Known free ligand and free metal concentrations and those calculated by FICS[a]

	Free ligand		Free metal	
pH	Known	Calculated	Known	Calculated
4.0	1.204×10^{-5}	1.202	3.414×10^{-5}	3.419
5.0	1.250×10^{-4}	1.246	2.732×10^{-7}	2.746
6.0	5.792×10^{-4}	5.732	4.314×10^{-9}	4.389
7.0	1.055×10^{-3}	1.044	7.151×10^{-10}	7.262
8.0	1.422×10^{-3}	1.415	1.959×10^{-10}	1.971
9.0	1.844×10^{-3}	1.836	2.463×10^{-11}	2.474
10.0	1.980×10^{-3}	1.973	2.498×10^{-12}	2.510

[a]For a system containing a diprotic ligand and the complexes ML, ML_2, ML_3, and $H_{-1}ML_2$. The known constants and those derived from these values are given in Table 3. The following conditions were used in the simulation: C_M = 0.90, 0.95, 1.00, 1.05, and 1.10×10^{-3} M with $C_L = 4.00\times10^{-3}$ M and C_L = 3.6, 3.9, 4.1, and 4.4×10^{-3} M with $C_M = 1.00\times10^{-3}$ M. The middle titration is $C_M = 1.00\times10^{-3}$ M and $C_L = 4.00\times10^{-3}$ M.

TABLE 2. The effect of dilution on free ligand and free metal concentrations calculated by FICS[a]

	Titrant	Free ligand		Free metal	
pH	volume[b] (ml)	Known	Calculated	Known	Calculated
3.0	—	2.756×10^{-15}	2.756	7.839×10^{-4}	7.839
4.0	—	1.863×10^{-12}	1.860	5.094×10^{-5}	5.104
5.0	—	9.127×10^{-10}	9.100	1.002×10^{-6}	1.007
6.0	—	5.443×10^{-8}	5.432	2.629×10^{-8}	2.641
7.0	—	9.124×10^{-7}	9.111	5.974×10^{-10}	5.997
8.0	—	9.805×10^{-6}	9.794	9.456×10^{-12}	9.493
9.0	—	9.083×10^{-5}	9.070	1.200×10^{-13}	1.206
10.0	—	5.000×10^{-4}	4.989	3.996×10^{-15}	4.022
3.0	0.3437	2.753×10^{-15}	2.753	7.832×10^{-4}	7.839
4.0	2.240	1.849×10^{-12}	1.868	5.092×10^{-5}	4.833
5.0	3.251	9.033×10^{-10}	9.141	1.003×10^{-6}	0.8804
6.0	5.458	5.355×10^{-8}	5.524	2.661×10^{-8}	2.225
7.0	6.300	8.937×10^{-7}	9.402	6.097×10^{-10}	4.916
8.0	6.682	9.591×10^{-6}	10.32	9.667×10^{-12}	7.545
9.0	6.818	8.881×10^{-5}	9.767	1.227×10^{-13}	0.9290
10.0	7.201	4.882×10^{-4}	5.474	4.092×10^{-15}	3.039

[a]For a system containing a triprotic ligand and the complexes HML, HML_2, and ML_2. The known constants and those derived from these values are given in Table 3. The titration conditions were: C_M = 0.99, 1.0, and 1.01×10^{-3} M with $C_L = 3.0\times10^{-3}$ M, and C_L = 2.99 and 3.01×10^{-3} $M$with $C_M = 1.00\times10^{-3}$ M. The middle titration is $C_M = 1.00\times10^{-3}$ M and $C_L = 3.00\times10^{-3}$ M.
[b]Initial volume was 300 ml.

with those derived from another. The constants which are known, for example, ligand protonation constants, must be derived correctly from the data. The existence of some species may be questioned if small or negative formation constants are produced, or if the agreement of values based on different mass balances is poor.

The next section will deal directly with the problem of assigning a model to the system.

A Model for Metal–Ligand Interactions

Titration methods do not in general provide information from which the model, or the types of complexes in a system, can be derived. In this respect, FICS has an advantage over other methods. Using [H], [L], and [M] the concentrations of proton, ligand, and metal whose chemical situation has not been determined (ΔC_H, ΔC_L, and ΔC_M) can be calculated. For example, given the total ligand concentration C_L, and the free ligand concentration [L], ΔC_L equals C_L − [L]. If the pH and protonation constants are known,

$$[9]\quad \Delta C_L = C_L - ([L] + \beta_1[H][L] + \beta_2[H]^2[L])$$

for a diprotic ligand.

Figure 3 is a combined plot of ΔC_H, ΔC_L, and ΔC_M for a system containing a triprotic ligand and complexes H_2ML, HM_2L, and M_2L_2.

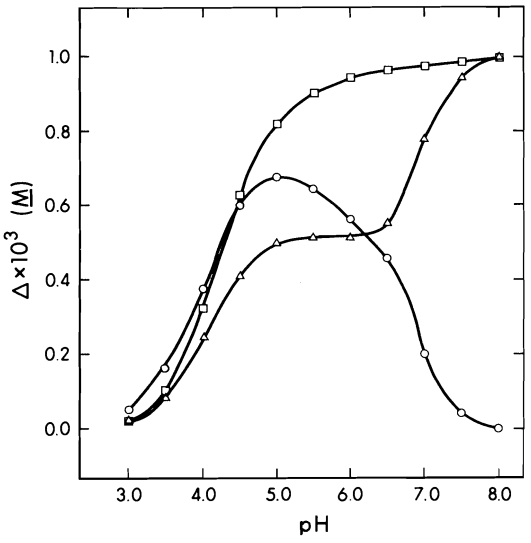

FIG. 3. ΔC_H, ○, ΔC_L, △, and ΔC_M, □, for a system containing a triprotic ligand and complexes H_2ML, HM_2L, and M_2L_2. See text for details of calculation.

Three distinct areas can be seen. (*1*) Below p*H* 3.5 there is a region where ΔC_H is about twice as large as ΔC_L and ΔC_M. (*2*) Near p*H* 6.0 ΔC_M is about twice as large as ΔC_H or ΔC_L. (*3*) Above p*H* 6.0 ΔC_H becomes zero and ΔC_L and ΔC_M are equal. Based upon (*1*) a complex of type H_2ML would be expected to minimize ΔC_H, ΔC_L, and ΔC_M if its concentration is about 1×10^{-4} *M* at p*H* 3.5. Using [H], [L], and [M] from p*H* 3.0 to 3.5, a formation constant of 1.2×10^{19} for H_2ML was calculated.

Figure 4 is a plot of ΔC_H, ΔC_L, and ΔC_M, where these quantities are calculated using the estimated value of the formation constant for H_2ML. For example

$$[10] \quad \Delta C_L = C_L - ([L] + [HL] + [H_2L] + [H_3L] + [H_2ML])$$

where $[H_2ML]$ equals $\beta_{H_2ML}[H]^2[M][L]$. If the series of species included in [10] completely accounts for all the ligand in solution, ΔC_L will be zero. This appears to be the case in the region near p*H* 3. However, in the p*H* region 4 to 5 a complex forms which contains approximately equal amounts of proton and ligand, and a larger amount of metal. A complex of the type HM_2L may best account for the observed ΔC_H, ΔC_L, and ΔC_M. This was not evident in Fig. 3 for the same p*H* range. Using [H], [L], and [M] data from p*H* 3 to 6, constants for H_2ML and HM_2L were found to be 1.02×10^{19} and 9.98×10^{17}

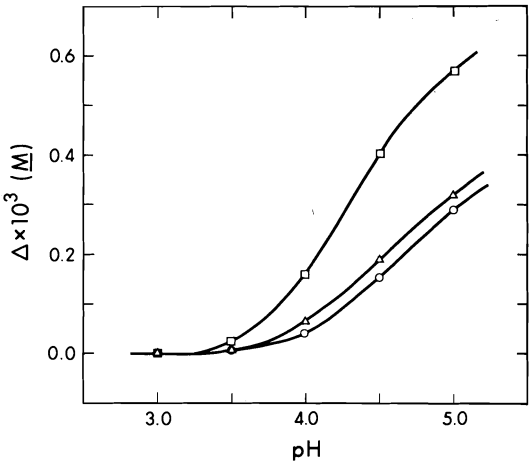

FIG. 4. ΔC_H, ○, ΔC_L, △, and ΔC_M, □, as in Fig. 3, except that the complex H_2ML is accounted for in the calculation of ΔC_H, ΔC_L, and ΔC_M. An estimated value of 1.2×10^{19} for β_{H_2ML} was used in the calculation.

respectively. Figure 5 is a plot of ΔC_H, ΔC_L, and ΔC_M using these estimated constants. The other major complex in solution must contain no protons, and equal numbers of ligands and metals. Inclusion of the species M_2L_2 yielded formation constants of 1.00×10^{21}, 9.97×10^{15}, 9.97×10^{9}, 9.93×10^{18}, 1.03×10^{18}, and 1.01×10^{17} for H_3L, H_2L, HL, H_2ML, HM_2L, and M_2L_2 respectively from the ligand mass balance and

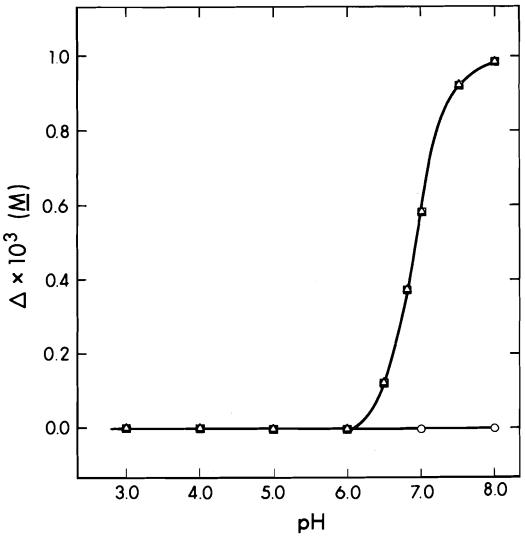

FIG. 5. ΔC_H, ○, ΔC_L, △, and ΔC_M, □, as in Fig. 3, except that the complexes H_2ML and HM_2L are accounted for in the calculation of ΔC_H, ΔC_L, and ΔC_M. Estimated values of 1.02×10^{19} and 9.98×10^{17} were used for β_{H_2ML} and β_{HM_2L}.

9.98×10^{18}, 1.00×10^{18}, and 1.01×10^{17} for H_2ML, HM_2L, and M_2L_2 respectively from the metal mass balance.

The Effect of Error on the FICS Method

This discussion will be limited to error introduced through the experimental procedure. The size of error due to the nature of data handling of the FICS method can be seen in Tables 1 and 2. The systems of simulated titrations were designed to be experimentally feasible, but without the error associated with the actual experiment. There has been no attempt to show that FICS can produce perfect [L]'s and [M]'s because this would require a set of titrations which could never actually be performed. At this point we will introduce those systematic and random errors which are inherent to the real experiment. The error in [L] and [M] will then include uncertainty arising from both sources, the FICS data handling and the imposed experimental error.

Dilution Error

Three separate types of error are introduced by dilution. First, in the experiments designed for the evaluation of $(dC_H/dC_L)_{C_M,pH}$, C_L is not constant but varies as titrant is added. This is easily compensated for in the evaluation by using C_L exactly as it is found at that pH, based upon volume of titrant added to that point. Each pH will have a unique set of C_L's through which the derivative is evaluated.

The second and third dilution problems are related to dilution of components other than C_L, and cannot be corrected in the data handling process. During a set of titrations designed to give the derivative $(dC_H/dC_L)_{C_M,pH}$, the C_M will vary through dilution. Assuming that all the titrations have equal dilution to a given pH, the derivative will be evaluated at a C_M different from C_M at pH_0.

The third type of error is implied above. All the titrations do not have equal dilution to a given pH, and consequently, at each pH, C_M will be different for the different titrations. The term $(dC_H/dC_L)_{C_M,pH}$ explicitly requires that the change in C_H with C_L be measured at constant pH and C_M.

These problems contribute significant error to the free ion concentrations. Table 2 shows [L] and [M] for a system containing a triprotic acid and complexes HML, HML_2, and ML_2. With a total dilution of 7.201 ml titrant into 300 ml, the free ligand concentration at pH 10.0 had about 10% error and the free metal concentration about 25%. Without dilution the error in [L] and [M] was only 0.5%. Table 3 summarizes formation constants derived from these two sets of free ion concentration data.

Error introduced by dilution cannot be corrected once the data have been taken. On the other hand, it is possible to experimentally ensure that C_M remains constant throughout a set of titrations, either by eliminating dilution by use of coulometric titration, or by simultaneous addition of titrant and a concentrated metal solution. We have found the latter, using computer operated instrumentation, to be a practical solution to this problem.

Error in pH Measurement

Unlike other pH titration methods, the FICS procedure does not require that the hydrogen ion concentration or the hydrogen ion activity be known to get accurate free ion concentrations for ligands and metals. The pH is merely a reference scale on which to first evaluate $(dC_H/dC_L)_{C_M,pH}$, and to finally integrate this quantity from pH_0 to pH. Its numerical value is not required in any stage of the calculation of [L] and [M]. However, the pH does enter into the calculation of formation constants.

If the electrodes are standardized using NBS activity buffers, then [L] and [M] are known at a series of p_aH values. The formation constants are calculated using the sets of p_aH, [L], and [M], and consequently are of a mixed activity, concentration type. If the electrodes are calibrated for H^+ concentration, the [L] and [M] are correct at those concentrations, and the derived β's are concentration formation constants.

The FICS method requires only that the pH electrode standardization be internally consistent and serious systematic error is avoided. Random errors in individual measurements will exist, however. These will give rise to exactly the same type of error as random errors in C_H, and will therefore be discussed in that section.

Error in the Initial Free Ligand and Free Metal Concentrations

The FICS method requires that [L] and [M] be known at pH_0, imposing restrictions which contradict many of the experimental requirements discussed above. In most cases complexation is only negligible at low pH, where protons successfully compete for ligand. Under these con-

TABLE 3. Actual formation constants and those calculated from p[M] and p[L] values obtained by the FICS method

Complex system	Formation constants		
	Actual	C_L Mass balance	C_M Mass balance
H_2L[a]	1.0×10^{10}	9.983×10^{9}	
HL	1.0×10^{6}	9.952×10^{5}	
ML	1.0×10^{6}	1.021×10^{6}	1.004×10^{6}
ML_2	1.0×10^{11}	9.978×10^{10}	9.948×10^{10}
ML_3	1.0×10^{15}	1.019×10^{15}	1.015×10^{15}
$H_{-1}ML_2$	1.0×10^{4}	1.004×10^{4}	1.002×10^{4}
H_3L[b]	1.0×10^{21}	1.0008×10^{21}	
H_2L	1.0×10^{16}	1.0062×10^{16}	
HL	1.0×10^{10}	9.9996×10^{9}	
HML	1.0×10^{17}	9.984×10^{16}	
HML_2	1.0×10^{25}	9.993×10^{24}	
ML_2	1.0×10^{18}	9.989×10^{17}	
H_3L[c]	1.0×10^{21}	9.893×10^{20}	
H_2L	1.0×10^{16}	1.073×10^{16}	
HL	1.0×10^{10}	1.215×10^{10}	
HML	1.0×10^{17}	1.056×10^{17}	
HML_2	1.0×10^{25}	1.044×10^{25}	
ML_2	1.0×10^{18}	9.647×10^{17}	

[a]Calculated from the p[M] and p[L] data in Table 1. The standard deviation of the fit to both the C_L and C_M mass balances is 0.12%.
[b]Calculated from the data with no dilution in Table 2.
[c]Calculated from the data with dilution in Table 2.

TABLE 4. Effect of systematic error in $p[L]_0$ and $p[M]_0$ on free ligand and free metal concentrations calculated by FICS[a]

pH	Initial concentrations of free ligand and free metal, $p[L]_0$ and $p[M]_0$[b]				
	6.439, 3.000[c]	6.460, 3.086	6.466, 3.115	6.469, 3.126	6.470, 3.131
			Free ligand		
4.0	1.29×10^{-5}	1.23	1.21	1.20	1.20
5.0	1.34×10^{-4}	1.27	1.26	1.25	1.25
6.0	6.14×10^{-4}	5.86	5.77	5.74	5.73
7.0	1.12×10^{-3}	1.07	1.05	1.05	1.04
8.0	1.52×10^{-3}	1.45	1.42	1.42	1.42
9.0	1.97×10^{-3}	1.88	1.85	1.84	1.84
10.0	2.11×10^{-3}	2.01	1.99	1.98	1.97
			Free metal		
4.0	4.62×10^{-5}	3.79	3.54	3.46	3.42
5.0	3.71×10^{-7}	3.05	2.85	2.78	2.75
6.0	5.39×10^{-10}	4.87	4.55	4.44	4.39
7.0	9.81×10^{-10}	8.06	7.53	7.34	7.26
8.0	2.66×10^{-10}	2.19	2.04	1.99	1.97
9.0	3.34×10^{-11}	2.74	2.57	2.50	2.47
10.0	3.39×10^{-12}	2.78	2.60	2.54	2.51

[a]See Table 1 for the model and the known free ligand and free metal concentrations.
[b]Correct $p[L]_0 = 6.470$ and $p[M]_0 = 3.131$ at $pH_0 = 3.00$.
[c]$p[L]_0$ and $p[M]_0$ assuming no complexation has occurred at pH_0.

ditions, C_H at pH_0 is large. This leads to difficulty in those regions of the pH titration where C_H is small. As the size of C_A and C_B (concentrations of added acid and base) increases, C_H loses significance at correspondingly larger values.

Table 4 illustrates the effect of error in $p[L]_0$ and $p[M]_0$ on [L] and [M] derived for the system

considered in Table 1. The far left column is the set of [L] and [M] calculated using $p[L]_0$ and $p[M]_0$ based upon the (incorrect) assumption that no interaction between ligand and metal has occurred. The error in [L] and [M] is significant.

The problem may be corrected by an iteration where (*1*) the $p[L]_0$ and $p[M]_0$ are calculated assuming no complexation and used in the FICS procedure to estimate p[L] and p[M], (*2*) the formation constants are then estimated, and (*3*) new $p[L]_0$ and $p[M]_0$ calculated on the basis of the calculated constants. Tables 4 and 5 show the effect of this iteration. Each $p[L]_0$ and $p[M]_0$ are based upon the [L], [M], and formation constants of the previous column. Each iteration gives better [L] and [M] values, and more reliable formation constants.

The method will fail if too much metal and ligand are complexed at pH_0, or if the complexes forming at low p*H* are not known. In these cases the titrations must be repeated beginning at lower pH_0. The C_H vs. C_L and C_H vs. C_M plots indicate the p*H* at which the complex starts to form; if no complex forms the slope of the C_H vs. C_L plot will equal the average protonation number of the ligand at that p*H* while that of the C_H vs. C_M plot will be zero.

Random Error

All measurements have some uncertainty associated with them. In order to evaluate the effects of random error on the FICS method we have imposed random noise of various magnitudes on the titration data. The experimental data are C_H as a function of p*H*. We will therefore restrict discussion to error in C_H, since an error in p*H* is equivalent to an error in C_H.

Two approaches have been considered, first a random error based on the absolute magnitude of C_H and, second, a random error of constant magnitude. It must be noted here, however, that error seldom is totally random, and conclusions based on studies of random errors are only qualitative in nature.

Table 6 summarizes results of the FICS method used on the system considered in Table 1, where random errors proportional to the size of C_H have been imposed on the titration data. The constants derived from the [L] and [M] from Table 6 are shown in Table 7. Considerable error develops in [L] and [M] when the random errors are larger than 0.5% of C_H. Similar con-

TABLE 5. Effect of systematic error in $p[L]_0$ and $p[M]_0$ on formation constants[a,b]

	Initial concentrations of free ligand and free metal, $p[L]_0$ and $p[M]_0$							
	6.439, 3.000		6.460, 3.086		6.466, 3.115		6.469, 3.126	
Complexes	Σ[L]	Σ[M]	Σ[L]	Σ[M]	Σ[L]	Σ[M]	Σ[L]	Σ[M]
H_2L	9.28×10^{9}		9.75×10^{9}		9.90×10^{9}		9.96×10^{9}	
HL	9.90×10^{5}		9.93×10^{5}		9.94×10^{5}		9.95×10^{5}	
ML	6.78×10^{5}	5.32×10^{5}	8.90×10^{5}	8.21×10^{5}	9.73×10^{5}	9.37×10^{5}	1.01×10^{6}	9.83×10^{5}
ML_2	6.06×10^{10}	7.02×10^{10}	8.45×10^{10}	8.84×10^{10}	9.42×10^{10}	9.55×10^{10}	9.80×10^{10}	9.82×10^{10}
ML_3	5.98×10^{14}	5.99×10^{14}	8.53×10^{14}	8.52×10^{14}	9.58×10^{14}	9.55×10^{14}	1.00×10^{15}	9.96×10^{14}
$H_{-1}ML_3$	6.01×10^{3}	6.48×10^{3}	8.47×10^{3}	8.65×10^{3}	9.47×10^{3}	9.52×10^{3}	9.86×10^{3}	9.86×10^{3}
Standard deviation of fit	0.13%	3.9%	0.12%	1.2%	0.12%	0.44%	0.12%	0.18%

[a]See Table 4 for the effect of systematic error in $p[L]_0$ and $p[M]_0$ on the free ligand and free metal concentrations used in calculating the formation constants.
[b]See Table 3 for the known formation constants.

TABLE 6. Effect of random error in C_H on free ligand and free metal concentrations calculated by FICS[a,b]

pH	Known free ligand	With random error in C_H ±0.5%	±1%	±2%	±5%
4.0	1.204×10^{-5}	1.21	1.21	1.32	1.50
5.0	1.250×10^{-4}	1.27	1.32	1.38	1.62
6.0	5.792×10^{-4}	5.86	6.00	6.14	6.80
7.0	1.055×10^{-3}	1.07	1.09	1.12	1.24
8.0	1.422×10^{-3}	1.45	1.47	1.51	1.68
9.0	1.844×10^{-3}	1.88	1.92	1.97	2.19
10.0	1.980×10^{-3}	2.01	2.06	2.14	2.42
	Known free metal				
4.0	3.414×10^{-5}	3.23	3.40	4.82	8.08
5.0	2.732×10^{-7}	2.52	2.91	3.95	6.80
6.0	4.314×10^{-9}	4.17	4.99	5.67	8.34
7.0	7.151×10^{-10}	6.95	8.27	9.50	10.42
8.0	1.959×10^{-10}	1.88	2.24	2.57	3.82
9.0	2.463×10^{-11}	2.37	2.70	3.25	4.91
10.0	2.498×10^{-12}	2.47	2.70	3.41	5.40

[a]The magnitude of the random error is proportional to the magnitude of C_H.
[b]From simulated titration data for the system considered in Table 1.

TABLE 7. Effect of random errors in C_H on formation constants [a,b]

Complexes	Known constants	With random error in C_H ±0.5% Σ[L][c]	±0.5% Σ[M][d]	±1% Σ[L]	±1% Σ[M]	±2% Σ[L]	±2% Σ[M]	±5% Σ[L]
H_2L	1.0×10^{10}	1.005		0.982		1.00		1.00
HL	1.0×10^{6}	1.026		0.909		1.01		1.08
ML	1.0×10^{6}	0.854	0.964	1.08	1.01	0.970	0.855	0.715
ML_2	1.0×10^{11}	1.059	1.101	1.06	0.951	0.259	0.388	−1.29
ML_3	1.0×10^{15}	0.982	0.985	0.753	0.755	0.652	0.674	3.21
$H_{-1}ML_2$	1.0×10^{4}	0.972	0.991	0.808	0.847	0.575	0.626	0.240
Standard deviation of fit		0.41%	0.99%	1.1%	2.1%	2.2%	3.8%	—

[a]The magnitude of the random error is proportional to the magnitude of C_H.
[b]From simulated titration data for the system considered in Table 1. See Table 6 for free ligand and free metal data.
[c]Calculated from ligand mass balance.
[d]Calculated from metal mass balance.

clusions result from the consideration of random error in C_H of a constant magnitude.

Several words of caution are appropriate. Systematic errors are considerably more serious than random errors. Therefore a systematic error of magnitude comparable to the random errors considered in Tables 6 and 7 will not give results as good as the results in Tables 6 and 7 indicate. In addition it must be kept in mind that the ligand to metal ratio, and so on, used in the simulated data, was chosen with all those factors discussed in the section on calculations given careful consideration. Conclusions arrived at in this section on errors cannot be applicable to situations where C_H is unnecessarily small, or severe curvature in the function of C_H vs. C_L exists.

Conclusions

The FICS method has several important advantages over most pH titration methods for the study of complex equilibria. The method provides free ion concentrations directly from the experiment. Moreover, they are derived for each component individually, that is, independent of the other components, and independent of the numerical value of the hydrogen ion

concentration. In contrast to most other methods, FICS derives free ligand and free metal concentrations completely independent of any preconceived model of interactions which may be occurring in solution. The free ligand and free metal concentrations are accurate even if a model for the system is never found.

The FICS procedure has been tested extensively on simulated titration data, and is applicable to systems containing a variety of species. Examples include hydroxy, protonated, polynuclear, and mixed ligand complexes. No attempt has been made to show that FICS will give completely exact [L] and [M]; rather, attention has been focused on each step of the procedure to find the most practical and reliable experimental method to use with FICS. In this respect it was found that situations where C_H is small and where the curvature of C_H vs. C_L is large must be avoided. Systems containing an excess of ligand appear to be most favorable. Under these conditions a series of relatively simple manipulations of the experimental data will give accurate free ion concentrations.

The availability of free ligand and free metal concentrations presents excellent possibilities for the logical deduction of the complexes existing in solution. For this purpose, the quantities ΔC_H, ΔC_L, and ΔC_M have been introduced, and applied to the deduction of a model from simulated titration data. Considerable information concerning the model is also potentially available from plots such as those in Figs. 1 and 2.

The results in this paper indicate, however, that proper use of this method requires careful design of the experiment. For example, significant error can result from dilution due to the systematic violation of the theoretical requirements of the FICS method. The requirement that $p[M]_0$ and $p[L]_0$ be known at pH_0 can be satisfied even though some complexation has occurred at pH_0 by use of an iterative procedure. This makes it possible to avoid extremely low pH values where precise measurement of pH, and thus C_H, can be difficult.

We have used the methods described in this paper in a study of the zinc complexes of aspartic acid and glutamic acid. The theoretical requirement that C_M and C_L remain constant for the evaluation of $(dC_H/dC_L)_{C_M,pH}$ and $(dC_H/dC_M)_{C_L,pH}$ has been satisfied by the addition of the required amount of a concentrated metal or a concentrated ligand solution with each addition of titrant. The results are in excellent agreement with literature values and will be presented in a future publication on the chemistry of these systems.

Acknowledgements

This research was supported in part by the National Research Council of Canada and the University of Alberta. Financial support to R.G. by a National Research Council of Canada Scholarship is gratefully acknowledged.

1. J. Bjerrum. Metal amine formation in aqueous solution. Dissertation. Copenhagen. 1941.
2. L. G. Sillén. Acta Chem. Scand. **16**, 159 (1962).
3. D. D. Perrin and I. G. Sayce. J. Chem. Soc. A, 82 (1967).
4. I. G. Sayce. Talanta, **15**, 1397 (1968).
5. P. Gans and A. Vacca. Talanta, **21**, 45 (1974).
6. R. Osterberg. Acta Chem. Scand. **14**, 471 (1960).
7. B. Sarkar and T. P. A. Kruck. Can. J. Chem. **51**, 3541 (1973).
8. W. A. E. McBryde. Can. J. Chem. **51**, 3573 (1973).

Determination of $\Delta H_{f298}^0(C_6F_5Br, g)$ from studies of the combustion of bromopentafluorobenzene in oxygen and calculation of $D[C_6F_5 — Br]$

MICHAEL J. KRECH

Department of Chemistry, Wilfrid Laurier University, Waterloo, Ont., Canada N2L 3C5

AND

STANLEY JAMES W. PRICE[1] AND HENRY J. SAPIANO

Department of Chemistry, University of Windsor, Windsor, Ont., Canada N9B 3P4

Received July 4, 1977

MICHAEL J. KRECH, STANLEY JAMES W. PRICE, and HENRY J. SAPIANO. Can. J. Chem. **55**, 4222 (1977).

The heat of formation of bromopentafluorobenzene has been determined through the use of the direct combustion method which has been applied to hexafluorobenzene, octafluorotoluene, and iodopentafluorobenzene. While a platinum lined bomb is normally used for these types of compounds a steel bomb had to be adopted in this work. The combustion of bromopentafluorobenzene in the steel bomb yields CO_2, CF_4, F_2, Br_2, and BrF_3. With a ten-fold excess of oxygen, the average CO_2 to CF_4 molar ratio is 7.29 ± 0.07. A material balance was obtained for carbon, fluorine, and bromine. The value of $\Delta H_{f298}^0(C_6F_5Br, g) = -711.6 \pm 16.7$ kJ mol^{-1} (-170.1 ± 4.0 kcal mol^{-1}) has been combined with $\Delta H_{f298}^0(C_6F_5, g) = -387.4$ kJ mol^{-1} (-92.6 kcal mol^{-1}) and $\Delta H_{f298}^0(Br, g) = 111.7$ kJ mol^{-1} (26.7 kcal mol^{-1}) to obtain a value for $D[C_6F_5—Br]$ of 435.9 kJ mol^{-1} (104.2 kcal mol^{-1}).

MICHAEL J. KRECH, STANLEY JAMES W. PRICE et HENRY J. SAPIANO. Can. J. Chem. **55**, 4222 (1977).

On a déterminé l'enthalpie de formation du bromopentafluorobenzène par l'utilisation de la méthode de combustion directe qui a été appliquée à l'hexafluorobenzène, à l'octafluorotoluène et à l'iodopentafluorobenzène. Alors qu'une bombe couverte de platine est généralement utilisée pour ce type de composé, on a adopté une bombe en acier dans le présent travail. La combustion du bromopentafluorobenzène dans la bombe d'acier conduit à la formation de CO_2, de CF_4, de F_2, de Br_2 et de BrF_3. Si on utilise 10 fois la quantité nécessaire d'oxygène, le rapport molaire moyen de CO_2 sur CF_4 est de 7.29 ± 0.07. On a obtenu une bonne balance de matériel pour le carbone, le fluor et le brome. On a combiné la valeur de $\Delta H_{f298}^0(C_6F_5Br, g) = -711.6 \pm 16.7$ kJ mol^{-1} (-170.1 ± 4.0 kcal mol^{-1}) avec la valeur de $\Delta H_{f298}^0(C_6F_5, g) = -387.4$ kJ mol^{-1} (-92.6 kcal mol^{-1}) et $\Delta H_{f298}^0(Br, g) = 111.7$ kJ mol^{-1} (26.7 kcal mol^{-1}) pour obtenir une valeur de 435.9 kJ mol^{-1} (104.2 kcal mol^{-1}) pour $D[C_6F_5—Br]$.

[Traduit par le journal]

Introduction

To date no thermodynamic study for the heat of formation of C_6F_5Br has been reported. The combustion of C_6F_5X (X = F, H, CH_3, Cl, OH) has been determined by Cox and co-workers (1, 2). These studies involve the placement of fluoro compounds in polyester film bags. To ensure complete combustion hydrogen containing organic materials were added to the crucible. An alternate and successful approach involves open dish combustion under anhydrous conditions and without any auxiliary materials (3–5). This method has been adopted for the combustion of bromopentafluorobenzene through the use of a steel crucible in a steel bomb.

[1]To whom correspondence should be addressed.

Experimental

Materials

(i) Bromopentafluorobenzene

C_6F_5Br obtained from the Imperial Smelting Corporation was purified by fractional distillation. The final product had the following physical properties (the values in parentheses are those reported by the manufacturer (6)): bp = 137°C (137°C), $n_D^{25} = 1.4483$ (1.4483). Analysis by gas chromatography (6 ft × $\frac{1}{8}$ in. od Durapak *n*-octane/Porasil C, 100–200 mesh, N_2 carrier, 60 cm^3/min, column temperature 120°C, flame ionization detection) showed the presence of a minor impurity which was found to represent a maximum of 0.05% of the sample.

Vapour pressure measurements were taken over the range 10–75°C using the same modified Ramsay–Young system previously employed for C_6F_6 (3), $C_6F_5CF_3$ (4), and C_6F_5I (5). Over 50 vapour pressure measurements were made over three independent runs. The data may be represented by

$$[1] \quad \log_{10} P\,(\text{cm}) = 7.2304 - 2278.4/T + 0.1142 \log_{10} T$$

The resulting heat of vaporization and average heat capacity differences (vapour − liquid) are $\Delta H_{298}{}^{0} = 43.05 \pm 0.21$ kJ mol^{-1} and $\langle \Delta C_p \rangle_{10.75°C} = 0.954$ J deg^{-1} mol^{-1}.

(ii) CO_2, CF_4, F_2, BrF_3, BrF_5

CO_2, CF_4, and F_2 were obtained from the Matheson Chemical Company and were used without further purification. BrF_5 and BrF_3 were obtained from the Air Products Chemical Company and Fluorchem Ltd., respectively. Both were stored as received in monel steel cylinders under their own vapour pressure. Before use the liquids were distilled into Pyrex traps and vacuum distilled. The vacuum distillation system used had taps equipped with Teflon barrels and Viton-O-rings and all joints and glass stopcocks were greased with halocarbon grease.

(iii) Bromine

Reagent A.C.S. bromine was dried over phosphorous pentoxide and vacuum distilled. A middle fraction was collected and stored under its own vapour pressure in a Pyrex tube.

(iv) Sodium Thiosulphate

Sodium thiosulphate pentahydrate (12.5 g) was dissolved in 1 ℓ of water that had been recently boiled and cooled. A few drops of chloroform were added as a preservative and the resulting solution was standardized with potassium iodate (7).

(v) Potassium Iodide

Reagent grade potassium iodide was used without further purification.

Apparatus and Calorimetric Procedure

The apparatus and procedure used for the main combustion process were identical to those used for C_6F_6 (3), C_7F_8 (4), and C_6F_5I (5). The sole exception was the use of a Parr model 1004 C steel bomb and steel crucible that contained the liquid C_6F_5Br.

The rate of loss of C_6F_5Br from the steel crucible in which it was weighed was 0.0207 mg s^{-1}. The time between weighing the crucible containing the liquid and closing the bomb was such that less than 0.04% of the total sample was lost by evaporation. The correction for the evaporation is estimated to be accurate to better than ±3%. The error generated by the correction procedure should therefore be less than ±0.001%.

Analysis of Reaction Products

The analytical procedures for CO_2, CF_4, and F_2 have been described elsewhere (3–5). Br_2 was either weighed and/or reduced with KI and titrated with standardized 0.05 *N* sodium thiosulphate. Quantitative analysis of BrF_3 was based on determination of F^- using a fluoride specific ion electrode in conjunction with an Orion 701 digital p*H* meter. Mass spectra were obtained using a Varian MAT CH5-DF spectrometer controlled by an INCOS computer system. Fluorine nmr spectra were obtained on a nmr JELCO C60 HL spectrometer and are reported in ppm with trifluoroacetic acid used as an internal standard. A Bauch and Lomb Spectronic 20 colorimeter was used to determine iron with 1,10-phenanthroline. Standards containing Fe(II) and Fe(III) were used. Both the ferrous and ferric iron were determined simultaneously. Only the ferrous complex absorbs at 515 nm and both complexes have identical absorption at 396 nm (the amount being additive) (8).

Results and Discussion

Preliminary combustions done in the platinum lined bomb resulted in the formation of a dark red to yellow–brown solid indicating possible formation of PtF_4. A noticeable loss in weight of the platinum crucible was observed after each combustion. Spot tests showed that platinum(IV) ions were formed (9).

Combustions were then extended to test the suitability of a steel bomb. It has been observed that combustion in this bomb with fluoroaromatic compounds produced the formation of a green coloration inside the bomb (10). This was shown to be iron(II) and iron(III) fluorides (9). A determination of the amount of Fe(II) and Fe(III) fluorides after combustion of C_6F_5Br was tested. A spectrophotometric determination (8) was used and the amount of iron fluorides found after combustion was 1.7 ± 0.01 mg. The correction to the heat of formation of C_6F_5Br caused by the formation of FeF_2 and FeF_3 would be less than 3.3 ± 0.5 kJ mol^{-1} per experiment. All subsequent combustions were therefore carried out using the steel bomb and steel crucible.

The combustion of C_6F_5Br led to the formation of products that were identified as CO_2, CF_4, F_2, Br_2, and BrF_3.

CO_2, CF_4, and F_2 were identified in the same manner as reported for the products of combustion of C_6F_6 (3), C_7F_8 (4), and C_6F_5I (5). Quantitative analysis of these products was carried out by gas chromatographic procedures similar to those previously used (3–5). In this study two types of columns were used. The first column was a 6 ft × ¼ in. od silica gel column (25°C, He carrier, 15 cm^3/min). Uncorrected retention times for O_2, CF_4, and CO_2 are 1 min 30 s, 3 min 12 s, and 12 min 36 s, respectively. In the first five runs in Table 1, the CO_2/CF_4 ratio was found through the use of this column. Calibrations were carried out using O_2–CF_4 and O_2–CO_2 mixtures. Use of pure CF_4 leads to a response factor that is low by 4.6%. The CO_2 calibration is uneffected. The net result is that, if the relative factor determined with pure CF_4 and CO_2 is used, a value for $\Delta H_{f298}{}^{0}(C_6F_5Br, g)$ is obtained that is about 17 kJ mol^{-1} too high.

TABLE 1. Combustion data and calculated enthalpy of formation for bromopentafluorobenzene§

Run number‡	Mass C_6F_5Br (g)	ΔT_{cor} (°C)	CO_2/CF_4* (by gc)	CO_2 collected (g)	BrF_3 collected (g)	Total F_2† collected (g)	% theoretical yields C(%)	F(%)	Br(%)	$\Delta H_{f298}^{0}(C_6F_5Br, g)$ (kJ mol^{-1})
1	1.504	0.7323	7.35	1.396			99			−707.4
2	1.527	0.7449	7.24	1.432		0.240	100	99	99	−717.1
3	1.553	0.7582	7.31	1.431		0.255	98	101	99	−702.4
4	1.769	0.8602	7.30	1.696			102			−711.6
5	1.763	0.8586	7.30	1.635			99		101	−707.9
6	1.308	0.6320	7.43	1.237	0.062	0.217	100	100	100	−719.2
7	1.220	0.5904	7.42	1.150	0.057	0.202	100	100	99	−715.4
8	1.040	0.5058	7.22	0.990	0.048	0.166	101	100		−714.6
9	1.508	0.7381	7.24	1.432		0.231	101	98		−715.8
10	1.686	0.8226	7.23	1.600	0.078	0.265	101	99	86	−705.8
11	1.638	0.7979	7.29	1.543	0.077	0.255	100	98	84	−704.9
12	1.386	0.6752	7.19		0.067				88	−712.5
13	1.391	0.6741	7.31						87	−718.7

*Molar ratio.
†From F_2 and BrF_3.
‡Runs 1 to 7 glass trap used to collect liquid products, runs 8 to 13 steel trap used to collect liquid products.
§Additional typical data (see ref. 19 for notation); ΔE, ign/J = 10.1, E(J) $(-\Delta t_c)$/J = −12 850.3, $\Delta E_c^0/M$(compound)/J g^{-1} = −8656.3.

The second column which was a 6 ft × $\frac{1}{4}$ in. od Porapak Q column (25°C, He carrier, 48 cm^3/min) was used to determine the CO_2/CF_4 ratio for the remaining runs. Uncorrected retention times for O_2, CF_4, and CO_2 are 1 min 3 s, 1 min 54 s, and 4 min 57 s, respectively. An improved separation between oxygen and tetrafluoromethane occurred using this column. Use of pure CF_4 leads to a response factor that is low by only 1%.

Condensable products (at −80°C) were collected in either a glass or stainless steel trap. To ensure all products volatile at 25°C were removed from the combustion bomb, the system was flushed with ultra high pure oxygen for 2 h and the bomb was then evacuated through the trap. The cold trap was allowed to come to room temperature. Two immiscible liquids were observed. The major portion (lower phase) had a characteristic colour of free bromine and the upper phase had a colorless to gray–yellow colour. Since a carbon balance had already been established the possibility of any halo-carbon products were unlikely and the fact that all the bromine oxides (11) are unstable at room temperature indicated that the remaining products would be halogen or interhalogen compounds such as Br_2, BrF, BrF_3, and BrF_5. BrF has not been isolated as of yet but there are indications that it does exist through spectroscopic studies.

By simple vacuum distillation the liquids were easily separated. The more volatile substance was dark red in colour and appeared to be free bromine. This was confirmed by mass spectral analysis using a MAT CH5 mass spectrometer. Major peaks were obtained at m/e 162, 160, and 158 with a peak height ratio of close to 1:2:1. In addition peaks of approximately equal height (about 7% of the m/e = 160 peak height) were observed at m/e = 81 and 79. Since the molecular constituents in order of increasing volatility at 25°C are BrF_3, Br_2, BrF_5, and BrF, any BrF_5 and/or BrF would have been collected in the 'bromine' fraction. In addition to the mass spectral analysis this fraction was tested by adding water to the distilled sample. If any halogen fluorides were present they would have reacted with water to form a complex mixture of HF, HBr, $HBrO_3$, Br_2, and O_2 (12). Fluoride analysis of this solution with a specific fluoride ion electrode proved to be negative.

Based on colour and volatility it appeared possible that the remaining liquid was BrF_3. The

TABLE 2. Comparison of $D[C_6F_5—X]$ values determined from thermochemistry with values derived from appearance potential studies

X	$D[C_6F_5—X]$ kJ mol^{-1} (kcal mol^{-1})	
	From thermochemistry*	From appearance potentials†
OH	608.8±12.6 (145.5±3.0)	
H	636.4±12.6 (152.1±3.0)	
F	642.7±12.6 (153.6±3.0)	629.3±8.4 (150.4±2.0)
Cl	543.9±12.6 (130.0±3.0)	531.8±8.4 (127.1±2.0)
Br	435.9±16.7 (104.2±4.0)	443.1±8.4 (105.9±2.0)
I	277.0± 4.2 (66.2±1.0)‡	277.0±4.2 (66.2±1.0)‡
CH_3	595.0±12.6 (142 ±3.0)	
CF_3	404.2±12.6 (96 ±3.0)	

*All values in this column are based on $\Delta H_{f298}^0(C_6F_5,g) = -387.4$ kJ mol^{-1} (-92.6 kcal mol^{-1}) determined from the kinetic value of $D(C_6F_5—I)$ and $\Delta H_{f298}^0(C_6F_5I,g) = -557.7 \pm 12.6$ kJ mol^{-1} (-133.3 ± 3.0 kcal mol^{-1}).
†Based on the kinetic value of $D(C_6F_5I)$ and differences in AP values.
‡Kinetic value.

liquid was distilled under vacuum into a carefully dried quartz capillary tube while the tube was immersed in liquid nitrogen. The capillary was then sealed under vacuum and removed for subsequent nmr fluorine analysis. The fluorine nmr analysis indicated a singlet peak corresponding to liquid BrF_3 at -55.2 ppm (literature value -54.3 ppm (13)) relative to trifluoroacetic acid.

The amount of Br_2 was analyzed by either weighing the sample collected in a small ampoule and/or by iodometric analysis (7). The BrF_3 was reacted with KI solution and analyzed for fluoride using the corresponding specific ion electrode. In three runs the BrF_3 fraction was also determined directly by weighing this fraction. Good agreement was obtained between specific ion and gravimetric determination.

From the material balance shown in Table 1 along with the average CO_2/CF_4 molar ratio, reaction 2 may be written to represent the combustion of bromopentafluorobenzene. However, as will be discussed later, it is unlikely that free bromine exists in the bomb.

$$[2]\quad C_6F_5Br + 5.276O_2 \rightarrow 5.276CO_2 + 0.724CF_4 + 0.923F_2 + 0.086BrF_3 + 0.457Br_2$$

In treating a complex mixture of products possible interactions between the compounds must be taken into account. No detectable heat of mixing was observed when F_2, O_2, CF_4, and CO_2 were mixed under anhydrous conditions (5).

However, a correction of -130 ± 13 kJ mol^{-1} is required for the interaction between Br_2, F_2, and BrF_3. Approximately -68.2 kJ mol^{-1} of this correction is due to reaction 3.

$$[3]\quad \tfrac{1}{2}F_2\,(g) + \tfrac{1}{2}Br_2\,(l) \rightleftharpoons BrF\,(g)$$

With the excess F_2 present the equilibrium should be far to the right (14). It should be noted that during the slow bleeding of the bomb over a period of 20 h to recover the combustion products for analysis, the BrF equilibrium shifts to the left resulting in quantitative conversion of BrF to Br_2 and F_2. In an all-metal system (steel traps) the reaction may be somewhat inhibited as indicated by the apparent slight shortfall in bromine recovery (Table 1). The shortfall was always accompanied by the appearance of a light yellow coloration in the F_2 absorbing solution in the bubbler.

In carrying out the thermochemical calculations the following heats of formation have been used: CO_2 (g), -393.512 kJ mol^{-1} (15); CF_4 (g), -933.0 kJ mol^{-1} (16); and BrF_3 (g), -255.60 kJ mol^{-1} (12).

Based on the preceding data and an estimated correction to standard state of 5.5 kJ mol^{-1}, $\Delta H_{f298}^0(C_6F_5Br, g) = -711.6 \pm 5.6$ kJ mol^{-1} with a standard deviation of 5.6 kJ mol^{-1}. However, when the uncertainty in the auxiliary experiments are taken into account the overall limit must be set at about ± 16 kJ mol^{-1}.

Defining $D(C_6F_5—X)$ as ΔH_{298}^0 for the reaction

$$[4]\quad C_6F_5X,g \rightarrow C_6F_5,g + X,g$$

and using the value for $\Delta H_{f298}^0(C_6F_5,g)$ as -387.4 ± 12 kJ mol^{-1} (5) and $\Delta H_f(Br,g) =$

111.7 kJ mol^{-1} (17) and the present determined value of $\Delta H_{f298}{}^{0}(C_6F_5Br,g) = -711.6 \pm 16.7$ kJ mol^{-1} will yield a value of $D(C_6F_5—Br)$ to be 435.9 kJ mol^{-1}.

In Table 2 a comparison is made between $D(C_6F_5X)$ values based on thermochemical methods and appearance potential methods (18). Agreement of the present value of $D(C_6F_5—Br)$ with the value estimated from the AP studies is well within the combined error limits.

Acknowledgements

The authors wish to thank Dr. W. F. Yared and B. Trudell for very helpful discussions and suggestions. This work has been supported by an operating grant from the National Research Council of Canada, which the authors gratefully acknowledge.

1. J. D. Cox, H. A. Gundry, and A. J. Head. Trans. Faraday Soc. **60**, 653 (1964).
2. J. D. Cox, H. A. Gundry, D. Harrop, and A. J. Head. J. Chem. Thermodyn. **1**, 77 (1969).
3. M. J. Krech, S. J. W. Price, and W. F. Yared. Can. J. Chem. **50**, 2935 (1972).
4. M. J. Krech, S. J. W. Price, and W. F. Yared. Can. J. Chem. **51**, 3662 (1973).
5. M. J. Krech, S. J. W. Price, and W. F. Yared. Can. J. Chem. **52**, 2673 (1974).
6. Highly fluorinated aromatic and alicyclic compounds. Imperial Smelting Company, St. Andrews Road, Avonmouth, Bristol BS11 9HP, England.
7. A. J. Vogel. Qualitative inorganic analysis. 3rd ed. Longman Group Ltd., London. 1961. p. 348.
8. H. H. Willard, L. L. Merritt, and J. A. Dean. Instrumental methods of analysis. 4th ed. D. Van Nostrand Company Inc., New York, NY. 1969. p. 104.
9. F. Feigl. Spot test in inorganic analysis. 3rd ed. Elsevier Pub. Co., New York, NY. 1954.
10. W. F. Yared. Ph.D. Thesis, University of Windsor, Windsor, Ontario. 1973.
11. N. V. Sidgwick. Chemical elements and their compounds. Vol. 2. Clarendon Press, Oxford, England. 1962.
12. L. Stein. J. Phys. Chem. **66**, 288 (1962).
13. J. W. Emsley, J. Feeney, and L. H. Sutcliffe. High resolution nuclear magnetic resonance spectroscopy. Vol. 2. 1st ed. Pergamon Press, London. 1966. p. 881.
14. L. Stein. J. Am. Chem. Soc. **81**, 1269 (1959).
15. F. D. Rossini *et al.* Selected values of chemical thermodynamic properties. Nat. Bur. Stand. (U.S.), Tech. Note No. 270-3. 1968.
16. E. Greenberg and W. H. Hubbard. J. Phys. Chem. **72**, 222 (1968).
17. R. C. Weast (*Editor*). Handbook of chemistry and physics. 51st ed. The Chemical Rubber Co., Cleveland, Ohio. 1970–1971. p. F163.
18. S. J. W. Price and H. J. Sapiano. Can. J. Chem. **52**, 4109 (1974).
19. J. Coops, R. S. Jessup, and K. Van Nes. *In* Experimental thermochemistry. Vol. 1. *Edited by* F. D. Rossini. Interscience, New York, NY. 1956.

Mercury(II) complexes of tris(*tert*-butyl)phosphine and tri(*o*-tolyl)phosphine

ELMER C. ALYEA, SHELTON A. DIAS, RAM G. GOEL, AND WILLIAM O. OGINI

Guelph–Waterloo Centre for Graduate Work in Chemistry, University of Guelph, Guelph, Ont., Canada N1G 2W1

Received June 15, 1977

ELMER C. ALYEA, SHELTON A. DIAS, RAM G. GOEL, and WILLIAM O. OGINI. Can. J. Chem. **55**, 4227 (1977).

Tris(*tert*-butyl)phosphine and tri(*o*-tolyl)phosphine form 1:1 complexes with mercury(II) halides and with mercury(II) thiocyanate. Physicochemical measurements, i.e. conductance, molecular weight determinations, infrared and Raman spectra indicate a dimeric structure of C_{2h} skeletal symmetry. The Hg—X and Hg—P stretching frequencies for all complexes have been assigned.

ELMER C. ALYEA, SHELTON A. DIAS, RAM G. GOEL et WILLIAM O. OGINI. Can. J. Chem. **55**, 4227 (1977).

La tris(*tert*-butyl)phosphine et la tris(*o*-tolyl)phosphine forment des complexes 1:1 avec les halogénures et le thiocyanate de mercure(II). Des mesures physicochimiques comme la conductivité, les déterminations de poids moléculaire et les spectres infrarouges et Raman indiquent que les complexes existent sous forme dimère avec une symétrie de squelette C_{2h}. On a fait l'attribution des fréquences de vibration Hg—X et Hg—P pour tous les complexes.

[Traduit par le journal]

Introduction

Mercury(II) salts are known (1) to form complexes with tertiary phosphines in the $HgX_2:PR_3$ ratios of 1:2, 1:1, 2:3, 2:4, and 3:2. Of these, the complexes of the type $(R_3P)_2HgX_2$ are the best characterized (1–7). The complex $(Ph_3P)_2Hg(SCN)_2$ has been shown by an X-ray diffraction study (6) to have a tetrahedral structure. A similar structure has been assigned (5) for the halide complexes $(Ph_3P)_2HgX_2$ on the basis of their infrared spectra in the low frequency region. Although the complexes of the type $(R_3P)HgX_2$ have been studied by several workers (1, 3, 7–10), their structures have not been well established. The complexes $(R_3P)HgX_2$ where X = halide and R = alkyl were found to be dimeric in solution and the dimeric *trans* structure as shown below was assigned by analogy with the structure established for the complex $(Et_3As)HgI_2$ by preliminary crystallographic analysis (1).

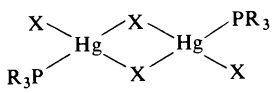

After the completion of this work, a preliminary report (11) on the crystal structures of the complexes $(R_3P)HgCl_2$ (R = Me, Et, or Ph) and $(Ph_3As)HgCl_2$ has appeared, which shows that the structures of the 1:1 complexes are markedly influenced by the nature of the phosphine. The complexes $(Ph_3P)HgCl_2$ and $(Ph_3As)HgCl_2$ are isostructural and consist of the expected chlorine-bridged centrosymmetric dimeric molecules. However, the complexes $(Me_3P)HgCl_2$ and $(Et_3P)HgCl_2$ have polymeric structures containing five-coordinate mercury atoms. Likewise, the crystal structure (12) of the complex $(Ph_3As)Hg(SCN)_2$ unexpectedly shows a trigonal coordination around mercury with two additional Hg---NCS contacts defining a distorted trigonal bipyramid geometry. A similar structure has also been suggested (8) for the complex $(Cy_3P)Hg(SCN)_2$[1] on the basis of a vibrational spectral study but an X-ray single-crystal analysis (13*a*) has established the structure as polymeric with trigonal pyramidal geometry at each mercury atom. Similarly, a recent X-ray single-crystal determination (14) has established that $(Ph_3P)Hg(NO_3)_2$ forms infinite chains via bridging nitrato groups; the coordination geometry about mercury may be described as very distorted tetrahedral or as distorted square pyramidal (if an additional weak Hg—O bond is included). In contrast, the crystal structure (13*b*) of $(Cy_3P)Hg(NO_3)_2$ is quite different, the molecule being dimeric with each mercury atom having a distorted square pyramidal coordination geometry.

[1] Cy_3P is tricyclohexylphosphine.

In order to evaluate the role of steric effects in metal complexes of tertiary phosphines we have undertaken a study of metal complexes of tertiary phosphines containing bulky substituents (13, 15–17). Recent studies (15*b*, 18) have clearly shown that the steric requirements of the substituents on phosphorus have a marked effect on the stereochemistry and the chemical reactivity of metal complexes of phosphorus ligands. In a previous paper (15*a*) we reported on the tris(*tert*-butyl)phosphine complexes of zinc(II) and cadmium(II). Herein we report on the synthesis, characterization, and vibrational spectra of tris(*tert*-butyl)phosphine and tri(*o*-tolyl)phosphine complexes of mercury(II) halides and mercury(II) thiocyanate.

Results and Discussion

Reaction of tris(*tert*-butyl)phosphine with mercury(II) halides or with mercury(II) thiocyanate in 2:1 mole ratio, in an aprotic solvent such as ether or dichloromethane, gave 1:1 complexes instead of the possible 2:1 complexes. The reaction of mercury(II) salts with tri(*o*-tolyl)phosphine also gave 1:1 complexes. Since less bulky tertiary phosphines such as tricyclohexylphosphine (8) and triphenylphosphine (5–7, 10) form both 1:1 and 2:1 complexes with mercury(II), the formation of only 1:1 complexes in the present work is evidently due to the large steric requirements of tris(*tert*-butyl)- and tri(*o*-tolyl)phosphines. A measure of the steric requirement of the phosphine ligands in terms of a "cone angle" has been proposed by Tolman (18). He estimated cone angles for $(o\text{-tolyl})_3P$, $Bu_3{}^tP$, Cy_3P, and Ph_3P to be 194°, 182°, 170°, and 145° respectively, using CPK molecular models. A crystallographic study (17) on the complex $[Bu_3{}^tPH][(Bu_3{}^tP)NiBr_3]$ showed that the Ni—$PBu_3{}^t$ cone angle is 180 ± 2°. X-ray structural studies (13) of several complexes have established that Tolman's estimates for the cone angle of PCy_3 (originally calculated as 179 ± 10°) are in good agreement with the observed range of experimentally derived cone angles.

The melting points, analytical, conductance, and molecular weight data for the complexes prepared in this work are given in Table 1. The conductance data clearly show that all the complexes behave as nonelectrolytes in nitromethane or dimethylsulfoxide. The molecular weight data for the tris(*tert*-butyl)phosphine complexes show their dimeric constitution in 1,2-dichloroethane. The molecular weights of the tri(*o*-tolyl)phosphine complexes could not be determined due to their insolubility in any solvent suitable for molecular weight measurements.

The infrared and Raman spectral data for the halide complexes in the region below 400 cm^{-1}, in the solid state, together with their assignments are shown in Tables 2 and 3. From a comparison of these infrared data with the infrared data reported for the $(Ph_3P)HgX_2$ complexes (5) it is clearly evident that the infrared frequencies associated with the vibrations involving the metal–halogen bonds in the complexes of tris(*tert*-butyl)phosphine, tri(*o*-tolyl)phosphine, and triphenylphosphine complexes are very similar. Thus, there can be little doubt that the mercury(II) halide complexes of tris(*tert*-butyl)-phosphine, tri(*o*-tolyl)phosphine, and triphenyl-phosphine are structurally similar.

A dimeric *trans*-tetrahedral structure of C_{2h} skeletal symmetry (*vide supra*) should give rise to only one infrared active and one Raman active frequency due to the stretching of the terminal mercury–halogen bonds. The Raman spectrum for each complex listed in Tables 2 and 3 showed only one band that can be assigned to the terminal mercury–halogen stretching frequency. Like the corresponding infrared frequency, this frequency is progressively decreased to lower wave numbers as X is changed from Cl to Br to I. For the chloride and the bromide complexes a Raman band due to a bridged Hg—X stretching mode is also observed. The Raman spectra of the tris(*tert*-butyl)phosphine complexes also show a strong band in the 123–110 cm^{-1} region. A similar Raman band is observed for the tri(*o*-tolyl)phosphine complexes in the 138 to 122 cm^{-1} region. Since no band is observed in these regions in the Raman spectra of the free phosphines, the above mentioned Raman bands are most likely due to the Hg—P stretching frequencies. As shown by the far infrared data (5) for tetrahedral $(Ph_3P)_2HgX_2$ complexes, the Hg—X bending frequencies are expected in the region below 80 cm^{-1}. Thus the combined infrared and Raman data for the present complexes are in complete accord with a dimeric tetrahedral structure of C_{2h} skeletal symmetry.

The assignments for the Raman bands in the region below 100 cm^{-1} cannot be made with certainty without polarization measurements.

TABLE 1. Melting points, analytical, conductance, and molecular weight data

Compound	Melting point (°C)	Calculated C%	Calculated H%	Found C%	Found H%	Λ_M* (Ω^{-1} cm^2 mol^{-1})	Molecular weight†
$(Bu_3^tP)HgCl_2$‡	257	30.44	5.71	30.32	6.05	0.59	942
$(Bu_3^tP)HgBr_2$	235	25.62	4.80	25.88	4.67	0.89	1124
$(Bu_3^tP)HgI_2$	228	21.95	4.11	21.63	4.33	1.2	1304
$(Bu_3^tP)Hg(SCN)_2$§	210	32.43	5.21	32.29	5.13	8.1	1048
$[(o\text{-Tolyl})_3P]HgCl_2$	298	43.80	3.68	43.59	3.87	2.5	—
$[(o\text{-Tolyl})_3P]HgBr_2$	303	37.94	3.18	38.41	3.71	2.5	—
$[(o\text{-Tolyl})_3P]HgI_2$‖	264	33.24	2.79	32.68	3.14	1.0	—
$[(o\text{-Tolyl})_3P]Hg(SCN)_2$¶	208	44.47	3.40	44.62	3.46	8.5	—

*For $10^{-3}M$ solutions, in nitromethane (Bu_3^tP complexes) or dimethylsulfoxide ($(o\text{-tolyl})_3P$ complexes).
†In 1,2-dichloroethane in the 10^{-4} to 10^{-3} M concentration range.
‡%Cl calcd.: 15.01; found: 15.26.
§%S calcd.: 12.36; found: 12.86. %N calcd.: 5.41; found: 5.47.
‖%I calcd.: 33.45; found: 32.75.
¶%N calcd.: 4.51; found: 4.37.

TABLE 2. Infrared and Raman spectral data* for $(Bu_3^tP)HgX_2$ complexes below 400 cm^{-1}†

$(Bu_3^tP)HgCl_2$		$(Bu_3^tP)HgBr_2$		$(Bu_3^tP)HgI_2$		
ir	R	ir	R	ir	R	Assignments
					392vw	
	376w		374w		374m	
	303s, 296s	300vw	298s		296s	
270s	266s					ν(Hg—Cl), terminal
			246w		242m	
	236w, 226w		230w		224w	
	206mw		204m		204m	
		178s	174vs			ν(Hg—Br), terminal
175s, b, 169s, b	162vw					ν(Hg—Cl), bridge
				140s	138s	ν(Hg—I), terminal
		134s				ν(Hg—Br, bridge
	123s		116vs		110vs	ν(Hg—P)
	92m				90sh	
	82m		82m			
	62m				50vs	

*In cm^{-1} for the solid state.
†ir, infrared; R, Raman; m, medium; s, strong; sh, shoulder; v, very; w, weak; ν, stretching.

Unfortunately, attempts to obtain Raman spectra in solution were not successful due to lack of solubility of the complexes in suitable solvents. The remaining Raman bands listed in Tables 2 and 3 are due to the internal vibrations of the coordinated phosphines.

In spite of several studies on tertiary phosphine complexes of mercury(II) little information is available on the Hg—P stretching frequencies. From the far-infrared spectral study (5) of the $(Ph_3P)_2HgX_2$ complexes the Hg—P stretching frequencies have been assigned in the range of 137 to 98 cm^{-1}. In a recent report (19) on trimethylphosphine complexes of mercury(II), the Hg—P stretching frequencies for the complexes $(Me_3P)HgX_2$ where X = halide or pseudohalide have been assigned in the 364 to 342 cm^{-1} region. Since the metal–phosphorus stretching frequencies (20) for the Ni(II) and Pd(II) complexes $(R_3P)_2MX_2$ have been found to be below 200 cm^{-1}, we believe that the assignments for the Hg—P stretching frequencies for the trimethylphosphine complexes of mercury(II) are erroneous. Our assignments for the Hg—P stretching frequencies for the tris(*tert*-butyl)-phosphine and the tri(*o*-tolyl)phosphine complexes are thus consistent with those for the $(Ph_3P)_2HgX_2$ complexes. Further support for

TABLE 3. Infrared and Raman spectral data* for $[(o\text{-tolyl})_3P]HgX_2$ complexes below 400 cm^{-1}†

$[(o\text{-Tolyl})_3P]HgCl_2$		$[(o\text{-Tolyl})_3P]HgBr_2$		$[(o\text{-Tolyl})_3P]HgI_2$		
ir	R	ir	R	ir	R	Assignments
390w		388w			387w	
382w		381w			379m	
270w		369w				
276vs	264vs	270s	270w	271m		ν(Hg—Cl), terminal
		257s				
	240wm		241w			
			220w		228w	
	211m		206wm		204w	
		189vs	180s			ν(Hg—Br), terminal
179s	181w					ν(Hg—Cl), bridging
				172w	178w	
				143s	140s	ν(Hg—I), terminal
		132vs	132s			ν(Hg—Br), bridging
	138s				122s	ν(Hg—P)
	103vs				93w	
	80vs		80s		80m	
	69s		67s		60w	
					51m	
					41m	
					32m	

*In cm^{-1} for the solid state.
†ir, infrared; R, Raman; m, medium; s, strong; sh, shoulder; v, very; w, weak; ν, stretching.

the proposed assignments is provided by the Raman data for the tertiary phosphine complexes of the halides of the main group elements. The In—P symmetric frequency for the complex $(Me_3P)_2InCl_3$ has been found (21) to be at 135 cm^{-1} by a single-crystal Raman polarization study. The Sn—P symmetric stretching frequency for the complex *trans*-$SnCl_4(PMe_3)_2$ has been reported (22) to be at 146 cm^{-1}. It is worth noting that the Hg—P stretching frequencies for the tris(*tert*-butyl)phosphine complexes as well as the tri(*o*-tolyl)phosphine complexes show a progressive decrease as X is changed from Cl to Br to I. A similar trend has been observed (15*a*) for the Zn—P and Cd—P stretching frequencies of the complexes with tris(*tert*-butyl)-phosphine.

The observed infrared and Raman frequencies due to the internal vibrations of the SCN groups for the complexes $(Bu_3^tP)Hg(SCN)_2$ and $[(o\text{-tolyl})_3P]Hg(SCN)_2$, in the solid state, are given in Table 4. By comparing these frequencies with the frequencies reported (23) for N-bonded, S-bonded, and bridged SCN groups, it can be concluded that both complexes contain S-bonded and/or bridging SCN groups. The observation of three ν(CN) frequencies for each compound suggests that each complex contains both S-bonded and bridging SCN groups. The infrared and Raman data for both compounds in the low frequency region, shown in Table 5, are also consistent with the presence of both S-bonded and bridging SCN groups. The infrared spectra of both complexes show medium to weak bands at ca. 270 and 250 cm^{-1}. Strong to medium bands in these regions are also observed in the Raman spectra. By comparison of these bands with the reported (24) infrared and Raman frequencies for $Hg(SCN)_2$ they can be assigned to the terminal Hg—SCN stretching

TABLE 4. Vibrational frequencies* due to the internal vibrations of the SCN groups for $(Bu_3^tP)Hg(SCN)_2$ and $[(o\text{-tolyl})_3P]Hg(SCN)_2$†

	$(Bu_3^tP)Hg(SCN)_2$		$[(o\text{-Tolyl})_3P]Hg(SCN)_2$	
	ir	R	ir	R
ν(CN)	2128sh 2112s 2063sh	2111ms	2116s, sh 2100vs 2050m, sh	2127s 2113s, sh 2102s, br
ν(CS)	750sh 740m	754m	758m, sh	‡
δ(SCN)	462sh 457m 443m 431m	460m 430w	462m 422m	‡

*In cm^{-1} for the solid state.
†ir, infrared; R, Raman; m, medium; s, strong; sh, shoulder; v, very; w, weak, ν, stretching.
‡Bands obscured by ligand bands.

TABLE 5. Infrared and Raman spectral data* for $(Bu_3{}^tP)Hg(SCN)_2$ and $[(o\text{-tolyl})_3P]Hg(SCN)_2$ below 400 cm^{-1}†

$(Bu_3{}^tP)Hg(SCN)_2$		$[(o\text{-Tolyl})_3P]Hg(SCN)_2$		
ir	R	ir	R	Assignment
380vw	380w	384m		
	336vw			
	303m			
270m }	268s }	267m }		
250m }	248m }	256s }	256s	ν(Hg—SCN), terminal
		234w }		
			211w	
	206w			
170m		183s }	170w	ν(Hg—SCN), bridge
		153s }		
	120vs		112s	ν(Hg—P)
	90s			
	56m		66m	

*In cm^{-1} for the solid state.
†ir, infrared; R, Raman; m, medium; s, strong; sh, shoulder; v, very; w, weak; ν, stretching.

frequencies. For both compounds another infrared band is observed at ca. 170–180 cm^{-1}. Since this band is not observed for the free phosphines it can be assigned to a bridging Hg—SCN stretching frequency. The assignment of this band to a Hg—SCN bending frequency can be ruled out because the Hg—SCN bending frequency for $Hg(SCN)_2$ is reported (24) to be at 148 cm^{-1}. The Raman spectra for both $(Bu_3{}^tP)Hg(SCN)_2$ and $[(o\text{-tolyl})_3P]Hg(SCN)_2$ show a strong band in the 120–112 cm^{-1} region. Following the assignments for the halide complexes, this band can be assigned to the Hg—P stretching frequency.

Although the Raman spectrum of neither compound could be examined in solution, the infrared measurement for the $(Bu_3{}^tP)Hg(SCN)_2$ complex in chloroform solution, in the ν(CN) spectral region, showed no change in the ν(CN) frequencies. It therefore appears that the solid state molecular geometry of this compound is maintained in solution. A dimeric formulation is compatible with the solution molecular weight determination and the assigned structures of the halides. The solid state infrared and Raman spectral bands assignable to thiocyanato modes for the $[(o\text{-tolyl})_3P]Hg(SCN)_2$ complex are nearly identical to those found for $(Cy_3P)Hg(SCN)_2$ (note that three Raman bands are observed in the ν(CN) region). The latter complex has a polymeric structure involving one thiocyanato bridge linking trigonal pyramidal mercury atoms (13*a*).

The proton nmr spectra for the tris(*tert*-butyl)phosphine complexes in dichloromethane show a doublet shifted downfield (δ = 1.63–1.65 ppm; $^3J_{P-H}$ = 15.0 Hz) as compared with the chemical shift of the free phosphine (δ = 1.30 ppm; $^3J_{P-H}$ = 10.0 Hz). A similar downfield shift (ca. 0.05 ppm) occurs for the methyl resonance in DMSO-d_6 solution of the tri(*o*-tolyl)phosphine complexes.

Experimental Section

Chemicals

Tri(*o*-tolyl)phosphine was prepared according to literature methods (25, 26), or obtained from Pressure Chemicals; other commercial samples were very impure. Tris(*tert*-butyl)phosphine was synthesized as previously described (16). Mercury(II) halides were obtained from Alfa Inorganics, Inc. $Hg(SCN)_2$ was prepared by a reported method (24). Solvents were purified and dried following standard procedures.

General Procedures

All operations involved in the preparation and purification of tris(*tert*-butyl)phosphine complexes were carried out either in a dry-box under an atmosphere of oxygen-free dry nitrogen or under vacuum. Elemental analyses were performed by M-H-W Laboratories, Garden City, Michigan. Molecular weights were measured with a Hitachi-Perkin-Elmer 115 osmometer. Melting points, conductance, infrared, Raman, and nmr spectra were measured as reported previously (16).

Preparation of Tris(tert-butyl)phosphine Complexes

(*a*) Tris(*tert*-butyl)phosphine (2.20 mmol) was added with stirring to a solution of mercury(II) halide (1.00 mmol) in 25 ml ether. The white solid formed was filtered off and recrystallized from a mixture of dichloromethane and petroleum ether. Yield: ca. 80%. The filtrate was concentrated to give a viscous liquid, which was found to be unreacted tris(*tert*-butyl)phosphine as shown by its ^1H nmr spectrum.

(*b*) A solution of 2.20 mmol Bu_3^tP in 10 ml dichloromethane was added with stirring to a suspension of 1.01 mmol $Hg(SCN)_2$ in 20 ml dichloroethane. A clear solution was formed after stirring for 6 h; upon concentrating the solution and adding petroleum ether to the concentrated solution the white $(Bu_3^tP)Hg(SCN)_2$ was precipitated. Recrystallization from dichloromethane yielded colourless needle-shaped crystals. Yield: 75%.

Preparation of Tri(o-tolyl)phosphine Complexes

(*a*) A 1.00 mmol solution of tri(*o*-tolyl)phosphine in 25 ml diethyl ether was slowly added to a stirred solution of 1.00 mmol mercury(II) halide in 25 ml diethyl ether (acetone for the bromide). After $\frac{1}{2}$ h reflux, the white precipitate was collected by filtration, washed with several portions of diethyl ether, and recrystallized from nitromethane or ethanol. The same products were obtained using excess $(o\text{-tolyl})_3P$. Yield: ca. 90%.

(*b*) A warm solution of 1.00 mmol tri(*o*-tolyl)phosphine in 30 ml ethanol was added dropwise to a stirred suspension of 1.00 mmol $Hg(SCN)_2$ in 30 ml of ethanol. The reaction mixture was refluxed for $\frac{1}{2}$ h and the white crystalline product collected by filtration. After washing with ethanol, recrystallization was effected from *n*-propanol. Yield: 96%.

Acknowledgement

Thanks are due to the National Research Council of Canada for financial support.

1. R. C. Evans, F. G. Mann, H. S. Peiser, and D. Purdie. J. Chem. Soc. 1209 (1940).
2. G. B. Deacon and B. O. West. J. Inorg. Nucl. Chem. **24**, 169 (1962).
3. G. E. Coates and D. Ridley. J. Chem. Soc. 166 (1964).
4. G. E. Coates and A. Lunder. J. Chem. Soc. 1875 (1965).
5. G. B. Deacon, J. H. S. Green, and D. J. Harrison. Spectrochim. Acta, Part A, **24**, 1921 (1968).
6. R. C. Makhija, A. L. Beauchamp, and R. Rivest. J. Chem. Soc. Dalton Trans. 2447 (1973).
7. S. C. Jain and R. Rivest. Inorg. Chim. Acta, **4**, 291 (1970).
8. F. G. Moers and J. P. Langhout. Recl. Trav. Chim. Pays-Bas, **92**, 996 (1973).
9. R. C. Cass, G. E. Coates, and R. G. Hayter. J. Chem. Soc. 4007 (1955).
10. A. R. Davis, C. J. Murphy, and R. A. Plane. Inorg. Chem. **9**, 423 (1970).
11. N. A. Bell, M. Goldstein, T. Jones, and I. W. Nowell. J. Chem. Soc. Chem. Commun. 1039 (1976).
12. R. C. Makhija, A. L. Beauchamp, and R. Rivest. J. Chem. Soc. Chem. Commun. 1043 (1972); J. Hubert, A. L. Beauchamp, and R. Rivest. Can. J. Chem. **53**, 3383 (1975).
13. (*a*) E. C. Alyea, G. Ferguson, and R. J. Restivo. J. Chem. Soc. Dalton Trans. In press; (*b*) E. C. Alyea, S. A. Dias, G. Ferguson, and P. Roberts. Inorg. Chem. **16**, 2329 (1977).
14. S. H. Whitlow. Can. J. Chem. **52**, 198 (1974).
15. (*a*) R. G. Goel and W. O. Ogini. Inorg. Chem. **16**, 1968 (1977); (*b*) R. G. Goel and R. G. Montemayor. Inorg. Chem. **16**, 2183 (1977).
16. E. C. Alyea, G. T. Fey, and R. G. Goel. J. Coord. Chem. **5**, 143 (1976).
17. E. C. Alyea, A. Costin, G. Ferguson, G. T. Fey, R. G. Goel, and R. J. Restivo. J. Chem. Soc. Dalton Trans. 1294 (1975).
18. (*a*) C. A. Tolman. J. Am. Trans. Chem. Soc. **92**, 2956 (1970); (*b*) C. A. Tolman. Chem. Rev. **77**, 313 (1977), and references cited therein.
19. H. Schmidbaur and K. H. Räthlein. Chem. Ber. **106**, 2491 (1973).
20. K. Shobatake and K. Nakamoto. J. Am. Chem. Soc. **92**, 3332 (1970).
21. G. A. Ozin. J. Chem. Soc. A, 1307 (1970).
22. I. R. Beattie and G. A. Ozin. J. Chem. Soc. A, 370 (1970).
23. A. H. Norbury. Adv. Inorg. Chem. Radiochem. **17**, 231 (1975), and references cited therein.
24. R. P. J. Cooney and J. R. Hall. Aust. J. Chem. **22**, 2117 (1969).
25. F. G. Mann and E. J. Chaplin. J. Chem. Soc. 527 (1933).
26. M. A. Bennett and P. A. Longstaff. J. Am. Chem. Soc. **91**, 6266 (1969).

Constituents of *Nauclea diderrichii*. Part IX. Conversion of sweroside to naucledal and 3-epinaucledal

JOHN PURDY AND STEWART MCLEAN

Department of Chemistry, University of Toronto, Toronto, Ont., Canada M5S 1A1

Received July 4, 1977

JOHN PURDY and STEWART MCLEAN. Can. J. Chem. **55**, 4233 (1977).

The aglucone of sweroside has been converted to naucledal and its epimer, 3-epinaucledal; the structure and stereochemistry of these products have been established through analysis of their nmr spectra. The course of the rearrangement has been studied and the intermediacy of a ring-opened isomer, seconaucledal, has been demonstrated. The relative amounts of naucledal and 3-epinaucledal produced from seconaucledal depend on the conditions of the cyclization.

JOHN PURDY et STEWART MCLEAN. Can. J. Chem. **55**, 4233 (1977).

On a transformé l'aglycone de la swéroside en naucléda l et en son épimère l'épi-3 naucléda l; on a pu établir la structure et la stéréochimie de ces produits par une analyse de leur spectra rmn. On a étudié l'évolution du réarrangement et on a démontré l'existence d'un isomère à cycle ouvert, le seconaucléda l, comme intermédiaire. Les quantités relatives de naucléda l et d'épi-3 naucléda l qui se forment à partir du seconaucléda l dépendent des conditions de la cyclisation.
[Traduit par le journal]

One of the neutral materials extracted from the bark of *Nauclea diderrichii* was a colorless syrup, the principal component of which was assigned the name naucledal (1). Although a homogeneous sample could not be obtained and the material appeared to be rather unstable, sufficient spectroscopic data could be obtained to allow the assignment of structural formula I to naucledal as a working hypothesis.

The secoiridoid glucoside, sweroside, has been assigned formula **1***a*, the structure and configuration of which appear to be on secure grounds (2). Examination of this structure led us to propose that a route to a product of formula I should be available through the aglucone (**1***b*) and a rearranged intermediate, II. In a preliminary report (3) we have shown that this transformation could, indeed, be carried out and that naucledal can be assigned the structure and relative configuration **2**. We now report on the details of this conversion.

Aliquots of a solution of the crystalline aglucone **1***b* (4) in pyridine-d_5 were subjected to a range of reaction conditions in which the amounts of water and acid added to the solution and the temperature were varied. The progress of the reaction was followed by nmr spectroscopy. Signals appropriate for the intermediate II (which we shall refer to as seconaucledal) and the product I appeared at rates that were markedly dependent on the reaction conditions; signals attributed to other reaction products, generally

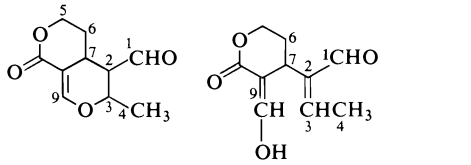

I II

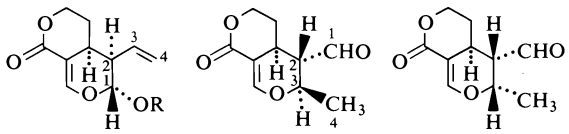

1*a* R = Glu
b R = H

2 **3**

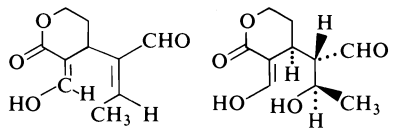

4 **5**

formed in smaller amounts, were also observed, and the composition of the reaction mixture depended on its history. The conditions that appeared optimum for the formation of I (aqueous pyridine at 100°C) were then applied on a preparative scale. Removal of the solvent *in vacuo* and chromatography of the residue afforded in 64% yield a product that closely resembled natural naucledal in spectroscopic and tlc behavior.

It became apparent, however, that neither the material obtained from the *Nauclea* extract nor

TABLE 1. The 220 MHz nmr spectrum of naucledal, **2**

Proton location†	Chemical shift (τ)	Multiplicity	Coupling constants (Hz)
1	0.10	d	$J^*_{1,2} = 2.8$
2	7.64	ddd	$J^*_{1,2} = 2.8, J^*_{2,3} = 10, J_{2,7} = 11$
3	5.80	dq	$J^*_{2,3} = 10, J^*_{3,4} = 6$
4	8.56	d	$J^*_{3,4} = 6$
5a,b	5.4–5.7	m	—
6a,b	7.9–8.1	m	—
7	7.04	dddd	$J_{2,7} = 11, J_{6a,7} = 12$ $J_{6b,7} = 4, J^*_{7,9} = 2.0$
9	2.27	d	$J^*_{7,9} = 2.0$

*Coupling constants established by spin–spin decoupling.
†See formula I for the complete numbering system. The relative areas of signals are in accord with the number of protons assigned to them. (Signals associated with isomers were also present (see text).)

TABLE 2. The 220 MHz nmr spectrum of 3-epinaucledal, **3**

Proton location†	Chemical shift (τ)	Multiplicity	Coupling constants (Hz)
1	0.17	d	$J_{1,2} = 0.5$
2	7.31	ddd	$J_{1,2} = 0.5, J_{2,3} = 4$ $J_{2,7} = 11$
3	5.00	dq	$J_{2,3} = 4, J^*_{3,4} = 7$
4	8.76	d	$J^*_{3,4} = 7$
5a,b	5.4–5.7	m‡	—
6a,b	7.9–8.1	m‡	—
7	7.04	m‡	—
9	2.31	d	$J_{7,9} = 2$

*Coupling constants established by spin–spin decoupling.
†See formula I for complete numbering system. The sample contained ~60% of **3** and ~40% of **2** (see Experimental). Assignments were made after subtracting the spectrum of **2** (see Table 1).
‡These multiplets appear to overlap completely the multiplets associated with **2**; the resolution of the signals suggests that the characteristics of those from **2** are very similar to those from **3**.

the rearrangement product from **1***b* was a single homogeneous substance, but consisted of a mixture of isomers that could not be completely separated. It was necessary, therefore, to use the close similarity of the ir spectra of the materials and a signal-to-signal comparison of their nmr spectra to judge the identity of components. It is desirable to reserve the name naucledal for the principal isomer obtained in the original isolation (1).

The rearrangement conditions described above produced material that corresponded most closely to the material isolated from *N. diderrichii*. The nmr spectrum showed that it consisted mainly of naucledal, but that an epimer was also present in smaller amounts. Examination of the original spectra showed that this epimer was also present in the material from *N. diderrichii*. The rearranged material afforded a crystalline oxime that was also a mixture of stereoisomers, but gave satisfactory results on microanalysis.

The material obtained from sweroside was then used to assign the structure and configuration of **2** to naucledal from a detailed examination of its 220 MHz nmr spectrum. The key data were the values of 11 and 10 Hz assigned to the coupling constants between the proton at C-2 and those at C-7 and C-3, respectively; details of the analysis are shown in Table 1. It was found that when the aglucone **1***b* was stirred in water with silica gel, naucledal and the epimer observed previously were again produced, but the product was much richer in the epimer (~60%), and a similar detailed examination of the 220 MHz nmr spectrum of this component was carried out. The analysis, which establishes that the molecule is an isomer of **2**, is recorded in Table 2. The proton at C-2 still shows the 11 Hz coupling to the C-7 proton, but its coupling to the C-3 proton is now 4 Hz. It follows that the compound is 3-epinaucledal, **3**. A careful examination of the nmr spectra of various product mixtures reveals the presence of other signals that can reasonably

be attributed to C-2 epimers of **2** and **3**, but the concentration of these isomers was never high enough to allow a thorough analysis of their spectra.

That naucledal, the dominant stereoisomer under conditions where equilibrium is approached, has the configuration of **2** with no axial substituents is in accord with expectations based on thermodynamics. It follows that mixtures rich in 3-epinaucledal, **3**, are formed under conditions where kinetic control is more important. It may be noted, however, that the antiviral natural product, elenolic acid, is structurally related to naucledal, but its stereochemistry corresponds to that of 3-epinaucledal, **3** (5). Moreover, Kelly and Schletter obtained isomerically pure methyl elenolate by a rearrangement similar in design to ours and apparently carried out under conditions very similar to those in which we obtained **2** as the dominant product.

The interconversion of **2** and **3** requires a retro-Michael reaction to afford an intermediate such as II, related to (if not identical with) the intermediate implicated in their formation from **1***b*. As was noted earlier, there is spectroscopic evidence for the presence of such an intermediate in some of the mixtures produced by rearrangement. In fact, under some conditions the intermediate, seconaucledal, appeared to be the principal product obtained from **1***b* and it could be methylated with diazomethane and acetylated with acetic anhydride. It was not possible to obtain any of these compounds in a sufficiently pure state for satisfactory characterization, but some spectroscopic data could be collected. These data, particularly from the nmr spectra, indicate that the intermediate exists, at least predominantly, as a single isomer. Some evidence bearing on the configuration of the double bonds at C-2 and C-8 was observed. In the related case of vallesiachotamine and its geometrical isomer, homoallylic coupling between the methyl group corresponding to C-4 and the proton at the site corresponding to C-7 was observed only in the isomer in which these two carbon centres were *trans* related (6). The absence of such coupling in seconaucledal and its derivatives provides evidence, albeit weak since only one isomer was observed, for placing the methyl and aldehyde groups in a *trans* relationship. The configuration at C-9 is even less secure, but under the conditions used to observe the ir spectrum, the values obtained for the stretching frequencies of the hydroxyl and carbonyl groups, as well as the shape of the spectroscopic envelopes they produce and their behavior on dilution, indicate that the hydroxyl is hydrogen-bonded to the lactone carbonyl. Formula **4** is thus the best available representation of the molecule. It may be noted, however, that while acetylation of seconaucledal appears to produce a single enol acetate, diazomethane converts it to a crude product which exhibits two distinct singlets characteristic of methyl ethers as well as smaller peaks that may also be associated with methyl ethers; it appears, therefore, that at least two isomeric enol ethers are formed, but it is possible that isomerization has occurred during their formation and isolation.

The conversion of sweroside to naucledal and 3-epinaucledal has allowed us to establish the structure and stereochemistry of the products and to identify them as constituents of *N. diderrichii*. It is, moreover, gratifying to find evidence that the rearrangement did, indeed, follow the predicted path through an intermediate of the anticipated type. However, more careful examination of the nature and behavior of seconaucledal raises questions about details of its role in the rearrangement. The C-9 hydroxyl group in **4** appears to have the wrong orientation for the required Michael addition at C-3, but this is a relatively minor point, since ready isomerization at this enolic centre can be anticipated. Of more significance is the apparent stability of the intermediate under a number of reaction conditions. As has been stated previously, the aglucone **1***b* rearranged rapidly to a mixture of **2** and **3** in hot aqueous pyridine. In dry pyridine, the intermediate **4** formed rapidly but was converted to ring-closed material very slowly, and under these conditions, it could be observed that the ratio of **3** to **2** in the product was highest in the early stages of ring closure. In pyridine containing an added acid, the intermediate again formed rapidly, but either failed to undergo ring closure or did so at a rate slower than that of reactions leading to its degradation.

These results can be best explained by postulating that **2** and **3** are not, in fact, formed from **4** by a simple Michael addition. The data from the reaction in dry pyridine suggest that the C-9 hydroxyl group is not an effective Michael donor (either for stereochemical reasons or because the lone-pair electrons are too delocalized). However, water catalyzes the ring closure, and it is

logical to propose that it does so by acting as a Michael donor itself and converting the unsaturated aldehyde to the aldol **5** (or its epimer); it is the hydroxyl group produced in this way that adds to C-9 in the Michael fashion and the subsequent elimination of a molecule of water leads to **2** (or **3**). In the presence of an acid, the unsaturated aldehyde in **4** remains unhydrated; in accord with this is the common observation that aldols undergo very ready dehydration in acidic media. The relative amounts of **2** and **3** formed when kinetic control is important may reflect factors influencing the stereochemistry of the hydration of **4** as well as those governing the cyclization process; when equilibration can occur, the thermodynamic arguments remain unchanged. Undoubtedly, we are describing only a portion of a larger and more complex equilibrium, but in the local area of interest, these proposals can explain all of the observations.

Experimental

Melting points were determined on a Thomas-Kofler micro hot stage. Infrared spectra were obtained on a Perkin-Elmer 337 spectrometer with samples dissolved in chloroform; the wavelengths (μm) of significant peaks are reported. A Unicam SP 1800 ultraviolet spectrometer was used; the solvent was methanol and the wavelengths (nm) of absorption peaks are reported. Routine nmr spectra (60 MHz) were obtained on a Varian T-60 spectrometer with samples dissolved in chloroform-*d* (containing tetramethylsilane) unless otherwise indicated; chemical shifts are reported on the τ scale and are followed in parentheses with an indication of the signal multiplicity (initial letter), the coupling constants (*J* in Hz) if determined, and the number of protons associated with the signal; in the spectra of impure samples the characteristics of complex signals could not be assigned with confidence, but rough values are quoted for completeness. The 220 MHz spectra were determined at the Canadian 220 MHz NMR Centre with a Varian HR-220 spectrometer; the results are reported in Tables 1 and 2. Samples rich in naucledal or 3-epinaucledal (see below) were dissolved in chloroform-*d* (containing tetramethylsilane); signals characteristic of the component of interest were identified by as many characteristics as possible: relative area, the change in relative areas with change in composition, and decoupling techniques. The circular dichroism measurement was made with a Roussel-Jouan Dichrographe II.

Sweroside Aglucone (1b)

Sweroside, isolated from local *Lonicera tatarica*, was cleaved with almond β-D-glucosidase according to the method of Linde and Ragab (4) and the aglucone was obtained as crystals, mp 121–123°C. The mp and spectroscopic data were in accord with literature values (4).

Rearrangement Reactions

Preliminary studies were carried out with solutions of the aglucone **1***b* in pyridine-d_5 (5 to 10 mg in 0.1 ml) containing variable amounts of water and acid (HCl or $MeSO_3H$). The nmr spectra of solutions at various temperatures were recorded and time-dependent changes were observed; of particular value for identifying components and judging their relative concentrations were the distinctive methyl doublets and the signals associated with the aldehyde groups and the β-proton of the alkoxyacrylate groups (see below). Typical results were the following.

(*i*) A solution of **1***b* in pyridine-d_5 containing 10% of water was heated to 105–110°C. The nmr spectrum was recorded at hour intervals for 6 h. After 1 h, signals associated with naucledal (~70%), seconaucledal (~20%) and 3-epinaucledal (~10%) were observed and only traces of the aglucone appeared to be present. Subsequent spectra showed little change in product composition.

(*ii*) A solution of **1***b* in dry pyridine-d_5 was heated to 105–110°C. After 3 h the aglucone had been converted to seconaucledal (~50%) and about equal amounts of naucledal and 3-epinaucledal. The composition of the reaction mixture then changed slowly with time, with the amount of naucledal increasing at the expense of the other components, and after about 1 day the composition corresponded to that produced in (*i*) above.

(*iii*) A solution of **1***b* in pyridine-d_5 containing 10% of a solution of 50% aqueous methanesulfonic acid was observed at room temperature. Signals associated with seconaucledal increased steadily with time at the expense of the aglucone. Complete conversion required about 2 days. No signals associated with naucledal or its epimer were observed, even when the solution was heated.

Preparative Scale

Naucledal (2)

A solution of sweroside aglucone (**1***b*, 70 mg) in 1 ml of 10% aqueous pyridine was heated at 100–110°C under nitrogen for 3 h. The solution was allowed to cool and the solvent was removed by evaporation under reduced pressure; addition of benzene to the residue and evaporation was then carried out repeatedly to ensure the complete removal of solvent. Preparative tlc on deactivated silica gel with elution by methylene chloride – acetone (9:1) led to a single band (R_f 0.3) which provided a yellow oil (45 mg) that was identical in all significant respects with the material obtained from *N. diderrichii* (1) (tlc, ir, uv, nmr, and ms); circular dichroism λ (MeOH) ($[\theta]_{max}$) 283 (10 550), 309 (−3690). Examination of its nmr spectrum showed that this material consisted of naucledal (**2**, ~90%) and 3-epinaucledal (**3**, ~10%) with traces of other epimers (see Tables 1 and 2). A sample was converted to a crystalline oxime, mp 175–183°C. *Anal.* calcd. for $C_{10}H_{13}O_4N$: C 56.86, H 6.20, N 6.63; found: C 56.90, H 6.31, N 6.68.

3-Epinaucledal (3)

The sample richest in **3** was prepared by stirring a solution of the aglucone **1***b* (20 mg) in 1 ml of water with silica gel (0.2 g, 70–230 mesh) for 24 h at room temperature. The silica gel was removed by filtration, washed with methanol, and the washings were combined with the aqueous solution. Evaporation under reduced pressure then afforded a yellow oil (20 mg) which consisted of **3** (~60%) and **2** (~40%) and traces of isomers (see Tables 1 and 2).

Seconaucledal

A solution of the aglucone **1***b* (34 mg) in 1 ml of pyridine containing about 0.1 ml of 40% aqueous

methanesulfonic acid was left at room temperature for 2 days and then heated to 70°C for 1 h. A further 20 ml of pyridine was added, and the volume of the solution was reduced to about 1 ml by distillation under reduced pressure to remove water. About 20 ml of dry ether was added and pyridinium salts were removed by filtration. The solvent was then removed on the rotary evaporator to provide crude seconaucledal as a gummy residue (32 mg). This material could not be purified satisfactorily because of its instability; under some conditions it readily cyclized to naucledal and 3-epinaucledal. Spectroscopic data: ir: 2.80, 3.0 (b, unchanged on dilution), 3.70, 5.92, 6.00, 6.22; uv: 245, 282 (shoulder); in base 285, reversed by acid; nmr: 0.78 (b s, 1), 1.4 (b, 1), 2.35 (m, 1), 3.20 (q, J = 7; 1, coupled to 7.95), 5.4–6.2 (complex, 2), 6.9–7.3 (m, 1), 7.7–8.2 (complex, 2), 7.95 (d, J = 7; 3, coupled to 3.20).

When seconaucledal was treated with an excess of diazomethane in ether at 0°C, a mixture of products, including some cyclized material, was obtained; peaks of equal height at 6.20 and 6.35 in the nmr spectrum indicated the presence of two methyl ethers; small satellite peaks were also observed. By preparative tlc on silica gel (9:1 methylene chloride – acetone elution), a single methyl ether was isolated, but this could not be purified further. Spectroscopic data: ir: 5.88, 6.22; nmr: 0.71 (b s, 1) 2.79 (d, J = 2; 1), 3.40 (q, J = 7; 1), ~7.9 (complex, 2), 8.00 (d, J = 7; 3).

When seconaucledal was treated with an excess of acetic anhydride and pyridine and the crude product from the standard isolation procedure was subjected to tlc on silica gel (9:1 methylene chloride – acetone elution), an impure acetate was obtained. Attempts at further purification were not fruitful (tlc on silica gel deactivated by water led to the formation of naucledal and seconaucledal). Spectroscopic data: ir: 5.61, 5.88, 5.92, 6.12, 6.20; nmr: 0.64 (b s, 1), 1.90 (d, 1), 3.31 (q, J = 7; 1), ~5.8 (complex, 3), 7.6–8.2 (complex, 2), 7.82 (s, 3), 7.93 (d, J = 7; 3).

Acknowledgments

We thank Dr. A. Grey for the 220 Hz nmr spectra and Dr. H. Boucher for the circular dichroism measurements. This research was supported by the National Research Council of Canada.

1. S. McLEAN and D. G. MURRAY. Can. J. Chem. **50**, 1496 (1972).
2. H. INOUYE, T. YOSHIDA, Y. NAKAMURA, and S. TOBITA. Tetrahedron Lett. 4429 (1968).
3. J. PURDY and S. McLEAN. Tetrahedron Lett. 2511 (1976).
4. H. H. A. LINDE and M. S. RAGAB. Helv. Chim. Acta, **50**, 991 (1961).
5. F. A. MacKELLAR, R. C. KELLY, E. E. van TAMELEN, and C. DORSCHEL. J. Am. Chem. Soc. **95**, 7155 (1973); R. C. KELLY and I. SCHLETTER. J. Am. Chem. Soc. **95**, 7156 (1973).
6. K. T. D. De SILVA, G. N. SMITH, and K. E. H. WARREN. Chem. Commun. 905 (1971).

Synthesis of proctolin, a pharmacologically active pentapeptide in insects

ALVIN NEIL STARRATT AND BRIAN ELLMAN BROWN

Agriculture Canada, Research Institute, University Sub Post Office, London, Ont., Canada N6A 5B7

Received June 20, 1977

ALVIN NEIL STARRATT and BRIAN ELLMAN BROWN. Can. J. Chem. **55**, 4238 (1977).

The synthesis of the pentapeptide H-Arg-Tyr-Leu-Pro-Thr-OH by the mixed anhydride procedure and by the pentafluorophenyl ester method is described. This synthetic peptide is identical to proctolin, a myotropic substance isolated from the cockroach, *Periplaneta americana* (L.).

ALVIN NEIL STARRATT et BRIAN ELLMAN BROWN. Can. J. Chem. **55**, 4238 (1977).

On décrit la synthèse du pentapeptide H-Arg-Tyr-Leu-Pro-Thr-OH par la procédure à anhydride mixte ainsi que par la méthode de l'ester pentafluorophényle. Ce peptide synthétique est identique à la proctoline, une substance myotropique isolée à partir de l'insecte *Periplaneta américana* (L.).

[Traduit par le journal]

Recently we reported the isolation of the myotropic substance proctolin from the cockroach, *Periplaneta americana* (L.), and its identification as H-Arg-Tyr-Leu-Pro-Thr-OH (1, 2).[1] Proctolin is a peptide of neural origin occurring in highest titre in nerves innervating the viscera (4). This peptide evokes contraction of the visceral musculature at threshold concentrations of about 10^{-9} *M*. Pharmacological and other lines of evidence suggest that proctolin functions as an excitatory neuromuscular transmitter in insect visceral muscle (4, 5). Although most of our studies have been limited to *P. americana*, it has been shown that proctolin occurs in a wide variety of insects (6). The synthesis of proctolin was undertaken to confirm the assigned structure and to provide sufficient material for further studies of its physiological role.

Proctolin was first synthesized in a stepwise manner by the mixed anhydride procedure using conditions for racemization-free coupling (7). The overall route is shown in Scheme 1. Reaction with the wrong moiety of the mixed anhydride can occur to a significant extent during coupling of amino acids to proline by this method (8). Therefore, to avoid a poor yield at the tripeptide stage and difficulties in purification expected from a synthesis commencing with the C-terminal amino acid of proctolin, we began by coupling Boc-Leu-OH to H-Pro-OMe. Treatment of the products with hydrogen chloride – acetic acid to remove the *tert*-butoxycarbonyl group yielded crystalline H-Leu-Pro-OMe·HCl. This substance was also obtained by the pentafluorophenyl ester method of coupling. Sequential addition of N-protected H-Tyr(Bzl)-OH and H-Arg(NO_2)-OH yielded the tetrapeptide, Z-Arg(NO_2)-Tyr(Bzl)-Leu-Pro-OMe. The acid from alkaline hydrolysis was coupled to H-Thr-OBzl by the mixed anhydride procedure and, with similar results, by the use of diphenylphosphoryl azide (9). Hydrogenolysis removed all the protecting groups yielding H-Arg-Tyr-Leu-Pro-Thr-OH which after purification was shown to be chromatographically, electrophoretically, and pharmacologically identical to natural proctolin (2).

Starting from threonine, the sequential synthesis of proctolin was also accomplished by the pentafluorophenyl ester method (10, 11) as outlined in Scheme 2. In some cases, the pentafluorophenyl esters were prepared immediately before the coupling step and used without purification. This did not appear to result in lower yields or products that were more difficult to purify. Occasionally, samples of the pentafluorophenyl ester of Boc-Arg(NO_2)-OH were partially converted during handling and storage to a less polar substance, probably a lactam analogous to that obtained when synthesis of the *p*-nitrophenyl ester of Z-Arg(NO_2)-OH was attempted (12). A significant amount of this substance was not observed, however, in samples of freshly prepared, crude ester. After removal of the *tert*-butoxycarbonyl group of the pentapeptide derivative with hydrogen chloride – acetic acid, other protecting groups were removed in one operation by catalytic hydrogenolysis. Puri-

[1]Abbreviations used are those recommended by the IUPAC–IUB Commission on Biochemical Nomenclature (3). PFP = pentafluorophenyl.

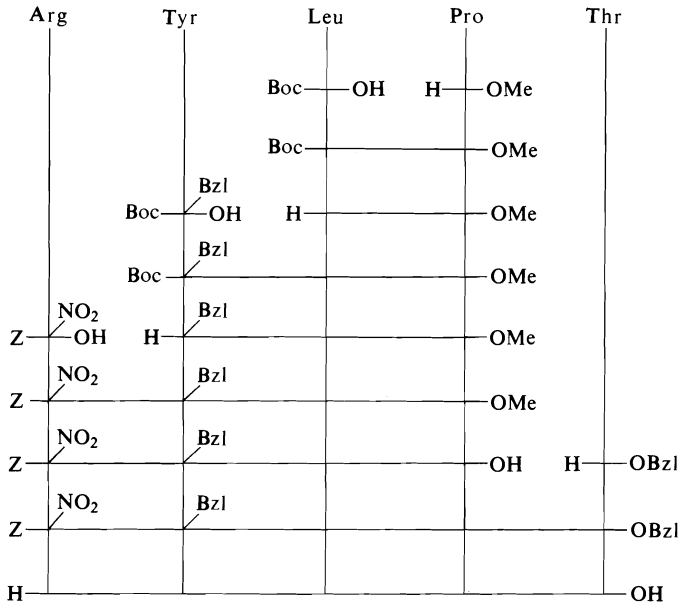

SCHEME 1

fication by ion-exchange chromatography and gel filtration yielded pure proctolin.

Peptides can usually be synthesized rapidly and efficiently by repeated addition of an excess of either the amino acid pentafluorophenyl esters or the mixed anhydrides to the peptide chain without purification of the intermediates (8, 11, 13). Proctolin has been synthesized in this manner by both methods. Although by-products were formed in each case during the coupling of Boc-

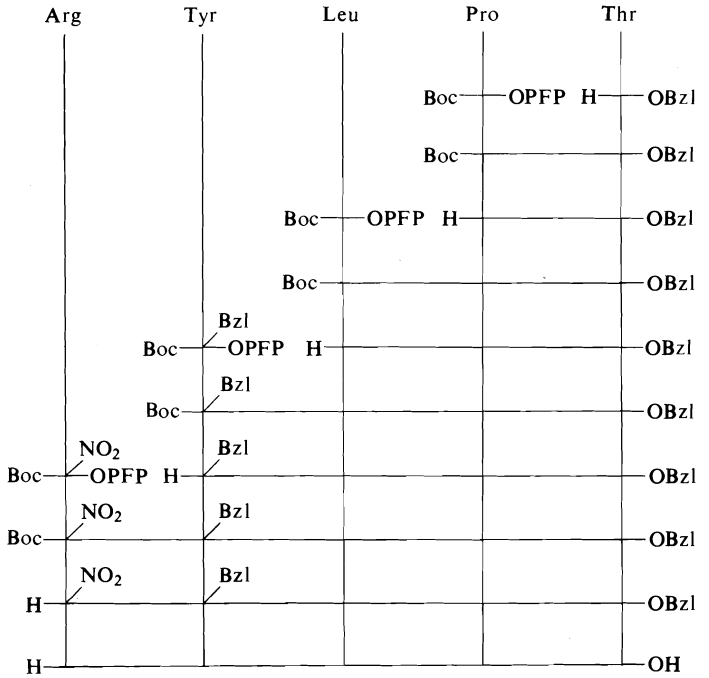

SCHEME 2

Arg(NO_2)-OH, the mixed anhydride procedure appeared to produce superior results in our hands. For the early steps in the synthesis of proctolin it is more convenient to use the pentafluorophenyl ester method since chain-lengthening can begin at the C-terminal end.

As well as confirming the structure of proctolin, the syntheses have furnished sufficient material for further physiological studies. In addition, intermediates useful in the synthesis of proctolin analogs have been characterized.

Experimental

The L-amino acids and derivatives used as starting materials were purchased from Pierce or Sigma Chemical Co. Dimethylformamide, dioxane, and tetrahydrofuran were passed through columns of basic alumina before use. The purity of amino acid and peptide derivatives was checked by thin-layer chromatography on Kieselgel DF-5 (Camag) plates using chloroform–methanol – acetic acid (85:10:5.5) and chloroform–methanol (19:1, 9:1, or 4:1). Spots were detected by use of ninhydrin and uv illumination. Melting points were determined on a Kofler hot stage and are uncorrected. Microanalyses were performed by Dr. C. Daessle, Montreal, and the amino acid analysis was carried out by the Amino Acid Analysis Laboratory, Chemistry and Biology Research Institute, Agriculture Canada, Ottawa.

Extracts containing completely protected peptides were washed successively with 1 *N* $KHCO_3$, water, 1 *M* citric acid, and water. In the case of products obtained by the pentafluorophenyl ester method, extracts were treated with *N*,*N*-diethylethylenediamine (11) prior to washing to remove unreacted active ester. All extracts were dried over magnesium sulfate and solvent was removed under reduced pressure at 30–35°C.

Removal of the tert-Butoxycarbonyl Group

The *tert*-butoxycarbonyl derivative was dissolved in 1.1 *N* hydrogen chloride in acetic acid. After approximately 30 min at room temperature, the reagent was removed under reduced pressure at 30–35°C.

Preparation of Pentafluorophenyl Esters

Pentafluorophenyl esters were prepared from *N*-protected amino acids by the method of Kisfaludy *et al.* (10).

H-Leu-Pro-OMe·HCl

(a) Mixed Anhydride Method

Isobutyl chloroformate (0.65 ml) was added to a solution of Boc-Leu-OH (1.15 g) and *N*-methylmorpholine (0.55 ml) in tetrahydrofuran (4 ml) at −15°C. The mixture was stirred for 2 min and then a cold solution of H-Pro-OMe·HCl (0.82 g) and *N*-methylmorpholine (0.55 ml) in dimethylformamide (3 ml) was added. After stirring for 1 h at approximately −15°C, the temperature was raised to 0°C and 2.5 *M* $KHCO_3$ added until a basic reaction was obtained. The solution was stirred for 30 min at 0°C, 75% saturated salt solution was then added, and the product was extracted into ethyl acetate. The extract was washed and dried and the solvent removed, yielding the crude product. Removal of the *tert*-butoxycarbonyl group and crystallization of the product from anhydrous ether – methanol yielded H-Leu-Pro-OMe·HCl (825 mg, 60%), mp 176–178°C (lit. (14) 177°C).

(b) Pentafluorophenyl Ester Method

N-Methylmorpholine (142 μl) was added to H-Pro-OMe·HCl (182 mg) in dioxane (5 ml) and the mixture was stirred for 10 min. Then Boc-Leu-OPFP (275 mg) was added and stirring was continued for 30 min. The solvent was removed and the product dissolved in ethyl acetate, washed, and dried. Removal of the *tert*-butoxycarbonyl group and crystallization of the product yielded H-Leu-Pro-OMe·HCl (220 mg, 71%), mp 182–183°C.

Boc-Tyr(Bzl)-Leu-Pro-OMe

Isobutyl chloroformate (285 μl) was added to a solution of Boc-Tyr(Bzl)-OH (881 mg) and *N*-methylmorpholine (260 μl) in tetrahydrofuran (3 ml) at −15°C. After 2 min a solution of H-Leu-Pro-OMe·HCl (470 mg) and *N*-methylmorpholine (185 μl) in dimethylformamide (2 ml) was added. The mixture was stirred for 1 h at approximately −15°C, unreacted mixed anhydride was destroyed, and the product was isolated as described for the preparation of Boc-Leu-Pro-OMe by the mixed anhydride method. Recrystallization of the product from ethyl acetate – light petroleum (60–80°C) yielded Boc-Tyr(Bzl)-Leu-Pro-OMe (725 mg, 72%), mp 91–93°C; $[\alpha]_D$ −43° (*c* 1.0, $CHCl_3$). *Anal.* calcd. for $C_{33}H_{45}N_3O_7$: C 66.53, H 7.61, N 7.05; found: C 66.82, H 7.40, N 7.09.

H-Tyr(Bzl)-Leu-Pro-OMe·HCl

Removal of the *tert*-butoxycarbonyl group of Boc-Tyr(Bzl)-Leu-Pro-OMe and recrystallization of the product from anhydrous ether – methanol yielded H-Tyr(Bzl)-Leu-Pro-OMe·HCl, mp 128–134°C; $[\alpha]_D$ −48° (*c* 1.0, $CHCl_3$). *Anal.* calcd. for $C_{28}H_{38}N_3O_5Cl$: C 63.20, H 7.20, N 7.90; found: C 62.74, H 7.27, N 8.28.

Z-Arg(NO$_2$)-Tyr(Bzl)-Leu-Pro-OMe

Isobutyl chloroformate (54 μl) was added to a solution of Z-Arg(NO_2)-OH (158 mg) and *N*-methylmorpholine (49 μl) in tetrahydrofuran (2 ml) at −15°C. After 2 min a solution of H-Tyr(Bzl)-Leu-Pro-OMe·HCl (170 mg) and *N*-methylmorpholine (35 μl) in dimethylformamide (2 ml) was added. The mixture was stirred for 1 h at −15°C, unreacted mixed anhydride was destroyed, and the product isolated as described for the preparation of Boc-Leu-Pro-OMe by the mixed anhydride method. Recrystallization from ethyl acetate yielded Z-Arg(NO_2)-Tyr(Bzl)-Leu-Pro-OMe (206 mg, 78%), mp 101–104°C; $[\alpha]_D$ −38° (*c* 1.0, $CHCl_3$). *Anal.* calcd. for $C_{42}H_{54}N_8O_{10}$: C 60.70, H 6.55, N 13.48; found: C 60.83, H 6.44, N 13.65.

Z-Arg(NO$_2$)-Tyr(Bzl)-Leu-Pro-OH

To a solution of Z-Arg(NO_2)-Tyr(Bzl)-Leu-Pro-OMe (328 mg) in methanol (4 ml) was added 0.5 *N* NaOH (2 ml). After 3.5 h at room temperature in a nitrogen atmosphere, the methanol was removed *in vacuo*. Water was added, the solution acidified with 1 *N* HCl, and the product extracted into ethyl acetate. Removal of the solvent yielded Z-Arg(NO_2)-Tyr(Bzl)-Leu-Pro-OH (255 mg, 78%). Thin-layer chromatography ($CHCl_3$–MeOH, 4:1) of the gummy material showed a single major spot, R_f 0.15, and traces of more polar material.

H-Thr-OBzl·HCl

This compound, mp 127–128°C (lit. (15) 125–126°C) was prepared by the method of Maclaren (16).

Boc-Pro-Thr-OBzl

Boc-Pro-OPFP (2.52 g) in dioxane (2 ml) was added to a mixture of H-Thr-OBzl·HCl (1.61 g) and *N*-methylmorpholine (868 μl) in dioxane (20 ml). After stirring for 1 h at room temperature, the solvent was removed *in vacuo*. The residue was dissolved in ethyl acetate and the solution was washed and dried. Recrystallization of the product from ether–hexane gave Boc-Pro-Thr-OBzl (2.24 g, 84%), needles, mp 88–90°C; $[\alpha]_D$ −54° (*c* 1.0, $CHCl_3$). *Anal.* calcd. for $C_{21}H_{30}N_2O_6$: C 62.05, H 7.44, N 6.89; found: C 62.00, H 7.49, N 6.66.

H-Pro-Thr-OBzl·HCl

Removal of the *tert*-butoxycarbonyl group of Boc-Pro-Thr-OBzl (2.17 g) and recrystallization of the product from anhydrous ether – methanol yielded H-Pro-Thr-OBzl·HCl (945 mg, 52%), mp 134–135°C; $[\alpha]_D$ −60° (*c* 1.0, $CHCl_3$). *Anal.* calcd. for $C_{16}H_{23}N_2O_4Cl$: C 56.05, H 6.76, N 8.17; found: C 55.63, H 7.07, N 8.26.

Boc-Leu-Pro-Thr-OBzl

Boc-Leu-OPFP, prepared from Boc-Leu-OH (346 mg) and used without purification, in dioxane (4 ml) was added to a mixture of H-Pro-Thr-OBzl·HCl (512 mg) and *N*-methylmorpholine (198 μl) in dioxane (5 ml). After stirring for 20 min at room temperature, water was added and the product was extracted into ethyl acetate. Recrystallization of the product (634 mg) from ether–hexane gave Boc-Leu-Pro-Thr-OBzl (140 mg), mp 68–70°C; $[\alpha]_D$ −89° (*c* 1.0, $CHCl_3$). *Anal.* calcd. for $C_{27}H_{41}N_3O_7$: C 62.41, H 7.95, N 8.09; found: C 62.11, H 8.18, N 8.51.

Boc-Tyr(Bzl)-Leu-Pro-Thr-OBzl

Boc-Tyr(Bzl)-OPFP (687 mg) in dioxane (3 ml) was added to a mixture of H-Leu-Pro-Thr-OBzl·HCl (486 mg), obtained by hydrolysis of the *tert*-butoxycarbonyl derivative, and *N*-methylmorpholine (140 μl) in dioxane (5 ml). After stirring for 20 min at room temperature the product was isolated. Addition of hexane to an ether solution of this material precipitated Boc-Tyr(Bzl)-Leu-Pro-Thr-OBzl (372 mg), mp 73–75°C; $[\alpha]_D$ −61° (*c* 1.0, MeOH). *Anal.* calcd. for $C_{43}H_{56}N_4O_9$: C 66.82, H 7.30, N 7.25; found: C 66.97, H 7.43, N 7.68.

Removal of the *tert*-butoxycarbonyl group yielded noncrystalline H-Tyr(Bzl)-Leu-Pro-Thr-OBzl·HCl.

H-Arg-Tyr-Leu-Pro-Thr-OH (Proctolin)

(a) From Z-Arg(NO₂)-Tyr(Bzl)-Leu-Pro-OH

(*1*). Isobutyl chloroformate (14 μl) was added to a stirred solution of Z-Arg(NO_2)-Tyr(Bzl)-Leu-Pro-OH (99 mg) and *N*-methylmorpholine (13 μl) in tetrahydrofuran (1 ml) at −15°C. After 2 min, a solution of H-Thr-OBzl·HCl (21 mg) and *N*-methylmorpholine (9 μl) in dimethylformamide (1.5 ml) was added and stirring was continued for 1 h. Unreacted mixed anhydride was destroyed and the product was isolated. Chromatography on a Kieselgel plate with chloroform–methanol – acetic acid (85:10:5.5) indicated the presence of a major product at R_f 0.61 and two minor products at R_f 0.49 and 0.40. For removal of the protecting groups, the crude peptide was dissolved in acetic acid – water (9:1) and 5% palladium-on-barium sulfate (1.5 times the weight of peptide derivative) added. The flask was flushed with nitrogen and hydrogen was bubbled slowly through the reaction mixture for approximately 24 h at room temperature. The solution was filtered and the solvent removed *in vacuo* yielding crude peptide (59 mg) indicated by bioassay (1) to contain 50 mg (89%) of proctolin.

(*2*). Diphenylphosphoryl azide (31 μl) in dimethylformamide (1.3 ml) was added to a stirred mixture of Z-Arg(NO_2)-Tyr(Bzl)-Leu-Pro-OH (99 mg) and H-Thr-OBzl·HCl (35 mg) in dimethylformamide (2 ml) at 0°C. Triethylamine (37 μl) was added and the mixture stirred at 0°C for 4.7 h and then at room temperature for 13 h. After addition of saturated salt solution, the product was extracted into ethyl acetate and the extract was washed and dried. Thin-layer chromatography indicated that the product consisted of the same components as obtained by the mixed anhydride method. Hydrogenolysis as described above yielded crude peptide shown by bioassay to contain 65 mg (84%) of proctolin.

(b) From H-Tyr(Bzl)-Leu-Pro-Thr-OBzl·HCl

Boc-Arg(NO_2)-OPFP, prepared from Boc-Arg(NO_2)-OH (255 mg) and used without purification, was dissolved in dioxane (3 ml) and added to a solution of H-Tyr(Bzl)-Leu-Pro-Thr-OBzl·HCl (358 mg) and *N*-methylmorpholine (62 μl) in dioxane (5 ml). After stirring for 1 h at room temperature and removal of the solvent, the residue was dissolved in ethyl acetate and the solution was washed and dried. The *tert*-butoxycarbonyl group was removed and the product partly purified by precipitation from methanol with ether. Thin-layer chromatography on Kieselgel with chloroform–methanol (4:1) indicated the presence of one major component, R_f 0.36, and several minor components. Hydrogenolysis of the hydrochloride as described above yielded crude peptide shown by bioassay to contain 250 mg (82%) of proctolin.

Purification of Proctolin

Crude proctolin was purified by ion-exchange chromatography (Rexyn 101, NH_4^+ form) and gel filtration (Sephadex G-15) as employed in the isolation of proctolin (1). The purified synthetic proctolin was homogeneous by paper and thin-layer chromatography and by high voltage paper electrophoresis and was chromatographically, electrophoretically, and pharmacologically identical to natural proctolin (2). Amino acid analysis of an acid hydrolysate (18 h at 110°C with constant boiling HCl in a sealed evacuated tube) showed the following molar ratio of amino acids: Arg, 0.97; Leu, 1.0; Pro, 0.99; Thr, 0.93; Tyr, 0.95

Comparison of the Mixed Anhydride and Pentafluorophenyl Ester Methods for Synthesis of Proctolin

Starting with H-Leu-Pro-OMe·HCl (4 mmol), the protected tetrapeptide Boc-Arg(NO_2)-Tyr(Bzl)-Leu-Pro-OMe was prepared by the mixed anhydride method as described above with the exception that a 1.4-fold excess of mixed anhydride was used at each stage (13). The product of each coupling was checked by tlc and used without further purification for the subsequent step. Hydrolysis of the ester and coupling of the product to H-Thr-OBzl (small excess) yielded Boc-Arg(NO_2)-Tyr(Bzl)-Leu-Pro-Thr-OBzl. After removal of the pro-

tecting groups, the overall yield of proctolin as determined by bioassay was 35%.

Similarly, beginning with H-Thr-OBzl·HCl (4 mmol), proctolin was synthesized by the pentafluorophenyl ester method as described above with the exception that a 1.5-fold excess of the Boc-amino acid pentafluorophenyl ester was used at each step and intermediates were not purified (11). Chromatography of the resulting protected pentapeptide, Boc-Arg(NO_2)-Tyr(Bzl)-Leu-Pro-Thr-OBzl, on Avicel with *n*-butanol – acetic acid – water (4:1:1) and on Kieselgel with *n*-butanol – acetic acid – ethyl acetate – water (1:1:1:1) showed the presence of one major ninhydrin-positive spot. After removal of the protecting groups, the overall yield of proctolin by this method as determined by bioassay was 40%.

Acknowledgments

We wish to thank Mrs. M. E. Stevens, Miss D. N. Mindenhall, and Mr. J. J. Jevnikar for valuable technical assistance.

1. B. E. Brown and A. N. Starratt. J. Insect Physiol. **21**, 1879 (1975).
2. A. N. Starratt and B. E. Brown. Life Sci. **17**, 1253 (1975).
3. IUPAC–IUB Commission on Biochemical Nomenclature. J. Biol. Chem. **247**, 977 (1972).
4. B. E. Brown. Science, **155**, 595 (1967).
5. B. E. Brown. Life Sci. **17**, 1241 (1975).
6. B. E. Brown. J. Insect Physiol. **23**, 861 (1977).
7. G. W. Anderson, J. E. Zimmerman, and F. M. Callahan. J. Am. Chem. Soc. **89**, 5012 (1967).
8. H. C. Beyerman, E. W. B. de Leer, and J. Floor. Recl. Trav. Chim. Pays-Bas, **92**, 481 (1973).
9. T. Shioiri, K. Ninomiya, and S. Yamada. J. Am. Chem. Soc. **94**, 6203 (1972).
10. L. Kisfaludy, M. Löw, O. Nyéki, T. Szirtes, and I. Schön. Justus Liebigs Ann. Chem. 1421 (1973).
11. L. Kisfaludy, I. Schön, T. Szirtes, O. Nyéki, and M. Löw. Tetrahedron Lett. 1785 (1974).
12. M. Bodanszky and J. T. Sheehan. Chem. Ind. London, 1268 (1960); R. Paul, G. W. Anderson, and F. C. Callahan. J. Org. Chem. **26**, 3347 (1961).
13. A. van Zon and H. C. Beyerman. Helv. Chim. Acta, **56**, 1729 (1973).
14. H. Determann and R. Köhler. Justus Liebigs Ann. Chem. **690**, 197 (1965).
15. E. Schnabel, H. Klostermeyer, and H. Berndt. Justus Liebigs Ann. Chem. **749**, 90 (1971).
16. J. A. Maclaren. Aust. J. Chem. **25**, 1293 (1972).

Kinetics of flowing dispersions. X. Oscillations in optical properties of streaming suspensions of spheroids

A. OKAGAWA AND S. G. MASON

Pulp and Paper Research Institute of Canada, Montreal, P.Q., Canada H3A 2A7

and

Department of Chemistry, McGill University, Montreal, P.Q., Canada H3A 2A7

Received June 24, 1977

A. OKAGAWA and S. G. MASON. Can. J. Chem. **55**, 4243 (1977).

Transients in angular light scattering and turbidity of dilute suspensions of nearly monodisperse spheroidal particles undergoing simple shear flow have been investigated by combining Rayleigh–Debye light scattering theory for single dielectric particles with fluid mechanical theory for the orientation distributions of particle assemblies in shear flow. Applying shear to an initially isotropic suspension causes the orientation distributions and thus the angular scattering coefficients to oscillate. Various geometrical arrangements are considered with a view to selecting those that will maximize such rheo-optical effects.

By calculating the optical scattering cross section of a single particle, the turbidity of a suspension is obtained; like the scattering coefficient, it undergoes oscillations that are damped by (*1*) the inevitable spread in particle shape and volume in real systems, (*2*) shear-induced particle interactions, and (*3*) rotary Brownian motion. The rates of damping, expressed as relaxation times, are considered for the three mechanisms acting alone or in concert.

Preliminary measurements of the turbidity of dilute suspensions of hardened human red blood cells confirm this general pattern of behavior. Apart from their intrinsic interest, such rheo-optical effects can be used to determine a number of useful properties of dispersions.

A. OKAGAWA et S. G. MASON. Can. J. Chem. **55**, 4243 (1977).

On a étudié les espèces de transition qui se produisent dans la diffusion de la lumière angulaire et la turbidité de suspensions diluées de particules sphéoridales presque monodispersées subissant un écoulement cisaillé simple; ces études ont été effectuées en combinant la théorie de la diffusion de la lumière de Raleigh–Debye pour des particules diélectriques simples avec la théorie de mécanique des fluides pour les distributions de l'orientation de groupements de particules subissant un écoulement cisaillé. L'application d'un cisaillement à une suspension initialement isotrope provoque une oscillation des distributions d'orientation et, donc, aussi des coefficients de diffusion angulaire. On a considéré divers arrangements géométriques afin de choisir ceux qui maximisent de tels effets rhéo-optiques.

En calculant la section droite de diffusion optique d'une particule simple, on obtient la turbidité de la suspension; on note que la turbidité subit, comme le coefficient de diffusion, des oscillations qui sont atténuées par: (*1*) l'inévitable dispersion de forme et de volume des particules dans le système réel; (*2*) les interactions de particules induites par le cisaillement et (*3*) par le mouvement rotatoire Brownien. On considère les taux d'atténuation, exprimés sous forme de temps de relaxation, pour les trois mécanismes agissant individuellement ou ensemble.

Des mesures préliminaires de turbidité de suspensions diluées de cellules rouges durcies de sang humain confirment ce comportement général. En plus de leur intérêt intrinsèque, on peut utiliser de tels effets rhéo-optiques pour déterminer un certain nombre de propriétés utiles des dispersions.

[Traduit par le journal]

Introduction

Many macroscopic properties of flowing suspensions depend on the motions of the individual particles and especially their rotations and the resulting orientations. Elsewhere the rheological (1) and electrical (2) properties have been examined. In this paper we consider optical properties, specifically angular light scattering and turbidity.

In the past the most commonly measured rheo-optical effect has been streaming birefringence, used to determine particle (or molecular) size and configuration in colloidal sols and polymer solutions (3–5). On the other hand, light scattering, while widely used in quiescent fluids, has received relatively little attention in streaming systems except by Diesslhost and Freundlich (6) and Heller, Peterlin, and co-workers (7–11), the latter workers deducing the statistical configuration of flowing macromolecules in dilute solutions. More re-

cently angular scattering (12) and turbidity (13, 14) measurements on dilute suspensions of human erythrocytes have been made in simple shear flow; the turbidity measurements (13, 14) exhibited damped oscillations from which it was inferred that cell shapes, size, and orientations could be determined.

In this paper we establish the theoretical foundations of the periodic optical properties of flowing dispersions by combining angular light scattering theory with that for the rotational motion of dilute and nearly monodisperse dispersions of spheroids in simple shear flow, and offer some corroboratory experimental evidence, which goes beyond that in refs. 13 and 14.

In our theory we assume that particles are much larger than the light wavelength and that their refractive index is close to that of suspending medium so that Rayleigh–Debye scattering theory (15) applies. Various geometrical arrangements of incident and scattered light beams relative to the flow field are considered with a view to optimizing the rheo-optical effects. The particle rotations and the resulting orientations in dilute suspensions are then expressed in various coordinate systems using the theory previously developed (1) for transient orientation distributions of spheroids. We thus show that the various angular scattering coefficients and the turbidity undergo oscillations, usually damped, with a frequency twice that of the particles rotating about the vorticity axis of the flow.

In our experiments, like some of those in ref. 13, dilute suspensions of hardened (i.e., rigid) red blood cells, which are biconcave discs, have been used to model oblate spheroids for which shape all of the numerical calculations from the theory are given. However, all of the light scattering equations are equally valid for prolate spheroids, including spheres. For reasons that will be seen later, some of the relations are purely formal in nature, while others (i.e., those dealing with relaxation times) are based on orientation distribution functions and are not applicable directly to light scattering. However, sufficient detail is given so that the theory can be readily used for numerical calculations of a variety of systems and geometries extending beyond those for which calculated or measured data are presented.

Angular Light Scattering

Light Scattering by Single Spheroids

When a particle of maximum linear dimension l suspended in a fluid is exposed to linearly polarized light of wavelength λ, the light may be absorbed and scattered by the particle; in this treatment we limit consideration to systems that do not absorb light, i.e., the optical dielectric constant (or refractive index) is not complex; we also assume that the particles are optically isotropic. When $l > \lambda$ and the particle refractive index n_B is close to that of the medium n_A, Rayleigh–Debye scattering occurs (15) for which the basic condition is

$$kl(m^2 - 1) \ll 1 \qquad [1]$$

where $k = 2\pi/\lambda$ is the wave number and $m = n_B/n_A$. The light scattering for this case is given by summation of the scattering by each volume element of the particle, which we take to be a spheroid whose surface is

$$\frac{x_1'^2}{a^2} + \frac{x_2'^2}{b^2} + \frac{x_3'^2}{b^2} = 1 \qquad [2]$$

where a, b are the semi-axes ($a \lessgtr b$ for oblate and prolate spheroids, and $a = b$ for a sphere) of revolution and the Cartesian coordinate system X_i' is fixed in the particle with X_1' on the axis of revolution. When the particle is placed in linearly polarized light of intensity I_0 directed along one of the Cartesian coordinate axes fixed in space as shown in Fig. 1, the scattered light intensity I_s at the scattering angle θ_0, ϕ_0 (the spherical polar coordinates for the scattered light with X_k as the polar axis) is given (15) by

$$I_s = \frac{I_0 V^2 k^4 (m^2 - 1)^2 (1 - \sin^2\theta_0 \sin^2\phi_0) R(\theta_0, \beta)}{16\pi^2 r^2} \qquad [3]$$

where $V = 4\pi ab^2/3$ and r is the distance from the particle to the light detector. The form factor $R(\theta_0, \beta)$ depends upon particle volume V, its shape, and orientation, and is given by

$$R(\theta_0, \beta) = \left[\frac{3(\sin u - u\cos u)}{u^3}\right]^2 \qquad [4]$$

where

$$u = 2kb \sin \tfrac{1}{2}\theta_0 [\sin^2\beta + (a/b)^2 \cos^2\beta]^{1/2} \qquad [5]$$

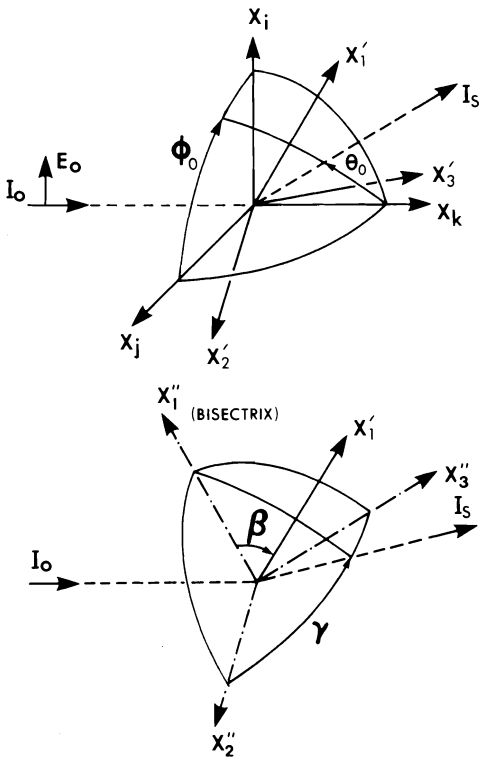

FIG. 1. Various coordinate systems for light scattering by a single spheroid whose axis of revolution is along X_1'. Top: The incident light I_0 polarized in the direction of X_i (indicated by E_0) is directed along X_k axis. The direction of the scattered light I_s is expressed by the spherical polar coordinates θ_0, ϕ_0 (relative to the incident light beam as polar axis). The numbering of $i, j, k = 1, 2, 3$ is determined by the geometrical arrangement of the optical and flow systems. Bottom: The orientation of X_1' relative to the Cartesian coordinates X_1'', X_2'', X_3'' is given by the spherical coordinates β, γ with the bisectrix (the axis bisecting the backward direction of incident beam I_0 and I_s) as the polar axis which is taken as X_1''.

where the orientation of particle is expressed by the spherical polar coordinates β and γ when the bisectrix (the axis which bisects the angle between I_0 and I_s in the plane containing them) is taken as the polar axis (Fig. 1, bottom). Since u is a function only of β, thus all particles of a given β have the same scattering pattern. It is usual to define the relative scattering intensity $I_r = I_s/I_s$ ($\theta_0 = 0$), so that from [3]

$$[6] \qquad I_r = (1 - \sin^2\theta_0 \sin^2\phi_0)R(\theta_0, \beta)$$

Thus I_r like $R(\theta_0, \beta)$ is also a function of the particle volume, shape, and orientation for a given scattering angle θ_0, ϕ_0.

Spheroids in the Simple Shear Flow

We now consider a single isolated spheroid when the fluid medium undergoes slow simple shear flow with velocity components v_i relative to the Cartesian coordinates X_i fixed in space

$$[7] \qquad \begin{aligned} v_1 &= v_2 = 0 \\ v_3 &= Gx_2 \end{aligned}$$

G being the velocity gradient (Fig. 2, top). The axis of revolution of the spheroid, whose orientation θ_1, ϕ_1 is now expressed relative to the polar axis X_1, rotates periodically in a fixed spherical elliptic orbit given by Jeffery's equations (1, 16):

$$[8a] \qquad \tan\theta_1 = \frac{C r_e}{(r_e^2 \cos^2\phi_1 + \sin^2\phi_1)^{1/2}}$$

$$[8b] \qquad \tan\phi_1 = r_e \tan(2\pi t/T + \kappa)$$

where $r_e = a/b$ is the axis ratio, C and κ are the orbit constant and phase angle respectively, and T is the period of one complete rotation about the vorticity axis X_1 given by

$$[9] \qquad T = 2\pi(r_e + r_e^{-1})/G$$

Since the particle rotates periodically with a frequency which is shape- but not size-dependent, I_r will vary periodically (but with twice the frequency of rotation because of fore–aft symmetry) in phase with the particle with an amplitude depending upon both the shape r_e and volume V of the particle and the geometrical arrangement of the optical system. As a guide for optimizing the measurement of I_s (and its oscillations), a number of geometries have been considered, all of which are experimentally realizable. These fall into two groups; one in which the bisectrix and the other in which the incident light coincide with one of the fixed coordinate axes X_i of the flow field. This classification yields six geometries as shown in Fig. 2, which we examine in detail below. In all cases, the incident and scattered light beams and their bisectrices are taken to lie on one of the X_iX_j planes and the electric field of the incident beam is normal to this plane (i.e., $\phi_0 = 0°$) so that

$$[10] \qquad I_r = R(\theta_0, \beta)$$

It thus becomes more convenient to express the particle orientation as β, γ the transformation equations of which from θ_1, ϕ_1, and θ_0 for the six cases are as listed in Table 2. In group I (Fig. 2, left), we consider scattering in the X_1X_2-plane with X_1 as bisectrix (I-A), in the X_2X_3-plane with X_2 as bisectrix (I-B), and in the X_2X_3-plane with X_3 as bisectrix (I-C). Since the bi-

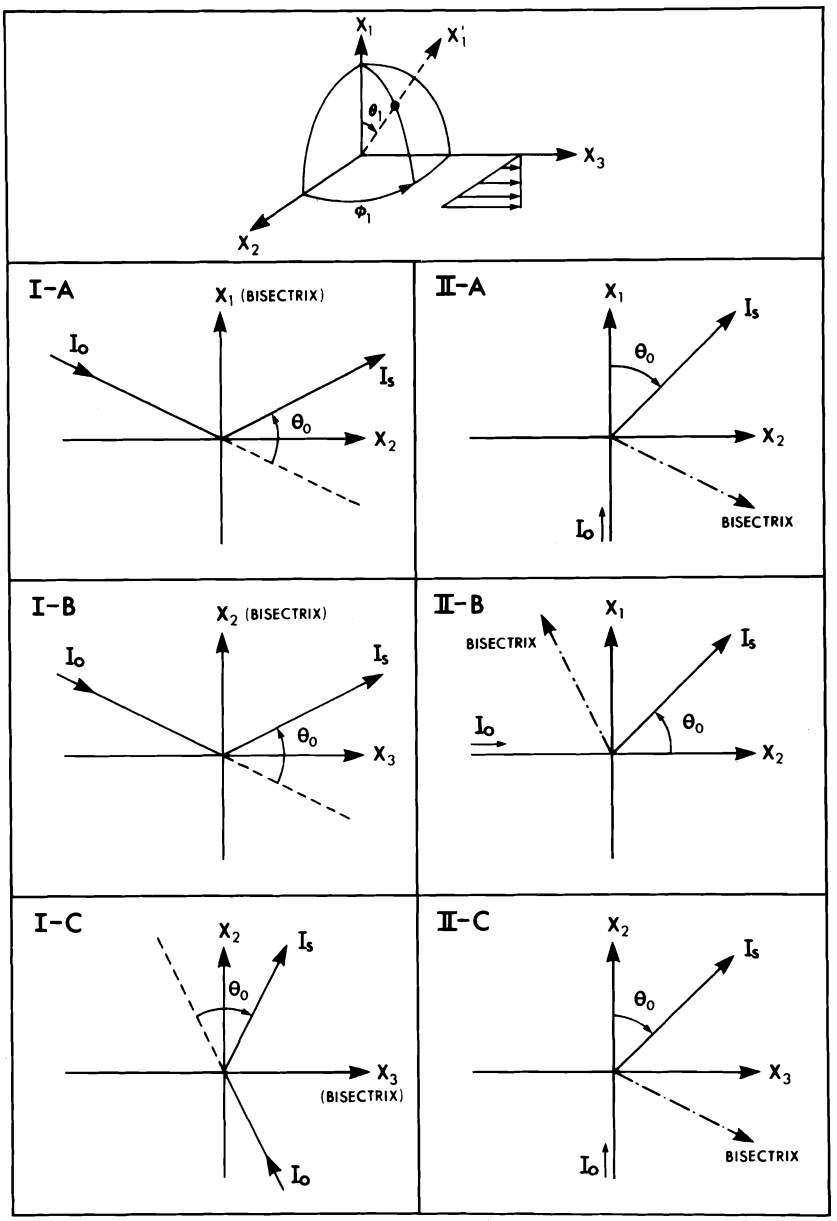

FIG. 2. Various feasible geometrical arrangements. In group I (A–C), the bisectrix between I_0 and I_s coincides with one of the space-fixed coordinate axes X_i, whereas in group II (A–C), I_0 itself coincides with one of X_i. I_s is considered only in the plane X_iX_j with the polarization of I_0 normal to this plane. At the top of the figure the spherical polar coordinates θ_1, ϕ_1 of the spheroidal axis are shown relative to the simple shear flow given by [7].

sectrix is the polar axis for β, γ and coincides with the Cartesian space coordinates X_i, the transformations are straightforward. For I-A, $\beta = \theta_1$ and $\gamma = \phi_1$, the variations of β and γ are thus identical to [8], whereas those of β and γ for the other two cases in group I depends upon the orbit constant C such that $\tan \gamma$ is limited to $\pm Cr_e$ for I-B and $\pm C$ for I-C.

On the other hand, in group II (Fig. 2, right) where the scattering is considered in the X_1X_2-plane with I_0 along the X_1 axis (II-A), in the X_1X_2-plane with I_0 along the X_2 axis (II-B), and

TABLE 1. Equations for transformation of coordinates and spheroid rotations for various geometries

Geometry (Fig. 2)	$\cos\beta$	$\tan\gamma$
I-A	$\cos\theta_1$	$\tan\phi_1$
I-B	$\sin\theta_1\cos\phi_1$	$\tan\theta_1\sin\phi_1$
I-C	$\sin\theta_1\sin\phi_1$	$\tan\theta_1\cos\phi_1$
II-A	$\sin\theta_1\cos\phi_1\cos\frac{\theta_0}{2} - \cos\theta_1\sin\frac{\theta_0}{2}$	$\frac{\cos\theta_1\cos\frac{\theta_0}{2} + \sin\theta_1\cos\phi_1\sin\frac{\theta_0}{2}}{\sin\theta_1\sin\phi_1}$
II-B	$\cos\theta_1\cos\frac{\theta_0}{2} - \sin\theta_1\cos\phi_1\sin\frac{\theta_0}{2}$	$\frac{\sin\theta_1\sin\phi_1}{\cos\theta_1\sin\frac{\theta_0}{2} + \sin\theta_1\cos\phi_1\cos\frac{\theta_0}{2}}$
II-C	$\sin\theta_1\sin\phi_1\cos\frac{\theta_0}{2} - \sin\theta_1\cos\phi_1\sin\frac{\theta_0}{2}$	$\tan\theta_1\cos\phi_1\cos\frac{\theta_0}{2} + \tan\theta_1\sin\phi_1\sin\frac{\theta_0}{2}$

	Variation of $\cos\beta$[a]	Variation of $\tan\gamma$[a]
I-A	$\left[\frac{r_e^2\cos^2\gamma + \sin^2\gamma}{C^2r_e^2 + r_e^2\cos^2\gamma + \sin^2\gamma}\right]^{1/2}$	$r_e\tan T^{*b}$
I-B	$\frac{Cr_e\cos\gamma}{(C^2r_e^2 + r_e^2\cos^2\gamma + \sin^2\gamma)^{1/2}}$	$Cr_e\sin T^*$
I-C	$\frac{Cr_e\sin\gamma}{(C^2r_e^2 + r_e^2\cos^2\gamma + \sin^2\gamma)^{1/2}}$	$C\cos T^*$
II-A	$\frac{C\cos\frac{\theta_0}{2}\cos T^* + \sin\frac{\theta_0}{2}}{[1 + C^2\{\cos^2 T^* + r_e^2\sin^2 T^*\}]^{1/2}}$	$\frac{\cos\frac{\theta_0}{2}\operatorname{cosec} T^*}{Cr_e} + \frac{\sin\frac{\theta_0}{2}\cot T^*}{r_e}$
II-B	$\frac{\cos\frac{\theta_0}{2} - C\sin\frac{\theta_0}{2}\cos T^*}{[1 + C^2\{\cos^2 T^* + r_e^2\sin^2 T^*\}]^{1/2}}$	$\frac{Cr_e\sin T^*}{\sin\frac{\theta_0}{2} + C\cos\frac{\theta_0}{2}\cos T^*}$
II-C	$\frac{C\{r_e\cos\frac{\theta_0}{2}\sin T^* - \sin\frac{\theta_0}{2}\cos T^*\}}{[1 + C^2\{\cos^2 T^* + r_e^2\sin^2 T^*\}]^{1/2}}$	$C\{r_e\sin\frac{\theta_0}{2}\sin T^* + \cos\frac{\theta_0}{2}\cos T^*\}$

[a]Calculated from [8] and the transformation equations in columns 2 and 3.
[b]$T^* = (2\pi t/T) + \kappa$.

in the X_2X_3-plane with I_0 along the X_2-axis (II-C), the transformations of θ_1, ϕ_1 to β, γ are more complicated and are functions of the scattering angle θ_0 (Table 1). The particle rotations expressed in terms of β and γ are also listed in the last two columns of Table 1.

Dilute Suspensions

If a suspension of identical spheroids is so dilute that there is no secondary scattering (i.e., by one particle from that scattered from another) the total scattering from the assembly is given by the summation, which from [10] becomes:[1]

$$[11]\qquad \overline{R(\theta_0, \beta)} = \int_0^{2\pi}\int_0^{\pi} R(\theta_0, \beta)p_t(\beta, \gamma)\,d\beta\,d\gamma$$

where $p_t(\beta, \gamma)\,d\beta\,d\gamma$ is the fraction of particles oriented in the interval $d\beta\,d\gamma$ at β, γ. We have previously shown theoretically for spheroids (1) and confirmed experimentally for rods and discs that behave like prolate ($r_e > 1$) and oblate ($r_e < 1$) spheroids (17) that, in an initially randomly oriented (or isotropic) dilute suspension of non-interacting spheroids when each particle retains its original orbit constant C and phase angle κ in flow [7], the time-dependent orientation probability distribution $p_t(\theta_1, \phi_1)$ is (1)

[1]Symbols with an overbar designate instantaneous number averages.

$$[12] \qquad p_t(\theta_1, \phi_1) = \frac{\sin \theta_1}{4\pi(\cos^2 \theta_1 + \chi^2 \sin^2 \theta_1)^{3/2}}$$

where

$$[13a] \qquad \chi^2 = \chi_1 \sin^2 \phi_1 + \chi_2 \sin \phi \cos \phi + \chi_3 \cos^2 \phi_1$$

$$[13b] \qquad \chi_1 = \tfrac{1}{2}[1 + r_e^{-2} + (1 - r_e^{-2}) \cos (4\pi t/T)]$$

$$[13c] \qquad \chi_2 = (r_e^{-1} - r_e) \sin (4\pi t/T)$$

$$[13d] \qquad \chi_3 = \tfrac{1}{2}[1 + r_e^2 + (1 - r_e^2) \cos (4\pi t/T)]$$

The transformation of $p_t(\theta_1, \phi_1)$ to $p_t(\beta, \gamma)$ can be made through the identity:

$$[14] \qquad p_t(\theta_1, \phi_1)\, d\theta_1\, d\phi_1 = p_t(\beta, \gamma)\, d\beta\, d\gamma$$

with the result:

$$[15] \qquad p_t(\beta, \gamma) = \frac{\sin \beta}{4\pi(F_1 \sin^2 \beta + F_2 \sin \beta \cos \beta + F_3 \cos^2 \beta)^{3/2}}$$

where F_1, F_2, and F_3 are explicit functions (the details of whose derivations like those in Table 1 are straightforward and hence omitted) of r_e, θ_0, γ, and t listed for all six cases in Table 2. Substituting [15] into [11], $\overline{R(\theta_0, \beta)}$ can be obtained by numerical integration over all possible orientations.

To illustrate, numerical integrations have been made for initially isotropic suspensions of oblate spheroids of $r_e = 0.4$, $b = 4.25$ μm with $n_B = 1.40$ in a fluid of $n_A = 1.44$, so that $(m^2 - 1) = 0.054$ and thus satisfying [1], which are exposed to linearly polarized incident light of $\lambda = 632.8$ nm in vacuum; these physical properties correspond closely to the experimental system described later. The calculated relative scattering intensities at various θ_0 over a semi-rotation $0 \leq t \leq T/2$ for the six geometries (Fig. 2) are shown in Fig. 3. Cases I-A and II-B exhibit only small amplitudes of oscillation in I_r during rotation whereas the other four cases clearly show appreciable amplitudes of frequency $2/T$. The scattering intensities at $t/T = 0.25$ are greater for cases I-B and II-A and lower for I-C and II-C than for random orientations (i.e., at $t = 0$ and $T/2$).

It is immediately clear from those calculations that geometries I-A and II-B are not suitable for studying particle orientation phenomena for this system, whereas the others are. At this stage it is not possible to generalize on the most suitable geometry to be used except to state that it will depend on (*1*) particle volume and shape, (*2*) the refractive indices n_A, n_B, and (*3*) the use of which the measurements are made. As will be seen in the following section the much simpler geometry used in turbidity measurements (and generally considered an anathema to most angular light scattering) is especially convenient for the oblate spheroids considered here.

Turbidity

Undamped Oscillations

The attenuation of light transmitted through a suspension of particles is given by the Beer–Lambert law (15)

$$[16] \qquad T_0 = I_t/I_0 = \exp(-\nu d)$$

where I_t is the transmitted intensity over the path length d and T_0 is the transmittance. The attenuation coefficient ν is the absorption coefficient when light is absorbed or the turbidity when it is scattered; as stated earlier only the latter case is considered here. Since we neglect secondary scattering, strictly speaking [16] is limited to low concentrations when only the linear term of the Taylor expansion is valid, i.e.,

$$[17] \qquad T_0 = 1 - \nu d$$

The turbidity ν (of dimension $[L]$) is a measure of the total energy removed from the primary beam by scattering, and can be written as

$$[18] \qquad \nu = N\overline{C_{sca}}$$

where N is the particle number concentration and $\overline{C_{sca}}$ (of dimension $[L^2]$) is the mean particle scattering cross section.

For a spheroid at θ_1, ϕ_1 (polar axis X_1) exposed to incident light directed along the X_2-axis and polarized in the X_1-direction (Fig. 4),

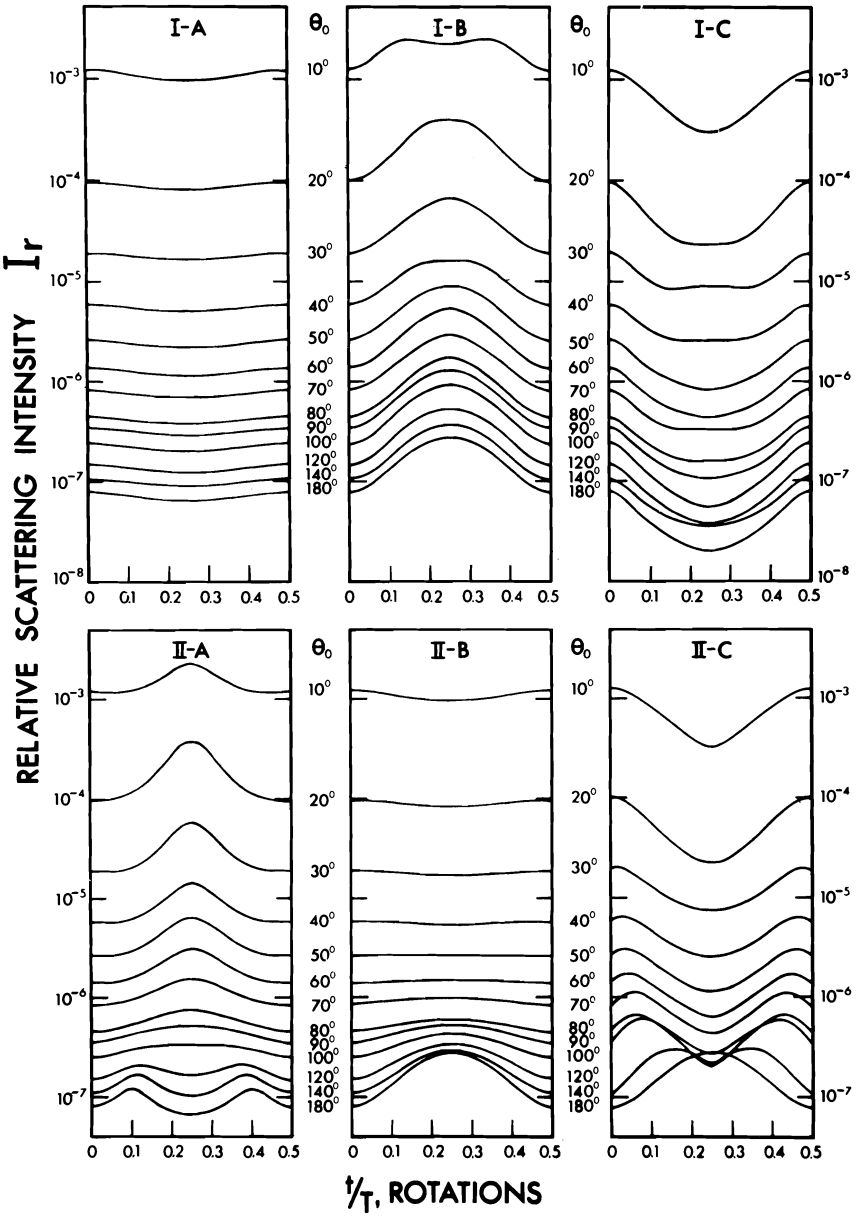

FIG. 3. Oscillation of relative scattering intensities I_r of a dilute suspension of oblate spheroids over a half-rotation in shear flow, for the various geometrical arrangements in Fig. 2 for $r_e = 0.4$ ($a = 1.2$ μm, $b = 4.25$, and $V = 91$ μm^3), $n_A = 1.44$, $n_B = 1.40$, and $\lambda = 632.8$ nm. The values at $t/T = 0$ and 0.5 are for random particle orientations and for a given θ_0 are identical for all cases. Equation 11 was integrated numerically using $p_t(\beta, \gamma)$ given by [15] and the values of F_i listed in Table 2.

scattering occurs over all values of θ_0, ϕ_0, the angular coordinates for the scattered light with X_2 taken as the polar axis. The scattering cross section is thus (15)

$$[19] \quad C_{sca} = \int_0^{2\pi} \int_0^{\pi} (I_s/I_0)\, r^2 \sin\theta_0 \, d\theta_0 \, d\phi_0$$

where I_s is given by [3], so that

$$[20] \quad C_{sca} = \frac{1}{16\pi^2} \int_0^{2\pi} \int_0^{\pi} V^2 k^4 (m^2 - 1)^2 (1 - \sin^2\theta_0 \sin^2\phi_0) R(\theta_0, \beta) \sin\theta_0 \, d\theta_0 \, d\phi_0$$

However, the angles β, γ of the bisectrix for a given θ_1, ϕ_1 vary with the scattering angles θ_0, ϕ_0 via the geometrical relations:

$$[21a] \quad \cos\beta = \cos\theta_1 \cos\tfrac{1}{2}\theta_0 \sin\phi_0 + \sin\theta_1 \cos\phi_1 \sin\tfrac{1}{2}\theta_0 - \sin\theta_1 \sin\phi_1 \cos\tfrac{1}{2}\theta_0 \cos\phi_0$$

$$[21b] \quad \tan\gamma = \frac{\sin\theta_1 (\cos\phi_1 \cos\tfrac{1}{2}\theta_0 \cos\phi_0 + \sin\phi_1 \sin\tfrac{1}{2}\theta_0)}{\cos\tfrac{1}{2}\theta_0 \sin\phi_0 \cos\beta - \cos\theta_1}$$

C_{sca} of a single particle can be conveniently compared with the geometrically projected area S_{13} on the plane normal to the incident beam (i.e., on the X_1X_3-plane) to yield the 'scattering efficiency':

$$[22] \quad Q_{sca} = C_{sca}/S_{13}$$

For a spheroid given by [2]

$$[23] \quad S_{13} = \pi ab[1 - \sin^2\theta_1 \cos^2\phi_1(a^2 - b^2)/a^2]^{1/2}$$

When $\theta_1 = 0$, $S_{13} = \pi ab$; and when $\theta_1 = 90°$, $\phi_1 = 0°$, $S_{13} = \pi b^2$; for an oblate spheroid ($r_e < 1$) these cases correspond to viewing it along the X_2-axis edge-on and face-on, respectively. Figure 5 shows numerical values of Q_{sca} for various orbit constants C for the oblate spheroids used in computing Fig. 3 when shear flow given by [7] is applied for a half-rotation starting at $\phi_1 = 0$ (i.e., $\kappa = 0$). When $C = 0$, (i.e., $\theta_1 = 0°$) the particle spins about its axis of revolution so that there is no change in C_{sca} and and S_{13}. When, on the other hand, $C = \infty$ (i.e., $\theta_1 = 90°$) it faces the incident light near $t = 0$ and $T/2$, and orients edge-on at $t = T/4$ so that Q_{sca} passes through a minimum and a maximum and like I_r oscillates with frequency $2/T$. It may appear paradoxical that the particle scatters more light when it is oriented edge-on to the incident light (when S_{13} is least) than when face-on (S_{13} greatest). This is confirmed by the experiments described below. From [22], $Q_{sca} = 1$ means that all of the light beam falling on the particle is removed by scattering. However, it is seen in Fig. 5 that Q_{sca} is often >1; this results from the disturbance of the light beam in regions away from the surface of the particle.

The mean value $\overline{C_{sca}}$ for an infinitely dilute suspension can be obtained from the orientation probability $p_t(\theta_1, \phi_1)$ using the relation

$$[24] \quad \overline{C_{sca}} = \int_0^{2\pi} \int_0^{\pi} C_{sca}\, p_t(\theta_1, \phi_1)\, d\theta_1\, d\phi_1$$

Values of $\overline{C_{sca}}$ calculated from [12], [20], and [24] for an initially random suspension of oblate spheroids of the system used in Figs. 3 and 5, and for the geometry of Fig. 4, are shown in Fig. 6. Since $p_t(\theta_1, \phi_1)$ is a periodic function of frequency $2/T$ (1), $\overline{C_{sca}}$ oscillates in synchronism and with constant amplitude reaching a minimum at $t = T/4$ when there is a preferred face-on orientation towards the X_2-axis (1), and a maximum at $t = 0$, $T/2$ when there is a preferred edge-on orientation and (as with a single particle) vice-versa for S_{13} (Fig. 6).

Damped Oscillations

The oscillations described above are modified by various factors not yet considered. Thus, direct measurements of particle orientation distributions (17) have shown that the oscillations decay with a characteristic relaxation time τ during which the amplitude is reduced to $1/e$ of its initial value.

The damping results from various mechanisms

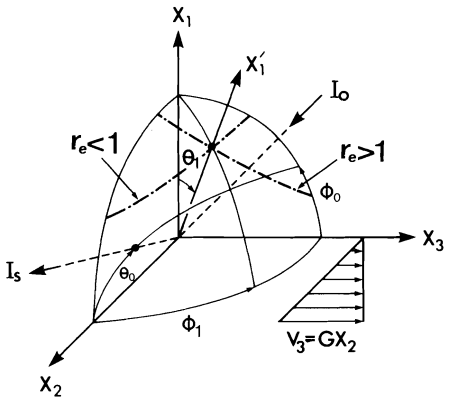

FIG. 4. Coordinate system for calculating the scattering cross section of a spheroid in the simple shear flow $v_3 = Gx_2$. The incident light beam is polarized in the X_1-direction and directed along the X_2-axis. The direction of the scattered light is expressed by the spherical angles θ_0, ϕ_0 (X_2 as polar axis) and the orientation of the axis of revolution of the spheroid by θ_1, ϕ_1 (X_1 as polar axis). The broken lines are the spherical elliptical orbits given by [8a] for oblate ($r_e < 1$) and prolate ($r_e > 1$) spheroids for arbitrarily chosen C's.

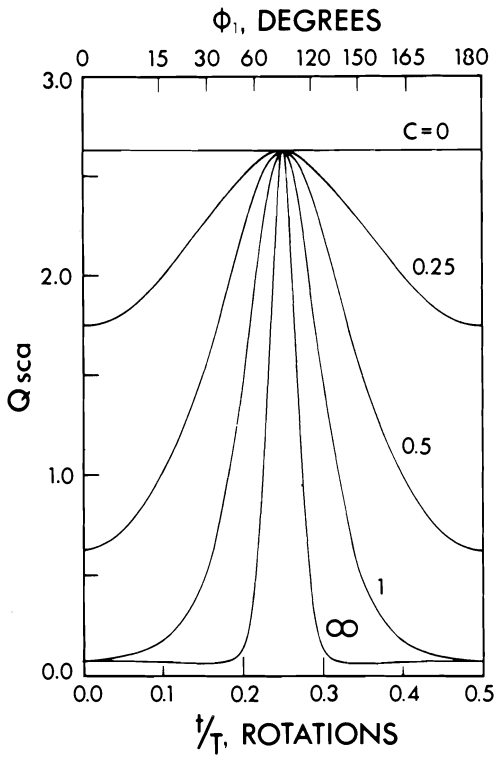

FIG. 5. Scattering efficiency Q_{sca} of a single oblate spheroid from the same system as in Fig. 3 rotating in simple shear flow at various orbit constants C for an initial $\phi_1 = 0$, $\kappa = 0$. When $C = 0$, the spheroid spins about its own axis, and is thus steadily oriented edge-on to the incident light so that Q_{sca} is constant. When $C = \infty$, it orients face-on at $t/T = 0$ and 0.5, but edge-on at $t/T = 0.25$ so that Q_{sca} alternates between a minimum and a maximum and vice-versa for S_{13} (see text). Thus when $0 < C \leq \infty$ Q_{sca}, like I_r (Fig. 3), oscillates with a frequency $2/T$.

(1, 17), but principally (*1*) variations in particle shape r_e, (*2*) shear-induced two-particle interactions, and (*3*) rotary Brownian motion, each with its own τ_i. Taking the effects to be additive the net τ for orientation distributions can be expressed[2]

$$[25] \qquad \frac{1}{\tau} = \frac{1}{\tau_1} + \frac{1}{\tau_2} + \frac{1}{\tau_3}$$

which can be rewritten in the dimensionless form

$$[26] \qquad T/\tau = b_1 + b_2 N + b_3 G^{-1}$$

[2]Equation 25 is based primarily on the redistribution of κ, i.e., 'rotational phase mixing' (18). Strictly speaking the equation should include a τ_4^{-1} for changes in orbit constants C [8*a*] due to shear-interactions; on the time and concentration scales for the systems considered here (1, 17) T/τ_4 is effectively zero.

TABLE 2. Equations for F_1, F_2, and F_3. See [15]

Geometry (Fig. 2)	F_1	F_2	F_3
I-A	$\chi_1 \sin^2\gamma + \chi_2 \sin\gamma\cos\gamma + \chi_3\cos^2\gamma$	0	1
I-B	$(\chi_1 - 1)\sin^2\gamma + 1$	$\chi_2 \sin\gamma$	χ_3
I-C	$(\chi_3 - 1)\sin^2\gamma + 1$	$\chi_2 \sin\gamma$	χ_1
II-A	$\left(\chi_3 \sin^2\frac{\theta_0}{2} + \cos^2\frac{\theta_0}{2}\right)\sin^2\gamma + \chi_2 \sin\frac{\theta_0}{2}\sin\gamma\cos\gamma + \chi_1\cos^2\gamma$	$2(\chi_3 - 1)\sin\frac{\theta_0}{2}\cos\frac{\theta_0}{2}\sin\gamma + \chi_2 \sin\frac{\theta_0}{2}\cos\gamma$	$\chi_3\cos^2\frac{\theta_0}{2} + \sin^2\frac{\theta_0}{2}$
II-B	$\left(\chi_3\cos^2\frac{\theta_0}{2} + \sin^2\frac{\theta_0}{2}\right)\cos^2\gamma + \chi_2\cos\frac{\theta_0}{2}\sin\gamma\cos\gamma + \chi_1\sin^2\gamma$	$2(1 - \chi_3)\sin\frac{\theta_0}{2}\cos\frac{\theta_0}{2}\cos\gamma - \chi_2\sin\frac{\theta_0}{2}\sin\gamma$	$\chi_3\sin^2\frac{\theta_0}{2} + \cos^2\frac{\theta_0}{2}$
II-C	$\left(\chi_1\sin^2\frac{\theta_0}{2} + \chi_2\sin\frac{\theta_0}{2}\cos\frac{\theta_0}{2} + \chi_3\cos^2\frac{\theta_0}{2}\right)\sin^2\gamma + \cos^2\gamma$	$(\chi_1 - \chi_3)\sin\theta_0\sin\gamma + \chi_2\cos\theta_0\sin\gamma$	$\chi_1\sin^2\frac{\theta_0}{2} - \chi_2\sin\frac{\theta_0}{2}\cos\frac{\theta_0}{2} + \chi_3\sin^2\frac{\theta_0}{2}$

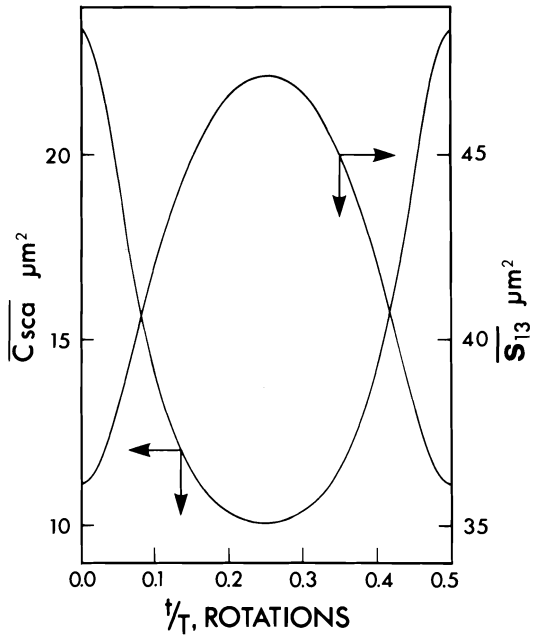

FIG. 6. Mean scattering cross section $\overline{C_{sca}}$ and mean projected area $\overline{S_{13}}$ for an initially isotropic dilute suspension of the system used in Figs. 3 and 5, when subjected to the simple shear flow shown in Fig. 4. The values were obtained by numerical integration of [24] using [20] with $p_t(\theta_1, \phi_1)$ given by [12], and show that $\overline{C_{sca}}$ and $\overline{S_{13}}$ behave oppositely, but with both oscillating with frequency $2/T$.

where b_1 is a known constant for spheroids and b_2 and b_3 are thus far calculable only for prolate spheroids ($r_e \gg 1$) (1, 17, 19), although for oblate spheroids ($r_e < 1$) they may be roughly estimated by analogy.

It is obvious that similar relations should apply to the damping of any orientation dependent property but, of course, with different values for the parameters b_i. However, the period of oscillation $T/2$ should be the same for all since it is determined by the particle rotation about the vorticity axis, is given by [9] using the mean value $\bar{r}_e$ (1), and is independent of V.

Considering now $\overline{C_{sca}}$ (or more generally I_r), damped oscillations of frequency $2/\overline{T}$ with a characteristic τ determined by $\bar{r}_e$ and $\overline{V}$ and their distributions should occur. The simplest general case to consider is that for which the distributions of r_e and V are independent, with the probability distribution $g(r_e, V)$ given by the product

$$[27] \qquad g(r_e, V) = g_1(r_e)g_2(V)$$

where $g_1(r_e)$ and $g_2(V)$ are the respective probability densities. The mean scattering cross section is then given by the formal relation:

$$[28] \quad (\overline{C_{sca}})_\sigma = \int_0^\infty \int_0^\infty \overline{C_{sca}}\, g_1(r_e)\, g_2(V)\, dr_e\, dV$$

where the subscript σ designates the spread in r_e, and $\overline{C_{sca}}$ is given by [24]; analogous equations will exist for I_r. In many situations, however, [27] will not apply and $g(r_e, V)$ will be more complicated and, indeed, may not be known; when it is, however, the optical properties can be calculated numerically by the use of equations given above.

We illustrate by numerically calculating $(\overline{C_{sca}})_\sigma$ for system considered in Figs. 3, 5, and 6, for simplicity taking $\tau_2^{-1} = \tau_3^{-1} = 0$ and particles of identical volume, but with a non-zero τ_1^{-1} resulting from a Gaussian distribution in r_e:

$$[29] \quad g_1(r_e) = \frac{1}{\sqrt{2\pi}\,\sigma_e} \exp\left[\frac{-(r_e - \bar{r}_e)^2}{2\sigma_e^2}\right]$$

where σ_e (= 0.07 (17.5%) corresponding to the experimental system) is the standard deviation in r_e.

As expected (Fig. 7), the calculated $(\overline{C_{sca}})_\sigma$ undergoes damped oscillations of frequency $2/T$ with the relative amplitude $A(t)$ at each quarter rotation decreasing nearly exponentially (although the scale in Fig. 7 is linear) from which $\tau_1/T = 0.875$. This is surprisingly close to the value (0.89) from the damped oscillations in orientation distribution using the earlier confirmed theory (1, 17) (see [30] below). At this stage of our knowledge this agreement between the two sets of τ_1 may be fortuitous because of the numerical values of r_e and σ_e selected for illustrations; however, the agreement in frequency, as already stated, is not. For the sake of brevity we will employ numerical values of b_1 based on the optical data presented in the experimental part which follows.

Experimental Part and Discussion

Methods

For turbidity measurements, suspensions of hardened human red blood cells (mean diameter 8.6 μm, thickness 2.5 μm) were used as convenient models of nearly mono-disperse oblate spheroids (20). They were suspended in aqueous glycerol (75% by volume) with a small amount of dissolved $SnCl_2$ to eliminate sedimentation. The density and viscosity of the medium were 1.29 g/ml and 0.125 Pa s, respectively. Particle concentrations determined by a hemacytometer ranged from 2×10^7 to 4×10^8 cells/ml corre-

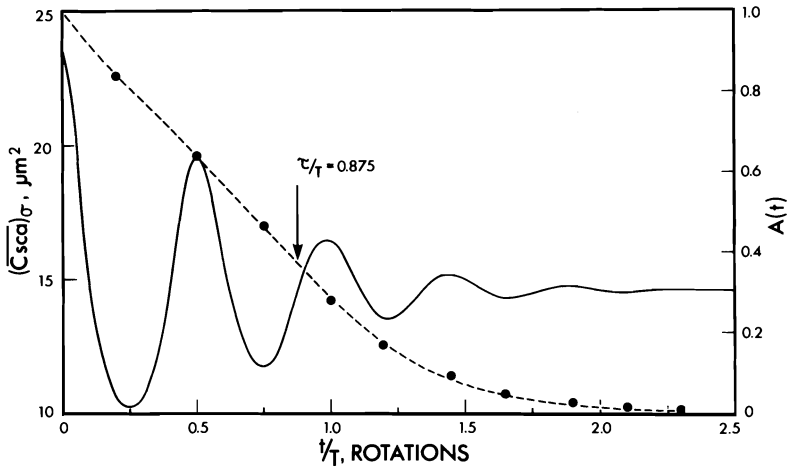

FIG. 7. Values calculated by numerical integration of [28] for the suspension considered in Figs. 3 to 6, but with a spread in r_e given by [29] with $\overline{r_e} = 0.4$, $\sigma_e = 0.07$, and $\tau_{2,3}^{-1} = 0$. The damping of the relative amplitude $A(t)$ whose values were determined at each peak and valley of $(\overline{C_{sca}})_\sigma$ is shown by the broken line yielding $\tau_1/T = 0.875$.

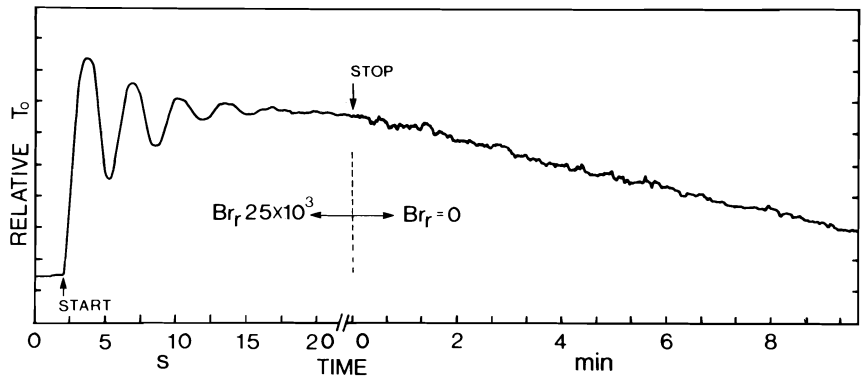

FIG. 8. Typical example of a recorder trace of the transmitted light intensity (arbitrary scale) for a suspension of hardened human red blood cells at $N = 4 \times 10^8/ml^{-1}$ and $G = 2.6\ s^{-1}$ over the interval marked START to STOP when damped oscillations occurred. The fluctuations in the decaying I_t after stopping shear appeared to be enhanced; this is due mainly to the expanded time scale.

sponding to volume fractions of 1.7×10^{-3} to 3.6×10^{-2} when the average volume of red blood cells is taken as 88 μm^3 (20). The refractive indices were $n_A = 1.44$ and $n_B = 1.40$, respectively, so that $m = 1.03$. The suspension was then placed between two parallel optically polished glass discs of diameter 12.7 cm separated by a gap of 1.6 mm, with the bottom one rotated at an adjustable constant angular velocity (21).

The turbidity was measured across the discs (i.e., along the X_2-axis) using a He–Ne laser (Spectra Physics Model 124A, $\lambda = 632.8$ nm with a beam diameter of 1.1 mm) and a power meter (Coherent Radiation Laboratory, Model 212) whose output was chart-recorded (Keithley Instruments, Model 370). All measurements were made in a constant temperature room at 21 ± 1°C.

Results and Discussion

A typical example of the changes in light transmission is given in Fig. 8. When shear was applied T_0 initially increased rapidly to a maximum and then experienced damped oscillations, with superimposed (and apparently random) fluctuations, which became more evident as the oscillations became smaller. When flow was stopped, T_0 decreased monotonically and asymptotically approached the initial value at $t = 0$.

The damped oscillations of T_0 parallel the theoretical calculation shown in Fig. 7, remembering ([16] to [18]) that a decrease in $\overline{C_{sca}}$corre-

TABLE 3. Measured parameters of oscillations in transmission coefficient[a]

N (ml^{-1})	τ/T at corresponding G			
	G (s)	τ/T	$b_1 + b_2N^b$	b_3 (s)[c]
2×10^7	2.6	0.93	0.67	1.09
	3.5	0.98		
	4.9	1.15		
1×10^8	2.5	0.80	0.81	1.13
	3.8	0.88		
	4.7	0.96		
4×10^8	2.2	0.66	1.10	0.90
	2.6	0.68		
	3.8	0.74		
	4.9	0.80		

[a]For these systems $\overline{TG} = 16.9 \pm 0.6$ when measured from the period of oscillation of T_0 as in Figs. 7 and 8.
[b]From intercepts $(T/\tau)_{G^{-1}=0}$ in Fig. 9 using [34].
[c]From slopes in Fig. 9 using [34].

sponds to an increase in T_0 and vice-versa. The periods of oscillation, which should correspond to $\overline{T}/2$, were measured from those tracings. As expected the product TG was found to be independent of N and G, and for some 50 measurements yielded $\overline{TG} = 16.9 \pm 0.6$; from [9] this yields a mean equivalent spheroidal axis ratio $\overline{r_e} = 0.44$, a value that compares reasonably well with $\overline{r_e} = 0.38 \pm 0.07$ obtained by direct microscopic observations of $\overline{TG}$ on a different sample of the rotating cells (20).

The amplitude $A(t)$ of the oscillations was generally found to decay nearly exponentially. Taking the height of the first peak as $A(0) = 1$, τ was determined as in Fig. 7. The dimensionless relaxation times τ/T thus obtained are listed in Table 3. Their reciprocals, which can be regarded as damping coefficients, are plotted against G^{-1} for various concentrations in Fig. 9 where it is seen that they vary linearly in accord with [26]. The slopes give b_3 and the intercepts at $G^{-1} = 0$, which correspond to orthokinetic conditions (22) when the effect of rotary Brownian motion are negligible (i.e., the rotary Brenner number $Br_r = \infty$ (22)), yield $b_1 + b_2N$ (Table 3). The intercepts $(T/\tau)G^{-1} = 0$ are linear with N (Fig. 9, top) from which, using [26], $b_1 = 0.68$ and $b_2 = 1.22 \times 10^{-7}$ ml^{-1}.

Using the analytic expression for b_1 of *orientation distributions* derived in ref. 1 for a distribution of r_e's given by [29] is:

$$[30] \qquad b_1 = \frac{\sqrt{8}\pi\sigma_e(1 - \overline{r_e}^2)}{\overline{r_e}(\overline{r_e}^2 + 1)}$$

and inserting the experimental value of b_1 for damping of transmission coefficients, $\sigma_e = 0.05$ for $\overline{r_e} = 0.44$. This is somewhat lower than the value (0.07) obtained by the direct microscopic measurements (20); however, in view of the differences to be expected in b_1 derived from optical measurements and those given for orientation distributions by [30], the fact our samples and those of Goldsmith and Marlow (20) were different, and that $g_1(r_e)$ and $g_2(V)$ are not strictly independent for blood cells (20), the agreement in the σ_e's is considered satisfactory. In the absence of a theory of two-body shear-interactions for oblate spheroids (1), it is premature to comment on our experimental value of b_2.

We now consider the effects of rotary Brownian motion which determines τ_3 in [25] by a relation of the type (17)

$$[31] \qquad \tau_3^{-1} \simeq \alpha D_r$$

where α is a parameter yet to be determined and D_r the rotary Brownian diffusion coefficient normal to X_1', which for an oblate spheroid ($r_e < 1$) is given by (23)

$$[32] \qquad D_r = \frac{k_0 T_1 r_e^2}{4\eta V(1 - r_e^4)}\left[1 + \frac{1 - 2r_e^2}{r_e\sqrt{1 - r_e^2}}\tan^{-1}\frac{\sqrt{1 - r_e^2}}{r_e^2}\right]$$

k_0 being the Boltzmann constant, T_1 the absolute temperature, and η the medium viscosity. The parameter $\alpha = 6$ for orientation distributions at $Br_r = G/2D_r = 0$ (i.e., at $G = 0$) (23). For finite, but very large Br_r, α is estimated to be proportional to r_e^4 for phase mixing (24) when $r_e \gg 1$. If an analogy can be made for oblate spheroids ($r_e < 1$) we may write

$$[33] \qquad \alpha = 6r_e^{-4}$$

For the system used in our experiments, $D_r = 5.2 \times 10^{-5}$ s^{-1}, so that from [31] the calculated $\tau_3 = 120$ s whereas the experimental τ_3 obtained from the measured mean value of $\overline{b_3} = 1.04$ s^{-1} (Table 3) is 16 s. At $G = 0$ (as in the last portion of Fig. 8 where the decay was due to rotary Brownian motion restoring random orientation) the measured $\tau_3 = 4 \times 10^2$ s and the calculated τ_3 from [31] and [32] with $\alpha = 6$ (23) is 3.2×10^3 s. In both cases the measured τ_3's are approxi-

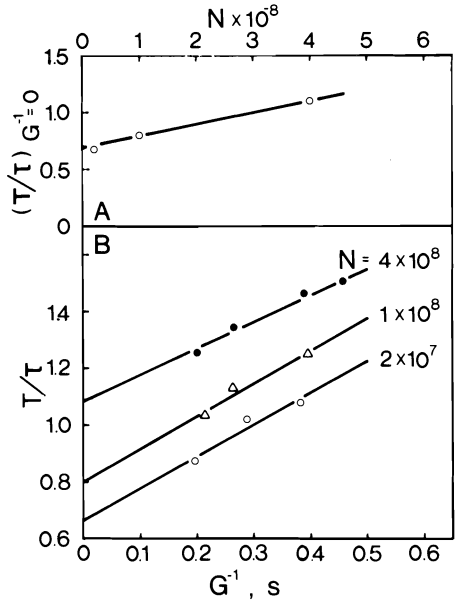

FIG. 9. Measured damping coefficients T/τ vs. G^{-1} at various N ml^{-1} (part *B*). The intercepts $(T/\tau)G^{-1} = 0$ vs. N are plotted in the upper half. From these plots of the experimental data, the constants b_i in [26] were evaluated (see Table 3 and text).

mately one order of magnitude smaller than those calculated. However, in view of the approximations that are inherent in applying [26] and [31] to turbidity data the difference between two values is not unreasonable.

The fluctuations, or scintillations (13), which are superimposed on the traces to T_0 (Fig. 9), are considered to be experimentally significant, and are not merely electronic noise and other random disturbances: it is significant that at $Br_r = \infty$ they, like the oscillations in T_0, can be perfectly reproduced on reversing flow (25) and for this reason cannot be random. On the other hand, at $Br_r = 0$, when Brownian motion predominates and one is dealing with purely perikinetic conditions (22), the scintillations are random. It is our belief that for $0 \leq Br_r \leq \infty$ they arise from statistical fluctuations in the number of particles sampled by the finite volume (1.5×10^{-3} ml) of the light beam; since only a small fraction of the total number are in orientations near maximum C_{sca}, the fluctuation in T_0 can be shown to be significant, e.g., 2.5% of T_0 at $N = 10^8$ (13).

Concluding Remarks

The theory and the preliminary experimental results presented here demonstrate some of the potentials of rheo-optical measurements in determining distributions of size and shape, especially when the particles scatter (rather than absorb) light and are reasonably monodisperse. Some related observations are the following:

(*1*) Damped oscillations in T_0 can occur with particles that absorb light, e.g., with hardened red blood cells like those used here but rendered absorbing by coating them with silver (25), under which conditions all of the light on a particle is removed from the beam and hence, as the analogue of [18],

$$[34] \qquad \nu = N\overline{S_{13}}$$

However, the oscillations in T_0 are now in phase with those of $\overline{S_{13}}$ instead of being 90° out of phase (as in Fig. 6), and thus show an initial drop to a minimum instead of rising to a maximum (as in Fig. 8). Q_{sca} is now a maximum when the cell is face-on to the beam, and a minimum when edge-on as expected intuitively.

(*2*) When σ_e becomes very large $\tau/T < 1/4$ and oscillations will not occur, i.e., the system is overdamped (1). Under these conditions monotonic changes of T_0 and I_r may be expected as we have already observed with highly heterodisperse suspensions of guanine (26) and kaolin (27) platelets, but with both systems recovering the original values on stopping shear as random orientations are restored by the appreciable D_r. Further complications undoubtedly arose from the optical anisotropy (birefringence) of the guanine crystals (26).

Further development of the theory (including a consideration of particles that are deformable in a flow) and of instrumental methods that incorporate a number of the geometries described in Fig. 2 have been planned or made and will be reported later. Additional optical phenomena which may prove fruitful for similar theoretical and experimental investigations are streaming dichroism and optical rotatory dispersion when Br_r is much greater, as in classical streaming birefringence studies (3).

Acknowledgements

The authors wish to thank Mr. K Sarantidis for assistance in the light transmission measurements, and Drs. H. L. Goldsmith and M. M. Frojmovic for preparation of the erythrocyte suspensions.

This work was supported by the Medical Research Council of Canada (Grant MA-4012).

1. A. OKAGAWA, R. G. COX, and S. G. MASON. J. Colloid Interface Sci. **45**, 303 (1973).
2. A. OKAGAWA, R. G. COX, and S. G. MASON. To be published.
3. J. T. EDSALL. Adv. Colloid Sci. **1**, 269 (1942).
4. R. CERF and H. A. SCHERAGA. Chem. Rev. **51**, 185 (1952).
5. H. G. JERRARD. Chem. Rev. **59**, 345 (1959).
6. H. DIESSLHOST and H. FREUNDLICH. Phys. Z. **17**, 117 (1916).
7. W. HELLER. Rev. Mod. Phys. **31**, 1072 (1959).
8. A. PETERLIN, W. HELLER, and M. NAKAGAKI. J. Chem. Phys. **28**, 470 (1958).
9. A. PETERLIN. J. Polym. Sci. **23**, 189 (1957).
10. M. NAKAGAKI and W. HELLER. J. Polym. Sci. **38**, 117 (1959).
11. W. HELLER, E. WADA, and L. A. PAPAZIAN. J. Polym. Sci. **47**, 481 (1960).
12. R. S. CHADWICK and I-DEE CHANG. J. Colloid Interface Sci. **42**, 516 (1973).
13. M. M. FROJMOVIC, A. OKAGAWA, and S. G. MASON. Biochem. Biophys. Res. Commun. **62**, 17 (1975).
14. M. M. FROJMOVIC. Biorheology, **12**, 193 (1975).
15. M. KERKER. The scattering of light and other electromagnetic radiation. Academic Press, New York, NY. 1969.
16. G. B. JEFFERY. Proc. R. Soc. London, Ser. A, **102**, 161 (1922).
17. A. OKAGAWA and S. G. MASON. J. Colloid Interface Sci. **45**, 330 (1973).
18. G. K. BATCHELOR. Ann. Rev. Fluid Mech. **6**, 227 (1974).
19. E. ANCZUROWSKI, R. G. COX, and S. G. MASON. J. Colloid Interface Sci. **23**, 547 (1967).
20. H. L. GOLDSMITH and J. MARLOW. Proc. R. Soc. London, Ser. B, **182**, 351 (1972).
21. S. G. MASON and H. L. GOLDSMITH. Biorheology, **12**, 181 (1975).
22. S. G. MASON. J. Colloid Interface Sci. **58**, 275 (1977).
23. H. BENOIT. Ann. Phys. **6**, 561 (1951).
24. E. J. HINCH and L. G. LEAL. J. Fluid Mech. **57**, 753 (1973).
25. A. OKAGAWA, G. ENNIS, and S. G. MASON. To be published.
26. M. SORRENTINO and S. G. MASON. J. Colloid Interface Sci. **41**, 178 (1972).
27. C. CERDA, A. OKAGAWA, and S. G. MASON. To be published.

Water-soluble lysine-containing polypeptides. IV. The synthesis, characterization, and circular dichroism spectra of sequential polypeptides formed from dipeptides of lysine and amino acids of increasing side chain size[1]

LEWIS A. SLOTIN,[2] DENIS R. LAUREN,[3] AND ROSS E. WILLIAMS[4]

Division of Biological Sciences, National Research Council of Canada, Ottawa, Ont., Canada K1A 0R6

Received June 6, 1977

LEWIS A. SLOTIN, DENIS R. LAUREN, and ROSS E. WILLIAMS. Can. J. Chem. **55**, 4257 (1977).

Several polypeptides have been synthesized which contain the alternating sequence lysyl-X, where X = gly, L-ala, D-ala, L-val, L-leu, and L-phe. The polypeptides have been characterized by gel filtration (molecular weight) and by circular dichroism spectroscopy (secondary structure).

LEWIS A. SLOTIN, DENIS R. LAUREN et ROSS E. WILLIAMS. Can. J. Chem. **55**, 4257 (1977).

Nous avons synthétisé plusieurs polypeptides qui contiennent la séquence alternée lysyl-X, ou X = gly, L-ala, D-ala, L-val, L-leu et L-phe. Les polypeptides ont été caractérises par des filtrations sur gel (poids moléculaire) et par des spectres du dichroisme circulaire (structure secondaire).

Introduction

The nuclei and chromosomes of eukaryotic organisms contain significant amounts of protein and nucleic acid. Many of the proteins are basic or cationic in nature and constitute a class of proteins known as the histones. Because of their cationic character these proteins interact strongly with cellular DNA (deoxyribonucleic acid) and have thus been postulated to play an integral role in chromosomal architecture and a smaller role in cellular regulation (1).

The nature of the association between these cationic proteins and cellular DNA may be simply electrostatic or may be coupled to a more complex sequence-dependent recognition process (2). In order to elucidate the role which the structure of the protein plays in these interactions, a number of synthetic models containing basic amino acids have been utilized (3–7). As an example, the homopolymers poly-(L-lysine) and poly-(L-arginine) have been used to study DNA – cationic protein interactions (3, 4). In order to extend the study of these latter model systems the synthesis, characterization, and DNA interaction study of a series of sequential lysine–glycine polypeptides has been reported (8). To continue in this approach the sequential polymers

poly-(L-lysgly)

poly-(L-lys-L-ala)

poly-(L-lys-D-ala)

poly-(L-lys-L-val)

poly-(L-lys-L-leu)

poly-(L-lys-L-phe)

have been synthesized.

In this paper we describe the synthesis of the monomer blocks used for the preparation of the polymers and the polymerization conditions used. The secondary structure and conformational mobility of the polypeptides has also been examined by circular dichroism (cd) spectroscopy.

Materials and Methods

All chemicals were of reagent grade and were used directly unless otherwise noted.

Optical rotations were measured on a Perkin-Elmer polarimeter Model 141 in a 1 dm microcell. Methanol (MeOH) or glacial acetic acid (HOAc) were used as solvents as noted. Melting points were taken on a Fisher-Johns melting point apparatus (heated block) and are uncorrected. Combustion analyses were determined on a Perkin-Elmer CHN analyzer, model 240. Amino acid analyses were done on a Beckman automatic analyzer, model 120. Amino acid hydrolyses were carried out in 6 *N* HCl at 110°C for 24 h.

Circular dichroism spectra were taken on a calibrated (9) Cary spectropolarimeter, model 61, in quartz cells (path length 0.05 cm). Reported ellipticities are based upon the lysine concentration (as determined by amino acid analysis). Ultraviolet spectra were taken on a Cary 14

[1]NRCC No. 16200.

[2]NRCC Research Associate, 1975–1977.

[3]NRCC Postdoctoral Fellow, 1971–1973.

[4]Address correspondence to this author.

recording spectrophotometer in quartz cells (path length 1 cm).

N^{ε}-Benzyloxycarbonyl(Cbz)-L-lysine was purchased from Pierce Chemicals, Rockford, Illinois. N^{α}-*tert*-Butyloxycarbonyl (Boc)-N^{ε}-Cbz-L-lysine, N^{α}-*tert*-Boc-phenylalanine, and N^{α}-*tert*-Boc-leucine monohydrate were purchased from Beckman Instruments Co., Palo Alto, California. L-Alanine was purchased from Bion Biochemicals, Oakville, Ontario, D-alanine from Nutritional Biochemicals Corporation, Cleveland, Ohio, and glycine from British Drug House, England. *N*-Hydroxysuccinimide (HOSu) and dicyclohexylcarbodiimide (DCC) were obtained from Fluka AG, Buchs, Switzerland.

N^{α}-*tert*-Boc-leucine monohydrate was rendered anhydrous by repeated dissolution in and evaporation from anhydrous benzene. Triethylamine (TEA) was distilled from *p*-toluenesulfonyl chloride and stored under nitrogen atmosphere. Dicyclohexylamine (DCHA) was distilled prior to use. Dimethylformamide (DMF) was purified by treatment with barium oxide, filtration, and vacuum distillation. Dimethoxyethane (DME) was purified by distillation from lithium aluminum hydride. Pyridine was purified by distillation from *p*-toluenesulfonyl chloride and then lithium aluminum hydride. Trifluoracetic acid (TFA) was purified by distillation from phosphorous pentoxide.

Polymer molecular weight (mw) distributions were established on the unblocked polymers by dialysis against 2% aqueous HOAc in Spectrapor dialysis tubing (#3 mw cutoff, 3500; #1 mw cutoff, 6000–8000; and #2 mw cutoff, 12 000 – 14 000) which had been pretreated as directed (sodium sulfide and dilute sulfuric acid). Dialyses were performed at room temperature for 18 h. Polymer molecular weights were also estimated by thin layer gel filtration on Sephadex G-100 (sodium phosphate, 0.002 *M*; sodium chloride, 0.05 *M*; p*H* 7.0) using ribonuclease, chymotrypsinogen, and ovalbumin as standards (10, 11). Detection was by trinitrobenzene – sulfonic acid treatment of a paper replica (12).

Monomer Preparation

The monomers used for the synthesis of the polypeptides were prepared according to the procedures outlined in Schemes 1 and 2. Elemental analyses, specific rotations ($[\alpha]_D$), and melting points are given in Tables 1[5,6] and 2. The general procedure for the preparation of Cbz
t-Boc-X-lys-dipeptides (Scheme 1) may be exemplified by the synthesis of N^{α}-*t*-Boc-phenylalanine-N^{ε}-Cbz-L-lysine DCHA salt. N^{ε}-Cbz-L-lysine (50 g, 0.18 mol) was suspended in anhydrous methanol (600 ml) and the mixture cooled in a Dry Ice – acetone bath. Thionyl chloride (42.4 ml, 0.59 mol) was added dropwise over 0.5 h with rapid stirring. Upon completion of addition the reaction clarified. The solution was then warmed to 0–5°C and stirred overnight during which time the temperature rose to ambient. The solvent was removed *in vacuo*

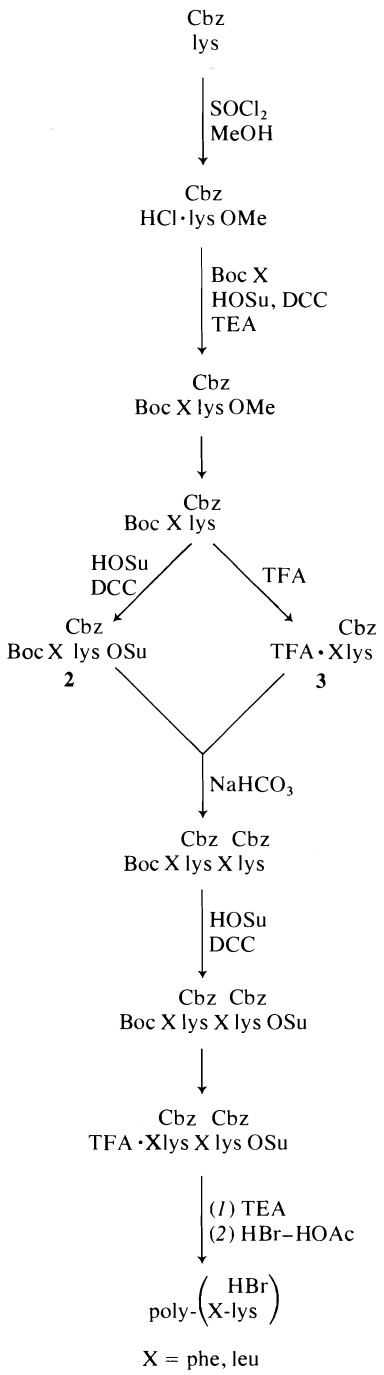

SCHEME 1

below 30°C and methanol–benzene (1:1, 400 ml) added and evaporated. The process was repeated three times. The residue was shaken with acetone (600 ml) and Cbz
HCl·lysOMe (50 g) collected by filtration. *t*-Boc-phenyl-

[5]All elemental analyses were within acceptable limits (C ±0.2%, H ±0.2%, N ±0.3%).

[6]Copies of Table 1 are available, at a nominal charge, from the Depository of Unpublished Data, CISTI, National Research Council of Canada, Ottawa, Ont., Canada K1A 0S2.

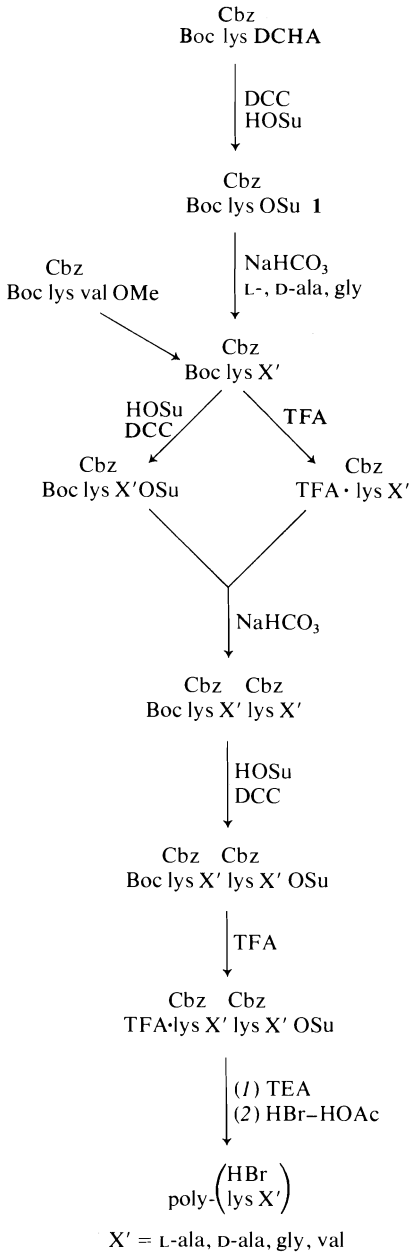

SCHEME 2

Cbz
alanine (45.5 g, 170 mmol) and HCl·lysOMe (56 g, 170 mmol) were dissolved in DME–DMF (2:3, 250 ml) and cooled in ice. *N*-Hydroxysuccinimide (19.5 g, 170 mmol) and triethylamine (23.6 ml, 170 mmol), followed by a cooled (0–5°C) solution of dicyclohexylcarbodiimide (DCC) in DME–DMF (2:3, 100 ml), were added. After stirring overnight, during which time the temperature reached ambient, the mixture was filtered and the precipitated dicyclohexylurea washed with cold methylene chloride (3 × 1 ℓ). The filtrate and washings were combined and concentrated *in vacuo*. The residue was dissolved in ethyl acetate (2 ℓ), filtered, and the filtrate washed successively with 0.1 *N* HCl (cold, 2 ℓ), 5% sodium bicarbonate (cold, 2 ℓ), and water (cold, 4 ℓ). The organic layer was dried over sodium sulfate, filtered, and evaporated *in vacuo*. The residue, *t*-Boc-
Cbz
phelysOMe (72.5 g, 79%) was recrystallized from ethyl acetate – petroleum ether (30–60°C).

Cbz
t-BocphelysOMe (40 g, 74 mmol) was dissolved in DME (300 ml) and cooled to 0–5°C. Cold 1 *N* NaOH (74 ml) was added and the temperature allowed to reach ambient over a period of 2 h. Cold (0–5°C) sodium bicarbonate (5%, 1 ℓ) was added and the mixture cooled in ice and then acidified to p*H* 2 with cold 1 *N* HCl. The aqueous solution was extracted with ethyl acetate (3 × 1 ℓ) and the organic phase dried over sodium sulfate and evaporated to dryness *in vacuo*. The product was taken up in ether (1 ℓ) and dicyclohexylamine (15.9 ml, 81 mmol) added. The solution was refluxed on a steam bath for 2 h, cooled to room temperature, and shaken overnight on a mechanical shaker. The DCHA salt was collected by filtration and washed with petrol (30–60°C) (yield 71%).

Cbz
t-BocleulysDCHA salt was prepared in a similar manner from *t*-Bocleu and HCl·lysOMe (yield 50%).

The general procedure for the preparation of *t*-
Cbz
Boclys-X dipeptides (Scheme 2) was identical to the re-
Cbz
ported (8) synthesis of N^{α}-*t*-BoclysglyDCHA from N^{α}-*t*-
Cbz
BoclysOSu and glycine in aqueous sodium bicarbonate
Cbz
(yield 91%). The couplings of N^{α}-*t*-BoclysOSu with L- and D-alanine were performed in an analogous fashion (yields: L 73%; D 63%). The dipeptide *t*-Boclysval was pre-
Cbz
pared from *t*-Boclys and HCl·valOMe by coupling with DCC in the presence of hydroxysuccinimide, hydrolysis of the methylester on DME–NaOH(aq.), and isolation of the acidic product (yield 90%).

The general procedure for the preparation of *t*-Boc-
Cbz Cbz Cbz Cbz
X-lys-X-lys or *t*-Boc-lys-X-lys-X tetrapeptides is exempli-
Cbz Cbz
fied by the synthesis of *t*-Boc-phe-lys-phe-lys and is as
Cbz
follows: N^{α}-*t*-Boc-phe-lysDCHA (15 g, 21.1 mmol) was dissolved in cold (0–5°C) ethyl acetate (250 ml). Cold (0–5°C) 0.1 *N* HCl (230 ml, 23 mmol) was added and the mixture stirred vigorously at 0–5°C for 10 min. The free acid was extracted into ethyl acetate (3 × 300 ml), dried over sodium sulfate, and filtered. The filtrate was divided into two equal fractions (*A* and *B*) and each was concentrated to dryness *in vacuo*. The residue from *A* was converted to its succinimide ester by dissolution in cold (0–5°C) DME–pyridine (95:5, 50 ml) followed by the addition of *N*-hydroxysuccinimide (1.2 g, 10.55 mmol) and DCC (2.28 g, 10.55 mmol). The mixture was stirred at 0–5°C for 6 h, filtered, and the filtrate concentrated

TABLE 2. Specific rotations and melting points of starting materials and monomer blocks

Compound[a]	$[\alpha]_D$ (deg)	mp (°C) (crystallization solvent)
Cbz HCl·lysOMe[b]	+15.0 (*c* 2.19, MeOH)	116–117 (Acetone)
HCl·valOMe[c]	+23.0 (*c* 2.04, MeOH)	173–174 (MeOH–ether)
Cbz *t*-BocphelysOMe	−7.78 (*c* 2.07, MeOH)	95–95.5 (EtOAc-petrol)
Cbz *t*-BocphelysDCHA	−3.28 (*c* 1.95, HOAc)	86.5–88 (Ether)
Cbz *t*-BocleulysDCHA	−12.76 (*c* 2.11, HOAc)	86–88 (Ether)
Cbz *t*-BoclysvalDCHA	−8.48 (*c* 1.87, HOAc)	74–76 (EtOAc-hexane)
Cbz *t*-Boclys-L-alaDCHA	−10.46 (*c* 2.14, HOAc)	134–135 (Ether)
Cbz *t*-Boclys-D-alaDCHA	−4.74 (*c* 1.96, HOAc)	135–138 (EtOAc-petrol)
Cbz *t*-BoclysglyDCHA	−7.34 (*c* 2.06, HOAc)	141–143 (EtOAc-petrol)
Cbz Cbz *t*-Bocphelysphelys	−12.60 (*c* 2.17, MeOH)	130–131 (EtOAc)
Cbz Cbz *t*-BocleulysleulysDCHA	−19.53 (*c* 1.93, HOAc)	103–105 (Ether)
Cbz Cbz *t*-Boclys-L-alalys-L-ala	−26.75 (*c* 2.29, MeOH)	161–164 (EtOAc)
Cbz Cbz *t*-Boclys-D-alalys-D-alaDCHA	−7.97 (*c* 1.71, HOAc)	114–116 (Ether)
Cbz Cbz *t*-Boclysglylysgly	−12.18 (*c* 2.05, MeOH)	103–105 (EtOAc)

[a]All optically active amino acids are of L configuration unless noted otherwise.
[b]Literature (13) mp 117°C, $[\alpha]_D$ +16.7° (*c* 2.0, MeOH).
[c]Literature (13) mp 175°C, $[\alpha]_D$ +23.5 ± 0.5° (*c* 2, MeOH).

to dryness *in vacuo*. The residue from *B* was treated with TFA–CH_2Cl_2 (1:1, 40 ml) and let stand at room temperature for 1 h. Excess ether was added and the solution concentrated *in vacuo*. The residue was triturated with ether until the TFA was removed. The residue was dissolved in *p*-dioxane (150 ml) and added to the succinimide ester from *A*. Water (50 ml) was added and the solution cooled (0–5°C). Sodium bicarbonate (1.77 g, 21.1 mmol) was added and the solution stirred at 0–5°C for 6 h. The product was extracted into ethylacetate (4 × 400 ml), dried over sodium sulfate, filtered, and concentrated to dryness *in vacuo*. The residue was recrystallized from ethyl acetate (5.17 g) (60%). The tetrapeptides (yields in parentheses) *t*-Boc-lys-val-lys-valDCHA (an uncharacterized oil 70%), *t*-Boc-leu-lys-leu-lysDCHA salt (54%), *t*-Boc-lys-L-ala-lys-L-ala (76%), *t*-Boc-lys-D-ala-lys-D-alaDCHA salt (83%), and *t*-Boc-lys-gly-lys-glyDCHA salt (75%) were prepared in a similar manner from *t*-Boc-lysvalDCHA, *t*-Boc-leu-lysDCHA, *t*-Boc-lys-L-alaDCHA, *t*-Boc-lys-D-alaDCHA, and *t*-Boc-lys-glyDCHA respectively.

Activation and Polymerization of the Monomer Blocks

N-Hydroxysuccinimide esters of the blocked peptides were prepared by coupling the free acid (liberated from its DCHA salt where necessary) with *N*-hydroxysuccinimide using DCC in ice cold DME–pyridine (95:5, v/v). After reaction (6 h at 0°C) the urea was filtered off and the solution evaporated. The residue was thoroughly dried and treated with an excess of TFA and methylene chloride (1:1, v/v) (approx. 10 ml/g) at room temperature for 2 h. The TFA salt was precipitated by addition of 10–20 volumes of ether by decantation. The product was transferred to a centrifuge tube (50 ml) in methylene chloride and the solvent evaporated by a stream of nitrogen.

The TFA–succinimide ester (approximately 1 g) was suspended in cold (0–5°C) DME to make the solution 1 *M* in monomer. Triethylamine (3 mol equiv./mol of monomer) was added and the mixture stirred rapidly with a glass rod. The polymerization was allowed to proceed in a desiccator ($CaCl_2$) at room temperature overnight after which the gel or viscous solution which resulted was diluted with DME to give a monomer concentration of 0.5 *M*. The polymerization was allowed to continue for an additional 6 days. The polymeric material was precipitated by addition of 10 volumes of acidified water (1 drop concentrated HCl per litre) and then recovered by centrifugation. The polymer was rewashed and then the precipitate washed first with isopropanol

(3 × 20 ml) and then with ether (3 × 20 ml). The residue was then dried *in vacuo* over calcium chloride at room temperature overnight.

Blocking Group Removal

Benzyloxycarbonyl (Cbz) blocking groups were removed from all polymers with saturated HBr – acetic acid (15). The hydrobromide salt was isolated by precipitation with ether. The HBr – acetic acid treatment was repeated in order to ensure complete removal of all blocking groups. The ether-insoluble salt was then washed with isopropanol–ether (1:10, 20 ml, 2×) and then dried *in vacuo* over $CaCl_2$. The extent of blocking group removal after the two HBr – acetic acid treatments could be estimated for all but the phenylalanine containing polymer by the residual benzyloxycarbonyl (Cbz) absorption at 254 nm (aqueous solution, approximately 2 mg/ml (ε_{254} 200 (16)). In all cases greater than 98% of all blocking groups were estimated to have been removed.

Isolation of High Molecular Weight Polymeric Material

Isolation of polymeric material was accomplished using Spectrapor 1 (mw cutoff 6000–8000) dialysis sacs except for the $(lysval)_n$ sample which was isolated using Spectrapor 3 (3500 mw cutoff). Dialyses of 50 ml volumes (polypeptide concentration approx. 50 mg/ml) were performed against 3.5 ℓ of 2% aqueous acetic acid for 4 h at room temperature followed by further dialysis against a fresh 2% aqueous acetic acid solution (3.5 ℓ) overnight. The contents of the sacs were then passed through Millipore filters (0.45 μ) and lyophillized.

Results and Discussion

Synthesis of Monomers and Polypeptides

The routes for the synthesis of the monomers and their polymerization are given in Schemes 1 and 2. The N^{α}-*t*-Boc-X-N^{ε}-Cbz-lysDCHA dipeptides (Scheme 1) were synthesized by coupling the N^{α}-*t*-Boc-X amino acid with HCl·N^{ε}-Cbz-lysOMe in the presence of dicyclohexylcarbodiimide and *N*-hydroxysuccinimide. Hydrolysis of the methyl ester, followed by treatment of the resulting acid with dicyclohexylamine (DCHA), gave the dipeptide DCHA salts. For the synthesis of the N^{α}-*t*-Boc-N^{ε}-Cbz-lys-X DCHA dipeptides (Scheme 2) the *N*-hydroxysuccinimide active esters **1** were coupled with D- or L-alanine or glycine in aqueous sodium bicarbonate solutions via a backing-off procedure (17). In both cases activation via the *N*-hydroxysuccinimide ester was used to minimize racemization (18, 19). The dipeptide Boclysval was prepared from Boclys(Cbz) and HClvalOMe by coupling with DCC, hydrolysis of the methyl ester and isolation of the acidic product. The DCHA salts could be obtained from the acidic products in good yields and were easily characterized compounds (Table 2). Conversion of the dipeptides into their corresponding tetrapeptides was accomplished by converting one half the material into the corresponding succinimide ester, **2**, while the other half was treated with trifluoroacetic acid to remove the N^{α}-*tert*-butyloxycarbonyl blocking group. The trifluoroacetate salt, **3**, was then coupled with **2** in the presence of triethylamine. Except for N^{α}-*t*-Boc-leu-N^{ε}-Cbz-lys-leu-N^{ε}-Cbz-lysDCHA and corresponding valine tetrapeptide all the tetrapeptides gave satisfactory combustion analyses. The leucine tetrapeptide, however, consistently gave a low carbon analysis. To further substantiate its structure, a molecular weight determination by end group titration (14) was determined to be within 1.5% of the calculated value and the product also had a leucine–lysine ratio of 0.98. N^{α}-*t*-Boc-N^{ε}-Cbz-lys-val-N^{ε}-Cbz-lys-val-DCHA was an oil which resisted all attempts at crystallization and its acid was used directly for the polymerization.

The choice of the tetrapeptide as the minimum size of monomer to be used in the polymerizations was determined by a comparison of the yields of unblocked polymeric material obtained from the polymerizations of phenylalanine-lysine di- and tetrapeptides respectively (Table 3). Dimethoxyethane was chosen as the polymerization solvent because higher yields of unblocked high molecular weight material were obtained when the polymerization of the TFA salt of phe-N^{ε}-Cbz-lys-phe-N^{ε}-Cbz-lysOSu was compared in DMF, DMSO, and DME (Table 3).

For the polymerization of other tetrapeptides, their acids were activated by conversion to their succinimide esters since it has been shown that good yields of polymeric material could be obtained using these esters (20–24). The *t*-Boc blocking group was removed and the resulting active ester trifluoroacetate (TFA) used for polymerization in dimethoxyethane (DME) solution. During polymerization the monomer concentration was kept high (~ 1 *M*) in order to reduce the formation of cyclic and low molecular weight material. After isolation the polymers were treated twice with HBr – acetic acid to ensure complete removal of all the benzyloxycarbonyl groups as evidenced by uv absorption at 254 nm. The resulting hydrobromide salts were isolated in good yields (30–50% yield based upon the amount of monomer used). Unblocked polymeric materials were finally

TABLE 3. Effects of monomer size and polymerization solvent on the preparation of high molecular weight poly-(L-lys-L-Phe)[a]

Monomer[c]	Polymerization solvent	Unblocked polymer	% retained 3500 mw	% retained 6000–8000 mw	% retained < 12 000 mw
Cbz TFAphelysOSu	DMF[b]	Poly-(L-lys-L-phe)	—	6	3
Cbz Cbz TFAphelysphelysOSu	DMF[b]	Poly-(L-lys-L-phe)	38	15	12
	DMF	Poly-(L-lys-L-phe)	34	14	6
	DME	Poly-(L-lys-L-phe)	59	33	23
	DMSO	Poly-(L-lys-L-phe)	31	13	7

[a]Dialyses were performed using dialysis tubing (Spectrapor 3, 1, and 2, nominal mw cutoff of 3500, 6000–8000 and 12 000 – 14 000 respectively). Percentages retained by the dialysis sacs were determined by dialyzing the polypeptide solutions (approx. 4 mg/ml) against 2% aqueous acetic acid for 18 h at room temperature and are based on the lysine concentration in solution before and after dialysis.
Cbz
[b]Polymerization in the presence of 0.01 mol equiv. of chain terminator HCl·lysOMe.
[c]All optically active amino acids are of the L configuration unless noted otherwise.

TABLE 4. Percentage retained on dialysis of the unblocked polypeptides and molecular weights of lysine-X polypeptides

Polymer	% retained by Spectrapor 1 dialysis sac[a]	Molecular weight[b]
Poly-(L-lys)	—	33 000 (78 000–8 200)
Poly-(L-lys-gly)	49	8 700 (21 700–2 300)
Poly-(L-lys-L-ala)	51	16 500 (33 500–4 100)
Poly-(L-lys-D-ala)	45	7 800 (21 500–1 800)
Poly-(L-lys-L-val)	10[c]	< 2 000 (5 400– < 2 000)
Poly-(L-lys-L-leu)	71	6 000 (13 200–2 200)
Poly-(L-lys-L-phe)	33	3 200 (9 500– < 2 000)

[a]Percentages retained by the dialysis sac were determined as noted in Table 3.
[b]Measured by gel filtration of the unblocked polypeptide on Sephadex G-100 in 0.002 *M* sodium phosphate, 0.05 *M* sodium chloride, p*H* 7.0 (10, 11). Ribonuclease, chymotrypsinogen, and ovalubumin were used as standards. Molecular weights were unaffected by increasing the sodium chloride concentration to 0.15 *M*. The molecular weight was taken as mid-point of a spot detected on paper replica by trinitrobenzenesulfonic acid – borate buffer treatment. Ranges are given in parentheses.
[c]Dialysis was done using Spectrapor 3 (3500 mw cutoff).

isolated by dialysis against dilute acetic acid (Table 4) and stored as lyophilized powders in a desiccator.

Previous reports have described the preparation of a high molecular weight poly-(L-lys-L-phe) (25) via the tetrapeptide monomer but little experimental detail and no characterization of the monomer blocks was reported. In addition a poly-(L-lys-L-ala) sample has been synthesized earlier by an alternate approach (26).

Polypeptide Molecular Weights

Molecular weight determinations of the unblocked polymeric material obtained by dialysis were checked by gel filtration on Sephadex G-100 (10, 11) (Table 4). This allowed us to determine the molecular weight distribution of each of the polymers. It should be noted the values obtained for poly-(L-lys-L-val), poly-(L-lys-L-leu), and poly-(L-lys-L-phe) may not be truly representative of their actual molecular weights. It is possible that these hydrophobic polymers interact with the gel employed or adopt non-globular-like conformations and thus reduce their mobility relative to the globular standards employed. Either effect would lead to molecular weight values much lower than reality.

Circular Dichroic Spectra

Circular dichroic spectra have been used to investigate the conformation of polypeptides and proteins (27). Circular dichroic spectra of polypeptides in the various standard conformations are available (28–30) and comparison of these with the circular dichroic spectra of the sequential lysine-X polypeptides would indicate which, if any, of the standard conformations the synthetic polypeptides adopt.

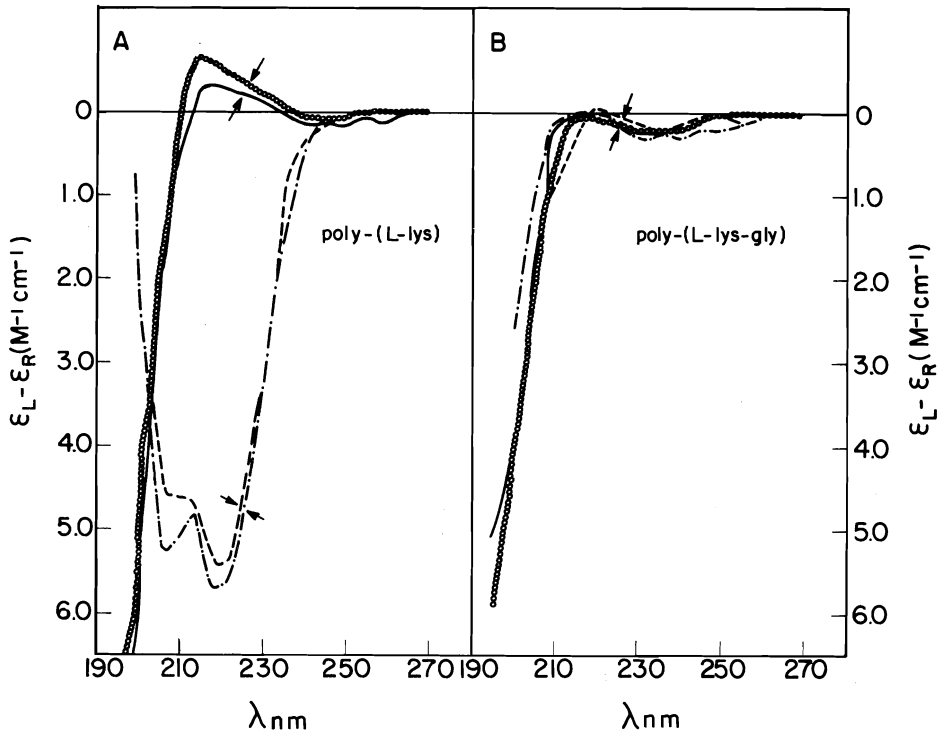

FIG. 1. Circular dichroic spectra of the unblocked poly-(L-lys) (A) and poly-(L-lysgly) (B) isolated by dialysis against dilute acetic acid (Spectrapor 1): (○) p*H* 7.0, 0.14 *M* KF; (—) p*H* 7.0, 1.0 *M* KF; (---) p*H* 12.0, 0.14 *M* KF; (-·-) p*H* 12.0, 1.0 *M* KF; arrows indicate wavelengths where ellipticities listed in Table 5 were taken.

Circular dichroic spectra under differing conditions of p*H* (7 and 12) and salt concentrations (0.14 and 1.0 *M*) have been taken of each of the polypeptides (Figs. 1–3). The ellipticities at specific wavelengths and based upon molar concentration of lysine are presented in Table 5.

The spectrum of poly-(L-lys) (Fig. 1A), at low and high salt (p*H* 7.0), is characteristic of an extended or disordered conformation (31–33) or 3_1 helix (34) and shows a slight decrease in ellipticity at 215 nm upon increasing the salt concentration from 0.14 to 1.0 *M* (35). When the p*H* of the solution was changed to 12 in order to neutralize the side chain charges, the poly-(L-lysine) conformation shifted to that of the α helix with the concomitant production of intense negative bands at 225 and 208 nm (36).

The conformation of poly-(L-lys-gly) (Fig. 1B) is one of a random coil over the complete salt and p*H* ranges examined. This is in accord with the poly-(L-lys-gly) synthesized from the dipeptide monomer and reported earlier (8). Thus poly-(L-lys-gly) would appear to be very flexible, lacking the rigidity observed in poly-(L-lys).

The spectrum of poly-(L-lys-L-ala) (Fig. 2A) at low salt and neutral p*H* is essentially the same as that seen for poly-(L-lys) (Fig. 1A). At neutral p*H* and high salt the poly-(L-lys-L-ala) polymer shows a slight tendency towards α-helix formation or random coil formation (34) either of which may be attributed to a greater charge separation making the electrostatic shielding of the salt more effective than that observed with poly-(L-lys). At p*H* 12 where the side chain charges are neutralized, poly-(L-lys-L-ala) adopts the typical α-helical conformation with the maximum ellipticities centered at 220 and 208 nm. Changing the salt concentration from 0.14 to 1.0 *M* at this p*H* had no effect. This conformational assignment is consistent with optical rotatory dispersion studies reported for poly-(L-lys-L-ala) of similar size (26) and closely resembles a series of poly-(L-lys-L-ala) random copolymers (37). Poly-(L-lys-L-ala-L-ala) (38) and poly-(L-lys-L-ala-L-ala-L-ala) (39, 40) show de-

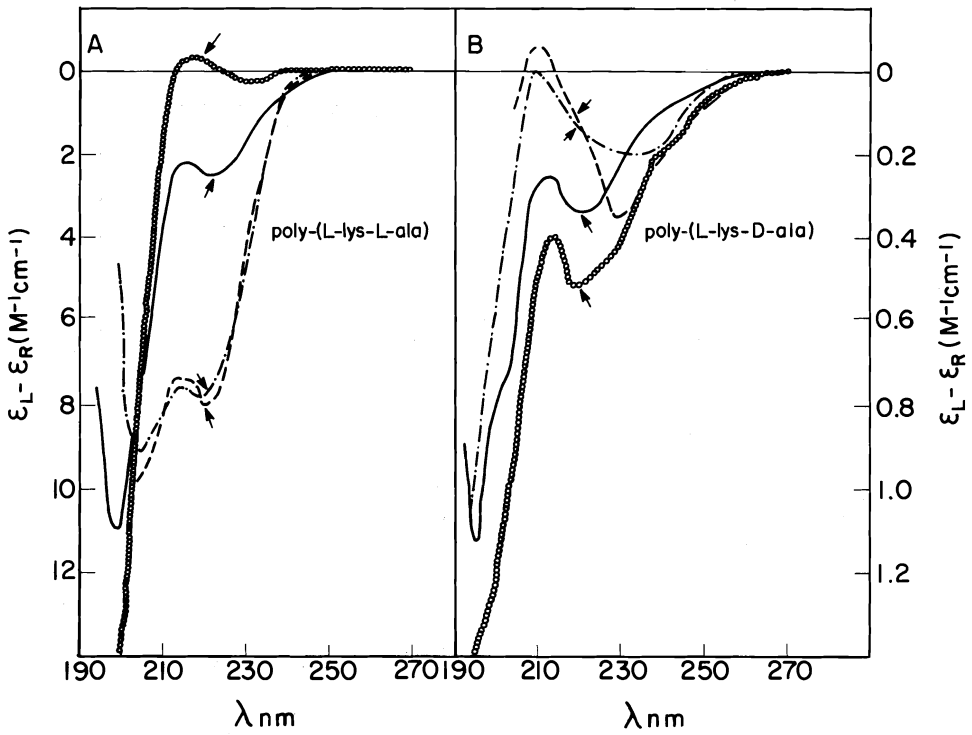

FIG. 2. Circular dichroic spectra of the unblocked poly-(L-lys-L-ala) (A) and poly-(L-lys-D-ala) (B) isolated by dialysis against dilute acetic acid (Spectrapor 1); symbols and details as in Fig. 1.

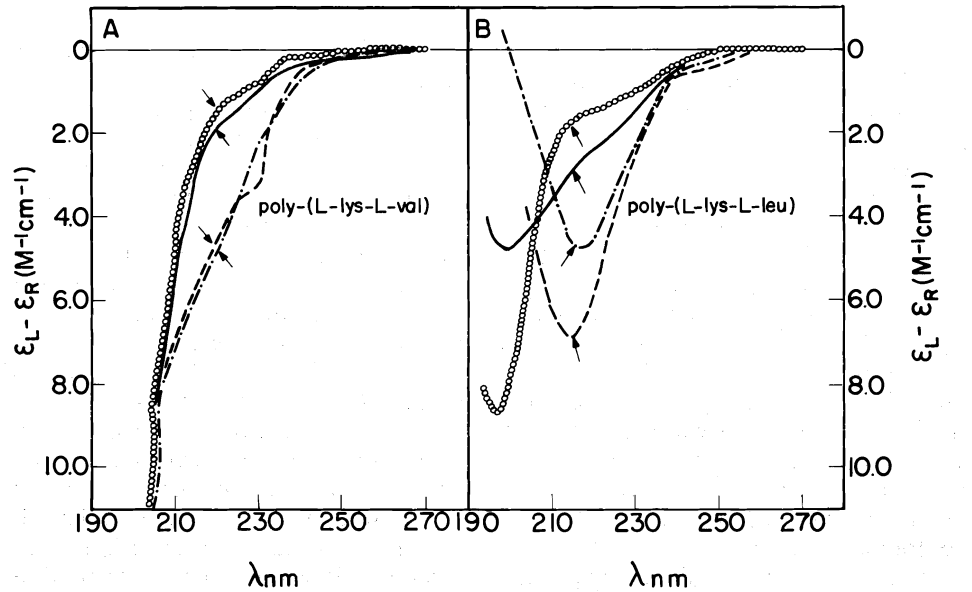

FIG. 3. Circular dichroic spectra of the unblocked poly-(L-lys-L-val) (A) and poly-(L-lys-L-leu) (B) isolated by dialysis against dilute acetic acid (Spectrapor 3 and Spectrapor 1 respectively); symbols and details as in Fig. 1.

TABLE 5. Circular dichroic ellipticities

		$\varepsilon_L - \varepsilon_R$[a]			
		0.14 *M* KF		1.0 *M* KF	
	λ (nm)	p*H* 7	p*H* 12	p*H* 7	p*H* 12.0
Poly-(L-lys)	225	+0.34	−4.90	+0.25	−5.17
Poly-(L-lys-gly)	225	−0.19	−0.13	−0.19	−0.13
Poly-(L-lys-L-ala)	220	+0.05	−8.34	−2.95	−8.18
Poly-(L-lys-D-ala)	220	−0.53	−0.18	−0.34	−0.18
Poly-(L-lys-L-val)	220	−1.48	−4.68	−1.91	−4.56
Poly-(L-lys-L-leu)	215	−1.67	−7.01	−2.95	−4.70
Poly-(L-lys-L-phe)	220	+1.31	−1.44	+0.50	−0.15

[a]The calculations of $\Delta\varepsilon$ ($\varepsilon_L - \varepsilon_R$) are based upon the number of moles of lysine in solution (approximately 2–4 × 10^{-3} *M*) as determined by hydrolysis and amino acid analysis. Spectra were first taken at p*H* 7 in Tris-HCl buffer, 0.01 *M*, at the salt concentrations noted. The solutions were then adjusted to p*H* 12 with concentrated sodium hydroxide (1 *N*) and the spectra measured. All polymeric materials used were obtained by dialysis of the unblocked polypeptides against dilute acetic acid.

finite tendencies towards α-helical conformations in conditions of low salt and neutral p*H* but this may be attributed to a more effective separation of positive charge than is possible with poly-(L-lys-L-ala).

The spectrum of poly-(L-lys-D-ala) (Fig. 2B) suggests that the polymer exists in a random coil conformation under all the salt and p*H* ranges examined. This is similar to that obtained for poly-(L-lys-gly) (Fig. 1B) and, thus, indicates this polypeptide is very flexible. There does appear to be a bathochromic shift of the negative band at 220 nm to 230 nm upon increasing the p*H* from 7.0 to 12.0 which is not seen in the poly-(L-lys-gly) spectrum. However, structural assignments based upon completely L-amino acid systems as references may not be applicable and final conclusions as to the solution conformation of poly-(L-lys-D-ala) must await further examination of more relevant models.

Poly-(L-lys-L-val) (Fig. 3A) is predominantly in a random coil conformation at low and high salt at neutral p*H*. Increasing the p*H* from 7.0 to 12.0 increases the ellipticity at 220 nm (Table 5), suggestive of a slight contribution from a β-like conformation.

Poly-(L-lys-L-leu) (Fig. 3B) is predominantly in a random coil conformation at low salt and neutral p*H*. Increasing the salt concentration did not affect the cd significantly but at p*H* 12 (low and high salt) the spectrum was characteristic of a β-structure. Random copolymers of poly-(L-lys-L-leu) show a similar tendency towards random coil conformation at low salt and neutral p*H* with the transition to a β-structure as the p*H* is raised (41, 42). However, in a series of random copolymers where the mole fraction of L-leucine went from 0 to 0.41, there was an apparent transition to α-helical conformation upon raising the p*H* above 9.8 at low salt (41).

At p*H* 12.0 and 0.14 *M* KF the spectrum of poly-(L-lys-L-phe) (Fig. 4) resembles that generated by a polypeptide adopting a β-structure and is similar in shape but weaker in intensity to that

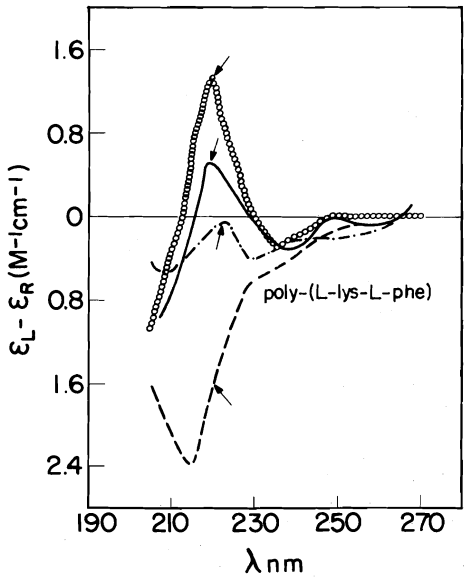

FIG. 4. Circular dichroic spectra of the unblocked poly-(L-lys-L-phe) isolated by dialysis against dilute acetic acid (Spectrapor 1); symbols and details as in Fig. 1.

reported by Seipke *et al.* (25). At neutral p*H* and 0.14 or 1.0 *M* salt the spectrum shows a slightly positive ellipticity centered at 220 nm which is in direct contrast to the reported cd spectrum of the Seipke copolymer in which a slightly negative ellipticity is evident at 225 nm. The spectrum recorded here (Fig. 4) more closely resembles the reported cd of a 1:1 random poly-(lys,phe) (43, 44). It is possible that the spectral differences among the various polypeptide preparations arise from a considerable difference in apparent molecular weights (70 000 vs. 3200), a phenomena which has been previously observed in the cd spectra of poly L-lysines of varying sizes (45). Although the spectrum resembles that generated by a β-structured polypeptide the assignment of one of the standard secondary conformations based upon the spectral appearance in the 215–220 nm region becomes quite difficult due to the contribution of the π–π^* transition of the phenylalanine chromphore (46).

Acknowledgements

The authors wish to express their thanks to M. Hector Seguin for the elemental microanalyses and to Miss Sandra Kielland and Mlle Marie Larue (NRCC Summer Student 1976) for their expert technical assistance.

1. R. J. DELANGE and E. L. SMITH. Ann. Rev. Biochem. **40**, 279 (1971).
2. N. C. SEEMAN, J. M. ROSENBERG, and A. RICH. Proc. Natl. Acad. Sci. USA, **73**, 804 (1976).
3. D. E. OLINS, A. L. OLINS, and P. H. VON HIPPEL. J. Mol. Biol. **24**, 157 (1967).
4. M. TSUBOI. *In* Conformation of biopolymers. Vol. 2. *Edited by* G. N. Ramachandran. Academic Press, New York, NY. 1967. p. 689.
5. K. WEHLING, H.-A. ARFMANN, K.-H. C. STANDKE, and K. G. WAGNER. Nucleic Acids Res. **2**, 799 (1975).
6. P. H. VON HIPPEL and J. D. MCGHEE. Ann. Rev. Biochem. **41**, 231 (1972) and references therein.
7. K. G. WAGNER and H.-A. ARFMANN. Eur. J. Biochem. **46**, 27 (1974) and references therein.
8. J. BROWN, J. R. LANGOIS, D. R. LAUREN, B. K. STOCHNOFF, and R. E. WILLIAMS. Can. J. Chem. **52**, 3140 (1974).
9. M. F. GILLEN and R. E. WILLIAMS. Can. J. Chem. **53**, 2351 (1975).
10. B. RADOLA. J. Chromatogr. **38**, 61 (1968).
11. B. G. JOHANSSON. *In* New techniques in amino acids peptide and protein analysis. *Edited by* A. Niederwieser and G. Pataki. Ann Arbor Science Publishers, Ann Arbor, MI. 1971. p. 249.
12. C. WILSON, R. F. KIBLER, and R. SHAPIRA. Anal. Biochem. **35**, 371 (1970).
13. R. A. BOISSONAS, S. GUTTMAN, R. L. HUGUENIN, P. A. JAQUENOD, and E. SANDRIN. Helv. Chim. Acta, **41**, 1867 (1958).
14. M. SELA and A. BERGER. J. Am. Chem. Soc. **77**, 1893 (1955).
15. J. P. GREENSTEIN and M. WINITZ. Chemistry of the amino acids. J. Wiley, New York, NY. 1961. p. 1245.
16. E. KATCHALSKI. *In* Methods in enzymology. Vol. 3. *Edited by* S. P. Colowick and N. O. Kaplan. Academic Press, New York, NY. 1957. p. 540.
17. G. W. ANDERSON, J. E. ZIMMERMAN, and F. M. CALLAHAN. J. Am. Chem. Soc. **86**, 1839 (1964).
18. J. E. ZIMMERMAN and G. W. ANDERSON. J. Am. Chem. Soc. **89**, 7151 (1967).
19. N. IZUMIYA, M. MURAKO, and H. AOYAGI. Bull. Chem. Soc. Jpn. **44**, 3391 (1971).
20. B. B. DOYLE, W. TRAUB, G. P. LORENZI, F. R. BROWN III, and E. R. BLOUT. J. Mol. Biol. **51**, 47 (1970).
21. G. P. LORENZI, B. B. DOYLE, and E. R. BLOUT. Biochemistry, **10**, 3046 (1971).
22. M. FRIDKIN, A. FRENKEL, and S. ARIELY. Biopolymers, **8**, 661 (1969).
23. G. RAMACHANDRAN, A. BERGER, and E. KATCHALSKI. Biopolymers, **10**, 1829 (1971).
24. V. A. SHIBNEV, T. P. CHUVAEVA, and K. T. POROSHIN. Izv. Akad. Nauk. SSR Ser. Khim. 121 (1970).
25. G. SEIPKE, H-A. ARFMANN, and K. G. WAGNER. Biopolymers, **13**, 1621 (1974).
26. G. SPACH, A. BRACK, and F. HEITZ. C.R. Acad. Sci. **265**, 19 (1967).
27. (*a*) I. TINOCO, JR. and C. R. CANTOR. *In* Methods of biochemical analysis. *Edited by* D. Glick. Wiley-Interscience, New York, NY. 1970. p. 81; (*b*) S. BEYCOCK. *In* Poly α-aminoacids. *Edited by* G. D. Fasman. M. Dekker, New York, NY. 1967. p. 293.
28. G. HOLZWORTH and P. DOTY. J. Am. Chem. Soc. **87**, 218 (1965).
29. G. D. FASMAN and J. POTTER. Biochem. Biophys. Res. Commun. **27**, 209 (1967).
30. W. B. GRATZER and D. A. COUBURN. Nature, **222**, 426 (1969).
31. D. G. DEARBORN and D. B. WETLAUFER. Biochem. Biophys. Res. Commun. **39**, 314 (1970).
32. M. L. TIFFANY and S. KRIMM. Biopolymers, **6**, 1379 (1968).
33. M. L. TIFFANY and S. KRIMM. Biopolymers, **8**, 347 (1969).
34. W. B. RIPPON and R. LAM. Int. J. Polym. Mater. **4**, 25 (1975).
35. M. L. TIFFANY. Physiol. Chem. Phys. **7**, 191 (1975).
36. Y. P. MEYER. Macromolecules, **2**, 624 (1969).
37. S. STOKROVA, J. SPONAR, M. HAVRANEK, B. SEDLACEK, and K. BLAHA. Biopolymers, **14**, 1231 (1975).
38. A. YARON, N. TAL (TURKELTAUB), and A. BERGER. Biopolymers, **11**, 2461 (1972).
39. D. B. WENDER, L. R. TREIBER, H. B. BENSUSAN, and A. G. WALTON. Biopolymers, **13**, 1929 (1974).
40. L. I. MAR'YASH, L. V. ABATUROV, and V. A. SHIBNEV. Stud. Biophys. **43**, 41 (1974).
41. C. R. SNELL and G. D. FASMAN. Biopolymers, **11**, 1723 (1972).
42. C. R. SNELL and G. D. FASMAN. Biochemistry, **12**, 1017 (1973).
43. E. PEGGION, A. S. VERDINI, A. COSANI, and E. SCOFFONE. Macromolecules, **3**, 194 (1970).
44. E. PEGGION, A. COSANI, M. TERBOJEVICH, and G. BORIN. Biopolymers, **11**, 633 (1972).
45. D. CARROLL. Biochemistry, **11**, 421 (1972).
46. J. DONOVAN. *In* Physical principles and techniques of protein chemistry. *Edited by* S. Leach. Academic Press, New York, NY. 1969. p. 109.

Erratum: An acidity function based on thiocarbonyl indicators

JOHN T. EDWARD, IVAN LANTOS, GARY D. DERDALL, AND SIN CHEONG WONG

Department of Chemistry, McGill University, Montreal, P.Q., Canada H3C 3G1

Received October 17, 1977

(Ref.: Can. J. Chem. **55**, 812 (1977))

Indicator No. 2 in Table 1 is incorrectly identified in the table, in line 3 of the Experimental section, and in the legend of Fig. 2. The compound used was 4,5-dimethyl-4-imidazoline-2-thione.